 © 1986 The Chemical Society of Japan Bull. Chem. Soc. Jpn., 59, 1—5 (1986)

The Cyclodextrin-Quinone Inclusion Compounds in an Aqueous Solution at 77 K. II. 9,10-Phenanthrenequinone and Acenaphthenequinone

Akira KUBOYAMA* and Sanae Y. MATSUZAKI
National Chemical Laboratory for Industry, Tsukuba Research Center,
Yatabe, Ibaraki 305
(Received February 23, 1985)

A complex formation between cyclodextrins (CD's) and the two *o*-quinones (9,10-phenanthrenequinone (PHQ) and acenaphthenequinone (ANQ)) in a water-ethylene glycol 1:1 mixture glassy solution at 77 K was investigated using the nπ* phosphorescence spectra of these quinones. It was considered on the basis of the observed results that PHQ forms a 1:1 complex with γ-CD and ANQ a 2:1 complex with β-CD. The structures of these complexes are discussed. It was found that complexes between γ-CD and the PHQ- and ANQ-naphthalene charge-transfer complexes are also formed.

Previously. we studied the complex formation[1] between CD's and the *p*-quinones (9,10-anthraquinonesulfonates and 1,4-naphthoquinones) in an aqueous solution at 77 K, using the nπ* phosphorescence spectra of the quinones.[2] *o*-Quinones show various characteristic organic reactions like *p*-quinones. The CD-*o*-quinone complex formation may play an important role in some of these reactions. Previously, we studied the nπ* phosphorescence spectra of the *o*-quinones,[3] 9,10-phenanthrenequinone (PHQ) and acenaphthenequinone (ANQ) in organic solvents at 77 K. These spectra are sensitive to the environment around the α-dicarbonyl groups and are thought to be useful in an investigation of complex formations between CD's and the quinones.

In this work complex formations between CD's and these *o*-quinones were investigated under the same conditions as those used in the previous work.[1] Naphthalene (NA), an electron-donor to the quinones was also used as a third component.[4] Heretofore, only one study[4a] of the complex formation between CD's and a charge-transfer complex has ever, to our knowledge, been reported.

Experimental

Measurements. The phosphorescence spectra, their excitation spectra and lifetimes were obtained using an Aminco 500 spectrofluorophotometer equipped with a phosphoroscope and a photon counter (PM tube 1P28) at 77 K.[2] The solvent of the water-ethylene glycol 1:1 mixture (H_2O-EG) which forms a glassy state at 77 K was mainly used. Two cooling-speeds of the sample solutions (fast and slow) were used.[2]

Materials. PHQ and ANQ were purchased from Tokyo Kasei Kogyo Co. PHQ and ANQ were purified by the zone-melting method and vacuum sublimation, respectively (mp 209.5—210.5 °C and 262 °C). Scintillation grade NA of Merk Co., α-, β-, and γ-CD of Tokyo Kasei Kogyo Co., nonfluorescent water of Dojin Yakukagaku Kogyo Co., ethylene glycol especially prepared for chromatography by Nakarai Chemical Co., spectrograde hexane of Tokyo Kasei Kogyo Co., spectrograde heptane of Dojin Yakukagaku Kogyo Co., and analytical grade 1-chlorobutane of Nakarai Chemical Co. were used without further purification.

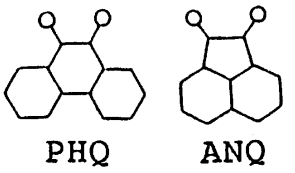

Fig. 1. PHQ and ANQ.

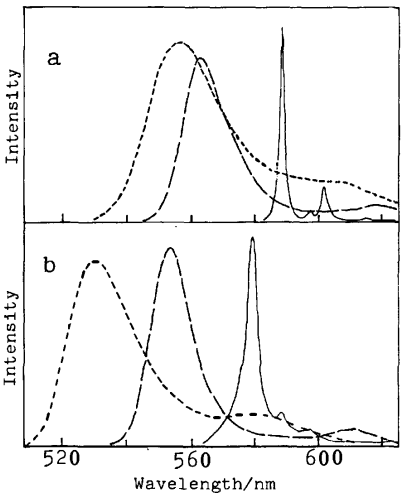

Fig. 2. Phosphorescence spectra of the *o*-quinones in solutions at 77 K.
a: 9,10-phenanthrenequinone, b: acenaphthenequinone, ——: heptane (a), hexane (b), — —: 1-chlorobutane, ----: H_2O-EG. The concentrations of the quinones in the solutions are all lower than 3×10^{-4} M (In all the figure captions M denotes mol dm^{-3}). In Fig. 2—7 all the solutions used are of the fast-cooling unless otherwise described. In Fig. 2—6 the phosphorescence spectra of 9,10-phenanthrenequinone and acenaphthenequinone were obtained at the 420 and 312 nm excitation, respectively, unless otherwise described.

Results and Discussion

As is seen in Fig. 2, the phosphorescence spectra of PHQ and ANQ are observable in an H_2O–EG solution at 77 K, but the phosphorescence intensity of PHQ is very weak. The phosphorescence spectra of these quinones may be assigned to the $n\pi^*$ spectra, as they clearly show a CO-stretching vibrational structure alone. Also, their observed lifetimes[5] are short. From these spectra, no spectral changes can be observed under the irradiation of the exciting light, and no concentration dependence can be observed.

A *b*-shift in the spectrum of the 1-chlorobutane solution compared with that in the normal paraffin solution is ca. 790 and 830 cm^{-1} in PHQ and ANQ, respectively. The shift in the H_2O–EG solution is ca. 990 and 1620 cm^{-1} in PHQ and ANQ, respectively (Table 1). This difference in the *b*-shift between PHQ and ANQ in the H_2O–EG solution can be explained as follows. The large *b*-shift in ANQ is due to the formation of a strong hydrogen bond between ANQ and water. On the other hand, the *b*-shift in PHQ indicates that the phosphorescence is due to the PHQ molecules forming a hydrogen bond with ethylene glycol. This bond is weaker than that between PHQ and water. The PHQ molecules forming the hydrogen bond with water show no phosphorescence because their T_1 state is $\pi\pi^*$, in contrast to that of the former.[5,6] The weakness of phosphorescence of PHQ in the H_2O–EG solution is perhaps due to the proportion of the PHQ molecules forming the hydrogen bond with ethylene glycol, being far smaller than that of the PHQ molecules forming the hydrogen bond with water. The phosphorescence spectra of these quinones show no change in the presence of α-CD.

In PHQ, a spectral change can be observed only in the presence of γ-CD. As is seen in Fig. 3, the broad 0-0 peak of the phosphorescence spectrum of the γ-CD complex shifts to the red by 180 cm^{-1} in comparison with that of the free PHQ molecules, and the second peak which is sharper than the 0-0 peak is

Table 1. Peak Wavelengths, λ, of the Phosphorescence Spectra

	Solvent	λ/nm
PHQ	Hexane	588.5, 602
	1-Chlorobutane	562.5
	H_2O–EG	556
(+γ-CD)[a]	H_2O–EG	562.5, 578
(+γ-CD+NA)[a]	H_2O–EG	573
ANQ	Heptane	579
	1-Chlorobutane	552.5
	H_2O–EG	529.5
(+β-CD)[a]	H_2O–EG	553, 571
(+γ-CD+NA)[a]	H_2O–EG	544, 548, ≈551, 561.5

a) For example, (+γ-CD) denotes the solution containing γ-CD. NA denotes naphthalene.

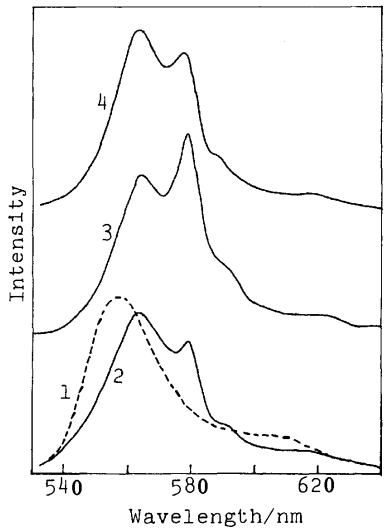

Fig. 3. Phosphorescence spectra of 9,10-phenanthrenequinone in the H_2O–EG solutions containing γ-CD at 77 K.
1: 2.4×10^{-4} M, 2: 1.2×10^{-4} M + γ-CD(1.9×10^{-3} M), 3 and 4: 2.4×10^{-4} M + γ-CD(3.7×10^{-3} M) (4:sector-speed slow).

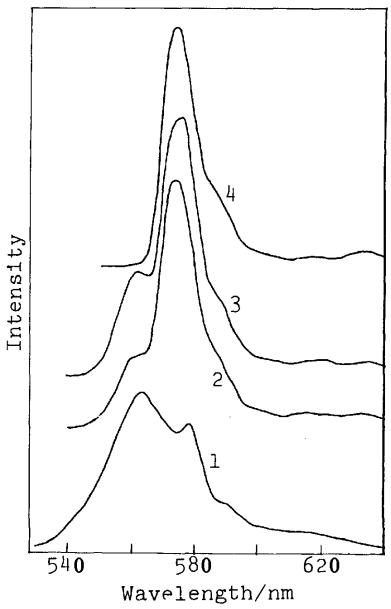

Fig. 4. Phosphorescence spectra of 9,10-phenanthrenequinone in the H_2O–EG solutions containing γ-CD and naphthalene at 77 K.
1: 1.2×10^{-4} M + γ-CD(1.9×10^{-3} M), 2 and 3: 8.6×10^{-5} M + γ-CD(1.3×10^{-3} M) + NA (5.8×10^{-5} M) (3: sector-speed slow), 4: 8.6×10^{-5} M + γ-CD(1.3×10^{-3} M) + NA(3.3×10^{-4} M) (In Fig. 4 and 6 NA denotes naphthalene).

observed at wavelengths longer by 450 cm^{-1} than the 0-0 peak. The relative intensity of the second peak to the 0-0 peak decreases with a decrease in the sector speed of the phosphoroscope. It increases a little in slow cooling compared to that with fast cooling. Furthermore, the relative intensity of the second peak increases considerably with a twofold increase in the concentration of both PHQ an γ-CD. From these results, the 0-0 and the second peak are thought to be due to a complex in the solution and a crystalline phase, respectively. The above-mentioned r-shift of the phosphorescence 0-0 peak of the complexes in comparison with that of the free PHQ molecules may be due to the weakening or destruction of the hydrogen bond between PHQ and ethylene glycol.

As is seen in Fig. 4, in the presence of γ-CD and NA, PHQ shows a relatively sharp phosphorescence 0-0 peak at wavelengths longer by 340 cm^{-1} than the above-mentioned 0-0 peak of the γ-CD–PHQ complex. This r-shift and sharpening of the spectrum is thought to be due to the formation of a complex between γ-CD and the PHQ–NA charge-transfer complex and may indicate a weakening of the beforementioned hydrogen bond between PHQ and ethylene glycol or γ-CD in the presence of NA. The intensity of this phosphorescence is considerably stronger than that of the γ-CD–PHQ complex, and its observed lifetime (4.7 ms) is close to that (5.5 ms)[3] of PHQ in the hexane solution. It is considerably shorter than that of the free PHQ molecules.[5]

In ANQ, as is seen in Fig. 5a, the phosphorescence spectrum shifts to the red by ca. 800 cm^{-1} and becomes sharper in the presence of β-CD, while in the presence of γ-CD, as is seen in the spectrum 1 of Fig. 6, a weak shoulder appears at almost the same position as the spectrum observed in the presence of β-CD in the phosphorescence spectrum of the free ANQ molecules. The large r-shift of the spectrum in the presence of β-CD might indicate that the beforementioned strong hydrogen bond between ANQ and water is considerably weakened or destroyed due to the complex formation. The observed phosphorescence lifetime (17 ms) is considerably shorter than that (26 ms) of the free ANQ molecules.[5,7]

As is seen in Fig. 5a, in the presence of β-CD the phosphorescence spectrum of the free ANQ molecules and a weak shoulder which is at wavelengths longer by ca. 570 cm^{-1} than the strong 0-0 peak of the complex appear clearly in fast cooling. From a comparison between the spectra in Fig. 5a and 5b it can be seen that the relative intensity of the phosphorescence spectrum of the complex to that of the free ANQ molecules is far weaker in the low-concentration solution of β-CD than that in the high-concentration solution. In the low-concentration solution it is considerably stronger in slow cooling than in fast cooling. Though in the low-

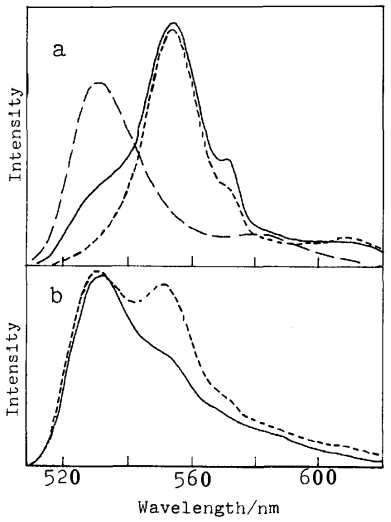

Fig. 5. Phosphorescence spectra of acenaphthenequinone in the H_2O–EG solutions containing β-CD at 77 K.
(a) ——: 7.4×10^{-5} M, ---- and ——: 7.4×10^{-5} M $+\beta$-CD(2.0×10^{-3} M)(----: slow cooling), (b) ---- and ——: 7.4×10^{-5} M$+\beta$-CD (6.7×10^{-4} M) (----: slow cooling).

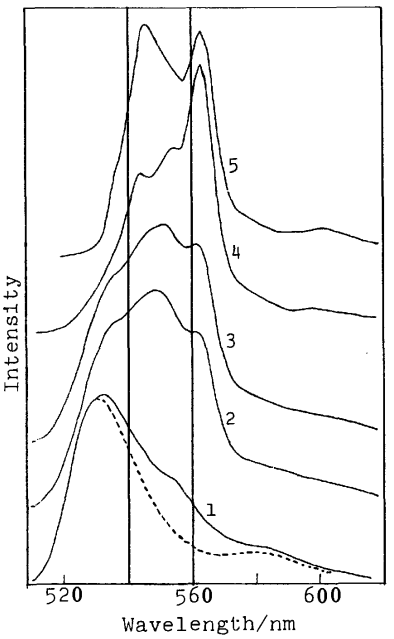

Fig. 6. Phosphorescence spectra of acenaphthenequinone in the H_2O–EG solutions containing γ-CD and naphthalene at 77 K at the 330 nm excitation.
1: 1.0×10^{-4} M$+\gamma$-CD(1.9×10^{-3} M), 2: 6.7×10^{-5} M $+\gamma$-CD (1.2×10^{-3} M)+NA (6.7×10^{-5} M), 3: 9.8×10^{-5} M$+\gamma$-CD(1.8×10^{-3} M)+NA(9.5×10^{-5} M), 4: 6.1×10^{-5} M$+\gamma$-CD(1.5×10^{-3} M)+NA(3.3×10^{-4} M), 5: 1.0×10^{-4} M$+\gamma$-CD(1.9×10^{-3} M)+NA(2.0×10^{-3} M). The dotted line spectrum is the same as the broken line spectrum in Fig. 5a.

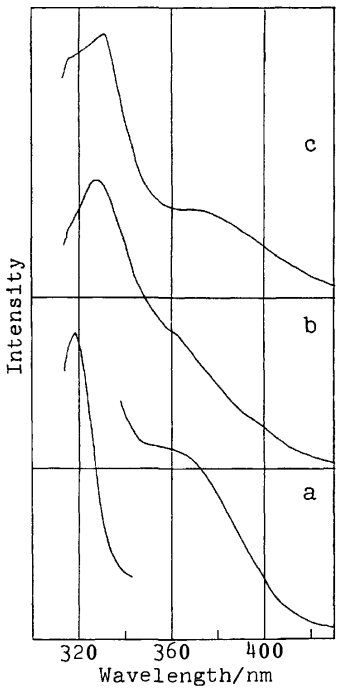

Fig. 7. Phosphorescence excitation spectra of acenaphthenequinone in the H_2O–EG solutions containing γ-CD and naphthalene at 77 K.
The solution used for the spectrum a is the same as that for the broken line spectrum in Fig. 5a, and the solution used for the spectrum b and c is the same as that for the spectrum 5 in Fig. 6. Monitoring wavelength: a 529 nm, b 561.5 nm, c 544 nm.

concentration solution the concentration of β-CD is three times lower than that in the high-concentration solution, the concentration of β-CD is one order higher than that of ANQ. On the other hand, no similar concentration-dependent features can be observed in the γ-CD–PHQ complex. These results suggest that the β-CD to ANQ ratio in the complex is not one-to-one but probably two-to-one, while that in the γ-CD–PHQ complex is one-to-one.

In the solution in which the concentrations of ANQ and β-CD are both about two times higher than those in the solution used for the solid-line spectrum in Fig. 5a, the relative intensity of the before-mentioned long-wavelength shoulder to the 0-0 peak of the complex in the spectrum obtained is close to that in the above-mentioned spectrum, contrary to the case of the γ-CD–PHQ system. In view of this result and the before-mentioned cooling-speed dependence of that relative intensity, the long-wavelength shoulder might not be due to the β-CD–ANQ complex in a crystalline phase but due to that in the solution, the structure of which is different from that of the complex showing the strong 0-0 peak, and in which the α-dicarbonyl group of ANQ is in more hydrophobic circumstances than that in the latter complex.

In the presence of NA, no shift in the phosphorescence spectrum of the β-CD–ANQ complex occurs, but the relative intensity of the phosphorescence spectrum of the free ANQ molecules to that of the complex markedly increases in the presence of NA. This result may be due to a decrease in the concentration of β-CD to form the complex with ANQ, resulting from a complex formation between β-CD and NA.[8] As is mentioned before, ANQ shows only a slight spectral change in the presence of γ-CD, while marked spectral changes are observed in the presence of NA in addition to that of γ-CD, as is seen in Fig. 6. These spectral changes are thought to be due to a complex formation between γ-CD and the quinone–NA charge-transfer complex. In the spectrum 2 two new peaks (one broad and one sharp peak) appear at 548 and 561.5 nm, respectively, in comparison with the spectrum 1. In the spectrum 3 and 4, another broad peak appears at ca. 551 nm. In the spectrum 4 and 5, a sharp peak appears at 544 nm. From a comparison between the spectra 2—5, it is thought that there are two kinds of the complexes, and that one of them shows the broad and the sharp peak at 548 and 561.5 nm in the solution and the crystalline phase, respectively, and the other one shows the broad and the sharp peak at ca. 551 and 544 nm in the solution and the crystalline phase, respectively. The latter complex is thought to be formed in the solutions containing NA in high concentrations, compared with the former complex. In the two excitation spectra of the above-mentioned two sharp peaks at 544 and 561.5 nm in Fig. 7, the two $\pi\pi^*$ absorption peaks at 328 and 325 nm, respectively, are at considerably longer wavelengths than that of the free ANQ molecules at 317 nm. This is thought to be due to a charge-transfer interaction between ANQ and NA in the γ-CD complexes.

As is mentioned before, since the phosphorescence spectra of the γ-CD–PHQ and β-CD–ANQ complex in the solution are at considerably shorter wavelengths and are far broader than those of these quinones in the normal paraffin solutions, the two α-dicarbonyl groups of these quinones in the complexes are thought not to be mostly in the hydrophobic cavity of the CD's; in other words, these complexes do not take the equatorial form.[9] This is reasonable in view of the α-dicarbonyl groups being hydrophilic. In view of the dimensions (ca. 11.6 and ca. 9.1 Å, respectively) of PHQ[10] and ANQ[11] along the direction perpendicular to the symmetry axis, the γ-CD–PHQ and β-CD–ANQ complexes cannot also take the axial form.[9,12] In these complexes the CD molecules are thought to partly cover the hydrophobic parts of the PHQ and ANQ molecules. In the complexes between γ-CD and the quinone–NA charge-transfer complexes also, the γ-CD molecules

are thought to partly cover the hydrophobic parts of the charge-transfer complexes.

References

1) A. Kuboyama and S. Y. Matsuzaki, *J. Inclusion Phenomena*, **2**, 755 (1984).

2) A. Kuboyama and S. Yabe, *Bull. Chem. Soc. Jpn.*, **40**, 2475 (1967); A. Kuboyama, ibid., **43**, 3373 (1970); **51**, 2771 (1978); A. Kuboyama and S. Y. Matsuzaki, ibid., **58**, 73 (1985).

3) A. Kuboyama and M. Anze, *Nippon Kagaku Kaishi*, **1972**, 229; A. Kuboyama and S. Matsuzaki, ibid., **1973**, 2249.

4) a) N. Kobayashi, A. Ueno, and T. Osa, *J. Chem. Soc., Chem. Commun.*, **1981**, 340; b) A. Ueno, K. Takahashi, Y. Mino, and T. Osa, ibid., **1981**, 194; K. Kano, I. Takenoshita, and T. Ogawa, *Chem. Lett.*, **1980**, 1035; *J. Phys. Chem.*, **86**, 1833 (1982); H. Kobashi, M. Takahashi, Y. Muramatsu, and T. Morita, *Bull. Chem. Soc. Jpn.*, **54**, 2815 (1981).

5) The observed phosphorescence lifetime (26 ms) of ANQ is considerably longer than those (12.5—15.5 ms) in organic solvents.[3] This may be due to a increase in the mixing of the close-lying $\pi\pi^*$ state with the phosphorescent $n\pi^*$ state accompanying with a decrease in the energy separation between the two states resulting from the strong hydrogen-bond formation between ANQ and water.[2,6] That of PHQ could not be accurately obtained because of the weakness of the phosphorescence intensity, but it was estimated to be close to those (8.7 and 8.3 ms respectively) in the ethanol and dioxane solutions from the correlation between the phosphorescence intensity and the sector-speed of the phosphoroscope.

6) A. Kuboyama and S. Y. Matsuzaki, *Bull. Chem. Soc. Jpn.*, **54**, 3635 (1981); *J. Nat. Chem. Lab. for Ind.*, **78**, 21 (1983).

7) This result may be mainly due to a decrease in the mixing of the close-lying $\pi\pi^*$ state with the phosphorescent $n\pi^*$ state in ANQ in the complex formation.

8) K. Harata and H. Uedaira, *Bull. Chem. Soc. Jpn.*, **48**, 375 (1975); N. Kobayashi, Y. Hino, A. Ueno, and T. Osa, ibid., **56**, 1849 (1983).

9) The symmetry axes of the CD and quinone in these complexes are at right angles.[8] In the axial form these two symmetry axes are the same.

10) A. Kuboyama, F. Kobayashi, and S. Morokuma, *Bull. Chem. Soc. Jpn.*, **48**, 2145 (1975).

11) T. C. W. Mak and J. Trotter, *Acta Crystallogr.*, **16**, 811 (1963).

12) The cavity diameters of β-, and γ-CD are taken as about 7.0 and 8.5 Å, respectively, in this work (M. L. Bender and M. Komiyama, "Cyclodextrin Chemistry," Springer-Verlag, Berlin (1978)).

 © 1986 The Chemical Society of Japan Bull. Chem. Soc. Jpn., 59, 7—11 (1986)

Kinetic Study of Liquid-Phase Esterification with Sulfonic Acid Cation-Exchange Resin of the Macroreticular Type. I. Heterogeneous-Pseudohomogeneous Resin Catalysis[1)]

Shoichi SHIMIZU* and Choichiro HIRAI
Department of Industrial Chemistry, College of Industrial Technology, Nihon University, Izumi-cho, Narashino, Chiba 275
(Received May 25, 1985)

The rates of the esterification of octanoic acid with 1-butanol catalyzed by macroreticular sulfonated ion-exchange resin were measured by the use of a batch reactor. The effects on the rate were investigated for variations in the amount of the catalyst, the temperature, and the reactant alcohol concentrations as well as those of water and butyl octanoate. From these data, it is considered that alcohol and water solvate the matrix-bound sulfo groups, and so this esterification system consists of a heterogeneous reaction catalyzed by un-ionized sulfo groups and a pseudo-homogeneous reaction catalyzed by solvated protons; in other words, catalysis by sulfonic acid resin is both heterogeneous and pseudo-homogeneous in liquid-phase esterification.

In organic reactions catalyzed by acids or bases, the use of ion-exchange resins as catalysts offers the following advantages over that of homogeneous catalysts:[2-4)] (1) the resins are easily separated from the reaction mixture, (2) undesirable side reactions are frequently avoided, (3) resin catalysis can afford a degree of selectivity unattainable in homogeneous catalysis, (4) resins permit operation in either continuous or batch processes, and (5) corrosion is eliminated or reduced significantly. Therefore, experimental studies of the use of resin as catalysts have been carried out on many reactions. The major groups of these reactions are acetal-formation, dehydration, esterification, etherification, hydration, hydrolysis, and isomerization. The range of practical application of ion-exchange catalysts has, consequently, been extended. Theoretical problems in ion-exchange catalysis have also been discussed in several reviews.[5-7)]

The esterification of acids with alcohols, which is one of the most active areas for the application of resin catalysis, has usually been catalyzed by the use of a sulfonic acid cation-exchanger and has been carried out in both gas[8-10)] and liquid phases.[11-22)] Kinetic studies of the esterification have been reported in numerous reports on the reaction. In gas-phase esterification, it is known that the experimental data agree well with the estimate obtained by the use of a Langmuir-Hinshelwood model, which demonstrates that the resin catalysis is heterogeneous.[8,10)] In the case of liquid-phase esterification, several authors have preferred Helfferich's classical explanation[23)] based on a pseudo-homogeneous system assumption,[11,13-21)] although others have reported that the kinetics of heterogeneous catalytic reactions provide a satisfactory fit of the data.[12,21)] At present, there is no unified opinion about the liquid-phase catalysis with sulfonic acid resin, as has been mentioned above. Gates and his co-workers, however, pointed out that an excess of water or alcohol can shift the catalytic species from the more active undissociated sulfonic acid (general acid catalysis) to the less active solvated proton (specific acid catalysis), which was substantiated by a series of fundamentally important investigations of the dehydration of 2-methyl-2-propanol,[24)] olefin and paraffin formation from butyl alcohols,[25)] and benzene propylation.[26)] Recently, Gomzi et al.[21)] studied the kinetics of the esterification of acetic acid with 1-butanol catalyzed by sulfonic acid resin of the standard type; they reported that the best model for explaining the reaction rate with a partially wet ion-exchanger (27% water contents) is obtained by assuming a pseudo-homogeneous system, while the kinetics of a dry one is best represented by a model derived from assumptions based on a heterogeneous system. However, in the report of Gomzi et al.[21)] the catalytic species in these reactions were not mentioned at all.

In this work we have measured the kinetics of the esterification of octanoic acid with 1-butanol catalyzed by macroreticular sulfonic acid resin (Amberlyst 15) in order to clarify the catalysis by the resin in liquid-phase esterification. Furthermore, this work should help to elucidate the selectivity behavior of the resin catalyst in relation to the alkyl-chain length of normal fatty acids, which was reported in the preceding paper.[22)]

Experimental

Catalyst Preparation and Materials. A macroporous sulfonated copolymer of styrene and divinylbenzene was prepared from commercial ion-exchange resin, Amberlyst 15. The resin, 0.59—0.84 mm particles, was washed with distilled water and cycled between the hydrogen and sodium forms according to a conventional column method. The hydrogen-form resin to be used as a catalyst was dried in an oven at a temperature below 110 °C to 5.81% water and then stored in a desiccator in sealed vials over silica gel. The ion-exchange capacity was 4.99 meq/g of dry resin.

Guaranteed reagent-grade octanoic acid and butyl

octanoate were used without further purification. The toluene and 1-butanol were purified by distillation, and then the former was dried over anhydrous magnesium sulfate.

Reaction-Rate Measurement. The esterification with an ion-exchanger as a catalyst was usually measured at 80±0.05 °C in a 100-ml three-necked flask equipped with a magnetic stirrer (about 250 rpm) and a condenser, and heated in an oil bath. In all experiments, the volume of the reaction mixture, consisting of octanoic acid, 1-butanol, and toluene as a diluent, was kept constant at 30 ml. A timer was started on the addition of the catalyst to the reactor, and 40-μl samples were removed by using a microsyringe at appropriate time intervals and then transferred to individual capped microtubes containing a toluene solution of hexadecane as an internal standard. For gas-chromatographic (GC) analysis, samples of about 1—2 μl were taken from these microtubes. The only product detected, except water, was butyl octanoate. Therefore, the rates were determined from the ester analyses. The molar concentrations of the ester in each original sample were obtained by determining the ratio of the areas of the ester peaks to that of the hexadecane peak and by comparing these with the calibration curves.

The instrument used to carry out the GC analyses and the operating conditions were described in detail in an earlier paper.[22]

Results

Catalyst Amount and Temperature Dependence of Apparent Rate Constant. For determining the order of octanoic acid, the half-life periods were measured under the following conditions: initial concentration of 1-butanol, 7.29 mol dm^{-3}; amount of resin, 1.50 g. Figure 1 shows that the dependence of the rate on the concentration of acid is first-order under these experimental conditions. In addition, it is confirmed, by a comparison with the order obtained in the preceding study,[22] that the toluene used as a diluent does not affect the order. The rate of reaction is represented by

$$r = k'_{obsd}[F]. \quad (1)$$

As is shown in Fig. 2, the pseudo-first-order rate constants, k'_{obsd}, were directly proportional to the amount of the resin catalyst. Hence, the specific rate constant, k_{obsd}, was introduced

$$k_{obsd} = k'_{obsd}/M. \quad (2)$$

The logarithm of k_{obsd} vs. the reciprocal of the absolute temperature, that is, the Arrhenius-type plot, is shown in Fig. 3. As can be seen from the figure, a good straight line was obtained. From the slope of this line, an apparent activation energy of about 14 kcal† mol^{-1} was estimated; this is consistent with the finding of a previous work[22] that neither bulk diffusion nor pore diffusion is a limiting step.

Effects of Alcohol, Water, and Ester. The influence of the concentration of 1-butanol upon the reaction rate is shown in Fig. 4, while the cases of water and butyl octanoate instead of 1-butanol are represented in Figs. 5 and 6 respectively. Water inhibited the reaction, as is shown by the results of Fig. 5, but the ester did not affect the rate over the present range of experimental conditions. In all the

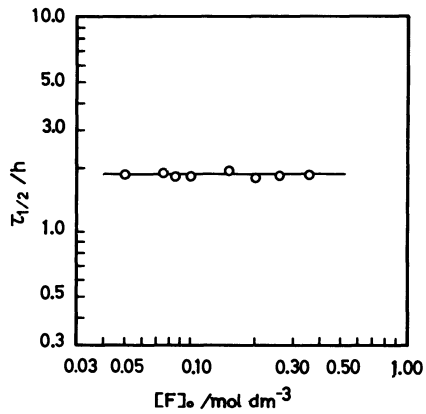

Fig. 1. Relationship between initial concentration of octanoic acid ($[F]_o$) and half life of esterification ($\tau_{1/2}$).

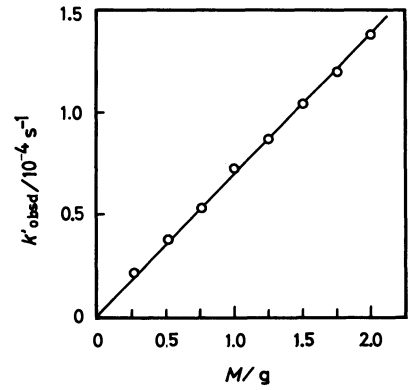

Fig. 2. Dependence of pseudo-first-order rate constant (k'_{obsd}) on amount of Amberlyst 15 (M).

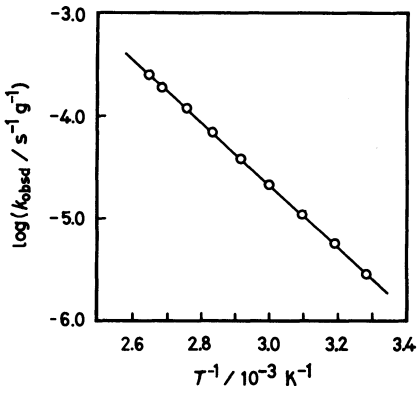

Fig. 3. Dependence of specific rate constant (k_{obsd}) on reaction temperature (T).

† 1 cal=4.184 J.

runs denoted in Figs. 4—6, the initial concentration of octanoic acid and the amount of resin were held constant at 0.150 mol dm^{-3} and 1.75 g respectively. The ester-concentration increments from 0.0200 to 0.0400 mol dm^{-3}, divided by the time required for the reaction progress, were set equal to the reaction rates for each solution composition at a conversion of 20% and were adopted as the kinetic data, since a short induction period appeared rarely and an initial reaction rate could not be employed.

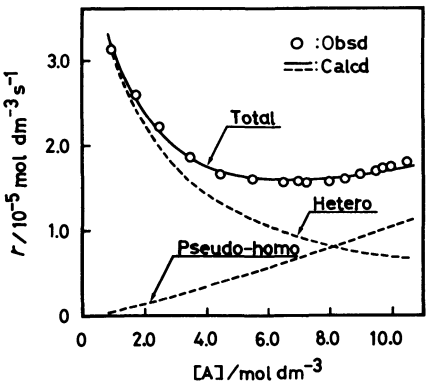

Fig. 4. Influence of concentration of 1-butanol ([A]) upon reaction rate (r).
[F]=0.120 mol dm^{-3}, [W]=0.030 mol dm^{-3}.

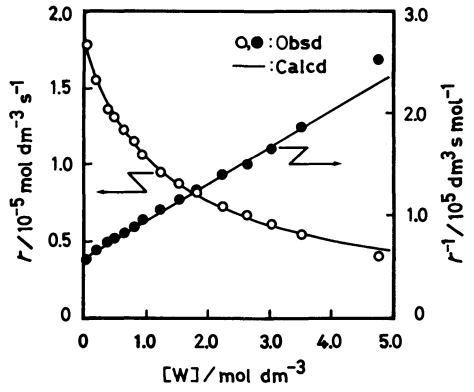

Fig. 5. Influence of concentration of water ([W]) upon reaction rate (r).
[F]=0.120 mol dm^{-3}, [A]=9.8 mol dm^{-3}.

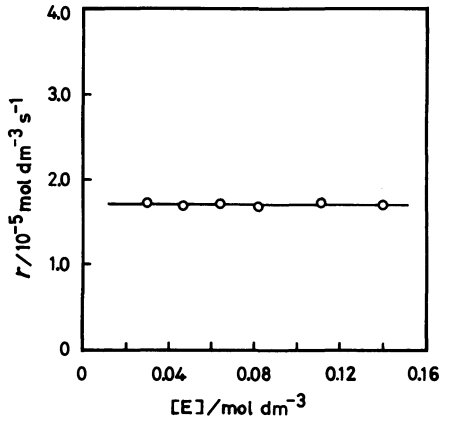

Fig. 6. Influence of concentration of butyl octanoate ([E]) upon reaction rate (r).
[F]=0.120 mol dm^{-3}, [A]=9.7 mol dm^{-3}.

Discussion

Evaluation of Effects of Resin Swelling and the Dielectric Constant of the Reaction Medium on the Rate. Amberlyst 15, which consists of aggreates of very small gelular microspheres, presumably consists of about 20% divinylbenzene.[27] At cross-linker levels above 12%, the resin matrix exhibits great resistance to swelling.[2] Therefore, it is considered[22,27,28] that the gelular microspheres are not greatly swollen by the reaction medium and that only the sulfo groups residing on the surface of the microspheres[29] are available for a catalytic reaction. This conclusion is supported by the curve shown in Fig. 4, for if 1-butanol causes a swelling of the microsphere gel network,[30] the number of directly accesible sulfo groups should decrease with the decrease in its concentration in a reaction solution, and the catalytic activity of the resin should consequently diminish. All this is contrary to the observed curve. From the above evaluation of the resin swelling, it seems that the assumption of Helfferich[23] can not be applied in this case.

The results obtained from Figs. 4 and 5 can not be used in the treatment of the solvent effects for a reaction between a neutral dipolar molecule and a positive ion as the rate-controlling step, because the plot of ln k_2 against $1/D$ is found to be nonlinear.

Nature of the Acid Site in the Resin and Kinetic Analysis. It is considered from Fig. 5 that the product water solvates the matrix-bound sulfo groups and then depresses the catalytic rate.[12,24,25,27,31] Appropriate polar molecules such as alcohol may also participate in a similar solvation to water.[32] Since the ester did not inhibit the reaction, and since the solvating power of the toluene used as a diluent is negligibly small, it is considered that water and alcohol behave as solvating agents under the present reaction conditions. These solvation equilibria may be written as

$$\alpha A + \text{Ⓟ-}SO_3H \overset{K_{sol}^{(A)}}{\rightleftarrows} \text{Ⓟ-}SO_3^-/\alpha A/H^+, \quad (3)$$

$$\beta W + \text{Ⓟ-}SO_3H \overset{K_{sol}^{(W)}}{\rightleftarrows} \text{Ⓟ-}SO_3^-/\beta W/H^+. \quad (4)$$

The solvated protons also become catalytic agents.[33] However, it is thought that the specific activity of the hydrated protons is negligible compared with that of those solvated with alcohol; therefore, this esterification system consists of a heterogeneous reaction catalyzed by matrix-bound sulfo groups which are not ionized and a pseudo-homogeneous reaction by

protons solvated with alcohol.

Based on these considerations and the fact that the reaction was first-order in its concentration of fatty acid, the following reaction mechanism may be assumed

$$F + Ⓟ\text{-}SO_3H \xrightarrow{k_{het}} Ⓟ\text{-}SO_3H \cdots F, \quad (5)$$

$$A + Ⓟ\text{-}SO_3H \cdots F \underset{}{\overset{K_{het}}{\rightleftarrows}} E + W + Ⓟ\text{-}SO_3H, \quad (6)$$

$$F + Ⓟ\text{-}SO_3^-/\alpha A/H^+ \overset{K^{(A)}_{phom}}{\rightleftarrows} Ⓟ\text{-}SO_3^-/\alpha A + HF^+, \quad (7)$$

$$A + HF^+ + Ⓟ\text{-}SO_3^-/\alpha A \xrightarrow{k^{(A)}_{phom}} E + W + Ⓟ\text{-}SO_3^-/\alpha A/H^+. \quad (8)$$

Reaction (5) corresponds to the chemisorption of octanoic acid on the acid site in the resin, and it appears that the fatty-acid molecule is associated with the un-ionized sulfo group by means of the formation of a doubly hydrogen-bonded structure:[34]

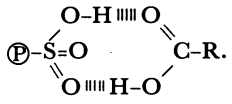

If the $Ⓟ\text{-}SO_3H \cdots F$ and HF^+ species are present in very small amounts, which implies $K_{het} \gg 1 \gg K^{(A)}_{phom}$, the following equation can be set up

$$[Cat] = [Ⓟ\text{-}SO_3H] + [Ⓟ\text{-}SO_3^-/\alpha A/H^+] + [Ⓟ\text{-}SO_3^-/\beta W/H^+]. \quad (9)$$

For the two equilibria (3) and (4), it is possible to write as follows:

$$[Ⓟ\text{-}SO_3^-/\alpha A/H^+] = K^{(A)}_{sol}[A]^{\alpha}[Ⓟ\text{-}SO_3H], \quad (10)$$

$$[Ⓟ\text{-}SO_3^-/\beta W/H^+] = K^{(W)}_{sol}[W]^{\beta}[Ⓟ\text{-}SO_3H]. \quad (11)$$

The substitution of (10) and (11) into (9) gives

$$[Ⓟ\text{-}SO_3H] = [Cat]/(1+K^{(A)}_{sol}[A]^{\alpha}+K^{(W)}_{sol}[W]^{\beta}). \quad (12)$$

The rate of the heterogeneous reaction which contains the chemisorption reaction (5) as its rate-determining step is represented by

$$r_{het} = k_{het}[F][Ⓟ\text{-}SO_3H]M. \quad (13)$$

Equation (13) may be transformed into

$$r_{het} = \frac{k_{het}[F][Cat]M}{1+K^{(A)}_{sol}[A]^{\alpha}+K^{(W)}_{sol}[W]^{\beta}}. \quad (14)$$

For the pseudo-homogeneous reaction, where only the protonated form of fatty acid HF^+ reacts with alcohol at a measurable rate, the rate equation is given by

$$r_{phom} = k^{(A)}_{phom}[A][HF^+][Ⓟ\text{-}SO_3^-/\alpha A]M. \quad (15)$$

Equilibrium (7) can be expressed by

$$[HF^+][Ⓟ\text{-}SO_3^-/\alpha A] = K^{(A)}_{phom}[F][Ⓟ\text{-}SO_3^-/\alpha A/H^+], \quad (16)$$

and by using Eqs. (10), (12), and (16) r_{phom} is given as follows:

$$r_{phom} = \frac{k^{(A)}_{phom}K^{(A)}_{phom}K^{(A)}_{sol}[F][A]^{\alpha+1}[Cat]M}{1+K^{(A)}_{sol}[A]^{\alpha}+K^{(W)}_{sol}[W]^{\beta}}. \quad (17)$$

Therefore, the total reaction rate is expressed by

$$r = \frac{\{k_{het}[F]+k^{(A)}_{phom}K^{(A)}_{phom}K^{(A)}_{sol}[F][A]^{\alpha+1}\}[Cat]M}{1+K^{(A)}_{sol}[A]^{\alpha}+K^{(W)}_{sol}[W]^{\beta}}. \quad (18)$$

The straight line in the plot of [W] vs. $1/r$ in Fig. 5 indicates that the sulfo groups are solvated by one molecule of water per group at values of [W]<4 mol dm^{-3}: $\beta=1$. Therefore, the data shown in Figs. 4 and 5 were compared with the values calculated from Eq. (18), in which $\beta=1$ had been substituted. In order to determine the optimum values of $k_{het}[Cat]$, $k^{(A)}_{phom}K^{(A)}_{phom}[Cat]$, $K^{(A)}_{sol}$, and $K^{(W)}_{sol}$ for integral values of the α exponent ranging from one to three, the sum of the squares of deviations of the predicted rates from the observed ones has been calculated with a computer. The most precise representation is given by

$$r = \frac{\{k_{het}[F]+k^{(A)}_{phom}K^{(A)}_{phom}K^{(A)}_{sol}[F][A]^2\}[Cat]M}{1+K^{(A)}_{sol}[A]+K^{(W)}_{sol}[W]}, \quad (19)$$

where the values of $k_{het}[Cat]$, $k^{(A)}_{phom}K^{(A)}_{phom}[Cat]$, $K^{(A)}_{sol}$, and $K^{(W)}_{sol}$ were 2.85×10^{-4} s^{-1} g^{-1}, 5.66×10^{-6} dm^3 mol^{-1} s^{-1} g^{-1}, 0.769 dm^3 mol^{-1}, and 5.30 dm^3 mol^{-1} respectively. In view of the polarity of 1-butanol and water, it seems reasonable that the equilibrium constant, $K^{(W)}_{sol}$, is greater than the $K^{(A)}_{sol}$.

When the values calculated from Eq. (19) are compared to the data in Figs. 4 and 5, the agreement between the observed and calculated values is satisfactory. These results give support to the assumptions that this esterification involves both the heterogeneous and pseudo-homogeneous catalyses and that, in the heterogeneous one, the rate-determining step is the chemisorption reaction of fatty acid. As may be seen from Fig. 4, at the lower alcohol concentrations the rate of the heterogeneous reaction catalyzed by the un-ionized sulfo groups[35] substantially governs the total reaction rate, while at the higher ones the rate is roughly equal to that of a pseudo-homogeneous reaction catalyzed by the solvated protons with alcohol.

It is considered that, since the positions of equilibria (3), (4), and (7) are affected by the reaction temperature, the activation energy for both the heterogeneous and pseudo-homogeneous reactions are different from the apparent one estimated from the slope of the straight line in Fig. 3. Furthermore, it is presumed that the selectivity behavior of the resin catalyst related to the alkyl-chain length of normal fatty acids, which was reported in the preceding paper,[22] is due to differences in the rate constant, k_{het}, for the heterogeneous chemisorption

reaction (5).

The authors are grateful to Messrs. Fujio Asaga, Katsuo Aikawa, Hiroyasu Oguma, and Masanori Suzuki for their experimental assistance. The present work was partially supported by a Grant-in-Aid from Nihon University.

Notation

A	1-Butanol
E	Butyl octanoate
F	Octanoic acid
W	Water
M	Amount of resin catalyst, g
T	Absolute temperature, K
D	Dielectric constant of reaction medium
r	Reaction rate, mol dm^{-3} s^{-1}
k'_{obsd}	Pseudo-first-order rate constant, s^{-1}
k_{obsd}	Pseudo-first-order rate constant per g of resin catalyst, s^{-1} g^{-1}
k_2	Specific rate constant, calculated by assuming that the esterification was second-order, dm^3 mol^{-1} s^{-1} g^{-1}
[Cat]	Number of sulfo groups participating in the reaction per g of resin catalyst, mol of sulfo groups g^{-1}
Ⓟ-SO_3H	Matrix-bound sulfo groups which are not ionized
Ⓟ-$SO_3^-/\alpha A/H^+$, Ⓟ-$SO_3^-/\beta W/H^+$	Solvent-separated ion pair
α,β	Number of molecules participating in solvation
r_{het}, r_{phom}	Rates of heterogeneous and pseudo-homogeneous reactions with ion-exchange resin, mol dm^{-3} s^{-1}
k_{het}, $k_{phom}^{(A)}$	Specific rate constants for the reactions represented by Eq. (5) and (8), s^{-1} (mol of -SO_3H groups participating in the reaction)$^{-1}$ and dm^{-3} mol^{-1} s^{-1} (mol of -SO_3H groups)$^{-1}$, respectively
$K_{sol}^{(A)}$, $K_{sol}^{(W)}$	Equilibrium constants for solvent-separated ion-pair formations (3) and (4), dm^3 mol^{-1} (α, β=1)
K_{het}, $K_{phom}^{(A)}$	Equilibrium constants for reactions (6) and (7), dm^3 mol^{-1} and no dimension, respectively

References

1) This work was presented in part at the 52nd National Meeting of the Catalysis Society of Japan, Sapporo, August 1983, Abstr., No. 4F20.

2) A. R. Pitochelli, "Ion Exchange Catalysis and Matrix Effects," Rohm & Haas, Philadelphia (1980).

3) H. Hisayama, "Kireto-jushi Ion-kokan-jushi," ed by N. Hojo, Kodan-sha, Tokyo (1976), Chap. 2, p. 175.

4) D. I. Saletan and R. R. White, *AIChE Symp. Ser.*, **48**, 59 (1952).

5) N. G. Polyanskii, *Russ. Chem. Rev.*, **31**, 496 (1962).

6) N. G. Polyanskii, *Russ. Chem. Rev.*, **39**, 244 (1970).

7) S. S. Bhagade and G. D. Nageshwar, *Chem. Petro-Chem. J.*, **9**, 3 (1978).

8) A. A. Yeramian, J. C. Gottifredi, and R. E. Cunningham, *J. Catal.*, **12**, 257 (1968).

9) K. Setinek and L. Beranek, *J. Catal.*, **17**, 306 (1970).

10) N. Takamiya, T. Fukuda, and J. Horii, *Nippon Kagaku Kaishi*, **1975**, 2069.

11) C. L. Levesque and A. M. Craig, *Ind. Eng. Chem.*, **40**, 96 (1948).

12) M. B. Bochner, S. M. Gerber, W. R. Vieth, and A. J. Rodger, *Ind. Eng. Chem., Fundam.*, **4**, 314 (1965).

13) R. Tartarelli, G. Stoppato, F. Morelli, A. Lucchesi, and M. Giorgini, *J. Catal.*, **13**, 108 (1969).

14) R. Tartarelli, G. Stoppato, F. Morelli, A. Lucchesi, and M. Giorgini, *J. Catal.*, **18**, 219 (1970).

15) R. Tartarelli, F. Piladi, G. Stoppato, and A. Lucchesi, *Chim. Ind. (Milan)*, **53**, 150 (1971).

16) P. Davini and R. Tartarelli, *Chim. Ind. (Milan)*, **53**, 1119(1971).

17) P. Davini and R. Tartarelli, *Chim. Ind. (Milan)*, **54**, 133 (1972).

18) P. Davini and R. Tartarelli, *Ann. Chim. (Rome)*, **62**, 444 (1972).

19) O. N. Sharma, G. D. Nageshwar, and P. S. Mene, *Indian J. Technol.*, **10**, 221 (1972).

20) G. D. Nageshwar, D. M. Pandharpurkar, and P. S. Mene, *Chem. Age India*, **26**, 365 (1975).

21) Z. Gomzi and S. Zrnčević, *Croat. Chem. Acta*, **53**, 25 (1980).

22) S. Shimizu, K. Ishii, and C. Hirai, *Yukagaku*, **30**, 771 (1981).

23) F. Helfferich, *J. Am. Chem. Soc.*, **76**, 5567 (1954).

24) B. C. Gates and W. Rodriguez, *J. Catal.*, **31**, 27 (1973).

25) R. Thornton and B. C. Gates., *J. Catal.*, **34**, 275 (1974).

26) R. B. Wesley and B. C. Gates, *J. Catal.*, **34**, 288 (1974).

27) H. W. Heath, Jr., and B. C. Gates, *AIChE J.*, **18**, 321 (1972).

28) O. Rodriguez and K. Setinek, *J. Catal.*, **39**, 449 (1975).

29) The surface sulfo groups in Amberlyst 15 may be about 4 mol % of the total: Ref. 2, p. 3.

30) Amberlyst 15, with a high ring substitution (about 90%), is swollen by polar solvents rather than by nonpolar ones: S. L. Regen, *J. Am. Chem. Soc.*, **98**, 6270 (1976).

31) V. J. Frilette, E. B. Mower, and M. K. Rubin, *J. Catal.*, **3**, 25 (1964).

32) D. C. Sherrington, "Polymer-supported Reactions in Organic Synthesis," ed by P. Hodge and D. C. Sherrington, John Wiley & Sons, New York (1980), Chap. 3, p. 175.

33) F. Ancillotti, M. M. Mauri, and E. Pescarollo, *J. Catal.*, **46**, 49 (1977).

34) B. C. Gates and G.-M. Schwab, *J. Catal.*, **15**, 430 (1969).

35) The proportion of the un-ionized sulfo groups is given by

$$[Ⓟ\text{-}SO_3H]/[Cat] = 1/(1+K_{sol}^{(A)}[A]+K_{sol}^{(W)}[W]).$$

For example, when the concentrations of 1-butanol are 2.00, 6.00, and 10.00 mol dm^{-3}, the proportions are calculated to be 0.371, 0.173, and 0.113 respectively. From these proportions and the values of r_{het} and r_{phom} for each solution composition, it is considered that the un-ionized sulfo groups are very active compared to the solvated protons with alcohol.

 © 1986 The Chemical Society of Japan Bull. Chem. Soc. Jpn., 59, 13—17 (1986)

Simulation of Absorption Spectra of Polyenes Produced in PVA Film by Heating and Kinetics of Polyenes Formation

Kazunori MARUYAMA, Michio TAKÉ, Nobuyuki FUJII, and Yoshié TANIZAKI*
Department of Materials Science and Technology, Technological University of Nagaoka, Nagaoka, Niigata 949-54
(Received June 24, 1985)

Characteristics of absorption spectra of heated PVA film could be simulated as combinations of absorption spectra of free polyenes corresponding to the type $-(CH=CH)_n-$ (n=1—13). The change in concentrations of polyenes produced in PVA films was calculated by means of simulation. Each polyene $-(CH=CH)_n-$ was assumed to be produced by a first order reaction with rate constant k_n with respect to the concentration of $-(CH=CH)_{n-1}-$. k_n values (n=1—13) at several temperatures were obtained. Arrhenius plots of k_n from straight lines, giving activation energies 57—63 kJ mol^{-1} for the reaction catalyzed by H_3PO_4 and 94—100 kJ mol^{-1} for that by H_2SO_4. The activation entropies are negative in both cases.

At the initial stage of heating, thermal decomposition of poly(vinyl alcohol) [PVA] leads to formation of polyene structures in main polymer chains.[1] The authors have already assigned peaks and bands in absorption and excitation spectra of heated PVA films to 0←0, 1←0, and 2←0 π-π* transitions of $-(CH=CH)_n-$ type polyenes and $-(CH=CH)_n-CO-$ type polyenones.[2] These types are distinguished from each other according as the spectrum is accompanied with a fine structure or not; the former shows a fine structure and the latter a broad band. Under certain conditions, the type of polyenes is preferentially produced. In such cases, a proper combination of absorption spectra of free polyenes is expected to reproduce the experimental spectrum, provided that the concentration of polyenones produced may be disregarded relative to that of polyenes. Moreover, by using the concentration of polyenes determined by simulation, a kinetic study on the polyenes formation is expected to be made.

The present purpose is to simulate absorption spectra of polyenes produced in heated PVA film and to try a kinetic study on the polyenes formation.

Experimental

The PVA used was a commercial one (Koso Chemical Co., Ltd.), of which the average polymerization degree was 1400 and the alkaline saponification was 99—100%. Ten grams of PVA powder was dissolved in distilled water of 200 cm^3 at 90 °C and the solution was poured on a horizontal plate of glass. After it was dried at room temperature for 10 d, a PVA film about 100 μm thick was obtained. This film was kept for 2 h at 80 °C, digested in a mixed solution of 0.1 M(1 M=1 mol dm^{-3}) $NaBH_4$ and 0.1 M NaOH for 1 d to reduce the carbonyl group contained, and then washed successively with 0.05 M HCl solution and with distilled water.

Subsequently, the PVA film was digested in 0.05 M H_3PO_4 or 0.05 M H_2SO_4 solution for 1 d and then dried at room temperature. The PVA film thus treated was fixed on a metal holder and heated in a heating compartment at a constant temperature in a 0.5 dm^3 min^{-1} flow of nitrogen. After a period of time, it was taken out from the compartment and cooled rapidly to room temperature by keeping the holder in contact with a metal plate, and then the absorption spectrum of the film was measured. The above-mentioned procedure from heating to absorption measurement was repeated until the maximum absorbance became 2.0.

Absorption spectra were measured on a Shimadzu UV-360 spectrophotometer, and simulation and kinetic calculation were carried out with a micro computer, an NEC model-N6300 system.

Results

Simulation. The solid line in Fig. 1 shows an example of absorption spectra of PVA film heated at 170 °C. The arrows in Fig. 1 indicate positions of 1←0 transition peaks for respective n values which were already assigned to π-π* transitions of polyenes, $-(CH=CH)_n-$, produced along polymer chains.[2]

A simulation for the spectrum was made as follows by combination of absorption spectra of free polyenes corresponding to $-(CH=CH)_n-$ with n=1—13. The absorption spectra of free polyenes[3-7] were shifted in wave number so that the 1←0 transition peaks were in accord with those assigned by the authors.[8] As for the absorption coefficients of polyenes, reported values[9] were used. Figure 2 shows examples of the shifted absorption spectra of $H(CH=CH)_nH$ used for the simulation where n=6 and 13.

In order to determine concentrations of 13 polyenes produced in the heated PVA film, the following 13 simultaneous equations were solved so that calculated absorbances at 13 wavelengths λ_m (m=1—13) agreed with those observed:

$$A_{obsd}(\lambda_m) = \sum_{n=1}^{13} C_n \cdot \varepsilon_n(\lambda_m) \cdot d \quad (\text{for } m=1\text{—}13), \qquad (1)$$

where $A_{obsd}(\lambda_m)$ is the absorbance observed at λ_m, C_n, and $\varepsilon_n(\lambda_m)$ are the concentration and molar absorption coefficient of $-(CH=CH)_n-$ at λ_m, respectively, and d is the film thickness.

The simulated spectrum is shown by the dotted

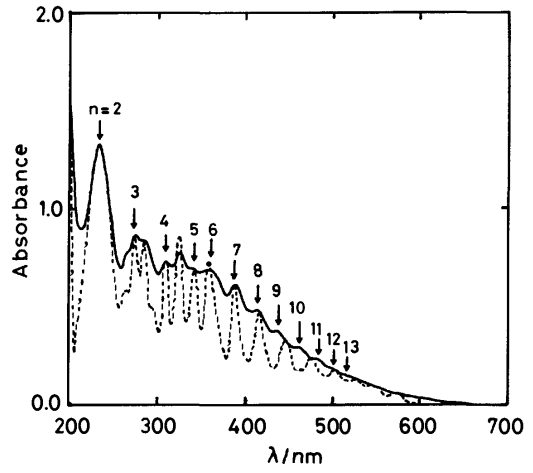

Fig. 1. Absorption spectrum of the heated PVA film (solid line) and that by simulation (dotted line). PVA film was digested in 0.05 M H_3PO_4 solution and heated at 170 °C for 40 min. n indicates conjugation number and arrows indicate 1←0 positions of $-(CH{=}CH)_n-$.

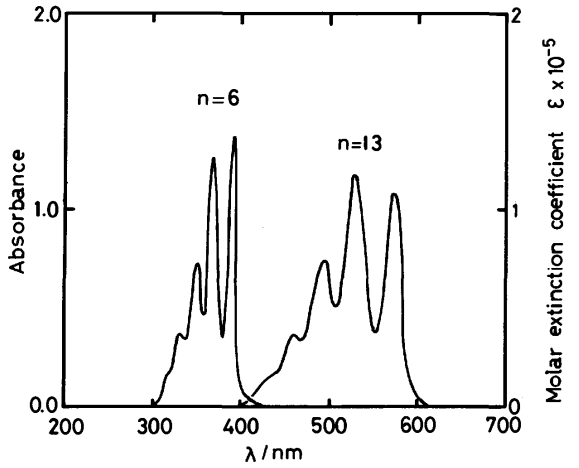

Fig. 2. Shifted absorption spectra of $H(CH{=}CH)_nH$. The concentration of each polyene is 1 mmol dm^{-3} and the film thickness is 100 μm.

line in Fig. 1. It is in good agreement with the observed absorption maxima in the region 200—400 nm.

Strictly speaking, the absorption spectra (solid lines) in Fig. 1 should be a mixture of spectra of polyenes and polyenones. But the concentrations of polyenones were disregarded for the simulation, because the excitation spectra of this sample film indicated that the intensities of polyenones were very low compared to those of polyenes.[2]

The concentrations of polyenes calculated by the present simulation, which are given in Fig. 3, are very low and decrease with increasing conjugation number n.

Kinetics. It has been pointed out that the concentrations of polyenones produced in the heated

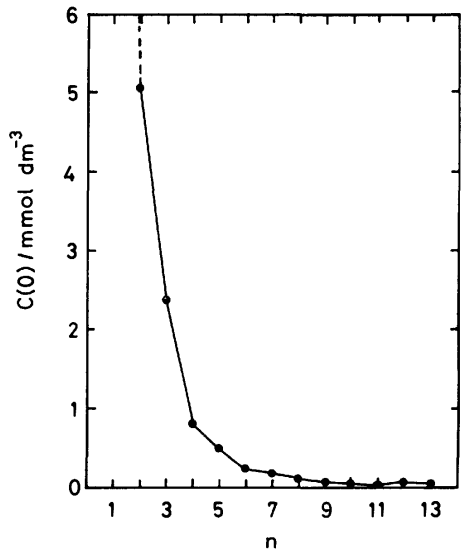

Fig. 3. Concentrations of calculated polyenes produced in the heated PVA film whose absorption spectrum is shown in Fig. 1. The concentration of monoene (n=1) is 2.95×10^{-1} mol dm^{-3}.

PVA film are much lower than that of polyenes when HCl, H_2SO_4, or H_3PO_4 is used as a catalyzer.[2] For such cases, therefore, a kinetic study on the polyenes formation could be made by repeating the heating process and absorption measurement as described in the Experimental section.

Figure 4 shows the change of absorption spectra of a PVA film with heating time at 170 °C. The concentrations of polyenes $-(CH{=}CH)_n-$ were determined from the well fitted simulation curves. The marks in Fig. 5 indicate the concentrations of polyenes thus obtained for n=2—6 against heating time. The concentration of each polyene increases rapidly according as the specimen is heated.

Since the concentrations of polyenes are very low at the initial stage of the heating, it is reasonable to consider that each polyene is formed by a dehydration of the PVA unit adjacent to the polyene as follows:

$$-(CH{=}CH)_{(n-1)}-CH_2CH(OH)- \xrightarrow{k_n} -(CH{=}CH)_n- + H_2O.$$

Accordingly, the concentration of PVA monomer unit $-CH_2CH(OH)-$, $C(0)$, is calculated by

$$C(0) = C(0)_0 - \sum_{n=1}^{13} n\cdot C(n), \qquad (2)$$

where $C(0)_0$ is the initial concentration of PVA unit, which was calculated to be 30.1 mol dm^{-3} from the volume and weight of PVA film before heating, and $C(n)$ is the concentration of $-(CH{=}CH)_n-$. Values of log $C(0)$ at various heating temperatures were plotted against heating time in Fig. 6. The plots give

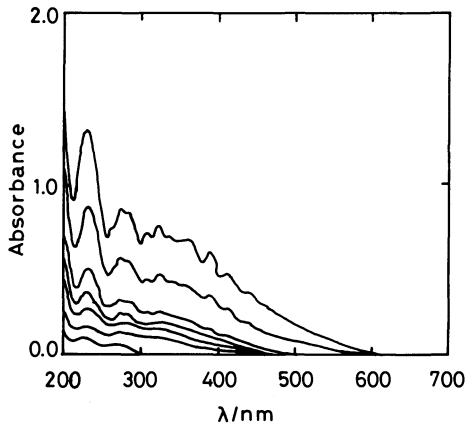

Fig. 4. Absorption spectra of PVA film (106 μm thick) which was digested in 0.05 M H_3PO_4 and heated at 170 °C for 0 (the lowest line), 5, 10, 15, 20, 30, and 40 min (the highest line) respectively.

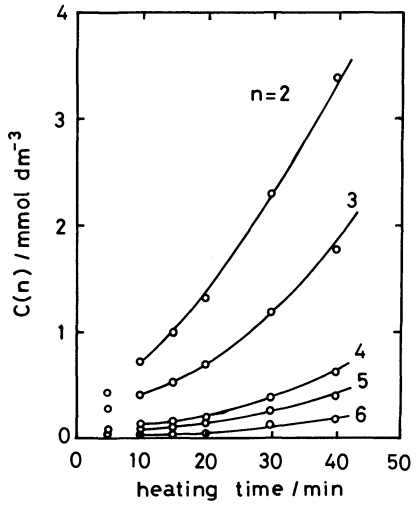

Fig. 5. Comparison of observed concentrations of polyenes (n=2—6) with calculated ones at 170 °C. Marks are experiments, lines are obtained by calculations using the rate constants shown in Table 1 and the concentrations of polyenes at 10 min of heating time as initial condition of the calculation.

straight lines in all cases for 160, 170, 180, and 190 °C. This indicates that the polyene formation is of the first order as a whole.

Assuming that each polyene of $-(CH{=}CH)_n-$ is formed by a first order consecutive reaction, we may handle the following 14 differential equations

$$\left.\begin{aligned} &d[C(0)]/dt = -\sum_{n=1}^{13} k_n[C(n-1)], \\ &d[C(n)]/dt = k_n[C(n-1)] - k_{n+1}[C(n)] \\ &\qquad\qquad (\text{for } n=1—12), \\ &d[C(13)]/dt = k_{13}[C(12)]. \end{aligned}\right\} \quad (3)$$

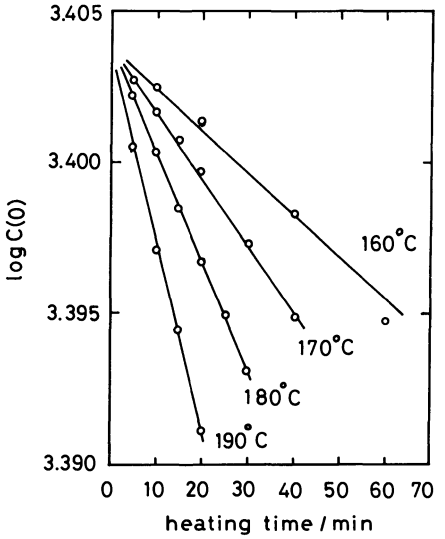

Fig. 6. Relation of log $C(0)$ and heating time at 160, 170, 180, and 190 °C.

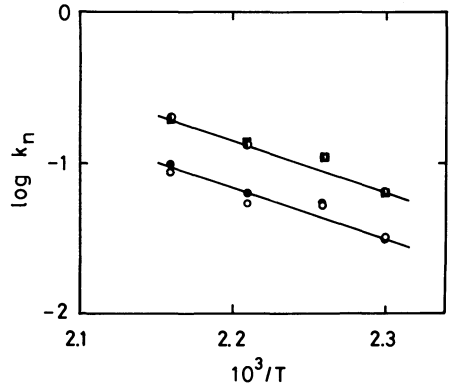

Fig. 7. Arrhenius plots of k_n for PVA film containing H_3PO_4. ○: k_3, ●: k_4, ◐: k_5, ■: k_6.

Such simultaneous differential equations could be solved numerically by the Runge-Kutta method with trial values for rate constants k_1—k_{13}. The most reliable rate constants k_1—k_{13} were determined by making calculated concentrations of polyenes fit experimental ones. The rate constants thus obtained are summarized in Table 1. The calculated curves in Fig. 5, which have been obtained by using the rate constants in Table 1, are in good agreement with the experimental concentrations of polyenes.

Figure 7 shows some of the Arrhenius plots for k_n (n=3—6). They make straight lines for respective rate constants and, therefore, activation energies of the polyenes formation can be calculated. They are summarized in Table 2 together with other activation parameters.

Tables 3 and 4 also shows rate constants k_1—k_{13} and activation parameters determined for the case using H_2SO_4 as a catalyst.

Table 1. Rate Constants for Polyenes Formation Catalyzed by H_3PO_4

Temp	Rate constant/min^{-1}			
°C	160	170	180	190
k_1	0.0001326	0.0002065	0.00033	0.000587
k_2	0.0006784	0.00107	0.00121	0.00211
k_3	0.0346	0.0532	0.052	0.0857
k_4	0.0307	0.0531	0.059	0.0974
k_5	0.0649	0.107	0.125	0.198
k_6	0.0613	0.106	0.128	0.190
k_7	0.112	0.181	0.22	0.31
k_8	0.060	0.174	0.21	0.29
k_9	0.120	0.178	0.21	0.30
k_{10}	0.12	0.20	0.24	0.30
k_{11}	0.22	0.25	0.38	0.56
k_{12}	0.10	0.31	0.28	0.35
k_{13}	0.05	0.09	0.10	0.17

Table 2. Activation Parameters for Polyenes Formation Catalyzed by H_3PO_4 at 175 °C

k_n	Act. E	Act. H_{448}	Act. S_{448}
	kJ mol^{-1}	kJ mol^{-1}	J mol^{-1} K^{-1}
k_3, k_4	57	53	−191
k_5, k_6	63	59	−174

Table 3. Rate Constants for Polyenes Formation Catalyzed by H_2SO_4

Temp	Rate constant/min^{-1}			
°C	100	111	120	130
k_1	0.0000369	0.000108	0.0001976	0.000592
k_2	0.000206	0.000648	0.001012	0.002845
k_3	0.0174	0.0512	0.07123	0.181
k_4	0.0167	0.0549	0.07513	0.197
k_5	0.043	0.122	0.1565	0.414
k_6	0.052	0.145	0.1855	0.502
k_7	0.0808	0.205	0.2715	0.766
k_8	0.0930	0.275	0.2668	0.828
k_9	0.0620	0.200	0.2255	0.675
k_{10}	0.0525	0.214	0.212	0.66
k_{11}	01610	0.453	0.368	1.25
k_{12}	0.6075	0.400	0.368	1.65
k_{13}	0.0191	0.075	0.081	0.25

Table 4. Activation Parameters for Polyenes Formation Catalyzed by H_2SO_4 at 115 °C

k_n	Act. E	Act. H_{388}	Act. S_{388}
	kJ mol^{-1}	kJ mol^{-1}	J mol^{-1} K^{-1}
k_3, k_4	100	97	−65
k_5, k_6	94	91	−71

Discussion

Simulation. As shown in Fig. 1, the simulated spectrum reproduces well the experimental one with respect to the number and wavelengths of peaks in the region 200—400 nm. Nevertheless, the simulated spectrum does not agree with the absorption minima. Two reasons for this disagreement are conceivable: One is that the broad bands of polyenones form the foundation of the spectrum although the concentrations of polyenones have been judged to be low from the excitation spectra, and the other is concerned with the matter of valleys of the spectrum, which is considered as the determinant. The valleys of the reported spectra of $H(CH{=}CH)_nH$[5] are deeper than those of $CH_3(CH{=}CH)_nCH_3$.[10] Considering that the polyenes in the PVA film are formed from part of the polymer chains, their spectra should resemble those of substituted polyenes, $CH_3(CH{=}CH)_nCH_3$, rather than $H(CH{=}CH)_nH$. In fact, the excitation spectrum of tetraene produced in the heated PVA film[2] shows shallower absorption minima than the reported spectrum of $H(CH{=}CH)_4H$[5] as shown in Fig. 8. The absorption spectra of $CH_3(CH{=}CH)_nCH_3$, however, could not be used for the present simulation, because the spectrum of each polyene described in the report is part of itself. For that reason, such a spectrum with very deep constrictions as shown in Fig. 2 was obliged to be adopted for all the polyenes under consideration.

In the longer wavelength region over 400 nm, the simulated spectrum does not reproduce the number and wavelengths of absorption peaks. One reason is that the absorption spectrum of octaene has been used for $-(CH{=}CH)_n-$ of n=9—13.

Kinetics. For evaluation of k_n, 30.1 mol dm^{-3} was used as the initial concentration of PVA monomer unit. Taking into consideration the free water remaining in the PVA film before heating, we should assign $C(0)_0$ a smaller value than 30.1 mol

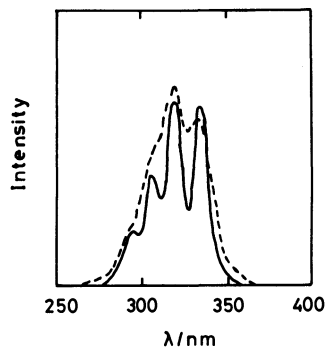

Fig. 8. Shifted absorption spectrum of $H(CH{=}CH)_4H$ (solid line) and the excitation spectrum of heated PVA film monitored at 383 nm (dotted line).

dm^{-3}. Further, the concentration of monoene, $C(1)$, is not so reliable as those for n=2—7, because the intensity of the absorption shoulder at 200 nm was adopted in the simulation instead of that of the absorption maximum of monoene. However, the unreliabilities of $C(0)_0$ and $C(1)$ influence only k_1 and k_2, having no effect on the other constants k_3—k_{13}. Because, for instance, if 25.0 mol dm^{-3} is used for $C(0)_0$ instead of 30.1 mol dm^{-3}, the value of k_1 is changed to 2.492×10^{-4} from 1.326×10^{-4} min^{-1}, but the k_2—k_{13} values are not changed and kept almost the same as shown in Table 1.

The values of k_8—k_{13} also are less reliable for the reason that the concentrations of polyenes for n=8—13 in PVA were calculated without using the absorption data for longer conjugate polyenes than tridecaene. For the same reason, there is a disagreement of the simulated spectrum with the experimental one in the longer wavelength region over 400 nm.

A few kinetic studies have been reported about the degradation of PVA by heating. Yamaguchi et al.[11] investigated the first order rate constant for degradation of PVA by the thermobalance method. According to their report, activation energies for degradation of commercial PVA powder are about 96—230 kJ mol^{-1}, which are affected by the polymerization degree, the degree of oxidation of PVA, and others. Perepelkin and Borodina[12] postulated that the change in transmittance of PVA film was dependent on the decrease in concentration of PVA monomer unit, and determined the activation energy to be 67—176 kJ mol^{-1} for the PVA film containing CH_3COONa and 192—263 kJ mol^{-1} without CH_3COONa. In the present study, as shown in Tables 2 and 4, the activation energies are 53—64 kJ mol^{-3} for the reaction catalyzed by H_3PO_4, and 94—100 kJ mol dm^{-3} for H_2SO_4, which are comparatively low, probably reflecting the effect of catalyzers.

The activation entropies in Tables 2 and 4 are negative, suggesting some sterical restriction operating in the transition state of the polyenes formation. The difference in numerical values of activation energy and entropy between Tables 2 and 4 may be taken to suggest a difference between the roles of H_3PO_4 and H_2SO_4 as catalysts.

References

1) C. A. Finch, "Poly Vinyl Alcohol," John Wily & Sons, New York (1973), p. 172.

2) The assignment of $-(CH=CH)_n-$ for n=2—5: K. Maruyama, H. Akahoshi, M. Kobayashi, and Y. Tanizaki, *Chem. Lett.*, **1983**, 1863; the assignment of the other polyenes and polyenones: K. Maruyama, H. Akahoshi, M. Kobayashi, and Y. Tanizaki, *Bull. Chem. Soc. Jpn.*, **85**, 2923 (1985).

3) The spectrum of *trans*-$(CH_3)CH=CH(CH_3)$ was cited from Ref. 4, the spectrum of $CH_3(CH=CH)_2CH_3$ being measured with a commercial product (Tokyo Kasei Co., Ltd.). The spectra of $H(CH=CH)_nH$ with n=3, 5, 6, and 8 were cited from Ref. 5; $H(CH=CH)_4H$, from Ref. 6 and $H(CH=CH)_7H$, from Ref. 7. No spectra of $H(CH=CH)_nH$ for n=9 and 11—13 have been reported, however the reported spectrum of decaene (n=10) is very similar to the shifted octaene (n=8). Therefore, the spectrum of octaene was used for these of polyenes of n=9—13.

4) G. F. Woods and L. H. Schwaltzman, *J. Am. Chem. Soc.*, **71**, 1396 (1941).

5) F. Sondheimer, D. A. Ben-Efrain, and R. Molovsky, *J. Am. Chem. Soc.*, **83**, 1675 (1961).

6) A. D. Mebane, *J. Am. Chem. Soc.*, **74**, 5227 (1952).

7) L. C. Jones, Jr. and L. W. Tayler, *Anal. Chem.*, **28**, 228 (1955).

8) Since the peak maximum of monoene, -CH=CH-, was not detected in the measured absorption range (190—800 nm) in this study, the spectrum of *trans*-$CH_3(CH=CH)$-CH_3 was used as it was, i. e., without any shifting applied for the simulation. Since both 0←0 and 1←0 transitions of tetraene and pentaene were observed in the experimental spectrum, the experimental spectra of $H(CH=CH)_nH$ (n=4 and 5) were shifted so that both the absorptions of 0←0 and 1←0 agreed with their experimental positions.

9) The molar absorption coefficent of $H(CH=CH)_4H$ was not described in Ref. 6; the molar coefficient of $CH_3(CH=CH)_4CH_3$ given in Ref. 10 was used. Since the molar absorption coefficient of heptaene reported for the 1←0 transition (33000) is so small compared with those of hexaene (127000) and octaene (112000), the average value (119500) for hexaene and pentaene was used as the absorption coefficient of heptaene.

10) P. Nayler and M. C. Whiting, *J. Chem. Soc.*, **1955**, 3037.

11) K. Yamaguchi, M. Amagasa, and S. Uchiyama, *Kobunshi Kagaku*, **18**, 26 (1961).

12) K. E. Perepelkin and O. O. Borodina, *Sov. Plast.*, (2), **1968**, 17.

Base-Catalyzed Hydrolysis of Acetylcholine Chloride in the Presence of Cationic and Nonionic Surfactants

Masayuki NAKAGAKI and Shoko YOKOYAMA*
Faculty of Pharmaceutical Sciences, Kyoto University, Yoshida-shimoadachi-cho, Sakyo-ku, Kyoto 606
(Received July 15, 1985)

The base-catalyzed hydrolysis of acetylcholine chloride (Ach) in the presence of cationic and nonionic surfactants was investigated. The rate of hydrolysis of Ach was determined by following the disappearance of Ach spectrometrically. At a constant pH of 9.0, addition of dodecyltrimethylammonium chloride (DTAC) at concentrations below the critical micelle concentration results in a large decrease in the apparent rate constant for the hydrolysis of Ach, k_{app}. The plot of k_{app} against the concentration ratio of DTAC to Ach ($C_{DTAC}/[D]_0$) gives a break point at $C_{DTAC}/[D]_0=1$. This is considered to be due to the formation of 1:1 complex between Ach and DTAC. In the presence of heptaoxyethylene dodecyl ether (HED)-DTAC mixed micelles, k_{app} decreases with the mole fraction of DTAC, in contradistinction to the usually presupposed electrostatic effect. This is because Ach molecule penetrates into the micellar phase and is shielded from the attack by OH^- for hydrolysis. The decrease of k_{app} has been successfully interpreted on the basis of the data on the distribution of Ach between the micellar and aqueous phases.

A number of studies[1-7] on the hydrolysis of acetylcholine chloride (Ach) have been carried out, particularly in relation to the effect of pH and temperature, salt effect, and the enthalpy of hydrolysis of Ach. Nogami et al.[8] have revealed the influence of sodium dodecyl sulfate (SDS), a surfactant, on the hydrolysis of Ach. The reaction in the presence of surfactants is also interesting from the viewpoint of micellar catalysis. No kinetic analysis of the hydrolysis in the presence of SDS has, however, been carried out yet.

A kinetic study on the base-catalyzed hydrolysis of Ach in the presence of anionic and nonionic surfactants has been reported in our previous paper,[9] in which the relevant rate constant is explained well by taking into consideration both the distribution of Ach between the aqueous and micellar phases and the electrostatic effect operating on the micelle surface.

In this paper, we report a further kinetic study on the base-catalyzed hydrolysis of Ach in the presence of a cationic surfactant and mixed micelles composed of cationic and nonionic surfactants; this study has been conducted by taking into account both the accurate critical micelle concentration (cmc) of surfactant in the presence of Ach[10] and the distribution of Ach between micellar and bulk phases.[11]

Experimental

Materials. Acetylcholine chloride (Ach) and heptaoxyethylene dodecyl ether (HED) are the same as those used for our previous paper.[9] Dodecyltrimethylammonium chloride (DTAC) obtained from Nakarai Chemicals Co. was purified as previously described.[10,11]

Method of Measurement. The rate of hydrolysis of Ach was obtained as the disappearance rate of Ach at pH 9.0 and 25 °C. The concentration of Ach was determined spectrometrically as previously described.[9,11]

Results

Effect of DTAC Concentration on the Hydrolysis of Ach. The apparent rate constant for the hydrolysis, k_{app}, is defined as

$$k_{app} = \frac{1}{t} \ln \frac{[D]_0}{[D]}, \quad (1)$$

where $[D]_0$ and $[D]$ are the concentrations of Ach at the beginning and at time t, respectively. Plots of $\ln([D]_0/[D])$ vs. t are shown in Fig. 1, where the percent hydrolyzed of Ach is also included on the right side of the ordinate. In all cases, good proportionality is observed. The hydrolysis of Ach in the presence of DTAC can, therefore, be characterized as a first order reaction. The relation between the rate constant evaluated from the slope shown in Fig. 1 and the concentration of DTAC is shown in Fig. 2. In Fig. 2, each curve has a break point and this point

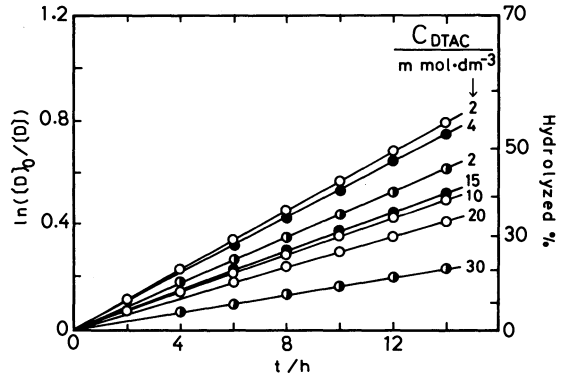

Fig. 1. Hydrolysis of Ach in the presence of DTAC. $\ln([D]_0/[D])$ vs. time.
Concentration of Ach $[D]_0$: ◑ 3, ○ 5, ● 10 mmol dm^{-3} pH: 9.0.

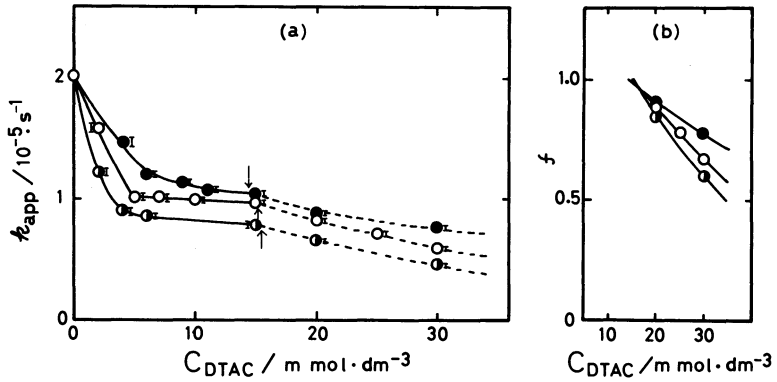

Fig. 2. Effect of DTAC on apparent rate constant for hydrolysis of Ach, k_{app}, with varying concentration of Ach (a) and distribution of Ach (b).[11]
$[D]_0$: ◑ 3, ○ 5, ● 10 mmol dm^{-3}. pH: 9.0.
Dotted line: theoretical curve for the rate in the aqueous phase expected from the distribution ratio shown in Fig. 2(b).

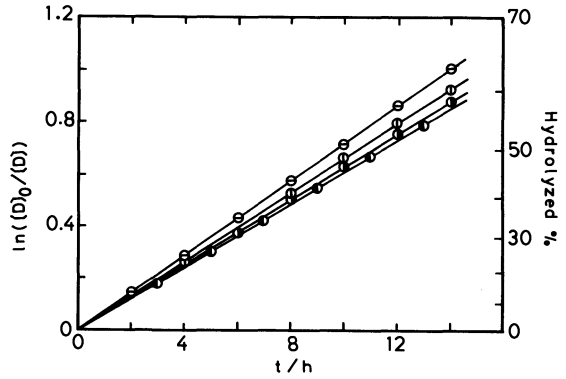

Fig. 3. Hydrolysis behavior of Ach in the presence of DTAC-HED mixed micelle (X_{DTAC}=0.2).
ln ([D]$_0$/[D]) vs. time.
Concentration of surfactants: ⊖ 2, ⓓ 10, ◑ 20, ◐ 30 mmol dm^{-3}. pH: 9.0. $[D]_0$: 5 mmol dm^{-3}.

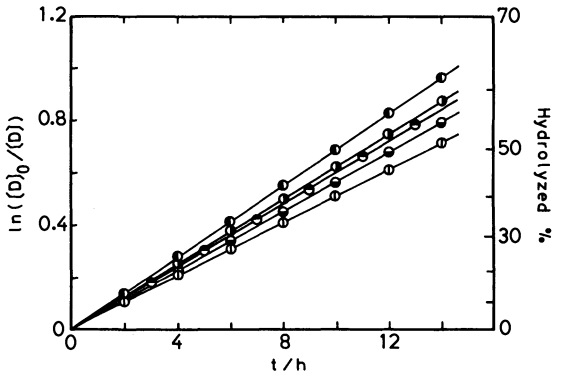

Fig. 5. Hydrolysis behavior of Ach in the presence of DTAC-HED mixed micelle systems.
ln ([D]$_0$/[D]) vs. time.
Mixed micelle systems at the total surfactant concentration of 20 mmol dm^{-3}: ◐ X_{DTAC}=0.1, ◑ X_{DTAC}=0.2, ◓ X_{DTAC}=0.4, ◒ X_{DTAC}=0.6, ⓓ X_{DTAC} =0.8. pH: 9.0. $[D]_0$: 5 mmol dm^{-3}.

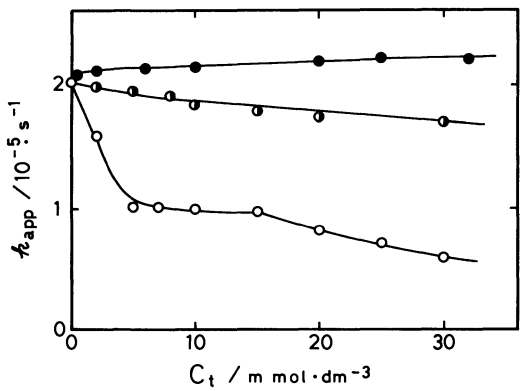

Fig. 4. Effect of surfactants on k_{app}.
Surfactants: ● HED alone,[9] ○ DTAC alone, ◑ HED-DTAC mixed system (X_{DTAC}=0.2). pH: 9.0. $[D]_0$: 5 mmol dm^{-3}.

is found to correspond to the cmc of DTAC in the presence of Ach: 14.4, 15.2, and 15.5 mmol dm^{-3} for Ach at 10, 5, and 3 mmol dm^{-3}, respectively.[10] The value of k_{app} decreases largely at the lower concentration region and again above the cmc.

We have carried out the present experiment very carefully. Therefore, the conclusion that the break points actually exist, may be drawn in conjunction with the experimental error (note that the error for the three measurements of hydrolysis rate is within ±1.5%, that for the distribution of Ach between the micellar and aqueous phases[11] being within ±2.0%) and the solubilization into the micelle.

Effect of DTAC-HED Mixed Micelles on the Hydrolysis of Ach. For the case of the presence of DTAC-HED mixed micelle (X_{DTAC}=0.2) with

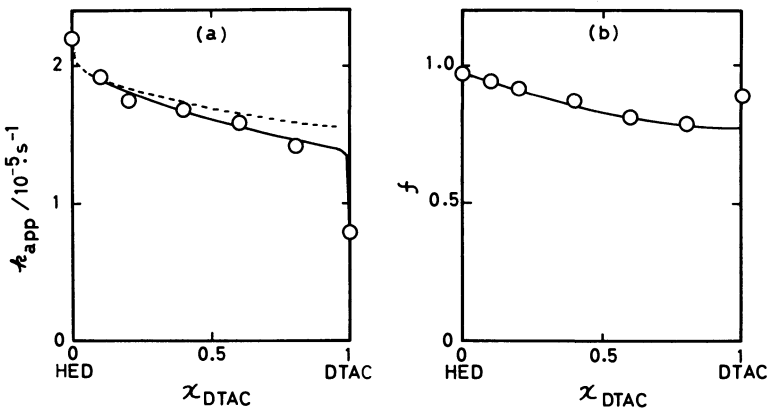

Fig. 6. Effect of HED–DTAC mixed systems on k_{app} (a) and distribution of Ach (b).[11]
(a) solid line: experimental curve.
dotted line: theoretical curve for the rate in the aqueous phase expected from the distribution ratio shown in Fig. 6(b).
(b) $f=[D_f]/[D_t]$, $[D_t]=[D_f]+[D_m]$
Total concentration of surfactants: 20 mmol dm^{-3}. pH: 9.0. $[D]_0$: 5 mmol dm^{-3}.

varying concentration, values of ln ($[D]_0/[D]$) for Ach of $[D]_0$=5 mmol dm^{-3} are plotted in Fig. 3 against t according to Eq. 1.

The values of k_{app} obtained from the plots shown in Fig. 3 are plotted in Fig. 4 against the total concentration of surfactants, C_t. The values of k_{app} in the presence of HED alone[9] and of DTAC alone are shown together in Fig. 4. In the presence of DTAC–HED mixed micelle (X_{DTAC}=0.2), no break point, unlike the case of DTAC alone, can be found because the value of cmc is as low as 0.1 mmol dm^{-3} for this system in the presence of 5 mmol dm^{-3} Ach.

On the other hand, the effect of the composition of DTAC–HED mixed systems at a total concentration of 20 mmol dm^{-3} was also examined. Plots of ln ($[D]_0/[D]$) vs. t are shown in Fig. 5, and the values of k_{app} obtained from Fig. 5 are given in Fig. 6(a). The value of k_{app} decreases with the mole fraction of DTAC.

Discussion

Effect of Concentrations of Ach and DTAC on the Hydrolysis of Ach. It is found from Fig. 2 that k_{app} decreases greatly in the lower concentration region below the cmc and that the inclination becomes the steeper, the lower the concentration of Ach. Therefore, the values of k_{app} are plotted against the concentration ratio of DTAC to Ach, ($C_{DTAC}/[D]_0$), in Fig. 7, and it is found that all the three curves in Fig. 2 give the same curve that has a break point at $C_{DTAC}/[D]_0$=1. This would indicate that Ach is stabilized by the formation of 1:1 complex with DTAC, because the attack of OH^- is suppressed. Furthermore, k_{app} decreases again above the point

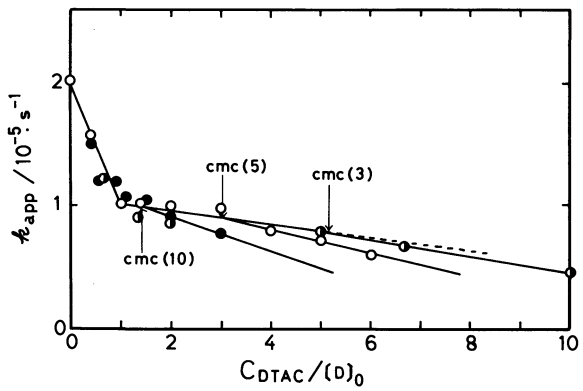

Fig. 7. Relation between k_{app} and concentration ratio of DTAC and Ach ($C_{DTAC}/[D]_0$).
$[D]_0$: ◑ 3, ○ 5, ● 10 mmol dm^{-3}.

corresponding to the cmc. Ach would form a complex with free ions of DTAC, and the complex would be solubilized into the micelle above the cmc.

The decrease of k_{app} above the cmc suggests that the rate of hydrolysis of Ach in the micellar phase is very small. This is considered to be due to the sequence that the acetyl group of Ach enters the palisade layer of the DTAC micelle[11] and is protected from the hydrolysis; hence the base-catalyzed hydrolysis of Ach in the DTAC micellar phase cannot be interpreted in terms of the electrostatic effect in contrast to the case[9] of Ach and sodium dodecyl sulfate.

Effect of DTAC-HED Mixed Micelles on the Hydrolysis of Ach. Ach is distributed between the micellar and bulk phases. The apparent rate constant, k_{app}, for the hydrolysis of Ach is, therefore, written as a sum of two terms

$$k_{app} = k(f) + k(m), \tag{2}$$

where $k(f)$ and $k(m)$ are the rates of hydrolysis in the aqueous and micellar phases, respectively. Equation 2 is rewritten as follows by taking into account the distribution ratio f between the aqueous and micellar phases and the concentrations of OH^-, $[OH^-]_f$, and $[OH^-]_m$:

$$\left.\begin{aligned} &k_{app} = k_{2\,app}[OH^-]_f = k_{2f}f[OH^-]_f + k_{2m}(1-f)[OH^-]_m \\ &\text{or} \\ &k(f) = k_{2f}f[OH^-]_f,\ k(m) = k_{2m}(1-f)[OH^-]_m, \end{aligned}\right\} \tag{3}$$

where $[OH^-]_f$ and $[OH^-]_m$ are the concentrations of hydroxide ion, k_{2f} and k_{2m} are the second order rate constants for the hydrolysis of Ach in the aqueous and micellar phases, respectively, and f is the distribution ratio of Ach in the aqueous phase, that is, $f=[D_f]/[D_t]$ where $[D_t]=[D_f]+[D_m]$ and $[D_f]$ and $[D_m]$ are the concentrations of Ach in the aqueous and micellar phases, respectively. When the total concentration of surfactants, C_t, is lower than the cmc, namely $C_t<$cmc, Eq. 3 reduces to

$$k_{2\,app} = k_{2f} \quad (\text{for } C_t<\text{cmc}), \tag{4}$$

since $f=1$ and $[OH^-]_m=0$.

The apparent rate constants for the hydrolysis of Ach in the presence of DTAC–HED mixed micelles are represented by the solid line in Fig. 6(a). The distribution ratios[11] of Ach in the aqueous phase, $f=[D_f]/[D_t]$, in the presence of DTAC–HED mixed micelles are given in Fig. 6(b).

If it is postulated that all DTAC molecules form mixed micelles with HED, the value of k_{2f} will be 2.02 $mol^{-1}\,dm^3\,s^{-1}$ as obtained from the result[9] in the absence of surfactant. The values of $k(f)=k_{2f}f[OH^-]_f$ are calculated and represented by the dotted line in Fig. 6(a), which indicates that the apparent rate of hydrolysis is nearly equal to the rate in the aqueous phase, implying that Ach in the micellar phase is not hydrolyzed with significant rate, i.e., $k_{2m}\approx 0$. This means that Ach molecules are bound so tightly to DTAC micelle[11] as to be prevented from hydrolysis. These are consistent with the result[11] that the binding constant for Ach to DTAC–HED mixed micelles increases, whereas f decreases with the mole fraction of DTAC in opposition to the expectation on the basis of the electrostatic repulsion between Ach cation and the mixed micelle caused to be charged positive by DTAC.

The small value of k_{app} in the presence of DTAC alone is due to both the existence of free DTAC and the occurrence of the interaction between Ach and DTAC in the aqueous phase.

The decrease of k_{app} with the mole fraction of DTAC is considered to be due to the decrease of f shown in Fig. 6(b). The deviation of the experimental result from the dotted line is considered to be due mainly to the existence of a small quantity of free DTAC in the aqueous phase. If the percentage of free DTAC to total added DTAC for the formation of mixed micelle is 5% at $X_{DTAC}=0.8$, the value of k_{app} is expected to be $1.424\times10^{-5}\ s^{-1}$ from the relationship between the rate constant and the concentrations of Ach and DTAC shown in Fig. 7, and the value thus obtained is consistent well with the experimental value; namely, when $(C_{DTAC}/[D]_0)\leqq 1$, the relation between k_{app} and $(C_{DTAC}/[D_f])$ is written as

$$k_{app} = k^0_{app} - 0.5\,k^0_{app}\frac{C_{DTAC}}{[D_f]} \quad \left(\text{for } \frac{C_{DTAC}}{[D_f]}\leqq 1\right), \tag{5}$$

because the value of k_{app} at $(C_{DTAC}/[D_f])=1$ is equal to $(1/2)k^0_{app}$ and the decrease of k_{app} is proportional to $(C_{DTAC}/[D_f])$ as can be seen in Fig. 7, where k^0_{app} is the value of k_{app} in the absence of free surfactant. By substituting $C_{DTAC}=20\times0.8\times0.05=0.8$ (mmol dm^{-3}), $[D_f]=5\times0.785=3.925$ (mmol dm^{-3}), and $k^0_{app}=k^0(f)=2.02\times10^{-5}\times0.785=1.586\times10^{-5}$ (s^{-1}), the value of k_{app} is obtained as $1.424\times10^{-5}\ s^{-1}$.

We have reported[12] that all sodium dodecyl sulfate molecules will form mixed micelles with HED. Although we have not studied the DTAC–HED system, it is reported[13] that the formation of mixed micelle with cationic surfactant is harder than that with anionic surfactant. Therefore, the presence of a small quantity of free DTAC is reasonable.

Finally, the values of $k(f)(=k_{2f}f[OH^-]_f)$ for the region above the cmc given by the dotted lines in Fig. 2(a) have been calculated by using the values of k_{2app} at the cmc as the values of k_{2f}. The dotted lines indicate that the apparent rate of hydrolysis decreases with decreasing value of f. This suggests that the complex formed between Ach and DTAC is solubilized into the micelle above the cmc. The existence of break point in Fig. 2(a) is, therefore, confirmed.

Conclusion

The apparent rate constant, k_{app}, for base-catalyzed hydrolysis of Ach is caused to decrease greatly by the presence of DTAC. This is considered to be due to Ach interacting with DTAC in the aqueous phase. In the presence of DTAC–HED mixed micelles, k_{app} decreases with the mole fraction of DTAC. The decrease of k_{app} is considered to be due to the sequence that the rate constant for the hydrolysis in the micellar phase is approximately zero and that the distribution ratio of Ach in the aqueous phase decreases with the mole fraction of DTAC. This

sequence is, in turn, caused by the sequence that the Ach molecule penetrates into the micelle and is shielded from the attack by OH^- for hydrolysis. It is concluded that the base-catalyzed hydrolysis of Ach in the positively charged micelle is not interpreted in terms of the electrostatic effect, in contrast to the acid-catalyzed hydrolysis of Ach in the negatively charged micelle.

References

1) M. A. Zoglio, H. V. Maulding, W. H. Streng, and W. C. Vincek, *J. Pharm. Sci.*, **64**, 1381 (1975).
2) J. Butterworth, P. P. Eley, and G. S. Stone, *Biochem. J.*, **53**, 30 (1953).
3) L. Larsson, *Acta. Chem. Scand.*, **8**, 1017 (1954).
4) K. B. Schowen, E. E. Smissman, and W. F. Stephan, *J. Med. Chem.*, **18**, 292 (1975).
5) R. P. Bell and M. Robson, *Trans. Faraday Soc.*, **60**, 893 (1964).
6) G. S. Annis and D. D. Eley, *Biochem. J.*, **53**, 34 (1953).
7) H. Hofmann, *Helv. Chim. Acta.*, **13**, 138 (1930).
8) H. Nogami, S. Awazu, and M. Iwatsuru, *Chem. Pharm. Bull.*, **11**, 1251 (1963).
9) M. Nakagaki and S. Yokoyama, *Bull. Chem. Soc. Jpn.*, submitted (No. 50368).
10) M. Nakagaki and S. Yokoyama, *Bull. Chem. Soc. Jpn.*, **58**, 753 (1985).
11) M. Nakagaki and S. Yokoyama, *Chem. Pharm. Bull.*, **33**, 2654 (1985).
12) M. Nakagaki, S. Yokoyama, and I. Yamamoto, *Nippon Kagaku Kaishi*, **1982**, 1865.
13) H. Lange and K. H. Beck, *Kolloid Z. Z. Polym.*, **251**, 424 (1973).

 © 1986 The Chemical Society of Japan Bull. Chem. Soc. Jpn., 59, 25—29 (1986)

Stability Constants and Some Other Properties of the Lanthanoid Nitrate Complexes with Tri-, Tetra-, and Pentaethylene Glycols

Yoshiyuki HIRASHIMA,* Koji KANETSUKI, Ikuo YONEZU, Noriyuki ISOBE, and Jiro SHIOKAWA
Department of Applied Chemistry, Faculty of Engineering, Osaka University, Yamada-oka, Suita, Osaka 565
(Received May 10, 1985)

The lanthanoid nitrate complexes of tri-, tetra-, and pentaethylene glycols (EO3, EO4, and EO5) exhibited anomalous stability trends attributed to structures similar to those of crown complexes. The stability constants of the EO4 and the EO5 complexes decreased with an increase in the atomic number of the lanthanoid in contrast to the lanthanoid complexes with most other ligands. A maximum stability was found at europium for EO3 complexes. The decomposition temperatures of EO3 complexes were higher than those of the corresponding EO4 and EO5 complexes. The yields of the solid complexes in reactions of the lanthanoids with EO5 decreased with an increase in the atomic number of the lanthanoid (with some exceptions). The separation factors observed for fractional precipitation using EO5 as the separating reagents were comparable to those reported regarding reagents practically used for lanthanoid separation.

Macrocyclic polyethers, so-called crown ethers and so on, have received increasing attention in recent years because of their specific interaction with several cations. Relatively few reports[1-5] are concerned with the interaction of noncyclic polyethers with cations. The lanthanoid complexes of polyethylene glycols and glymes have been synthesized by the present authors.[6-8] The mutual separation of lanthanoids by fractional precipitation using tetraethylene glycol has also been reported.[9] According to structure analyses,[10-12] polyethylene glycols in lanthanoid complexes form ring-like structures similar to those of crown compounds, and the mode of coordination of a nitrate ion varies with a change in the number of oxygen atoms in the polyethylene glycols.

It would be interesting to investigate the stability of lanthanoid nitrate complexes with polyethylene glycols since the selectivities of the glycols are expected to be unique, as those of the crown compounds.[13-15] This is due to a similar structure. This paper reports on the stability constants and some other properties of lanthanoid complexes with tri-, tetra-, and pentaethylene glycols.

Experimental

Materials. The lanthanoid nitrates and their complexes were prepared by the method described in a previous report.[8] The composition of the complexes used in this investigation was $Ln(NO_3)_3 \cdot HO(CH_2CH_2O)_nH$ (Ln: lanthanoid element, n=3, 4, or 5). Tri-, tetra-, and pentaethylene glycols were the same as those in the previous paper,[8] and are denoted as EO3, EO4, and EO5, respectively.

Measurements of Decomposition Temperature and Solubility of the Complexes. The decomposition temperatures of the complexes were determined on a Yanagimoto micro melting-point apparatus. The procedure for solubility measurements was as previously described.[8]

Determination of Stability Constants. The EO4 and EO5 Complexes: The stability constants of the EO4 and EO5 complexes were determined by measuring the solubilities of the complexes in ethyl acetate containing different concentrations of EO4 and EO5. The following equilibrium was attained in solutions. The complex partly dissociated into the parent nitrate and EOn (n=4 or 5).

$$Ln(NO_3)_3 \cdot EOn \rightleftharpoons Ln(NO_3)_3 + EOn \quad (1)$$

Therefore, the apparent solubility (S), which was observed directly, is regarded to be the sum of the solubility of the undissociated complex (S_0) and the concentration of $Ln(NO_3)_3$ ([M]) arising from the dissociation, that is $S = S_0 + [M]$. The value of S was varied with a change in the concentration of EO4 or EO5 because [M] is related to the concentration of EOn by Eq. 2 though S_0 is invariant.

$$K = \frac{S_0}{[M] \cdot [EOn]}, \quad (2)$$

where K and [EOn] represent the stability constant and the concentration of EOn, respectively. Equation 2 can be rewritten as Eq. 3 since $[M] = S - S_0$ and $[EOn] = [M] + L$.

$$K = \frac{S_0}{(S-S_0)(S-S_0+L)}, \quad (3)$$

where L is the initial concentration of EOn. Equation 4 is derived from Eq. 3.

$$S^2 + L \cdot S = S_0(2S+L) + (S_0/K - S_0^2) \quad (4)$$

A plot of $(S^2 + L \cdot S)$ against $(2S+L)$ gave values for S_0 and K.

The EO3 Complexes: The stability constants of the EO3 complexes were determined by measurements of apparent molecular weights in solutions, since a determination of stability by measuring the solubility was difficult, owing to the very large solubilities of the complexes. The measurement of the molecular weights were carried out by vapor osmometry. The stability constant was calculated using Eq. 5.

$$K = \frac{\alpha^2 \cdot C_0}{1-\alpha}, \quad (5)$$

where α and C_0 represent the degree of dissociation and the formal concentration of the complex dissolved in acetone, respectively. The value of α was calculated from the

observed molecular weight (M_o) and the formula weight (FW) of the complex using the equation $\alpha=(FW/M_o)-1$.

The stability constants of the EO3 complexes of some lanthanoids (La, Eu, and Lu) and yttrium were also determined by measurements of the proton NMR spectra of acetone-d_6 solutions. The signals of the oxyethylene protons of EO3 shifted upon complexing with metals. The relation between the dissociation degree of the complex (α) and the shift is expressed in Eq. 6.

$$\Delta a = (1-\alpha)\cdot\Delta A, \quad (6)$$

where Δa is the magnitude of the actually observed shift and ΔA is a value to be observed when all of the EO3 is complexed. A combination of Eq. 6 with Eq. 5 gives Eq. 7.

$$\Delta a = \Delta A - \sqrt{\Delta A/K}\cdot\sqrt{\Delta a/C_0} \quad (7)$$

A plot of Δa against $\sqrt{\Delta a/C_0}$ gave values for K and ΔA. The stability constants obtained by NMR measurement were roughly in accordance with those obtained by measurements of the molecular weight.

Determination of the Yield of the Solid Complexes. Ten cm^3 of a 0.05-M ethyl acetate solution of a hydrated lanthanoid nitrate was added to an equal volume of an ethyl acetate solution of EO5 in a 50-cm^3 flask with a glass stopper (1 M=1 mol dm^{-3}). The concentration of the EO5 solution was 0.025, 0.05, or 0.1 M. The water content of the mixed solution was adjusted to the desired value by dehydration or by the addition of water. The flask was shaken for 2 h in a water bath thermostatted at 25.0+0.5 °C. The complex was then deposited immediately after mixing or during the shaking. A solid complex was filtered out with sintered glass. The amounts of lanthanoid in the filtrate and in the solid complex were determined separately by EDTA titration. The yield of the solid complex (Y) was defined as

$$Y = (\mathrm{Ln})_s/((\mathrm{Ln})_s + (\mathrm{Ln})_f),$$

where $(\mathrm{Ln})_s$ and $(\mathrm{Ln})_f$ are the amounts of lanthanoid in the solid complex and filtrate, respectively.

Determination of the Separation Factor. The procedure for the determination of the separation factor was nearly the same as that for the determination of the yield, except the former treated the two-lanthanoid systems, which contained two different lanthanoids. The initial concentrations of individual lanthanoids and EO5 were all 0.0125 M. The separation factor between two lanthanoids (Ln1 and Ln2), $S_{Ln1,Ln2}$ is defined as follows:

$$S_{Ln1,Ln2} = \left(\frac{Ln\,1}{Ln\,2}\right)_s \Big/ \left(\frac{Ln\,1}{Ln\,2}\right)_f, \quad (8)$$

where (Ln1/Ln2) is the molar ratio of the two lanthanoids in the solid complex or filtrate. The amounts of individual lanthanoids in each phase were determined by absorption spectrophotometry, fluorescent X-ray analysis, or atomic absorption analysis.

Results and Discussion

Stability Constants of the Complexes. Figure 1 indicates that the stability constants of the EO4 and the EO5 complexes decreased with increasing atomic

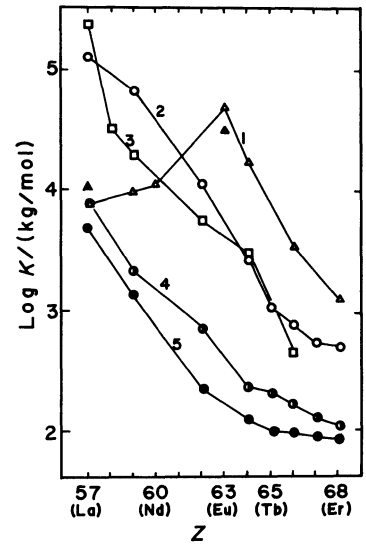

Fig. 1. Stability constants (K) of the lanthanoid nitrate complexes with EO3, EO4, and EO5.
1(△): EO3 complex (in acetone, ▲: Determined by NMR), 2(○): EO4 complex (in ethyl acetate), 3(□): EO5 complex (in ethyl acetate), 4(◑): EO4 complex (in ethyl acetate), 5(●): EO4 complex (in ethyl acetate). 1,2,3: $[H_2O]$=0.0 mol/kg, 4: $[H_2O]$ =0.14 mol/kg, 5: $[H_2O]$=0.28 mol/kg. Z: atomic number.

number of the lanthanoid and that those of the EO3 complexes exhibited a maximum at europium. The stability trends are considerably different from those of lanthanoid complexes, most other ligands showing higher stabilities for the heavier lanthanoids. Similar trends have been reported for complexes of crown compounds by Izatt et al.[13] and Massaux et al.[14,15] The stabilities of most other lanthanoid complexes depend mainly on the charge density of the lanthanoid ion, and accordingly increase with a decrease in the ionic radius. On the other hand, the specific selectivities of crown compounds for several cations have been explained on the basis of the concept of the fitness between the size of the cation and the cavity of the crown ether. The unique stability trends observed here are also considered to be attributed to the ring-like structures formed by the ligands.[10-12] The diameter of the cavity of the ring-like structure in an EO4 or EO5 complex was estimated to be about 270 pm by assuming that the conformation for C-C-O-C-C in the glycol is G-T-T-G (G: gauche, T: trans), which was reported to be the most stable one for poly(oxyethylene) derivatives in the metal complexes.[16] The cavity size is larger than the diameter of a La^{3+} ion (ca. 250 pm) which is the largest among the lanthanoid ions; correspondingly, the EOn chain in a lanthanoid complex is deformed from an ideal structure and is strained to maintain the Ln–O distance at a length suitable for coordination. The decrease in the ionic radius of the

lanthanoid increases the strain in the EO*n* chain and, hence, reduces the stability of the complex.

Triethylene glycol (EO3) in the complex surrounds only half of the lanthanoid ion and forms a ring-like structure with a bidentate nitrate. In addition, the distance between the two coordinating oxygens of the nitrate is rather short compared with those between the adjacent oxygens of EO*n*'s in the complexes. These situations make it possible for the coordinating oxygen atoms in the EO3 complexes to be located closer to the central metal ions without significant repulsion among the oxygen atoms or a serious strain in the glycol chain, than those in the EO4 or EO5 complexes. The contribution of the effect of charge density is, therefore, relatively large in the EO3 complexes as in the lanthanoid complexes with most other ligands. This is especially true for those of the lighter lanthanoids, while the effect of the strain in the EO3 chain becomes significant for complexes of heavier lanthanoids. The former effect increases and the latter decreases the stability with a decrease in the ionic radius of the lanthanoid. A maximum stability at europium is considered to result from a balancing of the above opposing effects.

The above results suggest that other noncyclic compounds, which would form ring-like structures in the complexes, could also exhibit specific selectivities for lanthanoids. The stability trends of the EO*n* complexes are different from those of many other lanthanoid complexes and demonstrate that the polyethylene glycols can be useful for lanthanoid separation, especially in a combined use with other separating reagents.

Figure 1 also demonstrates that the stability constants of the EO4 complexes decrease with an increase in the water concentration in a solution (curves 2, 4, and 5). A similar stability drop was also observed for EO3 and EO5 complexes, though only a qualitative investigation was carried out for a few of the complexes. The decrease in the stability is attributed to a competitive coordination of the water and the glycol to the lanthanoid, and necessitates the dehydration of the solution for a syntheses of some of the complexes.

Decomposition Temperature. All the complexes were decomposed to evolve gas (explosively) and to be blackened upon heating. As shown in Fig. 2, the decomposition temperature, T_d, of an EO3 complex is higher than those of the corresponding EO4 and EO5 complexes. This temperature became lower with an increase in the atomic number of the lanthanoid, except for lanthanum and praseodymium. The T_d of the EO4 complex became lower with an increasing atomic number of the lanthanoid from lanthanum to dysprosium (Z=66). It remained nearly constant for elements between dysprosium and lutetium. On the other hand, the T_d of the EO5

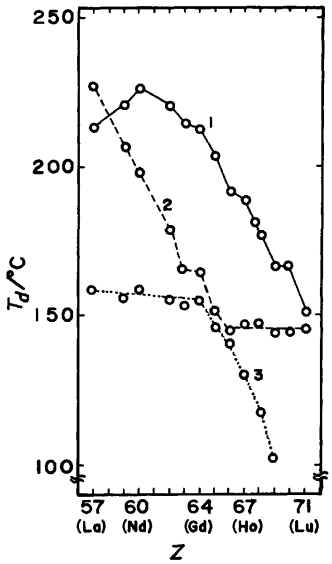

Fig. 2. Decomposition temperatures (T_d) of the lanthanoid nitrate complexes with EO3, EO4, and EO5. 1: EO3 complex, 2: EO4 complex, 3: EO5 complex. Z: atomic number.

complex between lanthanum and gadolinium is nearly constant, and it lowers from gadolinium complex to the heavier lanthanoid complexes. The difference in the decomposition trends of EO4 and EO5 complexes between the lighter and heavier lanthanoids is probably related to different crystal structures. This was previously suggested by a powder X-ray analysis.[8]

Fractional Precipitation. The use of tetraethylene glycol (EO4) in the fractional precipitation of lanthanoids was reported by the present authors.[9] From data regarding the solubilities and stability constants of the complexes, pentaethylene glycol (EO5) was also expected to be useful for the separation of lanthanoids. Figure 3 shows the yields of the solid complexes in a reaction of lanthanoid nitrates with EO5. The yield generally decreased with an increase in the atomic number of the lanthanoid, with a few exceptions, and increased with an increasing initial molar ratio of EO5 to the lanthanoid (EO5/Ln). When the molar ratio was two or unity the yields were nearly the same. They were higher than 95% for elements between lanthanum and gadolinium ((EO5/Ln)=2) or for elements from lanthanum to neodymium ((EO5/Ln)=1). When the molar ratio was 1/2, the yield for cerium, praseodymium, neodymium, and samarium was higher than 50% (ca. 60%), though the yield was not expected to exceed 50% assuming that only a 1:1 complex was deposited. The actual Ln/EO5 ratios in the solid complexes of these elements were larger than 1.0. It was in accordance with the report[8] that the ratio in the solid complex was larger than unity unless EO5

was always in excess. The yield for lanthanum was lower than 50% in contrast to those for the other elements (Ce–Sm). The unique behavior of the lanthanum complex is attributed to the fact that only the 1:1 complex is deposited for lanthanum even when the nitrate is in excess.

The yields decreased for all the lanthanoids with an increase in the water content of the solution, as is shown in Fig. 4. The effect of water was greater for lanthanoid with a higher atomic number; and therefore, the difference in the yield among individual lanthanoids was enhanced by the addition of water. The yield was higher than 90% for elements from lanthanum to holmium in an anhydrous system, and ranged from 97.8% (for lanthanum) to 0.6% (for holmium) in a system containing 0.125 M H_2O. In a system of 0.5-M water content, the yield became 0% for europium and heavier lanthanoids, but was still higher than 80% for lanthanum, cerium, and praseodymium.

The above variation in the yield is consistent with the solubility data regarding complexes previously reported,[8] since the larger solubility of the complex results in the lower yield. The solubility generally decreases with an increase in the atomic number of the lanthanoid and with an increase in the water content of the solution. The anomalous behavior at cerium or the lower yield of the cerium complex (compared with the yield of praseodymium complex) reflects the larger solubility of the cerium complex. The yields shown in Fig. 4 are lower than those estimated from the solubility data assuming that equilibrium is attained. The lower yields are attributed to the fact that the equilibria are not entirely reached within two hours because the yields increased when they were determined after three days or longer.

The difference in the yield among individual

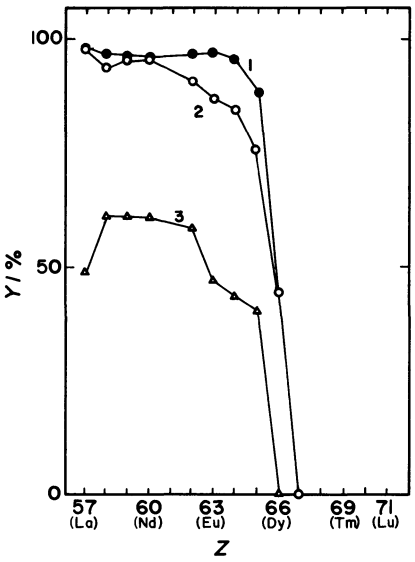

Fig. 3. Relationship between the yield (Y) of the solid EO5 complex and the atomic number (Z) of the lanthanoid.
Initial solution: $[Ln(NO_3)_3]=0.025$ M, $[H_2O]=0.125$ M.
1(●): EO5/Ln=2, 2(○): EO5/Ln=1, 3(△): EO5/Ln=1/2. Reaction time: 2 h.

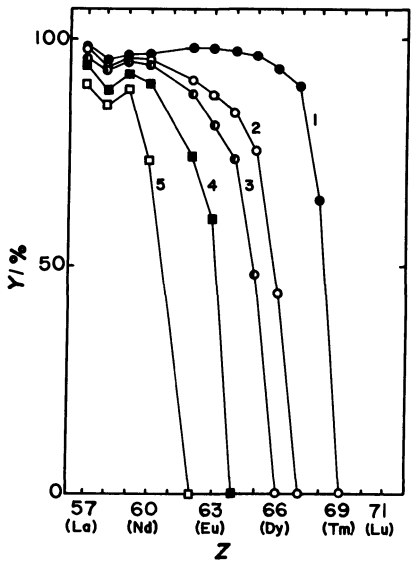

Fig. 4. Effect of the water content on the yield of the EO5 complex.
Initial solution; $[Ln(NO_3)_3]=[EO5]=0.025$ M.
1: $[H_2O]=0.0$ M, 2: $[H_2O]=0.125$ M, 3: $[H_2O]=0.25$ M, 4: $[H_2O]=0.375$ M, 5: $[H_2O]=0.5$ M. Reaction time: 2 h.

Table 1. Separation Factors($S_{Ln1, Ln2}$) for Several Couples of Lanthanoids

Reagent	$S_{Ln1, Ln2}$ for the pairs								
	La-Pr	Pr-Nd	Nd-Sm	Sm-Eu	Eu-Gd	Gd-Tb	Tb-Dy	Dy-Ho	Ho-Er
EO5[a]	1/1.53	1.34	2.48	1.72	1.70	1.71	1.75	1.76	1.74
EO5[b]	1/1.08	1.14	3.36	2.27	1.95	2.51	2.46	—	—
EO4[b]	4.71	1.99	5.50	2.94	2.05	—	—	—	—
EDTA[c]	10.81	2.0	3.1	1.4	1.02	4.8	2.25	3.6	1.8
D2EHPA[d]	6.72	1.7	5.0	2.2	1.6	3.2	2.0	2.1	2.1

a) Anhydrous system. b) System containing 0.0625 M H_2O. c) The values for EDTA were estimated from the stability constants of the complexes.[17] d) The values for D2EHPA were estimated from the distribution ratios.[18]

elements suggests the possibility of lanthanoid separation by fractional precipitation with EO5. The separation factors, $S_{Ln1,Ln2}$, were determined for several two-lanthanoid systems to evaluate the ability of EO5 for the separation of lanthanoids. Table 1 lists the separation factors obtained in this study, together with those reported for systems using EO4,[9] ethylenediaminetetraacetic acid (EDTA)[17] and bis(2-ethylhexyl) hydrogenphosphate (D2EHPA).[18] The value of $S_{Ln1,Ln2}$ were larger than unity except for the La-Pr, reflecting the trend of the yields that they were generally higher for lighter elements. The apparently anomalous value for a La-Pr pair is also reasonable considering that the yield of the lanthanum complex was lower than that of the praseodymium complex when EO5/Ln was 1/2. The separation factors observed for the systems containing water were higher than those for the anhydrous systems with two exceptions (La-Pr and Pr-Nd). The increase of the separation factors upon the addition of water is attributed to an enhancement of a difference in the yield among the individual elements described above. The separation factors obtained here were, like those for EO4, comparable to those for EDTA and D2EHPA which are the excellent reagents practically used for the separation of lanthanoids in ion-exchange and solvent-extraction processes, respectively. These results demonstrate that EO5 has an excellent separating ability.

The results also show that EO4 and EO5 are good precipitants for lanthanoid separation, though the loss of the solvent would be a serious problem regarding practical applications. A fractional precipitation may be favorable in some cases (for example, in the separation into two groups), since the procedure is simple and no special apparatus is required, though nowadays it is not popular because of the difficult procedures during multi-stage operation.

References

1) F. Vögtle and H. Sieger, *Angew. Chem.*, **89**, 410 (1977).
2) U. Heimann and F. Vögtle, *Angew. Chem.*, **90**, 212 (1978).
3) S. Yanagida, K. Takahashi, and M. Okahara, *Bull. Chem. Soc. Jpn.*, **50**, 1386 (1977); **51**, 1294, 3111 (1978).
4) F. Vögtle and U. Heimann, *Chem. Ber.*, **111**, 2257 (1978).
5) W. Rasshofer, G. Oepen, and F. Vögtl, *Chem. Ber.*, **111**, 419 (1978).
6) Y. Hirashima and J. Shiokawa, *Chem. Lett.*, **1979**, 463.
7) Y. Hirashima, K. Ito, and J. Shiokawa, *Chem. Lett.*, **1983**, 9.
8) Y. Hirashima, K. Kanetsuki, I. Yonezu, K. Kamakura, and J. Shiokawa, *Bull. Chem. Soc. Jpn.*, **56**, 738 (1983).
9) Y. Hirashima, Y. Moriwaki, and J. Shiokawa, *Chem. Lett.*, **1980**, 1181.
10) Y. Hirashima, K. Kanetsuki, J. Shiokawa, and N. Tanaka, *Bull. Chem. Soc. Jpn.*, **54**, 1567 (1981).
11) Y. Hirashima, T. Tsutsui, and J. Shiokawa, *Chem. Lett.*, **1981**, 1501.
12) Y. Hirashima, T. Tsutsui, and J. Shiokawa, *Chem. Lett.*, **1982**, 1405.
13) R. M. Izatt, J. D. Lamb, J. J. Christensen, and B. L. Haymore, *J. Am. Chem. Soc.*, **99**, 8344 (1977).
14) J. Massaux, J. F. Desreux, C. Delchambre, and G. Duyckaerts, *Inorg. Chem.*, **19**, 1893 (1980).
15) J. Massaux and J. F. Desreux, *J. Am. Chem. Soc.*, **104**, 2967 (1982).
16) R. Iwamoto, *Bull. Chem. Soc. Jpn.*, **46**, 1144 (1973).
17) E. J. Wheelwright, F. H. Spedding, and G. Schwartzenbach, *J. Am. Chem. Soc.*, **75**, 4196 (1953).
18) T. B. Pierce, P. F. Peck, and R. S. Hobbs, *J. Chromatogr.*, **12**, 81 (1963).

 © 1986 The Chemical Society of Japan Bull. Chem. Soc. Jpn., 59, 31—38 (1986)

Metal Complexes of Amino Acids. XV. Racemization and Deuteration of Bis(biguanide)sarcosinatocobalt(III) Complex

Hiroshi KAWAGUCHI,* Mizuki MATSUKI, Tomoharu AMA, and Takaji YASUI
Department of Chemistry, Faculty of Science, Kochi University,
Akebono-cho, Kochi 780
(Received June 11, 1985)

All four possible optical isomers ($\Delta(S)$, $\Delta(R)$, $\Lambda(S)$, and $\Lambda(R)$) of the bis(biguanide)sarcosinatocobalt(III) ion, $[Co(sar)(Hbg)_2]^{2+}$, were isolated and characterized by their absorption, CD, and ^1H NMR spectra. The optically active $[Co(sar)(Hbg)_2]^{2+}$ ion in a basic aqueous solution showed a loss of CD intensity due to racemizations at both the chiral cobalt center ($\Delta \rightleftarrows \Lambda$) and the asymmetric nitrogen center ($R \rightleftarrows S$). The rate of an $R \rightleftarrows S$ change was ca. 50 times slower than that of a $\Delta \rightleftarrows \Lambda$ change. The rate of deuteration (H→D) at the asymmetric nitrogen atom was slower than those of other sarcosinato complexes. The ratio k_{H-D}/k_{inv} was about 10^2—10^3. The rates of racemization ($\Delta \rightleftarrows \Lambda$) for the $[Co(amino\ acidato)(Hbg)_2]^{2+}$ ion series increased in the order L-valine<L-alanine<glycine<sarcosine.

The tris(biguanide)cobalt(III) ion, $[Co(Hbg)_3]^{3+}$ [where biguanide (imidodicarbonimidic diamide) has the chemical formula $NH_2C(=NH)NH-C(=NH)NH_2$], is more reactive compared with $[Co(N)_6]$ type complexes containing amino and/or imino nitrogens as donor atoms, such as $[Co(en)_3]^{3+}$.[1] The racemization of an optically active $[Co(Hbg)_3]^{3+}$ complex was investigated in an aqueous solution and a twist mechanism has been proposed on the basis of the fact that the value of the probability factor was very small from the point of view of a unimolecular type change.[2] However, another type study was conducted for *fac*-$[Co(Ph-Hbg)_3]^{3+}$, where Ph-Hbg is $C_6H_5-NHC(=NH)NH-C(=NH)NH_2$, in which a bond-rupture mechanism was proposed regarding the intramolecular racemization process.[3] Previously, we found that optically active $[Co(am)(Hbg)_2]^{2+}$ complexes (am denotes amino acidate anion) racemize more rapidly compared to $[Co(Hbg)_3]^{3+}$ and $[Co(am)_3]$ complexes.[4,5] $[Co(am)(Hbg)_2]^{2+}$ complexes are of interest from the point of view of the reaction mechanism.

On the other hand, the kinetics of racemization and deuteration at an asymmetric nitrogen in an aqueous solution have been studied for several cobalt(III) complexes containing sarcosine (Hsar)[6,7] or *N*-methylethylenediamine (Me-en).[8] For these complexes, deuteration rates were several orders of magnitude faster than racemization rates, and both reaction processes could be described by a similar rate law, $R=k[OH^-][complex]$. A mechanism which has been proposed by Buckingham and Sargeson to account for these results is shown in Scheme 1.[8] The reactivities (proton exchange and inversion) at secondary nitrogen centers in *mer*-$[Co(dien)_2]^{3+}$ [9] and $[CoX(trenen)]^{n+}$ [10] complexes were also studied and are discussed in connection with racemization and deuteration at the nitrogen centers of the complexes described above.

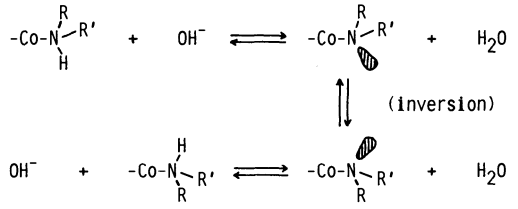

Scheme 1.

$[Co(sar)(Hbg)_2]^{2+}$ ion provides four possible optically active isomers ($\Delta(R)$, $\Lambda(R)$, $\Delta(S)$, and $\Lambda(S)$) arising from two chiral centers (cobalt and sarcosinate nitrogen). In this paper we describe the isolation of the four isomers, the kinetics of racemization at these two chiral centers, and the kinetics of deuteration at the nitrogen centers of coordinated sarcosinates. In addition, we also report on rate data regarding racemization for $[Co(am)(Hbg)_2]^{2+}$ complexes, where am is glycinate, L-alaninate, and L-valinate anions.

Experimental

Preparation, Separation, and Optical Resolution. Bis(biguanide)sarcosinatocobalt(III) Chloride: An isomeric mixture of bis(biguanide)sarcosinatocobalt(III) perchlorate was prepared according to the method described in a previous paper.[4]

About six grams of $[Co(sar)(Hbg)_2](ClO_4)_2$ was dissolved in warm water (ca. 50 cm^3). The solution was poured into a SP-Sephadex C-25 column (4.7 cm×90 cm, Ba^{2+} form) and the adsorbed band was developed with a 0.2 M (M=mol dm^{-3}) $BaCl_2$ solution. Developing was repeated on the same column using a micropump until the adsorbed band completely separated into two bands (E-1 and E-2 in the order of effluence). Each eluting solution from the two bands was concentrated to a small volume under reduced pressure at 35—40 °C. Then, methanol was added to the concentrated solution and deposited barium chloride was filtered off. The filtrate was again evaporated and the remaining $BaCl_2$ was eliminated by the addition of methanol to the concentrated solution by the same procedure as described above. Finally, the methanolic solution was evaporated almost to dryness and the complex was extracted with hot methanol. A crude complex,

obtained by evaporating the extracted solution to dryness, was recrystallized from a small amount of water after adding a mixture of methanol-ethanol (1:3). The deposited crystals were filtered and washed with a mixture of methanol-ethanol (1:3) containing a little water and then with ethanol. The crystals were dried in air.

$(-)^{CD}_{480}$-$\Lambda(S)$- and $(+)^{CD}_{480}$-$\Lambda(R)$-[Co(sar)(Hbg)$_2$]Br$_2$·C$_2$H$_5$OH·H$_2$O: A solution containing 5.0 g (0.0075 mol) of K_2Sb_2(d-tart)$_2$·3H$_2$O in ca. 150 cm^3 of warm water was slowly added to an aqueous solution containing 6.3 g (0.015 mol) of the E-1 racemate, $\Lambda(S)\Lambda(R)$-[Co(sar)(Hbg)$_2$]Cl$_2$, in ca. 150 cm^3 of water without scratching the side of the vessel. The mixed solution was kept in a refrigerator for 1—2 h. The diastereomer (sparingly soluble in water) became deposited in red needle-like crystals and was filtered and washed with ice-water until the color of the filtrate turned almost colorless. They were then dried in air. The yield was 6.1 g.

The diastereomer (powdered in a mortar) was suspended in ca. 150 cm^3 of warm water together with a Dowex 1-X8 resin (Br^- form, 150 cm^3 in wet). The mixture was stirred vigorously until the color of the solution changed to red, and then filtered. The same procedure was repeated several times until the diastereomer completely disappeared. All of the red solutions were combined and concentrated using a rotary evaporator. Methanol, ethanol, and a few drops of concentrated NaBr solution were added to this concentrated solution. Red needle-like crystals were filtered, washed with 80% ethanol, and dried under reduced pressure. The crystals were recrystallized from a little warm water upon adding a few drops of concentrated NaBr solution, methanol, and ethanol (in this order). The yield was 2.7 g. Found: C, 18.52; H, 4.91; N, 27.02%. Calcd for $CoC_9H_{28}N_{11}O_4Br_2$=$(-)^{CD}_{480}$-$\Lambda(S)$-[Co(sar)(Hbg)$_2$]Br$_2$·C$_2$H$_5$OH·H$_2$O: C, 18.86; H, 4.92; N, 26.88%. $\Delta\varepsilon_{560}$=+3.275, $\Delta\varepsilon_{480}$=−5.349.

The $(+)^{CD}_{480}$-$\Lambda(R)$ isomer was obtained as follows. The filtrate obtained upon a separation of the above diastereomer was evaporated under reduced pressure at 35—40 °C. A large amount of methanol was added to the concentrated solution. Deposited potassium chloride was filtered off and the filtrate was again evaporated to dryness. The obtained crude complex was dissolved in water, and then the chloride salt was converted to a bromide salt using a short column containing a Dowex 1-X8 resin (Br^- form). After a concentration of the bromide solution, a crude complex was obtained upon the addition of methanol and ethanol to the concentrated solution. Recrystallization was carried out by the same method as that for the $(-)^{CD}_{480}$-$\Lambda(S)$ isomer. The yield was 1.6 g. $(+)^{CD}_{480}$-$\Lambda(R)$-[Co(sar)(Hbg)$_2$]Br$_2$·C$_2$H$_5$OH·H$_2$O. $\Delta\varepsilon_{560}$=−3.350, $\Delta\varepsilon_{480}$=+5.405.

$(-)^{CD}_{485}$-$\Lambda(R)$- and $(+)^{CD}_{485}$-$\Lambda(S)$-[Co(sar)(Hbg)$_2$]Br$_2$·H$_2$O: The optical resolution of the E-2 racemate ($\Lambda(R)\Lambda(S)$-[Co(sar)(Hbg)$_2$]Cl$_2$) was made by the same method used for the E-1 isomer. The $(-)^{CD}_{485}$-$\Lambda(R)$ isomer was obtained from the less soluble diastereomer. Found: C, 15.97; H, 4.32; N, 29.27%. Calcd for $CoC_7H_{22}N_{11}O_3Br_2$=[Co(sar)(Hbg)$_2$]Br$_2$·H$_2$O: C, 15.95; H, 4.21; N, 29.23%. $\Delta\varepsilon_{563}$=+2.851, $\Delta\varepsilon_{485}$=−5.754. For the $(+)^{CD}_{485}$-$\Lambda(S)$ isomer, $\Delta\varepsilon_{563}$=−2.932, $\Delta\varepsilon_{485}$=+5.814.

Other complexes examined here were prepared and resolved according to a method described in the literature[4] and were found to be analytically pure. $(-)^{CD}_{478}$-[Co(gly)(Hbg)$_2$]Br$_2$·1.5H$_2$O ($\Delta\varepsilon_{478}$=−4.79), $(-)^{CD}_{473}$-[Co(L-ala)(Hbg)$_2$]I$_2$·H$_2$O ($\Delta\varepsilon_{473}$=−4.81), $(+)^{CD}_{475}$-[Co(L-ala)(Hbg)$_2$]Br$_2$ ($\Delta\varepsilon_{475}$=+5.19), $(-)^{CD}_{473}$-[Co(L-val)(Hbg)$_2$]Cl$_2$·1.5H$_2$O ($\Delta\varepsilon_{473}$=−5.67), $(+)^{CD}_{475}$-[Co(L-val)(Hbg)$_2$]Br$_2$·3.5H$_2$O ($\Delta\varepsilon_{475}$=+5.28).

Racemization. All the chemicals used were of a reagent grade, and deionized water was degassed before use. The racemization reactions (at the chiral cobalt center and at the asymmetric nitrogen center) were followed spectrophotometrically with the use of a JASCO J-22 spectropolarimeter. A reaction vessel with a jacket and a water-jacketed cell mounted in a cell holder of the spectropolarimeter were thermostated at a constant temperature (±0.1 °C) with circulating water from a constant-temperature bath. During the experiments, the temperatures of the reaction vessel and the cell were checked with a thermistor thermometer (Takara D-221), and the pH of the reaction solution in the vessel with a Toa TSC-10A pH meter. The reaction was started by adding a buffer solution (5.0 cm^3) with stirring to the complex solution (20.0 cm^3) in the reaction vessel. About 3 cm^3 of this solution was quickly transfered to the cell in order to record the loss of the CD intensity at a suitable wave-length (485 nm for the sarcosinato complex and 475 nm for the glycinato, L-alaninato, and L-valinato complexes). The following conditions were set. For the racemization at the chiral cobalt center; pH 7.5—9.0 (Na_2HPO_4-KH_2PO_4, H_3BO_3-NaCl-$Na_2B_4O_7$, and $NaHCO_3$-Na_2CO_3 buffers), complex concentration (1.2—3.6)×10^{-3} M, ionic strength 0.15—1.0 ($NaClO_4$), temperature 25—35 °C. For the racemization at the asymmetric nitrogen center of the $[Co(sar)(Hbg)_2]^{+2}$ complex; pH 9.0—10.1 ($NaHCO_3$-Na_2CO_3 buffer), complex concentration (2.0—3.0)×10^{-3} M, ionic strength 0.15 ($NaClO_4$), temperature 30—40 °C.

For both of the racemization processes, plots of $\ln[(L_0-L_{eq})/(L_t-L_{eq})]$ vs. time, where L represents CD intensity at the subscripted time, gave straight lines over three half-lives, from which the pseudo-first-order rate constant k' (s^{-1}) were obtained. Analyses of the kinetic data were carried out on an NEC-9801F computer using the least-squares methods. In each of the rate analyses, the value of the standard error was within ±2% of the rate constant.

Deuteration. The deuteration reactions were carried out for both the $\Delta(S)$- and $\Delta(R)$-$[Co(sar)(Hbg)_2]^{2+}$ complexes in D_2O solutions buffered with D_3BO_3-NaCl-$Na_2B_4O_7$, and were followed with a ^{1}H-NMR spectrometer (JEOL MH-100). All the solutions were 0.104 M in complex concentration. The reaction was started by an addition of 1.0 cm^3 of $Na_2B_4O_7$-D_2O(0.0015 M) to the complex solution in 1.0 cm^3 of D_3BO_3(0.2 M)-NaCl(0.045 M)-D_2O in a thermostat at a constant temperature (40, 45, or 50 °C). About 0.5 cm^3 aliquot of the reaction solution was quickly transfered to a NMR tube which was kept in the probe of the spectrometer throughout the run at a constant temperature (40, 45, or 50 °C). The pD of the reaction solution in the vessel was checked using a Toa TSC-10A pH meter. The formulae, pD=pH+0.4[11] and K_{D_2O}=0.195K_w[12], were used to evaluate [OD$^-$].

pH Titration. In order to obtain the pK_a value for the $[Co(am)(Hbg)_2]^{2+}$ complex, the complex solution (1.00×10^{-2} M) was titrated with carbonate-free sodium hydroxide in an atmosphere of nitrogen at 30.0 °C using a

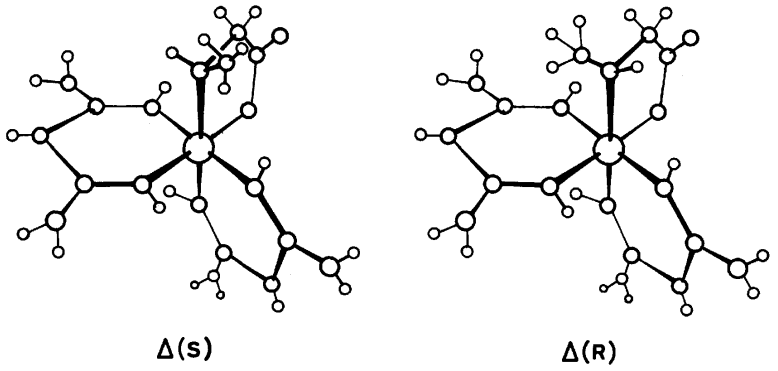

Fig. 1. Structures of $\Delta(S)$- and $\Delta(R)$-$[Co(sar)(Hbg)_2]^{2+}$.

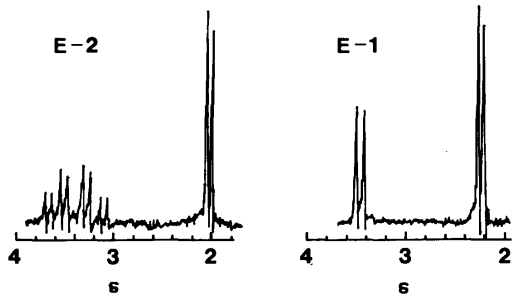

Fig. 2. ^1H NMR spectra of the E-1 ($\Delta(S)\Lambda(R)$) and E-2 ($\Delta(R)\Lambda(S)$) racemates of $[Co(sar)(Hbg)_2]^{2+}$ in D_2O.

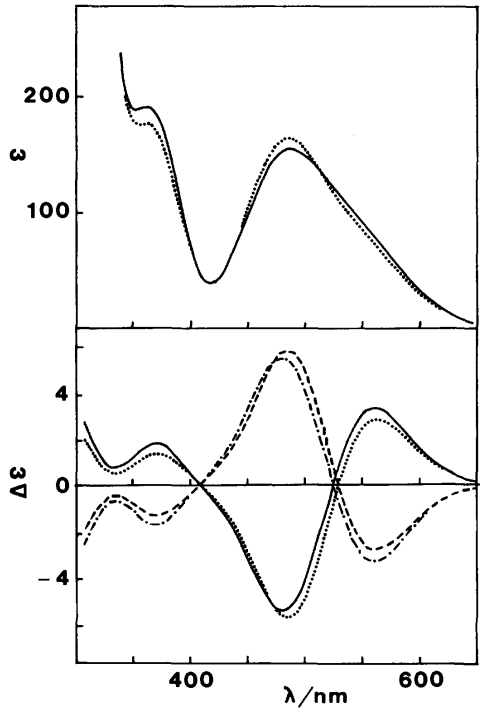

Fig. 3. Absorption and CD spectra of $[Co(sar)(Hbg)_2]^{2+}$ in water: $(-)^{CD}_{480}$-E-1 (——), $(+)^{CD}_{480}$-E-1 (—·—), $(-)^{CD}_{485}$-E-2 (·····), $(+)^{CD}_{485}$-E-2 (----).

Toa TSC-10A pH meter. The obtained titration data were analyzed using the method of Noyes.[13]

Results and Discussion

Four Isomers of the Bis(biguanide)sarcosinato-cobalt(III) Ion. The $[Co(sar)(Hbg)_2]^{2+}$ ion, which contains a chiral cobalt and an asymmetric nitrogen, gives four possible optical isomers ($\Delta(S)$, $\Delta(R)$, $\Lambda(S)$, and $\Lambda(R)$). Figure 1 shows two of the isomers, $\Delta(S)$ and $\Delta(R)$, that are different from each other only with respect to their configurations about the nitrogen atom. The cobalt-biguanide ring is a six-membered plane with π-electrons[14-16] and the cobalt-sarcosine ring is almost planar (within 6°).[17] The N-CH_3 group of the sarcosinato ligand is different in a chemical environment regarding the $\Delta(S)$ and $\Delta(R)$ configurations. The N-CH_3 group is perpendicular to one of the biguanide planes in the $\Delta(R)$ configuration, but is coplanar to that plane in the $\Delta(S)$ configuration. A similar situation is found for the $\Lambda(R)$ and $\Lambda(S)$ isomers which are antipodes of the $\Delta(S)$ and $\Delta(R)$, respectively.

The ^1H NMR spectra of the E-1 and E-2 racemates (measured in D_2O) are given in Fig. 2. As the deuteration of the NH proton of the sarcosinato ring is slow, even in neutral D_2O, N-CH_3 proton resonance is observed as a doublet signal due to coupling with the NH proton at 2.25 ppm (J=6 Hz) for E-1 and at 2.02 ppm (J=6 Hz) for E-2. The methyl signal of E-2 lies in a higher field than that of E-1. Hence, in E-2 the methyl group should be in a shielding position with respect to one of the biguanide rings with π-electrons; it occupies a position perpendicular to the biguanide plane. This indicates that the E-1 and E-2 racemates can be assigned to $\Delta(S)\Lambda(R)$ and $\Delta(R)\Lambda(S)$, respectively.

The -CH_2- moiety of the sarcosinato ring in E-1 gives a doublet signal centered at 3.48 ppm (J=8 Hz) while coupling with an NH proton. After a deuteration of the NH proton, the doublet signal

changes to a singlet one, indicating that the two protons of $-CH_2-$ are in same magnetic environment. However, the two protons of the $-CH_2-$ moiety in E-2 are in a different environment, and the resulting AB system is further coupled to the proton on the adjacent nitrogen atom to give an eight-line ABX spectrum: H_A=3.61, H_B=3.21 ppm ($J_{H_A-H_B}$=17, J_{NH-H_A}= 7, and J_{NH-H_B}=8 Hz).

The absorption and CD spectra for isomers of the $[Co(sar)(Hbg)_2]^{2+}$ complex are shown in Fig. 3 and their numerical data are listed in Table 1. The E-1 and E-2 racemates, which are diastereomeric to each other, show a slightly different absorption spectra in the first d-d band region. A similar behavior was observed for the diastereomers of the $[Co(sar)(en)_2]^{2+}$ complex.[7] In the first absorption band region, each of the four isomers of $[Co(sar)(Hbg)_2]^{2+}$ shows two CD bands of opposite signs with higher intensity in the higher energy side (Fig. 3). The CD curves of the

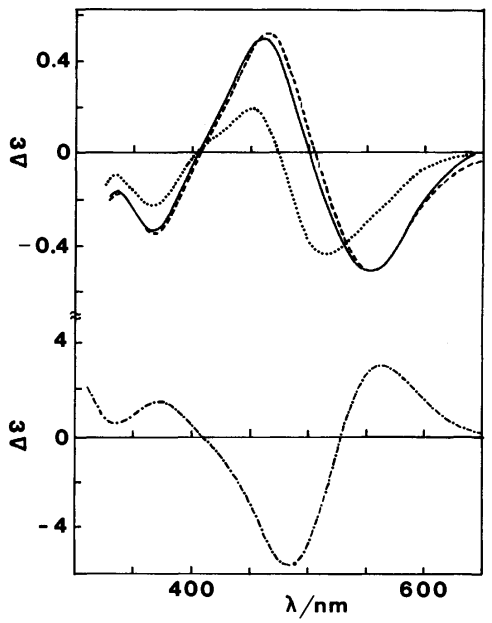

Fig. 4. Configurational and vicinal CD curves of $[Co(sar)(Hbg)_2]^{2+}$: $[\Lambda(R)+\Lambda(S)]/2$ (—·—), $[\Lambda(R)-\Lambda(S)]/2$ (·····). The CD curve of the reaction solution at the pseudo-equilibrium state (——), and the CD curve calculated for the mixture of the $\Lambda(R)$ and $\Delta(R)$ isomers with the $\Lambda(R)/\Delta(R)$ value of 1.22 (----).

$(-)^{CD}_{480}$-E-1 and $(+)^{CD}_{480}$-E-1 isomers are exactly symmetrical to each other, indicating that these isomers are in an enantiomeric relationship. The same relationship is found between the $(-)^{CD}_{485}$-E-2 and $(+)^{CD}_{485}$-E-2 isomers. Previously, the Λ configuration was assigned to $[Co(am)(Hbg)_2]^{2+}$ complexes which exhibited the same CD sign patterns as shown for the $(+)^{CD}_{480}$-E-1 and $(+)^{CD}_{485}$-E-2 isomers in Fig. 3.[4] From the CD and ^1H NMR data, the structures of four isomers of the isolated $[Co(sar)(Hbg)_2]^{2+}$ complex were assigned as follows: $(-)^{CD}_{480}$-E-1, $\Delta(S)$; $(+)^{CD}_{480}$-E-1, $\Lambda(R)$; $(-)^{CD}_{485}$-E-2, $\Delta(R)$; $(+)^{CD}_{485}$-E-2, $\Lambda(S)$.

The $(-)^{CD}_{436}$-$[Co(R\text{-}sar)(NH_3)_4]^{2+}$ ion shows three CD peaks of alternating sign (−, +, −) in the first absorption band region.[6] It is known that the "vicinal" CD curve of the $[Co(sar)(en)_2]^{2+}$ ion is quite similar to the CD curve of the $[Co(sar)(NH_3)_4]^{2+}$ ion.[7] As shown in Fig. 4, the halved difference of the CD curves of the $(-)^{CD}_{485}$-E-2 and $(-)^{CD}_{480}$-E-1 isomers of $[Co(sar)(Hbg)_2]^{2+}$, showing an R-vicinal contribution of asymmetric nitrogen, is similar to the CD spectrum of $[Co(R\text{-}sar)(NH_3)_4]^{2+}$ except for relative peak intensities. This similarity can be taken as additional evidence for our assignment of the absolute configuration of the isomers.

Racemization at the Cobalt Center of $[Co(sar)(Hbg)_2]^{2+}$ Ion. The optically active isomers of the $[Co(am)(Hbg)_2]^{2+}$ ions gradually lost their CD intensities in a weak basic aqueous solution without any change in their absorption spectra.[5] Figure 5 shows the time-course change of the CD intensities at 485 nm when $\Delta(R)$- and $\Lambda(R)$-$[Co(sar)(Hbg)_2]^{2+}$ ions were used as starting materials at pH 8.15 and 35.0 °C. After ca. 80 min, both of the isomers gave a weak residual CD with a positive sign. The loss of the residual CD was very slow under these conditions. However, a CD loss in the second step occurred at a considerable rate in the higher pH region.

A portion of the reaction solution mentioned above was neutralized with 0.1 M HCl at the pseudo-equilibrium state. The neutralized solution gave a CD curve that was slightly different from the vicinal CD (Fig. 4). If the neutralized solution contains only the $\Lambda(R)$ and $\Delta(R)$ isomers, the ratio $\Lambda(R)/\Delta(R)$ at the pseudo-equilibrium state can be calculated from the CD intensities at 485 nm in Figs. 3 and 5. The value

Table 1. Absorption (AB) and CD Data of the $[Co(sar)(Hbg)_2]^{2+}$ Complex in an Aqueous Solution

Complex	Config.		AB (ε)	CD ($\Delta\varepsilon$)	
			nm	nm	
$(-)^{CD}_{480}$-E-1	$\Delta(S)$	1st band	486(155)	560(+3.32)	480(−5.45)
		2nd band	361(191)	372(+1.78)	
$(-)^{CD}_{485}$-E-2	$\Delta(R)$	1st band	485(163)	563(+2.85)	485(−5.76)
		2nd band	361(177)	372(+1.78)	

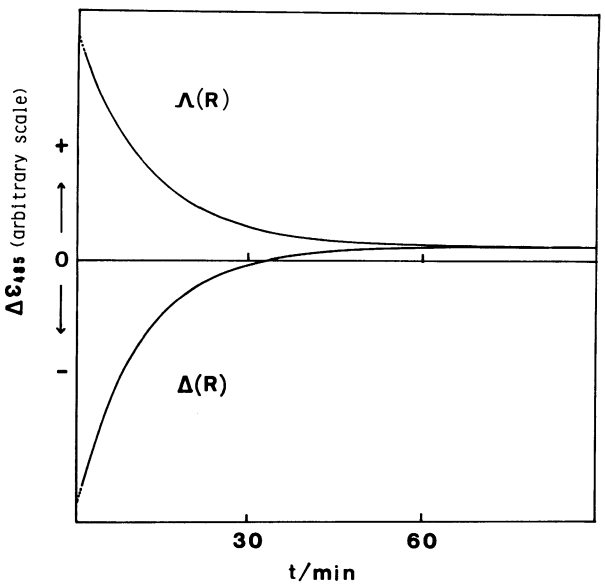

Fig. 5. The time-course change of the CD intensities of the $\Lambda(R)$- and $\Delta(R)$-$[Co(sar)(Hbg)_2]^{2+}$ ions measured at 485 nm (35.0 °C, pH=8.15, μ=0.15).

Table 2. The Rate Constants and the Activation Parameters for the $\Delta(R)\rightarrow\Lambda(R)$ Change of the $[Co(sar)(Hbg)_2]^{2+}$ Ion

Run	T / °C	pH[a]	$k'_{\Delta(R)-\Lambda(R)}$[b] / 10^{-4} s^{-1}	$k_{\Delta(R)-\Lambda(R)}$ / 10^2 M^{-1} s^{-1}	ΔH^{*}[c] / kJ mol^{-1}	ΔS^{*}[c] / JK^{-1} mol^{-1}
1	30.0	7.43	0.618	1.57	83.9±2.9	73.6±9.9
2	30.0	7.78	1.34	1.53		
3	30.0	8.14	3.13	1.55		
4	30.0	8.07	2.63	1.51	(μ=0.5)	
5	30.0	8.00	1.87	1.26	(μ=1.0)	
6	30.0	8.62	11.99	1.95	(higher pH)	
7	25.0	8.12	1.16	0.823		
8	26.3	8.12	1.46	1.01		
9	32.5	8.12	4.72	2.06		
10	35.0	8.15	7.57	2.56		

a) Phosphate buffer. b) Calculated from the values of both the pseudo-first-order rate constants (k') and the equilibrium constants ($\Delta(R)/\Lambda(R)$). The values of $\Lambda(R)/\Delta(R)$: 1.18 (run 4), 1.20 (run 5), 1.14 (run 6), 1.22 (other runs). c) Calculated from the data of $k_{\Delta(R)-\Lambda(R)}$ (at 30 °C). μ=0.15 except for the run of 4 and 5.

is estimated to be 1.22. The CD curve calculated for a mixture of the $\Lambda(R)$ and $\Delta(R)$ isomers with a $\Lambda(R)/\Delta(R)$ value of 1.22 coincides exactly with the spectrum of the neutralized reaction solution (Fig. 4). Moreover, in the present sarcosinato complex, both the "configurational effect" (Δ or Λ) and the "vicinal effect" (R or S) contribute to the observed CD spectrum in the d-d band region. Also, the "vicinal effect" makes a relatively small contribution to the observed CD. These considerations show that the large CD loss in the first step can be attributed to a racemization of $\Delta(R)\rightleftarrows\Lambda(R)$ and that the small CD loss in the second step can be attributed to a racemization of $R\rightleftarrows S$.

The progress of the $\Delta(R)\rightleftarrows\Lambda(R)$ change was followed by a loss of the CD intensity at 485 nm. Each of the $\Delta(R)$ and $\Lambda(R)$ isomers was used as a starting material under the same conditions, and the average value of the $[CD]_{eq}$ (CD intensity at the pseudo-equilibrium state) was used for a kinetic analysis. The values of the equilibrium constant ($\Lambda(R)/\Delta(R)$) are invariable within experimental error under conditions of pH 7.5—8.5 and 25—35 °C. The mean value is 1.22±0.03, indicating that the $\Lambda(R)$ isomer is favored. The value of $\Lambda(R)/\Delta(R)$ is reported to be 5.58 for the $[Co(sar)(en)_2]^{2+}$ complex. The stereoselectivity is smaller in the bis(biguanide)-cobalt(III) complex, since a smaller steric interaction might be expected because of the nearly planar biguanide chelate rings.

In Table 2, the rate constants, $k'_{\Delta(R)-\Lambda(R)}$, of the $\Delta(R)\rightarrow\Lambda(R)$ change, which are calculated from values of both the pseudo-first-order rate constants (k') and the equilibrium constants ($\Lambda(R)/\Delta(R)$), are summarized. The values of $k_{\Delta(R)-\Lambda(R)}(=k'_{\Delta(R)-\Lambda(R)}/[OH^-])$ are regarded as essentially constant in the lower pH region (<8.0); however, the values increase with a pH above ca. 8.5. Namely, the rate deviates from a first-order-relationship with $[OH^-]$ in a higher pH region. As the biguanide which is coordinated to a cobalt(III) ion dissociates its proton in a basic aqueous solution,[18] the following equilibrium is established for the $[Co(sar)(Hbg)_2]^{2+}$ ion:

$$[Co(sar)(Hbg)_2]^{2+} \overset{k_{a1}}{\rightleftharpoons} [Co(sar)(Hbg)(bg)]^{+} + H^{+} \overset{k_{a2}}{\rightleftharpoons} [Co(sar)(bg)_2] + 2H^{+} \quad (1)$$

(The pK_a values are listed in Table 3.) Deprotonation equilibrium was established much faster than the racemization equilibria of $\Delta\rightleftarrows\Lambda$ and $R\rightleftarrows S$. Therefore, the "$\Delta(R)\rightleftarrows\Lambda(R)$" change is described by Eq. 2.

$$\begin{bmatrix} \Delta(R)\text{-}[Co(sar)(Hbg)_2]^{2+} \\ +H^{+}\uparrow\downarrow-H^{+} \\ \Delta(R)\text{-}[Co(sar)(Hbg)(bg)]^{+} \\ +H^{+}\uparrow\downarrow-H^{+} \\ \Delta(R)\text{-}[Co(sar)(bg)_2] \\ \Delta(R) \end{bmatrix} \rightleftharpoons \begin{bmatrix} \Lambda(R)\text{-}[Co(sar)(Hbg)_2]^{2+} \\ +H^{+}\uparrow\downarrow-H^{+} \\ \Lambda(R)\text{-}[Co(sar)(Hbg)(bg)]^{+} \\ +H^{+}\uparrow\downarrow-H^{+} \\ \Lambda(R)\text{-}[Co(sar)(bg)_2] \\ \Lambda(R) \end{bmatrix} \quad (2)$$

The deviation of the data from a first-order-relationship with $[OH^-]$ may be explained by a

Table 3. Acid Dissociation Constants of the $[Co(am)(Hbg)_2]^{2+}$ Complexes (30.0 °C)

Complex	pK_{a1}	pK_{a2}
$[Co(sar)(Hbg)_2]^{2+}$	8.84±0.04	10.32±0.05
$[Co(gly)(Hbg)_2]^{2+}$	9.06±0.06	10.36±0.08
$[Co(L\text{-ala})(Hbg)_2]^{2+}$	9.07±0.05	10.41±0.04
$[Co(L\text{-val})(Hbg)_2]^{2+}$	9.04±0.02	10.37±0.03

Table 4. The Rate Constants and the Activation Parameters for the $\Lambda \rightarrow \Delta$ Change of the $[Co(am)(Hbg)_2]^{2+}$ Ions

am	T / °C	pH[a]	$k'_{\Lambda-\Delta}$[b] / 10^{-4} s^{-1}	$k_{\Lambda-\Delta}$ / 10^2 M^{-1} s^{-1}	$\Delta H^{\ddagger}$[c] / kJ mol^{-1}	$\Delta S^{\ddagger}$[c] / JK^{-1} mol^{-1}
gly	25.0	8.02	0.494	0.423		
	30.0	8.01	1.19	0.788	94.0±1.0	102±3
	35.0	7.73	1.58	1.48		
	30.0	8.76	9.60	1.16		
	30.0	8.80	15.3	1.61	(carbonate buffer)	
	30.0	8.89	30.4	2.67	(borate buffer)	
L-ala	25.0	8.02	0.192	0.183		
	30.0	8.01	0.510	0.338	96.3±1.7	102±6
	35.0	7.73	0.686	0.641		
L-val	25.0	8.02	0.094	0.0894		
	30.0	8.02	0.304	0.196	101 ±9	112±30
	35.0	8.02	0.721	0.345		

a) Phosphate buffer. μ=0.15 for all the runs. b) Calculated from the values of both the pseudo-first-order rate constants (k') and the equilibrium constants. c) Calculated from the data of $k_{\Lambda-\Delta}$ (at 30 °C).

higher reactivity of the higher order conjugate-base species which are expected to be present in considerable concentration in a higher pH region (>9.0). Similar deviations have been found regarding racemization rates for other (amino acidato)bis-(biguanide) complexes and for $[Co(Hbg)_3]^{3+}$ [19] and $[Co(Ph\text{-}Hbg)_3]^{3+}$ [3] complexes. Hereafter, we only discuss experimental data obtained in a lower pH region where the rate law is described as $R = k_{\Delta(R)-\Lambda(R)}[OH^-][complex]$.

The rate constants of the $\Lambda \rightarrow \Delta$ change for other (amino acidato)bis(biguanide)cobalt(III) complexes are summarized in Table 4. These data were obtained in a pH region where the rates show a first order dependence on $[OH^-]$. The diastereomeric equilibrium constants, $K = \Delta(L)/\Lambda(L)$, of [Co(L-amino acidato)$(Hbg)_2]^{2+}$, which were calculated from CD data in the d-d band region, were essentially constant under the present experimental conditions (25—35 °C, pH <8.5). The constants are 0.803±0.010 and 0.504±0.005 for the L-alaninato and L-valinato complexes, respectively. In Table 2, an increase in

Table 5. The Rate Constants and the Activation Parameters for the $R \rightleftarrows S$ Change of the $[Co(sar)(Hbg)_2]^{2+}$ Ion

Run	T / °C	pH[a]	k' / 10^{-4} s^{-1}	k_{rac}[b] / 10 M^{-1} s^{-1}	$\Delta H^{\ddagger}$[c] / kJ mol^{-1}	$\Delta S^{\ddagger}$[c] / JK^{-1} mol^{-1}
1	30.0	9.29	2.08	0.730	89.2±4.4	91.2±14.3
2	32.6	9.30	3.70	1.05		
3	35.0	9.29	5.60	1.38		
4	35.2	9.74	16.7	1.45		
5	35.2	9.82	19.7	1.42		
6	35.1	9.97	28.0	1.44		
7	35.2	10.04	32.0	1.39		
8	37.0	9.31	9.26	1.85		
9	39.8	9.31	12.7	2.15		

a) Carbonate buffer. μ=0.15. b) $k_{rac} = (k_{R-S} + k_{S-R}) = 2k_{inv}$. c) Calculated from the data of k_{rac}(at 30 °C).

ionic strength from 0.15 to 1.0 caused a decrease in the rates of the $\Delta(R) \rightarrow \Lambda(R)$ change (about 20%). Further, as shown for the case of the $[Co(gly)(Hbg)_2]^{2+}$ complex (Table 4), the rates of the $\Lambda \rightarrow \Delta$ change depend on the type of buffer and the rate decreases in the phosphate buffer. This result may be due to a difference in the formation constant of the ion pair between the complex and each of the buffer anions. It is supposed that the ion pair no longer reacts with OH^- at a rate comparable to that of the original complex. The same results were also obtained for the other complexes studied here.

Ray and Dutt proposed a twist mechanism for the racemization of the $[Co(Hbg)_3]^{3+}$ ion in a neutral aqueous solution on the basis of an abnormally lower probability factor; a large value of $\Delta S^{\ddagger}$ with a negative sign.[2] However, in the $[Co(am)(Hbg)_2]^{2+}$ series the activation entropies, $\Delta S^{\ddagger}$, are positive. The racemization rates for a series of the $[Co(am)(Hbg)_2]^{2+}$ ion increase in the order L-valine<L-alanine<glycine< sarcosine; an alkyl-substitution on the nitrogen atom of glycine increases the rate and an alkyl-substitution on the α-carbon atom decreases the rate. A higher reactivity of the sarcosinato complex is not favorable to the twist mechanism because the transition state of the twist mechanism for the sarcosinato complex is expected to be higher in energy than that for the glycinato complex due to the intramolecular repulsion. One of the possible mechanisms may be a bond-rupture mechanism through the conjugate-base species. However, it is not clear which bond severs, Co–O(sarcosine) or Co–N(biguanide).

Racemization and Deuteration at the Asymmetric Nitrogen Center. The racemization rates at the asymmetric nitrogen center ($R \rightleftarrows S$) in the $[Co(sar)(Hbg)_2]^{2+}$ ion were obtained from the CD loss of the second step at 485 nm. Kinetic data are summarized in Table 5. The constancy of $k_{rac} = k'/[OH^-]$

Table 6. The Rate Constants and the Activation Parameters for the Deuteration at the the Sarcosinato-N in the $[Co(sar)(Hbg)_2]^{2+}$ Ion

Isomer	T °C	pH[a]	k' 10^{-4} s^{-1}	k_{H-D} 10^3 M^{-1} s^{-1}	$\Delta H^{\neq}$ [b] kJ mol^{-1}	$\Delta S^{\neq}$ [b] JK^{-1} mol^{-1}
$\Delta(S)$	39.6	7.11	2.54	3.57	45.0±4.5	−0.48±14.7
	45.2	7.02	4.34	5.17		
	50.7	7.05	8.30	6.62		
$\Delta(R)$	39.6	6.98	5.48	10.4	48.4±2.3	−0.20± 7.7
	45.2	7.02	12.0	14.3		
	50.7	7.00	22.8	20.4		

a) Borate buffer. b) Calculated from the values of k_{H-D} (at 30 °C).

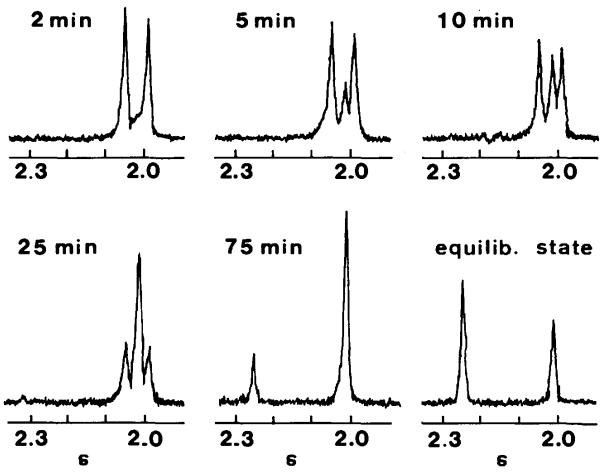

Fig. 6. Deuteration at the sarcosinato-N atom in the $\Delta(R)$-$[Co(sar)(Hbg)_2]^{2+}$ ion as followed by the collapse of the methyl doublet to a singlet (pD=6.98, 39.6 °C). An appearance of the singlet peak at 2.25 ppm is ascribed to the formation of the $\Lambda(R)$ isomer.

in a pH region of 9.0—10.0 (35 °C) indicates that the rate law is given by $R=k_{rac}[OH^-][complex]$. As the values of pK_{a1} and pK_{a2} (deprotonation equilibrium constants) are 8.84 and 10.32, respectively, this result shows that the rate of the $R\rightleftarrows S$ change for each of the species in deprotonation equation (1) is not greatly different. In Table 6, the rate constants for deuteration on the sarcosinato NH proton of $\Delta(S)$- and $\Delta(R)$-$[Co(sar)(Hbg)_2]^{2+}$ are listed. The kinetic data were obtained by following the collapse of the methyl doublet signal to a singlet as the NH proton exchanged with D^+. Part of a typical set of data for the $\Delta(R)$ isomer is shown in Fig. 6. Plots of $\ln[(\text{doublet peak height})_t/(\text{total peak height})]$ vs. time were linear for two half-lives. As the deuteration rates of NH protons observed in other complexes[6-10,20] show a first-order dependence on $[OD^-]$ concentration, the deuteration runs studied here were also analyzed according to the rate law $R=k_{H-D}[OD^-]\times[complex]$. In Table 6, the deuteration rate for the $\Delta(S)$ isomer is about 3 times slower than that for the $\Delta(R)$ isomer. The NH proton of the sarcosinato in the $\Delta(S)$ isomer, which lies in a position perpendicular to one of the biguanide rings, is more effectively hindered with the biguanide ring than in the $\Delta(R)$ isomer. Thus, the kinetic results described above can be interpreted if the rate-determining step is the nucleophilic attack of OD^- on the NH proton. (The rate of deuteration is faster enough than that of the $\Delta\rightleftarrows\Lambda$ change. See Tables 2 and 6.) The small rate constant of the $R\rightleftarrows S$ change compared with that of the deuteration implies that deuteration takes place with a substantial retention of the configuration.

The $[Co(sar)(en)_2]^{2+}$ complex shows no racemization at the cobalt center even in a basic aqueous solution.[7] In the $[Co(sar)(Hbg)_2]^{2+}$ ion, the rate of the $\Delta\rightleftarrows\Lambda$ change is faster than that of the $R\rightleftarrows S$ change. The rates of the $R\rightleftarrows S$ change and deuteration at the nitrogen center are ca. 10^4 and ca. 10^4—10^5 times slower than those for the $[Co(sar)(NH_3)_4]^{2+}$ ion, respectively. However, the ratio of k_{H-D}/k_{inv}, where the k_{H-D} and $k_{inv}(=k_{rac}/2)$ denote the rate constants of the deuteration and inversion at the asymmetric nitrogen center, is ca. 10^2—10^3 for the $[Co(sar)(Hbg)_2]^{2+}$ ion. Although both the rates of the inversion and the H→D change at the nitrogen center for $[Co(sar)(Hbg)_2]^{2+}$ are much slower than those of other sarcosinato complexes, the present kinetic results regarding the asymmetric nitrogen center can be interpreted by a mechanism proposed by Buckingham and Sargeson (Scheme 1).[6-10] Recently, the racemization at the asymmetric nitrogen center of $[Co(Me\text{-}en)(acac)_2]^+$, where the acac ring is also planar structure with π-electrons such as the biguanide ring, has been studied. It was found that the second rate constant is 1.2×10^{-2} M^{-1} s^{-1} for the $\Lambda(R\rightleftarrows S)$ change at 25.1 °C.[21] This value is about 10^4 times smaller than that of $[Co(Me\text{-}en)(NH_3)_4]^{3+}$. These results indicate that the racemization rate at the coordinated asymmetric nitrogen center is extremely affected by the natures of coexisting ligands such as Hbg or $acac^-$, both of which produce a planar chelate ring with π-electrons.

References

1) There are some exceptional complexes such as the $[Co(stn)]^{3+}$ * and macrocyclic(N)-cobalt(III) complexes**, which are much more reactive than $[Co(en)_3]^{3+}$.

* U. Sakaguchi, K. Tomioka, T. Kashihara, and H. Yoneda, *Inorg. Chem.*, **24**, 463 (1985).

** D. J. Royer, G. J. Grant, D. G. Van Derveer, and M. J. Castillo, *Inorg. Chem.*, **21**, 1902 (1982).

2) P. Ray and N. K. Dutt, *J. Indian Chem. Soc.*, **20**, 81

(1943).
3) S. Tachiyashiki and H. Nakayama, presented at the 26th Symposium on Coordination Chemistry, Sapporo, Japan, August, 1976.
4) H. Kawaguchi and B. E. Douglas, *J. Coord. Chem.*, **5**, 115 (1976).
5) H. Kawaguchi, T. Ama, and T. Yasui, presented at the 32th Symposium on Coordination Chemistry, Nagasaki, Japan, October, 1982.
6) B. Halpern, A. M. Sargeson, and K. R. Turnbull, *J. Am. Chem. Soc.*, **88**, 4630 (1966).
7) M. Fujita, Y. Yoshikawa, and H. Yamatera, *Bull. Chem. Soc. Jpn.*, **50**, 3209 (1977).
8) D. A. Buckingham, L. G. Marzilli, and A. M. Sargeson, *J. Am. Chem. Soc.*, **89**, 825 (1967); ibid., **89**, 3429 (1967); ibid., **90**, 6028 (1968).
9) G. H. Searle and F. R. Keene, *Inorg. Chem.*, **11**, 1006 (1972).
10) D. A. Buckingham, P. A. Marzilli, and A. M. Sargeson, *Inorg. Chem.*, **8**, 1595 (1969).
11) P. K. Glasoe and F. A. Long, *J. Phys. Chem.*, **64**, 188 (1960).
12) W. F. K. Wynne-Jones, *Trans. Faraday Soc.*, **32**, 1397 (1936).
13) A. A. Noyes, *Z. Phys. Chem.*, **11**, 495 (1893).
14) M. R. Snow, *Acta Crystallogr.,Sect. B*, **30**, 1850 (1974).
15) T. Tada, Y. Kushi, and H. Yoneda, *Bull. Chem. Soc. Jpn.*, **54**, 1538 (1981).
16) T. Tada, Y. Kushi, and H. Yoneda, *Bull. Chem. Soc. Jpn.*, **55**, 1063 (1982).
17) H. C. Freeman, M. R. Snow, I. Nitta, and K. Tomita, *Acta Crystallogr.*, **17**, 1463 (1964).
18) P. Ray, *Chem. Rev.*, **61**, 313 (1961).
19) Unpublished data.
20) U. Sakaguchi, K. Maeda, and H. Yoneda, *Bull. Chem. Soc. Jpn.*, **49**, 397 (1976) and references cited therein.
21) M. Kojima, U. Ouyang, and J. Fujita, presented at the 49th National Meeting of the Chemical Society of Japan, Tokyo, April, 1984, Abstr., No. 2O07.

 © 1986 The Chemical Society of Japan Bull. Chem. Soc. Jpn., 59, 39—42 (1986)

The Preparation and Properties of the Manganese(II) Ion-Selective Electrode

Junko MOTONAKA,* Hiroshi NISHIOKA,† Sanae IKEDA, and Nobuyuki TANAKA††
Technical College, The University of Tokushima, Minamijosanjima, Tokushima 770
†Himeji Institute of Technology, Shosha, Himeji 671-22
††Nippon Jimuki Co., Ltd., 12, 3-Chome, Kanda Ogawa-cho,
Chiyoda-ku, Tokyo 101
(Received June 20, 1985)

For the measurement of manganese(II)-ion activity, manganese(II) ion-selective electrodes were prepared and tested. As electrodes, heterogeneous membranes were prepared by dispersing sensitive materials, such as manganese sulfide, manganese borate, or manganese dibenzyldithiocarbamate, in silicone rubber, poly(vinyl chloride), or poly(vinyl acetate). A manganese chloride solution (0.1 mol dm^{-3}) was used as the internal reference solution, along with an Ag/AgCl internal reference electrode. The manganese(II) ion-selective electrodes thus made were then examined in terms of their response curves, response times, the effect of the pH, the variation in the response slopes with the temperature, and selectivity coefficients. The response time of the manganese dibenzyldithiocarbamate electrode was within 15 s in the concentration range of 10^{-8}—10^{-1} mol dm^{-3}. The response slope was 33.14 mV/pMn^{2+} in the linear part, and the coefficient of correlation was 0.999. The selectivity coefficients were examined by the separate-solution method.

In recent years, a number of books[1-3] and review articles[4-7] on various aspects of ion-selective electrodes have appeared. In spite of great recent progress in the study of ion-selective electrodes, however, very few manganese(II) ion-selective electrodes have been developed.[8-10] To measure the manganese-ion activity, several manganese(II) ion-selective electrodes have been prepared and tested.

Experimental

Apparatus and Reagents. A digital pH/mV meter, Model PT 3D (Toyo Kagaku Sangyo Co., Ltd.), was used to make the potential measurements (Fig. 1). All the reagents were of an analytical-reagent grade(Wako Pure Chemical Industries). Redistilled water was used in all experiments.

Manganese(II) Ion-Selective Electrode Preparation. Sensitive materials were synthesized as shown below. Manganese sulfide (type α) was formed by the addition of ammonium sulfide to manganese chloride and heated as Eq. 1. Manganese sulfide (type β+γ) was formed by the addition of hydrogen sulfide as in Eq. 2. Manganese hydrogenorthoborate was obtained by the addition of borax to manganese sulfate, while manganese dibenzyldithiocarbamate was obtained by the addition of sodium dibenzyldithiocarbamate to manganese chloride, as in Eqs. 3 and 4 respectively.

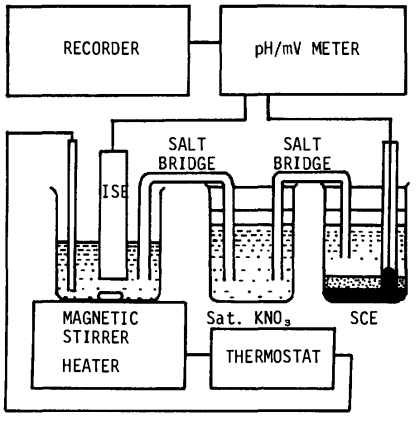

Fig. 1. Apparatus for measurement of potential.

$$(NH_4)_2S + MnCl_2 = MnS \text{ (type } \alpha) + 2NH_4Cl \quad (1)$$

$$H_2S + MnCl_2 = MnS \text{ (type } \beta+\gamma) + 2HCl \quad (2)$$

$$Na_2B_4O_7 + 2MnSO_4 + 5H_2O = 2MnH_4(BO_3)_2 + 2NaHSO_4 \quad (3)$$

(Borax) [Manganese hydrogen-orthoborate]

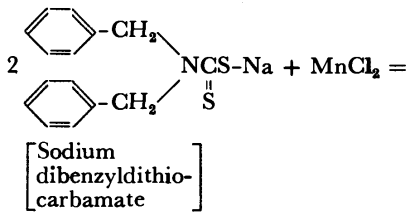

[Sodium dibenzyldithio-carbamate]

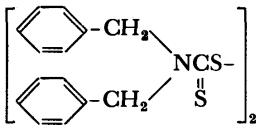

(4)

[Manganese dibenzyldithio-carbamate]

The analytical data on manganese dibenzyldithiocarbmate are shown in Table 1. The analytical data agree reasonably well with the calculated values.

Heterogeneous membranes were prepared with these manganese salts by using, at room temperature, vulcanized silicone rubber (Toshiba RTV silicone rubber), poly(vinyl

Table 1. Ultimate Analysis of Manganese Dibenzyldithiocarbamate

	H(%)	C(%)	N(%)	Ash(%)
Calcd	4.71	60.08	4.67	9.16
Found	4.54	58.64	4.53	10.41

chloride), or poly(vinyl acetate) as the matrix in a weight ratio of manganese salt to the matrix of 1 to 4. The membranes were left to stand in the air for at least 12 h. Then a suitable section (a circle with a radius of 7 mm) of the membranes was attached to the end of the glass tubing with epoxy-resin-series adhesive. A solution of 0.1 mol dm^{-3} manganese chloride was used as the internal reference solution. Finally the silver-silver chloride electrode was inserted. The manganese(II) ion-selective electrodes were conditioned in a 0.1 mol dm^{-3} manganese chloride solution for 12-h periods and then stored at room temperature in a 0.1 mol dm^{-3} manganese chloride solution. The structure of the manganese(II) ion-selective electrode is shown in Fig. 2.

An electrochemical cell is as follows:

$$\underbrace{\oplus Ag|AgCl,\ Mn^{2+},\ Cl^-|\begin{matrix}\text{Activity}\\\text{Sensitive}\\\text{Material}\end{matrix}}_{\text{Manganese(II) ion-selective electrode}}$$

$$\underbrace{|Mn^{2+},Cl^-|}_{\text{Sample solution}}\underbrace{|K^+,\ Cl^-,\ AgCl|Ag\ominus}_{\text{Reference electrode}}$$

Results and Discussion

Response Curve. The responses of 10 manganese ion-selective electrodes were examined. The manganese-ion activity was calculated by means of the Debye-Hückel limitting equation. Figure 3 shows the response of a manganese(II) ion-selective electrode, with manganese sulfide (type α) as the sensing material. The slope of the E vs. manganese-ion activity was 28.49 mV/decade in the linear part of 10^{-4} to 10^{-1} mol dm^{-3}, and the coefficient of correlation was 0.998. Figure 4 shows the response of a manganese(II) ion-selective electrode with manganese dibenzyldithiocarbamate. The slope of the E vs. manganese-ion activity was 33.14 mV/decade in the linear part of 10^{-6} to 10^{-1} mol dm^{-3}, and the coefficient cf correlation was 0.999.

Response Slope. The response slopes of manganese(II) ion-selective electrodes are summarized in Table 2. The response slopes of manganese sulfide (type α) in silicone rubber, manganese sulfide (type β+γ) in silicone rubber, manganese sulfide (type β+γ)-silver sulfide in poly(vinyl acetate), and manganese dibenzyldithiocarbamate in silicone rubber are close to the Nernstian slope (29.57 mV/decade at 25 °C). With these electrodes, the slopes of E vs. the manganese-ion activity in the linear parts were 28.49 mV/decade, 28.52 mV/decade, 28.85 mV/decade, and 33.14 mV/decade respectively. The lower limits of the linear range were 10^{-4} mol dm^{-3} for the electrode with manganese sulfide (type α) in silicone rubber, manganese sulfide (type β+γ) in silicone rubber, and manganese sulfide (type β+γ)-silver sulfide in poly(vinyl acetate), and 10^{-6} mol dm^{-3} for the electrode with manganese dibenzyldithiocarbamate in silicone rubber.

Response Time. The response times (according to the definition of IUPAC[11]) of the manganese(II) ion-selective electrodes were also considered (Figs. 5 and 6). The response times of the electrodes with manganese sulfide (type α) were within 15 s in

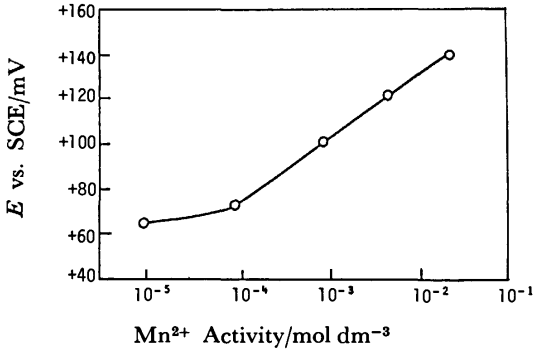

Fig. 3. Response of manganese(II) ion-selective electrode [manganese sulfide (type α)] to manganese ion.

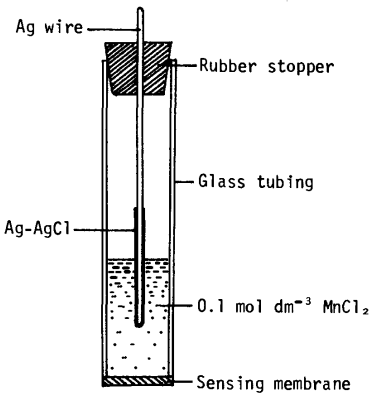

Fig. 2. Manganese(II) ion-selective electrode.

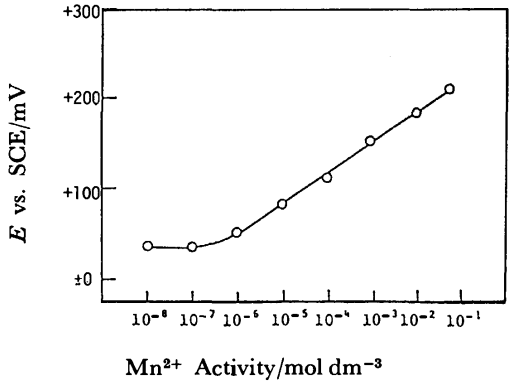

Fig. 4. Response of manganese(II) ion-selective electrode (manganese dibenzyldithiocarbamate) to manganese ion.

Table 2. Response Slopes and Coefficients of Correlation of Manganese(II) Ion-Selective Electrodes

Activity-sensitive material	Matrix	Response slope (mV/pMn^{2+})	Linear part (pMn^{2+})	Coefficient of correlation
MnS(α)	Silicone rubber	28.49	1—4	0.998
MnS(α)	Poly(vinyl chloride)	46.13	1—4	0.994
MnS(β+γ)	Silicone rubber	28.52	1—4	0.990
MnS(α)+Ag_2S	Silicone rubber	21.16	1—3	0.998
MnS(β+γ)+Ag_2S	Poly(vinyl acetate)	28.85	1—4	0.994
MnS(α)+C	Silicone rubber	6.61	1—3	0.981
$MnH_4(BO_3)_2$	Silicone rubber	22.44	1—3	1.000
Dowex 50W-X8	Silicone rubber	23.14	1—4	0.985
Amberlite CG-120	Silicone rubber	4.71	2—4	0.999
$[(C_6H_5\cdot CH_2)_2NCS_2]_2Mn$	Silicone rubber	33.14	1—6	0.999

Table 3. Selectivity Coefficients of Manganese(II) Ion-Selective Electrodes

Interfering ion	Selectivity coefficient[a]			
	MnS(α) electrode	MnS(β+γ) electrode	MnS(β+γ)-Ag_2S electrode	$[(C_6H_5\cdot CH_2)_2NCS_2]_2Mn$ electrode
Zn^{2+}	7.5×10^{-1}	9.9×10^{-1}	6.7×10^{-1}	5.8×10^{-3}
Cu^{2+}	4.7×10^{-1}	1.7	1.5	6.3×10^{-3}
Ni^{2+}	2.2	1.7	9.7×10^{-1}	1.3×10^{-2}
Cr^{3+}	5.3	6.7	4.2	6.8×10^{-3}
Pb^{2+}	3.1	3.0	9.7×10^{-1}	1.6×10^{-2}
Cd^{2+}	7.5	4.3	1.6	9.4×10^{-3}
Mg^{2+}	5.4×10^{-1}	5.4×10^{-1}	1.2	
Ca^{2+}	9.5×10^{-1}	8.8×10^{-1}	1.0	2.1×10^{-2}
Na^{+}	5.3×10^{-2}	9.2×10^{-2}	1.4×10^{-1}	2.6×10^{-3}
K^{+}	4.6×10^{-2}	6.6×10^{-2}	4.7×10^{-2}	4.2×10^{-2}
Al^{3+}				8.6×10^{-3}

a) Separate-solution method. The selectivity coefficients were calculated from the e.m.f. of a solution containing the manganese(II) ion, at activity 10^{-2} mol dm^{-3}, and a solution containing the interfering ion, at activity 10^{-2} mol dm^{-3}.

the concentration range of 10^{-3}—10^{-1} mol dm^{-3}, 1 min in 10^{-4} mol dm^{-3}, and 2 min in 10^{-5} mol dm^{-3}. The response time of the electrode with manganese dibenzyldithiocarbamate was within 15 s in the concentration range of 10^{-8}—10^{-1} mol dm^{-3}.

Effect of pH. Figure 7 shows the results obtained when the manganese ion was determined with a manganese(II) ion-selective electrode (manganese dibenzyldithiocarbamate) in solutions of various pH values obtained by adding nitric acid or sodium hydroxide. Manganese ions could be determined accurately at pH 2.5—5.5.

The Variation in the Response Slopes with the Temperature. The variation in response slopes with the temperature were also considered (Fig. 8). Over the range of 0—60 °C, the 10^{-2} mol dm^{-3} manganese ion could be determined with the manganese(II) ion-selective electrode [manganese sulfide (type α)]. The experimental value of 0.1095 mV/decade per 1 °C was in good agreement with the calculated value of 0.09922 mV/decade per 1 °C. Similar results were obtained with an electrode with manganese dibenzyldithiocarbamate.

Selectivity Coefficient. The selectivity coefficients of manganese(II) ion-selective electrodes to the several ions, such as the zinc ion, the copper ion, the nickel ion, the chromiun ion, and the lead ion, were examined by means of the separate-solution method (Table 3). The selectivity coefficients were calculated by the separate-solution method from the following relationship:

$$\log K_{MN}=\frac{E_2-E_1}{2.303RT/2F}$$

K_{MN} : Selectivity coefficient
E_1 : Electrode potential in the presence of the M ion
E_2 : Electrode potential in the presence of the N ion
M : Manganese ion
N : Interfering ion
R : Gas constant
T : Absolute temperature
F : Faraday's constant

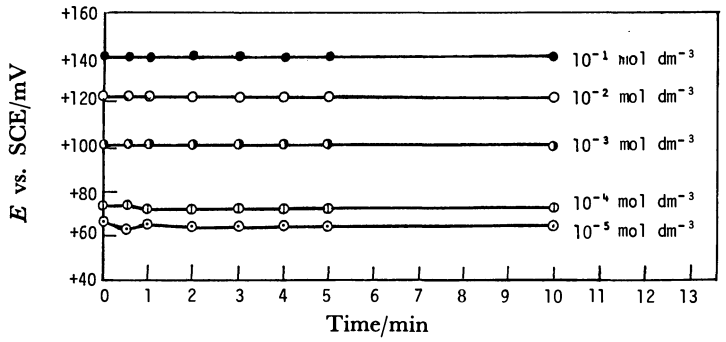

Fig. 5. Response time of manganese(II) ion-selective electrode [manganese sulfide (type α)].

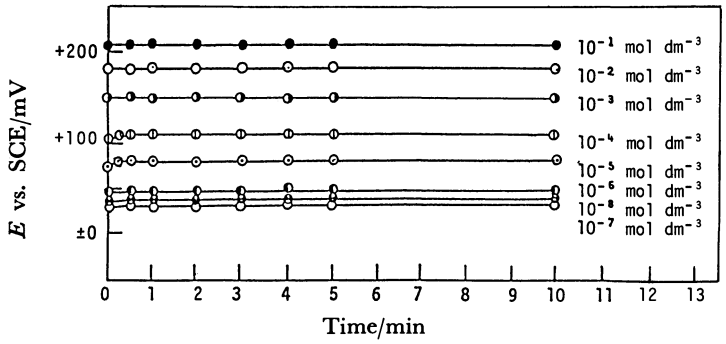

Fig. 6. Response time of manganese(II) ion-selective electrode (manganese dibenzyldithiocarbamate).

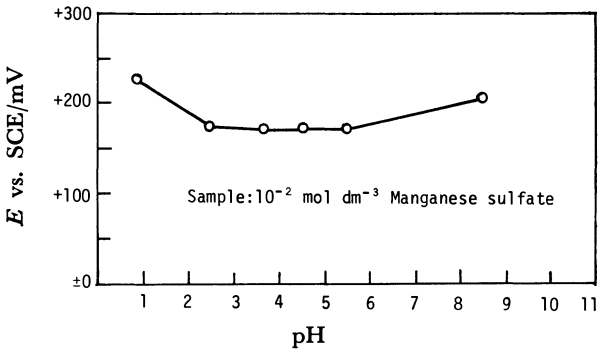

Fig. 7. Effect of pH on manganese(II) ion-selective electrode (manganese dibenzyldithiocarbamate).

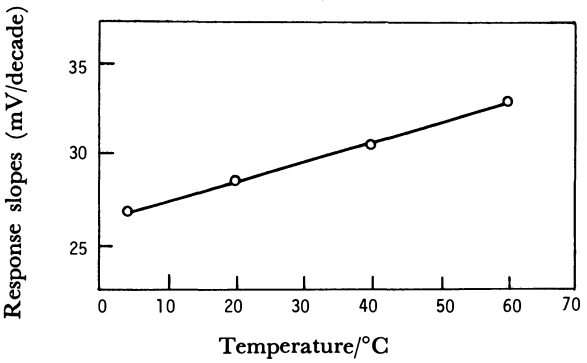

Fig. 8. The variation of response slopes by temperature on manganese(II) ion-selective electrode [manganese sulfide (type α)].

Four types of manganese(II) ion-selective electrodes [manganese sulfide (type α), manganese sulfide (type β+γ), manganese sulfide (type β+γ)-silver sulfide, and manganese dibenzyldithiocarbamate] were tested. The selectivities for monovalent cations (the sodium ion and the potassium ion) were better than those of divalent cations with the manganese sulfide (type α) and manganese sulfide (type β+γ) electrodes. The selectivity coefficients, 2.6×10^{-3}—4.2×10^{-2}, for interfering ions were obtained when the manganese dibenzyldithiocarbamate electrode was used. The electrode potentials were reproducible within 3 mV in 7—10 replicate runs.

References

1) G. J. Moody and J. R. D. Thomas, "Selective Ion Sensitive Electrodes," Merrow Publ., Watford, Hertfordshire, England (1971).
2) N. Iakshminarayanaiah, "Membrane Electrodes," Academic Press, New York (1976), p. 4.
3) J. Koryta and K. Stulik, "Ion-selective Electrodes," Cambridge University Press, Cambridge, London (1983).
4) E. Pungor, *Anal. Chem.*, **39**, 28A (1969).
5) W. Simon, *Pure Appl. Chem.*, **25**, 811 (1971).
6) J. Koryta, *Anal. Chim. Acta*, **61**, 329 (1972).
7) A. K. Covington, *Crit. Rev. Anal. Chem.*, **3**, 355 (1974).
8) Y. Su, *Henxi Huaxue*, **11**, 905 (1983).
9) D. Midgley and D. E. Mulcahy, *Talanta*, **32**, 7 (1985).
10) *Chem. Eng. News*, **63**, 56 (1985).
11) IUPAC, Anal. Chem. Div., Commission of Analytical Nomenclature, *Pure Appl. Chem.*, **48**, 127 (1976).

 © 1986 The Chemical Society of Japan Bull. Chem. Soc. Jpn., 59, 43—47 (1986)

Absolute Configuration and Circular Dichroism Spectrum of *all-cis*(NO_2,*N*,*O*)-(−)$^{CD}_{450}$[$Co(NO_2)_2(gly)_2]^-$ Complex

Shuhei FUJINAMI,* Hiroshi MIYAMAE,† Takahiro MIURA, and Koichi FUSHIMI†
Department of Chemistry, Faculty of Science, Kanazawa University, Kanazawa 920
†Department of Chemistry, Faculty of Science, Josai University,
Sakado, Saitama 350
(Received July 4, 1985)

An X-Ray analysis of *all-cis*(NO_2,*N*,*O*)-(−)$^{CD}_{450}$K[$Co(NO_2)_2(gly)_2]\cdot 1/2H_2O$ has been carried out. The crystal form is trigonal, $P3_121$, with a=10.747(1), c=18.589(4) Å and Z=6. The structure was refined by a block-diagonal least-squares method to a final R value of 0.047 for 3207 independent reflections with $|F_o|>3\sigma(|F_o|)$. The absolute configuration of the (−)$^{CD}_{450}$[$Co(NO_2)_2(gly)_2]^-$ ion has been determined to be $\Delta(R)$. By comparing the CD spectrum of $\Delta(R)$-[$Co(NO_2)_2(gly)_2]^-$ with that of a related $\Lambda(R)$-[$Co(NO_2)_2$(en)(ox)]$^-$ complex, the optical activities of these complexes have been concluded to be derived largely from helical distributions of chelate rings.

In a previous paper,[1] the CD spectrum of $\Lambda(R)$-*all-cis*(*C*,*N*,*O*)-(+)$^{CD}_{500}$[$Co(CN)_2(gly)_2]^-$ was reported and compared with that of $\Delta(R)$-*cis*-(−)$_{589}$[$Co(CN)_2$(ox)(en)]$^-$,[2] where the absolute configuration due to a helical ring pair is designated with Δ or Λ,[3] and the absolute configuration due to the distribution of donor atoms around a metal ion, with R or S.[4] The CD spectra of these complexes resemble each other due to the common R configuration. This result can not be anticipated from a dynamic coupling model regarding optical activity in transition metal complexes since the contribution from the chelate rings is usually evaluated by second-order perturbation[5] and that from the donor atoms by fourth-order perturbation.[6]

In order to clarify the optical activity derived from a chiral arrangement of donor atoms, we attempted to investigate the CD spectra of *all-cis*(NO_2,*N*,*O*)-[$Co(NO_2)_2(gly)_2]^-$ (*N* and *O* represent donor atoms of glycinato). This complex is composed of the same donor atoms as those of *cis*-[$Co(NO_2)_2$(ox)(en)]$^-$.[2] Since the ligand field strength of NO_2^- is weaker than that of CN^-, a CD spectral comparison between the dinitro complexes affords further information on the optical activity due to the arrangement of donor atoms. The *all-cis*(NO_2,*N*,*O*)-[$Co(NO_2)_2(gly)_2]^-$ complex has already been prepared by a reaction of $[Co(NO_2)_6]^{3-}$ with glycine, and resolved into optical antipodes with cinchonine by Celap et al.[7,8] However, the complex will later be prepared and optically resolved by other methods during this study. The absolute configuration of *all-cis*(NO_2,*N*,*O*)-(−)$^{CD}_{450}$[$Co(NO_2)_2(gly)_2]^-$ has been determined by an X-ray analysis in order to facilitate an analysis of the CD spectra.

Experimental

Preparation and Optical Resolution. One *cis*(NO_2) isomer of [$Co(NO_2)_2(gly)_2]^-$ has been isolated by Matsuoka et al.[9] In this study, the complex was prepared by a method described in the literature[9] with a few modification. Potassium nitrite (15 g, 0.18 mol) and glycine (15 g, 0.20 mol) were dissolved in 80 cm^3 of water. The solution was mixed with a solution containing $CoCl_2\cdot 6H_2O$ (10 g, 0.042 mol, in 30 cm^3 H_2O) and aerated for 12 h. Deposited orange needle-like crystals were filtered, and the filtrate was diluted to 3 dm^3 with water and poured onto a column of Dowex 1-X8 resin in Cl^- form (200—400 mesh, ϕ4×25 cm). The column was washed with water and the adsorbed species were eluted with 0.05 mol dm^{-3} KCl. Two bands, corresponding to univalent species, were collected in each fraction. The isomers are labelled E1 and E2 according to the order of elution. The fractions were concentrated with simultaneous removals of the eluting agent. After additions of ethanol, the solutions were kept in a refrigerator in order to precipitate the crystals. The absorption spectrum of the orange needle-like crystals deposited from the reaction mixture was identical with that of the E1 isomer. Found for E1: C, 14.14; H, 2.43; N, 16.51%. Calcd for K[$Co(NO_2)_2(C_2H_4O_2N)_2$]: C, 14.21; H, 2.38; N, 16.57%. Found for E2: C, 13.83; H, 2.61; N, 16.66%. Calcd for K[$Co(NO_2)_2(C_2H_4O_2N)_2]\cdot 0.5H_2O$: C, 13.84; H, 2.59; N, 16.14%. The infrared and absorption spectra of E1 were identical with those of the known isomer.[9]

The E2 isomer was optically resolved by the following procedure: (+)$^{CD}_{520}$[Co(ox)$(en)_2$]I (1.03 g, 2.6 mmol) and silver acetate (0.434 g, 2.6 mmol) were shaken in water (6.3 cm^3) at 60 °C for 10 min. Silver iodide was filtered and washed with 2 cm^3 of hot water and crystals containing the E2 isomer (1.35 g, 3.9 mmol) were dissolved in the above-mentioned filtrate combined with the washings. Upon scratching the wall of the vessel without cooling, an orange diastereoisomeric salt was separated. The mixture was allowed to stand for 15 min at room temperature; then the crystals were filtered. The less-soluble diastereoisomeric salt was repeatedly recrystallized from hot water (50 °C) until the $\Delta\varepsilon$ value became constant. The obtained salt was converted into potassium salt by column chromatography using Dowex 50W-X8 in a K^+ form (ϕ2×5 cm). The less-soluble diastereoisomeric salt contained (+)$^{CD}_{450}$[$Co(NO_2)_2$-$(gly)_2]^-$. The filtrate from which the less-soluble diastereoisomeric salt had been removed was also passed through a column, and a single crystal of K(−)$^{CD}_{450}$-[$Co(NO_2)_2(gly)_2]\cdot 0.5H_2O$ was obtained from the effluent and subjected to an X-ray analysis.

Spectral Measurement. Absorption and CD spectra

Table 1. Crystal Data

$K[Co(NO_2)_2(gly)_2]\cdot 1/2H_2O$	F.W.=317.2
Trigonal	Space group $P3_121$
a=10.747(1)	c=18.589(4) Å
Z=6	U=1859.3(4) Å^3
μ(Mo $K\alpha$)=1.79 mm^{-1}	D_x=1.699 g/cm^3

were recorded with a Hitachi 323 recording spectrophotometer and a JASCO J-40C automatic spectropolarimeter, respectively.

X-Ray Measurement. Crystal data are given in Table 1. Reflections were collected in a θ—2θ scan mode ($2\theta_{max}$=60°) with monochromated Mo $K\alpha$ radiation on a Rigaku AFC-5. 4187 reflections ($h\geqq 0$, $k\geqq 0$, $l\geqq 0$) were measured in which 3207 reflections, including Bijvoet pairs with $|F_o|\geqq 3\sigma(|F_o|)$, were used for a structural determination. Intensities were corrected for Lp factors, but not for absorption and extinction. Calculations were carried out on a FACOM M-160F computer at Josai University with the UNICS-III program.[10] Complex atomic scattering factors were taken from tables.[11]

Structure Determination. The structure was solved by heavy-atom and Fourier methods. Potassium atoms were located at only one special position (on a twofold axis), at the beginning. This is consistent with three K atoms per unit cell. Later, the remaining cation was found at a general position with 1/2 occupancy. One of the NO_2 groups exhibited two different orientations; each orientation was weighted at 0.5. A block-diagonal least-squares refinement with anisotropic thermal parameters for non-H atoms and isotropic parameters for H atoms reduced the R value to 0.047 (R_w=0.044 with $w=1/[\sigma^2+0.02(F_o)^2]$). The absolute structure was determined by comparing Bijvoet pairs. These are given in the F_o—F_c table.[12]

Results and Discussion

Spectral Characterization. There are five possible geometrical isomers in $[Co(NO_2)_2(gly)_2]^-$. Celap et al.[7] have isolated four isomers, except a *cis(NO$_2$)-trans(O)* isomer, from a reaction mixture of $[Co(NO_2)_6]^{3-}$ with glycine. Two isomers were isolated by column chromatography in this study. One isomer (E1) was identified with the *cis(NO$_2$)-trans(N)* isomer, and another isomer (E2) with the *all-cis(NO$_2$,N,O)* isomer from spectral data. The $(-)^{CD}_{450}$-*all-cis(NO$_2$,N,O)* isomer shows two CD peaks with opposite signs in the $^1A_{1g}\rightarrow{}^1T_{1g}$ (Oh) transition region (19400 cm^{-1}, $\Delta\varepsilon$=+0.3; 22400 cm^{-1}, $\Delta\varepsilon$=−1.4), as shown in Fig. 1.

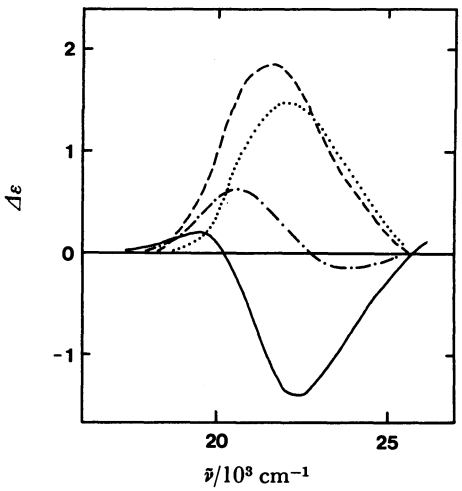

Fig. 1. CD spectra and calculated configurational curves.
a. *all-cis(NO$_2$,N,O)-Δ(R)*-$(-)^{CD}_{450}[Co(NO_2)_2(gly)_2]^-$ (——), b. *cis-Δ(R)*-$(+)_{589}[Co(NO_2)_2(ox)(en)]^-$ (----), c. $\Delta\varepsilon(R)=[\Delta\varepsilon(a)+\Delta\varepsilon(b)]/2$ (—·—), d. $\Delta\varepsilon(\Lambda)=[\Delta\varepsilon(b)-\Delta\varepsilon(a)]/2$ (·····).

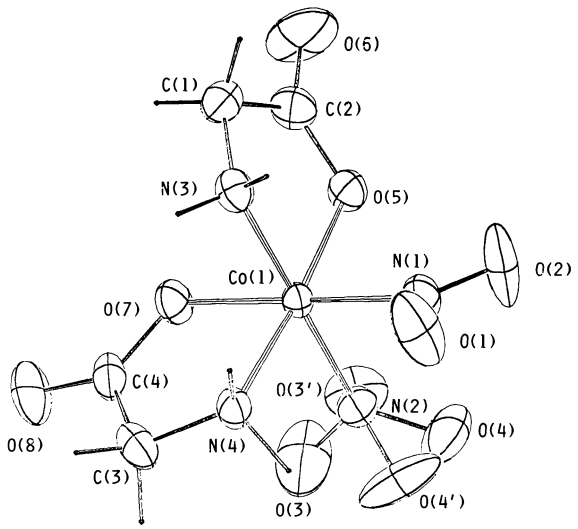

Fig. 2. Perspective view of the *all-cis(NO$_2$,N,O)*-$[Co(NO_2)_2(gly)_2]^-$ complex with atomic numbering.

Description of the Structure. Final atomic parameters are listed in Table 2. A perspective drawing of the complex anion is drawn in Fig. 2 with atomic numbering. Interatomic distances and angles are listed in Table 3. The geometrical arrangement of ligands around a cobalt ion coincides with the assignment based on spectral data; the cobalt ion is in an octahedral coordination with two bidentate glycinate ions and two unidentate nitro ions. Each of the chemically identical ligating atoms occupy cis positions on the octahedron, i.e. *all-cis(NO$_2$,N,O)*. The octahedral arrangement around a metal ion is much distorted, since there are discernible differences, even in the chemically identical bond distances around a metal ion. The differences, Co–N(NO_2), Co–N(gly), and Co–O are 0.025, 0.024, and 0.019 Å, respectively. The bond angles around a metal ion are spread at an octahedral face comprizing N(1), N(3), and N(4). The absolute configuration of helical chelate rings is described as Λ; accordingly the chiral arrangement of donor atoms, as R.

Table 2. Atomic Parameters. Positional Parameters are Multiplied by 10^4 (10^5 for Co). Thermal Parameters are Given by the Equivalent Temperature Factors (Å^2)

Atom	X	Y	Z	B_{EQV}
Co(1)	53117(8)	21979(8)	11783(4)	1.57(0.02)
K+(1)	0	2488(2)	1667	3.58(0.22)
K+(2)	670(4)	1038(4)	3648(2)	4.28(0.11)
O (1)	7943(6)	3313(7)	1803(3)	5.04(0.19)
O (2)	7048(7)	4658(6)	1944(3)	5.34(0.18)
O (3)	5345(18)	3156(14)	−176(6)	7.44(0.48)
O (3′)	4841(12)	3816(13)	154(5)	3.90(0.34)
O (4)	6823(13)	4774(11)	450(5)	4.79(0.33)
O (4′)	6961(11)	4245(15)	142(6)	5.50(0.39)
N (1)	6962(6)	3561(6)	1700(3)	2.67(0.12)
N (2)	5825(7)	3560(6)	400(3)	2.60(0.22)
O (5)	4112(5)	2814(5)	1638(2)	2.39(0.12)
O (6)	2138(7)	1941(7)	2291(4)	6.31(0.16)
N (3)	4704(6)	800(6)	1959(3)	2.26(0.15)
C (1)	3339(8)	592(8)	2233(4)	2.73(0.15)
C (2)	3150(8)	1841(8)	2044(4)	3.04(0.14)
O (7)	3668(5)	822(5)	663(2)	2.38(0.14)
O (8)	2964(6)	−701(6)	−255(3)	3.98(0.18)
N (4)	6335(6)	1401(6)	689(3)	2.48(0.19)
C (3)	5398(9)	404(9)	100(4)	3.38(0.21)
C (4)	3898(8)	119(7)	164(3)	2.49(0.17)
W (1)	101(25)	−2623(19)	1435(6)	6.54(0.57)
W (2)	−2247(12)	−559(12)	3941(7)	4.47(0.34)

Atomic Parameters.
Positional Parameters are Multiplied by 10^3

Atom	X	Y	Z	B
H(N31)	527(6)	102(6)	227(3)	1.3(0.9)
H(N32)	469(7)	3(7)	180(3)	3.2(1.2)
H(C11)	328(7)	55(8)	273(3)	3.4(1.1)
H(C12)	262(6)	−18(6)	201(3)	1.9(1.1)
H(N41)	738(7)	225(6)	48(3)	1.8(1.0)
H(N42)	682(12)	95(12)	120(5)	10.2(2.2)
H(C31)	540(8)	−53(7)	9(3)	3.4(1.4)
H(C32)	584(9)	73(9)	−40(4)	4.9(1.6)

One nitro group which occupies the site trans to the oxygen atom of glycinate ion ligates with a particular orientation. However, the other nitro group trans to the nitrogen atom of glycinate ion exhibits two different orientations in disorder. The geometry of the former nitro group is normal compared with related compounds,[13–15] while the bond angle, ∠ONO, of the latter group is somewhat smaller than that of the former group. The geometry of the glycinato groups is very similar to that observed in related complexes.[16] The bite angles of glycinate ions are 84.9 and 86.0°, and the dispositions of Co atom from mean planes of glycinate ions are 0.496(8) and 0.226(0) Å, respectively.

Crystal packing (viewed down a*) is illustrated in Fig. 3, and intermolecular distances are listed in

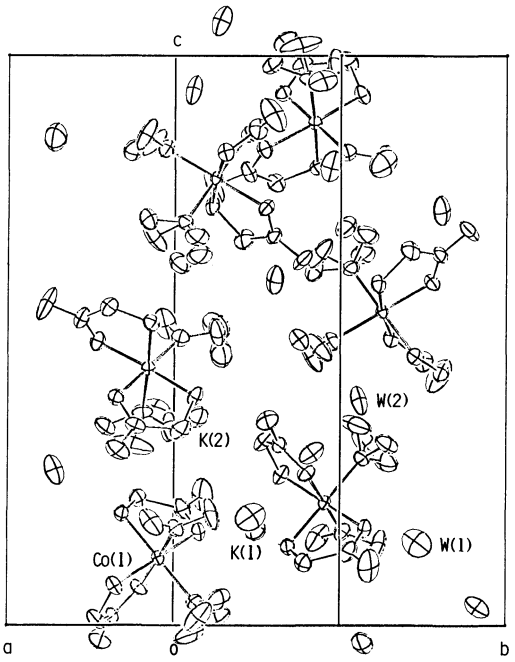

Fig. 3. Crystal packing diagram viewed down a*.

Table 3. Distances (l/Å) and Angles (ϕ/°) within the Complex Anion

Co(1)-N(1)	1.906(5)	N(1)-O(1)	1.225(11)
Co(1)-N(2)	1.931(5)	N(1)-O(2)	1.223(10)
Co(1)-O(5)	1.920(6)	N(2)-O(3)	1.174(12)
Co(1)-N(3)	1.951(5)	N(2)-O(4)	1.209(10)
Co(1)-O(7)	1.901(4)	N(2)-O(3′)	1.303(17)
Co(1)-N(4)	1.927(7)	N(2)-O(4′)	1.168(12)
N(3)-C(1)	1.461(11)	N(4)-C(3)	1.511(9)
C(1)-C(2)	1.495(14)	C(3)-C(4)	1.487(13)
C(2)-O(5)	1.286(7)	C(4)-O(7)	1.294(9)
C(2)-O(6)	1.234(13)	C(4)-O(8)	1.228(8)
N(1)-Co(1)-N(2)	89.7(2)	O(5)-Co(1)-N(3)	84.9(3)
N(1)-Co(1)-O(5)	92.0(3)	O(5)-Co(1)-N(3)	88.3(2)
N(1)-Co(1)-N(3)	92.2(2)	O(5)-Co(1)-N(4)	174.1(2)
N(1)-Co(1)-O(7)	179.4(3)	N(3)-Co(1)-O(7)	87.3(2)
N(1)-Co(1)-N(4)	93.6(3)	N(7)-Co(1)-N(4)	93.1(3)
N(2)-Co(1)-O(5)	93.4(3)	O(7)-Co(1)-N(4)	86.0(2)
N(2)-Co(1)-N(3)	177.4(3)		
N(2)-Co(1)-O(7)	90.8(2)		
N(2)-Co(1)-N(4)	88.5(3)		
Co(1)- N(1)-O(1)	118.9(5)		
Co(1)- N(1)-O(2)	121.5(6)		
O(1)- N(1)-O(2)	119.6(6)		
Co(1)- N(2)-O(3)	119.8(7)	Co(1)0N(2)-O(3′)	118.0(5)
Co(1)- N(2)-O(4)	121.6(6)	Co(1)-N(2)-O(4′)	126.8(9)
O(3)- N(2)-O(4)	117.2(8)	O(3′)-N(2)-O(4′)	115.1(10)
Co(1)- N(3)-C(1)	107.5(5)	Co(1)-N(4)-C(3)	109.3(6)
Co(1)- O(5)-C(2)	112.7(6)	Co(1)-O(7)-C(4)	116.1(4)
N(3)- C(1)-C(2)	110.9(5)	N(4)-C(3)-C(4)	110.9(7)
C(1)- C(2)-O(5)	117.0(8)	C(3)-C(4)-O(7)	116.2(6)
C(1)- C(2)-O(6)	120.8(6)	C(3)-C(4)-O(8)	120.6(7)
O(5)- C(2)-O(6)	122.2(9)	O(7)-C(4)-O(8)	123.2(8)

Table 4. Intermolecular Distances in a Unit Cell (Å)

		Symmetry operations:		i)	$-y$,	$x-y$,	$1/3+z$;
ii)	y,	x,	$-z$;	iii)	$-x$,	$-x+y$,	$1/3-z$;
iv)	$x-y$,	$-y$,	$2/3-z$;	v)	$-1+x$,	y,	z;
vi)	$-x+y$,	$-y$,	$-1+z$;	vii)	$1-x$,	$1-x+y$,	$1/3-z$;
viii)	$1-y$,	$x-y$,	$1/3+z$;	ix)	$1+y$,	x,	$-z$;
x)	$1+x$,	$1+y$,	z;	xi)	$1-x+y$,	$1-x$,	$2/3+z$;
xii)	$-x$,	$-x+y$,	$4/3-z$;	xiii)	$-x+y$,	$1-x$,	$-1/3+z$;
xiv)	$-x+y$,	$-x$,	$-1/3+z$,	xv)	y,	x,	$1-z$;
xvi)	$-x$,	$1-x+y$,	$4/3-z$;	xvii)	$1-x$,	$-x+y$,	$1/3-z$.

K(1)···O(6)	2.885(9)	K(2)···O(6)	2.874(8)
K(1)···O(8)^{i}	2.846(5)	K(2)···W(2)	2.773(2)
K(1)···O(8)^{ii}	2.846(5)	K(2)···O(8)^{i}	3.000(10)
K(1)···O(6)^{iii}	2.885(8)	K(2)···O(7)^{i}	3.144(10)
K(1)···W(2)^{iv}	2.776(12)	K(2)···W(1)^{i}	2.868(15)
K(1)···O(1)^{v}	2.775(8)	K(2)···O(6)^{iv}	3.272(10)
K(1)···W(2)^{vi}	2.776(16)	K(2)···W(2)^{iv}	2.884(17)
K(1)···O(1)^{vii}	2.775(7)	K(2)···C(4)^{i}	3.461(13)
O(1)···O(3)^{viii}	2.786(12)	O(4′)···O(2)^{xiii}	3.389(15)
O(1)···O(8)^{ix}	3.331(18)	O(4′)···N(1)^{xiii}	3.496(13)
O(2)···W(1)^{x}	3.258(18)	O(4′)···N(3)^{xiii}	3.337(15)
O(2)···O(3)^{viii}	3.405(21)	O(4′)···C(1)^{xiii}	3.370(16)
O(2)···O(4)^{viii}	3.389(14)	O(4′)···O(8)^{ix}	3.423(18)
O(2)···N(3)^{vii}	3.157(12)	O(4′)···C(3)^{ix}	3.293(15)
O(2)···C(1)^{vii}	3.403(14)	O(5)···N(2)^{xiv}	3.040(17)
O(2)···O(7)^{vii}	3.417(10)	O(5)···N(3)^{vii}	3.132(10)
O(2)···C(4)^{vii}	3.278(12)	O(5)···N(4)^{vii}	3.279(10)
O(3)···N(1)^{xi}	3.057(15)	O(6)···O(8)^{i}	3.289(13)
O(3)···N(3)^{xi}	3.008(14)	O(6)···W(2)^{xiv}	3.208(15)
O(3)···W(2)^{xii}	2.994(20)	O(6)···C(3)^{vii}	3.494(11)
O(3′)···N(3)^{xiii}	3.206(10)	O(7)···W(2)^{iii}	3.193(16)
O(3′)···W(2)^{xiv}	3.053(19)	O(8)···N(4)^{xv}	2.875(7)
O(3′)···N(2)^{ii}	3.254(18)	O(8)···W(2)^{xvi}	3.097(21)
O(4)···C(1)^{xiii}	3.420(13)	N(4)···C(2)^{xvii}	3.413(14)
O(4)···N(3)^{vii}	3.161(17)	C(4)···W(2)^{iii}	3.323(20)
O(4)···C(1)^{vii}	3.009(18)		

Table 4. The crystal comprises potassium cations, complex anions and water molecules in a complicated three-dimensional network of ionic and hydrogen bonds. Potassium ions are accomodated in two different environments in disorder. Half ions, K(1), are surrounded by eight oxygen atoms in a square prism while the remaining ions, K(2), by seven oxygen atoms in a monocapped octahedron. The low occupation of K(2) may be due to the short distance between the equivalent K(2) ions (2.58 Å). The K(1) ion exists near the O(1) atoms, as shown in Table 4, and an ionic bond is suggested to exist between them. On the other hand, there is no favorable atom near the oxygen atoms of the nitro group which ligates the site trans to the nitrogen atom of the glycinate ion. This is the reason for the disorder of the orientation in the nitro group.

Optical Activity of *all-cis(NO$_2$,N,O)*-[Co(NO$_2$)$_2$(gly)$_2$]$^-$. Two optical sources can be considered for the isomer as in *all-cis(C,N,O)*-[Co(CN)$_2$(gly)$_2$]$^-$;[1] a helical chelate rings and a chiral arrangement of donor atoms. The *cis*-[Co(NO$_2$)$_2$(ox)(en)]$^-$ complex also has two sources of optical activity. Since the absolute configuration of (+)$_{589}$[Co(NO$_2$)$_2$(ox)(en)]$^-$ has been assigned to $\Lambda(R)$,[2] the $\Delta(R)$-[Co(NO$_2$)$_2$(gly)$_2$]$^-$ isomer is pseudo-diastereoisomeric with the $\Lambda(R)$-[Co(NO$_2$)$_2$(ox)(en)]$^-$ isomer, judging from a description of the absolute configurations. Therefore, the contribution curve due to the R configuration can be formally evaluated by adding the two observed CD curves, as shown in Fig. 1. The resultant curve shows positive and negative peaks from the lower frequency, the positive one being dominant. The contribution curve due to the Λ configuration, which is calculated by subtraction (curve d in Fig. 1), exhibits a positive peak. The peak is twice as intense as the dominant peak in the R configurational contribution curve. Therefore, the helical ring pair is a more important optical source than the chiral arrangement of donor atoms in dinitro complexes.

The obtained result disagrees with that for the *all-cis*(C,N,O)-[$Co(C)_2(N)_2(O)_2$]-type complex in which most of the optical activity is derived from a chiral arrangement of donor atoms. These findings can be explained as follows; the difference in the ligand field strength between the cyano and the N donor atoms of glycinato is very large, while the difference between the nitro and the N donor atoms of glycinato is small. Consequently, the asymmetric field due to the donor atoms in dinitro complexes becomes weaker than that in dicyano complexes.

Atoh et al.[17] have found that *trans*(P,N)-[Co(acac)$(edpp)_2$]$^{2+}$ and [Co(acac)(en)(dppe)]$^{2+}$, which have two possibilities for the sources of optical activity (like the present complexes), exhibit CD spectra that are different from each other (edpp=(2-aminoethyl)diphenylphosphine; dppe=1,2-bis(diphenylphosphino)ethane). They concluded that the chiral arrangement of donor atoms is not the dominant source of the optical activity in the phosphine complexes. This fact can also be attributed to the ligand field strength of phosphine, similar to that of ethylenediamine.

Mason[6] has applied a dynamic coupling model to the optical activity of complexes with chiral arrangements of donor atoms. However, his application is incompatible with the present results. Though the dynamic coupling model demands that the optical activity is intimately related to polarizabilities of the donor atoms, the present results show that the optical activity derived from a chiral arrangement of donor atoms is intimately related to crystal field strengths of donor atoms rather than polarizabilities.

References

1) S. Fujinami and M. Shibata, *Bull. Chem. Soc. Jpn.*, **54**, 2939 (1981).
2) T. Ito and M. Shibata, *Inorg. Chem.*, **16**, 108 (1977).
3) *Inorg. Chem.*, **9**, 1 (1970).
4) R. S. Cahn, C. K. Ingold, and V. Prelog, *Angew. Chem., Int., Ed. Engl.*, **5**, 385 (1966).
5) S. F. Mason and R. H. Seal, *Mol. Phys.*, **31**, 755 (1976).
6) S. F. Mason, *Mol. Phys.*, **37**, 843 (1979).
7) M. B. Celap, J. K. Beattle, T. J. Janjic, and P. N. Radivojsa, *Inorg. Chem. Acta*, **10**, 21 (1974).
8) M. B. Celap, S. M. Nesic, M. J. Malinar, T. J. Janjic, and P. N. Radivojsa, *Glas. Hem. Drug., Beograd*, **39**, 559 (1975).
9) N. Matsuoka, J. Hidaka, and Y. Shimura, *Bull. Chem. Soc. Jpn.*, **39**, 1257 (1966).
10) T. Sakurai and K. Kobayashi, *Rikagaku Kenkyusho Hokoku* (*Rep. Inst. Phys. Chem. Res.* in Japanese) **55**, 69 (1979).
11) "International Tables for X-ray Crystallography," Kynoch Press, Birmingham, U.K. (1974), Vol. IV.
12) Anisotropic thermal parameters and list of F_o—F_c are deposited as Document No. 8601 at the office of the Editor of the Bulletin of the Chemical Society of Japan.
13) H. Shintani, S. Sato, and Y. Saito, *Acta Crystallogr., Sect. B*, **32**, 1184 (1976).
14) S. Ohba, K. Toriumi, S. Sato, and Y. Saito, *Acta Crystallogr., Sect. B*, **34**, 3535 (1978).
15) R. Herak, B. Prelesnik, LJ. Manojlovic-Muir, and K. W. Muir, *Acta Crystallogr., Sect. B*, **30**, 229 (1974).
16) D. A. Buckingham, P. J. Cresswell, R. J. Dellaca, M. Dwyer, G. J. Gainsford, L. G. Marzilli, I. E. Maxwell, W. T. Robinson, A. M. Sargeson, and K. R. Turnbull, *J. Am. Chem. Soc.*, **96**, 1713 (1974).
17) M. Atoh, I. Kinoshita, K. Kashiwabara, and J. Fujita, *Bull. Chem. Soc. Jpn.*, **55**, 3179 (1982).

Adsorption of Cobalt(II) Ions on Crystalline Hydrous Titanium Dioxide Fibers at 298 to 423 K

Yū Komatsu,* Yoshinori Fujiki, and Takayoshi Sasaki
National Institute for Research in Inorganic Materials, 1-1 Namiki,
Sakura-mura, Niihari-gun, Ibaraki 305
(Received July 26, 1985)

The distribution of cobalt(II) ions between crystalline hydrous titanium dioxide fibers and aqueous solutions has been investigated. The adsorption behavior of cobalt(II) ions is explained in terms of their ion exchange with hydrogen-ions in the fibers. The distribution coefficients of cobalt(II) ions, K_d, increased with increasing temperature at 298—373 K. Slopes of the plots of log K_d vs. pH for 398—423 K were ca. +1.6, which was somewhat lower than those for 298—373 K: +2.0. X-Ray powder diffraction patterns indicate that the fibers hold a layer structure up to 373 K but change to anatase or its precursor above this temperature.

Many papers have been published on the treatment of radioactive wastes with inorganic ion exchangers.[1-3] The previous work in this laboratory has demonstrated that crystalline hydrous titanium dioxide fibers, $H_2Ti_4O_9 \cdot nH_2O$,[4] adsorb alkali metal ions,[5] alkaline earth metal ions,[6] and divalent transition metal ions[7] in weak acid solutions at 298 K. The logarithm of distribution coefficient, log K_d, for each metal ion increases proportionally with the pH of the aqueous phase if the concentration of hydrogen ions in the solid phase is kept substantially constant.

Removal of cobalt(II) ions from cooling water is indispensable for safe operation in an atomic power plant. The present paper deals with the adsorption of cobalt(II) ions on the hydrous titanium dioxide fibers. Distribution coefficients of cobalt(II) ions were measured as a function of pH at 298—423 K; in addition, X-ray powder diffractometry was performed to obtain information about the chemical and structural changes of the solid phase.

Experimental

Titanium dioxide used was of 99.9% purity. Distilled and deionized water was used throughout this work. All the other reagents were of analytical grade.

Crystalline potassium tetratitanate fibers, $K_2Ti_4O_9$, were synthesized by a flux method.[4] The average size of the fibers was 1 mm in length and 0.01 mm in diameter.

Figure 1 shows the flow sheet of a process for synthesizing crystalline hydrous titanium dioxide fibers. About 15 g portion of the fibers was filled in a glass column with an inner diameter of 25 mm, and washed with 20 dm^3 of water to remove residual K_2MoO_4. Subsequently, 1 mol dm^{-3} hydrochloric acid was passed through the column to convert $K_2Ti_4O_9$ into an H^+ form according to the reaction:

$$K_2Ti_4O_9 + nH_2O + 2H^+ \rightarrow H_2Ti_4O_9 \cdot nH_2O + 2K^+. \quad (1)$$

The fibers were treated with the acid solution until the concentration of potassium ions in the effluent became less than 1×10^{-5} mol dm^{-3}. Potassium concentrations were measured by atomic absorption spectrophotometry. The resulting product was washed with water and dried over a saturated NaCl solution (relative humidity: 70%) to a constant weight.

Aqueous standard solutions of cobalt(II) ions were prepared by dissolving cobalt(II) chloride in water. The concentration of cobalt(II) ions was determined by EDTA titration.

Figure 2 gives the flow sheet of adsorption measurement of cobalt(II) ions on the fibers. Adsorption experiments were carried out in batchwise operations in an aluminium box thermostated at temperatures between 298 and 423 K. Twenty-cm^3 stoppered glass tubes (298—373 K) or teflon tubes (398—423 K) were used to equilibrate the solid (0.1 g) with the aqueous solutions (10 cm^3) containing cobalt(II) ions. The Teflon tubes were covered with an aluminium block to seal them tightly (Fig. 3). The initial concentration of cobalt(II) chloride was 1×10^{-4} mol dm^{-3},

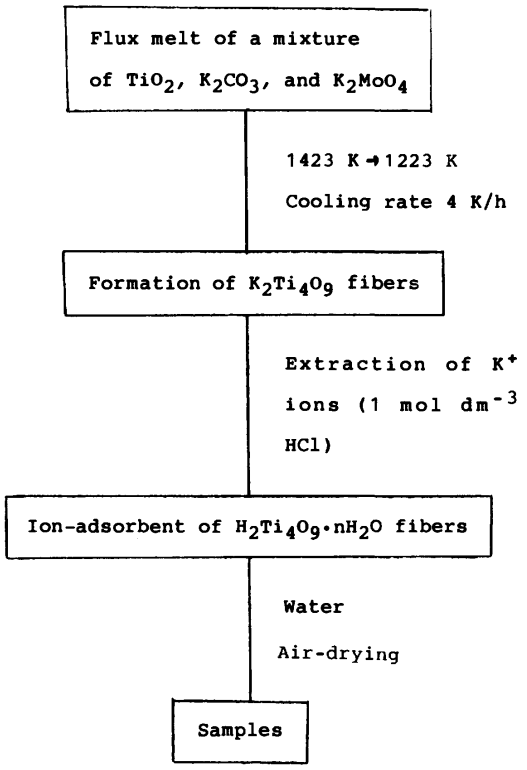

Fig. 1. Flow sheet of a process for synthesizing crystalline hydrous titanium dioxide fibers.

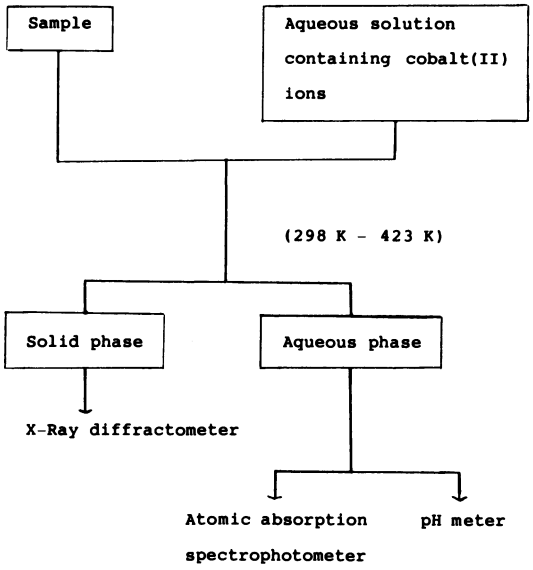

Fig. 2. Flow sheet of adsorption of cobalt(II) ions on the crystalline hydrous titanium dioxide fibers.

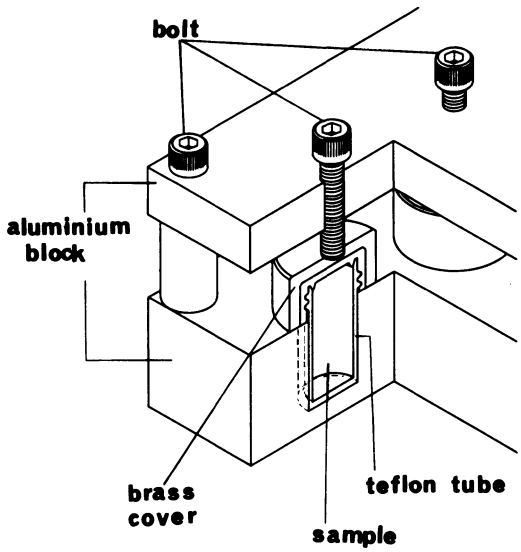

Fig. 3. Schematic diagram of the apparatus for ion exchange.

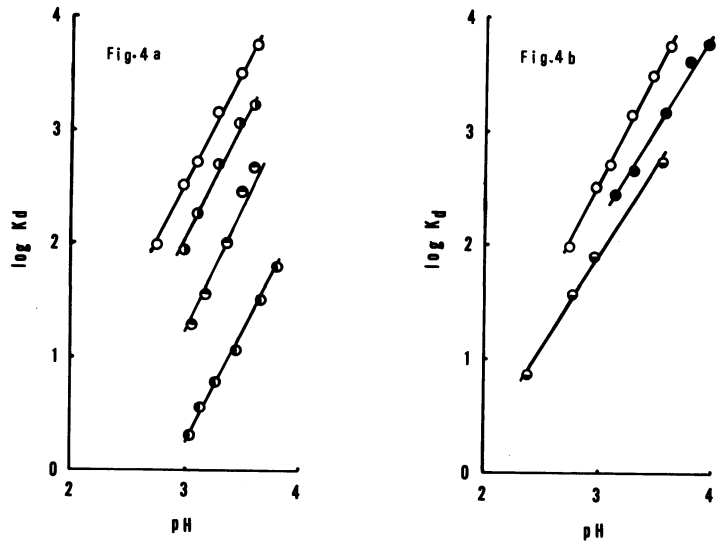

Fig. 4. Distribution coefficients of cobalt(II) ions as a function of pH in the aqueous phase at various temperatures.
The ion exchanger is 0.1 g of $H_2Ti_4O_9 \cdot nH_2O$. The aqueous solution is 10 cm^3 of hydrochloric acid solution with an initial cobalt(II) concentration of 1×10^{-4} mol dm^{-3}. Fig. 4a (◐: 298 K, ◓: 323 K, ◑: 348 K, and ○: 373 K). Fig. 4b (○: 373 K, ●: 398 K, and ◒: 423 K).

and the pH was adjusted with hydrochloric acid. The glass or teflon tubes were kept in the thermostated box, and shaken gently by hand once 1 d. The reaction times were 21 d (298 K), 10 d (323 K), or 4 d (348, 373, 398, and 423 K). Ion-exchange equilibrium was confirmed to be attained under these conditions. The fibers were separated by centrifugation for 10 min at 4000 rpm. The concentration of cobalt(II) ions in the aqueous solution was determined using a Hitachi 180—80 polarized Zeeman atomic absorption spectrophotometer. The pH of the solution was measured with a TOA HM-20E pH meter. X-Ray powder diffraction patterns were obtained by using a Rigaku Denki RAD-2B diffractometer with Cu $K\alpha$ radiation.

Results

The distribution coefficient, K_d, was calculated as

$$K_d = \frac{C_1/g}{C_2/cm^3}, \quad (2)$$

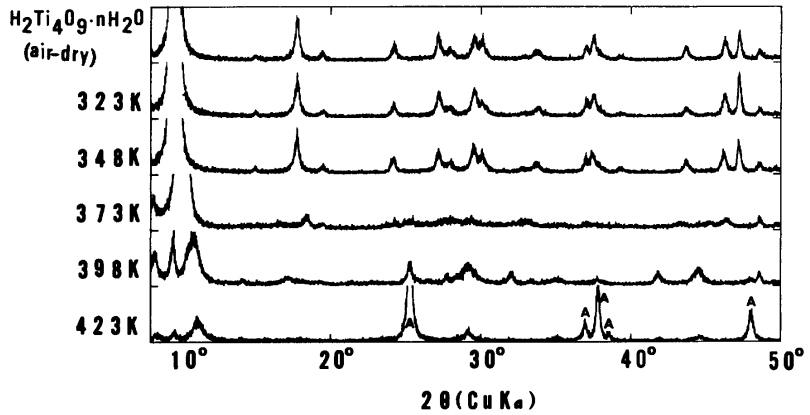

Fig. 5. X-Ray powder diffraction patterns of the solid samples treated with aqueous solutions at six different temperatures.
A: anatase.

where C_1 is the amount of adsorbed cobalt(II) ions per 1 g of the solid, and C_2 is the concentration of cobalt(II) ions per 1 cm^3 of the aqueous solution.

Figure 4 gives the plots of log K_d vs. pH in the aqueous phase for six different temperatures. In these experiments, the concentration of hydrogen ions in the solid phase was held substantially constant before and after the adsorption of cobalt(II) ions. The slopes of the log K_d–pH lines were about +2 below 398 K. Figure 4 also shows that the slopes of the lines for 398 and 423 K were somewhat lower than +2. X-Ray powder diffractometry was then applied to clarify the cause of the differences in slopes (Fig. 5).

The fibers treated below 373 K showed almost the same diffraction patterns as the original fibers. This fact indicates that the structure of the fibers remain virtually unchanged at 348 K or below. Therefore, the adsorption of cobalt(II) ions on the fibers under these conditions can be represented by the ion-exchange reaction:

$$m\mathrm{Co^{2+}(aq)} + \mathrm{H_2Ti_4O_9 \cdot nH_2O(s)} \rightarrow 2m\mathrm{H^+(aq)} + \mathrm{Co}_m\mathrm{H}_{2(1-m)}\mathrm{Ti_4O_9 \cdot nH_2O(s)}, \quad (3)$$

where the subscripts "aq" and "s" denote the aqueous and solid phases, respectively, and $0<m<1$.

The layer structure of the crystalline hydrous titanium dioxide is characterized by a very strong 200 reflection with an interplanar spacing, $d(200)$, of ca. 0.91 nm.[8] The corresponding peak of the solid treated at 373 K was observed at 0.86 nm; all the other peaks disappeared almost completely. The presence of this peak suggests that the poorly crystallized phase formed at 373 K has a layer structure similar to that of hydrous titanium dioxide.

The solids treated at 373 K or below remained fibrous, but those treated at 398—423 K turned powdery. The powdery samples showed X-ray diffraction patterns different greatly from those of fibrous ones. The three reflections appeared at 8° to 12°; furthermore, the peaks of anatase-type titanium dioxide appeared, and their intensities increased with an increase in temperature of the solution. That is, a part of hydrous titanium dioxide, $H_2Ti_4O_9 \cdot nH_2O$, dehydrates to give anatase under the above conditions:

$$\mathrm{H_2Ti_4O_9 \cdot nH_2O} \rightarrow 4\mathrm{TiO_2} + (n+1)\mathrm{H_2O}. \quad (4)$$

The three peaks described above are assigned to an intermediate phase which is formed in the course of conversion of hydrous titanium dioxide to anatase.

Table 1. Summary of the Values of $d(200)$ Determined by X-ray Powder Diffractometry and Distribution Coefficients of Cobalt(II) Ions at pH 3.0

Temperature / K	$d(200)$ / nm	K_d
298	0.91	0.22
323	0.91	1.36
348	0.91	2.10
373	0.86[a]	2.54
398	—	2.16
423	—	1.90

a) Strictly speaking, this peak cannot be assigned to the 200 reflection because this sample was not a crystalline material.

Discussion

The hydrous titanium dioxide fibers have a layer structure similar to that of potassium tetratitanate.[4] Table 1 summarizes the $d(200)$ values and distribution coefficients of cobalt(II) ions at pH 3.0. As the temperature was increased between 298 and 373 K, the

distribution coefficient also increased. At 373 K, the crystalline hydrous titanium dioxide fibers converted into the poorly crystallized phase with an interlayer distance considerably smaller than that of the crystalline fibers. The amount of adsorbed cobalt(II) ions must be influenced by the variations of both the temperature and structure of the fibers. It is, however, difficult to evaluate the extent to which these two factors affect the partition of cobalt(II) ions between the solid and aqueous phases.

The distribution coefficient of cobalt(II) ions reached a maximum at 373 K (Table 1). However, this temperature cannot be regarded as optimum for adsorption of cobalt(II) ions. As the temperature was raised above 373 K, the hydrous titanium dioxide changed into the intermediate phase and/or anatase to a greater extent with a result that the K_d values decreased with increasing temperature. In view of the fact that the layer structure is stable to heating in the air up to 573 K,[9] the presence of high-temperature solutions evidently accelerates both chemical and structural changes of the fibers in the closed tube. There is a fear of the unfavorable conversion of the poorly crystallized phase formed at 373 K into anatase or its precursor if minor modification in experimental conditions is made. On the other hand, the layer structure of the fibers remains almost unchanged below 373 K. Accordingly, a reaction temperature between 348 and 373 K is recommended especially when the fibers are used as an adsorbent for a long period. If the present fibers are used as an adsorbent for cobalt(II) ions, conditions under which $H_2Ti_4O_9 \cdot nH_2O$ does not change to other phases should be determined prior to adsorption runs.

The authors are very grateful to Professor Tatsuya Sekine of the Science University of Tokyo and Professor Mitsuo Abe of the Tokyo Institute of Technology for their valuable discussions during this work and to Mr. Yasuji Masuda, Dr. Takashi Akahane, Mr. Toshiaki Wada and Mr. Hajime Haneda of this institute for the assistance with the experimental work.

References

1) US-ERDA, Alternatives for managing wastes from reactors and post-fission operations in the LWR fuel cycle, ERDA-76—43 (1976).
2) T. Kanno and H. Mimura, *Nippon Genshiryoku Gakkai Shi*, **19**, 113 (1977).
3) M. Abe and K. Uno, *Sep. Sci. Technol.*, **14**, 355 (1979).
4) Y. Fujiki and N. Ohta, *Yogyo Kyokai Shi*, **88**, 111 (1980).
5) Y. Komatsu, Y. Fujiki, and T. Sasaki, *Bunseki Kagaku*, **31**, E225 (1982).
6) Y. Komatsu, Y. Fujiki, and T. Sasaki, *Bunseki Kagaku*, **32**, E33 (1983).
7) T. Sasaki, Y. Komatsu, and Y. Fujiki, *Sep. Sci. Technol.*, **18**, 49 (1983).
8) T. Sasaki, M. Watanabe, Y. Komatsu, and Y. Fujiki, *Inorg. Chem.*, **24**, 2265 (1985).
9) N. Ohta and Y. Fujiki, *Yogyo Kyokai Shi*, **88**, 1 (1980).

 © 1986 The Chemical Society of Japan Bull. Chem. Soc. Jpn., 59, 53—57 (1986)

The Ion-Association Sorption and Extraction of Metal Thiocyanate Complexes to Cellulose Acetate Polymer and Organic Solvents. Similarity in Distribution Mechanisms

Takashi HAYASHITA† and Makoto TAKAGI*
Department of Organic Synthesis, Faculty of Engineering, Kyushu University, Hakozaki, Higashi-ku, Fukuoka 812
(Received July 30, 1985)

The sorption and extraction of heavy metal thiocyanate complexes from an aqueous solution were studied for a cellulose acetate polymer and conventional organic solvents. The ease of metal sorption to solid cellulose acetate correlated well with the ease of metal extraction to liquid glycerol triacetate. The distribution behavior of ammonium thiocyanatozincate complexes was studied in detail and compared among cellulose acetate, isobutyl methyl ketone, and glycerol triacetate. The chemical processes involved in the metal distribution to the organic phase were found to be essentially the same for these three media. Thus, cellulose acetate was conveniently considered a polymer solvent. The results were discussed in relation to metal-selective hyperfiltration through cellulose acetate membranes.

In the course of our study of metal-selective separation by means of polymer membranes,[1-4] we outlined an idea of metal-selective hyperfiltration. The principle of metal separation is based on a metal-selective sorption of ion-association complexes to the membrane phase and a subsequent transport of the sorbed metal species through the membrane by some coupling processes with a solvent flow under hydraulic pressure.[3,4] The sorption of heavy metal thiocyanate complexes to polymers took place predominantly on polymers of medium polyarity, such as cellulose acetate (CA) and polyacrylonitrile. An equilibrium study indicated that the sorption obeys the Langmuir adsorption isotherm and the Nernstian distribution law at high and low metal loadings respectively. An analysis of the Nernstian-type distribution suggested that the nature of the sorption to the polymer (CA) is essentially similar to that of the conventional liquid–liquid extraction of the metal-complex species. The permeability under hydraulic pressure of metal thiocyanate and iodide complexes through CA membranes correlated well with the sorptivity of metal species, suggesting a solvent flow-coupled permeation by the sorbed metal species. The present paper includes an extended study of metal sorption on a polymer (CA) and its comparison with liquid–liquid extraction, since their understanding is essential for the development of metal-selective hyperfiltration membranes.

Experimental

Reagents. The cellulose acetate (acetyl content 39.8%; ASTM viscosity, 3s) was obtained from Eastman Chemicals. The other reagents were reagent-grade commercial products and were used without further purification. Cellulose acetate powders finer than 50 mesh were used in the sorption experiments.

Sorption and Extraction. Sorption experiments were done by the procedure previously described.[3] Liquid–liquid extraction was carried out in a conventional manner. Ten to fifteen min mechanical shaking was enough to attain equilibrium. The volumes of the organic and aqueous solutions after equilibration were measured. The concentrations of the metal complexes were determined by means of atomic absorption spectrophotometry with a Japan Jarrel Ash Co. AA-1 instrument.

The sorption and extraction of metal complexes were estimated by means of the degree of sorption (or extraction) (E) and the distribution ratio (D):

$$E=\frac{[M]_i-[M]_f}{[M]_i}\times 100 \quad (1)$$

$$D=\frac{[M]_i-[M]_f}{[M]_f}\times\frac{V_w}{W_m}, \quad (2)$$

where $[M]_i$ and $[M]_f$ are the initial and final metal concentrations respectively, in an aqueous solution; V_w is the volume of the aqueous solution (ml) after equilibrium, and W_m is either the weight of CA (g) or the volume of the organic solution (ml) after equilibrium. In this definition, the dimensions of the metal-distribution ratio are not the same for sorption (to CA) and extraction (to organic solvent). Therefore, where a clear distinction between the two distribution constants should be made, D' is used for the volume-based liquid-liquid distribution ratio. The weight-based D value may be converted to the volume-based D' value by dividing it by the density of the dry polymer (1.25 g/cm^3 for CA) at the first approximation. The D and D' values are thus not very different numerically, and one can use either value for a direct comparison of the effectiveness of metal sorption and extraction.

Results and Discussion

Previous studies indicated that the sorption of metal thiocyanate complexes took place readily for

† Present address: Department of Applied Chemistry, Faculty of Engineering, Kanagawa University, Kanagawa-ku, Yokohama 221.

Table 1. Extraction[a] and Sorption (%)[b] of Metal Thiocyanate Complexes

No.	Solvent	Fe^{3+}	Co^{2+}	Ni^{2+}	Cu^{2+}	Zn^{2+}	Pd^{2+}	Ag^{+}	Cd^{2+}	In^{3+}	Au^{3+}
1	TA	90	27	7.4	65	96	7.2	0.0	22	97	90
2	MIBK	100	96	0.0	87	100	33	0.0	23	100	100
3	DCE	0.0	0.8	2.6	0.0	0.0	0.0	0.0	0.0	0.0	0.0
4	CA	63	9.6	1.2	47	92	84	0.0	12	79	94

a) Ten ml of a 0.5 M (1 M=1 mol dm^{-3}) NH_4SCN solution containing 0.5 mM metal nitrate (pH 1.0, adjusted by HNO_3) were shaken with 10 ml of triacetin (TA), methyl isobutyl ketone (MIBK), and 1,2-dichloroethane (DCE). b) Twenty ml of a 0.5 M NH_4SCN solution containing 0.5 mM metal nitrate (pH 1.0, adjusted by HNO_3) were shaken with 2.0 g of CA powder. Data taken from Reference 4.

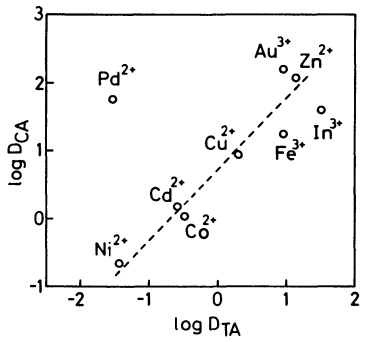

Fig. 1. Correlation between distribution ratios for the sorption and extraction of metal thiocyanate complexes. D_{CA}, distribution ratio in water–CA; D_{TA}, distribution ratio in water–TA. Conditions are similar to those in Table 1.

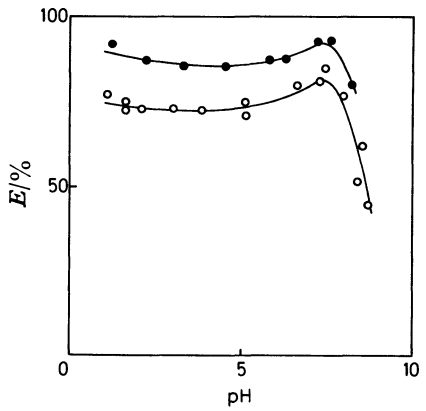

Fig. 2. Effect of pH on the sorption and extraction of zinc thiocyanate complexes. Sorption to CA (○): Twenty ml of 0.25 M NH_4SCN solution containing 0.5 mM $Zn(NO_3)_2$ were used. The pH was adjusted by adding HCl or KOH. The amount of CA was 2.0 g. Extraction to TA (●): 10 ml of 0.25 M NH_4SCN solution containing 0.5 mM $Zn(NO_3)_2$ were used. The volume of TA was 10 ml.

CA and polyacrylonitrile, but not for cellulose and poly(vinyl chloride).[3,4] In order to compare such sorption behavior with solvent-extraction systems, the extraction of metal thiocyanate complexes was investigated by using organic solvents of a related chemical structure. The results are shown in Table 1, along with the sorption data for CA. Oxygen-containing organic solvents, such as isobutyl methyl ketone (MIBK) and triacetin (TA, glycerol triacetate), have a high extraction ability. On the other hand, 1,2-dichloroethane shows little extraction ability. Such behavior is general in ion-association extraction systems.[5]

It is noteworthy that the sorption behavior of metal thiocyanate complexes on solid polymers correlates well with the liquid–liquid metal extraction. That is, CA effectively exhibits an "extraction" ability similar to those of oxygen-containing organic solvents, while poly(vinyl chloride) has little sorption ability, just like dichloroethane liquid–liquid extraction systems, Figure 1 shows the correlation of the distribution ratios between the sorption by cellulose acetate and the extraction by triacetin. The correlation is approximately linear except for palladium. This strongly suggests the similarity of metal-partition mechanisms between the solid polymer matrix and the structurally related organic solvent. The cause of the departure from the linearity for palladium is not apparent at present. It is possible, though, that a local micro-structure of the polymer matrix helps enhance the sorptivity of some particular metal complexes. A "cation chelation mechanism" has recently been described for the sorption of metal complexes by polyether-type polyurethane foam.[6,7]

The effect of the pH on the sorption and extraction of zinc thiocyanate complexes is shown in Fig. 2. The pH-E(%) profiles are quite similar for TA and CA. The E(%) values stay almost constant at pH 1—6 but drop sharply at pH>7.5. The latter effect is due to the hydrolysis of metal ions in the bulk solution.[3] As has been reported previously,[3,4] the zinc ion becomes sorbed on CA as ammonium thiocyanate complexes with an average composition of $(NH_4)Zn(SCN)_3$–$(NH_4)_2Zn(SCN)_4$ under weakly acidic conditions. The sorption and extraction were not studied under low pH conditions (pH<1) to avoid possible ester hydrolysis. However, the proton is known to act as a counter cation in such ion-association complexes as the trihydrated hydronium ion, and the

increase in proton concentration is considered to enhance the sorption and extraction,[8,9] which may, in fact, be reflected in the increased metal extractions in the lower pH region.

The relationship of the distribution ratio and the zinc concentration (total concentration) in an aqueous solution at equilibrium is shown in Fig. 3. The figure shows that the sorption and extraction ability for zinc thiocyanate complexes increases in this order; MIBK>CA>TA. The metal distribution ratio for cellulose acetate is about five times higher than that for the triacetin extraction system at an ammonium thiocyanate concentration of 0.5 M. The similar is the case at 0.25 M ammonium thiocyanate. Thus, CA is substantially a better sorbent or extraction solvent than is TA for collecting zinc(II) thiocyanate complexes from aqueous solutions. This is quite interesting because it means that a "solid" polymer can be a better "extraction solvent" than its liquid analogue.

Figure 3 also shows that the distribution ratio

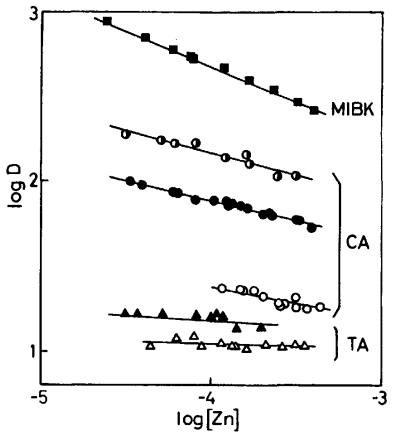

Fig. 3. Variation of zinc distribution ratio as a function of (total) zinc concentration in aqueous solution. Sorption to TA: Twenty ml of aqueous solution containing $Zn(NO_3)_2$ in various concentrations were shaken with 0.5—2.0 g CA. The aqueous solution contained NH_4SCN in concentrations 0.25 M (○), 0.50 M (●), and 0.75 M (◑). Extraction to TA and MIBK: Ten ml of aqueous solution containing $Zn(NO_3)_2$ in various concentrations were shaken with 5 ml TA or 2 ml MIBK. The aqueous solution contained NH_4SCN in concentrations 0.25 M (TA, △), 0.50 M (TA, ▲), and 0.50 M (MIBK, ■).

decreases as the aqueous zinc concentration increases. For conventional solvent-extraction systems, such behavior is usually considered to indicate the dissociation of extracted ion-association complexes in an organic solution, and it is particularly common for liquid-liquid extraction using solvents with a moderate dielectric constant.[10] It is conceivable that a similar dissociation reaction is taking place in the CA polymer matrix. In fact, Oren et al. studied the sorption behavior of metal halogeno complexes by using open-cell polyurethane foam and confirmed the dissociation of the extracted ion-association species in the foam.[11] However, in our sorption system, as we showed in a previous paper,[3] the polymer (CA) has a maximum sorption capacity (the maximum load of metal according to the Langmuir adsorption isotherm) for each ion-association-complex sorption system.[3] Therefore, the saturation effect, which should lead to a decrease in D similar to that observed in Fig. 3, may not be negligible under the relevant conditions. Calculations according to the Langmuir adsorption equilibria indicated, however, that the saturation effect is quite negligible under the conditions shown in Fig. 3. Thus, the behavior of CA, being in line with that of MIBK and TA (Fig. 3), further strengthens the idea that CA serves as a "polymer solvent" for the extraction of ion-association complexes.

The mechanism of the sorption of metal species to CA was compared with that of extraction to the organic solvent with a related structure (TA). Scheme 1 shows a simplified model of metal distribution. The sorption and extraction of ammonium thiocyanatozincate complexes were studied at a relatively low metal loading in the organic phase. Under such conditions, both sorption and extraction can be treated according to the Nernstian distribution law, which gives these expressions, 3—5:[3,4]

$$\log \beta D' = (n-2)\log[NH_4^+]_a + n\log[SCN^-]_a + \log K_a K_d' \quad (3)$$

$$D' = [(NH_4)_{n-2}Zn(SCN)_n]_o / ([Zn^{2+}]_a + [Zn(SCN)^+]_a + \cdots\cdots + [Zn(SCN)_m^{2-m}]_a) \quad (4)$$

$$\beta = 1 + K_1[SCN^-]_a + K_1K_2[SCN^-]_a^2 + \cdots\cdots + K_1K_2\cdots\cdots K_m[SCN^-]^m \quad (5)$$

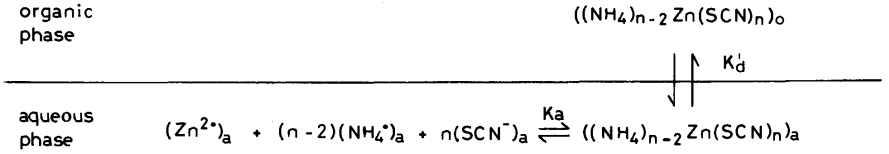

Scheme 1. Model for zinc thiocyanate complex distribution among organic and aqueous solutions.

where K_m stands for the mth successive complex formation constant in an aqueous solution.

Equation 3 indicates that the coordination number n of the extracted metal species can be determined from the plots of log $\beta D'$ vs. log $[SCN^-]_a$.

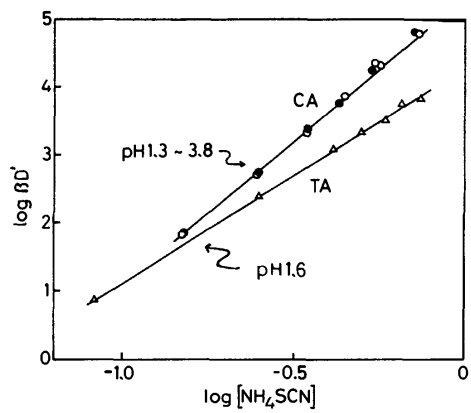

Fig. 4. Sorption and extraction of zinc thiocyanate complexes as a function of aqueous NH_4SCN concentration. Plots according to Equation 3. Sorption to CA (○,●): Twenty ml of aqueous NH_4SCN solution (○, pH 1.3; ●, pH 3.8. adjusted by HNO_3) containing 0.5 mM $Zn(NO_3)_2$ were used. The amount of CA was 2.0 g. Extraction to TA(△): Ten ml of aqueous NH_4SCN solution containing 0.5 mM $Zn(NO_3)_2$ (pH 1.6, adjusted by HNO_3) were used. The volume of TA was 10 ml.

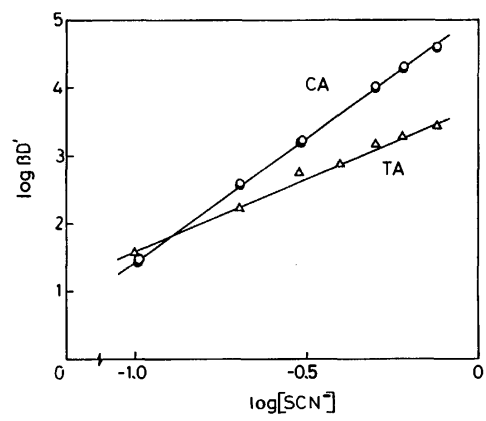

Fig. 5. Sorption and extraction zinc thiocyanate complexes as a function of aqueous SCN^- concentration. Plots according to Equation 3. Sorption to CA (○,●): Twenty ml of aqueous NH_4SCN solution (pH 1.6, adjusted by HNO_3) containing 0.5 mM $Zn(NO_3)_2$ were used. Total concentration of ammonium ion was adjusted to 0.75 M by NH_4NO_3. The amount of CA was 1.0 g (●) and 2.0 g (○). Extraction to TA (△): Twenty ml of aqueous NH_4SCN solution containing 0.5 mM $Zn(NO_3)_2$ (pH 1.6, adjusted by HNO_3) were used. Total concentration of ammonium ion was adjusted to 0.75 M by NH_4NO_3. The volume of TA was 5 ml.

Figure 4 shows one such plot, where the concentration of ammonium thiocyanate is varied (in this case, $[NH_4^+]_a=[SCN^-]_a=[NH_4SCN]_a$ in Equation 3). For the sorption on CA, the D' in Equation 3 was replaced by D. Figure 5 shows a similar plot, where $[NH_4^+]_a$ is maintained constant at 0.75 M and $[SCN^-]_a$ is varied. Figure 4 gives n values of 3.2 and 2.6 for the metal distributions to CA and TA respectively. Figure 5 similarly gives n values of 3.5 (CA) and 2.5 (TA). The sorbed or extracted metal species, therefore, seem to have average compositions of $(NH_4)_{1.2-1.5}Zn(SCN)_{3.2-3.5}$ in CA and $(NH_4)_{0.5-0.6}$-$Zn(SCN)_{2.5-2.6}$ in TA.

As regards the similarity (as extraction solvents) between CA and carbonyl group-containing solvents (MIBK and TA), it seemed that it would be interesting to obtain some insight into the solvation of the extracted metal complex in the solid polymer. A solvation number (m) or a number of solvent (S) molecules associated with the extracted complex species may be defined by Equation 6:

$$((NH_4)_{n-2}Zn(SCN)_n)_a + m(S)_o \quad ((NH_4)_{n-2}Zn(SCN)_n \cdot mS)_o \qquad (6)$$

where the suffixes "a" and "o" denote the aqueous and organic phases respectively. To obtain a rough measure of the m number, zinc thiocyanate complexes were extracted by an "inert" solvent, 1,2-dichloroethane, to which a variable concentration of MIBK or TA was added. Pure 1,2-dichloroethane does not extract the metal species at all, as shown in Table 1. A conventional manipulation then gives Expression 7 for the metal-distribution ratio (D) between the aqueous and the "active" solvent (S)-doped 1,2-dichloroethane phases:

$$\log D = m \log [S]_o + \text{constant} \qquad (7)$$

where $[S]_o$ stands for the molar concentration of the active solvent (MIBK or TA) in 1,2-dichloroethane.[12]

Equation 7 indicates that m is obtained as a slope of a linear plot, log D vs. $[S]_o$. Figure 6 shows such plots, from which the m value is determined to be 5.0 for both MIBK and TA. Although a TA molecule contains three carbonyl (or CH_3CO-) functional groups, it is most likely acting as a monofunctional carbonyl compound, as is MIBK. Since the nature of CA as an extraction solvent is between MIBK and TA (Fig. 3), it is quite probable that zinc thiocyanate complexes are stabilized by at least five carbonyl functional groups from CA in the polymer matrix.

In conclusion, there is now ample evidence that CA behaves just like ordinary carbonyl group-containing solvents, such as MIBK and TA, in "extracting" metal-complex species. Halogeno and pseudohalogeno complexes are especially easy to extract. Interestingly, CA membranes (including the

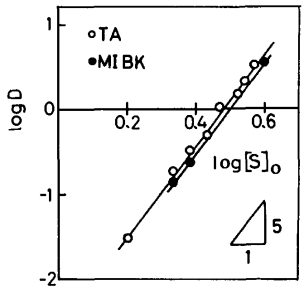

Fig. 6. Determination of solvation number according to Equation 7. Ten ml of 0.5 M NH_4SCN containing 0.5 mM $Zn(NO_3)_2$ were shaken with 10 ml of 1,2-dichloroethane containing TA or MIBK in variable concentration. The pH was adjusted to 1.0 by HNO_3.

hyperfiltration membrane) are quite similar to CA powders in such sorption properties.[13] In the light of these findings, it is no accident that CA membranes exhibit peculiar permeation characteristics to such metal complexes under hyperfiltration conditions.[1-4] At present, CA is the only polymer material which is a good sorbent for metal complexes and which can at the same time, be fabricated into hyperfiltration membranes. It is hoped that an understanding of the mechanism of metal sorption will give impetus to the development of a variety of polymer materials for the fabrication of metal-selective hyperfiltration membranes.

References

1) T. Hayashita, M. Takagi, and K. Ueno, *Sepn. Sci. Techn.*, **18**, 461 (1983).
2) Idem, ibid., **19**, 315 (1984).
3) T. Hayashita and M. Takagi, *Talanta*, **32**, 399 (1985).
4) T. Hayashita, M. Hamada, and M. Takagi, *Chem. Lett.*, **1985**, 829.
5) T. Sekine and Y. Hasegawa, "Solvent Extraction Chemistry," Dekker, New York (1977).
6) R. F. Hamon, A. S. Khan, and A. Chow, *Talanta*, **29**, 313 (1982).
7) S. J. Al-Bazi and A. Chow, ibid., **30**, 487 (1983).
8) R. L. Erickson and R. L. McDonald, *J. Am. Chem. Soc.*, **88**, 2099 (1966).
9) D. K. K. Liu, D. T. Shioshita, and R. L. McDonald, *J. Phys. Chem.*, **78**, 2572 (1974).
10) R. M. Diamond, ibid., **61**, 75 (1957).
11) J. J. Oren, K. M. Gough, and H. D. Gesser, *Can. J. Chem.*, **57**, 2032 (1979).
12) The expression can be derived in a manner similar to that of Expression 3. The constant includes the extraction equilibrium constant for Reaction 6 as well as those equilibrium constants in an aqueous solution concerning the formation of zinc thiocyanate complexes and ion-association complexes. The constant is also a function of the concentration of ammonium and thiocyanate ions in an aqueous solution. Therefore, if the concentrations of ammonium thiocyanate and an active solvent are in a large excess of the zinc ion, and if the ammonium thiocyanate concentration is kept constant, the metal distribution ratio D becomes a function of only $[S]_o$.
13) T. Hayashita and M. Takagi, unpublished results.

Chemistry of 1,2-Thiaphosphole 2-Sulfides. II. Reactions of 1,2-Thiaphosphole 2-Sulfides with Some Nucleophiles

Hideyuki TANAKA, Takao SAITO, and Shinichi MOTOKI*
Department of Chemistry, Faculty of Science, Science University of Tokyo,
Kagurazaka, Shinjuku-ku, Tokyo 162
(Received April 1, 1985)

5-*t*-Butyl-1,2-thiaphosphole 2-sulfides reacted with alcohols, thiols, and amines to give the 1,4-adducts, 2-alkoxy-, 2-(*p*-tolylthio)-, and 2-alkyl(aryl)amino-1,2-thiaphosphol-3-ene 2-sulfides, respectively. However, the reactions of 5-phenyl-1,2-thiaphosphole 2-sulfides with cyclohexyl- and arylamines afforded 1,2,3-dithiaphosphorins.

Previously, we reported the synthesis of 2,9-dithia-1-phosphabicyclo[4.3.0]nona-3,7-diene 1-sulfides **A** and their thermolysis generating 1,2-thiaphosphole 2-sulfides **B** and α,β-unsaturated thiones **C**.[1] The sulfides **B** are unique intermediates containing phosphorus and sulfur in their unsaturated heterocyclic ring, and they have been found to undergo cycloaddition reactions with various dienophiles.[1] Meanwhile, interest is being shown in π-bonded phosphorus compounds such as methylenephosphine sulfides, -(S=)P=C , and related compounds.[2] Their reactions with some alcohols (as nucleophile) were also reported recently.[3]

Accordingly, it appeared of interest to investigate further reactions of **B**. The reaction with some nucleophilic reagents is reported in the present paper.

Results and Discussion

Reactions of Phosphabicyclo Compounds 1 with Alcohols, Phenols, Thiols, and Amines. Treatment of **1** with alcohols (phenols) afforded no product on refluxing in benzene. However reactions took place readily in the presence of NEt_3 to give the 1,4-adducts (**5**) of alcohols toward **3** along with thione (**4**) dimers **6**[1,4] (Scheme 2, Table 1). The reaction of **1** with cyclohexanol was carried out in refluxing xylene in the presence of NPr^n_3, since the reaction was slow in refluxing benzene.

The elemental analyses and the mass spectra indicated that **5** were 1:1 adducts of **3** and the alcohols. The adducts **5** showed strong IR absorption due to the P-O linkage at about 1000 cm^{-1}. In the ^1H NMR spectra,[6] H-4 and H-5 protons resonated at δ=6.8—6.9 and 4.2—4.3 with the coupling constant 3.0—3.5 Hz and the H-4 proton exhibited a large H-P coupling constant (J_{HP}=50—55 Hz)(Table 2). The ^{13}C NMR spectra[7] showed a signal of the C-3 olefinic carbon at δ=140—142 with a large C-P coupling constant (J_{CP}=100—107 Hz), suggesting a direct bonding of the P-C(3). Chemical shifts of signals assigned to the C-4 and C-5 carbons and their coupling constants are summarized in Table 2.

The reactions of **1** with *p*-toluenethiol or primary and secondary amines gave similarly the 1,4-adducts **7** or **8** along with **6** (Table 1). The structures of **7** and **8** were determined as described above for **5**[6,7] and the ^1H and ^{13}C NMR spectral assignments are listed in Table 2.

Table 2 shows that the magnitudes of the C-P coupling constants $J_{C(3)P}$ of **5**, **7**, and **8** are in the order of **5**>**8**>**7**. This result is in accord with the observation, reported previously, that the C-P coupling constants ($^1J_{CP}$) of the structurally related phosphorus compounds, 3-phospholene 1-sulfides,

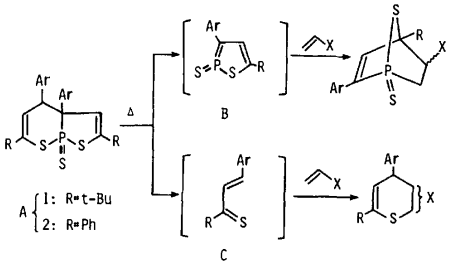

Scheme 1.

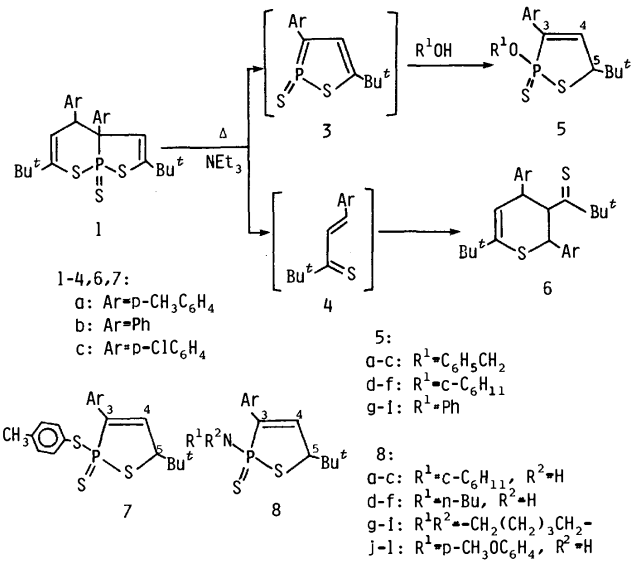

Scheme 2.

Table 1. Reactions of **1** with Alcohols, Phenols, Thiols, and Amines

Material	Reagent	Reaction time/h	Product[a]				
				Mp θ_m/°C	Yield/%		Yield/%
1a	$PhCH_2OH$	10	**5a**	115—118	54	**6a**	52
1b	$PhCH_2OH$	10	**5b**	107—109	36	**6b**	33
1c	$PhCH_2OH$	10	**5c**	113—116	38	**6c**	90
1a	*c*-$C_6H_{11}OH$	15[b]	**5d**	129—132	53	**6a**	72
1b	*c*-$C_6H_{11}OH$	20	**5e**	138—141	28	**6b**	35
1b	*c*-$C_6H_{11}OH$	15[b]	**5e**		40	**6b**	90
1c	*c*-$C_6H_{11}OH$	11[b]	**5f**	156—159	59	**6c**	89
1a	PhOH	10.5	**5g**	155—157	76	**6a**	90
1b	PhOH	12	**5h**	151—154	48	**6b**	90
1c	PhOH	12	**5i**	161—164	29	**6c**	90
1a	*p*-$CH_3C_6H_4SH$	10	**7a**	181—183	77	**6a**	80
1b	*p*-$CH_3C_6H_4SH$	10	**7b**	150—152	68	**6b**	49
1c	*p*-$CH_3C_6H_4SH$	10	**7c**	175—177	66	**6c**	80
1a	*c*-$C_6H_{11}NH_2$	13	**8a**	140—142	59	**6a**	61
1b	*c*-$C_6H_{11}NH_2$	12	**8b**	136—139	62	**6b**	92
1c	*c*-$C_6H_{11}NH_2$	12	**8c**	185—188	74	**6c**	56
1a	Bu^nNH_2	8	**8d**	117—119	59	**6a**	61
1b	Bu^nNH_2	8	**8e**	124—128	73	**6b**	82
1c	Bu^nNH_2	8	**8f**	118—120	59	**6c**	91
1a	$\overline{CH_2(CH_2)_4NH}$	7	**8g**	118—120	54	**6a**	61
1b	$\overline{CH_2(CH_2)_4NH}$	8	**8h**	113—116	50	**6b**	85
1c	$\overline{CH_2(CH_2)_4NH}$	8	**8i**	121—122	60	**6c**	98
1a	*p*-$CH_3OC_6H_4NH_2$	14	**8j**	137—140	11	**6a**	65
1b	*p*-$CH_3OC_6H_4NH_2$	14	**8k**	163—165	28	**6b**	65
1c	*p*-$CH_3OC_6H_4NH_2$	14	**8l**	158—161	21	**6c**	66

a) Colorless crystals (**6**; red oil). b) NPr^n_3/xylene reflux.

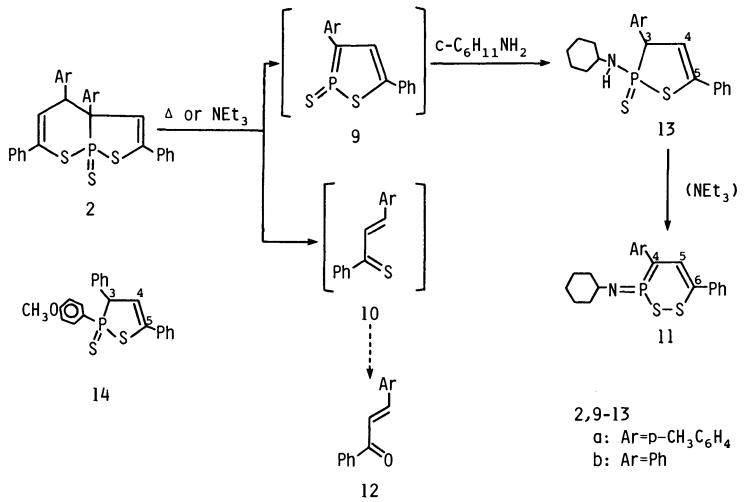

Scheme 3.

increase with the increasing electronegativity of the exocyclic heteroatom attached to the phosphorus atom.[8]

Reactions of Phosphabicyclo Compounds 2 with Amines. Phosphabicyclo compounds **2** are more reactive than **1** and the reactions with cyclohexylamine proceeded even at room temperature by addition of NEt_3. However, the products obtained

Table 2. ^1H and ^{13}C NMR Spectral Data of **5**, **7**, and **8** ($\delta(J/Hz)$)

Compound	H(4)	H(5)	J_{HH}	$J_{H(4)P}$	$J_{H(5)P}$	C(3)	C(4)	C(5)	$J_{C(3)P}$	$J_{C(4)P}$	$J_{C(5)P}$
5a	6.85	4.29	3.4	52.0	9.5	**141.8**	140.6	65.9	107.2	28.1	4.9
5b	6.88	4.28	3.5	54.0	9.5	141.7	141.4	65.8	101.3	28.1	6.1
5c	6.87	4.29	3.5	55.0	10.0	**141.0**	141.7	65.9	102.5	28.1	4.9
5d	6.83	4.28	3.0	54.0	9.1	142.1	139.8	65.9	102.5	28.1	4.9
5e	≃6.8[a]	4.29	3.2	≃54[a]	9.5	140.7	140.6	65.8	102.5	28.1	4.9
5f	6.83	4.29	3.0	54.0	9.8	141.2	141.1	66.0	103.0	28.1	4.9
5g	≃6.9[a]	4.35	3.2	≃50[a]	9.8	141.3	140.9	66.3	100.1	28.1	6.1
5h	≃6.9[a]	4.36	3.2	≃50[a]	9.3	**141.5**	141.7	66.3	100.1	28.1	4.9
5i	≃6.9[a]	4.37	3.1	≃50[a]	10.0	140.3	142.2	66.4	100.1	28.1	4.9
7a	6.64	4.43	2.0	55.0	≃0	137.1	139.7	66.3	72.2	24.4	3.7
7b	6.65	4.44	2.5	54.5	≃0	**141.7**	140.4	66.2	72.0	23.2	2.4
7c	6.65	4.44	2.5	54.0	≃0	140.8	140.8	66.3	66.2	23.5	2.9
8a	6.83	4.25	2.0	52.0	≃0	141.1	139.8	63.4	94.0	26.9	6.1
8b	6.83	4.31	2.0	52.0	≃0	141.7	140.8	63.5	90.3	25.6	4.9
8c	6.86	4.30	2.5	52.2	≃0	140.5	141.0	63.5	90.3	25.6	4.9
8d	6.76	4.30	3.5	52.0	≃0	141.1	140.4	63.5	89.1	26.9	4.9
8e	6.83	4.30	2.5	51.0	≃0	141.2	141.2	63.6	89.1	25.6	4.9
8f	6.82	4.30	2.5	51.0	≃0	140.1	141.5	63.6	90.3	25.6	4.9
8g	6.81	4.33	2.5	53.5	2.5	140.7	139.2	63.2	94.0	25.6	4.9
8h	6.86	4.36	2.0	53.0	2.5	141.3	140.3	63.5	94.0	25.6	4.9
8i	6.86	4.32	2.5	48.0	1.5	140.2	140.6	63.5	95.2	24.4	4.9
8j	6.88	4.27	2.0	54.0	≃0	141.3	140.6	63.9	89.1	26.9	6.1
8k	6.83	4.28	3.5	54.0	≃0	141.4	141.5	63.9	89.1	26.9	4.9
8l	6.84	4.28	2.5	52.5	≃0	140.5	141.9	64.0	92.8	25.6	6.1

a) Part of the signal of the double doublet is superimposed on Ar-H.

Table 3. Reactions of **2** with Amines

Material	Reagent	Reaction Conditions			Product[a]				
		Time	Solvent	Temp/°C	Mp θ_m/°C	Yield/%		Yield/%	
2a	*c*-$C_6H_{11}NH_2$	2 Week	NEt_3/C_6H_6	20—25	**11a**	264—265	34	**12a**	99
2a	*c*-$C_6H_{11}NH_2$	2 h	C_6H_6	80	**11a**		13	**12a**	99
					13a	196—198 (dec.)	46		
2b	*c*-$C_6H_{11}NH_2$	2 Week	NEt_3/C_6H_6	20—25	**11b**	272—274	39	**12b**	99
2b	*c*-$C_6H_{11}NH_2$	3 h	C_6H_6	80	**11b**		30	**12b**	99
					13b	190—192 (dec.)	43		
2a	*p*-$CH_3OC_6H_4NH_2$	2 Week	NEt_3/C_6H_6	20—25	**16a**	261—263	55	**17a**[b]	65
2b	*p*-$CH_3OC_6H_4NH_2$	2 Week	NEt_3/C_6H_6	20—25	**16b**	227—229	33	**17b**[c]	58
2a	*p*-$CH_3C_6H_4NH_2$	2 Week	NEt_3/C_6H_6	20—25	**16c**	208—210	16	**17c**[d]	97
2b	*p*-$CH_3C_6H_4NH_2$	2 Week	NEt_3/C_6H_6	20—25	**16d**	203—205	51	**17d**[e]	70

a) **11**, **16**, and **17**; red crystals, **13**; colorless crystals. b) mp 117—120 °C. c) mp 162—164 °C (lit,[10] 165 °C). d) mp 123—126 °C. e) mp 169—171 °C (lit,[10] 168—169 °C).

Table 4. ^1H NMR Spectral Data of **13** and **14** (δ (J/Hz))

Compound	H(3)	H(4)	J_{HH}	$J_{H(3)P}$	$J_{H(4)P}$
13a	4.88	6.35	4.0	15.0	36.0
13b	4.51	6.32	4.0	15.5	36.0
14	5.17	6.32	4.0	18.0	32.0

were chalcones **12** and 1,2,3-dithiaphosphorins **11** (Scheme 3, Table 3). When the reactions were carried out in refluxing benzene without NEt_3, **11**, **12**, and 1,2-adducts **13** of cyclohexylamine toward **9** were formed.

The ^1H and ^{13}C NMR spectra of **13a** were different from those of the 1,4-adducts **8**. Namely, the

Table 5. ^1H and ^{13}C NMR Spectral Data of **11** and **16** ($\delta(J/Hz)$)

Compound	H(5)	$J_{H(5)P}$	C(4)	C(5)	C(6)	$J_{C(4)P}$	$J_{C(5)P}$	$J_{C(6)P}$
11a	6.94	34.0	161.3	117.1	169.2	81.8	11.0	14.7
11b	6.94	34.0	160.9	118.1	169.1	82.4	11.8	14.7
16a	7.37	34.0	158.9	115.1	168.4	81.8	11.0	14.7
16b	7.42	34.2	160.7	116.2	167.6	81.8	11.0	14.7
16c	7.37	34.0	160.3	115.2	167.5	81.8	11.0	14.7
16d	7.42	34.0	163.0	116.3	165.9	79.4	10.3	16.2

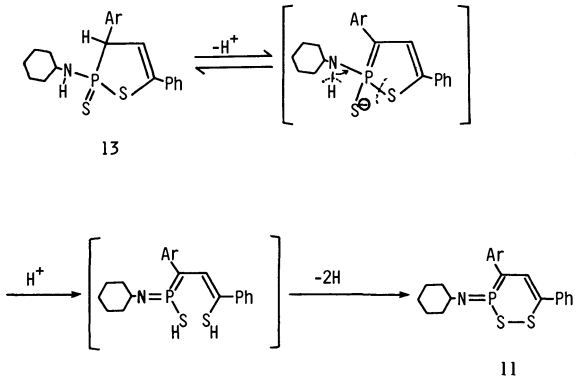

Scheme 4.

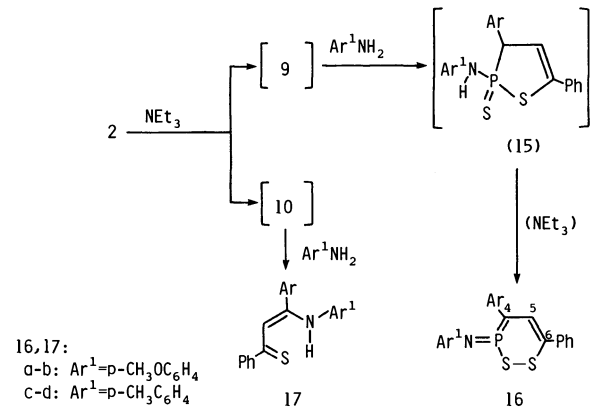

Scheme 5.

^1H NMR spectrum showed signals of the H-3 proton at δ=4.88 (J_{HH}=4.0 Hz, J_{HP}=15.0 Hz) and of the H-4 proton at δ=6.35 (J_{HH}=4.0 Hz, J_{HP}=36.0 Hz). These spectral patterns are similar to those of 1,2-thiaphosphol-4-ene 2-sulfide **14** reported previously[9] (Table 4). In the ^{13}C NMR spectrum, the resonance at δ=60.7 (J_{CP}=61.0 Hz) is assigned to the saturated C-3 carbon atom directly bonded to the phosphorus atom. Signals of the unsaturated carbons, C-4 and C-5, appeared at δ=120.4 (J_{CP}=4.9 Hz) and 141.8 (J_{CP}=11.0 Hz), respectively.

The mass spectrum of **11a** showed a molecular ion peak at *m/z* 397 [M$^+$] and an ion peak of [M$^+$ −2S] at *m/z* 333 as a base peak. The IR spectrum revealed no NH absorption band. The ^1H NMR spectrum exhibited a doublet of H-5 proton at δ=6.94 (J_{HP}=34.0 Hz) and the ^{13}C NMR spectrum displayed three signals at δ=161.3 (J_{CP}=81.8 Hz), 117.1 (J_{CP}= 11.0 Hz), and 169.2 (J_{CP}=14.7 Hz)(Table 5).

These spectral data support the proposed structures **11** and **13**. The compounds **11** were found to be very stable, probably due to the resonance stabilization of the dithiaphosphorin ring system. Treatment of **13** with NEt_3 produced **11** instead of the corresponding 1,4-adducts. A probable pathway for the formation of **11** from **13** is illustrated in Scheme 4.

The reactions of **2** with aromatic amines (*p*-anisidine, *p*-toluidine) afforded 3-amino-2-propene-1-thiones **17**[10] and 1,2,3-ditiaphosphorins **16** in contrast to the reactions with cyclohexylamine (Scheme 5, Table 3). This result is interesting but the dehydrogenation step to form **17** is still ambiguous.[11]

The accelerating effect of NEt_3 in these reactions is remarkable and the following three rationales can be considered: (1) The amine accelerates the dissociation of **A** into **B** and **C**. (2) The amine activates the nucleophiles. (3) The amine interacts with **A** at the positive center, the phosphorus atom, to activate **A** toward the nucleophiles. When the solution of **1** and the amine in benzene was heated in the absence of the nucleophiles, the solution turned greenish-blue. A benzene solution of **2** also colored even at room temperature on adding the amine. These observations suggest the generation of the monomeric thiones **C** (or dimers) and **B**. On the other hand, previously reported cycloaddition reactions of **A** with dienophiles (Scheme 1) were also found to be accelerated on addition of the amine. On the basis of these findings, the rationale (1) is considered to be most probable. However, the possibilities of (2) and (3) still remain, especially for the reactions of **1**.

Experimental

All melting points are uncorrected. IR spectra were measured on a Hitachi Model 260—10 spectrometer. ^1H and ^{13}C NMR spectra were recorded on a JEOL JNM-FX 100 spectrometer in $CDCl_3$ solution using Me_4Si as an internal standard (^1H; at 100 MHz, ^{13}C; at 25 MHz). ^{31}P NMR spectra were recorded at 40 MHz on a JEOL

JNM-FX 100 spectrometer using 85% H_3PO_4 as an external standard. Mass spectra were recorded on a Hitachi double focusing mass spectrometer (RMU-7M) operating at an ionizing potential of 70 eV. 2,9-Dithia-1-phosphabicyclo[4.3.0]nona-3,7-diene 1-sulfides **1** and **2** were prepared according to the previously described method.[1]

General Procedure for the Reactions of the Phosphabicyclo Compounds 1 or 2 with Nucleophilic Reagents (Alcohols, Phenols, Thiols, and Amines) to Afford 1,4- or 1,2-Adducts, 5, 7, 8, and 13: A solution of **1** (3 mmol) and a nucleophilic reagent (10 mmol) in 20 cm^3 of dry benzene (xylene) and 15 cm^3 of NEt_3 (NPr^n_3) was refluxed under a nitrogen atmosphere for 2—20 h until the phosphabicyclo compound **1** was consumed, as indicated by TLC (Reaction times are shown in Tables 1 and 3). After evaporation of the solvent the residue was chromatographed on silica gel (Wakogel C-200) with benzene–hexane (1:1) as an eluent to afford the adduct. Recrystallization from ethanol gave the adduct as colorless crystals. The reaction of **2** to afford **13** was carried out without NEt_3.

2-Benzyloxy-5-*t*-butyl-3-(*p*-tolyl)-1,2-thiaphosphol-3-ene 2-Sulfide (5a): IR (KBr) 2970, 1375, and 1000(P–O) cm^{-1}; ^1H NMR ($CDCl_3$) δ=1.07 (s, 9H), 2.35 (s, 3H), 4.29 (dd, 1H, J_{HH}=3.4 Hz, J_{HP}=9.5 Hz), 5.06—5.28 (m, 2H), 6.85 (dd, 1H, J_{HH}=3.4 Hz, J_{HP}=52.0 Hz), and 6.93—7.54 (m, 9H); MS *m/z* (rel intensity) 388 (M^+, 18), 332 (17), 282 (22), 241 (55), 225 (47), 192 (28), 91 (100), and 57 (24). Found: C, 64.68; H, 6.23%. Calcd for $C_{21}H_{25}OPS_2$: C, 64.92; H, 6.49%.

2-Benzyloxy-5-*t*-butyl-3-phenyl-1,2-thiaphosphol-3-ene 2-Sulfide (5b): IR (KBr) 2970, 1370, and 990(P–O) cm^{-1}; ^1H NMR ($CDCl_3$) δ=1.04 (s, 9H), 4.28 (dd, 1H, J_{HH}=3.5 Hz, J_{HP}=9.5 Hz), 5.06—5.28 (m, 2H), 6.88 (dd, 1H, J_{HH}=3.5 Hz, J_{HP}=54.0 Hz), and 7.00—7.68 (m, 10H); MS *m/z* (rel intensity) 374 (M^+, 16), 318 (17), 268 (25), 227 (42), 211 (30), 178 (37), 91 (100), and 57 (25). Found: C, 64.38; H, 6.40; S, 17.19%. Calcd for $C_{20}H_{23}OPS_2$: C, 64.14; H, 6.19; S, 17.12%.

2-Benzyloxy-5-*t*-butyl-3-(*p*-chlorophenyl)-1,2-thiaphosphol-3-ene 2-Sulfide (5c): IR (KBr) 2970, 1370, and 990(P–O) cm^{-1}; ^1H NMR ($CDCl_3$) δ=1.07 (s, 9H), 4.29 (dd, 1H, J_{HH}=3.5 Hz, J_{HP}=10.0 Hz), 5.06—5.28 (m, 2H), 6.87 (dd, 1H, J_{HH}=3.5 Hz, J_{HP}=55.0 Hz), and 7.16—7.60 (m, 9H); MS *m/z* (rel intensity) 408 (M^+, 13), 352 (18), 302 (16), 261 (44), 245 (19), 212 (29), 91 (100) and 57 (32). Found: C, 58.45; H, 5.35%. Calcd for $C_{20}H_{22}OPS_2Cl$: C, 58.74; H, 5.42%.

5-*t*-Butyl-2-cyclohexyloxy-3-(*p*-tolyl)-1,2-thiaphosphol-3-ene 2-Sulfide (5d): IR (KBr) 2960, 2940, 2860, 1370, and 980(P–O) cm^{-1}; ^1H NMR ($CDCl_3$) δ=1.10 (s, 9H), 1.14—2.18 (broad m, 10H), 2.36 (s, 3H), 4.28 (dd, 1H, J_{HH}=3.0 Hz, J_{HP}=9.1 Hz), 4.54—4.96 (broad m, 1H), 6.83 (dd, 1H, J_{HH}=3.0 Hz, J_{HP}=54.0 Hz), 7.14 (d, 2H, J_{HH}=8.0 Hz), and 7.48 (dd, 2H, J_{HH}=8.0 Hz, J_{HP}=1.5 Hz); MS *m/z* (rel intensity) 380 (M^+, 1), 299 (100), 242 (61), 225 (17), 209 (23), and 57 (21). Found: C, 63.36; H, 7.71%. Calcd for $C_{20}H_{29}OPS_2$: C, 63.13; H, 7.68%.

5-*t*-Butyl-2-cyclohexyloxy-3-phenyl-1,2-thiaphosphol-3-ene 2-Sulfide (5e): IR (KBr) 2960, 2940, 2855, 1365, and 980(P–O) cm^{-1}; ^1H NMR ($CDCl_3$) δ=1.11 (s, 9H), 1.16—2.20 (broad m, 10H), 4.29 (dd, 1H, J_{HH}=3.2 Hz, J_{HP}=9.5 Hz), 4.54—4.96 (broad m, 1H), ≈6.8 (dd, 1H, J_{HH}=3.2 Hz, J_{HP}≈54 Hz), and 6.92—7.70 (m, 5H); MS *m/z* (rel intensity) 366 (M^+, 1), 285 (100), 228 (49), 211 (13), 195 (18), and 57 (56). Found: C, 62.86; H, 7.66%. Calcd for $C_{19}H_{27}OPS_2$: C, 62.26; H, 7.43%.

5-*t*-Butyl-3-(*p*-chlorophenyl)-2-cyclohexyloxy-1,2-thiaphosphol-3-ene 2-Sulfide (5f): IR (KBr) 2970, 2950, 2860, 1370, and 985(P–O) cm^{-1}; ^1H NMR ($CDCl_3$) δ=1.11 (s, 9H), 1.14—2.36 (broad m, 10H), 4.29 (dd, 1H, J_{HH}=3.0 Hz J_{HP}=9.8 Hz), 4.54—4.92 (broad m, 1H), 6.83 (dd, 1H, J_{HH}=3.0 Hz, J_{HP}=54.0 Hz), 7.28 (d, 2H, J_{HH}=9.0 Hz), and 7.54 (dd, 2H, J_{HH}=9.0 Hz, J_{HP}=1.5 Hz); MS *m/z* (rel intensity) 400 (M^+, 2), 319 (100), 262 (45), 245 (9), 229 (14), and 57 (44). Found: C, 56.54; H, 6.12%. Calcd for $C_{19}H_{26}OPS_2Cl$: C, 56.92; H, 6.54%.

5-*t*-Butyl-2-phenoxy-3-(*p*-tolyl)-1,2-thiaphosphol-3-ene 2-Sulfide (5g): IR (KBr) 2970, 1370, and 900(P–O) cm^{-1}; ^1H NMR ($CDCl_3$) δ=1.07 (s, 9H), 2.39 (s, 3H), 4.35 (dd, 1H, J_{HH}=3.2 Hz, J_{HP}=9.8 Hz), ≈6.9 (dd, 1H, J_{HH}=3.2 Hz, J_{HP}≈50 Hz), 6.94—7.38 (m, 7H), and 7.64 (dd, 2H, J_{HH}=8.0 Hz, J_{HP}=1.5 Hz); MS *m/z* (rel intensity) 374 (M^+, 7), 318 (100), 281 (9), 225 (71), 192 (22), 161 (17), and 57 (35). Found: C, 64.13; H, 6.12%. Calcd for $C_{20}H_{23}OPS_2$: C, 64.14; H, 6.19%.

5-*t*-Butyl-2-phenoxy-3-phenyl-1,2-thiaphosphol-3-ene 2-Sulfide (5h): IR (KBr) 2970, 1370, and 905(P–O) cm^{-1}; ^1H NMR ($CDCl_3$) δ=1.07 (s, 9H), 4.36 (dd, 1H, J_{HH}=3.2 Hz, J_{HP}=9.3 Hz), ≈6.9 (dd, 1H J_{HH}=3.2 Hz, J_{HP}≈50 Hz), 6.88—7.50 (m, 8H), and 7.60—7.84 (m, 2H); MS *m/z* (rel intensity) 360 (M^+, 7), 304 (100), 267 (11), 211 (88), 178 (23), 147 (28), and 57 (56). Found: C, 63.62; H, 5.86; S, 17.72%. Calcd for $C_{19}H_{21}OPS_2$: C, 63.31; H, 5.87; S, 17.79%.

5-*t*-Butyl-3-(*p*-chlorophenyl)-2-phenoxy-1,2-thiaphosphol-3-ene 2-Sulfide (5i): IR (KBr) 2970, 1370, 905(P–O) cm^{-1}; ^1H NMR ($CDCl_3$) δ=1.08 (s, 9H), 4.37 (dd, 1H, J_{HH}=3.1 Hz, J_{HP}=10.0 Hz), ≈6.9 (dd, 1H, J_{HH}=3.1 Hz, J_{HP}≈50 Hz), 6.86—7.48 (m, 7H), and 7.70 (dd, 2H, J_{HH}=9.0 Hz, J_{HP}=1.7 Hz); MS *m/z* (rel intensity) 394 (M^+, 7), 338 (100), 301 (7), 245 (58), 212 (16), 181 (16), and 57 (84). Found: C, 57.88; H, 5.08%. Calcd for $C_{19}H_{20}OPS_2Cl$: C, 57.79; H, 5.10%.

5-*t*-Butyl-2-(*p*-tolylthio)-3-(*p*-tolyl)-1,2-thiaphosphol-3-ene 2-Sulfide (7a): IR (KBr) 2970 and 1375 cm^{-1}; ^1H NMR ($CDCl_3$) δ=0.81 (s, 9H), 2.29 (s, 3H), 2.41 (s, 3H), 4.43 (d, 1H, J_{HH}=2.0 Hz), 6.64 (dd, 1H, J_{HH}=2.0 Hz, J_{HP}=55.0 Hz), 6.96—7.40 (m, 6H), and 7.74 (d, 2H, J_{HH}=9.0 Hz); MS *m/z* (rel intensity) 404 (M^+, 14), 372 (2), 348 (3), 281 (60), 225 (100), 193 (61), 192 (33), 123 (11), and 57 (76). Found: C, 62.17; H, 6.04%. Calcd for $C_{21}H_{25}PS_3$: C, 62.34; H, 6.23%.

5-*t*-Butyl-3-phenyl-2-(*p*-tolylthio)-1,2-thiaphosphol-3-ene 2-Sulfide (7b): IR (KBr) 2975 and 1375 cm^{-1}; ^1H NMR ($CDCl_3$) δ=0.83 (s, 9H), 2.28 (s, 3H), 4.44 (d, 1H, J_{HH}=2.5 Hz), 6.65 (dd, 1H, J_{HH}=2.5 Hz, J_{HP}=54.5 Hz), 6.98—7.48 (m, 7H), and 7.74—7.92 (m, 2H); MS *m/z* (rel intensity 390 (M^+, 26), 358 (2), 334 (3), 267 (63), 211 (100), 178 (49), 123 (14), and 57 (91). Found: C, 61.23; H, 5.84; S, 24.55%. Calcd for $C_{20}H_{23}PS_3$: C, 61.51; H, 5.94; S, 24.63%.

5-*t*-Butyl-3-(*p*-chlorophenyl)-2-(*p*-tolylthio)-1,2-thiaphosphol-3-ene 2-Sulfide (7c): IR (KBr) 2970 and 1375 cm^{-1}; ^1H NMR ($CDCl_3$) δ=0.83 (s, 9H), 2.30 (s, 3H), 4.44 (d, 1H, J_{HH}=2.5 Hz), 6.65 (dd, 1H, J_{HH}=2.5 Hz, J_{HP}=54.0 Hz), 6.98—7.22 (m, 4H), 7.34 (d, 2H, J_{HH}=9.0 Hz), and 7.78 (d, 2H, J_{HH}=9.0 Hz); MS *m/z* (rel intensity) 424 (M^+, 6), 392 (1), 368 (1), 301 (15), 245 (27), 212 (12), 123 (12), and 57 (100). Found: C, 56.91; H, 5.32%. Calcd for $C_{20}H_{22}PS_3Cl$: C, 56.52; H, 5.22%.

5-*t*-Butyl-2-cyclohexylamino-3-(*p*-tolyl)-1,2-thiaphosphol-3-ene 2-Sulfide (8a): IR (KBr) 3260 (NH), 2970, 2940, 2850,

and 1365 cm^{-1}; ^1H NMR ($CDCl_3$) δ=0.80—1.80 (broad m, 9H), 1.11 (s, 9H), 1.84—2.12 (broad m, 1H), 2.35 (s, 3H), 3.02 (broad d, 2H, J_{HP}=12.0 Hz), 4.25 (d, 1H, J_{HH}=2.0 Hz), 6.83 (dd, 1H, J_{HH}=2.0 Hz, J_{HP}=52.0 Hz), 7.11 (d, 2H, J_{HH}=8.0 Hz), and 7.67 (d, 2H, J_{HH}=8.0 Hz); MS *m/z* (rel intensity) 379 (M^+, 1), 346 (4), 225 (7), 192 (5), 98 (100), and 57 (8). Found: C, 62.86; H, 8.14; N, 3.58%. Calcd for $C_{20}H_{30}NPS_2$: C, 63.29; H, 7.97; N, 3.69%.

5-*t*-Butyl-2-cyclohexylamino-3-phenyl-1,2-thiaphosphol-3-ene 2-Sulfide (8b): IR (KBr) 3200 (NH), 2970, 2940, 2850, and 1365 cm^{-1}; ^1H NMR ($CDCl_3$) δ=0.80—1.80 (broad m, 9H), 1.13 (s, 9H), 1.84—2.16 (broad m, 1H), 2.93 (broad d, 2H, J_{HP}=12.0 Hz), 4.31 (d, 1H, J_{HH}=2.0 Hz), 6.83 (dd, 1H, J_{HH}=2.0 Hz, J_{HP}=52.0 Hz), 7.12—7.40 (m, 3H), and 7.60—7.84 (m, 2H); MS *m/z* (rel intensity) 365 (M^+, 1), 332 (4), 211 (6), 178 (5), 98 (100), and 57 (11). Found: C, 62.58; H, 7.84; N, 3.53%. Calcd for $C_{19}H_{28}NPS_2$: C, 62.43; H, 7.72; N, 3.83%.

5-*t*-Butyl-3-(*p*-chlorophenyl)-2-cyclohexylamino-1,2-thiaphosphol-3-ene 2-Sulfide (8c): IR (KBr) 3300 (NH), 2970, 2940, 2860, and 1370 cm^{-1}; ^1H NMR ($CDCl_3$) δ=0.80—1.80 (broad m, 9H), 1.12 (s, 9H), 1.88—2.20 (broad m, 1H), 2.96 (broad d, 2H, J_{HP}=11.7 Hz), 4.30 (d, 1H, J_{HH}=2.5 Hz), 6.86 (dd, 1H, J_{HH}=2.5 Hz, J_{HP}=52.2 Hz), 7.26 (d, 2H, J_{HH}=9.0 Hz), and 7.70 (d, 2H, J_{HH}=9.0 Hz); ^{31}P NMR ($CDCl_3$) δ=90.3 (ddd, J_{PH}=52.2, 11.7, and 11.7 Hz); MS *m/z* (rel intensity) 399 (M^+, 1), 366 (3), 300 (1), 245 (4), 212 (5), 98 (100), and 57 (18). Found: C, 57.35; H, 6.95; N, 3.48; P, 7.28; S, 16.20%. Calcd for $C_{19}H_{27}NPS_2Cl$: C, 57.06; H, 6.80; N, 3.50; P, 7.74; S, 16.03%.

2-Butylamino-5-*t*-butyl-3-(*p*-tolyl)-1,2-thiaphosphol-3-ene 2-Sulfide (8d): IR (KBr) 3270 (NH), 2960, 2850, and 1365 cm^{-1}; ^1H NMR ($CDCl_3$) δ=0.70—1.62 (m, 7H), 1.12 (s, 9H), 2.35 (s, 3H), 2.72—3.08 (m, 3H), 4.30 (d, 1H, J_{HH}=3.5 Hz), 6.76 (dd, 1H, J_{HH}=3.5 Hz, J_{HP}=52.0 Hz), 7.13 (d, 2H, J_{HH}=9.0 Hz), and 7.58 (d, 2H, J_{HH}=9.0 Hz); MS *m/z* (rel intensity) 353 (M^+, 4), 320 (1), 296 (2), 281 (1), 225 (16), 192 (9), 72 (100), and 57 (13). Found: C, 61.00; H, 8.35; N, 3.81%. Calcd for $C_{18}H_{28}NPS_2$: C, 61.16; H, 7.98; N, 3.96%.

2-Butylamino-5-*t*-butyl-3-phenyl-1,2-thiaphosphol-3-ene 2-Sulfide (8e): IR (KBr) 3210 (NH), 2960, 2850, and 1360 cm^{-1}; ^1H NMR ($CDCl_3$) δ=0.64—1.62 (m, 7H), 1.12 (s, 9H), 2.68—3.20 (m, 3H), 4.30 (d, 1H, J_{HH}=2.5 Hz), 6.83 (dd, 1H, J_{HH}=2.5 Hz, J_{HP}=51.0 Hz), 7.19—7.44 (m, 3H), and 7.54—7.78 (m, 2H); MS *m/z* (rel intensity) 339 (M^+, 2), 306 (2), 282 (2), 267 (1), 211 (12), 178 (1), 72 (100), and 57 (17). Found: C, 60.13; H, 7.89; N, 4.27%. Calcd for $C_{17}H_{26}NPS_2$: C, 60.14; H, 7.72; N, 4.13%.

2-Butylamino-5-*t*-butyl-3-(*p*-chlorophenyl)-1,2-thiaphosphol-3-ene 2-Sulfide (8f): IR (KBr) 3280 (NH), 2960, 2860, and 1365 cm^{-1}; ^1H NMR ($CDCl_3$) δ=0.60—1.77 (m, 7H), 1.12 (s, 9H), 2.60—3.21 (m, 3H), 4.30 (d, 1H, J_{HH}=2.5 Hz), 6.82 (dd, 1H, J_{HH}=2.5 Hz, J_{HP}=51.0 Hz), 7.28 (d, 2H, J_{HH}=8.0 Hz), and 7.65 (d, 1H, J_{HH}=8.0 Hz); MS *m/z* (rel intensity) 373 (M^+, 2), 340 (1), 316 (1), 301 (1), 245 (6), 212 (6), 72 (100), and 57 (21). Found: C, 54.61; H, 6.83; N, 3.53%. Calcd for $C_{17}H_{25}NPS_2Cl$: C, 54.60; H, 6.74; N, 3.75%.

5-*t*-Butyl-2-piperidino-3-(*p*-tolyl)-1,2-thiaphosphol-3-ene 2-Sulfide (8g): IR (KBr) 2970, 2945, 2850, and 1370 cm^{-1}; ^1H NMR ($CDCl_3$) δ=1.10 (s, 9H), 1.24—1.76 (broad m, 6H), 2.34 (s, 3H), 3.06—3.54 (broad m, 4H), 4.33 (dd, 1H, J_{HH}=2.5 Hz, J_{HP}=2.5 Hz), 6.81 (dd, 1H, J_{HH}=2.5 Hz, J_{HP}=53.5 Hz), 7.09 (d, 2H, J_{HH}=7.5 Hz), and 7.55 (d, 2H, J_{HH}=7.5 Hz); MS *m/z* (rel intensity) 365 (M^+, 2), 332 (3), 225 (8), 192 (5), 84 (100), and 57 (8). Found: C, 62.78; H, 7.85; N, 3.60%. Calcd for $C_{19}H_{28}NPS_2$: C, 62.43; H, 7.72; N, 3.83%.

5-*t*-Butyl-3-phenyl-2-piperidino-1,2-thiaphosphol-3-ene 2-Sulfide (8h): IR (KBr) 2970, 2945, 2850, and 1365 cm^{-1}; ^1H NMR ($CDCl_3$) δ=1.13 (s, 9H), 1.20—1.83 (broad m, 6H), 2.94—3.58 (broad m, 4H), 4.36 (dd, 1H, J_{HH}=2.0 Hz, J_{HP}=2.5 Hz), 6.86 (dd, 1H, J_{HH}=2.0 Hz, J_{HP}=53.0 Hz), 7.18—7.50 (m, 3H), and 7.53—7.81 (m, 2H); MS *m/z* (rel intensity) 351 (M^+, 1), 318 (3), 294 (1), 211 (7), 178 (7), 84 (100) and 57 (10). Found: C, 61.60; H, 7.61; N, 3.71%. Calcd for $C_{18}H_{26}NPS_2$: C, 61.51; H, 7.40; N, 3.98%.

5-*t*-Butyl-3-(*p*-chlorophenyl)-2-piperidino-1,2-thiaphosphol-3-ene 2-Sulfide (8i): IR (KBr) 2970, 2945, 2850, and 1375 cm^{-1}; ^1H NMR ($CDCl_3$) δ=1.12 (s, 9H), 1.20—1.72 (broad m, 6H), 2.96—3.52 (broad m, 4H), 4.32 (dd, 1H, J_{HH}=2.5 Hz, J_{HP}=1.5 Hz), 6.86 (dd, 1H, J_{HH}=2.5 Hz, J_{HP}=48.0 Hz), 7.26 (d, 2H, J_{HH}=8.0 Hz), and 7.64 (d, 2H, J_{HH}=8.0 Hz); MS *m/z* (rel intensity) 385 (M^+, 1), 352 (2), 245 (3), 212 (4), 84 (100), and 57 (16). Found: C, 56.34; H, 6.66; N, 3.59; S, 16.33%. Calcd for $C_{18}H_{25}NPS_2Cl$: C, 56.02; H, 6.53; N, 3.63; S, 16.61%.

5-*t*-Butyl-2-(*p*-methoxyphenylamino)-3-(*p*-tolyl)-1,2-thiaphosphol-3-ene 2-Sulfide (8j): IR (KBr) 3150 (NH), 2960, and 1370 cm^{-1}; ^1H NMR ($CDCl_3$) δ=0.88 (s, 9H), 2.35 (s, 3H), 3.70 (s, 3H), 4.27 (d, 1H, J_{HH}=2.0 Hz), 5.14 (broad d, 1H, J_{HP}=7.0 Hz), 6.64 (d, 2H, J_{HH}=8.0 Hz), 6.84 (d, 2H, J_{HH}=8.0 Hz), 6.88 (dd, 1H, J_{HH}=2.0 Hz, J_{HP}=54.0 Hz), 7.14 (dd, 2H, J_{HH}=8.0 Hz, J_{HP}=3.0 Hz), and 7.72 (d, 2H, J_{HH}=8.0 Hz); MS *m/z* (rel intensity) 403 (M^+, 100), 371 (1), 346 (11), 281 (20), 250 (26), 225 (80), 192 (22), 123 (95), and 57 (40). Found: C, 62.33; H, 6.47; N, 3.45%. Calcd for $C_{21}H_{26}NOPS_2$: C, 62.51; H, 6.49; N, 3.47%.

5-*t*-Butyl-2-(*p*-methoxyphenylamino)-3-phenyl-1,2-thiaphosphol-3-ene 2-Sulfide (8k): IR (KBr) 3210 (NH), 2960, and 1365 cm^{-1}; ^1H NMR ($CDCl_3$) δ=0.88 (s, 9H), 3.70 (s, 3H), 4.28 (d, 1H, J_{HH}=3.5 Hz), 5.16 (broad d, 1H, J_{HP}=7.0 Hz), 6.64 (d, 2H, J_{HH}=9.0 Hz), 6.83 (dd, 1H, J_{HH}=3.5 Hz, J_{HP}=54.0 Hz), 6.83 (dd, 2H, J_{HH}=9.0 Hz, J_{HP}=2.0 Hz), 7.20—7.36 (m, 3H), and 7.70—7.88 (m, 2H); MS *m/z* (rel intensity) 389 (M^+, 68), 357 (1), 333 (6), 267 (18), 236 (15), 211 (76), 178 (17), 123 (100), and 57 (42). Found: C, 61.41; H, 6.37; N, 3.31%. Calcd for $C_{20}H_{24}NOPS_2$: C, 61.67; H, 6.21; N, 3.60%.

5-*t*-Butyl-3-(*p*-chlorophenyl)-2-(*p*-methoxyphenylamino)-1,2-thiaphosphol-3-ene 2-Sulfide (8l): IR (KBr) 3220 (NH), 2970, and 1370 cm^{-1}; ^1H NMR ($CDCl_3$) δ=0.88 (s, 9H), 3.72 (s, 3H), 4.28 (d, 1H, J_{HH}=2.5 Hz), 5.18 (broad d, 1H, J_{HP}=8.0 Hz), 6.66 (d, 2H, J_{HH}=9.0 Hz), 6.84 (dd, 1H, J_{HH}=2.5 Hz, J_{HP}=52.5 Hz), 6.84 (dd, 2H, J_{HH}=9.0 Hz, J_{HP}=2.0 Hz), 7.30 (d, 2H, J_{HH}=8.0 Hz), and 7.78 (dd, 2H, J_{HH}=8.0 Hz, J_{HP}=1.0 Hz); MS *m/z* (rel intensity) 423 (M^+, 55), 391 (2), 367 (5), 301 (9), 270 (9), 245 (35), 212 (10), 123 (100), and 57 (57). Found: C, 56.27; H, 5.48; N, 3.05; S, 15.48%. Calcd for $C_{20}H_{23}NOPS_2Cl$: C, 56.66; H, 5.47; N, 3.30; S, 15.12%.

2-Cyclohexylamino-5-phenyl-3-(*p*-tolyl)-1,2-thiaphosphol-4-ene 2-Sulfide (13a): IR (KBr) 3200 (NH), 2950, and 2860 cm^{-1}; ^1H NMR ($CDCl_3$) δ=0.96—2.20 (broad m, 10H),

2.36 (s, 3H), 3.08—3.64 (broad m, 2H), 4.88 (dd, 1H, J_{HH}=4.0 Hz, J_{HP}=15.0 Hz), 6.35 (dd, 1H, J_{HH}=4.0 Hz, J_{HP}=36.0 Hz), and 7.08—7.68 (m, 9H); MS *m/z* (rel intensity) 399 (M^+, 12), 366 (12), 300 (6), 238 (25), 237 (58), 205 (19), and 98 (100). Found: C, 66.40; H, 6.55; N, 3.21%. Calcd for $C_{22}H_{26}NPS_2$: C, 66.14; H, 6.56; N, 3.51%.

2-Cyclohexylamino-3,5-diphenyl-1,2-thiaphosphol-4-ene 2-Sulfide (13b): IR (KBr) 3175 (NH), 2940, and 2850 cm^{-1}; ^1H NMR ($CDCl_3$) δ=0.96—2.20 (broad m, 10H), 3.08—3.64 (broad m, 2H), 4.51 (dd, 1H, J_{HH}=4.0 Hz, J_{HP}=15.5 Hz), 6.32 (dd, 1H, J_{HH}=4.0 Hz, J_{HP}=36.0 Hz), and 7.08—7.60 (m, 10H); MS *m/z* (rel intensity) 385 (M^+, 5), 352 (9), 286 (6), 224 (4), 223 (100), and 98 (86). Found: C, 65.34; H, 6.36; N, 3.44; S, 16.63%. Calcd for $C_{21}H_{24}NPS_2$: C, 65.43; H, 6.27; N, 3.44; S, 16.63%.

6-*t*-Butyl-3-[*t*-butyl(thiocarbonyl)]-2,4-bis(*p*-tolyl)-3,4-dihydro-2*H*-thiin (6a): IR (neat) 2970 and 1370 cm^{-1}; ^1H NMR ($CDCl_3$) δ=1.08 (s, 9H), 1.24 (s, 9H), 2.18 (s, 3H), 2.30 (s, 3H), 3.73 (dd, 1H, J_{HH}=2.4, 6.4 Hz), 4.33 (dd, 1H, J_{HH}=2.4, 6.4 Hz), 4.58 (d, 1H, J_{HH}=6.4 Hz), 5.87 (d, 1H, J_{HH}=6.4 Hz), and 6.72—7.35 (m, 8H); MS *m/z* (rel intensity) 436 (M^+), 218 (27), 161 (100).

6-*t*-Butyl-3-[*t*-butyl(thiocarbonyl)]-2,4-diphenyl-3,4-dihydro-2*H*-thiin (6b): IR (neat) 2970 and 1370 cm^{-1}; ^1H NMR ($CDCl_3$) δ=1.07 (s, 9H), 1.25 (s, 9H), 3.77 (dd, 1H, J_{HH}=2.8, 6.4 Hz), 4.33 (dd, 1H, J_{HH}=2.8, 6.8 Hz), 4.63 (d, 1H, J_{HH}=6.8 Hz), 5.88 (d, 1H, J_{HH}=6.4 Hz), and 6.40—7.33 (m, 10H); MS *m/z* (rel intensity) 408 (M^+, 2), 204 (38), and 147 (100).

6-*t*-Butyl-3-[*t*-butyl(thiocarbonyl)]-2,4-bis(*p*-chlorophenyl)-3,4-dihydro-2*H*-thiin (6c): IR (neat) 2970, 1370, and 1100 (C=S) cm^{-1}; ^1H NMR ($CDCl_3$) δ=1.08 (s, 9H), 1.24 (s, 9H), 3.74 (dd, 1H, J_{HH}=4.0, 6.9 Hz), 4.43 (dd, 1H, J_{HH}=4.0, 11.0 Hz), 4.66 (d, 1H, J_{HH}=11.0 Hz), 5.87 (d, 1H, J_{HH}=6.9 Hz), and 6.40—7.20 (m, 8H); MS *m/z* (rel intensity) 476 (M^+), 238 (25), and 181 (100).

General Procedure for the Reactions of the Phosphabicyclo Compounds 2 with Amines to Afford 11, 16, and 17: A solution of **2** (3 mmol) and amine (10 mmol) in dry benzene (20 cm^3) and NEt_3 (15 cm^3) was stirred at room temperature under a nitrogen atmosphere until the phosphabicyclo compound **2** was consumed as indicated by TLC (2 weeks). The solvent was removed and the residue was chromatographed on silica gel (Wakogel C-200) with benzene–hexane (2:3) as an eluent. The solvent was evaporated and the residue was recrystallized to give the products as red crystals (**11**, **16**; from hexane–ethanol, **17**; from ethanol).

3-Cyclohexylimino-6-phenyl-4-(*p*-tolyl)-1,2,3-dithiaphosphorin (11a): IR (KBr) 2940 and 2850 cm^{-1}; ^1H NMR ($CDCl_3$) δ=0.84—2.56 (broad m, 9H), 2.40 (s, 3H), 4.40—4.80 (m, 2H), 6.94 (d, 1H, J_{HP}=34.0 Hz), 7.12—7.76 (m, 7H), and 8.06 (d, 2H, J_{HH}=9.0 Hz); MS *m/z* (rel intensity) 397 (M^+, 9), 364 (38), 333 (100), and 251 (33). Found: C, 66.73; H, 6.10; N, 3.34%. Calcd for $C_{22}H_{24}NPS_2$: C, 66.47; H, 6.09; N, 3.52%.

3-Cyclohexylimino-4,6-diphenyl-1,2,3-dithiaphosphorin (11b): IR (KBr) 2940 and 2860 cm^{-1}; ^1H NMR ($CDCl_3$) δ=0.90—2.48 (broad m, 9H), 4.28—4.80 (m, 2H), 6.94 (d, 1H, J_{HP}=34.0 Hz), 7.20—7.84 (m, 8H), and 8.04—8.36 (m, 2H); MS *m/z* (rel intensity) 383 (M^+, 15), 350 (41), 319 (57), and 237 (100). Found: C, 65.70; H, 5.92; N, 3.77%. Calcd for $C_{21}H_{22}NPS_2$: C, 65.77; H, 5.78; N, 3.65%.

3-(*p*-Methoxyphenylimino)-6-phenyl-4-(*p*-tolyl)-1,2,3-dithiaphosphorin (16a): ^1H NMR ($CDCl_3$) δ=2.44 (s, 3H), 3.83 (s, 3H), 6.80—7.00 (m, 2H), 7.16—7.68 (m, 9H), 7.37 (d, 1H, J_{HP}=34.0 Hz), and 8.20 (d, 2H, J_{HH}=9.0 Hz); MS *m/z* (rel intensity) 421 (M^+, 21), 357 (100), and 138 (52). Found: C, 65.83; H, 4.76; N, 2.90%. Calcd for $C_{23}H_{20}NOPS_2$: C, 65.54; H, 4.78; N, 3.32%.

3-(*p*-Methoxyphenylimino)-4,6-diphenyl-1,2,3-dithiaphosphorin (16b): ^1H NMR ($CDCl_3$) δ=3.84 (s, 3H), 6.80—7.00 (m, 2H), 7.20—7.70 (m, 10H), 7.42 (d, 1H, J_{HP}=34.2 Hz), and 8.12—8.40 (m, 2H); ^{31}P NMR ($CDCl_3$) δ=114.6 (d, J_{PH}=34.2 Hz); MS *m/z* (rel intensity) 407 (M^+, 4), 343 (100), and 138 (40). Found: C, 65.10; H, 4.41; N, 3.10; S, 15.28%. Calcd for $C_{22}H_{18}NOPS_2$: C, 64.85; H, 4.45; N, 3.44; S, 15.74%.

6-Phenyl-3-(*p*-tolylimino)-4-(*p*-tolyl)-1,2,3-dithiaphosphorin (16c): ^1H NMR ($CDCl_3$) δ=2.36 (s, 3H), 2.40 (s, 3H), 6.96—7.64 (m, 9H), 7.37 (d, 1H, J_{HP}=34.0 Hz), 8.09 (d, 2H, J_{HH}=9.0 Hz), and 8.18 (d, 2H, J_{HH}=8.0 Hz); MS *m/z* (rel intensity) 405 (M^+, 8), 371 (7), and 341 (100). Found: C, 68.70; H, 4.63; N, 3.10%. Calcd for $C_{23}H_{20}NPS_2$: C, 68.12; H, 4.97; N, 3.45%.

4,6-Diphenyl-3-(*p*-tolylimino)-1,2,3-dithiaphosphorin (16d): ^1H NMR ($CDCl_3$) δ=2.37 (s, 3H), 7.04—7.76 (m, 12H), 7.42 (d, 1H, J_{HP}=34.0 Hz), and 8.12—8.40 (m, 2H); MS *m/z* (rel intensity) 391 (M^+, 13), 357 (3), and 327 (100). Found: C, 67.49; H, 4.36; N, 3.58%. Calcd for $C_{22}H_{18}NPS_2$: C, 67.50; H, 4.63; N, 3.58%.

3-(*p*-Methoxyphenylamino)-1-phenyl-3-(*p*-tolyl)-2-propene-1-thione (17a): ^1H NMR ($CDCl_3$) δ=2.32 (s, 3H), 3.69 (s, 3H), 6.65 (d, 2H, J_{HH}=9.0 Hz), 6.78 (s, 1H), 6.83 (d, 2H, J_{HH}=9.0 Hz), 6.96—7.44 (m, 7H), 7.60—7.88 (m, 2H), and 15.85 (broad s, 1H); MS *m/z* (rel intensity) 359 (M^+, 61), 358 (82), 326 (9), and 252 (100). Found: C, 76.45; H, 5.90; N, 3.54%. Calcd for $C_{23}H_{21}NOS$: C, 76.85; H, 5.89; N, 3.90%.

3-(*p*-Methoxyphenylamino)-1,3-diphenyl-2-propene-1-thione (17b): ^1H NMR ($CDCl_3$) δ=3.68 (s, 3H), 6.62 (d, 2H, J_{HH}=9.0 Hz), 6.76 (s, 1H), 6.79 (d, 2H, J_{HH}=9.0 Hz), 7.29 (m, 8H), 7.68—7.80 (m, 2H), and 15.86 (broad s, 1H); MS *m/z* (rel intensity) 345 (M^+, 64), 344 (100), 312 (7), and 238 (89). Found: C, 76.51; H, 5.62; N, 3.88%. Calcd for $C_{22}H_{19}NOS$: C, 76.49; H, 5.54; N, 4.05%.

1-Phenyl-3-(*p*-tolylamino)-3-(*p*-tolyl)-2-propene-1-thione (17c): ^1H NMR ($CDCl_3$) δ=2.22 (s, 3H), 2.32 (s, 3H), 6.64—7.36 (m, 11H), 6.76 (s, 1H), 7.60—7.80 (m, 2H), and 15.81 (broad s, 1H); MS *m/z* (rel intensity) 343 (M^+, 60), 342 (96), 310 (12), and 252 (100). Found: C, 80.62; H, 6.11; N, 3.80%. Calcd for $C_{23}H_{21}NS$: C, 80.43; H, 6.16; N, 4.08%.

1,3-Diphenyl-3-(*p*-tolylamino)-2-propene-1-thione (17d): ^1H NMR ($CDCl_3$) δ=2.22 (s, 3H), 6.72 (d, 2H, J_{HH}=9.0 Hz), 6.77 (s, 1H), 6.90 (d, 2H, J_{HH}=9.0 Hz), 7.14—7.38 (m, 8H), 7.68—7.80 (m, 2H), and 15.83 (broad s, 1H); MS *m/z* (rel intensity) 329 (M^+, 49), 328 (78), 296 (11), and 238 (100). Found: C, 79.88; H, 5.79; N, 4.07%. Calcd for $C_{22}H_{19}NS$: C, 80.20; H, 5.81; N, 4.25%. The ^1H NMR spectrum is identical with that reported by Quiniou et al.[9]

The authors wish to thank Dr. Jun Uzawa for measuring the ^{31}P NMR spectra and also Messrs.

Toshiaki Kubota, Yoichi Sawayanagi, and Etsuji Takanobu for technical assistance.

References

1) H. Yamaguchi, S. Kametani, T. Karakasa, T. Saito, and S. Motoki, *Tetrahedron Lett.*, **23**, 1263 (1982); T. Uchida, K. Kozawa, T. Saito, and S, Motoki, *Bull. Chem. Soc. Jpn.*, **57**, 1985, 1990 (1984); H, Tanaka, S. Kametani, T. Saito S. Motoki, ibid., **58**, 667 (1985).

2) E. Niecke and D.-A. Wildbredt, *J. Chem. Soc., Chem. Commun.*, **1981**, 72; R. Appel, F. Knoll, and I. Ruppert, *Angew. Chem., Int. Ed. Engl.*, **20**, 731 (1981); R. Appel, F. Knoch, and H. Kunze, ibid., **23**, 157 (1984); M. Caira, R. H. Neilson, W. H. Watson, P. Wisian-Neilson, and Z.-M. Xie, *J. Chem. Soc., Chem. Commun.*, **1984**, 698.

3) M. Yoshifuji, J. Tagawa, and N. Inamoto, *Tetrahedron Lett.*, **1979**, 2415; B. Divisia, *Tetrahedron*, **1979**, 181; T. Kawashima, T. Tomita, and N. Inamoto, *Phosphorus and Sulfur*, **16**, 9 (1983); Th. A. van der Knaap, Th. C. Klebach, R. Lourens, M. Vos, and F. Bickelhaupt, *J. Am. Chem. Soc.*, **105**, 4026 (1983); E. Deschamps and F. Mathey, *J. Chem. Soc., Chem. Commun.*, **1984**, 1214.

4) The thione dimers **6** can not be obtained by thionation of 1-arylmethylene pinacolones under the reaction conditions as reported in the previous paper.[5]

5) T. Karakasa and S. Motoki, *J. Org. Chem.*, **43**, 4147 (1978).

6) G. Märkl and R. Potthast, *Tetrahedron Lett.*, **1968**, 1755; E. F. Moony, "Annual Reports on NMR Spectroscopy," Academic Press, New York (1973), Vol. 5B, p. 12; R. S. Macomber, G. A. Krudy, and M. Z. Amer, *J. Org. Chem.*, **48**, 1420 (1983).

7) G. A. Krudy and R. S. Macomber, *J. Org. Chem.*, **43**, 4656 (1978); K. Clausen, A. A. El-Barbary, and S.-O. Lawesson, *Tetrahedron*, **1981**, 1019; L. D. Quin, K. C. Caster, and S. B. Soloway, *J. Org. Chem.*, **49**, 2627 (1984).

8) G. W. Buchanan and V. L. Webb, *Org. Magn. Reson.*, **21**, 436 (1983).

9) S. Kametani, H. Ohmura, H. Tanaka, and S. Motoki, *Chem. Lett.*, **1982**, 793.

10) G. Duguay and H. Quiniou, *Bull. Soc. Chim. Fr.*, **1970**, 1918; E. Kleinpeter and M. Pulst, *J. Prakt. Chem.*, **322**, 575 (1980); H. Quiniou, *Phosphorus and Sulfur*, **10**, 1 (1981).

11) Treatment of thiochalcone (**10**) dimers with the aromatic amines (*p*-anisidine, *p*-toluidine) in the presence of NF_3 also afforded 3-amino-2-propene-1-thiones **17** in low yields.

Isopropylidenation of Raffinose[1)]

Toshiki OTAKE* and Junko TSUKAHARA
Department of Food and Nutrition, Yamanashi Gakuin Junior College,
2-4-5, Sakaori, Kofu 400
(Received April 23, 1985)

A reaction of raffinose with an excess amount of 2,2-dimethoxypropane and *p*-toluenesulfonic acid as a catalyst in *N,N'*-dimethylformamide, followed by acetylation, gave seven kinds of mono-, di, or tri-*O*-isopropylideneraffinose peracetates with at least five kinds of minor products. A reaction of raffinose with a limited amount of 2,2-dimethoxypropane gave a new isopropylidene derivative with some of the derivatives described above. The isopropylidenation occurred at 1′,2-, 2,3-, 2″,3″-, 3,4-, 3″,4″-, and 4″,6″-positions. The structures of these compounds were established by ^{1}H and ^{13}C NMR analyses.

The importance of cyclic acetals for the selective blocking of hydroxyl groups in carbohydrate chemistry has long been recognized.[2)] However isopropylidenation of nonreducing sugars like sucrose and raffinose with acetone and an acidic catalyst had been unsuccessful. In 1975, Khan and Mufti[3–5)] investigated the reaction of sucrose with a combination of DMP,*1 DMF,*2 and TSA*3 called reagent A. They obtained 4,6-*O*-isopropylidenesucrose and 1′,2:4,6-di-*O*-isopropylidenesucrose. The author[6)] has reported the isopropylidenation of 6,6′-di-*O*-palmitoylsucrose with reagent A. The main product was 1′,2-*O*-isopropylidene-6,6′-di-*O*-palmitoylsucrose.

Salam[7,8)] has reported that treatment of raffinose (**1**) with benzylidene bromide in pyridine followed by acetylation gave 3″,4″-*O*-benzylideneraffinose nonaacetate and 1′,2:4″,6″-di-*O*-benzylideneraffinose heptaacetate, and that treatment of **1** with reagent A yielded 4″,6″-*O*-isopropylideneraffinose in 21% yield. This paper will deal with mono-, di-, or tri-*O*-isopropylideneraffinose peracetates acetalated at 1′,2-, 2,3-, 2″,3″-, 3,4-, 3″,4″-, or 4″,6″-positions using reagent A.

Results and Discussion

Reaction of **1** with DMP in a molar ratio of 1:20 and TSA in DMF for 80 min, gave a mixture of isopropylidene(Ip) derivatives of **1**. By thin-layer chromatography(TLC), the complete consumption of **1** was confirmed. On a silica-gel TLC of the acetylation product of the above reaction mixture (developed four times with an admixture of diethyl ether and hexane (4:1 or 5:1)), at least seven spots were separately observed. They were designated in R_f's order (high to low) as **2** to **8**. After recycling column chromatography of the acetates about 35 times on an open column of silica gel eluted with a solvent system of diethyl ether and hexane or diisopropyl ether and hexane, the seven acetates were isolated as pure or almost pure forms on a TLC, and at least five minor components were also separated as almost pure forms. Yields of the seven acetates were 0.8 (**2**), 4.0 (**3**), 3.4 (**4**), 3.5 (**5**), 25.4 (**6**), 3.5 (**7**), and 5.5% (**8**), respectively. The major component was **6**. Compounds **3**, **6**, **7**, and **8** were crystallized as needles, respectively. From an elementary analysis, and ^{1}H and ^{13}C NMR analyses of acetyl methyl proton signals and methyl and quaternary carbon signals of the Ip-groups (Tables 1 and 2), the degree of isopropylidenation was estimated as shown in Table 3. Figure 1 shows schematic spectra of the acetates in the region of methyl and quaternary carbons of the Ip-group. By following common signals on the spectra of the eight compounds, at

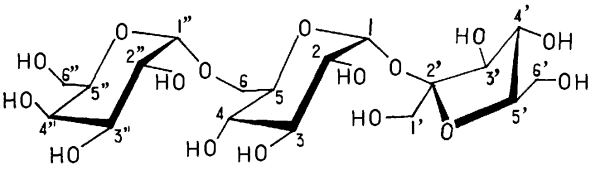

Table 1. ^{1}H Chemical Shifts(δ ppm) of the Ip- and Acetyl Groups of the *O*-Isopropylideneraffinose Peracetates

	Ip-methyl protons	Acetyl methyl protons
2	1.34, 1.40, 1.47(6H), 1.52, and 1.56.	2.08, 2.09, 2.12, 2.14, and 2.15.
3	1.27, 1.32, 1.48, and 1.50.	2.02, 2.05, 2.06, 2.10, 2.12, 2.14, and 2.24.
4	1.39, 1.42, 1.47(9H), and 1.54.	2.06, 2.07, 2.08, 2.10, and 2.14.
5	1.26, 1.47(9H), and 1.51.	2.01, 2.03, 2.08, 2.09, and 2.24.
6	1.27, 1.42, 1.46, and 1.49.	2.02, 2.05, 2.06, 2.07, 2.08, 2.12, and 2.24.
7	1.39, 1.42, 1.44 and 1.46.	2.08, 2.09(9H), and 2.12(9H)
8	1.38 and 1.43.	1.98, 2.00, 2.02, 2.05 2.06(6H), 2.07, 2.08, and 2.13.
9	1.31 and 1.49.	2.00, 2.04, 2.08, 2.09(6H), 2.10, 2.11, 2.13, and 2.15.

*1 2,2-Dimethoxypropane, *2 *N,N'*-Dimethylformamide, *3 *p*-Tolueneesulfonic acid.

least, six sets of signals were distinguished. Compound **9** will be described later. Each set consists of signals of two methyl carbons and one quaternary carbon in the same Ip-group. The Ip-groups corresponding to each set were designated as Ip-1 to Ip-6. The mean δ-values of the carbons in each Ip-group are as follows: Ip-1, δ=26.26, 27.82, and 109.85; Ip-2, δ=26.62, 26.81, and 111.02; Ip-3, δ=26.57, 26.68, 110.23; Ip-4, δ=23.93, 25.43, and 101.51; Ip-5, δ=26.20, 26.91, and 111.57; Ip-6, δ=18.50, 29.38, and 98.79. Possible assignments of the Ip-groups to each compound are as follows: **2**, Ip-1, Ip-2, and Ip-4; **3**, Ip-1, and Ip-4; **4**, Ip-2, Ip-4, and Ip-6; **5**, Ip-3, Ip-4, and Ip-6; **6**, Ip-4 and Ip-6; **7**, Ip-5 and Ip-6; **8**, Ip-6; **9**, Ip-1.

Table 2. ^{13}C Chemical Shifts(δ ppm) of the Ip-Group and C-1, C-1″, and C-2′ of the *O*-Isopropylideneraffinose Peraceates

	Ip-methyl carbons
2	24.02, 25.46, 26.34, 26.58, 26.76, and 27.92.
3	23.86, 25.39, 26.30, and 27.88.
4	18.52, 24.06, 25.48, 26.65, 26.85, and 29.40.
5	18.47, 23.79, 25.45, 26.57, 26.68, and 29.28.
6	18.51, 23.93, 25.39, and 29.40.
7	18.50, 26.20, 26.91, and 29.40.
8	18.49 and 29.40
9	26.51 and 27.73

	C-1	C-1″	C-2′	Quaternary carbons of the Ip-group
2	91.42	96.52	104.26	101.62, 109.88, and and 111.02.
3	90.54	96.49	104.58	101.53 and 109.89.
4	91.11	97.24	104.03	98.78, 101.52, and 111.02.
5	90.57	96.47	104.55	98.74, 101.41, and 110.23.
6	90.34	93.33	104.44	98.78 and 101.47.
7	90.25	96.79	103.05	98.80 and 111.57
8	89.96	96.66	104.36	98.84.
9	90.08	96.00	104.40	109.77.

Table 3. Degree of Isopropylidenation of Each Compound Estimated by Elementary Analysis and Numbers of Signals of Under-Lined Atoms on NMR Spectra

	Ip-degree	Numbers of signals		
		$C\underline{H}_3CO$	$(C\underline{H}_3)_2CO_2$	$(CH_3)_2\underline{C}O_2$
2	Tri	5	6	3
3	Di	7	4	2
4	Tri	5	6	3
5	Tri	5	6	3
6	Di	7	4	2
7	Di	7	4	2
8	Mono	9	2	1
9	Mono	9	2	1

The structure of each compound was established by ^{1}H NMR with the aid of the 180° pulse-τ-90° pulse method[9,10] or others. The signal of the free induction decay of the 90° pulse was recorded and Fourier-transformed. At a τ-value of 0.15 s, the intensity of methylene-proton signal was almost zero, and methine protons showed negative signals. At a τ-value of 0.30—0.35 s, the intensities of methine-proton signals were low (positive or negative) and methylene protons showed positive signals.

First-order analyses of the eight compounds are summarized in Tables 4-1 and 4-2. Signals of the glycosylated methylene (H-6a and H-6b), Ip-*O*-methylene and methine protons are in a region between 3.3 and 4.3 ppm. Signals of acetoxy-substituted methylene and methine protons adjacent to the methylene group (H-5, H-5′, and H-5″) are in a region between 4.3 and 4.5 ppm, while signals of anomeric and other acetoxy-substituted methine protons fall in a region over 4.6 ppm.[11,12]

From the high-field shifts of H-4″ and H-6″ (2H), **8** was estimated to be 4″,6″-*O*-isopropylideneraffinose nonaacetate. Two symmetric proton signals, centered on 5.25 ppm, are regarded as signals of H-2″ and H-3″. This pattern is caused by a similar environment of the two protons:

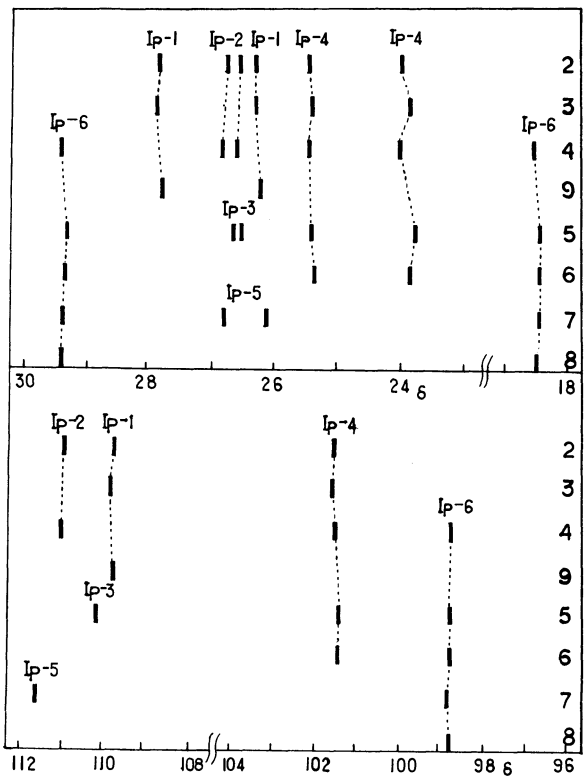

Fig. 1. Schematic ^{13}C NMR spectra of methyl (δ 18—30) and quaternary carbons (δ 96—112) of the Ip-group.

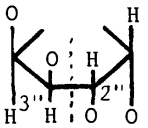

Other acetoxy-substituted methine signals (H-2, H-3, H-4, H-3′, and H-4′) were well analyzed, confirming the structure. Compounds having Ip-6 (**7**, **6**, **5**, and **4**) are also regarded as 4″,6″-*O*-isopropylidene derivatives. On a ^{1}H NMR spectrum of 6″-*O*-tritylraffinose decaacetate,[11] the coupling constants, $J_{5'',6''a}$ and $J_{5'',6''b}$ were 5 and 7 Hz, respectively. The small values of the corresponding coupling constants in the case of **8** may be caused by the rigid structure of the 4″,6″-*O*-Ip-ring.

In the case of **7**, the presence of a 4″,6″-*O*-isopropylidene group was confirmed by high-field shifts of the corresponding protons. A doublet and a triplet at 3.52 and 4.09 ppm were confirmed to be the signals of H-2 and H-3 by the decoupling method. Thus, **7** is expected to be 2,3:4″,6″-di-*O*-isopropylideneraffinose heptaacetate.

On a ^{1}H NMR spectrum of **6**, high-field shifts of H-1′ (2H) and H-2 were observed in addition to the high-field shifts of H-4″ and H-6″ (2H). Signals of acetoxy-substituted methine protons, H-3, H-4, H-3′, and H-4′ were wholly analyzed. A broad singlet of two protons centered on 5.25 ppm was assigned to the complex signals of H-2″ and H-3″. Thus, the main product **6** was confirmed to be 1′,2:4″,6″-di-*O*-isopropylideneraffinose heptaacetate. The Ip-4 type products, **2**, **3**, **4**, **5**, and **6** should be 1′,2-*O*-Ip-derivatives.

In the case of **5**, high-field shifts of H-1′ (2H), H-2, H-4″, and H-6″ (2H) were observed. All the signals involving acetoxy-substituted methine protons in a region over 4.6 ppm, H-3, H-4, H-3′, and H-4′ were wholly analyzed. At a τ of 0.15 s, in the 180° pulse-τ-90° pulse method, symmetric two-proton signals centered on 4.12 ppm were observed and assigned to the complex signals of H-2″ and H-3″. The assignments were supported by homonuclear correlated two-dimentional ^{1}H NMR.[13] A signal at 5.29 ppm (H-1″) correlated with a signal at 4.14 ppm

Table 4-1. Chemical Shifts (δ ppm) on ^{1}H NMR Spectra of the *O*-Isopropylideneraffinose Peracetates

	H-1 d	H-2 dd	H-3t(dd)		H-4t(dd)	H-6a dd	H-6b dd
2	6.20	3.96	3.80	or	3.35	3.85	3.72
3	6.12	3.84	5.31		5.11	3.74	3.52
4	6.17	3.96	3.79	or	3.30	3.76	3.69
5	6.16	3.85	5.30		5.16	3.81	3.67
6	6.16	3.78	5.33		5.04	3.79	3.53
7	5.71	3.52	4.09		5.21	3.77	3.63
8	5.67	4.82	5.46		5.06	3.78	3.54
9	5.63	4.78	5.43		5.09	3.69	3.49

	H-1′a d	H-1′b d	H-3′d	H-4′t(dd)	H-6′a dd	H-6′b dd
2	4.06	3.54	5.13	5.35	rd. 4.4	
3	4.04	3.53	5.16	5.37	rd. 4.4	
4	3.88	3.53	5.16	5.36	ca. 4.22	ca. 4.15
5	4.06	3.53	5.16	5.34	rd. 4.4	
6	3.86	3.53	5.19	5.38	4.53	4.27
7	4.27	4.07	rd. 5.46		rd. 4.4	
8	4.29	4.20	5.46	5.32	4.37	ca. 4.3
9	rd. 4.3		5.41	5.33	rd. 4.4	

	H-1″d	H-2″	H-3″	H-4″	H-5″	H-6″a dd	H-6″b dd
2	5.04	4.92 dd			rd. 4.3		
3	5.02	4.87 dd	4.38 dd			rd. 4.3	
4	5.19	ct. 5.30 m	3.79 bs	4.46 bs	4.09		3.89
5	5.29	ct. 4.12 m	3.46 bs	4.52 bs	4.17		3.90
6	5.19	ct. 5.27 m	3.72 bs	4.48 bs	4.08		4.01
7		rd. 5.2	3.71 bs	4.66 bs	4.07		3.84
8	5.17	ct. 5.25 m	3.72 bs	4.44 bs	4.10		3.85
9	4.97	4.85 dd	4.30 dd		rd. 4.2		

rd.: round, ct: centered on, bs: broad singlet, d: doublet, dd: doublet of doublets, t: triplet, m: multiplet.

Table 4-2. Coupling Constants(J Hz) on ^{1}H NMR Spectra of the *O*-Isopropylideneraffinose Peracetates

	1-2	2-3	3-4	4-5	5-6a	5-6b	6a-6b
2	3.8	10.4	10.0	10.0	5.0	ca. 2	10.4
3	3.4	9.6	10.0	10.0	4.0	ca. 2	12.0
4	3.5	9.8	9.8	9.8	5.6	ca. 2	9.0
5	3.8	9.5	9.5	9.5	4.0	ca. 2	10.6
6	3.5	9.8	9.8	9.8	5.0	ca. 3	ca.13
7	3.4	9.8	9.8	ca.10	3.8	2.3	8.8
8	4.0	10.4	10.4	10.4	5.2	2.5	11.0
9	3.8	10.0	10.0	10.0	3.8	ca. 2	12.0

	1′a-1′b	3′-4′	4′-5′	5′-6′a	5′-6′b	6′a-6′b
2	12.2	6.0	4.0	—	—	—
3	12.8	6.0	4.0	—	—	—
4	12.2	6.4	5.4	—	—	—
5	12.0	4.7	3.8	—	—	—
6	13.0	6.2	ca. 6	—	—	—
7	12.4	—	—	—	—	—
8	12.0	6.0	6.0	6.0	ca. 2	6.0
9	—	5.2	5.2	—	—	—

	1″-2″	2″-3″	3″-4″	4″-5″	5″-6″a	5″-6″b	6″a-6″b
2	3.4	8.4	—	—	—	—	—
3	3.6	7.8	—	—	—	—	—
4	4.0	—	ca. 1.5	ca. 1.5	ca. 1.5	ca. 1.5	13.5
5	2.8	—	ca. 1.5	ca. 1.5	ca. 1.5	ca. 1.5	13.6
6	3.5	—	ca. 1.5	ca. 1.5	ca. 1.5	0	12.8
7	—	—	ca. 1.5	ca. 1.5	ca. 1.5	ca. 1.5	12.6
8	2.5	—	ca. 1.5	ca. 1.5	ca. 1.5	ca. 1.5	12.4
9	3.3	8.0	—	—	—	—	—

to be assigned to H-2″, and a signal at 3.46 ppm (H-4″) correlated with a signal at 4.12 ppm to be assigned to H-3″. Thus, **5** was regarded as 1′,2:2″,3″:4″,6″-tri-*O*-isopropylideneraffinose pentaacetate, and Ip-3 is 2″,3″-*O*-Ip-group.

On a spectrum of **4**, high-field shifts of H-1′ (2H), H-2, H-3, H-4, H-4″, and H-6″ (2H) were recognized. In a region between 5.1 and 5.4 ppm, signals of acetoxy-substituted methine protons, H-1″, H-2″, H-3′, H-3″, and H-4′ were observed. The complex signals of H-2″ and H-3″ had almost the same symmetric pattern as that on the spectrum of **8**. Thus, **4** was recognized as 1′,2:3,4:4″,6″-tri-*O*-isopropylideneraffinose pentaacetate. Compound **2**, which also had an Ip-2 type Ip-group, was assumed to be a 3,4-*O*-isopropylidene derivative of **1**.

In the case of **3**, signals of five acetoxy-substituted methine protons, H-2″, H-3, H-3′, H-4, and H-4′ and an anomeric proton, H-1″ were observed in the region between 4.8 and 5.4 ppm. Signals of H-1′ (2H), H-2, and H-3″ were in a high field. Although the assignment of H-4″ could not be achieved due to the absence of an H-4″ signal in the region above 4.6 ppm, the high-field shift of H-4″ was clear. Thus, **3** is regarded to be 1′,2:3″,4″-di-*O*-isopropylideneraffinose heptaacetate, and Ip-1 is assumed to be a 3″,4″-*O*-isopropylidene group.

In the case of **2**, acetoxy-substituted methine protons were H-2″, H-3′ and H-4′. High-field shifts of H-1′ (2H), H-2, H-3, and H-4 were clearly recognized. Signals of H-3″ and H-4″ should be in the region between 4.3 and 4.5 ppm. Compound **2** was recognized as 1′,2:3,4:3″,4″-tri-*O*-isopropylideneraffinose pentaacetate.

In the above reaction, six types of isopropylidenation were observed. The main types were 4″,6″- and 1′,2-*O*-isopropylidenation. Isopropylidenations at 3′,4′-, and 4′,6′-positions were not found.

A reaction of **1** with DMP in a molar ratio of 1:6.5 in the presence of TSA in DMF for 80 min., also gave a mixture of Ip-derivatives without a free form of **1**. After recycling column chromatography of the corresponding acetates (about 30 times on a silica-gel column using the same method as for the former reaction), compounds, **3**, **6**, **8**, and **9** were isolated as pure or almost pure forms. A minor component and a mixture consisting of two components were also obtained. The yields of the four acetates were 1.7 (**3**), 11.3 (**6**), 10.6 (**8**), and 2.3% (**9**), respectively.

On ^{1}H and ^{13}C NMR spectra of **9**, 9 signals of acetyl methyl protons, 2 signals of Ip-methyl carbons and one signal of a quarternary carbon in an Ip-group were observed as shown in Table 1. Thus, **9** was estimated to be a mono-*O*-Ip-derivative, and the chemical shifts of the Ip-methyl carbons and the quaternary carbon in the Ip-group showed that **9** is 3″,4″-*O*-isopropylideneraffinose nonaacetate (Fig 1).

Table 5. Elementary Analysis, Optical Rotation ($[\alpha]_D^{20}$) in Chloroform, Melting Point, and R_f and R_2 on TLC of the *O*-Isopropylideneraffinose Peracetates

	Found (%) C	Found (%) H	$[\alpha]_D^{20}$	(c)	Mp(θ_m/°C)	R_f*	R_2*2
2	53.26	6.55	+ 59.50°	(1)	—	0.53	1.00
3	51.64	6.19	+ 78.16°	(1)	90—91	0.50	0.96
4	53.36	6.50	+ 82.67°	(1.5)	—	0.44	0.83
5	53.34	6.55	+ 75.33°	(1.5)	—	0.38	0.71
6	51.68	6.17	+104.00°	(1.5)	181—183	0.33	0.63
7	51.66	6.12	+113.58°	(1.5)	153—155	0.28	0.52
8	50.55	5.72	+115.46°	(1.5)	187—188	0.22	0.42
9	51.08	5.94	+122.27°	(1)	—	0.37	0.70

Calcd for $C_{39}H_{54}O_{21}$ (**8** and **9**): C, 50.76; H, 5.90%, for $C_{38}H_{54}O_{23}$ (**3**, **6**, and **7**): C, 51.94; H, 6.19%, for $C_{37}H_{54}O_{25}$ (**2**, **4**, and **5**): C, 53.23; H, 6.52%.

*1TLC was performed with diethyl ether–hexane (4:1) in a quadruplicated development.

*2R_2: migration length of **X**/ that of **2**.

In the acetoxy-substituted methine-proton region on a ^{1}H NMR spectrum of **9**, H-2, H-2″, H-3, H-3′, H-4, and H-4′ signals were observed. Due to an overlapping of the signals assignments of H-3″ and H-4″ could not be achieved; however **9** is difinitely regarded as a 3″,4″-*O*-Ip-derivative. Increases in mono-*O*-Ip-derivatives and decreases in tri-*O*-Ip-derivatives (compared to a high-DMP reaction) were reasonable.

Experimental

General Methods. Melting points were determined in capilary tubes and were uncorrected. Optical rotations were measured with a Japan Spectroscopic DIP-SL polarimeter. The ^{1}H and ^{13}C NMR spectra were recorded at 200 MHz (for ^{1}H) with a Varian XL-200 and at 300 MHz (for ^{1}H) with a Varian XL-300 spectrophotometer in deuteriochloroform with tetramethylsilane as an internal standard. With ^{1}H NMR, the spectral width was 2000 Hz (16000 data points) for the 200-MHz instrument and 4000 Hz (32000 data points) for the 300-MHz instrument. With ^{13}C NMR, the spectral width was 11574.1 Hz (16364 data points) and 16501.7 Hz (32000 data points). Acquisition times were 4.0 s for ^{1}H NMR and 0.7—0.97 s for ^{13}C NMR. Sixteen-times accumulation for ^{1}H NMR and 512-times accumulation for ^{13}C NMR were used. In the 180° pulse-τ-90° pulse method, the post delay (interval of the end of acquisition and 180° pulse) was 5 s, and the range of τ was 0.05—0.35 s TLC was performed on silica-gel plates (Art. 5554, DC-Alufolien Kieselgel 60 F_{254}, in a thickness of 0.2 mm, Merck) developed with a solvent system of 1-butanol–acetic acid–water (4:1:1.7) for the free Ip-derivatives and a solvent system of diethyl ether–hexane (4:1 or 5:1) in quadruplicated development for the *O*-isopropylideneraffinose peracetates. Open-column chromatography of the acetates was achieved on a silica-gel

column (Wakogel C-200, Wako Pure Chemical Ind. Ltd.) eluted with diethyl ether–hexane (4:1 or 5:1). Recycling took place 30—35 times. Samples added to the column were dissolved in chloroform. The weight of the adsorbent that was used was about 20 times that of the submitted sample and the volume of eluting solvent was about 30 times that of the adsorbent (vol/wt). The eluent was divided into 50—60 fractions. Each fraction was inspected by TLC, and the fractions having the same R_f values were collected and dried for further inspection. An admixture of diisopropyl ether and hexane (3:1) was applied for the separation of **4** and **5**.

Isopropylidenation of 1 and Acetylation of the Reaction Products. To a solution of **1** (5.0 g, 0.01 mol as dehydrated material), 0.5 g of TSA and 25 ml (d=0.85, ca. 0.2 mol) of DMP in a "high-DMP reaction" and 8 ml (0.065 mol) of DMP in a "low-DMP reaction" in 250 ml of DMF were added and each mixture was settled for 80 min at room temperature. The solution was then neutralized with IR-410(OH) resin, filtered, and concentrated. The resultant syrupy residue was then acetylated with acetic anhydride (12 ml) in pyridine (20 ml). The reaction mixture was concentrated to give a syrupy product. The product was dissolved in chloroform and added to a silica-gel column. After recycling chromatography above-described, each reaction product of the high- and low-DMP reaction was divided into the isolates, **2** to **8** in the high-DMP reaction, and **3**, **6**, **8**, and **9** in the low-DMP reaction. The combined yields of the high- and low-DMP reaction were 4.03 g (46%), and 2.42 g (26%), respectively.

Elementary Analysis and Physical Data of the *O*-Isopropylideneraffinose Peracetates. The elementary analysis and physical data of 1′,2:3,4:3″,4″-tri-*O*-isopropylideneraffinose pentaacetate (**2**), 1′,2:3″,4″-di-*O*-isopropylideneraffinose heptaacetate (**3**), 1′,2:3,4:4″,6″-tri-*O*-isopropylideneraffinose pentaacetate (**4**), 1′,2:2″,3″:4″,6″-tri-*O*-isopropylideneraffinose pentaacetate (**5**), 1′,2:4″,6″-di-*O*-isopropylideneraffinose heptaacetate (**6**), 2,3:4″,6″-di-*O*-isopropylideneraffinose heptaacetate (**7**), 4″,6″-*O*-isopropylideneraffinose nonaacetate (**8**), and 3″,4″-*O*-isopropylideneraffinose nonaacetate (**9**) were summarized in Table 1, 2, 4, and 5. The weights obtained and yields were as follows; (i) high-DMP reaction: **2** 72.1 mg (0.8%), **3** 348 mg (4.0%), **4** 297 mg (3.4%), **5** 302 mg (3.5%), **6** 2227 mg (25.4%), **7** 309 mg (3.5%), and **8** 479 mg (5.5%); (ii) low-DMP reaction: **3** 159 mg (1.7%), **6** 1066 mg (11.3%), **8** 1000 mg (10.6%), and **9** 215 mg (2.3%).

The authors wish to thank Mr. Katsuhiko Kushida, Varian Instrument Ltd., for determining the NMR spectra.

References

1) Presented in part at the 4th Japanese Carbohydrate Symposium, Tokyo, August (1981), Abstr., p. 74.
2) A. N. DeBelder, *Adv. Carbohyd. Chem.*, **20**, 219 (1965).
3) R. Khan and K. S. Mufti, *Carbohyd. Res.*, **43**, 247 (1975).
4) K. S. Mufti and R. Khan, British Patent 1437048 (1975).
5) R. Khan, K. S. Mufti, and M. R. Jenner, *Carbohyd. Res.*, **65**, 109 (1978).
6) T. Otake, *Hōkei Kenkyu (Yamanashi Gakuin University)* **11**, 825 (1978).
7) M. A. Salam, Ph. D. Thesis, Queen Elizabeth College, University of London, The United Kingdom, 1977.
8) E. B. Rathbone, "Developments in Food Carbohydrate-2," ed by C. K. Lee, Applied Science Publishers, London (1980), Chap. 3.
9) H. Y. Carr and E. M. Purcell, *Phys. Rev.*, **94**, 630 (1954).
10) J. R. Lyerla Jr. and G. C. Levy, "Topics in Carbon-13 NMR Spectroscopy," ed by G. C. Levy, Wiley Interscience, New York (1974), Chap. 3.
11) T. Suami, T.Otake, T. Nishimura, and T. Ikeda, *Carbohyd. Res.*, **26**, 234 (1973).
12) T. Suami, T. Otake, T. Ikeda, and R. Adachi, *Bull. Chem. Soc. Jpn.*, **50**, 1612 (1977).
13) G. A. Gray, Varian Instruments Application Report (Two-dimentional NMR on the XL-200), MAG 2626 4M681.

 © 1986 The Chemical Society of Japan Bull. Chem. Soc. Jpn., 59, 73—76 (1986)

Geometrical Isomerism of Phenylhydrazones of α-Keto Esters. II. *p*-Substituted Phenylhydrazones of Ethyl Pyruvate and 2,4-Dinitrophenylhydrazones of Some α-Keto Esters[1)]

Fumihide Ishibashi,* Takeo Nashima,* Junko Nishino, Ikuko Kobayashi, Yoshinori Ichihara, Yoshimi Kitagawa, Shigeko Sasaki, Masako Yoshikawa, Atsuko Matsuoka, and (late) Keiko Yamamoto

Department of Chemistry, Osaka Kyoiku University, Tennoji-ku, Osaka 543

(Received June 17, 1985)

Each geometrical isomer of various substituted phenylhydrazones of ethyl pyruvate and 2,4-dinitrophenylhydrazones of some α-keto esters was isolated in a pure state. Partial isomerizations of the *E*-isomers of the former hydrazones to the *Z*-isomers took place by keeping solutions of the hydrazones in organic solvents containing C, H, and Cl in the dark. An *E*- or *Z*-structure was assigned to each molecule on the basis of IR and ^{1}H NMR spectra. In all cases, isomers with higher R_f-values on a silica gel TLC (using benzene as a developing solvent) involved an intramolecular hydrogen bonding between the imino hydrogen and the ester carbonyl oxygen. Thus, the *Z*-structure was assigned. An *E*-structure was assigned to other isomers with lower R_f-values. The present assignment is, thus, entirely the same as that proposed in a previous investigation.

Previously, we[1)] reported on the isolation of each geometrical isomer of 2,4-dinitrophenylhydrazones (DNPHs) of some pyruvic esters. *E*- and *Z*-configurations were assigned to the isomers on the basis of IR, visible, and ^{1}H NMR spectroscopy, thus correcting Van Duin's[2)] assignment.

This investigation stimulated us to reexamine the geometry of some of the hitherto-known substituted phenylhydrazones of the α-keto esters. With regard to the hydrazones reported in the present paper, their separation into individual isomers and the assignment of an *E*- or *Z*-structure to each of the isomers have scarcely been described in the literature. The reported melting points of the hydrazones, in most cases, are probably those either of a mixture of *E*- and *Z*-isomers, or of the more stable isomer of the two.[3,4)]

In the present work, we report on the preparation of some *p*-substituted phenylhydrazones of ethyl pyruvate and DNPHs of ethyl glyoxylate and ethyl benzoylformate, the fractional isolation of each geometrical isomer of the above hydrazones, and structural assignments of an *E*- or *Z*-configuration, by means of the previously mentioned method.[1)] In addition, the relative stability of each isomer compared to its geometrical counterpart is also discussed.

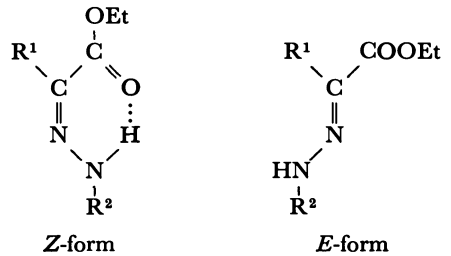

Z-form

E-form

R^1	R^2	R^1	R^2
1a=Me,	*p*-$CH_3C_6H_4$	**2a**=Me ,	2,4-$(NO_2)_2C_6H_3$
1b=Me,	C_6H_5	**2b**=H ,	2,4-$(NO_2)_2C_6H_3$
1c=Me,	*p*-ClC_6H_4	**2c**=C_6H_5,	2,4-$(NO_2)_2C_6H_3$
1d=Me,	*p*-$NO_2C_6H_4$		

Experimental

All the melting points are uncorrected. Visible and IR spectra were recorded on a Hitachi Recording Spectrophotometer ESP-3 and a Hitachi-Perkin-Elmer IR-Spectrometer-225, respectively. ^{1}H NMR spectra were recorded on a Hitachi-Perkin-Elmer R-20B operating at 60 MHz.

Geometrical isomers showing higher R_f-values on a silica gel TLC plate using benzene as the developing solvent are called α-isomers, and those with lower R_f-values are called β-ones for all the geometrical isomer pairs of hydrazones,† in common, studied in the present investigation.

Preparation of Ethyl 2-(*p*-Tolylhydrazono)propanoate (1a). **1a** was prepared from ethyl pyruvate, *p*-tolylhydrazine hydrochloride and sodium acetate in an aqueous ethanol solution according to the general procedure.

Fractional Isolation of Each Geometrical Isomer of 1a. Crude **1a** (11.0 g), as it was prepared, was treated with petroleum ether and an insoluble precipitate was separated by filtration. The filtrate was evaporated and the residue was chromatographed on silica gel using benzene as an eluting solvent. The α-isomer (1.3 g), obtained from the first eluting fraction, melted at 43.5—43.7 °C after recrystallization from aqueous methanol. The β-isomer was isolated from the second portion of the eluate which was combined with the precipitate obtained above (weight 9.3 g), and melted at 107.7—108 °C after recrystallization from petroleum ether containing a small volume of ethanol.

Partial Isomerization of the β-Isomer of 1a to the α-Isomer. A solution of 13.2 g of the β-isomer of **1a** in 55 ml of trichloroethylene was allowed to stand for 24 h in the dark. After removing the solvent, the residue was chromatographed on silica gel to yield 6.9 g and 5.6 g of the

† An isomer with a smaller retention volume (higher R_f-value) was called an α-isomer by Van Duin[2)] and an A-isomer by Moriwaki et al.[5)] The other isomer was called a β-isomer and a *B*-isomer, respectively.

α- and β-isomers, respectively. Partial isomerizations were also carried out in 1,2-dichloroethane and chloroform.

Preparation of Ethyl 2-(Phenylhydrazono)propanoate (1b) and Ethyl 2-(*p*-Chlorophenylhydrazono)propanoate (1c), Fractional Isolation of Each Geometrical Isomer of the Above Hydrazones, and Partial Isomerization of the β-Isomers of 1b and 1c to the Corresponding α-Isomers. The above operations were all carried out in essentially the same way as described for **1a**.

Preparation of Ethyl 2-(*p*-Nitrophenylhydrazono)propanoate (1d). **1d** was prepared in a yield of 70% by the reaction of ethyl pyruvate with *p*-nitrophenylhydrazine in 50% acetic acid according to the usual procedure. The product consisted exclusively of the β-isomer.

Partial Isomerization of the β-Isomer of 1d to the Corresponding α-Isomer. A solution of the β-isomer of **1d** in 1,2-dichloroethane was irradiated with sunlight for 24 h to yield a mixture of the isomers in an α to β ratio of 1:0.4.

Yields of the α- and β-isomers of **1** in the syntheses and results of partial isomerization of the β-isomers of **1** to the α-ones are summarized in Tables 1 and 2, respectively.

Preparation of Ethyl 2-(2,4-Dinitrophenylhydrazono)acetate (2b). **2b** was synthesized according to the method described by Cope et al.[3] After a separation of the crude product into the α- and β-isomers by means of chromatography, the ratio of the yields of the α-isomer to the β-one was ca. 3:1.

Preparation of Ethyl 2-Phenyl-2-(2,4-dinitrophenylhydrazono)acetate (2c). Ethyl benzoylformate, synthesized by the oxidation of mandelic acid with potassium permanganate and subsequent esterification, was treated with 2,4-dinitrophenylhydrazine either in an ethanol-sulfuric acid solution or in an aqueous hydrochloric acid solution. The ratios of the yield of the α-isomer to that of the β-one were 3.7:1 under the former reaction conditions and 1.8:1 under the latter ones, as determined after chromatographic separation of the crude products.

Table 1. Yields for the Synthesis of **1**

Compd	Yield/%	
	α	β
1a	12	86
1b	15	80
1c	9	81
1d	Trace	70

Table 2. Partial Isomerization of β-Isomers of **1** to the Corresponding α-Isomers

Compd	Conditions			Ratio α : β
	Solvent	Dark/Light	Hour	
1a	$CHCl_3$	In the dark	24	**1** : 1.2[b]
	$CHCl_3$: C_6H_6[a]	In the dark	72	1 : 6
	$CHBr_3$	In the dark	36	1 : 5
	CH_2Cl-CH_2Cl	In the dark	24	**1** : 0.6
	$CHCl$=CCl_2	In the dark	24	1 : 0.5
	$CHCl_3$	Sunlight	3	1 : 2.6[b]
	$CHCl$=CCl_2	Sunlight	3	1 : 1.3[b]
1b	$CHCl_3$	In the dark	2	**1** : 0.4
	$CHCl_3$: C_6H_6[a]	In the dark	72	No isomerization
	$CHBr_3$	In the dark	48	1 : 9
	CH_2Cl-CH_2Cl	In the dark	48	**1** : 0.9
	$CHCl$=CCl_2	In the dark	36	**1** : 1.4
	$CHCl_3$	Sunlight	2	1 : 1.8[b]
	$CHCl$=CCl_2	Sunlight	3	1 : 2.3[b]
1c	$CHCl_3$	In the dark	24	**1** : 1.4
	$CHCl_3$: C_6H_6[a]	In the dark	72	1 : 0.4
	$CHBr_3$	In the dark	48	**1** : 3
	CH_2Cl-CH_2Cl	In the dark	72	**1** : **1**
	$CHCl$=CCl_2	In the dark	48	**1** : 4
	$CHCl_3$	Sunlight	2	**1** : 2.5[b]
	$CHCl$=CCl_2	Sunlight	2	**1** : 1.7[b]
1d	$CHCl_3$	In the dark	72	No isomerization
	$CHBr_3$	In the dark	48	1 : 6
	CH_2Cl-CH_2Cl	In the dark	72	No isomerization
	$CHCl$=CCl_2	In the dark	72	No isomerization
	$CHCl_3$	Sunlight	36	1 : 1
	$CHCl_3$: C_6H_6[a]	Sunlight	48	1 : 4
	$CHBr_3$	Sunlight	6	**1** : **1**
	CH_2Cl-CH_2Cl	Sunlight	24	**1** : 0.5
	$CHCl$=CCl_2	Sunlight	48	**1** : 0.7

a) Chloroform : benzene = 1 : 9 (v/v). b) Significant degradation occurred.

Results and Discussion

Isolation of Geometrical Isomers. Since each of the *p*-substituted phenylhydrazones (**1a—d**) studied, when formed from the reactants, consisted overwhelmingly of the β-isomer (as seen in Table 1), the corresponding α-isomer was obtained as follows. In the case of **1a**, **1b**, or **1c**, the β-isomer was dissolved in organic solvents consisting of C, H, and halogen such as chloroform, 1,2-dichloroethane, trichloroethylene, bromoform, or chloroform–benzene, and left in the dark at room temperature. At a higher temperature (or with sunlight) the reaction was accompanied by a significant degradation of the hydrazones. A conversion of the β-isomer to α-one occurred so extensively that the isolation of the latter became facile by means of chromatography. It is quite interesting that when a sample of the β-isomer was dissolved in ethanol, benzene, carbon tetrachloride, or tetrachloroethylene and kept in the dark, no appreciable isomerization to the α-isomer was observed.

On the other hand, even if a solution of the β-isomer of **1d** in any one of the above solvents consisting of C, H, and halogen was left in the dark, no appreciable amount of the α-isomer was observed in the resulting equilibrium mixture. However, the irradiation of a 1,2-dichloroethane or trichloroethylene solution of **1d** with sunlight or UV light caused the equilibrium to shift toward the formation of the α-isomer.

In the preparation of **2c**, the ratio of the yield of

Table 3-a. Melting Points, Elementary Analyses, Crystalline Forms, and R_f-Values of *p*-Substituted Phenylhydrazones of Ethyl Pyruvate

Compd		Mp(θ_m/°C)[a]	Analysis(%) Found(Calcd) C	H	N	Formula	Crystalline form	R_f-value[b]
1a,	α	43.5— 43.7	65.14 (65.43	7.41 7.32	12.41 12.72)	$C_{12}H_{16}N_2O_2$	Needles	0.87
	β	107.7—108.0	65.15	7.70	12.66		Needles	0.19
1b,	α	31.7— 32.2[c]	64.32 (64.06	6.61 6.84	14.08 13.58)	$C_{11}H_{14}N_2O_2$	Prisms	0.79
	β	117.9—118.4[d]	64.19	7.08	13.34		Prisms	0.14
1c,	α	60.0— 61.0	54.79 (54.89	5.54 5.44	11.45 11.64)	$C_{11}H_{13}N_2O_2Cl$	Needles	0.86
	β	137.5—138.5	54.89	5.36	11.47		Needles	0.23
1d,	α	110.5—110.9	52.34 (52.59	5.05 5.22	16.95 16.73)	$C_{11}H_{13}N_3O_4$	Prisms	0.41
	β	191.8—192.7	52.68	4.85	16.74		Prisms	0.02

a) Uncorrected. b) TLC on silica gel using benzene as the developing solvent. c) Elguero et al.[6] reported 33—34 °C for the *Z*-isomer. d) Elguero et al.[6] reported 117—118 °C for the *E*-isomer.

Table 3-b. Melting Points, Elementary Analyses, Crystalline Forms, and R_f-Values of DNPHs of α-Keto Acid Ethyl Esters

Compd		Mp(θ_m/°C)[a]	Analysis(%) Found(Calcd) C	H	N	Formula	Crystalline form	R_f-value[b]
2b,	α	124.0—124.5[c]	42.27 (42.56	3.39 3.57	19.66 19.85)	$C_{10}H_{10}N_4O_6$	Plates	0.51
	β	134.0—135.0	42.40	3.44	19.61		Prisms	0.12
2c,	α	159.5—160.0[d]	53.80 (53.63	4.03 3.94	15.64 15.64)	$C_{16}H_{14}N_4O_6$	Prisms	0.57
	β	149.5—150.5	53.66	4.16	15.71		Scales	0.18

a) Uncorrected. b) TLC on silica gel using benzene as the developing solvent. c) Cope et al.[3] reported 125.0—125.5 °C for the sample of an unseparated isomer mixture. d) Stuart et al.[4] reported 151.5—152.0 °C for the sample of an unseparated isomer mixture.

the α-isomer to β-one was larger during a reaction in an ethanol–sulfuric acid solution than in an aqueous hydrochloric acid solution. The observation was similar to that seen in the case of **2a** reported in the previous investigation.[1]

In a solution of **2a—c** in methanol, ethanol or chloroform, no interconversion between the α- and β-isomers occurred in the dark.

Melting points, analytical data, crystalline forms and R_f-values for compounds **1** and **2** are listed in Tables 3-a and 3-b, respectively.

Assignment of *E*, *Z*-Structure. Data regarding visible, IR, and ^{1}H NMR spectra for **1** and **2** are listed in Table 4. Several points are seen from the Table. (1) Visible spectra for all the hydrazones, except for **2b**, show absorption maxima for the α-isomers at longer wavelengths than those for the corresponding β-isomers. In the case of **2b**, the absorption maximum for the α-isomer lies at a wavelength that is slightly shorter than that for β-one. (2) The extinction coefficient at the absorption maximum is greater for α-isomers of **1a**, **1b**, **1c**, and **2b** than for the corresponding β-one; the reverse is true for the remaining hydrazones. (3) The ester carbonyl stretching bands in the IR spectra in Nujol mulls appear at smaller wavenumbers for α-isomers of **1b**, **1d**, **2a**, and **2b** than for the corresponding β-ones. This is in agreement with results obtained in the previous study.[1] On the other hand, the reverse is true in the case of **1a**, **1c**, and **2c**. Those observations have not yet been consistently explained. (4) However, the imino stretching bands in Nujol mulls appear at smaller wavenumbers for α-isomers for all the hydrazones studied than those for the corresponding β-ones. (5) Furthermore, the IR spectra in 0.01 M (1 M=1 mol dm^{-3}) carbon tetrachloride solutions for all hydrazones without exception reveal both carbonyl and imino stretching absorptions at smaller wavenumbers for α-isomers than for the corresponding β-ones. The same results are obtained even at dilutions of 10 times. (6) Finally, chemical shifts (in ppm) shown by imino protons in the ^{1}H NMR spectroscopy are larger by about δ 1.9 to 4.4 for α-isomers for all the hydrazones studied than those for the corresponding β-isomers.

From all of the above observations, it can be said

Table 4. Visible, IR, and ^{1}H NMR Spectra for **1** and **2**

Compd	Visible in EtOH		IR						^{1}H NMR δ_{NH}	
			Nujol mull		0.01 M[a]		0.001 M[a]			
	λ_{max} nm	$\varepsilon \times 10^{-4}$	ν_{N-H} cm^{-1}	$\nu_{C=O}$ cm^{-1}	ν_{N-H} cm^{-1}	$\nu_{C=O}$ cm^{-1}	ν_{N-H} cm^{-1}	$\nu_{C=O}$ cm^{-1}		
1a, α(*Z*)	355	1.83	3250	1685	3260	1680	3261	1680	12.1[b]	12.1[c]
β(*E*)	332	2.16	3260	1674	3359	1705	3360	1704	7.7[b]	9.3[c]
1b, α(*Z*)	349	1.83	3250	1687	3268	1682[d]	3261	1679	12.1[b,e]	12.1[c]
β(*E*)	325	2.15	3310	1698	3364	1704[d]	3362	1706	7.7[b,e]	9.5[c]
1c, α(*Z*)	349	1.97	3270	1690	3256	1678	3261	1681	12.1[b]	12.1[c]
β(*E*)	329	2.30	3290	1680	3360	1704	3365	1706	9.0[b]	9.5[c]
1d, α(*Z*)	381	3.13	3250	1684	3260	1687	3261	1687	12.2[b]	12.4[c]
β(*E*)	373	2.95	3300	1690	—	—	3361[f]	1712[f]	10.3[b]	10.2[c]
2a, α(*Z*)[g]	360	2.62	3200	1697	3206	1700	3205	1701	14.1[h]	
β(*E*)[g]	348	2.37	3320	1723	3316	1714	3315	1714	11.1[h]	
2b, α(*Z*)	349	2.57	3205	1694	3208	1702	3210	1701	14.4[h]	
β(*E*)	350	2.58	3290	1712	3298	1725	3294	1710	11.4[h]	
2c, α(*Z*)	389	2.87	3180	1728	3210	1697	3210	1695	13.8[h]	
β(*E*)	354	2.60	3275	1694	3280	1722	3280	1720	11.3[h]	

a) In CCl_4. b) In CCl_4. c) In MeOH. d) Elguero et al.[6] reported 1675 and 1696 cm^{-1} in $CHCl_3$ solution for *Z*- and *E*-isomer, respectively. e) Elguero et al.[6] reported 14.03 and 7.8 ppm in $CDCl_3$ solution for *Z*- and *E*-isomer, respectively. f) Saturated solution (below 0.001 M). g) Previous data.[1] h) In $CDCl_3$.

that each α-isomer involves an intramolecular hydrogen bonding between the imino hydrogen and the ester carbonyl oxygen. Accordingly, it can be concluded that the *Z*-structure should be assigned to the α-isomer and the *E*-structure to the β-one. This conclusion is the same as that shown in the previous paper.

Recently, using our assignment method, Cracknell et al.[7] reported structural assignments of an *E*- or *Z*-structure to geometrical isomers of phenylhydrazones of benzocyclobutene-1,2-dione.

We also examined the behavior of ^{1}H NMR signals of an imino proton for **1** in a polar solvent such as methanol (**2** was insufficiently soluble in methanol). This was compared with that in a nonpolar solvent such as carbon tetrachloride (Table 4). By changing the solvent from carbon tetrachloride to methanol, the imino proton signal flattened somewhat as a result of an exchange of protons between the hydrazone and the solvent molecule. Also, the signal appeared at a lower magnetic field in methanol than in carbon tetrachloride. It is noted from this comparison that the imino proton signals exhibited almost the same tendency in a methanol solution as in a carbon tetrachloride solution. Thus, in the first place, the imino proton signals of all the *Z*-isomers appeared in either solution at a lower magnetic field than those of the corresponding *E*-isomer. This suggests that an intramolecular hydrogen bonding exists in the *Z*-isomer, but not in the *E*-isomer, even in a polar solvent. Secondly, in the case of *E*-isomers, as the electronegativity of the *p*-substituent in the phenyl group becomes larger, the imino proton signal appears at a lower magnetic field in both solvents. This observation might be rationally interpreted in terms of the normal effect of electronegativity on the chemical shift of a proton.

Stability to Isomerization. Each of the individual geometrical isomers studied in the present investigation did not isomerize as it was kept in a pure state either upon irradiation with UV light or upon heating the sample to cause melting. The latter observation is contrary to that made by Katsuki et al.[8] regarding the behavior of the DNPHs of a few of α-keto acids. Also, during recrystallization from methanol or ethanol in the dark (or under dim light) isomerization took place to such a slight extent that samples were obtained practically in pure states. Only for cases **1a**, **1b**, and **1c** did isomerization take place to an ultimate equilibrium in several organic solvents consisting of C, H, and halogen even in the dark.

References

1) Part I: T. Nashima, F. Ishibashi, M. Iwamoto, Y. Aihara, S. Anzai, and G. Yamano, *Bull. Chem. Soc. Jpn.*, **50**, 539 (1977).

2) H. Van Duin, *Recl. Trav. Chim. Pays-Bas*, **73**, 78 (1954).

3) A. C. Cope and D. L. Ross, *J. Am. Chem. Soc.*, **83**, 3854 (1961).

4) D. B. Stuart and R. M. Herbst, *J. Org. Chem.*, **6**, 867 (1941).

5) T. Moriwaki, H. Katsuki, and S. Tanaka, *Nippon Kagaku Zasshi*, **76**, 1367 (1955).

6) J. Elguero, R. Jacquier, and G. Tarrago, *Bull. Soc. Chim. Fr.*, **1966**, 2981.

7) M. E. Cracknell, M. C. Goodland, and J. F. W. McOmie, *Bull. Chem. Soc. Jpn.*, **56**, 965 (1983).

8) H. Katsuki, C. Tanegashima, M. Tokushige, and S. Tanaka, *Bull. Chem. Soc. Jpn.*, **45**, 813 (1972).

 © 1986 The Chemical Society of Japan Bull. Chem. Soc. Jpn., 59, 77—81 (1986)

Studies of Polystyrene-Based Ion-Exchange Fiber. V. Immobilization of Microorganism Cells by Adsorption on a Novel Fiber-Form Anion Exchanger†

Toshio YOSHIOKA* and Masaharu SHIMAMURA
Fibers Research Laboratories, Toray Industries, Inc.,
Sonoyama, Otsu 520
(Received June 19, 1985)

Immobilization of microorganism cells by adsorption on a new polystyrene-based ion-exchange fiber has been studied. Microorganism cells, such as yeasts, bacteria, and actinomycetes, were well adsorbed on the anion-exchange fibers through an electrostatic force. The adsorption capacity for the cells became much greater as the water-holding capacity of the fibers increased. The adsorption and desorption behavior of the cells was different between actinomycetes and yeasts, and also between strong and weak anion-exchange fibers. The enzyme activities of the immobilized actinomycetes containing glucose isomerase and yeasts containing L-aminolactam hydrolase were ca. 70 and 60% of those of the native cells respectively. The stability of the immobilized yeasts in the hydrolysis of DL-cyclic lysine anhydride was also investigated.

Recently immobilization of microorganism cells as well as enzymes has been intensively studied from a view point of their use as bioreactors in industry. Microorganism cells have been immobilized by adsorption on a support and entrapment in a matrix.[1-3]

In the previous paper,[4] we have reported that the polystyrene-based ion-exchange fiber, IONEX, can be used as a support for immobilization of some enzymes such as invertase and glucose isomerase. The ion-exchange fiber exhibits good capacity for adsorbing macromolecular ionic substances; this is attributable to its large surface area.[5-7] These findings led us to investigate the possible use of the ion-exchange fiber as the support for the immobilization of microorganism cells.[8] In the present paper, immobilization of some microorganism cells including yeasts and bacteria by adsorption on IONEX is described.

Experimental

Polystyrene for ion exchange as the predominant *sea* ingredient and polypropylene for reinforcement as the *island* ingredient were spun into composite filaments having an *islands-in-a-sea* type sectional structure shown in Fig. 1, by the conventional method.[5] Following the introduction of a crosslinking group, IONEX with various ion-exchange groups were prepared by the introduction of the corresponding ion-exchange group into the polystyrene part according to the procedure described in the previous paper.[5] The resulting fibers had a diameter of ca. 30 μm in the dry state. The ion-exchange capacities of the fibers were found to be ca. 90% of the theoretically calculated values. A cation IONEX in the Na form or an anion IONEX in the Cl form was immersed in a bath of deionized water at room temperature for a sufficient period of time to reach saturation. The fiber was centrifugally dehydrated at 3000 r.p.m. for five minutes. Immediately thereafter, the wet weight (W) of the fiber was measured. The water content of the fiber was determined from the following equation:

$$\text{Water content} = (W - W_0)/W_0,$$

where W_0 is the weight of the completely dry fiber. The water content means the water-holding capacity of the fiber and it was controlled by chosing the conditions of the crosslinking reaction.[5-7] The water content becomes higher as the degree of crosslinkage is lowered.

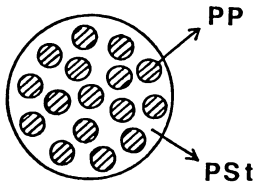

Fig. 1. Schematic cross section of composite fiber. PSt: polystyrene, *sea* ingredient; PP: polypropylene, *island* ingredient.

Actinomycetes with the activity of glucose isomerase (G-actinomycetes; *Streptomyces phaeochromogenus*) and yeasts (P-yeasts; *Saccharomyces cerevisiae*) were obtained from Nagase Sangyo Co., Ltd. and Nitushin Seifun Co., Ltd. (Japan) respectively. Yeasts with the activity of L-aminolactam hydrolase (H-yeasts; *Cryptoccus laurentii*), bacteria (R-bacteria; *Achromobacterobae*), and bacteria (E-bacteria; *Escherichica coli*) were kindly supplied from Basic Research Laboratories, Toray Ind., Inc. (Japan).

The adsorption of the microorganism cells was carried out by the following procedure. An ion exchanger of 100 mg in the Cl or Na form was added to 0.02—0.05% cell suspension, and the mixture was shaken at 20 °C for 1 h. The adsorption capacity of the microorganism cells to the ion exchanger was evaluated by measuring the concentration of the cells remaining in the suspension before and after the adsorption treatment by optical-density measurements at 550 nm. Glucose isomerase activity was determined as described in the previous paper.[4] One unit (U) of L-aminolactam hydrolase was defined as the amount of the enzyme which produced 1 μ mole of L-lysine per hour at 40 °C in 10 wt/vol% DL-cyclic lysine anhydride (CLA) solution of pH 8.0 containing 0.625 mM $MnCl_2$ (1 M=1

† A preliminary report of this work was presented in *Polym. Prepr. Jpn.*, **32**, 1855 (1983).

mol dm^{-3}).

Results and Discussion

Adsorption of Microorganism Cells. The first experiment was carried out using G-actinomycetes, H-yeasts, R-bacteria, and P-yeasts as the test microorganism cells to test whether microorganism cells were adsorbed on IONEX. The results are summarized in Table 1. E-Bacteria of 25 mg and 4 mg were also adsorbed from 0.115% cell suspension (20 °C, 4 h) on 100 mg of anion IONEX having a dimethylaminomethyl group with a water content of 7.0 and Amberlite IRA-938 respectively. It can be seen from Table 1 that the microorganism cells are not adsorbed on cation IONEX with a sulfo group, but well adsorbed on anion IONEX. They are slightly adsorbed on the macroreticular-type anion-exchange resin (Amberlite IRA-938). These results suggest that the outer walls of the microorganism cells are negatively charged and are adsorbed on anion exchangers by an electrostatic force.

Figure 2 shows the relation between the cell adsorption capacity and the water content of anion IONEX. The adsorption capacity was dependent on the water content of the fiber, but independent of the kind of anion-exchange group. The adsorption capacity of the actinomycetes and bacteria was lower than that of the yeasts. This can be ascribed to the difference in the cell size. The strong anion IONEX with water contents of 1.0 and 4.0 had adsorption capacities of 60 and 700 mg g^{-1} for P-yeasts respectively. The adsorption capacity of the yeasts on the fiber can be geometrically evaluated from their volumes and surface areas. We assume, as a first-order approximation, that the spherical yeasts with a diameter of 6 μm are most closely adsorbed on the surface of the cylindrical endless fiber with a variable

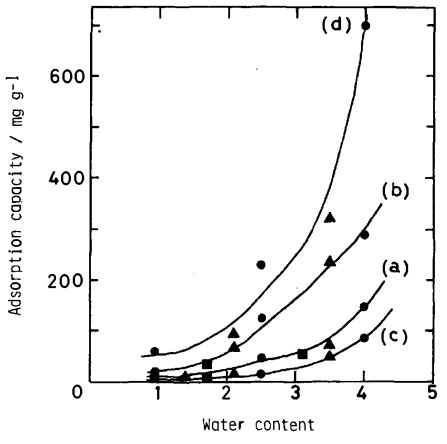

Fig. 2. Cell adsorption capacity vs. water content of anion IONEX. (a) G-Actinomycetes, (b) H-yeasts, (c) R-bacteria, (d) P-yeasts. ●: Trimethylammonio group, ■: dimethylamino group, ▲: amino group.

Table 1. Results of Microorganism Cell Adsorption on Various Exchangers

Exchanger[a]	Ionic group	Water content	G-Actinomycetes		H-Yeasts		R-Bacteria		P-Yeasts	
			Added[b]	Adsorbed[e]	Added[c]	Adsorbed[e]	Added[c]	Adsorbed[e]	Added[d]	Adsorbed[e]
			mg	mg	mg	mg	mg	mg	mg	mg
Strong anion IONEX	-φ-$CH_2\overset{+}{N}(CH_3)_3$	1.0	4	1.4	10	3.1	10	0.5	20	6.0
		2.5	12	4.8	10	9.1	10	1.8	50	23
		4.0	40	14.5	50	29.3	10	8.5	200	70
Weak anion IONEX	-φ-$CH_2\overset{+}{N}H(CH_3)_2$	3.1	8	5.3	—	—	—	—	—	—
	-φ-$CH_2\overset{+}{N}H_3$	3.5	10	7.2	30	23.4	10	8.4	100	32
Strong cation IONEX	-φ-SO_3^-	3.1	4	0.0	10	0.0	10	0.0	10	0.0
Amberlite IRA-938	-φ-$CH_2\overset{+}{N}(CH_3)_3$	2.7	—	—	10	1.7	10	0.5	10	2.1

a) 100 mg. b) 0.02% Suspension (0.05 M $NaHCO_3$, pH 8.2), (distilled water) for weak anion IONEX. c) 0.05% Suspension (0.05 M Tris buffer, pH 8.0), (distilled water) for weak anion IONEX. d) 0.05% Suspension (distilled water). e) 20 °C, 1 h.

diameter according to the water content (30 μm in dry state). The adsorption capacities for the fibers with water contents of 1.0 and 4.0 are calculated to be 680 and 1020 mg g^{-1} respectively. In the case of the yeasts, the experimental values of the adsorption capacity are generally lower than the calculated ones. This discrepancy is explained by assuming that the adsorption capacity is reduced by the repulsion between the cells, rather than that the adsorption capacity is not saturated because of the low concentration of the cells. On increasing the water content of the fiber, the adsorption capacity is considered to increase rapidly and to approach the calculated capacity since the adherent force of the cells to the fiber is enhanced by their affinity for water and it inhibits the repulsion between the cells.

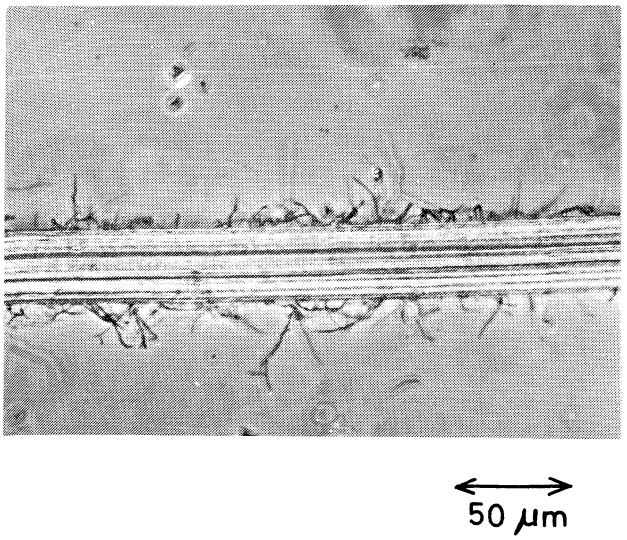

Fig. 3. Adsorption process of G-actinomycetes on strong anion IONEX in 0.05 M $NaHCO_3$ solution (pH 8.2).

Adsorption and Desorption Behavior of Microorganism Cells. Figure 3 presents the adsorption process of G-actinomycetes on the strong anion IONEX. The extreme part of the cells adheres on the fiber surface at first when the fiber is added to the cell suspension. The whole of the cell adheres on the fiber surface on shaking.

Figures 4 and 5 show G-actinomycetes and H-yeasts adsorbed on the strong anion IONEX. The yeasts were easily desorbed from the strong anion IONEX in a 10 wt% NaCl or lysine aqueous solution (Fig. 6). However, vigorous shaking was needed for desorption of G-actinomycetes even in 10 wt% NaCl. The results suggest that the ionic strength in a solution controls the adsorption and desorption properties for the cells in the case of a strong anion exchanger. The fiber is considered to shrink and lose the electrostatic force in a solution with a high ionic strength. The reason why this change of the

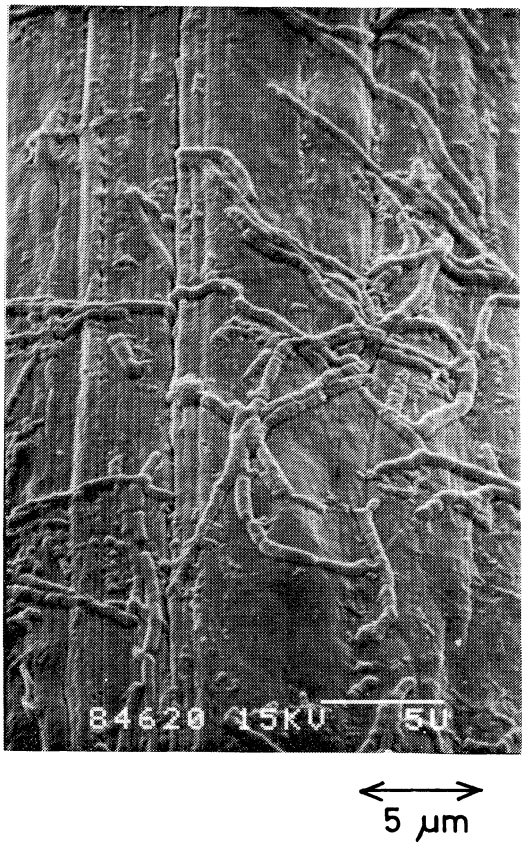

Fig. 4. Adsorption state of G-actinomycetes on strong anion IONEX of water content, 2.5.

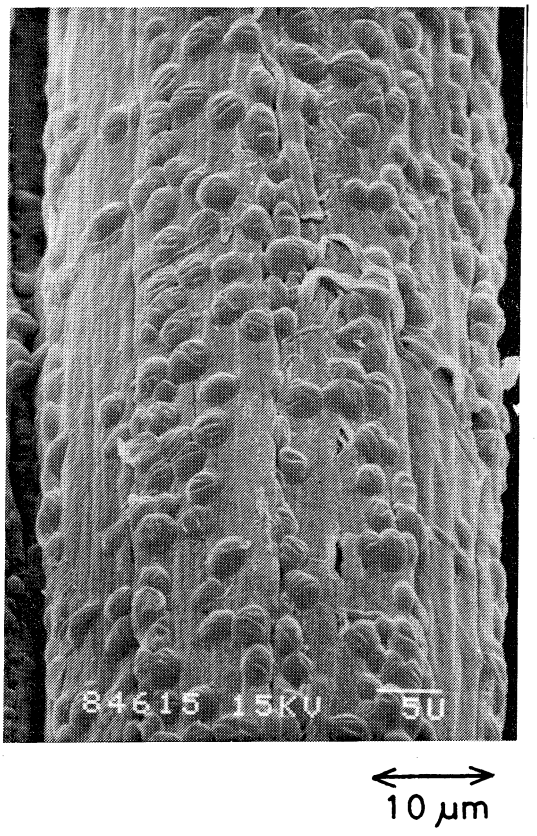

Fig. 5. Adsorption state of H-yeasts on strong anion IONEX of water content, 2.5.

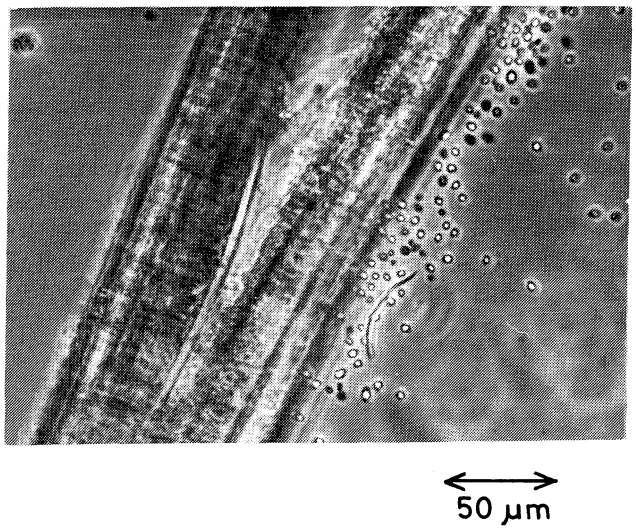

Fig. 6. Desorption process of H-yeasts from strong anion IONEX in 10 wt% NaCl solution.

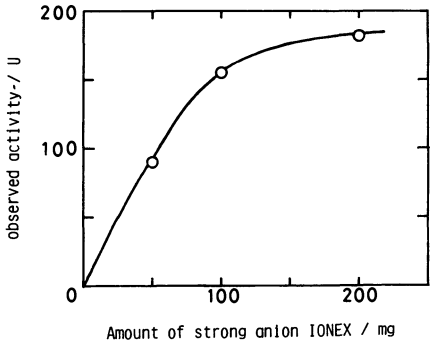

Fig. 7. Observed activity of glucose isomerase vs. amount of strong anion IONEX (water content, 4.0). Immobilization was carried out in 25 ml of 0.05 M $NaHCO_3$ (pH 8.2) containing G-actinomycetes of 260 U, 50 mg (20 °C, 1 h).

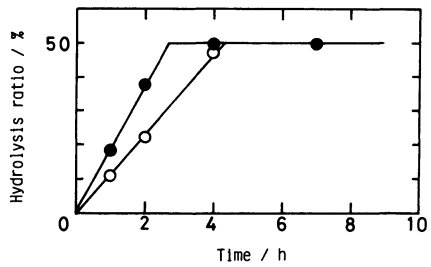

Fig. 8. Hydrolysis ratio of DL-CLA as a function of time. Native or immobilized cells were placed in 10 ml of 10 wt/vol% DL-CLA solution (pH 8.0) containing 0.625 mM $MnCl_2$ and shaken at 40 °C. ●: Native H-yeasts (17.5 mg), 1455 U, ○: immobilized H-yeasts (17.5 mg) on 500 mg of weak anion IONEX with amino group, 845 U.

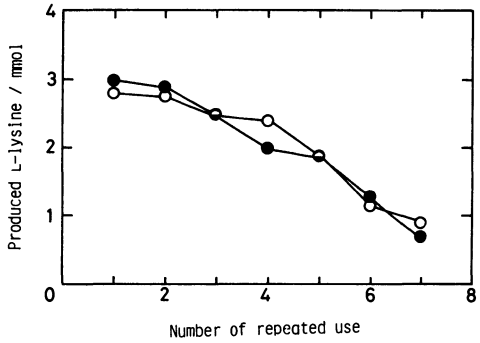

Fig. 9. Stability of immobilized H-yeasts in hydrolysis of DL-CLA by a repeated batch method. Immobilized H-yeasts (1.75 mg) on 25 mg of weak anion IONEX with amino group were placed in 8 ml of 10 wt/vol% DL-CLA solution (pH 8.0) containing 0.625 mM $MnCl_2$ and shaken at 40 °C for 40 h. 0.7 mg of native H-yeasts produced 2.45 mmol of L-lysine on the same conditions. The open and closed circles represent two separate experimental data.

electrostatic force does not readily cause the desorption of the actinomycetes can be attributed to the difference in the adsorption state. That is, the actinomycetes have a much larger contact area with the fiber than the yeasts, as seen in Figs. 4 and 5, so that the former is not so easily desorbed from the fiber as the latter. In the case of the weak anion IONEX, no appreciable desorption of the yeasts was observed in a 10 wt% lysine aqueous solution. They were partially desorbed from the fiber in a 10 wt% NaCl aqueous solution and extensively in a 1 M NaOH. Therefore, the adsorption and desorption properties of the cells for a weak anion exchanger are affected by the pH of a solution rather than by the ionic strength. This is considered to be due to the fiber shrinking more as the pH in a solution is raised. The adsorption and desorption properties for R-bacteria were the same as for H-yeasts.

Immobilization of Microorganism Cells.

Figure 7 shows the correlation between the amount of the strong anion IONEX and the glucose isomerase activity of the fiber when a fixed amount of G-actinomycetes is used in the immobilization. The activity yield was relatively high at ca. 70%.

The hydrolysis of DL-CLA was carried out by using the native H-yeasts with the activity of L-aminolactam hydrolase and the immobilized H-yeasts on the weak anion IONEX with the amino group, as is shown in Fig. 8. The activity yield was ca. 60%. Next, the stability of the immobilized H-yeasts in the hydrolysis of DL-CLA was investigated by a repeated batch method (40 °C, 40 h). The plots of the L-lysine produced vs. the number of repeated use are given in Fig. 9. It can be seen from Fig. 9 that the half life of the immobilized H-yeasts is ca. 240 h. The decrease in activity can be attributed to the inactivation of the enzyme since no appreciable desorption of the yeasts was observed during the reaction. The weak anion IONEX for the support can be repeatedly used by immobilizing new H-yeasts after the desorption

treatment in a 1 M NaOH aqueous solution when the activity of the immobilized H-yeasts decreases.

Conclusion

1. The microorganism cells are well adsorbed on anion-exchange fiber. On increasing the water content of the fiber as well as its surface area, the adsorption ability for the immobilization becomes much larger.
2. The adsorption and desorption behavior is dependent upon the kind of microorganism cells and also upon the basicity of the anion-exchange fiber.
3. The immobilization of the microorganism cells by adsorption on the fiber gives a high enzyme activity.

The authors would like to express their appreciation to Dr. Taturo Kawaguchi, Mr. Michihiko Tanaka, and Dr. Masaki Nishino for their continuous encouragement throughout this work. They are also much obliged to Mr. Kazuo Teramoto for his advice on the chemical treatments and to Mr. Seiichi Yoshikawa and other collaborators for the preparation of the composite fibers. The authors also wish to thank Toray Industries, Inc., for making this study possible.

References

1) T. Hattori and C. Furusaka, *J. Biochem.*, **48**, 831 (1960).
2) D. E. Johnson and A. Ciegler, *Arch. Biochem. Biophys.*, **130**, 384 (1969).
3) I. Takada, T. Tosa, and I. Chibata, *J. Solid-Phase Biochem.*, **2**, 225 (1977).
4) T. Yoshioka and M. Shimamura, *Polym. Prepr. Jpn.*, **32**, 1851 (1983); to be published in *Bull. Chem. Soc. Jpn.*
5) T. Yoshioka and M. Shimamura, *Bull. Chem. Soc. Jpn.*, **56**, 3726 (1983).
6) T. Yoshioka and M. Shimamura, *Bull. Chem. Soc. Jpn.*, **57**, 334 (1984).
7) T. Yoshioka, *Bull. Chem. Soc. Jpn.*, **58**, 2618 (1985).
8) T. Yoshioka, K. Teramoto, and M. Shimamura, Japanese Laid-open Patent 11288 (1979).

 © 1986 The Chemical Society of Japan Bull. Chem. Soc. Jpn., 59, 83—87 (1986)

A Novel Friedel-Crafts Type Reaction of 2-Chlorothiophene with Some Active Aromatic Compounds[1)]

Tyo Sone,* Ryoji Yokoyama, Yohko Okuyama, and Kazuaki Sato
Department of Applied Chemistry, Faculty of Engineering, Yamagata University, Yonezawa 992
(Received June 20, 1985)

2-Chlorothiophene (**1**) was found to easily react with certain active aromatic compounds (**2**) in the presence of $AlCl_3$ under mild conditions, yielding the corresponding 2-arylthiophenes (**3**) and 5-chloro-2,2′-bithienyl (**5**) as the main products. With compounds more reactive than **1**, the formation of **3** predominated. Reactions of **1** with aryl alkyl ethers, for example, afforded the corresponding **3** in 44—83% yields in one step.

It has been generally assumed that a chlorine atom that is directly attached to a thiophene ring is inert[2)] and cannot be replaced by an aryl group under Friedel-Crafts conditions as is true for aryl chlorides that are inert.

In contrast to this fact, Ramsey et al. have reported the polymerization of chlorothiophenes by $AlCl_3$–$CuCl_2$, which involves a nuclear coupling along with the elimination of HCl.[3)] We recently found that in the presence of a cation-exchange resin, 2-chlorothiophene (**1**) reacted with anisole (**2d**) to give 2-(*p*-methoxyphenyl)thiophene (**3d**) and its derivatives, although the yield was low.[4)] We also found that $AlCl_3$ catalyzed a Friedel-Crafts reaction involving 2,5-dichloro-3-(chloromethyl)thiophene with simple benzene derivatives and unexpectedly afforded corresponding 4-aryl-3-arylmethyl-2-chlorothiophenes as the major products.[5)]

These findings suggest that chlorothiophenes can be sufficiently activated to couple with reactive aromatic compounds (**2**) under appropriate acidic conditions. This prompted us to investigate an $AlCl_3$-catalyzed reaction of **1** with **2**. In the present paper we wish to report the results.

The reaction was carried out by adding one mole equiv of $AlCl_3$ to an equimolar mixture of **1** and **2** in CH_2Cl_2 under ice-cooling. This reaction was instantaneous in most cases (as shown by a color change and the evolution of HCl gas) and came to completion upon briefly heating at ca. 40 °C. Through the reaction with **2**, the corresponding 2-arylthiophenes (**3**) and 5-chloro-2,2′-bithienyl (**5**) were obtained as the main products. On occasions, the 2,4-diarylthiophenes (**4**) and its tetrahydrothiophene derivatives (**7**) were isolated from the products. In many cases, the presence of isomers due to the

Table 1. Reaction of 2-Chlorothiophene (**1**) with Aromatic Compounds (**2**)[a)]

	Ar–H (**2**)	Mole ratio **1**/**2**/$AlCl_3$	Yield/ %[b)] **3**	**4**	**5**	Bp ((θ_b/°C)/mmHg) or Mp (θ_m/°C)(lit,)
a:	C_6H_6	1:5:1	Tr[c)]		42	**5:** Bp 110—120/4 (100—110/3—4[4)])
b:	$C_6H_5CH_3$	1:5:1	3		25	**3b:** R=4-CH_3, R′=H; Mp 61—63 (63—64[15b)], 63—66[17)], 82—83[18b)])
c:	*m*-$C_6H_4(CH_3)_2$	1:3:1	20		34	**3c:** R=R′=2,4-$(CH_3)_2$; Bp 61—63/1×10^{-4}
d:	$C_6H_5OCH_3$	1:1:1	44	2	22	**3d:** R=4-OCH_3, R′=H; Mp 109—110 (110—111[4)], 107—108[16)])
		1:5:1	30	15	Tr	**4d:** R=4-OCH_3, R′=H; Mp 219—221 (204—205[9a)], 217—219[9b)])
		1:5:0.5	20	9		
e:	*o*-$CH_3C_6H_4OCH_3$	1:1:1	51[f)]	2[d)]	6	**3e:** R=CH_3, R′=OCH_3; Mp 58—67
f:	*m*-$CH_3C_6H_4OCH_3$	1:1:1	53[f)]	3[d)]	10	**3f:** R=CH_3, R′=OCH_3; Oil
g:	*m*-$C_6H_4(OCH_3)_2$	1:1:1	55	2[d)]	Tr	**3g:** R=R′=2,4-$(OCH_3)_2$; Bp 124—126/5×10^{-4}
		1:3:1	38	28[d)]	Tr	**7g:** R=R′=2,4-$(OCH_3)_2$; Mp 113—114
h:	$C_{10}H_8$[e)]	1:1:1	13[f)]		35	**3h:** Ar=naphthyl; Oil[h)]
i:	α-$C_{10}H_7OCH_3$[g)]	1:1:1	83		Tr	**3i:** R=4-OCH_3; Mp 50—51
j:	β-$C_{10}H_7OC_2H_5$[g)]	1:1:1	59		8	**3j:** R=2-OC_2H_5; Mp 58—59

a) Reaction conditions: 30 min under ice-cooling, then 60 min at room temperature, and additional 30 min at ca. 40 °C. b) Isolated yield based on **1** used. c) Trace. d) Contains the corresponding dihydro (**6**) and tetrahydro derivatives (**7**). e) Naphthalene. f) A mixture of the positional isomers. g) $C_{10}H_7$-: naphthyl. h) 2-(2-Naphthyl)thiophene (main component) was isolated from the mixture, mp 104—105 °C (lit,[15b)] 104—105 °C).

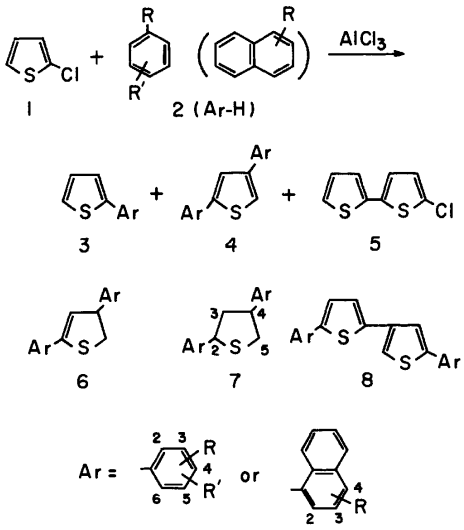

Scheme 1.

position of the substituent(s) on the aromatic ring, the dihydrothiophene derivatives (**6**) of **4**, and the coupling products of **3**, probably 5,5′-diaryl-2,3′-bithienyls (**8**),[6] were also suggested in the products (MS, NMR, and/or TLC). The results are summarized in Table 1.

The yields of the products and the product distribution depend on the relative reactivities of **2** and **1** towards electrophiles and the mole ratio of **2** to **1**. Thus, with substrates less reactive than **1**, predominantly the self-condensation of **1** occurred. For example, in a reaction with benzene (**2a**), **5** was obtained as the sole isolable product in ca. 40% yield, which had been prepared from 2-iodothiophene in seven steps.[7] With reactive substrates such as aryl alkyl ethers, the coupling of **1** with aromatic rings predominated, yielding **3** as expected. This sometimes further reacted with **2** (or **3**) to give **4**, **6**, and **7** (or **8**). An increasing mole ratio of **2** produced higher yields of **4** and its analogs.

The structures of the products were confirmed by their physical and spectral data, elemental analyses and/or direct comparisons with the authentic samples. Authentic samples of 2-(4-methoxy-1-naphthyl)- (**3i**) and 2-(2-ethoxy-1-naphthyl)thiophenes (**3j**) were conveniently prepared by Grignard cross-coupling between 2-thienylmagnesium iodide and the corresponding 1-iodo-4- or 1-iodo-2-alkoxynaphthalene using nickel(II) acetylacetonate as a catalyst.[8] Usually, compounds, **4**, **6**, and **7**, were obtained as mixtures from the products. The presence of the three compounds was readily shown by the MS spectra of the mixtures. It was difficult to separate the mixtures into their components, but 2,4-bis(*p*-methoxyphenyl)thiophene (**4d**) and 2,4-bis(2,4-dimethoxyphenyl)tetrahydrothiophene (**7g**) could be isolated from mixtures which were produced in

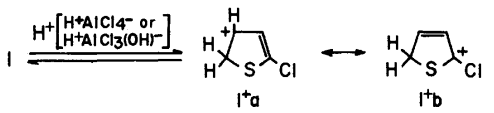

Scheme 2.

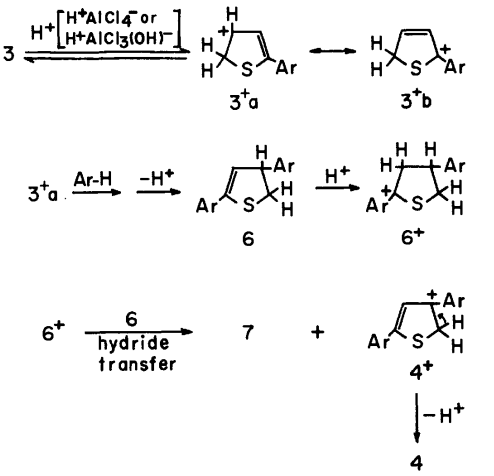

Scheme 3.

reactions of **1** with excess anisole (**2d**) and with excess resorcinol dimethyl ether (**2g**), respectively. The structure of **4d** was established by a comparison of its melting point and UV spectral data with that reported in the literature.[9] The structure of **7g** was assigned on the basis of spectral data and elemental analyses. The MS [*m/z* 360 (M^+, 100%)] and UV spectra [λ_{max} (MeOH) 231 (4.29), 277 (3.78)] suggested the presence of two dimethoxyphenyl units in the molecule of **7g**, neither of which was in conjugation. The ^{1}H NMR spectrum ($CDCl_3$) exhibited, besides a resonance involving six protons of the two aromatic groups, the characteristic peaks for a 2,4-disubstituted tetrahydrothiophene ring in the aliphatic region;[10] a two-proton multiplet (δ 1.93—2.63) and signals (δ 3.03 and 3.21) ascribable to the AB part of an ABX spin system corresponding to 3- and 5-methylene protons. A one-proton multiplet (centered at δ ca. 3.7) and a quartet (δ 5.02, the X part of the ABX system) were ascribable to the 4- and 2-methine groups, respectively. Although 2,4-disubstituted tetrahydrothiophenes exist in two diastereomeric forms, cis and trans, and in each case there are many conformational isomers as a result of the so-called pseudorotation, a detailed examination of the structure of **7g** was not further undertaken. An attempted dehydrogenation of **7g** to **4g** with chloranil was unsuccessful. The dihydrothiophene derivatives (**6**) could not be isolated, but the ^{1}H NMR spectra of the

mixtures showed the olefinic proton absorption (δ ca. 6.0) expected for **6**.[11]

A probable mechanism for the formation of **3** is shown in Scheme 2; this requires an initial protonation of **1** to form 2-chlorothiophenium ion **1**$^+$**b** as the electrophile. It is widely accepted that $AlCl_3$, when contacted with water in moist air, forms species such as $H^+AlCl_3(OH)^-$, which act as proton sources. In this reaction, once a small amount of **3** had been formed, the reaction could provide HCl, which, together with $AlCl_3$, would prompt a further reaction. Thiophenium ions produced from several thiophene derivatives have been observed directly by means of ^1H NMR spectroscopy.[12] We have also confirmed the presence of the ion **1**$^+$ in an $AlCl_3$-HCl-CH_2Cl_2 system at $-40\,^\circ C$ by a direct NMR spectroscopic observation.[13] With less reactive substrates than **1**, the carbonium ion **1**$^+$**b** attacks, instead of the substrate, another molecule of **1**, generating **5** as the main product. 100% Orthophosphoric acid (PPA) failed to cause a reaction with anisole at room temperature; this is probably due to the lower catalytic activity or a smaller acid strength of PPA than that of $H^+AlCl_3(OH)^-$ and/or $H^+AlCl_4^-$.

The protonation of **3** produces carbonium ions, **3**$^+$**a** and **3**$^+$**b**. An attack of **3**$^+$**a** upon an aromatic substrate, followed by proton elimination, gives the corresponding dihydrothiophene **6**. A hydride transfer from **6** to **6**$^+$ affords the tetrahydrothiophene **7** and the carbonium ion **4**$^+$, which then yields the 2,4-diarylthiophene **4** by the elimination of a proton (Scheme 3). Compound **8** can be formed analogously to **4**.

In conclusion, it was found that in the presence of $AlCl_3$ **1** was sufficiently activated to react with various active aromatic compounds under mild conditions, giving the corresponding 2-arylthiophenes (**3**) as the major products. The results are of interest not only from a theoretical viewpoint concerning the unusual reactivity of the chlorine atom of **1**, but also from a preparative one. Thus, a series of 2-arylthiophenes with alkoxyl group(s) on the aromatic ring not readily accessible by the known procedures[14] was prepared in one step by this reaction using **1** as a starting substance in moderate to good yields.

Experimental

All melting and boiling points are uncorrected. The NMR, UV, IR, and MS spectra were obtained on Hitachi R-22 (90 MHz, TMS as an internal reference), Hitachi EPU-2A, Hitachi EPI-S2, and Hitachi UMU (70 eV) spectrometers, respectively.

2-Chlorothiophene (**1**) was prepared by a method described in the literature.[19] Commercial $AlCl_3$ was used without special precautions against moisture. The authentic 5-chloro-2,2′-bithienyl (**5**),[4] 2-phenylthiophene (**3a**),[20] and 2-(*p*-methoxyphenyl)thiophene (**3d**)[4] were prepared according to the literature.

Reaction of 2-Chlorothiophene (1) with Resorcinol Dimetyl Ether (2g) (Typical Procedure). Pulverized $AlCl_3$ (2.7 g, 20 mmol) was added in portions to ice-cooled solutions of **1** (2.4 g, 20 mmol) and **2g** (2.8 g, 20 mmol) in CH_2Cl_2 (10 ml) over 2—3 min periods. Exothermic reactions occurred with the appearance of a coloration of the reaction mixtures. Also, the temperature of the mixtures rose to ca. 20 °C. The reaction mixtures were stirred in the ice-bath for 30 min, then at room temperature for 60 min, and finally at the reflux temperature of the solvent for additional 30 min. An evolution of HCl gas was observed during the reactions. Reaction mixtures were poured into ice-water (ca. 70 ml) and extracted with $CHCl_3$ (20 ml×3). The extracts were combined, washed successively with water, 5% $NaHCO_3$ solution, and water, and dried (Na_2SO_4). After the removal of the solvent and small amounts of the starting substances by distillation, the residues were chromatographed (silica gel/benzene–hexane (3:2)) to afford 2-(2,4-dimethoxyphenyl)thiophene (**3g**; 2.4 g) and an oily mixture (0.14 g) of 2,4-bis(2,4-dimethoxyphenyl)thiophene (**4g**), 2,4-bis(2,4-dimethoxyphenyl)dihydrothiophene (**6g**), and 2,4-bis(2,4-dimethoxyphenyl)tetrahydrothiophene (**7g**).

When **1** was reacted with three equivalent moles of **2g** in the presence of an equimolar amount of $AlCl_3$, the yield of the oily mixture increased; for the mixture, bp 215—220 °C/1×10^{-3} mmHg (1 mmHg≈133.322 Pa). MS *m/z* (rel. intensity) 356 (M$^+$ for **4g**, 100), 358 (M$^+$ for **6g**, 22), 360 (M$^+$ for **7g**, 37). Found: C, 66.82; H, 6.13%. The oily mixture was diluted with a mixture of MeOH and acetone and left standing in the cold to give **7g**.

3g: Colorless viscous oil, bp 124—126 °C/5×10^{-4} mmHg. MS *m/z* 220 (M$^+$, 100). UV λ_{max} (MeOH) 226 sh (4.07), 279—287 (4.09), 310 (4.05). ^1H NMR (CCl_4) δ=3.71, 3.80 (s, 3H each, OCH_3), 6.25—6.5 (m, 2H, Ar-H), 6.8—7.5 (m, 4H, Ar-H). Found: C, 65.53; H, 5.50%. Calcd for $C_{12}H_{12}O_2S$: C, 65.43; H, 5.49%.

7g: Colorless fine needles, mp 113—114 °C (from MeOH). MS *m/z* 360 (M$^+$, 100). UV λ_{max} (MeOH) 231 (4.29), 277 (3.78). ^1H NMR ($CDCl_3$) δ=1.93—2.63 (m, 2H, 3-H_aH_b), 3.03, 3.21 (ABX m J_{ab}=9.1 Hz, J_{a4}=5.7 Hz, J_{b4}=10.7 Hz, 2H, 5-H_aH_b), 3.58~ (m, overlapped partly with the OCH_3 peaks, 4-H), 3.76, 3.79 (s, 6H each, OCH_3) 5.02 (ABX q, $J_{a4}+J_{b4}$=16.4 Hz, 1H, 2-H), 6.38—6.56 (m, 4 H, Ar-H) 7.13—7.23, 7.50—7.59 (m, 1H each, Ar-H). Found: C, 66.55; H, 6.78%. Calcd for $C_{20}H_{24}O_4S$: C, 66.63; H, 6.71%.

Reaction with Anisole (2d). The reaction mixture which was obtained by the reaction of **1** (30 mmol) with 5 mol equiv of **2d** and 1 mol equiv of $AlCl_3$ was poured into ice-water. 2,4-Bis(*p*-methoxyphenyl)thiophene (**4d**; 1.4 g, mp 211—220 °C), thus precipitated, were filtered off and washed with $CHCl_3$ (10 ml). The organic layer was separated from the filtrate and combined with the washing. After the usual work-up and the removal of solvents and starting substances by distillation, the residue was chromatographed (silica gel/benzene–hexane (3:1)) to give 2-(*p*-methoxyphenyl)thiophene (**3d**; after recrystallization from MeOH, 1.7 g, mp 109—110 °C) and 2,4-bis(*p*-methoxyphenyl)tetrahydrothiophene (**7d**; 0.4 g, oil, MS *m/z* 300

(M^+, 20), ^1H NMR (CCl_4) δ=2.0—2.7 (m, 2H), 3.0—3.4 (m, 2H), 3.5~ (m, overlapped in part with the OCH_3 peaks), 3.82 (s, 6H), 4.4—4.9 (m, 1H), 6.7—7.6 (m, 8H)). The presence of the corresponding diarylbithienyl (**8d**) and 2,4-bis(*p*-methoxyphenyl)dihydrothiophene (**6d**) was also suggested to be in the product by an MS spectral analysis.

4d: Colorless leaflet, mp 219—221 °C (from *N,N*-dimethylformamide). MS *m/z* 296 (M^+, 100). UV λ_{max} (EtOH) 267 (4.60), 292 sh (4.28), 310 sh (3.98) (lit,[9a] 265 (4.56), 300—330 (4.18—4.04)).

Reaction with *o*-Methoxytoluene (2e). Chromatography (silica gel/benzene–hexane (1:2)) of the crude product gave an unseparable mixture of the two isomeric 2-(methoxytolyl)thiophenes (**3e**; mp 58—67 °C, the ratio= 85:15 (NMR)) together with small amounts of **5** and a mixture of the corresponding diarylthiophenes (**4e**; MS *m/z* 324 (M^+, 100)).

3e (as a mixture): Pale yellow crystals, mp 67—70 °C (from hexane). MS *m/z* 204 (M^+, 100). ^1H NMR (CCl_4) δ=2.11, 2.15 (s each, 3H, CH_3), 3.76 (s, 3H, OCH_3), 6.6—7.4 (m, 6H, Ar–H). Found: C, 70.31; H, 5.94%. Calcd for $C_{12}H_{12}OS$: C, 70.55; H, 5.92%.

Reaction with *m*-Methoxytoluene (2f). The crude products were chromatographed (silica gel/benzene–hexane (1:1)) to give an unseparable mixture of the two isomeric 2-(methoxytolyl)thiophenes (**3f**; oil, the ratio=70:30 (NMR)) together with small amounts of **5** and a mixture of the corresponding diarylthiophene (**4f**) and diaryldihydrothiophene (**6f**) (MS *m/z* 324 (M^+ for **4f**, 31), 326 (M^+ for **6f**, 26)).

3f (as a mixture): Pale yellow viscous oil, bp 100—110 °C/2×10^{-3} mmHg. MS *m/z* 204 (M^+, 86). ^1H NMR (CCl_4) δ=2.31 (s, 3H, CH_3), 3.74, 3.86 (s each, 3H, OCH_3), 6.5—7.5 (m, 6H, Ar–H). Found: C, 70.68; H, 5.91%. Calcd for $C_{12}H_{12}OS$: C, 70.55; H, 5.92%.

Reaction with 1-Methoxy- (2i) or 2-Ethoxynaphthalene (2j). The crude products were chromatographed (silica gel/hexane–$CHCl_3$ (3:1)) to afford 2-(4-methoxy-1-naphthyl)- (**3i**) or 2-(2-ethoxy-1-naphthyl)thiophene (**3j**), respectively. The IR spectra were identical with those of the authentic samples which were prepared as described below, and the mixed melting points exhibited no depression.

3i: Colorless plates, mp 50—51 °C (from MeOH). MS *m/z* 240 (M^+, 100). UV λ_{max} (MeOH) 218 (4.57), 238 sh (4.37), 310 (4.02). ^1H NMR ($CDCl_3$) δ=4.00 (s, 3H, OCH_3), 6.83 (d, 1H, Ar–H), 7.1—7.3 (m, 2H, Ar–H), 7.3—7.6 (m, 4H, Ar–H), 8.1—8.5 (m, 2H, Ar–H). Found: C, 75.15; H, 5.01%. Calcd for $C_{15}H_{12}OS$: C, 74.97; H, 5.03%.

3j: Pale yellow needles, mp 58—59 °C (from MeOH). MS *m/z* 254 (M^+, 100). UV λ_{max} (MeOH) 232 (4.71), 283 (3.80), 294 (3.81), 337 (3.60). ^1H NMR (CCl_4) δ=1.24 (t, *J*=6.6 Hz, 3H, $OCH_2\underline{CH_3}$), 4.04 (q, *J*=6.6 Hz, 2H, $O\underline{CH_2}CH_3$), 6.9—7.4 (m, 6H, Ar–H), 7.6—7.8 (m, 3H, Ar–H). Found: C, 75.85; H, 5.62%. Calcd for $C_{16}H_{14}OS$: 75.56; H, 5.55%.

Preparation of 2-(4-Methoxy-1-naphthyl)- (3i) and 2-(2-Ethoxy-1-naphthyl)thiophenes (3j) by the Grignard Cross-Coupling. The procedure was a modification of the method used for the preparation of arylnaphthalenes from iodonaphthalenes.[8] A solution of 2-iodothiophene (7.6 g, 36 mmol) in dry ether (40 ml) was added under a nitrogen atmosphere to magnesium turnings (0.87 g, 36 mmol) in a flask at such a rate that a gentle reflux was maintained (ca. 20 min). After an additional 1-h heating, the resulting Grignard solution was diluted with dry benzene (20 ml). To the refluxing solution was added a solution of 1-iodo-4-methoxynaphthalene[21] (3.4 g, 12 mmol) and nickel(II) acetylacetonate (31 mg) in dry benzene (20 ml). The reaction mixture was stirred for 1 h at the reflux temperature. After cooling, the mixture was treated with an aqueous NH_4Cl solution (20%, 100 ml), and the aqueous layer was extracted with benzene (20 ml×2). The combined organic layers were washed with water and dried. After a removal of the solvents, the crude reaction products were chromatographed (silica gel/hexane–$CHCl_3$ (3:1)) to give 2,2′-bithienyl (mp 32.5—33.5 °C; 0.8 g) and crude **3i** (mp 46—49 °C; 2.4 g, 88%) in order of decreasing R_f values. This was recrystallized from MeOH to afford the analytical sample (mp 50—51 °C).

2-(2-Ethoxy-1-naphthyl)thiophene (**3j**) was prepared similarly by the reaction of 2-thienylmagnesium iodide and 1-iodo-2-ethoxynaphthalene[22] in 75% yield. Mp 58—59 °C (from MeOH).

Preparation of 2-(2,4-Dimethylphenyl)thiophene (3c) by Gomberg Reaction. Compound **3c** was prepared by a reaction of thiophene with 2,4-dimethylbenzenediazonium acetate according to the procedure of Beaton et al.[18b] Purification of the crude product by chromatography (silica gel/CCl_4) followed by distillation afforded **3c** (13%) as a colorless oil. Bp 61—63 °C/1×10^{-4} mmHg. MS *m/z* 188 (M^+, 100). UV λ_{max} (EtOH) 229 (4.03), 268 (4.03); ^1H NMR (CCl_4) δ=2.29 (s, 3H, CH_3), 2.31 (s, 3H CH_3), 6.90—7.23 (m, 6H, Ar–H). Found: C, 76.40; H, 6.39%. Calcd for $C_{12}H_{12}S$: C, 76.55; H, 6.42%.

References

1) Acid-Catalyzed Reactions of Thiophene Nuclei. V. Presented in part at the 41st Annual Meeting of the Chemical Society of Japan, Suita, April 1980, Abstr. 2N10. Part IV, to be published (A part of the results has been reported in the preliminary form; T. Sone, M. Kubo, and T. Kanno, *Chem. Lett.*, **1982**, 1195).

2) For example, chlorine atom has been sometimes utilized as blocking group under Friedel-Crafts conditions in the syntheses of certain β-substituted thiophenes: a) S. Gronowitz, *Arkiv Kemi*, **8**, 441 (1956); b) D. W. H. MacDowell, T. B. Patrick, B. K. Frame, and D. L. Ellison, *J. Org. Chem.*, **32**, 1226 (1967).

3) J. S. Ramsey and P. Kovacic, *J. Polym. Sci.*, **A-1**, **7**, 127 (1969).

4) T. Sone, O. Shiromaru, S. Igarashi, E. Kato, and M. Sawara, *Bull. Chem. Soc. Jpn.*, **52**, 1126 (1979).

5) T. Sone, H. Kawasaki, S. Nagasawa, N. Takahashi, K. Tate, and K. Sato, *Chem. Lett.*, **1981**, 399.

6) Acid-catalyzed reaction of certain 2-arylthiophenes (**3**) has been known to afford the corresponding 5,5′-diaryl-2,3′-bithienyls (**8**); see Part IV of this series.[1]

7) R. F. Curtis and G. T. Phillips, *J. Chem. Soc.*, **1965**, 5134.

8) For example, a) R. F. Clough, P. Mison, and J. D. Roberts, *J. Org. Chem.*, **41**, 2252 (1976); b) E. Ibuki, S. Ozasa, Y. Fujioka, and H. Mizutani, *Bull. Chem. Soc. Jpn.*, **55**, 845 (1982).

9) a) M. Gindy, V. B. Baghos, E. A. Ghaly, *J. Ind. Chem. Soc.*, **53**, 490 (1976); b) W. E. Parham, E. T. Harper, R. S. Berger, *J. Am. Chem. Soc.*, **82**, 4932 (1960).

10) a) R. M. Dodson and P. D. Hammen, *J. Chem. Soc., Chem. Commun.*, **1968**, 1294; b) R. F. Curtis, D. M. Jones, and W. A. Thomas, *J. Chem. Soc.*, (*C*), **1971**, 234.

11) P. Y. Johnson, E. Koza, and R. E. Kohrman, *J. Org. Chem.*, **38**, 2967 (1973).

12) a) H. Hogeveen, *Rec. Trav. Chim. Pays-Bas*, **85**, 1072 (1966); b) L. I. Belen'kii, A. P. Yakubov, and Ya. L. Gol'dfarb, *Zh. Org. Khim.*, **11**, 424 (1975); c) L. I. Belen'kii, A. P. Yakubov, and I. A. Bessonava, *Zh. Org. Khim.*, **13**, 364 (1977); d) A. P. Yakubov, N. V. Grigor'eva, and L. I. Belen'kii, *Zh. Org. Khim.*, **14**, 641 (1978).

13) a) Y. Yokoyama, Y. Yamashita, K. Takahashi, and T. Sone, *Chem. Lett.*, **1981**, 813; b) Y. Yokoyama, Y. Yamashita, K. Takahashi, and T. Sone, *Bull. Chem. Soc. Jpn.*, **56**, 2208 (1983).

14) 2-Arylthiophenes with substituent(s) on the aromatic ring have been prepared by: a) The cyclization of the sodium salts of appropriately substituted benzoylpropionic acids with P_2S_3 or P_4S_7,[15] b) The coupling of 2-thienylcopper[16] or 2-thiophenecarboxylic acid[17] with iodoarenes, and c) The Gomberg reaction between arenediazonium salts and thiophene.[18] However, these methods require many steps and the yields are low.

15) a) A. Chrzaszczewska, *Roczniki Chem.*, **5**, 33 (1925); *Chem. Abstr.*, **20**, 1078 (1926); b) H. Wynberg, H. van Driel, R. M. Kellogg, and J. Butter, *J. Am. Chem. Soc.*, **89**, 3487 (1967).

16) M. Nilsson and C. Ullenius, *Acta Chem. Scand.*, **24**, 2379 (1970).

17) M. Nilsson and C. Ullenius, *Acta Chem. Scand.*, **22**, 1998 (1968).

18) a) M. Gomberg and W. E. Bachmann, *J. Am. Chem. Soc.*, **46**, 2339 (1924); b) C. M. Beaton, N. B. Chapman, K. Clarke, and J. M. Willis, *J. Chem. Soc.*, **1976**, 2355; c) M. G. Bartle, R. K. Mackie, and J. M. Tedder, *J. Chem. Soc., Chem. Commun.*, **1974**, 271; d) S. H. Korzeniowski, L. Blum, and G. W. Gokel, *Tetrahedron Lett.*, **1977**, 1871.

19) E. Campaigne and M. LeSuer, *J. Am. Chem. Soc.*, **70**, 415 (1948).

20) A. I. Kosak, R. J. F. Palchak, W. A. Steele, and C. M. Selwitz, *J. Am. Chem. Soc.*, **76**, 4450 (1954).

21) H. W. D. Stubbs and S. H. Tucker, *J. Chem. Soc.*, **1954**, 227; *Chem. Abstr.*, **49**, 2401 (1955).

22) L. Jurd, *Aust. J. Sci. Res.*, **2A**, 246 (1949); *Chem. Abstr.*, **45**, 2887e (1951).

 © 1986 The Chemical Society of Japan Bull. Chem. Soc. Jpn., 59, 89—91 (1986)

Replacement of the Activated Nitro Group by a Phenylthio Group

Hideyoshi MIYAKE* and Kimiaki YAMAMURA
Department of Chemistry, College of General Education, Kobe University,
Tsurukabuto, Nada-ku, Kobe 657
(Received June 22, 1985)

The nitro group, activated by a carbonyl group, alkoxycarbonyl group or a phenyl group, can be replaced by a phenylthio group in the reaction with benzenethiol or its potassium salt. This reaction proceeds in the electron transfer mechanism, and is applicable to the general syntheses of α-phenylthio ketones, α-phenylthio carboxylic esters and α-phenylthio alkylbenzenes from primary nitro compounds.

Primary aliphatic nitro compounds can be prepared in various methods.[1] Recently, the attractive methods of acylation,[2] alkoxycarbonylation,[3] and arylation[4] of the primary nitroalkanes have been reported, and those reactions proceed under mild conditions with high yields due to the strong electron withdrawing inductive effect and the electron acceptability of the nitro group. However, the target molecule in organic synthesis is usually nitro-free one. Therefore, the conversion of the nitro compound into nitro-free one has a considerable value. The replacement of the nitro group by hydrogen is the only useful method which is applicable to α-nitro ketone and α-nitro carboxylic ester.[5] We wish to describe the replacement of the nitro group by a phenylthio group. By this reaction, two-step conversion of primary nitro compound into α-phenylthio ketone, α-phenylthio carboxylic ester and α-phenylthio alkylbenzene become possible (Eq. 1).

$$\underset{\mathbf{1}}{R^1CH_2NO_2} \longrightarrow \underset{\mathbf{2}}{R^1CHNO_2} \longrightarrow \underset{\mathbf{3}}{R^1CHSPh} \qquad (1)$$
$$\quad\quad\quad

Table 2. Replacement of the Nitro Group by the Phenylthio Group Under Neutral Conditions (Eq. 3)

$R\text{-}NO_2$	AIBN(equiv)	Conditions[a]	Yield of 3/%[b]
2a	0.5	90 °C, 0.5 h,	**3a** 56
	0	90 °C, 2 h,	35
	0[c]	90 °C, 2 h,	0
$i\text{-PrCCH}_2\text{NO}_2$ **2b** (O)	0.5	90 °C, 1 h,	**3b** 69
$i\text{-PrC(O)-CH(NO}_2\text{)CH}_3$ **2c**	1	90 °C, 1 h,	**3c** 61
$-(CH_2)_{10}-C(O)-CH(NO_2)-$ **2d**	1	90 °C, 1 h,	**3d** 54
$CH_3C(O)-CH(NO_2)CH_3$ **2e**	1	90 °C, 1 h,	**3e** 47
$O_2NCH_2CO_2CH_3$ **2f**	1.5	130 °C, 0.5 h,	**3f** 55
$PhCH_2NO_2$ **2g**	1	120 °C, 1 h,	**3g** 65
$PhCH(NO_2)CH_2CH_2CH_3$ **2h**	1.5	120 °C, 1 h,	**3h** 13
$CH_3CH_2CH(NO_2)CO_2C_2H_5$ **2i**	1.5	120 °C, 1 h,	**3i** 7

a) 3 equiv of PhSH was used. b) Isolated yield. c) 0.1 equiv of *m*-DNB was added.

Replacement of the Nitro Group Under Basic Conditions. When potassium benzenethiolate was used instead of benzenethiol the replacement also proceeded. This method is favorable for the compounds which do not have the sensitive functionality to a nucleophile. The results are shown in the Table 3. The nitro compound, such as **4**, which was synthesized by the Michael addition of a nitro compound, did not give **5** by the reaction with PhS^-, because retro Michael type elimination predominated and it gave **6** in 61% yield (Eq.5). In order to avoid such elimination, the carbonyl group of **4** must be protected (**2j** in Table 3).

$$\underset{\textbf{4}}{PhCH(NO_2)CH_2CH_2C(O)CH_3} \not\longrightarrow \underset{\textbf{5}}{PhCH(SPh)CH_2CH_2C(O)CH_3} \qquad (5)$$

$$\textbf{4} \longrightarrow PhSCH_2CH_2C(O)CH_3\ 61\%\ (\textbf{6})$$

When the nitro compound has an alkoxycarbonyl group, reaction at lower temperatures and addition of AIBN are favorable to avoid the destruction of the alkoxycarbonyl group.

This basic procedure was not appropriate to the replacement of the nitro group of α-nitro ketone due to the nucleophilicity of PhS^- (see Eq. 2), and the yield of the sulfide was lower than that of the neutral procedure (Table 2).

Table 3. Replacement of the Nitro Group by the Phenylthio Group Under Basic Conditions (Eq. 4)

$R\text{-}NO_2$	Conditions	Yield of 3/%[e]
2g	100 °C 1 h	**3g** 77
	120 °C 2.5 h[a]	76
2h	120 °C 2 h	**3h** 72
2i	60 °C 2 h[b]	**2i** 58
$PhCH(NO_2)CH_2CH_2C(O)CH_3$ **2j**	80 °C 3.5 h	**3j** 74
2e	60 °C 1 h[c]	**2e** 17
	60 °C 1 h[c,d]	28

a) 0.1 equiv of *m*-DNB was added. b) 0.25 equiv of AIBN was added. c) 0.5 equiv of AIBN was added. d) Et_3N was used instead of *t*-BuOK. e) Isolated yield.

Mechanism. These reactions (neutral and basic) were accelerated by a small amount of radical initiator such as AIBN, and completely inhibited (neutral) or decelerated (basic) by a small amount of *m*-dinitrobenzene(*m*-DNB). These results and the solvent effect suggest the electron transfer mechanism, which was well established for the replacement of the nitro group.[1] Equations 6—9 show the mechanism of the replacement of the nitro group under basic conditions.

$$PhS^- + R\text{-}NO_2 \longrightarrow PhS\cdot + R\text{-}NO_2^{\cdot-} \quad (6)$$

$$R\text{-}NO_2^{\cdot-} \longrightarrow R\cdot + NO_2^- \quad (7)$$

$$R\cdot + PhS^- \longrightarrow R\text{-}SPh^{\cdot-} \quad (8)$$

$$R\text{-}SPh^{\cdot-} + R\text{-}NO_2 \longrightarrow R\text{-}SPh + R\text{-}NO_2^{\cdot-} \quad (9)$$

However, the mechanism of the reaction under neutral conditions is not apparent. We think, there are two possible mechanisms. One of them involves the equilibrium of Eq 10, followed by Eqs. 6—9. The other one involves the cation radical of benzenethiol which was suggested by Hashiyama and co-workers for the reaction with glycidate.[9] However, we cannot distinguish them up to the present and the mechanism is now under investigation.

$$RhSH \rightleftharpoons PhS^- + H^+ \quad (10)$$

$$PhSH + R\text{-}NO_2 \longrightarrow [PhSH^{\cdot+} + R\text{-}NO_2^{\cdot-}] \longrightarrow R\text{-}SPh + HNO_2 \quad (11)$$

Experimental

Materials. Nitro compounds were prepared according to the reported procedures.[1-4,10]

General Procedure for the Replacement of the Nitro Group by a Phenylthio Group Under Neutral Conditions. The nitro compound (3 mmol), benzenethiol (9 mmol) and AIBN (3 mmol) were dissolved in HMPT (7 ml) and the mixture was stirred at 90—130 °C for 0.5—1 h (see Table 2). The reaction mixture was poured into water and extracted with ether. The organic layer was washed with water, dried with $MgSO_4$, concentrated under reduced pressure, and purified by column chromatography on silica gel.

General Procedure for the Replacement of the Nitro Group by a Phenylthio Group Under Basic Conditions. Benezenethiol (9 mmol) and *t*-BuOK (4.5 mmol) were dissolved in HMPT (7 ml), and the nitro compound (3 mmol) was added to that solution and the mixture was stirred at appropriate temperature for 1—3.5 h (see Table 3). The reaction mixture was poured into 0.5 M HCl (30 ml (1 M=1 mol dm^{-3})) and extracted with ether. The organic layer was washed with water, dried with $MgSO_4$, concentrated under reduced pressure, and purified by column chromatography on silica gel.

Identification of the Sulfides. The sulfides were identified by ^1H NMR and IR spectra. Some of them (**3a**, **3b**, **3d**, **3e**, **3f**, **3g**, and **3i**) were compared with the data reported.[11,12]

2-Methyl-2-phenylthio-2-butanone (3c): ^1H NMR ($CDCl_3$) δ=1.05 (dd, 6H, J=7 Hz, 3 Hz), 1.04 (d, 3H, J=7 Hz), 2.7—3.2 (m, 1H), 3.85 (q, 1H, J=7 Hz), 7.0—7.7 (m, 5H); IR (neat) 2970, 1708, 1438, 1010 cm^{-1}; Anal. ($C_{12}H_{16}OS$) C, H.

1-Phenyl-1-(phenylthio)butane (3h): ^1H NMR ($CDCl_3$) δ=0.85 (t, 3H, J=6 Hz), 1.0—1.6 (m, 2H), 1.7—2.1 (m, 2H), 4.10 (t, 1H, J=7 Hz), 6.9—7.3 (m, 10H); IR (neat) 3060, 3030, 2960, 1480, 1453, 1438, 1050 cm^{-1}; Anal.($C_{16}H_{18}S$) C, H.

4,4-Ethylenedioxy-1-phenyl-1-(phenylthio)pentane (3i): ^1H NMR ($CDCl_3$) δ=1.30 (s, 3H), 1.5—2.3 (m, 4H), 3.7—3.9 (m, 4H), 4.10 (t, 1H, J=7 Hz), 7.0—7.5 (m, 10H); IR (neat) 2940, 1455, 1440, 1365 cm^{-1}; Anal.($C_{19}H_{22}O_2S$) C, H.

The present work was partially supported by the Research Aid of the Inoue Foundation for Science.

References

1) N. Kornblum, *Org. React.*, **12**, 101 (1962); N. Ono and A. Kaji, *Yuki Gosei Kagaku Kyokai Shi.*, **38**, 115 (1980); D. Seebach, E. W. Colvin, F. Lehr, and T. Weller, *Chimia*, **33**, 1 (1979).

2) R. L. Crumble, J. S. Nimitz, and H. S. Mosher, *J. Org. Chem.*, **47**, 4040 (1980); G. Rosini and R. Ballini, *Synthesis*, **1983**, 543.

3) M. V. Prostenik and I. Butula, *Angew. Chem., Int. Ed. Engl.*, **21**, 139 (1982).

4) M. E. Kurz, V. Baru, and P. Nguyen, *J. Org. Chem.*, **49**, 1603 (1984); H. Kurosawa, M. Sato, and H. Okada, *Tetrahedron Lett.*, **23**, 2965 (1982); R. P. Kozyrod and J. T. Pinhey, ibid., **22**, 783 (1981).

5) N. Ono, H. Miyake, R. Tamura, and A. Kaji, *Tetrahedron Lett.*, **22**, 1705 (1981); N. Ono, H. Miyake, and A. Kaji, *J. Chem. Soc., Chem. Commun.*, **1983**, 875.

6) M. Benn and A. C. M. Meesters, *J. Chem. Soc., Chem. Commun.*, **1977**, 597.

7) H. Feuer, J. K. Doty, and N. Kornblum, *J. Heterocyclic Chem.*, **15**, 1419 (1978); N. Kornblum, S. C. Carlson, and R. G. Smith, *J. Am. Chem. Soc.*, **101**, 647 (1979).

8) N. Ono, I. Hamamoto, T. Yanai, and A. Kaji, *J. Chem. Soc., Chem. Commun.*, **1985**, 523.

9) T. Hashiyama, H. Inoue, and M. Takeda, *J. Chem. Soc., Perkin Trans. 1*, **1985**, 421.

10) N. Kornblum, H. O. Larson, R. K. Blackwood, D. D. Mooberry, E. P. Oliveto, and G. E. Graham, *J. Am. Chem. Soc.*, **78**, 1497 (1956); N. Kornblum, R. K. Blackwood, and J. W. Powers, *J. Am. Chem. Soc.*, **79**, 2507 (1957).

11) I. Kuwajima, M. Shimizu, and H. Urabe, *J. Org. Chem.*, **47**, 837 (1982); P. Blatcher and S. Warren, *J. Chem. Soc., Perkin Trans. 1*, **1979**, 1074; G. Morel, E. Marchand, and A. Foucaud, *Synthesis*, **1980**, 918.

12) M. R. Detty and G. P. Wood, *J. Org. Chem.*, **45**, 80 (1980).

 © 1986 The Chemical Society of Japan Bull. Chem. Soc. Jpn., 59, 93—96 (1986)

Raman and Solid State NMR Study on an Inclusion Compound of Aspartame with Cyclodextrin

Shin-ichiro TAKAHASHI,* Ei-ichiro SUZUKI, Yusuke AMINO, Nobuya NAGASHIMA, Yoshifumi NISHIMURA,† and Masamichi TSUBOI†

Central Research Laboratories, Ajinomoto Co., Inc. Suzuki-cho, Kawasaki-ku, Kawasaki 210
†Faculty of Parmaceutical Sciences, The University of Tokyo,
Hongo, Bunkyo-ku, Tokyo 113
(Received June 24, 1985)

A crystal of inclusion compound of Aspartame (α-L-aspartyl-L-phenylalanine methyl ester, APM) with β-cyclodextrin (β-CD) was obtained from their aqueous solution. The Raman spectrum of this crystal indicates some differences from the spectral sum of APM and β-CD. An analysis of these spectral differences suggests that the phenyl moiety of APM is included in the cavity of β-CD in the inclusion compound. In addition, a Raman spectroscopic study of APM with ^{15}N-substitution and N-deuteration indicates that the peptide backbone of APM undergoes some conformational change on APM going into the inclusion compound. Solid state ^{13}C CP MAS- and gated-decoupling MAS-NMR spectra for the inclusion compound indicate that the phenyl ring rotates at a higher frequency than 270 MHz, that the Phe Cβ and phenyl ring C1 move at the frequency of about 270 MHz, and that the molecular motion of the other parts of APM occurs at lower frequency than 270 MHz.

APM (Scheme 1) is a dipeptide sweetener. We have recently succeeded in obtaining a crystal of an inclusion compound of APM with β-CD which has a higher dissolving rate into H_2O than APM itself. For finding out the mechanism of such a change in that property, a single crystal X-ray diffraction study of the inclusion compound would be powerful. Unfortunately, however, our attempt to obtain a sufficiently large crystal has not so far been successful. Other methods such as Raman spectroscopy[1,2] and solid-state ^{13}C NMR spectroscopy[3–5] may also be useful. We have used the Raman method to elucidate the inclusion mechanism of APM–β-CD and the solid-state ^{13}C NMR method to determine the rate of motion of APM molecule. Such studies would provide not only new pieces of information on the particular inclusion compound now in question but also data for constructing a general view of the CD inclusion compounds, in conjunction with comparison our results with others' for different guest molecules.

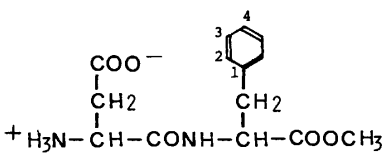

Scheme 1 APM

Experimental

Materials. Crystals of inclusion compound of APM with β-CD was prepared from their aqueous solutions, i.e., 6.7×10^{-2} M(=mol dm^{-3}) of APM and 5.5×10^{-2} M of β-CD in water were sealed in a flask and stirred gently at 60 °C for 15 min. The solution was cooled gradually and kept at 4 °C for two weeks. The crystals formed of the compound were precipitated, collected by filtration and dried in a desiccator at room temperature. The composition of this crystal was found by means of an amino acid analyzer, ^1H NMR and Karl Fischer's analysis to be 1:1:6 of APM:β-CD:water. Phenylalanine-^{15}N was obtained from SHOKO Co., Ltd. Phenylalanine-^{15}N methyl ester hydrochloride (**1**) was prepared by the thionyl chloride method. *N*-benzyloxycarbonyl-β-benzyl-L-aspartyl-L-phenylalanine-^{15}N methyl ester (**2**) was synthesized from β-benzyl-*N*-benzyloxycarbonyl-L-aspartate and **1** via dicyclohexylcarbodiimide in the presence of triethylamine in chloroform. α-L-Aspartyl-L-phenylalanine-^{15}N methyl ester (**3**) was prepared from **2** by hydrogenation at room temperature in the presence of 2% palladium charcoal in aqueous methanol. **3** was purified by YMC-PAK SH-343 column chromatography using methanol/0.1 M phosphate buffer pH 5.0 (30:70 by vol) as eluent. The fraction of **3** was collected, concentrated three times with a rotary evaporator, desalted by a SEP-PAK C18 cartridge, and lyophilyzed to dryness.

Apparatus. Raman spectra were recorded on a JASCO R-800 spectrometer. The 514.5 nm exciting line from an argon ion laser (NEC model GLS 3300) was used. Wavenumbers were calibrated against the spontaneous emission (521 cm^{-1}) of Ar^+.

Solid state ^{13}C NMR was recorded on a JEOL GX-270 spectrometer operating at 67.8 MHz and on a JEOL FX-60 spectrometer at 15.1 MHz.

Results

Raman spectra of the inclusion compound of APM with β-CD and their mechanical mixture are shown in Fig. 1. The Raman bands assigned to the APM molecule in the inclusion compound indicate some frequency differences from those of free APM. Thus the bands at 819, 1005, and 1197 cm^{-1} of free APM are shifted to 825, 1002, and 1207 cm^{-1}, respectively, and the bands at 747, 765, 890, and 971 cm^{-1} are caused to disappear. From a comparison with Raman bands of toluene,[6] the shifted bands can be assigned to the normal vibrations at ν_1, ν_{12}, and ν_{13} of monosub-

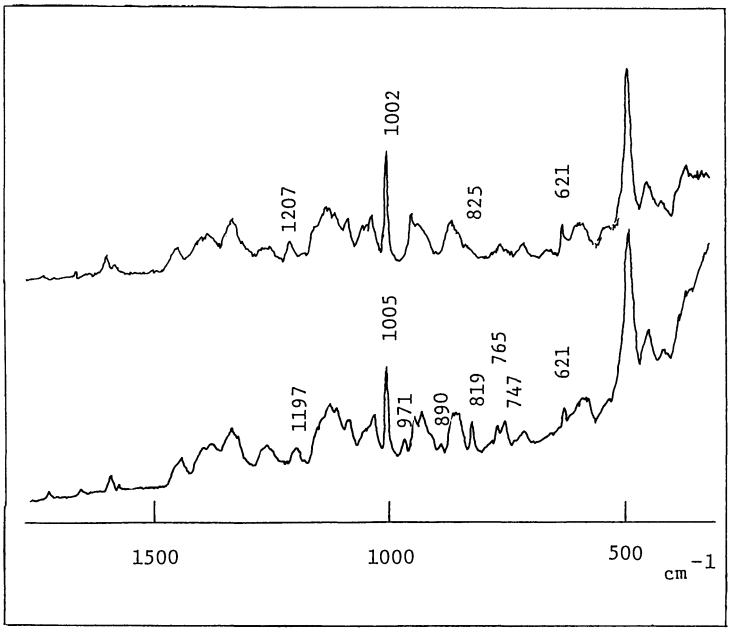

Fig. 1. Raman spectra of the inclusion compound of Aspartame with β-CD (top) and their mechanical mixture (bottom).

Table 1. Raman Bands/cm^{-1} of APM and the Inclusion Compound of APM with β-CD

APM	Inclusion compound	Assignment[a)]
819	825	ν_1
1005	1002	ν_{12}
1197	1207	ν_{13}
747	Disappear	
765	Disappear	
890	Disappear	
971	Disappear	

a) Normal vibration of monosubstituted benzene.

Table 2. Raman Bands/cm^{-1} in 600—100 cm^{-1} of APM and Its Derivatives

APM	Asp-Phe-^{15}N-OMe	N-deuterated APM
621	621	621
747	747	745
819	816	812
890	890	886
971	967	960
1005	1005	1004

stituted benzene, respectively. Results of such observations are summarized in Table 1. The observed shifts suggest that the phenyl ring of APM gets located in the cavity of β-CD on the formation of the inclusion compound. The Raman bands observed in the 600—1000 cm^{-1} range with Asp-Phe-^{15}N-OMe and N-deuterated APM are shown in Table 2. The band at 971 cm^{-1} of normal APM is shifted to 967 cm^{-1} on ^{15}N-substitution and to 960 cm^{-1} on N-deuteration. The band width of the 960 cm^{-1} line of N-deuterated APM has been found to increase and this is probably because the band of amide III is overlapping here. The Raman band around 940 cm^{-1} of polypeptides has been assigned to the backbone stretching vibration,[7] and its frequency is reported to be sensitive to the backbone conformation.[8-10] The ^{15}N and N-deuteration shifts of the band (971 cm^{-1}) indicate that it is assignable to this backbone stretching vibration. The disappearance of the band in the inclusion compound suggests that when APM is included in the cavity of β-CD, its backbone undergoes a conformational change.

The 67.8 MHz solid state ^{13}C CP MAS-NMR spectra of the inclusion compound crystal of APM with β-CD and their mechanical mixture are shown in Fig. 2. The observed resonances are assigned by comparing with the spectrum in aqueous solution. The line widths of resonances of the atoms in APM are found larger than those of β-CD in the inclusion compound, especially, the resonances of phenyl ring Cl and Phe Cβ are too broad to be detected. Figure 3a shows a 67.8 MHz ^{13}C gated-decoupling MAS-NMR spectrum of the inclusion compound. In general, resonances of nuclei of higher frequency motion shoud be sharper than those of lower one in this method. A comparison of Figs. 2 (upper) and 3a indicates that the resonances of the phenyl ring carbons except Cl become obviously sharper on gated-decoupling. This fact indicates that the phenyl ring in the cavity of β-CD is rotating rapidly, whereas the other part of the molecule is moving slowly Figure 3b shows a 15.1 MHz solid state ^{13}C CP

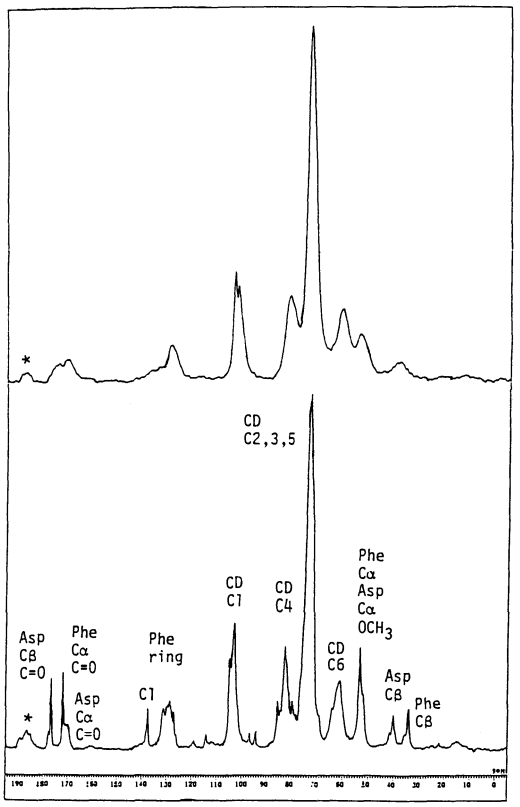

Fig. 2. 67.8 MHz solid state ^{13}C CP MAS-NMR spectra of the inclusion compound of APM with β-CD (top) and their mechanical mixture (bottom). (* denotes spinning side band)

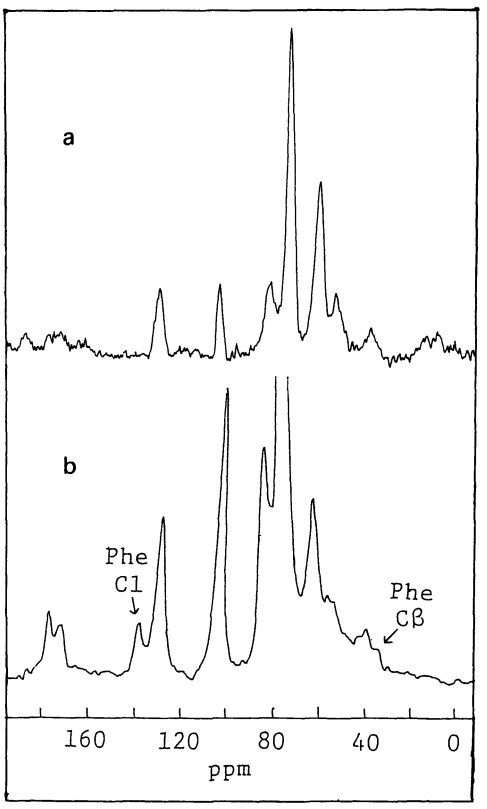

Fig. 3. (a) 67.8 MHz solid state ^{13}C gated-decoulping MAS-NMR spectrum of the inclusion compound of Aspartame with β-CD. (b) 15.1 MHz solid state ^{13}C CP MAS-NMR spectrum of the inclusion compound of Aspartame with β-CD.

MAS-NMR spectrum of the inclusion compound. The resonance of phenyl ring Cl carbon is now found sharper than that at 67.8 MHz, and the resonance of Cβ of Phe residue is detectable here, although its *S/N* ratio is very low. This phenomenon can be explained in terms of the formula proposed by Rothwell and Waugh.[11] In their paper the Hamiltonian of a two-spin system (I=^{1}H and S=^{13}C) is written as

$$H=-\omega_{0I}I_z-\omega_{0S}S_z-2\omega_1 I_x\cos\omega_{0I}t+d.d., \quad (1)$$

where ω_{0I} and ω_{0S} are the Larmor frequencies of I and S, respectively ω_1 is rf irradiation intensity, and *d.d.* is the term of the dipole-dipole interaction between I and S. If the motion of spin I takes place with a frequency ω_{0I} in the order of magnitude, the line width of the resonance of spin S should be large because I_x of the third term of Eq. 1 decays rapidly during the CP condition. Thus the large line widths of the resonances of Phe Cβ and phenyl ring Cl in 67.8 MHz ^{13}C NMR and the smaller one in 15.1 MHz indicate that the molecular motions of Phe Cβ and phenyl ring Cl occur at about 270 MHz (^{1}H Larmor frequency in 67.8 MHz ^{13}C NMR). In summary, it may be concluded that the phenyl ring is considered to rotate at higher frequencies than 270 MHz, that the Phe Cβ and phenyl ring Cl move at about 270 MHz, and that the molecular motions of the other parts of APM occurr at lower frequencies than 270 MHz in the inclusion compound.

Discussion

It is an interesting problem to find out what type and magnitude of distortions a guest molecule will undergo on being brought it into an inclusion compound with CD. Several pieces of information have been obtained on this point:[2-5] For example Sato et al.,[2] examined in 1979 some CD inclusion compounds of azo dyes in aqueous solutions. They detected frequency shifts for some Raman lines, and assigned them to Ph-N stretching and ring vibrations of the dye molecules having been brought into the inclusion compounds. There have been a number of reports on the broadening of signals of guest molecules in solid state ^{13}C NMR studies of their inclusion compounds with CD. In general, there may be two possible causes for such broadening: chemical shift dispersion and molecular mobility.[12]

Hall and Lim[13] demonstrated, by the deuterium quadrupolar echo method, that benzene-d_6 molecule is rapidly rotating around the six-fold symmetry axis in the cavity of CD where it is included.

By the use of the particular type of guest molecule, our present study has enlightened several new aspects of the problem. It should be pointed out, first of all, that our present study was made on a crystal in which 100% of the guest molecules are considered to be in the regular inclusion sites. At the same time, however, the guest molecules may be involved in an inter-molecular interaction, besides the interaction with CD, in such a crystal. In our present study some localized changes in the guest molecule have been suggested. Thus, the phenyl group is considered to be located in the CD cavity but seems to rotate rapidly in the cavity. The other part of the molecule seems to be moving slowly (<270 MHz), probably because this part is located outside the CD cavity and fixed by an inter-molecular interaction with the adjacent APM molecule. The inbetween portion, involving the Phe Cβ and Cl atoms, seems to be moving with a medium rate (close to 270 MHz). Probably because of its environmental change, on going from free to included APM, the Raman lines assignable to the phenyl group showed frequency shifts. Of them, the strong and sharp line at 1005 cm^{-1} is considered to be caused by the phenyl ring breathing vibration of the phenylalanine residue. This Raman line is always prominent in the Raman spectrum of a protein as long as it contains phenylalanine residues.[14] A review of such Raman spectra reveals that its frequency is generally insensitive to the conformation of the protein molecule and to the intra-molecular environment of the phenylalanine residue.[15] It is therefore noteworthy that this is shifted from 1005 to 1002 cm^{-1} on going from free to included APM. From this amount of frequency shift, as well as those given in Table 1, we shoud be able to derive a set of force constant changes of the phenyl group on going from free APM to the APM located in the CD cavity. This, however, is not yet to be done.

In conclusion, we have been able to ensure by Raman examination that the phenyl ring is included in the cavity of β-CD in the inclusion compound of APM with β-CD, and by solid state ^{13}C NMR that the phenyl ring rotates rapidly in the cavity.

We thank Dr. Kenzo Deguchi (JEOL NM Group Application Lab.) for the measurement of 67.8 MHz solid state ^{13}C NMR spectra and Dr. Tadashi Yoshida (Government Industrial Development Laboratory, Hokkaido) for the measurement of 15.1 MHz solid state ^{13}C NMR spectrum, and Professor Akiko Hirakawa (Univ. of Tokyo) for discussions.

References

1) H. Ueda and T. Nagai, *Chem. Pharm. Bull.*, **29**, 2710 (1981).
2) H. Sato, S. Higuchi, N. Teramae, and S. Tanaka, *Chem. Lett.*, **1979**, 299.
3) H. Saito and R. Tabeta, *Chem. Lett.*, **1981**, 713.
4) Y. Inoue, T. Okuda, and R. Chujo, *Carbohydr. Res.*, **116**, C5 (1983).
5) M. Okazaki and C. A. McDowell, *Chem. Phys. Lett.*, **102**, 20 (1983).
6) G. Varsanyi, "Assignment for Vibrational Spectra of Benzene Derivatives," Adam Hilgen, London (1974), Vol. 1.
7) P. Lagant, M. H. Loucheuxlefebvre, and G. Fleury, *Biopolymers*, **12**, 1267 (1983).
8) J. L. Koenig and B. Frushour, *Biopolymers*, **11**, 1871 (1972).
9) T. J. Yu, J. L. Lippert, and W. L. Peticolas, *Biopolymers*, **12**, 2161 (1973).
10) M. C. Chen and R. C. Lord, *J. Am. Chem. Soc.*, **96**, 4750 (1974).
11) W. P. Rothwell and J. S. Waugh, *J. Chem. Phys.*, **74**, 2721 (1981).
12) D. L. VanderHart, W. L. Earl, and A. N. Garroway, *J. Magn. Reson.*, **44**, 361 (1981).
13) L. D. Hall and T. K. Lim, *J. Am. Chem. Soc.*, **106**, 1858 (1984).
14) M. Tsuboi, in "Vibrational Spectroscopy-Modern Trends," ed by A. J. Barnes and W. J. Orville-Thomas, Elsevier Publishing Co., New York (1977), p. 405.
15) F. S. Parker, "Applications of Infrared, Raman, and Resonance Raman Spectroscopy in Biochemistry," Plenum Press, New York (1983).

 © 1986 The Chemical Society of Japan Bull. Chem. Soc. Jpn., 59,97—103(1986)

Selective Preparation of Fluorene Derivatives Using the *t*-Butyl Function as a Positional Protective Group[1)]

Shoji KAJIGAESHI,* Toshiya KADOWAKI, Akiko NISHIDA, and Shizuo FUJISAKI
Department of Industrial Chemistry, Faculty of Engineering, Yamaguchi University, Tokiwadai, Ube 755
(Received July 8, 1985)

Several 4-substituted 2,7-di-*t*-butylfluorene derivatives (**3**) were prepared by electrophilic substitutions of 2,7-di-*t*-butylfluorene (**1**). 4-Substituted fluorene (**4**), such as 4-bromo- (**4a**), 4-methyl (**4e**), and 4-acetylaminofluorene (**4j**), were obtained by the trans-*t*-butylations of **3**. Although we attempted to synthesize 1,8-disubstituted fluorene from 3,6-di-*t*-butylfluorene (**2**) which was derived from 2,2′-diiodo-4,4′-di-*t*-butyldiphenylmethane (**5**), by the same methods, we obtained only 2,7-disubstituted fluorene derivatives (**8**); it turned out electrophilic substitutions of **2** gave 2,7-disubstituted 3,6-di-*t*-butylfluorene derivatives.

It is difficult to prepare 4-substituted fluorenes by direct electrophilic substitutions on the fluorene ring because such substitutions occur predominantly at the 2- or 2,7-positions having the highest electron density. Therefore, 4-substituted fluorenes usually have been prepared via 4-fluorenonecarboxylic acid, the dehydrated fused-ring compound of diphenic acid, in a tedious synthetic procedure.[2)]

Recently, Tashiro[3)] have reported that many kinds of aromatic compounds can be selectively prepared by using *t*-butyl function as a positional protective group. We now report a convenient preparation of the 4-substituted fluorenes by electrophilic substitutions of 2,7-di-*t*-butylfluorene (**1**) and subsequent Lewis acid-catalyzed trans-*t*-butylations, using the Tashiro's method. Furthermore, we report also an attempted preparation of 1,8-disubstituted fluorenes by electrophilic substitutions of 3,6-di-*t*-butylfluorene (**2**) which is prepared from diphenylmethane via several steps.

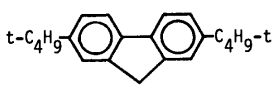

1

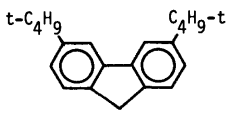

2

Results and Discussion

Electrophilic Substitutions of 2,7-Di-*t*-butylfluorene (1). Although starting material **1** has been prepared from the reaction of fluorene with *t*-butyl chloride in the presence of $AlCl_3$ in nitrobenzene/carbon disulfide,[4)] this method is not so appropriate because of contamination of 2-*t*-butylfluorene. Now we could obtained **1** by the $AlCl_3$/Nitromethane-catalyzed *t*-butylation[3)] of fluorene with 2,6-di-*t*-butyl-*p*-cresol in good yield under mild conditions.

The reactions of **1** with electrophiles afforded 4-substituted 2,7-di-*t*-butylfluorenes (**3**) regioselectively. In these reactions, the electrophilic attack to **1** did not occur at 1-, 3-, 6-, and 8-positions in the fluorene ring blocked by the bulky *t*-butyl groups. Thus, the reaction of **1** with bromine in the presence of iron powder in carbon tetrachloride gave 4-bromo-2,7-di-*t*-butylfluorene (**3a**). The reaction of **1** with iodine, periodic acid, and sulfuric acid in acetic acid/carbon tetrachloride at 70—80 °C gave 4-iodo-2,7-di-*t*-butylfluorene (**3b**). 4-Chloromethyl-2,7-di-*t*-butylfluorene (**3c**) was obtained by the $ZnCl_2$-catalyzed chloromethylation of **1** with chloromethyl methyl ether. The reaction of **1** with fuming nitric acid in acetic anhydride/acetic acid at −40 °C to −20 °C gave a

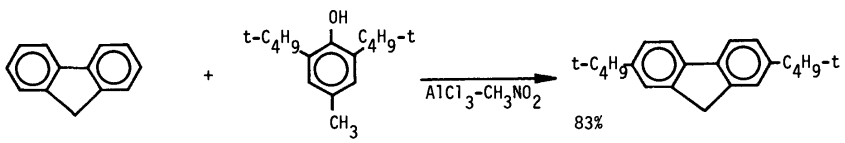

1

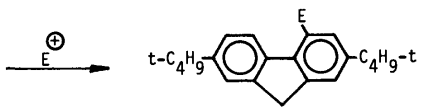

3

	E	Yield(%)
3a :	Br	95
3b :	I	87
3c :	CH_2Cl	62
3d :	NO_2	22

Scheme 1.

mixture of 4-nitro-2,7-di-*t*-butylfluorene (**3d**) and 7-nitro-2-*t*-butylfluorene. Compound **3d** was separated from the mixture by column chromatography over alumina (Scheme 1).

Attempts to synthesize 4-acetyl and 4-chloro derivatives of **1** were unsuccessful. Furthermore, any 4,5-disubstituted products were not obtained by the electrophilic substitutions of **1**. It seems that 4-substituent prevent further substitution of electrophile on 5-position owing to its steric hindrance.

Several derivatives **3** were also obtained from the subsequent reactions of **3c** and **3d**. The reduction of **3c** with $LiAlH_4$ in tetrahydrofuran afforded 4-methyl-2,7-di-*t*-butylfluorene (**3e**). The reaction of **3c** with NaCN in acetonitrile afforded 4-cyanomethyl-2,7-di-*t*-butylfluorene (**3f**), and subsequent hydrolysis of **3f** gave 4-carboxymethyl-2,7-di-*t*-butylfluorene (**3g**). 4-Hydroxymethyl-2,7-di-*t*-butylfluorene (**3h**) was also obtained by treating **3c** with $AgNO_3$ in water/acetone. And then, the reduction of **3d** with tin and hydrochloric acid in ethanol gave 4-amino-2,7-di-*t*-butylfluorene (**3i**). 4-Acetylamino-2,7-di-*t*-butylfluorene (**3j**) was obtained from **3i** and acetic anhydride.

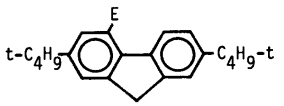

	E
3e :	CH_3
3f :	CH_2CN
3g :	CH_2COOH
3h :	CH_2OH
3i :	NH_2
3j :	$NHCOCH_3$

Trans-*t*-butylations of 3. $AlCl_3$-catalysed trans-*t*-butylations[3] of **3a, 3e,** and **3j** were carried out at 50 °C for 3—6 h in benzene to afford the desired 4-bromofluorene (**4a**), 4-methylfluorene (**4e**), and 4-acetylaminofluorene (**4j**), respectively (Scheme 2).

Compounds **4a**[5] and **4j**[6], have already been prepared from 4-fluorenonecarboxylic acid by means of successive conversion of the functional groups. However, our method is more useful because these compounds can be prepared in only three steps from fluorene as starting material which is easily available. Although **4e** have been obtained by passing 2,2-dimethylbiphenyl over Pd–charcoal at 450 °C,[7] the above preparative conditions are too severe as an experimental procedure in laboratory in comparison with our method.

While we tried to prepare other derivatives **4** from **3** except above **3a, 3e,** and **3j**, these products **4** were not obtained because the trans-*t*-butylation of **3** with $AlCl_3$ in benzene did not proceed satisfactory owing to the deficient electron densities in the fluorene ring substituted with electron-attractive groups, or the products were difficult to isolate from the reaction mixture.

Synthesis of 3,6-Di-*t*-butylfluorene (2). The preparations of 1,8-disubstituted fluorene are also difficult by direct electrophilic substitutions to the fluorene ring because of the same reason described about the preparation of 4-substituted fluorenes. From the facts that several **4**'s were obtained from **1**, we also expected that 1-substituted and 1,8-disubstituted 3,6-di-*t*-butylfluorenes may be obtained by electrophilic substitutions of **2** in which the bulky *t*-butyl groups should block 2-, 4-, 5-, and 7-positions in the fluorene ring.

Thus, 2,2′-diiodo-4,4′-di-*t*-butyldiphenylmethane (**5**) was prepared by iodination of 4,4′-di-*t*-butyldiphenylmethane[8] with iodine, periodic acid, and sulfuric acid in acetic acid, and then by heating **5** with activated copper powder[9] crude **2** was obtained in fairly good yield. Furthermore, in order to obtain pure **2**, the crude **2** was oxidized with bubbling oxygen in the *N,N*-dimethylformamide solution in the presence of Triton B to afford 3,6-di-*t*-butyl-9-fluorenone (**6**) which can be easily purified by recrystallization. And then **6** is reduced with $NaBH_4$ in ethanol to give 3,6-di-*t*-butyl-9-fluorenol (**7**). The pure **2** could be obtained by reduction of **7** with hydroiodic acid in acetic acid as colorless columnar crystals (Scheme 3).

Electrophilic Substitutions of 3,6-Di-*t*-butylfluorene (2). The reaction of **2** with *N*-bromosuccinimide in propylene carbonate at 70—75 °C gave a dibromo-substituted 3,6-di-*t*-butylfluorene (**8a**). Compound **8a** was also obtained from the reaction of **2**

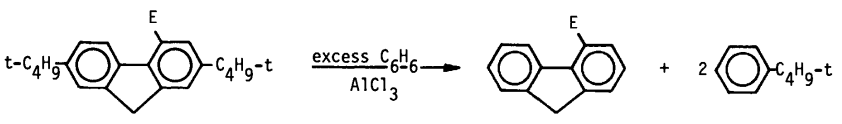

3

	E	Yield(%)
4a :	Br	45
4e :	CH_3	30
4j :	$NHCOCH_3$	94

Scheme 2.

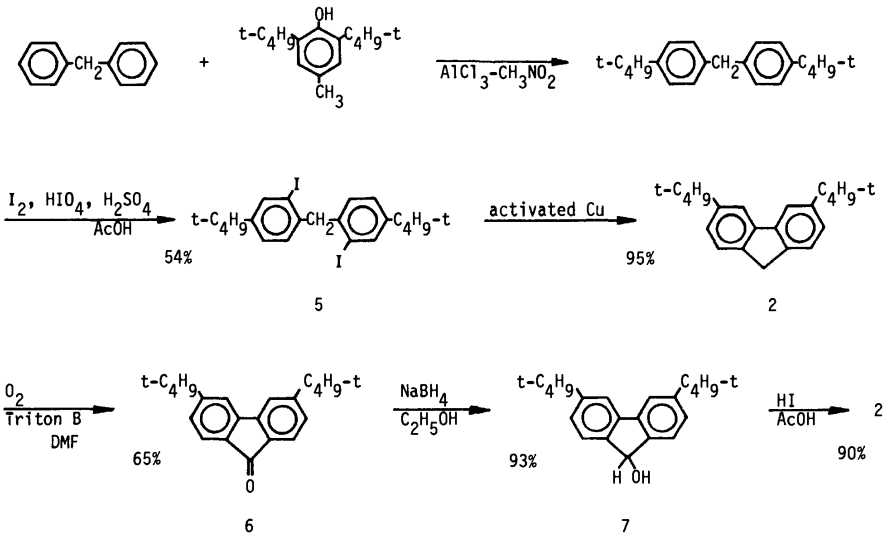

Scheme 3.

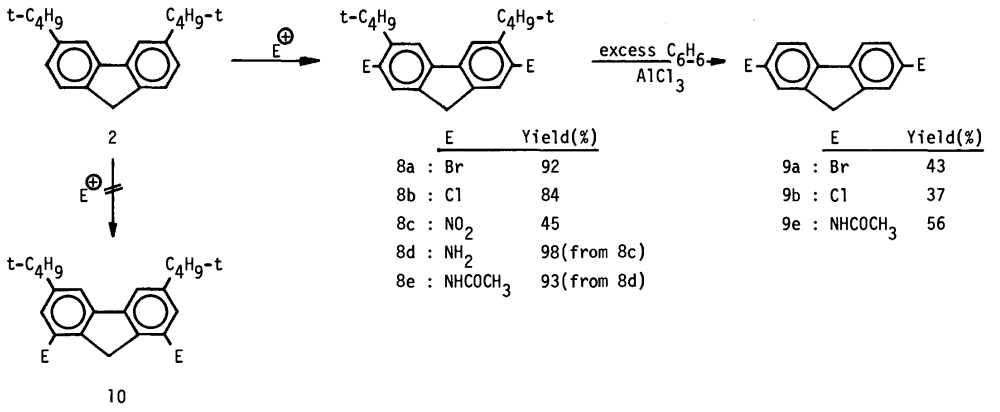

	E	Yield(%)
8a	Br	92
8b	Cl	84
8c	NO_2	45
8d	NH_2	98(from 8c)
8e	$NHCOCH_3$	93(from 8d)

	E	Yield(%)
9a	Br	43
9b	Cl	37
9e	$NHCOCH_3$	56

Scheme 4.

with bromine in carbon tetrachloride in the presence of iron powder. When **2** was treated with chlorine in carbon tetrachloride in the presence of iron powder, a dichloro-substituted 3,6-di-*t*-butylfluorene (**8b**) was obtained. The reaction of **2** with fuming nitric acid and sulfuric acid in acetic anhydride at 10—20 °C afforded a dinitro-substituted 3,6-di-*t*-butylfluorene (**8c**). Furthermore, the reduction of **8c** with zinc powder and aqueous $CaCl_2$ in ethanol gave a diamino-substituted 3,6-di-*t*-butylfluorene (**8d**). Then a bis(acetylamino)-substituted 3,6-di-*t*-butylfluorene (**8e**) was obtained by acetylation of **8d** with acetic anhydride. It could be confirmed that products, **8a, 8b, 8c, 8d,** and **8e** were all symmetrical-type compounds by their ^1H NMR spectra which showed only two singlets in aromatic regions.

Subsequently, the trans-*t*-butylations of **8a, 8b,** and **8e** were carried out in the usual way. However, all resultant products were 2,7-disubstituted fluorenes. That is, the reactions of **8a, 8b,** and **8e** with $AlCl_3$ in benzene at 50 °C gave 2,7-dibromofluorene[10] (**9a**), 2,7-dichlorofluorene[10] (**9b**), and 2,7-bis(acetylamino)-fluorene[11] (**9e**), which were identical with authentic samples, respectively.

Because it can not be considered that 1,8-groups of 1,8-disubstituted 3,6-di-*t*-butylfluorene (**10**) immigrate into the 2,7-positions under the treating conditions, the substitution reactions with electrophiles should proceed at the 2,7-positions. Thus we recognized the above compounds, **8a—e**, as 2,7-disubstituted 3,6-di-*t*-butylfluorenes. That is, it turned out that although the 2,7-positions in **2** have been blocked by bulky *t*-butyl groups the electrophilic attack to **2** occurs predominantly at 2,7-positions having the highest electron density,[12] rather than at the 1,8-positions which are not hindered sterically (Scheme 4).

Furthermore, ^1H NMR spectra of the acetylamino compounds, **3j, 4j, 8e,** and **9e**, in CF_3COOH showed two acetylmethyl signals due to the two conformers

which appear at room temperature on the NMR time scale by the restricted rotation around the N-CO bond. We have already investigated about the *cis*, *trans*-isomerism of the protonated ring-substituted acetanilides by measurements of their NMR spectra in CF_3COOH.[13]

Experimental

All melting points are uncorrected. NMR spectra were determined on a JEOL-MH-100 spectrometer with Me_4Si as internal standard. IR spectra were measured as KBr pellets on a Nippon Bunko IR-A spectrometer.

2,7-Di-*t*-butylfluorene (1). To a solution of fluorene (34.0 g, 0.2 mol) and 2,6-di-*t*-butyl-*p*-cresol (44 g, 0.2 mol) in nitromethane (300 ml) was added at 10—15 °C $AlCl_3$-nitromethane catalyst [$AlCl_3$ (40 g, 0.3 mol)/nitromethane (60 ml)] over a period of 40 min. After the reaction mixture was stirred for 15 min more, it was poured into a large amount of ice-water. The aqueous layer was extracted with ether and the combined organic phase was washed with water, and concentrated to remove nitromethane. The residue was dissolved in ether, washed with 10% NaOH solution to remove *p*-cresol, and then washed with water, dried over $MgSO_4$, and evaporated in vacuo to obtain a black oily product which was column-chromatographed on alumina using benzene as an eluent to give **1**; yield: 46 g (83%); colorless needles; mp 120—122 °C (from ethanol) (lit,[4] mp 122—123 °C). IR (KBr): 1257 cm^{-1} (*t*-C_4H_9); ^1H NMR ($CDCl_3$) δ=1.38 (18H, s, *t*-C_4H_9×2), 3.87 (2H, s, 9-CH_2), 7.39 (2H, d, J=7 Hz, 3- and 6-H), 7.58 (2H, s, 1- and 8-H), and 7.68 (2H, d, J=8 Hz, 4- and 5-H). Found: C, 90.45; H, 9.50%. Calcd for $C_{21}H_{26}$: C, 90.59; H, 9.41%.

4-Bromo-2,7-di-*t*-butylfluorene (3a). To a mixture of **1** (4.5 g, 16 mmol) and catalytic amount of iron powder in CCl_4 (20 ml) was added dropwise a solution of bromine (2.8 g, 18 mmol) in CCl_4 (5 ml) at 5—8 °C under stirring. After the reaction mixture was stirred for more 3 h at 15—20 °C, it was poured into water. The mixture was extracted with ether, and the ether solution was washed with 10% NaOH solution, dried over $MgSO_4$, and evaporated in vacuo to afford the residue which was recrystallized from ethanol to give **3a** as colorless needles; yield: 5.4 g (95%); mp 125—127 °C. IR (KBr): 1260 cm^{-1} (*t*-C_4H_9); ^1H NMR ($CDCl_3$) δ=1.39, 1.41 (each 9H, s, *t*-C_4H_9×2), 3.96 (2H, s, 9-CH_2), 7.48—7.72 (4H, m, H_{arom}), and 8.60 (1H, d, J=8Hz, 5-H). Found: C, 70.57; H, 7.03%. Calcd for $C_{21}H_{25}Br$: C, 70.58; H, 7.05%.

4-Iodo-2,7-di-*t*-butylfluorene (3b). To a solution of **1** (2.3 g, 8 mmol) and iodine (1.0 g, 4 mmol) in a 2:1 acetic acid-CCl_4 (12 ml) was added 98% H_2SO_4 (0.2 ml) and water (1.6 ml), and the mixture was heated for 3 h at 70—80 °C. After the reaction mixture was poured into water, it was extracted with ether. The ether solution was washed with $NaHSO_3$ solution to remove unreacted iodine, and washed with Na_2CO_3 solution and then with water, and dried over $MgSO_4$. The solution was evaporated in vacuo to leave the residue which was recrystallized from ethanol to give **3b** as yellow needles; yield: 2.8 g (87%); mp 109—110 °C. IR (KBr): 1260 cm^{-1} (*t*-C_4H_9); ^1H NMR ($CDCl_3$) δ=1.40 (18H, s, *t*-C_4H_9×2), 3.88 (2H, s, 9-CH_2), 7.44—7.92 (4H, m, H_{arom}), and 8.74 (1H, d, J=8 Hz, 5-H). Found: C, 62.34; H, 6.12%. Calcd for $C_{21}H_{25}I$: C, 62.38; H, 6.23%.

4-Chloromethyl-2,7-di-*t*-butylfluorene (3c). A mixture of **1** (7 g, 25 mmol), chloromethyl methyl ether (8 g, 0.1 mol), and $ZnCl_2$ (1.7 g, 13 mmol) was stirred for 20 min at room temperature. The reaction mixture was poured into water, extracted with ether, and dried over $MgSO_4$. The ether solution was evaporated in vacuo to give the residue which was recrystallized from hexane affording **3c** as colorless needles; yield: 5.1 g (62%); mp 90—93 °C. IR (KBr): 1260 cm^{-1} (*t*-C_4H_9); ^1H NMR ($CDCl_3$) δ=1.36 (18H, s, *t*-C_4H_9×2), 3.88 (2H, s, 9-CH_2), 5.00 (2H, s, CH_2Cl), 7.28—7.68 (4H, m, H_{arom}), and 9.94 (1H, d, J=8 Hz, 5-H). Found: C, 80.92; H, 8.23%. Calcd for $C_{22}H_{27}Cl$: C, 80.93; H, 8.33%.

4-Nitro-2,7-di-*t*-butylfluorene (3d). To a solution of **1** (2.3 g, 8 mmol) in acetic anhydride (40 ml) was added dropwise at −40—−20 °C a mixture of fuming HNO_3 (1 g) and acetic acid (1.15 g) over a period of 30 min under stirring. After the reaction mixture was stirred for 2 h more at −20—0 °C, it was poured into an ice-cold water. The precipitated solid was filtered, washed with water, and column chromatographed on alumina using petroleum benzine as an eluent to give **3d** in the second fraction; yield: 0.6 g (22%); yellow needles; mp 135—137 °C (from ethanol). IR (KBr): 1255 (*t*-C_4H_9), 1340, 1520 cm^{-1} (NO_2); ^1H NMR ($CDCl_3$) δ=1.36, 1.38 (each 9H, s, *t*-C_4H_9×2), 3.89 (2H, s, 9-CH_2), 7.34 (1H, d, J=8 Hz, 6-H), 7.49, 7.66, 7.80 (each 1H, s, H_{arom}), and 7.94 (1H, d, J=8 Hz, 5-H). Found: C, 77.77; H, 7.73; N, 4.05%. Calcd for $C_{21}H_{25}NO_2$: C, 77.98; H, 7.79; N, 4.33%.

4-Methyl-2,7-di-*t*-butylfluorene (3e). To a solution of **3c** (0.5 g, 1.5 mmol) in tetrahydrofuran (10 ml) was added a small portions of $LiAlH_4$ (0.07 g, 2 mmol) under stirring, and the mixture was refluxed for 5 h and then allowed to stand. To the solution was added a 3:2 tetrahydrofuran-water (2 ml) and then a few drops of diluted H_2SO_4. The reaction mixture was extracted with ether, washed with water, and dried over $MgSO_4$. The ether solution was evaporated in vacuo to give **3e** as colorless needles; yield: 0.38 g (87%); mp 133—135 °C (from ethanol). IR (KBr): 1260 cm^{-1} (*t*-C_4H_9); ^1H NMR ($CDCl_3$) δ=1.34 (18H, s, *t*-C_4H_9×2), 2.68 (3H, s, CH_3), 3.84 (2H, s, 9-CH_2), 7.06—7.54 (4H, m, H_{arom}), and 7.70 (1H, d, J=8 Hz, 5-H). Found: C, 90.08; H, 9.70%. Calcd for $C_{22}H_{28}$: C, 90.35; H, 9.65%.

4-Cyanomethyl-2,7-di-*t*-butylfluorene (3f). To a solution of **3c** (3.9 g, 12 mmol) in acetonitrile (60 ml) was added a solution of NaCN (1.2 g, 24 mmol) in water (3 ml). After the mixture was refluxed for 3 h, it was poured into water. The precipitated solid was filtered, washed with water, and recrystallized from ethanol to give **3f** as colorless crystals; yield: 3.1 g (83%); mp 186—187 °C. IR (KBr): 1260 (*t*-C_4H_9), 2240 cm^{-1} (CN); ^1H NMR ($CDCl_3$) δ=1.36 (18H, s, *t*-C_4H_9×2), 3.82 (2H, s, 9-CH_2), 4.04 (2H, s, CH_2CN), and 7.20—7.56 (5H, m, H_{arom}). Found: C, 86.81; H, 8.74; N, 4.23%. Calcd for $C_{23}H_{27}N$: C, 87.01; H, 8.57; N, 4.41%.

4-Carboxymethyl-2,7-di-*t*-butylfluorene (3g). To a solution of **3f** (3.7 g, 12 mmol) in ethylene glycol (60 ml) was added a solution of NaOH (4.8 g, 0.12 mol) in water (30 ml). The mixture was heated for 30 h at 150—160 °C with an oil bath and then poured into water. The precipitated solid was dissolved in hot water and filtered off under

heating. After the filtrate was acidified with hydrochloric acid, the resultant precipitate was filtered and recrystallized from hexane to give **3g** as colorless crystals; yield: 1.7 g (41%); mp 177—178 °C. IR (KBr): 1255 (t-C_4H_9), 1700 cm^{-1} (CO); ^1H NMR ($CDCl_3$) δ=1.36 (18H, s, t-C_4H_9×2), 3.88 (2H, s, 9-CH_2), 4.04 (2H, s, CH_2COOH), 6.36 (1H, br.s, COOH), 7.24, 7.55, 7.62 (each 1H, s, H_{arom}), 7.42, and 7.80 (each 1H, d, J=9 Hz, 5- and 6-H). Found: C, 81.96; H, 8.44%. Calcd for $C_{23}H_{28}O_2$: C, 82.10; H, 8.39%.

4-Hydroxymethyl-2,7-di-*t*-butylfluorene (3h). To a solution of **3c** (1.6 g, 5 mmol) in acetone (24 ml) was added a solution of $AgNO_3$ (2.3 g, 13 mmol) in water (10 ml). The mixture was refluxed for 12 h and then acetone was distilled. The residue obtained was extracted with ether, washed with water, and dried over $MgSO_4$. The ether solution was evaporated in vacuo to give **3h** as colorless needles; yield: 0.4 g (27%); mp 150—151 °C (from petroleum benzine). IR (KBr): 1265 (t-C_4H_9), 3280 cm^{-1} (OH); ^1H NMR ($CDCl_3$) δ=1.36 (18H, s, t-C_4H_9×2), 3.82 (2H, s, 9-CH_2), 5.04 (2H, s, CH_2OH), and 7.24—7.60 (5H, m, H_{arom}). Found: C, 85.43; H, 9.30%. Calcd for $C_{22}H_{28}O$: C, 85.66; H, 9.15%.

4-Amino-2,7-di-*t*-butylfluorene (3i). To a solution of **3d** (3.23 g, 10 mmol) and concentrated hydrochloric acid (d=1.19; 10 ml) in ethanol (50 ml) was gradually added tin powder (2.37 g). After the mixture was refluxed for 1 h, it was poured into a large amount of ice-cold water, basified with 10% NaOH solution and extracted with chloroform. The chloroform solution was washed with water, dried over $MgSO_4$, and evaporated in vacuo to give **3i** as pink prisms; yield: 2.8 g (95%); mp 148—150 °C (from methanol). IR (KBr): 1265 (t-C_4H_9), 3350, 3450 cm^{-1} (NH_2); ^1H NMR ($CDCl_3$) δ=1.36, 1.39 (each 9H, s, t-C_4H_9×2), 3.85 (2H, s, 9-CH_2), 4.01 (2H, br.s, NH_2), 6.68, 7.02, 7.52 (each 1H, s, H_{arom}), 7.33, and 7.55 (each 1H, d, J=9 Hz, 5- and 6-H). Found: C, 85.74; H, 9.29; N, 4.67%. Calcd for $C_{21}H_{27}N$: C, 85.95; H, 9.28; N, 4.77%.

4-Acetylamino-2,7-di-*t*-butylfluorene (3j). To a solution of **3i** (1.17 g, 4 mmol) in benzene (20 ml) was added acetic anhydride (0.8 ml). The mixture was stirred at 40—50 °C for 15 min and then poured into water. The resultant precipitate was filtered, washed with water, and recrystallized from hexane to give **3j** as colorless needles; yield: 1.3 g (95%); mp 189—190 °C. IR (KBr): 1270 (t-C_4H_9), 1650 (CO), 3230, 3300 cm^{-1} (NH); ^1H NMR (CF_3COOH) δ=1.42 (18H, s, t-C_4H_9×2), 2.18, 2.60 (total 3H, s, $COCH_3$), 3.73, 3,83 (total 2H, 9-CH_2), 7.17—7.68 (5H, m, H_{arom}), 8.85, and 9.70 (total 1H, br.s, NH). Found: C, 82.29; H, 8.74; N, 4.26%. Calcd for $C_{23}H_{29}NO$: C, 82.34; H, 8.71; N, 4.18%.

4-Bromofluorene (4a). A solution of **3a** (1.08 g, 3 mmol) and $AlCl_3$ (0.04 g, 0.3 mmol) in benzene (18 ml) was stirred at 50 °C for 6 h, and then the mixture was quenched with water. The organic layer was extracted with ether, washed with water, dried with $MgSO_4$, and evaporated in vacuo at 100 °C to leave t-butylbenzene. Compound **4a** was obtained from residue as colorless needles; yield: 0.33 g (45%); mp 55—57 °C (from methanol) (lit,[5] 59 °C). ^1H NMR ($CDCl_3$) δ=3.86 (2H, s, 9-CH_2), 6.96—7.56 (6H, m, H_{arom}), and 8.56 (1H, d, J=8 Hz, 5-H). Found: C, 63.59; H, 3.72%. Calcd for $C_{13}H_9Br$: C, 63.70; H, 3.70%.

4-Methylfluorene (4e). A solution of **3e** (0.58 g, 2 mmol) and $AlCl_3$ (0.03 g, 0.2 mmol) in benzene (12 ml) was stirred at 50 °C for 4 h, and then it was treated and worked up as described above to afford **4e** as colorless crystals; yield: 0.1 g (30%); mp 68—70 °C (from methanol) (lit,[7] 70.4—71.2 °C). ^1H NMR ($CDCl_3$) δ=2.73 (3H, s, CH_3), 3.93 (2H, s, 9-CH_2), and 7.17—7.98 (7H, m, H_{arom}). Found: C, 93.34; H, 6.65%. Calcd for $C_{14}H_{12}$: C, 93.29; H, 6.71%.

4-Acetylaminofluorene (4j). To a solution of **3j** (0.67 g, 0.2 mmol) in benzene (30 ml) was added $AlCl_3$ (0.87 g, 6.6 mmol). After the reaction mixture was stirred for 3 h at 50 °C, it was treated and worked up as described above to give **4j** as a light brown crystals; yield: 0.42 g (94%); mp 197—198 °C (from benzene) (lit,[6] 199—200 °C). IR (KBr): 1630, 1650 (CO), 3160, 3220 cm^{-1} (NH); ^1H NMR (CF_3COOH) δ=2.21, 2.64 (total 3H, s, $COCH_3$), 3.86, 3.97 (total 2H, s, 9-CH_2), 7.18—7.71 (7H, m, H_{arom}), 8.98, and 9.76 (total 1H, br.s, NH). Found: C, 80.40; H, 5.88: N, 6.38%. Calcd for $C_{15}H_{13}NO$: C, 80.69; H, 5.87; N, 6.27%.

2,2′-Diiodo-4,4′-di-*t*-butyldiphenylmethane (5). To a solution of 4,4′-di-t-butyldiphenylmethane (17.6 g, 63 mmol), periodic acid (7.6 g, 34 mmol), water (35 ml), and 98% H_2SO_4 (4.9 ml), and the mixture was poured into ice-water, it was extracted with ether. The ether solution was washed with $NaHSO_3$ solution to remove iodine, and washed with Na_2CO_3 and then with water, and dried over $MgSO_4$. The solution was evaporated in vacuo to leave the residue which was column-chromatographed on alumina using petroleum benzine as an eluent to give **5**; yield: 17.6 g (54%); colorless plates; mp 88—90 °C (from ethanol). IR (KBr): 1260 cm^{-1} (t-C_4H_9); ^1H NMR ($CDCl_3$) δ=1.28 (18H, s, t-C_4H_9×2), 4.20 (2H, s, CH_2), 6.76 (2H, d, J=8 Hz, 6- and 6′-H), 7.20 (2H, dd, J=2 and 8 Hz, 5- and 5′-H), and 7.76 (2H, d, J=2 Hz, 3- and 3′-H). Found: C, 46.61; H, 4.91%. Calcd for $C_{20}H_{24}I$: C, 46.35; H, 4.67%.

3,6-Di-*t*-butylfluorene (2) by Ullmann Reaction of 5. To melted **5** (30 g, 60 mmol) was added slowly the activated copper powder[13] (30 g, 0.47 mol) and the mixture was heated at 230 °C for 4 h. After cooling, the reaction mixture was extracted with acetone and the acetone solution was filtered to remove the copper powder. The filtrate was concentrated in vacuo to give crude **2** as oily material; yield: 30 g (95%).

3,6-Di-*t*-butylfluorenone (6). To a solution of crude **2** (15 g, 54 mmol) in dimethylformamide (150 ml) was added Triton B (4 ml), and oxygen gas was bubbled into the reaction mixture with heating at 90 °C. The above mixture was poured into the water, acidified with dil. hydrochloric acid, and extracted with benzene. The benzene solution was evaporated in vacuo to give **6** as yellow needles; yield: 10 g (65%); mp 208—209 °C (from petroleum benzine). IR (KBr): 1250 (t-C_4H_9), 1700 cm^{-1} (CO); ^1H NMR ($CDCl_3$) δ=1.36 (18H, s, t-C_4H_9×2), 7.16 (2H, dd, J=8 and 2 Hz, 2- and 7-H), 7.62 (2H, d, J=2 Hz, 4- and 5-H), and 7.64 (2H, d, J=8 Hz, 1- and 8-H). Found: C, 86.19; H, 8.41%. Calcd for $C_{21}H_{24}O$: C, 86.25; H, 8.27%.

3,6-Di-*t*-butyl-9-fluorenol (7). Sodium borohydride (7.5 g, 0.2 mol) was added to the solution of **6** (10.2 g, 35 mmol) in ethanol (400 ml). The mixture was heated and stirred for 30 min until **6** was dissolved perfectly. The reaction mixture was evaporated in vacuo, and to the residue was added water, and then it was extracted with

benzene. The benzene solution was washed with water, dried with $MgSO_4$, and evaporated in vacuo to give **7** as colorless prisms; yield: 9.6 g (93%); mp 120—123 °C (from ethanol). IR (KBr): 1255 (t-C_4H_9), 3240 cm^{-1} (OH); ^1H NMR ($CDCl_3$) δ=1.32 (18H, s, t-C_4H_9×2), 1.76 (1H, br.s, OH), 5.38 (1H, br.s, 9-H), 7.28 (2H, dd, J=8 and 2 Hz, 2- and 7-H), 7.48 (2H, d, J=8 Hz, 1- and 8-H), and 7.64 (2H, d, J=2 Hz, 4- and 5-H). Found: C, 85.48; H, 9.02%. Calcd for $C_{21}H_{26}O$: C, 85.66; H, 8.90%.

3,6-Di-*t*-butylfluorene (2) from 7. To a solution of **7** (13.2 g, 45 mmol) in acetic acid (550 ml) was added hydroiodic acid (57%, 53 g, 0.24 mol) and the mixture was refluxed for 2 h. The reaction mixture was poured into ice-cold water, extracted with ether. The ether solution was washed with $NaHSO_3$ solution, Na_2CO_3 solution, and water, and then dried with $MgSO_4$. The solution was evaporated in vacuo to leave the residue which was recrystallized from ethanol to give **2** as colorless prisms; yield: 11 g (90%); mp 82—83 °C. IR (KBr): 1260 cm^{-1} (t-C_4H_9); ^1H NMR ($CDCl_3$) δ=1.42 (18H, s, t-C_4H_9×2), 3.82 (2H, s, CH_2), 7.35 (2H, dd, J=8 and 2 Hz, 2- and 7-H), 7.48 (2H, d, J=8 Hz, 1- and 8-H), and 7.82 (2H, d, J=2 Hz, 4- and 5-H). Found: C, 90.34; H, 9.39%. Calcd for $C_{21}H_{26}$: C, 90.59; H, 9.41%.

2,7-Dibromo-3,6-di-*t*-butylfluorene (8a). a) To a solution of **2** (1.1 g, 4 mmol) in dry propylene carbonate (26 ml) was added NBS (1.4 g, 8 mmol) and the mixture was heated for 6 h at 70—75 °C under stirring. The reaction mixture was poured into water, and the precipitated solid was filtered, washed with water and recrystallized from ethanol; yield: 1.6 g (92%); colorless prisms; mp 177—180 °C. b) To a solution of **2** (0.28 g, 1 mmol) in carbon tetrachloride (4 ml) with a small amount of iron powder was added the solution of bromine (0.48 g, 3 mmol) in carbon tetrachloride (2 ml) dropwised for 20 min at 35—40 °C and the reaction mixture was stirred for more 30 min at the same temperature. After the mixture was poured into water, it was extracted with ether, washed with 10% NaOH solution and then water, dried with $MgSO_4$ and concentrated in vacuo to give **8a** as colorless prisms; yield: 0.35 g (80%); mp 177—180 °C. IR (KBr): 1240 cm^{-1} (t-C_4H_9); ^1H NMR ($CDCl_3$) δ=1.60 (18H, s, t-C_4H_9×2), 3.74 (2H, s, CH_2), 7.67 and 7.75 (each 2H, s, 1,8- and 4,5-H). Found: C, 57.63; H, 5.56%. Calcd for $C_{21}H_{24}Br_2$: C, 57.82; H, 5.55%.

2,7-Dichloro-3,6-di-*t*-butylfluorene (8b). Into a solution of **2** (0.56 g, 2 mmol) in carbon tetrachloride (8 ml) with a small amount of iron powder was bubbled chlorine gas for 30 min at 30 °C. After the reaction mixture was poured into water, it was extracted with ether, washed with 10% NaOH solution and water, and dried with $MgSO_4$. The ether solution was concentrated in vacuo to give **8b** as colorless prisms; yield: 0.58 g (84%); mp 155—157 °C (from ethanol). IR (KBr): 1240 cm^{-1} (t-C_4H_9); ^1H NMR ($CDCl_3$) δ=1.53 (18H, s, t-C_4H_9×2), 3.70 (2H, s, CH_2), 7.43 and 7.76 (each 2H, s, 1,8- and 4,5-H). Found: C, 72.42; H, 6.97%. Calcd for $C_{21}H_{24}Cl_2$: C, 72.62; H, 6.97%.

2,7-Dinitro-3,6-di-*t*-butylfluorene (8c). To a solution of **2** (1.4 g, 5 mmol) in acetic anhydride (26 ml) was added the mixture of fuming nitric acid (1.3 g, 20 mmol) and concd sulfuric acid (1.3 g) dropwised for 2 h at 15—20 °C. The precipitated solid as filtered, washed with water and then ether, and recrystallized from petroleum benzine to give **8c** as slight yellow crystals; yield: 0.8 g (45%); mp 246—247 °C. IR (KBr): 1240 (t-C_4H_9), 1350, 1515 cm^{-1} (NO_2); ^1H NMR ($CDCl_3$) δ=1.51 (18H, s, t-C_4H_9×2), 3.90 (2H, s, CH_2), 7.48 and 7.91 (each 2H, s, 1,8- and 4,5-H). Found: C, 68.55; H, 6.63; N, 7.44%. Calcd for $C_{21}H_{24}N_2O_4$: C, 68.46; H, 6.57; N, 7.60%.

2,7-Diamino-3,6-di-*t*-butylfluorene (8d). To a solution of **8c** (1.2 g, 3.3 mmol) in ethanol (78%, 50 ml) was added $CaCl_2$ aqueous solution (0.5 g, 0.7 ml) and zinc powder (14 g, 0.2 mol). After the mixture was refluxed for 2 h, zinc powder was filtered off. The filtrate was concentrated in vacuo to give **8d** as white crystals. This crystals were washed with water and dried under reduced pressure; yield: 1.0 g (98%); mp 185—188 °C (decomp). IR (KBr): 1240 (t-C_4H_9), 3360, 3470 cm^{-1} (NH_2); ^1H NMR ($CDCl_3$) δ=1.44 (18H, s, t-C_4H_9×2), 3.48 (4H, br.s, NH_2×2), 3.60 (2H, s, CH_2), 6.54 and 7.32 (each 2H, s, 1,8- and 4,5-H). This product was unstable in atmosphere so that it was analyzed as the acetyl compound (**8e**).

2,7-Bis(acetylamino)-3,6-di-*t*-butylfluorene (8e). To a solution of **8d** (0.8 g, 2.5 mmol) in benzene (10 ml) was added acetic anhydride (0.3 g, 2.8 mmol), and the mixture was stirred for 20 min at 40—50 °C. The precipitation solid was filtered and washed with benzene to give **8e** as white crystals; yield: 0.9 g (93%); mp 333—336 °C (decomp) (from chloroform). IR (KBr): 1240 (t-C_4H_9), 1650 (CO), 3240 cm^{-1} (NH); ^1H NMR (CF_3COOH) δ=1.56 (18H, s, t-C_4H_9×2), 2.30, 2.66 (total 6H, br.s, $COCH_3$), 3.94, 3.98 (total 2H, br.s, CH_2), 7.40, 8.16 (each 2H, br.s, 1,8- and 4,5-H), 9.23, 9.37, and 9.95 (total 2H, br.s, NH). Found: C, 76.41; H, 8.16; N, 7.13%. Calcd for $C_{25}H_{32}N_2O_2$: C, 76.49; H, 8.22; N, 7.14%.

Trans-*t*-butylation of 8. A solution of **8** (3 mmol) and $AlCl_3$ (8 mg, 0.6 mmol) in benzene (15 ml) was stirred at 50 °C for 30 min, and then the mixture was quenched with water. The organic layer was extracted with ether, washed with water, dried with $MgSO_4$, and evaporated in vacuo at 100 °C to leave t-butylbenzene.

2,7-Dibromofluorene (9a). Yield: 43%; colorless prisms mp 166—168 °C (from ethanol) (lit,[10] 167—168 °C). ^1H NMR ($CDCl_3$) δ=3.72 (2H, s, CH_2), 7.34, 7.42 (each 2H, d, J=9 Hz, 3,6- and 4,5-H), and 7.49 (2H, s, 1- and 8-H).

2,7-Dichlorofluorene (9b). Yield: 37%; colorless prisms mp 122—125.5 °C (from ethanol) (lit,[10] 126 °C). ^1H NMR ($CDCl_3$) δ=3.86 (2H, s, CH_2), 7.36 (2H, dd, J=2 and 8 Hz, 3- and 6-H), 7.51 (2H, d, J=2 Hz, 1- and 8-H), and 7.63 (2H, d, J=8 Hz, 4- and 5-H).

2,7-Bis(acetylamino)fluorene (9e). Yield: 56%; white crystals mp 285—286 °C (from ethanol) (lit,[11] mp 281 °C). IR (KBr): 1360 ($COCH_3$), 1650 (CO), 3040, 3220 cm^{-1} (NH); ^1H NMR (CF_3COOH) δ=2.40, 2.65 (total 6H, br.s, $COCH_3$), 3.98, 4.04 (total 2H, br.s, CH_2), 7.40 (2H, br.d, J=8 Hz, 3- and 6-H), 7.62 (2H, br.s, 1- and 8-H), and 7.77 (2H, br.d, J=8 Hz, 4- and 5-H).

The authors wish to thank Drs. Shigeki Nagai, Yoshiaki Ishida, and Mr. Tsuyoshi Arai, Ube Research Laboratory, Ube Industries LTD., for the elemental analyses.

References

1) A part of this work has been published as a preliminary report: S. Kajigaeshi, T. Kadowaki, A. Nishida, S. Fujisaki, and M. Noguchi, *Synthesis*, **1984**, 335.

2) E. H. Huntress, K. Pfister, and K. H. T. Pfister, *J. Am. Chem. Soc.*, **64**, 2845 (1942).

3) M. Tashiro, *Synthesis*, **1979**, 921.

4) M. Bruch, M. Grosse, and D. Rewicki, *Justus Liebigs Ann. Chem.*, **1976**, 74.

5) K. Suzuki, S. Kajigaeshi, and S. Kato, *Yuki Gosei Kagaku Kyokai Shi*, **16**, 304 (1958); *Chem. Abstr.*, **52**, 18339 (1958).

6) J. H. Weisburger, E. K. Weisburger, and H. P. Morris, *J. Am. Chem. Soc.*, **74**, 4540 (1952).

7) M. Orchin, and E. O. Woolfolk, *J. Am. Chem. Soc.*, **67**, 122 (1945).

8) M. Tashiro, T. Yamato, and G. Fukata, *J. Org. Chem.*, **43**, 1413 (1978).

9) E. C. Kleiderer and R. Adams, *J. Am. Chem. Soc.*, **55**, 4219 (1933).

10) F. Dewhurst and P. K. Shah, *J. Chem. Soc. (c)*, **1970**, 1737.

11) G. T. Morgan and R. W. Thomason, *J. Chem. Soc.*, **1926**, 2691.

12) M. G. Shishov, V. A. Obédkova, and N. L. Dýachenko, *Khim. Khim. Tekhnol.*, **25**, 24 (1982); *Chem. Abstr.*, **96**, 216929q (1982).

13) S. Fujisaki, K. Nagano, A. Nishida, and S. Kajigaeshi, *Nippon Kagaku Kaishi*, **1985**, 1411.

 © 1986 The Chemical Society of Japan Bull. Chem. Soc. Jpn., 59, 105—108 (1986)

Cerium or Ruthenium Catalyzed Oxidation of Alcohols to Carbonyl Compounds by Means of Sodium Bromate

Shigekazu KANEMOTO, Hiroki TOMIOKA, Koichiro OSHIMA,* and Hitosi NOZAKI
Department of Industrial Chemistry, Faculty of Engineering, Kyoto University, Yoshida, Kyoto 606
(Received August 22, 1985)

Sodium bromate has been found to be effective oxidant for oxidation of alcohols in the presence of cerium or ruthenium compounds in biphase reaction. Selective oxidation of secondary alcohols was performed in the presence of primary ones using cerium(IV) ammonium nitrate (CAN) or cerium(IV) sulfate (CS) as catalyst. For instance, treatment of 1,10-undecanediol with CS/$NaBrO_3$ provided 11-hydroxy-2-undecanone in 82% yield. Ruthenium catalyzed biphase oxidation of alcohols with sodium bromate provided the corresponding aldehydes or ketones in good to excellent yields.

Transition metal catalyzed oxidation of alcohols to carbonyl compounds has been widely studied.[1] A variety of oxidants such as *t*-butyl hydroperoxide,[2] bis(trimethylsilyl) peroxide,[3] chloramine-T[4] were employed with many transition metals. In contrast to these procedures with organic oxidants, there are few efficient methods using inorganic oxidants for the oxidation of alcohols because of their insolubility in organic solvents. Here we wish to report two methods which utilize sodium bromate as an oxidant: (1) Cerium(IV) ammonium nitrate catalyzed selective oxidation of secondary alcohols in the presence of primary ones and (2) ruthenium(III) chloride catalyzed oxidation of hydroxyls to carbonyl compounds.

(1) Cerium Catalyzed Selective Oxidation of Secondary Alcohols in the Presence of Primary Ones.[5] Although cerium(IV) ion oxidation of organic compounds has been widely studied, application of cerium(IV) ammonium nitrate (CAN) oxidation of alcohols to organic synthesis has been limited because of the large quantities of reagents required and the lack of generality of the reaction.[6] Here we wish to report that under CAN catalysis sodium bromate oxidizes secondary alcohols[11] into ketones in excellent yields and certain diols are thus converted into the expected keto alcohols with high selectivity.

Treatment of secondary alcohols with a suspension of sodium bromate in aq acetonitrile ($CH_3CN:H_2O$= 7:3 v/v) at reflux gave the corresponding carbonyl compounds in good to excellent yields. Variations in catalysts and oxidants have been examined with cyclododecanol as the substrate. Cerium(IV) ammonium nitrate and cerium(IV) sulfate[12] were equally active as catalyst, while cerium(III) chloride and cerium(IV) oxide were inactive. Sodium bromate was far superior to other oxidants tried. The results for the oxidation of cyclododecanol in aq CH_3CN in the presence of 10 mol% CAN with several oxidants are given in order of oxidant, reaction conditions, and % yield of cyclododecanone: *t*-BuOOH, 15 h at 80 °C, 13%; 30% H_2O_2, 5 h at 80 °C, 7%; *N*-methylmorpholine *N*-oxide, 5.5 h at 80 °C, 0%. Although the longer reaction period was required, the amount of cerium(IV) and sodium bromate could be reduced from 0.1 and 1.0 mol to 0.035 and 0.35 mol, respectively per 1.0 mol of cyclododecanol without decrease of the yield of cyclododecanone.

As shown in Table 1, wide variety of secondary alcohols could be easily oxidized to ketones. Primary alcohol, however, was recovered practically unchanged. On treatment of 1-dodecanol (1.0 mmol) with cerium(IV) sulfate[13] (0.035 mmol) and sodium bromate (0.35 mmol) in aq acetonitrile at reflux for 30 min[14] dodecanal was obtained in only 2% yield along with 92% recovery of starting alcohol. Olefinic moiety even in the remote position from hydroxyl group interrupts the oxidation (run 9).[15] It is worth noting that the oxidation proceeds smoothly even with the substrates undergoing C-C bond fission upon treatment with stoichiometric amount of CAN (run 4, 5, and 6).[10,16]

It was anticipated that the treatment of primary,

Table 1. Oxidation of Secondary Alcohols

$$\underset{(2.0\ \text{mmol})}{RR'CHOH} \xrightarrow[NaBrO_3\ (2.0\ \text{mmol}),\ \text{aq. } CH_3CN,\ 80\,^\circ C]{(NH_4)_2Ce(NO_3)_6\ (0.2\ \text{mmol})} RR'CO$$

Run	Alcohol	Reaction Time/h	Product	Yield/%[a]
1	4-Dodecanol	0.8	4-Dodecanone	94
2	Cyclododecanol	0.2	Cyclododecanone	98
3	4-*t*-Butylcyclohexanol	0.5	4-*t*-Butylcyclohexanone	86
4	PhCH(OH)C(O)Ph	4.5	PhC(O)C(O)Ph	66 (9)
5	Norborneol	0.3	Norcamphor	82[b]
6	Borneol	1.0	Camphor	77[b]
7	*l*-Menthol	0.3	*l*-Menthone	82[c]
8	3β-Cholestanol	0.8	3-Cholestanone	97[d]
9	11-Dodecen-2-ol	7.0	11-Dodecen-2-one	3(71)

a) Isolated yields unless otherwise stated. The figures in parentheses indicate the yields of recovered, unreacted alcohols. b) Glpc yields using internal standard. c) Contaminated by less than 1% of isomenthone. d) Because of solubility problem, $CH_3CN/H_2O/CH_2ClCH_2Cl$=2:2:1 system was used as a solvent.

Table 2. Selective Oxidation of Diols[a]

Alcohol 1.0 mmol	Ce Salt $\times 10^{-2}$ mmol	$NaBrO_3$ mmol	Reaction Time/h	Product	Yield[b] %
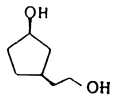	CAN (10)	1.0	0.5	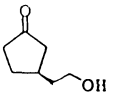	89
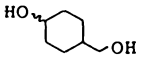	CAN (10)	1.0	0.25	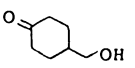	83
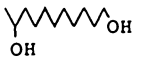	CS[c] (3.5)	1.0	2.0	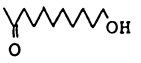	86
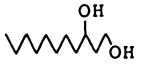	CS[c] (8)	0.8	19.0	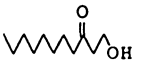	88
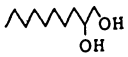	CS[c] (20)	2.0	24.0	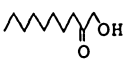	50
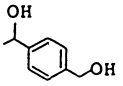	CAN (3.5)	0.35	1.5	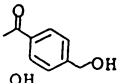	59
				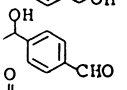	19
				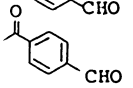	13
1-Dodecanol[d] 4-Dodecanol	CS[c] (3.5)	0.40	1.0	Dodecanal 4-Dodecanone	3 98
l-Menthol[d] Cyclododecanol	CAN (3.5)	0.45	1.0	*l*-Menthone Cyclododecanone	37 83
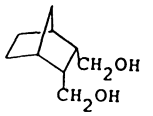	CAN (10)	1.0	6.5	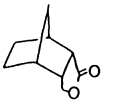	87

a) Reactions were performed on 1.0 mmol scale in aq CH_3CN at 80 °C. b) Isolated yields unless otherwise specified. The underlined figures refer to the yields determined by glpc relative to an internal standard. c) Cerium(IV) sulfate. d) Two hydroxy compounds (1.0 mmol each) were employed.

secondary diols with this technique would afford hydroxy ketones arising from selective oxidation at the secondary carbon.[17,18] This was indeed the case as demonstrated by the reactions summarized in Table 2. The selectivity was excellent except the case of 1-[*p*-(hydroxymethyl)phenyl]ethanol. In this particular substrate, the secondary hydroxyl group reacts only three times the rate of primary one.

The system is also effective for the oxidation of a primary, primary 1,4-diol. For instance, treatment of 2,3-bis(hydroxymethyl)bicyclo[2.2.1]heptane with cerium(IV) ammonium nitrate–sodium bromate provided the corresponding γ-lactone in a good yield. The reaction presumably proceeds via the lactol.

(2) Ruthenium Catalyzed Oxidation of Alcohols to Carbonyl Compounds. In recent years oxidation reactions using ruthenium as a key atom have been extensively developed. Among them, ruthenium complex, $RuCl_2(PPh_3)_3$ proved to be an efficient oxidant for chemoselective oxidation of primary alcohols.[18] Moreover, ruthenium catalyzed reactions with oxidants such as bis(trimethylsilyl) peroxide,[3] amine *N*-oxide,[4] *t*-butyl hydroperoxide,[19] hypervalent iodine compounds,[20] molecular oxygen,[21,22] have been reported. We chose sodium bromate as an oxidant which proved to be an effective and inexensive oxidant for oxidation of hydroxyl substrates to the corresponding carbonyl compounds.[23]

Secondary alcohols were added to a biphase solution of ruthenium trichloride hydrate and sodium bromate in water and 1,2-dichloroethane (H_2O:$ClCH_2CH_2Cl$=1:1 v/v). The mixture was heated at reflux to yield the corresponding carbonyl compounds in good to excellent yields (Reaction Conditions B). Variations in catalysts and reaction conditions have been examined with cyclododecanol as a substrate. Ruthenium trichloride hydrate, tris(triphenylposhine)ruthenium(II) dichloride, and dodecacarbonyltriruthenium(0) were equally active as catalyst and cyclododecanone was obtained quantita-

tively with each catalyst. Reaction was accelerated by phase transfer catalyst such as quaternary ammonium salt (Reaction Conditions A). For instance, cyclododecanol was easily oxidized to cyclododecanone even at 25 °C within 30 min (>99% yield), in the presence of tetrabutylammonium bromide. Some representative examples are shown in Table 3.

In contrast, $RuCl_3 \cdot nH_2O$ or $RuCl_2(PPh_3)_3$ catalyzed oxidation of primary alcohols resulted in the formation of the desired aldehydes in poor yields along with carboxylic acids and esters. Dodecacarbonyltriruthenium(0) catalyzed reaction (Reaction Conditions D), however, has solved this problem and converted primary alcohols into aldehydes in good yields. In the case of former ruthenium chloride compounds, hydrochloric acid generated during the reaction catalyzes the transformation of the resultant aldehydes into hemiacetals or gem-diols which are oxidized further to esters or carboxylic acids. The use of the buffer solution (pH=10) instead of water prevented these side reactions and provided us with a simple method for the selective formation of aldehydes (Reaction Conditions C).

Table 3. Oxidation of Alcohols with Ruthenium Compounds

Run	Alcohol	Conditions[a]	Reaction Time/h	Yield[b]/%
1	Cyclododecanol	A	0.5	>99
		B	1.0	97
2	4-Dodecanol	A	0.5	98
3	4-*t*-Butylcyclohexanol	A	0.5	97
4	*l*-Menthol	A	0.5	93
5	Borneol	A	0.5	98
6	Norborneol	A	0.5	98[c]
7	$PhCH(OH)CH_3$	A	0.5	93
8	11-Dodecen-2-ol	A	1.0	54[d]
		B	7.0	77
9	3β-Cholestanol	A	1.5	98
10	Carveol	B	1.5	78
11	2-Cyclohexen-1-ol	B	1.5	69[c]
12	1-Dodecanol	A	1.0	40[e]
		C	1.0	86
		D	1.0	88
13	10-Undecen-1-ol	C	1.2	70
14	2-Dodecen-1-ol	A	2.0	63
		B	2.5	80
15	Cyclohexylmethanol	C	2.5	97[c]
16	Geraniol	C	1.5	78
17	Benzyl alcohol	C	1.5	81

a) Reactions were performed under these conditions A: $RuCl_3 \cdot nH_2O$ (5.0 mol%), n-Bu_4NBr (3.0 mol%), H_2O/CH_2Cl_2=2 ml : 2 ml, 25 °C. B: $RuCl_3 \cdot nH_2O$ (5.0 mol%), H_2O/CH_2ClCH_2Cl=2 ml : 2 ml, 70 °C. C: $RuCl_3 \cdot nH_2O$ (5.0 mol%), a buffer solution/CH_2Cl-CH_2Cl=2 ml : 2 ml, 70 °C. The buffer solution (pH 10) is prepared by mixing equal volume of 0.2 M aq Na_2CO_3 and 0.2 M aq $NaHCO_3$. (M=1 mol dm^{-3}) D: $Ru_3(CO)_{12}$ (5.0 mol%), H_2O/CH_2ClCH_2Cl=2 ml: 2 ml, 70 °C. b) Isolated, purified yields unless otherwise noted. c) Glpc yields using an internal standard. d) Transformation of olefin to bromohydrin was observed (23%). e) Dodecanoic acid (20%) and dodecyl dodecanoate (22%) were also obtained.

Experimental

Infrared spectra of neat liquid film samples were determined on a Hitachi grating infrared spectrometer 215, or JASCO IR-810, mass spectra and exact mass on a Hitachi M-80. NMR spectra were recorded on a Varian EM-390, or Varian XL-200 spectrometer using TMS as an internal standard unless otherwise noted. Multiplicity is designed as s, singlet; d, doublet; t, triplet; q, quartet; m, multiplet. Preparative TLC plates were prepared with Merck kiesel-gel PF_{254}. Column chromatography was carried out with silica-gel (Wakogel C-200) at atmospheric pressure.

General Procedure for the Oxidation of Secondary Alcohols with Cerium(IV) Ammonium Nitrate (CAN)/$NaBrO_3$: Cyclododecanol (0.37 g, 2.0 mmol) and catalytic amount of CAN (0.11 g, 0.2 mmol) were added to a suspension of sodium bromate (0.30 g, 2.0 mmol) in aq acetonitrile (CH_3CN/H_2O=7/3 v/v, 12 ml). The whole was heated at reflux for 30 min and the resulting yellow suspension was diluted with ether (20 ml). After extraction with ether (10 ml×2), organic layer was washed with sat. $NaHCO_3$ and brine successively, and dried over sodium sulfate. Concentration and purification by preparative TLC (hexane–ethyl acetate=10:1) gave cyclododecanone (0.36 g, 98%).

Oxidation of 3-(2-Hydroxyethyl)cyclopentanol: The diol (0.23 g, 1.8 mmol) and CAN (0.1 g, 0.18 mmol) were added to a suspension of sodium bromate (0.27 g, 1.8 mmol) in aq acetonitrile. The whole was heated at reflux for 30 min and the solvent was removed under reduced pressure. The residue was diluted with ethyl acetate and poured into water. After extraction with ethyl acetate, the combined organic layer was dried over sodium sulfate. Concentration followed by purification by silica-gel column chromatography (hexane–ethyl acetate=3:1) gave 3-(2-hydroxyethyl)-cyclopentanone (0.20 g, 89%).

Oxidation of 1,10-Undecanediol with Cerium(IV) Sulfate (CS)/$NaBrO_3$: The diol (0.37 g, 2.0 mmol) and CS (0.07 g, 0.2 mmol) were added to a suspension of sodium bromate (0.3 g, 2.0 mmol) in aq acetonitrile (10 ml) and the whole was refluxed for 2 h. Extractive workup and purification by silica-gel column chromatography (hexane–ethyl acetate=2:1) gave 11-hydroxy-2-undecanone (0.32 g, 86%).

General Procedure for the Oxidation of Secondary Alcohols with $RuCl_3/NaBrO_3$ in the Presence of a Phase Transfer Reagent (Reaction Conditions A): Tetrabutylammonium bromide (ca. 10 mg) and a solution of cyclododecanol (0.18 g, 1.0 mmol) in dichloromethane (2.0 ml) were added successively to a solution of sodium bromate (0.15 g, 1.0 mmol) and ruthenium trichloride (0.01 g, 0.05 mmol) in deionized water (2.0 ml). The mixture was stirred at 25 °C and the alcohol was consumed completely within 30 min. The resulting dark brown solution was diluted with ether, then poured into ice cooled sat. sodium hydrogensulfite. After extraction with

ethyl acetate (20 ml×2), the combined organic layer was dried over sodium sulfate and concentrated. The residual oil was purified by silica-gel column chromatography (hexane–ethyl acetate=10:1) to yield cyclododecanone (0.18 g) quantitatively.

General Procedure for the Oxidation of Alcohols with $RuCl_3/NaBrO_3$ without a Phase Transfer Catalyst (Reaction Conditions B): A solution of cyclododecanol (0.18 g, 1.0 mmol) in 1,2-dichloroethane was added to a mixed solution of sodium bromate (0.15 g, 1.0 mmol) and ruthenium trichloride (0.01 g, 0.05 mmol) in deionized water (2.0 ml). The mixture was stirred at 70 °C for 3 h. Workup and purification by silica-gel column chromatography gave cyclododecanone in quantitative yield.

General Procedure for the Oxidation of Primary Alcohols with $RuCl_3 \cdot nH_2O/NaBrO_3$ (Reaction Conditions C): Sodium bromate (0.15 g, 1.0 mmol) and ruthenium trichloride (0.01 g, 0.05 mmol) were dissolved in the buffer solution (2.0 ml, pH=10). 1,2-Dichloroethane (1.0 ml) was added and the whole was stirred for 30 min at 25 °C. A solution of 1-dodecanol (0.19 g, 1.0 mmol) in 1,2-dichloroethane (1.0 ml) was added and the resulting mixture was stirred for 20 min at 70 °C. Workup and purification gave dodecanal in 86% yield.

General Procedure for the Oxidation of Primary Alcohols with $Ru_3(CO)_{12}/NaBrO_3$ (Reaction Conditions D): A solution of 1-dodecanol (0.19 g, 1.0 mmol) in 1,2-dichloroethane (2.0 ml) was added to a solution of dodecacarbonyltriruthenium(0) (0.01 g, 0.05 mmol of ruthenium element) and sodium bromate (0.3 g, 2.0 mmol) in deionized water (2.0 ml). The whole was stirred for 1 h at 70 °C and the mixture was poured into ice-cooled water and extracted with ethyl acetate. Purification by preparative TLC gave dodecanal (0.13 g) in 68% yield.

References

1) R. A. Sheldon, and J. K. Kochi "Metal-Catalyzed Oxidations of Organic Compounds," Academic Press, New York (1981).

2) G. Sosnovsky and D. J. Rawlinson, "Organic Peroxides," ed by D. Swern, Wiley-Interscience, New York, (1970), Vol. 2, Chap. 2.

3) S. Kanemoto, K. Oshima, S. Matsubara, K. Takai, and H. Nozaki, *Tetrahedron Lett.*, **24**, 2185 (1983).

4) K. B. Sharpless, K. Akashi, and K. Oshima, *Tetrahedron Lett.*, **1976**, 2503.

5) Preliminary account of this work has appeared: H. Tomioka, K. Oshima, and H. Nozaki, *Tetrahedron Lett.*, **23**, 539 (1982).

6) Stoichiometric CAN oxidation of benzylic alcohols[7] and cyclopropylmethanols[8] affords the carbonyl compounds, whereas 1,2-diarylethanols[9] and exo- and endo-bicyclo[2.2.1]heptan-2-ol[10] do not react in the expected way. The former substrates have been cleaved into benzaldehydes, while the latter into 3- and 4-cyclopenteneacetaldehydes as major products.

7) W. S. Trahanovsky, L. B. Young, and G. L. Brown, *J. Org. Chem.*, **32**, 3865 (1967).

8) L. B. Young, and W. S. Trahanovsky, *J. Org. Chem.*, **32**, 2394 (1967).

9) P. M. Nave and W. S. Trahanovsky, *J. Am. Chem. Soc.*, **90**, 4755 (1968).

10) W. S. Trahanovsky, P. J. Flash, and L. M. Smith, *J. Am. Chem. Soc.*, **91**, 5068 (1969).

11) The CAN–$NaBrO_3$ system has been reported to effect the oxidation of benzylic alcohols briefly. T-L. Ho, *Synthesis*, **1978**, 936. See also T-L. Ho, *Synth. Commun.*, **9**, 237 (1979).

12) H. L. Hintz and D. C. Johnson, *J. Org. Chem.*, **32**, 556 (1967).

13) The use of CAN instead of cerium(IV) sulfate under the same reaction conditions resulted in formation of dodecanoic acid in 30% yield in addition to recovered 1-dodecanol (60%). CAN was, however, as effective as cerium(IV) sulfate for the selective oxidation of primary, secondary diols (Table 2). Treatment of a mixture of 1-dodecanol and 4-dodecanol (1.0 mmol each) with CAN (0.1 mmol) and $NaBrO_3$ (1.0 mmol) gave 4-dodecanone in 98% yield together with recovered 1-dodecanol (95%).

14) Under the same reaction conditions, cyclododecanol was converted into cyclododecanone in 95% yield.

15) Allylic alcohol such as 2-cycloocten-1-ol was not easily oxidized and provided the corresponding enone in 9% yield contaminated by unidentified products after 1 h at reflux (45% of starting alcohol remained).

16) Benzoin splits into benzaldehyde and benzoic acid. T-L. Ho, *Synthesis*, **1972**, 560.

17) Y. Ueno and M. Okawara, *Tetrahedron Lett.*, **1976**, 4597; M. E. Jung and L. M. Speltz, *J. Am. Chem. Soc.*, **98**, 7882 (1976); M. E. Jung and R. W. Brown, *Tetrahedron Lett.*, **1978**, 2771; G. H. Posner, R. B. Perfetti, and A. W. Runquist, ibid., **1976**, 3499; M. A. Neirabeyeh, J. C. Ziegler, and B. Gross, *Synthesis*, **1976**, 811.

18) For preferential oxidation of primary over secondary hydroxyls see H. Tomioka, K. Takai, K. Oshima, and H. Nozaki, *Tetrahedron Lett.*, **22**, 1605 (1981).

19) Y. Watanabe, Y. Tsuji, and T. Ohta, 29th Symposium on Organometallic Chemistry (JAPAN) B-220.

20) P. H. J. Carlsen, T. Katsuki, V. S. Martin, and K. B. Sharpless, *J. Org. Chem.* **46**, 3936 (1981); P. Müller and J. Godoy, *Tetrahedron Lett.*, **22**, 2361 (1981).

21) R. Tang, S. E. Diamond, N. Meary, and F. Mares, *J. Chem. Soc., Chem. Commun.*, **1978**, 562; M. Matsumoto and S. Ito, ibid., **1981**, 907.

22) Dehydrogenative oxidation of alcohols with hydrogen acceptor such as α,β-unsaturated carbonyl compounds has been also studied. Y. Sasson and J. Blum, *Tetrahedron Lett.*, **1971**, 2167; Y. Sasson and G. L. Rempel, ibid., **1974**, 4133; idem, *Can. J. Chem.*, **52**, 3825, (1974); S. L. Regan and G. M. Whitesides, *J. Org. Chem.* **37**, 1832, (1972); S. Murahashi, K. Ito, T. Naota, and Y. Maeda, *Tetrahedron Lett.*, **22**, 5327, (1981).

23) Recently Moro-oka et al. independently reported the oxidation of secondary alcohols using ruthenium trichloride hydrate-sodium bromate system. They did not mention the oxidation of primary alcohols. Y. Yamamoto, H. Suzuki, and Y. Moro-oka, *Tetrahedron Lett.*, **26**, 2107 (1985).

 © 1986 The Chemical Society of Japan Bull. Chem. Soc. Jpn., 59, 109—116 (1986)

Polymer-Protected Metal Complex for Gas Separation. I. A Solution of Polystyrene-Protected Aluminium Copper(I) Halide as Water-Resistant Carbon Monoxide Absorbent

Hidefumi HIRAI,* Susumu HARA, and Makoto KOMIYAMA
Department of Industrial Chemistry, Faculty of Engineering,
The University of Tokyo, Hongo, Bunkyo-ku, Tokyo 113
(Received August 10, 1985)

Carbon monoxide absorbents composed of linear polystyrene (PSt), aluminium halide, copper(I) halide, and toluene are prepared. The toluene solutions of polystyrene-protected aluminium copper(I) chloride (PSt-$AlCuCl_4$) rapidly absorb CO at 20 °C under 1 atm (initial partial pressure of CO: 0.90 atm) and the equilibrium molar ratio of absorbed CO to the charged CuCl is 0.78. On the elevation of the temperature from 20 °C to 82 °C under 1 atm, the absorbed CO is released completely. The absorption-release cycles are repeated many times without measurable decrease in the absorbing capacity. The CO absorbing capacities of toluene solutions composed of aluminium halides, copper(I) halides, and polystyrene decrease as follows: $AlCl_3$-CuCl system> $AlBr_3$-CuBr system$\gg AlI_3$-CuI system=0. The CO absorbing activity of the toluene solution of PSt-$AlCuCl_4$ remains virtually unchanged on the contact of the solution with nitrogen gas containing 10 mol% water to the charged CuCl (water content: 9000 ppm), when the molar ratio of phenyl residue of polystyrene (number-averaged degree of polymerization: 420, 50, or 4.0) to $AlCuCl_4$ is unity or larger. This result is markedly in contrast with the fact that the activity of the toluene solution of $AlCuCl_4$ without polystyrene significantly (25%) decreases on the contact.

The importance of carbon monoxide (CO) as one of chief raw materials in chemical industry is increasing.[1,2] Carbon monoxide is usually produced as gas mixtures with nitrogen, hydrogen, oxygen, methane, carbon dioxide, and water[3] by steam reforming of hydrocarbons, partial oxidation processes, and coal gasification. Thus, separation of CO from gas mixtures is significant.

Copper liquor and cryogenic separation processes are known as CO separation methods.[3] Recently, a separating process using an absorbent, which takes advantage of selective complex formation of a double salt, aluminium copper(I) chloride ($AlCuCl_4$), with CO in toluene, has been proposed.[4] With this absorbent, CO is separated under mild conditions and the absorbent is stable against oxygen and carbon dioxide.[4,5] However, the CO absorbing activity of the absorbent rapidly and irreversibly decreases on the contact with gas mixture containing water, since $AlCuCl_4$ vigorously reacts with water as follows.[6,7]

$$H_2O + 2AlCuCl_4 \longrightarrow HCl + AlCuCl_4Al(OH)Cl_2 + CuCl \quad (1)$$

$$AlCuCl_4Al(OH)Cl_2 \xrightarrow{\Delta} HCl + AlCuCl_4AlOCl \quad (2)$$

Thus, the water content in feed gas mixtures must be reduced to 1 ppm or less by pretreatment for CO separation in industry.[4]

In a preliminary communication,[8] the authors showed that a solution composed of linear polystyrene (PSt), copper(I) chloride (CuCl), aluminium chloride ($AlCl_3$), and toluene reversibly absorbed CO under mild conditions and in addition was stable against water vapor.

This paper reports the results of detailed study on the toluene solutions of polystyrene-protected $AlCuCl_4$ (PSt-$AlCuCl_4$). The effects of the degree of polymerization and the amount of polystyrene on the water resistivity are revealed. The CO absorbing activities of the absorbents composed of $AlCuCl_4$ and other polymers are also shown. Furthermore, the infrared spectra of the PSt-$AlCuCl_4$ complex in the presence and the absence of CO are presented. The mechanism of protection of $AlCuCl_4$ by polystyrene in the CO absorbents is discussed.

Experimental

Materials. Linear polystyrene, purchased from Wako Pure Chemical Co. or prepared in toluene by use of benzoyl peroxide as initiator, was reprecipitated using the chloroform-methanol system and was dried in vacuo for 12 h at 60 °C. The number-averaged degrees of polymerization (DP_n) of these polystyrenes were 420 and 50, respectively, as estimated from the number-averaged molecular weight (M_n) and weight-averaged molecular weight (M_w): $M_n=4.4\times10^4$ and $M_w=1.5\times10^5$ for the first polystyrene, and $M_n=5.2\times10^3$ and $M_w=1.2\times10^4$ for the second one. The molecular weights were determined by gel permeation chromatography using columns of TSK-GEL, G5000H+G3000H, Toyo Soda Manufacturing Co. Styrene oligomer of DP_n 4.0, which contained oligomers of degrees of polymerization 2, 3, 4, 5, 6, 7, and 8 in 16, 27, 23, 16, 10, 5, and 3 mol%, respectively, was obtained from Toyo Soda Manufacturing Co.

Poly[oxy(2,6-dimethyl-1,4-phenylene)], $M_n=3.2\times10^4$ and $M_w=2.4\times10^5$, and polybutadiene (45% vinyl and 55% *cis* and *trans*-1,4), $M_n=4.5\times10^3$, respectively, were purchased from Scientific Polymer Products and Aldrich Chemical Co. Styrene-butadiene block copolymer composed of 41.6 wt% styrene part and 58.4 wt% butadiene part and hydrogenation product (Kraton-G 1650) of styrene-butadiene block copolymer composed of 30 wt% of styrene part and 70 wt%

of butadiene part were obtained from Asahi Chemical Industry Co. and Shell Co., respectively. Alternating copolymer of styrene and methyl methacrylate was prepared by photopolymerization in the presence of boron chloride.[9]

Aluminium chloride (Kishida Chemical Co.) was purified by sublimation. Copper(I) chloride (Koso Chemical Co.) was reprecipitated from an aqueous concentrated hydrochloric acid solution by the addition of distilled water, followed by washing successively with ethanol and diethyl ether, and then dried overnight in vacuo at 100 °C. Aluminium bromide, copper(I) bromide, aluminium iodide, and copper(I) iodide were commercially (guaranteed grades) obtained and were used without further purification. Titanium(IV) chloride and tin(IV) chloride were purified by distillation.

Toluene and benzene were distilled after being dried over metallic sodium. Chlorobenzene was dried over diphosphorus pentaoxide and was distilled.

Carbon monoxide and nitrogen gas, which had the purities of 99.95 and 99.999%, respectively, were passed through columns of molecular sieves 3A immediately before use.

Preparation of CO Absorbents. Carbon monoxide absorbents were prepared by heating polymer, aluminium halide, copper(I) halide, and aromatic solvent at 50 °C for 4 h. The charged molar ratio of CuCl to $AlCl_3$ was kept constant at unity unless otherwise noted.

For example, the preparation procedure for toluene solution of PSt-$AlCuCl_4$ was as follows. 2.08 g (20 mequiv in phenyl residue) of linear polystyrene, 2.67 g (20 mmol) of $AlCl_3$, 1.98 g (20 mmol) of CuCl, and 20 cm^3 (192 mmol) of toluene were placed in a 100 cm^3 flask and were heated at 50 °C for 4 h under dry nitrogen with stirring by use of a magnetic stirrer. The nitrogen in the flask was several times replaced with fresh dry nitrogen during the preparation.

Toluene solution of $AlCuCl_4$ without polystyrene was prepared in a similar manner as above, except for the absence of polystyrene.

Absorption and Release of CO. The absorption of CO by the absorbent, continuously stirred by use of a magnetic stirrer, from CO-N_2 mixture (the total pressure: 1 atm) was carried out at room temperature under 1 atm using the apparatus depicted in Fig. 1. The amount of absorbed CO was determined at room temperature under 1 atm by a gas burette (6) using toluene as leveling liquid (7). During the first 10 min, the CO-N_2 mixture was made to flow over the absorbent (1), stirred magnetically in the flask, by a gas-circulating pump (5) (Iwaki Co., BA-106TN). The initial partial pressure of CO was in the range of 0.8 to 1.0 atm and the decrease of the partial pressure of CO during CO absorption was at most 0.07 atm.

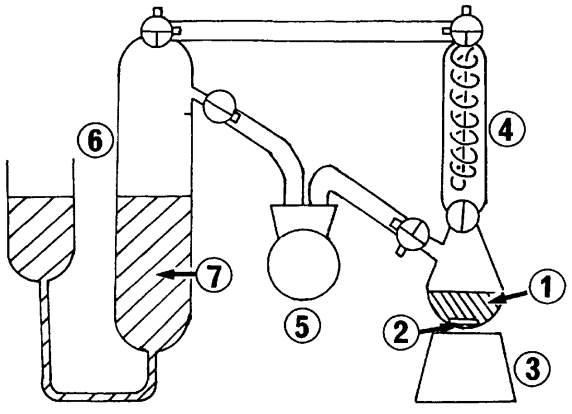

Fig. 1. Apparatus for measuring the amount of carbon monoxide absorbed by the absorbents or released from them; 1: CO absorbent, 2: rotor, 3: magnetic stirrer, 4: Dimroth condenser, 5: gas-circulating pump, 6: gas burette, 7: leveling liquid (toluene).

The release of CO from the absorbent was accomplished by heating the absorbent and the amount of released CO was determined by the gas burette ((6) in Fig. 1). Toluene vapor, produced from the absorbent on heating, was refluxed by a Dimroth condenser (4). After CO was released, the absorbent was cooled to room temperature under dry nitrogen, and then the second absorption by the absorbent was carried out by the same method as described above.

Contact of the Absorbent with Water Vapor. The contact of the absorbent with water vapor was effected by circulating 5000 or 10000 cm^3 of N_2 gas, containing 10 mol% water to the charged CuCl, over the absorbent for 10 min by use of a gas-circulating pump. During the contact, the absorbent was continuously stirred using a magnetic stirrer (Fig. 1, (3)). The N_2 gas containing water vapor was prepared by the introduction of distilled water into 5000 or 10000 cm^3 of evacuated vessel using a microsyringe, followed by the addition of dry nitrogen in an amount required to make the total pressure atmospheric.

After the contact with water, the gas phase in the flask was replaced by dry nitrogen, and then the following CO absorption was carried out.

Infrared Spectroscopy. Infrared spectra were taken with a Japan Spectroscopic Co. Model A-3 recording spectrophotometer by use of a KBr cell. Specimens were toluene solutions of PSt-$AlCuCl_4$ before and after the contact with CO under atmospheric pressure for 1 h.

Results

Preparation of CO Absorbent. The color of polystyrene (PSt) immediately changed from white to orange when aluminium chloride, copper(I) chloride, linear polystyrene, and toluene were mixed in a flask. The toluene solutions were reddish brown in the early stage of the preparation, and gradually became dark brown.

The CO absorbents were thoroughly homogeneous at the charged molar ratio unity of CuCl to $AlCl_3$. When the charged molar ratio of CuCl was larger than unity, however, CuCl in excess precipitated as white to gray powder in the mixture. In all the CO absorbents described hereinafter, the charged molar ratios of copper(I) halides to aluminium halides were maintained at 1.0.

Toluene and benzene solutions of $AlCuCl_4$ without

polystyrene were black and brown homogeneous solutions, respectively.

Chlorobenzene solutions of PSt-$AlCuCl_4$ were prepared from $AlCl_3$, CuCl, polystyrene, and chlorobenzene as homogeneous dark brown solutions. The charged molar ratio of phenyl residue in polystyrene to CuCl was 1.0. In the absence of polystyrene, however, considerable amounts of gray precipitates were formed under reddish brown solutions and homogeneous absorbents were not obtained.

Toluene solution of polystyrene-protected aluminium copper(I) bromide complex was prepared as homogeneous solution from aluminium bromide, copper(I) bromide, polystyrene, and toluene. In the case of polystyrene-protected aluminium copper(I) iodide complex in toluene, however, the resulting mixture was composed of precipitates and a reddish brown solution.

CO Absorbing and Releasing Activities of PSt-$AlCuCl_4$ Complex in Aromatic Solvents. Figure 2 shows the absorption of CO at 20 °C under 1 atm by the absorbent composed of 0.96 g (7.2 mmol) of $AlCl_3$, 0.72 g (7.3 mmol) of CuCl, 0.67 g, (6.4 mequiv in phenyl residue) of linear polystyrene (DP_n: 420), and 10 cm^3 (96 mmol) of toluene. As depicted by the open circles, the absorbent rapidly absorbs CO and the equilibrium molar ratio of the absorbed CO to the charged CuCl is 0.85. On the elevation of the temperature of the absorbent from 20 °C to 82 °C, almost all the absorbed CO is released in 5 min from the absorbent to the vapor phase.

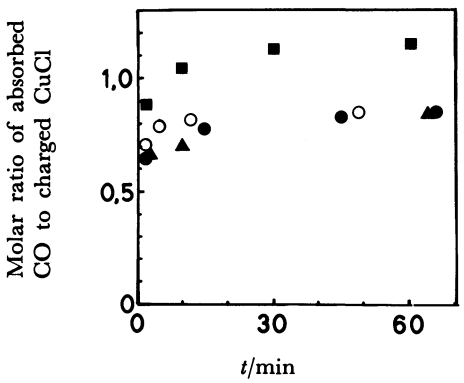

Fig. 2. Absorption of carbon monoxide at 20 °C under 1 atm by toluene or chlorobenzene solutions of polystyrene-$AlCuCl_4$: The first absorption by the toluene solution (○), the second absorption by the toluene solution which was heated to 82 °C to release CO after the first absorption (●), the third absorption by the toluene solution (▲); the first absorption by the chlorobenzene solution (■); For the toluene solution, $[AlCl_3]_0=[CuCl]_0=0.73$ and [phenyl residue of polystyrene (DP_n: 420)]$_0$=0.64 mol dm^{-3} in 10 cm^3 of toluene, and the initial $P_{CO}=1.0$ atm. For the chlorobenzene solution, $[AlCl_3]_0=[CuCl]_0=$ [phenyl residue of polystyrene (DP_n: 420)]$_0$=1.0 mol dm^{-3} in 22 cm^3 of chlorobenzene, and the initial volume of the gas mixture is 3000 cm^3 with initial pressures of CO and N_2, 0.9 and 0.1 atm, respectively.

In the second absorption, which is carried out after the cooling of the absorbent to 20 °C under dry nitrogen, the absorbent rapidly absorbs CO again as shown by the solid circles in Fig. 2. The equilibrium molar ratio of the absorbed CO to the charged CuCl is 0.85, which is exactly identical with the value (0.85) of the first absorption. The equilibrium molar ratio of the absorbed CO to the charged CuCl in the third absorption (the solid triangles) is also 0.85.

Table 1 shows the equilibrium molar ratios of the absorbed CO to the charged copper(I) halide for the various absorbents prepared from aluminium halides, copper(I) halides, polystyrene (DP_n: 420), and toluene. The absorbing capacities of the absorbents are as follows:

$AlCl_3$-CuCl system>$AlBr_3$-CuBr system $\gg$ AlI_3-CuI system=0.

Solid squares in Fig. 2 depict the absorption of CO by the chlorobenzene solution of PSt-$AlCuCl_4$ complex. The equilibrium molar ratio (1.15) of the absorbed CO to the charged CuCl is larger than the value (0.85) of the toluene solution even though the initial partial pressure of CO (0.9 atm) is smaller than the value (1.0 atm) for the toluene solution.

Effect of Water Vapor on CO Absorbing Activity of Toluene Solutions of PSt-$AlCuCl_4$ Complex. Open circles in Fig. 3 depict the absorption of CO from 1500 cm^3 of CO-N_2 mixture (initial partial pressure of CO: 0.80 atm) under 1 atm at 20 °C by the absorbent composed of 2.98 g (22.3 mmol) of $AlCl_3$, 2.22 g (22.4 mmol) of CuCl, 2.33 g (22.4 mequiv in phenyl residue) of polystyrene (DP_n: 420), and 15 cm^3 (144 mmol) of toluene. The absorption of CO is rapid and the equilibrium molar ratio of the absorbed CO to the charged CuCl is 0.71. On the elevation of the temperature from 20 °C to 95 °C,

Table 1. Molar Ratios of Equilibrium Amounts of the Absorbed CO to the Charged Copper(I) Halide for Toluene Solutions of Aluminium Halide (AlX_3) and Copper(I) Halides (CuX) with of without Polystyrene (PSt)[a)]

Absorbent	Halogen (X)		
	Cl	Br	I
PSt-AlX_3-CuX	0.78	0.45	0.00
AlX_3-CuX	0.83	0.45	—

a) CO absorbing conditions; at room temperature under 1 atm; the initial volume of the gas mixture is 3000 cm^3 and the initial pressures of CO and N_2 are 0.9 and 0.1 atm, respectively; $[AlX_3]_0=[CuX]_0=$ [phenyl residue of polystyrene]$_0$=1.0 mol dm^{-3}; the subscript 0 is used to designate the charged concentration; number-averaged degree of polymerization of polystyrene: 420.

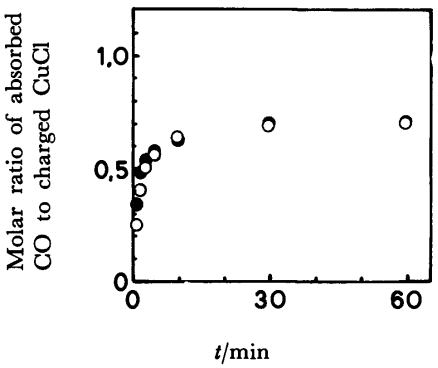

Fig. 3. Effect of water vapor on the CO absorbing activity of toluene solution of polystyrene-$AlCuCl_4$; the first absorption (○); the second absorption after the contact of the solution with 10 mol% water to the charged CuCl (●); CO absorbing conditions, 20 °C under 1 atm; the initial volume of the gas mixture is 1500 cm^3 and the initial pressures of CO and N_2 are 0.8 and 0.2 atm, respectively; $[AlCl_3]_0=[CuCl]_0=$[phenyl residue of polystyrene (DP_n: 420)]$_0$ $=1.5$ mol dm^{-3} in 15 cm^3 of toluene.

almost all the absorbed CO is released.

After being cooled to 20 °C under dry nitrogen, the absorbent is contacted with 5000 cm^3 of nitrogen containing 10 mol% water to the charged CuCl (water content: 9000 ppm) for 10 min. In the following CO absorption, the absorbent quickly absorbs CO from 1500 cm^3 of CO-N_2 mixture (initial pressure of CO: 0.80 atm), as shown by the solid circles in Fig. 3. The equilibrium molar ratio of the absorbed CO to the charged CuCl is 0.71, which is identical with the value (0.71) for the absorbent prior to the contact with water vapor. No decrease in the CO absorbing activity was detected at all even after the repeated (five times) contacts of the absorbent with water vapor. Thus, the water vapor exhibits no measurable deactivation effect on the absorbent containing polystyrene (DP_n: 420) equimolar in phenyl residue to the charged CuCl.

Table 2 shows the effects of the degree of polymerization and the amount of polystyrene used on the water resistivity of the toluene solution of PSt-$AlCuCl_4$ complex. Here, the ratio of the amount of CO absorbed by the absorbent after the contact with water vapor (10 mol% to the charged CuCl) to the value before the contact is used as an index of the water resistivity of the absorbents.

When the charged molar ratio of the phenyl residue of polystyrene (DP_n: 420) to CuCl is larger than unity, no decrease in the activity is observed after the contact with 10 mol% water to the charged CuCl. At the molar ratios 0.5 and 0.1, however, the CO absorbing activity decreases by 6 and 8%, respectively, after the contact. The decrease of the CO absorbing activity of the absorbents, even at the molar ratio 0.5 or 0.1, is much smaller than that

Table 2. Effects of the Degree of Polymerization and the Amount of Polystyrene (PSt) on the Water Resistivity of Toluene Solution of PSt-$AlCuCl_4$[a]

PSt		Water resistivity of the CO absorbent[d]
DP_n[b]	Charged amount[c]	
420	3.0	1.01
420	1.0	1.01
420	0.5	0.94
420	0.1	0.92
50	1.0	1.01
4	1.0	0.99
—	0	0.75

a) $[AlCl_3]_0=[CuCl]_0=1.0$ mol dm^{-3}. CO absorbing conditions: at room temperature under 1 atm; the initial volume of the gas mixture is 1500 cm^3 and the initial pressures of CO and N_2 are 0.8 and 0.2 atm, respectively. b) Number-averaged degree of polymerization. c) The charged molar ratio of phenyl residue in polystyrene to CuCl. d) The ratio of the equilibrium amount of the absorbed CO after the contact of the absorbent with water vapor to the value before the contact. The charged molar ratio of water to CuCl is 0.10.

(25%) of the toluene solutions of $AlCuCl_4$ without polystyrene.

At the charged molar ratio 1.0 of the phenyl residue of polystyrene to CuCl, no measurable decrease of the CO absorbing activity of the absorbents by the contact with water vapor is observed irrespective of the degree of polymerization (420, 50, and 4.0) of polystyrene.

CO Absorbing Activity and Water Resistivity of Toluene Solution of $AlCuCl_4$ without PSt. As shown by the open circles in Fig. 4, the toluene solution of $AlCuCl_4$ without polystyrene rapidly absorbs CO from 1500 cm^3 of CO-N_2 mixture (initial partial pressure of CO: 0.80 atm) at 20 °C under 1 atm and the equilibrium molar ratio of the absorbed CO to the charged CuCl is 0.68. Almost all the absorbed CO is released when the absorbent is heated to 80 °C. The CO absorbing activity remains constant on repeated absorption-release cycles, as long as sufficiently dried CO is used.

However, the activity of the absorbent without polystyrene rapidly decreases on the contact with water vapor. The equilibrium molar ratio (0.51) of the absorbed CO to the charged CuCl after the contact of the absorbent with N_2 gas containing 10 mol% water to the charged CuCl (the solid circles in Fig. 4) is much smaller than that (0.68) before the contact.

After the second contact with 10 mol% water to the charged CuCl, the equilibrium molar ratio of the absorbed CO to the charged CuCl is further decreased

to 0.30.

The activity of the absorbent without polystyrene did not change on the contact with oxygen. The contact was carried out under 1 atm of oxygen for 1 h at room temperature, while the absorbent was magnetically stirred.

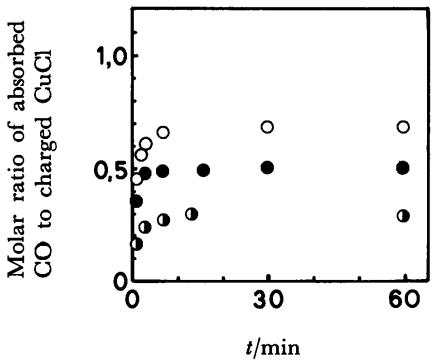

Fig. 4. Effect of water vapor on the CO absorbing activity of toluene solution of $AlCuCl_4$ without polystyrene; the first absorption (○); the second absorption after the contact of the solution with 10 mol% water to the charged CuCl (●); the third absorption after the second contact with 10 mol% water (◑); CO absorbing conditions, 20 °C under 1 atm; the initial volume of the gas mixture is 1500 cm^3 and the initial pressures of CO and N_2 are 0.8 and 0.2 atm, respectively; $[AlCl_3]_0=[CuCl]_0=1.5$ mol dm^{-3} in 19 cm^3 of toluene.

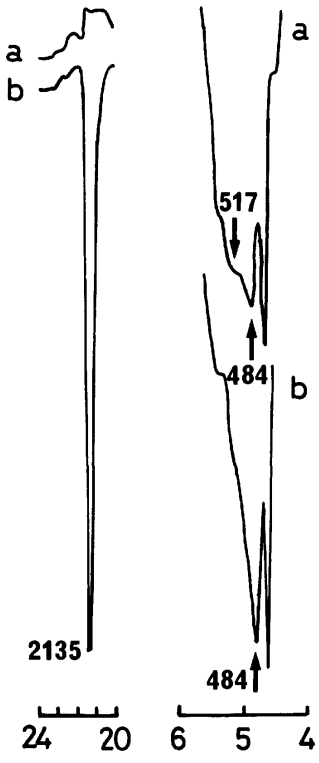

Fig. 5. Partial IR spectra of toluene solution of polystyrene–$AlCuCl_4$ before the contact with CO (a) and after the contact (b); $[AlCl_3]_0=[CuCl]_0=$[phenyl residue of polystyrene (DP_n: 420)]$_0=1.0$ mol dm^{-3}.

Infrared Spectra of the Solution of PSt-$AlCuCl_4$ with or without Absorbed CO. In the absence of CO, the solution of PSt–$AlCuCl_4$ exhibits a strong absorption at 484 cm^{-1} and a shoulder peak at 517 cm^{-1} as shown in Fig. 5, (a). All other signals are assignable to polystyrene and toluene.

When the absorbent absorbs CO, a strong and sharp absorption band appears at 2135 cm^{-1} and the band at 517 cm^{-1} weakens, as shown in Fig. 5, (b). The band at 2135 cm^{-1} is due to stretching vibration (ν_{CO}) of the absorbed CO. Otherwise, no change in the spectrum is observed on the CO absorption.

In benzene and chlorobenzene solutions of $AlCuCl_4$, ν_{CO} bands were observed at 2132 and 2135 cm^{-1}, respectively. No band assignable to the absorbed CO was observed for toluene itself without $AlCuCl_4$, which was stored under CO for 1 d.

CO Absorbents Composed of Various Polymers and $AlCuCl_4$. Homogeneous toluene solution of polymer–$AlCuCl_4$ complex was prepared using poly[oxy(2,6-dimethyl-1,4-phenylene)] or hydrogenated styrene-butadiene block copolymer (Kraton G) instead of polystyrene. These absorbents slowly absorbed CO as depicted by the open circles and solid circles in Fig. 6.

When polybutadiene, styrene-butadiene block copolymer, or alternating copolymer of styrene and methyl methacrylate were used, however, aggregates were formed and homogeneous solutions were not obtained. These aggregates showed no absorption of CO under 1 atm at 20 °C.

CO Absorbing Activities of the Absorbents with-

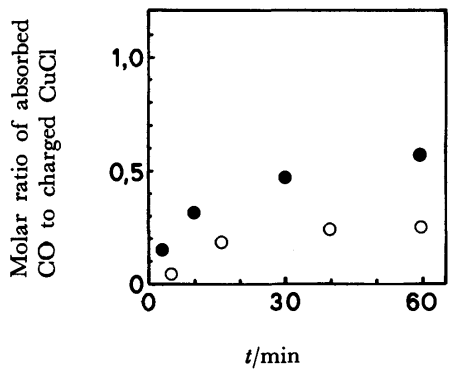

Fig. 6. Absorption of carbon monoxide at 20 °C under 1 atm CO by toluene solutions of $AlCuCl_4$ with poly[oxy(2,6-dimethyl-1,4-phenylene)] (○) or hydrogenated styrene-butadiene block copolymer (●): for the absorbent with poly[oxy(2,6-dimethyl-1,4-phenylene)], $[AlCl_3]_0=[CuCl]_0=1.3$ and [phenyl residue of the polymer]$_0=1.6$ mol dm^{-3} in 20 cm^3 of toluene; for the absorbent with hydrogenated styrene–butadiene block copolymer, $[AlCl_3]_0=[CuCl]_0=0.7$ and [phenyl residue of the polymer]$_0=0.25$ mol dm^{-3} in 40 cm^3 of toluene.

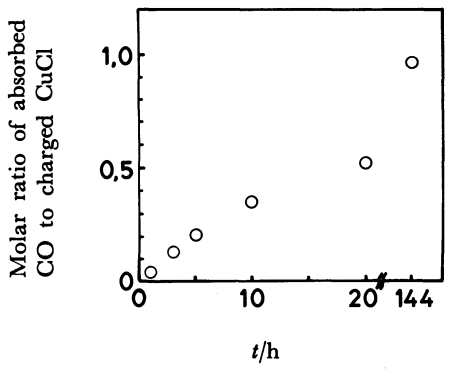

Fig. 7. Absorption of carbon monoxide at 20 °C under 1 atm CO by toluene suspension of CuCl composed of 25.0 mmol of CuCl and 20 cm^3 of toluene.

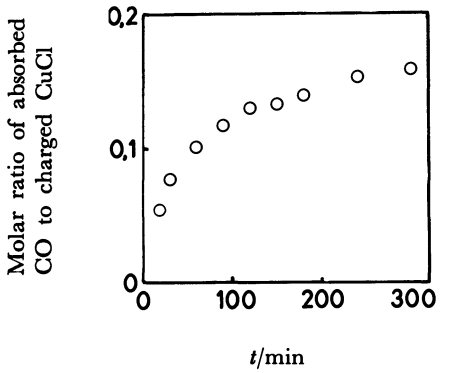

Fig. 8. Absorption of carbon monoxide at 30 °C under 1 atm by concentrated hydrochloric acid solution of CuCl composed of 3.0 mmol of CuCl and 20 cm^3 of aqueous HCl solution (12 mol dm^{-3}); the initial volume of the gas mixtures is 3000 cm^3 and the initial pressures of CO and N_2 are 0.9 and 0.1 atm, respectively.

out $AlCl_3$. In the absence of $AlCl_3$, CuCl does not dissolve in toluene either in the presence or the absence of polystyrene, and only toluene suspension of CuCl is obtained. The suspension without polystyrene slowly absorbs CO and the molar ratio of the absorbed CO to the charged CuCl is 0.04 at 60 min and 0.97 at 144 h under 1 atm at 20 °C, as shown in Fig. 7.

Concentrated hydrochloric acid solution of CuCl also slowly absorbs CO and the molar ratio of the absorbed CO to the charged CuCl is 0.10 at 60 min and 0.16 at 300 min, as shown in Fig. 8.

Dark reddish brown solution prepared from 0.85 g (8.2 mequiv in phenyl residue) of linear polystyrene (DP_n: 420), 1.55 g (8.2 mmol) of titanium(IV) chloride, 0.81 g (8.2 mmol) of CuCl, and 20 cm^3 of toluene did not absorb CO. Yellow solution from 0.95 g (9.1 mequiv in phenyl residue) of linear polystyrene (DP_n: 420), 2.39 g (9.2 mmol) of tin(IV) chloride, 0.91 g (9.2 mmol) of CuCl, and 20 cm^3 of toluene did not absorb CO either. In both cases, considerable amounts of precipitates were formed under homogeneous solutions.

Discussion

Formation of PSt-$AlCuCl_4$ Complex. Copper(I) chloride, which hardly dissolves in toluene alone, satisfactorily dissolves in toluene in the presence of $AlCl_3$ equimolar to CuCl. When the molar ratio of CuCl to $AlCl_3$ is larger than unity, CuCl present in excess forms precipitates. These results definitely show that CuCl and $AlCl_3$ form a double salt $AlCuCl_4$ in a molar ratio 1:1. Formation of $AlCuCl_4$ in toluene either in the presence or the absence of polystyrene was further confirmed by the infrared absorption band at 484 cm^{-1} (Fig. 5 (a)), which was assigned to antisymmetric stretching mode ν_a of $AlCl_4^-$ residue in $AlCuCl_4$.[10]

In the CO absorbents composed of polystyrene, $AlCl_3$, CuCl, and aromatic solvents, polystyrene and $AlCuCl_4$ form a polymer complex PSt-$AlCuCl_4$. This is shown by the fact that chlorobenzene solution of $AlCuCl_4$ was homogeneous only in the presence of polystyrene. Here, aromatic rings of polystyrene formed charge-transfer complexes with $AlCuCl_4$, which satisfactorily dissolved in chlorobenzene. In the absence of polystyrene, however, considerable portion of $AlCuCl_4$ precipitated, since the equilibrium constant for the charge-transfer complex formation between $AlCuCl_4$ and chlorobenzene was small due to small electron donating ability of chlorobenzene (ionization potential (I_p): 9.60 eV).[11] Toluene, which had a larger electron donating ability (I_p: 9.18 eV)[11] than chlorobenzene, efficiently formed charge-transfer complex with $AlCuCl_4$, resulting in a homogeneous toluene solution of $AlCuCl_4$ even in the absence of polystyrene.

The formation of the PSt-$AlCuCl_4$ complex has been further confirmed by a very strong charge-transfer band in the 380—500 nm region.[12] Such a charge-transfer band has not been found in a toluene solution of $AlCuCl_4$ without polystyrene.

Marked difference in absorption spectra between the $AlCuCl_4$-PSt system and the $AlCuCl_4$-toluene system indicates that the PSt-$AlCuCl_4$ complex involves interactions of two aromatic rings of polystyrene with $AlCuCl_4$. Probably an aromatic ring in polystyrene interacts with the Cu(I) ion in $AlCuCl_4$ and another aromatic ring interacts with the $AlCl_3$ part in the same $AlCuCl_4$ molecule.[11] The interaction between polystyrene and $AlCuCl_4$ is promoted by the chelate effect of these two types of interactions. The proposed conformation of the PSt-$AlCuCl_4$ complex is consistent with the result of crystallography on the $AlCuCl_4$-benzene complex,[13] where a benzene molecule interacts with the Cu(I)

ion in $AlCuCl_4$. Alternatively, two aromatic rings of polystyrene can interact with the two Cl atoms of the $AlCl_3$ part of $AlCuCl_4$ in the PSt-$AlCuCl_4$ complex.

When poly[oxy(2,6-dimethyl-1,4-phenylene)] and hydrogenated styrene-butadiene block copolymer were used in place of polystyrene, homogeneous solutions were obtained also by the interactions between the aromatic rings of the polymers and $AlCuCl_4$. Formation of the aggregates on the usage of polybutadiene and the alternating copolymer of styrene and methyl methacrylate, respectively, were associated with cross-linking of polybutadiene by cationic polymerization with $AlCl_3$ catalyst and the coordination of the ester groups in the alternating copolymer to $AlCl_3$.

CO Absorption by Solutions of PSt-$AlCuCl_4$ Complex. The frequency (2135 cm^{-1}) of the stretching vibration for the CO absorbed by the toluene solution of PSt-$AlCuCl_4$ (Fig. 5) is smaller than the value (2143 cm^{-1})[14] for free CO by about 10 cm^{-1}. This fact shows that CO absorption by the PSt-$AlCuCl_4$ absorbent is attributable to the coordination of CO to Cu(I) ion in $AlCuCl_4$. The coordination results in π-back donation from the Cu(I) ion to CO, reducing the bond order of C-O bond in CO.[14]

On the coordination of CO to the Cu(I) ion in $AlCuCl_4$, the aromatic ring of polystyrene or the toluene molecule, which is originally interacting with Cu(I) ion, is liberated from the Cu(I) ion and instead CO coordinates to the resultant unoccupied coordination site.[15] The larger equilibrium amount of the absorbed CO for the chlorobenzene solution of PSt-$AlCuCl_4$ than that for the toluene solution (Fig. 2) is consistent with this argument, since the ligand exchange from chlorobenzene to CO is easier than that from toluene to CO. The coordination of chlorobenzene to the Cu(I) ion in $AlCuCl_4$ is weaker than that of toluene, because of smaller electron donating ability (I_p=9.60 and 9.18 eV, respectively, for chlorobenzene and toluene).

Both the CO absorption rate and the amount of absorbed CO for the toluene solution of PSt-$AlCuCl_4$ complex (Fig. 2) are much larger than those of the concentrated hydrochloric acid solution of CuCl (Fig. 8). Formation of the double salt between $AlCl_3$ and CuCl decreases the electron density on the Cu(I) ion, which enhances the electron donation from CO to the Cu(I) ion, and promotes the coordination of CO to the Cu(I) ion.

The halogen dependence for the amount of CO absorbed by the toluene solutions of PSt-$AlCuX_4$ (Cl>Br $\gg$ I=0) (Table 1) is identical with that for the coordination of CO to copper(I) halides.[16] As the electronegativity of halogen decreases, the electron density on the Cu(I) ion in $AlCuCl_4$ increases and thus the capacity of CO absorption decreases.

In the coordination of CO to Cu(I) ion in $AlCuCl_4$, electron donation from CO to the Cu(I) ion makes predominant contribution, and the contribution of back donation from the Cu(I) ion to CO is less important. The ν_{CO} (2135 cm^{-1}) of the CO coordinating to the Cu(I) in $AlCuCl_4$ is larger than the ν_{CO} (2063 cm^{-1} in water,[17] and 2080 cm^{-1} in methanol)[18] of CO coordinating to CuCl. The back donation is suppressed by the decrease of electron density on the Cu(I) ion due to the formation of double salt $AlCuCl_4$.

In addition to the promotion of CO coordination to the Cu(I) ion by decreasing electron density on the ion, $AlCl_3$ in the solutions of PSt-$AlCuCl_4$ accelerates the CO absorption by dissolving CuCl, which is not soluble in toluene alone, with the formation of the double complex. CO absorption of homogeneous toluene solution of PSt-$AlCuCl_4$ complex (Fig. 2) is much faster than that by the toluene suspension of CuCl (Fig. 7).

Protection of $AlCuCl_4$ by PSt. The toluene solution of PSt-$AlCuCl_4$ shows no measurable deactivation on the repeated contacts with 10 mol% water to the charged CuCl (Fig. 3). This is markedly in contrast with significant decrease of the absorbing capacity of the toluene solutions of $AlCuCl_4$ without polystyrene. The amount of the $AlCuCl_4$ deactivated by water in the absence of polystyrene, estimated from the decrease in the CO absorbing capacity, is about twice in mole as large as that of the water (Fig. 4). This result is consistent with the irreversible reaction between $AlCuCl_4$ and water expressed by Eqs. 1 and 2.

No deterioration of the toluene solution of PSt-$AlCuCl_4$ on the contact with water vapor is probably due to the protection of $AlCuCl_4$ against water by the hydrophobic field of polystyrene. As described above, polystyrene and $AlCuCl_4$ form a polymer complex, in which two aromatic rings of polystyrene interact with one $AlCuCl_4$ molecule. The interactions of the two aromatic rings function cooperatively, and thus the interaction between aromatic ring and the $AlCl_3$ moiety is largely enhanced due to chelate effect. As the result, the $AlCl_3$ moieties, which otherwise rapidly react with water, are sufficiently protected by the aromatic rings of polystyrene. The water vapor remains in the gas phase here.[19]

In case of the toluene solution of $AlCuCl_4$ without polystyrene, however, protective effects of toluene on $AlCuCl_4$ are not so large, since the chelate effect does not take place. Water vapor promptly penetrates into the absorbent and hydrolyzes the $AlCuCl_4$.[19]

No dependence of the water-resistivity of CO absorbent on the degree of polymerization of polystyrene used (Table 2) indicates that the water resistivity of the absorbent is not attributable to the

increase of the viscosity of the absorbent resulting from the addition of polystyrene.

The proposed mechanism of water resistivity of the absorbent is also supported by the fact that water-resistive CO absorbent can be prepared by use of 1,3-diphenylpropane, a low molecular weight model of polystyrene, as solvent.[20]

References

1) "New Syntheses with Carbon Monoxide," ed by J. Falbe, Springer-Verlag, Berlin (1980).
2) "Chemicals from Synthesis Gas," ed by R. A. Sheldon, D. Reidel Publishing Co., Dordrecht (1983).
3) A. L. Kohl and F. C. Riesenfeld, "Gas Purification," 3rd ed, Gulf Publishing Co., Houston (1979).
4) D. J. Haase and D. G. Walker, *Chem. Eng. Prog.*, **70**, 74 (1974).
5) D. G. Walker, *Chemtech*, May, 308 (1975).
6) D. J. Haase, *Chem. Eng.*, August **4**, 52 (1975).
7) T. Inukai, *Sekiyu Gakkai Shi*, **20**, 317 (1977).
8) H. Hirai, M. Komiyama, and S. Hara, *Makromol. Chem., Rapid Commun.*, **2**, 495 (1981).
9) H. Hirai, K. Takeuchi, and M. Komiyama, *J. Polym. Sci., Polym. Chem. Ed.*, **19**, 2581 (1981).
10) C. Sourisseau and B. Pasquier, *Spectrochim. Acta*, **26A**, 1279 (1970).
11) G. F. Crable and G. L. Kearns, *J. Phys. Chem.*, **66**, 436 (1962).
12) H. Hirai, K. Kanaka, and M. Komiyama, *Polymer Preprints Japan*, **34**, 484 (1985).
13) R. W. Turner and E. L. Amma, *J. Am. Chem. Soc.*, **88**, 1877 (1966).
14) F. A. Cotton and G. Wilkinson, "Advanced Inorganic Chemistry", 4th ed, John Wiley and Sons, Inc. pp. 82—86 (1980).
15) H. Hirai, M. Nakamura, and M. Komiyama, *Bull. Chem. Soc. Jpn.*, **56**, 2519 (1983).
16) M. I. Bruce, *J. Organomet. Chem.*, **44**, 209 (1972).
17) J. O. Alben, L. Yen, and N. J. Farrier, *J. Am. Chem. Soc.*, **92**, 4475 (1970).
18) G. Rucci, C. Zanzottera, M. P. Lachi, and M. Camia, *J. Chem. Soc., Chem. Commun.*, **1971**, 652.
19) H. Hirai, M. Komiyama, and S. Hara, *Chem. Lett.*, **1981**, 1447.
20) H. Hirai, S. Hara, and M. Komiyama, *Chem. Lett.*, **1984**, 861.

 © 1986 The Chemical Society of Japan Bull. Chem. Soc. Jpn., 59, 117—120 (1986)

Reciprocal Space Expansion in the Analysis of X-Ray Scattering Intensities from Liquid Carbon Tetrachloride

Keiko NISHIKAWA* and Takao IIJIMA
Department of Chemistry, Faculty of Science, Gakushuin University,
Mejiro, Toshima-ku, Tokyo 171
(Received May 31, 1985)

The concept of "reciprocal space expansion" has been applied in the analysis of the X-ray scattering intensity from liquid carbon tetrachloride. The results obtained by using the bcc local lattice structure model show very good agreement with the experimental intensity in the small-s region, where ghost peaks are inevitably introduced by the "real space expansion" usually adopted.

The analysis of the X-ray scattering intensity from a liquid by constructing a "local lattice structure model" is usually carried out by means of the formulation put forward by Narten and his co-workers.[1,2] This formulation is based on the theory developed by Debye and Menke[3] and by Warren,[4] i.e., the expansion of the scattering intensity in terms of the interatomic distances, r_{ij}, in the real space (see Eq. 2). Therefore, hereafter, we will name Narten's expression for the "local lattice structure model" the "real space expansion."

This method was applied to liquid carbon tetrachloride.[5,6] The body-centered-cubic local lattice structure formed by the head-tail head-tail packing of the carbon tetrachloride molecules with a nearest neighbor distance of 5.9 Å accounted for the experimental intensity beyond s=1.2 Å^{-1} ($s=4\pi\sin\theta/\lambda$, 2θ: scattering angle, λ: wavelength of X-rays).

As was pointed out in a previous paper,[5] the limitations of the real space expansion for the local lattice structure model arise from the unreasonable connection of the discrete structure region and the continuum one, as the sudden onset of the continuum region inevitably leads to spurious peaks in the small-s region. The use of a larger discrete-structure region is, on the other hand, difficult practically because of the slow convergence of the real space expansion for small values of s. The small-s region, however, contains information on the long-range structure of liquids. Thus it is important to investigate the scattering intensities in this region more carefully.

In the case of the real space expansion of the bcc model for liquid carbon tetrachloride,[5] the ghost peak and valley appearing at 0.5 and 0.8 Å^{-1} respectively are distinguishable from the inherent peaks beyond $s\simeq$1.3 Å^{-1} (see Fig. 2(a)). However, in some simulation studies of the structure of liquids, ghost peaks may be misunderstood as inherent peaks. Moreover, due to the ghost peaks, the usefulness of the local lattice structure model itself has often been devaluated.[7,8]

To overcome the difficulty in the real space expansion, a method called "reciprocal space expansion" was applied to liquid carbon tetrachloride; the results were reported in a previous letter by the present authors.[6] The details are described in the present paper.

Formulation of the "Reciprocal Space Expansion"

The Poisson summation formula[10] states that, for the functions $\eta(\boldsymbol{k})$ and $\phi(\boldsymbol{r})$, that are mutually related by a Fourier transform, we have

$$\sum_{\mu}\phi(\boldsymbol{a}_{\mu})=\frac{1}{v}\sum_{\nu}\eta(\boldsymbol{b}_{\nu}), \tag{1}$$

where $\boldsymbol{a}_{\mu}$ is the lattice-point vector in real space, $\boldsymbol{b}_{\nu}$ is that in the corresponding reciprocal space, and v is the volume of the unit cell in the real space. The notations μ and ν are the representations of a set of three indices.

The total coherent scattering intensity per molecule, as formulated by the real space expansion, is given by,[5]

$$I=\sum_{i}\sum_{j}f_{i}f_{j}\frac{\sin(sr_{ij})}{sr_{ij}}\exp(-l_{ij}^{2}s^{2}/2), \tag{2}$$

where f_i is the atomic scattering factor of the i-th atom and l_{ij} is the root mean-square deviation of the mean interatomic distance, r_{ij}. The summation for j is over all atoms of the sample, while that for i is over the atoms of the central molecule. By employing the Prins relation, $l_{ij}^2=2Dr_{ij}$,[11] Eq. 2 becomes

$$I=\sum_{\alpha,\alpha'}\sum_{\mu}f_{\alpha}f_{\alpha'}\frac{\sin(s|\boldsymbol{a}_{\mu}+\boldsymbol{a}_{\alpha\alpha'}|)}{s|\boldsymbol{a}_{\mu}+\boldsymbol{a}_{\alpha\alpha'}|}\exp(-Ds^{2}|\boldsymbol{a}_{\mu}+\boldsymbol{a}_{\alpha\alpha'}|), \tag{3}$$

where $\boldsymbol{a}_{\mu}$ is the lattice-point vector and $\boldsymbol{a}_{\alpha,\alpha'}$ is the vector which connects α and α'-th atoms in a unit cell (see Fig. 1). Let us define $\phi(\boldsymbol{r})$ by means of the following relation:

$$\phi(\boldsymbol{r})=\exp(-Ds^{2}|\boldsymbol{r}+\boldsymbol{a}_{\alpha\alpha'}|)\frac{\sin(s|\boldsymbol{r}+\boldsymbol{a}_{\alpha\alpha'}|)}{s|\boldsymbol{r}+\boldsymbol{a}_{\alpha\alpha'}|}. \tag{4}$$

By the Fourier transform of the $\phi(\boldsymbol{r})$, $\eta(\boldsymbol{k})$ is given as follows, where $(\boldsymbol{r}+\boldsymbol{a}_{\alpha,\alpha'})$ is replaced by $\boldsymbol{r}'$,

$$\eta(\boldsymbol{k}) = \int \exp(-Ds^2r')\frac{\sin(sr')}{sr'}\exp(i\boldsymbol{k}\cdot\boldsymbol{r})d\boldsymbol{r}$$
$$= \int \exp(-Ds^2r')\frac{\sin(sr')}{sr'}\exp(i\boldsymbol{k}\cdot\boldsymbol{r}')\times\exp(-i\boldsymbol{k}\cdot\boldsymbol{a}_{\alpha\alpha'})d\boldsymbol{r}'$$
$$= \frac{2\pi Ds}{k}\left[\frac{1}{(Ds^2)^2+(s-k)^2}-\frac{1}{(Ds^2)^2+(s+k)^2}\right]\times\exp(-i\boldsymbol{k}\cdot\boldsymbol{a}_{\alpha\alpha'}), \quad (5)$$

k being the absolute value of $\boldsymbol{k}$. Accordingly, by the use of the Poisson sum formula given by Eq. 1,

$$I = \sum_{\alpha,\alpha'}\sum_{\nu}{}' f_\alpha f_{\alpha'}\exp(-i\boldsymbol{b}_\nu\cdot\boldsymbol{a}_{\alpha\alpha'})\times\frac{2\pi Ds}{vb_\nu}\left[\frac{1}{(Ds^2)^2+(s-b_\nu)^2}-\frac{1}{(Ds^2)^2+(s+b_\nu)^2}\right], \quad (6)$$

is derived. The prime over the summation sign denotes omission of the $\boldsymbol{\nu}$=(0 0 0) term[9].

Next, let us examine the term $\sum_{\alpha,\alpha'} f_\alpha f_{\alpha'}\exp(-i\boldsymbol{b}_\nu\cdot\boldsymbol{a}_{\alpha\alpha'})$ for the bcc model of carbon tetrachloride. The atoms numbered from 1 to 5 are included in the stoichiometric unit (a molecule) placed at the origin (see Fig. 1). Therefore, the summation for α is over the atoms numbered from 1 to 5, while the summation for α′ is over the atoms numbered from 1 to 10. Let $\boldsymbol{R}$ be the vector which connects the center of the molecule at the origin with that of the nearest neighboring molecule, which in this case is given by

$$\boldsymbol{R} = \left(\frac{a}{2},\frac{a}{2},\frac{a}{2}\right) \quad (7)$$

where a is the lattice constant of the bcc unit cell. Then, we obtain the following relation,

$$\sum_{\alpha=1}^{5}\sum_{\alpha'=1}^{10} f_\alpha f_{\alpha'}\exp(-i\boldsymbol{b}_\nu\cdot\boldsymbol{a}_{\alpha\alpha'}) = \sum_{\alpha=1}^{5}\sum_{\alpha''=1}^{5} f_\alpha f_{\alpha''}\exp(-i\boldsymbol{b}_\nu\cdot\boldsymbol{a}_{\alpha\alpha''})[1+\exp(-i\boldsymbol{b}_\nu\cdot\boldsymbol{R})], \quad (8)$$

where the first term in parentheses corresponds to the correlation among the atoms in the central molecule (1—5) and where the second term is that between the two molecules in a unit cell (1—5 and 6—10 in Fig. 1). With a little manipulation of Eq. 8, we have

$$\sum_{\alpha,\alpha'} f_\alpha f_{\alpha'}\exp(-i\boldsymbol{b}_\nu\cdot\boldsymbol{a}_{\alpha\alpha'}) = [f_C^2+4f_{Cl}^2+\sum_{i=2}^{5}2f_Cf_{Cl}\cos(\boldsymbol{b}_\nu\cdot\boldsymbol{a}_{C\text{-}Cl(i)}) + \sum_{\substack{j,k=2\\ j>k}}^{5}2f_{Cl}^2\cos(\boldsymbol{b}_\nu\cdot\boldsymbol{a}_{Cl(j)\text{-}Cl(k)})]\times[1+\exp(-i\boldsymbol{b}_\nu\cdot\boldsymbol{R})]. \quad (9)$$

Finally, we must consider the correction for the term of $\boldsymbol{a}_\mu=\boldsymbol{0}$. In Eqs. 3 and 6, the mean-square deviations of the intermolecular distances are also given by the Prins relation. It is necessary to replace them by the intramolecular mean-square amplitudes, which are known more exactly. Then, the correction term, ΔI_{intra}, becomes

$$\Delta I_{intra} = 8f_Cf_{Cl}[\exp(-l_{C\text{-}Cl}^2s^2/2)-\exp(-Dr_{C\text{-}Cl}s^2)]\frac{\sin(sr_{C\text{-}Cl})}{sr_{C\text{-}Cl}} + 12f_{Cl}^2[\exp(-l_{Cl\text{-}Cl}^2s^2/2)-\exp(-Dr_{Cl\text{-}Cl}s^2)]\frac{\sin(sr_{Cl\text{-}Cl})}{sr_{Cl\text{-}Cl}}, \quad (10)$$

where $l_{C\text{-}Cl}$ and $l_{Cl\text{-}Cl}$ are the root mean-square amplitudes for the distances $r_{C\text{-}Cl}$ and $r_{Cl\text{-}Cl}$, respectively.

From Eqs. 6, 9, and 10, the total coherent intensity of the bcc model for carbon tetrachloride is given by

$$I = \frac{1}{v}\sum_{\nu}{}'\frac{2\pi Ds}{b_\nu}\left[\frac{1}{(Ds^2)^2+(s-b_\nu)^2}-\frac{1}{(Ds^2)^2+(s+b_\nu)^2}\right]\times[f_C^2+4f_{Cl}^2+\sum_{j=2}^{5}2f_Cf_{Cl}\cos(\boldsymbol{b}_\nu\cdot\boldsymbol{a}_{C\text{-}Cl(j)}) + \sum_{\substack{j,k=2\\ j>k}}^{5}2f_{Cl}^2\cos(\boldsymbol{b}_\nu\cdot\boldsymbol{a}_{Cl(j)\text{-}Cl(k)})][1+\exp(-i\boldsymbol{b}_\nu\cdot\boldsymbol{R})] + \Delta I_{intra}. \quad (11)$$

For $\boldsymbol{b}_\nu$ expressed by $\left(\frac{2\pi h}{a},\frac{2\pi k}{a},\frac{2\pi l}{a}\right)$, the value in parentheses $[1+\exp(-i\boldsymbol{b}_\nu\cdot\boldsymbol{R})]$ is equal to 2 when $h+k+l$ is even and zero when $h+k+l$ is odd. This corresponds to the extinction rule of the bcc lattice.

In practical calculation the following values were used; the intramolecular parameters, $r_{C\text{-}Cl}$, $r_{Cl\text{-}Cl}$, $l_{C\text{-}Cl}$, and $l_{Cl\text{-}Cl}$, were the values obtained by means of gas electron diffraction,[12] the lattice constant of the bcc unit cell was 6.81,[5] and D was 0.036 Å.[5] (Note that the definition of D in Ref. 5 is that of $2D$ of the present paper.)

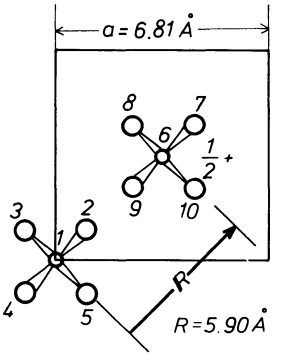

Fig. 1. The arrangement of carbon tetrachloride molecules in a bcc unit cell.

Results and Discussion

The results of the application to carbon tetra-

chloride based on the bcc local lattice structure are shown in Fig. 2(b). For comparison, the results of the "real space expansion" are shown in Fig. 2(a).[5] The total coherent intensity is adopted, because it distinguishes the discrepancy between the experimental and the simulated intensities in the small-s region. The dots represent the experimental intensities,[13] while the monotonically decreasing broken curves are the calculated self-scattering

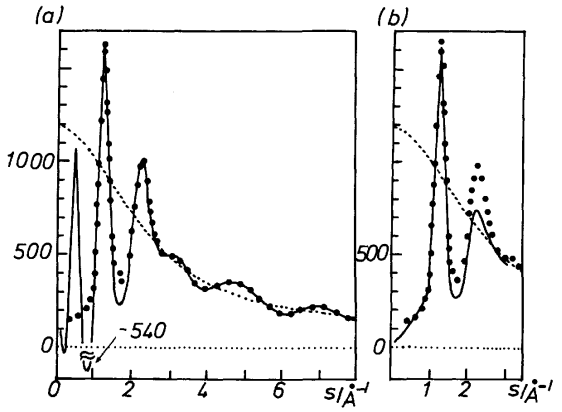

Fig. 2. Total coherent intensity (in electron unit) of liquid carbon tetrachloride. The curves described by dots are experimental intensity.[13]
(a): The solid curve is the calculated intensity based on the bcc model by the use of the "real space expansion."
(b): The solid curve is the calculated intensity based on the bcc model by the use of the "reciprocal space expansion."

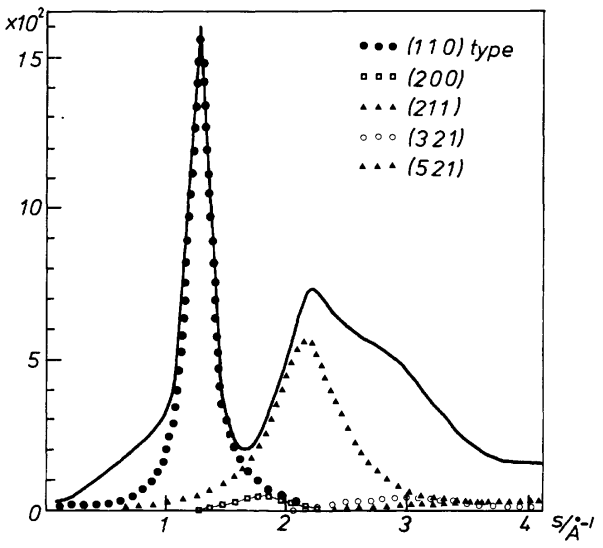

Fig. 3. contribution of each reciprocal lattice point. The solid curve is the calculated total coherent intensity. The Lorentzian-like curves are contributions from {1 1 0}, {2 0 0}, {2 1 1}, {3 2 1}, and {5 2 1} lattice points, respectively. The difference between the solid curve and the sum of the contributions from the reciprocal lattice points is the contribution of ΔI_{Intra}.

intensities. The solid curve in Fig. 2(a) is the calculated intensity based on the bcc model.[5] The agreement is very good up to $s \simeq 20$ Å^{-1}, although not shown in this figure. The intensity in the small-s region ($s < 1.2$ Å^{-1}), however, shows discrepancies, which are due to the inherent ghost peaks of the "real space expansion."

The solid curve in Fig. 2(b) is the intensity calculated by the use of the "reciprocal space expansion" based on the bcc model. In this calculation reciprocal lattice points up to $\nu=(6\ 0\ 0)$ ($b_\nu = 5.54$ Å^{-1}) are included. The calculated curve is in very good agreement with the experimental intensity in the region of s less than 1.5 Å^{-1}. However, the convergence becomes worse with the increase in the scattering parameter, s, contrary to the case with the "real space expansion."

Figure 3 shows the contribution of each reciprocal lattice point to the calculated total coherent intensity (solid curve). The Lorentzian-like curve with the peak at $s \simeq 1.3$ Å^{-1} is the contribution from the {1 1 0} reflections, which contain 12 equivalent reflections with the magnitude of b_ν 1.305 Å^{-1}. The next peak is due to the {2 0 0} reciprocal points, whose contribution is relatively small in this bcc structure. It should be noticed that the main feature of the total coherent intensity is almost entirely determined by the {1 1 0} and the {2 1 1} reflections; that is, the former form the first peak at $s = 1.3$ Å^{-1}, while the latter form the second peak at $s = 2.3$ Å^{-1}. The difference between the solid curve and the sum of the contributions from the reciprocal lattice points in the range of $s < 1$ Å^{-1} and $s > 2$ Å^{-1} is the contribution of ΔI_{intra} (see Eq. 11). As the magnitude of b_ν increases, the widths of the Lorentzian-like curves rapidly become wider. This corresponds to the fact that the convergence becomes worse with the increase in the scattering parameter, s. By the reciprocal space expansion, the intensities for s values ranging up to about 2 Å^{-1} can be well simulated. For some molecular liquids, the scattering intensity near $s \approx 0$ Å^{-1} has a finite value. This is caused by the density fluctuation of the liquids.[14] This fluctuation was not included in the present formulation by the local lattice structure model. Thus, the calculated intensity is not necessarily in agreement with the experimental values at $s \approx 0$ Å^{-1} for a liquid with large density fluctuations.[15]

With the use of both the "reciprocal space expansion" and the "real space expansion", the observed scattering intensity of liquid carbon tetrachloride is satisfactorily accounted for over the whole range of the parameter s on the basis of the bcc local lattice model.

In simulation studies for the diffaction intensity of liquids, there have been many cases where the calculated intensities can not simulate the observed

intensities. In these cases, there are two possibilities; one is that the structure model itself is not adequate, and the other is that the ghost peaks because of the inevitable result of the "real space expansion" are disturbing the inherent peaks. In this paper, the problem of the ghost peaks of the "real space expansion," which appears in the small-s region is solved by the introduction of the "reciprocal space expansion." By the use of both expansions, the application of the "local lattice structure model" becomes more promising in the study of the structure of liquids.

References

1) A. H. Narten, M. D. Danford, and H. A. Levy, *Discuss. Faraday Soc.*, **43**, 97 (1967).
2) A. H. Narten and H. A. Levy, *Science*, **165**, 447 (1969).
3) P. Debye and H. Menke, *Phys. Z.*, **31**, 797 (1930).
4) B. E. Warren, *Phys. Rev.*, **45**, 657 (1934).
5) K. Nishikawa and T. Iijima, *Bull. Chem. Soc. Jpn.*, **58**, 1215 (1985).
6) K. Nishikawa and Y. Murata, *Bull. Chem. Soc. Jpn.*, **51**, 441 (1978).
7) J. G. Powles, *Adv. Phys.*, **22**, 1 (1973).
8) N. Ohtomo and K. Arakawa, *Bull. Chem. Soc. Jpn.*, **51**, 1649 (1978).
9) T. Iijima and K. Nishikawa, *Chem. Phys. Lett.*, **115**, 522 (1985).
10) P. M. Morse and H. Feshbach, "Methods of Theoretical Physics," McGraw-Hill, New York (1953), p. 466.
11) J. Frenkel, "Kinetic Theory of Liquids," Dover Publications, New York (1955).
12) Y. Morino, Y. Nakamura, and T. Iijima, *J. Chem. Phys.*, **32**, 643 (1960).
13) K. Nishikawa and T. Iijima, *Bull. Chem. Soc. Jpn.*, **57**, 1750 (1984).
14) C. Croxton, "Introduction to Liquid State Physics," John Wiley & Sons, London (1975).
15) K. Nishikawa, *Bull. Chem. Soc. Jpn.*, to be published.

 © 1986 The Chemical Society of Japan Bull. Chem. Soc. Jpn., 59, 121—125 (1986)

Crystal and Molecular Structure of 3-Pyrazolone Derivatives. III.[1] 5-Amino-2-phenyl-4-(9*H*-thioxanthen-9-yl)-1,2-dihydro-3*H*-pyrazol-3-one

Michio KIMURA
Niigata College of Pharmacy, 5829 Kamishin'ei-cho, Niigata 950-21
(Received June 20, 1985)

The crystal and molecular structure of 5-amino-2-phenyl-4-(9*H*-thioxanthen-9-yl)-1,2-dihydro-3*H*-pyrazol-3-one has been determined by the X-ray diffraction method to establish the predominant tautomeric form of the 3-pyrazolone ring in the solid state. The title compound, $C_{22}H_{17}N_3OS$, crystallizes in the space group $P2_1/c$ with lattice parameters: a=18.179(4), b=8.333(1), c=11.961(7) Å, β=95.88(3)°, and Z=4. The 5-amino group is intramolecularly hydrogen-bonded to the sulfur atom of the thioxanthene ring (N-H···S=3.284 Å). In the packing structure, molecules are linked to each other through hydrogen bonds between the NH of amino and C=O groups [2.849 Å] and the NH moiety and C=O group [2.939 Å] of the 3-pyrazolone ring.

3-Pyrazolone derivatives have important uses in medicine as analgesics and antipyretics and in color photography as magenta dye-formers.[2] The tautomerism in 2,5-disubstituted 3-pyrazolone[3–6] has been the subject of much work since Konn's synthesis[7] appeared as the first example of this class. In the course of studying the reactivity of 5-methyl- and 5-amino-2-phenyl-1,2-dihydro-3*H*-pyrazol-3-one, which has three possible tautomeric forms (designated as the NH-, OH-, and CH-forms (**1a,b**, **2a,b**, and **3a,b** in Scheme 1)), according to the position of the labile proton), it has been reported that these 3-pyrazolone derivatives undergo dehydration at the 4-position of the active methylene of the 3-pyrazolone ring with the OH group of 9*H*-xanthen-9-ol or 9*H*-thioxanthen-9-ol to form the condensed products (**4a,b**).[8] Generally, 3-pyrazolone derivatives[3,5] exist predominantly as the CH-form in nonpolar solvents, while the other tautomers, the OH- and NH-form, are formed as the polar character of the solvent is increased. On the other hand, in the crystalline state, additional tautomeric forms are expected to emerge due to the strong hydrogen bonding or other intermolecular forces. X-ray diffraction studies have elucidated that the preferred tautomeric form in the solid state of 5-methyl-2-phenyl-1,2-dihydro-3*H*-pyrazol-3-one is a 1:1 mixture of the NH- and OH-form(**1a** and **2a**),[9] its condensed product 5-methyl-2-phenyl-4-(9*H*-thioxanthen-9-yl)-1,2-dihydro-3*H*-pyrazol-3-one (**4a**),[8] the NH-form, and 5-amino-2-phenyl-1,2-dihydro-3*H*-pyrazol-3-one, the CH-form (**3b**).[1]

The purpose of the present work is to establish the three-dimensional structure and the preferred tautomeric form of 5-amino-2-phenyl-4-(9*H*-thioxanthen-9-yl)-1,2-dihydro-3*H*-pyrazol-3-one in the crystal, and to compare them with those of 5-amino-2-phenyl-2,4-dihydro-3*H*-pyrazol-3-one(**3b**) In the packing structure of **3b**, the molecules are linked to each other by two kinds of hydrogen bonds between the NH_2 and CO groups (2.995 and 3.170 Å) to form a two-dimensional hydrogen bond network parallel to the ac-plane, while the different hydrogen bonds could be expected from the NH_2 and CO groups of the title compound (**4b**). One of the main goals of this work was to examine the possibility of the presence of strong intramolecular hydrogen bonds between the NH_2 group and other intramolecular hydrogen bond acceptors in **4b**, because there are three hydrogen bond donors (NH_2 and NH of the 3-pyrazolone ring) in contrast to one acceptor of the C=O group requiring two hydrogen donors.

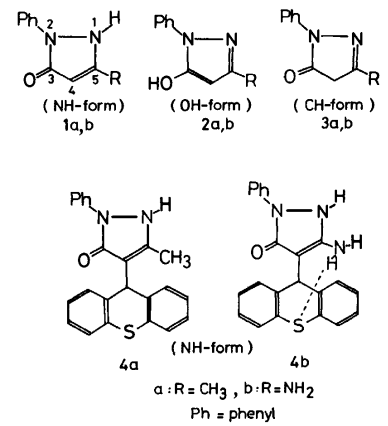

Scheme 1.

Experimental

The title compound (**4b**) was prepared by the method described previously,[8] and it was recrystallized by the slow evaporation of an EtOH-CH_3Cl solution at room temperature. The crystal used for the X-ray measurement was a cleaved piece with approximate dimensions of 0.20×0.25×0.30 mm. A preliminary examination of the crystal, carried out on a Rigaku automated, four-circle diffractometer, showed it to be monoclinic with the space group $P2_1/c$. The unit cell parameters at room temperature were refined by the least-squares fit using the Bragg angles of 24 reflections ($30° < 2\theta < 40°$).

Crystal Data: $C_{22}H_{17}N_3OS$, M 371.45, monoclinic, space group $P2_1/c$, a=18.179(4), b=8.333(1), c=11.961(7) Å, β=95.88(3)°, V=1802.3 Å^3, D_c=1.37 g cm^{-3} for Z=4, μ=16.8 cm^{-1}.

The intensity data were collected at room temperature on a diffractometer utilizing nickel-filtered Cu $K\alpha$ radiation (λ=1.54178 Å). The θ—2θ scan mode was employed. The scan rate was 6° min^{-1} in 2θ, and the scan range in θ was varied by 1.2°+0.15° tanθ. Backgrounds were counted for 5 s at both ends of the scan with an offset of 50% of the scan range from the calculated position of the $K\alpha$ peak. The intensities of the three standard reflections measured after every 57 reflections, showed a drop of 1% over the period of data collection, but no correction was made. A total of 2634 unique reflections was measured (2θ<125°), of which 2342 were observed. The standard deviations in the structure amplitudes, $\sigma(F_o)$, were derived from the counting statistics. Lorentz and polarization corrections were applied, but no absorption correction was made.

Solution and Refinement of the Structure

The structure was solved by the direct method (MULTAN),[10] determining the phases of the 200 reflections with $|E_o|$>1.84. The E-map computed from the phases with the largest combined figure of merit (2.65) revealed all the non-hydrogen atoms. The structure was refined by the block-diagonal least-squares method. The function minimized was $\sum w(|F_o|-|F_c|)^2$, where w=1 for 0<$|F_o|\leq$20 and $w=(20/|F_o|)^{-2}$ for $|F_o|$>20. An initial refinement using individual isotropic temperature factors for the non-hydrogen atoms led to a conventional $R=(\sum||F_o|-|F_c||)/\sum|F_o|$ of 0.117. After successive refinement with anisotropic temperature factors for the non-hydrogen atoms, all the hydrogen atoms were readily located in the difference Fourier map; these atoms were then included in the further refinement with isotropic temperature factors. The efinement was completed after 6 cycles. The final values of R and $R_w=(\sum w|F_o|-|F_c|)^2/\sum w|F_o|^2)^{1/2}$ were 0.048 and 0.050 respectively. At the final cycle, the largest shift of any parameters of the non-hydrogen atoms was less than 10% of the standard deviations, while that of the hydrogen atoms was 13%. The largest peak in the final difference map, 0.2e Å^{-3}, was located near the sulfur atoms. The final atomic positional and thermal parameters* are given in Table 1. The atomic scattering factors for the S, O, and C atoms were taken from "International Tables for X-Ray Crystallography," (1974)[11a] while the factors for H were those of Stewart, Davidson and Simpson.[12] Computations were performed using the crystallographic program system *UNICS*.[13]

Table 1. Final Atomic Parameters of Non-Hydrogen Atoms, with Estimated Standard Deviations in Parentheses

$$B_{eq}=\frac{1}{3}(U_{11}+U_{22}+U_{33})$$

Atoms	x	y	z	B_{eq}/Å^2
N 1	0.1360(2)	−0.1918(4)	0.5894(3)	4.3
N 2	0.1238(2)	−0.2372(4)	0.4751(3)	3.8
C 3	0.1747(2)	−0.1568(4)	0.4161(3)	3.4
C 4	0.2251(2)	−0.0761(4)	0.4960(3)	3.2
C 5	0.2017(2)	−0.1070(5)	0.5995(3)	3.8
O 6	0.1731(2)	−0.1624(3)	0.3117(2)	4.2
N 7	0.2304(2)	−0.0660(5)	0.7047(3)	6.0
C 8	0.2915(2)	0.0146(4)	0.4618(3)	3.3
C 9	0.3628(2)	−0.0811(4)	0.4857(3)	3.5
C10	0.3812(2)	−0.1957(5)	0.4078(3)	4.5
C11	0.4441(3)	−0.2905(5)	0.4286(4)	5.5
C12	0.4901(2)	−0.2714(5)	0.5271(4)	5.6
C13	0.4738(2)	−0.1568(5)	0.6047(3)	4.9
C14	0.4109(2)	−0.0615(4)	0.5834(3)	3.8
S 15	0.3957(1)	0.0841(2)	0.6860(1)	4.2
C16	0.3410(2)	0.2258(4)	0.6065(3)	3.7
C17	0.3424(3)	0.3824(5)	0.6480(3)	5.0
C18	0.3010(3)	0.5002(5)	0.5904(4)	6.4
C19	0.2593(3)	0.4621(5)	0.4903(4)	6.4
C20	0.2575(2)	0.3056(5)	0.4491(3)	4.9
C21	0.2977(2)	0.1838(4)	0.5076(3)	3.6
C22	0.0504(2)	−0.2805(4)	0.4321(3)	4.0
C23	−0.0094(2)	−0.2192(5)	0.4791(4)	6.0
C24	−0.0805(3)	−0.2615(6)	0.4334(5)	8.1
C25	−0.0901(3)	−0.3658(6)	0.3432(4)	7.5
C26	−0.0300(3)	−0.4277(7)	0.2985(4)	7.3
C27	0.0410(2)	−0.3866(5)	0.3430(3)	5.6

* Tables of the anisotropic thermal parameters, the coordinates of the hydrogen atoms, the observed and calculated structure factors and the bond distances involving hydrogen atoms are deposited at the Chemical Society of Japan, Document No. 8606.

Results and Discussion

The molecular structure and the atom labeling of **4b** are presented by the *ORTEP*[20] drawing in Fig. 1. The bond distances and angles are given in Table 2. The present study has shown that the predominant tautomeric form of the title compound in the solid state adopts the NH-form (**4b**). The structure of the benzene rings in the peripheral of the 3-pyrazolone and in the thioxanthene rings has normal values [C–C$_{(av)}$=1.381 and 1.392 Å, and C–C–C$_{(av)}$=120.0°]. In Fig. 2, the geometry of the 3-pyrazolone ring observed in **4b** is compared with those of **1a, 2a, 3b,** and **4a**.[1,8,9] As may be seen in Fig. 2, the C–C and C–N bond distances in the 3-pyrazolone ring reflect

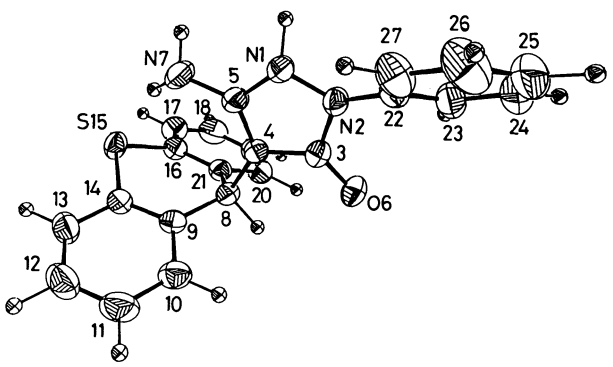

Fig. 1. Molecular structure (*ORTEP* drawing)[20] of the title compound (**4b**). Non-hydrogen atoms are drawn as thermal ellipsoids with 50 % probability level and hydrogen atoms as spheres of arbitrary radius.

Table 2. Bond Distances (l/Å) and Angles (ϕ/°) in **4b**, with Estimated Standard Deviations in Parentheses

(a)	Bond lengths for non-hydrogen atoms				
	N 1–N 2	1.414(4)	N 1–C 6	1.382(4)	N 2–C 3	1.392(4)
	N 2–C22	1.426(4)	C 3–O 6	1.247(4)	C 3–C 4	1.424(4)
	C 4–C 5	1.375(4)	C 4–C 8	1.517(4)	C 5–N 7	1.356(4)
	C 8–C 9	1.523(4)	C 8–C21	1.513(4)	C 9–C10	1.399(5)
	C 9–C14	1.396(4)	C10–C11	1.391(5)	C11–C12	1.384(5)
	C12–C13	1.385(5)	C13–C14	1.396(5)	C14–S15	1.767(3)
	S15–C16	1.759(3)	C16–C17	1.396(5)	C16–C21	1.397(4)
	C17–C18	1.378(5)	C18–C19	1.387(6)	C19–C20	1.394(5)
	C20–C21	1.397(5)	C22–C23	1.374(5)	C22–C27	1.382(5)
	C23–C24	1.395(5)	C24–C25	1.382(7)	C25–C26	1.365(6)
	C26–C27	1.389(6)				
(b)	Bond angles					
	C 5–N 1–N 2	105.7(2)	C22–N 2–C 3	125.8(3)		
	C22–N 2–N 1	117.7(2)	C 3–N 2–N 1	108.4(2)		
	C 4–C 3–O 6	129.6(3)	C 4–C 3–N 2	107.6(2)		
	O 6–C 3–N 2	122.8(3)	C 8–C 4–C 5	131.7(3)		
	C 8–C 4–C 3	122.0(2)	C 5–C 4–C 3	106.2(3)		
	N 7–C 5–C 4	131.6(3)	N 7–C 5–N 1	117.2(3)		
	C 4–C 5–N 1	111.2(3)	C21–C 8–C 9	112.9(2)		
	C21–C 8–C 4	113.4(2)	C 9–C 8–C 4	112.0(2)		
	C14–C 9–C10	117.8(3)	C14–C 9–C 8	122.9(3)		
	C10–C 9–C 8	119.3(3)	C11–C10–C 9	121.1(3)		
	C12–C11–C10	120.2(3)	C13–C12–C11	119.8(3)		
	C14–C13–C12	119.9(3)	S15–C14–C13	116.6(2)		
	S15–C14–C 9	122.2(2)	C13–C14–C 9	121.2(3)		
	C16–S15–C14	101.9(1)	C21–C16–C17	121.6(3)		
	C21–C16–S15	121.9(2)	C17–C16–S15	116.5(2)		
	C18–C17–C16	119.9(3)	C19–C18–C17	119.4(4)		
	C20–C19–C18	120.7(4)	C21–C20–C19	120.7(3)		
	C20–C21–C16	117.6(3)	C20–C21–C 8	118.7(3)		
	C16–C21–C 8	123.7(3)	C27–C22–C23	120.8(3)		
	C27–C22–N 2	118.6(3)	C23–C22–N 2	120.6(3)		
	C24–C23–C22	119.1(4)	C25–C24–C23	120.2(4)		
	C26–C25–C24	120.1(4)	C27–C26–C25	120.3(4)		
	C26–C27–C22	119.5(3)				

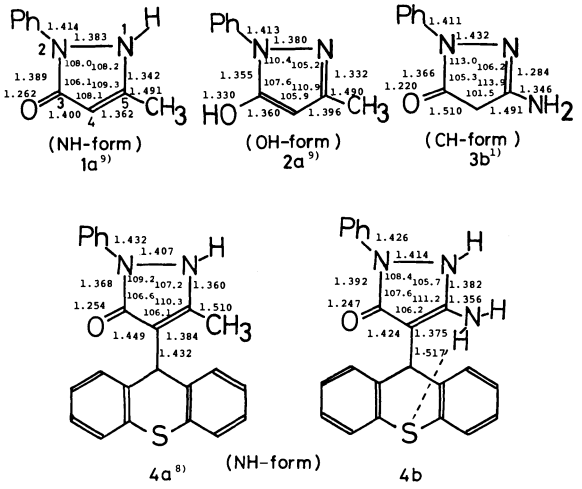

Fig. 2. The selected bond distances and angles of the 3-pyrazolone ring of **1a**, **2a**, **3b**, and **4a,b**. The stadard deviations are described in Table 2.

their predominant tautomeric forms, which are slightly shorter or longer than the normal value (1.44—1.53 and 1.35—1.36 Å respectively).[11b] The N1–C5, C4–C5, and C3–C4 bond distances are significantly different from each other in the NH-, OH-, and CH-forms (**1a**, **4a,b**, **2a**, and **3b**), showing the differences in the degree of the delocalization of the π electrons in the 3-pyrazolone ring. The C4–C5 bond distances are shorter in the NH-form (1.362, 1.384(6), and 1.375(4) Å for **1a**, **4a**, and **4b** respectively) than in the OH-form (1.396 Å for **2a**) and the CH-form (1.491(5) Å for **3b**), indicating the double-bond character of the C4–C5 in the NH-form. On the other hand, the short C3–C4 distances in the NH-form (1.400, 1.449(6), and 1.424(4) Å for **1a**, **4a**, and **4b** respectively), compared with the value of the single bond (1.510(5) Å) in the CH-form, appears to be caused by the conjugation with the C4–C5 double bond. The N1–C5 bond distances in the OH- and

CH-forms (1.332 and 1.284(5) Å for **2a**, and **3b** respectively) are shorter than the corresponding values of the NH-form (1.342, 1.360(6), and 1.382(4) Å for **1a**, **4a**, and **4b** respectively), reflecting their double-bond character. The N1–N2, N2–C3 (in the NH- and CH-form), and C3–OH bonds (in the OH-form) have typical single bond distances in the ranges of 1.383(5)—1.432(5), 1.355(5)—1.392(4), and 1.330(5) Å respectively. The C=O distances in the NH-form (**1a** and **4a,b**), 1.262, 1.254(6), and 1.247(4) Å respectively, are slightly longer than that (1.220(5) Å) in the CH-form(**3b**). These facts show the electron delocalization of the (O=C–C=C–) conjugation system in the NH-form.

Regarding the hydrogen bond, 5-methyl-2-phenyl-1,2-dihydro-3*H*-pyrazol-3-one exists in two crystallographycally independent molecules in the crystal, one in the NH-form (**1a**) and the other in the OH-form (**2a**), which are characterized by the hydrogen bonds of O–H···O (2.48 Å) and N–H···N (2.80 Å)[9] respectively. The **4a** molecules are packed with hydrogen bonds between the NH and CO groups (2.799(6) Å) to form endless chains along the c-axis in the crystal.[8] In the case of 5-amino-2-phenyl-2,4-dihydro-3*H*-pyrazol-3-one (**3b**), however, the molecules are linked together by two kinds of hydrogen bonds between the NH_2 and CO groups (2.955(5) and 3.170(5) Å) to form a network of hydrogen bonds parallel to the ac-plane.[1] It is shown that one NH of the amino group in **4b** is intramolecularly hydrogen bonded to the sulfur atom of thioxanthene (N–H···S= 3.284(3) Å). Another NH of the amino group forms an intermolecular hydrogen bond with the CO group of the neighbouring molecule (2.849(4) Å), which is also linked to the NH group of the 3-pyrazolone ring (2.939(3) Å) to form a sheet parallel to the ac-plane, as is shown in Fig. 3.

Scheme 2 shows the four chemical species (three neutral tautomers-**1a,b**, **2a,b**, and **3a,b**, and one cation-**5a,b**) in the equilibrium state in an acid solution. The structure of the 5-substituted 3-pyrazolone corresponding to **5a,b** has been established by IR, UV, and NMR spectroscopy,[14] which has shown that all three tautomeric form (OH-, NH-, and CH-forms) possess a common cation (**5a,b**). The complete equations for these equilibria have been given by a simple equation, because the CH-form is much less basic than the OH- and NH-forms.[15] As the molecular structures of **1a**, **2a**, **3b**, and **4a,b** have been established by the X-ray diffraction method, a plausible mechanism by which the tautomers are trapped in the crystal is as follows. Each NH- or OH-form is trapped in crystals by shifting the equilibrium from the common cation (**5a,b**) by electron transfer, as is shown in Scheme 2. The thioxanthene-bearing forms (**4a,b**) exist as the NH-form is a result of the removal of a proton from the protonated carbonyl group, as is shown in Scheme 2. The CH-form of **4a,b** can not participate in hydrogen bondings in crystals like the **1a** and **2a** types because of the low basicity of the pyridine-like nitrogen atom in the 3-pyrazolone ring.

The best least-squares planes, together with the displacement of atoms from the best planes and the dihedral angles between these planes were calculated. It is well known that the dihedral angle (butterfly angle) of the related thioxanthene nucleus is quite sensitive to alterations in the electronegativity of its substituents,[16] as may be seen in the change in the dihedral angle on going from phenothiazine (158.5°) to thioxanthen-9-ol (132.4°). The value (148.6°) of **4b** is in good agreement with the 143.4° value of **4a**

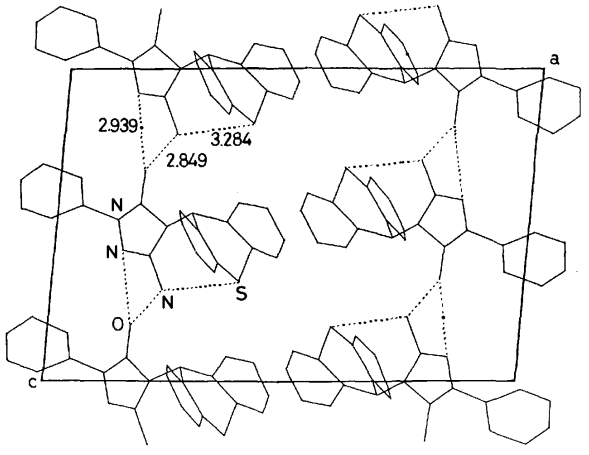

Fig. 3. Crystal structure projected along the b axis. Hydrogen bonds between molecules are shown by broken lines.

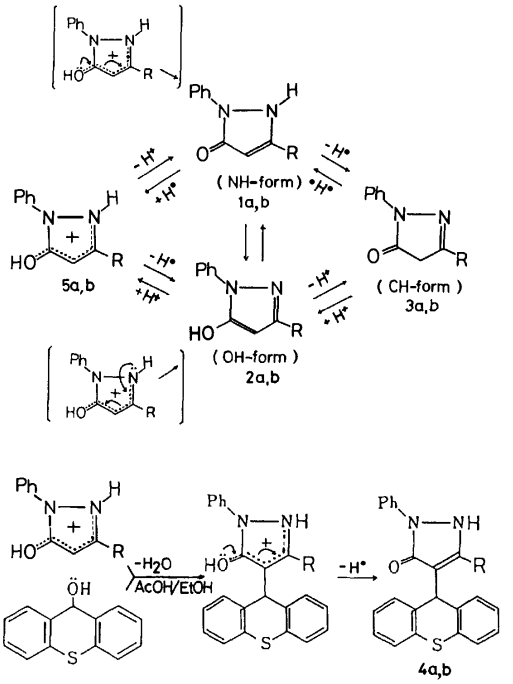

Scheme 2.

within the limits of experimental error. A final point of particular interest concernes the dihedral angles between the planes of 3-pyrazolone and phenyl rings; 47.0° for **4b**, which are to be compared with the values 47.8°, 23°, 38°, and 1.7° for **4a**, **1a**, **2a**, and **3b** respectively. These values show that the dihedral angles are different in spite of having the same tautomeric form, and that of the CH-form is significantly different. The conformation of the phenyl group in the present compounds may be mainly affected by the packing of molecules in the crystal.

The author is grateful to Professor Masao Kakudo, Professor Noritake Yasuoka, and the staff of the Crystallographic Research Center, Institute for Protein Research, Osaka University, for the use of the diffractometer and computing facilities. The author's thanks are also due to Professor Ichizo Okabayashi, Niigata College of Pharmacy, for his valuable discussions.

References

1) Part II: M. Kimura, I. Okabayashi, and N. Yasuoka, *Chem. Pharm. Bull.*, **32**, 318 (1984).

2) R. H. Wiley and P. Wiley, "Pyrazoles, Pyrazolines and Derivatives," Part 2, ed by A. Weissberger, John Wiley and Sons, New York (1964), Chapters 1 and 2.

3) G. A. Newman and P. J. S. Pauwels, *Tetrahedron*, **25**, 4605 (1969).

4) G. A. Newman and P. J. S. Pauwels, *Tetrahedron*, **26**, 1571 (1970).

5) A. R. Katritzky and F. W. Maine, *Tetrahedron*, **20**, 299 (1964).

6) A. R. Katritzky and F. W. Maine, *Tetrahedron*, **20**, 315 (1964).

7) A. Weissberger and D. Porter, *J. Am. Chem. Soc.*, **64**, 2133 (1942).

8) M. Kimura, I. Okabayashi, and N. Yasuoka, *Chem. Pharm. Bull.*, **31**, 3718, (1983).

9) F. Bechtel, J. Gaultier, and C. Hauw, *Cryst. Struct. Commun.*, **3**, 469 (1973).

10) G. Germain, P. Main, and M. M. Woolfson, *Acta Crystallogr., Sect. A*, **27**, 368 (1971).

11) a) "International Tables for X-Ray Crystallography," Kynoch Press, Birmingham, Vol. IV (1974), p. 71; b) ibid., Vol. III (1974), p. 275.

12) R. F. Stewart, E. R. Davidson, and W. T. Simpson, *J. Chem. Phys.*, **42**, 3175 (1965).

13) T. Ashida and N. Yasuoka, *UNICS-Osaka*, the Computation Center, Osaka Univ., 1979.

14) I. I. Grandberg, V. G. Vinokurov, V. S. Troitskaya, T. A. Ivanova, and V. A. Moskalenko, *Khim. Geterotsikl. Soedin.*, **1970**, 202.

15) J. Elguero, R. Jacquier, and G. Tarrago, *Bull. Soc. Chim. Fr.*, **1967**, 3780.

16) G. E. Martin, J. D. Korp, J. C. Turley, and L. Bernal, *J. Heterocycl. Chem.*, **15**, 721 (1978).

17) J. D. Bell, J. F. Blount, O. V. Briscoe, and H. C. Freeman, *J. Chem. Soc., Chem. Commun.*, **1968**, 1656. (monoclinic form); J. J. H. McDowell, *Acta Crystallogr., Sect. B*, **32**, 5 (1976); B. W. van de Waal and D. Feil, ibid., **33**, 314 (1977) (orthorhombic form).

18) S. Hosoya, *Acta Crystallogr., Sect. B*, **20**, 429 (1966).

19) A. L. Ternay, D. W. Chasar, and M. Sax, *J. Org. Chem.*, **32**, 2465 (1967).

20) C. K. Johnson, *ORTEP* II, Report ORNL-5138, Oak Ridge National Laboratory, Tennessee (1976).

 © 1986 The Chemical Society of Japan Bull. Chem. Soc. Jpn., 59, 127—132 (1986)

Crystal Structure and Physical Properties of (TTM-TTF)$I_{2.47}$

Peiji Wu,† Takehiko Mori,* Toshiaki Enoki, Kenichi Imaeda,
Gunzi Saito,†† and Hiroo Inokuchi
Institute for Molecular Science, Okazaki 444
†† Institute for Solid State Physics, The University of Tokyo, Roppongi, Tokyo 106
(Received June 28, 1985)

The X-ray crystal structure analysis of a novel organic conductor (TTM-TTF)$I_{2.47}$ (TTM-TTF: tetrakis-(methylthio)tetrathiafulvalene) shows that the donors with an almost flat structure are stacked face-to-face to form columns. The iodine lattice composed of I_3^- columns is incommensurate with the donor lattice. The measurements of resistivity, thermoelectric power, and ESR show a metal-insulator transition around 100 K. This transition is attributed to the Peierls type phase transition. The quasi-one-dimensional electronic structure is supported by the arrangement of the donor molecules in the crystal and the calculated anisotropy of transfer integrals.

It has been demonstrated that in organic conductors an enhancement in the dimensionality is required to stabilize the metallic states and to design organic superconductors. Among the organic conductors including BEDT-TTF (bis(ethylenedithio)tetrathiafulvalene), two-dimensional conductors which are metallic down to liquid helium temperature and even superconductors have been discovered.[1-3] The investigations of the crystal structures and electronic structures have indicated that the side-by-side intermolecular interaction of these BEDT-TTF compounds is comparable to a face-to-face interaction.[4-6] This characteristic property is considered to come from the four outer sulfur atoms attached to the tetrathiafulvalene(TTF) skeleton. For the purpose of developing organic donors directed toward organic superconductors, it is important to investigate the influence of the outer alkyl groups in other alkylthio-substituted TTF's on the dimensionality of the electronic systems.

As a part of the investigation of uncapped tetrakis(alkylthio)-substituted TTF (TTC_n-TTF) (Scheme), where "uncapped" means that each outer ethylene group of BEDT-TTF is replaced by two separated alkyl groups, we have prepared a variety of charge-transfer complexes including tetrakis(methylthio)tetrathiafulvalene (TTC_1-TTF=TTM-TTF).[7,8] Among them the iodine complex (TTM-TTF)I_x showed the highest conductivity. In the present report, we deal with the crystal structure, electric conductivity, thermoelectric power, ESR spectra, and electronic structure of this iodine complex.

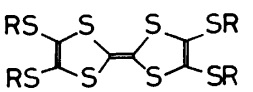

TTC_n-TTF R=C_nH_{2n+1}
TTM-TTF R=CH_3

Scheme.

† On leave from the Institute of Chemistry, Academia Sinica, Beijing, China.

Experimental

The iodine complex was prepared by the following three methods; (1) electrocrystallization of the donor with tetrabutylammonium triiodide as an electrolyte in a mixed solvent of benzene and methanol, (2) direct mixing of the donor and the electrolyte in dichloromethane and methanol, and (3) direct reaction of the donor with iodine molecules in dichloromethane and methanol.

X-Ray photographs with the use of Cu $K\alpha$ radiation confirmed that all these methods gave the same complex. The results of elemental analysis showed the iodine/donor ratio x to be close to 5/2 or 12/5. The exact estimation by means of an X-ray investigation indicated x=2.47. Anal. Calcd for $C_{10}H_{12}S_8I_{2.47}$: C, 17.11; H, 1.72; S, 36.53; I, 44.64. Found: C, 16.91; H, 1.73; S, 36.95; I, 44.67.

Oscillation photographs along the crystal needle axis displayed ununiformly spaced layer lines (Fig. 1), which indicated the presence of a superlattice structure characteristic of iodine complexes.[9] This superlattice structure was considered to be composed of donor and iodine subcells. Among these layer lines the scatterings from the iodine subcell were neglected in the course of the structure analysis.

The intensity data of the donor subcell were collected at room temperature with a Rigaku automated four circle diffractometer using monochromatized Mo $K\alpha$ radiation by the ω-2θ scan technique. Since the intense scatterings from the iodine subcell were neglected and the iodine subcell was approximately commensurate with the donor subcell, the accuracy of the intensity data was limited. Only 664 independent reflections of 2112 accessible reflections ($2\theta \leq 50°$) were recorded with sufficient accuracy ($|F_o| \geq 3\sigma(|F_o|)$). Cell parameters were determined from least squares applied to 25 reflections with $25° < 2\theta < 30°$.

In the course of the structure determination, first the b-axis projection, which corresponds to the projection along the crystal needle axis, was deduced from the Patterson systhesis using the $h0l$ reflections. Since the $h0l$ reflections of the donor subcell was common to that of the iodine subcell, the position of the iodine column in the b axis projection was also determined. Then the three-dimensional structure was derived from this projection. In

Table 1. Atomic Parameters

Atom	$X(\times10^4)$	$Y(\times10^3)$	$Z(\times10^4)$
I	287(3)	—	3589(4)
S(1)	1747(3)	437(3)	161(4)
S(2)	3045(3)	453(3)	971(3)
S(3)	1485(3)	763(3)	1215(4)
S(4)	2906(4)	799(3)	2094(4)
C(1)	2461(10)	293(10)	250(13)
C(2)	1996(11)	635(10)	948(14)
C(3)	2599(11)	625(9)	1332(13)
C(4)	781(16)	635(10)	523(21)
C(5)	3681(12)	684(8)	2363(15)

the three-dimensional structure analysis the iodine atoms were considered to be distributed randomly along the b direction. The three-dimensional structure was refined by the block diagonal least squares method. Anisotropic thermal parameters were adopted for non H atoms. Hydrogen atoms were not included in the refinement. Final refinement gave R=0.099 and R_w=0.126, where $w=1/[\sigma^2(F_o)+0.000225F_o^2]$. The positional parameters are listed in Table 1. The F_o—F_c table and the anisotropic temperature parameters are deposited as Document No. 8604 at the Office of this Bulletin.

The dc resistivity of the single crystal was measured by the four-probe method using gold paint. The anisotropy of the resistivity was measured by the combined use of the Montgomery method and the two-probe method. The thermoelectric power along the b axis was measured by attaching a single crystal with gold paint or carbon paint to two boron nitride heat sinks.[10] ESR data were obtained with an X-band spectrometer Varian E112 equipped with an Oxford Instruments ESR 9 continuous flow helium cryostat.

Results

Among the ununiformly spaced layer lines of the oscillation photograph along the crystal needle axis, the layer line with a spacing of 3.978 Å was attributed to the donor subcell, because the observed high conductivity suggests that the donor molecules form a columnar structure along the crystal needle axis. Weissenberg photographs and the investigation using a four-circle diffractometer determined the crystal data of the donor subcell to be: monoclinic, $C2/c$, a=24.78(1), b=3.978(2), c=22.65(1) Å, β=115.50(5)°, V=2015(2) Å^3, and Z=4. The b axis corresponds to the crystal needle axis.

Iodine species reported to exist in solids include I_2, I^-, I_3^-, I_5^-.[9] In addition to the scatterings from the donor subcell, the oscillation photograph along the b axis displayed layer lines at 0.233, 0.412, 0.823, 1.234, and 1.647 reciprocal lattice units of the donor subcell, b/d (Fig. 1). All these layer lines were composed of well-defined spots even at room temperature, and no diffuse layer was observed. This observation indicates the three-dimensional order of the iodine atoms.

The layer lines at 0.233 and 1.647 are weaker than the donor layer lines and the layer lines at 0.412 and 0.823 are weaker still. The layer line at 1.234 is comparable to that of the donor subcell and is attributed to the average spacing of the iodine atoms along the b axis. Since the resulting atom spacing 3.224 Å is shorter than twice of the I^- ionic radius, 4.3 Å, the presence of an I^- column is excluded. This is also consistent with the supposition that if the iodine existed as I^-, the charge on the donor should be unrealistically large.

The layer lines at 0.412, 0.823, 1.234, and 1.647 form a series with a lattice constant b'=9.670(6) Å. This lattice constant is three times as large as the above-mensioned iodine average spacing. It is documented that I_3^-, which is the most common iodine species, has a repeat period of 9.4—9.7 Å in the iodine column.[9] Therefore, this subcell spacing indicates the presence of the I_3^- column. The existence of the I_5^- column, which displays a repeat period of about 15.5 Å,[9] is excluded.

The layer line at 0.233 is not due to the two-fold structure of this iodine subcell which should appear at 3.978 Å/2×9.670 Å=0.206. This layer line is attributed to the convolution of the intense iodine layer line and the donor layer line, b/d=1.234—1.0= 0.234.

The ratio of b to b′ determines the iodine content to be $x=6b/b'$=2.468(3). The scatter of x among the samples prepared by different methods is too small to be detectable by X-ray investigations. The stoichiometry associated with x=2.47 is between TTM-TTF$_5$I$_{12}$ (x=2.4) and TTM-TTF$_2$I$_5$ (x=2.5); the iodine subcell is incommensurate with the donor subcell.

Since no additional scattering is found in the k=0 Weissenberg photograph, the iodine subcell corresponds to the donor subcell in the a*c* plane. The crystal data of the iodine subcell were determined by the combined use of Weissenberg photographs and a four circle diffractometer: triclinic, a'=24.97, b'=9.670, c'=48.95 Å, α'=111.55, β'=112.38, γ'=94.60°, and V=9827 Å^3. This subcell is related to the donor subcell by the equations: $\mathbf{a^{*\prime}=a^*}$, $\mathbf{b'//b}$, $\mathbf{2c^{*\prime}=c^*}$.

The 5th layer line of the iodine subcell at 2.06 was not clearly distinguishable from the second layer of the donor subcell. Moreover the iodine subcell gave poorer quality scatterings than did the donor subcell. Therefore analysis of the intensity data was not attempted for the iodine subcell.

The crystal structure is shown in Figs. 2 and 3. The donor molecule TTM-TTF is almost flat similarly to other TTM-TTF complexes such as (TTM-TTF)(HCBD) and (TTM-TTF)AsF$_6$,[7,8] although its neutral structure is strongly deformed to be nonplanar.[8] The donor molecules are stacked

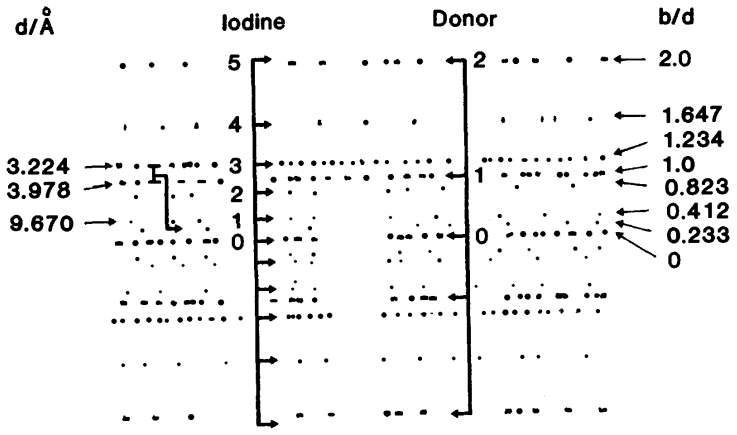

Fig. 1. Schematic representation of the oscillation photograph along the b axis. On the right side is shown b/d: the inverse of d (Å), multiplied by b=3.978 Å.

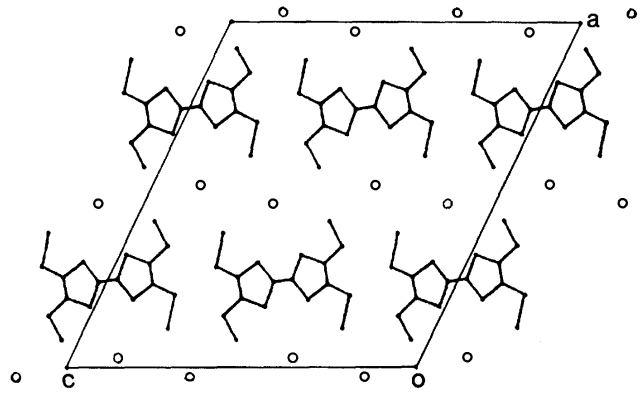

Fig. 2. Crystal structure: projection along the b axis. The white circles designate ioldine columns.

face-to-face to form a column along the b axis. The interplanar spacing is 3.58 Å and there is no shorter sulfur-to-sulfur contact than the van der Waals distance (3.7 Å) (Fig. 3). The mode of intermolecular overlap is, however, favorable to the orbital overlap (Fig. 4);[5] the adjacent molecules are displaced from each other by 1.37 Å along the long molecular axis.

There are comparatively short intercolumnar sulfur-to-sulfur contacts between the outer sulfur atoms (Fig. 3). The donor molecules form conducting sheets parallel to the bc plane in association with the short sulfur-to-sulfur contacts, and these sheets are separated from each other by the anions. The long axis of the molecule is almost parallel to this sheet.

This exhibits a striking contrast to the BEDT-TTF compounds. In all BEDT-TTF complexes whose crystal structures have been known so far, the molecular long axis is almost perpendicular to the sheet, and the intermolecular contacts at the molecular long sides are as important as the face-to-face interaction for the electron transfer.

As for TTM-TTF the terminal methyl groups extending to the direction perpendicular to the molecular long axis (see Fig. 2) block the contacts at the molecular long sides. In addition, the presence of the anions are also disadvantageous for the intermolecular interactions perpendicular to the molecular long axis in the ac plane. Since the outer sulfur atoms are instead exposed to the adjacent donors at the molecular short sides, the sheet of the donors extends through the contacts at the molecular short sides.

The b axis resistivity is shown in Fig. 5. The resistivity at room temperature is in the range of 7—10×10^{-3} Ωcm. The resistivity slightly decreases as the temperature is lowered down to 155 K, where it exhibits a broad minimum. Below 100 K the resistivity steeply increases in an activated manner with E_a=0.028 eV. The anisotropy of the resistivity is estimated to be $\rho_b:\rho_c:\rho_a=1:50:4000$.

The thermoelectric power is negative (−9 μV/K) at room temperature and decreases slightly to 155 K (−10 μV/K) (Fig. 6). Around this temperature the thermoelectric power has a broad minimum and increases below this temperature.

The magnetic susceptibility associated with the ESR intensity is almost constant from room temperature to 155 K (Fig. 7). In the temperature region between 155 and 100 K, the susceptibility decreases, but the temperature dependence is too gradual to be fitted to an activation-type formula. Below 100 K the susceptibility behaves in an activated manner with E_a=0.022 eV. This value agrees with the activation energy of the resistivity in this temperature region. Judging from the behavior of both the resistivity and the susceptibility, a metal-insulator transition is considered to take place at T_c=100 K.

The ESR linewidth is 56 G at room temperature and with a decrease in temperature decreases linearly

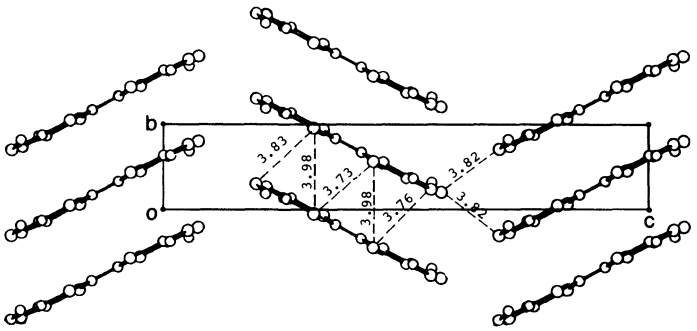

Fig. 3. Crystal structure: projection along the a axis and short intermolecular sulfur-to-sulrfur distances.

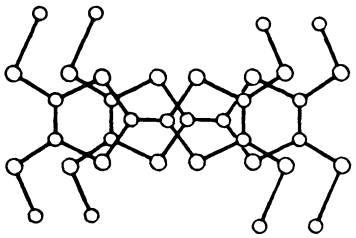

Fig. 4. Mode of the intracolumnar overlap of the TTM-TTF molecules.

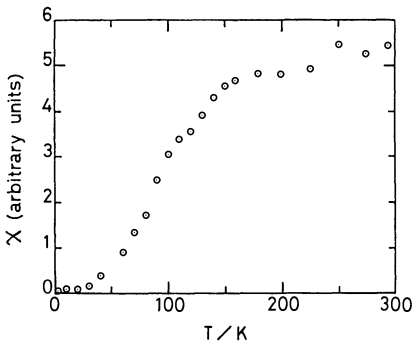

Fig. 7. Temperature dependence of the relative spin susceptibility χ.

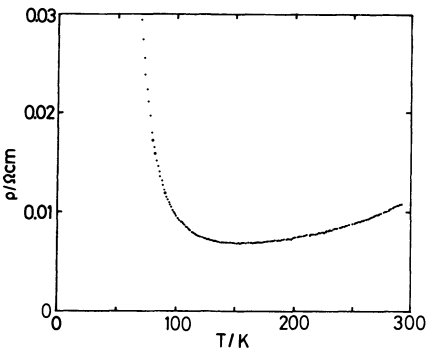

Fig. 5. Temperature dependence of the electrical resistivity ρ along the b axis.

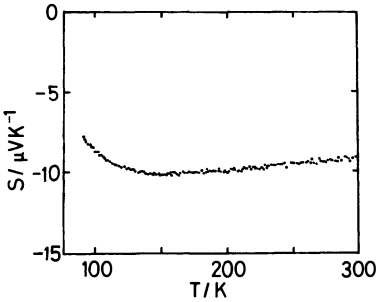

Fig. 6. Temperature dependence of the thermoelectric power S along the b axis.

like that of other halides and pseudohalides of TTF derivatives.[11] This large linewidth suggests the presence of conducting sheets where the spin relaxation is allowed through interchain hoppings. The g-value (H//a*) is almost constant (2.003) through all the measured temperature region, and is close to the free electron value.

Discussion

From the stoichiometry (TTM-TTF)$I_{2.47}$ and the presence of the I_3^- species established by the X-ray investigation, the charge on a donor molecule is estimated to be n=0.823. This value is consistent with that in the estimation from the intramolecular bond lengths of the donor.[4] In general TTM-TTF tends to be slightly more positively charged in charge-transfer complexes in comparison with BEDT-TTF.

In order to estimate the anisotropy of the electron transfer, intermolecular overlap integrals of the highest occupied molecular orbital (HOMO) have been calculated on the basis of molecular orbital calculations.[5,6] The intermolecular overlap in the column is -14.7×10^{-3} and the intercolumnar overlap along the c axis is 0.88×10^{-3}. If transfer integrals t are assumed to be proportional to the intermolecular

overlaps, the anisotropy of the transfer integrals are obtained, $t_c/t_b=0.06$.

In a quasi-one-dimensional band, the ratio of the conductivity is roughly proportional to the square of the transfer integrals,[12] $(\sigma_c/\sigma_b)\simeq(ct_c/2bt_b)^2$. Thus σ_c/σ_b is evaluated to be 0.03, in agreement with the observed anisotropy 0.02.

The dimensionality of this TTM-TTF complex is lower than that of ordinary BEDT-TTF complexes. Then it is convincing that the metal-insulator transition at $T_c=100$ K observed in the resistivity and the magnetic susceptibility is attributed to the Peierls type phase transition in the quasi-one-dimensional donor chain.

A surprising observation concerning this complex is the negative thermoelectric power at high temperatures. Halide and pseudohalide systems of the TTF family ordinarily show positive thermoelectric power, because of the hole carriers existing on the donors. In a simple tight-bindihg band the thermoelectric power changes its sign to the band center, which corresponds to the degree of charge transfer $n=1.0$. In (TTM-TTF)$I_{2.47}$, the relatively large degree of charge transfer $n=0.823$ causes the Fermi energy E_F near to the band center. Thus it is possible that the deviation of the energy band from the simple tight-binding band brings about a positive curvature at E_F in the band, leading to the negative thermoelectric power.

The negative thermoelectric power is, however, attributable to the presence of a pseudogap generated by the fluctuation in the iodine lattice. Since the iodine lattice has three-dimensional order even at room temperature, a pseudogap at E_F is induced by the periodical potential of the iodine atoms. The electronic structure at high temperatures is rather semimetallic or narrow-gap semiconductor-like than one-dimensional metallic. Such an electronic structure makes the thermoelectric power either positive or negative, depending on the difference of the carrier mobilities above and below the pseudogap.

The small increase in the resistivity and the gradual decrease in the spin susceptibility blow 155 K suggest the precursor effect of the Peierls transition. Since the iodine lattice is approximately commensurate with the donor lattice, the possibility remains that a lock-in transition may take place. The X-ray investigation which determined the average periodicity of the iodine lattice does not exclude the existence of minor iodine species other than I_3^-. Therefore, the degree of charge transfer may be changed a little from $n=0.823$, depending on temperature. Then the phase transition is possibly cooperated with the change of order in the iodine lattice and/or the degree of charge transfer. In order to confirm this speculation temperature-dependent investigation of charge transfer is desirable by means of X-ray analysis or Raman spectroscopy.

It has been suggested that the spread of the donor HOMO is related to the dimensionality of the complex.[13] As the ratio of the atomic populations of the HOMO between the outer sulfur atoms and the inner sulfur atoms P_2/P_1 increses, the dimensionality is enhanced through the increase in the transverse intermolecular overlap. The ratio P_2/P_1 is calculated to be 0.452 for TTM-TTF. This value is even larger than the 0.148 for BEDT-TTF and the 0.315 for BMDT-TTF which form conductors with two-dimensionality.[14] In TTM-TTF, however, the transverse interaction at the molecular long sides is inhibited by the methyl groups; the transverse interaction works only through the outer sulfur atoms at the molecular short sides. Thus the magnitude of the transverse interaction is small. This is the reason for the less than two-dimensional electronic structure of this TTM-TTF complex, in spite of a large P_2/P_1.

In conclusion (TTM-TTF)$I_{2.47}$ is recognized as a quasi-one-dimensional conductor with an incommensurate iodine superlattice. Since the iodine atoms have three-dimensional order, the electronic structure at room temperature is considered to be semimetallic or narrow-gap semiconductor-like. Thus the resistivity shows a slightly metallic temperature dependence, the spin susceptibility is almost constant, and the thermoelectric power shows a negative value with small temperature dependence. Around $T_c=100$ K a metal-insulator transition takes place, which is attributed to the Peierls type instability. The arrangement of the donor molecules in the crystal and the calculated anisotropy of the transfer integrals support a comparatively one-dimensional electronic structure of this complex.

The authors are grateful to Prof. H. Kobayashi and Dr. A. Kobayashi for helpful advice on the structure analysis.

References

1) G. Saito, T. Enoki, K. Toriumi, and H. Inokuchi, *Solid State Commun.*, **42**, 557 (1982).

2) S. S. P. Parkin, E. M. Engler, R. R. Schumaker, R. Lagier, V. Y. Lee, J. C. Scott, and R. L. Greene, *Phys. Rev. Lett.*, **50**, 270 (1983).

3) E. B. Yagubskii, I. F. Shchegolev, V. N. Laukhin, P. A. Kononovich, M. V. Kartsovnic, A. V. Zvarykina, and L. I. Buravov, *Pis'ma Zh. Eksp. Teor. Fiz.* **39**, 12 (1984).

4) H. Kobayashi, R. Kato, T. Mori, A. Kobayashi, Y. Sasaki, G. Saito, T. Enoki, and H. Inokuchi, *Mol. Cryst. Liq. Cryst.*, **107**, 33 (1983).

5) T. Mori, A. Kobayashi, Y. Sasaki, H. Kobayashi, G. Saito, and H. Inokuchi, *Bull. Chem. Soc. Jpn.*, **57**, 627 (1984).

6) T. Mori, A. Kobayashi, Y. Sasaki, H. Kobayashi. G. Saito, and H. Inokuchi, *Chem. Lett.*, **1984**, 957.

7) G. Saito, H. Kumagai, C. Katayama, C, Tanaka, J. Tanaka, P. Wu, T. Mori, T. Enoki, and H. Inokuchi, to be published.

8) C. Katayama, M. Honda, H. Kumagai, J. Tanaka, G. Saito, and H. Inokuchi, *Bull. Chem. Soc. Jpn.*, **58**, 2272 (1985).

9) P. Coppens, "*Extended Linear Chain Compounds I*," ed by J. S. Miller, Plenum (1982), p. 333.

10) P. M. Chaikin and J. F. Kwak, *Rev. Sci. Instrum.*, **46**, 218 (1975).

11) K. Carneiro J. C. Scott, and E. M. Engler, *Solid State Commun.*, **50**, 477 (1984).

12) J. F. Kwak, *Phys. Rev.*, **B26**, 4789 (1982).

13) T. Mori, A. Kobayashi, Y. Sasaki, R. Kato, and H. Kobayashi, *Chem. Lett.*, **1984**, 1335.

14) R. Kato, H. Kobayashi, T. Mori, A. Kobayashi, and Y. Sasaki, *Solid State Commun.*, **55**, 387 (1985).

 © 1986 The Chemical Society of Japan Bull. Chem. Soc. Jpn., 59, 133—137 (1986)

Thermal Stability of Electroless Nickel-Molybdenum-Phosphorus Alloy Films

Ichiro KOIWA, Masao NISHIKAWA, Keizo YAMADA, and Tetsuya OSAKA*
Department of Applied Chemistry, School of Science and Engineering,
Waseda University, Okubo, Shinjuku-ku, Tokyo 160
(Received July 12, 1985)

The structure and the electric resistivity of electroless Ni-Mo-P alloy films, which were plated from a caustic alkali citrate-glycolic acid bath, have been investigated. The phosphorus content in deposits and the deposition rate decreased with increasing Mo-complex concentration which was formed with sodium gluconate before constructing the bath. The crystallized structure and the formation of solid solutions between the Ni matrix and the codeposited Mo were indicated by X-ray diffraction measurments for high Mo-complex concentration range. On the other hand, amorphous states appeared for the Mo-complex concentration range lower than 0.002 mol dm^{-3}. In the range less than 0.002 mol dm^{-3} Mo-complex concentration, the resistivity of as-plated Ni-Mo-P films was higher than the binary Ni-P alloy film plated from the bath without the Mo-complex. In the higher Mo-complex concentration range, the resistivity immediately reached a constant value independently of the Mo-complex concentration. After 500 and 800 °C heat treatment under vacuum, the resistivity increased with increasing Mo-complex concentration. Moreover for the higher Mo-complex concentration range, the resistivity after heat treatment became higher than that of as-plated conditions, and the increased resistivity after the heat treatment depended on the Mo content in the deposits. Therefore, the codeposited Mo tended to increase the thermal stability of the films.

Recently, some workers applied electroless Ni-P plating films to thin film resistors[1,2] taking into account some advantages of mass production capability and good cost performance as compared with those prepared by PVD[3] and thick film[4] technologies. Since the amorphous Ni-P alloy film with high phosphorus content, easily produced by electroless plating method,[5,6] has high specific resistance and low temperature coefficient of resistivity,[7] it has been applied to the fields.

The structure of electroless Ni-P films[5,6,8-12] and the structure variation by heat treatment[13-15] have been studied, but satisfactorily thermally-stabilized amorphous Ni-P films have not been reported.

It is important to improve the thermal stability of electroless Ni-P plating films in view of their application to thin-film resistors. The codeposition of a higher-melting-metal into the Ni-P film is one of the candidates to improve the thermal stability of electroless Ni alloy films. Ternary alloy films of electroless Ni-W-P[16,17] and Ni-Mo-P[18,19] have already been reported. Their thermal variation is different from that of binary Ni-P alloy films, however, the study from this viewpoint has scarcely been reported and the thermal stability of the resistivity of the ternary alloy has not been discussed in detail.

This paper describes the correlation between the structure and the electric resistivity of electroless Ni-Mo-P alloy films and discusses the effect of molybdenum codeposition into Ni-P films.

Experimental

Electroless nickel-molybdenum-phosphorus alloy films were plated from a caustic alkali citrate-glycolic acid bath whose compositions and operating conditions were listed in Table 1. Molybdenum codeposition was easily formed by complexing sodium molybdate with sodium gluconate before constructing the bath as an analogy to the method by Mallory.[20] The solution of sodium molybdate which is complexed with sodium gluconate is designated Mo-complex in the text. The ninety-six w/o α-alumina ceramics (NGK Spark Plug Co. Ltd.) were used as a plating substrate except for the differential scanning calorimetry (DSC) measurement. For the DSC measurement, the catalyzed polyimide film (25KA, Torey Co. Ltd.) was used as substrate. The repeated two step process[21] was used for catalyzing the ceramics substrate, where the sensitizer and the activator are as follows; sensitizer: $SnCl_2 \cdot 2H_2O$ 1.0 g dm^{-3}, 37% HCl 1.0 ml dm^{-3}, and activator: $PdCl_2$ 0.1 g dm^{-3}, 37% HCl 0.1 ml dm^{-3}. The film thickness was adjusted to 2 μm by controlling the deposition time. The molybdenum and phosphorus contents shown as weight percentage (wt%) were determined by an inductively coupled argon plasma atomic emission spectrophotometer (ICAP-575 MarkII, Nippon Jarrell-Ash). The resistivity of the deposits on the alumina substrate was measured by the four-probe method. The structure of the deposits was determined using an X-ray diffractometer (RAD-IIA, Rigaku Denki Co. Ltd.). Thermal analysis was made with DSC (DSC-30, Shimadzu Co. Ltd.). The samples were prepared by grinding the deposits which were peeled off the polyimide substrate. The samples were heated from room temperature up to 500 °C at a constant rate of 10 °C/min, in a nitrogen atmosphere, using 10—20 mg

Table 1. Electroless Plating Bath Compositions and Operating Conditions

Chemicals	Concentration
$NaH_2PO_2 \cdot H_2O$	0.20 mol dm^{-3}
$C_3H_4(OH)(COONa)_3 \cdot 2H_2O$	0.10
$HOCH_2COOH$	0.20
$NiSO_4 \cdot 7H_2O$	0.10
Mo-complex	0—0.015

Bath temperature 90 °C, Bath pH 9.0 adjusted by NaOH.

sample weight. The heat treatment of the deposits was made under 2×10^{-3} Pa with 10 °C/min constant heating rate from room temperature to the setting temperature afterward the sample was maintained for one hour at the setting temperature.

Results and Discussion

Deposition Rate and Film Composition of Electroless Ni-Mo-P Alloy Films. The deposition rate and film composition at various Mo-complex concentration are shown in Fig. 1. The molybdenum content in the deposits increases with increasing the Mo-complex concentration up to 0.01 mol dm^{-3}, then it reaches a constant value. The maximum Mo content, 16.8 wt%, was obtained at 0.015 mol dm^{-3} Mo-complex concentration. The deposition rate decreases with increasing Mo-complex concentration and finally no deposition occurs at the region more than 0.015 mol dm^{-3} Mo-complex concentration. In contrast to Mo content behavior, the phosphorus content decreases with increasing the Mo-complex concentration. In particular, the phosphorus content remarkably decreases until 0.0025 mol dm^{-3} Mo-complex concentration, and the phosphorus content is depressed under 2 wt% at the region more than 0.0025 mol dm^{-3} Mo-complex concentration.

Structure and Resistivity of Electroless Ni-Mo-P Alloy Films. Figure 2 shows typical X-ray diffraction patterns of the deposits at various Mo-complex concentrations in the bath. As is seen in Fig. 2, the structure of the Ni-P alloy film without Mo-complex addition is in an amorphous state; only two peaks appear due to the Al_2O_3 substrate. In the region below 0.002 mol dm^{-3}, the structure of the Ni-Mo-P alloy films is in the same amorphous state as that of the Ni-P alloy film. On the other hand, at the region more than 0.002 mol dm^{-3} Mo-complex concentration, the structure of the Ni-Mo-P alloy films changes to a crystallized state. The structural change can be due to the remarkable decrease of the P content, as is seen in Fig. 1. Since the peaks of the Ni(111) and Ni(200) planes shift to the lower angle side as compared with the pure Ni value, the interplanar spacing of the Ni-Mo-P alloy can be widened by the molybdenum codeposition. The specific resistance, ρ, and the interplanar spacing, d, of Ni-Mo-P alloys are shown in Fig. 3 as a function of Mo-complex concentration. The ρ value increases with Mo-complex concentration up to 0.001 mol dm^{-3}, and it decreases to 0.0025 mol dm^{-3}. However, the ρ value becomes constant at 100 $\mu\Omega$ cm in the crystallized region above 0.0025 mol dm^{-3}. The d value of the crystallized Ni-Mo-P alloy films increases with increasing Mo-complex concentration. The increase in d value in the crystallized states

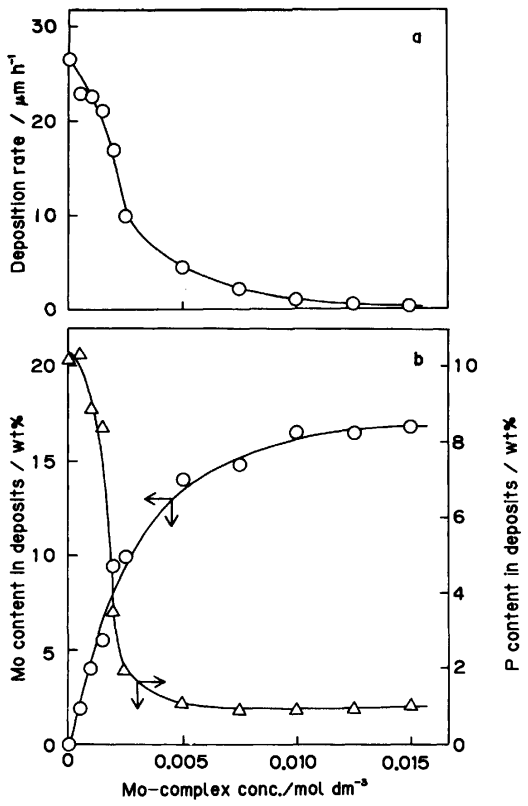

Fig. 1. Effect of Mo-complex concentration on deposition rate and film composition.

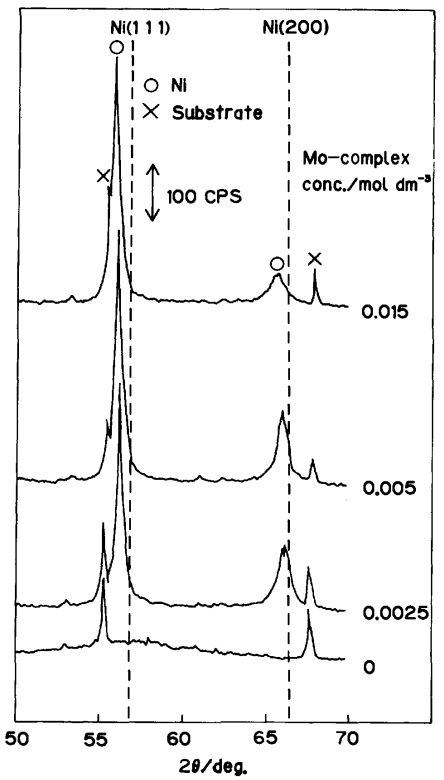

Fig. 2. X-Ray diffraction patterns for Ni-Mo-P alloy films with various Mo-complex concentrations using Fe target. Dashed lines show the peak positions of pure Ni.

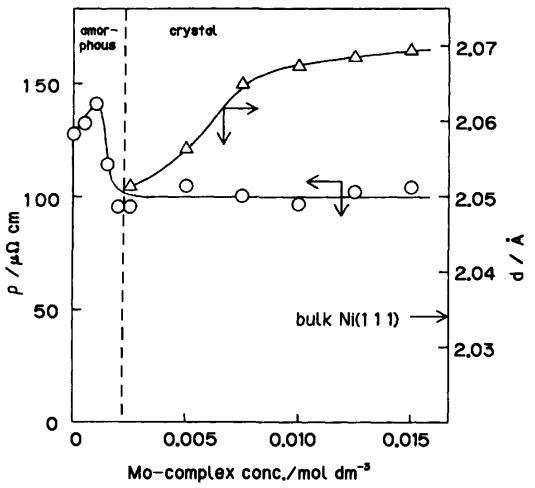

Fig. 3. Effect of Mo-complex concentration on specific resistance (ρ) and interplanar spacing (d) of Ni–Mo–P alloy films. Dashed line shows the phase change from amorphous to crystallized states.

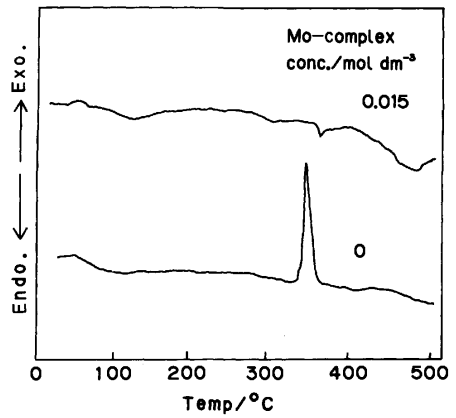

Fig. 4. DSC curves of Ni–P and Ni–Mo–P films.

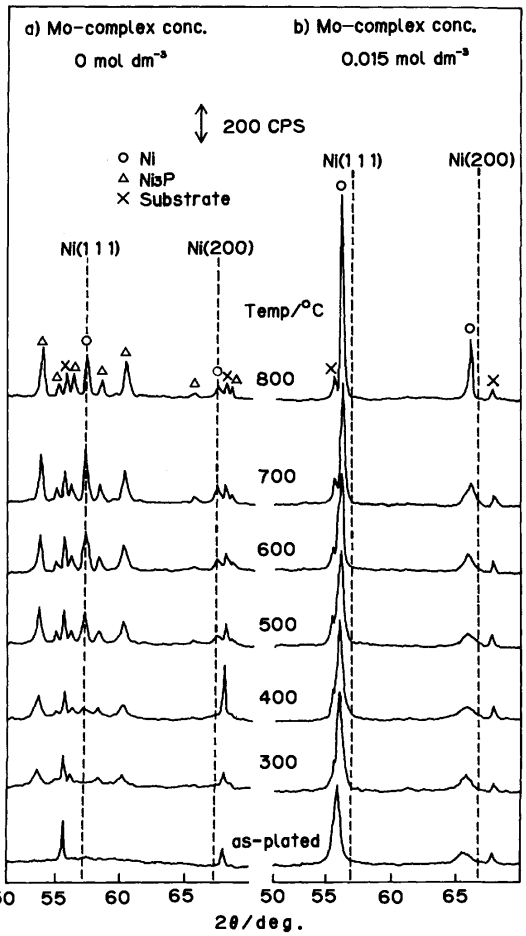

Fig. 5. X-Ray diffraction patterns for Ni–P and Ni–Mo–P alloy films at various annealing temperatures. Dashed lines show the peak positions of pure Ni.

corresponds to the increase in the Mo content with increasing Mo-complex concentration, but the ρ value of the films is independent of the increase in the Mo content. When considering that the ρ value of crystallized Ni–P alloy films with low phosphorus content generally becomes much lower than that of amorphous films,[22] the molybdenum codeposition into the Ni–P film might form a solid solution with a nickel matrix which results in the higher ρ value, in spite of the very low P content. The resistivity of as-plated Ni–Mo–P films, however, have no clear correlation with the Mo content.

Differential Scanning Calorimetry (DSC) Measurements. The DSC curves clearly show the difference between Ni–P and Ni–Mo–P deposits as is seen in Fig. 4. In the case of Ni–P film, there appears one clear exothermic peak around 350 °C, which coincides well with the previous studies.[13–15] In contrast to that of the Ni–P film, there is no obvious peak for Ni–Mo–P alloy films. In general, the exothermic peak is related to a structural change which affects the film properties such as the resistivity, and the magnetic and mechanical properties.[13–16] Therefore, the structure of an electroless Ni–Mo–P alloy film can be thermally more stable than that of a Ni–P alloy film.

Heat Treatment Effects on Properties of Electroless Ni–Mo–P Alloy Films. Figure 5 demonstrates typical X-ray diffraction patterns of the electroless Ni–P and the Ni–Mo–P alloy films after heat treatment at various temperatures. The amorphous Ni–P alloy film changes to a crystalline state and forms a Ni_3P compound on heat treatment at 300 °C. The structural change corresponds to the exothermic peak of the DSC curves as is seen in Fig. 4. The peak intensities of the Ni and Ni_3P increase with increasing heat treatment temperature. On the other hand, the electroless Ni–Mo–P alloy film, which has a crystalline structure at the as-plated conditions, maintains almost the same structure as that of an as-plated film up to 300 °C heat treatment. Moreover the peak intensities of the Ni(111) and Ni(200) plane gradually increase with the increase in the heat treatment temperature more than 300 °C. Therefore,

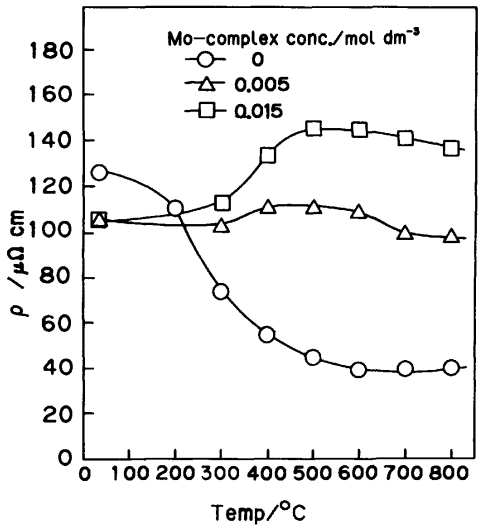

Fig. 6. Variation of specific resistance, ρ after heat treatment.

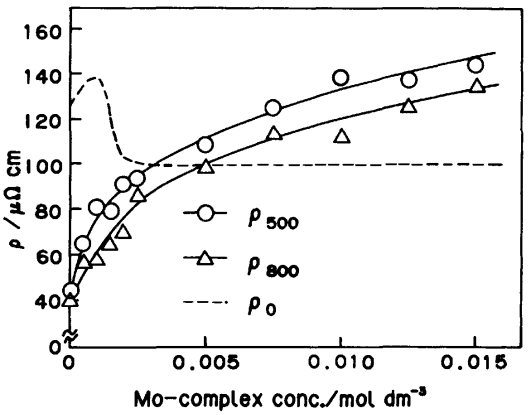

Fig. 7. Effect of Mo-complex concentration on resistivity after 500 and 800 °C heat treatment. Dashed line shows the resistivity, ρ_0 at as-plated conditions.

crystallization of electroless Ni-Mo-P alloy films is gradually proceeded by heat treatment. However, crystallization of Ni-Mo-P alloy film is much less than that of Ni-P alloy films, as has been reported previously.[13-15] The other peaks except for Ni(111) and Ni(200) planes are not observed for thermally-treated Ni-Mo-P films. The results coincide well with DSC measurement as is seen in Fig. 4. The molybdenum codeposition might inhibit the crystallization of a Ni matrix in contrast to the general Ni-P film with low phosphorus content.

Figure 6 illustrates the effect of heat treatment on the specific resistance (ρ) of Ni-Mo-P films. As is seen in Fig. 6, the resistivity of a Ni-P alloy film decreases remarkably with increasing heat treatment temperature. The decrease of Ni-P film resistivity starts in the lower heat treatment temperature range, and the decreased amount becomes larger with the increase in setting temperature. The results for a Ni-P film correspond well to those of the X-ray analysis as is shown in Fig. 5. On the other hand, the ρ value variation of electroless Ni-Mo-P alloy films is quite different from that of Ni-P alloy films, i.e., the ρ value variation is much smaller than that of a Ni-P alloy film. The resistivity of a Ni-Mo-P alloy film deposited from 0.005 mol dm^{-3} Mo-complex concentration bath is almost independent of the heat treatment temperature. Moreover, the resistivity of a Ni-Mo-P alloy film deposited from 0.015 mol dm^{-3} Mo-complex concentration bath increases with the heat treatment temperature and reaches a maximum around 500—600 °C. Such a tendency has not been observed for the binary electroless Ni-P and Ni-B alloy films. It can be concluded that the molybdenum codeposited into Ni-P film gives high stability against thermal treatment, and moreover that the Ni-Mo-P film of the higher Mo content shows the higher resistivity than that of as-plated one after heat treatment.

Figure 7 demonstrates the ρ value variation of Ni-Mo-P alloy films after heat treatment as a function of Mo-complex concentration. The resistivities after 500 °C and 800 °C heat treatments are denoted as ρ_{500} and ρ_{800}, respectively, and the dashed line indicates the resistivity value ρ_0 at as-plated conditions. The dashed line crosses solid lines of ρ_{500} and ρ_{800} values at 0.0035 and 0.005 mol dm^{-3} Mo-complex concentrations, respectively. It means that the ρ_{500} and ρ_{800} values become higher than the ρ_0 value at the region more than 0.0035 mol dm^{-3} and 0.005 mol dm^{-3} Mo-complex concentrations, respectively. The small difference of the degree of Ni matrix crystallization between 500 and 800 °C heat treatment can be observed as is seen in Fig. 5. In contrast to the poor correlation between the ρ_0 values and the Mo-complex concentration in the as-plated state, the resistivity of the heat treated Ni-Mo-P films increases with increasing Mo-complex concentration. Although no clear explanation is given for the ρ value variation of Mo codeposited Ni-P films, the molybdenum content plays one of the most important roles to determine the resistivity and the structure after heat treatment. Moreover, the codeposited molybdenum improves the thermal stability of resistivity, and it might be due to the fact that the codeposited molybdenum disturbes the structural change by heat treatment.

Conclusion

The characteristics of electroless Ni-Mo-P alloy films, which were prepared by addition of the Mo-complex into the bath, have been studied. The deposition rate and the phosphorus content decrease with increasing Mo-complex concentration. The structure of Ni-Mo-P alloy films is changed from amorphous to crystalline on increasing Mo-complex

concentration. X-Ray diffraction measurements indicate that codeposited Mo forms a solid solution with a Ni matrix. From DSC, X-ray diffraction and resistivity measurement, the Ni-Mo-P alloy film is thermally stabler than the Ni-P film. In general, a thin film resistor is actually used after heat treatment. The resistivity of the Ni-P film after heat treatment is changed abruptly by a structural transformation. Since the Ni-Mo-P films described in the text, show very stable resistivity against 400 °C heat treatment, electroless Ni-Mo-P alloy films have much advantage for the usage in thin film resistors. Under as-plated conditions, the correlation between resistivity and Mo content is not clear, however after heat treatment, the resistivity strongly depends on the Mo content, and the resistivity after heat treatment increases with increasing Mo content.

The authors wish to thank Professor Emeritus Dr. T. Yoshida, Waseda University, and Dr. K. Nihei and Mr. H. Sawai, the Research Labs, OKI Electric Industry Co. Ltd., for their encouragement of the work.

References

1) N. Miura, Y. Fuura, and A. Kazumi, *IEEE Trans. Components. Hybrids, Manuf. Technol.*, **CHMT-4**, 532 (1981).

2) J. Dearden, *Electrocomponent Sci. Technol.*, **3**, 103 (1976).

3) Y. Tokunaga, M. Yoshida, and M. Kizawa, *IEEE Trans. Components, Hybrids, Manuf. Technol.*, **CHMT-4**, 148 (1981).

4) N. Sinnadurai and K. J. Wilson, *IEEE Trans. Components, Hybrids, Manuf. Technol.*, **CHMT-5**, 308 (1982).

5) A. W. Goldstein, W. Rostoker, F. Schossberger, and G. Gutzeit, *J. Electrochem. Soc.*, **104**, 104 (1957).

6) J. P. Marton and M. Schlesinger, *J. Electrochem. Soc.*, **115**, 16 (1968).

7) P. J. Cote, *Solid State Commun.*, **18**, 1311 (1976).

8) A. H. Graham, R. W. Lindsay, and H. J. Read, *J. Electrochem. Soc.*, **109**, 1200 (1962).

9) A. H. Graham, R. W. Lindsay, and H. J. Read, *J. Electrochem. Soc.*, **112**, 401 (1965).

10) J. Diximer and K. Doi, *Compt. Rend.*, **257**, 2451 (1963).

11) B. G. Bagley and D. Turnbull, *J. Appl. Phys.*, **39**, 5681 (1968).

12) J.-P. Randin and H. E. Hinterman, *J. Electrochem. Soc.*, **115**, 480 (1968).

13) J.-P. Randin, P. A. Maire, E. Saurer, and H. E. Hintermann, *J. Electrochem. Soc.*, **114**, 442 (1967).

14) K. Masui, S. Maruno, and T. Yamada, *J. Jpn. Inst. Metals*, **41**, 1130 (1977).

15) K. Masui, M. Tachihara, T. Yamada, and T. Tsujimoto, *J. Jpn. Inst. Metals*, **44**, 124 (1980).

16) F. Pearlstein and R. F. Weightman, *Electrochem. Tech.*, **6**, 427 (1968).

17) K. Aoki and O. Takano, *Ex. Abstract the 58th Conf. of Metal Finishing Soc. Jpn.*, (1978), p. 52.

18) G. O. Mallory, *Plating and Surface Finishing*, **63**, No. 6, 34 (1976).

19) M. Schwartz and G. O. Mallory, *J. Electrochem. Soc.*, **123**, 606 (1976).

20) G. O. Mallory and T. R. Horhn, *Plating and Surface Finishing*, **66**, No. 4, 40 (1979).

21) L. G. Svendsen, T. Osaka, and H. Sawai, *J. Electrochem. Soc.*, **130**, 2252 (1983).

22) T. Osaka and I. Koiwa, *Kinzoku Hyomen Gijutsu*, **34**, 330 (1983).

 © 1986 The Chemical Society of Japan Bull. Chem. Soc. Jpn., 59, 139—144 (1986)

Kinetic and Equilibrium Studies of Complex Formation of Nickel(II) with Carboxylate Ligands at High Pressure. III. Nickel(II) Malonate and Nickel(II) Tartronate

Kiyotaka KOJIMA, Tohru INOUE,* Michiko IZAKI, and Ryosuke SHIMOZAWA
Department of Chemistry, Faculty of Science, Fukuoka University,
Nanakuma, Jonan-ku, Fukuoka 814-01
(Received August 16, 1985)

Kinetic and equilibrium measurements were carried out for the complexation reaction of nickel(II) malonate and nickel(II) tartronate in an aqueous solution at 20 °C and at pressures up to 100 MPa. The reaction volume, ΔV^0, and the activation volume, ΔV_f^*, for the complex formation were estimated from the pressure dependence of the stability constant and the rate constant. The results are as follows: $\Delta V^0=13.5\pm1.0$ cm^3 mol^{-1} and $\Delta V_f^*=14.7\pm0.5$ cm^3 mol^{-1} for nickel(II) malonate, and $\Delta V^0=13.3\pm0.7$ cm^3 mol^{-1} and $\Delta V_f^*=15.2\pm0.5$ cm^3 mol^{-1} for nickel(II) tartronate. The larger ΔV^0 value compared with those obtained for dicarboxylate ligands which form a monodentate complex coincides with that malonate and tartronate form a chelate complex with nickel(II) in an aqueous solution. By appropriately estimating the volume changes associated with the outer-sphere complex formation and first-bond formation, the overall volume profile for the complexation reaction was obtained. A Similar feature regarding the volume profile for the complexation of nickel(II) malonate and nickel(II) tartronate suggests that tartronate forms a bidentate chelate complex by two carboxyl groups rather than by carboxyl and hydroxyl groups.

The usefulness of the activation volume as a criterion for a mechanistic study has been progressively demonstrated since a high-pressure technique was combined with rapid-reaction techniques. Recently, many kinetic investigations have been reported for metal complexation reactions in solutions under high pressure in order to understand reaction mechanisms based on the activation volume.[1-3] Previously, we studied the complex formation reactions of nickel(II) with some carboxylate ligands in aqueous solutions under high pressure using a high-pressure pressure-jump technique.[4,5] In this present paper, we report the results obtained with nickel(II) malonate and nickel(II) tartronate systems.

In a preliminary communication,[6] we presented the kinetics of a nickel(II) malonate complexation reaction under high pressure, where only the pressure-jump relaxation data were available and the overall volume profile for the reaction could not be obtained because of the poor accuracy of the kinetically determined stability constants. Hence, in the present work, the stability constants at high pressure were determined independently.

A malonate ion has two carboxylato groups which can coordinate to a nickel(II) ion to form a six-membered chelate complex in an aqueous solution, while a tartronate ion has an additional hydroxyl group on α-carbon (see Scheme 1). Considering the molecular structure of a tartronate ion, there may be possible structures of the complex with nickel(II); six-membered chelate coordinated by two carboxyl oxygens, five-membered chelate coordinated by one carboxyl oxygen and one hydroxyl oxygen, and also tridentated chelate coordinated by two carboxyl oxygens and one hydroxyl oxygen. It will be shown below that the volume profile obtained in this study can serve to elucidate not only the rate-determining step of the reaction but also the structure of the complex.

Experimental

Reagents. Stock solutions of nickel(II) malonate and nickel(II) tartronate were prepared from nickel sulfate and respective acids according to a procedure described previously.[4] The concentration of the solution was determined by titrating with an EDTA solution standardized by a standard solution of zinc nitrate. Nickel sulfate (Wako Pure Chemicals, guaranteed grade), malonic acid (Wako Pure Chemicals, >98%), and tartronic acid (Aldrich Chemical Co., 98%) were used without further purification. Each sample solution was prepared by diluting the stock solution to the desired concentration. The pH's of the sample solutions were 6.9±0.1 for nickel(II) malonate and 6.0±0.1 for nickel(II) tartronate. In these pH ranges, most of the ligands were in a fully dissociated form, considering the pKa values of the acids; pKa$_1$=2.85 and pKa$_2$=5.67 for malonic acid,[7] and pKa$_1$=2.02 and pKa$_2$=4.24 for tartronic acid.[8]

Measurements. The stability constants of the complexes were determined from conductivity measurements according to the Fuoss-Kraus method.[9] The conductivity under high pressure was measured using a conductivity cell made by modifying an injector, which was immersed in a conventional high-pressure vessel. The concentration range of nickel(II) species employed for the conductivity measurements was 1×10^{-4}—1×10^{-3} mol dm^{-3}. Kinetic measurements were made using a high-pressure pressure-jump apparatus.[6] The concentration range of nickel(II) species for kinetic measurements was 5×10^{-4}—1×10^{-2} mol dm^{-3} for nickel(II) malonate and 5×10^{-4}—5×10^{-3} mol dm^{-3} for nickel(II) tartronate. The temperature was kept at 20.0±0.1 °C throughout the measurements and the pressure was maintained within ±0.5 MPa. As the concentration of the sample solution is expressed in molarity, in the case of measurements under pressure, corrections for the molar

concentration due to compression were made using the density data of water.[10]

Results

The complex formation reaction under consideration is represented in Scheme 1. Stability constants

$$Ni^{2+} + L^{2-} \rightleftharpoons NiL$$

L^{2-}: $CH_2(COO^-)_2$ (malonate) $CHOH(COO^-)_2$ (tartronate)

Scheme 1.

of the complexes, K, were determined from the conductivity data according to Eq. 1 using a computer iteration technique (detail of the procedure was described previously[4]).

$$\frac{F}{\Lambda} = \frac{1}{\Lambda^0} + \left(\frac{K}{(\Lambda^0)^2}\right)\left(\frac{\Lambda c\gamma_\pm^2}{F}\right), \quad (1)$$

where F is the conductivity coefficient (related to the degree of dissociation of the complex, α, by $\alpha=\Lambda/\Lambda^0F$), and other symbols have their usual meanings. Figures 1a and 1b show the plot of Eq. 1 for nickel(II) malonate and nickel(II) tartronate, respectively, at various pressures. Good linearity was observed for the whole pressure range. From the slope and intercept of these plots, the values of K were determined and are summarized in Table 1.

The present value of K for nickel(II) malonate at 0.1 MPa is in good agreement with a value found in the literature[11] ($K=1.26\times10^4$ mol^{-1} dm^3 at 25 °C and $I\rightarrow0$). For nickel(II) tartronate, the available literature value[8] is $K=2.82\times10^3$ mol^{-1} dm^3 at 20 °C and $I=0.1$. From this value, the stability constant at zero ionic strength is estimated to be 18.5×10^3 mol^{-1} dm^3 by using activity coefficient calculated from the Davies equation[12] ($\gamma_\pm\simeq0.39$ for a divalent electrolyte at $I=0.1$). Considerable disagreement is seen between this value and the present result at 0.1 MPa, the origin of which is not known.

The pressure dependence of the stability constant provides for an evaluation of the reaction volume for the complex formation according to the relation[13]

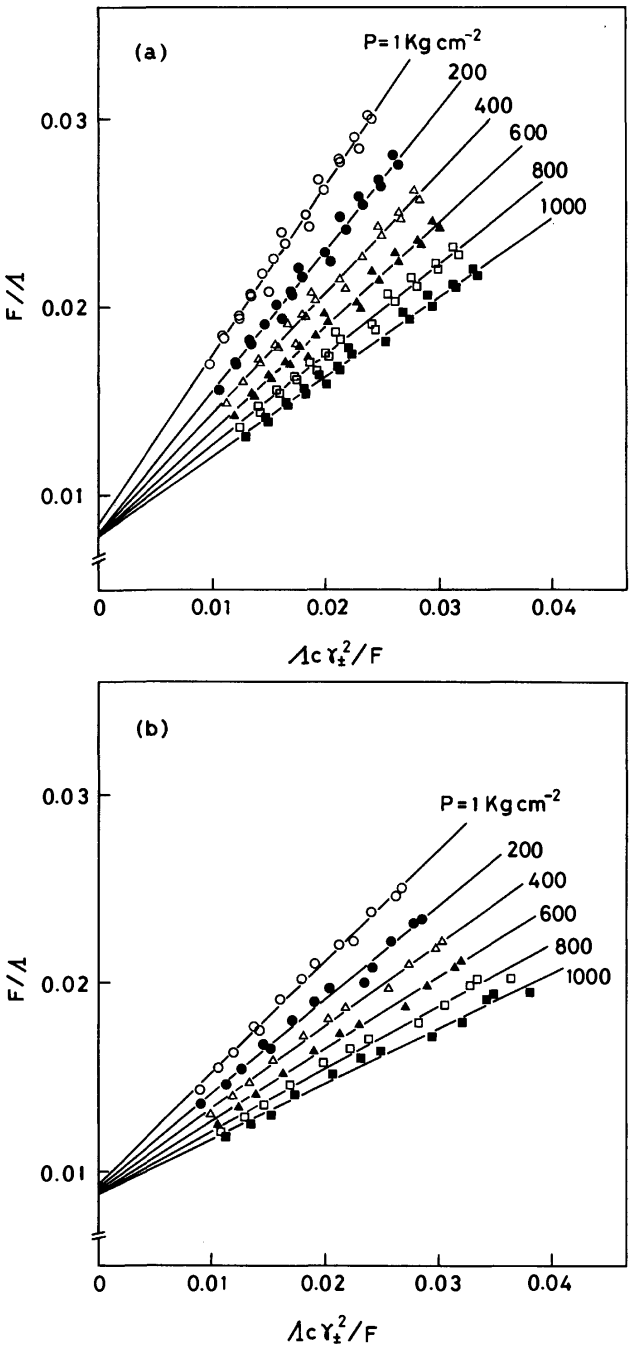

Fig. 1. Plot of conductivity data according to Eq. 1 for (a) nickel (II) malonate and (b) nickel (II) tartronate at 20 °C. Pressures are indicated in the figure.

Table 1. Stability Constants, K,[a] as a Function of Pressure at 20 °C and $I\rightarrow0$

	P/MPa					
	0.1	20	40	60	80	100
Nickel(II) malonate	12.3 (1.3)	11.2 (1.2)	10.4 (1.1)	9.21 (0.87)	7.90 (0.67)	6.84 (0.54)
Nickel(II) tartronate	6.77 (0.42)	5.93 (0.46)	5.37 (0.32)	4.94 (0.31)	4.12 (0.32)	3.80 (0.31)

a) In 10^3 mol^{-1} dm^3. Standard deviations estimated from the least-squares analysis are given in parentheses.

$$RT\left(\frac{\partial \ln K}{\partial P}\right)_T = -\Delta V^0 - RT\kappa_0, \quad (2)$$

where ΔV^0 is the reaction volume, i.e., the change in the partial molar volume at infinite dilution accompanied by the complex formation from a nickel(II) ion and ligand, κ_0 represents the solution compressibility, and other symbols have their usual meanings. In Eq. 2, $-RT\kappa_0$ is the correction term for the compression required when the concentration is expressed in terms of molarity and has a value of 1.1 $cm^3 mol^{-1}$[13a] for the present case. A plot of log K against pressure is shown in Fig. 2a, and log K shows a linear pressure dependence over the studied pressure range. From the slope of a straight line fitted using a least-squares method, the reaction volumes for nickel(II) malonate and nickel(II) tartronate were estimated according to Eq. 2. They are listed in Table 4 together with those obtained for other dicarboxylate ligands.

The rate constants for the complex formation reaction were determined from the pressure-jump relaxation data. The observed relaxation process was characterized by a single relaxation time in the measured concentration range. A reciprocal relaxation time for the reaction of Scheme 1 is given by Eq. 3.[14]

$$1/\tau = k_f[\gamma_\pm^2(c_{Ni}+c_L) + 1/K], \quad (3)$$

where k_f is the rate constant of the complex formation at zero ionic strength, c_{Ni} and c_L are the equilibrium concentration of nickel(II) and ligand ions, and $\gamma_\pm$ is the mean activity coefficient of the free ions at a given ionic strength.

The values of k_f were determined from the relaxation time using Eq. 3, where c_{Ni}, c_L, and $\gamma_\pm$ were calculated from the stability constant by a previously described procedure.[4] Some examples of the obtained results are shown in Table 2. The dissociation rate constants of the complex, k_d, were determined from the relation

$$k_d = k_f/K \quad (4)$$

The values of the rate constants, thus obtained, at various pressures are summarized in Table 3.

The activation volume of the reaction was estimated from the pressure dependence of the rate constant based on a relation analogous to Eq. 2.[13] Figures 2b and 2c show plots of log k_f and log k_d against pressure. In the studied pressure range, a linear relationship was obtained between the logarithm of the rate constant and the pressure. From the slope of the straight line (fitted by a least-squares method), the values of the activation volume for the complex formation, ΔV_f^*, and dissociation, ΔV_d^*, were estimated, and are listed in Table 4.

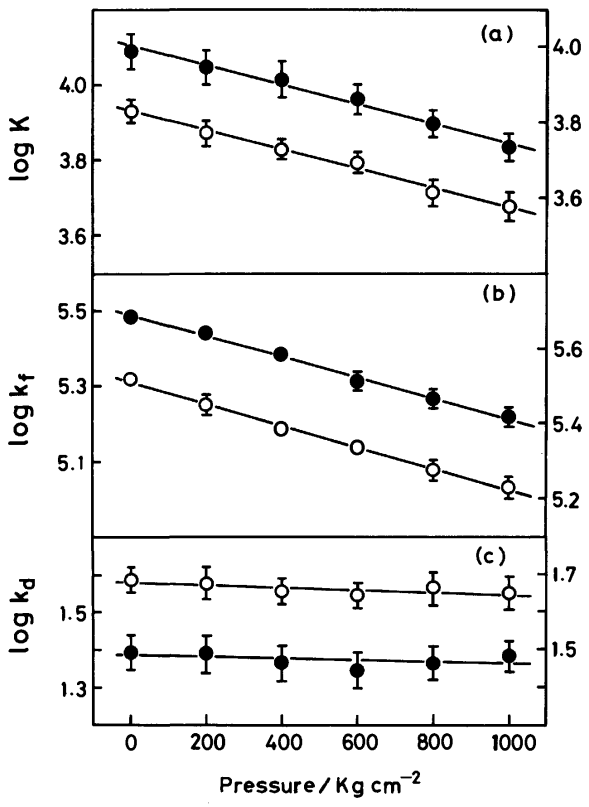

Fig. 2. Pressure dependence of (a) log K, (b) log k_f, and (c) log k_d at 20 °C: ●, nickel(II) malonate (left scale); ○, nickel(II) tartronate (right scale). Solid lines show the linear least-squares fits to the data points.

Discussion

It is considered that malonate ions form six-membered chelate complexes with nickel(II) ions in an aqueous solution, while succinate ions form monodentate complexes with nickel(II) ions rather than seven-membered chelate complexes. This may be justified from a comparison of the stability constant; the stability constant of nickel(II) succinate is much smaller than that of nickel(II) malonate. The glutarate ion and the adipate ion, which have longer methylene chains between two carboxyl groups, might also form a monodentate complexes. The difference in the structure of the complexes is reflected in the reaction volume. As can be seen in Table 4, succinate, glutarate, and adipate have similar values of ΔV^0 and are smaller than that for malonate.

The resultant volume change associated with the complex formation between metal ions and charged ligands may be divided into several contributions; i) the release of electrostriction due to the charge

Table 2. Relaxation Times and Rate Constants of Complex Formation for Nickel(II) Malonate and Nickel(II) Tartronate at 20 °C and $I \rightarrow 0$

$P=0.1$ MPa			$P=100$ MPa		
c[a] / 10^{-3} mol dm^{-3}	$1/\tau$ / s^{-1}	k_f / 10^5 mol^{-1} dm^3 s^{-1}	c[a] / 10^{-3} mol dm^{-3}	$1/\tau$ / s^{-1}	k_f / 10^5 mol^{-1} dm^3 s^{-1}
(a) Nickel(II) Malonate					
0.474	110	3.09	0.404	82.7	1.80
0.671	125	3.01	0.606	96.9	1.78
0.758	135	3.08	0.808	99.1	1.61
0.948	154	3.18	1.01	111	1.64
1.85	207	3.19	1.52	135	1.67
2.37	223	3.08	3.03	172	1.59
2.84	245	3.13	5.05	203	1.51
4.63	284	2.94	8.08	268	1.65
6.02	321	2.97	10.1	289	1.62
9.48	384	2.93			av. 1.65
		av. 3.06			
(b) Nickel(II) Tartronate					
0.578	172	3.27	0.578	135	1.85
0.771	202	3.41	0.771	150	1.84
0.962	215	3.30	1.16	151	1.57
1.16	231	3.28	1.35	186	1.82
1.35	244	3.25	1.54	187	1.74
1.54	248	3.12	1.93	200	1.69
1.93	317	3.63	2.31	222	1.75
2.31	312	3.31	2.89	238	1.71
2.89	327	3.16	3.28	227	1.55
3.28	365	3.34	3.86	249	1.59
3.86	398	3.40	4.43	265	1.61
4.43	382	3.09			av. 1.70
		av. 3.30			

a) Analytical concentration under atmospheric pressure.

Table 3. Rate Constants for the Complex Formation Reaction of Nickel(II) Malonate and Nickel(II) Tartronate as a Function of Pressure at 20 °C and $I \rightarrow 0$[a]

P/MPa	Nickel(II) malonate		Nickel(II) tartronate	
	$k_f/10^5$ / mol^{-1} dm^3 s^{-1}	k_d / 10 s^{-1}	$k_f/10^5$ / mol^{-1} dm^3 s^{-1}	k_d / 10 s^{-1}
0.1	3.06(0.09)	2.49(0.27)	3.30(0.15)	4.87(0.37)
20	2.76(0.14)	2.46(0.29)	2.82(0.17)	4.76(0.47)
40	2.42(0.10)	2.32(0.26)	2.43(0.12)	4.53(0.36)
60	2.05(0.12)	2.23(0.25)	2.18(0.10)	4.42(0.35)
80	1.84(0.10)	2.33(0.24)	1.90(0.12)	4.61(0.47)
100	1.65(0.09)	2.42(0.23)	1.70(0.11)	4.48(0.47)

a) Standard deviations estimated from the values at 9—13 different concentrations are shown in parentheses.

Table 4. Reaction Volumes, ΔV^0, and Activation Volumes, ΔV^*, for the Complex Formation of Nickel(II) with Carboxylate Ligands[a]

Ligands	ΔV^0	ΔV_f^*	ΔV_d^*
Succinate[b]	11.1±0.9	14.1±0.8	3.0±0.9
Glutarate	10.4±0.8[c]		
Adipate	11.2±0.7[c]		
Malonate	13.5±1.0	14.7±0.5	1.2±1.2
Tartronate	13.3±0.7	15.2±0.5	1.9±0.8

a) In cm^3 mol^{-1}; Errors are standard deviations estimated from the least-squares analysis. b) Ref. 4. c) Reaction volumes determined in our laboratory by the same method.

neutralization, ii) the elimination of solvated water around the coordinating group accompanied by the coordination bond formation to produce free water, iii) the difference in coordination bond length between a metal-water bond and a metal-ligand bond, and iv) for a chelating ligand, the increase of free volume, which is too small to be occupied by the solvent molecule, resulting from the formation of ring structure. The contributions from i), ii), and iv) are positive for volume increase in the system, while the sign of the contribution from iii) may depend on

the nature of metal-ligand bond. Since all ligands listed in Table 4 have the same electrical charge (−2), it can be regarded that contribution i) is the same for all ligands. The smaller values of ΔV^0 for a monodentate complex than for a chelate complex may be reasonable considering contributions ii) and iv).

The value of ΔV^0 for nickel(II) tartronate is essentially the same as that for nickel(II) malonate (Table 4). Malonate ions form six-membered chelate complexes coordinated by two carboxyl oxygens. For a chelate complex formed from a tartronate ion, three different structures may be expected; a six-membered chelate coordinated by two carboxyl oxygens, a five-membered chelate coordinated by one carboxyl oxygen and one hydroxyl oxygen, or a tridentate chelate coordinated by two carboxyl oxygens and one hydroxyl oxygen. That the ΔV^0 value of nickel(II) tartronate is comparable to that of nickel(II) malonate suggests that tartronate forms a six-membered chelate complex using two carboxyl oxygens. If tartronate forms a chelate using one carboxyl and one hydroxyl group or a tridentate chelate using two carboxyl and one hydroxyl groups, then a different ΔV^0 value from malonate should be expected from the contributions ii)—iv) described above; in fact, the reaction volume of 17.8 cm^3 mol^{-1} was obtained for nickel(II) malate which forms a chelate complex coordinated by one carboxyl and one hydroxyl groups.[15]

The metal complexation reaction has been generally interpreted in terms of a stepwise mechanism which was postulated by Eigen and discussed further by Wilkins.[16] For the bidentate chelate complex (as in the present case), this mechanism is represented by Scheme 2. In this scheme, I is a free ion, II is an

$$\underset{\text{I}}{Ni(H_2O)_6^{2+} + L\text{-}L^{2-}} \overset{K_{os}}{\rightleftharpoons} \underset{\text{II}}{(H_2O)_5Ni(H_2O)L\text{-}L} \overset{k_1}{\underset{k_{-1}}{\rightleftharpoons}} \underset{\text{III}}{(H_2O)_5Ni\text{-}L\text{-}L} + H_2O \overset{k_2}{\underset{k_{-2}}{\rightleftharpoons}} \underset{\text{IV}}{(H_2O)_4Ni\begin{pmatrix}L\\L\end{pmatrix}} + 2H_2O$$

Scheme 2.

outer-sphere complex, III is a monodentate complex with one end of the ligand left free, IV is a bidentate chelate complex, K_{os} is outer-sphere complex formation constant, and k's are the rate constants of the respective steps. Under the assumptions that I $\rightleftharpoons$ II is very rapid compared with other steps and that III is in a steady state, the overall rate constants are related to the rate constants of each step in Scheme 2 by the equations

$$k_f = K_{os}k_1\left(\frac{k_2}{k_2+k_{-1}}\right) \tag{5}$$

$$k_d = k_{-1}\left(\frac{k_{-2}}{k_2+k_{-1}}\right) \tag{6}$$

For the complex formation of nickel(II) malonate, the rate-determining step was assigned to the first-bond formation step (i.e., the formation of III) based on an analysis of the complexation rate constant.[17,18] This assignment is further supported from the present result that the activation volume ΔV_f^* for nickel(II) malonate is essentially the same as that for nickel(II) succinate for which the chelation process is lacking. This may also be the case for the complexation of nickel(II) tartronate, since ΔV_f^* is comparable to the other two ligands listed in Table 4. For a case in which the rate-determining step is the first-bond formation (i.e., $k_2 \gg k_{-1}$), Eqs. 5 and 6 are reduced to

$$k_f \simeq K_{os}k_1 \quad \text{and} \quad k_d \simeq k_{-1}/K_2, \tag{7}$$

where $K_2=k_2/k_{-2}$. Then, the overall activation volume can be approximately expressed by

$$\Delta V_f^* = \Delta V_{os}^0 + \Delta V_1^*, \tag{8}$$

$$\Delta V_d^* = \Delta V_{-1}^* - \Delta V_2^0, \tag{9}$$

where ΔV_{os}^0 and ΔV_2^0 are the reaction volumes for the outer-sphere complex formation and the chelate formation from monodentate intermediate, and ΔV_1^* and ΔV_{-1}^* are the activation volumes for the first bond formation and breaking.

The value of ΔV_{os}^0 is estimated to be approximately 7.2 cm^3 mol^{-1} for 2-2 electrolyte at 20 °C according to Hemmes[19] as mentioned in a previous paper.[4] Then, the values of ΔV_1^* can be estimated from Eq. 8 as follows; $\Delta V_1^*=7.5\pm0.5$ cm^3 mol^{-1} for nickel(II) malonate and 8.0 ± 0.5 cm^3 mol^{-1} for nickel(II) tartronate. These values show a close resemblance to the activation volume of the water exchange of the aquanickel(II) ion, $\Delta V_{H_2O}^*=7.2\pm0.3$ cm^3 mol^{-1}, obtained from a high-pressure NMR study.[20] This result suggests that the activated state for the first-bond formation process is the same as that for the water exchange process, where the bond between nickel(II) and leaving water molecule is loosened and somewhat lengthened.

The volume profile diagrams obtained for the complexation reaction of nickel(II) malonate and nickel(II) tartronate are shown in Fig. 3. The value of ΔV_1^0, which represents the volume difference between II and III, was estimated to be 4.3 cm^3 mol^{-1} from ΔV^0 and ΔV_{os}^0 for nickel(II) succinate.[4] This estimation is based on the facts that ΔV_1^0 corresponds to the volume change associated with the coordina-

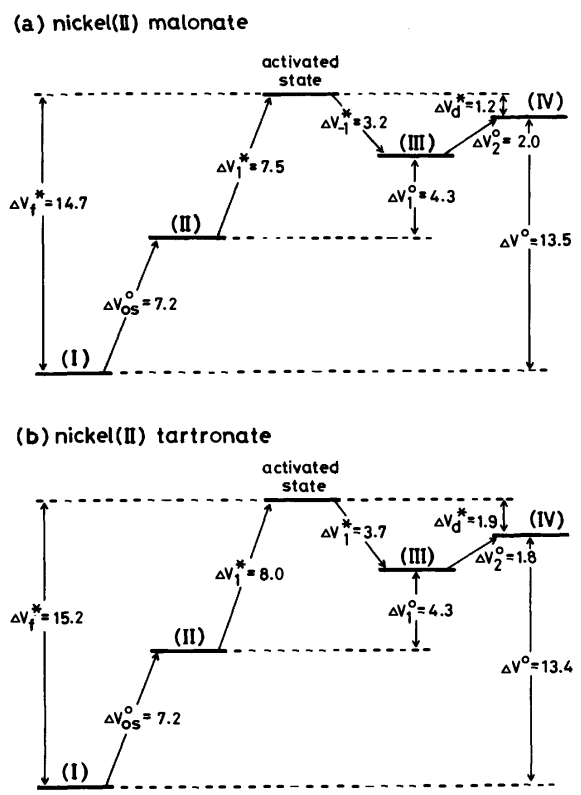

Fig. 3. Volume profile diagrams for the complex-formation reaction of nickel(II) malonate (a) and nickel(II) tartronate (b). I, II, III, and IV correspond to the species in Scheme 2. The values of volume change in $cm^3\ mol^{-1}$ are shown in the figure.

tion-bond formation by a carboxyl group after an outer-sphere complex forms, and nickel(II) succinate forms a monodentate complex coordinated by a single carboxyl group. An initial volume increase occurs due to the release of electrostriction upon forming the outer-sphere complex(II). It is followed by a volume increase due to the loosening of water-nickel(II) bonds to reach an activated state. Then, a volume decrease occurs upon going from the activated state to the monodentate complex(III) due to the completion of the coordination bond. It is again followed by a volume increase due to another coordination-bond formation to form a final chelate complex(IV). The positive ΔV_1^0 and ΔV_2^0 may be ascribed to the elimination of solvated water around the coordinating group due to the bond formation, which produces the free water and the resulting volume increase.

Features of the volume profiles for nickel(II) malonate and nickel(II) tartronate resemble each other. It is inferred from this result that the hydroxyl group on an α-carbon present in a tartronate ion has no significant role regarding both the mechanism of the complexation reaction and the final structure of the complex.

This work was supported financially in part by the Central Institute of Fukuoka University.

References

1) E. F. Caldin, M. W. Grant, and B. B. Hasinoff, *J. Chem. Soc., Faraday Trans. 1*, **68**, 2247 (1972); M. W. Grant, ibid., **69**, 560 (1973); M. W. Grant and C. J. Wilson, ibid., **72**, 1362 (1976); B. B. Hasinoff, *Can. J. Chem.*, **52**, 910 (1974); B. B. Hasinoff, ibid., **54**, 1820 (1976); B. B. Hasinoff, ibid., **57**, 77 (1979); E. F. Caldin and R. C. Greenwood, *J. Chem. Soc. Faraday Trans. 1*, **77**, 773 (1981).

2) S. Funahashi, K. Ishihara, and M. Tanaka, *Inorg. Chem.*, **20**, 51 (1981); K. Ishihara, S. Funahashi, and M. Tanaka, ibid., **22**, 194 (1983); K. Ishihara, S. Funahashi, and M. Tanaka, ibid., **22**, 2564 (1983); S. Funahashi, Y. Yamaguchi, and M. Tanaka, ibid., **23**, 2249 (1984).

3) P. J. Nichols, Y. Ducommun, and A. E. Merbach, *Inorg. Chem.*, **22**, 3993 (1983).

4) T. Inoue, K. Kojima, and R. Shimozawa, *Inorg. Chem.*, **22**, 3972 (1983).

5) T. Inoue, K. Sugahara, K. Kojima, and R. Shimozawa, *Inorg. Chem.* **22**, 3977 (1983).

6) T. Inoue, K. Kojima, and R. Shimozawa, *Chem. Lett.*, **1981**, 259.

7) E. Gelles and G. H. Nancollas, *J. Chem. Soc.*, **1956**, 4847.

8) E. Campi, *Ann. Chim. (Rome)*, **53**, 96 (1963).

9) R. M. Fuoss and C. A. Kraus, *J. Am. Chem. Soc.*, **55**, 476 (1933). R. M. Fuoss, ibid., **57**, 488 (1935).

10) P. W. Bridgman, "The Physics of High Pressure," G. Bell, London (1949).

11) V. S. K. Nair and G. H. Nancollas, *J. Chem. Soc.*, **1961**, 4367.

12) C. W. Davies, *J. Chem. Soc.* **1938**, 2093.

13) a) K. E. Weale, "Chemical Reactions at High Pressures," E. & F. N. Spon Ltd., London (1967); b) N. S. Isaacs, "Liquid Phase High Pressure Chemistry," John Wiley & Sons, New York (1981).

14) G. H. Czerlinski, "Chemical Relaxation," Marcel Dekker Inc., New York (1966).

15) The author's unpublished data.

16) M. Eigen and R. G. Wilkins, "Mechanisms of Inorganic Reactions," Adv. Chem. Ser. No. 49, American Chemical Society, Washington, DC (1965); R. G. Wilkins, *Acc. Chem. Res.*, **3**, 408 (1974).

17) J. L. Bear and C. T. Lin, *J. Phys. Chem.*, **72**, 2026 (1968).

18) F. P. Cavasino, *J. Phys. Chem.*, **69**, 4380 (1965); G. Calvaruso, F. P. Cavasino, and E. Di Dio, *J. Chem. Soc., Dalton Trans.* **1972**, 2632.

19) P. Hemmes, *J. Phys. Chem.*, **76**, 895 (1972).

20) Y. Ducommun, W. Earl, and A. E. Merbach, *Inorg. Chem.*, **18**, 2754 (1979); Y. Ducommun, K. E. Newman, and A. E. Merbach, ibid., **19**, 3696 (1980).

 © 1986 The Chemical Society of Japan Bull. Chem. Soc. Jpn., 59, 145—148 (1986)

Effect of Electrochemical Pretreatment on Catalytic Activity of Bismuth Ruthenate Electrodes for Oxygen Evolution in Alkaline Solution

Chiaki IWAKURA,* Toshiyuki EDAMOTO, and Hideo TAMURA
Department of Applied Chemistry, Faculty of Engineering, Osaka University,
Yamadaoka, Suita, Osaka 565
(Received August 28, 1985)

The catalytic activity of a film-type bismuth ruthenate electrode for oxygen evolution was greatly enhanced by the electrochemical pretreatment, including potential holding and cycling. On the other hand, any appreciable enhancement in catalytic activity was not observed for a pellet-type bismuth ruthenate electrode. Such an pretreatment effect was explained on the basis of the participation of higher valence Ru species in the oxygen evolution reaction, rather than the increase of surface area.

Metallic oxides with the pyrochlore structure such as bismuth and lead ruthenates ($Bi_2Ru_2O_7$, $Pb_2Ru_2O_{7-y}$) have been of increasing interest as electrode materials in recent years. Carcia et al.[1] have first reported that bismuth ruthenate thin film electrodes, prepared by rf sputtering directly onto heated Ti substrates, showed high activity for chlorine evolution. On the other hand, Horowitz et al.[2] have lately reported that in alkaline electrolyte bismuth and lead ruthenates, prepared mainly by the alkaline solution synthesis technique, displayed significantly lower polarizations than any other catalyst for oxygen evolution and were among the best for oxygen reduction. The oxygen reduction on bismuth and lead ruthenates, prepared by conventional solid state synthesis technique, has also been reported by Egdell et al.[3]

In the course of the studies on DSA-type metal oxide electrodes for oxygen evolution, we noticed that bismuth ruthenate film electrodes showed high catalytic activity for the reaction when they were pretreated electrochemically. The pretreatment included the potential holding and cycling. To date, the electrocatalytic activation of noble metal electrodes for oxygen and chlorine evolution reactions by potential cycling has been studied rather extensively.[4–10] However, many different interpretations have been proposed for the cause of the activity enhancement. The arguments seem to be principally divided into two groups: (1) Apparent activity enhancement by the increase in surface area and (2) intrinsic activity enhancement by the surface modification. This paper describes the work on the effect of electrochemical pretreatment on catalytic activity of bismuth ruthenate electrodes for oxygen evolution in alkaline solution, supporting the second view rather than the first view.

Experimental

Film- and pellet-types of bismuth ruthenate electrodes were used in this work. The film-type electrode ($Pt/Bi_2Ru_2O_7$) was prepared by a thermal decomposition method in the following way. First, a Pt substrate (2.5_4 cm^2) was mechanically polished with emery papers (≈#2000) and then degreased with a boiling 1 mol dm^{-3} KOH aqueous solution. Next, 0.05 cm^3 of (0.05 mol dm^{-3} $BiCl_3$ and 0.05 mol dm^{-3} $RuCl_3$)-containing 20 wt% HCl aqueous solution was applied to one side of the cleaned Pt substrate, dried at temperatures below 100 °C and then heated at 700 °C in air for 10 min. Such operations were repeated for 5 times. Finally, the resulting sample was heated at 700 °C for 1 h to decompose completely. On the other hand, the pellet-type electrode ($Bi_2Ru_2O_7$) was prepared by a coprecipitation method in the following way. First, the above mixed solutions of $BiCl_3$ and $RuCl_3$ were hydrolyzed by adding concentrated ammonia water. The resulting coprecipitate was washed thoroughly with distilled water and then dried at temperatures below 100 °C. Next, the dried sample was heated at 700 °C in air for 10 min, followed by grinding to powder with an agate mortar and a pestle. After such operations were repeated for 5 times, the powder was heated at 700 °C for 12 h. Finally, the heat-treated powder was mixed with 15 wt% of a binder (mp ca. 283 °C) and then pressed at 6000 kg cm^{-2} to form a pellet (1.3_3 cmϕ, ca. 0.05 mm thick). The pellet was heated at 240 °C and water-proofed by immersing in 10 wt% polystyrene-containing benzene solution. The X-ray diffraction patterns of the surface oxides of the electrodes thus obtained correspond to the formula $Bi_2Ru_2O_{7.3}$ as indicated in the ASTM card, however, the bismuth ruthenate electrodes will be represented by $Pt/Bi_2Ru_2O_7$ or $Bi_2Ru_2O_7$ in this paper because the oxygen content is still uncertain.

All electrochemical measurements, including cyclic voltammetry and polarization measurements, were carried out at 30 °C in 1 mol dm^{-3} KOH aqueous solution unless otherwise stated. The counter electrode used was a Pt plate with large surface area. A mercury (II) oxide electrode (Hg/HgO, 1 mol dm^{-3} KOH) was mainly used as the reference electrode.

The other experimental procedures and conditions will be described in the next section.

Results and Discussion

The film-type $Pt/Bi_2Ru_2O_7$ electrode was previously anodized at a constant potential (typically 0.7 V vs. Hg/HgO) for several tens minutes (typically 40 min). For each 10 min, the potential was cycled twice in the region between 0 and 0.7 V vs. Hg/HgO with a sweep rate of 0.1 V s^{-1} in order to check the catalytic

activity. However, the potential cycling should also be regarded as a part of the pretreatment because the pretreatment effect described later was not observed in the absence of the succeeding potential cycling (see Fig. 6) and because the same effect was observed when the potential cycling was continued for much longer time (say 50 min) without the preceding constant-potential anodization.

Typical cyclic voltammograms of the $Pt/Bi_2Ru_2O_7$ electrodes with and without pretreatment are shown in Fig. 1. It is evident that the current, or the catalytic activity, for oxygen evolution is appreciably enhanced by the pretreatment. Such a current enhancement phenomenon is not explicable by the change of surface area alone, because the surface area of the pretreated electrode was found to be only about 1.3 times that of the non-pretreated electrode as the result of the surface area determination both by Zn^{2+} ion adsorption method[11] and by cyclic voltammetry[12] and because the current enhancement was observed in alkaline solutions with relatively high pH values but scarcely in acidic solutions; for example, the electrode pretreated in 1 mol dm^{-3} KOH did not reveal any enhanced activity for oxygen evolution in 0.5 mol dm^{-3} H_2SO_4.

It can also be seen from Fig. 1 that the redox peaks at around 0.4 V vs. Hg/HgO become more conspicuous after pretreatment. The redox peaks may be attributable to either Ru^{4+}/Ru^{5+} or Ru^{4+}/Ru^{6+} as reported for the $Bi_2Ru_2O_7$[3] and $Ti/(RuO_2+TiO_2)$[13] electrodes, respectively, in alkaline solutions. The current enhancement factor, which was defined as the current density at a given potential (0.7 V vs. Hg/HgO) after pretreatment divided by the current density at the same potential before pretreatment, increased as the preanodization potential increased beyond ca. 0.4 V vs. Hg/HgO where the redox peaks appeared (see Fig. 1). Furthermore, a positive correlation was observed between the current enhancement factor and the charge passed in the redox peaks. These facts suggest the important role of the mixed valence Ru species in the pretreatment effect, in agreement with the view reported for the other kinds of electrodes.[4,7,8,10]

The film-type electrodes having different oxide compositions were prepared by changing the mole ratio of $BiCl_3$ to $RuCl_3$ while the total amount of them was kept constant at 1×10^{-5} mol cm^{-2}, and their catalytic activities for oxygen evolution were measured. Figure 2 shows the plots of current density at 0.7 V vs. Hg/HgO against Bi content in the oxide layer for the $Pt/Bi_xRu_{1-x}O_y$ ($0\leqslant x\leqslant 1$) electrodes with

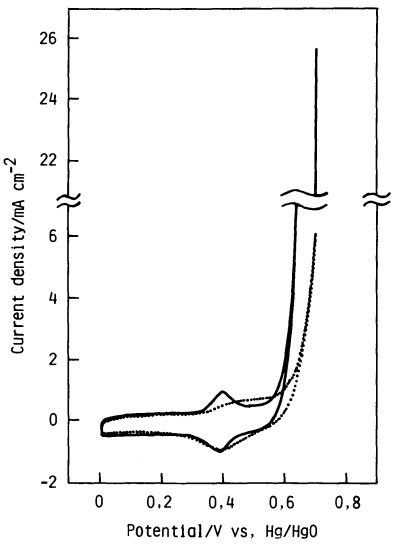

Fig. 1. Cyclic voltammograms of the film-type $Pt/Bi_2Ru_2O_7$ electrodes with (solid line) and without (dotted line) pretreatment, measured in 1 mol dm^{-3} KOH (sweep rate = 100 mV s^{-1}).

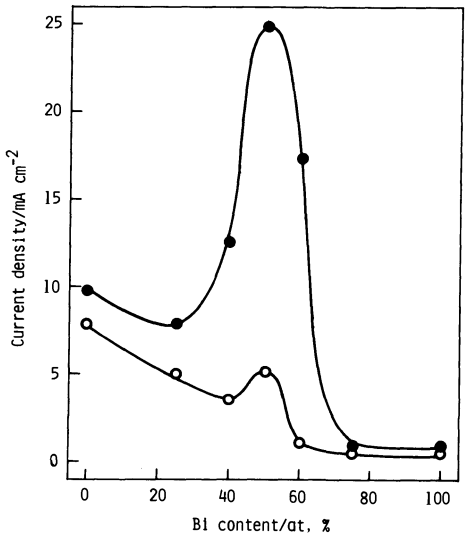

Fig. 2. Plot of current density at 0.7V vs. Hg/HgO against Bi content for the film-type $Pt/Bi_xRu_{1-x}O_y$ ($0\leqslant x\leqslant 1$) electrodes with (closed circle) and without (open circle) pretreatment.

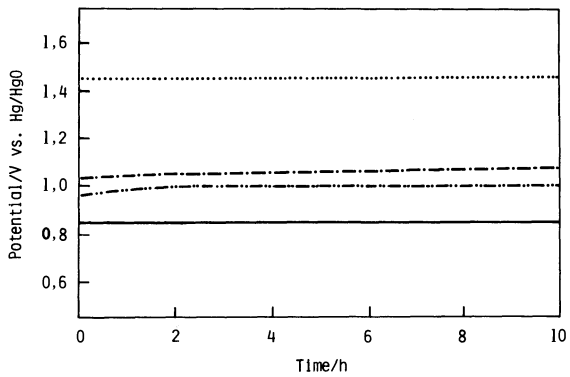

Fig. 3. Potential-time curves of the film-type $Pt/Bi_2Ru_2O_7$ and related electrodes under constant-current (0.1 A cm^{-2}) polarization in 1 mol dm^{-3} KOH. .....: Pt, —·—: $Pt/Bi_2Ru_2O_7$, —··—: Pt/RuO_2, ——: pretreated $Pt/Bi_2Ru_2O_7$.

and without pretreatment. The current for oxygen evolution has a maximum value at the oxide composition corresponding to $Bi_2Ru_2O_7$. It is to be noted that the catalytic activity for oxygen evolution of the $Pt/Bi_2Ru_2O_7$ electrode is rather low before pretreatment but is quite high after pretreatment, compared with that of the Pt/RuO_2 electrode. The superiority of the pretreated $Pt/Bi_2Ru_2O_7$ electrode over the Pt/RuO_2 electrode as well as the non-pretreated $Pt/Bi_2Ru_2O_7$ electrode in catalytic activity for oxygen evolution was confirmed by constant-current polarization measurements, as shown in Fig. 3 (see also Fig. 4). These findings suggest the special participation of Bi species in the pretreatment effect.

In contrast to the film-type $Pt/Bi_2Ru_2O_7$ electrode mentioned above, the pellet-type $Bi_2Ru_2O_7$ electrode showed no detectable pretreatment effect. Furthermore, the apparent redox peaks were observed on the cyclic voltammograms for the $Bi_2Ru_2O_7$ electrode even in the absence of pretreatment. Figure 4 shows galvanostatic polarization curves of the pellet-type electrodes together with the film-type electrodes. The pellet-type $Bi_2Ru_2O_7$ electrode exhibits the relatively high catalytic activity for oxygen evolution though it shows a steep rise in potential at high current densities, probably because of its low electrical conductivity. These observations are explained on the basis of the assumption that some Ru species exist in higher valence state on the surface of the as-prepared $Bi_2Ru_2O_7$ electrode, as well as the pretreated $Pt/Bi_2Ru_2O_7$ electrode.

The X-ray photoelectron spectroscopic (XPS) measurements were performed to get support for the above assumption. Figure 5 shows some XPS data obtained with the $Pt/Bi_2Ru_2O_7$ and $Bi_2Ru_2O_7$ electrodes. Evidently, the additional Bi peaks observed for the non-pretreated $Pt/Bi_2Ru_2O_7$ electrode in higher binding energies disappear in the case of the pretreated $Pt/Bi_2Ru_2O_7$ electrode, suggesting a valency change of Bi species in part from higher to lower oxidation states. Moreover, the Bi spectra of the pretreated $Pt/Bi_2Ru_2O_7$ electrode are similar to those observed for the $Bi_2Ru_2O_7$ electrode. On the other hand, the Ru spectra except for Ru $3d_{5/2}$ were unfortunately ambiguous for every electrode, due to the contamination by C 1s electron line at 285.0 eV. Though the further detail measurements are necessary, it appears more likely from the information obtained that the pretreatment effect is attributed to the formation of higher valence Ru species and the coexistence of Bi species may contribute to maintain the Ru species in higher valence state.

In order to prove the above view, the pretreatment effect was further examined with the other film-type electrodes ($Pt/Bi_{2-x}Co_xRu_2O_{7-y}$) prepared by partial substitution of Co^{2+} for Bi^{3+}.[14] As a result, the catalytic activity for oxygen evolution of these electrodes was found to be essentially high even before pretreatment and to increase with increasing Co content. The variation of current enhancement factor with preanodization time for the $Pt/Bi_{2-x}Co_xRu_{7-y}$ ($0 \leqslant x \leqslant 0.5$) electrodes is shown in Fig. 6. As expected, the current enhancement factor decreases with an increase in Co content. This can be explained by taking into account the valence change of Ru species by replacing Bi^{3+} with Co^{2+}, in addition to little contribution of Co oxide itself to the increased catalytic activity for oxygen evolution.

The mechanistic analysis was briefly done for the oxygen evolution reaction on the pretreated $Pt/Bi_2Ru_2O_7$ electrode and, as the result, the kinetics were found to be characterized by a Tafel slope of 0.042 V dec^{-1} and a reaction order with respect to OH^- ion of 1.12. It can therefore be presumed that the reaction mechanism as well as the rate-determining step is identical to that proposed for the

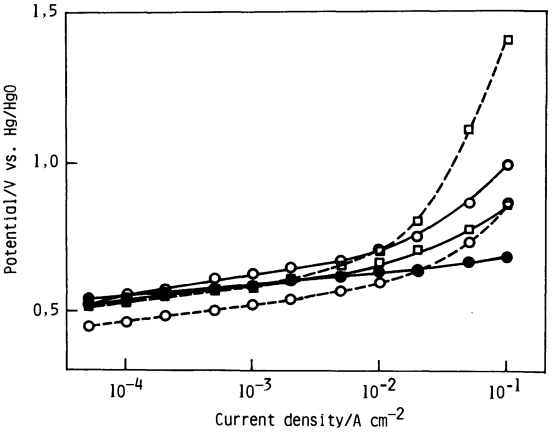

Fig. 4. Galvanostatic polarization curves of the film-type (solid line) and pellet-type(broken line) electrodes in 1 mol dm^{-3} KOH.
○: $Pt/Bi_2Ru_2O_7$, $Bi_2Ru_2O_7$, □: Pt/RuO_2, RuO_2,●: pretreated $Pt/Bi_2Ru_2O_7$.

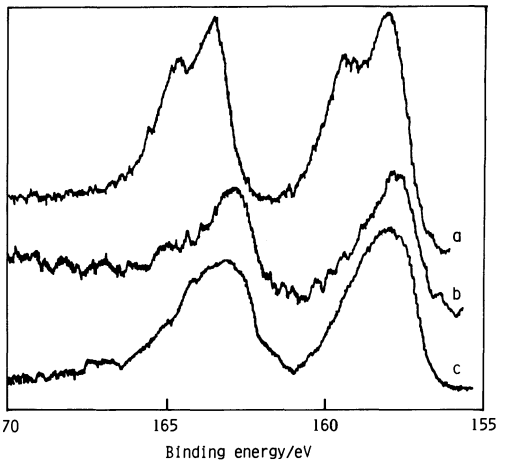

Fig. 5. XPS Bi $4f_{5/2,7/2}$ spectra of (a) $Pt/Bi_2Ru_2O_7$, (b) pretreated $Pt/Bi_2Ru_2O_7$ and (c) $Bi_2Ru_2O_7$ electrodes.

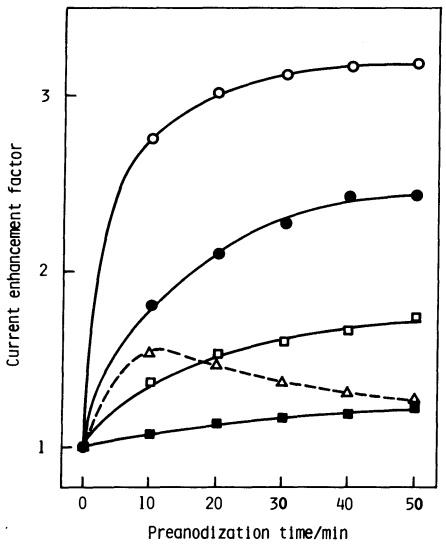

Fig. 6. Variation of current enhancement factor at 0.7V vs. Hg/HgO with preanodization time for the film-type $Pt/Bi_{2-x}Co_xRu_2O_{7-y}(0 \leqslant x \leqslant 0.5)$ electrodes.
○: $x=0$, ●: $x=0.1$, □: $x=0.2$, ■: $x=0.5$.
The broken line with triangles repersents a current enhancement factor vs. time curve for the $Pt/Bi_2Ru_2O_7$ electrode under constant-potential (0.7V vs.Hg/HgO) polarization.
The current enhancement factors are normalized to the values at a preanodization time of 0 min.

Ti/RuO_2 electrode,[15] in which the valence change of Ru species is virtually involved. According to such a mechanism, it is reasonable to expect that higher valence Ru species should cause modification of electron transfer rates and probably of adsorption of intermediates.

The authors wish to express their thanks to Toyo Soda Manufacturing Co, Ltd. for a financial support in a part of this work.

References

1) P. F. Carcia, R. B. Flippen, and P. E. Bierstedt, *J. Electrochem. Soc.*, **127**, 596 (1980).
2) H. S. Horowitz, J. M. Longo, and H. H. Horowitz, *J. Electrochem. Soc.*, **130**, 1851 (1983).
3) R. G. Egdell, J. B. Goodenough, A. Hamnett, and C. C. Naish, *J. Chem. Soc., Faraday Trans. 1*, **79**, 893 (1983).
4) S. Gottesfeld and S. Srinivasan, *J. Electroanal. Chem. Interfacial Electrochem.*, **86**, 89 (1978).
5) L. D. Burke and E. J. M. O'Sullivan, *J. Electroanal. Chem. Interfacial Electrochem.*, **97**, 123 (1979).
6) L. D. Burke and E. J. M. O'Sullivan, *J. Electroanal. Chem. Interfacial Electrochem.*, **117**, 155 (1981).
7) E. J. Frazer and R. Woods, *J. Electroanal. Chem. Interfacial Electrochem.*, **102**, 127 (1979).
8) J. Mozota, M. Vukovic, and B. E. Conway, *J. Electroanal. Chem. Interfacial Electrochem.*, **114**, 153 (1980).
9) J. Mozota and B. E. Conway, *J. Electrochem. Soc.*, **128**, 2142 (1981).
10) M. Vukovic, H. Angerstein-Kozlowska, and B. E. Conway, *J. Appl. Electrochem.*, **12**, 193 (1982).
11) A. Kozawa, *J. Inorg. Nucl. Chem.*, **21**, 315 (1961).
12) L. D. Burke and O. J. Murphy, *J. Electroanal. Chem. Interfacial Electrochem.*, **96**, 19 (1979).
13) L. D. Burke and O. J. Murphy, *J. Electroanal. Chem. Interfacial Electrochem.*, **109**, 199 (1980).
14) M. Schuler and S. Kemmler-Sack, *J. Less-Common Met.*, **102**, 105 (1984).
15) W. O'Grady, C. Iwakura, J. Huang, and E. Yeager, "Proceedings of the Symposium on Electrocatalysis," ed by M. W. Breiter, The Electrochemical Society, Inc., Princeton, New Jersey (1974), pp. 286—302.

 © 1986 The Chemical Society of Japan Bull. Chem. Soc. Jpn., 59, 149—154 (1986)

The Axial-Ligand Replacement of the [Tetrakis(1-methyl-4-pyridinio)-porphine]iron(III) Ion by the Cyanide Ion in a Highly Alkaline Aqueous Solution

Fumihiro ARIFUKU,* Kikujiro UJIMOTO, and Hirondo KURIHARA
Department of Chemistry, Faculty of Science, Fukuoka University,
Nanakuma, Jonan-ku, Fukuoka 814-01
(Received April 18, 1985)

The axial-ligand replacement of the [Tetrakis(1-methyl-4-pyridinio)porphine]iron(III) ion by the cyanide ion was investigated in a highly alkaline aqueous solution by means of the spectrophotometric method at 25 °C. In the course of the replacement, a protolytic equilibrium between monocyanomonoaqua- and monocyanomonohydroxo complex ions was observed; the p(K_a/mol dm^{-3}) value of the monocyanomonoaqua complex ion was found to be 12.2±1.1. In the formation of the dicyano complex ion, the rate-determining step was the second replacement of axial ligands, i.e., from the monocyano complex ion to the dicyano-complex ion; according as the pH is 11 or 13, the equilibrium constant was found to be 38.0 mol^{-1} dm^3 or 11.0, while the rate constant was 1.07×10^{-3} or 4.23×10^{-3} mol^{-3} dm^3 s^{-1}.

Iron porphyrin complexes are regarded as model compounds for studying the redox properties in the respiratory-electron-transport chain, which contains such elements as cytochromes.[1,2] In order to clarify the basic properties of iron porphyrins, we have been investigating the equilibrium situation and properties of the [Tetrakis(1-methyl-4-pyridinio)porphine]-iron(III) ion (abbreviated as Fe(III)-TMPyP) in aqueous solutions.[3] As a result of the investigation, it has been found that monomeric Fe(III)-TMPyP-$(H_2O)_2$, Fe(III)-TMPyP(OH)(H_2O), and Fe(III)-TMPyP$(OH)_2$ are, in turn, the predominant species in the solutions with pH values of pH<5.5, 5.5<pH<12 and pH>12 respectively; it has also been found that monomeric Fe(II)-TMPyP$(H_2O)_2$ and Fe(II)-TMPyP(OH)(H_2O) are predominant in the ranges of pH<11.5 and pH>11.5 respectively.

As subsequent experiments, we intended to investigate the effects of axial ligands on the redox potential. The cyanide ion was chosen as an axial ligand to investigate at first, because the preliminary experiments on the axial-ligand replacement of aqua- or hydroxo-Fe(III)-TMPyP ion by various ligands showed that only the addition of the cyanide ion induced shifts both in the position of the Soret band and in the redox potential of the central metal (Fe(III)/Fe(II)).

The substitution equilibria for various axial ligands of Fe(III)-TMPyP ions have previously been reported by Fleischer et al.,[4,5] Pasternack et al.,[6,7] Goff and Morgan,[8,9] and Weinraup et al.[10] However, for a monocyano Fe(III)-TMPyP ion in an aqueous solution, the kind of axial ligand at the trans position to CN^- can not be inferred from the descriptions in those papers or also in the paper relating to the axial-ligand replacement of Cr(III)-TMPyP by CN^-.[11]

The main purpose of the present paper is to infer the axial ligand at the trans position to the cyano group in the monocyano Fe(III)-TMPyP ion in an aqueous solution and to determine the equilibrium constant in the protolytic equilibrium between different monocyano ions and kinetic parameters for the axial replacement of the Fe(III)-TMPyP ion by the cyanide ion.

Experimental

Fe(III)-TMPyP perchlorate was prepared by metal insertion into TMPyP tetra(*p*-toluenesulfonate) (Dojindo Laboratories) with Mohr's salt according to the method of Hambright and Fleischer,[12] with a slight modification, and was stored in an about 3.5×10^{-4} mol dm^{-3} aqueous solution. All the other chemicals were of a guaranteed reagent grade (Wako Pure Chemical Industries) and were used without further purification.

The concentration of the Fe(III)-TMPyP stok solution was accurately determined spectrophotometrically by the use of a molar-absorption coefficient at 403 nm: 1.02×10^5 mol^{-1} dm^3 cm^{-1} at pH 2 and an ionic strength of 0.1 mol dm^{-3}.[6] Sample solutions were prepared by diluting the stock solution with deionized distilled water. The pH of the sample solution was then adjusted with a sodium hydroxide solution. The ionic strength was adjusted to 0.1 mol dm^{-3} with a sodium sulfate solution except when the pH was above 13.

A Hitachi 228 spectrophotometer was used for the spectrophotometric investigation. Measurements of the pH were made on a TOA HM-5B pH meter. The concentrations of the cyanide ion are expressed by the values calculated from the weight of the potassium cyanide dissolved.

The equilibrium constant and the number of protons transferred between the different monocyano complexes were obtained by spectrophotometric pH titration at a constant pCN; on the contrary, the formation constant and the number of cyanide ions transferred between monocyano and dicyano complexes were obtained by pCN titration at a constant pH.

The rate of cyano substitution was measured as follows. A small volume of a 1.00 mol dm^{-3} KCN aqueous solution, adjusted to the appropriate pH, was added quickly to a dilute Fe(III)-TMPyP aqueous solution adjusted to the

same pH as the KCN solution. The resulting mixed solution, which included a large excess of cyanide ions to Fe(III)-TMPyP, was stirred vigorously. Then, the time-course of the absorbance at the Soret peak of the dicyano complex in the mixed solution was followed on the spectrophotometer.

All the measurements were performed at 25 °C.

Results and Discussion

Time-Course of Absorption Spectra after the Addition of CN^-. Fe(III)-TMPyP species in aqueous solutions are predominantly present as a monoaquamonohydroxo complex at pH 11 and as a dihydroxo complex at pH 13.[3] A solution of potassium cyanide was added to a Fe(III)-TMPyP solution of pH 11 or 13. Figure 1 shows the time-course of the visible spectra of the Fe(III)-TMPyP solutions after the addition of KCN. The dotted lines represent the spectra of CN^--free solutions; the other lines are the spectra of the mixed solutions containing Fe(III)-TMPyP and KCN at concentrations of 1.00×10^{-5} mol dm^{-3} and 5.00×10^{-2} mol dm^{-3} respectively. At both pH 11 and 13, the Soret band shows the characteristic maximum absorption peaks for the species formed by the 1st or 2nd substitution by

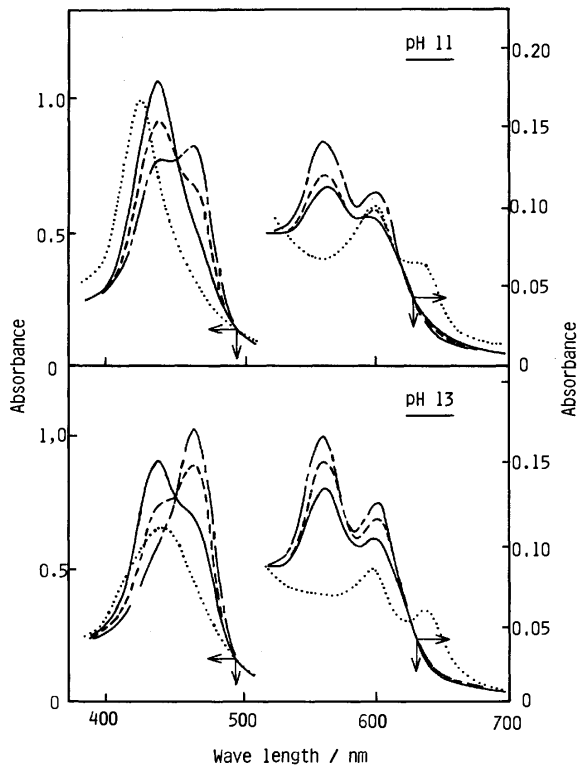

Fig. 1. The time-course of absorption spectra of Fe(III)-TMPyP aqueous solutions after addition of cyanide ion.
·····: No addition, ——: 2 min, — —: 30 min, — — —: 4 h 10 min (pH 11) or 2 h (pH 13).
Fe(III)-TMPyP: 1.00×10^{-5} mol dm^{-3}, KCN: 5.00×10^{-2} mol dm^{-3}.

CN^-. On the other hand, the Q (0—0 and 0—1) band shows the blue shift by ca. 20 nm due to the 1st substitution by CN^-, while, because of the 2nd substitution by CN^-, no shift, but an increase in the Q band, was observed. These spectral changes may be attributable to the following step-by-step substitution reactions, Eq. 1 or 2, at pH 11 or 13:

$$\underset{\text{(I)}}{\text{Fe(III)-TMPyP(H}_2\text{O)(OH)}} \rightleftharpoons \underset{\text{(II)}}{\text{Fe(III)-TMPyP(H}_2\text{O)}_2} \rightleftharpoons \underset{\text{(III)}}{\text{Fe(III)-TMPyP(CN)}_2}, \quad (1)$$

$$\underset{\text{(I')}}{\text{Fe(III)-TMPyP(OH)}_2} \rightleftharpoons \underset{\text{(II')}}{\text{Fe(III)-TMPyP(OH)(CN)}} \rightleftharpoons \underset{\text{(III)}}{\text{Fe(III)-TMPyP(CN)}_2}. \quad (2)$$

As may be seen in Fig. 1, the monocyano complexes, II and II', both have Soret bands with the same maximum absorption wavelength, 437 nm, and their Q band spectra are similar in shape.

The 2nd substitution is much slower than the 1st substitution. An electron-withdrawing property of CN^-, caused by back-donation to its empty antibonding π-orbital, probably makes the 2nd substitution slow down compared to the 1st step. Within two minutes after the addition of CN^-, the 1st step of substitution is almost complete, while the 2nd step seems to have proceeded slightly, as is shown in Fig. 1.

At pH 13, the absorption band of 437 nm (the Soret band of II') was scarcely observed after two hours, while at pH 11 the peak of 437 nm remained distinctly even after four hours. Such observation indicates that the 2nd step of substitution at pH 13 is faster than that at pH 11, even though the concentration of hydroxide ions in the pH 13 solution is about 100 times that in the pH 11 solution. If the II species is the same as II', the rate of the 2nd substitution step at pH 11 should be faster than that at pH 13. Therefore, in spite of the similarity in shape of the two absorption spectra, the II species differs from the II' species; they are identified as Fe(III)-TMPyP(H_2O)(CN) and Fe(III)-TMPyP(OH)(CN) respectively.

Acid-Dissociation Equilibrium of Fe(III)-TMPyP-(H_2O)(CN). Figure 2 shows the spectrophotometric pCN titration curves of Fe(III)-TMPyP obtained at the Soret-band maximum of the III species, 465 nm. A change in absorption attributable to an equilibrium between monocyano and dicyano complexes is observed in the pCN range from 1 to 3, and in the pCN range above 4 the absorption is gradually reduced with an increase in the value of pCN because of a dissociation equilibrium of

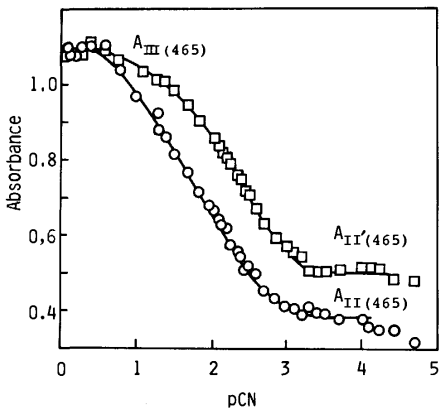

Fig. 2. Spectrophotometric pCN titration curves for Fe(III)-TMPyP in aqueous solutions at pH 11 (○) and 13 (□).
$A_{II(465)}$: Absorbance of monocyano complex at pH 11.
$A_{II'(465)}$: Absorbance of monocyano complex at pH 13.
$A_{III(465)}$: Absorbance of dicyano complex.
Fe(III)-TMPyP: 1.00×10^{-5} mol dm^{-3}.

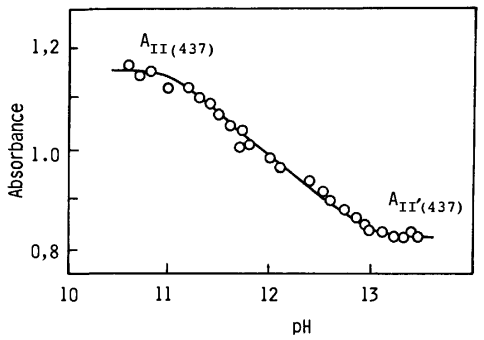

Fig. 3. Spectrophotometric pH titration curve at 437 nm for Fe(III)-TMPyP aqueous solutions containing cyanide ion.
Fe(III)-TMPyP: 1.00×10^{-5} mol dm^{-3}.
KCN: 3.00×10^{-4} mol dm^{-3}.

the two monocyano complexes. In this figure, $A_{III(465)}$ represents the absorbance at a high concentration of CN^-, while $A_{II(465)}$ and $A_{II'(465)}$ represent the absorbances at pH 11 and 13 respectively at a low concentration of CN^-, i.e., $3<pCN<4$. Although the average values of $A_{III(465)}$ obtained separately at pH 11 and 13 virtually agreed with each other, the values of $A_{II(465)}$ and $A_{II'(465)}$ differ from one another, suggesting a change in the monocyano complex species with the pH.

Therefore, a spectrophotometric pH titration of complex solutions of pCN 3.52 was carried out over the pH range from 10.5 to 13.5 at 437 nm, which was the Soret maximum wavelength of the II and II′ species. The monocyano complexes are the predominant species in solutions with this pCN value, as is shown in Fig. 2. Figure 3 shows the titration curve thus obtained, indicating the existence of the following equilibrium between the II and II′ species:

$$\underset{(II)}{Fe(III)\text{-}TMPyP(H_2O)(CN)} \overset{K_a}{\rightleftharpoons} \underset{(II')}{Fe(III)\text{-}TMPyP(OH)(CN)} + nH^+ \quad (3)$$

$$K_a = \frac{[II'][H^+]^n}{[II]} \quad (4)$$

The value of pK_a was obtained from the data in Fig. 3 using Eq. 5:

$$\log \frac{|A_{II(437)} - A_{(437)}|}{|A_{(437)} - A_{II'(437)}|} = n\cdot pH - pK_a \quad (5)$$

A plot of the left-hand side of Eq. 5 vs. pH gives a straight line, as is shown in Fig. 4. The values of $p(K_a/\text{mol dm}^{-3})$† and n were estimated to be 12.2±1.1 and 1.02±0.09 from the slope and the intercept respectively of this straight line. Since the n value is close to unity, the equilibrium between Fe(III)-TMPyP(H_2O)(CN) and Fe(III)-TMPyP(OH)(CN) consists of one proton-transfer step. The molar absorption coefficients of the II, II′, and III species at 437 and 465 nm were also obtained from the data in Figs. 2 and 3; they are listed in Table 1.

Formation Constant of Fe(III)-TMPyP(CN)$_2$. Figure 1 indicates that the first step of CN^- substitution is rapid enough and that the second step is the rate-determining step in the presence of a large excess of CN^- to the complex. Therefore, the concentrations of the I and I′ species can be ignored except for an extremely early stage of substitution. Then, the reactions observed at pH 11 and 13 are approximately represented by:

$$II + CN^- \underset{k_b}{\overset{k_f}{\rightleftharpoons}} III \quad (6)$$

and:

$$II' + CN^- \underset{k'_b}{\overset{k'_f}{\rightleftharpoons}} III + OH^- \quad (7)$$

Table 1. Molar-Absorption Coefficients at 437 and 465 nm of Monocyano and Dicyano Complexes at pH 11 and 13

Wavelength	437 nm	465 nm
pH 11		
ε_{II}/mol^{-1} dm^3 cm^{-1}	1.15×10^5	3.87×10^4
ε_{III}/mol^{-1} dm^3 cm^{-1}	—	1.10×10^5
pH 13		
$\varepsilon_{II'}$/mol^{-1} dm^3 cm^{-1}	8.30×10^4	5.06×10^4
ε_{III}/mol^{-1} dm^3 cm^{-1}	—	1.09×10^5

† K_a is the equilibrium constant in terms of concentration.

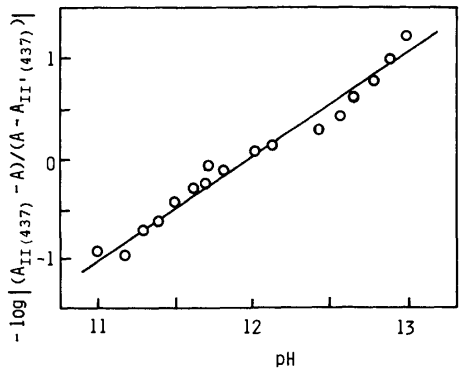

Fig. 4. Plot of left-hand side of Eq. 5 vs. pH.

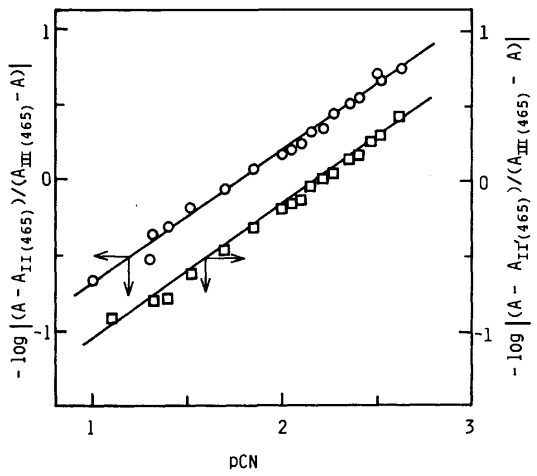

Fig. 5. Plots of left-hand sides of Eqs. 10 (○) and (11) (□) vs. pCN.

respectively, where k_f and k_f' are the formation rate constants of the III species and where k_b and k_b' are the rate constants of the reverse reactions. The values of the 2nd step-by-step formation constants of the III species at pH 11 and 13, as expressed by Eqs. 8 and 9, can be determined from the data in Fig. 2 and the molar absorption coefficient of the II and II′ species, by the use of Eqs. 10 and 11:

$$K = \frac{[\mathrm{III}]}{[\mathrm{II}][\mathrm{CN^-}]} = \frac{k_f}{k_b}, \tag{8}$$

$$K' = \frac{[\mathrm{III}][\mathrm{OH^-}]}{[\mathrm{II'}][\mathrm{CN^-}]} = \frac{k_f'}{k_b'}, \tag{9}$$

$$-\log\frac{|A_{(465)} - A_{\mathrm{II}(465)}|}{|A_{\mathrm{III}(465)} - A_{(465)}|} = pK + \mathrm{pCN}, \tag{10}$$

$$-\log\frac{|A_{(465)} - A_{\mathrm{II'}(465)}|}{|A_{\mathrm{III}(465)} - A_{(465)}|} = pK' + \log[\mathrm{OH^-}] + \mathrm{pCN}. \tag{11}$$

Figure 5 shows the linear relationship between the left-hand side of Eq. 10 or 11 and pCN. The transfer number of CN^- and the values of pK and pK' were obtained from the slope and the intercept at pCN=0 of these lines; they are listed in Table 2. The number of transferred CN^- at pH 11 is considerably smaller than unity.

Table 2. Equilibrium Constants and Number of Transfered Cyanide Ions between Monocyano and Dicyano Complexes at pH 11 and 13

	K/mol^{-1} dm^3	K'	n
pH 11	38.0	—	0.884
pH 13	—	11.0	0.919

Formation Rate Constant of the Dicyano Complex. Assuming Eq. 6 or 7 for the observed substitution, the formation rate or the III species is represented by:

$$\frac{d[\mathrm{III}]}{dt} = k_f[\mathrm{P}][\mathrm{CN^-}] - k_f\left([\mathrm{CN^-}] + \frac{1}{K}\right)[\mathrm{III}] \tag{12}$$

or:

$$\frac{d[\mathrm{III}]}{dt} = k_f'[\mathrm{P}][\mathrm{CN^-}] - k_f'\left([\mathrm{CN^-}] + \frac{[\mathrm{OH^-}]}{K'}\right)[\mathrm{III}], \tag{13}$$

where [P] is the total concentration of the complex species. In the presence of a large excess of CN^- to the complex species, therefore, the rate equation for substitution is expressed by Eq. 14 or 15 according as the pH value is 11 or 13:

$$\ln\left(\alpha - \frac{[\mathrm{III}]}{[\mathrm{P}]}\right) = \ln\alpha - k_f\beta t, \tag{14}$$

$$\ln\left(\alpha' - \frac{[\mathrm{III}]}{[\mathrm{P}]}\right) = \ln\alpha' - k_f'\beta' t, \tag{15}$$

where $\alpha = 1/(1+1/K[\mathrm{CN^-}])$, $\alpha' = 1/(1+[\mathrm{OH^-}]/K'[\mathrm{CN^-}])$, $\beta = 1/K + [\mathrm{CN^-}]$ and $\beta' = [\mathrm{OH^-}]/K' + [\mathrm{CN^-}]$.

If the formation constant of the III species and the molar-absorption coefficient of the monocyano and dicyano complexes are known, the concentration of the III species can be obtained from the observed absorbance at an appropriate wavelength using Eq. 16 or 17 according as the pH value is 11 or 13:

$$[\mathrm{III}] = \frac{\mathrm{Abs}}{\varepsilon_{\mathrm{II}}/K[\mathrm{CN^-}] + \varepsilon_{\mathrm{III}}} \tag{16}$$

or:

$$[\mathrm{III}] = \frac{\mathrm{Abs}}{\varepsilon_{\mathrm{II'}}[\mathrm{OH^-}]/K'[\mathrm{CN^-}] + \varepsilon_{\mathrm{III}}}, \tag{17}$$

where Abs is the absorbance at a certain wavelength and where $\varepsilon_{\mathrm{II}}$, $\varepsilon_{\mathrm{II'}}$, and $\varepsilon_{\mathrm{III}}$ are the respective molar-absorption coefficients of the II, II′ and III species at the same wavelength. Consequently, the rate constants, k_f and k_f' can be obtained by the use of Eqs.

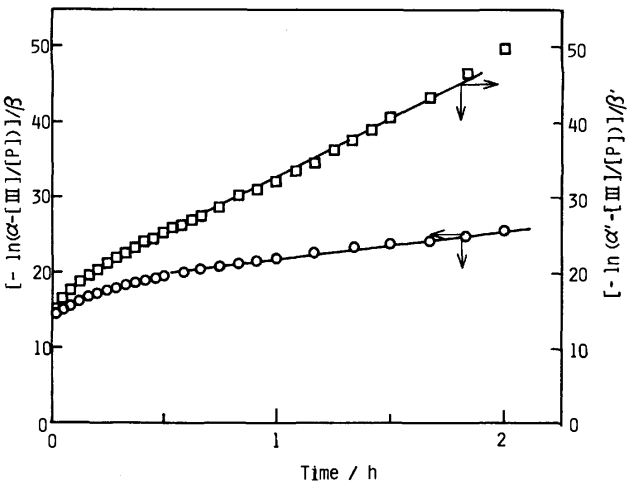

Fig. 6. Plots of $[-\ln(\alpha-[III]/[P])]/\beta$ vs. time (○ at pH 11) and $[-\ln(\alpha'-[III]/[P])]/\beta'$ vs. time (□ at pH 13).

14 and 15.

Figure 6 shows the plots of $[-\ln(\alpha-[III]/[P])]/\beta$ at pH 11 and $[-\ln(\alpha'-[III']/[P])]/\beta'$ at pH 13 against the reaction time t calculated from the data of the time-course of absorbance at 465 nm, the Soret maximum of the III species, after the addition of CN^- to a Fe(III)-TMPyP solution, in which the concentrations of the complex species and CN^- were 1.00×10^{-5} and 5.00×10^{-3} mol dm^{-3} respectively in a mixed solution. These lines show a good linearity except for the initial stage of reactions. The rate constants of formation were obtained from the slopes of these straight lines, and the rate constants of the reverse reaction, k_b and k_b' were calculated by the use of Eqs. 8 and 9. The values of the constants are listed in Table 3. The value of k_f' is almost four times that of k_f. This apparently indicates that the CN^- ion replaces the axial hydroxo ligand more easily than the axial aqua ligand in an aqueous solution, though this seems unreasonable because of the repulsion between the negative-charged ions. This finding may be interpreted in terms of the difference in the spin state of monocyano-complexes, as will be described in the next section.

Mechanisms of Substitution. The mechanism of the substitution of CN^- for the axial ligand of the Fe(III)-TMPyP species in a highly alkaline aqueous solution is summarized in Scheme 1. The solid lines express the main routes of substitution, while the dashed lines express the alternative routes.

Since the II and II′ species differ from one another, and since the pK_a value of the II species is 12.2 in the protolytic equilibrium between II and II′, the predominant monocyano species in aqueous solutions have been regarded as Fe(III)-TMPyP(H_2O)(CN) at pH 11 and Fe(III)-TMPyP(OH)(CN) at pH 13. It is considered hardly possible, because of the negative

Table 3. Rate Constants of the Axial Replacement of Monocyano and Dicyano Complexes

pH 11	
k_f/mol^{-1} dm^3 s^{-1}	1.07×10^{-3}
k_b/s^{-1}	2.82×10^{-5}
pH 13	
k_f'/mol^{-1} dm^3 s^{-1}	4.23×10^{-3}
k_b'/mol^{-1} dm^3 s^{-1}	3.83×10^{-4}

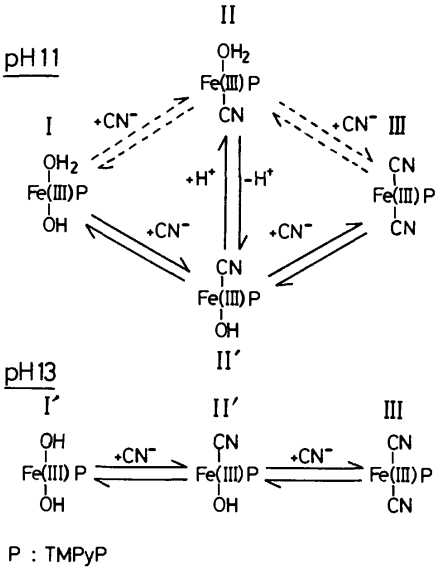

Scheme 1.

charge of the cyanide ion and the stronger donation of the hydroxo ligand than that of the aqua ligand, that the cyanide ion prefers to replace the hydroxo ligand rather than the aqua ligand of the monoaquamonohydroxo complex (I).[13,14] Therefore, the monohydroxomonocyano complex (II′) is probably formed first by the replacement of the species I; then the rapid protolysis[15] follows to give monoaquamonocyano complex (II) at pH 11.

In the 2nd substitution, the cyanide ion replaces the ligand at the trans position to the cyano-ligand of II′ more easily than that of II, as may be seen in Fig. 1 and Table 3. This behavior is presumably attributable to the difference in the spin states of monocyano-complexes; that is, the spin state of the II′ species, in comparison with that of II, is close to that of III.[16,17] Therefore, the 2nd substitution at pH 11 occurs via the II′ species as an intermediate; this species exists in a smaller quantity relative to the II species. Therefore, the value of the apparent rate constant, k_f, at pH 11 is smaller (seemingly by about one fourth) than the k_f' at pH 13. Similarly, it is probably ascribable to the similarity in the spin state between I′ and II′ species that the 1st substitution at pH 13 is faster than that at pH 11, as may be seen in

Fig. 1.

The authors wish to thank Miss Chie Fukuzawa for her technical collaboration and Professor Hiroko Shimada, Fukuoka University, for her valuable comments. The present work was partially supported by a Grant-in-Aid for Scientific Research (No. 57740327) from the Ministry of Education, Science and Culture, and a grant from the Central Research Institute of Fukuoka University.

References

1) E. B. Bowden and F. M. Hawkridge, *A. C. S. Advan. Chem.*, **201**, 159 (1982).
2) M. J. Eddowes and H. A. O. Hill, *A. C. S. Advan. Chem.*, **201**, 173 (1982).
3) H. Kurihara, F. Arifuku, I. Ando, M. Saita, R. Nishino, and K. Ujimoto, *Bull. Chem. Soc. Jpn.*, **55**, 3515 (1982).
4) E. B. Fleischer, J. M. Palmer, T. S. Srivastava, and A. Chattergee, *J. Am. Chem. Soc.*, **93**, 3162 (1971).
5) E. B. Fleischer and D. A. Fine, *Inorg. Chem. Acta*, **29**, 267 (1978).
6) R. F. Pasternack, H. Lee, P. Malek, and C. Spencer, *J. Inorg. Nucl. Chem.*, **39**, 1865 (1877).
7) R. F. Pasternack, B. S. Gillies, and J. R. Stahlbush, *J. Am. Chem. Soc.*, **100**, 2613 (1978).
8) H. Goff and L. O. Morgan, *Inorg. Chem.*, **15**, 2062 (1976).
9) H. Goff and L. O. Morgan, *Inorg. Chem.*, **15**, 2069 (1976).
10) D. Weinraup, P. Peretz, and M. Faraggl, *J. Phys. Chem.*, **86**, 1839 (1982).
11) J. G. Leipoldt, S. S. Basson, and D. R. Rabie *J. Inorg. Nucl. Chem.*, **43**, 3239 (1981).
12) P. Hambright and E. B. Fleischer, *Inorg. Chem.*, **9**, 1757 (1970).
13) K. R. Ashley, J. G. Leipoldt, and V. K. Joshi, *Inorg. Chem.*, **19**, 1608 (1980).
14) D. Thusius, *Inorg. Chem.*, **10**, 1106 (1971).
15) R. F. Pasternack and M. A. Cobb, *J. Inorg. Nucl. Chem.*, **35**, 4327 (1973).
16) J. Beetlestone and P. George, *Biochem.*, **3**, 707 (1964).
17) D. W. Smith and R. J. P. Williams, *Biochem. J.*, **110**, 297 (1968).

 © 1986 The Chemical Society of Japan Bull. Chem. Soc. Jpn., 59, 155—159 (1986)

The Synthesis, Magnetic, and Spectroscopic Properties of Binuclear Iron(III) Complexes Bridged by Pyrazine, 1,1′-Tetramethylenebis(imidazol), or Bis(pyridine) Compounds Exhibiting a Spin-Equilibrium Behavior

Shoichi Ohta, Chikako Yoshimura, Naohide Matsumoto, Hisashi Okawa,† and Akira Ohyoshi*

Department of Synthetic Chemistry, Faculty of Engineering, Kumamoto University, Kurokami 2-39-1, Kumamoto 860

†Department of Chemistry, Faculty of Science, Kyushu University, Hakozaki, Higashi-ku, Fukuoka 812

(Received June 5, 1985)

Five binuclear iron(III) complexes bridged by pyrazine, 1,1′-tetramethylenebis(imidazol), or bis(pyridine) compounds with the formula of $[LFe(Bge)FeL](BPh_4)_2$ have been prepared, and their spin-equilibrium behavior between high-spin($S=5/2$) and low-spin($S=1/2$) states has been investigated by means of the temperature dependences of the magnetic susceptibilities and the electronic spectra, where Bge denotes pyrazine, 1,1′-tetramethylenebis(imidazol), 4,4′-bipyridine, 4,4′-ethylenebis(pyridine), or 4,4′-vinylenebis(pyridine), L=bis(3-salicylideneaminopropyl)amine, and BPh_4^-=tetraphenylborate. The pyrazine complex is low-spin, while the bis(imidazole) and the bis(pyridine) complexes showed a spin-equilibrium between high-spin and low-spin states, accompanied by a striking thermochromism in both the solids and solutions.

Previously, we have shown that a series of iron(III) complexes with the general formula of $[FeXL]^{n+}$ ($n=0,1$) are a new family among spin-equilibrium iron(III) complexes.[1] In these complexes, the pentadentate ligand (L=bis(3-salicylideneaminopropyl)amine) is kept constant and the spin-state of iron(III) depends on the position of the sixth ligand X in the spectrochemical series; i.e., the chloro and azido complexes are high-spin, the complexes with imidazole or pyridine derivatives are spin-equilibrium, and the cyano complex is low-spin.

A number of mononuclear iron(III) complexes with spin-equilibrium, including our complexes, have been known.[1-9] However, to our knowledge, no binuclear iron(III) complex with spin-equilibrium has been reported. In this study, binuclear iron(III) complexes bridged by pyrazine, 1,1′-tetramethylenebis(imidazol), or bis(pyridine) compounds with the formula of $[LFe(Bge)FeL](BPh_4)_2$ were prepared, and their spin-equilibrium behavior was clarified by means of the temperature dependence of the magnetic susceptibilities and electronic spectra, in order to investigate the influence of the formation of binuclear species or the nature of the bridging ligand on the spin state of iron(III). The spin-equilibrium behavior of the binuclear complexes $[LFe(Bge)FeL](BPh_4)_2$ is compared with that of the corresponding mononuclear complexes $[FeXL](BPh_4)$. The schematic structures of the mononuclear $[FeXL]^{n+}$ ($n=0,1$) and binuclear $[LFe(Bge)FeL]^{2+}$ iron(III) complexes, along with the abbreviations used in this text, are shown in Fig. 1.

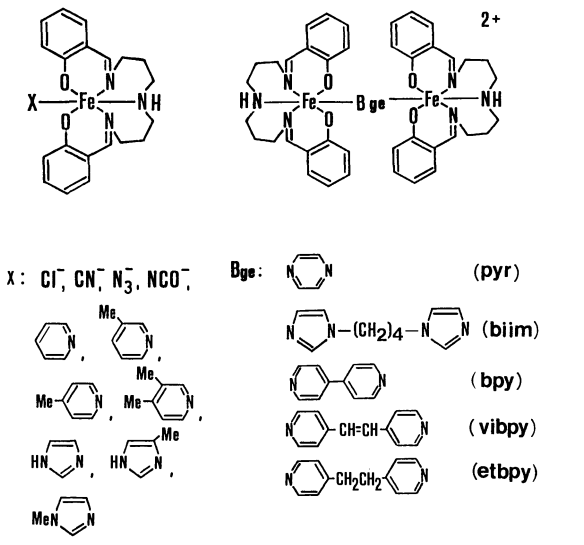

Fig. 1. Structures of mononuclear $[FeXL]^{n+}$ ($n=0,1$) and binuclear $[LFe(Bge)FeL]^{2+}$ iron(III) complexes: Bge=pyrazine(pyr), 1,1′-tetramethylenebis(imidazol) (biim), 4,4′-bipyridine(bpy), 4,4′-vinylenebis(pyridine) (vibpy), and 4,4′-ethylenebis(pyridine)(etbpy), where the abbreviations of bridging ligands Bge are given in parentheses.

Experimental

Physical Measurements. The melting points were measured on a Yanagimoto micromelting-point apparatus and uncorrected. The elemental analyses were performed by Mr. Shinichi Miyazaki at the Technical Service Center of Kumamoto University. The 100 MHz ^1H NMR spectrum was recorded on a JEOL MH 100 spectrometer; the solvent used was $CDCl_3$, and the shift measurements were made relative to $SiMe_4$. The thermogravimetric analysis was carried out on a Shimadzu TGC-20 microthermobalance at the heating rate of 5 °C min^{-1}, using ca. 20 mg of the sample. The electrical-conductivity measurements were carried out on a Denki Kagaku AOC-10 apparatus in dichloromethane solution on ca. 10^{-3} mol dm^{-3}. The reflectance spectra of the ground samples were measured on a Shimadzu UV-260 apparatus at the ambient temperature.

The temperature dependence of the electronic spectra in a dichloromethane solution was recorded with a Hitachi spectrophotometer 323, where the cell temperature was controlled by a circulating bath with a thermostat and where the sample temperature was monitored by means of a Yokogawa-Hokushin Denki digital multithermometer, Type 2572, and was kept constant within ±0.1 °C during the measurement. The magnetic susceptibilities were measured by the Faraday method in the temperature range from liquid nitrogen temperature to room temperature, according to a procedure reported previously.[10]

Syntheses. 1,1′-Tetramethylenebis(imidazol) Dihydrate. The bis(imidazole) was prepared according to the method in the literature[11] and was identified by means of elemental analysis, its mp, its ^{1}H NMR spectrum, and thermogravimetric analysis. Found: C, 53.16; H, 7.88; N, 24.80%. Calcd for $C_{10}H_{14}N_4 \cdot 2H_2O$: C, 53.08; H, 8.02; N, 24.76%. mp 56—71 °C (Ref. 58—75 °C), ^{1}H NMR ($CDCl_3$) δ=1.70 (4H, m, CH_2), 1.80 (4H, s, H_2O), 3.80 (4H, m, CH_2), 7.10 (6H, q, aromatic), mass loss 15.9 wt% (55—130 °C), Calcd for $2H_2O$:15.9 wt%.

[FeClL]. The chloro iron(III) complex as a starting material was prepared according to the method reported previously.[1]

Binuclear Iron(III) Complexes [LFe(Bge)FeL](Bph$_4$)$_2$. The binuclear iron(III) complexes bridged by pyrazine, 1,1′-tetramethylene-bis(imidazol), or bis(pyridine) compounds were obtained by mixing stoichiometric amounts of [FeClL] and the bridging ligand in a mole ratio of 2:1 and by then adding sodium tetraphenylborate to provide a counter anion, where pyrazine, 1,1′-tetramethylenebis(imidazol), 4,4′-bipyridine, 4,4′-ethylenebis(pyridine), and 4,4′-vinylenebis(pyridine) were used as bridging ligands. The syntheses of all the binuclear complexes are practically the same, so only the synthesis of the 4,4′-bipyridine complex [LFe(bpy)FeL](BPh$_4$)$_2$ will be described in detail as an example. To a solution of [FeClL] (2 mmol) in 50 cm^3 of methanol was added a solution of 4,4′-bipyridine (1 mmol). The mixture was warmed at 60 °C for 10 min and then filtered. The filtrate was added to a solution of sodium tetraphenylborate (2.5 mmol) in 10 cm^3 of methanol. The resulting crystals were filtered, washed with methanol and diethyl ether, and dried in vacuo.

Results and Discussion

Binuclear iron(III) complexes [LFe(Bge)FeL](BPh$_4$)$_2$ were prepared by mixing stoichiometric amounts of [FeClL] and the bridging ligand (Bge) in methanol and by then adding a slight excess of sodium tetraphenylborate. The elemental analytical data, melting points, molar electrical conductances in 10^{-3} mol dm^{-3} dichloromethane solutions, and colors in the solids and solutions at the ambient temperature and at the temperature of liquid nitrogen are summarized in Table 1. As shown in Table 1, the bis(pyridine) complexes showed a striking thermochromism both in the solids and solutions. On the other hand, the pyrazine complex showed no thermochromism in the solid state, and its green color is characteristic of low-spin complexes.[1]

The temperature dependences of the magnetic moments for the binuclear iron(III) complexes [LFe(Bge)FeL](BPh$_4$)$_2$ are shown in Fig. 2, where the magnetic moment per iron is given. As could be

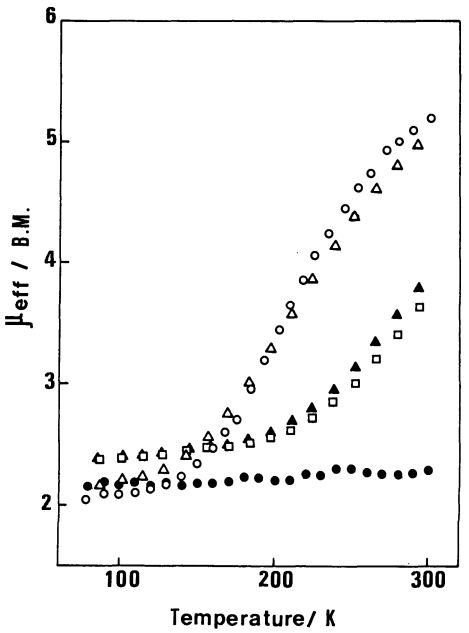

Fig. 2. Temperature dependences of effective magnetic moments for binuclear iron(III) complexes [LFe(Bge)FeL](BPh$_4$)$_2$, Bge: pyr (●), biim (○), bpy(△), vibpy(□), etbpy(▲).

Table 1. Elemental Analytical Data, Melting Points, Molar Electrical Conductances,[a] and Colors[b] at *ca.* 80 and 300 K in the Solids and Solutions[c]

Complex	C(%) Found(Calcd)	H(%) Found(Calcd)	N(%) Found(Calcd)	Mp θ_m/°C	a	Color solid	Color soln
[LFe(pyr)FeL](BPh$_4$)$_2$	73.52(73.42)	6.01(6.03)	7.43(7.45)	153—157	49.1	G-G	V-V
[LFe(biim)FeL](BPh$_4$)$_2$	72.70(72.87)	6.18(6.24)	8.71(8.67)	205—207	45.5	DV-G	V-BG
[LFe(bpy)FeL](BPh$_4$)$_2$	74.04(74.44)	6.05(5.99)	6.96(7.08)	200—205	45.7	DV-G	V-DG
[LFe(vibpy)FeL](BPh$_4$)$_2$	74.64(74.73)	6.23(6.02)	6.88(6.97)	235—240	60.8	DV-G	V-G
[LFe(etbpy)FeL](BPh$_4$)$_2$	74.56(74.64)	6.18(6.14)	6.94(6.96)	213—215	66.2	DV-G	V-G

a) Electrical conductance in ca. 10^{-3} mol dm^{-3} dichloromethane solutions/S mol^{-1} cm^2. b) Colors at 300 K (left) and 80 K (right); V, violet; DV, dark violet; BG, blue green; DG, dark green; G, green. c) In a dichloromethane solution.

predicted from its green color, the pyrazine complex [LFe(pyr)FeL](BPh4)2 is essentially low-spin, because the magnetic moment (ca. 2.2 BM) is in the expected range for low-spin (S=1/2) iron(III) complexes and is independent of the temperature. On the other hand, the magnetic moments for the bis(imidazole) and the bis(pyridine) complexes showed temperature dependence, indicating that the complexes exhibit a spin-equilibrium between high-spin(S=5/2) and low-spin (S=1/2) states. Since the spin-transition for these complexes takes place over a wide range of temperatures, the complexes, on the basis of König's criterion,[12] can be classified as forming a continuous type of spin-equilibrium complexes. The magnetic moments for the bis(imidazole) and 4,4′-bipyridine complexes [LFe(biim)FeL](BPh4)2 and [LFe(bpy)FeL](BPh4)2 increase gradually from a low-spin value (ca. 2.2 BM) at 80 K to a nearly high-spin value (ca. 5.3 BM) at 300 K, indicating that the spin-transition from the low-spin state to the high-spin state is almost completed in the temperature range studied. For the other two bis(pyridine) complexes, [LFe(etbpy)FeL](BPh4)2 and [LFe(vibpy)FeL](BPh4)2, the magnetic moments gradually increase from 2.3 BM at 80 K to ca. 3.7 BM at 300 K, suggesting that the spin-transition seems to be completed at a temperature higher than 300 K.

It is of interest to compare the magnetic behavior of the binuclear complexes [LFe(Bge)FeL](BPh4)2 with that of the corresponding mononuclear complexes [FeXL](BPh4). The magnetic behavior of the bis(imidazole) complex [LFe(biim)FeL](BPh4)2 can be compared with that of the mononuclear complexes with imidazole derivatives [FeXL](BPh4) (X=im, 1-meim, 2-meim). The bis(imidazole) complex showed the spin-transition between ca. 130 and 300 K, while [FeimL](BPh4) and [Fel-meimL](BPh4) are high-spin complexes between 80 and 300 K, and [Fe2-meimL](BPh4) showed the spin-transition between ca. 130 and 300 K.[1] The magnetic behavior of the bis(pyridine) complexes [LFe(Bge)FeL](BPh4)2 (Bge=bpy, etbpy, vibpy) can be compared with that of the mononuclear complexes [FeXL](BPh4) (X=py, 3-mepy, 4-mepy, 3,4-dmepy). The μ_{eff} vs. T curves for the [FeXL](BPh4) complexes (X=py, 3-mepy, 4-mepy, 3,4-dmepy) are roughly compatible with those for the [LFe(etbpy)FeL](BPh4)2 and [LFe(vibpy)FeL](BPh4)2 complexes, but are obviously different from that for [LFe(bpy)FeL](BPh4)2.

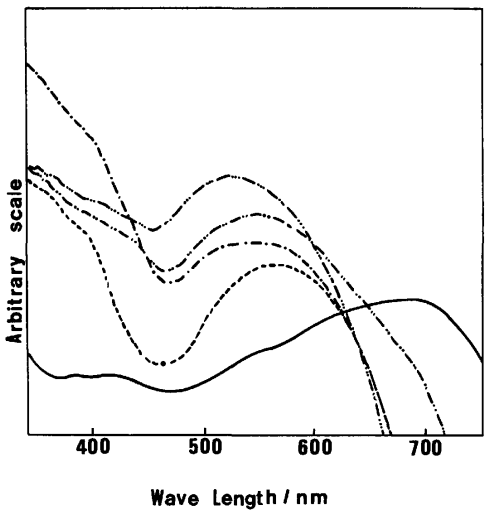

Fig. 3. Reflectance spectra for binuclear iron(III) complexes [LFe(Bge)FeL](BPh4)2, Bge: pyr(——), biim(—·····—), bpy(—·—·—), vibpy(—·—), etbpy(----).

The reflectance spectra for the binuclear complexes at the ambient temperature are shown in Fig. 3. The complexes exhibit an intense broad band in visible region. The pyrazine complex has the absorption maximum at 680 nm, while the bis(imidazole) and the bis(pyridine) complexes have the maxima around 550 nm. The results from the reflectance spectra are compatible with those from the magnetic moments at the ambient temperature.

The temperature dependence of the electronic spectra was measured in dichloromethane solutions. All the binuclear complexes except for the pyrazine complex showed thermochromic behavior. The pyrazine complex exhibits a green color in the solid and a violet color in the dichloromethane solution. The pyrazine complex showed no thermochromism in a solution, probably because the complex decomposes to form a penta-coordinated complex with the formula of [FeL](BPh4). Figure 4 shows the temperature dependence of the spectrum for [LFe(bpy)FeL](BPh4)2. The spectral patterns of the bis(pyridine) complexes are similar to each other and to those of the corresponding mononuclear complexes with pyridine derivatives.[1] At 16 °C, the spectrum for [LFe(bpy)FeL](BPh4)2 exhibits two absorptions, at 430 and 490 nm, with extinction coefficients of 8500 and 7100 $dm^3 mol^{-1} cm^{-1}$ attributable to the charge-transfer bands. With a lowering in the temperature, the absorption at 430 nm decreases in intensity and that at 490 nm shifts to a higher wavelength, accompanied by a decrease in the intensity. The temperature dependence of the electronic spectrum is probably due to the spin-equilibrium between high-spin and low-spin states, as is known for the well-characterized spin cross-over complexes.[1-9] The spectral changes are associated with two pseudo-isosbestic points at 400 and 510 nm, in which the latter is gradually displaced from 510 nm to a higher wavelength with a lowering in the temperature. The disagreement of the isosbestic points is attributable to the partial dissociation of 4,4′-bipyridine from the complex. When the spectrum was measured after having been left overnight, the absorbance was reduced by almost one

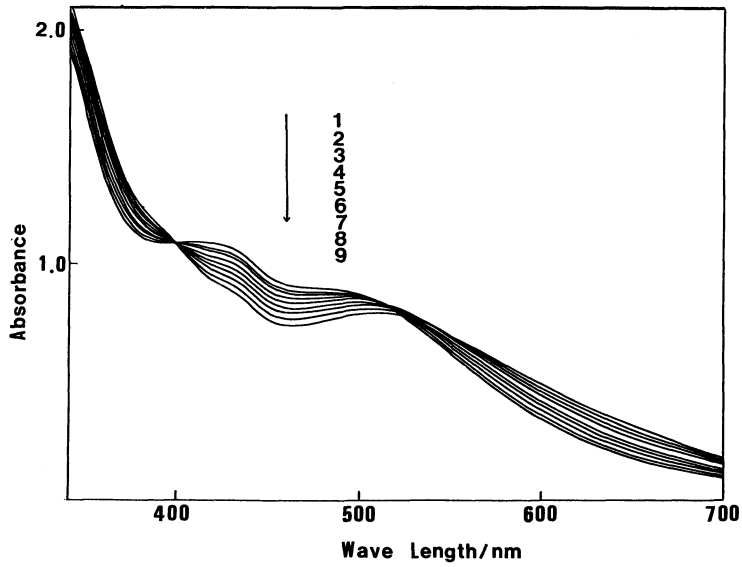

Fig. 4. Temperature dependence of electronic spectrum for $[LFe(bpy)FeL](BPh_4)_2$ in 1.257×10^{-4} mol dm^{-3} dichloromethane solution: (**1**: 16.0 °C, **2**: 13.0 °C, **3**: 10.0 °C, **4**: 7.0 °C, **5**: 4.0 °C, **6**: 1.0 °C, **7**: −2.0 °C, **8**: −5.0 °C, **9**: −8.0 °C).

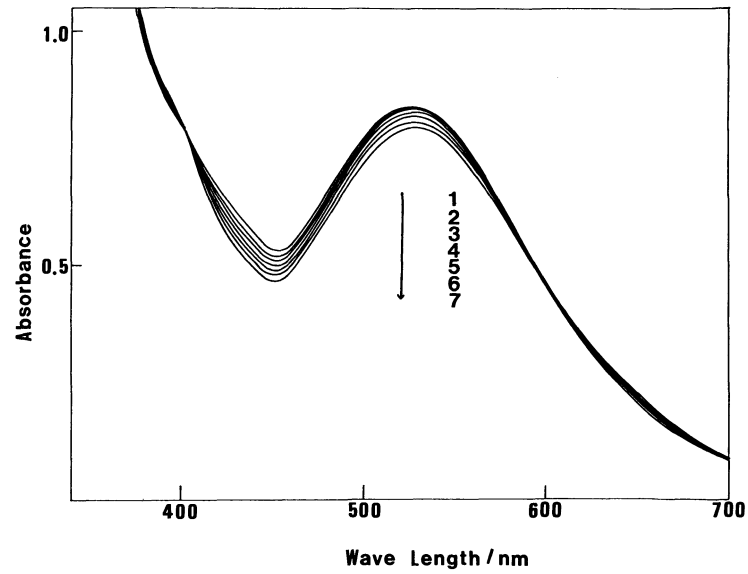

Fig. 5. Temperature dependence of electronic spectrum for $[LFe(biim)FeL](BPh_4)_2$ in 1.158×10^{-4} mol dm^{-3} dichloromethane solution: (**1**: 16.0 °C, **2**: 10.4 °C, **3**: 6.8 °C, **4**: 3.1 °C, **5**: −1.0 °C, **6**: −7.0 °C, **7**: −9.5 °C).

half, while the spectral pattern is consistent with that of the sample measured immediately after the preparation. Figure 5 shows the temperature dependence of the spectrum for the bis(imidazole) complex $[LFe(biim)FeL](BPh_4)_2$. The spectrum exhibits a band at 530 nm, which decreases in intensity with a lowering of the temperature. The spectrum changes with a set of isosbestic points at 400 and 595 nm.

We wish to thank Mr. Susumu Kohata at the Yatsushiro College of Technology for allowing us to use the Shimadzu UV-260 spectrophotometer (for the reflectance specta). This work was in part supported by a Grant-in-Aid for Scientific Research from the Ministry of Education, Science, and Culture (No. 59740300).

References

1) N. Matsumoto, S. Ohta, C. Yoshimura, S. Kohata, Y. Maeda, H. Okawa, and A. Ohyoshi, *J. Chem. Soc. Dalton*

Trans., in press.

2) E. Sinn, G. Sim, E. V. Dose, M. F. Tweedle, and L. J. Wilson, *J. Am. Chem. Soc.*, **100**, 3375 (1978).

3) M. F. Tweedle and L. J. Wilson, *J. Am. Chem. Soc.*, **98**, 4824 (1976).

4) R. A. Binstead, J. K. Beattie, T. G. Dewey, and D. H. Turner, *J. Am. Chem. Soc.*, **102**, 6642 (1980).

5) T. Ito, M. Sugimoto, H. Ito, K. Toriumi, H. Nakayama, W. Mori, and M. Sekizaki, *Chem. Lett.*, **1983**, 121.

6) E. Frank and C. R. Abeledo, *Inorg. Chem.*, **5**, 1453 (1976).

7) L. Cambi and L. Szego, *Ber. Dtsch. Chem. Ges.* **B64**, 2591 (1931).

8) H. Ohshio, Y. Maeda, and Y. Takashima, *Inorg. Chem.*, **22**, 2684 (1983).

9) Y. Maeda, Y. Takashima, N. Matsumoto, and A. Ohyoshi, *Inorg. Chem.*, in press.

10) M. Mikuriya, H. Okawa, and S. Kida, *Bull. Chem. Soc. Jpn.*, **54**, 2943 (1983).

11) W. Schütze and H. Schubert, *J. Prackt. Chem.*, **8**, 306 (1959).

12) E. König, G. Ritter, and S. K. Kulshreshtha, *Inorg. Chem.*, **23**, 1144 (1984).

 © 1986 The Chemical Society of Japan Bull. Chem. Soc. Jpn., 59, 161—167 (1986)

Kinetics of Axial Substitution of the Iron(II) Complex of 2,3,9,10-Tetraphenyl-1,4,8,11-tetraaza-1,3,8,10-cyclotetradecatetraene in Acetonitrile. Evidence for a Dissociative-Interchange Mechanism

Shigenobu FUNAHASHI, Naotaka UCHIYAMA, and Motoharu TANAKA*
Laboratory of Analytical Chemistry, Faculty of Science, Nagoya University, Chikusa-ku, Nagoya 464
(Received June 11, 1985)

The reaction of the iron(II) complex of 2,3,9,10-tetraphenyl-1,4,8,11-tetraaza-1,3,8,10-cyclotetradecatetraene ($[FeL(CH_3CN)_2]^{2+}$, **1**) with imidazole and thiocyanate ion in acetonitrile has been investigated spectrophotometrically at various temperatures and pressures. The axial substitution of **1** with imidazole is first order with respect to the concentration of the iron(II) complex and imidazole and the rate constant and the activation parameters are obtained as k (25.0 °C)=0.69 mol^{-1} kg s^{-1}, $\Delta H^{\ddagger}$=76±4 kJ mol^{-1}, $\Delta S^{\ddagger}$=7±13 J mol^{-1} K^{-1}, $\Delta V^{\ddagger}$=13.7±0.9 cm^3 mol^{-1}. It has been demonstrated that at higher concentration of imidazole there exists self-associated imidazole which does not react directly with the complex. The axial substitution of **1** with thiocyanate ion proceeds through the ion-association between **1** and SCN^- prior to the rate-determining step from the outer-sphere complex to the inner-sphere complex. The activation parameters for the rate-determining step were determined as follows: k^0 (25.0 °C and 0.1 MPa)=2.35 s^{-1}, $\Delta H^{\ddagger}$=86±2 kJ mol^{-1}, $\Delta S^{\ddagger}$=51±6 J mol^{-1} K^{-1}, $\Delta V^{\ddagger}$=10.1±0.2 cm^3 mol^{-1}. The positive activation volumes strongly indicate a dissociative character of the activation process.

Transition-metal complexes containing macrocyclic ligands have been investigated as models for biological molecules.[1,2] One particular interest in these model studies has been to elucidate mechanisms of solvent exchange and ligand substitution at the axial coordination site of metal complexes with macrocyclic ligands from biological interests.[3,4] There are a number of kinetic studies on axial ligand substitution reactions in six-coordinated iron(II) complexes with macrocyclic ligands,[5-21] including phthalocyanine[5-11] and porphyrins.[12-14] In such complexes the equatorial positions are occupied by four nitrogen atoms of the macrocyclic ligands and the axial sites by the ligands taking part in the relevant rate processes. Despite numerous studies, the reaction mechanism of axial substitution of iron complexes does not appear to have been proved decisively and there seems to be no mechanistic approach on the basis of the activation volumes.

We present here the results of a kinetic study on the substitution of axial acetonitrile by imidazole(Im) and thiocyanate ion in the iron(II) complex of 2,3,9,10-tetraphenyl-1,4,8,11-tetraaza-1,3,8,10-cyclotetradecatetraene ($[FeL(CH_3CN)_2]^{2+}$, **1**) at various temperatures and pressures. The overall reactions are represented by Eqs. 1 and 2.

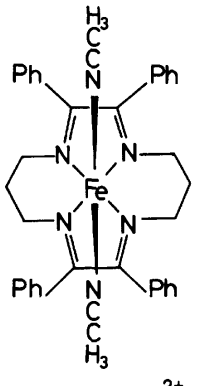

$[FeL(CH_3CN)_2]^{2+}$, **1**

$$\mathbf{1} + 2\mathrm{Im} \rightleftharpoons [FeL(Im)_2]^{2+} + 2CH_3CN \quad (1)$$

$$\mathbf{1} + 2SCN^- \rightleftharpoons FeL(SCN)_2 + 2CH_3CN \quad (2)$$

Experimental

Materials. **Acetonitrile**: Reagent grade acetonitrile (Wako Pure Chemical Industries, Ltd.) was refluxed over P_2O_5 (2 g dm^{-3}) for longer than 3 h and distilled under dry air. Furthermore, the distilled acetonitrile was refluxed over calcium hydride (Wako) (2 g dm^{-3}) in an argon atmosphere for longer than 3 h, distilled under argon, and stored in a dry box. The amount of water contained in acetonitrile was checked by the Karl-Fisher method and it was found to be less than 2×10^{-3} mol dm^{-3}.

Imidazole: Imidazole (Wako) was purified by sublimation in vacuo (3 mmHg, 80—100 °C).

Sodium Thiocyanate: Reagent grade sodium thiocyanate (Nakarai Chemicals) was recrystallized from methanol. The crystals were washed with diethyl ether and dried for 6 h under reduced pressure. The amount of water contained in the crystals was determined to be less than 0.015 wt%.

Anhydrous Sodium Perchlorate: A sodium perchlorate solution was prepared by neutralizing reagent grade 60% perchloric acid with reagent grade anhydrous sodium carbonate. Heavy-metal impurities in the sodium perchlorate solution were precipitated as hydroxides together with active carbon at pH 8.5. After concentration of the solution crystals of sodium perchlorate hydrates were obtained by cooling the solution. Sodium perchlorate was then crystallized twice from distilled water. Anhydrous sodium perchlorate was obtained by drying the obtained sodium perchlorate hydrates at 60 °C under reduced

pressure for more than 5 h.

[FeL(CH$_3$CN)$_2$](PF$_6$)$_2$: This complex was synthesized by a procedure similar to the literature method.[22] All operations were carried out under an argon atmosphere. Yielded dark purple crystals were washed with cold methanol and then with ether. The product was purified further by chromatography (Silica gel 2308, Merck; ϕ45 mm, h 270 mm column; eluent: dry nitromethane). Recrystallization from dry acetonitrile and dry diethyl ether gave purple crystals. Anal. Calcd for $C_{38}H_{38}N_6P_2F_{12}Fe$: C, 49.39; H, 4.14; N, 9.09; Fe, 6.04. Found: C, 49.36; H, 4.08; N, 8.94; Fe, 5.95±0.03. After decomposition of the complex by heating with sodium carbonate, iron was determined by the colorimetry with 1,10-phenanthlorine. ^{1}H NMR (acetone-d_6, Me$_4$Si): 1.62 ppm (m, 4H), 2.51 (m, 6H), 4.35 (m, 8H), 7.48 (m, 20H). Visible electronic spectrum (CH$_3$CN solution): λ_{max} (ε) 551 nm (8.83×10^3 mol^{-1} dm^3 cm^{-1}), 592 nm (1.78×10^4 mol^{-1} dm^3 cm^{-1}). Half-wave potential of Fe^{2+}/Fe^{3+} for the complex 1.48 V (ΔP=64 mV, 100 mV s^{-1}). IR (KBr pellet): 1340(m), 1320(m), 1270(m), 1115(w), 1080(w), 1030(w, axial CH$_3$CN), 845(s, PF$_6^-$), 710(s).

Measurement. The reaction was started by mixing the iron(II) complex solution with an imidazole or a thiocyanate ion solution. Reactions at atmospheric pressure were followed by a stopped-flow spectrophotometer (Type RA 401, Union Giken). Reactions at high pressure up to 200 MPa were measured with a high-pressure stopped-flow apparatus with spectrophotometric detection (Type FIT 3).[23,24]

Results

Reaction of 1 with Imidazole. Under conditions with a large excess of imidazole over the bis(acetonitrile) complex, during the reaction after mixing, we observed solutions having visible absorption spectra corresponding to those of the species $[FeL(Im)_2]^{2+}$, but not corresponding to $[FeL(CH_3CN)(Im)]^{2+}$. Moreover, the final change in absorbance was independent of the concentration of imidazole and proportional to the complex concentration. Therefore, under the present experimental conditions the reverse reaction is negligible for the kinetic study and the second ligation is much faster than the first ligation of imidazole. The axial substitution of the complex with imidazole was followed at 592 nm, the maximum wavelength of the complex. The first-order plots were linear at least for 3 half-lives. Rate constants obtained at a constant concentration of imidazole (C_{Im}=0.150 mol kg^{-1}) and various concentrations of the complex (C_{FeL}=2.68—5.91×10^{-5} mol kg^{-1}) were independent of the complex concentration. The rate law is thus given by

$$-d[\mathbf{1}]/dt = k_{0(Im)}[\mathbf{1}], \quad (3)$$

where $k_{0(Im)}$ is a conditional first-order rate constant. Rate constants $k_{0(Im)}$ were obtained at various concentrations of imidazole. The plots of $k_{0(Im)}$ against the total concentrations of imidazole, C_{Im}, are shown in Fig. 1.

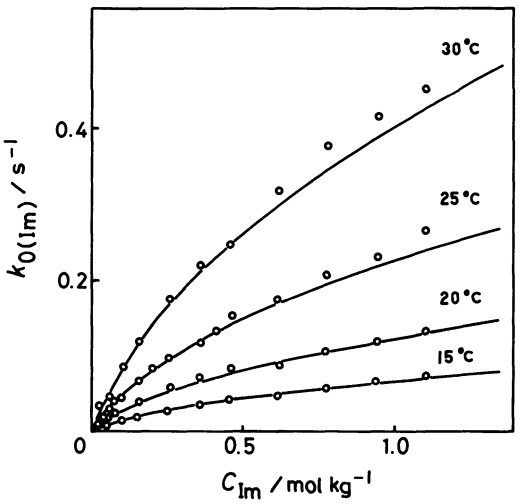

Fig. 1. Imidazole concentration dependence of first-order rate constants under atmospheric pressure at 15.0, 20.0, 25.0, and 30.0 °C. In Figs. 1—6, each point is an average of several runs. In Figs. 1, 3, 5, and 6, the soild lines were calculated by using the values obtained.

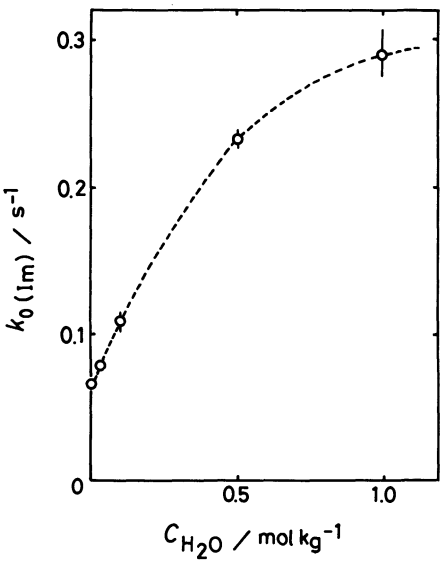

Fig. 2. Water effect on rate. C_{H_2O} is the concentration of added water. The rate constants were obtained at $C_{FeL}=5.90\times10^{-5}$ mol kg^{-1}, C_{Im}=0.150 mol kg^{-1}, and 25.0 °C.

The effect of water on the rate was checked by the addition of water (see Fig. 2). Rates drastically increase with increasing water concentration. However since water in the present reaction systems is less than 5×10^{-3} mol dm^{-3}, we believe with confidence that the presence of water, if any, does not affect our results. The rate was also not influenced by introduction of sodium perchlorate up to 0.2 mol kg^{-1}. The absence of any salt effect is

consistent with the imidazole reacting as free base.

Conditional first-order rate constants $k_{0(Im)}$ were determined at various temperatures and various pressures and they are shown as a function of imidazole concentrations in Figs. 1 and 3.

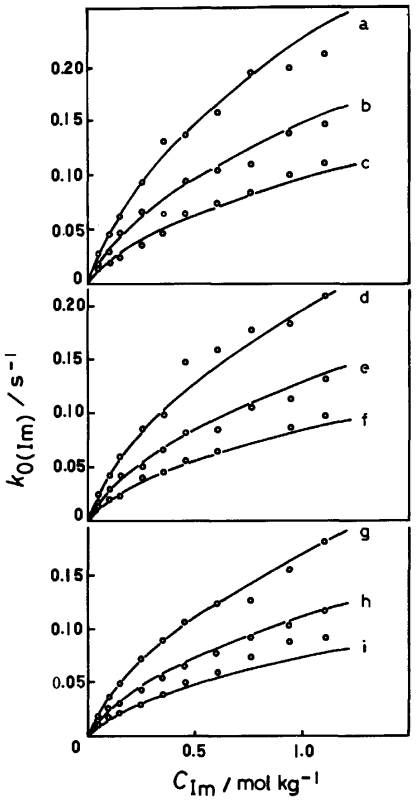

Fig. 3. Imidazole concentration dependence of first-order rate constants at 25.0 °C and nine different pressures. a: 0.1 MPa, b: 73.6 MPa, c: 147 MPa, d: 24.5 MPa, e: 98.1 MPa, f: 172 MPa, g: 49.0 MPa, h: 123 MPa, i: 196 MPa.

Reaction of 1 with Thiocyanate Ion. In a large excess of thiocyanate ion concentrations over the bis(acetonitrile) complex concentration, equilibrium 2 is much favored to the right and the reverse reaction is negligible. Under pseudo-first-order conditions, the axial substitution was followed at 732 nm, the maximum wavelength of the bis(thiocyanato) complex produced. The conditional first-

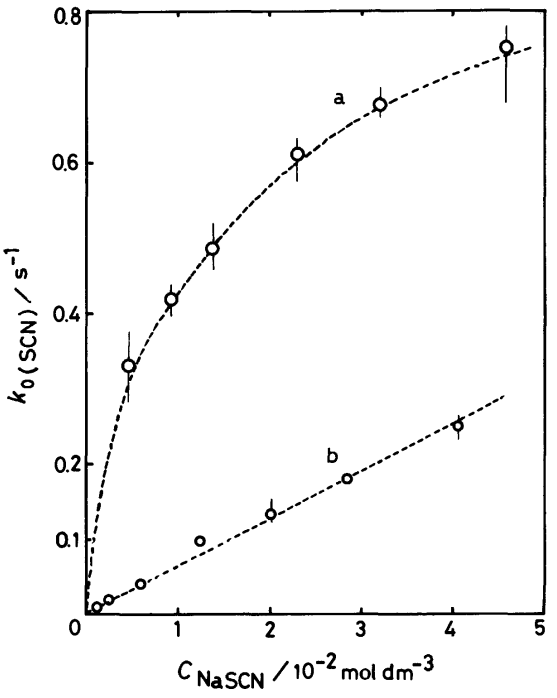

Fig. 4. Dependence of rate constant $k_{0(SCN)}$ on the total concentation of sodium thiocyanate (a) in the absence of and (b) in the presence of sodium perchlorate (C_{NaClO_4}=0.20 mol kg^{-1}).

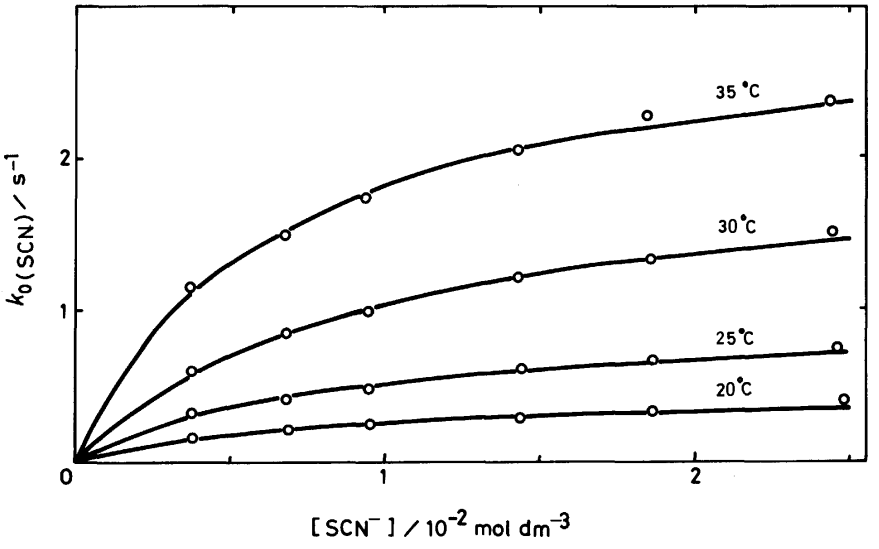

Fig. 5. Thiocyanate-ion concentration dependence of first-order rate constants at 20.0, 25.0, 30.0, 35.0, and 35.0 °C.

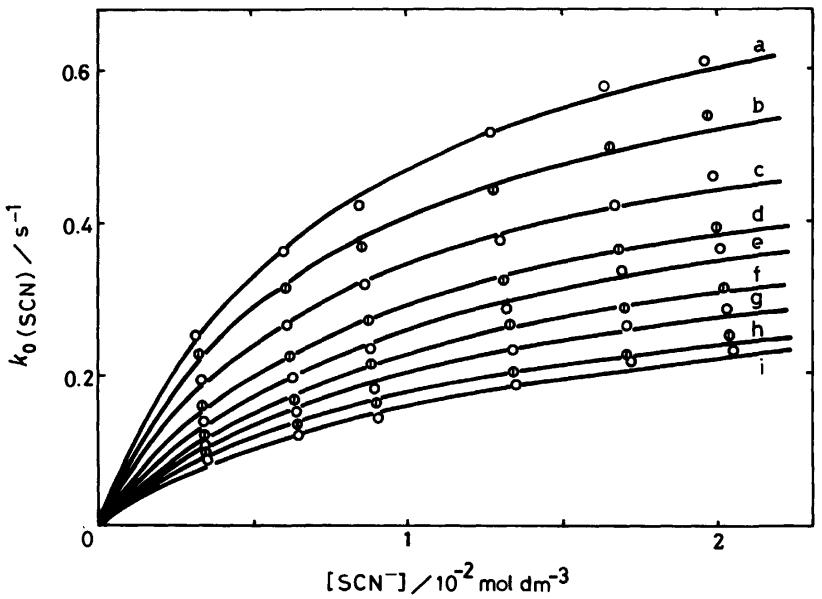

Fig. 6. Thiocyanate-ion concentration dependence of first-order rate constants at nine different pressure. a: 0.1 MPa, b: 24.5 MPa, c: 49.0 MPa, d: 73.6 MPa, e: 98.1 MPa, f: 123 MPa, g: 147 MPa, h: 172 MPa, i: 196 MPa.

order plots were excellently linear and the rate was confirmed to be first order with respect to the bis(acetonitrile) complex. Then we have

$$-\mathrm{d}[\mathbf{1}]/\mathrm{d}t = \mathrm{d}[\mathrm{FeL(SCN)_2}]/\mathrm{d}t = k_{0(\mathrm{SCN})}[\mathbf{1}], \quad (4)$$

where $k_{0(\mathrm{SCN})}$ is a conditional first-order rate constant involving the concentration of thiocyanate ion. Conditional first-order rate constants were obtained at various concentrations of thiocyanate ion both in the presence and in the absence of sodium perchlorate. As apparent from Fig. 4, in the presence of $NaClO_4$ the plot of $k_{0(\mathrm{SCN})}$ vs. the total concentration of sodium thiocyanate, C_{NaSCN}, gives a straight line through the origin, while in the absence of $NaClO_4$ the plot is leveled out with increasing thiocyanate concentration.

First-order rate constants $k_{0(\mathrm{SCN})}$ were determined as a function of thiocyanate ion concentrations at various temperatures and pressures. In Figs. 5 and 6 values of $k_{0(\mathrm{SCN})}$ are plotted as a function of the concentration of free thiocyanate ion, [SCN^-] (not the total concentration of sodium thiocyanate, C_{NaSCN}, see Discussion).

Discussion

In reaction systems showing a leveling of $k_{0(\mathrm{L})}$ with increasing concentration ([L]) of an incoming ligand, the plot of $k_{0(\mathrm{L})}^{-1}$ vs. $[\mathrm{L}]^{-1}$ gives sometimes a straight line. In this case $k_{0(\mathrm{L})}$ is expressed as follows:

$$k_{0(\mathrm{L})} = \frac{a[\mathrm{L}]}{1+b[\mathrm{L}]}. \quad (5)$$

However, the plot of $k_{0(\mathrm{L})}^{-1}$ vs. $[\mathrm{L}]^{-1}$ for the imidazole system in this work did not give a straight line. Data at higher concentration of imidazole were unable to fit to the function of Eq. 5. This behavior may be rationalized in terms of the known tendency for imidazole to make hydrogen bonding strongly with itself.[25,26] If the resulted dimer (Im_2) is assumed to be unreactive with the complex, it is possible to express the reaction as follows:

$$2\mathrm{Im} \overset{K}{\rightleftharpoons} \mathrm{Im_2}, \quad (6)$$

$$[\mathrm{FeL(CH_3CN)_2}]^{2+} + \mathrm{Im} \overset{k}{\longrightarrow} [\mathrm{FeL(CH_3CN)(Im)}]^{2+} + \mathrm{CH_3CN}, \quad (7)$$

$$[\mathrm{FeL(CH_3CN)(Im)}]^{2+} + \mathrm{Im} \overset{\text{fast}}{\longrightarrow} [\mathrm{FeL(Im)_2}]^{2+} + \mathrm{CH_3CN}, \quad (8)$$

where K refers to the dimerization constant of imidazole (Eq. 6), k is a second-order rate constant for the mono (imidazole) complex formation (Eq. 7), and the second imidazole reaction (Eq. 8) is very rapid. In a case where $C_{\mathrm{Im}} \gg C_{\mathrm{FeL}}$, we obtain

$$k_{0(\mathrm{Im})} = k\frac{\sqrt{8KC_{\mathrm{Im}}+1}-1}{4K}. \quad (9)$$

The $k_{0(\mathrm{Im})}$'s for a series of imidazole concentrations at 15, 20, 25, and 30 °C were fitted to Eq. 9 by a nonlinear least-squares program. The values of thermodynamic and activation parameters were obtained as follows: ΔH^{*}=74±3 kJ mol^{-1}, ΔS^{*}=0±9 J mol^{-1} K^{-1}, ΔH=−36±8 kJ mol^{-1}, and ΔS=−100±30 J mol^{-1} K^{-1}.

Since the plots of $\ln k$ and $\ln K$ against pressure showed linear relationships within experimental errors, the activation volume $\Delta V^{\ddagger}$ and the reaction volume ΔV can be accepted to be independent of pressure. Thus we can express k and K by Eqs. 10 and 11.

$$k = k^0 \exp(-\Delta V^{\ddagger} P/RT), \quad (10)$$

$$K = K^0 \exp(-\Delta V P/RT), \quad (11)$$

where k^0 and K^0 are constants at zero pressure, and then the conditional first-order rate constant is expressed as Eq. 12.

$$k_{0(\mathrm{Im})} = k^0 \exp(-\Delta V^{\ddagger} P/RT) \frac{\sqrt{8K^0 \exp(-\Delta V P/RT) C_{\mathrm{Im}} + 1} - 1}{4K^0 \exp(-\Delta V P/RT)} \quad (12)$$

Values of k^0, K^0, $\Delta V^{\ddagger}$, and ΔV were obtained by a nonlinear least-squares fit to all nine sets of data (201 data points): $k^0 = 0.686\ \mathrm{mol^{-1}\,kg\,s^{-1}}$, $\Delta V^{\ddagger} = 13.6 \pm 1.4\ \mathrm{cm^3\,mol^{-1}}$, $K^0 = 3.7\ \mathrm{mol^{-1}\,kg}$, $\Delta V = 1.6 \pm 4.2\ \mathrm{cm^3\,mol^{-1}}$. The final analysis of data by the least-squares program (SALS)[27] was carried out by applying simultaneously all data (341 data points) obtained at various temperatures and pressures. The parameters obtained are summarized in Table 1. The solid lines in Figs. 1 and 3 were depicted by the obtained values.

The activation volume of $13.7\ \mathrm{cm^3\,mol^{-1}}$ is considerably larger than that found for the CH_3CN exchange at Ni^{2+} ($7.3\ \mathrm{cm^3\,mol^{-1}}$), the most dissociative among solvent exchange reactions of bivalent transition metal ions.[28] Since the entering ligand, imidazole, has no charge, the electrostatic contribution to the volume change due to the interaction between the complex and imidazole is negligible. Therefore $\Delta V^{\ddagger}$ of $13.6\ \mathrm{cm^3\,mol^{-1}}$ points to a marked dissociative character of the reaction.

Figures 5 and 6 show also a falling-off of $k_{0(\mathrm{SCN})}$ with increasing concentration of the incoming ligand, $[SCN^-]$. We assume that the reaction of **1** with thiocyanate ion proceeds by the following processes:

$$\mathbf{1} + SCN^- \overset{K_{os}}{\rightleftharpoons} [FeL(CH_3CN)_2]^{2+}\cdots SCN^-, \quad (13)$$

$$[FeL(CH_3CN)_2]^{2+}\cdots SCN^- \xrightarrow{k} [FeL(CH_3CN)(SCN)]^+ + CH_3CN \quad (14)$$

$$[FeL(CH_3CN)(SCN)]^+ + SCN^- \xrightarrow{\text{fast}} FeL(SCN)_2 + CH_3CN. \quad (15)$$

Then, the conditional first-order rate constant is given by Eq. 16.

$$k_{0(\mathrm{SCN})} = \frac{kK_{os}[SCN^-]}{1 + K_{os}[SCN^-]} \quad (16)$$

The rate constant (k) of the unimolecular reaction may not be affected by ionic strength, I, while the association constant of the outer-sphere complex, K_{os}, varies as a function of ionic strength. For computation of K_{os} as described below we used the molar concentration calculated from the molal concentration with knowledge of the density of each solution at a certain temperature and pressure.[29] The ion association constant K_{NaSCN} of sodium thiocyanate in acetonitrile is available: thermodynamic constant $K_{\mathrm{NaSCN}} = 88\ \mathrm{mol\,dm^{-3}}$ at $I = 0\ \mathrm{mol\,dm^{-3}}$.[30] The ionic strength dependence of K_{NaSCN} is given by the following relations:[31]

$$K_{\mathrm{NaSCN}} = K_{\mathrm{NaSCN}} y_{\pm}^2, \quad \log y_{\pm} = -AI/(1 + BaI), \quad (17)$$

where $A = (DT)^{-3/2} \times 1.8246 \times 10^6$, $B = (DT)^{-1/2} \times 50.29 \times 10^8$, $y_{\pm}$ is a mean activity coefficient, D is the specific dielectric constant of acetonitrile of which the temperature and pressure dependence is available,[29] and a is the distance of the closest approach which is accepted to be 4×10^{-8} cm. Since, in the absence of sodium perchlorate, sodium thiocyanate exists in a very large excess (up to $5 \times 10^{-2}\ \mathrm{mol\,dm^{-3}}$), the ionic strength is controlled by the added sodium thiocyanate and then the ionic strength is given by Eq. 18.

$$I = \{-1 + (1 + 4K_{\mathrm{NaSCN}} C_{\mathrm{NaSCN}})^{1/2}\}/2K_{\mathrm{NaSCN}} \quad (18)$$

The ionic strength for each run was calculated by Eqs. 17 and 18. We have

$$k = \frac{kT}{h} \exp\left(-\frac{\Delta H^{\ddagger} - T\Delta S^{\ddagger}}{RT}\right) \quad (19)$$

K_{os} is given by Eq. 20[32]

$$K_{os} = \frac{4\pi N \text{å}^3}{3000} \exp\left\{-\frac{u(\text{å})}{kT}\right\}, \quad (20)$$

where $u(\text{å}) = z_1 z_2 e^2/\text{å}D - z_1 z_2 e^2 \kappa / D(1 + \kappa \text{å})$, $\kappa^2 = 8\pi N e^2 I / 1000 DkT$, å is the distance of the closest approach, and the other symbols have their usual meanings. The parameters ($\Delta H^{\ddagger}$, $\Delta S^{\ddagger}$, and å) from the data (187 data points) of temperature dependence of $k_{0(\mathrm{SCN})}$ were computed with knowledge of values of variables such as I, $[SCN^-]$, T, and $k_{0(\mathrm{SCN})}$ with use of Eqs. 16, 19, and 20 by a nonlinear least-squares program. We

Table 1. Thermodynamic and Activation Parameters According to Eq. 6, Eq. 7, and Eq. 14[a]

Eq. 6	Eq. 7	Eq. 14
$\Delta H = -23 \pm 12$	$\Delta H^{\ddagger} = 76 \pm 4$	$\Delta H^{\ddagger} = 86 \pm 2$
$\Delta S = -67 \pm 41$	$\Delta S^{\ddagger} = 7 \pm 13$	$\Delta S^{\ddagger} = 51 \pm 6$
$\Delta V = -1.3 \pm 2.7$	$\Delta V^{\ddagger} = 13.7 \pm 0.9$	$\Delta V^{\ddagger} = 10.1 \pm 0.2$

a) Enthalpy, entropy, and volume are given by the unit in $\mathrm{kJ\,mol^{-1}}$, $\mathrm{J\,mol^{-1}\,K^{-1}}$, and $\mathrm{cm^3\,mol^{-1}}$, respectively.

obtained the following values: $\Delta H^{\ddagger}=86\pm2$ kJ mol^{-1}, $\Delta S^{\ddagger}=51\pm6$ J K^{-1} mol^{-1}, and $\mathring{a}=(6.1\pm0.3)\times10^{-8}$ cm. With knowledge of values of I, [SCN$^-$], P, and $k_{0(SCN)}$ the parameters of k^0, $\Delta V^{\ddagger}$, and $\mathring{a}$ from the data (162 data points) of pressure dependence of $k_{0(SCN)}$ were estimated with use of Eqs. 10, 16, and 20 by a nonlinear least-squares best fit. The following values were determined: $k^0=2.35\pm0.05$ s^{-1}, $\Delta V^{\ddagger}=10.1\pm0.2$ cm^3 mol^{-1}, and $\mathring{a}=(6.9\pm0.2)\times10^{-8}$ cm. The $\mathring{a}$ value of 6—7$\times10^{-8}$ cm is reasonable judging from the molecular model. The fact that the entropy of activation and the activation volume are both positive is consistent with the dissociative character of the reaction.

In the presence of a large excess of sodium perchlorate the values of K_{os} and [SCN$^-$] become smaller than in the absence of sodium perchlorate. Moreover because of the equilibrium $Na^+ + SCN^- \rightleftarrows Na^+SCN^-$, [SCN$^-$] is proportional to C_{NaSCN} in the presence of a large excess of sodium perchlorate. Therefore the term K_{os}[SCN$^-$] should be smaller than unity in Eq. 16. In this case, $k_{0(SCN)}$ is, in fact, proportional to the thiocyanate ion concentration as seen in Fig. 4b. We can calculate the ion-association constant, K_{NaClO_4}, of sodium perchlorate in CH_3CN from the data at 25.0 °C and 0.1 MPa in Fig. 4. The value of K_{NaClO_4} is evaluated to be 45 ± 5 mol^{-1} dm^3 at $I=0.057\pm0.002$ mol dm^{-3} which is reasonable as compared to the K_{NaSCN} value of 59 mol^{-1} dm^3 at $I=0.057$ mol dm^{-3} obtained from Eq. 17.

Jones and Twigg have pointed out two possible mechanisms for the substitution of axially bound dimethyl sulfoxide (Me_2SO) by imidazole at an iron (II) phthalocyanine center in Me_2SO.[5] In order to distinguish the two mechanisms they have extended their study to higher concentration range of imidazole up to 1.45 mol dm^{-3},[6] without finding the curvature which we observed in this work. This seems reasonable because imidazole dimerizes to a lesser extent in Me_2SO which is much more basic than acetonitrile.[33]

Rates of exchange of acetonitrile solvent on hexasolventoiron(II) ion are available:[28b,34] $k=6.6\times10^5$ s^{-1} (25 °C), $\Delta H^{\ddagger}=41.4$ kJ mol^{-1}, $\Delta S^{\ddagger}=5.3$ J K^{-1} mol^{-1}, and $\Delta V^{\ddagger}=3$ cm^3 mol^{-1}.[28b] The exchange rate is about 6 orders of magnitude higher than that for axial substitution in $[FeL(CH_3CN)_2]^{2+}$ primarily due to the difference in activation enthalpy. This will result from the different state of the paramagnetic high-spin hexa(acetonitrile)iron(II) and diamagnetic low-spin $[Fe(II)L]^{2+}$ ions. The activation volume for axial substitution of $[Fe(II)L]^{2+}$ is larger than that for solvent exchange and $[FeL(CH_3CN)_2]^{2+}$ reacts more dissociatively than $[Fe(CH_3CN)_6]^{2+}$ does.

S. F. gratefully acknowledges financial support by a grant from the Kurata Foundation. Financial support from the Ministry of Education, Science, and Culture through a Grant-in-Aid for Scientific Research (No. 59430010) is gratefully acknowledged.

References

1) "The Coordination Chemistry of Metalloenzymes," ed by I. Bertini, R. S. Drago, and C. Luchinat, D. Reidel Publishing Company, Dordrecht, Holland (1983).
2) "Coordination Chemistry of Macrocyclic Compounds," ed by G. A. Melson, Plenum Press, New York (1979).
3) B. R. James, "The Porphyrins," ed by D. Dolphin, Academic Press, New York (1978), Vol. V, p. 205.
4) "The Biological Chemistry of Iron," ed by H. B. Dunford, D. Dolphin, K. N. Raymond, and L. Sieker, D. Reidel Publishing Company, Dordrecht, Holland (1982).
5) J. G. Jones and M. V. Twigg, *Inorg. Chem.*, **8**, 2120 (1969).
6) H. P. Bennetto, J. G. Jones, and M. V. Twigg, *Inorg. Chim. Acta*, **4**, 180 (1970).
7) D. V. Stynes and B. R. James, *J. Am. Chem. Soc.*, **96**, 2733 (1974).
8) D. A. Sweigart, *J. Chem. Soc., Dalton Trans.*, **1976**, 1476.
9) D. V. Stynes, *Inorg. Chem.*, **16**, 1170 (1977).
10) J. G. Jones and M. V. Twigg, *J. Chem. Soc., Dalton Trans.*, **1978**, 1709.
11) J. Martinsen, M. Miller, D. Trojan, and D. A. Sweigart, *Inorg. Chem.*, **19**, 2162 (1980).
12) D. V. Stynes and B. R. James, *J. Chem. Soc., Chem. Commun.*, **1973**, 325.
13) C. J. Weschler, D. L. Anderson, and F. Basolo, *J. Am. Chem. Soc.*, **97**, 6707 (1975).
14) B. R. James, K. J. Reimer, and T. C. T. Wong, *J. Am. Chem. Soc.*, **99**, 4815 (1877).
15) I. W. Pang and D. V. Stynes, *Inorg. Chem.*, **16**, 2192 (1977).
16) C. E. Holloway, D. V. Stynes, and C. P. J. Vuik, *J. Chem. Soc., Dalton Trans.*, **1979**, 124.
17) D. E. Hamilton, T. J. Lewis, and N. K. Kildahl, *Inorg. Chem.*, **18**, 3364 (1979).
18) N. K. Kildahl, T. J. Lewis, and G. Antonopoulos, *Inorg. Chem.*, **20**, 3952 (1981).
19) D. V. Stynes, Y. S. Hui, and V. Chew, *Inorg. Chem.*, **21**, 1222 (1982).
20) N. K. Kildahl, K. J. Balkus, Jr., and M. J. Flynn, *Inorg. Chem.*, **22**, 589 (1983).
21) A. Butler and R. G. Linck, *Inorg. Chem.*, **23**, 2227 (1984).
22) D. A. Baldwin, R. M. Pfeiffer, D. W. Reichgott, and N. J. Rose, *J. Am. Chem. Soc.*, **95**, 5152 (1973).
23) K. Ishihara, S. Funahashi, and M. Tanaka, *Rev. Sci. Instrum.*, **53**, 1231 (1982).
24) K. Ishihara, S. Funahashi, and M. Tanaka, *Inorg. Chem.*, **22**, 2564 (1983).
25) It has been reported that the ^{1}H NMR spectrum of imidazole in dichloromethane[26a] and in benzene[26b] is strongly dependent on the imidazole concentration and on the temperature. As the imidazole concentration decreases (from 1 mol dm^{-3} to 0.2 mol dm^{-3}) the N-H resonance broadens and moves upfield, while the C-H resonances show only very minor shifts. These changes have been ascribed to the formation of strongly hydrogen-bonded

agregates of imidazole in solution.
26) a) D. J. Doonan and A. L. Balch, *J. Am. Chem. Soc.*, **97**, 1403 (1975); b) N. Joop and H. Zimmermann, *Z. Elektrochem.*, **66**, 541 (1962).
27) T. Nakagawa and Y. Oyanagi, "SALS" (statistical analysis with least-squares fitting), Program Library, Nagoya University Computation Center, 1979.
28) a) Y. Yano, M. T. Fairhurst, and T. W. Swaddle, *Inorg. Chem.*, **19**, 3267 (1980); b) M. J. Sisley, Y. Yano, and T. W. Swaddle, *Inorg. Chem.*, **21**, 1141 (1982); c) T. W. Swaddle "Advances in Inorganic and Bioinorganic Mechanisms," ed by A. G. Sykes, Academic Press, New York (1983), Vol. 2, p. 96.
29) K. R. Srinivasan and R. L. Kay, *J. Sol. Chem.*, **6**, 357 (1977).
30) E. P. Grimsrud and B. Kratochvil, *J. Am. Chem. Soc.*, **95**, 4477 (1973).
31) R. A. Robinson and R. H. Stokes, "Electrolyte Solutions," 2nd Ed., Butterworths (1959).
32) R. M. Fuoss, *J. Am. Chem. Soc.*, **80**, 5059 (1958).
33) W. C. Barrette, Jr., H. W. Johnson, Jr., and D. T. Sawyer, *Anal. Chem.*, **56**, 1890 (1984).
34) R. J. West and S. F. Lincoln, *Aus. J. Chem.*, **24**, 1169 (1971).

 © 1986 The Chemical Society of Japan Bull. Chem. Soc. Jpn., 59, 169—174 (1986)

Studies of the Hydrous Tin(IV) Oxide Ion Exchanger. V. The Sodium Isotopic Exchange Rate between the Exchanger in the Na^+ Form and Aqueous Solutions

Yasushi INOUE,* Hiromichi YAMAZAKI, and Akira OSAWA
Department of Nuclear Engineering, Faculty of Engineering, Tohoku University, Aramaki, Sendai 980
(Received July 15, 1985)

The sodium isotopic exchange rate between the hydrous tin(IV) oxide ion exchanger in the Na^+ form and aqueous solutions was determined radiochemically. When the dried exchanger was used, the rate of the first step was controlled by the rate of the equilibration of water in the exchanger with the solutions, while the second step was found to be controlled by the diffusion of sodium ions in the particles (particle diffusion). When the exchanger had been sufficiently immersed in solutions in advance, the particle diffusion controlled the rate from the beginning. From the dependency of the rate of particle diffusion on the apparent particle size and the specific surface area of the exchanger, and on the sodium-ion concentrations in the solutions, the process controlling the rate is considered to be the diffusion in the primary particles, which are formed at the initial stage of precipitation and which aggregate to form the hydrous tin(IV) oxide gel. The diffusion constants and their activation energy (35±2 KJ mol^{-1}) were also evaluated.

The ion-exchange equilibrium, the effect of thermal treatment, and other important properties were previously studied on a hydrous tin(IV) oxide ion exchanger prepared by the method recommended by the present authors.[1] Although the investigation of ion-exchange kinetics is very important for understanding the ion-exchange mechanism of the material, there has been only a little information to date. The measurement of the isotopic exchange rate of cations between the corresponding salt forms of ion exchangers and aqueous solutions is especially interesting because it provides fundamental data which are useful for elucidating ion-exchange kinetics.

This paper will deal with the results of radiochemical experiments undertaken to measure the isotopic exchange rate of sodium ions between the hydrous tin(IV) oxide in the Na^+ form and aqueous solutions of sodium salts.

Experimental

Preparation of the Exchanger in the Na^+ Form Spiked with ^{22}Na. The hydrous tin(IV) oxide prepared by the method recommended previously was classified into three particle sizes by using Japan Industrial Standard sieves; it was then converted to the H^+ form by treating it with a 0.1 mol dm^{-3} HCl solution.[1] The exchanger was air-dried and stored in a desiccator containing a saturated NH_4Cl solution. Table 1 shows the particle size and some properties of each sample. The average particle radius was estimated by approximating the particle shape to a sphere by means of this equation: $4/3\pi r^3\rho N=W$, where ρ is the density of the sample, and N, the number of particles per W g, as counted under an optical microscope.

The exchanger in the H^+ form was converted to the Na^+ form by treating it with solutions, prepared by the desired combinations of NaCl and NaOH (pH 11), with the same compositions as those used for the rate measurement. The exchanger in the Na^+ form was then labeled with ^{22}Na by equilibrating it with a ^{22}Na solution having the same chemical compositions as the above solutions for about 2 d at room temperature. After having been washed with the solutions (free from ^{22}Na) used for converting to the Na^+ form, the exchanger was used for the rate measurement (wet system), or it was dried again to a constant weight over a saturated NH_4Cl solution and then also used for the experiments (dried system).

Apparatus and the Measurement of the Isotopic Exchange Rate. All the experiments were performed in a nitrogen atmosphere. The rate was measured in solutions with the same compositions as those used for converting the exchanger to the Na^+ form, by using the same apparatus as before.[2] Otherwise, an ion-exchange reaction occurs between H^+ and Na^+ ions, since the ion-exchange capacity for Na^+ strongly depends on the pH and on the concentration of the solution.[1] A 0.2-g to 0.5-g portion of the sample was placed in the cage and immesed in 200 cm^3 of a solution of a desired composition while the cage was being rotated. The frequency of revolution was measured

Table 1. Particle Size and Some Properties of the Samples

Particle size mesh[1]	Radius μm	Density g cm^{-3}	Ion-exchange Capacity[2] mmol g^{-1}	Composition[3] mol H_2O(mol Sn)$^{-1}$	Specific Surface Area m^2 g^{-1}
−70+100	86	3.52±0.08	1.160±0.008	2.14±0.02	174±8
−100+145	64	3.45±0.08	1.168±0.008		167±8
−145+200	45	3.48±0.08	1.165±0.008		178±8

1): Japan Industrial Standard mesh. 2): Exchange capacity for Na^+ at pH 11.0 (Ionic strength=0.10). 3): The water content was calculated from the weight loss at 850 °C.

with a Yokogawa, Model 2607, Photo Tachometer. The solution had been adjusted in advance to a constant temperature within ±0.1 °C. Aliquots of the solution (0.2 cm^3) were taken out at appropriate time intervals in order to measure the radioactivity with a well-type NaI(Tl) scintillation counter (Fuji Denki Model NHS-2). The time of contact of the exchanger with the solution was taken as the time elapsing between the immersion of the cage and the withdrawal of an aliquot of the solution. The fractional attainment of equilibrium, $F(t)=C_t/C_\infty$, was calculated from these results; here, C_t is the total radioactivity of the solution at time t and C_∞ at $t=\infty$. C_∞ was calculated by means of this equation: $C_\infty=CM/(M+m)$, where C is the initial total radioactivity of the exchanger, and m and M, the total amounts of Na^+ in the exchanger and in the solution respectively. Although the rate measurement is for a limited solution-volume condition, the infinite solution-volume approximation is closely obeyed under the present experimental conditions (less than 0.5 g of the exchanger per 200 cm^3 of the solutions).

The specific surface area of the sample was determined by the BET method (N_2 adsorption at −196 °C) using a Perkin-Elmer Shell Model 212D Sorptometer.

Results and Discussion

The sodium isotopic exchange rate was measured with two types of sample: (a) as dried and (b) wet. The results for each type of experiment will be described separately for convenience.

(1) Dried System. In order to ascertain the efficiency of agitation, the effect of the stirring rate on the half-exchange time was examined for pH-11 solutions of different NaCl concentrations. The time required for half-exchange ($t_{1/2}$) became shorter as the revolution rate increased, and reached a constant value at 1200 min^{-1}. Furthermore, it was confirmed that no particles were broken down during the agitation. On the basis of these results, a revolution rate of 1300 min^{-1} was adopted throughout the experiment for the dried system.

Figure 1 shows a comparison of the isotopic exchange rates in 0.01 mol dm^{-3} solutions of different sodium salts, indicating that no difference was observed in the rates between anions in the solution. This observation also held when the concentration of Na^+ was varied up to 1 mol dm^{-3}.

Figure 2 shows the influence of the sodium-ion concentration on the rate. When the concentration was higher than 0.5 mol dm^{-3}, the rate was independent of the concentration. When the concentration was less than 0.5 mol dm^{-3}, however, the rate increased with the concentration. It can be considered, from the dependence of the rate on the sodium-ion cencentration, that the rate is determined by either the diffusion of sodium ions in the adherent film (film diffusion) or by a chemical reaction at the exchange site. Since the sodium ions in the exchanger phase are in equilibrium with those in the solution phase, in the isotopic exchange reaction no concentration gradient of sodium ions exists in the film. Hence, the rate of the isotopic exchange would seem to be independent of the concentration of the sodium ion, unless the self-diffusion rate of sodium ions in solutions depends on the sodium-ion concentration. As the self-diffusion coefficients in NaCl solutions are almost constant in the concentration range lower than 1 mol dm^{-3}, the film diffusion cannot be the rate-controlling step. Furthermore, the chemical reacion in the exchanger does not appear to control the rate, because all the sodium ions in the exchanger exist as dissociated ions and, therefore, will exchange instantaneously with the incoming ions at the exchange sites.

When the exchange rate is controlled by the diffusion of ions within the particles (particle

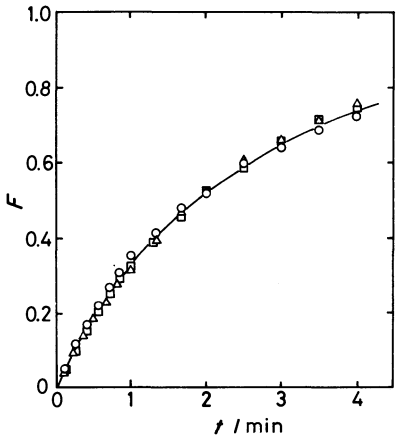

Fig. 1. Effect of diverse anions on the isotopic exchange rates (Dried system).
Sample, −70+100 mesh; Temperature, 5 °C; pH, 11.0, ○: 0.01 mol dm^{-3} Na(Cl,OH), △: 0.01 mol dm^{-3} $Na(NO_3,OH)$, □: 0.01 mol dm^{-3} $Na(ClO_4, OH)$.

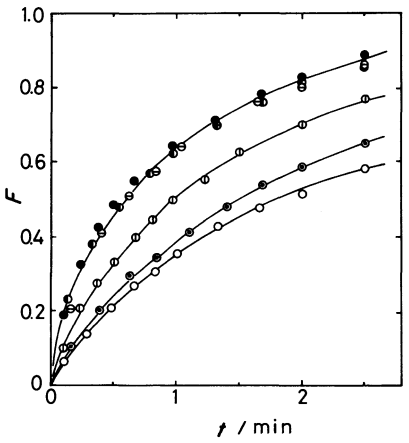

Fig. 2. Effect of Na^+ concentration on the isotopic exchange rates (Dried system).
Sample, −70+100 mesh; temperature, 5 °C; pH, 11.0; Na(Cl,OH) concd, ○: 0.01 mol dm^{-3}, ⊙: 0.05 mol dm^{-3}, ◑: 0.1 mol dm^{-3}, ◐: 0.5 mol dm^{-3}, ●: 1 mol dm^{-3}, ⊖: 2 mol dm^{-3}.

diffusion), the sodium-ion concentration of a solution does not affect the rate, provided that the structure of the exchanger is unchanged and the change in the ionic composition of the exchanger does not affect the self-diffusion coefficients of sodium ions in the particles. Figure 3 shows the composition of the exchanger as a function of the sodium-ion concentration of the solutions. This figure suggests a strong correlation between the $t_{1/2}$ and the exchange capacity of the samples; the $t_{1/2}$ markedly changed with the sodium-ion concentration in the range lower than 0.5 mol dm^{-3}, where the capacity changed with the concentration, while it was unchanged in the concentration range higher than 0.5 mol dm^{-3}, where the capacity was nearly constant. Therefore, it appears to the present authors that the isotopic exchange rate is controlled by the particle diffusion and that the diffusion coefficients are affected by the composition of the exchanger.

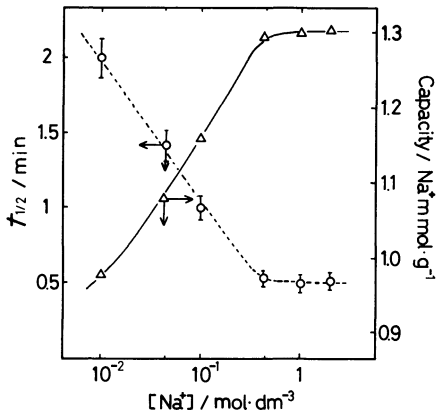

Fig. 3. Effect of Na^+ concentration on the half-exchange time and the exchange capacity (Dried system).
○: Half exchange time, △: Ion-exchange capacity for Na^+ at pH 11.0.

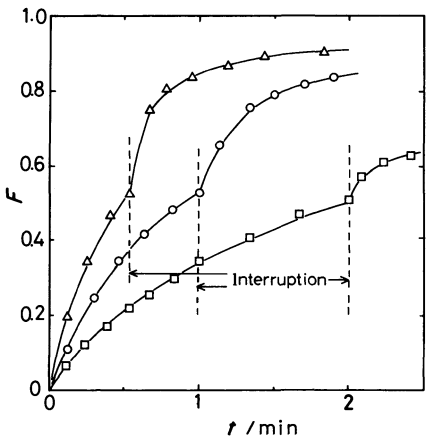

Fig. 4. Interruption test (Dried system).
Sample, −70+100 mesh; Temperature, 5 °C; pH, 11.0, □: 0.01 mol dm^{-3} Na(Cl,OH), ○: 0.1 mol dm^{-3} Na(Cl,OH), △: 1 mol dm^{-3} Na(Cl,OH).

Figure 4 shows the results of the method called "interruption test"; the exchangers were removed from the solution for 1 h and then reimmersed. In any concentration of sodium ions, the rate immediately after reimmersion was greater than that prior to the interruption. When these findings are combined with the above discussion, it can be concluded that, in solutions of any concentration, the rate is controlled by the particle diffusion.

When the isotopic exchange rates are controlled by the diffusion of ions in spherical exchangers immersed in a well-stirred solution of approximately an infinite volume, the fractional attainment of equilibrium can be obtained by solving this equation:[3]

$$F(t) = 1 - \frac{6}{\pi^2}\sum_{n=1}^{\infty}\frac{1}{n^2}\exp\left(-\frac{\pi^2 Dn^2 t}{r^2}\right), \quad (1)$$

where D is the self-diffusion coefficient of the ions in the exchanger and where r refers to the radius of the particles. When F is less than about 0.4, Eq. 1 is approximated by a simpler form:

$$F(t) = \frac{6}{r}\left(\frac{Dt}{\pi}\right)^{1/2}, \quad (2)$$

which gives a fairly good approximation.[4] Therefore, a plot of F against the square root of the contact time must give a straight line passing through the point of origin in the region of F less than 0.4.

Figure 5 shows the effect of the particle size on the rate. A linear relation with the same slope between F and $\sqrt{t}$ held, irrespective of the particle size, but the straight lines did not pass through the point of origin; the displacement of the intercept from the origin increased with the particle size. In order to clarify the rate of the initial portion of the exchange reaciton, the effect of the particle size on the rate was

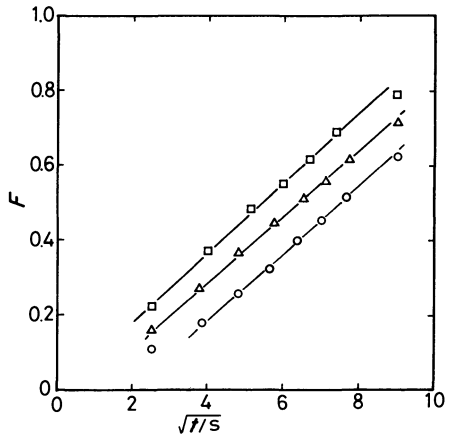

Fig. 5. Effect of particle size on the isotopic exchange rates (Dried system, I).
Temperature, 5 °C; 0.1 mol dm^{-3} Na(Cl,OH); pH, 11.0. Particle size/mesh; ○: −70+100, △: −100+145, □: −145+200.

measured under conditions of a slower rate (sodium-ion concentration, 0.01 mol dm^{-3}; revolution rate, 400 min^{-1}). The results are shown in Fig. 6. The F vs. $\sqrt{t}$ curves consist of two linear parts; the rate of exchange decreased with the particle size in the first step ($F<0.2$), but not in the second step. The latter step corresponds to the curves in Fig. 5. When the rate of this step is controlled by the particle diffusion, as has been claimed previously, the rate should depend on the particle size (Eq. 2). The experimental data, however, do not support this view. To solve the discrepancy, the specific surface area of each sample was determined; the results are shown in Table 1. This indicates that the surface areas of all the samples are the same, regardless of their apparent particle sizes. This can be understood by considering that the particles of the hydrous tin(IV) oxide are aggregates of the crystallites, subsequently called "primary particles," which have been produced at the beginning of precipitation, and that the surface area measured by the BET method is the internal surface attributable to the primary particles. If the diffusion of Na^+ within the primary particles is rate-controlling, the independence of the rate from the apparent particle size can be easily explained, since the size of the primary particles is irrelevant to the apparent particle sizes. When the shape of the primary particle is assumed to be spherical, the radius of the crystallite, r, can be calculated as $r=3/\rho S$, where ρ is the density (g cm^{-3}), and S, the specific surface area (cm^2 g^{-1}), of the exchanger. From the results in Table 1 the radius of the primary particle can be calculated to be $(4.9\pm0.3)\times10^{-7}$ cm.

Goodman and Gregg confirmed the existence of crystallites of hydrous tin(IV) oxide dried at 300 °C and determined their size ($1.5-8.0\times10^{-7}$ cm) with an electron microscope.[5] Heitner and Albu pointed out the possibility that hydrous thorium(IV) oxide is an aggregate of smaller units.[6] Hence, it is natural to consider that the particle of hydrous tin(IV) oxide consists of primary particles.

Provided the particle diffusion in the primary particles is rate-controlling, the ions should diffuse fast through the openings of the gel. In order for the ions to diffuse rapidly, these must be sufficient water in the openings. The water content of the dried sample is, however, less than that of the wet sample equilibrated with the test solutions, as is shown in Table 2. On the other hand, the rate of the penetration of the solution may reasonably be assumed to be faster into the smaller than into the larger particles. On the basis of these discussions, the rate of the first step is considered to be controlled by the rate of the equilibration of the water in the exchanger.

In conclusion, the rate of the exchange reaction on the dried system is initially controlled by the rate of the penetration of the solution into the particles, and subsequently by the diffusion rate of ions in the primary particles. In order to examine the latter step in detail, experiments were also carried out on the wet system.

(2) Wet System. In the wet system, the rate of

Table 2. Comparison of Water Contents of the Samples

Na^+-concentration of the solution	Water content[1]/wt%	
	Dried-sample[2]	Wet-sample[3]
0.01 mol dm^{-3}	18.3±0.1	19.5±0.1
0.1 mol dm^{-3}	18.0±0.1	19.5±0.1
1 mol dm^{-3}	17.8±0.1	19.4±0.1

1): Weight loss at 850 °C. 2): Dried over a saturated NH_4Cl solution. 3): Immediately after the separation from the Na^+ solution.

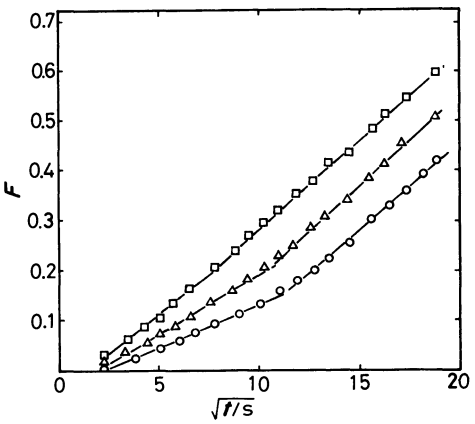

Fig. 6. Effect of particle size on the isotopic exchange rates (Dried system, II).
Temperature, 5 °C; Revolution rate, 400 min^{-1}; 0.01 mol dm^{-3} Na(Cl, OH); pH, 11.0. Particle size/mesh; ○: −70+100, △: 100+145, □: 145+200.

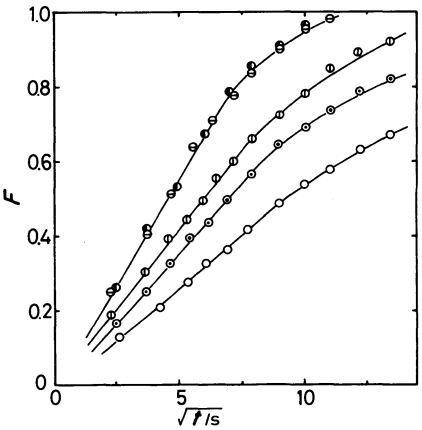

Fig. 7. Effect of Na^+ concentration on the isotopic exchange rates (Wet system).
Sample, −70+100 mesh; Temperature, 5 °C; pH, 11.0; Na(Cl, OH) concd, ○: 0.01 mol dm^{-3}, ⊙: 0.05 mol dm^{-3}, ◑: 0.1 mol dm^{-3}, ⊖: 0.5 mol dm^{-3}, ◐: 1 mol dm^{-3}.

Table 3. Effect of Temperature on Na^+ Self-diffusion Coefficient

Na^+ concentration in the solution / mol dm^{-3}	Temperature / °C	D / $m^2 s^{-1}$	E_a / KJ mol^{-1}	D_0 / $m^2 s^{-1}$
0.01	5.0	1.2×10^{-20}	35±2	4.7×10^{-14}
	20.0	2.1×10^{-20}		
	30.0	4.0×10^{-20}		
	40.0	6.8×10^{-20}		
1	5.0	5.3×10^{-20}	34±2	2.2×10^{-14}
	12.5	9.3×10^{-20}		
	20.0	1.2×10^{-19}		
	25.0	1.5×10^{-19}		

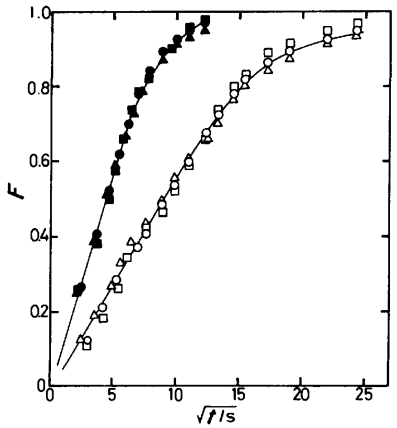

Fig. 8. Effect of particle size on the isotopic exchange rates (Wet system).
Temperature, 5 °C; pH, 11.0; Open marks: 0.01 mol dm^{-3} Na(Cl,OH), Filled marks: 1 mol dm^{-3} Na(Cl, OH). Particle size/mesh; ○●: −70+100, △▲: −100+145, □■: −145+200.

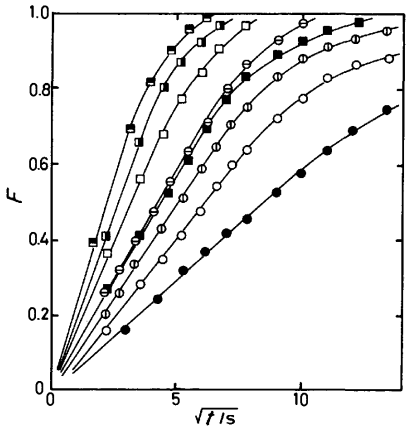

Fig. 9. Effect of temperature on the isotopic exchange rates (Wet system).
Sample, −70+100 mesh; 0.01 mol dm^{-3} Na(Cl,OH); pH, 11.0; ●: 5.0 °C, ○: 20.0 °C, ⊕: 30.0 °C, ⊖: 40.0 °C; 1 M Na(Cl,OH); pH, 11.0; ■: 5.0 °C, □: 12.5 °C, ◨: 20.0 °C, ⬒: 25.0 °C.

the exchange reaction became constant at a revolution rate greater than 1000 min^{-1}, irrespective of the sodium-ion concentration. Hence, a revolution rate of 1100 min^{-1} was adopted throughout the subsequent experiments.

Figure 7 indicates that the dependency of the rate on the sodium-ion concentration was similar to that for the dried system (Fig. 2) and that the straight lines between F and $\sqrt{t}$ in the F range smaller than about 0.5 passed through the point of origin. This relation means that the rate is controlled by the particle diffusion from the beginning of the reacion.

The effect of the particle size on the rate is shown in Fig. 8, which indicates that the rate is controlled by the diffusion of sodium ions within the primary particles, since it was independent of the particle size, in the same manner as in the second step in the dried system.

The fractional attainment of equilibrium against the square root of the time was studied in sodium-ion solutions of 0.01 and 1 mol dm^{-3} as a function of the temperature, as is shown in Fig. 9. The figure indicates that the rate of the exchange reaction increased with the temperature. The self-diffusion coefficients of sodium ions, D, were then evaluated by means of Eq. 2 from the slopes of the straight lines and the average radius of the primary particles. These values are summarized in Table 3. When log D was plotted against $1/T$, a good linearity was obtained. From the Arrhenius equation, $D = D_0 \exp(-E_a/RT)$, the activation energy, E_a, and the constant, D_0, were determined. As the activation energies obtained in solutions of 0.01 and 1 mol dm^{-3} agreed well with each other, the mechanism of the diffusion of sodium ions in the exchanger is considered to be unchanged by the compositions of the exchangers. The self-diffusion coefficients of sodium ions at 5 °C have been reported by Barrer and Rees, and by Dyer and Gill, to be 2.1×10^{-18} $m^2 s^{-1}$ in analcite and 2.0×10^{-17} $m^2 s^{-1}$ in crystalline zirconium(IV) phosphate respectively.[7,8] These values are larger than the present results. The $t_{1/2}$ is, however, considerably shorter for hydrous tin(IV) oxide (a few minutes) than for analcite and

crystalline zirconium(IV) phosphate (a few hours), because in the case of the hydrous tin(IV) oxide, the particle size practically controlling the exchange rate is smaller than the apparent particle size. Such a fast exchange rate for the hydrous tin(IV) oxide is of great practical value.

References

1) Y. Inoue and H. Yamazaki, *Bull. Chem. Soc. Jpn.*, **55**, 3782 (1982); **57**, 1534, 3437 (1984); **58**, 1292 (1985).

2) T. R. E. Kressman and J. A. Kitchener, *Faraday Discuss. Chem. Soc.*, **7**, 90 (1949).

3) F. Helfferich, "Ion Exchange," McGraw-Hill, New York (1963), Chap. 6.

4) G. E. Boyd, A. W. Adamson, and L. S. Myers, *J. Am. Chem. Soc.*, **69**, 2836 (1947).

5) J. F. Goodman and S. J. Gregg, *J. Chem. Soc.*, **1960**, 1162.

6) G. W. Heitner and A. Y. Albu, *J. Appl. Chem.*, **15**, 445 (1962).

7) R. M. Barrer and L. V. C. Rees, *J. Chem. Soc.*, **1959**, 709.

8) A. Dyer and J. S. Gill, *J. Inorg. Nucl. Chem.*, **39**, 665 (1976).

 © 1986 The Chemical Society of Japan Bull. Chem. Soc. Jpn., 59, 175—178 (1986)

Homogeneous Asymmetric Hydrogenation Using a Chiral Phosphinite Derivative of Carbohydrates as Ligand

Mitsuji YAMASHITA,* Mineaki KOBAYASHI, Motoyuki SUGIURA, Kenji TSUNEKAWA, Tatsuo OSHIKAWA, Saburo INOKAWA,† and Hiroshi YAMAMOTO†

Department of Chemistry, Faculty of Engineering, Shizuoka University, Hamamatsu 432

† Department of Chemistry, Faculty of Science, Okayama University, Okayama 700

(Received May 16, 1985)

Diphenylphosphinite derivatives of sugars were conveniently synthesized by the reaction of diphenylphosphinous chloride–triethylamine with sugar derivatives. Homogeneous asymmetric hydrogenations of several prochiral olefins, i.e., (*Z*)-α-acetylaminocinnamic acid, (*Z*)-α-benzoylaminocinnamic acid, itaconic acid, tiglic acid, and their esters, were carried out using rhodium(I) catalysts with the tervalent chiral phosphorus derivative of sugars. The highest optical yields for all the prochiral substrates investigated were obtained when di-μ-chloro-bis(cyclooctadiene)dirhodium(I) and methyl 2,3-*O*-isopropylidene-4-*O*-(diphenylphosphino)-α-L-rhamnopyranoside were used.

Homogeneous catalytic hydrogenation of olefins have been widely investigated since Wilkinson's work on chlorotris(triphenylphosphine)rhodium(I) was published.[1,2] Monosaccharides have several chiral carbon atoms in their skeletons, however, their application to homogeneous asymmetric hydrogenation of prochiral materials are found only in a few papers.[3–7] Bis-phosphinite of cellulose was used as a chiral ligand for a rhodium catalyst because of the more rigid conformation of the oxacylohexane ring than the cyclohexane ring of cyclohexane-1,2-diol.[8]

In our preceding paper we reported the asymmetric hydrogenation of a prochiral unsaturated acid such as (*Z*)-α-acetylaminocinnamic acid to afford the corresponding saturated acid in an optical yield of up to 67%, where 1,2:3,4-di-*O*-isopropylidene-6-*O*-(diphenylphosphino)-α-D-galactopyranose was revealed to be a good ligand.[9] The result suggested that the *O*-diphenylphosphino derivative of the carbohydrate afforded a higher optical yield than did the *C*-diphenylphosphino. In general, it is known that the nearer the chiral center is located to the ligand center the higher will be the optical yield on homogeneous asymmetric hydrogenation. Hence the synthesis of a dinuclear phosphorus ligand is more difficult than that of a mononuclear phosphorus ligand.[10,11] On the basis of the above standpoint much attention has been focussed on phosphinite derivatives of carbohydrate. The present paper deals with the facile synthesis of carbohydrates having a carbon–oxygen–phosphorus linkage on the hemiacetal ring and their successful application for asymmetric hydrogenation of olefins as an efficient ligand for the rhodium(I) catalyst.

Results and Discussion

Synthesis of Chiral Phosphinite Ligand from Carbohydrates. 1,2:5,6-Di-*O*-isopropylidene-3-*O*-(diphenylphosphino)-α-D-glucofuranose (**2**) was prepared from 1,2:5,6-di-*O*-isopropylidene-α-D-glucofuranose (**1**) by treatment with diphenylphosphinous chloride in the presence of triethylamine in 73% yield. Methyl 2,3-*O*-isopropylidene-4-*O*-(diphenylphosphino)-α-L-rhamnopyranoside (**4**) was synthesized by a reported method,[9] and was oxidized with hydrogen peroxide giving oxide **5** in quantitative yield (Scheme 1) for the purpose of confirmation of compound **4**.

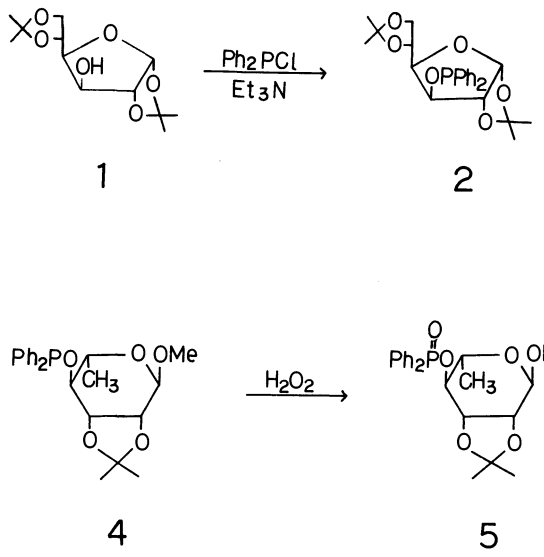

Asymmetric Hydrogenation of Prochiral Olefins. Asymmetric hydrogenation of prochiral olefins such as (*Z*)-α-acetylaminocinnamic acid, methyl (*Z*)-α-acetylaminocinnamate, (*Z*)-α-benzoylaminocinnamic acid, itaconic acid, dimethyl itaconate, and tiglic acid were carried out. The hydrogenation using glucose derivative **2** as the chiral ligand for di-μ-chloro-bis(cyclooctadiene)dirhodium(I) complex proceeded in 100% chemical yield for such a substrate as (*Z*)-α-acetylaminocinnamic acid to afford *N*-acetylphenylalanine. However, the optical yield was 10% with the *R* configuration, which did not improve over the previous work.[9] The results are shown in Table 1. The complex was not effective enough for the asymmetric hydrogenation.

The asymmetric hydrogenation of prochiral olefins

in the presence of di-μ-chloro-bis(cyclooctadiene)dirhodium(I) and rhamnose **4** gave the good results summarized in Table 2. Pure dimethyl (*S*)-methylsuccinate was prepared from dimethyl itaconate. Therefore, **4** should be a better ligand for the asymmetric hydrogenation than **2**. The asymmetric hydrogenation of (*Z*)-α-benzoylaminocinnamic and itaconic acids by chloro-bis(cyclooctene)rhodium(I) in the presence of chiral ligand **4** afforded the hydrogenation product in lower optical yields than

Table 1. Asymmetric Hydrogenation of Prochiral Olefins with $[(C_8H_{12})RhCl_2Rh(C_8H_{12})]$-Ligand **2**[a]

Substrate	Product	Chemical yield/%	$[\alpha]_D^{14}$/° (Solvent)	Optical yield/%	Configuration
(*Z*)-α-Acetylaminocinnamic acid	*N*-Acetylphenylalanine	100	−4.50 (*c* 1.0, EtOH)	10	(*R*)
Methyl (*Z*)-α-Acetylaminocinnamate	*N*-Acetylphenylalanine methyl ester	100	−1.60 (*c* 1.0, MeOH)	7	(*R*)
(*Z*)-α-Benzoylaminocinnamic acid	*N*-Benzoylphenylalanine	100	−4.29 (*c* 1.0, MeOH)	11	(*S*)
Itaconic acid	Methylsuccinic acid	100	−3.60 (*c* 1.0, EtOH)	21	(*S*)
Tiglic acid	2-Methylbutyric acid	100	−2.70 (*c* 1.0, EtOH)	14	(*R*)

a) The ratios of substrate to Rh(I) complex and of ligand **2** to Rh(I) complex were 25:1 and 4:1, respectively. All hydrogenations were carried out in 10 ml of benzene–ethanol (1:1, v/v) in the presence of 0.2 ml of triethylamine at room temperature under atmospheric pressure of hydrogen for 24 h.

Table 2. Asymmetric Hydrogenation of Prochiral Olefins with $[(C_8H_{12})RhCl_2Rh(C_8H_{12})]$-Ligand **4**[a]

Substrate	Product	Chemical yield/%	$[\alpha]_D^{14}$/° (Solvent)	Optical yield/%	Configuration
(*Z*)-α-Acetylaminocinnamic acid	*N*-Acetylphenylalanine	100	−22.1 (*c* 1.0, EtOH)	48	(*R*)
Methyl (*Z*)-α-Acetylaminocinnamate	*N*-Acetylphenylalanine methyl ester	96	− 8.70 (*c* 1.0, MeOH)	41	(*R*)
(*Z*)-α-Benzoylaminocinnamic acid	*N*-Benzoylphenylalanine	100	+31.1 (*c* 1.0, MeOH)	78	(*R*)
Itaconic acid	Methylsuccinic acid	100	−11.6 (*c* 4.3, EtOH)	68	(*S*)
Dimethyl itaconate	Dimethyl methylsuccinate	100	−17.0 (*c* 1.0, EtOH)[b]	100	(*S*)
Tiglic acid	2-Methylbutyric acid	100	−12.5 (*c* 1.0, EtOH)	65	(*R*)

a) The ratios of substrate to Rh(I) complex and of ligand **4** to Rh(I) complex were 25:1 and 4:1, respectively. All hydrogenations were carried out in 10 ml of benzene–ethanol (1:1, v/v) in the presence of 0.2 ml of triethylamine at room temperature under atmospheric pressure of hydrogen for 24 h. b) The value is for methylsuccinic acid, the hydrolysis product of dimethyl methylsuccinate.

Table 3. Asymmetric Hydrogenation of Prochiral Olefins with $[RhCl(C_8H_{14})_2]$-Ligand **4**[a]

Substrate	Product	Chemical yield/%	$[\alpha]_D^{14}$/° (Solvent)	Optical yield/%	Configuration
(*Z*)-α-Benzoylaminocinnamic acid	*N*-Benzoylphenylalanine	100	+3.40 (*c* 1.0, MeOH)	8	(*R*)
Itaconic acid	Methylsuccinic acid	100	−0.65 (*c* 4.3, EtOH)	4	(*S*)

a) The ratios of substrate to Rh(I) complex and of ligand **4** to Rh(I) complex were 25:1 and 2:1, respectively. All hydrogenations were carried out in 10 ml of benzene–ethanol (1:1, v/v) in the presence of 0.2 ml of triethylamine at room temperature under atmospheric pressure of hydrogen for 24 h.

that by di-μ-chloro-bis(cyclooctadiene)dirhodium(I) as shown in Table 3.

These results indicate that the efficiency of chiral phosphinite **4** is good enough for the asymmetric hydrogenation of prochiral olefins compared with the reported results using the ligand of carbohydrate derivatives.[9,12] This procedure seems to be a simple and efficient way for the asymmetric hydrogenation of prochiral olefins, especially for dimethyl itaconate, owing to the convenience in the ligand synthesis and to the improvement affording comparatively high optical yields.

Experimental

Measurements. ^{1}H-NMR spectra were measured on a Hitachi R-24 (60 MHz) spectrometer with tetramethylsilane as an internal standard, and IR spectra on a Japan Spectroscopic Co. Ltd. A-3 infrared spectrophotometer. Optical rotations were measured on Japan Spectroscopic Co. Ltd. DIP-4 digital polarimeter. Melting (measured by Yanagimoto micro melting apparatus) and boiling points are uncorrected.

Materials. The following materials were synthesized according to reported methods: (*Z*)-α-acetylaminocinnamic acid,[13] (*Z*)-α-benzoylaminocinnamic acid,[14] methyl (*Z*)-α-acetylaminocinnamate,[15] dimethyl itaconate,[15] 1,2:5,6-di-*O*-isopropylidene-α-D-glucofuranose (**1**),[16] methyl 2,3-*O*-isopropylidene-α-L-rhamnopyranoside (**3**),[17] diphenylphosphinous chloride (bp 110 °C/0.5 mmHg[18]),[19] chloro-bis(cyclooctene)rhodium(I),[20] di-μ-chloro-bis(cyclooctadiene)dirhodium(I),[21] and methyl 2,3-*O*-isopropylidene-4-*O*-(diphenylphosphino)-α-L-rhamnopyranoside (**4**).[9]

Preparation of 1,2:5,6-Di-*O*-isopropylidene-3-*O*-(diphenylphosphino)-α-D-glucofuranose (2). Reaction of diphenylphosphinous chloride (3.0 g) with glucose **1** (3.5 g) in triethylamine for 24 h at room temperature under nitrogen atmosphere followed by filtration and evaporation in vacuo gave compound **2** (4.4 g) in 73% yield. The purity was checked by TLC on silica gel (eluent; ethyl acetate:petroleum ether=**1**:**1** v/v, R_f=0.77); $[\alpha]_D^{14}$=−12.9° (*c* 0.65, MeOH). ^{1}H-NMR ($CDCl_3$) δ=1.25, 1.30, 1.45, 1.50 (4s, 12H, $2CMe_2$), 3.8—4.2 (m, 6H, $C_{2-6,6'}$-H), 6.00 (d, 1H, *J*=4.5 Hz, C_1-H), 7.1—7.9 (m, 10H, 2Ph); IR ν_{max}^{neat} (cm^{-1}) 1440 (P-Ph), 1040 (P-O-C); MS, *m/z*, 444 (M^+, $C_{24}H_{29}O_6P$).

Oxidation of Compound 4. Oxidation of compound **4** (0.11 g) with 30% hydrogen peroxide (0.034 ml) in chloroform (2 ml)-methanol (1 ml) overnight at room temperature followed by work-up with sodium thiosulfate afforded methyl 2,3-*O*-isopropylidene-4-*O*-(diphenylphosphinyl)-α-L-rhamnopyranoside (**5**, 0.12 g) in quantitative yield. The purity was confirmed by HPLC (eluent; chloroform:methanol=20:1, retention time 6.5 min). ^{1}H-NMR ($CDCl_3$) δ=1.24 (d, 3H, *J*=5.4 Hz, C_5-Me), 1.41, 1.51 (2s, 6H, CMe_2), 3.33 (s, 3H, OMe), 3.8—4.4 (m, 4H, C_{2-5}-H), 4.79 (s, 1H, C_1-H), 7.0—8.0 (m, 10H, 2Ph); IR ν_{max}^{neat} (cm^{-1}) 1442 (P-Ph), 1225 (P=O), 1030 (P-O-C).

Found: *m/z* 419.1661. Calcd for $C_{22}H_{28}O_6P$: M+1, 419.1622.

Asymmetric Hydrogenation of (*Z*)-α-Acetylaminocinnamic Acid with Di-μ-chloro-bis(cyclooctadiene)dirhodium(I) and Ligand 4. Asymmetric hydrogenation of (*Z*)-α-acetylaminocinnamic acid (500 mg) in anhydrous benzene (5 ml)-absolute ethanol (5 ml) was carried out using di-μ-chloro-bis(cyclooctadiene)dirhodium(I) (49 mg) and ligand **4** (160 mg) as catalyst in the presence of triethylamine (0.2 ml) under atmospheric pressure of hydrogen at room temperature for 24 h. Removal of the catalyst by passage through a column packed with ion-exchange resin Amberlite IRC-50 (H^+), followed by decolorization with activated charcoal and removal of the solvent in vacuo, gave *N*-acetylphenylalanine (100% conversion). The identification of the product was performed by ^{1}H-NMR, whose spectrum was as follows: ^{1}H-NMR ($CDCl_3$) δ=2.06 (s, 3H, COMe), 3.15 (d, 2H, *J*=6.0 Hz, $PhC\underline{H}_2$), 4.75 (t, 1H, *J*=6.0 Hz, CH), 7.1—7.4 (m, 5H, Ph); MS, *m/z*, 207 (M^+). The product had $[\alpha]_D^{14}$=−22.1° (*c*, 1.0, EtOH), which showed 48% optical yield of the *R* configuration.[22]

Removal of the catalyst from the hydrogenation mixture with ion-exchange resin Dowex 50 W (H^+) gave *N*-acetylphenylalanine methyl ester (100% conversion), which was esterified with eluent methanol.

Asymmetric Hydrogenation of Methyl (*Z*)-α-Acetylaminocinnamate with Di-μ-chloro-bis(cyclooctadiene)dirhodium(I) and Ligand 4. Asymmetric hydrogenation of methyl (*Z*)-α-acetylaminocinnamate (500 mg) was carried out by the same method as mentioned for (*Z*)-α-acetylaminocinnamic acid using ion exchange resine Dowex 50 W (H^+) gave *N*-acetylphenylalanine methyl ester (100% conversion); ^{1}H-NMR ($CDCl_3$) δ=2.07 (s, 3H, COMe), 3.15 (d, 2H, *J*=6.0 Hz, $PhC\underline{H}_2$), 3.75 (s, 3H, OMe), 4.6—4.9 (m, 1H, CH), 6.05 (bd, 1H, *J*=7.5 Hz, NH), 6.9—7.4 (m, 5H, Ph); MS, *m/z*, 221 (M^+, $C_{12}H_{15}NO_3$). The product showed $[\alpha]_D^{14}$=−8.70° (*c* 1.0, MeOH), which indicated 41% optical yield of the *R* configuration.[23]

Asymmetric Hydrogenation of Dimethyl Itaconate with Di-μ-chloro-bis(cyclooctadiene)dirhodium(I) and Ligand 4. Asymmetric hydrogenation of dimethyl itaconate (250 mg) in anhydrous benzene (5 ml)-absolute ethanol (5 ml) was carried out using di-μ-chloro-bis(cyclooctadiene)dirhodium(I) (32 mg) and ligand **4** (103 mg) as the catalyst in the presence of triethylamine (0.2 ml) under atmospheric pressure of hydrogen for 24 h at room temperature. Removal of the catalyst by passing a column packed with ion exchange resin Dowex 50 W (H^+), followed by decolorization with activated charcoal and removal of the solvent in vacuo, gave dimethyl methylsuccinate quantitatively, ^{1}H-NMR ($CDCl_3$) δ=1.15 (d, 3H, *J*=7.0 Hz, $C\underline{H}_3CH$), 2.1—3.3 (m, 3H, $CHCH_2$), 3.67 (s, 3H, $CHCO_2\underline{Me}$) 3.72 (s, 3H, CO_2Me). Alkaline hydrolysis of the ester at room temperature gave methylsuccinic acid, $[\alpha]_D^{14}$=−17.0° (*c* 1.0, EtOH), indicating 100% optical yield of the *S* configuration.[3,24] Treatment of methylsuccinic acid with diazomethane[25] in ether gave the dimethyl ester, $[\alpha]_D^{14}$=−6.1° (*c* 1.0, EtOH).[24]

Asymmetric hydrogenation of prochiral olefins with di-μ-chloro-bis(cyclooctadiene)dirhodium(I) and ligand **4** gave the corresponding product as shown in Table 2. The optical yields of the products were calculated based on the reported values of optical rotation for *N*-acetyl-(*S*)-phenylalanine, $[\alpha]_D^{26}$ +46.0° (*c* 1.0, EtOH);[22] *N*-acetyl-(*S*)-phenylalanine methyl ester, $[\alpha]_D^{25}$ +21.4° (*c* 2.0, MeOH);[23] *N*-benzoyl-(*S*)-phenylalanine, $[\alpha]_D^{27}$=−40.3° (*c* 1.0, MeOH);[26] (*R*)-methylsuccinic acid, $[\alpha]_D^{18}$ +17.01° (*c* 4.41, EtOH);[3,24]

dimethyl (*R*)-methylsuccinate, $[\alpha]_D^{25}$ +6.11° (neat);[24] and (*S*)-2-methylbutyric acid, $[\alpha]_D$ +19.33°.[28]

Asymmetric Hydrogenation of (*Z*)-α-Acetylaminocinnamic Acid with Chloro bis(cyclooctene)rhodium(I) and Ligand 4. Asymmetric hydrogenation of (*Z*)-α-acetylaminocinnamic acid (500 mg) in anhydrous benzene–absolute ethanol (1:1 v/v, 10 ml) was carried out using chlorobis(cyclooctene)rhodium(I) (27 mg) and ligand **4** (60 mg) as the catalyst in the presence of triethylamine (0.2 ml) under atmospheric pressure of hydrogen at room temperature for 24 h. Removal of the catalyst and work-up as described for the asymmetric hydrogenation with di-μ-chloro-bis(cyclooctadiene)dirhodium(I) gave *N*-acetylphenylalanine (100% conversion); $[\alpha]_D^{14}$=+3.40° (*c* 1.0, MeOH), indicating an optical yield 8% of the *R* configuration.

Results for asymmetric hydrogenation with chlorobis(cyclooctene)rhodium(I) and ligand **4** were summarized in Table 3.

Asymmetric Hydrogenation of (*Z*)-α-Acetylaminocinnamic Acid with Di-μ-chloro-bis(cyclooctadiene)dirhodium(I) and Ligand 2. Asymmetric hydrogenation of (*Z*)-α-acetylaminocinnamic acid (500 mg) in anhydrous benzene–absolute ethanol (1:1 v/v, 10 ml) was carried out using di-μ-chloro-bis(cyclooctadiene)dirhodium(I) (49 mg) and ligand **2** (178 mg) as the catalyst in the presence of triethylamine (0.2 ml) under atmospheric pressure of hydrogen at room temperature for 24 h. Removal of the catalyst and work-up as mentioned for asymmetric hydrogenation using ligand **4** gave *N*-acetylphenylalanine (100% conversion); $[\alpha]_D^{14}$=−4.50° (*c* 1.0, EtOH), optical yield of 10% of the *R* configuration.

The results obtained for several prochiral olefins are shown in Table 1.

References

1) J. A. Osborn, F. H. Jardine, J. F. Young, and G. Wilkinson, *J. Chem. Soc., A*, **1966**, 1711.

2) A. P. G. Kieboom and F. van Rantwijk, "Hydrogenation and Hydrogenolysis in Synthetic Organic Chemistry," Delft University Press, Rotterdam (1977), pp. 80—86.

3) T. Iwami, T. Yoshida, and M. Sato, *Nippon Kagaku Kaishi*, **1976**, 1652.

4) W. R. Cullen and Y. Sugi, *Tetrahedron Lett.*, **1978**, 1635.

5) Y. Sugi and W. R. Cullen, *Chem. Lett.*, **1979**, 39.

6) T. H. Johnson and G. Rangerjan, *J. Org. Chem.*, **45**, 62 (1980).

7) D. Lafont, D. Sinou, and G. Descotes, *J. Organomet. Chem.*, **169**, 87 (1979).

8) Y. Kawabata, M. Tanaka, and I. Ogata, *Chem. Lett.*, **1976**, 1213.

9) M. Yamashita, K. Hiramatsu, M. Yamada, N. Suzuki, and S. Inokawa, *Bull. Chem. Soc. Jpn.*, **55**, 2917 (1982).

10) W. S. Knowles and M. J. Sabacky, *J. Chem. Soc., Chem. Commun.*, **1968**, 1445.

11) Y. Inouye, "Fusei Yuki Gosei," Kagaku Dojin, Kyoto (1977), Chap. 8.

12) V. Čaplar, G. Comisso, and V. Šunjić, *Synthesis*, **1981**, 85.

13) R. M. Herbst and D. Shemin, *Org. Synth.*, Coll. Vol. II, 1 (1950).

14) H. B. Gillespie and H. R. Snyder, *Org. Synth.*, Coll. Vol. II, 489 (1950).

15) E. Rothstein, *J. Chem. Soc.*, **1949**, 1968.

16) O. Th. Schmidt, "Method in Carbohydrate Chemistry," ed by R. L. Whistler, M. L. Wolfrom, Academic Press Inc., New York (1963), Vol. 2, p. 318.

17) M. Yamashita, P. T. Long, M. Shibata, and S. Inokawa, *Carbohydr. Res.*, **84**, 35 (1980).

18) 1 mmHg=133.322 Pa.

19) M. P. Brown and H. B. Silver, *Chem. Ind. (London)*, **1961**, 24.

20) A. Van Der Ent and A. L. Onderlinden, *Inorg. Synth.*, **14**, 92 (1973).

21) J. Chatt and L. M. Veuanzi, *J. Chem. Soc.*, **1957**, 4735.

22) T. P. Dang, J.-C. Poulin, and H. B. Kagan, *J. Organomet. Chem.*, **91**, 105 (1975).

23) R. Glaser and B. Vainas, *J. Organomet. Chem.*, **121**, 249 (1976).

24) R. Rossi, P. Diversi, and G. Ingrosso, *Gazz, Chim. Ital.*, **98**, 1391 (1968).

25) Th. J. De Boer and H. J. Backer, *Org. Synth.*, Coll. Vol. IV, 250 (1963).

26) M. Goodman and L. Levine, *J. Am. Chem. Soc.*, **86**, 2918 (1964).

27) W. C. Christopfel and B. D. Vineyard, *J. Am. Chem. Soc.*, **101**, 4406 (1979).

28) Y. Asahina and T. Shimizu, *Nippon Yakugaku Kaishi*, **479**, 1 (1922).

Reactions of α-Polyhalo Ketone Tosylhydrazones with Sulfide Ion and Primary Amines. Cyclization to 1,2,3-Thiadiazoles and 1,2,3-Triazoles

Kunikazu SAKAI,* Nobuko HIDA, and Kiyosi KONDO
Sagami Chemical Research Center, Nishi-Ohnuma 4-4-1, Sagamihara, Kanagawa 229
(Received June 27, 1985)

Trichloroacetaldehyde tosylhydrazone acts as an excellent precursor of diazodithioacetate which is generated by treatment of the hydrazone with sulfide ion. This spontaneously cyclizes it to 5-mercapto-1,2,3-thiadiazole. The precursor also gives a 5-amino-1,2,3-triazole on reaction with an amine. α,α-Dichloro ketone tosylhydrazones similarly cyclize to give 1,2,3-thiadiazoles and 1,2,3-triazoles.

Heterocycles, such as 1,2,3-thiadiazoles and 1,2,3-triazoles are useful for various purposes such as modifiers of cephalosporin antibiotoics,[1] or precursors of herbicides[2] or insecticides.[3] For the synthesis of 1,2,3-heterocycles, such as 1,2,3-thiadiazoles and 1,2,3-triazoles, several methods have been developed. Among them, for example, is the preparation of 1,2,3-thiadiazoles by the 1,3-dipolar [2+3] cycloaddition of diazomethane with a thioketone as shown in Fig. 1.[4]

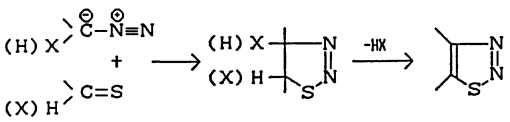

Fig. 1.

The synthesis of 1,2,3-heterocycles **3** was achieved by the intramolecular cyclization of the intermediate **2** as shown in Scheme 1. For the preparation of 1,2,3-thiadiazole **3** (X=S), diazothioacetate **2** (X=S) is considered as a potential precursor, because **2** (X=S) has the moieties of both the diazo and thiocarbonyl groups in the molecule, which are necessary for the cyclization to the 1,2,3-thiadiazole. However, the diazothioacetate **2** (X=S) is an unknown hypothetical compound, differing from the diazoacetate **2** (X=O). The intermediate **2** (X=S) is thought to be so labile that it will cyclize spontaneously to 1,2,3-thiadiazole **3** (X=S). Here, we chose the α-polyhalo ketone tosylhydrazone **1** as the precursor for the generation of the labile **2** (X=S) and cyclization to **3** (X=S). Similarly diazoacetamidinate **2** (X=NR′) will be generated from the common precursor **1** and **2** (X=NR′) will cyclize to 1,2,3-triazole **3** (X=NR′). Because, the trichloromethyl group in **1** is an equivalent of dithiocaboxylate, C(=S)-SNa, by treatment with Na_2S, and it is also an equivalent of amidine, C(=NR′)-NHR′, by the treatment with H_2NR'. On the other hand, the generation of a diazo group from tosyl hydrazone by treatment with base is well-known as the Bamford-Stevens reaction.[5] Thus, the treatment of **1** with sulfide ion or amine will induce concurrent or stepwise reactions, and will generate labile **2** which will spontaneously cyclize to **3**. Based on the above considerations and analysis, we have developed the intramolecular cyclization method successfully, and we will demonstrate the results of several reactions of α-polyhalo ketone tosylhydrazones with sulfide ion and amines to cyclize to 1,2,3-thiadiazole and 1,2,3-triazole, respectively.

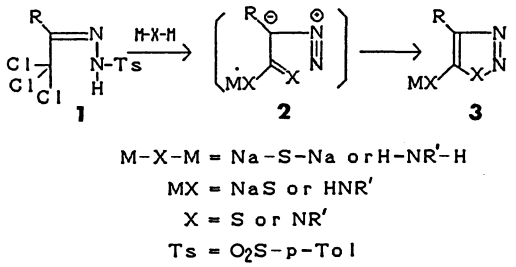

M-X-M = Na-S-Na or H-NR′-H
MX = NaS or HNR′
X = S or NR′
Ts = O_2S-p-Tol

Scheme 1.

Trichloroacetaldehyde tosylhydrazone (**4**), a precursor of the reactive intermediate **2** (X=S, MX=NaS), is a known compound and was prepared as described in the literature.[6] The cyclization reaction was carried out as follows: Into a solution of 3 equivalents of sodium sulfide nonahydrate ($Na_2S \cdot 9H_2O$) in 50% aqueous ethanol, hydrazone **4** was added. The solution was concentrated and the deposited crystals collected. Treatment of the crystals with benzyl bromide gave 5-benzylthio-1,2,3-thiadiazole (**7**) in 67% yield and benzyl *p*-tolyl sulfone (**8**) in 41% yield, as shown in Eq. 3. The result suggested that the deposited crystals were composed of sodium 1,2,3-thiadiazol-5-yl sulfide (**5**) and sodium *p*-toluenesulfinate (**6**). In practice, an attempt to separate them by fractional recrystallization from ethanol gave **5** and **6** in 60 and 84% yields. The reaction yielded the 1,2,3-thiadiazole **5** via intramolecular cyclization of the reactive intermediate **2** generated from the precursor **4**. This result encouraged us to extend the reaction using other bases, such as amines and hydroxide ion.

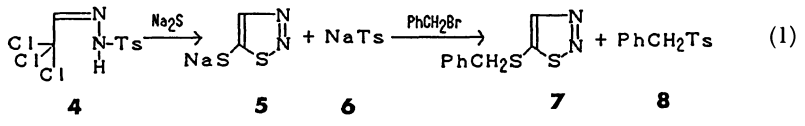

Accordingly, amines were allowed to react with **4**. Although treatment with aqueous ammonia provided no identified materials, a treatment with excess benzylamine in methanol gave 1-benzyl-5-benzylamino-1,2,3-triazole (**9**) in 30% yield, along with large amounts of mixed salts of benzylamine. With methylamine, 1-methyl-5-methylamino-1,2,3-triazole (**10**) was also afforded in 25% yield (Eq. 2).

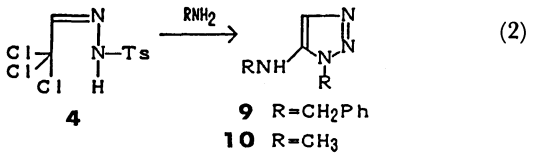

In the case of hydroxide ion, the expected reaction product of the precursor **4**, 1,2,3-oxadiazole, is known to be unstable, except for the case of sydnone.[7] In practice, treatment of **4** with sodium hydroxide solution gave no identified products.

We were next interested in the reaction of thioacetaldehyde **2** (X=S, MX=H) as the reactive intermediate. The precursor for the generation of **2** (X=S, MX=H) should be a dichloride, such as **11**. A precursor, α,α-dichloroacetone tosylhydrazone (**11**), was prepared by the same method as above for **4**.[6] By treatment of **11** with sodium sulfide, only a trace amount of 4-methyl-1,2,3-thiadiazole (**12**) was detected by NMR spectroscopy. This will be related to the volatility of the product **12**. On the other hand, reaction of **11** with excess benzylamine gave 1-benzyl-4-methyl-1,2,3-triazole (**13**), in a high yield of 84% as shown in Eq. 3. Allylamine likewise gave 1-allyl-4-methyl-1,2,3-triazole (**14**) in 83% yield. The precursor **11** also cyclized successfully.

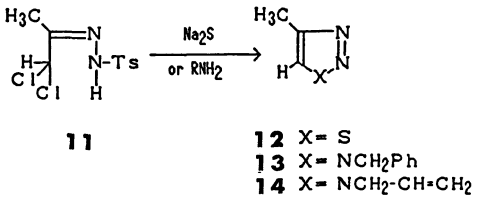

The preparation of two other α,α-dichloroketones, **15** and **18** was attempted by the cyclization reaction. By treatment with tosylhydrazine, 2,2-dichloro-1-indanone (**15**) gave 2-chloro-1-indenone tosylhydrazone (**16**) with simultaneous removal of hydrogen chloride (Eq. 4). The hydrazone **16** provided 2-chloro-1-diazoindene (**17**) as a common product, by reaction both with sodium sulfide and with benzylamine. The difficult substitution of sulfur or amine nucleophiles for a chlorine atom in **16** or **17** and stabilization of the diazo group by a benzene ring will lead to the isolation of the diazo compound **17**. On the other hand, when α,α-dichloroacetophenone (**18**) was treated with tosylhydrazine (Eq. 5), the compound isolated was unexpectedly cyclized 4-phenyl-1-(*p*-toluenesulfonamido)-1,2,3-triazole (**20**). This indicates that tosylhydrazone **19** was so labile that tosylhydrazine reacted with **19** to give **20**.

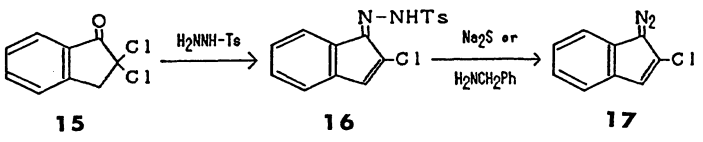

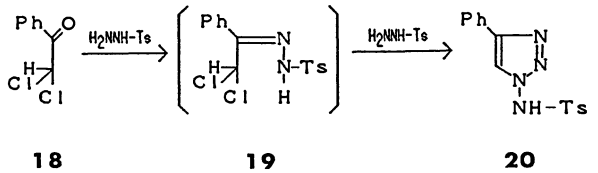

As a final example, 1,1-dichloro-2-(*p*-tolylsulfonylazo)ethene (**21**) was obtained from **4** by gentle treatment with triethylamine as reported by Bott[6] (Eq. 6). The 1,1-dichloroethenyl derivative **21** similarly cyclized to **5** by reaction with sodium sulfide; it was identified as the benzyl derivative **7**.

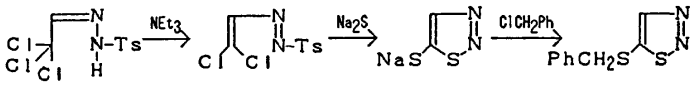

4 21 5 7 (6)

From the mechanistic view point, the production of 5-mercapto-1,2,3-thiadiazole (**5**) from **21** suggests that the reaction may proceed via the intermediate **21**. We can speculate that the course of the cyclization reaction is as shown in Scheme 2. According to

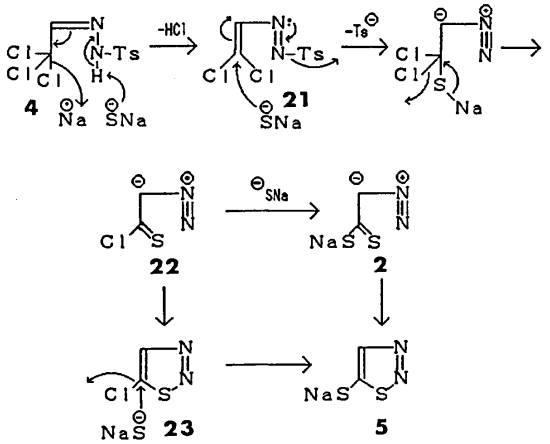

Scheme 2.

which, the reaction with Na_2S initiates a removal of hydrogen chloride from **4** to give a stable intermediate **21**. The addition of second sulfide ion for the substitution for chlorine atom in **21** by addition-elimination manner induces the simultaneous removal of toluenesulfinate ion to generate a diazomethane moiety to afford intermediate **22**. From **22** to the final product **5**, two routes are possible. One is that the reaction proceeds by the attack of a third sulfide ion to generate diazodithiocarboxylate **2** (X=S); alternatively cyclization may occur first, to give stable 5-chloro-1,2,3-thiadiazole (**23**). This is already known to easily substitute a sulfide ion for a chlorine atom,[8] although we could not detect it in the reaction mixture. The reaction of **4** with amines can take place by the same mechanism as shown above. However, generation of the diazo intermediate, **2** or **22**, in the course of the reaction still remains an uncertainty, because in the Bamford-Stevens reaction, the reaction conditions are generally *more drastic.*[5] *But in a particular case, such as a* monotosylhydrazone of α-diketone, it is known that the hydrazone easily gave an α-diazoketone by treatment with 0.1 M† sodium hydroxide solution at room temperature.[9] In this case the contribution of the α-carbonyl group is important for the genaration of diazo group under such mild conditions. Similarly the thiocarbonyl group may act a significant role for the smooth generation of the diazo moiety in **2** or **22**.

† 1 M=1 mol dm^{-3}.

Further detailed studies to clarify the intermediate role of the diazodithioacetate **2** are in progress.

Experimental

Measurements: All the melting points are uncorrected. NMR spectra were taken with Varian EM-390 and XL-100 instruments. Mass spectra were obtained with a Hitachi RMU-6MG instrument. IR were measured with a JASCO A-202 instrument.

Trichloroacetaldehyde Tosylhydrazone (4): This was prepared according to the method described in the literature from trichloroacetaldehyde and tosylhydrazine.[6]

Sodium 1,2,3-Thiadiazol-5-yl Sulfide (5) and Sodium *p*-Toluenesulfinate (6): To a solution of sodium sulfide ($Na_2S \cdot 9H_2O$) (18.0 g, 74.9 mmol) in 50% aqueous ethanol (40 ml) under ice-cooling, trichloroacetaldehyde tosylhydrazone (**4**) (6.31 g, 20.0 mmol) was added as powder portion wise over a period of 5 min. The stirring was continued at that temperature for 10 min and at room temperature for 1 h. The solution was then concentrated under reduced pressure at 50 °C to one third of the volume. The deposited precipitates of a mixture of **5** and **6** were collected by filtration after cooling with ice. The crystals, dried under reduced pressure in desiccator, were dissolved in ethanol (100 ml) and treated with active charcoal. Ethanol was distilled off by heating until the volume of the solution reduced to ca. 50 ml. On cooling with ice, precipitates of **6** were deposited and filtered off. The filtrate was concentrated again to a half. From the solution, **6** was crystallized again on cooling and filtered off. By complete removal of the solvent, 1.68 g of **5** was obtained (60% yield). All filtered **6** fractions were combined and totally 3.00 g of **6** was collected (84% yield).

5: IR (KBr disc); 3350, 1665, 1640, 1400, 1200, 1120, 1040, 870, 820 cm^{-1}; ^{1}H-NMR (D_2O, TSP deuterated) δ=8.2 (singlet).

5-Benzylthio-1,2,3-thiadiazole (7) and Benzyl *p*-Tolyl Sulfone (8): The dried crystalline mixture of **5** and **6** (1.00 g) obtained as above was dissolved in 50% aqueous ethanol (6 ml) and to this was added benzyl bromide (806 mg, 4.71 mmol) at room temperature. The solution was extracted with dichloromethane, after 1 h. The organic layer was washed with brine, dried over anhydrous sodium sulfate, and the solvent removed to leave 1.13 g of residue. Column chromatographic separation (silica gel, CH_2Cl_2) of the residue gave **7** (449 mg, 67% yield) and **8** (315 mg, 41% yield), respectively.

7: Mp 49—51 °C; ^{1}H-NMR ($CDCl_3$) δ=4.14 (2H, s), 7.30 (5H, s); MS (70 eV) *m/z* 208 (M^+, 2.3%), 180 (1.5%), 179 (5.3%), 147 (7.8%), 122 (15.1%), 91 (100%).

8: ^{1}H-NMR ($CDCl_3$) δ=2.39 (3H, s), 4.25 (2H, s), 6.95—7.55 (9H, m).

1-Benzyl-5-benzylamino-1,2,3-triazole (9): To a solution of trichloroacetaldehyde tosylhydrazone (**4**) (3.2 g, 10 mmol) in methanol (10 ml) under ice-cooling, was added a

solution of benzylamine (6.4 g, 60 mmol) in methanol (5 ml) dropwise. Stirring was continued at ice-water temperature for 2.5 h. Methanol was removed below 30 °C under reduced pressure. Benzene was added to the residue and the solid was crushed to a fine powder. Insoluble crystals of benzylamine salts (2.7 g) were removed by filtration and the benzene layer was washed with 1 M sodium hydroxide aqueous solution and brine. Removal of solvent after drying over anhydrous magnesium sulfate left a dark residue which was purified by column chromatography (silica gel, hexane: AcOEt=1:2) to afford **9** (0.77 g, 30% yield).

9: Mp 102—108 °C: ^{1}H-NMR (d_6-DMSO) δ=4.25 (2H, bt), 5.41 (2H, s), 6.50 (1H, bt), 6.81 (1H, s), 7.10—7.43 (10H, m): IR (KBr disc) 3050, 1670, 1600, 1500, 1450, 1290, 1240 cm^{-1}: MS (70 eV) m/z 264 (M^+, 83%), 236 (4.1%), 104 (26.0%), 91 (100%).

1-Methyl-5-methylamino-1,2,3-triazole (10): To a solution of 40% aqueous methylamine (4.7 g, 60 mmol) in water (15 ml) and methanol (10 ml) under ice-cooling, powdered trichloroacetaldehyde tosylhydrazone (**4**) (3.2 g, 10 mmol) was added portion wise. Stirring was continued at room temperature for 19 h and the product was extracted with chloroform. The organic layer was washed with brine, and dried over anhydrous magnesium sulfate. The residue (1.02 g) on removal of the solvent under reduced pressure was purified by column chromatography (silica gel, AcOEt) to give **10** (0.27 g, 25% yield).

10: Mp 61—63 °C: ^{1}H-NMR ($CDCl_3$) δ=2.83 (3H, s), 3.77 (3H, s), 4.91(1H, bs), 6.87 (1H, s): IR (KBr disc) 3050, 2810, 1440, 1310, 1280 cm^{-1}: MS (70 eV) m/z 112 (M^+, 44.6%), 83 (15.5%), 69 (41.0%), 55 (44.7%), 42 (100%).

α,α-Dichloroacetone Tosylhydrazone (11): To a solution of *p*-tosylhydrazine (6.7 g, 36 mmol) in propionic acid (30 ml), was added α,α-dichloroacetone (5.0 g, 39 mmol) and the reaction mixture was stirred at room temperature for 4 h. To this was added cyclohexane (30 ml) and the reaction mixture was cooled in ice bath. The white crystals which deposited were collected by filtration to give **11** (10 g, 94% yield).

11: Mp 137—138 °C (decomp): ^{1}H-NMR (d_6-DMSO) δ=1.85 (3H, s), 2.37 (3H, s), 7.40 (2H, m), 9.17 (1H, s), and 2.03 (3H, s), 2.37 (3H, s), 6.70 (1H, s), 7.40 (2H, m), 7.77 (2H, m): IR (KBr disc) 3230, 1600, 1340, 1170 cm^{-1}: MS (70 eV) m/z 294 (M^+, 2.3%), 155 (14.5%), 91 (100%).

Detection of 4-Methyl-1,2,3-thiadiazole (12): A solution of sodium sulfide ($Na_2S \cdot 9H_2O$)(3.00 g, 12.5 mmol) in water (7 ml) was covered with a layer of ether (12 ml), under ice-cooling, α,α-dichloroacetone tosylhydrazone (**11**) (1.48 g, 5.00 mmol) was added portion wise and stirring was continued for 19 h at that temperature. The ether layer was separated, washed with brine, and dried over anhydrous sodium sulfate. Ether was removed at atmospheric pressure at 55 °C to leave a trace of colorless residue. The ^{1}H-NMR of the residue revealed the signals due to 4-methyl-1,2,3-thiadiazole (**12**) at 2.85(s) and 8.20(s).

1-Benzyl-4-methyl-1,2,3-triazole (13): To a solution of α,α-dichloroacetone tosylhydrazone (**11**) (3.0 g, 10 mmol) in methanol (10 ml) under ice-cooling, was added a solution of benzylamine (5.3 g, 50 mmol) in methanol (5 ml) dropwise, followed by stirring at that temperature for 2 h. To the residue after removal of methanol under reduced pressure, benzene (10 ml) was added. The precipitates were crushed under ice-cooling, and removed by filtration. The benzene layer was washed with 1 M sodium hydroxide and brine, dried over anhydrous magnesium sulfate and the solvent removed leaving a dark residue. The residue was purified by column chromatography (silica gel, hexane: AcOEt=1:1) to afford **13** (1.46 g, 84% yield).

13: Mp 61—62 °C: ^{1}H-NMR ($CDCl_3$) δ=2.30 (3H, s), 5.43 (2H, s), 7.17 (1H, s), 7.21—7.37 (5H, m): IR (KBr disc) 3070, 2950, 1500, 1440, cm^{-1}: MS (70 eV) m/z 173 (M^+, 31.8%), 91 (100%), 65 (74.9%).

1-Allyl-4-methyl-1,2,3-triazole (14): To a solution of allylamine (2.9 g, 50 mmol) in methanol (15 ml), under ice-cooling, powdered dichloroacetone tosylhydrazone (**11**) was added portion wise. The mixture was stirred at that temperature for 4.5 h and at room temperature for 1.5 h. The solvent was removed under reduced pressure and replaced with dichloromethane. The solution was washed with 1 M sodium hydroxide and brine and dried over anhydrous magnesium sulfate. The residual oil on removal of solvent was purified by distillation (15 mmHg,† 100—160 °C) to give **14** (125 mg, 83%) as an oil.

14: ^{1}H-NMR ($CDCl_3$) δ=2.33 (3H, s), 4.90 (2H, dd), 5.25 (2H, m), 6.00 (1H, m), 7.30 (1H, d): IR (KBr plate) 3100, 2950, 1650, 1440, 1210, 1050, cm^{-1}: MS (70 eV) m/z 123 (M^+, 15.2%), 54 (36.1%), 41 (100%).

2,2-Dichloro-1-indanone (15): This was prepared according to the literature[10] from 1-indanone and copper(II) chloride.

2-Chloro-1-indenone Tosylhydrazone (16): 2,2-Dichloro-1-indanone (**15**) (0.54 g, 2.7 mmol) in ethanol (10 ml) was added to a solution of tosylhydrazine (0.50 g, 2.7 mmol) and 12 M hydrochloric acid (0.25 ml) and the mixture was stirred at room temperature for 20 h. The yellow crystals which deposited were collected by filtration. The filtrate was concentrated to half the volume and the crystals collected by filtration. Totally, 0.70 g of 2-chloro-1-indenone tosylhydrazone (**16**) was obtained (78% yield).

16: Mp 162—165 °C: ^{1}H-NMR (d_6-DMSO) δ=2.40 (3H, s), 6.87 (1H, s), 7.00—7.40 (5H, m): IR (KBr disc) 3450, 3250, 1600, 1345, 1170 cm^{-1}: MS (70 eV) m/z 332 (M^+, 2.1%), 176 (46.7%), 148 (93.8%), 113 (100%).

2-Chloro-1-diazoindene (17); Reaction of 16 with Benzylamine: A mixture of 2-chloro-1-indenone tosylhydrazone (**16**) (0.49 g, 1.5 mmol) and benzylamine (0.66 g, 5.9 mmol) in methanol (10 ml) was stirred under ice cooling for 1 h, at room temperature for 4 h, and finally at reflux temperature for 1 h. The solvent was removed under reduced pressure and to the residue was added a mixture of benzene and ether (v/v=1/1, 20 ml). The organic layer was washed with saturated sodium hydrogencarbonate solution and brine, and dried over anhydrous magnesium sulfate. Removal of the solvent under reduced pressure gave a residue which was separated by column chromatography (silica gel, hexane:AcOEt=1:1) to afford **16** (0.08 g, 16%) and 2-chloro-1-diazoindene (**17**) (0.07 g, 27% yield).

17: ^{1}H-NMR ($CDCl_3$) δ=6.30 (1H, s), 7.03—7.47 (4H, m): IR (KBr disc): 2100, 1505, 1430 cm^{-1}: MS (70 eV) m/z 176 (M^+, 41.7%), 148 (81.8%), 113 (100%).

2-Chloro-1-diazoindene (17); Reaction of 16 with Sodium

† 1 mmHg=133.322 Pa.

Sulfide: To a solution of sodium sulfide ($Na_2S \cdot 9H_2O$) (2.2 g, 9.0 mmol) in methanol (8 ml) was added 2-chloro-1-indenone tosylhydrazone (**16**) (1.0 g, 3.0 mmol) in methanol (10 ml) under ice-cooling and stirring was continued for 46 h at room temperature. The reaction mixture was filtered and the filtrate was concentrated until the precipitates began to deposit. The precipitates were collected by filtration. ^{1}H-NMR and IR spectra of the crystals showed that **17** was produced.

4-Phenyl-1-(*p*-toluenesulfonamido)-1,2,3-triazole (20): A mixture of α,α-dichloroacetophenone (**18**) (purchased from Aldrich Chemical Co.) (10.4 g, 60 mmol) and *p*-tosylhydrazine (5.6 g, 30 mmol) in ethanol (50 ml) was refluxed for 1 h. The crystals formed by concentration of the solution were collected by filtration after cooling with ice. The crystals of **20** were produced (1.94 g, 20% yield).

20: Mp 202—203 °C (decomp): Elemental analysis, Found: C, 57.43; H, 4.41; N, 17.58; S, 10.10%: Calcd for $C_{15}H_{14}N_4O_2S$: C, 57.31; H, 4.49; N, 17.82; S, 10.20%: ^{1}H-NMR (d_6-DMSO) δ=2.40 (3H, s), 7.17—7.87 (9H, m), 8.07 (1H, s): IR (KBr disc) 3050, 1600, 1480, 1370, 1170, 1090 cm^{-1}: MS (70 eV) *m/z* 314 (M^+, 3.8%), 171 (44.7%), 155 (52.5%), 145 (100%).

5-Benzylthio-1,2,3-thiadiazole (7) from 1,1-Dichloro-2-(*p*-tolylsulfonylazo)ethene (21): To a solution of sodium sulfide ($Na_2S \cdot 9H_2O$) (600 mg, 2.50 mmol) in water (1.0 ml) and ethanol (0.5 ml), was added 1,1-dichloro-2-(*p*-tolylsulfonylazo)ethene (**21**) (280 mg, 1.00 mmol) prepared by the method reported by Bott[6] from trichloroacetaldehyde tosylhydrazone (**4**) and triethylamine in dichloromethane at 0 °C in ethanol (0.5 ml) slowly at room temperature, and the reaction mixture was stirred for 1 h. The solution was cooled with ice and benzyl chloride was added (0.5 ml). After 1 h, ether was added and the organic layer was washed with brine, dried over anhydrous sodium sulfate, and the solvent removed under reduced pressure. Removal of excess benzyl chloride in vacuo at 60 °C gave **7** as orange crystals (94 mg, 45%).

References

1) G. E. Lewis and P. H. Nelson, *J. Med. Chem.*, **22**, 1214 (1979); America Cyanamide, *France Demande*, 2 488 258 (1982).

2) K. Hiratani and T. Nakagawa, *Japan Tokkyo Kokai Koho*, JP81-127,363 (1981).

3) Bayer A.-G., *Japan Tokkyo Kokai Koho*, JP77-116 464 (1977).

4) P. Demaree, M.-C. Doria, and J. M. Muchowski, *Can. J. Chem.*, **55**, 243 (1977); M. Uher, *Coll. Czech. Chem. Commun.*, **41**, 1182 (1976); W. E. Hymans, *J. Heterocycl. Chem.*, **13**, 1141 (1976); S. Hoff and A. P. Blok, *Recl. Trav. Chim. Pays-Bas*, **93**, 317 (1974); S. Holm and A. Senning, *Tetrahedron Lett.*, **1973**, 2389; B. M. Beck, *Liebigs Ann. Chem.*, **682**, 90 (1965).

5) R. H. Shapiro, *Organic Reactions*, **23**, 405 (1976).

6) K. Bott, *Chem. Ber.*, **108**, 402 (1975).

7) L. B. Clapp, "Comprehensive Heterocyclic Chemistry," ed by A. R. Katritzky and C. W. Rees, Pergamon Press (1984) Vol. 6. p. 366.

8) Dynamit Nobel A.-G. *Ger. Offen.*, 2 856 404 (1980).

9) A. T. Blomquist and F. W. Schlaefer, *J. Am. Chem. Soc.*, **83**, 4547 (1961).

10) V. A. Nefedov, *Zh. Obshch. Khim.*, **43**, 2016 (1973); *Chem. Abstr.*, **80**, 3288n (1974).

Synthesis of Gramicidin S (GS) Analogs, [3—4-δAva]-GS and [3—4,3′—4′-Bis(δAva)]-GS (δAva=5-Aminovaleric Acid)

Shosuke SOFUKU,* Yasutaro SUGIYAMA, and Ichiro MURAMATSU
Department of Chemistry, College of Science, Rikkyo University,
Nishi-Ikebukuro, Toshima-ku, Tokyo 171
(Received July 20, 1985)

Gramicidin S (GS) analogs, [δAva$^{3-4}$]-GS and [δAva$^{3-4,3'-4'}$]-GS, were synthesized. Both of these peptides are analogs in which one or two L-leucyl-D-phenylalanyl residues of GS are replaced by one or two 5-aminovaleric acid residues. The CD spectrum of the mono-substituted analog has two troughs as that of GS. However, this analog showed almost no antimicrobial activity. Moreover, the di-substituted analog showed a CD spectrum that is ascribed to a random structure and had no antimicrobial activity.

In previous reports,[1-3] we have described the syntheses and properties of four gramicidin S (GS) analogs containing 5-aminovaleric acid residue (δAva). All of them were cyclic peptides in which each sequence of two adjacent amino acid residues is replaced by one residue of 5-aminovaleric acid. Consequently, each amide group was substituted by an ethylene group which had the same number of members in the ring as that of natural GS, *cyclo*-(Val-Orn-Leu-D-Phe-Pro)$_2$, although the side chains inevitably were lacking. Thus, it can be elucidated whether or not the original amide group in the natural peptide takes part in the intramolecular hydrogen bond. One of the analogs, [δAva$^{4-5}$]-GS, had a similar CD spectrum to that of GS, and its conformation was confirmed by ^{1}H-NMR measurement.[4] This analog showed significant antimicrobial activity against some microorganisms.[5]

In view of these results, it became of interest to obtain information about the contributions of the amide bond and side chains in Leu-D-Phe sequence of GS. Hence we undertook the synthesis and

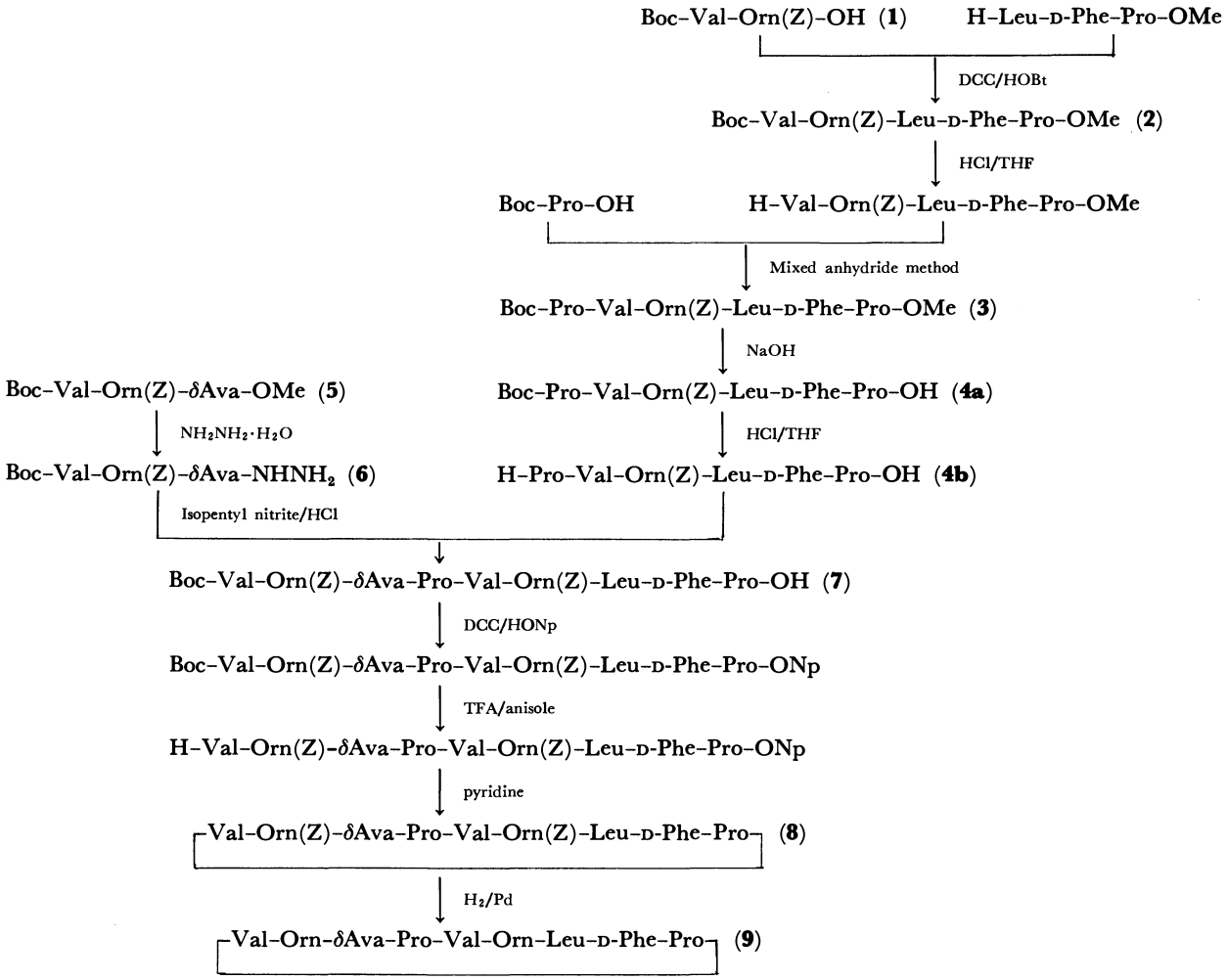

Fig. 1. Synthetic scheme for [δAva$^{3-4}$]-GS.

evaluation of the properties of [δAva$^{3-4}$]-GS and [δAva$^{3-4,3'-4'}$]-GS, as described in this paper.

Results and Discussion

The synthesis of [δAva$^{3-4}$]-GS is outlined in Fig. 1.[6] H-Leu-D-Phe-Pro-OMe was obtained by hydrogenolysis of oily Z-Leu-D-Phe-Pro-OMe which had been synthesized stepwise by the mixed anhydride method.[8] Peptides **2** and **3** were prepared by the conventional methods.[9] On the other hand, Boc-Val-Orn(Z)-δAva-OMe (**5**) was synthesized from Boc-Val-Orn(Z)-$NHNH_2$[10] and H-δAva-OMe[1] by the azide method[11] and converted to **6** by hydrazinolysis. Peptide **7** was synthesized from **4b** and **6** by the azide method.

The synthetic scheme of [δAva$^{3-4,3'-4'}$]-GS is also shown in Fig. 2. Peptide **10** was synthesized from **6** and H-Pro-OMe by the azide method. Deprotections of **10** gave **11** and **12**, respectively, which were then coupled with each other to afford **13** by the DCC-HOBt method. After purification by gel filtration on a Sephadex LH-20 with MeOH, the saponification of **13** gave **14**.

The intramolecular cyclizations of **7** and **14** were performed by the active ester method in dilute pyridine solution and the products (**8** and **15**) were purified by column chromatography. [δAva$^{3-4}$]-GS (**9**) and [δAva$^{3-4,3'-4'}$]-GS (**16**) were obtained by hydrogenolysis of **8** and **15**, respectively, and were confirmed by means of the DNSC (5-dimethylamino-1-naphthalenesulfonyl chloride) procedure[12] and paper electrophoresis.[1]

To obtain information on the conformation of [δAva$^{3-4}$]-GS and [δAva$^{3-4,3'-4'}$]-GS, CD and ORD spectra of the aqueous solutions were measured. The CD spectra of these analogs are shown in Fig. 3. The CD spectrum of the former analog has two troughs (207 and 215 nm) which are similar to those of GS although the molar ellipticity is smaller than that of GS, and the spectrum of the latter suggests a random structure. The ORD spectra of these analogs gave the same information. The minimum value in the ORD spectrum of [δAva$^{3-4}$]-GS was observed at 230 nm, the same as that of GS. The sequence of [δAva$^{3-4}$]-GS is the same as half that of GS, and this half can make the hydrogen bond maintain the β-turn, which has been indicated from the CD spectrum. From these results we predicted that [δAva$^{3-4}$]-GS may show antimicrobial activity against Gram-positive bacteria. However, as shown in Table 1, the mono-substituted analog had almost no activity, and the di-subsitituted analog had no activity at all. The partial sequence, -NH-$(CH_2)_4$-CO-Pro-Val, of these analogs corresponds to Gly-Pro-Val or D-X-Pro-Y of Type II′ in the rules for

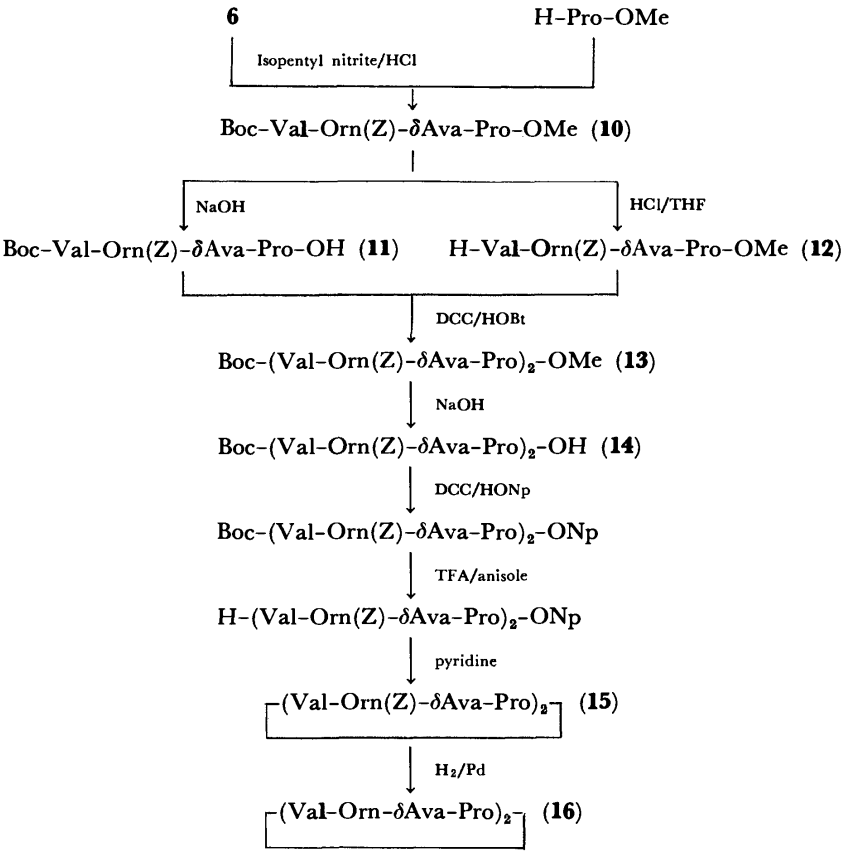

Fig. 2. Synthetic scheme for [δAva$^{3-4,3'-4'}$]-GS.

Table 1. Atimicrobial Activity of GS and its Analogs

Test organism	Minium inhibitory concentration[a]		
	GS	[δAva$^{3-4}$]-GS	[δAva$^{3-4,3'-4'}$]-GS
Sarcina lutea ATCC 9341	6.3	>100	>100
Micrococcus flavus ATCC 10240	3.1	50	>100
Corynebacterium diphtheriae P.W.8	1.6	50	>100
Bacillus subtilis ATCC 6633	6.3	>100	>100
Escherichia coli NIHJ-JC2	>100	>100	>100

a) The minimum concentration (μg/ml) was determined by the agar dilution method.

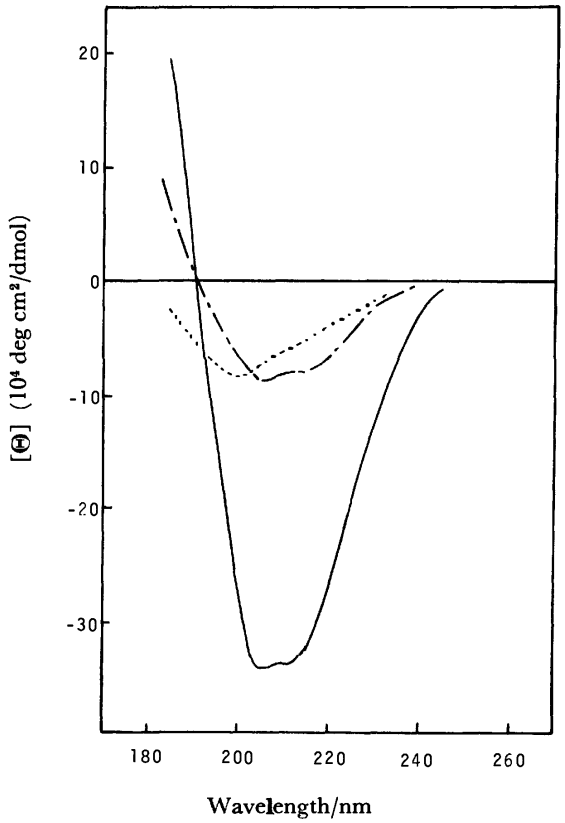

Fig. 3. CD spectra of GS·2HCl (——), [δAva$^{3-4}$]-GS·2HOAc (— — —), and [δAva$^{3-4,3'-4'}$]-GS·2HOAc (----) in water. Measurements were made using a 0.5mm quartz cell at room temperature.

β-turn proposed by Blout.[13] However, δAva has no carbonyl group at the γ-position and hence this part can not form the hydrogen bond as in the case of GS. [δAva$^{5-1'}$]-GS, in spite of the lack of an amide bond between Pro^5 and Val$^{1'}$, did exhibit some antimicrobial activity.[3] In the case of [δAva$^{4-5}$]-GS, this analog showed significant antimicrobial activity even though one of the side chains of D-phenylalanyl residues was lacking. The present results, together with these earlier findings, suggest the importance of both leucyl residue side chains in GS for the exhibition of antimicrobial activity.

Experimental

The melting points are uncorrected. The homogeneity of the synthetic compounds was confirmed by TLC on Merck silica gel F_{254} plates with following solvent systems (v/v): R_f^1, $CHCl_3$-MeOH-HOAc (9:1:1); R_f^2, *n*-BuOH-HOAc-pyridine-H_2O (4:1:1:2); R_f^3, *n*-BuOH-HOAc-H_2O (4:1:1); R_f^4, $CHCl_3$-MeOH-EtOAc (95:7:5). Amino acid analyses were performed with a JEOL automatic amino acid analyzer, after the samples had been hydrolyzed with constant-boiling HCl in evacuated sealed ampoules for 20 h at 110 °C. The molecular weight was determined with a Hitachi molecular weight apparatus model 115, using MeOH. CD spectrum was measured with a JASCO model J-20 spectrometer and is represented in term of molar ellipticity.

Boc-Val-Orn(Z)-OH (1). Boc-Val-Orn(Z)-OEt[7] (14.0 g, 28.4 mmol) was saponified in MeOH (150 ml) with 2.6 M† NaOH (44 ml) at room temperature for 20 min. The solution was neutralized with 5% citric acid and concentrated in vacuo to remove the MeOH. The aqueous phase was acidified with citric acid to pH 3 and extracted with EtOAc. The extract was dried over anhydrous Na_2SO_4 and evaporated in vacuo. The residue was recrystallized from EtOAc and hexane. Yield, 12.8 g (97.0%); mp 66—68 °C; $[\alpha]_D^{20}$ +16.2° (*c* 0.7, DMF).

Found: C, 59.27; H, 7.88; N, 9.32%. Calcd for $C_{23}H_{35}N_3O_7$: C, 59.34; H, 7.58; N, 9.03%.

Boc-Val-Orn(Z)-Leu-D-Phe-Pro-OMe (2). H-Leu-D-Phe-Pro-OMe·HCl was obtained in the theoretical yield by hydrogenolysis (Pd black in 50 ml of MeOH containing 1.8 ml of concd HCl) of oily Z-Leu-D-Phe-Pro-OMe[14] (7.8 g, 15 mmol) which had been synthesized stepwise by the mixed anhydride method from C-terminal. This deprotected peptide (15 mmol) and compound **1** (7.0 g, 15 mmol) were dissolved in THF (80 ml) containing *N*-methylmorpholine (1.75 ml, 15 mmol). Coupling was performed with DCC (3.1 g, 15 mmol) and HOBt (4.1 g, 30 mmol) at 0 °C for 2 h and room temperature overnight. After filtration of the insoluble materials, the filtrate was concentrated in vacuo. The EtOAc solution of the residue was washed successively with 5% citric acid, water, 5% $NaHCO_3$, and water, and dried over anhydrous Na_2SO_4. The solution was concentrated in vacuo and the residue was recrystallized from EtOAt and hexane. Yield, 7.3 g (58.3%); mp 159—162 °C; $[\alpha]_D^{20}$ −31.0° (*c* 1.0, DMF).

† 1 M=1 mol dm^{-3}.

Found: C, 62.92; H, 7.76; N, 10.50%. Calcd for $C_{44}H_{64}N_6O_{10}$: C, 63.14; H, 7.71; N, 10.04%.

Boc-Pro-Val-Orn(Z)-Leu-D-Phe-Pro-OMe (3). Compound **2** (5.57 g, 6.65 mmol) was dissolved in 2.3 M HCl/THF (29 ml) to remove the Boc-group. The solution was stirred at room temperature for 2 h and evaporated in vacuo. The oily residue was dried over NaOH pellets in vacuo and dissolved in DMF (20 ml) containing *N*-methylmorpholine (0.75 ml). The solution was added to the mixed anhydride solution which was prepared from Boc-Pro-OH (1.5 g, 7.0 mmol), ethyl chloroformate (0.83 ml, 8.6 mmol) and *N*-methylmorpholine (0.96 ml, 8.7 mmol) in DMF (30 ml) at −15 °C for 4 min. This reaction mixture was stirred at 0 °C 2 h and at room temperature overnight. After filtration of the mixture, the filtrate was evaporated in vacuo and the residue was triturated with water. The product was collected by filtration and washed on a funnel successively with 5% citric acid, water, 5% $NaHCO_3$ and water. The crude product was recrystallized from DMF and water. Yield, 5.45 g (87.0%); mp 208—209 °C; $[\alpha]_D^{20}$ −54.0° (*c* 1.0, DMF).

Found: C, 62.29; H, 7.60; N, 10.50%. Calcd for $C_{49}H_{71}N_7O_{11}\cdot 0.5H_2O$: C, 62.40; H, 7.69; N, 10.40%.

Boc-Pro-Val-Orn(Z)-Leu-D-Phe-Pro-OH (4a). Into the solution of **3** (5.2 g, 5.5 mmol) in THF (60 ml), 3.6 M NaOH (6.2 ml) was added. The reaction solution was stirred at room temperature for 3 h and neutralized with 5% citric acid. After removal of the solvent in vacuo, the residue was treated with 5% citric acid. The precipitate was filtered and washed with cold water on a funnel. The dried product weighed 5.15 g (100%). Mp 158—164 °C; $[\alpha]_D^{20}$ −52.5° (*c* 0.3, DMF).

Found: C, 61.98; H, 7.82; N, 10.05%. Calcd for $C_{48}H_{69}N_7O_{11}\cdot 0.5H_2O$: C, 62.05; H, 7.59; N, 10.55%.

Boc-Val-Orn(Z)-δAva-OMe (5). Boc-Val-Orn(Z)-$NHNH_2$[10] (2.5 g, 5.2 mmol) was converted to the corresponding azide with isopentyl nitrite (0.82 ml, 6.1 mmol) and 2.9 M HCl/dioxane (11.3 ml) in DMF (26 ml) at −30 °C for 15 min. Into the azide solution neutralized with Et_3N (4.8 ml) at −55 °C, the solution of H-δAva-OMe·HCl[1] (0.92 g, 5.5 mmol) and Et_3N (1.5 ml) in DMF (26 ml) was added and the reaction mixture was stirred at 0 °C for 3 d. After filtration of the insoluble materials, the filtrate was concentrated in vacuo. The AcOEt solution of the residue was treated in the same manner as described for **2**. The product was recrystallized from AcOEt and diethyl ether. Yield, 2.21 g (73.4%); mp 148—152 °C; $[\alpha]_D^{20}$ −21.3° (*c* 0.5, DMF).

Found: C, 59.78; H, 8.06; N, 10.22%. Calcd for $C_{29}H_{46}N_4O_8$: C, 60.19; H, 8.01; N, 9.68%.

Boc-Val-Orn(Z)-δAva-$NHNH_2$ (6). Compound **5** (20.2 g, 34.9 mmol) in MeOH (100 ml) was treated with 80% hydrazine hydrate (44 ml) at room temperature overnight. After evaporation of the solvent, the crystalline residue was collected on a funnel and washed with water several times. Dried crystals weighed 18.9 g (92.1%). Mp 163—165 °C.

Found: 57.03; H, 8.33; N, 13.88%. Calcd for $C_{28}H_{46}N_6O_7\cdot 0.5H_2O$: C, 57.22; H, 8.06; N, 14.30%.

Boc-Val-Orn(Z)-δAva-Pro-Val-Orn(Z)-Leu-D-Phe-Pro-OH (7). Into the solution of **6** (3.47 g, 6 mmol) in DMF (80 ml), 7.3 ml of 3.3 M HCl/THF was added and followed by isopentyl nitrite (0.9 ml, 6.7 mmol) at −15 °C. After 15 min, the reaction mixture was neutralized with Et_3N (3.4 ml) and the solution of the hydrochloride of **4b** obtained from **4a** (4.8 g, 5.2 mmol) by treatment with 2.5 M HCl/THF as described for **3** and Et_3N (0.77 ml) in DMF (40 ml) was added into the above azide solution. After the stirring for 3d at 0 °C, the filtrate was evaporated in vacuo and the residue was triturated with cold water. The product was washed on a funnel succesively with 5% citric acid, 5% $NaHCO_3$, and water. This product was purified by column chromatography on silica gel (Wakogel C-200, 3.6×40 cm) with $CHCl_3$–MeOH (97:3). The combined eluates were concentrated in vacuo and the residue was recrystallized from EtOH and diethyl ether. Yield, 2.55 g (35.9%); mp 197—200 °C; R_f[1] 0.40; $[\alpha]_D^{20}$ −28.71° (*c* 0.4, EtOH).

Found: C, 62.10; H, 7.87; N, 11.18%. Calcd for $C_{71}H_{103}N_{11}O_{16}$: C, 62.40; H, 7.60; N, 11.27%.

***Cyclo*-(Val-Orn(Z)-δAva-Pro-Val-Orn(Z)-Leu-D-Phe-Pro-) (8).** Into the solution of **7** (700 mg, 0.51 mmol) in DMF (25 ml), *p*-nitrophenol (219 mg, 1.6 mmol) and DCC (126 mg, 0.61 mmol) were added at 0 °C and the reaction mixture was stirred at room temperature overnight. After removal of the DCC, urea, and the solvent, the residue was recrystallized from MeOH–water and washed with diethyl ether. The *p*-nitrophenyl ester of **7** weighed 550 mg (72.5%), R_f[1] 0.89. Boc-group of this active ester (500 mg, 0.34 mmol) was removed with TFA (5 ml) containing anisole (0.8 ml) at 0 °C for 20 min. Evaporation of the TFA was carried out at 0 °C. An oily residue was crystallized by treatment with diethyl ether and decantation. A solution of this ester in DMF (10 ml) containing HOAc (0.1 ml) was added dropwise into pyridine (350 ml) at 58—60 °C for 2.5 h. After the stirring of the solution at 58—60 °C for 5 h, it was concentrated in vacuo. The residue was dissolved in MeOH–water (7:1) and passed succesively through columns of Dowex 1 (OH^-) and Dowex 50 (H^+). The oily product was obtained by concentration of the eluate and crystallized with diethyl ether. The recrystallization from MeOH and diethyl ether gave 77 mg (17.9%). R_f[1] 0.79; mp 165 °C; $[\alpha]_D^{18}$ −166.9° (*c* 0.6, MeOH); mol wt, found: 1240 (calcd for $C_{66}H_{93}N_{11}O_{13}$: 1247).

Found: C, 62.43; H, 7.76; N, 12.02%. Calcd for $C_{66}H_{93}N_{11}O_{13}\cdot H_2O$: C, 62.59; H, 7.56; N, 12.16%.

***Cyclo*-(Val-Orn-δAva-Pro-Val-Orn-Leu-D-Phe-Pro) (9).** Hydrogenolysis of **8** (80 mg, 0.063 mmol) was carried out in a mixture of MeOH (6 ml) containing 0.1 ml of 3 M HCl/THF and Pd black for 10 h at room temperature. After removal of the catalyst, an oily product was obtained by concentration of the filtrate in vacuo, and it was purified by chromatography on a Sephadex G-10 with 4% HOAc. The homogeneous fractions were collected and lyophilized and white crystalline peptide was obtained. Yield, 69 mg (94.9%); mp 168—169 °C; $[\alpha]_D^{22}$ −171.2° (*c* 0.3, EtOH); R_f[2] 0.63. Amino acid ratio: Val 1.89, Orn 1.91, Leu 1.02, Phe 1.02, Pro 2.07, δAva 1.09.

Found: C, 55.80; H, 8.07; N, 13.41%. Calcd for $C_{50}H_{81}N_{11}O_9\cdot 2HOAc\cdot 3H_2O$: C, 56.18; H, 8.29; N, 13.35%.

Boc-Val-Orn(Z)-δAva-Pro-OMe (10). Hydrazide **6** (3.86 g, 6.57 mmol) was converted to the corresponding azide with isopentyl nitrite (1.2 ml, 9 mmol) and 5M HCl/THF (5.3 ml) in DMF (30 ml) at −20 °C for 40 min. A solution of H-Pro-OMe·HCl (1.32 g, 8.0 mmol) and Et_3N (1.2 ml, 8.6 mmol) in DMF (20 ml) was added to the above azide solution previously neutralized with Et_3N (3.7 ml

26.6 mmol) at −50 °C. This reaction mixture was stirred at 0 °C for 3d and then added into 0.4% citric acid (750 ml), liberating an oily product. The product extracted in AcOEt was washed with water and dried over anhydrous Na_2SO_4. The solution was concentrated in vacuo and the residue was recrystallized from AcOEt and hexane. Yield, 3.93 g (88.5%); mp 87 °C; $[\alpha]_D^{20}$ −18.1° (*c* 0.7, DMF).

Found: C, 59.94; H, 8.09; N, 10.51%. Calcd for $C_{34}H_{53}N_5O_9$: C, 60.43; H, 7.90; N, 10.36%.

Boc-(Val-Orn(Z)-δAva-Pro)$_2$-OH (14). Saponification of **10** (1.96 g, 2.9 mmol) was carried out with 2.2 M NaOH (5.2 ml) in MeOH (20 ml) at room temperature for 6 h. After evaporation of the MeOH, the residue was treated with 5% citric acid and extracted with AcOEt. The oily product **11** (1.25 g, 1.9 mmol) was obtained in a 64% yield by concentration of the extract which was washed with water and dried over anhydrous Na_2SO_4. On the other hand, removal of the Boc-group of **10** (1.66 g, 2.5 mmol) was carried out with 2.3 M HCl/THF (24.5 ml) at room temperature for 2.5 h. After concentration of the reaction solution, the residual oily compound (**12**, 2.5 mmol) was dried over NaOH pellets in vacuo and used directly in the next step. The solution of above **11** and **12**·HCl in THF (30 ml) was neutralized with *N*-methylmorpholine (0.96 ml), followed by the additions of HOBt (0.5 g, 3.7 mmol) and DCC (0.42 g, 2.0 mmol). The coupling reaction proceeded at 0 °C overnight. After filtration of the insoluble materials, the filtrate was concentrated in vacuo. The residue was crystallized by treatment with water and washed successively with 5% citric acid, water, 5% Na_2CO_3, and water on a funnel. The crude product was purified by gel filtration on a Shephadex LH-20 with MeOH. The yield of **13** was 2.22 g (95.7%) and the amino acid analysis showed the composition within experimental error. Saponification of **13** (1.36 g, 1.1 mmol) was carried out with 1.3 M NaOH (4.4 ml) in DMF (30 ml) at room temperature for 2.5 h. The reaction solution was added into 0.5% citric acid (500 ml) at 0 °C. The precipitate was filtered off and recrystallized from MeOH and diethyl ether. Yield, 1.30 g (93.9%); mp 205.5—206.5 °C; $[\alpha]_D^{20}$ −23.8° (*c* 0.8, DMF); R_f^1 0.56.

Found: C, 58.11; H, 7.75; N, 11.10%. Calcd for $C_{61}H_{92}N_{10}O_{15}\cdot 3H_2O$: C, 58.17; H, 7.84; N, 11.12%.

***Cyclo*-(Val-Orn(Z)-δAva-Pro)$_2$ (15).** a) *p*-Nitrophenol (104 mg, 0.75 mmol) and DCC (152 mg, 0.74 mmol) were added into the solution of **14** (440 mg, 0.35 mmol) in DMF (10 ml) at 0 °C. After the stirring of the reaction mixture at room temperature overnight, it was filtered and the filtrate was concentrated in vacuo. The residual oily product was treated with a mixture of diethyl ether–hexane (1:1) and the crystalline *p*-nitrophenyl ester (292 mg, 0.22 mmol) of **14** was collected by decantation. In the same way as in the preparation of **8**, this active ester was used in the cyclization reaction after removal of the Boc-group. The product was dissolved in MeOH–water (7:1) and passed successively through columns of Dowex 1 (OH^-) and Dowex 50 (H^+). The eluent was removed under reduced pressure to give an oil. Chromatography on Sephadex LH-20 eluting with MeOH gave after recrystallization from aqueous MeOH 29 mg (11.5%) of **15**. Mp 202—204 °C; $[\alpha]_D^{22}$ −39.5° (*c* 0.3, MeOH); R_f^3 0.77, R_f^4 0.42; mol wt, found 1050 (calcd for $C_{56}H_{82}N_{10}O_{12}$: 1086).

Found: C, 58.87; H, 7.59; N, 11.33%. Calcd for $C_{56}H_{82}N_{10}O_{12}\cdot 3.5H_2O$: C, 58.46; H, 7.79; N, 12.17%. b) Compound **14** (1.25 g, 0.99 mmol), HOSu (245 mg, 2.13 mmol), 1-ethyl-3-(3-dimethylaminopropyl)carbodiimide (320 mg, 2.06 mmol) and 3 M HCl/dioxane (0.67 ml) were mixed in DMF (8 ml) at 0 °C and the reaction mixture was stirred at room temperature overnight. After concentration of this mixture under reduced pressure, an oily residue was crystallized by the treatment with water. The dried compound weighed 750 mg (58%). Removal of the Boc-group of this *N*-hydroxysuccinimide ester, the subsequent cyclization reaction and the purification were carried out just as described in the method a. This compound gave the same properties mentioned above. Yield, 87 mg (13.1%).

***Cyclo*-(Val-Orn-δAva-Pro)$_2$ (16).** Z-groups of **15** (64.8 mg, 0.056 mmol) in MeOH (20 ml) with 3.1 M HCl/THF (0.05 ml) were removed by hydrogenolysis over Pd black for 5 h. In the same manner as with **9**, crystalline product was obtained in a 62.1% yield (36.4 mg). Mp 182—190 °C; $[\alpha]_D^{23}$ −66.7° (*c* 0.2, H_2O); R_f^2 0.37. Amino acid ratio: Val 2.03, Orn 2.04, δAva 2.14, Pro 1.78.

Found: C, 50.29; H, 8.18; N, 13.76%. Calcd for $C_{40}H_{70}N_{10}O_8\cdot 2HOAc\cdot 6H_2O$: C, 50.46; H, 8.66; N, 13.37%.

The authors express their thanks to the staff of the research laboratories of Toyo Jozo Co. for performing the elemental analyses and the microbiological assays.

References

1) S. Sofuku, *Bull. Chem. Soc. Jpn.*, **46**, 968 (1973).
2) S. Sofuku, I. Muramatsu, K. Okada, and A. Hagitani, *Bull. Chem. Soc. Jpn.*, **48**, 2888 (1975).
3) S. Sofuku, A. Yoshida, H. Baba, and I. Muramatsu, *Bull. Chem. Soc. Jpn.*, **50**, 2143 (1977).
4) H. Naganawa, T. Takita, I. Muramatsu, S. Sofuku, and L. W. Cary, "Proceedings of the 10th Symposium on Peptide Chemistry," ed by J. Noguchi, Protein Research Foundation, Osaka, 1973, pp. 121—125.
5) I. Muramatsu, S. Sofuku, and A. Hagitani, *J. Antibiot.*, **25**, 189 (1972).
6) Abbreviations with no prefix indicate the L-amino acid residue and follow the IUPAC-IUB tentative nomenclature described in *J. Biol. Chem.*, **247**, 977 (1972). Abbreviations used are: Z, benzyloxycarbonyl; Boc, *t*-butoxycarbonyl; DCC, dicyclohexylcarbodiimide; HOBt, 1-hydroxybenzotriazole; HONp, *p*-nitrophenol; HOSu, *N*-hydroxysuccinimide; THF, tetrahydrofuran; DMF *N*,*N*-dimethylformamide; TFA, trifluoroacetic acid.
7) N. Izumiya, T. Kato, Y. Fujita M. Ohno, and M. Kondo, *Bull. Chem. Soc. Jpn.*, **37**, 1809 (1964).
8) G. W. Anderson, J. E. Zimmerman, and F. M. Callahan, *J. Am. Chem. Soc.*, **89**, 5012 (1967).
9) W. König and R. Geiger, *Chem. Ber.*, **103**, 788 (1970).
10) M. Ohno, T. Kato, S. Makizumi, and N. Izumiya, *Bull. Chem. Soc. Jpn.*, **39**, 1738 (1966).
11) J. Honzl and J. Rudinger, *Collect. Czech. Chem. Commun.*, **26**, 2333 (1961).
12) G. Pataki, "Techniques of Thin-Layer Chromatography in Amino Acid and Peptide Chemistry," 2nd English ed, Ann Arbor-Humphrey Science Publishers, Inc., Ann Arbor and London (1969), p. 145.

13) E. R. Blout, *Biopolymers*, **20**, 1901 (1981).

14) This compound was synthesized from H-Pro-OMe·HCl by a procedure reported by Ohno et al.[10] although the ethyl ester had been used in their procedure. Yield, 81%; oil; R_f 0.59 ($CHCl_3$–MeOH, 9:1).

 © 1986 The Chemical Society of Japan Bull. Chem. Soc. Jpn., 59, 191—199 (1986)

Photochemical Reactions of *N*-Methyl-1,2-naphthalenedicarboximide with Alkenes. Preferential Naphthazepinedione Formation

Yasuo KUBO,* Rie TODA, Kengo YAMANE, and Takeo ARAKI
Department of Chemistry, Faculty of Science, Shimane University,
Matsue, Shimane 690
(Received July 27, 1985)

Irradiation of benzene solutions of *N*-methyl-1,2-naphthalenedicarboximide (**1**) in the presence of alkenes (**2a,b,d—i**) gave two regio-isomers of naphthazepinediones (**3a,b,d—i** and **4a,b,d—i**). Stereospecificity of the naphthazepinedione formation was observed in the reaction with *cis*- and *trans*-2-butene (**2a** and **2b**). Naphthazepinediones (**3j** and **4j**) produced by the irradiation of **1** with ethyl vinyl ether (**2j**) underwent secondary photoreactions to give **7** and **8**, respectively. On the other hand, irradiation of **1** with 2,3-dimethyl-2-butene (**2k**) resulted in the formation of oxetanes (**13a,b**) and 1:1-adducts of **1** and **2k** at the carbonyl groups of **1** (**14** and **15a,b**). Irradiation of **1** with *cis*-stilbene (**2l**) afforded oxetanes (**22a,b**) and fragmentation products of oxetanes (**23a,b**, and **24**). Stern-Volmer slopes ($k_q\tau$) obtained from quenching of fluorescence of **1** by alkenes (**2a—e,k**) correlated to some extent with relative rates for disappearance of **1** in the reaction. Preferential formation of the naphthazepinedione was rationalized by the nature of the excited singlet state of **1** compared with those of other *N*-methylarenedicarboximides.

In recent years, photochemistry of imides has been the subject of intensive investigations.[1] Concerning the reactions with alkenes, there are remarkable differences between the photoreactions of alicyclic imides and arenedicarboximides (especially phthalimides). Aliphatic imides undergo effective intra-[2] or inter-molecular oxetane formation,[3] illustrating its normal $n\pi^*$ carbonyl photoreactivity. In contrast, phthalimides undergo alcohol-incorporated C–C coupling at the carbonyl carbon of phthalimides (electron transfer reaction),[4] insertion of alkene into C(=O)-N bond of the imide moiety,[5] and only in a few cases oxetane formation.[6] As there has been only a little information on the effects of arene structures in the photochemistry of arenedicarboximides,[7] our studies have been focused on the effects of extended π-conjugation systems. Recently we reported the photoreactions of three types of *N*-methylnaphthalenedicarboximides with alkenes in benzene, in which the arene structure played a crucial role in determining the reaction pathways.[8] The predominant reactions of *N*-methyl-1,8- and 2,3-naphthalenedicarboximides with alkenes were cycloaddition to the aromatic C=C bond (cyclobutane formation) and oxetane formation, respectively. This paper describes the details of the photoreactions of *N*-methyl-1,2-naphthalenedicarboximide (**1**) with a variety of alkenes in benzene. In contrast to other naphthalenedicarboximides, the predominant reaction of **1** is found to be insertion of the alkene into C(=O)-N bond of the imide moiety (naphthazepinedione formation) accompanied, in some cases, by other types of reactions depending on the structure of the alkene.

Results and Discussion

Naphthazepinedione Formation. The insertion of alkene into the C(=O)-N bond of **1**, naphthazepinedione formation, was a most typical reaction observed in the photochemistry of **1** and alkenes in benzene. For example, irradiation of a benzene solution of **1** (10 mM, 1 M=1 mol dm^{-3}) and cis-2-butene (**2a**) (100 mM) by a light of >320 nm (aq $CuSO_4$ filter) gave two regio-isomers of naphthazepinedione (**3a** and **4a**) (Eq. 1). The two isomers

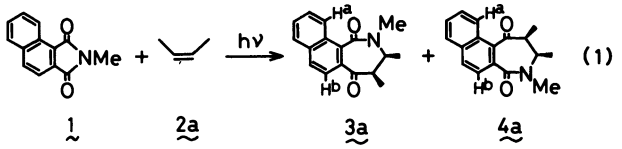

1 **2a** **3a** **4a**

were readily separated by column chromatography on silica gel to give 45% of **3a** and 29% of **4a**. Irradiation of **1** with *trans*-2-butene (**2b**) also gave **3b** (46%) and **4b** (33%) (Scheme 1). Other examples of

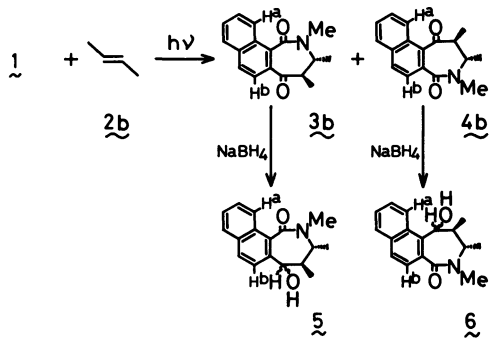

2b **3b** **4b** **5** **6**

Scheme 1.

photoreactions of **1** and alkenes (**2c—i**) are shown in Table 1. The results indicate that the naphthazepinedione formation is characteristic of the reaction with ethylenes substituted by two or three alkyl groups and with some ethylenes substituted by

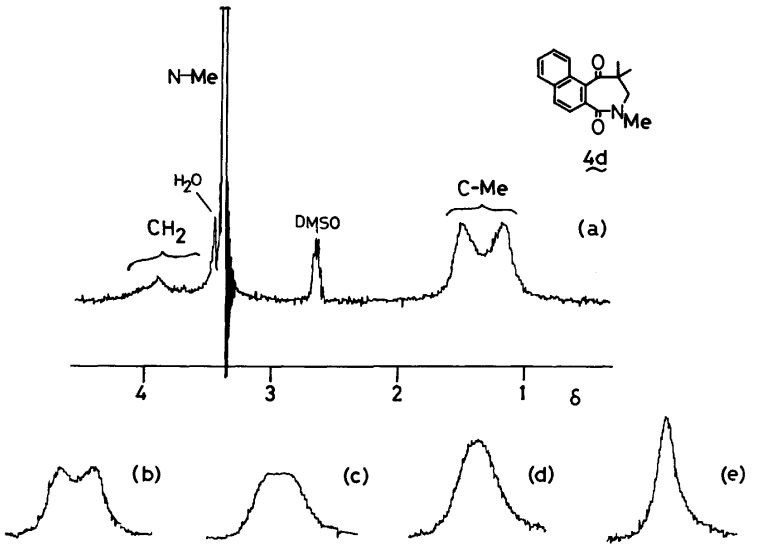

Fig. 1. ^{1}H NMR (100MHz) spectra of **4d** in CD_3SOCD_3. Temperature (calibrated by the spectra of 1,3-propanediol). a): Ambient temperature, b): 32.5 °C, c): 34.0 °C, d): 37.5 °C, e): 43.5 °C.

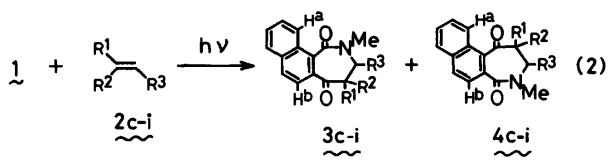

Table 1. Yields of Naphthazepinediones (**3c—i** and **4c—i**) from Photoreactions of **1** and Alkenes (**2c—i**) in Benzene[a]

R^1	R^2	R^3	2	3	Yield[b]/%	4	Yield[b]/%
n-C_4H_9-	H-	H-	**2c**	**3c**	0	**4c**	0
Me-	Me-	H-	**2d**	**3d**	53	**4d**	46
Me-	Me-	Me-	**2e**	**3e**	46	**4e**	31
H-	-$(CH_2)_3$-		**2f**	**3f**	40	**4f**	28
H-			**2g**	**3g**	40	**4g**	46
Ph-	H-	H-	**2h**	**3h**	54	**4h**	21
Ph-	Ph-	H-	**2i**	**3i**	41	**4i**	38

a) Reaction conditions: [**1**]=10 mM, [**2c—j**]=100 mM. b) Yields were based on consumed **1** (conversion: >70%).

phenyl groups. No reaction was observed in the photolysis of **1** with 1-hexene (**2c**), an ethylene substituted by one alkyl group.

The structures of the naphthazepinediones, including the position of the alkyl substituent of the azepine ring, were supported by the spectral resemblance to the benzo analogues obtained by the photoreactions of *N*-methylphthalimide with the alkenes.[5] ^{1}H NMR spectra of some naphthazepinediones show coalesced signals. As the most typical example the ^{1}H NMR spectra of **4d** are shown in Fig. 1. Although signals of *N*-methyl and aromatic protons are sharp, signals of two *C*-methyl and methylene protons are broad at ambient temperature. The broad doublet signals of the two *C*-methyl protons were coalesced at 34.0 °C [(c) in Fig. 1] and changed to a more sharp singlet at higher temperatures [(d,e)]. The spectral changes probably arise from flipping of the azepine ring.

The regiochemistry of the naphthazepinediones shown in the structural formula are deduced from the following three observations: ^{1}H NMR behavior of H^a and H^b in addition to the spectral features of the reduction products. First, the H^a signals (double doublets) of **4a,b,d—i** showed low field shift (δ= 8.38—8.55) relative to those of **3a,b,d—i** (δ=≈8). This fact suggests that the H^a is close to the ketone carbonyl groups, in accord with the observations that the ketone carbonyl group exerts a stronger deshielding effect on the peri-hydrogens than the lactam carbonyl group.[5b] Second, the H^b signals (doublet) of **4a,b,d—i** were observed at slightly higher fields compared with those of **3a,b,d—i**. Third, reduction of **3b** and **4b** with sodium borohydride gave **5** and **6**, respectively (Scheme 1). The H^a signal of **5** was considerably shifted to a lower field (δ=9.10) compared with that of **6** (δ=8.25), probably due to the deshielding effect by the lactam carbonyl group remained.

The yields of the regio-isomers (**3a,b,d—i**) are generally higher than those of the other isomers (**4a,b,d—i**) except for the reaction of **1** with **2g**. Attack of alkene to the less hindered C(=O)-N bond of **1** seems to predominate over that to the other

C(=O)-N bond. In the irradiation of **1** and **2e** the ratio of the yields of the products (**3e**:**4e**) remained almost constant over the concentration region of 50 mM to 1 M of **2e**. The result may indicate that the two regio-isomers arise from the same excited state of **1**, since in the photoreactions of phthalimides and alkenes a marked concentration dependency on the ratio of the yields of products is reported when the products are generated from the distinct excited states.[6c,d]

An important characteristic of the naphthazepinedione formation is stereochemical course of the reactions. Irradiation of **1** in the presence of **2a** and **2b** gave mixtures of **3a**+**4a** and **3b**+**4b**, respectively (Eq. 1 and Scheme 1). The facts that no detectable amounts of cis-trans isomerized products are observed in the irradiation of **1** with **2a** and **2b** obviously indicate the stereospecific formation of the naphthazepinedione, and suggest that the reaction occurs directly from the singlet excited state of **1**.

The stereochemistry of the products could be assigned by comparison of the coupling constants of the two methine hydrogens of the azepine ring with those of corresponding benzazepinediones, which were reported to be J=2.3 Hz for the cis-isomer and J=10.1 Hz for the trans-isomer.[5h] The products (**3a**, **3b**, and **4b**) had the coupling constants of J=3.2, 11.0, and 11.6 Hz, respectively, although the coupling constant of **4a** could not be determined. These coupling constants suggested the cis-stereochemistry for **3a** and trans-stereochemistry for **3b** and **4b** as shown in Scheme 1. The stereochemistry of the products corresponds to that of the alkenes (**2a**, **b**) used.

In the inter-[5e,h] and intramolecular[5i] photoreactions of phthalimides and alkenes, the stereospecificity of the benzazepinedione formation at the early stage of the photoreaction was already reported, but concomitant cis-trans isomerization of alkenes always occurred to give non-stereospecific mixtures of the products at a prolonged irradiation. No such cis-trans isomerization was observed in the photo reactions of **1** with **2a** and **2b**.

The mechanism of the cis-trans isomerization process in the reactions of phthalimides is not fully clarified.[5e] However, the isomerization may arise via a triplet biradical, an intermediate of the oxetane formation from the triplet excited state of **1**,[9] because the trans/cis ratio of 2-butene at the photosteady state is 4/1[5e] and oxetane formation has been known to occur from the triplet excited state of phthalimides.[6c,d] The fact that no isomerization is observed in the reaction of **1** seems to show a small contribution of the triplet excited state of **1** to the reaction of **1** with the alkenes.

Ethyl vinyl ether (**2j**) also reacted with excited **1** to give naphthazepinediones, but secondary photoreactions were observed at the same time. Prolonged irradiation of **1** and **2j** in benzene gave **7** (43%) and **8** (26%) which however were not the primary photoproducts (Scheme 2). One of the primary products (**3j**) was isolated by the photoreaction of shorter irradiation-time. Further irradiation of **3j** in benzene quantitatively gave **7** probably through intramolecular γ-hydrogen abstraction (**3j**→**9**), followed by elimination of acetaldehyde (**9**→**10**), and tautomerization of **10** (**10**→**7**) (Eq. 3). This type of reaction series

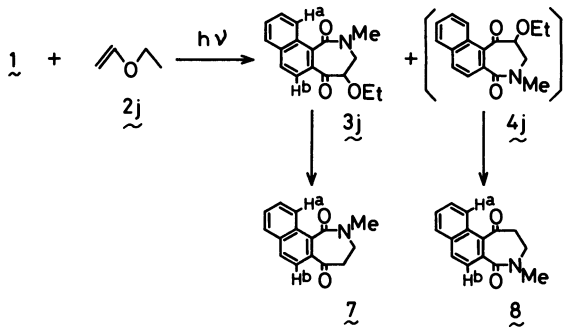

Scheme 2.

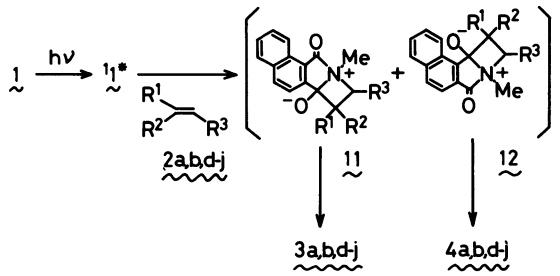

Scheme 3.

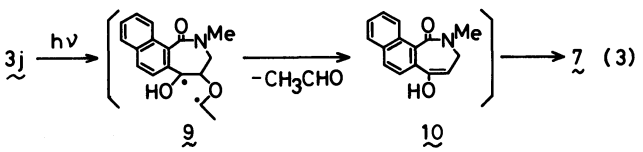

is familiar in photoreactions of benzazepinediones.[1,6a]

The naphthazepinedione formation may be rationalized by a mechanism (Scheme 3) similar to that of the benzazepinedione formation[5i] on the basis of the structures of the naphthazepinediones and the stereospecificity of the reaction. Thus, reaction of singlet excited state of **1** and alkene (**2a,b,d—j**) gave two regioisomers of intermediate (**11** and **12**) with retention of the stereochemisty of the alkene, and then C(=O)-N bond cleavage of **11** and **12** results in the formation of **3a,b,d—j** and **4a,b,d—j**, respectively.

Other Reactions. Besides the naphthazepinedione formation, two types of reactions were observed in the irradiation of **1** with 2,3-dimethyl-2-butene

(**2k**) and *cis*-stilbene (**2l**).

Irradiation of **1** and **2k** in benzene gave two regio-isomers of oxetane [**13a** (30%) and **13b** (8%)] and additional products [**14** (16%), **15a** (11%), and **15b** (9%)] (Eq. 4). The reaction is analogous to that of

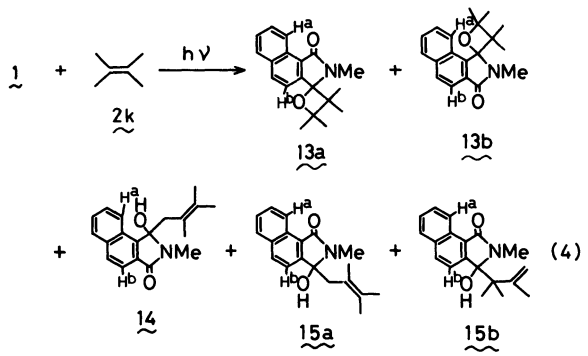

(4)

N-methylphthalimide and **2k**, and structures of the products were assigned from their spectral resemblance to the benzo analogues.[6d]

The regiochemistries of **13**—**15** were assigned on the ^{1}H NMR spectra. ^{1}H NMR spectra of the products showed characteristic double-doublets signals due to H^a in a lower field region of δ=8.47 to 9.19. The H^a signal of **13a** was shifted to a lower field (δ=9.19) compared with that of **13b** (δ=8.94) probably due to the deshielding effect from the lactam carbonyl group. The H^a signal of **15a** was likewise shifted to a lower field (δ=8.58) compared with that of **14** (δ=8.47). Attack of **2k** to the less hindered carbonyl group of **1** to give **13a** seems to predominate.

Formation of **14** and **15a, b** may be rationalized by a mechanism shown in Scheme 4, by referring the mechanism proposed by Mazzocchi and Klingler.[6d] First of all, an ion pair (**16**+**17**) is generated by electron transfer. Subsequent proton transfer gives two types of radical pairs (**18**+**19** and **20**+**19**) via path a and path b, respectively. The former pair couples to give **14** and the latter to **15a**. Another possibility is the collapsing of the ion pair (**16**+**17**) to a zwitter ionic intermediate (**21**) via path c, which converts to mainly **15b** by proton transfer.

Irradiation of **1** and **21** in benzene gave two stereoisomers of oxetane [**22a** (19%) and **22b** (19%)], a pair of unsaturated amides [**23a** (37%) and **23b** (15%)], and benzaldehyde [**24** (45%)] (Scheme 5). As reported in many cases,[10] the productions of **23a, b,** and **24** were rationalized by fragmentation of the oxetane precursor (**25**), i.e., carbonyl-alkene metathesis. Acid-catalyzed decomposition of **22a** or **22b** in methanol afforded **26** and **24** (Eq. 5).

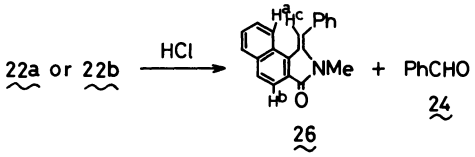

(5)

The configurations at the olefinic carbons in **23a, b** were assigned on the basis of the ^{1}H NMR spectra. First, the *N*-Me protons in **23a** were observed at a considerably higher field (δ=3.05) compared with those of **23b** (δ=3.37), probably due to the anisotropic shielding effect of the phenyl group. Second, the H^c signal of **23a** was shifted to a lower field (δ=6.83) compared with that of **23b** (δ=6.60), probably due to an anisotropic deshielding effect from the naphthyl ring current.

The positions of lactam carbonyl groups were assigned as follows: The H^a signals of **23a** (δ=9.11) and **23b** (δ=9.20) were significantly shifted to lower fields probably due to the deshielding effect of the lactam carbonyl groups, when compared with that of **26** (δ=8.55).

The regiochemistry of the oxetane precursor (**25**) of **23a, b** can be readily deduced from the structures of **23a, b**. The compound **26** was a regio-isomer of **23a, b** and its *Z*-configuration was suggested as follows: It has deshielded *N*-Me protons (δ=2.97) and shielded H^c proton (δ=7.2—7.7 mixed with arom H's). The structure of **26** allows to deduce the regiochemistry of **22a, b**.

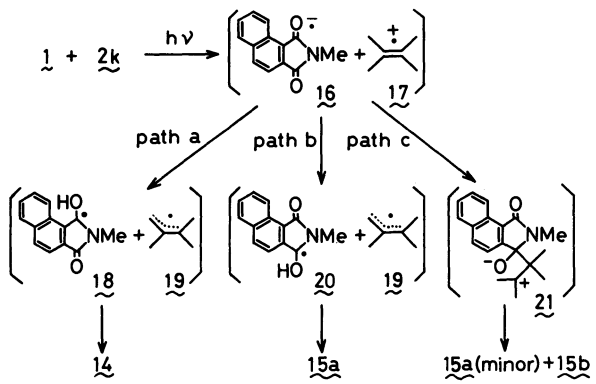

Scheme 4.

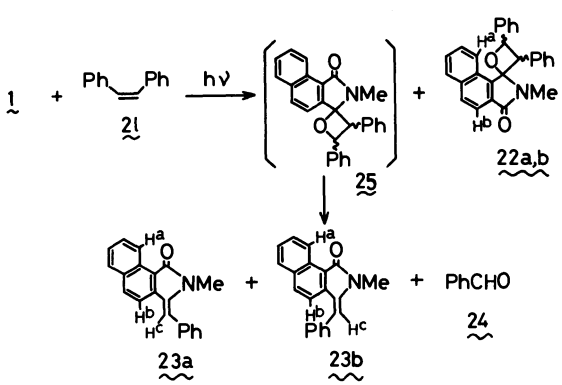

Scheme 5.

On the basis of these structures of the products, it is possible to suppose that **2l** attacks predominantly at the less hindered carbonyl group of **1**. The stereochemical course of the reaction, however, seems to be complicated by the concomitant cis-trans isomerization of the alkene (**2l**).

A common feature between **2k** and **2l** is that **2k** has the lowest ionization (oxidation) potential among the series of ethylenes substituted by alkyl groups (**2a—e, k**) and **2l** has the lowest among the series of ethylenes substituted by phenyl groups (**2h, i, l**). The requirement of dominant electron donor-acceptor interaction has been recognized in the oxetane formation from the $\pi\pi^*$ excited state.[10,11] In this connection the formation of **14** and **15a, b** in the reaction of **1** with **2k** is rationalized by the electron transfer mechanism (Scheme 4).

Nature of the Singlet Excited State of 1 and Fluorescence Quenching. The absorption spectrum of **1** in benzene showed a broad band around 344 nm (log $\varepsilon\approx4$), which were slightly shifted to longer wavelengths ($\approx$2 nm) in ethanol. The fluorescence spectrum of **1** was obtained by using a diluted benzene solution (1×10^{-5} M) to avoid concentration quenching. The spectrum showed a strong and broad band ($\lambda_{max.}$ 430 nm, lifetime 42.0 ns at 25 °C in air-saturated benzene). The fluorescence excitation spectrum was almost identical with the absorption spectrum. These data suggest that the lowest singlet excited state of **1** is $\pi\pi^*$ in character. The energy of the excited singlet state (E_S) estimated from the absorption and fluorescence spectra was 308 kJ mol^{-1}.

Addition of aliphatic alkenes (**2a, b, d, e, k**) to the air-saturated benzene solutions of **1** (ca. 1×10^{-5} M) resulted in reduction of the fluorescence of **1** without varying the shape and the position of the maximum emission. Stern-Volmer plots of the fluorescence quenching by the alkenes (**2a—e, k**) gave straight lines against concentration of the alkenes (**2a—e, k**). Fluorescence quenching rate constants (k_q) calculated from the Stern-Volmer slopes ($k_q\tau$) using the lifetime (τ) of the fluorescence of **1** are shown in Table 2 together with ionization potentials (I_P) of the alkenes (**2a—e, k**) and relative rates for disappearance of **1** in the photoreaction with the alkenes. A good correlation was obtained between the k_q values and the relative rates for disappearance of **1**, which may indicate that the efficiency of the reaction mainly depends on the rate of reaction with excited singlet state of **1**. A correlation between the k_q values and the I_P values of alkenes is poor. This is probably due to the steric effect of the alkyl substituents, especially 1,2-dialkyl substituents, on the stage of interaction with the singlet excited state of **1**.

In summary, the most characteristic type of the reaction of **1** and alkenes was found to be naphthazepinedione formation. Other types of reactions, i.e., oxetane formation and electron

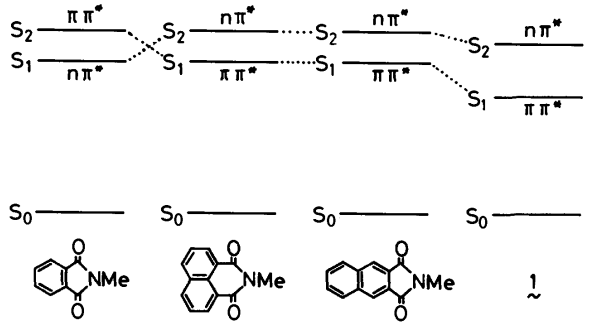

Fig. 2. Energy levels and nature of the singlet excited states of *N*-methylarenedicarboximides.

Table 2. Ionization Potentials (I_P) of Alkenes (**2a—e, k**), Stern-Volmer Slopes ($k_q\tau$) for the Fluorescence Quenching by Alkenes (**2a—e, k**),[a] Fluorescence Quenching Rate Constants (k_q),[b] and Relative Rates for Disappearance of **1** in the Photoreactions of **1** and Alkenes (**2a—e, k**) in Benzene[c]

Alkenes	I_p / eV	$k_q\tau$ / dm^3 mol^{-1}	k_q / dm^3 mol^{-1} s^{-1}	Relative rates for disapearance of **1**
2c	9.46[d]	0	0	0
2d	9.23[d]	0.23	5.5×10^6	1[f]
2a	9.12[e]	0.034	8.1×10^5	0.10
2b	9.11[e]	0.003	7.1×10^4	0.07
2e	8.68[d]	2.57	6.1×10^7	1.1
2k	8.53[d]	118	2.8×10^9	3.0

a) Conditions: [**1**]=1×10^{-5} M, at room temperature, in air-saturated benzene. b) Calculated from $k_q\tau$ using the lifetime (τ=42.0 ns) of the fluorescence of **1**. c) Reaction conditions: [**1**]=10 mM, [**2a—e, k**]=100 mM, conversion<20%. d) Ref. 5b. e) Ref. 12. f) Standard.

Table 3. Lifetimes of Fluorescence (τ)[a] and Energies of the Lowest Singlet Excited States (S_1) of *N*-Methylarenedicarboximides[b]

Imide	τ/ns	Energies of S_1/kJ mol^{-1}
N-Methylphthalimide	—	335[c]
N-Methyl-**1**,8-naphthalenedicarboximide	1.0	332
N-Methyl-2,3-naphthalenedicarboximide	5.9	332
1	42.0	308

a) Conditions: at 25 °C, in air-saturated benzene. b) Estimated from the absorption and fluorescence spectra. c) Ref. 13.

transfer reaction (hydrogen abstraction), were observed only in the reactions with special alkenes (**2k**, **l**). The predominant types of reaction are found to depend largely upon the arene structure of naphthalenedicarboximides. For instance, **1**, is advantageous for the naphthazepinedione formation, but this reaction was minor for *N*-methyl-1,8- and 2,3-naphthalenedicarboximides.[8]

The results of the structure-dependent photoreactions can be explained by considering the natures of the singlet energy levels as shown in Fig. 2. The energies of the lowest singlet excited states and the lifetimes of the fluorescence of *N*-methylarenedicarboximides are shown in Table 3. The lowest and the second singlet excited states of *N*-methylphthalimide, $n\pi^*$-S_1 and the $\pi\pi^*$-S_2, respectively, are shown by referring a literature.[13] Change in the arene moiety from benzene to naphthalene alters the nature of the S_1 states from $n\pi^*$ to $\pi\pi^*$. For three *N*-methylnaphthalenedicarboximides the $\pi\pi^*$-S_1 levels were supported by the strong fluorescence and the solvent effects. The energies of $\pi\pi^*$-S_1 for 1,8- and 2,3-derivatives are virtually the same as that of $n\pi^*$-S_1 for the phthalimide. Hence, $\pi\pi^*$-S_1 of the 1,8- and 2,3-derivatives can interact with $n\pi^*$-S_2 as in the case of the phthalimide. Shorter lifetimes of the fluorescence of 1,8- and 2,3-derivatives than that for **1** as shown in Table 3 may support the stronger interaction. The predominant reaction of the 2,3-derivative is found as oxetane formation caused from the $\pi\pi^*$-S_1 strongly interacted with $n\pi^*$-S_2. The $\pi\pi^*$-S_1 level of **1** is however lowered to a "pure and simple" $\pi\pi^*$ state due to the decrease of the interaction. This nature of S_1 may be responsible for the formation of naphthazepinediones as the main products from **1**.

Experimental

The mps were measured by a Yanagimoto micromelting point apparatus, and are uncorrected. ^{1}H NMR spectra were determined on a JEOL JNM-MH-100 (100 MHz) and a JEOL JNM-GX-400 spectrometer (400 MHz) in $CDCl_3$ solution. IR spectra were obtained with a Hitachi 260-50 spectrophotometer. Mass spectra were measured on a JEOL JMS-DX-300 apparatus. Fluorescence spectra and the lifetimes were recorded by a Hitachi 650-40 spectrophotometer and a HORIBA NAES-1100 time-resolved spectrofluorometer, respectively. Microanalyses were performed on a Yanagimoto CHN corder MT-2.

Materials. *N*-Methyl-1,2-naphthalenedicarboximide (**1**)[14] were prepared by the reaction of the 1,2-naphthalenedicarboxylic anhydride[15] with methylamine and purified by chromatography (eluant dichloromethane), then by recrystallization from ethanol. Alkenes (**2a—l**) were commercially available and purified by distillation for liquid materials and by recrystallization for solid materials.

General Procedure for Irradiation and Product Isolation. UV irradiation of 25 cm^3 of N_2 purged benzene solutions containing 10 mM of **1** and 100 mM of alkenes (**2a—l**) was carried out with an Eikosha PIH 300-W high-pressure Hg-lamp through aq $CuSO_4$ filter about 1 cm in thickness (>320 nm) at ambient temperature. The reaction was monitored by TLC (Merck, Kieselgel 60 F_{254}) analyses and ^{1}H NMR measurements. After evaporation of the solvent, the residue was subjected to column chromatography [Wakogel C-200 (silica gel, 74—149 μ)]. Dichloromethane–ether was used as the eluant for the separation of the products.

Irradiation of 1 and *cis*-2-Butene (2a). ***cis*-2,3,4-Trimethyl-3,4-dihydro-1*H*-naphth[1,2-*c*]azepine-1,5(2*H*)-dione (3a)**: Mp 145—147 °C; ^{1}H NMR (400 MHz) δ=1.38 (d, *J*=7.3 Hz, 3H, NCH*Me*), 1.41 (d, *J*=7.0 Hz, 3H, COCH*Me*) 2.85 (q of d, $J_{CH\text{-}CH}$=3.2 Hz, $J_{CH\text{-}Me}$=7.0 Hz, 1H, COC*H*Me), 3.14 (s, 3H, NMe), 4.68 (q of d, $J_{CH\text{-}CH}$=3.2 Hz, $J_{CH\text{-}Me}$=7.3 Hz, 1H, NC*H*Me), 7.5—7.6 (m, 2H, Arom H), 7.83 (d, *J*=8.6 Hz, 1H, C*H*CH^b), 7.8—7.9 (m, 2H, Arom H), 7.99 (d, *J*=8.6 Hz, 1H, H^b); IR (KBr) 1683 (ketone), 1635 (lactam), 1423, 1358, 762 cm^{-1}. Found: C, 76.61; H, 6.52; N, 5.26%; M$^+$, 267. Calcd for $C_{17}H_{17}NO_2$: C, 76.38; H, 6.41; N, 5.24%; M, 267.

***cis*-2,3,4-Trimethyl-3,4-dihydro-1*H*-naphth[2,1-*c*]-azepine-1,5(2*H*)-dione (4a)**: Mp 130—133 °C; ^{1}H NMR (400 MHz) δ=1.39 (d, *J*=7.3 Hz, 6H, NCH*Me*CH*Me*CO), 2.61 (m, 1H, COC*H*Me), 3.23 (s, 3H, NMe), 4.72 (m, 1H, NC*H*Me), 7.4—7.6 (m, 3H, Arom H), 7.8—7.9 (m, 1H, Arom H), 7.95 (d, *J*=8.6 Hz, 1H, H^b), 8.41 (dd, 1H, H^a); IR (KBr) 1682 (ketone), 1640 (lactam), 1403, 1328, 824 cm^{-1}. Found: C, 76.53; H, 6.57; N, 5.29%; M$^+$, 267. Calcd for $C_{17}H_{17}NO_2$: C, 76.38; H, 6.41; N, 5.24%; M, 267.

Irradiation of 1 and *trans*-2-Butene (2b). ***trans*-2,3,4-Trimethyl-3,4-dihydro-1*H*-naphth[1,2-*c*]azepine-1,5(2*H*)-dione (3b)**: Mp 177—180 °C; ^{1}H NMR (400 MHz) δ=1.18 (d, *J*=7.3 Hz, 3H, COCH*Me*), 1.35 (d, *J*=6.7 Hz, 3H, NCH*Me*), 3.09 (q of d, $J_{CH\text{-}CH}$=11.0 Hz, $J_{CH\text{-}Me}$=7.3 Hz, 1H, COC*H*Me), 3.10 (s, 3H, NMe), 4.03 (q of d, $J_{CH\text{-}CH}$=11.0 Hz, $J_{CH\text{-}Me}$=6.7 Hz, 1H, NC*H*Me), 7.5—7.6 (m, 2H, Arom H), 7.84 (d, *J*=8.6 Hz, 1H, C*H*CH^b), 7.8—7.9 (m, 2H, Arom H), 8.01 (d, *J*=8.6 Hz, 1H, H^b); IR (KBr) 1698 (ketone), 1640 (lactam), 1424, 1396, 846 cm^{-1}. Found: C, 76.58; H, 6.55; N, 5.29%; M$^+$, 267. Calcd for $C_{17}H_{17}NO_2$: C, 76.38; H, 6.41; N, 5.24%; M, 267.

***trans*-2,3,4-Trimethyl-3,4-dihydro-1*H*-naphth[2,1-*c*]azepine-1,5(2*H*)-dione (4b)**: Mp 151—154 °C; ^{1}H NMR (400 MHz) δ=1.11 (d, *J*=7.3 Hz, 3H, COCH*Me*), 1.33 (d, *J*=6.9 Hz, 3H, NCH*Me*), 2.97 (q of d, $J_{CH\text{-}CH}$=11.6 Hz, $J_{CH\text{-}Me}$=7.3 Hz, 1H, COC*H*Me), 3.14 (s, 3H, NMe), 4.11 (q of d, $J_{CH\text{-}CH}$=11.6 Hz, $J_{CH\text{-}Me}$=6.9 Hz, 1H, NC*H*Me), 7.39 (d, *J*=8.6 Hz, 1H, C*H*CH^b), 7.6—7.7 (m, 2H, Arom H), 7.87 (dd, 1H, Arom H), 7.97 (d, *J*=8.6 Hz, 1H, H^b), 8.45 (dd, 1H, H^a); IR (KBr) 1686 (ketone), 1642 (lactam), 1322, 1252, 768 cm^{-1}. Found: C, 76.49; H, 6.53; N, 5.28%; M$^+$, 267. Calcd for $C_{17}H_{17}CO_2$: C, 76.38; H, 6.41; N, 5.24%; M, 267.

Reduction of 3b and 4b. To a solution of 50 mg of **3b** in 20 cm^3 of ethanol was added 5 mg of sodium borohydride with stirring and the solution was kept overnight at room temperature. Then, the solution was poured into 10 cm^3 of 0.1 M-hydrochloric acid and extracted with 20 cm^3 of chloroform. The extract was washed several times with water and dried over magnesium sulfate. After

evaporation of the solvent, the residue was chromatographed (eluant dichloromethane–ether) to give **5** (60%).

Reduction of **4b** (50 mg) by sodium borohydride as described above gave **6** (60%).

5-Hydroxy-2,*r*-3,*t*-4-trimethyl-2,3,4,5-tetrahydro-1*H*-naphth[1,2-*c*]azepin-1-one (5): Mp 187—190 °C; ^{1}H NMR δ=1.02 (d, 3H, COCH*Me*), 1.10 (d, 3H, NCH*Me*), 2.1—2.5 (m, 1H, CH), 2.85 (s, 3H, NMe), 2.9—3.0 (m, 2H, *H*COH), 4.9—5.1 (m, 1H, NC*H*Me), 7.3—7.8 (m, 5H, Arom H), 9.10 (m, 1H, H^a); IR (KBr) 3220 (OH), 1612 (lactam), 1401, 842, 770 cm^{-1}. Found: C, 76.07; H, 7.25; N, 5.23%; M$^+$, 269. Calcd for $C_{17}H_{19}NO_2$: C, 75.81; H, 7.11; N, 5.20%; M, 269.

1-Hydroxy-*r*-2,*t*-3,4-trimethyl-2,3,4,5-tetrahydro-1*H*-naphth[2,1-*c*]azepin-5-one (6): Mp 260—262 °C; ^{1}H NMR δ=0.61 (d, 3H, NCH*Me*), 1.19 (d, 3H, COCH*Me*), 2.1—2.5 (m, 1H, CH), 2.8—3.0 (m, 2H, *H*COH), 3.05 (s, 3H, NMe), 4.5—4.7 (m, 1H, NC*H*Me), 7.2—7.9 (m, 5H, Arom H), 8.25 (m, 1H, H^a); IR (KBr) 3290 (OH), 1611 (lactam), 1401, 1088, 763 cm^{-1}. Found: C, 76.10; H, 7.28 N, 5.23%; M$^+$, 269. Calcd for $C_{17}H_{19}NO_2$: C, 75.81; H, 7.11; N, 5.20%; M, 269.

Irradiation of 1 and Isobutene (2d). 2,4,4-Trimethyl-3,4-dihydro-1*H*-naphth[1,2-*c*]azepine-1,5(2*H*)-dione (3d): Mp 149—151 °C; ^{1}H NMR δ=1.28 (d, 6H, CMe_2), 3.23 (s, 3H, NMe), 3.42 (s, 2H, CH_2), 7.4—8.0 (m, 5H, Arom H), 7.96 (d, 1H, H^b); IR (KBr) 1708 (ketone), 1652 (lactam), 1392, 1088, 778 cm^{-1}. Found: C, 76.57; H, 6.54; N, 5.29%; M$^+$, 267. Calcd for $C_{17}H_{17}NO_2$: C, 76.38; H, 6.41; N, 5.24%; M, 267.

2,2,4-Trimethyl-3,4-dihydro-1*H*-naphth[2,1-*c*]-azepine-1,5-(2*H*)-dione (4d): Mp 151—153 °C; ^{1}H NMR δ=0.8—1.7 (coalesced br s, 6H, CMe_2), 2.9—3.2 (coalesced br s, 1H, 1H of CH_2), 3.30 (s, 3H, NMe), 3.7—4.2 (coalesced br s, 1H, 1H of CH_2), 7.36 (d, 1H, C*H*CH^b), 7.4—7.7 (m, 2H, Arom H), 7.7—7.9 (m, 1H, Arom H), 7.89 (d, 1H, H^b), 8.48 (dd, J=3.9, 8.0 Hz, 1H, H^a); IR (KBr) 1705 (ketone), 1648 (lactam), 1475, 1403, 842, 774 cm^{-1}. Found: C, 76.48; H, 6.50; N, 5.27%; M$^+$, 267. Calcd for $C_{17}H_{17}NO_2$: C, 76.38; H, 6.41; N, 5.24%; M, 267.

Irradiation of 1 and 2-Methyl-2-butene (2e). 2,3,4,4-Tetramethyl-3,4-dihydro-1*H*-naphth[1,2-*c*]azepine-1,5(2*H*)-dione (3e): Mp 141—143 °C; ^{1}H NMR δ=0.98 (s, 3H, CMe), 1.22 (d, 3H, CH*Me*), 1.27 (s, 3H, CMe), 3.00 (s, 3H, NMe), 4.17 (q, 2H, C*H*Me), 7.3—7.8 (m, 5H, Arom H), 7.87 (d, 1H, H^b); IR (KBr) 1695 (ketone), 1646 (lactam), 1468, 1401, 841, 759 cm^{-1}. Found: C, 77.00; H, 6.95; N, 5.03%. Calcd for $C_{18}H_{19}NO_2$: C, 76.84; H, 6.81; N, 4.98%.

2,2,3,4-Tetramethyl-3,4-dihydro-1*H*-naphth[2,1-*c*]-azepine-1,5(2*H*)-dione (4e): Mp 136—138 °C; ^{1}H NMR δ=0.88 (s, 3H, CMe), 1.21 (d, 3H, CH*Me*), 1.22 (s, 3H, CMe), 3.04 (s, 3H, NMe), 4.18 (q, 2H, C*H*Me), 7.22 (d, 1H, C*H*CH^b), 7.4—7.6 (m, 2H, Arom H), 7.6—7.8 (m, 2H, Arom H), 7.81 (d, 1H, H^b), 8.40 (dd, 1H, H^a); IR (KBr) 1680 (ketone), 1642 (lactam), 1402, 1324, 833, 763 cm^{-1}. Found: C, 76.96; H, 6.90; N, 5.00%. Calcd for $C_{18}H_{19}NO_2$: C, 76.84; H, 6.81; N, 4.98%.

Irradiation of 1 and Cyclopentene (2f). 7,7a,8,9,10,10a,11,12-Octahydrocyclopenta[*b*]naphth[2,1-*e*]-azepine-7,12-dione (3f): Mp 156—159 °C; ^{1}H NMR δ=1.2—2.2 (m, 6H), 3.13 (s, 3H, NMe), 3.3—3.6 (m, 1H, COCH), 4.0—4.3 (m, 1H, NCH), 7.4—7.6 (m, 2H, Arom H), 7.7—7.9 (m, 3H, Arom H), 8.03 (d, 1H, H^b); IR (KBr) 1698 (ketone), 1636 (lactam), 1462, 1418, 1392, 763 cm^{-1}. Found: 77.57; H, 6.31; N, 5.04%. Calcd for $C_{18}H_{17}NO_2$: C, 77.39; H, 6.13; N, 5.01%.

7,8,8a,9,10,11,11a,12-Octahydrocyclopenta[*b*]naphth[1,2-*e*]-azepine-7,12-dione (4f): Mp 143—146 °C; ^{1}H NMR δ=1.3—2.4 (m, 6H), 2.8—3.2 (m, 1H, COCH), 3.24 (s, 3H, NMe), 4.1—4.5 (m, 1H, NCH), 7.36 (d, 1H, C*H*CH^b), 7.5—8.0 (m, 3H, Arom H), 8.00 (d, 1H, H^b), 8.38 (dd, 1H, H^a); IR (KBr) 1682 (ketone), 1638 (lactam), 1459, 1402, 1328, 763 cm^{-1}. Found: C, 77.20; H, 6.25; N, 4.87%. Calcd for $C_{18}H_{17}NO_2$: C, 77.39; H, 6.13; N, 5.01%.

Irradiation of 1 and 2-Norbornene (2g). 9,10,11,11a-Tetrahydro-8,11-methano-8*H*-benzo[*b*]naphth[2,1-*e*]-azepine-7,13(7a*H*,12*H*)-dione (3g): Mp 176—179 °C; ^{1}H NMR δ=1.0—2.0 (m, 6H), 2.8—3.0 (m, 1H), 3.0—3.3 (m, 2H), 3.14 (s, 3H, NMe), 3.9—4.1 (m, 1H, NCH), 7.5—7.8 (m, 2H, Arom H), 7.9—8.1 (m, 4H, Arom H); IR (KBr) 1711 (ketone), 1634 (lactam), 1372, 838, 762 cm^{-1}. Found: C, 78.72; H, 6.39; N, 4.63%. Calcd for $C_{20}H_{19}NO_2$: C, 78.66; H, 6.27; N, 4.59%.

9,10,11,12-Tetrahydro-9,12-methano-8a*H*-benzo-[*b*]naphth[1,2-*e*]azepine-7,13(8*H*,12a*H*)-dione (4g): Mp 153—156 °C; ^{1}H NMR δ=0.9—2.0 (m, 6H), 2.7—3.1 (m, 3H), 3.21 (s, 3H, NMe), 3.9—4.1 (m, 1H, NCH), 7.35 (d, 1H, C*H*CH^b), 7.5—7.8 (m, 2H, Arom H), 7.8—8.0 (m, 1H, Arom H), 8.01 (d, 1H, H^b), 8.55 (dd, 1H, H^a); IR (KBr) 1712 (ketone), 1624 (lactam), 1383, 1362, 1096, 763 cm^{-1}. Found: C, 78.83; H, 6.36; N, 4.61%. Calcd for $C_{20}H_{19}NO_2$: C, 78.66; H, 6.27; N, 4.59%.

Irradiation of 1 and Styrene (2h). 2-Methyl-4-phenyl-3,4-dihydro-1*H*-naphth[1,2-*c*]azepine-1,5(2*H*)-dione (3h): Mp 157—159 °C; ^{1}H NMR δ=3.15 (s, 3H, NMe), 3.49 (dd, J=2, 12 Hz, 1H, PhC*H*), 4.17 (t, J=12 Hz, 1H, 1H of CH_2), 4.35 (dd, J=2, 12 Hz, 1H, 1H of CH_2), 6.9—7.6 (m, 7H, Arom H), 7.7—7.9 (m, 3H, Arom H), 7.96 (d, 1H, H^b); IR (KBr) 1702 (ketone), 1652 (lactam), 1483, 1398, 774 cm^{-1}. Found: C, 80.14; H, 5.59; N, 4.50%; M$^+$, 315. Calcd for $C_{21}H_{17}NO_2$: C, 79.98; H, 5.43; N, 4.44%; M, 315.

4-Methyl-2-phenyl-3,4-dihydro-1*H*-naphth[2,1-*c*]azepine-1,5(2*H*)-dione (4h): Mp 144—147 °C; ^{1}H NMR δ=3.27 (coalesced br s, 3H, NMe), 3.3—3.8 (coalesced br s, 1H), 4.0—4.4 (coalesced br s, 2H), 7.0—8.0 (m, 9H, Arom H), 7.94 (d, 1H, H^b), 8.45 (dd, 1H, H^a); IR (KBr) 1682 (ketone), 1652 (lactam), 1398, 1258, 834, 754 cm^{-1}. Found: C, 80.20; H, 5.61; N, 4.42%; M$^+$, 315. Calcd for $C_{21}H_{17}NO_2$: C, 79.98; H, 5.43; N, 4.44%; M, 315.

Irradiation of 1 and 1,1-Diphenylethylene (2i). 4,4-Diphenyl-2-methyl-3,4-dihydro-1*H*-naphth[1,2-*c*]azepine-1,5-(2*H*)-dione (3i): Mp 195—198 °C; ^{1}H NMR δ=2.48 (s, 3H, NMe), 4.28 (br s, 2H, CH_2), 6.8—7.9 (m, 15H, Arom H), 7.96 (d, 1H, H^b); IR (KBr) 1712 (ketone), 1656 (lactam), 1483, 1401, 772, 713 cm^{-1}. Found: C, 83.01; H, 5.55 N, 3.46%. Calcd for $C_{27}H_{21}NO_2$: C, 82.84; H, 5.41; N, 3.58%.

2,2-Diphenyl-4-methyl-3,4-dihydo-1*H*-naphth[2,1-*c*]azepine-1,5(2*H*)-dione (4i): Mp 191—193 °C; ^{1}H NMR δ=2.53 (s, 3H, NMe), 3.62 and 5.04 (coalesced br ABq, 2H, CH_2), 7.12 (d, 1H, C*H*CH^b), 7.1—7.4 (m, 13H, Arom H), 7.5—7.7 (m, 1H, Arom H), 7.79 (d, 1H, H^b), 8.51 (dd, 1H, H^a); IR (KBr) 1690 (ketone), 1658 (lactam), 1456, 1402, 758, 716 cm^{-1}. Found: C, 82.92; H, 5.38; N, 3.40%. Calcd for $C_{27}H_{21}NO_2$: C, 82.84; H, 5.41; N, 3.58%.

Irradiation of 1 and Ethyl Vinyl Ether (2j). 4-Ethoxy-2-methyl-3,4-dihydro-1*H*-naphth[1,2-*c*]azepine-1,5-(2*H*)-dione (3j): Mp 141—143 °C; ^{1}H NMR δ=1.29 (t, 3H, OCH_2Me), 3.20 (s, 3H, NMe), 3.4—4.4 (m, 5H), 7.4—7.7 (m,

2H, Arom H), 7.7—8.0 (m, 3H, Arom H), 8.00 (d, J=9 Hz, 1H, H^b); IR (in $CHCl_3$) 1710 (ketone), 1646 (lactam), 1482, 1400, 1081 cm^{-1}. Found: C, 72.32; H, 6.21; N, 5.09%; M^+, 283. Calcd for $C_{17}H_{17}NO_3$: C, 72.06; H, 6.05; N, 4.94%; M, 283.

2-Methyl-3,4-dihydro-1*H*-naphth[1,2-*c*]azepine-1,5(2*H*)-dione (7): Mp 186—188 °C; ^1H NMR δ=3.23 (s, 3H, NMe), 3.0—3.4 (m, 2H, $COCH_2$), 3.6—3.8 (m, 2H, NCH_2), 7.5—7.7 (m, 2H, Arom H), 7.8—8.0 (m, 3H, Arom H), 8.03 (d, J=9 Hz, 1H, H^b); IR (KBr) 1690 (ketone), 1638 (lactam), 1493, 1392, 1256, 764 cm^{-1}. Found: C, 75.20; H, 5.69; N, 5.94%; M^+, 239. Calcd for $C_{15}H_{13}NO_2$: C, 75.30; H, 5.48; N, 5.85%; M, 239.

4-Methyl-3,4-dihydro-1*H*-naphth[2,1-*c*]azepine-1,5(2*H*)-dione (8): Mp 151—145 °C; ^1H NMR δ=2.9—3.1 (m, 2H, $COCH_2$), 3.28 (s, 3H, NMe), 3.6—3.8 (m, 2H, NCH_2), 7.5—7.7 (m, 3H, Arom H), 7.8—7.9 (m, 1H, Arom H), 7.98 (d, J=9 Hz, 1H, H^b), 8.41 (dd, 1H, H^a); IR (in $CHCl_3$) 1696 (ketone), 1646 (lactam), 1400, 1263, 828 cm^{-1}. Found: C, 75.57; H, 5.73; N, 5.90%; M^+, 239. Calcd for $C_{15}H_{13}NO_2$: C, 75.30; H, 5.48; N, 5.85%; M, 239.

Irradiation of 1 and 2,3-Dimethyl-2-butene (2k). 2,3′,3′,4′,4′-Pentamethylspiro[3*H*-benz[*e*]isoindole-3,2′-oxetan]-1(2*H*)-one (13a): Oil; ^1H NMR δ=1.05 (s, 3H, CMe), 1.25 (s, 3H, CMe), 1.53 (s, 3H, CMe), 1.63 (s, 3H, CMe), 3.24 (s, 3H, NMe), 7.4—7.9 (m, 4H, Arom H), 7.94 (d, J=9 Hz, 1H, H^b), 9.19 (dd, 1H, H^a); IR (oil) 1692 (lactam), 1372, 1356, 1068, 942, 783 cm^{-1}. Found: C, 77.53; H, 7.32; N, 4.47%; M^+, 295. Calcd for $C_{19}H_{21}NO_2$: C, 77.26; H, 7.17; N, 4.74%; M, 295.

2,3′,3′,4′,4′-Pentamethylspiro[1*H*-benz[*e*]isoindole-1,2′-oxetan]-3(2*H*)-one (13b): Mp 168—170 °C; ^1H NMR δ=0.89 (s, 3H, CMe), 1.12 (s, 3H, CMe), 1.67 (s, 3H, CMe), 1.77 (s, 3H, CMe), 3.32 (s, 3H, NMe), 7.3—7.9 (m, 5H, Arom H), 8.94 (dd, 1H, H^a); IR (KBr) 1698 (lactam), 1418, 1384, 1038, 776 cm^{-1}. Found: C, 77.30; H, 7.21; N, 4.81%; M^+, 295. Calcd for $C_{19}H_{21}NO_2$: C, 77.26; H, 7.17; N, 4.74%; M, 295.

1-(2,3-Dimethyl-2-butenyl)-1-hydroxy-2-methyl-1,2-dihydro-3*H*-benz[*e*]isoindol-3-one (14): Mp 191—193 °C; ^1H NMR δ=1.12 (s, 3H, CMe), 1.21 (s, 3H, CMe), 1.33 (s, 3H, CMe), 2.84 (s, 3H, NMe), 2.88 and 3.08 (ABq, J=14 Hz, 2H, CH_2), 3.97 (s, 1H, OH), 7.3—8.0 (m, 5H, Arom H), 8.47 (dd, 1H, H^a); IR (KBr) 3300 (OH), 1694 (lactam), 1440, 1411, 768 cm^{-1}. Found: C, 77.46; H, 7.30; N, 4.79%; M^+, 295. Calcd for $C_{19}H_{21}NO_2$: C, 77.26; H, 7.17; N, 4.74%; M, 295.

3-(2,3-Dimethyl-2-butenyl)-3-hydroxy-2-methyl-2,3-dihydro-1*H*-benz[*e*]isoindol-1-one (15a): Mp 124—127 °C; ^1H NMR δ=1.17 (s, 3H, CMe), 1.52 (s, 3H, CMe), 1.59 (s, 3H, CMe), 2.38 and 2.73 (ABq, J=14 Hz, 2H, CH_2), 2.62 (s, 3H, NMe), 4.64 (s, 1H, OH), 7.2—7.7 (m, 5H, Arom H), 8.58 (dd, 1H, H^a); IR (KBr) 3280 (OH), 1684 (lactam), 1381, 1360, 1018, 811 cm^{-1}. Found: C, 77.50; H, 7.28; N, 4.78%; M^+, 295. Calcd for $C_{19}H_{21}NO_2$: C, 77.26; H, 7.17; N, 4.74%; M, 295.

3-Hydroxy-2-methyl-3-(1,1,2-trimethyl-2-propenyl)-2,3-dihydro-1*H*-benz[*e*]isoindol-1-one (15b): Mp 122—125 °C; ^1H NMR δ=0.94 (s, 3H, CMe), 1.03 (s, 3H, CMe), 1.96 (s, 3H, =CMe), 2.41 (s, 3H, NMe), 4.31 (s, 1H, OH), 4.52 and 4.76 (two br s, 2H, $=CH_2$), 7.2—7.7 (m, 5H, Arom H), 8.72 (dd, 1H, H^a); IR (KBr) 3350 (OH), 1682 (lactam), 1386, 1362, 1080, 824 cm^{-1}. Found: C, 77.47; H, 7.24; N, 4.78%; M^+, 295. Calcd for $C_{19}H_{21}NO_2$: C, 77.26; H, 7.17; N, 4.74%; M, 295.

Irradiation of 1 and *cis*-Stilbene (2l). One Stereoisomer of 2-Methyl-3′,4′-diphenylspiro[1*H*-benz[*e*]isoindole-1,2′-oxetan]-3(2*H*)-one (22a): Mp 187—190 °C; ^1H NMR δ=2.87 (s, 3H, NMe), 5.61 (d, J=9 Hz, 1H, OCHC*H*Ph), 6.4—6.6 (m, 2H, Arom H), 6.85 (d, J=9 Hz, 1H, OC*H*Ph), 6.9—7.1 (m, 2H, Arom H), 7.3—8.2 (m, 10H, Arom H), 8.76 (dd, 1H, H^a); IR (KBr) 1718 (lactam), 1395, 968, 768, 714 cm^{-1}. Found: C, 83.02; H, 5.65; N, 3.61%; M^+, 391. Calcd for $C_{27}H_{21}NO_2$: C, 82.84; H, 5.41; N, 3.58%; M, 391.

Another Stereoisomer (22b): Mp 255—258 °C; ^1H NMR δ=2.89 (s, 3H, NMe), 5.43 (d, J=9 Hz, 1H, OCHC*H*Ph), 6.67 (d, J=9 Hz, 1H, OC*H*Ph), 6.9—7.1 (m, 2H, Arom H), 7.2—8.1 (m, 13H, Arom H), 8.26 (dd, 1H, H^a); IR (KBr) 1711 (lactam), 1382, 954, 764, 702 cm^{-1}. Found: C, 82.97; H, 5.42; N, 3.63%; M^+, 391. Calcd for $C_{27}H_{21}NO_2$: C, 82.84; H, 5.41; N, 3.58%; M, 391.

(*Z*)-3-Benzylidene-2-methyl-2,3-dihydro-1*H*-benz[*e*]-isoindol-1-one (23a): Mp 143—146 °C; ^1H NMR δ=3.05 (s, 3H, NMe), 6.83 (s, 1H, H^c), 7.1—7.9 (m, 9H, Arom H), 7.96 (d, 1H, H^b), 9.11 (dd, 1H, H^a); IR (KBr) 1682 (lactam), 1283, 824, 751, 708 cm^{-1}. Found: C, 84.36; H, 5.49; N, 4.98%; M^+, 285. Calcd for $C_{20}H_{15}NO$: C, 84.18; H, 5.30; N, 4.91%; M, 285.

(*E*)-3-Benzylidene-2-methyl-2,3-dihydro-1*H*-benz[*e*]-isoindol-1-one (23b): Mp 136—139 °C; ^1H NMR δ=3.37 (s, 3H, NMe), 6.60 (s, 1H, H^c), 7.0—8.0 (m, 10H, Arom H), 9.20 (dd, 1H, H^a); IR (KBr) 1697 (lactam), 1434, 828, 756, 702 cm^{-1}. Found: C, 84.41; H, 5.52; N, 4.87%. Calcd for $C_{20}H_{15}NO$: C, 84.18; H, 5.30; N, 4.91%.

Acid Decomposition of 22a and 22b. To a solution of 50 mg of **22a** in 20 cm^3 of methanol was added a few drops of hydrochloric acid. After 1 d, to the solution was added 30 cm^3 of chloroform and the solution was washed successively with water, and then dried over magnesium sulfate. After evaporation of the solvent, the residue was chromatographed (eluant dichloromethane) to give **26** (53%).

Acid decomposition of **22b** (50 mg) by hydrochloric acid as described above gave **26** (58%).

(*Z*)-1-Benzylidene-2-methyl-1,2-dihydro-3*H*-benz[*e*]-isoindol-3-one (26): Mp 166—168 °C; ^1H NMR δ=2.97 (s, 3H, NMe), 7.2—7.7 (m, 7H, Arom H+H^c), 7.8—8.0 (m, 3H, Arom H), 8.55 (dd, 1H, H^a); IR (KBr) 1710 (lactam), 1378, 1086, 784, 759, 703 cm^{-1}. Found: C, 84.05; H, 5.52; N, 4.91%; M^+, 285. Calcd for $C_{20}H_{15}NO$: C, 84.18; H, 5.30; N, 4.91%; M, 285.

The authors wish to express their thanks to Dr. Atsuhiro Osuka, Kyoto University, for his help in operating the 400 MHz-NMR. The present work was partially supported by a Grant-in-Aid for Scientific Research No. 60740276 from the Ministry of Education, Science and Culture.

References

1) For reviews see: P. H. Mazzocchi, "Organic Photochemistry," ed by A. Padwa, Marcel Dekker, New York (1981), Vol. 5, p. 421; Y. Kanaoka, *Acc. Chem. Res.*, **11**, 407 (1978).

2) K. Maruyama and Y. Kubo, *J. Org. Chem.*, **42**, 3215

(1977).

3) K. Maruyama, T. Ogawa, and Y. Kubo, *Chem. Lett.*, **1978**, 1107; Y. Kanaoka, K. Yoshida, and Y. Hatanaka, *J. Org. Chem.*, **44**, 664 (1979).

4) K. Maruyama, Y. Kubo, M. Machida, K. Oda, Y. Kanaoka, and K. Fukuyama, *J. Org. Chem.*, **43**, 2303 (1978); K. Maruyama and Y. Kubo, *Chem. Lett.*, **1978**, 851; P. H. Mazzocchi, S. Minamikawa, and P. Wilson, *Tetrahedron Lett.*, **1978**, 4361; K. Maruyama and Y. Kubo, *J. Am. Chem. Soc.*, **100**, 7772 (1978); M. Machida, K. Oda, K. Maruyama, Y. Kubo, and Y. Kanaoka, *Heterocycles*, **14**, 779 (1980); P. H. Mazzocchi and F. Khachik, *Tetrahedron Lett.*, **1981**, 4189; K. Maruyama and Y. Kubo, *J. Org. Chem.*, **46**, 3612 (1981); K. Maruyama and Y. Kubo, *J. Org. Chem.*, **51**, 1426 (1985).

5) a) P. H. Mazzocchi, M. Bowen, and N. Narian, *J. Am. Chem. Soc.*, **99**, 7063 (1977); b) P. H. Mazzocchi, S. Minamikawa, and M. Bowen, *J. Org. Chem.*, **43**, 3079 (1978); c) K. Maruyama and Y. Kubo, *Chem. Lett.*, **1978**, 769; d) Y. Kanaoka, K. Yoshida, and Y. Hatanaka, *J. Org. Chem.*, **44**, 664 (1979); e) P. H. Mazzocchi, S. Minamikawa, and P. Wilson, ibid., **44**, 1186 (1979); f) P. H. Mazzocchi, S. Minamikawa, P. Wilson, M. Bowen, and N. Narian, ibid., **46**, 4846 (1981); g) P. H. Mazzocchi, F. Khachik, P. Wilson, and R. Highet, *J. Am. Chem. Soc.*, **103**, 6498 (1981); h) P. H. Minamikawa, ibid., **48**, 2981 (1983); i) K. Maruyama, T. Ogawa, Y. Kubo, and T. Araki, *J. Chem. Soc., Perkin Trans. 1*, **1985**, 2025.

6) a) P. H. Mazzocchi, S. Minamikawa, and M. Bowen, *Heterocycles*, **9**, 1713 (1978); b) M. Machida, H. Takeuchi, and Y. Kanaoka, *Tetrahedron Lett.*, **1982**, 4981; c) P. H. Mazzocchi, L. Klingler, M. Edwards, P. Wilson, and D. Shook, ibid., **1983**, 143; d) P. H. Mazzocchi and L. Klingler, *J. Am. Chem. Soc.*, **106**, 7567 (1984).

7) Y. Kubo, T. Araki, and Y. Maruyama, *Chem. Lett.*, **1984**, 1909; P. H. Mazzocchi, C. Somich, and C. Ammon, *Tetrahedron Lett.*, **1984**, 3551.

8) Y. Kubo, S. Tojo, M. Suto, R. Toda, and T. Araki, *Chem. Lett.*, **1984**, 2075.

9) G. O. Schenck and R. Steinmetz, *Bull. Soc. Chim. Belg.*, **71**, 781 (1962).

10) G. Jones, II, "Organic Photochemistry," ed by A. Padwa, Marcel Dekker, New York (1981), Vol, 5, p. 1.

11) N. J. Turro, J. C. Dalton, K. Dawes, G. Frarrington, R. R. Hautala, D. Morton, N. Niemczyk, and N. Schore, *Acc. Chem. Res.*, **5**, 92 (1972); D. Creed and R. A. Caldwell, *J. Am. Chem. Soc.*, **96**, 7369 (1974); J. D. Coyle, *Chem. Rev.*, **78**, 97 (1978).

12) "Kagakubinran Kisohen II," Maruzen, Tokyo, (1975).

13) J. D. Coyle and G. L. Newport, *J. Chem. Soc., Perkin Trans. 2*, **1978**, 133.

14) C. Amith and D. Ginsburg, *Tetrahedron*, **29**, 1819 (1973); D. W. Jones and G. Kneen, *J. Chem. Soc., Perkin Trans. 1*, **1975**, 175.

15) M. S. Newman, B. Dhawan, M. M. Hashem, V. K. Khanna, and J. M. Springer, *J. Org. Chem.*, **41**, 3925 (1976).

 © 1986 The Chemical Society of Japan Bull. Chem. Soc. Jpn., 59, 201—206 (1986)

Preparations, NMR Spectra, and Electrochemical Properties of a (Ferrocenylcarbonyl)palladium(II) Complex and Its Derivatives with Some Chelate Groups Attached via Two Ligating Nitrogen Atoms

Masayoshi ONISHI,* Katsuma HIRAKI, Hatsumi KONDA, Yasuhiro ISHIDA, Yushichiro OHAMA, and Yuko UCHIBORI
Department of Industrial Chemistry, Faculty of Engineering, Nagasaki University, Bunkyo-machi, Nagasaki 852
(Received August 12, 1985)

Oxidative addition of (chloroformyl)ferrocene to $[Pd(PPh_3)_4]$ yielded a stable acylpalladium(II) compound of $[Pd(COFc)Cl(PPh_3)_2]$ (**1**), (Fc=ferrocenyl). Complex **1** was treated with alkali metal salts of poly(1-pyrazolyl)-borates (H_nBPz_{4-n}), (Pz=1-pyrazolyl) to give complexes $[Pd(COFc)(H_nBPz_{4-n})(PPh_3)]$, (**2**, n=0; **3**, n=1; and **4**, n=2), which retained the palladium-attached ferrocenylcarbonyl structure. Reaction of **1** with 1,10-phenanthroline (phen) afforded [Pd(COFc)Cl(phen)], whereas reaction with 2,2′-bipyridine gave $[\{Pd(COFc)Cl(PPh_3)\}_2]$ as an isolable material. Transformation of the ferrocenylcarbonyl moiety took place to the ferrocenyl group on palladium, in chlorine-abstraction from **1** with $AgClO_4 \cdot H_2O$ in CH_3CN. In the temperature-dependent ^{1}H-NMR spectra, fluxional behavior was observed for the poly(1-pyrazolyl)borate groups in **2** and **3**. Electrochemical experiments were carried out for **1**—**4** in CH_3CN using platinum working electrodes, and reversible one-electron redox-couples were detected, which were attributed to the process Fe(II)⇄Fe(III) in the ferrocenyl moiety. Furthermore, electron-withdrawing effects of the [poly(1-pyrazolyl)borato]palladiocarbonyl moieties from the Fe centers were compared among these complexes, in relation to their redox potentials.

Transition-metal acyl complexes have been regarded as models of intermediates for catalytic hydroformylation and carboxylation of olefins.[1-6] It would be still worthwhile to synthesize new stable acyl complexes and to study their chemical reactivity and stability of the acyl-metal σ-bonds, in relation to the properties of coexisting other ligands and to the character of alkyl or aryl groups in the acyl moiety. In the course of our study on the properties and applications of bimetallic complexes with ferrocene moieties,[7] we performed oxidative addition of (chloroformyl)ferrocene to tetrakis(triphenylphosphine)palladium(0) $[Pd(PPh_3)_4]$ to yield a stable complex of chloro(ferrocenylcarbonyl)bis(triphenylphosphine)palladium(II) $[Pd(COFc)Cl(PPh_3)_2]$ (Fc=ferrocenyl) (**1**), which involved the well-delocalized π-system of the ferrocenylcarbonyl group. The present paper deals with the syntheses, NMR spectra, and electrochemical properties of the complex **1** and its derivatives with some chelates attached via two ligating nitrogen atoms, including poly(1-pyrazolyl)-borate groups $[H_nBPz_{4-n}]^-$ (Pz=1-pyrazolyl).[8-10] Poly(1-pyrazolyl)borate groups are a versatile and interesting class of uninegative ligands, which have been shown to confer considerable stability on organometallic complexes and have a potentiality for novel fluxionality on the basis of NMR spectroscopy. Electrochemical properties of these groups seemed to be one of key clues to their interesting character. To our knowledge, there were no reports on the electrochemistry of transition-metal poly(1-pyrazolyl)-borate complexes except Trofimenko's brief mention on the polarographic data of $[M(H_nBPz_{4-n})_2]$ (M=Fe, Co, and Cu).[9]

Results and Discussion

Syntheses and Properties of (Ferrocenylcarbonyl)palladium(II) Complexes. When the zerovalent palladium compound $[Pd(PPh_3)_4]$ was added to a benzene solution of (chloroformyl)ferrocene, the color turned into orange and the resulting yellowish orange precipitates were found to be the (ferrocenylcarbonyl)palladium(II) complex **1**. In the IR spectrum, there were a strong ν(C=O) band at 1655 cm^{-1} and a medium ν(Pd-Cl) band at 303 cm^{-1}. The ^{13}C-NMR spectrum of **1** in CD_2Cl_2 showed a weak signal for the carbonyl carbon at δ=207.9. A large signal at δ=69.8 was attributed to the unsubstituted cyclopentadienyl group, and three resonances at δ=70.5, 71.1, and 73.1 were to the monosubstituted one. The phenyl carbons in the coordinated triphenylphosphine ligands resonated at δ=129.7 (1-C), 135.0 (2-C), 128.4 (3-C), and 132.3 (4-C).

Treatment of **1** with sodium or potassium salts of poly(1-pyrazolyl)borates $[H_nBPz_{4-n}]^-$ yielded (ferrocenylcarbonyl)[poly(1-pyrazolyl)borato]palladium(II) $[Pd(COFc)(H_nBPz_{4-n})(PPh_3)]$ (**2**, n=0; **3**, n=1; and **4**, n=2). Complexes **2** and **3** were considerably air-stable both in the solid states and in common organic solvents. On the other hand, complex **4** was slowly decomposed in halogenated solvents, and solubility in other organic solvents, such as benzene and THF was a little lower than those of **1**—**3**. Similar decomposition and low solubility of palladium complexes with the H_2BPz_2 group were reported previously.[9,10] Characteristic ν(C=O) bands were observed for **2**—**4** near 1650 cm^{-1} similarly to that of **1**, supporting retention of the palladium-attached ferrocenylcarbonyl structure in these complexes. The

Table 1. Yields, Analytical Data, and Properties of Complexes

Complex		Yield[a]	Found (Calcd)(%)			Mp[b]	ν(C=O)[c]
		%	C	H	N	θ_m/°C	cm^{-1}
[Pd(COFc)Cl(PPh_3)$_2$][d]	**1**	80[e]	64.26 (64.19)	4.55 (4.47)	0.00 (0.00)	165—170	1655
[Pd(COFc)(BPz_4)(PPh_3)]	**2**	46	57.02 (57.21)	4.23 (4.22)	12.95 (13.02)	192—196	1650
[Pd(COFc)($HBPz_3$)(PPh_3)]	**3**	41	57.15 (57.43)	4.46 (4.31)	10.29 (10.57)	174—180	1643
[Pd(COFc)(H_2BPz_2)(PPh_3)]	**4**	30	57.40 (57.69)	4.46 (4.43)	7.59 (7.69)	164—168	1648
[Pd(COFc)Cl(phen)][f]	**5**	53	52.02 (51.63)	3.29 (3.20)	4.89 (5.24)	188—191	1660
[{Pd(COFc)Cl(PPh_3)}$_2$][g]	**6**	42	56.84 (56.44)	4.20 (3.92)	0.00 (0.00)	185—188	1660

a) Based on **1**, unles noted elsewhere. b) Uncorrected value; with decomposition in a capillary tube. c) Measured in KBr disc. d) ν(Pd-Cl), 314(sh) and 303 cm^{-1}. e) Based on [Pd(PPh_3)$_4$]. f) ν(Pd-Cl), 322 (sh) and 311 cm^{-1}. g) Far IR data, 353(s), 326(m), 313(m), 302(m), and 264(m) cm^{-1}.

Table 2. ^{1}H-NMR Data of the (Ferrocenylcarbonyl)palladium(II) Complexes[a]

Complex	(η^5-C_5H_4)-CO-Pd		η^5-C_5H_5	1-Pyrazolyl group		
	(2-H, 5-H)	(3-H, 4-H)		3-H	4-H	5-H
1	4.40(bs)	4.06(t, 2.0)	3.64(s)	—	—	—
2[b]	3.95(bs)	3.95(bs)	3.95(bs)	7.24(d, 2.0)	6.32(bs)	d)
3	4.0 (bs)	3.7 (bs)	3.73(s)	7.36(bs)	6.17(t, 2.0)	7.69(d, 2.0)
4[c]	4.10(bs)	3.98(bs)	3.77(s)	5.81(bs) 6.13(dd, 2.0, 0.5)	5.58(t, 2.0) 6.00(dt, 2.0, 0.8)	8.07(d, 2.0) d)

a) Measured in $CDCl_3$ at 23 °C with the CW-type JNM-MH-100 spectrometer, unless stated otherwise; δ values from TMS; signal shape and coupling constants in Hz are given in the parentheses; abbreviations used, s=singlet, bs=broad singlet, dd=doublet of doublets d=doublet, t=triplet, dt=doublet of triplets. b) At 51 °C. c) In toluene-d^8; measured with the FT-type FX-90-Q spectrometer. d) Obscured by signals for PPh_3.

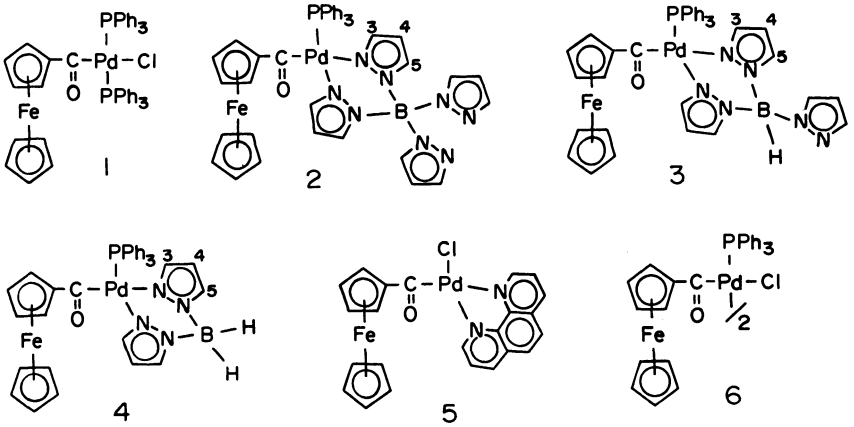

$HBPz_3$ group in **3** showed a ν(BH) band at 2450 cm^{-1}, and the H_2BPz_2 group in **4** gave a characteristic $\nu(BH_2)$ pattern consisting of a slightly resolved doublet at 2395 cm^{-1} and a weak band at 2280 cm^{-1}. Visible absorption spectra of **1**—**4** in CH_3CN showed a band around 460 nm, which was associated with the mixing of a charge-transfer type transition from the Fe atom to the antibonding orbitals on the cyclopentadienyl rings and a d-d type transition.[7]

In addition, complex **1** was treated with 1,10-phenanthroline (phen), and the complex [Pd(COFc)-Cl(phen)] (**5**) was formed through displacement of

two triphenylphosphine molecules. Complex **5** was very insoluble in benzene and dichloromethane, and a ^{1}H-NMR spectrum was not obtained. In case of the reaction with 2,2′-bipyridine (bpy), the expected compound [Pd(COFc)Cl(bpy)] was not isolated, and the reaction-mixture gave a very insoluble material (**6**). Although NMR measurement was not possible, the IR spectrum confirmed retention of the ferrocenylcarbonyl group and triphenylphosphine on palladium. The elemental analysis of **6** suggested its structure to be $[\{Pd(COFc)Cl(PPh_3)\}_2]$,[11] and one mole of triphenylphosphine remained coordinated to the palladium atom in the marked contrast to the case of phen.

Chlorine-abstraction from **1** in CH_3CN was performed with hydrated silver perchlorate in expectation of a cationic complex $[Pd(COFc)(NCCH_3)(PPh_3)_2]ClO_4$, and a pale yellow material (mp, 186 °C (decomp)) of (**7**)[14] was obtained from the reaction-mixture. The IR spectrum of **7** did not show any ν(C=O) bands. There was a strong band at 1095 cm^{-1} without any significant splitting, assignable to the T_2(ClO) stretching mode of an ionic perchlorate uncomplexed. Measurement of the ^{1}H-NMR spectrum indicated retention of the ferrocenyl group and triphenylphosphine in a ratio close to 1:2. The above evidence led us to believe that the ferrocenyl group migrated to the vacant coordination-site produced, followed by dissociation of carbon monoxide from palladium.[1,2] The resulting vacant site seemed to be occupied by a water molecule.

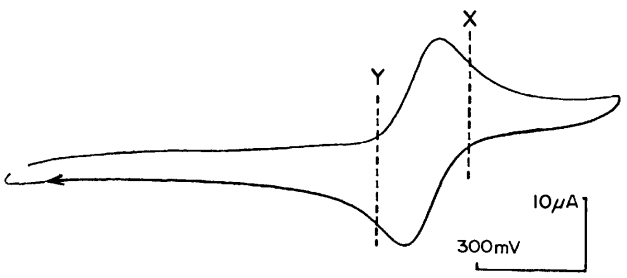

Fig. 1. Cyclic voltammogram of 10^{-3} mol dm^{-3} [Pd(COFc)(BPz_4)(PPh_3)] in CH_3CN at a scan rate of 100 mV/s.

Fluxional Behavior of (Ferrocenylcarbonyl)[poly(1-pyrazolyl)borato]palladium(II) Complexes. In ^{1}H-NMR spectra of **2** measured in $CDCl_3$ at 51 °C, four pyrazolyl groups in the BPz_4 ligand exhibited a slightly broad singlet (4H) at δ=6.32 for 4-H's and a doublet (4H) at δ=7.24 for 3-H's, as shown in Table 2. However, a signal for 5-H's was obscured by those for triphenylphosphine and was not determined explicitly. Upon cooling to −30 °C, the broad singlet for 4-H's separated into three triplets (1H, 2.0 Hz) at δ=5.71, 6.18, and 6.36, and one slightly broad singlet (1H) at δ=6.31. The 3-H protons resonated as three slightly broad singlets at δ=6.59 (2H), 6.77 (1H), and 7.06 (1H). Concerning 5-H's, two slightly broad singlets were observed at δ=7.71 (1H) and 7.93 (2H), whereas a signal of the remaining proton was not distinguished owing to overlapping with the aromatic protons in triphenylphosphine. At this temperature, coordination of the BPz_4 ligand to palladium was stereochemically rigid to give the four spectroscopically nonequivalent pyrazolyl groups. On the other hand at 51 °C, fluxional motion of the BPz_4 ligand averaged environments of all pyrazolyl groups leading to their spectroscopic equivalence.

As described previously,[15–17] the geometrical arrangement in the stereochemically rigid coordination has a square-planar structure about the central palladium atom and a boat conformation of the Pd-(pyrazolyl)$_2$-B six-membered ring. The fluxional motion for the spectroscopic equivalence of four pyrazolyl groups at high temperatures has been regarded as the "tumbling process", which involves coordination of the uncoordinated pyrazolyl group near the palladium atom, accompanied instantaneously by dissociation of the previously coordinated group and by inversion of the Pd-(pyrazolyl)$_2$-B ring.

As for the monosubstituted cyclopentadienyl group in **2**, a broad singlet at δ=3.95 was observed at 51 °C, which overlapped a signal of the unsubstituted cyclopentadienyl group.

^{1}H-NMR spectra of the [hydrotris(1-pyrazolyl)-

Table 3. Electrochemistry of Complexes **1**—**4** and Electronic Spectra of Their Oxidized Species

Complex	Electrochemical data[a]				Oxidized species	
	$E°$	ΔE_p	i_{pc}/i_{pa}	n[b]	λ_{max}	ε
	mV	mV		(Found)	nm	mol^{-1} dm^3 cm^{-1}
1	159	62	0.94	1.12	623	310
2	119	62	0.99	0.98	631	309
3	105	62	0.91	1.08	625	235
4	104	147	0.95	~1.0[c]	625	214

a) In CH_3CN; (n-Bu_4N)PF_6=0.1 mol dm^{-3}; complex=10^{-3} mol dm^{-3}; scan rate=100 mV/s; redox for the Fe(II)⇄Fe(III) couple; see the text and ref. 18. b) Number of electrons passed per complex, for anodic exhaustive electrolysis. c) Corresponding to the first step, see the text.

borato]palladium(II) **3** in $CDCl_3$ at 23 °C showed a triplet (3H) δ=6.17 for 4-H's, a slightly broad singlet (3H) at δ=7.36 for 3-H's, and a doublet (3H) at δ= 7.69 for 5-H's, indicating spectroscopic equivalence of all pyrazolyl groups and fluxional behavior of the $HBPz_3$ ligand. On cooling to −45 °C, the signals for pyrazolyl groups became broader gradually, but a slow-exchange limiting spectrum was not obtained. Similar difficult fixation of the fluxional motion of the $HBPz_3$ ligand on cooling was described previously in some [hydrotris(1-pyrazolyl)borato]palladium(II) complexes.[16,17]

^{1}H-NMR spectra of the [dihydrobis(1-pyrazolyl)-borato]palladium(II) **4** were measured in toluene-d^8 in the temperature range of 50 to −36 °C, and there was no spectral change observed. At 80 °C, the complex was decomposed slowly. Two 4-H protons at room temperature resonated as triplets at δ=5.58 and 6.00, and two 3-H protons did as a slightly broad singlet at δ=5.81 and a doublet at δ=6.13. Additional smaller coupling to ^{31}P nucleus was noticed for the signals at δ=6.00 and 6.13 in the FT-type NMR measurement, and suggested that protons for these two signals belonged to the pyrazolyl group at a trans position to the triphenylphosphine ligand. Concerning 5-H's, one proton appeared as a doublet at δ= 8.07, but the other one was obscured by overlapping with the signals of triphenylphosphine. As a whole, complex **4** did not show the fluxional motion involving bond-breaking process between palladium and pyrazolyl groups.

Electrochemistry of (Ferrocenylcarbonyl)palladium(II) Complexes. Acetonitrile solutions of complexes **1**—**4** were served for their electrochemical studies, containing 0.1 mol dm^{-3} (n-Bu_4N)PF_6 as supporting electrolyte. Working electrodes were a platinum disc and gauze for cyclic voltammetry and bulk electrolysis, respectively. Cyclic voltammogram in Fig. 1 shows a typical well-reversible redox-couple for **2**. The peak current ratio of i_{pc}/i_{pa} remained close to unity in the sweep rate of 200 to 10 mV/s, and the current function (proportional to $i_p/\sqrt{v}$) was also constant with the rate.[18] There was no current flow observed in the bulk electrolysis at the controlled potential Y in Fig. 1. On the other hand, the electrolysis at X resulted in an anodic current, which upon integration yielded charge consistent with one electron per molecule of the complex, and changed color of the solution from yellowish orange to dark brown. One-electron transfer was also confirmed by potential separation ΔE_p between oxidation and reduction peaks of the couple, which was very close to theoretical 59 mV. These findings indicated that the redox under consideration was electrochemically reversible and diffusion-controlled one-electron transfer, and that the oxidation product of **2** was stable during the time

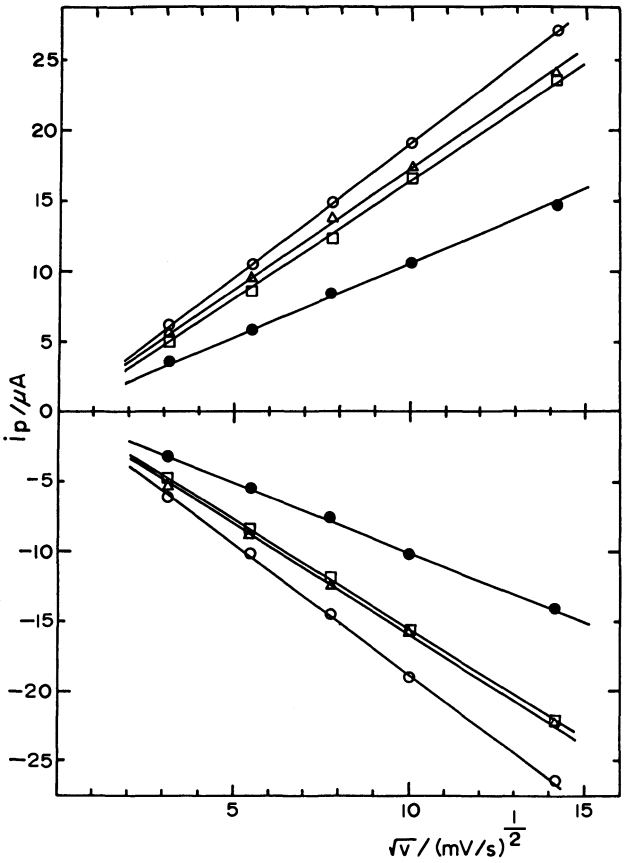

Fig. 2. Dependence of anodic and cathodic peak currents i_p of the Fe(III)/Fe(II) redoxes on the scan rate v. Concentration of complexes; 10^{-3} mol dm^{-3} ●: Complex **1**, ○: Complex **2**, △: Complex **3**, □: Complex **4**.

of the sweep.[19,20] Complexes **1** and **3** underwent analogous reversible one-electron oxidation, and the results are summarized in Table 3.

The corresponding redox-couple for **4** with the H_2BPz_2 group demonstrated that the peak current ratio i_{pc}/i_{pa} was nearly close to unity and the current function was also independent of the sweep rate similarly, whereas the peak separation ΔE_p was fairly larger than the theoretical 59 mV on the contrary. Thus, the redox couple of **4** was diffusion-controlled like the other complexes, but varying in the electrochemical reversibility, and was regarded as quasi-reversible.[19,20] Furthermore, the bulk electrolysis of **4** (10^{-3} mol dm^{-3}) was performed at a slightly more anodic potential than that of its oxidation peak, and the electrolysis was found to proceed in two steps. The current observed was ca. 9 mA at the beginning of the electrolysis and decayed following a manner of the first-order kinetics.[21] One electron passed per molecule of the complex for ca. 15 min and the current decreased to 1 mA. Then, the current was increased gradually again and approximately two more electrons passed additionally to reach

completion of the electrolysis.

Visible and near-infrared absorption spectra were observed after one-electron oxidation of the complexes **1**—**4**. In the region above 500 nm, each oxidized complex (including **4**) gave only one band detected around 625 nm. Since ferricinium cation $[Fe(C_5H_5)_2]^+$ was reported to have a characteristic band of a Ligand (e_{1u})→Fe (e_{2g}(3d)) transition at ca. 620 nm,[22] the band observed was attributable to a similar transition in the (ferrocenylcarbonyl)palladium complexes oxidized. Near-infrared absorption bands for light-induced intervalent electron-transfer were described for some heterobinuclear complexes upon oxidation,[23,24] which involved ferrocenyl groups as one component similarly to our complexes. The electron-transfer bands were expected in the range of 700 to 2000 nm, but such a band was not discernible in the spectra of **1**—**4** after one-electron oxidation.

On the basis of these results, the redox system under consideration was concluded to be the process of Fe(II)⇄Fe(III) in the ferrocenyl moiety. As for the bulk electrolysis of **4**, the Fe center was oxidized similarly at the first step and then some kinds of oxidative decomposition of the H_2BPz_2 group would occur as the second step. The oxidative decomposition of the H_2BPz_2 group seemed to be associable with some reducing ability of the group, suggested previously.[9,10]

When cyclic voltammograms of **1**—**4** were performed in a wider potential-range, an additional irreversible anodic wave appeared at a potential more than ca. 1300 mV, owing to oxidation of the Pd(II) sites.[23]

Formal redox potentials[18] $E°$ for the Fe(III)/Fe(II) couples of **1**—**4** were more anodic than that of ferrocene, and this was ascribed to electron-withdrawing effects of their palladiocarbonyl structures from the Fe redox centers. The effects of the four kinds of palladiocarbonyl structures were quite comparable. The ordering for the readiness of oxidation of the Fe centers was **4**≧**3**>**2**>**1**. Therefore, electron-withdrawing effects of the [poly(1-pyrazolyl)borato]palladiocarbonyl moieties from the Fe centers were smaller than that of the chloro(triphenylphosphine)palladiocarbonyl moiety. In addition, this parallelism indicated also that the [tetrakis(1-pyrazolyl)borato]-palladium moiety possessed greater ability for withdrawing electrons from the Fe center than the other poly(1-pyrazolyl)borate analogues, possibly owing to its larger electron-delocalization over the pyrazolyl groups.

Experimental

General Procedures and Materials. ^1H- and ^{13}C-NMR spectra were run on JEOL model FX-90-Q (FT type) and MH-100 spectrometers with tetramethylsilane as an internal standard. Temperatures of NMR samples were determined with methanol or 1,3-propanediol. IR spectra were obtained using Hitachi 285 and Shimadzu IR-450 spectrometers. Melting points were observed on a Yanagimoto MP-S3 microstage apparatus in capillary tubes and are uncorrected. Electronic spectra (260—2100 nm) were recorded on a Hitachi 323 UV-VIS-NIR spectrophotometer.

(Chloroformyl)ferrocene[25] and $M[H_nBPz_{4-n}]$ (M=Na and K)[9] were prepared according to the reported methods. Preparative and electrochemical operations were performed under dry nitrogen.

Preparation of $[Pd(COFc)Cl(PPh_3)_2]$ 1. The powder of $[Pd(PPh_3)_4]$ (850 mg) was added in portions to a benzene solution (20 cm^3) of (chloroformyl)ferrocene (230 mg) and the mixture was stirred for 24 h at ambient temperature. The resulting precipitates were collected and washed with diethyl ether. Yellowish orange microcrystals (520 mg) were obtained and characterized as **1**. Vis(CH_3CN) 450 nm (ε 625).

Preparation of $[Pd(COFc)(BPz_4)(PPh_3)]$ 2. A mixture of **1** (218 mg) and $K[BPz_4]$ (95 mg) in dichloromethane (20 cm^3) was stirred overnight. After concentration, the reaction mixture passed through a silica-gel column (200 mesh, 1.2×20 cm) to give a red fraction by eluting with dichloromethane–diethyl ether (2:1). The fraction was evaporated to dryness and the residue was recrystallized from dichloromethane and hexane, affording an orange powder (98 mg) of **2**. Vis(CH_3CN) 464 nm (ε 506).

Preparation of $[Pd(COFc)(HBPz_3)(PPh_3)]$ 3. Complex **1** (200 mg) was treated with $Na[HBPz_3]$ (63 mg) in dichloromethane (20 cm^3). After stirring for 24 h, the solvent was removed in vacuo. Then, the benzene extract was chromatographed on a silica-gel column, and a red fraction eluted by dichloromethane–diethyl ether (4:1) was evaporated to dryness. The resulting solid was recrystallized from diethyl ether and hexane to give orange microcrystals (74 mg) of **3**. Vis(CH_3CN) 464 nm (ε 441).

Preparation of $[Pd(COFc)(H_2BPz_2)(PPh_3)]$ 4. Potassium dihydrobis(1-pyrazolyl)borate $K[H_2BPz_2]$ (50 mg) was mixed with **1** (180 mg) in THF (20 cm^3), followed by stirring for 24 h at room temperature. The solvent was evaporated under reduced pressure and recrystallization of the residue from benzene and diethyl ether gave yellowish orange microcrystals (45 mg) of **4**. Vis(CH_3CN) 461 nm (ε 456).

Reaction of 1 with 1,10-Phenanthroline (phen). 1,10-Phenanthroline monohydrate (58 mg) was added to a benzene suspension (50 cm^3) of **1** (250 mg) and the mixture was stirred for 2 h. After concentration to a small volume, addition of hexane gave orange precipitates (81 mg) of **5**.

Reaction of 1 with 2,2′-Bipyridine (bpy). A mixture of **1** (250 mg) and 2,2′-bipyridine (50 mg) in benzene (50 cm^3) was stirred at ambient temperature for 2 h and the resulting precipitates were collected and washed with diethyl ether to afford pale yellow microcrystals (74 mg) of **6**.

Reaction of 1 with $AgClO_4$ in CH_3CN. An CH_3CN solution (5 cm^3) of $AgClO_4 \cdot H_2O$ (52 mg) was added dropwise to an CH_3CN suspension (20 cm^3) of **1** (200 mg). After stirring of the mixture for 2 h and evaporation under vacuum to dryness, recrystallization of the residue from dichloromethane and diethyl ether yielded pale yellow

microcrystals (130 mg), **7**.

Electrochemical Studies. Electrochemical experiments were carried out with a standard three-electrode electric circuit, using a Hokuto Denko HA-301 potentiostat and a HB-104 function generater. Acetonitrile test-solutions (20 cm^3) contained (ferrocenylcarbonyl)palladium complexes (10^{-3} mol dm^{-3}) and (n-Bu_4N)PF_6 (0.1 mol dm^{-3}) as the supporting electrolyte. The reference and auxiliary electrodes were separated from the test solution by a tube with glass frits, and the tube contained electrolytic solvent and the supporting electrolyte. Working electrodes were a Pt disc (3 mmϕ) and gauze (12 cm^2, 80 mesh) for cyclic voltammetry and bulk electrolysis, respectively. The auxiliary electrode was a Pb plate and the reference electrode was a Pt wire in a solution of [$Fe(C_5H_5)_2$] (0.01 mol dm^{-3}), [$Fe(C_5H_5)_2$]PF_6 (0.01 mol dm^{-3}), and (n-Bu_4N)PF_6 (0.1 mol dm^{-3}) in CH_3CN.

Electronic Absorption Spectra of 1—4 after One-electron Oxidation. The complexes **1**—**4** in nitrogen-deaerated acetonitrile solutions (10^{-3} mol dm^{-3}) were served for bulk electrolysis at appropriately controlled potentials. After one-electron oxidation, a syringe was used to transfer ca. 3 cm^3 of the solutions to a 10 mm quartz cuvette under nitrogen, taking care to avoid dilution with solvent in the auxiliary electrode compartment. Electronic absorption bands under consideration were observed within 5 min after completion of the electrolysis.[26] Molar absorptivities ε were evaluated from the absorbances obtained, and were based on the concentration of the complexes charged.

References

1) J. P. Collman and L. S. Hegedus, "Principles and Applications of Organotransition Metal Chemistry," University Science Books, Mill Valley (1980).

2) G. W. Parshall, "Homogeneous Catalysis," John Wiley & Sons, New York (1980).

3) J. K. Stille and P. K. Wong, *J. Org. Chem.*, **40**, 532 (1975).

4) K. Suzuki and M. Nishida, *Bull. Chem. Soc. Jpn.*, **46**, 2887 (1973).

5) K. Kudo, M. Sato, M. Hidai, and Y. Uchida, *Bull. Chem. Soc. Jpn.*, **46**, 2820 (1973).

6) P. Fitton, M. P. Johnson, and J. E. McKeon, *J. Chem. Soc., Chem. Commun.*, **1968**, 6.

7) M. Onishi, K. Hiraki, and A. Iwamoto, *J. Organomet. Chem.*, **262**, C-11 (1984).

8) A. Shaver, *J. Organomet. Chem. Libr.*, **3**, 157 (1977), and references cited therein.

9) S. Trofimenko, *J. Am. Chem. Soc.*, **89**, 3170 (1967), and references cited therein.

10) M. Onishi, K. Hiraki, T. Itoh, and Y. Ohama, *J. Organomet. Chem.*, **254**, 381 (1983), and references cited therein.

11) Similar structural transformations from [$PdRCl(PPh_3)_2$] to [{$PdRCl(PPh_3)$}$_2$] were described on the complexes with benzyl and cyanobenzyl groups for R.[12,13]

12) P. Fitton, J. E. McKeon, and B. C. Ream, *J. Chem. Soc., Chem. Commun.*, **1969**, 370.

13) P. Zanello, R. Seeber, A. Cinquantini, and R. Ros, *J. Inorg. Nucl. Chem.*, **43**, 1095 (1981).

14) Elemental analysis, Found: C, 56.73; H, 4.05%. The values were close to those calculated for [$PdFc(OH_2)$-$(PPh_3)_2$]$ClO_4 \cdot 1/2CH_2Cl_2$; C, 57.23; H, 4.34%.

15) M. Onishi, Y. Ohama, K. Sugimura, and K. Hiraki, *Chem. Lett.*, **1976**, 955.

16) M. Onishi, K. Sugimura, and K. Hiraki, *Bull. Chem. Soc. Jpn.*, **51**, 3209 (1978).

17) M. Onishi, K. Hiraki, M. Shironita, Y. Yamaguchi, and S. Nakagawa, *Bull. Chem. Soc. Jpn.*, **53**, 961 (1980).

18) v=scan rate; i_p=peak current; E_p=peak potential; i_{pc}/i_{pa}=ratio of peak cathodic and anodic currents; $\Delta E_p = E_{pa} - E_{pc}$, potential separation between anodic and cathodic peaks; E°=formal redox potential evaluated as $0.5(E_{pa}+E_{pc})$, for a reversible couple.

19) M. F. Joseph, J. A. Page, and M. C. Baird, *Organometallics*, **3**, 1749 (1984).

20) J. Edwin and W. E. Geiger, *Organometallics*, **3**, 1910 (1984).

21) A. J. Bard and L. R. Faulkner, "Electrochemical Methods, Fundamentals and Applications," John Wiley & Sons, New York (1980), Chap. 10.

22) S. B. Colbran, B. H. Robinson, and J. Simpson, *Organometallics*, **2**, 943 (1983), and references cited therein.

23) J. C. Kotz, E. E. Getty, and L. Lin, *Organometallics*, **4**, 610 (1985).

24) A. J. Deeming, "Comprehensive Organometallic Chemistry," ed by G. Wilkinson, F. G. A. Stone, and E. W. Abel, Pergamon Press, Oxford (1982), Vol. 4, Chap. 31—3, and references cited therein.

25) H. H. Lau and H. Hart, *J. Org. Chem.*, **24**, 280 (1959).

26) The times required for one-electron oxidation of **1**—**4** were ranged from 12 to 20 min. After one-electron oxidation, the electrolytic solutions were applied to the same electrolysis conditions for additional 10 min, and there was not a significant change of the electronic absorption spectra. In addition, reduction of the oxidized species occurred also at −500 mV with the passage of electricity close to 1 Faraday/mol, showing little decomposition of the species.

 © 1986 The Chemical Society of Japan Bull. Chem. Soc. Jpn., 59, 207—214 (1986)

Three-Dimensionally-Modified Tetracyanoquinodimethanes and Their Charge-Transfer Complexes with Tetrathiafulvalene Derivatives Having a Wide Range of Ionicity

Kazuhiro NAKASUJI,* Masakatsu NAKATSUKA, Hideki YAMOCHI,** Ichiro MURATA,* Shigeharu HARADA,† Nobutami KASAI,† Kimiaki YAMAMURA,†† Jiro TANAKA,††† Gunzi SAITO,††††,** Toshiaki ENOKI,†††† and Hiroo INOKUCHI††††

Department of Chemistry, Faculty of Science, Osaka University, Toyonaka, Osaka 560

† Department of Applied Chemistry, Faculty of Engineering, Osaka University, Suita, Osaka 565

†† Department of Chemistry, College of General Education, Kobe University, Nada-ku, Kobe 657

††† Department of Chemistry, Faculty of Science, Nagoya University, Chikusa-ku, Nagoya 464

†††† Institute for Molecular Science, Okazaki 444

(Received August 22, 1985)

Eight different 1:1 charge-transfer(CT) complexes were prepared using tetrahydrobarreleno-tetracyanoquinodimethane(THBTCNQ), dihydrobarreleno-tetracyanoquinodimethane(DHBTCNQ), monobenzobarreleno-tetracyanoquinodimethane(MBBTCNQ), and dibenzobarreleno-tetracyanoquinodimethane(DBBTCNQ) as tetracyanoquinodimethane(TCNQ)-type acceptors, and tetrathiafulvalene(TTF), bis(tetramethyene)-tetrathiafulvalene(OMTTF), and tetramethyl-tetrathiafulvalene(TMTTF) as TTF-type donors. The complexes can be classified into three distinct groups, I—III, on the basis of the magnitude of both the degree of CT and the electrical resistivity of compacted powders. Group-I complexes are characterized by a small band gap semiconductivity and moderate CT, group-II complexes by low conductivity and small CT, and group-III complexes by low conductivity and complete CT. The stacking mode of the three groups of complexes are discussed, by comparing the electronic absorption spectra of the three groups of CT complexes with those of the complexes for which the crystal structures are known. A crystal structure analysis of OMTTF-DBBTCNQ revealed that it is the first example of a highly ionic CT complex of a TTF-TCNQ type with a regular mixed stacking mode. These three groups of complexes containing bulky acceptor groups will be of theoretical interest in studying the crystal properties of organic CT complexes.

Highly-conducting organic charge-transfer (CT) complexes usually have the following structural and electronic properties in the solid state:[1] (a) a uniform segregated stacking of donors and acceptors and (b) an incomplete CT between the components. Several synthetic design criteria have been proposed for obtaining a high conductivity.[1,2] Generally, an effective overlap of the planar π-electron systems is required for an efficient charge transport. As a result, two-chain organic conductors composed of donor and acceptor components have been designed mainly with planar π-systems modified two-dimensionally. Therefore, three-dimensional modifications, which lead to a destruction of the molecular planarity, have not attracted much attention so far.[2b,3] In principle, however, such modifications will affect the following essential properties in the solid state: (i) The stacking mode of the component molecules, (ii) the ionicity, and (iii) intra- and interstack interactions. We started the first systematic study regarding these points by selecting tetrathiafulvalene (TTF) and tetracyanoquinodimethane (TCNQ) as basic skeletons. These are the most widely investigated donors and acceptors. In this paper we describe the preparations and properties of the three groups of CT complexes (having a wide range of ionicity) and stress that small band gap semiconductors (including a relatively highly conducting complex (ρ=2.5×10^{-2} Ω cm)) can be prepared even from TCNQ having bulky groups. A rare example of highly ionic complexes with a mixed stacking mode was also prepared.[4]

Results and Discussion

A) Classification of CT Complexes. In this study, we aimed at obtaining rigid, bulky modifications with small electronic perturbations on TCNQ (**1a**). To this end, four barreleno-TCNQ's, **1b**, **1c**, **1d**,[5] and **1e**,[6] were synthesized in which a TCNQ moiety was incorporated into the rigid barrelene skeleton.[7] The new acceptors, **1b** and **1c**, were

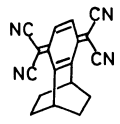
THBTCNQ
1b

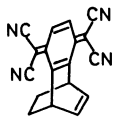
DHBTCNQ
1c

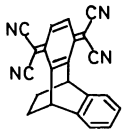
MBBTCNQ
1d

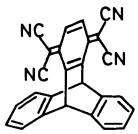
DBBTCNQ
1e

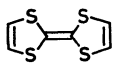
TTF
2a

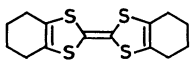
OMTTF
2b

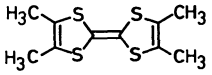
TMTTF
2c

** Present address: The Institute for Solid State Physics, The University of Tokyo, Roppongi, Minato-ku, Tokyo 106.

prepared by the Acker and Hertler procedure[8] for the synthesis of TCNQ (Scheme 1). The first half-wave reduction potentials ($E^{r}_{1/2}$) of **1b—e** show that the acceptor strength increases gently and gradually with an increasing unsaturation in the barrelene moieties[9] (Table 1). However, the difference of $E^{r}_{1/2}$ between TCNQ **1a** and both extremes **1b** or **1e** is only +0.07 V or −0.05 V, respectively. Thus, the electronic perturbation of TCNQ caused by an introduction of bridged segments is fairly small as judged from their $E^{r}_{1/2}$ values.

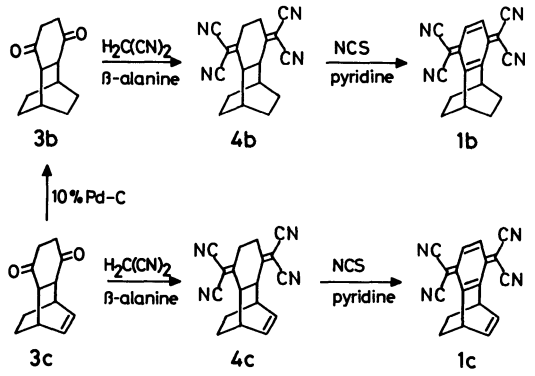

Scheme 1.

Table 1. Redox Potentials of Donors(**1a—e**) and Acceptors(**2a—c**) (V vs. SCE)[a]

	1b	**1c**	**1a**	**1d**	**1e**	**2a**	**2b**	**2c**
$E^{r}_{1/2}$	0.11	0.14	0.18	0.18	0.23			
$E^{o}_{1/2}$						0.33	0.26	0.25

a) Measured by cyclic voltammetry in 0.1 mol dm^{-3} Et_4NClO_4/CH_3CN at a Pt electrode.

Eight different 1:1 CT complexes were prepared using **1b—e** as acceptors and molecules of the TTF family, namely TTF (**2a**), bis(tetramethylene)-TTF (OMTTF, **2b**), and tetramethyl-TTF (TMTTF, **2c**) as donors. Their selected physical properties are compiled in Table 2. The difference between the oxidation potential ($E^{o}_{1/2}$) of donor and the reduction potential ($E^{r}_{1/2}$) of acceptor, i.e., $\Delta E^{o,r}=E^{o}_{1/2}-E^{r}_{1/2}$, is a convenient experimental measure to predict the degree of CT for a complex.[1b,2b,2d] Such intermolecular HOMO-LUMO gap, $\Delta E^{o,r}$ values, for the eight complexes are in a narrow range (+0.02—+0.22 V) since the electronic perturbation resulting from a three-dimensional modification was nearly negligible. Therefore, we expected that the ground states of all these complexes were in incomplete CT states. The degree of CT, Z, for each complex was determined by both the infrared[10] and Raman[11] spectra. We obtained values for Z (Table 2) using the frequency shifts, $\Delta\omega$, between neutral molecules and ion-radical salts for these spectra (Tables 3 and 4). The two methods which reflect the electronic structure of both the acceptor and the donor components yield estimated Z values in good agreement each other. Interestingly, the values of Z for the complexes are in a wide range (0.1—1.0) despite the narrow range of the $\Delta E^{o,r}$ values.

These CT complexes can be classified into three distinct groups, I—III, on the basis of the magnitude of both the degree of CT, and the electrical resistivity, ρ, of compacted powders. The apparent activation energies E_a for semiconduction ($\rho=\rho_0\exp(-E_a/kT)$) are also given. Group I, II, and III complexes are characterized by a relatively high conductivity with a moderate CT (small band gap semiconducting complex), a low conductivity with a small CT

Table 2. Classification and Selected Physical Properties of Eight 1 : 1 CT Complexes

	Group I (SBGSC)[a]		Group II (Nonionic)			Group III (Ionic)		
CT Complex	**2a-1b** TTF-THBTCNQ	**2a-1c** TTF-DHBTCNQ	**2b-1b** OMTTF-THBTCNQ	**2b-1c** OMTTF-DHBTCNQ	**2c-1c** TMTTF-DHBTCNQ	**2b-1d** OMTTF-MBBTCNQ	**2b-1e** OMTTF-DBBTCNQ	**2c-1e** TMTTF-DBBTCNQ
$\Delta E^{o,r}$, V	+0.22	+0.19	+0.15	+0.12	+0.11	+0.08	+0.03	+0.02
IR, cm^{-1}	2179	2177	2208	2209	2204	2180	2175	2176
(Z)[b]	(0.76)	(0.84)	(0.11)	(0.13)	(0.24)	(0.92)	(1.00)	(0.97)
Raman, cm^{-1}	1444	1445	1510	1503	1500	1415	1422	1427
(Z)[b]	(0.74)	(0.75)	(0.22)	(0.28)	(0.31)	(0.98)	(0.93)	(0.92)
ρ_{RT}, Ω cm[c]	2.8 2.5×10^{-2} [d]	13	6.8×10^{5}	5.5×10^{7}	4.2×10^{6}	2.1×10^{6}	2.2×10^{7}	2.8×10^{3}
E_a, eV	0.095 0.045[d]	0.14	0.39	0.44	0.36	0.34	0.64	0.30
$h\nu_{CT}$ (obsd), cm^{-1}	4100	3700	5300	5100	4500	5600	6300	Shoulder
$h\nu_{CT}$ (calcd), cm^{-1} [b]	4900	5200	5200	5000	4900	6000	6500	6500

a) Small band gap semiconductor. b) See text. c) Compacted powder measurements. d) Single crystal measurement.

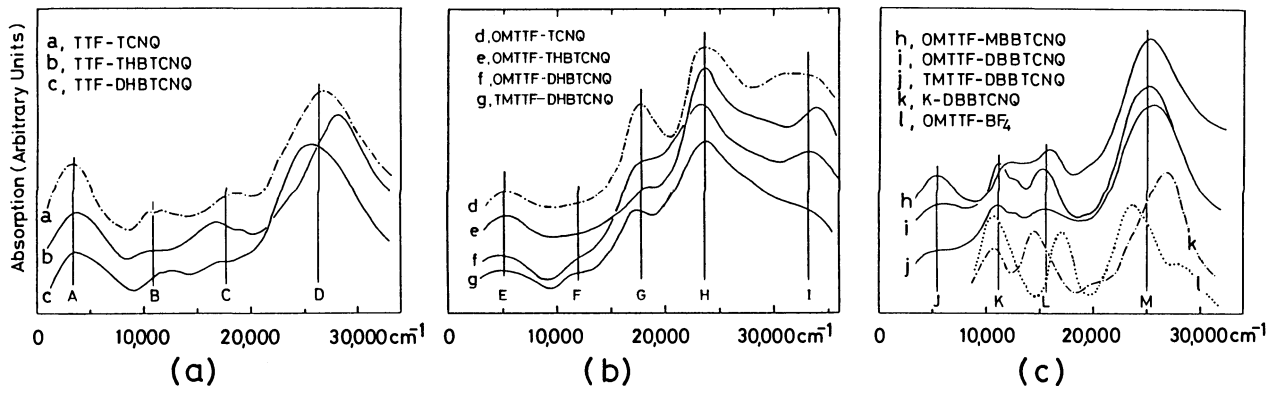

Fig. 1. Absorption spectra of three distinct groups of CT complexes as powders dispersed in KBr.

Table 3. Infrared Frequencies ($\omega_{C\equiv N}$, cm^{-1}) of Acceptors

	1a[b]	1b	1c	1d	1e
Neutral	2227	2213	2215	2216	2217
Anion radical[a]	2183	2168	2170	2177	2175
$\Delta\omega$	44	45	45	39	42

a) K salts. b) Ref. 10.

Table 4. Raman Frequencies ($\omega_{C=C}$, cm^{-1}) of Donors

	2a[b]	2b	2c[b]
Neutral	1518	1537	1537
Cation radical[a]	1420	1413	1418
$\Delta\omega$	98	124	119

a) BF_4 salts. b) Ref. 11.

(nonionic complex), and a low conductivity with a complete CT (ionic complex), respectively.

B) Electronic Spectra and Prediction of Stacking Mode. The stacking modes of the components are essential for understanding the solid-state properties of CT complexes. One of the group-III complexes, bis(tetramethylene)tetrathiafulvalene(OMTTF)-dibenzobarrelenotetracyanoquinodimethane(DBBTCNQ), crystallizes in a monoclinic lattice. However, group-I complex crystals are not suitable for X-ray structure analyses and group-II complexes gradually decomposed upon X-ray irradiation. Therefore, we estimated the stacking mode by comparing the electronic spectra of the three groups of CT complexes with those of the complexes for which the crystal structures are known. We will discuss the electronic spectra of powdered samples since they provide useful information, particularly for cases of CT complexes composed of TTF or TCNQ skeletons.[12]

For group-I complexes, we selected TTF-TCNQ as a reference complex. The two requisites, (a) and (b), for the highly conducting organic complexes, TTF-TCNQ for example, can be substantiated by the detection of a very low energy absorption band at about 3000 cm^{-1}. This was determined to be an intrastack CT transition in a segregated stack with an incomplete CT (intraband transition).[12a,13] Figure 1(a) shows the solid-state electronic spectra of TTF-THBTCNQ and TTF-DHBTCNQ as well as that of TTF-TCNQ. In addition to the similarity of the spectra between TTF-TCNQ and group-I complexes in bands B, C, and D, the presence of band A at about 4000 cm^{-1} suggests that the group-I complexes possess a segregated stacking mode. The electrical resistivity for a single crystal of TTF-THBTCNQ ($\rho=2.5\times10^{-2}$ Ω cm) is fairly low and about two orders of magnitude smaller than that for a compacted powder sample. Such small resistivity and activation energy also support the prediction of a segregated stacking mode for the group-I complexes, although more data are needed to make this argument conclusive.

Group-II complexes are characterized by their nonionic nature. Such properties closely resemble those of OMTTF-TCNQ. We estimated the value of Z as 0.25 for OMTTF-TCNQ using the nitrile stretching frequency (2216 cm^{-1}). The crystal structure shows a mixed stack of alternating donor and acceptor components.[14] As shown in Fig. 1(b)[15] we found a weak CT transition for OMTTF-TCNQ (curve d) at 5100 cm^{-1} (band E). The strong absorption bands H and I are nearly identical with the molecular absorption of neutral TCNQ and OMTTF, respectively: this is consistent with the small degree of CT of the complex. These spectral features are recognized exactly in group-II complexes (Fig. 1(b)). Hence, we expect that group-II complexes possess a mixed stacking mode.

Group-III complexes are characterized by an almost completely ionic nature. In agreement with

the complete CT, the absorption bands K, L, and M of group-III complexes were also found in the ionic salts of corresponding components, K-MBBTCNQ, K-DBBTCNQ and OMTTF-BF_4 (Fig. 1(c)). Furthermore, an additional band at 6000 cm^{-1} (band J) was observed for each of the group-III complexes, which can be assigned to a back CT transition between the anion and the cation radicals.[16] These results strongly suggest a mixed stacking mode of this group. The crystal structure of OMTTF-DBBTCNQ actually contains a mixed stacking donor and an acceptor (vide infra).

The single-crystal polarized reflection-spectra revealed that the CT band E of OMTTF-TCNQ and J of OMTTF-DBBTCNQ proved to be a transition polarized along the c-axis. This is very close to the stacking direction of the donor and the acceptor.[17] Furthermore, OMTTF-TCNQ is shown to be mostly nonionic with two CT configurations in which the lowest energy one contributes to the ground state only to a small extent, and OMTTF-DBBTCNQ to be ionic with only one CT configuration in the ground state by means of the analysis of the crystal and electronic structure.

Recently, Torrance et al. showed the simple linear relationship[16] between the energies of the CT transition ($h\nu_{CT}$) and the intermolecular HOMO-LUMO gap ($\Delta E^{o,r}$): $h\nu_{CT,neutral}=\Delta E^{o,r}+0.5$; $h\nu_{CT,ionic}=0.83-\Delta E^{o,r}$ (eV). Using this equation, we calculated the $h\nu_{CT}$ values for each complex of the three groups. These are summarized in the last two rows of Table 2 together with the observed values. The agreement is good for both the nonionic group II and the ionic group III complexes, considering the simplicity of the approximation. In addition, the calculated value for OMTTF-TCNQ (5000 cm^{-1}) is also in good agreement with the observed one (5100 cm^{-1}) (vide supra). However, for the ionic group I complexes, the agreement is relatively poor. This also supports our estimation for the stacking mode as a segregated but not a mixed type.

C) Crystal Structure of OMTTF-DBBTCNQ. OMTTF-DBBTCNQ contains a solvent molecule, benzene (see experimental section). As shown in Fig. 2, the donor and the acceptor form mixed stacking columns along the c-axis with alternating the two components. The acceptors arrange themselves in a columnar array so as to release any unfavorable steric repulsion between the bulky dibenzo-barreleno moiety on TCNQ. The mean separation distance between the π-electron frameworks of the donor and acceptor is 3.46 Å. The dihedral angle between the two planes is about 1.26°. The overlapping mode and a view of the interstack interaction are depicted in Fig. 3. The two components are shifted from the direct overlap mode as found in OMTTF-TCNQ,[14] in which the symmetry plane perpendicular to the long axis coincides nearly with each other. Interestingly, there exist no short interstack interactions of the S···S and S···N types. The shortest S···N contact distance is 4.69 Å, and is much longer than the sum of the appropriate van der Waals radii. Thus, the mixed columns in OMTTF-DBBTCNQ are completely

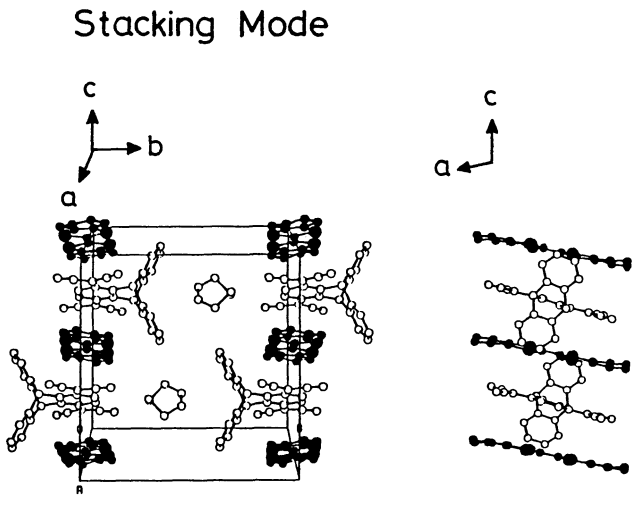

Fig. 2. Two views of the molecular packing in the crystal structure of OMTTF-DBBTCNQ-C_6H_6; (left) a view along a* axis, and (right) a view along b axis.

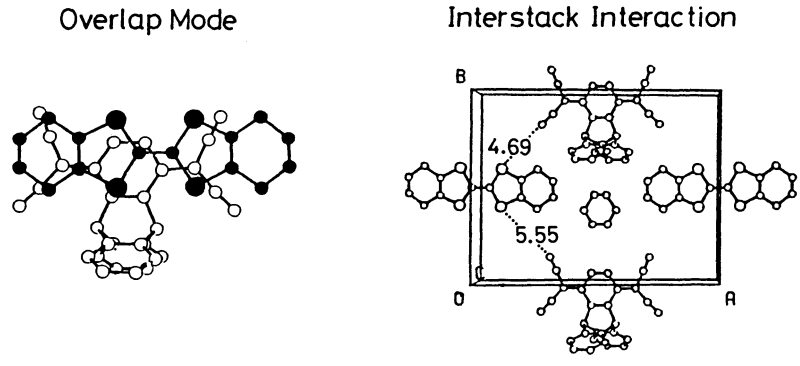

Fig. 3. Overlap mode; (left) viewed along the normal to the TCNQ plane. Interstack interaction; (right) viewed along c axis.

Table 5. Typical Examples of Mixed Stacking Mode Complexes of TTF-TCNQ Type

	Z[a]	Interplanar spacing (Å)	Overlap mode	Interstack S···N distance (Å)
OMTTF-TCNQ[b]	0.25[c]	3.53	Direct	3.36
TMTSF-TCNQ[d]	0.21[e]	3.5	Direct	3.56
DBTTF-TCNQ[f,g]	0.25[f]	3.30	Shifted	
	0.47[g]	3.4		3.48
DBTTF-TCNQF$_2$[g]	0.65[g]	3.4	Shifted	3.47
OMTTF-DBBTCNQ[c]	1.0[c]	3.46	Shifted	4.69

a) Values determined by IR procedure. b) Ref. 14. c) This work. d) Ref, 18. e) Ref. 10. f) H. Kobayashi and J. Nakayama, *Bull. Chem Soc. Jpn.*, **54**, 2408 (1981). g) Ref 20.

Table 6. Degree of CT Determined from TCNQ Geometries[a]

	Ratio[b] $c/(b+d)$	Calculated CT (Z)
TCNQ^0 [a]	0.476	0.00
TCNQ$^-$ [a]	0.500	1.00
OMTTF-TCNQ	0.474	−0.08[c]
OMTTF-DBBTCNQ	0.502	1.08

a) Ref. 18. b) Bond lengths were averaged over assumed mmm symmetry. c) Bond lengths used in this calculations were taken from Ref. 14.

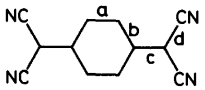

Table 7. Comparison of Bond Lengths (Å) in TTF Skeleton of Neutral and Ionic States

	a[d]	Δa	b[d]	Δb
TTF[a]	1.349		1.757	
TTF$^+$ClO$_4^-$ [b]	1.404	0.055	1.713	−0.044
OMTTF[c]	1.326		1.759	
OMTTF-TCNQ[c]	1.330	0.004	1.758	−0.001
OMTTF-DBBTCNQ	1.388	0.062	1.716	−0.043

a) W. F. Cooper, N. C. Kenny, J. N. Edmonds, A. Nagel, F. Wudl, and P. J. Coppens, *J. Chem. Soc., Chem. Commun.*, **1971**, 889, b) K. Yakushi, S. Nishimura, T. Sugano, and H. Kuroda, *Acta Crystallogr.*, **B36**, 358 (1980). c) Ref. 14. d) Bond lengths were averaged over assumed mmm symmetry.

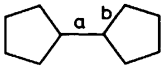

isolated from each other (Table 5).

Applying the bond-length-ratio procedure of Kistenmacher et al.,[18] we calculated the degree of CT as shown in Table 6. For OMTTF-DBBTCNQ, the calculated Z is 1.08, which indicates a complete charge transfer. This value is consistent with the Z determined by IR and Raman procedures. Furthermore, the donor geometry also suggests a strong ionic nature (Table 7). Thus, the difference in the central double-bond length between OMTTF and OMTTF in the complex, 0.062 Å, is comparable to that between TTF and TTF-ClO$_4$, 0.055 Å. The same procedure for OMTTF-TCNQ leads to the result that there is no charge on the donor or the acceptor. This is in good agreement with an estimation by the IR procedure.

Conclusion

Usually, the ionicity of CT complexes can be controlled by selecting the donor-acceptor combination so as to change the $\Delta E^{o,r}$ values to a large extent. It should be noted that we prepared the three groups of CT complexes with a wide range of ionicity using the three dimensionally modified TCNQ's, despite the small electronic perturbation on the acceptor and the narrow range of $\Delta E^{o,r}$ values. However, another important feature in this study is that the $\Delta E^{o,r}$ values are kept small at a positive region near zero, the so-called neutral-ionic boundary.[16] Therefore, our results indicate that, in these conditions, the solid-state properties are influenced to a large extent by small steric and/or electronic perturbations in the three-dimensional modifications which influence the intra- and interstack interactions in the complexes.

Recently, Soos et al. presented experimental and theoretical aspects regarding ionicity and paramagnetism of strong organic CT complexes. One of their important results was that TMPD-TCNQF$_4$ is the first highly ionic ($Z \geq 0.9$) and paramagnetic organic CT complex to be found with a regular mixed stacking mode.[19] Although OMTTF-DBBTCNQ is found to be another example of such a highly ionic CT complex, the complex is, to best of our knowledge, the first example for the TTF-TCNQ type complexes. The Z value of 0.65 of DBTTF-TCNQF$_2$[20] is the most strong ionicity known so far in mixed-stacking mode complexes of the TTF-TCNQ type (Table 5). Interestingly, although the acceptor

strengths of MBBTCNQ and DBBTCNQ are close to that of TCNQ and much weaker than that of $TCNQF_4$,[21] the group III complexes are complete CT.

In addition, relatively highly-conducting complexes were also prepared, although our modification leads to the TCNQ's carrying the bulky groups. All these results will be of theoretical interest in studying the crystal properties of organic CT complexes.[22] Finally, this study may open an unexplored area for chemical modifications to design molecular conductors, since many variations of the barrelene skeleton are possible.[23] Furthermore, if such molecules with bulky groups pack in a crystal as shown schematically in **5**, a segregated stacking mode of CT complexes

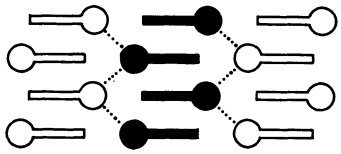

5

will be formed. This is our model for future studies concerning new effects of three-dimensional modifications on intra- and interstack interactions, that is, the enhancement of low dimensionality and introduction of a new types of interstack interactions.

Experimental

General. All the melting points are uncorrected. Infrared spectra and electronic spectra were recorded on JASCO DS-402G and Hitachi 340 spectrometers, respectively. Each IR spectrum was calibrated with indene as the standard. Laser Raman spectra were recorded with Ar^+ (514.8 nm) excitation by using a JASCO R-800 spectrometer for samples of KBr disks or powders. Proton NMR spectra were measured by using Varian XL-100-15 and JEOL JNM-PMX-60 spectrometers. All chemical shifts are reported in parts per million (δ) relative to internal tetramethylsilane. The cyclic voltammetry was carried out at room temperature under nitrogen using Yanagimoto P-1100. The electrical resistances for the compacted pellet and the single crystal were measured with two probe and four probe methods, respectively.

Preparation of the Acceptors. 5,8-Bis(dicyanomethylene)-1,4,4a,6,7,8a-hexahydro-1,4-ethanonaphthalene (4c). A mixture of 1,4,4a,6,7,8a-hexahydro-1,4-ethanonaphthalene-5,8-dione (**3c**)[24] (2.99 g, 15.7 mmol), malononitrile (3.12 g, 47.2 mmol) and β-alanine (18 mg, 0.20 mmol) in 3.5 mL of water was stirred for 9 h at 70 °C. The crude product was recrystallized from acetonitrile to give 3.06 g (68%) of **4c** as yellow prisms: Mp 244—245 °C; ^1H NMR (CD_2Cl_2) δ=1.67 (4H, m, H-5,6), 2.88 (6H, br s, H-1,4,9,10), 3.49 (2H, br s, H-7,12), 6.33 (2H, q-like, H-2,3); IR (KBr) 2230 cm^{-1}. Found: C, 75.46; H, 4.97; N, 19.72%. Calcd for $C_{18}H_{12}N_4$: C, 75.51; H, 4.93; N, 19.57%.

1,2,3,4,4a,6,7,8a-Octahydro-1,4-ethanonaphthalene-5,8-dione (3b). The hydrogenation of **3c** with 10% Pd-C in methanol gave **3b** (93%) which continued to produce **4b**.

5,8-Bis(dicyanomethylene)-1,2,3,4,4a,6,7,8a-octahydro-1,4-ethanonaphthalene (4b). A mixture of **3b** (20 g, 0.104 mol), malononitrile (16.5 g, 0.25 mol) and β-alanine (250 mg) in 5 mL of water was stirred for 3 d at 65—75 °C. The crude product was recrystallized from acetonitrile–benzene to give **4b** (37%) as colorless needles: Mp 167—168 °C, IR (KBr) 2230 cm^{-1}; Found: C, 74.65; H, 5.53; N, 19.38%. Calcd for $C_{18}H_{16}N_4$: C, 74.98; H, 5.59; N, 19.43%.

5,8-Bis(dicyanomethylene)-1,4-dihydro-1,4-ethanonaphthalene (dihydrobarreleno-TCNQ, DHBTCNQ) (1c). A mixture of **4c** (1.01 g, 3.51 mmol), *N*-chlorosuccinimide (1.61 g, 12.0 mmol), pyridine (1.15 mL, 14.2 mmol) and dichloromethane (60 mL) was refluxed for 4 h. After the usual workup, the crude product was purified by column chromatography on silica gel. Elution with dichloromethane yielded 0.72 g (73%) of **1c** as red solids which was recrystallized from methanol: Red needles, mp 171.5—173.5 °C; ^1H NMR ($CDCl_3$) δ=1.63 (4H, AA'BB', H-5,6), 5.31 (2H, br s, H-1,4), 6.52 (2H, q-like, H-2,3), 7.41 (2H, s, H-9,10); IR (KBr) 2215 cm^{-1}; UV λ_{max} (CH_3CN) 248 (log ε 3.71), 380 (sh, 4.46), 401 (4.59), 460 nm (sh, 3.98).

5,8-Bis(dicyanomethylene)-1,2,3,4-tetrahydro1,4-ethanonaphthalene (tetrahydrobarreleno-TCNQ, THBTCNQ) (1b). The title compound was prepared as described above (67%): Golden yellow needles (recrystallized from C_6H_6–C_6H_{12}), mp 195—197 °C (decomp); ^1H NMR ($CDCl_3$) δ=1.65 (8H, m, H-2,3,5,6), 4.24 (2H, br s, H-1,4), 7.43 (2H, s, H-9,10); IR (KBr) 2213 cm^{-1}; UV λ_{max} (CH_3CN) 244 (log ε 3.68), 402 nm (4.61). Found: C, 76.10; H, 4.24; N, 19.61%. Calcd for $C_{18}H_{12}N_4$: C, 76.04; H, 4.25; N, 19.71%.

Preparation of Charge-Transfer Complexes. All CT complexes described in this paper were prepared by

Table 8. Solvents Used for the Preparation of Eight CT Complexes and Their Properties

	2a–1b	2a–1c	2b–1b	2b–1c	2c–1c	2b–1d	2b–1e	2c–1e
Solvent	CH_3CN	CH_3CN	C_6H_6	C_6H_6	CH_3CN/C_6H_6	Cl–C_6H_5	C_6H_6	C_6H_6
Yield/%	78	32	69	81	25	84	80	80
Appearance	Black needles	Deep-violet needles	Reddish-purple needles	Purple needles	Deep-violet needles	Dark-green needles	Dark-purple needles	Deep-purple needles
Mp (θ_m/°C) (decomp)	148	138	180	178	161	179	170	193

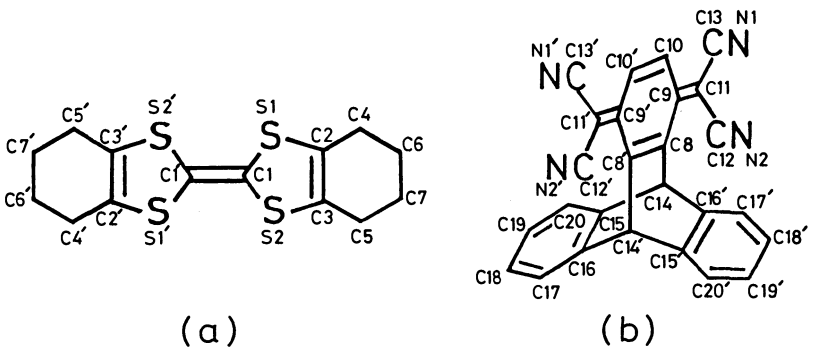

Fig. 4. Atomic numbering scheme of OMTTF-DBBTCNQ. OMTTF (a) and DBBTCNQ (b) lie on the center of symmetry and the two-fold axis, respectively.

Table 9. Crystallographic Data for OMTTF-DBBTCNQ-C_6H_6

Formula	$C_{40}H_{28}N_4S_4\ C_6H_6$
Formula wt	771.0
Crystal system	Monoclinic
Space group	*C2/c*
a, Å	18.535(2)
b, Å	14.417(2)
c, Å	14.906(3)
β, deg	98.89(1)
V, Å^3	3935.3(9)
Z	4
Scan type	θ—2θ
Max 2θ, deg	120
No. of reflections	2380 with $F_{obsd} \geq 2\sigma(F)$
R	0.091

Table 10. Selected Interatomic Distances (*l*/Å) and Angles (deg) in OMTTF-TCNQ

Bond Legths(*l*/Å)		Bond Angles(ϕ/°)	
C(1)-C(1′)	1.390(8)	C(1′)-C(1)-S(1)	123.3(4)
C(1)-S(1)	1.715(6)	C(1′)-C(1)-S(2)	122.0(4)
C(1)-S(2)	1.716(6)	S(1)-C(1)-S(2)	114.6(3)
S(1)-C(2)	1.724(6)	C(1)-S(1)-C(2)	96.6(3)
S(2)-C(3)	1.745(7)	C(1)-S(2)-C(3)	95.4(3)
C(2)-C(3)	1.329(9)	S(1)-C(2)-C(3)	116.2(5)
		S(2)-C(3)-C(2)	117.1(5)
C(8)-C(8′)	1.377(7)	C(8′)-C(8)-C(9)	122.3(4)
C(8)-C(9)	1.418(7)	C(8′)-C(8)-C(14)	112.9(4)
C(9)-C(10)	1.431(7)	C(9)-C(8)-C(14)	124.8(4)
C(9)-C(11)	1.416(7)	C(8)-C(9)-C(10)	115.2(5)
C(10)-C(10′)	1.356(8)	C(8)-C(9)-C(11)	127.3(5)
C(11)-C(13)	1.408(8)	C(10)-C(9)-C(11)	117.5(5)
C(11)-C(12)	1.393(9)	C(9)-C(10)-C(10′)	122.5(5)
N(1)-C(13)	1.149(9)	C(9)-C(11)-C(12)	127.5(5)
N(2)-C(12)	1.170(10)	C(9)-C(11)-C(13)	119.6(5)
		C(12)-C(11)-C(13)	112.9(5)
		C(11)-C(12)-N(2)	175.7(7)
		C(11)-C(13)-N(1)	179.6(7)

mixing solutions of donors and acceptors at 20—40 °C. The complexes usually precipitated out immediately. The 1:1 stoichiometries of donors and acceptors were determined by elemental analyses which agree with calculated values within ±0.4% for C, H, N, and S. In the case of OMTTF-DBBTCNQ, solvent molecule, benzene, was included in the crystals; elemental analysis and crystal-structure analysis indicated the molecular ratio of the components, OMTTF:DBBTCNQ:benzene, to be 1:1:1. The solvents used for the preparation of the complexes and their properties are summarized in Table 8.

Crystal Structure Analysis of OMTTF-DBBTCNQ. X-Ray data were collected on a Rigaku four-circle diffractometer of the Crystallographic Research Center, Institute for Protein Research, Osaka University. Ni-filtered Cu $K\alpha$ radiation was provided by a Rigaku rotating anode X-ray generator operated at 40 kV and 200 mV. Crystallographic data are given in Table 9. The structure was solved by direct method, using the program MULTAN 78, and refined by the block-diagonal anisotropic least-squares methods to final *R* value of 0.091. The hydrogen atoms were not included in the refinement. The atomic numbering scheme, bond lengths, and bond angles are shown in Fig. 4 and Table 10, respectively. Tables of structure factors, atomic and thermal parameters, bond lengths and angles are deposited as Document No. 8605 at the Office of the Editor of Bull. Chem. Soc. Jpn.

We are grateful to Professor Robert M. Metzger (University of Mississippi) for a critical reading of a part of the manuscript. We thank Dr. Tadaoki Mitani for valuable discussions and Dr. Kenichi Imaeda for his technical assistance on resistivity measurements. The research at Osaka was partially supported by the Grant-in-Aid for Special Research Project on Properties of Molecular Assemblies (No. 58118003) from the Ministry of Education Science and Culture.

References

1) a) J. H. Perlstein, *Angew. Chem., Int. Ed. Engl.*, **16**, 519 (1977); b) J. B. Torrance, *Acc. Chem. Res.*, **12**, 79 (1979); c) R.

M. Metzger, *Ann. N. Y. Acad. Soc.*, **313**, 145 (1978); d) R. M. Metzger, *Top. Curr. Phys.*, **26**, 80 (1981).

2) a) A. F. Garito and A. J. Heeger, *Acc. Chem. Res.*, **7**, 232 (1974); b) R. C. Wheland and J. L. Gillson, *J. Am. Chem. Soc.*, **98**, 3916 (1976). R. C. Wheland, ibid., **98**, 3926 (1976); c) J. B. Torrnace, J. J. Mayerle, V. Y. Lee, and K. Bechgaard, ibid., **101**, 4747 (1979); d) G. Saito and J. P. Ferraris, *Bull. Chem. Soc. Jpn.*, **53**, 2141 (1980); e) F. Wudl, *J. Am. Chem. Soc.*, **103**, 7064 (1981); f) S. S. Shaik, ibid., **104**, 5328 (1982); g) D. O. Cowan, A. Kini, L-Y. Chiang, K. Lerstrup, and D. R. Talham, *Mol. Cryst. Liq. Cryst.*, **86**, 1 (1982); h) K. Nakasuji, M. Nakatsuka, and I. Murata, *Yuki Gosei Kagaku Kyokai Shi*, **41**, 204 (1983) and references cited therein.

3) a) E. M. Engler, V. V. Patel, J. R. Andersen R. R. Schumaker, and A. A. Fukushima, *J. Am. Chem. Soc.*, **100**, 3769 (1978); b) L. B. Coleman, F. G. Yamagishi, A. F. Garito, A. J. Heeger, D. J. Dahm, M. G. Miles, and J. D. Wilson, *Phys. Lett.*, **51A**, 412 (1975).

4) Part of this paper has been published: I. Murata and K. Nakasuji, *Mol. Cryst. Liq. Cryst.*, **125**, 19 (1985).

5) K. Yamamura, K. Nakasuji, H. Yamochi, I. Murata, and S. Inagaki, *Chem. Lett.*, **1983**, 627.

6) K. Yamamura, T. Nakazawa, and I. Murata, *Angew. Chem., Int. Ed. Engl.*, **19**, 543 (1980).

7) Abbreviations for TCNQ derivatives: THBTCNQ, tetrahydro-barreleno-TCNQ; DHBTCNQ, dihydrobarreleno-TCNQ; MBBTCNQ, monobenzobarreleno-TCNQ; and DBBTCNQ, dibenzobarreleno-TCNQ. See experimental section for the systematic names.

8) D. S. Acker and W. R. Hertler, *J. Am. Chem. Soc.*, **84**, 3370 (1962).

9) These results are consistent with a study of the tropylium ions incorporated into a barrelene skeleton, see: a) H. Yamochi, K. Nakasuji, T. Nakazawa, and I. Murata, *Chem. Lett.*, **1982**, 459; b) T. Nakazawa, Y. Niimoto, K. Kubo, and I. Murata, *Angew. Chem., Int. Ed. Engl.*, **19**, 545 (1980); c) T. Nakazawa, K. Kubo, and I. Murata, ibid., **20**, 189 (1981).

10) J. A. Chappell, A. N. Bloch, W. A. Bryden, M. Maxfield, T. O. Poehler, and D. O. Cowan, *J. Am. Chem. Soc.*, **103**, 2442 (1981).

11) a) S. Matsuzaki, T. Moriyama, and K. Toyoda, *Solid State Commun.*, **34**, 857 (1980); b) R. Bozio and C. Pecile, "The Physics and Chemistry of Low Dimensional Solids," ed by L. Alcacer, D. Reidel Publishing Co. Dordrecht, Holland (1980), p. 165.

12) a) J. B. Torrance, B. A. Scott, and F. B. Kaufman, *Solid State Commun.*, **17**, 1369 (1975); b) J. B. Torrance, B. A. Scott, B. Welber, F. B. Kaufman, and P. E. Seiden, *Phys. Rev.*, **B19**, 730 (1979).

13) J. Tanaka, M. Tanaka, T. Kawai, T. Takabe, and O. Maki, *Bull. Chem. Soc. Jpn.*, **49**, 2358 (1976).

14) D. Chasseau, J. Gaultier, J. M. Farbe, and L. Giral, *Acta Crystallogr., Sect. B*, **38**, 1632 (1982).

15) The powdered samples dispersed in KBr were prepared with care to avoid some decompositions: strong grind of complexes with KBr sometimes gave small absorptions near the region of F.

16) J. B. Torrance, J. E. Vazquez, J. J. Mayerle, and V. Y. Lee, *Phys. Rev. Lett.*, **46**, 253 (1981).

17) These results and the magnetic properties have been published, S. Akhtar, J. Tanaka, K. Nakasuji, and I. Murata, *Bull. Chem. Soc. Jpn.*, **58**, 2279 (1985).

18) T. J. Kistenmacher, T. J. Emge, A. N. Bloch, and D. O. Cowan, *Acta Crystallogr., Sect. B*, **38**, 1193 (1982).

19) Z. G. Soos, H. J. Keller, K. Ludolf, J. Queckborner, and D. Wehe, *J. Chem. Phys.*, **74**, 5287 (1981).

20) T. J. Emge, F. M. Wiygul, J. S. Chappell, A. N. Bloch, J. P. Ferraris, D. O. Cowan, and T. J. Kistenmacher, *Mol. Cryst. Liq. Cryst.*, **87**, 137 (1982).

21) E. C. Chen and W. E. Wentworth, *J. Chem. Phys.*, **63**, 3183 (1975).

22) For leading references, see: a) R. M. Metzger and A. N. Bloch, *J. Chem. Phys.*, **63**, 5098 (1975); b) F. M. Wiygue, R. M. Metzger, and T. J. Kistenmacher, *Mol. Cryst. Liq. Cryst.*, **107**, 115 (1984); c) J. B. Torrance and B. D. Silverman, *Phys. Rev.*, **B15**, 788 (1977); d) B. D. Silverman and S. L. Laplaca, *J. Chem. Phys.*, **69**, 2585 (1978); e) Z. G. Soos and S. Mazumdar, *Phys. Rev.*, **B18**, 1991 (1978); f) Ref. 2f.

23) See for example, a) S. Inagaki, K. Yamamura, K. Nakasuji, T. Nakazawa, and I. Murata, *J. Am. Chem. Soc.*, **103**, 2093 (1981); b) K. Nakasuji, H. Yamochi, I. Murata, K. Yamamura, and S. Inagaki, *J. Org. Chem.*, **48**, 2384 (1983), and references cited therein.

24) a) R. C. Cookson, R. R. Hill, and J. Hudec, *J. Chem. Soc.*, **1964**, 3043; b) K. Alder and G. Stein, *Justus Liebigs Ann. Chem.*, **501**, 247 (1933).

 © 1986 The Chemical Society of Japan Bull. Chem. Soc. Jpn., 59, 215—219 (1986)

Perfluoropropylation of Furans, Thiophenes, and Pyridines with Bis(heptafluorobutyryl) Peroxide

Hideo SAWADA,† Masato YOSHIDA, Hidehiko HAGII,† Kazuyoshi AOSHIMA,† and Michio KOBAYASHI*

† Chemicals and Explosives Research Laboratory, Nippon Oil & Fats Co., Ltd., Taketoyo, Chita-gun, Aichi, 470-23

Department of Chemistry, Faculty of Science, Tokyo Metropolitan University, Fukazawa, Setagaya-ku, Tokyo, 158

(Received June 14, 1985)

Bis(heptafluorobutyryl) peroxide (**1**) smoothly reacted with furans and thiophenes under mild conditions to regioselectively give 2-perfluoropropylfurans and thiophenes in high yields. Mechanistically, reactions with furans or thiophenes are considered to be initiated by one-electron transfers from substrates to **1**. On the other hand, the perfluoropropylation of pyridine was proceeded by the usual free-radical substitution to a pyridinium salt by a heptafluoropropyl radical produced by the homolytic decomposition of **1**.

Recently, remarkable attention have been focused on fluoroalkyl-containing compounds due to their unique properties. However, the introduction of fluoroalkyl groups is not easy since the usual methods for alkylation can not be applied to perfluoroalkylation due to the high electronegativity of perfluoroalkyl groups. Especially, an exploration of electrophilic perfluoroalkylating agents is desired since reactions involving a perfluoroalkyl cation as an intermediate are very limited.[1] We have been studying the perfluoroalkylation of nucleophilic substrates with bis(heptafluorobutyryl) peroxide **1** via an electron-transfer process (shown in Scheme 1) and the heptafluoropropylation of electron-rich benzenes, naphthalene, anthracene, and electron-rich olefins has been achieved.[2,3]

$$\mathrm{Nu{:} + (C_3F_7CO_2)_2 \longrightarrow Nu^{\ddagger} + (C_3F_7CO_2)_2^{\cdot-}}$$
$$\longrightarrow \mathrm{Nu^{\ddagger} + C_3F_7{\cdot} + C_3F_7CO_2^- + CO_2}$$
$$\longrightarrow \mathrm{Nu{+}C_3F_7 + C_3F_7CO_2^- + CO_2}$$

Scheme 1.

In this paper, we wish to report on reactions involving bis(heptafluorobutyryl) peroxide with such heteroaromatic compounds as furans, thiophenes, and pyridines.

Results and Discussion

Two moles of furan or thiophene per mol of **1** were added to a solution of **1** in Freon-113. The mixture was degassed by a freeze-thaw cycle, sealed in an ampoule and kept at 40 °C for 3 h. Regioselectively 2-substituted furan or thiophene with a perfluoropropyl group was obtained in 98% yield and a substantial amount of perfluorobutyric acid was also formed. Several substituted furans and thiophenes

Table 1. Reactions of Furans, Thiophenes with Bis(heptafluorobutyryl) Peroxide in Freon-113 at 40 °C for 3 h

			Peroxide	Yield of the products/%[a]		
X	R	mmol	mmol	**2**	**3**[b]	$C_3F_7CO_2H$
O	H	2	4	Trace[c]	8[d]	52[c]
O	H	2	2	32[c]	2	88
O	H	4	2	98	0	98
O	CH_3	4	2	64	4[e]	108
O	CH_3OCO	4	2	17	0	93
S	H	4	2	98	0	99
S	CH_3	4	2	92	4	98
S	Cl	4	2	78	0	102
S	Br	4	2	44	0	89

a) The yields of products are based on peroxide. b) Bis(perfluoropropyl)furans, thiophenes 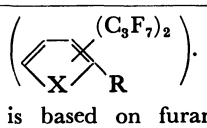 .

c) Considerable amounts of polymeric compounds were obtained. d) The yield of product is based on furan.
e) Trace amount of 2-methyl-3,4,5-tris(perfluoropropyl)furan was also formed.

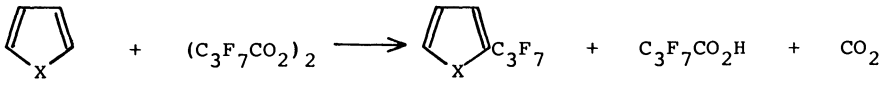

(X = O, S) 1 2

were also reacted with **1** and the results are summarized in Table 1. The production of perfluorobutyric acid, not heptafluoropropane (C_3F_7H), should be important from the viewpoint of synthetic chemistry; the produced perfluorobutyric acid could be recovered as a sodium salt and used again for the synthesis of peroxide **1**.

Hitherto, the direct perfluoroalkylation of heteroaromatic compounds has been carried out thermally or photochemically using perfluoroalkyl iodides.[4,5] However, these processes require high temperatures or irradiation for long periods of time. Recently, Umemoto et al. reported the perfluoroalkylation of various aromatic compounds with perfluoroalkylphenyliodonium trifluoromethanesulfonate(FITS) under mild conditions.[6] Now, peroxide **1** has also been shown to be an excellent reagent for the perfluoropropylation of furans and thiophenes under very mild conditions.

A plausible reaction mechanism for perfluoroalkylation with **1** is shown in Scheme 2; the reaction is initiated by one-electron transfers from substrates to peroxide **1**. The reactions of benzoyl peroxide with thiophene or furan via an electron-transfer process have been reported.[7,8] In an MO calculation for the substituted benzoyl peroxides, an electron-withdrawing substituent lowers the O-O antibonding energy level.[9] Thus, the energy level of the O-O antibonding of peroxide **1** should be lower than that of benzoyl peroxide due to the high electronegativity of perfluoroalkyl group. Thus, the mechanism shown in Scheme 2 involving an electron-transfer process is reasonable.[10]

The rate of decomposition of **1** should be accelerated in the presence of furans and thiophenes if the reaction is initiated by one-electron transfers from furans or thiophenes to **1**. The decomposition of **1** was followed by iodometry in the presence or absence of 5 mol of thiophenes or furan per mol of **1** and shown to be markedly accelerated by adding thiophenes or furan. The rate of decomposition of **1** was not affected by $C_3F_7CO_2H$. The results are summarized in Table 2.

When pyridine was added to a solution of **1** in

Table 2. Apparent First-Order Rate Constants for the Thermal Decomposition of 0.02 mol/l $(C_3F_7CO_2)_2$ in the Presence of 0.10 mol/l 2-Substituted Thiophenes or Furan in Freon-113

2-Substituted thiophene, furan	Temp °C	$k_d/10^{-4}$ s^{-1}	$\Delta H^{\neq}$ kJ mol^{-1}	$\Delta S^{\neq}$ JK^{-1} mol^{-1}
Thiophene	5.0	0.74±0.03	87.70	−8.03
	10.0	1.47±0.02		
	15.0	2.57±0.05		
	20.0	5.61±0.11		
Methyl-thiophene	5.0	4.24±0.17	73.93	−42.55
	7.5	6.27±0.18		
	10.0	7.57±0.18		
	15.0	13.79±0.49		
Chloro-thiophene	5.0	1.25±0.08	77.57	−40.12
	10.0	2.18±0.02		
	15.0	3.84±0.05		
	20.0	7.40±0.14		
Furan	15.0	9.84±0.34		
None	15.0	0.08±0.00	100.71	7.57
	20.0	0.16±0.00		
	25.0	0.33±0.00		
	30.0	0.66±0.01		
$C_3F_7CO_2H$ (0.02 mol/l^{-1})	15.0	0.10±0.00	94.64	−11.51
	20.0	0.20±0.00		
	25.0	0.37±0.01		
	30.0	0.77±0.02		

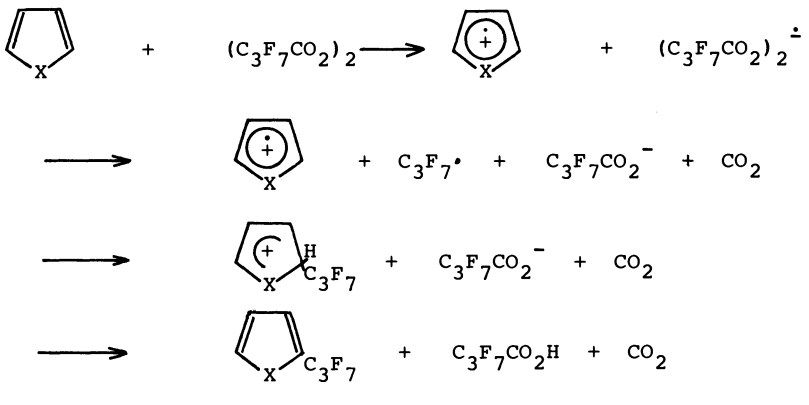

X = O, S

Scheme 2.

Freon-113, the solution turned to reddish-brown at once; the solution was maintained at 40 °C for 6 h under N_2, and the products were analyzed. Perfluoropropylpyridines were not detected and pyridinium heptafluorobutyrate and pyridine *N*-oxide heptafluorobutyrate were obtained. The reaction proceeded even at −20 °C to give pyridine heptafluorobutyrate and pyridine *N*-oxide heptafluorobutyrate. This means that the nucleophilic attack of an *N*-lone pair of pyridine on an O-O bond of **1** may be more preferential than an electron-transfer reaction from the π-orbital of pyridine to **1** observed in reactions with furan or thiophene. A similar nucleophilic attack of an *N*-lone pair on an O-O bond of benzoyl peroxides has been reported.[11]

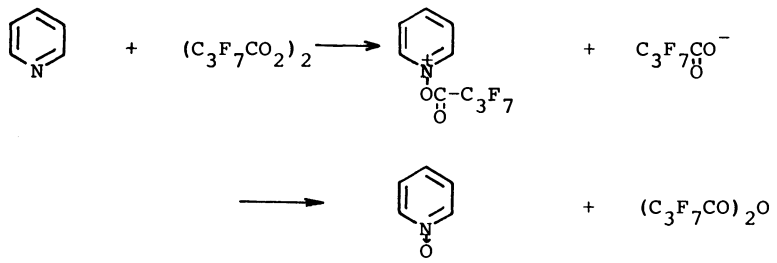

The thermal decomposition of benzoyl peroxide in pyridine gives a mixture of 2-, 3-, and 4-phenylpyridine due to the substitution of a phenyl radical to pyridine;[12] however similar reactions with *m*-nitrobenzoyl peroxides gave an abnormally high yield of the nitrobenzoic acid and pyridine *N*-oxide.[11] The nucleophilic attack should compete more effectively with homolytic substitution when the peroxide contains powerful electron-withdrawing substituents.[11]

We have attempted a reaction with pyridinium heptafluorobutyrate which has no lone pair on the nitrogen atom with **1** in Freon-113. The results are summarized in Table 3. In the reaction of pyridinium heptafluorobutyrate with **1**, perfluoropropylpyridines were obtained. Almost the same regioselectivities ($\alpha:\beta:\gamma$=21:18:22) were observed in the perfluoropropylation of pyridinium salt, suggesting a free-radical character of this reaction as shown in Scheme 3.[13]

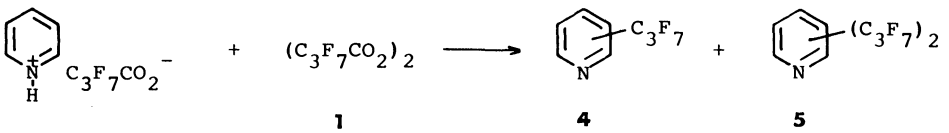

1 **4** **5**

Experimental

Measurement. ^{1}H-NMR spectra were taken with a JEOL JNM-MH-100 (100 MHz) spectrometer. ^{13}C-NMR spectra were taken with a JEOL FX-60 FT-NMR spectrometer. A GC analysis was performed on Shimadzu GC-4APTF gas chromatograph. IR spectra were recorded on a JASCO A-3 spectrophotometer. GC-IR spectra were taken with a Shimadzu GC-IR-VGS-1 spectrophotometer. The Mass spectra were taken with a JEOL JMS-D300 spectrometer and a JEOL DX-500 spectrometer.

Materials. Bis(heptafluorobutyryl) peroxide was prepared from heptafluorobutyryl chloride and hydrogen peroxide in the presence of aqueous sodium hydroxide in

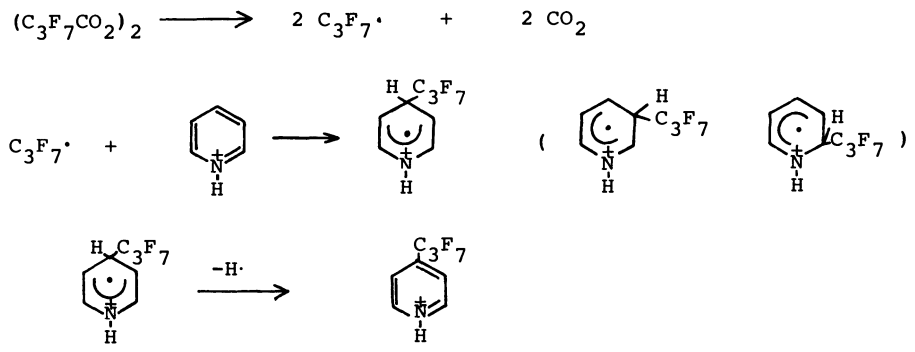

Scheme 3.

Table 3. Reaction Products for the Perfluoropropylation of Pyridinium Compounds with Bis(heptafluorobutyryl) Peroxide in Freon-113

	Reagent/mmol		Temp/Time	Yield of the products/%[a]	
	$PyH^+RCO_2^-$	Peroxide	°C/h	**4**	**5**
$R=C_3F_7$	2[b]	2	40/ 3	18	6
$=C_3F_7$	2[b]	4	40/ 6	59[c]	14
$=CH_3$	20	20	40/20	0	0
$=C_3F_7$	2[d]	5	40/ 8	29	6

a) The yields of products are based on the pyridine consumption. b) Pyridinium heptafluorobutyrate. c) Isomer composition: $\alpha:\beta:\gamma=42:36:22$. d) 2,6-Lutidinium heptafluorobutyrate.

Freon-113 by a method described in the literature.[14]

Reaction with Furans and Thiophenes. A solution containing 2 mmol of bis(heptafluorobutyryl) peroxide and 4 mmol of furans or thiophenes in 30 g of Freon-113 was degassed and kept at 40 °C for 3 h in a sealed tube. The solution was washed with 20 mL of water. The organic layer was analyzed by GLC using internal standards and $C_3F_7CO_2H$ in aqueous layer was determined by titration.

The 2-perfluoropropylfurans and thiophenes were isolated by distillation of the reaction mixture, which was obtained by scaled-up reactions under similar conditions, and identified by IR, ^{1}H-NMR, ^{13}C-NMR, and GC-MS.

2-Perfluoropropylfuran: ^{1}H-NMR ($CDCl_3$) δ=6.60 (1H, m), 6.93 (1H, m), 7.74 (1H, m); IR (cm^{-1}) 1355 (CF_3), 1230 (CF_2); ^{13}C-NMR ($CDCl_3$) δ=111.0, 113.9, 145.9; MS *m/z* 236 (M^+), 217, 167, 148, 117, 69, 39. Exact MS: *m/z* 236.0062. Calcd for $C_7H_3F_7O$: 236.0072.

2-Perfluoropropylthiohene: ^{1}H-NMR ($CDCl_3$) δ=7.08 (1H, m), 7.34 (1H, m), 7.57 (1H, m); IR (cm^{-1}) 1350 (CF_3), 1230 (CF_2); ^{13}C-NMR ($CDCl_3$) δ=127.5, 130.2, 130.3 (t, J_{CCCF}=6.1 Hz); MS *m/z* 252 (M^+), 233, 133. Exact MS: *m/z* 251.9811. Calcd for $C_7H_3F_7S$: 251.9844.

2-Methyl-5-perfluoropropylfuran: ^{1}H-NMR ($CDCl_3$) δ= 2.24 (3H, s), 5.86 (1H), 6.42 (1H); IR (cm^{-1}) 1350 (CF_3), 1255 (CF_2); ^{13}C-NMR ($CDCl_3$) δ=13.4, 107.4, 115.0 (t, J_{CCCF}=3.7 Hz), 156.7; MS *m/z* 250 (M^+), 231, 131. Exact MS: *m/z* 250.0186. Calcd for $C_8H_5OF_7$: 250.0229.

2-Methyl-3,4,5-tris(perfluoropropyl)furan: MS *m/z* 586 (M^+).

2-Methyl-5-perfluoropropylthiophene: ^{1}H-NMR ($CDCl_3$) δ=2.54 (3H, s), 6.80 (1H), 7.26 (1H); IR (cm^{-1}) 1350 (CF_3), 1230 (CF_2); ^{13}C-NMR ($CDCl_3$) δ=15.0, 125.7, 130.3 (t, J_{CCCF}=6.1 Hz), 145.5; MS *m/z* 266 (M^+), 147, 96. Exact MS: *m/z* 265.9989. Calcd for 266.0000.

2-Methyl-bis(perfluoropropyl)thiophene: MS *m/z* 434 (M^+), 415, 315, 265, 144.

2-Methyl-bis(perfluoropropyl)furan: MS *m/z* 418 (M^+), 130.

2-Methoxycarbonyl-5-perfluoropropylfuran: ^{1}H-NMR ($CDCl_3$) 3.72 (3H, s), 6.65 (1H), 6.93 (1H); ^{13}C-NMR ($CDCl_3$) δ=50.8, 115.3, 118.0, 158.1; IR (cm^{-1}) 1740 (C=O), 1355 (CF_3), 1230 (CF_2); MS *m/z* 294 (M^+), 263, 175. Exact MS: *m/z* 294.0128. Calcd for $C_9H_5O_3F_7$: 294.0127.

2-Chloro-5-perfluoropropylthiophene: ^{1}H-NMR ($CDCl_3$) δ=7.20 (1H), 7.46 (1H); IR (cm^{-1}) 1350 (CF_3), 1230 (CF_2); ^{13}C-NMR ($CDCl_3$) δ=126.6, 129.9 (t, J_{CCCF}=6.1 Hz), 135.9. MS *m/z* 288, 286 (M^+), 169, 167, 69. Exact MS: *m/z* 285.9447. Calcd for $C_7H_2F_7SCl$: 285.9453.

2-Bromo-5-perfluoropropylthiophene: ^{13}C-NMR ($CDCl_3$) δ=118.2, 130.3, 130.7; IR (cm^{-1}) 1345 (CF_3), 1230 (CF_2). Exact MS: *m/z* 329.8952. Calcd for $C_7H_2F_7SBr$: 329.8949.

Kinetics of the Reaction with Thiophenes or Furan. Solutions of 0.02 mol/l $(C_3F_7CO_2)_2$ and 0.10 mol/l thiophenes or furan in degassed sealed tubes were immersed in a constant-temperature bath. Each sample tube was removed after appropriate time intervals and immediately immersed in the Dry Ice-acetone bath to quench the reaction; the amount of the residual $(C_3F_7CO_2)_2$ was estimated by iodometric titration. Apparent first-order rate constants were obtained from the initial slopes of the plot of the logarithm of the peroxide concentration against time.

Reaction Products with Pyridine. A solution containing 100 mmol of pyridine and 20 mmol of $(C_3F_7CO_2)_2$ in 400 g of Freon-113 in a 500-mL flask was deaerated with N_2. The flask was immersed in a bath at −20 °C for 3 d. The solution was then concentrated by evaporating the solvent under reduced pressure. A white solid (4.61 g) was obtained by the recrystallization of the residue from 2-propanol and identified as pyridinium heptafluorobutyrate on the basis of the following data; mp 54—56 °C (lit,[15] 56—58 °C), IR (cm^{-1}) 1660 (C=O), 1350 (CF_3), 1220 (CF_2); ^{1}H-NMR ($CDCl_3$) δ=8.11 (2H, m), 8.58 (1H, m), 9.14 (2H, m), 16.76 (1H, s). NaOH was added to the alcohol solution and the solution was stirred at room temperature for 3 h. After removing the alcohol, diethyl ether was added and the precipitated solid was removed. From the ether solution pyridine *N*-oxide was obtained and identified by IR, ^{1}H-, and ^{13}C-NMR.

Reaction Products with Pyridinium Heptafluorobutyrate. A solution containing 2 mmol of pyridinium heptafluorobutyrate and 4 mmol of $(C_3F_7CO_2)_2$ in 30 g of Freon-113 was stirred under N_2 at 40 °C for 6 h. The solution was then diluted with 20 mL of 5% aqueous NaOH and 20 mL of water. The organic layer was analyzed by GLC using the internal standard. The products were identified by GC-MS and isomer composition of perfluoropropylpyridines were determined by GC-IR.

Perfluoropropylpyridine: IR (cm^{-1}) 1350 (CF_3), 1230 (CF_2); MS *m/z* 247 (M^+), 228, 128, 78, 69; CI-MS *m/z* 248 (M^++1).

Bis(perfluoropropyl)pyridine. MS *m/z* 396 (M^+-19), 296, 177, 69; CI-MS *m/z* 416 (M^++1).

GC-IR (aromatic C-H bend). 2-Perfluoropropyl pyridine 750 cm^{-1} (745 cm^{-1}), 3-Perfluoropropylpyridine 780, 710 cm^{-1} (779, 714 cm^{-1}), 4-Perfluoropropylpyridine 818, 740 cm^{-1} (818, 737 cm^{-1}). Values in parenthese are perfluorodecylpyridines.[4a]

2,6-Dimethylperfluoropropylpyridine. MS *m/z* 275 (M^+) 256, 156.

2,6-Dimethylbis(perfluoropropyl)pyridine. MS *m/z* 324 ($M^+-C_2F_5$), 205, 69; CI-MS *m/z* 444 (M^++1).

The authors wish to express their thanks to Mr. Shigehiko Yamaguchi at Tsukuba Central Research Laboratory of Nippon Oil & Fats Co., Ltd. for GC-MS spectrometric measurement.

References

1) T. Umemoto, *Yuki Gosei Kagaku Kyokai Shi*, **41**, 251 (1983).

2) M. Yoshida, H. Amemiya, M. Kobayashi, H. Sawada, H. Hagii, and K. Aoshima, *J. Chem. Soc., Chem. Commun.*, **1985**, 234.

3) M. Yoshida, K. Moriya, H. Sawada, and M. Kobayashi, *Chem. Lett.*, **1985**, 755.

4) a) A. B. Cowell and C. Tamborski, *J. Fluorine Chem.*, **17**, 345 (1981); b) G. V. D. Tiers, *J. Am. Chem. Soc.*, **82**, 5513 (1960); c) E. S. Huyser and E. Bedard, *J. Org. Chem.*, **29**, 1588 (1964).

5) Y. Kobayashi, I. Kumadaki, and A. Ohsawa, *Chem. Pharm. Bull.*, **26**, 1247 (1978).

6) T. Umemoto, Y. Kuriu, and H. Shuyama, *Chem. Lett.*, **1981**, 1633.

7) C. E. Griffin and K. R. Martin, *J. Chem. Soc., Chem., Commun.*, **1965**, 154.

8) K. E. Kolb and W. A. Black, *J. Chem. Soc., Chem. Commun.*, **1969**, 1119.

9) O. Kikuchi, *Yuki Gosei Kagaku Kyokai Shi*, **37**, 678 (1979).

10) The electron-transfer reactions between peroxide **1** and methoxybenzenes were reported; C. Zhao, G. M. El-Taliawi, and C. Walling, *J. Org. Chem.*, **48**, 4908 (1983).

11) a) D. H. Hey, K. S. Y. Liang, and M. J. Perkins, *J. Chem. Soc., C*, **1967**, 2679. b) K. H. Pausacker, *Aust. J. Chem.*, **11**, 200 (1958).

12) D. H. Hey, C. J. M. Stirling, and G. H. Williams, *J. Chem. Soc.*, **1955**, 3963.

13) Radical decomposition of peroxide **1** was reported in our previous paper; M. Yoshida, M. Kobayashi, H. Sawada, H. Hagii, and K. Aoshima, *Nippon Kagaku Kaishi*, **1985**, 1958.

14) C. Zhao, R. Zhou, H. Pan, X. Jin, Y. Qu, C. Wu, and X. Jiang, *J. Org. Chem.*, **47**, 2009 (1982).

15) Mp of pyridinium heptafluorobutyrate obtained by the reaction of pyridine with heptafluorobutyric acid. When pyridine *N*-oxide was reacted with heptafluorobutyric acid at room temperature, pyridine *N*-oxide heptafluorobutyrate (mp 29—30 °C from 2-propanol) was obtained.

 © 1986 The Chemical Society of Japan Bull. Chem. Soc. Jpn., 59, 221—227 (1986)

A Convenient Synthesis of Ethyl 3-(2,2-Dihaloethenyl)-2,2-dimethylcyclopropanecarboxylates and Its Modifications for cis-Isomer Enrichment[1)]

Kiyohide MATSUI,* Akira NEGISHI, Yuriko TAKAHATAKE, Kikuo SUGIMOTO, Tamotsu FUJIMOTO, Toshiyuki TAKASHIMA, and Kiyosi KONDO
Sagami Chemical Research Center, Nishi-Ohnuma 4-4-1, Sagamihara, Kanagawa 229
(Received July 19, 1985)

A synthesis of the title compounds **5** involves the reaction between 3-methyl-2-buten-1-ol and triethyl orthoacetate to produce ethyl 3,3-dimethyl-4-pentenoate, which is followed by the addition of various carbon tetrahalides to the double bond. The reaction of resulting adducts with a base affords **5** in high yields. Stereoselective preparation of the cis-isomer was achieved by the following two methods: First one involves selective transformation of ethyl 4-bromo-6,6,6-trichloro-3,3-dimethylhexanoate to ethyl 6,6,6-trichloro-3,3-dimethyl-4-hexenoate (**8a**) with piperidine followed by the selective conversion of **8a** to *cis*-2,2-dichloroethenyl compound (*cis*-**5a**). Second one is based on the stereoselective cyclization of ethyl 4,6,6,6-tetrachloro-3,3-dimethylhexanoate (*t*-BuONa/solvent/HMPA) to ethyl *cis*-2,2-dimethyl-3-(2,2,2-trichloroethyl)cyclopropanecarboxylate which is transformed into *cis*-**5a** without cis-trans isomerization.

The esters of 3-(2,2-dihaloethenyl)-2,2-dimethylcyclopropanecarboxylic acid belong to the most important class of agricultural insecticides at present.[2)] Particularly, 3-phenoxybenzyl ester of the dichloroethenyl analog (permethrin, **1a**) exibits higher activity than natural pyrethroids, moderate stability under natural conditions, and in additon, low mammalian toxicity.[3,4)] Furthermore, one optical isomer of α-cyano-3-phenoxybenzyl ester of the *cis*-dibromoethenyl analog (decamethrin, **1b**) has been known as the most powerful insecticide so far reported.[5)]

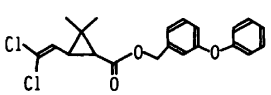

permethrin (1a)
(*cis*-, *trans*- and racemic mixture)

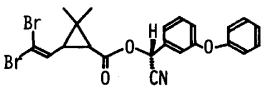

decamethrin (1b)

The known methods to prepare the acid moiety of these potent artificial pyrethroids include the followings:[6)] (1) The construction of substituted ethenyl groups by the Wittig reaction of 3-formyl-2,2-dimethylcyclopropanecarboxylate with phosphonium ylides.[7)] (2) Reaction of diazoacetates with appropriate dienes.[8)] (3) Rearrangement of substituted α-halocyclobutanones.[9)] (4) Other methods to construct ethenylcyclopropanes, for example, cyclization of 4-haloalkanoates,[10)] the Michael addition of allylic sulfones to 3-methyl-2-butenoates,[11)] addition of allenic carbenes,[12)] and addition of phosphonium ylides to 4-oxobutenoates.[13)] These methods were, however, difficult to apply to industrial production of the target compounds by following reasons: The starting materials are not readily available, the reagents required are expensive and/or the operation is tedious. Furthermore, these methods usually afforded a mixture of cis- and trans-isomers (cis/trans= 50/50—10/90).

This paper details a new and industrially acceptable method for the synthesis of ethyl 3-(2,2-dihaloethenyl)-2,2-dimethylcyclopropanecarboxylates and its modification for the stereochemically controlled preparation of the corresponding *cis*-dichloroethenyl compound.[14,15)]

The method developed herein is based on the reaction between 3-methyl-2-buten-1-ol (**2**) and triethyl orthoacetate to produce ethyl 3,3-dimethyl-4-pentenoate (step 1), and the subsequent addition of a carbon tetrahalide to the double bond (step 2). The dehydrohalogenation and cyclization of the resulting halide with a base (step 3) afford the desired cyclopropanecarboxylate **5**, as shown in the following scheme.

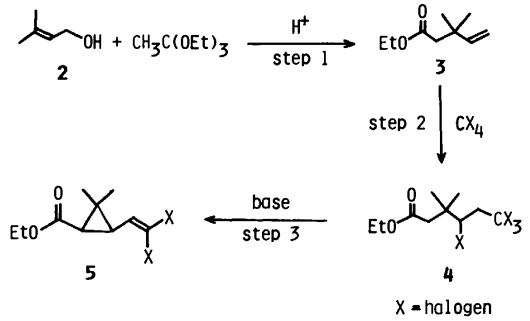

Scheme 1.

Preparation of Ethyl 3,3-Dimethyl-4-pentenoate 3 (Step 1). The pentenoate **3** was obtained by heating a mixture of 3-methyl-2-buten-1-ol (**2**) and triethyl orthoacetate (TEOA) in the presence of acidic catalyst under the removal of ethanol formed as the reaction proceeded.[16,17)]

The effect of various acidic catalysts on the yield of **3** was studied. Table 1 shows clearly that phosphoric acid is the best catalyst from the viewpoint of the yield and the reaction rate. When phenol was used as the catalyst, 3-methyl-2-butenyl phenyl ehter was obtained as a by-product. The formation of another by-product, i.e., 3-methyl-2-butenyl 3,3,-dimethyl-4-pentenoate (**6**), was observed in all cases in the range

Table 1. Effect of Acidic Catalysts on Preparation of 3[a]

Catalyst[b]	Reaction time	Yield of 3
	h	%
Phenol	25	76
H_3PO_4	6	81
Oxalic acid	27	65
$(CH_3)_2CHCO_2H$	23	70
$Hg(OAc)_2$	23	69
Hydroquinone	23	51

a) Molar ratio of 2:TEOA=1:2. b) The amount of the catalyst was 5.0 mol% based on 2 except for case of H_3PO_4 (1.0 mol%).

of 5—20% yields. The amount of **6** depended on the molar ratio of **2**/TEOA. The increase of the ratio of TEOA to **2** clearly suppressed the formation of **6** to improve the yield of **3** remarkably up to 89%.

Ethyl bis(3-methyl-2-butenyl) orthoacetate or tris(3-methyl-2-butenyl) orthoacetate would be the precursor of **6**. The possibility of transesterification of **3** giving **6** was excluded by the fact that heating **3** with **2** in the presence of an acidic catalyst did not afford **6**.

Thus, in order to attain the maximum yield of **3**, an excess of TEOA (preferably more than three equivalents to **2**) should be used in the presence of phosphoric acid. Most of the excess orthoacetate can be recovered by fractional distillation.

Addition of Carbon Tetrahalide to 3 (Step 2). The addition was first investigated either in the presence of a radical initiator or under irradiation.[18]

Heating a solution of **3** and AIBN in bromotrichloromethane at 104 °C for 10 h successfully induced the desired addition reaction to afford ethyl 4-bromo-6,6,6-trichloro-3,3-dimethylhexanoate (**4a**) in 89% yield. Similarly, ethyl 4,6,6,6-tetrachloro-3,3-dimethylhexanoate (**4b**) was obtained in 86% yield by refluxing a solution of **3** in carbon tetrachloride in

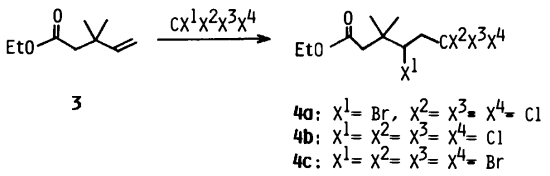

3

4a: X^1= Br, X^2= X^3= X^4= Cl
4b: X^1= X^2= X^3= X^4= Cl
4c: X^1= X^2= X^3= X^4= Br

the presence of BPO. Addition of carbon tetrabromide to **3** was effected by heating them with AIBN or under irradiation of visible light to afford ethyl 4,6,6,6-tetrabromo-3,3-dimethylhexanoate (**4c**) in 60% yield.

Furthermore, other radical initiators, such as transition metal-amine complexes,[19,20] were found to be good alternatives in carbon tetrachloride case. For example, heating a mixture of DMF and $FeCl_3 \cdot 6H_2O$–$BuNH_2$ complex in carbon tetrachloride at 100 °C for 15 h afforded the desired adduct **4b** in 90% yield. Other than above complex, $FeCl_2$–$BuNH_2$, CuCl–$BuNH_2$, and $Cu(CN)_2$–$BuNH_2$ were found to be also effective. In carbon tetrabromide case, the use of these metal complexes resulted low yields of **4c**.

Preparation of Ethyl 3-(2,2-Dihaloethenyl)-2,2-dimethylcyclopropanecarboxylate (5) (Step 3). This simultaneous cyclization and dehydrohalogenation were successfully achieved by treating the adduct **4** with an appropriate base as shown in Table 2. A wide variety of bases could be utilized for the preparation of dichloroethenyl compound **5a**. In the case of the tetrabromo adduct **4c**, the use of too strong bases such as *t*-BuOK and a high reaction temperature should be avoided because of decomposition of the resulting cyclopropanecarboxylate **5c**. The cis/trans ratio of **5** changed with the reaction conditions used. In general, the use of EtONa or EtOK as a base favored the formation of trans-isomer of **5**.

There was observed the formation of ethyl 2-haloethynyl-3,3-dimethylcyclopropanecarboxylate (**7**) (2—15% yields). The amount of formation of **7** increased when the reaction was carried out at high

Table 2. Preparation of 5 from Adduct 4

Adduct	Base	Solvent	Temp	Time	Product	Cis/trans	Yield
			°C	h			%
4a	*t*-BuOK	THF	60	4	**5a**	45/55	70
4b	*t*-BuOK	THF	22	3			
			60	3.5	**5a**	50/50	73
4b	*t*-BuONa	THF	5	3	**5a**	50/50	92
4b	EtONa	EtOH	22	1			
			80	1.5	**5a**	34/66	94
4b	EtOK	EtOH	22	2			
			80	1.5	**5a**	26/74	96
4b	$NaNH_2$	THF-EtOH	22	5.5	**5a**	50/50	94
4b	EtONa	Heptane	98	22	**5a**	24/76	68
4c	EtONa	EtOH	22	18	**5b**	20/80	79

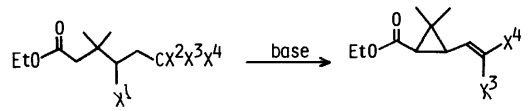

4a: X^1= Br, X^2= X^3= X^4= Cl
4b: X^1= X^2= X^3= X^4= Cl
4c: X^1= X^2= X^3= X^4= Br

5a: X^3= X^4= Cl
5b: X^3= X^4= Br

temperature or in protic solvents. In general, the reaction with the tetrabromo adduct **4c** gave more amount of the acetylenic compound, i.e., **7b** (10—15%) as compared with the case of the chloro analog (2—10%).

With respect to the reaction mechanism, we observed the formation of three intermediates **8a, 9b,** and **10a** at the beginning of the reaction of **4b** with a base. In the reaction of **4c**, detectable intermediates were only **9c** and **10b**. The ratio of the intermediates formed changed with the reaction conditions. In general, the use of *t*-alkoxide as a base favored the formation of **10**, while the reaction with ethoxide resulted in the predominant formation of **8** and **9**.

As the reaction proceeded, these intermediates formed were gradually converted to **5**. Among the intermediates, the intermediate **9** was found to be the most reactive. The rate of disappearance of **8a** was considerably lower in protic solvents than that in aprotic solvents, while the intermediate **10** was converted into **5** at a moderate rate in both solvents.

7a: X^4= Cl
7b: X^4= Br

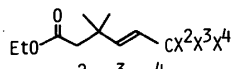

8a: X^2= X^3= X^4= Cl
8b: X^2= X^3= X^4= Br

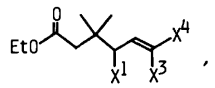

9a: X^1= Br, X^3= X^4= Cl
9b: X^1= X^3= X^4= Cl
9c: X^1= X^3= X^4= Br

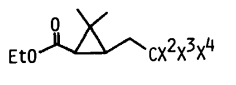

10a: X^2= X^3= X^4= Cl
10b: X^2= X^3= X^4= Br

Stereoselective Preparation of *cis*-5a. The title stereocontrolled preparation becomes interesting target because cis-isomer of above new artificial pyrethroids usually exhibit enhanced insecticidal activity than trans-isomers.[21] To this end, we intended to modify the above process. At the beginning of the reaction at step *3*, three intermediates **7, 8,** and **9** were produced and were gradually converted into **5**. In order to examine the stereochemical aspect of this reaction, we planned to isolate **8a** and **9b** by the treatment of **4a** or **4b** with amines.

Fortunately, selective dehydrohalogenation was achieved. For example, the compound **8a** was prepared by treating **4a** with piperidine in benzene or DMF in 75—85% yields, whereas treatment of **4b** with pyrrolidine in toluene or DMF afforded **9b** in 87—90% yields.[22]

Cyclization of **8a** or **9b** to **5a** was carried out using a variety of bases and solvents. Typical results are summarized in Table 3. Under all conditions examined (run 1—5), the compound **9b** was transformed mainly into *trans*-**5a**. In contrast, the cis/trans ratio of **5a** derived from **8a** changed significantly depending on the reaction conditions. The treatment of **8a** with EtONa in refluxing benzene (run 6) gave **5a** with an isomer ratio of ca. 50/50, while the use of $NaNH_2$ increased the cis content to some extent (run 7). This result suggests that absence of alcohol may favor the formation of *cis*-**5a**.[23] Therefore, the ethanol formed was removed from the reaction mixture as quickly as possible by distillation to afford cis-rich **5a** (run 9). The presence of THF accelerated the cyclization, favoring formation of the cis-isomer (cf. run 7 and 8). As a result, the cyclopropane **5a** of 90% cis content was attained (run 10).

Alternative approach involving stereoselective preparation of *cis*-**10a** from **4b** was also studied. Treatment of **4b** with *t*-BuONa or *t*-BuOK gave **10a** selectively. The cis/trans ratio of the product

Table 3. Cyclization of Intermediates **8a** and **9b** to **5a**

Run	Starting material	Base	Solvent	Temp °C	Yield %	cis/trans
1	**9b**	EtONa	EtOH	25	92	22/78
2	**9b**	EtONa	Benzene	80	≃100	13/87
3	**9b**	*t*-BuONa	Hexane	60	94	17/83
4	**9b**	*t*-BuOK	Toluene	25	78	13/87
5	**9b**	$NaNH_2$	THF	25	98	29/71
6	**8a**	EtONa	Benzene	80	94	54/46
7	**8a**	$NaNH_2$	Benzene	80	88	66/34
8	**8a**	$NaNH_2$	THF	60	98	71/29
9	**8a**	EtONa	Benzene	(80)[a]	92	79/21
10	**8a**	EtONa	Hexane/THF	(60)[a]	94	90/10

a) Ethanol formed during the reaction was removed as an azeotropic mixture.

Table 4. Stereoselective Cyclization of **4b** to **10a**

Run	Base	Solvent	Temp °C	Yield %	cis trans
1	*t*-BuONa	Benzene/ *t*-BuOH	80	74	30/70
2	*t*-BuONa	*t*-BuOH/ HMPA	4—8	86	73/27
3	*t*-BuONa	THF/HMPA	−26	81	79/21
4	*t*-BuONa	Hexane/ HMPA	−60	88	88/12

changed dramatically depending on the solvent and reaction temperature employed. The cyclization in a mixture of benzene and *t*-butyl alcohol at the reflux temperature afforded *trans*-**10a** as the main product (cis/trans=30/70).[24] In contrast, cis-rich **10a** was obtained by carrying out the reaction in hexane in the presence of HMPA at low temperature. Table 4 shows some typical results. The observed stereoselective cyclization of **4b** to **10a** may be attributed to a solvent effect in favor of kinetic control, as no isomerization between *cis*-**10a** and *trans*-**10a** was observed under these conditions. It is worthy to note that the preferential cyclization of γ-halo ester to *cis*-cyclopropanecarboxylate is unprecedented, though the predominant formation of trans-isomer was well-known in the preparation of chrysanthemic acid.[10]

The cyclopropane **10a** (cis/trans=30/70) was transformed into **5a** (cis/trans=28/72) by treating with a base such as EtONa or DBU. Furthermore, the treatment of **10a** (cis/trans=75/25) with NaOH afforded the corresponding carboxylic acid of **5a** (cis/trans=75/25). The original stereochemical integrity was thus retained during these transformations.[25]

In contrast to **4a** and **4b**, tetrabromo adduct **4c** gave **9c** as sole product upon the treatment with DABCO or DBU. Cyclization of **9c** with bases afforded *trans*-**5b** mainly in high yields. When **4c** was treated with a *t*-butoxide ion in a common solvent, such as THF or benzene, *trans*-**10b** was produced again. The highest cis content (50%) of **5b** was obtained upon the successive treatment of **4c** with $NaNH_2$ and DBU in a mixture of *t*-butyl alcohol and hexane, hereby **10b** being the responsible intermediate (glpc).

Experimental

General. All the melting points and boiling points are uncorrected. IR spectra were recorded on a Hitachi EPI-G3 grating spectrophotometer. NMR spectra were measured with Varian HA-100 spectrometer and Hitach-Perkin-Elmer R-20B using TMS as an internal standard. Mass spectra were recorded on Hitachi RMU-6E mass spectrometer (70eV). Analytical determinations by glpc were performed on a Hitachi 163 gas chromatograph (5 mm o.d.×1 m, 2% EGA on Uniport B or diasolid ZS).

General Procedure for the Examination of the Reaction Conditions of Step 1. A catalyst (5.0 mol% except for the case of H_3PO_4 (1.0 mol%)) was added to a mixture of 3-methyl-2-buten-1-ol (**2**)[27] (4.3 g, 50 mmol) and cited amount of TEOA in Tables 1 and 2 at room temperature. The mixture was heated to 140—150 °C under removal of ethanol. The yield of ethyl 3,3-dimethyl-4-pentenoate (**3**) was determined by glpc, decahydronaphthalene being used as an internal standard.

Large Scale Preparation of the Pentenoate 3. A mixture of 43 g (0.50 mol) of **2**, 0.24 kg (1.5 mol) of TEOA and 3.4 ml (50 mmol) of phosphoric acid was heated at 140 °C with stirring for 14 h under removal of ethanol. After excess TEOA was removed, the residue was distilled to give 66 g (85%) of **3**, bp 74—78 °C/55 mmHg† (lit,[17] 35—45 °C (bath)/0.1 mmHg). ^1H NMR (CCl_4) δ=5.86 (dd, 1H), 5.1—4.7 (m, 2H), 4.06 (q, 2H), 2.19 (s, 2H) 1.22 (t, 3H), 1.12 (s, 6H). The elemental analysis gave a satisfactory result.

Ethyl 4-Bromo-6,6,6-trichloro-3,3-dimethylhexanoate (4a). Fifty milligrams of AIBN was added to a solution of 1.6 g (10 mmol) of **3** in 5.0 ml of bromotrichloromethane. The mixture was heated at 104 °C for 10 h. After the unreacted bromotrichloromethane was removed, the residue was distilled to give 3.2 g (89%) of **4a**, bp 102—105 °C/0.1 mmHg. IR (neat): 1730, 1225, 1200, 1155, 1035, 960, 805, 710, 655 cm^{-1}. ^1H NMR (CCl_4) δ=4.49 (dd, 1H), 4.08 (q, 2H), 3.4—3.15 (m, 2H), 2.60 (d, 1H), 2.23 (d, 1H), 1.23 (t, 3H), 1.23 (s, 3H), 1.13 (s, 3H). MS *m/z*: 353 (M^+), 41 (base). Found: C, 33.83; H, 4.35%. Calcd for $C_{10}H_{16}BrCl_3O_2$: C, 33.88; H, 4.55%.

Ethyl 4,6,6,6-Tetrachloro-3,3-dimethylhexanoate (4b). A mixture of 6.2 g (40 mmol) of **3**, 50 ml of carbon tetrachloride and 50 mg of BPO was heated at 80 °C for 20 h under argon atmosphere. After having been cooled to room temperature, the reaction mixture was washed with aq $NaHCO_3$ and water. The mixture was dried ($MgSO_4$) and distilled to give 11 g (86%) of **4b**, bp 107—108 °C/0.15 mmHg. IR (neat): 1730, 1180, 1130, 1090, 975, 800, 685 cm^{-1}. ^1H NMR (CCl_4) δ=4.37 (dd, 1H), 4.07 (q, 2H), 3.40—2.85 (m, 2H), 2.56 (d, 1H), 2.22 (d, 1H), 1.27 (t, 3H), 1.22 (s, 3H), 1.13 (s, 3H). MS *m/z*: 308 (M^+), 46 (base). Found: C, 38.91; H, 5.07; Cl, 45.84%. Calcd for $C_{10}H_{16}Cl_4O_2$: C, 38.74; H, 5.20; Cl, 45.74%.

Addition of Carbon Tetrabromide to 3. **a) Using AIBN as a Radical Initiator:** Fifty milligrams of AIBN was added to a mixture of 1.6 g (10 mmol) of **3** and 3.3 g (10 mmol) of carbon tetrabromide. The mixture was heated at 120 °C for 5 h under argon atmosphere. The crude product was purified by chromatography (silica-gel column) to give 3.0 g (60%) of ethyl 4,6,6,6-tetrabromo-3,3-dimethylhexanoate (**4c**). IR (neat): 1735, 1220, 1150, 1032, 610 cm^{-1}. ^1H NMR (CCl_4) δ=4.35 (q, 1H), 4.07 (q, 2H), 3.55 (m, 2H), 2.61 (d, 1H), 2.27 (d, 1H), 1.32 (s, 3H), 1.28 (t, 3H), 1.21 (s, 3H). MS *m/z*: 324 (M^+), 88 (base). Found: C,

† 1 mmHg≈133.3 Pa.

24.87; H, 3.25; Br, 65.60%. Calcd for $C_{10}H_{16}Br_4O_2$: C, 24.62; H, 3.31; Br, 65.51%.

b) Addition under Irradiation: A mixture of **3** (0.78 g) and carbon tetrabromide (3.3 g) continuously purged with argon, was irradiated with a 100 W sunlight lamp for 10 h at room temperature. The resulting darkbrown oil was purified by chromatography (silica-gel column) to give **4c** (1.5 g).

Ethyl 3-(2,2-Dichloroethenyl)-2,2-dimethylcyclopropanecarboxylate (5a). The THF solution of **4a** [0.71 g (2.0 mmol)] (5 ml) was added dropwise to 0.45 g of *t*-BuOK in 15 ml of THF and the mixture was heated under reflux for 2 h. After an additional 0.11 g of *t*-BuOK was added, the mixture was heated under reflux for 1 h. The mixture was poured into aq NH_4Cl and extracted with ether. The ether extract was dried ($MgSO_4$) and concentrated in vacuo. Distillation gave 0.35 g (74%) of **5a**, bp 80—83 °C/0.8 mmHg (lit,[8] 119—120 °C/15 mmHg). IR (neat): 1730, 1182 cm^{-1}. ^1H NMR (CCl_4) δ=6.22 (d, *cis*-H) 5.56 (d, *trans*-H) (total 1H, cis/trans=45/55), 4.05 (bq, 2H), 2.35—1.4 (m, 2H), 1.4—1.05 (m, 9H). MS *m/z*: 236 (M^+), 91 (base). Found: C, 50.44; H, 5.83; Cl, 29.63%. Calcd for $C_{10}H_{14}Cl_2O_2$: C, 50.65; H, 5.95; Cl, 29.90%. The cis- and trans-isomers could be separated by chromatography (silica-gel column). The ^1H NMR spectra of them are identical with those reported.[28] The fore-cut (45 mg) at the above distillation was composed with **5a** and ethyl *trans*-2-(2-chloroethynyl)-3,3-dimethylcyclopropanecarboxylate (**7a**). The acetylenic ester **7a** was alternatively prepared from **5a** by the treatment with NaH in THF-HMPA at room temperature for 14—26 h. *trans*-**7a** (from *trans*-**5a**): Bp 66 °C/1 mmHg. Yield 75%. IR (neat): 2220, 1735, 1280, 1170, 1050 cm^{-1}. ^1H NMR (CCl_4) δ=4.04 (q, 2H), 1.81 (d, 1H), 1.58 (d, 1H), 1.28 (s, 3H), 1.24 (t, 3H), 1.20 (s, 3H). MS *m/z*: 200 (M^+), 127 (base). Found: C, 59.95; H, 6.48; Cl, 17.42. Calcd for $C_{10}H_{13}ClO_2$: C, 59.86; H, 6.53; Cl, 17.67. *cis*-**7a** (from *cis*-**5a**): Yield 28%. ^1H NMR (CCl_4) δ=4.04 (q, 2H), 1.58 (s, 2H), 1.30 (s, 3H), 1.23 (t, 3H), 1.16 (s, 3H). MS *m/z*: 200 (M^+), 127 (base).

The formation of the intermediates **8a** and **10a** was observed at the beginning of the reaction by glpc analysis.

Cyclopropanecarboxylate 5a from the Carbon Tetrachloride adduct 4b. Typical Procedure 1 (*t*-BuONa/THF): A suspension of 4.2 g (22 mmol) of *t*-BuONa in 80 ml of dry THF was cooled to 5 °C. A solution of 3.1 g (10 mol) of the adduct **4b** in 20 ml of dry THF was added dropwise to the above susepnsion and the mixture was stirred at ca. 5 °C for 3 h. The mixture was neutralized with dry HCl in ether and filtered. The filtrate was diluted with ether, washed with water and dried ($MgSO_4$). Distillation gave 2.2 g (92%) of a mixture of *cis*- and *trans*-**5a**, bp 73—78 °C/0.6 mmHg. The cis/trans ratio was 50/50 based on NMR analysis.

Typical Procedure 2 (EtONa/EtOH): To an ethanolic EtONa (prepared from Na metal (1.0 g, 44 mmol) and dry ethanol (80 ml)) was added dropwise, while cooling with ice, 20 ml of an ethanolic solution containing 6.2 g (20 mmol) of **4b**. The mixture was stirred for 1 h at room temperature, then heated under reflux for 1.5 h. The mixture was worked up and distillation of the crude product gave 4.5 g (94%) of **5b**, bp 72—74 °C/0.4 mmHg. The cis/trans ratio was 34/66 based on the glpc analysis (2% EGA, 120 °C).

Ethyl 3-(2,2-Dibromoethenyl)-2,2-dimethylcyclopropanecarboxylate (5b). An ethanolic solution (5 ml) of EtONa (0.62 g) was added dropwise to 1.5 g (3 mmol) of **4c** in 16 ml of dry ethanol under ice cooling. The mixture was warmed to room temperature and stirred for 6 h. An additional 2.5 ml of ethanolic EtONa (about 0.3 g) was added, and the mixture was stirred for another 12 h. The mixture was worked up and distillation gave 0.77 g (79%) of **5b**, bp 98—101 °C/0.4 mmHg (lit,[29] 95—97 °C/0.4 mmHg). IR (neat): 1725, 1223, 1175 cm^{-1}. ^1H NMR (CCl_4): δ=6.72 (bd, *cis*-H), 6.10 (d, *trans*-H) (total 1H, cis/trans=2/8), 4.10 (q, 2H), 2.3—1.5 (m, 2H), 1.5—1.1 (m, 9H). MS *m/z*: 253, 41 (base). Found: C, 37.07; H, 4.40; Br, 49.27%. Calcd for $C_{10}H_{14}Br_2O_2$: C, 36.84; H, 4.33; Br, 49.02%. The fore-cut (74 mg) was mainly composed with *trans*-**7b**. Yield 10%. IR (neat): 2220, 1735 cm^{-1}. ^1H NMR (CCl_4): δ=4.05 (q, 2H), 2.0—1.4 (m, 2H), 1.5—1.0 (m, 9H). MS *m/z*: 245 (M^+), 41 (base).

Ethyl 4,6,6-Trichloro-3,3-dimethyl-5-hexenoate (9b). A solution of pyrrolidine (0.71 mg) in toluene was added to a toluene solution of **4b** (1.6 g). The mixture was stirred at 100—110 °C for 4 h and worked up. Distillation gave 1.2 g (87%) of **9b**, bp 87—90 °C/0.12 mmHg. IR (neat): 1735, 1613, 1220, 1035, 880 cm^{-1}. ^1H NMR (CCl_4) δ=5.96 (d, 1H), 4.85 (d, 1H), 4.06 (q, 2H), 2.41 (d, 1H), 2.23 (d, 1H), 1.23 (t, 3H), 1.11 (s, 6H). Found: C, 44.18; H, 5.39; Cl, 38.65%. Calcd for $C_{10}H_{15}Cl_3O_2$: C, 43.90; H, 5.53; Cl, 38.87%.

Ethyl 6,6,6-Trichloro-3,3-dimethyl-4-hexenoate (8a). Piperidine (5.1 g, 60 mmol) was added dropwise to a solution of ethyl 4-bromo-6,6,6-trichloro-3,3-dimethylhexanoate (**4a**) (11 g, 30 mmol) in benzene (45 ml) at room temperature. The mixture was refluxed for 5 h, diluted with ether, and washed (water, 1 M HCl(1 M=1 mol dm^{-3}), aq $NaHCO_3$, water) and dried ($MgSO_4$). Distillation afforded 7.0 g (85%) of **3a**, bp 82—83 °C/0.5 mmHg. IR (neat): 1730, 1615, 1225, 1175, 1030 cm^{-1}. ^1H NMR (CCl_4) δ=6.26 (d, 1H, *J*=15 Hz), 5.96 (d, 1H, *J*=15 Hz), 4.01 (q, 2H), 2.26 (s, 2H), 1.21 (t, 3H), 1.19 (s, 6H). Found: C, 44.12; H, 5.35; Cl, 38.11%. Calcd for $C_{10}H_{15}Cl_3O_2$: C, 43.90; H, 5.53; Cl, 38.87%.

Rearrangement of 8a to 9b. A solution of **8a** (1.1 g, 4 mmol) in xylene was heated at 130 °C for 5 h under argon atmosphere. The solution was concentrated in vacuo and the residue was distilled to give 0.93 g of a colorless oil which was composed of **9b** (90%) and a by-product (10%). The by-product separated by chromatography (silica-gel column) was identified to be 4-(2,2-dichloroethenyl)-2,2-dimethyl-4-butenolide. Mp 26.5—28.0 °C (lit,[30] 27.0—28.0 °C). IR (neat): 1790, 1625, 1235, 1160, 1000, 920 cm^{-1}. ^1H NMR (CCl_4) δ=5.50 (d, 1H), 4.78 (d, 1H), 2.33 (d, 1H), 2.25 (d, 1H), 1.21 (s, 3H), 1.05 (s, 3H).

Ethyl 3-(2,2-Dichloroethenyl)-2,2-dimethylcyclopropanecarboxylate (5a) from 8a and 9b (Typical Procedures). From Ethyl 4,6,6-Trichloro-3,3-dimethyl-5-hexenoate (9b). A solution of 0.55 g (2.0 mmol) of **9b** in dry ethanol (2.0 ml) was added dropwise to a solution of Na methal (57 mg, 2.5 mmol) in dry ethanol (10 ml). The mixture was stirred at room temperature for 5 h, cooled with ice and then neutralized by adding dry HCl in ether. The mixture was concentrated to one-tenth its original volume and diluted with ether. The mixture was poured into ice water,

and the ethereal layer was washed (aq $NaHCO_3$, brine) and dried ($MgSO_4$). Distillation gave 0.44 g (92%) of **5a**, bp 75—76 °C/0.25 mmHg. cis/trans=22/78 (glpc, 2% EGA).

From Ethyl 6,6,6-Trichloro-3,3-dimethyl-4-hexenoate (8a). **a) $NaNH_2$/THF**: A solution of the compound **8a** (0.41 g, 1.5 mmol) in dry THF (1.5 ml) was added dropwise to a suspension of $NaNH_2$ (78 mg, 2 mmol) in 20 ml of dry THF. The mixture was heated under reflux with stirring for 5 h poured into ice-water. The aqueous mixture was extracted with ether, washed (aq $NaHCO_3$, brine) and dried ($MgSO_4$). Distillation afforded 0.35 g (98%) of **5a**, bp 72—74 °C/0.2 mmHg. cis/trans=71/29 (glpc).

b) EtONa/Hexane-THF: Dry THF (6 ml) was added to a hexane suspension (20 ml) of EtONa (15 mmol). Then, a solution of **8a** (2.7 g, 9.9 mmol) in hexane (4 ml) was added dropwise to the suspension at the boiling temperature. Ethanol formed was azeotropically removed during the reaction. After 8 h the reaction mixture was worked up as described above. Distillation gave 2.2 g (94%) of **5a**, bp 77—80 °C/0.3 mmHg. cis/trans=90/10 (glpc).

Ethyl 2,2-Dimethyl-3-(2,2,2-Trichloroethyl)cyclopropanecarboxylate (10a). **a) *t*-BuONa/PhH**: To a mixture of *t*-BuOH (60 ml) and dry benzene (30 ml) was added portionwise Na metal (0.28 g, 12 mmol). The resulting mixture was heated under reflux until Na metal disappeared. A benzene solution (5 ml) of **4b** (3.1 g, 10 mmol) was added dropwise and the mixture was stirred for 2 h. Then, the reaction mixture was acidified by introducing dry HCl, diluted with water and extracted with ether. The ethereal layer was washed (aq $NaHCO_3$, brine) and dried ($MgSO_4$). Distillation afforded 2.0 g (74%) of **10a**, bp 78—80 °C/0.1 mmHg. cis/trans=30/70 (glpc). IR (neat): 1730, 1180, 1135, 765 cm^{-1}. ^1H NMR spectrum of trans-isomer (CCl_4) δ=4.08 (q, 2H), 2.85—2.65 (m, 2H), 1.72 (bq, 1H), 1.36 (d, 1H), 1.24 (t, 3H), 1.24 (s, 3H), 1.20 (s, 3H). ^1H NMR spectrum of cis-isomer (CCl_4) δ=4.06 (q, 2H), 3.2—2.95 (m, 2H), 1.7—1.5 (m, 2H), 1.26 (t, 3H), 1.24 (s, 6H). Found: C, 43.80; H, 5.41; Cl, 38.87%. Calcd for $C_{10}H_{15}Cl_3O_2$: C, 43.90; H, 5.53; Cl, 38.87%.

b) *t*-BuONa/Hexane-HMPA: Powdered *t*-BuONa (7.2 g, 75 mmol) was added portionwise to a solution of **4b** (16 g, 52 mmol) and HMPA (10 ml) in dry hexane (50 ml) at −60 °C over a period of 50 min. The mixture was stirred for additional 7 h under cooling and for 12 h at room temperature. Then the mixture was worked up. Distillation gave 12 g (88%) of **10a**, bp 80—83 °C/0.5 mmHg. cis/trans=88/12 (glpc).

Attempted Isomerization between *cis*- and *trans*-10a. **a) *t*-BuONa/Hexane-HMPA**: Powdered *t*-BuOK (30 mg) was added to a solution of *trans*-**10a** (0.54 g) and HMPA (0.40 ml) in hexane (2.0 ml) at −60 °C. The mixture was stirred for 5 h at the temperature and then for 15 h at room temperature. Glpc analysis showed no trans-cis isomerization of **10a** at each temperature.

b) LDA/THF: A solution of LDA in THF (0.40 ml, 0.20 mmol) was added to a solution of *cis*-**10a** (0.54 g) in dry THF (2.0 ml) at −10 °C. The mixture was stirred for 6 h at the temperature and then for 12 h at room temperature. Glpc analysis indicated no cis-trans isomerization.

Ethyl 3-(2,2-Dichloroethenyl)-2,2-dimethylcyclopropanecarboxylate (5a) from 10a. A solution of **10a** (cis/trans=30/70) (2.7 g, 9.9 mmol) in dry ethanol (20 ml) was added dropwise to an ethanolic NaOEt (prepared from Na metal (0.25 g, 11 mmol) and dry ethanol (80 ml)). The mixture was heated under reflux for 5 h. The reaction mixture was worked up as described above. Distillation afforded 1.9 g (80%) of **5a**, bp 75—76 °C/0.25 mmHg. cis/trans=28/72 (glpc).

3-(2,2-Dichloroethenyl)-2,2-dimethylcyclopropanecarboxylic Acid from 4a. A solution of **4a** (cis/trans=75/25) (9.6 g, 35 mmol) in ethanol (5 ml) was added dropwise to a solution of NaOH (6.0 g, 0.15 mmol) in water (30 ml) and ethanol (5 ml). The mixture was heated at 100 °C for 5 h under vigorous stirring. The reaction mixture was washed with ether. The aqueous layer was acidified with concd HCl and extracted with ether–AcOEt (2:1). The latter organic layer was washed with brine and dried ($MgSO_4$). Distillation gave 6.3 g (86%) of the desired acid as a viscous oil, bp 105 °C/0.3 mmHg. cis/trans=75/25 (glpc after esterification with CH_2N_2).

Ethyl 4,6,6-Tribromo-3,3-dimethyl-5-hexenoate (9c). An ethanolic solution of EtONa (prepared from Na metal (94 mg, 4.1 mmol) and dry ethanol (5 ml)) was added dropwise to an ice-cooled solution of ethyl 4,6,6,6-tetrabromo-3,3-dimethylhexanoate (**4c**) (2.0 g, 4.1 mmol) in dry ethanol (10 ml). After 2 h the reaction mixture was worked up as described above. Distillation afforded 0.85 g (51%) of **9c**, bp 130—133 °C/0.3 mmHg. IR (neat): 1730, 1600, 1225, 1150, 1030 cm^{-1}. ^1H NMR (CCl_4) δ=6.64 (d, 1H), 4.95 (d, 1H), 4.12 (q, 2H), 2.38 (bd, 2H), 1.4—1.1 (m, 9H). Found: C, 29.78; H, 3.65; Br, 58.67%. Calcd for $C_{10}H_{15}Br_3O_2$: C, 29.51; H, 3.71; Br, 58.91%.

Ethyl 3-(2,2-Dibromoethenyl)-2,2-dimethylcyclopropanecarboxylate (5b). **a) EtONa/EtOH**: A solution of **4c** (0.41 g, 1.0 mmol) in dry ethanol (1.5 ml) was added dropwise to an ethanolic EtONa (prepared from Na metal (30 mg, 1.3 mmol) and dry ethanol (5 ml)) at room temperature. After 3 h the reaction mixture was worked up and distillation gave 0.27 g (83%) of **5b**, bp 95—98 °C/0.3 mmHg. cis/trans=20/80 (NMR).

b) *t*-BuONa and DBU/*t*-BuOH-Hexane: To an ice-cooled solution of **4c** (9.8 g, 20 mmol) in *t*-BuOH (40 ml) and hexane (20 ml), $NaNH_2$ (1.2 g, 31 mmol) was added portionwise. The mixture was stirred for 1 h at 4—5 °C and for 1 h at room temperature. Then, DBU (3.1 g, 21 mmol) was added to the mixture at 4—5 °C. The mixture was stirred at room temperature for 45 min then heated under reflux for 5 h. After acidified with 1 M HCl, the mixture was evaporated in vacuo. The residue was extracted with ether and the ethereal solution was washed (aq $NaHCO_3$, brine) and dried ($MgSO_4$). Distillation gave 5.7 g (87%) of **5b**, bp 88 °C/0.1 mmHg. cis/trans=50/50 (NMR).

References

1) Preliminary accounts: a) K. Kondo, K. Matsui, and A. Negishi, ACS Symposium Series No. 42, "Synthetic Pyrethroids," ed by M. Elliott, (1977) p. 128; b) K. Kondo, T. Takashima, A. Negishi, K. Matsui, T. Fujimoto, K. Sugimoto, C. E. Hatch III, and J. S. Baum, *Pestic. Sci.*, **11**, 180 (1980).

2) M. Elliott and N. F. Janes, *Chem. Soc. Rev.*, **7**, 473 (1978); *Chem. International*, **1979**, 5.

3) M. Elliott, A. W. Farnham, N. F. Janes, P. H. Needham, and D. A. Pulman, *Nature (London)*, **244**, 456 (1973).

4) M. Elliott, A. W. Farnham, N. F. Janes, P. H. Needham, D. A. Pulman, and J. H. Stevenson, *Nature (London)*, **246**, 169 (1973).

5) M. Elliott, A. W. Farnham, N. F. Janes, P. H. Needham, D. A. Pulman, *Nature (London)*, **248**, 710 (1974).

6) For reviews on the synthesis of acid moiety of pyrethroid: a) D. Arlt, M. Jautelat, and R. Lantzsch, *Angew. Chem. Intern. Ed. Engl.*, **20**, 703 (1981); b) K. Matsui and K. Kondo, *Kagaku No Ryoiki*, **36**, 514 (1982).

7) M. Elliott, N. F. Janes, and D. A. Pulman, *J. Chem. Soc., Perkin Trans. 1*, **1974**, 2470.

8) J. Farkas, P. Kourim, and F. Sorm, *Collect. Czech. Chem. Commun.*, **24**, 2230 (1959).

9) P. Martin, H. Greuter, and D. Bellus, *J. Am. Chem. Soc.*, **101**, 5853 (1979).

10) M. Juria, S. Julia, and M. Langlois, *Bull Soc. Chim. Fr.*, **1964**, 1007, 1476, 1487.

11) L. Velluz, J. Martel, and G. Nomine, *C. R. Acad. Sci., Ser. C*, **268**, 2199 (1969).

12) R. W. Mills, R. D. H. Murray, and R. A. Raphael, *J. Chem. Soc., Perkin Trans. 1*, **1973**, 133.

13) M. J. Devos, L. Hevesi, P. Bayet, and A. Krief, *Tetrahedron Lett.*, **1976**, 3911.

14) Stereoselective synthesis of cis-isomer: N. Itaya, T. Matsuo, N. Ohno, T. Mizutani, F. Fujita, and H. Yoshioka, ACS Symposium Series No. 42, "Synthetic Pyrethroids," ed by M. Elliott, (1977) p. 45.

15) Stereospecific synthesis of cis-isomer: C. E. Hatch III, J. S. Baum, T. Takashima, and K. Kondo, *J. Org. Chem.*, **45**, 3281 (1980).

16) W. S. Johnson, L. Wertheman, W. B. Bartlett, T. J. Brockson, T. Li, D. J. Faulkner, and M. R. Petersen, *J. Am. Chem. Soc.*, **92**, 741 (1970).

17) J. H. Babler, A. J. Tortorello, *J. Org. Chem.*, **41**, 885 (1976).

18) G. Sosnovsky, "Free Radical Reactions in Preparative Organic Chemistry", Macmillan Co., New York, (1964).

19) M. Asscher and D. Vofsi, *J. Chem. Soc.*, **1961**, 2261; **1963**, 1887; T. Suzuki and J. Tsuji, *J. Org. Chem.*, **35**, 2982 (1970); H. Matsumoto, T. Nakano, and Y. Nagai, *Tetrahedron Lett.*, **1973**, 5147.

20) D. J. Burton and L. J. Kehoe, *J. Org. Chem.*, **35**, 1339 (1970).

21) M. Eliott, A. W. Farnham, N. F. Janes, P. H. Needham, and D. A. Pulman, *Pestic. Sci.*, **6**, 537 (1975).

22) The trans stereochemistry of the olefinic linkage in **3a** was assigned by ^{1}H NMR spectrum (coupling constant between the two olefinic protons=15 Hz).[26]

23) The reaction of **8a** with NaOEt in ethanol proceeded very slowly to give **5a** (cis/trans=20/80). Thus, the presence of ethanol retarded the conversion of **8a** to **5a** and favored the formation of trans-rich **5a**.

24) Y. Nakada, R. Endo, S. Muramatsu, J. Ide, and Y. Yura, *Bull. Chem. Soc. Jpn.*, **52**, 1511 (1979).

25) The cis-trans isomerization of **5a** did not occur by the treatment with base (*t*-BuOk/THF-*t*-BuOH or EtONa/EtOH). Note that the isomerization of *cis*-chrysanthemate or its analogs to the corresponding trans-isomer occurs readily: M. Julia, S. Julia, B. Bemont, and G. Tchenoff, *C. R. Acad. Sci., Ser. C*, **248**, 242 (1959).

26) W. Reeve and L. W. Fine, *Can. J. Chem.*, **1963**, 2231.

27) J. Tanaka, T. Katagiri, and S. Yamada, *Nippon Kagaku Zasshi*, **87**, 877 (1966); C. A. Vernon, *J. Chem. Soc.*, **1954**, 2504; R. H. Dewolfe and W. G. Young, *Chem. Rev.*, **56**, 795 (1956).

28) P. E. Burt, M. Eliott, A. W. Farnham, N. F. Janes, P. H. Needham, and D. A. Pulman, *Pestic. Sci.*, **5**, 791 (1974).

29) D. G. Brown, O. F. Bodenstein, and S. J. Norton, *J. Agric. Food Chem.*, **21**, 767 (1973).

30) T. Matsuo, N. Itaya, and O. Magara, Jpn. Kokai Tokkyo Koho, 51-125358 (1976).

 © 1986 The Chemical Society of Japan Bull. Chem. Soc. Jpn., 59, 229—234 (1986)

Catalytic Action of Iron and Manganese Ions in the Photochemically-Induced Oxidation of D-Fructose with Atmospheric Oxygen

Koji ARAKI* and Shinsaku SHIRAISHI*
Institute of Industrial Science, The University of Tokyo,
7-22-1, Roppongi, Minato-ku, Tokyo 106
(Received July 20, 1985)

D-Fructose is susceptible to photochemically-induced oxidation by atmospheric oxygen in the presence of a catalytic amount of iron or manganese cations in a neutral to weakly basic pH range. Metal hydroxide does not precipitate from a solution in this pH range because of the high sequestering ability of D-fructose. Upon irradiation of Pyrex-filtered light, D-fructose degraded into D-erythrose and other fragments. This reaction is shown to proceed by coupling with an oxidation-reduction cycle involving a metal cation, i.e., the photooxidation of D-fructose by M(III) and the subsequent reoxidation of the resultant M(II) by atmospheric oxygen.

It is well recognized that trace amounts of transition metal cations like Cu(II), Mn(II), and Fe(III) often play key roles in many biological activities.[1] Among them, the ability of saccharides to sequester metals in aqueous solutions has been drawing considerable interest because of their physiological and chemical importance and the possible applications of metal-saccharide systems to clinical use.[2-4] However, the photochemical properties of metal-saccharide systems are not yet well understood. Recent reports from our and other laboratories have shown that the photochemically-induced oxidation of monosaccharides by transition metals leads to a degradation of saccharides with selective C–C bond cleavage.[5-8] For instance, the photooxidation of D-fructose in an acidic $FeCl_3$ solution causes a C_2—C_3 bond cleavage of D-fructose via the formation of an Fe(III)–D-fructose complex to give D-erythrose in nearly 90% yield.[7] In a preceding letter, we showed that D-fructose and D-glucose are susceptible to photochemically-induced oxidation by atmospheric oxygen in the presence of a catalytic amount of transition-metal ions in the neutral pH range.[9] The catalytic action of transition metals for the oxidation and oxygenation of organic substrates with atmospheric oxygen is a subject of current interest.[10] Thus, the results of our research might have physiological and chemical importance. Therefore, we further extended our study to clarify the role of metal ions in this type of reaction. Here, we wish to report on more detailed aspect of the catalytic action of iron and manganese ions in the photochemically-induced oxidation of D-fructose in neutral to weakly basic solution.

Experimental

Materials. D-Erythrose and D-fructose were obtained from Aldrich Chem. Co. and Wako Pure Chem. Ind. Ltd., respectively. Other chemicals were also obtained commercially, and some of them were purified by conventional methods prior to use.

Photoirradiation. Sample solutions were freshly prepared using deionized water. The pH of solutions were adjusted to appropriate values by the addition of a concd NaOH solution. Photoirradiation was carried out at 20 °C by one of the following three methods.

1) 70 ml of a solution whose pH was initially adjusted to 9.6 was placed in a reaction vessel and internally irradiated by a 100 W high-pressure mercury lamp (Type UM-102, Ushio Electric Inc.) through a Pyrex-made water jacket. During irradiation, the solution was magnetically stirred and air was continuously bubbled from the bottom of the vessel. As the pH of the solution gradually decreased during photoirradiation, small amounts of concd NaOH solution were added every hour during irradiation to keep the solution within the pH range 6 to 9.6.

2) 500 ml of the solution was placed in a larger reaction vessel fitted with a pH electrode and irradiated using the same procedure described above. The pH of the solution was monitored by a TOA HM-20B pH meter and was kept constant during irradiation by a controlled addition of a 2 M[11] NaOH solution with a HSM-10A pH stat (Toa Electronics Ltd.).

3) 3 ml of the solution in a quartz cell was degassed by three freeze-thaw cycles and then irradiated by light of a known wavelength and energy (1—2.3×10^{-2} W) in a JASCO CRM-FA spectro-irradiator with a 2 kW Xenon lamp.

Analyses of the Irradiated Solutions. Syrup obtained from the irradiated solution was analyzed by previously described methods; D-fructose by high-performance liquid chromatography and D-erythrose by gas-liquid chromatography after acetylation of the syrup.[7] D-Erythrose could also be isolated from the syrup by column chromatography with anion-exchange resins (Hitachi Gel #3019N, Hitachi Ltd.; 300×20 mm; CH_3OH). Formic acid in the solution was determined according to a method of Isbell et al.[12] The irradiated solution was treated with cation-exchange resins (Amberlite IR-120, H^+-form, Rohm & Haas) and then extracted three times with ether. The amount of ether-extractable acid, which was identified to be formic acid after converting to *p*-bromophenacyl formate (mp 99—101 °C; lit, 99—100 °C[13]), was determined by titration with a 0.2 M NaOH solution.

Other Measurements. UV-visible spectra were recorded by a JASCO UVIDEC-505 spectrophotometer at 20 °C and electron-spin-resonance (ESR) spectra were measured at room temperature by a JEOL JES-FE3X

spectrometer operated in the X band.

Titration of 30 ml metal-D-fructose solutions were carried out pH-metrically at 25 °C by the addition of 0.1 M NaOH at a rate of 0.5 ml min^{-1} under an anaerobic atmosphere or 0.13 ml min^{-1} under an aerobic atmosphere.

Results

Photoirradiation in the Presence of Metal Salts. Though addition of concd NaOH solutions to acidic $FeCl_3$, $MnCl_2$, or $CuCl_2$ solutions usually resulted in a formation of a colloidal precipitate of metal hydroxide, no precipitate was formed in the presence of a large excess of D-fructose. The solutions remained clear even in the weakly acidic to basic pH range, demonstrating the ability of D-fructose to sequester metal cations in aqueous media.

Seventy millilitre of a solution containing D-fructose (2.8×10^{-2} mol) and a catalytic amount of metal chloride (1.4×10^{-4} mol) was irradiated by Pyrex-filtered light (method 1, see Experimental section). The pH of the solution initially adjusted to 9.6 was kept within the range between 6 to 9.6 during irradiation. Though the formation of a brown colloidal precipitate was observed at the end of irradiation in the presence of $FeCl_3$ or $FeCl_2$, no precipitate was formed even after 24 h of irradiation in the presence of $MnCl_2$. Irradiation in the presence of $CuCl_2$ led to the deposition of metallic copper on the surface of the water jacket at an early stage of the reaction and no light was transmitted to the solution thereafter. Results are summarized in Table 1. Though D-erythrose was the main oxidation product, its yield markedly decreased in the case of $MnCl_2$. No reaction proceeded without photoirradiation or in the absence of any of the metal salts or oxygen.

Oxidation-reduction Cycle of Iron and Manganese Ions. We showed in a preceding letter that the irradiation of an $FeCl_3$–D-fructose solution at pH 9.6 under anaerobic conditions caused the reduction of Fe(III) into Fe(II) and a subsequent aeration of the irradiated solution led to the oxidation of Fe(II) to Fe(III) again.[9] Spectral changes shown in Fig. 1(a) confirm the photoreduction and subsequent oxidation of Fe(II) ion. Similar experiments were carried out for the $MnCl_2$–D-fructose system. A $MnCl_2$ (2×10^{-3} M)–D-fructose (0.4 M) solution was adjusted

Table 1. Photoirradiation in the Presence of Metal Chloride at 20 °C

Metal Chloride	Irradiation Time/h	D-Fructose Oxidized 10^{-3} mol	D-Erythrose Formed 10^{-3} mol
$FeCl_3$[a]	12	9.1	6.7 (74%)[b]
$FeCl_2$[a]	12	8.5	6.2 (73%)
$MnCl_2$[a]	24	15.4	8.7 (56%)
$CuCl_2$	6	0	0

A 70 ml of the D-Fructose(2.8×10^{-2} mol)–metal chloride (1.4×10^{-4} mol) solution was irradiated by the method 1.

a) Ref. 9, b) Conversion based on the D-fructose oxidized (mol%).

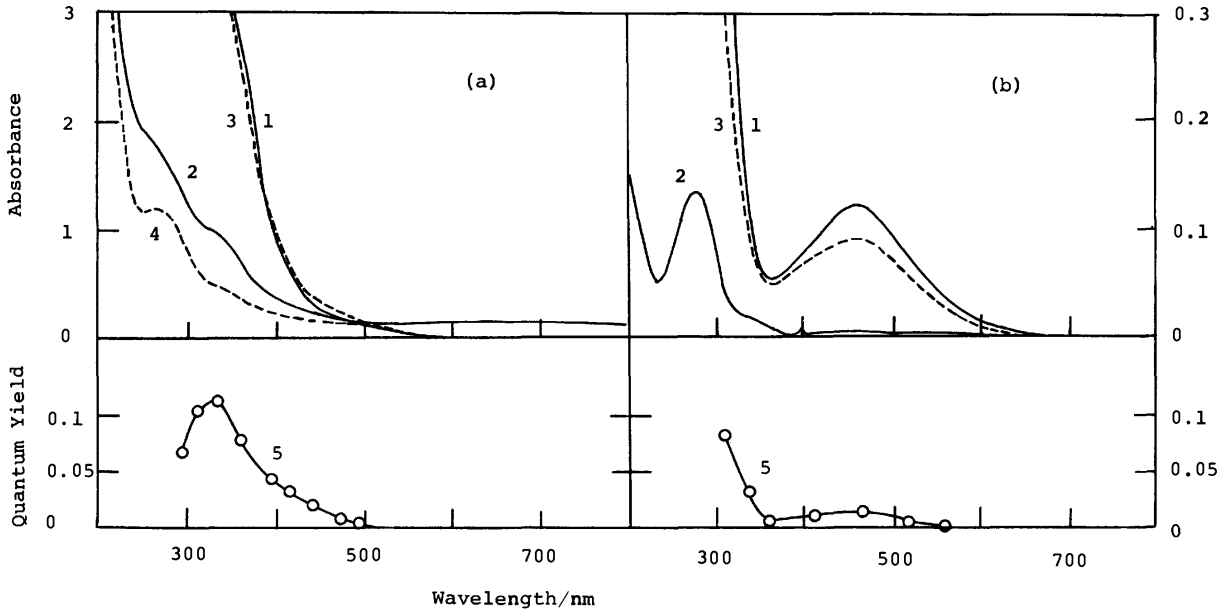

Fig. 1. Absorption and Action Spectra of (a) $FeCl_3$ (2×10^{-3} M)- and (b) $MnCl_2$ (2×10^{-3} M)–D-Fructose (4×10^{-1} M) Sloutions at pH 9.6 and 20 °C.
Initial solution(1) was irradiated for 30 min under anaerobic conditions(2), and then the solution was aerated(3). Spectrum (4)represents the $FeCl_2$(2×10^{-3} M)–D-fructose (4×10^{-1} M) solution at pH 9.6 prepared under anaerobic conditions, and curves(5) shows the quantum yields of the reduction of M(III) at different wavelengths.

to pH 9.6 by the addition of concd NaOH under an aerobic atmosphere. The colorless solution became slightly reddish and the d-d transition-band characteristics for the high-spin Mn(III) state were observed at 400—500 nm (Fig. 1(b)).[14] No signal was observed in the ESR spectrum of the solution, further supporting the formation of Mn(III) species.[15] Photoirradiation after deaerating the solution gave a clear colorless solution, showing practically no absorption in the visible region. The ESR spectrum of the irradiated solution showed a sextet signal, confirming the formation of a high-spin octahedral Mn(II) complex.[15] The aeration of the irradiated solution again made the solution faintly reddish and the ESR signal disappeared. Thus, it was shown that a photochemically-induced reduction of Mn(III) to Mn(II) and subsequent oxidation to Mn(III) by atmospheric oxygen does take place in the presence of a large excess of D-fructose in a weakly basic pH range without forming any precipitate. The action spectrum of the reduction of Mn(III) obtained by method 3 is also shown in Fig. 1(b).

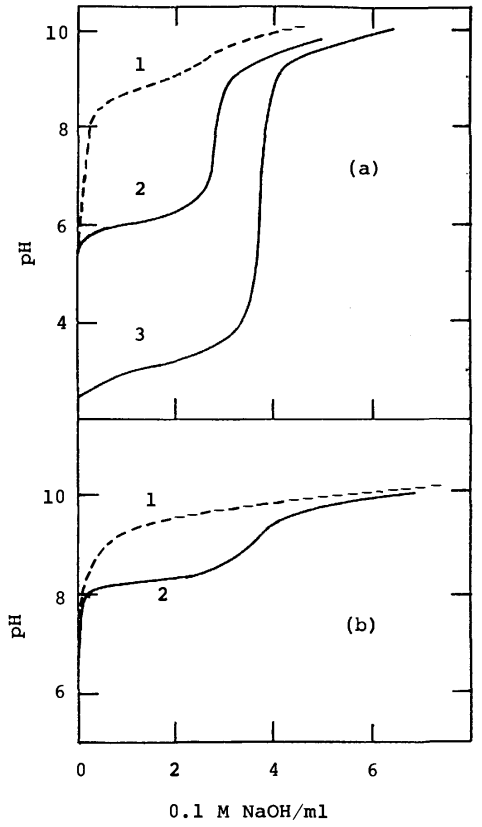

Fig. 2. Titration Curves of Metal Chloride(4×10^{-3} M)-D-fructose(8×10^{-1} M) Solutions(30 ml) by 0.1 M NaOH at 25 °C.
(a): 1. $FeCl_2$ under anaerobic, 2. $FeCl_2$ under aerobic, and 3. $FeCl_3$ under aerobic atmosphere. (b): 1. $MnCl_2$ under anaerobic, and 2. $MnCl_2$ under aerobic atmosphere.

To study the oxidation process of Fe(II) and Mn(II) further, $FeCl_3$-, $FeCl_2$-, and $MnCl_2$-D-fructose solutions were titrated using a 0.1 M NaOH solution under anaerobic or aerobic atmosphere (Fig. 2). When $FeCl_2$ was titrated in an oxygenated solution, Fe(II) was oxidized to Fe(III) at around pH 6. However, the oxidation of Mn(II) was observed only above pH 8 under similar conditions.

Effect of pH on the Reaction. Since the pH of a solution is an essential factor for the photochemically-induced oxidation of monosaccharide in the presence of transition-metal ions, the effect of pH on the reaction was further studied for $FeCl_3$-D-fructose systems. For this purpose, 500 ml of the $FeCl_3$(1×10^{-3} mol)-D-fructose(2×10^{-1} mol) solution was irradiated for 120 h with a controlled addition of a small amount of 2 M NaOH in order to maintain the pH of the solution more strictly (method 2). Without the addition of 2 M NaOH, the pH of the solution (initially adjusted to 9.6) decreased to about 3 after 12 h of irradiation. The irradiation of a solution whose pH was below 6.8 resulted in the formation of a colloidal precipitate within 24 h. The amounts of 2 M NaOH required to maintain the initial pH of the solution during irradiation are shown in Fig. 3 and the irradiation results are summarized in Table 2. A considerable amount of 2 M NaOH was consumed to maintain the pH of the solution and the yield of D-erythrose in the oxidation products markedly decreased, especially when irradiated at a higher pH. This suggested the formation of acids as oxidation products. Formic acid was detected from the ether-extract of the irradiated solution.

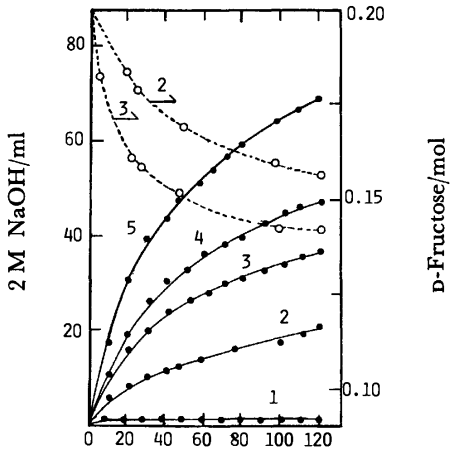

Fig. 3. Time Cource of the Photooxidation of D-Fructose (2×10^{-1} mol/500 ml) by Method 2 in the Presence of $FeCl_3$ (1×10^{-3} mol) at 1. pH 6.8, 2. pH 7.2, 3. pH 7.8, 4. pH 8.4 and 5. pH 9.0.
(—●—): 2 M NaOH required to maintain the initial pH, and (—○—): D-fructose.

Table 2. Effect of pH on the Photochemically-Induced Oxidation of D-Fructose in the Presence of $FeCl_3$ at 20 °C

pH	D-Fructose oxidized 10^{-3} mol	D-Erythrose[a] $/10^{-3}$ mol	NaOH consumed $/10^{-3}$ mol	Formic Acid $/10^{-3}$ mol
6.8	49	27 (55%)	5	5
7.2	44	18 (41%)	42	12
7.8	54	18 (33%)	74	19
8.4	80	12 (15%)	99	31
9.0	92	6 (7%)	133	38

A 500 ml of the D-fructose(0.2 mol)-$FeCl_3$(1×10^{-3} mol) solution was irradiated by the method 2 (see Experimental) for 120 h.

a) Conversions based on the D-frucotse oxidized are given in parentheses(mol%).

Discussion

Catalytic Action of Iron and Manganese Ions. Titration curves in Fig. 2 show that Fe(III) exists as $[Fe^{III}(OR^-)_3]$ at neutral to weakly basic pH in the presence of a large excess of D-fructose, where OR^- represents OH^- or a dissociated form of D-fructose. Fe(II) is supposed to exist as Fe^{2+} or to some extent as $[Fe^{II}(OR^-)]^+$ at around pH 9. These results are essentially the same as those in the absence of D-fructose (pK_a=6 for $[Fe^{III}(OH^-)_2]^+ + OH^- \rightleftarrows [Fe^{III}(OH^-)_3]$, and pK_a=9.2 for $Fe^{2+} + OH^- \rightleftarrows [Fe^{II}(OH^-)]^+$).[16,17] However, no precipitate was formed in this pH range in the presence of D-fructose, and both Fe(III) and Fe(II) remained in the solution.

The oxidation of Fe(II) by atmospheric oxygen in the presence of D-fructose was shown to take place at an appreciable rate above pH 6 in the dark (Fig. 2). This result is consistent with the fact that the oxidation-reduction potential of Fe(III)/Fe(II) decreased at a higher pH of the solution. Several studies have shown that the rate of oxidation of Fe(II) strongly depends on the hydroxide ion concentration. The half-lives of Fe^{2+} in an air-saturated solution at pH 8 is estimated to be 45 s.[17,18] This oxidation process can be written as follows at a neutral pH,

$$2Fe^{2+} + 1/2O_2 + 6HOR \longrightarrow 2[Fe^{III}(OR^-)_3] + 4H^+ + H_2O,$$

where ROH represents H_2O or D-fructose. Therefore, the pH of the solution decreases upon the oxidation of Fe(II).

When D-fructose is degraded by a photochemically-induced oxidation with Fe(III) in a acidic medium under either an aerobic or an anaerobic atmosphere, 2 mol of Fe(III) is required to oxidize 1 mol of D-fructose into D-erythrose.[7] The irradiation of D-fructose solutions at a neutral pH in the presence of a small amount of $FeCl_3$ also caused the degradation of D-fructose, mostly into D-erythrose. However, the amount of D-fructose oxidized or D-erythrose formed is much more than that of Fe(III) (Table 1). The reaction requires the presence of oxygen, a small amount of iron ions, and irradiation with light. Irradiation in the absence of oxygen caused only a reduction of Fe(III) into Fe(II) without a detectable decrease in D-fructose. This was because the amount of iron ion in a solution was quite small compared to that of D-fructose. Therefore, the reaction was concluded to involve a photochemically-induced oxidation with atmospheric oxygen by coupling with the oxidation-reduction cycle of iron ions (Scheme 1). Little difference was observed for reactions in the presence of different iron species at the beginning ($FeCl_3$ and $FeCl_2$). Also Fe(II) was shown to be oxidized to Fe(III) by atmospheric oxygen at an appreciable rate at neutral pH. These facts further support the mechanism shown above, and the results shown in Fig. 1(a) also confirm that the oxidation-reduction cycle of iron is operative and repeatable. The photochemical process of the reaction was the reduction of Fe(III) into Fe(II) with a concomitant oxidation of D-fructose to D-erythrose. The highest quantum yield of the process was observed at 300—350 nm, showing that the exitation of the ligand-to-metal charge transfer (LMCT) band of Fe(III) was the key step of the process.[19] The results are substantially the same as those of reactions in acidic media.[7]

It was noted in relation to the results shown in

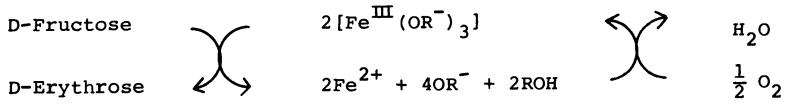

Scheme 1.

Table 2 that the irradiation of a solution whose pH was below 6.8 resulted in the formation of a colloidal precipitate. In this pH range, Fe(III) was supposed to exist in part as $[Fe^{III}(OR^{-})_2]^{+}$ in the solution, and the relative instability of this species toward hydrolysis compared to that of $[Fe^{III}(OR^{-})_3]$ may have been responsible for the precipitate formation.

It was also shown that manganese ions underwent a photoreduction from Mn(III) to Mn(II) and a subsequent reoxidation to Mn(III) due to atmospheric oxygen in the presence of a large excess of D-fructose at a weakly basic pH without the formation of any precipitate. Mn(III) and other higher oxidation states of manganese ion were interpreted to be involved in biological electron-transfer reactions.[20] However, relatively few Mn(III) complexes are known to be stable and soluble in aqueous solutions due to their high affinity toward hydroxide ions.[21,22] D-Fructose showed a good sequestering ability toward Mn(III), and Mn(III) species were formed with an appreciable rate above pH 8 under an aerobic atmosphere and remained in solution. The action spectrum of the reduction of Mn(III) at 260—650 nm showed that light of shorter wavelengths was more effective though a small maximum was observed at a region corresponding to the d-d transition band of Mn(III) (Fig. 1(b)). As the LMCT band of the Mn(III) species has been reported to be at 200—220 nm with a large extinction coefficient,[14] the excitation of the LMCT band is suggested to be most effective for the reduction of Mn(III), being consistent with that of Fe(III).

Effect of PH on the Catalytic Action of $FeCl_3$. The photooxidation of D-fructose by Fe(III) in an acidic media shows a high selectivity and gives D-erythrose in a nearly 90% yield via the formation of a D-fructose–Fe(III) complex.[7] As the reoxidation of Fe(II) does not proceed at an appreciable rate in an acidic solution, the pH of a solution should be kept above 6 for the oxidation-reduction cycle of iron ions to operate. However, the selectivity of the reaction to yield D-erythrose markedly decreased at a higher pH (Table 2). Though the yield of D-erythrose still complised more than a half of D-fructose oxidized at pH 6.8, the formation of formic acid and other acid products predominated in a more basic pH range. Aldonic acids, formic acid, and other acid products along with carbon dioxide were the common oxidation products of aldoses and ketoses with oxygen in highly alkaline solutions or with hydrogen peroxide.[23,24] Hydroxyl radical is thought to be involved in these reactions. The autoxidation of cellulose in alkaline conditions is known to be more extensive in the presence of transition-metal cations, and the photoirradiation of a cellulose-transition metal system leads to the formation of radical species.[25,26] Therefore, a free-radical process might be involved in the formation of acid products rather than a direct electron transfer from D-fructose to the Fe(III) via a complex formation. And this process becomes more dominant at a higher pH.

Thus, a catalytic amount of transition-metal cations in neutral to weakly basic solutions is shown to cause the photochemically-induced degradation of D-fructose in the presence of atmospheric oxygen. Cox et al. have noted that the presence of Fe(II) in freshly opened ampoules of "Imferon" (the ferric-dextran preparation frequently used for the treatment of iron-defficient anemia) is responsible for the hypotensive side effect of this preparation and that an exposure to the atmosphere abolishes this side effect.[27] This observation may be understood from the results presented here, i.e., the reduction of Fe(III) during the storage and reoxidation of Fe(II) by atmospheric oxygen in the presence of dextran. Furthermore, the results might have a wide variety of biological and physiological importance,[28] since saccharides and transition-metal cations are widely distributed in nature.

References

1) "Inorganic Biochemistry," ed by G. L. Eichhorn Elsevier, Amsterdam (1973).

2) J. Briggs, P. Finch, M. C. Matulewics, and H. Weigel, *Carbohydr. Res.*, **97**, 181 (1981).

3) H. Shioi, S. Yano, K. Toriumi, T. Ito, and S. Yoshikawa, *J. Chem. Soc., Chem. Commun.*, **1983**, 201.

4) S. A. Barker, P. J. Somers, and J. Stevenson, *Carbohydr. Res.*, **36**, 331 (1974).

5) K. Araki, M. Sakuma, and S. Shiraishi, *Chem. Lett.*, **1983**, 665.

6) T. Sato, K. Takahashi, and S. Ichikawa, *Chem. Lett.*, **1983**, 1589.

7) K. Araki, M. Sakuma, and S. Shiraishi, *Bull. Chem. Soc. Jpn.*, **57**, 997 (1984).

8) T. Sato, K. Takahashi, and S. Ichikawa, *Nippon Kagaku Kaishi*, **1984**, 119.

9) K. Araki, and S. Shiraishi, *Chem. Lett.*, **1984**, 267.

10) D. W. Reichgott, N. J. Rose, *J. Am. Chem. Soc.*, **99**, 1813 (1977).

11) 1 M=1 mol dm^{-3}.

12) H. S. Isbell, H. L. Frush, and E. T. Martin, *Carbohydr. Res.*, **26**, 287 (1973).

13) T. Kubota, and T. Matsuura, *Nippon Kagaku Zasshi*, **72**, 482 (1951).

14) C. F. Wells, and G. Davies, *J. Chem. Soc., A*, **1967**, 1858.

15) A. Abragram, and B. Bleaney, "Electron Paramagnetic Resonance of Transition Ions," Clarendon Press, Oxford (1970).

16) C. M. Flynn, Jr., *Chem. Rev.*, **84**, 31 (1984).

17) G. K. Johnson, and J. E. Bauman, Jr., *Inorg. Chem.*, **17**, 2774 (1978).

18) K. Goto, H. Tamura, and M. Nagayama, *Inorg. Chem.*, **9**, 963 (1970).

19) A. W. Adamson, W. L. Waltz, E. Zinato, D. W. Watts,

P. D. Fleishauer, and R. D. Lindholm, *Chem. Rev.*, **68**, 541 (1968).
20) M. Pick, J. Rabani, F. Yost, and I. Fridovich, *J. Am. Chem. Soc.*, **96**, 7329 (1974).
21) C. F. Wells, *Nature*, **205**, 693 (1965).
22) K. D. Magers, C. G. Smith, and D. T. Sawyer, *Inorg. Chem.*, **17**, 515 (1978).
23) H. S. Isbell, H. L. Frush, *Carbohydr. Res.*, **28**, 295 (1973).
24) B. Warshowsky, and W. M. Sandstrom, *Arch. Biochem. Biophys.*, **37**, 46 (1952).
25) D. Entwistle, E. H. Cole, and N. S. Wooding, *Text. Res. J.*, **19**, 527 (1949).
26) N-S. Hon, *J. Polym. Sci., Polym. Chem. Ed.*, **13**, 1933 (1975).
27) J. S. G. Cox, R. E. King, and G. F. Reynolds, *Nature*, **207**, 1202 (1965).
28) K. Araki, H. Ishida, S. Shiraishi, The 1984 International Chemical Congress of Pacific Basin Societies, Honolulu, Hawaii, Dec. 1984, Abstr., 04B22.

 © 1986 The Chemical Society of Japan Bull. Chem. Soc. Jpn., 59, 235—238 (1986)

The Asymmetric Ullmann Coupling Reaction of (*S*)-2,2′-Bis(1-bromo-2-naphthoyloxy)-1,1′-binaphthyl Revisited. Formation of 24-Membered Optically Pure Cyclic Dimer as Well as 12-Membered Cyclic Monomer

Sotaro MIYANO,* Shigeru HANDA, Masayuki TOBITA, and Harukichi HASHIMOTO
Department of Applied Chemistry, Faculty of Engineering, Tohoku University, Aramaki-Aoba, Sendai 980
(Received August 28, 1985)

The copper-promoted Ullmann reaction of the title diester proceeded with high stereoselectivity to give 24-membered optically pure cyclic dimer of (*S,S,S,S*)-configuration as well as 12-membered monomeric cycle of (*S,S*)-configuration. The reaction also gave reduced, open-chain dimer enriched in (*S,R,S*)-diastereomer over (*S,S,S*)-counterpart (17% d.e.). Stereochemical course to the cyclic dimer was discussed considering the result that the intermolecular Ullmann coupling of chiral alcohol esters of 1-bromo-2-naphthoic acid poorly induced axial chirality in the joining of the two naphthyl units.

Recently, much attention has been centered on the asymmetric reaction by the use of axially chiral biaryls as the chirality-recognizing auxiliaries,[1] and thus there has been an increasing interest in the construction of the requisite atropisomeric biaryl skeleton via a route other than optical resolution of the racemate.[2]

In our previous papers,[3] we have reported that the Ullmann reaction of axially chiral 1,1′-binaphthyl-2,2′-diol diester (*S*)-**1** proceeds with complete diastereoselectivity to give intramolecularly coupled 12-membered monomeric cycle (*S,S*)-**2** in a 36% isolated yield without formation of (*S,R*)-diastereomer (Scheme 1). It was also implied that 24-membered cyclic dimer **4**, which was obtained only in a small amount from the reaction conducted under dilution conditions, was likely to have a rather high diastereomeric purity (87—100% d.e.) of (*S,S,S,S*)-configuration.[3b] Here we wish to report that the cyclic dimer is obtainable in a 10% yield as a precipitate from a benzene solution of an Ullmann reaction mixture in essentially optically pure state, and also wish to discuss the stereochemical course of the copper-promoted coupling reaction of (*S*)-**1** to the cyclic dimer.

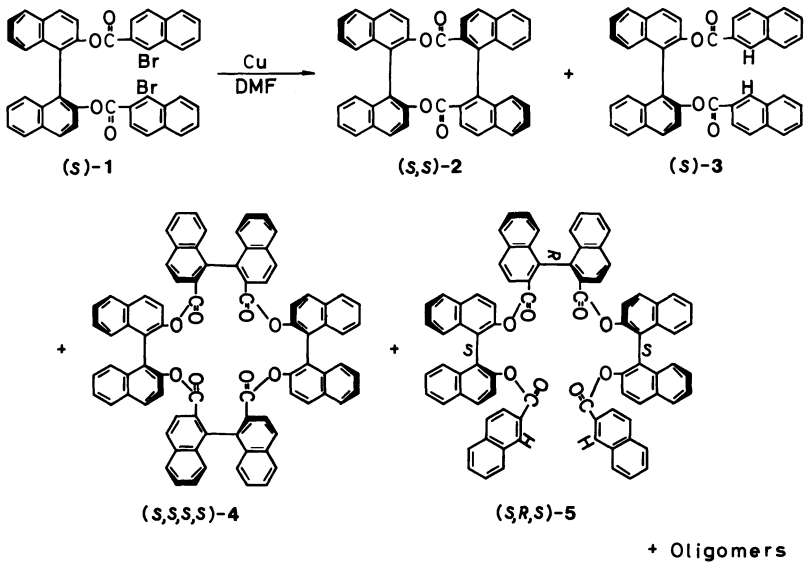

Scheme 1.

Results and Discussion

Isolation of Optically Pure Cyclic Dimer (*S,S,S,S*)-4. In order to gain more information on the stereochemistry of the cyclic dimer, here again we repeated the copper-promoted Ullmann reaction of (*S*)-**1** under conditions intended to promote the intermolecular coupling; a mixture of (*S*)-**1** and an activated copper powder in a small volume of DMF was heated at gentle reflux with vigorous stirring. Debromination was completed within 5 h, and HPLC of the crude reaction mixture showed the presence of several components which had the

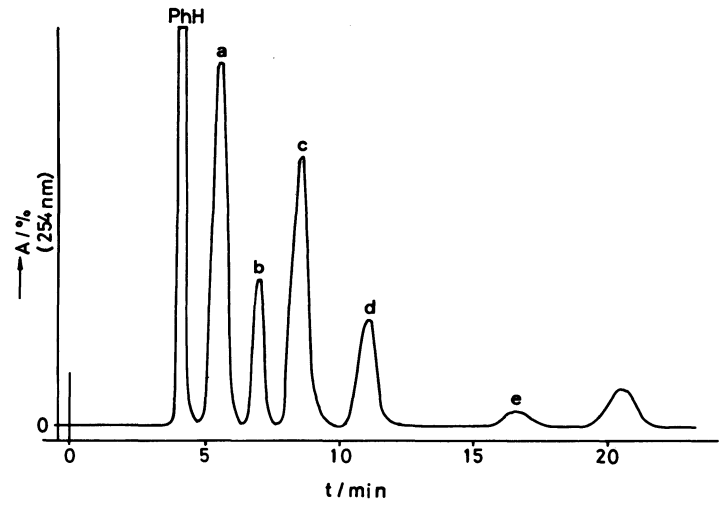

Fig. 1. HPLC of the Ullmann reaction mixture of (*S*)-**1**.
Conditions: microcolumn (0.5 mm (i.d.) × 10 cm) packed with JASCOSIL SC-01 eluted with 2% aq CH_3CN (8 μl/min). **a**, (*S,S*)-**2**; **b**, (*S*)-**3**; **c**, (*S,S,S,S*)-**4**; **d**, (*S,S,S*)- and (*S,R,S*)-**5**; **e**, tentative cyclic trimer(s).

retention volumes identical to those of, in the order of elution, (*S,S*)-**2**, (*S*)-**3**, cyclic dimer **4** obtained in the previous work,[3b] and open-chain dimer **5** (Fig. 1). The authentic sample of **5** was comprised of a 52:48 mixture of (*S,S,S*)- and (*S,R,S*)-**5**,[4] showing that these diastereomers were not differentiated on the HPLC conditions. The component eluting the 5 th on HPLC (**e** in Fig. 1) was tentatively assigned to cyclic trimer(s) (see Experimental).

Attempted cryoscopy of the Ullmann reaction mixture in benzene was unsuccessful because of the deposition of a white precipitate on cooling a rather dilute solution. Unexpectedly but to our pleasure, we found that the precipitate showed only one peak on HPLC which had the same retention volume as that of the cyclic dimer **4**. Thus, the component of $[\alpha]_{436}^{24}$ −293±4° (PhH) was isolated in a 10% yield by standing a benzene solution of the reaction mixture at ambient temperature for 2 d followed by filtration of the precipitate deposited. The benzene filtrate was then subjected to silica-gel chromatographies to allow the isolation of (*S,S*)-**2** (12%), an extra amount of cyclic dimer **4** of $[\alpha]_{436}^{24}$ −296±3° (PhH) (1.2%), and open-chain dimer **5** (3.6%).

Discrepancies in optical rotations of the samples of **4** recovered above and the one obtained in the previous work by a column chromatography ($[\alpha]_{436}^{24}$ −291° (PhH)) should be regarded within the limits of the experimental error accompanying the measurement of them. These samples showed IR spectra superimposable on each other. From these results there seemed to be little chance that concentration of a particular stereoisomer among the possible cyclic dimers **4** had occurred during the isolation process.

Stereochemistry of the precipitated cyclic dimer **4** was unequivocally established to be optically pure (*S,S,S,S*)-**4** as follows: Treatment of the sample with lithium aluminium hydride (LAH) gave only two diols, (*S*)-1,1′-binaphthyl-2,2′-diol ((*S*)-**6**) and (*S*)-2,2′-bis(hydroxymethyl)-1,1′-binaphthyl ((*S*)-**7**). Optical

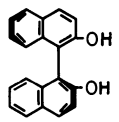

(*S*)-**6**

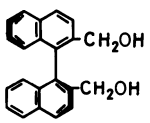

(*S*)-**7**

rotations of these diols compare well with those claimed for enantiomerically pure specimens.[5] The homochirality of (*S*)-**7** was further confirmed by ^1H NMR study of the α-methoxy-α-(trifluoromethyl)-phenylacetic acid (MTPA) ester in the presence of Eu(fod)$_3$ shift reagent.

Stereochemical Course of the Ullmann Reaction of (*S*)-1 to (*S,S,S,S*)-4. Reaction path to cyclic dimer **4** inevitably requires initial bimolecular coupling of (*S*)-**1** to open-chain dibromo dimer **8**. It may be reasonable to assume that this kind of intermolecular coupling should afford a diastereomer mixture of (*S,S,S*)- and (*S,R,S*)-**8** (Eq. 1), the former being slightly in excess as a closely related coupling of (*S*)-**9** to **5** induced (*S*)-axial chirality only in a 4% diastereomeric excess (Eq. 2).[4] It was also reported that *C*-chiral alcohol esters (**10**) of 1-bromo-2-naphthoic acid poorly induced axial chirality in the Ullmann coupling of the two naphthyl units.[6]

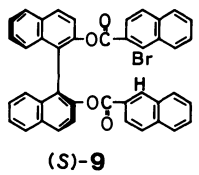

(S)-9

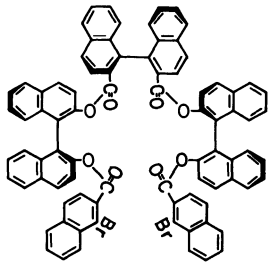

(S,S,S)-8

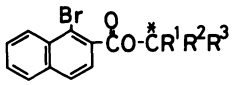

10

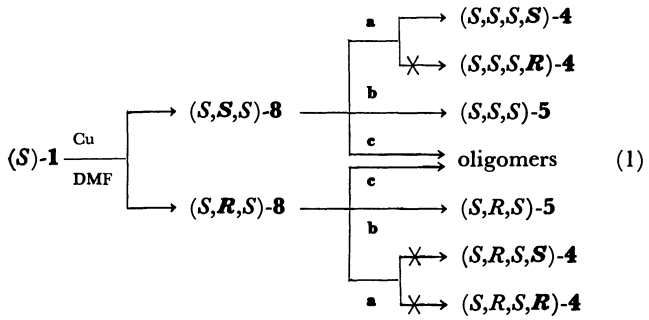

(1)

a: Intramolecular coupling, **b**: Reduction, **c**: Intermolecular reactions. (Bold italic letter indicates newly formed 1,1′-binaphthyl linkage in the said reaction.)

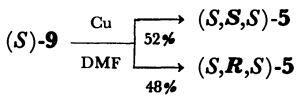

(2)

A rational conclusion deduced from the argument above is that intramolecular cyclization of **8** is allowed only for (*S,S,S*)-diastereomer to (*S,S,S,S*)-**4** without forming (*S,S,S,R*)-**4**, but not allowed for (*S,R,S*)-**8** which should give (*S,R,S,S*)- or (*S,R,S,R*)-**4** (Eq. 1). Although it is not easy to unequivocally explain the exclusive formation of (*S,S,S,S*)-**4**, inspection of the CPK molecular models of the intermediate dibromo dimers **8** and the possible cyclic dimers **4** gives some indication.

Conformationally identical 1,1′-binaphthyl axes in (*S,S,S*)-**8** seem to bring the two bromine substituents in a position to allow ring closure to cyclic dimer, while in (*S,R,S*)-**8** the coupling sites are disposed rather separated each other by intervening three 1,1′-binaphthyl moieties.

The models also show that (*S,S,S,S*)-**4** has the most symmetrical, and the least sterically crowded structure among the four possibilities; four sets of 1,1′-binaphthyl moieties are all staggered to each other as schematically illustrated in Fig. 2, which is a top view looking down along the axes of four 1,1′-binaphthyl linkages where the hatched naphthalene rings locate closer to the eyes.

On the other hand, naphthalene planes **a** and **b**, and **c** and **d** in (*S,S,S,R*)-**4** are respectively disposed face to face to each other in a close vicinity, thus imposing steric repulsion between the edges of the rings **c** and **e** (Fig. 3). Similar situation to this is valid for the (*S,R,S,S*)-counterpart. The (*S,R,S,R*)-disposition seems to be the least comfortable because every naphthalene ring faces to another causing four sets of collision among edges of the eight naphthalene rings (Fig. 4).

Stereochemistry of Open-chain Dimer 5. Treatment of the recovered **5** with LAH gave (*S*)-**6**, 2-naphthalenemethanol **11**, and **7**. On the basis of the

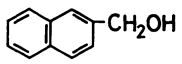

11

optical rotation of the diol **7**, the diastereomeric excess of the open-chain dimer **5** should be 17% enriched in (*S,R,S*)-**5** over (*S,S,S*)-diastereomer.[7] This stereochemical bias in **5** is qualitatively understandable as follows: Among the plausible reactions of the dibromo dimers **8** are intramolecular ring closure to cyclic dimers **4** and reduction to open-chain dimers **5**, as well as further intermolecular reactions to oligomeric products (Eq. 1). Assuming that the other conditions are equal, (*S,R,S*)-**8** should have more chance than (*S,S,S*)-**8** to be reduced to the open-chain dimer ((*S,R,S*)-**5**), because it lacks the exit to the corresponding cyclic dimer **4** as stated above.

In conclusion, we have shown here that 24-membered optically pure cyclic dimer (*S,S,S,S*)-**4** is

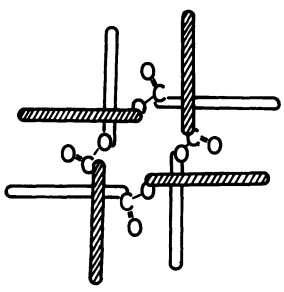

Fig. 2. (*S,S,S,S*)-4.

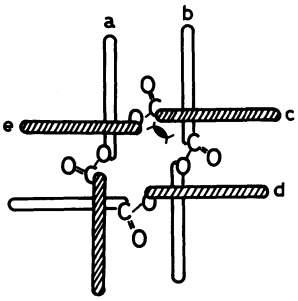

Fig. 3. (*S,S,S,R*)-**4**.

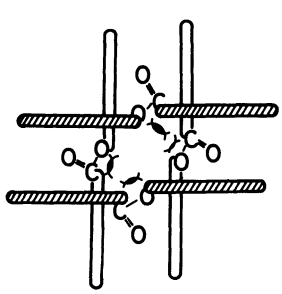

Fig. 4. (*S,R,S,R*)-**4**.

easily obtainable in a 10% yield as a precipitate from a benzene solution of an Ullmann reaction mixture of (*S*)-**1**. Recently, macrocyclic compounds with chiral cavity such as chiral crown ethers and cyclodextrins have been receiving considerable attention because of their high ability for chiral recognition of guest molecules.[8] CPK molecular models show that the 24-membered (*S,S,S,S*)-**4** confines a cavity just fit to accommodate a molecule of the size of benzene nucleus (Fig. 2), and investigation of the host-guest interaction involving the cycle is now under way.

Experimental

General directions are given in Ref. 3b. A JASCO FAMILIC-100 instrument was routinely utilized for the HPLC analyses of various binaphthyl derivatives encountered in this study using a 0.5 mm(i.d.)×10 cm microcolumn packed with JASCOSIL SC-01 (ODS) eluted with CH_3CN–H_2O.

(*S*)-**1** was prepared as before[3b] from (*S*)-**6** ($[\alpha]_D^{22}$ −34.8° (*c* 0.985, THF)) and 1-bromo-2-naphthoyl chloride; mp 178—179 °C (uncor.); $[\alpha]_D^{22}$ +34.3° (*c* 1.13, acetone).

Ullmann Reaction of (*S*)-1. To a mixture of (*S*)-**1** (3.00 g, 3.99 mmol) and activated copper powder (prepared from 3.0 g of Cu (47 mg-atom)) was added 20 ml of DMF. The mixture was magnetically stirred and heated to gentle reflux under nitrogen. After 5 h reaction, the mixture was worked up as before[3b] to give a pale yellow organic residue, 2.31 g (97.7% yield calculated as **2**), $[\alpha]_D^{24}$ −48.6° (*c* 0.803, PhH).

Isolation of (*S,S,S,S*)-4 by Precipitation: A 1.25 g sample of the Ullmann product was dissolved in 30 ml of hot benzene. The solution was allowed to stand for 2 d at ambient temperature to give a white precipitate. The material settled out was recovered by filtration, washed with small portions of benzene, and dried in vacuo (≈100 °C/10^{-1} mmHg) to give (*S,S,S,S*)-**4** as a white powder; 0.133 g (0.112 mmol); $[\alpha]_{436}^{24}$ −293±4° (*c* 0.152, PhH); IR (KBr) 1745 cm^{-1}. Found: C, 84.81; H, 4.43%. Calcd for $C_{84}H_{48}O_8$: C, 85.12; H, 4.08%.

The cyclic dimer (57 mg) was boiled with 0.1 g of LAH in 30 ml of ether for 5 h. After usual work-up, products were separated by preparative TLC (silica gel, $CHCl_3$/AcOEt(4/1)).

(*S*)-**6**: 21 mg; $[\alpha]_D^{24}$ −34.3° (*c* 1.14, THF).

(*S*)-**7**: 25 mg; $[\alpha]_{546}^{24}$ −83.2° (*c* 1.25, acetone). MTPA esters of (*S*)-**7** and racemic **7** were prepared by treatment with (*R*)-MTPA chloride. ^{1}H NMR studies of the esters in $CDCl_3$ in the presence of varying amounts of Eu(fod)$_3$ indicated that the (*S*)-**7** should be more than 98% e.e.[3b]

Stereochemistry of (*S,R,S*)-5: The benzene filtrate, which had been removed of the precipitate of (*S,S,S,S*)-**4**, was subjected to a silica-gel column chromatography ($CHCl_3$ (1% EtOH)) to give 0.157 g of (*S,S*)-**2**, $[\alpha]_D^{24}$ −452° (*c* 0.613, PhH) (lit,[3b] −457.6° (*c* 0.507, PhH)).

Column effluent fractions which were mostly comprised of cyclic dimer **4** and open-chain dimer **5** were further subjected to TLC separation (silica gel, $CHCl_3$ (1% EtOH)) to give (*S,S,S,S*)-**4** (15 mg, $[\alpha]_{436}^{24}$ −296±3° (*c* 0.147, PhH)) and (*S,R,S*)-**5** (46 mg). The latter was treated with LAH to give (*S*)-**6** (18 mg, $[\alpha]_D^{24}$ −34.2° (*c* 0.352, THF), (*S*)-**7** (11 mg, $[\alpha]_{546}^{24}$ +14.6° (*c* 0.518, acetone), and **11** (6 mg).

Similar preparative TLC of another fraction of the column effluent gave the component corresponding to **e** in Fig. 1, 14 mg, $[\alpha]_D^{24}$ +26.3° (*c* 0.909, PhH), which was tentatively assigned to cyclic trimer(s) on the basis of the HPLC elution pattern, a chemical transformation, and IR spectral studies: The cyclic structure was confirmed by the fact that LAH treatment of the sample gave only two spots on TLC (silica gel, $CHCl_3$/AcOEt(4/1)) which corresponded to (*RS*)-**6** (R_f 0.18) and (*RS*)-**7** (R_f 0.67), respectively. IR absorption (KBr disk) of the ester carbonyl function was precisely compared with those of cyclic monomer and dimer as follows, and it seemed that release of ring strain reduced the absorption frequency of the cyclic trimer(s).

(*S,S*)-**2**	1752.4 cm^{-1}
(*S,S,S,S*)-**4**	1744.7 cm^{-1}
Tentative cyclic trimer(s)	1742.9 cm^{-1}

We are grateful for support of this work by Takeda Science Foundation.

References

1) Recent examples; a) K. Yamamoto, H. Fukushima, Y. Okamoto, K. Hatada, and M. Nakazaki, *J. Chem. Soc., Chem. Commun.*, **1984**, 1111; b) Y. Kawakami, J. Hiratake, Y. Yamamoto, and J. Oda, ibid., **1984**, 779; c) R. Noyori, I. Tomino, Y. Tanimoto, and M. Nishizawa, *J. Am. Chem. Soc.*, **106**, 6709 (1984); d) K. Tani, T. Yamagata, S. Akutagawa, H. Kumobayashi, T. Taketomi, H. Takaya, A. Miyashita, R. Noyori, and S. Otsuka, ibid., **106**, 5208 (1984); e) A. Miyashita, H. Takaya, T. Souchi, and R. Noyori, *Tetrahedron*, **40**, 1245 (1984).

2) Recent examples; a) F. Sannicolo, *Tetrahedron Lett.*, **26**, 119 (1985); b) J. M. Wilson and D. J. Cram, *J. Org. Chem.*, **49**, 4930 (1984); c) K. Yamamoto, H. Fukushima, and M. Nakazaki, *J. Chem. Soc., Chem. Commun.*, **1984**, 1490; d) A. I. Meyers and D. G. Wettlaufer, *J. Am. Chem. Soc.*, **106**, 1135, (1984).

3) a) S. Miyano, M. Tobita, M. Nawa, S. Sato, and H. Hashimoto, *J. Chem. Soc., Chem.. Commun.*, **1980**, 1233; b) S. Miyano, M. Tobita, and H. Hashimoto, *Bull. Chem. Soc. Jpn.*, **54**, 3522 (1981).

4) The sample was in fact comprised of a 52:48 mixture of (*R,R,R*)- and (*R,S,R*)-**5**, as it was obtained in Ref. 3b by the Ullmann reaction of (*R*)-**9**. For the sake of clarity, however, we will discuss here as if the reaction had been carried out with (*S*)-**9**.

5) See Ref. 3b: (*S*)-**6**: $[\alpha]_D^{22}$ −35.0° (*c* 1.18, THF). (*S*)-**7**: $[\alpha]_{546}^{24}$ −86.0° (*c* 1.43, acetone).

6) S. Miyano, M. Tobita, S. Suzuki, Y. Nishikawa, and H. Hashimoto, *Chem. Lett.*, **1980**, 1027.

7) The (*S,S,S*)-**5** in Scheme 3 in Ref. 3b) should now be read (*S,R,S*)-**5**.

8) "Inclusion Compounds," ed by J. L. Atwood, J. E. D. Davies, and D. D. MacNicol, Academic Press, London (1984) Vol. 2.

 © 1986 The Chemical Society of Japan Bull. Chem. Soc. Jpn., 59, 239—242 (1986)

The Crystal and Molecular Structure of 12-Bromo[2.2][2.2]triple-Layered Paracyclophane

Yosuke KOIZUMI, Toshihiro TOYODA, Kunio MIKI,† Nobutami KASAI,†,* and Soichi MISUMI*
The Institute of Scientific and Industrial Research, Osaka University,
Ibaraki, Osaka 567
† Department of Applied Chemistry, Faculty of Engineering, Osaka University,
Suita, Osaka 565
(Received August 29, 1985)

The molecular structure of 12-bromo[2.2][2.2]paracyclophane has been determined by means of X-ray diffraction. The crystal is orthorhombic, space group *Pbcn*, a=12.768(1), b=11.515(1), c=13.074(1) Å, Z=4. The structure was solved by the heavy-atom method, and refined anisotropically by the block-diagonal least-squares procedure; R=0.062. The Br-C····C-H axis of the central benzene ring lies on a crystallographic two-fold axis. The outer benzene rings take a boat form, and the central benzene ring is twisted.

Among the molecular structures of multi-layered paracyclophane, only that of tetramethyl quadruple-layered paracyclophane has been reported, hitherto.[1] As to the structure of triple-layered ones, a preliminary result on isomers of tetramethyl triple-layered paracyclophanes has been presented, but the structure was reported disordered.[2] This paper deals with the first example of the molecular structure of a triple-layered one, 12-bromo[2.2][2.2]paracyclophane, determined by means of X-ray diffraction. A brief sketch of the structure has been described previously.[3]

Experimental

Crystal Data. $C_{26}H_{25}Br$, M=417.42, orthorhombic, space group *Pbcn*(No. 60, absent reflections, $0kl$: $k=2n+1$, $h0l$: $l=2n+1$, $hk0$: $h+k=2n+1$), a=12.768(1), b=11.515(1), c=13.074(1) Å, V=1922.1(2) Å^3, D_m=1.42 g cm^{-3}(by floatation in an aqueous solution of $ZnBr_2$), D_c=1.46 g cm^{-3} for Z=4.

Colorless octahedral crystal with approximate dimensions of 0.4×0.5×0.6 mm was mounted on a Rigaku automated, four-circle diffractometer. Zr-filtered Mo $K\alpha$ radiation(λ=0.71069 Å) was used.

Intensity data were collected by the θ—2θ scan technique at a 2θ rate of 2° min^{-1}. The scan range was from $\{2\theta(\alpha_1)-1.0\}$ to $\{2\theta(\alpha_2)+1.0\}$°. Backgrounds were counted for 15 s at both ends of a scan. Three standard reflections measured after every 50 reflections to monitor the stability and orientation of the crystal showed no significant decay throughout the data collection. A total of 1762 reflections was observed out of 2520(sin θ/λ<0.7). Usual Lorentz and polarization corrections were made but absorption correction was ignored [μ(Mo)=23.5 cm^{-1}].

Structure Solution and Refinement

Since the space group is *Pbcn* and the unit cell contains four molecules, the molecule must lie on a special position, either two-fold axis or a center of symmetry. The structure was established by the heavy-atom method. The position of the bromine atom was found by the Patterson function. All the carbon atoms could be located on a Fourier map computed by using approximate phases based on the bromine atom. The structure was refined anisotropically by the block-diagonal least-squares procedure (*HBLS* V).[4] The function minimized was $\sum(\Delta F)^2$. Hydrogen atoms were located on a difference Fourier map, which were included in the refinement with isotropic temperature factors. The R value converged to 0.062. Final atomic parameters are listed in Table 1.††

Atomic scattering factors were taken from International Tables for X-Ray Crystallography.[5] Computations were done mainly on a NEAC 2200—500 computer at the Computation Center, Osaka University, and at the final stage an ACOS 850 computer was used at the Crystallographic Research Center, Institute for Protein Research, Osaka University.

Table 1. Final Atomic Coordinates of Non-hydrogen Atoms with Equivalent Isotropic Temperature Factors[6]

Atom	x	y	z	B_{eq}/Å^2
Br	0.5000	0.56717(8)	0.2500	4.72
C(1)	0.3195(4)	0.4014(6)	0.1642(4)	3.93
C(2)	0.2313(4)	0.3803(5)	0.2467(5)	3.93
C(3)	0.2730(4)	0.3312(5)	0.3461(4)	3.12
C(4)	0.3289(4)	0.3999(5)	0.4139(4)	3.25
C(5)	0.4024(4)	0.3503(5)	0.4794(4)	3.23
C(6)	0.4199(4)	0.2307(5)	0.4791(3)	2.94
C(7)	0.3466(4)	0.1621(5)	0.4284(4)	3.31
C(8)	0.2749(4)	0.2120(5)	0.3620(4)	3.27
C(9)	0.5253(4)	0.1836(5)	0.5112(4)	3.77
C(10)	0.5989(4)	0.1614(6)	0.4158(4)	4.00
C(11)	0.5616(4)	0.2251(5)	0.3215(4)	3.10
C(12)	0.5781(4)	0.3436(5)	0.3059(3)	3.04
C(13)	0.5000	0.4005(6)	0.2500	2.80
C(14)	0.5000	0.1659(7)	0.2500	3.32

†† Tables of anisotropic temperature factors, coordinates of hydrogen atoms, and observed and calculated structure factors are kept at the Chemical Society of Japan, Document No. 8612.

Results and Discussion

The molecular structure(*ORTEP*)[7] is drawn in Fig. 1 with the numbering scheme of non-hydrogen atoms. Bond distances and bond angles are given in Fig. 2. The molecule has a two-fold axis symmetry. The Br, C(13), C(14), and H(14) atoms lie on a crystallographic two-fold axis. Three benzene rings are displaced slightly in a helical way from the eclipsed position (Fig. 3a). The C(5)–C(4) and C(12)–(13) bonds projected onto the least-squares plane of the central benzene ring make an angle of 4.1°, and similarly the C(12)–C(13) and C(4′)–C(3′) bonds form 6.4°.

The outer benzene ring has a boat form (Fig. 3b). The bending angle p_1, i.e. the dihedral angle between the plane defined by the C(4), C(5), C(7), and C(8) atoms (Plane 1) and that formed by the C(3), C(4), and C(8)(Plane 2) is 12.0°, and the p_2, the dihedral angle between the plane made by the C(5), C(6), and C(7) atoms (Plane 3) and the Plane 1 is 12.1°. These are approximately equal to the corresponding angles in [2.2]paracyclophane [12.6°][8] and its derivatives[9,10] and tetramethyl quadruple-layered paracyclophane [12.5 and 12.9°].[1] The C(2)–C(3) bond makes an angle q_1 of 11.0° with the Plane 2, and the C(6)–C(9) bond an angle q_2 of 11.7° with the Plane 3. These values are almost the same as those of the [2.2]paracyclophanes. Six C–C bond distances in the outer ring are equal and have normal values [av. 1.393 Å]. Among the bond angles, the C(4)-C(3)-C(8) and C(5)-C(6)-C(7) angles [117.3(5) and 117.0(5)°], which are the angles at the bow and stern of the boat form, are smaller than 120°, whereas the other four angles have normal values [120.4(5) to 121.0(5)°].

The central benzene ring is twisted. The dihedral angle between the plane defined by the C(11), C(12), C(13), and C(14) atoms and that by the C(11′), C(12′), C(13), and C(14) is 5.1°. Bond distances in this ring seem normal, however, inner angles at the C(11) [117.6(5)°] and C(12) atoms [115.3(6)°] are much smaller, whereas that at the C(13)[124.1(6)] is larger than 120°. The C(1)–C(12′) bond bends by 6.6° away from the plane defined by the C(11′), C(12′), and C(13) and the C(10)–C(11) bond by 4.7° away from the C(11)-C(12)-C(14) plane (Fig. 3(b_2)).

In the ethylene bridges, two C_{sp^3}–C_{sp^3} bonds are equal in length[1.578(8) and 1.582(8) Å], which are comparable to those in 4,7-dimethy[2.2]paracyclophane[1.587(12) Å],[9] 4,7,13,16-tetramethyl[2.2]paracyclophane[1.580(10) Å],[9] and tricarbonylchromium complex of [2.2]paracyclophane[1.595(4) Å].[10] Torsional angles around the C(1)–C(2) and C(9)–C(10) bonds are 12.5 and 17.6°, respectively.

Because of the deformation of the outer and central benzene rings closest nonbonded atomic distances between these rings are observed between the C(6) and C(11) atoms [2.744(7) Å] and between the C(3) and C(12′)[2.754(7) Å] (Fig 3(b_2)). The nonbonded

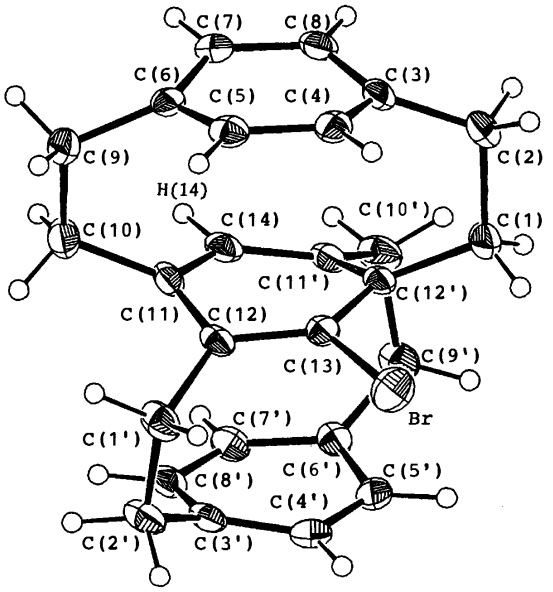

Fig. 1. A perspective view[7] of the molecule. The numbering scheme of non-hydrogen atoms are given. Non-hydrogen atoms are drawn as thermal ellipsoids with 30% probability level, and hydrogen atoms as spheres with $B=1.0$ Å^2.

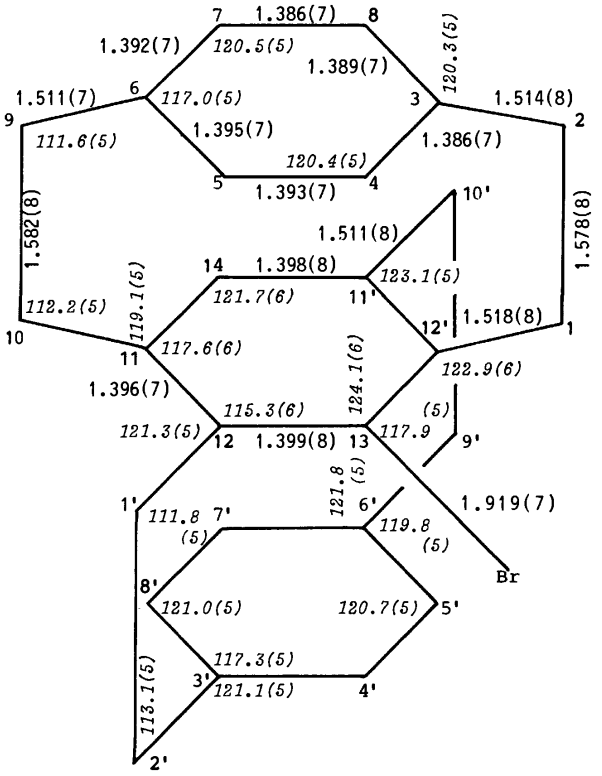

Fig. 2. Selected bond lengths and bond angles with estimated standard deviations in parentheses.

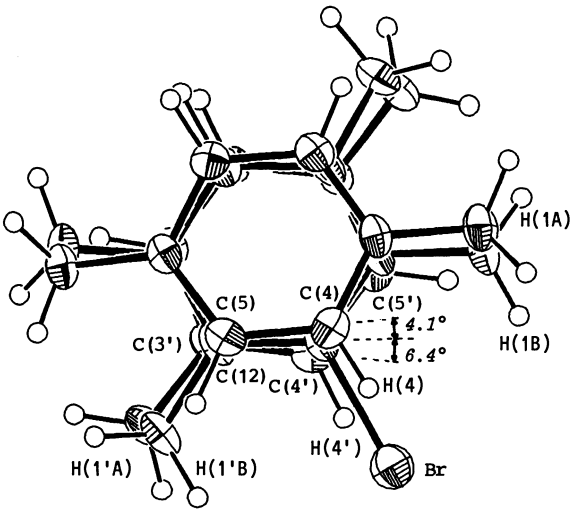

(a)

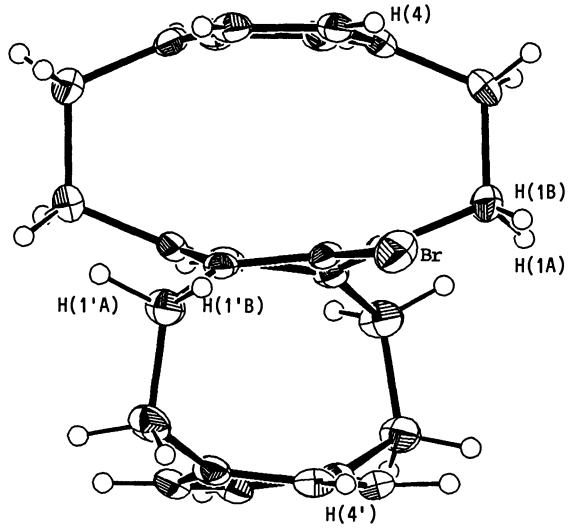

(b$_1$)

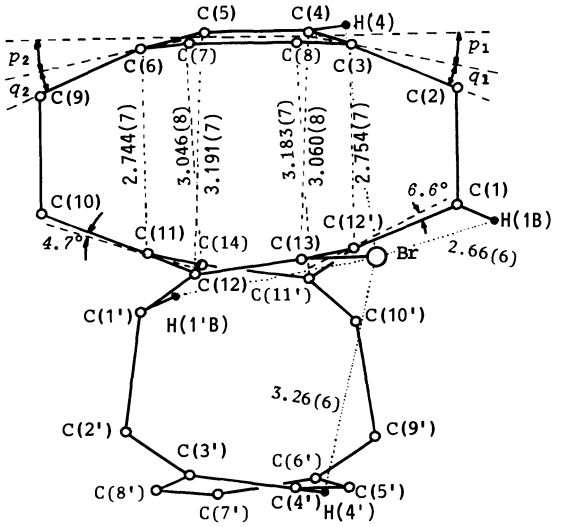

(b$_2$)

Fig. 3. Projections of the molecule.
(a): Projected along the C(6)→C(11) vector.[7] (b$_1$): Projected along the normal to the plane defined by the C(6), C(11), and C(12′) atoms.[7] (b$_2$): Schematic drawing of (b$_1$) with nonbonded atomic distances between the outer and central benzene rings[l/Å]. p, q, and other angles are also given.

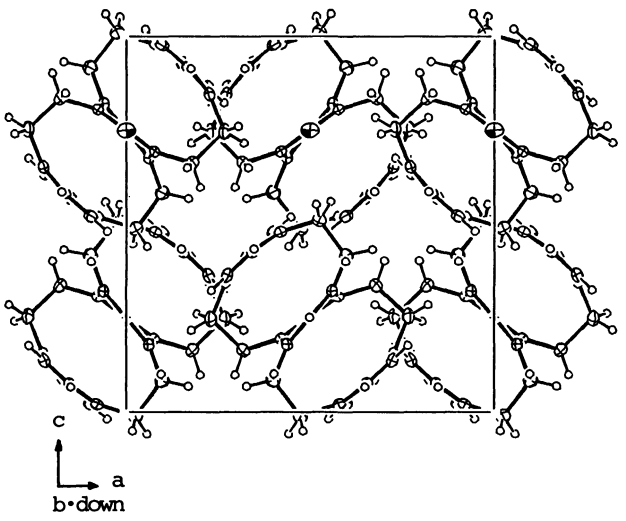

Fig. 4. Crystal structure projected along the b axis.[7]

distance between the Br and the pseudo-gem proton, H(4) is a large value, 3.26(6) Å, which is equal to or rather larger than the ordinary van der Waals contact. In other words, the Br substitution provides little effect on the geometry of the present hydrocarbon, triple-layered paracyclophane. Among the nonbonded Br···H distances the closest is 2.66(6) Å of Br···H(4).

Crystal Structure. The packing of molecules in the crystal is shown in Fig. 4. Molecules are packed rather loosely. The closest intermolecular contact is observed between C(4)(x, y, z) and C(10)(−0.5+x, 0.5−y, 1−z)[3.753(8) Å].

References

1) H. Mizuno, K. Nishiguchi, T. Toyoda, T. Otsubo, S. Misumi, and N. Morimoto, *Acta Crystallogr., Sect. B*, **33**, 329 (1977).

2) Y. Kai, N. Yasuoka, and N. Kasai, Annual Meeting Crystallogr. Soc. Jpn., Nagoya, Nov. (1974), Abst. No. 29P-17.

3) T. Otsubo, H. Horita, Y. Koizumi, and S. Misumi, *Bull. Chem. Soc. Jpn.*, **53**, 1677 (1980).

4) T. Ashida, *HBLS* V, "The Universal Crystallographic Computing System-Osaka," The Computation Center, Osaka Univ. (1973), pp. 55—61.

5) "International Tables for X-Ray Crystallography," Vol. IV, Kynoch Press, Birmingham (1974), p. 71.

6) W. C. Hamilton, *Acta Crystallogr.*, **12**, 609 (1959).

7) C. K. Johnson, *ORTEP* II, Report ORNL-5138, Oak Ridge National Laboratory, Tennessee (1976).

8) H. Hope, J. Bernstein, and K. N. Trueblood, *Acta Crystallogr., Sect. B*, **28**, 1733 (1972).

9) H. Goto, Y. Kai, N. Yasuoka, and N. Kasai, Abst. 10th Symposium on Structural Organic Chemistry, Matsuyama (1977), p. 219.

10) Y. Kai, N. Yasuoka, and N. Kasai, *Acta Crystallogr., Sect. B*, **34**, 2840 (1978).

 © 1986 The Chemical Society of Japan Bull. Chem. Soc. Jpn., 59, 243—247 (1986)

Effect of Pressure on the Pre-Steady-State Kinetics of the Hydrolysis of *p*-Nitrophenyl Pivalate Catalyzed by α-Chymotrypsin

Syoichi MAKIMOTO, Keizo SUZUKI, and Yoshihiro TANIGUCHI*
Department of Chemistry, Faculty of Science and Engineering, Ritsumeikan University, Kita-ku, Kyoto 603
(Received July 10, 1985)

The pre-steady-state of the hydrolysis of *p*-nitrophenyl pivalate (pNPT) catalyzed by α-chymotrypsin (α-CHT) in Tris buffer solutions was measured up to 2.4 k bar at 25 °C. The reaction was initiated by substrate binding, and followed by acylation and deacylation processes. From the pressure dependence on the dissociation constants (K_s), the volume change ΔV_{K_s} was -14 ± 1 cm^3 mol^{-1}. From the pressure dependence on the rate constants (k_{acyl} and k_{deacyl}) of the acylation and deacylation processes, the activation volumes $\Delta V^{\neq}_{acyl}$ and $\Delta V^{\neq}_{deacyl}$ were -24 ± 1 and -2 ± 1 cm^3 mol^{-1}, respectively. The reaction mechanisms of α-CHT are discussed in terms of the reaction and activation volumes.

α-Chymotrypsin (α-CHT) is a well-known endoproteinase which hydrolyzes the peptide bonds at the C end of hydrophobic amino acid residues. It also catalyzes the cleavage of amides of individual amino acids and all other carboxylic acid derivatives, in addition to that of polymeric amides. A number of kinetic studies of this enzyme have been performed on the overall reaction rates (k_{cat}/K_M) or the steady-state kinetic parameters (k_{cat}, K_M).[1,2] However, the parameters by themselves are not sufficient to represent the microscopic rate or equilibrium constant for the elementary reactions of this enzyme. In order to obtain an insight into the mechanism of an α-CHT catalysis, the thermodynamic parameters[3] of individual reaction rate processes, as shown by Eq. 1, are necessary, especially through pre-steady-state kinetic measurements.

$$E + S \underset{K_s}{\rightleftharpoons} ES \xrightarrow{k_{acyl}} ES' + P_1 \xrightarrow{k_{deacyl}} E + P_2. \quad (1)$$

Here E, S, ES, ES′, P_1, and P_2 denote an enzyme, a substrate, an enzyme-substrate complex, an acyl-enzyme, a first leaving group, and a second leaving group, respectively, and K_s, k_{acyl}, and k_{deacyl} represent the dissociation constant of the ES complex, the acylation rate constant, and the deacylation rate constant, respectively.

Activation volumes or reaction volumes, evaluated from the pressure dependence of chemical reactions, are useful parameters for determining the differences in the reaction mechanisms.[4] From recent studies of trypsin,[5] carboxypeptidase A,[6] thermolysin,[7] and α-CHT[8] catalysis, it has been shown that these parameters also provide important information on enzyme reactions.[9]

Regarding the studies concerning the reaction mechanism of an enzyme under high pressure, the effects on pressure inactivation must be removed from the pressure effect on the reaction rate, as an enzyme protein becomes inactivated by a high-pressure treatment. Miyagawa and Suzuki[10] indicated that there is no loss of the activity of α-CHT in a pH 7.8 Tris buffer solution up to 3 kbar from measurements of enzyme activity after a pressure treatment. It has been clarified that α-CHT undergoes a reversible pressure inactivation from the rate of the hydrolysis of phenyl esters catalyzed by α-CHT up to 3 kbar.[8a] Therefore, it is necessary to check the true active enzyme concentration ($[E]_a$) directly under high pressure in order to study the reaction mechanism. These $[E]_a$ values can be stoichiometrically determined[11] by means of the pre-steady-state kinetics in the hydrolysis of *p*-nitrophenyl ester catalyzed by α-CHT.

In the present work, first the $[E]_a$ values at each pressure up to 2.4 kbar at 25 °C were determined from the measurements of the pre-steady-state in a hydrolysis reaction of *p*-nitrophenyl pivalate (pNPT) catalyzed by α-CHT. After the removal of the effect on the pressure inactivation of the enzyme, the reaction mechanism of α-CHT is discussed in terms of the volume change during substrate binding and the activation volumes of the acylation and deacylation processes.

Experimental

Materials. α-Chymotrypsin (α-CHT)(3× crystallized, Sigma Chemical Co.) was used without further purification. *p*-Nitrophenyl pivalate (pNPT) was recrystallized five times from hexane, mp 94.5—95.2 °C (lit,[12] 94—95 °C). The demineralized water was distilled. Acetonitrile was distilled over diphosphorus pentaoxide before use.

Apparatus and Procedure. The method for measuring the rate of hydrolysis reactions under high pressure has been described in a previous report.[13] The rate was measured at pH 7.8 in a 0.005 M† Tris-HCl buffer solution up to 2.4 kbar at 25±0.5 °C. The pressure dependence on the pH value was negligible, since the volume change of the dissociation process was -1 cm^3 mol^{-1}.[14] The rate of the hydrolysis of the pre-steady-state was determined by a change in the optical density (400 nm). This was attributable to the λ_{max} of the *p*-nitrophenolate ion formed as a product, monitored by means of a Hitachi 340 type

† 1 M=1 mol dm^{-3}.

spectrophotometer. It takes 45 seconds (on the average) for a compression up to a certain experimental pressure after mixing an ester and α-CHT solutions in a high-pressure cell.

Stock solutions of the enzyme (9.0×10^{-4} M) were prepared daily in a 0.01 M sodium acetate buffer. Each enzyme solution that was stored below 4 °C during use, was stable for at least 48 h.[11] Total substrate concentrations ($[S]_o$ were varied from 7.5×10^{-6} to 2.5×10^{-5} M, and the total enzyme concentration ($[E]_o$) was 4.5×10^{-6} M.

Results

The equilibrium and rate constants (K_s, K_M, k_{acyl}, and k_{deacyl}), determined by assuming a pre-steady-state, and $[E]_a$ values were analyzed by the following modified Bender's method.[11] Under the conditions of $[E]_o \ll [S]_o$, and $k_{acyl} \gg k_{deacyl}$ for a *p*-nitrophenyl ester substrate,[11] a typical plot of P_1 formation at each pressure as a function of time (t), obtained by spectrophotometry, is shown in Fig. 1. It can be represented by an equation of the form:

$$P_1 = At + B(1-e^{-Ct}) \tag{2}$$

$$A = \frac{k_{deacyl}[E]_a[S]_o}{[S]_o+K_M} + k_s([S_o]-[E_o]) \tag{3}$$

$$B = \frac{[E]_a[S]_o^2}{([S]_o+K_M)^2} \tag{4}$$

$$C = \frac{k_{acyl}[S]_o}{[S]_o+K_s} \tag{5}$$

$$K_M = K_s k_{deacyl}/k_{acyl}. \tag{6}$$

Here k_s denotes the rate constant of the spontaneous hydrolysis of the ester. The K_s and k_{acyl} are obtained by the least-squares method from Lineweaver-Burk plots (Eq. 7, Fig. 2) of the obtained C from the curvature of the initial "burst" of P_1 (Fig. 1).

$$\frac{1}{C} = \frac{K_s}{k_{acyl}}\cdot\frac{1}{[S]_o} + \frac{1}{k_{acyl}}. \tag{7}$$

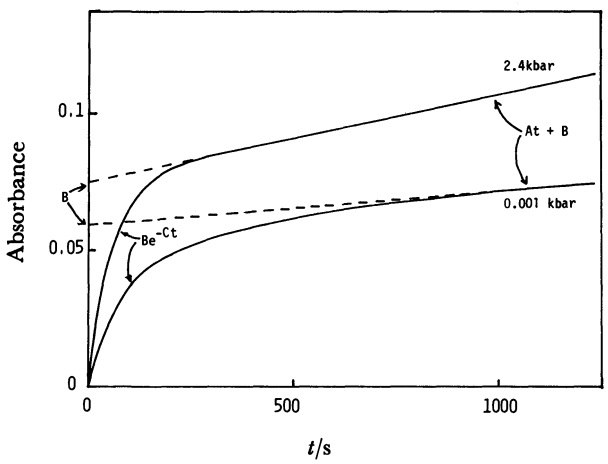

Fig. 1. The α-CHT-catalyzed hydrolysis of pNPT at 25 °C and two pressures, pH 7.8 (0.005 M Tris). Each ester concentration is 2.5×10^{-5} M.

K_M and k_{deacyl} are obtained by the same method (Eq. 8, Fig. 3) of the obtained A from a part of the straight line in Fig. 1.

$$\frac{1}{D} = \frac{1}{A-k_s([S]_o-[E]_o)} = \frac{K_M}{k_{deacyl}[E]_a}\cdot\frac{1}{[S]_o} + \frac{1}{k_{deacyl}[E]_a}. \tag{8}$$

On the other hand, B can be obtained from the intercept by extrapolating the above straight line (Fig. 1). As K_M values, being independent of $[E]_a$,

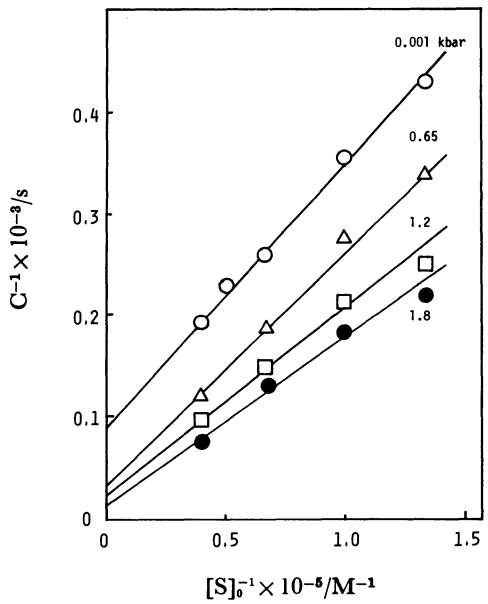

Fig. 2. Lineweaver-Burk plots for the hydrolysis of pNPT in the acylation process, pH 7.8 (0.005 M Tris).

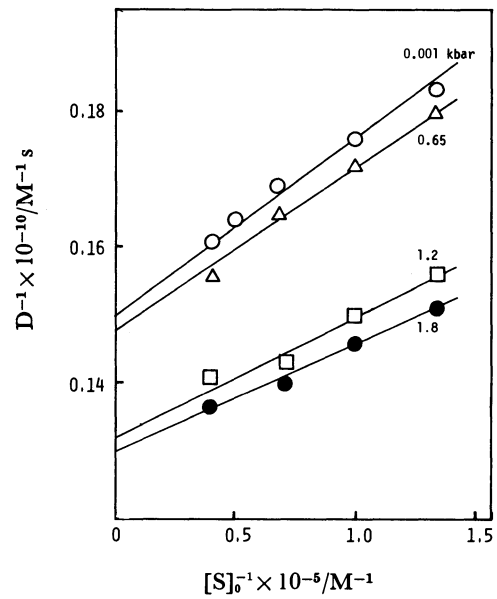

Fig. 3. Lineweaver-Burk plots for the hydrolysis of pNPT in the deacylation process, pH 7.8 (0.005 M Tris).

Table 1. $[E]_a$ and E_p at Various Pressures and 25 °C[a]

	P/kbar				
	0.001	0.65	1.2	1.8	2.4
$10^6[E]_a$/mol kg^{-1} [b]	3.84	3.71	3.71	3.77	3.92
E_p[c]/%	85	82	82	84	87

a) pH 7.8, 0.005 M Tris. b) ±0.1. c) ±2.

Table 2. Kinetic Parameters of the Hydrolysis of pNPT Catalyzed by α-CHT at Various Pressures and 25 °C[a]

P/kbar	$10^4 k_{deacyl}$/s^{-1}	$10^2 k_{acyl}$/s^{-1}	$10^6 K_M$/M	$10^5 K_s$/M
0.001	1.33	1.19	1.89	3.37
0.65	1.35	2.33	1.57	5.19
1.2	1.51	4.05	1.40	7.61
1.8	1.54	6.54	1.23	10.3

a) pH 7.8, 0.005 M Tris. ±0.05.

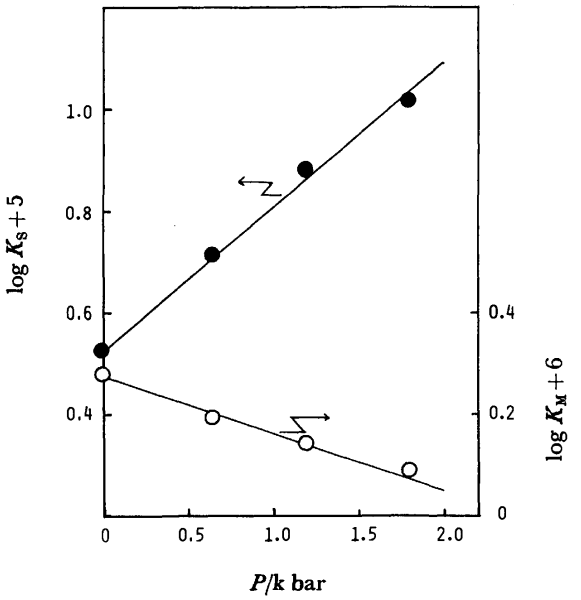

Fig. 4. Log K_S and log K_M vs. pressure at 25 °C.

(1.23×10^{-6} M—1.89×10^{-6} M) at each pressure are smaller than an $[S]_0$ value of 2.5×10^{-5} M. The B value corresponds to $[E]_a$ in Eq. 4. The values of $[E]_a$ and the enzyme purity (E_p) (calculated from the ratio of $[E]_a$ to the $[E]_0$ at each pressure) are summarized in Table 1. These values tell us that there is no loss in activity of α-CHT within ±5% by a compression of up to 2.4 kbar. The rate constants, corrected by the $[E]_a$ and the values of K_M and K_s at each pressure, are shown in Table 2.

From the linear relations of the logarithms of K_s, K_M, k_{acyl}, and k_{deacyl} vs. the pressure established for pNPT in Figs. 4 and 5, the volume changes (ΔV_{K_s} and ΔV_{K_M}) and the activation volumes ($\Delta V^{\ddagger}_{acyl}$ and $\Delta V^{\ddagger}_{deacyl}$) accompanying each process are summarized in Table 3.

Table 3. Volume Changes and Activation Volumes for α-CHT Catalysis at 25 °C[a]

cm^3 mol^{-1}			
ΔV_{K_s}	ΔV_{K_M}	$\Delta V^{\ddagger}_{acyl}$	$\Delta V^{\ddagger}_{deacyl}$
−14±1	6±1	−24±1	−2±1

a) pH 7.8, 0.005 M Tris.

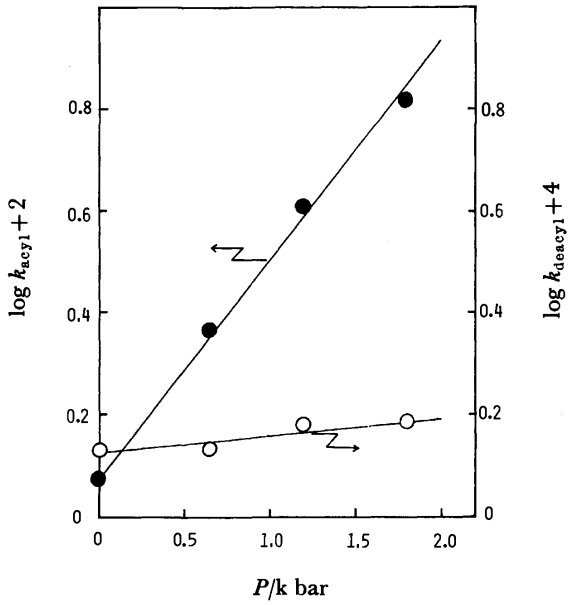

Fig. 5. Log k_{acyl} and log k_{deacyl} vs. pressure at 25 °C.

Discussion

The established overall enzyme reaction of α-CHT with a tetrahedral intermediate (ET, ET′) in the acylation or deacylation step is given by Eq. 9.

$$E + S \underset{K_s}{\rightleftharpoons} ES \overset{k_1}{\underset{k_{-1}}{\rightleftharpoons}} ET \xrightarrow{k_2} \underset{+\ P_1}{ES'} \overset{k_3}{\underset{k_{-3}}{\rightleftharpoons}} ET' \xrightarrow{k_4} E + P_2 \quad (9)$$

(k_{acyl} over the first arrow; k_{deacyl} over the second)

As the k_1 step is rate limiting in the acylation process of a p-nitrophenyl ester substrate,[15] the observed k_{acyl} is given by Eq. 10.

$$k_{acyl} = k_1. \quad (10)$$

While, in a deacylation step, the rate constant is given by Eq. 11,

$$k_{deacyl} = K_3 k_4, \quad (11)$$

where $K_3 = k_3/k_{-3}$.

Substrate Binding. The volume change accompanying the formation of a Michaelis complex ($-\Delta V_{K_s}$) is 14 cm^3 mol^{-1}. This value is discussed in

terms of the weak intermolecular interactions of noncovalent bonds (ΔV_{inter}) and of the conformational change of the enzyme itself (ΔV_{conf}) for the incorporation of pNPT in a binding site.

$$-\Delta V_{K_s} = \Delta V_{Inter} + \Delta V_{conf}. \quad (12)$$

The driving force of the incorporation of pNPT into the binding site is mainly the hydrophobic interaction between pNPT and α-CHT. The size of the binding site is approximately 1.0—1.2 nm×0.55—0.65 nm×0.33—0.45 nm determined by the X-ray study of Steiz et al.[16] The van der Waals radius of the pivaloyl group over 0.5 nm[17] is too large to incorporate it into a binding site of this enzyme at a depth of 0.33—0.45 nm. This pocket corresponds to the radius of the isopropyl group which removes the methyl group from the pivaloyl group. Therefore, we consider that a hydrophobic interaction between the binding site of α-CHT and the isopropyl group can be formed. The volume change accompanying the transfer of an isopropyl group from the water medium (the process of the formation of hydrophobic interaction) is 3.03 $cm^3\,mol^{-1}$. This was determined from the difference in the corresponding volume change (between 5.47 cm^3mol^{-1} for isobutyl alcohol and 2.44 $cm^3\,mol^{-1}$ for methyl alcohol). These were determined from the density data of an aqueous alcohol solution.[18]

Therefore, the value of ΔV_{conf} is 11 $cm^3\,mol^{-1}$, accompanying the incorporation of a nonspecific substrate like pNPT into α-CHT. On the other hand, in our previous paper[8b] it was reported that ΔV_{conf} is negligibly small during the incorporation of a specific substrate as *N*-Ac-L-Trp-amide (ATA). The difference in ΔV_{conf} between nearly zero for ATA and about 11 $cm^3\,mol^{-1}$ for pNPT obtained in this work may be considered to be the specific (ATA)-nonspecific (pNPT) substrate with a bulky pivaloyl group.

Acylation Process. Taniguchi and Suzuki[8a] reported that the $\Delta V^{\neq}_{acyl}$ for the hydrolysis of 2-valeryloxy- and 2-heptanoyloxy-benzoic acids catalyzed by α-CHT are −20 and −21 $cm^3\,mol^{-1}$, respectively. A $\Delta V^{\neq}_{acyl}$ of −24 $cm^3\,mol^{-1}$, found in our work, agrees with the above data. From Eq. 10, $\Delta V^{\neq}_{acyl}$ corresponds to the volume change for the process from ES to ET. The k_1 process is characterized by a large decrease in volume in contrast to a volume increase of 15 $cm^3\,mol^{-1}$ for the k_2 process[8b] in acylation. According to the single-proton-transfer (SPT) mechanism[19] (Fig. 6), the following four interactions may be mainly formed at the transition state in a k_1 process.

(1) The formation of a covalent bond between the oxygen atom of Ser-195 and the carbonyl carbon atom of the substrate, (2) the charge concentration at the carbonyl oxygen atom of the substrate and at the nitrogen atom of the imidazole ring of His-57, the formation of two hydrogen bonds (H-bonds) (3) between the oxygen atom of Ser-195 and nitrogen atom of imidazole ring of His-57, and (4) between the nitrogen atom of above ring and the oxygen atom of Asp-102, take place simultaneously. It is reported that the volume changes accompanying the formation of each interaction for model systems are −10 cm^3mol^{-1} for covalent bond,[20] −5 $cm^3\,mol^{-1}$ for H-bonding,[8b] and −5.5 $cm^3\,mol^{-1}$ for charge concentration,[8b] respectively. Accordingly, the large negative volume change of −24 $cm^3\,mol^{-1}$ is considered to correspond to the sum of the volume decreases for interactions (1)—(4).

Deacylation Process. The $\Delta V^{\neq}_{deacyl}$ (−2 $cm^3\,mol^{-1}$) is consistent with the data of Lockyer et al.[21] (−2 $cm^3\,mol^{-1}$). It is reported[21] that the values of $\Delta V^{\neq}_{deacyl}$ for other *p*-nitrophenyl esters are −6—−4 for acetate and −3 $cm^3\,mol^{-1}$ for isobutylate. From an average volume change of −4 $cm^3\,mol^{-1}$, the slightly negative volume decrease takes place in the deacylation process. From Eq. 11, the $\Delta V^{\neq}_{deacyl}$ is given by Eq. 13.

$$\Delta V^{\neq}_{deacyl} = \Delta V_{K_3} + \Delta V^{\neq}_{4}. \quad (13)$$

According to the SPT mechanism, we showed the initial state (ES′) of the deacylation process, ET′, and the expected transition state in Fig. 7. Interactions of (1)—(8) may be possible to form between ES′ and the transition state through the ET′. Because a volume change of −4 cm^3mol^{-1} is small, in spite of the

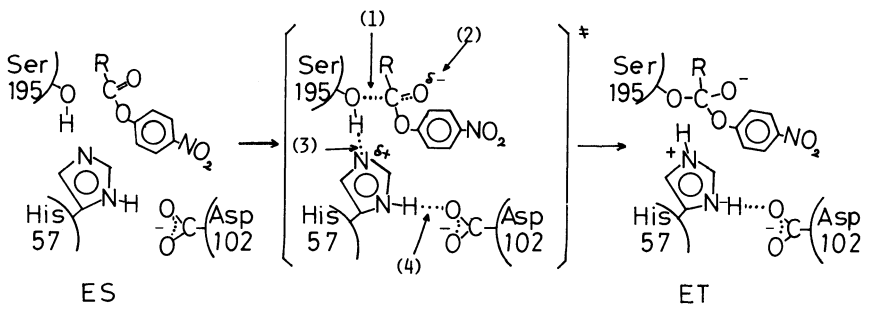

Fig. 6. Schematic drawing of the reaction mechanism of α-CHT on the process of ET formation.

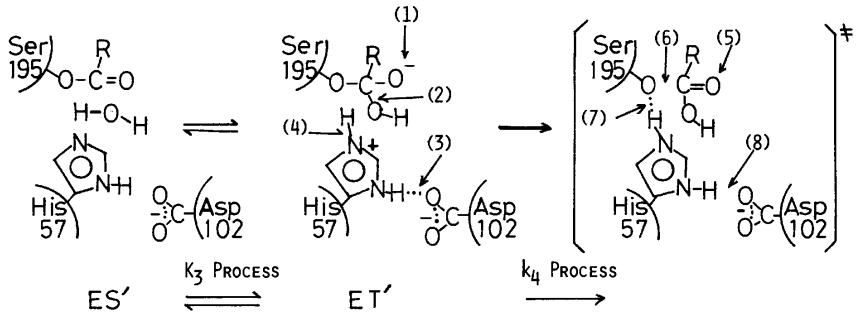

Fig. 7. Schematic drawing of the reaction mechanism of α-CHT on the process of deacylation.

formation of many interactions, the volume changes for some interactions are expected to cancell each other. Those interactions are considered to be (1)—(8) interactions, except (7) in Fig. 7, for the following reason.

At first, there was no contribution from the volume change during (1) hydration and (5) dehydration at the carbonyl oxygen atom for a reverse reaction, and (3) the formation and (8) the cleavage of one H-bond between the nitrogen atom of imidazole ring of His-57 and the oxygen atom of Asp-102. Also, similar volume changes may be expected to (2) [the formation of a covalent bond between the oxygen atom of H_2O and the carbonyl carbon atom of the substrate], and (6) [the cleavage of a covalent bond of ET′ for the formation/cleavage of C-O covalent bond]. The volume change for (4) [a proton transfer between the oxygen atom of H_2O and the nitrogen atom of imidazole of His-57, accompanying a cleavage/formation of a H-bond], may be cancelled out. Accordingly, the volume change for (7) [the formation of a H-bond between the oxygen atom of Ser-195 and nitrogen atom of imidazole ring of His-57] is considered to correspond to the experimental value of $-4\ cm^3\ mol^{-1}$.

References

1) M. L. Bender and F. J. Kézdy, *Annu. Rev. Biochem.*, **34**, 49 (1965).

2) D. M. Ingles and J. R. Knowles, *Biochem. J.*, **104**, 369 (1967).

3) M. Dixon and E. C. Webb, "Enzymes," 2nd ed., Longmans, London (1971), p. 150.

4) T. Asano, Abstracts of the 23rd High Pressure Conference of Japan (1982), p. 358.

5) S. Kunugi, M. Fukuda, and N. Ise, *Biochim. Biophys. Acta.*, **704**, 107 (1982).

6) M. Fukuda, S. Kunugi, and N. Ise, *Bull. Chem. Soc. Jpn.*, **56**, 3308 (1983).

7) S. Kunugi and M. Fukuda, *Eur. J. Biochem.* **142**, 565 (1984).

8) a) Y. Taniguchi and K. Suzuki, *Bull. Chem. Soc. Jpn.*, **53**, 1709 (1980); b) S. Makimoto, K. Suzuki, and Y. Taniguchi, *J. Phys. Chem.*, **88**, 6021 (1984).

9) K. J. Laidlar and P. S. Bunting, "The Chemical Kinetics of Enzyme Action," 2nd ed., Oxford University Press, London (1973).

10) K. Miyagawa and K. Suzuki, *Rev. Phys. Chem. Jpn.*, **32**, 51 (1963).

11) M. L. Bender, F. J. Kézdy, and F. C. Wedler, *J. Chem. Ed.*, **44**, 84 (1967).

12) L. E. McDonald and A. K. Balls, *J. Biol. Chem.*, **227**, 727 (1959).

13) Y. Taniguchi, S. Makimoto, and K. Suzuki, *J. Phys. Chem.*, **85**, 2218 (1981).

14) R. C. Neuman, Jr., W. Kauzmann, and A. Zipp, *J. Phys. Chem.*, **77**, 2689 (1973).

15) M. Caplow, *J. Am. Chem. Soc.*, **91**, 3639 (1969).

16) T. A. Steiz, R. Henderson, and M. Blow, *J. Mol. Biol.*, **46**, 337, (1969).

17) A. Bondi, *J. Phys. Chem.*, **68**, 441 (1964).

18) M. E. Friedman and H. A. Scheraga, *J. Phys. Chem.*, **69**, 3795 (1965).

19) L. Polger and M. L. Bender, *Proc. Natl. Acad. Sci. U. S. A.*, **64**, 1335 (1969).

20) T. Asano and W. J. le Noble, *Chem. Rev.*, **78**, 407 (1978).

21) G. D. Lockyer, Jr., D. Owen, D. Crew, and R. C. Neuman, Jr., *J. Am. Chem. Soc.*, **96**, 7303 (1974).

 © 1986 The Chemical Society of Japan Bull. Chem. Soc. Jpn., 59, 249—253 (1986)

The Regulation of Emulsion Polymerization with Fluorocarbon-Hydrocarbon Emulsifiers Mixture

Kazufumi KATO,* Kunio ESUMI, and Kenjiro MEGURO
Department of Applied Chemistry and Institute of Colloid and Interface Science,
Science University of Tokyo, Kagurazaka, Shinjuku-ku, Tokyo 162
(Received July 10, 1985)

The emulsion polymerization of styrene using a mixture of sodium dodecyl sulfate (SDS) and lithium fluorooctane sulfonate (LiFOS) has been studied. The polymerization rate decreased upon increasing the mole fraction of LiFOS, and was dependent on the solubilized amount of styrene in mixed surfactant solutions of SDS and LiFOS. The particle size increased upon increasing the mole fraction of LiFOS on the whole, and the molecular weight of the polymer formed in latices decreased upon increasing the mole fraction of LiFOS. Furthermore, the molecular-weight distribution of the latex polymer formed in mixed emulsifier solutions was considerably wider than that of the latex polymer formed in a single-emulsifier solution. It was confirmed from the above results that LiFOS had a repressive effect on the polymerization rate, and that it affected the number of particles and the molecular weight in the emulsion-polymerization process.

In the process of emulsion polymerization, the emulsifier plays an important role for the following two reasons: 1) It offers sites for polymerization, as does the micelle being acted upon for the solubilization of a monomer, and 2) It produces a stability of the synthetic latex, which has been influenced by the nature of the emulsifiers being used in the synthesis.[1-3] During emulsion polymerization, mixtures of emulsifiers have been generally used. However, a systematic study regarding the effect of emulsifier mixtures on emulsion polymerization was limited to nonion-nonion or nonion-anion hydrocarbon type surfactant systems.[4-6]

Recently, fluorocarbon surfactants have been given attention due to their peculiar natures: A low affinity for both water and oil and a good resistance against acidic, alkaline, oxidative, and reductive reagents. The surface tension of fluorocarbon surfactants is lower than that of hydrocarbon surfactants at an air-water interface, and fluorocarbon surfactants have higher surface activities.[7-11]

Suzuki et al. investigated the effect of the addition of a fluorocarbon surfactant on the micellization of hydrocarbon surfactants using the solubilization of the keto-enol tautomerism of *p*-benzoylacetanilide. They observed that the addition of a fluorocarbon surfactant was effective to expulse any materials solubilized in the micelles of a hydrocarbon surfactant by forming a mixed micelle.[12] This expulsive effect of a fluorocarbon surfactant would be interesting for the study of emulsion polymerization and, in particular the process of nucleation for a latex particle.

In this work, the emulsion polymerization of styrene in the presence of mixtures of fluorocarbon and hydrocarbon surfactants was studied by measuring the polymerization rates, particle sizes and molecular-weight distributions. The emulsifiers employed were sodium dodecyl sulfate (SDS) and lithium fluorooctanesulfonate (LiFOS).

Experimental

Materials. Potassium fluorooctane sulfonate ($C_8F_{17}SO_3K$) was repeatedly washed with water to remove water-soluble impurities, then dried at 80 °C. To prepare a lithium salt of fluorooctane sulfonate, fluorooctanesulfonic acid ($C_8F_{17}SO_3H$) was obtained by the distillation of the potassium salt in the presence of sulfuric acid (95%, guaranteed grade sample) at 180 °C, 10 mmHg. Then, it was neutralized by lithium hydroxide. Thus obtained lithium fluorooctane sulfonate ($C_8F_{17}SO_3Li$; LiFOS) was purified by repeated crystallization from dioxane after an extraction with ethanol. The purity of this sample was confirmed by an elemental analysis and by a surface tension measurement.

Sodium dodecyl sulfate (SDS) for biochemical use (Wako Pure Chemical Industries Ltd.) was purified by crystallization twice from ethanol, and was carefully dried in vacuo for 60 h before use. The purity of the sample was confirmed by the same method mentioned above.

Styrene was distilled twice under a dried nitrogen atmosphere, and was stored in a refrigerator under nitrogen before use.

For an initiator, potassium peroxodisulfate ($K_2S_2O_8$) was an analytical grade supplied by Wako Pure Chemical Industries Ltd.

Water was purified by a Milli-Q Water-Purification System.

Procedure. Each emulsion polymerization run was made using a batch process in a one-liter glass reactor fitted with a metal screw, thermometer and facilities for charging and sampling. A typical polymerization recipe is shown in Table 1. Emulsifiers (SDS and LiFOS) were mixed by two

Table 1. Emulsion Polymerization Recipe

Ingredients	Grams	Moles
Styrene	50	0.48
Water	250	13.9
Potassium peroxodisulfate	0.2	0.00755
Emulsifiers (SDS, LiFOS)	—	0.02

procedures. In the first procedure, while maintaining the same total moles of the emulsifiers, the mixed ratios of SDS and LiFOS were varied shown in Table 1.

In the second procedure, surfactant mixtures were prepared by adding various quantities of LiFOS to a definite quantity of SDS, whereas the total concentration of the mixed emulsifiers changed in each reaction system. Before the polymerization, water and emulsifiers were added to the reactor at room temperature, then a styrene monomer was added. After that, the reaction flask was immersed in a constant temperature bath which was adjusted to 60±1 °C under a nitrogen atmosphere. The mixture was stirred at 250 min^{-1}. After rising up the temperature to 60 °C, an initiator was added to the contents in the reactor.

The samples for determinations of conversion, particle size, and molecular-weight distribution were collected with pipettes at fixed intervals. The procedure for the determination of the conversion was as follows. To terminate the polymerization reaction, 5 cm^3 of a *p*-benzoquinone methanol solution (1.5 g dm^{-3}) as an inhibitor was added to 5 cm^3 samples in glass bottles. Then, the unreacted styrene monomer, methanol, and water were evaporated at 70 °C and the conversion percentages of styrene to polystyrene were estimated by measuring the dried samples on the assumption that the (monomer+polymer)/water was constant throughout the reaction.

In order to determine the particle sizes and the molecular-weight distributions after a reaction time of 90 min, the samples were rapidly cooled in cold water (0 °C). Particle sizes and size distributions were determined by transmission electron microscopy (TEM) and by submicron particle sizer (MARVERN AUTOSIZER MODEL-700). Measurements were carried out under the following conditions: The temperature was 25.0 °C, the refractive index was 1.33, and the viscosity was 0.8909cP.

The weight-average molecular-weights and the molecular weight distributions of each polystyrene latex sample were determined using gel permeation chromatography.

The solubilized amounts of ethylbenzene as a substitute for styrene in the mixed surfactant solutions were measured by means of a spectrophotometer at a wavelength of 262.6 nm at 25 °C.

Results and Discussion

Before the emulsion polymerization of styrene in the presence of SDS and LiFOS, it was necessary to confirm the stability of the emulsion particles being prepared with an aqueous mixture of LiFOS and SDS in the polymerization process. In order to evaluate the stability of the emulsion particles in each surfactant component, a percentage of coagulum was used which was estimated by the ratio of coagulum to the total amount of residue in a defined volume for each emulsion after a 90 min reaction time during the polymerization process. From the above experiments, only a few visible coagulums were observed and the coagulation ratios were below 1% for every mixed ratio of the emulsifiers. This result suggests that mixtures of SDS and LiFOS at every ratio were suitable for the stabilization of the emulsion polymerization of styrene.

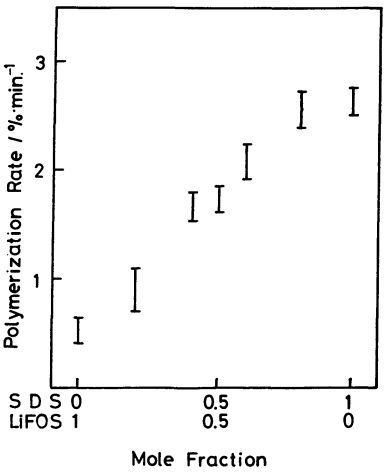

Fig. 1. The polymerization rate with mole fraction of emulsifiers; Lithium fluorooctane sulfonate (LiFOS) and sodium dodecyl sulfate (SDS), Temperature; 60 °C.

Polymerization Rate. In the first procedure, in the presence of mixtures of various mole fractions of SDS and LiFOS, the time-conversion curves in the emulsion polymerization of styrene were obtained. The polymerization rates (% min^{-1}) were calculated from the time-conversion curves in the initial period, and the results are shown in Fig. 1. The polymerization rate with SDS alone was 2.8% min^{-1} and that with LiFOS alone was 0.5% $min.^{-1}$ The polymerization rate decreased upon increasing the mole fraction of LiFOS. This result suggests that LiFOS has a depressive effect on the polymerization rates.

In the polymerization of styrene in the presence of a water-soluble initiator, the polymerization sites are considered to be in the water phase. However, a styrene monomer is only slightly soluble in water. Thus, the solubilization phenomenon of styrene in surfactant micelles became important for providing an initiation site for polymerization. Indeed, an emulsion polymerization using a styrene nearly occurred above the critical micelle concentration (cmc) in an aqueous surfactant solution.

The solubilizing power of the surfactant and the solubilized amount of monomer affect the polymerization rate in the emulsion polymerization, and it has been supported that the polymerization rate is proportional to the solubilizing power of various surfactant solutions.[13] In this work, it was assumed that the solubilized amount of ethylbenzene was similar to that of styrene in several aqueous solutions of SDS or LiFOS. The solubilized amounts of ethylbenzene were increased in proportion to the concentration of the aqueous surfactant solutions

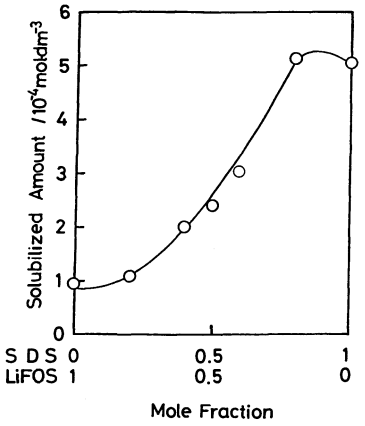

Fig. 2. Solubilized amount of ethylbenzene in mixed surfactant aqueous solution; 20 mmol dm^{-3}, Surfactants; SDS and LiFOS, Temperature; 25 °C.

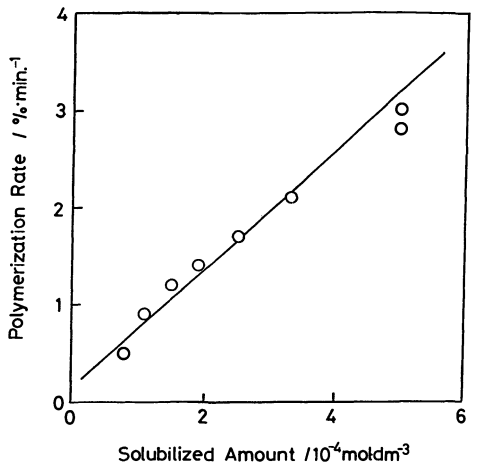

Fig. 3. Polymerization rate as a function of solubilized amount of ethylbenzene at various molar ratios of SDS and LiFOS.

above their cmc. Here, the cmc of an aqueous solution of SDS was 7.9 mmol dm^{-3} and that of an aqueous solution of LiFOS was 6.5 mmol dm^{-3}.

The solubilized amounts of ethylbenzene at total concentrations of 20 mmol dm^{-3} are shown in Fig. 2 as a function of the mole fraction. The solubilized amount in a SDS aqueous solution was about 52 mmol dm^{-3} and that in a LiFOS solution was 8 mmol dm^{-3}, whereas the solubilizing power of SDS was seven times as large as that of LiFOS. The solubilized amount of ethylbenzene decreased upon increasing the mole fraction of LiFOS, but had a maximum value at 0.8 of the mole fraction of LiFOS.

Figure 3 shows the relationship between the polymerization rates and the solubilized amounts at various mole fractions of SDS and LiFOS. As the polymerization rate is proportional to the solubilized amount, it is clear that the polymerization rate in the emulsion polymerization of styrene was influenced by the solubilized amount of styrene in the mixed-surfactant solution.

As a second procedure, an emulsion polymerization of styrene was carried out using mixed emulsifiers prepared by adding various quantities of LiFOS to a definite quantity of SDS. The obtained results are shown in Fig. 4. In this procedure, every condition in the emulsion polymerization pathway was the same as that in the first procedure except for the concentration of the emulsifiers.

These results indicate that by adding a small amount of LiFOS to SDS, the polymerization rate increases, however, a further addition of LiFOS causes the polymerization rate to decrease, compared with that for SDS alone. During the first stage, an acceleration of the polymerization rate by adding LiFOS can be correlated with an increase in the total amount of emulsifiers in the reaction system. On the other hand, a deacceleration of polymerization rate

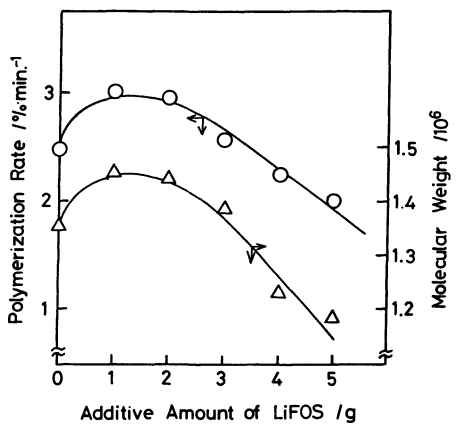

Fig. 4. The effect of additive amount of LiFOS to SDS (6.0 g) on polymerization rate and molecular weight.

occurred upon a further addition of LiFOS, in spite of an increase in the total amount of the emulsifiers. This result was almost similar to one shown in Fig. 2; the polymerization rate decreased upon increasing the mole fraction of LiFOS. This fact seems to be attributed to the expulsive effect, that added LiFOS expelles styrene radicals from the micelles in aqueous surfactants solutions, resulting in a depression of the polymerization rate.[12]

Particle Size and Particle Number Concentration. By electron micrography, the number-average particle diameter (D_n) and the polydispersity (D_w/D_n) were determined, respectively. By light scattering, the z-average particle diameter (D_z) and the polydispersity index (Pusey's Q factor) which gave an indication of the breadth of the size distribution, were determined.[14,15] These results are shown in Table 2.

The particle size of latex formed with various mixed ratios of SDS and LiFOS, which was

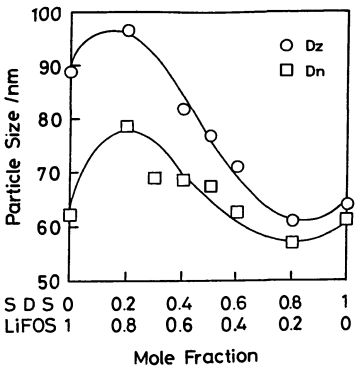

Fig. 5. The change of latex particle size with molar ratio of SDS and LiFOS; Total emulsifiers mole (0.02 mol), (○): z-average diameter, (□): number-average diameter.

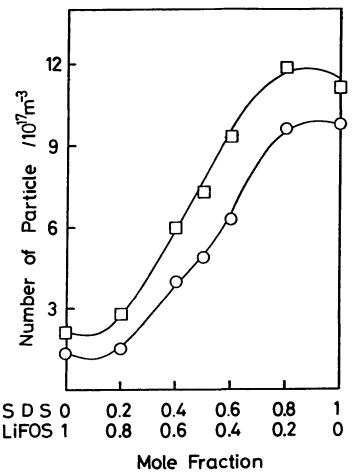

Fig. 6. Number of particles vs. mole fraction of SDS and LiFOS at total moles (0.02 mol), (○): Number of particles from z-average diameter, (□): Number of particles from number-average diameter.

Table 2. Particle Size and Size Distribution as a Function of Molar Ratio of SDS and LiFOS

Mole fraction		Light scattering method		Electron micrography method	
SDS	LiFOS	D_z/nm	Q.f	D_n/nm	D_w/D_n
1.0	0	64.0	0.074	61.2	1.15
0.8	0.2	61.0	0.092	56.9	1.11
0.6	0.4	71.1	0.06	62.5	1.13
0.5	0.5	76.8	0.04	67.3	1.11
0.4	0.6	81.9	0.082	67.9	1.06
0.3	0.7	79.4	0.076	67.9	1.04
0.2	0.8	97.0	0.076	78.9	1.07
0	1.0	88.3	0.12	61.2	1.09

determined by both methods, has a relatively narrow distribution. From this result, the latices were determined to be exceedingly monodispersed spheres. The change in the latex particle size with the mole fraction of the emulsifiers is shown in Fig. 5.

There are many methods for measuring the particle size, and each determined average diameter provides a difference in size. The difference between the number-average diameter and the z-average diameter is caused by measurement method.[16] According to Wesslaw's experiment, the light scattering method has an upper limit in its application for a determination of the particle size; for instance, 400 nm to the size of polystyrene particles.[17]

It can be seen from Fig. 5 that all sizes are less than 400 nm. The z-average particle diameter vs. the mole fraction curve indicates, on the whole, that the particle size becomes large upon increasing the mole fraction of LiFOS. This is because the polymerization rates decrease upon increasing the mole fraction of LiFOS. Namely, when the polymerization rate is slow, the period during which the emulsion droplets and polymer particles coexist is prolonged. As a result, latex particle sizes continuously increase up to the depletion of droplets of the monomer.

Although the tendency described above regarding the z-average diameter was also observed for the number average diameters, it became much smaller. Especially, the higher the mole fraction of LiFOS was, the greater the gap between the number-average diameter and the z-average diameter became. This difference resulted from an apparent increase in the average diameter, determined by the light scattering which is capable of detecting the particle being coalesced in a suspended state.

There was a minimum value for both the average diameters at 8:2 of molar ratio of SDS and LiFOS. The z-average diameter was 56.9 nm and the number-average diameter was 61.0 nm at this mole fraction. At the same molar ratio of surfactant solutions of two emulsifiers, the solubilized amount and the polymerization rate were maximum. Thus, it was proven that the particle size increased if the mixed emulsifiers contained a small amount of LiFOS. At a high mole fraction of LiFOS, the average diameters of the latices became smaller since the polymerization rate was so slow that particle nucleation could not sufficiently progress.

The number of particles formed per cubic meter of the aqueous phase (N) was calculated from the z-average diameter or the number-average diameter, and the conversion rates. A diagram of the particle numbers plotted against the mixed emulsifiers is shown in Fig. 6. It was found that the number of particles calculated from the z-average diameter and the number-average diameter behaved similarly to each other upon a change in the mole fractions of the emulsifiers. Since latex particles are dispersed in a suspended state, the z-average diameter determined by

Table 3. The Change of Weight-average Molecular Weight (M_w) and Molecular Weight Distribution (M_w/M_n) with Mole Fraction of SDS and LiFOS

SDS : LiFOS		M_w ($\times 10^{+6}$)	M_w/M_n
0	1.0	0.812	2.69
0.2	0.8	1.090	9.33
0.4	0.6	1.266	7.84
0.5	0.5	1.347	6.71
0.6	0.4	1.223	6.20
0.8	0.2	1.458	6.44
1.0	0	1.475	3.56

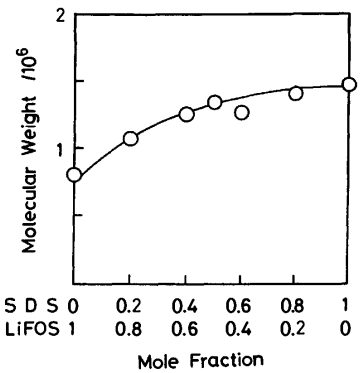

Fig. 7. The change of weight-average molecular weight with mole fraction of SDS and LiFOS.

light scattering should be used to determine the number of particles. From these results, it can be seen that the number of particles increases all over upon increasing the mole fraction of SDS. Also, it has a maximum at a molar ratio of 8:2 for SDS to LiFOS. These results can be explained by the same reasoning as mentioned above regarding particle size changes.

Molecular Weight and Its Distribution. The molecular weight of a formed latex polymer was measured after being dissolved in tetrahydrofuran by gel permeation chromatography (GPC). The same samples that were used for the particle-size measurement were used again. The weight-average molecular weights (M_w) and molecular weight distributions (M_w/M_n) of several polymer latices were calculated using Shimadzu Chromatopac C-R2AX.

Table 3 shows the weight-average molecular weights (M_w) and the molecular weight distributions (M_w/M_n), and Fig. 7 shows the change in the weight-average molecular weight with the mole fraction of mixed surfactant solutions of SDS and LiFOS. From M_w/M_n for the molecular weight distribution of the formed latices shown in Table 3, it was found that the breadth of the molecular weight distribution of the latices formed with mixed emulsifiers of SDS and LiFOS were rather broadened, compared with that of latices formed with single emulsifiers of SDS or LiFOS. These results demonstrate that the composition of emulsion and micelle in the mixed surfactant solution of SDS and LiFOS has a much wider distribution than that in a single emulsifier.

The change in the weight-average molecular weight of latex polymer against the mole fraction of a mixed surfactant solution of SDS and LiFOS is shown in Fig. 7. The molecular weight decreases upon increasing the mole fraction of LiFOS, in agreement with changes in the polymerization rate. As shown in Fig. 4, the molecular weight of the polymer latices formed with the mixed emulsifiers prepared by adding various quantities of LiFOS to a definite quantity of SDS, decreased upon adding LiFOS. The result agreed with the behavior of the polymerization rates. These results indicate that the addition of LiFOS to SDS in a mixed surfactant solution decreases the molecular weight of the latices. Accordingly, the addition of LiFOS has a repressive effect on the growth of the molecular weight of the latex polymer.

References

1) W. V. Smith and R. H. Ewart, *J. Chem. Phys.*, **16**, 592 (1948).
2) R. N. Haward, *J. Polym. Sci.*, **4**, 273 (1949).
3) F. K. Hansen and J. Ugelstad, *J. Polym. Sci. Polym. Chem. Ed.*, **16**, 1953 (1978).
4) G. G. Greth and J. E. Wilson, *J. Appl. Polym. Sci.*, **5**, 136, (1961).
5) S. Muroi, *Kogyo-Kagaku*, **68**, 1785 (1965).
6) S. S. Medvedev, I. A. Gritskova, L. V. Zuikov, L. I. Sedakowa, and G. D. Berejnol, *J. Macromol. Sci. Chem.*, **A7(3)**, 725 (1973).
7) "Fluorine Chemistry," ed by J. H. Simons, Academic Press Inc., (1964), Vol. 5, p. 370.
8) N. O. Brace, *J. Org. Chem.*, **27**, 4491 (1962).
9) P. Mukerjee and A. Y. S. Yang, *J. Phys. Chem.*, **80**, 1388 (1976).
10) K. Sinoda, M. Hato, and T. Hayashi, *J. Phys. Chem*, **76**, 909 (1981).
11) J. H. Hildebrand, M. j. Pransnitz, and L. R. Scott, "Regular and Related Solutions," Van Nostrand-Reinhold, New York (1970).
12) T. Suzuki, K. Esumi, and K. Meguro, *J. Colloid Interface Sci.*, **93(1)**, 205 (1983).
13) I. M. Kolthoff, E. J. Meehan, and C. W. Car, *J. Polym. Sci.*, **6**, 73 (1951).
14) P. N. Pusey, "Industrial Polymer; Characterisation by Molecular Weights," ed by Green and Dietz, Transcripta Books, London (1973).
15) S. W. Provencher, J. Hendrix, L. De Maeyer, and N. Paulussen, *J. Chem. Phys.*, **69**, 4273 (1978).
16) S. H. Maron, C. Moore, and A. S. Powell, *J. Apple. Phys.*, **23**, 900 (1952).
17) H. Wesslaw, *Macromol. Chem.*, **69**, 213 (1963).

 © 1986 The Chemical Society of Japan Bull. Chem. Soc. Jpn., 59, 255—258 (1986)

Crystal and Molecular Structures of the Adduct of Fluoreno[9,1-*bc*]pyrylium-3-olate with Methyl Cinnamate and the Dimer of Fluoreno-[9,1-*bc*]pyrylium-3-olate

Keiichi FUKUYAMA,* Hideo FUJITA, Shigeru TOKUSHIMA, Tomitake TSUKIHARA, Yukiteru KATSUBE,† and Tadayuki MOTOYAMA§,††

Faculty of Engineering, Tottori University, Koyama-cho, Tottori 680

§ Department of Chemistry, College of General Education, Osaka University, Toyonaka, Osaka 560

(Received July 12, 1985)

The molecular structures of the adduct of fluoreno[9,1-*bc*]pyrylium-3-olate with methyl cinnamate (**1**), $C_{25}H_{18}O_4$, and the dimerized product of fluoreno[9,1-*bc*]pyrylium-3-olate (**2**), $C_{30}H_{16}O_4$, have been determined by the X-ray diffraction method. In the adduct (**1**), the phenyl ring is situated above the fluorene ring with a dihedral angle of 64°. The product **2** has a dimeric structure with a head-to-head type *anti*-configuration, and a local two-fold symmetry. Both crystals belong to a triclinic system with a space group $P\bar{1}$. The cell constants for **1** are a=13.287(4), b=8.794(3), c=8.797(3) Å, α=109.78(3), β=82.17(3), γ=88.58(3)°, and those for **2** are a=10.401(2), b=12.425(3), c=8.564(2) Å, α=103.77(4), β=108.76(4), γ=95.06(4)°. The structure of **1** was refined to R=0.067 for 2141 reflections, and that of **2** to R=0.058 for 2301 reflections.

Pyrylium-3-olate(**5**), formed by an intramolecular carbene–carbonyl reaction of **4**, has a resonance contribution of carbonyl ylide. It has been known that **5** is an unstable and reactive species and that it undergoes a 1,3-dipolar cycloaddition reaction with acetylenic, olefinic and carbonyl compounds.[1-3] When **5** was reacted with methyl cinnamate, a 1:1 adduct(**1**) was obtained in a 66% yield.[2] The structure of **1** was assigned on the bases of an elementary analysis and NMR data.[3] $Cu(acac)_2$-catalysed decomposition of 1-diazoacetylfluorenone(**3**) in the absence of dipolarophile in absolute benzene at 80 °C yielded a crystalline compound(**2**) quantitatively (Scheme).[3] The elemental analysis and mass spectrum for **2** showed a dimeric structure. Among four possible configurations for the dimer(**2**), an NMR study rejected two *syn*-configurations. In order to confirm the structure of **1** as well as to determine either of the two *anti*-configurations, X-ray analyses of **1** and **2** were undertaken.

Results and Discussion

The molecular structures of **1** and **2** drawn by DCMS-3[4] are shown in Fig. 1. The selected bond lengths and angles are given in Table 1.[5] The present X-ray analyses have established the molecular structures of **1** and **2**. In contrast to the case of 2-benzothiopyrylium-4-olate, where it gave a head-to-tail type dimer with a *syn*-configuration,[6] fluoreno [9,1-*bc*]pyrylium-3-olate(**5**) gave a dimer (**2**) with a head-to-head type *anti*-configuration. Hence, the structural formula of **6** in Ref. 3 should be revised. The structure of **2** shows that the dimerization of **5** occurred through a bond formation between the equivalent atoms in **5**. As pyrylium-3-olate, with a carbonyl ylide resonance structure, behaves as 4π component in cycloaddition, a concerted thermal [π4s+π4s] process is not allowed for the facile dimerization of **5** according to the rule of the conservation of orbital symmetry.[7] We presume that the dimer was formed by a two-step mechanism. The transition state to *syn*-dimer, in which the carbonyl groups lie above each other, is unfavored over that of an *anti*-dimer in terms of the dipolar or electrostatic repulsion between the carbonyl groups. This electronic effect might result in the exclusive formation of an *anti*-dimer.

As seen from Fig. 1, molecule **2** has a local 2-fold symmetry. The lengths and angles of the equivalent bonds within a molecule are similar (Table 1). The six-membered ring, through which the 2-fold axis passes, has a chair form. The two six-membered rings comprizing C(7), C(8), C(9), C(14), C(15), and O(1) in **2** have envelope form; the former five atoms lie on a mean plane with an rms deviation of 0.05 Å and O(1) deviates from the plane by about 0.68 Å for each ring. The two fluorene rings of **2** are slightly bent; the dihedral angles between the two benzene rings in each fluorene ring are 16 and 15°, respectively. The proton signal exhibiting an up-field shift in the NMR spectrum of **2** might be that of the hydrogen atoms bonded to C(5A) and C(5B), which are located above the aromatic ring.

The structure of **1** shows features that are similar to those observed in **2**. The fluorene ring is bent to the same extent as in **2**; the dihedral angle between the two benzene rings is 13°. The dihedral angle between the fluorene and phenyl rings is 64°. The six-membered ring of C(7), C(8), C(9), C(14), C(15), and O(1) also takes an envelope form; the O(1) deviated by 0.79 Å from the mean plane through the former five atoms. The coupling constants of the

† Present address: Institute for Protein Research, Osaka University, Suita, Osaka 565.

†† Present address: Maruho Co. Ltd., Nakatsu 1-chome 6-24, Oyodo-ku, Osaka 531.

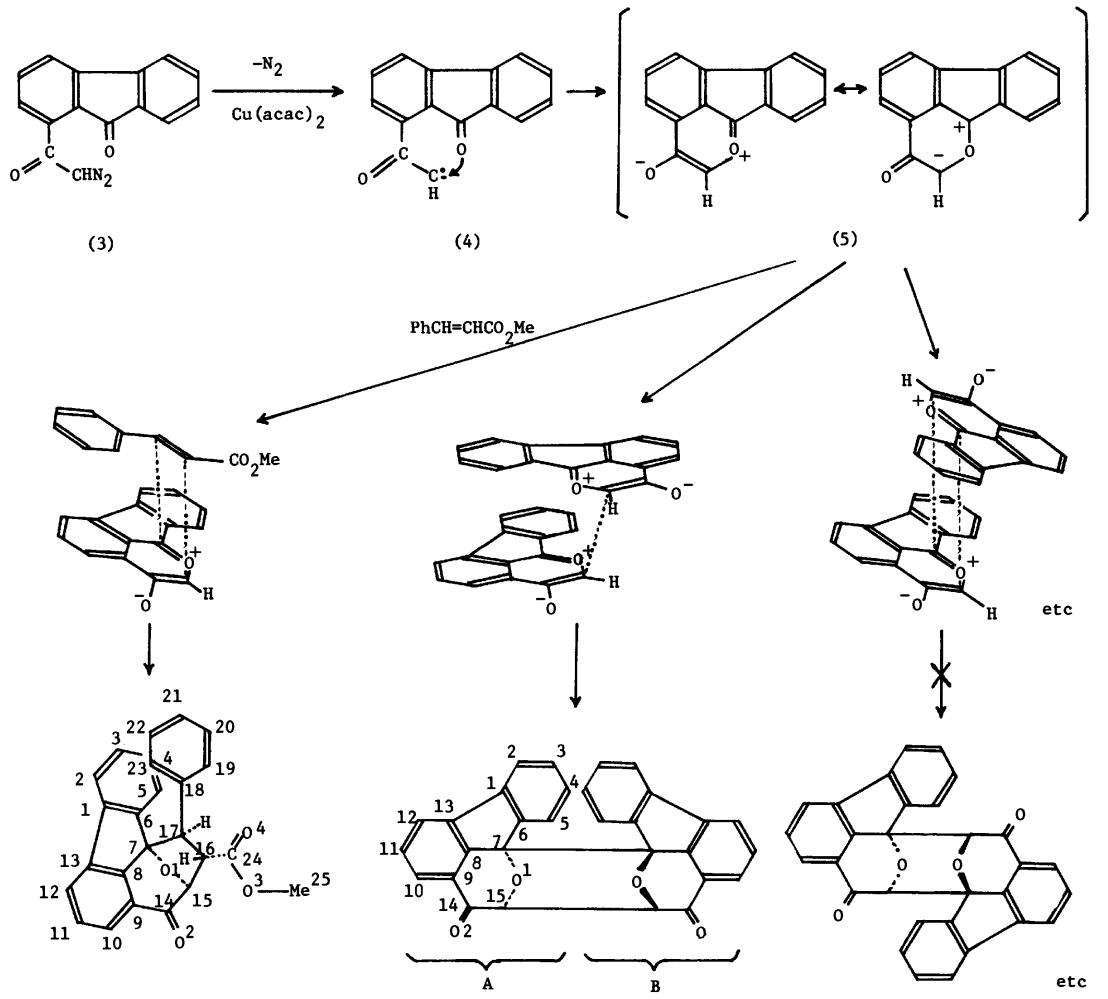

Scheme

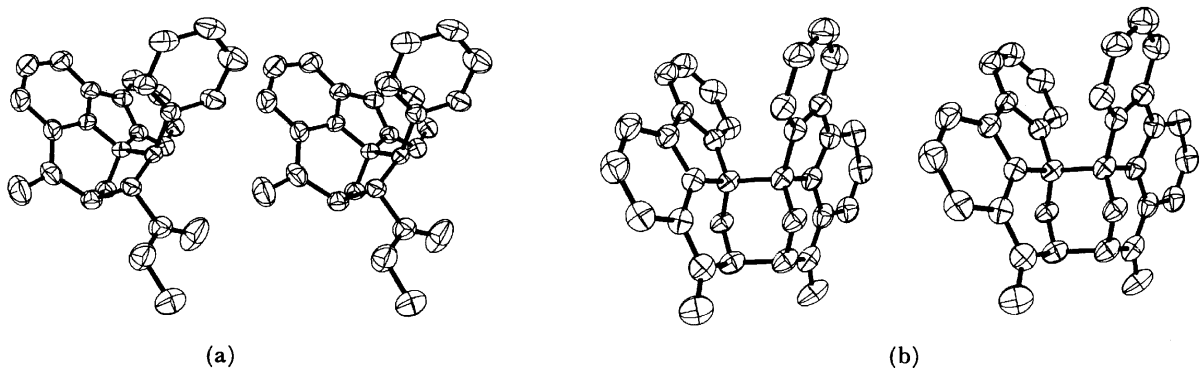

Fig. 1. Stereoscopic views of (a) the adduct **1** and (b) the dimer **2.**
The hydrogen atoms are omitted from the figures for the sake of clarity.

Table 1. Selected Bond Lengths and Angles with Estimated Standard Deviations in Parentheses

(a) Bond lengths (l/Å)			
	1	**2**	
		A[a]	B[a]
C (1)-C (2)	1.390(7)	1.396(5)	1.382(5)
C (1)-C (6)	1.405(6)	1.401(4)	1.400(4)
C (1)-C(13)	1.481(7)	1.475(4)	1.474(4)
C (2)-C (3)	1.388(8)	1.384(5)	1.382(5)
C (3)-C (4)	1.378(8)	1.386(5)	1.367(6)
C (4)-C (5)	1.398(8)	1.389(5)	1.401(5)
C (5)-C (6)	1.374(7)	1.391(4)	1.384(4)
C (6)-C (7)	1.508(6)	1.510(4)	1.521(4)
C (7)-C (8)	1.478(6)	1.494(4)	1.489(4)
C (7)-O (1)	1.447(5)	1.443(4)	1.433(3)
C (7)-C (7')[c]	—	1.582(4)[b]	
C (8)-C (9)	1.386(6)	1.381(4)	1.386(4)
C (8)-C(13)	1.378(6)	1.398(4)	1.383(4)
C (9)-C(10)	1.408(8)	1.399(5)	1.391(5)
C (9)-C(14)	1.466(7)	1.476(5)	1.474(5)
C(10)-C(11)	1.365(8)	1.389(6)	1.381(5)
C(11)-C(12)	1.397(8)	1.392(5)	1.405(5)
C(12)-C(13)	1.399(7)	1.383(5)	1.393(5)
C(14)-C(15)	1.548(7)	1.542(5)	1.541(5)
C(14)-O (2)	1.217(7)	1.211(5)	1.216(4)
C(15)-O (1)	1.443(5)	1.437(4)	1.448(4)
C(15)-C(15')[c]	—	1.523(5)[b]	
(b) Bond angles (ϕ/°)			
	1	**2**	
		A[a]	B[a]
C (2)-C (1)-C (6)	120.3(4)	120.5(3)	120.2(3)
C (2)-C (1)-C(13)	131.0(5)	130.3(3)	131.1(3)
C (6)-C (1)-C(13)	108.6(4)	109.1(3)	108.6(3)
C (1)-C (2)-C (3)	118.6(5)	118.2(3)	118.5(3)
C (2)-C (3)-C (4)	120.7(5)	121.1(4)	121.5(4)
C (3)-C (4)-C (5)	121.1(5)	121.3(3)	121.2(4)
C (4)-C (5)-C (6)	118.4(5)	117.9(3)	117.3(3)
C (1)-C (6)-C (5)	120.8(4)	120.9(3)	121.4(3)
C (1)-C (6)-C (7)	109.0(4)	109.3(3)	109.6(3)
C (5)-C (6)- C(7)	130.1(4)	129.7(3)	129.0(3)
C (6)-C (7)-C (8)	102.2(4)	101.7(2)	101.3(2)
C (6)-C (7)-O (1)	117.0(4)	114.7(2)	114.1(2)
C (6)-C (7)-C (7')[c]	—	112.3(2)	111.8(2)
C (8)-C (7)-O (1)	108.3(3)	108.0(2)	108.3(2)
C (8)-C (7)-C (7')[c]	—	112.0(2)	112.0(2)
O (1)-C (7)-C (7')[c]	—	108.1(2)	109.1(2)
C (7)-C (8)-C (9)	123.9(4)	125.1(3)	124.4(3)
C (7)-C (8)-C(13)	112.2(4)	111.6(3)	112.2(3)
C (9)-C (8)-C(13)	123.6(4)	122.9(3)	122.7(3)
C (8)-C (9)-C(10)	117.5(5)	118.3(3)	118.3(3)
C (8)-C (9)-C(14)	114.9(4)	115.4(3)	115.3(3)
C(10)-C (9)-C(14)	127.4(5)	126.1(3)	125.8(3)
C (9)-C(10)-C(11)	118.8(5)	118.2(3)	119.1(3)
C(10)-C(11)-C(12)	123.5(6)	123.2(4)	122.4(4)
C(11)-C(12)-C(13)	117.8(5)	118.3(3)	117.9(3)
C (1)-C(13)-C (8)	106.7(4)	106.5(3)	107.2(3)
C (1)-C(13)-C(12)	134.6(5)	134.6(3)	133.4(3)
C (8)-C(13)-C(12)	118.4(4)	118.4(3)	119.0(3)
C (9)-C(14)-C(15)	114.9(4)	116.4(3)	117.2(3)
C (9)-C(14)-O (2)	125.6(5)	124.9(3)	124.6(3)
C(15)-C(14)-O (2)	119.6(5)	118.8(3)	118.3(3)
C(14)-C(15)-O (1)	112.1(4)	115.8(3)	114.6(3)
C(14)-C(15)-C(15')[c]	—	108.2(3)	108.5(3)
O (1)-C(15)-C(15')[c]	—	107.8(3)	106.7(3)
C (7)-O (1)-C(15)	101.5(3)	108.9(2)	109.2(2)

a) A and B represent halves of the **2** molecule. b) The value between the atoms related by the local two-fold axis within a molecule. c) Prime represents the atom of the other half within the molecule.

methine protons (J=1.7 Hz and J=6.9 Hz) seem to be consistent with ∠H-C(15)-C(16)-H=−99° and ∠H-C(16)-C(17)-H=146°, respectively.

Experimental

The formations and isolations of **1** and **2** have been reported.[3] ^{1}H NMR of **2** ($CDCl_3$) δ=4.42 (s, 2H), 6.32 (d, 2H), 6.8—8.0 (m, 12H).

Crystal Data. Adduct(**1**); $C_{25}H_{18}O_4$, M=382.4, triclinic, $P\bar{1}$, a=13.287(4), b=8.794(3), c=8.797(3) Å, α=109.78(3), β=82.17(3), γ=88.58(3)°, V=955.4 Å^3, Z=2, D_o=1.33 g/cm^3. D_c=1.33 g/cm^3. Dimer(**2**); $C_{30}H_{16}O_4$, M=440.5, triclinic, $P\bar{1}$, a=10.401(2), b=12.425(3), c=8.564(2) Å, α=103.77(4), β=108.76(4), γ=95.06(4)°, V=1001.4 Å^3, Z=2, D_o=1.46 g/cm^3, D_c=1.46 g/cm^3.

Crystallographic Measurements. The unit-cell constants and intensities of both crystals were measured with Ni-filterd Cu $K\alpha$ radiation on a Rigaku four-circle diffractometer. The intensities were measured with a θ-2θ scan technique up to 2θ=120° for **1** and 2θ=108° for **2**. The backgrounds for each reflection were measured for 5 s at both ends of the scan range. Reflections which were monitored every 100 reflections showed no significant variation in intensity during data collection. The intensities were corrected for the Lorentz and polarization factors.

Structure Determination of 1. The structure was solved by the vector-search method,[8] followed by a successive Fourier synthesis. Out of 2829 independent reflections, 2141 reflections whose intensities were greater than $3\sigma(I_o)$ were used for the refinement. The block-diagonal least-squares refinement[9] was made with anisotropic temperature factors for non-hydrogen atoms. The hydrogen atoms were located in the difference Fourier synthesis and included in a refinement with the isotropic temperature factors. Five of the strongest reflections were corrected for the extinction effect(g=3.7×10^{-6}). The weighting scheme used in the final cycle of the refinement was w=1.0 for $0<F_o\leqq 20$ and $w=[1.0+0.2(F_o-20)]^{-1}$ for $F_o>20$. The final R value was 0.067 for 2141 reflections. The final atomic parameters are given in Table 2.[5]

Structure Determination of 2. The solution and refinement of the structure of **2** was done in the same way as that of **1**. The weighting scheme used in the final cycle of the refinement was w=0.4 for F_o=0, w=1.0 for $0<F_o\leqq 7$, and $w=[1.0+0.36(F_o-7)]^{-1}$ for $F_o>7$. However, six of the

Table 2. Final Atomic Coordinates and Equivalent Temperature Factors of the Adduct (**1**)

$$B_{eq} = \frac{4}{3}\sum_i\sum_j \beta_{ij}a_ia_j$$

	x	y	z	B_{eq}/Å^2
C (1)	0.2376(3)	−0.1393(5)	0.2915(5)	3.7
C (2)	0.2800(4)	−0.2973(6)	0.2124(6)	5.1
C (3)	0.3679(4)	−0.3450(6)	0.2589(7)	5.3
C (4)	0.4113(4)	−0.2387(6)	0.3825(6)	4.8
C (5)	0.3701(3)	−0.0789(5)	0.4613(6)	3.9
C (6)	0.2829(3)	−0.0313(5)	0.4165(5)	3.3
C (7)	0.2243(3)	0.1323(5)	0.4746(5)	3.2
C (8)	0.1328(3)	0.0955(5)	0.3939(5)	3.1
C (9)	0.0441(3)	0.1967(5)	0.4402(6)	3.7
C(10)	−0.0371(4)	0.1451(7)	0.3522(7)	4.8
C(11)	−0.0245(4)	−0.0004(7)	0.2271(7)	5.4
C(12)	0.0628(5)	−0.1064(6)	0.1868(6)	4.8
C(13)	0.1425(3)	−0.0573(5)	0.2769(5)	3.8
C(14)	0.0434(3)	0.3404(6)	0.5864(6)	4.1
C(15)	0.1442(3)	0.3605(5)	0.6587(5)	3.6
C(16)	0.2240(3)	0.4234(5)	0.5504(5)	3.2
C(17)	0.2865(3)	0.2669(5)	0.4359(5)	2.8
C(18)	0.3098(3)	0.2502(5)	0.2582(5)	3.1
C(19)	0.4095(4)	0.2051(6)	0.1771(6)	4.2
C(20)	0.4341(4)	0.1936(6)	0.0141(6)	5.2
C(21)	0.3608(4)	0.2275(6)	−0.0674(5)	4.9
C(22)	0.2614(4)	0.2699(6)	0.0108(5)	4.5
C(23)	0.2357(3)	0.2821(5)	0.1724(5)	3.8
C(24)	0.2892(3)	0.5407(5)	0.6553(5)	3.9
C(25)	0.2917(4)	0.8118(6)	0.8351(6)	5.6
O (1)	0.1914(2)	0.2072(3)	0.6488(3)	3.5
O (2)	−0.0283(2)	0.4405(4)	0.6521(5)	5.6
O (3)	0.2379(2)	0.6828(4)	0.7345(4)	5.0
O (4)	0.3750(3)	0.5147(5)	0.6678(6)	7.5

Table 3. Final Atomic Coordinates and Equivalent Temperature Factors of the Dimer (**2**)

$$B_{eq} = \frac{4}{3}\sum_i\sum_j \beta_{ij}a_ia_j$$

	x	y	z	B_{eq}/Å^2
C (1A)	0.2181(3)	−0.1007(3)	0.5319(4)	3.6
C (2A)	0.1552(4)	−0.0605(3)	0.6503(4)	4.5
C (3A)	0.1520(4)	−0.1195(3)	0.7677(4)	5.0
C (4A)	0.2123(4)	−0.2144(3)	0.7707(4)	4.6
C (5A)	0.2735(3)	−0.2564(3)	0.6523(4)	3.8
C (6A)	0.2749(3)	−0.1989(2)	0.5318(3)	3.2
C (7A)	0.3259(3)	−0.2277(2)	0.3832(4)	3.1
C (8A)	0.3225(3)	−0.1218(2)	0.3293(4)	3.3
C (9A)	0.3961(3)	−0.0899(3)	0.2342(4)	3.9
C(10A)	0.3823(4)	0.0123(3)	0.1943(4)	4.6
C(11A)	0.2981(4)	0.0777(3)	0.2562(4)	4.9
C(12A)	0.2337(4)	0.0498(3)	0.3644(4)	4.4
C(13A)	0.2488(3)	−0.0507(2)	0.4051(4)	3.6
C(14A)	0.4915(3)	−0.1647(3)	0.1964(4)	4.1
C(15A)	0.5061(3)	−0.2620(3)	0.2806(4)	3.8
O (1A)	0.4659(2)	−0.2481(2)	0.4287(2)	3.4
O (2A)	0.5568(3)	−0.1553(2)	0.1046(3)	5.9
C (1B)	0.0106(3)	−0.4019(3)	0.2404(4)	3.5
C (2B)	−0.1277(3)	−0.4063(3)	0.2173(4)	4.5
C (3B)	−0.1964(3)	−0.3312(3)	0.1413(4)	4.8
C (4B)	−0.1305(3)	−0.2538(3)	0.0897(4)	4.9
C (5B)	0.0094(3)	−0.2481(3)	0.1105(4)	3.9
C (6B)	0.0782(3)	−0.3232(2)	0.1867(3)	3.2
C (7B)	0.2298(3)	−0.3330(2)	0.2333(3)	3.0
C (8B)	0.2311(3)	−0.4381(2)	0.2880(3)	3.2
C (9B)	0.3341(3)	−0.5024(2)	0.2967(4)	3.4
C(10B)	0.3203(4)	−0.6003(3)	0.3465(4)	4.2
C(11B)	0.2033(4)	−0.6315(3)	0.3798(4)	4.8
C(12B)	0.0932(4)	−0.5719(3)	0.3555(4)	4.4
C(13B)	0.1078(3)	−0.4744(2)	0.3047(4)	3.4
C(14B)	0.4383(3)	−0.4681(3)	0.2267(4)	3.9
C(15B)	0.4178(3)	−0.3694(3)	0.1464(4)	3.7
O (1B)	0.2775(2)	−0.3492(2)	0.0913(2)	3.3
O (2B)	0.5380(2)	−0.5125(2)	0.2276(3)	5.0

strongest reflections (which seemed to be affected by the extinction effect) were omitted from the refinement. The final R value was 0.058 for 2301 independent reflections. The final stomic parameters are given in Table 3.[5] The atomic scattering factors were taken from the International Tables for X-ray Crystallography.[10]

We wish to thank Dr. Masashi Hamaguchi for his cordial guidance and suggestions, Masanori Yoshida and Hiromasa Tahara for technical assistance, and Miwako Irie for the preparation of this manuscript.

References

1) E. F. Ullman and J. E. Milks, *J. Amer. Chem. Soc.*, **86**, 3814 (1964).

2) T. Motoyama, Doctoral thesis, Osaka University (1978).

3) T. Ibata, T. Motoyama, and M. Hamaguchi, *Bull. Chem. Soc. Jpn.*, **49**, 2298 (1976). (The structure of the dimer **2** was erroneously reported.)

4) A. Takenaka, *DCMS*-3, Tokyo Institute of Technology (1977).

5) The atomic parameters of hydrogen atoms, anisotropic temperature factors, bond lengths and angles other than those listed in Table 1, selected torsion angles of **2**, and the list of observed and calculated structure factors(×10) for both crystals are deposited as Document No. 8611 at the Chemical Society of Japan.

6) K. Undheim and S. Baklien, *J. Chem. Soc., Perkin Trans. 1*, **1975**, 1366.

7) R. B. Woodward and R. Hoffmann, *Angew. Chem. Internat. Edn.*, **81**, 797 (1969).

8) I. Tanaka, *RICS*, UNICS-Nagoya ed. by T. Ashida, Department of Applied Chemistry, Nagoya Univ. (1981), p. 37.

9) T. Ashida, *HBLS*-V, The Universal Crystallographic Computing System-Osaka, The Computation Center, Osaka Univ. (1973), p. 55.

10) "International Tables for X-Ray Crystallography," Vol. IV, Kynoch Press, Birmingham (1974).

Photocatalytic Isomerization of Butenes over TiO_2. Photo-Formed Active Species and Characteristics of Reaction

Masakazu Anpo,* Masaaki Yabuta, Sukeya Kodama, and Yutaka Kubokawa
Department of Applied Chemistry, College of Engineering, University of Osaka Prefecture, Sakai, Osaka 591
(Received July 16, 1985)

It has been found that UV irradiation of powdered TiO_2 catalysts in the presence of butene molecules leads to both cis-trans and double bond shift isomerization reactions with high efficiency. In the photocatalytic isomerization the reactivity of 2-butene is much higher than that of 1-butene, being in contrast to the feature in the thermal isomerization. The addition of O_2 or NO molecules leads to the complete inhibition of photocatalytic isomerization of butenes. The effect of adsorbed water on the photocatalytic isomerization has been investigated. From these results together with the ESR measurements under UV irradiation of TiO_2 at 77 K in the presence of butene as well as O_2 or NO, the following conclusion emerges: The interaction of the photo-formed O^- species or $[Ti^{3+}\text{-}O^-]$ pairs results in opening of the C=C bond of butene, i.e. formation of a radical species, which acts as the intermediate in the photocatalytic isomerization. The O^- as well as surface OH^- species participates in the hydrogen shift, i.e. the double bond shift isomerization. Thus, the reaction mechanism which has been proposed for the photocatalytic isomerization of butene over ZnO has been confirmed over TiO_2.

Photocatalysis of powdered semiconductors has received much attention from the standpoint of photochemistry of solid surfaces as well as the possibility of utilization of solar energy. However, most studies have been mainly made with the reactions associated with the photodecomposition of water over metal loaded semiconductors.[1] In order to understand the true nature of the photocatalysis, it seems necessary to investigate the photocatalytic reactions other than the oxidation and reduction reactions. As an approach along this line, a number of workers have investigated the isomerization of alkenes over metal sulfides such as CdS[2] and ZnS[3] as well as metal oxides,[4] indicating that photocatalytic isomerization reactions proceed with higher efficiency than other photocatalytic reactions such as H_2 evolution reaction from water. In these systems only the cis-trans isomerization, i.e. geometrical isomerization proceeds.

As described previously,[5] we have found out that the double bond shift isomerization as well as geometrical isomerization of butenes is markedly enhanced over TiO_2 and ZnO under UV irradiation (band gap light). We have also proposed the mechanism for photocatalytic isomerization over ZnO catalyst on the basis of detection of reaction intermediate species by using ESR.[6] However, in the case of ZnO, the isomerization proceeds significantly in the dark even at 273 K, suggesting that separation of the photocatalytic isomerization seems to be very difficult. Accordingly, in the present work, with TiO_2 where the isomerization scarcely proceeds in the dark at room temperature, we have investigated the photocatalytic isomerization by ESR techniques as well as product analysis.

Experimental

Materials. The TiO_2 was obtained from Japan Aerosil Co. (P-25, Degussa, BET surface are: 40 m^2/g, average particle size: 0.029 μm, purity: >97%). Pure rutile type TiO_2 from Ishihara Industry Co. (BET surface area: 7.5 m^2/g, average particle size: 0.1—0.2 μm). The reactant gases (1-butene, *cis*-2-butene, and *trans*-2-butene) as well as NO gases were of extra pure grade from Takachiho Kagakukogyo Co. (purity of 1-butene: >99.1%, *cis*-2-butene: >98.9%, *trans*-2-butene: >99.8%, respectively). They were used without further purification. Commercial tank oxygen was purified by low-temperature distillation. Deionized double-distilled water was degassed by alternate freezing and thawing in vacuo. Deuterium dioxide of 99.9 mol% isotopical purity (E. Merk, Darmstadt) were used without further purification.

Apparatus and Procedure. Details of the apparatus and procedure were described in our previous papers.[5,6] The quartz cell having a volume of ca. 43 cm^3 was connected to a conventional vacuum system. Ultimate vacua of 1.33×10^{-3} Pa (1×10^{-5} Torr) were attainable. The sample of 0.3 g (P-25) or 0.6 g (rutile) was subjected to oxygen treatment at 833 K, followed by evacuation at the same temperature. The TiO_2 powder was spread on the quartz cell window, having a surface area of about 32 cm^2. The reactant butene was introduced onto the catalysts, its pressure being adjusted in the range of about 4.0 kPa (30 Torr). Then UV irradiation was carried out at 313 K using a Toshiba SHL-100UV Hg lamp with a color filter (Toshiba UV-D33S; $\lambda\cong260$—420 nm) and a water filter. Analysis of the reaction products was made by gas chromatography. Isotopic analysis of butenes was carried out with Hitachi RME-6E mass spectrometer using low-voltage electrons in just sufficient amount to produce an ion of the parent mass. ESR measurements were carried out at 77 K with a JSE-ME-1 (X-band) spectrometer. Mn^{2+} ions in MgO powders were used for *g*-values and sweep calibration. UV irradiation for ESR measurements was carried out by using a 500 W Hg lamp with a color filter (Toshiba UV-29; $\lambda\geq280$ nm).

Results and Discussion

1. Photocatalytic Isomerization of 2-Butenes over

TiO_2. As shown in Fig. 1, UV irradiation of TiO_2 in the presence of *trans*-2-butene leads to the formation of 1-butene as well as *cis*-2-butene. The yield of 1-butene increases with UV irradiation time, while that of *cis*-2-butene passes through a maximum and then slowly decreases. The rate of 1-butene formation (double bond shift isomerization) is much larger than that of *cis*-2-butene formation (geometrical isomerization). As shown in Fig. 2, similar results were obtained with *cis*-2-butene. As described previously,[5,6] no skeletal isomerization, i.e. formation of isobutene was detected. The amount of photo-formed products other than butene isomers was negligible, although small amounts of butenes were irreversibly adsorbed onto the catalysts.

The initial rates of the photoisomerization determined from the slopes of the plots of the amount reacted vs. reaction time are shown in Table 1, which includes the rates of the isomerization in the dark. It is clear that the isomerization in the dark is much slower than the photoisomerization. Furthermore, as shown in Fig. 1 after the UV irradiation ceased, no isomerization occurred. It is concluded, therefore, that the isomerization of 2-butene in the dark hardly takes place over TiO_2 at around 313 K, i. e., the observed photoisomerization of 2-butene is not associated with the thermal effect by UV irradiation. Thus, a much higher reactivity of 2-butene as compared with 1-butene shown in Table 1 has been established. Such features are completely different from those of the isomerization in the dark where 1-butene is more reactive than 2-butene.

2. Effect of the Addition of O_2 or NO Molecules upon the Photoisomerization. The addition of NO molecules leads to the complete inhibition of photoisomerization of *cis*-2-butene and *trans*-2-butene. Figure 3 shows the results for *trans*-2-butene. The inhibition was also observed in the dark isomerization of 1-butene. Lunsford et al.[7] have found that the addition of NO molecules leads to the inhibition of the dark isomerization of butene over Al_2O_3. Lunsford et al.[8] and Che et al.[9] showed that on the surface of Al_2O_3 and TiO_2 the paramagnetic NO molecules interact with exposed Al and Ti ions, respectively, by using ESR.

A similar inhibition of photoisomerization of *cis*-2-butene as well as of *trans*-2-butene was observed with the addition of oxygen. In this case the photooxidation reactions took place in place of photoisomerization. Details of the photooxidation of alkenes such as butenes have been reported elsewhere.[10]

3. ESR Measurements of the Catalysts. In connection with the inhibition of the photocatalytic isomerization caused by added O_2 or NO, ESR measurements have been carried out. The addition of O_2 onto the TiO_2 catalyst degassed at high temperature leads to the formation of O_2^- anion radicals having *g*-values, $g_1=g_{zz}=2.020$, $g_2=g_{yy}=2.0106$, and $g_3=g_{xx}=2.0046$, being in good agreement with those given in many literatures.[11] This species is very stable

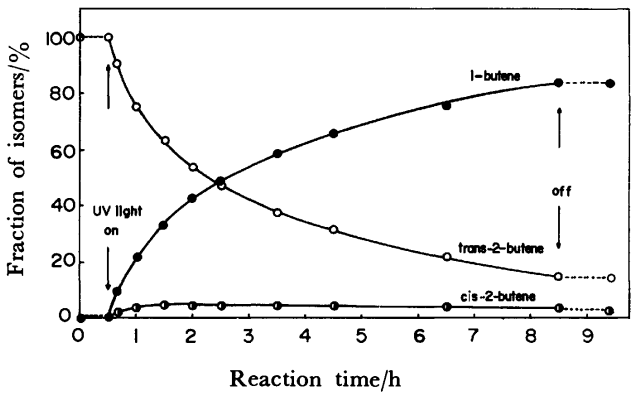

Fig. 1. Photocatalytic isomerization of *trans*-2-butene over TiO_2 catalyst at 313 K. Amount of used TiO_2 (P-25) is 0.3 g. Initial pressure of *trans*-2-butene is 4.0 kPa (30 Torr).

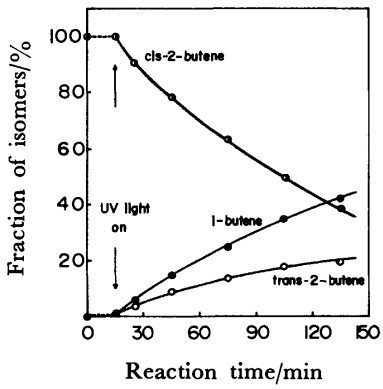

Fig. 2. Photocatalytic isomerization of *cis*-2-butene over TiO_2 catalyst at 313 K. Amount of used TiO_2 (P-25) is 0.3 g. Initial pressure of *cis*-2-butene is 4.0 kPa (30 Torr).

Table 1. Rates of Isomerization of Butenes over TiO_2 at 313 K

Catalyst	Condition	Temperature K	Initial rate/10^{-9} mol s^{-1}					
			cis→*trans*	*cis*→1	*trans*→*cis*	*trans*→1	1→*cis*	1→*trans*
TiO_2 (P-25)[a]	Under UV	313	15.3	16.9	4.12	13.5	2.61	0.68
TiO_2 (rutile)[b]	Under UV	313	5.46	18.2	3.92	9.00	0.64	0.09
TiO_2 (P-25)[a]	Dark	313	0.127	0.122	0.065	0.063	2.60	0.65

Initial pressure of butenes: 4.0 kPa (30 Torr). a) Amount of used TiO_2=0.3 g, b) Amount of used TiO_2=0.6 g.

even at higher temperature (up to around 373 K). Figure 4 shows the new ESR signal which appears by UV irradiation of TiO_2 at 77 K in the presence of O_2. This new signal is obtained as a differential spectrum by subtracting the spectrum of before UV irradiation from the spectrum of after UV irradiation at 77 K. This new ESR signal having g_1=2.0080 and g_2=2.0015 could be assigned to the O_3^- anion radicals, since the shape and paramagnetic parameters of the spectrum are in good agreement with those for the O_3^- anion radicals on TiO_2.[12] This suggests that the following reaction occurs on the TiO_2 under UV irradiation.

$$O^- + O_2 \rightarrow O_3^-,$$

where O^- is the photo-formed hole center. Details of the photo-formed O_3^- have been described in the previous papers.[10,13]

Figure 5 shows the ESR spectrum of the NO molecules adsorbed onto TiO_2 degassed at high temperature. As reported by a number of workers,[8-10] NO molecules adsorbed onto the solid surface shows the ESR spectrum due to partially quenching of the spin-orbit coupling. The ESR spectrum characterized by g_1=2.003 and g_2=1.920 is assigned to NO radicals coordinated with exposed Ti^{4+} ions on the surfaces.[9] This radical species can be easily removed from the surface by degassing the catalyst at around 300 K, being in agreement with previous works.[8,9,14] The high concentration of NO molecules on the surface results in the rather poorly resolved spectrum. On UV irradiation of the TiO_2 containing NO essentially no change was observed with the signal due to the radicals. Recently, Pichat et al.[15] have reported that NO molecules photodecompose over TiO_2 through the interaction with the O^- hole center as follows:

$$O^- + NO_{ad}^- \longrightarrow N_{ad} + O_{ad} + O^{2-}.$$

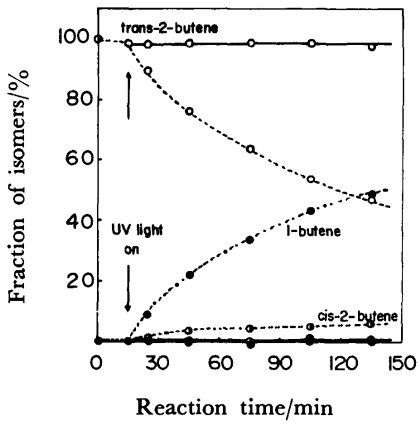

Fig. 3. Effect of the addition of NO molecules upon the photocatalytic isomerization of *trans*-2-butene over TiO_2 catalyst at 313 K. Amount of used TiO_2 (P-25) is 0.3 g. Pressures of *trans*-2-butene and NO molecule are 4.0 and 0.67 kPa, respectively. Solid lines: in the presence of NO molecules; dotted lines: in the absence of NO molecules.

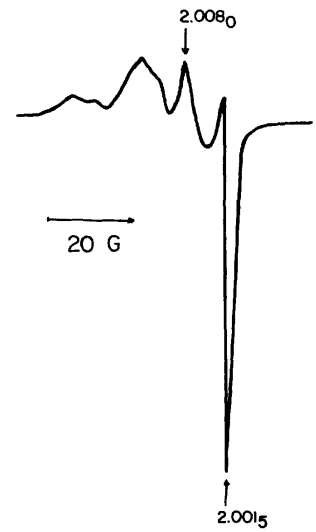

Fig. 4. ESR spectrum of photo-formed O_3^- anion radicals on TiO_2 catalyst at 77 K. Initial pressure of O_2 onto TiO_2 (rutile) is 0.33 kPa (2.5 Torr). UV irradiation was carried out at 77 K by using 500 W Hg lamp (λ>280 nm). Amount of photo-formed O_3^- anion radicals: 2×10^{-6} mol/g.

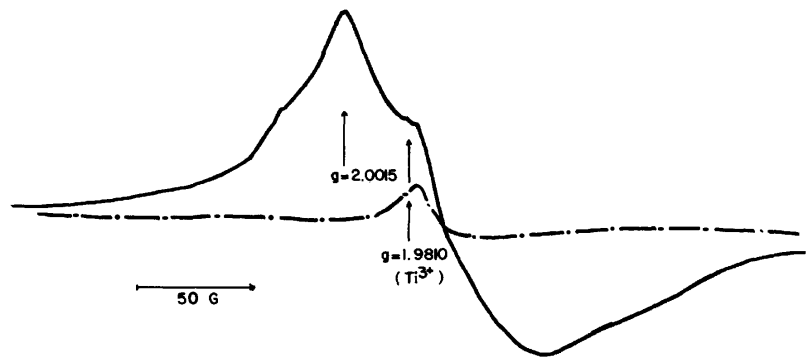

Fig. 5. ESR spectrum of adsorbed NO molecules on TiO_2 catalyst at 77 K. ESR spectra were recorded at 77 K. Amount of adsorbed NO: 2.1×10^{-5} mol/g.

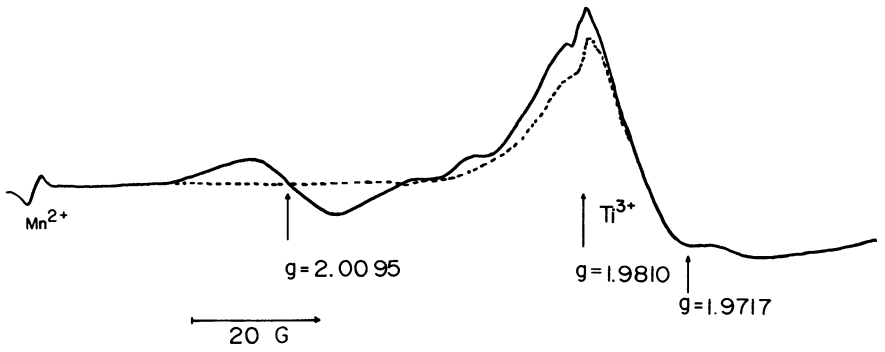

Fig. 6. ESR spectrum obtained before and after UV irradiation of TiO_2 catalyst at 77 K in the presence of adsorbed 1-butene. ESR spectra were recorded at 77 K. UV irradiation was carried out at 77 K for 30 min. Amount of adsorbed 1-butene: 1.1×10^{-5} mol/g. Dotted line: before UV irradiation; solid line: under UV irradiation.

Furthermore, as described in the previous paper,[6] the interaction of NO with photo-formed O^- species has been established. From the above considerations the following conclusions emerge: UV irradiation of TiO_2 results in formation of O^- or $[Ti^{3+}-O^-]$ pairs, although the O^- species is not detected directly by ESR, probably because of its short lifetime even at 77 K and/or incomplete removal of the degeneracy of the p-orbitals in this species, as suggested by Kazansky;[16] the O^- species thus formed interacts with NO or O_2 molecules in a manner similar with ZnO. Thus, the inhibition of the photocatalytic isomerization by added NO and O_2 is explicable.

The TiO_2 sample degassed at 833 K exhibited the ESR signal due to the Ti^{3+} ions and the O^- ions in the bulk at 77 K. The addition of butene molecules onto the catalyst at 300 K induced a slight increase in the signal due to the Ti^{3+} ions. This suggests that some fraction of Ti^{3+} ions interact with butene molecules. As shown in Fig. 6, the UV irradiation of TiO_2 in the presence of butenes at 77 K leads to the increase in the Ti^{3+} signal with UV irradiation time. Simultaneously, a broad signal with g=2.0095 appears. This signal is very unstable, and disappeared completely on raising the catalyst temperature to about 180 K. Although it is not possible to assign the species, the increase in the Ti^{3+} ion signal suggests that this unstable species might be formed through the reaction of butene with photo-formed O^- hole center. The occurrence of the photoreaction is in good agreement with the results obtained by Volodin et al.[17] who investigated the photoreduction of TiO_2 in the temperature range or 90—400 K. As shown in the preceding paper,[6] formation of a radical species has been demonstrated clearly by ESR under UV irradiation of ZnO in the presence of 1-butene at 77 K. The poorly resolved ESR spectrum may arise from the high concentration of butene adsorbed on the surface at 77 K and/or mixing of several type of radical species.

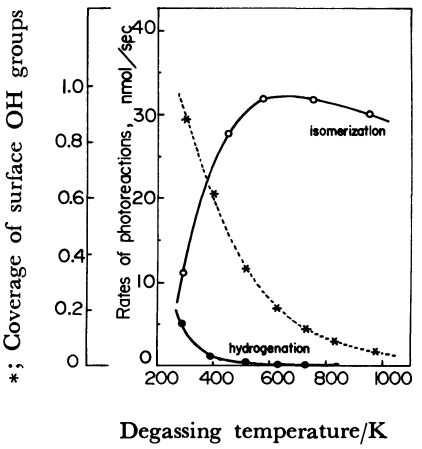

Fig. 7. Effect of the adsorbed H_2O upon the photocatalytic isomerization of *cis*-2-butene and the photocatalytic hydrogenation of $CH_3-C\equiv CH$ over TiO_2 catalyst at 313 K. H_2O vapor was adsorbed at 313 K until a pressure of 1.3 kPa (10 Torr) was reached, after which the degassing of the catalyst was carried out at each temperatures for 30 min. Initial pressure of *cis*-2-butene or $CH_3-C\equiv CH$ is 4.0 kPa (30 Torr). Coverage of H_2O was difined as ([amount of adsorbed H_2O]-[amount of desorbed H_2O])/[amount of adsorbed H_2O]. Amount of used TiO_2 (P-25): 0.3 g.

4. Effect of Remaining Water Adsorbed on the Photocatalytic Isomerization. The effect of the adsorbed water on the photocatalytic isomerization has been investigated in order to obtain further information on the active sites for the reaction. As shown in Fig. 7, the rates of photoisomerization reaction increases, passing through a maximum and then decreases. While, the increase in the degassing temperature results in the decrease in the yields of photohydrogenation of $CH_3-C\equiv CH$ (or *cis*-2-butene) where simultaneous activation of alkyne (or alkene) and H_2O is involved.[18]

When photo-formed O^- species plays a significant role in the photocatalytic isomerization, its rate is expected to increase with increasing the degassing

temperature, since the concentration of the presence of O^- species (i.e. O^{2-} ions) becomes larger. The presence of a maximum rate suggests that the surface OH^- groups is involved in the photocatalytic isomerization. From the results in Fig. 7, it is clear that on the surface of TiO_2 containing water (wet surfaces) UV irradiation leads to the photohydrogenation reactions, where simultaneous activation of alkyne (or alkene) and H_2O is involved, while on the surfaces of TiO_2 (dry surfaces) the double bond shift isomerization (1,3-hydrogen shift) occurs with high efficiency.

In order to obtain information on the role of surface OH^- groups in the photocatalytic isomerization reactions, the photoisomerization reactions of *cis*-2-butene have been undertaken over TiO_2 catalysts, which was subjected to pretreatment with D_2O followed by evacuation at 773 K. As shown in Fig. 8, deuterium substitution has no effect on the rates of double bond shift isomerization as well as cis-trans isomerization reactions. Table 2 shows the results of the distribution of D-atom in the photo-formed products and the reactant. It is clear that D-atom is incorporated into the photo-formed 1-butene, though its extent is not high. On the other hand, within the experimental error no D-atom incorporation is observed with *cis*- and *trans*-2-butene. Thus, participation of surface OH^- species in the photocatalytic isomerization is confirmed.

5. Mechanism for the Photocatalytic Isomerization of Butene. It has been reported by many workers that with TiO_2 catalysts degassed at higher temperatures (at around 900 K), the isomerization of butene proceeds via π-allyl carbanion intermediates.[19] In this mechanism the key step is abstraction of hydrogen from butene molecules, which is easier with 1-butene than with 2-butene. Such feature has been established as the characteristic of the dark isomerization. As described above, in the photocatalytic isomerization of butenes the reactivity of 2-butene is much higher than that of 1-butene, product distribution being completely different from that predicted from thermodynamic equilibrium. These clearly indicate not only that the photocatalytic isomerization reaction is kinetically controlled, as described in the previous paper,[6] but also that the active species associated with the photocatalytic isomerization is quite different from that in the dark isomerization reactions. The results of the ESR and inhibition studies described above clearly demonstrate that the interaction of photo-formed O^- species or $[Ti^{3+}-O^-]$ pair with butene molecules is involved in its photocatalytic isomerization.

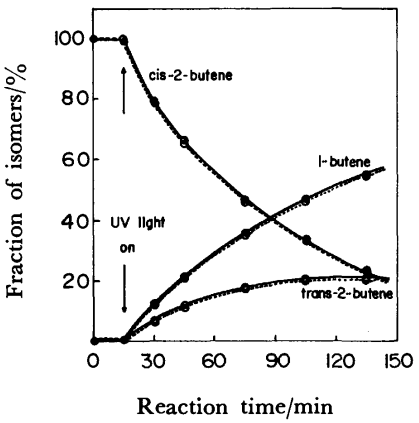

Fig. 8. Effect of the D_2O pretreatment of TiO_2 catalyst upon the photocatalytic isomerization of *cis*-2-butene over TiO_2 at 313 K. D_2O vapor was introduced onto the catalyst, kept for enough time, and then degassed at 453 K. This treatment was repeated several times. Solid lines: treated with H_2O; dotted lines: treated with D_2O. Amount of used TiO_2 (P-25): 0.3 g.

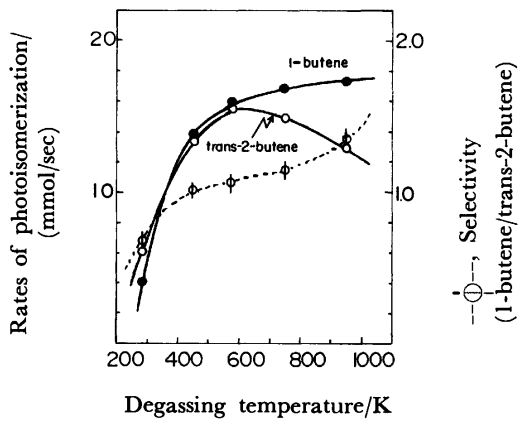

Fig. 9. Effect of the adsorbed H_2O upon the rate of photocatalytic isomerization and the selectivity of isomerization over TiO_2 at 313 K. Experimental condition is same to Fig. 7.

Table 2. Distribution of D-Atom in the Products Formed from the Photocatalytic Isomerization of *cis*-2-Butene over TiO_2 at 313 K

	Before photoreaction/%	After photoreaction/%		
	cis-2-butene	*cis*-2-butene	1-butene	*trans*-2-butene
$m/e^-=56$	96.11	92.46	84.94	93.12
$m/e^-=57$	3.89	7.54	15.06	6.88
Conversion of exchange (%)		3.65	11.17	2.99

D_2O vapor was adsorbed at 313 K until a pressure of 1.3 kPa (10 Torr) was reached, after which the evacuation was carried out at 453 K.

Recently, we have reported that the charge transfer excited states, complex, $[Mo^{5+}-O^-]^*$, of supported MoO_3 catalyst easily react with alkenes resulting in the fission of C=C bond of alkene molecule.[4b,20] It is likely, therefore, the closely existent electron and hole state, $[Ti^{3+}-O^-]$, of TiO_2 reacts with butene molecule to produce a corresponding radical species resulting from the opening of the C=C bond of butene in a manner similar to that with MoO_3 catalyst. As shown in Fig. 6, the ESR studies suggest that the photo-formed O^- species interacts with a butene molecule to form a radical species, though the spectrum is not well resolved due to high concentration of adsorbed butene.

Accordingly, it might be concluded that the photocatalytic isomerization of butene over TiO_2 proceeds according to a mechanism similar to that proposed for ZnO in the preceding paper:[6] Butene interacts with photo-formed O^- species to form a radical species. When this reverts to butene, the cis-trans isomerization will occur. The presence of H atom appears to be prerequisite for the occurrence of the double bond migration. Consequently, the more acidic the surface OH^- groups as well as the larger concentration of electron available for the neutralization of protons, the more efficient double bond migration results. As shown in Fig. 9, with increasing degassing temperature of TiO_2, the reactivity towards 1-butene formation monotonously increases. This suggests that supply of protons, i.e. the acidity of surface OH^- groups is not important in bringing about double bond migration. Accordingly, the increase in the selectivity towards 1-butene formation may be attributed to the increase in the concentration of electrons available for the neutralization of protons. Further study is necessary to clarify the nature of such an increase in the selectivity towards 1-butene formation.

References

1) "Photoelectrochemistry, Photocatalysis, and Photoreactions," ed by M. Schiavello, D. Reidel Publ. Co., Boston, (1984), and references therein; M. Anpo and Y. Kubokawa, *Hyomen Kagaku*, **4**, 200 (1983), and references therein.

2) H. Al-Ekabi and P. de Mayo, *J. Chem. Soc., Chem. Commun.*, **1984**, 1231; A. Matsumoto, M. Anpo, S. Kodama, and Y. Kubokawa, unpublished data; M. Meyer, C. Wallberg, K. Kurihashi, and J. H. Fender, *J. Chem. Soc., Chem. Commun.*, **1984**, 90; D. H. M. W. Thewissen, E. A. van der Zouwen-Assink, K. Timmer, A. H. A. Tinnemans, and A. Mackor, ibid, **1984**, 941.

3) S. Yanagida, T. Azuma, H. Kawakami, aud H. Sakurai, *J. Chem. Soc., Chem. Commun.*, **1984**, 21; S. Yanagida, H. Kawakami, K. Hashimoto, T. Sakata, C. Pac, and H. Sakurai, *Chem. Lett.*, **1984**, 1449; A. Matsumoto, M. and H. Sakurai, *Chem. Lett.*, **1984**, 1449; A. Matsumoto, M.

4) a) A. Morikawa, M. Hattori, K. Yagi, and K. Otsuka, *Z. Phys. Chem.* (Frankfurt am Main), **104**, 309 (1977); b) Y. Kubokawa and M. Anpo in "Adsorption and Catalysis on Oxide Surfaces," ed by M. Che and G. C. Bond, Elsevier, Amsterdam (1985), p. 127.

5) S. Kodama, M. Yabuta, and Y. Kubokawa, *Chem. lett.*, **1982**, 1671.

6) S. Kodama, M. Yabuta, M. Anpo, and Y. Kubokawa, *Bull. Chem. Soc., Jpn.*, **58**, 2307 (1985).

7) W. N. Delgass, G. L. Haller, R. Kellerman, and J. H. Lunsford, "Spectroscopy in Heterogeneous Catalysis," Academic Press, New York (1979), p. 183; J. H. Lunsford, L. W. Zingery, and M. P. Rosynek, *J. Catal.*, **38**, 179 (1975).

8) K. M. Wang and J. H. Lunsford, *J. Phys. Chem.*, **73**, 2069 (1969); J. H. Lunsford, ibid., **72**, 4163 (1968).

9) M. Che, C. Naccache, and B. Imelik, *J. Catal.*, **24**, 328 (1972); M. Priment, M. Che, C. Naccache, M. V. Mathieu, and B. Imelik, *J. Chim. Phys. Physico. Chim.*, **67**, 1629 (1970).

10) Y. Kubokawa, M. Anpo, and C. Yun, Proc. 7th Intern. Congr. Catalysis, Tokyo, B-36 (1980); M. Anpo, T. Fujii, S. Suzuki, and Y. Kubokawa, *J. Phys. Chem.*, **88**, 2572 (1984).

11) M. Che and A. J. Tench, *Adv. Catal.*, **32**, 1 (1983), and references therein.

12) V. V. Nikisha, C. A. Surin, B. N. Shelimov, and V. B. Kazansky, *React. Kinet. Catal. Letters*, **1**, 141 (1974); M. Anpo, N. Aikawa, Y. Kubokawa, M. Che, C. Louis, and E. Giamello, *J. Phys. Chem.*, in press.

13) Y. Kubokawa and M. Anpo, *Shokubai*, **23**, 189 (1981).

14) J. H. Lunsford, *J. Phys. Chem.*, **72**, 2141 (1968); *J. Chem. Phys.*, **46**, 4347 (1967).

15) H. Courbon and P. Pichat, *J. Chem. Soc., Faraday Trans. 1*, **80**, 3175 (1984).

16) S. A. Surin, V. V. Nikisha, B. N. Shelimov, and V. B. Kazansky, *Khimi. Vys. Energ.*, **8**, 43 (1974); V. V. Nikisha, B. N. Shelimov, and V. B. Kazansky, *Kinet. Katal.*, **15**, 676 (1974).

17) A. M. Volodin, A. E. Cherkashin, and V. S. Zakharenko, *React. Kinet. Catal. Letters*, **11**, 235 (1979).

18) M. Anpo, N. Aikawa, S. Kodama, and Y. Kubokawa, *J. Phys. Chem.*, **88**, 2569 (1984); M. Anpo, N. Aikawa, and Y. Kubokawa, ibid., **88**, 3998 (1984).

19) C. C. Chang, W. C. Conner, and R. J. Kokes, *J. Phys. Chem.*, **77**, 1957 (1973); M. Itoh, H. Hattori, and K. Tanabe, *J. Catal.*, **35**, 225 (1974).

20) M. Anpo, I. Tanahashi, and Y. Kubokawa, *J. Chem. Soc., Faraday Trans. 1*, **78**, 2121 (1982); M. Anpo and Y. Kubokawa, *J. Catal.*, **75**, 204 (1982); M. Anpo, T. Suzuki, F. Tanaka, S. Yamashita, and Y. Kubokawa, *J. Phys. Chem.*, **88**, 5778 (1984); M. Anpo and Y. Kubokawa, *Rep. Asahi Glass Found. Ind. Technol.*, **42**, 99 (1983).

Determination of the Equilibrium and Kinetic Parameters for the Surface-Redox Reaction of Hydroquinone Moiety of Adsorbed Adriamycin by Means of Numerical Simulation of d.c. Voltammogram

Tomonori KONSE, Kenji KANO, and Tanekazu KUBOTA*
Gifu Pharmaceutical University, 6-1 Mitahora-higashi 5-Chome, Gifu 502
(Received August 2, 1985)

Electrochemical equilibrium and kinetic parameters for a redox reaction caused by the hydroquinone moiety of adriamycin adsorbed on a pyrolytic graphite electrode have been determined by means of a numerical simulation of the quasi-reversible d.c. voltammograms using a theory regarding a two-step one-electron surface-redox reaction, since the electron-transfer rate constant is so small that the reversible d.c. wave can not be obtained and an analysis by a.c. voltammetry is difficult. The voltammogram was also analyzed from the viewpoint of a one-step two-electron surface-redox reaction mechanism taking into account the interaction parameters between adsorbed molecules. The analyses in terms of both mechanisms mentioned above reveal that the redox system considered here occurs through a two-step process.

The anthracycline antibiotics adriamycin and daunomycin are highly effective antitumore agents.[1] These drugs, including many new analogues and derivatives, have a dihydroxyanthraquinone structure, i.e. they contain two commonly electroactive sites: a reducible quinone moiety and an oxidizable hydroquinone moiety. The redox reaction of the quinone moiety of these drugs have been intensively investigated using various techniques, including electrochemical, in an attempt to correlate the behavior to the physiological activity of the drugs.[2-7] However, there are only a few articles concerning the redox reaction of the hydroquinone moiety. Baldwin et al.[4] have reported on a surface-redox wave of the hydroquinone moiety of adriamycin adsorbed on a carbon paste electrode. However, their analysis of the electrochemical behavior was only qualitative. One of the reasons may be related to the quasi-reversible character resulting from the small value of the electron-transfer rate constant. This character makes it difficult to estimate the equilibrium and kinetic parameters which would be obtained by an analysis of the reversible d.c. waves and a.c. voltammograms, respectively.[8,9]

In a previous paper[7] we presented a theory pertinent to the quasi-reversible d.c. voltammogram of a two-step surface-redox reaction ($O_{ad}+e \rightleftarrows S_{ad}$, $S_{ad}+e \rightleftarrows R_{ad}$), and derived a new method for determining the electrochemical equilibrium and kinetic parameters by means of a numerical simulation of d.c. voltammograms (i.e. non-linear least-squares curve fitting by the numerical calculation of current-potential curves). This new method was successfully applied to the analysis of the surface-redox reaction for the quinone moiety of adriamycin adsorbed on a basal-plane pyrolytic graphite electrode (BPGE). An excellent agreement between the equilibrium and kinetic parameters obtained from this technique and those obtained from reversible d.c. voltammograms and a.c. voltammograms indicates that the present method is very useful for determining the electrochemical parameters.

In principle, our d.c.-wave-simulation method can be employed even for surface-redox systems where the electron-transfer rate constants are so small that a direct analysis of the reversible d.c. and a.c. voltammograms is experimentally difficult. In this paper, our simulation method has been applied to the analysis of the surface-redox system of the hydroquinone moiety of adriamycin adsorbed on a BPGE. Furthermore, we have derived the theoretical equations regarding the quasi-reversible voltammetry of a one-step two-electron surface-redox mechanism ($O_{ad}+2e \rightleftarrows R_{ad}$), where the parameters describing the mutual interactions between adsorbed molecules have been taken into consideration. Then, the voltammogram was also analyzed based on the theory of a one-step mechanism. A comparison of the simulation results derived from both the mechanisms, i.e. two-step and one-step, suggests that the surface-redox system considered here obeys the above two-step mechanism.

Theoretical Treatment of Quasi-Reversible d.c. Voltammetry of Surface-Redox Reaction

At first, let us consider a one-step n-electron surface-redox reaction:

$$O_{ad} + ne \rightleftharpoons R_{ad}, \quad (1)$$

under the condition that all the electrochemical species are strongly adsorbed or immobilized on the electrode surface. Then,

$$\Gamma_o + \Gamma_r = \Gamma_t = \text{const.}, \quad (2)$$

where Γ_j's (j=o, r, and t) are the surface concentrations of O_{ad}, R_{ad}, and the total. In the following, our assumption is that the interaction between the adsorbed molecules can be expressed by using Frumkin's a-parameters (a_{ij}; i, j=O or R) and, thus, the surface activity of O_{ad} and R_{ad}, a_o and a_r, is given

by[15]

$$a_o = \Gamma_o \exp[-a_{OO} f\theta_t - a_{OR}(1-f)\theta_t] \quad (3)$$

$$a_r = \Gamma_r \exp[-a_{RR}(1-f)\theta_t - a_{RO} f\theta_t], \quad (4)$$

where $f=\Gamma_o/\Gamma_t$, and $\theta_t=\Gamma_t/\Gamma_m$, Γ_m being the maximum surface concentration. Theoretical studies regarding "reversible" d.c. voltammetry[8,11,12] and a.c. voltammetry[8] have been already reported for this type of redox system. Our formulation is, therefore, for "quasi-reversible" d.c. voltammetry.

Assuming that a surface-redox reaction occurs exclusively for adsorbed molecules and that the current-potential-surface activity characteristics can be given by the Butler-Volmer equation,[8,13] we can write:

$$i/nFA = d\Gamma_o/dt \quad (5)$$

$$= k_s a_r B_r^{-1} \exp[(1-\alpha)nF(E-E_o)/RT] - k_s a_o B_o^{-1} \exp[-\alpha nF(E-E_o)/RT], \quad (6)$$

where E_o stands for the standard redox potential of the redox couple O/R in the bulk solution, B_j (j=o,r) is the adsorption coefficient of species j at E_o, and k_s is the electron-transfer rate constant at the standard surface-redox potential, E_o'. The E_o'[8,11,12] and the electrode potential, E, are expressed by:

$$E_o' = E_o + (RT/nF) \times [\ln(B_r/B_o) - (a_{OO} - a_{RR} + a_{OR} - a_{RO})\theta_t/2] \quad (7)$$

$$E = E_i + vt. \quad (8)$$

Putting $\alpha=0.5$, a combination of Eqs. 2 to 8 leads to:

$$\psi = df_o/d\rho = m\{(1-f)\rho^{0.5} \exp(-G\theta_t/4) \exp(Jf\theta_t) - f\rho^{-0.5} \exp(G\theta_t/4) \exp[(J-G)f\theta_t]\}, \quad (9)$$

where $\psi = iRT/n^2F^2vA\Gamma_t$, $m=k_{sap}RT/nFv$, $k_{sap}=k_s \times (B_oB_r)^{-0.5}\exp[-(a_{RR}+a_{OR})\theta_t/2]$, $\rho=\exp[nF(E-E_o')/RT]$, $G=a_{OO}+a_{RR}-a_{OR}-a_{RO}$, and $J=a_{RR}-a_{RO}$. The current-potential characteristics for linear sweep voltammetry are, thus, obtained by solving Eq. 9. A standard fourth-order Runge-Kutta method was applied to resolve differential equation 9.[14] The initial conditions are $f=0$ at $\rho\to 0$ for the anodic curve and $f=1$ at $\rho\to\infty$ for the cathodic curve. To perform a numerical simulation of the d.c. voltammograms, a BASIC program was rewritten by modifying our program[7] to satisfy the above theoretical treatment. The parameters to be refined are generally k_{sap}, G (or $G\theta_t$), and J (or $J\theta_t$). When a reversible wave is obtained, the G value can be estimated from the peak current or the half-peak width of the "reversible" wave.[15] In such a case, the number of parameters will be diminished to two, k_{sap} and J.

On the other hand, in a previous paper[7] we have reported on a theoretical treatment of the quasi-reversible voltammetry for the two-step n-electron surface-redox reaction:

$$O_{ad} + ne \rightleftharpoons S_{ad} \quad \text{(1st step)}$$

$$S_{ad} + ne \rightleftharpoons R_{ad} \quad \text{(2nd step)}, \quad (10)$$

where a homogeneous interaction between the adsorbed molecules was assumed. The theoretical equations for this case are briefly given below for a comparison with those of the foregoing one-step mechanism. In this case, Eqs. 2, 5, and 6 must be rewritten as follows:

$$\Gamma_o + \Gamma_s + \Gamma_r = \Gamma_t = \text{const.}, \quad (11)$$

$$i = i(1) + i(2) \quad (12)$$

$$i(1)/nFA = d\Gamma_o/dt = k_{sap}(1)\{\Gamma_s \exp[(1-\alpha_1)nF(E-E_{o1}')/RT] - \Gamma_o \exp[-\alpha_1 nF(E-E_{o1}')/RT]\} \quad (13)$$

$$i(2)/nFA = -d\Gamma_r/dt = k_{sap}(2)\{\Gamma_r \exp[(1-\alpha_2)nF(E-E_{o2}')/RT - \Gamma_s \exp[-\alpha_2 nF(E-E_{o2}')/RT]\}, \quad (14)$$

where $i(j)$, $k_{sap}(j)$, and α_j are, respectively, the faradaic currents, the apparent rate constants at the formal standard surface-redox potentials E_{oj}', and the electron-transfer coefficients at the j-th steps (j=1 and 2). Here we define the semiquinone formation constant, K, as follows:

$$K = [S_{ad}]^2/[O_{ad}][R_{ad}] = \exp[nF(E_{o1}'-E_{o2}')/RT]. \quad (15)$$

The standard surface-redox potential, E_o', corresponding to the redox couples O_{ad}/R_{ad} is given by

$$E_o' = (E_{o1}'+E_{o2}')/2. \quad (16)$$

Equations 15 and 16 are introduced in Eqs. 13 and 14, and the resulting differential equations were numerically solved by combining them with Eqs. 8, 11, and 12. We can, thus, obtain the current-potential characteristics. In general, the parameters to be refined by a numerical simulation are $k_{sap}(1)$, $k_{sap}(2)$, K, α_1, and α_2. As we have already verified for the case of the surface-redox reaction of the quinone moiety of adsorbed adriamycin,[7] if the conditions $k_{sap}(1)=k_{sap}(2)$ and $\alpha_1=\alpha_2=0.5$ are experimentally satisfied, the parameters to be used are only two, $k_{sap}(=k_{sap}(1)=k_{sap}(2))$ and K. In addition, if the K values can be estimated from the reversible d.c. wave,[9] then only the k_{sap} needs to be refined.

Experimental

Adriamycin hydrochloride, which was donated from Kyowa Hakko Kogyo Co., and all other chemicals used

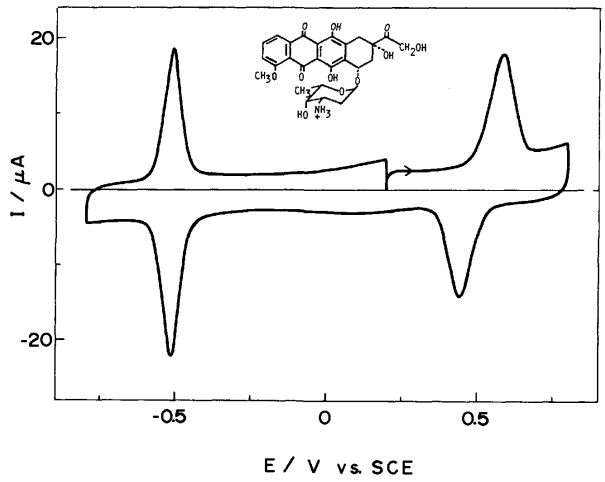

Fig. 1. Cyclic d.c. voltammograms of adriamycin adsorbed on a BPGE. Voltage scanning was done with $v=200$ mV s^{-1}. Before the measurement of cyclic voltammogram the 3.68×10^{-6} mol dm^{-3} adriamycin solution was first stirred for 1 min, then left for 1 min at $E_i=0.2$ V at 25 °C (pH=4.54, acetate buffer, $I=0.5$).

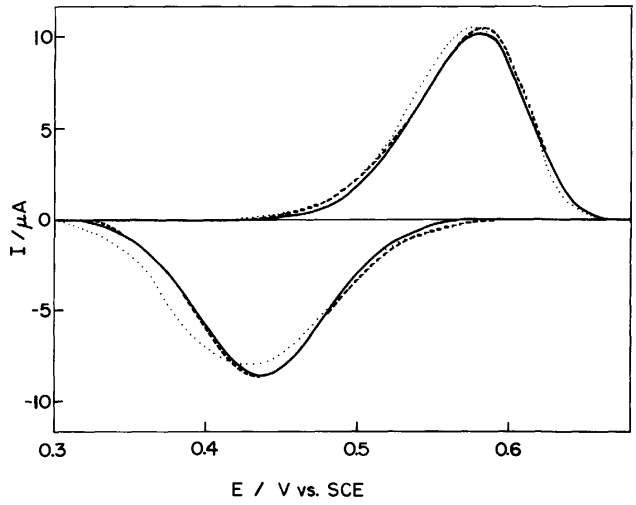

Fig. 2. Cyclic d.c. voltammograms of adriamycin adsorbed on a BPGE. Voltage scanning was done with $v=200$ mV s^{-1} under the same conditions as those in Fig. 1. The current is corrected for the base current. The broken line represents the regression curve calculated under the conditions of $k_{sap}(1)=9.49$ s^{-1}, $k_{sap}(2)=1.50$ s^{-1}, $K=0.06$, $\alpha_1=0.35$, and $\alpha_2=0.30$ for the case of the two-step mechanism. The dotted line shows the regression curve calculated under the conditions of $k_{sap}=0.187$ s^{-1}, $G\theta_t=-3.82$, and $J\theta_t=-1.20$ for the case of one-step mechanism. $E_o'=0.466$ V, $Q=4.845$ μC, and the "geometric" area of the electrode was 0.126 cm^2.

have been described elsewhere.[5-7] The electrochemical measurements and the preparation of BPGE (used as working electrodes) were, for the most part, performed as described in a previous paper.[7] The BPGE were freshly cleaved with a razor blade just before use. In the course of an analysis of the d.c. cyclic voltammograms, the base current was subtracted to determine the faradaic one. The calculation was carried out with an NEC 9801 personal computer. The computer-aided numerical simulations were done mostly performed, for the most part, as described in a previous paper.[7]

Results and Discussion

In Fig. 1 is shown a cyclic d.c. voltammogram of the adriamycin adsorbed on a BPGE in acetate buffer (pH 4.54). The voltammogram was recorded from the initial potential E_i=0.20 V to the switching potentials E_s's=0.80 and −0.80 V at a sweep rate $v=200$ mV s^{-1}, a saturated calomel electrode, SCE, being used as a reference electrode. One pair of the d.c. anodic and cathodic reversible waves at −0.50 V can be ascribed to the surface-redox reaction of the quinone moiety of adsorbed adriamycin.[3,5,6] Another pair of the quasi-reversible anodic and cathodic waves was observed at 0.60 and 0.45 V, respectively, and can be ascribed to a surface-redox reaction of the hydroquinone moiety of the substance.[4] The peak-separations of the anodic and cathodic waves on the two redox systems tell us that the electron-transfer rate constant of the hydroquinone moiety is considerably smaller than that of the quinone moiety. Actually, in a phase-selective a.c. voltammetry, the imaginary component pertinent to the redox system of the hydroquinone moiety was too small, even at the frequency as low as 100 Hz. Therefore, the analysis was difficult.

The solid line in Fig. 2 shows the d.c. voltammogram recorded from E_i=0.20 V to E_s=0.80 V at $v=200$ mV s^{-1} under the same conditions as those in Fig. 1. In Table 1 are listed the peak potentials ($E_{p,a}$, $E_{p,c}$), peak currents ($i_{p,a}$, $i_{p,c}$), half-peak widths ($\Delta E_{p/2,a}$, $\Delta E_{p/2,c}$), peak-separations ($\Delta E_p=E_{p,a}-E_{p,c}$), and $(E_{p,a}+E_{p,c})/2$ at various v, here subscripts a and c indicate anodic and cathodic waves, respectively. Upon decreasing v, ΔE_p became smaller. However, ΔE_p did not converge to zero, even at v=5 mV s^{-1}, i.e. a so-called d.c. reversible wave can not be recorded. On the other hand, the shape of the anodic wave is obviously not symmetrical with that of a cathodic one at a given v. Also, the $(E_{p,a}+E_{p,c})/2$ values shift to the cathodic side with an increasing v. These circumstances are very different from those for the quinone moiety. In the following analysis of the voltammograms, E_o' was estimated to be 0.496 V by extrapolating the v vs. $(E_{p,a}+E_{p,c})/2$ relation to v=0 within a sweep rate of 5 to 50 mV s^{-1}.

These cyclic voltammograms were then analyzed from the viewpoint of a two-step one-electron surface-redox mechanism while assuming a homogeneous interaction between the adsorbed mole-

Table 1. Scan-Rate Dependence of the Peak Potential, Peak Current, Half-Peak Width, Peak Separation, and the Average of Peak Potential of d.c. Voltammogram of Adriamycin Adsorbed on a Pyrolytic Graphite Electrode at pH 4.54

v / mV s^{-1}		$E_{p,a}$ / V vs. SCE	$E_{p,c}$ / V vs. SCE	$i_{p,a}$[a] / μA	$i_{p,c}$[a] / μA	$\Delta E_{p/2,a}$ / mV	$\Delta E_{p/2,c}$ / mV	ΔE_p / mV	$(E_{p,a}+E_{p,c})/2$ / V vs. SCE
5	Obsd	0.502	0.492	0.39	−0.38	55	55	10	0.497
10	Obsd	0.509	0.488	0.78	−0.71	55	60	21	0.503
	Calcd[b]	0.509	0.485	0.78	−0.80	56	54	24	0.497
		(0.508)	(0.489)	(0.51)	(−0.46)	(91)	(105)	(19)	(0.499)
20	Obsd	0.522	0.483	1.50	−1.34	61	66	39	0.503
	Calcd[b]	0.518	0.478	1.43	−1.48	62	59	40	0.498
		(0.520)	(0.481)	(1.05)	(−0.88)	(88)	(109)	(39)	(0.506)
50	Obsd	0.540	0.470	3.19	−3.11	74	72	70	0.505
	Calcd[b]	0.537	0.464	3.05	−3.13	74	70	73	0.501
		(0.541)	(0.464)	(2.63)	(−2.07)	(88)	(118)	(77)	(0.506)
100	Obsd	0.560	0.452	5.75	−5.51	81	84	108	0.506
	Calcd[b]	0.557	0.451	5.49	−5.29	82	84	106	0.504
		(0.558)	(0.446)	(5.23)	(−4.01)	(87)	(119)	(112)	(0.502)
200	Obsd	0.580	0.436	10.20	−8.57	83	103	144	0.508
	Calcd[b]	0.581	0.436	10.33	−8.67	87	103	145	0.509
		(0.576)	(0.428)	(10.39)	(−7.93)	(88)	(120)	(148)	(0.505)

a) The current values are normarized to $Q=4.845$ μC, assuming that i_p is proportional to Q in the narrow Q range. b) Calculated according to the theory of two-step one-electron mechanism under the conditions of $k_{sap}(1)=9.49$ s^{-1}, $k_{sap}(2)=1.50$ s^{-1}, $K=0.06$, $\alpha_1=0.35$, and $\alpha_2=0.30$ at $E_o'=0.496$ V and $Q=4.845$ μC. The values in the parentheses denote the calculated ones according to the theory of one-step two-electron mechanism under the conditions of $k_{sap}=0.187$ s^{-1}, $G\theta_t=-3.82$, and $J\theta_t=-1.20$.

cules.[7] A direct estimation of K from a reversible wave[9] is impossible in this case, and the unsymmetrical shape and the v dependence of $(E_{p,a}+E_{p,c})/2$ of the quasi-reversible waves indicate that $k_{sap}(1)\neq k_{sap}(2)$ and/or α_1, $\alpha_2\neq 0.5$.[7] For a numerical simulation of the voltammogram in Fig. 2, the following five parameters were used: $k_{sap}(1)$, $k_{sap}(2)$, K, α_1, and α_2. After repeated simulation trials, the parameters finally refined were: $k_{sap}(1)=9.49\pm1.06$ s^{-1}, $k_{sap}(2)=1.50\pm0.07$ s^{-1}, $K=0.060\pm0.009$, $\alpha_1=0.35\pm0.02$, and $\alpha_2=0.30\pm0.02$ at $Q=4.845$ μC.[16] The resultant regression curve is depicted in Fig. 2 as a broken curve. The fitting of the curves seems to be quite good. On the other hand, a numerical simulation with the three parameters, $k_{sap}(1)$, $k_{sap}(2)$, and K, was also undertaken while assuming $\alpha_1=\alpha_2=0.5$. However, the resulting regression curve did not reproduce very well the experimental one.[17]

In general, attention is necessary in a least-squares analysis based on a statistical treatment. This is in case that the parameters used are sufficiently large in number compared to those of observed points, and/or the collinearity among the parameters is large. In these cases there occurs some possibility that the refined parameter values themselves, thus derived, may be physically meaningless, though the regression curve, itself, results in a good reproduction of the observed one.[18] In order to check the validity of the parameters refined during this study, we calculated the values of $E_{p,a}$, $E_{p,c}$, $i_{p,a}$, $i_{p,c}$, $\Delta E_{p/2,a}$, $\Delta E_{p/2,c}$, ΔE_p, and $(E_{p,a}+E_{p,c})/2$ at various v by using the refined parameters described above, and compared them with the observed values. Table 1 gives the results. The calculated values and the observed values agreed well with each other.

In turn, Brown and Anson, and Kakutani et al. reported (independently) that the redox reactions of 9,10-phenanthrenequinone adsorbed on a pyrolytic graphite electrode[11] and of flavin-adenine dinucleotide adsorbed on a mercury electrode[19] can be reasonably explained by a one-step two-electron surface-redox system by taking account of heterogeneous interactions between the adsorbed molecules. Now, we would like to consider this reaction in terms of a one-step two-electron surface-redox system, since the K value (0.06) estimated above is very small. A numerical simulation was undertaken by using three parameters; k_{sap}, $G\theta_t$, and $J\theta_t$. A simulation of the voltammogram at $v=200$ mV s^{-1} (Fig. 2) resulted in $k_{sap}=0.187\pm0.02$ s^{-1}, $G\theta_t=-3.82\pm0.02$, and $J\theta_t=-1.20\pm0.15$: the regression curve is shown in Fig. 2 by a dotted curve. Also, the values of E_p, i_p, $\Delta E_{p/2}$, ΔE_p, and $(E_{pa}+E_{pc})/2$ were calculated numerically using the estimated parameters (listed in parentheses in Table 1). Although the fitting of the regression curve to the observed voltammogram is good at $v=200$ mV s^{-1}, the discrepancy between the observed and calculated values is obvious as can be seen in

Table 1. This is especially true for i_p and $\Delta E_{p/2}$ at a decreasing v. These results indicate that this redox system is not well described in terms of the one-step surface-redox reaction, even if the heterogeneous interactions between the adsorbed species are taken into account. As a result, it may be safely said that the redox reaction obeys the two-step mechanism; then, the above five parameters, refined on the basis of the two-step mechanism, can be considered to be physically significant.

It is interesting to compare the values of the equilibrium and kinetic parameters obtained for the hydroquinone moiety of the adsorbed adriamycin with those of the quinone moiety. First of all, the E'_o value of the hydroquinone part is more positive (by 1 V) than that of the quinone part (−0.498 V at pH 4.54[7]). The oxidation and the reduction of adriamycin occur at the hydroquinone and the quinone parts, respectively; thus, the hydroquinone part in the HOMO and the quinone part in the LUMO may play an important role in the oxidation and the reduction processes, respectively. Now, the difference in the above two E'_o values can be easily understood on the basis of the well-known energy-level order. In our case, however, deprotonation and protonation are coupled with the oxidation and the reduction of the hydroquinone and quinone moieties, respectively. This is because of a redox reaction in an aqueous medium. These circumstances would make it possible to reduce the difference in the two E'_o values in comparison with those expected from the HOMO and LUMO energy difference, which is correlated directly for the case of a nonaqueous medium.[20] Secondly, the semiquinone formation reaction ($O_{ad}+R_{ad}\rightarrow 2S_{ad}$) of the hydroquinone moiety in adriamycin is thermodynamically up-hill as in the case of the quinone moiety. The estimated K value (0.06) for the hydroquinone moiety corresponds to +7.0 kJ mol^{-1} in the free energy change of this reaction, $\Delta G°$, which is about 2 times as large as that of the quinone moiety (K=0.211[7]). This stability difference between the semiquinone species produced from the hydroquinone and the quinone parts might be attributable to an intramolecular hydrogen bond. In case of the semiquinone formation reaction of the quinone moiety, two hydrogen bonds formed between carbonyl groups and hydroxyl groups in adriamycin are kept in the electron transfer process. On the other hand, any one of the two hydrogen bonds should be removed due to a one-electron oxidation of the hydroquinone moiety. As a result, we can easily understand that the semiquinone species derived from the quinone part is more stable than that from the hydroquinone part. Finally, let us consider the rate constant values of $k_{sap}(1)$ and $k_{sap}(2)$. These $k_{sap}(1)$ and $k_{sap}(2)$ for the hydroquinone moiety are less than one-fiftieth and one-three hundredth of those of the quinone moiety ($k_{sap}(1)=k_{sap}(2)=5.16\times10^2$ s^{-1} at Q=4.845 μC[7,21]), respectively. The small value of k_{sap} for the hydroquinone moiety may also, in part, be ascribed to an intramolecular hydrogen-bond breakdown and/or formation in the process of a semiquinone formation equilibrium, as has been described above. This is because the activation barrier for proceeding to the semiquinone species seems to be higher for the hydroquinone moiety than for the quinone moiety, under the assumption that the barrier height is in parallel to the above-mentioned $\Delta G°$ values (chemical non-crossing rule[22]). Here note that $k_{sap}(1)$ is 6 times as large as $k_{sap}(2)$[23,24] and also α_1=0.35 and α_2=0.30 for the case of the hydroquinone moiety. This unsymmetrical nature was not observed for the hydroquinone moiety in the acetate buffer (pH 4.54) containing 9.1% *N,N*-dimethylformamide (v/v) as well as the quinone moiety in the acetate buffer.[5,7] In the former case, the analysis of the voltammograms indicates that $k_{sap}(1)=k_{sap}(2)=5.16\pm0.67$ s^{-1}, K=0.072±0.046, $\alpha_1=\alpha_2$=0.5, and E'_o=0.514 V at Q=2.301 μC. This kind of solvent effect on the kinetic parameters may also suggest the significance of inter- and intramolecular hydrogen bonds in the redox reaction. Additional work will be postponed to a future study.

We may now say, as a conclusion, that the present numerical simulation, based on a theory pertinent to the quasi-reversible d.c. voltammogram in terms of the two-step surface-redox mechanism, can be safely applied to estimate the electrochemical equilibrium and the kinetic parameters of the surface-redox system, of which the rate constants are so small that an observation of the d.c. reversible wave and the application of a.c. voltammetry are difficult. In addition, we believe that this technique can also be applied to surface-redox systems coupled with succeeding irreversible chemical reactions, such as redox reactions of the adsorbed adriamycin in neutral and alkaline media.[3,6] This is because the effect of the succeeding chemical reaction may be excluded by increasing the sweep rate,[6] then, the so-called quasi-reversible d.c. voltammograms are recorded.

We are grateful to Kyowa Hakko Kogyo Co. for kindly supplying the adriamycin. This work was supported in part by a Grant-in-Aid for Scientific Research (No. 59390012) from the Ministry of Education, Science and Culture.

References

1) A. Di. Marco, F. Arcamore, and F. Zunino, "Antibiotics III-Mechanism of Action of Antimicrobial and Antitumor Agents," ed by J. W. Corcoran and F. E. Hahn, Springer, New York (1975), pp. 101—128; S. Neidle, "Topics in Antibiotic Chemistry," ed by P. G. Sammes, John

Wiley & Sons, New York (1978), Vol. 2, pp. 240—278.

2) N. R. Bachur, S. L. Gordon, and M. V. Gee, *Mol. Pharmacol.*, **13**, 901 (1977); L. W. Lown, S. K. Sim, K. C. Majumdar, and R. Y. Chang, *Biochem. Biophys. Res. Commun.*, **76**, 705 (1977); B. Kalyanaraman, E. Perez-Reyes, and R. P. Mason, *Biochim. Biophys. Acta*, **630**, 119 (1980); S. Sato, M. Iwaizumi, K. Handa, and Y. Tamura, *Gann*, **68**, 603 (1977); J. W. Lown and H.-H. Chen, *Can. J. Chem.*, **59**, 3212 (1981).

3) G. M. Rao, J. W. Lown, and J. A. Plambeck, *J. Electrochem. Soc.*, **125**, 534, 540 (1978); C. Molinier-Jumel, B. Malfoy, J. A. Reynaud, and G. Aubel-Sadron, *Biochem. Biophys. Res. Commun.*, **84**, 441 (1978); V. Malatesta, S. Penco, N. Sacchi, L. Valentine, A. Vigevani, and F. Arcamone, *Can. J. Chem.*, **62**, 2845 (1984).

4) R. P. Baldwin, D. Packeff, and T. M. Woodcock, *Anal. Chem.*, **53**, 540 (1981); E. N. Chaney, Jr. and R. P. Baldwin, *Anal. Chem.*, **54**, 2556 (1982).

5) K. Kano, T. Konse, N. Nishimura, and T. Kubota, *Bull. Chem. Soc. Jpn.*, **57**, 2383 (1984).

6) K. Kano, T. Konse, and T. Kubota, *Bull. Chem. Soc. Jpn.*, **58**, 424 (1985).

7) K. Kano, T. Konse, and T. Kubota, *Bull. Chem. Soc. Jpn.*, **58**, 1879 (1985).

8) T. Kakutani and M. Senda, *Bull. Chem. Soc. Jpn.*, **52**, 3236 (1979).

9) T. Kakutani and M. Senda, *Bull. Chem. Soc. Jpn.*, **53**, 1942 (1980).

10) B. B. Damaskin, O. A. Petri, and V. V. Batrakov, "Adsorption of Organic Compounds on Electrodes", Plenum Press, New York (1971).

11) A. P. Brown and F. C. Anson, *Anal. Chem.*, **49**, 1589 (1977).

12) E. Laviron, *J. Electroanal. Chem.*, **52**, 395 (1974); D. F. Smith, K. Millman, K. Kuo, and R. W. Murray, *J. Electroanal. Chem.*, **95**, 217 (1979).

13) E. Laviron, *J. Electroanal. Chem.*, **101**, 19 (1979).

14) H. Margenau and G. M. Mupphy, "The Mathematics of Physics and Chemistry," the 2nd Japanese, ed by T. Sato and M. Kunimune, Kyoritsu Press, Tokyo (1961), p. 534.

15) See Eqs. 25—28 of Ref. 8.

16) In simulation of voltammogram in Fig. 2, the observed currents were measured at every 10 mV from 0.490 V to 0.630 V for the anodic wave (15 points) and from 0.550 V to 0.360 V for the cathodic wave (20 points). The observed current was normarized to an average value of Q pertinent to the anodic and cathodic waves, which were determined by measuring the area under the waves.

17) The regression curve shows that $E_{p,a}$=0.576 V, $E_{p,c}$=0.428 V, $i_{p,a}$=9.00 μA, $i_{p,c}$=−8.50 μA, $\Delta E_{p/2,a}$=98.1 mV, and $\Delta E_{p/2,c}$=104.8 mV. The discrepancy between the observed and calculated values is observed especially for $E_{p,c}$, $i_{p,a}$, and $\Delta E_{p/2,a}$ (see Table 1).

18) T. Nakagawa and Y. Oyanagi, "Analysis of Experimental Data by Least-Squares Method—Program SALS," (in Japanese), Applied Mathematics Series, Vol. 7, Tokyo Univ. Press, Tokyo (1982), Chap. 7; T. Kubota, J. Hanamura, K. Kano, and B. Uno, *Chem. Pharm. Bull.*, **33**, 1488 (1985) and references cited therein.

19) T. Kakutani, I. Katasho, and M. Senda, *Bull. Chem. Soc. Jpn.*, **56**, 1761 (1983). They concluded that the surface-redox reaction of flavin-adenine dinucleotide is brought about by way of the two-step one-electron system at θ_t<0.83 (Γ_t=5×10^{-11} mol cm^{-2}) and of the one-step two-electron system at θ_t=0.83−1.

20) H. Miyazaki, T. Kubota, and M. Yamakawa, *Bull. Chem. Soc. Jpn.*, **45**, 780 (1972); T. Kubota, H. Miyazaki, K. Ezumi, and M. Yamakawa, *Bull. Chem. Soc. Jpn.*, **47**, 491 (1974); T. Kubota, H. Miyazaki, M. Yamakawa, K. Ezumi, and Y. Yamamoto, *Bull. Chem. Soc. Jpn.*, **52**, 1588 (1979).

21) The k_{sap} of the quinone moiety depends on the total surface coverage θ_t.[7] This k_{sap} value was estimated by interpolating the logk_{sap} vs. θ_t plot (Fig. 6 in Ref. 7) to θ_t=0.277 (Q=4.845 μC).

22) T. Nagata, "Introduction to Quantum Biology," (in Japanese), Tokyo Univ. Press, Tokyo (1975), p. 24.

23) Armstrong et al.[23] reported that the rate constant of the first step one-electron transfer would be smaller than that of the second step one-electron transfer for the oxidized flavodoxin. In connection with their report we may say that our analytical method of voltammograms gives clearly the electron-transfer rate constants of the first and second steps separately, though the application is limited to only the redox reaction of surface-attached species. Our method then seems to be very useful.

24) F. A. Armstrong, H. A. O. Hill, B. N. Oliver, and N. J. Walton, *J. Am. Chem. Soc.*, **106**, 921 (1984). See also: S. G. Meyhew, V. Massey, *Biochim. Biophys. Acta*, **315** 181 (1973).

 © 1986 The Chemical Society of Japan Bull. Chem. Soc. Jpn., 59, 271—276 (1986)

The Structure of Liquid *N*-Methylformamide by Means of X-Ray Diffraction and Ab Initio LCGO-MO-SCF Calculations

Hitoshi Ohtaki,* Sumiko Itoh, and Bernd M. Rode†
Department of Electronic Chemistry, Tokyo Institute of Technology at Nagatsuta, 4259 Nagatsuta-cho, Midori-ku, Yokohama 227
† Institute of Inorganic and Analytical Chemistry, The University of Innsbruck, Innrain 52a, Innsbruck A-6020, Austria
(Received August 29, 1985)

The liquid structure of *N*-methylformamide (NMF) has been investigated by the X-ray diffraction method and the ab initio MO-SCF method. The structure parameters within a molecule were obtained as follows: C=O: 122(1) pm, C(methyl)-N: 145(2) pm, C(carbonyl)-N: 134(2) pm, N···O: 222(4) pm, C(methyl)···O: 278(6) pm. The intermolecular hydrogen-bonded N···O distance was estimated to be 298(11) pm. A linear and flexible chain structure was proposed for the liquid structure of NMF on the basis of scattered intensity data by the X-ray diffraction method and of interaction energies and geometries of hydrogen-bonded NMF molecules calculated by the ab initio MO calculations.

N-Methylformamide (NMF) is a methyl-substituted derivative of formamide (FA), and many physicochemical properties of NMF show intermediate values between those of formamide and *N,N*-dimethylformamide (DMF). Some properties of FA, NMF, and DMF are compared in Table 1. In spite of the increasing order of the molecular weight from FA to DMF, the boiling points, melting points and viscosities of the compounds decrease in the order FA>NMF>DMF. The trend indicates that intermolecular interaction energies may decrease in the same order. However, it must be noted that the relative dielectric constant of NMF is extremely large, 64% larger than that of FA, although the dipole moment of NMF is only 15% larger.

In previous papers we studied the liquid structures of FA[1] and DMF[2] by the X-ray diffraction method in combination with MO-SCF calculations for interaction energies between molecules and concluded that the former liquid has a relatively strong hydrogen-bonded structure through -CHO···H_2N- interactions, while the latter has an almost random structure due to weak intermolecular interactions.

In the present study we aim at determining the liquid structure of NMF in order to compare the structures of FA and DMF and to explain physicochemical properties of the amides on the basis of structural information of the liquids.

The structural investigation of NMF is also an interesting subject for biochemists, because the molecule has the -OC-NH- moiety which is found in peptides. Thus the definition of the cis- and trans-forms of an NMF molecule is given on the basis of the -CO-NH- bond in peptides (Fig. 1).

Infrared spectroscopic studies in the liquid phase[3,4] and in carbon tetrachloride solutions[5] revealed that the trans-isomer was predominant in the liquid and in the solution phase. The result agreed with that found in the gas phase by using infrared[6] and microwave[7] spectroscopies and the electron diffraction method.[8] NMR spectra obtained in the liquid phase[9] and measurements for the dipole moment of NMF in dioxane solutions[10] indicated that 90—92% of NMF molecules were present in the trans-form. Theoretical calculations[11] supported the more stable conformation of the trans-form than the cis-form of

Table 1. Some Physicochemical Properties of Formamide (FA), *N*-Methylformamide (NMF) and *N,N*-Dimethylformamide (DMF)[a]

	$HCONH_2$	$HCONH(CH_3)$	$HCON(CH_3)_2$
Molecular weight	45.041	59.068	73.095
Boiling point (θ_b/°C)	210.5	180—185	153.0
Melting point (θ_m/°C)	2.55	−3.8	−60.43
Viscosity/cP (25 °C)[b]	3.302	1.65	0.802
Relative dielectric constant	111.0 (20 °C)	182.4 (25 °C)	36.71 (25 °C)
Dipole moment (10^{-30} C m)	11.2 (30 °C)	12.9 (25 °C)	12.9 (25 °C)
Donor number	24	—	26.6
Acceptor number	39.8	—	16.0

a) Data are taken from "Techniques of Chemistry, II, Organic Solvents," J. A. Riddick and W. B. Bunger, Ed., Wiley-Interscience, New York (1970), except for the donor and acceptor numbers, which are quoted from "The Donor-Acceptor Approach to Molecular Interactions" V. Gutmann, Plenum Press, New York (1978). b) 1 cP = 10^{-3} N s m^{-2}.

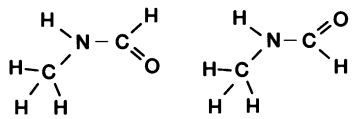

trans cis

Fig. 1. *N*-Methylformamide: Definition of trans- and cis-forms.

NMF molecules. Therefore, it seems to be generally accepted that most NMF molecules exist in the trans-form in the gas and liquid phases. However, since no diffraction study has so far been examined for NMF in the condensed phase, we try to confirm the molecular conformation of NMF in the liquid state by using the X-ray diffraction method.

The energy for the hydrogen-bonds between NMF molecules was estimated by the ab initio LCGO-MO-SCF method in order to compare the strength of the intermolecular interactions in NMF with those in FA and DMF.

Experimental

Reagents. Commercially available NMF of analytical grade was dehydrated with molecular sieves and distilled in a dry nitrogen atmosphere under a reduced pressure.

X-Ray Scattering Measurements. X-Ray scattering measurements were carried out with a JEOL θ—θ diffractometer by using LiF monochromatized Mo $K\alpha$ radiation (λ=71.07 pm) at (25±2) °C. The range of the scattering angle (2θ) was from 4 to 127°. Times spent to accumulate 80000 counts were recorded over the whole angle range. The methods of data corrections and treatments were essentially the same as those described previously.[12,13] The scattering and correction factors were quoted from the literature.[14]

The reduced intensities $i(s)$ were obtained from the following equation:

$$i(s)_{obsd} = K \cdot I_{corr}(s) - \sum n_i[\{f_i(s)+\Delta f_i'\}^2+(\Delta f_i'')^2], \quad (1)$$

where n_i is the number of atom i in a stoichiometric volume V, and $f_i(s)$ denotes the atomic scattering factor at angle s. $\Delta f_i'$ and $\Delta f_i''$ are the real and imaginary parts of the anomalous dispersion of atom i, respectively. I_{corr} denotes the measured scattering intensity corrected for the back ground, absorption, polarization, multiple scattering and incoherent scattering. K is a factor for converting measured intensities to the absolute ones and was obtained by the high angle method and the Krogh-Moe-Norman method.[15,16] The radial distribution function $D(r)$ was then obtained by Eq. 2

$$D(r) = 4\pi r^2\rho_0 + 2r\pi^{-1}\int_{s_{min}}^{s_{max}} s \cdot i(s) \cdot M(s) \cdot \sin(sr)ds \quad (2)$$

where ρ_0 is the average electronic density of sample solution. s_{max} and s_{min} correspond to the maximum and minimum values of s for the Fourier transform, which are 15.7×10^{-2} and 0.6×10^{-2} pm^{-1}, respectively. $M(s)$ is a modification function and is given as follows:

$$M(s) = [\sum n_i\{(f_i(0)+\Delta f_i')^2+(\Delta f_i'')^2\}/ \sum n_i\{(f_i(s)+\Delta f_i')^2+(\Delta f_i'')^2\}] \cdot \exp(ks^2), \quad (3)$$

and the damping factor k is set to be 100 pm^2.

Theoretical reduced intensities were calculated according to Eq. 4:

$$i(s)_{calcd} = \sum n_j[\sum\sum n_{pq}\{(f_p(s)+\Delta f_p')(f_q(s)+\Delta f_q') + \Delta f_p''\Delta f_q''\} \cdot \sin(sr_{pq})/(sr_{pq}) \cdot \exp(-b_{pq}s^2)] - [4\pi R_j^3/(3V)] \cdot [3\{\sin(sR_j)-sR_j\cos(sR_j)\}/(sR_j)^3] \cdot \exp(-B_js^2) \cdot \{\sum n_i(f_i(s)+\Delta f_i') \cdot \sum n_j(f_j(s)+\Delta f_j') + \sum n_i\Delta f_i''\sum n_j\Delta f_j''\}, \quad (4)$$

where r_{pq}, b_{pq}, and n_{pq} stand for the distance, the temperature factor and the frequency factor of the p-q atom pair, respectively. R_j denotes the distance from an atom j beyond which a continuous electron distribution is assumed. A parameter B_j is introduced to avoid a sudden emergence of a continuous electron distribution at R_j. The program *KURVLR*[17] was employed for the intensity calculations. Structural parameters of each atom-pair in the system were determined by employing the least-squares method to measured intensities. The error-square sum $U=\sum w(s)\{i(s)_{obsd}-i(s)_{calcd}\}^2$ was minimized by using the program *NLPLSQ*[18], where the weighting function $w(s)$ is given to proportional to $\cos\theta/I(s)_{obsd}^2$.

Data Analysis

The procedure for determining the structural parameters of each atom-pair in the system was performed on the following assumptions:

(1) The initial structural parameters within an NMF molecule, which will be refined by the least-squares method, are assumed to be the same as those found in a DMF molecule; C=O: 122 pm, C(carbonyl)–N: 134 pm, C(methyl)–N: 145 pm. The temperature factors for these three bonds are first assumed to be 0.3×10^2 pm^2.

(2) The N–H and C(methyl)–H and C(carbonyl)–H bond distances are assumed to be 103, 109, and 109 pm, respectively, and these temperature factors are 0.1×10^2 pm^2.

(3) The methyl group has a tetrahedral form. Nonbonding interactions of H atoms are neglected except for the 3N···H and 3H···H interactions.

After corrections for spurious peaks, the experimental $s \cdot i(s)$ curve was compared with theoretical curves of the cis- and trans-isomers of NMF by using the first term of Eq. 4. The theoretical curve calculated for the trans-form showed a better agreement than that obtained from the cis-form (see Fig. 2). Intermolecular interactions were then taken into account for the least-squares fitting of the experimental data to the theoretical ones. Each molecule was assumed to link with other molecules through the –NH···OCH– hydrogen-bond. The

least-squares refinement of the data was performed for the trans- and cis-conformations of NMF molecules. In the course of the calculations a continuous electron distribution was assumed. The results are depicted in Fig. 3 for the trans- and cis-forms of NMF molecules. It is obvious from the figure that the curve calculated on the basis of the trans-conformation of NMF molecules gave a much better agreement with the experimental curve than that of the cis-conformation.

The radial distribution curve $D(r)-4\pi r^2\rho_0$ of NMF is shown in Fig. 4. The first peak at 120 pm corresponds to the C–N and C=O bonds within an NMF molecule, and the second peak around 230 pm is ascribed to the N···O and C···C nonbonding interactions within a molecule. The difference of the contribution of the isomeric conformations is expected to appear at about 280 pm for the trans-

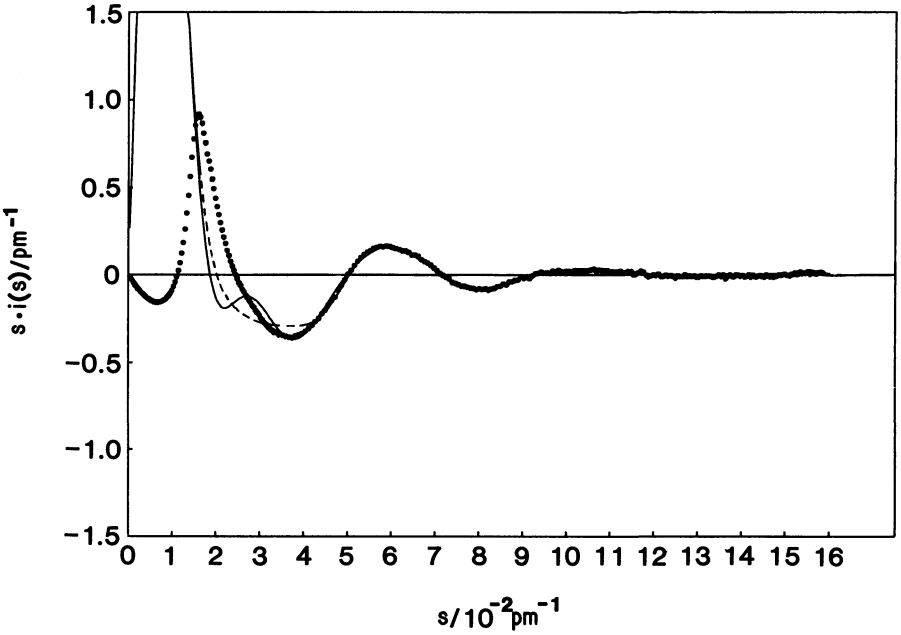

Fig. 2. Comparison between observed (circles) and the calculated $s\cdot i(s)$ corresponding to cis-(broken line) and trans-(solid line) forms. The contributions of the intermolecular N···O interaction are included.

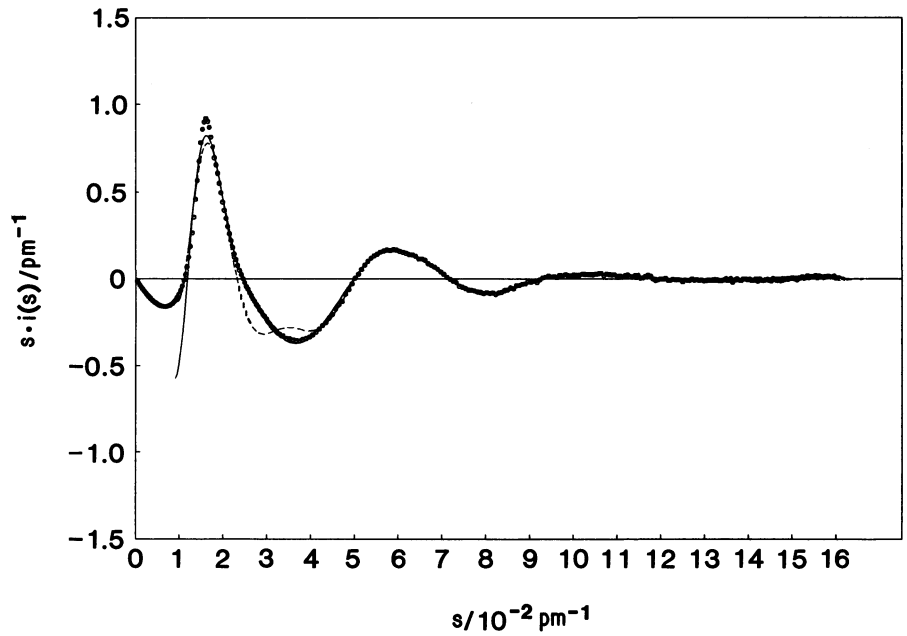

Fig. 3. Experimental (circles) and the theoretical $s\cdot i(s)$ curves for the chain structures consisting of the trans-isomer (solid line) and the cis-isomer (dashed line).

isomer and 350 pm for the cis-isomer due to the nonbonding interaction of C(methyl)···O within a molecule. On the supposition that the cis-isomer was predominant, the peak at 300 pm should be attributed only to the intermolecular N···O interaction and it was required to increase in the number of the hydrogen bonds per molecule to be 3. But even at that time, the theoretical $s \cdot i(s)$ curve showed the manifest discrepancy with the experimental one at about 4×10^{-2} pm^{-1} of s.

Therefore, we concluded that most NMF molecules in the liquid have the trans-conformation, as have been found in previous works.[4-11] The final results thus obtained for the structure parameters of NMF are listed in Table 2, together with those of FA and DMF.

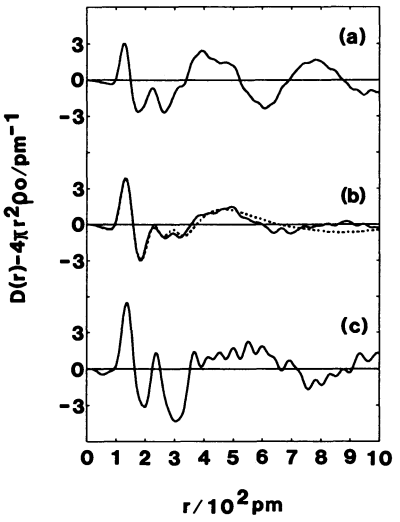

Fig. 4. Experimentally obtained $D(r)-4\pi r^2\rho_0$ curve of three amides. (a) Formamide, (b) *N*-Methylformamide. The dashed line represents calculated curve from the linear chain model structure of the trans-form molecules and the continuous electron distribution by using parameters in Table 2. (c) *N*,*N*-Dimethylformamide.

Table 2. The Structure Parameters of Liquid FA, NMF and DMF. r and b Denote the Distance and the Temperature Factor, Respectively. The Values in Parentheses are Their Standard Deviations

	FA[1]	NMF		DMF[2]
	r/pm	r/pm	b/10² pm²	r/pm
C=O	124 (1)	122 (1)	0.2 (1)	124 (2)
N-C(CO)	133 (1)	134 (2)	0.4 (2)	135 (3)
N-C(CH_3)	—	145 (2)	0.2 (1)	145 (2)
N···O	225 (2)	222 (4)	0.7 (3)	225 (6)
C(CH_3)···C(CO)	—	248 (4)	0.7 (3)	238 (10)
C(CH_3)···C(CH_3)	—	—	—	257 (15)
C···O	—	278 (6)	1.5 (7)	274 (12) 364 (16)
N···O(inter)	305 (5) 292[a] 310[b]	298 (11)	3.6 (20)	—

a) Ref. 20. b) Ref. 21.

Theoretical Treatment

Stabilities of the cis- and trans-conformations of an NMF molecule, as well as the interaction energies between molecules through the -NH···OCH- hydrogen bond, were investigated by the ab initio LCGO-MO-SCF method with the minimal basis sets. The bond lengths within an NMF molecule were kept at the values experimentally obtained by the present X-ray diffraction study as shown in Table 2. Total energies for the cis- and trans-conformations, both being examined for the staggered and eclipsed orientations, are shown in Table 3. The stabilities were in the order, trans(staggered)>trans(eclipsed)>cis(eclipsed)>cis (staggered), which agreed well with the result found by Sugawara, et al., using the STO-4l-G basis set.[11] The energy differences between the trans- and cis- forms were about 11 kJ mol^{-1} (0.00431 hartrees), which may be compared with the energy difference calculated by Sugawara et al. (5.7 kJ mol^{-1}).[11]

Interaction energies between NMF molecules were calculated by assuming some plausible geometries of NMF dimers which consisted of molecules of trans(staggered)-form, except for the cyclic dimer which must be constructed from molecules of the cis-form. The results are summarized in Table 4. For the calculation the counterpoise correction[19] had been performed. The energy of the hydrogen bond was the largest in the type D3 in Table 4. The cyclic dimer (D5) has the smallest interaction energy per hydrogen bond among the models examined.

Table 3. Energies of Monomers of NMF

Number	Model		Energy/hartree
M1	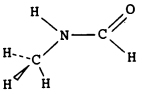	(cis eclipsed)	−176.47569
M2	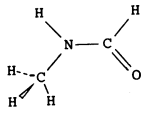	(trans eclipsed)	−176.47679
M3	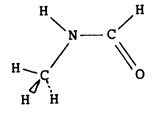	(trans staggered)	−176.48000
M4	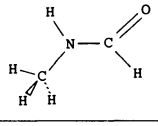	(cis staggered)	−176.47523

1 hartree=2625.34 kJ mol^{-1}.

Table 4. Energies of Hydrogen-bonds E_h for Various Dimers of NMF

Number	Model	E_h/kJ (per H-bond)
D1	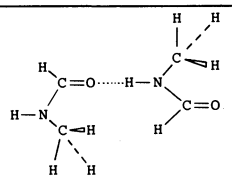	−22.16
D2	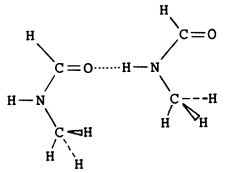	−22.16
D3	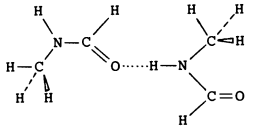	−26.76
D4	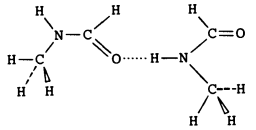	−26.35
D5	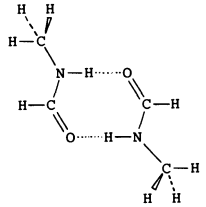	−18.40

Furthermore, the interaction energy was additive when another NMF molecule was combined with a linear dimer to form a trimer with elongation of the same conformation of the type from D1 to D4.

Intensities $s \cdot i(s)$ calculated from the models D1 to D4 gave very similar curves and all fitted well the experimental curve. Figure 3 shows the $s \cdot i(s)$ curve for the chain structure consisting of the D3 units and the continuous electron distribution are also included.

Discussion

The radial distribution curve $D(r)-4\pi r^2\rho_0$ of NMF is shown in Fig. 4, together with the curves of FA and DMF for comparison. The calculated radial distribution curve (broken line) for the chain structure using the structural parameters given in Table 2 for NMF and a continuous electron distribution satisfactory agreed with the experimental curve. In the case of NMF, the peak due to the hydrogen bonded N-(H)···O interaction appears at about 300 pm at almost the same position of that of FA, but no significant corresponding peak was observed in the case of DMF. The obtained N-(H)···O distance for NMF is compared with the value for FA[1,20,21] in Table 2. The hydrogen-bond distances are not appreciably changed between NMF and FA.

The radial distribution curve of NMF indicates a practically random distribution of molecules at a long distance $r>500$ pm, which is similar to the curve of DMF, in spite of the existence of relatively strong

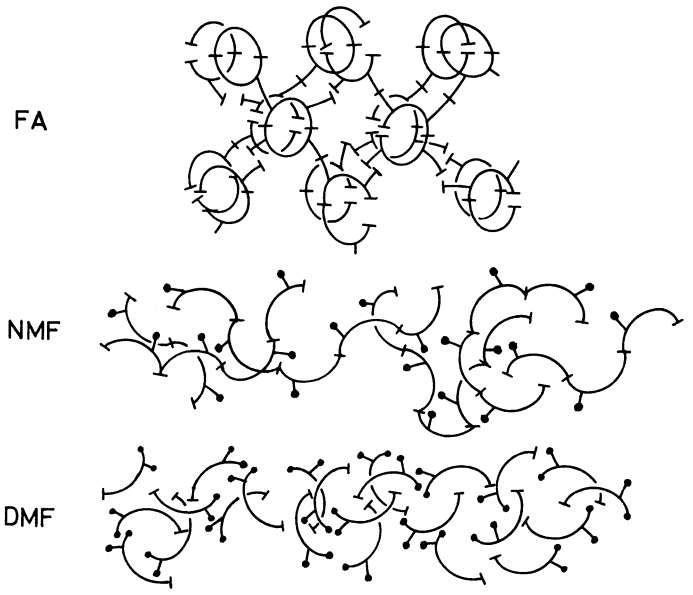

Fig. 5. Models for the liquid structures of formamide, *N*-methylformamide and *N*,*N*-dimethylformamide. —• indicates $-CH_3$, ≺ and ≺● represent $-N\langle^{H}_{H}$ and $-N\langle^{H}_{CH_3}$, respectively. ⌒ shows a hydrogen-bond between molecules.

hydrogen bonds in the system. On the contrary, FA has a three-dimensional hydrogen-bonded structure consisting of ring-dimer and chain moieties,[22] which has long-range order correlations over the ranges 350—500 pm and 700—850 pm. The energies of the hydrogen bonds in FA and NMF were estimated to be similar (E_h=−68.8[1] and −59.8 kJ mol^{-1} without the counterpoise corrections).

From the experimental results obtained by the X-ray diffraction studies and theoretical estimations for energies of hydrogen-bonds in FA,[1,22] NMF, and DMF,[2] we propose the liquid structure of these compounds as follows:

(1) Formamide has a three-dimensional structure containing the ring and chain moieties. The energy for the hydrogen-bond may be the largest among the three systems. Therefore, FA has a high boiling point and a high melting point and a large viscosity. According to most investigations from vibrational spectroscopies, however, the liquid FA has been proposed to have a chain structure.[23] This suggests that FA has a chain-like structure as the V-structure, but the time and space averaged structure (D-structure) shows a more or less crystal-like three-dimensional arrangement of molecules. So the life time of the chain moieties is suggested to be longer than that of the ring ones. A relatively high dielectric constant of FA is explained in terms of the relatively large dipole moment and the ordered structure. The ratio of the dielectric constants of FA to NMF was smaller than that expected from their dipole moments, which should be ascribed to the formation of ring-dimers in the liquid formamide in which the dipole moment is cancelled each other.

(2) *N*-Methylformamide has a hydrogen-bonded chain structure without the formation of a net-work structure. The chain may be so flexible that long-range ordered structure could not be seen from the diffraction method. Ring-dimer units hardly form in the system. The lower viscosity of NMF than FA may be explained by a slightly smaller value of the energy of the hydrogen-bond between NMF molecules, flexibility of the chain structure, and probably also by the absence of a net-work structure. The donor number and acceptor number of NMF have not been determined, but they may be similar to the corresponding values of FA.

(3) *N*,*N*-Dimethylformamide has a practically random structure, although DMF molecules interact each other through weak -HCO···HCO- hydrogen bonds. Therefore, the boiling and melting points of DMF are lower than those of FA and NMF. In spite of a larger molecular volume of DMF than those of the other two liquids, viscosity of DMF is smaller because of weaker intermolecular interactions. The relative dielectric constant is also much smaller than those of the other two solvents because of the random structure of DMF in the liquid state.

Models for the structures of FA, NMF, and DMF are depicted in Fig. 5.

The work has partially been financially supported by the Grant-in-Aid for Scientific Research (No 57470054) from the Ministry of Education, Science and Culture of Japan and the Austrian Ministry for Science and Research (Erl. Zl. 18.854/6-10/81). Computer calculations were done at the Tokyo Institute of Technology at Nagatsuta and at the University of Innsbruck.

References

1) H. Ohtaki, A. Funaki, B. M. Rode, and G. J. Reibnegger, *Bull. Chem. Soc. Jpn.*, **56**, 2116 (1983).
2) H. Ohtaki, S. Itoh, T. Yamaguchi, S. Ishiguro, and B. M. Rode, *Bull. Chem. Soc. Jpn.*, **56**, 3406 (1983).
3) T. Miyazawa, T. Shimanouchi and S. Mizushima, *J. Chem. Phys.*, **24**, 408 (1956).
4) I. Suzuki, *Bull. Chem. Soc. Jpn.*, **35**, 540 (1962).
5) R. A. Russell and H. W. Thompson, *Spectrochim. Acta.* **8**, 138 (1956).
6) T. Miyazawa, *J. Mol. Spectrosc.*, **4**, 155 (1960).
7) R. A. Elzaro, *Diss. Abstr. Int. B* **34**, 1052 (1973).
8) M. Kitano and K. Kuchitsu, *Bull. Chem. Soc. Jpn.*, **47**, 631 (1974).
9) L. A. LaPlanche and M. T. Rogers, *J. Am. Chem. Soc.*, **86**, 337 (1964).
10) M. J. Aroney, R. J. W. Le Fevre, and A. N. Singh, *J. Chem. Soc.*, **3**, 3179 (1965).
11) Y. Sugawara, A. Y. Hirakawa, M. Tsuboi, S. Kato, and K. Morokuma., *Chem. Phys.*, **62**, 339 (1981).
12) H. Ohtaki, M. Maeda, and S. Ito, *Bull. Chem. Soc. Jpn.*, **47**, 2217 (1974).
13) E. Andersson, O. Lindqvist, and T. Yamaguchi, *Acta Chem. Scand., Ser. A*, **35**, 591 (1981).
14) "International Tables for X-Ray Crystallography," Kynoch Press, Birmingham (1974), Vol. 4; D. T. Cromer and J. B. Mann, *J. Chem. Phys.*, **47**, 1892 (1967); D. T. Cromer, *J. Chem. Phys.*, **50**, 4857 (1969).
15) J. Krogh-Moe, *Acta Crystallogr.*, **9**, 951 (1956).
16) N. Norman, *Acta Crystallogr.*, **10**, 370 (1957).
17) G. Johansson and M. Sandström, *Chem. Scr.*, **4**, 195 (1973).
18) H. Ohtaki, T. Yamaguchi, and M. Maeda, *Bull. Chem. Soc. Jpn.*, **49**, 701 (1976).
19) The counterpoise correction method gives more precise results because of taking into consideration the basis set superposition error.
20) E. Kálmán, I. Serke, G. Pálinkás, M. D. Zeidler, F. J. Wiesmann, H. Bertagnolli, and P. Chieux, *Z. Naturforsch.*, **38a**, 231 (1983).
21) M. Miyake, O. Kaji, N. Nakagawa, and T. Suzuki, *J. Chem. Soc., Faraday Trans. 2*, **81**, 277 (1985).
22) H. Ohtaki and S. Itoh, *Z. Naturforsch.*, in press.
23) For example, O. F. Nielsen, P.-A. Lund, and E. Praestgaard, *J. Chem. Phys.*, **77**, 3878 (1982); H. Siegbahn, L. Asplund, P. Kelfve, K. Hamrin, L. Karlsson, and K. Siegbahn, *J. Electron Spectrosc. Relat. Phenom.*, **5**, 1059, (1974).

Green and Brown Isomers of the ((*S*)-1-Amino-2-propanethiolato-*N*,*S*)(1,4,7,10-tetraazacyclododecane)cobalt(III) Ion and Crystal Structure of the Green Isomer

Masaaki KOJIMA, Kyoko NAKABAYASHI, Shigeru OHBA,† Satoshi OKUMOTO,† Yoshihiko SAITO,† and Junnosuke FUJITA*

Department of Chemistry, Faculty of Science, Nagoya University, Chikusa-ku, Nagoya 464
† Department of Chemistry, Faculty of Science and Technology, Keio University, Hiyoshi 3, Kohoku-ku, Yokohama 223

(Received July 18, 1985)

The $[Co(S\text{-apS})(cyclen)]^{2+}$ (*S*-apS=(*S*)-1-amino-2-propanethiolate ion, cyclen=1,4,7,10-tetraazacyclododecane) complex was prepared and separated into two isomers (green and brown) by column chromatography. The crystal structure of the green isomer, $[Co(S\text{-apS})(cyclen)]ZnCl_4 \cdot H_2O$ was determined by X-ray analysis. Crystal data are as follows: monoclinic, space group $P2_1$, a=9.382(2), b=13.124(3), c=8.934(2) Å, β=91.08(3)°, and Z=2. The complex ion has a cis-octahedral geometry with the cyclen ligand coordinated in a folded, butterfly-like configuration and the bidentate *S*-apS ligand in a δ-gauche form. One of the two "planar" NH hydrogens of the macrocycle with respect to the *S*-apS ligand is directed opposite the *S*-apS chelate ring (exo), while the other "planar" and the remaining two "apical" NH hydrogens are directed to the *S*-apS ring (endo). The green isomer can be represented by *endo*(S,NH), where NH denotes the planar NH hydrogen cis to the sulfur atom. The other brown isomer was assigned as the *exo*(S,NH) configuration, where the S and NH_2 coordination sites of *S*-apS in the green isomer are interchanged with each other, remaining the configuration of the macrocycle unchanged. Reversible isomerization between the two isomers occurred in aqueous solution and the kinetics was studied at 25.4 °C in the pH range of 5.98—6.97. The isomerization obeyed a rate law of the form, $R=k[OH^-]\cdot[complex]$, and was suggested to take place with synchronous inversion at the two nitrogen atoms of the macrocycle. The relative abundance of the two isomers at equilibrium is 1.0, and the forward and reverse second-order rate constants at 25.4 °C are 6.5×10^3 mol^{-1} dm^3 s^{-1}.

In the course of circular dichroism (CD) studies of cobalt(III) complexes containing a chiral aminoalkanethio(or seleno)late-*N*,*S*(or *Se*) chelate ligand,[1] we have obtained two isomers (green and brown) of $[Co(S\text{-apS})(cyclen)]^{2+}$ (*S*-apS=(*S*)-1-amino-2-propanethiolate ion, cyclen=1,4,7,10-tetraazacyclododecane). To our knowledge, no isomers of metal-cyclen complex have been reported. The isomers are stable in acidic solution, but easily isomerize to each other in basic solution. This report is concerned with the structures, absorption and CD spectra, and isomerization reactions of these isomers.

Experimental

Preparation of $[Co(S\text{-apS})(cyclen)]ZnCl_4$ (brown isomer) and $[Co(S\text{-apS})(cyclen)]ZnCl_4 \cdot H_2O$ (green isomer). An aqueous solution (10 cm^3) containing cyclen$\cdot 2H_2SO_4$[2] (0.737 g, 2.00 mmol) and NaOH (0.32 g, 8.00 mmol) was deoxygenated by bubbling nitrogen, and then added to a deoxygenated aqueous solution (5 cm^3) of $CoCl_2 \cdot 6H_2O$ (0.397 g, 1.67 mmol) with stirring. To the resulting brownish orange solution was added a deoxygenated aqueous solution (5 cm^3) containing (*S*,*S*)-$(NH_2CH_2CH(CH_3)S\text{-})_2 \cdot 2HCl$[3,4] (0.212 g, 0.835 mmol) and NaOH (0.067 g, 1.67 mmol). The mixture was stirred under an atmosphere of nitrogen for 4 d at 30 °C, and then filtered to remove a small amount of insoluble substance. The brown filtrate was diluted with water (500 cm^3) and applied on a column (ϕ2.7 cm×30 cm) of Dowex 50 W×2 (200—400 mesh, H^+ form). By elution with 2 mol dm^{-3} HCl, a green and a brown band developed in this order. The eluate containing the green band was collected and evaporated to a small volume under reduced pressure. To the concentrate was added $ZnCl_2$ (0.5 g) in 3 mol dm^{-3} HCl (1 cm^3) to precipitate dark brown tetrachlorozincate of the complex. The precipitate was collected by filtration and washed with acetone. Yield: 0.2 g. Found: C, 23.81; H, 5.61; N, 12.60%. Calcd for $C_{11}H_{30}N_5Cl_4CoOSZn$: C, 24.17; H, 5.53; N, 12.81%.

The eluate containing the brown band was treated by the same method to yield brown plates. Yield: 0.15 g. Found: C, 24.82; H, 5.28; N, 13.19%. Calcd for $C_{11}H_{28}N_5Cl_4CoSZn$: C, 25.00; H, 5.34; N, 13.25%.

When the reaction product was chromatographed with a column of SP-Sephadex C-25 and an eluent 0.1 mol dm^{-3} Na_2SO_4—0.01 mol dm^{-3} HCl, the order of elution was reversed; the brown isomer being eluted faster than the green one.

Spectral Measurements. Absorption spectra were recorded on a Hitachi 323 or a JASCO 610B spectrophotometer, and circular dichroism (CD) spectra on a JASCO J-40CS spectropolarimeter.

Kinetic Measurements. The rate of the change in absorption spectrum was measured for a phthalate buffer solution (pH range: 5.98—6.97) of each isomer (ca. 3×10^{-3} mol dm^{-3}) at 25.4 °C. The change in absorption spectrum was recorded in the region of 800—400 nm. The reaction was followed at least three half-lives.

Crystal Structure Determination. A dark brown crystal was ground into approximate sphere 0.45 mm in diameter and mounted on an automated Rigaku four-circle diffractometer AFC-5. The cell dimensions were refined based on 20 2θ values ($20<2\theta<28°$) with λ(Mo Kα)=0.71073 Å. The crystal data are: $[Co(C_3H_8NS)(C_8H_{20}N_4)]^{2+}[ZnCl_4]^{2-} \cdot H_2O$, F.W.=546.5, monoclinic, space group $P2_1$, a=9.382(2), b=13.124(3), c=8.934(2) Å and β=91.08(3)°, V=1099.9(4) Å^3, Z=2, D_m(ether/bromoform)=1.65, D_x=1.65 Mg m^{-3}, μ=2.46 mm^{-1}. Intensity measurement was performed to 2θ=55° by θ—2θ scan technique with scan speed 6° min^{-1} (θ). The

ratio of structure factors of five standard reflections, $|F_o|/|F_o|_{initial}$, was from 0.98 to 1.06. 2814 reflections were measured and 2573 reflections with $|F_o|>3\sigma(|F_o|)$ were regarded as observed, of which 2423 reflections were unique. Lorentz-polarization and absorption corrections were applied (0.447≦transmission factor≦0.457). The structure was solved by Patterson-Fourier method. The atomic parameters were refined by block-diagonal least squares. The function minimized was $\Sigma w||F_o|-|F_c||^2$, $w^{-1}=\sigma^2(|F_o|)+(0.015|F_o|)^2$. After the introduction of anisotropic thermal parameters (R=0.050), 9 among 28 hydrogen atoms were found from the difference synthesis and others were calculated (R=0.039). The difference synthesis at this stage of the refinement showed a peak of 1.7 eÅ^{-3} with three satellite peaks of 0.7—1.0 eÅ^{-3}, suggesting positional disorder of the water of crystallization. D_m indicated one water molecule for each asymmetric unit. O(W)1 atom was included in the calculation with 0.25 occupancy factor tentatively (R=0.034). Anisotropic thermal parameter of the O(W)1 atom became non-positive definite. Thus, O(W)2, O(W)3, and O(W)4 atomic positions which separate from the most populated O(W)1 position with distances from 0.88(5) to 1.14(3) Å were added. The population parameters of four O(W) atoms were estimated by the trial and error method in such a way that each isotropic thermal parameter took nearly equal value. The R value reduced to 0.028, wR=0.035 and S=1.6.[5] All the shifts in the final cycle of the refinement were less than 0.6σ for non-hydrogen atoms except O(W). Maximum and minimum height in the final difference synthesis was 0.5 and −0.4 eÅ^{-3}. The calculations were carried out on a FACOM M-380R computer at Keio University with UNICS III program system.[6]

The absolute structure was determined by the anomalous-scattering technique. The enantiomeric structure gave R=0.032, wR=0.040 and could be rejected at the 0.005 significance level by the Hamilton test.[7] The absolute configuration of optically active apS in the present complex cation, which was obtained from $(+)_{589}$-apS·HCl,[1] was determined to be S in agreement with the assignment based on the isomer distribution and CD spectra of [Co(apS){(*R*,*R*)-1,2-cyclohexanediamine}$_2$]$^{2+}$ and related complexes.[1]

Results and Discussion

Preparation and Characterization of the Complexes. The [Co(*S*-apS)(cyclen)]$^{2+}$ complex was prepared by oxidizing Co^{II}–cyclen species with the disulfide according to the method for analogous aminoalkanethiolate-*N*,*S* complexes of cobalt(III).[8,9] The complex was separated into two isomers (green and brown) by column chromatography on Dowex 50W×2 (eluent: 2 mol dm^{-3} HCl) or on SP-Sephadex C-25 (eluent: 0.1 mol dm^{-3} Na_2SO_4—0.01 mol dm^{-3} HCl). The isomers are stable in acidic water and show no measurable change in absorption and CD spectra, but isomerize in neutral or alkaline solution to give an equilibrium mixture of the two isomers (vide infra).

The structure of the green isomer was determined by the X-ray method to be *endo*(S,NH) isomer of configuration I (vide infra, Figs. 1 and 2). We could not obtain good crystals of the brown isomer suitable for X-ray analysis. However, this isomer can be assigned to the other isomer of configuration I, *exo*(S,NH) from comparisons of the behavior in column chromatography, and the absorption and CD spectra with those of two isomers of [Co(*S*-apS)(tren)]$^{2+}$[1] (tren=tris(2-aminoethyl)amine). The steric relations of the sulfur and amine hydrogen atoms of the p- and t-isomers of [Co(*S*-apS)(tren)]$^{2+}$ can be compared to those of the *exo*(S,NH) and *endo*(S,NH) isomers of [Co(*S*-apS)(cyclen)]$^{2+}$, respectively (Fig. 2). The *exo*(S,NH) isomer of the cyclen complex and the p-isomer of the tren complex have two sets of three N–H bonds capable of forming hydrogen bonds with a sulfate ion. Thus, the isomers will be eluted faster in column chromatography than the other isomers (*endo*(S,NH) and t-isomers), since the former isomers will form a stronger ion pair with a sulfate ion than the latter ones which have no such a set of three N–H bonds.[10] The brown isomer of the cyclen complex and p-

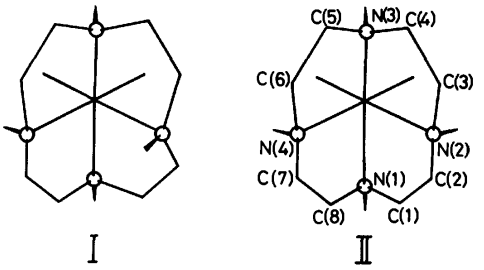

Fig. 1. Two possible configurations for cis-octahedral complexes of cyclen.

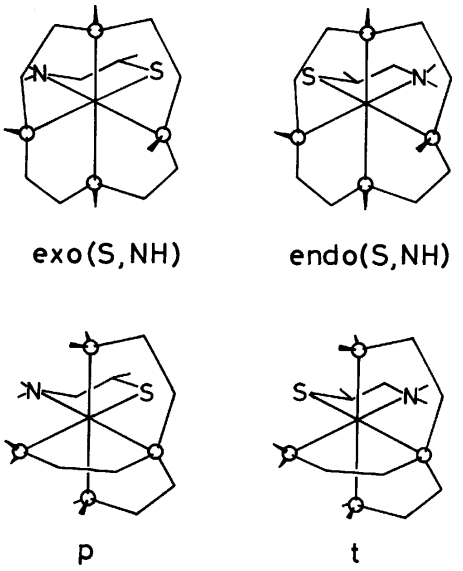

Fig. 2. Structures of *exo*(S, NH)- and *endo*(S, NH)-[Co(*S*-apS)(cyclen)]$^{2+}$, and *p*- and *t*-[Co(*S*-apS)(tren)]$^{2+}$.

isomer of the tren complex[1] are eluted faster than the other respective isomers. Thus the brown isomer can be assigned to the *exo*(S,NH) isomer. Similarity of the absorption and CD spectra between the *exo*(S,NH) and p-isomers, and between the *endo*(S,NH) and t-isomers support the assignment. The relative intensities of the two absorption components in the first absorption band region are considerably different between the two pairs of the complexes; the brown and p-isomers exhibit only a weak shoulder around 17000 cm^{-1}, while the green (*endo*(S,NH)) and t-isomers show a rather strong, distinct band in this region (Fig. 3 and Table 1). The CD spectral pattern of the green isomer resembles that of the t-isomer in the d-d absorption band region. On the other hand, the brown isomer shows a CD spectrum rather different from that of *p*-[Co(*S*-apS)(tren)]$^{2+}$. However, there is something in common between them; the spectra are weak in magnitude and complicated in pattern, and seem to consist of several components with opposite signs. Thus, all these results support the assignment of the brown isomer to *exo*(S,NH).

Figure 1 shows the two possible configurations (I and II) for cis-octahedral complexes of cyclen. Several Co^{III}-cyclen complexes have been prepared, and all of the cobalt(III) complexes whose structures have been determined by X-ray crystallography have configuration I.[2,11,12] Configuration II was found only in [NiBr(H_2O)(Me2cyclen)]Br (Me2cyclen=1,7-dimethyl-1,4,7,10-tetraazacyclododecane), where the two methyl groups are attached to the two "apical" nitrogen atoms (N(1) and N(3) in Fig. 1).[13] On the other hand, the Me2cyclen ligand takes configuration I in [Co(CO_3)(Me2cyclen)]ClO_4.[14] ^{13}C NMR spectroscopy suggests that Co^{III}-cyclen and Co^{III}-Me2cyclen complexes in solution also assume configuration I.[2,14] Examination of molecular models indicates that when a complex with cyclen (or Me2cyclen) has configuration II, steric interactions occur between the methylene groups of the macrocycle (C(3)···C(6) and C(2)···C(7) in Fig. 1). The interactions will increase as the M-N bond distances decrease. On the other hand, configuration I does not have such interactions between the methylene groups. Thus, the shorter bond distance of Co-N than Ni-N will be responsible for the preference of configuration I over II in Co^{III}-cyclen (or Co^{III}-Me2cyclen) complexes. If the brown isomer were configuration II, the strain energy would be large and the relative abundance of the isomer at equilibrium would become small. The fact that the ratio of the brown to green isomer is 1.0 also supports the assignment for the brown isomer. A similar isomerism to the *exo*(S,NH) and *endo*(S,NH)

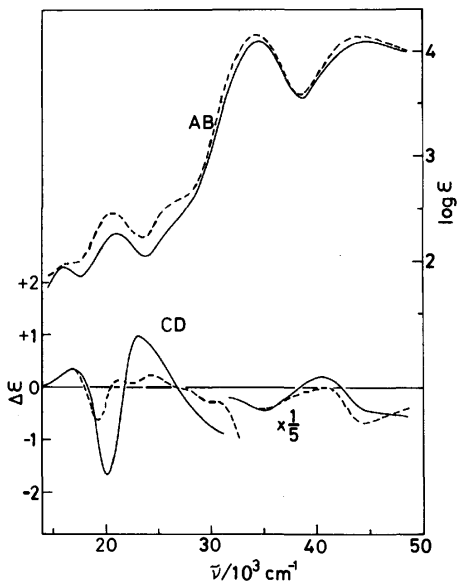

Fig. 3. Absorption (AB) and CD spectra of the green (——) and the brown (----) isomers of [Co(*S*-apS)-(cyclen)]$^{2+}$ in 0.01 mol dm^{-3} $HClO_4$.

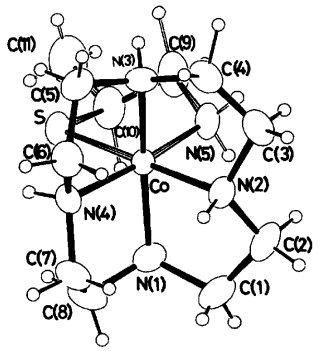

Fig. 4. An ORTEP drawing of the complex cation with thermal ellipsoids scaled at the 50% probability level.[17] Hydrogen atoms are represented by circles of radius 0.08 Å.

Table 1. Absorption (AB) and CD Spectral Data of the Isomers of [Co(*S*-apS)(cyclen)]$^{2+}$ in 0.01 mol dm^{-3} $HClO_4$

Isomer	AB: $\tilde{\nu}_{max}/10^3$ cm^{-1}($\log(\varepsilon/mol^{-1}$ dm^3 $cm^{-1})$)	CD: $\tilde{\nu}_{ext}/10^3$ cm^{-1}($\Delta\varepsilon/mol^{-1}$ dm^3 cm^{-1})
exo(S,NH) (brown isomer)	16.7(sh, 1.99), 20.6(2.44), 26.7(sh, 2.56), 34.1(4.15), 44.2(4.15)	16.7(+0.36), 19.3(−0.63), 21.4(+0.15), 24.5(+0.22), 27.2(sh, −0.02), 29.5(sh, −0.28), 35.0(−2.16), 44.0(−3.40)
endo(S,NH) (green isomer)	16.0(1.95), 21.0(2.27), 26.3(sh, 2.33), 34.5(4.10), 44.5(4.10)	17.0(+0.34), 20.2(−1.68), 23.2(+1.00), 35.1(−2.18), 40.7(+1.14)

isomers of [Co(*S*-apS)(cyclen)]$^{2+}$ was found in *trans*-(O,X)-[CoX(amino acidato)(dien)]$^{+}$ (X^{-}=CN^{-}, NO_2^{-}, Cl^{-}; dien=diethylenetriamine).[15]

Structure of [Co(*S*-apS)(cyclen)]$ZnCl_4 \cdot H_2O$ (green isomer). Final atomic coordinates and bond lengths and angles are listed in Tables 2 and 3. Figure 4 is a perspective drawing of the complex cation. This is the *endo*(S,NH) isomer (Fig. 2) in agreement with the prediction based on the order of elution in column chromatography and spectral data. Edge-on views of the five-membered chelate rings are shown in Fig. 5. The cyclen ligand has a pseudo-mirror symmetry through N(2)-Co-N(4) plane.

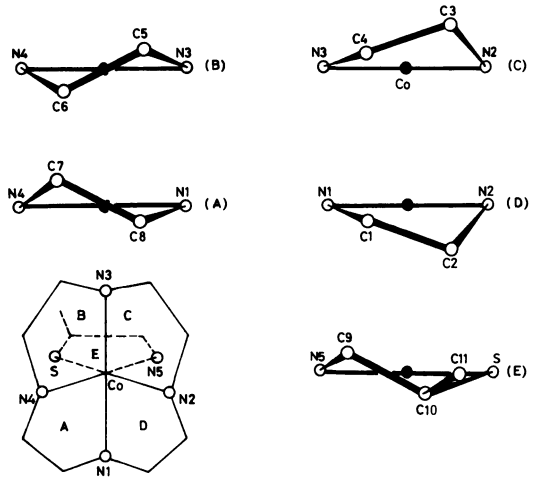

Fig. 5. Edge-on views of the five-membered chelate rings. The black circles stand for the Co atom.

Table 2. Positional Parameters ($\times 10^4$; for O(W) $\times 10^3$) and Equivalent Isotropic Temperature Factors

Atom	*X*	*Y*	*Z*	B_{eq}(Å^2)
Zn	17438(5)	0*	24307(5)	3.0
Co	46480(5)	57631(5)	25282(5)	1.9
Cl (1)	3491(1)	1222(1)	2434(1)	3.6
Cl (2)	1960(2)	−961(1)	325(2)	5.7
Cl (3)	−340(2)	762(2)	2550(2)	8.1
Cl (4)	2161(2)	−1064(1)	4387(2)	5.3
S	5675(1)	7300(1)	2536(1)	2.7
N (1)	4418(4)	5679(3)	338(4)	2.9
N (2)	3815(4)	4375(3)	2499(4)	2.7
N (3)	4389(3)	5660(3)	4713(4)	2.6
N (4)	2832(3)	6500(3)	2500(4)	2.5
N (5)	6643(4)	5218(3)	2598(4)	3.0
C (1)	4062(6)	4599(4)	−153(5)	4.0
C (2)	4297(5)	3869(4)	1113(6)	3.7
C (3)	4214(5)	3861(4)	3907(6)	3.6
C (4)	4000(5)	4581(4)	5162(5)	3.6
C (5)	3236(5)	6375(4)	5112(5)	3.3
C (6)	2095(4)	6304(4)	3917(5)	3.3
C (7)	2089(5)	6312(4)	1041(5)	3.4
C (8)	3257(5)	6396(5)	−103(5)	3.8
C (9)	7765(5)	5981(4)	2972(7)	4.4
C(10)	7502(5)	6933(4)	2146(6)	3.8
C(11)	8512(5)	7777(5)	2572(7)	5.0
O(W)1†	88(1)	360(1)	209(1)	8.1
O(W)2	69(2)	383(2)	329(3)	7.9
O(W)3	82(4)	411(3)	145(4)	8.8
O(W)4	102(4)	320(4)	127(4)	9.4

* This parameter was used to define the origin of *b* and listed without e.s.d. † Population parameters of the disordered hydrate O atoms: O(W)1, 0.40; O(W)2, 0.26; both O(W)3 and O(W)4, 0.17.

Table 3. Bond Lengths (l/Å) and Bond Angles (ϕ/°)

Zn	-Cl (1)	2.293(1)	Cl(1)	-Zn	-Cl (2)	108.3(1)
Zn	-Cl (2)	2.277(2)	Cl(1)	-Zn	-Cl (3)	108.5(1)
Zn	-Cl (3)	2.200(2)	Cl(1)	-Zn	-Cl (4)	108.5(1)
Zn	-Cl (4)	2.265(2)	Cl(2)	-Zn	-Cl (3)	112.6(1)
Co	-S	2.235(1)	Cl(2)	-Zn	-Cl (4)	106.2(1)
Co	-N (1)	1.968(4)	Cl(3)	-Zn	-Cl (4)	112.6(1)
Co	-N (2)	1.982(4)	S	-Co	-N (1)	95.3(1)
Co	-N (3)	1.976(4)	S	-Co	-N (2)	177.6(1)
Co	-N (4)	1.959(3)	S	-Co	-N (3)	96.9(1)
Co	-N (5)	2.004(4)	S	-Co	-N (4)	85.9(1)
S	-C(10)	1.820(5)	S	-Co	-N (5)	85.4(1)
N (1)	-C (1)	1.519(7)	N(1)	-Co	-N (2)	84.2(2)
N (1)	-C (8)	1.487(7)	N(1)	-Co	-N (3)	164.8(2)
N (2)	-C (2)	1.483(6)	N(1)	-Co	-N (4)	86.3(1)
N (2)	-C (3)	1.470(6)	N(1)	-Co	-N (5)	95.5(2)
N (3)	-C (4)	1.518(6)	N(2)	-Co	-N (3)	83.9(2)
N (3)	-C (5)	1.481(6)	N(2)	-Co	-N (4)	96.4(1)
N (4)	-C (6)	1.476(6)	N(2)	-Co	-N (5)	92.3(2)
N (4)	-C (7)	1.487(6)	N(3)	-Co	-N (4)	85.6(1)
N (5)	-C (9)	1.486(6)	N(3)	-Co	-N (5)	94.4(2)
C (1)	-C (2)	1.495(7)	N(4)	-Co	-N (5)	171.3(1)
C (3)	-C (4)	1.483(7)	Co	-S	-C(10)	99.7(2)
C (5)	-C (6)	1.500(6)	Co	-N (1)	-C (1)	111.0(3)
C (7)	-C (8)	1.516(7)	Co	-C (1)	-C (8)	107.1(3)
C (9)	-C(10)	1.470(8)	C(1)	-N (1)	-C (8)	111.0(4)
C(10)	-C(11)	1.502(8)	Co	-N (2)	-C (2)	107.2(3)
			Co	-N (2)	-C (3)	108.5(3)
			C(2)	-N (2)	-C (3)	115.6(4)
			Co	-N (3)	-C (4)	111.1(3)
			Co	-N (3)	-C (5)	107.4(3)
			C(4)	-N (3)	-C (5)	110.3(3)
			Co	-N (4)	-C (6)	108.9(3)
			Co	-N (4)	-C (7)	108.8(3)
			C(6)	-N (4)	-C (7)	120.2(3)
			Co	-N (5)	-C (9)	115.1(3)
			N(1)	-C (1)	-C (2)	110.5(4)
			N(2)	-C (2)	-C (1)	107.6(4)
			N(2)	-C (3)	-C (4)	108.6(4)
			N(3)	-C (4)	-C (3)	111.0(4)
			N(3)	-C (5)	-C (6)	107.7(4)
			N(4)	-C (6)	-C (5)	105.1(3)
			N(4)	-C (7)	-C (8)	104.2(4)
			N(1)	-C (8)	-C (7)	108.1(4)
			N(5)	-C (9)	-C(10)	110.4(4)
			S	-C(10)	-C (9)	106.2(4)
			S	-C(10)	-C(11)	110.4(4)
			C(9)	-C(10)	-C(11)	113.6(4)

Chelate rings A and B take a gauche, and C and D an envelope conformation. The geometry of cyclen is almost identical with those in cobalt(III) complexes investigated by X-ray analysis up to the present.[2,11,12] The hydrogen bonds listed in Table 4 do not seem to affect the conformation of the five-membered chelate rings of cyclen. In other Co^{III}-cyclen complexes, Co–N bond lengths involving N atoms on the pseudo-mirror plane (N(2) and N(4) atoms in the present complex) are by 0.02—0.04 Å shorter than others. However, the Co–N(2) bond is longer by 0.023(4) Å than Co–N(4) owing to the trans influence of the S atom.[16] The five-membered chelate ring formed by *S*-apS is δ-gauche to make the C(10)–C(11) bond in an equatorial position. The Co–N(5) bond is lengthened to avoid the short H···H contacts between the cyclen and *S*-apS ligands (see Fig. 6). A projection of crystal structure along *b* is shown in Fig. 7. Arrangement of the complex cation and $ZnCl_4^{2-}$ is NaCl type. There is an approximate

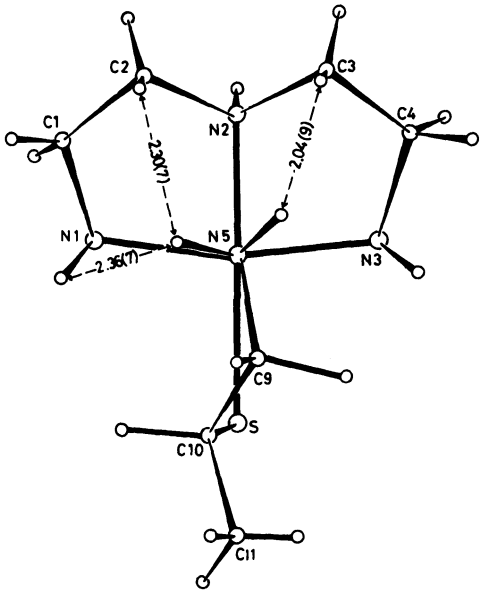

Fig. 6. The complex cation viewed along the line through the Co and N(5) atoms showing non-bonded H···H interactions between cyclen and *S*-apS ligands less than 2.4 Å, twice the van der Waals radius of the hydrogen atom.

Table 4. Intermolecular Hydrogen Bonds (Distances in Å)

A···H–B (symmetry code)	A···B	A···H	H···B
Cl(1)···H(N1)–N(1) (i)	3.268(4)	2.37(5)	1.04(5)
Cl(1)···H(N3)–N(3) (ii)	3.287(4)	2.51(4)	0.83(4)
Cl(2)···H(N5)1–N(5) (iii)	3.325(4)	2.50(5)	0.87(5)
Cl(4)···H(N5)2–N(5) (iv)	3.351(4)	2.58(6)	0.88(7)

Symmetry code: (i) $1-x$, $-1/2+y$, $-z$, (ii) $1-x$, $-1/2+y$, $1-z$, (iii) $1-x$, $1/2+y$, $-z$, (iv) $1-x$, $1/2+y$, $1-z$.

oblate spheroidal hollow, which accomodates a disordered water molecule. The shortest interatomic distance involving the hydrate O atom is 3.03(3) Å for O(W)3···Cl(2) ($-x$, $y+\frac{1}{2}$, $-z$) and only by 0.24 Å shorter than the sum of van der Waals radii.

Isomerization Reactions. Figure 8 shows a typical set of absorption spectra (800—400 nm) obtained at intervals after the brown isomer had been dissolved in water at pH 6.27 and 25.4 °C. The spectra gave an isosbestic point at 597 nm and showed a large absorbance change at 480 nm, and this wavelength was used to follow the rate. In every kinetic run, the plot of $\ln(A_t-A_\infty)$ vs. time at a constant pH gave a straight line for at least three half-lives, where A_t and A_∞ represent the absorbance at time t and at infinite time at 480 nm, respectively. The slope gave the pseudo first-order rate constant, k_{obsd}. The $k_{obsd}/[OH^-]$ ($=k_{iso}$) values are constant at 25.4 °C in the pH range of 5.98—6.97, indicating that the reaction is first-order in $[OH^-]$. The values of k_{obsd} and k_{iso} are listed in Table 5, the average value of k_{iso} being 1.3×10^4 mol^{-1} dm^3 s^{-1} at 25.4 °C. After the isomers had been equilibrated at 25.4 °C, the isomer distribution was analyzed by means of chromatography. The formation ratio of the brown to green isomer was 1.0, and no indication was observed for the formation of other isomers. The runs starting from either of the isomers gave the same result within the experimental

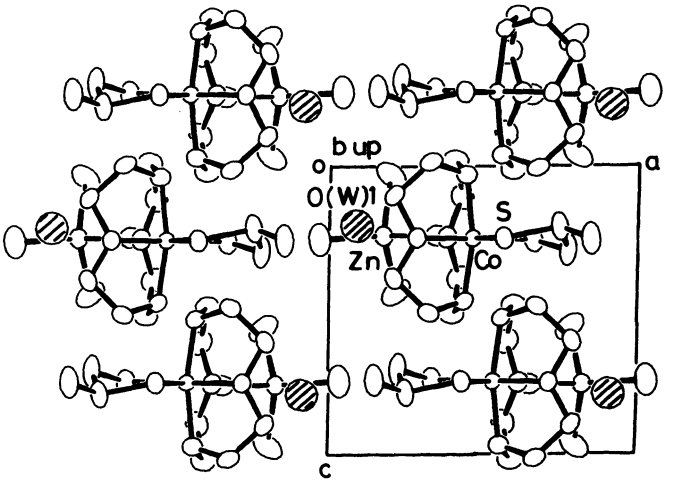

Fig. 7. A projection of the crystal structures along *b*. The hatched circles denote the O(W)1 atom. Other O(W) atoms were not drawn for simplicity.

Table 5. Rate Constants for the Isomerization of [Co(*S*-apS)(cyclen)]$^{2+}$ at 25.4 °C

pH	k_{obsd}/s^{-1}	k_{iso}/mol^{-1} dm^3 s^{-1}
5.98	$(1.22\pm0.03)\times10^{-4}$	$(1.28\pm0.03)\times10^4$
6.27	$(2.36\pm0.05)\times10^{-4}$	$(1.27\pm0.03)\times10^4$
6.74	$(7.2\pm0.2)\times10^{-4}$	$(1.31\pm0.03)\times10^4$
6.97	$(1.25\pm0.03)\times10^{-3}$	$(1.35\pm0.03)\times10^4$

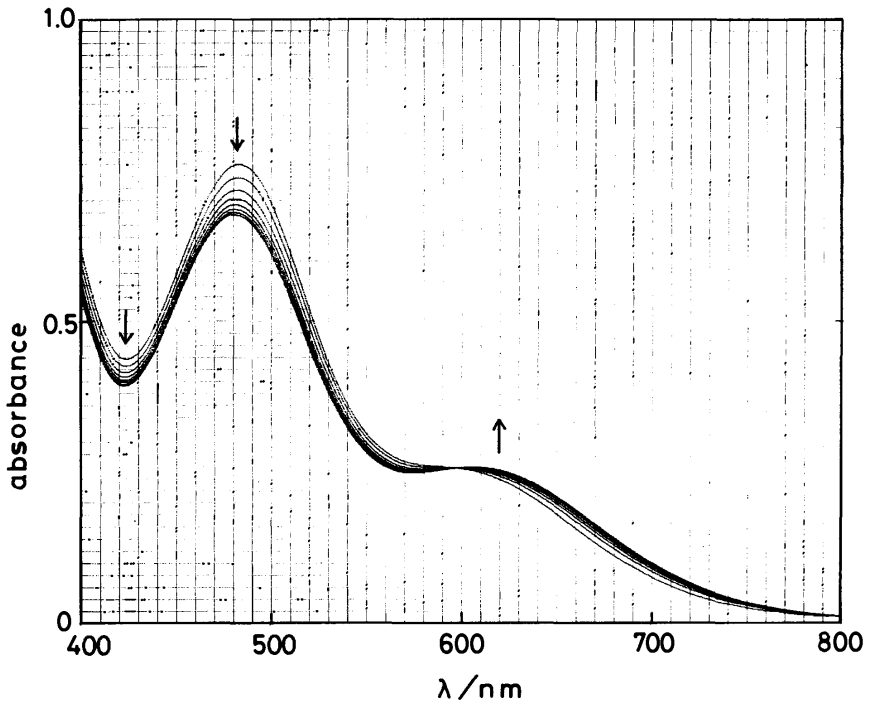

Fig. 8. Time-course changes of absorption spectrum of the brown isomer of $[Co(S\text{-apS})(cyclen)]^{2+}$ in an aqueous solution at pH 6.27 and 25.4 °C (recorded intervals: 20 min). Trends of spectral changes with time are shown by arrows.

error. The absorption and CD spectra of the equilibrated mixture agree well with those of an equimolar mixture of the two isomers. From these observations, the reaction can be expressed as

$$\text{brown isomer } (exo(\text{S,NH})) \underset{k_{-1}}{\overset{k_1}{\rightleftharpoons}} \text{ green isomer } (endo(\text{S,NH})).$$

The forward and reverse second-order rate constants, k_1 and k_{-1}, are related to the rate constant, k_{iso}, and to the equilibrium constant, K, as follows:

$$k_{iso} = k_1 + k_{-1} \qquad K = \frac{k_1}{k_{-1}}.$$

From the k_{iso} and K values, the values k_1 and k_{-1} are calculated to be 6.5×10^3 mol^{-1} dm^3 s^{-1} ($k_1=k_{-1}=0.5k_{iso}$).

Inversion at an asymmetric nitrogen atom is known to be proportional to the hydroxide ion concentration[18] and the reversible isomerization is considered to occur between the two isomers (*exo*(S,NH) and *endo*(S,NH)) of configuration I. The observations decsribed above strongly suggest that the isomerization is resulted from the synchronous inversion at the two nitrogen atoms of the cyclen ring (N(2) and N(4) in Fig. 4). The isomerization can be compared to the racemization of *mer*-$[Co(dien)_2]^{3+}$. In *mer*-$[Co(dien)_2]^{3+}$, the molecular dissymmetry arises from the stereochemical relationship between the two trans NH bonds of the secondary amine nitrogen atoms in the two dien ligands. A rate constant, 2.4×10^2 mol^{-1} dm^3 s^{-1}, for the recemization of *mer*-$[Co(dien)_2]^{3+}$[19] at 35 °C is ca. 10^2 times as small as those obtained above for the isomerization of $[Co(S\text{-apS})(cyclen)]^{2+}$. An investigation is being undertaken to elucidate the effect of the sulfur donor atom on the rate of inversion at nitrogen.

Configuration II (Fig. 1) can be a possible intermediate for the isomerization reaction. The facts that (1) during the course of isomerization the absorption spectra give an isosbestic point, (2) the equilibrated mixture gives only two bands in column chromatography, and (3) only configuration I has been found by X-ray crystallography in the cobalt(III)-cyclen complexes suggest that configuration II is not stable in $[Co(S\text{-apS})(cyclen)]^{2+}$. Thus we conclude that isomerization does not involve formation of any intermediate in measurable amounts.

The present work was partially supported by a Grant-in-Aid for Scientific Research No. 58470032 from the Ministry of Education, Science and Culture.

References

1) K. Nakabayashi, K. Doi, M. Kojima, and J. Fujita, *Bull. Chem. Soc. Jpn.*, **57**, 989 (1984). The S atoms in the p- and t-isomers are trans to the primary (p) and tertiary (t) tren amine nitrogens, respectively.

2) N. Matsumoto, A. Hirano, T. Hara, and A. Ohyoshi, *J. Chem. Soc., Dalton Trans.*, **1983**, 2405.

3) T. C. Owen, *J. Chem. Soc., C*, **1967**, 1374.

4) J. R. Piper and T. P. Johnstone, *J. Org. Chem.*, **29**, 1657 (1964).

5) Tables of the coordinates of hydrogen atoms, the anisotropic thermal parameters of the non-hydrogen atoms, bond lengths and bond angles involving hydrogen atoms, and observed and calculated strucrure factors are kept as Document No. 8613 at the Chemical Society of Japan.

6) T. Sakurai and K. Kobayashi, *Rikagaku Kenkyusho Hokoku*, **55**, 69 (1979).

7) W. C. Hamilton, *Acta Crystallogr.*, **18**, 502 (1965).

8) D. L. Nosco and E. Deutsch, *Inorg. Synth.*, **21**, 19 (1982).

9) R. H. Lane, F. A. Sedor, M. J. Gilroy, P. F. Eisenhardt, J. P. Bennett, Jr., R. X. Ewall, and L. E. Bennett, *Inorg. Chem.*, **16**, 93 (1977).

10) Y. Yoshikawa and K. Yamasaki, *Inog. Nucl. Chem. Lett.*, **6**, 523 (1970); K. Sakakibara, Y. Yoshikawa, and H. Yamatera, *Bull. Chem. Soc. Jpn.*, **52**, 2725 (1979); K. Nakajima, M. Kojima, and J. Fujita, *Chem. Lett.*, **1982**, 925.

11) Y. Iitaka, M. Shina, and E. Kimura, *Inorg. Chem.*, **13**, 2886 (1974).

12) J. H. Loehlin and E. B. Fleischer, *Acta Crystallogr., Sect. B*, **32**, 3063 (1976).

13) M. Ciampolini, M. Micheloni, N. Nardi, P. Paoletti, P. Dapporto, and F. Zanobini, *J. Chem. Soc., Dalton Trans.*, **1984**, 1357.

14) J. Giusti, S. Chimichi, M. Ciampolini, M. Sabat, and D. Masi, *Inorg. Chim. Acta*, **88**, 51 (1984).

15) K. Ohkawa, J. Fujita, and Y. Shimura, *Bull. Chem. Soc. Jpn.*, **45**, 161 (1972).

16) R. C. Elder, L. R. Florian, R. E. Lake, and A. M. Yacynych, *Inorg. Chem.*, **12**, 2690 (1973).

17) C. K. Johnson (1965). ORTEP. Report ORNL-3794. Oak Ridge National Laboratory, Tennessee.

18) B. Halpern, A. M. Sargeson, and K. R. Turnbull, *J. Am. Chem. Soc.*, **88**, 4630 (1966); W. G. Jackson and A. M. Sargeson, "Rearrangements in Ground and Excited States," ed by P. de Mayo, Academic Press, New York (1980), Vol. 2, p. 273.

19) F. R. Keene and G. H. Searle, *Inorg. Chem.*, **11**, 148 (1972). The second-order rate constant for the racemization of *mer*-$[Co(dien)_2]^{3+}$ was calculated from the half-lives for racemization at pH 7.42 and 8.10.

 © 1986 The Chemical Society of Japan Bull. Chem. Soc. Jpn., 59, 285—294 (1986)

Syntheses, Characterization, and Structures of (Monomethyl Carbonato)-Nickel(II), -Copper(II), and -Cobalt(II) Complexes with Tetraazacycloalkanes Obtained from CO_2 Uptake

Masako KATO† and Tasuku ITO*
Department of Applied Molecular Science, Institute for Molecular Science,
Okazaki National Research Institutes, Okazaki 444
(Received August 14, 1985)

A new series of monomethyl carbonato complexes of nickel(II), cobalt(II), and copper(II) containing tetraazacycloalkanes (L) have been synthesized and characterized: Ni(L)(O_2COCH_3)(ClO_4) (L=[14]aneN$_4$ (**1**); L=[15]aneN$_4$ (**2**); L=*iso*-[14]aneN$_4$ (**3**); L=*RSRS*-Me$_4$[14]aneN$_4$ (**4**)), [Ni(*RRSS*-Me$_4$[14]aneN$_4$)(O_2COCH_3)$_2$]·$HNEt_3ClO_4$ (**5**), Cu([**14**]aneN$_4$)(O_2COCH_3)(ClO_4) (**6**), [Cu(Me$_4$[14]aneN$_4$)(O_2COCH_3)](ClO_4)·CH_3OH (**7**), and Co(L)(O_2COCH_3)(ClO_4) (L=[15]aneN$_4$ (**8**); L=Me$_4$[14]aneN$_4$ (**9**)), where [14]aneN$_4$=1,4,8,11-tetraazacyclotetradecane, [15]aneN$_4$=**1**,4,8,12-tetraazacyclopentadecane, *iso*-[14]aneN$_4$=**1**,4,7,11-tetraazacyclotetradecane, Me$_4$[14]-aneN$_4$=1,4,8,11-tetramethyl-1,4,8,**11**-tetraazacyclotetradecane, *RSRS*-=1*RS*,4*SR*,8*RS*,**11***SR*-, and *RRSS*-=1*RS*, 4*RS*,8*SR*,11*SR*-. These compounds have been obtained through CO_2 uptake reaction in basic methanol from the corresponding four-coordinate complex, [M(L)](ClO_4)$_2$. X-Ray structures of three compounds, **4**, **5**, and **6**, have been determined. Compound **4** is a five-coordinate complex with the trigonal bipyramidal geometry (Type II), in which $CH_3OCO_2^-$ is coordinated in a unidentate fashion. Compound **5** is a tetragonally distorted six-coordinate complex with two unidentate $CH_3OCO_2^-$ at axial sites (Type III). Compound **6** is also a tetragonally distorted six-coordinate complex but the $CH_3OCO_2^-$ ligand bridges two neighboring [Cu([14]aneN$_4$)]$^{2+}$ to form a linear chain structure (Type I). All the monomethyl carbonato complexes synthesized are classified into these three types on the basis of IR and/or electronic spectral data, supplemented with the X-ray results. Efficiency of the CO_2 uptake depends strongly on the coordination structure which is controlled by a combination of metal ion and tetraazacycloalkane. Differences in reactivity among the complexes of various metal ions and factors influencing the efficiency have been discussed in connection with the zinc(II) system which undergoes the most effective CO_2 uptake of this type.

Recently we reported facile CO_2 uptake by zinc(II) complexes containing tetraazacycloalkanes (L).[1] In the system, CO_2 is taken up very easily, in certain cases spontaneously from the air, as monoalkyl carbonate ion in alcohol (ROH) under mild conditions to give Zn(L)(O_2COR)(ClO_4). It is thought that square-planar coordination of a tetraazacycloalkane with an appropriate cavity size leaves the Zn^{2+} ion coordinately unsaturated and that it makes the effective uptake reaction possible. Therefore, coordination structure controlled by a combination of tetraazacycloalkane and metal ion is an important factor for such the CO_2 uptake. In this paper, we synthesized a new series of monomethyl carbonato complexes using various divalent metal ions, Co^{2+}, Ni^{2+}, and Cu^{2+}, and tetraazacycloalkanes shown below[2] in order to compare efficiency of the CO_2

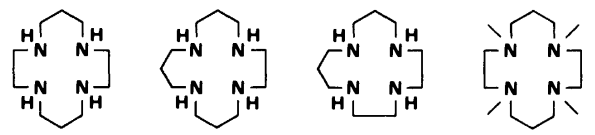

uptake and to explore its factors. Aiming to investigate structural factors, single crystal X-ray analyses have been also carried out on three monomethyl carbonato complexes, [Ni(*RSRS*-Me$_4$[14]-aneN$_4$)(O_2COCH_3)](ClO_4),[3] [Ni(*RRSS*-Me$_4$[14]aneN$_4$)(O_2COCH_3)$_2$]·$HNEt_3ClO_4$,[3] and Cu([14]aneN$_4$)(O_2COCH_3)(ClO_4), which have different coordination geometries.

† Present address: Department of Chemistry, Faculty of Science, Kyoto University, Kyoto 606.

Experimental

Materials. The tetraazacycloalkanes, [14]aneN$_4$, [15]aneN$_4$, and Me$_4$[14]aneN$_4$, were purchased from Strem Chemical Inc. *Iso*-[14]aneN$_4$ was prepared according to the literature.[4] Starting nickel(II) complexes, [Ni(L)](ClO_4)$_2$ (L=[14]aneN$_4$, [15]aneN$_4$, *iso*-[14]aneN$_4$, *RSRS*-Me$_4$[14]-aneN$_4$), were prepared from the free ligands L and Ni(ClO_4)$_2$·$6H_2O$ in methanol and recrystallized from water or methanol. [Ni(*RRSS*-Me$_4$[14]aneN$_4$)](ClO_4)$_2$ was prepared by *N*-methylation of the complex, [Ni([14]aneN$_4$)](ClO_4)$_2$.[5] [Cu([14]aneN$_4$)](ClO_4)$_2$ was obtained as follows. A methanolic solution of [14]aneN$_4$ was mixed with an equimolar amount of $CuCl_2$ in methanol under stirring. After a while, addition of a methanolic solution of $NaClO_4$ to this solution gave purple precipitate, which was recrystallized from hot methanol containing a small amount of 2,2-dimethoxypropane or $NaOCH_3$. On cooling, red-purple needles came out of the solution. The same procedure was applied to the synthesis of [Cu([15]-aneN$_4$)](ClO_4)$_2$ to give blue-violet crystals. The blue-violet complex, [Cu(Me$_4$[14]aneN$_4$)](ClO_4)$_2$, was prepared by the reaction of Cu(ClO_4)·$6H_2O$ and Me$_4$[14]aneN$_4$ in methanol. FSO_3CH_3 was purchased from Wako Pure Chemical Industries, Ltd.

Ni(L)(O_2COCH_3)(ClO_4) (1, L=[14]aneN$_4$; 2, L=[15]aneN$_4$; 3, L=*iso*-[14]aneN$_4$): CO_2 gas was bubbled into a methanol solution (50—100 cm^3) of Ni(L)(ClO_4)$_2$ (1 mmol)

containing NEt_3 (1 mmol) at room temperature. After a while, a precipitate began to come out of the solution, but a stream of CO_2 was passed through the solution further for several hours. Pale pink, blue, and purple products of **1**, **2**, and **3**, were filtered and washed with methanol. Yield 89, 83, and 72% for **1**, **2**, and **3**, respectively. Found for **1**: C, 33.29; H, 6.39; N, 12.97%. Calcd for $NiClO_7N_4C_{12}H_{27}$: C, 33.25; H, 6.28; N, 12.92%. Found for **2**: C, 34.52; H, 6.16; N, 12.38%. Calcd for $NiClO_7N_4C_{13}H_{29}$: C, 34.89; H, 6.53; N, 12.52%. Found for **3**: C, 33.53; H, 6.37; N, 13.16%. Calcd for $NiClO_7N_4C_{12}H_{27}$: C, 33.25; H, 6.28; N, 12.92%.

[Ni(*RSRS*-Me$_4$[14]aneN$_4$)(O$_2$COCH$_3$)](ClO$_4$) (4) and [Ni(*RRSS*-Me$_4$[14]aneN$_4$)(O$_2$COCH$_3$)$_2$]·HNEt$_3$ClO$_4$ (5): When a stream of CO_2 was bubbled through a methanolic solution (50 cm^3) of Ni(*RSRS*-Me$_4$[14]aneN$_4$)(ClO$_4$)$_2$ (1 mmol) in the presence of an excess of NEt_3, color of the solution turned green immediately from pink-red. The solution was rotoevaporated to ca. 10 cm^3 and stood for a few days at −20 °C under CO_2 atmosphere to give green crystals of **4**. The blue complex **5** was prepared in a similar way from [Ni(*RRSS*-Me$_4$[14]aneN$_4$)](ClO$_4$)$_2$. Compound **5** was also obtained from the green methanolic solution containing [Ni(*RSRS*-Me$_4$[14]aneN$_4$)](ClO$_4$)$_2$, a large excess of NEt_3, and saturated CO_2 via configurational change of Me$_4$[14]aneN$_4$, when the solution was allowed to stand for several weeks. Found for **4**: C, 38.94; H, 6.79; N, 11.54%. Calcd for $NiClO_7N_4C_{16}H_{35}$: C, 39.25; H, 7.09; N, 11.44%. Compound **5** could not be analyzed because it decomposed rapidly in the air, but its composition is unambiguous from the X-ray analysis (vide infra).

Cu(L)(O$_2$COCH$_3$)(ClO$_4$)·*n*CH$_3$OH (6, L=[14]aneN$_4$, *n*=0; 7, L=Me$_4$[14]aneN$_4$, *n*=1): These complexes were prepared from [Cu(L)](ClO$_4$)$_2$ in the same way as described for **4**. Compounds **6** and **7** are purple and blue, respectively, and **7** was obtained as methanol solvate. Found for **6**: C, 32.61; H, 6.15; N, 12.51%. Calcd for $CuClO_7N_4C_{12}H_{27}$: C, 32.88; H, 6.21; N, 12.78%. Found for **7**: C, 38.78; H, 7.47; N, 10.64%. Calcd for $CuClO_8N_4C_{17}H_{39}$: C, 38.29; H, 7.47; N, 10.62%.

Co([15]aneN$_4$)(O$_2$COCH$_3$)(ClO$_4$) (8): A methanolic solution (50 cm^3) of [15]aneN$_4$ (5 mmol) was added to a methanolic solution (50 cm^3) of Co(ClO$_4$)$_2$·6H$_2$O (5 mmol) under a nitrogen atmosphere. Color of the solution turned red brown. After refluxing for 2 h, an excess of NEt_3 was added to the filtered solution and then CO_2 was bubbled through the solution. Pink-red crystals formed were filtered and stored under a nitrogen atmosphere to avoid air oxidation. Found: C, 34.56; H, 6.38; N, 12.28%. Calcd for $CoClO_7N_4C_{13}H_{29}$: C, 34.87; H, 6.53; N, 12.51%.

[Co(Me$_4$[14]aneN$_4$)(O$_2$COCH$_3$)](ClO$_4$) (9): A methanol solution (80 cm^3) of Me$_4$[14]aneN$_4$ (10 mmol) was added dropwise to a stirred methanol solution (50 cm^3) of Co(ClO$_4$)$_2$·6H$_2$O (10 mmol) under bubbling CO_2 at room temperature. Color of the solution became red purple and concomitantly white precipitate, presumably a salt of perchloric acid and Me$_4$[14]aneN$_4$, came out. When an excess of NEt_3 was added into the reaction mixture and CO_2 bubbling was continued, the white precipitate dissolved again and then red-purple precipitate of **9** was obtained. Yield 80%. Found: C, 39.21; H, 7.19; N, 11.43%. Calcd for $CoClO_7N_4C_{16}H_{35}$: C, 39.23; H, 7.20; N, 11.44%.

Measurements. Infrared spectra were recorded on a Jasco IR-810 or a Hitachi 295 spectrometer. Electronic spectra were measured on a Hitachi 340 spectrophotometer. Solid state spectra were taken as nujol mulls mounted between polyethylene films. ^{1}H NMR spectra were obtained on a JEOL JNM-GX400 spectrometer at 400 MHz.

Magnetic susceptibility measurements on cobalt(II) complexes were carried out at 77 K by the Hartshorn bridge method[6] (operating at 300 Hz). Tutton's salt, [Mn(OH$_2$)$_6$]-SO$_4$·(NH$_4$)$_2$SO$_4$, was used as a standard.

X-Ray diffraction data were obtained on a Rigaku AFC-5 four-circle diffractometer with use of graphite-monochromatized Mo $K\alpha$ radiation. Diffraction data were collected at room temperature for **4** and **6** but at 168 K under a nitrogen stream for **5** because it decomposed rapidly in the air at room temperature. The low-temperature measurement was made with an attached Rigaku variable-temperature apparatus using a cold nitrogen gas stream method. The procedures used for data collection were standard and have been described previously.[7] The intensity data were corrected for Lorentz-polarization effects and for absorption.

Solution and Refinement of the Structures. The structure of **4** was solved by a standard Patterson and Fourier method, whereas the direct method was used for **5** and **6**. All the structures were refined by the block-diagonal least-squares technique. The atomic scattering factors for non-hydrogen atoms were taken from Ref. 8 and those for hydrogen from Stewart, Davidson, and Simpson.[9] The effects of anomalous dispersion for non-hydrogen atoms were corrected. The weights (w) were taken as $w=[\sigma^2_{count}+(0.015|F_o|)^2]^{-1}$. All the hydrogen atoms were located by difference syntheses. Non-hydrogen and hydrogen atoms were refined anisotropically and isotropically, respectively. Calculations of the refinements for all the compounds converged smoothly.[10] All the calculations were carried out on a HITAC M-200H computer at the Computer Center of the Institute for Molecular Science with the Universal Crystallographic Computation Program System UNICS III[11] and MULTAN 78.[12]

Results

Synthesis and Characterization. Table 1 lists compounds prepared in this study along with their IR data. Monomethyl carbonato complexes are obtained by bubbling CO_2 through methanolic solutions of [M(L)](ClO$_4$)$_2$ (M=Ni^{2+}, Cu^{2+}, and Co^{2+}) containing NEt_3 as a base (Eq. 1).

$$CH_3OH + CO_2 + NEt_3 \rightleftharpoons CH_3OCO_2^- + HNEt_3^+$$
$$M(L)^{2+} + nCH_3OCO_2^- \longrightarrow M(L)(O_2COCH_3)_n^{m+} \quad (1)$$
$$(n=1,\ m=1 \text{ or } n=2,\ m=0).$$

Addition of NEt_3 was necessary in these systems, although, in some zinc(II) systems, the CO_2 uptake reaction proceeds under base-free conditions. In the systems of the nickel(II) complexes with [14]aneN$_4$ and [15]aneN$_4$, CO_2 is taken up from the air spontaneously in the presence of an equivalent amount of NEt_3 and the monomethyl carbonato

Table 1. IR Data of $-OCO_2^-$ Group (cm^{-1})[a]

Compound	$\nu_1(OCO_2)$[b]	$\nu_2(OCO_2)$[b]	$\pi(OCO_2)$[c]	$\Delta\nu$[d]
Ni([14]aneN$_4$)(O_2COCH_3)(ClO_4) (**1**)	1614 vs	1306 m, 1320 s	810 w	294
Ni([15]aneN$_4$)(O_2COCH_3)(ClO_4) (**2**)	1620 vs	1312 s	812 m	308
Ni(*iso*-[14]aneN$_4$)(O_2COCH_3)(ClO_4) (**3**)	1618 s	1316 s, 1330 m	814 w	302
[Ni(*RSRS*-Me$_4$[14]aneN$_4$)(O_2COCH_3)](ClO_4) (**4**)	1636 w, 1676 s	1310 s	816 m	366
[Ni(*RRSS*-Me$_4$[14]aneN$_4$)(O_2COCH_3)$_2$]·$HNEt_3$·ClO_4 (**5**)	1648 s, 1672 s	1306 m	815 w	366
Cu([14]aneN$_4$)(O_2COCH_3)(ClO_4) (**6**)	1646 vs	1300 vs	816 s	346
[Cu(Me$_4$[14]aneN$_4$)(O_2COCH_3)](ClO_4) (**7**)	1660 vs	1306 vs	806 s	354
Co([15]aneN$_4$)(O_2COCH_3)(ClO_4) (**8**)	1620 vs	1316 vs	808 m	304
[Co(Me$_4$[14]aneN$_4$)(O_2COCH_3)](ClO_4) (**9**)	1630 m, 1670 s	1306 vs	806 s	364

a) vs=very strong, s=strong, m=medium, and w=weak. b) Stretching. c) Out-of-plane bending. d) $\Delta\nu=\nu_1-\nu_2$.

Table 2. Electronic Spectral Data for (Monomethyl Carbonato)Nickel(II) Complexes[a]

Compd	$\tilde{\nu}/10^3\ cm^{-1}$			
1	9.7	15.6	19.6	29.5
2	9.5 sh	12.5	17.6	27.8
3	11.5 sh	14.7	18.4	28.2
4	9.4	15.4	20.4	25.4
5	8.6	12.0	16.5	26.7

a) sh=shoulder.

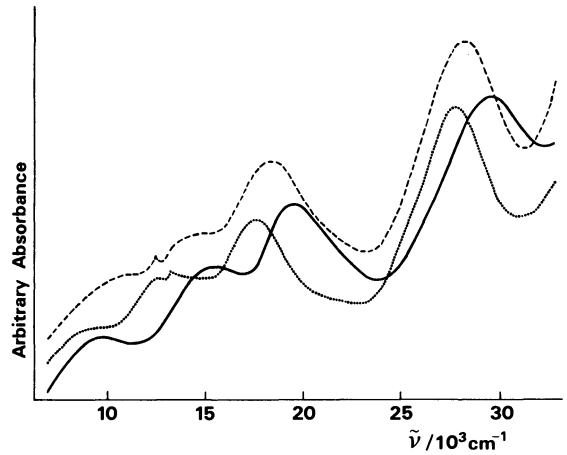

Fig. 1. Electronic absorption spectra (in methanol) of Ni([14]aneN$_4$)(O_2COCH_3)(ClO_4) (**1**) (——), Ni([15]aneN$_4$)(O_2COCH_3)(ClO_4) (**2**) (·····), and Ni(*iso*[14]aneN$_4$)(O_2COCH_3)(ClO_4) (**3**) (----).

complexes were isolated as a single product.

In contrast with the nickel(II) systems, the reactivity of $[Cu(L)]^{2+}$ toward monomethyl carbonate ions was so weak that only the starting complex, $[Cu(L)](ClO_4)_2$, was recovered when an equimolar amount of NEt_3 was present in the solution. However, when a large excess of NEt_3 was added, (monomethyl carbonato)copper(II) complexes, **6** and **7**, were successfully isolated. But we failed to isolate a desired product from $[Cu([15]aneN_4)](ClO_4)_2$ even in the presence of a large excess of NEt_3.

As to cobalt(II) complexes, it may be worth while pointing out the following observation. The cobalt(II) complex with [15]aneN$_4$ was easily oxidized by air, so that the reaction was carried out under a nitrogen atmosphere. On the other hand, the cobalt(II) complex with Me$_4$[14]aneN$_4$ was extraordinarily air stable and it underwent the uptake reaction in the air smoothly.

We pointed out previously for the zinc(II) system that stretching vibrational bands (ν_1 and ν_2) of the $-OCO_2$ group reflect a coordination mode of the monomethyl carbonato ligand.[1a] That is, in the case of unidentate $CH_3OCO_2^-$, the ν_1 band appears at higher frequencies than that of bridged $CH_3OCO_2^-$. In addition, the intensity of ν_2 is strong as compared with ν_1 in unidentate $CH_3OCO_2^-$, and vice versa in bridged $CH_3OCO_2^-$. Similar trends were also observed for the present nickel(II)- and cobalt(II)-monomethyl carbonato complexes (Table 1). The frequency difference between ν_1 and ν_2 was as much as 360 cm^{-1} in compounds **4**, **5**, and **9**, while it was at most 300 cm^{-1} in **1**—**3** and **8**. Thus, complemented with the relative band intensities, the $CH_3OCO_2^-$ ligands in complexes with Me$_4$[14]aneN$_4$ are assigned to unidentate coordination and those in other compounds to bridged coordination. However, it was difficult for copper(II) complexes to assign the coordination mode from IR data because they do not show a distinct tendency.

As shown in Fig. 1 and Table 2, the ligand field electronic spectrum of nickel(II) complex, **1**, **2**, **3**, or **5** consists of four bands except for a sharp peak due to spin-forbidden transition around 13000 cm^{-1}. Each spectrum shows clearly the splitting typical of tetragonal nickel(II) complexes in the lowest energy region (8000—15600 cm^{-1}).[13] The lowest and the second lowest energy bands are assigned to $^3E_g \leftarrow {}^3B_{1g}$ and $^3B_{2g} \leftarrow {}^3B_{1g}$, respectively, which arise from the tetragonal splitting of $^3T_{2g} \leftarrow {}^3A_{2g}$ in Oh symmetry. Thus compounds **1**, **2**, **3**, and **5** have coordination geometry of the *trans*-NiO_2N_4 type. The spectral

pattern of green compound **4** is quite different from others and indicates a five-coordinate structure.

Nujol mull solid state electronic spectra of (monomethyl carbonato)copper(II) complexes, **6** and **7**, show one broad absorption band at 19000 and 14300 cm^{-1}, respectively. The d-d band position is at lower energy than those of the corresponding square-planar four-coordinate complexes, $[Cu(L)]^{2+}$.[14] This indicates the occurrence of an axial interaction of the fifth or sixth ligand with the Cu^{2+} ion although coordination geometry of the copper(II) complexes is not clear from the electronic spectra.[15]

(Monomethyl carbonato)cobalt(II) complexes, **8** and **9**, are pale pink and red purple in color, respectively. Their electronic spectral patterns are quite different ($\tilde{\nu}_{max}/10^3$ cm^{-1}: 19.7 and 22.1 for **8**; 6.9, 13.5, 18.6, 19.9, and 20.7 for **9**). The spectral pattern of **8** resembles those of high spin octahedral cobalt(II) complexes, $[Co(OH_2)_6]^{2+}$ and $[Co(NH_3)_6]^{2+}$. On the other hand, the spectral pattern of **9** is very similar to that of high-spin five-coordinate complexes with the trigonal bipyramidal geometry, $[Co(tbcyclen)X]^+$ (X=Cl, NCS; tbcyclen=1,4,7,10-tetrabenzil-1,4,7,10-tetraazacyclododecane)[16] and $[Co(MSBen\text{-}N(C_2H_5)_2(NCS)_2]$ (MSBen-$N(C_2H_5)_2$=Schiff base derived from o-(methylthio)benzaldehyde and *N,N*-diethylethylenediamine)[17]. But the pattern of **9** differs clearly from that of a low-spin five coordinate complex having the trigonal bipyramidal geometry, [Co(CR)X]Y (X, Y=Cl, Br, I etc., CR=2,12-dimethyl-3,7,11,17-tetraazabicyclo[11.3.1]heptadeca-1(17),2,11,13,15-pentaene.[18] Magnetic moments for **8** and **9** have been found to be 4.09 and 4.21 μ_B, respectively. These results indicate that compound **8** is a high spin six-coordinate complex whereas **9** is a high spin five-coordinate complex.

X-Ray Structure. Partinent crystallographic parameters and final *R* indices for three analyzed compounds, **4**, **5**, and **6**, are summarized in Table 3. Their positional and thermal parameters for non-hydrogen atoms are given in Tables 4-6, respectively. Figure 2 shows X-ray structures and Table 7 lists relevant bond distances and angles.

[Ni(*RSRS*-Me_4[14]aneN$_4$)(O_2COCH_3)](ClO_4) (**4**) was found to be a mononuclear five-coordinate complex with the trigonal bipyramidal geometry (Fig. 2(a)). The macrocycle is folded and the $CH_3OCO_2^-$ ligand is coordinated in a unidentate fashion. The overall structure of **4** is essentially the same as that of the corresponding zinc(II) complex, [Zn(Me_4[14]aneN$_4$)(O_2COCH_3)](ClO_4)[1b]. All the four methyl groups of the Me_4[14]aneN$_4$ ligand are disposed toward the same side as the $CH_3OCO_2^-$ ligand. A main difference between these two structures is as follows: An angle subtended at the Ni atom by two axial bonds, Ni–N(2) and Ni–N(4), is 171.2(2)°, which is much wider than the corresponding angle of the zinc complex (166.2(1)°); Apical bonds (Ni–N(2) and Ni–N(4)) are similar in length to the in-plane ones in the nickel complex, while the formers are longer by

Table 3. Crystallographic Parameters

	4	**5**	**6**
Formula	$NiClO_7N_4C_{16}H_{35}$	$NiClO_{10}N_5C_{24}H_{54}$	$CuClO_7N_4C_{12}H_{27}$
F_w	489.63	666.87	438.37
Cryst syst	Triclinic	Monoclinic	Monoclinic
Space group	$P\bar{1}$	*Aa*	$P2_1/n$
a/Å	11.375(1)	23.909(5)	12.303(3)
b/Å	12.415(1)	12.221(2)	15.498(3)
c/Å	8.323(1)	11.134(2)	9.649(2)
α/deg	109.082(8)	90	90
β/deg	98.74(1)	94.51(2)	94.18(2)
γ/deg	87.19(1)	90	90
V/Å^3	1097.9(2)	3243(1)	1835.0(6)
Z	2	4	4
d_c/g cm^{-3}	1.48	1.365	1.59
d_m/g cm^{-3}	1.47	—	1.57
Cryst size/mm	0.36×0.44×0.72	0.64×0.40×0.37	0.64×0.08×0.08
Scan range	1.4+0.5 tan θ	1.2+0.5 tan θ	1.3+0.5 tan θ
μ/mm^{-1}	1.050	0.740	1.425
2θ range/deg	2—55	2—55	2—55
Unique data[a]	3771	2983	1558
No. of variables	403	587	344
R	0.052	0.048	0.042
R_w	0.075	0.063	0.052

a) $|F_o| > 3\sigma(|F_o|)$.

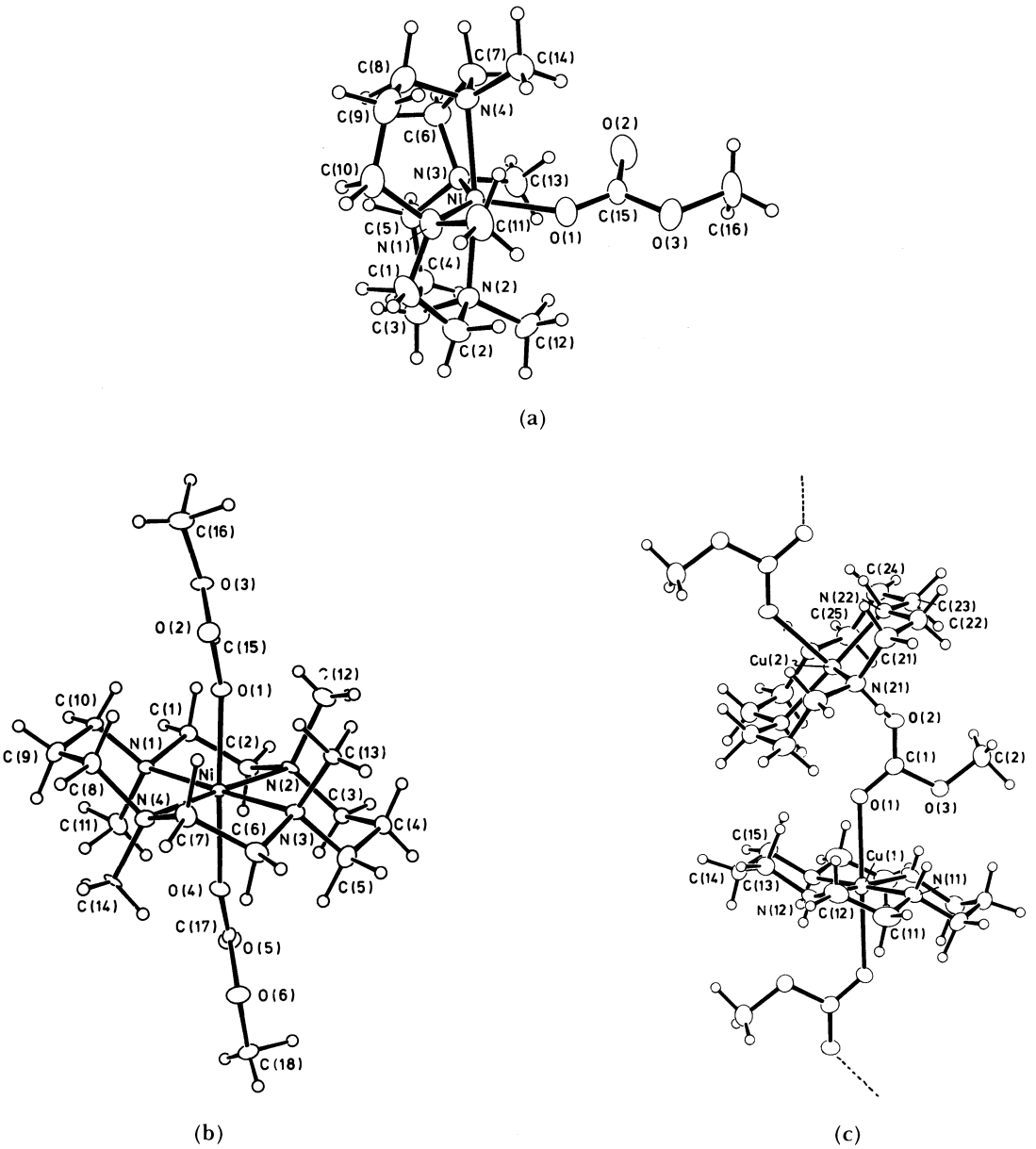

Fig. 2. ORTEP view of the structure, (a): [Ni(*RSRS*-Me_4[14]aneN$_4$)(O_2COCH_3)](ClO_4) (**4**), (b): [Ni(*RRSS*-Me_4[14]aneN$_4$)(O_2COCH_3)$_2$]·$HNEt_3ClO_4$ (**5**), (c): Cu([14]aneN$_4$)(O_2COCH_3)(ClO_4) (**6**).

ca. 0.1 Å in the zinc complex. Although the in-plane coordination bond lengths are not much different between the nickel and zinc complexes, deviations of the in-plane coordination bond angles from 120° are larger in the nickel complex than in the zinc complex.

As shown in Fig. 2(b), the structure of **5** is of the *trans*-NiO_2N_4 type with the macrocycle in a plane and with two unidentate $CH_3OCO_2^-$ occupying the axial sites. This 2:1 complex (two $CH_3OCO_2^-$'s per a metal ion) is the first example among about twenty monoalkyl carbonato complexes of M(II)–tetraaza-cycloalkane we prepared. There is an approximate inversion center at the nickel atom, although all the atoms in the complex cation are crystallographically independent. The overall skeletal structure of the macrocycle is the same as that of the most strain-free form of the [14]aneN$_4$ ligand, five- and six-membered chelate rings being in the gauche and chair conformations, respectively. The average Ni–N distance is 2.163(9) Å and is comparable to a reported value (2.16(1) Å) for [Ni_2(*RRSS*-Me_4[14]aneN$_4$)$_2$(N_3)$_3$]I.[3a] But it is about 0.1 Å longer than those found in high-spin complexes without N-methyl groups, *trans*-[NiX_2([14]aneN$_4$)].[19] This is the outcome of the *N*-methylation of [14]aneN$_4$ which causes a decrease in the ligand field strength. Monomethyl carbonato ligands are oriented parallel to the fence of the CH_3 groups on the same side, avoiding mutual steric interactions (Fig. 2(b)). Angles of Ni–O(1)–C(15) and

Table 4. Atomic Parameters for [Ni(*RSRS*-Me_4[14]aneN$_4$)-(O_2COCH_3)](ClO$_4$) (**4**)[a]

Atom	x	y	z	B_{eq}[b]
Ni	21456(4)	24187(4)	4045(6)	2.4
Cl	6008(1)	2080(1)	-2619(2)	4.0
O(1)	888(3)	2346(3)	1789(4)	4.8
O(2)	-372(4)	3763(4)	1723(6)	6.3
O(3)	-571(3)	2609(3)	3242(5)	5.1
O(4)[c]	6556(5)	2558(5)	-879(6)	8.5
O(5)[c]	6037(7)	2843(5)	-3504(8)	13.0
O(6)[c]	6541(7)	1065(5)	-3389(8)	13.0
O(7)[c]	4823(5)	1848(6)	-2613(9)	11.7
N(1)	2599(3)	662(3)	-232(5)	3.6
N(2)	3464(3)	2633(3)	2615(4)	3.3
N(3)	2570(3)	4034(3)	255(4)	2.9
N(4)	1041(3)	2202(3)	-1996(4)	3.5
C(1)	3701(4)	623(4)	916(7)	4.5
C(2)	3659(4)	1453(4)	2698(6)	4.2
C(3)	4618(4)	3101(4)	2492(6)	4.1
C(4)	4527(4)	4271(4)	2284(6)	4.2
C(5)	3877(4)	4288(4)	579(6)	3.6
C(6)	2127(4)	3962(4)	-1543(6)	4.0
C(7)	949(4)	3368(5)	-2138(7)	4.5
C(8)	1588(5)	1416(5)	-3467(6)	4.7
C(9)	1805(5)	230(5)	-3406(7)	5.6
C(10)	2825(5)	126(4)	-2046(7)	4.5
C(11)	1670(4)	-41(4)	79(8)	4.7
C(12)	3074(5)	3328(5)	4283(6)	4.7
C(13)	1956(4)	5003(4)	1431(7)	4.4
C(14)	-200(4)	1797(5)	-2116(7)	5.0
C(15)	23(4)	2943(4)	2211(6)	3.5
C(16)	-1637(5)	3251(6)	3709(8)	6.0

a) Positional parameters are multiplied by 10^4 except for positional parameter of Ni, for which the values are multiplied by 10^5. b) $B_{eq}=4/3(\sum_i\sum_j a_i a_j \beta_{ij})$, where the a_i's are the unit-cell edges in direct space. c) Perchlorate oxygen atom.

Table 5. Atomic Parameters for [Ni(*RRSS*-Me_4[14]aneN$_4$)-(O_2COCH_3)$_2$]·$HNEt_3ClO_4$ (**5**)[a]

Atom	x	y	z	B_{eq}[b]
Ni	0	2497(1)	0	1.2
Cl	2513(2)	1260(1)	-2475(4)	3.2
O(1)	-356(2)	2732(4)	-1767(4)	1.9
O(2)	-1101(2)	3672(4)	-2527(4)	2.2
O(3)	-686(2)	2327(3)	-3603(3)	2.0
O(4)	397(2)	2312(4)	1755(4)	2.2
O(5)	1136(2)	1308(4)	2601(4)	2.5
O(6)	725(2)	2626(4)	3616(4)	2.7
O(7)[c]	2997(3)	588(5)	-2333(7)	5.9
O(8)[c]	2009(4)	687(1)	-2700(11)	12.3
O(9)[c]	2531(7)	1841(5)	-1506(10)	17.9
O(10)[c]	2630(4)	1993(7)	-3457(11)	11.1
N(1)	-58(2)	747(4)	-282(4)	1.5
N(2)	805(2)	2429(4)	-776(4)	1.4
N(3)	73(2)	4240(4)	234(4)	1.6
N(4)	-789(2)	2604(4)	823(4)	1.8
N(5)	2723(2)	-4106(5)	-2592(5)	2.5
C(1)	396(3)	582(5)	-1123(5)	1.7
C(2)	929(3)	1192(5)	-718(5)	1.8
C(3)	1271(2)	3011(5)	-68(5)	1.5
C(4)	1149(3)	4233(6)	66(6)	2.3
C(5)	641(3)	4527(6)	833(7)	3.0
C(6)	-365(3)	4450(5)	1119(6)	2.3
C(7)	-901(3)	3792(6)	717(6)	2.2
C(8)	-1218(3)	1960(5)	9(6)	2.5
C(9)	-1109(3)	732(5)	-140(6)	2.3
C(10)	-622(3)	433(5)	-861(5)	1.4
C(11)	84(3)	64(5)	826(6)	2.2
C(12)	817(3)	2793(6)	-2135(6)	2.6
C(13)	-37(3)	4978(5)	-809(5)	2.0
C(14)	-818(3)	2266(5)	2038(5)	1.7
C(15)	-732(3)	2995(5)	-2578(5)	1.5
C(16)	-1143(3)	2501(6)	-4553(6)	3.0
C(17)	760(2)	2049(5)	2558(5)	1.6
C(18)	1114(3)	2465(7)	4607(6)	3.0
C(19)	2418(3)	-3129(6)	-3154(8)	3.5
C(20)	2488(8)	-2055(6)	-2500(15)	4.9
C(21)	2677(4)	-5100(7)	-3418(8)	3.8
C(22)	2086(5)	-5503(9)	-3770(17)	10.2
C(23)	2555(4)	-4324(6)	-1312(7)	3.3
C(24)	2844(5)	-5330(9)	-851(13)	8.5

a) Positional parameters are multiplied by 10^4. b) See footnote in Table 4 for B_{eq}. c) Perchlorate oxygen atom.

Ni-O(4)-C(17) widen up to 156.4(4)° and 158.9(4)°, respectively.

The crystal structure of Cu([14]aneN$_4$)(O_2COCH_3)(ClO$_4$) (**6**) is isostructural with Zn([14]aneN$_4$)(O_2COCH_3)(ClO$_4$). As shown in Fig. 2(c), the $CH_3OCO_2^-$ ligand bridges adjacent Cu([14]aneN$_4$) units, forming a linear chain along the a axis. Two independent copper atoms (Cu(1) and Cu(2)) are situated at a crystallographic inversion center. Intramolecular hydrogen bonds operate between NH of [14]aneN$_4$ and the O(3) atom of the $CH_3OCO_2^-$ ligand (O(3)···HN(12)=2.40(6) Å, O(3)···HN(11)=2.60(6) Å), as in the zinc complex.

Discussion

Nickel(II) Complexes. Three types of coordination structures (I—III) are found in (monomethyl carbonato)nickel(II) complexes. Type I is a linear-chain structure with the bridging monomethyl carbonato ligand. Compounds **1**, **2**, and **3** are assigned to this type from IR and electronic spectral data. The second type (II) is a mononuclear five-coordinate structure with the unidentate monomethyl carbonato ligand and is found for compound **4**. These two types have been already known in zinc(II) complexes.[1] Type III, which is a mononuclear six-coordinate complex containing two unidentate $CH_3OCO_2^-$, has been newly found for compound **5**. As to the CO_2 uptake reaction, compounds with the structural type I were the most effective in the nickel(II) complexes as well as in the zinc(II) systems.[1] CO_2 is taken up spontaneously from the air in the system of this type to form desired monomethyl carbonato complexes. In complexes

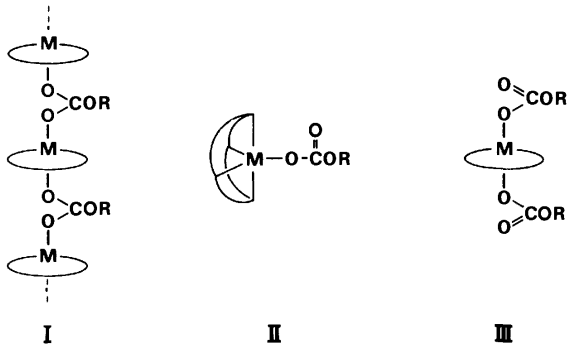

I II III

Table 6. Atomic Parameters for $Cu([14]aneN_4)(O_2COCH_3)(ClO_4)$ (**6**)[a]

Atom	x	y	z	B_{eq}[b]
Cu(1)	5000	5000	0	2.8
Cu(2)	0	5000	0	2.8
Cl	2095(2)	6679(2)	-3908(2)	4.5
O(1)	2960(4)	4841(3)	-207(5)	3.5
O(2)	1374(4)	4452(3)	-1325(5)	4.1
O(3)	2952(4)	4302(3)	-2323(5)	3.9
O(4)[c]	2245(8)	6667(9)	-2485(8)	15.3
O(5)[c]	1129(6)	6243(6)	-4353(8)	10.1
O(6)[c]	2143(10)	7442(7)	-4498(14)	18.2
O(7)[c]	2948(9)	6241(10)	-4269(13)	18.3
N(11)	4898(5)	5684(4)	-1781(6)	3.4
N(12)	4812(4)	6140(4)	946(6)	3.4
N(21)	38(4)	6105(4)	-1128(6)	3.1
N(22)	-1123(4)	4592(4)	-1490(6)	3.0
C(1)	2367(6)	4542(5)	-1202(7)	3.1
C(2)	2335(7)	3941(6)	-3486(8)	5.0
C(11)	5031(7)	6606(5)	-1374(9)	4.9
C(12)	4452(7)	6765(5)	-122(9)	4.5
C(13)	4126(6)	6133(6)	2143(8)	4.8
C(14)	4506(7)	5497(6)	3283(8)	5.3
C(15)	4388(7)	4579(6)	2857(7)	4.9
C(21)	-938(6)	6094(5)	-2125(8)	4.2
C(22)	-1069(6)	5193(5)	-2670(7)	4.1
C(23)	-1080(6)	3680(5)	-1912(7)	3.8
C(24)	-1147(6)	3074(5)	-689(9)	4.3
C(25)	-156(6)	3077(5)	346(8)	4.3

a) Positional parameters are multiplied by 10^4. b) See footnote in Table 4 for B_{eq}. c) Perchlorate oxygen atom.

with $Me_4[14]aneN_4$, steric constraints provided by *N*-methyl groups of $Me_4[14]aneN_4$ prevent monomethyl carbonato ligand from bridge coordination, giving structural type II or III. The $Me_4[14]aneN_4$ ligand in the *RSRS*-form folds easily to afford the type II structure, whereas *RRSS*-$Me_4[14]aneN_4$ cannot fold to form the type III complex.

As was mentioned in the experimental section, compound **5** was produced also from the solution of **4** through the nitrogen configuration inversion of $Me_4[14]aneN_4$ from *RSRS*- to *RRSS*-form. The electronic spectrum of a methanol solution of **4** containing an excess of NEt_3 and saturated CO_2 was found to change with time. The absorption maximum of the original solution at 681 nm shifted gradually toward higher frequencies, that is, toward the absorption band of **5** and reached an equilibrium position. The more NEt_3 was added, the larger and faster the band shifted. Moore et al. reported that the *RSRS*- and *RRSS*-isomers of $[Ni(Me_4[14]aneN_4)]^{2+}$ are interconvertible, and that the conversion occurs at a relatively slow rate in DMSO or DMF but rapidly in the presence of a strongly coordinating amine such as propylamine.[20] In our case, however, reverse reaction, i.e., conversion from **5** to **4** was not observed. An absorption spectrum of **5** in methanol did not change at all at least for a month. Compound **5** decomposes rapidly in the air liberating CO_2, although it is stable in a nitrogen atmosphere or in a vacuum.[21] The instability of **5** is reflected in bond angles of Ni-O-C in the monomethyl carbonato ligands. The corresponding angle in other monomethyl carbonato[1b] or carbonato complexes[22] is in the range of 122—136°, which are close to 120° expected for the oxygen atom in the sp^2 hybridization. However, the angles in **5** (157.7° in average) are by far larger.

The monomethyl carbonato ligand was successfully converted into dimethyl carbonate by treating with FSO_3CH_3 in $CDCl_3$. The formation of dimethyl carbonate was easily followed by ^1H NMR. The conversion efficiency in the present nickel(II) complexes was not much different from the case of zinc(II) complexes described previously.[1a]

Copper(II) Complexes. IR data of the (monomethyl carbonato)copper(II) complexes did not provide definite evidence for structural information. It is because an interaction of $CH_3OCO_2^-$ with $[Cu(L)]^{2+}$ is very weak. In fact, the X-ray structure of $Cu([14]aneN_4)(O_2COCH_3)(ClO_4)$ (**6**) demonstrates clearly the weakness of the interaction. As described previously, the crystal structure of **6** is isomorphous with the Zn analogue, $Zn([14]aneN_4)(O_2COCH_3)(ClO_4)$, which has been found to be one of the most effective system as to the efficiency of the CO_2 uptake among about 20 systems explored in a series of our studies. In the zinc structure, one of the Zn atoms takes an out-of-plane position,[1b] but such an out-of-plane displacement has not been found in **6** in spite of the constrained coordination environment. The double of the Cu···Cu separation (12.303(3) Å) corresponds to the length of the a axis, and is slightly longer than that of the zinc complex (12.128(2) Å). These structural informations show that the Cu-O interaction is rather weak. The Cu-O distances are as large as 2.351(6) and 2.516(5) Å, while the Zn-O lengths are 2.143(3) and 2.227(3) Å. This difference is consistent with the observation that the $CH_3OCO_2^-$ uptake by the zinc complex takes place much easier. The occurrence of such a weak interaction in copper(II) complexes was observed spectrally in a methanol solution. A d-d band of $[Cu(L)]^{2+}$ shifts to lower energies as the concentration of NEt_3 increases. Such a spectral change was observed for all the copper(II) complexes studied, $[Cu(L)](ClO_4)_2$ (L=$[14]aneN_4$, $[15]aneN_4$, and $Me_4[14]aneN_4$). The spectral change indicates that a monoalkyl carbonato adduct exists in equilibrium with the starting $[Cu(L)]^{2+}$. The d-d band shift upon addition of a large excess of NEt_3 was as much as 2400 cm^{-1} for compound **7**, whereas it was only 800 cm^{-1} for **6**. Complemented by structural data for other $Me_4[14]aneN_4$ complexes, this may indicate that the coordination geometry about Cu in **7** is of the trigonal bipyramidal type. An interaction between Cu^{2+} and $CH_3OCO_2^-$ is stronger in **7** than in **6**.

Table 7. Relevant Bond Lengths(Å) and Angles(°)

[Ni(RSRS-Me_4[14]aneN_4)(O_2COCH_3)](ClO$_4$) (4)

Ni	-O(1)	1.991(4)		O(1)	-C(15)	1.226(6)	
Ni	-N(1)	2.126(4)		O(2)	-C(15)	1.255(7)	
Ni	-N(2)	2.142(4)		O(3)	-C(15)	1.342(6)	
Ni	-N(3)	2.132(4)		O(3)	-C(16)	1.450(8)	
Ni	-N(4)	2.135(4)					
O(1)	-Ni	-N(1)	95.4(2)	N(2)	-Ni	-N(4)	171.7(2)
O(1)	-Ni	-N(2)	89.8(2)	N(3)	-Ni	-N(4)	85.0(2)
O(1)	-Ni	-N(3)	118.5(2)	Ni	-O(1)	-C(15)	133.4(4)
O(1)	-Ni	-N(4)	98.5(2)	C(15)	-O(3)	-C(16)	115.9(5)
N(1)	-Ni	-N(2)	85.0(2)	O(1)	-C(15)	-O(2)	127.4(5)
N(1)	-Ni	-N(3)	145.9(2)	O(1)	-C(15)	-O(3)	113.6(4)
N(1)	-Ni	-N(4)	93.7(2)	O(2)	-C(15)	-O(3)	118.9(5)
N(2)	-Ni	-N(3)	91.5(1)				

[Ni(RRSS-Me_4[14]aneN_4)(O_2COCH_3)$_2$]·$HNEt_3$·ClO$_4$ (5)

Ni	-O(1)	2.101(4)		O(2)	-C(15)	1.214(8)	
Ni	-O(4)	2.117(5)		O(3)	-C(15)	1.415(7)	
Ni	-N(1)	2.165(5)		O(3)	-C(16)	1.477(8)	
Ni	-N(2)	2.172(5)		O(4)	-C(17)	1.239(7)	
Ni	-N(3)	2.151(5)		O(5)	-C(17)	1.274(8)	
Ni	-N(4)	2.165(6)		O(6)	-C(17)	1.380(8)	
O(1)	-C(15)	1.265(7)		O(6)	-C(18)	1.400(8)	
O(1)	-Ni	-O(4)	176.9(2)	N(2)	-Ni	-N(4)	178.0(2)
O(1)	-Ni	-N(1)	89.0(2)	N(3)	-Ni	-N(4)	87.4(2)
O(1)	-Ni	-N(2)	86.5(2)	Ni	-O(1)	-C(15)	156.4(4)
O(1)	-Ni	-N(3)	90.1(2)	C(15)	-O(3)	-C(16)	113.2(5)
O(1)	-Ni	-N(4)	94.9(2)	Ni	-O(4)	-C(17)	158.9(4)
O(4)	-Ni	-N(1)	92.7(2)	C(17)	-O(6)	-C(18)	121.3(5)
O(4)	-Ni	-N(2)	90.9(2)	O(1)	-C(15)	-O(2)	128.2(5)
O(4)	-Ni	-N(3)	88.2(2)	O(1)	-C(15)	-O(3)	109.5(5)
O(4)	-Ni	-N(4)	87.6(2)	O(2)	-C(15)	-O(3)	122.3(5)
N(1)	-Ni	-N(2)	87.3(2)	O(4)	-C(17)	-O(5)'	131.5(6)
N(1)	-Ni	-N(3)	178.2(2)	O(4)	-C(17)	-O(6)	113.4(6)
N(1)	-Ni	-N(4)	94.2(2)	O(5)	-C(17)	-O(6)	114.9(5)
N(2)	-Ni	-N(3)	91.2(2)				

Cu([14]aneN_4)(O_2COCH_3)(ClO$_4$) (6)

Cu(1)	-O(1)	2.352(5)		Cu(2)	-N(22)	2.010(6)	
Cu(1)	-N(11)	2.032(6)		O(1)	-C(1)	1.226(9)	
Cu(1)	-N(12)	2.023(5)		O(2)	-C(1)	1.252(8)	
Cu(2)	-O(2)	2.515(5)		O(3)	-C(1)	1.393(9)	
Cu(2)	-N(21)	2.015(6)		O(3)	-C(2)	1.423(9)	
O(1)	-Cu(1)	-N(11)	88.2(2)	Cu(1)	-O(1))	-C(1)	131.0(5)
O(1)	-Cu(1)	-N(12)	89.0(2)	Cu(2)	-O(2)	-C(1)	128.3(5)
N(11)	-Cu(1)	-N(12)	85.6(2)	C(1)	-O(3)	-C(2)	116.2(6)
O(2)	-Cu(2)	-N(21)	89.1(2)	O(1)	-C(1)	-O(2)	129.6(7)
O(2)	-Cu(2)	-N(22)	88.6(2)	O(1)	-C(1)	-O(3)	117.5(6)
N(21)	-Cu(2)	-N(22)	85.6(2)	O(2)	-C(1)	-O(3)	112.8(6)

Cobalt(II) Complexes. Cobalt(II) complexes, **8** and **9**, are classified to types I and II, respectively, from the spectral and magnetic susceptibility data. Compound **8** is easily oxidized to the tervalent state and this enables discussion on the structure of **8**. When an aqueous solution of compound **8** acidified with HCl was stirred in the air, brown solid was produced. The product was identified as the most stable isomer of *trans*-[$Co^{III}Cl_2$([15]aneN_4)](ClO$_4$), in which one five-membered and three six-membered chelate rings adopt a gauche-skew-chair-chair conformational sequence.[23] Since nitrogen configurations would be retained in the process of the oxidation, the skeletal structure of [15]aneN_4 in compound **8** is considered to be the same. This overall conformation is different from that found for the corresponding zinc(II) complex in [{Zn([15]-aneN_4)}$_3$(O_2COCH_3)$_2$](ClO$_4$)$_4$, which has the [15]aneN_4 ligand in a gauche-chair-skew-chair conformation.[1b] On the other hand, compound **9** was found to be very stable in the air. The trigonal bipyramidal geometry characteristic of this particular macrocycle prevents Co(Me$_4$[14]aneN_4)$^{2+}$ from the air oxidation. To our knowledge, compound **9** is the first example that assumes a high-spin five coordinate structure in tetraaza macrocyclic cobalt(II) complexes.

Comparison of Metal Ions from the Viewpoint of the CO_2 Uptake. Among tetraazacycloalkane complexes of various metal ions studied, the zinc complexes are the most superior in the efficiency of the CO_2 uptake as monoalkyl carbonate ion. As discussed in detail in the previous paper,[1] coordinately unsaturated situation introduced by square-planar coordination of a tetraazacycloalkane ligand is the most important in the case of the zinc(II) systems. The uptake reaction by the nickel(II) systems was not so effective as the zinc(II) systems. A Ni^{2+} ion has $3d^8$ valence electron configuration and a square-planar four-coordinate structure is one of the stable geometries for nickel(II) complexes. That is, axial sites of starting nickel(II) complexes with tetraazacycloalkane are supposed to be not so reactive as those of the zinc(II) complexes. It is well known that nickel(II) complexes with tetraazacycloalkanes (L) exists in a coordinating solvent or in the presence of coordinating anions as an equilibrium mixture between square-planar four-coordinate species and five- or six-coordinate species (Eq. 2). Thermodynamic parameters of the equilibrium

$$[Ni(L)]^{2+} + nX \rightleftharpoons [Ni(L)X_n]^{m+} \quad (2)$$
$$n=1 \text{ or } 2;\ m=0\text{—}2,$$

in aqueous solution ($X=H_2O$) have been reported for various tetraaza macrocycles. The position of the equilibrium depends strongly on the kind of the in-plane ligand. For example, in the case of L=[14]aneN$_4$, only 28% of the complex exists as six-coordinate species at room temperature, while, in the case of L=[15]aneN$_4$, six-coordinate species amounts to as much as 99%.[24] A position of the equilibrium of Eq. 2 has been known to be affected by an electronic factor, that is, ligand field strength of the in-plane ligand. We tried to correlate an equilibrium constant with efficiency in the uptake of monoalkyl carbonate ion. But such a correlation was not observed in the present system. A steric factor contributes more strongly than the electronic one. In fact, the following facts are noted between [Ni(*RRSS*-Me$_4$[14]aneN$_4$)]$^{2+}$ and [Ni([14]aneN$_4$)]$^{2+}$: in aqueous solution, the former favors six-coordination over four-coordination and vice versa in the latter, while compound **5** containing the *RRSS*-Me$_4$[14]aneN$_4$ ligand is so unstable that it returns to the four-coordinate complex rapidly in the air.[21] However, the electronic effect on the uptake reaction was indeed noted in the case where ligand field strength of the macrocyclic ligand is by far stronger and, therefore, the equilibrium of Eq. 2 is shifted far to the left. [Ni(Me$_2$[13]dienatoN$_4$)]$^+$ (Me$_2$[13]dienatoN$_4$= 11,13-dimethyl-1,4,7,10-tetraazacyclotrideca-10,12-diene)[25] is such an example and it did not afford a monomethyl carbonato complex. One more fact that deserves a brief comment on the nickel(II) system, is that a nickel(II) complex containing linear tetramines such as 3,2,3-tet (3,2,3-tet=4,7-diazadecane-1,10-diamine) instead of tetraazacycloalkane undergoes the uptake of monomethyl carbonate ion. A zinc(II) complex having 3,2,3-tet never undergoes such a reaction. Possibly, this is due to the difference in coordination behavior between nickel(II) and zinc(II). Ni(3,2,3-tet)$^{2+}$ prefers a square-planar geometry and has coordinately unsaturated nature. On the other hand, Zn(3,2,3-tet)$^{2+}$ assumes a tetrahedrally distorted geometry which is more stable than a square planar form, and therefore it does not undergo further ligand uptake.

The uptake efficiency of the copper(II) complexes was the lowest among the metal ions studied. This originates from the inherently weak reactivity of axial sites of tetragonal copper(II) complexes. As described previously, the X-ray structure of compound **6** demonstrates clearly such a situation.

The cobalt(II) system is disadvantageous to the formation of monomethyl carbonato complexes because cobalt(II) complexes with four nitrogen donors are generally susceptible to oxidation. However, the Co([15]aneN$_4$) complex underwent the uptake reaction smoothly under oxygen-free conditions. The Co(Me$_4$[14]aneN$_4$) system is an exception. It forms a five-coordinate cobalt(II) complex with an extra unidentate ligand (X), CoX(Me$_4$[14]aneN$_4$)$^+$, which is exceptionally stable to oxidation. Cobalt(II) complexes resemble zinc(II) complexes in the point that they can take many different types of coordination geometries.[26] It seems that the efficiency of the cobalt complexes is not much different from that of the zinc complexes under oxygen free conditions.

References

1) a) M. Kato and T. Ito, *Inorg. Chem.*, **24**, 504 (1985); b) M. Kato and T. Ito, ibid., **24**, 509 (1985).

2) [14]aneN$_4$=1,4,8,11-tetraazacyclotetradecane, [15]aneN$_4$= 1,4,8,12-tetraazacyclopentadecane, *iso*-[14]aneN$_4$=1,4,7,11-tetraazacyclotetradecane, Me$_4$[14]aneN$_4$=1,4,8,11-tetramethyl-1,4,8,11-tetraazacyclotetradecane.

3) For [Ni(Me$_4$[14]aneN$_4$)]$^{2+}$, two configurational isomers are known [a) F. Wagner, M. T. Mocella, M. J. D'Aniello, Jr., A. H. -J. Wang, E. K. Barefield, *J. Am. Chem. Soc.*, **96**, 2625 (1974); b) M. J. D'Aniello, M. T. Mocella, F. Wagner, E. K. Barefield, and I. C. Paul, *J. Am. Chem. Soc.*, **97**, 192 (1975)]. One contains the Me$_4$[14]aneN$_4$ ligand with coordinated nitrogens in the 1*RS*,4*SR*,8*RS*,11*SR*-form, the other in the 1*RS*,4*RS*,8*SR*,11*SR*-form. These ligands are abbreviated as *RSRS*-Me$_4$[14]aneN$_4$ and *RRSS*-Me$_4$[14]aneN$_4$, respectively, throughout this paper.

4) L. Sabatini and L. Fabbrizzi, *Inorg. Chem.*, **18**, 438 (1979).

5) F. Wagner and E. K. Barefield, *Inorg. Chem.*, **15**, 408 (1976).

6) a) Y. Hirshberg and E. Fischer, *Rev. Sci. Instrum.*, **30**, 197 (1959); b) L. S. Nelson, *Rev. Sci. Instrum.*, **30**, 655 (1956).

7) M. Sugimoto, J. Fujita, H. Ito, K. Toriumi, and T. Ito, *Inorg. Chem.*, **22**, 955 (1983).

8) "International Tables for X-ray Crystallography," Kynoch Press, Birmingham (1974), Vol IV.

9) R. F. Stewart, E. R. Davidson, and W. T. Simpson, *J. Chem. Phys.*, **42**, 3175 (1965).

10) Tables of hydrogen atomic coordinates, thermal parameters for non-hydrogen atoms, full bond lengths and angles, and complete F_o—F_c data for compound **4**, **5**, and **6** are deposited as Document No. 8614 at the office of the Editor of the Bulletin of the Chemical Society of Japan.

11) T. Sakurai, K. Kobayashi, *Rikagaku Kenkyusho Hokoku*, **55**, 69 (1979).

12) P. Main, S. E. Hull, L. Lessinger, G. Germain, J-P. Declercq, and M. M. Woolfson (1978). MULTAN 78. A System of Computer Programmes for the Automatic Solution of Crystal Structure from X-ray Diffraction Data. Univ. of York, England and Louvain, Belgium.

13) a) D. A. Rowley and R. S. Drago, *Inorg. Chem.*, **7**, 795 (1968); b) L. Y. Martin, C. R. Sperati, and D. H. Busch, *J. Am. Chem. Soc.*, **99**, 2968 (1977).

14) Absorption maximum of a square-planar complex, $[Cu(L)](ClO_4)_2$ in methanol appears at 19800 and 16700 cm^{-1} for L=[14]aneN$_4$ and Me$_4$[14]aneN$_4$, respectively.

15) N. F. Curtis, *Coord. Chem. Rev.*, **3**, 3 (1968).

16) C. M. Sarther and E. L. Blinn, *Inorg. Chem.*, **15**, 3083 (1976).

17) L. Sacconi and G. P. Speroni, *Inorg. Chem.*, **7**, 295 (1968).

18) K. M. Long and D. H. Busch, *Inorg. Chem.*, **9**, 505 (1970).

19) T. Ito, M. Kato, and H. Ito, *Bull. Chem. Soc. Jpn.*, **57**, 2641 (1984).

20) P. Moore, J. Sachinidis, and G. R. Willey, *J. Chem. Soc., Chem. Commun.*, **1983**, 522.

21) The resulting product is orange in color indicating a four-coordinate nickel(II) complex. When this change was followed by IR spectra, bands at 1670 and 1306 cm^{-1} due to the monomethyl carbonate group disappeared gradually and a new peak appeared at 1630 cm^{-1}. This band suggested an existence of hydrogencarbonate ion. In fact, analytical data of the product was consistent with [Ni(Me$_4$[14]aneN$_4$)](O$_2$COH)(ClO$_4$): Found: C, 38.10; H, 7.04; N, 11.79%. Calcd for $NiClO_7N_4C_{15}H_{33}$: C, 37.88; H, 6.99; N, 11.78%. Therefore, the decomposition of **5** is considered to be induced by the reaction with moisture, as shown below.

$$[Ni(Me_4[14]aneN_4)(O_2COCH_3)_2]\cdot HNEt_3ClO_4 \xrightarrow[H_2O]{CO_2,\ 2CH_3OH,\ NEt_3} [Ni(Me_4[14]aneN_4)](O_2COH)(ClO_4).$$

22) D. A. Palmer and R. V. Eldik, *Chem. Rev.*, **83**, 651 (1983).

23) Y. Hung, L. Y. Martin, S. C. Jackels, A. M. Tait, and D. H. Busch, *J. Am. Chem. Soc.*, **99**, 4029 (1977).

24) L. Fabbrizzi, *J. Chem. Soc., Dalton Trans.*, **1979**, 1857.

25) J. A. Cunningham and R. E. Sievers, *J. Am. Chem. Soc.*, **95**, 7183 (1973).

26) In fact, the similarity of coordination modes between Co^{2+} and Zn^{2+} is often used in studies of zinc enzymes such as carbonic anhydrase and carboxypeptidase, Zn^{2+} ion being replaced by Co^{2+} ion in order to make it possible to investigate by means of visible absorption spectra.

 © 1986 The Chemical Society of Japan Bull. Chem. Soc. Jpn., 59, 295—300 (1986)

Flow Injection Analysis of Cobalt(II) by Catalytic Oxidations of Stilbazo and Pyrocatechol Violet

Toshio Deguchi,* Atsuya Higashi, and Isao Sanemasa
Department of Chemistry, Faculty of Science, Kumamoto University,
Kurokami 2-39-1, Kumamoto 860
(Received September 4, 1985)

Catalytic oxidations of ten organic dyes with an aromatic-hydroxyl or -amino functional group have been studied in the presence of metal ions such as cobalt(II), copper(II), and vanadium(V). Of these dyes, six were found to be effectively oxidized and decolorized specifically by one of these metals. 4,4′-Bis(3,4-dihydroxyphenylazo)stilbene-2,2′-disulfonic acid diammonium salt (Stilbazo) and 3,3′,4′-trihydroxyfuchsone-2″-sulfonic acid (Pyrocatechol Violet) were found to be promising for determining trace amounts of cobalt(II). The optimum analytical conditions have been studied for these two compounds with the aid of a flow injection analysis technique. The both reagents can be used to determine cobalt(II) down to 1 ppb.

It is well known that some metal ions, particularly transition metals with different oxidation states, catalyze the oxidation reactions of an arylamine, phenol, or some dyestuffs.[1] Indeed, a number of catalytic methods using a suitable oxidant such as H_2O_2 or BrO_3^- have been reported which permit trace analysis of some transition metal ions.[2-5] Concerning with the cobalt(II) determination, the following organic chromogenic substances have been so far used; Alizarin,[6] 3-(4-sulfophenylazo)-4,5-dihydroxy-2,7-naphthalenedisulfonic acid,[7] Gallocyanine,[8] chromotropic acid,[9] diphenylcarbazone,[10] Tiron,[11] gallic acid,[12] Luminol.[13] The last two have been used for the chemiluminescent reactions, and they are generally very sensitive. The other substances have been used for the photometric method. The organic chromogenic substances listed above are helpful to search for organic dyes with similar functional group(s) that might be expected to provide new catalytic systems.

Ten kinds of organic dyes were chosen, and the possibility of their metal-catalyzed oxidations have been investigated in view of trace analyses of cobalt(II), copper(II), and vanadium(V). 4,4′-Bis(3,4-dihydroxyphenylazo)stilben-2,2′-disulfonic acid diammonium salt (Stilbazo) and 3,3′,4′-trihydroxyfuchsone-2″-sulfonic acid (Pyrocatechol Violet) appeared promising for the determination of trace amounts of cobalt(II).

A flow injection analysis (FIA) technique was employed to find the optimum analytical conditions for these two organic dyes. The technique makes many different types of analysis be easily performed by controlling reaction conditions such as mixing of reactants at a fixed rate, reaction time, and temperature of reactant, and hence, particularly suitable for kinetic method of analysis which generally takes advantage of the difference between an indicator reaction (a reaction in the absence of the metal in question) and a catalytic reaction. By the use of FIA technique, an indicator reaction can be monitored continuously and the output signal is to be recorded as a baseline on a chart, and if a catalytic reaction does take place, it appears as a signal on the baseline.

Experimental

Reagents and Materials. Distilled and deionized water was used throughout. Commercially available 1000 ppm standard solutions of cobalt(II) and the other metal ions were diluted with water (a little acidic if necessary) to prepare the working solutions. Dotite 2,2′-dihydroxyazobenzene, Stilbazo, Pyrogallol Red, Pyrocatechol Violet, Beryllon II, and di-SNADNS-4 and Wako Pure Chemical's Evans Blue, Bismarck Brown, *m*-Cresol Purple, and Cresol Red were dissolved in water to give suitable concentrations. Potassium bromate and hydrogen peroxide (30%) were used as oxidants. Buffer solutions were prepared according to the literature;[14] CH_3COOH/CH_3COONa (pH 3—6), Na_2HPO_4/KH_2PO_4 (pH 6—8) and Na_2CO_3/$NaHCO_3$ or Na_2CO_3/NaOH (pH 9—12).

Apparatus. The FIA manifold employed in determining cobalt(II) with Stilbazo or Pyrocatechol Violet as a chromogenic substance is shown in Fig. 1. The system was

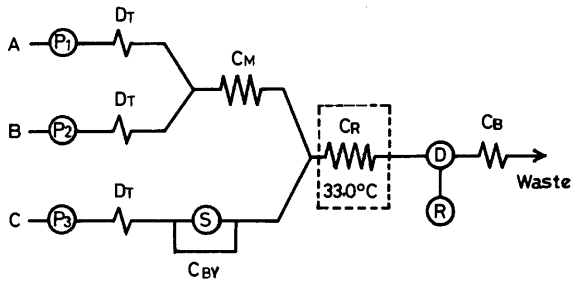

Fig. 1. Block diagram of FIA for determinations of cobalt(II) by catalytic oxidations of Stilbazo and Pyrocatechol Violet.
A: Stilbazo or Pyrocatechol Violet-hydrogen peroxide reagent solutions, B: buffer solution, C: distilled deionized water, P_1–P_3: pump, flow rates being fixed at 1 $cm^3\ min^{-1}$ (P_1), 1 $cm^3\ min^{-1}$ (P_2), and 2 $cm^3\ min^{-1}$ (P_3). D_T: damper tube(30 cm long, 2 mm i.d.), C_M: mixing coil (5 m long, 0.5 mm i.d.), C_{BY}: bypass coil (3 m long, 0.5 mm i.d.), C_R: reaction coil (4 m long, 0.5 mm i.d.), C_B: back-pressure coil(2 m long, 0.5 mm i.d.), S: sample injector(62 μl), D: detector, R: recorder.

built from Teflon tubing (i.d., 0.5 mm), Teflon connectors, two reciprocating pumps (Kyowa Seimitsu KHU-52, P_3, and KHU-W-52, double-plunger type, P_1, P_2), a spectrophotometer (Kyowa Seimitsu KLC-2290)(D), equipped with a flow-through cell (volume 8 μl, optical path-length 10 mm), a six-way loop valve injector (Seishin VHU-6)(S), and a recorder (Rikadenki R-22) (R). Elastic PVC tubes (Technicon 061 116-0536-15) of ca. 30 cm length, D_T, were placed immediately after each pump so that the pumping pulse was completely eliminated. A bypass coil, C_{BY}, which acts as a damper of sample injection shock, and a back-pressure coil, C_B, which serves to prevent the liberation of gas dissolved in reactant and carrier solutions upon heating, were incorporated into the system. The symbols, C_M and C_R, denote mixing and reaction coils, respectively.

Results and Discussion

Metal Ion-Catalized Oxidations of Organic Dyes. A suitable concentration of each chromogenic substance was prepared in pH 4 or pH 11 buffer solution in the presence of an oxidant (1.0×10^{-3} mol dm^{-3} $KBrO_3$ or 3.3% H_2O_2). To this solution a known volume of 1000 ppm metal standard solution was added with the aid of a micropipette so that the concentration of metal ion of interest became 1 ppm, and then the absorbance of the solution was followed as a function of standing time at room temperature or at an elevated temperature, if necessary. The results are summarized in Table 1. These substances listed in the Table were almost completely decolorized within 30 s in the presence of 1 ppm metal specified in the Table, while it took 30 min or more in the absence of the metal. A typical absorbance change with standing time is illustrated for Stilbazo-cobalt(II) system in Fig. 2, where the cobalt(II) concentration is lowered to 5 ppb for the sake of convenience of measuring the absorbance change with time.

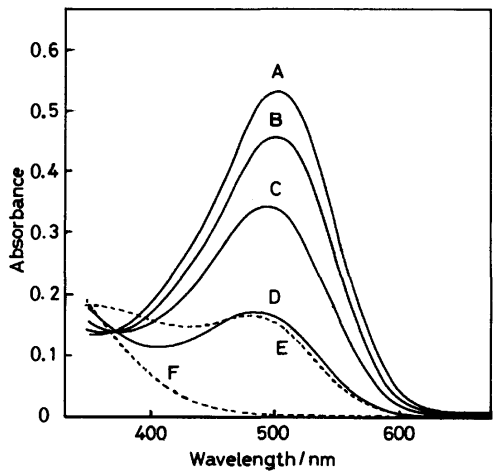

Fig. 2. Absorption spectra change with standing time. Solid line: reagent mixture of Stilbazo(1.0×10^{-5} mol dm^{-3}) and hydrogen peroxide(0.5%) at pH 11.7; A, 1.5 min; B, 15 min; C, 30 min; D, 40 min. Broken line: reagent mixture in the presence of 5 ppb cobalt at pH 11.7; E, 1.5 min; F, 15 min.

Concerning with cobalt(II) determination, Stilbazo, Pyrocatechol Violet, Pyrogallol Red, and Evans Blue are expected to be of potential utility. Among them, the first two seem better since Evans Blue is only effective at a fairly high temperature and Pyrogallol Red is of limited solubility in water.

The optimum conditions for determining trace amounts of cobalt(II) will be discussed in detail below. The experiments were carried out by using the FIA system shown in Fig. 1. The peak height recorded on a chart, which corresponds to a difference of absorbances between a metal blank and a metal-catalyzed reaction zone is a measure of analytical sensitivity.

Stilbazo Method—Effects of Operational Conditions—. The effects on the peak height were studied of such conditions as pH (9—12), concentrations of Stilbazo (4.8×10^{-5}—1.4×10^{-4} mol dm^{-3}) and hydrogen peroxide (0.05—0.6%), temperature (33, 43, 53, and 63 °C), and the FIA manifold including flow rate (P_1=P_2, 0.5—1.0 cm^3 min^{-1}; P_3, 1.0—2.0 cm^3 min^{-1}), tube length of the reaction coil (2—8 m), and sample volume (62, 91, and 110 μl). The peak height was found to (i) increase almost linearly with pH above 10, (ii) increase as the concentrations of Stilbazo and H_2O_2 increase (the peak hight become constant at Stilbazo concentrations greater than 9.6×10^{-5} mol dm^{-3} and at H_2O_2 concentrations greater than 0.15% at pH 11.9), (iii) increase by 1.4, 1.9, and 2.4 times as the temperature is raised from 33 °C to 43, 53, and 63 °C, respectively, (iv) increase with the tube length of the reaction coil to become constant at length greater than 6 m, but a longer coil tends to lead to broad peaks because of an increased axial dispersion of the sample zone, (v) increase as the flow rate decreases, but at the same time, there observed is the pronounced tailing of the peaks probably due to the adsorption of the reaction product onto the inside of the Teflon tube.

Stilbazo Method—Recommended Procedure for Cobalt(II) Determination—. Two solutions A and B are prepared; A: Stilbazo (9.6×10^{-5} mol dm^{-3})-H_2O_2 (0.15%), B: Na_2CO_3 (0.05 mol dm^{-3})-NaOH (0.006 mol dm^{-3}) mixed solution to give pH 11.9. Solutions A and B are both made to flow at the same flow rate of 1.0 cm^3 min^{-1}, while water at a flow rate of 2.0 cm^3 min^{-1}. A 62 μl portion of sample solutions which contain cobalt(II) higher than 1 ppb is injected via the loop valve injector into the carrier stream of water and mixed with the reagent stream before entering the reaction coil of 4 m which has been immersed in a thermostated bath (33 or 53 °C), and the absorbance is measured at 503 nm. A negative peak appears as a result of absorbance change due to the decolorization of Stilbazo.

Table 1. Metal Ion Catalysis in the Oxidative Decolorization of Organic Dyes

Compound examined	Oxidant	Catalyst	pH	Temperature	Color change of solution
Stilbazo 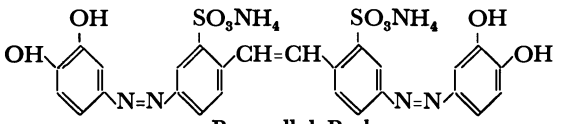	H_2O_2	Co(II)	11	Room temp	Red ⟶ Colorless
Pyrogallol Red 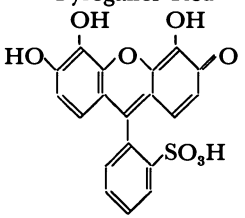	H_2O_2	Co(II)	11	Room temp	Purple ⟶ Colorless
	BrO_3^-	V(V)	4	Room temp	Orange ⟶ Colorless
Evans Blue 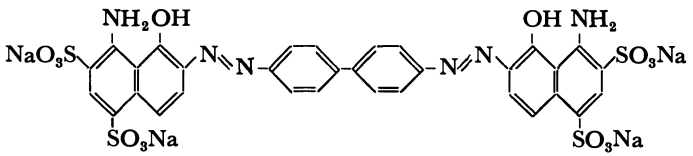	H_2O_2	Co(II)	11	70 °C	Blue ⟶ Colorless
m-Cresol Purple 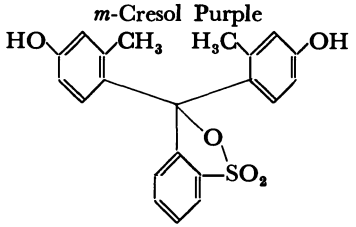	H_2O_2	Cu(II)	11	70 °C	Red ⟶ Colorless
Cresol Red 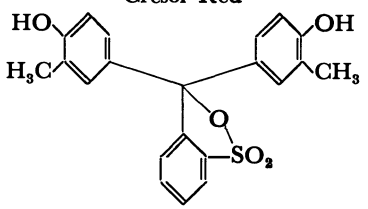	H_2O_2	Cu(II)	11	70 °C	Red ⟶ Colorless
Pyrocatechol Violet 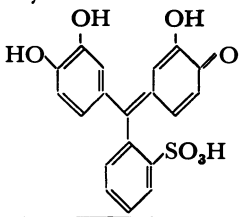	H_2O_2	Co(II)	11	Room temp	Violet ⟶ Colorless[a]

a) This system was studied by a batchwise technique (Ref. 15).

Stilbazo Method—FIA Responses—. Figure 3 shows typical FIA responses obtained under the recommended procedure. It will be seen that cobalt(II) down to 1 ppb can be determined. A dip is observed in front of each peak, which is caused by an injection shock. The relative standard deviation observed for analysis of 60 ppb cobalt was 0.7% (n=13), and a sampling rate of 60 samples/h was achieved.

Stilbazo Method—Interferences—. Sample solutions containing 50 ppb cobalt(II) and various concentrations of foreign ions were injected according to the recommended procedure mentioned above (the temperature of bath was set at 33 °C). The results are shown in Table 2. Zinc(II) and cadmium(II) exhibited serious interferences when present above 500 ppb. The interferences, however, were completely eliminated up to 1 ppm concentration of these metals by making a 500 ppm sodium citrate solution flow instead of water. The serious interference by EDTA is due to its stable complex formation with cobalt(II). The other ions examined have no or only slight interference so far as their concentrations do not exceed 100 to 200 times the cobalt(II) concentration.

Pyrocatechol Violet Method—Effects of Operational Conditions—. The optimum conditions were

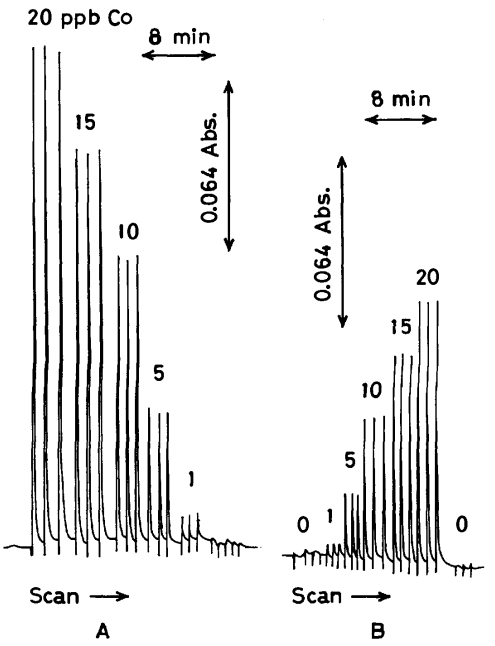

Fig. 3. Typical responses for cobalt(0–20 ppb) by FIA with Stilbazo (9.6×10^{-5} mol dm^{-3})–hydrogen peroxide(0.15%) system at 53 and 33 °C.
Experimental conditions: A, 53 °C; B, 33 °C; pH, 11.9. Other conditions and manifold as in Fig. 1.

Table 2. Effect of Diverse Ions on the Determination of 50 ppb Cobalt in the Catalytic Oxidation of Stilbazo at 33 °C

Foreign ion	Concentration/ppm	Relative error/%	Foreign ion	Concentration/ppm	Relative error/%
Al(III)	10	−4.8	Mg(II)	2	5.9
	5	0		1	3.0
Ag(I)	10	12	Ca(II)	5	11
	5	1.7		1	2.3
Cr(III)	5	−5.1	NH_4^+	50	1.8
	1	−2.6		10	1.9
Cr(VI)	10	0	F^-	50	0
Se(IV)	50	5.4	Cl^-	50	1.8
	10	0	Br^-	50	0
Fe(III)	1	−2.7	I^-	50	0
Ni(II)	5	−17	NO_3^-	50	0
	2	0	NO_2^-	50	−3.0
Mn(II)	0.5	−1.0	SO_4^{2-}	50	5.5
Cu(II)	1	0.9		10	0
Zn(II)	1	25	PO_4^{3-}	50	2.8
	0.5	14	Citrate	50	5.5
	1	0.8*		10	0
Cd(II)	1	17	Tartrate	50	0
	0.5	9.2	Oxalate	50	9.1
	1	0*		10	0
V(V)	10	2.9	Acetate	50	0
Pb(II)	10	0	EDTA	1	−100

* These values were obtained when pumping a 500 ppm of citrate aqueous solution through the pump(P_3). A negative relative error(%) means that the peak hights of 50 ppb cobalt in the presence of the diverse ions are lower than those for 50 ppb cobalt only.

studied by changing the concentration of Pyrocatechol Violet (4.0×10^{-5}—4.0×10^{-4} mol dm^{-3}) and that of H_2O_2 (0.075—0.55%) and pH (9—12). The peak height was found to (i) increase with the concentration of Pyrocatechol Violet up to 3.0×10^{-4} mol dm^{-3} and then decrease gradually beyond this concentration, (ii) increase with H_2O_2 concentration and become constant at 0.3% H_2O_2, (iii) increase with pH and remain constant above pH 11.8, and (iv) increase by 1.4 and 1.8 times as the temperature is raised from 33 °C to 42 and 51 °C, respectively.

Pyrocatechol Violet Method—Recommended Procedure for Cobalt(II) Determination—. Two solutions A and B are prepared; A: Pyrocatechol Violet (3.0×10^{-4} mol dm^{-3})-H_2O_2 (0.3%), B: the same solution as that used in the Stilbazo method (pH=11.8). Just in the same way and at the same flow rates as the Stilbazo method, solutions A and B and water are made to flow and a 62 μl portion of sample solutions is injected and the absorbance is measured at 585 nm.

Pyrocatechol Violet Method—FIA Responses—. Figure 4 shows typical responses obtained under the recommended procedure. The sensitivity of the cobalt(II) determination is approximately in the same order as that of the Stilbazo method. The relative standard deviation observed for analysis of 25 ppb cobalt was 0.5% (n=10), and a sampling rate of 60 samples/h was achieved.

Pyrocatechol Violet Method—Interferences—. Sample solutions containing 50 ppb cobalt(II) and various concentrations of foreign ions were injected (the temperature of bath was set at 33 °C). The results are shown in Table 3. In contrast to the Stilbazo method, zinc(II) and cadmium(II) do not interfere seriously, while iron(III) and manganese(II) exhibit serious interferences. The other ions examined show only slight interferences when present 100 to 200 times the cobalt(II) concentration.

The present paper is concerned with the cobalt(II) determinations based on the catalytic oxidations of Stilbazo and Pyrocatechol Violet. We had thought that these organic substances had not been used for the cobalt(II) analysis. On writing this paper,

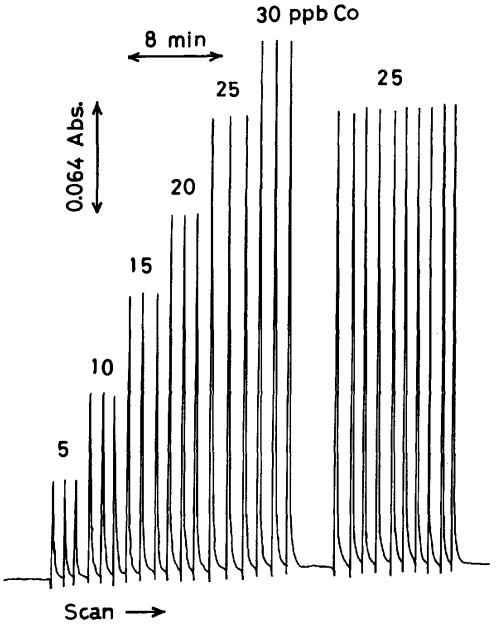

Fig. 4. Typical responses for cobalt(5—30 ppb) by FIA with Pyrocatechol Violet(3.0×10^{-4} mol dm^{-3})-hydrogen peroxide(0.3%) system at 33 °C.
Buffer solution: pH 11.8. Other conditions and manifold as in Fig. 1.

Table 3. Effect of Diverse Ions on the Determination of 50 ppb Cobalt in the Catalytic Oxidation of Pyrocatechol Violet at 33 °C

Foreign ion	Concentration/ppm	Relative error/%	Foreign ion	Concentration/ppm	Relative error/%
Al(III)	2	3.0	V(V)	50	−4.6
	5	6.0	Mg(II)	2	3.6
Cr(III)	5	0.6		5	18
Fe(III)	2	−25	Ca(II)	2	3.0
	5	−35		5	9.0
Ni(II)	5	−3.0	NH_4^+	50	2.4
	10	−15	F^-	50	2.9
Zn(II)	10	3.1	Cl^-	50	2.3
Cd(II)	2	−2.0	NO_2^-	50	3.0
	5	−6.9	NO_3^-	50	2.3
Cu(II)	2	−2.6	SO_4^{2-}	50	3.1
	5	−8.3	Citrate	50	1.7
Pb(II)	10	−4.0	Tartrate	50	2.9
Mn(II)	2	−14	Oxalate	50	0
	5	−25	Acetate	50	1.2

A negative relative error(%) means that the peak hights of 50 ppb cobalt in the presence of the diverse ions are lower than those for 50 ppb cobalt only.

however, we found the latter reagent used for the same purpose in a batchwise technique.[15] The analytical conditions such as H_2O_2 concentration and pH are almost the same between the present work and the literature, but the concentration of Pyrocatechol Violet employed by the literature[15] is lower by one order of magnitude than the present conditions. According to the literature,[15] cobalt(II) of 0.0065 ppb can be determined. The sensitivity is higher by two orders of magnitude than that attained in the present work using FIA technique and almost comparable to that obtained based on chemiluminescence methods.[12,13] The literature method, however, seems much laborious and time-consuming since it needs measurements of reaction rates and calculations of rate constants.

The sensitivity for the cobalt(II) analysis attained in the present work using Stilbazo and Pyrocatechol Violet appears to be comparable to that reported by investigators who used aromatic chromogenic substances with two 1,3-, or 1,4-dihydroxyl group.[8]

References

1) P. R. Bontchev, *Talanta*, **17**, 499 (1970).
2) K. Hirayama and T. Sawaya, *Nippon Kagaku Kaishi*, **1976**, 1401.
3) T. Yamane and T. Fukasawa, *Anal. Chim. Acta*, **119**, 389 (1980).
4) K. Hirayama and N. Unohara, *Nippon Kagaku Kaishi*, **1981**, 98.
5) J. L. Ferrer-Herranz and D. Perez-Bendito, *Anal. Chim. Acta*, **132**, 157 (1981).
6) K. B. Yatsimirskii, "Kinetic Method of Analysis," Pergamon, Oxford (1966), p. 98.
7) T. Yamane, *Anal. Chim. Acta*, **130**, 65 (1981).
8) K. Hirayama and N. Unohara, *Nippon Kagaku Kaishi*, **1978**, 1498.
9) T. Yamane, *Nippon Kagaku Kaishi*, **1982**, 93.
10) I. F. Dalmanov, N. M. Ushakova, and V. M. Peshkova, *Zh. Anal. Khim.*, **28**, 1131 (1973); *Chem. Abstr.*, **79**, 100167j (1973).
11) C. Maekoya, F. Mizuniwa, K. Usami, and K. Osumi, *Nippon Kagaku Kaishi*, **1983**, 1023.
12) M. Yamada, T. Komatsu, S. Nakahara, and S. Suzuki, *Anal. Chim. Acta*, **155**, 259 (1983).
13) J. L. Burguera, A. Townshend, and S. Greenfield, *Anal. Chim. Acta*, **114**, 209 (1980).
14) "Kagaku Binran (Kisohen)," 2nd ed, ed by Chemical Society of Japan, Tokyo (1975), p. 1490.
15) T. J. Janjic and G. A. Milovanovic, *Glas. Hem. Drus., Beograd*, **37**, 173 (1972); *Chem. Abstr.*, **78**, 168149q (1973).

The Crystal and Molecular Structures of Bis(ethylenedithio)-tetrathiafulvalene

Hayao KOBAYASHI,* Akiko KOBAYASHI,† Yukiyoshi SASAKI,† Gunzi SAITO,††,α and Hiroo INOKUCHI††

Department of Chemistry, Faculty of Science, Toho University, Funabashi, Chiba 274

† Department of Chemistry, Faculty of Science, The University of Tokyo, Hongo, Bunkyo-ku, Tokyo 113

†† Institute for Molecular Science, Okazaki 444

(Received May 10, 1985)

Synopsis. The X-ray crystal structure analysis of a sulfur containing π-donor molecule, bis(ethylenedithio)-tetrathiafulvalene, (BEDT-TTF) shows that the BEDT-TTF molecule is nonplanar and that the crystal is composed of pairs of BEDT-TTF.

Recent discoveries of the superconductivities of the organic conductors based on a sulfur containing π-donor molecule, bis(ethylenedithio)tetrathiafulvalene (abbreviated as BEDT-TTF hereafter) have aroused a considerable interest.[1] The crystals of BEDT-TTF compounds show a characteristic two-dimensional (abbreviated as 2-D hereafter) array of BEDT-TTF,[2] whereas the molecular metals so far reported have 1-D stacks of planar π-donor and/or acceptor molecules. The examination of the intermolecular overlap integrals of HOMO, from which the conduction bands are formed, indicates 2-D properties of BEDT-TTF compounds.[2-4] Moreover, β-$(BEDT\text{-}TTF)_2PF_6$ has an open Fermi surface perpendicular to the direction approximately parallel to the averaged molecular plane of BEDT-TTF, which shows definitely an important role of the 2-D intermolecular interactions in the organic conductors.[5,6]

In this paper, we will report the crystal structure of the neutral BEDT-TTF molecule.

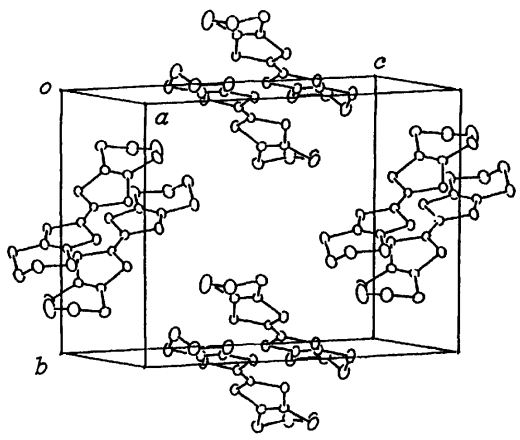

Fig. 1. The crystal structure of BEDT-TTF.

α Present address: Institute for Solid State Physics, The University of Tokyo, Roppongi, Minato-ku, Tokyo 106.

Results and Discussion

Crystal Data: $C_{10}H_8S_8$, M=384.7, monoclinic, space group, $P2_1/c$, a=6.614(11), b=13.985(2), c=16.646(3) Å, β=109.55(2)°, U=1449.6 Å^3, Z=4, D_x=1.76 g cm^{-3}, μ(Mo $K\alpha$)=11.6 cm^{-1}. Intensities were measured by the θ—2θ scan technique on a Rigaku automated four-circle diffractometer with Mo $K\alpha$ radiation (2θ<55°) and were corrected for usual Lorentz and polarization effects, but not for the absorption. The maximum dimension of the crystal used was 0.3 mm. The structure was solved by the direct method and refined by the least-squares procedure (currently R=0.052), using 2262 reflections ($|F_o|>3\sigma(|F_o|)$). The hydrogen atoms were refined isotropically, but the temperature factors of two of them became very large (10 Å^2 and 8 Å^2), which is probably due to the large thermal motion of the ethylene groups. Therefore, the hydrogen atoms were omitted in the final refinement. The atomic coordinates are given in Table 1.[7] The crystal structure is shown in Fig. 1.

The crystal is composed of the pairs of BEDT-TTF molecules. Similar paired structure of BEDT-TTF has also been found in the crystals of BEDT-TTF monocation salts ((BEDT-TTF)X(THF); X=ClO_4 or ReO_4).[8] The bond lengths and angles are shown in

Table 1. Atomic Parameters of BEDT-TTF

	x	y	z	B_{eq}/Å^2
S(1)	0.2564(2)	0.3834(1)	0.0163(1)	3.6
S(2)	0.6211(2)	0.3592(1)	−0.0457(1)	4.0
S(3)	0.0050(2)	0.5067(1)	−0.1531(1)	3.7
S(4)	0.3704(2)	0.4826(1)	−0.2142(1)	2.6
S(5)	0.4054(2)	0.2299(1)	0.1475(1)	5.4
S(6)	0.8167(2)	0.2029(1)	0.0790(1)	3.8
S(7)	−0.2917(2)	0.5081(1)	−0.3143(1)	5.9
S(8)	0.1430(2)	0.5522(1)	−0.3884(1)	3.2
C(1)	0.3599(7)	0.4049(3)	−0.0667(3)	2.8
C(2)	0.2581(7)	0.4554(4)	−0.1353(3)	2.8
C(3)	0.4421(7)	0.2937(4)	0.0634(3)	3.3
C(4)	0.6073(8)	0.2816(4)	0.0353(3)	2.8
C(5)	−0.0354(7)	0.5356(4)	−0.2599(3)	3.3
C(6)	0.1290(7)	0.5240(4)	−0.2879(4)	2.7
C(7)	0.6767(11)	0.2173(7)	0.2197(4)	5.9
C(8)	0.8566(10)	0.2210(6)	+0.1904(4)	4.9
C(9)	−0.2893(9)	0.5803(5)	−0.4221(4)	5.8
C(10)	−0.0933(10)	0.6255(5)	−0.4309(3)	6.9

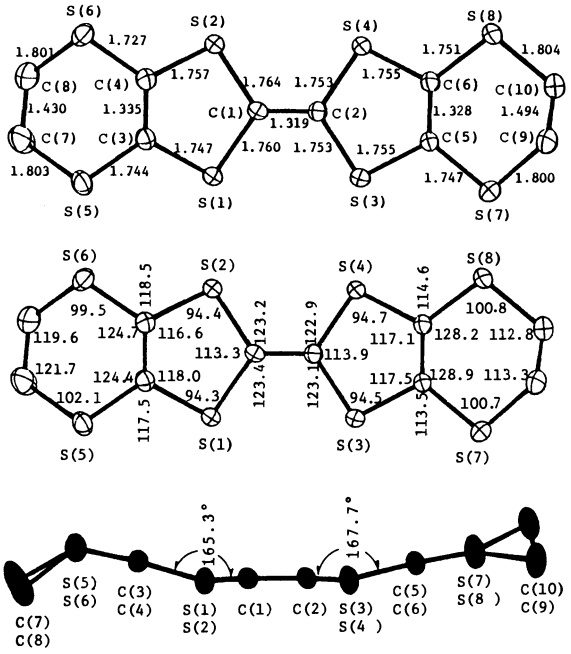

Fig. 2. Molecular structure of BEDT–TTF. Estimated standard deviations of bond lengths are 0.007—0.012 Å and those of bond angles are 0.6—1.0°.

Fig. 2. The mean bond length of C–S in the TTF skeleton is 1.751 Å and that of C=C is 1.327 Å. The structure analyses of several BEDT-TTF salts show that the C=C bonds become longer and the C–S bonds become shorter with the increasing formal charge(ρ) of BEDT-TTF$^{+\rho}$ molecule: r(C=C)=1.33 Å(ρ=0), 1.35(ρ=0.5), 1.38(ρ=1); r(C–S)=1.751(ρ=0), 1.745(ρ=0.5), 1.724(ρ=1). This is due to the symmetry of HOMO of BEDT-TTF which has nodal planes on the every C–S bond.

The BEDT-TTF molecule is nonplanar. The molecule is composed of three planes of tetrathio-substituted ethylene moieties (Fig. 2). The mode of overlapping of the paired molecules is shown in Fig. 3a. Despite of the pair structure of BEDT-TTFs, the shortest S···S distance (3.69 Å) is almost equal to the van der Waals distance (3.70 Å). Closer intermolecular contacts are found along the a axis (Fig. 3b). The sulfur atoms play a central role for the formation of the characteristic transverse intermolecular contacts. As described before, the side-by-side arrangement of BEDT-TTF is a common structural feature of the conducting BEDT-TTF salts. It is of interest that similar arrangement is also found even in the insulating neutral BEDT-TTF crystal.

Calculations were carried out partly on PANAFACOM U1300 computer of Toho University and mainly on HITAC M-200H computer at the Computer Center of The University of Tokyo, using the local version of the UNICS.[9]

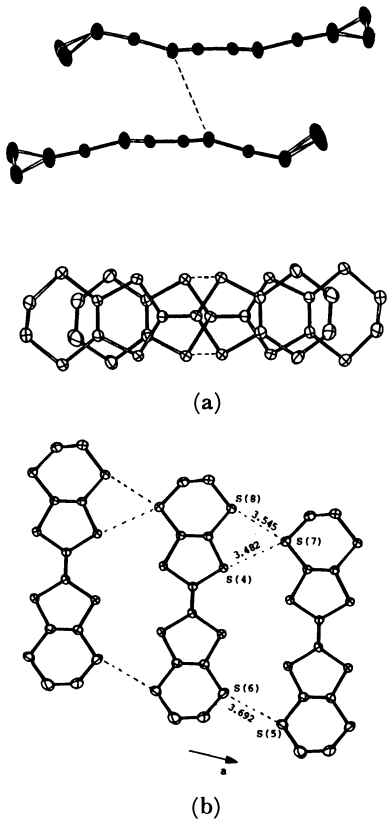

Fig. 3. (a) The mode of overlapping of the paired BEDT-TTFs. The dotted line indicates the short S···S contact (3.69 Å). (b) Molecular arrangement along the a axis.

References

1) S. S. Parkin, E. M. Engler, R. R. Schumaker, R. Lagier, V. V. Y. Lee, J. C. Scott, and R. L. Greene, *Phys. Rev. Lett.*, **50**, 270 (1983); E. B. Yagubskii, I. F. Shchegolev, V. N. Laukhin, P. S. Kononovich, V. F. Kaminskii, A. K. Kartosovnik, A. V. Zvarykina, and L. I. Buravov, *Zh. Eksp. Teor., Fiz. Pis'ma*, **39**, 12 (1984); J. M. Williams, H. H. Wang, M. A. Beno, T. J. Emge, L. M. Sowa, P. T. Copps, F. Behroozi, L. N. Hall, K. D. Carlson, and G. W. Crabtree, *Inorg. Chem.*, **23**, 3839 (1984); K. Murata, M. Tokumoto, H. Anzai, H. Bando, G. Saito, K. Kajimura, and T. Ishiguro, *J. Phys. Soc. Jpn.*, in press.

2) H. Kobayashi, T. Mori, R. Kato, A. Kobayashi, Y. Sasaki, G. Saito, T. Enoki, and H. Inokuchi, *Mol. Cryst. Liq. Cryst.*, **107**, 33 (1984).

3) T. Mori, A. Kobayashi, Y. Sasaki, H. Kobayashi, G. Saito, and H. Inokuchi, *Bull. Chem. Soc. Jpn.*, **57**, 627 (1984).

4) G. Saito, T. Enoki, K. Toriumi, and H. Inokuchi, *Solid State Commun.*, **42**, 557 (1982).

5) H. Kobayashi, R. Kato, T. Mori, A. Kobayashi, Y. Sasaki, G. Saito, and H. Inokuchi, *Chem. Lett.*, **1983**, 759.

6) T. Mori, A. Kobayashi, Y. Sasaki, R. Kato, and H. Kobayashi, *Solid State Commun.*, **53**, 627 (1985).

7) The anisotropic thermal parameters and the list of the structure factors are deposited at the Office of the Chemical Society of Japan (Document No. 8607)

8) H. Kobayashi, R. Kato, T. Mori, A. Kobayashi, Y. Sasaki, G. Saito, and H. Inokuchi, *Chem. Lett.*, **1984**, 183.

9) "The Universal Crystallographic Computation Program System (UNICS)," ed by T. Sakurai, Crystallographic Society of Japan, Tokyo (1967).

Solid-State NMR Studies on Pillar-Interlayered Naturally-Occurring Montmorillonite

Mutsuyoshi MATSUMOTO,*,† Minoru SUZUKI, (the late) Hiroshi TAKAHASHI, and Yasukazu SAITO
Institute of Industrial Science, The University of Tokyo,
22-1, Roppongi 7-Chome, Minato-ku, Tokyo 106
(Received June 21, 1985)

Synopsis. Solid-state MAS NMR spectroscopy on naturally occurring montmorillonite has revealed that the Fe(III), contained in the octahedral layer, exerts a greater influence on octahedral Al nuclei than on tetrahedral ones. The same trend is observed in a more pronounced manner with the material intercalated with $[AlO_4Al_{12}(OH)_{24}(OH_2)_{12}]^{7+}$ cations. Mechanisms of selective peak broadening in solid-state NMR spectra are discussed.

Pillar interlayered montmorillonite (abbreviated as PILM hereafter) has attracted considerable interest since its well-defined pore structure of molecular dimension suggests promising wide applications as adsorbents[1] and catalyst supports.[2] The layer distance of PILM (ca. 0.9 nm), as determined by X-ray diffraction, is consistent with the size of $[AlO_4Al_{12}OH)_{24}(OH_2)_{12}]^{7+}$ cation introduced.[3] Direct evidence for the Al_{13} structure present in the interlayer of clay minerals was given by Plee et al.[4] with solid-state MAS ^{27}Al NMR.

The Fe(III) constituent in naturally occurring montmorillonite may exert a paramagnetic influence on solid-state MAS NMR. In the present study, Kunipia-G montmorillonites with and without the Al_{13} pillar have been examined in order to elucidate the limitation in quantitative analysis.

Kunipia-G Na-montmorillonite (abbreviated as Na-Mont), supplied from Kunimine Ind. Co., Ltd., was intercalated with Al_{13} cations and dried in an oven overnight at 393 K as previously described.[5,6] Chemical analysis was carried out by atomic absorption spectroscopy. The basal spacing was enlarged to 1.80 nm by the pillar substance, as confirmed by X-ray diffraction. Solid-state MAS ^{27}Al NMR spectra were recorded at 70.28 MHz on a JEOL FX270 NMR spectrometer. The spinning frequency of rotor was 3—4 kHz. All measurements were carried out at room temperature with $[Al(H_2O)_6]^{3+}$ as an external standard. The peak intensity was calculated by integration of the principal peak and of its spinning side bands. In deconvolving overlapping peaks, it was assumed that both the tetrahedral and octahedral Al ions would give symmetrical NMR spectra.

The crystal unit of Na-Mont is formulated according to Brindley and Sempels[7] as

$$[Na_{0.38}Ca_{0.03}Mg_{0.01}][Al_{1.59}Fe^{3+}_{0.10}Mg_{0.31}][Si_{3.86}Al_{0.14}]O_{10}(OH)_2nH_2O, \quad (1)$$

where these brackets are arranged in the order: the exchangeable cation sites, the octahedral layer ones, and the tetrahedral layer ones. As for PILM, the composition of the exchangeable cation sites is changed into

$$[(Al_{1.16}O_{0.55})^{+0.38}Ca_{0.01}Mg_{0.02}], \quad (2)$$

where the interlayered alumina is represented as

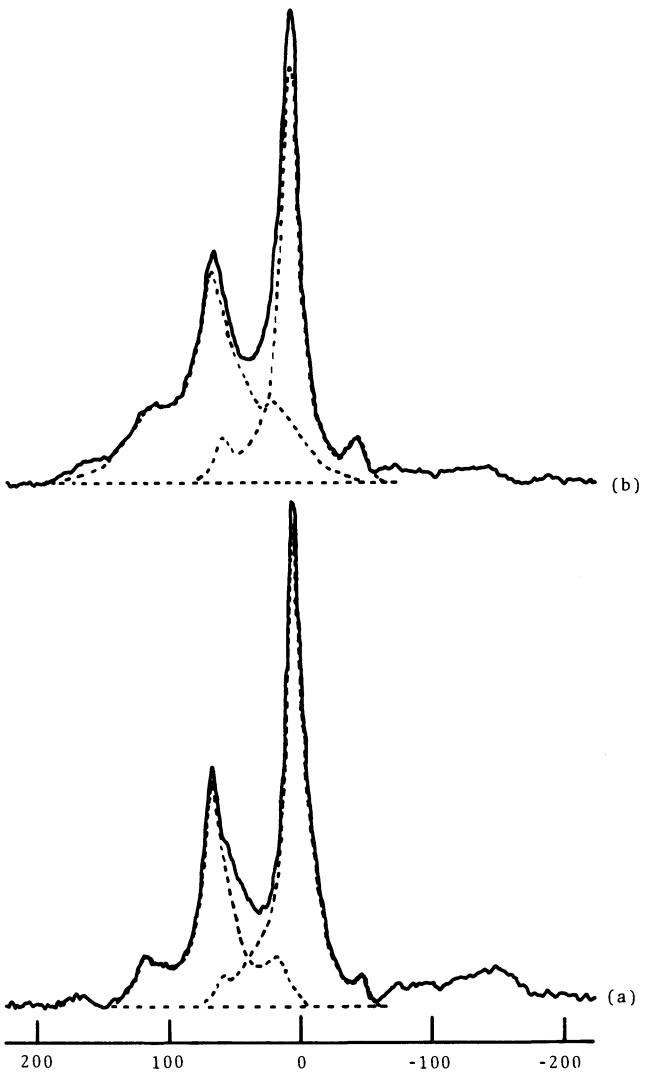

Fig. 1. Solid-state MAS ^{27}Al NMR spectra of Na-Mont (a) and PILM (b). The observed spectra are the full lines. The dotted lines are the deconvolved patterns. Resonance frequency: 70.28 MHz. Standard for δ: $[Al(H_2O)_6]^{3+}$.

† Present address: National Chemical Laboratory for Industry, 1-1, Higashi, Yatabe-machi, Tsukuba-gun, Ibaraki 305.

$(Al_{1.16}O_{0.55})^{+0.38}$.

The solid-state MAS ^{27}Al NMR spectra of Na-Mont and PILM are shown in Fig. 1 with deconvolved patterns indicated by the dotted lines. The chemical shift assignments already made for the octahedral and tetrahedral Al ions[8] are aptly applied to the peaks of 5.4 (Na-Mont) and 7.4 (PILM) ppm and of 67.0 (Na-Mont) and 66.0 (PILM) ppm, respectively.

The numbers of Al nuclei in the tetrahedral and octahedral coordinations per unit structure of Na-Mont, (Al_{tet}) and (Al_{oct}), respectively, are given from formula 1 as

$$(Al_{tet}) = 0.14, \quad (3)$$

$$(Al_{oct}) = 1.59. \quad (4)$$

The peak intensity ratio of Al_{tet}/Al_{oct} for Na-Mont should be obtained as

$$\alpha(Al_{tet})/\beta(Al_{oct}) = 0.50, \quad (5)$$

where α and β are positive coefficients which become unity when the Al nuclei involved are all detected by NMR spectroscopy. From Fig. 1, the value of β/α is obtained as 0.18. This magnitude far less than unity has certainly resulted from a rather difficult NMR detection for octahedral Al nuclei.

It is to be noted that the paramagnetic Fe(III) constituent of the naturally occurring montmorillonite is concentrated in the octahedral layer,[7] and that Al atoms are contained in the tetrahedral layer only in a small amount. Selective peak broadening due to electron-spin relaxation[9] would therefore be operative more efficiently for Al_{oct} in the same layer than for diluted Al_{tet} in a different layer.

The numbers of interlayered Al nuclei in the tetrahedral and octahedral coordinations, $\langle Al_{tet}\rangle$ and $\langle Al_{oct}\rangle$, respectively, are given from formula 2 as

$$\langle Al_{tet}\rangle + \langle Al_{oct}\rangle = 1.16. \quad (6)$$

The intensity ratio of the peak at 66.0 ppm (Al_{tet}) to that at 7.4 ppm (Al_{oct}) in Fig. 1 leads to the relationship

$$[\alpha(Al_{tet}) + \gamma\langle Al_{tet}\rangle]/[\beta(Al_{oct}) + \delta\langle Al_{oct}\rangle] = 1.3, \quad (7)$$

where γ and δ are positive coefficients not greater than unity.

The ratio of $\langle Al_{tet}\rangle/\langle Al_{oct}\rangle$ of the Al_{13} cation itself is equal to 1/12. By substituting Eqs. 3—6 in Eq. 7 we obtain

$$[\alpha(0.14) + \gamma(1/13)(1.16)]/$$
$$[\alpha(0.14)(1/0.50) + \delta(12/13)(1.16)] = 1.3, \quad (8)$$

which is simplified to

$$\delta/\gamma = 0.07 - 0.17\alpha/\gamma. \quad (9)$$

Apparently, δ/γ should be smaller than 0.07, whatever the values of α and γ may be.

Since supporting evidence for the Al_{13} structure has been obtained by solid-state NMR spectroscopy for interlayered hectorite,[4] the small magnitude of 0.07 ought to be understood in terms of the paramagnetic influence due to Fe(III) centers on the close octahedral Al nuclei of the pillar. In addition to this, the distortion factor, which has been pointed out for interlayered hectorite as becoming dominant on calcination,[4] must be taken into consideration. Moreover, any structural transformations, leading to increasing the tetrahedral sites, might occur in the pillar species partially.

Quantitative analysis of naturally occurring clay minerals by solid-state NMR spectroscopy should be undertaken with precaution against these intrinsic factors.

References

1) J. Shabtai, F. E. Massoth, M. Tokarz, G. M. Tsai, and J. McCauley, "Proc. 8th Intern. Congr. Catal.," Verlag Chemie, Berlin (1984), Vol. IV, p. 735 and references therein.

2) J. Shabtai, R. Lazar, and A. G. Oblad, "Proc. 7th Intern. Congr. Catal.," ed by T. Seiyama and K. Tanabe, Kodansha Ltd., Tokyo (1980), p. 828 and references therein.

3) D. E. W. Vaughan, "Proc. 5th Intern. Conf. Zeolites," ed by L. V. Rees, Heyden & Son Ltd., London (1980), p. 94.

4) D. Plee, F. Borg, L. Gatineau, and J. J. Fripiat, *J. Am. Chem. Soc.*, **107**, 2362 (1985).

5) M. Matsumoto, S. Shinoda, H. Takahashi, and Y. Saito, *Bull. Chem. Soc. Jpn.*, **57**, 1795 (1984).

6) M. Matsumoto, M. Suzuki, H. Takahashi, and Y. Saito, *Bull. Chem. Soc. Jpn.*, **58**, 1 (1985).

7) G. W. Brindley and R. E. Sempels, *Clay Miner.*, **12**, 229 (1977).

8) D. Müller, W. Gessner, H. J. Behrens, and G. Scheler, *Chem. Phys. Lett.*, **79**, 59 (1981).

9) A. Abragam, "The Principles of Nuclear Magnetism," Oxford Univ. Press, London (1961), Chap. 6, p. 194.

Substituent Effects in the Acid-Catalyzed Hydrolysis of Cyclic Acetals of Benzophenones

Shinya UENO, Takumi OSHIMA, and Toshikazu NAGAI*
Institute of Chemistry, College of General Education, Osaka University,
Toyonaka, Osaka 560
(Received July 18, 1985)

Synopsis. Eight 2,2-diaryl-1,3-dioxanes were prepared and the kinetic substituent effects regarding acid-catalyzed hydrolysis were studied in 80% dioxane-water(v/v) at 30 °C. The log k were well correlated with the Yukawa-Tsuno equation; log $k/k_0=-2.92(\sigma^0+0.385\Delta\bar{\sigma}_R{}^+)$($r$=0.999).

There have been numerous investigations on the acid-catalyzed hydrolysis of acetals from a mechanistic point of view.[1-3] It is generally accepted that the acetals hydrolyze by an A1 mechanism; pre-equilibrium protonation, rate-determining oxocarbenium ion formation, and fast degradation into carbonyl compound and alcohol (Scheme 1). As one part of the experimental evidence that supports the mechanism, a number of data have been collected related to kinetic substituent effects for the hydrolysis of a variety of acetals.[2] However, little is known about the cyclic acetals of benzophenones, especially with six-membered and higher ring sizes,[4] probably because of difficulties in a synthesis by traditional methods.[5]

Recently, we have discovered a facile synthetic method for cyclic and acyclic acetals of benzophenone using a redox reaction of diphenyldiazomethane(DDM) with 2,3-dichlore-5,6-dicyanobenzoquinone(DDQ) in the presence of suitable alcohols.[6-8] This discovery prompted us to synthesize cyclic acetals of benzophenones with a series of substituents and to obtain further information concerning the structure-reactivity relationship regarding the hydrolysis of acetals.

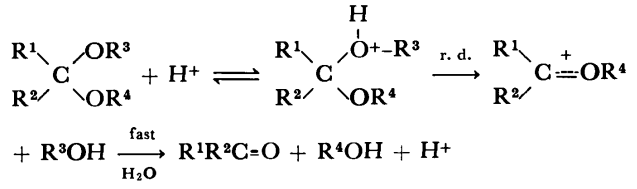

Scheme 1.

Table 1. Preparation and Hydrolysis of 2,2-Diaryl-1,3-dioxanes (**1a—h**)

Acetals	Substituents	Yields/%[a]	Mp θ_m/°C	$10^4\,k_{obsd}$ (s^{-1})[b]
1a	p-OCH_3	62	52—53	51.0
1b	p-CH_3	52	76—78	17.1
1c	m-CH_3	61	67—69	6.96
1d	p-Ph	46	154—156	4.99
1e	H	84	113—115	1.36
1f	p-Cl	55	60—61	1.13
1g	m-Cl	56	75—77	0.311
1h	m-NO_2	58	oil	0.0396

a) Isolated yields by column chromatography(Al_2O_3). b) All rates were measured in 80% dioxane-water at 30 °C under the constant HCl concentration(0.2 mol dm^{-3}).

Results and Discussion

The eight m- and p-substituted 2,2-diaryl-1,3-dioxanes (**1a—h**) were prepared and the rates of acid-catalyzed hydrolyses of these six-membered cyclic acetals were determined in 80% dioxane-water (by volume) at 30 °C (Table 1). When various values of

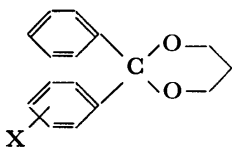

X=	X=
1a; p-OCH_3	**1e**; H
1b; p-CH_3	**1f**; p-Cl
1c; m-CH_3	**1g**; m-Cl
1d; p-Ph	**1h**; m-NO_2

log k were correlated with the standard Hammett σ and the Brown σ^+, the σ substituent constants gave a better result (ρ=−3.10, r=0.997) than σ^+, (ρ=−2.19, r=0.974). It can be corroborated, however, that the resonance substituent effects moderately contribute to the stabilization of the transition state as evaluated from the value of the resonance reaction constant (R=0.385) in the satisfactory Yukawa-Tsuno equation.[9]

$$\log k/k_0 = -2.92(\sigma^0+0.385\Delta\bar{\sigma}_{R^+}) - 0.05 \quad (n=8,\ r=0.999)$$

In Table 2, the Hammett parameters have been collected for the hydrolysis of **1** and related cyclic acetals. The hydrolysis of **1** provided a larger negative ρ value, accompanied by increased resonance effects than that of the corresponding five-membered cyclic acetals, 2,2-diaryl-1,3-dioxolanes(**2**),[10] though a straightforward comparison is somewhat ambiguous because of the change in the solvent composition. Whereas, monoaryl substituted 1,3-dioxolanes(**3**) were more subject to both polar and resonance effects than **1**.[11]

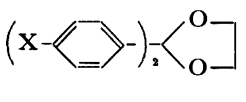

2

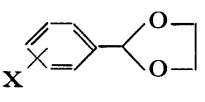

3

Table 2. Hammett Parameters for Hydrolysis of **1**, **2**, and **3**

Substrates	ρ	R	No. of substituents	Solvent	r	T/C°	Ref.
1	−2.92	0.385	8	80% Dioxane	0.999	30	This work
2[a]	−2.08[b]	0.240[b]	4	20% Dioxane	0.998	25	10
3	−3.28[b]	0.457[b]	5	50% Dioxane	0.999	30	11

a) The σ^+ and σ^0 values used are the sums of the values for the two substituents. b) Original data were treated according to Yukawa-Tsuno equation.

Experimental

Materials. 1,4-Dioxane was refluxed over metal sodium and fractionated. The substituted diphenyldiazomethanes(DDMs) were synthesized by the oxidation of the corresponding benzophenone hydrazones with yellow mercury oxide as has been described.[12] Also, solid DDMs were purified by recrystallization from petroleum ether or ether. The melting points of these DDMs have been reported elsewhere.[13] The *m*-NO_2 substituted DDMs had a mp of 53—54 °C (lit,[14]; oil). The acetals (**1a—h**) were produced by a reaction of DDMs with DDQ in the presence of 1,3-propanediol according to our previous methods.[8] The structures of **1a—h** were confirmed by IR, NMR, and elemental analyses. The yields and mp are collected in Table 1.

Kinetic Measurements. The rates of hydrolysis of **1a—h** were measured in 80% dioxane-water(v/v) at a constant acid(HCl) concentration(0.200 mol dm^{-3}). The rates were measured spectrophotometrically with a JASCO UVIDEC 505 spectrophotometer by following the increase in absorption due to the benzophenone at constant temperature maintained by circulating water from a Haake constant temperature circulating bath. Pseudo-first-order rate constants (k_{obsd}) were determined from logarithmic plots of ($A_\infty - A_t$) against time. These were linear over 3 half-times.

References

1) E. H. Cordes, *Progr. Phys. Org. Chem.*, **4**, 1 (1967).
2) E. H. Cordes and H. G. Bull, *Chem. Rev.*, **74**, 581 (1974).
3) R. G. Bergstrom, "The Chemistry of Ethers, Crown Ethers, Hydroxy Groups and Their Sulphur Analogues," ed by S. Patai, John Wiley and Sons, London (1980), Chap. 20.
4) O. Ceder, *Arkiv. Kemi.*, **6**, 523 (1954).
5) E. Schmitz and I. Eichhorn, "The Chemistry of the Ether Linkage," ed by S. Patai, John Wiley and Sons, London (1967), Chap. 7.
6) T. Oshima, R. Nishioka, and T. Nagai, *Tetrahedron Lett.*, **1980**, 3319.
7) T. Oshima, R. Nishioka, S. Ueno, and T. Nagai, *J. Org. Chem.*, **47**, 2114 (1982).
8) S. Ueno, T. Oshima, and T. Nagai, *J. Org. Chem.*, **49**, 4060 (1984).
9) Y. Yukawa, Y. Tsuno, and M. Sawada, *Bull. Chem. Soc. Jpn.*, **39**, 2274 (1966).
10) R. H. DeWolfe, K. M. Ivanetich, and N. F. Perry, *J. Org. Chem.*, **34**, 848 (1969).
11) T. H. Fife and L. K. Jao, *J. Org. Chem.*, **30**, 1492 (1965).
12) L. I. Smith and K. L. Howard, *Org. Synth.*, Coll. Vol. III, 351.
13) T. Oshima, A. Yoshioka, and T. Nagai, *J. Chem. Soc., Perkin Trans. 2*, **1978**, 1283.
14) R. Curci, F. D. Furia, and F. Marcuzzi, *J. Org. Chem.*, **36**, 3374 (1971).

A Novel Rearrangement of Protonated 2-Bromo-5-methylthiophene

Yukihiro YOKOYAMA, Yukihide YAMASHITA, Kensuke TAKAHASHI,* and Tyo SONE†
Department of Applied Chemistry, Nagoya Institute of Technology, Gokiso-cho, Showa-ku, Nagoya 466
† Department of Applied Chemistry, Faculty of Engineering, Yamagata University, Jonan, Yonezawa 992
(Received July 19, 1985)

Synopsis. A novel rearrangement of protonated 2-bromo-5-methylthiophene was observed in HSO_3F by means of ^1H NMR spectroscopy.

Recently we reported that well resolved ^1H NMR spectra of the cations formed from chloro- and bromothiophenes were observed in HSO_3F or HCl–$AlCl_3$-Solvent system.[1-4] We extended the observation to protonated 2-bromo-5-methylthiophene, as shown in Scheme 1. The experimental procedures were the same as those described in a previous report.[4]

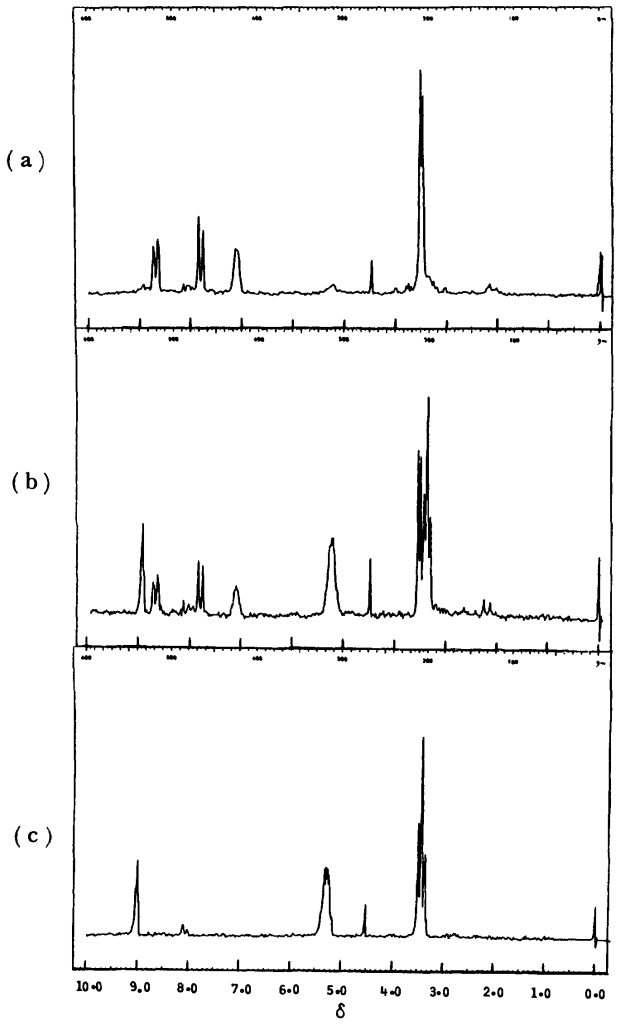

Fig. 1. ^1H NMR spectra of protonated 2-bromo-5-methylthiophene in HSO_3F at 60 MHz; (a) at −50 °C, (b) at −30 °C, and (c) at 10 °C.

Typical examples of ^1H NMR spectra are shown in Fig. 1. The protonation of 2-bromo-5-methylthiophene gave a mixture of the two cations, 5H- and 2*H*-2-bromo-5-methylthiophenium ions at −70 °C. The former ion then underwent an irreversible 2,5-hydrogen shift and changed almost completely to the latter ion at about −50 °C (Fig. 1a), as in the case of 2-chloro-5-methylthiophenium ion.[4] When the temperature was raised to about −30 °C, however, another peculiar rearrangement appeared on the ^1H NMR spectra (Fig. 1b). This rearrangement was accomplished at about 10 °C as shown in Fig. 1c, which showed the presence of only one cation, 2*H*-4-bromo-5-methylthiophenium ion.[5] Evidence of the cation was also obtained from another route. That is, the spectral data of the cation are consistent with those observed for the cation produced from the protonation of 3-bromo-2-methylthiophene in HSO_3F, which was stable and gave an almost unchanged spectrum from −70 to 10 °C. The spectral data were also different from those obtained from the protonation of 4-bromo-2-methylthiophene in HSO_3F, which was stable from −70 to 30 °C. After the ^1H NMR measurement was carried out at 10 °C (Fig. 1c), the sample solution was poured into water and an aqueous solution was extracted by diethyl ether. Then, after the solvent was distilled off, the residue was checked by ^1H NMR. ^1H NMR spectral data were consistent with those of 2-methyl-3-bromothiophene. The spectral data of the ions are given in Table 1.

Two facts must be noted. First, the rearrangement

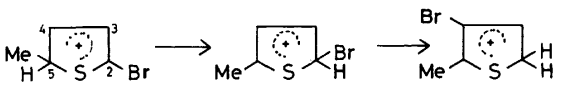

Scheme 1.

Table 1. ^1H Chemical Shifts of Protonated Bromomethylthiophenes in HSO_3F

Substituents	Temp °C	Chemical shift, ppm			
		2-H	3-H	4-H	5-H
2H, 2-Br, 5-Me	−50	7.11	8.68	7.80	(3.49)[a]
5H, 2-Br, 5-Me	−70	—	8.01	8.87	5.29 (2.11)
2H, 3-Br, 5-Me	−30	5.28	—	8.06	(3.31)
2H, 4-Br, 5-Me	−10	5.26	8.97	—	(3.40)

a) The values in parentheses are the chemical shifts of methyl protons.

proceeded with three clearly separated stages as given in Scheme 1 and only one species of the cation existed in a solution at a specific temperature (Fig. 1a or Fig. 1c). The mechanism of this novel rearrangement is not clear at present. However, this fact strongly suggests that the rearrangement involves an intramolecular process.[6] Second, the 2*H*-2-bromo-5-methylthiophenium ion does not rearrange to a more stable 2*H*-3-bromo-5-methylthiophenium ion, but to a 2*H*-4-bromo-5-methylthiophenium ion.

References

1) Y. Yokoyama, Y. Yamashita, K. Takahashi, and T. Sone, *Chem. Lett.*, **1981**, 813.

2) Y. Yokoyama, Y. Yamashita, K. Takahashi, and T. Sone, presented at the 20th Symposium on NMR Spectroscopy of the Chemical Society of Japan, Tokyo, Nov. 1981, Preprint p. 207.

3) Y. Yamashita, A. Yoshino, K. Takahashi, and T. Sone, 46th National Meeting of the Chemical Society of Japan, Niigata, Octber 1982, Abstr., No. 4P15.

4) Y. Yokoyama, Y. Yamashita, K. Takahashi, and T. Sone, *Bull. Chem. Soc. Jpn.*, **56**, 2208 (1983).

5) An unknown signal appeared at 4.5 ppm in Fig. 1, but this is not attributed in the cations in problem.

6) In the case of intermolecular proesses, which were observed in the acid-catalyzed reactions of bromothiophenes, several species of the products were obtained in the reaction mixture. For example, R. M. Kelogg, A. P. Schaap, E. T. Harper, and H. Wynberg, *J. Org. Chem.*, **33**, 2902 (1968).

Photoinduced Hydrogen Evolution with Hydrogenase Using Bipyridinium Salts as Electron Carriers

Ichiro OKURA,* Hiroki FUJIE, Shigetoshi AONO, Tatsuya KITA, and Naruhiko KAJI
Department of Chemical Engineering, Tokyo Institute of Technology, Meguro-ku, Tokyo 152
(Received July 30, 1985)

Synopsis. Photoinduced hydrogen evolution was carried out by using bipyridinium salts as electron carriers. Hydrogen evolution rate strongly depends on the type of bipyridinium salt. The order of the rate values undergoes a change by the change in the rate-determining step.

Photochemical redox systems have been proposed for solar-energy utilization.[1,2] The systems illustrated in Scheme 1, consisting of a photosensitizer (S), an electron donor (D), and an electron carrier (C), have been able to evolve hydrogen from water in the presence of hydrogenase.

The electron carrier employed almost exclusively in these studies is methylviologen, except for a few cases.[3,4] In this paper we hope to describe that some bipyridinium salts are more suitable electron carriers than methylviologen when the rate-determining step for this reaction is the photoreduction of bipyridinium salts.

Experimental

The hydrogenase from *Desulfovibrio vulgaris* (Miyazaki type) was purified according to Yagi's method.[5] The bipyridinium salts used in this experiment are listed in Fig. 1. Compounds A, B, and C were synthesized according to the literature.[6,7] The concentration of hydrogenase is not known, but it has the ability to release 19.8×10^{-6} mol of hydrogen in the following system: hydrogenase (0.5 ml)–methylviologen (1.7×10^{-4} mol dm^{-3})–$Na_2S_2O_4$ (3.8×10^{-3} mol dm^{-3}) in 6.0 ml of a 0.02 mol dm^{-3} phosphate buffer (pH 7.0) at 30 °C for 30 min. The sample solution, which consisted of zinc meso-tetraphenylporphyrintrisulfonate (Zn-TPPS$_3$), an electron carrier, 2-mercaptoethanol (RSH) as an electron donor, and hydrogenase in a phosphate buffer (pH 7.0), was deaerated by repeated freeze-pump-thaw cycles. In the photolysis with continuous irradiation, the sample in a Pyrex cell equipped with a magnetic stirrer was irradiated with light from a 200-W tungsten lamp. Light of wavelengths shorter than 390 nm was cut off by a Toshiba L-39 filter.

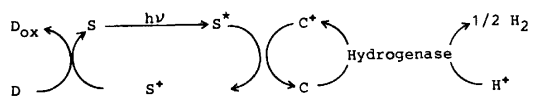

Scheme 1.

Results and Discussion

When an aqueous solution containing RSH, Zn-TPPS$_3$, bipyridinium salt, and hydrogenase was irradiated, hydrogen evolution at a stationary rate was observed, as is shown in Fig. 2. In these experiments an excess amount of hydrogenase was used to make the photoreduction of electron carriers the rate-determining step of the hydrogen evolution. It is evident that all the compounds shown in Fig. 1 can serve as electron carriers for photoinduced hydrogen evolution. The hydrogen-evolution rate of the system for the B electron carrier was much greater than that for methyl viologen. Under the reaction conditions where the rate-determing step of hydrogen evolution is the step of the photoreduction of electron carriers, the bipyridinium salts with low redox potentials will be favorably photoreduced. The order of the rate values, however, does not always coincide with the order of the redox potentials of the bipyridinium salts. The above results are not explained by the electrostatic effect. MV and B are positively charged, and A and C are neutral in the oxidized form. Positively charged bipyridinium salts do not always have high activity, as is shown in the case of MV. As we reported previously,[8] the back reaction (recombination of the oxidized Zn-TPPS$_3$ and reduced bipyridinium salt) may play a part in the photoinduced hydrogen evolution reaction in these systems.

By the increase in the Zn-TPPS$_3$ concentration, the rate-determining step of photoinduced hydrogen evolution is changed from the photoreduction of

MV: R = CH_3 (-0.44 V)

A : R = $(CH_2)_3SO_3^-$ (-0.46 V)

B : R = CH_3 (-0.72 V)

C : R = $(CH_2)_3SO_3^-$ (-0.75 V)

Fig. 1. Electron carriers. (Values in parenthese indicate the redox potentials vs. NHE).

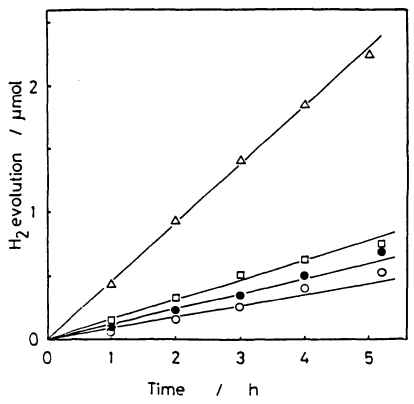

Fig. 2. Time dependence of hydrogen evolution by irradiation at 30 °C. To the solution containing RSH (2.26×10^{-1} mol dm^{-3}), Zn-TPPS$_3$ (1.00×10^{-6} mol dm^{-3}), and bipyridinum salt (8.3×10^{-5} mol dm^{-3}) 0.5 ml of hydrogenase was added and adjusted to 6.5 ml with 0.02 mol dm^{-3} phosphate buffer (pH 7.0). Bipyridinium salts are labelled in Fig. 1; ●: MV, ○: A, △: B, □: C.

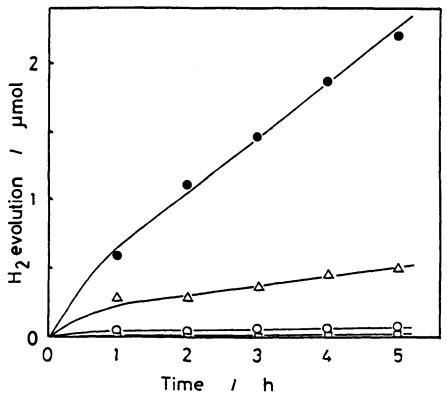

Fig. 3. Time dependence of hydrogen evolution by irradiation at 30 °C. To the solution containing RSH (2.27×10^{-1} mol dm^{-3}), Zn-TPPS$_3$ (1.00×10^{-6} mol dm^{-3}), and bipyridinium salt (8.3×10^{-5} mol dm^{-3}) 0.5 ml of hydrogenase was adjusted to 6.5 ml with 0.02 mol dm^{-3} phosphate buffer (pH 7.0). Bipyridinium salts are labelled in Fig. 1; ●: MV, ○: A, △: B, □: C.

bipyridinium salts to hydrogen evolution by reduced bipyridinium salts. Figure 3 shows the photoinduced hydrogen evolution in the region of higher concentrations of Zn-TPPS$_3$ compared with Fig. 2. In the experimental conditions of Fig. 3, it was confirmed that the rate-determining step of hydrogen evolution was the step of water reduction by reduced bipyridinium salt, for the hydrogen-evolution rate was proportional to the amount of hydrogenase used. Methylviologen shows a remarkably high activity for photoinduced hydrogen evolution. The high activity of methylviologen may be caused by the fact that methylviologen is a better substrate of the hydrogenase than are other bipyridinium salts.

From the above results, it is apparent that the photoinduced hydrogen evolution rate with the systems shown in Scheme 1 depends greatly on the type of bipyridinium salt and that the order of the rate values undergoes a change with a change in the rate-determining step.

We wish to express our appreciation to Professor Tominaga Keii and Professor Yoshio Ono for their stimulating and helpful discussions.

References

1) J. R. Darwent, P. Douglas, A. Harriman, G. Porter, and M.-C. Richoux, *Coord. Chem. Rev.*, **44**, 83 (1982), and the references cited therein.

2) J. Kiwi, K. Kalyanasundaram, and M. Gratzel, *Struct. Bonding (Berlin)*, **49**, 37 (1982), and the references cited therein.

3) O. Johansen, A. Launikonis, J. Loder, A. W. H. Mau, W. H. F. Sasse, J. P. Swift, and D. Well, *Aust. J. Chem.*, **34**, 981 (1981).

4) E. Amouyal and B. Zidler, *Isr. J. Chem.*, **22**, 117 (1982).

5) T. Yagi, *J. Biochem.*, **68**, 649 (1970).

6) K. J. Schmalzl and L. A. Summers, *Aust. J. Chem.*, **30**, 657 (1977).

7) R. F. Homer and T. E. Tolinson, *J. Chem. Soc.*, **1960**, 2498.

8) I. Okura, N. Kaji, S. Aono, T. Kita, and A. Yamada, *Inorg. Chem.*, **24**, 451 (1985).

The Crystal Structure of a Squarylium Dye, 2,4-Bis(1,3,3-trimethyl-2-indolinylidenemethyl)cyclobutenediylium-1,3-diolate

Yoshinori KOBAYASHI,* Midori GOTO, and Masayasu KURAHASHI
National Chemical Laboratory for Industry, Yatabe-machi, Ibaraki 305
(Received August 6, 1985)

Synopsis. The crystal structure of 2,4-bis(1,3,3-trimethyl-2-indolinylidenemethyl)cyclobutenediylium-1,3-diolate has been determined. The space group is $P2_1/c$, with a=9.5115(4), b=15.712(1), c=15.174(1) Å, β=96.138(5)°, and Z=4. The molecule adopts the trans conformation.

With interest increasing in squarylium dyes as materials for effective photovoltaic devices, much attention has been paid to their solid-state structure. According to Morel et al.,[1] devices with squarylium dyes containing indoline rings have an especially high short-circuit-photocurrent yield. In order to reveal the structural feature of such compounds, an X-ray determination of the title compound (Fig. 1) was performed.

Experimental

The compound was provided by Tatsuo Sekiguchi of this laboratory. Purple needle-like crystals were obtained from a 1,2-dichloroethane solution. The cell dimensions and diffraction intensities were measured on a Rigaku AFC-4 four-circle diffractometer by using graphite-monochromated Mo $K\alpha$ radiation (λ=0.71069 Å) at room temperature. 1541 independent reflections with 2θ values up to 55° ($|F_o| \geqq 3\sigma(|F_o|)$) were used for the analysis. No correction was made for absorption.

Crystal Data: $C_{28}H_{28}N_2O_2$; M=424.54; monoclinic; space group $P2_1/c$; a=9.5115(4), b=15.712(1), c=15.174(1) Å, β=96.138(5)°; D_x=1.252 g cm^{-3} for Z=4. The structure was solved by the *MULTAN* 78 program.[2] The positions of the hydrogen atoms were obtained from the difference Fourier synthesis. The structural parameters were refined by the full-matrix least-squares method, using the *UNICS* III system.[3] Anisotropic thermal parameters were assumed for the non-hydrogen atoms, and isotropic parameters, for the hydrogen atoms. The final refinement, employing the weighting scheme of $w=(0.012|F_o|^2-0.562|F_o|+7.949)^{-1}$, led to the R value of 0.077. All the computations were carried out on a FACOM M-380 computer.

Results and Discussion

An *ORTEP* diagram[4] displaying the molecular structure is shown in Fig. 2. Table 1 lists the final atomic coordinates of the non-hydrogen atoms.[5]

The central four-membered ring (I) is planar within the limit of experimental error of 0.005 Å.

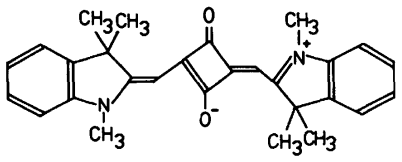

Fig. 1. One of the resonance structures of the title compound.

The indoline rings (II and III) are planar within 0.03 Å and 0.06 Å respectively. The molecule is slightly folded at the C(3) atom and is twisted along the C(16)-C(17) bond. The II and III rings make angles of 7.8° and 24.6° respectively with the I ring. The molecule is roughly planar and adopts the trans conformation.

The bond lengths of C(2)-C(3), C(3)-C(4), C(16)-C(17), and C(17)-C(18) fall in the range of those of the conjugated C-C bonds. The shorter bond lengths of N(1)-C(4) and N(2)-C(18) compared with the corresponding bonds in *N*-thioacetylindoline[6] and 3-hydroxy-2,3-diphenylindoline[7] indicate that these

Table 1. Fractional Atomic Coordinates(×10^4) and Equivalent Isotropic Thermal Parameters, with Estimated Standard Deviations in Parentheses

	x	y	z	B_{eq}/Å^2
O(1)	7177(7)	228(3)	3803(4)	5.2(2)
O(2)	8537(7)	2049(4)	6043(4)	5.2(2)
N(1)	6360(7)	3484(4)	3057(4)	4.1(2)
N(2)	9090(7)	−1276(4)	6779(4)	4.0(2)
C(1)	7537(9)	713(5)	4421(6)	4.1(2)
C(2)	7584(8)	1633(5)	4494(5)	3.7(2)
C(3)	7065(9)	2204(5)	3824(6)	3.9(3)
C(4)	6998(9)	3078(5)	3779(5)	3.8(2)
C(5)	7544(9)	3739(5)	4463(5)	3.9(2)
C(6)	7157(9)	4559(5)	3972(5)	4.1(3)
C(7)	7372(9)	5396(6)	4241(6)	4.8(3)
C(8)	6855(12)	6036(6)	3652(7)	5.7(4)
C(9)	6110(13)	5825(6)	2843(8)	5.8(4)
C(10)	5899(11)	4999(6)	2585(6)	4.7(3)
C(11)	6434(9)	4373(5)	3153(5)	3.9(3)
C(12)	5737(16)	3091(8)	2242(7)	5.2(3)
C(13)	6803(13)	3699(7)	5308(7)	4.8(3)
C(14)	9134(11)	3662(7)	4694(8)	5.3(4)
C(15)	8165(9)	1567(5)	5433(6)	4.0(2)
C(16)	8139(8)	632(5)	5361(6)	3.8(2)
C(17)	8626(10)	53(5)	6012(6)	4.1(3)
C(18)	8471(8)	−810(5)	6095(5)	3.5(2)
C(19)	7502(8)	−1408(5)	5485(5)	3.7(2)
C(20)	7584(8)	−2210(5)	6025(5)	3.4(2)
C(21)	6899(9)	−2977(5)	5884(6)	4.2(3)
C(22)	7205(11)	−3621(6)	6492(6)	4.8(3)
C(23)	8155(11)	−3527(6)	7220(7)	5.1(3)
C(24)	8863(11)	−2768(6)	7372(6)	4.6(3)
C(25)	8545(8)	−2110(5)	6770(5)	3.7(2)
C(26)	10099(14)	−939(9)	7475(8)	5.4(3)
C(27)	6028(9)	−1067(6)	5284(6)	3.9(3)
C(28)	8202(11)	−1567(6)	4621(6)	4.0(3)

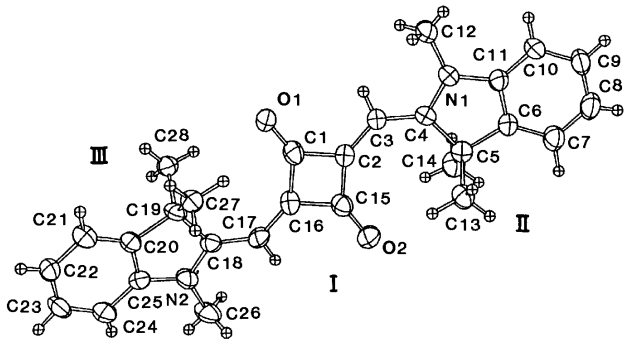

Fig. 2. Perspective view of the molecule showing the atom numbering scheme for the non-hydrogen atoms. Atoms are represented by thermal ellipsoids at 40% probability level. Hydrogen atoms are drawn at an arbitrarily small size. Selected bond lengths (l/Å) and angles (ϕ/°) are: C(2)-C(3) 1.404(12), C(3)-C(4) 1.377(12), C(16)-C(17) 1.385(12), C(17)-C(18) 1.372(12), N(1)-C(4) 1.353(11), N(2)-C(18) 1.353 (10), C(1)-C(2)-C(3) 125.1(8), C(3)-C(2)-C(15) 144.1(8), C(2)-C(4) 133.2(8), C(1)-C(16)-C(17) 143.8(8), C(15)-C(16)-C(17) 126.8(8), C(16)-C(17)-C(18) 133.1(8).

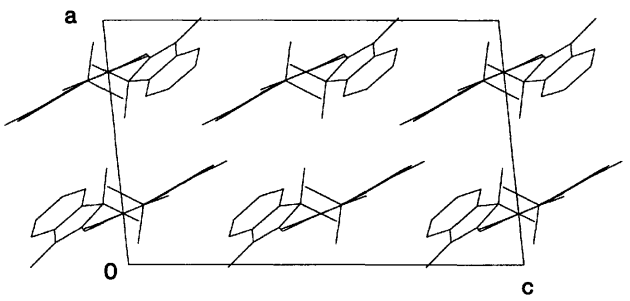

Fig. 3. Crystal structure projected along the b axis.

bonds are also involved in conjugation. The enlargement of the C(3)-C(2)-C(15), C(2)-C(3)-C(4), C(1)-C(16)-C(17), and C(16)-C(17)-C(18) angles is due to the repulsive interactions between oxygen atoms and methyl carbons, C(13), C(14), C(27), and C(28). Such interactions are suggested by the short intramolecular distances of O(1)···C(27)=3.30(1), O(1)···C(28)=3.19(1), O(2)···C(13)=3.21(1), and O(2)···C(14)=3.34(1) Å.

The crystal structure is displayed in Fig. 3. Although several short intermolecular contacts are found (O(2)···C(24)=3.27(1), C(1)···C(27)=3.51(1), and C(15)···C(28)=3.46(1) Å), the molecules are held together by van der Waals forces. The twist of the III ring from the I ring probably results from the crystal packing.

The authors would like to express their thanks to Dr. Tatsuo Sekiguchi for synthesizing the compound. They are also grateful to Drs. Yasujiro Kawabata and Kazumasa Honda for their helpful discussions.

References

1) D. L. Morel, E. L. Stogryn, A. K. Ghosh, T. Feng, P. E. Purwin, R. F. Shaw, C. Fishman, G. R. Bird, and A. P. Piechowski, *J. Phys. Chem.*, **88**, 923 (1984).

2) P. Main, S. E. Hull, L. Lessinger, G. Germain, J. P. Declercq, and M. M. Woolfson, *MULTAN* 78, "A System of Computer Programmes for the Automatic Solution of Crystal Structures from X-Ray Diffraction Data," University of York, York, England (1978).

3) T. Sakurai and K. Kobayashi, *Rep. Inst. Phys. Chem. Res.*, **55**, 69 (1978).

4) C. K. Johnson, *ORTEP* II, Report ORNL-5138, Oak Ridge National Laboratory, Tennessee, USA (1976).

5) The lists of observed and calculated structure factors, the atomic parameters for the hydrogen atoms, and the anisotropic thermal parameters for the non-hydrogen atoms are deposited at the Chemical Society of Japan as Document No. 8603.

6) H. W. Schmalle and O. Jarchow, *Acta Crystallogr., Sect. B*, **34**, 1371 (1978).

7) C. Berti, L. Greci, M. Poloni, G. D. Andreetti, G. Bocelli, and P. Sgarabotto, *J. Chem. Soc., Perkin Trans. II*, **1980**, 339.

X-Ray Structure of 5-Chloro-1-thia-5-boracyclooctane

Akio FURUSAKI,* Zhou WEIKE,† and Akira SUZUKI†
Department of Chemistry, Faculty of Science, Hokkaido University,
Kita-ku, Sapporo 060
† Department of Applied Chemistry, Faculty of Engineering, Hokkaido University,
Kita-ku, Sapporo 060
(Received September 4, 1985)

Synopsis. 5-Chloro-1-thia-5-boracyclooctane has been prepared by the hydroboration of diallyl sulfide with a chloroborane–dimethyl sulfide complex and its structure containing a sulfur–boron dative bond has been examined in detail by an X-ray crystallographic analysis.

As a part of a study on the development of useful cyclic hydroborating agents such as 9-borabicyclo-[3.3.1]nonane, 5-chloro-1-thia-5-boracyclooctane (**1**)

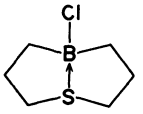

1

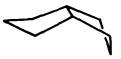

2

was synthesized. In the present paper, we wish to report on the X-ray structure determination and molecular geometry of this new heterocyclic compound.

Experimental

Preparation of 5-Chloro-1-thia-5-boracyclooctane. In a 300-ml flask cooled in a Dry Ice–acetone bath was placed a mixture of diallyl sulfide (23.0 g, 201 mmol) and pentane (100 ml). A chloroborane–dimethyl sulfide complex (200 mmol) prepared by Brown's procedure[1] was added dropwise to the vigorously-stirred solution over a period of 2 h, the temperature being kept below −20 °C. The reaction mixture was warmed to 20 °C and was stirred for another 2 h at this tempeature. After removal of the solvent, the residue was heated to 150 °C and was then distilled under reduced pressure to give 5-chloro-1-thia-5-boracyclooctane (27.56 g, 84.8% yield) as colorless crystals: Mp 50.5—51.5 °C; IR (CCl_4) 864, 1034, 1052, 1140, 1283, 1423, and 2590 cm^{-1}; ^1H NMR ($CDCl_3$) δ=1.06 (4H, t, J=7 Hz), 1.99 (4H, q, J=7 Hz), 2.59 (2H, t, J=7 Hz), and 3.02 (2H, t, J=7 Hz); MS (70 eV) m/z (%) 164 (2.85, M^+ for $BC_6H_{12}SCl^{37}$), 162 (7.65, M^+ for $BC_6H_{12}SCl^{35}$), 127 (9.85, M^+–Cl), 122 (9.94, $BC_6H_{12}SCl^{37}$-42), 120 (27.9, $BC_6H_{12}SCl^{35}$-42), and 42 (100, $CH_2CH_2CH_2$). The absence of any peak in the m/z 250—900 region indicates that this product is a monomer. Found: C, 43.70; H, 7.53; S, 19.63; Cl, 21.67%. Calcd for $BC_6H_{12}SCl$: C, 44.35; H, 7.44; S, 19.73; Cl, 21.82%.

X-Ray Measurement. A single crystal with dimensions of about 0.3×0.4×0.5 mm^3 was used. Because of the instability to air, the sample was sealed in a glass capillary tube filled with nitrogen gas. The crystallographic data were as follows: $BC_6H_{12}SCl$, mol wt 162.48, monoclinic, space group $P2_1/n$, a=11.383(7), b=11.055(5), c=6.586(5) Å, β=90.97(5)°, Z=4, D_c=1.302 g cm^{-3}, μ(Mo $K\alpha$)=6.15 cm^{-1}. The unit-cell dimensions and diffraction intensities were measured on a Rigaku four-circle diffractometer at the High-Brilliance X-Ray Laboratory of Hokkaido University, using graphite-monochromated Mo $K\alpha$ radiation. The ω—2θ scan technique was applied at an ω scan rate of 4° min^{-1}; the background was counted for 10 s at each end of the scan range. Three standard reflections, measured at intervals of every 100 reflections, showed a slight decrease in intensity with the course of data collection; the final-intensity/initial-intensity ratios were 0.93—0.94. The intensities were corrected for this damage to the sample as well as for the Lorentz and polarization factors, but not for the absorption or the extinction effect. In the range of 2θ values up to 50°, 1138 independent structure factors above the $3\sigma(F)$ level were selected for the structure determination.

Structure Determination

The structure was solved by the Monte Carlo direct method,[2] using the 10 reflections with the greatest $|E|$ values as the starting set. The fourth-generated random-phase set led to the correct solution; an E-map based on 301 phases revealed the locations of all the non-hydrogen atoms. The structure was refined by the block-diagonal least-squares method with anisotropic thermal parameters. After all the hydrogen atoms had been located in a difference Fourier map, further full-matrix least-squares refinements were performed including the hydrogen atoms with isotropic temperature factors and the anomalous dispersion effects of the chlorine and sulfur atoms. For these refinements, the following weighting scheme was used:

$$w=1/\{\sigma(F)^2\exp(c_1X^2+c_2Y^2+c_3XY+c_4X+c_5Y)\},$$

where $X=|F_o|$ and $Y=\sin\theta/\lambda$. The c_1, c_2, c_3, c_4, and

Table 1. The Final Atomic Parameters and Estimated Standard Deviations

Atom	10^4x	10^4y	10^4z	B_{eq}[a]/Å^2
S(1)	1860(1)	4775(1)	1804(1)	3.87
C(2)	3197(4)	4092(5)	856(8)	5.17
C(3)	4085(5)	4147(7)	2539(10)	7.09
C(4)	3544(4)	3767(5)	4498(8)	5.33
B(5)	2274(4)	4371(4)	4755(6)	3.51
C(6)	1192(4)	3520(4)	5302(7)	4.56
C(7)	912(5)	2759(5)	3426(8)	5.34
C(8)	764(4)	3571(5)	1639(7)	5.08
Cl	2315(1)	5843(1)	6195(2)	5.37

a) $B_{eq}=8\pi^2(u_1^2+u_2^2+u_3^2)/3$, where u_i is the root-mean-square deviation in the i-th principal axis of the thermal ellipsoid.

c_5 coefficients were evaluated from the $(\Delta F)^2$ distribution; c_1=−0.418×10^{-3}, c_2=29.8, c_3=0.241, c_4=0.388×10^{-2}, and c_5=−35.9. The final R value was 0.050. The final atomic parameters are listed in Table 1.[3]

The calculations were done on a HITAC M-280H computer at the Hokkaido University Computing Center using our own programs. The atomic scattering factors and anomalous dispersion corrections were taken from the International Tables.[4]

Results and Discussion

The obtained molecular structure is depicted in Fig. 1. The molecule has a bicyclo[3.3.0]octane skeleton where an eight-membered ring is bridged by a dative bond formed between the S(1) and B(5) atoms. As Fig. 2 shows, of the two five-membered rings, one (S(1), C(2), C(3), C(4), and B(5)) adopts an envelope conformation; the C(3) atom deviates remarkably from the C(2)–S(1)–B(5)–C(4) mean plane onto the opposite side to the C(6) and C(8) atoms. On the other hand, the remaining ring has a half-chair conformation with an approximate two-fold rotation axis through the S(1) atom; however, this conformation is not very different from the envelope one where the C(7) atom deviates from the C(8)–S(1)–B(5)–C(6) plane onto the same side as the C(2) and C(4) atoms. Accordingly, it may be said that the conformation of the present bicyclic system as a whole resembles the most stable C_s conformation of *cis*-bicyclo[3.3.0]octane (**2**).[5]

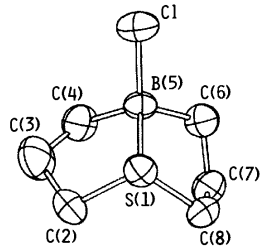

Fig. 1. A perspective view of the 5-chloro-1-thia-5-boracyclooctane molecule. Each non-hydrogen atom is represented as a thermal ellipsoid enclosing a 50% probability.

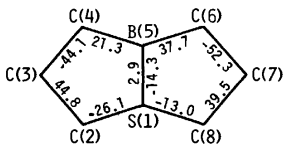

Fig. 2. The torsion angles (ϕ/°). The torsion angles relevant to atoms which form the same ring are given in the ring. The e.s.d.'s are 0.3—0.7°.

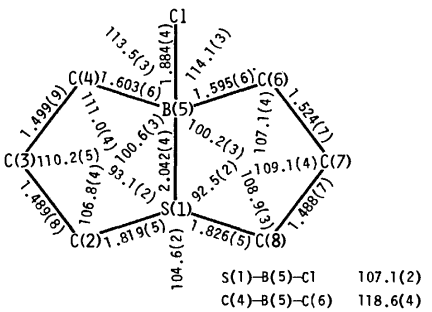

Fig. 3. The bond distances (l/Å) and angles (θ/°) and estimated standard deviations.

As Fig. 3 shows, the S(1)–B(5) bond distance is considerably longer than the S–B distances (av. 1.927 Å) in the adamantane-like compound $[CH_2(SBH_2)_2]_2$[6] in which each of the sulfur and boron atoms forms two equivalent S–B bonds. Such a long bond distance (2.04(2) Å) has already been found for the S–B dative bonds by which the two 3,4-diethyl-2,5-diiodo-1,2,5-thiadiborolene molecules form a centrosymmetric dimer.[7] The average (1.599 Å) of the B(5)–C(4) and B(5)–C(6) bond ditances lies midway between the B(sp^2)–C(sp^3) distance (1.570(4) Å) in dimethyl(methylthio)borane[8] and the B(sp^3)–C(sp^3) distance (av 1.632 Å) in lithium tetramethylborate,[9] whereas the B(5)–Cl bond distance is somewhat longer than the B(sp^3)–Cl distance (av. 1.864 Å) in boron trichloride–trimethylamine complex.[10] The S(1)–C(2) and S(1)–C(8) bond distances are almost equal to the standard S–C(sp^3) distance (1.82 Å).

References

1) H. C. Brown and N. Ravindran, *Inorg. Chem.*, **16**, 2938 (1977).
2) A. Furusaki, *Acta Crystallogr., Sect. A*, **35**, 220 (1979).
3) The tables of the anisotropic temperature factors and hydrogen parameters and the F_o—F_c table are kept at the Chemical Society of Japan (Document No. 8608).
4) "International Tables for X-Ray Crystallography," Kynoch Press, Birmingham (1974), Vol. IV.
5) N. L. Allinger, M. T. Tribble, M. A. Miller, and D. H. Wertz, *J. Am. Chem. Soc.*, **93**, 1637 (1971).
6) H. Binder, W. Diamantikos, K. Dermentzis, and H. Hausen, *Z. Naturforsch., Teil B*, **37**, 1548 (1982).
7) F. Zettler, H. Hess, W. Siebert, and R. Full, *Z. Anorg. Allg. Chem.*, **420**, 285 (1976).
8) K. Brendhaugen, E. W. Nilssen, and H. M. Seip, *Acta Chem. Scand.*, **27**, 2965 (1973).
9) W. E. Rhine, G. Stucky, and S. W. Peterson, *J. Am. Chem. Soc.*, **97**, 6401 (1975).
10) P. H. Clippard, J. C. Hanson, and R. C. Taylor, *J. Cryst. Mol. Struct.*, **1**, 363 (1971).

Synthesis and Complexing Ability of New Type of Macrobicyclic Compounds

Yohji NAKATSUJI, Takashi KIKUI, Isao IKEDA, and Mitsuo OKAHARA*
Department of Applied Chemistry, Faculty of Engineering, Osaka University,
Yamada-oka, Suita, Osaka 565
(Received July 2, 1985)

Synopsis. New types of macrobicyclic compounds were synthesized from monoaza crown ethers bearing two hydroxyl groups and their complexing abilities regarding alkali metal cations were investigated.

Lipophilic monoaza crown ethers are good synthetic ionophores for the active transport of cations since they have a basic nitrogen atom as a constituent of the ring.[1] In order to improve selectivity toward a specific cation, it is necessary to design the structure of ionophores. From this viewpoint, we are reporting on the syntheses of new monoaza cryptands.[2,3]

Monoaza crown ethers (**1**)[4] bearing two hydroxyl groups, which were prepared by reactions between oligoethylene glycol diglycidyl ether and ammonia (or an appropriate primary amine), were treated with tri- or tetraethylene glycol ditosylate (**2**) in the presence of *t*-BuONa to give cryptands (**3**), generally as pale-yellow oils in fair yields (Scheme). As another route to lipophilic cryptands, *N*-unsubstituted derivatives **3a** (m=1, n=2) and **3b** (m=n=2) were easily alkylated by 1-bromodecane to afford **3h** and **3d**, respectively.

It is noteworthy that the new "Shell-shaped" cryptands **3** showed fairly good complexing abilities and selectivities in comparison with the starting crowns **1**. Derivatives with 15—17 (**3d** and **3g**) and 18—17 (**3e**) membered rings possessed selectivities

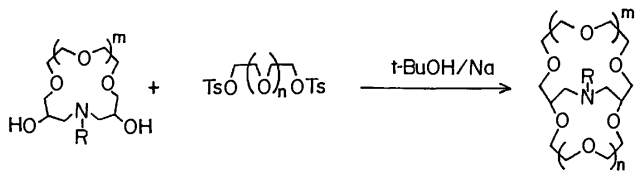

1 **2** **3**

Scheme 1.

regarding Na^+ and K^+, respectively (Table 1). A comparison of the stability constants of **3g** with those of **3d** seems to show a contribution of the electron-donating side arm to complexation.[5] Although these compounds were mixtures of stereoisomers and their separations have, so far, not been successful, the ease of preparation should be useful when they are practically used as complexing agents or carriers for a variety of cations.

Experimental

The ^{1}H-NMR spectra were taken at 100 MHz on a JEOL JNM-PS-100 spectrometer using tetramethylsilane as the internal standard. The infrared spectra were obtained on a Hitachi 260-10 spectrometer. The mass spectra were measured with a Hitachi RMU-6E mass spectrometer at an ionization potential of 70 eV.

2,5,8,11,14,17,20-Heptaoxa-23-azabicyclo[10.9.3]-tetracosane (3a): To a solution of sodium *t*-butoxide (Na: 1.0 g, 0.0435 mol) in *t*-butyl alcohol (160 ml), 1,4,7-trioxa-11-azacyclotetradecane-9,13-diol[4] (**1a**) (R=H, m=1, 4.71 g, 0.02 mol) was added and the mixture was then refluxed for 1 h. Triethylene glycol ditosylate (**2b**) (n=2, 9.17 g, 0.02 mol) in dioxane (40 ml) was added dropwise to the resulting mixture at 40 °C over a 2-h period and the mixture was further stirred for another 12 h. Insoluble matter was removed by filtration and the solvent was evaporated. The crude product was distilled in a Kugelrohr apparatus under reduced pressure (150—155 °C/0.01 Torr: 1 Torr=133.3 Pa) to give **3a** as a pale-yellow oil (2.61 g, 37%); ^{1}H-NMR ($CDCl_3$) δ=2.19 (s, 1H), 2.6—3.3 (m, 4H), 3.3—4.0 (m, 26H); MS, m/z (rel intensity) 349 (M^+, 10), 320 (9), 244 (20), 218 (20), 118 (36), 87 (58), 45 (100); IR (neat) 3320, 2855, 1455, 1350, 1245, 1100 cm^{-1}.

Found: C, 55.04; H, 9.07; N. 3.94. Calcd for $C_{16}H_{31}NO_7$: C, 55.00; H, 8.94; N, 4.01.

3,6,9,12,15,18,21,24-Octaoxa-26-azabicyclo[12.10.3]-heptacosane (3b): Bp 165—170 °C/0.006 Torr (Kugelrohr); ^{1}H-NMR ($CDCl_3$) δ=2.3—3.2 (m, 6H), 3.3—4.1 (m, 29H); MS, m/z (rel intensity) 393 (M^+, 8), 364 (7), 288 (13), 202 (15), 88 (39), 45 (100); IR (neat) 3320, 2875, 1460, 1355, 1255,

Table 1. Complexing Ability of Macrobicyclic Compounds

	Macrobicyclic Compound R	m	n	ring size	log K'[6,a] Na^+	log K'[6,a] K^+	Extraction Data[7,b] Li^+	Na^+	K^+	Rb^+	Cs^+
3d	n-$C_{10}H_{21}$	2	2	(15—17)	2.57	2.44	13	25	13	7	7
3e	n-$C_{10}H_{21}$	2	3	(18—17)	2.84	3.66	6	19	45	29	24
3f	n-$C_4H_9(OCH_2CH_2)_2$	1	2	(15—14)	3.33	2.98	27	38	18	8	8
3g	n-$C_4H_9(OCH_2CH_2)_2$	2	2	(15—17)	3.40	3.14	27	45	29	15	12
(1b)	n-$C_4H_9(OCH_2CH_2)_2$	1	—	(14)	1.26	<1	2	0	1	0	3
(1e)	n-$C_{10}H_{21}$	2	—	(17)	1.34	1.91	10	7	9	6	9

a) In MeOH, at 25 °C. b) Picrate, CH_2Cl_2/H_2O, 22 °C.

1155 cm^{-1}.

Found: C, 54.69; H, 9.10; N, 3.50. Calcd for $C_{18}H_{35}NO_8$: C, 54.94; H, 8.97; N, 3.56.

26-Ethyl-3,6,9,12,15,18,21,24-octaoxa-26-azabicyclo-[12.10.3]-heptacosane (3c): Bp 160—165 °C/0.004 Torr (Kugelrohr); ^{1}H-NMR ($CDCl_3$) δ=0.98+1.02 (t+t, 3H), 2.3—2.8 (m, 6H), 3.3—4.1 (m, 30H); MS, *m/z* (rel intensity) 421 (M^+, 5), 232 (40), 216 (36), 72 (100), 58 (54); IR (neat) 2880, 1455, 1355, 1255, 1125 cm^{-1}.

Found: C, 56.95; H, 9.48; N, 3.39. Calcd for $C_{20}H_{39}NO_8$: C, 56.99; H, 9.33; N, 3.32.

26-Decyl-3,6,9,12,15,18,21,24-octaoxa-26-azabicyclo-[12.10.3]-heptacosane (3d): Bp 175—180 °C/0.005 Torr (Kugelrohr); ^{1}H-NMR ($CDCl_3$) δ=0.87 (t, 3H), 1.0—1.6 (m, 16H), 2.1—3.1 (m, 6H), 3.4—4.1 (m, 30H), MS, *m/z* (rel intensity) 533 (M^+, 11), 406 (100), 376 (25), 344 (16), 328 (19), 184 (35), 170 (28), 144 (26); IR (neat) 2925, 2810, 1465, 1350, 1250, 1115 cm^{-1}.

Found: C, 62.67; H, 10.73; N, 2.69. Calcd for $C_{28}H_{55}NO_8$: C, 63.01; H, 10.39; N, 2.62.

29-Decyl-2,5,8,11,14,17,20,23,26-nonaoxa-29-azabicyclo-[13.12.3]triacontane (3e): Bp 185—190 °C/0.002 Torr (Kugelrohr); ^{1}H-NMR ($CDCl_3$) δ=0.87 (t, 3H), 1.0—1.6 (m, 16H), 2.3—3.1 (m, 6H), 3.2—4.1 (m, 34H); MS, *m/z* (rel intensity) 576 (M^+—1, 7), 450 (100), 420 (17), 328 (16), 184 (31), 170 (21), 144 (21); IR (neat) 2910, 2855, 1470, 1350, 1250, 1120 cm^{-1}.

Found: C, 62.08; H, 10.38; N, 2.49. Calcd for $C_{30}H_{59}NO_9$: C, 62.36; H, 10.29; N, 2.42.

23-[2-(2-Butoxyethoxy)ethyl]-2,5,8,11,14,17,20-heptaoxa-23-azabicyclo[10.9.3]tetracosane (3f): Bp 165—170 °C/0.005 Torr (Kugelrohr); ^{1}H-NMR ($CDCl_3$) δ=0.90 (t, 3H), 1.2—1.8 (m, 4H), 2.6—3.1 (m, 6H), 3.4—4.1 (m, 34H); MS, *m/z* (rel intensity) 493 (M^+, 1), 450 (100), 332 (21), 248 (23), 230 (16), 188 (19); IR (neat) 2880, 1465, 1355, 1255, 1120 cm^{-1}.

Found: C, 58.38; H, 9.81; N, 3.23. Calcd for $C_{24}H_{47}NO_9$: C, 58.39; H, 9.60; N, 2.84.

26-[2-(2-Butoxyethoxy)ethyl]-3,6,9,12,15,18,21,24-octaoxa-26-azabicyclo[12.10.3]heptacosane (3g): Bp 175—180 °C/0.005 Torr; ^{1}H-NMR ($CDCl_3$) δ=0.89 (t, 3H), 1.1—1.7 (m, 4H), 2.5—3.1 (m, 6H), 3.4—4.1 (m, 38H); MS, *m/z* (rel intensity) 536 (M^+—1, 1), 406 (100), 376 (11), 349 (8), 274 (18), 188 (17); IR (neat) 2880, 1460, 1350, 1255, 1120 cm^{-1}.

Found: C, 57.82; H, 9.68; N, 2.64. Calcd for $C_{26}H_{51}NO_{10}$: C, 58.08; H, 9.56; N, 2.61.

Alkylation of Unsubstituted Cryptands (3a and 3b): A mixture of cryptand **3b** (1.0 g, 0.0025 mol), 1-bromodecane (0.60 g, 0.0027 mol), and powdered sodium carbonate (0.20 g, 0.0019 mol) in dioxane (10 ml) was stirred for 12 h at 80 °C. Insoluble matter was removed by filtration and the solvent was concentrated. The residue was dissolved in hexane (50 ml). The hexane-soluble part was concentrated and distilled in a Kugelrohr apparatus (175—180 °C/0.005 Torr) to give **3d** in 63% yield. All analytical data regarding this compound were coincident with those described above. Compound **3h** was prepared by a reaction of **3a** with 1-bromodecane using the same procedure with a 64% yield; bp 160—165 °C/0.003 Torr (Kugelrohr); ^{1}H-NMR ($CDCl_3$) δ=0.87 (t, 3H), 1.1—1.5 (m, 16H), 2.1—3.1 (m, 6H), 3.4—4.3 (m, 26H) MS, *m/z* (rel intensity) 489 (M^+, 14), 362 (100), 248 (30), 184 (36), 170 (34), 100 (95), 45 (73); IR (neat) 2915, 2850, 1465, 1350, 1250, 1120 cm^{-1}.

Found: C, 63.47; H, 10.54; N, 2.84. Calcd for $C_{26}H_{51}NO_7$: C, 63.77; H, 10.50; N, 2.86.

References

1) K. Matsushima, H. Kobayashi, Y. Nakatsuji, and M. Okahara, *Chem. Lett.*, **1983**, 701.

2) C. G. Krespan, *J. Org. Chem.*, **45**, 1177 (1980).

3) B. Son, B. P. Czech, and R. A. Bartsch, *Tetrahedron Lett.*, **26**, 1787 (1985).

4) T. Kikui, H. Maeda, Y. Nakatsuji, and M. Okahara, *Synthesis*, **1984**, 74.

5) A. Masuyama, Y. Nakatsuji, I. Ikeda, and M. Okahara, *Tetrahedron Lett.*, **22**, 4665 (1981).

6) H. K. Frensdorff, *J. Am. Chem. Soc.*, **93**, 600 (1971).

7) C. J. Pedersen, *Fed. Proc., Fed. Am. Soc. Exp. Biol.*, **27**, 1305 (1968).

A Positive Halogen Mediated Ring-Opening Reaction of 2-(α-Phenylthiobenzyl)cycloalkanol Derivatives

Masateru YASUMURA,* Ken TAKAKI, Takao TAMURA, and Kenji NEGORO
Department of Applied Chemistry, Faculty of Engineering, Hiroshima University,
Saijo, Higashi-Hiroshima 724
(Received July 4, 1985)

Synopsis. A new ring-opening reaction of the title cycloalkanols (**1** and **3**) takes place upon treatment with *N*-chloro-succinimide and triethylamine to give ω-oxo α,β-unsaturated sulfides (**2**) in fairly good yields.

Halosulfonium salts are useful synthetic intermediates and have been used in alcohol oxidation,[1] alkaloid synthesis,[2] and many other reactions. However, in spite of their fascinating properties, sulfide derivatives, having internal nucleophiles such as hydroxyl and amino groups, have rarely been employed as substrates for halosulfonium chemistry.[3] Therefore, we undertook to study a reaction of 2-(α-phenylthiobenzyl)cycloalkanol derivatives (**1** and **3**) with a positive halogen with the hope that the internal hydroxyl group would participate in the halosulfonium center and control the reaction course and stereochemistry of the reaction. In this note we wish to describe an interesting ring-opening reaction of the cycloalkanols (**1** and **3**) with *N*-chloro-succinimide.

trans-2-(α-Phenylthiobenzyl)cyclohexanol (**1c**), a 2:1 mixture of threo and erythro isomers, was allowed to react with *N*-chlorosuccinimide (NCS), followed by treatment with triethylamine to give 7-phenyl-7-phenylthio-6-heptenal (**2c**). The product was labile but isolated rapidly by MPLC in 75% yield as a mixture of (*E*)- and (*Z*)-isomers (2:1). The structure of **2c** was determined by spectral data and by a comparison with an authentic sample. The results are summarized in Table 1. Similarly, aldehydes (**2a** and **2e**) were obtained in 10 and 64% yields, respectively. The ring-opening reaction of the tertiary substrates (**1b**, **1d**, and **1f**) took place to afford ketones (**2b**, **2d**, and **2f**). In every case, the (*E*)-isomers were the major products from the *trans*-cycloalkanols (**1**) as shown in the Table 1. On the other hand, *cis*-2-(α-phenylthiobenzyl)cyclopentanol (**3a**) (threo:erythro, 1:1) and *cis*-1-methyl-2-(α-phenylthiobenzyl)cyclohexanol (**3d**) (threo:erythro, 1:3), were also converted to ω-oxo α,β-unsaturated sulfides (**2a** and **2d**) in 60 and 68% yields, respectively. Interestingly, the stereochemistry of the products was just reversed (*E*:*Z*=1:3 in both cases). Although the stereoselectivity of the present reaction is low, these results suggest that *trans*-cycloalkanols (**1**) are changed mainly to (*E*)-isomers and *cis* derivatives (**3**) mainly to (*Z*)-isomers.

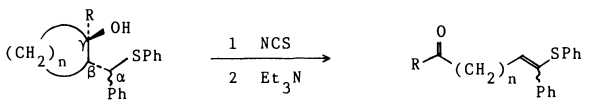

1 **2**

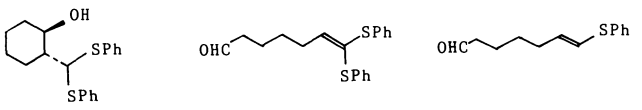

4 **5** **6**

Semmelhack has reported a Grob-type ring-opening reaction of *trans*-2[bis(phenylthio)methyl]-cyclohexanol derivatives by a metal catalyst to give ω-oxo α,β-unsaturated sulfides.[4] This result prompted us to carry out a reaction of bis(phenylthio)-compound (**4**) with NCS and triethylamine. The reaction gave the ketene thioacetal (**5**), in contrast to

Table 1. Synthesis of ω-oxo α,β-Unsaturated Sulfides (**2**) from 2-(α-Phenylthiobenzyl)cycloalkanol Derivatives (**1**)

n	R	Substrate	Ratio of threo/erythro[a]	Product	Yield[b] %	Ratio of *E*/*Z*[c]
3	H	**1a**	3 : 2	**2a**	10	3 : 1
3	Me	**1b**	2 : 1	**2b**	36	2 : 1
4	H	**1c**	2 : 1	**2c**	76	7 : 3
4	Me	**1d**	1 : 1	**2d**	67	3 : 1
5	H	**1e**	1 : 1	**2e**	64	3 : 2
5	Me	**1f**	3 : 2	**2f**	63	3 : 2

a) Threo and erythro indicate a stereochemical relation between C_α and C_β of **1**. b) Isolated yield. c) Stereochemistry of **2** which was determined on the basis of δ value of vinyl proton (^{1}H NMR) as previously described.[10]

the metal-catalyzed reaction in which the α,β-unsaturated sulfide (**6**) was obtained. However, the yield was low (14%, isolated), presumably due to the decomposition of the product during workup.[5]

The ring-opening reaction mediated by NCS could be explained as follows. Cycloalkanols (**1**, **3**, and **4**) are converted to five-membered oxasulfonium salts (**7**) by a reaction with NCS,[6] which undergo a cycloelimination reaction induced by α-proton abstraction[7] to give ω-oxo α,β-unsaturated sulfides (**2**) or ketene thioacetal (**5**).

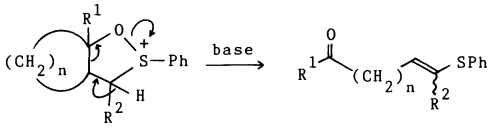

7

2 (R^2=Ph)
5 (R^2=SPh)

Experimental

General. *IR spectra were recorded with a Hitachi* 215 using liquid films. ^{1}H NMR spectra were obtained on a JEOL PMX-60 for a solution in $CDCl_3$ with Me_4Si as the internal standard. Mass spectra were taken with a Hitachi RMU-6D at 70 eV. Microanalyses were determined on a Yanagimoto CHN-Corder.

Material. *trans*-2-(α-Phenylthiobenzyl)cycloalkanols (**1a—f**) were prepared from the corresponding cycloalkene oxides and α-lithiobenzyl phenyl sulfide[8] (≈80%). *cis*-Cycloalkanols (**3a** and **3d**) were obtained by a base-catalyzed thiophenol addition to the corresponding 2-benzylidenecycloalkanones, followed by the reaction with $NaBH_4$ or MeMgI and separation from the trans isomer in 43 and 13% yields, respectively. *trans*-2-[Bis(phenylthio)methyl]cyclohexanol (**4**) was prepared by the reaction of cyclohexene oxide with bis(phenylthio)methyllithium in 80% yield.[8]

General Procedure for the Ring Opening Reaction of 1, 3, and 4. To a stirred solution of NCS (10 mmol) in dry dichloromethane (20 ml) was added an equimolar amount of the hydroxyl sulfide (**1**, **3**, or **4**) under N_2 with cooling (−40 °C). After 3 h, triethylamine (15 mmol) in dichloromethane (5 ml) was added dropwise and allowed to react at room temperature for 3 h. The reaction mixture was quenched with brine (10 ml), extracted with ether, and dried over anhydrous magnesium sulfate. The extract was concentrated in vacuo to give a crude product (**2** or **5**), which was purified by a MPLC (SiO_2, benzene–ethyl acetate 10:1 v/v as an eluent). Several data for the purified ring-opening products, ω-oxo, α,β-unsaturated sulfides (**2a—f**) and ketene thioacetal (**5**), are shown below.

2a: IR 1730 cm^{-1}; ^{1}H NMR δ=1.42—2.87 (m, 6H), 5.93 (t, *J*=7 Hz, 0.75 H), 6.33 (t, *J*=7 Hz, 0.25 H), 6.82—7.65 (m, 10H), 9.45—9.78 (m, 1H); MS, *m/z* 282 (M$^+$). Found: C, 76.38; H, 6.32%. Calcd for $C_{18}H_{18}OS$: C, 76.56; H, 6.42%.

2b: IR 1720 cm^{-1}; ^{1}H NMR δ=1.08—2.61 (m, 9H, at δ=2.01 acetyl methyl), 6.30 (t, *J*=7 Hz, 0.67 H), 6.78 (t, *J*=5 Hz, 0.33H), 6.42—7.72 (m, 10H); MS, *m/z* 296 (M$^+$). Found: C, 76.54; H, 6.77%. Calcd for $C_{19}H_{20}OS$: C, 76.99; H, 6.80%.

2c: IR 1730 cm^{-1}; ^{1}H NMR δ=1.17—1.90 (m, 4H), 2.83—3.40 (m, 4H), 6.02 (t, *J*=7 Hz, 0.7H), 6.35 (t, *J*=7 Hz, 0.3H), 6.77—7.42 (m, 10H), 9.53—9.77 (m, 1H); MS, *m/z* 296 (M$^+$). Found: C, 76.70; H, 6.80%. Calcd for $C_{19}H_{20}OS$: C, 76.99; H, 6.80%.

2d: IR 1715 cm^{-1}; ^{1}H NMR δ=1.27—2.80 (m, 11H, at δ=2.07 acetyl methyl), 6.03 (t, *J*=7 Hz, 0.75H), 6.35 (t, *J*=7 Hz, 0.25H), 7.00—7.42 (m, 10H); MS, *m/z* 310 (M$^+$). Found: C, 77.17; H, 7.11%. Calcd for $C_{20}H_{22}OS$: C, 77.38; H, 7.14%.

2e: IR 1730 cm^{-1}; ^{1}H NMR δ=1.12—1.92 (m, 6H), 1.92—2.78 (m, 4H), 6.05 (t, *J*=7.5 Hz, 0.6H), 6.35 (t, *J*=7.5 Hz, 0.4H), 6.92—7.40 (m, 10H), 9.55—9.75 (m, 1H); MS, *m/z* 310 (M$^+$). Found: C, 77.38; H, 7.13%. Calcd for $C_{20}H_{22}OS$: C, 77.38; H, 7.14%.

2f: IR 1715 cm^{-1}; ^{1}H NMR δ=0.86—2.73 (m, 13H, at δ=2.07 acetyl methyl), 6.06 (t, *J*=7 Hz, 0.6H), 6.36 (t, *J*=7 Hz, 0.4H), 6.73—7.66 (m, 10H); MS, *m/z* 324 (M$^+$). Found: C, 77.70; H, 7.42%. Calcd for $C_{21}H_{24}OS$: C, 77.73; H, 7.45%.

5: IR 1720 cm^{-1}; ^{1}H NMR δ=1.35—1.81 (m, 4H), 2.20—2.64 (m, 4H), 6.23 (t, *J*=7.4 Hz, 1H), 7.07—7.40 (m, 10H), 9.62 (t, *J*=1.5 Hz, 1H); MS, *m/z* 328 (M$^+$), Found: C, 69.29; H, 6.14%. Calcd for $C_{19}H_{20}OS_2$: C, 69.47; H, 6.14%.

Preparation of Authentic Samples 2c and 5. An authentic sample of **2c** was synthesized by the Peterson olefination of aldehydic acid ester ($EtO_2C(CH_2)_4CHO$) with α-phenylthio-α-(trimethylsilyl)toluene ($PhSCH(SiMe_3)Ph$)[9] and butyllithium (30%), followed by reduction ($LiAlH_4$) (80%) and PCC oxidation (80%): (Z)-**2c** (δ=6.35) predominated over *E*-isomer (δ=6.02) (9:1). Similar sequence using $(PhS)_2CHSiMe_3$[11] gave an authentic sample of **5** (δ=6.23) in 23% yield.

References

1) E. J. Corey and C. U. Kim, *J. Am. Chem. Soc.*, **94**, 7586 (1972); *J. Org. Chem.*, **38**, 1233 (1973); *Tetrahedron Lett.*, **1974**, 287.

2) P. G. Gassman, J. J. Roos, and S. J. Lee, *J. Org. Chem.*, **49**, 717 (1984).

3) Y. Ueno, T. Miyano, and M. Okawara, *Bull. Chem. Soc., Jpn.*, **53**, 3615 (1980).

4) M. F. Semmelhack and J. C. Tomesch, *J. Org. Chem.*, **42**, 2657 (1977).

5) The ketene thioacetal product (**5**) was more unstable than the vinyl sulfides (**2**) to give, along with **5**, unidentified compounds upon chromatography.

6) E. Vilsmaier and W. Sprugel, *Justus Liebigs Ann. Chem.*, **747**, 151 (1971).

7) M. G. Pattett and A. B. Holmes, *J. Chem. Soc., Perkin Trans. 1*, **1983**, 1243.

8) J. G. Smith, *Synthesis*, **1984**, 629.

9) D. J. Ager, *J. Chem. Soc., Perkin Trans. 1*, **1983**, 1131.

10) M. Mikolajczyk, S. Grzejzczak, A. Chefczynska, and A. Zatorski, *J. Org. Chem.*, **44**, 2967 (1979).

11) D. Seebach, M. Kolb, and B. T. Grobel, *Chem. Ber.*, **106**, 2277 (1973); D. J. Ager, *J. Org. Chem.*, **49**, 168 (1984).

Thermal Dimerization of 10-Methyleneanthrone

Kiyoichi HIRAKAWA,* Eriko OGIUE, Jiro MOTOYOSHIYA, and Toshio KAKURAI
Department of Chemistry, Faculty of Textile Science and Technology, Shinshu University, Ueda, Nagano 386
(Received July 15, 1985)

Synopsis. The thermal reaction of the title compound (**1**) gave three dimeric products which were formed via a path involving two competitive reactions, Diels-Alder and radical dimerization.

10-Methyleneanthrone (**1**) is a certain member of a class of compounds which are called "quinone methides." This system is, as a rule, unstable and is subject to reactions which form dimers, trimers, and polymers, because of the possibility that the aromatization of the cyclohexadienone portion of the molecule might supply a strong driving force for reactions.[1] However, **1** is stable and shows no tendency toward spontaneous aromatization under ordinary conditions. Such a low probability of the central ring's becoming aromatic makes its quinone methide character weak. For that reason, its chemistry has received much attention. It has been known that the base-[2] and phosphite-induced,[3,4] autoxidative,[3,5] and ketone-sensitized photochemical reactions[6] of **1** give Diels-Alder dimeric products, a dimeric peroxide, and a reductive dimeric product, respectively. Also, we previously reported that the acid-induced reaction of **1** leads to a dimeric dispiro compound, which thermally rearranged with a synchronous ring expansion.[7,8] We investigated the previously unnoticed thermal reaction of **1** and found that it undergoes thermal dimerization.

Heating compound **1** without solvent at 150 °C led to dimeric products, spiro[anthrone-10,3′(2′*H*)-benz[*de*]anthrone] (**2**), 10,10′-(1,2-ethanediyl)bisanthrone (**3**), and 10,10′-(1,2-ethanediylidene)bisanthrone (**4**) in 27, 12, and 4% yields, respectively. In a similar treatment at 180 °C, red and violet products (formulas $C_{46}H_{26}O_3$ and $C_{62}H_{34}O_4$) were obtained bisides the dimeric products, but have not yet been identified. Compounds **2** and **4** were identified by a comparison with authentic samples.[6,7] **3** was isolated as the keto rather than the enol-tautomer, the structure of which was confirmed by comparison with a sample prepared independently by the acid-induced hydrolysis of 10,10′-(1,2-ethanediyl)bis[9-anthracenol] diacetate, the reductive acetylation product of **1** with zinc and acetic anhydride. The IR spectrum of **3** indicates absorption for the carbonyl group (1665 cm^{-1}) and no hydroxy function. Its ^1H NMR spectrum reveals a triplet of H-10 and −10′ (δ 1.48). A heat treatment of **1** in refluxing xylene gave only **2**; **1** in refluxing *o*-dichlorobenzene yielded **2** along with minor products **3** and **4**. Anthraquinone was isolated in all runs and resulted from the autoxidation of **1**.

A conceivable mechanism for the thermal reaction of **1** is shown in the scheme. There would be two

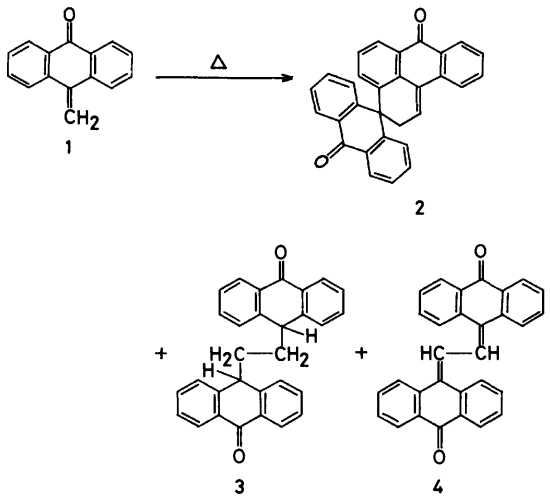

competing reactions in which **1** could be consumed. One is a Diels-Alder dimerization in which **1** behaves both as a dienophile and as a diene, followed by an isomerization to **5**. Compound **5** is unstable and leads to **2** by autoxidation.[7] The other is dimerization involving the formation of biradical **7** whose disproportionation leads to **8** and **4**. Compound **8** isomerizes to a more stable keto-tautomer **3**.[9] The Diels-Alder dimerization was predominant to the radical one. The former path is supported by the following facts. The reaction of **1** in a low-boiling-point solvent such as xylene gave only **2** and in acetic anhydride afforded only **6**, acetate of **5**. Thus, at a reaction temperature below

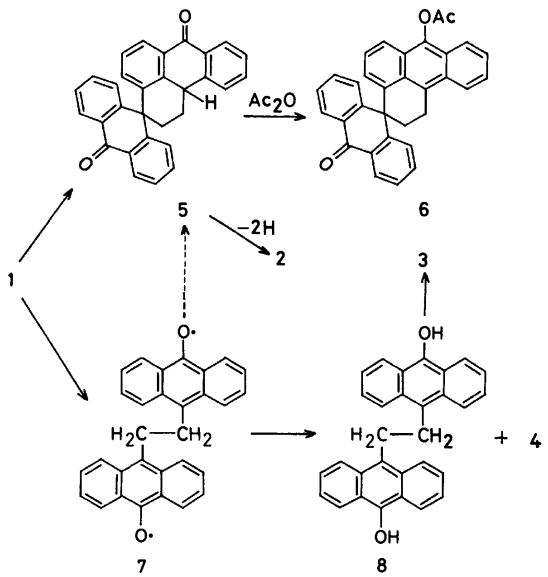

ca. 140 °C, **1** undergoes the Diels-Alder dimerization (exclusively). No ESR signal was detected in the reaction mixture of **1** while refluxing xylene and acetic anhydride under nitrogen. Also, **3** was not detected in any reaction products at 140 °C even in a solvent labile on hydrogen abstraction, such as decalin. Therefore, it seems unlikely that the formation of **2** involves an alternative path via the intramolecular cyclization of **7** to **5**. The latter would readily be rationalized both by the formation of **3** and **4** and by the concomitant appearance of a multiline ESR signal which might be attributable to **7** in the thermal reaction of **1** without solvent under nitrogen.

10-Methyleneanthrone (**1**) behaves as a quinone methide as well as an olefin (diene or dienophile). Such a fact shows the comparative isolation of the ethylenic bond from the carbonyl group in the molecule.

Experimental

Thermal Reaction of 10-Methyleneanthrone (1). (a) Without solvent. Finely ground **1**[3] (2.06 g,10 mmol) was heated at its melting point (148 °C) in a sealed test tube for 15 min. The reaction mixture was chromatographed on silica with benzene and then with chloroform. The first fraction (benzene) contained anthraquinone (0.04 g, 2%). The second (benzene) consisted of spiro[anthrone-10,3′(2′*H*)-benz[*de*]anthrone] (**2**) (0.55 g, 27%), light yellow microcrystals (from benzene-hexane), mp 298—300 °C, identical with an authentic specimen.[7] The third (benzene) afforded 10,10′-(1,2-ethanediyl)bisanthrone (**3**) (0.24 g, 12%), colorless microcrystals (from chloroform-hexane), mp 249—251 °C (lit,[6] 245—246 °C), identical with an authentic specimen prepared independently by the method described below. The fourth eluate (chloroform) gave 10,10′-(1,2-ethanediylidene)bisanthrone (**4**) (0.08 g, 4%), orange-red microcrystals (from chloroform), mp 290—292 °C, identical with an authentic specimen.[10]

(b) In an inert solvent. A solution of **1** (1.03 g, 5 mmol) in xylene, *o*-dichlorobenzene, or decalin (30 ml) was heated under nitrogen for 30 h. The solvent was distilled off under reduced pressure, and the residue was chromatographed on silica. The results of analyses of the isolated products are as follows. The product mixture from the reaction of **1** in xylene (bp of the solution: 141 °C) gave **1** (70%) and **2** (7%). *o*-Dichlorobenzene (at 181 °C): **1** (42%), **2** (10%), **3** (1%), and **4** (trace). Decalin (at 140 °C): **1** (68%) and **2** (6%). Decalin (at 191 °C): **1** (47%), **2** (9%), **3** (1%), and **4** (trace).

(c) In acetic anhydride. A solution of **1** (1.03 g, 5 mmol) in acetic anhydride (30 ml) was heated under reflux for 1 d (bp of the solution: 139 °C). After cooling, the resulting mixture was poured into water. The crystals were collected, washed with water, and chromatographed (benzene as eluant). The first fraction gave unchanged **1** (0.85 g, 82%), and the second afforded 7′-acetoxy-1′,2′-dihydrospiro[anthrone-10,3′-[3*H*]benz[*de*]anthracene] (**6**) (0.11 g, 11%) as yellow microcrystals, mp 282—283 °C, identical with an authentic specimen.[7]

Preparation of 3. A mixture of **1** (2.06 g, 10 mmol) and zinc dust (6 g) in acetic anhydride (40 ml) was stirred and heated under reflux for 5 h. The hot mixture was filtered, and the filtrate was poured into water; the precipitate was chromatographed on silica (benzene as eluant). The first eluate afforded 9-acetoxy-10-methylanthracene (0.03 g, 1%) as light yellow needles, mp 167—169 °C (lit, 167 °C), identical with an authentic specimen.[11] The second gave 10,10′-(1,2-ethanediyl)bis[9-anthracenol] diacetate (2.17 g, 87%), light yellow needles, mp 300—302 °C (lit,[6] 295—297 °C).

A solution of the diacetate (**1**.00 g, 2 mmol) in sulfuric acid (20 ml) was allowed to stand at room temperature for 30 min. The mixture was poured into ice water (200 g), and the precipitate was collected and washed with water. Recrystallization from chloroform-hexane gave **3** (0.67 g, 81%) as colorless microcrystals, mp 261—262 °C. Its spectral data were identical to those of a specimen of **3** obtained from the ketone-sensitized photochemical dimerization of **1**.[6]

Referencens

1) H.-U. Wagner, "The Chemistry of the Quinonoid Compounds," ed by S. Patai, Wiley-Interscience, New York (1973), Chap. 8; P. Gruenanger, "Methoden der Organichen Chemie (Huoben-Weyl)," ed by E. Mueller, Georg Thieme Verlag, Stuttgart (1979), Vol 7/3b, p. 395; O. Bayer, ibid., Vol 7/3c, p. 294.

2) A. N. Al-Kafaji, Ph. D. Thesis, University of Texas, Austin, Texas (1966).

3) W. H. Starnes, Jr., *J. Org. Chem.*, **35**, 1974 (1970).

4) M. M. Sidky, M. R. Mahran, and W. M. Abdo, *J. Prakt. Chem.*, **316**, 377 (1974).

5) A. Mustafs and A. N. Islam, *J. Chem. Soc.*, **1949**, S 81.

6) H.-D. Becker, D. Sanchez, and A. Arvidsson, *J. Org. Chem.*, **44**, 4247 (1979).

7) K. Hirakawa and S. Nakazawa, *J. Org. Chem.*, **43**, 1804 (1978).

8) H.-D. Becker and D. Sanchez, *J. Org. Chem.*, **44**, 1787 (1979).

9) Z. Majerski and N. Trinajstć, *Bull. Chem. Soc. Jpn.*, **43**, 2648 (1970).

10) E. Clar, *Ber.*, **72**, 2134 (1939).

11) E. de B. Barnett and M. A. Matthews, *Ber.*, **59**, 767 (1926).

Preparation of Optically Active Piperazines from Ethyl (*S*)-2-(2-Alkyl-1-aziridinyl)acetates

Nobuhide YAHIRO* and Shigekazu ITO
Department of Industrial Chemistry, Chiba Institute of Technology,
Tsudanuma, Narashino, Chiba 275
(Received August 8, 1985)

Synopsis. Reaction of ethyl (*S*)-2-(2-alkyl-1-aziridinyl) acetates with boron trifluoride etherate in a large excess of ethylamine or ammonia gives the corresponding optically active piperazines in good yields. These piperazines retain the configuration of the starting aziridines.

Optically active piperazine derivatives are usually prepared by dimerization of optically active aziridines,[1] by optical resolution of racemic piperazines,[2] or by cyclization of optically active amino acid derivatives,[3,4] but these processes are inconvenient because they involve complicated procedures. It was reported[5] that optically active aziridines react with amines under the catalytic action of boron trifluoride etherate ($BF_3 \cdot OEt_2$) to give optically active diamines:

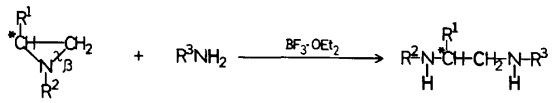

R^1; C_2H_5, *i*-C_4H_9, R^2; H, C_2H_5, R^3; H, C_2H_5

The ring-opening reaction of an optically active aziridine (R^2=alkyl) with a nucleophilic reagent was found to proceed by β-cleavage (CH_2–N) to give the corresponding diamine retaining the configuration of the starting aziridine.[6,7] If ethyl (*S*)-2-(2-isobutyl-1-aziridinyl)acetate (**1**) is used in the above reaction, 3,6-diaza-1-ethoxy-4-isobutyl-1-octanone (R^1=*i*-C_4H_9, R^2=$CH_2COOC_2H_5$, R^3=C_2H_5) is expected to be produced. But the reaction of **1** with a large excess of ethylamine was found to give (*S*)-*N*-ethyl-2-(2-isobutyl-1-aziridinyl)acetamide (**2**) and (*S*)-1-ethyl-5-isobutyl-2-piperazinone (**3**) but no optically active diamines. In a similar procedure, optically active 2-(2-isobutyl-1-aziridinyl)acetamide (**4**) and 5-isobutyl-2-piperazinone (**5**) were prepared from **1** and ammonia:

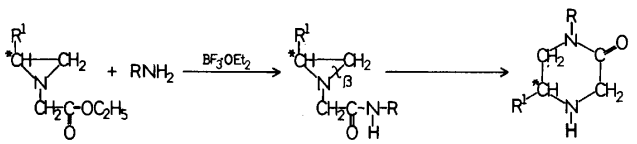

R^1=*i*-C_4H_9, **1**
R^1=C_2H_5, **9**

R^1=*i*-C_4H_9, R=C_2H_5, **2**
R^1=*i*-C_4H_9, R=H, **4**
R^1=R=C_2H_5, **10**

R^1=*i*-C_4H_9, R=C_2H_5, **3**
R^1=*i*-C_4H_9, R=H, **5**
R^1=R=C_2H_5, **11**

The configuration and structure of **5** were confirmed by direct comparison with an authentic sample. Optically active 2-isobutylpiperazine (**6**) was prepared by the reduction of **5** with lithium aluminium hydride ($LiAlH_4$). To determine the stereochemistry of **6**, (*S*)-2-isobutylpiperazine (**8**) was prepared by the reduction of (*S*)-3-isobutyl-2,5-piperazinedione (**7**)[3] with $LiAlH_4$:

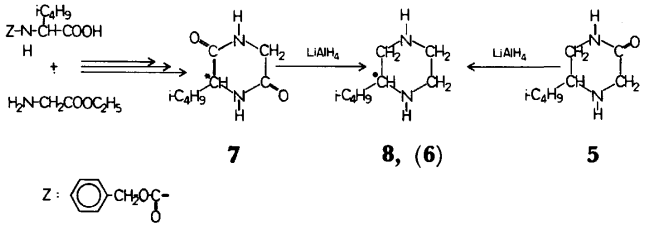

7 **8**, (**6**) **5**

Z:

Compounds **6** and **8** showed identical ORD, CD, and IR spectra and retention times in GLC. **6**: ORD (MeOH) $[\Phi]_{205}$ +2790° and $[\Phi]_{220}$ +320°, in a positive simple dispersion curve; CD (MeOH) $[\theta]_{205}$ −350 and $[\theta]_{220}$ −110, in a negative simple dispersion curve; $[\alpha]_D^{15}$ +7.0° (*c* 2.33, EtOH); IR (neat) 3225 and 1520 cm^{-1}. **8**: ORD (MeOH) $[\Phi]_{205}$ +2850° and $[\Phi]_{220}$ +320°, in a positive simple dispersion curve; CD (MeOH) $[\theta]_{205}$ −360 and $[\theta]_{220}$ −110, in a negative simple dispersion curve; $[\alpha]_D^{15}$ +6.8° (*c* 1.07, EtOH); IR (neat) 3225 and 1520 cm^{-1}. In due course of these experiments, an effort was made in vain to determine the configuration and structure of piperadinones **3** and **5** since neither of these isomers was formed as expected. On the other hand, the reaction of **2** with $BF_3 \cdot OEt_2$ in a large excess of ethylamine was found to give **3** in a good yield. The fact that **2** and **4** gave optically active **3** and **5** with retained configuration, respectively, suggests occurrence of an intramolecular nucleophilic displacement of an intermediate acetamide derivative:

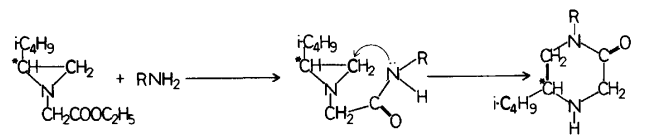

R; H, C_2H_5

Similarly, (*S*)-*N*-ethyl-2-(2-ethyl-1-aziridinyl)acetamide (**10**) and (*S*)-1,5-diethyl-2-piperazinone (**11**) were prepared from ethyl (*S*)-2-(2-ethyl-1-aziridinyl) acetate (**9**) and ethylamine.

Experimental

Materials. Ethylamine, ammonia, and $BF_3 \cdot OEt_2$ were commercial materials and were purified before use. (*S*)-2-Isobutylaziridine, with $[\alpha]_D^{25}$ −19.6° (*c* 2.02, EtOH) and bp 127—130 °C, was converted to **1**, with yield 89%, $[\alpha]_D^{25}$ +23.6° (*c* 2.63, EtOH), and 109—111 °C/17 mmHg (1 mmHg=133.322 Pa), by treating it with ethyl chloroacetate and triethylamine.[8] In a similar procedure, **9** was prepared by the reaction of (*S*)-2-ethylaziridine, with $[\alpha]_D^{25}$ −23.0° (*c* 1.54, EtOH) and bp 89—90 °C, with ethyl chloroacetate. **9**: yield 86%; bp 87—90 °C/18 mmHg; $[\alpha]_D^{25}$ +4.5° (*c* 1.02, MeOH).

Amide and Piperazine Derivatives. A large excess of ethylamine (5.4 g, 0.12 mol) and **1** (3.7 g, 0.02 mol) were placed in a stainless steel tube cooled in a Dry Ice–methanol bath, and $BF_3 \cdot OEt_2$ (0.4 cm^3) was added to the mixture. The stainless steel tube was sealed and allowed to stand at 95—98 °C. After 72 h, the reaction mixture was dissolved in benzene and washed with 10% sodium hydroxide solution. The organic layer was dried over anhydrous magnesium sulfate and the solution was distilled under reduced pressure. The product **3** (2.8 g, 76%) was obtained as colorless liquid: $[\alpha]_D^{25}$ +79.0° (*c* 0.61, EtOH); bp 106—107 °C/2 mmHg, ORD (MeOH) $[\Phi]_{300}$ +730°, $[\Phi]_{248}^{peak}$ +1880°, $[\Phi]_{243}^{trough}$ +1840°, and $[\Phi]_{220}$ +11800°, in a positive abnormal dispersion curve; CD (MeOH) $[\theta]_{223}^{trough}$ −3700 with crossover point 217 nm; IR (neat) 3275, 2940, 1635, 1496, 1465, 1430, 1304, 1213, 1164, and 791 cm^{-1}. Calcd for $C_{10}H_{20}N_2O$: C, 65.18; H, 10.94; N, 15.20%. Found: C, 64.87; H, 10.96; N, 15.19%.

In a similar procedure, **2** was prepared by the reaction of **1** with ethylamine at room temperature for 24 h. From the crude mixture (**2** and **3**), **2** was obtained by a fractional distillation: yield 54%; bp 78—80 °C/1 mmHg, $[\alpha]_D^{20}$ +31.9° (*c* 1.40, EtOH); ORD (MeOH) $[\Phi]_{300}$ +110° and $[\Phi]_{215}$ +2250°, in a positive simple dispersion curve; CD (MeOH) $[\theta]_{210}^{trough}$ −1350; IR (neat) 3300, 3050, 2960, 1650, 1535, 1332, 1293, 1251, 1168, and 828 cm^{-1}. Calcd for $C_{10}H_{20}N_2O$: C, 65.18; H, 10.94; N, 15.20%. Found: C, 64.68; H, 10.95; N, 15.33%. Compounds **4** and **5** were prepared from **1** and ammonia in similar procedures. Each product was purified by column chromatography (developing solvent MeOH/acetone) on silica gel. **4**: yield 58%; mp 78—81 °C; $[\alpha]_D^{20}$ +42.1° (*c* 0.27, MeOH); ORD (MeOH) $[\Phi]_{300}$ +570° and $[\Phi]_{215}$ +1580°, in a positive simple dispersion curve; CD (MeOH) $[\theta]_{216}^{trough}$ −650 with crossover point 205 nm; IR (KBr) 3390, 3180, 3045, 2950, 1630, 1463, 1412, 1396, 1327, 1234, 1170, 867, 782, and 705 cm^{-1}. **5**: yield 42%; mp 77—79 °C, $[\alpha]_D^{20}$ +80.9° (*c* 0.21, MeOH); ORD (MeOH) $[\Phi]_{300}$ +430°, $[\Phi]_{263}^{peak}$ +810°, $[\Phi]_{242}^{trough}$ +680°, and $[\Phi]_{220}$ +9800°, in a positive abnormal dispersion curve; CD (MeOH) $[\theta]_{221}^{trough}$ −5650 with crossover point 214 nm; IR (KBr) 3210, 2945, 1692, 1653, 1493, 1462, 1365, 1117, 916, 830, and 786 cm^{-1}. Calcd for $C_8H_{16}N_2O$: C, 61.51; H, 10.32; N, 17.93%. Found: C, 61.08; H, 10.34; N, 18.01%.

Compounds **10** and **11** were prepared from **9** and ethylamine. **10**: yield 65%; bp 88—89 °C/4 mmHg; $[\alpha]_D^{20}$ +11.2° (*c* 0.91, EtOH); ORD (MeOH) $[\Phi]_{300}$ +70° and $[\Phi]_{215}$ +1340°, in a positive simple dispersion curve; CD (MeOH) $[\theta]_{213}^{trough}$ −790; IR (neat) 3375, 3048, 2960, 1652, 1534, 1375, 1295, 1253, 1168, and 828 cm^{-1}. **11**: yield 70%, bp 104—105 °C/3 mmHg; $[\alpha]_D^{20}$ +82.8° (*c* 1.44, EtOH); ORD (MeOH) $[\Phi]_{300}$ +450°, $[\Phi]_{247}^{peak}$ +1150°, $[\Phi]_{243}^{trough}$ +1100°, and $[\Phi]_{220}$ +7200°, in a positive abnormal dispersion curve; CD (MeOH) $[\theta]_{223}^{trough}$ −2250 with crossover point 215 nm; IR (neat) 3290, 2965, 1637, 1496, 1458, 1430, 1305, 1215, 1171, 830, and 791 cm^{-1}. Calcd for $C_8H_{16}N_2O$: C, 61.51; H, 10.32; N, 17.93%. Found: C, 61.03; H, 10.39; N, 18.16%.

Reduction of 7. A solution of **7** (1.7 g, 0.01 mol) in 25 cm^3 of diethyl ether was added to a diethyl ether solution (25 cm^3) of $LiAlH_4$ (0.43 g, 0.011 mol) at 0 °C. The mixture was stirred for 48 h and the reaction was terminated by adding water. The organic layer was dried over anhydrous magnesium sulfate and the solution was concentrated under reduced pressure. The product **8** was purified by sublimation: yield 64%; mp 85—87 °C (hygroscopic); $[\alpha]_D^{15}$ +6.8° (*c* 1.07, EtOH).

The authors are grateful to Professor Masaya Yanagita for his valuable discussion and comments. This work was partially supported by a Grant-in-Aid for Scientific Research No. 60750846 from the Ministry of Education, Science and Culture.

References

1) S. Tsuboyama, K. Tsuboyama, S. Tanji, and M. Yanagita, *Nippon Kagaku Kaishi*, **1976**, 540.
2) F. B. Kipping and W. J. Pope, *J. Chem. Soc.*, **1926**, 1076.
3) J. C. Sheehan and D. N. McGregor, *J. Am. Chem. Soc.*, **84**, 3000 (1962).
4) T. Fujii and K. Okawa, *Bull. Chem. Soc. Jpn.*, **39**, 1598 (1966).
5) Y. Minoura, M. Takebayashi, and C. C. Price, *J. Am. Chem. Soc.*, **81**, 4689 (1959).
6) K. Tsuboyama, S. Tsuboyama, and M. Yanagita, *Bull. Chem. Soc. Jpn.*, **40**, 2954 (1967).
7) N. Yahiro and K. Asakawa, *Kobunshi Ronbunshu*, **39**, 507 (1982).
8) K. Tsuboyama and S. Tsuboyama, 30th National Meeting of the Chemical Society of Japan, Osaka, April 1974, Abstr., p. 1589.

Synthesis of Unusual Aromatic L-Amino Acids by Asymmetric Hydrogenation of Cyclic Dehydrodipeptides

Haruhiko Aoyagi,* Fumio Horike, Atsuko Nakagawa, Sayuri Yokote, Namgyu Park, Yoshihide Hashimoto, Tetsuo Kato, and Nobuo Izumiya
Laboratory of Biochemistry, Faculty of Science, Kyushu University 33, Hakozaki, Higashi-ku, Fukuoka 812
(Received August 31, 1985)

Synopsis. To prepare L-Tyr(Me) and L-Amp (L-2-amino-5-(*p*-methoxyphenyl)pentanoic acid), their precursors cyclo(-⊿Tyr(Me)-L-Ala-) and cyclo(-⊿Amp-L-Ala-) were hydrogenated in *N,N*-dimethylformamide. The content of LL isomers in the hydrogenated products was over 94%. Mild acid hydrolysis of the hydrogenated products and subsequent recrystallization gave pure L-Tyr(Me) and L-Amp.

Unusual aromatic amino acids L-Tyr(Me)[1] and L-Amp were found in puromycin[2] and Cyl-2,[3] and AM-toxin I,[4] respectively. Both amino acids had been synthesized by us and others.[5-7] However, preparation of Ac-DL-Amp and its enzymatic resolution in the synthesis of L-Amp were troublesome and time-consuming.[7] Recently we developed a simple method for preparation of optically pure α-amino acids by asymmetric hydrogenation of cyclo(-⊿aminoacyl-L-aminoacyl-),[8] and could prepare L-2-amino-5-phenylpentanoic acid which is a constituent of AM-toxin II and its homologs in moderate yields.[9] Therefore, we intended to apply the method for preparation of L-Tyr(Me) and L-Amp. Some modification, however, seemed necessary because the method contained acid hydrolysis in the final step which might cause partial decomposition of the methoxy moiety of the L-Tyr(Me) and L-Amp side chains.[7]

We investigated hydrolytic conditions of cyclo(-L-Tyr(Me)-L-Ala-) (**1**) using the mixture of 1—6 M HCl (1 M=1 mol dm^{-3}) and dioxane[10] as a preliminary experiment. As shown in Table 1, the conditions of 1 M HCl-dioxane (1:1), 110 °C and 72 h were adequate for **1**. Almost complete hydrolysis and negligible demethylation of the Tyr(Me) residue were observed. The conditions selected for cyclo(-L-Amp-L-Ala-) (**2**) were 0.5 M HCl-dioxane (1:1), 110 °C and 96 h.

Scheme 1 shows the route for preparation of L-Tyr(Me) and L-Amp. Compound **3** was converted into **4a** in 52% and **4b** in 40%, respectively. According to our previous papers,[8,9] Pd black and DMF were used for hydrogenation, and chiral induction (%) in hydrogenation was determined by HPLC. While the chiral induction of cyclo(-⊿phe-L-Ala-) was previously found to be of temperature dependence,[9] **4a** showed unexpectedly uniform chiral induction of about 95% between 0 °C and 50 °C. The high chiral induction of 97% at 20 °C was observed in the case of **4b**. Acid hydrolysis of the hydrogenated products (**5a** and **5b**) under the conditions found above followed by neutralization of the hydrolysates gave crude products. Pure L-Tyr(Me) and L-Amp were obtained after recrystallization in 66% from **4a** and 56% from **4b**, respectively. The total yield (34%) of L-Tyr(Me)

Table 1. Hydrolysis and Demethylation of Cyclo(-L-Tyr(Me)-L-Ala-)

Solvent	Time	Hydrolysis	Demethylation
	h	%	%
6 M HCl-dioxane[a]	24	99	24
2 M HCl-dioxane[a]	24	90	6
1 M HCl-dioxane[a]	24	69	<1
1 M HCl-dioxane[a]	72	98	2

[a] Ratio of 1—6 M HCl and dioxane is 1:1 (v/v); Temperature, 110 °C.

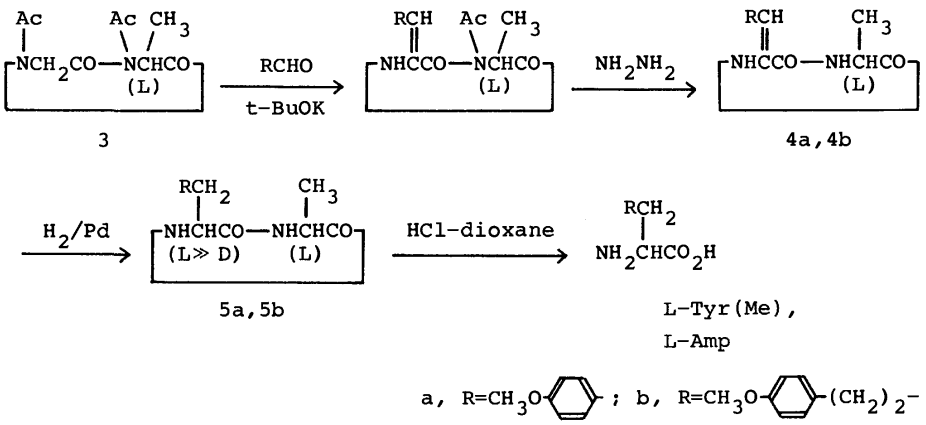

Scheme 1.

in the present work was lower than the reported one (62%).[6] The higher yield in the latter is due to simple modification of natural L-Tyr. On the other hand, the yield (22%) of L-Amp was comparable to that (24%) described before,[7] indicating that the present method is useful in cases where optically active natural amino acids are not available as starting materials.

Experimental

Optical rotation was measured with a Union high sensitivity polarimeter PM-71. HPLC was carried out with a Hitachi 635A liquid chromatograph and monitered at 210 nm. Amino acid analysis was performed with a Hitachi amino acid analyzer KLA-5. Thin-layer chromatography was carried out on Merck silica gel G with the following solvent systems: R_f^1, $CHCl_3$-MeOH (9:1); R_f^2, $CHCl_3$-MeOH-AcOH (95:5:1).

Cyclo(-L or D-aminoacyl-L-Ala-). Authentic samples were prepared from the corresponding Z-dipeptide-OMe according to the literature.[9] All the compounds afforded satisfactory results of elemental analysis. Cyclo(-L-Tyr(Me)-L-Ala-) (**1**): Yield, 80%; mp 274—276 °C (decomp); $[\alpha]_D^{20}$ −4.8° (*c* 1, DMF); R_f^1=0.35. Cyclo(-D-Tyr(Me)-L-Ala-) (**6**): Yield, 73%; mp 235—237 °C (decomp); $[\alpha]_D^{20}$ −17.2° (*c* 0.5, DMF); R_f^1=0.34, R_f^2=0.65. Cyclo(-L-Amp-L-Ala-) (**2**): Yield, 88%; mp 211—213 °C; $[\alpha]_D^{19}$ −31.0° (*c* 0.5, DMF); R_f^2=0.34. Cyclo(-D-Amp-L-Ala-) (**7**): Yield, 61%; mp 204—206 °C; $[\alpha]_D^{19}$ −3.5° (*c* 0.5, DMF); R_f^2=0.41.

Cyclo(-ΔTyr(Me)-L-Ala-) (4a). Compound **3** was allowed to react with *p*-methoxybenzaldehyde in the presence of *t*-BuOK. Cyclo(-ΔTyr(Me)-*N*-Ac-L-Ala-) obtained was treated with $NH_2NH_2 \cdot H_2O$ to give **4a** using the same procedure in the literature;[8] yield, 52%; mp 254—257 °C (decomp); $[\alpha]_D^{22}$ −17.0° (*c* 1, DMF); R_f^1=0.47. Found: C, 63.11; H, 5.77; N, 11.50%. Calcd for $C_{13}H_{14}N_2O_3$: C, 63.40; H, 5.73; N, 11.38%.

Cyclo(-ΔAmp-L-Ala-) (4b). This compound was prepared from **3** and 3-(*p*-methoxyphenyl)propionaldehyde; yield, 40%; mp 231-233 °C; $[\alpha]_D^{20}$ −17.5° (*c* 0.5, DMF); R_f^1=0.40. Found: C, 65.42; H, 6.66; N, 10.26%. Calcd for $C_{15}H_{18}N_2O_3$: C, 65.67; H, 6.61; N, 10.21%.

Acid Hydrolysis of Authentic Samples. A mixture of **1** and Lys·HCl (5 μmol each) was heated in a sealed tube with 1—6 M HCl-dioxane (1:1) at 110 °C for certain intervals. Lys·HCl was used as a standard for determination of hydrolysis percentage by comparison with Ala formed in hydrolysis. Amino acid analysis and calculation of demethylation were carried out as described before.[7] The results are shown in Table 1. A similar procedure was applied for **2**.

HPLC of Authentic Samples. The separation of DL and LL isomers of cyclo(-Tyr(Me)-Ala-) was performed under the following conditions: column, LiChrosorb RP-8 (4×250 mm); eluent, H_2O-CH_3CN (95:5); flow rate, 1.0 ml/min. Elution volume and relative intensity were determined as 44 ml and 99% for **6**, and 51 ml and 100% for **1**. The conditions on the separation of DL and LL isomers of cyclo(-Amp-Ala-) were as follows: column, LiChrosorb RP-18 (4×150 mm); eluent, H_2O-CH_3CN-*i*-PrOH (14:1:1); flow rate,. 1.0 ml/min. Eluent volume and intensity were 22.5 ml and 94% for **7**, and 31.2 ml and 100% for **2**.

Determination of Chiral Induction in Hydrogenation of Cyclic Dehydrodipeptides. Compound **4a** (7.4 mg, 30 μmol) in absolube DMF (8 ml) was hydrogenated in the presence of Pd black (ca. 10 mg) at 0 °C for 10 h, and an aliquot was applied to HPLC. The ratio of the DL and LL isomers in cyclo(-Tyr(Me)-Ala-) was 2.5:97.5 after correction of the apparent ratio by relative intensity. Therefore, the chiral induction (%) was calculated as 95%, and those at 25 °C and 50 °C were 97% and 94%, respectively. The chiral induction of **4b** was 97% at 20 °C.

Preparation of L-Amino Acids. **L-Tyr(Me)**: Hydrogenated product of **4a** (1.23 g, 5 mmol) was hydrolyzed with 1 M HCl-dioxane (1:1, 150 ml) at 110 °C for 3 d and evaporated in vacuo. The residue was dissolved in water (10 ml) and the solution was neutralized with Et_3N. The resulting solid was collected and washed with cold water. Dissolution of the crude product in 6 M HCl and neutralization with Et_3N gave pure L-Tyr(Me); yield, 0.65 g (66%); $[\alpha]_D^{25}$ −6.2° (*c* 1, 1 M HCl) (lit,[5] $[\alpha]_D^{29}$ −5.9° (*c* 2, 1 M HCl)). Found: C, 61.49; H, 6.71; N, 7.27%. Calcd for $C_{10}H_{13}NO_3$: C, 61.52; H, 6.71; N, 7.18%.

L-Amp: This was prepared from **4b** as described above except for hydrolysis with 0.5 M HCl-dioxane (1:1) for 4 d; yield, 56%; $[\alpha]_D^{22}$ +30.8° (*c* 1, 5 M HCl-DMF (1:1)) (lit,[7] $[\alpha]_D^{21}$ +31.8° (*c* 2, 5 M HCl-DMF). Found: C, 64.71; H, 7.61; N, 6.08%. Calcd for $C_{12}H_{17}NO_3$: C, 64.55; H, 7.68; N, 6.27%.

References

1) Abbreviations: Amp, 2-amino-5-(*p*-methoxyphenyl)-pentanoic acid; Δ, α,β-dehydro; DMF, *N*,*N*-dimethylformamide; Et_3N, triethylamine; HPLC, high-performance liquid chromatography; Tyr(Me), *O*-methyltyrosine.

2) C. W. Waller, P. W. Fryth, B. L. Hutchings, and J. H. Williams, *J. Am. Chem. Soc.*, **75**, 2025 (1953).

3) A. Hirota, A. Suzuki, and S. Tamura, *Agric. Biol. Chem.*, **37**, 1185 (1973).

4) T. Ueno, T. Nakashima, Y. Hayashi, and H. Fukami, *Agric. Biol. Chem.*, **39**, 1115 (1975).

5) L. Davies and H. T. Clarke, *J. Am. Chem. Soc.*, **54**, 1630 (1932).

6) N. Izumiya and A. Nagamatsu, *Bull. Chem. Soc. Jpn.*, **25**, 265 (1952).

7) Y. Shimohigashi, S. Lee, and N. Izumiya, *Bull. Chem. Soc. Jpn.*, **49**, 3280 (1976).

8) T. Kanmera, S. Lee, H. Aoyagi, and N. Izumiya, *Int. J. Peptide Protein Res.*, **16**, 280 (1980).

9) Y. Hashimoto, H. Aoyagi, M. Waki, T. Kato, and N. Izumiya, *Int. J. Peptide Protein Res.*, **21**, 11 (1983).

10) Y. Shimohigashi and N. Izumiya, *Int. J. Peptide Protein Res.*, **12**, 7 (1978).

Mass Spectra of Tetrahydrofuran Derivatives

Hajime NAGANO,* Makiko IJIRI, Xiao Hong XU, and Michio SHIOTA
Department of Chemistry, Faculty of Science, Ochanomizu University,
Otsuka, Bunkyo-ku, Tokyo 112
(Received September 6, 1985)

Synopsis. Mass spectra of 2-(4,5-dialkyloxacyclopent-2-yl)-2-propanols exhibited a characteristic cleavage of tetrahydrofuran ring yielding an ion at *m/z* 102 ($C_5H_{10}O_2$) and/or an ion ($M^+-C_5H_{10}O_2-H$).

In the course of structure determination of magydardienediol, a diterpene isolated from *Magydaris panacifolia* (Vahl) Lange (Umbelliferae), we found a new characteristic mass spectral cleavage of tetrahydrofurans (**1**) derived from the diterpene.[1] The cleavage yielded ions at *m/z* 250 ($M^+-C_5H_{10}O_2$) and at *m/z* 167 ($M^+-C_5H_{10}O_2-CH_2CH_2CH=C(CH_3)_2$) as intense peaks. The other possible structure 2-(5-alkyl-5-methyloxacycopent-2-yl)-2-propanol expected for **1** was disproved as the mass spectra of tetrahydrofurans of the general type are well known to show an ion at *m/z* 143.[2] This difference in fragmentations shows that mass spectroscopy is efficient for the discrimination of these tetrahydrofurans.

We report here the mass spectral fragmentations of tetrahydrofurans (**2—5**) which verify the cleavage of tetrahydrofuran ring mentioned above.

Tetrahydrofurans **2—5** were prepared from 5α-cholestan-3-one, 5-undecanone, cyclooctanone, and androsterone, respectively ((i) $LiN(i\text{-}Pr)_2$, $(CH_3)_2C=CHCH_2Br$, (ii) $NaBH_4$, (iii) *m*-chloroperbenzoic acid, H^+).

Mass spectrum of **2**, mp 132—134 °C, obtained at an electron beam energy of 70 eV showed a prominent peak at *m/z* 102 (relative intensity 52%) due to ion **a** ($C_5H_{10}O_2^+$). The formation of ion **a**, which was scarcely observed in the spectrum of **1**, firmly established the fragmentation process of tetrahydrofuran ring as shown in Scheme. At a lower electron beam energy (25 eV) the cleavage occurred predominantly to give the base peak at *m/z* 102 and loss of water from the molecular ion to a lesser extent. The predominancy of tetrahydrofuran ring cleavage over other fragmentations was also shown in the spectrum of **1** obtained at 18 eV (*m/z* 250 (54%) and 167 (100)).

Mass spectra of diastereomeric mixtures, **3a**, **3b**, **4a**, and **4b**, also showed an intense peak at *m/z* 102 (70 eV: **3a**(58%), **3b**(57), **4a**(53), and **4b**(53); 25 eV: **3a**(81%), **3b**(88), **4a**(87), and **4b**(100)).

In the spectra of **5** (diastereomeric mixture) fragment ions at *m/z* 273 (70 eV (77%) and 25 eV (67); $M^+-C_5H_{10}O_2-H$) and 255 (70 eV (70%), 25 eV (100); $M^+-H_2O-C_5H_{10}O_2-H$) were observed as predominant peaks, whereas the intensities of ion **a** were moderate (70 eV (21%) and 25 eV (20)). The tendency for charge to reside on the methoxycarbonyl group in **1** and the hydroxyl group at C-3 in **5** may decrease the intensities of ion **a**. In the spectra of **4a** and **4b** a fragment ion ($M^+-C_5H_{10}O_2-H$) was also observed as an intense peak at *m/z* 109 (70 eV: **4a**(72%) and **4b**(75); 18 eV: **4a**(54%) and **4b**(46)).

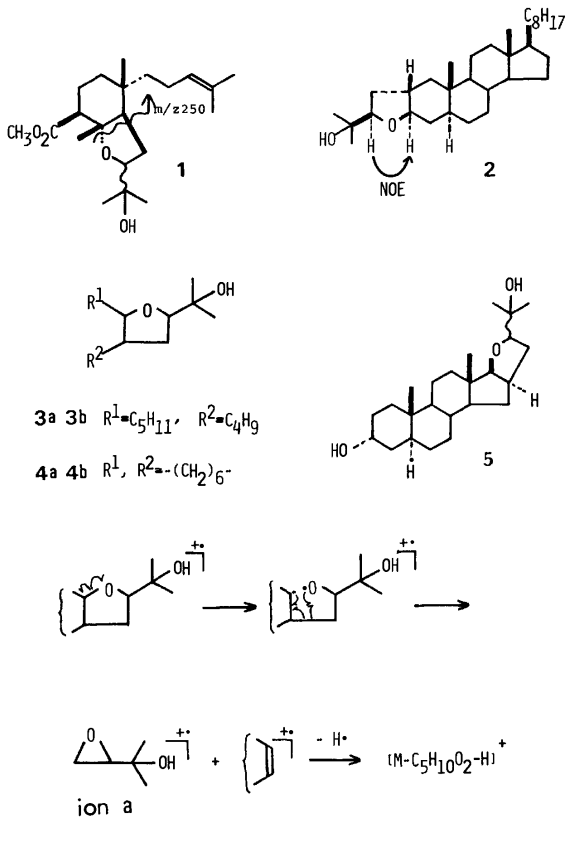

Scheme

Experimental

Mass spectra were measured on a JEOL DX-300 spectrometer using direct inlet system. NMR Spectra were recorded on a JEOL GX270 spectrometer in $CDCl_3$.

2α-(3-Methyl-2-butenyl)-5α-cholestan-3-one. To a solution of the enolate of 5α-cholestan-3-one (569 mg) prepared using $LiN(i\text{-}Pr)_2$ (1.5 mmole) in dry THF (5 ml) and HMPA (0.2 ml) was added a solution of 4-bromo-2-methyl-2-butene (249 mg) in THF (1 ml) at −78 °C and the solution was stirred for 3 h. After work-up as usual the product was submitted to preparative TLC to give 2α-(3-methyl-2-butenyl)-5α-cholestan-3-one (31 mg), mp 115.5—116.5 °C; IR (KBr) 1708 cm^{-1}; ^1H NMR δ=1.59 (3H, s, Me), 1.69 (3H, s, Me), and 5.06 (1H, t, *J*=6.7 Hz); ^{13}C NMR δ=45.85 (C-1), 48.07 (C-2), 45.03 (C-4), and 46.85 (C-5); Found: *m/z* 454.4141. Calcd for $C_{32}H_{54}O$: M, 454.4173.

2α-(3-Methyl-2-butenyl)-5α-cholestan-3β-ol. The above ketone (30 mg) was reduced with $NaBH_4$ (17 mg) in

ethanol to give 3β-ol (21 mg), mp 97—98 °C; IR (KBr) 3350 cm^{-1}; ^1H NMR δ=3.29 (1H, ddd, J=10.5, 10.5, and 5 Hz, 3α-H); Found: m/z 456.4416. Calcd for $C_{32}H_{56}O$: M, 456.4331.

Tetrahydrofuran 2. A solution of the 3β-ol (21 mg) and *m*-chloroperbenzoic acid (18 mg) in CH_2Cl_2 was allowed to stand at room temperature and then treated with dilute HCl to give **2** (7.6 mg); IR (KBr) 3520 and 3440 cm^{-1}; ^1H NMR δ=1.15 (3H, s, Me), 1.22 (3H, s, Me), 3.09 (1H, ddd, J=10.5, 10.5, and 4 Hz, 3α-H), and 3.83 (1H, dd, J=9 and 3.5 Hz, CH–O); HRMS: m/z 454.4170 (Calcd for $C_{32}H_{54}O$, M−H_2O, m/z 454.4173) and 102.0777 (Calcd for $C_5H_{10}O_2$, 102.0681).

Tetrahydrofurans 3a and 3b. A diastereomeric mixture of tetrahydrofurans derived similarly from 5-undecanone was separated into two fractions, **3a** (a mixture of two less polar diastereomers) and **3b** (a mixture of two polar diastereomers) using silica gel column chromatography. **3a**: an oil, IR (neat) 3450 cm^{-1}; ^1H NMR δ=0.89 (6H, m, Me), 1.105 (1.5H, s, Me), 1.109 (1.5H, s, Me), 1.21 (3H, s, Me), 3.46 (1H, m), and 3.73 (1H, m); MS (70 eV): m/z 241 (5%, M^+−Me), 238 (6, M^+−H_2O), and 153 (23, M^+−$C_5H_{10}O_2$–H); HRMS: m/z 197.1940 (Calcd for $C_{13}H_{25}O$, M−C_3H_7O, 197.1905), 153.1654 (Calcd for $C_{11}H_{21}$, 153.1644), and 102.0692 (Calcd for $C_5H_{10}O_2$, 102.0681). **3b**: an oil, IR (neat) 3450 cm^{-1}; ^1H NMR δ=0.89 (6H, m, Me), 1.10 (3H, s, Me), 1.20 (1.8H, s, Me), 1.23 (1.2H, s, Me), 3.69 (0.4H, dd, J=9.7 and 5.6 Hz), 3.78 (0.6H, t, J=7.5 Hz), and 3.91 (1H, m); MS: m/z 241 (4%), 238 (4) and 153 (19); HRMS: m/z 197.1928 and 102.0696.

Tetrahydrofurans 4a and 4b. A diastereomeric mixture of tetrahydrofurans derived from cyclooctanone was separated into two fractions, **4a** (a mixture of two less polar diastereomers) and **4b** (a mixture of two polar diastereomers). **4a**: an oil, IR (neat) 3450 cm^{-1}; ^1H NMR δ=1.10 (1.8H, s, Me), 1.11 (1.2H, s, Me), 1.21 (3H, s, Me), 3.5—3.85 (1.4H, m), 4.13 (0.6H, m); MS: m/z 212 (M^+, 0.3%); HRMS: m/z 194.1733 (Calcd for $C_{13}H_{22}O$, M−H_2O, 194.1671), 109.1011 (Calcd for C_8H_{13}, 109.1016), and 102.0693 (Calcd for $C_5H_{10}O_2$, 102.0681). **4b**: an oil, IR (neat) 3450 cm^{-1}; ^1H NMR δ=1.10 (3H, s, Me), 1.20 (3H, s, Me), 3.71 (1H, t, J=7.5 Hz), and 4.04 (1H, m); MS: m/z 212 (M^+, 1%); HRMS: m/z 197.1556, 109.1020, and 102.0707.

Tetrahydrofurans 5. The spectral data of **5** (a mixture of diastereomers), colorless plates, mp 199.5—200.5 °C, are as follows. IR (KBr) 3350 cm^{-1}; ^1H NMR δ=0.73 (1.8H, s, 18-H or 19-H), 0.78 (4.2H, s, 18-H and 19-H), 1.08 (1.8H, s, Me), 1.14 (1.2H, s, Me), 1.18 (1.8H, s, Me), 1.25 (1.2H, s, Me), 2.18 (1H, br s, OH), 2.29 (1H, br s, OH), 2.65 (1H, m,), 3.81 (0.4H, dd, J=11.3 and 4.4 Hz,), and 3.9—4.1 (2.6H, m); HRMS: m/z 376.2983 (Calcd for $C_{24}H_{40}O_3$, M, 376.2977), 273.2176 (Calcd for $C_{19}H_{29}O$, 273.2217), 255.1401 (Calcd for $C_{17}H_{19}O_2$, 255.1384), and 102.0735 (Calcd for $C_5H_{10}O_2$, 102.0681).

References

1) H. Nagano, M. Tori, M. Shiota, and J. de Pascual Teresa, *Bull. Chem. Soc. Jpn.*, **57**, 2971 (1984).

2) C. R. Enzell, R. A. Appleton, and I. Wahlberg, "Biochemical Applications of Mass Spectrometry," ed by G. R. Waller, John Wiley (1972), Chap. 13, p. 372.

^{13}C NMR Spectra of 1,3-Dithiolan-2-ylium Ions and 2-Alkylidene-1,3-dithiolanes

Tadashi OKUYAMA* and Takayuki FUENO
Faculty of Engineering Science, Osaka University, Toyonaka, Osaka 560
(Received September 9, 1985)

Synopsis. ^{13}C NMR spectra of various 2-substituted 1,3-dithiolan-2-ylium perchlorates **5** as well as 2-alkylidene-1,3-dithiolanes **6** are measured. Chemical shifts induced by protonation of **6** to form **5** are compared with those found with the unsaturated analogues, 1,3-dithiolylium ions, implying the aromatic charge delocalization in the latter ions.

1,3-Dithiolylium ion **1** is an unsaturated five-membered ring cation which possesses potential aromatic sextet. The stability of this ion is usually attributed to this 6π-electron delocalization (**1a**).[1] The NMR

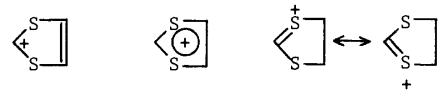

1 **1a** **1b**

spectral data of this class of cations have been considered to support this view in one paper[2] while the other workers[3] rationalized the observed ^{13}C chemical shifts only by the sulfur conjugation (**1b**). The former paper[2] examined both ^{1}H and ^{13}C NMR spectra of **1** and the saturated analogue, 1,3-dithiolanylium ion **2**, as well as their neutral precursors. The signal of 2-H of **1** appeared at a lower field than that of **2**, whereas the chemical shift of 2-C of **1** is much smaller than that of **2**, suggesting the aromatic ring current and charge delocalization in **1**. On the other hand, the latter workers[3] compared ^{13}C NMR spectra of 2-substituted derivatives of **1** with those of their deprotonated derivatives; e. g., **3** and **4**. Chemical shift differences between **3**

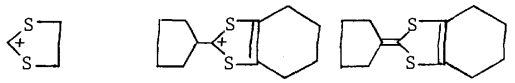

2 **3** **4**

and **4** were found to be much greater at 2-C than at 4-C.

In the present investigation, we have measured ^{13}C NMR spectra of substituted 1,3-dithiolan-2-ylium ions **5** and 2-alkylidene-1,3-dithiolanes **6** in order to examine the conclusion deduced from the similar comparison between **3** and **4**. Perchlorates of **5** were

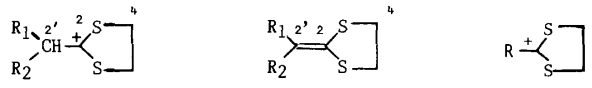

5 **6** **5**

a, $R_1=R_2=H$ **b**, $R_1=H$, $R_2=CH_3$ **e**, $R=(CH_3)_3C$
c, $R_1=R_2=CH_3$ **d**, $R_1=H$, $R_2=C_6H_5$ **f**, $R=C_6H_5$
g, $R=p\text{-}CH_3OC_6H_4$

prepared from acyl chlorides and 1,2-ethanedithiol and converted to **6** by the treatments with triethylamine.[4] ^{13}C FT NMR spectra were recorded at 27 °C on a JNM-FX 100 spectrometer operating at 25.05 MHz.[5] Spectra of **5** and **6** were measured as 5—10% solutions in CF_3COOH-CF_3COOD and $CDCl_3$, respectively. Results are summarized in Table 1.

Table 1. ^{13}C Chemical Shifts of **5** and **6**[a]

No.	R(R_1, R_2)	2-C	4-C	2-C′[b]	Others
2[c]	H	221.4	46.4		
5a	CH_3	245.0	47.8	24.4	
5b	CH_3CH_2	253.4	46.8	34.0	15.6
5c	$(CH_3)_2CH$	259.1	46.8	41.7	28.5
5e	$(CH_3)_3C$	264.1	46.5	48.5	32.8
5d	$C_6H_5CH_2$	242.6	46.8	45.2	130.5, 131.5, 135.0
5f	C_6H_5	234.6	45.4	143.3	132.0, 132.3, 144.0
5g	$p\text{-}CH_3OC_6H_4$	225.5	44.2	126.6	57.9, 118.1, 136.8, 174.3
6a	(H, H)	144.3	38.4	99.3	
		(100.7)	(9.4)	(−74.9)	
6b	(H, CH_3)	135.2	36.9, 37.2	110.6	9.3
		(118.2)	(9.7)	(−76.6)	
6c	(CH_3, CH_3)	127.1	37.9	119.1	24.2
		(132.0)	(8.9)	(−77.4)	
6d	(H, C_6H_5)	137.8	35.4, 39.5	115.5	125.5, 127.0, 128.0, 137.1
		(104.8)	(9.3)	(−70.3)	

a) ppm downfield from internal TMS. Values in parentheses show the chemical shift differences between **5** and **6**. b) The carbon next to 2-C. c) Taken from reference 2.

Assignments of signals were made by comparisons with those of relevant compounds.

Resonance of 2-C of dithiolanylium ions **5** occurs at the lowest field reflecting a positive charge. Among the chemical shifts of 2-C of **5**, the largest is that of **5e** (R=*t*-Bu), decreasing in the order **5e**(*t*-Bu)>**5c**(*i*-Pr)>**5b**(Et)>**5a**(Me)>**5d**($PhCH_2$). This order coincides with that of electron-donating ability of alkyl groups to the positive center, e. g., in terms of the σ_p^+ substituent constants, and indicates decreasing order of the charge density at the positive carbon. The 2-phenyl and 2-(*p*-methoxyphenyl) cations (**5f** and **5g**) have the 2-C signals at still higher field.

2-Alkyl-1,3-dithiolanylium ion **5** is formed by protonation of 2-alkylidene-1,3-dithiolane **6**. The protonation causes large downfield (100—132 ppm) and upfield (70—77 ppm) shifts at 2-C and 2-C′ (the carbon next to 2-C), respectively, as given in parentheses in Table 1. The chemical shift of 4-C (5-C) changes only by about 9 ppm. The upfield shift of 2-C′ must mostly be due to the hybridization change from sp^2 to sp^3. The downfield shifts at 2-C and 4-C come primarily from a positive charge of the cation **5**. Similar changes in the chemical shifts of the unsaturated analogues (**3** and **4** and related dithiole derivatives) were found to be 74—89, −74—81, and 28 ppm at 2-C, 2-C′, and 4-C, respectively.[3] The changes at 2-C′ are much the same between the dithiole and dithiolane derivatives (70—80 ppm upfield shift), as expected for the same hybridization change. However, downfield shifts at 2-C and 4-C of dithiolylium ions are 30—40 ppm smaller and about 20 ppm larger than those of dithiolanylium ions, respectively. This indicates that the charge density in dithiolylium ion **1** is smaller at 2-C while greater at 4-C as compared with that in dithiolanylium ion **2**. That is, the positive charge in **1** delocalizes extensively involving the 4 and 5 carbons.

^{13}C NMR data presented by Meier et al.[3] should be taken as indicating that the positive charge delocalizes over the whole ring system of dithiolylium ion (**1a**), contrary to their conclusion.

References

1) See for reviews, H. Prinzbach, and E. Futterer, *Adv. Heterocycl. Chem.*, **7**, 39 (1966); N. Lozac'h and M. Stavaux, ibid., **27**, 151 (1980).

2) K. Sakamoto, N. Nakamura, M. Ōki, J. Nakayama, and M. Hoshino, *Chem. Lett.*, **1977**, 1133.

3) U. Timm, U. Plücken, H. Petersen, and H. Meier, *J. Heterocycl. Chem.*, **16**, 1303 (1979).

4) T. Okuyama, W. Fujiwara, and T. Fueno, *Bull. Chem. Soc. Jpn.*, in press.

5) We thank Y. Terawaki for recording the spectra.

Gas-Chromatographic Measurements of Atmospheric Sulfur Hexafluoride

Michio HIROTA* and Hisafumi MURAMATSU
Meteorological Research Institute, 1-1 Nagamine, Yatabe-machi, Tsukuba-gun, Ibaraki 305
(Received July 19, 1985)

Synopsis. From air samplings on aircraft in February and December 1982 and in February 1983, and from gas-chromatographic measurements, the background volume mixing ratio of sulfur hexafluoride(SF_6) over Japan was found to be about (0.72±0.13) ppt, where ppt=10^{-12}. Since the first observation by Lovelock in 1970 (0.03 ppt), SF_6 seems to have been increasing steadily.

Sulfur hexafluoride(SF_6) is a very stable compound which has been used for gas insulation since the 1960's[1]; it has also been used as an atmospheric tracer because a electron-capture detector(ECD) has very high sensitivity for it.

With the increasing use of SF_6, it is being accumulated in the atmosphere; its background volume mixing ratio was about 0.5 ppt in 1978.[2] Because its use as a tracer for long-range-transport experiments is not considered to be suitable, it is being replaced by C_6F_{12} and C_8F_{16}.[2] However, it can still be used as a tracer of global atmospheric circulation like CF_2Cl_2, $CFCl_3$,[3] and ^{85}Kr.[4] Furthermore, it has the anvantage that, like them, its emission is due only to man's activities.

In this paper, our preliminary findings regarding its vertical distribution in the troposphere and the time trend of its background volume mixing ratio will be reported.

Experimental

The details of our air sampling and gas-chromatographic measurements have been described in Refs. 5 and 6. Therefore, except for some changes, only a brief description will be presented here.

Sampling of Air. Air samples were collected on an aircraft (Aerocommander 685 or Cessna 404) by means of an air pump (NRK, UP-2) into stainless steel cylinders (0.3 l, Nupro SS-4JB or B-4H valves were used). The SF_6 concentration was almost constant for several months in the cylinder.

Gas-Chromatographic Measurements. SF_6 was analyzed using a Shimadzu Gas Chromatograph GC-6AM equipped with an ECD. The sample air in the cylinder was transferred into a gas sampling tube (Shimadzu MGS-4, 2 ml) and then into a glass column (3 m×5 mm o.d., 90 °C) filled with molecular sieve 5A (30—60 mesh). An ECD (^{63}Ni 10 mci) was used at 300 °C. Ultra-pure N_2(>99.9995%), which had been passed through a drier tube filled with molecular sieve 5A(1/16″ pellets), was used as the carrier gas at a flow rate of 30 ml $min.^{-1}$

SF_6 was eluted before CF_2Cl_2 and O_2. Though CF_3Cl has nearly the same retention time as SF_6, its sensitivity was about 10^2 times lower.

A reference gas was made by diluting pure SF_6 (Takachiho, >99.8%) with ultra-pure N_2 into a *tedlar* bag (20 l). The SF_6 in the *tedlar* bag was constant in a few days. By a two-step static dilution, a reference gas of SF_6 in N_2 was made. The peak height of SF_6 was proportional to the amount of SF_6 in the range from 0 to 0.33×10^{-12} g, which was equal to the amount of 25 ppt SF_6 in a 2-ml sample air. The error in repeated measurements at 1.0 ppt was ±10%. In practice, the volume mixing ratios of SF_6 were calculated from those of CF_2Cl_2[7] by making use of the fact that the peak height of SF_6 was about 20 times (20.8±0.6) higher than that of CF_2Cl_2, which was eluted about 20 s after SF_6. In the measurement of the sensitivity ratio, a mixed gas of 10 ppt SF_6 and 400 ppt CF_2Cl_2 in N_2 was used. The detection limit was 0.3 ppt (S/N~1).

Results and Discussion

The vertical distribution of SF_6 in February 1982 is shown in Fig. 1. In every flight, the Cessna 404 took off and landed at Haneda Airport. The flight courses ranged from Sendai to Hachijo-jima. As with CF_2Cl_2 and $CFCl_3$,[7] higher mixing ratios were often observed over urban areas up to an altitude of 2 km. Above 2 km, nearly constant mixing ratios were observed; the mean value (0.64 ppt) for 17 samples was considered as the background mixing ratio in the troposphere. Subsequent air samplings were performed on 20 and 21 December 1982 over the Kanto Mountains and on 7 February 1983 between Hamamatsu and Nii-Jima. Above 2 km, the mean values and standard deviations were 0.85 and 0.06 ppt for 7 samples in December 1982 and 0.83 and 0.07 ppt for 5 samples in February 1983. The mean value for the total of 29 samples and its standard deviation were 0.72 and 0.13 ppt. The increase in the mean value from February 1982 to December 1982 and February 1983 seems attributable mostly to the experimental uncertainties.

The background mixing ratios of SF_6 which were obtained in both this study and earlier works are shown in Fig. 2. The (a) value, which was obtained for the first time by Lovelock in 1970, was 0.03 ppt.[8] Observations after Lovelock have shown that the atmospheric SF_6 is increasing steadily.

The (b), (d), (g), (i), (j), and (l) values were obtained by aircraft observations. Except for the lower values of (e), (h), and (k), which were obtained in Antarctica or in the southern hemisphere, samples were obtained in the mid-latitude of the northern hemisphere. The values of this study((i), (j), and (l)) were in agreement with a higher value of Rasmussen and Khalil (0.75 ppt, (k)) which was obtained in the Pacific Northwest(≈45° N).[15]

The main sink for atmospheric SF_6 would be photodecomposition by solar ultraviolet radiation in the upper atmosphere. The rate of this process, however, must be very slow in the stratosphere, as SF_6 is photoionized only in the wavelength region below 81 nm.[16-18]

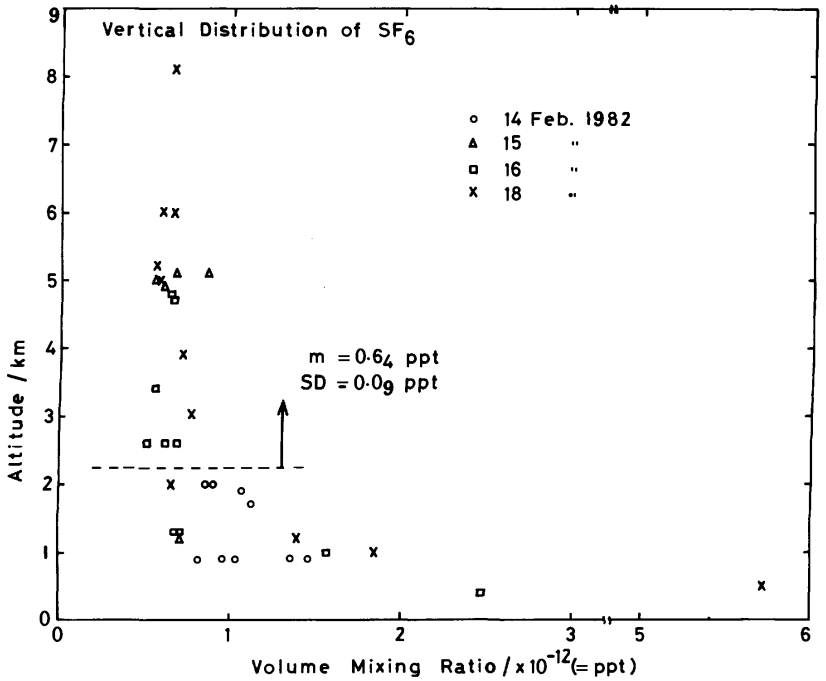

Fig. 1. Vertical distribution of SF_6.
Cessna 404 was used. Flight courses ranged from Sendai to Hachijo-jima.

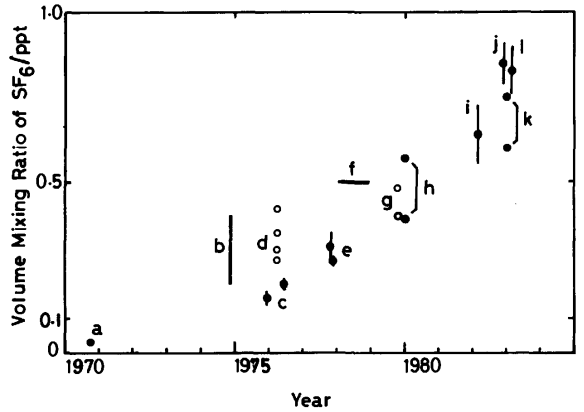

Fig. 2. Volume mixing ratios of SF_6.
○: individual value, ●: mean value and standard deviation.
In (b) and (f), only approximate values were reported. Individual values in (i) are shown in Fig. 1. In (j) and (l), samples were collected around Kanto Mts., and between Hamamatsu and Nii-jima.
(a): Lovelock,[8] (b): Elias et al.,[9] (c): Singh et al.,[10] (d): De Bortori and Pecchio.,[11] (e): Singh et al.,[12] (f): Pack et al.,[2] (g): Leifer et al.,[13] (h): Rasmussen et al.,[14] (i),(j), and (l): this study, (k): Rasmussen and Khalil[15].

The emission rate of SF_6 from gas-insulation instruments is not known. If the global mean mixing ratio is assumed to be about 0.5 ppt(≈1980), the total amount of SF_6 in the atmosphere is about 1.3×10^7 kg, assuming that the total air is 5.137×10^{18} kg.[19] The total world use was estimated to be 2.5—4.5×10^6 kg/year about 1980.[20] From these facts and also the development of SF_6 production since 1960's, a rather large part of the SF_6 may be supposed to have been released into the atmosphere in the several years since its production.

In this study, CF_2Cl_2 was used as the standard because a very dilute reference gas, such as SF_6, was not needed. However, the ratio in the senstivities of SF_6 and CF_2Cl_2 is not necessarily independent of the experimental conditions, and so further improvements are now in progress.

References

1) "Special Issue on SF_6 Gas Insulated Electric Apparatus," *J. Inst. Elec. Eng. Jpn.*, **97**, 327—405 (1977).
2) D. H. Pack, G. J. Ferber, J. L. Heffter, K. Telegadas, J. K. Angell, W. H. Hoecker, and L. Machta, *Atmos. Environ.*, **12**, 425 (1978).
3) For example, P. Hyson, P. J. Fraser, and G. I. Pearman, *J. Geophys. Res.*, **85**, 4443 (1980); P. D. Guthrie, C. H. Jackman, J. R. Herman, and C. J. McQuillan, ibid., **89**, 9589 (1984).
4) W. Weiss, A. Sittkus, H. Stockburger, H. Sartorius, and K. O. Münnich, *J. Geophys. Res.*, **88**, 8574 (1983).
5) H. Muramatsu, M. Hirota, and Y. Makino, *Bull. Chem. Soc. Jpn.*, **55**, 117 (1982).
6) M. Hirota, H. Muramatsu, Y. Makino, Y. Toyama, and T. Sasaki, *Tech. Rep. Met. Res. Inst.*, (1982) No. 6, Chap. 1, p. 5.
7) M. Hirota, H. Muramatsu, Y. Makino, T. Sasaki, and Y. Toyama, *J. Meteor. Soc. Jpn.*, **62**, 158 (1984).
8) J. E. Lovelock, *Nature*, **230**, 379 (1971).
9) L. Elias, M. McCooeye, and G. Gardner, *Geophys. Res. Lett.*, **3**, 17 (1976).
10) H. B. Singh, L. Salas, H. Shigeishi, and A. Crawford, *Atmos. Environ.*, **11**, 819 (1977).

11) M. De Bortoli and E. Pecchio, *Atmos. Environ.*, **10**, 921 (1976).
12) H. B. Singh, L. J. Salas, H. Shigeishi, and E. Scribner, *Sci*, **203**, 899 (1979).
13) R. Leifer, R. Larsen, and L. Toonkel, *Geophys. Res. Lett.*, **9**, 755 (1982).
14) R. A. Rasmussen, M. A. K. Khalil, and R. W. Dalluge, *Sci.*, **211**, 285 (1981).
15) R. A. Rasmussen, and M. A. K. Khalil, *Antarctic J. U. S.*, **18**, 250 (1983).
16) E. D. Nostrand and A. B. F. Dunkan, *J. Am. Chem. Soc.*, **76**, 3377 (1954).
17) J. A. Simpson, C. E. Kuyatt, and S. R. Mielczarek, *J. Chem. Phys.*, **44**, 4403 (1966).
18) V. H. Dibeler and J. A. Walker, *J. Chem. Phys.*, **44**, 4405 (1966).
19) K. E. Trenberth, *J. Geophys. Res.*, **86**, 5238 (1981).
20) "Encyclopedia of Chemical Technology," 3rd. Ed, John Wiley & Sons (1980), Vol. 10.

The Structure of Diaquatris(1,1,1-trifluoro-2,4-pentanedionato)neodymium(III)-Acetone (1/1)

Masao NAKAMURA, Reiko NAKAMURA, Kiyofumi NAGAI, Mamoru SHIMOI, Shuji TOMODA, Yoshito TAKEUCHI, and Akira OUCHI*
Department of Chemistry, College of Arts and Sciences, The University of Tokyo, Komaba, Meguro-ku, Tokyo 153
(Received July 27, 1985)

Synopsis. The crystal and molecular structure of the title complex was determined by means of the single-crystal X-ray diffraction method. The crystal of $NdC_{18}H_{22}O_9F_9$, F.W. 697.59, is orthorhombic, with a space group *Pbna*, a=22.068(5), b=22.293(4), c=11.020(2) Å, U=5421(2) Å^3, Z=8, D_m=1.72(3), D_x=1.71 Mg m^{-3}, and μ(Mo $K\alpha$)=20.46 cm^{-1}. The central metal atom is octa-coordinated, being ligated with six β-diketonato and two water oxygen atoms, and is in a dodecahedral geometry. Two configurational isomers co-exist in the crystal, with the respective occupancy factors of 74 and 26%. In these isomers, the two chelate rings span in different ways; although the positions of all ligating oxygen atoms are the same, the chelates span two m-edges in one isomer and two g-edges in the other one.

Although the structures of some β-diketonato complexes of lanthanoids(III) have already been reported, the coordination geometry and the spanned edges of the chelate rings have been found to be diverse. For example, in $M(acac)_3(H_2O)_2$ (where M=La, Pr, or Nd; Hacac=2,4-pentanedione), the central metal atom is in a square-antiprism geometry (octa-coordinated), and the chelate ligands span square edges.[1-3] On the other hand, in $Nd(tta)_3(Ph_3PO)_2$ (where Htta=4,4,4-trifluoro-1-(2-thienyl)-1,3-butanedione; Ph_3PO=triphenylphosphine oxide), the central metal is in a dodecahedral geometry (octa-coordinated), and the ligands span one m-edge and two g-edges.[a,4] In $NH_4Pr(tta)_4\cdot H_2O$ and $(C_9H_8N)[Ce(tta)_4]$, all the ligands span g-edges and m-edges respectively.[5,6] Although 1,1,1,-trifluoro-2,4-pentanedione (Htfa) is a ligand which gives several interesting types of complexes,[7,8] few structural data about its lanthanoid complexes have yet been reported. Therefore, we have determined the structure of the title complex by the single-crystal X-ray diffraction technique.

Experimental

Single-Crystal X-Ray Analysis. The crystals of the title complex were obtained by the slow evaporation of the complex in an acetone-water mixed solvent (4:1=v/v). (The crude product was obtained by a reaction between the metal hydroxide and Htfa, as was the isomorphous lanthanum(III) complex.) Anal. ($MC_{18}H_{22}O_9F_9$, where M=La, or Nd), M, C, H. The crystal used for the structure determination was about 0.3×0.3×0.2 mm^3 in size, and was used without shaping. The reflections in the range of $3°<2\theta<60°$ were collected on a Rigaku AFC-6A automated four-circle diffractometer, with graphite-monochromated Mo $K\alpha$ radiation, by means of the ω—2θ scan technique (scan speed 4° min^{-1}; scan width, 1.30+0.5 tanθ°). The intensities were corrected for Lorentz and polarization factors, but no correction was made for absorption and extinction. Among the 8731 independent reflections collected, 3611 with $|F_o|>3\sigma(|F_o|)$ were used for the structure determination. All the calculations were carried out on a HITAC M-280H computer at the Computer Center of the University of Tokyo, using the local version of the UNICS.[9] The scattering factors were taken from Ref. 10.

The structure was solved by the heavy-atom method. It was found that the crystal is composed of mixture of two configurational isomers. As is shown in Fig. 2, except for the common ligand (**1**), the Type A complexes include the ligands of F(21, 22A, 23A), C(21, 22A, 23A, 24A, 25), and O(21, 22) (**2A**) and F(31A, 32, 33A), C(31, 32A, 33A, 34A, 35), and O(31, 32) (**3A**), while the Type B complexes include those of F(21, 22B, 23B), C(21, 22B, 23B, 34B, 35), and O(21, 32) (**2B**) and F(31B, 32, 33B), C(31, 32B, 33B, 24B, 25), and O(31, 22) (**3B**). The probabilities of the occupancy of both types of complexes were first approximately assigned from the intensities of the atoms belonging to the respective types of ligands, and were then refined by means of the full-matrix least-squares procedure; the final occupancy factors for the type A and B complexes are 73.6(18)% and 26.4% respectively.

At the final refinement process, the positions of the seven fluorine atoms as well as the two acetone carbon atoms were fixed assuming B_{iso}=11.0. For the other atoms, except for O(AC) and C(Al), the anisotropic temperature factors were applied; the final R value[11] thus obtained was 0.066.

NMR Measurements. ^{1}H-NMR and ^{13}C-NMR spectra of the isomorphous lanthanum(III) complex were obtained by means of a Varian EM 390 NMR spectrometer and a JEOL FX90Q Fourier Transform NMR spectrometer, using the acetone-d_6 solution and TMS as the internal standards.[a]

Results and Discussion

The selected interatomic distances and bond angles are shown in Table 1.[12] A perspective drawing of the complexes in Type A is shown in Fig. 1. The schematic presentation showing the positions of the ligating atoms and of the spanning ligands, together with the numbering scheme of the ligands is shown in Fig. 2.[12]

. The central metal atom is octa-coordinated and is in a little deformed dodecahedral geometry. The chelating ligand **1**, which spans an m-edge, is common to both types of the species, while the other two ligands span in different ways; in Type A species, the ligands, **2A** and **3A**, span m-edges, but in

a) The isomorphism was checked from their powder X-ray diffraction patterns.

Table 1. Selected Bond Lengths and Bond Angles, with Estimated Standard Deviations in Parentheses

Bond length	l/Å	Bond length	l/Å	Bond length	l/Å
Nd-O(11)	2.411(8)	Nd-O(12)	2.393(8)	Nd-O(21)	2.366(9)
Nd-O(22)	2.460(8)	Nd-O(31)	2.372(8)	Nd-O(32)	2.455(8)
Nd-O(W1)	2.477(10)	Nd-O(W2)	2.498(9)	O(11)-C(12)	1.260(15)
O(12)-C(14)	1.264(15)	C(12)-C(13)	1.383(18)	C(13)-C(14)	1.386(15)
O(21)-C(22A)	1.20(2)	O(22)-C(24A)	1.32(2)	C(22A)-C(23A)	1.40(3)
C(23A)-C(24A)	1.43(3)	O(31)-C(32A)	1.23(2)	O(32)-C(34A)	1.283(19)
O(32A)-C(33A)	1.39(3)	C(33A)-C(34A)	1.40(2)	O(21)-C(22A)	1.11(4)
O(32)-C(34A)	1.30(4)	C(22B)-C(23B)	1.46(6)	C(23B)-C(34B)	1.27(6)
O(31)-C(32B)	1.17(5)	O(22)-C(24B)	1.32(4)	C(32B)-C(33B)	1.42(7)
C(33B)-C(24B)	1.36(6)	O(AC)···O(W1^{i})	2.736(19)		
Bond angle	ϕ/°	**Bond angle**	ϕ/°	**Bond angle**	ϕ/°
O(11)-Nd-O(12)	70.5(3)	O(21)-Nd-O(22)	70.7(3)	O(31)-Nd-O(32)	70.5(3)
O(21)-Nd-O(32)	72.3(3)	O(31)-Nd-O(22)	72.7(3)	O(W1)-Nd-O(W2)	67.9(3)
O(11)-Nd-O(21)	97.9(3)	O(11)-Nd-O(31)	143.5(3)	O(11)-Nd-O(22)	74.9(3)
O(11)-Nd-O(32)	145.4(3)				

Key to the symmetry operation: i, x, y, 1+z.

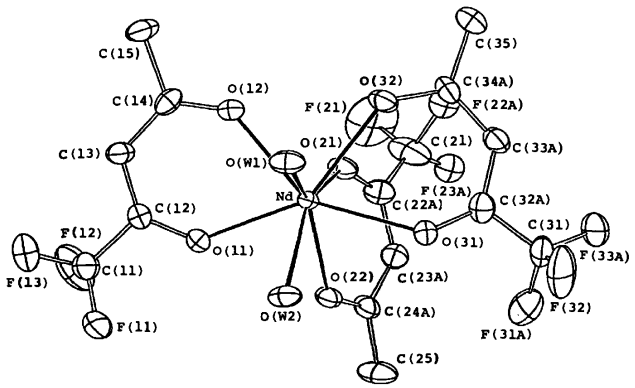

Fig. 1. A perspective drawing of Type A complex with the numbering scheme.

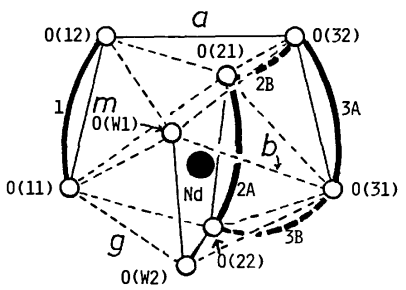

Fig. 2. Schematic presentation of the complex about the coordination geometry, with the numbering scheme of the chelating ligands (**1**, **2A**, and **3A** for Type A, and **1**, **2B**, and **3B** for Type B complex, respectively).

the Type B species, the ligands, **2B** and **3B**, span g-edges. In the chelate ring **1**, the two Nd-O bond lengths, 2.411(8) and 2.393(8) Å, are not much different from each other. On the other hand, in all the other chelate rings, the Nd-O(n1) lengths are shorter than the corresponding Nd-O(n2) ones. The Nd-O bond lengths to the coordinated water oxygen atoms are longer than those to the β-diketonato oxygen atoms. In view of the positions of O(11), O(21), and O(31), the trifluoromethyl groups of the ligands may be said to take the positions most separated from each other around the metal atom. Although the positions of all the atoms of the ligands were found, their thermal parameters, especially those of the fluorine atoms, were relatively large, probably because they are distributed around the most probable positions, respectively.

The NMR data of the isomorphous lanthanum(III) complex are as follows: ^{1}H-NMR (acetone d_6), δ=2.00 (9H, s, CH_3 of tfa), 2.10 (6H, s, CH_3 of acetone), 4.01 (4H, s, H_2O), 5.68 (3H, s, CH). ^{13}C-NMR (acetone-d_6), δ=28.8 (m, CH_3 in acetone), 29.9 (m, CH_3 in acetone-d_6), 96.1 (d, J_{CH}=146 Hz, CH), 169.1 (q, J_{CF}=31 Hz, CO(CF_3 side) of tfa), 197.3 (s, CO(CH_3 side) of tfa), 206.9 (s, CO of acetone), 120.1 (q, J_{CF}=290 Hz, CF_3). Judging from these data, the β-diketone in this complex can be said to be of the enol-type. As the peaks are all sharp, and as no splittings were found, a rapid exchange of the ligands can be expected between the two types of species in the solution at the ambient temperature (25 °C).

References

1) T. Phillips, D. E. Sands, and W. F. Wagner, *Inorg. Chem.*, **7**, 2295 (1968).
2) L. Yung-Hua, M. Chih-Sheng, and H. Yen, *Acta Chim. Sinica*, **34**, 33 (1976).
3) L. A. Aslanov, M. A. Porai-Koshits, and M. O. Dekaprilevich, *Zh. Strukt. Khim.*, **12**, 470 (1971).
4) J. G. Leipoldt, L. D. C. Bok, S. S. Basson, A. E.

Laubsher, and J. S. van Vollenhoven, *J. Inorg. Nucl. Chem.*, **39**, 301 (1977).

5) R. A. Lalancette, M. Cefola, W. C. Hamilton, and J. La Placa, *Inorg. Chem.*, **6**, 2127 (1967).

6) A. T. McHail and P. S. W. Tschang, *J. Chem. Soc., Dalton Trans.*, **1974**, 1165.

7) R. C. Mehrotra, R. Bohra, and D. P. Gaur, "Metal β-Diketonates and Allied Derivatives," Acad. Press, New York (1978), pp. 62, 75, 109.

8) F. Ebina, A. Ouchi, Y. Yoshino, S. Sato, and Y. Saito, *Acta Crystallogr., Sect. B*, **34**, 1512 (1978).

9) "The Universal Crystallographic Computation Program System (UNICS)," ed by T. Sakurai, Crystallographic Society of Jpn., Tokyo (1967).

10) "International Tables for Crystallography," Kynoch Press, Birmingham (1974), Vol. IV, pp. 92, 150.

11) $R=\sum||F_o|-|F_c||/\sum|F_o|$.

12) A perspective drawing of the complex B, the crystal packing diagram, the final atomic and thermal parameters, the final F_o-F_c table, and some additional data about the bond lengths and bond angles are deposited as Document No. 8602 at the Office of the Bull. Chem. Soc. Jpn.

Preparation and Thermal Isomerization of β-Arylthio α,β-Unsaturated Thioketone Dimer

Takayuki KARAKASA, Sadayoshi SATSUMABAYASHI,* and Shinichi MOTOKI†
Nippon Dental University, 1-9-20, Fujimi, Chiyoda-ku, Tokyo 102
†Department of Chemistry, Faculty of Science, Science University of Tokyo, Kagurazaka, Shinjuku-ku, Tokyo 162
(Received June 24, 1985)

Synopsis. β-Arylthio α,β-unsaturated thioketone dimer, 3,6-diphenyl-4-arylthio-3-[2-(arylthio)ethenyl]-3,4-dihydro-1,2-dithiin, has been prepared. Thermal isomerization of 3,4-dihydro-1,2-dithiin (aryl=phenyl) afforded 6-phenyl-2,4-bis(phenylthio)-3-thiobenzoyl-3,4-dihydro-2*H*-thiopyran.

Several types of acyclic α,β-unsaturated thioketones have been reported. For example, aliphatic (**1**)[1] or aromatic (**4**)[2,3] α,β-unsaturated thioketone is unstable at room temperature and exists in the dimeric form (**2**, **3**, or **5**). In contrast, β-thioxo enamines (**6**)[4] and α-(thioacyl)ketene dithioacetals (**7**)[5] are relatively stable and exist in monomeric forms. These results suggest that the thermal stability of acyclic α,β-unsaturated thioketone is influenced by the substituent groups, particularly heteroatoms (N or S), on the β-position.[4]

As a continuation of our investigation of α,β-unsaturated thioketones,[3,6] we have examined the preparation of β-arylthio α,β-unsaturated thioketone (**9**) in order to investigate the influence of the β-arylthio group on the stability of the α,β-unsaturated thioketone (**9**), and it was found that the thioketone **9** readily dimerized into 3,4-dihydro-1,2-dithiin compounds (**10** and **12**) at room temperature and the dimer **10a** or **12a** isomerized to the thermodynamically more stable dimer, the 3,4-dihydro-2*H*-thiopyran derivative (**13a**), at elevated temperature.

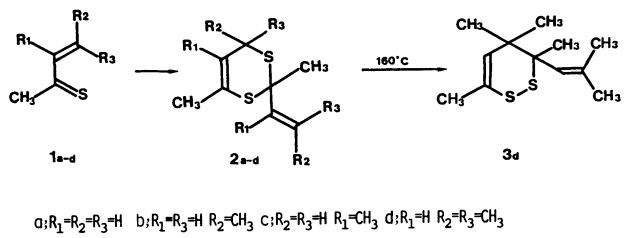

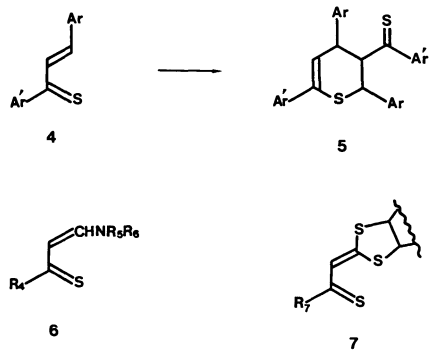

The reaction of 1-phenyl-3-phenylthio-2-propene-1-one (**8a**) with P_4S_{10} gave two products together with a large amount of tarry matter.

In the ^{1}H-NMR spectrum of one product, doublets at δ 6.13 (J=14.8 Hz) and 6.70 (J=14.8 Hz) were assigned to olefinic protons in an *E*-configuration. An assignment of the C-4 proton to the axial position is supported by the coupling constant (J=3.2 Hz) between the C-4 and the C-5 protons.[7,8] The ^{13}C-NMR spectrum exhibited two alkyl carbon signals at δ 55.2 (s) and 58.4 (d). These spectral data are in agreement with the proposed structure **10a** or **11a**. A treatment of this product with Raney nickel (W-2) gave 1,4-diphenylhexane. Therefore, this product was determined to be the 3,4-dihydro-1,2-dithiin structure **10a**.

The ^{1}H-NMR spectrum of the other product showed three olefinic protons at δ 6.33 and one methine proton at δ 4.42. In the ^{13}C-NMR spectrum appeared two alkyl carbon signals. However, it could not be determined whether the product was the 3,4-dihydro-1,2-dithiin or the 4*H*-1,3-dithiin structure.

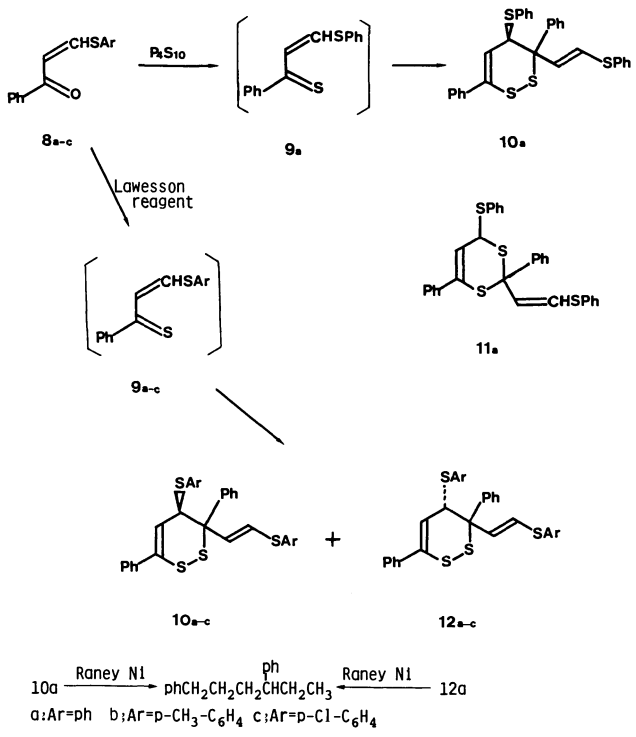

On the other hand, when **8a** was treated with Lawesson reagent while refluxing carbon disulfide, **10a** and **12a** were obtained. The structural assignment of **12a** is based on the ^{1}H-NMR spectrum and its conversion into 1,4-diphenylhexane by a Raney nickel reduction. The assignment of a C-4 proton to the equatorial position is supported by the larger coupling constant (J=5.2 Hz) between the C-4 and the C-5 protons than that of **10a** and in comparison with that of the analogous 3,4-dihydro-1,2-dithiin in the literature.[8]

3,4-Dihydro-1,2-dithiin was unstable during the course of isolation by column chromatography and recrystallization. Thus, the isolated yields were low. The thionation of other ketones **8b** and **8c** with Lawesson reagent afforded **12b** and **10c**, respectively. However, it was not possible to isolate **10b** and **12c** due to the ease of decomposition.

We observed that the color of solution (hexane, chloroform, etc) **10** or **12** turned from pale yellow to green upon heating. Thus, 3,4-dihydro-1,2-dithiin **10a** or **12a** was refluxed in hexane to give 3,4-dihydro-2*H*-thiopyran **13a** in moderate yield, respectively. The molecular ion (m/z 512) was observed in the mass spectrum. The ^{13}C-NMR spectrum exhibited a characteristic thiocarbonyl carbon signal at δ 235.5 and three methine carbon signals. Desulfurization of the dihydrothiopyran gave 2-methyl-1,5-diphenylpentane. Therefore, this compound was assigned to the proposed structure **13a**.

It would be probable that 3,4-dihydro-1,2-dithiin **10** and **12** formed by the cyclodimerization of **9** and the thermal unstable 3,4-dihydro-1,2-dithiin isomerized to the thermodynamically more stable dihydrothiopyran via a retro-Diels-Alder reaction at an elevated temperature (Scheme 1). The β-arylthio group, especially when there was only one sulfur atom, did not contributed to the stabilization of monomer **9**.

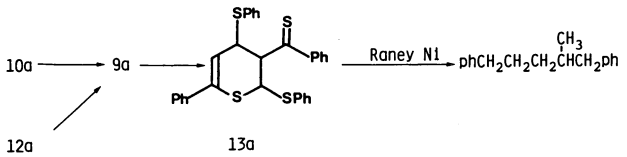

Scheme 1.

Experimental

All melting points were uncorrected. ^{1}H-NMR spectra were determined on a JEOL JNM PMX60SI or FX-100 spectrometer and ^{13}C-NMR spectra were recorded on a JEOL JNM-FX-100 spectrometer. Me_4Si was used as an internal standard. Mass spectra were measured on a Hitachi mass spectrometer RMU-7M or a JEOL JMS-DX300 or JMA-3100 mass spectrometer. 2,4-Bis(4-methoxyphenyl)-1,3-dithia-2,4-diphosphetane 2,4-disulfide (Lawesson reagent) was obtained commercially. All 1-phenyl-3-arylthio-2-propene-1-ones (**8**) were prepared according to the method of Engelhard et al.[9]

Thionation with P_4S_{10}. A suspension of 1-phenyl-3-phenylthio-2-propene-1-one **8a** (2.4 g), P_4S_{10} (1.0 g), and triethylamine (1.0 ml) in carbon disulfide (80 ml) was stirred at room temperature for 6 d. The solvent was evaporated and the residue was chromatographed on a Florisil gel by using benzene–hexane (1:1) as the eluent.

The first fraction was determined to be 3,6-diphenyl-4-phenylthio-3-[2-(phenylthio)ethenyl]-3,4-dihydro-1,2-dithiin **10a**: yellow rhombic crystals. Mp 102—104 °C. yield 3.9%. MS (22 eV) m/z: 256 ($M^+/2$, 5.8), 179 (100), 147 (3.9), 121 (11.7), 110 (18). ^{1}H-NMR ($CDCl_3$) δ=4.58 (1H, d, J=3.2 Hz), 6.13 (1H, d, J=14.8 Hz), 6.50 (1H, d, J=3.2 Hz), 6.70 (1H, d, J=14.8 Hz), 7.10—7.67 (20H, m). ^{13}C-NMR ($CDCl_3$) δ=55.2 (s), 58.4 (d), 126.3, 127.1, 127.5, 127.8, 128.4, 128.8, 129.1, 132.4, 135.0, 136.6, 137.8, 141.3. Found: C, 70.00; H, 4.72%. Calcd for $C_{30}H_{24}S_4$: C, 70.27; H, 4.66%.

The second fraction: yellow silky needles. Mp 116—117.5 °C. yield 1.8%. MS (22 eV) m/z: 256 ($M^+/2$,8), 179 (100), 147 (64), 121 (18), 115 (10), 110 (10), 103 (11). ^{1}H-NMR ($CDCl_3$) δ=4.42 (1H, d, J=4.8 Hz), [6.33 (d, J=4.8 Hz), 6.33 (s) total 3H], 7.23—7.70 (20H, m). ^{13}C-NMR ($CDCl_3$) δ=55.5 (d), 63.9 (s), 123.3, 125.9, 126.6, 127.0, 127.3, 127.9, 128.5, 128.9, 129.1, 129.8, 132.1, 132.6, 135.7, 135.9, 138.0, 138.3. Found: C, 70.03; H, 4.66%. Calcd for $C_{30}H_{24}S_4$: C, 70.27; H, 4.66%.

Thionation with Lawesson Reagent. A suspension of **8a** (2.4 g) and Lawesson reagent (2.0 g) in carbon disulfide (20 ml) was refluxed for 5 h under a nitrogen atmosphere. The solvent was removed using a rotary evaporator and the residue was passed through a short column of Florisil gel using benzene–hexane (1:1) as the eluent to give a mixture of **10a** and **12a** (yield 46%). The mixture was chromatographed on Florisil gel using benzene–hexane (1:3) as the eluent.

10a: Yield 13% (recrystallized from benzene–hexane).

12a: Yellow silky needles (recrystallized from benzene–ethanol). Mp 99.5—101.5 °C. yield 7.8%. ^{1}H-NMR ($CDCl_3$) δ=4.27 (1H, d, J=5.2 Hz), 6.23 (1H, d, J=15.2 Hz), 6.40 (1H, d, J=15.2 Hz), 6.52 (1H, d, J=5.2 Hz), 6.97—7.45 (20H, m). ^{13}C-NMR ($CDCl_3$) δ=57.1 (d), 58.4 (s), 126.1, 126.3, 126.8, 127.0, 127.3, 127.7, 127.8, 128.3, 128.6, 128.7, 128.9, 129.1, 129.8, 132.2, 134.0, 134.6, 136.0, 136.5, 138.0, 139.4. Found: C, 70.11; H, 4.57%. Calcd for $C_{30}H_{24}S_4$: C, 70.27; H, 4.66%.

4-(*p*-Methylphenylthio)-3,6-diphenyl-3-[2-(*p*-methylphenylthio)ethenyl]-3,4-dihydro-1,2-dithiin 12b: Mp 108—109 °C. yield 8%. MS (20 eV) m/z: 416 (2), 385 (6), 293 (30), 179 (100). ^{1}H-NMR ($CDCl_3$) δ=2.27 (6H, s), 4.22 (1H, d, J=5.2 Hz), 6.14 (1H, d, J=15.2 Hz), 6.50 (1H, d, J=15.2 Hz), 6.55 (1H, d, J=5.2 Hz), 6.85—7.47 (18H, m). Found: C, 71.01; H, 5.22%. Calcd for $C_{32}H_{28}S_4$: C, 71.07; H, 5.22%.

***p*-(Chlorophenylthio)-3,6-diphenyl-3-[2-(*p*-chlorophenylthio)ethenyl]-3,4-dihydro-1,2-dithiin 10c**: Mp 122—126 °C. yield 22%. MS (20 eV) m/z: 436, 408, 406, 404, 320, 318, 298, 296, 180, 144. ^{1}H-NMR ($CDCl_3$) δ=4.52 (1H, d, J=3.2 Hz), 6.10 (1H, d, J=16.0 Hz), 6.43 (1H, d, J=3.2 Hz), 6.57 (1H, d, J=16.0 Hz), 6.93—7.60 (18H, m). Found: C, 61.59; H, 3.82%. Calcd for $C_{30}H_{22}Cl_2S_4$: C, 61.95; H, 3.81%.

Reduction of 10a with Raney Nickel. To a suspension of freshly prepared W-2 Raney nickel[10] (≃10 g) in ethanol (20 ml) was added 1,2-dithiin **10a** (1.0 g) in benzene (20 ml). The mixture was stirred overnight at room temperature. The mixture was chromatographed on Wakogel C-200 using hexane as the eluent to give 1,4-diphenylhexane: yield 0.3 g (65%). MS (20 eV) m/z: 238 (M^+, 23), 131 (69), 119 (23), 105 (19), 91 (100). ^{1}H-NMR ($CDCl_3$) δ=0.62—2.63 (12H, m), 7.08 (10H). ^{13}C-NMR ($CDCl_3$) δ=12.3, 29.5, 29.9, 36.1, 47.9, 125.7, 125.9, 127.9, 128.3, 128.5, 142.7, 145.8.

Reduction of 12a with Raney Nickel. 1,4-Diphenylhexane: yield 94%.

Reduction of 13a with Raney Nickel. To a suspension of freshly prepared W-2 Raney nickel[10] (≃10 g) in benzene (100 ml) was added dihydrothiopyran **12a** (0.5 g). The mixture was stirred overnight at room temperature. Purification of the mixture by preparative TLC (Merk 5744) using benzene-hexane (1:3) as the eluent gave 2-methyl-1,5-diphenylpentane: yield 73 mg (31%). MS (70 eV) *m/z*: 238 (M^+, 17), 147 (12), 131 (12), 91 (100). ^{1}H-NMR ($CDCl_3$) δ=0.83 (3H, d), 1.17—1.93 (5H, m), 2.13—2.80 (4H, m), 7.10 (10H, s). ^{13}C-NMR ($CDCl_3$) δ=19.3 (t), 29.1 (t), 34.9 (d), 36.1 (t), 36.3 (t), 43.6 (t).

Thermal Isomerization of 10a. A suspension of **10a** (1.145 g) in hexane (100 ml) was refluxed for 9 h under a nitrogen atmosphere. The resulting deep-blue precipitate was collected by filtration and washed with ethanol. The precipitate was recrystallized from benzen-hexane to give 6-phenyl-2,5-bis(phenylthio)-3-thiobenzoyl-3,4-dihydro-2*H*-thiopyran **13a** as a deep blue needles: Mp 128—129 °C. yield 0.894 g (78%). MS (FD) *m/z*: 512 (M^+). ^{1}H-NMR ($CDCl_3$) δ=[4.46 (J=3.6, 7.0, and 0.2 Hz), 4.50 (J=3.6, 4.0, and 0.2 Hz) total 2H], 5.09 (1H, J=7.0, 0.2, and 0.1 Hz), 6.20 (1H, J=4.0, 0.2, and 0.1 Hz), 7.08—7.56 (20H, m). ^{13}C-NMR ($CDCl_3$) δ=47.2 (d), 51.2 (d), 55.6 (d), 119.5, 126.4, 126.5, 127.4, 128.9, 129.1, 129.4, 131.9, 132.1, 132.9, 133.7, 134.4, 135.6, 138.2, 145.8, 235.5. Found: C, 70.30; H, 4.56%. Calcd for $C_{30}H_{24}S_4$: C, 70.27; H, 4.66%.

Thermal Isomerization of 12a. **13a**: yield 53%.

References

1) W. J. Bailey and M. Izogawa, *Am. Chem. Soc. Div. Polymer Chem. Preprints* **14**, 300 (1973); H. G. Giles, R. A. Marty, and P. deMayo, *J. Chem. Soc., Chem. Commun.*, **1974**, 409; H. G. Giles, R. A. Marty, and P. deMayo, *Can. J. Chem.*, **54**, 537 (1976); P. Beslin, D. Lagain, and J. Vialle, *Tetrahedron Lett.*, **1979**, 2677; P. Beslin, D. Lagain, J. Vialle, and C. Monot, *Tetrahedron*, **37**, 3839 (1981): P. Beslin, *J. Heterocyclic Chem.*, **20**, 1753 (1983).

2) J. P. Pradere, G. Bouet, and H. Quiniou, *Tetrahedron Lett.*, **1972**, 3471.

3) T. Karakasa and S. Motoki, *J. Org. Chem.*, **43**, 4147 (1978).

4) H. Quiniou, *Phosphorus and Sulfur*, **10**, 1 (1981): V. A. Usov and M. G. Voronkov, *Sulfur Reports*, **2**, 39 (1982) and refereces therein.

5) R. Okazaki, K. Okawa, and N. Inamoto, *J. Chem. Soc., Chem. Commun.*, **1971**, 843; R. Okazaki, F. Ishii, K. Ozawa, and N. Inamoto, *Chem. Lett.*, **1972**, 9; F. Ishii, K. Okawa, and N. Inamoto, *J. Chem. Soc., Perkin Trans. 1*, **1975**, 270.

6) T. Karakasa and S. Motoki, *J. Org. Chem.*, **44**, 4151 (1979); T. Karakasa, H. Yamaguchi, and S. Motoki, ibid, **45**, 927 (1980); T. Karakasa and S. Motoki, *Chem. Lett.*, **1980**, 879.

7) P. M. Henrichs and C. H. Chen, *J. Org. Chem.*, **44**, 3591 (1979).

8) J-P. Guemas and H. Quiniou, *Sulfur Letters*, **2**, 121 (1984).

9) N. Engelhard and A. Kolb, *Justus Liebigs Ann. Chem.*, **673**, 136 (1964).

10) R. Mozingo, *Org. Synth.*, Coll. Vol. **3**, 181 (1954).

Selective Electrolytic Cleavage of a Side-Chain Carbon-Sulfur Bond of Heterocyclic Compounds. Formation of Di-2-thienyl Disulfides and 2-Mercaptothiazoles

Toshio FUCHIGAMI,* Zaghloul El-Shahat KANDEEL,† and Tsutomu NONAKA
Department of Electronic Chemistry, Graduate School at Nagatsuta,
Tokyo Institute of Technology, Nagatsuta, Midori-ku, Yokohama 227
†Department of Chemistry, Faculty of Science, Cairo University, Giza, A. R. Egypt
(Received April 22, 1985)

Synopsis. Highly selective cleavage of a side-chain carbon-sulfur bond of thiophene and thiazole derivatives containing acyl, cyano, and ethoxycarbonyl groups was successfully performed by electroreduction to provide the corresponding disulfides and thiols respectively in excellent to good yields.

In the course of our intensive synthetic studies of heterocyclic compounds,[1,2] we found a facile synthesis of 2-acyl-3-aminothiophene derivatives (**3**) from two equiv of α-halo ketones (**2**) and sodium cyanophenyldithioacetate (**1**) in the presence of triethylamine (Scheme 1).[3] Even though equimolar amounts of **1** and **2** were used in this reaction, **3** was always obtained and any 2-acyl-3-amino-5-mercapto-4-phenylthiophenes (**4**) were not formed.

It is well known that the desulfurization of phenacyl sulfides[4] and phenacyl sulfoxides[5] can be easily achieved by chemical reduction with zinc/AcOH or alminum amalgam to provide the corresponding ketones.

Since the molecular structure of **3** is similar to phenacyl sulfides, its chemical reduction was first carried out in a manner similar to that reported.[4,5] However, our attempts to obtain **4** were not successful.

Recently, electrochemical methods have been shown

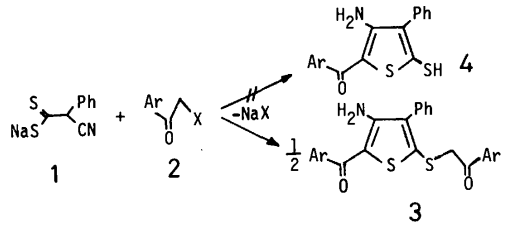

Scheme 1.

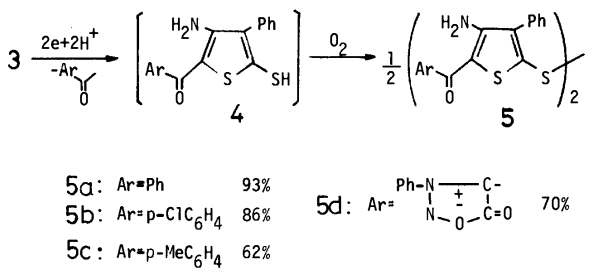

Scheme 2.

to be useful for the deprotection of sulfur moieties for organic synthesis, especially for that of natural products.[6,7] These facts prompted us to attempt the electroreduction of **3**. After several attempts, the constant current electroreduction was successfully carried out at a mercury cathode in DMF containing phenol as a proton source to give rise to **4**. In these electrolyses, after slightly excess of theoretical amount of electricity ($2.2\times96480\ C\ mol^{-1}$) had been passed, the cell voltage was found to increase remarkably and the electrolysis was stopped.

As shown in Scheme 2, the electroreduction proceeded smoothly and cleanly, and the desired **4** could be obtained as the corresponding disulfide (**5**) in good yields. The structure of **5** was determined mainly by the mass spectra together with IR and elemental analysis. The disulfide **5** showed its molecular ion peak and/or its fragments such as M^+-S, M^+-SH, and $M^+/2$. These fragmentation is well known to be characteristic of diaryl disulfides.[8]

Although a typical mesoionic compound, sydnone is interesting for its chemical, physical, and biological properties, its synthesis seems to be limitted, because the sydnone ring is unstable to acid, alkali, and heat.[9] Since the sydnone ring is also easily reduced chemically and electrochemically to decomposition products,[10] no report of the preparative electroreduction of sydnone compounds has been published except for one reported by us[11] and only a few papers deal with polarography of sydnones.[12] From this point, the electroreduction of a sydnone derivatives of **3** was also attempted. It was found that the selective reduction proceeded without any decomposition of the sydnone ring to provide pure **5d** without purification. The isolated disulfides **5** seem to be formed during the work-up by the air-oxidation of **4** once formed by the electroreduction.

At the second stage of this study, we applied this electrochemical technique to other heterocyclic compounds such as thiazoles. Three thiazole derivatives (**6**)[13] were chosen as model compounds. A highly selective electroreduction of **6** proceeded to provide the corresponding 2-mercaptothiazoles (**7**) in good yields as shown in Scheme 3. It is noticeable that disulfides **5** were always obtained as the products from thiophene derivatives **3** whereas thiols **7** were derived from thiazoles **6** in the electroreduction. In these electrolyses, reasonable amount of acetophenone derivatives, acetonitrile, and ethyl acetate were detected in the catholyte by GC analysis and any further reduction did not occur. From these results,

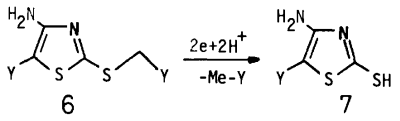

6 7

7a : Y=PhCO 69%
7b : Y=CN 53%
7c : Y=EtOCO 70%

Scheme 3.

the electroreduction seemed to proceed via a two-electron step.

Although **3** and **6** contain other reducible groups such as carbonyl, nitrile, and ester groups, only reductive cleavage of the C-S bond took place selectively.

Since the reduction proceeded selectively and efficiently under quite mild conditions and did not need any reducing reagent, this clean electrochemical method seems to have a potential utility for organic synthesis.

Experimental

Starting Material. Thiophene and thiazole derivatives (**3** and **6**) were prepared using the method reported previously[3] and according to the reference.[13]

General Electrolytic Procedure. An H-type electrolytic cell divided with a glass filter diaphragm was used. A mercury pool (area 7.1 cm^2) and a platinum plate were used as a cathode and anode, respectively. The catholyte was 40 ml of 0.1 mol dm^{-3} $NaClO_4$-DMF solution containing 1.5 mmol of thiophenes **3** or thiazoles **6** together with 3.0 mmol of phenol. The constant current (0.57 A dm^{-2}) was passed at ca. 20 °C.

Analysis and Isolation of Products. After the electrolysis, the catholyte was evaporated under reduced pressure below 60 °C. The residue was mixed with water and neutralized. The resulting precipitated product was collected by filtration, washed with water or ether, and dried. The catholyte was subjected to gas chromatography (PEG 20M) for analysis of acetophenones, acetonitrile, and ethyl acetate.

Bis(4-Amino-5-benzoyl-3-phenyl-2-thienyl) Disulfide (5a): Mp 174 °C (from ethanol). IR (KBr) 3500, 3300 (νNH) and 1590 cm^{-1} (νC=O). MS *m/z* 620 (M^+), 588 (M^+-S), 587 (M^+-SH), 310 ($M^+/2$), and 105 ($PhCO^+$). Found: C, 65.79; H, 3.69; N, 4.52%. Calcd for $C_{34}H_{24}N_2O_2S_4$: C, 65.78; H, 3.90; N, 4.51%.

Bis[4-amino-5-(*p*-chlorobenzoyl)-3-phenyl-2-thienyl] Disulfide (5b): Mp 138 °C (from DMF). IR (KBr): 3450, 3300 (νNH) and 1580 cm^{-1} (νC=O). MS *m/z* 660 (M^++4−S), 658 (M^++2−S), 656 (M^+-S), 655 (M^+-SH), 346 (M^++4/2), 345 (M^++2/2), 344 ($M^+/2$), 141, and 139 (p-$ClC_6H_4CO^+$). Found: C, 59.16; H, 3.23; N, 4.45%. Calcd for $C_{34}H_{22}N_2S_4Cl_2$: C, 59.21; H, 3.21; N, 4.08%.

Bis[4-Amino-5-(*p*-toluoyl)-3-phenyl-2-thienyl] Disulfide (5c): Mp 136 °C (from EtOH-DMF). IR (KBr): 3500, 3300 (νNH), 1605 and 1580 cm^{-1} (νC=O). MS *m/z* 616 (M^+-S), 615 (M^+-SH), 325 ($M^+/2+H$), and 120 (p-$MeC_2H_4CHO^+$). ^1H NMR (acetone-d_6) δ=2.44 (s, 6H, CH_3), 3.08 (broad s, 4H, NH_2), and 7.28—7.92 (m, 18H, Ar-H). Found: C, 66.54; H, 4.49; N, 4.32%. Calcd for $C_{36}H_{28}N_2O_2S_4$: C, 66.64; H, 4.35; N, 4.32%.

Bis[4-Amino-5-(3-phenyl-4-sydnonylcarbonyl)-3-phenyl-2-thienyl] Disulfide (5d): Mp 194 °C (decomp). IR (KBr): 3480, 3320 (νNH), 1775 (νC=O of a sydnone ring), and 1580 cm^{-1} (νC=O). MS *m/z* 478 (M^+-PhN-CO-NO-PhN—C-(N±C=O, O⁻)), 438 (M^+- PhN—C-(N±C=O, O⁻) — PhN—C-CO(N±C=O, O⁻)), and 189 (PhN—C-CO⁺ (N±C=O, O⁻)). Found: C, 57.61; H, 3.30; N, 10.54%. Calcd for $C_{38}H_{24}N_6O_6S_4$: C, 57.86; H, 3.07; N, 10.65%.

4-Amino-5-benzoyl-2-mercaptothiazole (7a): Mp 231 °C (from ethanol). IR (KBr): 3400, 3300 (νNH) and 1640 cm^{-1} (νC=O). MS *m/z* 236 (M^+), 235 (M^+-H), 159 (M^+-Ph), 130 ($M^+-H-PhCO$), and 105 ($PhCO^+$). Found *m/z* 236.0039. Calcd for $C_{10}H_8N_2OS_2$: 236.0077.

4-Amino-5-cyano-2-mercaptothiazole (7b): Mp 202—203 °C (from ethanol). IR (KBr): 3320, 3220, 3100 (νNH) and 2220 cm^{-1} (νC=N). MS *m/z* 157 (M^+), 130 (M^+-HCN), and 98 ($M^+-HCN-S$). Found: C, 30.60; H, 1.81; N, 26.73%. Calcd for $C_4H_3N_3S_2$: C, 30.56; H, 1.81; N, 26.73%.

4-Amino-5-ethoxycarbonyl-2-mercaptothiazole (7c): Mp 192 °C (from ethanol). IR (KBr): 3400, 3320, 3220 (νNH) and 1670 (νC=O). MS *m/z* 204 (M^+), 176 ($M^+-C_2H_4$), 159 (M^+-EtO), and 130 ($M^+-H-EtOCO$). Found: C, 35.56; H, 3.83; N 13.61%. Calcd for $C_6H_8N_2O_2S_2$: C, 35.28; H, 3.95; N, 13.71%.

We are grateful for valuable discussion with Profs. H.-J. Tien and M.-Y. Yeh of National Cheng Kung University, Taiwan, Republic of China, and thank Dr. Y. Fujimoto, Tokyo Institute of Technology and Mitsubishi Chemical Industry for MS and Hi-MS measurement.

References

1) T. Fuchigami and T. Nonaka, *J. Org. Chem.*, **48**, 3340 (1983); T. Fuchigami, M.-Y. Yeh, T. Goto, T. Nonaka, and H.-J. Tien, *Bull. Chem. Soc. Jpn.*, **57**, 116 (1984).

2) Z. E. Kandeel, K. M. H. Hilmy, F. M. A. Razek, and M. H. Elnagdi, *Chem. Ind. (London)*, **1984**, 33.

3) T. Fuchigami, Z. E. Kandeel, and T. Nonaka, *Bull. Chem. Soc. Jpn.*, **58**, 2441 (1985).

4) G. A. Russel and G. J. Mikol, *J. Am. Chem. Soc.*, **88**, 5498 (1966); M. A. McKerrey and P. Ratananukul, *Tetrahedron Lett.*, **24**, 117 (1983).

5) E. J. Corey and M. Chaykovsky, *J. Am. Chem. Soc.*, **86**, 1639 (1964); *J. Am. Chem. Soc.*, **87**, 1345 (1965).

6) M. Platen and E. Stekhan, *Tetrahedron Lett.*, **21**, 511 (1980); T. Mandai, H. Yasunaga, M. Kawada, and J. Otera, *Chem. Lett.*, **1984**, 715; M. Kimura, S. Matsubara, and Y. Sawaki, *J. Chem. Soc., Chem. Commun.*, **1984**, 1619; A. Kunugi, A. Muto, and T. Hirai, *J. Chem. Soc. Jpn.*, **1984**, 1821.

7) Very recently, Kunugi et al. have reported the polarographic study on the electroreduction of phenacyl sulfides in aqueous ethanol and anhydrous acetonitrile solutions. They have also carried out controlled potential macroelectrolyses of the phenacyl sulfides to provide acetophenone and the corresponding arylthiols and/or diaryl disulfides in moderate yields: *Bull. Chem Soc. Jpn.*, **58**, 1262 (1985).

8) H. Budzikiewicz, C. Djerassi, and D. H. Williams, "Mass Spectrometry of Organic Compounds," Holden-Day

Inc., San Francisco (1967), p. 292.

9) F. H. C. Stewart, Chem. Rev., **64**, 129 (1964); M. Ota and H. Kato, "Non-benzenoid Aromatics," Academic Press, New York (1969), Vol. 1, p. 117; C. G. Newton and C. A. Ramsden, *Tetrahedron*, **38**, 2965 (1982).

10) For example, electroreduction of 4-nitrosydnones to 4-aminosydnones was unsuccessful because the reduction of the ring is easier than that of the nitro group: H.-J. Tien, T. Nonaka, and T. Fuchigami, unpublished results.

11) 4-(Bromoacetyl)sydnone is easily reduced at a cathode to provide 1,4-bis(4-sydnonyl)butane and 4-acetylsydnone without any decomposition of the sydnone ring: T. Fuchigami, T. Goto, M.-Y. Yeh, T. Nonaka, and H.-J. Tien, *Bull. Chem. Soc. Jpn.*, **57**, 1362 (1984).

12) P. Zuman, *Collection. Czech. Chem. Commun.*, **25**, 3245, 3252, 3265 (1960).

13) K. Gewald, P. Blauschmidt, and R. Mayer, *J. Prak. Chem.*, **35**, 97 (1967).

Reaction of Tri-*n*-butyltin ω-Haloalkoxide (*n*-$Bu_3SnO(CH_2)_nX$) with Isothiocyanate

Akio BABA, Ikuya SHIBATA,* Hiroki KASHIWAGI, and Haruo MATSUDA
Department of Applied Chemistry, Faculty of Engineering, Osaka University,
2-1 Yamadaoka, Suita, Osaka 565
(Received August 8, 1985)

Synopsis. Tri-*n*-butyltin ω-haloalkoxides are useful reagents for the preparation of sulfur-containing five- and six-membered cyclic compounds combined with isothiocyanates.

We have recently reported the novel use of tri-*n*-butyltin ω-haloalkoxides (*n*-$Bu_3SnO(CH_2)_nX$ n=2,3 X=Cl, Br, I) (**1**). They are useful reagents yielding a variety of five- and six-membered heterocyclic compounds by combination with isocyanates or carbodiimides.[1] An important feature of this reaction is that **1** can be regarded as a synthon of oxiranes or oxetanes.[2] Nevertheless, in some cases, several types of compounds different from the cycloadducts of heterocumulenes with oxiranes can be obtained.

The cycloaddition of isothiocyanates to oxiranes has been investigated,[3] but in these cases, cycloadducts were obtained only by using activated isothiocyanates such as benzoyl and acetyl isothiocyanate. In other isothiocyanates such as aromatic and aliphatic isothiocyanates, no sulfur-containing cycloadduct has been obtained because of the isomerization from oxathiolanimines to oxazolidinones in the presence of oxiranes, moreover, the formation of by-products was often a problem.[4]

As a part of continuing study on synthetic use of **1**, we wish herein to report the reaction of **1** with isothiocyanates (**2**), thereby preparing five- and six-membered sulfur- containing cyclic compounds under mild condition (Scheme 1).

Treatment of *n*-$Bu_3SnO(CH_2)_2X$ with PhNCS gave a mixture of *N*-phenyl-1,3-oxathiolan-2-imine **3** and 3-phenyl-1,3-oxazolidin-2-thione **4**. The proportion of these products appeared to be dependent on the nature of substrates and solvents as shown in Table 1. The order of the reactivity of halogen species in **1** was Cl<Br<I, and the proportion of **4** was decreased in this order (entries 1, 3, and 4). The use of the chloride in hexane induced the predominant formation of **4a** (entry 1), which has not been obtained even from the cycloaddition of activated isothiocyanates to oxiranes.[3] Meanwhile, DMF, when used as a solvent,

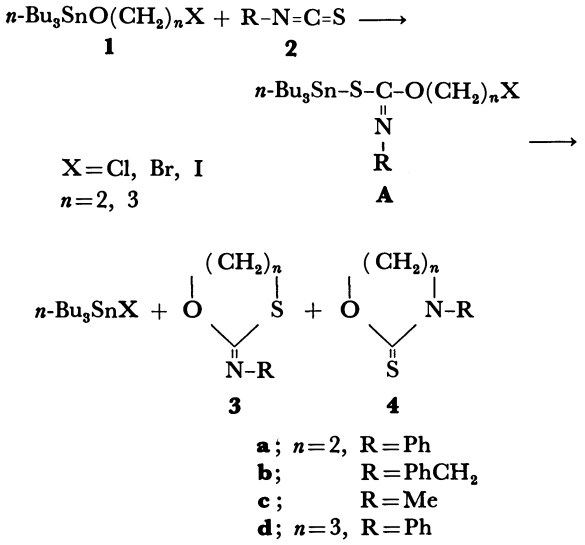

Scheme 1.

Table 1. Reactions between *n*-$Bu_3SnO(CH_2)_nX$ and Isothiocyanates[a]

Entry	1		2	Solv. (ml)	Isolated yield/ %	3/4 Ratio[b]
	n	X	R			
1	2	Cl	Ph	Hexane (10)	43	7/93
2	2	Cl	Ph	DMF (5)	90[c]	49/51
3	2	Br	Ph	Hexane (10)	68	17/83
4	2	I	Ph	Hexane (10)	80	34/66
5	2	I	Ph	DMF (5)	100[c]	83/17
6	2	Br	$PhCH_2$	Hexane (10)	41	68/32
7	2	Br	$PhCH_2$	DMF (5)	91	77/23
8	2	Br	Me	Hexane (10)	15	20/80
9	2	Br	Me	DMF (5)	33	90/10
10	2	I	Me	DMF (5)	56	100/0
11	3	Br	Ph	Hexane (10)	14	0/100
12	3	Br	Ph	DMF (5)	57	0/100
13	3	I	Ph	Hexane (15)	73	0/100

a) **1** 10 mmol, **2** 8 mmol, Temp. 40 °C, Time 1 h, b) Determined by GLC, c) 25 °C.

accelerated the reaction, and the proportion of **3a** was greater than in hexane (entries 2 and 5). Similar effects of DMF were observed in the reactions with alkyl isothiocyanates, although, the reactivity of which was low (entries 6—10).

At the initial stage of the reaction, isothiocyanates were added to **1** exothermically, and the IR absorption band of ν NCS immediately disappeared and the new band around 1600 cm^{-1} (C=N) was recognized.[5] In the case of isocyanates, two types of adducts were considered.[1] However, because of the great affinity of tin toward sulfur atoms,[6] the addition of **1** may take place only across the C=S group of RNCS as described by Davies et al.,[7] giving **A** as an intermediate (Scheme 1). In next stage, the intramolecular alkylation at the sulfur atom and at the nitrogen atom gives **3** and **4**, respectively. Although the formation of **4** was generally predominant, DMF increased the proportion of **3**. This is explained by the coordination of DMF to the tin atom in **A** as a Lewis base. The basicity of the sulfur atom adjacent to the tin is thus increased, therefore, the intramolecular S-alkylation is accelerated, giving **3** predominantly. This is not the case, however, in the case of tri-*n*-butyltin γ-halopropoxides (*n*-$Bu_3SnO(CH_2)_3X$). Compound **4d** was produced in a higher selectivity than *n*-$Bu_3SnO(CH_2)_2X$ even when DMF was used (entries 11—13).

Alternatively, the isomerization of initially formed **3** to **4** catalyzed by *n*-Bu_3SnI which is a by-product of the reaction of **1** with **2**, can be considered. However, no isomerization was recognized by the treatment of **3c** with an equimolar *n*-Bu_3SnI at 40 °C for 1 h, and **3c** was recovered quantitatively.

On the other hand, treatment of **3c** with an equimolar *n*-Bu_3SnI at 100 °C for 1 h induced the formation of the thiazolidinone **5** in 50% yield as described by Sakai et al.[8]

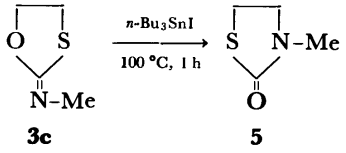

3c **5**

In this case, formation of **4c** could not be recognized. We thus conclude that no isomerization of **3** to **4** occurred under present conditions.

Experimental

***N*-Phenyl-1,3-oxathiolan-2-imine (3a).** *n*-$Bu_3SnO(CH_2)_2I$ (4.61 g, 10 mmol) and PhNCS (1.08 g, 8 mmol) were stirred under dry N_2 on cooling, then heat was evolved about 40 °C. The infrared spectrum showed the disappearance of the characteristic absorption band of ν NCS at 2100 cm^{-1} and the presence of a new band around 1600 cm^{-1}. After additional 5 min, DMF (5 ml) was added and the stirring was continued for 1 h at 25 °C. The addition of excess amounts of hexane on cooling induced 1.79 g of white precipitates immediately, which were filtered, washed with hexane and dried in vacuo. The precipitates contained *N*-phenyl-1,3-oxathiolan-2-imine **3a** as a mixture with **4a** (100%, **3a**:**4a**=83:17, entry 5). The **3**/**4** ratio was determined by GLC. Analytically pure sample of **3a** was obtained by column chromatography (Silica gel, $CHCl_3$). Compound **4a** was obtained as the major product from the reaction of *n*-$Bu_3SnO(CH_2)_2Cl$ (entry 1). Spectral data for **3a** was as follows; mp 65—67 °C (lit,[8] mp 65—65.5 °C); IR (KBr) 1035, 1110, 1640 cm^{-1}; ^1H NMR ($CDCl_3$) δ=3.40 (t, 2H, $C\underline{H}_2S$), 4.50 (t, 2H, $C\underline{H}_2O$), 6.90—7.50 (m, 5H, phenyl).

Following compounds were isolated similarly.

***N*-Benzyl-1,3-oxathiolan-2-imine (3b)**: Bp 113—115 °C/10^{-3} mmHg; IR (neat) 1060, 1660 cm^{-1}; MS *m/z* 193 (M^+); ^1H NMR ($CDCl_3$) δ=3.40 (t, 2H, $C\underline{H}_2S$), 4.40 (t, 4H, $C\underline{H}_2N$, $C\underline{H}_2O$), 7.20—7.40 (m, 5H, phenyl); ^{13}C NMR ($CDCl_3$) δ=31.7, 58.0, 68.8, 126.7, 127.5, 128.2, 139.4, 163.1.

***N*-Methyl-1,3-oxathiolan-2-imine (3c)**: Bp 66—67 °C/2 mmHg(1 mmHg=133.322 Pa) (lit,[8] bp 117—118 °C/20 mmHg); IR (neat) 1050, 1670 cm^{-1}; ^1H NMR ($CDCl_3$) δ=3.00 (s, 3H, $C\underline{H}_3N$), 3.40 (t, 2H, $C\underline{H}_2S$), 4.30 (t, 2H, $C\underline{H}_2O$).

3-Phenyl-1,3-oxazolidin-2-thione (4a): Mp 97 °C (lit,[9] 95.5 °C); IR (KBr) 1180, 1300, 1430, 1495 cm^{-1}; ^1H NMR ($CDCl_3$) δ=4.20 (t, 2H, $C\underline{H}_2N$), 4.60 (t, 2H, $C\underline{H}_2O$), 7.20—7.60 (m, 5H, phenyl).

3-Benzyl-1,3-oxazolidin-2-thione (4b): Mp 90—91 °C; IR (KBr) 1160, 1330, 1520 cm^{-1}; MS *m/z* 193 (M^+); ^1H NMR ($CDCl_3$) δ=3.60 (t, 2H, $C\underline{H}_2N$), 4.50 (t, 2H, $C\underline{H}_2O$), 4.82 (s, 2H, $PhC\underline{H}_2N$), 7.30—7.40 (m, 5H, phenyl); ^{13}C NMR ($CDCl_3$) δ=47.2, 52.0, 65.9, 128.1, 128.3, 128.8, 134.5, 188.0.

3-Methyl-1,3-oxazolidin-2-thione (4c): Bp 120 °C/0.3 mmHg (lit,[10] bp 127 °C/0.4 mmHg); IR (neat) 1180 cm^{-1}; ^1H NMR ($CDCl_3$) δ=3.21 (s, 3H, $C\underline{H}_3N$), 3.82 (t, 2H, $C\underline{H}_2N$), 4.52 (t, 2H, $C\underline{H}_2O$).

3-Phenyl-1,3-oxazine-2-thione (4d): Mp 138—139 °C; MS *m/z* 193 (M^+); IR (KBr) 1300, 1320, 1480, 1500 cm^{-1}; ^1H NMR ($CDCl_3$) δ=2.10—2.40 (m, 2H, $C\underline{H}_2$), 3.70 (t, 2H, $C\underline{H}_2N$), 4.50 (t, 2H, $C\underline{H}_2O$), 7.20—7.50 (m, 5H, phenyl); ^{13}C NMR ($CDCl_3$) δ=21.4, 50.7, 67.7, 126.6, 127.8, 129.4, 145.5, 187.1.

The Isomerization of 3: Oxathiolanimine **3c** (0.56 g, 5 mmol) and *n*-Bu_3SnI (2.08 g, 5 mmol) were stirred under N_2 in a 50 ml round bottomed flask, after 1 h at 100 °C, the GLC analysis showed the disappearance of **3c**, and 3-methyl-1,3-thiazolidin-2-one **5** was formed in 50% yield, this was purified by column chromatography (silica gel, $CHCl_3$) and distillation: bp 65 °C/10^{-3} mmHg (lit,[8] 73—75 °C/0.2 mmHg); IR (neat) 1240, 1690 cm^{-1}; ^1H NMR ($CDCl_3$) δ=2.88 (s, 3H, $C\underline{H}_3N$), 3.30 (t, 2H, $C\underline{H}_2S$), 3.60 (t, 2H, $C\underline{H}_2N$).

References

1) A. Baba, H. Kishiki, I. Shibata, and H. Matsuda, *Organometallics*, **4**, 1329 (1985).

2) B. Delmond, J. C. Pommier, and J. Valade, *J. Organomet. Chem.*, **35**, 91, (1972); B. Delmond, J. C. Pommier, and J. Valade, *J. Organomet. Chem.*, **47**, 337 (1973).

3) R. Feinauer, M. Jacobi, and K. Hamann, *Chem. Ber.*, **98**, 1782 (1965).

4) V. S. Etlis, A. P. Sineokov, and G. A. Razuvaev, *Zh. Obshch. Khim.*, **34**, 4018 (1964); *Chem. Abstr.*, **62**, 9132 (1965); V. S. Etlis, A. P. Sineokov, and G. A. Razuvaev, *Zh, Obshch. Khim.*, **34**, 4090 (1964); *Chem. Abstr.*, **62**, 10423 (1965).

5) The intermediate **A** may also exist in the presence of DMF, because the IR absorption around 1600 cm^{-1} (C=N) was confirmed even in the presence of bases.

6) See, for example; A. K. Sawyer, "Organotin Compounds Vol. 2," Marcel Dekker, New York (1971), p. 297; E. Negishi,

"Organometallics in Organic Synthesis Vol. 1," John Wiley & Sons, New York (1980), p. 394; A. G. Davies and P. J. Smith, "Comprehensive Organometallic Chemistry Vol. 2," Pergamon Press (1982), p. 519.

7) A. J. Bloodworth, A. G. Davies, and S. C. Vasishtha, *J. Chem. Soc. (C)*, **1967**, 1309.

8) S. Sakai, H. Niimi, Y. Kobayashi, and Y. Ishii. *Bull. Chem. Soc. Jpn.*, **50**, 3271 (1977).

9) T. Mukaiyama, I. Kuwajima, and K. Mizui, *J. Org. Chem.*, **31**, 32 (1966).

10) S. Sakai, Y. Asai, Y. Kiyohara, K. Itoh, and Y. Ishii, *Organometal. Chem. Synth.*, **1**, 45 (1970/1971).

X- and Q-Band ESR Studies of Binuclear Copper(II) Complexes with 3-Alkyl-2-pyridone Bridging Ligands

David M. L. GOODGAME,† Yuzo NISHIDA, and Richard E. P. WINPENNY†
† Department of Chemistry, Imperial College, London SW7 2AY, U. K.,
Department of Chemistry, Faculty of Science, Kyushu University 33, Fukuoka 812
(Received August 26, 1985)

Synopsis. The ESR spectra of polycrystalline samples of bis(*N*,*N*-dimethylformamide)tetrakis(3-ethyl-2-pyridonato)dicopper(II) and its 3-methyl-2-pyridone analogue have been measured at X-band (≈9.5 GHz) and Q-band (≈34 GHz) frequencies. The spectra are characteristic of S=1 species and the parameters (g_z 2.30, g_{xy} 2.05 and $D\approx0.29\,cm^{-1}$) are discussed in terms of the known binuclear structure.

Many binuclear copper(II) complexes are known in which two copper(II) ions are bridged by four carboxylato groups.[1,2] Analogous compounds in which nitrogen atoms are the donor atoms in the bridging unit are fewer in number,[3] and those in which the four bridges each contain one N and one O donor atom are even rarer[4] though they are well-established for other metal ions.[5]

Two complementary techniques have been customarily employed to study the electronic nature of such binuclear copper(II) compounds with the classic copper(II) acetate structure. Studies of the temperature dependence of the magnetic susceptibility generally show that the pair of copper(II) atoms are antiferromagnetically coupled, giving an $S=0$ ground state and $S=1$ level $|2J|$ above this. Application of the Bleaney and Bowers equation[6] permits evaluation of $|2J|$ and, for powder samples, an average g value. Measurement of the ESR spectra arising from those molecules within the thermally accessible $S=1$ state and application of the spin Hamiltonian (1) permit derivation of the zero-field splitting

$$\mathscr{H} = g\beta B.\hat{S} + D\hat{S}_z^2 + E(\hat{S}_x^2-\hat{S}_y^2) - 2D/3 \quad (1)$$

parameters D and E and the g values g_x, g_y, g_z if $E\neq0$, or g_z and g_{xy} if $E=0$.

It has recently been shown by X-ray methods[4] that bis(*N*,*N*-dimethylformamide)tetrakis(3-ethyl-2-pyridonato)dicopper(II) has a structure of the copper(II) acetate type but with N,O donor atom bridges. This has afforded us the opportunity of comparing the ESR parameters for such a bridging unit with those of bridges containing only O or N atoms as donors.

Experimental

The complexes $[Cu_2(3\text{-ethyl-pyr})_4(dmf)_2]$ and its 3-methyl-2-pyridone analogue were prepared as described previously.[4] Their ESR spectra were obtained as polycrystalline samples at room temperature using Varian E12 X-band (≈9.5 GHz) and Bruker ER200 Q-band (≈34 GHz) spectrometers.

Results and Discussion

The X- and Q-band ESR spectra of $[Cu_2(3\text{-ethyl-pyr})_4(dmf)_2]$ are shown in Figs. 1 and 2 respectively.

Solution of the spin Hamiltonian (1) for the situation where $D<h\nu$ and $E=0$ yields four allowed ($\Delta m_s=1$) transitions at resonance field B_{z1}, B_{z2}, B_{xy1}, and B_{xy2} given by:[7]

$$B_{z1} = (g_e/g_z)|B_0-D'| \qquad B_{z2} = (g_e/g_z)(B_0+D')$$
$$B_{xy1}^2 = (g_e/g_{xy})^2B_0(B_0-D') \qquad B_{xy2}^2 = (g_e/g_{xy})^2B_0(B_0+D')$$

where $B_0=h\nu/g_e\beta$ and $D'=D/g_e\beta$. In addition the formally forbidden $\Delta m_s=2$ transition between the $|-1\rangle$ and $|+1\rangle$ levels, the so-called half-field transition, is often observed.

Assignments of the observed transitions in Figs. 1 and 2 are summarized in Table 1 for the parameters $g_{xy}=2.05$, $g_z=2.30$, and $D=0.287\,cm^{-1}$. The values of B_{z2} and B_{xy2} are such that the transitions are virtually coincident at Q-band frequency (calculated values of 13,203 and 13,230 gauss respectively at 33.90 GHz). Consequently the low intensity B_{z2} band is hidden by the much stronger B_{xy2} band. Changing the microwave frequency to X-band enables a clear separation of these transitions to be made (Fig. 2). Conversely, the B_{z1}, B_{xy1}, and $\Delta m_s=2$ transitions could not have been unambiguously assigned from the X-band results alone because of appreciable band

Table 1. ESR Data for the Complexes[a]

	$[Cu(3\text{-ethyl-pyr})_2(dmf)]_2$		$[Cu(3\text{-methyl-pyr})_2(dmf)]_2$	
At 33.90 GHz				
	Observed	Calcd[b]	Observed	Calcd[c]
$\Delta m_s=2$	5368	d)	5388	d)
B_{z1}	7875	7858	7859	7850
B_{xy1}	10163	10206	10187	10201
B_{z2}	e)	13203	e)	13212
B_{xy2}	13255	13230	13239	13234
At 9.503 GHz				
$\Delta m_s=2$	f)	d)	f)	d)
B_{z1}	≈300	279	≈250	270
B_{xy1}	≈1000	1019	≈1000	1003
B_{xy2}	4520	4572	4550	4575
B_{z2}	5580	5625	5580	5633

a) Resonance fields in gauss(=10^{-4} T). b) Calculated for $g_z=2.30$, $g_{xy}=2.05$, $D=0.287\,cm^{-1}$. c) Calculated for $g_z=2.30$, $g_{xy}=2.05$, $D=0.288\,cm^{-1}$. d) Not calculated. e) Hidden by stronger B_{xy2} band. f) Not resolved from nearby $\Delta m=1$ band.

Table 2. Comparison of D and $|2J|$ Values for Some Binuclear Copper(II) Complexes

Complex[a]	Bridge donor atoms	Cu-Cu/Å	D/cm^{-1}	$2J$/cm^{-1}	Ref.
$Cu(CH_3CO_2)_2H_2O$	4O	2.615	0.34	286	1
$Cu(CH_3CO_2)_2\cdot$quin	4O	2.642	0.341	320	1
$Cu(CH_3CO_2)_2\cdot NCS^-$	4O	2.643	0.34	305	1, 8
$Cu(HCO_2)_2\cdot NCS^-$	4O	2.716	0.44	485	1, 8
$Cu(3\text{-Et-pyr})_2\cdot$dmf	2O, 2N	2.550	0.287	395	4, b
$Cu(ad)_2\cdot 4H_2O$	4N	2.947	0.121	257	3
$Cu(adH)_2(ClO_4)_2\cdot 2H_2O$	4N	2.951	0.110	300	10, 11
$Cu(adH)_2Cl_2\cdot 3H_2O$	4N	3.066	0.127	270	12, 13

a) quin=quinoline; 3-Et-pyr=3-ethyl-2-pyridone anion; dmf=*N*,*N*-dimethylformamide; ad=adenine anion. b) This work.

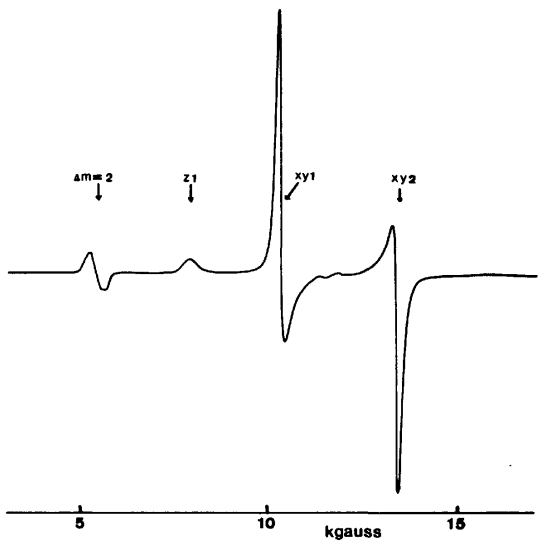

Fig. 1. Q-band ESR spectrum of $[Cu_2(3\text{-Et-pyr})_4(dmf)_2]$(kgauss=$10^{-1}$T).

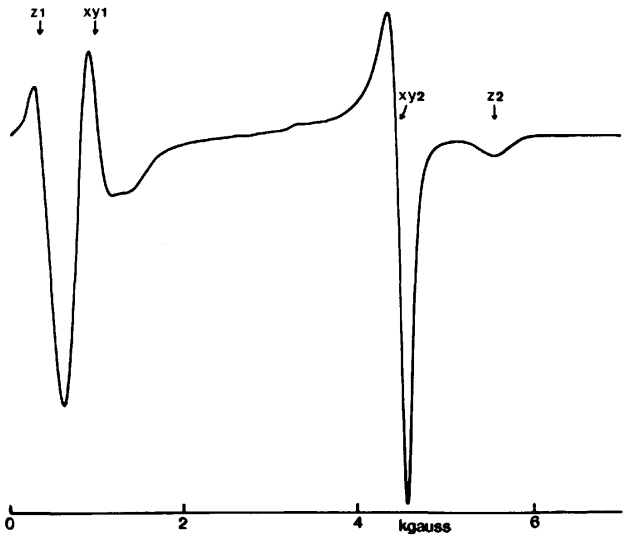

Fig. 2. X-band ESR spectrum of $[Cu_2(3\text{-Et-pyr})_4(dmf)_2]$(kgauss=$10^{-1}$T).

overlap at that frequency. However these transitions are clearly resolved and readily assigned at Q-band frequency. The advantage of measuring such spectra at more than one microwave frequency is well demonstrated by these results.

The observation that E=0, or at least too small to be evident in any splitting of the B_{xy1} and B_{xy2} bands, is in good agreement with the results of the X-ray structural determination.[4] The pairs of N and O donor atoms from the four pyridone bridges are arranged in cis-dispositions about each Cu atom and the angular and bond-length deviations from axial symmetry are small.

The ESR spectra of $[Cu_2(3\text{-methyl-pyr})_4(dmf)_2]$ are virtually identical to those disussed above, and the derived parameters and assignmens are listed in Table 1. This close similarity tallies well with the reported[4] agreement of their magnetic properties. Moreover the average g value (2.15) derived from the temperature dependence of their magnetic susceptibilities[4] is close to that (2.14) we obtain from the ESR spectra by using the expression: $g_{av}^2=(g_z^2+2g_{xy}^2)/3$.

The D values we observe ($\approx$0.29 cm^{-1}) are somewhat smaller than those (0.33—0.44 cm^{-1}) generally found for copper(II) carboxylate dimers[1,2,8] but they are larger than the values (0.1—0.19 cm^{-1}) reported[3,9] for analogous copper(II) dimers with nitrogen donor atoms in the bridges (see Table 2). It is interesting to note in this context that Brookes and Martin found $D\approx$0.27 cm^{-1} for $Cu(CH_3CO_2)L\cdot X$, where L represents the anion of 1,7-diazaindene and X=1,7-diazaindene or pyridine.[3]

The observed D value, $D_{obs}=D_{dd}+D_{exch}$, where D_{dd} arises from dipole-dipole interaction, and D_{exch} from exchange. D_{dd}, which is expected to be negative, is approximately calculated[14] from the equation based on a point dipole model, $R^3=0.65g_z^2/D_{dd}$, where R is the copper-copper distance. Use of the equation yields D_{dd}=0.207 cm^{-1}, and therefore D_{exch}=0.494 cm^{-1} for $[Cu_2(3\text{-ethyl-pyr})_2(dmf)_2]$($R$=2.55 Å). Rough correlations between D_{exch} and $|2J|$, the energy separation between the singlet ground state and the triplet first-excited state, have sometimes been made,[2,14] by means of the equation, $D_{exch}=-2J[(g_z\text{-}2)^2/4\text{-}(g_{xy}\text{-}2)^2]/8$. Use of this equation predicts a value of $|2J|$ of 198 cm^{-1}, whereas the experimental value[4] is 395

cm^{-1}. The difference between the calculated and the experimental values may be due to the approximations assumed in deriving the equations, and also to the fact that the singlet-triplet splitting is not simply related to the strength of the exchange interaction, as pointed out elsewhere.[2,15,16]

References

1) J. Catterick and P. Thornton, *Adv. Inorg. Radiochem.*, **20**, 291 (1977).
2) J. L. Meier, C. E. Coughenour, J. A. Carlisle, and G. O. Carlisle, *Inorg. Chim. Acta*, **106**, 159 (1985).
3) R. W. Brookes and R. L. Martin, *Inorg. Chem.*, **14**, 528 (1975).
4) Y. Nishida and S. Kida, *Bull. Chem. Soc. Jpn.*, **58**, 383 (1985).
5) F. A. Cotton and R. A. Walton "Multiple Bonds between Metal Atoms", John Wiley & Sons, New York (1982).
6) B. Bleaney and K. D. Bowers, *Proc. Roy. Soc.* **A214**, 451 (1952).
7) E. Wasserman, L. C. Snyder, and W. A. Yager, *J. Chem. Phys.*, **41**, 1763 (1964).
8) D. F. Marsham, Ph. D. Thesis, London University, 1969.
9) D. M. L. Goodgame and S. V. Waggett, *Biochem. Biophys. Res. Commun.*, **42**, 63 (1971).
10) A. Terzis, A. N. Beauchamp, and R. Rivest, *Inorg. Chem.*, **12**, 1166 (1973).
11) R. W. Duerst, S. J. Baum, and G. F. Kokoszka, *Nature*, **222**, 666 (1969).
12) K. A. Price, Ph. D. Thesis, London University, 1971.
13) P. de Meester, D. M. L. Goodgame, K. A. Price, and A. C. Skapski, *Nature*, **229**, 191 (1971).
14) N. D. Chasteen and R. L. Belford, *Inorg. Chem.*, **9**, 169 (1970).
15) P. J. Hay, J. C. Thibeault, and R. Hoffmann, *J. Am. Chem. Soc.*, **97**, 4884 (1975).
16) Y. Nishida, M. Takeuchi, K. Takahashi, and S. Kida, *Chem. Lett.*, **1985**, 631.

Pretreatments of Porous Silica for Improving the Activity of a Nickel-Loaded Catalyst

Masahiko Arai, Yutaka Ikushima, and Yoshiyuki Nishiyama*
Chemical Research Institute of Non-Aqueous Solutions, Tohoku University, Katahira, Sendai 980
(Received July 15, 1985)

Nickel catalysts supported on porous silicas treated with water, ethanol, and 1-butanol were found to be more active than that supported on untreated silica for ethane hydrogenolysis and furan hydrogenation. To elucidate the reason for the activation, some surface properties of the treated silicas were examined. The treatments decreased the surface area and increased the volume of the macropores, the surface density of hydroxyl groups, and the heat of immersion in water per unit surface area. The state of nickel on the support was examined by temperature programed desorption(TPD) of hydrogen, X-ray diffraction(XRD), and scanning electron microscopy/X-ray microanalysis. The dispersion measured by XRD was not appreciably altered by the treatments, but the TPD showed more hydrogen desorbed above 150 °C from nickel on the treated supports. The activation of nickel by pretreatment of the support was ascribed to the increase of those nickel atoms which dispersed finely over the support by the increased number of surface hydroxyl groups. This was based on the number of hydroxyl groups per unit surface area. The nickel catalyst supported on the pretreated silicas showed greater thermal stability.

It is well established that the activities of supported metal catalysts are influenced by the surface properties of the supports, so that the choice of the support material is important for the preparation of the catalysts.[1] Therefore some surface modifications of the support can improve the activity of the catalysts loaded on it. Previously, we have reported that nickel and platinum catalysts loaded on porous silicas pretreated with water and alcohols are more active than those on untreated silicas.[2,3] As the impregnation of the active metal species was done from aqueous solutions, it was our anticipation that alcohol treatment, which would be expected to give the surface a hydrophobic nature, would lead to a lower dispersion of the active metal. Contrary to this anticipation, the catalytic activities of metals on alcohol treated silicas were found to be higher than those on untreated silica. As a follow-up of the previous work, the present study was undertaken to clarify the reason for the activation by the pretreatment of the support. In doing so, temperature programed desorption of hydrogen was extensively used to characterize the state of nickel on the support, as it seems to be more relevant to examine those metals which are active in catalysis.[2]

A number of researches on surface modifications of silica as well as other metal oxides have been reported in the literature.[4—10] Their concern of these authors, however, is more with the actions of modified surfaces as adsorbents and solid acid catalysts. There was little attempt made to use modified materials as supports for the metal catalyst.

Experimental

A porous silica material was used, Silbead-N obtained from Mizusawa Industrial Chemicals, Ltd. It was powdered to 32—60 mesh and treated with water at 280 °C, ethanol at 280 °C, and 1-butanol at 250 °C. Detailed procedures of these treatments were described previously.[2,3] The silica was characterized before and after the treatments by the following means. (i) The surface area was measured by the nitrogen BET method. (ii) The pore size distribution was determined by the Cranston-Inkley method using a nitrogen adsorption isotherm[11] and by a mercury porosimetry (Shimadzu-Micromeritics Pore Sizer 9300). (iii) FT-IR diffuse reflectance spectra were obtained using a mixture of the silica (ca. 5 wt%) and potassium bromide with a JEOL JIR-100 spectrometer. (iv) The heat of immersion in either water or hexane was measured at 22 °C using a Tokyo Riko TCC-21 calorimeter.

Using the treated and untreated silicas, supported nickel (5 wt%) catalysts were prepared by impregnation with nickel nitrate from its aqueous solution. The impregnated samples were vacuum dried and reduced in flowing hydrogen at 350 °C for 16 h. The state of the nickel dispersion was examined by temperature programed desorption (TPD) of hydrogen, X-ray diffraction line broadening (XRD), and scanning electron microscopy/X-ray microanalysis (SEM-XMA). For TPD, using a 5 mm i.d. quartz tube reactor operated at atmospheric pressure, ca. 0.3 g of the catalyst was exposed to flowing hydrogen of 48 ml min^{-1} at room temperature for 20 min. The adsorbed hydrogen was then desorbed by linear heating at 30 °C min^{-1} in an argon carrier at a flow rate of 40 ml min^{-1}. The catalytic activity was examined for ethane hydrogenolysis at 350 °C and furan hydrogenation at 110 and 200 °C with ethane and furan partial pressures of 16.0 and 27.7 kPa, respectively. The apparatus and procedures for the TPD and the activity test were described in detail previously.[2,3]

In the following sections, the water-, ethanol-, and 1-butanol-treated and untreated silicas will be referred to as SI(W), SI(E), SI(B), and SI(U), respectively.

Results

Effects of Treatments of Silica on the Surface Properties.

(1) Surface Area and Porosity. The BET surface area, pore volumes, and XRD data as well as the heat of immersion of the silicas are summarized in Table 1. The treatments caused the surface area to decrease to less than 1/5 of the initial value. The pores in SI(U) were mostly smaller than 5 nm in diameter and the treatments enlarged the pore diameter. Compared with

Table 1. Characterization of Treated and Untreated Silicas

	SI(U)	SI(W)	SI(E)	SI(B)
Surface area (m^2/g)	680.0	74.3	98.1	131.2
Pore volume (ml/g)				
diameter<5 nm	0.202	0.052	0.010	0.020
5—30 nm	0.021	0.063	0.142	0.220
XRD[a] 2θ (deg)	23.8	21.6	22.0	22.2
d (nm)	0.37	0.41	0.40	0.40
Heat of immersion				
in water (J/m^2)	0.218	0.616	0.422	0.417
in hexane (J/m^2)	0.246	0.335	0.200	0.276

a) A Cu $K\alpha$ ray was used. d is the corresponding interlayer spacing.

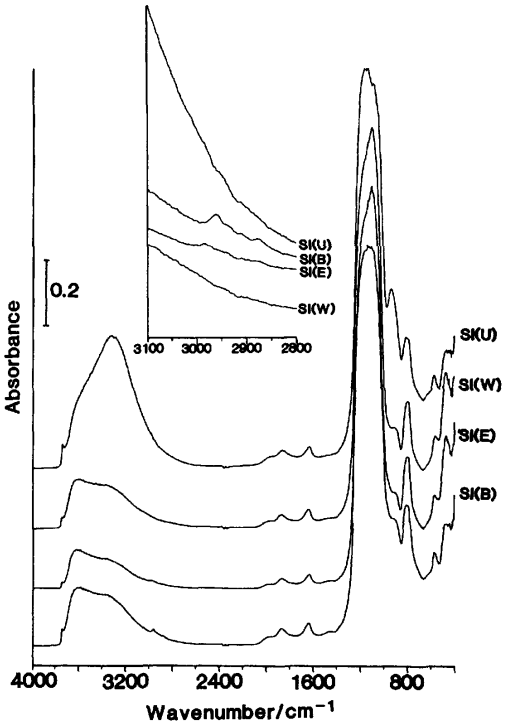

Fig. 1. FT-IR spectra for treated and untreated silicas.

SI(U), the total pore volumes of SI(W) and SI(E) were smaller by factors of 0.6—0.7 while that of SI(B) was comparable. The mercury porosimetry showed the absence of macropores larger than 30 nm even in the treated silicas. The observed maximum pore diameter was 20 nm for SI(E) and SI(B) and 30 nm for SI(W).

The XRD showed an increase in the interlayer spacing, d, with the treatments, the order of d being SI(W)>SI(E)≥SI(B)>SI(U). This suggests that the treatments caused a growth of cristobalite- and/or tridymite-like structure in the silica.

(2) Infrared Absorption Spectra. In Fig. 1, FT-IR spectra for the treated and untreated silicas are compared. The intensity of absorption of the sharp peak at 3750 cm^{-1}, of the broad band between 3600 and 2800 cm^{-1}, and of the weak band at 870 cm^{-1} was decreased by the treatments. These absorptions can be

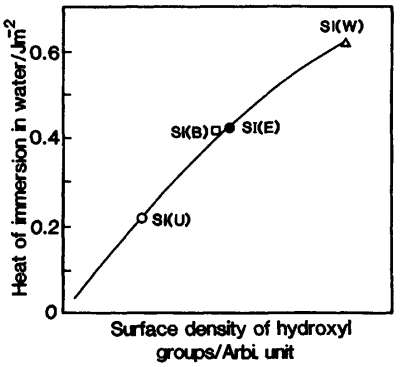

Fig. 2. A plot of heat of immersion in water versus relative surface density of hydroxyl groups.

assigned to surface hydroxyl groups. Thus the number of hydroxyl groups on the treated silicas was smaller than that on the untreated silica when compared on a unit weight basis. However, as the surface area was decreased by the treatments, the number of hydroxyl groups in unit surface area increased (see Fig. 2). In addition, the spectra of SI(E) and SI(B) have absorption bands at 1450 and 2950 cm^{-1}, which can be assigned to methyl and methylene groups. These indicate the exchange of some hydroxyl groups with alkoxyl groups on the silica surface.

(3) Heat of Immersion in Water and Hexane. The heat of immersion per unit surface area is presented in Table 1. The surface treatments caused the heat of immersion in water to increase by factors of about 3 and 2 for the water and alcohol treatments, respectively. Figure 2 shows a plot of the heat of immersion in water against the relative density of surface hydroxyl groups from FT-IR. The latter was obtained by graphically integrating the absorbance between 2600 to 3800 cm^{-1} in Fig.1 and then normalizing to the absorbance at 1640 cm^{-1} assigned to a silicon-oxygen overtone vibration.[12,13] The correlation indicates that the surface hydrophilicity was associated with the surface hydroxyl groups for the present silicas and that, contrary to expectation, the treatment by alcohols rendered the silica more hydrophilic nature. On the other hand, the heat of immersion in hexane per unit surface area was only slightly changed. It was increased by the water and 1-butanol treatments but it was decreased by the ethanol treatment.

Effect of Silica Pretreatments on the Catalytic Properties of Supported Nickel.

(1) Metal Dispersion. Figure 3 shows TPD spectra of hydrogen adsorbed on the nickel catalysts on SI(U), SI(W), and SI(B). In the present TPD experiment, the heating of the catalyst was restricted to below 350 °C to avoid thermal effects on the nickel dispersion during repeated measurements. It was found that the catalysts on the treated silicas could, as a whole, adsorb larger amount of hydrogen than that on SI(U). After the heat treatment in hydrogen at 500 and 700 °C, the total

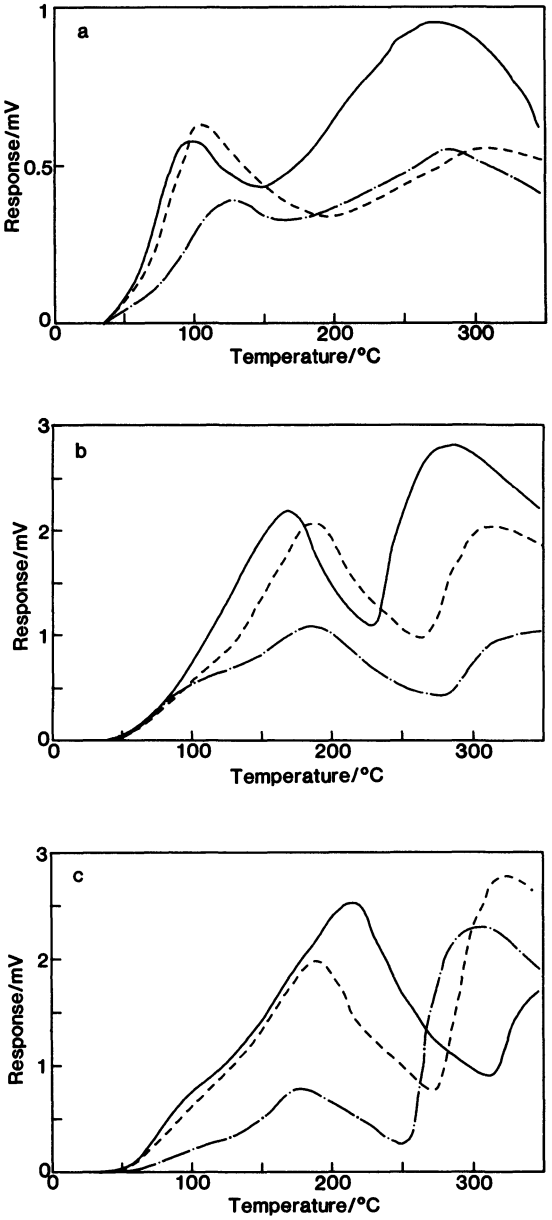

Fig. 3. TPD spectra of hydrogen adsorbed on (a) Ni/SI(U), (b) Ni/SI(W), and (c) Ni/SI(B). ——: as reduced, – – –: heated in hydrogen at 500°C for 1 h, —·—: heated in hydrogen at 700°C for 1 h.

amount of hydrogen desorbed in the TPD decreased for all the catalysts used. However, the amounts of hydrogen desorbed from nickel on the treated silicas were larger or, at least, comparable to that from the catalyst on SI(U) without the heat treatment although the TPD patterns were different.

Table 2 presents mean crystallite sizes of the supported nickel obtained by XRD, including the influence of heat treatment in hydrogen at 700°C for 1 h. It shows that the nickel crystallites in the catalysts as prepared had similar sizes although the supports used were different in the surface area, porosity, and hydrophilicity as noted above. On heat treatment, the crystallites in all the catalysts grew but the extent of growth was larger

Table 2. Mean Nickel Crystallite Size[a)]

H.T.T.[b)]	Support			
	SI(U)	SI(W)	SI(E)	SI(B)
As reduced (350°C)	7.3	6.5	7.1	6.3
700°C	8.8	14.8	11.3	11.2

a) Determined by an XRD line broadening, in nm. b) Heat treatment temperature. The treatment was performed in a flowing hydrogen for 1 h.

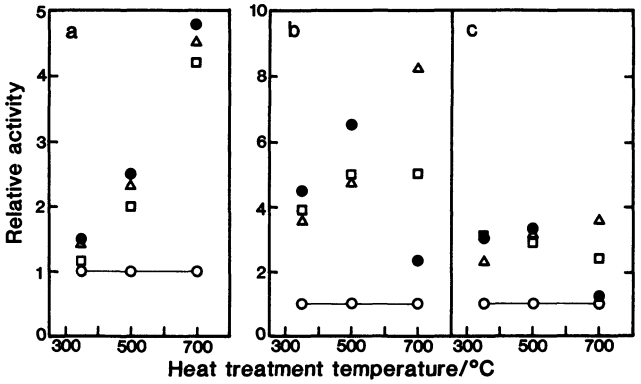

Fig. 4. Relative activities of (△) Ni/SI(W), (●) Ni/SI(E), and (□) Ni/SI(B) to (○) Ni/SI(U) for ethane hydrogenolysis at 350°C (a) and furan hydrogenation at 110°C (b) and at 200°C (c).

for the treated silicas than that for SI(U).

To see whether or not the surface pretreatment of the support caused some irregular distribution of nickel at the time of impregnation, the radial distribution of nickel on the cleaved surface of a catalyst particle was examined by SEM-XMA. The nickel distribution was found to be uniform within experimental error for all the catalysts on SI(U), SI(W), SI(E), and SI(B).

(2) Catalytic Activity. Figure 4 shows the catalytic activities of nickel supported on the treated silicas in ethane hydrogenolysis and furan hydrogenation relative to those of nickel on untreated silica. For the SI(U)-supported catalyst, the heat treatment in hydrogen at 500°C decreased the activity in ethane hydrogenolysis at 350°C by 44% and those in furan hydrogenation at 110 and 200°C by 35 and 22%, respectively; the treatment at 700°C decreased it in the same order, by 80, 68, and 60%. Though the heat treatment deactivated all the catalysts examined, those on surface-modified silicas were more stable against thermal deactivation than that on SI(U) as seen in Fig. 4.

Discussion

It is noteworthy that the structure of the silica was altered by the autoclave treatments with such alcohols as ethanol and 1-butanol as well as with water. Namely, the treatments decreased the surface area by factors less than 1/5 while they increased the volume of the pores in the range of 5-30 nm in diameter. Previous workers

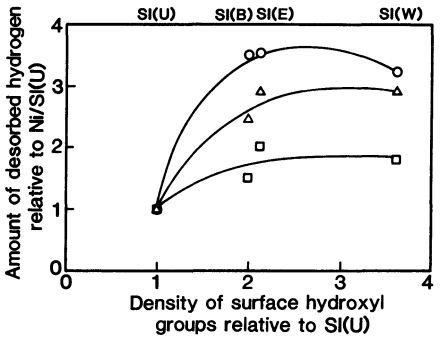

Fig. 5. Correlation between hydrogen adsorbability of supported nickel and density of surface hydroxyl groups of the supports. ○: Desorbed at 150—250 °C, △: 150—300 °C, □: 25—350 °C.

showed that the hydrothermal treatment of oxide gels including alumina and silica-alumina resulted in the change of surface area and pore structure, and it varied their catalytic properties.[10,14] On our treatments, the extent of the structural change is thought to be associated with the penetrability of the treating agent into the silica gel structure. The solvents penetrated into unstable gel caused some rearrangement of its structural units, resulting in a partial crystallization as indicated by the XRD measurements, thereby reducing its surface area.

Along with the structural change, there occurred chemical change of the silica surface on the treatments. They increased the density of hydroxyl groups on the surface. The larger heat of immersion of treated silicas in water on unit surface area basis than that of untreated one is mainly due to the increased density of the surface hydroxyl groups. Some of the surface hydroxyl groups were replaced with alkoxyl groups by the alcohol treatments as expected, but their effect on the surface properties seems small.

An interesting finding is that the pretreatments of the silica enhanced the catalytic activity of supported nickel in spite of a concurrent significant decrease in the surface area of the silica. One probable explanation is that the larger density of the hydroxyl groups on the silica surface resulted in a higher dispersion of nickel, as evidenced by the TPD of hydrogen. Figure 5 shows the plot of the amount of hydrogen desorbed against the density of surface hydroxyl groups from the FT-IR spectra, both in relative values to SI(U). It suggests that the amount of hydrogen retained on the catalyst has some correlation with the surface hydroxyl groups on the support. The hydrogen adsorbability can be related with the catalytic activity in either hydrogenolysis or hydrogenation.[2] Dispersion of nickel estimated from XRD gave no reasonable correlation with the catalytic activity. It is therefore inferred that well-dispersed nickel atoms play a main role in the catalysis and those in larger crystallites have small activity.

For all the catalysts examined, the heat treatment in hydrogen at 500 and 700 °C caused deactivation due to the sintering of the nickel crystallites as evidenced by the XRD measurements. At treatment temperatures of 500 and 700 °C, there is a possibility of an occurrence of strong nickel-support interaction, e. g., the formation of a nickel-support complex.[15,16] Nickel atoms on the treated silicas were more stable than those on the untreated one, which suggested a stronger interaction with the treated supports.

Part of the enhanced activities of the catalysts on the pretreated supports may be ascribed to their increased pore diameter, which would favor the diffusion of reactants and products in the catalyst. The contribution of pores in activity enhancement needs further study.

The present study was done using a particular kind of silica gel, so that it is natural to ask whether the pretreatments of the support are applicable to other substances as well. An additional study using two aluminas indicated that the effectiveness of the pretreatments depended on the substance used; a catalyst with Neobead-C (Mizusawa Industrial Chemicals, Ltd.) was activated by the pretreatment of the support though the extent of the activation was less marked, whereas the other with JRC-ALO-1 (Catalysis Society of Japan) was not activated to any appreciable extent.

References

1) D. L. Trimm, "Design of Industrial Catalysts," Elsevier, Amsterdam (1980), p. 91.
2) Y. Ikushima, M. Arai, and Y. Nishiyama, *Appl. Catal.*, **11**, 305 (1984).
3) M. Arai, K. Kato, H. Saito, and Y. Nishiyama, *Nippon Kagaku Kaishi*, **1985**, 1016.
4) J. A. Hockey, *Chem. Ind. (London)*, **1956**, 57.
5) R. L. Burwell, Jr., *CHEMTECH*, **4**, 370 (1974).
6) H. Utsugi, H. Horikoshi, and T. Matsuzawa, *J. Colloid Interface Sci.*, **50**, 154 (1975).
7) N. G. Newman and W. Hertl, *J. Chromatogr.*, **65**, 467 (1972).
8) S. Okazaki and T. Kanno, *Nippon Kagaku Kaishi*, **1973**, 1285.
9) A. V. Tench, D. Giler, and J. F. J. Kibblewhite, *Trans. Faraday Soc.*, **67**, 854 (1971).
10) S. Furuyama, O. Murashita, Y. Yukumoto, and T. Morimoto, *Bull. Chem. Soc. Jpn.*, **53**, 3039 (1980).
11) R. W. Cranston and F. A. Inkley, *Adv. Catal.*, **2**, 143 (1957).
12) H. A. Benesi and A. C. Jones, *J. Phys. Chem.*, **63**, 179 (1959).
13) H. Heyne and F. C. Tompkins, *Trans. Faraday Soc.*, **63**, 1274 (1967).
14) M. Inoguchi, *SHOKUBAI*, **20**, 144 (1978).
15) R. B. Shalvoy, P. J. Reucroft, and B. H. Davis, *J. Catal.*, **56**, 336 (1979).
16) A. L. Hausberger, K. Atwood, and C. B. Knight, *Adv. Chem. Ser.*, **146**, 47 (1975).

 © 1986 The Chemical Society of Japan Bull. Chem. Soc. Jpn., 59, 351—354 (1986)

The Photochemical Formation of the π-Cation Radical from Chloro(5,10,15,20-tetraphenylporphyrinato)cobalt(III) in Aerated Dichloromethane

Kiyoko YAMAMOTO,* Mikio HOSHINO, Masahiro KOHNO,† and Hiroaki OHYA-NISHIGUCHI††
The Institute of Physical and Chemical Research(RIKEN), Wako, Saitama 351-01
†JEOL Ltd., Akishima, Tokyo 196
††Department of Chemistry, Faculty of Science, Kyoto University, Sakyo-ku, Kyoto 606
(Received July 15, 1985)

Chloro(5,10,15,20-tetraphenylporphyrinato)cobalt(III), Co^{III}(tpp)Cl, in an aerated dichloromethane(DCM) solution undergoes photooxidation to produce the porphyrin π-cation radicals, $Co^{III}(tpp)^{+\cdot}Cl_2$. The formation mechanism of the π-cation radical was investigated by means of optical absorption and ESR spectroscopy: Co^{III}(tpp)Cl in DCM decomposes photochemically to yield Co^{II}(tpp) and chlorine atoms, which then abstract hydrogen atoms from DCM molecules to yield solvent radicals, $\cdot CHCl_2$, and HCl. The solvent radicals react with oxygen molecules, resulting in the generation of peroxyl radicals, which then oxidize Co^{III}(tpp)Cl to produce the π-cation radicals, $Co^{III}(tpp)^{+\cdot}Cl_2$.

In an earlier paper[1] we reported that chloro (5, 10, 15, 20-tetraphenylporphyrinato)cobalt(III), Co^{III}(tpp)Cl, in chlorinated hydrocarbon solutions is converted, partially and reversibly, into a π-cation radical of (tetraphenylporphyrinato)cobalt(III), $Co^{III}(tpp)^{+\cdot}Cl_2$, by thermal and light activations. Such behavior of Co^{III}(tpp)Cl is considered to be closely related to the enzymatic reactions of natural metalloporphyrins. In previous papers,[2,3] we reported that crystals of Co^{III}(tpp)Cl always contain a small amount of the π-cation radical and Co^{II}(tpp). This fact suggests that these oxidation and reduction products are easily formed in the process of preparing Co^{III}(tpp)Cl. The elucidation of the redox behavior of Co^{III}(tpp)Cl is expected to give useful information for an understanding of the functions of peroxidases in vivo.[4] In the present study, we examined in detail the effects of air and light on the redox behavior of Co^{III}(tpp)Cl by using optical absorption and ESR techniques. It was found from these experiments that Co^{III}(tpp)Cl in aerated DCM solutions is efficiently oxidized by irradiation of $\lambda<500$ nm to produce π-cation radicals, $Co^{III}(tpp)^{+\cdot}Cl_2$. The photochemical formation mechanism of $Co^{III}(tpp)^{+\cdot}Cl_2$ is discussed on the basis of optical and ESR measurements of the irradiated DCM solutions.

Experimental

Materials. Chloro(5, 10, 15, 20-tetraphenylporphyrinato) cobalt(III), Co^{III}(tpp)Cl, was prepared by the method previously reported[5] (Found C, 72.66; H, 3.98; N, 7.71; Co, 8.29; Cl. 4.90%).

High-purity dichloromethane (DCM) supplied from Merck Co., Inc., was used as the solvent. The concentration of Co^{III}(tpp)Cl was ca. 1.5×10^{-3} mol dm^{-3} throughout this study.

Instruments. The optical-absorption spectra were recorded on a HITACHI 330 spectrophotometer. The ESR spectra were measured by means of a JEOL FE-2XG spectrometer.

Measurements. Two portions of Co^{III}(tpp)Cl in aerated DCM solutions were preserved, in a light room or in a dark room, over a period of one month. At about one-week intervals, the optical absorption and ESR spectra of the stored solutions were measured. The spectra of Co^{III}(tpp)Cl in deaerated DCM solutions stored in the light room over the period of one week were also measured. For an examination of the effects of light on the photochemical reaction, Co^{III}(tpp)Cl in aerated DCM solutions was irradiated by using a 500 W mercury lamp as a light source, with and without cut-off filters.

The unstable radicals generated from the solvent molecules by UV irradiation were examined by means of a spin-trapping method. Nitrosodurene(3 mg), a spin-trapping reagent, was added to neat DCM(1 cm^3) in vacuo, and the mixture was irradiated.

Results and Discussion

The Optical Absorption and ESR Spectral Changes of Co^{III}(tpp)Cl in Aerated DCM Solutions Preserved in the Light Room. The optical absorption spectrum of Co^{III}(tpp)Cl[6] in DCM has a Soret band at 406 nm (ε=112000), a Q band at 543.5 nm (ε=13200), a small peak at 900 nm (ε=330), and an absorption shoulder at 1080 nm (ε=250). When the aerated DCM solution of Co^{III}(tpp)Cl was preserved in the light room for one month, the optical-absorption spectrum changed, as is shown in Fig. 1. The intensities of the absorption bands of Co^{III}(tpp)Cl gradually decreased with the preservation time, and broad absorption bands around 620 and 680 nm appeared. When methanol was added to the preserved solution, the broad absorption bands disappeared.

Since the solids of Co^{III}(tpp)Cl used for the present study contain a small amount of the π-cation radical, $Co^{III}(tpp)^{+\cdot}Cl_2$, the ESR spectrum observed for the solution of Co^{III}(tpp)Cl immediately after preparation showed a weak signal due to the π-cation radical.[1,2,7] The ESR signal increased in intensity with the preservation time. When methanol was added to the solution, the signal disappeared immediately.

On the other hand, the optical absorption spectra of Co^{III}(tpp)Cl in aerated DCM solutions preserved in the dark room did not show any appreciable changes except for a slight decrease in the absorption intensity around

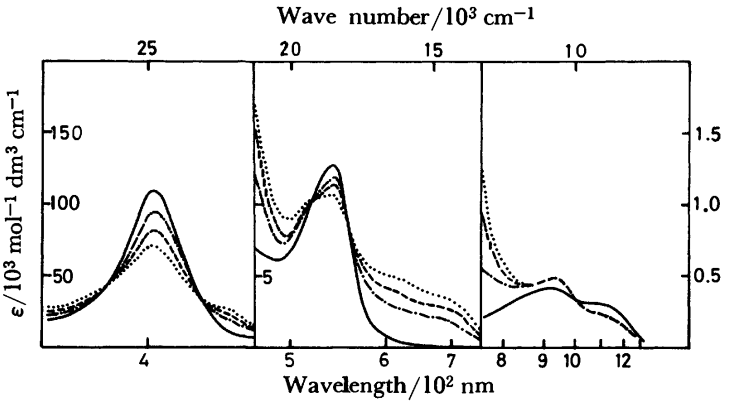

Fig. 1. Absorption spectral changes observed for aerated DCM solutions of Co^{III}(tpp)Cl preserved in the light room. Measured immediately after preparation (——), and measured after preservation for 6 (-·-·-·-), 13 (----), and 17 (·····) days in the light room.

580—720 nm. The ESR spectra of the solutions showed a considerable decrease in the signal intensity of $Co^{III}(tpp)^{+\cdot}Cl_2$. This reveals that the π-cation radical decomposes thermally, while Co^{III}(tpp)Cl does not, so long as the solution is preserved in a dark room.

From these results, we may conclude that: (1) The absorption bands around 620 and 680 nm observed for the preserved solution are to be ascribed to the π-cation radicals, $Co^{III}(tpp)^{+\cdot}Cl_2$, and (2) the π-cation radical is produced photochemically when the aerated DCM solution of Co^{III}(tpp)Cl is preserved in a light room.

Participation of Solvent Radicals in the Formation of $Co^{III}(tpp)^{+\cdot}Cl_2$. The photochemical decomposition of chlorinated hydrocarbons is well-established. In order to examine the participation of the solvent radicals in the photochemical reactions, an aerated DCM solution of Co^{III}(tpp)Cl was irradiated by a mercury lamp without and with a cut-off filter transmitting the light of $\lambda>360$ nm. Since DCM molecules absorb only the light of $\lambda<360$ nm, Co^{III}(tpp)Cl can be selectively irradiated by the use of this filter.

Figure 2 shows the ESR signal intensity of $Co^{III}(tpp)^{+\cdot}Cl_2$, represented as a function of the irradiation time. The formation rate of $Co^{III}(tpp)^{+\cdot}Cl_2$ observed for the aerated solution irradiated without a filter becomes faster than that irradiated with the filter ($\lambda>360$ nm). This result indicates that the photooxidation of Co^{III}(tpp)Cl in DCM occurs by the photolysis of both Co^{III}(tpp)Cl and DCM, as will be discussed later.

The aerated DCM solution of Co^{III}(tpp)Cl was also irradiated by the use of a mercury lamp with a cut-off filter transmitting the light of $\lambda>500$ nm. No increase in the ESR signal intensity of $Co^{III}(tpp)^{+\cdot}Cl_2$ was observed. From this observation, we may conclude that the Q-band excitation gives no oxidation product, $Co^{III}(tpp)^{+\cdot}Cl_2$.

Detection of Solvent Radicals Generated from Neat DCM. Radicals generated by the direct photolysis of neat DCM in vacuo were examined by using the spin-trapping method. When the mixture was irradiated by the use of a mercury lamp without a filter, the ESR spectrum shown in Fig. 3 was obtained. The following ESR parameters were obtained for the generated radical: One nitrogen (a_N=1.37 mT) and two hydrogen (a_H=0.86 mT) nuclei. The radical was identified as a spin adduct of nitrosodurene with the $\cdot CH_2Cl$ radical. This result clearly indicates that DCM molecules undergo the C–Cl bond cleavage upon UV irradiation to produce $\cdot CH_2Cl$ radicals and chlorine atoms.

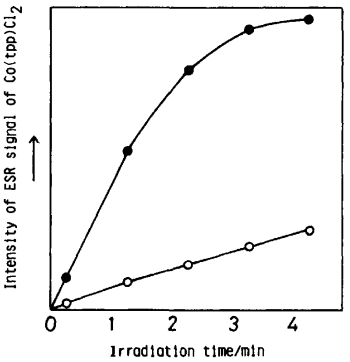

Fig. 2. ESR signal intensity of $Co^{III}(tpp)^{+\cdot}Cl_2$ generated from Co^{III}(tpp)Cl in aerated DCM solutions by irradiation with the light of $\lambda>360$ nm (○) and without filter (●).

The Optical Absorption and ESR Spectral Changes of Co^{III}(tpp)Cl in Degassed DCM Solutions Preserved in the Light Room. As is shown in Fig. 4, the optical absorption spectrum observed for the degassed DCM solution of Co^{III}(tpp)Cl preserved for one week in the light room showed a red shift of the Soret band and a blue shift of the Q band. The spectrum of pure Co^{II}(tpp) in DCM shows a Soret band at 409.5 nm (ε=295000), a Q band at 527.5 nm (ε=16200), and a band at 860 nm (ε=140). The spectral changes in Fig. 4 may be interpreted in terms of the photochemical formation of Co^{II}(tpp) by the photodissociation of the

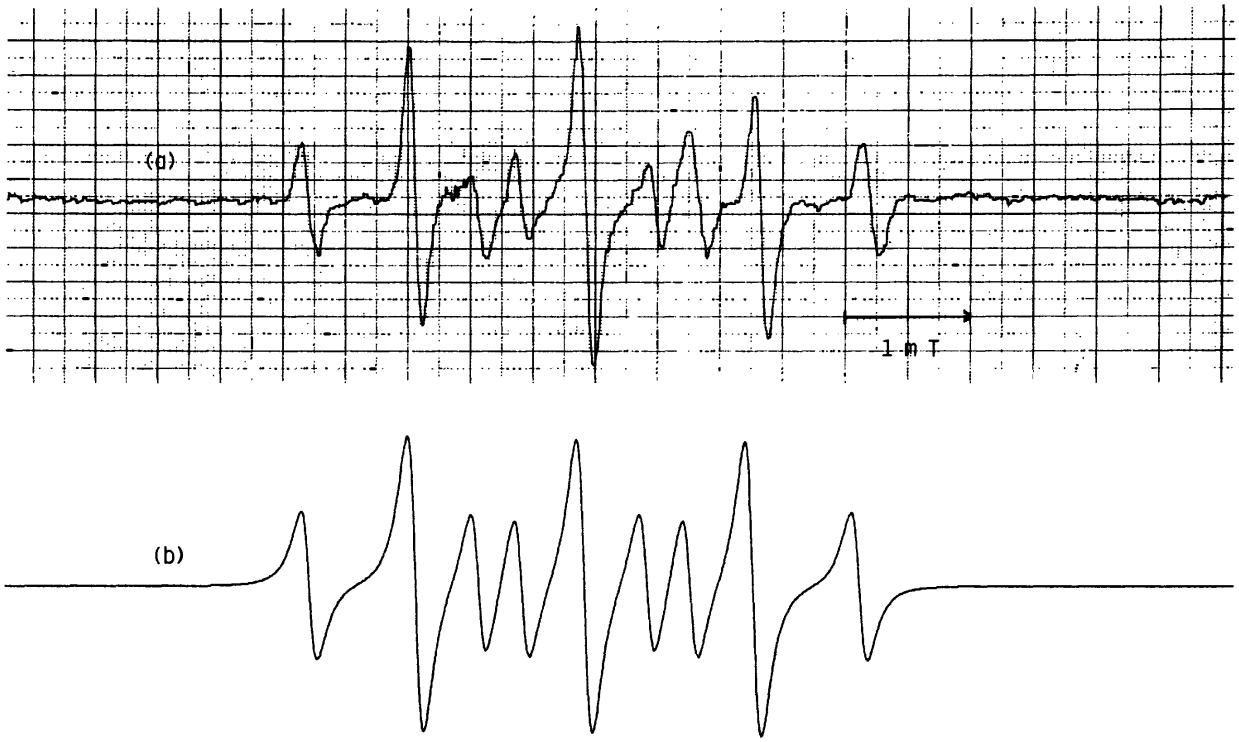

Fig. 3. ESR spectrum of spin adduct of nitrosodurene with $\cdot CH_2Cl$ radical. Observed (a) and simulated (b) spectra.

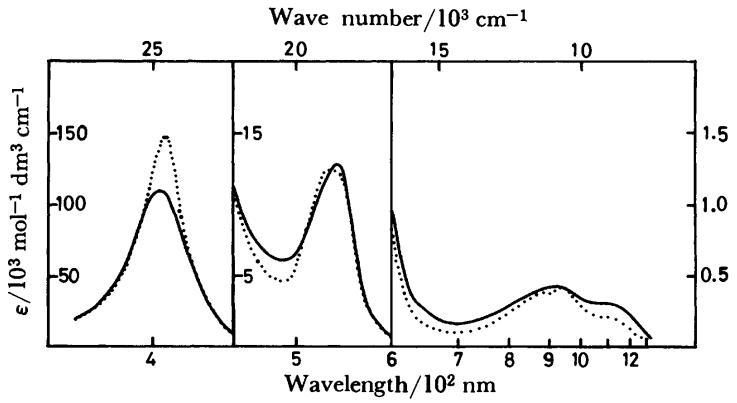

Fig. 4. Absorption spectral changes observed for degassed DCM solutions of Co^{III}(tpp)Cl preserved in the light room. Measured immediately after preparation (——) and after preservation for 7 days (·····) in the light room.

chlorine atom from Co^{III}(tpp)Cl. In fact, the ESR spectrum measured for the degassed solution stored in the light room for one week shows an increase in the signal intensity of Co^{II}(tpp).[8] No formation of the π-cation radical was observed in the degassed conditions.

Oxidation Mechanism of Co^{III}(tpp)Cl in Aerated DCM Solutions. The photoinduced homolytic Co–Cl bond cleavage of Co^{III}(tpp)Cl gives rise to the formation of Co^{II}(tpp) and chlorine atoms:[9]

$$Co^{III}(tpp)Cl \xrightarrow{h\nu} Co^{II}(tpp) + Cl\cdot \quad (1)$$

The occurrence of this reaction is demonstrated by the result that the concentration of Co^{II}(tpp) in the degassed DCM solutions of Co^{III}(tpp)Cl increases with the preservation time in the light room. The formation of the chlorine atoms in Co^{III}(tpp)Cl solutions was also detected by using another spin-trapping method.[10] Subsequently, the chlorine atoms abstract hydrogen atoms from DCM molecules to yield solvent radicals, $\cdot CHCl_2$, and hydrochloric acid:

$$Cl\cdot + CH_2Cl_2 \longrightarrow \cdot CHCl_2 + HCl \quad (2)$$

In the aerated solutions, the solvent radicals react with oxygen molecules, forming peroxyl radicals,

$CHCl_2O_2\cdot$. They oxidize $Co^{III}(tpp)Cl$ to produce π-cation radicals, $Co^{III}(tpp)^{+\cdot}Cl(CHCl_2O_2)$, which are then converted into the stable π-cation radicals of $Co^{III}(tpp)^{+\cdot}Cl_2$, presumably as a result of axial-ligand substitution.[1,11]

$$\cdot CHCl_2 + O_2 \longrightarrow [CHCl_2O_2\cdot] \quad (3)$$

$$[CHCl_2O_2\cdot] + Co^{III}(tpp)Cl \longrightarrow Co^{III}(tpp)^{+\cdot}Cl(CHCl_2O_2) \quad (4)$$

$$Co^{III}(tpp)^{+\cdot}Cl(CHCl_2O_2) + HCl \longrightarrow Co^{III}(tpp)^{+\cdot}Cl_2 + CHCl_2O_2H \quad (5)$$

It should be noted here that the formation of the peroxyl radicals is essential to give the π-cation radicals.

As revealed from the spin-trapping study, solvent molecules, CH_2Cl_2, undergoes photodecomposition with the light of $\lambda<360$ nm:

$$CH_2Cl_2 \xrightarrow{h\nu} Cl\cdot + \cdot CH_2Cl \quad (6)$$

The solvent radicals produced by the photolysis of DCM molecules may also react with oxygen molecules, forming peroxyl radicals:

$$\cdot CH_2Cl + O_2 \longrightarrow CH_2ClO_2\cdot \quad (7)$$

The radicals also oxidize $Co^{III}(tpp)Cl$ to form $Co^{III}(tpp)^{+\cdot}Cl_2$.

$$CH_2ClO_2\cdot + Co^{III}(tpp)Cl \longrightarrow Co^{III}(tpp)^{+\cdot}Cl(CH_2ClO_2) \quad (8)$$

$$Co^{III}(tpp)^{+\cdot}Cl(CH_2ClO_2) + HCl \longrightarrow Co^{III}(tpp)^{+\cdot}Cl_2 + CH_2ClO_2H \quad (9)$$

Thus, the fast formation rate of the $Co^{III}(tpp)^{+\cdot}Cl_2$ radical observed for the conditions without a filter (Fig. 2) is conducted with the two oxidation mechanisms described above. When we use the filter absorbing the light of $\lambda<360$ nm, the first five reactions (1—5) dominate the formation of the π-cation radical.

According to Reaction (1), $Co^{III}(tpp)Cl$ decomposes photochemically to produce $Co^{II}(tpp)$. However, we can not detect $Co^{II}(tpp)$ in the aerated DCM solution of $Co^{III}(tpp)Cl$ upon irradiation. This fact suggests that the oxidant radicals, such as $CHCl_2O\cdot$, $CH_2ClO\cdot$, and $HO\cdot$, which are produced from $CHCl_2O_2H$ and CH_2ClO_2H, oxidize $Co^{II}(tpp)$ to reproduce $Co^{III}(tpp)Cl$.

Conclusion

Studies on the mechanism of the formation of the porphyrin π-cation radicals, $Co^{III}(tpp)^{+\cdot}Cl_2$, from $Co^{III}(tpp)Cl$ in aerated DCM solutions in the light room have revealed that: (1) $Co^{III}(tpp)Cl$ undergoes the homolytic cleavage of the Co–Cl bond in $Co^{III}(tpp)Cl$ upon Soret-band excitation to yield $Co^{II}(tpp)$ and chlorine atoms; (2) the hydrogen abstraction of the chlorine atoms from DCM molecules produces solvent radicals, which then react with oxygen molecules to form oxidant radicals; (3) oxidant radicals are also formed by the photolysis of aerated DCM, and (4) these oxidant radicals oxidize $Co^{III}(tpp)Cl$ to produce $Co^{III}(tpp)^{+\cdot}Cl_2$.

References

1) K. Yamamoto, M. Kohno, and H. Ohya-Nishiguchi, *Chem. Lett.*, **1981**, 255.
2) M. Kohno, H. Ohya-Nishiguchi, K. Yamamoto, and T. Sakurai, *Bull. Chem. Soc. Jpn.*, **56**, 822 (1983).
3) M. Kohno, H. Ohya-Nishiguchi, K. Yamamoto, and T. Sakurai, *Bull. Chem. Soc. Jpn.*, **57**, 932 (1984).
4) W. D. Hewson and L. P. Hager, "Peroxidases, Catalases, and Chloroperoxidase," in "The Porphyrins," ed by D. Dolphin, Academic Press Inc., New York (1979), Vol. 7, p. 295, and the other references cited therein.
5) T. Sakurai, K. Yamamoto, H. Naito, and N. Nakamoto, *Bull. Chem. Soc. Jpn.*, **49**, 3042 (1976).
6) K. Yamamoto, *Sci. Papers Inst. Phys. Chem. Res.*, **71**, 111 (1977).
7) H. Ohya-Nishiguchi, M. Kohno, and K. Yamamoto, *Bull. Chem. Soc. Jpn.*, **54**, 1923 (1981).
8) J. M. Assour, *J. Chem. Phys.*, **43**, 2477 (1965).
9) M. Hoshino, K. Yasufuku, S. Konishi, and M. Imamura, *Inorg. Chem.*, **23**, 1982 (1984).
10) M. Kohno, *Bull. Chem. Soc. Jpn.*, to be published.
11) K. Ichimori, H. Ohya-Nishiguchi, N. Hirota, and K. Yamamoto, *Bull. Chem. Soc. Jpn.*, **58**, 623 (1985).

 © 1986 The Chemical Society of Japan Bull. Chem. Soc. Jpn., 59, 355—361 (1986)

A Study of the Zero Field Splittings of the Lowest Excited Triplet States of Substituted Benzenes and Related Molecules by Optical Detection of Magnetic Resonance, Electron Paramagnetic Resonance, and Molecular Orbital Calculations

Shin-ichi NAGAOKA,*,†,††,††† Edward T. HARRIGAN,†4 Masayo NODA,†,†5,†6
Noboru HIROTA,*,†,†4 and Jiro HIGUCHI*,†7
†Department of Chemistry, Faculty of Science, Kyoto University, Sakyo-ku, Kyoto 606
††Division of Chemistry, Research Institute of Applied Electricity, Hokkaido University, Kita-ku, Sapporo 060
†4Department of Chemistry, State University of New York at Stony Brook, Stony Brook, New York 11794, U.S.A.
†5Tokai Women's College, Kagamigahara, Gifu 504
†6Tokai Women's Junior College, Kagamigahara, Gifu 504
†7Department of Chemistry, Faculty of Engineering, Yokohama National University, Hodogaya-ku, Yokohama 240
(Received July 30, 1985)

The zero field splittings of a series of substituted benzenes and related molecules have been examined by means of optical detection of magnetic resonance (ODMR), electron paramagnetic resonance (EPR), and molecular orbital (MO) calculations. It is experimentally shown that D and E values vary remarkably depending on the type of molecule despite the similarlity in the molecular size. In particular, E varies from $+0.038$ cm^{-1} for phenylacetylene to -0.0597 cm^{-1} for aniline reflecting large differences in the spin distributions. The calculation of the zero field splittings of the molecules studied here on the basis of the Pariser-Parr-Pople-type MO's can give the values reasonably close to those obtained experimentally with a few exceptions. On the basis of the obtained results the natures of the T_1 states of substituted benzenes are characterized from the zero field splittings.

The zero field splittings (ZFS's) of the lowest excited triplet (T_1) states of aromatic molecules have been studied extensively for more than two decades.[1–18] Since in most molecules ZFS's are determined by spin-spin interactions between two unpaired electrons, the ZFS's reflect spin distributions which are directly related to the electronic wave functions of the T_1 states. One would hope to extract useful information about electronic structures of the T_1 states from the analysis of ZFS's. Yet, use of ZFS's in elucidating the electronic structures of the T_1 states of aromatic molecules has been limited so far in spite of numerous experimental data accumulated. This is due partly to the fact that the ZFS's are often not very sensitive to structural changes. In the present work we have attempted to analyze the ZFS's of substituted benzenes and related molecules with a hope of utilizing the ZFS's to characterize the electronic structures of the T_1 states.

Substituted benzenes form an attractive group of molecules for a detailed study of ZFS, because their ZFS's are markedly dependent on the nature of substituent.[2–18] This situation is quite different from the cases of other hydrocarbons such as naphthalene.[19] The triplet states of substituted benzenes are often classified as having quinonoidal (Q) or antiquinonoidal (AQ) structures. The ZFS's are expected to vary depending on whether the T_1 state is of Q type or of AQ one and an examination of the ZFS's may be helpful in characterizing their electronic structures.

The main purposes of the present work are the following. First, we compare the ZFS's of various substituted benzenes in order to find general qualitative trends. For this purpose we have supplemented the existing data by conducting optical detection of magnetic resonance (ODMR) and electron paramagnetic resonance (EPR) experiments on a series of substituted benzonitriles, anilines, and anisoles. On the basis of the obtained results we attempt to characterize the natures of the T_1 states of substituted benzenes from the ZFS's. Second, we calculate the ZFS's of the representative systems by using the semiempirical Pariser-Parr-Pople-type molecular orbitals (MO's) to see whether or not such calculations reproduce the experimentally obtained ZFS's adequately. Substituted benzenes which we examine here are divided into two groups, one having electron-attracting mesomeric groups such as -CCH, -CN, and -CHO, and the other having electron-donating inductive substituents such as $-NH_2$ and $-OCH_3$. The effects of weakly perturbing substituents such as F, Cl, and CH_3 were examined in benzonitrile, aniline, and anisole. We also studied other related molecules such as benzofuran, indole, and indazole as the examples of the molecules with very strongly mesomeric groups.

Experimental

Sample Preparation. 1,4-Dibromobenzene (DBB) was purified by recrystallization from ethanol followed by zone refining. All of the solid guest samples were purified by recrystallization and all the liquid samples were purified by distillation. Mixed crystals containing small amounts of guest molecules were grown using the standard Bridgman method starting from the melts containing approximately 2 wt% of the guest molecules.

ODMR and EPR Measurements. The ZFS's (D's and E's) of benzonitriles, anilines, and anisoles were determined from the microwave frequencies corresponding to the transitions among the zero field (ZF) spin sublevels observed by the zero field optical detection of magnetic resonance (ZFODMR)

†††Present address: Institute for Molecular Science, Myodaiji, Okazaki 444.

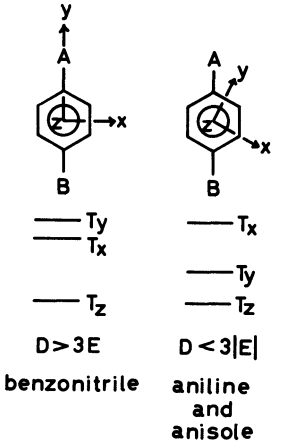

Fig. 1. Direction of axes and ZFS's of the molecules investigated in this work.

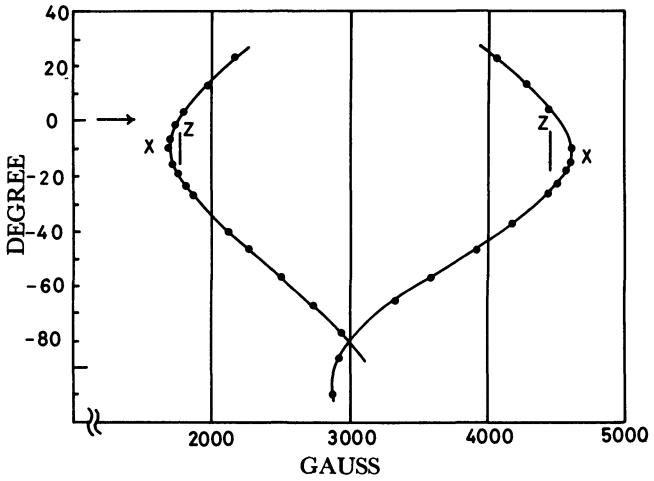

Fig. 2. Angular dependence of the EPR signals of 4-methylanisole in DBB. Magnetic field was rotated in the x-y plane of the molecule.

experiments at about 1.8 K. The experimental setup and procedures are essentially the same as those described in a previous paper.[20] The ODMR experiments were normally made under steady state illumination using the fast passage technique. The lifetimes of the substituted benzenes in DBB host range from 5 to 100 ms and we swept the frequency region of 0.1—0.5 GHz within 0.1—2 s. Normally three ODMR transitions were detected with good S/N ratios. In order to determine the sublevel schemes we also performed the EPR experiments of single crystal on a few anilines and anisoles at 4.2 K. The experimental setup and the method are similar to those described previously.[6]

Experimental Results and Qualitative Interpretation

Experimental Results. The ZFS's, D's and E's, of the molecules studied here are determined from the ZF transition energies using the spin Hamiltonian,

$$H_s = D\left(S_z^2 - \frac{1}{3}S^2\right) + E(S_x^2 - S_y^2). \quad (1)$$

When the z axis is taken perpendicular to the molecular plane, the bottom sublevel is the z sublevel. In the cases of benzonitriles and phenylacetylene with the C_{2v} symmetry we take the x and y axes as shown in Fig. 1. Then the order of the sublevels becomes y, x, and z from the top. In these molecules it is known that $T_y - T_x < T_x - T_z$ and $D > 3E$.[5] In the ortho- and meta-substituted benzonitriles the y directions are not exactly parallel to the C-CN direction. However, the above sublevel scheme is considered to be correct in all the benzonitriles studied here.

On the other hand, whether D is larger than $3|E|$ is not certain in anisoles and anilines. In most aromatic molecules D is usually larger than $3|E|$. $D > 3|E|$ was found in the case of 4-chloroaniline in xylene (X),[3,8] but the same molecule gives $D < 3|E|$ in the 1,4-dichlorobenzene (DCB) host.[8,14] Kothandaraman and Tinti also concluded $D < 3|E|$ for 4-chloroanisole.[3] One cannot make an a priori assumption about the relative magnitudes of D and $3|E|$. Here we have examined the EPR spectra of 4-methylanisole in the DBB host (Fig. 2). We have obtained the values for the field strengths of the Z stationary points, 4465 and 1755 G (1 G=10^{-4} T). These values are in good agreements with the values calculated from the D and E determined by the ODMR experiments on the assumption of $D < 3|E|$. This assignment is also confirmed by the observation that the field separation between the two in-plane stationary peaks is larger than that for the Z stationary peaks. These observations definitely show $D < 3|E|$ for 4-methylanisole. $D < 3|E|$ was also found for 4-chloroanisole[3] 4-chloroaniline, and 2-fluoroaniline in DBB.[14] Here we calculated D's and E's of other anilines and anisoles by assuming $D < 3|E|$.

Another remarkable point about the T_1 states of anilines and anisoles is the spin axis rotation whose occurrence has been confirmed in the cases of aniline in X,[11] 4-fluoroaniline in DBB,[14] and 4-chloroaniline in DCB.[14] It is quite probable that the spin axis rotation is also taking place in anilines and anisoles studied here. If this is the case, the x and y axes deviate from the molecular symmetry axes as shown in Fig. 1. The order of the sublevels determined for aniline is x, y, and z from the top and this is assumed for all anilines and anisoles studied here. The ZFS's determined in this work are tabulated in Table 1 together with those of other related systems.

The values of the ZFS's determined by the present ODMR experiments agree reasonably well with those determined by EPR at 4.2 K. However, the ZFS's determined by the ODMR experiments do not necessarily agree with the values determined by the EPR experiments at 77 K. For instance, EPR at 77 K gives D=0.1371 cm^{-1} for benzonitrile in DBB,[5] while ODMR at about 1.8 K gives D=0.1430 cm^{-1} for the same system. The ZFS's of the substituted benzenes also depend on the nature of the matrix. D and E values of aniline in DBB are considerably different from those obtained in X.[11]

General Trend of ZFS. We first discuss some notable observations about the ZFS's of substituted benzenes. Despite the similarities of the molecular size the ZFS's vary remarkably depending on the substituent. D observed here ranges from 0.1472 cm^{-1} in 4-fluorobenzonitrile to 0.1040 cm^{-1} in 4-fluoroaniline. E ranges from +0.0380 cm^{-1} in phenylacetylene to −0.0597 cm^{-1} in aniline. However, the variations of D and E in the same type of molecules are much smaller. From the results given in Table 1 we conclude the following.

1) Even weakly perturbing substituents such as F, Cl, and CH_3 affect D considerably, but their effect on E is relatively small.

Table 1. Experimental Results of E_T's, D's, and E's

Number	Guest	Host[a]	E_T	D	E	Reference
			cm^{-1}	cm^{-1}	cm^{-1}	
1	Aniline	DBB	27601	0.1160	(−)0.0597[b]	Present work
2		X	27659	0.1229	(−)0.0352[b]	11
3	2-Fluoroaniline	DBB	27285	0.1126	−0.0435[c]	Present work
4	4-Fluoroaniline	DBB	26838	0.1040	−0.0533[c]	Present work[d]
5	4-Chloroaniline	DCB	26938	0.1220	−0.0500[c]	14
6		X	26514	0.1171	±0.0338[e]	3
7	4-Toluidine	DBB	26795	0.1119	(−)0.0533[b]	Present work
8	4-Fluoroanisole	X	27563	0.1220	(−)0.0562[b]	3
9	4-Chloroanisole	X	27377	0.1323	(−)0.0569[b]	3
10	4-Methylanisole	DBB	27278	0.1236	(−)0.0537[b]	Present work
11	Benzonitrile	DBB	26882	0.1430	0.0106	Present work[f]
12	2-Fluorobenzonitrile	DBB	26788	0.1405	0.0117	Present work
13	3-Fluorobenzonitrile	DBB	26553	0.1370	0.0191	Present work
14	4-Fluorobenzonitrile	DBB	27229	0.1472	0.0073	Present work
15	4-Chlorobenzonitrile	DBB	25840[g]	0.1319	0.0045	15
16	2-Tolunitrile	DBB	26246	0.1325	0.0206	Present work
17	3-Tolunitrile	DBB	26143	0.1231	0.0050	Present work
18	4-Tolunitrile	DBB	26702	0.1344	0.0070	Present work
19	Phenylacetylene	DBB	25120	0.1339	0.0380	5
20	Benzaldehyde	BAC	25456	0.1381	0.0089	9, 10, 13, 17
21	Benzofuran	DBB	24570	0.1076	0.0530	6
22	Indole	DBB	24155	0.0978	0.0453	6
23	Benzimidazole	BAC	26539	0.1123	0.0270	18
24	1*H*-Indazole	BAC	23590	0.1077	0.0293	18
25	2*H*-Indazole	BAC	20903	0.0983	0.0120	16
26	Purine	BAC	26409	0.1042	0.0608	18

a) DBB, X, DCB, and BAC denote 1,4-dibromobenzene, xylene, 1,4-dichlorobenzene, and benzoic acid, respectively. b) The sign of the E parameter seems to be negative by analogy. c) The sign of the E parameter was determined by means of single crystal EPR. d) EPR at 4.2 K gives $D=0.102\,cm^{-1}$ and $E=-0.0535\,cm^{-1}$ for 4-fluoroaniline in DBB.[14] The value of the ZFS of 4-fluoroaniline in this table is determined by the ODMR experiment, and agrees well with the value determined by EPR. e) The sign of the E parameter was not determined. f) EPR at 77 K gives $D=0.1371\,cm^{-1}$ and $E=0.0072\,cm^{-1}$ for benzonitrile in DBB.[5] The value of the ZFS of benzonitrile in this table is determined by the ODMR experiment. As mentioned in the text, the ZFS's determined by the ODMR experiments do not necessarily agree with the values determined by the EPR experiments at 77 K. g) Present work.

2) D's of benzonitriles are relatively large compared with those of anilines and anisoles.

3) $|E|$'s of anilines and anisoles are similar and quite large, while $|E|$'s of benzonitriles are rather small.

In Fig. 3 we plot D vs. S_0—T_1 transition energy (E_T) for a series of benzonitriles, anilines and anisoles. Brinen and Orloff noted that there is a linear relation between D and E_T for a large number of polyacenes.[21] We have extrapolated their plot to the region of large E_T which is shown by a dotted line in Fig. 3. It is seen that the points for benzonitriles are located above the extrapolated Brinen Orloff line, but D's for anilines and anisoles are located below. For a series of benzonitriles D vs. E_T plot gives an approximately linear relation, but the slope is much steeper than that for the Brinen Orloff plot. It is interesting to note that the D values of benzonitriles with mesomeric substituents, polyacences (extrapolated Brinen Orloff line), and aniline and anisoles with mainly inductive substituents decrease in that order.

A detailed analysis of the ZFS's of benzene and benzene derivatives by Godfrey, Kern, and Karplus showed that the main factors determining the magnitude of D are the extent of configurational mixing and the extent of delocalization of unpaired electrons.[22] The former tends to increase D, whereas the latter to decrease D. It was shown that D calculated for the benzene triplet state with a single configuration can be very small, being $0.1\,cm^{-1}$, but a small amount of configurational mixing can increase the D drastically. In the present systems benzonitriles and phenylacetylene with more delocalization of unpaired electrons into the substituents have larger D values than anilines and anisoles with less delocalization. Therefore the main factor determining the variation of D in the present systems appears to be the extent of the configurational mixing.

In the aromatic hydrocarbons such as naphthalene, substitution by weakly perturbing substituents hardly affects D.[19] In the molecules studied here D is rather sensitive to the substitution by them. Even fluorine substitution causes a significantly large change in D. Furthermore the change in D caused by the mono fluoro substitution depends on the location of the substitution: D (para)>D (ortho)>D (meta) in benzonitrile, while D (ortho)>D (para) in aniline. It was also found that fluorine substitution at the para position produces a blue shift of E_T in benzonitrile, but a red shift in aniline. Thus the effect of fluorine substitution is opposite in these two types of molecules. These observations seem to indicate that substitution by weakly perturbing substituents changes the extent of configurational mixing considerably in the present systems.

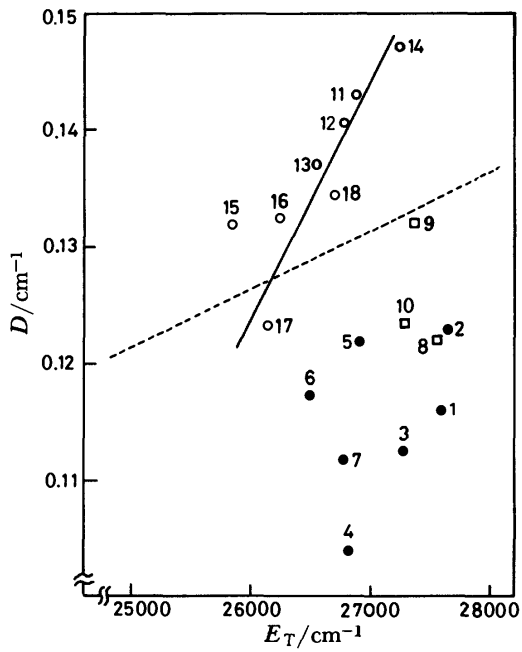

Fig. 3. Plots of D vs. E_T for a series of benzonitriles (○), anilines (●), and anisoles (□). The numbers near the data points correspond to those in Table 1. The dotted line shows the extrapolated Brinen Orloff plot.[21]

The previous investigations have shown that benzonitrile and phenylacetylene have Q structures,[5] while anilines and anisoles have AQ ones.[11,14] Anilines and anisoles studied here all have large $|E|$ values. It seems that substituted benzenes with AQ structures have large $|E|$ values.

Calculation of ZFS

The ZFS's in the lowest excited triplet states of the representative benzene derivatives have been calculated using the semiempirical Pariser-Parr-Pople-type LCAO-MO's.[23,24] The ZFS's of benzofuran, indole, 1*H*- and 2*H*-indazoles, benzimidazole, and purine were also calculated for comparison. Many calculations on the ZFS's of several molecules in their triplet states have been made successfully with various degrees of approximations.[25-34] One of the present authors (J. H.) also obtained good agreements between the observed ZFS's and the calculated ones for aromatic hydrocarbons.[25] We have used a similar procedure in the present calculation.

Method and Procedure. The ZFS's were evaluated from the electron spin-spin interactions, using the standard and simple approximation with only Coulomb-type integrals.[35-38] The spin-orbit interactions were ignored. The ZFS parameters, D and E, can be expressed as,

$$D = \frac{3\mu_0 g^2\beta^2}{16\pi hc}\left\langle \frac{r_{12}^2 - 3z_{12}^2}{r_{12}^5} \right\rangle, \quad (2)$$

$$E = \frac{3\mu_0 g^2\beta^2}{16\pi hc}\left\langle \frac{x_{12}^2 - y_{12}^2}{r_{12}^5} \right\rangle, \quad (3)$$

where r_{12} is the distance between two unpaired electrons. The wave functions were constructed by including configurations arising from all the single excitations relative to the ground state. For all of the molecules studied here, the overlap integrals and the electron spin-spin interactions were calculated by using double-zeta atomic orbitals by Clementi.[39]

The information obtained from the present calculation for the directions of the principal axes of the ZF tensors is not complete.[40] In fact, we cannot determine whether the direction of the principal axis of the ZF tensor corresponds to, for example,

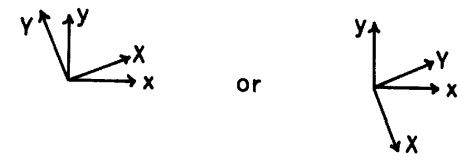

where (x, y) and (X, Y) denote sets of the in-plane axes for the coordinate system of the molecule and for the principal axis system of the ZF tensor, respectively. This means that the absolute sign of E cannot be determined from the calculation. We therefore deduced the directions of the principal axes of the ZF tensors and the signs of E's from the experimental results.

For benzaldehyde, benzonitrile, and phenylacetylene, two-center electron repulsion integrals were estimated by the method suggested by Nishimoto.[41-43] Since the detailed knowledge of the molecular geometry is not required, two-center core integrals (β) were calculated by the method of variable β approximation[43] using the following parameters reported previously.[5,13]

Benzaldehyde:

$(-0.51P - 2.12)$ eV for C-C(ring),

$(-0.55P - 2.80)$ eV for C=O,

$(-0.51P - 1.70)$ eV for C(ring)-C(formyl group).

Benzonitrile:

$(-0.51P - 2.12)$ eV for C-C(ring),

$(-0.53P - 2.60)$ eV for C≡N,

$(-0.51P - 1.72)$ eV for C(ring)-C(cyano group).

Phenylacetylene:

$(-0.51P - 2.12)$ eV for C-C(ring),

$(-0.51P - 2.40)$ eV for C≡C,

$(-0.51P - 1.72)$ eV for C(ring)-C(ethynyl group),

where P is the bond order. In the calculations of these molecules, the ionization potentials (I's) and electron affinities (A's) for C, O, and N were taken as 86% of the values for free atoms[44] following Nishimoto (C $tr^1tr^1tr^1\pi$: I=9.60 eV, A=0.00 eV, N $tr^2tr^1tr^1\pi$: I=12.14 eV, A=1.53 eV, O $tr^2tr^2tr^1\pi$: I=15.22 eV, A=2.12 eV).[5,42] The UHF calculations using these parameters have been made previously for benzaldehyde,[13] benzonitrile,[5] and phenylacetylene[5] with satisfactory results for

spin distributions. We checked our program and procedure with naphthalene. The result of the calculation (D=0.101 cm^{-1} and E=-0.010 cm^{-1}) agreed well with the experimental result for naphthalene (D= 0.1006 cm^{-1} and E=−0.0138 cm^{-1}).[45]

The above method is not applicable to the molecules with odd π orbitals. Therefore, in the calculations of aniline, anisole, benzofuran, indole, 1*H*- and 2*H*-indazoles, benzimidazole, and purine, two-center electron repulsion integrals and β's were evaluated by using Ohno-Klopman-type[46] and Wolfsberg-Helmholtz-type[47] approximations, respectively. β for benzene was assumed to be −2.39 eV.

In the calculations of the molecules with odd π orbitals, we adopted either of the following two kinds of parameters (parameter A and B). In parameter A, we used the values given by Hinze and Jaffe[44] (C trtrtrπ: I=11.16 eV, A=0.03 eV, N tr^{2}trtrπ: I=14.12 eV, A=1.78 eV, O tr^{2}tr^{2}trπ: I=17.70 eV, A=2.47 eV) and by Dewar and Morita[48] (N trtrtrπ: I=28.59 eV, A= 11.96 eV, O tr^{2}trtrπ: I=33.90 eV, A=15.30 eV).

As described later, parameter A does not satisfactorily reproduce the observed trend of ZFS in the calculations of *N*-heterocyclic molecules with N trtrtrπ. The reason for this may be explained by the following fact. N tr^{2}trtrπ and N trtrtrπ provide one and two π electrons to π molecular orbitals, respectively. However, since in a conjugated system the π electron density on N trtrtrπ decreases substantially from 2 owing to the π electron delocalization, while the σ electron density on N trtrtrπ is estimated to increase largely from 3.[49] Thus, the value of semiempirical parameters, such as the one-center repulsion integral (I−A), for N trtrtrπ are considered to become close to those for N tr^{2}trtrπ. As a result, the observed trend of ZFS may not be reproduced with parameter A. Accordingly, in parameter B the value of I−A for N trtrtrπ is tentatively assumed to be equal to that for N tr^{2}trtrπ given by Hinze and Jaffe (I−A=12.34 eV).[44] On the other hand, since N tr^{2}trtrπ and N trtrtrπ provide one and two π electrons to π molecular orbitals, the electric fields for electrons on N tr^{2}trtrπ and N trtrtrπ approximate to those of N^+ and N^{2+}, respectively. The value of A for N^{2+} is considered to be equal to that of I for N^+. It may not be unreasonable, thus, to assume that the value of A for N trtrtrπ is nearly the same as that of I for N tr^{2}trtrπ given by Hinze and Jaffe.[44] In parameter B, for N trtrtrπ we used the value thus determined (I=26.45 eV, A=14.11 eV) and for C trtrtrπ and N tr^{2}trtrπ we used the same values as those in parameter A.

The ZFS of aniline was calculated for the conformation in which the benzene ring is hexagonal (H), Q, AQ, or skewed-antiquinonoidal (SAQ) form. The geometries of the benzene rings for the H, Q, and AQ conformations were taken from the results by Fujimura et al.[50] The geometry of the SAQ conformation was assumed to be the same as that of 4-fluoroaniline which had been predicted from the EPR study.[14] The effect of the methyl group in anisole was not taken into account in the present calculation. The ZFS of anisole was calculated with the same geometry as that of the SAQ conformation of aniline.

The geometries of indole, 1*H*-indazole, benzimidazole, and purine were taken from the results of the X-ray diffraction.[51–53] The geometries of the benzene and pyrazole moieties in 2*H*-indazole were assumed to be the same as those of the benzene ring in 1*H*-indazole and of pyrazole ring given in the reference,[51] respectively. The ZFS of benzofuran was calculated with the same geometry as that of indole.

Results and Discussion. The results of the calculations for E_T's, the D's and E's, and the directions of the in-plane principal axes of the ZF tensors (θ) are summarized in Table 2. Here θ denotes the angle between the short axis of the molecule and the principal axis of the top sublevel. It is seen

Table 2. Calculated E_T's, ZFS's, and Directions of Principal Axes of ZF Tensors

					Parameter A				Parameter B			
	E_T	D	E	θ	E_T	D	E	θ	E_T	D	E	θ
	10^4 cm^{-1}	cm^{-1}	cm^{-1}		10^4 cm^{-1}	cm^{-1}	cm^{-1}		10^4 cm^{-1}	cm^{-1}	cm^{-1}	
Benzaldehyde	2.50	0.129	0.011	31[a]								
Benzonitrile	2.45	0.124	0.010	90								
Phenylacetylene	2.40	0.122	0.029	90								
Aniline H					2.41	0.124	0.004	90	2.49	0.131	0.003	90
Q					2.27	0.110	0.020	90	2.37	0.118	0.026	90
AQ					2.42	0.128	−0.027	0	2.46	0.130	−0.032	0
SAQ					2.50	0.116	−0.011	−52	2.61	0.126	−0.010	−47
Anisole SAQ					2.62	0.129	−0.009	−51				
Benzofuran					2.31	0.109	−0.047	−36				
Indole					2.26	0.102	0.030	−19	2.32	0.107	0.041	−35
1*H*-Indazole					2.48	0.107	0.029	−13	2.60	0.116	0.038	−25
2*H*-Indazole					2.36	0.104	0.025	−10	2.13	0.099	0.018	−13
Benzimidazole					2.49	0.111	0.027	3	2.57	0.117	0.029	13
Purine					2.59	0.097	0.064	43	2.58	0.100	0.080	45

a) In benzaldehyde the principal axis of the top sublevel is nearly parallel to the C=O direction.

that the main characteristics of the observed results (Table 1) are reproduced reasonably well by these calculations with a few exceptions.

The calculated ZFS of benzaldehyde is consistent with the observed value in benzoic acid (BAC) host,[9,10,13,17] although it is very different from those obtained in many other hosts.[4,7] In the present calculation the second order effect of the spin-orbit interaction was ignored, though this effect is known to make a large contribution to the ZFS of benzaldehyde in many hosts.[4,7] In the BAC host, however, the contribution of the spin-orbit interaction is very small owing to the effect of the hydrogen bonding formation between benzaldehyde and BAC.[9,10,13,17]

The calculated D values of benzonitrile and phenylacetylene are considerably smaller than that of benzene.[25] As described in the preceding section, the smaller value of D is related to the situation that one of the singly-excited configurations relative to the ground state dominates over the other configurations in the wave function of the lowest excited triplet state. In fact, the main configuration was calculated to be dominant in benzonitrile and phenylacetylene. However, the calculated D's are somewhat smaller than the observed values. This may indicate that the present calculation underestimates the configurational mixing. The calculated E values of benzonitrile and phenylacetylene are in good agreement with the observed values. The D values calculated for aniline and anisole are in reasonable agreement with the observed values.

Although the observed absolute value of E of aniline is rather large,[11] the calculated one for the H conformation is very small. We examined the influence of distortion from H symmetry upon the ZFS of aniline for the Q, AQ, and SAQ conformations. For the Q conformation the calculated sign of the E parameter is the same as those of benzonitrile and phenylacetylene and contradicts the observation. For the AQ conformation the sign does not contradict the observation, but the calculated $|E|$ is somewhat small. From the angular dependence of the EPR signals of aniline and anisole derivatives, it was indicated that the geometries of these molecules in the lowest excited triplet states are distorted to the SAQ conformations.[11,14] The experimental results show that $|E|$'s of these molecules are relatively large. However, the calculated $|E|$ values of the SAQ conformations are still rather small. Thus the present calculation does not reproduce correctly E's of aniline and anisole.

The ZFS's of indole, indazole, and benzimidazole are reproduced well by the present calculation with parameter B. As to the observed values of E, benzofuran, indole, 1*H*- and 2*H*-indazoles, benzimidazole, and purine are divided into two groups.[6,16,18] In benzofuran, indole, and purine, $D<3|E|$,[6,18] while in 1*H*- and 2*H*-indazole and benzimidazole, $D>3|E|$.[6,16,18] This trend of the ZFS parameters is well reproduced in the present calculation with parameter B, whereas with parameter A, $D>3|E|$ was obtained for indole. The observed values of D and E of 1*H*-indazole are considerably larger than those of 2*H*-indazole.[16] This trend is also reproduced in the calculation with parameter B more clearly than with parameter A.

Summary and Conclusions

We have examined the ZFS's of a series of substituted benzenes. It is experimentally shown that D and E values vary remarkably depending on the type of molecule despite the similarity in the molecular size. In particular, E varies from $+0.038\,cm^{-1}$ for phenylacetylene to $-0.0597\,cm^{-1}$ for aniline reflecting large differences in the spin distributions. Generally speaking, the calculation of the ZFS's of substituted benzenes based on the Pariser-Parr-Pople-type MO's can give the values reasonably close to those obtained experimentally, but some more subtle points such as the difference in D between benzonitrile and aniline and large $|E|$'s of aniline and anisole are not reproduced in the present calculation. In the case of molecules with odd π orbitals we have examined two sets of parameters A and B. It was found that parameter B satisfactorily explains the observed trend of ZFS.

References

1) S. P. McGlynn, T. Azumi, and M. Kinoshita, "Molecular Spectroscopy of the Triplet States," Prentice Hall, New Jersey (1969); M. A. El-Sayed, "Double Resonance Techniques and the Relaxation Mechanisms Involving the Lowest Triplet State of Aromatic Compounds," in "Excited States," ed by E. C. Lim, Academic Press, London (1974), Vol. 1, pp. 35—78; D. W. Pratt, "Magnetic Properties of Triplet States," in "Excited States," ed by E. C. Lim, Academic Press, London (1979), Vol. 4, pp. 137—236.

2) E. T. Harrigan, T. C. Wong, and N. Hirota, *Chem. Phys. Lett.*, **14**, 549 (1972).

3) G. Kothandaraman and D. S. Tinti, *Chem. Phys. Lett.*, **19**, 225 (1973).

4) T. H. Cheng and N. Hirota, *Mol. Phys.*, **27**, 281 (1974).

5) N. Hirota, T. C. Wong, E. T. Harrigan, and K. Nishimoto, *Mol. Phys.*, **29**, 903 (1975).

6) E. T. Harrigan and N. Hirota, *J. Am. Chem. Soc.*, **97**, 6647 (1975).

7) E. T. Harrigan and N. Hirota, *Mol. Phys.*, **31**, 663, 681 (1976).

8) N. Nishi and M. Kinoshita, *Bull. Chem. Soc. Jpn.*, **49**, 1221 (1976).

9) N. Hirota, M. Baba, Y. Hirata, and S. Nagaoka, *J. Phys. Chem.*, **83**, 3350 (1979).

10) Y. Hirata and N. Hirota, *Mol. Phys.*, **39**, 129 (1980).

11) H. M. van Noort, Ph. J. Vergragt, J. Herbich, and J. H. van der Waals, *Chem. Phys. Lett.*, **71**, 5 (1980).

12) Y. Asahi and N. Hirota, *Mol. Phys.*, **41**, 1211 (1980).

13) S. Nagaoka and N. Hirota, *J. Chem. Phys.*, **74**, 1637 (1981).

14) Y. Asahi and N. Hirota, *Mol. Phys.*, **45**, 1245 (1982).

15) Y. Asahi and N. Hirota, *Bull. Chem. Soc. Jpn.*, **55**, 1379

(1982).
16) M. Noda and N. Hirota, *J. Am. Chem. Soc.*, **105**, 6790 (1983).
17) S. Nagaoka and N. Hirota, *Bull. Chem. Soc. Jpn.*, **56**, 3381 (1983).
18) M. Noda, S. Nagaoka, and N. Hirota, *Bull. Chem. Soc. Jpn.*, **57**, 2376 (1984).
19) B. Smaller, E. C. Avery, and J. R. Remko, *J. Chem. Phys.*, **46**, 3976 (1967).
20) T. H. Cheng and N. Hirota, *J. Chem. Phys.*, **56**, 5019 (1972).
21) J. S. Brinen and M. K. Orloff, *Chem. Phys. Lett.*, **1**, 276 (1967).
22) M. Godfrey, C. W. kern, and M. Karplus, *J. Chem. Phys.*, **44**, 4459 (1966).
23) R. Pariser and R. G. Parr, *J. Chem. Phys.*, **21**, 466, 767 (1953).
24) J. A. Pople, *Trans, Faraday Soc.*, **49**, 1375 (1953).
25) J. Higuchi, *Bull. Chem. Soc. Jpn.*, **54**, 2864 (1981).
26) References cited in Ref. 25.
27) J. A. Kooter and J. H. van der Waals, *Mol. Phys.*, **37**, 1015 (1979).
28) D. Feller, T. Borden, and E. R. Davidson, *J. Chem. Phys.*, **74**, 2256 (1981).
29) C. Mijoule, *Chem. Phys., Lett.*, **80**, 593 (1981).
30) H. Vogler, *Mol. Phys.*, **43**, 83 (1981).
31) A. G. Motten, E. R. Davidson, and A. L. Kwiram, *J. Chem. Phys.*, **75**, 2603 (1981).
32) M. R. Taherian, W. H. Fink, and A. H. Maki, *J. Phys. Chem.*, **86**, 2586 (1982).
33) R. S. Hutton and H. D. Roth, *J. Am. Chem. Soc.*, **104**, 4458 (1982).
34) D. A. Case, *Chem. Phys. Lett.*, **109**, 66 (1984).
35) Y. Gondo and A. H. Maki, *J. Chem. Phys.*, **50**, 3270 (1969).
36) Y. Gondo and A. H. Maki, *J. Chem. Phys.*, **50**, 3638 (1969).
37) Y. Gondo and Y. Kanda, *Bull. Chem. Soc. Jpn.*, **43**, 3943 (1970).
38) S. A. Boorstein and M. Gouterman, *J. Chem. Phys.*, **41**, 2776 (1964).
39) E. Clementi, "Tables of Atomic Functions" [supplement to *IBM J. Res. Develop.*, **9**, 2 (1965)] Table 45-01.
40) See Eq. 12 in Ref. 35.
41) K. Nishimoto, *Theor. Chim. Acta*, **5**, 207 (1966).
42) K. Nishimoto, *Theor. Chim. Acta*, **7**, 74 (1968).
43) K. Nishimoto and L. S. Forster, *Theor. Chim. Acta*, **3**, 407 (1965).
44) J. Hinze and H. H. Jaffe, *J. Am. Chem. Soc.*, **84**, 540 (1962).
45) C. A. Hutchison, Jr. and B. W. Mangum, *J. Chem. Phys.*, **29**, 952 (1958).
46) K. Ohno, *Theor. Chim. Acta*, **2**, 219 (1964); G. Klopman, *J. Am. Chem. Soc.*, **86**, 4550 (1964); **87**, 3300 (1965).
47) M. Wolfsberg and L. Helmholz, *J. Chem. Phys.*, **20**, 837 (1952).
48) M. J. S. Dewar and T. Morita, *J. Am. Chem. Soc.*, **91**, 796 (1969).
49) In an SCF calculation of pyrrole by Clementi et al. [E. Clementi, H. Clementi, and D. R. Davis, *J. Chem. Phys.*, **46**, 4725 (1967)], the gross charge obtained is $\sigma^{3.7513}\pi^{1.6589}$ for N trtrtrπ.
50) Y. Fujimura, H. Yamaguchi, and T. Nakajima, *Bull. Chem. Soc. Jpn.*, **45**, 384 (1972).
51) A. Escande and J. Lapasset, *Acta Crystallogr., Sect. B*, **30**, 2009 (1974).
52) A. Escande and J. L. Galigne, *Acta Crystallogr., Sect. B*, **30**, 1647 (1974).
53) M. Spencer, *Acta Crystallogr.*, **12**, 59 (1959).

 © 1986 The Chemical Society of Japan Bull. Chem. Soc. Jpn., 59, 363—366 (1986)

Structure and Optical Spectrum of $(TMTTF)_2IO_4$. The Role of Coulomb Interaction

Kyuya YAKUSHI,* Sukekazu ARATANI, Koichi KIKUCHI, Hiroyuki TAJIMA, and Haruo KURODA
Department of Chemistry, Faculty of Science, The University of Tokyo, Hongo, Bunkyo-ku, Tokyo 113
(Received September 4, 1985)

The semiconductive $(TMTTF)_2IO_4$ salt was prepared by using the electrochemical method. The crystal structure was determined to be isomorphous to the metallic $(TMTTF)_2X$ salts. The polarized infrared reflectance spectra of $(TMTTF)_2IO_4$ and $(TMTTF)_2BF_4$ were measured and were interpreted on the basis of the extended Hubbard model.

Over the past few years, the bis(tetramethyltetrathiafulvalenium) salts [$(TMTTF)_2X$] have been widely studied.[1] All of these salts exhibit a metallic character as regards the temperature dependence of electrical resistivity near room temperature.[2] On the other hand, the optical spectra of $(TMTTF)_2PF_6$ and $(TMTTF)_2Br$ do not show a Drude-like spectral shape, but show a shape which suggests the localization of charges due to the Coulomb interaction.[3] We found a new semiconductive TMTTF salt, $(TMTTF)_2IO_4$, which has an isomorphous structure to other $(TMTTF)_2X$ salts. Although this salt is a semiconductor, its optical spectrum was found to be very similar to that of the metallic $(TMTTF)_2PF_6$, showing a non Drude-like spectral shape. These facts suggest that the Coulomb interaction cannot be neglected also in the metallic $(TMTTF)_2PF_6$, and if this is the case, the transfer integrals, which were given for $(TMTTF)_2PF_6$ from the analysis of its reflectance data by use of the Drude model, should be reexamined by taking account of the Coulomb interaction. In this paper we describe the characteristic structure of the TMTTF column of $(TMTTF)_2IO_4$, and estimate the band parameters of the extended Hubbard model through the analysis of the reflectance spectrum. The reflectance spectrum of the metallic $(TMTTF)_2BF_4$ was also measured for the purpose of comparison.

Experimental

The single crystals of $(TMTTF)_2IO_4$ and $(TMTTF)_2BF_4$ were obtained in the tetrahydrofuran solutions of $(n\text{-}Bu_4N)BF_4$ and $(n\text{-}Bu_4N)IO_4$ by using the electrochemical method. The temperature of the electrochemical cell was controlled to be 0 °C and the constant current, 5 μA, was applied for 2 d. The largest crystal thus obtained was of the dimension of $5\times1\times0.2\,mm^3$ for $(TMTTF)_2BF_4$ and $20\times2.5\times0.5\,mm^3$ for $(TMTTF)_2IO_4$. The low frequency electrical resistivity was measured along the a-axis by using a standard four-probe method. The electrical contacts were made by 20 μm gold wires with carbon paint onto the (001) crystal face. The reflectance measurement on the (001) crystal faces was conducted over the spectral range from 720 cm^{-1} to 25000 cm^{-1} by using the microspectrophotometric technique. The intensities of X-ray diffraction were collected with Rigaku automated diffractometer using Mo $K\alpha$ radiation in the range of 2θ from 2° to 60°. The 1107 independent diffractions which are larger than three times of the standard deviations were used for the analysis. The full-matrix-least-squares refinement reduced the R-value to 0.079.

Results and Discussion

The temperature dependence of the electrical conductivity of $(TMTTF)_2IO_4$ is shown in Fig. 1. The electrical behavior is semiconductive throughout the observed temperature region below 300 K. The room-temperature dc conductivity along the a-axis was ≈10 $\Omega^{-1}cm^{-1}$. The activation energy around 150 K was obtained to be 0.09 eV, which is about twice the values of other $(TMTTF)_2X$ salts. Among the $(TMTTF)_2X$ salts, $(TMTTF)_2IO_4$ is the first example which exhibits the semiconductive behavior at room temperature.

The crystal of $(TMTTF)_2IO_4$ belongs to the triclinic system, the space group $P\bar{1}$, the lattice constants being a=7.226(6) Å, b=7.664(3) Å, c=13.226(4) Å, α=81.99(3)°, β=96.54(4)°, γ=106.68(5)°, Z=1. The final values of the fractional coordinates were listed in Table 1. The crystal structure is isomorphous to other $(TMTTF)_2X$ salts as shown in Fig. 2, in which the two orientations, of IO_4 occupying the center of symmetry are drawn separately although those two orientations are randomly distributed. The intrastack S–S distances are significantly shorter than the interstack S–S distances.

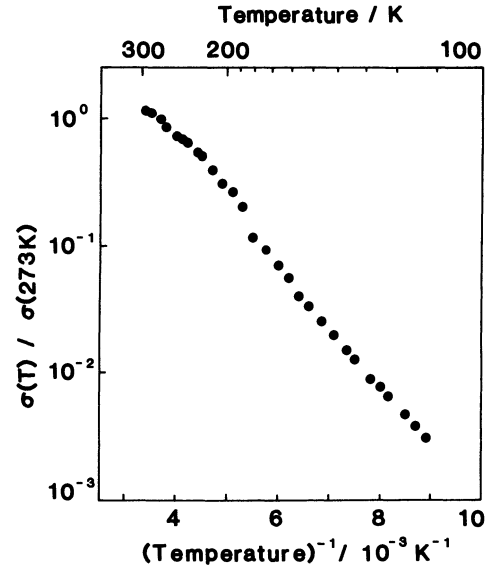

Fig. 1. Temperature dependence of the electrical conductivity.

Table 1. Fractional Atomic Coordinates ($\times 10^4$) of $(TMTTF)_2IO_4$. The e.s.d.'s are Given in Parentheses

Atom	x	y	z	$B_{eq}(A^2)$[a]
I	0000(0)	5000(0)	5000(0)	6.3
S1	3435(7)	3140(6)	1017(4)	4.1
S2	2514(8)	−545(6)	2115(4)	4.1
S3	2720(8)	1424(6)	−1135(4)	4.2
S4	1853(7)	−2261(6)	−55(4)	3.9
C1	2817(25)	825(22)	924(13)	3.3
C2	2483(28)	62(21)	33(15)	4.0
C3	3600(27)	2971(27)	2370(15)	4.4
C4	3128(28)	1265(23)	2863(14)	4.2
C5	2169(24)	−406(23)	−1885(13)	3.4
C6	1738(27)	−2078(24)	−1392(12)	3.6
C7	4176(31)	4751(25)	2828(14)	5.1
C8	3157(35)	803(27)	4026(13)	5.9
C9	2241(32)	177(25)	−3039(13)	4.8
C10	1226(30)	−3894(24)	−1852(14)	4.8
O1	260(108)	3184(55)	4484(39)	15.3
O2	1661(137)	6110(77)	5441(44)	18.0
O3	−1977(83)	5051(91)	4986(53)	15.3
O4	−320(113)	3630(56)	6228(32)	18.3

a) $B_{eq}=(4/3)\sum_{ij}\beta_{ij}(a_i a_j)$.

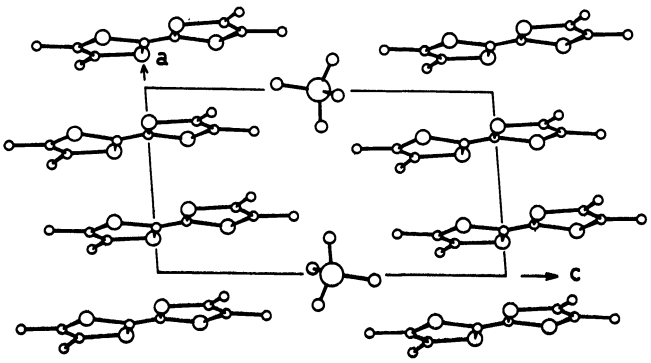

Fig. 2. Crystal structure of $(TMTTF)_2IO_4$ projected along the b-axis.

This result indicates that this salt possesses a strong one-dimensional nature like other $(TMTTF)_2X$ salts. The TMTTF molecules are stacking diadically along the a-axis. The interplanar spacings between the TMTTF molecules are listed in Table 2 together with the corresponding values of other $(TMTTF)_2X$ salts. In a $(TMTTF)_2X$ crystal, the semiconductive gap is introduced by the periodic potentials,[5] the difference of the transfer integrals,[5] and the nearest-neighbor Coulomb interaction, V,[6] if the on-site Coulomb repulsion, U, is very large as compared with the average transfer integral, t. The difference of the transfer integrals increases with the increase of the value of the difference between the interplanar spacings, $(d2-d1)$, found in a TMTTF stack, while the normalized Coulomb interaction, V/t, increases with the increase of the average spacing. The most characteristic feature of the semiconductive $(TMTTF)_2IO_4$ is that it shows the largest average spacing among the $(TMTTF)_2X$ salts hitherto investigated. This fact suggests that the Coulomb interaction, V, is

Table 2. Inter-Planar Spacings in the TMTTF Stack[a]

Anion	$d1$	$d2$	$d2-d1$	$(d1+d2)/2$
Br	3.50	3.53	0.03	3.52
I	3.50	3.54	0.04	3.52
SCN	3.49	3.56	0.07	3.53
NO_3	3.50	3.57	0.07	3.54
BF_4	3.54	3.56	0.02	3.55
ClO_4	3.52	3.59	0.07	3.56
PF_6	3.52	3.62	0.10	3.57
ReO_4	3.57	3.59	0.02	3.58[b]
AsF_6	3.54	3.64	0.10	3.59
IO_4	3.58	3.63	0.05	3.61[c]

a) The values of $d1$ and $d2$ except for IO_4 and BF_4 salts are given in Ref. 4. b) Ref. 12. c) This work.

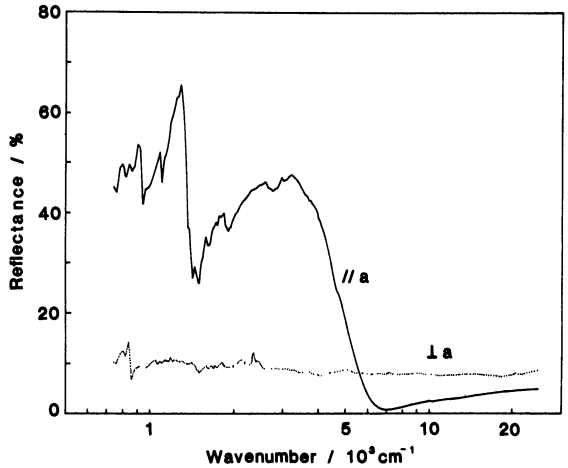

Fig. 3. Polarized reflectance spectrum on the (001) crystal face of the $(TMTTF)_2IO_4$ single crystal.

playing a dominant role in opening the band gap in $(TMTTF)_2IO_4$, although other effects may also contribute to the magnitude of the gap.

The reflectance spectrum of $(TMTTF)_2IO_4$ is shown in Fig. 3. The dispersion in the infrared region is completely polarized along the stacking axis. The spectrum is very similar to that of $(TMTTF)_2PF_6$, which was reported by Jacobsen et al.[3] We calculated the optical conductivity spectrum through the Kramers-Kronig transformation of the reflectance data. The spectrum thus obtained is shown in Fig. 4 together with the spectrum of $(TMTTF)_2BF_4$, which is known to be metallic. Four prominent peaks, A, B, C, and D were observed in the infrared region. The maximum position of the peak A is 2300 cm^{-1} for $(TMTTF)_2IO_4$ and 2100 cm^{-1} for $(TMTTF)_2BF_4$. This broad band is assignable to the charge-transfer transition from $TMTTF^{\circ}$ to $TMTTF^{+}$ or interband transition between the subbands separated mainly by Coulomb energy, V. The positions of peaks, B, C, and D are 1180 cm^{-1}, 1080 cm^{-1}, and 900 cm^{-1} both for $(TMTTF)_2IO_4$ and $(TMTTF)_2BF_4$. These peaks correspond to the a_{1g} vibrational transitions of TMTTF mixed with the charge-transfer excitation.[7] The total oscillator strength, which can be the measure of the

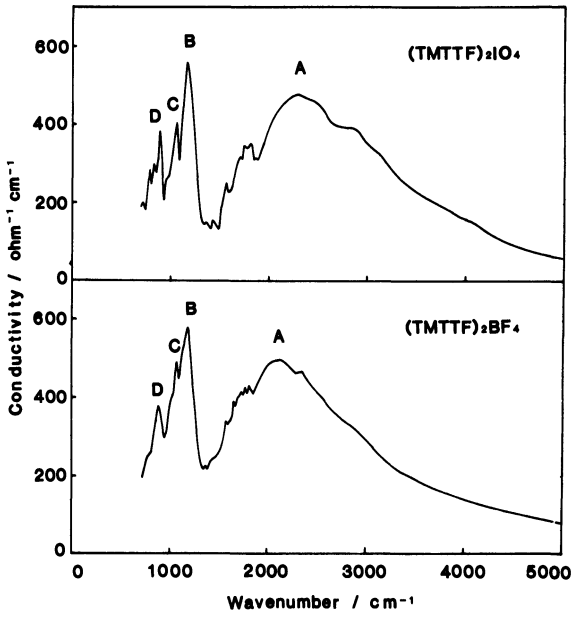

Fig. 4. Conductivity spectra in the infrared region.

magnitude of transfer integral, was obtained by the numerical integration of the conductivity curve from 0 to 10000 cm^{-1}, where the conductivity curve in the region from 720 cm^{-1} to 0 cm^{-1} was drawn by a smooth extrapolation to the dc conductivity at zero frequency. The oscillator strengths thus obtained were about 0.4 both for $(TMTTF)_2IO_4$ and $(TMTTF)_2BF_4$. This value is slightly smaller in comparison with alkali-metal-TCNQ salt, which gave the oscillator strength value of about 0.5.[8,9]

We should consider that the band-gap in $(TMTTF)_2IO_4$ arises from the electron-electron Coulomb interactions, since the one-electron theory predicts a metallic state without a gap for a diadically stacked TMTTF column. If the on-site Coulomb repulsion, U, is much larger than the average transfer integrals, t, the band-gap is introduced by the periodic potentials due to anions, by the nonequivalent transfer integrals in the diadically stacked column, and/or by the nearest-neighbor Coulomb repulsion, V. As we have already mentioned, the crystal structure of $(TMTTF)_2IO_4$ suggests the importance of V for opening a semiconductive gap. The difference of the two kinds of transfer integrals is rather small and is not likely to be the main factor. Thus, let us make a rough estimation of the band parameters, U, V, and t within the framework of the extended Hubbard model. In the case $U \gg t$, the exact solution of the 3/4-filled extended Hubbard chain predicts that $V/2t=1$ is the boundary between a metal and a semiconductor.[6] Thus, we can consider that $V>2t$ in $(TMTTF)_2IO_4$, because it is semiconductive at room temperature. No theory is known to predict the excitation energy and the oscillator strength of the optical transition in such a case. However, we could estimate the parameters in the following way. Mazumdar and Soos calculated the band structure of a one-dimensional chain in the limit of $V \gg 2t$, and concluded the optical gap to be $V+2t^2/V$.[6] Since the electronic transition (peak A) appears at about 0.3 eV, we should consider that $2t<V<0.3$ eV. From the magnetic susceptibility study, Delhaes et al.[10] proposed that $(U-V)/4t \simeq 2$ for the $(TMTTF)_2X$ salts. If we assume this relation for $(TMTTF)_2IO_4$, we obtain the following relations: $U<1.5$ eV and $2t<V<0.3$ eV. Thus the parameters in $(TMTTF)_2IO_4$ are likely to be comparable with those of K·TCNQ[8] and Rb·TCNQ[9], and consistent also with the powder optical spectrum of TMTTF-Br.[11] As shown in Fig. 4, the optical conductivity spectrum of the semiconductive $(TMTTF)_2IO_4$ is quite similar to that of the metallic $(TMTTF)_2BF_4$. This fact indicates that the band structures of these two salts are similar to each other. Mortensen et al. proposed from their thermopower studies that the apparent metallic behavior observed for several $(TMTTF)_2X$ salt comes not from the absence of a band gap but from the narrowness of their semiconductive gap.[12] According to their model, we can consider that the difference between the semiconductive $(TMTTF)_2IO_4$ and other metallic $(TMTTF)_2X$ salts exists only in the magnitude of the band gap. The similarity of the reflectance spectrum between $(TMTTF)_2BF_4$ and $(TMTTF)_2IO_4$, shown in the present study, indeed supports their model.

We thank Dr. A. Kobayashi and Dr. K. Ichida for their kind assistance to the crystal structure analysis. This work was supported by the Grant-in-Aid for the Special Project Research on "The Properties of Molecular Assemblies"(No.59112002) from the Ministry of Education, Science and Culture.

References

1) See "Proceedings of the International Conferences on the Physics and Chemistry of Organic Metals" [*J. Phys. (Paris) Colloq.* **44**, C3 (1983)].

2) P. Delhaes, C. Coulon, J. Amiell, S. Flandrois, E. Toreilles, J. M. Fabre, and L. Giral, *Mol. Cryst. Liq. Cryst.*, **50**, 43 (1979).

3) C. S. Jacobsen, D. B. Tanner, and K. Bechgaard, *Phys. Rev.* **B28**, 7019 (1983).

4) B. Liautard, S. Peytavin, G. Brun, and M. Maurin, *J. Phys. (Paris) Colloq.* **44**, C3-951 (1983).

5) R. Bosio, M. Meneghetti, and C. Pecile, *J. Chem. Phys.*, **76**, 5782 (1982).

6) S. Mazumdar and Z. G. Soos, *Phys. Rev.*, **B23**, 2810 (1981).

7) M. J. Rice, V. M. Yartsev, and C. S. Jacobsen, *Phys. Rev.*, **B21**, 3437 (1980).

8) K. Yakushi, T. Kusaka, H. Kuroda, *Chem. Phys. Lett.*, **68**, 139 (1979).

9) K. Yakushi, S. Miyajima, T. Kusaka, H. Kuroda, *Chem. Phys. Lett.*, **114**, 68 (1985).

10) P. Delhaes, C. Coulon, J. Amiell, S. Flandrois, E. Toreilles, J. M. Fabre and L. Giral, *Mol. Cryst. Liq. Cryst.*, **50**,

43 (1972).
11) J. B. Torranace, B. A. Scott, B. Welber, F. B. Kaufman, and P. E. Seiden, *Phys. Rev.*, **B19**, 730 (1979).
12) K. Mortensen, E. M. Conwell, and J. M. Fabre, *Phys. Rev.*, **B28**, 5856 (1983).

Preparation of Polymer-Protected Colloidal Dispersions of Copper

Hidefumi HIRAI,* Hidehiko WAKABAYASHI, and Makoto KOMIYAMA
Department of Industrial Chemistry, Faculty of Engineering, The University of Tokyo, Hongo, Bunkyo-ku, Tokyo 113
(Received September 5, 1985)

Colloidal copper dispersions are prepared by reducing copper(II) ions in water with sodium tetrahydroborate or hydrazine in the presence of various protective polymers. The polymers are poly(*N*-vinyl-2-pyrrolidone), poly(vinyl alcohol), poly(methyl vinyl ether), poly(potassium vinyl sulfate), dextrin, amylopectin, methylamylopectin, methylcellulose, ethylcellulose, and (2-hydroxyethyl)cellulose. The dispersions are black, reddish dark brown, or reddish brown homogeneous solutions, and are stable under nitrogen at room temperature for more than three months. Electron diffraction experiments indicate that copper atoms in the colloidal particles are arranged in an ordered way, which is almost identical with that in a crystal of bulk copper metal. At the charged molar ratio 40 of the monomeric residue of the protective polymer to copper(II) ion, the average diameters of the copper particles, prepared by use of sodium tetrahydroborate, range from 50 to 150 Å, depending on the polymer used. With the use of poly(*N*-vinyl-2-pyrrolidone) as protective polymer, the size of the copper particles monotonously increases with increase in the degree of polymerization of the polymer and also with decrease in the amount of the polymer.

Colloidal dispersions of noble metals such as rhodium, ruthenium, and platinum were prepared by reduction of the corresponding metal salts in the presence of protective polymers, using molecular hydrogen,[1,2] hydrazine,[3] formaldehyde,[4] sodium tetrahydroborate,[5] and alcohols[6–9] as reducing agents. These dispersions exhibited high and selective catalytic activities in hydrogenation of olefins and nitro groups. However, information on the preparation of colloidal dispersions of non-noble metals and their properties has been rather scant.

Papavassiliou and Kokkinakis[10] prepared a colloidal copper dispersion by reducing copper(II) sulfate with hydrazine in the presence of gelatin. However, concurrent precipitation took place in the reduction, and homogeneous solution was obtained only after the removal of large particles of copper by centrifugation. No information on the size of copper particles was presented there.

In a preliminary communication,[11] the authors reported that homogeneous colloidal dispersions of copper could be prepared by reducing copper(II) sulfate with sodium tetrahydroborate in the presence of poly(*N*-vinyl-2-pyrrolidone) or poly(vinyl alcohol). The resulting colloidal dispersions were highly active and selective in the hydration of acrylonitrile to acrylamide.

This paper will report preparation of colloidal copper dispersions using various kinds of protective polymers, copper salts, and reducing agents. Results of electron microscopy on the colloidal particles will be described. Furthermore, effects of degree of polymerization of protective polymers and their amounts on the size of colloidal particles will be shown.

Experimental

Materials. Poly(*N*-vinyl-2-pyrrolidone)s, amylopectin, methylcellulose (degree of methylation, 2.0), (2-hydroxyethyl)cellulose (degree of hydroxyethylation, 1.6) (from Tokyo Kasei Kogyo Co.), poly(vinyl alcohol)s (from Pure Chemicals Co.), dextrin (from Kanto Chemicals), and ethylcellulose (degree of ethylation, 1.0, from Nakarai Chemicals) were repeatedly (2—5 time) reprecipitated from aqueous solutions with the addition of acetone. Poly(potassium vinyl sulfate), β-cyclodextrin (from Nakarai Chemicals), poly(methyl vinyl ether) (from Tokyo Kasei Kogyo Co.), poly(acrylic acid), poly(2-acrylamido-2-methyl-1-propanesulfonic acid) (from Aldrich Chemical Co.), and a copolymer of methyl vinyl ether and maleic acid (methyl vinyl ether composition 0.62, from Scientific Polymer Products) were used without further purification. Soluble nylon, in which 30% of the hydrogens in the α-methylene groups with respect to the carbonyl groups in nylon 6 were substituted with diethylamino groups, was kindly provided by Toray Chemical Co. Poly(aminoethylene)[12] and methylamylopectin[13] were prepared according to the literatures. The degree of methylation with respect to glucose unit in the methylamylopectin was 1.1 as determined by ^{1}H-NMR spectroscopy.

Copper(II) sulfate from Yoneyama Chemical Co. was recrystallized three times from aqueous solution. Copper(II) chloride, copper(II) nitrate, and copper(II) acetate were obtained from Koso Chemical Co. Doubly distilled water was degassed by boiling under a reduced pressure.

Sodium tetrahydroborate (Koso Chemical Co.) was stored over silica gel and was dissolved in water immediately before use. Hydrazine hydrate and aqueous formaldehyde solution (37 wt%) were obtained from Nakarai Chemicals and Yoneyama Chemical Co., respectively. Nitrogen gas and hydrogen gas, which had purities higher than 99.9995 and 99.999%, respectively, were purchased from Nippon Sanso Co.

Preparation of Colloidal Copper Dispersion. Copper salts and various amounts of polymers were dissolved in water, and were stirred magnetically at 80 °C under nitrogen for 1 h. The stirring was made at 25 °C instead of 80 °C only for the case of poly(methyl vinyl ether), since this polymer dissolved in water at 25 °C but not at 80 °C. Then, aqueous solution of sodium tetrahydroborate, hydrazine, or formaldehyde was added to the resulting solution at 25 °C. Reduction using molecular hydrogen was carried out at 80 °C for 20 h under hydrogen pressure 37 atm.

Preparation with the use of methanol containing alkali as reducing agent was carried out as follows. Copper salts and

Table 1. Preparation of Colloidal Copper Dispersions by Reduction of Copper(II) Sulfate with Sodium Tetrahydroborate in the Presence of Various Polymers[a)]

Polymer	Degree of polymerization	Colloid	
		Color	Average particle diameter/Å
Poly(*N*-vinyl-2-pyrrolidone)	6300		b)
	3240		100
	1440	Reddish dark brown	60
	360		b)
	90		50
Poly(vinyl alcohol)	2000		b)
	1500		150
	360		b)
Poly(methyl vinyl ether)	570		b)
Poly(potassium vinyl sulfate)	b)	Black	b)
Dextrin	b)		90
Amylopectin	b)		100
Methylamylopectin	b)		b)
Methylcellulose	140		100
Ethylcellulose	b)	Reddish dark brown	b)
(2-Hydroxyethyl)cellulose	b)		b)

a) $[CuSO_4]_0=5.0\times10^{-3}$ mol dm^{-3}; [monomeric residue of protective polymer]$_0=2.0\times10^{-1}$ mol dm^{-3}; $[NaBH_4]_0=1.0\times10^{-2}$ mol dm^{-3}; Suffix 0 refers to the charged concentration. b) Not determined.

polymers were dissolved in 1: 1 methanol–water mixture, and the solutions were stirred magnetically at 80 °C for 1 h, and then aqueous solution of sodium hydroxide was added. The solution was further kept at 80 °C for 10 min.

Electron Microscopy. Electron micrographs of the colloids were measured on a Hitachi Model HU-12A electron microscope operated at 100 kV. Sample films were prepared under nitrogen from the colloidal dispersions on collodion films coated with a carbon layer, by evaporating the solvent to dryness.

Absorption Spectroscopy. Absorption spectra of the colloidal dispersions were taken under nitrogen on a Hitachi Model 340 spectrometer at 25 °C using 1 cm quartz cell.

Results

Preparation of Colloidal Copper Dispersions Using Sodium Tetrahydroborate as Reducing Agent. As shown in Table 1, homogeneous colloidal copper dispersions were successfully prepared by reducing copper(II) sulfate with sodium tetrahydroborate in the presence of various polymers as protective polymers. The protective polymers were poly(*N*-vinyl-2-pyrrolidone) (PVP), poly(vinyl alcohol), poly(methyl vinyl ether), poly(potassium vinyl sulfate), dextrin, amylopectin, methylamylopectin, methylcellulose, ethylcellulose, and (2-hydroxyethyl)cellulose. Here, the charged molar ratio of monomeric residue of the polymer to copper(II) sulfate was kept constant at 40.

The resulting colloidal copper dispersions were highly stable under nitrogen. For example, neither change in color nor precipitation was detected, when the colloidal dispersion with PVP of viscosity-averaged degree of polymerization (DP) 3240 was kept under nitrogen at room temperature for more than three months. On contacts with oxygen, however, the dispersions turned into yellow in a few minutes.

Stable colloidal copper dispersion was obtained even at the charged molar ratio 5 of monomeric residue of PVP (DP=3240) to copper(II) sulfate. At the charged molar ratio 1.0, however, the dispersion was less stable and considerable amounts of black precipitates were formed in 1 h.

In contrast with the formation of homogeneous colloidal dispersions in the presence of these protective polymers, black precipitates were rapidly formed in their absence. The precipitation took place immediately after the addition of sodium tetrahydroborate to an aqueous solution of copper(II) sulfate.

When poly(ethylene oxide) and β-cyclodextrin were used as protective polymers, copper particles rapidly coaggregated, and black precipitates were formed in a few minutes under virtually colorless supernatant. No reduction of copper(II) sulfate occured in the presence of poly(acrylic acid), poly(2-acrylamido-2-methyl-1-propanesulfonic acid), or the copolymer of methyl vinyl ether and maleic acid, even after the addition of sodium tetrahydroborate. Poly(aminoethylene) and soluble nylon did not dissolve in aqueous solutions containing copper(II) sulfate due to gelation.

In addition to copper(II) sulfate, copper(II) chloride, copper(II) acetate, and copper(II) nitrate were reduced with sodium tetrahydroborate in the presence of PVP, yielding homogeneous reddish dark brown, dark brown, and dark brown colloidal dispersions, respectively. The dispersion prepared from copper(II) nitrate was rather unstable, and gradually turned into yellowish green even under nitrogen.

Figure 1 shows the absorption spectrum of the colloidal copper dispersion prepared from copper(II) sulfate and PVP (DP=3240). A peak is clearly observed at

Table 2. Effects of Reducing Agents on the Formation of Colloidal Copper Dispersions Using PVP (DP=3240) as Protective Polymer[a)]

Reducing agent	Charged concentration of reducing agent (10^{-2} mol dm^{-3})	Colloid	
		Formation	Color
Sodium tetrahydroborate	*1.0*	*Yes*	*Reddish dark brown*
Hydrazine	3.3	Yes	Reddish brown
Molecular hydrogen	—[b)]	No (no reduction)	—
Ethanol	—[c)]	No (no reduction)	—
Methanol/NaOH	—[d)]	No (precipitation)	—
Formaldehyde	3.3	No (gelation)	—

a) $[CuSO_4]_0=5.0\times10^{-3}$ mol dm^{-3} and [monomeric residue of PVP]$_0=2.0\times10^{-1}$ mol dm^{-3}; solvent was water unless otherwise noted. b) Reduction was carried out at 80°C, hydrogen pressure 37 atm for 20 h. c) Copper(II) sulfate (0.15 mmol) was refluxed in 50 cm^3 ethanol for 2 h. d) Copper(II) chloride (0.15 mmol) was refluxed in 50 cm^3 of 1:1 methanol-water mixture containing sodium hydroxide (0.45 mmol) for 1 h.

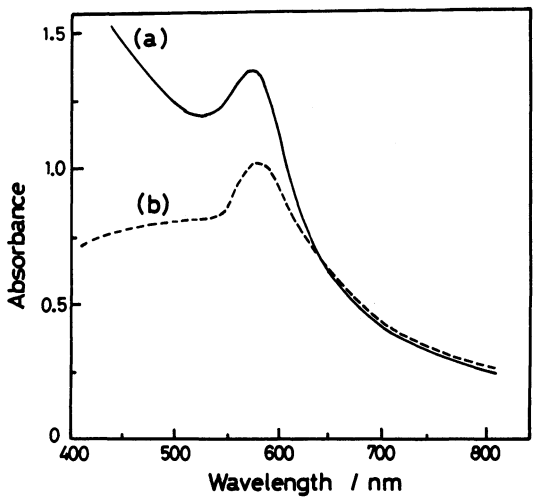

Fig. 1. Absorption spectra for the colloidal copper dispersions prepared by reduction of copper(II) sulfate in the presence of PVP (DP=3240) using (a) sodium tetrahydroborate and (b) hydrazine: $[CuSO_4]_0=5.0\times10^{-3}$, [monomeric residue of PVP]$_0=2.0\times10^{-1}$, $[NaBH_4]_0=1.0\times10^{-2}$, and [hydrazine]$_0=3.3\times10^{-2}$ mol dm^{-3}.

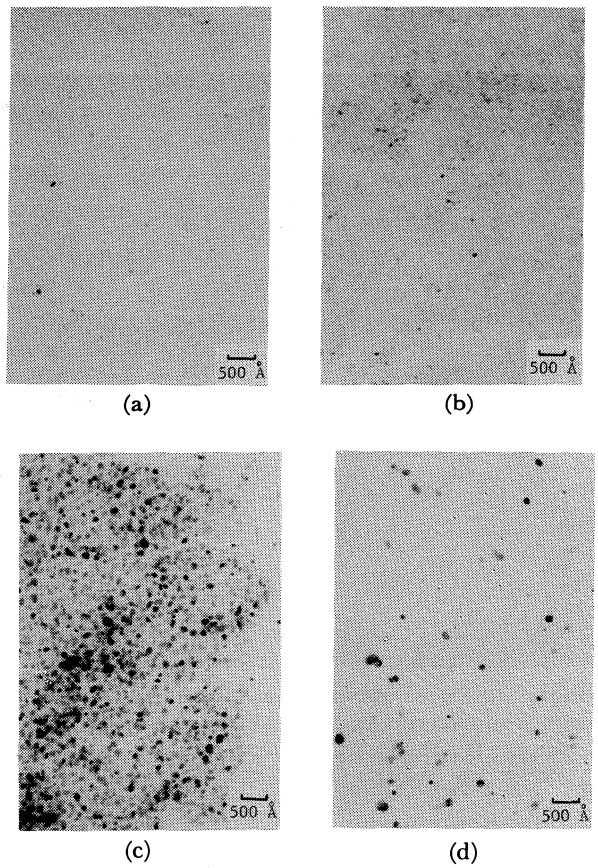

Fig. 2. Electron micrographs of colloidal copper dispersions prepared by reduction of copper(II) sulfate with sodium tetrahydroborate in the presence of (a) PVP (DP=1440), (b) PVP (DP=90), (c) dextrin, or (d) methylcellulose (×100000); $[CuSO_4]_0=5.0\times10^{-3}$, $[NaBH_4]_0=1.0\times10^{-2}$, and [monomeric residue of polymer]$_0=2.0\times10^{-1}$ mol dm^{-3}.

570 nm. Otherwise, the optical density increases with decrease in wavelength, which is ascribed to light scattering by the colloidal copper particles.

Preparation of Colloidal Copper Dispersions Using Various Reducing Agents. Table 2 shows the results of the treatment of copper(II) sulfate with various reducing agents in the presence of PVP (DP=3240). Homogeneous dispersion of copper is prepared with the use of hydrazine as well as sodium tetrahydroborate. The color of the dispersion obtained with hydrazine is reddish brown. As shown in Fig. 1, the dispersion exhibits an absorption miximum at 580 nm.

Colloidal dispersion can not be prepared with the use of the other four reducing agents. Ethanol exhibits no reducing activity on copper(II) sulfate under refluxing conditions. Hydrogen shows no reducing activity at 80°C under 37 atm either.

Refluxing of alkaline methanol-water mixture (1:1 in volume) containing copper(II) chloride for 10 min turns the color of the solution into pale reddish brown, indicating that a small amount of copper(II) ion is reduced. On prolonged reaction, however, brown precipitates are formed. The addition of formaldehyde to an aqueous solution of copper(II) sulfate and PVP results in gelation.

Electron Microscopy on Colloidal Copper Particles. Figure 2 shows the electron micrographs of the copper

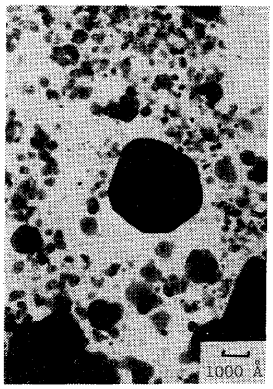

Fig. 3. Electron micrograph of copper precipitates prepared by reduction of copper(II) sulfate in the absence of polymers (×50000); $[CuSO_4]_0=5.0\times10^{-3}$ and $[NaBH_4]_0=1.0\times10^{-2}$ mol dm^{-3}.

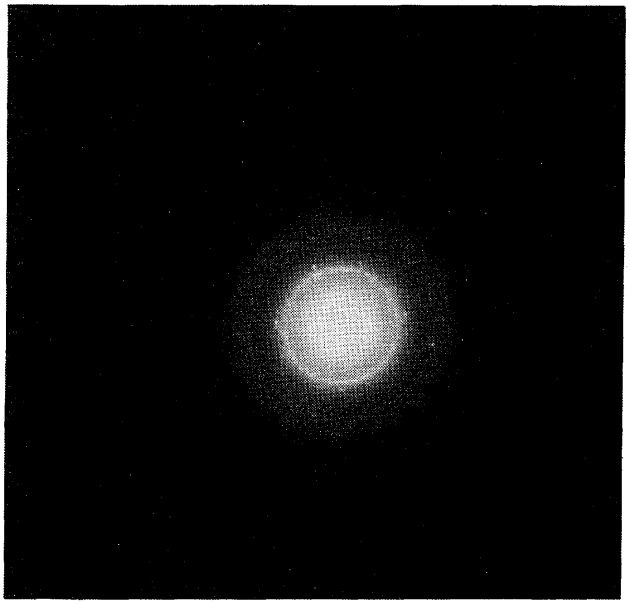

Fig. 4. Selected area electron diffraction pattern of the colloidal copper dispersion obtained by reducing copper(II) sulfate with sodium tetrahydroborate in the presence of dextrin; $[CuSO_4]_0=5.0\times10^{-3}$, $[NaBH_4]_0=1.0\times10^{-2}$, and [monomeric residue of dextrin]$_0=2.0\times10^{-1}$ mol dm^{-3}.

colloids prepared by reduction of copper(II) sulfate with sodium tetrahydroborate in the presence of various polymers. Highly dispersed particles without any aggregation are observed. For the colloid with PVP (DP=1440), for example, the particle size is distributed from 20 to 190 Å, and the average particle diameter is 100 Å. The average diameter depends on the polymer used, ranging from 50 Å for the colloid with PVP (DP=90) to 150 Å for the one with poly(vinyl alcohol) (DP=1500), as listed in Table 1.

In contrast, the diameters of the copper particles in the precipitates, obtained by the reduction of copper(II) sulfate with sodium tetrahydroborate in the absence of the polymers, were widely distributed from 40 to 3500 Å (Fig. 3).

Table 3. Selected Area Electron Diffraction on the Colloidal Copper Dispersion Prepared by Reducing Copper(II) Sulfate with Sodium Tetrahydroborate in the Presence of Dextrin[a)]

Relative radius (r) of Debye-Scherrer ring	Relative ratio for $1/r$	Copper crystal[b)]	
		Lattice[c)] spacing (A)	Relative lattice spacing
1.00	1.93	2.09(111)	1.92
1.17	1.66	1.81(200)	1.66
1.63	1.18	1.28(220)	1.17
1.93	1.00	1.09(311)	1.00

a) $[CuSO_4]_0=5.0\times10^{-3}$ mol dm^{-3}, $[NaBH_4]_0=1.0\times10^{-2}$ mol dm^{-3}, and [monomeric residue of dextrin]$_0=2.0\times10^{-1}$ mol dm^{-3}. b) Values from Ref. 14. c) Numbers in parentheses refer to *hkl* values.

Fig. 5. Electron micrograph of colloidal copper dispersion prepared by reduction of copper(II) sulfate with hydrazine in the presence of PVP (DP=3240) (×100000); $[CuSO_4]_0=5.0\times10^{-3}$, [hydrazine]$_0=3.3\times10^{-2}$, and [monomeric residue of PVP]$_0=2.0\times10^{-1}$ mol dm^{-3}.

Figure 4 depicts a selected area electron diffraction pattern for the particles in the colloidal copper dispersion prepared by reducing copper(II) sulfate in the presence of dextrin. The diffraction experiment has been carried out for the inside of a circle, which is located exactly at the center of the picture (c) in Fig. 2 and has diameter of around 400 nm. Clearly split and distinct Debye-Scherrer rings are observed. Virtually identical patterns are observed also for the dispersions with PVP and poly(vinyl alcohol). As shown in Table 3, the relative ratios for the reciprocals of the radii of the four rings are almost perfectly identical with the relative values for the lattice spacing in pure crystal of bulk copper metal.

Figure 5 shows the electron micrograph of the colloidal copper dispersion prepared by using hydrazine as reducing agent. Copper particles are much larger than those in the dispersions prepared by using sodium tetrahydroborate, and the particle diameters range from 200 Å to 1600 Å.

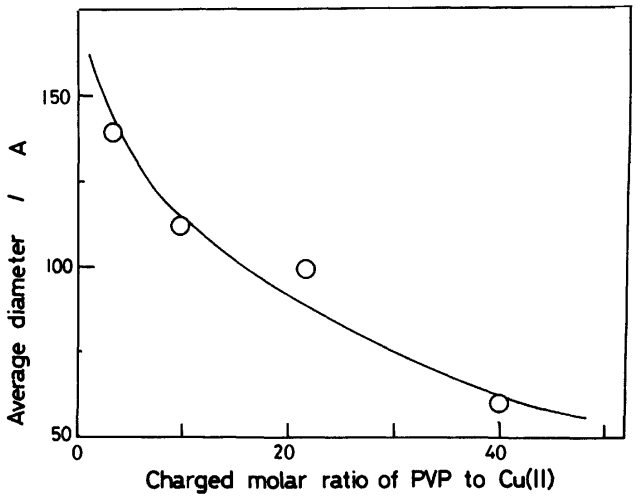

Fig. 6. Dependence of the average diameter of copper particles on the amount of PVP (DP=1440) for the colloidal dispersion prepared by reduction of copper(II) sulfate with sodium tetrahydroborate; $[CuSO_4]_0=5.0\times10^{-3}$ and $[NaBH_4]_0=1.0\times10^{-2}$ mol dm^{-3}.

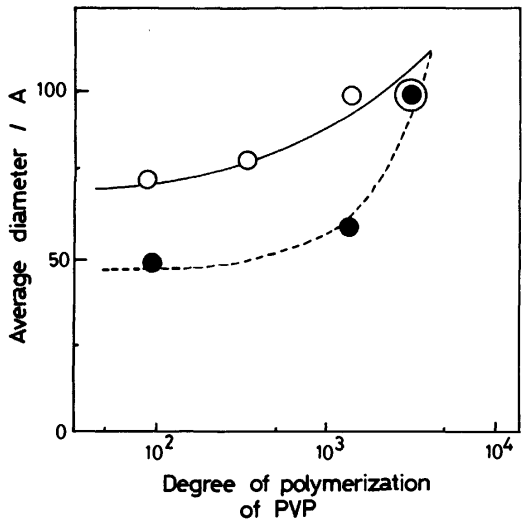

Fig. 7. Dependence of the average diameter of colloidal copper particles on the degree of polymerization of PVP for the colloidal dispersion prepared by reduction of copper(II) sulfate with sodium tetrahydroborate; [monomeric residue of PVP]$_0=1.0\times10^{-1}$ (○) or 2.0×10^{-1} mol dm^{-3} (●); $[CuSO_4]_0=5.0\times10^{-3}$ and $[NaBH_4]_0=1.0\times10^{-2}$ mol dm^{-3}.

Effects of Amount of Poly(*N*-vinyl-2-pyrrolidone) and Its Degree of Polymerization on Size of Copper Particles. As depicted in Fig. 6, the average diameter of copper particles, determined by electron microscopy, monotonously decreases with increase in the charged molar ratio of monomeric residue of PVP to copper(II) sulfate.

Figure 7 shows the plots of the average diameter of copper particles vs. the degree of polymerization of PVP. The particle size increases with increasing degree of polymerization for both the charged molar ratios 20 (○) and 40 (●) of the monomeric residue of PVP to copper(II) sulfate.

Discussion

Formation of Colloidal Copper Particles. Clearly split Debye-Scherrer rings in electron diffraction pattern in Fig. 4, which are virtually identical with those for a crystal of bulk copper metal, show that the colloidal copper particles prepared in the present study are not simple aggregates of copper atoms. Instead, the copper atoms in the particles with diameters of 20—250 Å show face-centered cubic packing in the same way as those in the copper metal. In addition, the lattice constants for the colloidal particles are almost identical with those for bulk copper metal.

Formation of copper boride is ruled out by these facts as well as by successful preparation of colloidal dispersion using hydrazine as reducing agent (Table 2).

The positions of absorption maxima (570 and 580 nm, respectively) for the colloidal copper dispersions prepared by reducing copper(II) sulfate with sodium tetrahydroborate and hydrazine in the presence of PVP (Fig. 1) is almost identical with that (580 nm) for the copper dispersion prepared by using gelatin as protective polymer.[10] The dispersion with gelatin was prepared by reduction of copper(II) sulfate with hydrazine in the presence of gelatin, followed by the removal of large copper particles by centrifugation. These absorption maxima are attributable to excitation of surface plasmon in copper particles.

Protective Polymers. The polymers successfully used as protective polymers for the preparation of colloidal copper dispersions have *N*-substituted amide, alcoholic, ethereal, or sulfate groups in the side chains (Table 1). On the formation of colloidal dispersions, the polymers first form complexes with copper(II) ions using these functional groups. Then copper(II) ions in the polymer complexes are reduced to zero valence states by sodium tetrahydroborate or hydrazine. Stability of the dispersion is attributable to the inhibition of the direct contacts of the metal particles by the polymers, which are located on the surface of the particles.[15]

Steric factors are also important for the polymers to function effectively as protective polymers. Quite a small protecting activity of poly(ethylene oxide) with alkoxyl groups in the polymer main chains, which is in contrast with sufficient protecting activity of poly(methyl vinyl ether) with alkoxyl groups in the side chains, is due to steric hindrance. β-Cyclodextrin, possessing rings composed of seven or fourteen hydroxyl groups with diameter of 6—8 Å, has a poor activity also due to steric hindrance, although poly(vinyl alcohol) shows effective protection. Soluble nylon, which has *N*-unsubstituted amide groups in the main chains and probably interacts with copper(II) ions more strongly than PVP with *N*-substituted amide groups, forms gel

with copper(II) ions.

No reduction of copper(II) ions in the presence of poly(acrylic acid), poly(2-acrylamido-2-methyl-1-propanesulfonic acid), and the copolymer of methyl vinyl ether and maleic acid is associated with the acidity of the polymer complex solution. Here, sodium tetrahydroborate added is largely used for the reactions with protons. This interpretation is consistent with the successful preparation of a colloidal dispersion using poly(potassium vinyl sulfate).

Reducing Agents. Sodium tetrahydroborate and hydrazine effectively reduce copper(II) ions, yielding colloidal copper dispersions. No reducing activity of ethanol and molecular hydrogen on copper(II) ions is in contrast with successful preparation of colloidal dispersions of noble metals from the salts using them as reducing agents.[1,2,6-9] This is attributable to much more negative oxidation-reduction potential (+0.34 eV[16]) for copper(II) ions than those for noble metals. The values for palladium(II), silver(I), and gold(III) ions, for example, are +0.92, +0.83, and +1.50 eV, respectively.[16]

Size of Colloidal Copper Particles. The size of colloidal copper particles should increase with increase in the relative rate of combination of copper atoms with copper particles, with respect to the rate of coverage of surface of copper particles by protective polymers. Thus, the particle size decreases with increasing amount of the protective polymer (Fig. 6). The decrease of the particle size with decreasing degree of polymerization of the protective polymer (Fig. 7) is associated with more rapid and effective coverage of the particles by the polymer of smaller degree of polymerization. This argument is consistent with the fact that the protecting activity of PVP on colloidal dispersions of silver increases with decreasing degree of polymerization.[17]

The authors would like to thank Mr. Koichi Adachi for valuable assistance in the electron microscope measurements.

References

1) C. Paar and C. Amberger, *Chem. Ber.*, **37**, 124 (1904).
2) A. Skita and W. A. Meyer, *Chem. Ber.*, **45**, 3579 (1912).
3) L. D. Rampino and F. F. Nord, *J. Am. Chem. Soc.*, **63**, 2745 (1941).
4) R. Zsigmondy, *Z. Anal. Chem.*, **40**, 697 (1901).
5) K. N. Machalov, A. T. Groisberg, and N. A. Palikhov, *Tr. Kazan. Khim-Tekhnol. Inst.*, **1969**, No. 40 (Pt. 1), 150; *Chem. Abstr.*, **75**, 40844h (1971).
6) H. Hirai, *J. Macromol. Sci. Chem.*, **A13**, 633 (1979).
7) H. Hirai, Y. Nakao, and N. Toshima, *J. Macromol. Sci. Chem.*, **A12**, 1117 (1978).
8) H. Hirai, Y. Nakao, and N. Toshima, *J. Macromol. Sci. Chem.*, **A13**, 727 (1979).
9) H. Hirai, H. Chawanya, and N. Toshima, *Makromol. Chem., Rapid Commun.*, **2**, 99 (1981).
10) G. C. Papavassiliou and Th. Kokkinakis, *J. Phys.*, **F, 4**, L67 (1974).
11) H. Hirai, H. Wakabayashi, and M. Komiyama, *Chem. Lett.*, **1983**, 1047.
12) H. Tanaka and R. Senju, *Kobunshi Ronbunshu*, **33**, 309 (1976).
13) W. N. Haworth, *J. Chem. Soc.*, **107**, 8 (1915).
14) "Powder Diffraction File, Sets 1-5 (Revised)," Inorganic Volume, No. PDIS-5iRB," ed by L. G. Berry, Joint Committee on Powder Diffraction Standard, Swarthmore (1974).
15) H. Hirai, H. Wakabayashi, and M. Komiyama, *Makromol. Chem., Rapid Commun.*, **5**, 381 (1984).
16) "Lange's Handbook of Chemistry," ed by J. A. Dean, 12th Ed., McGraw-Hill Book Company, New York (1979).
17) B. Jirgensons, *Makromol. Chem.*, **6**, 30 (1951).

 © 1986 The Chemical Society of Japan Bull. Chem. Soc. Jpn., 59, 373—379 (1986)

Valence Coordinate Contributions to Zero-Point Energy Shifts Due to Hydrogen Isotope Substitutions

Takao Oi*,† and Takanobu Ishida
Department of Chemistry, State University of New York, Stony Brook, New York 11794, U.S.A.
(Received September 18, 1985)

The orthogonal approximation method for the zero-point energy (ZPE) developed previously has been applied to analyze the shifts in the ZPE, δ(ZPE), due to monodeuterium substitutions in methane, ethylene, ethane and benzene in terms of elements of $\boldsymbol{F}$ and $\boldsymbol{G}$ matrices. The δ(ZPE) can be expressed with a reasonable precision as a sum of contributions of individual valence coordinates and correction terms consisting of the first-order interactions between the coordinates. A further refinement in the precision is achieved by a set of small number of second-order terms, which can be estimated by a simple procedure.

The zero-point energy, ZPE, of a molecule is of fundamental interest since it represents the minimum energy of the vibrating system with respect to the minimum in the potential energy surface. In the field of chemistry of isotopes, the ZPE differences between isotopically substituted molecules, δ(ZPE), are very important in the theoretical consideration of isotope effects on equilibria and also on reaction rates.

In a previous paper,[1] we developed an approximation for the ZPE expressed in terms of the first-order and second-order traces of the vibrational $\boldsymbol{H}$ matrix ($\boldsymbol{H}\equiv\boldsymbol{FG}$), i.e., Tr($\boldsymbol{H}$) and Tr($\boldsymbol{H}^2$), on the basis of a method of orthogonal expansion,

$$\mathrm{ZPE}=\frac{\hbar}{2}\lambda_{\max}^{1/2}[f\beta_0+(\beta_1/\lambda_{\max})\mathrm{Tr}(\boldsymbol{H})+(\beta_2/\lambda_{\max}^2)\mathrm{Tr}(\boldsymbol{H}^2)], \tag{1}$$

where $\lambda_{\max}$ is the largest vibrational eigenvalue of the molecule, f is the number of internal degree of freedom, and the coefficients β_0, β_1, and β_2 are simple functions of λ_0, a reference eigenvalue for a normalization purpose (Sometimes, $\eta\equiv\lambda_0/\lambda_{\max}$ is used in place of λ_0.), and ξ, the range of λ_i/λ_0 for the purpose of expansion. An advantage of this approximation method is that contributions of individual elements of the $\boldsymbol{F}$ and $\boldsymbol{G}$ matrices to the ZPE and/or to the δ(ZPE) can be explicitly estimated, and thus the method can provide an analytical means to study correlation of the ZPE and δ(ZPE) with molecular structures and molecular forces.

The method was since tested for the ZPE's of normal paraffins[2] and for the δ(ZPE) due to the deuterium-for-hydrogen substitutions in some molecules,[3] and a linear frequency sum rule was derived.[3] Now it seems to be a due course to apply the method to study in detail relationships between δ(ZPE) and the elements of $\boldsymbol{F}$ and $\boldsymbol{G}$ matrices.

In this paper we report on an analysis of correlation between internal valence coordinates and the ZPE shifts for monodeuterium substitutions, i.e., the d_1/d_0 pairs, in methane, ethylene, ethane and benzene. A simple equation is presented which yields the δ(ZPE) with a reasonable precision.

Computation

The isotope shift in ZPE, δ(ZPE), is defined as the ZPE of the lighter of two isotopic species of the pair minus the ZPE of the heavier. Thus, δ(ZPE) for the pair, d_1/d_0, is ZPE(d_0)−ZPE(d_1). In this paper we will treat the contributions of various valence coordinates and interactions between them to the shift in the sum of the frequencies, expressed in units of wavenumbers, $\delta\sum\omega_i$. From Eq. 1, we have

$$\delta\sum\omega_i\simeq\omega_{\max}[\beta_1\delta\sum(\lambda_i/\lambda_{\max})+\beta_2\delta\sum(\lambda_i/\lambda_{\max})^2], \tag{2}$$

where $\omega_{\max}=\lambda_{\max}^{1/2}/2\pi c$, and δ denotes the difference in the quantity that follows it between the two isotopic molecules, d_0 and d_1. If one uses the conventional units for the elements of $\boldsymbol{F}$ and $\boldsymbol{G}$ matrices so that the eigenvalues are in units of mdyn Å^{-1}amu^{-1} (1 mdyn=1×10^{-8}N, 1 Å=1×10^{-10} m, and 1 amu=1.66057×10^{-27} kg), Eq. 2 becomes

$$\delta\sum\omega_i\simeq\beta_1'\delta\sum\lambda_i+\beta_2'\delta\sum\lambda_i^2, \tag{3}$$

where

$$\beta_1'\equiv\beta_1/\sigma\omega_{\max},\ \beta_2'\equiv\beta_2/\sigma^2\omega_{\max}^3, \tag{4a,b}$$

and

$$\sigma\equiv 4\pi^2c^2/10^5N_0 \tag{5}$$

in which c is the speed of light in cm/s and N_0 the Avogadro's number.

The term of $\sum\lambda_i$ is the first-order term and that of $\sum\lambda_i^2$ is the second-order term. Each can be explicitly written in terms of the elements of $\boldsymbol{F}$ and $\boldsymbol{G}$ matrices, which forms the basis of our present study. Due to the Born-Oppenheimer approximation, an $\boldsymbol{F}$ matrix of a chemical species is common to all isotopic molecules. Because hydrogen is always a terminal atom (with exceptions of hydrogen-bonded structures), any motion of a hydrogen atom in a molecule does not vary many valence coordinates. Thus, many $\boldsymbol{G}$ matrix elements in $\sum\lambda_i$ and $\sum\lambda_i^2$ cancel between the isotopic pair d_1/d_0.

Let us denote the first-order term by S_1. Then,

$$S_1\equiv\beta_1'\delta\sum\lambda_i=\beta_1'[\sum_i f_{ii}\delta g_{ii}+2\sum_{i>j}\sum f_{ij}\delta g_{ij}], \tag{6}$$

†Present address: Department of Chemistry, Faculty of Science and Technology, Sophia University, 7-1, Kioicho, Chiyodaku, Tokyo 102.

Table 1. Second-Order Terms of $\delta\sum\lambda_i^2$, $A_m \equiv a_m \sum \bar{F}\delta\bar{G}$ [a]

Type(m)	a_m	$\delta\bar{G}$	$\bar{F}$	Summation [b]
1	1	$\delta(g_{ii}^2)$	f_{ii}^2	Over all coordinate number i
2	2	$\delta(g_{ii}g_{jj})$	f_{ij}^2	Over all distinct combinations of different coordinate numbers i and j
3	4	$\delta(g_{ij}g_{ij})$	$f_{ii}f_{ij}$	(same as above)
4a	2	$\delta(g_{ij}^2)$	$f_{ii}f_{jj}$	(same as above)
4b	2	$\delta(g_{ij}^2)$	f_{ij}^2	(same as above)
5	4	$\delta(g_{ii}g_{jk})$	$f_{ij}f_{ik}$	Over all distinct combinations of different coordinate numbers i, j, and k
6	4	$\delta(g_{ij}g_{ik})$	$f_{ii}f_{jk}+f_{ij}f_{ik}$	(same as above)
7	4	$\delta(g_{ij}g_{kl})$	$f_{ii}f_{jk}+f_{ik}f_{jl}$	Over all distinct combinations of different coordinate numbers i, j, k, and l

a) $\sum_m A_m = \delta\sum\lambda_i^2$. b) When more than one subscript are involved, all permutations of the same combination are counted once, except for Type 3 terms for which both $\delta(g_{ii}g_{ij})f_{ii}f_{ij}$ and $\delta(g_{jj}g_{ij})f_{jj}f_{ij}$ have to be separately considered.

where f_{ii} and g_{ii} are the diagonal elements of $\boldsymbol{F}$ and $\boldsymbol{G}$ matrices, respectively, for the i-th coordinate, while f_{ij} and g_{ij} are the off-diagonal elements of $\boldsymbol{F}$ and $\boldsymbol{G}$ matrices, respectively, representing the interactions between the i-th and j-th coordinates. δg_{ii} and δg_{ij} are the isotopic differences in g_{ii} and g_{ij}, respectively, i.e., the lighter (g_{ii} and g_{ij}) minus the heavier (g_{ii} and g_{ij}). The double summation in Eq. 6 is taken over all different combinations of different coordinates i and j.

Similarly, the second-order term S_2 is

$$S_2 \equiv \beta_2'\delta\sum\lambda_i^2 = \beta_2'\sum_{m=1}^{7}A_m, \tag{7}$$

where each A_m[4] is in the form of a product of a force constant factor, $\bar{F}$, and a geometric factor, $\delta\bar{G}$ as defined in Table 1.

At this point, let us define the kinds (or the types) of coordinate and the kinds (or the types) of interaction between coordinates. What follows is more or less generally presumed in papers on chemistry of isotopes, but it is essential for the present work to spell it out. A valence coordinate system of a molecule consists of a set of groups of equivalent coordinates. Then, each of such groups is a kind (or a type). Due to the isotope-independence of $\boldsymbol{F}$ matrix, the equivalence of coordinates for the present purpose is considered unaffected by a change of molecular symmetry by an isotopic substitution. A complete set of kinds of coordinate of a given chemical species is, therefore, found by examining the most symmetric isotopic species. Thus, ethane may be said to consist of five kinds (or types) of coordinates if redundancies are freely built into the coordinate system to preserve the highest possible symmetry; C-H stretching, C-C stretching, H-C-H bending, H-C-C bending, and HC-CH torsion. We will denote the kinds (or types) of coordinate with subscripts p and q, in order to distinguish them from the coordinate numbers for which the subscripts i, j, k, and l will be used.

The interaction (pq) between two kinds of coordinate, p and q, is the sum of all equivalent interactions between all coordinates i of kind p and all coordinates j of kind q. p may be equal to q in an interaction (pq), while i cannot be equal to j in an interaction (ij). It should be noted that not all interactions between the coordinates of kind p and those of kind q are necessarily identical. In such cases, an appropriate notation will be used to uniquely define the relative positions of two coordinates involved.

To examine the various terms included in Eqs. 6 and 7 from the viewpoint of the kinds of coordinate and of interaction, it may be useful to decompose these equations into the quantities, T, defined below.

$T_1(p)$: Sum of all terms of the form $f_{ii}\delta g_{ii}$, where i is a coordinate of kind p, multiplied by β_1'. $f_p \equiv f_{ii}$.

$T_1(pq)$: Sum of all terms of the form $2\beta_1' f_{ij}\delta g_{ij}$, $i>j$, where i is a coordinate of kind p and j is a coordinate of kind q. $f_{pq}\equiv f_{ij}$.

$T_2^m(p)$: Take the sum of all second-order terms of type m (cf: Table 1) involving the diagonal force constant f_{ii}, where i is a coordinate of kind p, and multiply the sum with β_2'. Then, $T_2^m(p)$ for $m=1$ is equal to the product, and $T_2^m(p)$ for all other terms containing another force constant beside f_{ii} is one-half of the product.

$T_2^m(pq)$: Take the sum of all second-order terms of type m involving the interaction constant f_{ij}, where i is a coordinate of kind p and j is a coordinate of kind q, and multiply the sum with β_2'. $T_2^m(pq)$ is equal to the product for types 2 and 4b, and one-half the product for all other types containing another constant beside f_{ij}. For $m=6$ and 7, the rule applies to each term of force constant product.

$T_2(p)$: Total second-order contribution of the coordinates of kind p to $\delta\Sigma\omega_i$.

$T_2(pq)$: Total second-order contribution of the interactions of kind pq to $\delta\Sigma\omega_i$.

$T_2(m)$: Total contribution of the second-order interactions of type m to $\delta\Sigma\omega_i$.

$T(p)$: Total contribution of the coordinates of kind p to $\delta\Sigma\omega_i$.

$T(pq)$: Total contribution of the interactions of kind pq to $\delta\Sigma\omega_i$.

Relationships among $\delta\Sigma\omega_i$, S_1, S_2, and various T's are easily understood. Whenever a second-order term contains a product of two different force constants, each half of the term is attributed to each of the participating force constants.

The various contributions, T, to $\delta\Sigma\omega_i$ were calculated for the d_1/d_0 pairs of methane, ethylene, ethane and benzene. The $\boldsymbol{F}$ matrices and the approximation parameters used are noted in the footnotes of Tables 2—6. The expansion coefficients β_1' and β_2' were computed from Eqs. 4a,b. The parameters ξ and η

Table 2. Major Contributions to $\delta\sum\omega_i$ in CH_3D/CH_4[a]

(1)	(2)	(3)	(4)	(5)	(6)	(7)	(8)	(9)	(10)
Coordinate type (p) or Interaction type (pq)	f_p or f_{pq} /mdyn Å^{-1}	n_p or n_{pq}	$T_1(p)$[b] or $T_1(pq)$	$T_2(p)$[b] or $T_2(pq)$	$T(p)$[b] or $T(pq)$	(4)[c] / (2)×(3)	$T_2^1(p)$[b]	$T_2^m(p)$ or $T_2^m(pq)$, $m\neq1$[f]	(4)+(8)[b]
C-H stretch	4.918	1	1137.4	−202.1	935.3	231.3	−202.4		935.1
			(92.4)	(−16.4)	(76.0)		(−16.4)		(75.9)
HCH bend[g]	0.370	3	256.7	−11.8	244.9	231.3	−8.1	[3]=−3.4; [4]=−1.5	248.5
			(20.8)	(−1.0)	(19.9)		(−0.7)	(−0.3) (−0.1)	(20.2)
(HCH)×(HCH); adjacent[g]	−0.0779	3	54.1	−2.9	51.2	−231.3	0.0	[2]=−1.5; [3]=−3.2; [5]=2.2	54.1
			(4.4)	(−0.2)	(4.2)		(0.0)	(−0.1) (−0.3) (0.2)	(4.4)
Total (approx)[d]			1448.2	−216.8	1231.4		−210.5		1237.7
			(117.6)	(−17.6)	(100.0)		(−17.1)		(100.5)
Total (exact)[e]			1448.2	−216.4	1231.8		−210.5		1237.7
			(117.6)	(−17.6)	(100.0)		(−17.1)		(100.5)

a) $\boldsymbol{F}$ matrix is taken from Hartshorn and Shiner.[5] The *c1* approximation[1] is used; k=0.77, ξ=3.614329, η=1.274406, ω_{max}=3022.31 cm^{-1} and $\delta\sum\omega_i$(exact)=1231.45 cm^{-1}. b) All T terms are in cm^{-1}. The numbers in parentheses below the wavenumber values are percent of $\delta\sum\omega_i$(exact). c) In units of Å mdyn^{-1}cm^{-1}. d) The sum of the contributions tabulated. e) The sum of all contributions, both tabulated and not tabulated. Contributions whose absolute magnitudes are less than 0.1% of $\delta\sum\omega_i$(exact) are not tabulated. f) Number in the brackets is the type of interaction, m. See Table 1 for the definition of interaction types. g) All bending coordinates are weighted by the equilibrium C-H bond length. The adjacent bends are two bends which share a C-H bond.

Table 3. Major Contributions to $\delta\sum\omega_i$ in $CHD{=}CH_2/CH_2{=}CH_2$ (All Vibrations)[a]

(1)	(2)	(3)	(4)	(5)	(6)	(7)	(8)	(9)	(10)
Coordinate type (p) or Interaction type (pq)	f_p or f_{pq} /mdyn Å^{-1}	n_p or n_{pq}	$T_1(p)$[b] or $T_1(pq)$	$T_2(p)$[b] or $T_2(pq)$	$T(p)$[b] or $T(pq)$	(4)[c] / (2)×(3)	$T_2^1(p)$[b]	$T_2^m(p)$ or $T_2^m(pq)$, $m\neq1$[f]	(4)+(8)[b]
CH stretch	5.026	1	1311.9	−322.8	989.1	261.0	−322.7		989.2
			(102.0)	(−25.1)	(76.9)		(−25.1)		(76.9)
HCH bend	0.598	1	156.1	−9.5	146.6	261.0	−11.0		145.1
			(12.1)	(−0.7)	(11.4)		(−0.9)		(11.3)
H_2CC pw[g]	1.133	1	73.9	−2.4	71.6	65.3	−3.1		70.8
			(5.7)	(−0.2)	(5.6)		(−0.2)		(5.5)
H_2CC op[g]	0.802	1	52.3	−1.4	51.0	65.3	−1.5		50.8
			(4.1)	(−0.1)	(4.0)		(−0.1)		(3.9)
H_2C-CH_2 t[g]	0.626	1	40.8	−1.3	39.6	65.3	−1.4		39.4
			(3.2)	(−0.1)	(3.1)		(−0.1)		(3.1)
(CH)×(pw); w/ common CH	±0.300	0	0.0	−3.7	−3.7	—	0.0	[2]=−1.5; [3]=−2.4	0.0
			(0.0)	(−0.3)	(−0.3)		(0.0)	(−0.1) (−0.2)	(0.0)
(CH)×(pw); w/o common CH	±0.608	0	0.0	−3.5	−3.5	—	0.0	[2]=−7.0; [3]=3.0	0.0
			(0.0)	(−0.3)	(−0.3)		(0.0)	(−0.5) (0.2)	(0.0)
Total (approx)[d]			1635.1	−344.4	1290.7		−339.6		1295.4
			(127.1)	(−26.8)	(100.3)		(−26.4)		(100.7)
Total (exact)[e]			1635.1	−348.2	1286.9		−339.6		1295.4
			(127.1)	(−27.1)	(100.0)		(−26.4)		(100.7)

a) $\boldsymbol{F}$ matrix is taken from Stern, Van Hook and Wolfsberg.[6] The *c1* approximation[1] is used; k=0.24, ξ=2.756151, η=1.392833, ω_{max}=3110.79 cm^{-1} and $\delta\sum\omega_i$(exact)=1286.64 cm^{-1}. b)—f) See the footnotes b)—f) of Table 2, respectively. g) Two HCH bends and two H_2CC in-plane wags (pw) are each weighted by the equilibrium C-H bond length, R_{CH}, two out-of-plane wags (op) are each weighted by $R_{CH}\cos\alpha$, and the torsion (t), as defined by Arnett and Crawford,[7] is weighted by $R_{CH}\sin\alpha$, where α is one half the equilibrium angle H-C-H.

used for each chemical species correspond to the value of the weighting parameter k[1] that makes the approximation, Eq. 3, almost exact for the d_1/d_0 pair of the molecule.

Results and Discussion

Results of calculations have been summarized in

Table 4. Major Contributions to $\delta\sum\omega_i$ in C_2H_5D/C_2H_6[a]

(1)	(2)	(3)	(4)	(5)	(6)	(7)	(8)	(9)	(10)
Coordinate type (p)	f_p /mdyn Å^{-1}	n_p	$T_1(p)$[b]	$T_2(p)$[b]	$T(p)$[b]	$\frac{(4)}{(2)\times(3)}$[c]	$T_2^1(p)$[b]	$T_2^m(p)$, $m\neq1$[f]	(4)+(8)[b]
C-H stretch	4.704	1	1251.5	−295.5	956.0	266.1	−295.6		955.9
			(94.9)	(−22.4)	(72.5)		(−22.4)		(72.5)
HCH bend[g]	0.451	2	240.5	−15.4	225.1	266.5	−12.9	[4]=−2.8	227.6
			(18.2)	(−1.2)	(17.1)		(−1.0)	(−0.2)	(17.3)
HCC bend[g]	0.532	1	141.9	−5.8	136.0	266.5	−4.4	[4]=−1.5	137.5
			(10.8)	(−0.4)	(10.3)		(−0.3)	(−0.1)	(10.4)
HC-CH τ[g]	0.00672	1	2.0	−0.1	1.9	299.7	−0.0	[4]=−0.1	2.0
			(0.2)	(−0.0)	(0.1)		(−0.0)	(−0.0)	(0.2)
Total (approx)[d]			1635.9	−316.8	1319.1		−312.9		1322.9
			(124.0)	(−24.0)	(100.0)		(−23.7)		(100.3)
Total (exact)[e]			1635.9	−316.6	1319.3		−312.9		1322.9
			(124.0)	(−24.0)	(100.0)		(−23.7)		(100.3)

a) $\boldsymbol{F}$ matrix used is Schachtschneider and Snyder's VFF(V).[8] The *c1* approximation[1] is used; k=0.30, ξ=2.901508, η=1.370426, ω_{max}=2968.70 cm^{-1} and $\delta\sum\omega_i$(exact)=1319.28 cm^{-1}. b)—f) See the footnotes b)—f) of Table 2, respectively. g) All bending coordinates and the torsion (τ) are weighted by the equilibrium C-H bond length. The torsion is as defined by Wilson, Decius, and Cross.[9]

Table 5. Major Contributions to $\delta\sum\omega_i$ in Benzene-d_1/Benzene-d_0 (Planer Vibrations Only)[a]

(1)	(2)	(3)	(4)	(5)	(6)	(7)	(8)	(9)	(10)
Coordinate type (p)	f_p /mdyn Å^{-1}	n_p	$T_1(p)$[b]	$T_2(p)$[b]	$T(p)$[b]	$\frac{(4)}{(2)\times(3)}$[c]	$T_1^2(p)$[b]	$T_2^m(p)$, $m\neq1$[f]	(4)+(8)[b]
C-H stretch[g]	5.063	1	1202.3	−236.3	966.1	237.5	−235.7		966.7
			(103.3)	(−20.3)	(83.0)		(−20.2)		(83.0)
HCC_2 pw[g]	0.870	1	206.5	−6.3	200.1	237.5	−7.8	[3]=1.5	198.7
			(17.7)	(−0.5)	(17.2)		(−0.7)	(0.1)	(17.1)
Total (approx)[d]			1408.8	−242.6	1166.2		−243.5		1165.3
			(121.0)	(−20.8)	(100.2)		(−20.9)		(100.1)
Total (exact)[e]			1408.8	−244.5	1164.3		−243.5		1165.3
			(121.0)	(−21.0)	(100.0)		(−20.9)		(100.1)

a) $\boldsymbol{F}$ matrix is taken from Crawford and Miller.[10] The *c1* approximation[1] is used; k=0.55, ξ=3.332543, η=1.309823, ω_{max}=3083.78 cm^{-1} and $\delta\sum\omega_i$(exact)=1164.06 cm^{-1}. b)—f) See the footnotes b)—f) of Table 2, respectively. g) The coordinate system consists of six C-H stretchings, six C-C stretchings, six CCC bendings and six in-plane wags (pw). The pw's are weighted by the equilibrium C-H bond length and CCC bends are weighted by the equilibrium C-C bond length.

Tables 2—6. Each entry of the terms T, i.e., the columns 4, 5, 6, 8, 9, and 10 in these tables, shows the magnitude of the term in cm^{-1} and, in parentheses, percent of the exact value of $\delta\Sigma\omega_i$, $\delta\Sigma\omega_i$(exact). The exact value was calculated from the eigenvalues obtained by solving vibrational secular equations. For clarity, only the coordinate and interaction types (column 1) for which the magnitude of the first-order or second-order term (column 4 or 5) is more than 0.1% of the $\delta\Sigma\omega_i$(exact) have been tabulated. Columns 4 and 5 tabulate the totals of the first-order and second-order terms, respectively, and column 6 is the sum of columns 4 and 5. Columns 7—10 will be used for detailed examination of individual contributions contained in columns 4—6.

From their definitions, $T_1(p)$ and $T_1(pq)$ may be written as

$$T_1(p) = \beta_1' n_p f_p \delta g_p, \tag{8}$$

and

$$T_1(pq) = 2\beta_1' n_{pq} f_{pq} \delta g_{pq}, \tag{9}$$

where n_p and n_{pq} are, respectively, the numbers of non-vanishing δg_{ii}, in which i is a member of p, and the number of non-vanishing δg_{ij} in which (ij) is a member of the interaction type (pq) (column 3). Because hydrogen is a terminal atom, n_p is usually unity. The larger value of n_p is possible only when two or more coordinates of the same kind share the substituted hydrogen atom (SHA).

The "Total" under the columns 4, 5, 6, 8, and 10 are, respectively, S_1 (Eq. 6), S_2 (Eq. 7), $\delta\Sigma\omega_i$ (Eq. 3), $T_2(1)$, and $S_1+T_2(1)$. A difference between "Total (approx)" and

Table 6. Major Contributions to $\delta\sum\omega_i$ in Benzene-d_1/Benzene-d_0 (Out-of-plane Vibrations Only)[a]

(1)	(2)	(3)	(4)	(5)	(6)	(7)	(8)	(9)	(10)
Coordinate type (p) or Interaction type (pq)	f_p or f_{pq} /mdyn Å^{-1}	n_p or n_{pq}	$T_1(p)$[b] or $T_1(pq)$	$T_2(p)$[b] or $T_2(pq)$	$T(p)$[b] or $T(pq)$	(4)[c] / (2)×(3)	$T_2^1(p)$[b]	$T_2^m(p)$ or $T_2^m(pq)$, $m\neq1$[f]	(4)+(8)[b]
HCC_2 op[g]	0.378	1	243.9	−32.6	211.3	645.2	−42.3	[3]=9.7	201.6
			(114.2)	(−15.3)	(98.9)		(−19.8)	(4.6)	(94.3)
(op)×(t);[g]	±0.0875	0	0.0	4.0	4.0	—	0.0	[2]=−3.6; [3]=−10.1;[5]=−2.4	0.0
sharing 3C's			(0.0)	(1.9)	(1.9)		(0.0)	(−1.7) (4.7) (−1.1)	(0.0)
(op)×(op);[g]	−0.0570	0	0.0	−2.3	−2.3	—	0.0	[2]=−2.3; [3]=−3.0; [5]=3.0	0.0
sharing 2C's			(0.0)	(−1.1)	(−1.1)		(0.0)	(−1.1) (−1.4) (1.4)	(0.0)
(op)×(t);[g]	±0.0430	0	0.0	0.7	0.7	—	0.0	[2]=−0.9; [3]=2.7; [5]=−1.2	0.0
sharing 2C's			(0.0)	(0.3)	(0.3)		(0.0)	(−0.4) (1.3) (−0.5)	(0.0)
Total (approx)[d]			243.9	−30.2	213.7		−42.3		201.6
			(114.2)	(−14.1)	(100.0)		(−19.8)		(94.3)
Total (exact)[e]			243.9	−30.2	213.7		−42.3		201.6
			(114.2)	(−14.1)	(100.0)		(−19.8)		(94.3)

a) $\boldsymbol{F}$ matrix is taken from Miller and Crawford.[11] The *cl* approximation[1] is used; k=1.4, ξ=4.193083, η=1.209680, ω_{max}=993.44 cm^{-1} and $\delta\sum\omega_i$(exact)=213.67 cm^{-1}. b)—f) See the footnotes b)—f) of Table 2, respectively. g) The coordinate system consists of six HCC_2 out-of-plane wags (op) and six CC-CC torsions (t) as defined in Wilson, Decius, and Cross.[9] The op's are weighted by the equilibrium C-H bond length and t's are weighted by the equilibrium C-C bond length.

"Total (exact)" is a sum of the small contributions which were individually not tabulated due to the 0.1% criterion.

In the following we will first itemize important observations one would make on these tables and then discuss each feature separately.

Observations. (1) On $\delta\Sigma\omega_i$: $\delta\Sigma\omega_i$ is within 0.1% of $\delta\Sigma\omega_i$(exact) if all contributions are counted. It is within 0.1% for all molecules, except ethylene (100.3%) and the planar vibrations of benzene (100.2%), when only those tabulated in these tables are summed up.

(2) On few entries for interaction types (pq) in column 1: Except for methane, ethylene and benzene (out-of-plane vibrations), there is no entry for the interactions in column 1, which means that $T_1(pq)$ and $T_2(pq)$ for the interaction forces do not individually contribute more than 0.1% of $\delta\Sigma\omega_i$(exact) in most cases.

(3) On the relative magnitudes of entries in columns 4, 5, and 6: By far the largest contributor is the H-X stretching coordinate. The following inequalities generally hold on the absolute magnitudes among various terms; a) $T_1(p)\gg T_2(p)$ and $T_1(pq)\gg T_2(pq)$, b) T_1(H-X stretch)$\gg T_1$(bend)$\gg T_1$(out-of-plane motion), c) many $T_1(pq)$'s vanish, and when they do not, T_1(bend)$\gg T_1(pq)$, and d) T_2(HX stretch)$\gg T_2$(p$\neq$HX-stretch).

(4) On the "Totals" for the columns: a) The S_1 and $T_2(1)$ entries (columns 4 and 8) for "approx" are respectively identical to the "exact", and b) the difference between "approx" and "exact" of S_2 (column 5) is equal to that of $\delta\Sigma\omega_i$ (column 6).

(5) On column 10: $S_1+T_2(1)$ is within 0.7% of $\delta\Sigma\omega_i$(exact) except for the out-of-plane vibrations of benzene. The sources of the errors for all molecules are identified in column 9.

First-Order Terms. Every type of coordinate that includes the SHA in the coordinate definition makes a positive contributions, $T_1(p)$, to the first-order term. The number n_p of non-vanishing δg_p (Eq. 8) is more than unity only when more than one equivalent bending coordinate share the SHA, as exemplified by methane and ethane. Expressions for $T_1(p)$ can be easily obtained. It is seen that column 7 in Tables 2—6 gives $\beta_i'\delta g_p$ (Eq. 8) and, β_i' being common to all coordinate types of a given molecule, the difference in $T_1(p)/n_pf_p$ is the difference in δg_p. For every molecule studied, all bending coordinates except CCC bends in benzene are weighted by the equilibrium C-H bond length. For stretching and angle-bending coordinates, therefore, the numbers under column 7 are equal to $\beta_i'\delta\mu_H$. For the wagging and torsional coordinates in ethylene, 65.3 for the coordinate types pw, op, and t is simply 261/4. The value for the out-of-plane wag for benzene seems to be out of place at a first glance, but actually it is not. The unusually large value is due to the artifact that the out-of-plane vibrations have been isolated for the purpose of this analysis, thus making ω_{max} for this group of motions small (993 cm^{-1}). In fact, the products of these values of $\beta_1\delta\mu_H/(\sigma\omega_{max})$ and ω_{max} fall in a relatively narrow range between 7 and 8 in units of 10^5 Å mdyn^{-1} for all molecules tested, and variation of the values is due to the difference in the k-values used for the different molecules.

The first-order contribution of an interaction type (pq) does not vanish only if 1) there is at least one member coordinate i of kind p and at least one member

coordinate j of kind q, such that $s_{iH} \cdot s_{jH} \neq 0$, where s_{iH} is the s-vector[9] for the motion of the SHA in the coordinate i, and 2) f_{ij} for such a pair ij is non-zero. Thus, δg_{pq} vanishes whenever one of p and q is a stretching coordinate.

The most common interaction type that makes a finite contribution to the first-order term is one between two bending coordinates that share the SHA.

The fact that the "Total (approx)" and "Total (exact)" for S_1 are identical for all molecules studied is accidental due to two major reasons. The first is lack of appropriate f_{ij} in the $\boldsymbol{F}$ matrix used. For instance, the interactions such as (HCH)×(in-plane wag)$_{adj.}$, in ethylene, (HCH)×(HCC)$_{adj.}$, in ethane do not contribute to the first-order term simply because the corresponding interaction constants are, somewhat strangely, missing from the particular $\boldsymbol{F}$ matrices used. The second reason is lack of adjacent bending coordinates. For example, there is no entry for the (HCC)×(HCC)$_{adj.}$ interaction in column 1 for the in-plane vibrations of benzene, due to the fact that coordinate system used happens to include six wags rather than, say, twelve HCC bends. However, the difference between the "approx" and "exact" can be made assuredly negligible as long as one includes all the important interactions for which f_{pq}'s are large.

Second-Order Contributions by Diagonal Elements of $\boldsymbol{F}$ Matrix. It is clear from Table 1 that the diagonal elements of $\boldsymbol{F}$ matrix may contribute to the second-order terms only through Types 1, 3, 4a, and 6. Further, it can be shown that $\delta(g_{ii}^2)$ does not vanish if and only if the corresponding δg_{ii} is non-zero and that $\delta(g_{ij}^2)$ does not vanish if and only if the corresponding δg_{ij} is non-zero. Therefore, the number of non-vanishing $\delta(g_{ii}^2)$ is n_p, where p is the kind of coordinate of which i is a member. The number of non-vanishing $\delta(g_{ij}^2)$ is n_{pq}, where pq is the kind of interaction of which ij is a member.

It is thus evident that $T_2^1(p)$ is always non-zero for every p which has a member involving the SHA. Furthermore, they are the largest second-order term, because both of its geometric and force constant factors involve the diagonal elements only. Because the bond-stretching force constants are larger than the bending force constants, usually by one order of magnitude, T_2^1(H–X stretch) is by far the most important contributor of all $T_2^1(p)$'s. $T_2^1(p)$ is always nagative, because β_2' is negative.

As explained earlier, many g_{ij} $(i \neq j)$ are zero, and many $\delta(g_{ij})$ vanish for monodeuterium substitutions. $T_2^3(p)$ is non-zero, only if g_{ij} and f_{ij} are both non-zero at least one coordinate i of kind p that contains the SHA and for at least another coordinate j $(i \neq j)$. Note that j may be another member of p. $T_2^{4a}(p)$ does not vanish, only if there is another coordinate j sharing the SHA with i, such that $s_{iH} \cdot s_{jH} \neq 0$. Again, j may be another member of p. The probability of non-zero $T_2^6(p)$ due to any f_{ii} is so low that we can safely disregard this term.

The sum of S_1 and $\Sigma T_2^1(p)$ (column 10 of Tables 2—6) is within 0.7% of $\delta\Sigma\omega_i$(exact) for all molecules studied with the exception of out-of-plane vibration of benzene. This offers a possibility of a means for a quick approximate calculation for δ(ZPE). A further refinement can be made if one is able to locate all major correction terms to this approximation, namely, all large terms among $T_2^m(p)$ and $T_2^m(pq)$, $m \neq 1$ (column 9, Tables 2—6).

Second-Order Contributions by Off-Diagonal Elements of $\boldsymbol{F}$ Matrix. From Table 1, it is seen that an off-diagonal element f_{ij} may make a non-vanishing contribution in all but those for $m=1$ and 4a. Due to the stringent requirements for the existence of non-zero $T_2^6(pq)$ and $T_2^7(pq)$, we can safely ignore these terms. Similarly, the likelihood of occurrence of non-zero $T_2^5(pq)$ is small and, even if it does occur, its magnitude will be small due to the fact that it contains a product of two off-diagonal force constants and one off-diagonal $\boldsymbol{G}$ matrix element. This leaves us with three types: $T_2^2(pq)$, $T_2^3(pq)$, and $T_2^{4b}(pq)$.

For a given (non-zero) f_{pq}, the process of finding major contributing terms among $T_2(m)$, $m \neq 1$, is a rather simple task once $\boldsymbol{F}$ and $\boldsymbol{G}$ matrices become available, because one can eliminate a major portion of all possible second-order terms on the basis of vanishing δg_{ii} and δg_{ij}: When a δg_{ii} or a δg_{ij} vanishes, the corresponding $\delta(g_{ii}^2)$ or $\delta(g_{ij}^2)$ also does.

Among the non-vanishing terms of $T_2^2(pq)$, $T_2^3(pq)$ and $T_2^{4b}(pq)$, the term $T_2^3(pq)$ tends to be the largest, especially when the members i and j share the SHA because, then, the geometric factors g_{ii} and g_{ij} would become comparable. One should note that Type 3 $(m=3)$ terms contains both $f_{ii}f_{ij}\,\delta(g_{ii}g_{ij})$ and $f_{jj}f_{ij}\,\delta(g_{jj}g_{ij})$ which are different from each other. For a given (ij) both possibilities should be explored.

A Simple Correlation Formula

As noted earlier in this paper, column 10 in Tables 2—6 suggests that an approximation,

$$\delta\Sigma\omega_i \simeq S_1 + T_2(1), \tag{10}$$

gives a precision of 0.7% or better in all molecules tested except the out-of-plane vibrations of benzene. The error for the latter is unusually large simply because the major contribution for this case, $T(op)$, comes from the weak out-of-plane motion, thus making other small second-order terms $T_2(m)$, $m \neq 1$, relatively significant. The foregoing example shows that the process of estimating such a correction term is not a laborious task, even for the relatively large correction.

We made similar correlation study for some other molecules, which we did not report here, and obtained the result that Eq. 10 is a good approximation of Eq. 3.

Equation 10 may be rewritten as

$$\delta(\text{ZPE}) \simeq \frac{\hbar c}{2}\{[\beta_1'\sum_i f_{ii}\delta g_{ii} + \beta_2'\sum_i f_{ii}^2\delta g_{ii}^2] + 2\beta_1'\sum_{i>j}\sum f_{ij}\delta g_{ij}\}. \tag{11}$$

The terms within the brackets represent the contribution of various valence coordinates (diagonal elements), and the last term under the double sum is the contribution of interactions between the coordinates. It has been shown that the first-order interaction terms usually vanish, unless there are more than one adjacent bending coordinates sharing the SHA and the corresponding interaction force constant is non-zero.

Equation 11 thus implies that, usually, a fair result can be obtained only by considering the diagonal elements of $\boldsymbol{F}$ and $\boldsymbol{G}$ matrices. This result is consistent with the result by Wolfsberg's perturbation approximation.[12] His approximation for ZPE consists of a zeroth-order term, $\hbar(f_{ii}g_{ii})^{1/2}/2$, and a correction term which consists of the off-diagonal elements as well as the diagonal ones. This zeroth-order term gives an excellent approximation, and the correction term is usually very small.

The fact that the second-order terms $T_2(m)$, $m\neq1$ in our present approximation are relatively small can be understood from Eq. 2. Every ratio λ_i/λ_{max} in Eq. 2 is much smaller than unity, except for the H-X stretching eigenvalues. The ratios for all bending modes usually lie in the range below $0.25\lambda_{max}$.[2,3] The squares of such ratios are much smaller quantities than λ_i/λ_{max}. As we have shown in this paper, a large majority of the non-vanishing terms $T_2(m)$, $m\neq1$, may be regarded as correction terms for the eigenvalues of bending modes. Since the stretching modes are well accounted for within S_1 and $T_2(1)$, the terms of $T_2(m)$, $m\neq1$, are thus second-order corrections for the small eigenvalues, and one expects such corrections to be very small. One may also reason for the smallness of these terms on the basis of relative magnitudes of $\delta\overline{G}$ and $\overline{F}$ tabulated in Table 1.

It is thus reasonable to make a general statement that Eq. 11 is a simple way to correlate the δ(ZPE) for the monodeuterium substitution and the molecular structures and forces.

Conclusion

The shift in the zero-point energy due to monodeuterium substitutions can be expressed, with the precision which is usually better than 1%, by the relation,

$$\delta(\mathrm{ZPE}) \simeq \frac{\hbar c}{2}\{[\beta'_1\sum_i f_{ii}\delta g_{ii} + \beta'_2\sum_i f_{ii}^2\delta g_{ii}^2] + 2\beta'_1\sum_{i>j}\sum f_{ij}\delta g_{ij}\}.$$

A further refinement in the precision can be achieved by a relatively simple process of estimating major correction terms among the second-order terms of Types 3, 4, and 2.

We gratefully acknowledge the partial support for this work by the Office of Basic Energy Sciences, U. S. Department of Energy, Contract No. DE-AC08-80ER10612.

References

1) T. Oi and T. Ishida, *J. Phys. Chem.*, **87**, 1067 (1983).
2) T. Oi and T. Ishida, *J. Phys. Chem.*, **88**, 1507 (1984).
3) T. Oi and T. Ishida, *J. Phys. Chem.*, **88**, 2057 (1984).
4) T. Ishida and J. Bigeleisen, *J. Chem. Phys.*, **64**, 4775 (1976).
5) S. R. Hartshorn and V. J. Shiner, Jr., *J. Am. Chem. Soc.*, **94**, 9002 (1972).
6) M. J. Stern, W. A. Van Hook, and M. Wolfsberg, *J. Chem. Phys.*, **39**, 3179, (1963).
7) R. L. Arnett and B. L. Crawford, Jr., *J. Chem. Phys.*, **18**, 118 (1950).
8) J. H. Schachtschneider and R. G. Snyder, *Spectrochim. Acta*, **19**, 117 (1963).
9) E. B. Wilson, Jr., J. C. Decius, and P. C. Cross, "Molecular Vibrations," McGraw-Hill, New York (1955).
10) B. L. Crawford, Jr. and F. A. Miller, *J. Chem. Phys.*, **17**, 249 (1949).
11) F. A. Miller and B. L. Crawford, Jr., *J. Chem. Phys.*, **14**, 282 (1946).
12) M. Wolfsberg, *Z. Naturforsch. A*, **18**, 216 (1963).

 © 1986 The Chemical Society of Japan Bull. Chem. Soc. Jpn., 59, 381—384 (1986)

The Solvent Extraction of Alkaline Earth Metal Ions with Nonionic Surfactants

Yukio SAKAI,*,† Hiroshi NAKAMURA,†† Makoto TAKAGI,†† and Keihei UENO†††

†Faculty of Education, Miyazaki University, Funatsuka, Miyazaki 880

††Department of Organic Synthesis, Faculty of Engineering, Kyushu University, Hakozaki, Higashi-ku, Fukuoka 812

†††Department of Industrial Chemistry, Kumamoto Institute of Technology, Ikeda, Kumamoto 860

(Received July 26, 1985)

The extraction of alkaline earth metal ions has been investigated using a mixture of polyethylene glycol mono-*p*-nonylphenyl ether (PEGP; average number of oxyethylene group, 10) and 4-(1,1-dimethyl-3,3-dimethylbutyl)-2,5-dinitrophenol (2,5-dinitro-4-*t*-octylphenol, DNP; HL) in 1,2-dichloroethane. The metal extraction takes place with one molecule of deprotonated DNP (L^-) and an extraneous monoanion (X^-) for neutralization of the dicationic charge of the metal ion. The ease of extraction generally follows the order, $Ba^{2+}>Sr^{2+}>Ca^{2+}\gg Mg^{2+}$. The nature of the anion present in the aqueous phase strongly affects the extractability. For barium, the extractability decreases in the order $ClO_4^->SCN^->I^->Cl^->NO_3^-$. The composition of the extracted complexes for barium and strontium ions proportional to the metal is metal : PEGP : L^- : X^- = 1 : 1 : 1 : 1. The overall extraction constants were estimated.

Nonionic surfactant molecules with noncyclic poly(oxyethylene) chains are known to form cationic complexes with alkali and alkaline earth metal ions. The complexes can be extracted into organic solvents by forming ion pairs with suitable counter anions. Such extractions have successfully been applied to the evaluation of complexation equilibrium constants between metal ions and poly(oxyethlene) derivatives[1-3] as well as to the determination of poly(oxyethlene)-chain-containing nonionic surfactants.[4,5] The nature of the counter anion strongly influences the extractablity of such cationic complexes. Yanagida et al.[1] investigated the extractability of potassium complexes from poly(oxyethylene) derivatives and showed that the extractability varies with the anion in the order $SCN^->I^->>Br^->NO_3^->Cl^-$.

For the extraction of alkaline earth metal ions, however, only a few systematic investigations on the effect of anion have been reported.

On the other hand, a carrier mediated transport of metal ions through membranes continues to be a major concern in biological cell membrane studies as well as in industrial metal separation technology.[6] For alkaline earth metal ions, so far a combination of a lipophilic (counter) anion such as picrate and a lipophilic neutral complexing ligand such as poly(oxyethylene)-chain-containing surfactant or crown ether has been a preferred method, and few systems have a potential for the selective separation of alkaline earth metal ions on a large scale.

In the present study, a proton dissociable lipophilic molecule, 4-(1,1-dimethyl-3,3-dimethylbutyl)-2,5-dinitrophenol(2,5-dinitro-4-*t*-octylphend, DNP; HL) is used in combination with a poly(oxyethylene)-chain-containing, surfactant type neutral ligand (polyethylene glycol mono-*p*-nonylphenyl ether, PEGP; average number of oxyethylene group, 10) for the extraction alkaline earth metals. The basic features in the metal extraction equilibrium has been elucidated.

Experimental

Reagent. *p-tert*-Octylphenol was purchased from Wako Pure Chemicals Co. LTD., and dicyclohexano-18-crown-6 (DCH18C6) from Nakarai Chemicals Co. LTD. DNP was synthesized as described below. 1,2-Dichloroethane was of analytical reagent grade and used as received. Other reagents used were of the best available quality.

Synthesis of DNP. *p-tert*-Octylphenol (5.0 g) was dissolved in a mixture of chloroform (25 ml) and acetic acid (25 ml). Concentrated nitric acid (4 ml) was added dropwise with stirring at room temperature. The mixture was stirred for 30 min, then diluted with 50 ml of chloroform and washed with distilled water. The chloroform layer was dried and evaporated, and the residue was purified by passage through a silica gel column with chloroform as eluent. Yellow crystals yield 4.8 g (67%), mp 48—49 °C. Found: C, 56.76; H, 6.73; N, 9.41%. Calcd for ($C_{14}H_{20}N_2O_5$): C, 56.75; H, 6.80; N, 9.45%. H NMR ($CDCl_3$) δ=0.80 (9H, CH_3), 1.45 (6H, CH_3), 1.78 (2H, $-CH_2-$), 8.18 (2H, aromatic H).

Properties of DNP. DNP is sparingly soluble in water and readily soluble in organic solvents. The absorption spectrum of DNP in 1,2-dichloroethane shows a maximum at 360 nm, with a molar absorptivity at this wavelength of 6500 $dm^3\,mol^{-1}\,cm^{-1}$. The deprotonated anion in dichloroethane shows an absorption maximum at 460 nm with a molar absorptivity of 8500 $dm^3\,mol^{-1}\,cm^{-1}$. The proton dissociation constant of DNP (HL) was determined photometrically to be $10^{-4.5}$ in a 1: 3 (v/v) dioxane: water mixture.

Extraction Study. An aqueous solution (7 ml) containing 0.10 mol dm^{-3} alkaline earth metal salt and a pH buffer (diethanolamine-HCl) was placed in a 50-ml glass stoppered centrifuge tube. To this was added 7 ml of 1,2-dichloroethane containing 6×10^{-6}—1×10^{-4} mol dm^{-3} PEGP (or DCH18C6) and 5×10^{-6}—1×10^{-4} mol dm^{-3} DNP. The aqueous and organic solutions were equilibrated by shaking for 20 min at 25 °C. The tube was centrifuged for phase separation (3000 rpm for 15 min). The absorbances of both the organic and the aqueous phases were measured at 300-450 nm on a double beam spectrophotometer (Hitachi UV-200 type) in a 10 mm quartz cell.

Results and Discussion

The extraction equilibrium may be formulated by the following general reaction:

$$M^{2+} + n(PEGP)_o + m(HL)_o + (2-m)X^- \rightleftharpoons (M(PEGP)_nL_mX_{2-m})_o + mH^+ \quad (1)$$

where the suffix "o" refers to the species in the organic phase. The overall extraction constant K_{ex} is then defined by Eq. 2, which can be rewritten in a logarithmic form by Eq. 3, where D stands for the conventional distribution ratio of the metal ion between the two phases.

$$K_{ex} = \frac{[M(PEGP)_nL_mX_{2-m}]_o[H^+]^m}{[M^{2+}][PEGP]_o^n[HL]_o^m[X^-]^{2-m}} \quad (2)$$

$$\log D = n\log[PEGP]_o + m\log[HL]_o - m\log[H^+] + (2-m)\log[X^-] + \log K_{ex} \quad (3)$$

The special case where $m=1$, the ratio (Q) of the dissociated (L^-) and undissociated (HL) phenol concentrations in the organic phase is given by Eq. 4 in logarithmic form.

$$\log Q = \log\frac{[M(PEGP)_nLX]_o}{[HL]_o} = -\log[H^+] + n\log[PEGP]_o + \log[X^-] + \log[M^{2+}] + \log K_{ex}. \quad (4)$$

Both the D and Q values are readily obtained experimentally under various extraction conditions.

Figure 1 shows the dependence of the log Q values on the pH. As the pH of the aqueous phase is increased, the fraction of the L^- species or the extent of metal extraction increases, due to the facilitated dissocitation of HL. The extractability among alkaline earth metal ions decreases in the order $Ba^{2+}>Sr^{2+}>Ca^{2+}\gg Mg^{2+}$. The extraction of magnesium ion is negligibly small and hence is not shown in Fig. 1. In accordance with Eq. 4, all plots in Fig. 1 give straight lines having a slope of 1.0. This means that only one molecule of L^- is involved in the metal species extracted.

The dashed line in Fig. 1 indicates the extraction of calcium chloride with DNP alone (i.e., in the absence of PEGP). In this case, it is probable that DNP anion L^- acts as a bidentate chelating ligand to occupy the two coordination sites on calcium. It is interesting that here again the slope of the plot is 1.0, indicating that an anionic species (most probably Cl^-) other than L^- is involved in the extracted calcium species. This is probably related to the present extraction conditions, i.e., the presence of a large excess of metal chloride salt in aqueous solution as compared with a spectrometric concentration of the extractant phenol in the organic phase. The metal extraction ability of DNP when used by itself is poor, and calcium shown in Fig. 1 is the most easily extractable among the alkaline earth metals.

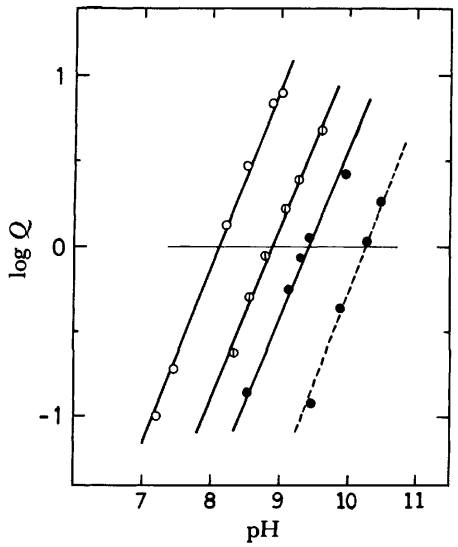

Fig. 1. Influence of pH on log Q for extraction of alkaline earth metal ions. Concentrations before equilibration: organic phase, $[PEGP]_o=5.0\times10^{-4}$ mol dm^{-3}, $[DNP]_o=6.9\times10^{-5}$ mol dm^{-3}; aqueous phase, $[MCl_2]=0.12$ mol dm^{-3}.
○, Ba^{2+}; ⊕, Sr^{2+}; ●, Ca^{2+}; dashed line, Ca^{2+} in the absence of PEGP.

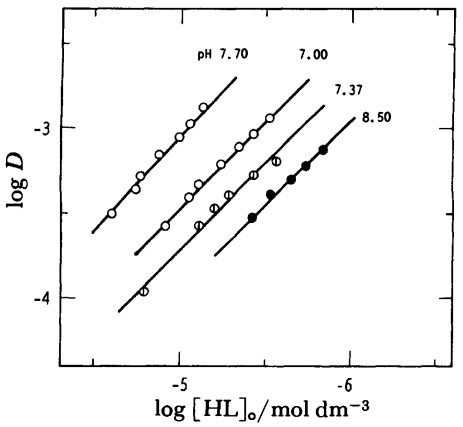

Fig. 2. Plots of distribution ratio (log D) against log $[HL]_o$ at constant pH. $[HL]_o$ stands for free DNP in organic phase. Concentrations before equilibration: organic phase, $[PEGP]_o=0.005$ mol dm^{-3}, $[DNP]_o=5.0\times10^{-6}$—1×10^{-4} mol dm^{-3}; aqueous phase, $[M(ClO_4)_2]=0.10$ mol dm^{-3}.
○, Ba^{2+}; ⊕, Sr^{2+}; ●, Ca^{2+}.

That the extracted species contain equimolecular amounts of metal ion and DNP anion has also been confirmed by the metal extraction at varying DNP concentration and constant pH. The results are shown in Fig. 2, where log D is plotted against log $[DNP]_o$. A linear relationship with a slope of 1.0 was obtained in every case.

Figure 3 shows the dependence on the concentration of PEGP for the extraction of alkaline earth metal ions.

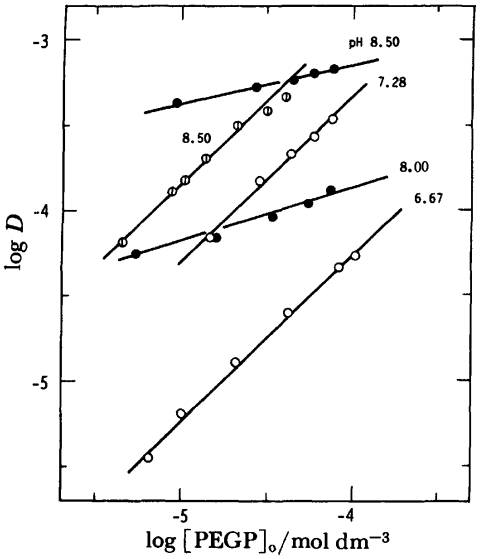

Fig. 3. Plots of distribution ratio (log D) against log [PEGP]$_0$ at constant pH. Concentrations before equilibration: organic phase, [DNP]$_0$=5.0×10^{-4} mol dm^{-3}, [PEGP]$_0$=6.0×10^{-6}—10^{-4} mol dm^{-3}; aqueous phase, [MCl_2]=0.10 mol dm^{-3}. ○, Ba^{2+}; ⊙ Sr^{2+}; ●, Ca^{2+}.

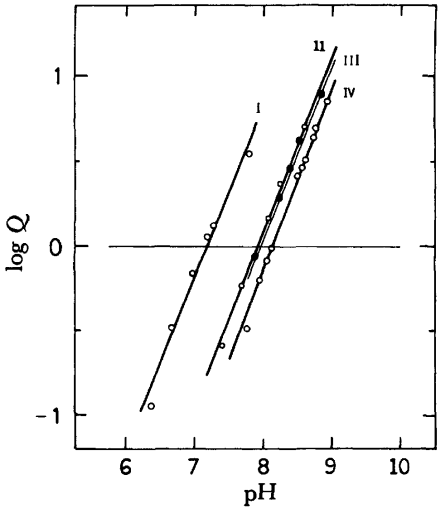

Fig. 4. Influence of pH on log Q for extraction of barium salts. Concentrations before equilibration: organic phase, [PEGP]$_0$=5.0×10^{-4} mol dm^{-3}, [DNP]$_0$=6.9×10^{-5} mol dm^{-3}; aqueous phase, [$Ba(ClO_4)_2$]=0.10 mol dm^{-3} (I), [$Ba(SCN)_2$]=0.087 mol dm^{-3} (II), [BaI_2]=0.103 mol dm^{-3} (III), [$Ba(NO_3)_2$]=0.101 mol dm^{-3} (IV).

The distribution of metal ions increases linearly with an increase in the concentration of PEGP. The slope of the plot of log D against log [PEGP]$_0$ gives a value for n in Eq. 3. As can be seen in Fig. 3, the values of the slopes for barium and strontium ions are 1.0, which indicates that both ions react with PEGP to form complexes having a composition of metal ion to PEGP ratio of 1 to 1. Considering the conformation suggested for the polyethylene glycol complex,[7,8] it is possible that the complexes in the present study assume a similar helical conformation.

On the other hand, the dependence of the calcium extraction on the PEGP concentration is different from that of barium and strontium ions; the slopes for calcium ion are 0.32 and 0.23 at pH 8.0 and 8.5 respectively (Fig. 3). The difference seems to arise from the difference in solvation by water for these ions. The calcium ion is strongly hydrated, so that the water molecule coordinated to the calcium ion are not replaced effectively by PEGP molecules, while both barium and strontium ions are easily encircled by the oxygen atoms of the poly(oxyethylene) chain in PEGP by replacing the hydration water molecules.

Finally, the effect of inorganic anions was investigated for the extraction of barium. The results are shown in Fig. 4, where log Q is plotted against pH. The extraction is influenced by the nature of the inorganic anion present in the aqueous phase. The extractability decreases in the order ClO_4^->SCN^->I^->Cl^->NO_3^-. The sequence is comparable with that observed for the extraction of alkali metal ions with poly (oxyethylene) derivatives[1] and DCH18C6.[9] The sequence is also compatible with the crystal ionic radius for these anions.[10] As may be expected, the bulkier anions are less hydrophilic and therefore promoted to be transferred into the organic phase. The effect of pH on log Q for various barium salts are similar, and a good linear relationship between pH and log Q (slope, 1.0) holds for each metal salt, as is expected from Eq. 4. This fact indicates that a barium ion is accompanied by an in oganic anion as well as by a DNP anion when extracted into the organic phase.

Based on the experimental results obtained above, the overall extraction constants for alkaline earth metal ions were calculated. The results are summarized in Table 1. Recently, Motomizu et al.[11] reported the extraction constants of inorganic anions with the Zephilamine cation. By comparing the extraction constants obtained in the present study with those reported, it is revealed that the difference among the extraction constants for the accompanied inorganic anions (in barium extraction) is very small in this study. The separation factor between perchlorate and chloride is only 6.3 in the present study, in contrast to about 1000 in the extraction with Zephilamine. From the investigation on the effect of organic anion on the extractability of sodium, potassium and calcium ions with DCH18C6, Jawaid et al.[12] concluded that the efficiency of the extraction increases with the hydrohobicity of the counter anion, while the selectivity among the accompanied anions decreases. The low anion selectivity in the present study is probably due to the high lipophilicity of DNP anion which plays a dominant role on the nature of the ion-pair complex formed in the organic phase.

In contrast to the ion-pair complex with the quater-

Table 1. Extraction of Alkaline Earth Metal Salts by DNP at 25°C. $-\log K_{ex}$[a)]

Neutral extractant	$Ba(ClO_4)_2$	$Ba(SCN)_2$	BaI_2	$Ba(NO_3)_2$	$BaCl_2$	$SrCl_2$	$Sr(ClO_4)_2$	$CaCl_2$
PEGP	2.2	2.8	2.9	3.1	3.0	3.6	3.1	(7.6)[b)]
DCH18C6	—	—	—	—	3.1	3.6	—	4.4

a) K_{ex} in $mol^{-2}dm^6$ according to Eq. 2. b) Composition of extracted species is Ca^{2+}:10PONPE:DNP:X^-=1:(0.2—0.3):1:1.

nary ammonium ion where there can be no direct chemical bond between the cationic center and anion, it is also possible that ion-pair complex in the present study can involve some kind of direct coordinate bond between the metal center and the accompanied anion X^-. Such a bond formation would be favored between a hard acid (alkaline earth metal ion) and a hard base (Cl^-), and helps to enhance the extractability of a chloro complex rather than an iodo or thiocyanato complex. This leads to a lowered extraction selectivity between lipophilic and hydrophilic anions. The importance of direct interaction between the alkali metal cation and the anionic group is well documented in the extraction of crown ether complexes.[13)]

In Table 1, the extraction constants with DCH18C6 are also shown. These constants were calculated on the assumption that the extraction of alkaline earth metal ions with the crown ether proceeds by the same mechanism as the extraction with PEGP. The validity of the assumption was partly justified by the plots of log Q against pH, which indicated linear relationships with a slope of 1.0 (Eq. 4). It can be seen that the extraction constants for barium and strontium ions with PEGP are close to those with DCH18C6. The similarity suggests that the extraction is governed by the nature of the counter anion rather than that of the neutral ligand, PEGP. An extracted metal species contains generally

In summary, DNP is an effective extractant for alkaline earth metal ions when used in combination with PEGP. An extracted metal species contains generally one molecule each of deprotonated DNP, inorganic monoanion, and PEGP. The extractability of the metal complex follows the order of the lipophilicity of the ions: $Ba^{2+}>Sr^{2+}>Ca^{2+}\gg Mg^{2+}$ and $ClO_4^-> SCN^->I^->Cl^->NO_3^-$. The present study, however, is limited by the use of a spectrophotometric concentration measurement ($<5\times10^{-4}$ mol dm^{-3}) of DNP and a similar concentration of PEGP. Extraction at much higher reagent concentration is still open to further research.

References

1) S. Yanagida, K. Tanaka, and M. Okahara, *Bull. Chem. Soc. Jpn.*, **50**, 1386 (1977).
2) A. M. Y. Jaber, G. J. Moody, and J. D. R. Thomas, *J. Inor. Nucl. Chem.*, **39**, 1689 (1977).
3) L. Favretto, B. Stancher, and F. Tunis, *Analyst*, **101**, 241 (1979).
4) L. Favretto and F. Tunis, *Analyst*, **101**, 198 (1976).
5) L. Favretto, B. Stancher, and F. Tunis, *Analyst*, **103**, 955 (1978); **105**, 1254 (1978).
6) M. Takagi, "Fundamentals of Carrier-mediated Transport," in "Fundamentals of Membrane Technology," ed by the Japan Society of Membrane Science, Kitami Shobo, Tokyo (1983), pp. 73—82.
7) D. L. Hughes, C. L. Mortimer, D. G. Parsons, M. R. Truter, and J. N. Wingfield, *Inorg. Chim. Acta*, **21**, L23 (1977).
8) Y. Hirashima, K. Kanetsuki, J. Shiokawa, and N. Tanaka, *Bull. Chem. Soc. Jpn.*, **54**, 1567 (1981).
9) Y. Takeda, "The Solvent Extraction of Metal Ions by Crown Compounds" in "Host Guest Complex Chemistry III" in "Topics in Current Chemistry," ed by F. L. Boschke, Springer-Verlag, Berlin (1984), Vol. 121, pp. 1—38.
10) R. Kiriyama and H. Kiriyama, "Kouzou Mukikagaku I," Kyoritsu Shuppan, Tokyo (1977), p. 239.
11) S. Motomizu, S. Hamada and K. Toei, *Bunseki Kagaku*, **32**, 649 (1983).
12) M. Jawaid and F. Ingman, *Talanta*, **25**, 91 (1978).
13) M. Takagi and K. Ueno, "Crown Compounds as Alkali and Alkaline Earth Metal Ion Selective Chromogenic Reagents" in "Host Guest Complex Chemistry III" in "Topics in Current Chemistry," ed by F. L. Boschke, Springer-Verlag, Berlin (1984), Vol. 121, pp. 39—65.

Cobalt(III)-Peroxo Complexes Containing 1,2-Bis(dimethylphosphino)ethane (dmpe) or 1,3-Bis(dimethylphosphino)propane (dmpp). Molecular Structures of $[Co(O_2)(dmpe)_2]B(C_6H_5)_4$ and $[Co(O_2)(dmpp)_2]BF_4 \cdot H_2O$

Tomoji Ohishi, Kazuo Kashiwabara, Junnosuke Fujita,* Shigeru Ohba,† Toshio Ishii,†† and Yoshihiko Saito†
Department of Chemistry, Faculty of Science, Nagoya University, Chikusa-ku, Nagoya 464
†Department of Chemistry, Faculty of Science and Technology, Keio University, Hiyoshi 3, Kohoku-ku, Yokohama 223
††Chiba Institute of Technology, Tsudanuma 2, Narashino, Chiba 275
(Received September 6, 1985)

Monomeric (yellow) and dimeric (red) cobalt(III)-dioxygen complexes containing 1,2-bis(dimethylphosphino)ethane (dmpe) have been prepared from $[Co(dmpe)_2]^+$ and $[Co(dmpe)_2]^{2+}$, respectively, by air oxidation. The 1,3-bis(dimethylphosphino)propane (dmpp) complex afforded only the monomeric dioxygen complex by either preparative method. The crystal structures of $[Co(O_2)(dmpe)_2]B(C_6H_5)_4$ (**1**) and $[Co(O_2)(dmpp)_2]BF_4 \cdot H_2O$ (**2**) have been determined by X-ray analysis. Crystal data for **1**; monoclinic, $P2_1/a$, a=18.011(12), b=18.761(10), c=11.455(6) Å, β=107.78(4)°, V=3686(4) Å^3, Z=4, and R=0.064. Crystal data for **2**; orthorhombic, $Pbcn$, a=14.540(5), b=13.123(4), c=13.138(2) Å, V=2507(1) Å^3, Z=4, and R=0.076. The complex ions in both **1** and **2** have a trigonal-bipyramidal coordination geometry when the O_2 group bonded to the Co atom in the side-on form at a coordination site of the trigonal plane is assumed to be a unidentate ligand. Bond lengths, Co–O (1.858(7)—1.881(4) Å) and O–O (1.414(12) and 1.425(6) Å), and O–O stretching frequencies (877 and 862 cm^{-1}) indicate that both **1** and **2** are the peroxo complexes. The monomeric dioxygen complexes react immediately with SO_2 and with concd HCl to afford $[Co(SO_4)(dmpe \text{ or } dmpp)_2]^+$ and *cis*-$[CoCl_2(dmpe \text{ or } dmpp)_2]^+$, respectively. The red dimeric *trans*-$[(dmso)(dmpe)_2Co(\mu\text{-}O_2)Co(dmpe)_2(dmso)](BF_4)_4$ (dmso=dimethyl sulfoxide) complex was isolated and characterized.

Only a few monomeric cobalt(III)-dioxygen complexes have been known, in contrast to a large number of dimeric cobalt(III)-dioxygen complexes.[1] Vaska et al.[2,3] prepared $[Co(O_2)(dpee)_2]^+$ (dpee=*cis*-$(C_6H_5)_2PCHCHP(C_6H_5)_2$) and determined the molecular structure by X-ray analysis. Gray et al.[4] studied the chemical properties, formation mechanisms, and absorption spectra of this complex in some detail. In the present paper, we report new complexes of the same type, $[Co(O_2)(dmpe \text{ or } dmpp)_2]^+$ (dmpe=$(CH_3)_2PCH_2CH_2P(CH_3)_2$, dmpp=$(CH_3)_2PCH_2CH_2CH_2P(CH_3)_2$). These new complexes are highly reactive to SO_2 and HCl to afford $[Co(SO_4)(dmpe \text{ or } dmpp)_2]^+$ and *cis*-$[CoCl_2(dmpe \text{ or } dmpp)_2]^+$, respectively, while $[Co(O_2)(dpee)_2]^+$ is unreactive to SO_2 and much less reactive to HCl. In order to examine their different reactivities, we have determined the molecular structures of $[Co(O_2)(dmpe)_2]^+$ and $[Co(O_2)(dmpp)_2]^+$ and compared them with that of $[Co(O_2)(dpee)_2]^+$. A new dimeric cobalt(III)-dioxygen complex, *trans*-$[(dmso)(dmpe)_2Co(\mu\text{-}O_2)Co(dmpe)_2(dmso)]^{4+}$, and two related complexes, $[Co(CO_3)(dmpe)_2]^+$ and *trans*-$[Co(H_2O)_2(dmpe)_2]^{3+}$ are also described. A preliminary report on $[Co(O_2)(dmpe)_2]^+$ has been published.[5]

Experimental

The dmpe[6] and dmpp[7] ligands were prepared according to the literatures and handled under a nitrogen atmosphere until they formed cobalt(III) complexes. All solvents used for the preparations were deoxygenated by bubbling nitrogen for 20 min immediately before use. Absorption, ^{1}H NMR and IR spectra were recorded on a Hitachi 323 spectrophotometer, a Jeol JNM-PMX 60 spectrometer and a Jasco A-3 spectrophotometer, respectively.

Preparation of Complexes. $[Co(O_2)(dmpe)_2]BF_4$ and $[Co(O_2)(dmpe)_2]B(C_6H_5)_4$ (1). The complexes were prepared by the methods reported in a previous paper.[5]

$[Co(^{18}O_2)(dmpe)_2]BF_4$. The complex was prepared by a method similar to that for $[Co(O_2)(dmpe)_2]BF_4$.[5] The complex was yielded by exposing an ethanol solution of $[Co(dmpe)_2]^+$ to $^{18}O_2$ gas (Prochem. Co., 99% pure), instead of bubbling air.

$[Co(O_2)(dmpp)_2]BF_4 \cdot H_2O$ (2). Method a). To an ethanol solution (50 cm^3) of $Co(BF_4)_2 \cdot 6H_2O$ (588 mg, 1.73 mmol) was added an ethanol solution (5 cm^3) of dmpp (707 mg, 4.31 mmol) with stirring. After stirring for 30 min, air was bubbled into the solution for 10 h. A small amount of a white precipitate (probably the phosphine oxide) was filtered off, and the filtrate was concentrated to ca. 10 cm^3 under reduced pressure. The concentrate was chromatographed using a column (ϕ 2.5 cm×20 cm) of Toyopearl TSK-GEL. By elution with ethanol, a yellow and a pink ($Co(BF_4)_2$) band appeared. The eluate containing the yellow band was collected and concentrated to ca. 20 cm^3 under reduced pressure. To the concentrate was added diethyl ether (50 cm^3), and the solution was allowed to stand at −10 °C for 10 h, yielding yellow-orange crystals which were filtered and air-dried. Yield: 384 mg(43%). Found: C, 31.79; H, 7.28%. Calcd for $C_{14}H_{38}BCoF_4O_3P_4$: C, 32.09; H, 7.30%.

Method b). The same dmpp dioxygen complex was also yielded by a method similar to that for the dmpe complex.[5] To an ethanol solution (50 cm^3) of $Co(BF_4)_2 \cdot 6H_2O$ (1.37 g, 3.71 mmol) was added an ethanol solution (5 cm^3) of dmpp (1.06 g, 6.45 mmol) with stirring. After 1 h an ethanol solution (3 cm^3) of $NaBH_4$(140 mg, 3.71 mmol) was added to the solution. The solution was stirred for 30 min, and then air was bubbled into the solution for 10 h. The resulting solution was concentrated to ca. 10 cm^3, yielding a yellow precipitate. It was dissolved in ethanol (10 cm^3), diethyl ether (30 cm^3) was added, and the solution was allowed to stand at −10 °C for 10 h to give yellow-orange crystals. Yield: 660 mg(35%).

The complex is soluble in ethanol and acetonitrile. It is also soluble in water, but slowly decomposes to give Co(II)

species.

[(dmso)(dmpe)$_2$Co(μ-O$_2$)Co(dmpe)$_2$(dmso)](BF$_4$)$_4$. Air was bubbled into a dimethyl sulfoxide (dmso) solution (30 cm^3) of [Co(dmpe)$_2$](BF$_4$)$_2$[5] (1.06 g, 1.99 mmol) for 10 h. A red precipitate was obtained, filtered, and dissolved in dmso (5 cm^3). The solution was chromatographed with a column (ϕ 2.5 cm×20 cm) of Toyopearl TSK-GEL. By elution with dmso, a main red and a minor yellow (probably [Co(dmpe)$_2$]$^{2+}$) bands developed. The eluate containing the red band was collected and mixed with ethanol to give a red precipitate. It was filtered, washed with a mixture of ethanol and diethyl ether (1:1), and air-dried. Yield: 460 mg(37%). Found: C, 26.93; H, 6.28; P, 20.43%. Calcd for $C_{14}H_{38}B_2CoF_8O_2P_4S$: C, 26.82; H, 6.11; P, 19.76%. The complex is soluble in dmso, but hardly in other common solvents such as water or ethanol.

[Co(CO$_3$)(dmpe)$_2$]ClO$_4$·1.5NaClO$_4$·H$_2$O. To *trans*-[CoCl$_2$(dmpe)$_2$]ClO$_4$[8] (840 mg, 1.6 mmol) in a mixture (100 cm^3) of methanol and water (2:1) was added K_2CO_3(335 mg, 2.42 mmol) in water (2 cm^3). The color of the solution immediately changed from blue to orange-yellow. After stirring for 4 h, the solution was diluted with water (2 dm^3) and applied on a column (ϕ 5 cm×20 cm) of SP-Sephadex C-25. The column was washed thoroughly with water, and the adsorbed product was eluted with 0.2 mol dm^{-3} NaClO$_4$ to give a main yellow and a small blue band (the starting complex). The eluate containing the yellow band was collected and concentrated to ca. 30 cm^3 under reduced pressure. Further concentration was carried out in a desiccator over P_4O_{10} to afford yellow crystals, which were filtered, washed with a mixture (50 cm^3) of methanol and diethyl ether (1:1), and air-dried. Yield: 940 mg(80%). Found: C, 21.03; H, 5.38%. Calcd for $C_{13}H_{34}Cl_{2.5}CoNa_{1.5}O_{14}P_4$: C, 21.15; H, 4.91%. The complex is soluble in water, methanol and ethanol, but not in diethyl ether.

***trans*-[Co(H$_2$O)$_2$(dmpe)$_2$](ClO$_4$)$_3$·2H$_2$O.** To an aqueous solution (20 cm^3) of [Co(CO$_3$)(dmpe)$_2$]ClO$_4$·1.5NaClO$_4$·H$_2$O (2.19 g, 2.97 mmol) was added dropwise 60% perchloric acid (5 cm^3) with stirring. The solution was warmed at 50 °C for 2 h, and then concentrated slowly in a desiccator over P_4O_{10} to yield red crystals, which were filtered, washed with a mixture (100 cm^3) of ethanol and diethyl ether (1:1), and air-dried. Yield: 1.85 g(86%). Found: C, 19.52; H, 5.22%. Calcd for $C_{12}H_{40}Cl_3CoO_{16}P_4$: C, 19.76; H, 5.53%. The complex decomposes slowly to cobalt(II) species in neutral water, although it is stable in water acidified with HClO$_4$. This complex was assigned to the trans isomer from the ^{1}H NMR spectrum.

Reaction of [Co(O$_2$)(dmpe or dmpp)$_2$]$^+$ with SO$_2$. SO_2 gas was bubbled into an ethanol solution (50 cm^3) of [Co(O$_2$)(dmpe)$_2$]BF$_4$ (100 mg, 0.2 mmol) for 10 min. The color of the solution changed immediately from yellow to red-orange. The solution was concentrated to ca. 5 cm^3. On addition of diethyl ether (30 cm^3) the concentrate afforded an orange precipitate, which was filtered and dissolved in a mixture (2 cm^3) of acetonitrile and ethanol (1:1). The solution was applied on a column (ϕ 1.5 cm×20 cm) of Toyopearl TSK-GEL, and the adsorbed product was eluted with a mixture of acetonitrile and ethanol (1:5). The eluate containing the orange band was collected and concentrated to ca. 5 cm^3 under reduced pressure. To the concentrate was added diethyl ether (20 cm^3), and the mixture was allowed to stand at −10 °C for 10 h, yielding orange crystals of [Co(SO$_4$)(dmpe)$_2$]BF$_4$·2H$_2$O, which were filtered and washed with a mixture (20 cm^3) of diethyl ether and ethanol (2:1). Yield: 80 mg(70%). Found: C, 24.97; H, 6.31%. Calcd for $C_{12}H_{36}BCoF_4O_6P_4S$: C, 24.93; H, 6.28%. The complex was identical with that prepared from *trans*-[Co(H$_2$O)$_2$(dmpe)$_2$](ClO$_4$)$_3$·2H$_2$O and Na_2SO_4.

The [Co(O$_2$)(dmpp)$_2$]BF$_4$·H$_2$O complex reacted similarly with SO_2 to afford [Co(SO$_4$)(dmpp)$_2$]BF$_4$. Yield: 52%. Found: C, 29.46; H, 5.81%. Calcd for $C_{14}H_{36}BCoF_4O_4P_4S$: C, 29.49; H,

Table 1. Experimental Conditions and Refinement Details

	1	2
Chemical formula	[Co(O$_2$)(C$_6$H$_{16}$P$_2$)$_2$][B(C$_6$H$_5$)$_4$]	[Co(O$_2$)(C$_7$H$_{18}$P$_2$)$_2$]BF$_4$·H$_2$O
Formula weight	710.5	524.1
Density, D$_x$ and D$_m$ (Mg m^{-3})	1.28, 1.25(2)	1.38, 1.41(2)
μ(Mo $K\alpha$) (mm^{-1})	0.664	0.969
Habit of crystals	Thin tabular (100)	Prisms surrounded by (100), (011), and (00$\bar{1}$)
Size of specimen (mm^3)	0.1×0.5×0.5	0.4×0.5×0.6
Number of reflections and 2θ range (°) for measuring lattice parameters	20 23<2θ<31	25 40<2θ<45
2θ_{max} (°)	55	55
Range of h, k, and l	−21≦h≦18, 0≦k≦19, 0≦l≦12	0≦h≦20, 0≦k≦17, 0≦l≦18
Systematic absences	$h0l$, h odd; $0k0$, k odd	$hk0$, $h+k$ odd; $h0l$, l odd; $0kl$, k odd
Variation of $\|F_o\|$ of n standard reflections, $\sum(\|F_o\|/\|F_o\|_{initial})/n$	n=3 0.96—1.00	n=5 0.94—1.00
Number of reflections measured	12127	3530
Number of unique reflections observed [$\|F_o\|>3\sigma(\|F_o\|)$]	2421	2346
Absorption correction	No	0.630≦transmission factor≦0.694
R	0.064	0.076
wR	0.068	0.119
$w^{-1}=\sigma^2(\|F_o\|)+(c\|F_o\|)^2$	c=0.015	c=0.03
S	2.4	3.2
$(\Delta\rho)_{min}$ and $(\Delta\rho)_{max}$ in final difference synthesis (e Å^{-3})	−0.63, 0.62	−1.0, 1.6
$(\Delta/\sigma)_{max}$	0.5	0.8

6.36%.

Reaction of $[Co(O_2)$(dmpe, dmpp, or dpee)$_2]^+$ with concd HCl. Both solid and dissolved $[Co(O_2)$(dmpe or dmpp)$_2]^+$ in ethanol reacted immediately with concd HCl at 0 °C to afford red *cis*-$[CoCl_2$(dmpe or dmpp)$_2]^+$. The same *cis*-dichloro complexes were prepared from $[Co(CO_3)$(dmpe or dmpp)$_2]^+$ with concd HCl.[9] The $[Co(O_2)$(dpee)$_2]^+$ complex reacted slowly with concd HCl at 0 °C to give a mixture of red *cis*-and green *trans*-$[CoCl_2$(dpee)$_2]^+$. The relative yield of the trans isomer increased with the reaction temperature. The $[Co(CO_3)$(dpee)$_2]ClO_4$ complex[4] afforded only the *trans*-dichloro complex by reaction with concd HCl even at below 0 °C.[9]

Crystal Structure Determination. Experimental conditions are listed in Table 1. Densities of the crystals were measured by flotation in aqueous solutions of KI. Intensity measurements were performed by a Rigaku AFC-5 four-circle diffractometer with Mo $K\alpha$ radiation (λ=0.70926 Å) monochromatized by a graphite plate. A crystal of **2** was sealed in a glass capillary with the mother liquid. The space group was uniquely determined from the Laue group and systematic absences. The intensity of reflections of **1** decreased rapidly with 2θ, and most of the reflections with $2\theta>40°$ were not observed. Corrections were made for Lorentz and polarization effects. Absorption correction was applied for **2** but not for **1**. The position of Co was deduced from the Patterson function, but the structure of **1** could not be solved by the heavy atom method because the location of Co near y=0 or 1/2 lacked the phase-determining power for reflections with $h+k$ odd in the case of $P2_1/a$. The structure was solved by direct methods with MULTAN78.[10] Starting with the positions of Co, four P and O atoms, those of the other non-hydrogen atoms were determined from the Fourier synthesis and refined by block-diagonal least-squares with anisotropic thermal parameters using UNICS III computation program system.[11] The function minimized was $\sum w||F_o|-|F_c||^2$. Complex neutral-atom scattering factors were taken from International Tables for X-Ray Crystallography.[12] The positions of 8 among 52 H atoms were found on the difference synthesis and others were calculated. Final R was 0.064 for 2421 observed unique reflections.[13] The atomic parameters of the non-hydrogen atoms are presented in Table 2.

The general position of space group *Pbcn* is eightfold. The Co atom of **2** must be on the fourfold position. Consequently the Co atom must lie on the twofold axis, because the complex does not have a center of symmetry. The position of the Co atom was deduced from the Patterson function and the orientation of the CoO_2P_4 octahedron around the twofold axis was determined by the R factor method, where the geometry of **1** was utilized. All of non-hydrogen atoms were found on the Fourier synthesis and all the H atoms except those of the water molecule were found on the difference synthesis. Positional disorder of the F atoms of BF_4^- was found. The B atom lies on the twofold axis. The population parameters for the two sets of F atoms, (F(1), F(2)) and (F(01), F(02)) were estimated to be 0.7 and 0.3, respectively by the trial and error method in such a way that the isotropic thermal parameters took nearly equal value. The F(01) atom could not be found on the difference synthesis so that it was omitted. Final R was 0.076 for 2346 unique reflections.

Results and Discussion

Preparation. Gray et al.[4] prepared $[Co(O_2)$(dpee)$_2]^+$ by two methods; one is oxidation of $[Co$(dpee)$_2]^+$ with O_2, and the other oxidation of $[Co$(dpee)$_2]^{2+}$ with air. In the present study, either oxidation of $[Co(dmpp)_2]^+$ or $[Co(dmpp)_2]^{2+}$ with air yielded $[Co(O_2)(dmpp)_2]^+$, while $[Co(O_2)(dmpe)_2]^+$ was only formed from $[Co(dmpe)_2]^+$. Oxidation of $[Co$(dmpe)$_2]^{2+}$ with air in dmso afforded a red complex whose chemical composition is $CoO(dmpe)_2(dmso)(BF_4)_2$. The $[Co(O_2)$(dmpe or dmpp)$_2]^+$ complexes are yellow in color and contain the O_2^{2-} group bonded to the Co^{3+} ion in the side-on form (vide infra). The ^{1}H NMR spectrum of the red complex in d_6-dmso is quite similar to that of *trans*-$[CoCl_2(dmpe)_2]^+$ [8] in the region of signals due to dmpe, and shows a singlet signal at 3.37 ppm assignable to the methyl protons of coordinated dmso.[14] In the IR spectrum the complex exhibits a strong band at 917 cm^{-1} which can be assigned to the S–O stretching vibration of dmso coordinated through the oxygen atom.[14] The *trans*-$[CoCl_2(dmpe)_2]^+$ complex shows no strong absorption in this region. Thus we assumed the red complex to be a dimeric μ-peroxo complex where the dmso and μ-peroxo groups occupy the trans positions to each other. No dimeric μ-peroxo cobalt(III) complex is formed with dpee and dmpp. Gray et al.[4] suggested that the dimeric μ-peroxo dpee complex is unstable for steric repulsions of the bulky dpee ligands with a solvent molecule coordinated at the position trans to the μ-peroxo group. The dmpe ligand is less bulky than dpee[15] and may be sterically favorable for formation of the dimeric μ-peroxo complex. The dmpp complex does not form the dimeric μ-peroxo complex. The instability of the dimeric dmpp complex will also be attributable to the steric reasons, since the six-membered dmpp chelate ring should be more bulky than the five-membered dmpe chelate ring and will have larger steric repulsions with other ligands. We have also attempted to prepare the dioxygen complex of 1, 2-bis(dibutylphosphino)ethane (dbpe) by two different methods described above. Both reactions proceeded quite similarly to those for dmpp and afforded only the monomeric dioxygen complex, $[Co(O_2)(dbpe)_2]^+$. The pure complex could not be isolated because the complex was highly soluble in common solvents, but the formation of only the monomer was confirmed by the ^{1}H NMR and absorption spectra. The dimeric μ-peroxo complex of bulky dbpe will also be unstable for steric reasons. Bosnich et al.[16] reported that *o*-phenylenebis(dimethylarsine) (diars) and *meso*- and *rac*-$\{(CH_3)_2AsCH_2CH_2CH_2As(C_6H_5)CH_2-\}_2$ (tetars) form both monomeric peroxo and dimeric μ-peroxo cobalt(III) complexes.

The monomeric dioxygen complexes of dmpe, dmpp and dbpe are stable in organic solvents such as alcohols

Table 2. Fractional Coordinates ($\times 10^4$, $\times 10^5$ for Co, $\times 10^3$ for F) and Equivalent Isotropic Thermal Parameters

	Atom	x	y	z	B_{eq}/Å^2
(1)					
	Co	18531 (8)	49248 (7)	61991 (13)	2.6
	P(1)	1591 (2)	6083 (2)	6184 (3)	3.9
	P(2)	3077 (2)	5234 (2)	6551 (3)	4.6
	P(3)	2000 (2)	3747 (2)	6082 (3)	4.3
	P(4)	1609 (2)	4705 (2)	7935 (3)	4.2
	O(1)	894 (4)	4773 (4)	5009 (7)	4.3
	O(2)	1486 (4)	4972 (4)	4498 (6)	4.3
	C(1)	2404 (8)	6532 (7)	5784 (13)	6.7
	C(2)	3147 (7)	6206 (7)	6591 (18)	9.4
	C(3)	1455 (7)	3338 (6)	7002 (13)	6.1
	C(4)	1677 (8)	3745 (7)	8272 (13)	7.0
	C(5)	726 (7)	6336 (6)	5007 (12)	5.5
	C(6)	1573 (8)	6579 (7)	7520 (13)	6.5
	C(7)	3864 (7)	5003 (8)	7821 (13)	7.4
	C(8)	3425 (8)	4994 (8)	5260 (13)	7.5
	C(9)	2928 (7)	3312 (6)	6647 (14)	7.1
	C(10)	1570 (8)	3378 (6)	4614 (12)	6.0
	C(11)	590 (7)	4891 (7)	7829 (12)	6.2
	C(12)	2157 (8)	5062 (8)	9377 (11)	7.1
	B	4816 (7)	2500 (7)	10023 (12)	3.2
	C(13)	4692 (5)	2958 (5)	11195 (9)	2.6
	C(14)	4203 (6)	3557 (6)	11030 (11)	4.2
	C(15)	4057 (6)	3918 (6)	11969 (11)	4.6
	C(16)	4404 (7)	3712 (6)	13142 (12)	5.0
	C(17)	4889 (7)	3123 (7)	13393 (10)	4.9
	C(18)	5018 (6)	2765 (6)	12372 (9)	3.6
	C(19)	5046 (5)	3052 (5)	9059 (9)	3.0
	C(20)	4910 (6)	2922 (6)	7834 (9)	3.9
	C(21)	5155 (7)	3383 (7)	7047 (11)	6.2
	C(22)	5530 (6)	4001 (6)	7490 (12)	5.2
	C(23)	5675 (7)	4152 (7)	8675 (12)	5.6
	C(24)	5436 (7)	3684 (6)	9454 (10)	4.3
	C(25)	4027 (6)	2062 (5)	9339 (9)	2.7
	C(26)	3291 (6)	2185 (5)	9471 (9)	2.8
	C(27)	2632 (6)	1827 (6)	8834 (10)	3.7
	C(28)	2646 (6)	1294 (6)	7991 (11)	4.2
	C(29)	3367 (6)	1150 (6)	7830 (10)	4.1
	C(30)	4027 (6)	1515 (6)	8470 (10)	3.6
	C(31)	5562 (6)	1968 (5)	10573 (9)	2.9
	C(32)	6338 (6)	2186 (6)	10844 (9)	3.5
	C(33)	6965 (6)	1749 (6)	11422 (11)	4.6
	C(34)	6846 (6)	1067 (6)	11768 (10)	4.5
	C(35)	6085 (7)	831 (6)	11491 (11)	4.7
	C(36)	5454 (6)	1263 (6)	10905 (10)	3.7
(2)					
	Co	50000	16436 (7)	25000	2.5
	B	5000	6228 (11)	2500	6.1
	P(1)	3511 (1)	1481 (1)	2075 (1)	3.3
	P(2)	5244 (1)	2663 (1)	1190 (1)	3.2
	O	4803 (3)	318 (3)	2997 (3)	4.0
	C(1)	2912 (4)	2560 (5)	1499 (5)	4.4
	C(2)	3377 (4)	2982 (5)	555 (4)	4.5
	C(3)	4299 (5)	3510 (5)	794 (5)	4.7
	C(4)	3329 (5)	464 (5)	1156 (5)	4.9
	C(5)	2761 (4)	1136 (6)	3130 (5)	4.8
	C(6)	6169 (5)	3596 (5)	1179 (5)	5.2
	C(7)	5465 (5)	1901 (6)	66 (5)	5.1
	OW	1379 (3)	3649 (4)	3308 (5)	6.8
	F(1)	552 (1)	679 (1)	195 (1)	14.6
	F(2)	433 (1)	582 (1)	184 (1)	14.8
	F(02)	546 (2)	579 (2)	174 (2)	12.2

and acetonitrile, but slowly decompose in water to give cobalt(II) species. No liberation of oxygen from the complexes was observed by bubbling nitrogen into organic solutions of the complexes. Uptake of O_2 is irreversible in these complexes.

Molecular Structure. Perspective drawings of complexes **1** and **2** are shown in Fig. 1. Bond distances and bond angles are listed in Table 3. The dioxygen group in each complex coordinates to the cobalt atom in the side-on form. $[Co(O_2)(dmpe)_2]^+$ **1** has a pseudo twofold axis passing through the Co and the midpoint of the O(1)–O(2) bond axis, and the coordination geometry can be described as a trigonal-bipyramid when the O_2 group is regarded as a unidentate ligand. A similar trigonal-bipyramidal structure was report-

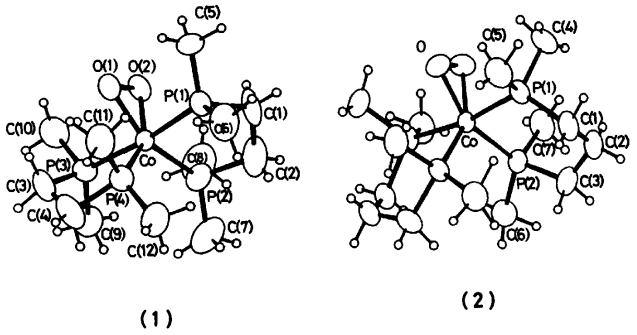

Fig. 1. ORTEP drawings of the complex cations **1** and **2** with thermal ellipsoids scaled at the 50% probability level.[17] H atoms are represented by circles of radius 0.08 Å.

Table 3. Bond Distances (l/Å) and Angles (ϕ/°)

(**1**)							
	Co	-P(1)	2.222(4)	P(1)	-Co	-P(2)	86.7(1)
	Co	-P(2)	2.194(4)	P(1)	-Co	-P(3)	174.4(2)
	Co	-P(3)	2.234(4)	P(1)	-Co	-P(4)	95.1(2)
	Co	-P(4)	2.202(4)	P(1)	-Co	-O(1)	89.8(2)
	Co	-O(1)	1.866(7)	P(1)	-Co	-O(2)	86.5(2)
	Co	-O(2)	1.858(7)	P(2)	-Co	-P(3)	98.1(1)
	P(1)	-C(1)	1.864(16)	P(2)	-Co	-P(4)	110.5(1)
	P(1)	-C(5)	1.785(12)	P(2)	-Co	-O(1)	145.9(2)
	P(1)	-C(6)	1.799(15)	P(2)	-Co	-O(2)	101.3(2)
	P(2)	-C(2)	1.827(14)	P(3)	-Co	-P(4)	85.9(1)
	P(2)	-C(7)	1.747(12)	P(3)	-Co	-O(1)	84.6(2)
	P(2)	-C(8)	1.829(17)	P(3)	-Co	-O(2)	89.7(2)
	P(3)	-C(3)	1.815(16)	P(4)	-Co	-O(1)	103.6(2)
	P(3)	-C(9)	1.794(12)	P(4)	-Co	-O(2)	148.2(2)
	P(3)	-C(10)	1.763(13)	O(1)	-Co	-O(2)	44.6(3)
	P(4)	-C(4)	1.838(14)	Co	-P(1)	-C(1)	105.2(5)
	P(4)	-C(11)	1.835(14)	Co	-P(1)	-C(5)	113.6(4)
	P(4)	-C(12)	1.776(12)	Co	-P(1)	-C(6)	123.9(5)
	O(1)	-O(2)	1.414(12)	C(1)	-P(1)	-C(5)	105.3(6)
	C(1)	-C(2)	1.50(2)	C(1)	-P(1)	-C(6)	101.2(7)
	C(3)	-C(4)	1.58(2)	C(5)	-P(1)	-C(6)	105.4(6)
				Co	-P(2)	-C(2)	109.0(4)
				Co	-P(2)	-C(7)	127.0(4)
				Co	-P(2)	-C(8)	111.1(5)
				C(2)	-P(2)	-C(7)	101.2(6)
				C(2)	-P(2)	-C(8)	103.2(7)
				C(7)	-P(2)	-C(8)	102.7(7)
				Co	-P(3)	-C(3)	106.8(5)
				Co	-P(3)	-C(9)	122.9(4)
				Co	-P(3)	-C(10)	114.8(4)
				C(3)	-P(3)	-C(9)	102.0(6)
				C(3)	-P(3)	-C(10)	103.3(6)
				C(9)	-P(3)	-C(10)	104.7(6)
				Co	-P(4)	-C(4)	110.7(5)
				Co	-P(4)	-C(11)	112.1(4)
				Co	-P(4)	-C(12)	124.1(4)
				C(4)	-P(4)	-C(11)	101.6(6)
				C(4)	-P(4)	-C(12)	101.1(6)
				C(11)	-P(4)	-C(12)	104.5(6)
				Co	-O(1)	-O(2)	67.4(4)
				Co	-O(2)	-O(1)	68.0(5)
				P(1)	-C(1)	-C(2)	106.5(9)
				P(2)	-C(2)	-C(1)	110.4(9)
				P(3)	-C(3)	-C(4)	107.5(8)
				P(4)	-C(4)	-C(3)	107.3(9)

Table 3. (Continued)

(2)							
	Co	-P(1)	2.246(2)	P(1)	-Co	-P(2)	91.1(1)
	Co	-P(2)	2.208(2)	P(1)	-Co	-O	81.5(1)
	Co	-O	1.881(4)	P(2)	-Co	-O	148.8(1)
	P(1)	-C(1)	1.827(7)	Co	-P(1)	-C(1)	119.3(2)
	P(1)	-C(4)	1.819(7)	Co	-P(1)	-C(4)	112.0(2)
	P(1)	-C(5)	1.821(7)	Co	-P(1)	-C(5)	114.3(2)
	P(2)	-C(3)	1.842(7)	C(1)	-P(1)	-C(4)	103.0(3)
	P(2)	-C(6)	1.819(7)	C(1)	-P(1)	-C(5)	102.9(3)
	P(2)	-C(7)	1.812(7)	C(4)	-P(1)	-C(5)	103.6(3)
	C(1)	-C(2)	1.517(8)	Co	-P(2)	-C(3)	117.8(2)
	C(2)	-C(3)	1.541(9)	Co	-P(2)	-C(6)	122.2(2)
	O	-O′	1.425(6)	Co	-P(2)	-C(7)	109.2(2)
				C(3)	-P(2)	-C(6)	98.2(3)
				C(3)	-P(2)	-C(7)	103.6(3)
				C(6)	-P(2)	-C(7)	103.5(3)
				P(1)	-C(1)	-C(2)	114.2(4)
				C(1)	-C(2)	-C(3)	112.7(5)
				P(2)	-C(3)	-C(2)	115.8(4)
				P(1)	-Co	-P(1′)	169.1(1)
				O	-Co	-O′	44.6(2)
				P(2)	-Co	-P(2′)	105.5(1)

ed for $[Co(O_2)(dpee)_2]^+$.[3] The O_2 ligand and P(2) and P(4) atoms form an equatorial plane, to which the P(1)-Co-P(3) axis is approximately perpendicular. The P(2) and P(4) atoms deviate by 0.03 and −0.02 Å, respectively from the plane formed by the Co, O(1) and O(2) atoms. The P(1) and P(3) atoms are 2.22 Å distant from the plane. The O-O bond distance (1.414(12) Å) is nearly the same as the values found in $[Co(O_2)(dpee)_2]^+$ (1.420(10) Å)[3] and *Δ-cis β*-$[Co(O_2)(RR$-tetars$)]^+$ (1.420 (10) Å).[18] These O-O distances are in the range of the reported values for a peroxide ion.[1] The O(1) and O(2) atoms are at essentially the same distance from the Co, and the Co-O distances (1.866(7), 1.858(7) Å) are similar to those for $[Co(O_2)(dpee)_2]^+$ (1.871(7), 1.902(7) Å)[3] and for *Δ-cis β*-$[Co(O_2)(RR$-tetars$)]^+$ (1.862(6), 1.867(7) Å)[18]. These facts indicate that the Co-O and O-O distances are not greatly affected by other ligands in a complex. The dmpe chelate ring takes a gauche conformation. The average Co-P bond distance, 2.213 (4) Å, is by 0.04—0.06 Å shorter than those in *Λ*-$[Co(en)_2(dmpe)]^{3+}$ (2.256(3) Å; en=$NH_2CH_2CH_2NH_2$)[19] and *trans(P, N)*-$[Co(edmp)_2(dmpe)]^{3+}$ (2.277(4) Å; edmp=$(CH_3)_2PCH_2CH_2NH_2$).[20] The average P-Co-P chelate angle (86.3(1)°) is by 2—4° larger than those of *Λ*-$[Co(en)_2(dmpe)]^{3+}$ (84.2(1)°) and *trans(P,N)*-$[Co(edmp)_2(dmpe)]^{3+}$ (82.7(1)°). The axial Co-P bond distances in **1** are longer by ca. 0.03 Å on average than those in the equatorial plane. It may be accounted for by trans influence of the mutually trans P donating atoms.[21] Two methyl groups C(5) and C(10) of **1** are placed over and under the O_2 group. The distance from the Co atom to the midpoint of the peroxide ion is 1.73(1) Å, which is comparable with the P-CH_3 bond length.

The structure of $[Co(O_2)(dmpp)_2]^+$ (**2**) is very similar to complex **1**. Complex **2** has a crystallographic twofold axis passing through the Co atom and the midpoint of the O-O bond. The trigonal-bipyramid around the Co atom is slightly deformed. The P(2) atom deviates by 0.37 Å from the plane formed by the Co, O, and O' atoms, and the P(1) atom is apart from the plane by 2.21 Å. All the O-O, Co-O, and Co-P bond distances are slightly longer than those of complex **1**, though not significant in view of the e.s.d.'s. The six-membered chelate ring formed by dmpp adopts a chair conformation. The C(1), C(2), and C(3) atoms of the chelate skeleton are shifted by 0.89, 0.47, and 0.89 Å, respectively from the plane through the Co, P(1) and P(2) atoms. There is no short contact between the two methyl groups C(4) and C(7), although P(1)-C(4) and P(2)-C(7) bonds are axial to the six-membered ring. Interatomic distances C(4)···C(7) and P(1)···P(2) are 3.91(1) and 3.18(2) Å, respectively.

IR Spectra. In Fig. 2 are shown IR spectra of $[Co(O_2)(dmpe)_2]BF_4$ and $[Co(^{18}O_2)(dmpe)_2]BF_4$ in the O-O stretching frequency region. The medium intensity band at 877 cm^{-1} of the O_2 complex shows the isotope shift; the $^{18}O_2$ complex gives a new band at 827 cm^{-1}. Other bands remain unchanged. The value of shift agrees well with that calculated for the O-O stretching vibration ($\Delta\nu$=50 cm^{-1}). For $[Co(O_2)(dmpp)_2]^+$, a similar medium intensity band is observed at 862 cm^{-1}. The corresponding *cis*-$[CoCl_2($dmpe or dmpp$)_2]^+$ complexes show no such bands in this region. Thus the bands at 877 cm^{-1} of the dmpe and 862 cm^{-1} of the dmpp complex can be assigned to the O-O stretching vibration. Gray et al.[4] assigned the band at 909 cm^{-1} of the dpee complex to the O-O stretching vibration. These frequencies are in the range of the reported values for a peroxide ion.[1,22]

Absorption Spectra. Figure 3 shows absorption spectra of the dioxygen complexes of dmpe, dmpp and

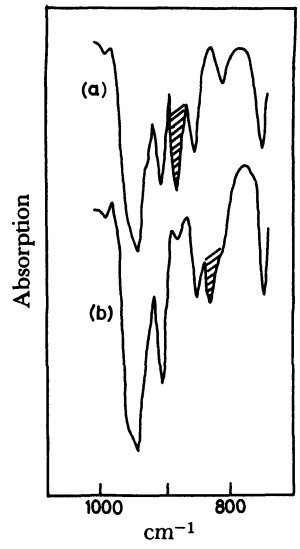

Fig. 2. IR spectra of $[Co(O_2)(dmpe)_2]BF_4$ (a) and $[Co(^{18}O_2)(dmpe)_2]BF_4$ (b).

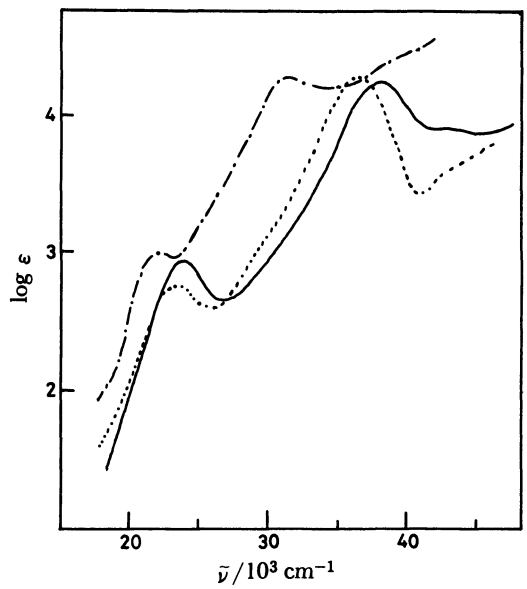

Fig. 3. Absorption spectra of $[Co(O_2)(dmpe)_2]BF_4$ (———), $[Co(O_2)(dmpp)_2]BF_4$ (·····) and $[Co(O_2)(dpee)]BF_4$ (—·—·—) in CH_3CN.

dpee. Gray et al.[4] assigned the band at 21000 cm^{-1} and the shoulder around 26000 cm^{-1} of the dpee complex to the first ($^1A \rightarrow {}^1T_1$) and the second ($^1A \rightarrow {}^1T_2$) ligand field bands, respectively, from a comparison with the spectrum of $[Co(CO_3)(dpee)_2]^+$ which has the same *cis*-$[CoO_2P_4]$ chromophore. The spectra of the dmpe and dmpp complexes are similar in pattern to that of the dpee complex, giving a peak at ca. 24000 cm^{-1} and a shoulder around 30000 cm^{-1} in the ligand field band region. The peak positions shift to high energy in the order of dpee<dmpp< dmpe complexes. This order coincides with the ranking of these phosphine ligands in the spectrochemical series.[23] Thus we have assigned the bands at 23750 cm^{-1} (log ε=2.95) of the dmpe complex and 23250 cm^{-1} (log ε=2.77) of the dmpp complex to the first ligand field band. It is not clear whether the shoulder absorption around 30000 cm^{-1} is the second ligand field band. In Fig. 4 are compared the spectrum of $[Co(O_2)(dmpe)_2]^+$ with those of $[Co(CO_3)(dmpe)_2]^+$ and $[Co(SO_4)(dmpe)_2]^+$. The latter two complexes exhibit two distinct absorption bands in the region of 20000 to 28000 cm^{-1} ($[Co(CO_3)(dmpe)_2]^+$ in water: 23530(2.96), 27100(2.98); $[Co(SO_4)(dmpe)_2]^+$ in CH_3CN: 21740(2.92), 25130(2.99) in cm^{-1} (log ε)). The two bands of each complex can be assigned to the ligand field bands, although the energy separation between them is much smaller than those of Co(III) amine complexes. The energy difference between the two ligand field bands in $[Co(CO_3)(dmpe)_2]^+$ (3750 cm^{-1}) is smaller than the half of the difference in $[Co(CO_3)(en)_2]^+$ (8250 cm^{-1}).[24] It is known that the energy differences between the two ligand field bands of phosphine[25] and arsine[16,26] cobalt(III) complexes are markedly reduced. No distinct band is observed for $[Co(O_2)(dmpe)_2]^+$ in the region of the second ligand field band of $[Co(CO_3)(dmpe)_2]^+$, although the first absorption bands of the two complexes are very similar both in intensity and peak position. When the shoulder around 30000 cm^{-1} of $[Co(O_2)(dmpe)_2]^+$ is assigned to the second ligand field band, the energy difference from the first ligand field band seems to be too large for a phosphine complex. Bosnich et al.[16] reported the absorption and CD spectra of an optically active peroxo tetrarsine complex, *Δ-cis β*-$[Co(O_2)(RR\text{-tetars})]^+$. The complex shows an absorption spectral pattern very similar to that of $[Co(O_2)(dmpe)_2]^+$ in the ligand field band region, and exhibits rather strong CD corresponding to the first ligand field band and fairly weak CD in the region from the absorption minimum to the high

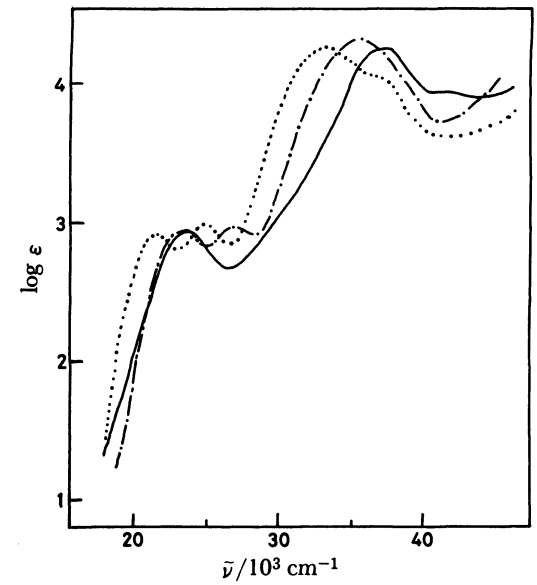

Fig. 4. Absorption spectra of $[Co(O_2)(dmpe)_2]BF_4$ (———), $[Co(CO_3)(dmpe)_2]ClO_4$ (—·—·—) and $[Co(SO_4)(dmpe)_2]BF_4$ (·····) in CH_3CN.

energy side. If the weak CD corresponds to the second ligand field band ($^1A \rightarrow {}^1T_2$) of Co(III), such a CD pattern is acceptable as a cobalt(III) complex. The second ligand field band would be so weak that it is hidden by adjacent strong absorption, although the reason is unknown. The ligand field absorption spectra of $[Co(O_2)(dmpe)_2]^+$ and $[Co(O_2)(dmpp)_2]^+$ could be understood in the same manner as that of the tetars complex.

The peroxo-bis(diphosphine) complexes show strong absorption bands in the region of 30000 to 40000 cm^{-1}. Gray et al.[4] assigned the band at 31000 cm^{-1} of $[Co(O_2)(dpee)_2]^+$ to a ligand-to-metal charge transfer transition of the type $\sigma(P) \rightarrow d\sigma^*(Co)$. The corresponding strong band is observed at 38000 cm^{-1} (log ε=4.36) and 36000 cm^{-1} (log ε=4.29) for $[Co(O_2)(dmpe)_2]^+$ and $[Co(O_2)(dmpp)_2]^+$, respectively. These bands are largely shifted to the high energy side compared with that of the dpee complex. Similar P-to-Co charge transfer bands of complexes, $[Co(en)_2(N\text{-}P)]^{3+}$ ($N\text{-}P=NH_2CH_2CH_2P(C_6H_5)_2$ or $NH_2CH_2CH_2P(CH_3)_2$)[27] and *trans*-$[Co(CN)_4(P)_2]^-$ ($P=P(C_6H_5)_3$, $P(C_6H_5)_2(CH_3)$ or $P(C_6H_5)(CH_3)_2$)[28] show a similar large shift to high energy by replacing a phenyl group on P with a methyl group.

The *trans*-$[(dmso)(dmpe)_2Co(\mu\text{-}O_2)Co(dmpe)_2(dmso)]^{4+}$ complex shows two medium intensity bands at 20000 cm^{-1} (log ε=2.93) and 25000 cm^{-1} (log ε=2.64) and a stron g band at 36000 cm^{-1} (log ε=4.67)(Fig. 5). The former two bands can be assigned to the two ligand field transitions of cobalt(III), since the spectral pattern quite resembles that of *trans*-$[Co(dmso)_2(dmpe)_2]^{3+}$ which was generated from *trans*-$[Co(H_2O)_2(dmpe)_2]^{3+}$ in dmso. While such distinct ligand field bands of a μ-peroxo cobalt(III) complex have been observed for $[(CH_3CN)(diars)_2Co(\mu\text{-}O_2)Co(diars)_2(CH_3CN)]^{4+}$[16] and $[X(cyclam)Co(\mu\text{-}O_2)(cyclam)X]^{n+}$ (X= a unidentate ligand such as H_2O or Cl^-; cyclam=1,4,8,11-tetraazacyclotetradecane),[29] a large number of amine complexes such as $[(NH_3)(en)_2Co(\mu\text{-}O_2)Co(en)_2(NH_3)]^{4+}$ show a broad, unresolved spectrum in the ligand field region.[30]

The *trans*-$[Co(H_2O)_2(dmpe)_2]^{3+}$ complex exhibits the first ligand field band split into two components, a shoulder around 20000 cm^{-1} (log ε = ca. 2.4) and a band at 23300 cm^{-1} (log ε = 2.80), and the second ligand field band at 27000 cm^{-1} (log ε = 2.96). The splitting of the first ligand field band can be anticipated from a *trans*-$[CoO_2P_4]$ chromophore. However, neither the present μ-peroxo complex nor *trans*-$[Co(dmso)_2(dmpe)_2]^{3+}$ show such splitting of the first ligand field band. Further studies will be needed for elucidating the absorption spectra of the cobalt(III) phosphine complexes.

Reactivity of Dioxygen Complexes. Both monomeric peroxo complexes of dmpe and dmpp in ethanol solutions react immediately with SO_2 at room temperature to afford $[Co(SO_4)(dmpe \text{ or } dmpp)_2]^+$, which were isolated as the tetrafluoroborate. The $[Co(O_2)(dbpe)_2]^+$ complex also reacts with SO_2, but the

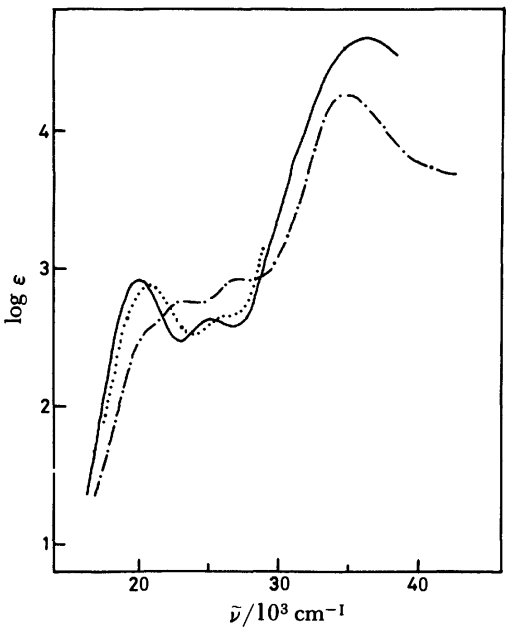

Fig. 5. Absorption spectra of $[(dmso)(dmpe)_2Co(\mu\text{-}O_2)Co(dmpe)_2(dmso)]^{4+}$ in dmso (——), and *trans*-$[Co(H_2O)_2(dmpe)_2]^{3+}$ in 0.5 mol dm^{-3} $HClO_4$ (—·—·—) and in dmso (·····).

sulfato complex could not be isolated because it decomposed to give Co(II) species during the course of isolation. Similar reactions have been reported for dioxygen complexes of cobalt(III). The $[Co(O_2)(diars)_2]^+$ complex reacts with SO_2, but the product (probably sulfato complex) can not be isolated because of the instability in the presence of SO_2.[16] Some μ-peroxo amine complexes such as $[(en)_2Co(\mu\text{-}NH_2, \mu\text{-}O_2)Co(en)_2]^{3+}$ yield μ-sulfato complexes by reaction with SO_2.[31]

On the other hand, $[Co(O_2)(dpee)_2]^+$ is quite inert toward SO_2. As described in Molecular Structure, the bond distances and angles of the Co-O_2 moiety are similar among the dmpe, dmpp and dpee complexes. As described previously the O_2^{2-} ion is surrounded by substituents on the axial P donor atoms of diphosphine ligands. The peroxide ion in $[Co(O_2)(dpee)_2]^+$ might be protected by the surrounding bulky phenyl groups against the attack of SO_2. Bulkiness of substituents on the axial P donor atoms in the $[Co(O_2)(diphosphine)_2]^+$ complex seems to be an important factor for the reactivity of the ligating peroxide ion. Thus the remarkable difference in reactivity toward SO_2 between the dpee complex and the other dmpe and dmpp complexes may be attributable to steric factors rather than electronic factors.

The peroxo complexes of dmpe and dmpp react instantly with concd HCl at 0 °C to afford red *cis*-$[CoCl_2(diphosphine)_2]^+$, while the same reaction of the dpee complex takes place very slowly and gives a mixture of green *trans*- and red *cis*-$[CoCl_2(dpee)_2]^+$. This indicates also the less reactivity of the dpee

complex. The formation of *trans*-$[CoCl_2(dpee)_2]^+$ may be related with the fact that *cis*-$[CoCl_2(dpee)_2]^+$ in ethanol isomerizes to the trans isomer (half-life=1.07 h at 53.3 °C) much faster than does *cis*-$[CoCl_2(dmpe)_2]^+$ (half-life=148 h at 55.0 °C). Detailed isomerization studies for these dichloro complexes will be reported elsewhere.

The authors wish to thank the Ministry of Education, Science and Culture for Scientific Research Grant-in-Aid No. 60470046. They are also indebted to the Institute for Solid State Physics, The University of Tokyo for the use of a FACOM M-160F computer and to the Institute for Molecular Science for the use of a HITAC M-180 computer .

References

1) a) M. H. Gubelmann and A. F. Williams, *Struct. Bonding*, **55**, 1 (1983); b) E. C. Niederhoffer, J. H. Timmons, and A. E. Martell, *Chem. Rev.*, **84**, 137 (1984).

2) L. Vaska, L. S. Chen, and M. V. Miller, *J. Am. Chem. Soc.*, **93**, 6671 (1971).

3) N. W. Terry, E. L. Amma, and L. Vaska, *J. Am. Chem. Soc.*, **94**, 653 (1972).

4) V. M. Miskowski, J. L. Robbins, G. S. Hammond, and H. B. Gray, *J. Am. Chem. Soc.*, **98**, 2477 (1976).

5) T. Ohishi, K. Kashiwabara, and J. Fujita, *Chem. Lett.*, **1984**, 1917.

6) *Inorg. Synth.*, Vol. XV, p.188.

7) J. C. Cloyd, Jr. and D. W. Meek, *Inorg. Chim. Acta*, **6**, 480 (1972).

8) T. Ohishi, K. Kashiwabara, and J. Fujita, *Chem. Lett.*, **1981**, 1371.

9) T. Ohishi, K. Kashiwabara, and J. Fujita, 34th Symposium on Coordination Chemistry, Japan (Nagaoka), 1984, Abstr. No. 2A09, p.254.

10) P. Main, S. E. Hull, L. Lessinger, G. Germain, J. P. Declercq, and M. M. Woolfson (1978). MULTAN78. "A System of Computer Programs for the Automatic Solution of Crystal Structures from X-ray Diffraction Data." Univs of York, England, and Louvain, Belgium.

11) T. Sakurai and K. Kobayashi, *Rikagaku Kenkyusho Hokoku*, **55**, 69 (1979).

12) "International Tables for X-Ray Crystallography," Kynoch Press, Birmingham (1974), Vol. IV, p. 71, 148.

13) Tables of the anisotropic thermal parameters of the non-hydrogen atoms, the coordinates of H atoms and observed and calculated structure factors are kept as Document No. 8615 at the Chemical Society of Japan.

14) T. V. Ohalloran and J. M. Malin, *J. Inorg. Nucl. Chem.*, **41**, 117 (1979).

15) C. A. Tolman, *Chem. Rev.*, **77**, 313 (1977).

16) B. Bosnich, W. G. Jackson, S. T. D. Lo, and J. W. McLaren, *Inorg. Chem.*, **13**, 2605 (1974).

17) C. K. Johnson (1965). ORTEP. Report ORNL-3794, Oak Ridge National Laboratory, Tennessee.

18) D. B. Crump, R. F. Stepaniak, and N. C. Payne, *Can. J. Chem.*, **55**, 438 (1977).

19) S. Ohba, Y. Saito, T. Ohishi, K. Kashiwabara, and J. Fujita, *Acta Crystallogr., Set. C*, **39**, 49 (1983).

20) T. Ohishi, S. Ohba, K. Kashiwabara, Y. Saito, and J. Fujita, *Bull. Chem. Soc. Jpn.*, **57**, 877 (1984).

21) M. Atoh, K. Kashiwabara, H. Ito, T. Ito, and J. Fujita, *Bull. Chem. Soc. Jpn.*, **57**, 3139 (1984), and references therein.

22) L. Vaska, *Acc. Chem. Res.*, **9**, 175 (1976).

23) a) K. Kashiwabara, I. Kinoshita, T. Ito, and J. Fujita, *Bull. Chem. Soc. Jpn.*, **54**, 725 (1981); b) T. Ohishi, K. Kashiwabara, and J. Fujita, *Bull. Chem. Soc. Jpn.*, **56**, 1553 (1983); c) K. Katoh, H. Sugiura, K. Kashiwabara, and J. Fujita, *Bull. Chem. Soc. Jpn.*, **57**, 3580 (1984).

24) Y. Shimura and R. Tsuchida, *Bull. Chem. Soc. Jpn.*, **29**, 311 (1956).

25) T. Ohishi, K. Kashiwabara, and J. Fujita, *Bull. Chem. Soc. Jpn.*, **56**, 3441 (1983).

26) W. G. Jackson, J. W. McLaren, and B. Bosnich, *Inorg. Chem.*, **22**, 2842 (1983).

27) I. Kinoshita, K. Kashiwabara, J. Fujita, K. Matsumoto, and S. Ooi, *Bull. Chem. Soc. Jpn.*, **54**, 2683 (1981).

28) K. Kashiwabara, K. Katoh, T. Ohishi, J. Fujita, and M. Shibata, *Bull. Chem. Soc. Jpn.*, **55**, 149 (1982).

29) B. Bosnich, C. K. Poon, and M. L. Tobe, *Inorg. Chem.*, **5**, 1514 (1966).

30) Y. Sasaki, J. Fujita, and K. Saito, *Bull. Chem. Soc. Jpn.*, **44**, 3373 (1971).

31) a) K. Garbett and R. D. Gillard, *J. Chem. Soc. (A)*, **1968**, 1725. b) C. H. Yang, D. P. Keeton, and A. G. Sykes, *J. Chem. Soc. Dalton Trans*, **1974**, 1089.

 © 1986 The Chemical Society of Japan Bull. Chem. Soc. Jpn., 59, 395—398 (1986)

A Study on the Mechanism of the Dimerization of Quinazoline Compounds Catalyzed by Cyanide Ions

Ayako GOTO* and Takeo HIGASHINO
Shizuoka College of Pharmacy, 2-2-1, Oshika, Shizuoka 422
(Received May 22, 1985)

It was shown that an intermediate, 4,4′(3*H*,3′*H*)-biquinazolinylidene (**2a**) was isolated in the formation process of 4,4′-biquinazolinyl (**3a**) which was obtained from the reaction of quinazoline (**1a**) with potassium cyanide, and **2a** was readily oxidized to **3a** by oxygen in air. The dimerization process was studied kinetically by NMR method. The result showed that the process was essentially similar to that of the benzoin condensation. The introduction of a methyl group into the C^2-position of **1a** resulted in a lowering of the reaction rate because the activation energy of 2-methylquinazoline (**1b**) dimerization became higher compared with that of **1a** dimerization.

It has been reported by Higashino et al.[1,2] that the chemical properties of the C^4-atom of quinazoline ring system are similar to those of carbonyl carbon. These properties were observed in the following reactions; i) the reaction of quinazoline(**1a**) with cyanide ions caused a dimerization,[1] ii) the benzoin-type condensation between quinazoline(**1a**) and aromatic aldehydes in the presence of cyanide ions resulted in the formation of α-aryl-4-quinazolinmethanol,[1] and iii) the benzilic acid-type rearrangement of aryl 4-quinazolinyl ketones proceeded in the presence of sodium hydroxide in dimethyl sulfoxide.[2]

Armarego and Willette[3] found that quinazoline (**1a**) reacted with cyanide ions to give 4,4′-biquinazolinyl(**3a**), and Higashino et al.[1] reported that this dimerization involved a benzoin-type condensation and oxidation. However, since an intermediate could not be isolated in the formation process of 4,4′-biquinazolinyl(**3a**), its mechanism is unknown. We studied its dimerization mechanism of quinazoline compounds in order to obtain useful information with respect to the carbonyl-like properties of the C^4-atom of quinazoline.

In this paper, we report that a benzoin-type condensation product, 4,4′(3*H*, 3′*H*)-biquinazolinylidene (**2a**), was isolated and the reaction process was investigated in detail by NMR technique.

Experimental

Infrared(IR) spectrum was recorded on a Jasco IRA-1 grating infrared spectrophotometer. The ^1H NMR and ^{13}C NMR spectra were measured at 90 MHz and at 21 °C on a JEOL TNM-FX90QFT NMR spectrophotometer. Mass spectra were obtained on a JEOL JMS-D100 mass spectrometer. The samples were vaporized in a direct inlet system at 190 °C. Ultraviolet spectra were measured in dimethyl sulfoxide (DMSO) on a Shimadzu Recording Spectrophotometer UV-360.

Materials. Dimethyl sulfoxide and potassium cyanide were of the reagent grade. Dimethyl-d_6 sulfoxide was obtained from Merck.

Quinazoline(**1a**) was synthesized according to the method of Higashino.[4] After the crude **1a** was distilled under 15—20 mmHg (1 mmHg=133.322 Pa) and the fraction boiling at 115—125 °C was collected, it was twice passed through a column of alumina. The elution with benzene gave the pure compound, mp 48 °C, white needles. 2-Methylquinazoline(**1b**) was synthesied by the method described in the previous paper.[5] The crude **1b** was purified by the same manner as **1a** to give the pure compound, light yellow, needles, mp 41 °C.

4,4′(3*H*, 3′*H*)-Biquinazolinylidene (2a). A mixture of 3.8 mmol of **1a** and 7.7 mmol of KCN in 2 cm³ of DMSO was allowed to stand overnight under nitrogen atmosphere. The reaction mixture was poured into an ice-H_2O mixture. The separated crystals were collected and washed thoroughly with methanol and dried under reduced pressure. The crystals, mp 217—218 °C, were obtained as needles in a 70% yield. The compound **2a** had molecular formula, $C_{16}H_{12}N_4$ (*m/z*, 260(M^+)). The NMR spectrum was as follows; NMR (DMSO-d_6) $\delta(^1H)$=6.69—7.16 (8H, m), 8.73 (2H, d, J=8.0 Hz), and 6.3 (2H, bs). $\delta(^{13}C)$=113.2, 126.5, 138.0 (each s), 122.1, 127.0, 128.3, 129.0, 140.5 (each d). When **2a** was heated or allowed to stand overnight in air, it was readily oxidized to **3a**.

Oxidation of 2a with $K_3[Fe(CN)_6]$. A solution of 500 mg of $K_3[Fe(CN)_6]$ in 5 cm³ of H_2O was added to a mixture of 120 mg of **2a**, 10 cm³ of benzene and 1 cm³ of 50% NaOH, and the mixture was vigorously shaken for 1 h at room temperature. The benzene solution was dried over Na_2SO_4 and evaporation of the benzene gave **3a**.

2,2′-Dimethyl-4,4′(3*H*,3′*H*)-biquinazolinylidene (2b). The NMR data of **2b** in the reaction mixture were as follows; NMR (DMSO-d_6, 90 MHz) $\delta(^1H)$=2.60 (6H, s), 6.67—7.12 (6H, m) and 8.87 (2H, d, J=7.8 Hz). $\delta(^{13}C)$=112.8, 121.1, 125.9, 138.8 (each s), 121.6, 126.7, 128.8, 147.3 (each d), and 21.2 (q).

2,2′-Dimethyl-4,4′-biquinazolinyl (3b). The dimer, **3b**, mp 219 °C, was prepared by the same method described by Armarego and Willette.[3] The yield was 25%.

3,4-Dihydro-4-quinazolinecarbonitrile. 3,4-Dihydro-4-quinazolinecarbonitrile was synthesized according to the method of Higashino.[4]

Kinetics of Dimerization. The reaction mixture was made by mixing equal volumes (0.2 cm³) of KCN-DMSO-d_6 solution and DMSO-d_6 solution of quinazoline compound (**1**) in an NMR tube and air was replaced with N_2 after degassing. The concentrations of KCN and **1** in a mixture of 0.2 cm³ of KCN-DMSO-d_6 and 0.2 cm³ of **1**-DMSO-d_6 are represented as mol dm^{-3}. Temperature equilibration was done outside the NMR probe in a thermostat at a constant temperature±0.1 °C. These reactions were followed by integration of the signal of the hydrogen atom at C^4-position of **1a** or **1b**. The errors of integration of the hydrogen atom observed by using CH_2Cl_2

as the standard were ±1.2% for **1a** and ±2.6% for **1b**, respectively. Rate constants were calculated by a least-square computer.

Results and Discussion

Although Higashino et al.[1] assumed that 3,4-dihydro-4,4′-biquinazoline (**2′**) (Chart 2) was a formal benzoin-type condensation product for **1a**, **2′** could not be isolated. Furthermore, it is yet unknown whether the oxidation step is caused by oxygen in atmosphere or by **1a** which may act as the hydride ion acceptor to form a reduction product such as 3,4-dihydroquinazoline.

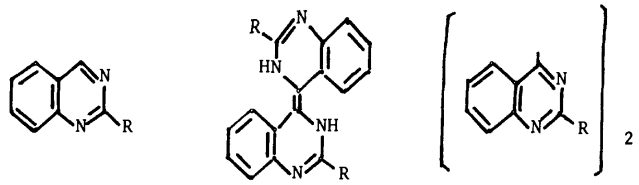

1a: R = -H **2a**: R = -H **3a**: R = -H
1b: R = -CH_3 **2b**: R = -CH_3 **3b**: R = -CH_3

Chart 1.

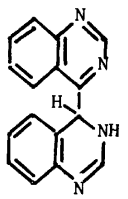

3,4-Dihydro-4,4′-biquinazoline (**2′**)

Chart 2.

When a dried dimethyl sulfoxide solution of **1a** containing potassium cyanide was allowed to stand under nitrogen atmosphere at room temperature, **2′** was not obtained, but the isomer, 4,4′(3*H*, 3′*H*)biquinazolinylidene (**2a**) was isolated. The structure of **2a** was elucidated by the spectra data (see Experimental) and the following chemical procedures. Compound **2a** was easily oxidized to **3a** not only with $K_3[Fe(CN)_6]$, but also by atmospheric oxygen at room temperature. The structure of **2a** was suggested as (*E*)-form as shown in Chart 1 on the basis of the following facts: (*E*)-Form corresponds to *trans*-stilbene and (*Z*)-form to *cis*-stilbene. Rizebos and Havinga[6] reported that *trans*-stilbene showed a longer wavelength shift of the absorption maximum (λ_{max} 295 nm, ε 27000) than *cis*-stilbene (λ_{max} 280 nm, ε 10500) because the hydrogen atoms at the ortho-positions of *cis*-stilbene interact mutually and the stilbene cannot exist in a coplanar structure either. On the other hand, Armarego and Willette[3] reported that the ultraviolet spectrum of 4,4′-biquinazolinyl(**3a**) is similar to that of **1a**, due to the restricted rotation about the 4,4′-bonds; the two halves of the molecule are not coplanar and the chromophores are not highly conjugated with one another. If the compound, **2a**, corresponds to (*Z*)-form, the hydrogen atoms at C^5-and $C^{5'}$-positions interact mutually and also it can hardly maintain a coplanar structure. However, the absorption maximum of **2a** in DMSO is at 414 nm (ε 9680), and is remarkably longer than that of **3a** (λ_{max} 320 nm, ε 7110 in DMSO). Therefore, this fact suggests that the double bonds of **2a** may be highly conjugated by maintaining a coplanar structure and it seems reasonable to assume that **2a** is in (*E*)-form.

Since the above result proved that the dimerization of **1a** in the presence of potassium cyanide gave **2a** which was oxidized to **3a**, the reaction process for the formation of **2** is assumed to be as shown in Scheme 1, which is similar to the benzoin condensation process: *N*-anion (**A-1**) formed by addition of cyanide ions to **1** would rearrange readily to carbanion (**A·2**) by a prototropic shift. Nucleophilic addition of **A-2** to quinazoline provides an intermediate *N*-anion, **A-3**, which rearranges readily to *N*-anion (**A·4**) and is finally converted to product **2** by rapid loss of CN^-. The process represented in Scheme 1 is also summarized as represented in Eqs. 1 and 2,

$$Q + C \underset{k_{-1}}{\overset{k_1}{\rightleftharpoons}} \textbf{A-2} \qquad (1)$$

$$\textbf{A-2} + Q \xrightarrow{k_2} P + C \qquad (2)$$

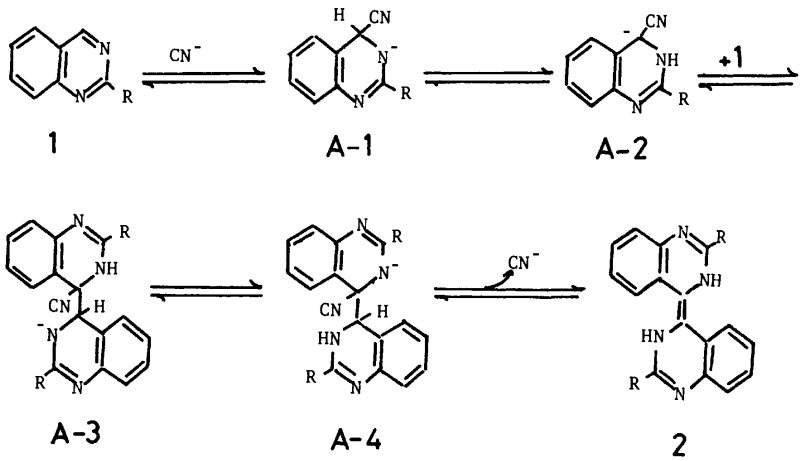

Scheme 1.

where [Q] refers to free quinazoline and C to free cyanide ions. **A·2** is the carbanion in Scheme 1, and P stands for product **2**. The presence of carbanion **A·2** is suggested from the following reasons: Hydrogen cyanide adds easily to quinazoline to produce 3,4-dihydro-4-quinazolinecarbonitrile. When 3,4-dihydro-4-quinazolinecarbonitrile in DMSO-d_6 was mixed with quinazoline and potassium hydroxide under nitrogen atmosphere in an NMR tube, the presence of **2a** was observed in the NMR diagram. This corresponds to the fact that α-hydroxyphenylacetonitrile was mixed with benzaldehyde and a base to give benzoin.[10]

Figure 1 shows the NMR diagram of the reaction mixture (0.4 cm^3) of **1a** (3.72×10^{-1} mol dm^{-3}) and KCN (4.55×10^{-2} mol dm^{-3}) in DMSO-d_6 at 25 min (A) and at 300 min (B) after mixing under nitrogen atmosphere, respectively. Since Fig. 1 shows only the presence of **1a** as the starting material and **2a** as the reaction product, it is possible to follow the reaction process kinetically by determing the time dependence of the signal of the hydrogen atom at C^4-position of quinazoline represented as * in Fig. 1. The rate constant may be derived, using a steady-state approximation in a similar manner as benzoin condensation.[7-10] That is to say, if $k_{-1}\gg k_2$, the following rate expression can be derived,

$$d[P]/dt = \frac{k_1k_2}{k_{-1}}[Q][C_0], \qquad (3)$$

where [Q] refers to free quinazoline concentration and C_0 to cyanide ion concentration. The second order rate plots with respect to quinazoline are shown in Fig. 2. Although ^{1}H NMR method may be less accurate than other spectrophotometric methods, the second order plots were fairly linear ($r>0.98$) in all cases. This is in agreement with the result that benzoin condensation is kinetically second order in benzaldehyde.[7-10] Therefore, it suggests that the process of Eq. 2, that is, addition of carbanion, **A·2**, to the carbon at C^4-position of quinazoline is rate-determing, corresponding to the result that addition of carbanion, [ArC(CN)OH]$^-$, to the carbonyl carbon of benzaldehyde is rate-determining in benzoin condensation.[7-10] It seems also reasonable to consider that the chemical properties of C^4-atom of the quinazoline ring system are similar to those of carbonyl carbon.

Furthermore, the dimerization process of **1b** was investigated in order to clarify the effect of methyl group at C^2-position of **1** on the dimerization. When **1b** was allowed to react under the same experimental conditions as the quinazoline dimerization, only 2,2′-dimethyl-4,4′-biquinazolinyl(**3b**) was obtained. The intermediate, 2,2′-dimethyl-4,4′(3*H*,3′*H*)-biquinazolinylidene(**2b**) could not be isolated because it was readily oxidized, compared with **2a**. Figure 3 shows ^{1}H NMR spectra of the reaction mixture (0.4 cm^3) of **1b** (3.17×10^{-1} mol dm^{-3}) and KCN (5.3×10^{-2} mol dm^{-3}) in

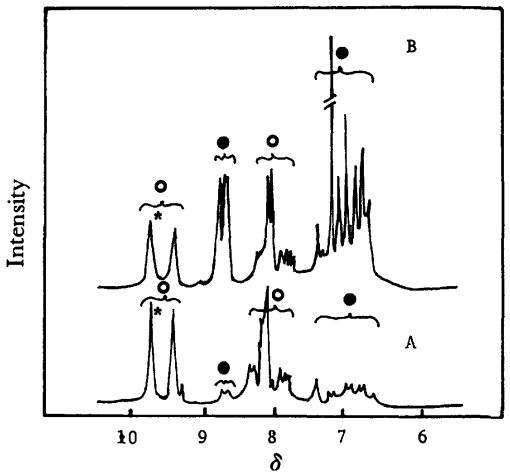

Fig. 1. ^{1}H NMR Spectra of the reaction mixture of quinazoline (**1a**) catalyzed by KCN in DMSO-d_6 at 21 °C.
○: **1a**, ●: **2a**, A: 25 min, B: 300 min.

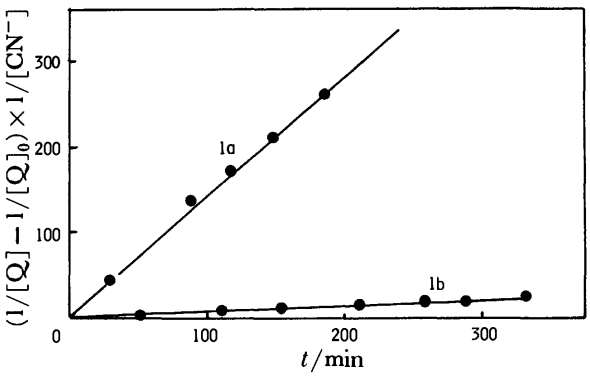

Fig. 2. Second order plots for the dimerization of quinazoline (**1a**) and 2-methylquinazoline (**1b**) at 25 °C.

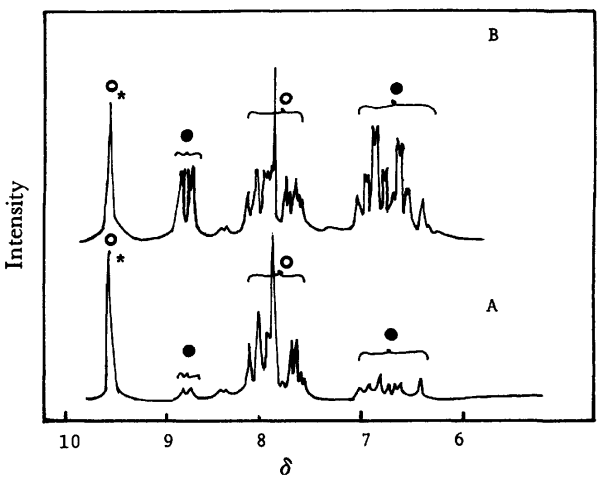

Fig. 3. ^{1}H NMR Spectra of the reaction mixture of 2-methylquinazoline (**1b**) catalyzed by KCN in DMSO-d_6 at 21 °C.
○: **1b**, ●: **2b**, A: 280 min, B: 1500 min.

Table 1. Kinetic and Thermodynamic Parameters for the Dimerization of **1**

Parameter	**1a**	**1b**
k/(mol dm^{-3})$^{-2}$ min^{-1} at 25 °C	1.20±0.09	$7.18\times10^{-2}\pm0.88\times10^{-2}$
ΔE^*/kJ mol^{-1}	1.02×10	2.39×10
ΔG^*/kJ mol^{-1} at 25 °C	5.71×10	6.42×10
ΔH^*/kJ mol^{-1}	5.24	1.90×10
ΔS^*/J mol^{-1} T^{-1}	-1.74×10^2	-1.52×10^2

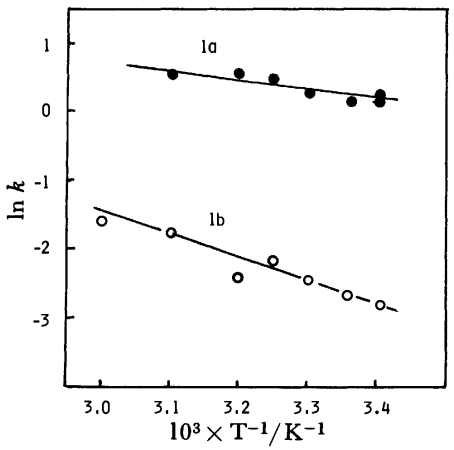

Fig. 4. Plots of ln k against T^{-1}.

DMSO-d_6 at 280 min (A) and at 1500 min (B) after mixing, respectively. Since the presence of **1b** and **2b** was observed by the NMR spectra shown in Fig. 3, the dimerization process of **1b** can be followed by ^{1}H NMR methods described above for the dimerization of **1a**. The rate was estimated by following the signal of hydrogen at C^4-position of **2b** represented as * in Fig. 3. Figure 2 shows second order rate plots for the **1b** dimerization, indicating that the rate of **1b** is lower than that of **1a**. Kinetic parameters were determined from the temperature-dependency of the rate constant, k. Plots of ln k vs. T^{-1} show an approximately linear relationship in the temperature ranges 20—45 °C for **1a** and 20—60 °C for **1b** (Fig. 4). Activation parameters, ΔE^*, ΔG^*, ΔH^*, and ΔS^* were determined (Table 1). The value of ΔE^* for the **1a** dimerization was smaller than that for the **1b** dimerization. In comparison with the parameters of benzoin condensation in methanol at 44—66 °C ($\Delta G^{\ddagger}_{298}$=94.1 kJ mol^{-1}, ΔH^*=41.8 kJ mol^{-1}, and ΔS^*=−75 J mol^{-1} T^{-1}), the values of ΔH^* and ΔG^* for both quinazolines were low. It is interesting because the reactivity of quinazoline compounds is suggested to be higher than that of benzaldehyde in regard to the benzoin condensation. Activation enthalpy, ΔH^*, for **1b** is much higher than that for **1a**, while ΔS^* at 25 °C is essentially the same. It is expected that the electrophilicity of the C^4-position of **1a** is higher than that of **1b** because electron density at the C^4-position of **1b** will increase due to the electron-donating effect of the methyl group. This expectation is compatible with the above result of activation parameters.

In conclusion, the present quantitative study verified that the dimerization process of **1** is essentially similar to the benzoin condensation process.

The authors are grateful to Professor E. Hayashi and Dr. M. Uchida of Shizuoka College of Pharmacy for many valuable discussion.

References

1) T. Higashino, M. Goi, and E. Hayashi, *Chem. Pharm. Bull.*, **22**, 2493 (1974).
2) T. Higashino, M. Takemoto, and E. Hayashi, *Chem. Pharm. Bull.*, **33**, 1351 (1985).
3) W. L. F. Armarego and R. E. Willette, *J. Chem. Soc.*, **1965**, 1258.
4) T. Higashino, *Yakugaku Zasshi*, **80**, 245 (1960).
5) T. Higashino, H. Kokubo, A. Goto, M. Takemoto, and E. Hayashi, *Chem. Pharm. Bull.*, **32**, 3690 (1984).
6) G. Rizebos and E. Havinga, *Rec. Trav. Chim.*, **80**, 446 (1961).
7) H. G. Bredig and E. Stern, *Z. Elektrochem.*, **10**, 582 (1904).
8) E. Stern, *Z. Phys. Chem.*, **50**, 513 (1905).
9) J. P. Kuebrich, R. L. Schowen, M. Wary and M. E. Lupes, *J. Am. Chem. Soc.*, **43**, 1214 (1971).
10) A. Lapworth, *J. Chem. Soc.*, **83**, 995 (1903).

Studies of Polystyrene-Based Ion-Exchange Fiber. IV. A Novel Fiber-Form Material for Adsorption and Immobilization of Biologically-Active Proteins†

Toshio YOSHIOKA* and Masaharu SHIMAMURA
Fibers Research Laboratories, Toray Industries, Inc., Sonoyama, Otsu 520
(Received June 12, 1985)

A new polystyrene-based ion-exchange fiber (IONEX) has a large surface area per unit weight and has been studied for its ability to adsorb and immobilize biologically-active proteins. A strong cation IONEX was found to be able to effectively adsorb hemoglobin and albumin, invertase, and glucose isomerase were readily adsorbed to a strong anion IONEX. The adsorption of these proteins to IONEX was found to take place through an electrostatic force. The adsorption capacity for proteins became exceedingly large (ca. 300 mg g^{-1}) with an increase in the water-holding capacity of the fiber. The activities of the invertase and glucose isomerase immobilized to the fiber exhibited 40—50 and 75—80%, respectively, of those of native enzymes. A continuous inversion of sucrose was also carried out using immobilized invertase. From these results, this fibrous ion exchanger with a high water-holding capacity is considered to be an excellent material for the adsorption and immobilization of proteins.

In other papers we have reported the preparation methods, fundamental characteristics, and acid-base catalytic properties of a polystyrene-based ion-exchange fiber (IONEX).[1-3] The ion-exchange fiber has a large surface area and, accordingly, is expected to have a large capacity for adsorbing macromolecular ionic substances.

Recently, the immobilization of enzymes has been intensively studied and some immobilized emzymes have been used in industry. There have been many investigations regarding methods for immobilizing enzymes, such as bonding to a supporter, entrapping in a crosslinked gel, and crosslinking by a bi- or multifunctional reagent.[4] An immobilization of enzymes to an ion-exchange fiber based on poly(vinyl alcohol) has also been examined and several reports have been published.[5-7] We have undertaken an investigation regarding the immobilization of emzymes using IONEX while considering the following advantages:[8]

(1) The capacity for adsorbing macromolecular proteins is expected to be large since IONEX has a large surface area per unit weight.

(2) The yield of the activity is expected to be high because immobilization probably occurs on the surface through ionic bonding. Thus, steric hindrances for the active site of proteins and for the diffusion of the substrates would be smaller.

(3) IONEX exhibits a high mechanical strength and, thus, it can be utilized in various forms, such as a cut fiber, a knitted fabric, a woven fabric, a braid, a felt, a nonwoven fabric, and a paper.

In the present report, the adsorption and immobilization of some proteins and enzymes to IONEX are described. The importance of the water-holding capacity of the fiber for protein adsorption and enzyme immobilization is also described.

†A preliminary report of this work was presented in *Polym. Prepr. Jpn.*, **32**, 1851 (1983).

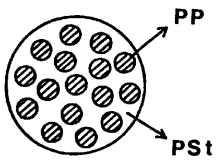

Fig. 1. Schematic cross section of composite fiber. Pst: polystyrene as *sea* ingredient; PP: polypropylene as *island* ingredient.

Experimental

Polystyrene to be converted into an ion exchanger (as the predominant *sea* ingredient) and polypropylene for reinforcement (as the *island* ingredient) were spun into composite filaments having an *islands-in-a-sea* type sectional structure (Fig. 1) by the conventional method. A cation IONEX with sulfo groups and an anion IONEX with trimethylammonio groups were prepared by the introduction of crosslinking groups and corresponding ion-exchange groups into the polystyrene part according to the procedures described in a previous paper.[1] The capacity of strong acidic- and basic-type IONEX was ca. 2.5 mequiv g^{-1}. A cation IONEX in the Na form or an anion IONEX in the Cl form was immersed in deionized water at room temperature for a sufficient period in order to reach an equilibrium water sorption. The fiber was centrifugally dehydrated at 3000 r.p.m. for five minutes, and then, the wet weight (W) was determined immediately. The water content of the fiber was determined using the following equation:

$$\text{Water content} = (W - W_0)/W_0,$$

where W_0 is the dry weight of the fiber. The water content means the water-holding capacity of a fiber. The content was controlled by choosing the conditions of the crosslinking reaction.[1-3] The water content becomes higher as the degree of crosslinking is lowered.

Hemoglobin and albumin from bovine blood and invertase from *Candia utilis* were obtained from Sigma Co. and Seikagaku Kogyo Co., Ltd., respectively. Glucose isomerase was extracted by the lysozyme methods from *Streptomyces*

phaeochromogenus supplied by Nagase Sangyo Co., Ltd. The adsorption capacity of the fiber for proteins was evaluated by measuring the concentrations of the proteins in solutions before and after an adsorption treatment by means of the copper-Folin[9] or optical-density (at 270 nm) methods. The amount of the enzyme adsorbed to the fiber (A) was calculated by subtracting the activity of the enzyme which remained unadsorbed from the activity of the added enzyme. The yield of the activity (B/A) was determined by measuring the activity of the enzyme immobilized to the fiber (B). One unit (U) of invertase activity was defined as the amount of enzyme which produced 1 μ mole of glucose per minute at 30°C in a 10 wt% sucrose solution containing a 0.01 M (1 M=1 mol dm^{-3}) phosphate buffer of pH 5.0. The activity of the native invertase was 170 U mg^{-1}. On the other hand, one unit (U) of glucose isomerase activity was defined as the amount of enzyme which produced 1 mg of fructose per hour at 60°C in a 0.5 M glucose solution (pH 8.2) containing 0.05 M $NaHCO_3$ and 0.01 M $MgSO_4$. The amount of glucose or fructose produced was determined by the polarimetric methods.[10]

Results and Discussion

Adsorption of Hemoglobin and Albumin. The adsorption of hemoglobin and albumin was carried out by the following procedures. A strong cation exchanger (20—100 mg in the Na form) was added to 10 ml of a 0.1% hemoglobin (isoelectric point; pH 6.9, molecular weight; ca. 70000) solution containing a 0.05 M phosphate buffer of pH 6.6. The mixture was then shaken at 30°C for 3 h. Similarly, a strong anion exchanger (20—100 mg in the Cl form) was added to 10 ml of a 0.1% albumin (isoelectric point; pH 4.7, molecular weight; ca. 70000) solution containing a 0.05 M phosphate buffer of pH 7.0; then, the mixture was shaken at 30°C for 3 h. The results of hemoglobin adsorption to cation exchangers and albumin adsorption to anion exchangers are summarized in Tables 1 and 2, respectively.

The adsorption capacity of a cation IONEX for hemoglobin was apparently dependent on its water content. IONEX with a water content of 1.5 exhibited an adsorption capacity of less than 20 mg g^{-1}. In contrast, IONEX with the highest water content among those tested exhibited a capacity of 300 mg g^{-1}. The granular cation-exchange resins, Amberlite IR-120B and IR-200C, and the crushed resin, Powdex PCH, were also examined for their capacity to adsorb hemoglobin. These resins had a water content in a range from 0.9 to 1.6 and showed adsorption capacities similar to that of IONEX with the lowest water content. In the case of albumin, protein was readily adsorbed to an anion IONEX having a trimethylammonio group as the ion-exchange site. The adsorption capacity was again dependent on the water content. Macroreticular-type granular anion-exchange resins, such as Amberlite IRA-900, IRA-904, and IRA-938, showed low adsorption capacities of 12—40 mg g^{-1}. Gel-type granular anion-exchange resins, Amberlite IRA-400 and IRA-401, and the crushed resin, Powdex PAO, exhibited no appreciable adsorption capacities for albumin.

Table 1. Results of Hemoglobin Adsorption to Cation Exchangers in Na Form

Cation exchanger	Water content	Adsorption capacity[a] mg g^{-1}
IONEX	1.5	<20
	3.0	50
	5.0	300
Amberlite IR-120B	0.9	<20
Amberlite IR-200C	0.9	<20
Powdex PCH	1.6	<20

a) 0.1% Hemoglobin solution containing 0.05 M phosphate buffer (pH 6.6), 30°C, 3 h.

Table 2. Results of Albumin Adsorption to Anion Exchangers in Cl Form

Anion exchanger		Water content	Adsorption capacity[a] mg g^{-1}
IONEX		1.5	30
		2.5	200
		3.5	300
Amberlite	IRA-400	0.8	<10
	IRA-401	1.6	<10
	IRA-900	1.6	13
	IRA-904	1.4	40
	IRA-938	2.7	12
Powdex PAO		1.4	<10

a) 0.1% Albumin solution containing 0.05 M phosphate buffer (pH 7.0), 30°C, 3 h.

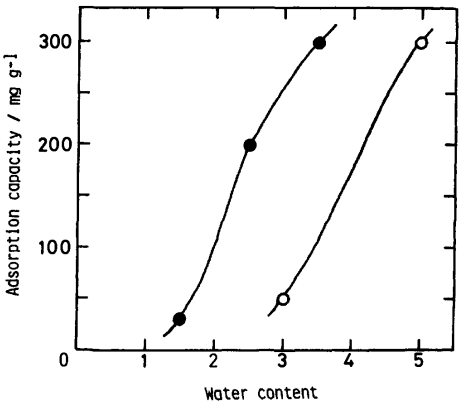

Fig. 2. Water content dependence of protein adsorption capacity of IONEX. Adsorption was carried out at 30°C for 3 h in 0.1% protein solution containing 0.05 M phosphate buffer.
○: Hemoglobin adsorbed to cation IONEX at pH 6.6, ●: albumin adsorbed to anion IONEX at pH 7.0.

The dependences on the water content of the adsorption capacities of IONEX for the proteins are shown in Fig. 2. Apparently, water in the polystyrene network of IONEX plays an important role in macromolecular protein's ability to have access to the ion-exchange site. In fact, IONEX comprises a polystyrene network crosslinked between the phenyl

Table 3. Results of Invertase Immobilization to Anion IONEX in Cl Form by Batch Method

Water content	Amount of IONEX	Adsorbed[a] enzyme (*A*)	Observed activity (*B*)	Yield of activity (*B/A*)
	mg	U	U	%
1.5	250	610	230	38
	500	1170	460	39
	1000	2125	860	40
2.5	50	625	350	56
	150	1940	1025	53
	500	2125	1140	54

a) Enzyme added: 2125 U, 12.5 mg (50 ml of 0.01 M phosphate buffer, pH 5.0), 20°C, 2 h.

groups by methylene linkages. The lattice of the network becomes wider as the degree of crosslinking is decreased; that is, the water content of the fiber increases, and thus, a macromolecule can diffuse into the network and more easily interact with the ion-exchange sites.

The higher adsorption capacity of IONEX (diameter; ca. 30 μm), compared with gel-type granular resins (diameter; ca. 500 μm) or with crushed resins (particle size; 37—250 μm) with similar water contents, would come from the larger surface area of IONEX. The surface areas of IONEX with a water content of 1.5—5.0 were 2.0—2.5 $m^2 g^{-1}$, as determined by the BET methods using nitrogen gas. On the other hand, the surface areas of the crushed resins and the gel-type granular resins were 0.5—0.8 $m^2 g^{-1}$ and less than 0.1 $m^2 g^{-1}$, respectively. In addition, the lattice sizes of the polystyrene network of IONEX are presumably larger than those of the usual styrene-divinylbenzene-based resins. This also contributes, at least in part, to the larger adsorption capacity of IONEX.

When a fiber which had adsorbed albumin was washed with distilled water and then treated with 10 wt% NaCl, more than 90% of the adsorbed protein was released. These results indicate that a protein is adsorbed to the fiber through an electrostatic force.

Immobilization of Some Enzymes. The results described above suggest the possibility of IONEX as an excellent material for the immobilization of enzymes. In order to prove this possibility, the immobilization of two enzymes, invertase and glucose isomerase, to IONEX was investigated with special reference to their activities.

Invertase (isoelectric point; pH 3.8, molecular weight; 270000) was first immobilized to an anion IONEX with two different water contents (1.5 and 2.5) by the following methods. A fixed amount of the anion IONEX in the Cl form was added to 50 ml of a 0.01 M phosphate buffer solution (pH 5.0) containing 2125 U of invertase. The mixture was shaken at 20°C for 2 h. Then, the fiber to which the enzyme was adsorbed was washed five times with distilled water and stored in the same buffer solution.

As expected, invertase was readily adsorbed to the anion IONEX and its adsorption capacity for this

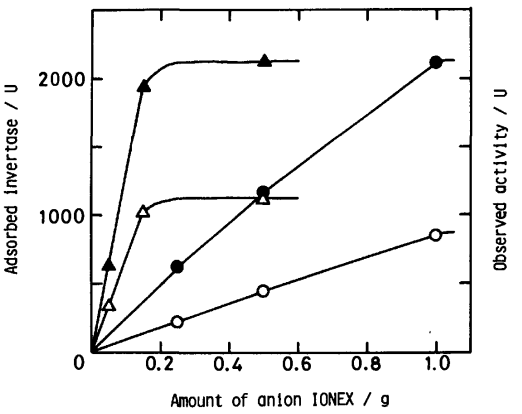

Fig. 3. Adsorbed invertase and observed activity vs. amount of anion IONEX in Cl form. Immobilization was carried out in 50 ml of 0.01 M phosphate buffer solution (pH 5.0) containing invertase of 2125U (20°C 2h). ●: Adsorbed invertase, ○: observed activity (water content of IONEX=1.5), ▲: adsorbed invertase, △: observed activity (water content of IONEX=2.5).

enzyme was greater when the water content of the ion exchanger was higher (Table 3). When the water content was 1.5, the increase in the amount of the adsorbed enzyme was almost linear to the amount of IONEX (see Fig. 3) up to 1.0 g under the conditions used. In contrast, when the water content was 2.5, saturation occured in the vicinity of 0.2 g. These results indicate that the capacity for immobilization increases by five times when the water content of the fiber increases from 1.5 to 2.5. This fact is attributable to the difference in the crosslinked structure described above. The reasons that the yield of the activity is lower than 100% are considered to be (1) that the enzyme is inactivated during the immobilization process, (2) that the active site of the immobilized enzyme is sterically hindered, and (3) that the diffusion of the substrate to the active site of the immobilized enzyme is hampered. The yield of the activity was enhanced from ca. 40% to ca. 50% when the water content of the fiber was increased from 1.5 to 2.5 (Table 3). These results may indicate that two effects, (2) and (3), are eliminated by a loosening of the crosslinked structure.

Invertase was also immobilized to anion exchangers

Table 4. Results of Invertase Immobilization to Anion Exchangers in Cl Form by Column Method

Anion exchanger	Water content	Packed[a] amount	Adsorbed[b] enzyme (*A*)	Observed activity (*B*)	Yield of activity (*B*/*A*)
		mg	U	U	%
IONEX	1.5	500	600	265	44
	2.5	150	1700	865	51
Amberlite IRA-900	1.4	1500	600	260	43

a) Column diameter: 7.5 mm. b) Enzyme added: 2125 U, 12.5 mg (50 ml of 0.01 M phosphate buffer, pH 5.0), 20 °C, 1 h.

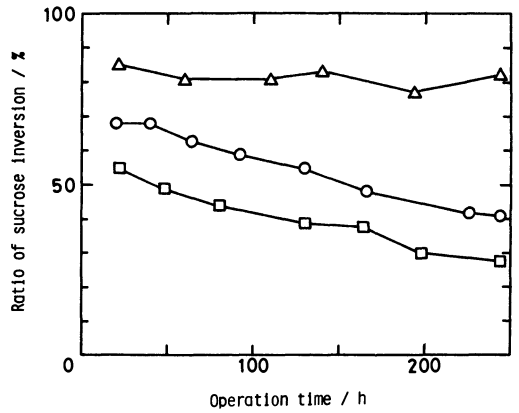

Fig. 4. Stability of immobilized invertase to continuous inversion of sucrose by a column method. 10 wt% Sucrose solution containing 0.01 M phosphate buffer of pH 5.0 was passed through the column (7.5 mmϕ) filled with the immobilized invertase at a flow rate of 50 ml h^{-1} at 25 °C.
○: 500 mg of anion IONEX with water content of 1.5 (265U). △: 150 mg of anion IONEX with water content of 2.5 (865U), □: 1500 mg of Amberlite IRA-900 (260U).

by a column method as follows. Anion exchangers were packed into a jacketed glass column with an inside diameter of 7.5 mm. The enzyme solution described above was circulated through the column at 20 °C for 1 h. The results are summarized in Table 4.

The column method gave results similar to the batch method, except that the amounts of adsorbed enzyme for IONEX with water contents (1.5 and 2.5) decreased to 55 and 85%, respectively. The decrease in the amounts of adsorbed enzyme may imply that some parts of IONEX are not utilized because of an irregular flow. The macroreticular-type resin, Amberlite IRA-900, has only one third as large an effective capacity for immobilizing invertase per unit weight as IONEX with a water content of 1.5.

Figure 4 shows the dependence on operation time of the ratio of sucrose inversion when the substrate solution was continuously passed through each column at 25 °C. The activity of an IONEX column with a water content of 2.5 decreased more slowly than that of an IONEX column with a water content of 1.5 and an IRA-900 column. The inversion ratio was not improved, although an enzyme solution with twice the decreased activity was circularly passed through each column. This fact indicates that the decrease in activity can be attributed to the inactivation of the enzyme, but not to the release of the enzyme.

Table 5. Results of Glucose Isomerase Immobilization to Anion IONEX of Water Content 4.0 in Cl Form

Amount of IONEX	Adsorbed[a] enzyme (*A*)	Observed activity (*B*)	Yield of activity (*B*/*A*)
mg	U	U	%
10	160	125	78
20	294	235	80
40	337	253	75

a) Enzyme added: 344 U (2 ml, pH 8.0), 20 °C, 6 h.

The immobilization of glucose isomerase was then examined by the following methods. A fixed amount of the anion IONEX with a water content of 4.0 in the Cl form was added to 2 ml of an extract solution (pH 8.0) of glucose isomerase. The mixture was shaken at 20 °C for 6 h. Then, the fiber to which the enzyme was adsorbed was washed five times with distilled water. The results of glucose isomerase immobilization are listed in Table 5.

Glucose isomerase was also readily adsorbed to the anion IONEX and the amount of the adsorbed enzyme was directly proportional to the amount of IONEX (up to 20 mg) under the conditions used. The yield of the activity was very high, that is, in the range from 75 to 80%. This shows that the enzyme is very stable, that the active site of the immobilized enzyme is not sterically hindered, and that the diffusion of glucose to the immobilized enzyme is not hampered.

Conclusion

1. The water content of the ion-exchange fiber as well as its surface area is very important for protein adsorption and enzyme immobilization. The adsorption capacity becomes much larger as the water content increases.

2. The immobilization of the enzymes by adsorption to the fiber gives high yields of the activity, that is, 40—50% for invertase and 75—80% for glucose isomerase.

3. The yield of the activity is improved as the water content of the fiber is increased.

The authors would like to express their appreciation to Dr. Tatsuro Kawaguchi, Mr. Michihiko Tanaka, and Dr. Masaki Nishino for their continuous encouragement throughout this work. They are also much obliged to Mr. Kazuo Teramoto for his advice on the chemical treatments and to Mr. Seiichi Yoshikawa and other collaborators for the preparation of the composite fibers. The authors also wish to thank Toray Industries, Inc., for making this study possible.

References

1) T. Yoshioka and M. Shimamura, *Bull. Chem. Soc. Jpn.*, **56**, 3726 (1983).
2) T. Yoshioka and M. Shimamura, *Bull. Chem. Soc. Jpn.*, **57**, 334 (1984).
3) T. Yoshioka, *Bull. Chem. Soc. Jpn.*, **58**, 2618 (1985).
4) L. Goldstein and G. Maneche, "Immobilized Enzyme Principles," Academic Press, New York (1976), pp. 25—30.
5) A. Yamauchi, T. Suehiro, M. Suzuki, M. Uzumaki, M. Takashio, and N. Fujii, Japanese Laid-open Patent 138624 (1979).
6) H. Ichijo, T. Suehiro, A. Yamauchi, S. Ogawa, M. Sakurai, and N. Fujii, *J. Appl. Polym. Sci.*, **27**, 1665 (1982).
7) H. Ichijo, *J. Appl. Polym. Sci.*, **28**, 1447 (1983).
8) T. Yoshioka, K. Teramoto, and M. Shimamura, Japanese Laid-open Patent 15019 (1979).
9) O. H. Lowry, N. J. Rosebrough, A. L. Farr, and R. J. Randall, *J. Biol. Chem.*, **193**, 265 (1951).
10) G. Bodamer and R. Kunin, *Ind. Eng. Chem.*, **43**, 1082 (1951).

 © 1986 The Chemical Society of Japan Bull. Chem. Soc. Jpn., 59, 405—410 (1986)

Regioselective Preparation of Allylic Sulfones by Palladium-Catalyzed Reactions of Allylic Nitro Compounds with Sodium Benzenesulfinate

Noboru ONO,* Isami HAMAMOTO, Takashi KAWAI, Aritsune KAJI, Rui TAMURA,*,† and Masato KAKIHANA†
Department of Chemistry, Faculty of Science, Kyoto University, Kyoto 606
†Department of Chemistry, The National Defence Academy, Yokosuka 239
(Received June 26, 1985)

Treatment of allylic nitro compounds with sodium benzenesulfinate in the presence of 5 mol% of $Pd(PPh_3)_4$ in *N,N*-dimethylformamide (DMF) at 20—70 °C for 1—10 h resulted in the formation of allylic sulfones with predominance of kinetically controlled products. The product distribution is mainly controlled by the electronic nature of substituents of an allyl unit, and the isomerization to the thermodynamically-stable isomers is negligible. On the other hand, the palladium-catalyzed sulfonylation of allylic acetates with sodium benzenesulfinate is accompanied by the isomerization to give the thermodynamically-controlled products selectively. These results can be explained by assuming that allylic nitro compounds are more reactive to the palladium catalyst than allylic acetates and sulfones.

Allylic sulfones are useful synthetic intermediates because of ability of the sulfonyl group as an activating group for generation of an adjacent carbanion[1] and as a leaving group in substitution reactions[2] and elimination reactions.[3] Allylic sulfones have been prepared so far by following four methods as described in the recent paper,[1] method A: The displacement of allylic halides with sodium benzenesulfinate, method B: The oxidation of the corresponding allylic sulfides, method C: The replacement of an allylic hydroxyl group with sulfone with sodium benzenesulfinate,[4] method D: Oxidation of allyl sulfoxides formed via rearrangement of allyl sulfenates. We now wish to report a new method for the preparation of allylic sulfones.

Recently we have reported that allylic nitro compounds can serve as allylic electrophiles in the palladium-catalyzed allylic alkylation or amination,[5,6] and in the substitution reactions with dialkylcuprates[7] or sodium benzenethiolate.[8] In our previous communications, we reported that allylic nitro compounds were converted into allylic sulfones on treatment with sodium benzenesulfinate in the presence of 5 mol% of $Pd(PPh_3)_4$.[8,9] This provides a useful addition to the above four methods, for some kinds of allylic nitro compounds are more readily available than other conventional allylic electrophiles and the reaction gives the kinetically-controlled products.[8,9] In this paper we wish to report additional experimental data for this reaction which further extend its synthetic utility.

Results and Discussion

Cyclic allylic nitro compounds (**1**), which were readily prepared by the amine-catalyzed reaction of nitroalkanes with cycloalkanones,[10] reacted with sodium benzenesulfinate in the presence of 5 mol% of $Pd(PPh_3)_4$ to give the corresponding sulfones (**2** and **2′**) with predominance of the endo isomer. The results are summarized in Table 1.

Table 1. Preparation of Cyclic Allylic Sulfones (**2**)[a]

Run	R	*n*	Temp/°C	Time/h	Product,	Yield/%
1	H	2	20	10	**2a**,	70[b]
2	H	3	70	1	**2b**,	85[b]
3	H	3	20	10	**2b**,	70
4	Me	3	20	15	**2c**,	75
5	H	4	70	1	**2d**,	92
6	H	5	70	1	**2e**,	76

a) The reaction was carried out in DMF in the presence of $Pd(PPh_3)_4$ (5 mol%). b) The regio-isomer (**2′**) was also formed in 2—3% yield.

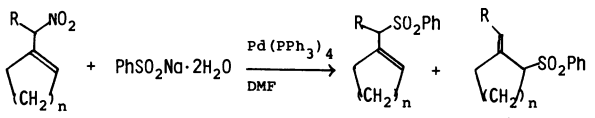

1 **2** **2′** (1)

DMF = *N,N*-Dimethylformamide

Acyclic allylic nitro compounds are also readily prepared in the same way using carbonyl compounds and nitroalkanes as cyclic cases.[10] α-Nitro olefins, which are prepared by dehydration of β-nitro alcohols[11] or nitration of olefins,[12] can be used as allylic nitro compounds because α-nitro olefins are readily isomerized on treatment with bases. A series of acyclic allylic nitro compounds (**3**) were prepared either by the base-catalyzed isomerization of 2-nitro-2-butene or by the introduction of a vinyl group into secondary nitroalkanes via the Michael addition of nitroalkanes to phenyl vinyl sulfoxide and the subsequent thermolysis.[5,6]

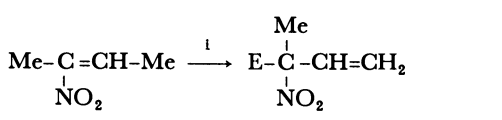

3 (2)

i) Et_3N (0.1 equiv), CH_3CN, E (H^+, HCHO, CH_2=CH-COOMe, CH_2=CH-C(=O)-Me)

Table 2. Preparation of Acyclic Allylic Sulfones (**4**, **5**)

Run	R	3	Temp/°C	Time/h	Product,	Yield/%	4/5
7	Me	**3a**	20	10	**4a**,	75	100/0
8	n-C_6H_{13}	**3b**	20	15	**4b**,	96	95/5
9	CH_2CH_2COOMe	**3c**	20	10	**4c**,	79	95/5
10	$CH_2CH_2C(=O)Me$	**3d**	20	15	**4d**,	80	95/5
11	Ph	**3e**	20	15	**4e**+**5e**	76	53/47
12	CH_2OAc	**3f**	20	15	**4f**+**5f**	95	51/49
13	COOEt	**3g**	20	15	**5g**,	87	0/100
14	H	**3h**	20	15	**4h**+**5h**	60	25/75

The reaction was carried out by stirring a mixture of **3** (1 mmol), $PhSO_2Na \cdot 2H_2O$ (2 mmol), and $Pd(PPh_3)_4$ (0.05 mmol) in DMF (10 ml).

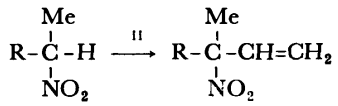

3 (3)

ii) $CH_2=CH-SOPh$, DBU, CH_3CN, 25 °C, 24 h, then thermolysis

Allylic nitro compounds (**3**) underwent the palladium-catalyzed denitro-sulfonylation with sodium benzenesulfinate in the similar way as in the reaction of **1** to give allylic sulfones, **4** and **5**, in good yields. The results are summarized in Table 2.

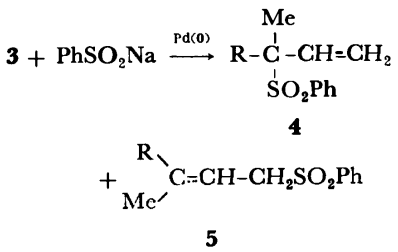

4 + **5** (4)

The product distribution was mainly controlled by the nature of substituents (R) in **3** and was a little affected by the reaction conditions. When R was an electron-donating group such as alkyl groups, the substitution reaction took place at the more hindered site to give the thermodynamically less stable isomer, **4**, regioselectively. When R was an electron-withdrawing group, the reverse regioselectivity was observed and **5** was obtained selectively.

Allylic sulfones are readily isomerized to the thermodynamically more stable isomers by the palladium catalyst.[4] In fact, stirring a mixture of **4d** and $Pd(PPh_3)_4$ (5 mol%) in DMF at room temperature resulted in clean isomerization to **5d**.

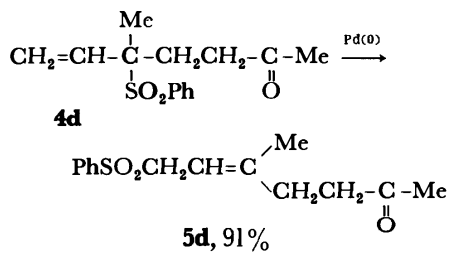

5d, 91% (5)

Nevertheless, **4d** was selectively obtained by the reaction of **3d** with sodium benzenesulfinate in the presence of $Pd(PPh_3)_4$. On the other hand, the palladium-catalyzed sulfonylation of allylic acetates was accompanied by the isomerization to give the thermodynamically-controlled products selectively. For example, treatment of linaryl acetate (**6**) with sodium benzenesulfinate in DMF at 70 °C in the same way as the reaction of **3** resulted in the exclusive formation of **5i**. This fact indicates that sodium nitrite which is liberated during the reaction suppresses the isomerization of the product, **4**. So the reaction was carried out in the presence of sodium nitrite (1 equiv). The results are summarized in Tables 3 and 4. Thus, addition of sodium nitrite is very effective to suppress the isomerization of the product in the sulfonylation of allylic nitro compounds and allylic acetates.

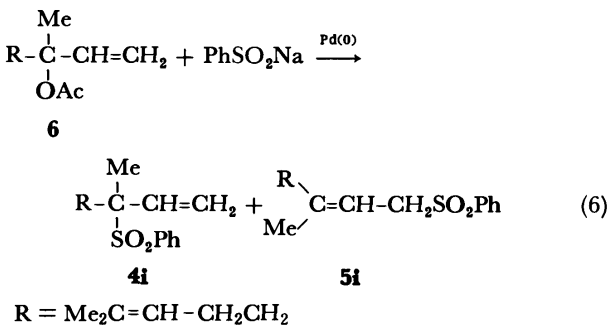

R = $Me_2C=CH-CH_2CH_2$ (6)

The sulfonylation of allylic nitro compounds (**3**) gives the kinetically-controlled product essentially when the isomerization can be ignored. However, the isomerization may occur to some extent during the sulfonylation of **3**. If the isomerization of **4** to **5** competes with the sulfonylation of **3**, the ratio of **4**/**5** may be affected by various factors. So the reaction of **3** with sodium benzenesulfinate was carried out under various conditions. The results are summarized in Tables 2 and 4. Concentration, temperature, and the nature of catalyst affect the ratio of **4**/**5** slightly. However, the reaction time does not affect the ratio of **4**/**5** (Run 19, 20). Namely, the isomerization occurs at the initial stage of the reaction. As the reaction

Table 3. Sulfonylation of Linaryl Acetate (**6**)

Run	Catalyst	Temp/°C	Time/h	Yield/%	Ratio of **4i**/**5i**
15	$Pd(PPh_3)_4$	70	3	**5i**, 76	0/100
16	$Pd(PPh_3)_4$+$NaNO_2$	70	3	**4i**+**5i**, 72	80/20

Table 4. Effects of Reaction Conditions on the Ratio of **4**/**5**[a]

Run	**3**	DMF, ml	Additive	Temp/°C	Time/h	Yield/%	**4**/**5**[b]
8	**3b** (1 mmol)	10	NONE	20	15	96	95/5
17	**3b** (1 mmol)	10	Ph_3P (0.04 mmol)	20	15	79	88/12
18	**3b** (1 mmol)	10	dppe[c] (0.04 mmol)	20	15	70	77/23
9	**3c** (1 mmol)	10	NONE	20	10	79	95/5
19	**3c** (1 mmol)	2	NONE	25	21	d	82/18
20	**3c** (1 mmol)	2	NONE	25	168	64	82/18
21	**3c** (1 mmol)	2	$NaNO_2$ (1 mmol)	25	21	79	100/0
22	**3d** (1 mmol)	2	NONE	25	24	d	78/22
23	**3d** (1 mmol)	5	NONE	25	24	d	85/15
10	**3d** (1 mmol)	10	NONE	20	15	80	95/5
24	**3d** (1 mmol)	2	NONE	70	1	91	75/25
25	**3d** (1 mmol)	2	$NaNO_2$ (1 mmol)	25	21	83	75/25

a) The reaction was carried out under Ar in the presence of $Pd(PPh_3)_4$ (5 mol%). b) The ratio of **4**/**5** was determined by GLC and NMR. c) $Ph_2PCH_2CH_2PPh_2$. d) Yields were not determined.

proceeds, sodium nitrite is liberated, which deactivates the palladium catalyst to generate a new palladium catalyst which catalyzes the sulfonylation of **3** but is inert to the isomerization of **4**.[13] Consequently, when the reaction was carried out in the presence of sodium nitrite (1 equiv), the isomerization could be completely suppressed to give **4** as a sole product. When the reaction was carried out at higher temperature (Run 24) or in a highly concentrated solution (Run 22, 23), it proceeds fast and the selectivity between the sulfonylation and the isomerization becomes low.

Thus, kinetically-controlled products are readily prepared from the reaction of allylic nitro compounds and thermodynamically-controlled products are obtained from the reaction of allylic acetates. It is rather difficult to get the kinetically-controlled products by the palladium-catalyzed sulfonylation of allylic acetates as shown in Table 3. It might be expected that pure **4i** might be obtained if the reaction is carried out at low temperature in the presence of sodium nitrite. However, allylic acetates were less reactive than allylic nitro compounds, and the reaction did not proceed well in the presence of sodium nitrite at low temperature.

All these facts strongly suggest that allylic nitro compounds are more reactive toward the palladium catalyst than allylic acetates or allylic sulfones. To confirm this hypothesis, the competition reaction of **7** (X=NO_2, OAc, tosyl) was carried out. The mixture of the allylic nitro compound and another electrophile was treated with sodium benzenesulfinate in the presence of $Pd(PPh_3)_4$ and the relative reactivity was estimated by measuring the amount of **7** using ^{1}H-NMR. The approximate order of relative reactivity of **7** is summarized in Table 5. Thus, higher reactivity of

Table 5. Relative Reactivity of Allylic Electrophiles (**7**)

X	Rel. Rate
NO_2	1
OAc	0.5
Ts	0.3

allylic nitro compounds than other allylic electrophiles was verified.

$$Me_2C(X)\text{-}CH{=}CH_2 + PhSO_2Na \xrightarrow{Pd(0)} \mathbf{4} + \mathbf{5} \qquad (7)$$

7 (X = NO_2, OAc, Ts)

Another type of competition reaction was carried out; 4-acetoxy-2-methyl-1-nitro-2-butene (**8**) was treated with sodium benzenesulfinate in the presence of $Pd(PPh_3)_4$ in DMF or tetrahydrofuran (THF)–MeOH. The results are summarized in Eq. 8. When the reaction was carried out in THF–MeOH, the acetoxyl group was selectively displaced to give **9** in 52% yield. When the reaction was carried out in DMF, both groups were displaced to give **10**. Namely, the acetoxyl group is more readily displaced than the nitro group in the reaction of Eq. 8.

$$O_2N\text{-}CH_2\text{-}C(Me){=}CHCH_2OAc + PhSO_2Na \xrightarrow{\text{THF-MeOH}} O_2N\text{-}CH_2\text{-}C(Me){=}CH\text{-}CH_2SO_2Ph \quad \mathbf{9} \qquad (8)$$

$$PhSO_2Na \xrightarrow{\text{DMF}} PhSO_2CH_2\text{-}C(Me){=}CH\text{-}CH_2SO_2Ph \quad \mathbf{10}$$

The regiochemistry of the present sulfonylation can be explained by the mechanism shown in Scheme 1, which has been proposed by Tsuji and Trost for the palladium-catalyzed allylic alkylation of allylic acetates or related reactions.[14] Three key-steps are involved there, step a: π-complexation of double bonds with PdLn, step b: elimination of X from this complex to form π-allylpalladium complex, step c: nucleophilic attack to this π-allyl complex.

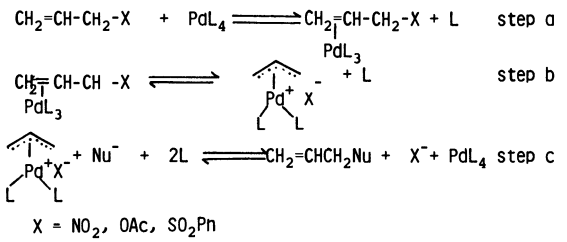

Scheme 1. The Mechanism of Palladium-Catalyzed Allylation

As the nitro group is a stronger electron-accepting group than the acetoxyl and sulfonyl groups, allylic nitro compounds are more reactive than other allylic electrophiles at step a. On the other hand, the acetoxyl group is a better leaving group than other allylic electrophiles at step b. The palladium catalyst may be used preferably for the sulfonylation of allylic nitro compounds rather than for the isomerization of allylic sulfones until the reaction is complete. As the palladium catalyst is deactivated by sodium nitrite when the reaction is complete, the sulfonylation of allylic nitro compounds gives the kinetically-controlled product selectively.

When allylic electrophiles have both the nitro and acetoxyl groups at the allylic positions as compound **8**, the regiochemistry of the leaving group is determined only at step b, and the acetoxyl group is more readily displaced by nucleophiles than the nitro group.

Product distribution is intrinsically controlled by the nature of substituents of an allyl unit. Although the steric effect plays an important role for the control of the regiochemistry of the palladium-catalyzed allylic alkylation,[15] the steric effect is a minor factor in the present sulfonylation as shown in Table 2. The regiochemical results are understood in terms of the electronic effects of the substituents of **3**. The palladium atom in the reaction intermediates may be unsymmetrically bonded to the allylic system depending on the substituents. When R is an electron-donating group, palladium lies close to the γ-carbon (intermediate A), and when R is an electron-withdrawing group, palladium lies close to the α-carbon (intermediate B).[16] The former intermediates causes the external nucleophilic attack to occur at the more weakly bonded α-carbon and the latter do it at the γ-position.[4] Hegedus and his co-workers have proposed that some kinds of palladium-assisted allylic aminations and alkylations may proceed via the σ-allyl complex rather than the cationic π-allyl complex. The regiochemical data of the present sulfonylation can also be explained by assuming that the reaction proceeds via the σ-allyl complex.[17] However, it is very difficult to distinguish these mechanisms at the present stage by the regiochemical data only.

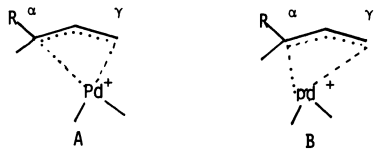

Although the utility of the present method is well demonstrated in Tables 1 and 2, it should be emphasized that allylic nitro compounds can be used both as nucleophiles and electrophiles. Namely, electrophiles (E) and nucleophiles (Nu) can be introduced stepwise as shown in Eq. 9. The regiochemistry of both steps is well-controlled as discussed here. Considering these merits, the present method provides a useful addition to the exisiting methods for the preparation of allylic sulfones.[1]

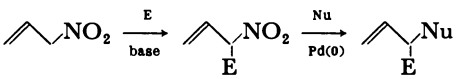

(9)

E = Electrophiles Nu = Nucleophiles

Experimental

Preparation of Allylic Nitro Compounds. Cyclic allylic nitro compounds were prepared by heating a solution of cycloalkanones, nitroalkanes, and amines in benzene at 80 °C according to the literature.[10] Acyclic allylic nitro compounds, **3a**,[18] **3b**, **3e**, and **3g**,[6] were prepared by the Michael addition of the corresponding nitro compounds to phenyl vinyl sulfoxide and the subsequent thermolysis. **3b**: IR (neat) 1340, 1540 cm^{-1}, ^1H NMR ($CDCl_3$) δ=0.92 (3H,m), 1.3 (8H, m), 1.62 (3H, s), 2.0 (2H, m), 5.24 (1H, d, J=17 Hz), 5.28 (1H, d, J=10 Hz), 6.20 (1H, dd, J=17 and 10 Hz). **3e**: IR (neat) 1360, 1540 cm^{-1}, ^1H NMR ($CDCl_3$) δ=2.04 (3H, s), 5.26 (1H, d, J=17 Hz), 5.48 (1H, d, J=10 Hz), 6.60 (1H, dd, J=17 and 10 Hz), 7.4 (5H, m). Other allylic nitro compounds, **3c**,[6] **3d**, and **3f** were prepared by the isomerization of 2-nitro-2-butene. **3d**: IR (neat) 1700, 1530, 1350 cm^{-1}, ^1H NMR ($CDCl_3$) δ=1.61 (3H, s), 2.08 (3H, s), 2.12—2.48 (4H, m), 5.12 (1H, d, J= 10 Hz), 5.22 (1H, d, J=17 Hz), 6.12 (1H, dd, J=17 and 10 Hz). All these compounds were prepared in 70—80% yields according to the literatures.[6,18] Compound **3f** was prepared as follows: A solution of 2-nitro-2-butene (3.03 g, 30 mmol), 35%-HCHO (5.14 g, 60 mmol), and triethylamine (0.303 g, 3 mmol) in 20 ml of acetonitrile was kept at room temperature for 24 h. The reaction mixture was poured into water and extracted with diethyl ether. The usual work-up followed by distillation with Kugelrohr gave 2-methyl-2-nitro-3-buten-1-ol, 3.15 g (80%), bp 110 °C/1 mmHg (1 mmHg=133.322 Pa). This alcohol (0.74 g, 5.65 mmol) was dissolved in 10 ml of benzene and to this solution was added acetic anhydride (0.58 g, 5.65 mmol), 3 ml of pyridine and 4-

(dimethylamino)pyridine (70 mg) and the resulting mixture was stirred at room temperature for 15 h. The usual work-up followed by column chromatography (silica gel/benzene-hexane) gave **3f**, 0.86 g (88%). IR (neat) 1730, 1540, 1370 cm^{-1}, ^1H NMR ($CDCl_3$) δ=1.72 (3H, s), 2.01 (3H, s), 5.48 (2H, q, J=10 Hz), 5.52 (1H, d, J=10 Hz), 5.54 (1H, d, J=17 Hz), 6.10 (1H, dd, J=10 and 17 Hz). Found: C, 45.74; H, 6.84; N, 10.38. Calcd for $C_5H_9NO_4$ (alcohol): C, 45.79; H, 6.92; N, 10.68.

Preparation of 1-(Phenylsulfonylmethyl)cyclopentene (2a). A mixture of 1-(nitromethyl)cyclopentene (0.381 g, 3 mmol), sodium benzenesulfinate dihydrate (0.60 g, 3 mmol), and $Pd(PPh_3)_4$ (20 mg) in 11 ml of DMF was stirred at 20 °C under Ar for 10 h and then poured into water. The product was extracted with diethyl ether and the organic layer was washed with brine and water, dried with anhydrous magnesium sulfate. After the solvent was evaporated, the residue was subjected to column chromatography (silica gel/hexane-ethyl acetate) to give **2a**, 0.466 g (70%), mp (from benzene-hexane) 95—96 °C. IR ($CHCl_3$) 1313, 1152 cm^{-1}, ^1H NMR ($CDCl_3$) δ=1.86 (2H, m), 2.28 (2H, m), 2.37 (2H, m), 3.92 (2H, s), 5.50 (1H, br), 7.50—7.90 (m, 5H). Found: C, 64.70; H, 6.32. Calcd for $C_{12}H_{14}O_2S$: C, 64.84; H, 6.35. Following compounds were prepared by this procedure.

2b: Mp 63—65 °C. IR ($CHCl_3$) 1315, 1155 cm^{-1}, ^1H NMR ($CDCl_3$) δ=1.38—1.58 (4H, m), 1.86 (2H, m), 2.00 (2H, m), 3.61 (2H, s), 5.33 (1H, br), 7.44—7.83 (5H, m). Found: C, 65.92; H, 6.84. Calcd for $C_{13}H_{16}O_2S$: C, 66.07; H, 6.82.

2c: IR (neat)1310, 1155 cm^{-1}, ^1H NMR ($CDCl_3$) δ=1.44 (3H, d, J=7 Hz), 1.4—2.2 (8H, m), 3.60 (1H, q, J=7 Hz), 5.34 (1H, br), 7.40—7.82 (5H, m). MS, found; M^+, 250.1047. Calcd for $C_{14}H_{18}O_2S$: M^+, 250.1056.

2d: Mp 48—49.5 °C. IR ($CHCl_3$) 1657, 1310, 1155 cm^{-1}, ^1H NMR ($CDCl_3$) δ=1.41 (2H, m), 1.53 (2H, m), 1.80 (2H, m), 2.02 (2H, m), 2.25 (2H, m), 3.73 (2H, s), 5.50 (1H, t, J=6.5 Hz), 7.52—7.92 (5H, m). Found: C, 67.12; H, 7.19. Calcd for $C_{14}H_{18}O_2S$: C, 67.17; H, 7.25.

2e: Mp 64—65.5 °C. IR ($CHCl_3$) 1658, 1316, 1151 cm^{-1}, ^1H NMR ($CDCl_3$) δ=1.2—1.71 (8H, m), 1.84—2.40 (4H, m), 3.72 (2H, s), 5.42 (1H, t, J=8.2 Hz), 7.40—7.97 (5H, m). Found: C, 68.52; H, 7.60. Calcd for $C_{15}H_{20}O_2S$: C, 68.15; H, 7.62.

Preparation of 3-Phenylsulfonyl-3-methyl-1-butene (4a). A mixture of 3-methyl-3-nitro-1-butene (**3a**, 0.115 g, 1 mmol), sodium benzenesulfinate dihydrate (0.24 g, 1.2 mmol), and $Pd(PPh_3)_4$ (40 mg) in 10 ml of DMF was stirred at 20 °C under Ar for 10 h. The usual work-up followed by column chromatography (silica gel/hexane-ethyl acetate) gave **4a**, 0.157 g (75%). IR (neat) 1300, 1135 cm^{-1}, ^1H NMR ($CDCl_3$) δ=1.68 (3H, s), 5.08 (1H, d, J=17 Hz), 5.26 (1H, d, J=10 Hz), 6.01 (1H, dd, J=17 and 10 Hz), 7.42—7.86 (5H, m). The spectra of **5a** was also detected slightly. The ratio of **4a**/**5a** was determined by GLC to be 98/2. Following acyclic allylic sulfones (**4** or **5**) were prepared by this procedure.

4b: IR (neat) 1300, 1150 cm^{-1}, ^1H NMR ($CDCl_3$) δ=0.88 (3H, t, J=7 Hz), 1.32 (3H, s), 1.0—1.4 (8H, m), 1.8—2.04 (2H, m), 5.00 (1H, d, J=16 Hz), 5.31 (1H, d, J=10 Hz), 5.90 (1H, dd, J=16 and 10 Hz), 7.36—7.86 (5H, m). The ratio of **4b**/**5b** was determined by NMR and GLC to be 95/5. Found: C, 68.44; H, 8.64. Calcd for $C_{16}H_{24}O_2S$: C, 68.53; H, 8.63.

4c: Mp 72—75 °C. IR ($CHCl_3$) 1735, 1298, 1147 cm^{-1}, ^1H NMR ($CDCl_3$) δ=1.35 (3H, s), 2.22—2.39 (4H, m), 3.66 (3H, s), 5.08 (1H, d, J=17 Hz), 5.38 (1H, d, J=11 Hz), 5.91 (1H, dd, J=17 and 11 Hz), 7.38—7.99 (5H, m). Found: C, 59.90; H, 6.65. Calcd for $C_{14}H_{18}O_4S$: C, 59.55; H, 6.43.

4d: Mp 82—84 °C. IR ($CHCl_3$) 1715, 1302, 1148 cm^{-1}, ^1H NMR ($CDCl_3$) δ=1.34 (3H, s), 2.13 (3H, s), 2.20 (2H, m), 2.48 (2H, m), 5.06 (1H, d, J=17 Hz), 5.35 (1H, d, J=11 Hz), 5.91 (1H, dd, J=17 and 11 Hz), 7.95—7.35 (5H, m). Found: C, 62.84; H, 6.73. Calcd for $C_{14}H_{18}O_3S$: C, 63.13; H, 6.81.

4e, 5e: Treatment of **3e** (0.16 g, 0.9 mmol) in the same way as the preparation of **4a** gave the mixture of **4e** and **5e** (the ratio of **4e**/**5e**=53/47), 0.177 g (72%). Mp 117—120 °C. IR ($CHCl_3$) 1310, 1155 cm^{-1}, ^1H NMR ($CDCl_3$) δ=1.64 (Me of **5e**, s), 1.82 (Me of **4e**, s), 3.96 (CH_2 of **5e**, d, J=8 Hz), 5.32 (CH=C of **4e**, m), 5.64 (C=CH, of **5e**, t, J=8 Hz), 6.65 (C=CH of **4e**), 7.08—7.84 (10H, m). Found: C, 70.23; H, 5.91. Calcd for $C_{16}H_{16}O_2S$: C, 70.56; H, 5.92.

4f, 5f: Treatment of **3f** (0.173 g, 1 mmol) gave the mixture of **4f** and **5f** (**4f**/**5f**=51/49), 0.254 g (95%). IR (neat) 1740, 1310, 1060 cm^{-1}, ^1H NMR ($CDCl_3$) δ=1.36 (s, Me of **5f**), 1.44 (s, Me of **4f**), 1.98 (s, Ac of **4f**), 2.01 (s, Ac of **5f**), 3.90 (m, CH_2 of **5f**), 4.3—4.5 (m, CH_2O- of **4f**, **5f**), 5.22 (1H, d, J=17 Hz), 5.40 (1H, d, J=10 Hz), 5.3—5.5 (CH=C of **5f**), 5.94 (1H, dd, J=17 and 10 Hz). MS, found: M^+ 268.0736. Calcd for $C_{13}H_{16}SO_4$: 268.0767.

5g: Treatment of **3g** (0.173 g, 1 mmol) in the same way as the preparation of **4a** gave **5g**, 0.234 g (87%). No **4g** was detected in GLC and NMR. *E*/*Z* ratio was determined by GLC and NMR to be 97/3. IR (neat) 1730, 1290, 1170 cm^{-1}, ^1H NMR ($CDCl_3$) δ=1.28 (3H, t, J=7 Hz), 1.60 (3H, s), 4.01 (2H, d, J=7 Hz), 4.22 (2H, q, J=7 Hz), 6.66 (1H, t, J=8 Hz), 7.44—7.96 (5H, m). MS, found: M^+ 268.0747. Calcd for $C_{13}H_{16}SO_4$: 268.0767.

4h, 5h: A mixture of 2-nitro-2-butene (0.101 g, 1 mmol), sodium benzensulfinate dihydrate (0.4 g, 2 mmol), $Pd(PPh_3)_4$ (58 mg), dppe (20 mg), and triethylamine (0.101 g, 1 mmol) in 4 ml of DMF was stirred at 70 °C under Ar for 2 h. The usual work-up followed by column chromatography (silica gel/benzene-hexane) gave the mixture of **4h** and **5h** (**4h**/**5h**=25/75), 0.117 g (60%). IR (neat) 1305, 1150 cm^{-1}. The GLC analysis showed that the products consists of **5h** consisted of two isomers, (*E*)-**5h** and (*Z*)-**5h**, (*E*/*Z*=75/25). ^1H NMR ($CDCl_3$) δ=1.34 (Me of (*Z*)-**5h**, d, J=7 Hz), 1.42 (Me of **4h**, d, J=7 Hz), 1.65 (Me of (*E*)-**5h**), 3.7—3.9 (CH-SO_2Ph or CH_2SO_2Ph of **4h** or **5h**), 5.06—6.0 (CH=C of **4h** and **5h**), 7.4—7.9 (5H, m). The spectral data of this mixture are in good agreement with those of the literature where this sulfone was prepared by the reaction of crotyl chloride with sodium benzenesulfinate.[1] MS, found: M^+ 196.0546. Calcd for $C_{10}H_{12}O_2S$: 196.0548.

Palladium-Catalyzed Isomerization of 4d to 5d. A mixture of **4d** (0.133 g, 0.5 mmol) and $Pd(PPh_3)_4$ (0.029 g) in 2 ml of DMF was stirred at 25 °C under Ar for 30 h and poured into water. After the usual work-up, the crude product was subjected to column chromatography (silica gel/hexane-ethyl acetate) to give *E*-**5d**, 0.097 g (73%) and *Z*-**5d**, 0.024 g (18%). (*E*)-**5d**: Mp 79—81 °C, IR ($CHCl_3$) 1714, 1311, 1149 cm^{-1}, ^1H NMR ($CDCl_3$) δ=1.35 (3H, s), 2.16 (3H, s), 2.27 (2H, t, J=7 Hz), 2.51 (2H, t, J=7 Hz), 3.80 (2H, d, J=8 Hz), 5.19 (1H, t q, J=2 and 8 Hz), 7.52—7.90 (5H, m). Found: C, 63.06; H, 6.83. Calcd for $C_{14}H_{18}O_3S$: C, 63.13; H, 6.81. (*Z*)-**5d**: colorless oil, ^1H NMR ($CDCl_3$) δ=1.25 (3H, s), 2.16 (2H, t, J=8 Hz), 2.18 (3H, s), 2.42 (2H, t, J=8 Hz), 3.90 (2H, d, J=8 Hz), 5.28 (1H, t, J=8 Hz), 7.53—7.95 (5H, m).

Sulfonylation of Linaryl Acetate (6). A mixture of linaryl acetate (0.196 g, 1 mmol), $PhSO_2Na \cdot 2H_2O$ (0.22 g,

1.1 mmol), and $Pd(PPh_3)_4$ (58 mg) in 3 ml of DMF was stirred at 70 °C under Ar for 3 h. The usual work-up followed by column chromatography (silica gel/hexane–ethyl acetate) gave **5i**,[4] 0.211 g (76%). The *E*/*Z* ratio was determined by GLC to be 74/26. IR (neat) 1310, 1150 cm^{-1}, ^1H NMR ($CDCl_3$) δ=1.30 (3H, s), 1.58 (3H, s), 1.65 (3H, s), 1.98 (4H, m), 3.82 (2H, d, J=8 Hz), 5.1 (2H, m), 7.5—7.9 (5H, m). The same reaction was carried out in the presence of $NaNO_2$ (0.069 g, 1 mmol) under the same reaction conditions as above. The mixture of **4i** and **5i**, 0.203 g (73%), was obtained. The ratio of **4i**/**5i** was determined by GLC to be 80/20.

Effects of Reaction Conditions on the Ratio 4/5 A mixture of **3** (1 mmol), $PhSO_2Na \cdot 2H_2O$ (1.2 mmol), and $Pd(PPh_3)_4$ (0.059 g) in DMF (2—10 ml) was stirred under various conditions as in Table 4. The product, which was isolated by the procedures described in the preparation of **4a**, was analyzed by GLC and NMR. The yields are in the range of 70—90% in every case. The results are summarized in Table 4.

Effects of Ligands on the Ratio of 4/5. A mixture of **3b** (0.185 g, 1 mmol), $PhSO_2Na \cdot 2H_2O$ (0.24 g, 1.2 mmol), $Pd(PPh_3)_4$ (0.059 g), and dppe (0.035 g) in 5 ml of DMF was stirred at 20 °C for 15 h under Ar. The usual work-up followed by column chromatography gave the mixture of **4b** and **5b**, 0.196 g (70%). The reaction in the presence of Ph_3P (0.090 g) was carried out in the same way. The product was analyzed by GLC and NMR.

Preparation of 4c and 4d by the Reaction of 3c and 3d in the Presence of Sodium Nitrite. A mixture of $Pd(PPh_3)_4$ (0.058 g, 0.05 mmol) and sodium nitrite (0.069 g, 1.0 mmol) in DMF (4 ml) was stirred at 25 °C under Ar for 30 min. To the resulting mixture was added $PhSO_2Na \cdot 2H_2O$ (0.22 g, 1.1 mmol) and **3c** (0.188 g, 1 mmol) and stirred at 25 °C for 21 h and then poured into water. The usual work-up followed by column chromatography (silica gel/hexane–ethyl acetate) gave **4c**, 0.22 g (79%), mp 72—75 °C. The same procedure using **3d** (0.172 g, 1 mmol) gave **4d**, 0.22 g (83%), mp 82—84 °C.

Competition Reaction of Allylic Electrophiles (7). To a mixture of **7** (X=NO_2, 1 mmol) and **7** (X=OAc, 1 mmol) in 5 ml of DMF was added $PhSO_2Na \cdot 2H_2O$ (1 mmol) and $Pd(PPh_3)_4$ (58 mg) and the resulting mixture was stirred at 20 °C. After 3 h and 6 h, a portion of the reaction mixture was poured into water and extracted with diethyl ether and the organic components were analyzed by NMR. The same reaction was carried out by using **7** (X=NO_2) and **7** (X=Ts). The reactivity was estimated by the peak at δ 1.60 (Me, X=NO_2), 2.02 (OAc, X=OAc), and 2.30 (Me, X=Ts). The results are summarized in Table 5.

Sulfonylation of 4-Acetoxy-2-methyl-1-nitro-2-butene (8).[19] A mixture of **8** (0.52 g, 3 mmol), $PhSO_2Na \cdot 2H_2O$ (0.60 g, 3 mmol), and $Pd(PPh_3)_4$ (70 mg) in 10 ml of THF and 2 ml of MeOH was stirred at 20 °C under Ar for 20 h. The usual work-up followed by column chromatography (silica gel/hexane–ethyl acetate) gave **9**, 0.52 g (52%). Mp 50—52 °C. IR ($CHCl_3$) 1550, 1357, 1305, 1150 cm^{-1}, ^1H NMR ($CDCl_3$) δ=1.42 (3H, s), 3.92 (2H, d, J=8 Hz), 4.83 (2H, s), 5.64 (1H, br t, J=8 Hz), 7.40—7.88 (5H, m). Found: C, 51.66; H, 4.90; N, 5.36. Calcd for $C_{11}H_{13}NO_4S$: C, 51.75; H, 5.13; N, 5.49. The same reaction was carried out in 12 ml of DMF to give **10**, 0.53 g, (42%). Mp 136—138 °C. IR ($CHCl_3$) 1310, 1150 cm^{-1}, ^1H NMR ($CDCl_3$) δ=1.55 (3H, s), 3.82 (4H, d, J=8 Hz), 5.30 (1H, br t, J=8 Hz), 7.44—7.96 (10H, m). Found: C, 58.13; H, 5.10. Calcd for $C_{17}H_{18}O_4S_2$: C, 58.26; H, 5.18.

This work was supported by a Scientific Research Grant from the Ministry of Education, Science, and Culture.

References

1) B. M. Trost and N. R. Schmuff, *J. Am. Chem. Soc.*, **107**, 396 (1985) and references therein.

2) B. M. Trost and M. R. Ghadiri, *J. Am. Chem. Soc.*, **106**, 7260 (1984) and references therein.

3) T. Mandai, T. Yanahi, K. Araki, Y. Morisaki, M. Kawada, and J. Otera, *J. Am. Chem. Soc.*, **106**, 3670 (1984) and references therein.

4) K. Inomata, T. Yamamoto, and H. Kotake, *Chem. Lett.*, **1981**, 1357; G. P. Boldrini, D. Savoia, E. Tagliavini, C. Trombini, and A. Umani-Ronchi, *J. Organomet. Chem.*, **268**, 97 (1984).

5) R. Tamura and L. S. Hegedus, *J. Am. Chem. Soc.*, **104**, 3727 (1982); R. Tamura, K. Hayashi, Y. Kai, and D. Oda, *Tetrahedron Lett.*, **24**, 4437 (1984).

6) N. Ono, I. Hamamoto, and A. Kaji, *J. Chem. Soc., Chem. Commun.*, **1982**, 821; N. Ono, I. Hamamoto, and A. Kaji, *Bull. Chem. Soc. Jpn.*, **58**, 1863 (1985).

7) N. Ono, I. Hamamoto, and A. Kaji, *J. Chem. Soc., Chem. Commun.*, **1984**, 274.

8) N. Ono, I. Hamamoto, T. Yanai, and A. Kaji, *J. Chem. Soc., Chem. Commun.*, **1985**, 523.

9) R. Tamura, K. Hayashi, N. Kakihana, M. Tsuji, and D. Oda, *Tetrahedron Lett.*, **26**, 851 (1985); R. Tamura, K. Hayashi, M. Kakihana, M. Tsuji, and D. Oda, *Chem. Lett.*, **1985**, 229.

10) Houben-Weyl, "Methoden der Organischen Chemie," Vol. X, Part I. 4h Ed., ed by Stuttgart (1971), pp. 336—338; D. H. R. Barton, W. B. Motherwell, and S. Z. Zard, *Bull. Soc. Chim. Fr., II*, **1983**, 61.

11) J. Melton and J. E. McMurry, *J. Org. Chem.*, **40**, 2138 (1975) and references therein.

12) E. J. Corey and E. Estricher, *J. Am. Chem. Soc.*, **100**, 6294 (1978).

13) The activity of the catalyst is affected by various additives involving $NaNO_2$, air or phophine ligands. The ratio of **4**/**5** is affected by the activity of the catalyst, for isomerization of **4** to **5** takes place during the reaction.

14) J. Tsuji, "Organic Synthesis with Palladium Compounds," Springer-Verlag, Berlin, Heiderberg, New York,1980; B. M. Trost and T. R. Verhoeven, *J. Am. Chem. Soc.*, **102**, 4730 (1980).

15) E. Keinan and M. Sakai, *J. Chem. Soc., Chem. Commun.*, **1984**, 648.

16) E. Keinan and Z. Roth, *J. Org. Chem.*, **48**, 1769 (1983).

17) B. Åkermark, G. Åkermark, L. S. Hegedus, and K. Zetterberg, *J. Am. Chem. Soc.*, **103**, 3037 (1981).

18) R. Tanikaga, H. Sugihara, K. Tanaka, and A. Kaji, *Synthesis*, **1977**, 299.

19) P. A. Wehrli and B. Scher, *J. Org. Chem.*, **42**, 2939 (1977).

α-D-Glucosylation by 6-O-Acetyl-2,3,4-tri-O-benzyl-D-glucopyranose Using Trimethylsilyl Triflate and Pyridine. Synthesis of α-Maltosyl and α-Isomaltosyl α-D-Glucosides[1]

Shinkiti KOTO,* Kazuo YAGO,† Shonosuke ZEN, Fumiya TOMONAGA,† and Shigehiko SHIMADA†
School of Pharmaceutical Sciences, Kitasato University, Shirokane, Minato-ku, Tokyo 108
†Department of Pharmacy, Kitasato University Hospital, Kitasato, Sagamihara 228
(Received July 3, 1985)

The D-glucosylation of methyl 2,3,4-tri-O-benzyl-α-D-glucopyranoside and methyl 2,3,6-tri-O-benzyl-β-D-glucopyranoside by 2,3,4,6-tetra-O-benzyl-α-D-glucopyranose using pyridine and excess trimethylsilyl triflate was carried out in dichloromethane, 1,2-dimethoxyethane, and acetonitrile. In a given solvent, the selectivity of the reaction varied depending on the type of hydroxyl group of the glucosyl acceptors. The D-glucosylation of these acceptors with 6-O-acetyl-2,3,4-tri-O-benzyl-D-glucopyranose employing this reagent system in dichloromethane proceeded with good α-selectivity irrespective of the type of the hydroxyl group. This α-D-glucosylation was applied for the synthesis of O-α-D-glucopyranosyl-(1→4)- and -(1→6)-α-D-glucopyranosyl α-D-glucopyranosides from α,α-trehalose.

Traditional glycosylation is performed with the aid of various heavy-metal compounds.[2] Several methods are, however, free from the use of such materials.[3,4] The desiloxane-promoted condensation between a 1-O-silyl derivative of 2,3,4,6-tetra-O-benzyl-α-D-glucopyranose (**1**) as a D-glucosyl donor and a silylated alcohol as its acceptor is catalyzed by strong acids such as sulfonic acids,[5] as well as a Lewis acid like trimethylsilyl triflate (TMSOTf).[6,7] Since trimethylsilyl triflate[8] is a powerful silylation reagent for a hydroxy compound, a mixture of excess trimethylsilyl triflate and a base such as pyridine (Py) was expected to bring about a condensation between **1** and an alcohol (Eq. 1) in which G denotes a 2,3,4,6-tetra-O-benzyl-D-glucosyl residue or appropriate equivalents.

$$\mathrm{GOH} + \mathrm{ROH} \xrightarrow[-2\mathrm{TfOH}\cdot\mathrm{Py}]{(2+x)\mathrm{TMSOTf}+2\mathrm{Py}} (\mathrm{GOTMS} + \mathrm{ROTMS}) \xrightarrow[-\mathrm{TMS_2O}]{x\mathrm{TMSOTf}} \mathrm{GOR} \qquad (1)$$

The results of the D-glucosylation of the protected glucosides **2** and **3** with **1** (prescribed by Eq. 1) is summarized in Table 1. The value of x, the excess of trimethylsilyl triflate (Eq. 1), was sufficient at 1.5 for the primary alcohol **2** (Entry 1) and at 2 for the secondary alcohol **3** (Entry 4) to react in dichloromethane at 0°C. Glucosylation in this solvent, however, showed poor selectivity. On the other hand, the glucosylation of **3** (Entry 5) in 1,2-dimethoxyethane exhibited a good α-selectivity but the reaction was slow. The reaction of **2** (Entry 2) in 1,2-dimethoxyethane, however, did not show any selectivity. The glucosylation of **2** (Entry 3) in acetonitrile[4] showed only moderate β-selectivity. A similar selectivity, however, was not observed in the reaction of **3** (Entry 6) in acetonitrile. Such a weak solvent-dependency of the selectivity is in contrast to the remarkable dependence of the selectivity observed in a coupling reaction between glucosyl fluoride and silylated alcohol in the presence of trimethylsilyl triflate.[4]

Expectedly,[7] in the absence of an acceptor, **1** underwent self-condensation[5] to give **9** and **10** (Entry 7).

6-O-Acetyl-2,3,4-tri-O-benzyl-D-glucopyranose (**4**), readily derived from 1,6-anhydro-β-D-glucopyranose (levoglucosan), has been used as an α-D-glucosyl donor in dehydrative glucosylation.[9] This compound was again effective for α-D-glucosylation in the glucosylation of **2** and **3** using the above-described reagent mixture (Entries 8 and 9). The α-selectivity (86%) of the glucosylation of the primary alcohol was improved

Table 1. Results of D-Glucosylation by Protected D-Glucoses Using Pyridine and Excess Trimethylsilyl Triflate

Entry	Donor GOH (equiv)	Acceptor ROH (0.1 mmol)	Solv. (0.5 ml)	Py (equiv)	TMSOTf (equiv)	x[a]	Temp °C	Time h	Glucosides GOR %(α/β)
1	**1** (1.0)	**2**	CH_2Cl_2	2.5	4.0	1.5	0	4.5	**5+6** 90(43/57)
2	**1** (1.1)	**2**	$(CH_2OMe)_2$	2.6	4.6	2.0	0	4.5	**5+6** 48(48/52)
3	**1** (1.1)	**2**	MeCN	2.6	4.6	2.0	0	4.5	**5+6** 81(32/68)
4	**1** (1.3)	**3**	CH_2Cl_2	2.8	4.9	2.1	0	4.5	**7+8** 78(57/43)
5	**1** (1.3)	**3**	$(CH_2OMe)_2$	2.8	4.9	2.1	0	6	**7+8** 31(82/18)
6	**1** (1.3)	**3**	MeCN	2.8	4.9	2.1	5	3	**7+8** 68(42/58)
7	**1** (1.0)	**1**	CH_2Cl_2	2.4	4.3	1.9	0	6	**9+10** 79(45/55)
8	**4** (1.1)	**2**	CH_2Cl_2	2.6	4.1	1.5	0	4.5	**11+12** 89(86/14)
9	**4** (1.3)	**3**	CH_2Cl_2	2.8	4.9	2.1	0	4.5	**13+14** 72(86/14)

a) x=TMSOTf(equiv)−Py(equiv) (cf. Eq. 1).

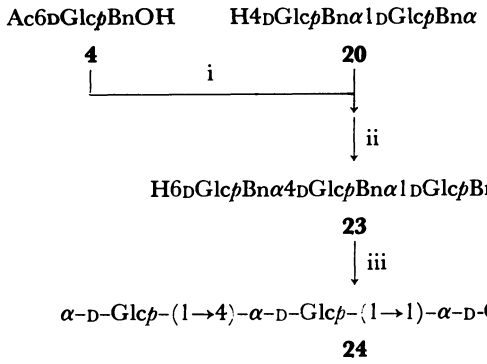

Fig. 1. Synthetic Scheme of α-Maltosyl α-D-Glucoside (**24**); Bn=—CH_2Ph (cf. Ref. 19 for the code-expression of the protected carbohydrates).

compared to the previously reported method (69%).[9]

The α-D-glucosylation described so far was then applied to the synthesis of *O*-α-D-glucopyranosyl-(1→4)- and -(1→6)-α-D-glucopyranosyl α-D-glucopyranosides (**24** and **28**) as illustrated in Fig. 1 for the case of **24**. Various kinds of unsymmetrical α,α-trehaloses have been synthesized in view of biological interests.[10-12] A short-time treatment of a solution of α,α-trehalose (**15**) in dimethyl sulfoxide with 2,2-dimethoxypropane in the presence of *p*-toluenesulfonic acid, followed by acetylation, gave the monoisopropylidene derivative **17** in a 57% yield. This compound was transformed into the hexabenzyl derivative **19**, which was then converted into a heptabenzyl derivative **20** via controlled benzylation. The heptabenzyl derivative **21** was prepared via tritylation of **19**. Glucosylation of **20** and **21** with **4** gave the corresponding α-glucosides **22** and **26** with good selectivity. A deprotection of these compounds afforded the unsymmetrical derivatives, **24** and **28**, of trehalose, and their C-13 were consistent with their proposed structure.

Experimental[13,14]

Compounds **5**,[15] **6**,[16] **7**,[13] **8**,[13] **9**,[5] and **10**[5] were identified with those prepared before.

Procedure for Glucosylation. Pyridine and trimethylsilyl triflate (Aldrich) were successively injected into a stirring mixture of a donor and an acceptor in a solvent at −45°C. The temperature was allowed to increase to the temperature specified in Table 1 and below. The reaction was continued for an appropriate duration. After the addition of triethylamine equimolar to trimethylsilyl trilfate, the mixture was concentrated and chromatographed using toluene–2-butanone system (gradient elution).

Methyl *O*-(6-*O*-Acetyl-2,3,4-tri-*O*-benzyl-α- and -β-D-glucopyranosyl)-(1→6)-2,3,4-tri-*O*-benzyl-α-D-glucopyranosides (11 and 12). Compound **11**, mp 80—82°C, $[\alpha]_D^{20}$ +56° (*c* 2.1, $CHCl_3$), R_f=0.35 (toluene/2-butanone=10/1), δ_C($CDCl_3$, TMS) 97.3 and 98.2 (the anomeric carbons). Compound **12**, $[\alpha]_D^{20}$ +29° (*c* 0.5, $CHCl_3$), R_f=0.33, δ_C($CDCl_3$, TMS) 98.2

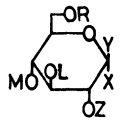

Cpd.	X	Y	Z	L	M	R
1	OH	H	Bn	Bn	Bn	Bn
2	OMe	H	Bn	Bn	Bn	H
3	H	OMe	Bn	Bn	H	Bn
4	OH,	H	Bn	Bn	Bn	Ac
5	OMe	H	Bn	Bn	Bn	αG
6	OMe	H	Bn	Bn	Bn	βG
7	H	OMe	Bn	Bn	αG	Bn
8	H	OMe	Bn	Bn	βG	Bn
11	OMe	H	Bn	Bn	Bn	αG′
12	OMe	H	Bn	Bn	Bn	βG′
13	H	OMe	Bn	Bn	αG′	Bn
14	H	OMe	Bn	Bn	βG′	Bn

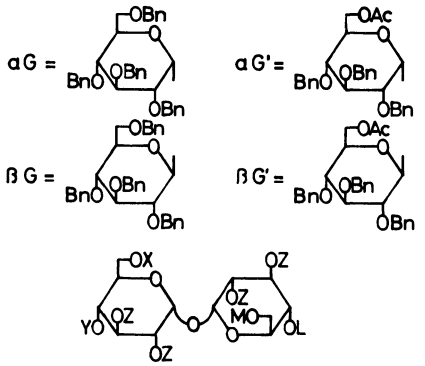

Cpd.	X	Y	Z	L	M
9	Bn	Bn	Bn	Bn	Bn
15	H	H	H	H	H
16	Me	Me	Ac	Me	Me
17	Me	Me	Ac	Ac	Ac
18	Ac	Ac	Ac	Ac	Ac
19	H	H	Bn	Bn	Bn
20	Bn	H	Bn	Bn	Bn
21	H	Bn	Bn	Bn	Bn

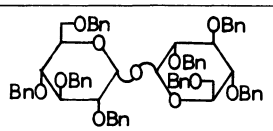

10

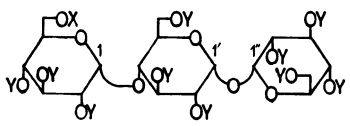

22 X = Ac, Y = Bn **24** X = Y = H

23 X = H, Y = Bn **25** X = Y = Bz

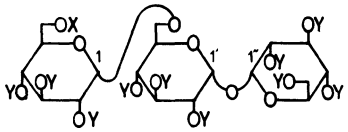

26 X = Ac, Y = Bn **28** X = Y = H

27 X = H, Y = Bn

and 104.1 (the anomeric carbons).

Found: **11**, C, 72.79, H, 6.64%. **12**, 72.81, H, 6.64%. Calcd for $C_{57}H_{62}O_{12}$: C, 72.90, H, 6.65%.

Methyl O-(6-O-Acetyl-2,3,4-tri-O-benzyl-α- and -β-D-glucopyranosyl)-(1→4)-2,3,6-tri-O-benzyl-β-D-glucopyranoside(13 and 14). Compound **13**, $[\alpha]_D^{20}$ +33° (*c* 1.3, $CHCl_3$), R_f= 0.38 (toluene/2-butanone=10/1), δ_C($CDCl_3$, TMS) 96.8 and 104.9 (the anomeric carbons). Compound **14**, $[\alpha]_D^{20}$ +10° (*c* 0.6, $CHCl_3$), R_f=0.33, δ_C($CDCl_3$, TMS) 102.5 and 104.9 (the anomeric carbons).

Found: **13**, C, 73.17, H, 6.69%. **14**, C, 73.15, H, 6.75%. Calcd for $C_{57}H_{62}O_{12}$: C, 72.90, H, 6.65%.

2,3-Di-O-benzyl-α-D-glucopyranosyl 2,3,4,6-Tetra-O-benzyl-α-D-glucopyranoside (19). A solution of **15** (Tokyo Kasei, 1.0 g, 2.9 mmol), *p*-toluenesulfonic acid monohydrate (100 mg) in dimethyl sulfoxide (19 ml) was treated with 2,2-dimethoxypropane (1.0 ml) at room temperature for 55 min. After the addition of triethylamine (1.5 ml), the mixture was evaporated at 85°C to give a syrup which was then treated with acetic anhydride (12 ml) and pyridine (24 ml) at room temperature. Chromatography using toluene–2-butanone system (gradient) afforded **16** (0.21 g, 12%), **17** (1.06 g, 57%), mp 80—81°C, $[\alpha]_D^{20}$ +141° (*c* 0.6, $CHCl_3$) (lit,[11] mp 79—80°C, $[\alpha]_D$ +150.5° (*c* 1.1, $CHCl_3$)), and **18** (0.61 g, 31%).

The monoisopropylidene derivative **17** (530 mg, 0.84 mmol) was heated in benzyl chloride (10.5 ml) containing potassium hydroxide (2.5 g) at 130°C for 1.0 h. Filtration and evaporation at 95°C gave a yellow oil, which was heated in 80% aq acetic acid (40 ml) at 90°C for 15 min. Evaporation and chromatography using toluene-2-butanone system (gradient) gave **19** (484 mg, 66% from **17**), $[\alpha]_D^{20}$ +92° (*c* 0.6, $CHCl_3$) (lit,[11] [α]+90° (*c* 3.09, $CHCl_3$)).

2,3,6-Tri-O-benzyl-α-D-glucopyranosyl 2,3,4,6-Tetra-O-benzyl-α-D-glucopyranoside (20). A mixture of **19** (484 mg, 0.55 mmol), silver oxide (1.66 g), anhydrous calcium sulfate (1.66 g), and benzyl bromide (0.66 ml) in chloroform (7.2 ml) was stirred at room temperature overnight.[17] Chromatography using hexane–acetone system (gradient) gave **9** (33.7 mg), **20** (387 mg, 73%), $[\alpha]_D^{20}$ +89° (*c* 1.2, $CHCl_3$), δ_C($CDCl_3$, TMS) 94.5 (2C, the anomeric carbons), **21** (72 mg, 14%), $[\alpha]_D^{20}$ +96° (*c* 1.4, $CHCl_3$), δ_C($CDCl_3$, TMS) 94.3 and 94.5 (the anomeric carbons).

Found: **20**, C, 74.42, H, 6.42%. **21**, C, 74.76, H, 6.49%. Calcd for $C_{61}H_{64}O_{11}$: C, 75.29, H, 6.63%.

2,3,4-Tri-O-benzyl-α-D-glucopyranosyl 2,3,4,6-Tetra-O-benzyl-α-D-glucopyranoside (21). A solution of **19** (70.2 mg, 0.080 mmol), and trityl chloride (120 mg) in pyridine (0.7 ml) was kept standing for 3 h at 65°C. After the addition of triethylamine (1 ml) and toluene (1 ml), the mixture was evaporated to dryness. The residue was heated in benzyl chloride (2.8 ml) containing potassium hydroxide (1.0 g) at 130°C for 2 h. After filtration and evaporation, the residue obtained was heated in aq acetic acid (80%, 4 ml) at 95°C for 0.5 h. Chromatography (toluene–2-butanone) gave **21** (60.0 mg, 78%).

O-(6-O-Acetyl-2,3,4-tri-O-benzyl-α-D-glucopyranosyl)(1→4)-2,3,6-tri-O-benzyl-α-D-glucopyranosyl 2,3,4,6-Tetra-O-benzyl-α-D-glucopyranoside (22). D-Glucosylation of **20** (143.2 mg, 0.15 mmol) with **4** (94.2 mg, 0.19 mmol) in the presence of pyridine (33.4 μl) and trimethylsilyl triflate (156.4 μl) in dichloromethane (1.4 ml) was conducted at 5 °C for 6 h. Chromatography (toluene–2-butanone, gradient) gave the impure β-anomer (ca. 20 mg, R_f=0.53 (toluene/2-butanone=10/1), δ_C($CDCl_3$, TMS) 103.2) and **22** (161.0 mg, 76%), $[\alpha]_D^{20}$ +81° (*c* 0.4, $CHCl_3$), R_f=0.49, δ_C($CDCl_3$, TMS) 94.0, 94.6, and 97.3 (the anomeric carbons). Found: C, 75.25, H, 6.57%. Calcd for $C_{90}H_{94}O_{17}$: C, 74.67, H, 6.54%.

O-(6-O-Acetyl-2,3,4-tri-O-benzyl-α-D-glucopyranosyl)-(1→6)-2,3,4-tri-O-benzyl-α-D-glucopyranosyl 2,3,4,6-Tetra-O-benzyl-α-D-glucopyranoside (26). Condensation between **4** (55.6 mg, 0.11 mmol) and **21** (100.0 mg, 0.10 mmol) in the presence of pyridine (21.6 μl) and trimethylsilyl triflate (91.4 μl) in dichloromethane (1.0 ml) at 5°C for 6 h, followed by chromatography (toluene–2-butanone, gradient) gave the impure β-anomer (ca. 10 mg, R_f=0.47 (toluene/2-butanone=10/1), δ_C($CDCl_3$, TMS) 103.2) and **26** (118 mg, 79%), $[\alpha]_D^{20}$ +93° (*c* 0.7, $CHCl_3$), R_f=0.43, δ_C($CDCl_3$, TMS) 94.3 (2C), and 97.4 (the anomeric carbons). Found: C, 75.13, H, 6.51%. Calcd for $C_{90}H_{94}O_{17}$: C, 74.67, H, 6.54%.

O-(2,3,4-Tri-O-benzyl-α-D-glucopyranosyl)-(1→4)-2,3,6-tri-O-benzyl-α-D-glucopyranosyl 2,3,4,6-Tetra-O-benzyl-α-D-glucopyranoside (23). A solution of **22** (50.3 mg, 0.035 mmol) in methanol (2 ml) and acetone (1 ml) was treated with 1.5M (1M=1 mol dm^{-3}) sodium methoxide in methanol (0.3 ml) at room temperature overnight. After neutralization with acetic acid, evaporation and chromatography (toluene–2-butanone) furnished **23** (30.2 mg, 62%), $[\alpha]_D^{20}$ +95° (*c* 1.6, $CHCl_3$), δ_C($CDCl_3$, TMS) 94.1, 94.7, and 97.1 (the anomeric carbons). Found: C, 75.19, H, 6.63%. Calcd for $C_{88}H_{92}O_{16}$: C, 75.19, H, 6.60%.

O-(2,3,4-Tri-O-benzyl-α-D-glucopyranosyl)-(1→6)-2,3,4-tri-O-benzyl-O-D-glucopyranosyl 2,3,4,6-Tetra-O-benzyl-α-D-glucopyranoside (27). Similar deacetylation of **26** (58.2 mg, 0.04 mmol) gave **27** (55 mg, 97%), $[\alpha]_D^{20}$+101° (*c* 1.5, $CHCl_3$), δ_C($CDCl_3$, TMS) 94.4 (2C) and 97.5 (the anomeric carbons). Found: C, 75.01, H, 6.50%. Calcd for $C_{88}H_{92}O_{16}$: C, 75.19, H, 6.60%.

O-α-D-Glucopyranosyl-(1→4)-α-D-glucopyranosyl α-D-Glucopyranoside (24). Hydrogenation of **23** (53.6 mg, 0.038 mmol) over palladized charcoal (10%, 40 mg) in acetic acid (6 ml) under 340 kPa of hydrogen at room temperature overnight, followed by chromatography (chloroform/methanol=1/1), gave **24** (17 mg, 81%), $[\alpha]_D^{20}$+169° (*c* 0.4, H_2O), δ_H(D_2O, TMS(ext.)) 5.61 (2H, d, *J*=3.6 Hz, H-1, H-1′), 5.85 (1H, d, *J*=3.0 Hz, H-1″), δ_C(D_2O, TMS(ext.))[18] 61.7 (3C, C-6, -6′, and -6″), 70.6 (C-4), 70.9 (C-4″), 72.0 (C-2′), 72.1 (C-2″), 72.3 (C-2), 73.0 (C-5), 73.4 (C-5″), 73.8 (C-5′), 73.9 (C-3″), 74.1 (C-3′), 74.3 (C-3), 78.2 (C-4′), 94.5 (C-1″), 94.7 (C-1′), and 101.0 (C-1). Found: C, 42.59, H, 6.19%. Calcd for $C_{18}H_{32}O_{16}$: C, 42.86, H, 6.39%.

Benzoylation of **24** (5.1 mg, 0.01 mmol) with benzoyl chloride (1 ml) and pyridine (2 ml) gave the perbenzoate **26** (13.7 mg, 82%), mp 118—119°C, $[\alpha]_D^{20}$ +202° (*c* 0.8, $CHCl_3$) (Found: C, 69.06, H, 4.64%); lit,[12] mp 121—122°, $[\alpha]_D^{21}$+217° (*c* 0.7, $CHCl_3$).

O-α-D-Glucopyranosyl-(1→6)-α-D-glucopyranosyl α-D-Glucopyranoside (28). Similar hydrogenation of **27** (70.6 mg, 0.05 mmol) gave **28** (15.2 mg, 60%), $[\alpha]_D^{20}$+144° (*c* 0.6, H_2O), δ_H(D_2O, TMS(ext.)) 5.41 (1H, d, *J*=3.6 Hz, H-1″), 5.61 (2H, d, *J*=3.5 Hz, H-1, H-1′), δ_C($CDCl_3$TMS(ext.))[18] 61.7 (2C, C-6 and C-6″), 66.6 (C-6′), 70.8 (C-4), 70.9 (2C, C-4′ and -4″), 71.8 (C-2′), 72.2 (2C, C-2 and -2″), 72.7 (C-5), 73.1 (C-5′), 73.4 (C-5″), 73.8 (C-3″), 74.1 (C-3′), 74.4 (C-3), 94.6 (2C, C-1′ and -1″), and 99.0 (C-1). Found: C, 42.76, H, 6.13%. Calcd for $C_{18}H_{32}O_{16}$: C, 42.86, H, 6.39%.

References

1) Presented at the 50th National Meeting of the Chemical Society of Japan, Tokyo, April. 1985.

2) A. F. Bochkov and G. E. Zaikov, Chemistry of the *O*-Glycosidic Bond. Formation and Cleavage, Engl. Ed., Pergamon, London (1979).

3) N. K. Kochetkov, A. F. Bochkov, T. A. Sokolovskaya, and V. I. Snyatkova, *Carbohydr. Res.*, **16**, 17 (1971); R. -A. Boigegrain, B. Castro, and B. Gross, *Bull. Soc. Chim. Fr.* **1974**, 2623; R. U. Lemieux, K. B. Hendriks, R. V. Stick, and K. James, *J. Am. Chem. Soc.*, **97**, 4056 (1975); G. Grynkiewicz, *Carbohydr. Res.*, **53**, C11 (1977); J. Leroux and A. S. Perlin, ibid., **67**, 163 (1978), S. Shoda and T. Mukaiyama. *Chem. Lett.*, **1979**, 847; R. R. Schmidt and J. Michel, *Angew. Chem., Int. Ed.*, **19**, 731 (1980); R. R. Schmidt, U. Moering, M. Reichrath, *Tetrahedron Lett.*, **21**, 3565 (1980); A. A. Pavia, J. -M. Rocheville, and S. N. Ung, *Carbohydr. Res.*, **79**, 79 (1980); T. Ogawa, K. Beppu, and S. Nakabayashi, ibid., **93**, C6 (1981); H. Lönn, *Carbohydr. Res.*, **139**, 105 (1985).

4) S. Hashimoto, M. Hayashi, and R. Noyori, *Tetrahedron Lett.*, **25**, 1379 (1984).

5) S. Koto, N. Morishima, and S. Zen, *Bull. Chem. Soc. Jpn.*, **52**, 784 (1979).

6) L. -F. Tietze, R. Fischer, and H. -J. Guder, *Tetrahedron Lett.*, **23**, 4661 (1982).

7) J. Yoshimura, K. Hara, T. Sato, and H. Hashimoto, *Chem. Lett.*, **1983**, 319.

8) M. Schmeisser, P. Sartori, and B. Lippsmeier, *Chem. Ber.*, **103**, 868 (1970).

9) S. Koto, N. Morishima, Y. Kihara, S. Suzuki, S. Kosugi, and S. Zen, *Bull. Chem. Soc. Jpn.*, **56**, 188 (1983).

10) C. K. Lee, "Developments in Food Carbohydrate-2," ed by C. K. Lee, Appl. Sci. Publ. Ltd., London (1980), p. 1; S. Koto, S. Inada, and S. Zen, *Bull. Chem. Soc. Jpn.*, **54**, 2728 (1981) and the references cited therein; F. Percheron and E. Guilloux, *Bull. Soc. Chim. Biol.*, **46**, 543 (1964).

11) J. Defaye, H. Driguez, B. Henrissat, J. Gelas, and E. Bar-Guilloux, *Carbohydr. Res.*, **63**, 41 (1978).

12) K. Yokose, K. Ogawa, Y. Suzuki, I. Umeda, and Y. Suhara, *J. Antibiot.*, **36**, 1166 (1983).

13) S. Koto, N. Morishima, M. Owa, and S. Zen, *Carbohydr. Res.*, **130**, 73 (1984).

14) S. Koto, N. Morishima, K. Takenaka, C. Uchida, and S. Zen, *Bull. Chem. Soc. Jpn.*, **58**, 1464 (1985).

15) S. Koto, N. Morishima, R. Kawahara, K. Ishikawa, and S. Zen, ibid., **55**, 1092 (1982).

16) S. Koto, Y. Hamada, S. Zen, *Chem. Lett.*, **1975**, 587.

17) H. Paulsen and C. Kolár, *Chem. Ber.*, **114**, 306 (1981).

18) P. E. Pfeffer, K. M. Valetine, and F. W. Parrish, *J. Am. Chem. Soc.*, **101**, 1265 (1979).

19) S. Koto, N. Morishima, C. Kusuhara, S. Sekido, T. Yoshida, and S. Zen., *Bull. Chem. Soc. Jpn.*, **55**, 2995 (1982).

 © 1986 The Chemical Society of Japan Bull. Chem. Soc. Jpn., 59, 415—421 (1986)

A Simple and Efficient Synthesis of Optically Active (+)-4-Demethoxydaunomycinone[1)]

Yoshikazu KIMURA, Michiyo SUZUKI, Teruyo MATSUMOTO, Rumiko ABE, and Shiro TERASHIMA*
Sagami Chemical Research Center, Nishi-Ohnuma, Sagamihara, Kanagawa 229
(Received July 18, 1985)

Diels-Alder reaction of 2-chloro-1,3-butadiene with anthracene-**1**,4,9,10-tetrone was found to occur exclusively at the external ($C_{2,3}$) double bond, giving the adduct in an excellent yield. The adduct was elaborated to 5,12-dihydroxy-1,2,3,4-tetrahydro-2,6,11-naphthacenetrione. The conventional cyanohydrin formation of this sample followed by acid hydrolysis gave (±)-2,5,12-trihydroxy-6,11-dioxo-1,2,3,4-tetrahydro-2-naphthacenecarboxylic acid. The racemic acid was found to be cleanly resolved by forming a salt with (−)-*N*-methylephedrine, furnishing optically pure (*R*)-carboxylic acid. Successive treatments of the (*R*)-carboxylic acid with *N*,*N*′-carbonyldiimidazole and methylmagnesium bromide in the presence of trimethylsilyl triflate readily produced optically pure (*R*)-(−)-7-deoxy-4-demethoxydaunomycinone, the key synthetic intermediate of (+)-4-demethoxydaunomycinone.

The anthracycline antibiotics, adriamycin (**1a**) and daunorubicin (**1b**), are important antitumor agents with clinical effectiveness against various types of human solid tumors and leukemias.[2,3)] However, their utilization for cancer chemotheraphy is hampered by various undesired side effects, the most notable and serious one of which is dose-related cardiotoxicity. Based on extensive studies on analogues of **1a**, **b**,[2)] 4-demethoxyanthracyclines, 4-demethoxyadriamycin (**1c**) and 4-demethoxydaunorubicin (**1d**) have been developed as unnatural anthracyclines which could show more improved therapeutic properties than natural **1a**, **b**. Since unnatural **1c**, **d** are obtainable only by chemical synthesis, numerous synthetic efforts have been devoted to 4-demethoxyanthracyclinones (**2c**, **d**), the aglycones of 4-demethoxyanthracyclines.[4)]

In connection with our continuing synthetic studies on optically active **2c**,**d**,[1,5–10)] we have hitherto developed various preparation methods of optically active (*R*)-(−)-7-deoxy-4-demethoxydaunomycinone ((*R*)-(−)-**14**) by featuring asymmetric synthesis[5,6,10,11)] or optical resolution.[1,7,8,9,12)] The optically active α-hydroxy ketone ((*R*)-(−)-**14**) is anticipated to place a central position in the synthesis of optically active **2c**, **d**,[4a,b)] since introduction of the C_7-hydroxyl group (anthracycline numbering) into (*R*)-(−)-**14** can be achieved in a highly stereoselective manner[8)] and optically active **2d** can be readily converted to optically active **2c** by sequential bromination and substitution.[6,8)] However, considering various impracticalities including uses of expensive reagents and/or chiral sources,[5,6,8)] reactions at low or high temperatures,[6)] and also substantial loss of optical integrities observed in the synthesis of (*R*)-(−)-**14**,[6,7)] the previously explored synthetic methods[1,4–10)] seem not to be adequate for a large scale preparation of (*R*)-(−)-**14**.

We have now developed another synthetic scheme for optically pure (*R*)-(−)-**14**, starting from cheap and readily available 1,4-dihydroxyanthracene-9,10-dione (quinizalin) (**3**).

This report deals with the exploration of this novel synthetic route which is considered to be more practical and efficient than the previously reported methods[1,5–10)]

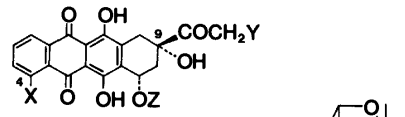

	X	Y
a:	OMe	OH
b:	OMe	H
c:	H	OH
d:	H	H

Commercially available **3** was oxidized with lead tetraacetate to give anthracene-1,4,9,10-tetrone (**4**) in 58% yield according to the reported method.[13)] The Diels-Alder reaction of **4** with 2-chloro-1,3-butadiene (chloroprene) as an enophile regiospecifically occurred at the external $C_{2,3}$-double bond, giving a 79% of 2-chloro-1,4,4a,12a-tetrahydronaphthacene-5,6,11,12-tetrone (**5a**). TLC and NMR analyses of the crude product clearly disclosed complete absence of the undesired Diels-Alder adduct which might result from the attack of chloroprene on the internal $C_{4a,9a}$-double bond of **4**. While 2-acetoxy-1,3-butadiene which had been employed as an excellent enophile in the synthesis of natural anthracyclinones (**2a**, **b**)[14)] afforded a 58% yield of the desired adduct in the Diels-Alder reaction with **4**, this diene could only be prepared in less than 10% yield according to the reported method by our hands.[15)] 2-Acetoxy-1,3-butadiene could be also prepared from methyl vinyl ketone in 38% yield by simultaneous metallation with lithium diisopropylamide and acylation with acetic anhydride. However, it is obvious that this synthetic method is not applicable to a large scale preparation of 2-acetoxy-1,3-butadiene. Therefore, chloroprene seems to be one of the best enophile for the construction of desired tetracyclic ring system such as **5a** because of its superior regioselectivity and ready availability.[16)] Since **5a** was found to be fairly unstable, it was immediately aromatized with anhyd sodium acetate in acetic acid to afford the

dihydroxyanthraquinone **6a** in 91% yield. Hydrolysis of the vinylic chloride functionality was readily accomplished with concd sulfuric acid, giving rise to 5,12-dihydroxy-1,2,3,4-tetrahydronaphthacene-2,6,11-trione (**7**)[16b,17] in 98% yield.

According to the conventional method, **7** was smoothly converted to (±)-2,5,12-trihydroxy-6,11-dioxo-1,2,3,4-tetrahydro-2-naphthacenecarboxylic acid ((±)-**9**). Thus, treatment of **7** with potassium cyanide and hydrochloric acid in acetic acid yielded the unstable cyanohydrin **8**, which without isolation was subjected to acid hydrolysis to afford (±)-**9** in 83% yield.

With a large quantity of (±)-**9** in hand, the optical resolution of (±)-**9** was first attempted. After several unsuccessful attempts, (−)-*N*-methylephedrine was found to be the best optically active amine, being neccessary for the salt formation with (±)-**9**. Treatment of (±)-**9** with (−)-*N*-methylephedrine (1.2 equiv) in ethanol gave the crude salt of (*R*)-**9** in 51% (102%)[19] yield. Two recrystallizations of the crude salt from ethanol containing a small amount of (−)-*N*-methylephedrine (0.2 equiv to the amount of the salt)[20] afforded the pure salt of (*R*)-**9** in 31% (62%)[19] yield which showed the constant melting point and optical rotation, mp 217.5—220 °C, $[\alpha]_D^{20}$ −12.0° ($CHCl_3$). The optically pure acid ((*R*)-**9**) was readily regenerated in a quantitative yield by stirring a suspension of the pure salt in aqueous hydrochloric acid. Unfortunately, the optical rotation of (*R*)-**9** could not be measured because of its extremely low solubility to almost all solvents.

While the absolute configuration and optical purity of optically active **9** could be determined by the successful synthesis of (*R*)-(−)-**14** (vide infra), the independent determination of these physical indices was examined at this stage by transforming optically active **9** into its derivatives. Thus, esterification of optically active **9** in a mixture of methanol and dimethyl sulfoxide[21] using a catalytic amount of concd sulfuric acid gave the corresponding (−)-methyl ester ((−)-**10**) in 91% yield, $[\alpha]_D^{20}$ −55.0° ($CHCl_3$), after purification by column chromatography. Further methylation of the phenolic hydroxyl groups of (−)-**10** with potassium carbonate and dimethyl sulfate in acetone, followed by purification by column chromatography, produced the (+)-dimethoxy ester ((+)-**11**) in 90% yield, $[\alpha]_D^{20}$ +11.7° ($CHCl_3$).[22] Measurement of the NMR spectrum of (+)-**11** in the presence of chiral shift reagent clearly disclosed that optically active **9** produced by the resolution was optically pure (100% ee). In order to determine the absolute configuration, (+)-**11** was further hydrolyzed under alkaline conditions to give the (+)-dimethoxy acid ((+)-**12**)[5,23] in 82% yield, $[\alpha]_D^{20}$ +16.9° ($CHCl_3$). Since (+)-**12** showing $[\alpha]_D^{20}$ +14.0° ($CHCl_3$) had been reported to belong to (*R*)-series,[5] optically active **9** was definitely established to belong to (*R*)-configuration.

Since determination of the absolute configuration and optical purity of optically active **9** was completed as mentioned above, our next attention was focused on the elaboration of (*R*)-**9** to (*R*)-(−)-**14**. At the outset, the synthesis of (*R*)-(−)-**14** from (*R*)-**9** seemed to be simply accomplished by employing one of the reported methods which could afford a methyl ketone from the corresponding acid. However, this was found to be quite refractory. After several unsuccessful attempts employing (±)-**9** as a substrate,[24] the reaction of the (±)-*N*-acylimidazole ((±)-**13**) in situ produced from (±)-**9**[25] with methylmagnesium bromide was turned out to be promising. Thus, the reaction of (±)-**9** with *N,N'*-carbonyldiimidazole (2.0 equiv) in tetrahydrofuran containing hexamethylphosphoric triamide furnished (±)-**13**. Without isolation, (±)-**13** was immediately treated with trimethylsilyl trifluoromethanesulfonate (trimethylsilyl triflate) (1 equiv) at −20 °C, then with methylmagnesium bromide at −40 °C, giving (±)-**14** in 65% yield. By applying the developed sequential reactions to (*R*)-**9**, optically pure (*R*)-(−)-**14**, $[\alpha]_D^{20}$ −90.3° ($CHCl_3$) was obtained in 58% overall yield from (*R*)-**9** by way of (*R*)-**13**.

In order to clearly elucidate several notable aspects of the explored one pot synthesis of (*R*)-(−)-**14** from (*R*)-**9**, some preliminary results obtained by using (*R*)- and (±)-**9** are summarized in Table 1. Absence of hexamethylphosphoric triamide and/or trimethylsilyl

Table 1. Preparation of (*R*)-(−)- or (±)-**14** from (*R*)- or (±)-**9** by Way of (*R*)- or (±)-**13**

Run	**9**	Solvent[a]	Additive[b]	Reaction[c] Temp/°C	Yield of (*R*)-(−)-[d] or (±)-**14**/%
1	(*R*)-	THF-HMPA[e]	TMSOTf	−40	58
2	(*R*)-	THF	TMSOTf	−40	44
3	(*R*)-	THF	—	−20	23[f]
4	(±)-	THF-HMPA[e]	TMSOTf	−40	65
5	(±)-	THF-HMPA[e]	BF_3·OEt_2	−20	51
6	(±)-	THF-HMPA[e]	—	−20	40[f]
7	(±)-	THF	—	−20	25[f]

a) Tetrahydrofuran (THF), hexamethylphosphoric triamide (HMPA). b) Trimethylsilyl triflate (TMSOTf), boron trifluoride etherate (BF_3·OEt_2). c) Reaction temperature in the reaction with methylmagnesium bromide. The *N*-acylimidazole ((*R*)- or (±)-**13**) was prepared at room temperature. d) Based on (*R*)- or (±)-**9**. e) The volume ratio of THF to HMPA was 50:1. f) NMR analysis showed that this sample was contaminated with the (*R*)-(−)- or (±)-methyl ester of (*R*)-(−)- or (±)-**9** ((*R*)-(−)- or (±)-**10**) ((*R*)-(−)- or (±)-**9**/(*R*)-(−)- or (±)-**10**=9/1—4/1) (see text).

triflate in the reaction medium significantly decreased the yield of (*R*)-(−)- or (±)-**14** (see runs 1—3).
Addition of the Grignard reagent to (*R*)- or (±)-**13** began to occur at −20 °C in the absence of trimethylsilyl triflate, affording a low yield of (*R*)-(−)- or (±)-**14** (see runs 1, 3 and 4, 6). In this case, the reaction product ((*R*)-(−)- or (±)-**14**) was accompanied by a significant amount of the methyl ester ((*R*)-(−)- or (±)-**10**) ((*R*)-(−)- or (±)-**14**/(*R*)-(−)- or (±)-**10**=9/1—4/1). While the formation mechanism of (*R*)-(−)- or (±)-**10** from (*R*)- or (±)-**9** is quite obscure, the amount of (*R*)-(−)- or (±)-**10** seems to be proportional to the temperature at which the Grignard reagent was added to a solution of (*R*)- or (±)-**13**. In the reaction carried out at −40 °C, no formation of undesired (*R*)-(−)- or (±)-**10** was definitely ascertained by NMR analysis of the crude reaction product. When methylmagnesium iodide was employed as a Grignard reagent in place of methylmagnesium bromide, the tertiary alcohol ((±)-**15**) was formed in 74% yield. It is noteworthy that a negligible amount of (*R*)- or (±)-**15**, usually less than 3% yield, was produced even though a large excess of methylmagnesium bromide was employed as a Grignard reagent. This may be explained by the assumption that the magnesium salt produced by the reaction of methylmagnesium iodide is more unstable than that formed by employing methylmagnesium bromide and liberates (*R*)-(−)- or (±)-**14** in the reaction medium.

By accumulating these results described above, we have finally succeeded in preparing (*R*)-(−)- or (±)-**14** directly from (*R*)- or (±)-**9** in ca. 60% yield. Numerous synthetic approaches to anthracyclinones hitherto reported, terminate at or proceed through 1,2,3,4-tetrahydro-2,6,11-naphthacenetrione derivatives.[4,14,16b,17,26] Therefore, the explored process is anticipated to hold promise for adding the racemic or optically active C_9-α-hydroxy ketone moiety to those tetracyclic systems.

As mentioned in the introduction part, the methods for converting (*R*)-(−)-**14** to optically pure **2d**, then to optically pure **2c**, have been firmly established by us.[6,8] Accordingly, the developed overall scheme to (*R*)-(−)-**14** which can be characterized by its operational simplicity and directness is expected to facilitate a large scale preparation of optically pure **2c**, **d** more readily than the previously reported method.[4-10]

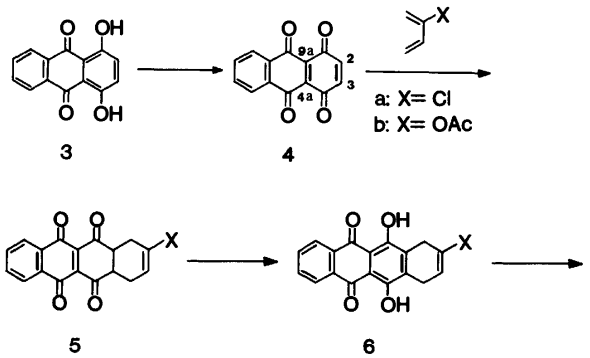

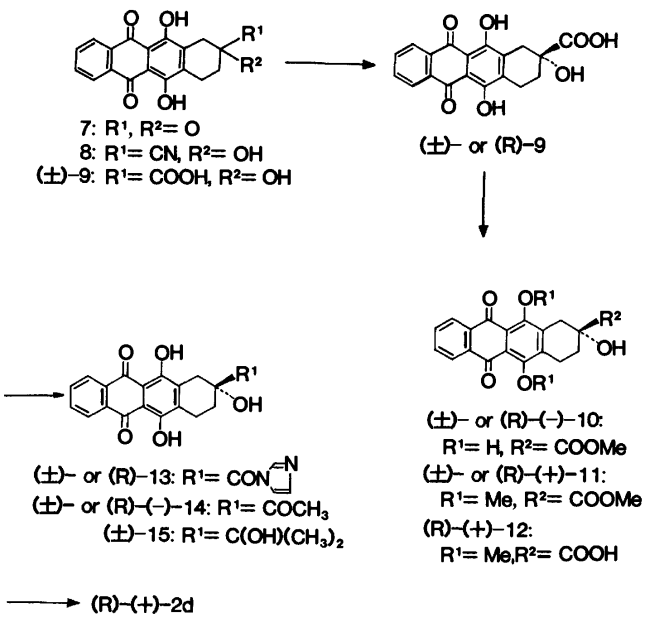

Scheme 1.

Experimental

General. All melting points were determined with a Yamato MP-21 melting point apparatus and were uncorrected. IR spectral measurements were carried out with a JASCO A-202 diffraction grating infrared spectrometer. NMR spectra were recorded with a Varian EM-390 spectrometer (90 MHz) and a Varian XL-100A spectrometer (100 MHz). All signals were expressed as ppm downfield from TMS, used as an internal standard (δ-value). Mass s_ectra were taken with a Hitachi RMU-6MG mass spectrometer. Measurements of optical rotation were performed with a Union PM-201 automatic digital polarimeter and Horiba SEPA-200 automatic digital polarimeter. Wakogel C-200 and Kieselgel 60 (Merck) were used as an adsorbent for column chromatography. All reactions were carried out using anhydrous solvents. Especially tetrahydrofuran, ether, and dioxane freshly distilled from sodium benzophenone ketyl, and dichloromethane, acetone, and pyridine freshly distilled from calcium hydride were used. Lead tetraacetate purchased from Wako Pure Chemical Industries, Ltd., was used for a reaction without further purification. Following abbreviations are used for solvents and reagents: acetic acid (AcOH), benzene (C_6H_6), chloroform ($CHCl_3$), dichloromethane (CH_2Cl_2), dimethyl sulfoxide (DMSO), ether (Et_2O), ethyl acetate (EtOAc), ethanol (EtOH), hexamethylphosphoric triamide (HMPA), hexane (C_6H_{14}), methanol (MeOH), tetrahydrofuran (THF).

Anthracene-1,4,9,10-tetrone (Quinizalin Quinone) (4). A mixture of **3** (31.9 g, 0.133 mol) and lead tetraacetate (purity 90%) (98.4 g, 0.200 mol) in AcOH (80 mL) are stirred in a mortal for 30 min. The brown precipitate was collected by filtration, washed with AcOH and H_2O, and dried over P_2O_5 in vacuo to give crude **4** (26.6 g, 84%). This was added to nitrobenzene (400 mL), and the mixture was stirred for 2 h at 70 °C, then filtered through a pad of celite. The filtrate was concentrated in vacuo below 70 °C until crystals appeared. After cooling to room temperature, the crystals were collected by filtration, washed with Et_2O, then dried in

vacuo to afford pure **4** (18.2 g, 58%), mp 210—212°C (decomp) (lit,[13] mp 208—210°C (decomp)). IR (KBr): 1700, 1685, 1645, 1595 cm^{-1}. ^1H NMR ($CDCl_3$) δ=6.87 (s, 2H, C<u>H</u>=C<u>H</u>), 7.70—8.15 (m, 4H, Ar).

2-Chloro-1,4,4a,12a-tetrahydronaphthacene-5,6,11,12-tetrone (5). Chloroprene (9.80 g, 0.111 mol) was added to a suspension of **4** (mp 210—212°C) (16.2 g, 0.068 mol) in a mixture of C_6H_6 and xylene (5 : 1) (170 mL). After reflux for 3 h, additional amount of chloroprene (3.53 g, 0.040 mol) was added to the mixture, then the whole suspension was heated at reflux for 1 h. After cooling, the crystals were collected by filtration, washed with Et_2O, then dried over P_2O_5 in vacuo, to give pure **5** (17.6 g, 79%), mp 232—234°C (decomp). A part of this sample was recrystallized from xylene to give an analytical sample of **5**, mp 232—234°C (decomp). IR (KBr): 1710, 1665, 1595 cm^{-1}. ^1H NMR ($CDCl_3$) δ=2.34—2.83 (m, 4H, 1-H_2+4-H_2), 3.39—3.81 (m, 2H, 4a-H+12a-H), 5.88 (m, 1H, C<u>H</u>=CCl), 7.76—8.22 (m, 4H, Ar). Found: C, 66,23; H, 3.34; Cl, 10.61%. Calcd for $C_{18}H_{11}O_4Cl$: C, 66.17; H, 3.39; Cl, 10.85%.

2-Chloro-5,12-dihydroxy-1,4-dihydro-6,11-naphthacenedione (6). The powdered tetrone (**5**) (mp 232—234°C (decomp)) (19.6 g, 60.0 mmol) was added to a mixture of anhyd sodium acetate (100 mg, 1.22 mmol) in AcOH (200 mL) over 15 min. After reflux for 30 min, the red crystals were collected by filtration, washed successively with H_2O, MeOH, and Et_2O, then dried over P_2O_5 in vacuo, to afford pure **6** (17.9 g, 91%), mp 285.5—286.5°C. A part of this sample was recrystallized from toluene to give an analytical sample of **6**, mp 285.5—286.5°C. IR (KBr): 1625, 1590 cm^{-1}. ^1H NMR ($CDCl_3$) δ=3.44—3.82 (m, 4H, 1-H_2+4-H_2), 6.00—6.13 (m, 1H, C<u>H</u>=CCl), 7.77—8.50 (m, 4H, Ar), 13.41 (s, 1H, ArO<u>H</u>), 13.42 (s, 1H, ArO<u>H</u>). Found: C, 65.95; H, 3.38; Cl 10.86%. Calcd for $C_{18}H_{11}O_4Cl$: C, 66.17; H, 3.39; Cl, 10.85%.

5,12-Dihydroxy-1,2,3,4-tetrahydro-2,6,11-naphthacenetrione (7). The vinylic chloride (**6**) (mp 285.5—286.5°C) (17.4 g, 53.3 mmol) was gradually added to a stirred concd H_2SO_4 (170 mL). The reaction mixture was stirred for 1 h under an exclusion of moisture ($CaCl_2$ tube), then poured onto ice-H_2O (3 L). The aqueous mixture was kept standing at room temperature for 3 d. Red powderlike crystals were collected by centrifugation and suspended in AcOH (250 mL). The acidic suspension was heated at reflux for 2 h with stirring. After cooling, the red powderlike crystals were collected by filtration, washed with MeOH, and dried over P_2O_5 in vacuo, to give **7** (16.1 g, 98%), mp > 250°C (decomp). A part of this sample was recrystallized from AcOH to give an analytical sample of **7**, mp > 250°C (decomp) (lit,[16b] mp 313—315°C, lit,[17a] mp>310°C (decomp), lit,[17b] mp> 300°C, lit,[17c] mp 296—298°C (decomp)). IR (KBr): 1730, 1620, 1585 cm^{-1}. ^1H NMR ($CDCl_3$) δ=2.68 (t, J=7 Hz, 2H, 3-H_2), 3.30 (t, J=7 Hz, 2H, 4-H_2), 3.70 (s, 2H, 1-H_2), 7.78—8.02 (m, 2H, Ar), 8.30—8.52 (m, 2H, Ar), 13.40 (s, 1H, ArO<u>H</u>), 13.50 (s, 1H, ArO<u>H</u>). Found: C, 69.92; H, 4.01%. Calcd for $C_{18}H_{12}O_5$: C, 70.13; H, 3.92%.

(±)-2-Cyano-2,5,12-trihydroxy-1,2,3,4-tetrahydro-6,11-naphthacenedione (8). Potassium cyanide (15.8 g, 24.3 mmol) was added to a suspension of **7** (mp > 250°C) (5.00 g, 16.2 mmol) in a mixture of EtOH (130 mL) and THF (170 mL) at 0°C with stirring. After stirring for 20 min, AcOH (20 mL) was added dropwise to the reaction mixture at 0°C. The whole mixture was stirred for 30 min at 0°C, then overnight at room temperature. The mixture was poured onto 3% HCl (1 L). The red powder was collected by filtration, washed with H_2O, and dried over P_2O_5 in vacuo, to afford crude **8** (4.50 g, 83%). IR (KBr): 3400, 2240, 1630, 1595, 1417, 1377, 1253, 1105, 1077, 1008, 797, 739 cm^{-1}. ^1H NMR ($(CD_3)_2CO$) δ=2.34 (t, J=6.5 Hz, 2H, 3-H_2), 3.06 (m, 2H, 4-H_2), 3.18 (d, J=18.4 Hz, 1H, one of 1-H), 3.45 (d, J=18.4 Hz, 1H, one of 1-H), 5.93 (brs, 1H, OH), 8.05 (m, 2H, Ar), 8.38 (m, 2H, Ar), 13.42 (s, 1H, ArO<u>H</u>), 13.47 (s, 1H, ArO<u>H</u>).

(±)-2,5,12-Trihydroxy-6,11-dioxo-1,2,3,4-tetrahydro-2-naphthacenecarboxylic Acid ((±)-9). A mixture of **8** (3.66 g, 10.9 mmol) AcOH (37 mL), and concd HCl (9 mL) was refluxed for 4.5 h. Additional amount of concd HCl (9 mL) was added to the mixture, and the whole mixture was heated at reflux for 5.5 h. After cooling, the red powder was collected by filtration, washed with H_2O, then dried over P_2O_5 in vacuo, to afford crude (±)-**9** (3.63 g, 94%). This was recrystallized from nitrobenzene to give pure (±)-**9**, mp 251—252°C (lit,[25] 253—258°C). IR (KBr): 3400, 3250, 1730, 1625, 1590 cm^{-1}. ^1H NMR ($(CD_3)_2SO$) δ=1.80—2.20 (m, 2H, 3-H_2), 2.57—3.00 (m, 4H, 1-H_2+4-H_2), 7.80—8.35 (m, 4H, Ar), 13.29 (s, 1H, ArO<u>H</u>), 13.31 (s, 1H, ArO<u>H</u>). Found: C, 64.03; H, 3.98%. Calcd for $C_{19}H_{14}O_7$: C, 64.41; H, 3.98%.

(*R*)-2,5,12-Trihydroxy-6,11-dioxo-1,2,3,4-tetrahydro-2-naphthacenecarboxylic Acid ((*R*)-9). Optical Resolution of (±)-9: A mixture of (±)-**9** (mp 251—252°C) (10.0 g, 28.2 mmol) and (−)-*N*-methylephedrine[17] (mp 85—86°C, $[\alpha]_D^{20}$ −30.2° (*c* 4.48, MeOH)) (6.07 g, 33.9 mmol) in EtOH (2 L) was heated at reflux for 2 h. After the hot solution was filtered, the filtrate was concentrated to a half volume and kept standing overnight at room temperature. The red crystals were collected by filtration to afford the crude salt of (*R*)-**9** (7.72 g, 51% (102%)[19]), mp 200—204°C, $[\alpha]_D^{20}$ −64.0° (*c* 0.10, $CHCl_3$). The salt was twice recrystallized from EtOH containing (−)-*N*-methylephedrine of 0.2 equiv to the total amount of the salt,[20] affording the pure *N*-methylephedrine salt of (*R*)-**9** as a red powder (4.71 g, 31% (62%)[19]), mp 217.5—220°C, $[\alpha]_D^{20}$ −12.0° (*c* 0.05, $CHCl_3$). IR (KBr): 3420, 1625, 1595 cm^{-1}. Found: C, 67.50; H, 5.60; N, 2.35%. Calcd for $C_{30}H_{31}NO_8$: C, 67.53; H, 5.86; N, 2.63%. The pure *N*-methylephedrine salt of (*R*)-**9** (1.17 g, 2.19 mmol) was added to stirred 3.6% HCl (350 mL), and the mixture was stirred at room temperature for 17 h. The red powder was collected by filtration, washed with dil HCl and H_2O, and dried over KOH at 100°C in vacuo, to give optically pure (*R*)-**9** (0.776 g, 100%), mp > 280°C. IR (KBr): 3450, 1730, 1625, 1590 cm^{-1}. MS *m/z*: 354 (M^+), 336, 291.

(±)-Methyl 2,5,12-Trihydroxy-6,11-dioxo-1,2,3,4-tetrahydronaphthacene-2-carboxylate ((±)-10). A mixture of (±)-**9** (mp 251—252°C) (506 mg, 1.43 mmol) and concd H_2SO_4 (7 drops) in MeOH (50 mL) and DMSO (10 mL) was heated at reflux for 4 h with stirring. After cooling, the reaction mixture was poured onto satd $NaHCO_3$ and extracted with EtOAc. The combined ethyl acetate extracts were washed with H_2O and satd NaCl, then dried over $MgSO_4$. Filtration and concentration in vacuo gave crude (±)-**10** as a red solid (524 mg, 100%), mp 198.5—199.5°C. This was recrystallized from toluene to afford pure (±)-**10**, mp 211.5—213.5°C. IR (KBr): 3470, 1743, 1620, 1590 cm^{-1}. ^1H NMR ($CDCl_3$) δ=1.95—2.20 (m, 2H, 3-H_2), 2.80—3.20 (m, 4H, 1-H_2+4-H_2), 3.09 (brs, 1H, OH), 3.84 (s, 3H, CH_3), 7.70—7.90 (m, 2H, Ar), 8.20—8.40 (m, 2H, Ar), 13.43 (s, 2H, ArO<u>H</u> ×2). MS *m/z*: 368 (M^+). Found: C, 65.23; H, 4.39%. Calcd for $C_{20}H_{16}O_7$: C, 65.22; H, 4.38%.

(*R*)-(−)-Methyl 2,5,12-Trihydroxy-6,11-dioxo-1,2,3,4-tetra-

hydronaphthacene-2-carboxylate ((*R*)-(−)-10). Treatments of (*R*)-**9** (mp > 280°C) (350 mg, 0.99 mmol) in the same manner as described for (±)-**10** gave crude (*R*)-(−)-**10** (345 mg, 95%) after concentration of the ethyl acetate extracts. This was purified by silica-gel column chromatography (C_6H_6/EtOAc=5/1—3/1) to afford pure (*R*)-(−)-**10** (293 mg, 81%) as red crystals, mp 206.5—210°C, $[\alpha]_D^{20}$ −55.0° (*c* 0.10, $CHCl_3$). A part of this sample was recrystallized from toluene to give an analytical sample of (*R*)-(−)-**10**, mp 210.5—211.5°C, $[\alpha]_D^{20}$ −60.0° (*c* 0.10, $CHCl_3$). IR (KBr): 3470, 1734, 1620, 1590 cm^{-1}. NMR spectrum of this sample was identical with that of (±)-**10**. Found: C, 65.21; H, 4.20%. Calcd for $C_{20}H_{16}O_7$ C, 65.22; H, 4.38%.

(±)-Methyl 2-Hydroxy-5,12-dimethoxy-6,11-dioxo-1,2,3,4-tetrahydronaphthacene-2-carboxylate ((±)-11). Anhyd potassium carbonate (150 mg, 1.09 mmol) and dimethyl sulfate (137 mg, 1.09 mmol) were added to a suspension of (±)-**10** (mp 198.5—199.5°C) (100 mg, 0.27 mmol) in Me_2CO (12 mL). After reflux for 5.5 h, the reaction mixture was filtered and the filtrate was concentrated in vacuo. The residue was dissolved in EtOAc, and the ethyl acetate solution was washed successively with satd $NaHCO_3$, H_2O, and satd NaCl, then dried over $MgSO_4$. Filtration and concentration in vacuo gave crude (±)-**11** (97.6 mg, 91%), which was purified by silica-gel column chromatography (Et_2O) to afford pure (±)-**11** as a yellow solid (78.6 mg, 73%), mp 152 and 186°C. A part of this sample was triturated with Et_2O to give an analytical sample of (±)-**11**, mp 152 and 186°C. IR (KBr): 3540, 1728, 1675 cm^{-1}. ^1H NMR ($CDCl_3$) δ=1.90—2.20 (m, 2H, 3-H_2), 2.90—3.20 (m, 4H, 1-H_2+4-H_2), 3.16 (brs, 1H, OH), 3.84 (s, 3H, CO_2Me), 3.86 (s, 3H, OMe), 3.91 (s, 3H, OMe), 7.63—7.82 (m, 2H, Ar), 8.05—8.30 (m, 2H, Ar). MS *m/z*: 396 (M^+). Found: C, 66.56; H, 5.07%. Calcd for $C_{22}H_{20}O_7$: C, 66.66; H, 5.09%.

(*R*)-(−)-Methyl 2-Hydroxy-5,12-dimethoxy-6,11-dioxo-1,2,3,4-tetrahydronaphthacene-2-carboxylate ((*R*)-(+)-11). Treatments of (*R*)-(−)-**10** (mp 206.5—210°C, $[\alpha]_D^{20}$ −55.0° (*c* 0.10, $CHCl_3$)) (50.0 mg, 0.14 mmol) in the same manner as described for (±)-**11** gave (*R*)-(+)-**11** as a yellow solid (48.5 mg, 90%) after purification by silica-gel chromatography, mp 152—154°C, $[\alpha]_D^{20}$ +11.7° (*c* 0.22, $CHCl_3$)[22] (lit,[5] mp 154—155°C). IR (KBr): 3540, 1728, 1675 cm^{-1}. ^1H NMR spectrum of this sample was identical with that of (±)-**11**. NMR spectrum of (*R*)-(+)-**11** measured in the presence of chiral shift reagent tris[3-(heptafluoropropylhydroxymethylene)-*d*-camphorato]europium(III) (Eu(hfc)$_3$) exhibited the methyl ester as a singlet at δ=6.07. Since NMR spectrum of (±)-**11** measured under the same conditions as described for (*R*)-(+)-**11** showed two singlets at δ=5.82 and 6.07, the optical purity of optically active **9** produced by the optical resolution was established to be 100% ee.

(*R*)-(+)-2-Hydroxy-5,12-dimethoxy-6,11-dioxo-1,2,3,4-tetrahydro-2-naphthacenecarboxylic Acid ((*R*)-(+)-12). Three percent potassium hydroxide (0.50 mL, 0.27 mmol) was added to a mixture of (*R*)-(+)-**11** (mp 152—154°C, $[\alpha]_D^{20}$ +11.7° (*c* 0.22, $CHCl_3$)) (70 mg, 0.18 mmol) in THF (1.4 mL) and MeOH (2.0 mL), and the mixture was stirred at room temperature for 3 h. After concentration in vacuo, the residue was diluted with satd NaCl, and the aqueous solution was washed with EtOAc. The aqueous layer was acidified (pH=2) with concd HCl, saturated with NaCl, then extracted with EtOAc. The combined organic extracts were washed with satd NaCl, dried over $MgSO_4$, and concentrated in vacuo, affording crude (*R*)-(+)-**12** (55.2 mg, 82%) as a yellow solid. Recrystallization of this sample from C_6H_{14}–EtOAc gave pure (*R*)-(+)-**12**, mp 202—207°C, $[\alpha]_D^{20}$+16.9° (*c* 0.20, $CHCl_3$) (lit,[5] mp 200—201°C, $[\alpha]_D^{20}$+13.6° (*c* 0.430, $CHCl_3$); lit,[23] mp 200—205°C, $[\alpha]_D^{20}$+14.0° (*c* 0.20, $CHCl_3$)). IR (KBr): 3440, 1715, 1675 cm^{-1}. ^1H NMR ($CDCl_3$) δ=1.92—2.29 (m, 2H, 3-H_2), 2.93—3.37 (m, 4H, 1-H_2+4-H_2), 3.91 (s, 3H, OMe), 3.94 (s, 3H, OMe), 5.76 (brs, 2H, O<u>H</u>+COO<u>H</u>), 7.60—7.84 (m, 2H, Ar), 8.00—8.30 (m, 2H, Ar). MS *m/z*: 382 (M^+), 319. Found: C, 65.32; H, 4.74%. Calcd for $C_{21}H_{18}O_7$–0.25H_2O: C, 65.20; H, 4.82%.

(±)-7-Deoxy-4-demethoxydaunomycinone ((±)-14). A mixture of (±)-**9** (mp 251—252°C) (52.7 mg, 0.15 mmol) and *N,N'*-carbonyldiimidazole (48.6 mg, 0.30 mmol) in THF (10 mL) containing HMPA (0.2 mL) was stirred at room temperature for 18 h to give a solution of (±)-**13**. Trimethylsilyl triflate (0.03 mL, 0.16 mmol) was added to the solution of (±)-**13** cooled at −20°C, and stirring was continued at −20°C for 15 min. After cooling at −40°C, an ethereal solution of methylmagnesium bromide (3 M[1] solution, 0.50 mL, 1.5 mmol) was added to the stirred reaction mixture. After stirring was continued at the same temperature for 2 h, additional amount of the ethereal solution of methylmagnesium bromide (3 M solution, 0.2 mL, total 0.7 mL, 2.1 mmol) was added to the reaction mixture. After being stirred at −40°C for 1 h, the reaction mixture was poured onto a vigorously stirred mixture of 1 M HCl (50 mL) and EtOAc (50 mL) to quench the reaction. The upper organic phase was separated, washed with satd NaCl, then dried over $MgSO_4$. Filtration and concentration in vacuo gave a red residue, which was purified by filtration through a short silica-gel column (C_6H_6/EtOAc=9/1) to give (±)-**14** as a red solid (34.0 mg, 65%), mp 194—198°C. Recrystallization of this sample from C_6H_6 gave a pure sample of (±)-**14** as a red minute crystals (29.3 mg, 56%), mp 213—215°C (lit,[6] mp 214—216°C). IR and NMR spectra of this sample were identical with those reported.[6]

(*R*)-(−)-7-Deoxy-4-demethoxydaunomycinone ((*R*)-(−)-14). Treatments of (*R*)-**9** (mp > 280°C) (50.5 mg, 0.14 mmol) in the same manner as described for (±)-**14** gave (*R*)-(−)-**14** as a red solid (29.1 mg, 58%), after extractive isolation with EtOAc and purification by filtration through a short silica-gel column, mp 195—203°C, $[\alpha]_D^{20}$ −85.7° (*c* 0.105, $CHCl_3$). This sample was recrystallized from C_6H_6 to afford pure (*R*)-(−)-**14** as a red minute crystals (23.3 mg, 46%), mp 214—216°C, $[\alpha]_D^{20}$ −90.6° (*c* 0.106, $CHCl_3$) (lit,[8] mp 218—219°C, $[\alpha]_D^{20}$−90.3° (*c* 0.106, $CHCl_3$)). IR and NMR spectra of this sample were superimposable on those of the authentic sample.[8]

(±)-2-Hydroxy-2-(1-hydroxy-1-methylethyl)-1,2,3,4-tetrahydro-6,11-naphthacenedione ((±)-15). A mixture of (±)-**9** (mp 251—252°C) (201 mg, 0.568 mmol) and *N,N'*-carbonyldiimidazole (185 mg, 1.14 mmol) in THF (40 mL) containing HMPA (0.8 mL) was stirred at room temperature for 18.5 h, to give a solution of (±)-**13**. Trimethylsilyl triflate (0.12 mL, 0.621 mmol) was added to the solution of (±)-**13** cooled at −40°C, and stirring was continued at −40°C for 20 min. An ethereal solution of methylmagnesium iodide (3 M solution, 1.9 mL, 5.70 mmol) was added to the reaction mixture at the same temperature. After stirring for 2 h, additional amount of the ethereal solution of methylmagnesium iodide (3M solution, 1.9 mL, 5.70 mmol) was added to the reaction mixture at −40°C. A reaction temper-

[1] 1 M = 1 mol dm^{-3}.

ature was gradually raised up to −20 °C, then the whole mixture was stirred at −20 °C for 5 h. Extractive isolation followed by purification by silica-gel column chromatography (C_6H_6/EtOAc=5/1) in the same manner as described for (±)-**14** afforded pure (±)-**15** (155 mg, 74%), mp 234.5—237.5 °C. IR (KBr): 3525, 1620, 1588 cm^{-1}. ^1H NMR ($CDCl_3$) δ=1.36 (s, 3H, CH_3), 1.42 (s, 3H, CH_3), 1.5—3.1 (m, 8H), 7.55—7.85 (m, 2H, Ar), 8.05—8.33 (m, 2H, Ar), 13.32 (s, 1H, ArOH), 13.36 (s, 1H, ArOH). MS *m/z*: 368 (M^+), 310.

The authors are grateful to Showa Neoprene K.K. for generous supply of 2-chloro-1,3-butadiene.

References

1) Part of this work has been the subject of two preliminary communications. a) Y. Kimura, M. Suzuki, T. Matsumoto, R. Abe, and S. Terashima, *Chem. Lett.*, **1984**, 473; b) M. Suzuki, T. Matsumoto, R. Abe, Y. Kimura, and S. Terashima, ibid, **1985**, 57.

2) a) F. Arcamone, Lloydia, **40**, 45 (1977); b) F. Arcamone, "Topics in Antibiotic Chemistry," ed by P. G. Sammes, Ellis Horwood, Chichester, England (1978), Vol. 2, pp. 98—239; c) F. Arcamone, "Anticancer Agents Based on Natural Product Models," ed by J. M. Cassady and J. D. Douros, Academic Press, New York (1980), pp. 1—41; d) F. Arcamone, "Doxorubicin Anticancer Antibiotics," Academic Press, New York (1981); e) M. B. Naff, J. Plowman, and V. L. Narayanan, "Anthracycline Antibiotics," ed by H. S. El Khadem, Academic Press, New York (1982), pp. 1—57.

3) a) T. Oki, *Hakko To Kogyo*, **37**, 1187 (1979); b) K. Ohta and K. Ohkuma, *Saisin Igaku*, **36**, 1060 (1981); c) T. Oki and T. Takeuchi, *Yuki Gosei Kagaku Kyokai Shi*, **40**, 2 (1982).

4) a) T. R. Kelly, *Ann. Rep. Med. Chem.*, **14**, 288 (1979); b) S. Terashima, *Yuki Gosei Kagaku Kyokai Shi*, **40**, 20 (1982); c) M. J. Broadhurst, C. H. Hassall, and G. J. Thomas, *Chem. Ind. (London)*, **1985**, 106.

5) S-s. Jew, S. Terashima, and K. Koga, *Chem. Pharm. Bull.*, **27**, 2351 (1979).

6) N. Tanno and S. Terashima, *Chem. Pharm. Bull.*, **31**, 811, 821 (1983).

7) K. Tamoto and S. Terashima, *Chem. Pharm. Bull.*, **32**, 4328, 4340 (1984).

8) K. Tamoto, M. Sugimori, and S. Terashima, *Tetrahedron*, **40**, 4617 (1984).

9) M. Suzuki, Y. Kimura, and S. Terashima, *Chem. Lett.*, **1984**, 1543.

10) M. Suzuki, Y. Kimura, and S. Terashima, *Chem. Lett.*, **1985**, 367.

11) For asymmetric synthesis of optically active anthracyclinones other than ours, see, a) R. C. Gupta, P. A. Harland, and R. J. Stoodley, *Tetrahedron*, **22**, 4657 (1984); b) D. Domingnez and M. P. Cava, *J. Org. Chem.*, **48**, 2820 (1983).

12) For synthesis of optically active anthracyclinones by optical resolutions, see, a) F. Arcamone, L. Bernardi, P. Giardino, B. Patelli, A. Di Marco, A. M. Casazza, G. Pratesi, and P. Raggiani, *Cancer Treat. Rep.*, **60**, 829 (1976); F. Arcamone, L. Bernardi, B. Patelli, and A. Di Marco, *Ger. Offen*, 2601785 (1976); F. Arcamone, L. Bernardi, B. Patelli, and A. Di Marco, Japan Kokai Tokkyo Koho, JP 59-231037; b) D. Domingnez, R. J. Ardecky, and M. P. Cava, *J. Am. Chem. Soc.*, **105**, 1608 (1983); c) M. J. Broadhurst, C. H. Hassall, and G. J. Thomas, *J. Chem. Soc., Perkin Trans. 1*, **1982**, 2239, 2249; d) J. S. Swenton, J. Freskos, G. W. Morrow, and A. D. Sercel, *Tetrahedron*, **40**, 4625 (1984); e) A. V. R. Rao, J. S. Yadav, K. B. Reddy, and A. R. Mebandale, ibid, **22**, 4643 (1984).

13) a) O. Dimroth and V. Hilcken, *Ber.*, **54**, 3050 (1921); b) M. Chandler and R. J. Stoodley, *J. Chem. Soc., Perkin Trans. 1*, **1980**, 1007.

14) A. S. Kende, Y-g. Tsay, and J. E. Mills, *J. Am. Chem. Soc.*, **98**, 1967 (1976).

15) a) H. J. Hagemeyer, Jr., and D. C. Hull, *Ind. Eng. Chem.*, **41**, 2929 (1949); b) M. Petrzilka and J. I. Greyson, *Synthesis*, **1981**, 753.

16) For extensive studies on Diels-Alder reactions of anthradiquinones and various dienes, see, a) T. R. Kelly, R. N. Goerner, Jr., J. W. Gillard, and B. K. Prazak, *Tetrahedron Lett.*, **1976**, 3869; b) W. W. Lee, A. P. Martinez, T. H. Smith, and D. W. Henry, *J. Org. Chem.*, **41**, 2296 (1976).

17) a) F. Farina and P. Parados, *Tetrahedron Lett.*, **1979**, 477; b) D. N. Gupta, P. Hodge, and N. Khan, *J. Chem. Soc., Perkin Trans. 1*, **1981**, 689; c) Y. Tamura, M. Sasho, S. Akai, A. Wada, and Y. Kita, *Tetrahedron*, **40**, 4539 (1984).

18) a) K. Nakajima, *Nippon Kagaku Zasshi*, **81**, 1476 (1960); b) T. Mashiko, S. Terashima, and S. Yamada, *Yakugaku Zasshi*, **100**, 319 (1980).

19) This yield was calculated based on (*R*)-**9** originally contained in (±)-**9**.

20) Existence of a small amount of (−)-*N*-methylephedrine (ca. 0.2 equiv to the total amount of the salt of (*R*)-**9**) was indispensable for improving purity of the salt of (*R*)-**9** by repeated recrystallizations.

21) When the esterification was carried out in the absence of dimethyl sulfoxide, only 64% yield of (−)-**10** was obtained under the similar reaction conditions. This might be due to extremely low solubility of optically active **9** in methanol.

22) This sample showed the following optical rotations in solvents other than chloroform: $[\alpha]_D^{20}$ 0.0° (*c* 0.22, Me_2CO), $[\alpha]_D^{20}$ −5.2° (*c* 0.23, MeOH), $[\alpha]_D^{20}$ −13.1° (*c* 0.25, EtOH), and $[\alpha]_D^{20}$ −23.5° (*c* 0.22, C_6H_6). Although $[\alpha]_D^{20}$ −7.8° (*c* 0.613, Me_2CO) was previously reported for this compound,[5] this rotation value should be corrected.

23) N. Ohashi, M. Muramatsu, N. Tanno, and K. Ishizumi, Japan Kokai Tokkyo Koho, JP 58-77844.

24) Before developing the efficient one-pot preparation method of (*R*)-(−)-**14** reported here, the following multi-step syntheses were found to produce (±)-**14** from (±)-**9** in rather low overall yields. Thus, esterification of (±)-**9** (concd H_2SO_4 in methanol and dimethyl sulfoxide) followed by protection of the C_9-hydroxyl group (dihydropyran-pyridinium *p*-toluenesulfonate in tetrahydrofuran or trimethylsilyl triflate-triethylamine in tetrahydrofuran) and reaction with sodium methylsulfinyl methanide in tetrahydrofuran, gave the corresponding C_9-*O*-protected methylsulfinyl ketone in ca. 60% overall yields. Successive reductive cleavage of the methylsulfinyl ketones (aluminum-amalgam in tetrahydrofuran or Raney-Ni in ethanol) and deprotection of the C_9-*O*-protective groups (pyridinium *p*-toluenesulfonate in ethanol, 50% acetic acid in ethyl acetate or 10% hydrochloric acid in tetrahydrofuran, etc.) gave (±)-**14** in 18—25% yields. On the other hand, (±)-**9** was converted to the corresponding thiol ester in 67% yield by treating with ethanethiol, magnesium ethoxide, and *N*,*N*′-carbonyldiimidazole in tetrahydrofuran. Reaction of thiol ester with lithium dimethylcuprate(I) in tetrahydrofuran at −40°C gave (±)-**14** in 23% yield.

25) H. A. Staab, *Angew. Chem., Int. Ed. Engl.*, **1**, 351 (1962).

26) For other representative anthracyclinone syntheses which terminate at or proceed through 1,2,3,4-tetrahydronaphthacene-2,6,11-trione derivatives, see, a) J. P. Gesson, J. C. Jacquesy, and M. Mondon, *Tetrahedron Lett.*, **21**, 3351 (1980); b) J. G. Bauman, R. B. Barbei, R. D. Gless, and H. Rapoport, *Tetrahedron Lett.*, **21**, 4777 (1980); c) E. Vedejs, W. H. Miller, and J. R. Pribish, *J. Org. Chem.*, **48**, 3613 (1983); d) M. Watanabe, H. Maenosono, and S. Furukawa, *Chem. Pharm. Bull.*, **31**, 2662 (1983); e) T. R. Kelly, L. Ananthasubramanian, K. Borab, J. W. Gillard, R. N. Goerner, Jr., P. F. King, J. M. Lyding, W. G. Tsang, and J. Vaya, *Tetrahedron*, **40**, 4569 (1984); f) M. Braun, *Tetrahedron*, **40**, 4585 (1984); g) R. C. Gupta, D. A. Jackson, and R. J. Stoodley, *J. Chem. Soc., Perkin Trans. 1*, **1985**, 525.

 © 1986 The Chemical Society of Japan Bull. Chem. Soc. Jpn., 59, 423—431 (1986)

Novel Glycosidation of 4-Demethoxyanthracyclinones by the Use of Trimethylsilyl Triflate. Syntheses of Optically Active 4-Demethoxydaunorubicin and 4-Demethoxyadriamycin[1)]

Yoshikazu KIMURA, Michiyo SUZUKI, Teruyo MATSUMOTO, Rumiko ABE, and Shiro TERASHIMA*
Sagami Chemical Research Center, Nishi-Ohnuma, Sagamihara, Kanagawa 229
(Received July 18, 1985)

Optically pure (+)-4-demethoxydaunorubicin has been prepared by a novel glycosidation reaction of (+)-4-demethoxydaunomycinone with (−)-3-*N*-trifluoroacetyl-1,4-bis(*O*-*p*-nitrobenzoyl)-L-daunosamine in the presence of trimethylsilyl triflate, followed by sequential *O*- and *N*-deprotection reactions. Total synthesis of optically pure (+)-4-demethoxyadriamycin has been also accomplished by two different synthetic schemes, starting from (+)-4-demethoxydaunorubicin or by way of (+)-3′-*N*-trifluoroacetyl-4-demethoxyadriamycin. (+)-4-Demethoxyadriamycin prepared by our hands was fully characterized by its spectral properties.

In the preceding paper,[2)] we have succeeded in exploring the simple and efficient synthetic scheme of optically pure (+)-4-demethoxydaunomycinone ((+)-**1a**). With a large quantity of (+)-**1a** in hand, our next efforts were focused on the elaboration of (+)-**1a** to unnatural 4-demethoxyanthracyclines, (+)-4-demethoxyadriamycin ((+)-**4d**–HCl) and (+)-4-demethoxydaunorubicin ((+)-**4a**–HCl). However, while an efficient glycosidation process is indispensable to the synthesis of unnatural anthracyclines such as (+)-**4a**, **d**–HCl, only a limited number of methods has been explored for glycosidation reaction in anthracycline area.

The reported methods of glycoside formation generally consist of the reactions of anthracyclinones, 1) with 1-halo-amino sugar derivatives in the presence of mercury(II) salt (Koenigs-Knorr reactions)[3)] or silver triflates,[4)] 2) with glycals derived from amino sugar derivatives in the presence of *p*-toluenesulfonic acid,[5)] 3) with 1-*O*-acyl amino sugar derivatives in the presence of tin(IV) chloride,[6a)] or *p*-toluenesulfonic acid.[6b,c)] However, these reactions seem not to be applicable to a large scale preparation of anthracyclines due to rather low yields,[3–6)] uses of unstable 1-halo amino sugar derivatives[3,4)] and toxic[3)] or expensive reagents,[4)] and lack of stereoselectivity resulting in the formation of α- and β-anomers.[3,5,6)]

We have recently explored the novel glycosidation method in which 4-demethoxyanthracyclinones are allowed to react with 1-*O*-acyl-L-daunosamine derivatives in the presence of trimethylsilyl trifluoromethanesulfonate (trimethylsilyl triflate) (TMSOTf).[1a)] This novel method has been found to produce the α-glycosides as sole reaction products which can be elaborated to optically pure (+)-**4a**–HCl and (+)-**4d**–HCl. In this full account, we wish to report the detailed procedure of the explored glycosidation reaction and the efficient synthetic schemes to (+)-**4a**–HCl and (+)-**4d**–HCl.

Development of the Novel Glycosidation Reaction and Its Application to the Synthesis of (+)-4-Demethoxydaunorubicin ((+)-4a–HCl). In order to obtain an authentic sample of (+)-3′-*N*-trifluoroacetyl-4-demethoxydaunorubicin ((+)-**3a**), and moreover, to evaluate the reported glycosidation method which could afford the desired α-glycoside most efficiently,[4b,c)] the reactions of (+)-**1a** with 1-chloro-L-daunosamine derivatives (**5a**, **b**) in the presence of silver trifluoromethanesulfonate (triflate) were examined by our hands. Treatment of optically pure (+)-**1a**[2)] with 3-*N*-trifluoroacetyl-4-*O*-*p*-nitrobenzoyl-L-daunosamyl chloride (**5a**)[3a,4b)] or 3-*N*:4-*O*-bis(trifluoroacetyl)-L-daunosamyl chloride (**5b**)[3b–d,4a)] in the presence of silver triflate, followed by 4′-*O*-deprotection under mild alkaline conditions or methanolysis, was found to give (+)-3′-*N*-trifluoroacetyl-4-demethoxydaunorubicin ((+)-**3a**) in 49 or 56% yield with 47 or 43% recovery of starting (+)-**1a**, respectively. These yields are very close to those reported.[4b,c)] With an aim to improve the yield of (+)-**3a** with decrease of the recovery of (+)-**1a**, uses of further equivalents of **5a**, **b** and/or silver triflate and additions of organic or inorganic bases to the glycosidation medium were examined.[7)] However, these attempts turned out to be ineffective for obtaining

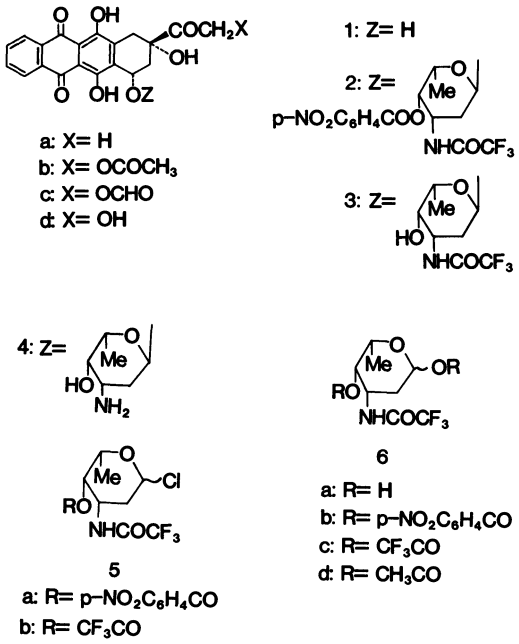

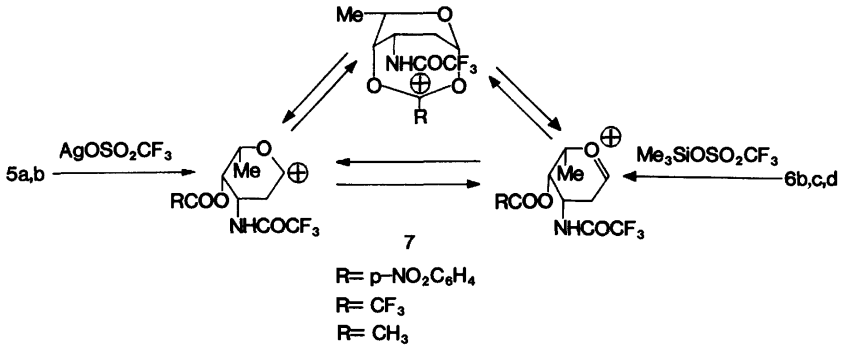

better yields of (+)-**3a** than those described above.

After accumulating numerous unsuccessful results, a combination of (−)-3-*N*-trifluoroacetyl-1,4-bis(*O*-*p*-nitrobenzoyl)-L-daunosamine ((−)-**6b**) and TMSOTf was found to be quite promising for the glycosidation of (+)-**1a** to afford an almost quantitative yield of the desired α-glycoside, (−)-3′-*N*-trifluoroacetyl-4′-*O*-*p*-nitrobenzoyl-4-demethoxydaunorubicin ((−)-**2a**). Thus, TMSOTf (2.0—2.5 equiv) was added to a suspension of (−)-**6b**[3a] (1.2—1.3 equiv) and granulated molecular sieves 4A[8] in a mixture of dichloromethane and ether (1:1—3:1) at −40 °C, and the whole mixture was stirred at 0—5 °C to give a clear solution. Then, a dichloromethane solution of (+)-**1a**[2] (1 equiv) was added dropwise to the clear solution cooled at −15 °C. The glycosidation reaction proceeded smoothly at −15 °C to produce (−)-**2a** as a sole reaction product. After completion of the reaction, usual extractive isolation followed by filtration through a short silica-gel column gave pure (−)-**2a**[4b] in 99.5% yield, mp 171—173 °C, $[\alpha]_D^{20}$ −89.7° (dioxane). No formation of the undesired β-glycoside was definitely ascertained by the NMR spectra which exhibited the C_1'-proton as a singlet at 5.70 ppm (W_H=6.0 Hz). The α-glycoside ((−)-**2a**) was successfully elaborated to (+)-**4a**–HCl according to the reported method.[4b] Thus, mild hydrolysis with 0.1 M[†] sodium hydroxide in a mixture of methanol and dichloromethane selectively effected 4′-*O*-deprotection, resulting in the formation of (+)-**3a**[4b] in 83% yield, mp 151—153 °C, $[\alpha]_D^{20}$ +190° (dioxane). Further treatment of (+)-**3a** with 0.1 M sodium hydroxide followed by salt formation with hydrogen chloride afforded (+)-**4a**–HCl[3b,4a,b] in 77% yield, mp 184—187 °C (decomp), $[\alpha]_D^{20}$ +188° (methanol). These physical data were almost identical with those reported.[3b,4a,b] The glycoside (+)-**4a**–HCl also showed the same spectral properties as those reported.[4b]

Next, in order to examine the scope and limitation of the explored glycosidation reaction, uses of trialkylsilyl triflate and L-daunosamine derivatives other than those employed above were attempted. Triethylsilyl triflate could be similarly used as an activating reagent of (−)-**6b**, giving (−)-**2a** in 95% yield. However, the reaction of (+)-**1a** with (−)-**6b** in the presence of *t*-butyldimethylsilyl triflate afforded (−)-**2a** in only 7% yield. When (−)-3-*N*-trifluoroacetyl-1,4-bis(*O*-trifluoroacetyl)-L-daunosamine ((−)-**6c**)[3b] or *N*-trifluoroacetyl-1,4-di-*O*-acetyl-L-daunosamine (**6d**) were subjected to the glycosidation under the same conditions as those described above and the formed unstable 4′-*O*-acyl-α-glycosides were immediately hydrolyzed under mild alkaline conditions, (+)-**3a** could be obtained in 61 or 70% overall yield, respectively.

Precise reaction mechanism of the novel glycosidation is presently obscure. As mentioned above, we have already observed that the glycosidation of (+)-**1a** with **5a**, **b** in the presence of silver triflate, followed by 4′-*O*-deprotection, exclusively produced (+)-**3a** in moderate yields with recovery of (+)-**1a**. This glycosidation reaction has been explained to proceed through the cationic species **7**. Since formation of the same cationic species **7** can be reasonably expected for the explored glycosidation, the observed higher yields of (+)-**3a** might be explained by the assumption that the reactivity of **7** derived from **6b**—**d** and TMSOTf is amplified more than that derived from **5a**, **b** and silver triflate. Exclusive formation of the desired α-glycoside ((−)-**2a**) may be due to a combination of the usual steric and anomeric effects.

The developed glycosidation reaction has the following novel characteristics: 1) Almost quantitative yield of the α-glycoside ((−)-**2a**) can be obtained by using (−)-**6b** as a daunosamine derivative. 2) 1,4-Di-*O*-acyl-L-daunosamine derivatives (**6b**—**d**) show larger stability under an air and are more feasible than **5a**, **b**, and (−)-**6b** is the best amino sugar component in the light of the exclusive formation of the desired α-glycoside ((−)-**2a**). 3) TMSOTf is commercially available[9] and is more inexpensive than silver triflate. 4) Presence of ether in the reaction medium is necessary for obtaining a good yield of the glycoside. When the glycosidation is carried out by omitting ether from a reaction solvent, the yield of (−)-**2a** dramatically decreases to 20%. This might be explained by the assumption that ether can effectively stabilize a cationic species such as **7** by chelation with the lone pair of oxygen atom.[10] 5) A role of molecular sieves 4A is quite obscure, but in the absence of molecular sieves 4A, the glycosidation affords only 27% of (−)-**2a**.[11]

[†] 1 M=1 mol dm^{-3}.

As detailed above, we have succeeded in exploring the highly efficient glycosidation reaction of (+)-**1a**. Taking into account various novel aspects, the developed glycosidation reaction might be considered to be one of the best preparation methods of anthracyclines among those hitherto reported.[3-6]

Synthesis of (+)-4-Demethoxyadriamycin ((+)-4d-HCl). The natural adriamycin is well known to display more favorable therapeutic profiles than daunorubicin[13,14] against various types of human cancers. Similar more improved anticancer activities can be foreseen for unnatural **4d**-HCl than for (+)-**4a**-HCl. Therefore, synthesis of optically pure **4d**-HCl was examined by two different synthetic schemes.

One synthetic route is the elaboration of (+)-**4a**-HCl to optically pure **4d**-HCl according to the same synthetic scheme as that reported by Arcamone et al.[4a,15] By subjecting (+)-**4a**-HCl to the reported synthetic operations such as successive acetalization and bromination with triethoxymethane[16] and bromine in a mixture of methanol, dioxane, and dichloromethane, deacetalization with 0.25 M hydrobromic acid, substitution with sodium formate, hydrolysis with 5% sodium hydrogencarbonate, and salt formation with hydrogen chloride, we obtained the compound showing mp 186—189 °C (decomp) and $[\alpha]_D^{20}$ +185° (methanol) in 30% overall yield. Although the melting point of this sample was almost identical with that reported for **4d**-HCl (mp 186—189 °C (decomp)),[15] the spectral profiles (IR, NMR, MS) were found to be inconsistent with the expected structure. Especially the NMR spectrum showed a singlet at 8.40 ppm which could be assigned as a formyl group, and the molecular weight could be determined as 541 based on its MS spectrum. These spectral properties clearly suggested that this sample was not the right compound (**4d**-HCl) but (+)-14-formyloxy-4-demethoxydaunorubicin hydrochloride ((+)-**4c**-HCl). The reason why (+)-**4c**-HCl was obtained instead of the expected **4d**-HCl should be insufficient hydrolysis of the formate with 5% sodium hydrogencarbonate. As expected, further hydrolysis of (+)-**4c**-HCl with 0.1 M sodium hydroxide followed by salt formation with hydrogen chloride, readily produced desired (+)-**4d**-HCl, mp 225—228 °C (decomp) and $[\alpha]_D^{20}$ +187° (methanol). Full spectral (IR, NMR, MS) properties of this sample strongly supported the structure of (+)-**4d**-HCl.

Taking into account the result obtained above, the improved procedure for preparing (+)-**4d**-HCl from (+)-**4a**-HCl was deviced by minor modifications of the original synthetic scheme.[4a,15] Thus, successive acetalization and bromination of (+)-**4a**-HCl with trimethoxymethane and bromine in a mixture of methanol and dioxane followed by removal of the acetal by transacetalization with acetone,[16,17] substitution of the α-bromo ketone with sodium formate, hydrolysis of the formate with 0.1 M sodium hydroxide in methanol, and salt formation with hydrogen chloride, gave (+)-**4d**-HCl in 49% overall yield.[19]

In order to confirm the structure of (+)-**4d**-HCl, another synthesis of (+)-**4d**-HCl was next attempted. According to the reported method,[20] (+)-14-acetoxy-4-demethoxydaunomycinone ((+)-**1b**), mp 187—188.5 °C, $[\alpha]_D^{20}$ +181° (dioxane), was prepared from (+)-**1a** in 70% overall yield by sequential bromination of (+)-**1a** with pyridinium tribromide and substitution of the bromide with potassium acetate. Glycosidation of (+)-**1b** with (−)-**6b** in the presence of TMSOTf by the same manner as that described for (−)-**2a** readily gave the desired (−)-α-glycoside ((−)-**2b**) as a sole product in 99% yield, mp 167—170 °C, $[\alpha]_D^{20}$ −53.5° (dioxane). No formation of the undesired β-glycoside was also ascertained by the NMR analysis of the reaction product. However, simultaneous hydrolysis of the 4′- and 14-ester functions with 10% potassium carbonate (pH≈10) afforded only crude (+)-3′-*N*-trifluoroacetyl-4-demethoxyadriamycin ((+)-**3d**) in 39% yield.

Since (+)-**3d** seems to be unstable under the basic conditions (pH≈10) which is required to hydrolyze the acetoxyl group, a formyl group that can be more easily removed than an acetyl group was selected as a protective group of the 14-hydroxymethyl function. Bromination of (+)-**1a** with pyridinium tribromide, followed by substitution of the bromide with tetrabutylammonium formate,[21] gave (+)-14-formyloxy-4-demethoxydaunomycinone ((+)-**1c**) in 78% overall yield, mp 183—185 °C, $[\alpha]_D^{20}$+153° (dioxane). Glycosidation of (+)-**1c** with (−)-**6b** in the presence of TMSOTf similarly produced the corresponding α-glycoside (**2c**) as a sole product.[22] Immediate hydrolysis of **2c** with 0.1 M sodium hydroxide in methanol (pH≈8) effected the removal of the 14-*O*-formyl and 4′-*O*-*p*-nitrobenzoyl groups, giving (+)-**3d** in 73% overall yield, mp 143—148 °C, $[\alpha]_D^{20}$ +170° (dioxane).

After simultaneous protection of the C_9- and C_{14}-hydroxylic functions of (+)-**3d** by treating with trimethoxymethane,[23] the formed protected glycoside was directly treated with 0.1 M sodium hydroxide to remove C_3′-*N*-trifluoroacetyl group, then with 0.25 M hydrochloric acid to cleave the protective group(s) derived from trimethoxymethane, affording (+)-**4d**-HCl in 40% overall yield from (+)-**3d**, mp 226—229 °C (decomp), $[\alpha]_D^{20}$+190° (methanol). Spectral (IR, NMR, MS) behavior of this sample were completely identical with that of (+)-**4d**-HCl prepared from (+)-**4a**-HCl.

Based on exploration of the novel glycosidation reaction and various modifications of the reported reactions, we have succeeded in the total syntheses of (+)-**4a**-HCl and (+)-**4d**-HCl starting from (+)-**1a**. Taking into account numerous novel aspects delineated in this report, the developed overall processes seem to hold promise not only for 4-demethoxyanthracyclines but also for the whole family of natural and unnatural anthracyclines.

Experimental

General. All melting points were determined with a Yamato MP-21 melting point apparatus and a Yanaco micro melting point apparatus and were uncorrected. IR spectral measurements were carried out with a JASCO A-202 diffraction grating infrared spectrometer. NMR spectra were measured with a Varian EM-390 spectrometer (90 MHz) and a Varian XL-100A spectrometer (100 MHz). All signals were expressed as ppm downfield from TMS used as an internal standard (δ-value). Mass spectra were taken with a Hitachi RMU-6MG mass spectrometer and a Hitachi M-80A mass spectrometer (SIMS). Measurements of optical rotations were performed with a Union PM-201 automatic digital polarimeter and a Horiba SEPA-200 automatic digital polarimeter. Wakogel C-200 and Kieselgel 60 (Merck) were used as an adsorbent for column chromatography. All reactions were performed using anhyd solvents. Especially, tetrahydrofuran, ether, and dioxane freshly distilled from sodium benzophenone ketyl, and dichloromethane, acetone, and pyridine freshly distilled from calcium hydride were used. Trimethylsilyl trifluoromethanesulfonate purchased from Petrarch System Inc. (Chisso) was used without further purification. Triethylsilyl trifluoromethanesulfonate and *t*-butyldimethylsilyl trifluoromethanesulfonate were purchased from Aldrich Chemical Co. and used without further purification. Pyridinium tribromide purchased from Tokyo Kasei Kogyo Co. Ltd. was used after three repeated recrystallizations from acetic acid. The following abbreviations are used for solvents: acetic acid (AcOH), acetone (Me_2CO), benzene (C_6H_6), chloroform ($CHCl_3$), dichloromethane (CH_2Cl_2), ethanol (EtOH), ether (Et_2O), ethyl acetate (EtOAc), hexane (C_6H_{14}), methanol (MeOH), tetrahydrofuran (THF).

(−)-3-*N*-Trifluoroacetyl-1,4-bis(*O*-*p*-nitrobenzoyl)-L-daunosamine ((−)-6b). Prepared from (−)-**6a**[24] (mp 146—147 °C, $[\alpha]_D^{20}$ −127.2° (*c* 0.10, MeOH)) (lit,[3a] mp 146—147 °C) in 82% yield according to the reported method,[3a] mp 201—202 °C, $[\alpha]_D^{20}$ −117° (*c* 0.029, Me_2CO) (lit,[3a] mp 202—203 °C, $[\alpha]_D^{21}$ −125° (*c* 0.03, 95% EtOH)). IR and NMR ($(CD_3)_2SO$) spectra were identical with those reported in the literature.[3a] ^{1}H NMR ($CDCl_3$) δ=1.27 (d, *J*=6 Hz, 3H, CH_3), 2.26 (d, *J*=3 Hz, 1H, 2-*ax*-H), 2.34 (d, *J*=3 Hz, 1H, 2-*eq*-H), 4.46 (q, *J*=6 Hz, 1H, 5-H), 4.47—5.02 (m, 1H, 3-H), 5.58 (brs, 1H, 4-H), 6.51 (brd, *J*=8 Hz, 1H, NH), 6.72 (brs, W_H=6 Hz, 1H, 1′-H), 8.24—8.50 (m, 8H, Ar). Since the C_1-anomeric proton appeared as a broad singlet at δ 6.72 (W_H=6 Hz) in the NMR spectrum in $CDCl_3$, it appeared evident that (−)-**6b** solely consisted of the α-anomer.

(−)-3-*N*-Trifluoroacetyl-1,4-bis(*O*-trifluoroacetyl)-L-daunosamine ((−)-6c). Prepared from (−)-**6a**[24] (mp 146—147 °C, $[\alpha]_D^{20}$ −127.2° (*c* 0.10, MeOH)) in 51% yield according to the literature,[3c] mp 133.5—135 °C, $[\alpha]_D^{20}$ −69.5° (*c* 0.12, Me_2CO) (lit,[3c] mp 132—134 °C). IR and NMR spectra of this sample were identical with those reported in the literature.[3c] Based on the NMR spectrum in which the C_1-anomeric proton appeared as a broad singlet at δ 6.53 (W_H=6 Hz), (−)-**6c** was considered to solely consist of the α-anomer.

3-*N*-Trifluoroacetyl-1,4-di-*O*-acetyl-L-daunosamine (6d). Acetic anhydride (1 mL, 10.6 mmol) was added to (−)-**6a**[24] (mp 146—147 °C, $[\alpha]_D^{20}$ −127.2° (*c* 0.10, MeOH)) (105 mg, 0.49 mmol) in pyridine (2 mL) with stirring at room temperature. After the stirring was continued overnight, the reaction was quenched by adding H_2O to the mixture. Usual extractive isolation with $CHCl_3$ followed by purification by silica-gel chromatography (EtOAc/C_6H_6=1/4), furnished **6d** as a white caramel (126.6 mg, 87%). ^{1}H NMR ($CDCl_3$) δ= 1.15 (d, *J*=6 Hz, 1.5H, CH_3), 1.22 (d, *J*=6 Hz, 1.5H, CH_3), 1.60—2.05 (m, 2H, 2-H_2), 2.12 (s, 3H, $COCH_3$), 2.20 (s, 3H, $COCH_3$), 3.66—4.00 (m, 1H, 5-H), 4.05—4.35 (m, 1H, 3-H), 5.00—5.20 (m, 1H, 4-H), 5.80 (dd, *J*=9 and 3 Hz, 0.5 H, 1-*ax*-H), 6.28 (brs, W_H=6 Hz, 0.5H, 1-*eq*-H), 6.40—6.80 (brs, 1H, NH). Based on this NMR spectrum, it appeared evident that **5d** was a mixture of the α- and β-anomers (α/β=1). This sample was immediately used without separation of these two anomers.

3-*N*-Trifluoroacetyl-4-*O*-*p*-nitrobenzoyl-L-daunosamyl Chloride (5a). Prepared by treating (−)-**6b** (mp 201—202 °C, $[\alpha]_D^{20}$ −117° (*c* 0.029, Me_2CO)) with hydrogen chloride in Et_2O according to the literature.[4b] ^{1}H NMR ($CDCl_3$) δ= 1.20 (d, *J*=6 Hz, 3H, CH_3), 2.10—2.48 (m, 2H, 2-H_2), 4.48 (q, *J*=6 Hz, 1H, 5-H), 4.64—5.03 (m, 1H, 3-H), 5.33—5.53 (m, 1H, 4-H), 6.20—6.56 (m, 2H, 1-H+NH), 8.24 (s, 4H, Ar). This sample was directly used without further purification.

3-*N*:4-*O*-Bis(trifluoroacetyl)-L-daunosamyl Chloride (5b). Prepared by treating (−)-**6c** (mp 133.5—135 °C, $[\alpha]_D^{20}$ −69.5° (*c* 0.12, Me_2CO)) with hydrogen chloride in Et_2O according to the reported method.[3c] NMR spectrum of this sample was identical with that reported.[3c]

(+)-3′-*N*-Trifluoroacetyl-4-demethoxydaunorubicin ((+)-3a). a) **Glycosidation of (+)-1a with (−)-6b by the Use of TMSOTf:** TMSOTf (0.12 mL, 0.62 mmol) was added to a stirred suspension of (−)-**6b** (mp 201—202 °C, $[\alpha]_D^{20}$ −117° (*c* 0.029, Me_2CO)) (159 mg, 0.29 mmol) and molecular sieves 4A (0.8 g) in a mixture of CH_2Cl_2 (12 mL) and Et_2O (10 mL) at −40 °C under an argon atmosphere. The whole mixture was stirred at 0 °C for 1 h to give a clear solution, which was cooled at −15 °C. A solution of (+)-**1a**[2] (mp 184—185 °C, $[\alpha]_D^{20}$ +154° (*c* 0.10, dioxane)) (85 mg, 0.23 mmol) in CH_2Cl_2 (25 mL) was added to the stirred reaction mixture cooled at −15 °C. After stirring at −15 °C for 5 h, the whole mixture was poured onto a two-layer mixture of satd $NaHCO_3$ (150 mL) and EtOAc (80 mL) with vigorous stirring to quench the glycosidation reaction. Progress of the glycosidation could be readily monitored by TLC analysis (SiO_2: EtOAc/C_6H_6=1/4). The organic layer was separated, washed with satd NaCl (50 mL×2), then dried over $MgSO_4$. Filtration and concentration in vacuo gave a residue, which was filtered through a short silica-gel column (EtOAc/C_6H_6=1/4) to give (−)-**2a** as an orange solid (170 mg, 99.5%). The purified sample was triturated with C_6H_{14} containing a small amount of $CHCl_3$, giving pure (−)-**2a** as an orange solid (157 mg, 92%), mp 171—173 °C, $[\alpha]_D^{20}$−89.7° (*c* 0.078, dioxane) (lit,[4b] mp 171—175 °C, $[\alpha]_D^{20}$ −89.8° (*c* 0.1, dioxane)). ^{1}H NMR ($CDCl_3$) δ=1.25 (d, *J*=6 Hz, 3H, 6′-Me), 1.98—2.38 (m, 4H, 2′-H_2+8-H_2), 2.45 (s, 3H, $COCH_3$), 3.00 (d, *J*=19 Hz, 1H, 10-*ax*-H), 3.36 (d, *J*=19 Hz, 1H, 10-*eq*-H), 4.22 (s, 1H, 9-OH), 4.32—4.66 (m, 2H, 3′-H+5′-H), 5.36 (brs, 1H, 7-H), 5.51 (m, 1H, 4′-H), 5.70 (brs, W_H=6 Hz, 1H, 1′-H), 6.24 (brd, *J*=7 Hz, 1H, NH), 7.76—7.94 (m, 2H, Ar), 8.20—8.48 (m, 6H, Ar), 13.35 (s, 1H, ArO*H*), 13.68 (s, 1H, ArO*H*). These spectral properties were identical with those reported.[4b] Found: C, 55.87; H, 4.17; N, 3.94%. Calcd for $C_{35}H_{29}F_3N_2O_{13}$·0.5H_2O: C, 55.89; H, 4.02; N, 3.72%.

Sodium hydroxide (0.1 M) (2.5 mL) was added to a solution of (−)-**2a** (mp 171—173 °C, $[\alpha]_D^{20}$ −89.7° (*c* 0.078, dioxane)) (189.0 mg, 0.25 mmol) in CH_2Cl_2 (1.5 mL) and MeOH (100 mL) with stirring at 0 °C under an argon atmosphere. The deep purple solution produced was stirred at 0 °C for 30 min. Glacial AcOH was added to the reaction mixture until the color of the solution became bright orange. Ethyl acetate (150 mL) and satd NaCl (150 mL) were successively added to the reaction mixture. The separated organic layer was washed with satd NaCl (50 mL×2), and dried over $MgSO_4$. Filtration and concentration in vacuo gave an orange residue, which was purified by silica-gel column chromatography (CH_2Cl_2/Me_2CO=9/1) to give pure (+)-**3a** as an orange crystalline solid (120 mg, 83%), mp 151—153 °C, $[\alpha]_D^{20}$ +190° (*c* 0.10, dioxane) (lit,[3b] mp 155—157 °C, $[\alpha]_D^{20}$ +188° (*c* 0.1, dioxane); lit,[4b] mp 155—156 °C, $[\alpha]_D^{20}$ +190° (*c* 0.1, dioxane)). IR (KBr): 3530, 3475, 1720 cm^{-1}. ^1H NMR ($CDCl_3$) δ=1.34 (d, *J*=7 Hz, 3H, 6′-Me), 1.80—2.38 (m, 4H, 2′-H_2+8-H_2), 2.43 (s, 3H, $COCH_3$), 2.99 (d, *J*=19 Hz, 1H, 10-*ax*-H), 3.34 (dd, *J*=19 and 1.5 Hz, 1H, 10-*eq*-H), 3.62—3.78 (m, 1H, 4-H), 4.32 (s, 1H, 9-OH), 4.10—4.42 (m, 2H, 3′-H+5′-H), 5.30 (dd, *J*=4 and 2 Hz, 1H, 7-H), 5.54 (brd, *J*=3 Hz, 1H, 1′-H), 6.67 (brd, *J*=8 Hz, 1H, NH), 7.81—7.93 (m, 2H, Ar), 8.35—8.47 (m, 2H, Ar), 13.38 (s, 1H, ArO*H*), 13.66 (s, 1H, ArO*H*). These spectra were identical with those reported.[4b]

b) Glycosidation of (+)-1a with (−)-6c by the Use of TMSOTf: Treatments of (+)-**1a**[2] (mp 184—185 °C, $[\alpha]_D^{20}$ +154° (*c* 0.10, dioxane)) (10.6 mg, 0.029 mmol) with (−)-**6c** (mp 133.5—135 °C, $[\alpha]_D^{20}$ −69.5° (*c* 0.12, Me_2CO)) (15.5 mg, 0.036 mmol) in the presence of TMSOTf (0.02 mL, 0.10 mmol) in the same manner as that described in **a**), gave the crude glycoside. This was immediately hydrolyzed with 0.1 M NaOH in MeOH to afford (−)-**3a** (10.0 mg, 61%). This sample showed an almost identical NMR spectrum with that of the pure sample obtained in **a**).

c) Glycosidation of (+)-1a with 5d by the Use of TMSOTf: Treatments of (+)-**1a**[2] (mp 184—185 °C, $[\alpha]_D^{20}$ +154° (*c* 0.10, dioxane)) (5.4 mg, 0.015 mmol) with **6d** (6.0 mg, 0.020 mmol) in the presence of TMSOTf (0.01 mL, 0.050 mmol) in the same manner as that described in **a**), followed by hydrolysis with 0.1 M NaOH and purification by silica-gel chromatography (CH_2Cl_2/Me_2CO=9/1), gave (+)-**3a** (6.2 mg, 70%). NMR spectrum of this sample was almost identical with that of pure (+)-**3a** obtained in **a**).

d) Glycosidation of (+)-1a with (−)-6b by the Use of Triethylsilyl Triflate: The same treatments of (+)-**1a**[2] (mp 184—185 °C, $[\alpha]_D^{20}$ +154° (*c* 0.10, dioxane)) (10.3 mg, 0.028 mmol) as those described in **a**), afforded (−)-**2a** (19.6 mg, 95%) after extractive isolation and purification by column chromatography. This was similarly identified by spectral (IR, NMR) comparisons.

e) Glycosidation of (+)-1a with (−)-6b by the Use of *t*-Butyldimethylsilyl Triflate: The same treatments of (+)-**1a**[2] (mp 184—185 °C, $[\alpha]_D^{20}$ +154° (*c* 0.10, dioxane)) (4.3 mg, 0.012 mmol) as those described in **a**), gave (−)-**2a** (0.50 mg, 7%), with recovery of (+)-**1a** (3.9 mg, 90%). NMR spectrum of (−)-**2a** was almost identical with that of pure (−)-**2a** obtained in **a**).

f) Glycosidation of (+)-1a with 5a by the Use of Silver Triflate: According to the reported method,[4b] a solution of silver triflate (22.0 mg, 0.086 mmol) in Et_2O (1 mL) was added to a mixture of (+)-**1a**[2] (mp 184—185 °C, $[\alpha]_D^{20}$ +154° (*c* 0.10, dioxane)) (20.9 mg, 0.057 mmol) and **5a** (26.7 mg, 0.075 mmol) in THF (4 mL) with stirring at room temperature. After being stirred at room temperature for 1 h with protection from a light, the mixture was diluted with EtOAc (20 mL), and washed with satd $NaHCO_3$ (30 mL). After drying over $MgSO_4$, filtration through a pad of celite and concentration in vacuo gave the crude product containing (−)-**2a**. Without purification, the crude glycoside ((−)-**2a**) was dissolved in a mixture of MeOH (20 mL) and CH_2Cl_2 (2 drops), and 0.1 M NaOH (0.4 mL) was added to the methanolic solution with stirring at 0 °C. After stirring at 0 °C for 20 min, the reaction was worked up in a similar manner as that described in **a**), giving a mixture of (+)-**3a** and (+)-**1a** as a red caramel after concentration of the ethyl acetate extracts. Separation by column chromatography (EtOAc/C_6H_6=1/4, then, 1/1) gave almost pure (+)-**1a** (9.8 mg, 47%) and (+)-**3a** (16.5 mg, 49%). Both samples were identified with the authentic samples by spectral (NMR) comparisons, respectively.

g) Glycosidation of (+)-1a with 5b by the Use of Silver Triflate: According to the reported method,[4a] a solution of silver triflate (20.0 mg, 0.078 mmol) in Et_2O (1 mL) was added to a mixture of (+)-**1a**[2] (mp 184—185 °C, $[\alpha]_D^{20}$ +154° (*c* 0.10, dioxane)) (20.0 mg, 0.054 mmol) and **5b** (22.0 mg, 0.067 mmol) in CH_2Cl_2 (3 ml) with stirring at room temperature. After stirring at the same temperature for 1.5 h, a solution of silver triflate (20.0 mg, 0.078 mmol) in Et_2O (1 mL) was further added to the reaction mixture, and the stirring was continued for 1 h. Usual extractive isolation followed by methanolysis in MeOH (20 mL) at 50 °C for 1 h, gave a crude mixture of (+)-**1a** and (+)-**3a**. This was separated by silica-gel column chromatography (EtOAc/C_6H_6=1/4, then 1/1), giving almost pure (+)-**1a** (8.5 mg, 43%) and (+)-**3a** (18.0 mg, 56%). Both samples were identified with the authentic samples by spectral (NMR) comparisons, respectively.

(+)-4-Demethoxydaunorubicin Hydrochloride ((+)-4a-HCl). A deep purple solution of (+)-**3a** (mp 151—153 °C, $[\alpha]_D^{20}$ +190° (*c* 0.10, dioxane)) (95.7 mg, 0.17 mmol) in 0.1 M NaOH (20 mL) was stirred at room temperature for 20 min under an argon atmosphere. After the acidity of the solution was adjusted to be pH 8 with 5 M HCl, the neutralized solution was extracted with $CHCl_3$ until a chloroform extract showed no orange color of the reaction product (ca. 70 mL×5). The combined chloroform layers were washed with H_2O (50 mL), and dried over Na_2SO_4. Filtration and concentration in vacuo gave an orange residue which was dissolved in a small amount of $CHCl_3$ and MeOH (9/1). After 0.25 M hydrogen chloride in MeOH was added to the resulting solution until the acidity became pH 3—5, Et_2O (30 mL) was added to the acidic solution to give (+)-**4a**-HCl as an orange powder (69.7 mg, 77%), mp 184—185 °C (decomp), $[\alpha]_D^{20}$ +188° (*c* 0.10, MeOH) (lit,[3b] mp 183—185 °C, $[\alpha]_D^{20}$ +205° (*c* 0.1, MeOH); lit,[4b] mp 172—174 °C (decomp), $[\alpha]_D^{20}$ +187° (*c* 0.1, MeOH)). IR (KBr): 3350, 1715, 1625, 1590, 1410, 1235, 1120, 985 cm^{-1}. ^1H NMR ($(CD_3)_2SO$) δ=1.18 (d, *J*=6 Hz, 3H, 6′-Me), 1.70—2.24 (m, 4H, 2′-H_2+8-H_2), 2.30 (s, 3H, $COCH_3$), 3.00 (brs, 2H, 10-H_2), 3.54—3.70 (brs, 1H, 4′-H), 4.24 (q, *J*=6 Hz, 1H, 5′-H), 5.00 (brs, W_H=8 Hz, 1H, 7-H), 5.32 (brs, W_H=6 Hz, 1H, 1′-H), 5.47 (d, *J*=6 Hz, 1H, 4′-OH), 5.58 (s, 1H, 9-OH), 7.75—8.05 (brs, 3H, NH_3), 7.95—8.12 (m, 2H, Ar), 8.20—8.42 (m, 2H, Ar), 13.36 (brs, 1H, ArO*H*), 13.54 (brs, 1H, ArO*H*). These IR and NMR spectra were identical with those reported.[4b] MS (SIMS) *m/z*: 498 (MH^+). Found: C, 56.34; H, 5.32; N, 2.42%. Calcd for $C_{26}H_{28}ClNO_9$-H_2O: C, 56.58; H, 5.48; N, 2.54%.

(+)-14-Acetoxy-4-demethoxydaunomycinone ((+)-1b). The same treatments of (+)-**1a**[2] (mp 184—185 °C, $[\alpha]_D^{20}$ +154° (*c* 0.10, dioxane)) (74 mg, 0.20 mmol) as those reported[19] gave (+)-**1b** as an orange solid (60 mg, 70%) after extractive isolation with CH_2Cl_2 and purification by column chromatography (EtOAc/C_6H_6=1/4). Recrystallization from a mixture of C_6H_6, Et_2O, and C_6H_{14} gave pure (+)-**1b** as orange crystals, mp 187—188.5 °C, $[\alpha]_D^{20}$ +181° (*c* 0.104, dioxane). IR (KBr): 3500, 3450, 1745, 1735, 1623, 1587 cm^{-1}. ^1H NMR ($CDCl_3$) δ=2.08 (dd, *J*=15 and 4.5 Hz, 1H, 8-*ax*-H), 2.21 (s, 3H, $COCH_3$), 2.51 (dt, *J*=15 and 2 Hz, 1H, 8-*eq*-H), 3.00 (d, *J*=19 Hz, 1H, 10-*ax*-H), 3.31 (dd, *J*=19 and 2 Hz, 1H, 10-*eq*-H), 3.43 (brs, 1H, 7-OH), 4.69 (s, 1H, 9-OH), 5.17 (d, *J*=18 Hz, 1H, one of 14-H), 5.38 (brs, 1H, 7-H), 5.42 (d, *J*=18 Hz, 1H, one of 14-H), 7.76—8.01 (m, 2H, Ar), 8.24—8.48 (m, 2H, Ar), 13.19 (s, 1H, ArO*H*), 13.52 (s, 1H, ArO*H*). MS *m/z*: 426 (M^+). Found: C, 61.86; H, 4.28%. Calcd for $C_{22}H_{18}O_9$: C, 61.97; H, 4.26%.

(+)-14-Formyloxy-4-demethoxydaunomycinone ((+-1c). A mixture of (+)-**1a**[2] (mp 184—185 °C, $[\alpha]_D^{20}$ +154° (*c* 0.10 dioxane)) (100 mg, 0.27 mmol) and pyridinium tribromide (100 mg, 0.30 mmol) in THF (10 mL) was stirred at room temperature for 2 h. A solution of tetrabutylammonium formate[21] (488 mg, 1.70 mmol) in THF (13 mL) was added to the reaction mixture. After stirring for 10 min at room temperature, the whole mixture was diluted with CH_2Cl_2 (150 ml), washed with satd NaCl (100 mL×3), then dried over $MgSO_4$. Filtration and concentration in vacuo followed by purification by a short silica-gel column (EtOAc/C_6H_6=1/4) gave crude (+)-**1c** as an orange solid (102.3 mg, 92%). Recrystallization from a mixture of $CHCl_3$, MeOH, and Et_2O gave an analytical sample of (+)-**1c** (86.7 mg, 78%), mp 183—185 °C, $[\alpha]_D^{20}$ +153° (*c* 0.11, dioxane). IR (KBr): 1735, 1720, 1625, 1590 cm^{-1}. ^1H NMR ($CDCl_3$) δ=2.14 (ddd, *J*=15, 5 and 2 Hz, 1H, 8-*ax*-H), 2.53 (dt, *J*=15 and 2 Hz, 1H, 8-*eq*-H), 3.02 (d, *J*=19 Hz, 1H, 10-*ax*-H), 3.34 (brs, 1H, 7-OH), 3.38 (dd, *J*=19 and 2 Hz, 1H, 10-*eq*-H), 4.69 (s, 1H, 9-OH), 5.26 (d, *J*=18 Hz, 1H, one of 14-H), 5.39 (brs, 1H, 7-H), 5.53 (d, *J*=18 Hz, 1H, one of 14-H), 7.78—7.98 (m, 2H, Ar), 8.24 (s, 1H, OC*H*O), 8.30—8.52 (m, 2H, Ar), 13.30 (s, 1H, ArO*H*), 13.63 (s, 1H, ArO*H*). MS *m/z*: 412 (M^+). Found: C, 59.24; H, 3.87%. Calcd for $C_{21}H_{16}O_9$-0.75H_2O: C, 59.23; H, 4.14%.

(+)-3′-*N*-Trifluoroacetyl-4-demethoxyadriamycin ((+)-3d).
a) Glycosidation of (+)-1b with (−)-6b by the Use of TMSOTf: TMSOTf (0.08 mL, 0.41 mmol) was added to a suspension of (−)-**6b** (mp 201—202 °C, $[\alpha]_D^{20}$ −117° (*c* 0.029, Me_2CO)) (90.0 mg, 0.166 mmol) and granulated molecular sieves 4A[8] (0.8 g) in a mixture of CH_2Cl_2 (9 mL) and Et_2O (3 mL) with stirring at −40 °C under an argon atmosphere. The whole mixture was stirred at 0 °C for 1 h, then cooled to −15 °C. A solution of (+)-**1b** (mp 187—188.5 °C, $[\alpha]_D^{20}$ +181° (*c* 0.104, dioxane)) (56.9 mg, 0.134 mmol) in CH_2Cl_2 (17 mL) was added to the stirred reaction mixture. After being stirred at −15 °C for 3.5 h, the whole mixture was poured onto a two-layer mixture of satd $NaHCO_3$ (100 mL) and EtOAc (50 mL) with vigorous stirring to quench the glycosidation reaction. The organic layer was separated, washed with satd NaCl (50 mL×2), then dried over $MgSO_4$. Filtration and concentration in vacuo gave a residue, which was filtered through a short silica-gel column (EtOAc/C_6H_6=1/4) to give almost pure (−)-**2b** as an orange solid (105.5 mg, 99%). The glycoside ((−)-**2b**) was further triturated with $CHCl_3$, then with C_6H_{14} to give pure (−)-**2b** (91.3 mg, 85%), mp 167—170 °C, $[\alpha]_D^{20}$ −53.5° (*c* 0.097, dioxane). IR (KBr): 3500, 3350, 1730 cm^{-1}. ^1H NMR ($CDCl_3$) δ=1.30 (d, *J*=6 Hz, 6′-Me), 2.00—2.68 (m, 4H, 2′-H_2+8-H_2), 2.22 (s, 3H, $COCH_3$), 3.10 (d, *J*=19 Hz, 1H, 10-*ax*-H), 3.44 (dd, *J*=19 and 1.5 Hz, 1H, 10-*eq*-H), 4.39 (s, 1H, 9-OH), 4.35—4.60 (m, 2H, 3′-H+5′-H), 5.10 (d, *J*=19 Hz, 1H, one of 14-H), 5.40 (brs, 1H, 7-H), 5.44 (d, *J*=19 Hz, 1H, one of 14-H), 5.54 (brs, 1H, 4′-H), 5.74 (brs, W_H=6 Hz, 1H, 1′-H), 6.31 (brd, *J*=8 Hz, 1H, NH), 7.80—7.98 (m, 2H, Ar), 8.20—8.50 (m, 6H, Ar), 13.33 (s, 1H, ArO*H*), 13.69 (s, 1H, ArO*H*). Found: C, 54.55; H, 3.86; N, 3.71%. Calcd for $C_{37}H_{31}F_3N_2O_{15}$-H_2O: C, 54.28; H, 4.06; N, 3.57%.

Ten percent potassium carbonate (0.12 mL) was added to (−)-**2b** (mp 167—170 °C, $[\alpha]_D^{20}$ −53.5° (*c* 0.097, dioxane)) (23.5 mg, 0.029 mmol) in MeOH (12 mL) at 0 °C. The deep purple solution produced was stirred at 0 °C for 4 h. Glacial AcOH was added to the reaction mixture until the color of the solution became bright orange. Usual extractive isolation and purification by silica-gel thin-layer chromatography ($CHCl_3$/Me_2CO=2/1) gave (+)-**3a** as an orange solid (6.9 mg, 39%), mp 132—135 °C. NMR spectrum of this sample was almost identical with that of (+)-**3a** obtained in **b**).

b) Glycosidation of (+)-1c with (−)-6b by the Use of TMSOTf: TMSOTf (0.10 mL, 0.52 mmol) was added to a suspension of (−)-**6b** (mp 201—202 °C, $[\alpha]_D^{20}$ −117° (*c* 0.029. Me_2CO)) (133 mg, 0.25 mmol) and granulated molecular sieves 4A[8] (0.75 g) in a mixture of CH_2Cl_2 (8 mL) and Et_2O (6 mL) with stirring at −40 °C under an argon atmosphere. The whole mixture was stirred at 3—5 °C for 1 h to give a clear solution. After cooling to −15 °C, a solution of (+)-**1c** (mp 183—185 °C, $[\alpha]_D^{20}$ +153° (*c* 0.11, dioxane)) (77.9 mg, 0.19 mmol) in THF (25 mL) was added to the reaction mixture with stirring, and the stirring was continued for 7 h at −10 °C. Extractive isolation in the same manner as described for (−)-**2a** gave crude **2c** as an orange solid in an almost quantitative yield. This was immediately subjected to deprotection reaction of the C_{14}-formyloxy and C_4′-*p*-nitrobenzoyl groups.[21]

Sodium hydroxide (0.1 M) (2 mL) was added to a solution of crude **2c** in a mixture of THF (1 mL) and MeOH (80 mL) with stirring at 0 °C under an argon atmosphere. After stirring at 0 °C for 20 min, the purple reaction mixture was neutralized to pH 7 with AcOH (1 drop). The resulting mixture was diluted with satd NaCl (100 mL) and EtOAc (100 mL). The upper organic layer was separated, washed with satd NaCl (100 mL), then dried over $MgSO_4$. Filtration and concentration in vacuo, followed by purification by filtration through a short silica-gel column ($CHCl_3$/Me_2CO=19/1→9/1) afforded pure (+)-**3d** as an orange solid (84.1 mg, 73% overall yield), mp 143—148 °C, $[\alpha]_D^{20}$ +170° (*c* 0.11, dioxane). IR (KBr): 3450, 1725, 1630, 1590, 1410 cm^{-1}. ^1H NMR ($CDCl_3$) δ=1.32 (d, *J*=7 Hz, 3H, 6′-Me), 1.80—2.38 (m, 4H, 2′-H_2+8-H_2), 2.97 (t, *J*=6 Hz, 1H, 14-OH), 3.08 (d, *J*=19 Hz, 1H, 10-*ax*-H), 3.30 (dd, *J*=19 and 1 Hz, 1H, 10-*eq*-H), 3.62—3.78 (m, 1H, 4′-H), 4.10—4.30 (m, 2H, 3′-H+5′-H), 4.38 (s, 1H, 9-OH), 4.79 (d, *J*=6 Hz, 2H, 14-H_2), 5.33 (dd, *J*=4 and 2 Hz, 1H, 7-H), 5.55 (d, *J*=4 Hz, 1H, 1′-H), 6.66 (brd, *J*=10 Hz, 1H, NH), 7.81—7.96 (m, 2H, Ar), 8.36—8.48 (m, 2H, Ar), 13.34 (s, 1H, ArO*H*), 13.65 (s, 1H, ArO*H*). Found: C, 53.84; H, 4.80; N, 2.21%. Calcd for $C_{28}H_{26}F_3NO_{11}$-H_2O: C, 53.59; H, 4.50; N, 2.23%.

(+)-14-Formyloxy-4-demethoxydaunorubicin Hydrochloride ((+)-4c-HCl). Attempted Preparation of (+)-4d-HCl According to the Reported Method:[15] Bromine (0.76 M

CH_2Cl_2 soln) (0.05 mL, 0.038 mmol) and 0.25 M hydrogen chloride in MeOH (0.1 mL) were added to a suspention of (+)-**4a**-HCl (mp 184—187 °C, $[\alpha]_D^{20}$ +188° (*c* 0.10, MeOH)) (20.0 mg, 0.037 mmol) and triethoxymethane (0.02 mL, 0.16 mmol) in a mixture of MeOH (0.3 mL) and dioxane (0.75 mL), and the whole mixture was stirred at room temperature for 1 h. A mixture of C_6H_{14} (2 mL) and Et_2O (4 mL) was added to the reaction mixture to precipitate the crude bromo acetal as an orange powder. The crude bromo acetal was collected by decantation and dried in vacuo.[16] After 0.25 M hydrobromic acid (3 mL) and dioxane (3 mL) were added to the crude bromo acetal, the whole mixture was stirred at room temperature for 22 h to liberate the α-bromo ketone.[17] A solution of sodium formate (220 mg, 3.24 mmol) in H_2O (2.2 mL) was added to the stirred solution of the α-bromo ketone. After stirring at room temperature for 24 h, the reaction mixture was diluted with 5% $NaHCO_3$ (50 mL) and extracted successively with a mixture of MeOH and $CHCl_3$ (1/2) (50 mL) and $CHCl_3$ (50 mL×4). The combined organic extracts were washed with H_2O (50 mL), and dried over Na_2SO_4. Filtration and concentration in vacuo gave a residue, which was dissolved in a mixture of MeOH and $CHCl_3$ (1/9) (2 mL). After addition of 0.25 M hydrogen chloride in MeOH (0.10 mL), Et_2O (15 mL) was added to the acidic solution to precipitate (+)-**4c**-HCl as a bright orange solid (6.0 mg, 30%), mp 186—189 °C (decomp), $[\alpha]_D^{20}$ +185° (*c* 0.040, MeOH). IR (KBr): 3400, 1725, 1620, 1590 cm^{-1}. ^1H NMR ($(CD_3)_2SO$) δ=1.18 (d, *J*=6 Hz, 3H, 6′-Me), 1.69—2.00 (m, 2H, 2′-H_2), 2.02—2.32 (m, 2H, 8-H_2), 2.92 (d, *J*=19 Hz, 1H, 10-*ax*-H), 3.20 (d, *J*=19 Hz, 1H, 10-*eq*-H), 3.44—3.69 (m, 2H, 3′-H+4′-H), 4.10—4.40 (m, 1H, 5′-H), 5.01 (brs, W_H=8 Hz, 1H, 7-H), 5.34 (brs, 3H, 14-H_2+1′-H), 5.46 (d, *J*=6 Hz, 1H, 4′-OH), 5.74 (s, 1H, 9-OH), 7.88 (brs, 3H, NH_3), 7.96—8.12 (m, 2H, Ar), 8.24—8.46 (m, 2H, Ar), 8.40 (s, 1H, C*H*O), 13.36 (brs, 1H, ArO*H*), 13.56 (brs, 1H, ArO*H*). MS (SIMS) *m/z*: 542 (MH^+).

(+)-4-Demethoxyadriamycin Hydrochloride ((+)-4d-HCl).

a) Preparation of (+)-4d-HCl from (+)-4c-HCl: Sodium hydroxide (0.1 M) (0.25 mL) was added to a solution of (+)-**4c**-HCl (mp 186—189 °C (decomp), $[\alpha]_D^{20}$ +185° (*c* 0.040, MeOH)) (12.2 mg, 0.021 mmol) in MeOH (10 mL) at 0 °C. The deep purple solution produced was stirred for 20 min at 0 °C. The reaction mixture was diluted with $CHCl_3$ (50 mL) and satd NaCl (50 mL). The chloroform layer was separated, and the aqueous layer was further extracted with $CHCl_3$ (50 mL×3). The combined organic extracts were washed with H_2O (50 mL×2), and dried over Na_2SO_4. Concentration in vacuo gave a residue, which was dissolved in a mixture of MeOH and $CHCl_3$ (1/9) (3 mL). After addition of 0.25 M hydrogen chloride in MeOH (0.15 mL), Et_2O (15 mL) was added to the acidic solution to precipitate (+)-**4d**-HCl as a bright orange solid (7.7 mg, 67%), mp 225—228 °C (decomp). NMR spectrum of this sample was almost identical with that of (+)-**4d**-HCl obtained in **c**).

b) Preparation of (+)-4d-HCl from (+)-4a-HCl by the Improved Method: A solution of (+)-**4a**-HCl (mp 184—187 °C (decomp), $[\alpha]_D^{20}$ +188° (*c* 0.10, MeOH)) (106 mg, 0.20 mmol) and trimethoxymethane (0.11 mL, 1.1 mmol) in a mixture of MeOH (2.7 mL) and dioxane (4.2 mL) was stirred at room temperature for 15 min under an argon atmosphere. Bromine (0.86 M CH_2Cl_2 soln) (0.39 mL, 0.34 mmol) was added to the reaction mixture. After stirring at room temperature for 1 h, the reaction mixture was poured onto Et_2O (60 mL) to precipitate the crude bromo acetal as an orange powder. The crude bromo acetal was collected by decantation and dried in vacuo.[16] Anhyd Me_2CO (45 mL) was added to the crude bromo acetal, and the mixture was stirred at room temperature for 1 h to liberate the α-bromo ketone.[17] A solution of sodium formate (266 mg, 3.9 mmol) in H_2O (3.3 mL) was added to the solution of the α-bromo ketone. After stirring at room temperature for 15 h, the mixture was concentrated in vacuo to give crude **3c** as an orange solid. Sodium hydroxide (0.1 M) (1.0 mL) was added to a solution of crude **3c** in MeOH (100 mL) and the mixture was stirred at 0—5 °C for 10 min. After addition of $CHCl_3$ (200 mL) and satd NaCl (200 mL), the lower organic layer was separated, and the aqueous layer was further extracted with $CHCl_3$ (100 mL×3). The combined organic extracts were washed with H_2O (100 mL×2), dried over Na_2SO_4, filtrated, then concentrated in vacuo. The residue was dissolved in a mixture of MeOH and $CHCl_3$ (1/9) (15 mL). After addition of 0.25 M hydrogen chloride in MeOH (0.50 mL), the acidic solution was diluted with Et_2O (50 mL) to give (+)-**4d**-HCl as bright orange powderlike crystals (54.0 mg, 49%), mp 225—228 °C (decomp), $[\alpha]_D^{20}$ +187° (*c* 0.030, MeOH). IR, NMR, and MS spectra of this sample were identical with those of (+)-**4d**-HCl obtained in **c**). Found: C, 53.63; H, 4.91; N, 2.09%. Calcd for $C_{26}H_{28}ClNO_{10}$-1.5H_2O: C, 54.12; H, 5.42; N, 2.43%.

c) Preparation of (+)-4d-HCl from (+)-3d: A mixture of (+)-**3d** (mp 143—148 °C, $[\alpha]_D^{20}$ +170° (*c* 0.11, dioxane)) (12.0 mg, 0.02 mmol), trimethoxymethane (1 mL), and *d*-10-camphorsulfonic acid (2 mg) in THF (3 mL) was stirred at room temperature for 2 h. The reaction mixture was poured onto 5% $NaHCO_3$ (50 mL), and extracted with EtOAc (50 mL×2). The combined organic extracts were successively washed with 5% $NaHCO_3$ (30 mL), satd NaCl (30 mL), and H_2O (30 mL), dried over Na_2SO_4, filtered, then concentrated in vacuo, giving an orange caramel which conceivably consisted of the cyclic orthoester.[23] Sodium hydroxide (0.1 M) (3 mL) was added to the concentrated residue with stirring under an argon atmosphere, and the mixture was further stirred for 45 min. The mixture was neutralized to pH 8 with 5 M HCl, and extracted with $CHCl_3$ (30 mL×5). The combined chloroform extracts were washed with H_2O (50 mL×2), dried over Na_2SO_4, filtered, then concentrated in vacuo. The residue was dissolved in a mixture of MeOH (3 mL) and 0.25 M HCl (1 mL), and the whole mixture was stirred at room temperature for overnight. After concentration in vacuo, MeOH (15 mL) was added to the residue. The methanolic solution was filtered to remove a small amount of insoluble materials, and the filtrate was concentrated in vacuo to a small volume. Addition of Et_2O (5 mL) to the concentrated methanolic solution gave (+)-**4d**-HCl as orange powderlike crystals (4.3 mg, 40%), mp 226—229 °C (decomp), $[\alpha]_D^{20}$ +190° (*c* 0.042, MeOH). IR (KBr): 3400, 1725, 1620, 1590 cm^{-1}. ^1H NMR ($(CD_3)_2SO$) δ=1.16 (d, *J*=6 Hz, 3H, 6′-Me), 1.70—2.00 (m, 2H, 2′-H_2), 2.00—2.30 (m, 2H, 8-H_2), 3.02 (s, 2H, 10-H_2), 3.40—3.68 (m, 2H, 3′-H+4′-H), 4.21 (q, *J*=6 Hz, 1H, 5′-H), 4.60 (brd, *J*=5 Hz, 2H, 14-H_2), 4.82 (d, *J*=5 Hz, 1H, 4′-OH), 5.01 (brs, W_H=8 Hz, 1H, 7-H), 5.34 (brs, W_H=6 Hz, 1H, 1′-H), 5.47 (s, 1H, 9-OH), 7.83 (brs, 3H, NH_3), 7.90—8.10 (m, 2H, Ar), 8.22—8.42 (m, 2H, Ar), 13.36 (brs, 1H, ArO*H*), 13.58 (brs, 1H, ArO*H*). MS (SIMS) *m/z*: 514 (MH^+). Found: C, 53.32; H, 5.03; N, 2.35%. Calcd for $C_{26}H_{28}ClNO_{10}$-1.75H_2O: C, 53.70; H, 5.46; N, 2.41%.

The authors are grateful to Dr. S. Penco, Farmitalia

Carlo Erba, for providing us with the spectral (IR, NMR, MS) data of 4-demethoxyadriamycin hydrochloride and for many valuable suggestions.

References

1) Part of this work has been the subject of two preliminary communications: a) Y. Kimura, M. Suzuki, T. Matsumoto, R. Abe, and S. Terashima, *Chem. Lett.*, **1984**, 501; b) Y. Kimura, M. Suzuki, and S. Terashima, *Chem. Lett.*, **1984**, 2113.

2) Y. Kimura, M. Suzuki, T. Matsumoto, R. Abe, and S. Terashima, *Bull. Chem. Soc. Jpn.*, **59**, 415 (1986).

3) a) T. H. Smith, A. N. Fujiwara, W. W. Lee, H. Y. Wu, and D. W. Henry, *J. Org. Chem.*, **42**, 3653 (1977); b) F. Arcamone, L. Bernardi, P. Giardine, B. Patelli, A. DiMarco, A. M. Casazza, G. Pratesi, and P. Reggini, *Cancer Treat. Rep.*, **60**, 829 (1976); c) Japan Kokai Tokkyo Koho, JP 59-231037; d) Japanese Patents, 5833880, 5840555, and 5840557; e) F. Arcamone, S. Penco, and A. Vigevani, *Cancer Chemother. Rep., Part 3*, **6**, 123 (1975).

4) a) F. Arcamone, L. Bernardi, B. Patelli, P. Giardino, A. DiMarco, A. H. Casazza, C. Soranzo, and G. Pratesi, *Experientia*, **34**, 1255 (1978); b) M. J. Broadhurst, C. H. Hassall, and G. J. Thomas, *J. Chem. Soc., Perkin Trans. 1*, **1982**, 2249; c) Japan Kokai Tokkyo Koho, JP 57-53497.

5) a) H. Umezawa, Y. Takahashi, M. Kinoshita, H. Naganawa, K. Tatsuta, and T. Takeuchi, *J. Antibiot.*, **33**, 1581 (1980); Japan Kokai Tokkyo Koho, JP 50-149663; b) Japanese Patent, 5840556.

6) a) H. S. El Khadem and D. Matsuura, *Carbohydr. Res.*, **101**, c 1 (1982); b) J. Boivin, A. Montagnac, C. Monneret, and M. Pais, ibid, **85**, 223 (1980); c) J. Biovin, C. Monneret, and M. Pais, *Tetrahedron*, **37**, 4219 (1981).

7) Various organic or inorganic bases such as pyridine, diphenylamine, 1,1,3,3-tetramethylurea, potassium carbonate, cesium carbonate, and aluminum oxide have been used by expecting that these bases could trap trifluoromethanesulfonic acid produced with the progress of glycosidation reaction.

8) Granulated molecular sieves 4A freshly dried over free flame under an argon stream should be used. No glycoside formation occurred at all when powdered molecular sieves 4A was employed.

9) TMSOTf can also be readily prepared by heating a mixture of trimethylsilyl chloride and trifluoromethanesulfonic acid. See, H. Emde, D. Domsch, H. Feger, U. Frick, A. Götz, H. H. Hergott, K. Hofmann, W. Kober, K. Krägeloh, T. Oesterle, W. Steppan, W. West, and G. Simchen, *Synthesis*, **1982**, 1.

10) A. C. West and C. Schuerch, *J. Am. Chem. Soc.*, **95**, 1333 (1973); R. M. Williams and A. O. Stewart, *Tetrahedron Lett.*, **24**, 2715 (1983).

11) Molecular sieves 4A is anticipated to trap trifluoromethanesulfonic acid produced with progress of the glycosidation reaction. However, in the case when 1,1,3,3-tetramethylurea which had been reported to behave as an acid scavenger[12] was employed instead of molecular sieves 4A, the glycosidation did not occur at all.

12) S. Hanessian and J. Banoub, *Carbohydr. Res.*, **53**, c 13 (1977); T. Ogawa, K. Beppu, and S. Nakabayashi, ibid, **93**, c 6 (1981).

13) F. Arcamone, *Lloydia*, **40**, 45 (1977).

14) See the preceding paper,[2] Ref. 2.

15) a) F. Arcamone, L. Bernardi, P. Giardino, and A. DiMarco, British Patent, 151168; Japanese Patent, 5736919; b) A. DiMarco, A. M. Casazza, F. Giuliani, G. Pratesi, F. Arcamone, L. Bernardi, G. Franchi, P. Giardino, B. Patelli, and S. Penco, *Cancer Treat. Rep.*, **62**, 375 (1978).

16) Direct bromination of the C_{14}-position of (+)-**4a**-HCl with bromine did not occur at all. However, the dimethyl acetal derived from (+)-**4a**-HCl was found to be readily brominated with bromine to afford the desired bromo acetal (i).

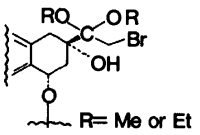

(i)

17) This novel transacetalization method was first introduced by Umezawa et al., in their preparation of 4′-*O*-tetrahydropyranyladriamycin and adriamycin hydrochloride.[18]

18) Japan Kokai Tokkyo Koho, JP 56-156300. Transacetalization of the bromo acetal (i) with acetone readily produced the α-bromo ketone (ii). This operation which could be carried out under neutral conditions is anticipated to be more favorable than the reported method[15] with aqueous hydrobromic acid.

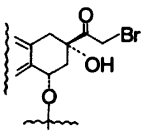

(ii)

19) After our preliminary communication was subjected for publication,[1b] we informed our results to Drs. F. Arcamone and S. Penco, Farmitalia Carlo Erba. Replying to our letter, Dr. Penco kindly provided us IR, NMR, and MS spectra of their sample of **4d**-HCl. While the melting point and optical rotation of their sample on which those spectral properties had been recorded were not informed to us, we found that the spectra of the Falmitalia's sample were completely identical with those of our (+)-**4d**-HCl. Recently, Dr. Penco generously wrote to us that the melting point of their **4d**-HCl measured with a differential scanning calorimetry was in the range of 270—277 °C, and that the measurement of the optical rotation could not be carried out because of the intense color of **4d**-HCl.

20) K. Tamoto, M. Sugimori, and S. Terashima, *Tetrahedron*, **40**, 4617 (1984).

21) E. J. Corey and S. Terashima, *Tetrahedron Lett.*, **1972**, 111.

22) Purification and identification of this protected α-glycoside were not attempted.

23) Umezawa et al. first introduced this novel protection method in their preparation of 11-deoxy-4-demethoxyadriamycin.[5a] According to the report, the protected glycoside

is anticipated to mainly consist of the cyclic orthoester (**iii**).

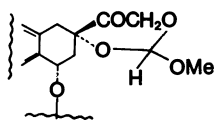

(iii)

24) Optically pure (−)-**5a** was prepared by the modification of the well-known Horton's method. See, Y. Kimura, T. Matsumoto, M. Suzuki, and S. Terashima, *Bull. Chem. Soc. Jpn.*, **59**, 663 (1986).

 © 1986 The Chemical Society of Japan Bull. Chem. Soc. Jpn., 59, 433—437 (1986)

The Diels-Alder Reactions of 2-Alkyl-5-methoxy-4-(*p*-nitrophenyl)oxazoles with Ethylenic, Acetylenic, and Azo-Type Dienophiles

Toshikazu IBATA,* Shuji NAKANO, Hiroyuki NAKAWA, Jiro TOYODA, and Yasushi ISOGAMI
Institute of Chemistry, College of General Education, Osaka University, Toyonaka, Osaka 560
(Received July 20, 1985)

The Diels-Alder reactions of 2-methyl- and 2-ethyl-5-methoxy-4-(*p*-nitrophenyl)oxazoles with *N*-methyl-, *N*-ethyl-, and *N*-phenylmaleimides gave endo- and exo-adducts. When the reactions were carried out in an acetonitrile solution containing a small amount of water as an impurity, *N*-substituted 3-hydroxy-2-(*p*-nitrophenyl)-4,5-pyridinecarboximides were obtained via the decomposition of the Diels-Alder adducts, while the methanol was eliminated. The decomposition might be catalyzed by contaminated water at the initial stage of the reaction. The adducts of *N*-phenylmaleimide and *N*-ethylmaleimide were shown to undergo the retro-Diels-Alder reaction on heating at 80°C to give the starting maleimides and oxazole. Diethyl azodicarboxylate and 4-phenyl-3*H*-1,2,4-triazole-3,5(4*H*)-dione gave the corresponding single adducts. A reaction with dimethyl acetylenedicarboxylate gave *p*-nitrobenzonitrile (**10**), dimethyl 2-methyl-5-methoxy-3,4-furandicarboxylate (**11**), and tetramethyl 3,5-epoxy-3-methoxy-5-methyl-1,4-cyclohexadiene-1,2,4,5-tetracarboxylate (**12**), although the expected adduct was not isolated. These products were explained on the basis of the Diels-Alder reaction, followed by the retro-Diels-Alder reaction, thus affording **10** and **11**, which gave **12** upon cycloaddition with the second molecule of DMAD.

The cycloaddition of the five-membered aromatic heterocycles has been recognized to be one of the most convenient methods of synthesizing six-membered heterocycles.[1] Since the early work of Kondrat'eva,[2] the Diels-Alder reactions of oxazoles with ethylenic dienophiles have been studied extensively in connection with the pathway of synthesizing vitamin B_6.[3] In general, the determination of the stereochemistry of the cycloaddition is important for the mechanistic investigation of the reaction. However, scarcely no stereochemical research into the Diels-Alder reaction of oxazoles has been done because of the instability of the adducts.[4] Recently the present authors have reported a general method of synthesizing oxazoles by the BF_3-catalyzed decomposition of diazo carbonyl compounds in the presence of excess nitriles to give various types of oxazoles.[5] Of the oxazoles obtained, we chose 5-methoxy-2-methyl-4-(*p*-nitrophenyl)oxazole (**1A**) and 2-ethyl-5-methoxy-4-(*p*-nitrophenyl)oxazole (**1B**) as azadiene components of the Diels-Alder reaction for the following reasons: First, a high Diels-Alder reactivity of the oxazoles can be expected because of the electron-releasing effect of the methoxyl group on C-5,[3b,6] second, a high stability of the cycloadducts may possibly be attained by the introduction of the *p*-nitrophenyl group. The retro-Diels-Alder reaction of the adducts was also studied.

Results and Discussion

Reactions with Ethylenic Dienophiles. *N*-Substituted maleimides have been recognized as having high reactivity as dienophiles in the Diels-Alder reactions. The refluxing of an acetonitrile solution of 5-methoxy-2-methyl-4-(*p*-nitrophenyl)oxazole (**1A**) and two molar equivalents of *N*-ethylmaleimide (**2b**) for 50 h gave three products after silica-gel column chromatography of the reaction mixture. The first and successively eluted products were determined to be the expected Diels-Alder adducts on the basis of the analytical and spectral data. The IR spectra of the two products showed absorptions ascribable to the imide carbonyl near 1700 cm^{-1} and to the nitro group at 1535 and 1340 cm^{-1}, and also showed similar absorption patterns in the fingerprint region. The first product (mp 159.0—161.0 °C) has signals of the methyl and methylene protons of the *N*-ethyl group at δ 0.48 (t) and 3.14 (q) respectively in the ^1H NMR spectrum; they are considerably higher (by 0.5—0.7 ppm) than those signals of the second product at δ 1.20 (t) and 3.57 (q). The high field of the *N*-ethyl group of the first product might be attributed to the shielding effect derived from the ring-current anisotropy of the *p*-nitrophenyl group. This indicates that the adduct is the endo-adduct (**3b**). Therefore, the second product may be assigned to the exo-adduct (**4b**). The appearance of methine protons of **3b** in a lower field (δ 3.50 (d) and 3.62 (d)) than those of **4b** at δ 2.96 (d) and 3.07 (d) is also in accord with the above assignment, assuming a deshielding effect of the bridged oxygen in the endo-adduct (**3b**).[7] The X-ray structural analysis of **4b** supported the above determination.[9]

The third product was found to have a molecular formula corresponding to that of the CH_3OH elimination from the adducts, **3b** or **4b**. The ^1H NMR spectrum lacked signals of the methoxyl and methine protons observed in **3b** and **4b** but showed signals of methyl at δ 2.84, *N*-ethyl at δ 1.21 (t) and 3.75 (q), and hydroxyl at δ 7.98, besides the ABq signals of the *p*-nitrophenyl group. The IR spectrum had absorptions of the imide carbonyl group at 1690 cm^{-1}, the hydroxyl group at 3350, and the nitro group at 1505 and 1340 cm^{-1}. These spectroscopic data show that the third product is *N*-ethyl-3-hydroxy-6-methyl-2-(*p*-nitrophenyl)-4,5-pyridinecarboximide (**5b**).

The Diels-Alder adducts between 5-alkoxyoxazoles and ethylenic dienophiles, which have structures like **3b** and **4b**, have already been reported to give 3-

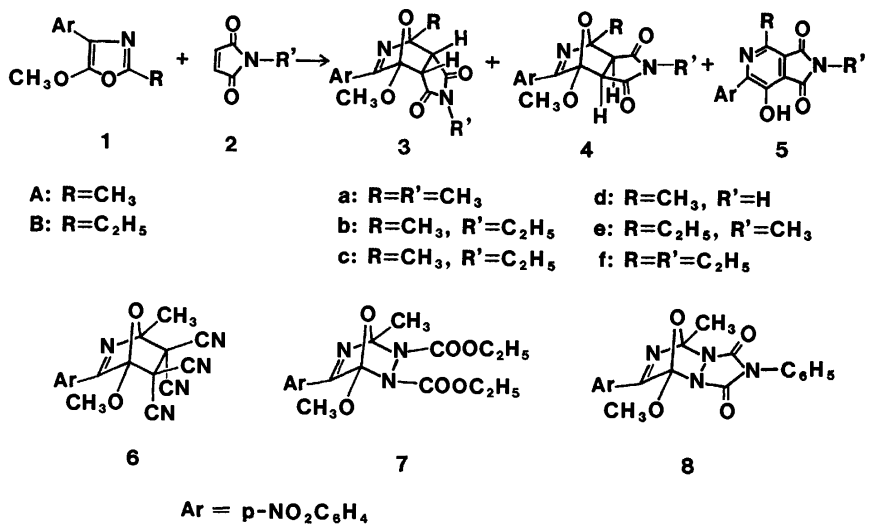

Scheme 1.

Table 1. Product Ratios of the Diels-Alder Reactions of Oxazoles (**1**) with *N*-Substituted Maleimides

Run	R	R'	Solvent	Temp	Time	Product Yield/%		
				°C	h	**3**	**4**	**5**
a-1	CH_3	CH_3	Acetonitrile	80	50	58	32	—
a-2			Acetonitrile[a)]	80	50	32	—	43
a-3			Toluene	100	70	54	29	—
b-1		C_2H_5	Acetonitrile	80	24	58	29	—
b-2			Acetonitrile[a)]	60	100	35	5	50
b-3			Acetonitrile[a)]	80	50	51	3	41
b-4			Acetonitrile[a)]	100	24	41	11	44
b-5			Acetonitrile[a)]	100	6	66	13	20
c-1		C_6H_5	Benzene	40	240	43	17	—
c-2			Benzene	80	50	13	21	—
c-3			Toluene	100	24	6	3	—
d		H	Acetonitrile[a)]	80	100	21	—	21[b)]
e	C_2H_5	CH_3	Acetonitrile	80	50	53	21	—
f		C_2H_5	Acetonitrile	80	50	96	3	—

a) The acetonitrile used in this reaction was stored for months after distillation. b) Unreacted **1A** was recovered in 33% yield.

hydroxypyridine derivatives upon treatment with acid.[3a,3c)] The treatment of **3b** and **4b** with *p*-toluenesulfonic acid in a benzene solution readily gave **5b**. The formation of **5b** in the Diels-Alder reaction of **1A** and *N*-ethylmaleimide may also be attributed to the second attack of a protic species such as H_2O, contained in the reaction mixture, on the **3b** and **4b** produced by the cycloaddition. In order to confirm this point, the reaction was examined under various reaction conditions, with differing solvents, reaction temperatures, and reaction times (Runs bl—b5). The results show that the formation of **5b** is greatly affected by the solvent and the reaction time, but only slightly by the reaction temperature. When the reaction was carried out using a freshly distilled solvent, no decomposition to give **5b** was observed. These results suggest that the H_2O present in the solvent might function as a protic species to catalyze the decomposition of **3b** or **4b** formed at the outset. Once the decomposition started, the methanol and **5b** produced might work as catalysts. Quite similar results were obtained in the reaction of **1A** with *N*-methylmaleimide. 2-Ethyl-5-methoxy-4-(*p*-nitrophenyl)-oxazole (**1B**) also showed similar behavior in the reactions with *N*-substituted maleimides.

The preference for the endo-adducts formation in these reactions may be explained by the endo rule.[8)] However, a larger endo/exo ratio (96:3) than usual was observed in the reaction of **1B** and *N*-ethylmaleimide (Run f). One of possible explanation is as follows. The CPK-model inspection of the adducts (**3f** and **4f**) indicated that the exo-adduct (**4f**) has a steric repulsion between the C-ethyl group and imide carbonyl. This may indicate that the steric repulsion between these two groups in the transition state to the exo-adduct lowers the rate of the addition and that the *N*-ethyl substitution strengthens this tendency.

On the other hand, *N*-phenylmaleimide (**2c**) gave

Table 2. ^{1}H NMR Data of Cycloadducts and 3-Hydroxypyridines[a)]

Compounds	O-CH_3	C-CH_3	C-CH_2CH_3	N-CH_3	N-CH_2CH_3	Methine[b)]	J
3a	3.61	2.09	—	2.55	—	3.55, 3.67	7.5
4a	3.54	2.01	—	3.04	—	3.04, 3.14	6.3
3b	3.60	2.07	—	—	0.48 (t), 3.14 (q)	3.50, 3.62	7.8
4b	3.54	2.01	—	—	1.20 (t), 3.60 (q)	3.05, 3.15	6.6
3c	3.63	2.14	—	—	—	3.65, 3.78	7.6
4c	3.57	2.07	—	—	—	3.13, 3.25	6.5
3d	3.49	1.91	—	—	—	2.75 (s)	—[c)]
3e	3.62	—	1.22 (t), 2.38 (q)	2.54	—	3.64 (s)	—
4e	3.60	—	1.33 (t), 2.37 (q)	3.09	—	3.12, 3.25	6.0
3f	3.64	—	1.23 (t), 2.46 (m)	—	0.50 (t), 3.14 (q)	3.65 (s)	—
4f	3.52	—	1.20 (t), 2.29 (m)	—	1.29 (t), 3.06 (q)	3.49, 3.66	7.2
5a	—	2.83	—	3.18	—	—	—[d)]
5b	—	2.84	—	—	1.31 (t), 3.75 (q)	—	—[d)]
5c	—	2.91	—	—	—	—	—[d)]
5d	—	2.72	—	—	—	—	—

a) Signals of the aromatic protons were omitted. b) Methine protons showed doublet signals unless otherwise cited. c) A singlet NH signal was at δ=3.27. d) Singlet OH signals of **5a**, **5b**, and **5c** were observed at δ=7.98, 8.03, and 8.18 respectively.

small amounts of both endo- and exo-adducts at 80 °C, and the yields decreased with the increase in the reaction temperature (100 °C). In order to clarify the course of the addition, the proceeding of the reaction between equivalent molar amounts of **1A** and **2c** was traced by monitoring the proton NMR in an NMR tube at 25 and 80 °C in C_6D_6. As a result, the rates of the formation of the endo-adduct were found to be faster than that of the exo-adduct. However, the tracing was interrupted during the course of the reaction because of the crystallization of the adducts in the NMR tube. The reaction of **1A** with *N*-ethylmaleimide (**2b**) exhibited a monotonous increase in the yields of the adducts at 25 °C, without any interruption by the crystallization of the adducts (Fig. 1a). However, at 80 °C the yield of the endo-adduct reached its maximum after 10 h and then decreased gradually, while the yield of the exo-adduct increased constantly, as is shown in Fig. 1b. This indicates that the endo-adduct is converted into the exo-adduct, probably via the retro-Diels-Alder reaction as described below.

The ratio between the adducts (**3**+**4**) and the remaining oxazole (**1A**) depends upon the reaction temperature, showing smaller values at higher temperatures. The ratios were also found to be larger for the reactions of **2b** with **1A** than for the corresponding reactions of **2c**, even though the reaction rates were faster for **2c** than for **2b** at various temperatures. The depressions of the yields of the adducts at higher temperatures may be explained on the assumption that the equilibrium between the Diels-Alder reaction and the retro-Diels-Alder reaction declines to the side of the reactants at higher temperatures.

The reaction of the oxazole (**1A**) and tetracyanoethylene gave a colorless product, which showed an absorption of the ester carbonyl group in its IR spectrum at 1758 cm^{-1}. This indicates that the product is not the expected Diels-Alder adduct (**6**), but the

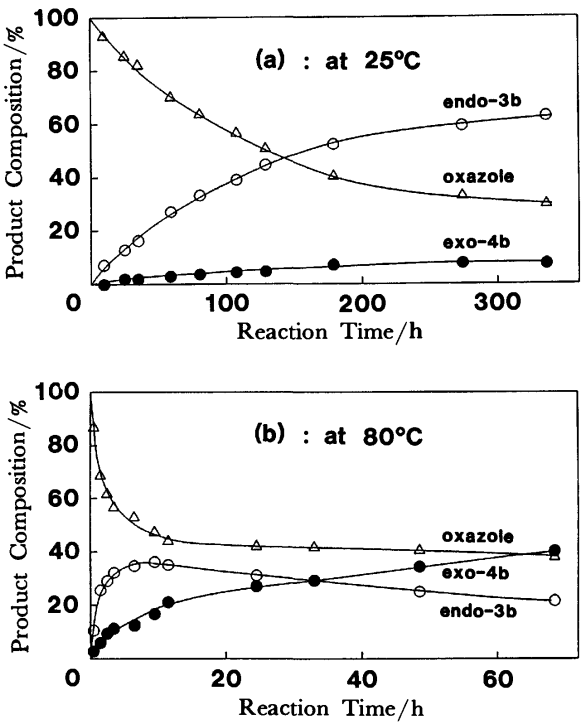

Fig. 1. Changes in the Product Composition during the Reaction of **1A** with **2b** at 25 °C (a) and 80 °C (b).

oxazole-ring-opened product obtained via the step-by-step reaction of **1A** and TCNE.[10] The results of the detailed examination of this reaction will be described elsewhere. Dimethyl fumarate and dimethyl maleate gave no adduct, the reactions with **1A** resulting in the recovery of the starting materials, even under such drastic reaction conditions as at 110 °C for 100 h in toluene.

Reactions with Azo-Type Dienophiles. The azo-type compounds have been reported to have higher Diels-Alder reactivities than the corresponding

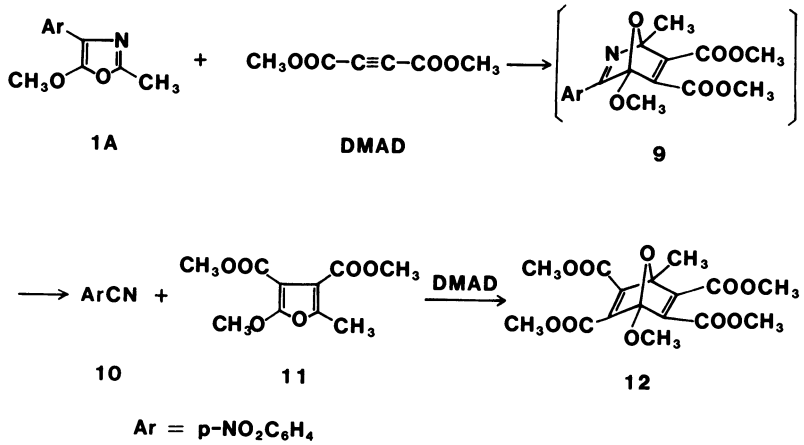

Scheme 2.

ethylenic dienophiles.[11] Similar results were observed in the Diels-Alder reaction of oxazoles. That is diethyl azodicarboxylate[12] was found to react readily with the oxazole (**1A**) in a benzene solution at 80 °C within 48 h to give an adduct (**7**) in a fairly good yield (91%). 4-Phenyl-3*H*-1,2,4-triazole-3,5(4*H*)-dione, which is one of the most reactive dienophiles,[11b] also gave an adduct (**8**) in a high yield. However, azobenzene gave no adduct.

Reaction with Acetylenic Dienophile. As a typical example of acetylenic dienophiles, dimethyl acetylenedicarboxylate was treated with the oxazole (**1A**) in toluene at 110 °C for 50 h. This reaction did not give the expected Diels-Alder adduct (**9**)[12,13] but *p*-nitrobenzonitrile (**10**), dimethyl 2-methoxy-5-methyl-3,4-furandicarboxylate (**11**), and tetramethyl 3,5-epoxy-3-methoxy-5-methyl-1,4-cyclohexadiene-1,2,4,5-tetracarboxylate (**12**) in yields of 86, 20, and 25%, respectively. The reaction may be explained by the retro-Diels-Alder reaction of the adduct (**9**) to give *p*-nitrobenzonitrile and the furan derivative (**11**),[12, 13] followed by the second Diels-Alder reaction of DMAD on the furan (**11**) to produce the adduct (**12**).[13,14] When the reaction was carried out under milder conditions, at 100 °C for 24 h, *p*-nitrobenzonitrile and furandicarboxylate (**11**) were isolated in 30 and 34% yields respectively, along with 61% of the unreacted oxazole (**1A**). Further attempts to isolate the adduct **9** by conducting the reaction at the low temperature of 50 °C were also unsuccessful.

Retro-Diels-Alder Reaction. In order to explain the low yields of the Diels-Alder adducts between the oxazole (**1A**) and *N*-phenylmaleimide, we studied the retro-Diels-Alder reaction of the adducts **3c** and **4c** to reproduce the starting materials. During the recrystallization of the endo-adduct (**3c**), separated by the column chromatograhy of the reaction mixture, yellow crystals of *N*-phenylmaleimide (**2c**) were isolated in a pure state. When the decompositions of **3c** and **4c** were traced by means of NMR spectroscopy in a DMSO solution at 80 °C, the intensities of the signals of **3c** and **4c** decreased, with an accompanying increase in the intensities of the signals of **1A** at δ 2.41 (s, CH_3) and 4.12 (s, OCH_3) and the methine signal of **2c** at δ 7.13. After 200 h, both reaction systems gave mixtures of **1A** (**2c**), **3c**, and **4c** in about a 7:1:2 ratio. In these measurements, the thermal retro-Diels-Alder reactions of **3c** was found to be faster than that of **4c**. This may be explained by the steric repulsion in the endo-adduct. These types of retro-Diels-Alder reactions were also found for the adducts of *N*-methyl- and *N*-ethylmaleimides. However, the rates of the decomposition of these adducts were not so rapid as those of the *N*-phenylmaleimide adducts.

Experimental

The melting points were measured with a Yanagimoto Melting-point Apparatus and are presented without correction. The IR spectra were recorded on a Perkin-Elmer model 983. The ^{1}H NMR spectra were recorded in a $CDCl_3$ solution at 90 MHz on a Varian Spectrometer model EM390, using TMS as the internal standard.

Materials. 2-Alkyl-5-methoxy-4-(*p*-nitrophenyl)oxazoles were prepared by the BF_3-catalyzed decomposition of methyl (*p*-nitrophenyl)diazoacetate in the presence of acetonitrile or propionitrile, as has been described in a previous paper.[15]

5-Methoxy-2-methyl-4-(*p*-nitrophenyl)oxazole (1A): Pale yellow crystals; yield, 75%; mp 122.0—123.0 °C; ^{1}H NMR δ=2.43 (s, CH_3), 4,12 (s, OCH_3), 7.85 and 8.20 (ABq, Ar). Found: C, 56.56, H, 4.29; N, 11.90%. Calcd for $C_{11}H_{10}N_2O_4$: C, 56.41; H, 4.30; N, 11.96%.

2-Ethyl-5-methoxy-4-(*p*-nitrophenyl)oxazole (1B): Pale yellow needles; yield, 84%; mp 96.0—97.0 °C; ^{1}H NMR δ=1.36 (t, CH_3), 2.76 (q, CH_2), 4.13 (s, OCH_3), 7.92 and 8.23 (ABq, Ar). Found: C, 58.26, H, 4.87; N, 11.27%. Calcd for $C_{12}H_{12}N_2O_4$: C, 58.06; H, 4.87; N, 11.29%.

General Procedure of the Diels-Alder Reaction of 1 with Maleimides. A solution of **1** (2.0 mmol) and maleimide (2.5 mmol) in acetonitrile (or toluene) was heated at 60—110 °C for several hours, as shown in Table 1. After the evaporation of the solvent under reduced pressure, the products were separated by silica-gel column chromatography,

Table 3. Melting Points and Analytical Data of the Reaction Products

Compound	Mp θ_m/°C	Found (%)			Calcd (%)			Molecular Formula
		C	H	N	C	H	N	
3a	191—192	55.63	4.30	12.07	55.65	4.38	12.17	$C_{16}H_{15}N_3O_6$
4a	188—189	55.68	4.34	12.02				
3b	159—161	56.94	4.75	11.68	56.82	4.77	11.70	$C_{17}H_{17}N_3O_6$
4b	155—156	56.82	4.77	11.70				
3c	179—180	62.16	4.13	10.20	61.91	4.21	10.32	$C_{21}H_{17}N_3O_6$
4c	173—174	61.71	4.20	10.27				
3d	190—192	54.34	3.93	12.71	54.38	3.96	12.69	$C_{15}H_{13}N_3O_6$
3e	129—130	56.98	4.78	11.53	56.82	4.77	11.70	$C_{17}H_{17}N_3O_6$
4e	177—178	57.00	4.73	11.59				
3f	158—159	58.07	5.12	11.20	57.90	5.13	11.25	$C_{18}H_{19}N_3O_6$
5a	287—289	57.43	3.49	13.35	57.51	3.54	13.41	$C_{15}H_{11}N_3O_5$
5b	197—199	58.78	3.96	12.73	58.71	4.00	12.84	$C_{16}H_{13}N_3O_5$
5c	244—245	64.17	3.42	11.10	64.00	3.49	11.20	$C_{20}H_{13}N_3O_5$
5d	287—289	56.02	3.05	14.30	56.19	3.03	14.04	$C_{14}H_9N_3O_5$
7	116—117	50.26	4.91	13.77	50.00	4.94	13.72	$C_{17}H_{29}N_4O_8$
8	166—167	55.98	3.67	17.16	55.74	3.69	17.11	$C_{19}H_{15}N_5O_6$
11	60—63	52.71	5.29	—	52.63	5.30	—	$C_{10}H_{12}O_6$

using benzene as the eluent.

Reaction of 1A with Diethyl Azodicarboxylate. A benzene solution of **1A** (0.23 g, 1.0 mmol) and diethyl azodicarboxylate (0.17 g, 1.0 mmol) was heated at 80 °C for 48 h. After the usual treatment, an adduct (**7**) was isolated: yield, 0.37 g; 91%; mp 116—117 °C; IR 1751 (ester C=O), 1523, and 1353 cm^{-1} (NO_2); ^1H NMR δ=1.30 (t, CH_3), 1.33 (t, CH_3), 2.46 (s, CH_3), 3.76 (s, OCH_3), 4.29 (q, CH_2), 7.81 and 8.22 (ABq, Ar).

Reaction of 1A with 4-Phenyl-3*H*-1,2,4-triazole-3,5(4*H*)-dione. A toluene solution of **1A** (0.47 g, 2.0 mmol) and 4-phenyl-1,2,4-triazoline-3,5-dione (0.35 g, 2.0 mmol) was heated at 100 °C for 9 h to give an adduct (**8**; 0.56 g, 69%): Pale yellow crystals; IR(KBr) 1730 (ring C=O), 1515, and 1355 cm^{-1} (NO_2); ^1H NMR δ=2.50 (s, CH_3), 3.73 (s, OCH_3), 7.45 (s, Ph), 7.86 and 8.39 (ABq, Ar).

Reaction of 1A with Dimethyl Acetylenedicarboxylate. A toluene solution of **1A** (0.70 g, 3.0 mmol) and DMAD (0.85 g, 6 mmol) was heated at 120 °C for 50 h. After the evaporation of the toluene under reduced pressure, the reaction products were separated by silica-gel column chromatograhy to isolate three products. The first fraction was assigned to *p*-nitrobenzonitrile (0.38 g, 86%) on the basis of a comparison of the spectral data with those of an authentic sample. The second fraction was characterized dimethyl 5-methoxy-2-methyl-3,4-furandicarboxylate (**11**): Colorless crystals; yield, 0.14 g; 20%; mp 60—63 °C; IR(KBr) 1705 cm^{-1} (ester C=O); ^1H NMR δ=2.38 (s, CH_3), 3.79 (s, OCH_3), 3.83 (s, OCH_3), and 4.06 (s, OCH_3). The third fraction was tetramethyl 3,5-epoxy-3-methoxy-5-methyl-1,4-cyclohexadiene-1,2,4,5-tetracarboxylate (**12**): Colorless oil; yield, 0.28 g; 25%; IR(liquid film) 1710 cm^{-1} (ester C=O); ^1H NMR δ=1.92 (s, 3H, CH_3), 3.61 (s, 3H, OCH_3), 3.80 (s, 6H, OCH_3), and 3.84 (s, 6H, OCH_3).

References

1) a) H. C. van der Plas, "Ring Transformations of Heterocycles," Academic Press: London (1973), p. 314; Vol 1; b) A. R. Katritzky, "Advances in Heterocyclic Chemistry," Academic Press: New York (1974); Vol 17.

2) G. Ya. Kondrat'eva, *Khim. Nauk. Prom.*, **2**, 666 (1958).

3) a) E. E. Harris, R. A. Firestone, K. Pfister, III, R. R. Boettcher, F. J. Cross, R. B. Currie, M. Monaco, E. R. Peterson, and W. Reuter, *J. Org. Chem.*, **27**, 2705 (1962); b) C. N. Huang and G. Ya. Kondrat'eva, *Isv. Akad. Nauk SSSR, Otd. Khim. Nauk*, **1962**, 525; c) R. A. Firestone, E. E. Harris, and W. Reuter, *Tetrahedron*, **23**, 943 (1967).

4) J. I. Levin and S. M. Weinreb, *J. Org. Chem.*, **49**, 4325 (1984); for an exception, see: T. Matsuo and T. Miki, *Chem. Pharm. Bull.*, **20**, 669 (1972).

5) T. Ibata and R. Sato, *Bull. Chem. Soc. Jpn.*, **52**, 3597 (1979).

6) R. Lakhen and B. Ternai, "Advances in Heterocyclic Chemistry," Academic Press: New York (1974); Vol 17, p. 183.

7) Similar deshielding effects of bridged oxygen have been observed in the endo-adducts of 2-benzopyrylium-4-olates with ethylenic dipolarophiles or aldehydes: T. Ibata, K. Jitsuhiro, and Y. Tsubokura,, *Bull. Chem. Soc. Jpn.*, **54**, 240 (1981); T. Ibata and J. Toyoda, *Bull. Chem. Soc. Jpn.*, **58**, 1787 (1985).

8) The results of the X-ray analysis will be published elsewhere.

9) K. Alder and G. Stein, *Angew. Chem.*, **50**, 510 (1937).

10) T. Tsuji and S. Nishida, *Acc. Chem. Res.*, **17**, 56 (1984).

11) a) R. C. Cookson, S. S. H. Gilani, and I. D. R. Stevens, *Tetrahedron Lett.*, **1962**, 615; b) J. Sauer, *Angew. Chem., Int. Ed. Engl.*, **6**, 16 (1967).

12) R. Grigg, R. Hayes, and J. L. Jackson, *J. Chem. Soc., (D)*, **1969**, 1167.

13) R. Grigg and J. L. Jackson, *J. Chem. Soc., (C)*, **1970**, 552.

14) a) A. W. McCulloch, B. Stanovik, D. G. Smith, and A. G. McInnes, *Can. J. Chem.*, **47**, 4319 (1969); b) P. J. Abbott, R. M. Acheson, R. F. Flowerday, and G. W. Brown, *J. Chem. Soc., Perkin Trans. 1*, **1974**, 1177.

15) T. Ibata, T. Yamashita, M. Kashiuchi, S. Nakano, and H. Nakawa, *Bull. Chem. Soc. Jpn.*, **57**, 2450 (1984).

Perfluoroalkylations of Carbanions with (Perfluoroalkyl)-phenyliodonium Triflates (FITS Reagents)

Teruo UMEMOTO* and Yoshihiko GOTOH
Sagami Chemical Research Center, Nishi-Ohnuma 4-4-1, Sagamihara, Kanagawa 229
(Received August 29, 1985)

FITS reagents reacted with primary alkylmagnesium halides in THF at −78 °C to give the corresponding perfluoroalkyl(R_f)-alkanes in moderate to good yields. But an alkyl-lithium or -copper gave a poor yield of the R_f-product. The reaction of FITS with secondary or tertiary alkylmagnesium halides resulted in low yields of the products. Alkynyl-lithiums or -magnesium halides produced R_f-alkynes in favorable yields. The reaction with aryl or vinylmagnesium halide was complex and the yields of R_f derivatives were low. FITS also reacted smoothly with enolate anions of active methylene compounds such as 2-methyl-1,3-cyclopentanedione, ethyl 2-methylacetoacetate, and ethyl 2-oxocyclopentanecarboxylate in a polar solvent to afford *O*- and *C*-perfluoroalkylation products in moderate yields, ratios *O*-/*C*-Rf products depending on the reaction temperature. Anions of diethyl 2-methylmalonate and 2-nitropropane afforded *C*-R_f-compounds only.

There have been many investigations on perfluoroalkylations of organic compounds, but the perfluoroalkylations of carbanions have never been reported.[1] This may be because it was very difficult to generate electrophilic perfluoroalkyl(R_f) species, since the R_f group has an extraordinary high electronegativity.[2] We have developed (perfluoroalkyl)-phenyliodonium triflates (FITS reagents) as useful electrophilic perfluoroalkylating agents[3,4] and partly described the perfluoroalkylations of carbanions in the preliminary report.[5] After that, *C*-perfluoroalkylations of β-diketones in liquid ammonia and of 2-nitropropyl anion with iodoperfluoroalkanes under irradiation were reported by L. M. Yagupol'skii's group[6] and A. E. Feiring,[7] respectively. This paper describes perfluoroalkylations of a variety of carbanions, and *O*- and *C*-perfluoroalkylations of active methylene compounds with FITS reagents.

Results and Discussion

Reaction of Grignard Reagents with FITS. FITS reacted with several kinds of Grignard reagents to give perfluoroalkyl derivatives in varying yields.

$$R_f\text{-}\underset{\underset{\text{Ph}}{|}}{\text{I}}\text{-OTf} + \text{RMgX} \longrightarrow R_f\text{-R} + \text{PhI} \qquad (1)$$

FITS-*m* (1) (2)

(R_f=*n*-C_mF_{2m+1})

Iodobenzene was formed in 70—95% isolated yield as another product. The reaction conditions of FITS-8 with octylmagnesium bromide are shown in Table 1. The best yield (52%) was obtained when FITS was added dropwise into a solution of an equivalent amount of the magnesium bromide in THF at −78 °C (Run 1). The reaction seemed to be fast, though the reaction mixture was stirred for 2 h. The reverse addition decreased the yield in some degree (Run 2) and there was no change in the yield at lower temperatures (Run 3). FITS-8 reacted with octylmagnesium chloride under the same conditions as in Run 1 to yield the product in a 58% yield. The yield was somewhat better than that of the bromide (52%). The results and reaction conditions of the reaction with several kinds of Grignard reagents are summarized in Table 2. No difference in reactivity among different carbon numbers of the *n*-R_f groups of FITS was observed. On the other hand, there was a significant difference between primary and secondary or tertiary Grignard reagents, and the secondary and tertiary reagents remarkably hindered the reaction (Run 6 and 7). Reactions of FITS-8 with Grignard reagents of sp^2 carbons, *p*-tolylmagnesium chloride and vinylmagnesium bromide, yielded complex mixtures, from which *p*-(perfluorooctyl)toluene and (perfluorooctyl)-ethylene were isolated in low yields, respectively, along with a small amount of (perfluorooctyl)-benzene. No formation of (perfluorooctyl)benzene

Table 1. Reaction of FITS with Alkylmagnesium Bromide
FITS-8(1 equiv) + *n*-$C_8H_{17}MgBr$(1 equiv) ⟶ *n*-C_8F_{17}-C_8H_{17}

Run	Solv.	Temp/°C	Time/h	Yield/%[a]
1	THF	−78	2	52
2[b]	THF	−78	2	41
3	THF	−100	2	53
4	Et_2O	−78	2	43
5	Toluene	−78	2	29
6	Hexane	−78	2	23
7	THF-HMPA (95:5)[c]	−78	0.5	38
		−78→0	0.5	

a) Isolated yields. b) Reverse addition; Grignard reagent was added to a mixture of FITS-8 in THF. c) HMPA=hexamethylphosphoric triamide.

Table 2. Reaction of FITS with Grignard Reagents
FITS-m + RMgX ⟶ R-R_f (R_f=n-C_mF_{2m+1})

Run	FITS-m	RMgX	Temp/°C	Time/h	Yield/%
1	m=8	n-$C_8H_{17}MgCl$	−78	2	58[a]
2	m=8	n-$C_{12}H_{25}MgCl$	−78→−10	2	55[a]
3	m=6	n-$C_{12}H_{25}MgCl$	−78	2	50[a]
4	m=4	n-$C_{12}H_{25}MgCl$	−78	2	48[a]
5	m=3	n-$C_{12}H_{25}MgCl$	−78	2	55[a]
6	m=8	Cyclohexyl-MgCl	−78	2	10[a]
7	m=8	1-Adamantyl-MgCl	−78	2	9[a]
8	m=8	$PhCH_2MgCl$	−78	2	38[a]
9	m=3	$PhCH_2MgCl$	−78	1.5	63[b]
10	m=3	$PhCH_2MgCl$	−110	2	82[b]
11	m=2	p-Xylyl-MgCl	−78	1	58[b]
12	m=8	CH_2=$CHCH_2MgBr$	−30	2	40[b]
13	m=8	p-Tolyl-MgCl	−78	2	8[b](17)[d]
14	m=8	CH_2=CHMgBr	−78	2	8[c](2)[d]

a) Isolated yields. b) GLC yields. c) NMR yields. d) GLC yields of (perfluorooctyl)benzene.

Table 3. Effect of Metal in Organometallic Compounds
FITS-8 + R-M ⟶ R-R_f

Run	R-M	Yield/%
1	n-$C_8H_{17}MgCl$	58
2	$(n$-$C_8H_{17})_2CuMgBr$	38
3	n-$C_8H_{17}Cu$	26
4	n-$C_8H_{17}MgCl$/cat. CuI	33
5	n-$C_8H_{17}Li$	9

was observed with sp^3 or sp carbon Grignard reagents.

We examined the reaction of FITS with other organometallic compounds and showed the results in Table 3. It is worth noting that the reaction with the lithium salt was complex and the yield was very low. Grignard reagents provided the best yield of all the organometallic compounds used.

Reaction of Acetylides with FITS. FITS-8 reacted with an equimolar lithium salt of phenylacetylene in THF at −78°C to give Rf-compound **4** (R=Ph) in favorable yield (Run 1 in Table 4).

$$\text{FITS-}m + \underset{\mathbf{3}}{\text{R-C}\equiv\text{CM}} \longrightarrow \underset{\mathbf{4}}{\text{R-C}\equiv\text{C-R}_f} \quad (2)$$

M=Li, MgX

Elevated temperature, excess of the lithium salt, or the reverse addition method resulted in lowering the yield (Runs 2, 3, and 4 in Table 4). Interestingly, it was found that β-(perfluorooctyl)styrene was formed in 11, 9, and 4% yields in Runs 2, 3, and 4, respectively, which was proved to be a 1:1 mixture of cis and trans isomers by comparison with authentic samples. At present the mechanism of the formation of the R_f-styrene is quite unclear. Table 5 shows the results of the reactions with several kinds of acetylides under similar conditions as in Run 1 in Table 4. It is interesting that there was no difference between the lithium salt and the magnesium chloride of phenylacetylene in contrast to the great difference between octyllithium and octylmagnesium chloride. Furthermore, it is worth noting that the acetylides (sp carbanions) afforded good yields of the products, while the reactions of vinyl or aryl anions (sp^2 carbanions) were complex and their yields were low.

Reaction of Enolate Anions of Active Methylene Compounds with FITS. FITS was allowed to react with sodium salt of 2-methyl-1,3-cyclopentanedione **5** in DMF at 0°C for 3h, giving *O*- and *C*-perfluoroalkylated compounds **6** and **7** in 26 and 7% yields, respectively. The ^{19}F chemical shifts of α-CF_2

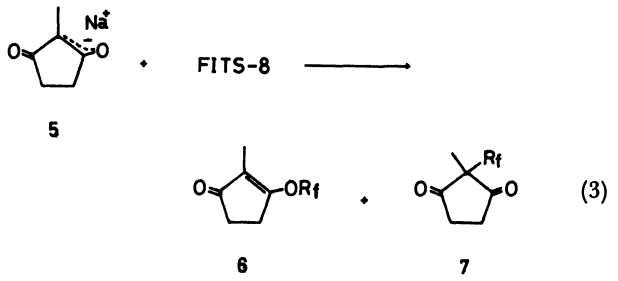

(3)

groups clearly reflect the structural difference between **6** and **7**. The CF_2 group bonding to the oxygen atom in **6** appears at 80.1 ppm as a multiplet, while the CF_2 bonding to the carbon atom in **7** at 112.8 ppm. The effect of solvents and reaction temperature on the perfluoroalkylation was investigated and the results are summarized in Table 6. The reaction was exothermic and other products were tarry materials. Polar solvents such as DMF and DMSO were needed for the alkylation. The reaction at room temperature in DMF or DMSO afforded only the *O*-R_f-product **6**. With a lowering of the temperature, **6** decreased, while the *C*-R_f-product **7** increased. In hydrocarbon system, a similar temperature-dependent change of the ratios of *O*/*C*-alkylation was observed in butylation of an enolate anion of ethyl acetoacetate with butyl halides.[8] The above results are very different from the photo-reaction of β-diketones with iodoperfluoroalkanes in liquid

Table 4. Reaction of FITS with Lithium Phenylacetylide

$$\text{FITS-8} + \text{PhC}{\equiv}\text{CLi} \xrightarrow[\text{in THF}]{0.5\text{ h}} \text{PhC}{\equiv}\text{C-C}_8\text{F}_{17}$$

Run	FITS-8	PhC≡CLi	Temp/°C	Yield/%
1	1 equiv	1 equiv	−78→−30	66
2[a]	1 equiv	1 equiv	−78→−30	37(11)[b]
3	1 equiv	1.5 equiv	−78→−30	35(9)[b]
4	1 equiv	1 equiv	−40	47(4)[b]

a) Reverse addition; Acetylide was added to a mixture of FITS-8 in THF. b) Figures in parentheses are the yields of β-(perfluorooctyl)styrene (cis/trans=1/1).

Table 5. Reaction of FITS with Acetylides

$$\text{FITS-}m + \text{R-C}{\equiv}\text{C-M} \xrightarrow[\text{in THF}]{} \text{R-C}{\equiv}\text{C-R}_f\ (R_f{=}n\text{-}C_mF_{2m+1})$$

Run	FITS-m	Acetylides	Temp/°C	Time/h	Yield/%
1	m=8	PhC≡CLi	−78→−30	0.5	66[a]
2	m=6	PhC≡CLi	−78→−30	0.5	53[a]
3	m=3	PhC≡CLi	−78→−30	0.5	44[b]
4	m=2	PhC≡CLi	−78	1	56[b]
5	m=2	PhC≡CMgCl[c]	−78	1	58[b]
6	m=8	n-C_6H_{13}C≡CLi	−78→−30	0.5	60[a]
7	m=6	n-C_6H_{13}C≡CLi	−78	1	70[b]
8[d]	m=2	n-C_6H_{13}C≡CLi	0	1	50[a]

a) Isolated yields. b) GLC yields. c) The magnesium chloride was prepared by treating phenylacetylene with a ethereal solution of benzylmagnesium chloride in THF. d) The reaction was carried out by adding an ethereal solution of 1-octynyllithium to a mixture of FITS-2 in pentane at 0°C.

Table 6. Reaction of **5** with FITS-8[a]

Run	Solv.	Temp/°C	Yield/%		Ratio
			6(O-R_f)	**7**(C-R_f)	**6/7**
1	DMF	R.t.	27	0	
2	DMF	0	26	7	3.7
3	DMF	−30	19	16	1.2
4	DMF	−55	7	31	0.23
5	DMSO	R.t.	20	0	
6	THF	−30	Trace	0	

a) Reaction time 3 h.

ammonia, which gave only C-R_f-products.[6]

Similarly FITS reacted with enolate anions of β-keto esters **8** and its cyclic ester **11** in DMF at 0°C to afford C-R_f-compounds **10** and **13** as major products along with a small amount of O-R_f-compounds **9** and **12**, respectively. Both the keto esters showed analogous behavior and it is in contrast to the case of the β-diketone **5** in which the O-product **6** was a main product at 0°C. The C-products **10** and **13** increased further at lower temperatures.

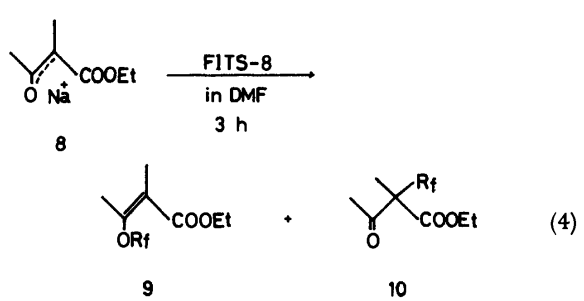

(4)

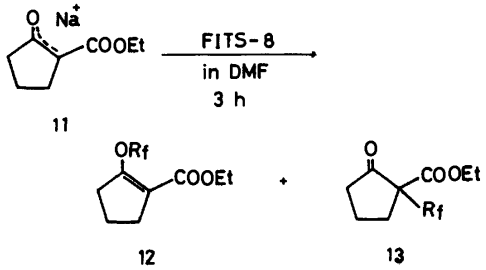

(5)

Temp/°C	**9**	**10**	**12**	**13**
0	8%	28%	8%	20%
−55	5%	36%	6%	29%

Sodium salt of diethyl 2-methylmalonate **14** reacted exothermically with FITS-8 at room temperature for 1 h to produce only a C-R_f-compound **15a** in a 24% yield. Other products were tarry materials, so their assignment was not made. In this reaction, the effect of the R_f groups was examined by using FITS-8 and -3, and FITS(F)-3*i*[9] (Eq. 6).

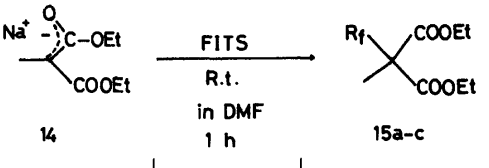

(6)

	R_f	Yield/%
15a	n-C_8F_{17}	24
15b	n-C_3F_7	20
15c	i-C_3F_7	3

Table 7. Reaction of **16** with FITS-8[a)]

Run	**16**	Solv.	Yield of **17**/%
1	M=Na	DMSO	43
2	M=Na	DMF	33
3	M=Na	Et_2O	22
4	M=Li	DMSO	49
5	M=Li	DMF	51
6	M=Li	Et_2O	18

a) Reaction time; 1 h, temp; room temperature.

Similar yields were obtained in the cases of FITS-8 and -3 having primary R_f, but FITS(F)-3*i* bearing perfluoroisopropyl group gave a very low yield of **15c**. Thus, the secondary R_f group strongly hindered the desired reaction.

The reaction of FITS-8 with 2-nitro-2-propanide anion **16** was run in several solvents at room temperature for 1 h. The reaction occurred exothermically and yielded 2-R_f-2-nitropropane **17** only in varying yields. The results are summarized in Table 7. Polar solvents gave better yields and the lithium

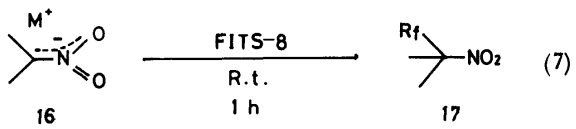

(7)

salt in the polar solvents afforded somewhat better yields than the sodium salt.

FITS-8 was also treated with an enolate anion of acetophenone under several conditions to give a mixture of α-(perfluorooctyl)acetophenone and its dehydrofluorination product, 2-fluoro-2-(perfluoroheptyl)vinyl phenyl ketone in low yields (<17%). Therefore, the reaction of FITS with enol silyl ethers was much better as a synthetic method of α-(perfluoroalkyl) ketones because high yields were obtained and the reaction procedure was simple.[10)]

Experimental

^{19}F Chemical shifts are given in ppm upfield from $CFCl_3$ as an internal standard. A gas chromatograph with a column of 10% SE-30 on Chromosorb WAW DMCS was used for the isolation or analysis of the products. FITS reagents were prepared by the method described previously.[3)] Reaction solvents were purified and dried by the usual methods. All the reactions were done under argon atmosphere.

Note: FITS reagents decomposed soon in diethyl ether or sooner in THF at room temperature. Therefore, if necessary, FITS must be dissolved in the solvents at −78 °C.

Reaction of FITS with Grignard Reagents. Typical Procedure: Into a solution of 1.4 mmol of Grignard reagent (0.4—0.8 mmol ml^{-1} of THF or diethyl ether) in 13 ml of THF at −78 °C, was added 1.3 mmol of FITS reagent in several portions with stirring. After the reaction mixture was stirred at −78 °C for additional 2 h, it was quenched with aq ammonium chloride and extracted with pentane. The extract was dried with magnesium sulfate and concentrated. The desired R_f-compound was seperated from iodobenzene as another product by column chromatography of the residue on silica gel using pentane as an eluent and then distilled.

Grignard reagents were prepared from the halides in THF or diethyl ether by the usual method. The organocopper compounds used as shown in Table 3 were prepared by the methods reported.[11)]

The reaction with Grignard reagents was carried out at different temperatures in different solvents as shown in Tables 1 and 2.

In the case of the reaction of FITS-8 with benzylmagnesium chloride, the residue resulting from the extraction with ether was treated with Raney Ni (W-2)[12)] in ethanol to reduce iodobenzene to benzene, because it was difficult to seperate the R_f-product from iodobenzene by column chromatography or distillation. After the reduction, the resulting residue was distilled to give (1*H*, 1*H*-heptadecafluorononyl)benzene in a 38% yield.

The yields of the volatile R_f-products were determined by NMR or gas chromatography. Spectral data and elemental analyses of new compounds are summarized in Table 8.

Reaction of FITS with Acetylides. Typical Procedure: Into a solution of 1.32 mmol of an alkyne in 8 ml of THF at −78 °C, was dropwise added a solution of 1.32 mmol of butyllithium in 0.96 ml of hexane with stirring. The solution was stirred for additional 10 min and 1.32 mmol of FITS reagent was added in several portions into it at −78 °C. After the reaction mixture was stirred for additional 5 min at −78 °C, it was warmed to −30 °C for a period of 25 min, quenched with aq ammonium chloride, and extracted with pentane. The extract was dried with magnesium sulfate and concentrated. The residue was column-chromatographed on silica gel using pentane to give the R_f-alkyne. The yields of the volatile R_f-products were determined by NMR or gas chromatography of the concentrated extracts, as shown in Table 5. The spectral data and elemental analyses of the products are shown in Table 8.

Reaction of FITS with Enolate Anions 5, 8, 11, and 14. Typical Procedure: A solution of 2-methyl-1,3-cyclopentanedione (168 mg, 1.5 mmol) in 8 ml of DMF was added dropwise into a mixture of sodium hydride (1.7 mmol) and 5 ml of DMF with stirring. The reaction mixture was stirred for an additional 15 min at room temperature and cooled to −55 °C. Then FITS-8 (772 mg, 1 mmol) was added into the solution of the enolate anion. After an additional stirring for 3 h at −55 °C, the mixture was quenched with 3 mol dm^{-3} hydrochloric acid and extracted with ether. The organic layer was washed with water, dried with magnesium sulfate, and concentrated. Two isomers were separated by column chromatography on silica gel using a mixture of pentane and ether as an eluent and then each distillation gave 38 mg (7%) of **6** and 163 mg (31%) of **7**. Products **9** and **15c** were isolated by gas chromatography after column chromatography. Products **15a** and **15b** were isolated by column chromatography only. The results are shown in Table 6 and in Eqs. 4—6.

Reaction of FITS with 16. Typical Procedure: Sodium or lithium 2-nitro-2-propanide was prepared according to the method described in the literature.[13)] FITS-8 (1.33 mmol) was added into a solution of **16** (2.00 mmol) in 10 ml of DMF at room temperature with stirring. After an additional stirring for 1 h, some water was added into the reaction mixture and the mixture was extracted with ether. The post-

Table 8. Properties of Products

Compd[a]	Bp(θ_b/°C)/mmHg[b] [Mp (θ_m/°C)]	^{1}H-NMR (δ, in $CDCl_3$)	^{19}F-NMR (in $CDCl_3$)	IR (Method)	m/z	Anal (%) Found (Calcd)	
						C	H
2							
n-C_8H_{17}-R_{f_8}	95—7/1.5	0.90(3H, m), 1.30 (12H, m),1.80—2.20(2H, m)	80.3(3F, m), 112.5 (2F, m), 120.0(8F, m), 121.9(2F, m), 124.5 (2F, m)	—	532 (M^+)	36.38 (36.10)	3.36 (3.22)
n-$C_{12}H_{25}$-R_{f_8}	160/6[b]	0.90(3H, m), 1.30 (20H, m), 1.80—2.30(2H, m)	81.5(3F, t, J=10Hz), 114.8(2F, m), 122.3 (6F, m), 123.2(2F, m), 124.0(2F, m), 126.6 (2F, m)	—	—	—	—
n-$C_{12}H_{25}$-R_{f_6}	170/25[b]	0.90(3H, m), 1.30 (20H, m),1.80—2.30(2H, m)	81.9(3F, t, J=10Hz), 114.8(2F, m), 122.4 (2F, m), 123.4(2F, m), 124.0(2F, m), 126.7 (2F, m)	—	488 (M^+)	44.31 (44.27)	5.11 (5.16)
n-$C_{12}H_{25}$-R_{f_4}	150/25[b]	0.90(3H, m), 1.30 (20H, m), 1.80—2.30(2H, m)	81.7(3F, t, J=10Hz), 115.0(2F, m), 125.0 (2F, m), 126.6(2F, m)	—	388 (M^+)	49.54 (49.48)	6.57 (6.49)
n-$C_{12}H_{25}$-R_{f_3}	200/30[b]	0.90(3H, m), 1.30 (20H, m), 1.80—2.30(2H, m)	81.3(3F, t, J=10Hz), 115.8(2F, m), 128.4 (2F, s)	—	—	—	—
R_{f_8}-Cyclohexane	120/20[b]	0.90—1.40(5H, m), 1.40—2.20 (6H, m)	81.4(3F, t, J=10Hz), 118.5(2F, m), 121.0 (2F, m), 122.3(6F, m) 123.1(2F, m), 126.6 (2F, m)	—	501 (M^+−1)	33.23 (33.48)	2.09 (2.21)
1-R_{f_8}-Adamantane	[54—55]	1.74(6H, m), 1.94 (6H, m), 2.08 (3H, m)	81.4(3F, t, J=10Hz), 118.6(2F, m), 122.2 (8F, m), 123.1(2F, m), 126.6(2F, m)	—	554 (M^+)	39.09 (38.93)	2.69 (2.90)
$PhCH_2$-R_{f_8}	100/0.3[b] [37.5—38.5]	3.30(2H, t, J=18 Hz), 7.10—7.45 (5H, m)	81.4(3F, t, J=10Hz), 110.8(2F, t, J=15Hz), 121.7(2F, m), 122.4(6F, m), 123.2(2F, m), 126.6 (2F, m)	—	510 (M^+)	35.28 (35.31)	1.26 (1.38)
$PhCH_2$-R_{f_3}	Oil	3.28(2H, tt, J= 18.9, 1.5Hz), 7.25 (5H, bs)	81.05(3F, t, J=10Hz), 114.3(2F, m) 127.6 (2F, m)	—	260 (M^+)	—	—
p-Xylyl-R_{f_2}	[13—15]	2.30(3H, s), 3.30 (2H, t, J=18Hz), 7.20(4H, s)	85.1(3F, s), 117.3 (2F, t, J=18Hz)	—	224 (M^+)	53.54 (53.58)	4.07 (4.05)
CH_2=$CHCH_2$-R_{f_8}	130/140	2.82(2H, dt, J=6, 18Hz), 5.03—5.45 (2H, m), 5.55—6.03(1H, m)	81.3(3F, t, J=10Hz), 113.6(2F, m), 122.4 (6F, m), 123.5(4F, m), 126.6(2F, m)	1650(C=C) (neat)	460 (M^+)	—	—
4							
PhC≡C-R_{f_8}	120/2[b]	7.20—7.65(5H, m)	81.4(3F, t, J=10Hz), 97.5(2F, m), 121.4 (2F, m), 122.2(4F, m), 122.9(4F, m), 126.5 (2F, m)	2250(C≡C) (neat)	520 (M^+)	36.74 (36.94)	0.97 (0.97)

Table 8. (Continued)

Compd[a]	Bp(θ_b/°C)/mmHg[b] [Mp (θ_m/°C)]	^{1}H-NMR (δ, in $CDCl_3$)	^{19}F-NMR (in $CDCl_3$)	IR (Method)	m/z	Anal (%) Found (Calcd) C	H
PhC≡C-R_{f_6}	140/25[b]	7.15—7.80(5H, m)	81.5(3F, t, J=10 Hz), 97.5(2F, m), 121.6 (2F, m), 123.0(4F, m), 126.5(2F, m)	2250(C≡C) (neat)	420 (M^+)	40.15 (40.02)	1.15 (1.20)
PhC≡C-R_{f_3}	135/110[b]	7.4(5H, m)	80.7(3F, tt, J=8.5, 0.5Hz), 98.7(2F, tq, J=8.5, 6.0Hz), 127.3 (2F, tq, J=6.0, 0.5Hz)	2240(C≡C) (neat)	270 (M^+)	49.20 (48.91)	1.90 (1.87)
PhC≡C-R_{f_2}	Oil	7.3—7.7(5H, m)	85.8(3F, t, J=4.5 Hz), 101.6(2F, q, J= 4.5Hz)	2250(C≡C) (neat)	220 (M^+)	54.47 (54.56)	2.23 (2.29)
n-C_6H_{13}C≡C-R_{f_8}	Oil	0.90(3H, m), 1.20—1.75(8H, m), 2.33(2H, m)	81.5(3F, t, J=10 Hz), 96.6(2F, m), 121.5 (2F, m), 122.3(4F, m), 123.1(4F, m), 126.6(2F, m)	2340(C≡C) (neat)	527 (M^+−1)	36.32 (36.38)	2.41 (2.48)
n-C_6H_{13}C≡C-R_{f_6}	Oil	0.8—1.0(3H, m), 1.1—1.7(8H, m), 2.30(2H, t, J= 6Hz)	81.4(3F, t, J=10 Hz), 96.6(2F, m), 121.8 (2F, m), 123.2(4F, m), 126.6(2F, m)	2250(C≡C) (neat)	429((M^++1) 427(M^+−1)	39.35 (39.27)	3.08 (3.06)
n-C_6H_{13}C≡C-R_{f_2}	Oil	0.87(3H, t, J= 6Hz), 1.00—1.78 (8H, m), 2.00— 2.45(2H, m)	86.1(3F, t, J=2 Hz), 100.9(2F, q, J=2 Hz)	2260(C≡C) (neat)	213 (M^+−CH_3)	—	—
6	160/14	1.60(3H, s), 2.47—2.70(2H, m), 2.70—3.00(2H, m)	80.1(2F, m), 81.4 (3F, t, J=10Hz), 122.4(6F, m), 123.3 (2F, m), 125.6(2F, m), 126.8(2F, m)	1730(C=O), 1690(C=C) (neat)	530 (M^+)	31.63 (31.71)	1.25 (1.33)
7	150/11 [44.5—45.5]	1.48(3H, s), 2.90(4H, m)	81.3(3F, t, J=10Hz), 112.8(2F, m), 117.4 (2F, m), 122.4(6F, m), 123.4(2F, m), 126.8(2F, m)	1740(C=O) (KBr)	530 (M^+)	31.77 (31.71)	1.37 (1.33)
9	Oil	1.33(3H, t, J=7Hz), 1.88(3H, s), 2.36 (3H, m), 4.26(2H, q, J=7Hz)	80.1(2F, bs), 81.3 (3F, t, J=10Hz), 122.4(6F, m), 123.3 (2F, m), 125.5(2F, m), 126.7(2F, m)	1730(C=O), 1670(C=C) (neat)	562 (M^+)	31.83 (32.04)	1.75 (1.94)
10	180/14	1.30(3H, t, J=7Hz), 1.63(3H, s), 2.33 (3H, s), 4.28(2H, q, J=7Hz)	81.4(3F, t, J=10Hz), 108.8(2F, m), 116.8 (2F, m), 122.3(6F, m), 123.3(2F, m), 126.8(2F, m)	1760(ester), 1740(C=O) (neat)	563 (M^++1)	32.01 (32.04)	1.97 (1.97)
12	170/15	1.25(3H, t, J=7Hz), 1.83—2.20(2H, m), 2.50—2.90(4H, m), 4.18(2H, q, J=7Hz)	80.7(2F, bs), 81.3 (3F, t, J=10Hz), 122.5(6F, m), 123.3 (2F, m), 125.5(2F, m), 126.7(2F, m)	1710(C=O), 1670(C=C) (neat)	575 (M^++1)	33.29 (33.46)	1.78 (1.90)
13	190/15 [54]	1.30(3H, t, J=7Hz), 1.80—3.00(6H, m), 4.27(2H, q, J=7Hz)	81.3(3F, t, J=10Hz), 109.0(1F, AB system, J=295Hz, FA), 111.9 (1F, AB system J=295Hz, FB), 118.0(2F, m), 122.4 (6F, m), 123.2(F, m), 126.7(2F, m)	1760(ester), 1740(C=O) (KBr)	574 (M^+)	33.68 (33.46)	2.07 (1.90)

Table 8. (Continued)

Compd[a]	Bp[b] (θ_b/°C) [Mp (θ_m/°C)]	^{1}H-NMR (δ, in $CDCl_3$)	^{19}F-NMR (in $CDCl_3$)	IR (Method)	*m/z*	Anal (%) Found (Calcd) C	H	N
15a	Oil	1.30(6H, t, J=6Hz), 1.73(3H, s), 4.20 (4H, q, J=6Hz)	81.3(3F, t, J=10Hz, 109.4(2F, m), 116.5 (2F, m), 122.3(6F, m), 123.2(2F, m), 126.6(2F, m)	1750(ester) (KBr)	592 (M^+)	32.32 (32.45)	2.13 (2.21)	
15b	Oil	1.30(6H, t, J=6Hz), 1.70(3H, s), 4.25 (4H, q, J=6Hz)	81.7(3F, t, J=10Hz), 110.0(2F, m), 120.8 (2F, t, J=5Hz)	1750(ester) (KBr)	342 (M^+)	38.52 (38.61)	3.72 (3.83)	
15c	Oil	1.30(6H, t, J=6Hz), 1.75(3H, s), 4.23 (4H, q, J=6Hz)	70.0(6F, s), 173.4 (1F, s)	1750(ester) (neat)	342 (M^+)	—	—	
						C	H	N
17	[73—74]	1.83(6H, s)	81.5(3F, t, J=10Hz), 115.6(2F, m), 118.6 (2F, m), 122.2(6F, m), 123.3(2F, m), 126.7 (2F, m)	1560(NO_2) 1345(NO_2) (KBr)	461 (M^+-NO_2)	25.76 (26.05)	1.25 (1.19)	2.72 (2.76)

a) R_{fm}=*n*-C_mF_{2m+1}. b) Bath temperature °C/mmHg. Distillation was carried out by using a glass tube oven.

treatment was carried out in a similar manner as above. Column chromatography of the resulting residue on silica gel gave **17** as crystals. The results are summarized in Table 7.

References

1) For example; a) W. A. Sheppard and C. M. Sharts, "Organic Fluorine Chemistry," W. A. Benjamin, Inc., New York (1969); b) P. Tarrant, *J. Fluorine Chem.*, **25**, 69 (1984); c) L. M. Yagupol'skii, I. I. Maletina, N. V. Kondratenko, and V. V. Orda, *Synthesis*, **1978**, 835; d) Y. Kobayashi, K. Yamamoto, I. Kumadaki, *Tetrahedron Lett.*, **1979**, 4071; e) N. O. Brace, *J. Org. Chem.*, **44**, 1964 (1979); f) T. Kitazume and N. Ishikawa, *Chem. Lett.*, **1981**, 1679; **1982**, 137; **1982**, 1453; g) V. I. Popov, V. N. Boiko, and L. M. Yagupol'skii, *J. Fluorine Chem.*, **21**, 365 (1982); h) T. Fuchikami and I. Ojima, *Tetrahedron Lett.*, **25**, 303 (1984); i) M.Yoshida, K. Moriya, H. Sawada, and M. Kobayashi, *Chem. Lett.*, **1985**, 755.

2) J. E. Huheey, *J. Phys. Chem.*, **69**, 3284 (1965).

3) T. Umemoto, Y. Kuriu, H. Shuyama, O. Miyano, and S. Nakayama, *J. Fluorine Chem.*, **20**, 695 (1982) and its full paper, ibid., **31**, 37 (1986).

4) T. Umemoto, *Yuki Gosei Kagaku Kyokai Shi*, **41**, 251 (1983) and references cited therein.

5) T. Umemoto and Y. Kuriu, *Tetrahedron Lett.*, **22**, 5197 (1981).

6) L. M. Yagupol'skii, G. I. Matyushecheva, N. V. Pavlenko, and V. N. Boiko, *J. Org. Chem. USSR*, **18**, 10 (1982).

7) A. E. Feiring, *J. Org. Chem.*, **48**, 347 (1983).

8) G. Brieger and W. M. Pelletier, *Tetrahedron Lett.*, **1965**, 3555.

9) FITS(F)-3*i*=heptafluoroisopropyl-*p*-fluorophenyliodonium triflate.[3,4]

10) T. Umemoto, Y. Kuriu, S. Nakayama, and O. Miyano, *Tetrahedron Lett.*, **23**, 1471 (1982).

11) G. H. Posner, *Org. Reactions*, **22**, 253 (1975).

12) R. Mozingo, *Org. Syn.*, Coll. Vol. **3**, 181 (1955).

13) N. Kornblum, S. D. Boyd, and N. Ono, *J. Amer. Chem. Soc.*, **96**, 2580 (1974).

 © 1986 The Chemical Society of Japan Bull. Chem. Soc. Jpn., 59, 447—452 (1986)

Synthesis and Reactivity of *N*-Trifluoromethyl-*N*-nitrosotrifluoromethanesulfonamide as a New Type of Trifluoromethylating Agent

Teruo UMEMOTO* and Akira ANDO†
Sagami Chemical Research Center, Nishi-Ohnuma 4-4-1, Sagamihara, Kanagawa 229
(Received September 21, 1985)

N-Trifluoromethyl-*N*-nitrosotrifluoromethanesulfonamide (TNS-Tf) was synthesized in a 58% yield by the reaction of trifluoronitrosomethane with hydroxylamine followed by the treatment with trifluoromethanesulfonyl fluoride in the presence of a base. TNS-Tf was demonstrated to be an effective trifluoromethylating agent photochemically or thermally for aromatics, thiols, disulfides, and uridine derivatives. The insertion reaction by two trifluoromethyl groups of TNS-Tf to the sulfur-sulfur bonds was observed in the reaction with disulfides having electron-withdrawing groups, giving 2 mols of trifluoromethylthio compounds. Furthermore, TNS-Tf served as a good reagent for mild and convenient in situ generation of trifluoromethylcopper complex which converted iodoaromatics to trifluoromethyl-substituted aromatics in good yields. Similarly, *N*-trifluoromethyl-*N*-nitrosononafluoro-1-butanesulfonamide (TNS-Nf) was synthesized in a 36% yield. The examination of the reactivity indicated that this type of *N*-nitroso sulfonamides became to be sources of both perfluoroalkyl radicals contained.

Much attention has been riveted to trifluoromethyl-containing compounds in the fields of medicine and agricultural chemicals because of the attractive effect of the trifluoromethyl groups on biological activity.[1] Therefore, there have been many investigations for introduction of trifluoromethyl groups into organic compounds. There have been two essential approaches, conversion of trichloromethyl or carboxy groups to trifluoromethyl groups with HF,[2,3] SbF_5,[4] or SF_4[5] and direct introduction of trifluoromethyl groups with trifluoromethyl iodide[6-17] or bromide,[18] trifluoroacetic acid or its salt.[19-21] However, the studies on the syntheses of new reactive trifluoromethylating agents were little reported.[22] Previously we presented the synthesis of *N*-trifluoromethyl-*N*-nitrosobenzenesulfonamide (TNS-B) as a new photochemical trifluoromethylating agent.[23] However the yields for trifluoromethylation were somewhat low and TNS-B was too thermal stable to act as a thermal reagent. In order to enhance the reactivity, we altered it according to our idea that the more the electronegativity of phenyl group of TNS-B rises the more the reactivity increases. Although we replaced the phenyl group of TNS-B with *p*-nitro- or 2,4-dinitrophenyl,[24] their reactivities were rather low. Thus, we expected a great variation in the reactivity by replacement of the aryl group with a perfluoroalkyl group because of its extraordinary high electronegativity.[25] As a result, we could develop a novel and effective trifluoromethylating agent. This paper describes the synthesis and reactivity of *N*-trifluoromethyl-*N*-nitrosotrifluoromethanesulfonamide (TNS-Tf) as a new type of trifluoromethylating agent.

Results and Discussion

TNS-Tf was synthesized in a 58% yield by the reaction of trifluoronitrosomethane with hydroxylamine in DMF/Et_2O (4/1) at −65 °C followed by the treatment with trifluoromethanesulfonyl fluoride at −65—−60 °C for 20 h in the coexistence of sodium hydride.

$$CF_3NO \xrightarrow[-65^{\circ}C]{NH_2OH} [CF_3N{=}NOH] \xrightarrow[NaH]{R_fSO_2F} CF_3{-}\overset{\overset{N=O}{|}}{N}{-}SO_2R_f$$

TNS-Tf (R_f=CF_3)
TNS-Nf (R_f=*n*-C_4F_9)

When trifluoromethanesulfonyl chloride was used instead of the fluoride, TNS-Tf could not be synthesized. TNS-Tf is colorless volatile liquid (mp 3.2—4 °C). Since it is stored in acetonitrile at room temperature for a long time, TNS-Tf can easily and safely be treated as an acetonitrile solution (1—0.5 mol dm^{-3}).

TNS-Tf was found to be a useful photochemical or thermal trifluoromethylating agent for aromatics, thiols, disulfides, and uridine derivatives. The reactions proceeded with evolution of gas. The photochemical reaction was carried out in acetonitrile by using a high pressure Hg lamp and biacetyl as a sensitizer. The results are summarized in Table 1. The trifluoromethylation smoothly took place in the case of electron-rich aromatic compounds and the substitution occurred preferentially at electron-rich positions as shown in Run 2. In this way, TNS-Tf has electrophilic nature. In addition, the trifluoromethylation showed a high *ortho-para* substitution ratio as shown in the reaction of acetanilide (*o*/*p*=4/1). It is in sharp contrast to classical electrophilic substitution of acetanilide (*o*/*p*=1/19 in the nitration).[26] Our method was successfully applied to the preparation of trifluoromethylated dopamine derivative (Run 6), whereas the trifluoromethylation with gaseous trifluoromethyl iodide needed an excess of the substrate and the yield was low.[27] The reaction with such activated aromatics as *p*-*t*-butylphenol and *p*-dimethoxybenzene was accompanied with the formation of considerable amount of

†Present address; Faculty of Pharmaceutical Sciences, Setsunan University, 45-1 Nagaotoge-cho, Hirakata, Osaka 573-01.

Table 1. Photochemical Trifluoromethylation with TNS-Tf

Run[a]	Substrate	Molar equiv of TNS-Tf	Time h	Product[b]	Yield[c] %	^{19}F-NMR[d]
1	Benzene	0.29	3	$PhCF_3$	49[e]	—
2	Naphthalene	1.0	3.5	CF_3-Naphthalene	41[e]	60.1(α)
				(α:β-isomers)	(8.7:1)	63.1(β)
3	*p*-*t*-Butylphenol	1.0	5	2-CF_3-4-*t*-Butylphenol	65[f,g]	61.3
				2,6-Bis(CF_3)-4-*t*-butylphenol	17[f](34)[h]	61.2
4	*p*-Dimethoxybenzene	1.0	2.8	2-CF_3-1,4-Dimethoxybenzene	60[e]	62.9
				Bis(CF_3)-1,4-dimethoxybenzene[i]	16[e](32)[h]	63.4
						55.9
5	Acetanilide	1.0	4.5	CF_3-Acetanilide	49[e]	60.7(*o*)
				(*o*:*m*:*p*-isomers)	(8:1:2)	63.3(*m*)
						62.5(*p*)
6	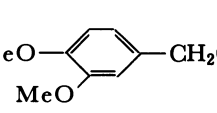	1.25	13	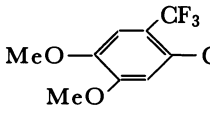	62[f]	57.8
7	n-$C_7H_{15}SH$	1.0	2	n-$C_7H_{15}SCF_3$[m]	43[f]	41.6
8	$HSCH_2COOH$	1.0	4	CF_3SCH_2COOH[n]	86[f]	42.0
9	$HSCH_2CH_2COOH$	1.0	4	$CF_3SCH_2CH_2COOH$[d]	89[f]	41.5
10	(n-$C_{10}H_{21}S$)$_2$	1.0	6.5	n-$C_{10}H_{21}SCF_3$[p]	36[f]	41.3
11	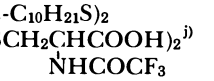	1.2	4.5	$CF_3SCH_2CHCOOH$	82[f]	40.9(CF_3S) 76.1($COCF_3$)
12	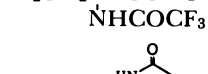	1.25	5	$CF_3SCH_2CH_2CHCOOCH_3$	71[f]	41.4(CF_3S) 76.1($COCF_3$)
13	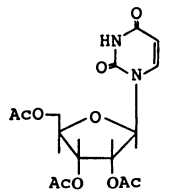	1.2	1.25	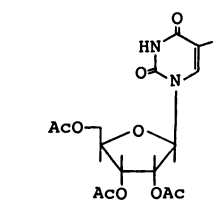	30[f]	63.8

a) Acetonitrile was used as a solvent except for Run 10 where acetone was used. b) See the experimental section for spectral data of new compounds. The known compounds were spectroscopically in agreement with authentic samples or spectral data reported. c) Yields were calculated on the basis of substrates except for Run 1 in which the yield was on the basis of TNS-Tf. d) Chemical shifts (ppm, upfield from $CFCl_3$ as an internal standard) of trifluoromethyl groups are given. e) ^{19}F-NMR yields. f) Isolated yields. g) 2,6-Bis(CF_3)-4-*t*-butylphenol as another product was isolated in a 17% yield based on the substrate (34% based on TNS-Tf). h) Yields were calculated based on TNS-Tf. i) 2,3-Bis(CF_3)-1,4-dimethoxybenzene and 2,5-bis(CF_3)-1,4-dimethoxybenzene were produced in 7 and 9% ^{19}F-NMR yields based on the substrate, respectively (14 and 18% based on TNS-Tf). Their spectral data are shown in the experimental section. j) This starting material was prepared by treating L-cystine with trifluoroacetic anhydride in trifluoroacetic acid at −10 to +10 °C. k) This starting material was prepared by treating DL-homocystine in the same manner as the case of j) followed by esterification with diazomethane. l) Ref. 24. m) Bp 60 °C/20 mmHg (1 mmHg=133.322 Pa). n) Bp 125 °C/21 mmHg [lit, 88—88.5 °C/15 mmHg, V. V. Boiko, G. M. Shchupak, and L. M. Yagupol'skii, *J. Org. Chem. USSR*, **13**, 972 (1977)]. o) Bp 120 °C/17 mmHg (lit, 108 °C/22 mmHg, J. F. Harris, Jr., USP 3522293). p) BP 106 °C/17 mmHg. q) Ref. 15.

bis(trifluoromethyl)aromatics (34% in Run 3 and 32% in Run 4, based on TNS-Tf). Accordingly, the total yields of trifluoromethylated aromatics in Runs 3 and 4 were 99 and 92% based on TNS-Tf, respectively. It indicated that TNS-Tf is an effective source of trifluoromethyl groups. Deactivated aromatics such as methyl benzoate did not give any trifluoromethylated products. Photochemical decomposition of TNS-Tf itself occurred. TNS-Tf could not trifluoromethylate such nitrogen-containing compounds as pyridine and aniline because TNS-Tf was decomposed by them.

The reaction of mercaptoacetic and 3-mercaptopropionic acids with TNS-Tf afforded (trifluoromethylthio) acetic and -propionic acids in 86 and 89% isolated yields, respectively. It is in contrast to the reaction of the phenyl analogue TNS-B, of which reaction with 3-mercaptopropionic acid yielded only a trace of the product. 1-Heptanethiol, an easily oxidizable thiol, gave a moderate yield of the product. Until now, trifluoromethylation of thiols was the photochemical or thermal action of trifluoromethyl iodide on the thiols under basic conditions.[8,15] TNS-Tf afforded a useful method for thiols or products which are unstable to basic conditions (for example Runs 9, 11, and 12).

TNS-Tf was a good reagent for the conversion of disulfides to trifluoromethylthio compounds. The yields were calculated according to the following equation. Actually the reaction of 2.73 mmol of TNS-

$$\mathbf{R\text{-}S\text{-}S\text{-}R} + \text{TNS-Tf} \longrightarrow 2\,\mathbf{CF_3\text{-}S\text{-}R}$$

Table 2. Thermal Trifluoromethylation with TNS-Tf

Run[a]	Substrate	Molar equiv of TNS-Tf	Temp °C	Time h	Product	Yield[b] %
1[c]	*t*-Butylphenol	1.0	110	22	2-CF_3-4-*t*-butylphenol[c]	69
2	$(n\text{-}C_{10}H_{21}S)_2$	1.5	80	1.5	$n\text{-}C_{10}H_{21}SCF_3$	23
3	$(SCH_2CH_2COOH)_2$	1.0	80	23	$CF_3SCH_2CH_2COOH$	47

a) Acetonitrile was used as a solvent. b) Isolated yields which were calculated on the basis of substrates. c) In addition, 2,6-bis(trifluoromethyl)-4-*t*-butylphenol was isolated in 15.5% yield.

Table 3. Preparation of 1-Trifluoromethylnaphthalene from 1-Iodonaphthalene by CF_3 Copper Complex Generated In Situ from TNS-Tf and Copper

Run	Solvent	Temp/°C	Time/h	Yield/%[b]
1	$HMPA/CH_3CN(5/2)$[a]	100	18	86
2	$NMP/CH_3CN(5/2)$[a]	100	19	93
3	$DMF/CH_3CN(5/2)$[a]	100	19	88
4	CH_3CN	Reflux	19	52

a) The amount of acetonitrile is that of acetonitrile solution (0.5 mol dm^{-3}) of TNS-Tf used. b) ^{19}F-NMR yields.

Tf with 2.28 mmol of *N*-trifluoroacetylcystine gave 3.75 mmol of the product (82% based on the disulfide, Run 11). In this way, two trifluoromethyl groups of TNS-Tf were consumed in the insertion reaction. The trifluoromethionine derivative was prepared in a 71% yield by TNS-Tf (Run 12), whereas the yield by TNS-B was 30% only. This insertion reaction followed by hydrolysis provided an effectual method for the preparation of trifluoromethionine, a competitive inhibitor of methionine activation,[28] compared with the known method[29] starting from acrylaldehyde and gaseous trifluoromethanethiol because of easiness of operation, availability of the amino acid as a starting material, high yield, and short steps.

TNS-Tf is the first to make it possible to trifluoromethylate the uridine derivative directly, giving the biologically interesting 5-trifluoromethyluridine derivative (Run 13).[1] Our method is advantageous compared with the stepwise synthesis.[17]

The thermal trifluoromethyaltion with TNS-Tf was accomplished by heating an equimolar mixture of TNS-Tf and a substrate in acetonitrile in a sealed tube. The results are shown in Table 2 and are similar to the photochemical reaction.

Interestingly, it was found that an exothermic reaction occurred with evolution of gas when a solution (0.5 mol dm^{-3}) of TNS-Tf (1 equimol) in acetonitrile was added dropwise into a mixture of activated copper powder (2 equimol) in such solvents as HMPA, NMP, DMF, and acetonitrile at room temperature. This is a good example for high reactivity of TNS-Tf. The reaction mixture resulted in an almost homogeneous brown solution. Iodonaphthalene (0.4 equimol) was added into the brown solution and the reaction mixture was heated to give trifluoromethylnapthalene in a high yield without the formation of naphthalene. Advantageously, no reduction of iodine atom by copper occurred. It is due to the complete reaction of TNS-Tf with copper. Reduction of aromatic iodides by copper was reported in the trifluoromethylation with trifluoromethyl iodide and copper.[10] The results and reaction conditions are shown in Table 3. These facts

$$\text{TNS-Tf} \xrightarrow[\text{R.t.}]{\text{Cu}} CF_3\text{–Cu Complex} \xrightarrow[\Delta]{\text{ArI}} \text{Ar–}CF_3$$

suggested that the reaction of TNS-Tf with copper formed trifluoromethylcopper complex, because it has been well-known that trifluoromethylcopper reacted with iodoaromatics to give trifluoromethyl compounds.[12,30] There have been many reports about the methods for the formation of the copper.[6,7,10,12,21,30] It was demonstrated that trifluoromethylcopper in situ generated afforded high yields and wide application for the preparation of trifluoromethyl compounds, compared with the copper transiently formed.[12,30] The reaction of trifluoromethylcopper complex generated in situ from TNS-Tf with several kinds of haloaromatics was carried out and the results are summarized in Table 4. Trifluoromethyl compounds were prepared from iodo compounds in good yields, while bromo compounds gave poor yields of the products under our conditions. Dodecyl iodide did not afford the corresponding trifluoromethyl compound under our conditions, although it was reported that trifluoromethylcopper in situ generated from trifluoromethyl iodide and copper in HMPA at 120 °C was treated with decyl iodide to give 1,1,1-trifluoroundecane in a 48% yield.[12] Our method using TNS-Tf is advantageous in generating in situ the copper complex conveniently under very mild conditions compared with the known methods which needed high tempearture or pressure reaction and removal of excess or remaining copper by filtration in a dry box.[12,30]

Table 4. Trifluoromethylation of Haloaromatics by CF_3 Copper Complex from TNS-Tf

Run	Haloaromatics	Method[a]	Product[b]	Yield/%[c]
1	*p*-Iodonitrobenzene	A	*p*-CF_3-nitrobenzene	68
2	*p*-Iodoanisole	A(B)	*p*-CF_3-anisole	71(66)
3	*m*-Iodoanisole	B	*m*-CF_3-anisole	72
4	*o*-Iodoanisole	B	*o*-CF_3-anisole	88
5	*p*-Iodochlorobenzene	B	*p*-CF_3-chlorobenzene	74
6	*p*-Iodobromobenzene	B	*p*-CF_3-bromobenzene	53
7	*p*-Bromoanisole	A	*p*-CF_3-anisole	5
8	1-Bromonaphthalene	A(B)	1-CF_3-naphthalene	16(3)

a) Method A=Run 1 in Table 3, B=Run 2 in Table 3. b) Spectral data of products were in agreement with authentic samples. c) ^{19}F-NMR yields.

Table 5. Photochemical or Thermal Reaction with TNS-Nf

Run[a]	Substrate	Molar equiv of TNS-Nf	Condition	Time/h	Product[b]	Yield/%[c]
1	*p*-*t*-Butylphenol	1.0	*hν*	18	2-CF_3-4-*t*-butylphenol	25
					2-C_4F_9-4-*t*-butylphenol	20
2	*p*-*t*-Butylphenol	0.8	100°C	7.5	2-CF_3-4-*t*-butylphenol	22
					2-C_4F_9-4-t-butylphenol	42
3	*p*-Dimethoxybenzene	1.0	*hν*	18	2-CF_3-1,4-dimethoxybenzene	30
					2-C_4F_9-1,4-dimethoxybenzene	25
4	*p*-Dimethoxybenzene	0.8	100°C	13	2-CF_3-1,4-dimethoxybenzene	11
					2-C_4F_9-1,4-dimethoxybenzene	47

a) All the reactions were carried out in acetonitrile. b) See the experimental section for spectral data of new compounds. c) Isolated yields which were calculated on the basis of TNS-Tf.

We also synthesized *N*-trifluoromethyl-*N*-nitrosononafluoro-1-butanesulfonamide (TNS-Nf) in a 36% yield in a similar manner as TNS-Tf. The results of the thermal and photochemical reactions with *p*-*t*-butylphenol and *p*-dimethoxybenzene are shown in Table 5. In every case, two kinds of products, trifluoromethyl and nonafluorobutyl compounds were formed, indicating that both trifluoromethyl and nonafluorobutyl radicals were generated from TNS-Nf, probably, by homolytic fission. It suggested that both trifluoromethyl groups in TNS-Tf participated in the trifluoromethylation. The mass spectrum of the gas evolved from the photoreaction of TNS-Tf with *p*-*t*-butylphenol in acetonitrile (Run 3 in Table 1) indicated that nitrogen and hexafluoroethane were contanined in the gas as main components but dinitrogen monoxide wasn't. The formation of nitrogen and hexafluoroethane suggested the isomerization of TNS-Tf to the azo compound followed by decomposition

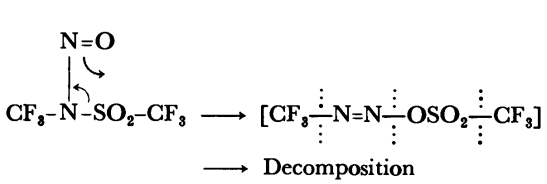

through the homolytic cleavage. It was reported that hydrocarbon analogues of nitrososulfonamides, *N*-alkyl-*N*-nitrosotoluenesulfonamides, easily isomerized to the corresponding azo compounds which decomposed through heterolytic fission.[31] Although the acetonitrile solution didn't contain triflic acid after the reaction, the solution became acidic. Probably it is due to the formation of sulfur trioxide as a by-product. It was reported that trifluoromethanesulfonyloxyl radical easily decomposed to release sulfur trioxide.[32]

Experimental

Melting and boiling points were uncorrected. ^1H NMR spectra were determined with a Varian HA-100 NMR spectrometer or a Varian EM 390 NMR spectrometer. ^{19}F NMR spectra were determined with a Varian XL-100A NMR spectrometer or a Hitachi R-20B NMR spectrometer. ^{19}F Chemical shifts are given in ppm upfield from trichlorofluoromethane as an internal standard. IR spectra were measured on a Jasco A-202 diffraction grating infrared spectrometer. Mass spectra were recorded on a Hitachi RMU-6MG spectrometer at 70 eV. GLC analyses were carried out with Ohkura 802 Gas Chromatograph, using a column (2 mm×3 m) packed with Silicone SE-30 (10%) on Chromosorb WAW DMCS. Riko Kagaku UVL-400P Hg lamp was used for the photoreaction. *N*,*N*-Dimethylformamide (DMF) used was distilled on a small amount of triphenylchlorosilane to remove amines contained, after drying with molecular sieve 3A.

Material. Trifluoronitrosomethane was prepared according to our method reported previously.[33]

Caution. Neat TNS-Tf or TNS-Nf must not be allowed to stand at room temperature because of possible violent decomposition and can be stored for a long time (more than one year) in a deep freezer (−20°C). As mentioned earlier, TNS-Tf can easily and safely be treated as an acetonitrile solution (1—0.5 mol dm^{-3}) at room temperature.

***N*-Trifluoromethyl-*N*-nitrosotrifluoromethanesulfonamide (TNS-Tf).** At −65 °C, trifluoronitrosomethane (16.1 g, 0.163 mol) was blown into a solution of hydroxylamine which was prepared by the treatment of hydroxylamine hydrochloride (10.9 g, 0.156 mol) with potassium *t*-butoxide (17.5 g, 0.156 mol) in 207 ml of a mixture of DMF/diethyl ether (4/1). An excess of the nitrosomethane was removed by flowing argon. After the introduction of 25.0 g (0.165 mol) of trifluoromethanesulfonyl fluoride, sodium hydride (50% in oil, 8.25 g, 0.172 mol) was added in several portions. All operations described above were performed at −65—−60 °C. The mixture was stirred for 20 h at −65 °C and warmed to −50 °C. At this temperature, pentane (20 ml) was added and then the mixture was allowed to warm to −20 °C. The mixture was poured into water and extracted with pentane (60 ml×3). The pentane solution was washed with water, dried ($MgSO_4$), and filtered. The filtrate (room temperature) was transfered to a trap cooled to −78 °C by trap-to-trap distillation in vacuo to remove high boiling materials (nujol and others) from the filtrate. Then the distillate was cooled to −90 °C—−100 °C. TNS-Tf crystallized from the solution and then was isolated as colorless crystals by removing the solvent with a syringe at the low temperature. Further purification by the trap-to-trap method in vacuo from −78 °C to −196 °C gave 22.3 g of colorless volatile crystals (58%); mp 3.2—4 °C; ^{19}F NMR ($CDCl_3$, ppm) 69.7 (3F, m, N-CF_3), 76.5 (3F, bs, SO_2CF_3); IR (neat, cm^{-1}) 1545 (N=O), 1415 (SO_2). Elemental analysis was not done because of instability at room temperature.

***N*-Trifluoromethyl-*N*-nitrosononafluoro-1-butanesulfonamide (TNS-Nf).** Trifluoronitrosomethane was allowed to react with hydroxylamine followed by the treatment with nonafluoro-1-butanesulfonyl fluoride in the same manner as the case of TNS-Tf. The reaction mixture was extracted with diethyl ether. The ethereal layer was washed with water till the aqueous layer was neutral (pH 6—7), dried ($MgSO_4$), filtered and then concentrated on an ice bath by using an aspirator. The residue (yellow oil) was purified by the trap-to-trap method at low temperature to give TNS-Nf as colorless liquid in a 36% yield. ^{19}F NMR ($CDCl_3$, ppm) 69.4 (3F, bs, CF_3N), 81.0 (3F, m, CF_3), 109.9 (2F, m, CF_2), 120.0 (2F, m, CF_2), 125.3 (2F, m, CF_2); IR (Neat, cm^{-1}) 1540 (N=O), 1420 (SO_2). Elemental analysis was not done because of instability at room temperature.

Photochemical Trifluoromethylation with TNS-Tf or -Nf. A Typical Experimental Procedure: A solution of 75 mg (0.50 mmol) of 4-*t*-butylphenol, 43.2 mg (0.50 mmol) of biacetyl, and 127.9 mg (0.52 mmol) of TNS-Tf in 2 ml of acetonitrile was degassed by a freeze-thaw cycle, sealed in a Pyrex tube equipped with a stopcock, and was irradiated under water bath cooling for 5 h with a 400W high pressure Hg lamp. The reaction mixture was chromatographed over silica gel (10% Et_2O/pentane) to give 24.9 mg (17%) of 2,6-Bis(CF_3)-4-*t*-butylphenol and 71 mg (65%) of 2-CF_3-4-*t*-butylphenol.

2,6-Bis(CF_3)-4-*t*-butylphenol: Oil; ^1H NMR ($CDCl_3$) δ=1.33 (9H, s, 3×CH_3), 5.93 (1H, broad peak, OH), 7.68 (2H, bs, ArH); ^{19}F NMR ($CDCl_3$, ppm) 61.2 (s, CF_3).

2,5-Bis(CF_3)-1,4-dimethoxybenzene: Mp 131—132 °C; ^1H NMR (CCl_4) δ=3.88 (6H, s, 2×CH_3), 7.13 (2H, s, ArH); ^{19}F NMR (CCl_4, ppm) 63.4 (s, CF_3); MS (*m/z*) 274 (M^+).

2,3-Bis(CF_3)-1,4-dimethoxybenzene: Mp 71—74 °C; ^1H NMR (CCl_4) δ=3.83 (6H, s, 2×CH_3), 7.08 (2H, s, ArH); ^{19}F NMR (CCl_4, ppm) 55.9 (s, CF_3); MS (*m/z*) 274 (M^+).

***N*-Acetyl-*O,O'*-dimethyl-6-CF_3-dopamine:** Mp 118.5—120.5 °C; ^1H NMR ($CDCl_3$) δ=1.95 (3H, s, CH_3CO), 2.93 (2H, t, $ArCH_2$), 3.48 (2H, m, CH_2N), 3.88 (3H, s, OCH_3), 3.90 (3H, s, OCH_3), 5.70 (1H, broad peak, NH), 6.81 (1H, bs, ArH), 7.07 (1H, s, ArH); IR (KBr, cm^{-1}) 3350 (NH), 1640 (C=O); MS (*m/z*) 291 (M^+).

***N*-Trifluoroacetyl-*S*-trifluoromethylcysteine:** Mp 69—72 °C; ^1H NMR ($CDCl_3$) δ=3.27—3.73 (2H, m, CH_2), 4.80—5.07 (1H, m, CH), 7.10—7.40 (1H, m, NH), 9.77 (1H, bs, COOH); IR (Nujol, cm^{-1}) 3325 (NH), 1720 (C=O).

***N*-Trifluoroacetyltrifluoromethionine Methyl Ester (*N*-Trifluoroacetyl-*S*-trifluoromethylhomocysteine):** Oil; ^1H NMR ($CDCl_3$) δ=2.27 (2H, m, CH_2), 2.93 (2H, t, *J*=7.5 Hz, CH_2), 3.80 (3H, s, OCH_3), 4.72 (1H, dt, *J*=6.0, 7.5 Hz, CH), 7.42 (1H, d, *J*=7.5 Hz, NH); IR (Neat, cm^{-1}) 3350 (NH), 1750 (sh) (C=O), 1720 (C=O). Found: C, 30.52; H, 2.85; N, 4.52%. Calcd for $C_8H_9NO_3SF_6$: C, 30.68; H, 2.90; N, 4.47%.

4-*t*-Butyl-2-C_4F_9-phenol: Oil; ^1H NMR (CCl_4) δ=1.33 (9H, s, 3×CH_3), 5.48 (1H, m, OH), 6.86 (1H, d, *J*=8.7 Hz, ArH), 7.30 (1H, d, *J*=2.4 Hz, ArH), 7.42 (1H, dd, *J*=8.7, 2.4 Hz, ArH); ^{19}F NMR (CCl_4, ppm) 81.0 (3F, t, *J*=10 Hz, CF_3), 107.6 (2F, m, CF_2), 122.3 (2F, m, CF_2), 125.3 (2F, m, CF_2); IR (Neat, cm^{-1}) 3450 (OH).

1,4-Dimethoxy-2-C_4F_9-benzene: Oil; ^1H NMR (CCl_4) δ=3.75 (3H, s, OCH_3), 3.78 (3H, s, OCH_3), 6.91 (3H, m, ArH); ^{19}F NMR (CCl_4, ppm) 81.4 (3F, bs, CF_3), 107.6 (2F, m, CF_2), 121.7 (2F, m, CF_2), 125.9 (2F, m, CF_2); IR (Neat, cm^{-1}) 2850 (OCH_3), 1590 (Ar), 1510 (Ar).

Thermal Trifluoromethylation with TNS-Tf or -Nf. A Typical Procedure: A solution of 300 mg (2.0 mmol) of 4-*t*-butylphenol and 491 mg (2.0 mmol) of TNS-Tf in 10 ml of acetonitrile was degassed by a freeze-thaw cycle, sealed in a Pyrex tube, and was heated at 110 °C for 22 h. The reaction mixture was cooled, poured into water, and extracted with diethyl ether. The ethereal layer was dried ($MgSO_4$) and concentrated in vacuo. The residue was chromatographed over silica gel (10% Et_2O/pentane) to give 88.7 mg (15.5%) of 2,6-bis(CF_3)-4-*t*-butylphenol and 300.4 mg (69%) of 2-CF_3-4-*t*-butylphenol.

Hydrolysis of *N*-Trifluoroacetyltrifluoromethionine Methyl Ester to Trifluoromethionine(*S*-trifluoromethylhomocysteine). 2 mol dm^{-3} Sodium hydroxide (1.5 ml) was dropwise added to a solution of 0.35 g of *N*-trifluoroacetyltrifluoromethionine methyl ester in 4 ml of methanol. The mixture was stirred for 5 h at room temperature. After evaporation of the solvent, a small amount of water was added to the residue and the solution was neutralized to pH=ca. 6 with hydrochloric acid. The resulting white precipitates were collected by filtration and washed with acetone. Yield 0.17 g (75%). Recrystallization from methanol gave pure crystals; mp 224—225 °C (with decomp) (lit, mp 229 with decomp),[29] ^{19}F NMR (CD_3OD, ppm) 40.9 (s, CF_3). Found: C, 29.74; H, 3.91; N, 6.78%. Calcd for $C_5H_8NO_2SF_3$: C, 29.56; H, 3.97; N, 6.89%.

Trifluoromethylation of Aromatic Iodides by Using TNS-Tf and Copper. A Typical Procedure: TNS-Tf (4 ml, 0.5 mol dm^{-3} in acetonitrile, 2.0 mmol) was dropwise added to a mixture of 250 mg (3.93 mmol) of activated copper powder[34] and 10 ml of dry *N*-methylpyrrolidinone (NMP) at room temperature under argon atmosphere. Then the mixture was stirred for 3 h at room temperature. 1-Iodonaphthalene (200 mg, 0.788 mmol) was added to the resulting brown solution which was almost homogeneous, and the mixture

was heated at 100 °C for 19 h. After addition of water and ether to the cooled reaction mixture, the resulting solution was filtered through Celite layer, and extracted with ether. Combined ethereal layer was washed with water, dried ($MgSO_4$), and concentrated at 40—50 °C under atmosphere. To the remaining crude product was added $CClBr_2CF_3$ (145.9 mg, 0.528 mmol) as an internal standard, and then the yield of 1-CF_3-naphthalene based on the relative intensity of ^{19}F NMR signal was 0.491 mmol (93%).

References

1) "Biomedical Aspects of Fluorine Chemistry," ed by R. Filler and Y. Kobayashi, Kodansha Ltd., Tokyo (1982).
2) A. E. Feiring, *J. Org. Chem.*, **44**, 2907 (1979).
3) A. Marhold and E. Klauke, *J. Fluorine Chem.*, **18**, 281 (1981).
4) J. H. Simons and C. J. Lewis, *J. Amer. Chem. Soc.*, **60**, 492 (1938).
5) G. A. Boswell, Jr., W. C. Ripka, R. M. Scribner, and C. W. Tullock, *Org. Reactions*, Vol. 21, 1 (1974).
6) Y. Kobayashi and I. Kumadaki, *Tetrahedron Lett.*, **1969**, 4095.
7) V. C. R. McLoughlin and J. Thrower, *Tetrahedron*, **25**, 5921 (1969).
8) V. N. Boiko, G. M. Shchupak, and L. M. Yagupol'skii, *J. Org. Chem., USSR*, **13**, 972 (1977).
9) D. Cantacuzene, C. Wakselman, and R. Dorme, *J. Chem. Soc., Perkin Trans. 1*, **1977**, 1365.
10) K. Hosokawa and K. Inukai, *Nippon Kagaku Kaishi*, **1977**, 1163.
11) Y. Kobayashi, I. Kumadaki, A. Ohsawa, S. Murakami, and T. Nakano, *Chem. Pharm. Bull.*, **26**, 1247 (1978).
12) Y. Kobayashi, K. Yamamoto, and I. Kumadaki, *Tetrahedron Lett.*, **1979**, 4071.
13) Y. Kobayashi and I. Kumadaki, *J. Chem. Soc., Perkin Trans. 1*, **1980**, 661.
14) T. Kitazume and N. Ishikawa, *Chem. Lett.*, **1981**, 1337, 1679; ibid, **1982**, 137, 1453.
15) V. I. Popov, V. N. Boiko, and L. M. Yagupol'skii, *J. Fluorine Chem.*, **21**, 365 (1982).
16) T. Fuchikami and I. Ojima, *Tetrahedron Lett.*, **25**, 303 (1984).
17) Y. Kobayashi, I. Kumadaki, and K. Yamamoto, *J. Chem. Soc., Chem. Commun.*, **1977**, 536.
18) N. J. O'Reilly, M. Maruta, and N. Ishikawa, *Chem. Lett.*, **1984**, 517.
19) C. J. Brook, P. L. Coe, A. E. Pedler, and J. C. Tatlow, *J. Chem. Soc., Perkin Trans. 1*, **1978**, 202.
20) L. Hein and D. Cech, *Z. Chem.*, **17**, 415 (1977).
21) K. Matsui, E. Tobita, M. Ando, and K. Kondo, *Chem. Lett.*, **1981**, 1719.
22) L. M. Yagupol'skii, V. N. Kondratenko, and G. N. Timofeeva, *J. Org. Chem., USSR*, **20**, 115 (1984).
23) T. Umemoto and O. Miyano, *Tetrahedron Lett.*, **23**, 3929 (1982).
24) T. Umemoto and O. Miyano, *J. Fluorine Chem.*, **22**, 91 (1983); *Nippon Kagaku Kaishi*, **1985**, 2205.
25) J. E. Huheey, *J. Phys. Chem.*, **69**, 3284 (1965).
26) L. F. Fieser and M. Fieser, "Textbook of Organic Chemistry," Maruzen Company, Ltd., Tokyo (1952), p. 442.
27) K. L. Kirk, H. Kimoto, and S. Fujii, 7th Symposium on Fluorine Chemistry of Japan (Okayama), Oct. 14, 1981, Abstract pp. 8—9; Kimoto reported that *N*-acetyl-*O*,*O'*-dimethyl-6-CF_3-dopamine was synthesized in a 32% yield (based on CF_3I) by irradiating the solution of *N*-acetyl-*O*,*O'*-dimethyldopamine (2 molar equiv), CF_3I (1 molar equiv), and Et_3N (1 molar equiv) in methanol for 3 d using a low pressure Hg lamp.
28) W. A. Zygmunt and P. A. Tavormina, *Can. J. Microbiol.*, **12**, 143 (1966).
29) R. L. Dannley and R. G. Taborsky, *J. Org. Chem.*, **22**, 1275 (1957).
30) V. N. Kondratenko, E. P. Vechirko, and L. M. Yagupol'skii, *Synthesis*, **1980**, 932.
31) E. H. White, *J. Amer. Chem. Soc.*, **77**, 6011 (1955).
32) J. Foropoulos, Jr., and D. D. DesMarteau, *Inorg. Chem.*, **23**, 3720 (1984).
33) T. Umemoto and H. Tsutsumi, *Bull. Chem. Soc. Jpn.*, **56**, 631 (1983).
34) R. Q. Brewster and T. Groening, *Org. Synth.*, Coll. Vol. 2, 445 (1948).

 © 1986 The Chemical Society of Japan Bull. Chem. Soc. Jpn., 59, 453—456 (1986)

Isolation of Dithiolanylium Salts and Their Conversion to Ketene Dithioacetals and Ortho Esters

Tadashi Okuyama,* Wataru Fujiwara, and Takayuki Fueno
Faculty of Engineering Science, Osaka University, Toyonaka, Osaka 560
(Received September 6, 1985)

Various 2-substituted 1,3-dithiolan-2-ylium perchlorates (**1**) were prepared by the reaction of 1,2-ethanedithiol with acyl chlorides in the presence of perchloric acid. Treatments of **1** with triethylamine gave 2-alkylidene-1,3-dithiolane (**2**) when the 2-substituent was a primary or secondary alkyl group. 2-Aryl derivatives of **1** were converted to ortho esters by the reaction with methanol in the presence of silver nitrate. 1,3-Dithian-2-ylium perchlorates and 2-alkylidene-1,3-dithianes were also prepared similarly from 1,3-propanedithiol.

We previously described a simple method of preparation of 2-methyl-1,3-dithiolan-2-ylium perchlorate from the reaction of 1,2-ethanedithiol with acetic anhydride in the presence of perchloric acid (Eq. 1).[1] This is extended to a general procedure by using an acyl chloride as one of starting materials (Eq. 2).

$$2(CH_3CO)_2O + HSCH_2CH_2SH + HClO_4 \longrightarrow \underset{\textbf{1a}}{CH_3\text{-}C_3H_4S_2^+}\,ClO_4^- + 3CH_3CO_2H \quad (1)$$

$$RCOCl + HSCH_2CH_2SH + HClO_4 \longrightarrow \underset{\textbf{1}}{R\text{-}C_3H_4S_2^+}\,ClO_4^- + HCl + H_2O \quad (2)$$

1 **a**, R = CH_3 **e**, R = $C_6H_5CH_2$
b, R = C_2H_5 **f**, R = C_6H_5
c, R = $(CH_3)_2CH$ **g**, R = *p*-$CH_3OC_6H_4$
d, R = $(CH_3)_3C$

The isolated salts can easily be converted to ketene dithioacetals when R is a primary or secondary alkyl group (Eq. 3) and to ortho esters when R is an aryl group (Eqs. 4 and 5).

$$\mathbf{1} + Et_3N \longrightarrow \underset{\textbf{2}}{R'R''C_3H_2S_2} + Et_3NHClO_4 \quad (3)$$

2 **a**, R′ = R″ = H
b, R′ = H, R″ = CH_3
c, R′ = R″ = CH_3
d, R′ = H, R″ = C_6H_5

$$\mathbf{1} + CH_3OH + Et_3N \longrightarrow \underset{\textbf{3}}{RC(OCH_3)S_2H} + Et_3NHClO_4 \quad (4)$$

$$\mathbf{3} + 2CH_3OH + 2AgNO_3 + 2Et_3N \longrightarrow \underset{\textbf{4}}{RC(OCH_3)_3} + AgSCH_2CH_2SAg + 2Et_3NHNO_3 \quad (5)$$

Results and Discussion

When equimolar amounts of 1,2-ethanedithiol and isobutyryl chloride were mixed together at room temperature, reaction gradually proceeded with some evolution of HCl gas. Pyridine was added in the final stage of the reaction to neutralize the mixture. A main product isolated was 2-isopropylidene-1,3-dithiolane (**2c**) instead of the thiocarboxylate expected. The monothio ester initially formed is cyclized.[2] The cyclization must be catalyzed by the HCl which is produced in the initial reaction (Eq. 6), although it partly escapes as a gas from the mixture.

$$RCOCl + HSCH_2CH_2SH \longrightarrow RCOSCH_2CH_2SH$$
$$+ HCl \rightleftharpoons R\text{-}C(^{+}OH)(HS)\text{-}S\text{-}C_2H_4 + Cl^- \rightleftharpoons R\text{-}CH(HO)\text{-}S\text{-}C_2H_4^+$$
$$+ Cl^- \rightleftharpoons R\text{-}CH(^{+}H_2O)\text{-}S\text{-}C_2H_4 + Cl^- \rightleftharpoons \underset{\textbf{1}}{R\text{-}C_3H_4S_2^+} + Cl^- + H_2O \quad (6)$$

The pyridine must have acted as a base to abstract a proton from the β carbon of the carbocation but not to neutralize the HCl in the above example.

In order to isolate the carbocation as a salt from this reaction, perchloric acid (70%) was added to compensate the HCl escaped and to facilitate the cyclization. Carbenium perchlorates are usually more stable than the chlorides. Acetic anhydride was used to remove the water and to dissolve the salt. Dry ether was then added to reprecipitate the pure salt. Organic impurities which are soluble in ether are removed in this stage. All the treatments can satisfactorily be done in air and the yellow crystals obtained are practically pure as judged from the NMR spectra.

Salts of dithio carbocations were previously prepared either by hydride transfer from dithioacetals to trityl cation[3] or by dissociation of ortho thio esters.[4–6] The present new procedure involves acid-catalyzed cyclization of thiocarboxylates derived from the dithiol.

Cyclization of acyl derivatives has been used to prepare oxo carbocations.[7,8] In these cases, cyclizing agents may promote formation of the primary carbocations which attack the carbonyl oxygen (Eqs. 7 and 8).

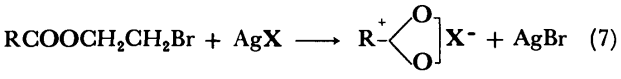

$$RCOOCH_2CH_2Br + AgX \longrightarrow R\text{-}\overset{+}{C}(O)O]X^- + AgBr \quad (7)$$

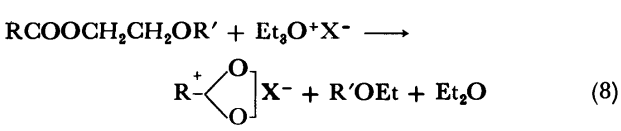

$$RCOOCH_2CH_2OR' + Et_3O^+X^- \longrightarrow R\text{-}\overset{+}{C}(O)O]X^- + R'OEt + Et_2O \quad (8)$$

In the sulfur analogue, the mercapto group is nucleophilic enough even in strongly acidic media to attack the carbonyl carbon which is activated by acid catalysis. A closely related example found in the literature is formation of 1,3-benzodithiolylium salts from the reaction of 1,2-benzenedithiol with acyl chlorides (Eq. 9).[9]

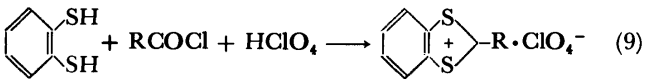

$$\text{1,2-benzenedithiol} + RCOCl + HClO_4 \longrightarrow \text{1,3-benzodithiolylium}\cdot ClO_4^- \quad (9)$$

These unsaturated carbocations are considered to be stable because of aromatic 10π electron delocalization and have been isolated by various methods.[10]

When the dithio carbocations (**1a—c**) carrying a primary or secondary alkyl group were treated with methanol, the deprotonated product **2** was obtained as a main product rather than the methanol adduct **3**. Deprotonation from the β carbon occurs more easily than the nucleophilic reaction. This is not unexpected since we have found from kinetic investigations that deprotonation competes well with hydration in aqueous solution[11–15] and even the former predominates in some cases.[16]

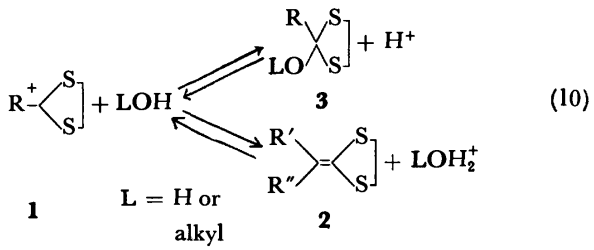

$$\underset{\mathbf{1}}{R\text{-}\overset{+}{C}(S)S]} + LOH \rightleftharpoons \underset{\mathbf{3}}{R\text{-}C(OL)(S)S} + H^+ \quad (10)$$

$$\mathbf{1} + LOH \rightleftharpoons \underset{\mathbf{2}}{R'R''C(S)S} + LOH_2^+$$

L = H or alkyl

Thus, ketene dithioacetals **2** were prepared quantitatively (as seen by NMR spectra of crude product mixtures) by treating **1** with bases, tertiary amines. Typical procedures are given in Experimental Section.

Ketene dithioacetals are used as versatile intermediates for organic syntheses but general procedures for syntheses of this class of compounds are rather elaborate.[17,18] The present simple procedure starting from readily available reagents would be useful.

The recent two reports[19,20] of new methods for preparation of aryl ortho esters prompted us to examine the possibility of the carbocations **1** leading to this class of compounds. The carbocation **1** derived from benzoyl chloride gave the 2-methoxy derivative **3** by reaction with methanol (Eq. 4).[21] This cyclic ortho thioester **3** could be converted to trimethyl ortho ester **4** by the treatment with two equivalents of $AgNO_3$ in methanol in the presence of excess base (Eq. 5). This is a modification of the method of Breslow[19] where ortho trithioesters are used as a starting material. The present method requires a smaller amount (2/3) of $AgNO_3$ and is much simpler than that of Breslow[19] since preparation of ortho trithioesters is very cumbersome with formation of a large amount of gel during workup which arises from metal halide used.[22] The intermediate ortho thio ester **3** is not necessarily isolated in the present procedure. The carbocation salts **1**, which are just filtered, washed with ether, and still wet, can directly be treated with $AgNO_3$ in methanol to afford the final ortho ester **4** in a satisfactory yield. The 2-*t*-butyl cation **1d** gave the ortho ester **4d** in a low yield.

Derivatives of 1,3-dithiane seem to be prepared in a similar way. Reaction of 1,3-propanedithiol with isobutyryl chloride afforded a 1,3-dithian-2-ylium ion which absorbs light at 311 nm. The salt was then converted to 2-isopropylidene-1,3-dithiane by treatment with triethylamine. Other examples were not examined in detail but brief preliminary experiments seem to give in general satisfactory results.

Experimental

Typical procedures are given below. Other derivatives were obtained in the same way. Spectral data and boiling points are summarized in Tables 1 and 2. Temperatures are not

Table 1. Spectral Data of 2-Substituted 1,3-Dithiolan-2-ylium Perchlorates

No.	Substituent	NMR Chemical Shift/ppm[a]	λ_{max}/nm ($10^4\varepsilon$)[b]
	H[c]	4.50(s, 4H), 11.35(s, 1H)	333(0.76)
1a	CH_3	3.22(s, 3H), 4.57(s, 4H)	330(0.80)
1b	C_2H_5	1.62(t, 3H), 3.45(q, 2H), 4.46(s, 4H)	329(0.79)
1c	$(CH_3)_2CH$	1.63(d, 6H), 3.74(m, 1H), 4.47(s, 4H)	331(0.70)
1d	$(CH_3)_3C$	1.68(s, 9H), 4.46(s, 4H)	331(0.77)
1e	$C_6H_5CH_2$	4.40(s, 4H), 4.57(s, 2H), 7.4(broad s, 5H)	332(0.78)
1f	C_6H_5	4.48(s, 4H), 7.6—8.1(m, 5H)	342(2.65)
1g	*p*-$CH_3OC_6H_4$	4.12(s, 3H), 4.36(s, 4H), 7.20(d, 2H), 8.25(d, 2H)	402

a) From internal TMS in CF_3CO_2D(H). b) In $HClO_4$ solution. c) Ref. 21.

Table 2. Boiling Points and Spectral Data of 2-Alkylidene-1,3-dithiolanes ( )

R′	R″	Yield/%[a]	Bp/°C(mmHg)	NMR Chemical Shift/ppm[b]	λ_{max}/nm($10^4\varepsilon$)[c]
H	H	36	55(9)	3.31(s, 4H), 5.00(s, 2H)[d]	243(0.75)
H	CH_3	55	85(10)	1.71(d, 3H), 3.25(s, 4H), 5.40(q, 1H)	235(0.75)
CH_3	CH_3	63	80—81(4)	1.80(s, 6H), 3.31(s, 4H)	230(0.78)
H	C_6H_5	48	143—145(2)	3.1—3.6(m, 4H), 6.49(s, 1H), 7.0—7.4(m, 5H)	304(1.88)

a) Based on the acyl chloride used. b) In CCl_4. c) In aqueous solution. d) In CS_2.

corrected. Proton NMR spectra were recorded on a JNM C60-HL spectrometer.

2-Ethyl-1,3-dithiolan-2-ylium Perchlorate (1b). To an ice-cooled mixture of propionyl chloride (25 mmol) and 1,2-ethanedithiol (25 mmol), 70% perchloric acid (2.5 ml) was added dropwise under stirring. After 5-h reaction on an ice bath, acetic anhydride (15 ml) was added carefully (exothermic) to the viscous mixture. Dry ether (ca. 50 ml) was then added to precipitate the product, which was collected on a sintered-glass filter, washed three times with ether, and dried under reduced pressure. The yellow crystals obtained (4.8 g, 80%) were practically pure as seen by the NMR spectroscopy (Table 1).

2-Phenyl-1,3-dithiolan-2-ylium Perchlorate (1f). 1,2-Ethanedithiol (25 mmol) was added to benzoyl chloride (25 mmol) and stirred on an ice bath for 1 h. Then, 70% perchloric acid (3 ml) was added to the mixture. Stirring was continued for another 1 h at 0 °C. The solidified mixture was dissolved with acetic anhydride (15 ml) and reprecipitated by adding dry ether (50 ml). The yellow crystals were collected on a sintered-glass filter, washed with ether, and dried under vacuum. Yield was 6.2 g (88%).

2-Ethylidene-1,3-dithiolane (2b). The salt of **1b** prepared from 25 mmol of propionyl chloride was dissolved in dry acetonitrile (30 ml). The wet salt was used without drying. The solution was added to excess triethylamine (6 ml). The products were taken up in ether, washed with water, and dried over $MgSO_4$. After the evaporation of the ether, the remaining liquid was distilled. Yield, 1.8 g (55%). Anal. ($C_5H_8S_2$) C, H.

Trimethyl *p*-Methoxyorthobenzoate (4g). The perchlorate **1g**, which was prepared from *p*-methoxybenzoyl chloride (25 mmol) and still wet with ether, was dissolved in acetonitrile (30 ml), and methanol (100 ml) and triethylamine (14 ml) were added to the solution. The solution of silver nitrate (7 g) in acetonitrile (50 ml) was then introduced under stirring. After 10-h stirring at room temperature, precipitates were removed by filtration and the filtrate was concentrated to ca. 20 ml on a rotary evaporator. The products were taken up in ether, washed with aqueous $NaHCO_3$, dried over $MgSO_4$, and distilled. Yield, 2.8 g (53%). Bp 114—116 °C (5 mmHg†) [lit,[23] 114—115 °C (5 mmHg)].

Trimethyl Orthopivalate (4d). A solution of $AgNO_3$ (20 mmol) in CH_3CN (20 ml) was added to a solution of triethylamine (3.5 ml) and 2-*t*-butyl-2-methoxy-1,3-dithiolane **3d** (10 mmol) prepared from **1d**[24] in methanol (50 ml). After 12-h of stirring at room temperature, precipitates were filtered away and the filtrate was concentrated to ca. 10 ml. The products were taken up in ether, washed with aqueous $NaHCO_3$, and dried over $MgSO_4$. After evaporation of the ether, the residues were distilled with a Kugelrohr. The fraction collected at the oven temperature of ca. 80 °C and 50 mmHg was solidified on cooling (yield 0.1 g). ^1H NMR (CCl_4) δ=0.92 (s, 9H), 3.36 (s, 9H). Anal. ($C_8H_{18}O_3$) C, H.

2-Isopropylidene-1,3-dithiane. To a mixture of isobutyryl chloride (10 mmol) and 1,3-propanedithiol (10 mmol), 70% $HClO_4$ (1 ml) was added under stirring at room temperature. After 15-h stirring, acetic anhydride (10 ml) and then dry ether (50 ml) were added. Yellow precipitates collected on a sintered-glass filter were washed with ether and dissolved in CH_3CN (20 ml). The solution was added to triethylamine (3 ml). Workup in a similar way to **2b** and the Kugelrohr distillation gave 0.88 g (55%) of the fraction boiling at ca. 95 °C and 5 mmHg. ^1H NMR and IR spectra agree with those reported.[25]

†1 mmHg=133.322 Pa.

References

1) T. Okuyama, *Tetrahedron Lett.*, **23**, 2665 (1982).

2) In order to obtain monothioester base should be added in advance although a considerable amount of bis(thioester) $RCOSCH_2CH_2SCOR$ is inevitably formed. Pure mono ester can be obtained by hydrolysis of the isolated salt **1**.

3) E. J. Corey and S. W. Wallinsky, *J. Am. Chem. Soc.*, **94**, 8932 (1972).

4) R. A. Olofson, S. W. Wallinsky, J. P. Marino, and J. L. Jernow, *J. Am. Chem. Soc.*, **90**, 6554 (1968).

5) K. Sakamoto, N. Nakamura, M. Ōki, J. Nakayama, and M. Hoshino, *Chem. Lett.*, **1977**, 1133.

6) L. Hevesi, S. Desauvage, B. George, G. Evrard, P. Blanpain, A. Michel, S. Harkema, and G. J. van Hummel, *J. Am. Chem. Soc.*, **106**, 3784 (1984).

7) H. Meerwein, V. Hederich, and K. Wunderlich, *Arch. Pharmaz.*, **291/63**, 541 (1958).

8) D. J. Raber and W. C. Guida, *Syntheses*, **1974**, 808.

9) L. Sodar and R. Wizinger, *Helv. Chim. Acta*, **42**, 1739 (1959) ; R. Wizinger and D. Dürr, ibid., **46**, 2167 (1963); P. Appriou and R. Guglielmetti, *Bull. Soc. Chim. Fr.*, **1974**, 510.

10) See for reviews, H. Prinzbach and E. Futterer, *Adv. Heterocycl. Chem.*, **7**, 39 (1966); N. Lozac'h and M. Stavaux, ibid., **27**, 151 (1980).

11) T. Okuyama and T. Fueno, *J. Am. Chem. Soc.*, **102**, 6590 (1980); **105**, 4390 (1983).

12) T. Okuyama, S. Kawao, and T. Fueno, *J. Am. Chem. Soc.*, **105**, 3320 (1983).

13) T. Okuyama, S. Kawao, and T. Fueno, *J. Org. Chem.*, **49**, 85 (1984).

14) T. Okuyama, S. Kawao, W. Fujiwara, and T. Fueno, *J. Org. Chem.*, **49**, 89 (1984).

15) T. Okuyama, *J. Am. Chem. Soc.*, **106**, 7134 (1984).

16) T. Okuyama, M. Toyoda, and T. Fueno, *Can. J. Chem.*,

in press.
17) M. Kolb, "The Chemistry of Ketene, Allene and Related Compounds, Part 2," ed by S. Patai, Wiley, New York (1980), Chap. 16.
18) Y. Nagao, K. Seno, and E. Fujita, *Tetrahedron Lett.*, **1979**, 4403.
19) R. Breslow and P. S. Pandey, *J. Org. Chem.*, **45**, 740 (1980).
20) R. A. McClelland, G. Patel, and P. W. K. Lam, *J. Org. Chem.*, **46**, 1011 (1981).
21) T. Okuyama, W. Fujiwara, and T. Fueno, *J. Am. Chem. Soc.*, **106**, 657 (1984).
22) L. C. Rinzema, J. Stoffelsma, and J. F. Arens, *Recl. Trav. Chin. Pays-Bas*, **78**, 354 (1959).
23) H. Kwart and M. B. Price, *J. Am. Chem. Soc.*, **82**, 5123 (1960).
24) T. Okuyama and T. Fueno, *J. Am. Chem. Soc.*, **107**, 4224 (1985).
25) D. Seebach, M. Kolb, and B.-T. Gröbel, *Chem. Ber.*, **106**, 2277 (1973).

 © 1986 The Chemical Society of Japan Bull. Chem. Soc. Jpn., 59, 457—463 (1986)

α,β-Epoxy Sulfoxides as Useful Intermediates in Organic Synthesis. III.[1] A Novel Synthesis of α-Amino Ketones and α-Amino Aldehydes by Aminolysis of α,β-Epoxy Sulfoxides

Tsuyoshi SATOH, Youhei KANEKO, Kiichi SAKATA, and Koji YAMAKAWA*
Faculty of Pharmaceutical Sciences, Science University of Tokyo, Ichigaya-funagawara-machi, Shinjuku-ku, Tokyo 162
(Received September 7, 1985)

Aminolysis of α,β-epoxy sulfoxides, easily prepared from 1-chloroalkyl phenyl sulfoxides or chloromethyl phenyl sulfoxide and carbonyl compounds, with alkyl- or arylamines afforded α-amino ketones or α-amino aldehydes in good yields. Treatment of thus obtained α-arylamino ketones with weak Lewis acid led to 2,3-disubstituted indoles.

α-Amino ketones (**5**) are valuable synthetic intermediates for drugs[2,9] or useful as building blocks for nitrogen containing heterocyclic compounds.[3] In contrast to the impressive development of the methods for the synthesis of β-amino ketones, such as Mannich reaction[4] or Michael addition of amines to α,β-unsaturated carbonyl compounds,[5] only limited numbers of methods for the preparation of α-amino ketones (**5**) are reported. Five main methods have so far been reported but they have some drawbacks. The S_N2 type displacement of α-halo ketones with amines[3,6] is useful only when regioselectively halogenated carbonyl compounds are easily available and at the same time, this reaction usually gives relatively poor yields. Reduction of acyl cyanides[7] gives only α-acylmethylamines and the Neber rearrangement[8] gives only α-amino ketones having no substituent on the nitrogen atom. Aminolysis of enediol silyl ethers[2] was reported to give less than 45% yield of α-amino ketones. Aminolysis of α,β-epoxy ethers,[9] which are synthesized from α-halo ketones, seems to be a relatively good method but only synthesis of phenyl α-amino ketones was reported.

As a consequence of the usefulness of α-amino ketones, exploration of a new procedure for the synthesis of them from readily available precursors is still required. Recently we have reported a method for the synthesis of ketones, aldehydes, and α-sulfenylated carbonyl compounds from α,β-epoxy sulfoxides (**4**).[1,10] Here we report, in detail, a new and efficient method for a synthesis of α-amino ketones and α-amino aldehydes[11] from α,β-epoxy sulfoxides and an application of this method to a synthesis of 2,3-disubstituted indoles.

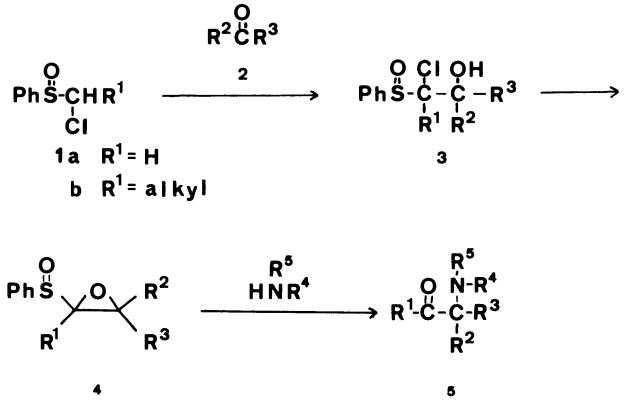

Scheme 1.

Results and Discussion

Synthesis of α-Alkylamino Ketones and α-Alkylamino Aldehydes. α,β-Epoxy sulfoxides (**4**)[12] are very easily prepared in good overall yields from *chloromethyl phenyl sulfoxide* (**1a**) *or 1-chloroalkyl* phenyl sulfoxides (**1b**) and carbonyl compounds (**2**) through chlorohydrins (**3**). Few synthetic methods have already been reported[13] by using α,β-epoxy sulfoxides. We have found that the β-carbon of α,β-epoxy sulfoxides (**4**) is highly reactive to various alkyl- and arylamines to afford α-amino ketones (**5**) in good to excellent yields.[11]

Seven types of α,β-epoxy sulfoxides (**4a—g**) are selected to clarify the reactivity of **4** with various amines. The epoxides **4a—c** and **4g** have two isomers, which are expressed as L and P,[14] respectively, but the stereochemistries have not yet been determined. The epoxide (**4g**) used in this study is a mixture of L and P.

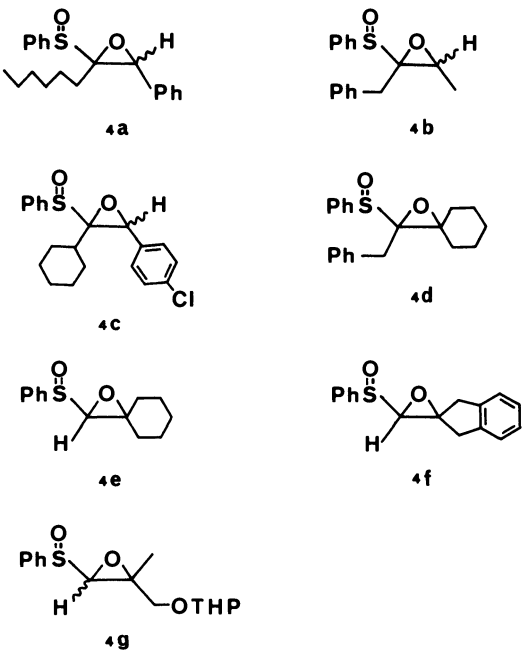

Table 1. α-Amino Ketones and Aldehydes from α,β-Epoxy Sulfoxides with Aliphatic Amines

Run	Epoxy Sulfoxide	Amine[a]	Solvent	Temp	Time	α-Amino Ketone	Yield[b] %
1	4a L	A	—	r.t.	3 h	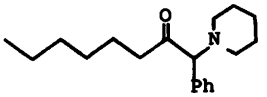 5a	97
	P	A	—	r.t.	21 h		100
2	4a L	B	—	r.t.	4 h	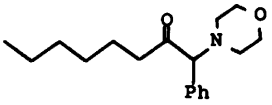 5b	100
	P	B	—	r.t.	23 h		99
	P	B	—	80°C	90 min		90
	P	B	DMSO	80°C	100 min		100
	P	B	HMPA	80°C	150 min		94
3	4a L	C	HMPA	r.t.	27 h	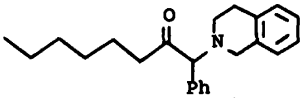 5c	89
	P	C	HMPA	110°C	40 min		100
4	4b L	A	—	r.t.	20 min	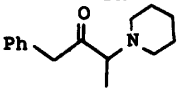 5d	92
	P	A	—	r.t.	2.5 h		100
5	4c L	A	—	100°C	2 h	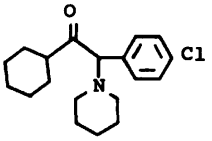 5e	97
	P	A	—	100°C	12 h		85
6	4c L	D	—	80°C	1 h	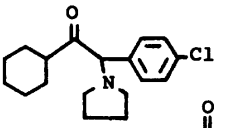 5f	100
	P	D	—	80°C	6 h		85
7	4c L	C[c]	DMSO	100°C	7 h	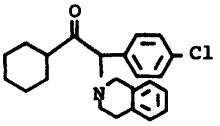 5g	94
	P	C[c]	DMSO	100°C	20 h		80
8	4d	A	—	100°C	6 h	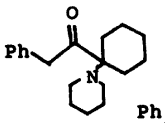 5h	76
9	4d	D	—	80°C	4 h	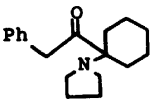 5i	100
10	4a L	E	—	r.t.	8 d	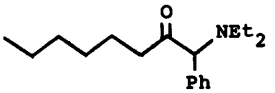 5j	96
	P	E[d]	DMSO	50°C	31 h		44
11	4a L	F[e]	DMSO	60°C	3 h	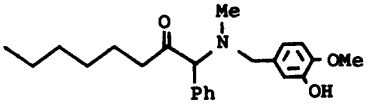 5k	53
	P	F[e]	DMSO	60°C	5 h		52
12	4a L	G[d]	DMSO	55°C	1 h	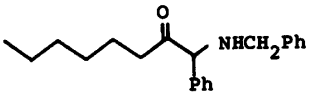 5l	72
	P	G[d]	DMSO	55°C	1 h		73
13	4b P	F[f]	DMSO	r.t.	8 h	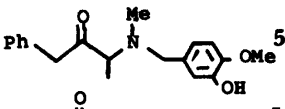 5m	80
14	4b P	E	—	r.t.	3 d	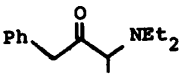 5n	96
15	4e	A	—	90°C	2 h	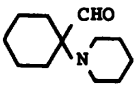 5o	78
16	4f	A	—	90°C	1 h	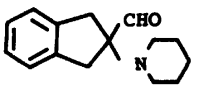 5p	83

Table 1. (Continued)

Run	Epoxy Sulfoxide	Amine[a]	Solvent	Temp	Time	α-Amino Ketone	Yield[b] %
17	**4g**	A	—	r.t.	1 d	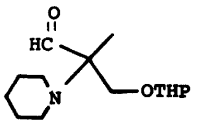	**5q** 71

a) A: piperidine, B: morpholine, C: 1,2,3,4-tetrahydroisoquinoline, D: pyrrolidine, E: diethylamine, F: *N*-methyl-3-hydroxy-4-methoxybenzylamine, G: benzylamine. b) Isolated yields after silica gel column chromatography. c) Forty equivalents of amine was used and the concentration of the epoxy sulfoxide was 0.07 M. d) Forty-five equivalents of amine was used. e) Three equivalents of amine was used. f) Five equivalents of amine was used.

The reaction was simply conducted in an amine without solvent or in dimethyl sulfoxide (DMSO) or hexamethylphosphoric triamide (HMPA) as a solvent (0.5M† concentration of epoxy sulfoxide and 10 equivalents of amines are used unless otherwise noted) under nitrogen atmosphere.

The results of the reaction of α,β-epoxy sulfoxides (**4**) with aliphatic amines are summarized in Table 1. As shown in Table 1, aliphatic amines especially cyclic amines are very reactive to α,β-epoxy sulfoxides (**4**) giving α-amino ketones under the mild conditions in good to excellent yields. Isomers L and P showed some differences in the reactivity toward the amines but these differences are not essential problem for the practical use of this method. The epoxide having a cyclohexane ring in R^1 (**4c**) reacted slowly with amines than those having normal alkyl groups in R^1 (**4a** and **b**) due to a steric hindrance on the β-carbon of the epoxide by cyclohexyl group (see runs 1—7). The dipolar aprotic solvents known to be effective for nucleophilic bimolecular reactions[15] were used but we did not observe any solvent effect. The other conditions reported to be effective for opening of epoxides, such as the reaction with aminosilanes[16] or the reaction at alumina surface[17] were not effective in this reaction.

The results of the reaction of α,β-epoxy sulfoxides with acyclic alkylamines are summarized in runs 10 to 14. As acyclic amines are known to be less nucleophilic than cyclic amines, these reactions required much longer reaction time than those in cyclic amines and the yields were moderate to good (compare runs 1—4 with runs 10—14). The amine having a phenolic hydroxyl group, *N*-methyl-3-hydroxy-4-methoxybenzylamine, also reacted with **4a** and **b** to afford **5k** and **5m**, respectively, in moderate to good yields (runs 11 and 13). Monoalkylamines usually gave a complex mixture but only benzylamine afforded an α-benzylamino ketone (**5l**) in about 70% yield (run 12). Runs 15 to 17 show the results of the reaction of α-unsubstituted α,β-epoxy sulfoxides (**4e—g**) with piperidine to afford α-piperidino aldehydes (**5o—q**). Such complex amino aldehydes are usually very difficult to obtain but the present procedure gave α-piperidino aldehyde under the mild conditions without any problem in 70—80% yields.

Synthesis of α-Arylamino Ketones, Aldehydes and an Application of the Procedure to a Synthesis of 2,3-Disubstituted Indoles. Table 2 shows the results of the reaction of **4a**, **b**, **e**, **f** with arylamines. Since usually arylamines have a lower nucleophilic property than that of alkylamines, the reaction of arylamines with **4** required a higher temperature but the yields are still very good. α-Anilino aldehydes (**5x**) and (**5y**) were also obtained in excellent yields. In these cases it is noteworthy that aniline was very reactive to **4e** and **4f** (see Table 1, runs 15 and 16)

The present procedure has proved of value by transforming the products to heterocyclic compounds according to Scheme 2. α-Arylamino ketones have already been transformed to tetrahydrocarbazoles[3b] or substituted indoles[3c,18] but in these cases, α-arylamino ketones were derived from α-chloro ketones in about 50% yield. In our study, *N*-(1-methyl-2-oxo-3-phenylpropyl)aniline (**5u**) was heated with magnesium

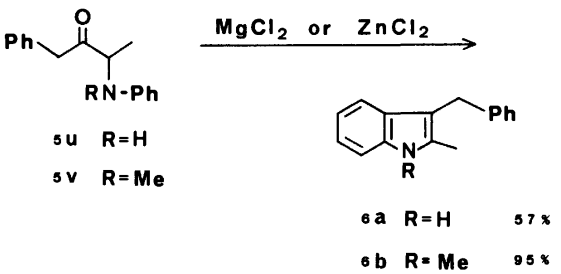

Scheme 2.

chloride in Ethylcellosolve at 130°C for 1.5 h to afford 3-benzyl-2-methylindole (**6a**; mp 89—90°C)[19] in 57% yield. Similarly, **5v** was heated with zinc chloride (in this case magnesium chloride was not effective) in Ethylcellosolve at 120°C for 3 h to give 3-benzyl-1,2-dimethylindole (**6b**; mp 54—55°C)[20] in 95% yield. Since, the α,β-epoxy sulfoxide (**4b**) was synthesized from benzyl bromide, chloromethyl phenyl sulfoxide, and acetaldehyde in three steps in over 90% yield[10a] the indole (**6b**) was synthesized from these three components and *N*-methylaniline in five steps overall

† 1 M=1 mol dm^{-3}.

Table 2. α-Arylamino Ketones and Aldehydes from α,β-Epoxy Sulfoxides with Arylamines[a)]

Run	Epoxy sulfoxide	Amine[a)] (equiv)	Temp	Time	α-Arylamino Ketone or Aldehyde	Yield[b)] %
1	**4a** L	H (50)	100°C	1 h	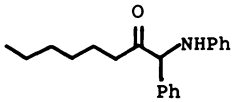 **5r**	97
	P	H (50)	100°C	2 h		81
2	**4a** L	I (90)	100°C	2 h	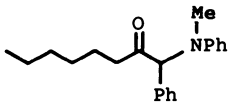 **5s**	73
	P	I (90)	100°C	2 h		56
3	**4a** L	J (5)	100°C	3 h	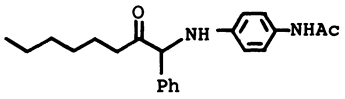 **5t**	63
	P	J (5)	100°C	5 h		47
4	**4b** L	H (5)	100°C	20 min	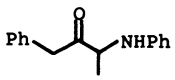 **5u**	99
	P	H (5)	100°C	30 min		96
5	**4b** L	I (5)	100°C	1 h	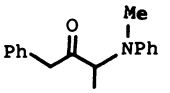 **5v**	95
	P	I (5)	100°C	2.5 h		88
6	**4b** L	K (5)	100°C	15 min	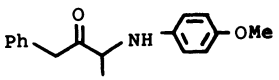 **5w**	81
	P	K (5)	100°C	30 min		70
7	**4e**	H (50)	r.t.	2 d	**5x**	84
8	**4f**	H (50)	r.t.	3 h	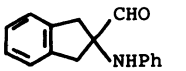 **5y**	100

a) H: aniline, I: *N*-methylaniline, J: *p*-aminoacetanilide, K: *p*-anisidine. All reactions were conducted in HMPA under nitrogen atmosphere. b) Isolated yields after silica-gel chromatography.

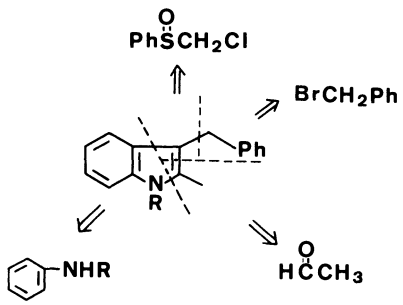

Fig. 1.

in about 80% yield (see Fig 1).

In conclusion a novel and versatile procedure for a synthesis of α-amino ketones and α-amino aldehydes has been developed from α,β-epoxy sulfoxides. In regard to the accessibility of the starting materials, the simplicity and mildness of the operation, and high yields of the products, the present method offers a simple and useful approach to α-amino ketones and α-amino aldehydes and at the same time this process contributes to the nitrogen containing heterocyclic chemistry.

Experimental

All melting points are uncorrected. Infrared (IR) spectra were measured directly on a NaCl plate or in KBr disks with a Hitachi 215 spectrometer. ^{1}H Nuclear magnetic resonance (NMR) spectra were measured in $CDCl_3$ solution with a JEOL FX-100 spectrometer using Me_4Si as an internal standard. Electron impact mass spectra (MS) were obtained on a Hitachi M-80 double focusing spectrometer at 70 eV by direct insertion. Silica gel BW-127ZH (Fuji-Devison) containing 2% fluorescence reagent 254 and quartz column were used for column chromatography and the products having ultraviolet (UV) absorption were detected by UV irradiation.

Materials. All α,β-epoxy sulfoxides (**4**) used in this study were reported in references 1 and 10. DMSO, HMPA, and all amines except *N*-methyl-3-hydroxy-4-methoxybenzylamine were dried over CaH_2 and distilled before use.

General Procedure for the Preparation of α-Amino Ketones and α-Amino Aldehydes by Aminolysis of α,β-Epoxy Sulfoxides with Amines. Method A: The α,β-epoxy sulfoxide (**4**) (0.1 mmol) was dissolved in 2 ml of an amine in dry flask under N_2 atmosphere. This reaction mixture was stirred at the appropriate temperature till the starting

material disappeared. The amine was distilled off under reduced pressure at room temperature and the residue was purified by silica-gel column chromatography with a mixture of hexane and ethyl acetate as an eluent.

Method B: The α,β-epoxy sulfoxide (**4**) (0.1 mmol) was dissolved in 0.2 ml of DMSO or HMPA in dry flask under N_2 atmosphere. To the solution was added an amine (1 mmol) and the reaction mixture was stirred at the appropriate temperature till the starting material disappeared. The reaction mixture was diluted with 50 ml of ethyl acetate and the solution was washed twice with water followed by sat. aq NaCl. The solution was dried over Na_2SO_4 and the solvent was evaporated under reduced pressure. The residue was purified by silica-gel column chromatography with a mixture of hexane and ethyl acetate as an eluent. In the cases of arylamines, usually the R_f values of the amines are very close to the products. The products were purified by silica-gel column chromatography followed by preparative thin-layer chromatography (Merck Kieselgel 60 F_{254}; 0.25 mm).

1-Phenyl-1-piperidino-2-octanone (5a). Colorless oil; IR (neat): 1710 (CO) cm^{-1}; ^1H NMR δ=0.82 (3H, t, J=6 Hz), 1.0—1.8 (14H, m), 2.1—2.6 (6H, m), 4.87 (1H, s), 7.1—7.5 (5H, m); MS m/z (%): 287 (M^+, trace), 286 ($[M-H]^+$, trace), 174 ($[M-C_7H_{13}O]^+$, 100); Found: m/z 286.2160. Calcd for $C_{19}H_{28}NO$: ($[M-1]^+$) 286.2169.

1-Phenyl-1-morphorino-2-octanone (5b). Colorless oil; IR (neat): 1720 (CO) cm^{-1}; ^1H NMR δ=0.82 (3H, t, J=6 Hz), 1.0—1.6 (8H, m), 2.3—2.5 (4H, m), 3.6—3.8 (4H, m), 3.93 (1H, s), 7.2—7.4 (5H, m); MS m/z (%): 289 (M^+, trace), 288 ($[M-H]^+$, 0.1), 176 ($[M-C_7H_{13}O]^+$, 100); Found: m/z 288.1947. Calcd for $C_{18}H_{26}NO_2$: ($[M-1]^+$) 288.1961.

***N*-(2-Oxo-1-phenyloctyl)-1,2,3,4-tetrahydroisoquinoline (5c).** Colorless oil; IR (neat): 1710 (CO) cm^{-1}; ^1H NMR δ=0.82 (3H, t, J=6 Hz), 1.0—1.6 (8H, m), 2.4—3.0 (6H, m), 3.59 (2H, s), 4.10 (1H, s), 6.78—7.12 (4H, m), 7.2—7.5 (5H, m); MS m/z (%): 335 (M^+, trace), 334 ($[M-H]^+$, trace), 305 (trace), 222 ($[M-C_7H_{13}O]^+$, 100).

1-Phenyl-3-piperidino-2-butanone (5d). Colorless oil; IR (neat): 1720 (CO) cm^{-1}; ^1H NMR δ=1.11 (3H, d, J=7 Hz), 1.3—1.8 (6H, m), 2.3—2.6 (4H, m), 3.29 (1H, q, J=7 Hz), 3.82, 3.94 (each 1H, d, J=15 Hz), 7.24 (5H, bs); MS m/z (%): 230 ($[M-H]^+$, trace), 218 (6), 112 ($[M-C_8H_7O]^+$, 100); Found: m/z 230.1541. Calcd for $C_{15}H_{20}NO$: ($[M-1]^+$) 230.1543.

2-(4-Chlorophenyl)-1-cyclohexyl-2-piperidinoethanone (5e). Colorless oil; IR (neat): 1720 (CO) cm^{-1}; ^1H NMR δ=1.0—1.8 (16H, m), 2.2—2.6 (5H, m), 4.04 (1H, s), 7.27 (4H, s); MS m/z (%): 319 (M^+, trace), 318 (trace), 208 ($[M-C_7H_{11}O]^+$, 100).

2-(4-Chlorophenyl)-1-cyclohexyl-2-(1-pyrrolidinyl)ethanone (5f). Colorless crystals; mp 136—137 °C (AcOEt-hexane); IR (KBr): 1720 (CO) cm^{-1}; ^1H NMR δ=0.7—1.9 (14H, m), 1.1—1.7 (5H, m), 4.05 (1H, s), 7.31 (4H, s); MS m/z (%): 304 ($[M-H]^+$, trace), 194 ($[M-C_7H_{11}O]^+$, 100).

***N*-(1-(4-Chlorophenyl)-2-cyclohexyl-2-oxoethyl)-1,2,3,4-tetrahydroisoquinoline (5g).** Colorless crystals; mp 113—114 °C (AcOEt-hexane); IR (KBr): 1720 (CO) cm^{-1}; ^1H NMR δ=0.8—1.9 (10H, m), 1.4—2.0 (5H, m), 3.61 (2H, bs), 4.31 (1H, s), 6.8—7.2 (4H, m), 7.41 (4H, s); MS m/z (%): 367 (M^+, trace), 366 ($[M-H]^+$, trace), 256 ($[M-C_7H_{11}O]^+$, 100); Found: C, 74.89; H, 7.09; N, 3.84%. Calcd for $C_{23}H_{26}ClNO$: C, 75.08; H, 7.12; N, 3.81%.

1-Phenyl-2-(1-piperidinocyclohexyl)ethanone (5h). Colorless crystals; mp 79—82 °C (AcOEt-hexane); IR (KBr): 1715 (CO) cm^{-1}; ^1H NMR δ=0.8—2.1 (16H, m), 2.4—2.6 (4H, m), 3.90 (2H, s), 7.1—7.5 (5H, m); MS m/z (%): 284 ($[M-H]^+$, trace), 166 ($[M-C_8H_7O]^+$, 100).

1-Phenyl-2-[1-(1-pyrrolidinyl)cyclohexyl]ethanone (5i). Colorless oil; IR (neat): 1710 (CO) cm^{-1}; ^1H NMR δ=1.1—2.2 (14H, m), 2.5—2.8 (4H, m), 3.87 (2H, s), 7.1—7.4 (5H, m); MS m/z (%): 270 ($[M-H]^+$, trace), 152 ($[M-C_8H_7O]^+$, 100).

***N,N*-Diethyl-2-oxo-1-phenyloctylamine (5j).** Colorless oil; IR (neat): 1710 (CO) cm^{-1}; ^1H NMR δ=0.83 (3H, t, J=6 Hz), 0.98 (6H, t, J=7 Hz), 2.3—2.8 (6H, m), 4.36 (1H, s), 7.2—7.4 (5H, m); MS m/z (%): 275 (M^+, trace), 162 ($[M-C_7H_{13}O]^+$, 100); Found: m/z 275.2240. Calcd for $C_{18}H_{29}NO$: M, 275.2247.

***N*-Methyl-*N*-(2-oxo-1-phenyloctyl)-3-hydroxy-4-methoxybenzylamine (5k).** Colorless oil; IR (neat): 3420 (OH), 1710 (CO) cm^{-1}; ^1H NMR δ=0.83 (3H, t, J=6 Hz), 1.0—1.6 (8H, m), 2.15 (3H, s), 2.4—2.6 (2H, m), 3.34, 3.54 (each 1H, d, J=13 Hz), 3.93 (3H, s), 4.18 (1H, s), 6.80—6.96 (3H, m), 7.2—7.5 (5H, m); MS m/z (%): 256 ($[M-C_7H_{13}O]^+$, 2.5), 137 ($[M-C_{15}H_{22}NO]^+$, 6), 120 (100).

***N*-Benzyl-2-oxo-1-phenyloctylamine (5l).** Colorless oil; IR (neat): 3350 (NH), 1710 (CO) cm^{-1}; ^1H NMR δ=0.82 (3H, t, J=6 Hz), 1.0—1.6 (8H, m), 2.30 (2H, t, J=7 Hz), 3.61, 3.73 (each 1H, d, J=13 Hz), 4.39 (1H, s), 7.32, 7.36 (each 5H, s); MS m/z (%): 308 ($[M-H]^+$, trace), 202 ($[M-C_7H_9N]^+$, 2), 196 ($[M-C_7H_{13}O]^+$, 100).

***N*-Methyl-*N*-(1-methyl-2-oxo-3-phenylpropyl)-3-hydroxy-4-methoxybenzylamine (5m).** Colorless oil; IR (neat): 3340 (OH), 1720 (CO) cm^{-1}; ^1H NMR δ=1.09 (3H, d, J=7 Hz), 2.15 (3H, s), 3.42 (1H, q, J=7 Hz), 3.48, 3.52 (each 1H, d, J=13 Hz), 3.89 (3H, s), 3.90, 3.94 (each 1H, d, J=13 Hz), 6.79 (2H, d, J=1 Hz), 6.96 (1H, bt, J=1 Hz), 7.0—7.3 (5H, m); MS m/z (%): 312 ($[M-H]^+$, trace), 311 ($[M-H_2]^+$, trace), 194 ($[M-C_8H_7O]^+$, 42), 137 ($[M-C_{11}H_{14}NO]^+$, 100).

3-Diethylamino-1-phenyl-2-butanone (5n). Colorless oil; IR (neat): 1725 (CO) cm^{-1}; ^1H NMR δ=1.04 (6H, t, J=7 Hz), 1.05 (3H, d, J=7 Hz), 2.48 (4H, m), 3.49 (1H, q, J=7 Hz), 3.86, 3.99 (each 1H, d, J=15 Hz), 7.1—7.4 (5H, m); MS m/z (%): 219 (M^+, 3), 218 ($[M-H]^+$, 26), 100 ($[M-C_8H_7O]^+$, 100).

***N*-(1-Formylcyclohexyl)piperidine (5o).** Colorless oil; IR (neat): 1725 (CO) cm^{-1}; ^1H NMR δ=1.0—2.1 (14H, m), 2.4—2.7 (4H, m), 9.33 (1H, s); MS m/z (%): 166 ($[M-CHO]^+$, 100).

2-Piperidino-2-indancarbaldehyde (5p). Colorless crystals; mp 87—89 °C (AcOEt-hexane); IR (KBr): 1710 (CO) cm^{-1}; ^1H NMR δ=1.3—1.8 (6H, m), 2.4—2.6 (4H, m), 3.14, 3.28 (each 2H, d, J=16 Hz), 7.18 (4H, s), 9.75 (1H, s); MS m/z (%): 229 (M^+, trace), 200 ($[M-CHO]^+$, 100), 115 ($[M-C_6H_{12}NO]^+$, 19); Found: C, 78.34; H, 8.34; N, 6.03%. Calcd for $C_{15}H_{19}NO$: C, 78.56; H, 8.35; N, 6.11%.

2-Methyl-2-(*N*-piperidino)-3-tetrahydropyranyloxypropanal (5q). Colorless oil; IR (neat): 1740 (CO) cm^{-1}; ^1H NMR δ=1.14 (3H, s), 1.3—1.9 (12H, m), 2.4—2.6 (4H, m), 3.4—4.1 (4H, m), 4.60 (1H, m, $W_{1/2}$=6 Hz), 9.49 (1H, s); MS m/z (%): 254 ($[M-H]^+$, trace), 226 ($[M-CHO]^+$, 100).

***N*-(2-Oxo-1-phenyloctyl)aniline (5r).** Colorless crystals; mp 84—85 °C (AcOEt-hexane); IR (KBr): 3410 (NH), 1715 (CO) cm^{-1}; ^1H NMR δ=0.83 (3H, t, J=6 Hz), 1.0—1.7 (8H, m), 2.44 (2H, t, J=7 Hz), 5.00 (1H, s), 6.48—6.76 (3H, m), 6.98—7.22 (2H, m), 7.26—7.56 (5H, m); MS m/z (%): 295 (M^+, trace), 182 ($[M-C_7H_{13}O]^+$, 100); Found: m/z 295.1930. Calcd for $C_{20}H_{25}NO$: M, 295.1934.

***N*-Methyl-*N*-(2-oxo-1-phenyloctyl)aniline (5s).**

Colorless oil; IR (neat): 1720 (CO) cm^{-1}; ^1H NMR δ=0.84 (3H, t, J=6 Hz), 1.0—1.8 (8H, m), 2.49 (2H, t, J=7 Hz), 2.82 (3H, s), 5.49 (1H, s), 6.64—6.85 (3H, m), 7.0—7.4 (7H, m); MS m/z (%): 309 (M^+, trace), 105 ([M−$C_{14}H_{20}O$]$^+$, 100).

***N*-Acetyl-*N'*-(2-oxo-1-phenyloctyl)-*p*-phenylenediamine (5t).** Colorless crystals; mp 108—109 °C (AcOEt-hexane); IR (KBr): 3400, 3330 (NH), 1710 (CO) cm^{-1}; ^1H NMR δ=0.82 (3H, t, J=6 Hz), 1.0—1.7 (8H, m), 2.06 (3H, s), 2.43 (2H, t, J=7 Hz), 4.97 (1H, d, J=4 Hz, +D_2O gave singlet signal), 6.4—6.6 (2H, m), 6.8—7.5 (7H, m); MS m/z (%): 352 (M^+, 2), 239 ([M−$C_7H_{13}O$]$^+$, 100); Found: m/z 352.2134. Calcd for $C_{22}H_{28}N_2O$: M, 352.2148.

***N*-(1-Methyl-2-oxo-3-phenylpropyl)aniline (5u).** Colorless prisms; mp 71—72 °C (AcOEt-hexane); IR (KBr): 3420 (NH), 1715 (CO) cm^{-1}; ^1H NMR δ=1.41 (3H, d, J=7 Hz), 3.84 (2H, s), 4.19 (1H, q, J=7 Hz), 6.24—7.45 (10H, m); MS m/z (%): 239 (M^+, 4), 120 ([M−C_8H_7O]$^+$, 100); Found: C, 79.94; H, 7.18; N, 5.70%. Calcd for $C_{16}H_{17}NO$: C, 80.30; H, 7.16; N, 5.85%.

***N*-Methyl-*N*-(1-methyl-2-oxo-3-phenylpropyl)aniline (5v).** Colorless oil; IR (neat): 1730 (CO) cm^{-1}; ^1H NMR δ=1.25 (3H, d, J=7 Hz), 2.74 (3H, s), 3.79 (2H, s), 4.46 (1H, q, J=7 Hz), 6.68—6.92 (3H, m), 7.04—7.40 (7H, m); MS m/z (%): 253 (M^+, 3), 134 ([M−C_8H_7O]$^+$, 100); Found: m/z 253.1440. Calcd for $C_{17}H_{19}NO$: M, 253.1465.

***N*-(1-Methyl-2-oxo-3-phenylpropyl)-*p*-anisidine (5w).** Colorless needles; mp 82—84 °C (AcOEt-hexane); IR (KBr): 3420 (NH), 1710 (CO) cm^{-1}; ^1H NMR δ=1.38 (3H, d, J=7 Hz), 3.75 (3H, s), 3.83 (2H, s), 4.12 (1H, q, J=7 Hz), 6.40—6.85 (4H, m), 7.08—7.40 (5H, m); MS m/z (%): 269 (M^+, 7), 150 ([M−C_8H_7O]$^+$, 100); Found: C, 75.46; H, 7.14; N, 5.06%; M^+, 269.1395. Calcd for $C_{17}H_{19}NO_2$: C, 75.81; H, 7.11; N, 5.20%; M, 269.1413.

***N*-(1-Formylcyclohexyl)aniline (5x).** Colorless oil; IR (neat): 3390 (NH), 1735 (CO) cm^{-1}; ^1H NMR δ=1.1—2.0 (10H, m), 6.5—7.4 (5H, m), 9.67 (1H, s); MS m/z (%): 203 (M^+, 5), 174 ([M−CHO]$^+$, 100).

2-Anilino-2-indancarbaldehyde (5y). Colorless oil; IR (neat): 3410 (NH), 1725 (CO) cm^{-1}; ^1H NMR δ=3.38, 3.54 (each 2H, d, J=16 Hz), 6.4—7.2 (5H, m), 7.24 (4H, s), 9.76 (1H, s); MS m/z (%): 237 (M^+, 7), 208 ([M−CHO]$^+$, 100).

3-Benzyl-2-methylindole (6a). To a 20 ml dry flask was added 38 mg (0.4 mmol) of dry $MgCl_2$ and 0.5 ml of Ethylcellosolve followed by 18 μl (0.2 mmol) of aniline. The atmosphere of the flask was evacuated and replaced with nitrogen. The suspension was stirred and heated at reflux for 15 min to give colorless clear solution. To this solution was added a solution of *N*-(1-methyl-2-oxo-3-phenylpropyl)aniline (**5u**) (36 mg; 0.15 mmol) in 0.2 ml of Ethylcellosolve and the reaction mixture was stirred and heated at 130 °C for 1.5 h. The reaction mixture was diluted with ethyl acetate and washed with water. The organic layer was dried over Na_2SO_4 and the solvent was evaporated and the residue was chromatographed on a silica-gel column (hexane : AcOEt = 20:1) to afford 19 mg (57%) of **6a** as yellow crystals. Recrystallization from AcOEt-hexane gave colorless prisms, mp 89—90 °C. IR (KBr): 3500 (NH) cm^{-1}; ^1H NMR δ=2.32 (3H, s), 4.09 (2H, s), 7.02—7.64 (10H, m); MS m/z (%): 221 (M^+, 100), 206 ([M−CH_3]$^+$, 27), 144 ([M−C_6H_5]$^+$, 43); Found: m/z 221.1194. Calcd for $C_{16}H_{15}N$: M, 221.1203.

3-Benzyl-1,2-dimethylindole (6b). To a 20 ml dry flask was added 230 mg (1.68 mmol) of dry $ZnCl_2$ and 1 ml of Ethylcellosolve and the atmosphere of the flask was replaced with nitrogen as described above. The suspension was stirred and heated at 100 °C for 10 min to give colorless clear solution. To this was added a solution of *N*-methyl-*N*-(1-methyl-2-oxo-3-phenylpropyl)aniline (**5v**) (62 mg; 0.24 mmol) in 0.5 ml of Ethylcellosolve and the reaction mixture was stirred and heated at 120 °C for 3 h. The work-up as described above gave a crude product, which was purified by silica-gel column chromatography (hexane:AcOEt=40:1) gave 55 mg (95%) of **6b** as light yellow crystals. Recrystallization from ethanol gave colorless prisms, mp 54—55 °C (lit,[20] 56.6—57 °C). IR (KBr): 740, 705 (aromatic) cm^{-1}; ^1H NMR δ=2.35 (3H, s), 3.65 (3H, s), 4.11 (2H, s), 6.92—7.50 (9H, m), MS m/z (%): 235 (M^+, 100), 220 ([M−CH_3]$^+$, 39), 158 ([M−C_6H_5]$^+$, 94); Found: m/z 235.1346. Calcd for $C_{17}H_{17}N$: M, 235.1360.

The authors are grateful to Professor O. Hoshino and Dr. H. Hara of this department and Professor B. Zwanenburg, University of Nijmegen, for their helpful discussions and to Dr. S. Saito, Tanabe Seiyaku Co., Ltd., for elemental analysis and Miss. Sawabe, Mrs. Yamatani and Miss Khim of this laboratory for NMR and MS measurements. This work was supported in part by a Grant-in-Aid for Scientific Research No. 59771658 from the Ministry of Education, Science and Culture.

References

1) Part II: T. Satoh, T. Kumagawa, and K. Yamakawa, *Bull. Chem. Soc. Jpn.*, **58**, 2849 (1985).

2) H. M. Fischler, H. G. Heine, and W. Hartman, Ger. Offen. 2145419; *Chem. Abstr.*, **78**, 159051z (1973).

3) a) D. Mayer, "Houben-Weyl, Methoden der Organischen Chemie," 4 th ed, Vol. 7/2c, p. 2251 (Thieme, Stuttgart 1977); b) E. Campaigne and R. D. Lake, *J. Org. Chem.*, **24**, 478 (1959); c) R. E. Walkup and J. Linder, *Tetrahedron Lett.*, **26**, 2155 (1985).

4) M. Tramontini, *Synthesis*, **1973**, 703.

5) Y. Ogata, A. Kawasaki, and I. Kishi, *J. Chem. Soc., B*, **1968**, 703.

6) S. L. Friess and H. D. Baldridge, *J. Am. Chem. Soc.*, **78**, 2482 (1956); H. Berbalk, K. Eichinger, and E. Deeker, *Monatsh. Chem.*, **107**, 401 (1976).

7) C. G. Stuckwisch, *J. Org. Chem.*, **37**, 318 (1972); A. Pfaltz and S. Anwar, *Tetrahedron Lett.*, **25**, 2977 (1984).

8) H. E. Baumgarten and J. M. Petersen, *J. Am. Chem. Soc.*, **82**, 459 (1960); C. Obrien, *Chem. Rev.*, **64**, 81 (1964).

9) Y. J. L'Italien, U. S. 3171858; *Chem. Abstr.*, **62**, 14575c (1965); A. Wander, Swiss 401054; *Chem. Abstr.*, **65**, 3835e (1966); C. L. Stevens and R. W. Fleming, Fr. 1447116; *Chem. Abstr.*, **66**, 104826c (1967); H. Schulz, E. Jassmann, and R. Kowarsch, Ger, (East) 50619; *Chem. Abstr.*, **67**, 21614b (1967); C. L. Stevens and C. H. Chang, *J. Org. Chem.*, **27**, 4392 (1962); C. L. Stevens, R. D. Elliot, and B. L. Winch, *J. Am. Chem. Soc.* **85**, 1464 (1963); C. L. Stevens, M. E. Munk, and C. H. Chang, *J. Org. Chem.*, **29**, 3146 (1964); C. L. Stevens, A. Thuillier, and F. A. Daniher, ibid, **30**, 2962 (1965); C. L. Stevens, A. B. Ash, A. Thuillier, J. H. Amin, A. Balys, W. E. Dannis, J. P. Dickerson, R. P. Glinski, H. T. Hanson, M. D. Pillai, and J. W. Stoddard, ibid., **31**, 2593 (1966); C. L. Stevens, A. Thuillier, K. G. Taylor, F. A. Daniher, J. P. Dickerson, H. T. Hanson, N. A. Nielsen, N. A. Tikotkar, and R. M. Weier,

ibid., **31**, 2601 (1966).

10) T. Satoh, Y. Kaneko, T. Izawa, K. Sakata, and K. Yamakawa, *Bull. Chem. Soc. Jpn.*, **58**, 1983 (1985).

11) A part of this study was reported as a communication: T. Satoh, Y. Kaneko, K. Sakata, and K. Yamakawa, *Chem. Lett.*, **1985**, 585.

12) T. Durst, *J. Am. Chem. Soc.*, **91**, 1034 (1969); T. Durst, K-C. Tin, F. de Reinach-Hirtzbach, J. M. Decesare, and M. D. Ryan, *Can. J. Chem.*, **57**, 258 (1978).

13) D. F. Tavares, R. E. Estep, and M. Blezard, *Tetrahedron Lett.*, **1970**, 2373; V. Reutrakul and W. Kanghae, ibid., **1977**, 1377; D. F. Taber and B. P. Gunn, *J. Org. Chem.*, **44**, 450 (1979).

14) The reaction of **1** and **2** gave diastereomeric mixture of chlorohydrin (**3**), in which less polar and polar ones on silica-gel plate are expressed as L and P, respectively. The epoxy sulfoxide (**4**) derived from L-chlorohydrin is expressed as **4**-L. Details see references 1 and 10.

15) A. J. Parker, *Chem. Rev.*, **69**, 1 (1969); E. Juarestl and J. D. Reyna, *Tetrahedron Lett.*, **25**, 3521 (1984).

16) A. Papini, A. Ricci, M. Taddei, G. Seconi, and P. Dembech, *J. Chem. Soc., Perkin Trans. 1*, **1984**, 2261.

17) G. H. Posner, D. Z. Rogers, C. M. Kinzig, and G. M. Gurria, *Tetrahedron Lett.*, **1975**, 3597; G. H. Posner and D. Z. Rogers, *J. Am. Chem. Soc.*, **99**, 8208, 8214 (1977).

18) R. C. Elderfield, "Heterocyclic Compounds," John Wiley and Sons, New York, (1952), Vol. 3, pp. 1—274.

19) T. Hino and M. Nakagawa, *J. Am. Chem. Soc.*, **91**, 4598 (1969).

20) R. W. Huffman and T. C. Bruice, *J. Am. Chem. Soc.*, **89**, 6243 (1967).

 © 1986 The Chemical Society of Japan Bull. Chem. Soc. Jpn., 59, 465—470 (1986)

Fluorescence and Circular Dichroism Studies on Host-Guest Complexation of γ-Cyclodextrin Bearing Two 2-Naphthyl Moieties

Akihiko UENO,* Fumio MORIWAKI, Tetsuo OSA,* Fumio HAMADA, and Koichi MURAI
Pharmaceutical Institute, Tohoku University, Aobayama, Sendai 980
Department of Fuel Chemistry, Mining College, Akita University, Gakuen-cho, Tegata, Akita 010
(Received September 17, 1985)

Host-guest complexation of γ-cyclodextrin bearing two 2-naphthyl moieties (**1**) has been studied by circular dichroism and fluorescence spectroscopic methods. The exciton coupling band observed in the naphthalene ^1L_a transition region shows that the two naphthyl moieties of **1** take a chiral orientation in the cavity. The guest binding of **1** changes the circular dichroism pattern, finally affording a negative band, but hardly influences the fluorescence pattern in which excimer emission is predominant. These phenomena suggest that a guest molecule is included in the cavity of **1** by extruding two naphthyl moieties from the cavity so as to make the moieties to act as hydrophobic caps. Dimethyl sulfoxide(DMSO) was found to be effective to change both fluorescence and circular dichroism patterns, increasing monomer-like emission and converting the exciton coupling pattern to a simple negative band. These results suggest that the two naphthyl moieties are not in proximal positions in DMSO-rich solutions.

Cycloamyloses (cyclodextrins, CDs) are a series of cyclic oligomers consisting of six or more α-1,4-linked D-glucopyranose units. The number of glucopyranose unit is designated by a Greek letter: α for six, β for seven, γ for eight, and so on. The smaller α- and β-CDs have been widely utilized for various purposes because of their remarkable property of forming inclusion complexes with a variety of small molecules.[1] However, the use of γ-CD has not been frequent due to its large cavity size in addition to the factor of its commercial unavailability. In recent reports of spectroscopic studies,[2-4] it was suggested that γ-CD can include two molecules of benzene or naphthalene derivatives in marked contrast to α-and β-CDs which form 1:1 host-guest complexes. The unique property of γ-CD places the basis for using γ-CD as a molecular flask which facilitates reactions by involving two reactants as shown by excimer[2] or charge-transfer complex[3] formation and dimerization.[5]

As a new extension of our works, we have prepared several γ-CD derivatives, which bear a covalently attached aromatic moiety,[6] and observed that the moiety acts as a spacer which enables the γ-CD derivatives to form 1:1 host-guest complexes by narrowing the large γ-CD cavity (Scheme 1). The complexation

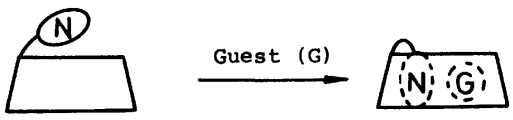

N: Naphthalene

Scheme 1.

behavior of the γ-CD derivatives may be regarded as an induced-fit type of complexation since the host changes the location of the appended moiety so as to be suited for guest binding.

We now wish to describe here another induced-fit type of complexation which was observed for γ-CD bearing two 2-naphthyl moieties (**1**). The preliminary study on the complexation behavior of **1** showed that orientation and location of the appended naphthyl moieties changed by guest binding.[7] In addition to the detailed features of the binding behavior, this work is concerned with the conformational changes induced by dimethyl sulfoxide (DMSO).

Results

We prepared the compound **1** via azobenzene-capped γ-CD as shown in Scheme 2. Figure 1 shows the absorption and circular dichroism spectra of **1** in an aqueous 10% DMSO solution. The circular dichroism spectrum reveals a peak around 282 nm and a trough around 258 nm in the naphthalene ^1L_a transition region. The exciton coupling pattern indicates that the two 2-naphthyl moieties of **1** form a pair with a chiral geometry in the cavity of **1**. The spectral pattern in shorter wavelengths (^1B_b transition region) may be a decisive indicator for determining the direction of the chirality since the ^1B_b transition occurs along the long axis of naphthalene ring. However, as the measurements in the shorter wavelengths could not be achieved due to the absorption of DMSO, we used aqueous 10% ethylene glycol solutions for the purpose. The circular dichroism spectrum of this solution shows a trough at 234 nm with the molar ellipticity of 29000 and a peak at 217 nm with the molar ellipticity of 158000 associated with the naphthalene ^1B_b transition. Although the spectrum has unballanced intensities between positive and negative bands, the pattern may be regarded as that of the exciton coupling of counter-clockwise orientation of the two naphthyl moieties.[8] Its deformed shape might be due to the electronic interaction between ^1B_b and ^1L_a transitions within the naphthyl pair. The circular dichroism pattern in the ^1L_a transition region of this aqueous 10% ethylene glycol solution is the same as that of the aqueous 10%

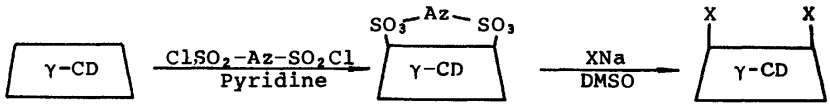

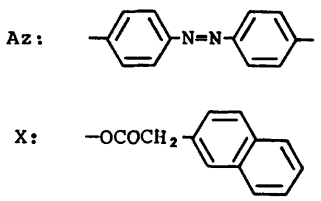

Scheme 2.

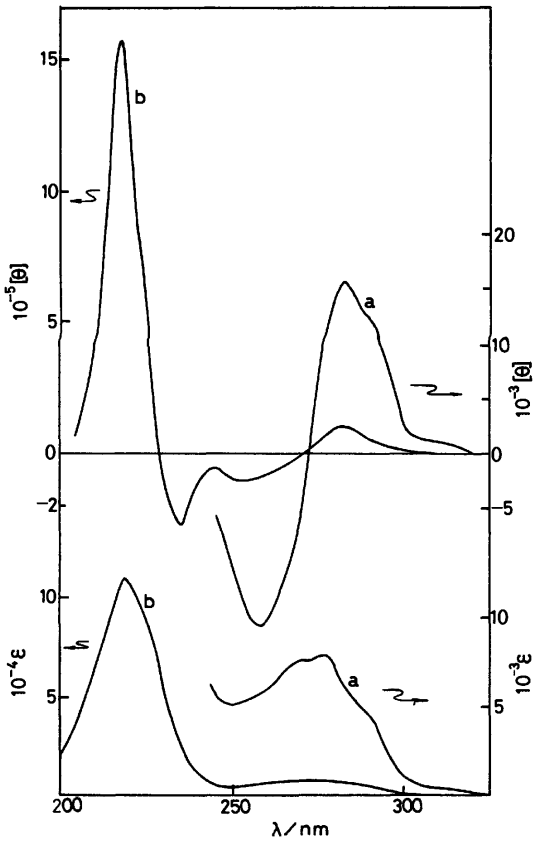

Fig. 1. Circular Dichroism (top) and absorption (bottom) spectra of **1** in aqueous 10% DMSO solution (a) and in aqueous 10% ethylene glycol solution (b). Concentrations of **1** were 6.53×10^{-5} and 7.66×10^{-6} mol dm^{-3} for the spectra a and b, respectively.

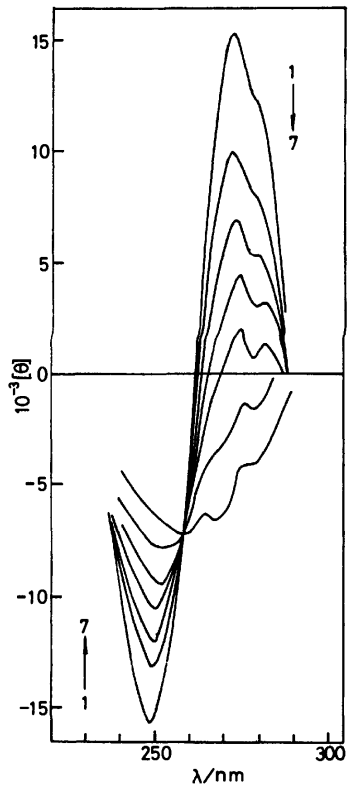

Fig. 2. Circular dichroism spectra of **1** in aqueous 10% DMSO solutions (6.53×10^{-5} mol dm^{-3}) at various cyclododecanol concentrations (1, 0.0; 2, 2.02×10^{-5}; 3, 4.04×10^{-5}; 4, 6.05×10^{-5}; 5, 8.07×10^{-5}; 6, 1.21×10^{-4}; 7, 1.81×10^{-4} mol dm^{-3}).

DMSO solution. Therefore, the orientation of the two naphthyl moieties involved in the cavity of **1** should be the same in both solutions.

The intensity of the positive peak of the exciton coupling band in the naphthalene ^1L_a transition region diminishes with increasing guest concentration. Figure 2 shows the variation of the circular dichroism pattern in the case of cyclododecanol. It is noted that the spectra have an isoellipticity point at 268 nm, this confirming that two forms of **1**, free and complexed ones are present in the present system.

The guest-induced variations of the molar ellipticity were used to obtain binding constants (K) of **1**. It was reported that the binding constant is given by Eq. 1 when circular dichroism intensity changes by guest.[9]

$$K=\frac{\theta_h-\theta_x}{(\theta_x-\theta_c)\left[C_g-C_h\dfrac{\theta_h-\theta_x}{\theta_h-\theta_c}\right]} \quad (1)$$

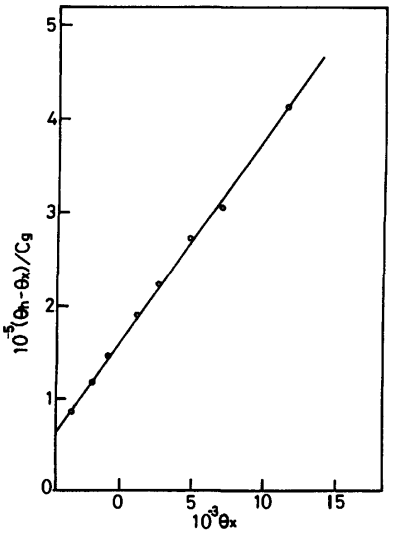

Fig. 3. The plot of $(\theta_h-\theta_x)/C_g$ as a function of θ_x in the system of **1** and cyclohexanol.

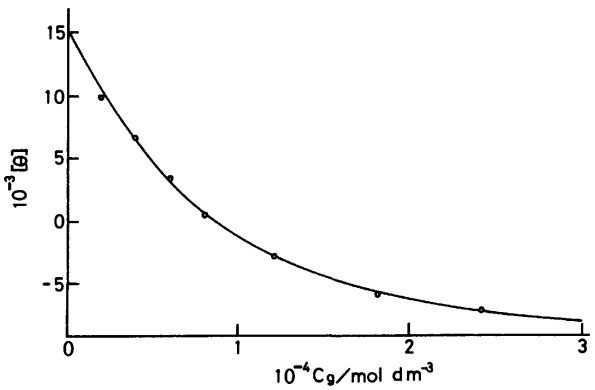

Fig. 4. The plot of $[\theta]_{282}$ of **1** in aqueous 10% DMSO solutions as a function of cyclododecanol concentration (solid line is the calculated curve for K=2.6×10^4 mol^{-3} dm^3).

Here, θ=molar ellipticity (the molar ellipticity at 282 nm in this study), θ_x for sample, θ_h for host alone, θ_c for complex, C_h=total host concentration, and C_g=total guest concentration. When guest is in large excess, we used Eq. 2 which derives from Eq. 1.

$$\frac{\theta_h-\theta_x}{C_g} = K\theta_x - K\theta_c \qquad (2)$$

Figure 3 shows the plot of $(\theta_h-\theta_x)/C_g$ againtst θ_x in the case of cyclohexanol guest. When guest is not in large excess, a curve-fitting method was used as an alternative method. Figure 4 shows the curve-fitting data for cyclododecanol guest. The binding constants obtained by these methods are listed in Table 1. The binding constants in aqueous 10% DMSO solutions are roughly in the order of guest sizes, ranging from 21.7 mol^{-1} dm^3 for cyclohexanol to 26000 mol^{-1} dm^3 for cyclododecanol. DMSO was found to influence the circular dichroism pattern of **1**, decreasing the intensity of the peak around 282 nm and finally giving a negative band around 275 nm (Fig. 5). The effect of DMSO content on guest binding was checked by using (−)-borneol as guest. Figure 6 shows the (−)-borneol-

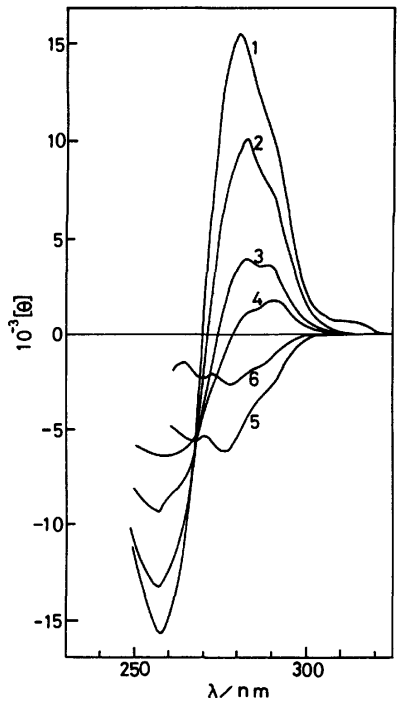

Fig. 5. Circular dichroism spectra of **1** (6.53×10^{-4} mol dm^{-3}) at various DMSO contents (1, 10; 2, 15; 3, 20; 4, 25; 5, 70; 6, 100%).

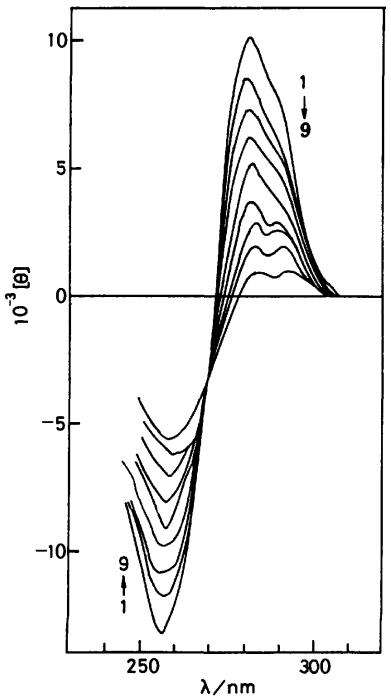

Fig. 6. Circular dichroism spectra of **1** in aqueous 15% DMSO solutions (7.54×10^{-5} mol dm^{-3}) at various (−)-borneol concentrations (1, 0.0; 2, 1.00×10^{-4}; 3, 2.00×10^{-4}; 4, 3.00×10^{-4}; 5, 4.00×10^{-4}; 6, 5.39×10^{-4}; 7, 6.98×10^{-4}; 8, 8.97×10^{-4}; 9, 11.9×10^{-4} mol dm^{-3}).

Table 1. Binding Constant of **1** at 25°C[a)]

Guest	Solvent	K/mol^{-1}dm^{3}[b)]
Cyclohexanol	10% DMSO	21.7
(−)-Menthol	10% DMSO	329
1-Adamantanecarboxylic acid	10% DMSO	507
(−)-Borneol	10% DMSO	795
	15% DMSO	1000
	20% DMSO	1500
	25% DMSO	1500
Cyclododecanol	10% DMSO	26000[c)]

a) Values were obtained by the plot of $(\theta_h-\theta_x)/C_g$ vs. θ_x except for the value for cyclododecanol which was obtained by the curve-fitting method. b) Errors are within ±15%. c) 9730 mol^{-1}dm^{3} in Ref. 7.

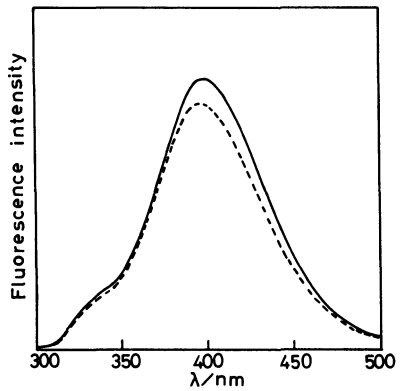

Fig. 7. Fluorescence spectra of **1** in aqueous 10% DMSO solutions (6.53×10^{-5} mol dm^{-3}) in the absence (——) and presence (----) of cyclodoecanol (2.41×10^{-4} mol dm^{-3}). Excitation wavelength is 290 nm.

dependent variation of the circular dichroism pattern of **1** in aqueous 15% DMSO solutions. The binding constans obtained in the range of 10—25% of DMSO are also shown in Table 1. The binding increased wtih increasing DMSO content until 20% DMSO. It should be noted that the analysis was limited to the solutions below 25% DMSO because of the depressed circular dichroism intensity.

Figure 7 shows the fluorescence spectra of **1** in aqueous 10% DMSO solutions, alone and in the presence of cyclododecanol. The spectra exhibit a predominant excimer emission around 400 nm and a shoulder of normal fluorescence around 330 nm. In contrast to the drastic circular dichroism changes, the fluorescence pattern was found to be hardly influenced by guest binding. However, marked changes of the fluorescence pattern was caused by increasing DMSO content (Fig. 8). This result suggests that the two naphthyl moieties of **1** in the DMSO-rich solutions are difficult to be held in the γ-CD cavity of **1** due to the weakened hydrophobic driving force.

Discussion

The synthesis of **1** was performed via γ-CD capped

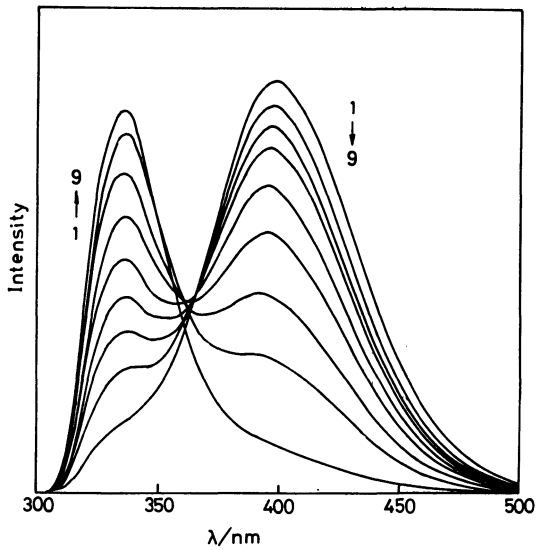

Fig. 8. Fluorescence spectra of **1** (7.54×10^{-5} mol dm^{-3}) at various DMSO contents (1, 10; 2, 20; 3, 30; 4, 40; 5, 50; 6, 60; 7, 70; 8, 80; 9, 100%).

by azobenzene-4,4′-disulfonate moiety. Therefore, the positions of the two naphthyl moieties are those of primary hydroxyls sulfonated by azobenzene-4,4′-disulfonyl dichloride. When glucose units of CD ring are denoted by A, B, C, D, etc., in the order, primary hydroxyl groups of A and D glucopyranose units of β-CD were reported to be selectively sulfonated by stilbene-4,4′-disulfonyl dichloride.[10)] Similar selectivity may be expected here. The examination of Corey-Pauling-Koltun models of the present system shows that substitution is most likely to occur at A-D and A-E positions of γ-CD. However, in spite of our efforts to observe the isomeric forms of **1**, there was no indication of mixing of the isomers. Furthermore, the circular dichroism spectra of **1** at various guest concentrations had an isoellipticity point and could be analyzed based on a simple 1:1 stoichiometry, so the physical nature of the isomers should be very similar even if the present sample is composed of two isomeric forms.

We have examined guest-induced circular dichroism variations for aqueous 10% DMSO solutions. Guest binding of **1** cancelled the exciton coupling in the 250—300 nm region (Fig. 2), this phenomenon indicating that the chiral orientation of the naphthyl pair was lost by forming inclusion complexes. In contrast to this marked variation of the circular dichroism pattern, the excimer emission was hardly influenced by guest binding. These results indicate that the two naphthyl moieties are still close in the complexes. It was reported that γ-CD bearing a naphthyl moiety showed an induced-fit type of complexation (Scheme 1).[6a)] In the system, the naphthyl moiety was fixed in the cavity together with a guest molecule. If similar type of complexation occurs in the present system, the complex

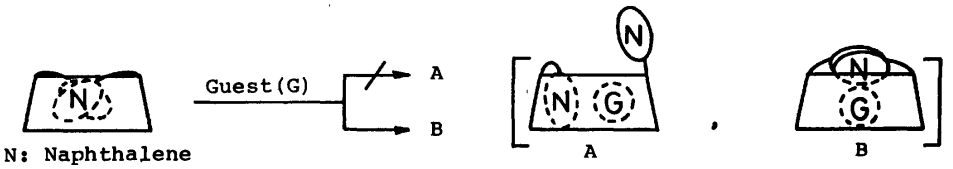

Scheme 3.

A should be formed (Scheme 3). However, the excimer emission from the complexes is not consistent with the structure A in which the face-to-face interaction between the two naphthyl moieties is not allowed. Thus, the structure B is the form which may be supported by both circular dichroism and fluorescence data. The two naphthyl moieties are likely to contact with the included guest molecule as flexible caps. It is interesting that **1** accommodates only one guest molecule in the cavity in spite of the fact that the γ-CD cavity itself is large enough to include two molecules of smaller guests. The hydrophobic naphthyl caps seem to contribute to form such 1:1 complexes.

The DMSO-enhanced binding ability of **1**, which was observed below 25% DMSO, is worthy to note since DMSO in aqueous solutions usually tends to decrease the binding ability of CDs. In the present system, the two naphthyl moieties seem to be so tightly involved in the cavity when water content is high that they are hard to be replaced by a guest molecule. Consequently, the proposed mechanism for the DMSO-enhanced binding is that DMSO increased the mobility of the naphthyl moieties so as to make the cavity suited for guest accommodation.

The fluorescence data indicate that the two naphthyl moieties are close to each other both in free and complex forms of **1** when DMSO content is low, but are located apart in pure DMSO. Figure 9 shows the plots of excimer-monomer ratio and circular dichroism intensity at 282 nm against DMSO content. It is obvious that exciton coupling is more sensitive to DMSO than excimer emission. This result suggests that the two naphthyl moieties are located still in the cavity after loosing the chiral orientation and then extruded outward from the cavity with increasing DMSO content. Thus, three forms with different geometries as illustrated below are likely to be present.

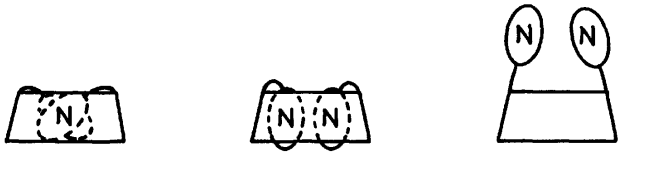

I (tense) II (quasi-tense) III (relaxed)

The two naphthyl moieties are tightly and loosely bound to the cavity in the tense and the quasi-tense forms, respectively, whereas not bound in the relaxed form.

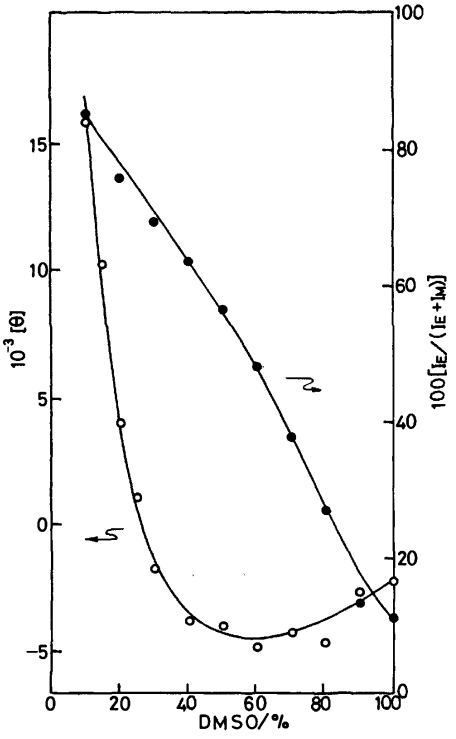

Fig. 9. Plots of excimer-monomer fluorescence ratio (I_M and I_E are intensities at 335 and 400 nm, respectively) and the molecular ellipticity at 282 nm of **1** (7.54×10^{-5} mol dm^{-3}) as a function of DMSO content.

The important aspect of the modified γ-CDs such as those bearing one and two naphthyl moieties is that native γ-CD, which is a rigid host, can be converted to flexible hosts. On this basis, various modified γ-CDs with different guest-selectivity may be designed and construction of new enzyme models, which are capable of induced-fit type of substrate binding, is now in progress.

Experimental

Materials. γ-CD was kindly gifted from Nihon Shokuhin Kako Ltd. The following commercially available guaranteed reagents were used without further purification; *p*-nitrobenzenesulfonic acid, cyclohexanol, (−)-menthol, 1-adamantanecarboxylic acid, (−)-borneol, and cyclododecanol. DMSO was Dotite-spectrosol grade.

Measurements. The circular dichroism, UV and fluorescence spectra were measured at 25 °C using a JASCO J-400X spectrodichrometer, a Shimadzu UV-250 spectrophotometer and a Shimadzu RF-500 spectrofluorophotom-

eter, respectively. The circular dichroism intensities were expressed as molar ellipticity (in degree $cm^2 dmol^{-1}$) on the basis of the total concentration of **1**. Due to the poor solubility of **1** in pure water, DMSO-containing aqueous solutions were used as solvents.

Disodium Azobenzene-4,4′-disulfonate (2). Sodium hydroxide solution (63.2 g in 150 ml H_2O) was added dropwise to the solution of *p*-nitrobenzenesulfonic acid (20.0 g, 0.0985 mol) and water (135 ml). The mixed solution was heated at 50 °C and then D-glucose solution (126 g, 0.699 mol and 150 H_2O) was added dropwise. Air was introduced into the resultant solution at room temperature for 10 h. The precipitates were collected by filtratioin, washed with 15% NaCl solution (100 ml), and recrystallized from 50% ethanol solution to give 9.6 g (25%) of **2**: ^{1}H NMR (D_2O) δ=8.14 (8H, m, Ar). Found: C, 36.46; H, 1.87; N, 7.23%. Calcd for $C_{12}H_8N_2O_6S_2Na_2$: C, 36.65; H, 2.05; N, 7.13%.

Azobenzene-4,4′-disulfonyl Dichloride (3). Thionyl chloride (8 ml) was added dropwise to the stirred suspension of **2** (9.0 g, 0.0233 mol) in *N,N*-dimethylformamide (150 ml). After vigorous stirring for 1 h, the solution was poured into ice water (280 ml). The precipitates were collected, washed with ether, and recrystallized from benzene to give 6.4 g of **3** (73%): mp 223—225 °C; ^{1}H NMR ($CDCl_3$) δ=8.20 (8H, m, Ar); IR (KBr) 1377, 1183, 655, 582, and 528 cm^{-1}; R_f=0.5 (2:1 hexane-acetone). Found: C, 38.19; H, 1.84; N, 7.24. Calcd for $C_{12}H_8S_2O_4N_2Cl_2$: C, 38.00; H, 2.13; N, 7.39.

***trans*-Azobenzene-4,4′-disulfonyl γ-CD (4).** To a stirred solution of dry γ-CD (4.0 g, 3.08 mmol) in dry pyridine (100 ml), azobenzene-4,4′-disulfonyl dichloride (1.40 g) 3.7 mmol) was added, and then heated at 60 °C for 1 h. After cooling the reaction mixture, pyridine was removed by evaporation under reduced pressure. Water addition to the residue followed by evaporation was repeated several times until no pyridine odor was detected. The resultant oily residue was dissolved in a small amount of water and subjected to Sephadex G-15 column chromatography. Recrystallization from methanol afforded the product (0.69 g, 13%) as orange powder: R_f=0.40 (5:1 CH_3CN-H_2O); Found: C, 42.93; H, 5.89; N, 1.45. Calcd for $C_{60}H_{86}N_2O_{44}S_2 \cdot 4H_2O$: C, 43.01; H, 5.66; N, 1.67.

Bis(2-naphthylacetyl) γ-CD. A mixture of **4** (0.515 g, 0.307 mmol), sodium 2-naphthylacetate (0.265 g, 1.28 mmol), and DMSO (10 ml) was stirred at 80 °C for 5 h. After cooling, the reaction mixture was poured into 500 ml of acetone. The precipitates were collected by filtration and subjected to Sephadex G-15 column chromatography. Recrystallization from water gave the desired product (0.12 g, 23%): R_f=0.48 (5:1 CH_3CN-H_2O); ^{1}H NMR (DMSO-d_6, 60 °C) δ=3.1—3.8 (48H, m, CD protons other than C_1H and OH), 4.0—4.5 (6H, m, O_6H), 4.8—4.9 (8H, br. s, C_1H), 5.8 (16H, br. s, O_2H, O_3H), 7.2—7.9 (14H, m, Ar); UV (9:1 H_2O-DMSO) (ε) 277 nm (7900); IR (KBr): 1735 cm^{-1} (CO). Found: C, 50.73; H, 6.12. Calcd for $C_{72}H_{96}O_{42} \cdot 4H_2O$: C, 50.70; H, 6.15.

We thank Dr. N. Harada of Chemical Research Institute of Non-Aqueous Solutions of this university for his variable comments about our circular dichroism results. This work was supported by Grant-in-Aid (No. 58118007) for Special Project Research from the Ministry of Education, Science and Culture.

References

1) M. L. Bender and M. Komiyama, "Cyclodextrin Chemistry," Springer-Verlag (1978).

2) A. Ueno, K. Takahashi, and T. Osa, *J. Chem. Soc., Chem. Commun.*, **1980**, 921; N. Kobayashi, R. Saito, Y. Hino, A. Ueno, and T. Osa, ibid., **1982**, 706; N. Kobayashi, R. Saito, Y. Hino, A. Ueno, and T. Osa, *J. Chem. Soc., Perkin Trans. 2*, **1983**, 1031; A. Harada and S. Nozakura, *Polym. Bull.*, **8**, 141 (1982); T. Yorozu, M. Hoshino, and M. Imamura, *J. Phys. Chem.*, **86**, 4426 (1982); K. Kano, I. Takenoshita, and T. Ogawa, *Chem. Lett.*, **1982**, 321; J. Emert, D. Kodali, and R. Catena, *J. Chem. Soc., Chem. Commun.*, **1981**, 758; N. J. Turro T. Okubo, and G. C. Weed, *Photochem. Photobiol.*, **35**, 325 (1982); N. Kobayashi, Y. Hino, A. Ueno, and T. Osa, *Bull. Chem. Soc. Jpn.*, **56**, 1849 (1983); R. A. Yellin and D. F. Eaton, *J. Phys. Chem.*, **87**, 5051 (1983); M. Itoh and Y. Fujiwara, *Bull. Chem. Soc. Jpn.*, **57**, 2261 (1984).

3) N. Kobayashi, A. Ueno, and T. Osa, *J. Chem. Soc., Chem. Commun.*, **1981**, 340; N. Kobayashi, R. Saito, A. Ueno, and T. Osa, *Makromol. Chem.*, **184**, 837 (1983).

4) A. Ueno, K. Takahashi, Y. Hino, and T. Osa, *J. Chem. Soc., Chem. Commun.*, **1981**, 194; K. Kano, I. Takenoshita, and T. Ogawa, *J. Phys. Chem.*, **86**, 1833 (1982); K. Takamura, S. Inoue, and F. Kusu, *Chem. Lett.*, **1983**, 233; H. Hirai, N. Toshima, S. Uenoyama, *Bull. Chem. Soc. Jpn.*, **58**, 1156 (1985).

5) T. Tamaki, *Chem. Lett.*, **1984**, 53.

6) a) A. Ueno, Y. Tomita, and T. Osa, *J. Chem. Soc., Chem. Commun.*, **1983**, 976; b) A. Ueno, Y. Tomita, and T. Osa, *Tetrahedron Lett.*, **1983**, 5245; c) A. Ueno, Y. Tomita, and T. Osa, *Chem. Lett.*, **1983**, 1635; d) A. Ueno, F. Moriwaki, Y. Tomita, and T. Osa, *Chem. Lett.*, **1985**, 493.

7) A. Ueno, F. Moriwaki, T. Osa, F. Hamada, and K. Murai, *Tetrahedron Lett.*, **26**, 3339 (1985).

8) N. Harada and K. Nakanishi, "Circular Dichroic Spectroscopy, Exciton Coupling in Organic Stereochemistry," Tokyo-Kagaku-Dojin, Tokyo (1982).

9) M. P. Mack, R. R. Hendrixson, R. A. Palmer, and R. G. Ghirardelli, *J. Am. Chem. Soc.*, **98**, 7830 (1976).

10) I. Tabushi, K. Yamamura, and T. Nabeshima, *J. Am. Chem. Soc.*, **106**, 5267 (1984).

 © 1986 The Chemical Society of Japan Bull. Chem. Soc. Jpn., 59, 471—477 (1986)

Oxidation of Lipids. XII. Inhibition of Oxidation of Soybean Phosphatidylcholine and Methyl Linoleate in Aqueous Dispersions by Uric Acid

Etsuo NIKI,* Mitsuo SAITO, Yasuyuki YOSHIKAWA, Yorihiro YAMAMOTO, and Yoshio KAMIYA
Department of Reaction Chemistry, Faculty of Engineering, The University of Tokyo, Hongo, Bunkyo-ku, Tokyo 113
(Received September 18, 1985)

The activity of uric acid as a chain-breaking antioxidant was studied in the oxidations of methyl linoleate micelles and soybean phosphatidylcholine liposomes in aqueous dispersions at 37°C. Uric acid was found to act as a radical scavenger. Uric acid located in an aqueous phase could trap the radicals in an aqueous phase, but it could not scavenge radicals within the lipid region of micelles and liposomal membranes. The kinetics of the oxidations of lipids in aqueous dispersions inhibited by uric acid was discussed.

Toxicity caused by oxygen and its active species has received much attention recently in connection with its pathological effects and aging.[1-11] Aerobic organisms have an array of protective mechanisms both for preventing the formation of active oxygen species and lipid peroxidation and for repairing oxidative damage. Enzymes such as superoxide dismutase and glutathione peroxidase play an important role in the protective systems. Chain-breaking antioxidants are also important and it has been reported[12] that vitamin E is the most potent and probably the only lipid soluble, chain-breaking antioxidant in erythrocyte membranes. Water soluble ascorbic acid also acts as an antioxidant.[13-17]

Uric acid may be another water soluble antioxidant. In 1963, Matsushita[18] found that uric acid was as effective antioxidant as α-tocopherol in the oxidation of linoleic acid in water at 37°C. Kellogg and Fridovich[19] observed that urate inhibited hemolysis of erythrocytes caused by xanthine oxidase-acetaldehyde system. Recently, Ames[20] suggested that uric acid may play a role in protecting man from oxygen radical toxicity. More recently, on the other hand, Kittridge and Willson[21] have shown that urate does not always show a protective effect against free radicals. In the course of our study on the oxidation of lipids and its inhibition, we have measured the activity of uric acid as a chain-breaking antioxidant. This paper shows convincingly that uric acid can scavenge peroxyl radicals.

Experimental

Materials. Commercial soybean phosphatidylcholine (PC) purchased from Daigo Chemicals Co. (Osaka) was purified by alumina and silica-gel columns. The purified PC gave only one spot on thin-layer chromatography and no conjugated diene was observed before oxidation. The composition of fatty acids in PC measured by gas-liquid chromatography after hydrolysis and esterification with HCl-methanol was as follows: palmitic acid 12.1%, stearic acid 1.6, oleic acid 9.6, linoleic acid 69.6, and linolenic acid 7.1 mol%. Methyl linoleate was obtained from Sigma Chemical Co. (St. Louis) and Tokyo Kasei Kogyo Co. (Tokyo) and purified by silica-gel column.

2,2′-Azobis(2-amidinopropane) dihydrochloride (AAPH) and 2,2′-azobis(2,4-dimethylvaleronitrile) (AMVN) were used as water-soluble and oil-soluble radical initiators, respectively, in order to generate initiating free radicals at a constant rate outside or within liposomes or micelles as requested. Both AAPH and AMVN were obtained from Wako Chemicals (Tokyo) and used as received. The rate of chain initiation was determined by the conventional method[22-24] from the induction period observed by the addition of a chain breaking antioxidant.

The rate of radical generation from AAPH in an aqueous phase was measured using a water soluble vitamin E model, 2-carboxy-2,5,7,8-tetramethyl-6-chromanol (CTMC), as a radical scavenger, whereas the rate of chain initiation in the lipid phase was measured using 2,6-di-*t*-butyl-4-methylphenol incorporated into lipid region of micelles or liposomes as a chain-breaking antioxidant.

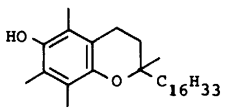

α-tocopherol

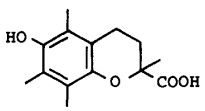

CTMC

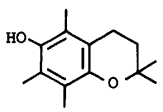

PMC

Uric acid, hypoxanthine, xanthine, purine, L-histidine, indole, and Triton X-100 were of the highest grade available commercially and used without further purification. *d*-α-Tocopherol and its models, CTMC and 2,2,5,7,8-pentamethyl-6-chromanol (PMC), were kindly supplied from Eisai Co. (Tokyo). 2,6-Di-*t*-butyl-4-methylphenol was recrystallized from ethanol.

Pure water was usually used for aqueous dispersion. In some experiments, the effect of pH of the medium was studied. Table 1 shows the buffer system used in this study.

Procedures. The liposome was prepared as follows. PC and oil soluble additives were dissolved in chloroform and the solution was taken into a small flask. The solvent was removed to obtain a thin film. An appropriate amount of 0.1 M NaCl (M=mol dm^{-3}) aqueous solution containing, when necessary, water-soluble additives was added and the film was slowly peeled off by shaking to obtain a white, milky liposome solution. An aliquot of the liposome solution was taken into a reaction vessel and immersed in a water bath which was carefully thermostated at the desired temperature.

The micelle was prepared as follows. Oil soluble additives were dissolved in benzene and the solution was taken into a 30 ml Pyrex glass ampoule. The ampoule was connected to

Table 1. Preparation of Buffer Solutions

pH	Buffer system
3.0	0.02 M Na_2HPO_4 4.11 ml+0.1 M Citric acid 15.89 ml
5.0	0.02 M Na_2HPO_4 10.30 ml+0.1 M Citric acid 9.70 ml
7.0	0.02 M Na_2HPO_4 16.47 ml+0.1 M Citric acid 3.53 ml
9.0	(0.2 M H_3BO_3+2 M KCl) 63 ml+0.2 M Na_2CO_3 37 ml+H_2O 100 ml

Table 2. Inhibition of Oxidation of Methyl Linoleate (LH) Micelle by Uric Acid (UA) in 10 mM Triton X-100 Aqueous Dispersions under Air at 37°C

[LH][a]	[AAPH]	[UA]	R_i(aq)[b]	t_{inh}[c]	R_{inh}	R_i(lipid)[d]	R_p	$(kcl)_p$[e]	$r^{2,f}$	k_{inh}/k_6
mM	mM	μM	nM/s	s	μM/s	nM/s	μM/s			
116	19.1	0	24.8	0		15.5	1.83	118		
114	18.5	10.5	24.1	1125	n.d.[g]	15.0	1.48	99		
111	17.8	25.5	23.1	2025	0.134	14.5	1.58	109	0.0036	12.1×10^5
108	17.7	37.3	23.0	3225	0.184	14.4	1.43	99	0.0081	3.4×10^5
106	17.3	48.7	22.5	3945	0.120	14.0	0.905	65	0.0081	2.7×10^5
88.0	19.1	205	24.8	8700	0.055	15.5	0.883	57	0.0009	4.8×10^5

a) Concentration of methyl linoleate in total aqueous dispersions. The concentration of neat methyl linoleate is 3.02 M. b) Rate of free radical generation in aqueous phase, $R_i(aq)=1.30\times10^{-6}$[AAPH]. c) Induction period. d) Rate of initial lipid radical production in micelles in the absence of uric acid; $R_i(lipid)=8.12\times10^{-7}$[AAPH]. e) Kinetic chain length in the absence of uric acid or after the induction period. f) $r^2=k_6[LH]/(k_{inh}[IH]+(1+\alpha)k_6[LH])$=(rate of reaction 6)/(rate of reactions 4+5+6), see text. g) n.d.=not determined.

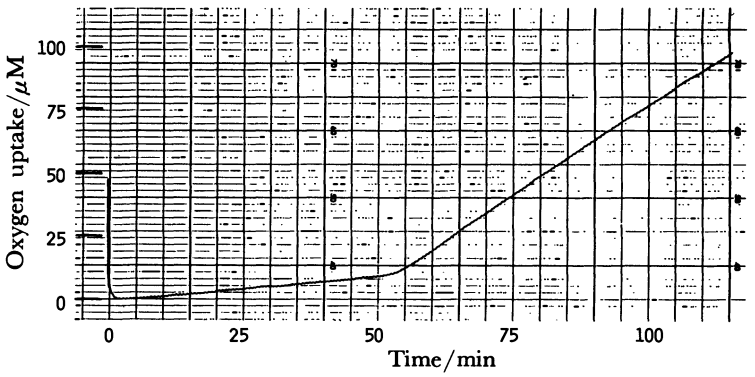

Fig. 1. Rate of oxygen uptake during the oxidation of 0.108 M methyl linoleate in 0.01 M Triton X-100 aqueous dispersion at 37°C under air in the presence of 17.7 mM AAPH and 37.3 μM uric acid. Oxygen uptake was followed by pressure transducer.

a water aspirator and benzene was removed at room temperature. Appropriate amount of methyl linoleate was added and oil-soluble materials were dissolved and then 0.01 M aqueous Triton X-100 containing, when necessary, water-soluble additives was added into the ampoule and shaken vigorously on Vortex mixer for two minutes.

The oxidation was carried out under air at 37°C. The reaction mixture was agitated with a magnetic stirrer. The rate of oxygen uptake was measured in an automatic recording gas absorption apparatus with either a pressure transducer or oxygen electrode and the rate of consumption of α-tocopherol was followed at 294 nm with high-performance liquid chromatography (HPLC) as reported previously.[15]

Results and Discussion

Oxidation of Methyl Linoleate Micelles in Aqueous Dispersion and Its Inhibition by Uric Acid. Methyl linoleate was oxidized in aqueous dispersions using Triton X-100 as a surfactant. In the absence of radical initiator, the rate of oxidation was quite slow, but the addition of AAPH induced the oxidation and methyl linoleate was oxidized at a constant rate without any noticeable induction period. When uric acid was added to the aqueous phase, the oxidation was suppressed quite markedly and after some induction period the rate of oxidation increased as shown in Fig. 1. The rate of oxidation after the induction period was as large as that in the absence of uric acid.

The pertinent results are shown in Table 2. The induction period was proportional to the uric acid concentration. The quantitative evaluation of the data in Table 2 will be discussed later in the text.

Figure 2 shows the results of oxidation of methyl linoleate micelles in aqueous dispersions of different

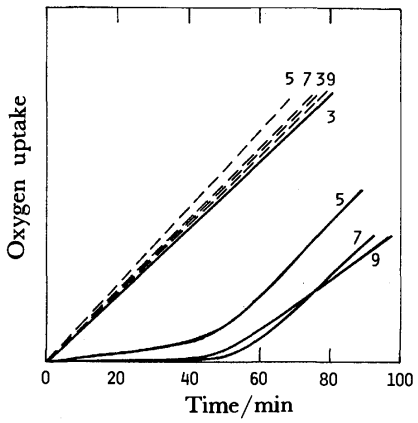

Fig. 2. Effect of pH of the medium on the inhibition of oxidation of 0.11 M methyl linoleate by 51 μM uric acid in 0.01 M Triton X-100 aqueous dispersion at 37°C under air initiated with 18 mM AAPH.
——: with uric acid, ----: without uric acid.

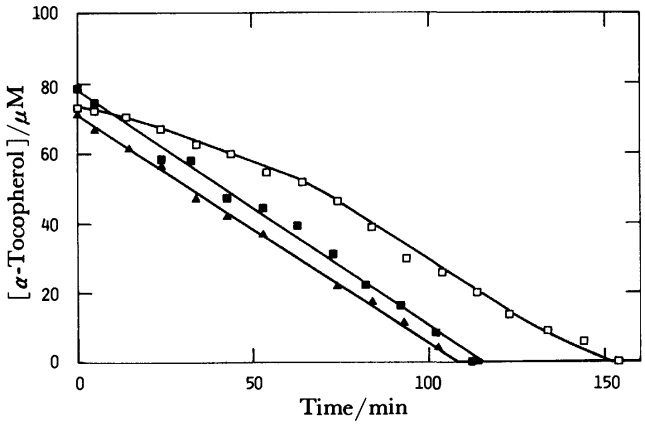

Fig. 3. Rate of disappearance of α-tocopherol during the oxidation of methyl linoleate micelle in 0.010 M Triton X-100 aqueous dispersion at 37°C under air.
■: [α-tocopherol]=78.7 μM; [uric acid]=none; [AMVN]=13.0 mM, ▲: [α-tocopherol]=71.3 μM; [uric acid]=49.9 μM; [AMVN]=10.9 mM, □: [α-tocopherol]=73.0 μM; [uric acid]=38.3 μM; [AAPH]=17.6 mM.

pH in the presence and absence of uric acid. It shows that pH of the medium has little effect in the absence of uric acid but that the antioxidant activity of uric acid depends on pH and it is not effective as an antioxidant at pH 3.

Although uric acid was an effective antioxidant, hypoxanthine, xanthine, purine, and L-histidine which have similar structures as uric acid did not suppress the oxidation of methyl linoleate in aqueous dispersions initiated with AAPH. Xanthine was not effective as an antioxidant over the pH range between 3 and 9. Indole did not suppress the oxidation of methyl linoleate in benzene solution initiated with AMVN.

Similarly, AMVN located in methyl linoleate micelles in Triton X-100 aqueous dispersions induced the oxidation. AMVN generates initiating free radicals

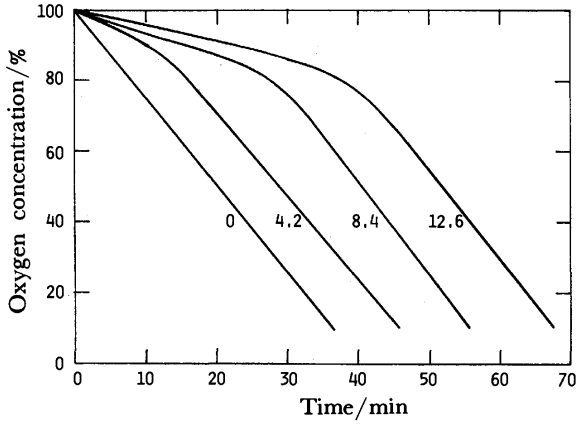

Fig. 4. Inhibition of oxidation of 1.95 mM soybean PC liposome by uric acid in 0.1 M NaCl aqueous dispersion at 37°C under air initiated with 10 mM AAPH. Rate of oxygen uptake was followed by oxygen electrode. Number show the concentration of uric acid in μM.

in the lipid region of micelles. Interestingly, however, uric acid could not suppress the oxidation when it was initiated with AMVN, suggesting that uric acid located in an aqueous phase can not scavenge radicals that are present in the lipid region of micelles, as observed for ascorbic acid.[15,16]

Figure 3 shows the rate of decay of α-tocopherol in the presence and absence of uric acid during the oxidation of methyl linoleate micelles in aqueous dispersions initiated with AAPH or AMVN. In the absence of uric acid, α-tocopherol disappeared linearly with time. In the presence of uric acid, the rate of decay of α-tocopherol was suppressed when the oxidation was initiated with AAPH, whereas uric acid had little effect on the rate of α-tocopherol consumption when the oxidation was initiated with AMVN.

Oxidation of Soybean PC Liposomes and Its Inhibition by Uric Acid. The results are summarized in Table 3 and in Fig. 4. Substantially the same results were obtained as in the oxidation of methyl linoleate micelles in aqueous dispersions. Both AAPH and AMVN induced the oxidation of soybean PC liposomes. Uric acid suppressed the oxidation initiated with AAPH, but it could not suppress the oxidation efficiently when it was induced by AMVN. The induction period was proportional to the concentration of uric acid.

Quantitative Evaluation of Antioxidant Activity of Uric Acid. The oxidation of lipids initiated with AAPH (A-N=N-A) proceeds by the following mechanism.[15-17,25,26]

Initiation:

$$\text{A-N=N-A} \xrightarrow{k_d} [\text{A}\cdot\ \text{N}_2\ \cdot\text{A}] \longrightarrow (1-e)\text{A-A} \quad (1)$$

$$\searrow\ 2e\text{A}\cdot \quad (2)$$

$$\text{A}\cdot + \text{O}_2 \xrightarrow{k_3} \text{AO}_2\cdot \quad (3)$$

Table 3. Inhibition of Oxidation of Soybean PC Liposomes by Uric Acid under Air at 37°C[a)]

[PC][b)]	[AAPH][c)]	[UA]	t_{inh}	R_{inh}[d)]	R_p[e)]	$(kcl)_p$[f)]	$r^{2,g)}$	k_{inh}/k_6
mM	mM	μM	s	nM/s	nM/s			
1.95	10.0	0	0		87.4	29		
1.95	10.0	4.21	820	44.5	87.8	29	0.0441	1.0×10^4
1.64	10.0	7.87	1610	22.2	61.5	20	0.0081	2.5×10^4
1.95	10.0	8.42	1660	29.6	94.1	31	0.1000	2.3×10^4
1.95	10.0	12.6	2350	23.1	91.9	30	0.0049	3.1×10^4

a) Concentrations are for total aqueous dispersions. b) Concentration of neat soybean PC is 1.16 M. c) $R_i(aq)=1.30\times10^{-6}$[AAPH]$=1.30\times10^{-8}$ M/s. $R_i(lipid)=3.06\times10^{-9}$ M/s. d) Rate of oxidation during the induction period. e) Rate of oxidation after induction period. f) Kinetic chain length after induction period. g) Same as footnote f in Table 2.

$$AO_2\cdot + IH \xrightarrow{k_{inh}} \text{stable products} \quad (4)$$

$$AO_2\cdot + AO_2\cdot \xrightarrow{k_t} \text{stable products} \quad (5)$$

$$AO_2\cdot + LH \xrightarrow{k_6} AOOH + L\cdot \quad (6)$$

Propagation:

$$L\cdot + O_2 \xrightarrow{k_7} LO_2\cdot \quad (7)$$

$$LO_2\cdot + LH \xrightarrow{k_p} LOOH + L\cdot \quad (8)$$

Termination:

$$2LO_2\cdot \xrightarrow{k_t} \text{non-radical products} \quad (9)$$

The water soluble AAPH generates geminate radicals by its thermal decomposition, a portion of which recombine within the solvent cage (reaction 1) but rest of them escape from the solvent cage and become free radicals (reaction 2). They rapidly interact with oxygen to give peroxyl radicals (reaction 3). The peroxyl radicals are either scavenged by an antioxidant (IH) that is present in the aqueous phase (reaction 4), interact with another peroxyl radical to give stable products (reaction 5), or attack micelles or liposomes and abstract active, doubly-allylic hydrogens from lipids (LH) (reaction 6) to initiate free radical chain oxidation (reactions 7 and 8). As shown above, the uric acid in the aqueous phase can not scavenge radicals in the lipid region and therefore the chains are terminated by bimolecular interactions of lipid peroxyl radicals (reaction 9). Thus the oxidation proceeds by a free radical chain mechanism and one initiating radical can produce many lipid peroxides.

When the rate of chain initiation is constant, that is, when the new chains are started at a constant rate, the steady state treatment can be applied for the reaction sequence 1 to 9.

The rate of free radical generation in an aqueous phase from AAPH, $R_i(aq)$, is given by

$$R_i(aq) = 2ek_d[AAPH] = n[CTMC]/t_{inh} \quad (10)$$

where e is the efficiency of free radical production and k_d is the rate constant for the unimolecular decomposition of AAPH. The rate of radical generation in an aqueous phase can be determined from the induction period (t_{inh}) produced by CTMC. The stoichiometric number (n) of peroxyl radicals trapped by each CTMC was assumed to be 2.[15,25,27)]

On the other hand, the rate of chain initiation, that is, the rate of initial radical generation in the lipid phase, $R_i(lipid)$, was determined from the induction period produced by 2,6-di-*t*-butyl-4-methylphenol incorporated into lipid phase of micelles or liposomes.[22,23,24)] The constant n was taken as 2.[15,22,23)] If all the free radicals from AAPH produced in an aqueous phase attack micelles or liposomes, then $R_i(aq)=R_i(micelle)=R_i(liposome)$.

$$R_i(lipid) = n[IH(lipid)]/t_{inh} \quad (11)$$

The steady state treatment for the above reactions 1 to 9 gives Eqs. 12 to 14,

$$[AO_2\cdot] = \frac{R_i(aq)}{k_{inh}[IH] + (1+\alpha)k_6[LH]} \quad (12)$$

$$[LO_2\cdot] = \left(\frac{k_6[AO_2\cdot][LH]}{2k_t}\right)^{1/2} \quad (13)$$

$$= \left\{\frac{k_6[LH]}{2k_t}\cdot\frac{R_i(aq)}{k_{inh}[IH] + (1+\alpha)k_6[LH]}\right\}^{1/2} \quad (14)$$

where

$$\alpha = 2k_5[AO_2\cdot]^2/k_6[AO_2\cdot][LH] \quad (15)$$

The rate of oxidation during the induction period (R_{inh}) is given by Eqs. 16 to 18,

$$R_{inh} = k_3[A\cdot][O_2] + k_7[L\cdot][O_2] \quad (16)$$

$$= R_i(aq) + k_6[AO_2\cdot][LH] + k_p[LO_2\cdot][LH] \quad (17)$$

$$= R_i(aq) + r^2R_i(aq) + rk_p[LH]\left(\frac{R_i}{2k_t}\right)^{1/2} \quad (18)$$

where

$$r = \left(\frac{k_6[\mathrm{LH}]}{k_{\mathrm{inh}}[\mathrm{IH}] + (1+\alpha)k_6[\mathrm{LH}]}\right)^{1/2} \quad (19)$$

and k_{inh}, k_p, and k_t are the rate constants for scavenging by uric acid of peroxyl radicals derived from AAPH, propagation reaction 8, and termination reaction 9, respectively.

In the absence of an antioxidant or after the induction period, where [IH]=0, $r=(1/(1+\alpha))^{1/2}$, and the rate of oxidation (R_p) is given by Eq. 20.

$$R_p = R_i(\mathrm{aq}) + \frac{1}{1+\alpha}R_i(\mathrm{aq}) + k_p[\mathrm{LH}]\left(\frac{R_i(\mathrm{aq})}{2(1+\alpha)k_t}\right)^{1/2} \quad (20)$$

Equations 18 and 20 gives Eq. 21

$$r = \left\{\frac{R_{\mathrm{inh}}}{R_i(\mathrm{aq})} + \left(\frac{(1+\alpha)^{1/2}R_q}{2R_i(\mathrm{aq})}\right)^2 - 1\right\}^{1/2} - \frac{(1+\alpha)^{1/2}R_q}{2R_i(\mathrm{aq})} \quad (21)$$

where

$$R_q = R_p - R_i(\mathrm{aq}) - \frac{1}{1+\alpha}R_i(\mathrm{aq}) \quad (22)$$

The constant α is the ratio of the rate of reaction 5 to that of reaction 6; that is, the ratio of $AO_2\cdot$ radicals that interact with each other to those that attack lipids. The value $1/(1+\alpha)$ gives the ratio of free $AO_2\cdot$ radicals generated in the aqueous phase that attack lipids in micelles or liposomes in the absence of an antioxidant in the aqueous phase (Eq. 23), and this can be obtained from R_i(aq) and the rate of chain initiation in the lipid phase, R_i(lipid), obtained from Eq. 11. On the other hand, the values of r^2 show the fraction of free $AO_2\cdot$ radicals generated in an aqueous phase that attack lipid in micelles or liposomes instead of being scavenged by uric acid and reacting with another $AO_2\cdot$ radicals.

Since R_i(aq), R_i(lipid), R_{inh}, and R_p can be measured experimentally, and α is calculated from Eq. 24, r can be calculated from Eqs. 21 and 22. Equation 19 gives Eq. 25 and, if k_6 is known, k_{inh} can be obtained.

$$\frac{1}{1+\alpha} = \frac{k_6[\mathrm{AO_2\cdot}][\mathrm{LH}]}{2k_5[\mathrm{AO_2\cdot}]^2 + k_6[\mathrm{AO_2\cdot}][\mathrm{LH}]} \quad (23)$$

$$= \frac{R_i(\mathrm{lipid})}{R_i(\mathrm{aq})} \quad (24)$$

$$\frac{k_{\mathrm{inh}}}{k_6} = \left(\frac{1}{r^2} - 1 - \alpha\right)\frac{[\mathrm{LH}]}{[\mathrm{IH}]} \quad (25)$$

Figure 5 shows the plot of induction period observed in the presence of uric acid and CTMC. The induction period was proportional to the concentration of antioxidant and inversely proportional to that of

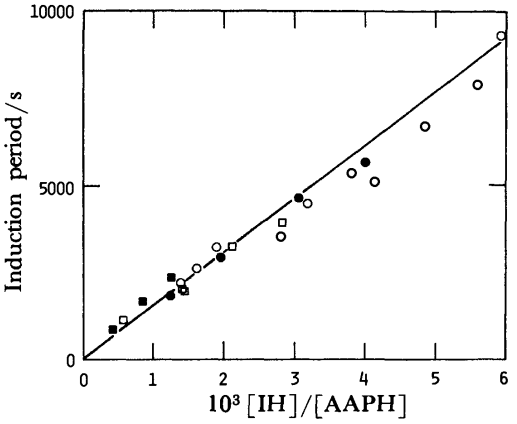

Fig. 5. Plot of induction period as a function of [antioxidant]/[AAPH] observed in the oxidations of methyl linoleate micelles and soybean phosphatidylcholine liposomes in aqueous dispersions initiated with AAPH and inhibited by uric acid and 2-carboxy-2,5,7,8-tetramethyl-6-chromanol (CTMC) at 37°C.

	Uric acid	CTMC
Micelles	□	○
Liposomes	■	●

AAPH as expected from Eq. 10. It is noteworthy that the same induction periods were observed in micelle and liposome systems. Furthermore, CTMC and uric acid gave substantially the same induction period, suggesting that both of them have same n values. Since the value of n for CTMC may reasonably be assumed to be 2,[15,25,27] the n value for uric acid must be also 2. The rate of free radical generation in an aqueous phase was obtained from Fig. 5 as

$$R_i(\mathrm{aq}) = 1.30 \times 10^{-6}[\mathrm{AAPH}] \quad (\mathrm{s^{-1}}) \quad (26)$$

In Tables 2 and 3 are shown the rates of oxidation of methyl linoleate micelles and soybean phosphatidylcholine liposomes during and after the induction period. The values of r^2 calculated from Eq. 21 are also included in Tables 2 and 3. They show that substantially all of the peroxyl radicals derived from AAPH are scavenged by uric acid before they attack lipids in micelles and liposomes. The ratio of rate constants, k_{inh}/k_6, calculated for micelle and liposome systems from Eq. 25 is also included in Tables 2 and 3 respectively. Since r values are obtained from Eq. 21 as a small difference between large numbers, these values may contain considerable error, but the average values of k_{inh}/k_6 are obtained as 5.8×10^5 and 2.2×10^4 for micelle and liposome systems respectively.

The difference between R_i(aq), R_i(micelle), and R_i(liposome) is interesting. The rates of radical production in aqueous phase are similar in micelles

and in liposome systems as shown in Fig. 5. The ratio is R_i(aq): R_i(micelle): R_i(liposome)=1.30×10^{-6}: 8.12×10^{-7}: 3.06×10^{-7}=1:0.62:0.24, when the lipid concentrations in total aqueous dispersions are about 110 and 2 mM for micelle and liposome systems respectively. This shows that under these conditions, considerable amounts of the radicals generated in an aqueous phase are terminated and only small fraction of the free radicals attack lipids and initiate chain oxidation even in the absence of an antioxidant in the aqueous region. In other words, the structure of liposomal membranes is by itself effective in protecting from the attack of oxygen radicals.

If we consider the concentration difference, it may be said that liposomes are more readily attacked than micelles by oxygen radicals. The higher k_{inh}/k_6 for micelle systems than that for liposome systems must be also ascribed to less accessibility of peroxyl radicals to lipids in micelles than to those in liposomes. These results are consistent with the previous finding that ascorbic acid can interact, although less readily than in homogeneous solution, with peroxyl radicals in liposomes whereas it can not interact with peroxyl radicals in micelles,[28] and that ascorbic acid, cysteine, and glutathione located in aqueous phase interact faster with galvinoxyl radical located in liposomes than they do with galvinoxyl located in micelles in Triton X-100 aqueous dispersions.[29] It may be noteworthy, however, that the reactivity of lipids in micelles toward radicals in aqueous phase must depend on the surfactant.

Synergistic Inhibition with Vitamin E. Ascorbic acid inhibits the oxidation synergistically in combination with vitamin E.[14,15,28,30-40] It has been shown[14,15,28,38-40] that ascorbic acid reacts with vitamin E radical to regenerate vitamin E. It was examined whether uric acid could interact with vitamin E radical and inhibit the oxidation synergistically. That the rate of disappearance of α-tocopherol during the oxidation initiated with AAPH was suppressed by uric acid (Fig. 3) must be due to the trapping by uric acid of radicals from AAPH rather than the trapping of substrate peroxyl radicals and/or α-chromanyloxyl radical from α-tocopherol and it does not necessarily indicate the interaction of uric acid with α-chromanyloxyl radical.

It has been found[28] previously that ascorbic acid in an aqueous phase can interact with chromanyloxyl radical from 2,2,5,7,8-pentamethyl-6-chromanol (PMC) located in micelles and that ascorbic acid can contribute to the inhibition of the oxidation of methyl linoleate micelles in aqueous dispersions in the presence of PMC even though the oxidation is initiated with AMVN and ascorbic acid can not scavenge lipid peroxyl radicals in the oil region. However, uric acid did not show any synergistic activity in the similar oxidation of methyl linoleate micelles in the presence of PMC initiated with AMVN. The above results and Fig. 3 suggest either that uric acid does not interact with chromanoxyl radical at all or that its rate is not fast enough to compete with the interaction of chromanoxyl radical with peroxyl radical.

This study was supported in part by Grant-in-Aid for Scientific Research from the Ministry of Education, Science and Culture.

References

1) "Tocopherol, Oxygen, and Biomembranes," ed by C. de Duve and O. Hayaishi, Elesvier, Amsterdam (1978).
2) "Oxygen Free Radicals and Tissue Damage," (Chiba Foundation Symp. 65), Excerpta Medica, Amsterdam (1979).
3) "Biochemical and Clinical Aspects of Oxygen," ed by W. S. Caughey, Academic Press, New York (1979).
4) "Autoxidation in Food and Biological Systems," ed by M. G. Simic and M. Karel, Plenum Press, New York (1980).
5) "Age Pigments," ed by R. S. Sohal, Elsevier/North Holland Biomedical Press, Amsterdam (1981).
6) "Free Radicals, Lipid Peroxidation and Cancer," ed by D. C. H. McBrien and T. F. Slater, Academic Press, London (1982).
7) "Lipid Peroxides in Biology and Medicine," ed by K. Yagi, Academic Press, New York (1982).
8) "Oxy Radicals and Their Scavenger Systems," ed by G. Cohen and R. A. Greenwald, Elsevier Biomedical, New York (1983).
9) "Oxygen Radicals in Chemistry and Biology," ed by W. Bors, M. Saran, and D. Tait, Walter de Gruyter, Berlin (1984).
10) W. A. Pryor, *Ann. New York Acad. Sci.*, **393**, 1 (1982).
11) B. Halliwell and J. M. C. Gutteridge, *Biochem. J.*, **219**, 1 (1984).
12) G. W. Burton, A. Joyce, and K. U. Ingold, *Arch. Biochem. Biophys.*, **221**, 281 (1983).
13) W. M. Cort, "Ascorbic Acid: Chemistry, Metabolism, and Uses," ed by P. A. Seib, and B. M. Tolbert, American Chemical Society, Washington, D. C. (1982), p. 533.
14) E. Niki, T. Saito, and Y. Kamiya, *Chem. Lett.*, **1983**, 631.
15) E. Niki, T. Saito, A. Kawakami, and Y. Kamiya, *J. Biol. Chem.*, **259**, 4177 (1984).
16) Y, Yamamoto, S. Haga, E. Niki, and Y. Kamiya, *Bull. Chem. Soc. Jpn.*, **57**, 1260 (1984).
17) Y, Yamamoto, E. Niki, Y, Kamiya, and H. Shimasaki, *Biochim. Biophys. Acta*, **795**, 332 (1984).
18) S. Matsushita, F. Ibuki, and A. Aoki, *Arch. Biochem. Biophys.*, **102**, 446 (1963).
19) E. W. Kellogg, III, and I. Fridovich, *J. Biol. Chem.*, **252**, 6721 (1977).
20) B. N. Ames, R. Cathcart, E. Schwiers, and P. Hochstein, *Proc. Natl. Acad. Sci. U. S. A.*, **78**, 6858 (1981).
21) K. J. Kittridge, and R. L. Willson, *FEBS Lett.*, **170**, 162 (1984).
22) C. E. Boozer, G. S. Hammond, and J. N. Sen, *J. Am. Chem. Soc.*, **77**, 3233 (1955).
23) G. W. Burton, and K. U. Ingold, *J. Am. Chem. Soc.*, **103**, 6472 (1981).
24) E. Niki, Y. Kamiya, and N. Ohta, *Bull. Chem. Soc. Jpn.*, **42**, 3220 (1969).

25) L. R. C. Barclay and K. U. Ingold, *J. Am. Chem. Soc.*, **103**, 6478 (1981).
26) Y. Yamamoto, E. Niki, and Y. Kamiya, *Bull. Chem. Soc. Jpn.*, **55**, 1548 (1982).
27) L. R. C. Barclay, S. J. Locke, J. M. MacNeil, J. Van Kessel, G. W. Burton, and K. U. Ingold, *J. Am. Chem. Soc.*, **106**, 2479 (1984).
28) E. Niki, A. Kawakami, Y. Yamamoto, and Y. Kamiya, *Bull. Chem. Soc. Jpn.*, **58**, 1971 (1985).
29) J. Tsuchiya, T. Yamada, E. Niki, and Y. Kamiya, *Bull. Chem. Soc. Jpn.*, **58**, 326 (1985).
30) C. Golumbic, and H. A. Mattill, *J. Am. Chem. Soc.*, **63**, 1279 (1941).
31) A. L. Tappell, *Geriatrics*, **23**, 97 (1968).
32) W. M. Cort, *J. Am. Oil Chem. Soc.*, **51**, 321 (1974).
33) A. H. Nathanus and A. E. Kitabchi, *Biochim. Biophys. Acta*, **399**, 244 (1975).
34) L. H. Chen, M. S. Lee, W. F. Hsing, and S. H. Chen, *Int. J. Nutr. Res.*, **50**, 156 (1980).
35) H.-W. Leung, M. J. Vang, and R. D. Mavis, *Biochim. Biophys. Acta*, **664**, 266 (1981).
36) L. J. Machlin, and E. Gabriel, *Ann. New York Acad. Sci.*, **355**, 98 (1980).
37) L. R. C. Barclay, S. J. Locke, and J. M. MacNeil, *Can. J. Chem.*, **61**, 1288 (1983).
38) J. E. Packer, T. F. Slater, and R. L. Willson, *Nature*, **278**, 737 (1979).
39) E. Niki, J. Tsuchiya, R. Tanimura, and Y. Kamiya, *Chem. Lett.*, **1982**, 789.
40) M. Scarpa, A. Rigo, M. Maiorino, F. Ursini, and C. Gregolin, *Biochim. Biophys. Acta*, **801**, 215 (1984).

 © 1986 The Chemical Society of Japan Bull. Chem. Soc. Jpn., 59, 479—482 (1986)

Addition Reaction of 1,4-Dibromo-2,5-piperazinedione with 3,4-Dihydro-2*H*-pyran

Kuniaki ITOH* and Akira SERA
Department of Science of Material Reaction, Division of Science of Materials, Graduate School of Science and Technology, Department of Chemistry, Faculty of Science, Kobe University, Kobe 657
(Received May 4, 1985)

Reaction of 1,4-dibromo-2,5-piperazinedione (**1**) with 3,4-dihydro-2*H*-pyran (**2**) under irradiation gave 1 : 1- and **1** : 2-addition products (**3**,**4**) and corresponding secondary products (**5**—**7**). The adducts were considered to be produced separately by photoinduced free radical addition as well as concomitant ionic addition reactions.

Reactions of *N*-bromosuccinimide (NBS) with olefins are characterized as allylic brominations and additions to double bonds.[1] The majority of the NBS-reactions have been postulated to involve a free radical chain mechanisms, though different chain transfer species participate: a bromine atom[1] or a succinimidyl radical[2-4] according to the reaction conditions. Incremona and Martin[5] however, claimed that reactions of *N*-bromotetrafluorosuccinimide (NBTFS) with olefins were considerably different from those of NBS, and proposed an ionic reaction pathway for these reactions. The ionic reactivity of NBTFS was attributed to the electron-withdrawing inductive effect of the fluorine substituent of NBTFS. We have reported that irradiation of 1,4-dibromo-2,5-piperazinedione (**1**) with cyclohexene or 1-alkenes in acetonitrile gave addition products produced by a free radical mechanism. The reactions were rationalized by taking into account an initial attack of the 2,5-dioxo-1-piperazinyl radical in the olefinic double bonds to give stable radical intermediates.[6,7] However, minor intervention of a concomitant ionic addition mechanism could not be ruled out. In this paper, we describe the reaction of **1** with 3,4-dihydro-2*H*-pyran (**2**) which is more susceptible to ionic addition reactions than cyclohexene or 1-alkenes. The addition reaction of **1** to **2** was suggested to proceed by two pathways, a free radical and an ionic process, to give two types of addition products, respectively.

Results and Discussion

The photoreaction of 1,4-dibromo-2,5-piperazinedione (**1**) with 3,4-dihydro-2*H*-pyran (**2**) was carried out in acetonitrile using a high pressure mercury lamp. The photolysate was separated by silica-gel column

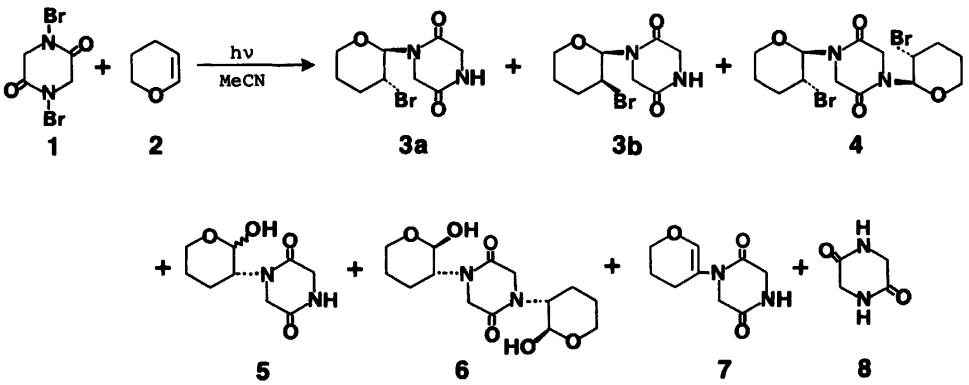

Scheme 1.

Table. Product Distribution of Addition of 1,4-Dibromo-2,5-piperazinedione (**1**) to 3,4-Dihydro-2*H*-pyran (**2**) in Acetonitrile under Irradiation[a]

Entry	1,2-Epoxybutane mmol	Temperature	Reaction time/h	Yield/%[b] 3a	3b	4	5	6	7	8
1	—	Room temp	3	———			Trace		———	44
2	40	Room temp	3	8	4	2	7	8	9	42
3[c]	40	Room temp	3	9	5	2	3	4	5	51
4	40	0°C	3	7	4	4	12	12	15	32
5[d]	40	Room temp	3	5	2	———	Trace	———	2	75[e]
6[d]	40	Room temp	24	15	7	6	2	2	4	55

a) A solution of **1** (10 mmol) and **2** (100 mmol) in acetonitrile (50 cm^3) was irradiated in the presence of the addendum given in the Table. b) Isolated yields are given as averages of three experiments, and on the basis of **1** employed. c) In the presence of hydroquinone (2 mmol). d) Under dark conditions. e) Contained a considerable amount of **1**.

chromatography and the structures of the products were determined by elemental and spectroscopic analyses. The results are summarized in Table.

Irradiation of **1** with **2** in acetonitrile gave only 2,5-piperazinedione (**8**) as an isolable product accompanied by a large amount of polymeric products. The dione **8** was derived from **1** by either hydrogen abstraction of the 2,5-dioxo-1-piperazinyl radical intermediate or protonation on the corresponding anion.[6] The polymeric products may come from **2** via the well-known acid catalyzed polymerization. When the reaction was performed in the presence of 1,2-epoxybutane (a hydrogen bromide scavenger), the formation of the polymers was greatly depressed. In the presence of 1,2-epoxybutane, the reaction gave a considerable amount of addition products (Scheme 1). These adducts consisted of bromine-containing 1:1- and 1:2-adducts (**3** and **4**), hydroxyl group-containing 1:1- and 1:2-adducts (**5** and **6**). A substituted 3,4-dihydro-2*H*-pyran (**7**) was also produced. The bromine-containing 1:1-adduct (**3**) was rechromatographed to give isomers **3a** and **3b** (approx. 2:1).

Both **3a** and **3b** had a bromine substituent (MS), and an NH group (IR and NMR). They gave similar NMR and IR spectra which demonstrated the presence of a 2,5-dioxo-1-piperazinyl group at C_1 of the respective tetrahydropyran ring. That is, both adducts showed characteristic infrared absorptions (1690, 1445—1460, 1190—1215 cm^{-1}) of a 2,5-piperazinedione moiety, and their NMR spectra showed signals of protons on bromine-bearing carbon atoms (C_2 of the tetrahydropyran ring) [**3a**; δ=4.0—4.6, m, and **3b**; δ=4.56, br.], and those on C_1 of the tetrahydropyran ring [**3a**; δ=5.43, d, J=10 Hz (axial-H_1/axial-H_2), and **3b**; δ=5.19, J=2 Hz (axial-H_1/equatorial-H_2)]. Treatment of **3a** and **3b** with tributyltin hydride led to the same reduced product, 1-(2-tetrahydropyranyl)-2,5-piperazinedione. This observation indicated that these two 1:1-adducts are a pair of stereoisomers at the bromine-bearing carbon atom. From these results, the stereochemistry was deduced as trans for the major isomer **3a** and cis for the minor isomer **3b**.[8] The bromine containing 1:2-adduct (**4**) bore two bromine atoms (MS), and showed no NH absorption on its IR spectrum. The features of the NMR spectra of **4** were similar to those of **3a**. Thus the structure of **4** was determined as *trans,trans*-1,4-bis(3-bromo-2-tetrahydropyranyl)-2,5-piperazinedione. Neither the trans, cis, nor the cis, cis isomer was isolated.

On the other hand, the adducts **5** and **6** were determined to be 3-substituted 2-hydroxytetrahydropyran derivatives by the following spectroscopic analysis. The presence of hydroxyl groups in **5** and **6** was characterized by their IR absorption (ν_{OH} 3400 cm^{-1}) and MS peaks (M^+-H_2O and M^+-2H_2O). The adduct **5** consisted of two isomers; which were hardly separated on TLC. The NMR spectra of **5** showed complex signals indicating that it contained two configurational isomers. That is, there were two hemiacetal hydroxylic groups at δ=6.29 (a doublet, coupled with an adjacent methine proton with J=4.5 Hz) and at δ=6.42 (another doublet, coupled with another adjacent methine proton with J=6 Hz). Two respective hemiacetal methine protons were also observed at δ=4.79 (dd, J=2 and 4.5 Hz) and at δ=4.57 (dd, J=6 and 8 Hz). The former was presumed to be an equatorial hemiacetal methine proton and the latter to be an axial hemiacetal methine proton, and their coupling constants indicated the presence of axial protons on C_2, to which an equatorial 2,5-piperadinedione moiety was attached. The NMR spectra also indicated a hemiacetal structure for the 1:2-adduct **6**. The methine protons resonated at δ=4.70 as a double doublet with J=6 and 12 Hz, which may be assigned to axial protons on C_1 with adjacent axial protons on C_2 as mentioned above. The spectra of **7** were also found to be consistant with the structure given in Scheme 1.

The position of the bromine substituent(s) of the bromine-containing adducts (**3** and **4**) suggested that a species to attack the double bond of **2** was either a bromine cation to give a 3-bromo-1-tetrahydropyranyl cation, or a bromine radical to give a corresponding radical. In the presence of hydroquinone, the reaction gave **3** and **4** in almost unchanged yields, while the yields of **5**—**7** were considerably depressed. In addition, the reactions in the dark[9] afforded **3** and **4** in increased yields, while **5**—

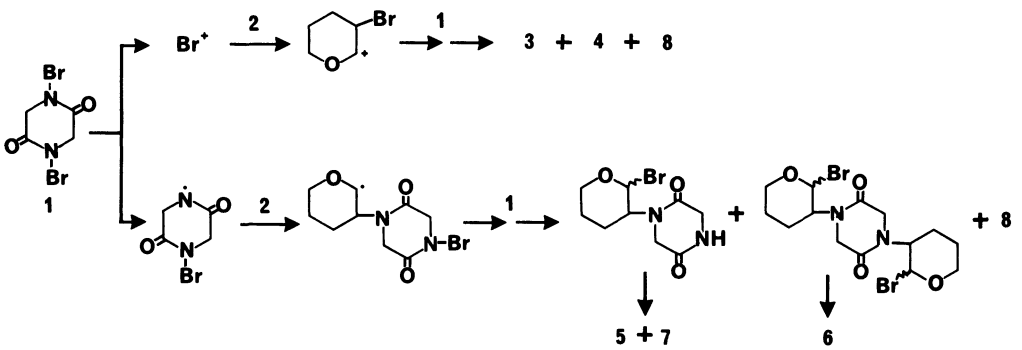

Scheme 2.

7 in highly decreased yields. These observations may rule out the radical addition mechanism for the formation of **3** and **4**. Thus the bromine cation produced by heterolysis of the N–Br bond of **1** added to **2** to give the 3-bromo-1-tetrahydropyranyl cation, which in turn reacted with the 2,5-dioxo-1-piperazinyl anion to afford the adducts **3** and **4**. In the reaction of **1** with cyclohexene in acetonitrile under similar conditions, 2-acetylamino-1-bromocyclohexane was isolated. This was thought to be derived by a Ritter-type addition of the 2-bromocyclohexyl cation to acetonitrile.[6] However, in the present reactions, no 2-acetylamino-3-bromotetrahydropyran, a corresponding Ritter-type product, was detected.

On the other hand, the hydroxyl group-containing adducts (**5** and **6**), and the dihydropyran derivative (**7**) were presumed to be secondary products derived from other bromine-containing adducts produced through a radical addition of **1** to **2**. We had previously shown that the radical reactions of **1** with cyclohexene and 1-alkenes revealed a solvent dependent product distributions.[6,7] In carbon tetrachloride, which is a poor solvent for **1** (under essentially heterogeneous conditions), allylic bromination and bromine addition to the double bonds were the dominant processes. Contrarily, in acetonitrile (a good solvent for **1**) the radical addition of **1** to the double bonds became the main reaction path, in which the 2,5-dioxo-1-piperazinyl radical added initially to the less substituted carbon atoms of the respective double bonds to give more stable radical intermediates.[7] Tedder and Walton[10] reported that addition of a radical to a vinyl ether gave preferentially a 1-alkoxy-1-alkyl radical. Accordingly, a primary radical expected from addition of the 2,5-dioxo-1-piperazinyl radical to **2** should be a 3-(4-bromo-2,5-dioxo-1-piperazinyl)-2-tetrahydropyranyl radical. The radical thus formed would abstract a bromine atom from **1** to give 1-(2-bromo-3-tetrahydropyranyl)-2,5-piperazinedione (not isolated). 1,4-Bis(2-bromo-3-tetrahydropyranyl)-2,5-piperazinedione (not isolated) woubd be produced in a similar manner. We had observed previously that 1- and 1,4-bis(2-bromoalkyl)-2,5-piperazinediones are spontaneously hydrolyzed during chromatographic separation to give corresponding 2-hydroxyalkyl derivatives.[7] Participation of the neighboring N-function was responsible for the observed ease of hydrolysis. In the present cases, the bromine substituents of the above mentioned bromotetrahydropyranyl-2,5-piperazinediones were undoubtedly more easily hydrolyzed to give **5** and **6**, because of the hemiacetal character of the bromine-bearing carbon atoms. The substituted 3,4-dihydro-2*H*-pyran (**7**) was considered to be formed by concomitant dehydrobromination of 1-(2-bromo-3-tetrahydropyranyl)-2,5-piperazinedione.

It was suggested that in the reaction of 1,4-dibromo-2,5-piperazinedione (**1**) with 3,4-dihydro-2*H*-pyran (**2**) the two processes, the radical addition and the ionic addition, were operating concurrently to give the corresponding adducts (Table). In dark conditions, the ionic addition predominated, but the radical addition was not completely depressed. Hydroquinone decreased the yields of the radical addition products, whereas those of the ionic addition products remained unchanged. Low temperature seemed to favor the radical addition process as described in the case of NBS.[4]

Experimental

3,4-Dihydro-2*H*-pyran and 1,2-epoxybutane were dried over Molecular Sieve 4A and distilled over copper(I) chloride prior to use. Acetonitrile was dried over calcium hydride and distilled. 1,4-Dibromo-2,5-piperazinedione was prepared according to the procedure reported earlier.[11] IR spectra (KBr) were recorded with JASCO IR-A-1 and -3 spectrometers. NMR spectra were measured on JEOL JMN-PMX-60 and-PS-100 specrometers using tetramethylsilane as the internal standard. Mass spectra were obtained by an ESCO EMD-05A spectrometer. Irradiation was carried out using a Halos EHB-WU high pressure mercury arc lamp (100 W).

Reaction of 1,4-Dibromo-2,5-piperazinedione (1) with 3,4-Dihydro-2*H*-pyran (2) in the Presence of 1,2-Epoxybutane. A typical experimental procedure is described. Irradiation of a mixture containing 2.72 g (10 mmol) of **1**, 8.41 g(100 mmol) of **2**, and 1,2-epoxybutane (2.88 g, 40 mmol) in acetonitrile (50 cm^3) was carried out for 3 h at room temperature with stirring. The resulted mixture was filtered to give 2,5-piperazinedione (**8**). The filtrate was evaporated to a syrup, which was separated on a silica-gel column using benzene–acetone (4:1) as eluant. Yields are given in Table as an average of three experiments on the basis of **1** employed. Physical constants of respective products are shown below.

***trans*-1-(3-Bromo-2-tetrahydropyranyl)-2,5-piperazinedione (3a):** Mp 195 °C (decomp). IR; 3200, 1690, 1450, 1330, 1215, 1060, and 720 cm^{-1}. ^1H NMR (DMSO-d_6); δ=1.4—2.3 (4H, m, $-(CH_2)_2-$), 3.4—4.3 (2H, m, O-CH_2-), 3.77 (4H, s, ring H), 4.0—4.6 (1H, m, -CHBr-), 5.43 (1H, d, J=10 Hz, O-CH-N), and 8.00 (1H, s, NH). MS (*m/z*); 278, 276(M^+), 197, 169, 115, and 114. Found: C, 39.04; H, 4.67%. Calcd for $C_9H_{13}BrN_2O_3$; C, 39.01; H, 4.73.

***cis*-1-(3-Bromo-2-tetrahydropyranyl)-2,5-piperazinedione (3b):** Mp 175 °C (decomp). IR; 3200, 1690, 1670, 1460, 1320, 1205, 1080, and 760 cm^{-1}. ^1H NMR (DMSO-d_6); δ=1.3—2.4 (4H, m, $-(CH_2)_2-$), 3.4—4.3 (2H, m, O-CH_2-), 3.79—3.91 (centers) (2H, AB-quartet, J=2 Hz, ring H), 4.56 (1H, broad, -CHBr-), 5.19 (1H, d, J=2Hz, O-CH-N), and 7.97 (1H, s, NH). MS (*m/z*); the same as those of **3a**. Found: C, 39.05; H, 4.84%. Calcd; see above.

1,4-Bis(3-bromo-2-tetrahydropyranyl)-2,5-piperazinedione (4): Mp 185 °C (decomp). IR; 1690, 1445, 1310, 1190, 1060, and 710 cm^{-1}. ^1H NMR (DMSO-d_6); δ=1.5—2.8 (8H, m, $-(CH_2)_2-$), 3.4—3.8 (4H, m, O-CH_2-), 3.95 (4H, s, ring H), 4.0—4.6 (2H, m, -CHBr-), and 5.42 (2H, d, J=9 Hz, O-CH-N). MS (*m/z*); 442, 440, 438(M^+), 361, 359, 240, 197, 165, 112, and 111. Found: C, 38.30; H, 4.86%. Calcd for $C_{14}H_{20}Br_2N_2O_4$; C, 38.21; H, 4.58%.

1-(2-Hydroxy-3-tetrahydropyranyl)-2,5-piperazinedione (5): Mp 162—164 °C. IR; 3400, 3200, 1635, 1460, 1325, and 1060

cm^{-1}. ^1H NMR (DMSO-d_6); δ=1.2—2.1 (4H, m, $-(CH_2)_2-$), 3.2—4.3 (2H, m, $O-CH_2-$), 3.69 (2H, s, ring H), 3.74 (2H, AB quartet, J=4 Hz, ring H), 4.0—4.3 (1H, m, -CH-N), 4.57 and 4.79 (1H, two dd, J=6 and 8 Hz; 2 and 4.5 Hz, -CH-OH), 6.29 and 6.42 (1H, two d, J=4.5 and 6 Hz, OH), and 7.85 (1H, s, NH).. MS (*m/z*); 196 (M^+-H_2O), 166, 112, 84, and 56. Found: C, 50.36; H, 6.74%. Calcd for $C_9H_{14}N_2O_4$; C, 50.46; H, 6.59%.

1,4-Bis(2-hydroxy-3-tetrahydropyranyl)-2,5-piperazinedione (6): Mp 185 °C (decomp). IR; 3400, 3230, 1670, 1460, 1325, and 1060 cm^{-1}. ^1H NMR (DMSO-d_6); δ=1.1—2.2 (8H, m, $-(CH_2)_2-$), 3.3—4.3 (4H, m, $O-CH_2-$), 3.83 (4H, s, ring H), 4.0—4.3 (2H, m, -CH-N), and 4.70 (2H, dd, J=6 and 12 Hz, -CH-OH). MS (*m/z*); 296 (M^+-H_2O), 278 (M^+-2H_2O), 196, 166, 112, 84, 56. Found: C, 53.19; H, 6.75%. Calcd for $C_{14}H_{22}N_2O_6$; C, 53.49; H, 7.05%.

1-(3,4-Dihydro-2*H*-pyran-5-yl)-2,5-piperazinedione (7): Mp 210 °C (decomp). IR; 3220, 1660, 1460, 1325, and 1090 cm^{-1}. ^1H NMR (DMSO-d_6); δ=1.5—2.4 (4H, m, $-(CH_2)_2-$), 3.73 (2H, d, J=1 Hz, ring H), 3.90 (2H, s, ring H), 3.7—4.0 (2H, m, $O-CH_2-$), 6.49 (1H, t, J=1 Hz, O-CH=), and 7.49 (1H, s, NH). MS (*m/z*), 196(M^+), 166, 112, and 84. Found; C, 54.83; H, 6.25%. Calcd for $C_9H_{12}N_2O_3$; C, 55.09; H, 6.16%.

Reduction of 1,4-Bis(3-bromo-2-tetrahydropyranyl)-2,5-piperazinedione (4) with Tributyltin Hydride. The compound **4** (108 mg, 0.24 mmol), tributyltin hydride (180 mg, 0.62 mmol), and AIBN (20 mg) were dissolved in 50 cm^3 of benzene, and the mixture was kept in an atmosphere of nitrogen at 80 °C for 3 h. The solvent was evaporated off and the residue was chromatographed on a silica-gel column using benzene-acetone (4:1) to give 1,4-bis(2-tetrahydropyranyl)-2,5-piperazinedione in 75% yield: Mp 138—140 °C. IR: 1670, 1470, 1330, 1200, 1180, and 1080 cm^{-1}. ^1H NMR ($CDCl_3$); δ=1.3—2.1 (12H, m, $-(CH_2)_3-$), 3.3—4.3 (4H, m, $O-CH_2-$), 3.92 (4H, d, J=3 Hz, ring H), and 5.40 (2H, t, J=6 Hz, O-CH-N). MS (*m/z*); 282(M^+), 199, 115, 114, and 85. Found: C, 59.20; H, 8.00%. Calcd for $C_{14}H_{22}N_2O_4$; C, 59.56; H, 7.85%.

From 1-(3-bromo-2-tetrahydropyranyl)-2,5-piperazinedione (**3a** and **3b**) 1-(2-tetrahydropyranyl)-2,5-piperazinedione was produced. Mp 183—185 °C. IR; 3220, 1700, 1660, 1320, 1200, 1050, and 730 cm^{-1}. ^1H NMR ($CDCl_3$); δ=1.2—2.2 (6H, m, $-(CH_2)_3-$), 3,5—4.4 (2H, m, $O-CH_2-$), 3.95 (4H, s, ring H), 5.45 (1H, t, J=5 Hz, O-CH-N), and 7.20 (1H, s, NH). MS (*m/z*); 198(M^+), 169, 115, 114, and 85. Found: C, 54.40; H, 7.18%. Calcd for $C_9H_{14}N_2O_3$; C, 54.53; H, 7.12%.

References

1) J. S. Pizey, "Synthetic Reagents," Ellis Horword Ltd., Chichester (1974), Vol. II, Chapt. 1.

2) J. C. Day, M. G. Katsaros, W. D. Kocher, A. E. Scott, and P. S. Skell, *J. Am. Chem. Soc.*, **100**, 1950 (1978).

3) R. L. Tlumak and P. S. Skell, *J. Am. Chem. Soc.*, **104**, 7267 (1982).

4) F.-L. Lu, Y. M. A. Naguib, M. Kitadani, and Y. L. Chow, *Can. J. Chem.*, **57**, 1967 (1979).

5) J. H. Incremona and J. C. Martin, *J. Am. Chem. Soc.*, **92**, 627 (1970).

6) K. Itoh, *Bull. Chem. Soc. Jpn.*, **56**, 1705 (1983).

7) K. Itoh, H. Yamada, and A. Sera, *Bull. Chem. Soc. Jpn.*, **57**, 2140 (1984).

8) The reaction of NBS with **2** was reported to yield a small amount (7%) of isomeric 3-bromo-2-succinimidotetrahydropyrans. However, their stereochemistry was not given; C. D. Hurd, J. Moffat, and L. Rosnati, *J. Am. Chem. Soc.*, **77**, 2793 (1955), and J. R. Shelton and C. Cialdella, *J. Org. Chem.*, **23**, 1128 (1958).

9) The reaction was not completed under dark conditions for 3 h (entry 5 in the Table); therefore the reaction was carried out for 24 h.

10) J. M. Tedder and J. C. Walton, *Tetrahedron*, **36**, 701 (1980).

11) A. Sera, H. Yamada, and K. Itoh, *Bull. Chem. Soc. Jpn.*, **53**, 219 (1980).

Synthesis of Sydnone Compounds Substituted by Heteroatom Groups at the 4-Positions

Toshio FUCHIGAMI,* Ching-Sy CHEN, Tsutomu NONAKA,* Mou-Yung YEH,† and Hsien-Ju TIEN†
Department of Electronic Chemistry, Graduate School at Nagatsuta, Tokyo Institute of Technology, Nagatsuta, Midori-ku, Yokohama 227
†Department of Chemistry, National Cheng Kung University, Tainan, Taiwan, Republic of China
(Received May 8, 1985)

A general method for the introduction of heteroatoms to the 4-position of a sydnone ring was developed. Various 4-alkylthio- and 4-arylthiosydnones were prepared in excellent yields by the reaction of 3-aryl-4-lithiosydnones (**2**) with dialkyl and diaryl disulfides. Treatment of **2** with diaryl diselenides, diphenylphosphinous chloride, and arsenic trichloride provided 3-aryl-4-(arylseleno)sydnones, (3-aryl-4-sydnonyl)diphenylphosphine and tris(3-aryl-4-sydnonyl)arsine, respectively, in good yields. It was also found that the reactivity of sydnonyl anions derived from **2** was quite different in some cases from that of the corresponding ordinary aromatic analogues, though the sydnone ring has a somewhat aromatic nature.

Sydnone is a typical mesoionic compound and has been investigated extensively because of its unique electronic structure and biological activity.[1]

As a part of a broad program to study on the synthesis of sydnone compounds and their properties, we reported the synthesis of sydnone derivatives having various kinds of heterocyclic groups at the 4-positions from derivatives of sydnone-4-carboxylic acid[2,3] and 4-(haloacety)sydnones.[4-7]

Although a number of sydnone derivatives have been prepared, relatively few studies on the direct substitution by heteroatoms at the 4-position have been reported.[8-14] All attempts to introduce electron-donating substituents such as hydroxyl, alkoxyl, and amino groups at this position have been unsuccessful so far. Recently, Masuda and Okutani have successfully introduced methylthio and phenylthio groups, i.e. analogues of an alkoxyl group, to the 4-position of sydnones by the use of dimethyl sulfoxide and methyl phenyl sulfoxide, respectively.[10] However, their method has limitation and some problems, because the yields are low except for a few cases and the reaction conditions are not so mild. Since the sydnone ring is unstable to acid, alkali, heat, oxidation, and reduction, the successful synthesis of sydnone derivatives requires quite mild reaction conditions in general. Although 4-lithiosydnone (**2**) can be easily prepared from sydnone (**1**) and butyllithium, very few synthetic studies using **2** have been reported: Especially, very few sydnone derivatives substituted by heteroatoms have been prepared from **2**.[13,14]

From these aspects, at first, a general method for the introduction of sulfur and its analogue, selenium, to the 4-position was developed using **2** as the starting material in this work. And then, some attempts to introduce phosphorus, arsenic, antimony, and tin atoms were also made.

Results and Discussion

Synthesis of 4-Alkylthio- and 4-Arylthiosydnone Compounds (3). It is known that carbanions readily react with disulfides to provide the corresponding sulfides.[15] This method seems suitable for the introduction of thio groups to carbon atoms which have active hydrogens. This prompted us to explore the possibilities of direct introduction of alkylthio and arylthio groups to the 4-position of a sydnone ring by the reaction of 4-lithiosydnone (**2**) with various disulfides. We found that the initial lithiation of sydnones and the subsequent reaction of the resulting **2** with disulfides could be run in sequence in THF below −50°C.

As shown in Table 1, 4-alkylthio- and arylthiosydnone compounds (**3**) were successfully prepared in excellent yields. Bis(2-Benzothiazolyl) disulfides provided 4-(2-benzothiazolylthio)-sydnone (**3d**) in a good yield whereas dimorpholino disulfide did not and large amount of the starting sydnone was recovered. This unsuccessful result may be attributable to higher electron density on the sulfur atoms compared with those of the other disulfides. The higher electron density may be due to the presence of the electron-donating morpholino groups. Two possible

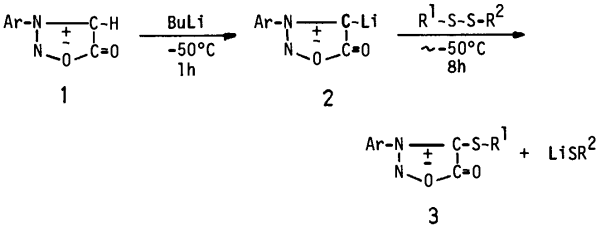

Scheme 1.

products, 4-(2-naphthylthio)sydnone (**3e**) and 4-sydnonyl thiocyanate, were expected to be formed from **2** and 2-naphthalenesulfenyl thiocyanate, however **3e** was obtained as a sole product in a good yield as shown in Scheme 2.

This procedure seems to be an excellent general method for the preparation of 4-alkylthio- and arylthiosydnone derivatives, since the reaction proceeds

Table 1. Synthesis of 4-Thiosydnone Compounds (3)

Compd (3) No.	Ar	R^1	R^2	Yield[a] %	Mp θ_m/°C
3a	Ph	Me	Me	87	101—102 (101.5—102.0)[10]
3b	Ph	Ph	Ph	93	65.0—65.5
3c	Ph	*p*-Tolyl	*p*-Tolyl	98	91—92
3d	Ph	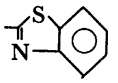	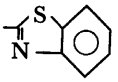	95	107—108
3e	Ph	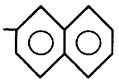	CN	92	134—135 (decomp)
3f	Ph			0	—
3g	*p*-Tolyl	Me	Me	90	90.5—91.5
3h	*p*-Tolyl	Ph	Ph	100	—[b]
3i	*p*-Tolyl	*p*-Tolyl	*p*-Tolyl	98	87.5—88.5
3j	*p*-Tolyl			0	—

a) Crude yield. b) Brown viscous oil.

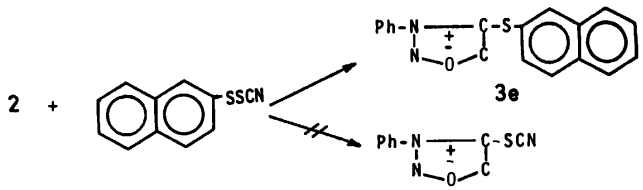

Scheme 2.

under quite mild conditions and almost pure products can be directly obtained.

Synthesis of 4-(Arylseleno)sydnones (4). We extended this process for the preparation of 4-(arylseleno)sydnones (**4**) and 4-(phenyltelluro)sydnone (**5**) using diaryl diselenide and diphenyl ditelluride, respectively. As shown in Tables 2, **4** was obtained in a good yield whereas **5** was not. Although disulfide, diselenide, and ditelluride are analogues, the reactivity of ditelluride to **2** was found to be quite different.

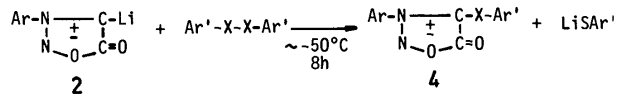

4a : Ar=Ph, Ar'=Ph, X=Se
4b : Ar=p-Tolyl, Ar'=Ph, X=Se
5 : Ar=Ph, Ar'=Ph, X=Te

Scheme 3.

Introduction of Phosphorus Atoms to the 4-Positions of Sydnones. Since it is known that aryllithiums react with various kinds of phosphorus acid esters and halophosphorus compounds to give the corresponding compounds having a C–P bond, the following reactions were examined using **2** as shown in

Table 2. Synthesis of Sydnone Derivatives (4—7)

Compound	Yield[a] %	Mp θ_m/°C
4a	99	83—84
4b	100	90—91
5	0	—
6a	92	175—176
6b	97	164.5—165
7a	99	92
7b	100	91

a) Crude yield.

Scheme 4. 4-Lithiosydnone **2** did not react with the

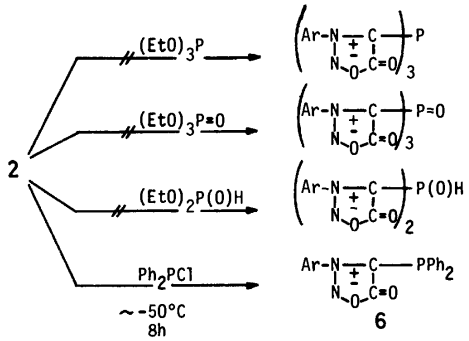

6a : Ar=Ph,
6b : Ar=p-Tolyl

Scheme 4.

phosphorus acid esters used, whereas diphenylphosphinous chloride reacted with **2** to provide 4-(diphenylphosphino)sydnone (**6**) in a good yield. These unsuccessful results may indicate that the reactivity of 4-sydnonyl anion is lower than that of ordinary aryl

anions.

Introduction of Arsenic Atom to the 4-Positions of Sydnones. Since diarylphosphinous chloride and phosphorus trichloride[13] reacted smoothly with **2**, the reaction of **2** with arsenic trichloride was successfully attempted in a similar manner to provide the corresponding tri(4-sydnonyl)arsine (**7**) which is a compound containing three sydnone rings bound to the same central arsenic atom.

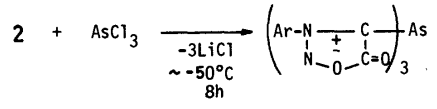

7a : Ar=Ph
7b : Ar=p-Tolyl

Scheme 5.

Attempts to Introduce Tin and Antimony to the 4-Positions of Sydnones. It is known that **2** reacts with chlorotrimethylsilane to give 4-sydnonylsilane.[14] In a similar manner, the reactions of **2** with tin(II) chloride, trimethyltin chloride, antimony trichloride, and antimony pentachloride were carried out. However, all attempts were unsuccessful. Since ordinary aryllithium readily reacts with halostannanes, the unsuccessful result also clearly indicates that the nucleophilicity of 4-sydnonyl anion is weaker than that of ordinary aryl anions.

The new types of sydnone compounds thus prepared are expected to be pharmacologically active and screening tests of several biological activities of these sydnones are currently under investigation.

Experimental

^{1}H NMR spectra were recorded at 60 MHz on a Varian EM-360 spectrometer using $CDCl_3$ and Me_4Si as a solvent and an internal standard, respectively. IR spectra were obtained on a Hitachi 295 infrared spectrometer. Electron impact mass spectra were determined at 30 eV on a JEOL JMS-D100 mass spectrometer by direct introduction via solid probe.

Typical Procedure for the Synthesis of 4-Alkylthio- and Arylthiosydnones (3). Synthesis of 4-Methylthio-3-phenyl-sydnone (3a): To a stirred suspension of 6.2 mmol of 4-phenylsydnone in 10 ml of anhydrous THF was added dropwise 6.5 mmol of a solution of butyllithium in hexane (15%, 4 ml) below −50 °C. After about 1 h of stirring, a solution of 6.2 mmol of diphenyl disulfide in 5 ml of THF was added dropwise to the resulting brown solution below −50 °C. After additional 8 h of stirring, the reaction mixture was poured into ice-water. The precipitating colorless pure product, **3a** was collected by filtration, washed with water, and dried. The yield was 1.15 g; IR (KBr): 3060 (νCH of Ph), 2950 (νCH of Me), 1790, and 1770 cm^{-1} (νC=O). *m/z* 208 (M^+) and 150 (M^+−NO-CO). ^{1}H NMR: δ=2.20 (s, 3H, CH_3) and 7.67 (s, 5H, C_6H_5). Found: C, 51.99; H, 3.96; N, 13.50; S, 15.69%. Calcd for $C_9H_8N_2O_2S$: C, 51.91; H, 3.87; N, 13.45; S, 15.40%.

3-Phenyl-4-(phenylthio)sydnone (3b): A yellow solid (from ethanol). IR (KBr): 3060 (νCH of Ph) and 1770 cm^{-1} (νC=O). *m/z* 270 (M^+) and 212 (M^+−NO-CO). ^{1}H NMR δ=7.16 (s, 5H, C_6H_5S) and 7.60 (s, 5H, C_6H_5). Found: C, 62.32; H, 3.68; N, 10.44; S, 11.65%. Calcd for $C_{14}H_{10}N_2O_2S$: C, 62,21; H, 3.73; N, 10.36; S, 11.86%.

3-Phenyl-4-(*p*-tolylthio)sydnone (3c): A pale yellow solid (from ethanol). IR (KBr): 3070 (νCH of aromatic), 2930 (νCH of Me), 1790 and 1770 cm^{-1} (νC=O). *m/z* 284 (M^+) and 226 (M^+−NO-CO). ^{1}H NMR δ=2.30 (s, 3H, CH_3), 7.07 (s, 4H, *p*-MeC_6H_4), and 7.30—7.80 (m, 5H, C_6H_5). Found: C, 63.33; H, 3.97; N, 9.76; S, 11.18%. Calcd for $C_{15}H_{12}N_2O_2S$: C, 63.36; H, 4.25; N, 9.85; S, 11.28%.

4-(2-Benzothiazolylthio)-3-phenylsydnone (3d): Colorless needles (from ethanol-acetone). IR (KBr): 3070 (νCH of aromatic), 1795, and 1775 cm^{-1} (νC=O). *m/z* 239 (M^+−NO-CO). ^{1}H NMR δ=7.00—8.00 (m, aromatic C-H). Found: C, 55.08; H, 2.71; N, 12.65; S, 19.65%. Calcd for $C_{15}H_9N_3O_2S$: C, 55.03; H, 2.77; N, 12.84; S, 19.59%.

4-(2-Naphthylthio)-3-phenylsydnone (3e): The product **3e** was obtained as a pale yellow solid, which contains ethanol of crystallization after recrystallization from ethanol. IR (KBr): 3070 (νCH of aromatic), 1785, and 1765 cm^{-1} (νC=O). *m/z* 320 (M^+), 262 (M^+−NO-CO), and 46 ($EtOH^+$). ^{1}H NMR δ=1.27 (t, 3H, CH_3CH_2OH), 1.67 (s, 1H, CH_3CH_2OH), 3.75 (CH_3CH_2OH), and 7.10—8.10 (m, 12H, aromatic C-H). Found: C, 65.36; H, 4.82; N, 7.41%. Calcd for $C_{20}H_{18}N_3O_3S$: C, 65.56; H, 4.95; N, 7.63%.

4-Methylthio-3-(*p*-tolyl)sydnone (3g): Colorless prisms (from ethanol). IR (KBr): 3070 (νCH of aromatic), 2930 (νCH of Me), and 1770 cm^{-1} (νC=O). *m/z* 222 (M^+) and 164 (M^+−NO-CO). ^{1}H NMR δ=2.28 (s, 3H, CH_3S), 2.53 (s, 3H, *p*-$CH_3C_6H_4$), and 7.47 (s, 4H, *p*-MeC_6H_4). Found: C, 53.75; H, 4.59; N, 12.36%. Calcd for $C_{10}H_{10}N_2O_2S$: C, 54.04; H, 4.53; N, 12.60%.

4-Phenylthio-3-(*p*-tolyl)sydnone (3h): After reaction, the reaction mixture was poured into ice-water and was repeatedly extracted with dichloromethane. The extracts were dried over anhydrous sodium sulfate and then evaporated to give pure **3h** as brown viscous oil. IR (KBr): 3070 (νCH of aromatic), 2930 (νCH of Me), and 1780 cm^{-1} (νC=O). *m/z* 284 (M^+) and 226 (M^+−NO-CO). ^{1}H NMR δ=2.40 (s, 3H, CH_3), 7.13 (s, 5H, C_6H_5), and 7.26 (s, 4H, *p*-MeC_6H_4). Found: C, 63.23; H, 4.18; N, 9.92; S, 11.27%. Calcd for $C_{15}H_{12}N_2O_2S$ C, 63.36; H, 4.25; N, 9.85; S, 11.28%.

3-(*p*-Tolyl)-4-(*p*-tolylthio)sydnone (3i): A yellow solid (from ethanol). IR (KBr): 3070 (νCH of aromatic), 2930 (νCH of Me), 1790, and 1775 cm^{-1} (νC=O). *m/z* 298 (M^+) and 240 (M^+−NO-CO). ^{1}H NMR δ=2.30 (s, 3H, *p*-$CH_3C_6H_4S$), 2.50 (s, 3H, *p*-$CH_3C_6H_4$), 7.10 (s, 4H, *p*-MeC_6H_4S), and 7.30 (s, 4H, *p*-MeC_6H_4). Found: C, 64.20; H, 4.54; N, 9.32; S, 10.83%. Calcd for $C_{16}H_{14}N_2O_2S$: C, 64.41; H, 4.73; N, 9.39; S, 10.75%.

Synthesis of 4-(Arylseleno)sydnones (4). 3-Phenyl-4-(phenylseleno)sydnone (4a): In a manner similar to the synthesis of **3**, **4a** was obtained using diphenyl diselenide. A yellow solid (from ethanol). IR (KBr): 3075 (νCH of aromatic) and 1770 cm^{-1} (νC=O). *m/z* 318 (M^++2), 316 (M^+), 260 (M^++2−NO-CO), and 258 (M^+−NO-CO). ^{1}H NMR δ=7.20 (broad s, 5H, C_6H_5Se) and 7.35—7.75 (m, 5H, C_6H_5). Found: C, 53.03; H, 3.05; N, 8.73%. Calcd for $C_{14}H_{10}N_2O_2Se$: C, 53.01; H, 3.18; N, 8.83%.

4-Phenylseleno-3-(*p*-tolyl)sydnone (4b): A pale yellow solid (from ethanol). IR (KBr): 3070 (νCH of aromatic), 2930 (νCH of Me), 1780, and 1760 cm^{-1} (νC=O). *m/z* 332 (M^++2),

330(M^+), 274 (M^++2−NO-CO), and 272 (M^+−NO-CO). ^{1}H NMR δ=2.50 (s, 3H, CH_3), and 7.10—7.50 (m, 9H, aromatic C-H). Found: C, 54.48; H, 3.53; N, 8.35%. Calcd for $C_{15}H_{12}N_2O_2Se$: C, 54.39; H, 3.65; N, 8.46%.

Diphenyl(3-phenyl-4-sydnonyl)phosphine (6a). In a manner similar to the synthesis of **3** and **4**, **6a** was obtained using chlorodiphenylphosphine and 4-lithio-3-phenylsydnone. White yellow plates [from ethanol-acetone (2:1)]. IR (KBr): 3070 (νCH of phenyl) and 1760 cm^{-1} (νC=O). *m/z* 346 (M^+), 288 (M^+−NO-CO), and 185 (Ph_2P^+). ^{1}H NMR δ=7.40 (m,10H, C_6H_5P) and 7.55 (s, 5H, C_6H_5). Found: C, 69.62; H, 4.17; N, 7.83%. Calcd for $C_{20}H_{15}N_2O_2P$: C, 69.36; H, 4.37; N, 8.09%.

Diphenyl[3-(*p*-tolyl)-4-sydnonyl]phosphine (6b). Colorless needles [from ethanol-acetone (2:1)]. IR (KBr): 3070 (νCH of aromatic), 1780, and 1760 cm^{-1} (νC=O). *m/z* 360 (M^+), 302 (M^+−NO-CO), and 185 (Ph_2P^+). ^{1}H NMR δ=2.47 (s, 3H, *p*-$CH_3C_6H_4$) and 7.00—7.70 (m, 14H, aromatic C-H). Found: C, 70.09; H, 4.49; N, 7.65%. Calcd for $C_{21}H_{17}N_2O_2P$: C, 70.00; H, 4.75; N, 7.77%.

Tris(3-Phenyl-4-sydnonyl)arsine (7a). In a manner similar to the synthesis of **3**, **7a** was obtained using arsenic trichloride and 4-lithio-3-phenylsydnone. A pale yellow solid [from ethanol-acetone (2:1)]. IR (KBr): 3060 (νC-H of Ph), 1785, and 1760 cm^{-1} (νC=O). ^{1}H NMR δ=7.37—7.87 (m, C_6H_5]. Found: C, 51.57; H, 2.54; N, 15.21%. Calcd for $C_{24}H_{15}N_6O_6As$: C, 51. 63; H, 2.71; N, 15.05%.

Tris[3-(*p*-Tolyl)-4-sydnonyl]arsine (7b). A colorless solid [from ethanol-acetone (2:1)]. IR (KBr): 3070 (νCH of aromatic), 2940 (νCH of Me), 1790, and 1750 cm^{-1} (νC=O). ^{1}H NMR δ=2.47 (s, 9H, CH_3) and 7.30 (s, 12H, *p*-MeC_6H_4). Found: C, 54.18; H, 2.31; N, 13.95%. Calcd for $C_{27}H_{21}N_6O_6As$: C, 54.01; H, 2.53; N, 14.00%.

References

1) F. H. C. Stewart, *Chem. Rev.*, **64**, 129 (1964); M. Ohta and H. Kato, "Non-benzenoid Aromatics," Academic Press, New York (1969), Vol. 1, p. 117; C. G. Newton and C. A. Ramsden, *Tetrahedron*, **38**, 2965 (1982).

2) M. -Y. Yeh, T. Nonaka, T. Goto, M. -C. Hsu, T. Fuchigami, and H. -J. Tien, *Bull. Chem. Soc. Jpn.*, **56**, 3535 (1983).

3) T. Fuchigami, M. -Y. Yeh, T. Goto, T. Nonaka, and H. -J. Tien, *Bull. Chem. Soc. Jpn.*, **57**, 116 (1984).

4) H. -J. Tien and M. Ohta, *Bull. Chem. Soc. Jpn.*, **45**, 2944 (1972).

5) H. -J. Tien, K. Kanda, A. Chinone, and M. Ohta, *Bull. Chem. Soc. Jpn.*, **46**, 3304 (1973).

6) a) T. Fuchigami, M. -Y. Yeh, T. Nonaka, and H. -J. Tien, *Bull. Chem. Soc. Jpn.*, **56**, 3851 (1983); b) T. Fuchigami, T. Goto, M. -Y. Yeh, T. Nonaka, and H. -J. Tien, *Bull. Chem. Soc. Jpn.*, **57**, 1362 (1984).

7) a) T. Fuchigami, Z. E. Kandeel, and T. Nonaka, *Bull. Chem. Soc. Jpn.*, **58**, 2441 (1985); b) T. Fuchigami, Z. E. Kandeel, and T. Nonaka, *Bull. Chem. Soc. Jpn.*, **59**, 338 (1986).

8) W. Baker, W. D. Ollis, and V. D. Poole, *J. Chem. Soc.*, **1949**, 307.

9) C. V. Greco and B. P. O'Reilly, *J. Heterocycl. Chem.*, **7**, 1433 (1970).

10) K. Masuda and T. Okutani, *Tetrahedron*, **30**, 409 (1974).

11) B. G. Ugarker, B. V. Badami, and G. S. Puranik, *Arch. Pharm.*, **312**, 977 (1979).

12) H. Kato and M. Ohta, *Bull. Chem. Soc. Jpn.*, **30**, 210 (1957).

13) N. Suciu and Gh. Mihai, *Tetrahedron*, **24**, 37 (1968).

14) H. Dickopp, *Tetrahedron Lett.*, **46**, 4403 (1971).

15) a) E. Marchand, G. Morel, and A. Foucaud, *Synthesis*, **1978**, 360; b) W. R. Bowman, and G. D. Richardson, *Tetrahedron Lett.*, **1977**, 4519; c) J. I. Grayson and S. Warren, *J. Chem. Soc., Perkin Trans. 1*, **1977**, 1; d) M. Asaoka, K. Miyake, and H. Takei, *Bull. Chem. Soc. Jpn.*, **51**, 3008 (1978).

Preparation of Sydnone Compounds Substituted by Thio and Seleno Functional Groups at the 4-Positions

Toshio FUCHIGAMI,* Ching-Sy CHEN, Tsutomu NONAKA, Mou-Yung YEN,† and Hsien-Ju TIEN†
Department of Electronic Chemistry, Graduate School at Nagatsuta, Tokyo Institute of Technology, Nagatsuta, Midori-ku, Yokohama 227
†Department of Chemistry, National Cheng Kung University, Tainan, Taiwan, Republic of China
(Received July 11, 1985)

The introduction of thio and seleno functional groups to the 4-position of a sydnone ring was successfully attempted using 4-lithiosydnones (**2**) and 4-bromosydnones (**3**) as starting compounds. The reaction of **2** with tetraalkylthiuram disulfides, bis[alkoxy(thiocarbonyl)] disulfides, and bis[alkylthio(thiocarbonyl)] disulfides provided 4-sydnonyl dithiocarbamates, *O*-alkyl *S*-(4-sydnonyl) dithiocarbonates, and dialkyl 4-sydnonyl trithiocarbonates, respectively in good yields. In addition, treatment of **2** with thiocyanogen and selenocyanogen gave rise to bis(4-sydnonyl) sulfides (**11**) and bis(4-sydnonyl) selenides (**12**), respectively. These products, **11** and **12** were also formed by the reaction of **3** with potassium thiocyanate and selenocyanate, respectively. Furthermore, it was found that **3** reacted with selenourea and potassium *O*-ethyl dithiocarbonate under heating to provide **12** and **11**, respectively. It was also found that the reactivity of these sydnone compounds **2** and **3** was quite different in many cases from that of the corresponding ordinary aromatic analogues, though the sydnone ring has a somewhat aromatic nature.

Although a typical mesoionic compound, sydnone (**1**) has been investigated extensively because of its unique electronic structure and biological activities, a few studies on the direct substitution by heteroatoms and hetero functional groups at the 4-position have been reported.[1)]

In our previous paper,[2)] we have reported a general method for the introduction of heteroatoms such as sulfur, selenium, phosphorus and arsenic to the 4-position. For example, we found that 4-thio and 4-selenosydnone compounds were successfully prepared by the reaction of 4-lithiosydnones (**2**) with disulfides and diselenides, respectively. In these cases, reaction proceeded under mild conditions and almost pure products could be obtained directly. Since sydnones are known to be unstable to acid, alkali, heat, oxidation, and reduction, quite mild reaction conditions are necessary for the successful synthesis of sydnone derivatives in general.[3)] Therefore, the previous method for the introduction of thio and seleno groups seems to be applicable to more complicated disulfides and selenides bearing carbonyl, thiocarbonyl, and cyano groups to provide sydnone compounds having hetero functional groups containing sulfur and selenium atoms.

4-Bromosydnones (**3**) are easily prepared by both chemical and electrochemical halogenation of 4-unsubstitued sydnones.[4)] Although **3** is known to be useful starting compounds for the preparation of sydnone derivatives, only one paper dealing with the reaction of **3** with heteroatom compounds such as hydrogen sulfide, thiophenol, and thiourea has been reported.[5)]

From these aspects, preparation of sydnone compounds substituted by hetero functional groups at the 4-positions was attempted using **2** and **3** as starting materials.

Results and Discussion

Preparation of Sydnones Having Thiocarbonylthio Groups at the 4-Positions. It was found that the initial lithiation of sydnones (**1**) and the subsequent reaction of the resulting 4-lithiosydnones (**2**) with tetraalkylthiuram disulfides, bis[alkoxy(thiocarbonyl)] disulfides, and bis[alkylthio(thiocarbonyl)] disulfides could be run in sequence in THF below −50 °C (Scheme 1).

As shown in Table 1, 4-sydnonyl dithiocarbamates (**4**), *O*-alkyl-*S*-(4-sydnonyl) dithiocarbonates (**5**), and alkyl 4-sydnonyl trithiocarbonates (**6**) were successfully prepared in good yields.

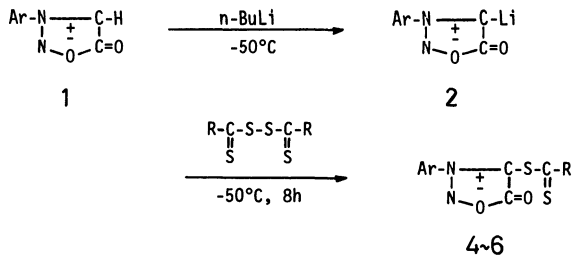

Scheme 1.

The structures of the products **4**, **5**, and **6** were confirmed by elemental analyses and various spectral studies. In the IR spectra, C–H absorption bands (3140—3160 cm^{-1}) of the starting **1** disappeared after the reaction, while those of thiocarbonyl groups (1050—1200 cm^{-1}) newly appeared. In the MS spectra, most sydnone derivatives showed their molecular ion peaks together with their characteristic fragment peaks due to the elimination of CO and NO. The sydnones bearing an isopropyl group showed fragment peaks due to elimination of the isopropyl group but did not show their molecular ion peaks.

It is known that the reaction of ordinary aryllithiums

Table 1. Preparation of Sydnone Compounds **4**, **5**, and **6**

Compd	Ar	R	Yield[a] %	Mp θ_m/°C	IR (KBr) $\nu_{C=O}$/cm^{-1}	IR (KBr) $\nu_{C=S}$/cm^{-1}
4a	Ph	Me_2N	99	148—150	1790 1775	1150
4b	Ph	*i*-Pr_2N	95	151—152	1795 1775	1150
4c	*p*-Tolyl	Me_2N	92	156—158	1795 1775	1160
4d	*p*-Tolyl	*i*-Pr_2N	100	118—119	1780	1150
5a	Ph	*i*-PrO	84	75—76	1790	1090
5b	*p*-Tolyl	*i*-PrO	74	95—96	1790 1770	1090
6	*p*-Tolyl	MeS	82	100—101	1785 1770	1080

a)Crude yield.

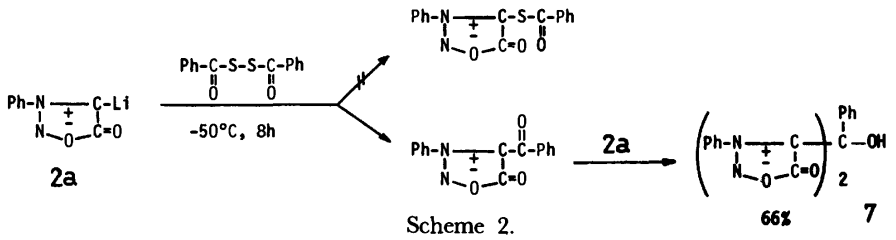

Scheme 2.

with such sulfides always gives a mixture of products because of a competing nucleophilic attack at both the sulfur atoms of the disulfide bond and the carbon atoms of the thiocarbonyl group. Recently, Cava et al.[6] have reported that an aryllithium reacts exclusively at a disulfide bond of tetraisopropylthiuram disulfide to provide aryl dithiocarbamate because the thiocarbonyl group is highly hindered to nucleophilic attack. From these points, it is noticeable that the reaction always took place at the disulfide bond selectively, regardless of the bulkiness of the alkyl substituents in the case of **2**. These results indicate that the reactivity of 4-sydnonyl anions is different from that of ordinary aryl anions.

Next, we extended this process to the preparation of 4-(benzoylthio)sydnone. The reaction was carried out in a similar manner using equimolar **2a** and dibenzoyl disulfide. However, no expected product was obtained and Phenylbis(3-phenyl-4-sydnonyl)methanol (**7**) was formed in a low yield. In this case, a large amount of the disulfide was recovered. Since **7** should be stoichiometrically formed from two mole of **2a** and one mole of the disulfide, the reaction was carried out using two equiv of **2a** to provide **7** in a moderate yield.

It is noticeable that 4-sydnonyl anions attack at a carbonyl group but do not attack the thiocarbonyl group of the disulfides used in these reactions. In order to confirm this fact further, the reaction of **2** with carbon disulfide was examined. However, the reaction did not proceed at all, though it is well-known that **2** readily reacts with carbon dioxide to provide 4-sydnonecarboxylic acid in a good yield.[7] Since carbon disulfide is much more reactive to nucleophiles than carbon dioxide, the reactivity of 4-sydnonyl anions is quite unique.

Since dithiocarbamates are known to be easily hydrolyzed by alcoholic alkali to give the corresponding thiols,[6] hydrolysis of **4**, **5**, and **6** were attempted in order to obtain 4-mercaptosydnone (**8**) which are hitherto unknown compounds. However, our attempts were unsuccessful owing to the decomposition of the sydnone ring.

Reaction of 4-Lithiosydnones (2) with Thiocyanogen and Selenocyanogen. Since the reaction of **2** with disulfides bearing a thiocarbonyl group was found to be useful for the introduction of thiocarbonylthio groups to the 4-positions of sydnones, we applied this procedure to the preparation of 4-sydnonyl thio- and selenocyanates (**9** and **10**) from thio- and selenocyanogens. Thio- and selenocyanogens were generated from potassium thio- and selenocyanates and bromine in dry THF at −50°C and the resulting solution was directly used for the reaction with **2**. When the solution of thiocyanogen was added gradually to the solution of **2** [procedure (a)], bis(4-sydnonyl) sulfide (**11**) was unexpectedly formed instead of 4-sydnonyl thiocyanate (**9**). In order to obtain the desired **9**, the reverse procedure (b) was attempted as follows: **2** was added to the solution of thiocyanogen, however the same product, **11** was obtained. No remarkable differene in the yield of **11** was observed between these two procedures employed.

In a similar manner, the reaction of **2** with seleno-

Table 2. Reaction of 4-Lithiosydnone (**2**) with Thiocyanogen and Selenocyanogen

Compd	Ar	X	Procedure	Yield[a] %	Mp θ_m/°C	IR (KBr) $\nu_{C=O}$/cm^{-1}
11a	Ph	S	(a)	57	165—166 (164—165)[5] (169—171)[14]	1780, 1750
11a	Ph	S	(b)	51	165—166	1780, 1750
11b	*p*-Tolyl	S	(b)	42	218—219 (201—203)[14]	1770
12a	Ph	Se	(a)	34	180—181	1770, 1750
12b	*p*-Tolyl	Se	(a)	64	209—211 (decomp)	1770, 1750

a) After recrystallization.

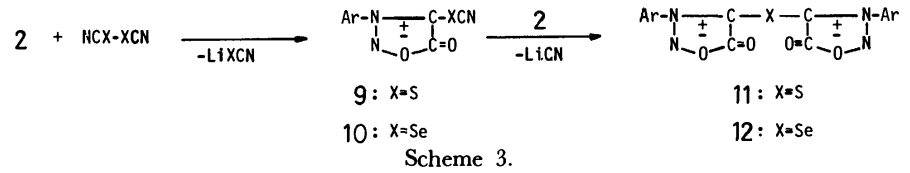

Scheme 3.

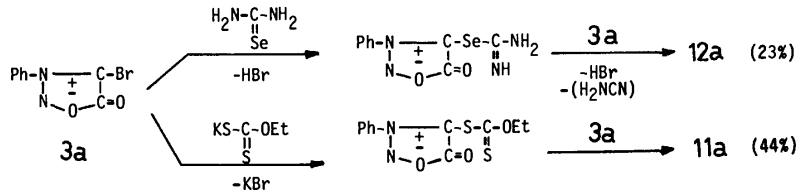

Scheme 4.

cyanogen also provided bis(4-sydnonyl) selenide (**12**) in a moderate yield as shown in Table 2.

Aryl tellurocyanates are known to be unstable and disproportionate to diaryl tellurides and tellurium dicyanate in some cases,[8] whereas aryl thio- and selenocyanates are stable and such disproportionation has not been reported. A probable mechanism for the reaction involves the formation of 4-sydnonyl thio- and selenocyanates (**9** and **10**) as primary products, which reacted further with 4-sydnonyl anions to give rise to **11** and **12**, respectively.[9]

These results clearly indicate that the reactivity of 4-sydnonyl anions is quite different from that of ordinary aromatic analogues though the sydnone ring has a somewhat aromatic nature.

Reaction of 4-Bromosydnone (3) with Selenourea. 4-Bromo-3-phenylsydnone (**3a**) was found to react with selenourea under refluxing in ethanol to give bis(3-phenyl-4-sydnonyl)selenide (**12a**). During the reaction, the precipitation of selenium metal was observed. Since ordinary aryl bromides do not react with selenourea, this reaction seems to be quite interesting.

Kato and Ohta found that 4-iodo- and bromosydnones have weak oxidizing power whereas 4-chlorosydnone does not.[5,10] Since oxidative deselenylation of selenourea is known to take place very often as well as that of thiourea, the elimination of selenium metal clearly indicates that the bromosydnone **3a** acted as oxidizing reagent in this reaction.

Table 3. Reaction of 4-Bromosydnone (**3**) with Potassium Thiocyanate and Selenocyanate

Compd	Ar	X	Reaction time/h	Yield[a] %
11a	Ph	S	4	61
11b	*p*-Tolyl	S	6.5	51
12a	Ph	Se	8	54
12b	*p*-Tolyl	Se	24	50

a) After recrystallization.

Reaction of 4-Bromosydnone with Potassium Thio- and Selenocyanates and Potassium *O*-Ethyl Dithiocarbonate. Because the thio- and selenocyanation of sydnones from **2** and thio- and selenocyanogen was unsuccessful, the reaction of **3** with potassium thio- and selenocyanates was attempted in order to obtain **9** and **10**, respectively. However, the reaction in DMF under heating provided sulfides **11** and selenides **12** instead of the desired products (**9** and **10**) as shown in Scheme 5. The results are summarized in Table 3.

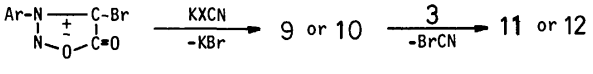

Scheme 5.

In our earlier work,[11] we found that *N*-[α-(chloroimino)benzyl]sulfilimine easily reacted with potassium thiocyanate to provide heterocyclic sulfilimine. Although this sulfilimine has a positive halogen, such elimination of the cyanate ion was not observed.

The products **11** and **12** seem to be formed by the further reaction of 4-sydnonyl thio- or selenocyanates (**9** or **10**) once formed with additional 4-bromosydnones as shown in Scheme 5.

It was found that the sulfide **11a** was also formed by the reaction of **3a** with potassium *O*-ethyl dithiocarbonate in a similar manner. The reaction may proceed similarly to the reaction of the thio- and selenocyanate ions (Secheme 4).

It was reported that the bromine atom of bromomalonic acids could be substituted by the thiocyanate ion, although their bromine atom has a positive character.[12] These unusual reactions (Schemes 4 and 5) have never been known in the case of the corresponding ordinary aryl bromides, therefore it can be stated that 4-bromosydnone **3** has quite intriguing reactivities.

The new type of sydnone compounds thus prepared are expected to be pharmacologically active and screening tests of several biological activities of these sydnones are currently under investigation.

Experimental

NMR spectra were recorded at 60 MHz on a Varian EM-360 spectrometer using Me_4Si as an internal standard. IR spectra were obtained on a Hitachi 295 infrared spectrometer. Electron impact mass spectra were determined at 30 eV on a JEOL JMS-D100 mass spectrometer by direct introduction via solid probe.

Typical Procedure for the Preparation of Sydnones Having Thiocarbonylthio Groups at the 4-Positions (4, 5, and 6). 3-Phenyl-4-sydnonyl Dimethyldithiocarbamate (4a): To a stirred suspension of 1.00 g (6.2 mmol) of 3-phenylsydnone in 10 ml of anhydrous THF, under a dry nitrogen atmosphere, was added dropwise 4.0 ml (6.5 mmol) of a solution of butyllithium in hexane (15%) below −50 °C. After about 1 h of stirring, a solution of 1.48 g (6.2 mmol) of tetramethylthiuram disulfide in 7 ml of THF was added dropwise to the resulting brown solution below −50 °C. After additional 8 h of stirring, the yellow-brown reaction mixture was poured into ice-water. The pricipitated yellow solid was collected by filtration, washed with water, and dried: yield 1.71 g (99%); mp 145—147 °C. Recrystallization from ethanol provided 1.55 g (89%) of the pure product **4a** as yellow plates: Mp 148—150 °C; NMR ($CDCl_3$) δ=3.30 (s, 3H, $C\underline{H}_3$), 3.35 (s, 3H, $C\underline{H}_3$), and 7.63 (s, 5H, $C_6\underline{H}_5$); MS, *m/z* 281 (M^+) and 223 (M^+−NO-CO). Found: C, 46.98; H, 3.92; N, 14.93; S, 22.47%. Calcd for $C_{11}H_{11}N_3O_2S_2$: C, 46.96; H, 3.94; N, 14.93; S, 22.79%.

3-Phenyl-4-sydnonyl Diisopropyldithiocarbamate (4b): A yellow solid (from ethanol); ^1H NMR ($CDCl_3$) δ=1.31 (d, 12H, $C\underline{H}_3$), 4.0—5.0 (m, 2H, C<u>H</u>), and 7.63 (s, 5H, $C_6\underline{H}_5$); MS, *m/z* 337 (M^+), 294 (M^+−*i*-Pr), and 236 (M^+−*i*-Pr-NO-CO). Found: C, 53.37; H, 5.71; N, 12.32; S, 18.98%. Calcd for $C_{15}H_{19}N_3O_2S_2$: C, 53.39; H, 5.67; N, 12.45; S, 19.00%.

3-(*p*-Tolyl)-4-sydnonyl Dimethyldithiocarbamate (4c): A yellow solid (from ethanol); ^1H NMR ($CDCl_3$) δ=2.45 (s, 3H, *p*-$C\underline{H}_3C_6H_4$), 3.35 (s, 3H, $NC\underline{H}_3$), 3.40 (s, 3H, $NC\underline{H}_3$), 7.30 (d, 2H, Ar-H), and 7.50 (d, 2H, Ar-H); MS, *m/z* 295 (M^+) and 149 (M^+−NO-CO-C(S)NMe_2). Found: C, 48.98; H, 4.77; N, 14.10; S, 21.65%. Calcd for $C_{12}H_{13}N_3O_2S$: C, 48.80; H, 4.44; H, 14.23; S, 21.71%.

3-(*p*-Tolyl)-4-sydnonyl Diisopropyldithiocarbamate (4d): Pale pink plates (from ethanol); ^1H NMR ($CDCl_3$) δ=1.40 (d, 12H, $CH(C\underline{H}_3)_2$), 2.45 (s, 3H, *p*-$C\underline{H}_3C_6H_4$), 4.10—4.90 (br. m, 2H, C<u>H</u>), 7.30 (d, 2H, Ar-H), and 7.50 (d, 2H, Ar-H); MS, *m/z* 308 (M^+−*i*-Pr), and 250 (M^+−*i*-Pr-NO-CO). Found: C, 54.87; H, 6.12; N, 11.73; S, 18.45%. Calcd for $C_{16}H_{21}N_3O_2S_2$: C, 54.68; H, 6.02; N, 11.96; S, 18.24%.

***O*-Isopropyl *S*-(3-phenyl-4-sydnonyl) Dithiocarbonate (5a):** A yellow solid (from ethanol); ^1H NMR (DMSO-d_6) δ=1.28 (d, 6H, $C\underline{H}_3$), 5.50 (m, 1H, C<u>H</u>), and 7.70 (s, 5H, $C_6\underline{H}_5$); MS, *m/z* 253 (M^+−*i*-Pr), and 195 (M^+−*i*-Pr-NO-CO). Fond: C, 48.62; H, 4.02; N, 9.46; S, 21.39%. Calcd for $C_{12}H_{12}N_2O_3S_2$: C, 48.63; H, 4.08; N, 9.45; S, 21.64%.

***O*-Isopropyl *S*-[3-(*p*-Tolyl)-4-sydnonyl] Dithiocarbonate (5b):** A yellow solid (from ethanol); ^1H NMR ($CDCl_3$) δ=1.33 (d, 6H, $CH(C\underline{H}_3)_2$), 2.50 (s, 3H, *p*-$C\underline{H}_3C_6H_4$), 5.57 (m, 1H, C<u>H</u>), and 7.37 (s, 4H, Ar-<u>H</u>); MS, *m/z* 310 (M^+), 267 (M^+−*i*-Pr), and 209 (M^+−*i*-Pr-NO-CO). Found: C, 50.32; H, 4.53; N, 8.98; S, 20.96%. Calcd for $C_{13}H_{14}N_2O_3S_2$: C, 50.31; H, 4.55; N, 9.03; S, 20.66%.

Methyl [3-(*p*-Tolyl)-4-sydnonyl] Trithiocarbonate (6): A yellow solid (from ethanol); ^1H NMR ($CDCl_3$) δ=2.40 (s, 3H, *p*-$C\underline{H}_3C_6H_4$), 2.70 (s, 3H, $C\underline{H}_3S$), and 7.40 (s, 4H, Ar-<u>H</u>); MS, *m/z* 298 (M^+) and 240 (M^+−NO-CO). Found: C, 44.22; H, 3.26; N, 9.49; S, 32.32%. Calcd for $C_{11}H_{10}N_2O_2S_3$: C, 44.28; H, 3.38; N, 9.39; S, 32.23%.

Phenylbis(3-phenyl-4-sydnonyl)methanol (7): In a manner similar to the preparation of **4—6**, **7** was obtained in 66% yield using two equiv of 4-lithio-3-phenylsydnone and dibenzoyl disulfide. Recrystallization from ethanol provided pure **7** as a pale yellow solid (58%); mp 199—201 °C (decomp) (lit,[13] mp 203—205 °C); IR (KBr): 3240 (νOH), 3070 (νCH of aromatic), 1790 and 1710 cm^{-1} (νC=O); ^1H NMR ($CDCl_3$) δ=6.15 (s, 1H, O<u>H</u>), 7.10 (s, 5H, $C_6\underline{H}_5COH$), and 7.20—7.60 (m, 10H, $C_6\underline{H}_5$). Found: C, 64.48; H, 3.51; N, 13.06%. Calcd for $C_{23}H_{16}N_4O_5$: C, 64.48; H, 3.76; N, 13.08%.

Reaction of 4-Lithiosydnones (2) with Thiocyanogen and Selenocyanogen. General Procedure (a). To a stirred solution of 6 mmol of 4-lithiosydnone **2** in 10 ml of THF under dry nitrogen atmosphere below −50 °C, was added dropwise a solution of thiocyanogen or selenocyanogen in 15 ml of THF, which was prepared by the treatment of potassium thiocyanate or selenocyanate (20—24 mmol) with 10—12 mmol of bromine below −50 °C. After ca. 8h of stirring, the colored (violet or orange color) reaction mixture was poured into a large amount of ice-water. After the mixture had been allowed to stand for 1h, the resulting precipitates were collected by filtration and washed with water. The crude product was dissolved in ethanol-acetone (10:1) and the solution was treated with activated charcoal powder. The solution was concentrated and the remaining solution was allowed to stand overnight. The precipitated pure product was obtained by filtration.

Bis(3-phenyl-4-sydnonyl)sulfide (11a): ^1H NMR ($CDCl_3$) δ=7.40—7.93 (m, $C_6\underline{H}_5$). MS, *m/z* 354 (M^+), 296 (M^+−NO-

CO), and 238 (M^+—2NO-2CO). Found: C, 54.17; H, 2.63; N, 15.66; S, 8.94%. Calcd for $C_{16}H_{10}N_4O_4S$: C, 54.24; H, 2.84; N, 15.81; S, 9.05%.

Bis[3-(*p*-tolyl)-4-sydnonyl]sulfide (11b): ^{1}H NMR ($CDCl_3$) δ=2.50 (s, 6H, CH_3), 3.37 (d, 4H, Ar-H), and 7.70 (d, 4H, Ar-H). MS, *m/z* 324 (M^+—NO-CO) and 266 (M^+—2NO-2CO). Found: C, 56.40; H, 3.61; N, 14.59; S, 8.50%. Calcd for $C_{18}H_{14}N_4O_4S$: C, 56.54; H, 3.69; N, 14.65; S, 8.38%.

Bis(3-phenyl-4-sydnonyl)selenide (12a): ^{1}H NMR ($CDCl_3$) δ=7.40—8.10 (m, C_6H_5). MS, *m/z* 402, 400 (M^+) and 344, 342 (M^+—NO-CO). Found: C, 47.83; H, 2.23; N, 13.93%. Calcd for $C_{16}H_{10}N_4O_4Se$: C, 47.90; H, 2.51; N, 13.96%.

Bis[3-(*p*-tolyl)-4-sydnonyl]selenide (12b): ^{1}H NMR ($CDCl_3$) δ=2.55 (s, 6H, CH_3), 7.43 (d, 4H, Ar-H), and 7.73 (d, 4H, Ar-H). MS, *m/z* 430, 428 (M^+) and 372, 370 (M^+—NO-CO). Found: C, 50.27; H, 3.13; N, 13.02%. Calcd for $C_{18}H_{14}N_4O_4Se$: C, 50.36; H, 3.29; N, 13.05%.

Reaction of 4-Bromo-3-phenylsydnone (3a) with Selenourea. To a stirred solution of 1.90 g (7.8 mmol) of **3a** in 20 ml of anhydrous ethanol was added 1.00 g (8.1 mmol) of selenourea and the mixture was refluxed for 8 h. After cooling, the precipitating selenium metal (0.44 g, 69%) was filtered. The filtrate was concentrated and the remaining solution was allowed to stand overnight. The resulting precipitates were collected by filtration and 0.36 g (23%) of pure **12a** was obtained as a yellow solid.

Reaction of 4-Bromosydnones (3) with Potassium Thiocyanate and Selenocyanate. General Procedure. A stirred mixture of 4.1 mmol of **3** and 4.1 mmol of potassium thiocyanate or selenocyanate in 10 ml of anhydrous DMF was heated at 80—90 °C. After 1—1.5h (reaction with potassium thiocyanate) or 4—6h (reaction with selenocyanate) of heating, the reaction mixture was cooled and poured into ice-water. The precipitated solid was collected by filtration and recrystallized from ethanol-acetone (10:1) to provide pure **11** or **12** (Table 3).

Reaction of 4-Bromo-3-phenylsydnone (3a) with Potassium *O*-Ethyl Dithiocarbonate. To a stirred solution of 1.00 g (4.2 mmol) of **3a** in 15 ml of anhydrous DMF was added 0.67 g (4.2 mmol) of potassium *O*-ethyl dithiocarbonate and then the mixture was heated at 80—90 °C. After ca. 0.5h, potassium bromide began to precipitate. After 4h, the reaction mixture was cooled and was poured into ice-water and then the precipitates were collected by filtration; 0.32 g (44%); mp 156—150 °C. Recrystallization from ethanol provided 0.30 g (41%) of pure **11a** as a yellow solid.

We are grateful for valuable discussion with Dr. Haruo Matsuyama of Tokyo Metropolitan University.

References

1) a) F. H. C. Stewart, *Chem. Rev.*, **64**, 129 (1964); b) M. Ohta and H. Kato, "Non-benzenoid Aromatics," Academic Press, New York (1969), Vol. 1, p. 117; c) C. G. Newton and C. A. Ramsden, *Tetrahedron*, **38**, 2965 (1982).

2) T. Fuchigami, C. -S. Chen, T. Nonaka, M. -Y. Yeh, and H. -J. Tien, *Bull. Chem. Soc. Jpn.*, **59**, 483 (1986).

3) a) M. -Y. Yeh, T. Nonaka, T. Goto, M. -C. Hsu, T. Fuchigami, and H. -J. Tien, *Bull. Chem. Soc. Jpn.*, **56**, 3535 (1983); b) T. Fuchigami, M. -Y. Yeh, T. Nonaka, and H. -J. Tien, *Bull. Chem. Soc. Jpn.*, **56**, 3851 (1983); c) T. Fuchigami, M. -Y. Yeh, T. Goto, T. Nonaka, and H. -J. Tien, *Bull. Chem. Soc. Jpn.*, **57**, 116 (1984); d) T. Fuchigami, T. Goto, M. -Y. Yeh, T. Nonaka, and H. -J. Tien, *Bull. Chem. Soc. Jpn.*, **57**, 1362 (1984); e) T. Fuchigami, Z. E. Kandeel, and T. Nonaka, *Bull. Chem. Soc. Jpn.*, **58**, 2441 (1985); f) M. -Y. Yeh, H. -J. Tien, T. Fuchigami, and T. Nonaka, *J. Chinese Chen. Soc.*, in press; g) T. Fuchigami, Z. E. Kandeel, and T. Nonaka, *Bull. Chem. Soc. Jpn.*, **59**, 338 (1986).

4) H. -J. Tien, T. Nonaka, and T. Sekine, *Chem. Lett.*, **1979**, 283.

5) H. Kato and M. Ohta, *Bull. Chem. Soc. Jpn.*, **30**, 210 (1957).

6) K. -Y. Jen and M. P. Cava, *Tetrahedron Lett.*, **23**, 2001 (1982).

7) C. V. Greco, M. Pesce, and J. M. Franco, *J. Heterocycl. Chem.*, **3**, 391 (1966).

8) L. Engman, *J. Org. Chem.*, **48**, 2920 (1983).

9) Hitherto, only few examples of nucleophilic reaction of carbanions with thiocyanates have been reported: M. Makosza and M. Fedorynski, *Synthesis*, **1974**, 274; N. X. Hu, Y. Aso, T. Otsubo, and F. Ogura, *Chem. Lett.*, **1985**, 603.

10) They also found that **3** reacted with thiourea to give bis(3-phenyl-4-sydnonyl) sulfide, however they did not observe desulfurization.

11) T. Fuchigami and K. Odo, *Bull. Chem. Soc. Jpn.*, **50**, 1791 (1977).

12) E. Bullmann and E. Madson, *Ann.*, **403**, 341 (1913).

13) N. Suciu and Gh. Mihai, *Tetrahedron*, **24**, 37 (1968).

14) V. A. Kozinskii, S. I. Burmistrov, and O. V. Mikheeva, *Zh. Org. Khim.*, **12**, 1572 (1976).

Efficient Synthesis of a New Amino Acid, (2*S*,3*R*,4*R*)-4-Chloro-3-hydroxyproline

Sannamu Lee,* Yasushi Kodera,† Kosaku Noda,†† Haruhiko Aoyagi, Tetsuo Kato, and Nobuo Izumiya
Laboratory of Biochemistry, Faculty of Science, Kyushu University 33, Higashi-ku, Fukuoka 812
†Department of Chemistry, Faculty of Science, Fukuoka University, Jonan-ku, Fukuoka 814-01
††Laboratory of Biochemistry, Fukuoka Women's University, Higashi-ku, Fukuoka 813
(Received September 12, 1985)

An unusual new amino acid, (2*S*,3*R*,4*R*)-4-chloro-3-hydroxyproline, was stereospecifically synthesized through a four-intermediate from Boc-3,4-dehydro-L-proline. The obtained product was stable in a mild alkaline solution.

The 3,4-disubstituted prolines occur in natural cyclic peptide toxins, e.g., virotoxin[1] and cyclochlorotine.[2] The two diastereomeric 3,4-dihydroxy-L-prolines in virotoxin were synthesized from *N*-tosyl-3,4-dehydro-L-proline methyl ester by Kahl and Wieland.[3] (2*S*,3*S*,4*R*)-Dichloroproline in cyclochlorotine has neither been isolated in a free state nor synthesized because of its instability under acid hydrolytic and mild basic conditions. In the course of studying the structure-activity relationship of cyclochlorotine, we found that both chlorine moieties in 3,4-dichloroproline are essential regarding toxic activity,[4] although attempts to synthesize 3,4-dichloroproline were unsuccesful.

Here, we report the synthesis of an interesting proline derivative, (2*S*,3*R*,4*R*)-4-chloro-3-hydroxyproline (**1**) through a stereoselective route (Scheme 1). The phenacyl group, which is deprotected by zinc powder in an aqueous acetic acid, was selected for the protection of the carboxyl group in order to avoid alkaline conditions.[5] Boc-3,4-dehydro-L-proline (**2**) was converted to its phenacyl ester (**3**) in high yield. Compound **3** was treated with *m*-chloroperbenzoic acid and an obtained crude product was purified by silica gel chromatography to give the corresponding epoxide (**4**). The stereochemistry in this epoxide was not directly clarified but a TLC of the reaction mixture showed only two main spots of the epoxide and the starting material, except for a few trace spots. This result suggests that the configuration of the obtained epoxide is a 2,3-*trans* form in consideration of the stereoselective epoxidation of *m*-chloroperbenzoic acid.[6] A treatment of **4** with 2-chloro-3-ethylbenzoxazolium tetrafluoroborate was expected to give Boc-3,4-dichloro-L-proline phenacyl ester,[7] but yielded Boc-3-hydroxy-4-chloro-L-proline phenacyl ester (**5**) instead. A deprotection of the phenacyl group using zinc powder in acetic acid gave Boc-3-hydroxy-4-chloro-L-proline (**6**), which was converted to 3-hydroxy-4-chloro-L-proline (**1**) with HCl in dioxane. Compound **5** was treated with HCl in dioxane to

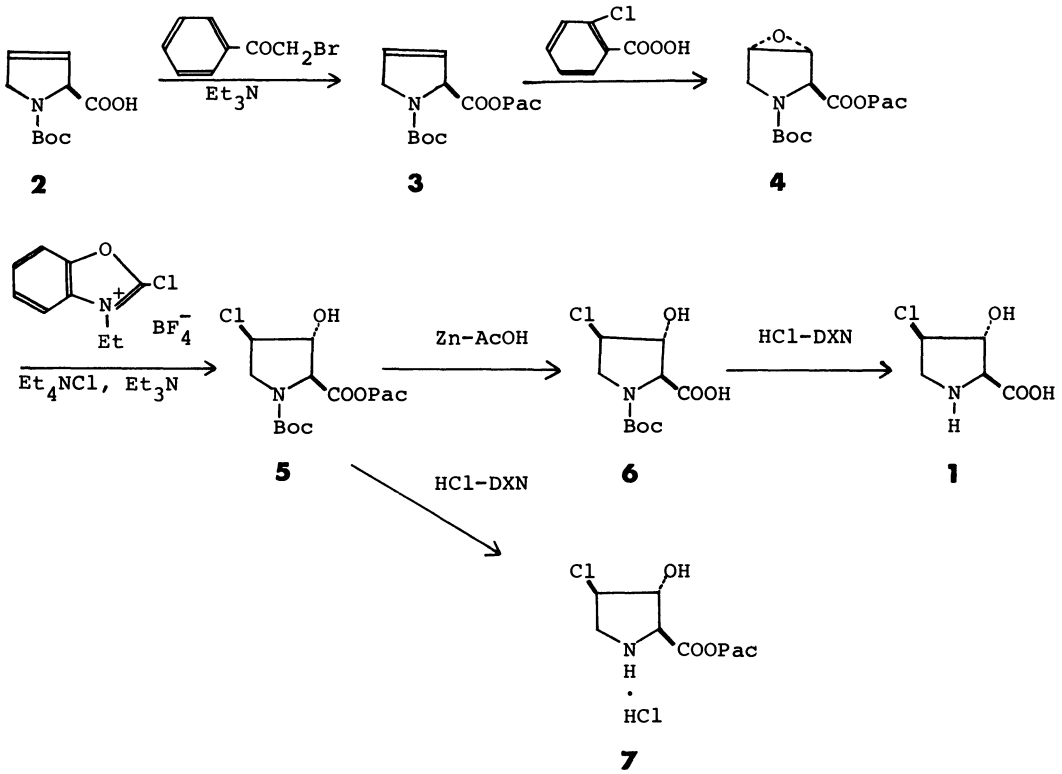

Scheme 1.

Table 1. Chemical Shifts (δ) and Coupling Constants of **1** and Comparison with 3,4-Dihydroxy-L-proline (**8**)

H[a)]	δ of **1** (in DMSO-d_6)	Coupling constant (Hz)			
			1 (in DMSO-d_6)	(2*S*,3*R*,4*R*)-**8**[3)] (in D_2O)	(2*S*,3*S*,4*S*)-**8**[3)] (in D_2O)
2	4.13	J(2, 3)	1.5	1.5	4.0
3	4.58	J(3, 4)	1.1	1.3	1.3
4	4.50	J(4, 5a)	1.5	1.5	
5a	3.55	J(4, 5b)	4.2	3.5	4.0
5b	3.78	J(5a, 5b)	13.4	12.4	12.9

a) Protones of **1** were defined as described below.

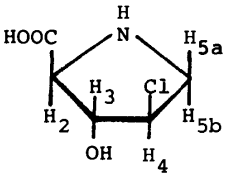

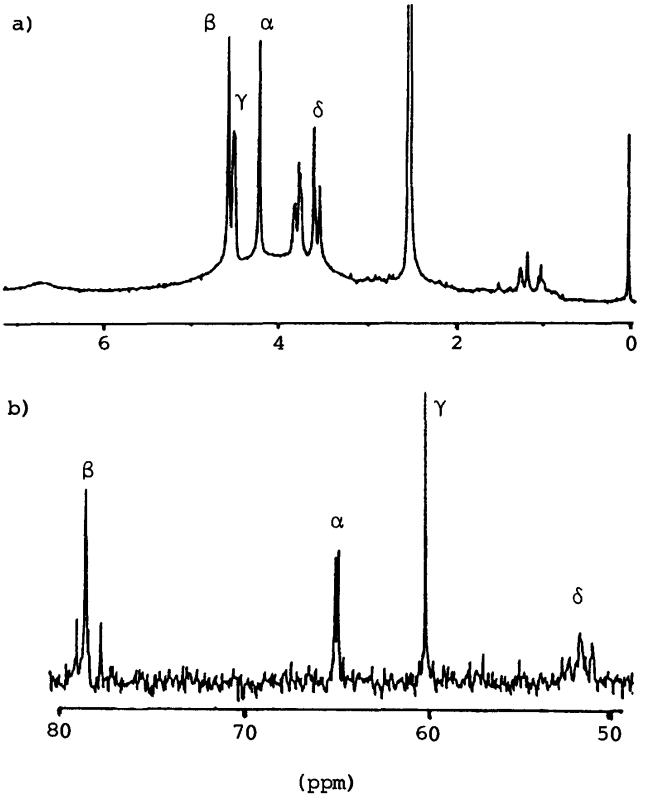

Fig. 1. ^{1}H-NMR spectrum of **1** (a) and ^{13}C-NMR spectrum of **1** resulting from selective irradiation of γH (b). The peak of δC showed a coupling with γH.

give 3-hydroxy-4-chloro-L-proline phenacyl ester (**7**). Compounds **6** and **7** can be used as acid and amine components, respectively, in a peptide synthesis.

The substituted positions of 3-hydroxy and 4-chloro groups in the proline was determined by a ^{13}C{^{1}H} selective decoupling technique of NMR (Fig. 1). The stereochemistry of 3-hydroxy and 4-chloro groups was determined to be 2,3-*trans* and 3,4-*trans*, respectively, compared to the coupling constants of 3,4-dihydroxy-L-proline diastereoisomer (Table 1). These results suggest that the ring opening of epoxide **3** arose from its trans side, attacking (exclusively) position 4.

This 3-hydroxy-4-chloro-L-proline was stable under ammoniacal alkaline conditions the same conditions under which dichloroproline in cyclochlorotine decomposes to a pyrrole derivative with the release of hydrogen chloride.[2)] This result means that 3-hydroxy-4-chloro-L-proline derivatives can be used for a conventional peptide synthesis. Proline analogs with a variety of functional groups have been developed for use in peptide and protein chemistry since proline often plays an important role for maintaining conformation and biological activities. This new amino acid may be useful for structure-activity studies as a proline analog having both hydrophobic and hydrophilic functional groups.

Experimental

All the melting points are uncorrected. TLC was carried out on silica gel G (Merck). Optical rotations were measured on a Union high-sensitivity polarimeter PM-71. ^{1}H and ^{13}C NMR spectra were recorded in a DMSO-d_6 solution on a JEOL FX-200 spectrometer at 29°C. Tetramethylsilane was used as an internal reference; sample concentration, 10—30 mg ml^{-1}. Amino acid analyses were performed using a Yanagimoto automatic analyzer LCA-8.

Boc-3,4-dehydro-L-proline Phenacyl Ester (3): To a solution of Boc-3,4-dehydro-L-proline (**2**)[8)] (6.39 g, 30 mmol) and Et_3N (4.06 ml) in EtOAc was added phenacyl bromide (5.77 g, 29 mmol) at room temperature. Stirring was continued for 6 h and the precipitate was filtered off. The filtrate was diluted with EtOAc (100 ml). The solution was washed with water, 4% $NaHCO_3$ and water, and dried over Na_2SO_4. The filtrate was evaporated in vacuo to give an yellow oil; yield, 9.47 g (98%); R_f=0.66 ($CHCl_3$–EtOH, 9:1).

***Trans*-Boc-3,4-epoxy-L-proline Phenacyl Ester (4):** To a solution of **3** (9.47 g, 28 mmol) and 2,6-di-*t*-butyl-*p*-cresol in $CHCl_3$ (100 ml), *m*-chloroperbenzoic acid (6.79 g, 28 mmol of 80% assay) dissolved in $CHCl_3$ (50 ml) was added dropwise over a period of 2 h with vigorous stirring. The mixture

was heated to reflux for 3 h. The content of the flask was cooled in an ice bath and the precipitate was removed by filtration. The filtrate was washed with 10% $NaHSO_3$, 4% $NaHCO_3$, and water, and dried over Na_2SO_4. The filtrate was then evaporated to give an oil (9.80 g). A solution of the oil in $CHCl_3$ was applied to a silica gel column (4×62 cm); cyclohexane–EtOAc (4:1) was used as an eluant and a 7.5 ml fraction was collected. Fractions 358—490 were collected and evaporated to produce an oil; yield, 2.12 g (22%); R_f=0.35 (cyclohexane–EtOAc, 4:1). A portion of starting material **3** (4.01 g) was recovered from fractions 235—335.

Boc-(2*S*,3*R*,4*R*)-4-chloro-3-hydroxyproline Phenacyl Ester (5): To a stirred suspension of **4** (335 mg, 1 mmol), tetraethylammonium chloride (165 mg, 1 mmol) and 2-chloro-3-ethylbenzoxazolium tetrafluoroborate (269 mg, 1 mmol) in CH_2Cl_2 (4 ml) was added (dropwise) a solution of Et_3N (0.17 ml) in CH_2Cl_2 (2 ml) at 0 °C under a nitrogen atmosphere.[7] The resulting mixture was stirred at room temperature for 48 h. After evaporation of the solvent, the residue was applied to a LiChroprep Si 60 (40—63 μm) column (1×20 cm); $CHCl_3$–EtOAc (9:1) was used as an eluant, 2 ml fraction. Fractions 10—13 were collected and evaporated to give an oil; yield 120 mg (32%); R_f=0.58 ($CHCl_3$–EtOAc, 9:1).

Boc-(2*S*,3*R*,4*R*)-4-chloro-3-hydroxyproline (6): To a stirred solution of **5** (250 mg, 0.67 mmol) in 90% acetic acid was added zinc powder (30 mg) at room temperature. After 2 h, the precipitate was filtered off, and the filtrate was evaporated in vacuo. The residue was acidified with 10% citric acid and extracted with EtOAc. The extract was dried over Na_2SO_4 and evaporated to give an oil; yield 150 mg (84%). R_f=0.17 ($CHCl_3$–MeOH, 5:1).

(2*S*,3*R*,4*R*)-4-Chloro-3-hydroxyproline Phenacyl Ester Hydrochloride (7): Compound **5** (690 mg, 1.8 mmol) was treated with 3.5 M HCl (1 M=1 mol dm^{-3}) in dioxane (5.1 ml) for 2 h and the solution was evaporated. The obtained product was collected with the aid of ether. Recrystallization from MeOH–ether gave 463 mg (80%); mp 168—169 °C; R_f=0.38 ($CHCl_3$–MeOH, 9:1).

Found: C, 48.73; H, 4.83; N, 4.29%. Calcd for $C_{13}H_{15}O_4NCl_2$: C, 48.76; H, 4.72; N, 4.37%.

(2*S*,3*R*,4*R*)-4-Chloro-3-hydroxyproline (1): Compound **6** (30 mg, 0.1 mmol) was treated with 4.7 M HCl in dioxane (2 ml) for 2 h at room temperature. The solution was evaporated. The residual oil was applied to a Dowex 50 (H^+ form); 10% pyridine was used as an eluant. The fraction containing the product was evaporated to give a solid; yield, 12 mg (68%); $[\alpha]_D^{20}$ −18.1° (*c* 0.25, MeOH); R_f=0.34 (1-butanol–AcOH–pyridine–H_2O, 4:1:1:2).

Found: C, 34.39; H, 5.15; N, 7.75%. Calcd for $C_5H_8O_3NCl \cdot 1/2H_2O$: C, 34.39; H, 5.19; N, 8.02%.

Stability of 1: To a solution of **1** (5.0 mg) in water (2 ml), Et_3N was added to adjust at pH 10.5. The solution was left to stand for 2 d at room temperature. An aliquot of the solution was applied on the amino acid analyzer (column size; 0.4×12.5 cm, pH of buffer solution; 3.25). Only a single peak of **1**, eluted for 6.0 min (cf Pro, at 12 min), was detected.

References

1) A. Buku, H. Faulstich, T. Wieland, and J. Dabrowski, *Proc. Natl. Acad. Sci. U. S. A.*, **77**, 2370 (1980).

2) M. Sato and T. Tatsuno, *Chem. Pharm. Bull. (Tokyo)*, **16**, 2182 (1966); H. Yoshida, K. Nakatsu, M. Sato, and T. Tatsuno, *Chem. Lett.*, **1973**, 1391.

3) J. U. Kahl and T. Wieland, *Liebigs Ann. Chem.*, **1981**, 1445.

4) S. Lee, K. Noda, H. Aoyagi, T. Kato, and N. Izumiya, *Int. J. Peptide Protein Res.*, in press.

5) N. Izumiya, T. Kato, H. Aoyagi, and M. Waki, "Principle and Practice of Peptide Synthesis" Maruzen, Tokyo (1985), p. 52.

6) H. O. House, "Modern Synthetic Reaction," Benjamin, New York (1972), p. 302.

7) Y. Echigo, Y. Watanabe, and T. Mukaiyama, *Chem. Lett.*, **1977**, 1013.

8) J. R. Dormoy, B. Castro, G. Chappuis, U. S. Fritschi, and P. Grogg, *Angew. Chem. Int. Ed. Engl.*, **19**, 742 (1980).

Oxidation of Lipids. XIII. Antioxidant Activities of α-, β-, γ-, and δ-Tocopherols

Etsuo NIKI,* Jyunichi TSUCHIYA, Yasuyuki YOSHIKAWA, Yorihiro YAMAMOTO, and Yoshio KAMIYA
Department of Reaction Chemistry, Faculty of Engineering, The University of Tokyo, Hongo, Tokyo 113
(Received September 18, 1985)

The antioxidant activities of α-, β-, γ-, and δ-tocopherols were studied. They were all effective as antioxidant in the oxidations of methyl linoleate in homogeneous solution. When one of the four tocopherols was used alone, they were consumed at the same rate and they suppressed the oxidation for the same period. However, the stabilities of chromanyloxyl radicals derived from the corresponding tocopherols varied considerably and decreased in the order α>β≅γ>δ -chromanyloxyl radicals. α-Tocopherol reacts quite rapidly with β-, γ-, and δ-chromanyloxyl radicals to give α-chromanyloxyl radical and β-, γ-, and δ-tocopherols respectively. Accordingly, when the four tocopherols were used together, α-tocopherol was consumed first, then β- and γ-tocopherols were consumed, and δ-tocopherol began to decrease after most of α-, β-, and γ-tocopherols were depleted.

The non-enzymatic, random peroxidations of biological molecules and foods by molecular oxygen have received much attention recently in connection with their pathological, toxicological, clinical, and nutritional effects.[1-12] Tocopherols (vitamin E) have been accepted to function as potent antioxidant by scavenging peroxyl radicals and interrupting free radical chain reactions. In a series of our study on the oxidation of lipids and its inhibition, we have studied in this work on the relative antioxidant activities of α-, β-, γ-, and δ-tocopherols.

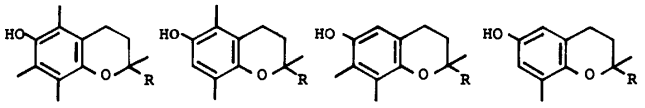

R: $C_{16}H_{33}$-

α-Tocopherol β-Tocopherol γ-Tocopherol δ-Tocopherol

Experimental

Natural *d*-α-, *d*-β-, *d*-γ-, and *d*-δ-tocopherols provided by Eisai Co. Ltd. were used as received. Commercial methyl linoleate was purified by silica-gel column before use. Dimyristoyl phosphatidylcholine (PC) was used as received from Sigma Chemicals. 2,2'-Azobis(2,4-dimethylvaleronitrile) (AMVN) was used as a radical initiator in order to generate initiating free radicals at a constant and known rate. The rate of chain initiation was determined by the conventional method[13-15] as reported previously[16,17] using 2,6-di-*t*-butyl-4-methylphenol as an antioxidant. Commercial galvinoxyl and 2,2-diphenyl-1-picrylhydrazyl were used as received.

Liposome was prepared as reported previously[18,19] and subjected to sonication with a Branson Sonifier Model 185 to obtain a unilamellar vesicles. The oxidation was carried out at 37°C under air in a Pyrex glass ampoule immersed in a water bath. The reaction mixture was agitated with a magnetic stirrer. The rate of oxygen uptake was followed with a pressure transducer and the rate of consumption of tocopherols was followed with high performance liquid chromatography at 294 nm. Electron spin resonance (ESR) spectra were recorded on a X-band JEOL FE1X spectrometer at room temperature.

Results and Discussion

The rate of spontaneous oxidation of methyl linoleate was quite small, but the oxidation proceeded smoothly in the presence of AMVN without any noticeable induction period and a constant rate of oxygen uptake was observed. When tocopherol was added to the reaction mixture, the oxidation was suppressed markedly and a clear induction period was observed. Figures 1 and 2 show the results of oxidation of methyl linoleate initiated with AMVN in the presence of α-tocopherol and γ-tocopherol respectively. The dotted line in Fig. 1 shows the oxygen uptake in the absence of tocopherol. Figures 1 and 2 show that α-tocopherol and γ-tocopherol were consumed linearly with time and when all of tocopherols were depleted, the induction period was over and a fast oxidation took place. It is noteworthy that the rate of oxidation after the induction period is similar to that in the absence of tocopherol. Similar results

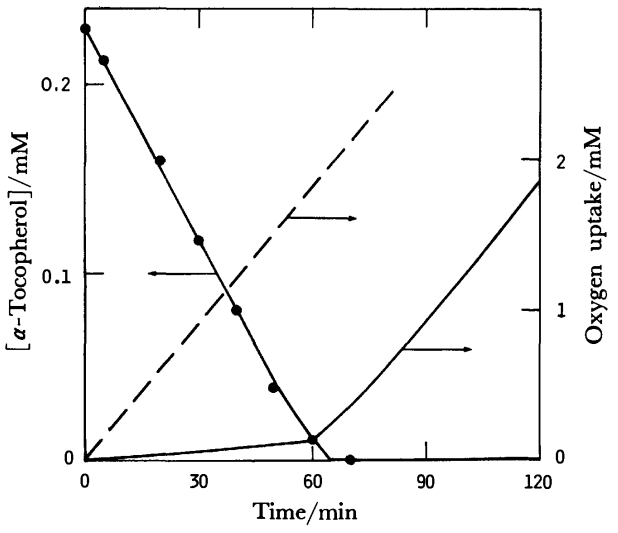

Fig. 1. Rates of oxygen uptake and α-tocopherol decay in the oxidation of 144 mM methyl linoleate in benzene under air at 37°C initiated with 30.0 mM AMVN. The dotted line show the oxygen uptake in the absence of α-tocopherol.

Table 1. Inhibition of Oxidation of Methyl Linoleate (LH) by Tocopherols (TOC) in Benzene at 37°C Under Air

[LH]	[AMVN]	TOC_1	TOC_2	t_{inh}	R_p	t_{inh}[AMVN]	10^5R_p
mM	mM	mM	mM	s	nM/s	[TOC]	$[LH][AMVN]^{1/2}$
144	19.3	0		0	790		3.95
144	30.0	α 0.230		3680	950	4.80×10^5	3.81
137	28.8	β 0.262		4510	868	4.96×10^5	3.73
137	28.9	γ 0.234		3820	870	4.72×10^5	3.74
137	28.9	δ 0.271		4820	837	5.14×10^5	3.60
144	30.3	α 0.230	β 0.274	8170	1130	4.91×10^5	4.51
144	30.4	α 0.230	γ 0.245	7530	914	4.82×10^5	3.64
144	30.5	α 0.230	δ 0.284	8700	918	5.16×10^5	3.65
144	30.4	γ 0.245	δ 0.284	9190	899	5.28×10^5	3.58
148	31.1	β 0.282	γ 0.176	7430	1040	5.05×10^5	3.98
140	29.6	β 0.300	γ 0.328	11120	915	5.24×10^5	3.80
144	30.4	β 0.307	δ 0.307	10220	823	5.06×10^5	3.28

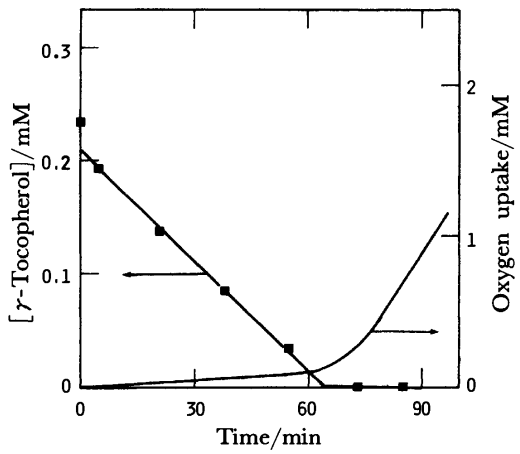

Fig. 2. Rates of oxygen uptake and γ-tocopherol disappearance in the oxidation of 137 mM methyl linoleate in benzene under air at 37°C initiated with 28.9 mM AMVN.

have been observed for β-and δ-tocopherols. The pertinent results are summarized in Table 1.

The oxidation of methyl linoleate (LH) initiated with AMVN (A-N=N-A) and inhibited by tocopherol (IH) proceeds by the following reaction mechanisms,[14,16-18,20]

$$\text{A-N=N-A} \longrightarrow [\text{A}\cdot\text{N}_2\cdot\text{A}] \longrightarrow (1-e)\text{A-A} \quad (1)$$
$$\searrow\ 2e\text{A}\cdot, \quad (2)$$

$$\text{A}\cdot + \text{O}_2 \longrightarrow \text{AO}_2\cdot, \quad (3)$$

$$\text{AO}_2\cdot + \text{LH} \xrightarrow{\text{O}_2} \text{AOOH} + \text{LO}_2\cdot, \quad (4)$$

Propagation:

$$\text{LO}_2\cdot + \text{LH} \xrightarrow{k_p} \text{LOOH} + \text{L}\cdot, \quad (5)$$

$$\text{L}\cdot + \text{O}_2 \longrightarrow \text{LO}_2\cdot \quad (6)$$

Termination;

$$\text{LO}_2\cdot + \text{IH} \xrightarrow{k_{inh}} \text{LOOH} + \text{I}\cdot, \quad (7)$$

$$(n-1)\text{LO}_2\cdot + \text{I}\cdot \longrightarrow \text{stable products}, \quad (8)$$

$$\text{LO}_2\cdot + \text{LO}_2\cdot \xrightarrow{k_t} \text{stable products}, \quad (9)$$

where e is the efficiency of free radical generation from AMVN, n is the stoichiometric number of peroxyl radicals trapped by each antioxidant, and k_p, k_{inh}, and k_t are the rate constants for reactions 5, 7, and 9 respectively.

The rate of chain initiation, R_i, is given by Eq. 10,

$$R_i = 2ek_d[\text{AMVN}], \quad (10)$$

where k_d is the rate constant for unimolecular decomposition of AMVN. The induction period, t_{inh}, is given by Eq. 11.

$$t_{inh} = n[\text{IH}]/R_i = n[\text{IH}]/2ek_d[\text{AMVN}] \quad (11)$$

Table 1 also shows the results of oxidation of methyl linoleate inhibited by the combination of two types of tocopherols. Figure 3 shows the plot of induction period as a function of $[IH]/R_i$. Table 1 and Fig. 3 show that the induction period is proportional to the total concentration of tocopherols independent of their types and inversrly proportional to the rate of chain initiation or the concentration of AMVN as expected from Eq. 11.[21]

The rate of oxidation in the absence of antioxidant or after the induction period is given by Eq. 12.

$$R_p = k_p[\text{LH}](R_i/2k_t)^{1/2} \quad (12)$$

The data in the last column of Table 1 show that Eq. 12 holds for all tocopherols.

Figure 4 shows the rates of disappearance of α-tocopherol and γ-tocopherol during the oxidation of methyl linoleate in benzene in the presence of both α- and γ-tocopherols. Figure 5 shows the similar results

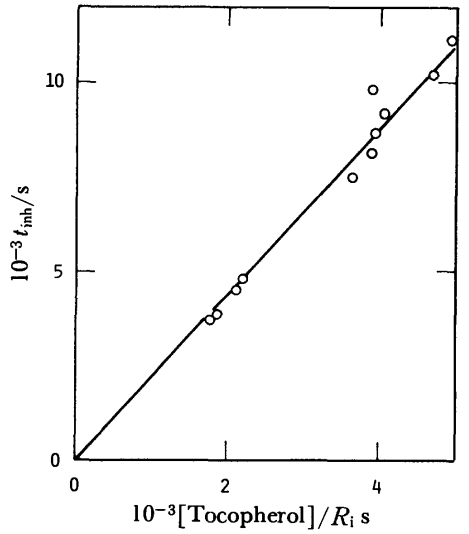

Fig. 3. Plot of induction period as a function of [tocopherol]/R_i for the oxidations of methyl linoleate in benzene under air at 37 °C initiated with AMVN.

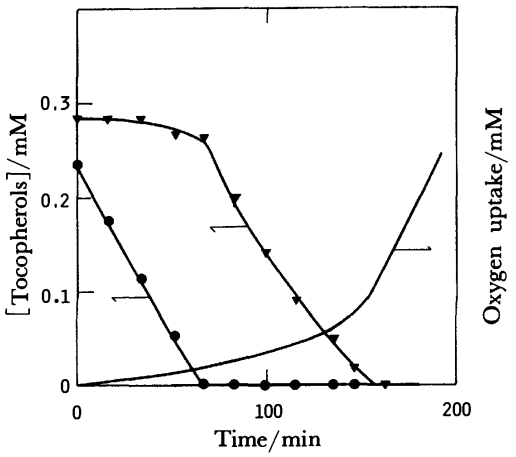

Fig. 5. Oxygen uptake and disappearance of α-(●) and δ-(▼) tocopherols during the oxidation of 144 mM methyl linoleate in benzene initiated with 30.5 mM AMVN inhibited by 0.230 mM α-tocopherol and 0.284 mM δ-tocopherol.

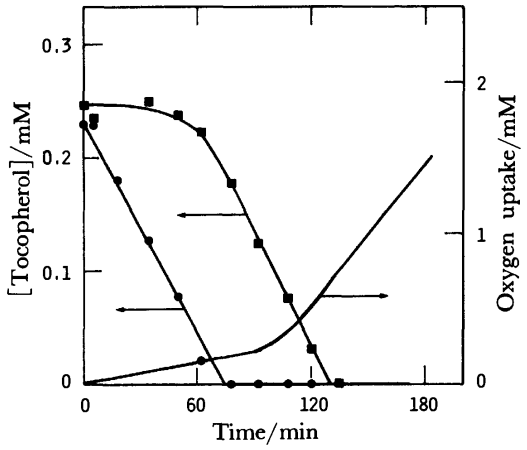

Fig. 4. Rates of oxygen uptake and disappearance of α-(●) and γ-(■) tocopherols in the oxidation of 144 mM methyl linoleate in benzene under air at 37 °C initiated with 30.4 mM AMVN.

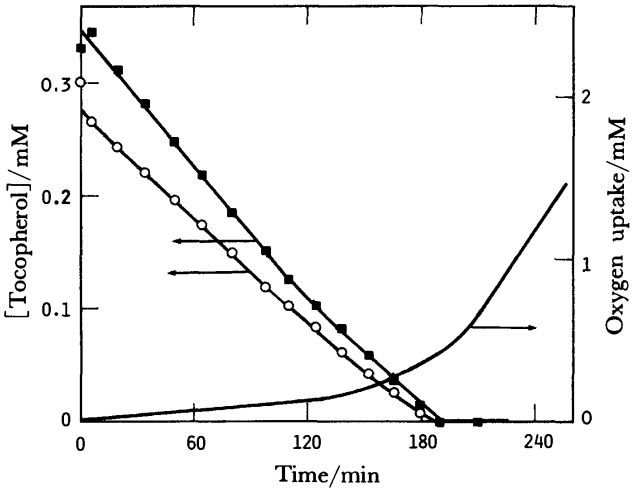

Fig. 6. Rates of oxygen uptake and β-(○) and γ-(■) tocopherols disappearance in the oxidation of 140 mM methyl linoleate in benzene under air at 37 °C initiated with 29.6 mM AMVN.

observed in the oxidation of methyl linoleate inhibited by both α- and δ-tocopherols. These results show that only α-tocopherol disappeared first linearly while γ- or δ-tocopherol remained almost unchanged at first and then they disappeared after α-tocopherol was depleted. When all tocopherols disappeared, the induction period was over and a fast oxidation took place. On the other hand, Fig. 6 shows that β- and γ-tocopherols disappeared at a similar rate when both of them were present together.

Figure 7 shows the rate of disappearance of four tocopherols during the oxidation of methyl linoleate in benzene. It can be seen that α-tocopherol disappeared first, then β- and γ-tocopherols disappeared at a similar rate, and finally δ-tocopherol followed. Interestingly, β- and γ-tocopherols were not consumed when appreciable amount of α-tocopherol was present, while most of δ-tocopherol remained until α-, β-, and γ-tocopherols were depleted.

The above results suggest that four tocopherols behave similarly as antioxidant when only one of them is present alone but also that the stabilities of tocopherols and/or chromanyloxyl radicals derived therefrom differ considerably.

The stabilities of chromanyloxyl radicals were studied by ESR. It has been observed that each tocopherol has its own specific ESR spectrum.[23-26] Chromanyloxyl radicals were generated as previously reported[26,27] by the interaction of tocopherol with galvinoxyl radical. The ESR spectrum of galvinoxyl radical disappeared instantaneously when it was reacted with α-tocopherol, and α-chromanyloxyl

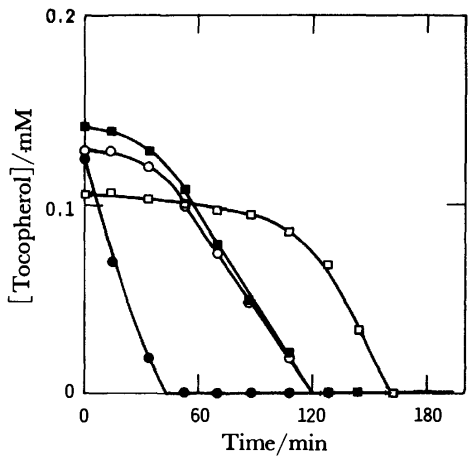

Fig. 7. Rates of disappearance of tocopherols during the oxidation of 144 mM methyl linoleate in benzene under air at 37°C initiated with 30.1 mM AMVN. Initial concentrations of tocopherols are: α(●)=0.124 mM, β(○)=0.130 mM, γ(■)=0.141 mM, γ(□)=0.105 mM.

radical was observed. β-, γ-, and δ-Tocopherols also reacted with galvinoxyl similarly. The rates of interactions between galvinoxyl and tocopherols in homogeneous solution were too fast to follow by a conventional method.

The rate of interactions between galvinoxyl radical incorporated into dimyristoyl PC liposomes and tocopherol incorporated into different dimyristoyl PC liposomes was followed by ESR. Galvinoxyl radical disappeared much more slowly than in homogeneous system and the pseudo first order rate constant was obtained as 10.1×10^{-4}, 5.44×10^{-4}, 5.00×10^{-4}, and 4.76×10^{-4} s^{-1} at 30°C for α-, β-, γ-, and δ-tocopherols respectively. Burton and Ingold[14] measured the reactivities of four tocopherols toward polystyrenylperoxyl radical and observed that the reactivities decreased in the same order of $\alpha>\beta\cong\gamma>\delta$ -tocopherols.

The interactions of tocopherol with chromanyloxyl radicals were also studied. The chromanyloxyl radical was prepared by the interaction of the corresponding tocopherol with 2,2-dipheyl-1-picrylhydrazyl. When α-tocopherol was prepared at first and then β-, γ-, or δ-tocopherol was added, no change in ESR spectrum was observed. On the other hand, when β-chromanyloxyl radical was first prepared and then α-tocopherol was added to the solution, β-chromanyloxyl radical disappeared quite rapidly and it was replaced by α-chromanyloxyl radical as shown in Fig. 8. Similar results were observed for the interactions of γ- and δ-chromanyloxyl radicals with α-tocopherol.

The above results suggest that both the reactivities of tocopherols toward peroxyl and phenoxyl radicals and stabilities of chromanyloxyl radicals decrease in the order of $\alpha>\beta\cong\gamma>\delta$. When, for example, both α- and γ-tocopherols are present, α-tocopherol scavenges the peroxyl radical predominantly, while γ-tocopherol scavenges peroxyl radicals more slowly but

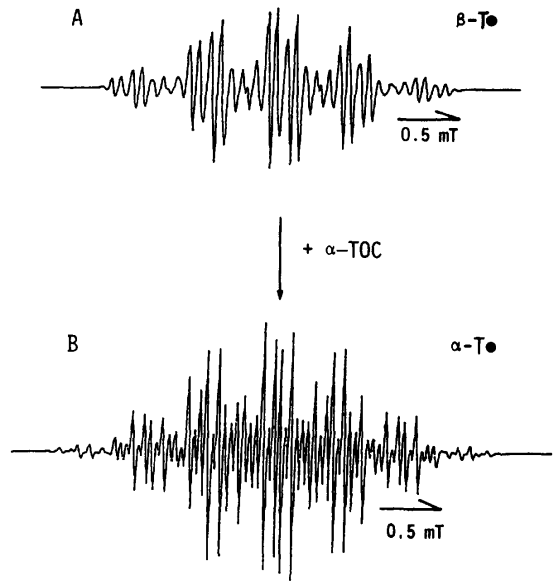

β-T• + α-TOC ⟶ β-TOC + α-T•

Fig. 8. Change of ESR spectrum observed when β-chromanyloxyl radical was interacted with α-tocopherol.
A: ESR spectrum of β-chromanyloxyl radical, B: ESR spectrum observed when α-tocopherol was added to the solution containing β-chromanyloxyl radical.

γ-chromanyloxyl radical formed by the interaction of γ-tocopherol with peroxyl radical must react with α-tocopherol rapidly to give γ-tocopherol and α-chromanyloxyl radical. Accordingly, only α-tocopherol must be consumed at first, while γ-tocopherol remains almost unchanged.

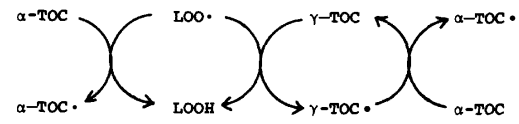

This study was supported in part by Grant-in-Aid for Scientific Research from the Ministry of Education, Science and Culture.

References

1) "Tocopherol, Oxygen, and Biomembranes," ed by C. de Duve and O. Hayaishi, Elsevier, Amsterdam (1978).
2) "Oxygen Free Radicals and Tissue Damage" (Chiba Foundation Symp. 65), Excerpta Medica, Amsterdam (1979).
3) "Biochemical and Clinical Aspects of Oxygen," ed by W. S. Caughey, Academic Press, New York (1979).
4) "Autoxidation in Food and Biological Systems," ed by M. G. Simic and M. Karel, Plenum Press, New York (1980).
5) "Age Pigments," ed by R. S. Sohal, Elsevier/North Holland Biomedical Press, Amsterdam (1981).
6) "Free Radicals, Lipid Peroxidation and Cancer," ed by

D. C. H. McBrien and T. F. Slater, Academic Press, London (1982).

7) "Lipid Peroxides in Biology and Medicine," ed by K. Yagi, Academic Press, New York (1982).

8) "Oxy Radicals and Their Scavenger Systems," ed by G. Cohen and R. A. Greenwald, Elsevier Biomedical, New York (1983).

9) "Oxygen Radicals in Chemistry and Biology," ed by W. Bors, M. Saran, and D. Tait, Walter de Gruyter, Berlin (1984).

10) W. A. Pryor, *Ann. New York Acad. Sci.* **393**, 1 (1982).

11) B. Halliwell and J. M. C. Gutteridge, *Biochem. J.*, **219**, 1 (1984).

12) "Free Radicals in Biology," ed by W. A. Pryor, Academic Press, New York (1976—1984), Vol. I—VI.

13) C. E. Boozer, G. S. Hammond, and J. N. Sen, *J. Am. Chem. Soc.*, **77**, 3233 (1955).

14) G. W. Burton and K. U. Ingold, *J. Am. Chem. Soc.*, **103**, 6472 (1981).

15) E. Niki, Y. Kamiya, and N. Ohta, *Bull. Chem. Soc. Jpn.*, **42**, 3220 (1969).

16) Y. Yamamoto, E. Niki, and Y. Kamiya, *Bull. Chem. Soc. Jpn.*, **55**, 1548 (1982).

17) E. Niki, T. Saito, A. Kawakami, and Y. Kamiya, *J. Biol. Chem.*, **259**, 4177 (1984).

18) Y. Yamamoto, E. Niki, Y. Kamiya, and H. Shimasaki, *Biochim. Biophys. Acta*, **795**, 332 (1984).

19) J. Tsuchiya, T. Yamada, E. Niki, and Y. Kamiya, *Bull. Chem. Soc. Jpn.*, **58**, 326 (1985).

20) L. R. C. Barclay and K. U. Ingold, *J. Am. Chem. Soc.*, **103**, 6478 (1981).

21) It may be noteworthy that the stoichiometric numbers n for the hindered phenols with alkyl substituents on both ortho positions are close to 2, whereas those for non-hindered phenols are smaller than 2.[22] The results of Table 1 and Fig. 3 suggest that the values of n for α-, β-, γ-, and δ-tocopherols are same within experimental error under the present reaction conditions. It has been found previously[17] that α-tocopherol and 2,6-di-*t*-butyl-4-methylphenol have same n values. These results may be attributed to the high concentration of peroxyl radicals in the present oxidation initiated with AMVN. If the concentration of peroxyl radical is smaller and the chromanoxyl radical has longer lifetime, the n values for β-, γ-, and δ-tocopherols may be smaller than that for α-tocopherol.

22) E. C. Horswill, J. A. Howard, and K. U. Ingold, *Can. J. Chem.*, **44**, 985 (1966).

23) W. Boguth and H. Niemann, *Biochim. Biophys. Acta*, **248**, 121 (1971).

24) T. Ozawa, A. Hanaki, S. Matsumoto, and M. Matsuo, *Biochim. Biophys. Acta*, **531**, 72 (1978).

25) K. Mukai, N. Tsuzuki, K. Ishizu, S. Ouchi, and K. Fukuzawa, *Chem. Phys. Lipids*, **29**, 129 (1981).

26) J. Tsuchiya, E. Niki, and Y. Kamiya, *Bull. Chem. Soc. Jpn.*, **56**, 229 (1983).

27) E. Niki, A. Kawakami, M. Saito, Y. Yamamoto, J. Tsuchiya, and Y. Kamiya, *J. Biol. Chem.*, **260**, 2191 (1985).

 © 1986 The Chemical Society of Japan Bull. Chem. Soc. Jpn., 59, 503—506 (1986)

Synthesis of Selenoxides by Oxidation of Selenides with *t*-Butyl Hypochlorite, and Its Application for Synthesis of Optically Active Selenoxide

Michio KOBAYASHI,* Hiromi OHKUBO, and Toshio SHIMIZU
Department of Chemistry, Faculty of Science, Tokyo Metropolitan University, Fukazawa, Setagaya-ku, Tokyo 158
(Received September 18, 1985)

An effective synthesis of selenoxides by the oxidation of selenides with *t*-butyl hypochlorite in the presence of methanol and pyridine followed by hydrolysis is descrived. This oxidation method is particularly effective for the oxidation of selenides which possess electron-withdrawing groups. A synthesis of partially optically active selenoxide with bulky substituents can be achieved using a novel oxidation method.

The oxidation of organic selenides to selenoxides has been carried out using several oxidizing reagents, such as hydrogen peroxide,[1] ozone,[2] peracetic acid,[1] dinitrogen tetraoxide,[3] (dichloroiodo)benzene,[4] *N*-chlorosuccinimide,[5] *t*-butyl hypochlorite[5] and sodium periodate.[4] Among these, sodium periodate is most widely used in laboratories. However, the oxidation of diaryl selenides by this reagent is retarded or completely prevented by the presence of strong electron-withdrawing groups. Ozone is effective in this respect, but its oxidation tends to go beyond the stage of the selenoxides. Nothing is known regarding the oxidation of a selenide substituted with electron-withdrawing groups in the case of oxidation with positive halogenating species. We report here a new synthesis of various selenoxides with an electron-withdrawing substituent through a reaction of selenides and *t*-butyl hypochlorite in the presence of methanol and pyridine followed by hydrolysis.

There had been no example of an optically active selenoxide for a long time. The difficulty of an optical resolution of selenoxide is due to its facile racemization through achiral hydrates.[6] In 1970, optically active selenoxide was isolated for the first time using steroidal systems.[7] Recently, partially optically active selenoxides were synthesized by Davis et al.[8] We also report here on the synthesis of optically active selenoxide using a novel oxidation technique.

Results and Discussion

To a solution of selenide in dichloromethane or acetonitrile were added an equimolar pyridine and an excess amount of methanol. An equimolar *t*-butyl hypochlorite in the same solvent was added slowly

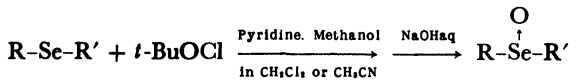

1 2

Scheme 1.

to a stirred solution of the selenide at −25 °C. Stirring continued for 40 min at −25 °C. The mixture was hydrolyzed by an addition of a sodium hydroxide solution. Results are shown in Table 1. By the present method, 4,4′-dinitrodiphenyl selenide (**1g**), which could not be oxidized by sodium periodate,[4] was oxidized to 4,4′-dinitrodiphenyl selenoxide (**2g**) in 90% yield. Nitro-substituted diaryl selenides (**1f** and **1h**) were also oxidized to the corresponding selenoxides (**2f** and **2h**) in good yields, respectively. Methyl *p*-(phenylseleno)benzoate (**1i**), which possesses an electron-withdrawing carboxyl group on an aromatic ring, was similarly oxidized to the corresponding selenoxide **2i** in good yields. By oxidation with sodium periodate, **1i** gave **2i** in only 22% yield. Even selenoxides (**2c** and **2d**) with bulky substituents were obtained in good yields. An undesired oxidation of selenoxide to selenone was not occur with the present method. Both methanol and pyridine play important roles to ensure good yields of selenoxides, since the yield of 4,4′-dinitrodiphenyl selenoxide (**2g**) decreases in the absence of pyridine (Table 2). Also, the yields of 4,4′-dinitrodiphenyl selenoxide (**2g**) and 2,4-dinitrodiphenyl selenoxide (**2h**) were greatly decreased in the absence of both methanol and pyridine. The present reaction is thought to proceed via an intermediary selenonium salt **5**. The formation of this type of

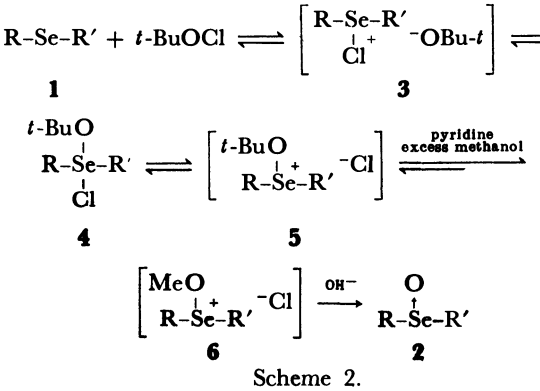

Scheme 2.

selenonium salt was reported in a reaction of diphenyl selenide with *t*-butyl hypochlorite.[10] An equilibrium seems to exist among the starting materials, **3**, selenurane **4** and **5**. The addition of excess methanol and pyridine may cause a shift the equilibrium toward the right, resulting in the formation of a selenonium salt

Table 1. Oxidation of Selenides to Selenoxides

	Product	Reaction Conditions: Solvent	Reaction temperature	Reaction time/min	Selenoxides: Yield %	MS. m/z (M^+) (^{80}Se)	Mp θ_m/°C	IR (KBr) (Se=O) (cm^{-1})
(2a)	$CH_3-\overset{\overset{O}{\uparrow}}{Se}-Ph$	CH_3CN	−25°C	40	80	188	—[b]	810 (neat)
(2b)	$CH_3-\overset{\overset{O}{\uparrow}}{Se}-C_6H_4-CH_3$	CH_3CN	−25°C	40	93	202	106—107.5	810
(2c)	$CH_3-\overset{\overset{O}{\uparrow}}{Se}-Ar$[a]	CH_3CN CH_2Cl_2 CH_2Cl_2	−25°C −25°C r.t.	40 40 60	90 94 66	314	153.5—155[c]	810
(2d)	$CH_3-C_6H_4-\overset{\overset{O}{\uparrow}}{Se}-Ar$[a]	CH_3CN	−25°C	40	91	390	147—148.5	820
(2e)	$Ph-\overset{\overset{O}{\uparrow}}{Se}-C_6H_4-OCH_3$	CH_3CN	−25°C	40	99	280	133.5—134.5	820
(2f)	$Ph-\overset{\overset{O}{\uparrow}}{Se}-C_6H_4-NO_2$	CH_2Cl_2 CH_3CN	−40°C −25°C	40 40	98 93	295	134.5—135.5	825
(2g)	$O_2N-C_6H_4-\overset{\overset{O}{\uparrow}}{Se}-C_6H_4-NO_2$	CH_2Cl_2	−25°C	40	90	340	207.5—208.5[d]	830
(2h)	$Ph-\overset{\overset{O}{\uparrow}}{Se}-C_6H_3(NO_2)-NO_2$	CH_2Cl_2	−25°C	40	94	340	134.5 (decomp)	830
(2i)	$Ph-\overset{\overset{O}{\uparrow}}{Se}-C_6H_4-COOCH_3$	CH_3CN CH_2Cl_2	−25°C −25°C	40 40	94 96	308	160—161	825

a) Ar=2,4,6-triisopropylphenyl. b) Isolated as an oil. 53—54°C (reported[9]). c) 136—138°C (reported[8]). d) 206°C (reported[4]).

Table 2. Oxidation of Selenides to Selenoxides in the Absence of Pyridine and Methanol[a]

Product	Solvent	Pyridine / Selenide b)	Methanol / Selenide b)	Yield %
(2b)	CH_3CN	1	1.2	93
	CH_3CN	—	—	98
(2g)	CH_2Cl_2	1	>2	90
	CH_2Cl_2	—	>2	51[c]
	CH_2Cl_2	—	—	33[d]
(2h)	CH_2Cl_2	1	>2	94
	CH_2Cl_2	—	—	71[e]
(2i)	CH_2Cl_2	1	>2	96
	CH_2Cl_2	—	—	94

a) All reactions were carried out at −25°C and for 40 min. b) mol mol^{-1}. c) 44% of selenide was recovered. d) 60% of selenide was recovered. e) 13% of selenide was recovered.

6, the hydrolysis of which gives selenoxide **2** in good yield.

Recently, Davis et al. reported the synthesis of partially optically active selenoxides by kinetic differentiation during the formation of selenimides.[8] We have attempted to synthesize the optically active selenoxide, the selenium moiety of which was flanged by two bulky substituents to prevent racemization, by an application of the present oxidation method. To a solution of 2,4,6-tri-*t*-butyldiphenyl selenide (**7**) in dry dichloromethane was added equimolar pyridine and excess amounts of (−)-2-octanol (twentyfold of the selenide). An equimolar *t*-butyl hypochlorite in dichloromethane was slowly added to the stirred solution at −40°C. Stirring continued for 2 h at −40°C. After hydrolysis and extraction, (−)-2-octanol was removed in vacuo (30°C/10^{-3}—10^{-4} mmHg (1 mmHg=133.322pa)) and the remaining selenoxide **8** was recrystallized from dichloromethane–hexane. Mp 133.5—134°C. $[\alpha]_D^{32}$ +1.73° (*c* 0.948, CH_2Cl_2). The CD spectrum shows the positive Cotton effect at 291 nm. An enantiomeric excess

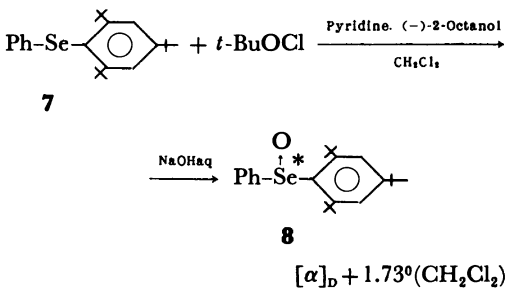

Seheme 3.

of 1.0% was estimated by HPLC using an optically active column. This enantioselectivity suggests the presence of (−)-1-methylheptyloxyselenonium salt as an intermediate. When (+)-2-octanol was used, selenoxide with a negative optical rotation ($[\alpha]_D^{33}$ −0.428°) was obtained. The racemization of **8** was found to be very slow in neutral solvents at room temperature.

Experimental

All melting points were determined on a Yamato MP-21. IR spectra were recorded on a Hitachi 260-10 spectrometer, ^{1}H-NMR spectra with TMS as an internal standard on a JEOL JNM-PMX60$_{SI}$, CD spectrum on a JASCO J-40A, and Mass spectra on a JEOL JMS-DX300 mass spectrometer. The optical rotation was measured on a JASCO DIP-140 digital polarimeter. Silica-gel TLC and column chromatography were performed on a Merck Kieselgel 60F$_{254}$ and a Wako Wakogel C-200, respectively. Organic solvents were purified and dried by the usual procedures.

Materials. The starting materials (**1a**, **1b**, **1c**, **1f**, **1g**, and **1h**) are all well known compounds.[8,11-14]

***p*-Tolyl 2,4,6-Triisopropylphenyl Selenide (1d):** Compound **1d** was prepared from bis(2,4,6-triisopropylphenyl)-diselenide and *p*-tolylmagnesium bromide. Yield=68%. Mp 59.5—61 °C. IR (KBr) ν=800, 1015, 1560, 1590, 2800—3100 cm^{-1}. ^{1}H-NMR ($CDCl_3$) δ=1.08 (12H, d, J=6.6 Hz, CH_3 of ortho isopropyl), 1.22 (6H, d, J=6.6 Hz, CH_3 of para isopropyl), 2.16 (3H, s, CH_3 of tolyl), 2.4—3.0 (1H, m, para methine), 3.66 (2H, hep., J=6.6 Hz, ortho methine), 6.90 (4H, s, aromatic protons of tolyl), 7.03 (2H, s, aromatic protons of triisopropylphenyl). Found: m/z 374.1512 (^{80}Se), Calcd for $C_{22}H_{30}{}^{80}Se$: 374.1512.

2-Methoxydiphenyl Selenide (1e): Compound **1e** was prepared from diphenyl diselenide and *o*-methoxyphenyl-magnesium bromide. Yield=59%. Bp 143—145 °C/2 mmHg. IR (liq. firm) ν=740, 1020, 1245, 1470, 1575, 2800—3100 cm^{-1}. ^{1}H-NMR ($CDCl_3$) δ=3.78 (3H, s, CH_3), 6.6—7.7 (9H, m, aromatic protons). Found: m/z 264.0076 (^{80}Se), Calcd for $C_{13}H_{12}O^{80}Se$: 264.0053.

Methyl *p*-(Phenylseleno)benzoate (1i): Compound **1i** was prepared by the esterification of *p*-(phenylseleno)-benzoic acid which was obtained by a reaction of benzeneselenol, potassium hydroxide and *p*-iodobenzoic acid.[15] Yield=67%. Mp 78—79 °C. IR (KBr) ν=1700(C=O) cm^{-1}. ^{1}H-NMR ($CDCl_3$) δ=3.85 (3H, s, OCH_3), 7.2—7.7 (5H, m, aromatic protons of phenyl), 7.32 and 7.83 (4H, ABq, J=8.2 Hz, aromatic protons of *p*-substituted benzene ring). Found: m/z 292.0002 (^{80}Se), Calcd for $C_{14}H_{12}O_2{}^{80}Se$: 292.0002.

2,4,6-Tri-*t*-butyldiphenyl Selenide (7): Compound **7** was prepared by a reaction of 2,4,6-tri-*t*-butylphenyllithium and benzeneselenenyl bromide in THF and purified by recrystallization from hexane-ethanol. Yield=28% (based on 2,4,6-tri-*t*-butyl-1-bromobenzene). Mp 127.5—128 °C. IR (KBr) ν=730, 1470, 2800—3000 cm^{-1}. ^{1}H-NMR ($CDCl_3$) δ=1.35 (9H, s, para *t*-butyl), 1.48 (18H, s, ortho *t*-butyl), 6.4—7.1 (5H, m, aromatic protons of phenyl), 7.49 (2H, s, aromatic protons of tri-*t*-butylphenyl). Found: m/z 402.1812 (^{80}Se), Calcd for $C_{24}H_{34}{}^{80}Se$: 402.1825.

Typical Procedure for the Oxidation of Selenide. To a solution of selenide (1.0 mmol) in dichloromethane (30 ml) was added an equimolar pyridine and an excess amount of methanol (ca.5 mmol). The solution was cooled to −25 °C under dry nitrogen. An equimolar *t*-butyl hypochlorite in dichloromethane (5 ml) was slowly added to the stirred solution and stirring continued for 40 min at −25 °C. A sodium hydroxide solution (2 mmol in 5 ml of water) was added to the mixture at this temperature with stirring. Then, the resulting mixture was allowed to become room temperature and the organic layer was separated. The aqueous phase was extracted with dichloromethane. The combined organic extract was concentrated and the remaining product was purified either by silica-gel column chromatography or by recrystallization. When acetonitrile was used as a solvent, extraction was carried out after the evaporation of acetonitrile. Among the resulting selenoxides, **2a**, **2c**, and **2g** are known compounds.[5,8,9]

Methyl *p*-Tolyl Selenoxide (2b): Mp 106—107.5 °C. IR (KBr) ν=810 (Se=O), 1400, 1490, 2900—3100 cm^{-1}. ^{1}H-NMR ($CDCl_3$) δ=2.34 (3H, s, CH_3 of tolyl), 2.51 (3H, s, CH_3-Se), 7.25 and 7.55 (4H, ABq, J=8.4 Hz, aromatic protons). Found: m/z 201.9892 (^{80}Se), Calcd for $C_8H_{10}O^{80}Se$: 201.9896.

***p*-Tolyl 2,4,6-Triisopropylphenyl Selenoxide (2d):** Mp 147—148.5 °C. IR (KBr) ν=810, 820(Se=O), 1460, 2850—3000 cm^{-1}. ^{1}H-NMR ($CDCl_3$) δ=0.88, 1.18, 1.22 (18H, d, J=6.6 Hz, CH_3 of isopropyl), 2.30 (3H, s, CH_3 of tolyl), 2.5—3.1 (1H, m, para methine), 3.72 (2H, hep., J=6.6 Hz, ortho methine), 7.01 (2H, s, aromatic protons of triisopropyl-phenyl), 7.18 and 7.42 (4H, ABq, J=8.1 Hz, aromatic protons of tolyl). Found: m/z 390.1464 (^{80}Se), Calcd for $C_{22}H_{30}O^{80}Se$: 390.1461.

2-Methoxydiphenyl Selenoxide (2e): Mp 133.5—134.5 °C. IR (KBr) ν=770, 820(Se=O), 1020, 1040, 1230, 1270, 1310, 1470 cm^{-1}. ^{1}H-NMR ($CDCl_3$) δ=3.81 (3H, s, CH_3), 6.8—8.0 (9H, m, aromatic protons). Found: m/z 279.9977 (^{80}Se), Calcd for $C_{13}H_{12}O_2{}^{80}Se$: 280.0002.

4-Nitrodiphenyl Selenoxide (2f): Mp 134.5—135.5 °C. IR (KBr) ν=744, 825(Se=O), 847, 1344(NO_2), 1516(NO_2)cm^{-1}. ^{1}H-NMR ($CDCl_3$) δ=7.3—7.8 (5H, m, aromatic protons of phenyl), 7.82 and 8.22 (4H, ABq, J=9.0 Hz, aromatic protons of nitrophenyl). Found: m/z 294.9753 (^{80}Se), Calcd for $C_{12}H_9NO_3{}^{80}Se$: 294.9747.

2,4-Dinitrodiphenyl Selenoxide (2h): Mp 134.5 °C(decomp). IR (KBr) ν=730, 830(Se=O), 915, 1079, 1340(NO_2), 1526(NO_2), 1602 cm^{-1}. ^{1}H-NMR ($CDCl_3$) δ=7.3—7.9 (5H, m, aromatic protons of phenyl), 8.7—9.1 (3H, m, aromatic protons of dinitrophenyl). Found: m/z 339.9662 (^{80}Se), Calcd for $C_{12}H_8N_2O_5{}^{80}Se$: 339.9598.

Methyl *p*-(Phenylseleninyl)benzoate (2i): Mp 160—161 °C. IR (KBr) ν=739, 761, 825(Se=O), 1204, 1269, 1435, 1585, 1724(C=O) cm^{-1}. ^{1}H-NMR ($CDCl_3$) δ=3.92 (3H, s, OCH_3), 7.4—7.6 (5H, m, aromatic protons of phenyl), 7.81 and 8.15 (4H, ABq, J=7.6 Hz, aromatic protons of *p*-(methoxycarbonyl)phenyl). Found: m/z 307.9933 (^{80}Se), Calcd for $C_{14}H_{12}O_3{}^{80}Se$: 307.9951.

(+)-2,4,6-Tri-*t*-butyldiphenyl Selenoxide (8): To a solution of 2,4,6-tri-*t*-butyldiphenyl selenide (**7**) (0.75 mmol) in dry dichloromethane (13 ml), was added equimolar pyridine and an excess amount of (−)-2-octanol (15 mmol). The solution was cooled to −40 °C under dry nitrogen. An equimolar *t*-butyl hypochlorite (0.75 mmol) in dry dichloromethane (2 ml) was slowly added to the stirred solution and stirring was continued for 2 h at −40 °C. A sodium hydroxide solution (1.5 mmol in 5 ml of water) was added to the mixture at this temperature with stirring.

Then, the resulting mixture was allowed to become room temperature and the organic layer was separated. The aqueous phase was extracted with dichloromethane. The resulting selenoxide **8** was purified by recrystallization from dichloromethane–hexane after the removal of (−)-2-octanol in vacuo (30 °C/10^{-3}—10^{-4} mmHg). Chemical Yield=54%. Mp 133.5—134 °C. $[\alpha]_D^{32}$ +1.73 °(*c* 0.948, CH_2Cl_2). $[\theta]_{291}$ +236 (Methanol). IR (KBr) ν=745, 840(Se=O), 1360, 1585, 2800—3100 cm^{-1}. ^{1}H-NMR ($CDCl_3$) δ=1.35 (9H, s, para *t*-butyl), 1.45 (18H, s, ortho *t*-butyl), 6.7—7.3 (5H, m, aromatic protons of phenyl), 7.46 (2H, s, aromatic protons of tri-*t*-butylphenyl). Found: *m/z* 418.1818 (^{80}Se), Calcd for $C_{24}H_{34}O^{80}Se$: 418.1774. The enantiomeric excess was determined by HPLC on an optically active column (Bakerbond chiral phase HPLC column DNBPG/Aminopropylsilica; 25 cm×4.6 mm; using hexane: 2-propanol=95:5 as eluent.

References

1) E. S. Gould and J. M. McCullough, *J. Am. Chem. Soc.*, **73**, 3196 (1951).
2) G. Ayrey, D. Barnard and D. T. Woodbridge, *J. Chem. Soc.*, **1962**, 2089.
3) R. Paetzold, U. Lindner, G. Bochmann, and P. Reich, *Z. Anorg. Allg. Chem.*, **352**, 295 (1967).
4) M. Cinquini, S. Colonna, and R. Giovini, *Chem. Ind. (London)*, **1969**, 1737.
5) M. R. Detty, *J. Org. Chem.*, **45**, 274 (1980).
6) M. Ōki and H. Iwamura, *Tetrahedron Lett.*, **1966**, 2917.
7) D. N. Jones, D. Mundy, and R. D. Whitehouse, *J. Chem. Soc., Chem. Commun.*, **1970**, 86.
8) F. A. Davis, J. M. Billmers, and O. D. Stringer, *Tetrahedron Lett.*, **1983**, 3191.
9) D. G. Foster, *Rec. Trav. Chim. Pays-Bas*, **45**, 447 (1935).
10) N. Ya. Derkach, N. P. Tishchenko, and V. G. Voloshchuk, *Zh. Org. Khim.*, **14**, 958 (1978).
11) H. M. Gilow and G. L. Walker, *J. Org. Chem.*, **32**, 2580 (1967).
12) L. Chierici, H. Lumbroso, and R. Passerina, *Boll. Sci. Fac. Chim. Ind. Bologna*, **12**, 127 (1954).
13) T. G. Back, S. Collins, and R. G. Kerr, *J. Org. Chem.*, **46**, 1564 (1981).
14) L. M. Litvinenko and R. S. Cheshko, *Zh. Obshch. Khim.*, **30**, 3682 (1960).
15) K. Šindelář , E. Svátek, J. Metyšová, J. Metyš, and M. Protiva, *Collect. Czech. Chem. Commun.*, **34**, 3792 (1969). 3792 (1969).

 © 1986 The Chemical Society of Japan Bull. Chem. Soc. Jpn., 59, 507—510 (1986)

Immobilization of β-Cyclodextrin on Silica Gel**

Shinsaku SHIRAISHI,* Makoto KOMIYAMA,† and Hidefumi HIRAI†
The Institute of Industrial Science, The University of Tokyo, Roppongi, Minato-ku, Tokyo 106
†Department of Industrial Chemistry, Faculty of Engineering, The University of Tokyo, Hongo, Bunkyo-ku, Tokyo 113
(Received September 21, 1985)

β-Cyclodextrin (β-CyD) was covalently immobilized on silica gel by chlorination of silica gel with thionyl chloride or silicon tetrachloride, followed by the reaction of the resulting chlorinated silica gel with β-CyD in pyridine. The amounts of the immobilized β-CyD were 8×10^{-5} to 1.4×10^{-4} mol per 1 g of the β-CyD–silica gel composites. On heating, the composites did not exhibit weight decrease up to 250 °C. The β-CyD in the composites formed 1 : 1 complex with phenol in aqueous solutions, and the equilibrium constant for the dissociation of the complex was 6×10^{-3} mol dm^{-3} at 25 °C. The immobilized β-CyD exhibited catalytic activity in the cleavage of 4-nitrophenyl acetate at 25 °C, pH 8.7.

Cyclodextrins (CyDs), cyclic oligomers of 6—8 glucose molecules, form inclusion complexes with various guest compounds. The magnitude of the complex formation is largely dependent on the structure of guest compound.[1,2] CyDs exhibit specific catalyses in the selective syntheses of various chemicals such as 4-chloroanisole,[3] vitamin K analogs,[4] 4-hydroxybenzaldehydes,[5] 4-hydroxybenzoic acids,[6] and 3-indolecarbaldehyde.[7]

Many works have been carried out on the immobilization of CyDs using organic materials either as cross-linking agents or as supports. Gels, prepared by the reactions of CyDs with epichlorohydrin or diisocyanates, were successfully used for column chromatography[8–13] and selective catalyses.[14–18] CyDs immobilized on polyacrylamide gels as supports were effective for column chromatography.[19] Water-soluble polymers containing CyDs were also prepared.[20]

However, there have been a few reports on the immobilization of CyDs on inorganic supports. Fujimura et al.[21] immobilized CyDs to silica gel by the reaction of aminated silica gel with CyD tosylate. Kawaguchi et al.[22] also immobilized CyDs on silica gel by condensation of carboxylated silica gel with CyDs having amino groups by use of 1-ethyl-3-[3-(dimethylamino)propyl]carbodiimide. Both methods require synthesis of modified CyD prior to immobilization.

In this paper, a simpler immobilization of CyDs on silica gel, which does not involve synthesis of modified CyDs, is reported. Silica gel is first chlorinated with thionyl chloride or silicon tetrachloride, and then is reacted with intact β-CyD. Thermal stabilities and binding properties of the β-CyD-silica gel composites are shown. Furthermore, the catalytic activity of the immobilized β-CyD in the cleavage of 4-nitrophenyl acetate is described.

Experimental

Materials. β-CyD was recrystallized from water, and was dried at 110 °C in vacuo. Silica gel (average diameter, 60 μm; surface area, 370 m^2 g^{-1}; average pore diameter, 130 Å; total pore volume, 0.96 dm^3 g^{-1}) was obtained from Iatron Co. and was dried at 110 °C in vacuo. Pyridine was distilled over metallic magnesium ribbon after prolonged refluxing over the same. All other reagents were dried and purified in usual ways.

Immobilization of β-Cyclodextrin on Silica Gel. Immobilization of β-CyD on the silica gel was carried out as depicted in Scheme 1. First, silica gel was added to thionyl chloride or silicon tetrachloride with or without benzene as solvent, and the mixture was refluxed for 5—20 h. The resulting solids were washed with dry benzene, and were dried at 110 °C in vacuo. Then, the solids were reacted with β-CyD in pyridine at 80 °C for 10 h. After the reactions, the solids were repeatedly washed with water, soaked in water for a week, and then dried in vacuo at 110 °C. The contents of β-CyD in the β-CyD–silica gel composites were estimated either from the carbon contents on elemental analyses or from the decrease of weight on thermogravimetric analyses (see Results and Discussion Section). The values determined by these two methods were identical with each other within 1%.

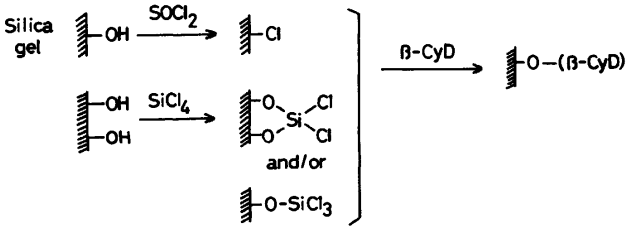

Scheme 1.

Characterization of β-CyD–Silica Gel Composite. Thermogravimetric analyses were made on a Shimadzu Model DT-30 Thermal Analyzer. Surface area (by BET method), pore volume, and pore size (by the Inkley method) were obtained by the analyses of the nitrogen isotherms measured by using an Orr Surface-Area Pore-Volume Analyzer 2100 D (Micromeritics Co.).

Determination of Equilibrium Constant for Complex Formation between β-Cyclodextrin Immobilized on Silica Gel and Phenol. The β-CyD-silica gel composite (100 mg) was added to 3 cm^3 aqueous solution of phenol (the concentration p_o). The mixture was vigorously shaken, and then was incubated at 25 °C for 30 min. The equilibrium concentration (p) of phenol in aqueous medium in the presence of the β-CyD–silica gel composite was determined

**A part of this paper was preliminarily presented at the 26th International Congress of Pure and Applied Chemistry, Tokyo (1977). Abstracts, Session I, p. 260.

Table 1. Immobilization of β-CyD to Silica Gel

Code	Silica gel	β-CyD	Chlorination of silica gel		Amount of β-CyD in β-CyD-silica gel composite	
	g	g	Agent[a)]	Reaction time/h	wt% in composite	10^{-4} mol per 1 g composite
A-1	18	5	$SOCl_2$(60)	20	16.0	1.4
A-2	18	4	$SOCl_2$(60)	5	10.4	0.88
A-3	18	5	$SOCl_2$/benzene (40/40)	10	15.0	1.3
A-4	20	5	$SiCl_4$/benzene (10/50)	10	9.4	0.83

a) The numbers in parentheses refer to the amounts used (in cm^3).

spectroscopically at 270 nm.

The equilibrium constant K_d for the dissociation of the complex was determined by plotting p vs. $p/(p_0-p)$ according to Eq. 1,

$$p = c_0 \cdot p/(p_0-p) - K_d. \quad (1)$$

Here, c_0 is the amount of the immobilized β-CyD, which is charged per unit volume of specimen. Equation 1 is obtained from Eq. 2, which is based on the assumption that the immobilized β-CyD form 1:1 complex with phenol.

$$K_d = p \cdot [c_0 - (p_0-p)]/(p_0-p). \quad (2)$$

The equilibrium constant for the dissociation of the complex between unmodified β-CyD and phenol in homogeneous solution at 25 °C was determined spectroscopically at 280 nm, according to the method in the literature.[23)]

Kinetics. To a quartz cell, a required amount of β-CyD-silica gel composite and 3 cm^3 of pH 8.7 Tris buffer solution were added at 25 °C. After a thermoequilibrium was attained, 20×10^{-3} cm^3 or less of a stock solution of 4-nitrophenyl acetate in acetonitrile was charged, and the mixture was vigorously stirred. The cleavage was followed by the release of 4-nitrophenol at 400 nm. The rate constants were determined by using usual first-order equation.

Results and Discussion

Immobilization of β-Cyclodextrin on Silica Gel. As shown in Table 1, β-CyD was successfully immobilized on silica gel according to Scheme 1, using either thionyl chloride or silicon tetrachloride as chlorinating agent of silica gel. The amounts of the immobilized β-CyD were 8×10^{-5} to 1.4×10^{-4} mol per 1 g of the β-CyD-silica gel composites. The resulting composites were fine and white particles, as long as purities and dryness of the reagents used, especially of pyridine, were sufficiently high. Otherwise, the particles turned to tan to dark brown color on the treatments.

There were no substantial changes observed either in the scanning electron micrographs of the particles or in the surface area of the particles before and after the treatments.

Figure 1 (a) depicts a thermogravimetric curve for the β-CyD-silica gel composite (code A-1 in Table 1). The composite is stable even at elevated temperatures, and no decomposition is detected up to 250 °C.

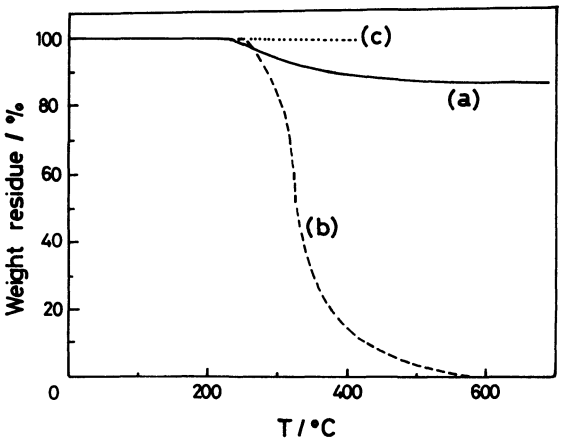

Fig. 1. Thermogravimetric analyses on (a) the β-CyD-silica gel composite (code A-1), (b) β-CyD, and (c) silica gel: the heating rate, 5 °C min^{-1} under air.

Neither color change of the composite nor its softening is observed here. A weight loss due to the oxidative degradation of the β-CyDs in the composites starts at 250 °C and almost ends up at 630 °C, when the heating rate is 5 °C min^{-1}. From the difference between the weight residue at 250 °C and the value at 630 °C, the amount of the β-CyD in the composite is estimated to be 16 wt%. This value satisfactorily agrees with that (15.0 wt%) calculated from the carbon content (6.65%) on elemental analysis.

β-CyD itself starts oxidative degradation at 260 °C, which completes at 580 °C (Fig. 1 (b)).

Virtually identical thermogravimetric curves were obtained for all the other composites A-2, A-3, and A-4, except for the difference in the magnitude of weight loss due to the difference in the amount of the β-CyD immobilized on the silica gel.

Covalent attachment of the β-CyD to silica gel was confirmed by the absence of loss of the β-CyD moieties on repeated washing of the composites with water or 0.002 M hydrochloric acid (1 M=1 mol dm^{-3}). The amount of the β-CyD was determined by thermogravimetric analyses on these specimens.

The largest value for the immobilization of β-CyD (1.4×10^{-4} mol per 1 g of the composite, code A-1) corresponds to occupation of 380 A^2 surface of the silica gel by one β-CyD molecule: the silica gel has surface

Table 2. Equilibrium Constant K_d for the Dissociation of the Complex between the β-CyD Immobilized to Silica Gel and Phenol in Aqueous Solution at 25°C

β-CyD-silica gel composite	K_d	Amount of β-CyD/10^{-6} mol[a)]	
	10^{-3} mol dm^{-3}	Charged	Kinetically determined
A-2	6.5±1.9	8.8	7.3±2.0
A-4	6.6±0.8	8.3	8.0±0.6
Intact β-CyD (Non-immobilized)	1.6±0.3	—	—

a) Amount of β-CyD in 3 cm^3 for specimen.

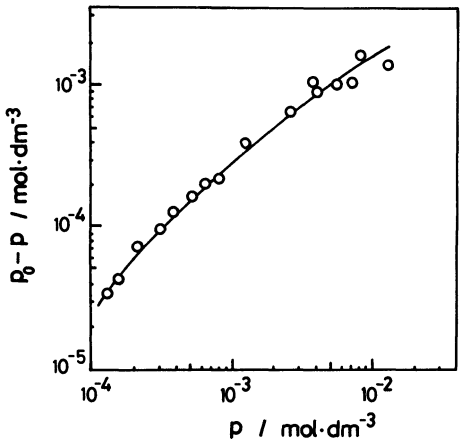

Fig. 2. Plot of (p_0-p) vs. p for the complex formation between the β-CyD immobilized on silica gel and phenol in aqueous solution at 25°C: 100 mg of the composite A-2, which contained 8.8×10^{-6} mol of β-CyD, was added to 3 cm^3 of phenol solution with the charged concentration p_0, and the equilibrium concentration p of phenol in aqueous medium was measured.

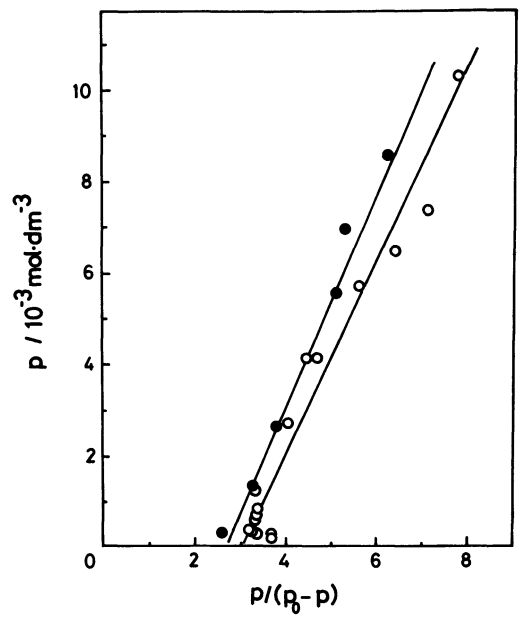

Fig. 3. Plots of p vs. $p/(p_0-p)$ for the complex formation between the β-CyD immobilized on silica gel and phenol in aqueous solution at 25°C: ○, composite A-2 (the charged amount of β-CyD, 8.8×10^{-6} mol); ●, the composite A-4 (the charged amount of β-CyD, 8.3×10^{-6} mol); Definition of p and p_0 as well as the experimental methods should be referred to the footnote in Fig. 2.

area of 370 m^2 per 1 g. This value is only 2.1 fold larger than the molecular cross-section area (184 A^2) of β-CyD, perpendicular to the longitudinal axis of the cavity. The outer diameter of β-CyD is 15.3 A.[2] Thus, the surface of the silica gel is largely covered by β-CyD molecules in the composites.

Complex Formation between the β-Cyclodextrin Immobilized on Silica Gel and Phenol. When the β-CyD-silica gel composite was mixed with aqueous phenol solution and the mixture was vigorously shaken, the concentration of phenol in the aqueous medium rapidly decreased. This shows that the β-CyD immobilized to silica gel forms complex with phenol and takes it out of the aqueous medium. Usually equilibrium was attained in less than 20 min.

Figure 2 depicts the plot of (p_0-p) vs. p. Here, 100 mg of the composite A-2, which contained 8.8×10^{-6} mol of β-CyD, was added to 3 cm^3 of aqueous phenol solution of the charged concentration p_0, and the equilibrium concentration p of phenol in the aqueous medium was measured. Logarithm of (p_0-p), which corresponds to the amount of phenol forming complex with the immobilized β-CyD, asymptotically increases with logarithm of p, the equilibrium concentration of phenol in the solution.

In Fig. 3, p is plotted against $p/(p_0-p)$ according to Eq. 1 for the complex formation of phenol with the immobilized β-CyDs in the composites A-2 and A-4. For both of the composites, linearities of the plots are satisfactorily fine. These results confirm that the β-CyDs immobilized on the silica gel form 1:1 complexes with phenol. Cooperativity of two immobilized β-CyD molecules or more in the complex formation is not detected.

Table 2 lists the equilibrium constants K_d for the dissociation of the complex between the β-CyD immobilized on silica gel and phenol in aqueous solution at 25°C. The K_d values for the immobilized β-CyDs in both of the composites A-2 and A-4, determined from the intercepts on the ordinate (see Eq. 1), are almost identical with each other. About 4 fold larger K_d values for these immobilized β-CyDs, compared with the value for intact β-CyD, are associated with larger steric hindrance on the complex formation.

Table 3. Catalytic Activity of the β-CyD Immobilized to Silica Gel in the Cleavage of 4-Nitrophenyl Acetate[a)]

Catalyst	Amount of β-CyD/10^{-6} mol	Pseudo-first order rate constant of cleavage/10^{-4} s^{-1}
β-CyD–silica gel composite		
A-2 (100 mg)	8.8	1.5
A-3 (60 mg)	7.8	1.9
A-4 (100 mg)	8.3	1.9
A-4 (300 mg)	24.9	2.4
Intact β-CyD (9.4 mg)	8.3	2.9
(Non-immobilized) (11.2 mg)	9.9	3.2
(Non-immobilized) (28.3 mg)	24.9	5.8
Silica gel (100 mg)	0.0	1.2
None	0.0	1.2

a) Catalysts were added to 3 cm^3 of pH 8.7 Tris buffer solution. The charged concentration of 4-nitrophenyl acetate was 3.3×10^{-5} mol dm^{-3}.

The amounts of the immobilized β-CyD in the specimens, determined from the slopes of the straight lines in Fig. 3 are in good agreements with the charged amounts, estimated from the compositions of the β-CyD–silica gel composites. This fact shows that β-CyDs were successfully immobilized on the silica gel in their intact forms and also confirms the validity of the procedures employed in the present study for the determination of K_d values.

Catalytic Activity of the β-Cyclodextrin Immobilized on Silica Gel. The cleavage of 4-nitrophenyl acetate in the presence of the β-CyD–silica gel composites obeyed first-order kinetics. This result rules out a possibility that diffusion of the substrate to the vicinity of the immobilized β-CyD is rate-determining.

As shown in Table 3, all the β-CyD–silica gel composites exhibit catalytic activities for the cleavage of 4-nitrophenyl acetate. The activity is definitely attributed to the functions of the immobilized β-CyD, since the silica gel alone has no catalytic activity at all.

The catalytic activities of the immobilized β-CyDs are 2—4 fold smaller than that of intact β-CyD. This is associated with smaller substrate-binding constant, as shown in Table 2. Kinetic determination of the catalytic rate constants and the substrate binding constants was not successful, due to small magnitude of acceleration.

Conclusion

β-Cyclodextrin was covalently immobilized on silica gel as support. The resulting composites were stable up to 250 °C, where most of organic supports or organic polymers were hard to be used due to decomposition or deformation. The immobilized β-cyclodextrins exhibited both binding and catalytic activities.

The authors are indebted to Mr. Tatsuro Tsuru, Institute of Industrial Science, The University of Tokyo, for the measurement of nitrogen isotherms and to Mr. Fumio Tsuji for his technical assistance.

References

1) M. L. Bender and M. Komiyama, "Cyclodextrin Chemistry," Springer-Verlag, Berlin (1978).
2) J. Szejtli, "Cyclodextrins and Their Inclusion Complexes," Akadémiai Kiadó, Budapest (1982).
3) R. Breslow and P. Campbell, *J. Am. Chem. Soc.*, **91**, 3085 (1969).
4) I. Tabushi, K. Yamamura, K. Fujita, and H. Kawakubo, *J. Am. Chem. Soc.*, **101**, 1019 (1979).
5) M. Komiyama and H. Hirai, *J. Am. Chem. Soc.*, **105**, 2018 (1983).
6) M. Komiyama and H. Hirai, *J. Am. Chem. Soc.*, **106**, 174 (1984).
7) M. Komiyama and H. Hirai, *Makromol. Chem., Rapid Commun.*, **2**, 757 (1981).
8) N. Wiedenhof, J. N. J. J. Lammers, and C. L. van Panthaleon van Eck, *Staerke*, **21**, 119 (1969).
9) N. Wiedenhof, *Staerke*, **21**, 163 (1969).
10) J. L. Hoffman, *J. Macromol. Sci. Chem.*, **A7**, 1147 (1973).
11) A. Harada, M. Furue, and S. Nozakura, *J. Polym. Sci., Polym. Chem. Ed.*, **16**, 189 (1978).
12) Y. Mizobuchi, M. Tanaka, and T. Shono, *J. Chromatogr.*, **194**, 153 (1980).
13) B. Zsadon, M. Szilasi, F. Tüdös, and J. Szejtli, *J. Chromatogr.*, **208**, 109 (1981).
14) R. Breslow, H. Kohn, and B. Siegel, *Tetrahedron Lett.*, **1976**, 1645.
15) M. Komiyama, I. Sugiura, and H. Hirai, *J. Inclusion Phenomena*, **2**, 823 (1984).
16) M. Komiyama, I. Sugiura, and H. Hirai, *Polym. J.*, **17**, 1225 (1985).
17) M. Komiyama, I. Sugiura, and H. Hirai, *J. Mol. Catal.*, submitted.
18) M. Komiyama and H. Hirai, *Polym. J.*, in press.
19) M. Tanaka, Y. Kawaguchi, M. Nakae, Y. Mizobuchi, and T. Shono, *J. Chromatogr.*, **246**, 207 (1982).
20) A. Harada, M. Furue, and S. Nozakura, *Macromolecules*, **9**, 701 (1976).
21) K. Fujimura, T. Ueda, and T. Ando, *Anal. Chem.*, **55**, 446 (1983).
22) Y. Kawaguchi, M. Tanaka, M. Nakae, K. Funazo, and T. Shono, *Anal. Chem.*, **55**, 1852 (1983).
23) R. L. VanEtten, J. F. Sebastian, G. A. Clowes, amd M. L. Bender, *J. Am. Chem. Soc.*, **89**, 3242 (1967).

The Cerium(IV) Ammonium Nitrate Oxidation of 5-Hydroxy-2-methoxytropone to Bitropolonyl Derivatives and One-Step Synthesis of 3-Methoxy-*p*-tropoquinone

Akira MORI, Yasutoshi ISAYAMA,† and Hitoshi TAKESHITA*
Research Institute of Industrial Science, 86, Kyushu University, Kasuga-koen, Kasuga, Fukuoka 816
†Graduate School of Engineering Sciences, 39, Kyushu University, Kasuga-koen, Kasuga, Fukuoka 816
(Received September 30, 1985)

Unlike the benzenoid equivalent, *p*-methoxyphenol, the cerium(IV) ammonium nitrate (CAN)-oxidation of 5-hydroxy-2-methoxytropone gave C-C coupling products. On the other hand, either by thallium(III) nitrate (TTN) or CAN at 50 °C, 5-hydroxytropolone, a free tropolone, gave 3-methoxy-*p*-tropoquinone together with *p*-tropoquinone and 8-oxabicyclo[3.2.1]octenone derivatives, but no dimeric product.

We have recently developed a practical method for preparing *p*-tropoquinone mono- and diacetals by thallium(III) nitrate (TTN) oxidation of 2-alkoxy-5-hydroxytropones,[1] useful intermediates for various functionalized troponoids. This one-pot type preparation of acetals from 2-alkoxy-5-hydroxytropones was favored since it takes advantage of a two-electron oxidation (type I) path. According to the path of a one-electron oxidation (type II), the different behaviors were considered regarding the oxidation of 5-hydroxytropolone (**1**). With a stoichiometric amount of silver acetate,[2] it yielded 2,10-dihydroxydicyclohepta[*b*,*d*]furan-3,9-dione (**2**) through a coupling of the semiquinone radical intermediate (**A**). However, with two moles of the agent, it afforded *p*-tropoquinone (**3**). Indeed, the yields of the tropoquinones were generally better than those produced through a reaction with 2,3-dichloro-5,6-dicyano-*p*-benzoquinone (DDQ).[3]

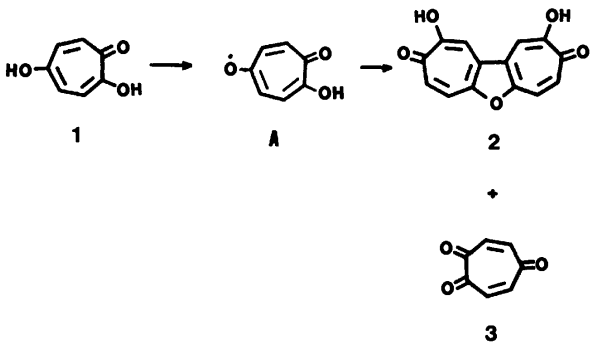

Scheme 1.

Accordingly, the oxidation of 2-alkoxy-5-hydroxytropones by a type-II agent, such as cerium(IV) ammonium nitrate (CAN),[4] should be worthwhile. Moreover, although it has already been noticed that the metal salt-induced oxidation of free tropolone derivatives at 0 °C is ineffective due to the formation of insoluble metal salts,[1] the reaction has been produced by heating at 50 °C in methanol. The results are described on the following pages.

Results and Discussion

During the oxidation of 5-hydroxy-2-methoxytropone (**4**) with two equivalents of CAN in anhydrous methanol, an instantaneous oxidation occurred to give two crystalline dimeric condensates (**5** and **6**) along with 2,10-dimethoxydicyclohepta[*b*,*d*]furan-3,9-dione (**7**),[5] *p*-tropoquinone dimethyl acetal (**8**)[1,6] and its methanol adduct (**9**).[1]

The dimer (**5**) showed three methoxyl groups on the sp^3-carbons and seven olefinic protons in the ^1H NMR spectrum. Also there were four carbonyl signals in the ^{13}C NMR. All these factors are consistent with our formulation.

The other dimer, **6**, yellow needles, exhibited only eight signals in the ^{13}C NMR, indicating a symmetrical structure. In the ^1H NMR, there were overlapping signals for four methoxyl groups on the sp^3-carbons and six olefinic protons. Therefore, a newly formed C–C bond must be at C-4 and C-4′. Also, **6** was bi(3,3-dimethoxy-4,7-dioxo-1,5-cycloheptadienyl). This corresponds to the bis-monoacetal of hitherto unknown biquinone, bi(*p*-tropoquinonyl) (**B**).

Particularly, this oxidation was sensitive to water. When the CAN-oxidation of **4** was carried out in methanol containing a trace amount of water, a new dimeric product (**10**) was obtained together with **5**, **7**, **8**, and **9**. The ^1H NMR spectrum of **10** revealed signals due to two methoxyl groups, five olefinic protons, and three protons on the sp^3-carbons. The coupling parameters observed in the signals [3.09 (Ha, dd, J=15, 2.5 Hz), 3.42 (Hb, ddd, J=15, 7.5, 1 Hz), 5.06 (Hc, dd, J=7.5, 2.5 Hz), and 6.73 (Hd, dd, J=12.5, 1 Hz)] indicated an arrangement of these four protons as shown in the scheme. Other than **7**, **10** was the only fully-conjugated tropone derivative among the oxidation products. The seven-membered rings of all other products contained a sp^3-carbon, such as an acetal group or a tertiary ether. The formation of **10** under moistened conditions illustrates the important role of a proton in the following step of the reaction; e.g., a coupling of the intermediate, **C** (an analog of **A**) to **D** at C-2 and C-4 via the type II-process, can be readily aromatized to a 5-hydroxy-2-methoxytropone (**E**). The subsequent CAN-oxidation of **E** should give the dimethyl acetal, **5**. However, in the presence of water, **E** was intramolecularly cyclized to **10**. Therefore, a further oxidation of **10** (as well as **7**), having no free hydroxyl group, was slow under these conditions.

Also, CAN was preferentially co-ordinated with water to prevent the further oxidation.

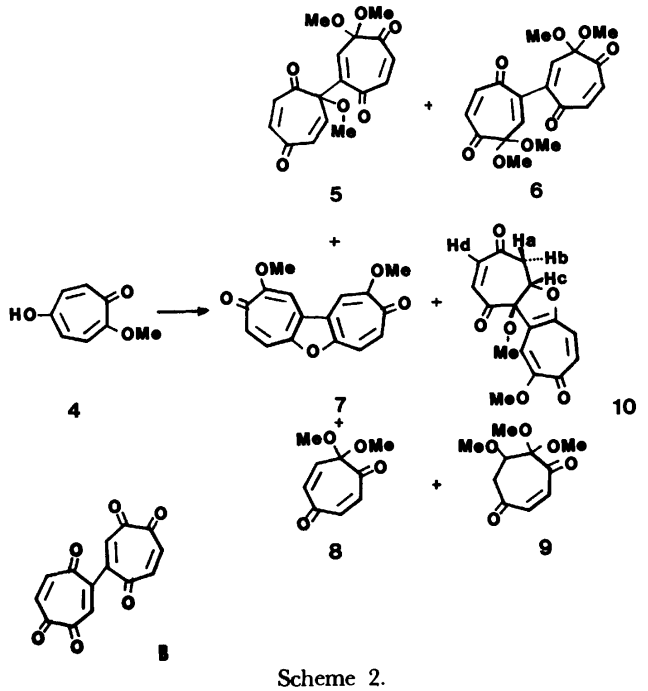

Scheme 2.

It is possible to classify the products into three categories, i.e., i) monomeric products (**8** and **9**), ii) C-2–C-4′ condensates (**5** and **10**), and iii) C-4–C-4′ condensates (**6** and **7**). The relative yields of these products showed a dependence on several conditions. Under anhydrous conditions, they were 22% for i), 9% for ii), and 48% for iii). In the presence of water, they were 19% for i), 44% for ii), and 20% for iii). Thus, there was a predominance of iii) in an anhydrous media and ii) in the presence of water.

In order to obtain **B**, a hydrolysis of **6** under various conditions has been attempted, but none of the products have been identified. Presumably, **B** is too reactive under the reaction conditions to form complex mixtures. Other transformations attempted so far with these dimeric products were unsatisfactory; i.e., a Thiele reaction in a mixture of acetic anhydride and acetic acid, a zinc reduction in acetic acid, and hydrolysis with perchloric acid in aqueous acetone all gave intractable mixtures.

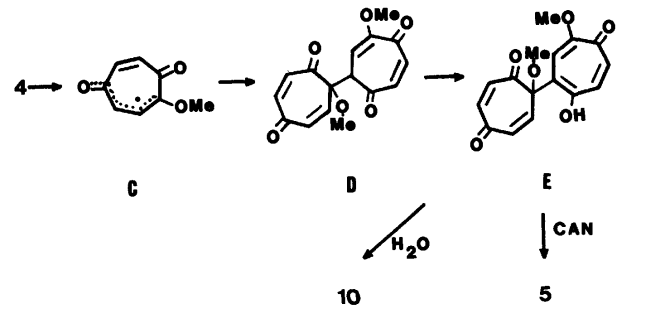

Scheme 3.

Next, a CAN oxidation of **1** was carried out at room temperature in methanol. A new product (**11**) was identified along with **3**. The ^{1}H NMR spectrum of **11** showed signals attributable to a methylene group, two methoxyl groups, two vicinal vinylic protons on the six-membered ring, and a proton on the sp^3-carbon bearing an oxygen function. Therefore, **11** should be an 8-oxabicyclo[3.2.1]octenone derivative.

For a comparison, the TTN-oxidation of **1** was also carried out in methanol at 50°C to obtain two new products (**12** and **13**). According to spectral evidence, the former, **12**, was 3-methoxy-*p*-tropoquinone. Although its yield was not very high, a one-step preparation should be useful from a practical point of view.[1] The structure of **13** was identified to be a methylated derivative of **11** from NMR spectral evidence; the ^{1}H NMR spectrum of **13** showed a close resemblance to that of **11** except for the presence of an additional methoxyl methyl singlet. Also, a comparison of the ^{13}C NMR chemical shifts led to the same conclusion (see Experimental). Interestingly, a TTN-oxidation of **3** in methanol gave **11** together with **13**. Thus, it is clear that **3** is a precursor of these oxidation products.

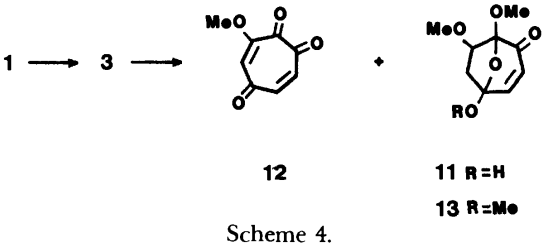

Scheme 4.

It should be mentioned that, unlike **4**, the TTN-oxidation of **1** formed no dimers. In other words, for the oxidation of **1**, there is no difference between the oxidizing agents (TTN and CAN) in this respect. This means that the transformations of an intermediate (**A**) to **3** by a one-electron oxidation process is rather easier than the C–C coupling process. This is parallel to the previous results regarding silver salt-oxidation, another one-electron oxidizing process of **1**.[2] With a stoichiometric amount of the reagent, it gave **3** in good yield; but, with a smaller amount, it also gave the C-4–C-4′ coupling product, **2** (Scheme 1).

In conclusion, the major products formed in the CAN-oxidation of **4** were the C–C coupling products. These differed remarkably to those formed in a TTN oxidation. This difference results from the nature of the oxidizing agent, as has been mentioned. It is noteworthy that, as has been reported, the CAN-oxidation of 4-methoxyphenol in methanol gave 4,4-dimethoxy-2,5-cyclohexadienone in 65% yield.[7] No other paper has described any accompanied C–C coupling product until a recent study by Maruyama

et al. They reported such a C-C coupling which gave a benzoquinonoid crown ether derivative.[8] In a contrast a facile C-C bond formation in the troponoids may be attributable to the presence of an adjacent carbonyl group which helps to delocalize an unpaired electron. Accordingly, the semiquinone radicals of tropoquinones would be more stable than those of benzoquinones to enable the intermolecular reaction. Otherwise, quinone acetals, e.g., **8**, should be formed by a reaction with CAN and the solvent-caged methanol. It would be interesting to investigate the electrochemical behaviors by the cyclic voltammetry of the tropoquinones. This would determine whether this is reflected to it or not. Such research will be published in due course.

Experimental

All the mps were measured by means of a Yanagimoto Micro-mp Apparatus and are uncorrected. Elemental analyses were performed by Miss S. Hirashima of the Research Institute of Industrial Science, Kyushu University. The NMR spectra were measured by means of a JEOL FX 100 Spectrometer in $CDCl_3$ solutions and the chemical shifts measured were expressed in δ units from the internal Me_4Si. The mass spectra were measured by means of a JEOL OISG-2 Spectrometer. The UV spectra were measured by means of a Hitachi 124 Spectro photometer in MeOH. The IR spectra were taken in either as KBr disks or as an inserted liquid film between NaCl plates using a Jasco IR-A 102 Spectrometer.

CAN-Oxidation of 4. a) To an anhydrous MeOH solution (6 cm^3) of **4** (100 mg), carefully desiccated CAN (721 mg) was added at 0°C. After 1 h, the mixture was warmed to 20—25°C and stirred for another 30 min. The mixture was then diluted with water, extracted with $CHCl_3$, and chromatographed on a silica-gel column with AcOEt-hexane (1:4) to give **5** [a yellow oil, 9.6 mg; 9%. Found: M.W., 332.0901 (M^+). Calcd for $C_{17}H_{16}O_7$: 332.0895. ^1H NMR δ=3.16 (3H, s), 3.28 (3H, s), 3.30 (3H, s), 6.40 (1H, d, J=12 Hz), 6.43 (2H, d, J=1.5 Hz), 6.44 (1H, s), and 6.74 (1H, d, J=12 Hz). ^{13}C NMR δ=50.7, 50.9, 53.7, 88.8, 103.0, 132.6, 133.5, 134.7, 135.6, 135.8, 137.8, 138.2, 144.1, 189.5, 191.5, 192.1, and 192.4, IR ν: 2950, 1710, 1660, 1620, and 1450 cm^{-1}], **8** (15.5 mg; 13%), and **9** (12.6 mg; 9%), which were identical with authentic samples,[1] together with **6** [yellow needles, mp 100°C (decomp), 12.0 mg; 10%. Found: C, 59.71; H, 5.09%. Calcd for $C_{18}H_{18}O_8$: C, 59.66; H, 5.01%. ^1H NMR δ= 3.28 (12H, s), 6.40 (2H, d, J=13 Hz), 6.43 (2H. s). and 6.58 (2H, d, J=13 Hz). ^{13}C NMR δ=50.8 (4C), 103.0 (2C), 132.3 (2C), 135.8 (2C), 138.2 (2C), 143.8 (2C), 191.4 (2C), and 191.6 (2C). IR ν: 1710, 1660, 1450, 1160, and 1050 cm^{-1}. UV λ_{max}^{MeOH}: 229 nm(ε=17800) and 380 (900)].

On the other hand, the aqueous washings were acidified with dil HCl, and extracted with 1-butanol; the solvent was evaporated in vacuo to leave **7** (colorless crystals, mp 226—228°C (lit,[5] mp 227—230°C), 35.5 mg; 38%.).

b) To an MeOH solution (3 cm^3) of **4** (80 mg), CAN (577 mg), fresh but not further purified, was added all at once at 0°C. After 1 h, the mixture was warmed to 20—25°C and stirred for an additional 30 min. The mixture was diluted with water, extracted with $CHCl_3$, washed with $NaHCO_3$, and chromatographed on a silica-gel column to give **8** (9.6 mg; 10%), **9** (9.1 mg; 8%), **5** (5.2 mg; 6%), and **10** [pale yellow needles, mp 150—150.5°C. 30.2 mg; 38%. Found: M. W., 302.0786 (M^+). Calcd for $C_{16}H_{14}O_6$: 302.0789. ^1H NMR δ=3.09 (1H, dd, J=15, 2.5 Hz), 3.35 (3H, s), 3.42 (1H, ddd, J=15, 7.5, 1 Hz), 3.85 (3H, s), 5.06 (1H, dd. J=7.5, 2.5 Hz), 6.31 (1H, s), 6.37 (1H, dd, J=12.5, 1 Hz), 6.74 (1H, d. J=12.5 Hz), 7.02 (1H, d, J=13 Hz), and 7.26 (1H, d, J=13 Hz). ^{13}C NMR δ=44.8. 52.0, 56.5, 78.8, 97.4, 107.2, 118.4, 125.2, 135.4, 139.8, 140.2, 158.9, 161.0, 178.9, 193.7, and 194.1. IR ν: 1710, 1670, 1560, 1510, 1450, 1320, 1240, and 1070 cm^{-1}. UV λ_{max}^{MeOH}: 234 nm (ε=22700), 336 (8700), 359 (7600), 377 (7950), and 395 (6900)].

From the aqueous washings, **7** (14.9 mg; 20%) was obtained by extraction with 1-butanol.

CAN-Oxidation of 1. To an MeOH solution (2 cm^3) of **1** (70 mg), CAN (280 mg) was added, and stirred at 20—25°C for 15 min. The mixture was then diluted with water, extracted with $CHCl_3$, and chromatographed on a silica-gel column with AcOEt-hexane (1:4) to give **3** (15.3 mg; 22%) and **11** [a colorless oil, 10.2 mg; 10%. Found: M. W., 200.0696 (M^+). Calcd for $C_9H_{12}O_5$: 200.0686. ^1H NMR δ=2.20 (1H, dd, J=13.5, 2.5 Hz), 2.53 (1H, dd, J=13.5, 10 Hz), 3.26 (3H, s), 3.45 (3H, s), 4.07 (1H, dd, J=10, 2.5 Hz), 6.28 (1H, d, J=9 Hz), and 7.26 (1H, d, J=9 Hz). ^{13}C NMR δ=39.6, 52.5, 58.8, 83.3, 104.2, 104.8, 128.4, 155.0, and 194.4. IR ν: 3400, 1703, and 1610 cm^{-1}].

TTN-Oxidation of 1. To an MeOH solution (5 cm^3) of **1** (200 mg), TTN (950 mg) was added. After 20 min, the reaction mixture was warmed at 50°C and stirred for 2 h. The mixture was then diluted with water, extracted with $CHCl_3$, and chromatographed on a silica-gel column with AcOEt-hexane (1:3) to give **12** [colorless crystals, mp 121—123°C, 43.5 mg; 18%. Found: m/z, 138.0310 (M^+—28). Calcd for $C_7H_6O_3$: 138.0315. ^1H NMR δ=3.80 (3H, s), 5.93 (1H, s), 6.61 (1H, d, J=13.5 Hz), and 6.79 (1H, d, J=13.5 Hz). ^{13}C NMR δ=56.2, 107.7, 134.4, 137.2, 158.6, 181.6, and 187.3 (2C). IR ν: 1680, 1640, and 1590 cm^{-1}. UV $\lambda_{max}^{CHCl_3}$: 255 nm (ε=14000), 286 (550), 356 (1100)], and **13** [a colorless oil, 18.6 mg; 6%. Found: M. W., 214.0836 (M^+). Calcd for $C_{10}H_{14}O_5$: 214.0840. ^1H NMR δ=1.97 (1H, dd, J=13.5, 2.5 Hz), 2.53 (1H, dd, J=13.5, 10 Hz), 3.26 (3H, s), 3.47 (3H, s), 3.50 (3H, s), 3.98 (1H, dd, J=10, 2.5 Hz), 6.22 (1H, d, J=10 Hz), and 7.22 (1H, d, J=10 Hz). ^{13}C NMR δ=40.2, 52.3, 53.7, 58.6, 82.9, 105.3, 109.0, 131.2, 153.0, and 192.1. IR ν: 1740, 1710, 1610, 1560, and 1450 cm^{-1}. UV λ_{max}^{MeOH}: 219 nm (ε=6050)].

TTN-Oxidation of 3. To an MeOH solution (2 cm^3) of **3** (178 mg), TTN (575 mg) was added and stirred at 20—25°C for 10 min. After stirring at 50°C for 1 h, the mixture was diluted with water and extracted with $CHCl_3$. Silica-gel column chromatography with AcOEt-hexane (2:3) yielded **12** (28.2 mg; 13%) and **11** (42 mg; 16%).

We would like to thank The Ministry of Education, Science, and Culture for a Grant-in-Aid for Scientific Research to A. M. (No. 60470025).

References

1) H. Takeshita, A. Mori, and Y. Isayama, *Bull. Chem. Soc. Jpn.*, **58**, 1678 (1985).

2) H. Takeshita, T. Kusaba, and A. Mori, *Chem. Lett.*, **1982**, 701; *Bull. Chem. Soc. Jpn.*, **55**, 1659 (1982).

3) S. Itô, Y. Shoji, H. Takeshita, M. Hirama, and K. Takahashi, *Tetrahedron Lett.*, **1975**, 1075.
4) W. S. Trahanovsky and L. B. Young, *J. Chem. Soc.*, **1965**, 5777; P. Jacob, III, P. S. Callery, A. T. Shulgin, and N. Castagnoli, Jr., *J. Org. Chem.*, **41**, 3627 (1976).
5) T. Kusaba, A. Mori, and H. Takeshita, *Bull. Chem. Soc. Jpn.*, **58**, 515 (1985).
6) A. Mori and H. Takeshita, *Kyushu Daigaku Sogo Rikogaku Kenkyuka Hokoku*, **3**, 125 (1981).
7) W. Dürckheimer and L. A. Cohen, *Biochemistry*, **3**, 1948 (1964).
8) K. Maruyama, H. Sohmiya, and H. Tsukube, *Tetrahedron Lett.*, **26**, 3583 (1985).

 © 1986 The Chemical Society of Japan Bull. Chem. Soc. Jpn., 59, 515—523 (1986)

Transformation between Lamellar and Nonlamellar Aggregates Formed with Synthetic Peptide Lipids†

Yukito MURAKAMI,* Jun-ichi KIKUCHI, Toshihiko TAKAKI, and Katsuya UCHIMURA
Department of Organic Synthesis, Faculty of Engineering, Kyushu University, Hakozaki, Higashi-ku, Fukuoka 812
(Received September 30, 1985)

The morphological behavior of various combinations of the following synthetic lipids was investigated in the aqueous dispersion state by means of electron microscopy, differential scanning calorimetry, and fluorescence polarization spectroscopy as well as by turbidity and X-ray diffraction measurements: $N^+C_5Ala2C_n$ and $N^+(H)C_5Ala2C_n$ as cationic, $(SO_3^-)C_5Ala2C_n$ as anionic, and QC_5Ala2C_n as nonionic (n=14, 16). Aqueous dispersions of various combinations of cationic and anionic lipids at the equimolar ratio afforded nonlamellar aggregates, having highly ordered and three-dimensional network structure with repeating distances in the 70—130 Å range, above their phase transition temperatures (T_m). However, any slight loss of the fractional balance retained at the equimolar ratio led to the formation of bilayer aggregates. Under such conditions that allow the formation of nonlamellar aggregates, the high microscopic homogeneity of cationic and anionic lipid molecules was attained, originating from the intramembrane electrostatic interaction between cationic and anionic head moieties to form highly developed ion-pair clusters on the aggregate surface. Meanwhile, the nonlamellar phase appeared above T_m was spontaneously transformed into the normal bilayer phase below T_m as confirmed by electron microscopy and turbidity measurements. The nonlamellar phase was also characterized by the low-angle X-ray diffraction method and was consistent with the highly developed domain with the face-centered cubic lattice.

The polymorphic phase behavior has been found to arise by changing compositions and properties of membrane-forming lipids in the aqueous dispersion state.[1] In contrast with extensive studies on the bilayer phase, characterization of the nonbilayer ones, such as inverted hexagonal (H_{II}), lipidic particle (LIP), and inverted cubic (C_{II}) phases, has been limited to systems composed of naturally occurring lipids up to the present time.[2] In connection with dynamic functions of biomembranes, the correlations between lipid compositions and morphological transitions between bilayer and nonbilayer phases pose major unsolved subjects.[2,3] In this regard, simple model systems composed of synthetic lipids may make useful contributions toward general understanding of biological phenomena. Although various bilayer-forming lipids have been prepared,[4] synthetic lipids capable of forming nonbilayer aggregates under diluted conditions in aqueous media have been scarcely treated. Recently, we have found that a series of ionic peptide lipids involving an amino acid residue interposed between a polar head group and an aliphatic double-chain segment form bilayer membranes (vesicles and/or lamellae) in the aqueous dispersion state.[5] On the other hand, nonionic lipids having the quinoyl group as a polar head have been confirmed to form nonlamellar network aggregates when they were dispersed in aqueous media.[6] As described in our preliminary communication,[7] the similar morphology was also observed for equimolar mixtures of cationic and anionic peptide lipids.

In order to understand the molecular basis for formation of nonlamellar aggregates, the morphological behavior of various combinations of the following synthetic lipids was investigated in the aqueous dispersion state: $N^+C_5Ala2C_n$ and $N^+(H)C_5Ala2C_n$ as cationic, $(SO_3^-)C_5Ala2C_n$ as anionic, and QC_5Ala2C_n as nonionic (n=14, 16).

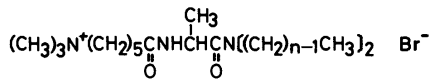

$N^+C_5Ala2C_n$ (n=14,16)

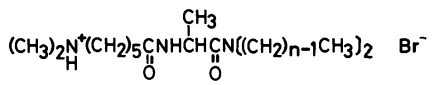

$N^+(H)C_5Ala2C_n$ (n=14,16)

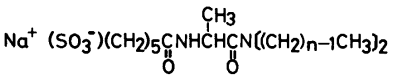

$(SO_3^-)C_5Ala2C_n$ (n=14,16)

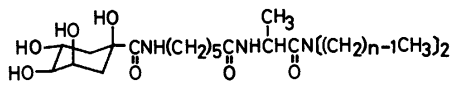

QC_5Ala2C_n (n=14,16)

Experimental

Materials. 1,6-Diphenyl-1,3,5-hexatriene (DPH) was obtained from Nakarai Chemicals as a guaranteed reagent and used without further purification. The preparation of the following lipids has been reported previously: *N,N*-ditetradecyl-N^α-[6-(trimethylammonio)hexanoyl]-L-alaninamide bromide ($N^+C_5Ala2C_{14}$),[5c] *N,N*-dihexadecyl-N^α-[6-(trimethylammonio)hexanoyl]-L-alaninamide bromide ($N^+C_5Ala2C_{16}$),[5c] sodium *N,N*-ditetradecyl-N^α-(6-sulfohexanoyl)-L-alaninamide [$(SO_3^-)C_5Ala2C_{14}$],[6b] sodium *N,N*-dihex-

†Contribution No. 778 from this Department.

adecyl-N^{α}-(6-sulfohexanoyl)-L-alaninamide [$(SO_3^-)C_5Ala2C_{16}$],[6b] *N,N*-ditetradecyl-N^{α}-[6-(quinoylamino)hexanoyl]-L-alaninamide (QC_5Ala2C_{14}),[6a)#] and *N,N*-dihexadecyl-N^{α}-[6-(quinoylamino)hexanoyl]-L-alaninamide (QC_5Ala2C_{16}).[6b)#]

***N,N*-Ditetradecyl-N^{α}-[6-(dimethylamino)hexanoyl]-L-alaninamide (NC_5Ala2C_{14}).** This material was prepared in a manner similar to that reported for the synthesis of *N,N*-didodecyl-N^{α}-[6-(dimethylamino)hexanoyl]-L-alaninamide,[5b] and isolated as the hydrobromide salt [$N^+(H)C_5Ala2C_{14}$]: a white glassy solid, final mp 123 °C; $[\alpha]_D^{25}$ −15.0° (*c* 1.01, ethanol); IR (KBr) 2920 and 2850 (CH), and 1640 cm^{-1} (C=O); ^{1}H-NMR ($CDCl_3$, TMS) δ=0.88 [6H, br t, $(CH_2)_{13}C\underline{H}_3$], 1.0—2.0 [57H, m, $CH_2(C\underline{H}_2)_{12}CH_3$, $CH(C\underline{H}_3)$, and $CH_2(C\underline{H}_2)_3CH_2CO$], 2.28 [2H, br t, CH_2CO], 2.81 [6H, s, $(C\underline{H}_3)_2HN^+$], 2.9—3.8 [6H, m, N^+CH_2 and $NC\underline{H}_2(CH_2)_{12}CH_3$], 4.80 [1H, m, $C\underline{H}(CH_3)$], and 6.83 [1H, d, CONH].

Found: C, 66.40; H, 11.42; N, 5.75. Calcd for $C_{39}H_{79}N_3O_2\cdot$HBr: C, 66.63; H, 11.47; N, 5.98.

***N,N*-Dihexadecyl-N^{α}-[6-(dimethylamino)hexanoyl]-L-alaninamide (NC_5Ala2C_{16}).** This material was prepared in a manner as described above and isolated as the hydrobromide salt [$N^+(H)C_5Ala2C_{16}$]: a white glassy solid, final mp 126 °C; $[\alpha]_D^{25}$ −20.8° (*c* 1.01, ethanol); IR (KBr) 2920 and 2850 (CH), and 1640 cm^{-1} (C=O); ^{1}H-NMR ($CDCl_3$, TMS) δ=0.87 [6H, br t, $(CH_2)_{15}C\underline{H}_3$], 1.0—2.0 [65H, m, $CH_2(C\underline{H}_2)_{14}CH_3$, $CH(C\underline{H}_3)$, and $CH_2(C\underline{H}_2)_3CH_2CO$], 2.25 [2H, br t, CH_2CO], 2.80 [6H, s, $(C\underline{H}_3)_2HN^+$], 2.9—3.7 [6H, m, N^+CH_2 and $NC\underline{H}_2(CH_2)_{14}CH_3$], 4.79 [1H, m, $C\underline{H}(CH_3)$], and 6.77 [1H, d, CONH].

Found: C, 68.16; H, 11.80; N, 5.55. Calcd for $C_{43}H_{87}N_3O_2\cdot$HBr: C, 68.03; H, 11.68; N, 5.54.

Preparation of Molecular Aggregates. As for mixed lipid systems, chloroform solutions of two different lipids were mixed at appropriate molar ratios and evaporated to dryness to give thin films. Each film placed in 2 mL of deionized and distilled water was subjected to vortex mixing with glass beads at room temperature (ca. 20 °C) for 1—10 min to afford an aqueous dispersion sample. Whenever necessary, the dispersion sample was subsequently sonicated with a probe-type (W-220F, Heat Systems-Ultrasonics) or a bath-type sonicator (Bransonic 12, Yamato Scientific Co.) and allowed to stand for 20 min at room temperature.

Analyses and Measurements. Elemental analyses were performed at the Microanalysis Center of Kyushu University. Melting points were measured with a Yanagimoto MP-S1 apparatus (hot-plate type). IR spectra were recorded on a JASCO IR-810 spectrophotometer. ^{1}H-NMR spectra were taken on a Hitachi R-24B or a Hitachi Perkin-Elmer R-20 spectrometer. Turbidity measurements were run at 400 nm on a Hitachi 340 or a Union Giken SM-401 high sensitivity spectrophotometer with a cell of 1.0-mm path length. A Daini Seikosha SSC-560U calorimeter was used for differential scanning calorimetry (DSC). The phase transition temperature (T_m, temperature at a peak maximum of DSC thermogram) and the enthalpy change for phase transition (ΔH) were determined in the same manner as reported previously.[6b] Electron micrographs were taken on a JEOL JEM-200B electron microscope installed at the Research Laboratory for High Voltage Electron Microscopy of Kyushu University. The negatively stained samples for the measurements were prepared in a manner as described previously.[6b]

The fluorescence polarization measurements were carried out on a Union Giken FS-501A fluorescence polarization spectrophotometer equipped with a Sord microcomputer M200 Mark II; the emission at 450 nm originated from DPH was monitored upon excitation at 366 nm with a slit width of 3.5 nm for both excitation and emission sides. The steady-state fluorescence anisotropy (r_s) was calculated by Eq. 1, where I is the fluorescence intensity, and the subscripts v and h refer to the orientations, vertical and horizontal, respectively, for the excitation and analyzer polarizers in this sequence. C_f is the grating correction factor, given by I_{hv}/I_{hh}.

$$r_s=(I_{vv}-C_fI_{vh})/(I_{vv}+2C_fI_{vh}) \quad (1)$$

The nickel-filtered Cu $K\alpha$ radiation (λ=1.5418 Å) from a Rigaku Rotaflex RU-200 X-ray generator was used for X-ray diffraction measurements. Each sample was sealed up in a specimen holder equipped with mica windows, and a low-angle diffraction pattern was recorded on a Fuji X-ray film 150; a sample—film distance being set at 200 mm.

Results

Electron Microscopy. We have previously reported aggregate morphology of the following individual lipids in aqueous media: $N^+C_5Ala2C_n$,[5c] $(SO_3^-)C_5Ala2C_n$,[6b] and QC_5Ala2C_n.[6] Additional lipids having the amino group, NC_5Ala2C_n (n=14, 16), were prepared in this work and found to behave as cationic lipids under acidic conditions (below pH 6) that allow the amino head moiety to be protonated, $N^+(H)C_5Ala2C_n$.[8] The cationic $N^+(H)C_5Ala2C_n$ was found to constitute multilayered aggregates, bent lamellae and vesicles (Fig. 1A), in the aqueous dispersion state and single-walled vesicles in the diameter range 200—1000 Å (Fig. 1B) after treated with a probe-type sonicator for 2 min at 30 W.

When equimolar amounts of a cationic lipid, $N^+(H)C_5Ala2C_{16}$, and an anionic one, $(SO_3^-)C_5Ala2C_{14}$, were dispersed in water at pH 4.0 and 20 °C, the formation of nonlamellar aggregates was detected by electron microscopy with the negative staining technique; highly ordered network structure with a repeating distance of 100 Å (Fig. 2A). Similar aggregates with repeating distances in the 70—130 Å range were observed in aqueous dispersions of the following combinations of cationic and anionic lipids at the equimolar ratio above their phase transition temperatures; $N^+C_5Ala2C_{14}$–$(SO_3^-)C_5Ala2C_{14}$,[7] $N^+C_5Ala2C_{16}$–$(SO_3^-)C_5Ala2C_{16}$, $N^+(H)C_5Ala2C_{14}$–$(SO_3^-)C_5Ala2C_{14}$, $N^+(H)C_5Ala2C_{14}$–$(SO_3^-)C_5Ala2C_{16}$ (Fig. 2B), and $N^+(H)C_5Ala2C_{16}$–$(SO_3^-)C_5Ala2C_{16}$. Such characteristic morphological behavior was also confirmed by the freeze-fracture electron microscopy as typically shown for the $N^+C_5Ala2C_{14}$–$(SO_3^-)C_5Ala2C_{14}$ system; close

Quinoyl is the conventional name for 1,3,4,5-tetrahydroxy-[1*R*-(1α, 3α, 4α, 5β)]cyclohexylcarbonyl.

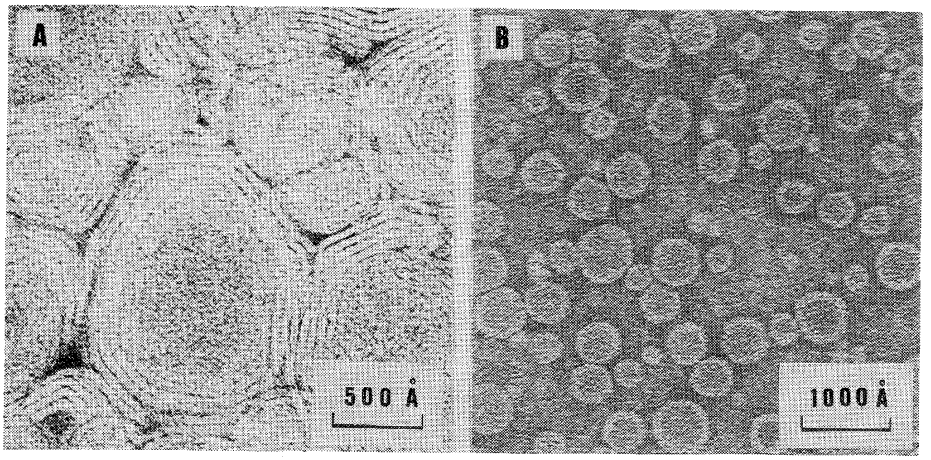

Fig. 1. Electron micrographs negatively stained with uranyl acetate: A, 5 mmol dm^{-3} aqueous dispersion of $N^+(H)C_5Ala2C_{14}$; B, 5 mmol dm^{-3} aqueous solution of $N^+(H)C_5Ala2C_{16}$ sonicated for 2 min with a probe-type sonicator at 30 W.

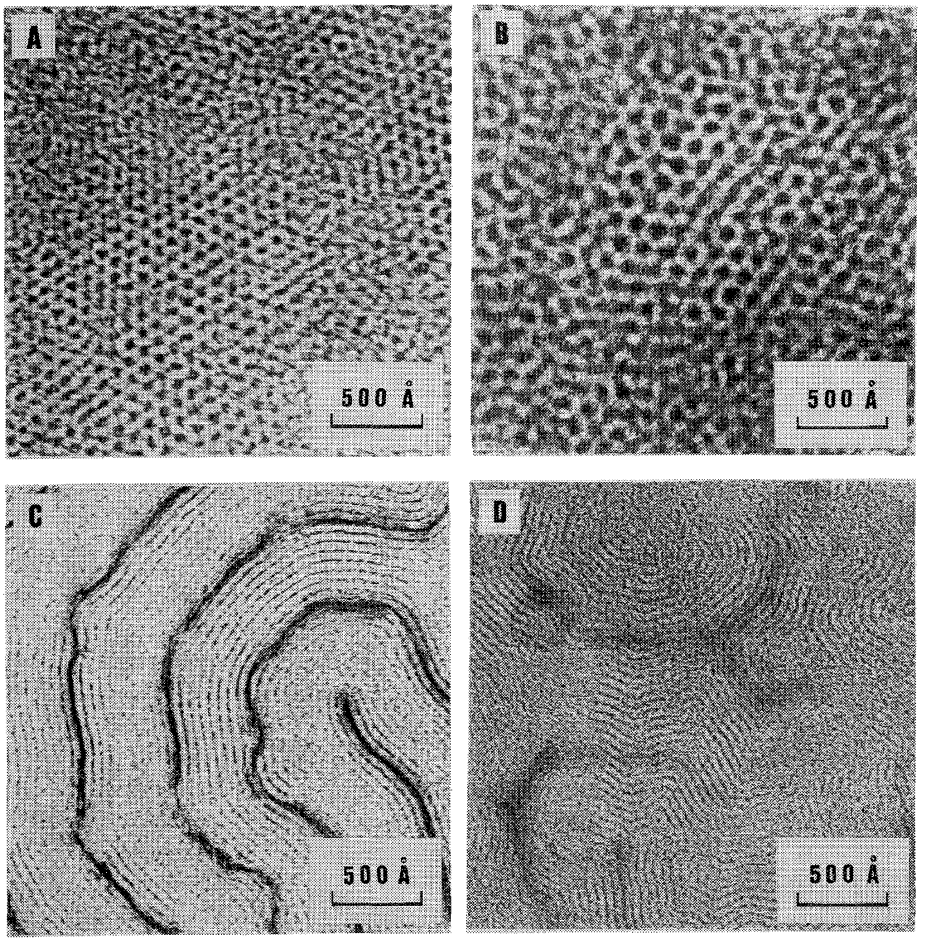

Fig. 2. Electron micrographs for equimolar mixtures (2.5 mmol dm^{-3} each) of two peptide lipids with the following combinations in the dispersion state, as negatively stained with uranyl acetate: A, $N^+(H)C_5Ala2C_{16}$ and $(SO_3^-)C_5Ala2C_{14}$; B, $N^+(H)C_5Ala2C_{14}$ and $(SO_3^-)C_5Ala2C_{16}$; C, $N^+(H)C_5Ala2C_{14}$ and $N^+C_5Ala2C_{16}$; D, QC_5Ala2C_{14} and $(SO_3^-)C_5Ala2C_{16}$.

packing of globular aggregates.[7] On the other hand, other mixed lipid systems, containing two kinds of peptide lipids at the equimolar ratio, formed normal bilayer aggregates in the aqueous dispersion state; e.g., $N^+C_5Ala2C_n$-$N^+(H)C_5Ala2C_n$ (Fig. 2C), N^+-C_5Ala2C_n-QC_5Ala2C_n, $N^+(H)C_5Ala2C_n$-QC_5Ala2C_n,

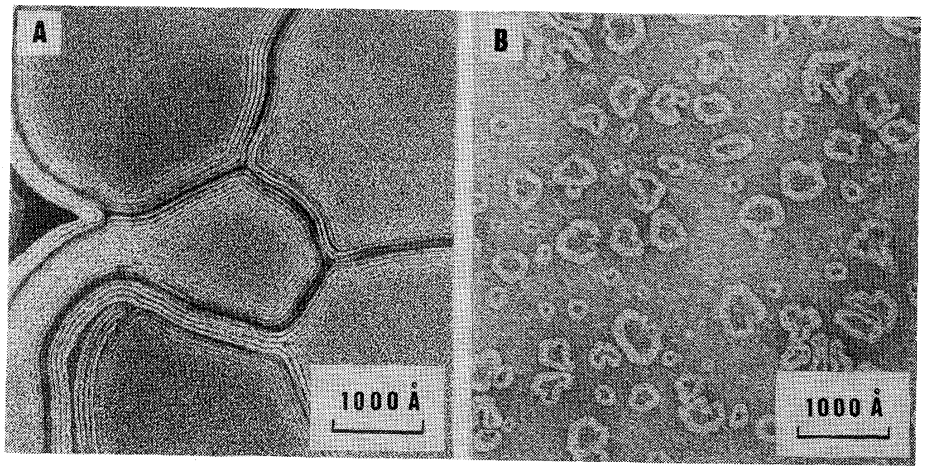

Fig. 3. Electron micrographs for a mixture of $N^+(H)C_5Ala2C_{14}$ (3.75 mmol dm^{-3}) and $(SO_3^-)C_5Ala2C_{14}$ (1.25 mmol dm^{-3}), as negatively stained with uranyl acetate: A, aqueous dispersion; B, aqueous solution sonicated for 60 min with a bath-type sonicator at 30 W.

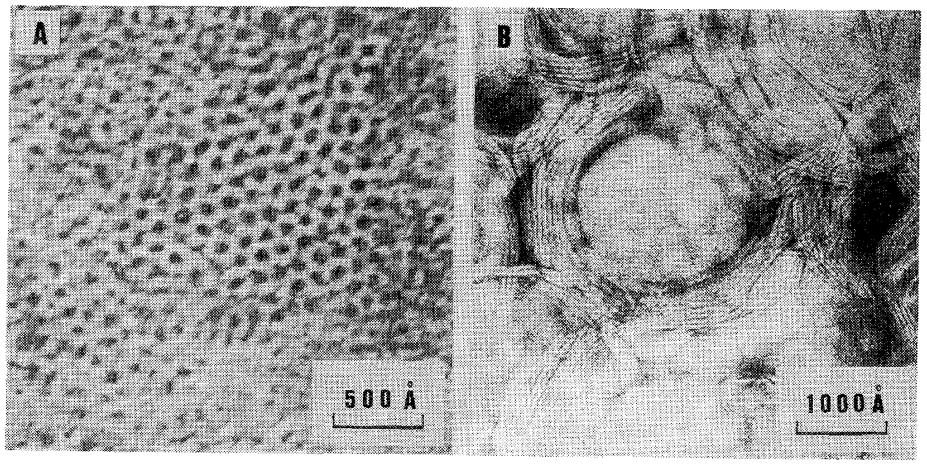

Fig. 4. Electron micrographs for an equimolar mixture (2.5 mmol dm^{-3} each) of $N^+C_5Ala2C_{16}$ and $(SO_3^-)C_5Ala2C_{16}$ in the dispersion state, as negatively stained with uranyl acetate: A, prepared at 50°C; B, prepared at 5°C.

and QC_5Ala2C_n-$(SO_3^-)C_5Ala2C_n$ (Fig. 2D). As for the systems composed of cationic and anionic lipids, any slight loss of the fractional balance retained at the equimolar ratio leads to the formation of bilayer aggregates. For example, bent lamellae were observed in an aqueous dispersion of $N^+(H)C_5Ala2C_{14}$ and $(SO_3^-)C_5Ala2C_{14}$ at the 3:1 molar ratio (Fig. 3A) and converted into single-walled vesicles in the diameter range 200—600 Å upon sonication with a bath-type sonicator for 60 min at 30 W (Fig. 3B). It needs to be noted that the aggregate morphology is subjected to change by the temperature range adopted for investigation, even if both cationic and anionic lipids were mixed exactly at the equimolar ratio, and the nonlamellar network aggregates were observed above the gel-liquid crystalline phase transition temperature. For example, the $N^+C_5Ala2C_{16}$-(SO_3^-)-C_5Ala2C_{16} system, T_m at 27.0°C (vide infra), formed nonbilayer and bilayer aggregates at 50 and 5°C, respectively, in the dispersion state as shown in Fig. 4.

Differential Scanning Calorimetry (DSC). The phase transition parameters (maximum temperature, T_m; enthalpy change, ΔH) for the bilayer aggregates formed with individual ionic lipids in the aqueous dispersion state are linearly correlated with the size of double-chain segment,[5c] and the nature of the head group segments has little effect on the parameters.[6b] The T_m and ΔH values for the cationic bilayer aggregates composed of $N^+(H)C_5Ala2C_n$ at pH 6 are 1.3°C and 17.6 kJ mol^{-1} for n=14 and 24.8°C and 27.6 kJ mol^{-1} for n=16, respectively. These values are comparable to those observed for other ionic bilayer aggregates having the same double-chain segments.[6b]

The phase transition parameters for the mixed lipid systems are listed in Table 1. It is clear that the T_m value is primarily dependent on the size and combination of the double-chain segments. The aggregate composed of two different lipids having the same double-chain segment shows a T_m value comparable to those for the aggregates of individual lipids, whereas the aggregate

Table 1. Phase Transition Parameters for Homogeneous Lipid Mixtures in Aqueous Dispersion

Mixed lipid system[a]	T_m/°C (ΔH/kJ mol^{-1})[b]			
	$m=n=14$	$m=14$, $n=16$	$m=16$, $n=14$	$m=n=16$
$N^+(H)C_5Ala2C_m/N^+C_5Ala2C_n$	2.0 (18.4)		16.1	25.3 (31.4)
$N^+C_5Ala2C_m/QC_5Ala2C_n$		13.9	14.2 (26.8)	
$QC_5Ala2C_m/(SO_3^-)C_5Ala2C_n$	2.3 (12.6)	15.3 (17.6)	14.3 (20.1)	
$N^+C_5Ala2C_m/(SO_3^-)C_5Ala2C_n$	4.9 (13.0)		15.5 (25.5)	27.0 (25.9)
$N^+(H)C_5Ala2C_m/(SO_3^-)C_5Ala2C_n$	4.3 (13.4)	14.2 (18.0)		27.0 (27.2)

a) Concentration of each lipid, 2.5 mmol dm^{-3}. b) ΔH values are given in parentheses. Each system without ΔH showed a broad peak which makes it difficult to evaluate the accurate value.

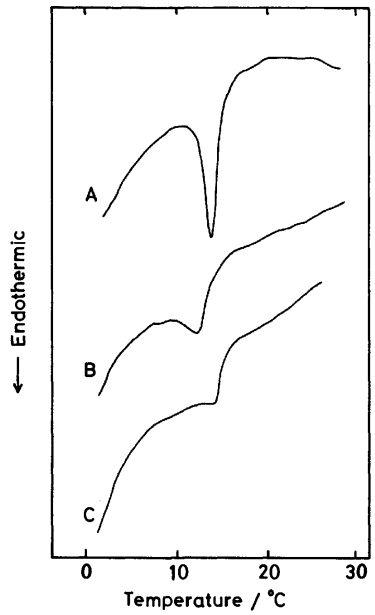

Fig. 5. DSC thermograms for equimolar mixtures (2.5 mmol dm^{-3} each) of two peptide lipids with the following combinations in the dispersion state: A, $N^+C_5Ala2C_{16}$ and $(SO_3^-)C_5Ala2C_{14}$; B, $N^+(H)$-C_5Ala2C_{16} and $N^+C_5Ala2C_{14}$; C, $N^+C_5Ala2C_{14}$ and QC_5Ala2C_{16}.

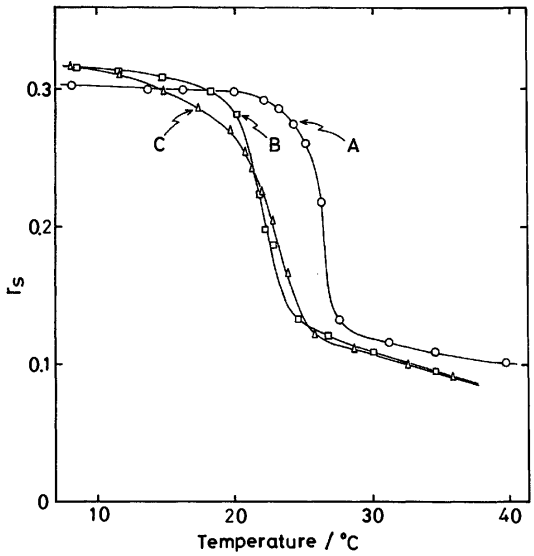

Fig. 6. Correlations of steady-state fluorescence anisotropy r_s with temperature for DPH (1.0×10^{-7} mol dm^{-3}) embedded in the following aggregates at pH 6.0: A, an equimolar mixture (2.5 mmol dm^{-3} each) of $N^+(H)C_5Ala2C_{16}$ and $(SO_3^-)C_5Ala2C_{16}$; B, 5 mmol dm^{-3} $N^+(H)C_5Ala2C_{16}$; C, 5 mmol dm^{-3} $(SO_3^-)C_5Ala2C_{16}$.

formed with an equimolar mixture of two kinds of lipids having different double-chain segments provides a phase transition peak in an intermediate region between intrinsic peaks of the individual aggregates. The ΔH values for the mixed lipid systems, which involve single species of the double-chain segments, are nearly identical with those for the corresponding bilayer aggregates of individual lipids.

The electrostatic interaction mode effective in the polar aggregate domain is reflected on the DSC thermographic pattern when the aggregate is composed of two kinds of peptide lipids having different double-chain segments. As shown in Fig. 5, the 1:1 cationic-anionic lipid system exhibits a sharp phase transition peak as compared with those for other mixed lipid systems. This undoubtedly indicates that highly homogeneous mixing of the cationic and anionic lipids is attained and consequently the surface charge is effectively neutralized without phase separation through formation of tight ion-pairs.

Fluorescence Polarization Spectroscopy. The steady-state fluorescence anisotropy (r_s) of 1,6-diphenyl-1,3,5-hexatriene (DPH) embedded in various aggregates is shown in Fig. 6 for selected cases as a function of temperature. The T_m value for an equimolar mixture of $N^+(H)C_5Ala2C_{16}$ and $(SO_3^-)C_5Ala2C_{16}$ was obtained from the inflection range (27 °C) and is in good agreement with that evaluated by DSC. The extent of variation of r_s for the mixed lipid system is comparable to those for the individual lipid systems over a whole temperature range studied.

Turbidity Measurements. The nonlamellar aggregates formed with both cationic and anionic lipids together provide largely developed domains (2000—20000 Å)[7] as reflected on the extent of turbidity which is appreciably larger than those observed for individual bilayer membranes in the dispersion state. Correlations of turbidity with temperature for aqueous dispersions of some mixed lipid systems are shown in Fig. 7. The bilayer aggregates, composed of $N^+C_5Ala2C_{16}$-$N^+(H)C_5Ala2C_{16}$ and (SO_3^-)-C_5Ala2C_{16}-QC_5Ala2C_{16}, do not undergo any turbidi-

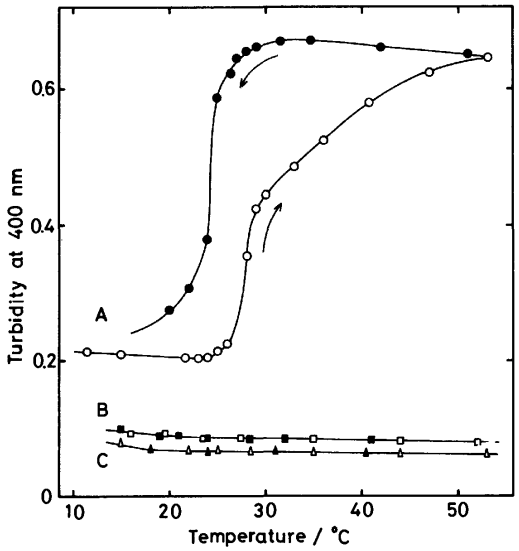

Fig. 7. Correlations of turbidity with temperature for equimolar mixtures (2.5 mmol dm^{-3} each) of two peptide lipids with the following combinations in the dispersion state: A, $N^+(H)C_5Ala2C_{16}$ and $(SO_3^-)C_5Ala2C_{16}$; B, $N^+(H)C_5Ala2C_{16}$ and $N^+C_5Ala2C_{16}$; C, QC_5Ala2C_{16} and $(SO_3^-)C_5Ala2C_{16}$. The values observed in heating and cooling processes are indicated with open and closed circles, respectively, and the measurements were carried out after incubation for 30 min at respective temperatures.

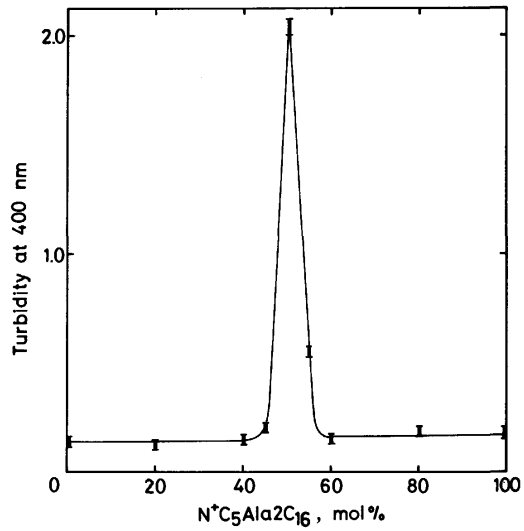

Fig. 8. Correlation of lipid composition with turbidity in the dispersion state for the homogeneously mixed system of $N^+C_5Ala2C_{16}$ and $(SO_3^-)C_5Ala2C_{16}$ at 30°C; total lipid concentration, 5.0 mmol dm^{-3}.

ty change over the whole temperature range regardless of the phase transition. On the other hand, turbidity of the $N^+(H)C_5Ala2C_{16}$–$(SO_3^-)C_5Ala2C_{16}$ system is subjected to change in a sigmoidal manner with a hysteresis effect as shown in Fig. 7. The inflection range for turbidity change apparently corresponds to the phase transition temperature, and the turbidity observed below T_m is comparable to that for the bilayer aggregates. A similar correlation of turbidity with temperature was observed for the aqueous dispersion of $N^+C_5Ala2C_{16}$ and $(SO_3^-)C_5Ala2C_{16}$, mixed at the equimolar ratio.

As for the mixed lipid system composed of $N^+C_5Ala2C_{16}$ and $(SO_3^-)C_5Ala2C_{16}$, its turbidity at 30°C (above T_m) is much sensitive to the lipid composition; the normal bilayer aggregates were spontaneously formed when the composition loses the fractional balance, retained at the equimolar ratio of both lipids, to any slight extent (Fig. 8). The extent of turbidity of the same mixed lipid system was independent of the lipid composition below T_m and comparable to that observed for the bilayer aggregates. The identical correlation of turbidity with lipid composition was also observed for the $N^+C_5Ala2C_{14}$–$(SO_3^-)C_5Ala2C_{14}$ system at 21°C (above T_m).

X-Ray Diffraction Measurements. The low-angle X-ray diffraction technique was applied to the mixed lipid system composed of $N^+C_5Ala2C_{14}$ and $(SO_3^-)C_5Ala2C_{14}$ at room temperature (15±5°C). An equimolar mixture of the lipids in water (the weight fraction of the total lipid quantity, 0.40) showed four diffractions consistent with spacings of 88, 75, 53, and 43 Å (Fig. 9A). This spacing ratio ($1:\sqrt{3}/2:\sqrt{3}/\sqrt{8}:1/2$) rules out the occurrence of lamellar and hexagonal phases since these requires the ratios of 1:1/2:1/3:1/4 and $1:1/\sqrt{3}:1/\sqrt{4}:1/\sqrt{7}$, respectively.[9] The present spacing ratio is in conformity with diffractions from (111), (200), (220), and (222) planes of the face-centered cubic (fcc) lattice having a lattice constant (a), 152 Å. The (111) plane of the fcc lattice is the closest packed one, and the distance between the nearest neighbors in the plane ($a/\sqrt{2}$, 108 Å) is referred to the repeating distance of elements (internal aqueous compartments; see Fig. 10) and in good agreement with the values evaluated by electron microscopy.[7] When the weight fraction of the total lipid quantity in water was reduced to 0.20, the $a/\sqrt{2}$ value was slightly increased to give 111 Å. Meanwhile, a mixture of $N^+C_5Ala2C_{14}$ and $(SO_3^-)C_5Ala2C_{14}$ at a molar ratio of 45:55 in water (the weight fraction of the total lipid quantity, 0.17) afforded a single diffraction with spacing of 52 Å (Fig. 9B), which corresponds to the bilayer thickness evaluated from the CPK molecular models.

Discussion

In the course of our studies on model membranes composed of synthetic peptide lipids,[5,6] we have emphasized that the hydrogen-belt domain[10] constructed with amino acid residues in the intramembrane phase contributes much to the morphological stability of such aggregates. The tight intramembrane hydrogen-bonding interaction, which leads to the formation of the hydrogen-belt domain, was confirmed by various spectroscopic measurements.[6b,11] The cationic peptide lipids such as $N^+C_5Ala2C_n$ (n=12—18)

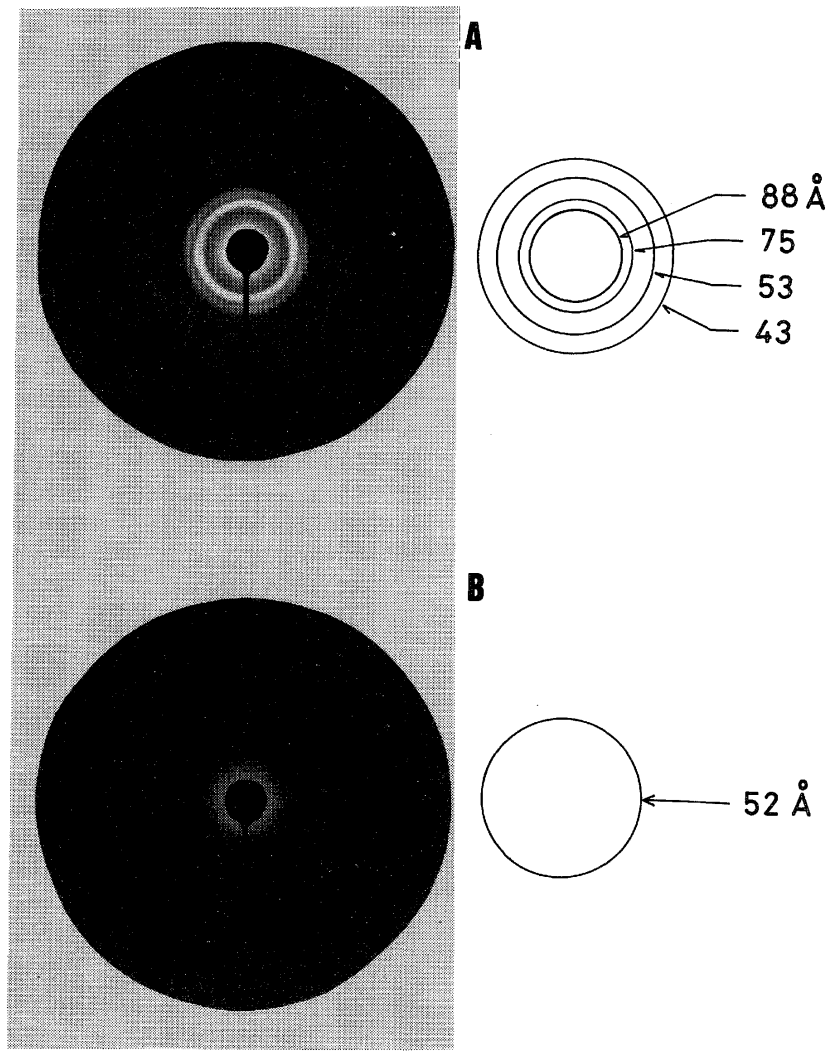

Fig. 9. X-Ray diffraction patterns for the following samples dispersed in water: A, an equimolar mixture of $N^+C_5Ala2C_{14}$ and $(SO_3^-)C_5Ala2C_{14}$ (weight fraction of the total lipid species, 0.40); B, a mixture of $N^+C_5Ala2C_{14}$ and $(SO_3^-)C_5Ala2C_{14}$ at the 45:55 molar ratio (weight fraction of the total lipid species, 0.17).

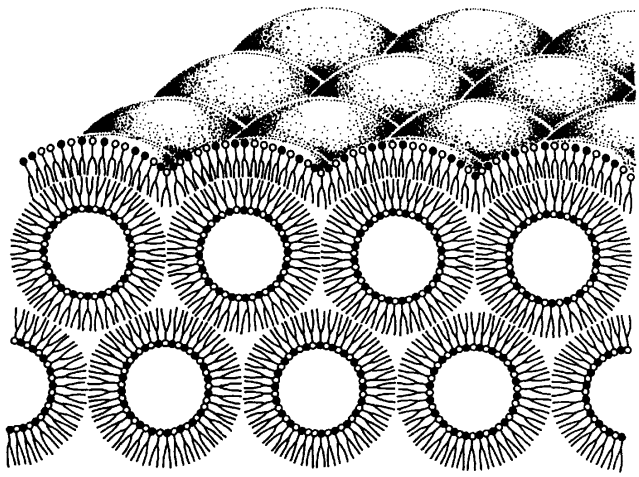

Fig. 10 Schematic representation of the nonlamellar aggregates formed with cationic (O–<) and anionic (●–<) lipids mixed at the equimolar ratio in water. The cross section corresponds to the (111) plane of the fcc lattice.

form multiwalled bilayer aggregates in the aqueous dispersion state, which are then transformed into single-walled vesicles upon sonication.[5c] Such single-walled vesicles are morphologically stable enough to inhibit fusion or aggregation under ordinary conditions.[5c] Regardless of the nature of amino acid residues and ionic head moieties placed in synthetic peptide lipids, the phase transition parameters for these aggregates in the aqueous dispersion state are primarily dependent on the length of the hydrophobic double-chain segment.[6b] On the other hand, nonionic peptide lipids having the quinoyl residue as a polar head moiety, QC_5Ala2C_n, form nonlamellar assemblies with the highly ordered and three-dimensional network arrangement of small aqueous compartments.[6a] Since the phase transition enthalpy (ΔH) and the fluorescence polarization parameter (r_s) obtained with DPH in the gel state for these aggregates are smaller than those for bilayer aggregates having the same double-

chain segments,[6b] the nonlamellar phase seems to be stable regardless of the phase transition.

As for the mixed peptide lipid systems, the bilayer phase is predominantly present under conditions that the total surface charge of the aggregate is not completely neutralized. On the other hand, the nonlamellar phase, schematically shown in Fig. 10, appears in the aqueous dispersions of cationic and anionic lipids mixed at the 1:1 molar ratio above T_m (Figs. 2 and 3). Under the latter conditions, the aggregates retain the high microscopic homogeneity of cationic and anionic lipid molecules (Fig. 5). The achievement of such microscopic homogeneity must be originated from the intramembrane electrostatic interaction between cationic and anionic head moieties to form highly developed ion-pair clusters on the membrane surface. Furthermore, the nonlamellar phase appeared above T_m in the mixed system of cationic and anionic lipids was spontaneously transformed into the normal bilayer phase below T_m as confirmed by the negative staining electron microscopy (Fig. 4). Since the nonlamellar domain is much more extensively developed than the bilayer one, the morphological transition between them was also reflected on turbidity change, accompanied with a hysteresis loop as shown in Fig. 7. In the light of the above observations, the gel to liquid-crystalline transition, which takes place in the hydrophobic domain, is thermodynamically required for transformation of the bilayer phase into the nonbilayer one. The liquid-crystalline bilayer phase, which would appear between the bilayer gel phase and the nonbilayer phase,[1a] was not detected by DSC, fluorescence polarization, and turbidity measurements under ordinary conditions.

It has been proposed that the aggregate morphology, which is favored thermodynamically in aqueous media, is theoretically rationalized in view of the dynamic packing mode of lipid molecules by introducing the critical packing parameter, $v/(a_0 l_c)$; where v, a_0, and l_c are the hydrocarbon volume, optimal surface area, and critical chain length of a lipid molecule, respectively.[12] According to this concept, the nonlamellar structure requires $v/(a_0 l_c)>1$, whereas the bilayer structure is favored under the conditions $1/2<v/(a_0 l_c)<1$. As we have previously discussed, the a_0 value is the primary factor which acts to develop the aggregate morphology observed for QC_5Ala2C_n.[6b] On the other hand, the 1:1 cationic-anionic lipid system develops the bilayer phase in the gel state. Therefore, the average a_0 value seems to be larger than that for QC_5Ala2C_n. However, the critical packing parameter must become larger than 1 in the temperature range above T_m by increasing the v value. This effect is plausibly brought about by defrosting the rotational motion of the hydrophobic double-chain segment.

The formation of *lipidic particles* or *lipidic intramembranous particles* has been detected in various aqueous lipid mixtures and in total lipid extracts under physiological conditions by means of electron microscopy.[2] Globular aggregates are arranged in three-dimensional quasi-crystalline manners and associated to afford various lipidic particles, showing large variation in shape, size, and packing behavior, as observed for the following mixed lipid systems: cardiolipin and egg phosphatidylcholine in the presence of calcium ions,[3a] monogalactosyldiacylglycerol and digalactosyldiacylglycerol,[3f] cardiolipin and chlorpromazine,[13] dioleoylphosphatidic acid and chlorpromazine,[13] and dilinoleoylphosphatidylethanolamine and egg phosphatidylcholine.[14] The lipidic particle phase has been suggested to consist of spherical aggregates of inverted micelles arranged in a closely packed organization[13] or to involve inverted micelles sandwiched in between lipid bilayers.[3f] These two concepts on morphological behavior have been subjected to some debate.[14,15] An aggregation mode for the system composed of dilinoleoylphosphatidylethanolamine and egg phosphatidylcholine at the 85:15 molar ratio in the quasi-crystalline state, in fact, was consistent with an isotropic cubic phase[14] in a manner as observed for systems composed of ordinary detergents such as potassium carboxylates and quaternary ammonium halides bearing a long alkyl chain[16] and of monoglycerides such as 1-monoolein and 1-monostearin,[17] all being based on the X-ray diffraction method. Such lipidic particles have been often observed in an intermediate step during the phase transition between lamellar and inverted hexagonal (H_{II}) phases.[14,18] The globular aggregates formed with an equimolar mixture of cationic and anionic lipids in the present study apparently constitute a highly developed quasi-crystalline phase with the face-centered cubic lattice. However, this phase remains stable in the aqueous dispersion state without being transformed into the H_{II} phase under the present conditions. The previous studies with mixed lipid systems, which allow the formation of lipidic particles, claimed that one of the mixed lipid species at least needs to prefer to constitute the H_{II} phase for each mixed system when it is dispersed in water alone.[2] However, this concept must be revised since lipidic particles are also formed with two kinds of lipids which constitute individually normal bilayer aggregates in the aqueous dispersion state. Thus, the formation of globular aggregates is primarily controlled by the critical packing parameter, which is subjected to change by the intramembrane interaction mode among the polar head moieties and/or the rotational freedom of the hydrophobic double-chain segment of lipid species. However, the molecular basis for the formation of various three-dimensional quasi-crystalline phases, such as inverted hexagonal and inverted cubic, needs to be clarified by employing appropriate synthetic lipids. Since it has been suggested that lipidic particles assume important roles in membrane fusion and trans-membrane transport,[2]

the present nonbilayer systems may provide useful means for clarifying those mechanisms.

We are grateful to professor Tisato Kajiyama of Kyushu University for the X-ray diffraction measurements. The present work was supported in part by a Grant-in-Aid for Scientific Research from the Ministry of Education, Science, and Culture (No. 58430016).

References

1) a) P. R. Cullis and B. De Kruijff, *Biochim. Biophys. Acta*, **559**, 399 (1979); b) S. W. Hui, T. P. Stewart, and L. T. Boni, *Chem. Phys. Lipids*, **33**, 113 (1983).

2) A. J. Verkleij, *Biochim. Biophys. Acta*, **779**, 43 (1984).

3) a) A. J. Verkleij, C. Mombers, W. J. Gerritsen, L. Leunissen-Bijvelt, and P. R. Cullis, *Biochim. Biophys. Acta*, **555**, 358 (1979); b) R. G. Miller, *Nature (London)*, **287**, 166 (1980); c) S. W. Hui, T. P. Stewart, and L. T. Boni, *Science*, **212**, 921 (1981); d) E. L. Bearer, N. Düzgünes, D. S. Friend, and D. Papahadjopoulos, *Biochim. Biophys. Acta*, **693**, 93 (1982); e) B. Kachar and T. S. Reese, *Nature (London)*, **296**, 464 (1982); f) P. J. Quinn and W. P. Williams, *Biochim. Biophys. Acta*, **737**, 223 (1983).

4) J. H. Fendler, "Membrane Mimetic Chemistry," John Wiley, New York (1982), Chap. 6 and 12.

5) a) Y. Murakami, A. Nakano, and K. Fukuya, *J. Am. Chem. Soc.*, **102**, 4253 (1980); b) Y. Murakami, A. Nakano, and H. Ikeda, *J. Org. Chem.*, **47**, 2137 (1982); c) Y. Murakami, A. Nakano, A. Yoshimatsu, K. Uchitomi, and Y. Matsuda, *J. Am. Chem. Soc.*, **106**, 3613 (1984).

6) a) Y. Murakami, A. Nakano, J. Kikuchi, T. Takaki, and K. Uchimura, *Chem. Lett.*, **1983**, 1891; b) Y. Murakami, J. Kikuchi, T. Takaki, K. Uchimura, and A. Nakano, *J. Am. Chem. Soc.*, **107**, 2161 (1985).

7) Y. Murakami, J. Kikuchi, T. Takaki, and K. Uchimura, *J. Am. Chem. Soc.*, **107**, 3373 (1985).

8) The pH effect on the aggregate morphology of NC_5Ala2C_n will be reported elsewhere. In the present work, this lipid was used under acidic conditions below pH 6 so as to behave as a cationic one [$N^+(H)C_5Ala2C_n$].

9) V. Luzzati, H. Mustacchi, A. Skoulios, and F. Husson, *Acta Cryst.*, **13**, 660 (1960).

10) H. Brockerhoff, "Bioorganic Chemistry," ed by E. E. van Tamelen, Academic Press, New York (1977), Vol. 3, Chap. 1.

11) a) Y. Murakami, Y. Aoyama, A. Nakano, T. Tada, and K. Fukuya, *J. Am. Chem. Soc.*, **103**, 3951 (1981); b) Y. Murakami, A. Nakano, and A. Yoshimatsu, *Chem. Lett.*, **1984**, 13.

12) a) J. N. Israelachvili, D. J. Mitchell, and B. W. Ninham, *J. Chem. Soc., Faraday Trans. 2*, **72**, 1525 (1976); b) J. N. Israelachvili, S. Marčelja, and R. G. Horn, *Quart. Rev. Biophys.*, **13**, 121 (1980).

13) A. J. Verkleij, R. De Maagd, J. Leunissen-Bijvelt, and B. De Kruijff, *Biochim. Biophys. Acta*, **684**, 255 (1982).

14) S. W. Hui and L. T. Boni, *Nature (London)*, **296**, 175 (1982).

15) W. P. Williams, A. Sen, A. P. R. Brain, P. J. Quinn, and M. J. Dickens, *Nature (London)*, **296**, 175 (1982).

16) V. Luzzati and F. Reiss-Husson, *Nature (London)*, **210**, 1351 (1966).

17) G. Lindblom, K. Larsson, L. Johansson, K. Fontell, and S. Forsén, *J. Am. Chem. Soc.*, **101**, 5465 (1979).

18) R. van Venetië and A. J. Verkleij, *Biochim. Biophys. Acta*, **645**, 262 (1981).

 © 1986 The Chemical Society of Japan Bull. Chem. Soc. Jpn., 59, 525—533 (1986)

Stereoselective Preparation of Acyclic *syn*-β-Amino Alcohols from β-Hydroxy Ketones via the Corresponding *O*-Benzyl Oximes

Koichi NARASAKA,* Yutaka UKAJI, and Shigeru YAMAZAKI
Department of Chemistry, Faculty of Science, The University of Tokyo, Hongo, Bunkyo-ku, Tokyo 113
(Received October 2, 1985)

Reduction of β-hydroxy ketone *O*-benzyl oximes with lithium aluminum hydride in the presence of sodium or potassium methoxide afforded the corresponding *syn*-β-amino alcohols in highly stereoselective manner. A lythraceae alkaloid, lasubine II, was synthesized stereoselectively by applying this method.

Over the years there have been a large number of efforts directed to control chiral induction in acyclic precursors, and various studies which demonstrate the synthetically useful level of stereocontrol have been published for diastereoselection between adjacent carbon atoms (1,2-relationships).[1] Only a limited number of method, however, have been published to regulate 1,3-chiral induction in acyclic systems,[1b,2,3] leaving this area still in a relatively primitive state of development.

Concerning 1,3-chiral induction of acyclic systems, we have studied and briefly reported the stereoselective preparation of β-amino alcohols from β-hydroxy ketones.[4] In this paper, the results of the stereoselective preparation of *syn*-β-amino alcohols via β-hydroxy ketone *O*-benzyl oximes are reported in detail with the revised mechanism.

Previously one of the authors found that β-hydroxy ketones are stereoselectively reduced with sodium borohydride via boron chelates giving *syn*-1,3-diols.[5] Then we turned our interest to the stereoselective preparation of β-amino alcohols from β-hydroxy imines, hydrazones, or oximes, by stereoselective reduction directed by the hydroxyl group.

Among β-hydroxy imines, hydrazones, and oximes, we chose to use β-hydroxy ketone *O*-benzyl oximes. *O*-Benzyl oximes **2** are readily prepared almost quantitatively from β-hydroxy ketones **1**. They are very stable and easily handled as compared with the corresponding imines. Also it was found that the reactivity of *O*-benzyl oximes toward the reduction with lithium aluminum hydride (LAH) exceeded that of the corresponding dimethylhydrazones.

Various β-hydroxy ketones **1** were prepared by aldol reactions between aldehydes and methyl ketones, and converted to the corresponding *O*-benzyl oximes by the treatment with *O*-benzylhydroxylamine hydrochloride and pyridine in refluxing methanol.[6] The resulting *O*-benzyl oximes **2** were equilibrium mixtures of *syn*- and *anti*-isomers *syn*-**2** and *anti*-**2**,[7] which were separated by column chromatography.

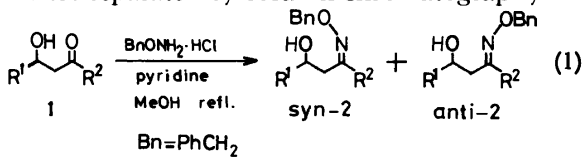

(1)

Then the stereoselectivity of the reduction with LAH was examined based on the following hypothesis. The reaction of **2** with LAH would generate the aluminum alcoholate **3**, and the intramolecular reduction would proceed through cyclic transition states T_1 or T_2 (Fig. 1). The steric interaction between R^1 and R^2 would destabilize the transition state T_2, hence the reduction might be expected to proceed through the transition state T_1 to result in the formation of a *syn*-β-amino alcohol **4**.[8]

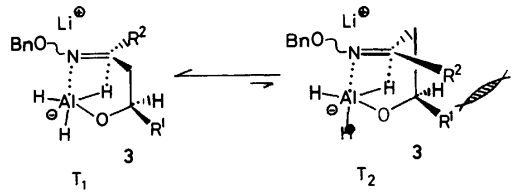

Fig. 1.

Each isomer *syn*-**2** or *anti*-**2** was reduced with an excess amount of LAH in THF between 0 °C and room temperature, and the results are listed in Table 1. From *syn*-*O*-benzyl oximes *syn*-**2**, *syn*-amino alcohols **4** were obtained in high stereoselectivity. In comparison with the high stereoselectivity in the reduction of *syn*-*O*-benzyl oximes *syn*-**2**, the reduction of *anti*-*O*-benzyl oximes *anti*-**2** proceeded only in moderate selectivity. When the reduction of *anti*-*O*-benzyl oxime *anti*-**2a** was tried at lower temperature (ca. −10 °C), the selectivity toward the *syn*-amino alcohol **4a** was found to increase to 89% from 77% but was still not sufficiently high. At the temperature below −10 °C, unfortunately the reduction hardly proceeded.

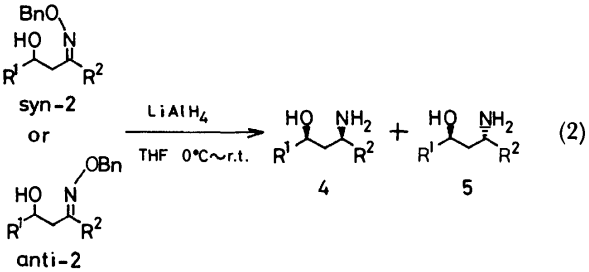

(2)

During this study, it was found that when sodium methoxide was added to the reaction mixture a significant effect on the stereoselectivity and the acceleration of the LAH reduction was observed. As

Table 1. Reduction of *O*-Benzyl Oximes **2** with LAH between 0°C and Room Temperature

	R^1	R^2	Ratio of **4**:**5** from *syn*-**2**	(Total yield/%) from *anti*-**2**
a	*n*-Bu	*n*-Bu	95: 5 (87)[a]	77:23 (96)[a]
b	*i*-Bu	*i*-Bu	95: 5 (77)[a]	77:23 (83)[a]
c	$PhCH_2CH_2$	$PhCH_2CH_2$	91: 9 (85)[b]	79:21 (96)[b]
d	$PhCH_2CH_2$	CH_3	88:12 (78)[c]	78:22 (85)[c]
e	Ph	CH_3	88:12 (74)[c]	85:15 (82)[c]
f	Ph	Ph	85:15 (82)[c]	88:12 (74)[c]

a) Isomeric ratio was determined by GLC (OV-101). b) Isomeric ratio was determined by the isolation of *syn*- and *anti*-amino alcohols. c) Isomeric ratio was determined by the conversion to the corresponding acetates.

mentioned before, the reduction of *anti*-**2a** with LAH occurred at ca. −10°C and did not proceed at −78°C. On the other hand, in the presence of sodium methoxide the LAH reduction of the C=N bond in *anti*-**2a** occurred even at −78°C. After the reduction of C=N bond in *anti*-**2a** was completed, the reaction temperature was gradually raised to 0°C to completely convert the resulting half reduced intermediate, *O*-benzylhydroxylamine derivative, to β-amino alcohol and benzyl alcohol. Furthermore, it is important to note that *syn*-amino alcohol **4a** was obtained in excellent stereoselectivity (**4a**:**5a**=95:5) by this procedure (Eq. 3).

The reaction of *syn*-**2a** with LAH was also examined in the presence of sodium methoxide. Although *syn*-*O*-benzyl oxime *syn*-**2a** was scarcely reduced below 0°C by the treatment with LAH, the presence of sodium methoxide was so effective that the reduction of C=N bond proceeded at −30°C. And the *syn*-amino alcohol **4a** was also obtained in excellent selectivity (**4a**:**5a**=95:5).

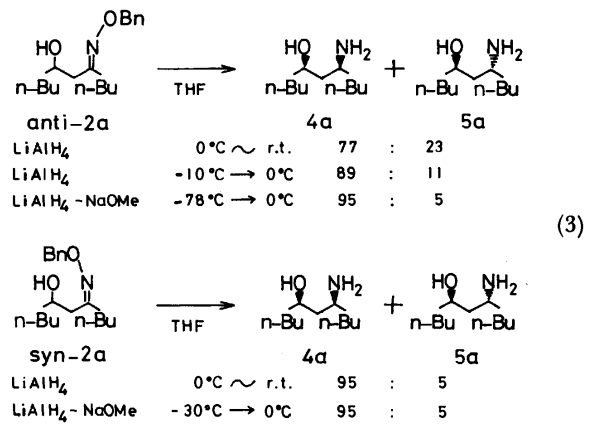

(3)

These results prompted us to examine the prepatation of β-amino alcohol from a mixture of *syn*- and *anti*-*O*-benzyl oxime **2a** by the reduction with LAH-sodium methoxide. A mixture of *syn*- and *anti*-**2a** was treated with 15 molar amounts of LAH in the presence of 10 molar amounts of sodium methoxide at −78°C. After the consumption of *anti*-**2a** was evidenced by TLC, the reaction temperature was gradually raised to 0°C and stirred overnight. In excellent stereoselectivity (96%), *syn*-amino alcohol **4a** was obtained. When the reduction was performed employing 7.5 molar amounts of LAH and 5 molar amounts of sodium methoxide, the selectivity was slightly decreased (*syn*-**2a**:*anti*-**2a**=94:6). Further, the reduction did not proceed at −78°C with 5 molar amount of LAH and 2.5 molar amounts of sodium methoxide. Hence, the reduction of various *O*-benzyl oximes **2** were investigated using 15 molar amounts of LAH and 10 molar amounts of sodium methoxide, and the results are summarized in Table 2. Generally, the selectivity toward *syn*-amino alcohols **4** is quite excellent. Only in the cases that subsituent (R) is (or are) phenyl group(s), the selectivity is decreased but still high.

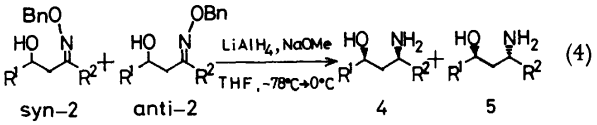

(4)

The stereochemistry of the products were confirmed by ^{13}C NMR spectra and the conversion of amino alcohols **4** and **5** to cyclic urethanes **8** and **9**. According to the empirical rule of ^{13}C NMR spectra of a β-amino alcohol, the chemical shift of the methine carbon adjacent to the hydroxyl group is observed at the lower field in the case of a *syn*-amino alcohol **4** as compared with an *anti*-isomer **5**.[9]

Furthermore, the relative reactivity in the cyclization of urethanes of each isomers **6** and **7** indicated the stereochemistry. Treatment of amino alcohols **4** and **5** with methyl chloroformate and triethylamine gave the corresponding urethanes **6** and **7**, respectively. The *syn*-urethanes **6** were easily converted to the cyclic urethanes **8** at room temperature by treatment with sodium hydride in benzene. On the other hand, the cyclization of *anti*-urethanes **7** did not occurred at room temperature but at the temperature of refluxing benzene. The inferior reactivity of the *anti*-isomers **7** is due to the disfavored transition state of the cyclization in which the R^2 group should orient to the pseudo-axial direction (Fig. 2). The relative stereochemistry of **4e** and **5e** determined by this way was agreed with the stereochemical assignment determined by ^{13}C NMR spectra.[9]

Instead of sodium methoxide, potassium methoxide was also found to be effective for the stereocontrol of

Table 2. Reduction of *O*-Benzyl Oximes **2** with LAH–NaOMe

	R^1	R^2	(*syn*-**2**:*anti*-**2**)	Ratio of **4**:**5** (Total yield/%)
a	*n*-Bu	*n*-Bu	(52:48)	96: 4 (92) 97: 3 (92)[a] 91: 9 (quant.)[b]
b	*i*-Bu	*i*-Bu	(55:45)	95: 5 (92)
c	$PhCH_2CH_2$	$PhCH_2CH_2$	(51:49)	94: 6 (89)
d	$PhCH_2CH_2$	CH_3	(34:66)	97: 3 (94)
e	Ph	CH_3	(28:72)	90:10 (97) 92: 8 (93)[a]
f	Ph	Ph	(82:18)	90:10 (81)

a) Potassium methoxide was used. b) Lithium methoxide was used.

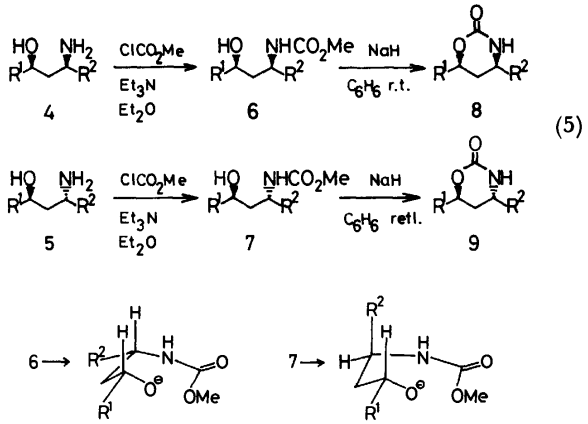

(5)

Fig. 2.

the LAH reduction. However, the slightly inferior selectivity was observed when lithium methoxide was employed (Table 2).

In the previous report,[4b] we supposed that the enhanced selectivity and reactivity by the addition of methoxide may be due to the formation of a sodium alcoholate **10** by an equilibrium between the aluminum alcoholate **3**. In order to ascertain this assumption, the sodium alcoholate *anti*-**10a** generated in situ by treatment of the *anti*-*O*-benzyl oxime *anti*-**2a** with sodium hydride in THF was reduced with LAH. But the reduction did not proceed at −78 °C but −20 to 0 °C, and the products ratio of *syn*- and *anti*-amino alcohols (**4a**:**5a**=80:20) was not so excellent as compared with the result in Table 2. Consequently, it was indicated that the sodium alcoholate **10** is not the actual intermediate in the reduction of *anti*-*O*-benzyl oxime *anti*-**2** in the presence of sodium methoxide.

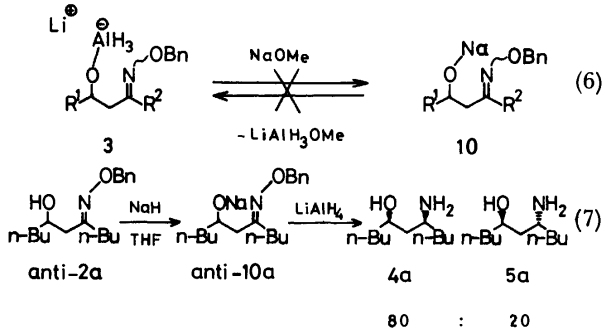

(6)

(7)

Next, the confirmation of the intramolecular reduction via the intermediate aluminum alcoholate **3** was examined by the reduction of *syn*- and *anti*-*O*-benzyl oximes after the protection of the hydroxyl groups as silyl ethers. The *t*-butyldimethylsilyl ethers of *syn*-**2b** and *anti*-**2b** were treated with LAH, but the reduction did not occur even at room temperature.

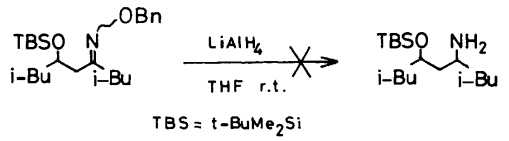

(8)

These observations may indicate that the formation of the intermediate aluminum alcoholate **3** is indispensable for the reduction of the C=N bond and the reduction may proceed by the intramolecular fashion as shown in Fig. 1. Coordination of methoxide to the aluminum of this intermediate **3**[10] may increase the nucleophilicity of the hydride, and the reduction proceeds at the lower temperature resulting *syn*-β-amino alcohol **4** in excellent stereoselectivity.

As mentioned, it was noted that the reduction of *O*-benzyl oximes with LAH in the presence of sodium or potassium methoxide provides a highly stereoselective method for the preparation of *syn*-β-amino alcohols starting from β-hydroxy ketones. The present method has a wide applicability to prepare various *syn*-β-amino alcohols because β-hydroxy ketones are readily prepared by directed aldol reactions.[11]

In these years, much efforts have been concentrated in the stereoselective preparation of β-amino alcohols, and several selective methods have been developed by the reduction of isoxazolines[9,12] and enaminones[3a] the iodocyclocarbamation of a homoallylamine,[3b] the intramolecular Michael addition of *O*-carbamates,[3c] the sulfoxide-mediated intramolecular hydroxylation of a remote olefin,[13] and the Grignard reaction of β-alkoxy imines.[3d] The present method affords the alternative procedure for the preparation of unprotected *syn*-β-amino alcohols.

As an efficient and practical method for the preparation of acyclic *syn*-β-amino alcohols was established, a new synthetic route to a lythraceae alkaloid, lasubine

II,[14] was investigated by applying this method.[15] Lythraceae alkaloids have been generally synthesized by the condensation of isopelletierine with aromatic aldehydes[16] or the [2+3] cycloaddition of tetrahydropyridine *N*-oxide.[17] In our synthetic strategy an acyclic key intermediate, a *syn*-β-amino alcohol **16**, was prepared firstly, and the successive cyclization processes afforded a bicyclic lasubine II (**22**) in a stereoselective manner.

Veratraldehyde was converted to a 1,3-dithiane **11**,[18] which was alkylated with 2-bromo-1,1-dimethoxyethane and the product **12** was hydrolyzed with concd hydrochloric acid to an aldehyde **13**. The aldol reaction between the aldehyde **13** and the kinetic lithium enolate of 5-hexen-2-one afforded a β-hydroxy ketone **14** in 80% yield. At this stage, the whole carbon skeleton required for the synthesis of lasubine II was arranged.

The aldol product **14** was converted to a *O*-benzyl oxime **15** as a mixture of almost equal amount of *syn*- and *anti*-isomers. The *O*-benzyl oxime **15** was reduced with LAH in the presence of potassium methoxide. During this reaction, the reaction temperature should be carefully controlled. After the reduction mixture was stirred at −78 °C overnight, the temperature was gradually raised to −15 °C during 5 h and the mixture was stirred for 12 h at −15 °C. When the reaction temperature was raised above −15 °C, the cleavage of dithioacetal group was observed. After the hydrolysis, the *syn*-β-amino alcohol **16** was isolated in 65% yield.[19]

For the construction of a octahydroquinolizine skeleton, the hydrolysis of dithioacetal group of **16** was investigated but did not afford the fruitful result. Therefore, the amino group of **16** was protected as a *t*-butylcarbamate **17** and then the dithioacetal group was hydrolyzed with *N*-chlorosuccinimide and silver nitrate in aqueous acetonitrile to give a hydroxy ketone **18** in 73% yield. The deprotection of the amino group with trifluoroacetic acid in dichloromethane spontaneously yielded a labile cyclic imine **19**, which was submitted to the successive reduction without isolation. Treatment of **19** with LAH in the presence of sodium methoxide in THF afforded the *cis*-2,6-disubtituted piperidine **20** stereoselectively.[20–22]

Hydroboration of **20** with bis(1,2-dimethylpropyl)-borane and the successive oxidation with alkaline hydrogen peroxide afforded a diol **21**. The regioselective tosylation of the primary hydroxyl group in **21** was carried out employing *p*-toluenesulfonyl chloride and pyridine at −20 °C to give (±)-lasubine II (**22**).

Thus the stereoselective synthesis of lasubine II has been achieved via an acyclic intermediate, demonstrating a new and useful strategy for the preparation of lythraceae alkaloids.

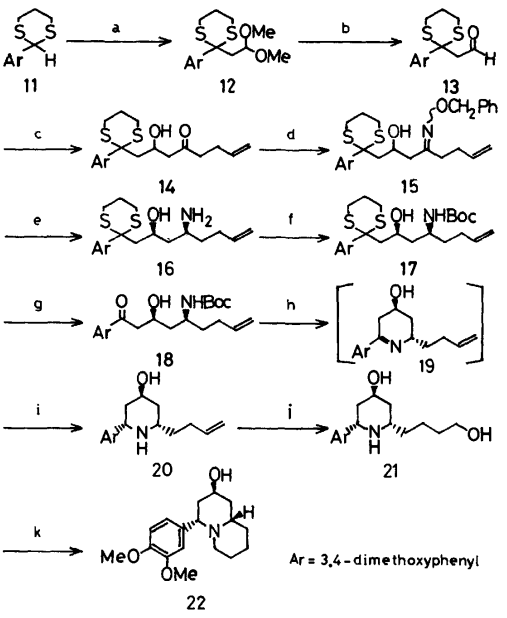

Scheme 1. Total Synthesis of (±)-Lasubine II.
(a): 1) *n*-BuLi, 2) $BrCH_2CH(OMe)_2$; 84%, (b): H_3O^+; 76%, (c): $CH_2=C(OLi)CH_2CH_2CH=CH_2$; 80%, (d) $PhCH_2ONH_2 \cdot HCl$, pyridine; quant., (e): $LiAlH_4$, KOMe; 65%, (f): Boc-S; 77%, (g): NCS, $AgNO_3$, H_2O; 73%, (h): CF_3COOH, (i): $LiAlH_4$, NaOMe; 60% from **18**, (j): 1) bis(1,2-dimethylpropyl)borane; 2) H_2O_2, NaOH; 87%, (k): *p*-TsCl, pyridine; 70%.

Experimental

All the melting points are uncorrected. The IR spectra were determined on a Hitachi Model 260-30 spectrometer. The ^1H NMR spectra were recorded with a Hitachi R-24B, a Varian EM-390, and a JEOL GX-400 spectrometers, and ^{13}C NMR spectra were measured with a JEOL FX-90Q spectrometer in $CDCl_3$ with tetramethylsilane as an internal standard. The MS spectra were taken on a JEOL JMS-D300. Benzene was distilled and dried over sodium wire. Tetrahydrofuran (THF) and diethyl ether were freshly distilled from sodium benzophenone ketyl. Pyridine and dichloromethane were distilled from CaH_2 and stored over Molecular Sieve. Purification of products was performed by column chromatography on silica gel (Wakogel C-200 or Merck, Art. 9385 Kieselgel 60, 230—400 mesh), preparative TLC on silica gel (Wakogel B-5F) or on aluminum oxide (Merck, Art. 1103 Aluminiumoxid 60 PF_{254}, Typ E), and Chromatotron on aluminum oxide (Merck, Art. 1092 Aluminiumoxid GF_{254}, Typ E).

β-Hydroxy ketones **1a—f** were prepared by the aldol reaction of kinetic lithium enolates of the corresponding methyl ketones with aldehydes, and purified by column chromatography on silica gel. Further details of the reaction procedure are described in the preparation of **14**.

Preparation of 7-Benzyloxyimino-5-undecanol (2a). A solution of 7-hydroxy-5-undecanone (604 mg, 3.2 mmol) and *O*-benzylhydroxylamine hydrochloride (574 mg, 6.6 mmol) in pyridine (0.5 mL) and methanol (8 mL) was refluxed for 30 min.[6] After the most of methanol was removed in vacuo, water was added to the residue and was extracted with CH_2Cl_2. The separated organic layer was dried over Na_2SO_4 and was

condensed under reduced pressure. Purification by column chromatography on silica gel (hexane:ethyl acetate=15:1, v/v) gave the *syn*-*O*-benzyl oxime *syn*-**2a** (473 mg, 50%) and the *anti*-oxime *anti*-**2a** (431 mg, 46%).[23]

***syn*-7-Benzyloxyimino-5-undecanol (*syn*-2a)**: IR (neat) 3430, 1635 cm^{-1}. ^{1}H NMR δ=0.60—1.58 (16H, m), 1.93—2.52 (3H, m), 2.30 (1H, d, *J*=1.6 Hz), 2.42 (1H, d, *J*=4.0 Hz), 3.48—4.03 (1H, m), 4.93 (2H, s), 7.17 (5H, s).

***anti*-7-Benzyloxyimino-5-undecanol (*anti*-2a)**: IR (neat) 3460, 1635 cm^{-1}. ^{1}H NMR δ=0.60—1.68 (16H, m), 1.98—2.45 (2H, m), 2.13 (2H, d, *J*=4.8 Hz), 3.18 (1H, br s), 3.53—4.02 (1H, m), 4.92 (2H, s), 7.17 (5H, s).

Preparation of the other *O*-benzyl oximes **2b—f** was carried out by the same procedure.

***syn*-6-Benzyloxyimino-2,8-dimethyl-4-nonanol (*syn*-2b)**: IR (neat) 3420, 1630 cm^{-1}. ^{1}H NMR δ=0.80 (12H, d, *J*=6.2 Hz), 0.95—2.58 (9H, m), 3.57—4.13 (1H, m), 4.92 (2H, s), 7.13 (5H, s).

***anti*-6-Benzyloxyimino-2,8-dimethyl-4-nonanol (*anti*-2b)**: IR (neat) 3440, 1630 cm^{-1}. ^{1}H NMR δ=0.83 (12H, d, *J*=6.2 Hz), 0.95—2.02 (4H, m), 2.02—2.32 (4H, m), 3.18 (1H, d, *J*=3.6 Hz), 3.65—4.18 (1H, m), 4.93 (2H, s), 7.18 (5H, s).

***syn*-5-Benzyloxyimino-1,7-diphenyl-3-heptanol (*syn*-2c)**: IR (neat) 3430, 1630 cm^{-1}. ^{1}H NMR δ=1.43—1.93 (2H, m), 2.18—2.98 (9H, m), 3.52—4.03 (1H, m), 4.93 (2H, s) 7.02, (10H, s), 7.13 (5H, s).

***anti*-5-Benzyloxyimino-1,7-diphenyl-3-heptanol (*anti*-2c)**: IR (neat) 3430, 1630 cm^{-1}. ^{1}H NMR δ=1.37—1.88 (2H, m), 2.03 (2H, d, *J*=6.0 Hz), 2.30—2.92 (6H, m), 3.00—3.30 (1H, m), 3.52—4.12 (1H, m), 4.98 (2H, s), 7.12 (10H, s), 7.24 (5H, s).

***syn*-5-Benzyloxyimino-1-phenyl-3-hexanol (*syn*-2d)**: IR (neat) 3410, 1635 cm^{-1}. ^{1}H NMR δ=1.35—1.90 (2H, m), 1.77 (3H, s), 2.30—2.85 (5H, m), 3.47—4.02 (1H, m), 4.88 (2H, s), 6.97 (5H, s), 7.07 (5H, s).

***anti*-5-Benzyloxyimino-1-phenyl-3-hexanol (*anti*-2d)**: IR (neat) 3440, 1645 cm^{-1}. ^{1}H NMR δ=1.37—1.87 (2H, m), 1.70 (3H, s), 2.10 (2H, d, *J*=6.0 Hz), 2.33—2.82 (2H, m), 2.92—3.15 (1H, m), 3.48—4.03 (1H, m), 4.87 (2H, s), 7.00 (5H, s), 7.09 (5H, s).

***syn*-3-Benzyloxyimino-1-phenyl-1-butanol (*syn*-2e)**: IR (neat) 3400, 1630 cm^{-1}. ^{1}H NMR δ=1.60 (3H, s), 2.53 (1H, d, *J*=2.0 Hz), 2.68 (1H, d, *J*=4.0 Hz), 2.97 (1H, br s), 4.65—5.03 (1H, m), 4.90 (2H, s), 7.12 (5H, s), 7.18 (5H, s).

***anti*-3-Benzyloxyimino-1-phenyl-1-butanol (*anti*-2e)**: IR (neat) 3430, 1640 cm^{-1}. ^{1}H NMR δ=1.42 (3H, s), 2.43 (2H, d, *J*=6.4 Hz), 3.40 (1H, d, *J*=3.0 Hz), 4.83 (1H, dd, *J*=3.0, 6.4 Hz), 4.95 (2H, s), 7.20 (5H, s), 7.22 (5H, s).

***syn*-3-Benzyloxyimino-1,3-diphenyl-1-propanol (*syn*-2f)**: IR (neat) 3420 cm^{-1}. ^{1}H NMR δ=2.47 (1H, d, *J*=6.0 Hz), 3.07 (1H, s), 3.18 (1H, d, *J*=3.4 Hz), 4.80—5.25 (1H, m), 5.15 (2H, s), 7.00—7.68 (10H, m), 7.28 (5H, s).

***anti*-3-Benzyloxyimino-1,3-diphenyl-1-propanol (*anti*-2f)**: IR (neat) 3430, 1620 cm^{-1}. ^{1}H NMR δ=2.75 (2H, d, *J*=6.4 Hz), 3.32—3.50 (1H, m), 4.72—5.07 (1H, m), 4.98 (2H, s), 7.12 (5H, s), 7.15 (5H, s), 7.20 (5H, s).

Stereoselective Reduction of a Mixture of the *O*-Benzyl Oximes *syn*-2a and *anti*-2a. To a THF (135 mL) solution of LAH (30 mmol) and sodium methoxide (1.08 g, 20 mmol) was added a 52:48 mixture of *syn*-**2a** and *anti*-**2a** (total 583 mg, 2 mmol) in THF (6 mL) at −78 °C under an argon atmosphere, and stirred for 6 h at −78 °C. After the complete consumption of *anti*-**2a** was indicated by TLC analysis, the reaction mixture was gradually warmed to 0 °C during 6 h and stirred for 18 h at 0 °C. The mixture was quenched with sat. aqueous sodium sulfate (8.8 mL) and the resulting precipitate was filtered off. The condensed filtrate was purified by preparative TLC on aluminum oxide (CH_2Cl_2: methanol=20:1, v/v) to give *syn*-7-amino-5-undecanol (**4a**) and the *anti*-isomer **5a** (total 343 mg, 92%) in the ratio of 96:4, respectively.

***syn*-7-Amino-5-undecanol (4a)**: IR (neat) 3370, 3300 cm^{-1}. ^{1}H NMR δ=0.60—1.75 (20H, m), 2.38—3.03 (1H, m), 2.93 (3H, br s), 3.47—3.97 (1H, m). ^{13}C NMR δ=73.00 (>CHOH).

***anti*-7-Amino-5-undecanol (5a)**: IR (neat) 3370, 3300 cm^{-1}. ^{1}H NMR δ=0.62—1.73 (20H, m), 2.57—3.22 (1H, m), 2.80 (3H, br s), 3.52—4.03 (1H, m). ^{13}C NMR δ=69.13 (>CHOH).

The stereoselective reduction of **2b—f** was carried out by the same procedure, and the elemental analyses were performed after the conversion to the corresponding cyclic urethanes **8** and **9**.

***syn*-6-Amino-2,8-dimethyl-4-nonanol (4b)**: IR (neat) 3370, 3290 cm^{-1}. ^{1}H NMR δ=0.85 (12H, d, *J*=6.0 Hz), 0.92—2.02 (8H, m), 2.52—3.02 (1H, m), 3.10 (3H, br s), 3.50—3.98 (1H, m). ^{13}C NMR δ=70.78 (>CHOH).

***anti*-6-Amino-2,8-dimethyl-4-nonanol (5b)**: IR (neat) 3370, 3290 cm^{-1}. ^{1}H NMR δ=0.83 (12H, d, *J*=6.2 Hz), 0.92—2.02 (8H, m), 2.85—3.48 (1H, m), 3.10 (3H, br s), 3.48—4.12 (1H, m). ^{13}C NMR δ=66.01 (>CHOH).

***syn*-5-Amino-1,7-diphenyl-3-heptanol (4c)**: IR (neat) 3370, 3290 cm^{-1}. ^{1}H NMR δ=1.38—2.00 (6H, m), 2.45—3.38 (5H, m), 3.05 (3H, br s), 3.53—4.02 (1H, m), 7.20 (10H, s). ^{13}C NMR δ=72.06 (>CHOH).

***anti*-5-Amino-1,7-diphenyl-3-heptanol (5c)**: IR (neat) 3370, 3300 cm^{-1}. ^{1}H NMR δ=1.37—1.92 (6H, m), 2.33—2.85 (4H, m), 2.50 (3H, br s), 2.82—3.35 (1H, m), 3.57—4.10 (1H, m), 7.12 (10H, s). ^{13}C NMR δ=68.67 (>CHOH).

***syn*-5-Amino-1-phenyl-3-hexanol (4d) and the *anti*-Isomer 5d**: IR (neat) 3370, 3290 cm^{-1}. ^{1}H NMR δ=1.03 (3H, d, *J*=6.0 Hz), 1.17—1.83 (4H, m), 2.43—3.18 (3H, m), 3.05 (3H, br s), 3.43—3.95 (1H, m) 7.08 (5H, s). ^{13}C NMR δ=67.93 (>CHOH, *anti*), 71.29 (>CHOH, *syn*).

The amino alcohol **4d** and **5d** could not be separated by TLC on aluminum oxide. The ratio was determined by the transformation to the corresponding acetates.

General Procedure for Acetylation of Amino Alcohols. To a CH_2Cl_2 (5 mL) solution of a mixture of *syn*- and *anti*-amino alcohols (ca. 100 mg) were added acetic anhydride (0.2 mL), pyridine (0.5 mL) and a catalytic amount of 4-(dimethylamino)pyridine under an argon atmosphere, and the resulting mixture was stirred at room temperature overnight. After evaporation of the excess acetic anhydride, pyridine and CH_2Cl_2 in vacuo, the residue was purified by preparative TLC on silica gel to afford the corresponding acetates.

***syn*-5-Acetamido-3-acetoxy-1-phenylhexane**: IR (neat) 3300, 1735, 1645 cm^{-1}. ^{1}H NMR δ=1.03 (3H, d, *J*=6.7 Hz), 1.42—2.12 (4H, m), 1.80 (3H, s), 1.92 (3H, s), 2.30—2.73 (2H, m), 3.50—4.27 (1H, m), 4.53—5.00 (1H, m), 5.80—6.27 (1H, m), 7.08 (5H, s).

***anti*-5-Acetamido-3-acetoxy-1-phenylhexane**: IR (neat) 3290, 1735, 1640 cm^{-1}. ^{1}H NMR δ=1.05 (3H, d, *J*=6.8 Hz), 1.45—2.22 (4H, m), 1.88 (3H, s), 1.94 (3H, s), 2.32—2.77 (2H, m), 3.63—4.17 (1H, m), 4.57—5.12 (1H, m), 5.17—5.65 (1H, m), 7.07 (5H, s).

***syn*-3-Amino-1-phenyl-1-butanol (4e) and the *anti*-Isomer 5e**: IR, ^{1}H NMR, and ^{13}C NMR spectra were identical with

those of lit.[9] IR (neat) 3360, 3280 cm^{-1}. ^{1}H NMR δ=1.13 (3H, d, J=7.2 Hz), 1.50—1.78 (2H, m), 2.67—3.53 (1H, m), 3.17 (3H, br s), 4.91 (1H, dd, J=6.0, 9.6 Hz). ^{13}C NMR δ=71.74 (>CHOH, *anti*), 74.96 (>CHOH, *syn*). The isomer ratio was determined by the conversion to the acetates.

***syn*-3-Acetamido-1-acetoxy-1-phenylbutane**: IR (neat) 3300, 1720, 1645 cm^{-1}. ^{1}H NMR δ=1.08 (3H, d, J=6.6 Hz), 1.58—2.25 (2H, m), 1.85 (3H, s), 2.00 (3H, s), 3.52—3.98 (1H, m), 5.40—5.98 (1H, m), 5.72 (1H, t, J=7.0 Hz), 7.30 (5H, s).

***anti*-3-Acetamido-1-acetoxy-1-phenylbutane**: IR (neat) 3300, 1715, 1640 cm^{-1}. ^{1}H NMR δ=1.08 (3H, d, J=6.8 Hz), 1.70—2.40 (2H, m), 1.82 (3H, s), 2.00 (3H, s), 3.67—4.48 (1H, m), 5.43—5.75 (1H, m), 5.68 (1H, dd, J=8.4, 9.0 Hz), 7.22 (5H, s).

***syn*-3-Amino-1,3-diphenyl-1-propanol (4f) and the *anti*-Isomer 5f**: IR, ^{1}H NMR and ^{13}C NMR spectra were well agreed with those of lit.[9] IR (KBr) 3360, 3280 cm^{-1}. ^{1}H NMR δ=1.65—2.15 (2H, m), 3.12 (3H, br s), 3.82—4.17 (1H, m), 4.62—5.00 (1H, m), 7.12 (5H, s), 7.16 (5H, s). ^{13}C NMR δ=71.78 (>CHOH, *anti*), 74.95 (>CHOH, *syn*). The ratio of *syn* to *anti* was also determined by the transformation to the acetates.

***syn*-3-Acetamido-1-acetoxy-1,3-diphenylpropane**: IR (neat) 3290, 1735, 1645 cm^{-1}. ^{1}H NMR δ=1.62—2.72 (2H, m), 1.80 (3H, s), 1.90 (3H, s), 4.63—5.15 (1H, m), 5.48 (1H, t, J=6.8 Hz), 6.13—6.67 (1H, m), 7.12 (5H, s), 7.17 (5H, s).

***anti*-3-Acetamido-1-acetoxy-1,3-diphenylpropane**: IR (neat) 3320, 1735, 1650 cm^{-1}. ^{1}H NMR δ=1.82 (3H, s), 1.90 (3H, s), 2.03—2.47 (2H, m), 4.73—4.92 (1H, m), 5.55—5.97 (1H, m), 5.62 (1H, dd, J=6.0, 8.4 Hz), 7.17 (10H, s).

Transformation of 4a to *cis*-Cyclic Urethane 8a. To an ether (6 mL) solution of *syn*-amino alcohol **4a** (113 mg, 0.69 mmol) and triethylamine (96 mg, 0.95 mmol) was added dropwise a solution of methyl chloroformate (68 mg, 0.72 mmol) in ether (3 mL) under an argon atmosphere and then stirred for 90 min at room temperature. To the mixture was added ice and the resulting solution was extracted with CH_2Cl_2. The separated organic layer was dried over Na_2SO_4 and condensed under reduced pressure. Purification by preparative TLC on silica gel (hexane: ethyl acetate=1:1, v/v) gave *syn*-7-methoxycarboxylamino-5-undecanol **6a** (113 mg, 76%). Next, a benzene (3 mL) solution of **6a** was added to a suspension of sodium hydride (55% dispersion in mineral oil) (23 mg, 0.52 mmol) in benzene (3 mL) under an argon atmosphere, and the mixture was stirred at room temperature for 3 h. Sat. aqueous NH_4Cl was added and the mixture was extracted with CH_2Cl_2. After being dried over Na_2SO_4, the CH_2Cl_2 solution was condensed in vacuo. The residue was purified by preparative TLC on silica gel (hexane: ethyl acetate=1:1, v/v) to give the cyclic urethane **8a** (90 mg, 70% from **4a**).

***cis*-4,6-Dibutyltetrahydro-2*H*-1,3-oxazin-2-one (8a)**: Mp 73.5—74.5 °C (H_2O-methanol). IR (KBr) 3250, 3130, 1680 cm^{-1}. ^{1}H NMR δ=0.57—2.12 (20H, m), 3.02—3.62 (1H, m), 3.85—4.03 (1H, m), 6.06—6.93 (1H, m). Found: C, 67.85; H, 10.87; N, 6.58%. Calcd for $C_{12}H_{23}NO_2$: C, 67.56; H, 10.87; N, 6.57%.

Transformation of 5a to *trans*-Cyclic Urethane 9a. *anti*-Urethane **7a** was obtained by the same procedure for **6a** (quant.). To a suspension of sodium hydride (55% dispersion in mineral oil) (4 mg, 0.08 mmol) in benzene (3 mL) was added a benzene (3 mL) solution of **6a** (18 mg, 0.07 mmol) under an argon atmosphere, and the mixture was refluxed for 30 min. After cooling to room temperature, sat. aqueous NH_4Cl was added and the solution was extracted with CH_2Cl_2. The extracts were dried over Na_2SO_4 and condensed in vacuo. Purification by preparative TLC on silica gel (hexane:ethyl acetate=1:1, v/v) afforded the cyclic urethane **9a** (12 mg, 72% from **5a**).

***trans*-4,6-Dibutyltetrahydro-2*H*-1,3-oxazin-2-one (9a)**: IR (neat) 3260, 3130, 1710 cm^{-1}. ^{1}H NMR δ=0.62—2.27 (20H, m), 3.08—3.60 (1H, m), 3.97—4.47 (1H, m), 5.83—6.17 (1H, m). Found: m/z 213.1689. Calcd for $C_{12}H_{23}NO_2$: M, 213.1727.

Transformation of other amino alcohols **4b—e**, **5b—e** to cyclic urethanes was carried by the same method described above. By the treatment with methyl chloroformate and triethylamine, a mixture of *syn*- and *anti*-β-amino alcohols **4d** and **5d**, **4e**, and **5e** were converted *syn*- and *anti*-urethane **6d** and **7d**, **6e** and **7e**, respectively, which were separated by preparative TLC.

***cis*-4,6-Bis(2-methylpropyl)tetrahydro-2*H*-1,3-oxazin-2-one (8b)**: Mp 94.5—95.0 °C. IR (KBr) 3260, 3130, 1680 cm^{-1}. ^{1}H NMR δ=0.93 (12H, d, J=6.2 Hz), 1.05—2.10 (8H, m), 3.28—3.68 (1H, m), 4.07—4.12 (1H, m), 6.40—6.80 (1H, m). Found: m/z 213.1713. Calcd for $C_{12}H_{23}NO_2$: M, 213.1727.

***trans*-4,6-Bis(2-methylpropyl)tetrahydro-2*H*-1,3-oxazin-2-one (9b)**: IR (neat) 3260, 3135, 1705 cm^{-1}. ^{1}H NMR δ=0.93 (12H, d, J=6.2 Hz), 1.07—2.10 (8H, m), 3.33—3.72 (1H, m), 4.15—4.57 (1H, m), 5.95—6.28 (1H, m). Found: m/z 213.1695. Calcd for $C_{12}H_{23}NO_2$: M, 213.1727.

***cis*-4,6-Diphenethyltetrahydro-2*H*-1,3-oxazin-2-one (8c)**: Mp 112.0—113.0 °C (ether-ethyl acetate). IR (KBr) 3250, 3130, 1705 cm^{-1}. ^{1}H NMR δ=1.65—2.27 (6H, m), 2.50—3.02 (4H, m), 3.18—3.60 (1H, m), 3.93—4.33 (1H, m), 6.85 (1H, br s), 7.22 (10H, s). Found: C,77.68; H, 7.51; N, 4.52%. Calcd for $C_{20}H_{23}NO_2$: C, 77.64; H, 7.49; N, 4.53%.

***trans*-4,6-Diphenethyltetrahydro-2*H*-1,3-oxazin-2-one (9c)**: IR (neat) 3250, 3130, 1705 cm^{-1}. ^{1}H NMR δ=1.55—2.25 (6H, m), 2.48—3.10 (4H, m), 3.28—3.70 (1H, m), 4.10—4.53 (1H, m), 6.48—6.77 (1H, m), 7.19 (5H, s), 7.22 (5H, s). Found: m/z 309.1752. Calcd for $C_{20}H_{23}NO_2$: M, 309.1729.

***cis*-4-Methyl-6-phenethyltetrahydro-2*H*-1,3-oxazin-2-one (8d)**: Mp 121.5—122.5 °C (hexane-toluene). IR (KBr) 3240, 3125, 1700 cm^{-1}. ^{1}H NMR δ=1.22 (3H, d, J=6.0 Hz), 1.28—1.63 (1H, m), 1.73—2.18 (3H, m), 2.67—3.02 (2H, m), 3.28—3.77 (1H, m), 4.02—4.38 (1H, m), 6.97—7.43 (1H, m), 7.23 (5H, s). Found: C, 71.24; H, 7.54; N, 6.29%. Calcd for $C_{13}H_{17}NO_2$: C, 71.20; H, 7.82; N, 6.39%.

***trans*-4-Methyl-6-phenethyltetrahydro-2*H*-1,3-oxazin-2-one (9d)**: IR (KBr) 3250, 3140, 1710 cm^{-1}. ^{1}H NMR δ=1.20 (3H, d, J=6.6 Hz), 1.50—2.32 (4H, m), 2.65—2.92 (2H, m), 3.42—3.82 (1H, m), 4.08—4.48 (1H, m), 6.37—6.57 (1H, m), 7.20 (5H, s). Found: m/z 219.1217. Calcd for $C_{13}H_{17}NO_2$: M, 219.1257.

***cis*-4-Methyl-6-phenyltetrahydro-2*H*-1,3-oxazin-2-one (8e)**: Mp 154.0—155.0 °C (benzene), lit, 152—153 °C.[9] IR (KBr) 3240, 3120, 1690 cm^{-1}. ^{1}H NMR δ=1.23 (3H, d, J=6.3 Hz), 1.57—1.92 (1H, m), 1.87—2.33 (1H, m), 3.52—3.93 (1H, m), 5.24 (1H, dd, J=2.1, 11.7 Hz), 6.65 (1H, br s), 7.34 (5H, s).

***trans*-4-Methyl-6-phenyltetrahydro-2*H*-1,3-oxazin-2-one (9e)**: Mp 101.0—102.5 °C. IR (KBr) 3240, 3130, 1725 cm^{-1}. ^{1}H NMR δ=1.27 (3H, d, J=6.3 Hz), 1.73—2.37 (2H, m), 3.32—3.67 (1H, m), 5.46 (1H, dd, J=4.2, 6.8 Hz), 6.61 (1H, br s), 7.33 (5H, s). Found: m/z 191.0940. Calcd for $C_{11}H_{13}NO_2$: M, 191.0945.

Total Synthesis of Lasubine II. **2-(2,2-Dimethoxy-**

ethyl)-2-(3,4-dimethoxyphenyl)-1,3-dithiane (12). To a solution of 2-(3,4-dimethoxyphenyl)-1,3-dithiane (**11**)[18] (2.00 g, 7.80 mmol) in THF (40 mL) was added *n*-BuLi (7.15 mmol) in hexane (6.3 mL) at −42 °C under an argon atmosphere was stirred for 2.5 h at −15 °C.[23] At −78 °C a THF (6 mL) solution of 2-bromo-1,1-dimethyoxyethane (1.17 g, 6.50 mmol) was added, and then gradually warmed to 0 °C. After stirred for 24 h at 0 °C, the reaction mixture was quenched with sat. aqueous NH_4Cl and the organic layer was extracted with ether. The separated organic layer was dried over Na_2SO_4 and was condensed under reduced pressure. Purification by column chromatography (hexane:ethyl acetate=5:1, v/v) gave the dimethyl acetal **12** (1.88 g, 84%). ^1H NMR δ=1.69—2.09 (2H, m), 2.12—2.40 (2H, m), 2.50—2.80 (4H, m), 3.13 (6H, s), 3.77 (6H, s), 4.08—4.39 (1H, m), 6.50—6.92 (1H, m), 7.08—7.50 (2H, m).

2-Formylmethyl-2-(3,4-dimethoxyphenyl)-1,3-dithiane (13). To a THF (80 mL) solution of **12** was slowly added concd HCl (20 mL). In a few minutes, the solution was turned to yellow and hydrolysis was completed. The reaction mixture was extracted with ether and the organic layer was washed with 4% aqueous $NaHCO_3$ and brine, dried over Na_2SO_4, and concentrated in vacuo to leave an oily residue. The residue was chromatographed on silica gel with hexane–ethyl acetate (8:1, v/v) as an eluting solvent to yield the aldehyde **13** (1.39 g, 76%). IR (neat) 1720 cm^{-1}. ^1H NMR δ=1.65—2.04 (2H, m), 2.54—2.83 (4H, m), 2.89 (2H, d, *J*=3.6 Hz), 3.76 (6H, s), 6.58—6.80 (1H, m), 7.09—7.40 (2H, m), 9.52 (1H, d, *J*=3.6 Hz). Found: *m/z* 298.0678. Calcd for $C_{14}H_{18}O_3S_2$: M, 298.0695.

2-(2-Hydroxy-4-oxo-7-octenyl)-2-(3,4-dimethoxyphenyl)-1,3-dithiane (14). To a solution of lithium diisopropylamide (5.7 mmol) in THF (50 mL) was added a solution of 5-hexen-2-one (0.50 g, 5.2 mmol) in THF (5 mL) at −78 °C under an argon atmosphere, and the mixture was stirred for 1 min at −78 °C. A THF (5 mL) solution of the aldehyde **13** (1.39 g, 4.5 mmol) was added. Immediately, the reaction mixture was quenched with sat. aqueous NH_4Cl and was extracted with ether. The combined ether extracts were washed with brine, dried over Na_2SO_4, and condensed under reduced pressure. Purification by column chromatography (hexane : ethyl acetate=3:1—1:1, v/v) gave the β-hydroxy ketone **14** (1.45 g, 80%). IR (neat) 3530, 1710, 1640 cm^{-1}. ^1H NMR δ=1.48—2.83 (15H, m), 3.77 (6H, s), 3.90—4.37 (1H, m), 4.58—5.05 (2H, m), 5.23—5.94 (1H, m), 6.56—6.83 (1H, m), 7.10—7.44 (2H, m). Found: *m/z* 396.1375. Calcd for $C_{20}H_{28}O_4S_2$: M, 396.1427.

***O*-Benzyl Oxime of β-Hydroxy Ketone 14.** A solution of β-hydroxy ketone **14** (1.31 g, 3.3 mmol) and *O*-benzylhydroxylamine hydrochloride (0.63 g, 3.9 mmol) in pyridine (0.6 mL) and methanol (45 mL) was refluxed for 5 h. After removal of the solvents in vacuo, water was added to the residue and was extracted with CH_2Cl_2. The separated organic layer was dried over Na_2SO_4 and was condensed under reduced pressure. Purification by column chromatography on silica gel (hexane: ethyl acetate=2:1, v/v) gave the ca. 1:1 mixture of *syn*- and *anti*-*O*-benzyl oxime **15** (1.66 g, quant.). IR (neat) 3530, 1640 cm^{-1}. ^1H NMR δ=1.57—2.80 (15H, m), 3.70 (6H, s), 3.85—4.25 (1H, m), 4.42—5.00 (2H, m), 4.86 (2H, s), 5.15—5.92 (1H, m), 6.50—6.78 (1H, m), 7.07 (5H, s), 7.10—7.37 (2H, m). Found: *m/z* 501.1961. Calcd for $C_{27}H_{35}NO_4S_2$: M, 501.2006.

***syn*-β-Amino Alcohol 16.** To a suspension of potassium methoxide (5.21 g, 74 mmol) in THF (400 mL) was added a THF (82 mL) solution of LAH (111 mmol) under an argon atmosphere and the mixture was stirred for 15 min at −78 °C. To that solution was added the *O*-benzyl oxime **15** (3.71 g, 7.4 mmol) in THF (100 mL) dropwise and the reaction mixture stirred overnight at −78 °C, then gradually warmed to −15 °C for 5 h, and stirred for 12 h at −15 °C. The reaction was carefully quenched with sat. aqueous Na_2SO_4 (32 mL) and the resulting precipitate was filtered off. The condensed filtrate was purified by Chromatron on aluminum oxide (CH_2Cl_2: methanol=25:1, v/v) to give *syn*-β-amino alcohol **16** (2.94 g, 65%). IR (neat) 3380, 3300, 1640 cm^{-1}. ^1H NMR δ=0.77—1.42 (4H, m), 1.48—2.25 (6H, m), 2.38—2.90 (5H, m), 2.72 (3H, br s), 3.58—4.09 (1H, m), 3.75 (6H, s), 4.57—5.07 (2H, m), 5.29—6.00 (1H, m), 6.60—6.83 (1H, m), 7.12—7.50 (2H, m). ^{13}C NMR δ=24.84, 27.57, 27.74, 29.90, 39.14, 43.53, 51.49, 53.25, 55.80, 55.96, 57.50, 69.15 (>CHOH), 110.81, 112.00, 114.82, 121.27, 134.35, 137.98, 147.87, 148.84. Found: *m/z* 397.1708. Calcd for $C_{20}H_{31}NO_3S_2$: M, 397.1744.

Protection of Amino Alcohol 16 with *t*-Butoxycarbonyl Group. To a CH_2Cl_2 (20 mL) solution of amino alcohol **16** (1.43 g, 3.6 mmol) was added *O*-*t*-butyl *S*-(4,6-dimethyl-2-pyrimidinyl) thiocarbonate (1.74 g, 7.2 mmol) and stirred overnight.[25] The reaction mixture was quenched with water and extracted with CH_2Cl_2. The combined extracts were washed with brine and dried over Na_2SO_4. After the solvent was removed in vacuo, the residue was chromatographed on silica gel by using hexane–ethyl acetate (1:1, v/v) to give *t*-butoxycarbonylamino alcohol **17** (1.38 g, 77%). IR (neat) 3370, 1700, 1640 cm^{-1}. ^1H NMR δ=1.12—1.73 (4H, m), 1.42 (9H, s), 1.73—2.95 (11H, m), 3.18—4.13 (2H, m), 3.83 (6H, s), 4.40—5.13 (3H, m), 5.37—6.10 (1H, m), 6.68—6.95 (1H, m), 7.28—7.52 (2H, m). Found: *m/z* 497.2244. Calcd for $C_{25}H_{39}NO_5S_2$: M, 497.2269.

Hydroxy Ketone 18. To an acetonitrile (15 mL)–water (1.5 mL) solution of *N*-chlorosuccinimide (178 mg, 1.34 mmol) and silver nitrate (225 mg, 1.50 mmol) was added an acetonitrile (5 mL) solution of **17** (166 mg, 0.33 mmol) at −42 °C and stirred for 1 h at that temperature.[26] To the mixtrure was added sat. aqueous Na_2SO_3 (1 mL) and stirred for 1 min. After addition of sat. aqueous Na_2CO_3 (1 mL), the reaction mixture was stirred for 1 min and brine (1 mL) was added. The resulting precipitate was filtered off and the filtrate was extracted with ether. The combined extracts were washed with brine and dried over $MgSO_4$. Concentration in vacuo and purification by preparative layer chromatography on silica gel (hexane: ethyl acetate=1:1, v/v) gave the hydroxy ketone **18** (99 mg, 73%). IR (neat) 3370, 1690 cm^{-1}. ^1H NMR δ=1.02—2.29 (6H, m), 1.30 (9H, s), 2.85—3.13 (2H, m), 3.57 (1H, br s), 3.77—4.23 (2H, m), 3.76 (6H, s), 4.38—5.04 (3H, m), 5.29—6.00 (1H, m), 6.68 (1H, d, *J*=8.6 Hz), 7.08—7.52 (2H, m). Found: *m/z* 407.2216. Calcd for $C_{22}H_{33}NO_6$: M, 407.2306.

(2S*,4S*,6S*)-6-(3-Butenyl)-2-(3,4-dimethoxyphenyl)-4-piperidinol (20). To a 1:1 mixture of trifluoroacetic acid and CH_2Cl_2 (1 mL) was added the hydroxy ketone **18** (104 mg, 0.23 mmol) at 0 °C. After being stirred for 10 min, the reaction mixture was quenched with 28% aqueous ammonia and extracted with CH_2Cl_2. The extracts were washed with water then brine and immediately condensed in vacuo under 20 °C. The residue, dissolved in THF (5 mL), was added to the suspension of sodium methoxide (175 mg, 3.2 mmol) and LAH (THF soln 1.2 mL, 1.6 mmol) in THF (5 mL) at −78 °C under an argon atmosphere.

The reaction mixture was stirred at −78°C for 1 h, at −42°C for 1 h, at −18°C for 1 h, and at 0°C overnight.[21] The reaction mixture was quenched with sat. aqueous Na_2SO_4 (0.5 mL) and the resulting precipitate was filtered off. After dried over Na_2SO_4, the filtrate was condensed under reduced pressure and the oily residue was purified by preparative TLC on aluminum oxide (CH_2Cl_2: methanol=40:1 v/v) to furnish *cis*-2,6-disubstituted piperidine **20** (40 mg, 60%). IR (neat) 3400, 1640 cm^{-1}. ^1H NMR δ=1.05—1.90 (6H, m), 1.79 (2H, br s), 1.90—2.34 (2H, m), 2.91—3.42 (1H, m), 3.86 (3H, s), 3.88 (3H, s), 4.01 (1H, dd, J=3.9, 10.2 Hz), 4.18—4.38 (1H, m), 4.75—5.13 (2H, m), 5.52—6.10 (1H, m), 6.71—7.00 (3H, m). ^{13}C NMR δ=30.12, 36.03, 39.03, 41.52, 50.98, 55.55, 55.99, 65.58, 11.57, 111.49, 114.66, 118.91, 137.76, 138.41, 148.25, 149.08. Found: m/z 291.1784. Calcd for $C_{17}H_{25}NO_3$: M, 291.1832.

(2S*,4S*,6S*)-6-(4-Hydroxybutyl)-2-(3,4-dimethoxyphenyl)-4-piperidinol (21). To a THF (0.7 mL) solution of B_2H_6 (1.28 mmol) was added 2-methyl-2-butene (180 mg, 2.56 mmol) in THF (5 mL) at −15°C and stirred for 2 h at 0°C under an argon atmosphere.[27] To the mixture was added a THF (6 mL) solution of **20** (93 mg, 0.32 mmol) and stirred for 45 min at that temperature. To the solution were added a few drops of water, then 3 M aqueous NaOH (1 mL (1 M=1 mol dm^{-3})), and 30% hydrogen peroxide (2 mL). After stirred for 1 h the mixture was extracted with chloroform, then washed with 1% aqueous Na_2CO_3, sat. aqueous Na_2SO_3, and brine. The organic layer was dried over Na_2SO_4 and condensed in vacuo. The residue was purified by preparative TLC on aluminum oxide (CH_2Cl_2: methanol=20:1, v/v) to give the diol **21** (86 mg, 87%). IR (neat) 3350 cm^{-1}. ^1H NMR δ=1.03—1.90 (10H, m), 2.18 (3H, br s), 2.68—3.20 (1H, m), 3.26—3.60 (2H, m), 3.70 (3H, s), 3.73 (3H, s), 3.80—4.28 (2H, m), 6.64—6.85 (3H, m). Found: m/z 309.1913. Calcd for $C_{17}H_{27}NO_4$: M, 309.1938.

(±)-Lasubine II (22). To a solution of the diol **21** (86 mg, 0.28 mmol) in pyridine (2 mL) was added *p*-toluenesulfonyl chloride (167 mg, 0.88 mmol) at −20°C under an argon atmosphere and stirred for 1.5 h at −20°C. After stirred overnight at 0°C, the reaction was quenched with ice and extracted with ethyl acetate. The extracts were washed 0.1 M aqueous NaOH, dried over Na_2SO_4, and condensed in vacuo. The residue was purified by preparative TLC on aluminum oxide (CH_2Cl_2 : methanol=20:1) to afford (±)-lasubine II (57 mg, 70%). IR ($CHCl_3$) 3610, 2930 cm^{-1}. ^1H NMR δ=1.26—1.91 (12H, m), 2.39—2.42 (1H, m), 2.69 (1H, d, J=11.60 Hz), 3.31 (1H, dd, J=3.36, 11.60 Hz), 3.86 (3H, s), 3.88 (3H, s), 4.00—4.21 (1H, m), 6.78—6.91 (3H, m). MS, m/z (relative intensity) 291(M^+, 472), 164 (332), 154 (434). Found: m/z 291.1878. Calcd for $C_{17}H_{25}NO_3$: M, 291.1833. ^1H NMR (400 MHz) and IR spectra of the synthetic (±)-lasubine II (**22**) was identical with those of the natural lasubine II. Mass spectrum also completely agreed with those values reported by C. Kibayashi.[17]

The authors are grateful to Professor Teruaki Mukaiyama for valuable discussion during this work. We are indebted to Professor Kaoru Fuji for his kind gift of ^1H NMR (400 MHz) and IR spectra of natural lasubine I and II, and also thank Dr. Tatsushi Murae for performing high-resolution mass spectra.

References

1) a) P. A. Bartlett, *Tetrahedron*, **36**, 2 (1980); b) M. T. Reetz, *Angew. Chem., Int. Ed. Engl.*, **23**, 556 (1984); c) "Asymmetric Synthesis," ed by J. D. Morrison, Academic Press, Inc., New York (1984), Vol. 3.

2) P. A. Bartlett and K. K. Jernstedt, *J. Am. Chem. Soc.*, **99**, 4829 (1977); T. Fukuyama, B. Vranesic, D. P. Negri, and Y. Kishi, *Tetrahedron Lett.*, **1978**, 2741; D. A. Evans, J. Bartroli, and T. Godel, ibid., **23**, 4577 (1982); M. Hirama and M. Uei, ibid., **23**, 5307 (1982).

3) a) Y. Matsumura, J. Fujiwara, K. Maruoka, and H. Yamamoto, *J. Am. Chem. Soc.*, **105**, 6312 (1983); b) Y. F. Wang, T. Izawa, S. Kobayashi, and M. Ohno, ibid., **104**, 6465 (1982); c) M. Hirama, T. Shigemoto, Y. Yamazaki, and S. Ito, ibid., **107**, 1797 (1985); d) Y. Yamamoto, T. Komatsu, and K. Maruyama, *J. Chem. Soc., Chem. Commun.*, **1985**, 814.

4) a) K. Narasaka and Y. Ukaji, *Chem. Lett.*, **1984**, 147; b) K. Narasaka, S. Yamazaki, and Y. Ukaji, ibid., **1984**, 2065.

5) K. Narasaka and F. C. Pai, *Chem. Lett.*, **1980**, 1415; *Tetrahedron*, **40**, 2233 (1984).

6) H. Feuer and D. M. Braunstein, *J. Org. Chem.*, **34**, 1817 (1969).

7) In this report, the isomer *syn*-**2** whose benzyloxyl group is *syn* to the hydroxyl group is presented as the *syn*-*O*-benzyl oxime, and the other isomer *anti*-**2** is called the *anti*-*O*-benzyl oxime.

8) The relative stereochemistry of β-amino alcohols is presented according to the Masamune's nomenclature using *syn* and *anti* terms; S. Masamune, S. A. Ali, D. L. Snitman, and D. S. Garvey, *Angew. Chem., Int. Ed. Engl.*, **19**, 557 (1980).

9) V. Jäger and V. Buss, *Justus Leibigs Ann. Chem.*, **1980**, 101.

10) J. W. Akitt and R. H. Duncan, *J. Magn. Reson.*, **15**, 162 (1974).

11) T. Mukaiyama, "Organic Reactions," ed by W. G. Dauben, John Wiley & Sons, Inc., New York (1982), Vol. 28, Chap. 3.

12) A. P. Kozikowski and Y. Y. Chen, *J. Org. Chem.*, **46**, 5248 (1981).

13) F. M. Hauser, S. R. E. Ellenberger, J. C. Clardy, and L. S. Bass, *J. Am. Chem. Soc.*, **106**, 2458 (1984).

14) For the isolation of lasubine II, see: K. Fuji, T. Yamada, E. Fujita, and H. Murata, *Chem. Pharm. Bull.*, **26**, 2515 (1978).

15) Preliminary work of the synthesis of (±)-lasubine II has been briefly reported as a communication: K. Narasaka, S. Yamazaki, and Y. Ukaji, *Chem. Lett.*, **1985**, 1177.

16) W. M. Golebiewski and J. T. Wrobel, "The Alkaloids," ed by R. G. A. Rodrigo, Academic Press, Inc., New York (1981), Vol. 18, Chap. 4.

17) H. Iida, M. Tanaka, and C. Kibayashi, *J. Org. Chem.*, **49**, 1909 (1984) and the references cited therein.

18) H. Raumz, *Arzneim.-Forsch.*, **28**, 2048 (1978).

19) The *anti*-β-amino alcohol was not detectable by ^{13}C NMR spectrum.

20) The *trans*-2,6-disubstituted piperidine was not detectable by ^{13}C NMR spectrum.

21) K. Maruoka, T. Miyazaki, M, Ando, Y. Matsumura, S. Sakane, K. Hattori, and H. Yamamoto, *J. Am. Chem. Soc.*,

105, 2831 (1983).

22) Attempt for the preparation of *trans*-2,6-disubsituted piperidine by the reduction of **19** using LAH and trimethylaluminum,[21] however, resulted in affording only *cis*-2,6-disubstituted piperidine **20**.

23) The stereochemical assignment of *syn*- and *anti*-*O*-benzyl oximes was due to the ^{1}H NMR spectra and the transformation to the isoxazolines. In ^{1}H NMR spectra, chemical shifts of methylene protones (-CH(OH)-C<u>H</u>$_2$-C=N-) of *syn*-*O*-benzyl oximes *syn*-**2** appears at lower fields than those of *anti*-**2**, see: G. J. Karabatsos and N. Hsi, *Tetrahedron*, **23**, 1079 (1967). The *syn*-isomers *syn*-**2** were transformed to the corresponding isoxazolines by treatment with methanesulfonyl chloride and triethylamine. However, the *anti*-isomers *anti*-**2** were not converted to isoxazolines.

24) D. Seebach and E. J. Corey, *J. Org. Chem.*, **40**, 231 (1975).

25) T. Nagasawa, K. Kuroiwa, K. Narita, and Y. Isowa, *Bull. Chem. Soc. Jpn.*, **46**, 1269 (1973).

26) E. J. Corey and B. W. Erickson, *J. Org. Chem.*, **36**, 3553 (1971).

27) H. C. Brown and A. W. Moerikofer, *J. Am. Chem. Soc.*, **83**, 3417 (1961).

Studies on β-Turn of Peptides. XII.[1] Synthetic Confirmation of Weak Activity of [D-Pro$^{5,5'}$]-Gramicidin S Predicted from β-Turn Preference of Its Partial Sequence

Kazuki SATO, Rika KATO, and Ukon NAGAI*
Mitsubishi-Kasei Institute of Life Sciences, 11 Minamiooya, Machida, Tokyo 194
(Received October 5, 1985)

[D-Pro$^{5,5'}$]-Gramicidin S was synthesized to confirm a prediction that D-D sequence at the corner position had low preference for β-turn. The analog showed much weaker activity than gramicidin S and also showed different CD spectra from those of gramicidin S. The results indicate that the analog can not take stable, gramicidin S-like, β-sheet conformation.

In the previous papers, we reported that the CD spectra of *N*-(2,4-dinitrophenyl)tetrapeptide *p*-nitroanilides reflected well the β-turn preference of the tetrapeptide sequences.[2-4] β-Turn preferences of the tetrapeptides related to the β-turn part sequences of gramicidin S (GS), *cyclo*(-Val$^{1,1'}$-Orn$^{2,2'}$-Leu$^{3,3'}$-D-Phe$^{4,4'}$-Pro$^{5,5'}$-)$_2$, [5] which was well known to take β-sheet conformation with two β-turns (Fig. 1),[6-8] had good correlation with antibiotic activities of the GS analogs having similar tetrapeptides sequences at their β-turn parts.[1,3] The GS analogs having D-D sequences at 4—5 and 4′—5′ positions were predicted not to take GS-like β-sheet conformation from the result that Dnp-Leu-D-Ala-D-Leu-Val-pNA showed much weaker CD bands than Dnp-Leu-D-Ala-Leu-Val-pNA did.[3] To confirm this prediction, we synthesized [D-Pro$^{5,5'}$]-GS which had D-Phe-D-Pro sequences at 4—5 and 4′—5′ positions.

Results and Discussion

Synthesis of [D-Pro$^{5,5'}$]-GS (8). [D-Pro$^{5,5'}$]-GS was synthesized according to a scheme shown in Fig. 2. In a cyclization reaction, a pentapeptide with D-Pro at the C-terminus was chosen as a precursor, because many GS analogs had been synthesized in satisfactory results by a similar strategy.[9,10] Boc-Val-Orn(Z)-Leu-D-Phe-D-Pro-OH (**4**) was prepared by azide coupling of Boc-Val-Orn(Z)-Leu-N_2H_3[11] and H-D-Phe-D-Pro-OH (**3**), and converted to its active ester (**5**). Cyclization of H-Val-Orn(Z)-Leu-D-Phe-D-Pro-OSu (**6**) derived from **5** by acid treatment was carried out in anhydrous pyridine at the final concentration of 3 mM (1 M=1 mol dm^{-3}). After usual work-up,[12] a mixture of the crude cyclized peptides was applied to a column of Sephadex LH-20 (Fig. 3). The product obtained from the major peak (peak A) was determined to be cyclic dimer by FAB-MS measurement (M$^+$, 1141) after hydrogenolysis. Peak-B fractions afforded cyclic trimer (M$^+$, 1711) after hydrogenolysis. It is interesting that cyclization of pentapeptide active ester af-

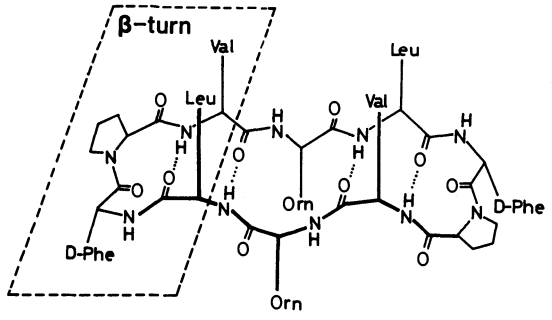

Fig. 1 β-Sheet conformation of gramicidin S.

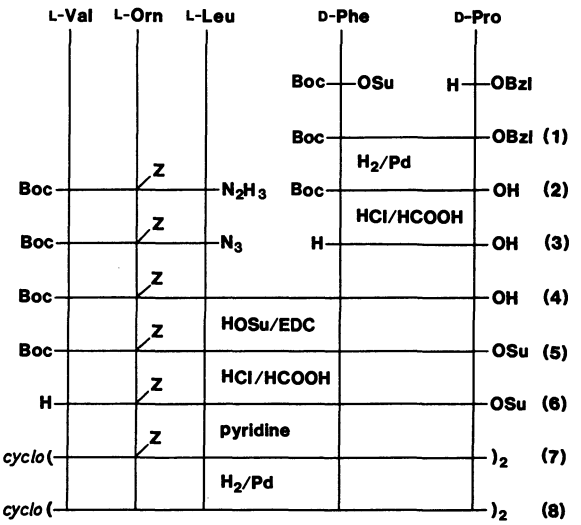

Fig. 2. Synthetic scheme of [D-Pro$^{5,5'}$]-GS (**8**).

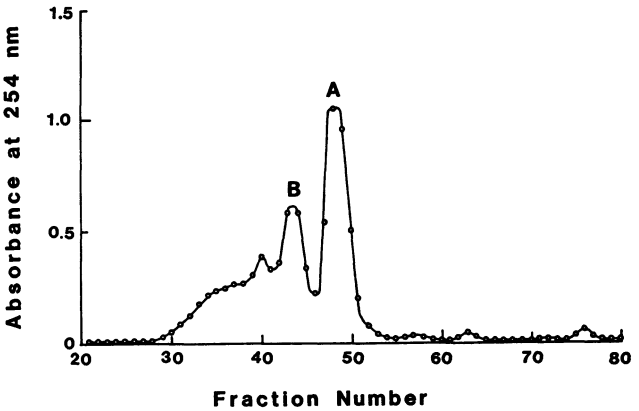

Fig. 3. Elution profile of crude cyclized peptides. For detail, see experimental section.

Table 1. Antibiotic Activity of GS and Its Analog (Minimum Inhibitory Concentration, μg/ml)

Strain	GS	[D-Pro$^{5,5'}$]-GS
Staphylococcus aureus MCI-1380	3.13	100
Bacillus subtilis marfurg 168	1.56	25
Escherichia coli C-600	>100	>100

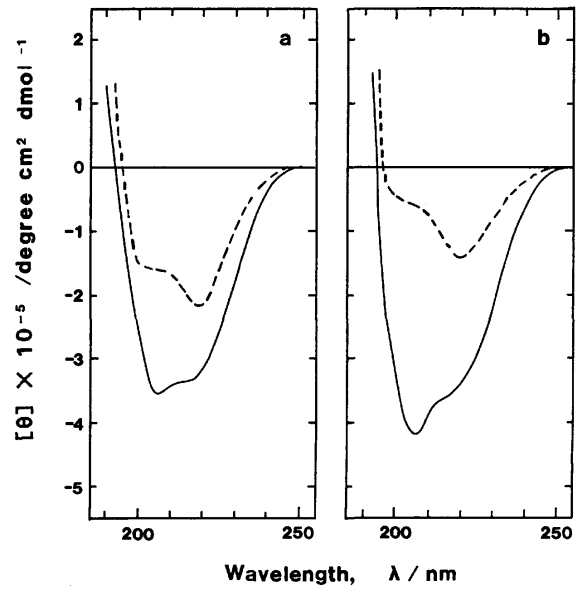

Fig. 4. CD spectra of GS and its analog measured at 25°C in (a) H_2O and in (b) MeOH solutions.
——: GS, ----: [D-Pro$^{5,5'}$]-GS.

forded much polymeric products and almost no cyclic monomer, since there are few papers which reported the absence of cyclic monomerization of pentapeptides.[10,13]. The results suggest that the sequence of [D-Pro$^{5,5'}$]-GS is unsuitable for compact, folded conformation.

Biological Activity. The antibiotic activity of the synthesized analog was compared with that of GS. The minimum concentration of the compound necessary for the complete inhibition of growth of several microorganisms was determined by a dilution method using a nutrient agar (Table 1). The analog showed much weaker activity than GS indicating that Pro at 5, 5′ position could not be replaced with D-Pro without affecting on its activity.

CD Spectra. In many GS analogs, good correlation was observed between their CD spectra and activities.[11,14] CD spectra of [D-Pro$^{5,5'}$]-GS and GS were measured in H_2O and in MeOH solutions (Fig. 4). The analog showed different CD patterns from those of GS in both solutions and also showed larger solvent dependence of CD intensities than GS did. These results suggested that the analog did not take stable,

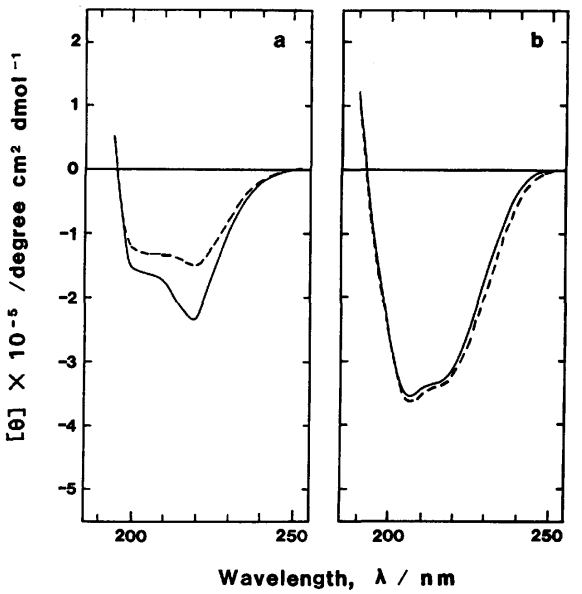

Fig. 5. Temperature dependence of CD spectra of (a) [D-Pro$^{5,5'}$]-GS and (b) GS in H_2O solution.
——: 10°C, ----: 85°C.

GS-like, β-sheet conformation. The large temperature dependence of CD spectra of the analog also suggested that the analog had flexible conformation (Fig. 5).

Structure-Activity Relationship. The decreased activity of the analog is considered to be caused by the conformational change as described above. And it is quite reasonable to consider that the conformational change is caused by the reluctance of D-Phe-D-Pro sequence to take stable, GS-like, β-turn conformation.

Present study proves that CD spectra of the chromophoric derivatives of tetrapeptides are useful for predicting the conformation and activity of bioactive peptides such as GS in which β-turn conformation plays an important role for its activity.

Experimental

All the melting points were uncorrected. Thin-layer chromatographies were carried out on Merck silica gel 60 F_{254} plates with the following solvent systems, the ratio in parentheses after the solvent system being indicated by vol: R_f^1, $CHCl_3$-MeOH (5:1); R_f^2, $CHCl_3$-MeOH-AcOH (95:5:1); R_f^3, *n*-BuOH-AcOH-pyridine-H_2O (4:1:1:2); R_f^4, *n*-BuOH-AcOH-H_2O (4:1:5, organic). Optical rotations were measured on a JASCO DIP-360 digital polarimeter. FAB-MS spectra were measured on a JEOL HX-100 mass spectrometer.

Boc-D-Phe-D-Pro-OBzl (1). To a chilled solution of H-D-Pro-OBzl·HCl (1.21 g, 5 mmol) in $CHCl_3$ (20 ml) were added TEA (0.7 ml, 5 mmol) and Boc-D-Phe-OSu (1.81 g, 5 mmol). After being stirred overnight at room temperature, the solution was evaporated under reduced pressure. The residue was dissolved in EtOAc and washed succesively with 10% citric acid, 4% $NaHCO_3$, and H_2O, and the solution was dried over anhydrous Na_2SO_4. After evaporation of the

solvent, the residue was crystallized by addition of ether and recrystallized from EtOAc-ether; yield, 1.76 g (78%); mp 104—108 °C; $[\alpha]_D^{24}$ 50.2° (*c* 0.7, MeOH); R_f^1=0.83, R_f^2=0.73, R_f^3=0.86, R_f^4=0.87.

Found: C, 68.97; H, 7.11; N, 6.37%. Calcd for $C_{26}H_{32}O_5N_2$: C, 69.01; H, 7.13; N, 6.19%.

Boc-D-Phe-D-Pro-OH (2). Compound **1** (769 mg, 1.7 mmol) dissolved in MeOH (20 ml) was hydrogenated in the presence of Pd-black (ca. 200 mg) for 5 h at room temperature. After filtration of catalyst, the filtrate was evaporated to leave an colorless oil which was used for the next reaction without further treatment; yield was quantitative; R_f^1=0.36, R_f^2=0.21, R_f^3=0.58, R_f^4=0.65.

H-D-Phe-D-Pro-OH·HCl (3·HCl). Compound **2** (616 mg, 1.7 mmol) was dissolved in 0.1 M hydrogen chloride in formic acid (26 ml). The solution was allowed to stand at room temperature for 30 min and evaporated. The desired product was collected by filtration with the aid of ether and used for the next reaction without further treatment; yield was quantitative; R_f^3=0.48, R_f^4=0.38.

Boc-Val-Orn(Z)-Leu-D-Phe-D-Pro-OH (4). To a solution of Boc-Val-Orn(Z)-Leu-N_2H_3[11] (541 mg, 0.91 mmol) in DMF (5 ml) were added 2 M hydrogen chloride in EtOAc (1.4 ml) and isopentyl nitrite (0.14 ml, 1.0 mmol) at −60 °C. After being left to stand at −20 °C for 10 min, the solution was cooled again to −60 °C and neutralized with TEA (0.38 ml, 2.73 mmol). To the mixture was added a chilled solution of **3**·HCl (508 mg, 1.7 mmol) and TEA (0.48 ml, 3.4 mmol) in DMF (3 ml). The reaction mixture was stirred at 5 °C for 2 d and then evaporated. Addition of 10% citric acid to the residue gave a white precipitate. The crude product (794 mg, >100%) dissolved in MeOH (2 ml) was applied to a column (3×170 cm) of Sephadex LH-20 and eluted with MeOH, each 12 ml fraction being collected. The fractions (No. 49—55) containing the desired product detected by UV absorption and TLC were collected and evaporated, and the residue was recrystallized from MeOH-ether; yield, 518 mg (69%); mp 116—120 °C; $[\alpha]_D^{24}$ −15.6° (*c* 0.6, MeOH); R_f^1=0.30, R_f^2=0.66, R_f^3=0.70, R_f^4=0.77.

Found: C, 62.11; H, 7.67; N, 9.98%. Calcd for $C_{43}H_{62}O_{10}N_6 \cdot 0.5H_2O$: C, 62.08; H, 7.63; N, 10.10%.

Boc-Val-Orn(Z)-Leu-D-Phe-D-Pro-OSu (5). To a chilled solution of **4** (411 mg, 0.5 mmol) and HOSu (115 mg, 1 mmol) in DMF (4 ml) was added a solution of EDC·HCl (192 mg, 1 mmol) in $CHCl_3$ (1 ml). After being stirred at 5 °C overnight, the solution was evaporated under reduced pressure. The precipitate fromed by the addedion of chilled H_2O was collected by filtration and dried in vacuo over P_2O_5. The product was used for next reaction without further treatment; yield 441 mg (96%); R_f^1=0.79, R_f^2=0.21.

H-Val-Orn(Z)-Leu-D-Phe-D-Pro-OSu·HCl (6·HCl). Compound **5** (441 mg, 0.48 mmol) was dissolved in 0.1 M hydrogen chloride in formic acid (7.2 ml). The solution was allowed to stand at room temperature for 30 min and evaporated to leave an oil which was crystallized by addition of ether. The product was used for the next reaction without further treatment; yield 390 mg (90%); R_f^1=0.25.

***Cyclo*[-Val-Orn(Z)-Leu-D-Phe-D-Pro-]$_2$ (7).** A solution of **6**·HCl (390 mg, 0.46 mmol) in DMF (5 ml) was added dropwise into pyridine (148 ml) at room temperature. The final concentration was 3 mM. The reaction mixture was stirred overnight and evaporated. The residue was dissolved in mixture (36 ml) of MeOH-H_2O (5:1, by vol.), and applied to columns (1.6×10 cm each) of Dowex 50 (H^+ form) and Dowex 1 (OH^- form). The columns were washed with the same solvent (100 ml) and the combined effluent was evaporated to leave a white solid, which was collected with the aid of H_2O. The crude product (198 mg, 61%) dissolved in MeOH (2 ml) was applied to a column (3×170 cm) of Sephadex LH-20 and eluted with MeOH, each 12 ml fraction being colleted (Fig. 3). The fractions (No. 47—51) containing the desired product were collected and evaporated. The product was recrystallized from MeOH-EtOAc-ether; yield 65 mg (20%); mp 148—153 °C; $[\alpha]_D^{24}$ −42.6° (*c* 0.2, MeOH); R_f^1=0.76, R_f^2=0.12, R_f^3=0.95, R_f^4=0.92.

Found: C, 63.30; H, 7.34; N, 11.59%. Calcd for $C_{76}H_{104}O_{14}N_{12} \cdot H_2O$: C, 63.14; H, 7.53; N, 11.63%.

***Cyclo*(-Val-Orn-Leu-D-Phe-D-Pro-)$_2$·2HCl ([D-Pro$^{5,5'}$]-GS·2HCl) (8·2HCl).** Compound **7** (48 mg, 0.03 mmol) dissolved in 0.02 M hydrogen chloride in MeOH (3 ml) was hydrogenated in the presence of Pd-black (ca. 100 mg) for 3 h at room temperature. After filtration of catalyst, the filtrate was evaporated and the residue was recrystallized from MeOH-ether; yield, 30 mg (83%); mp 251—255 °C; $[\alpha]_D^{24}$ −40.9° (*c* 0.7, MeOH); R_f^3=0.62, R_f^4=0.15; MS (FAB), *m/z* 1141 ($C_{60}H_{92}O_{10}N_{12}$, M^+).

Found: C, 55.78; H, 7.71; N, 12.95%. Calcd for $C_{60}H_{92}O_{10}N_{12} \cdot 2HCl \cdot 4H_2O$: C, 56.02; H, 7.99; N, 13.07%

Paper Electrophoresis. Electrophoresis was carried out with Whatman No. 1 paper and a solvent system of formic acid-AcOH-MeOH-H_2O (1:3:6:10, by vol., pH 1.8) for 2 h at 500 V/30cm. [D-Pro$^{5,5'}$]-GS showed single spot and the mobility was as follows: [D-Pro$^{5,5'}$]-GS, 7.3 cm; GS, 7.5 cm.

CD Measurements. CD spectra were recorded on a JASCO J-40 spectropolarimeter in 0.1 mM solution using a cell of 1 mm pass length.

Microbiological Assays. The minimum concentration of the compounds necessary for the complete inhibition of growth of several microorganisms was determined by a dilution method using a nutrient agar "Eiken" Sensitivity Test Agar E-MC10.

We thank Miss Manami Oku of our institute for measurement of FAB-MS spectra and the members of Analysis Center of Mitsubishi Chemical Industries Ltd. for elemental analysis.

References

1) For part XI, see K. Sato, M. Tamaki, and U. Nagai, *Bull. Chem. Soc. Jpn.*, **58**, 3661 (1985).

2) K. Sato, M. Kawai, and U. Nagai, *Biopolymers*, **20**, 1921 (1981).

3) K. Sato, M. Kawai, and U. Nagai, *Bull. Chem. Soc. Jpn.*, **56**, 1527 (1983).

4) K. Sato, U. Nagai, and T. Higashijima, *Bull. Chem. Soc. Jpn.*, **56**, 1657 (1983).

5) The abbreviations used in this paper are those recommended by IUPAC-IUB: *Eur. J. Biochem.*, **138**, 9 (1984). Additional abbreviations: EDC-1-ethyl-3-(3-dimethylaminopropyl)carbodiimide; pNA, *p*-nitroanilide; DMF, *N,N*-dimethylformamide; TEA, triethylamine; GS, gramicidin S. Amino acids are of L-configuration unless otherwise mentioned.

6) D. C. Hodgkin and B. M. Oughton, *Biochem. J.*, **65**, 752, (1957).

7) A. Stern, W. A. Gibbons, and L. C. Craig, *Proc. Natl. Acad. Sci. U.S.A*, **61**, 734, (1968).
8) M. Ohnishi and D. W. Urry, *Biochem. Biophys. Res. Commun.*, **36**, 194, (1969).
9) R. Schwyzer and P. Sieber, *Helv. Chim. Acta*, **41**, 2186 (1958).
10) N. Izumiya, T. Kato, H. Aoyagi, M. Waki, and M. Kondo, "Synthetic Aspects of Biologically Active Cyclic Peptides-Gramicidin S and Tyrocidines," Kodansha, Tokyo and Halsted Press, New York (1979), pp. 15—47.
11) M. Kawai and U. Nagai, *Biopolymers*, **17**, 2649, (1978).
12) K. Sato and U. Nagai, *Bull. Chem. Soc. Jpn.*, **56**, 3329, (1983).
13) R. Nagata, M. Waki, M. Kondo, H. Aoyagi, T. Kato, S. Makisumi, and N. Izumiya, *Bull. Chem. Soc. Jpn.*, **40**, 963 (1967).
14) Ref. 10, pp. 78—97.

 © 1986 The Chemical Society of Japan Bull. Chem. Soc. Jpn., 59, 539—543 (1986)

Rearrangement Approaches to Cyclic Skeletons. III. Practical Route to *cis*-Bicyclo[4.3.0]non-4-en-7-ones Based on Photochemical [1,3] Acyl Migration of Bicyclo[3.2.2]non-6-en-2-ones[1]

Tadao UYEHARA,* Yasuhiro KABASAWA, Toshiaki FURUTA, and Tadahiro KATO
Department of Chemistry, Faculty of Science, Tohoku University, Aramaki-Aoba, Sendai 980
(Received October 7, 1985)

1-Methoxybicyclo[3.2.2]non-6-en-2-ones and the related compounds were derived I) from the Diels-Alder type 1,4-addition products of tropones with ethylene by selective reduction of the α,β-unsaturated carbonyl part (hydrosilylation followed by hydrolysis) and/or II) from bicyclo[2.2.2]oct-5-en-2-ones a) by the ring-enlargement utilizing Tieffeneau-Demjanov type conditions (1, TMS-CN; 2, $LiAlH_4$; 3, $NaNO_2$-AcOH) and/or b) by the related ring-expansion using trimethylsilyldiazomethane and boron trifluoride etherate. These bridged compounds were transformed into the respective [1,3] acyl migration products, *cis*-bicyclo[4.3.0]non-4-en-7-ones, in practical yields by direct irradiation through a Pyrex filter.

The photochemical behavior of tricyclo[2.2.2]oct-5-en-2-ones (**1**) has been investigated extensively.[3] The triplet-sensitized oxa-di-π-methane rearrangement of them into tricyclo[3.3.0.$0^{2,8}$]octan-3-ones (**3**) is particularly noticeable as a key reaction of syntheses of bi- and tricyclopentanoid natural products. On the other hand, there are only a few studies on the photochemical reaction of the higher homologs, bicyclo[3.2.2]non-6-en-2-ones (**4**).[4] As a part of our program to develop methods for stereoselective syntheses of [*m*–*n*] fused-ring natural products from bicyclic systems, we were interested in photochemical reactions of **4**.

As is analogized from those reactions of **1**, the expected products from ketones **4** are the [5—6] fused-ring compounds (**5**) and/or the related tricyclic ketones (**6**). The C_2–C_9 bond of **6** will be cleaved to give the [5—6] fused-ring compounds which are different from **5**. Thus, whichever photochemical rearrangement is predominant we can get [5—6] fused-ring compounds.

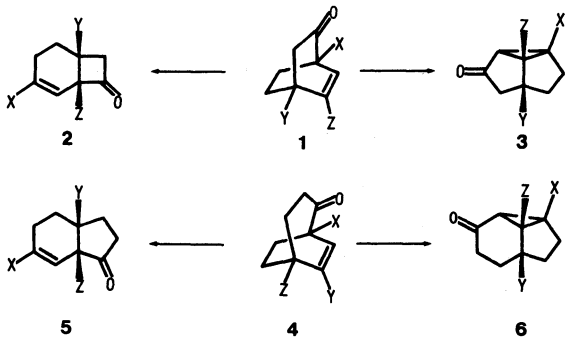

	X	Y	Z
a	H	H	H
b	Me	H	H
c	OMe	H	H
d	OMe	Me	H
e	OMe	H	Me
f	OMe	Me	Me

Results and Discussion

Syntheses of Bicyclo[3.2.2]non-6-en-2-ones. Already, we have reported that photochemical transformation of bicyclo[3.2.2]nona-3,6-dien-2-ones (**7**) into the C_7-disubstituted bicyclo[4.1.0]hept-2-enes is a practical synthetic method for [3—6] fused-ring sesquiterpenes such as sesquicarene[5] and isosesquicarene.[2] Bicyclononadienones **7a** and **7c** are the products of Diels-Alder reaction of tropones and ethylene.[6] Hydrosilylation of **7a** and **7c** with triethylsilane in the presence of Wilkinson's complex followed by hydrolysis[7] gave bicyclo[3.2.2]non-6-en-2-ones **4a** and **4c** in 47 and 84% yields, respectively. Another route to **4c** is sequential treatment of bicyclo[2.2.2]oct-5-en-2-one **1c**[8] with 1) cyanotrimethylsilane in the presence of a catalytic amount of zinc iodide, 2) lithium aluminium hydride, and 3) sodium nitrite in aqueous acetic acid (method A in Table 1). This Tieffeneau-Demjanov ring expansion[9] is useful to prepare the C_5-bridgehead methyl derivative (**4d**) from **1d**.[8] When 1-methylbicyclo[2.2.2]octenone **1b**[10] was treated similarly, the desired ketone (**4b**) was obtained along with a small amount of the regioisomer, 1-methylbicyclo-[3.2.2]non-6-en-3-one (**8**).[11]

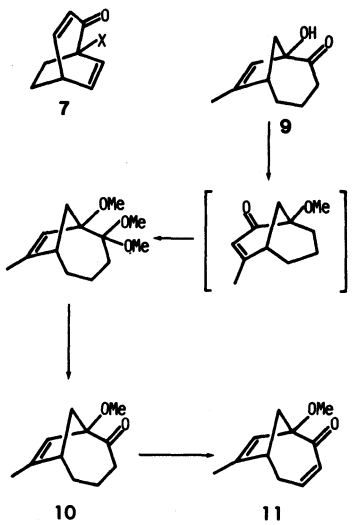

However, a similar treatment of **1e**[12] gave the unexpected compound, 1-hydroxybicyclo[4.2.1]non-7-en-2-one (**9**), instead of **4e**. Treatment of **9** with trimethyl orthoformate in the presence of TsOH gave the trimethoxy derivative. Acetal exchange of the product with acetone yielded **10**. The enone was transformed into the α,β-unsaturated ketone (**11**) by palladium-catalyzed oxidation[13] of the enol trimethylsilyl ether of **10**. Proton-NMR spectra of **11** suggest this compound consists of the four-, two-, and one- carbon bridges.

Hydroxy ketone **9** is derived presumably from the hydroxylamine **12** which should give diazonium ion **13**. The 1,3-shift of the ethano bridge of **13** is not extravagant because of the additional stabilization of the resulting carbonium ion (**14**) with its methyl group. It is reasonable that ketone **9** is thermodynamically more stable than the valence isomer (**15**) since we can convert the former into **10**.

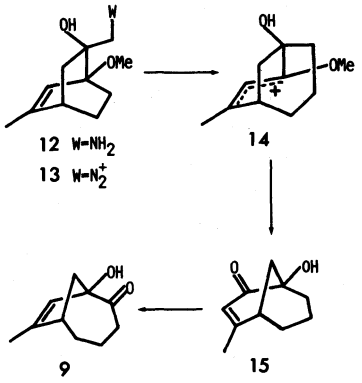

Ring enlargement of **1e** was accomplished by utilizing of trimethylsilyldiazomethane and BF_3-etherate (below −72 °C) to give **4e** on desilylation with potassium carbonate in methanol[14] (method B in table 1). Table 1 shows this Tiffeneau-Demjanov type homologation is a general method to obtain bicyclo[3.2.2]non-6-en-2-ones from respective bicyclo[2.2.2]oct-5-en-2-ones. As observed in monocyclic systems,[14] the methylene carbon migrates in preference to the other in this bridged bicyclic system.

Photochemical Reactions of Bicyclo[3.2.2]non-6-en-2-ones. Table 2 shows the conditions and the results of these photoreactions. As reported previously,[4] direct irradiation of **4a** through a Pyrex filter gave mainly the [1,3] acyl migration product (**5a**). The minor products of the reaction were undefined aldehydes. Formation of these is presumably due to the hydrogen abstraction process of the diradical which mainly turns into **5a**. When acetone was used as the solvent, the product (**6a**) via the oxa-di-π-methane rearrangement was obtained competitively with **5a**. The tricyclic structure of **6a** is supported by its spectral characteristics which clearly show the presence of the six-membered ring ketone conjugated with a three-membered ring: IR (CCl_4) 1690 (C=O) cm^{-1}.

The photochemical behavior of the bridgehead methyl derivative (**4b**) is very similar to that of **4a**.

Table 1. Tieffeneau-Demjanov Ring Enlargements of Bicyclo[2.2.2]oct-6-en-2-ones

Substrate	Method[a]	Product	Yield/%
1b	A	**4b**[b]	49
1c	A	**4c**	64
1c	B	**4c**	73
1d	A	**4d**	64
1d	B	**4d**	80
1e	A	**9**	40
1e	B	**4e**	73
1f	B	**4f**	71

a) Described in the text. b) With 4.5% of **8**.

Table 2. Photochemical Rearrangement of Bicyclo[3.2.2]non-6-en-2-ones

Substrate	Solvent	Concentration	Time	Products
		mol dm^{-3}	h	%
4a	Hexane	0.012	2	**5a** (53)
4a	Acetone	0.039	5.5	**5a** (18), **6a** (18)[a]
4b	Hexane	0.025	3.5	**5b** (55)
4b	Acetone	0.020	3.5	**5b** (28), **6b** (23)[b]
4c	THF	0.010	4	**5c** (55)
4c	Acetone	0.031	4	**16** (64)
4d	Hexane	0.018	6	**5d** (56)
4d	THF	0.010	4	**5d** (56)
4d	Acetone	0.023	6.5	**5d** (41)
4e	THF	0.010	4	**5e** (47)
4f	THF	0.010	4	**5f** (50)

a) Ketone **4a**, 37%, was recovered. b) With 18% of recovery of **4b**.

In contrast with these, only the respective [1,3] acyl migration products (**5d—f**) were obtained from the substrates (**4d—f**) possessing a methoxyl group at the bridgehead position by irradiation in acetone. When the reaction of **4c** was carried out in acetone, a mixture of the isomeric diketones (**16**) was obtained. However, the HPLC analysis of the irradiated acetone solutions indicated that the primary product derived from **4c** is the [1,3] acyl migration product (**5c**).

The respective [1,3] acyl migration products (**5c—f**) are obtained in practical yields by direct irradiation of the bridged ketones (**4c—f**) in hexane or THF. As is analogized from the reactivity of **4c** in acetone, these enol methyl ethers are less stable compounds. However, the ethylene acetals (**17e—f**) derived selectively by acetal exchange are remarkably stable compounds.

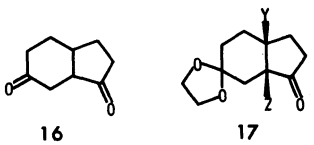

Thus, the most useful process among the photochemical conversions of bicyclo[3.2.2]non-6-en-2-ones is the [1,3] acyl rearrangement to give bicyclo[4.3.0]non-4-en-7-ones. The products derived from the substrates having a methoxyl group at the bridgehead

position are synthetically versatile compounds because that they have a masked ketone in the six-membered ring and a carbonyl group itself in the five-membered ring. An application of this [1,3] acyl migration to a natural product synthesis has already been reported.[1]

In contrast with the cases of bicyclo[2.2.2]oct-5-en-2-ones,[3] the oxa-di-π-methane rearrangement dose not predominate over the [1,3] acyl migration when acetone was used as the solvent. The [1,2] migration process disappears when the irradiation of the substrate having a methoxyl group at the bridgehead was carried out in acetone.

In order to understand the photochemistry of these homoconjugated systems generally, the chemistry of an additional bridged system, bicyclo[3.2.1]oct-6-en-2-ones, is under investigation. Preliminary results indicate that 1) the processes via S_1 (n-π^*), T (π-π^*), and T (n-π^*) give the products due to hydrogen abstraction, oxa-di-π-methane rearrangement, and [1,3] acyl migration, respectively, and 2) the energy difference between T (π-π^*) and T (n-π^*) is not large.[15] These results and the mechanistic studies of the reactions described in this paper will be reported in due course.

Experimental

General. Melting and boiling points are uncorrected. UV (in cyclohexane) and IR spectra (in CCl_4, unless otherwise mentioned) were recorded on Hitachi Model 323 and 215 spectrometers, respectively. ^1H NMR spectra (in CCl_4, unless otherwise noted) were obtained on JEOL JNM-PMX60, Varian EM-390 90 MHz, or Varian XL-200 NMR spectrometers, using tetramethylsilane as an internal standared. ^{13}C NMR spectra (in $CDCl_3$) were recorded on a JEOL FX 90Q NMR spectrometer. The mass spectral studies were conducted using a Hitachi M-52 spectrometer. Tetrahydrofuran and ether were distilled from benzophenone ketyl under argon, immediately prior to use. Dichloromethane was distilled from P_2O_5 and stored on 4A molecular sieves. Wilkinson's complex[16] and *N*-nitroso-*N*-trimethylsilylmethylurea[17] were prepared by using literature procedures. All reactions were monitored by analytical TLC using E. Merck precoated silica gel $60F_{254}$ plates. Column chromatography was carried out with E. Merck silica gel 60 (70—230 mesh ASTM). Analytical HPLC was performed on a Warters Associates Model R-401 liquid chromatograph using a 25 cm×4 mm stainless-steel column packed with Lichrosorb SI 100. Analytical VPC was carried out using a Hitachi 663-50 gas chromatograph, outfitted with a 3 m×3 mm stainless-steel column packed with 10% FFAP on 60/80 Uniport B.

Preparation of Bicyclo[3.2.2]non-6-en-2-one (4a). A flask containing of a mixture of 2.65 g (19.8 mmol) of bicyclo-[3.2.2]nona-3,6-dien-2-one (**7a**), ca. 10 mg of Wilkinson's complex, and 3.47 ml (21.7 mmol) of triethylsilane, was heated at 60 °C under argon for 4 d with stirring. The mixture was diluted with 20 ml of pentane, and filtered through a Celite layer. After removal of the solvent, the remaining oil (5.38 g) was treated with 0.6 g of K_2CO_3 in a mixture of 15 ml each of acetone, methanol, and water for 1 h. The solution was diluted with water, and extracted with ether. The extracts were combined, washed with two portions of water and with saturated brine, and then dried over $MgSO_4$. Removal of the volatiles by Kugelrohr distillation (100 °C/23—30 Torr (1 Torr=133.322 Pa)) gave 1.25 g (47%) of **4a** as colorless oil. **4a**: UV 289 (sh, ε 82), 298 (88), and 308 nm (72); IR 1700 (s) cm^{-1}. The 2,4-DNP derivative of **4a**: mp 149.5—150.5 °C (decomp). Found: C, 57.19; H, 5.08; N, 17.89%. Cacld for $C_{15}H_{16}N_4O_4$: C, 56.91; H, 5.10; N, 17.71%.

Preparation of 1-Methoxybicyclo[3.2.2]non-6-en-2-one (4c). a) Reduction of 1-Methoxybicyclo[3.2.2]nona-3,6-dien-2-one (7c). A mixture of 2.08 g (12.69 mmol) of **7c**, ca. 10 mg of [Rh(PPh_3]Cl, and 3.04 ml (19.0 mmol) of triethylsilane was heated at 60 °C overnight under argon. A similar workup to that employed for the synthesis of **4a** gave 3.37 g of a colorless oil. Chromatography (70 g of silica gel, 10:1—5:1 hexane, ethyl acetate) of the oil gave 1.78 g (84%) of **4c**: Colorless oil; UV 302 nm (ε103); IR 1715 (s) cm^{-1}. ^1H NMR δ=6.20 (H_6, dd, J=9.3, and 7.2 Hz), 5.87 (H_7, broad d, J=9.3 Hz), 3.22 (3H, s), 2.68 (H_5, m), 2.5—2.0 (2H, m), and 2.0—1.5 (6H, m); ^{13}C NMR δ=205.0 (s), 135.7 (d), 131.1 (d), 83.7 (s), 51.6 (q), 39.1 (t), 31.9 (t), 30.8 (d), 28.9 (t), and 22.7 (t); MS (13.5 eV) *m/z* (rel intensity) 166 (M^+, 55) and 110 (100). Found: C, 71.97; H, 8.65%. Calcd for $C_{10}H_{14}O_2$: C, 72.25; H, 8.49%.

b) Ring Enlargement of 1-Methoxybicyclo[2.2.2]oct-5-en-2-one (1c). (As a General Procedure for Method A). To a mixture of 2.40 g (15.77 mmol) of **1c** and ca. 10 mg of zinc iodide was added 2.3 ml (16.56 mmol)of cyanotrimethylsilane (TMSCN) at 0 °C, under argon, and the mixture was allowed to stand overnight at room temperature. After recognition of the end of the reaction from the disappearance of **1c**, the reaction mixture was diluted with 10 ml of dry ether, and the solution was added via a canula into a suspension of 0.9 g (23.66 mmol) of $LiAlH_4$ in 40 ml of dry ether at 0 °C. After stirring overnight at room tempetrature, this reaction mixture was treated successively with 0.9 ml of water, 0.9 ml of 15% aqueous NaOH, and 2.7 ml of water. A granular precipitate was filtered with K_2CO_3, and the filtrate was concentrated in vacuo to give 3.34 g of a pale yellow oil. To a solution of this oil in aqueous acetic acid, prepared from 4.7 ml of AcOH and 24 ml water, was added a solution of 1.63 g (23.64 mmol) of sodium nitrite in 7.9 ml of water over a period of 3 h using an Eyela Model MP-101 micro tube pump. After stirring overnight, the reaction mixture was diluted with water and extracted with three portions of ether. The extracts were combined, washed successively with saturated aqueous Na_2CO_3 and NaCl solutions, and dried over $MgSO_4$. Evaporation of the solvent gave 1.98 g of a yellow oil. Chromatography of the oil using 80 g of silica gel (10:1 hexane, ethyl acetate) gave 1.67 g (64%) of pure **4c**.

c) Ring Enlargement of 1-Methoxybicyclo[2.2.2]oct-5-en-2-one (1c) Using $TMSCHN_2$ and BF_3 Etherate. (As General Procedure for Method B). In a flask equipped with a Dry Ice condenser and a efficient magnetic stirrer were placed 4.59g (25.67 mmol) of *N*-nitroso-*N*-trimethylsilylmethylurea and 20 ml of pentane. To the mixture was added 8.8 ml of 20% aqueous potassium hydroxide solution at 0 °C. After 1.5 h stirring at 0 °C, the organic layer was diluted with pentane, separated, washed with water, and dried over Na_2SO_4. This solution was concentrated carefully to ca. 15 ml, and diluted with 30 ml of dichloromethane. To a solution of 1.56 g (10.3 mmol) of **1c** in 38 ml dichloromethane

was added 1.96 ml (15.34 mmol) of BF_3-etherate at −78 °C under argon and the mixture was stirred for 5 min. To this reaction mixture was added that $TMSCHN_2$ solution over a period of 1.5 h below −73 °C. After 30 min stirring, to the solution was added 40 ml of saturated aqueous $NaHCO_3$ solution. The mixture was allowed to warm to room temperature with stirring, and the organic layer was separated, washed with saturated brine, dried over $MgSO_4$, and concentrated in vacuo. Chromatography (40 g of silica gel, 8:1 hexane, ethyl acetate) of the remaining oil (2.2 g) gave 1.24 g (73%) of pure **4c**.

1-Methylbicyclo[3.2.2]non-6-en-2-one (4b): Colorless oil; UV 240 (sh, ε 62), 288 (sh, 91), 297 (102), and 303 nm (sh, 91); IR 1710 (s) cm^{-1}. ^1H NMR δ=6.21 (H_6, dd, J=8.9 and 7.5 Hz), 5.64 (H_7, d, J=8.9 Hz), 2.8—2.3 (3H, m), 2.0—1.2 (6H, m), and 1.11 (3H, s); MS (25 eV) m/z (rel intensity) 150 (M^+, 81) and 106 (100). The 2,4-DNP derivative of **4b**: Mp 138—139 °C. Found: C, 58.13; H, 5.46; N, 16.87%. Calcd for $C_{16}H_{18}N_4O_4$: C, 58 17; H, 5.49; N, 16.96%.

1-Methoxy-6-methylbicyclo[3.2.2]non-6-en-2-one (4d): Colorless oil; UV 293 (sh, ε 100), 301.5 (177), 311 (100), and 322 nm (sh, 65); IR 1715 (s) cm^{-1}. ^1H NMR δ=5.84 (1H, d, J=9.0 Hz), 5.76 (1H, dd, J=9.0 and<1.0 Hz), 3.18 (3H, s), 2.6—2.1 (3H, m), 2.0—1.3 (5H, m), and 1.16 (3H, s): ^{13}C NMR δ=204.6 (s), 140.7 (d), 130.2 (d), 83.5 (s), 51.6 (q), 39.7 (t), 39.3 (t), 34.9 (s), 30.9 (t), 29.0 (t), and 29.0 (q); MS (25 eV) m/z (rel intensity) 180(M^+, 14) and 124 (100). The 2,4-DNP derivative of **4d**: Mp 156—156.5 °C. Found: C, 56.82; H, 5.74; N, 15.50%. Calcd for $C_{17}H_{20}N_4O_5$: C, 56.66; H, 5.59; N, 15.55%.

1-Methoxy-5-methylbicyclo[3.2.2]non-6-en-2-one (4e): Mp 38.5—39.5 °C; UV 292 (sh, ε 141), 320 (174), 311 (169), and 323 nm (sh, 98); IR 1715 (s) cm^{-1}; ^1H NMR δ=5.45 (1H, s), 3.19 (3H, s), 2.6—2.1 (4H, m), 1.83 (3H, d, J=1.5 Hz), and 2.0—1.5 (5H, m); ^{13}C NMR δ=205.5 (s), 145.1 (s), 123.7 (d), 83.8 (s), 51.5 (q); MS (25 eV) m/z (rel intensity) 194 (M^+, 4) and 138 (100). DNP derivative of **4e**: Mp 131.5—132.5 °C. Found: C, 56.63; H, 5.65; N, 15.52%. Calcd for $C_{17}H_{20}N_4O_5$: C, 56.66; H, 5.59; N, 15.55%.

1-Methoxy-5,6-dimethylbicyclo[3.2.2]non-6-en-2-one (4f): Colorless oil; UV 292 (sh, ε 141), 302 (179), 312 (174), and 323 nm (sh, 102); IR 1710 (s) cm^{-1}; ^1H NMR δ=5.49 (1H, broad s), 3.18 (3H, s), 1.79 (3H, d, J=1.5 Hz), 2.5—1.3 (8H, m), and 1.12 (3H, s); ^{13}C NMR δ=205.4 (s), 146.5 (s), 124.7 (d), 83.8 (s), 51.4 (q), 39.1 (t), 39.0 (t), 37.3 (s), 31.7 (t), 26.3 (q), and 19.1 (q); MS (25 eV) m/z (rel intensity) 194 (M^+, 4) and 138 (100). Found: C, 74.10; H, 9.46%. Calcd for $C_{12}H_{18}O_2$: C, 74.19; H, 9.34%.

1-Methylbicyclo[3.2.2]non-6-en-3-one (8): Colorless oil; IR 1695 (s) cm^{-1}; ^1H NMR δ=6.14 (1H, dd, J=9.0 and 7.1 Hz), 5.95 (1H, d, J=9.0 Hz), 2.57 (1H, m), 2.4—2.25 (4H, m), 1.9—1.6 (4H, m), and 1.13 (3H, m); MS (13.5 eV) m/z (rel intensity) 150 (M^+, 81), 108 (100), and 93 (71). The 2,4-DNP derivative of **8**: Mp 140—141 °C. Found: C, 58.36; H, 5.68; N, 16.95%. Calcd for $C_{16}H_{18}N_4O_4$: C, 58.17; H, 5.49; N, 16.96%.

1-Hydroxy-7-methylbicyclo[4.2.1]non-7-en-2-one (9): Mp 71—72 °C; IR 1695 (s) cm^{-1}; ^1H NMR ($CDCl_3$) δ=5.14 (1H, broad s), 4.07 (1H, broad s), 1.74 (3H, d, J=1.5 Hz), 3.3—1.3 (9H, m); ^{13}C NMR δ=212.7 (s), 147.9 (s), 127.9 (d), 88.8 (d), 46.9 (d), 44.3 (t), 40.5 (t), 30.6 (t), 20.6 (t), and 15.1 (q); MS (25 eV) m/z (rel intensity) 116 (M^+, 34) and 109 (100). Found: C, 42.56; H, 8.64%. Calcd for $C_{10}H_{14}O_2$: C, 72.26; H, 8.49%.

Preparation of 1-Methoxy-7-methylbicyclo[4.2.1]non-7-en-2-one (10): To a solution of 280.4 mg (1.68 mmol) of **9** and 1.8 ml (16.4 mmol) of trimethyl orthoformate in dry dichloromethane was added a catalytic amount of TsOH at room temperature under argon. The resulting deep blue solution was allowed to stand overnight, and diluted with 20 ml of ether. The solution was successively washed with saturated aqueous $NaHCO_3$ solution, water, and saturated brine, and dried over $MgSO_4$. Evaporation of the solvents gave 373.6 mg of a yellow oil. To a solution of this oil in 5 ml of acetone was added a catalytic amount of TsOH, and the resulting deep blue solution was allowed to stand for 40 min. A similar workup to that used previously gave 291.5 mg of a yellow oil. Purification by chromatography (12 g of silica gel, 5:1 hexane, ethyl acetate) gave 232.5 mg (77%) of **10**: Colorless oil; IR 1710 (s) cm^{-1}. ^1H NMR δ=5.15 (1H, m), 3.11 (3H, s), 2.98 (1H, m), 2.5—2.2 (2H, m), 2.2—2.0 (2H, m), 1.70 (3H, d, J=1.5 Hz), 2.0—1.2 (4H, m); ^{13}C NMR δ=209.8 (s), 148.4 (s), 126.3 (d), 95.0 (s), 51.9 (q), 47.2 (d), 42.8 (t), 40.5 (t), 31.0 (t), 21.2 (t), and 15.1 (q). The 2,4-DNP derivatve of **10**: Mp 172—172.5 °C. Found: C, 56.38; H, 5.75; N, 15.43%. Calcd for $C_{17}H_{20}N_4O_5$: C, 56.66; H, 5.59; N, 11.55%.

Preparation of 1-Methoxy-7-methylbicyclo[4.2.1]nona-3,7-dien-2-one (11). The enol trimethylsilyl ether of **10** was prepared by treating with LDA and then with TMSCl at −78 °C. To a mixture of 87.9 mg of palladium acetate (0.39 mmol), 43 mg (0.39 mmol) of p-benzoquinone, and 1 ml of acetonitrile, prepared under argon, was added a solution of 195.2 mg (0.78 mmol) of the enol ether in 2 ml of acetonitrile at room temperature. After stirring overnight, the reaction mixture was poured in 0.5 M hydrochloric acid (1 M=1 mol dm^{-3}) and extracted with ether. The combined extracts were washed successively with saturated aqueous $NaHCO_3$ solution, water, and saturated brine, and dried over $MgSO_4$. Concentration followed by chromatography (8 g of silica gel, 5:1 hexane, ethyl acetate) gave 55.8 mg (40%) of **11**: Colorless oil; IR 1680 (s) cm^{-1}. ^1H NMR δ=5.87 (H_4, dtd, $J_{4,3}$=13.5, $J_{4,5}$=3.0, and $J_{4,6}$=0.7 Hz), 5.62 (H_3, ddd, $J_{3,4}$=13.5, $J_{3,5}$=2.3, and 1.5 Hz), 5.34 (H_8, q, J=1.5 Hz), 3.21 (OCH_3, s), 3.00 (H_6, m), 2.58 (H_5, 2H, m), 2.21 (H_9, 1H, d, $J_{9,6}$=1.5 Hz), 2.17 (H_9, 1H, s), and 1.73 (CH_3, dd, $J_{,8}$=1.5 and $J_{,6}$=0.75 Hz); MS (25 eV) m/z (rel intensity) 178 (M^+, 14) and 110 (100).

Photoreaction of 4a (General Procedure). A solution of 156.9 mg (1.15 mmol) of **4a** in 100 ml of hexane was placed in an immersion well equipped with a Pyrex filter and degassed by sonication. Irradiation of the solution under nitrogen using a 100-W Rikou high pressure Hg lamp for 2 h resulted in more than 95% conversion. From the crude photolysate (126.9 mg), 83.0 mg (53%) of **5a** was isolated by column chromatography (4 g of SiO_2, 15:1 hexane, ether).

***cis*-Bicyclo[4.3.0]non-4-en-7-one (5a):** Colorless oil; UV 236 (ε 631), 292 (49), 302 (56), 312.5 (47), and 325 nm (22); IR 1740 (s) cm^{-1}. ^1H NMR δ=5.8—5.5 (2H, m) and 2.7—1.2 (10H, m); MS (13.5 eV) m/z (rel intensity) 136 (M^+, 88), 118 (100), and 92 (55). The 2,4-DNP derivative of **5a**: Mp 150—152 °C. Found C, 56.98; H, 5.15; N, 17.66%. Calcd for $C_{15}H_{16}N_4O_4$: C, 56.96; H, 5.10; 17.71%.

4-Methyl-*cis*-bicyclo[4.3.0]non-4-en-7-one (5b): Colorless oil; IR 1740 (s) cm^{-1}; ^1H NMR δ=5.3 (1H, m), 1.70 (3H, broad s), and 2.7—1.1 (10H, m); MS (25 eV) m/z 150 (100), 132 (54), 106 (92), and 94 (96). The 2,4-DNP derivative of **6a**; Mp 142—164 °C (decomp). Found; C, 58.08; H, 5.54; N, 16.90%. Calcd for $C_{16}H_{18}N_4O_4$: C, 58.17; H, 5.49; N, 16.96%.

4-Methoxy-*cis*-bicyclo[4.3.0]non-4-en-7-one (5c): Colorless oil; IR 1745 (s) and 1665 (m) cm^{-1}; ^1H NMR δ=4.49 (1H,

broad d, J=4.5 Hz), 3.19 (3H, s), 2.8—1.3 (10H, m); MS (25 eV) m/z (rel intensity) 166 (M^+, 56) and 110 (100).

4-Methoxy-1-methyl-*cis*-bicyclo[4.3.0]non-4-en-7-one (5d): Colorless oil; UV 240 (sh, ε 1050), 270 (sh, 1050), 280 (1380), 292 (1200), and 315 (sh, 200); IR 1740 (s) cm^{-1}; ^1H NMR δ=4.48 (1H, d, J=4.5 Hz), 3.49 (3H, s), 2.3—1.3 (9H, m), and 1.13 (3H, s); MS (25 eV) m/z (rel intensity) 180 (M^+, 43) and 124 (100).

4-Methoxy-6-methyl-*cis*-bicyclo[4.3.0]non-4-en-7-one (5e): Mp 50.5—52 °C; IR 1745 (s) and 1665 (m) cm^{-1}; ^1H NMR δ=4.15 (1H, broad s), 3.43 (3H, s), 2.4—1.5 (9H, m), and 1.04 (3H, s): ^{13}C NMR δ=221.7 (s), 156.2 (s), 95.3 (d), 54.1 (q), 49.3 (s), 41.8 (d), 36.0 (t), 24.0 (t), 22.7 (t), and 22.4 (t); MS (25 eV) m/z (rel intensity) 180 (M^+, 32) and 124 (100).

4-Methoxy-1,6-dimethyl-*cis*-bicyclo[4.3.0]non-4-en-7-one (5f): Colorless oil; IR 1735 (s) and 1660 (w) cm^{-1}; ^1H NMR δ=4.09 (1H, broad s), 3.45 (3H, s), 2.3—1.8 (5H, m), 0.95 (3H, s), and 0.91 (3H, s); MS (25 eV) m/z (rel intensity) 194 (M^+, 94) and 148 (100).

Tricyclo[4.3.1.$0^{2,9}$]nonan-3-one (6a): Colorless oil; UV 206.5 (ε 20300), 274 (sh, 26), 281.5 (28), and 291 nm (sh, 24); IR 1690 (s) cm^{-1}; ^1H NMR δ=2.9—0.8 (m); MS (25 eV) m/z (rel intensity) 136 (M^+, 30), 118 (37), 108 (35), 92 (64), 80 (60), and 79 (100). The 2,4-DNP derivative of **6a**: Mp 156—161 °C (decomp). Found: C, 56.93; H, 5.05; N, 17.76%. Calcd for $C_{14}H_{16}N_4O_4$: C, 56.96; H, 5.10; N, 17.71%.

9-Methyltricyclo[4.3.1.$0^{2,9}$]nonan-3-one (6d): Colorless oil; IR 1680 (s) cm^{-1}; ^1H NMR δ=2.8—1.4 (11H, m) and 1.30 (3H, s); ^{13}C NMR δ=210.1 (s), 42.8 (s), 40.5 (d), 40.1 (d), 36.2 (t), 35.8 (t), 34.6 (t), 34.3 (d), 31.9 (t), and 24.2 (q); MS (25 eV) m/z (rel intansity) 150 (M^+, 49) and 79 (100). The 2,4-DNP derivative of **6b**: Mp 167—169 °C. Found: C, 57.86; H, 5.49; N, 16.86%. Calcd for $C_{16}H_{18}N_4O_4$: C, 58.17; H, 5.49; N, 16.96%.

Bicyclo[4.3.0]nona-3,9-diones (16m and 16n). **16m:** Colorless oil; IR 1745 (s) and 1720 (s) cm^{-1}; ^{13}C NMR δ=215.0 (s), 209.1 (s), 54.6 (d), 41.6 (d), 40.9 (t), 40.6 (t), 38.3 (t), 29.9 (t), and 26.7 (t); MS (25 eV) m/z (rel intensity) 152 (M^+, 100).

16n: Colorless oil; IR 1745 (s) and 1720 (s) cm^{-1}; ^{13}C NMR δ=217.3 (s), 209.3 (s), 49.2 (d), 39.3 (t), 36.7 (t), 34.9 (d), 34.5 (t), 29.9 (t), 27.6 (t), and 25.5 (t); MS (25 eV) m/z (rel intensity) 152 (M^+, 100).

Pereparation of 1-Methylspiro[bicyclo[4.3.0]nonane-3,2'-[1,3]dioxolan]-9-one (17e). To a solution of 55.4 mg (0.31 mmol) of **5e** in 0.5 ml each of 2-ethyl-2-methyl-1,3-dioxolane and benzene was added 3 mg of TsOH, and the mixture was allowed to stand for 2 d at room temperature. This mixture was diluted with ether, washed successively with saturated aqueous $NaHCO_3$ and NaCl solutions, and dried over $MgSO_4$. Concentration followed by chromatography (10 g of SiO_2, 10:1 hexane, ethyl acetate) gave 42.3 mg (65%) of **17e** as colorless prisms. **17e:** Mp 71—73 °C; IR (KBr) 1730 (s) cm^{-1}; ^1H NMR δ=4.0—3.6 (4H, m), 3.4—1.4 (10H, m), 1.20 (1H, d, J=14.3 Hz), and 0.97 (3H, s); MS (13.5 eV) m/z (rel intensity) 210 (M^+, 48), 182(16), and 99 (100). Found: C, 68.31; H, 8.92%. Calcd for $C_{12}H_{18}O_3$: C, 68.55; H, 8.62%.

Preparation of 1,6-Dimethylspiro[bicyclo[4.3.0]nonane-3,2'-[1,3]dioxolan]-9-one (17f). A similar procedure to that was used for the synthesis of **17e** gave 56.6 mg (76%) of **17f** starting from 64.2 mg (0.33 mmol) of **4f**. **17f:** Mp 58—60 °C; IR (KBr) 1728 (s) cm^{-1}; ^1H NMR δ=4.0—3.65 (4H, m), 3.4—1.3 (9H,m), 1.15 (d, J=14.3 Hz), 1.02 (3H, s), and 0.81 (3H, s); MS (25 eV) m/z (rel intensity) 224 (M^+, 17) and 99 (100). Found: C, 69.61; H, 8.98%. Calcd for $C_{13}H_{20}O_3$: C, 69.82; H, 9.08%.

References

1) A portion of this work has been published as a preliminary communication: T. Uyehara, Y. Kabasawa, T. Kato, and T. Furuta, *Tetrahedron Lett.*, **26**, 2343 (1985). Part II in this series is Ref. 2.

2) T. Uyehara, J. Yamada, T. Kato, and F. Bohlmann, *Bull. Chem. Soc. Jpn.*, **58**, 861 (1985).

3) M. Demuth and K. Schaffner, *Angew. Chem., Internat. Ed. Engl.*, **21**, 820 (1982).

4) L. A. Paquette, R. P. Henzel, and R. F. Eizenber, *J. Org. Chem.*, **38**, 3257 (1973).

5) T. Uyehara, J. Yamada, K. Ogata, and T. Kato, *Bull. Chem. Soc. Jpn.*, **58**, 211 (1985); *J. Chem. Soc., Chem. Commun.*, **1983**, 17.

6) T. Uyehara and Y. Kitahara, *Chem. Ind. (London)*, **1971**, 354; *Bull. Chem. Soc. Jpn.*, **52**, 3355 (1979).

7) I. Ojima, T. Kogure, M. Nihonyanagi, and Y. Nagai, *Bull. Chem. Soc. Jpn.*, **45**, 3506 (1972).

8) D. A. Evans, W. L. Scott, and L. K. Truesdale, *Tetrahedron Lett.*, **1972**, 121.

9) P. A. S. Smith and D. R. Baer, *Organic Reaction*, **11**, 157 (1960).

10) R. P. Gregson and R. N. Mirrington, *Aust. J. Chem.*, **29**, 2037 (1976).

11) L. G. Kozar, R. D. Clark, and C. H. Heathcock, *J. Org. Chem.*, **42**, 1386 (1977).

12) S. A. Monti, S. C. Chen, Y. L. Yang, S. S. Yuan, and O. P. Bourgeois, *J. Org. Chem.*, **43**, 4062 (1978).

13) Y. Ito, T. Hirao, and T. Saegusa, *J. Org. Chem.*, **43**, 1011 (1978).

14) N. Hashimoto, T. Aoyama, and T. Shioiri, *Chem. Pharm. Bull.*, **30**, 119 (1982).

15) T. Uyehara, T. Matsuoka, Y. Kabasawa, M. Akamatsu, and T. Kato, 50th National Meeting of the Chemical Society of Japan, Tokyo, April 1985, Abstr., No. 3038.

16) J. A.Osborn and G. Wilkinson, *Inorganic Synth.*, **10**, 67 (1967).

17) D. Seyferth, H. Menzel, A. W. Dow, and T. C. Flood, *J. Organomet. Chem.*, **44**, 279 (1972).

Catalytic Hydration of Unsaturated Nitriles to Unsaturated Amides Using Colloidal Copper Dispersions

Hidefumi HIRAI,* Hidehiko WAKABAYASHI, and Makoto KOMIYAMA
Department of Industrial Chemistry, Faculty of Engineering, The University of Tokyo, Hongo, Bunkyo-ku, Tokyo 113
(Received October 25, 1985)

Homogeneous hydrations of unsaturated nitriles such as acrylonitrile, methacrylonitrile, and crotononitrile to the corresponding unsaturated amides have been carried out in water at 80°C by use of colloidal copper dispersions as catalysts. The dispersions are prepared by reduction of copper(II) sulfate, copper(II) chloride, and copper(II) acetate with sodium tetrahydroborate in the presence of various polymers. The dispersions with poly(*N*-vinyl-2-pyrrolidone), poly(vinyl alcohol), methylamylopectin, methylcellulose, ethylcellulose, and (2-hydroxyethyl)-cellulose exhibit much larger catalytic activities than the copper precipitates prepared by reduction of the copper salts with sodium tetrahydroborate in the absence of the polymers. For all the catalytic reactions with the colloidal dispersions, selectivity for the unsaturated amides is 100% and formation of any by-products is not detected at all. Electron microscopy shows that no significant structural change occurs in the dispersions during the catalytic hydration. The catalytic activity monotonously increases with increasing amount of poly(*N*-vinyl-2-pyrrolidone) up to the charged ratio 20 of the monomeric residue to copper(II) ion, showing saturation at the ratio larger than 20. When the degree of the polymerization of poly(*N*-vinyl-2-pyrrolidone) is varied at a fixed residual molar ratio 40, the activity shows a maximum at the degree of polymerization 1440. The results are interpreted both by the change in the size of the colloidal copper particles and by the difference in the magnitude of the interactions between the polymers and the copper particles.

Hydration of unsaturated nitriles such as acrylonitrile and methacrylonitrile to the unsaturated amides such as acrylamide and methacrylamide (Eq. 1) is important in

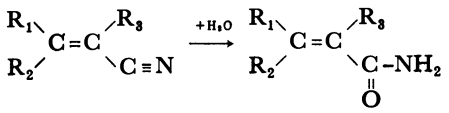
(1)

industry.[1,2] Many heterogeneous catalysts, most of which contain transition metals or their salts, have been reported.[1-6] Copper metal supported on silica,[3] magnesia,[3] or γ-alumina[4] showed high activity and high selectivity in the hydration of acrylonitrile to acrylamide. However, there have been few reports on homogeneous catalysts for selective hydrations of unsaturated nitriles to unsaturated amides.

Previously,[7] the authors showed that stable colloidal dispersions of copper metal could be prepared by the reduction of copper(II) sulfate with sodium tetrahydroborate in the presence of various polymers. The resulting colloidal dispersions were highly active and selective homogeneous catalysts for the hydration of acrylonitrile to acrylamide, as reported in a preliminary communication.[8]

This paper reports the catalytic activities of the colloidal copper dispersions, prepared by the reduction of copper salts in the presence of various polymers, for the hydration of acrylonitrile, methacrylonitrile, and crotononitrile to the corresponding unsaturated amides. Effects of the amounts of the protective polymers and their degrees of polymerization on the catalytic activities of the dispersions are described. Furthermore, dependence of the catalytic activity on the size of the colloidal copper particles is shown.

Experimental

Materials. Poly(*N*-vinyl-2-pyrrolidone)s, amylopectin, methylcellulose (degree of methylation 2.0), (2-hydroxyethyl)cellulose (degree of hydroxyethylation 1.6) (from Tokyo Kasei Kogyo Co.), poly(vinyl alcohol)s (from Junsei Pure Chemicals Co.), ethylcellulose (degree of ethylation 1.0) (from Nakarai Chemicals), and dextrin (from Kanto Chemicals) were repeatedly (2—5 times) reprecipitated from aqueous solutions with acetone. Methylamylopectin was prepared according to the literature,[9] and had a degree of methylation 1.1, as determined by ^{1}H-NMR spectroscopy.

Copper(II) sulfate from Yoneyama Chemical Co. was recrystallized from water twice. Copper(II) chloride, copper(II) acetate, copper(II) nitrate, and sodium tetrahydroborate were obtained from Koso Chemical Co.

Acrylonitrile was distilled after being washed successively with aqueous sodium hydroxide solution, aqueous phosphoric acid solution, and pure water. Methacrylonitrile and crotononitrile were purified by distillation.

Water was doubly distilled and then was degassed by boiling under a reduced pressure.

Nitrogen gas, which had a purity higher than 99.9995%, was purchased from Nippon Sanso Co.

Preparation of Colloidal Copper Dispersions.[7] Typical procedure for the preparation of colloidal copper dispersions is as follows. Copper(II) sulfate or the other copper salts (0.15 mmol) and various amounts of protective polymers were stirred in 22 cm^3 of water at 80°C under nitrogen for 1 h. Then sodium tetrahydroborate (0.30 mmol) in 3 cm^3 of water was added at 25°C. The color of the solution changed immediately, and colloidal copper dispersions were obtained as black or reddish dark brown homogeneous solutions.

Catalytic Hydration of Unsaturated Nitriles Using Colloidal Copper Dispersions. The hydrations of acrylonitrile, methacrylonitrile, and crotononitrile were carried out at 80°C under nitrogen by adding the corresponding nitrile (9.1 mmol) to the colloidal copper dispersions. Product analyses were made with gas chromatography (Tenax GC

Table 1. Catalytic Activities of Colloidal Copper Dispersions Protected by Various Polymers in the Hydration of Acrylonitrile[a)]

Polymer	Degree of polymerization	Average diameter of copper particles/A	Acrylamide formation	
			Yield[b)] mol%	Selectivity %
Poly(*N*-vinyl-2-pyrrolidone)	6300	c)	20.8	100
	3240	100	25.4	100
	1440	60	27.3	100
	360	c)	24.3	100
	90	50	7.5	100
Poly(vinyl alcohol)	2000	c)	8.6	100
	1500	150	6.0	100
	360	c)	6.9	100
Poly(potassium vinyl sulfate)	c)	c)	3.5	92[d)]
Dextrin	c)	90	0.5	100
Amylopectin	c)	100	0.2	100
Methylamylopectin	c)	c)	8.1	100
Methylcellulose	140	100	21.2	100
Ethylcellulose	c)	c)	20.2	100
(2-Hydroxyethyl)cellulose	c)	c)	21.7	100
None[e)]	—	g)	0.3	97[f)]

a) Reaction conditions: 80°C, 2h; $[Cu]_0=5.0\times10^{-3}$, $[\text{acrylonitrile}]_0=3.0\times10^{-1}$, and [monomeric residue of polymer]$_0=2.0\times10^{-1}$ mol dm^{-3}. b) The value with respect to the charged acrylonitrile. c) Not determined. d) By-products were ethylene cyanohydrin and another unidentified product. e) Catalysis by the copper precipitates. f) By-product was ethylene cyanohydrin. g) The value was not estimated, since the particle diameters were widely distributed from 40 to 3500A.

column, 2 m×3 mm glass column, 170°C).

Electron Microscopy. Electron micrographs of the colloids were obtained by a Hitachi Model HU-12A electron microscopy operated at 100 kV. Sample films were prepared from the colloidal dispersions on collodion films coated with a carbon layer by evaporating the solvent to dryness.

Results

Catalytic Hydrations of Unsaturated Nitriles Using Colloidal Copper Dispersions. Table 1 shows the catalytic activities of the colloidal copper dispersions, prepared by the reduction of copper(II) sulfate with sodium tetrahydroborate in the presence of various polymers, for the hydration of acrylonitrile in water at 80°C. The dispersions with poly(*N*-vinyl-2-pyrrolidone) (PVP), poly(vinyl alcohol), poly(potassium vinyl sulfate), methylamylopectin, methylcellulose, ethylcellulose, and (2-hydroxyethyl)cellulose exhibit much larger catalytic activities than the copper precipitates obtained by the reduction of copper(II) sulfate with sodium tetrahydroborate in the absence of the polymers. For example, the yield (27.3 mol%) of acrylamide for the colloidal copper dispersion with PVP of viscosity-averaged degree of polymerization (DP) 1440 is about 90 fold larger than that (0.3 mol%) for the copper precipitates.

The catalytic activity of the dispersion with methylamylopectin is 40 times as large as that with amylopectin. The dispersions with methylcellulose, ethylcellulose, and (2-hydroxyethyl)cellulose show 40 fold larger catalytic activities than the dispersion with dextrin. Measurement of the catalytic activity of the dispersion with cellulose has not been successful yet due to poor solubility of cellulose in water.

In the catalytic hydration of acrylonitrile using all the colloidal copper dispersions, except for the one with poly(potassium vinyl sulfate), the product was acrylamide alone. Either the formation of ethylene cyanohydrin due to hydration of the C-C double bond in place of the C-N triple bond, or the formation of acrylic acid, due to hydrolysis of acrylonitirle or acrylamide, was not detected at all. In contrast, the reaction using the copper precipitates, prepared by the reduction of copper(II) sulfate in the absence of the polymers, yielded considerable amount of ethylene cyanohydrin, resulting in the selectivity 97% for acrylamide.

When the colloidal copper dispersion with poly(potassium vinyl sulfate) was used as catalyst, ethylene cyanohydrin was produced as by-product together with an unidentified by-product.

The open circles in Fig. 1 show the time-conversion curve for the catalytic hydration of acrylonitrile using the colloidal copper dispersion with PVP (DP=1440). The yield of acrylamide monotonously increases with reaction time, attaining 68 mol% at 15 h. Up to this yield, the reaction satisfactorily follows first-order equation, and the selectivity for acrylamide is 100%.

The catalytic rate for the colloidal copper dispersion is more than 50 fold larger than that for the copper precipitates-PVP suspension system (the closed circles in Fig. 1). In the suspension system, the copper precipitates were first prepared by reducing copper(II) sulfate with sodium tetrahydroborate in the absence

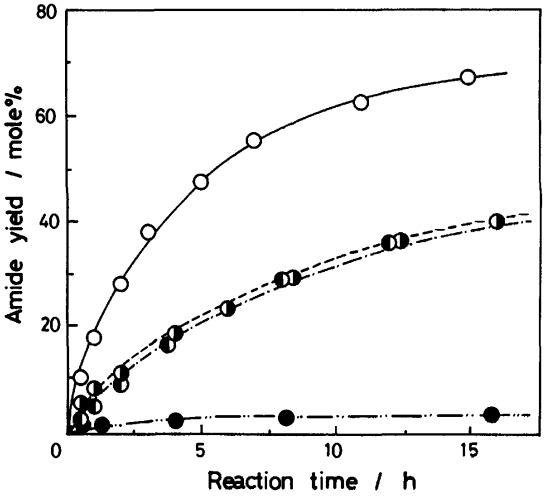

Fig. 1. Time course for the selective hydration of acrylonitrile (○), methacrylonitrile (◑), and crotononitrile (◐) catalyzed by the colloidal copper dispersion with PVP (DP=1440): 80 °C; $[Cu]_0=5.0\times10^{-3}$, [unsaturated nitrile]$_0=3.0\times10^{-1}$, and [monomeric residue of PVP]$_0=2.0\times10^{-1}$ mol dm^{-3}; the closed circles refer to the catalysis by the suspension composed of copper precipitates and PVP (details are described in the text.).

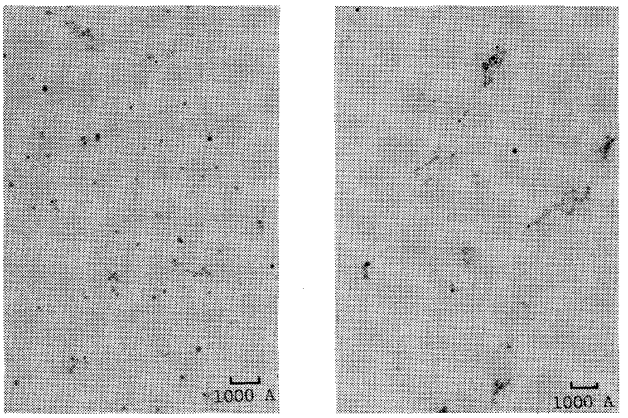

Fig. 2. Electron micrographs of the colloidal copper dispersions prepared by use of PVP (DP=1440) at the charged ratio 20 of the monomeric residue with respect to copper(II) sulfate; (a) before the catalytic hydration; (b) after the catalytic hydration of acrylonitrile at 80 °C for 2 h.

of PVP, and then they were charged to the reaction mixture together with PVP. The amount of PVP added was exactly identical with that used for the preparation of the colloidal dispersion. With the catalysis by the copper precipitates-PVP suspension system, considerable amount of ethylene cyanohydrin was formed as by-product, and the selectivity for acrylamide was 97%. This is significantly in contrast with 100% selectivity achieved by the colloidal copper dispersions.

The colloidal copper dispersions also catalyzed the hydrations of methacrylonitrile and crotononitrile to the corresponding unsaturated amides (◑ and ◐ in Fig. 1). The selectivities are 100% for both of the reactions. The rates for these methyl-substituted acrylonitriles are about 1/2 of the value for acrylonitrile itself.

Stability of Colloidal Copper Dispersion in the Catalytic Hydration. Catalytic hydration of acrylonitrile using the colloidal copper dispersion, prepared with the use of PVP, proceeded homogeneously throughout the reaction time. Neither precipitation nor change in color of the dispersion was perceived. Figure 2 shows the electron micrographs of the dispersion with PVP (DP=1440), before and after the hydration. In both of the electron micrographs, dispersion of colloidal copper particles is fine, In addition, the average diameter (100 A) of the particles after the hydration is exactly identical with that (100 A) before it. Thus, no significant structural change in the colloidal dispersion occurs during the catalytic reaction.

The colloidal copper dispersions with poly(potassium vinyl sulfate), dextrin, amylopectin, methylamylopectin, methylcellulose, ethylcellulose, and (2-hydroxyethyl)cellulose were also stable during the catalytic hydration. In the reaction using the dispersion with poly(vinyl alcohol), however, considerable amounts of black precipitates were formed during the reaction.

Effect of Copper Species on the Catalytic Activity of Colloidal Copper Dispersion. Table 2 lists the catalytic activities of the colloidal copper dispersions prepared by the reduction of various copper salts with sodium tetrahydroborate in the presence of PVP (DP=1440). The dispersions prepared from copper(II) sulfate and copper(II) chloride show high catalytic activities and 100% selectivity for acrylamide. No precipitation and color change are found during the catalytic reactions here.

The dispersion from copper(II) acetate exhibits also 100% selectivity, although the catalytic activity is slightly smaller. This dispersion is less stable than the ones from copper(II) sulfate and copper(II) chloride, and black precipitates are formed in the course of the catalytic reaction.

In the case of the colloidal copper dispersion prepared from copper(II) nitrate, the color of the dispersion gradually changed from dark brown to yellowish green. Ethylene cyanohydrin is formed as by-product, and both the yield and the selectivity for acrylamide are low.

Dependence of the Catalytic Activity of the Colloidal Copper Dispersion on the Amount and the Degree of Polymerization of Protective Polymer. Figure 3 shows the plot of the catalytic activity of the colloidal copper dispersions for the hydration of acrylonitrile vs. the amount of PVP (DP=1440) used for the preparation of the dispersion. The activity gradually increases with increase in the charged ratio of the monomeric residue of PVP to copper(II) sulfate, up to the ratio 20. At the ratio larger than 20, however, the activity is almost independent of the amount of PVP.

Table 2. Catalytic Activities of Colloidal Copper Dispersions Prepared by the Reduction of Various Copper Salts in the Presence of PVP (DP=1440)[a)]

Copper salt	Color of colloidal dispersion	Acrylamide formation	
		Yield/mole%[b)]	Selectivity/%
$CuSO_4 \cdot 5H_2O$	Reddish dark brown	28.1	100
$CuCl_2 \cdot 2H_2O$	Reddish dark brown	26.8	100
$Cu(OCOCH_3)_2$	Dark brown	17.2	100
$Cu(NO_3)_2$	Dark brown[c)]	0.4	81[d)]

a) Reaction conditions: 80°C, 2h; $[Cu]_0=5.0\times10^{-3}$, $[acrylonitrile]_0=3.0\times10^{-1}$, and [monomeric residue of PVP]$_0=1.0\times10^{-1}$ mol dm^{-3}. b) Value with respect to the charged acrylonitrile. c) The color gradually changed to yellowish green during the catalytic reaction. d) By-product was ethylene cyanohydrin.

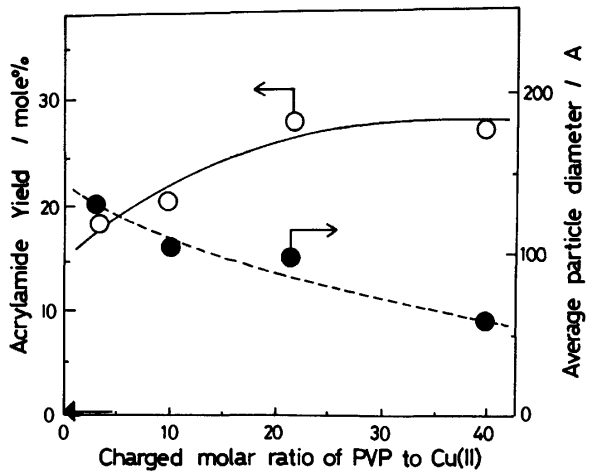

Fig. 3. Plots of the catalytic activity (○) of the colloidal copper dispersion in the hydration of acrylonitrile and the average diameter (●) of the colloidal copper particles as functions of the amount of PVP (DP=1440) used for the preparation of the dispersion: reaction conditions, 80°C, 2h; $[Cu]_0=5.0\times10^{-3}$ and $[acrylonitrile]_0=3.0\times10^{-1}$ mol dm^{-3}, the arrow refers to the result for the catalysis by the copper precipitates prepared in the absence of PVP.

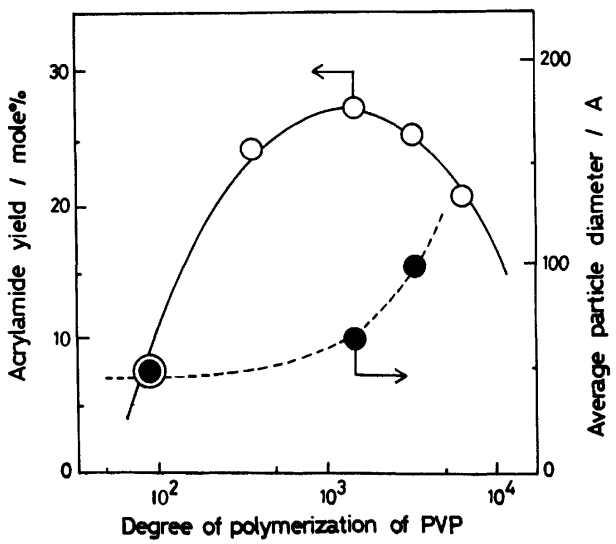

Fig. 4. Plots of the catalytic activity (○) of the colloidal copper dispersion in the hydration of acrylonitrile and the average diameter (●) of the colloidal copper particles as functions of the degree of polymerization of PVP: the charged ratio of the monomeric residue of PVP to copper(II) sulfate was kept constant at 40; reaction conditions, 80°C, 2h; $[Cu]_0=5.0\times10^{-3}$ and $[acrylonitrile]_0=3.0\times10^{-1}$ mol dm^{-3}.

Even at the ratio 3 of monomeric residue of PVP to copper(II) sulfate, the dispersion is stable throughout the reaction time. The activity of this dispersion is about 50 times as large as that, shown by the arrow in Fig. 3, of the copper precipitates prepared without PVP.

In Fig. 4, the catalytic activity of the colloidal copper dispersion is plotted against the degree of polymerization (DP) of PVP. Here, the ratio of monomeric residue of PVP to copper(II) sulfate is kept constant at 40. The activity increases with increasing degree of polymerization below DP 1440. Above DP 1440, however, the activity decreases with increasing degree of polymerization.

The closed circles in Figs. 3 and 4 show the average diameters of colloidal copper particles, determined by electron microscopy, for the corresponding dispersions. The average particle diameter decreases with increasing amount of PVP (Fig. 3) and with decreasing degree of polymerization of PVP (Fig. 4). Relationship between the catalytic activity and the average particle diameter will be discussed in the Discussion Section.

Discussion

Catalytic Activities of the Colloidal Copper Dispersions for the Hydration of Unsaturated Nitriles to Unsaturated Amides. The higher catalytic activities of the colloidal copper dispersions than the copper precipitates (Table 1) is mainly attributable to the fact that the effective surface area of copper metal is larger due to smaller particle diameter. The diameter of all the particles in the colloidal copper dispersion with PVP (DP=1440), exhibiting the largest catalytic activity, for example, are between 20 to 190 A, as described previously.[7] However, the particle diameter in the copper precipitates, prepared in the absence of polymer, ranges from 40 to 3500 A. Here, dominant part of the charged copper atoms is used for the

Table 3. Comparison of the Catalytic Activity for Colloidal Copper Dispersion Using PVP (DP=3240) with the Value for Copper on Silica-Magnesia in the Hydration of Acrylonitrile[a)]

	Amount of the charged copper in the catalyst	Acrylamide formation		Rate of formation of acrylamide per the charged copper g·atom
		Yield	Selectivity	
	10^{-4} g·atom	mol%	%	mol dm^{-3} min
Colloidal copper dispersion[b)]	1.4	7.2	100	0.31
Copper on silica-magnesia[c)]	47.2	21	97	0.027

a) Reaction conditions: 80°C, 30 min; $[\text{acrylonitrile}]_0=1.8\times10^{-1}$ mol dm^{-3}. b) [monomeric residue of PVP]$_0$/[Cu]$_0$=20. c) Date from Ref. 3.

formation of large particles, resulting in small value of the total surface area. The catalytic activity of the precipitates is small even in the suspension system formed by the addition of PVP (● in Fig.1).

In addition, the colloidal copper catalysts are more active than the copper precipitates, since the reactions proceed homogeneously and thus the contacts between the copper metal particles and the unsaturated nitriles are much more efficient. The catalytic activity of the dispersion prepared from copper(II) acetate, which shows precipitation of copper particles during the reaction, is about 2/3 of the values of the dispersions from copper(II) sulfate and copper(II) chloride, which are homogeneous throughout the reactions (Table 2).

Table 3 shows the comparison of the catalytic activity of the homogeneous colloidal copper catalyst with the value of a heterogeneous catalyst, copper supported on silica-magnesia.[3)] Reaction conditions are identical with each other except for the fact that the amount of copper used in the colloidal copper catalyst is about 34 fold smaller than that used in the heterogeneous catalyst. The rate of formation of acrylamide per the charged copper atom for the colloidal copper catalyst is 11 fold larger than the value for the heterogeneous catalyst. The selectivity for acrylamide is 100% for the colloidal catalyst, whereas the selectivity is 97% for the heterogeneous catalyst. Thus, the colloidal copper catalyst is superior to the heterogeneous catalyst, at least with respect to the catalytic activity and selectivity.

Selective catalyses by the colloidal copper dispersion are probably associated with absence or minimal amount of lattice defects, suppressing undesired side reactions. As shown by the previous electron diffraction experiments,[7)] the copper atoms in the colloidal copper particles are arranged in an ordered way, which is almost identical with that in the crystal of bulk copper metal. Selective catalyses by the colloidal dispersions of noble metals such as rhodium and palladium in the hydrogenation of olefins and dienes have been known.[10,11)]

Factors Governing the Catalytic Activity of Colloidal Copper Dispersion. The increase of the catalytic activity of the colloidal copper dispersion with increasing amount of PVP at the charged ratio 20 or smaller of monomeric residue of PVP to copper(II) sulfate (Fig. 3) is ascribed to increase in the surface area of copper particles due to decrease in the particle size. The increase of the activity with decreasing degree of polymerization of PVP at the DP 1440 or larger (Fig. 4) is also attributed to increasing surface area. The protective polymers protect fine colloidal copper particles from mutual coaggregation both in the preparation of the colloidal dispersion and in the catalytic hydration, providing effective contacts between the copper particles and the substrates unsaturated nitriles.

The catalytic activities of the colloidal copper dispersions are also dependent on the magnitude of the interactions between the polymers and the colloidal copper particles.[12)] The stronger interactions reduce the catalytic activities by competitive suppression of the interactions of the substrates unsaturated nitriles with the copper particles. The 4 fold decrease in the catalytic activity with decreasing degree of polymerization from 1140 to 90, in spite of decreasing average particle diameter from 60 to 50 A (Fig. 4), is attributable to this effect. The magnitude of the interactions of PVP with colloidal metal particles increases with decreasing degree of polymerization.[13)] Increase of the residual molar ratio of PVP with respect to copper(II) sulfate from 20 to 40 shows virtually no increase in the catalytic activity (Fig. 3), since enhancement of the competitive suppression by PVP on the interactions of the nitriles with the copper particles compensates the acceleration due to decrease in the average particle diameter from 100 to 60 A.

Large catalytic activities of the dispersions with methylamylopectin, methylcellulose, ethylcellulose, and (2-hydroxyethyl)cellulose than the values for the dispersions with dextrin and amylopectin (Table 1) are also consistent with the arguments. Alkylation of the hydroxyl groups prevents hydrogen bondings between the monomeric residues in the polysaccharides, resulting in more flexible and stretching conformations of the polymers. Thus, the surface of the copper metal particles in the dispersions protected by these alkylated polysaccharides is more favorable for the unsaturated nitriles to make interactions than the surface in the dispersions protected by the polymers with rigid and compact conformations.

With the use of the polymers such as poly(ethylene oxide) and β-cyclodextrin, which interact with the colloidal copper particles too weakly, no colloidal copper dispersions are obtained. Only copper precipitates are formed on the reduction of copper(II) sulfate with sodium tetrahydroborate in the presence of these polymers.[7]

The authors would like to thank Koichi Adachi for his valuable assistance in electron microscopy measurements.

References

1) D. C. MacWilliams, "Kirk-Othmer: Encyclopedia of Chemical Technology," 3rd ed., ed by H. F. Mark, Wiley-Interscience, New York, (1978), Vol. 1, p. 298.

2) E. Otsuka, T. Takahashi, F. Matsuda, and N. Hashimoto, *Kagaku Kogaku*, **38**, 626 (1974).

3) H. Hayashi, H. Nishi, Y. Watanabe, and T. Okazaki, *J. Catal.*, **69**, 44 (1981).

4) H. Miura, T. Hattori, K. Keitoku, K. Sugiyama, and T. Matsuda, *Nippon Kagaku Kaishi*, **1982**, 692.

5) H. Miura, K. Sugiyama, S. Kawakami, T. Aoyama, and T. Matsuda, *Chem. Lett.*, **1982**, 183.

6) F. Nozaki, T. Sodesawa, and T. Yamamoto, *J. Catal.*, **84**, 267 (1983).

7) H. Hirai, H. Wakabayashi, and M. Komiyama, *Bull. Chem. Soc. Jpn.*, **59**, 367 (1986).

8) H. Hirai, H. Wakabayashi, and M. Komiyama, *Chem. Lett.*, **1983**, 1047.

9) W. N. Haworth, *J. Chem. Soc.*, **107**, 8 (1915).

10) H. Hirai, *J. Macromol. Sic.-Chem.*, **A13**, 633 (1979).

11) H. Hirai, H. Chawanya, and N. Toshima, *Makromol. Chem., Rapid Commun.*, **2**, 99 (1981).

12) H. Hirai, H. Wakabayashi, and M. Komiyama, *Makromol. Chem., Rapid Commun.*, **5**, 381 (1984).

13) B. Jirgensons, *Makromol. Chem.*, **6**, 30 (1951).

Electrolytic Recovery of Silver from Photographic Fixing Solutions with a Fluidized Bed Electrode

Isao SEKINE* and Hiroyuki ISHII
Faculty of Science and Technology, Science University of Tokyo, Yamazaki, Noda, Chiba 278
(Received January 17, 1985)

For an effective electrolytic recovery of silver from photographic fixing solutions, polarization measurements and potentiostatic electrolysis were carried out using active carbon as a fluidized bed electrode. The optimum conditions, determined by the electrolytic recovery, required a static bed height was 4 mm, a bed expansion rate 14%, and an initial set potential −0.84 V vs. SCE. The current efficiency in this case was about 75%, and the limiting concentration for recovery of silver was about 5 ppm. The electrolytic duration for recovery of the silver was reduced to about half by enlarging the electrolytic cell. Other products formed during the electrolysis were hydrogen sulfide (H_2S) and silver sulfide (Ag_2S). When silver deposited under the optimum conditions was dissolved in 5M-HNO_3 (1M=1mol dm^{-3}) of 100 ml, the recovery efficiency of the silver was about 75%.

Electrolytic recovery of metals with a fluidized bed electrode is favorable in dilute solutions. It is also known to be more effective than a fixed bed electrode.[1-4] Active carbon, which has an ability for physical adsorption and a better conductivity, has rarely been used in electrolytic recovery as material for a bed electrode.

In the present work, the effective electrolytic recovery of silver in the photographic fixing solution was investigated using active carbon. The various kinds of photographic fixing solutions contain relatively large amount of silver ion. Therefore, the recovery of silver is important from the viewpoint of saving natural resources. Moreover, the optimum conditions for carrying out effective potentiostatic electrolysis were determined by measuring the cathodic polarization curve and by electrolysis. Factors are the static bed height, the bed expansion rate, and the initial set potential. The effect of scale up of the electrolytic cell and the recovery efficiency of silver were also investigated. The product deposited on the cathode was identified by X-ray diffraction.

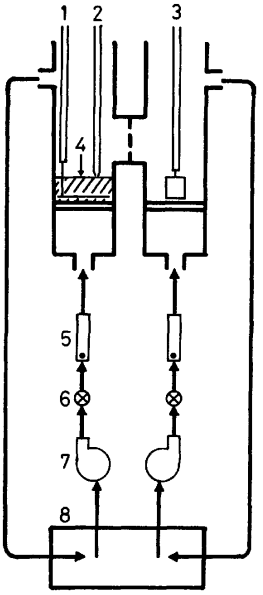

Fig. 1. Apparatus for electrolytic recovery of Ag. 1: Working electrode (Pt wire), 2: Reference electrode (SCE), 3: Counter electrode (Pt plate), 4: Fluidized bed electrode (active carbon), 5: Flow meter, 6: Valve, 7: Pump, 8: Tank in water bath.

Experimental

Cell and Electrode. The cell for the electrolytic recovery is shown in Fig. 1. The cell is made of acrylic resin. It has an H-type structure with an inside diameter of 26 mm or 18 mm. The diameter of both the inlet and the outlet for the solution was 7 mm. Anolyte and catholyte were divided by a diaphragm to prevent the electrolyte from mixing by natural convection. The electrolyte was filtered through a porous acrylic resin plate interposed at a point 35 mm up from the inlet through which the solution flows into the cell. The average particle diameter of the active carbon used as a fluidized bed electrode was 1.53 mm. The active carbon was used after immersion in distilled water for more than one day. The cathode was a spiral platinum wire of 0.5 mm diameter used as a feeder electrode on the porous acrylic resin plate, and the active carbon was placed on the feeder electrode. The anode was a platinum plate of 15×10 mm. Both anode and cathode were subsequently washed with ethanol, 1M-HNO_3 and 1M-HCl. The reference electrode was a saturated calomel electrode (SCE).

Electrolyte. The electrolyte was prepared by diluting tenfold a photographic fixing solution with distilled water. The electrolyte with a volume of 1 dm^3 was pumped to the cell from a tank maintained at 30 °C; the flow rate was controlled by a Teflon valve and was determined through a flow meter. Moreover, the electrolyte was circulated from the outlet of the cell to the tank, after it had fluidized the active carbon.

Polarization Measurement and Electrolysis. The measurements of the polarization curves were carried out by the potentiostatic method. The potential was changed stepwise from a natural electrode potential (NEP) to a less noble potential at a scan rate of 50 mV min^{-1}. The electrolytic recovery of silver was also carried out for 6 h by the potentiostatic method.

Concentration Determination of Silver Ion. The concentration of silver ion in the solution was determined by atomic absorption analysis. In this analysis, air-acetylene was used as a flame, and the wavelength of irradiation was 3281 Å for Ag. The concentration of silver ion was determined from

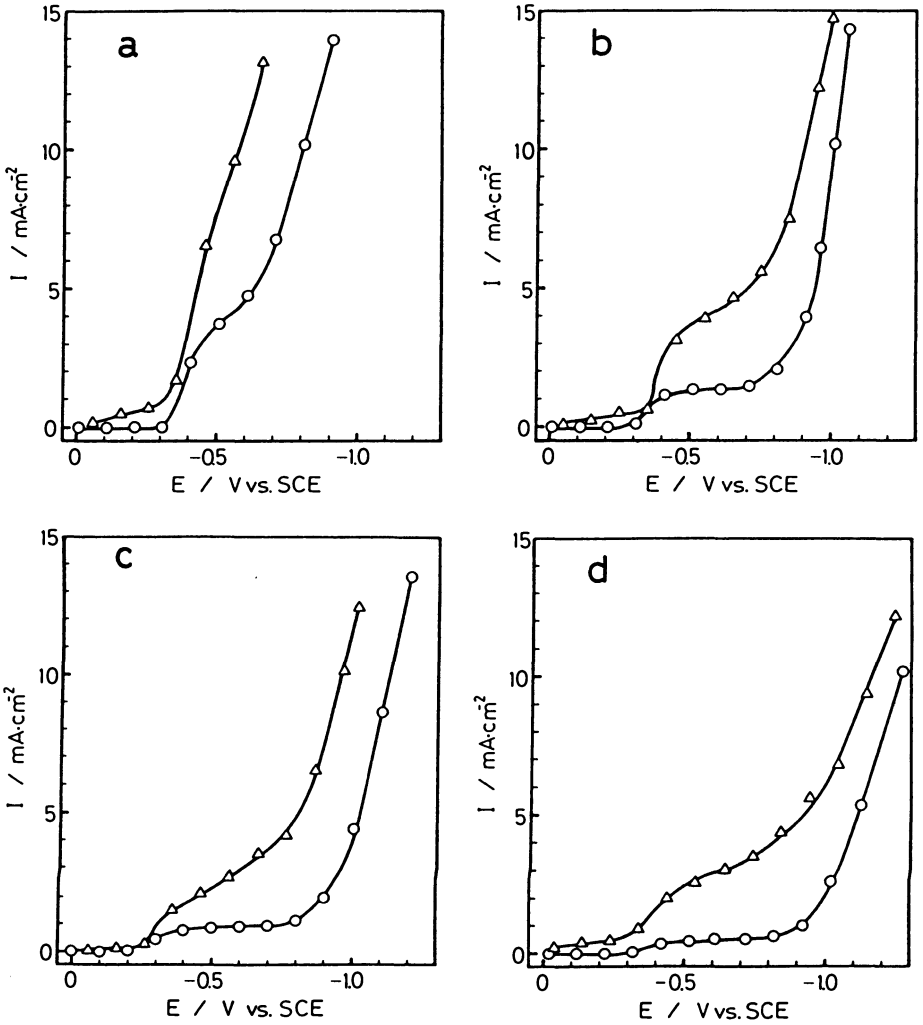

Fig. 2. Current density vs. potential curves for various dilution ratios, (a): 1/2, Ag^+ 2850 ppm, (b): 1/5, Ag^+ 1140 ppm, (c): 1/10, Ag^+ 570 ppm, (d): 1/20, Ag^+ 285 ppm.
—○—: feeder, —△—: 4 mm, 14%.

the calibration curve.

Analysis of Silver Sulfide. Silver sulfide as another product was deposited like a halo on the surface of the granular active carbon. This product was identified by X-ray diffraction. The wavelength of the irradiating X-ray was 1.9373 Å (Fe $K\alpha$).

Recovery Efficiency of Silver. To obtain the recovery efficiency of silver, the electrolysis was carried out under optimum conditions with a static bed height of 4 mm, a bed expansion rate of 14%, a set potential of −0.84 V vs. SCE and an electrolytic duration of 3 h. The amount of silver recovered from the photographic fixing solutions by electrolysis was about 0.5 g. In this case, the recovery of silver was stopped before the concentration of silver ion reached the lower limited value of about 5 ppm, because a large amount of silver sulfide was formed. The silver deposited on the active carbon was dissolved in 5M-HNO_3 of 100 ml for 2 h with stirring. The recovery efficiency of silver was obtained by the ratio of the dissolved silver (g) to the deposited silver (g).

Results and Discussion

Polarization Measurements. (I) Effect of Concentration: In the cell having an inside diameter of 26 mm, the polarization curves for the photographic fixing solutions diluted 2, 5, 10, and 20 times with water are shown in Fig. 2. These data were obtained by measurement under the following conditions: The static bed height of fluidized bed electrode was 4 mm, the bed expansion rate 14%, and the solution temperature 30±0.5 °C. In the case of the feeder electrode only, the flow rate of solution was 0.3 dm^3 min^{-1}. The current density on both the fluidized bed and the feeder electrode increases only with increasing concentration of silver. This can be explained by the fact that the bulk concentration of silver ion is directly proportional to the current. When the concentration of silver ion in the photographic fixing solution increases from 285 ppm in 20 times dilution to 2850 ppm in twofold dilution, the specific conductivity increases from 7500 to 53900 $\mu S\,cm^{-1}$, so that the current increases. Throughout the potential range, the current on the fluidized bed electrode is greater than that on the feeder electrode. Consequently, the

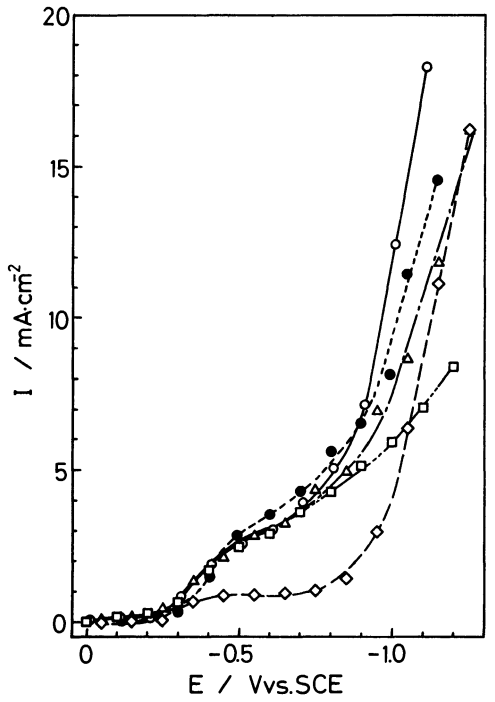

Fig. 3. Current density vs. potential curves for various static bed heights at expansion of 14%.
—○—: 4 mm, -·-△-·-: 8 mm, —-□—-: 12 mm, —◇—: feeder, ----●----: 4 mm (inside diameter of 18 mm).

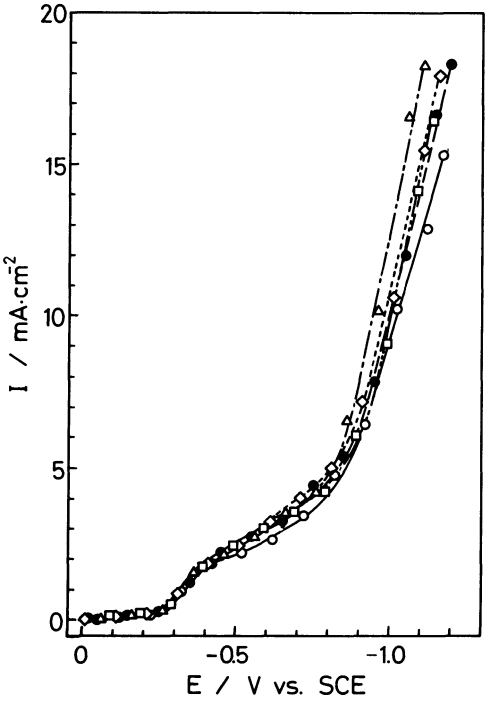

Fig. 4. Current density vs. potential curves for various bed expansions at bed height of 4 mm.
—○—: 10%, —△—: 14%, —-□—-: 17%, ---◇---: 20%, --●--: 30%.

fluidized bed would act as an effective electrode. However, the fluidized bed electrode was found to work effectively when the photographic fixing solution was diluted with water more than 10 times and the static bed height was 12 mm. This can be explained by the fact that the shape of the polarization curves obtained under these conditions resembled that in Fig. 2.

(II) Effect of the Static Bed Height: In a cell having an inside diameter of 26 mm, the polarization curves for static bed heights of 4, 8, and 12 mm, and for a feeder electrode only are shown in Fig. 3. These data were obtained at an expansion rate of the bed of 14% and a solution temperature of 30±0.5 °C. The current density decreases with increasing static bed height. As the ohmic drop in the fluidized bed electrode increases with increasing amount of active carbon, the decrease of the current density would be ascribed to the spread of potential distribution in the bed. When the static bed height was 4 mm, a fluidized bed electrode was more effective than a feeder electrode over all potential ranges. This current density was approximately the same as that with a small cell of 18 mm inside diameter. The optimum static bed height of the cells having inside diameters of 18 and 26 mm was 4 mm.

(III) Effect of Bed Expansion: In the cell having an inside diameter of 26 mm, the polarization curves for bed expansion rates of 10, 14, 17, 20, and 30% at a static bed height of 4 mm and a solution temperature of 30±0.5 °C are shown in Fig. 4. In all cases, a small difference in the current density was observed at less noble potentials than −0.8 V vs. SCE. However, the current density in the noble potential range less than −0.9 V increased steeply. These phenomena can be attributed to the evolution of H_2S and H_2.[5] In the less noble potential range below −0.8 V, the current density shows the highest value at a bed expansion rate of 14%. The current value is approximately the same at 17 and 20%, and lowest at 10 and 30%. In the case of a bed expansion rate smaller than 14%, the current density was small because the effective surface area of electrode was not spread sufficiently. In the range of 14—20%, the transfer to the cathode surface of the Ag^+ ion is promoted by the rotatory motion of the active carbon particles themselves, and the collision numbers among the particles as well as between the particles and the feeder are considerably increased. The charge transfer reaction is believed to proceed smoothly. Also, the thickness of the diffusion layer became smaller because of the flow of electrolyte; hence the current density increased.[6] Above 20%, the conductivity of the fluidized bed electrode deteriorates because the space rate of active carbon particles is increased. The amount of active carbon serving as an electrode was gradually diminished. As the resistance of the bed became progressively greater with increasing bed expansion rate, the current density is inferred to become smaller.[7] The current density with the cell of inside diameter of 26 mm did not differ significantly

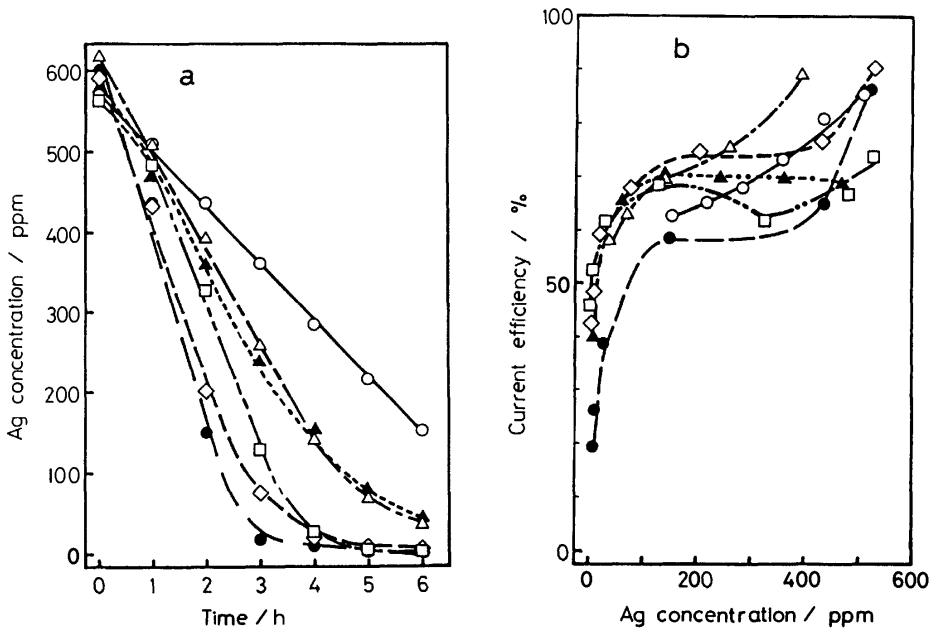

Fig. 5. (a) Change of concentration of silver ion as a function of time, and (b) current efficiency vs. concentration curves for various initial set potentials at bed bed height of 4 mm and expansion of 14%.
—○—: −0.60 V, —△—: −0.70 V, —□—: −0.80 V, —◇—: −0.84 V, —●—: −0.85 V, —▲—: −0.84 V (inside diameter of 18 mm).

from that for the cell of 18 mm inside diameter.

Macroelectrolysis. (1) Effect of Initial Set Potential: The relationship between the concentration of silver ion and the electrolytic duration at various set potentials is shown in Fig. 5(a), and the current efficiency in this case is shown in Fig. 5(b). These data were obtained for a static bed height of 4 mm, bed expansion rate of 14%, and solution temperature of 30±0.5 °C with the cell of inside diameter of 26 mm. The electrolytic duration for recovery of silver became much shorter as the set potential shifts to a less noble potential. The concentration of silver ion decreased linearly from about 600 ppm to about 100 ppm by electrolysis. At a concentration below about 100 ppm, the electrolytic duration for recovery of silver gradually increased. On enlarging the inside diameter of cell, the electrolytic duration for recovery of silver ion up to 50 ppm took about 5.8 h at the inside diameter of 18 mm, but it could be reduced to about 3.5 h in a cell of 26 mm diameter. On the other hand, at concentrations of silver ion up to about 100 ppm the current efficiency increased steeply with increasing concentration. At a concentration of silver ion above about 100 ppm, it was independent of the concentration and reached a value of about 60—75%. The low current efficiency in the concentration range up to about 100 ppm can be ascribed to the diffusion of silver ion in the dilute solution.[8] Such a tendency was similar to that described by Walker et al. for the electrolytic recovery of copper.[9] Moreover, the low current efficiency was due to the formation of other products such as H_2S and Ag_2S. The evolution of H_2S was observed at concentrations below about 100 ppm of silver ion, and at a negative set potential lower than −0.8 V vs. SCE. The H_2S evolution reaction[5] is considered to occur by

$$S_2O_3^{2-} + 2H_2O + 2e^- \longrightarrow H_2S + SO_3^{2-} + 2OH^- \quad (1)$$

Furthermore, a black powder was deposited on the cathode at all set potentials as the concentration of the silver ion decreased. The black powder was shown to be Ag_2S by X-ray diffraction analysis. The deposition reaction of silver from photographic fixing solutions is given as

$$Ag^+ + 2S_2O_3^{2-} \rightleftharpoons [Ag(S_2O_3)_2]^{3-} \quad (2)$$

$$Ag(S_2O_3)_2^{3-} + e^- \longrightarrow 2S_2O_3^{2-} + Ag \quad (3)$$

Then, this reaction competes further with the formation of silver sulfide as follows:[10]

$$H_2S \rightleftharpoons H^+ + HS^- \quad (4)$$

$$H_2S + 2[Ag(S_2O_3)_2]^{3-} \longrightarrow Ag_2S + 2H^+ + 4S_2O_3^{2-} \quad (5a)$$

or

$$HS^- + 2[Ag(S_2O_3)_2]^{3-} \longrightarrow Ag_2S + H^+ + 4S_2O_3^{2-} \quad (5b)$$

From both the recovery time and the current efficiency, it is concluded that the optimum set potential was −0.84 V vs. SCE, and that the limiting concentration of recovery was about 5 ppm. Further, when the inside

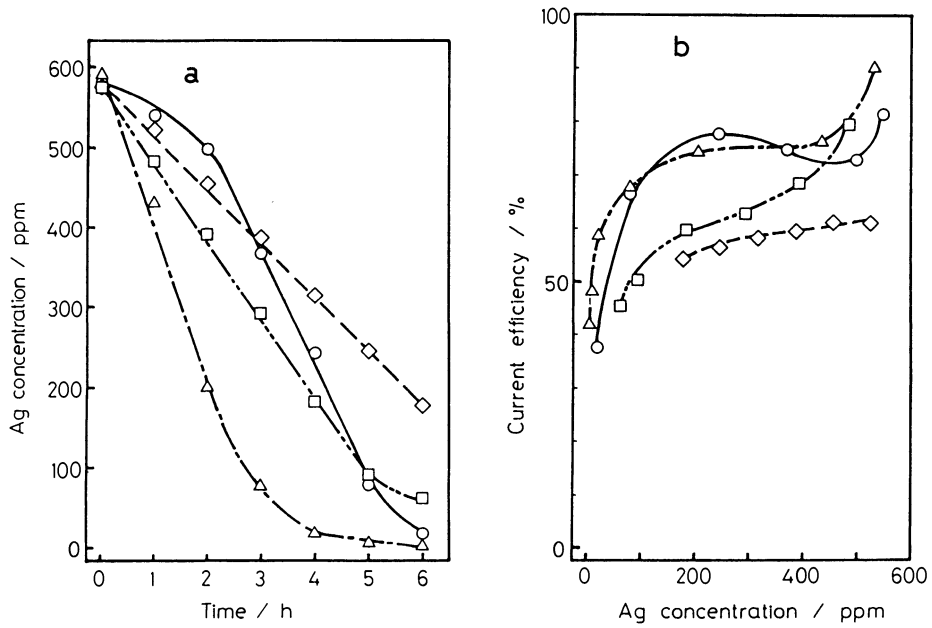

Fig. 6. (a) Change of concentration of silver ion as a function of time, and (b) current efficiency vs. concentration curves for various static bed heights at set potential of −0.84 V vs. SCE and expansion of 14%.
—○—: feeder only, —△—: 4 mm, —□—: 8 mm, —◇—: 12 mm.

diameter of the cell is enlarged from 18 mm to 26 mm, the electrolytic duration for recovery of silver became fairly short. However, the current efficiency for 26 mm was similar to that for 18 mm. In actual electrolysis, the electrolytic duration for recovery was found to be shorter as the electrode surface area is larger in the experimental range.

(II) Effect of Static Bed Height: In the cell having an inside diameter of 26 mm, the relationship between the concentration of silver ion and the electrolytic duration in various static bed heights is shown in Fig. 6(a). The current efficiency in such a run is shown in Fig. 6(b). The bed expansion rate was 14%, the initial set potential −0.84 V vs. SCE, and the solution temperature 30 °C. The electrolytic duration for recovery became shorter as the static bed height decreased. As shown in Fig. 3, the current density at less noble potential than −0.7 V vs. SCE became smaller in the order of 4, 8, and 12 mm of the bed height. Hence, the electrolytic duration for recovery was found to correspond to the result of the polarization measurement. The dependence of the electrolytic duration for recovery on the static bed height would be ascribed to the IR-drop as described previously. The electrolytic duration for recovery with the feeder electrode only was longer than that for the others with in about three hours. As seen in Fig. 3, the current density with the feeder electrode only was much smaller than that with the fluidized bed electrode. These results show that the electrolytic duration for recovery was long at the beginning of electrolysis. The value of the current efficiency decreased in the order of 4, 8, and 12 mm. However, silver sulfide was observed to produce in any bed height. Consequently, the optimum static bed height was 4 mm. The electrolytic duration for recovery of silver with the cell of inside diameter of 26 mm became shorter with decreasing static bed height resembling that obtained with the cell of inside diameter of 18 mm. Hence, the electrolytic duration for recovery was reduced as the inside diameter of the cell increased.

(III) Effect of Bed Expansion Rate: In the cell having an inside diameter of 26 mm, the relationship between the concentration of silver ion and the electrolytic duration in various bed expansion rates is shown in Fig. 7(a). The current efficiency in electrolysis with static bed height of 4 mm, set potential of −0.84 V vs. SCE, and solution temperature of 30± 0.5 °C is shown in Fig. 7(b). The electrolytic duration for recovery of silver was found to be almost independent of the bed expansion rate over the range of the experiment. Such a result would follow from the polarization curve in Fig. 4, because the current density did not change remarkably at various bed expansion rates. However, the current efficiency was optimal in a bed expansion rate of 14%. This may be ascribed to the increase of the effective surface area of the electrode, the decrease of the thickness of the diffusion layer, and the decrease of the bed resistance, as discussed above. At all bed expansion rates, H_2S and Ag_2S were observed to form as the concentration of silver ion decreased. From these results, it is concluded that the optimum bed expansion rate is 14%.

Yield of Silver. When silver deposited on active

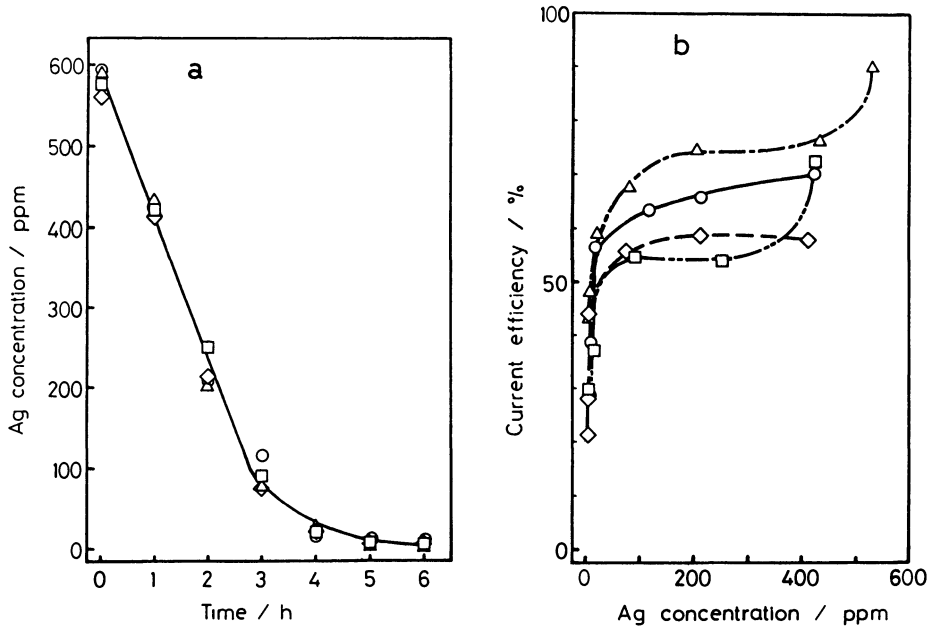

Fig. 7. (a) Change of concentration of silver ion as a function of time, and (b) current efficiency vs. concentration curves for various bed expansion rates at set potential of −0.84 V vs. SCE and bed height of 4 mm.
—○—: 10%, —-△—-: 14%, —--□—--: 20%, --◇--: 30%.

carbon was dissolved in 100 ml of 5M-HNO_3, the yield was about 75%. Silver of 25% could not be recovered, this may be attributed to the silver deposited inside of active carbon not being completely dissolved, and to silver isolated from the surface of the electrode as powdery Ag_2S being deposited on the inside of the pump, valve, and flowmeter.

The authors wish to thank Mr. Takashi Sugiyama for carrying out some of the experiments.

References

1) G. Kreysa, S. Pionteck, and E. Heitz, *J. Appl. Electrochem.*, **5**, 305 (1975).
2) G. Kreysa, *Electrochim. Acta*, **25**, 813 (1980).
3) S. Morooka and Y. Kato, *Kagaku Kohgaku*, **44**, 611 (1980).
4) Z. Ogumi, *Kagaku*, **34**, 316 (1978).
5) A. Tasaka, A. Itani, M. Koyama, and Y. Ohnishi, *Denki Kagaku*, **49**, 623 (1981).
6) M. Fleischmann, J. W. Oldfield, and D. F. Porter, *J. Electroanal. Chem.*, **29**, 244 (1971).
7) B. J. Sabacky and J. W. Evans, *J. Electrochem. Soc.*, **126**, 1182 (1979).
8) F. Hine, "Denki Kagaku Hanno Sousa to Denkaiso Kohgaku," Kagakudojin, Kyoto (1979), p. 68.
9) A. T. S. Walker and A. A. Wragg, *Chemical Engineering Science*, **35**, 405 (1980).
10) J. V. Zee and J. Newman, *J. Electrochem. Soc.*, **124**, 707 (1977).

Phase Transition of *N*-Acyl Amino Acids with Different Acyl Group

Shigeyoshi MIYAGISHI,* Seiichi MATSUMURA, Tsuyoshi ASAKAWA, and Morie NISHIDA
Department of Industrial Chemistry, Faculty of Technology, Kanazawa University, Kanazawa 920
(Received May 13, 1985)

The solid-liquid phase transitions of *N*-acyl amino acids with different acyl groups were investigated using a differential scanning calorimeter and an infrared spectrophotometer. The enthalpy and entropy changes of the transition increased by 3—5 kJ mol^{-1} and 8—10 J K^{-1}mol^{-1}, respectively, for an additional methylene group in *N*-acylglycine, and 7 kJ mol^{-1} and 18 J K^{-1}mol^{-1}, respectively, in the *N*-acyl-L-alanine series. The same thermodynamic quantities of *N*-acylvalines were only slightly dependend on the acyl chain length, while they varied irregularly for the *N*-acylleucine series. Both the enthalpy and entropy were smaller for the L-form than for its racemic isomer in the *N*-acylleucines (C_{12} and above) and *N*-acylvalines. The differences of the thermodynamic quantities between the L- and DL-forms seems to result mainly from the difference of the molecular packing in the solid state.

Chirality of molecules is one of the most important factors in determining the molecular packing in the solid state. For compounds with the long hydrocarbon chain, it is known that both the packing of the chains[1] and the degree of hydrogenbonding[1,2] depend on the chirality. Tachibana and his coworkers[1,3-5] found that 12-hydroxyoctadecanoic acid exhibited a chirality effect in a monolayer state, as well as in the solid state. Such chiral aggregation phenomena have often been found in monolayers,[6-10] ion aggregations,[11] micelles,[12,13] and liquid crystals.[14-16] It has also been reported that the liquid state of racemic 2-octanol differs considerably from that of the enantiomers in its physical properties.[17] Our previous paper[18] concerning the phase transition of *N*-acyl amino acids indicated that the chirality effect depended on the amino acid residue.

In the present work, the dependence of the chirality effect on an acyl group was examined with a differential scanning calorimeter and an infrared spectrophotometer.

Experimental

N-Acyl amino acids were prepared and purified according to a procedure described previously.[13,18,19] *N*-acylglycines were recrystallized from a mixture of ethanol and petroleum ether, and the other *N*-acyl amino acids were recrystallized from a mixed solvent of diethylether and petroleum ether. A differential scanning calorimeter (Daini Seikosha DSC,

Table 1. Properties of *N*-Acyl Amino Acids

	Transition Point			Melting Point		
	T_t/K	ΔH_t/kJ mol^{-1}	ΔS_t/J mol^{-1}K^{-1}	T_m/K	ΔH_f/kJ mol^{-1}	ΔS_f/J mol^{-1}K^{-1}
N-Dec-Gly				387.6	42.2	109
N-Dodec-Gly[a]				393.1	48.4	123
N-Tetradec-Gly	379.6	6.8	17.9	396.6	47.4	120
N-Hexadec-Gly	384.6	4.5	11.7			
	366.1	5.6	15.2	393.1	56.5	144
N-Dodec-L-Ala[a]				356.1	37.6	106
N-Tetradec-L-Ala				367.1	52.3	143
N-Hexadec-L-Ala				374.1	65.3	174
N-Dec-L-Val	378.1	21.3	56.4	380.6	15.4	40.4
N-Dodec-L-Val[a]				380.1	33.1	87.1
N-Tetradec-L-Val	334.6	14.9	14.2	365.1	20.6	56.4
N-Hexadec-L-Val	349.1	29.1	83.4	366.6	54.8	70.0
N-Dec-DL-Val				358.1	63.1	176
N-Dodec-DL-Val[a]				364.6	64.4	177
N-Tetradec-DL-Val				370.1	68.1	184
N-Hexadec-DL-Val				375.1	80.5	214
N-Oct-L-Leu	357.1	7.6	21.4	398.1	29.3	73.7
N-Dec-L-Leu	343.1	1.2	3.4	383.1	27.5	68.8
N-Dodec-L-Leu				383.1	33.5	87.4
N-Tetradec-L-Leu				377.6	32.4	85.8
N-Hexadec-L-Leu				367.1	46.1	126
N-Oct-DL-Leu	353.6	6.8	19.3	367.1	27.2	74.2
N-Dec-DL-Leu				357.1	28.9	81.0
N-Dodec-DL-Leu	341.1	28.9	84.8	356.6	31.0	86.9
N-Tetradec-DL-Leu	320.1	1.8	5.5	349.6	54.8	157
N-Hexadec-DL-Leu	333.1	4.3	12.8	355.1	60.6	171

a) From Ref. 18.

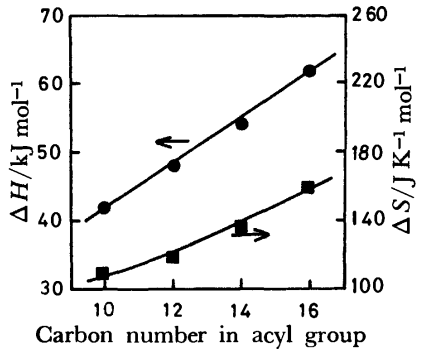

Fig. 1. Enthalpies and entropies of fusion of *N*-acylglycines.

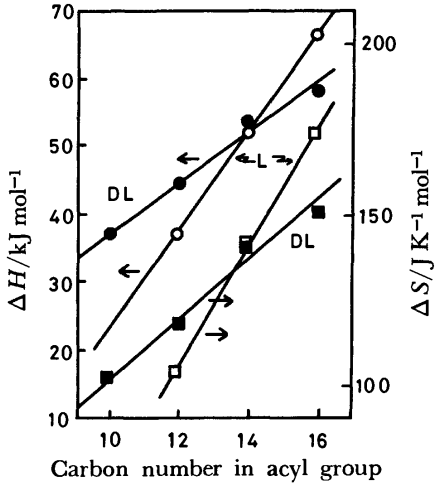

Fig. 2. Enthalpies and entropies of fusion of *N*-acylalanines.
The data of the racemic derivatives were cited from Ref. 18.

model SSC/560S) was used for measurements of the transition temperatures and their enthalpies under the same conditions as described previously.[18] Infrared(IR) spectra were recorded on a JASCO A202 spectrophotometer.

Results and Discussion

Thermal Analysis. The phase-transition temperatures, enthalpies, and entropies of the *N*-acyl amino acids are given in Table 1. The table shows that several *N*-acyl amino acids undergo a transition below the melting point. No distinct correlation existed between the thermodynamic quantities of the transition and the structure of the compound. If this transition is considered as a partial melting, the total enthalpy corresponding to a change from the solid to the liquid state should be the sum of the enthalpy of fusion and the transition enthalpy. Such summation should be true also for the entropy. The total enthalpy and entropy are plotted in Figs.1—4.

The total enthalpy(ΔH) and total entropy(ΔS) increased with the length of an acyl group in the *N*-acylglycine and *N*-acyl-L-alanine series. The increment

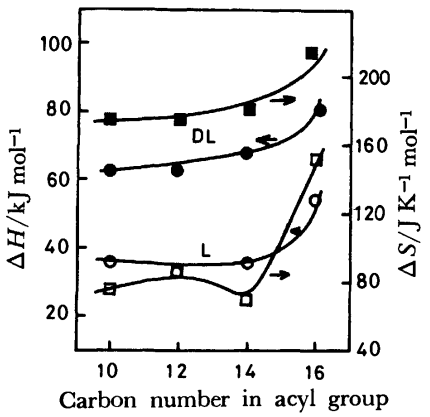

Fig. 3. Enthalpies and entropies of fusion of *N*-acylvalines.

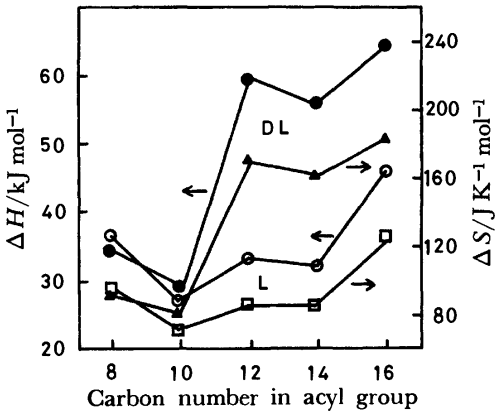

Fig. 4. Enthalpies and entropies of fusion of *N*-acylleucines.

per methylene group in ΔH and ΔS was 3—5 kJ mol^{-1} and 8—10 J K^{-1} mol^{-1}, respectively for the glycine derivatives. These figures are compatible with the corresponding values (4 kJ mol^{-1} and 9 J K^{-1} mol^{-1}) for normal paraffins,[20] monoglycerides,[21] and the racemic *N*-acylalanines.[18] The acyl groups in the monoglycerides and the racemic *N*-acylalanines were concluded to behave in the same manner as a normal alkane when they melted. Therefore, the acyl groups of the *N*-acylglycines seem to behave in the same manner as normal paraffins in regard to the phase transition.

For the L-alanine series, ΔH and ΔS increased by 7 kJ mol^{-1} and 18 J K^{-1} mol^{-1} respectively for each additional methylene group, as seen in Fig. 2. These values were abnormally large as compared with those of the racemic isomer.[18] This result implies a possibility for the acyl groups of the L-isomers to interact attractively with each other in the solid state or to do so repulsively in the liquid state.

In the *N*-acylvaline series, ΔH and ΔS increased slightly with the chain length of the acyl group (Fig. 3). The magnitude of their increments were small suggesting that the methylene chains were fusible or melted in the solid state. The change occuring in the amino acid part of the molecule may contribute to most

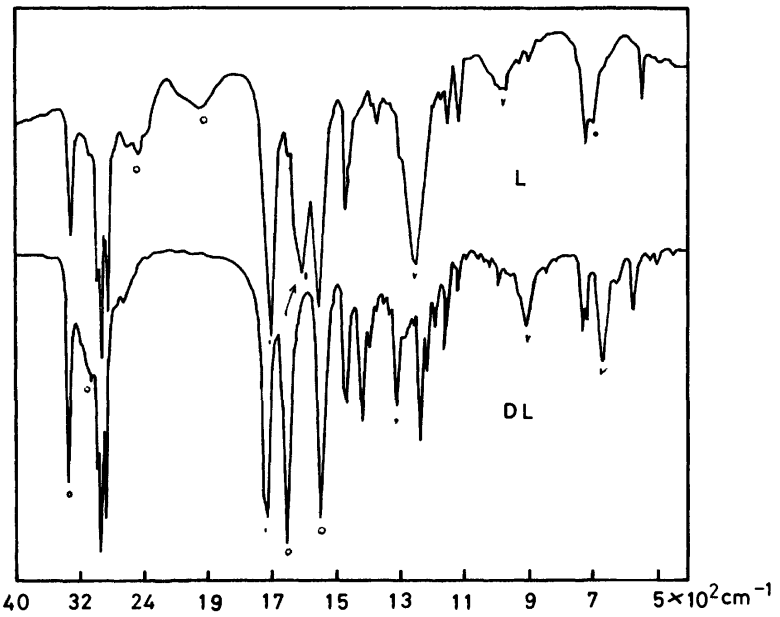

Fig. 5. IR spectra of *N*-tetradecanoyl-L-valine and -DL-valine.

of ΔH and ΔS, when the *N*-acylvalines undergo a transition from solid to liquid. The relation of the thermodynamic quantities with the acyl group was more complicated in the *N*-acylleucines. The enthalpy and the entropy varied in a zigzag form with the length of the acyl group (Fig. 4). Therefore we must consider that the acyl group and the amino acid part in the molecule interact strongly with each other when the phase transition occurs and the influence becomes larger as the molecular structure becomes more complicated.

Next we shall consider the chirality effect. In the alanine series, ΔH and ΔS increased linearly with the chain length of the acyl group, however, a difference was observed in the slope between the chiral and racemic series. For the compounds with the acyl chain shorter than a tetradecanoyl group, the racemic compounds gave larger ΔH and ΔS than the corresponding L-isomers, while *N*-hexadecanoyl-L-alanine had large values compared with its racemic isomer (Fig. 2). The differences between the values of the L- and DL-forms were smaller in the alanine series than in the valine and leucine series (as seen in Figs. 2—4).

Every racemic *N*-acylvalines gave larger ΔH and ΔS than the optically active isomers (as be seen in Fig. 3). In the *N*-acylleucine series, octanoyl and decanoyl derivatives respectively gave nearly identical values for both the chiral and racemic isomers, while the racemic derivatives with a longer acyl chain had large ΔH and ΔS compared with the chiral isomer. The experimental results indicate that if the liquid state is taken as the standard, the racemic form is thermally more stable and more ordered in the solid state than the chiral form, in the case of the *N*-acylvalines and the *N*-acylleucines (except for C_8 and C_{10}). Therefore the chirality effect depends not only on the structure of the amino acid residue but also on the chain length of the acyl group.

The specific heat of fatty acid (C_6—C_{25}) is 2.13—2.42 $J\,g^{-1}\,K^{-1}$ in the liquid state and 1.88—2.09 $J\,g^{-1}\,K^{-1}$ in the solid state,[22a] although the values of the specific heat of the *N*-acyl amino acids are not known. If the values for the *N*-acyl amino acids can be assumed to be similar to those of the fatty acids, the difference of the specific heat between the liquid and solid states is about 0.3 $J\,g^{-1}\,K^{-1}$. For the *N*-decanoyl valines (the melting point is 380.5 and 355 K for the L- and DL-forms), we get the value of 2 $kJ\,mol^{-1}$ (=0.3×(380—355)×271.4) as the enthalpy change due to the temperature difference. This value is negligibly small compared with the difference found in Fig. 3. This fact reveals that the differences between the thermodynamic quantities of the L- and DL-forms have some other origin.

IR Spectra. Information about the solid state is available from the measurement of its IR spectrum, because the spectrum is known to depend on its crystal structure. The IR spectra of the *N*-acyl amino acids were measured in KBr pellets in order to examine a difference of the solid state between the L- and DL-forms. Both the optically active and racemic *N*-acylalanines gave almost identical absorption characteristics except for the region from 600 to 700 cm^{-1}. The band at 690 cm^{-1} is ascribed to O-C=O angle deformation and the band at 640 cm^{-1} may be the C=O bending mode of the CONH group.[23] These two bands were replaced by a single band at 650 cm^{-1} in the racemic form.

Figure 5 shows that there is a significant difference between the spectra of the *N*-acyl-L-valine and -DL-valine. The strong bands at 1710, 1310, 900, and 660 cm^{-1} in the racemic form are associated with a carboxyl group.[24] The C=O stretching band at

1710 cm^{-1} and the C-OH stretching band at 1310 cm^{-1} in the racemic form shifted to 1700 and 1250 cm^{-1}, respectively, in the chiral form. The OH bending band at 900 cm^{-1} and the O-C=O angle deformation band at 680 cm^{-1} shifted to 980 and 695 cm^{-1}, respectively. On the other hand, the bands at 3310, 3100, 1650, and 1550 cm^{-1} in the DL-form are ascribed to amide A, B, I, and II bands respectively.[25] The amide A, B, and II bands are mainly associated with the N-H vibration, while the amide I band is largely a C=O stretching vibration. The amide I band at 1650 cm^{-1} in the DL-form shifted to 1600 cm^{-1} in the L-form, but the amide A, B, and II bands scarcely changed. The broad band near 3100 cm^{-1} in the racemic form was ascribed to hydrogenbonded OH vibration. The corresponding band in the L-form overlapped with the methyl and methylene stretching bands. In addition, two broad bands were observed at 1900 and 2500 cm^{-1} in the L-form.

It is well known that the hydrogenbonded OH band shifts to a lower frequency when the hydroxyl groups form multiple hydrogenbonding.[25] Furthermore the amide A and I bands shift to the low frequency direction and the amide II band to a higher frequency side when the strength of the hydrogenbonds increase owing to intermolecular association.[25] Chen and Parthasarathy[26] found from X-ray studies that short intermolecular hydrogenbonds between the carboxyl OH group and the *N*-acyl oxygen atom are an important feature for *N*-acyl amino acids and link the molecules in a head-to-tail fashion in an infinite chain. These facts suggest the following two possibilities. The small shift of the amide A, B, and II bands suggests that there is little difference in the contribution of the NH group to the hydrogenbonding between the L- and DL-forms. Some of the differences between the L- and DL-forms may result from a difference in the hydrogenbonding between the carboxyl OH group and the oxygen atom of the *N*-acyl group. However, the difference between the IR spectra seen in Fig. 5 is too large to be due to only the difference in the hydrogenbonding force. It is well known that the frequency of the amide I bands depends on the molecular conformation.[23,27,28] The authors reported in the previous paper[18] that the DL-derivatives of the *N*-acyl amino acids form racemic compounds in the solid state. Usually the IR spetrum and the crystal structure of the racemic compound differ significantly from those of the racemic mixture and the optically active isomers. We should also take into account the difference in the molecular packing between the L- and DL-forms. The optically active *N*-acyl amino acids gave different X-ray diffraction patterns from those of the racemic isomers.[29,30] The fatty acids usaully have an anti-parallel packing of the molecules in their solid states.

Therefore we assume two possibilities about the molecular packing in the L-form. The first case is the formation of a dimer or a molecular packing relatively similar to it. This dimer may be formed due to hydrogen bonding between the carboxyl OH group in one molecule and the *N*-acyl oxygen atom in the other molecule, and these molecules may be linked in an anti-parallel fashion to each other. In addition, such molecular packing can make the skeletal plane of the hydrocarbon chain parallel with its neighbors and enables us to explain a single peak at 720 cm^{-1} (see later). The second possibility is the formation of a similar bilayer structure as that found in the long chain fatty acids except for the hydrogen bonding. The hydrogenbonds in the latter case are formed between the carboxyl groups, but those in the *N*-acyl-L-valine may be formed between the carboxyl OH group and the *N*-acyl oxygen atom. In addition the bilayer structure may be linked to each other by the hydrogenbonds. In the racemic form the molecule has a different chirality from its neighbors. The valine residue group in the *N*-acylvaline may take up a trans position with respect to its NH group and thereby may prevent strong interaction between its *N*-acyl oxygen atom and the carboxyl group in its neighboring molecule compared with that in the L-from.

The IR spectrum of *N*-hexadecanoyl-L-valine was different from those of the other chiral *N*-acylvalines. Its spectrum was similar to those of the racemic derivatives in the region above 1500 cm^{-1} and was different in the regions of the methylene rocking and wagging bands. Furthermore the bands associated with the carboxyl group and the amide group had the same frequency and shape as those of the racemic isomer. *N*-Hexadecanoyl-L-valine seems to be different from the other *N*-acyl-L-valines in the solid state and to give larger thermodynamic quantities than the other (see Fig. 3). The spectra of the racemic *N*-acylvalines were almost the same as each other. This probably suggests that the racemic derivatives have closely similar crystal forms.

In the racemic *N*-acylvaline series, the methylene rocking vibration gives rise to split components at 715 and 725 cm^{-1}. In the L-forms a single rocking band which overlapped the carboxyl angle deformation band, was observed (Fig. 5). The *N*-acylglycines and *N*-acylleucines also exhibited a splitting of the methylene rocking band. On the other hand, the alanine derivatives gave a sharp single band at 720 cm^{-1} (Fig. 6). Such splitting of the methylene rocking band has been found in fatty acids,[24] normal paraffins,[31,32] 12-hydroxyoctadecanoic acid,[1] polyethylene,[33] and lithium *n*-hexadecanoate,[34] and is related to a hydrocarbon chain packing in the crystal. In the powder X-ray diffraction pattern of *N*-dodecanoyl-DL-valine,[30] the peaks at 4.11 and 3.72 A are in good agreement with those in the B- and C-forms of octadecanoic acid and the C-form dodecanoic acid, in which the methylene chain skeletal plane is nearly perpendicular to its neighbors in the orthorhombic subcell.[35]

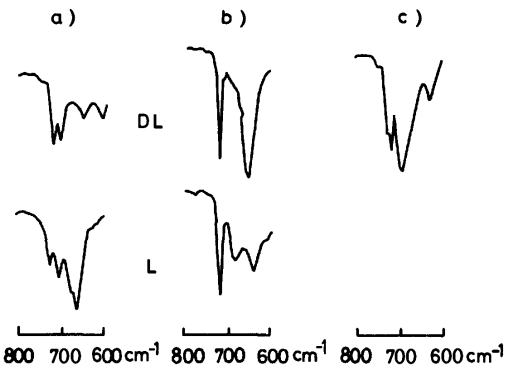

Fig. 6. Comparison of IR spectrum between L- and DL-isomers.
a) *N*-Tetradecanoylleucines, b) *N*-Tetradecanoylalanines, and c) *N*-Tetradecanoylglycine.

This agreement supports the nearly perpendicular packing of the methylene chains in *N*-dodecanoyl-DL-valine. Therefore the splitting in the methylene rocking band can be explained by such packing of the methylene chains. In its L-form, the peak corresponding to the hexagonal subcell packing of the methylene chains was not detected in the powder X-ray diffraction pattern.[30] Thus the parallel packing of the skeletal plane of the methylene chain may give the single peak at 720 cm^{-1}.

N-Octanoyl- and *N*-decanoyl-DL-leucines gave the same spectrum as those of the *N*-acyl-L-leucines. The spectra of the other racemic *N*-acylleucines differed from those of the chiral isomers. In the region above 1500 cm^{-1}, the consideration of the comparison of the L- and DL-forms in the valine derivatives was also applicable to the leucine series. In other regions, a band at 660 cm^{-1} in the L-form was replaced by two bands at 650 and 610 cm^{-1} in the DL-form, and the OH bending band at 920 and 970 cm^{-1} were replaced by a single band at 940 cm^{-1}.

The above results indicate that the *N*-acyl amino acids with large difference between the L- and DL-forms in the thermodynamic quantities also exhibit big differences in their IR spectra. The differences found in the IR spectra reflects that of the solid state, because the measurement of the spectra was done at room temperature. Analogy between the results of the thermal analysis and the spectral data indicates that the differences of the thermodynamic quantities between the L- and DL-forms result mainly from the difference of the molecular packing in the solid state.

References

1) T. Tachibana, T. Yoshizumi, and K. Hori, *Bull. Chem. Soc. Jpn.*, **52**, 34 (1979).
2) M. Iwahashi, Y. Watanabe, T. Watanabe, and M. Muramatsu, *Bull. Chem. Soc. Jpn.*, **57**, 1446 (1984).
3) T. Tachibana and H. Kambara. *J. Colloid Interface Sci.*, **28**, 173 (1968).
4) T. Tachibana and H. Kambara, *Bull. Chem. Soc. Jpn.*, **42**, 3422 (1969).
5) T. Tachibana and K. Hori, *J. Colloid Interface Sci.*, **61**, 398 (1977).
6) E. M. Arnett, J. Chao, B. Kinzig, M. Stewart. and O. Thompson. *J. Am. Chem. Soc.*, **100**, 5575 (1978).
7) E. M. Arnett and O. Thompson. *J. Am. Chem. Soc.*, **103**, 968 (1981).
8) E. M. Arnett, J. Chao, B. J. Kinzig, M. V. Stewart, O. Thompson, and R. J. Verbiar, *J. Am. Chem. Soc.*, **104**, 389 (1982).
9) Y. Shibazaki and K. Fukuda, *Kobunshi*, **26**, 702 (1977).
10) K. Fukuda, Y. Shibazaki, and H. Nakahara, *J. Macromol. Sci. Chem.*, **15**, 999 (1981).
11) E. M. Arnett and S. P. Zingg, *J. Am. Chem. Soc.*, **103**, 1221 (1981).
12) R. Yoshida, M. Takehara, and K. Sakamoto, *Yukagaku*, **29**, 538 (1975).
13) S. Miyagishi and M. Nishida, *J. Colloid Interface Sci.*, **65**, 380 (1978).
14) K. Sakamoto, *Mol. Cryst. Liq. Cryst.*, **59**, 59 (1980).
15) A. S. Tracey and K. Radley, *J. Phys. Chem.*, **88**, 6044 (1984).
16) A. S. Tracey and K. Radley, *Mol. Cryst. Liq. Cryst.*, **122**, 77 (1985).
17) C. J. McGinn, *J. Phys. Chem.*, **65**, 1896 (1961).
18) S. Miyagishi, S. Matsumura, K. Murata, T. Asakawa, and M. Nishida, *Bull. Chem. Soc. Jpn.*, **58**, 1019 (1985).
19) S. Miyagishi. Y. Ishibai, T. Asakawa, and M. Nishida, *J. Colloid Interface Sci.*, **103**, 169 (1985).
20) R. H. Aranow, L. Witten, and D. H. Andrews, *J. Phys. Chem.*, **62**, 812 (1958).
21) T. Maruyama, I. Niiya, M. Imamura, and T. Matsumoto. *Yukagaku*, **26**, 104 (1977).
22) a: K. Inaba and J. Hirano, "Shibosan Kagaku," Sachi Shobo, Tokyo (1981), p. 67; b: p. 49.
23) T. Miyazawa, Y. Masuda, and K. Fukushima, *J. Polym. Sci.*, **62**, S64, (1962).
24) R. F. Holland and J. R. Nielsen. *J. Mol. Spectroscopy*, **9**, 436 (1962).
25) T. Miyazawa, "Infrared Absorption Spectra," ed by Kinki Kogyo-Kai, Asakura Shoten, Tokyo (1964), Chap. 1.
26) C. Chen and R. Parthasarathy, *Acta Crystallogr., Sect. B*, **33**, 3332 (1977).
27) T. Miyazawa, *J. Chem. Phys.*, **32**, 1647 (1960).
28) T. Miyazawa and E. R. Blout, *J. Am. Chem. Soc.*, **83**, 712 (1961).
29) M. Takehara, H. Moriyuki, I. Yoshimura, and S. Yoshida, *J. Am. Oil Chem. Soc.*, **49**, 143 (1972).
30) S. Miyagishi, unpublished data.
31) J. R. Nielsen and C. E. Hathaway, *J. Mol. Spectroscopy*, **10**, 366 (1963).
32) G. Ungar and N. Masic, *J. Phys. Chem.*, **89**, 1036 (1985).
33) J. R. Nielsen and C. E. Holland, *J. Mol. Spectroscopy*, **6**, 394 (1961).
34) V. Busico, A. Ferraro, and M. Vacatello, *J. Phys. Chem.*, **88**, 4055 (1984).
35) M. Goto, *Yukagaku*, **19**, 583 (1970).

 © 1986 The Chemical Society of Japan Bull. Chem. Soc. Jpn., 59, 563—567 (1986)

In Situ X-Ray Observation on the Intercalation of Weak Interaction Molecules into Perovskite-Type Layered Crystals $(C_9H_{19}NH_3)_2PbI_4$ and $(C_{10}H_{21}NH_3)_2CdCl_4$

Yuri I. Dolzhenko,† Tamotsu Inabe, and Yusei Maruyama*
†Department of Physical Chemistry, Kharkov Polytechnical Institute, Kharkov, 310002, U.S.S.R.
Department of Molecular Assemblies, Institute for Molecular Science, Myodaiji, Okazaki 444
(Received August 5, 1985)

The intercalation-deintercalation process of weak interaction organic molecules such as 1-chloronaphthalene and *o*-dichlorobenzene into highly oriented polycrystalline $(C_{10}H_{21}NH_3)_2CdCl_4$ films and hexane into $(C_9H_{19}NH_3)_2PbI_4$ single crystals has been observed in situ by using X-ray technique. The process is highly reversible. Increasing of interlayer spacing is in reasonable agreement with the size of the intercalated molecules and corresponds to the parallel orientation of aromatic ring planes or hexane chains in between two paraffin layers of the host crystals.

Intercalation phenomena of layered compounds have been known for a long time, and a considerable variety of host lattices that can incorporate atomic or molecular guest species have been investigated, e.g. graphite, clay minerals, layered cyanides, layered dichalcogenides and so on.[1] The attention paid to these compounds began to grow significantly about fifteen years ago, when it was found that some physical properties of layered materials, for example such as superconductivity or cooperative lattice distortions, etc., can be modified significantly by intercalation.[2] On the other hand, intercalated phases show potential technological significance. Their application as reversible electrodes for high-energy-density batteries,[3] and their efficiency as heterogeneous catalysts[4] are well known.

Both academic and technological aspects of intercalation chemistry stimulate an effort to understand the structure, bonding and formation of these compounds in more detail and attempts to synthesize new layered materials and intercalation compounds with interesting structures and properties. During the past few years the range of layered compounds which can be intercalated has been extended to such materials as the almost insulating semiconductor, PbI_2,[5,6] metallic and electron donor type lattice, Ag_2F,[7] black phosphorus (which has both electron-donating and accepting potentiality),[8] and others.[1]

Possible new candidates for intercalation process studies are perovskite-type layered structures of the general formula, $(C_nH_{2n+1}NH_3)_2MCl_4$, where $M=Cu^{2+}$, Mn^{2+}, Cd^{2+}, Fe^{2+}, Pd^{2+}, Co^{2+}, or Zn^{2+}. Great interest has been shown in these compounds during the past decade since they exhibit a large variety of structural and magnetic phase transitions.[9-11] Some of these compounds, for example $(C_{10}H_{21}NH_3)_2CdCl_4$, are considered as crystalline models of lipid bilayer membranes.

In this communication, we wish to report the first brief results of organic molecules intercalation into $(C_nH_{2n+1}NH_3)_2MX_4$(X: halogen) layered materials, namely 1-chloronaphthalene (hereafter $C_{10}H_7Cl$) and *o*-dichlorobenzene ($C_6H_4Cl_2$) into $(C_{10}H_{21}NH_3)_2CdCl_4$ (C_{10}-$CdCl_4$) and hexane into $(C_9H_{19}NH_3)_2PbI_4$ (C_9-PbI_4), recently obtained by us.

Experimental

A highly oriented polycrystalline film of C_{10}-$CdCl_4$ in 0.05 mm thickness was obtained by slow cooling on the surface of a hot aqueous solution, which contains $C_{10}H_{21}NH_3$ and $CdCl_2$ in the amounts of reaction stoichiometry, acidized with a few drops of aqueous HCl solution. The film was scooped onto a glass plate and dried. The film so obtained has the same c-parameter of the lattice as that already reported for a single crystal.[10] The phase transition temperatures also correspond to the reported ones.

C_9-PbI_4 single crystals were recently synthesized in our laboratory using a silica-gel technique.[12] We believe this is the first example of $(C_nH_{2n+1}NH_3)_2MX_4$ family with M=Pb and X=I. The crystal has a dark orange square-like shape of $3\times3\times0.1$ mm^3. The details of the synthesis and complete characterization of this compound will be published elswhere soon. Here we only want to note that the C,H-chemical analysis corresponds to the assigned formula within an error of 0.05%.

By TGA it is established that in the region of 290—310 °C C_9-PbI_4 decomposes by a few steps involving melting and loses about 50% of its weight, this is in reasonable agreement with the reaction, $(C_9H_{19}NH_3)_2PbI_4 \rightarrow 2C_9H_{19}NH_3I + PbI_2$. X-Ray diffraction patterns of the remainder correspond to pure PbI_2. By optical reflectance and DSC measurements it was found that C_9-PbI_4 undergoes two phase transitions at 315 and 240 K. Under a polarizing microscope it seems that the higher temperature transition is an order-disorder one as in C_{10}-$CdCl_4$ and similar compounds. At this transition temperature the interlayer spacing changed discontinuously from 19.88 Å to 21.83 Å. The full structure determination of C_9-PbI_4 crystals is currently in progress and will be published elsewhere.

In situ X-ray analysis was carried out with the use of a Rigaku Geiger-flex Model 2027 X-ray diffractometer (with copper target). A C_9-PbI_4 single crystal of about 4 mm^2 or C_{10}-$CdCl_4$ film of approximately 5 mm^2 was mounted on a glass plate. The c-axis direction of the crystals was perpendicular to the glass surface. In the case of $C_{10}H_7Cl$, the intercalation-deintercalation process was easily observed by X-ray diffraction in the following procedure. One or two

drops of $C_{10}H_7Cl$ were dropped on the C_{10}-$CdCl_4$ film and it was kept under these conditions for about 5 min. Then, excess liquid was removed by absorbing with filter paper and the glass plate was set in the diffractometer for observation. At this stage of the procedure, $C_{10}H_7Cl$ was still continuing to intercalate into C_{10}-$CdCl_4$, but that amount of $C_{10}H_7Cl$ was enough to observe all the phases of the intercalation-deintercalation process. Deintercalation proceeded after a short time of heating.

In the case of hexane and $C_6H_4Cl_2$ in situ intercalation was carried out by vapor evaporation of the liquid impregnated in cotton mounted on the back side of the glass plate. The scanning was limited only to the region of strong reflections, i.e. $2\theta=5°$—$25°$ for C_{10}-$CdCl_4$ and $2\theta=15°$—$33°$ for C_9-PbI_4. Because of the high vapor pressure of hexane, we had to use rapid scanning and a short time-constant. In spite of that, the recorded diffractograms were highly reproducible and clear. All measurements were carried out at room temperature.

Results and Discussion

1) Intercalation into C_{10}-$CdCl_4$. According to Ref. 10, C_{10}-$CdCl_4$ consists of $[CdCl_4]^{2-}$ layers sandwiched between alkylammonium chains as is shown in a simplified form in Fig. 1 (a). The ammonium end of each chain is linked to the layer by weak hydrogen bonding, N-H····Cl.

Successive changes of X-ray diffraction patterns by exposing to $C_{10}H_7Cl$ are shown in Fig. 2. As one can easily see in Fig. 2 (a), after a 5 min exposure the intensities of the host crystal diffractions decrease remarkably and a well defined series of new (001) lines appear (marked with arrows). During the intercalation process (Fig. 2 (b), (c)), the intensities of the original lines are continuously decreasing while new ones are increasing in the same manner until full intercalation is achieved (Fig. 2 (d)). During deintercalation the diffraction patterns change inversely. The diffraction patterns for the completely $C_{10}H_7Cl$ deintercalated C_{10}-$CdCl_4$ polycrystalline film is shown in Fig. 2 (f). $C_6H_4Cl_2$ intercalation-deintercalation process for

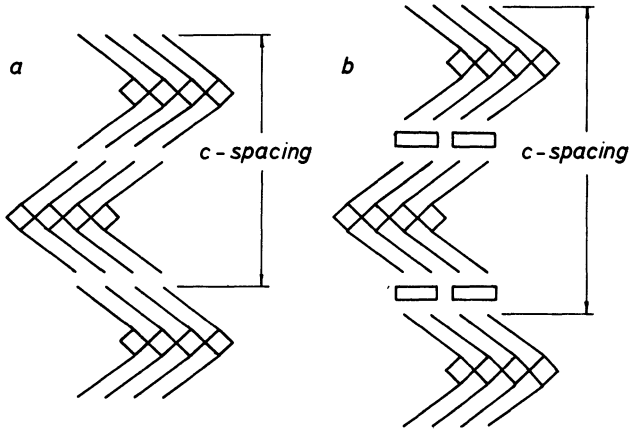

Fig. 1. Simplified schematic representation of nonintercalated (a) and intercalated (b) structures of C_{10}-$CdCl_4$.

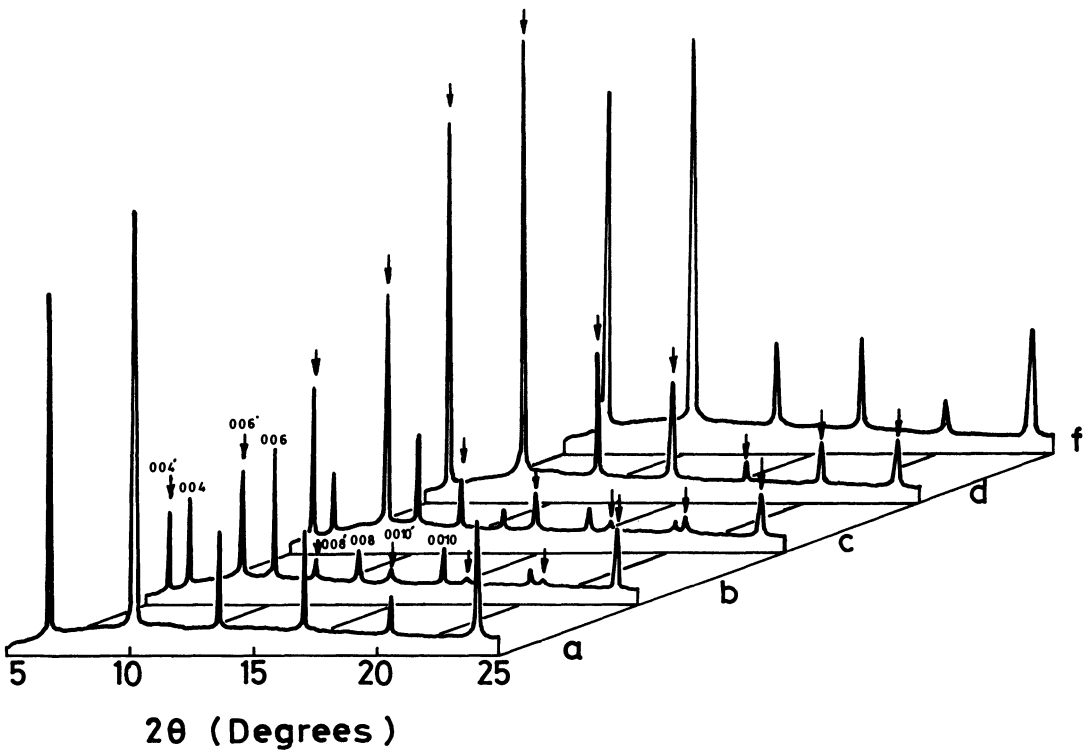

Fig. 2. X-Ray diffraction patterns of C_{10}-$CdCl_4$ during defferent phases of intercalation-deintercalation process with $C_{10}H_7Cl$. Pure C_{10}-$CdCl_4$ (a), successive phases of partially intercalated situation (b, c), fully intercalated (d), and completely deintercalated sample (f). The lines corresponding to the intercalated phases are marked with arrows. All diffraction patterns are recorded at the same sensitivity which equals to 20 kcps for the full scale.

C_{10}–$CdCl_4$ is observed in a same manner. By intercalation C_{10}–$CdCl_4$ c-spacings increased from 51.62 Å to 59.1 Å for $C_{10}H_7Cl$ and to 58.9 Å for $C_6H_4Cl_2$. In order to understand these differences and to know the exact positions of the intercalated molecules further investigations are required. The first brief results of interlayer increasing, i.e. 3.75 Å for $C_{10}H_7Cl$ and 3.65 Å for $C_6H_4Cl_2$ per one C_{10}–$CdCl_4$ layer, are in reasonable aqreement with the thickness of the aromatic rings and suggest the parallel orientation of the aromatic rings of guest molecules with the layer planes of the host crystal (Fig. 1 (b)).

The process was highly reversible. After three cycles of this procedure for the same C_{10}–$CdCl_4$ film, there was no significant change in the diffraction patterns and, surprisingly, even sharper lines were observed. For the first cycle of $C_{10}H_7Cl$ intercalation-deintercalation into C_{10}–$CdCl_4$, it took about 6 h and for the next two cycles only about 2 h. $C_6H_4Cl_2$ intercalation into C_{10}–$CdCl_4$ is remarkably faster and even for the first full cycle it required only about one hour and a half.

2) Intercalation into C_9–PbI_4. Although the full structural analysis of C_9–PbI_4 has not yet been solved, all observations of this compound suggest that C_9–PbI_4 has a similar structure to the C_{10}–$CdCl_4$ crystalline matrix in which the organic bilayers are embedded. The size of the I_6 octahedra the center of which is occupied by the Pb^{2+} ion is assumed to be the same as in PbI_2.[13] Further we suppose that for the best orientation of the N–H····I bonding, the N-atoms of the alkylammonium chains are occupying the A sites of a perovskite-type layer and lie in approximately the same plane with unshared I atoms of I_6 octahedra similarly to C_{10}–$CdCl_4$. On these assumptions the thickness of the $[PbI_4]^{2-}$ layer is estimated to be 6.45 Å and the $C_9H_{19}NH_3^+$ chain length which is rising above and below the $[PbI_4]^{2-}$ layer is calculated to be as long as 13.33 Å, based on the same assumptions as in Ref. 14. For this arrangement and taking into account that the C_9–PbI_4 interplanar spacing is as long as 19.88 Å at room temperature, we can conclude that the direction of the alkylammonium chain is tilted about 60° with respect to the normal to the octahedra layer. The following calculations are all made on these assumptions.

In the case of C_9–PbI_4 single crystals it was easy to observe the intercalation-deintercalation process. On dropping the C_9–PbI_4 crystal into hexane the color immediately changed from dark orange to yellow, and it turned back to original color after removing the crystal from the hexane. Deintercalated crystals have a slightly deformed shape, but do not lose their integrity even after keeping for one week in hexane, and they do not lose their weight during prolonged washing on a filter with hexane.

By watching with the naked eye or a polarizing microscope it is possible to observe the introduction of such solvents as hexane, benzene, dichloromethane, dichlorobenzene, chloronaphthalene or any other soft enough solvents from the view point of intermolecular interactions. In the case of more polar and/or potentially H-bonding solvents such as tetrahydrofuran, ethanol, acetone, we observed solvation but not molecular inclusion. In the case of the introduction of $C_{10}H_7Cl$ or $C_6H_4Cl_2$, we could observe only a decrease in the intensities of the host crystal diffraction lines and disordered pattern. No lines corresponding to a new interlayer spacing appeared. Only with such a weak solvent as hexane and with fresh C_9–PbI_4 single crystals could we observe new interlayer spacings clearly and unambiguously. These results are represented in Fig. 3. The first X-ray scanning started at about 10 s after exposing the crystal to hexane vapor (Fig. 3 (b)). The

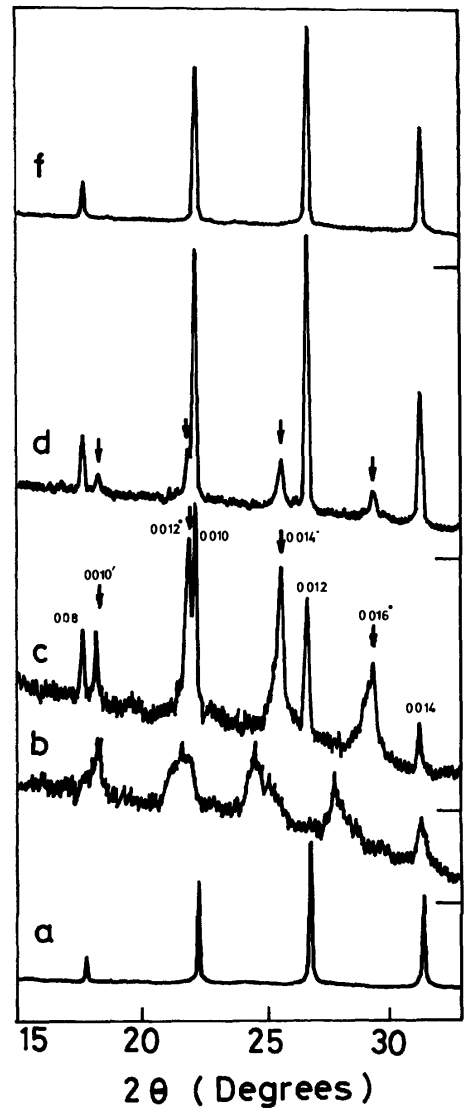

Fig. 3. X-Ray diffraction patterns of C_9–PbI_4 during different phases of hexane intercalation-deintercalation process. The lines corresponding to the intercalated phases are marked with arrows. X-Ray diffractometer full scale sensitivities correspond to 40 kcps for (a), 4 kcps for (b, c), 10 kcps for (d), and 20 kcps for (f).

diffracted patterns consist of a group of diffuse lines. We did not try to index these lines because of the nonequilibrium situation and the co-existence of multistates in this scanning. From this result we can presume only one conclusion, that the hexane intercalation into C_9-PbI_4 crystal passes through rather highly disordered states with some average interlayer spacings. On the contrary, for the next scanning (Fig. 3 (c)) the starting point was ≈5 min after the process had begun and it is clearly to be seen that these are two series of diffraction lines. One series corresponds to the host C_9-PbI_4 interlayer spacing pattern with decreased intensities, while other lines (marked with arrows) correspond to an interlayer spacing as long as 24.27 Å, or in other words a 4.36 Å increase per one C_9-PbI_4 layer. This value is reasonably close to the paraffinic chain diameter and suggests the parallel orientation of hexane chains with respect to the host crystal layers.

For the next scanning (Fig. 3 (d)), the intensities of the host crystal lines are increassing while the intensities of the new series of lines are decreasing and a completely deintercalated picture occurs after one hour (Fig. 3 (f)).

It is not impossible to observe the second cycle of hexane intercalation-deintercalation into C_9-PbI_4, but the recorded diffraction patterns become diffuse and not so clear due to the much more rapid rate of the process and a tendency to disordering.

3) General Discussion. The process we observed seems similar to the already reported results of organic molecules inclusion into paraffin layers of nickel cyanide-normal alkylamine layered systems.[15,16] However, there is a clearly distinguishable difference between these cases. In the reported case, no sharp dependence of the interlayer spacing on the amount or size of the excessively introduced amines was observed. Matsunaga clearly observed new interlayer spacings, but they did not correspond to the size of the excessively introduced molecules.[16] In our investigation all observed interlayer spacings are very clearly defined and in reasonable agreement with the size of the intercalated molecules.

As we interpret it, the main reason for such a difference between the observed processes lies in our host material structures. In their case only one layer of normal alkylamine molecules exists in between two crystalline nickel cyanide layers. Accordingly excessively introduced organic molecules penetrate inside the paraffin layer with changing of the packing coefficient of the amine molecules.[16] This pocess seems like a two-dimensional solvation with respect to the paraffin layers, or solvated intercalation with respect to the nickel cyanide layers.[17] In our cases of C_{10}-$CdCl_4$ and C_9-PbI_4 the crystals consist of organic bilayers in between two $[MX_4]^{2-}$ layers. In this case organic molecules presumably penetrate not inside but in between the alkylammonium layers retaining the full structure of C_{10}-$CdCl_4$ or C_9-PbI_4 layers perfectly unchanged. This behavior as well as reversibility are the main requirements for the exact definition of intercalation (see, for example, Ref. 17).

We believe that the existence of organic bilayers and the softness or weakness in view of intermolecular interaction forces of introduced organic molecules are the main reasons for the existence of the observed intercalation without breaking the host crystal framework structure. To our knowledge this type of introduction of molecules is reported here for the first time.

If we combine the results obtained here and reported before,[15,16] it is possible to imagine three steps of interaction processes for such layered materials and organic solvents. (i) For strong host matrixes and weak interaction guest molecules—intercalation with clearly defined new interlayer spacings corresponding to the size of the guest molecules. (ii) An intermediate situation with molecular inclusion inside paraffin layers. (iii) For weak matrixes and strong solvents-solvation leading to homogeneous solutions, for example, C_9-PbI_4 solvation in tetrahydrofuran and so on.

We belive that each member of the $(C_nH_{2n+1}NH_3)_2MX_4$ family can be intercalated with appropriate organic solvents. Moreover, we cannot exclude the possibility for similar process as secondary intercalation of long amine intercalated transition metal dichalcogenides in which an amine bilayer structure is present.

Finally, we want to note that it is difficult to imagine any charge transfer especially in the case of hexane intercalation. Thus, we believe that we really observe pure van der Waals intercalation.

We want to thank Prof. M. Sato for useful discussion. This work was done during a stay of Y. I. Dolzhenko at the Institute for Molecular Science. He would like to express his thanks to the Authorities of IMS of Okazaki National Institutes and special thanks to his host scientist Prof. Y. Maruyama for the possibility to pursue this work.

References

1) "Intercalation Chemistry," ed by M. S. Whittingham and A. J. Jacobson, Academic Press (1982).
2) F. R. Gamble, J. H. Osieck, M. Cais, R. Pisharody, F. J. Disalvo, and T. M. Geballe, *Science*, **174**, 493 (1971).
3) M. S. Whittingham, *Progr. Solid State Chem.*, **12**, 41 (1978).
4) L. B. Ebert, *J. Mol. Catalysis*, **15**, 275 (1982).
5) V. M. Koshkin, *Latv. PSR Zinat. Akad. Vestis, Fiz. Teh. Zinat. Ser.*, **1981**, 90.
6) A. M. Ghoryeb, C. C. Coleman, and A. S. Yoffe, *J. Phys. C. Solid State Phys.*, **17**, L715 (1984).
7) A. P. Mil'ner, Yu. R. Zabrodskii, V. M. Koshkin, V. V. Kukol, E. B. Yagubskii, and G. D. Guseinov, *Zh. Strukt. Khim.*, **21**, 93 (1980).
8) Y. Maruyama, unpublished result.
9) R. Kind, *Ber. Bunsenges. Phys. Chem.*, **87**, 248 (1983).

10) R. Kind, S. Plesuko, H. Arend, R. Blinc, B. Zeks, J. Selinger, B. Lozar, J. Slak, A. Levstik, C. Filipic, V. Zagar, G. Lahajar, F. Milia, and G. Chapuis, *J. Chem. Phys.*, **71**, 2118 (1979).
11) J. Etxebarria, J. Fernandez, M. A. Arriandiaga, and M. J. Tełło, *J. Phys. C; Solid State Phys.*, **18**, L13 (1985).
12) E. A. Ziger, "Rost i svoistva kristallov," Kharkov (1980), p. 8.
13) R. W. G. Wyckoff, "Crystal Structure," John Wiley, New York (1963), Vol. 1, p. 269.
14) Ref. 1, p. 239.
15) Y. Mathey, R. Setton, and C. Mazieres, *Can. J. Chem.*, **55**, 17 (1976).
16) K. Takayanagi and Y. Matsunaga, *Nippon Kagaku Kaishi*, **1983**, 277.
17) Ref. 1, p. 315.

Nanosecond Laser Photolysis of *N*-Methylindole in Acetonitrile

Nobuaki KANAMARU and Jiro TANAKA
Department of Chemistry, Faculty of Science, Nagoya University, Furo-cho, Chikusa-ku, Nagoya, Aichi 464
(Received August 19, 1985)

Nanosecond laser photolysis (nslp) of *N*-methylindole (NMI) was investigated using XeCl laser (308 nm) so that excitation is performed at the red edge of the first absorption band. At least three transient absorptions were observed i.e. those to be ascribed to $S_n \leftarrow S_1$, $T_n \leftarrow T_1$ transitions and ion-pair like species with peaks at ≈ 700 nm, ≈ 460 nm, and ≈ 380 nm, respectively. The transient absorptions were found to be produced by monophotonic processes. The lifetimes of the triplet state and the ion pair were determined to be ≈ 3.1 μs and ≈ 29 μs, respectively, in degassed solutions. Transient photoconductivity (tpc) measured on the same system indicated that there are both rise and decay components. Its fastest decay component of ≈26 μs is close to that of the transient absorption ascribed to the ion pair. This result provides another example of monophotonic electron ejection through fluorescent states of aromatic amines in polar solvents, such as, acetonitrile.

Potophysics and photochemistry (especially photoionization) of indole and its derivatives including tryptophan have been the subjects of intensive research. As for photophysics, the nature of fluorescent states in polar solvents has been discussed by many people and recent consensus on assignment is to an ^1L_a/CT state,[1] where a CTTS (charge transfer to solvent) state[2-4] seems to be involved. This seems to be related to a red edge excitation effect[5] in photophysical behaviors which indicates a strong interaction of a solute molecule with solvent molecules in the excited states. Although phenomena of this kind are usually interpreted by a solvent cage effect,[5,6] possible contribution of the CTTS state[2] cannot be neglected. As for photochemistry, photoionization i.e., electron ejection from indoles to the solvent, was of a great concern. This phenomenon has partly been connected with biological interests.[7]

In this labolatory, photoionization mechanisms of aromatic amines in polar solvents such as acetonitrile (AN) have been studied for years.[8] In the case of 8-anilino-1-naphthalenesulfonate (1,8-ANS), a biphotonic ionization mechanism was elucidated where the CTTS state is suggested to be an intermediate state.[9] In case of *N,N,N′,N′*-tetramethyl-*p*-phenylenediamine (TMPD) in acetonitrile (AN), a monophotonic ionization through a fluorescent level was confirmed where a major product is an ion pair between $TMPD^+$ and AN^-.[10] The latter conclusion is made on the basis of the following three kinds of experiments: fluorescence lifetime measurements (including solvent and temperature effects), ns and ps laser photolysis (nslp and pslp), and the transient photoconductivity measurements.

Recently, there are several publications concerning the monophotonic ionization of aromatic amines in polar solvents. Nogami et al.[11] have studied monophotonic ionization of *N,N,N′,N′*-tetramethyl-1,6-pyrenediamine (TM-1,6-PDA) in acetonitrile by nslp and tpc measurements, and therefrom, proposed the existence of a long-lived ion pair based on the slow rise time (several μs) of photocurrent, in spite of the rapid (≲50 ns) appearence of a cation-like absorption. Hirata et al.[12] did more detailed experiments on the acetonitrile solution of bis(dimethylamino)tetrahydropyrene (BDATP) by using a ps laser. In this case, the rise time of cation-like absorption was found to be ≈2 ns in agreement with the lifetime of fluorescence, while the rise time of photocurrent was found to be ≈9 ns. Thus, monophotonic ionization from fluorescent level through an ion-pair state was proposed. Experiments on *N,N,N′,N′*-tetramethylbenzidine (TMB) were also performed by Hirata et al.[13] In this case, the lifetime of the ion pair was ≈ 4.5 μs. The same group[14] also published the results on TMPD in acetonitrile which gave almost the same data as ours[10] but with some different interpretations.

The photophysical and photochemical schemes proposed in the studies mentioned in the above two paragraphs were not conclusive, e.g., as regards to the mechanism of the ion-pair formation. For instance, in comparing the time dependence of photocurrents with that of transient absorptions, the heterogeneity of the electrode reactions had to be taken into account, i.e., the mobilities of the charge carriers and also the electrode potential working on the ion pair.[10] As for the transient photoconductivity in polar solvents, no established theory is available in contrast to the case of nonpolar solvents.[15]

The aim of the present study is to add more data on this subject so that a clearer identification of the ion pair could be made. A new aspect is that the molecules are excited at the red edge of the 0, 0 band of NMI. Since a fluorescent level is directly excited, a possible mechanism of direct monophotonic ionization before vibrational relaxation may be eliminated.

Experimental

Apparatus and Procedure. The experimental methods of nslp are practically the same as those described in the previous paper[10] except for the fact that a XeCl laser (Lumonics TE 430-2, λ=308 nm and τ=≈ 8 ns, used at ≈ 20 mJ output) replaced a N_2 laser. In case of tpc the size of electrodes was 5×5 mm^2, the separation between them being 2 mm, so that a wider area was illuminated to avoid a biphotonic ionization due to a strong laser light. A 5.1 kΩ

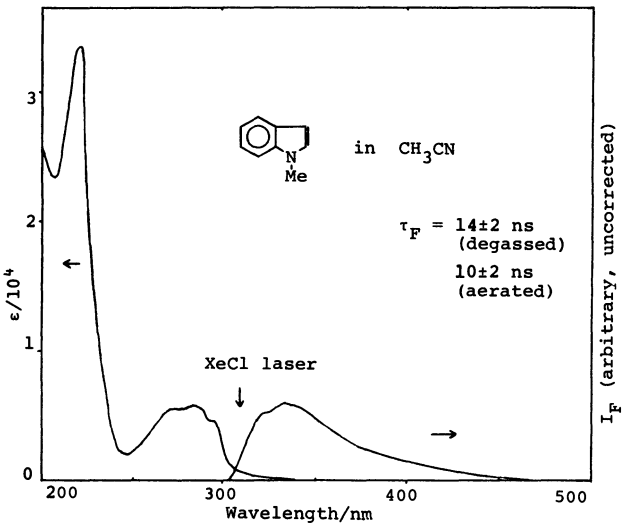

Fig. 1. Absorption and fluorescence spectra of *N*-methylindole in acetonitrile.

termination had to be used because of a small current yield. This caused ≈ 0.5 μs rise time of the system. All the experiments were done at ≈ 25 °C.

Materials. NMI purchased from Tokyo Kasei was vacuum distilled. Spectrograde acetonitrile from Nakarai Chem. was used without further purification.

Results and Discussion

Absorption and Fluorescence. Figure 1 shows the absorption and fluorescence spectra of NMI in acetonitrile. The first peak at ≈ 295 nm is ascribed to the 0, 0 band of the S_1 (^1L_b)←S_0 transition,[1] while the fluorescence is ascribed to the S_1'(^1L_a/CT)→S_0 transition.[1] Also shown in the figure is the location of excitation by the laser which is exactly at the red edge of the first absorption band. Namely, only molecules which are in the solvent cages similar to those of the emitting levels S_1'(^1L_a/CT) are selected by the laser light. Therefore, practically no vibrational relaxation, and little solute-solvent relaxation is required for the optically prepared excited state to reach the fluorescent state. The fluorescence lifetimes in the degassed and aerated solutions were determined to be τ_F°=14±2 ns and τ_F=10±2 ns, respectively. The difference is ascribed to the diffusion-controlled quenching of the fluorescing S_1' state by oxygen: $k_q \approx 10^{10}M^{-1}s^{-1}$ by $k_q[O_2]$=$(k_F+k_{nr}+k_q[O_2])-(k_F+k_{nr})=1/\tau_F-1/\tau_F^\circ=1/(10\times10^{-9})-1/(14\times10^{-9}) \approx 3\times10^7$ (s^{-1}) with [O_2] assumed to be $\approx10^{-3}$ M[1] (The solubility data is not available for the AN solution.). Here, k_F and k_{nr}, respectively, are the radiative and nonradiative decay rates of the S_1' state.

Nanosecond Laser Photolysis. Typical result of nslp on the degassed solution of NMI (6.5×10^{-3}M) is shown in Fig. 2. Time-resolved spectra at t=0, 50 ns and 0.1, 0.5, 4, 16 μs after laser excitation are given by dashed lines in the figure. The shorter-wavelength portions (≤610 and ≤410 nm) of the spectra at t=0 and 50 ns are not available due to interference by the scattered light mainly of fluorescence. The decay curve at each wavelength was represented by the sum of three exponential curves from which "component" spectra i.e., pre-exponential factors, A_s, A_m, and A_ℓ as functions of wavelengths were obtained as shown by the solid lines in the figure with lifetimes τ_s, τ_m, and τ_ℓ, respectively. The component spectra A_m and A_ℓ are similar to those of T_n←T_1 absorptions and of the cation radicals of indole derivatives, respectively, given in the literatures.[3,7,16] Therefore, the former is safely ascribed to the T_1 state of NMI, while the latter is ascribed to the ion pair between NMI^+ and AN^- rather than a free NMI^+, because its decay is described almost by a single-exponential curve. Oxygen effects are also explained by these assignments. The lifetime of the short-lived component has a wide distribution around the mean value of 40 ns compared to the other two, with the minimum value corresponding to the fluorescence lifetime. This fact indicates the existence of species other than S_1' state of NMI. A possible candidate for this species might be (free) AN^-[17] as in the case of TMPD.[10] However, the spectral shapes of the short-lived components could not be determined uniquely, so that any decisive assignment is not presented. Therefore, the spectra at 0 ns may be regarded as the sum of $S_n^{(\prime)}$←S_1' absorption and that of the other species, and the A_s spectra should be taken as a difference spectrum between those of before and after decay of the short-lived species.

The transient absorption intensity depends upon the intensity of the laser (I_{exc}): The plots at the wavelengths and times where the absorbance (A) exceeds 0.01, showed that A is proportional to I_{exc} in the region of $0.2\times I_{max} \leq I_{exc} \leq 0.7\times I_{max}$($I_{max}$≈20 mJ), while for $I_{exc}>0.7\times I_{max}$, a saturation effect was observed. However, the spectral shapes and the shapes of the decay curves did not depend on I_{exc}. Therefore, all the species observed can be safely regarded to be produced monophotonically. Generally speaking, even if $A \propto I_{exc}$, under the condition that the molar absorption coefficient (ε) at the exciting wavelength of the sample is very small (in this case $\varepsilon<10^3$ at 308 nm) we can not completely deny the possibility of a biphotonic process if ε of a possible intermediate for the process is very large. However, assignment to the ion pair instead of NMI^+ would rule out this possibility, because no report is available which indicates the biphotonic formation of an ion pair through the S_1 state.

The effect of aeration on the same solution was observed as that shown in Fig. 3. The presentation is practically the same as that in Fig. 2. Comparison of the components between Figs. 2 and 3 indicate that apparently the yields of the major species (S_1' and T_1 states and the ion pair) are not influenced by the introduction of air (oxygen) and only lifetimes are shortened by O_2. Small changes in the yields may not be

[1] 1 M=1 mol dm^{-3}.

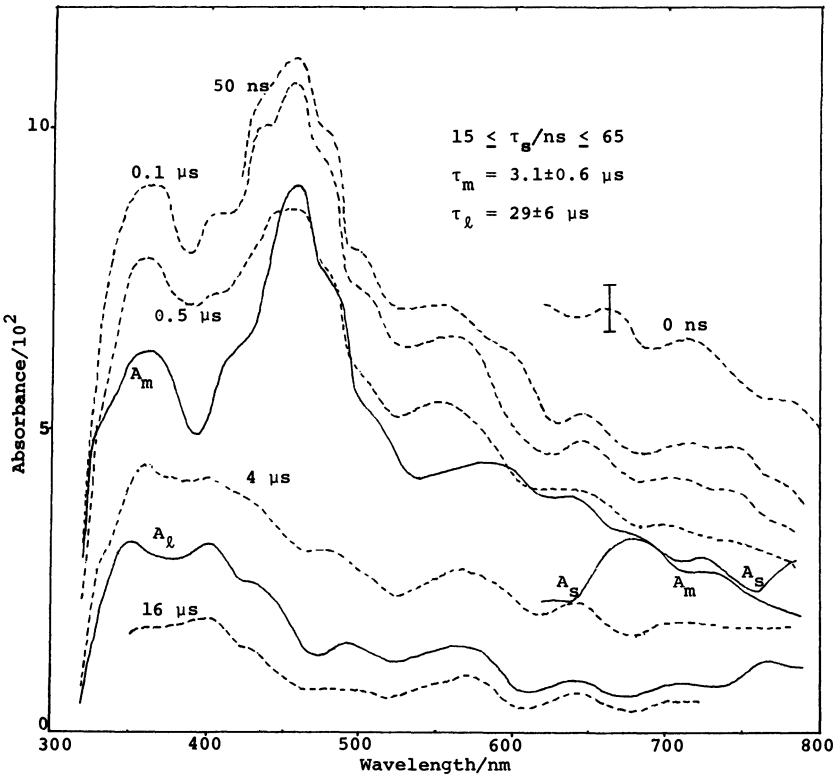

Fig. 2. Nanosecond laser photolysis of a degassed acetonitrile solution (6.5×10^{-3} M) of *N*-methylindole: Time-resolved and decomposed spectra.

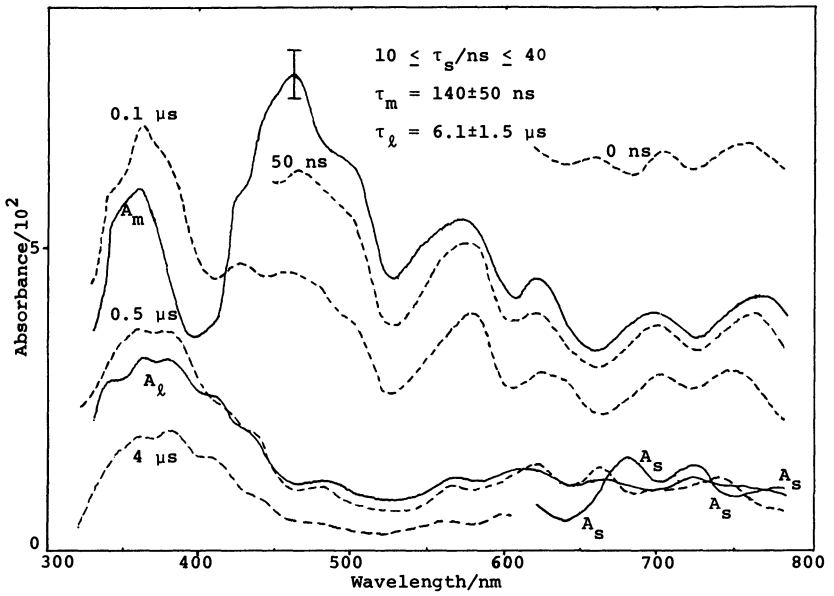

Fig. 3. Nanosecond laser photolysis of an aerated acetonitrile solution (6.5×10^{-3} M) of *N*-methylindole: Time-resolved and decomposed spectra.

consistent with fluorescence-lifetime shortening by oxygen. This fact, however, is rationalized if we assume that both intersystem-crossing and electron-ejection rates increased to the same extent (≈40%). Namely, the ion pair formed in the aerated solution might be due to the ion pair between NMI^+ and O_2^- possibly formed through an exciplex, $NMI^+\cdots O_2^-$ rather than that between NMI^+ and AN^-. There are some discrepancies between the two figures in the wavelength region of $\lambda>500$ nm. These may be interpreted by assuming another component with a lifetime of ≈ 100 ns in the case of the aerated solution. However, a spectral shape for this component is difficult to be determined uniquely because its lifetime is very close to that of the triplet state. The decreased lifetime of the short-lived component is interpreted as (diffusion-controlled)

Table 1. Time Behavior of Photoconductivity of 2×10^{-3} M NMI in N_2 Bubbled and Aerated(in Parenthesis) Acetonitrile Solutions, Respectively

	r	d_1	d_2	d_3
τ_j/μs	1.6±0.3	26±5	400±100	$>10^3$
	(1.3±0.3)	(8±2)	(180±40)	($>10^3$)
$i_j^\circ/\sum_k i_{d_k}^\circ$	−1.00±0.10	0.60±0.10	0.12±0.02	0.28±0.06
	(−0.95±0.10)	(0.60±0.10)	(0.15±0.03)	(0.25±0.05)

quenching of the S_1' state (vide supra) and another species like AN^- by oxygen. The quenching rate of the T_1 state, $k_q'[O_2]=(k_{nr}'+k_q'[O_2])-k_{nr}'=1/\tau_m-1/\tau_m^\circ=1/(140\times10^{-9})-1/(3.1\times10^{-6})=7\times10^6$ (s^{-1}) is just reasonable. Here $\tau_m^\circ=1/k_{nr}'$ is an intrinsic lifetime of the T_1 state. The decay rate of the long-lived component can be interpreted by two alternative schemes or their compromises (e.g. by assuming an equilibrium between them); (1) as the decay rate $k_d=1/\tau_\ell\approx1.6\times10^5$ (s^{-1}) of the ion pair, $NMI^+\cdots O_2^-$, or (2) by the quenching rate, k_q'' of $NMI^+\cdots AN^-$ by oxygen with $k_q''[O_2]=1/\tau_\ell-1/\tau_\ell^\circ=1/(6.1\times10^{-6})-1/(29\times10^{-6})\approx1.3\times10^5$ (s^{-1}). Both these numbers are not unusual for these processes. Although quenching (lifetime shortening) of the ion pairs by oxygen was not clearly demonstrated for the other systems,[11-14] nslp experiments on aminonaphthalenes (naphthalenamines and naphthalenediamines)[18] and *N,N,N',N'*-tetramethyl-2,7-pyrenediamine[19] done in this laboratory presented similar results.

Transient Photoconductivity. In order to obtain more and complementary informations on the scheme, transient photoconductivity was measured for the nitrogen-bubbled and air-saturated acetonitrile solutions of NMI. Its time profile was analyzed as a sum of one or two exponential rise and three exponential decay curves:

$$i_p(t)=\sum_j i_j^\circ e^{-t/\tau_j};\ \{j\}=(c, r, d_1, d_2, d_3).$$

Here, τ_c corresponds to the time constant of the detection system ($\approx$ 0.5 μs). i_p values were proportional to I_{exc} in the region $0.2\times I_{max}\lesssim I_{exc}\lesssim I_{max}$ indicating that the chemical species responsible for the photoconductivity is ascribed to that formed by a monophotonic process. The yield of photocurrent i.e., that of the radicals was estimated to be $\Phi_i\approx0.05$ which is more than one order of magnitude lower than that of TMPD ($\Phi_i\approx0.8$), but comparison was not easy due to large difference and a possible contribution of the biphotonic process in the latter case. The photocurrent yields were almost the same for the nitrogen-bubbled and air-saturated solutions. i_j°, normalized for $i_{d_1}^\circ+i_{d_2}^\circ+i_{d_3}^\circ\equiv1$, and τ_j values for $j=r$, d_1, d_2, and d_3 are given in Table 1, while $i_c^\circ=1-i_r^\circ$ with $\tau_c=0.5$ μs. Since the analysis was made by assuming the sum of five (or four) exponential functions (no deconvolution was made), the actual τ_r values are expected to be slightly less than those given in the table but definitely more than τ_c. This kind of facts have been usually taken as evidences of the ion pairs formed by photo-irradiation and then dissociated with time constants τ_r's (The process with τ_r was not found in nslp experiments and it has been explained by a resemblance of the spectra of the cation and the ion pair.).[11-13] If we apply the above judgement to the present system, the decay portion of the photoconductivity has to be ascribed to the decay behaviors of free ionic species such as NMI^+, AN^-, and some scavengers' anions (X_i^-). However, we regard the process with τ_r rather as the evidence of the formation of the ion pair which dissociates at electrode surfaces by the applied field: The major decay portion of the photoconductivity is governed by the decay of the ion pair existing in the liquid phase which is the origin of the transient absorption in the nslp experiment. This assessment is supported by the following facts: (1) Long-lived (with O_2 effect) transient species (identified to the ion pair) were observed in both nslp (nearly single exponential τ_ℓ component) and tpc (non-exponential but $\tau_{d_1}\sim\tau_\ell$) experiments. (2) Rises (τ_r) were observed in the case of tpc [correspondent to the dissociation rate(s) of the ion pair at the electrode(s) ($1/\tau_r$) which is larger than the intrinsic decay rate of the ion pair ($1/\tau_\ell$)]. (3) The yield of the ion pair $\Phi_{i.p.}$ is estimated to be $\approx$0.1 by this assessment from $\Phi_i\approx0.05$ which is consistent with $\Phi_{i.p.}\approx0.2$ as is estimated from nslp data assuming $\varepsilon_{TT}\approx\varepsilon_{i.p.}$ and $\Phi_F\approx0.1$. (4) Therefore, the longer-lived portion of tpc (τ_{d_2} and τ_{d_3}) has to be ascribed to the heterogeneity of the tpc experiment, i.e., differences in the diffusion rates of the ionic species (freed at the electrodes) and so on.

The above judgement underscores the need of careful examinations of the complementary experimental data of nslp and tpc experiments for elucidating the photoionization mechanisms including ion pairs.

Since presence of the ion pair as a unique chemical species is well established, some comments will be added on the results of TMPD photolysis in acetonitrile solutions[10] which have some differences from those of the present system: (1) The 0.7 μs decay component in the transient photoconductivity ascribed to free $TMPD^+$ is absent in the transient absorption. This fact can be interpreted by assuming that the charge of AN^- taken at the anode is compensated by the $TMPD^+$ arrived at the cathode with the time constant of 0.7 μs. (2) The decrease in the photocurrent corresponding to the ion pair by aeration can be easily explained if we assume that an ion pair with O_2 is formed which

may be less dissociative at the electrodes. This kind of O_2 effect was not observed for NMI solutions because dissociation of $NMI^+\cdots AN^-$ is less feasible ($\tau_r \lesssim 1.6\,\mu s$) than that of $TMPD^+\cdots AN^-$ ($\tau_r < 10$ ns).

In concluding this paper, one candidate for the scheme of the aerated system is given below:

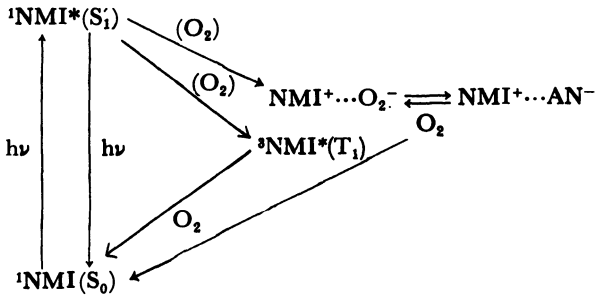

The scheme for the oxygen-free system is almost obvious.

References

1) S. R. Meech, D. Phillips, and A. G. Lee, *Chem. Phys.*, **80**, 317 (1983) and references therein.

2) T. B. Truong, *J. Chem. Phys.*, **77**, 5375 (1982) and references therein.

3) L. I. Grossweiner, A. M. Brendzel, and A. Blum, *Chem. Phys.*, **57**, 147 (1981).

4) E. F. Gudgin-Templeton and W. R. Ware, *J. Phys. Chem.*, **88**, 4626 (1984).

5) T. Ikeyama, T. Azumi, T. Murao, and I. Yamazaki, *Chem. Phys. Lett.*, **96**, 419 (1983) and references therein.

6) N. Kanamaru, *Sci. Papers IPCR*, **71**, 85 (1977); *Bull. Chem. Soc. Jpn.*, **55**, 3093 (1982).

7) E. Amouyal, A. Bernas, and D. Grand, *J. Chem. Soc., Faraday Disc.*, **74**, 147 (1982) and references therein.

8) J. Tanaka and N. Kanamaru, "Relaxation of Charge Transfer Excited States of Aromatic Amines in Polar Solvents" in "Studies in Physical and Theoretical Chemistry Vol. 36, Biomolecules; Electronic Aspects," ed by C. Nagata, M. Hatano, J. Tanaka, and H. Suzuki, Japan Sci. Soc. Press, Tokyo, pp. 169—180.

9) H. Nakamura, J. Tanaka, N. Nakashima, and K. Yoshihara, *Chem. Phys. Lett.*, **77**, 419 (1981).

10) S. Nakamura, N. Kanamaru, S. Nohara, H. Nakamura, Y. Saito, J. Tanaka, M. Sumitani, N. Nakashima, and K. Yoshihara, *Bull. Chem. Soc. Jpn.*, **57**, 145 (1984).

11) T. Nogami, T. Mizuhara, N. Kobayashi, M. Aoki, T. Akashi, Y. Shirota, H. Mikawa, and M. Sumitani, *Bull. Chem. Soc. Jpn.*, **54**, 1559 (1981).

12) Y. Hirata, N. Mataga, Y. Sakata, and S. Misumi, *J. Phys. Chem.*, **86**, 1508 (1982); **87**, 1493 (1983).

13) Y. Hirata, M. Takimoto, and N. Mataga, *Chem. Phys. Lett.*, **97**, 569 (1983).

14) Y. Hirata and N. Mataga, *J. Phys. Chem.*, **87**, 1680 (1983).

15) H. T. Choi, D. S. Sethi, and C. L. Braun, *J. Chem. Phys.*, **77**, 6027 (1982) and references therein.

16) C. Pernot and L. Lindqvist, *J. Photochem.*, **6**, 215 (1976/77) and references therein.

17) I. P. Bell, M. A. Rogers, and H. D. Burrows, *J. Chem. Soc., Faraday Trans., 1*, **73**, 315 (1977).

18) N. Kanamaru, K. Isogai, S. Suzuki, M. Suzuki, and J. Tanaka, to be submitted.

19) K. Hosokawa, N. Kanamaru, J. Tanaka, N. Nishikawa, Y. Sakata, and S. Misumi, preliminary results.

 © 1986 The Chemical Society of Japan Bull. Chem. Soc. Jpn., 59, 575—579 (1986)

Sulfur K-Edge Absorption Spectra of Na_2SO_4, Na_2SO_3, $Na_2S_2O_3$, and $Na_2S_2O_x$ (x=5—8)

Hideo SEKIYAMA,[†,††] Nobuhiro KOSUGI,[†] Haruo KURODA,[†] and Toshiaki OHTA*,[††]
[†]Department of Chemistry, Faculty of Science, The University of Tokyo, Hongo, Bunkyo-ku, Tokyo 113
[††]Photon Factory, National Laboratory for High Energy Physics, Oho, Tsukuba, Ibaraki 305
(Received August 24, 1985)

X-Ray absorption spectra of the sulfur K-edges of SO_4^{2-}, SO_3^{2-}, $S_2O_3^{2-}$, and $S_2O_x^{2-}$ (x=5—8) were measured with synchrotron radiation. The spectra show similarly strong absorption bands which originate in bound-state transitions to antibonding 3p-type orbitals and in shape resonances related to 3d-type orbitals. The K-edge spectrum for the terminal sulfur atom in $S_2O_3^{2-}$, however, shows only a bound-state transition. Differences in chemical environments and bonding around the X-ray absorbing atoms are discussed to interpret the spectra.

K- and L-shell X-ray absorption spectra for molecules such as SO_4^{2-},[1] SF_6,[1,2] and SiF_4,[3] where electronegative ligand atoms surround a central atom, show resonance-like bands below and above the ionization threshold and quite weak Rydberg series. Nefedov[4] and Dehmer[5] first introduced the concept of effective potential barrier in interpreting X-ray absorption spectra of molecules in which a B, S, or Si atom is bonded with two or more electronegative atoms. When an excited electron is within the cage of electronegative atoms near an electropositive atom, the electron experiences net attraction due to the partially screened nucleus of the central atom; when an excited electron is at a long distance, the electron undergoes only the Coulomb attraction by the molecular ion. At intermediate distances the potential constitutes a barrier due to electronegative atoms located there. The barrier in this case is primarily a pseudopotential barrier rather than the centrifugal barrier which is known in context with high angular momentum states of atoms[6] and molecules.[7] The effective potential barrier separates excited states into outer- and inner-well states. In the inner-well region, there exist bound and quasi-bound states below and above the ionization threshold, respectively. Transitions to inner-well states are of strong tendency to occur because of the large overlap between the wavefunctions of the initial and final states. On the other hand, Rydberg transitions are considerably or completely suppressed because Rydberg orbitals are in the outer-well region.

The effective potential barrier is only a qualitative concept and is not a rigorously physical model. Recently, the orgin of the resonance-like absorption near the inner-shell ionization threshold is interpreted in terms of shape resonance[7] or multiple-scattering resonance[8] within the framework of a rigorous theory of potential scattering. The molecular orbital theory is also powerful for predicting the energy position and transition probability of quasibound-state resonances as well as bound-state resonances.[3,9] In all cases, the chemical environment and bonding around an X-ray absorbing atom contribute dominantly to the origin of resonances.

Ion SO_4^{2-} is a typical cage-like molecule and its inner shell absorption spectra have been studied both experimentally[1] and theoretically.[5,10] There exist various kinds of stable sulfur-containing oxyanions. It is thus interesting to measure X-ray absorption spectra of several derivatives of SO_4^{2-} and to investigate how the deformation of the cage-like structure with T_d symmetry can be reflected on absorption spectra. Relative to SO_4^{2-}, SO_3^{2-} can be regarded as a one-ligand-free ion and $S_2O_3^{2-}$ as a one-ligand-exchange ion.

In the present work, we measured sulfur K-edge absorption spectra for SO_4^{2-}, SO_3^{2-}, and $S_2O_3^{2-}$ as well as their S 2p XPS spectra and interpret the ligand effect on resonance-like bands; i.e., transitions to bound and quasi-bound states. Furthermore, we measured absorption spectra for $S_2O_x^{2-}$ (x=5—8) and analyse them by comparison with spectra for SO_4^{2-}, SO_3^{2-}, and $S_2O_3^{2-}$.

Experimental

All samples for measurements were polycrystalline powders of sodium salts: Na_2SO_3, Na_2SO_4, $Na_2S_2O_3$, $Na_2S_2O_5$, $Na_2S_2O_6\cdot 2H_2O$, $Na_2S_2O_7$, and $Na_2S_2O_8$. They were obtained from Wako Pure Chemical Industry Co. and were not purified any further. The sample of $Na_2S_2O_7$ contained ≈10% $NaHSO_4$.

Sulfur K-edge absorption spectra were measured with a UHV compatible double crystal monochromator[11] at the Soft X-Ray Station (BL-11B) of the Photon Factory in the National Laboratory for High Energy Physics. Ge(111) was used as a monochromatizing crystal and its energy resolution was about 1 eV around the sulfur K-edge (≈2.5 KeV). Absorption spectra were obtained by collecting total electrons from the samples, which had been coated on oxidized aluminium plates. The photon energy was calibrated with the first intense peak (2469.8 eV) in the sulfur K-edge absorption spectrum of NiS powder.[12]

Sulfur 2p XPS spectra were measured with a laboratory ESCA spectrometer VG ESCALAB. Mg $K\alpha$ line (1253.6 eV) was used as an excitation source. Samples coated on scotch tape were used. Binding energies of spectra were calibrated with the Au $4f_{7/2}$ peak (83.8 eV) from gold evaporated on samples.

Results and Discussion

SO_4^{2-} and SO_3^{2-}. In the absorption spectrum for Na_2SO_4 shown in Fig. 1, there exist an intense peak (indicated as A) and two broad bands (indicated as B and C). Nefedov and Fomichev[1] also measured the sulfur K- and $L_{2,3}$-edge absorption spectra for Na_2SO_4. But the K-edge spectrum for SO_4^{2-} obtained in the present work shows a much better resolution than that by Nefedov and Fomichev.[1] Ion SO_4^{2-} belongs to the T_d point group, and there are two unoccupied valence (antibonding) orbitals, a_1^* of 3s character and t_2^* of 3p character; the intense peak A is assigned not to S 1s-a_1^* (dipole forbidden) but to S 1s-t_2^* dipole allowed transition. Following previous investigations,[1,2,5] the K- and $L_{2,3}$-shell absorption spectra can be placed on a common relative energy scale referenced to the location of respective inner-shell ionization potentials. Based on Dehmer's interpretation of the $L_{2,3}$ spectrum for ion SO_4^{2-} [5] and on the theoretical interpretation of the Si K-edge absorption spectrum for the isoelectronic molecule SiF_4 (cited in Ref. 3), the peaks B and C in the K spectrum for SO_4^{2-} shown in Fig. 1 are transitions to 3d-like e* and t_2^* orbitals, respectively. In the T_d symmetry, however, the e* orbital does not have a p component and peak B cannot be assigned only to a 1s-e* transition. We should appreciate a contribution from a 1s-t_2^* transition to peak B. Thus, it is necessary to reinterpret the origin of peak C as well as peak B.

The spectrum for Na_2SO_3 is also shown in Fig. 1. Ion SO_3^{2-} has a trigonal-pyramidal C_{3v} structure with a sulfur atom at the apex. There are two valence-type unoccupied orbitals: e* of $3p\pi$ character and a_1^* of 3s and $3p\sigma$ character. Transitions from S 1s to these orbitals are both dipole-allowed; the most intense peak indicated as A can be assigned to a transition to the e* valence orbital and the second peak B to a transition to the a_1^* orbital. Furthermore, there are one a_1^* and two e* orbitals of 3d character. The a_1^* orbital of 3d character with a large contribution from 3p is directed toward the region where there is no ligand or no potential barrier; the transition to a_1^* becomes lower in energy and stronger in intensity. The third peak C can be assigned to the transition to the d-like a_1^* orbital. Other d-type (e*) shape resonance are observed in the higher energy region similarly to the case of SO_4^{2-}.

$S_2O_3^{2-}$ and $S_2O_5^{2-}$. In the absorption spectrum for $Na_2S_2O_3$ shown in Fig. 2, several bound-state transitions are observed. Ion $S_2O_3^{2-}$, belonging to the C_{3v} point group, is considered as SO_3^{2-} coordinated with one more sulfur atom. There are inequivalent sulfur atoms (central and terminal); the terminal sulfur atom is negative (formal oxidation number −2) and the central sulfur atom highly positive (formal oxidation number +6). This explains well the S 2p XPS spectrum

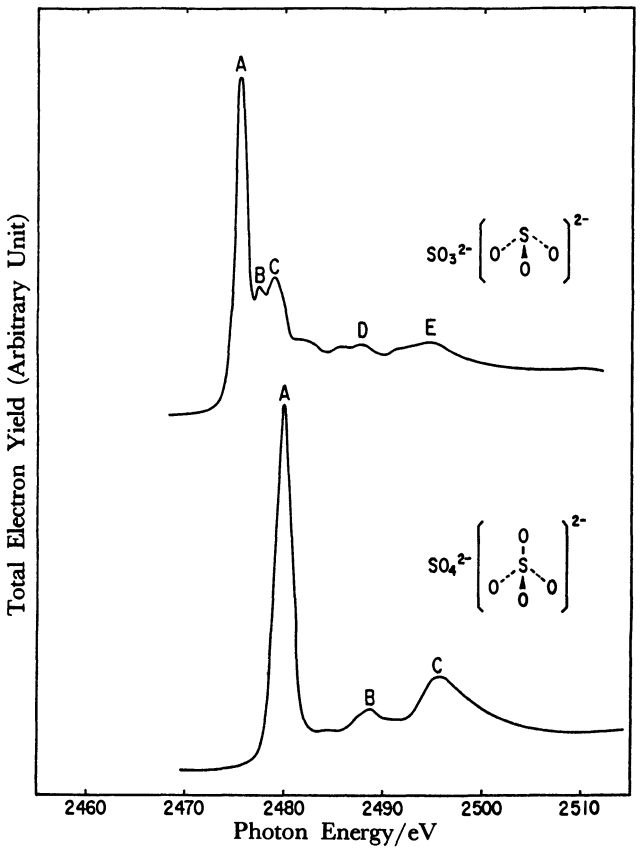

Fig. 1. Sulfur K-edge absorption spectra of Na_2SO_4 and Na_2SO_3.

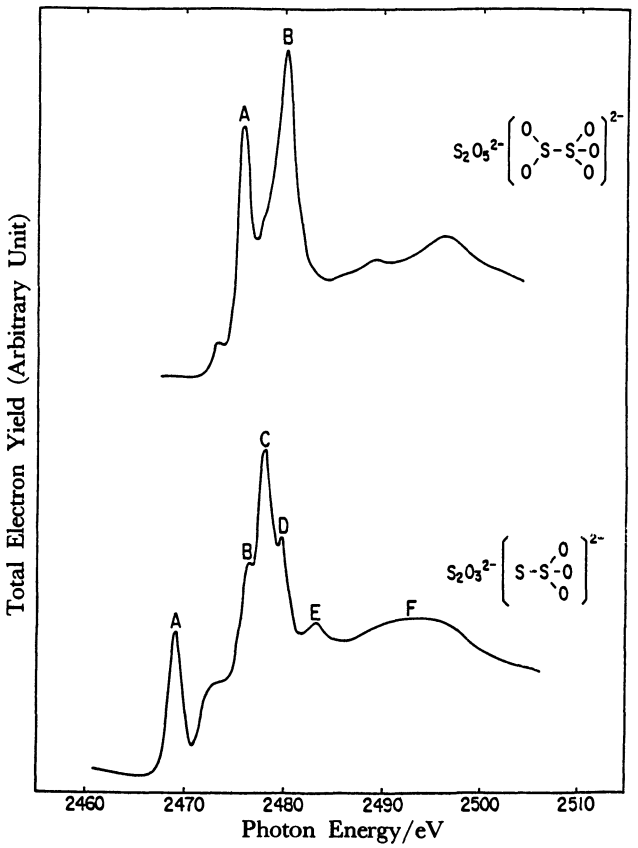

Fig. 2. Sulfur K-edge absorption spectra of $Na_2S_2O_3$ and $Na_2S_2O_5$.

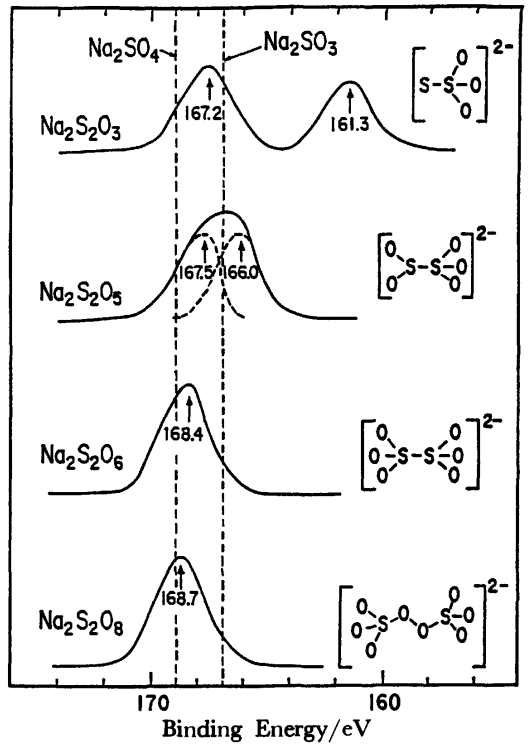

Fig. 3. Sulfur 2p XPS spectra of Na_2SO_4, Na_2SO_3, $Na_2S_2O_3$, and $Na_2S_2O_x$ (x=5—8).

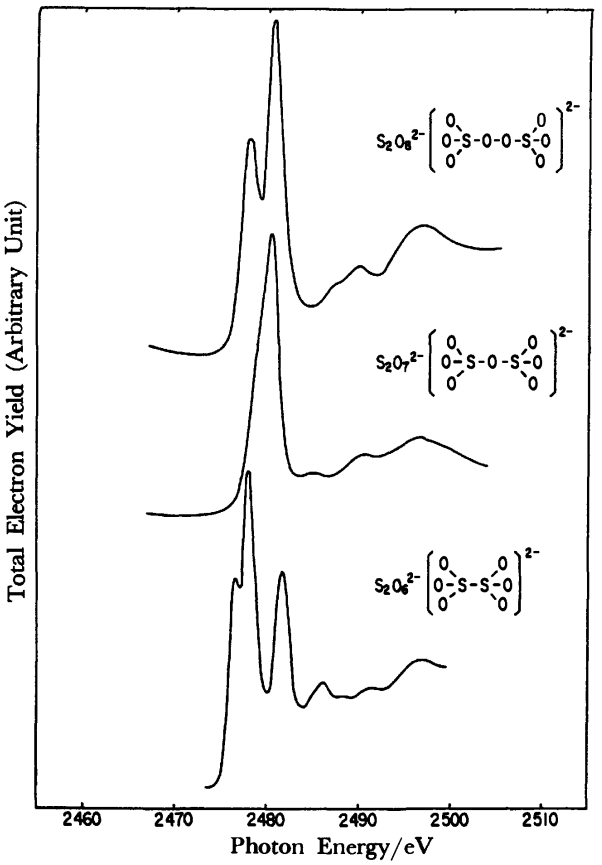

Fig. 4. Sulfur K-edge absorption spectra of $Na_2S_2O_6$, $Na_2S_2O_7$, and $Na_2S_2O_8$.

shown in Fig. 3, where the lower energy peak at 161.3 eV corresponds to the terminal S 2p peak and the peak at 167.2 eV to the central S 2p. Siegbahn et al.[13] reported the S 1s XPS spectrum for $Na_2S_2O_3$, where the difference between the binding energies of the two sulfur atoms is 7.0 eV, larger than the S 2p chemical shift (5.9 eV). The energy difference between peaks A and B in the S K-edge absorption spectrum is 7.2 eV as shown in Fig. 2; therefore, peaks A and B correspond to the transitions to the same lowest unoccupied orbital from the terminal and the central S 1s orbitals, respectively. Based on a simple molecular orbital calculation, there are three antibonding orbitals, $13a_1$* (terminal $3p\sigma$ and central $3p\sigma$), 9e* (central $3p\pi$), and $14a_1$* (central 3s and $3p\sigma$); the peaks A and B are associated with the transitions to the $13a_1$* orbital. The broad band at about 2475 eV between A and B is considered as an onset of the terminal S 1s ionization. It should be noted that the spectrum of the terminal S K-edge shows no shape resonances because the terminal sulfur atom is not affected by the potential barrier. Peaks C and D are assigned to the transitions from central S 1s to 9e* and $14a_1$*, respectively. They may correspond to the peaks A and B observed in the spectrum for Na_2SO_3 (Fig. 1); the energy separation of C and D for $S_2O_3^{2-}$ is the same as that of A and B for SO_3^{2-}. But C and D for $S_2O_3^{2-}$ shift to the higher energy by about 2.5 eV than A and B for SO_3^{2-}, probably due to the electrostatic effect by the terminal sulfur. Peak E observed for $S_2O_3^{2-}$ is attributed to a d-type shape resonance, which may correspond to peak C for SO_3^{2-}; it is noted that the resonance E of $S_2O_3^{2-}$ is weaker in intensity and higher in energy than the resonance C of SO_3^{2-}, probably due to the chemical bonding with the negative sulfur atom. These results indicate that the peak position and intensity of the d-type shape resonances are very sensitive to the surroundings of the X-ray absorbing atom.

The S K-edge spectrum for $Na_2S_2O_5$ is also shown in Fig. 2. In the XPS spectrum shown in Fig. 3, a broad 2p band is observed. This band has two components associated with $-SO_2$ and $-SO_3$ as indicated by the broken lines, as was previously investigated by Siegbahn et al.[13] In the S K-edge spectrum, the two intense peaks A and B correspond to transitions associated with $-SO_2$ species and $-SO_3$ species, respectively. The energy separation between peaks A and B is 4.4 eV and is larger than the S 1s chemical shift, ≈2 eV, which is estimated from the formal oxidation numbers of $-S(III)O_2$ and $-S(V)O_3$.[13] These two peaks may be attributed to transitions to different final orbitals.

$S_2O_6^{2-}$, $S_2O_7^{2-}$, and $S_2O_8^{2-}$. The absorption spectra of S K-edge of $Na_2S_2O_6$, $Na_2S_2O_7$ and $Na_2S_2O_8$ are shown in Fig. 4. Ions $S_2O_x^{2-}$ (x=6—8) have equivalent sulfur atoms.

The chemical environment of the sulfur atoms in $S_2O_6^{2-}$ is similar to that of the central sulfur atom in

Table 1. Assignments of the Absorption Spectra of S K-Edge of Na_2SO_4, Na_2SO_3, and $Na_2S_2O_3$

SO_4^{2-} energy/eV		Transition
2479.9	A	S 1s→t_2*
2488.7	B	d-type shape resonance
2495.6	C	d-type shape resonance

SO_3^{2-} energy/eV		Transition
2475.5	A	S 1s→e*
2477.5	B	→a_1*
2478.9	C	d-type shape resonance
2487.6	D	d-type shape resonance
2494.6	E	d-type shape resonance

$S_2O_3^{2-}$ energy/eV		Transition
2469.2	A	Terminal S 1s→a_1* (Terminal, central S 3pσ)
2476.4	B	Central S 1s→a_1* (Terminal, central S 3pσ)
2478.0	C	→e_1* (Central S 3pπ)
2479.8	D	→a_1* (Central S 3s and 3pσ)
2483.2	E	d-type shape resonance
2493.2	F	d-type shape resonance

Table 2. Assignments of the Absorption Spectra of S K-Edge of $Na_2S_2O_5$, $Na_2S_2O_6$, $Na_2S_2O_7$, and $Na_2S_2O_8$

$S_2O_5^{2-}$ energy/eV		Transition
2475.8	A	S1s→3p (−SO_2)
2480.2	B	→3p (−SO_3)
2489.2		d-type shape resonance
2495.9		d-type shape resonance

$S_2O_6^{2-}$ energy/eV	Transition
2476.5	S 1s→3pσ (S-S)
2477.8	→3pπ (S-O)
2481.7	→3pσ (S-O)
2486.0	d-type shape resonance
2491.2	d-type shape resonance
2496.7	d-type shape resonance

$S_2O_7^{2-}$ energy/eV	Transition
2480.5	S 1s→3p
2490.5	d-type shape resonance
2496.5	d-type shape resonance

$S_2O_8^{2-}$ energy/eV	Transition
2478.2	S 1s→3pσ
2480.7	→3pπ
2486.9	d-type shape resonance
2489.8	d-type shape resonance
2496.7	d-type shape resonance

$S_2O_3^{2-}$. Therefore, in the spectrum for $S_2O_6^{2-}$ shown in Fig. 4, three intense peaks arising from 1s→3p bound-state transitions can be interpreted as corresponding to peaks B, C, and D of the spectrum for $S_2O_3^{2-}$ shown in Fig. 2.

The spectrum for $S_2O_7^{2-}$ closely resembles that for SO_4^{2-}, because each sulfur atom in $S_2O_7^{2-}$ is surrounded by four oxygen atoms. The most intense peak can be considered as a transition from S 1s to t_2*-like (local symmetry) orbital of S 3p character. However, the peak has a shoulder structure at the lower energy side, which may come from ≈10% impurity of $NaHSO_4$ or from a nearly forbidden transition to a_1*-like (local symmetry) orbital of 3s character.

It is expected that the spectrum for $S_2O_8^{2-}$ should resemble that for SO_4^{2-} because of similar chemical environment and bonding to each other. However, two intense peaks are observed, which should be 1s→3p bound-state transitions. It may be reasonable to understand that the higher energy peak is a transition to a t_2*-like (local symmetry) orbital and that the lower one is a transition to an a_1*-like (local symmetry) orbital with a large mixing with t_2* (local symmetry) due to considerable symmetry-lowering in comparison with SO_4^{2-} and $S_2O_7^{2-}$.

Conclusion

Tables 1 and 2 summarize the present results of absorption spectra of S K-edge of Na_2SO_4, Na_2SO_3, $Na_2S_2O_3$, and $Na_2S_2O_x$ (x=5—8) together with the present interpretations. In the spectra for SO_4^{2-}, SO_3^{2-}, and $S_2O_3^{2-}$, there are remarkable differences in 1s→3p bound-state transitions and d-type shape resonances. Especially, the peak position and intensity of the d-type shape resonances are very sensitive to the surroundings of the X-ray absorbing atom. The spectra for $S_2O_x^{2-}$ (x=5—8) can be interpreted on the analogy of those for SO_4^{2-}, SO_3^{2-}, and $S_2O_3^{2-}$.

The authors wish to thank Dr. Mitsuyuki Soma in the National Institute for Environmental Studies for his help in the measurement of the XPS spectra, and Mr. Yoshinori Kitajima in the University of Tokyo for valuable discussion.

References

1) V. I. Nefedov and V. A. Fomichev, *J. Struct. Chem.*, **9**, 107, 217 (1968).

2) A. P. Hitchcock and C. E. Brion, *Chem. Phys.*, **33**, 55

(1978) and references therein.
3) H. Friedrich, B. Pittel, P. Rabe, W. H. E. Schwarz, and B. Sonntag, *J. Phys. B*, **13**, 25 (1980) and references therein.
4) V. I. Nefedov, *J. Struct. Chem.*, **11**, 277 (1970).
5) J. L. Dehmer, *J. Chem. Phys.*, **56**, 4496 (1972).
6) A. R. P. Rau and U. Fano, *Phys. Rev.*, **167**, 7 (1968).
7) J. L. Dehmer and D. Dill, *Phys. Rev. Lett.*, **35**, 213 (1975); *J. Chem. Phys.*, **65**, 5327 (1976).
8) A. Bianconi, M. Dell'Ariccia, P. J. Durham, and J. B. Pendry, *Phys. Rev.* **B26**, 6502 (1982).
9) S. Iwata, N. Kosugi, and O. Nomura, *Jpn, J. Appl. Phys.*, **17**, Suppl. 17-2, 109 (1978).
10) G. L. Bendazzoli and P. Palmieri, *Theor. Chim. Acta*, **36**, 77 (1974).
11) T. Ohta, P. M. Stefan, M. Nomura, and H. Sekiyama, to be published.
12) Y. Fujino, C. Sugiura, and S. Kiyono, *Technol. Rep. Tohoku Univ.*, **35**, 55 (1970).
13) K. Siegbahn, C. Nordling, A. Fahlmann, R. Nordberg, K. Hamrin, J. Hedmann, G. Johansson, T. Bergmark, S.-E. Karlsson, I. Lindgren, and B. Lindberg, *ESCA-Atomic, Molecular and Solid State Spectroscopy by means of Electron Spectroscopy, Almqvist and Wiksells, Uppsala*, **1967**.

 © 1986 The Chemical Society of Japan Bull. Chem. Soc. Jpn., 59, 581—585 (1986)

Crystal Structures of Trimethylammonium Hexaiodotellurate(IV) and Heptaiodotellurate(IV)

Hideko KIRIYAMA,* Yukiko MIZUHASHI, and Junji OOTANI
Department of Chemistry, Faculty of Science, Kobe University, Nada, Kobe 657
(Received August 30, 1985)

Crystal structures of the title compounds were determined by X-ray diffraction method. The crystal data and the final R values are: $[(CH_3)_3NH]_2TeI_6$, cubic, $Pa3$, a=13.210(2) Å, V=2305.2(9) Å^3, Z=4, R=0.057 for 263 observed unique reflections and $[(CH_3)_3NH]_2TeI_7$, tetragonal, $P4/nmm$, a=13.921(3), c=6.224(2) Å, V=1206.4(8) Å^3, Z=2, R=0.051 for 553 reflections. The structure of hexaiodo complex is a modified K_2PtCl_6 type. The discrete $[TeI_6]^{2-}$ octahedra are practically regular with a Te-I distance of 2.952(2) Å. The trimethylammonium cations lie on the unit cell triad axes and form trifurcated, weak hydrogen bonds of NH···3I. In contrast, the Te^{IV} coordination in the heptaiodo complex is an elongated octahedron with Te-I(1)=2.934(1) and Te-I(2)=3.124(4), 3.100(4) Å. These TeI_6 octahedra form linear trans TeI_5 chains running along c by sharing each pair of opposite vertices. Extra iodine atoms also stack along c with nearly equidistant I-I separations of 3.091(6) and 3.133(6) Å. The trimethylammonium cation is distributed randomly over four configurations in a cavity formed by two $[TeI_5]_n^{n-}$ and two $[I]_{2n}^{n-}$ columns. Thus, the chemical constitution of the heptaiodo complex can be expressed as di-trimethylammonium *catena*-μ-iodo-tetraiodo tellurate(1-) *catena*-diiodide(1-), $[(CH_3)_3NH]_{2n}^{2n+}[TeI_5]_n^{n-}[I]_{2n}^{n-}$.

A series of methylammonium hexahalometallate(IV), $[(CH_3)_nNH_{4-n}]_2MX_6$ where M=Pd, Pt, Sn, Te, X=Cl, Br, I and n=1, 2, 3, 4 has been widely studied so far by means of X-ray diffraction, NMR, NQR, dielectric and thermal analyses in view of structural chemistry focussed on their phase transitions and molecular dynamics.[1-5] Our preliminary report on $(CH_3NH_3)_2TeCl_6$ suggested that tellurate complexes of the series, especially their iodo analogs would be somewhat different from other hexahalometallates in nature.[6] In order to ascertain this suggestion the system of methylammonium hexaiodotellurate(IV), $[(CH_3)_nNH_{4-n}]_2TeI_6$ has been studied by X-ray diffraction and ^{1}H NMR measurements. In this paper, the X-ray results obtained for n=3 are described.

The X-ray powder patterns showed that trimetylammonium (abbreviated as Me_3NH hereinafter) hexaiodotellurate is isostructural with the corresponding hexachlorotellurate complex.[7] Thus, it was found that the structure is an antifluorite type in principle, but the crystal symmetry is lowered from $Fm3m$ to $Pa3$ owing to the presence of Me_3NH^+ cations. At the beginning of the work it was desired to determine the geometry of $[TeI_6]^{2-}$ ion more accurately than those in the literature.[8] Because the Me_3NH complex evidently contains discrete $[TeI_6]^{2-}$ anions, its crystal structure was analyzed by X-ray diffraction.

During preliminary attempts to grow single crystals of $(Me_3NH)_2TeI_6$ suitable for structure determination, a novel complex of formula $(Me_3NH)_2TeI_7$ was obtained by chance. Therefore, the heptaiodo complex was also subjected to an X-ray analysis in order to elucidate such a unique chemical constitution as well as the role of extra iodine atoms.

Experimental

Preparation. A saturated aqueous solution of trimethylammonium iodide added dropwise to a hydrogen iodide solution of tellurium dioxide in a stoichiometric molar ratio yielded black precipitates. The product was cubic from its X-ray powder patterns and was a hexaiodotellurate complex of $(Me_3NH)_2TeI_6$ from elemental analyses. The precipitate was dissolved into a hot, dilute HI solution and then brown-black prismatic crystals were grown from the solution held at ca. 50 °C for several days. These crystals were not identical to the source material of $(Me_3NH)_2TeI_6$, as evidenced by the X-ray powder pattern, and confirmed to correspond to $(Me_3NH)_2TeI_7$ by careful, chemical analyses.

Found: C, 6.62; H, 1.84; N, 2.55; I, 79.14%. Calcd for $C_6H_{20}N_2TeI_7$: C, 6.34; H, 1.77; N, 2.47; I, 78.19%.

To avoid such a change in composition, solvents and temperatures were varied upon recrystallization, and the pure hexaiodo complex was successfully recrystallized only from absolute ethanol solution not including HI acid at an optimum temperature near 50 °C. Thus obtained single crystals of $(Me_3NH)_2TeI_6$ were black, octahedral and less than 70 μm, these being used for the present study.

X-Ray Structure Determination. As the X-ray analytical methods used were almost the same for both complexes, the following description is made mainly for $(Me_3NH)_2TeI_7$ and briefly for $(Me_3NH)_2TeI_6$.

$(Me_3NH)_2TeI_7$: The density was measured by pycnometry with petroleum at 20 °C; the lattice parameters and the space group ($P4/nmm$ from systematic absences: $hk0$, $h+k=2n+1$) were previously determined with a Weissenberg camera; crystal 0.12×0.12×0.20 mm^3 in size was mounted with c coincident with the goniostat axis; Rigaku AFC-4 diffractometer, graphite-monochromatized Mo$K\alpha$ radiation, 40 kV-200 mA; unit cell parameters were refined by least-squares methods on the basis of 25 2θ values ($18° < 2\theta < 28°$, λ=0.71069 Å); intensity measurement was performed up to 2θ=55° ($0 \le h \le 12$, $0 \le k \le 18$, $-8 \le l \le 8$), ω—2θ scan technique, scan rate 4° min^{-1} (ω); all intensities were corrected for some X-ray damage (8.2% decay) by a factor of $a\exp(bN)$, where a=1.0043 and b=0.00011 obtained by least-squares on the basis of the intensity variation of three standard reflections (502, 060, and 004) every 50 reflections through experiments and N the ordinal number of measurements; 1523 reflections including 722 equivalent ones were measured, $R_{int}=\sum||F_o|-\langle|F_o|\rangle|/\sum|F_o|$=0.031, 248 weak reflections classified as unobserved [$|F_o| < 3\,\sigma(F_o)$], 553 observed unique reflections used for the structure determination;

Lorentz-polarization factors and absorption were corrected, empirical absorption correction factors on F 0.9986—1.0595; [9] the positions of Te and I were deduced from a Patterson map, starting with these positions the other non-H atoms were determined from electron density maps and refined by full-matrix least-squares on F with anisotropic thermal parameters for Te and I, and isotropic ones for N and C; the H atoms were not found from difference maps, and omitted in the refinement, $\sum w(|F_o|-|F_c|)^2$ minimized for 31 parameters, $w=[\sigma^2(F_o)]^{-1}$; final R=0.051, R_w=0.044, and goodness of fit $S=[\sum w(|F_o|-|F_c|)^2/(m-n)]^{1/2}$=1.74, where m is the number of unique reflections and n the number of refined parameters, ratio of maximum least-squares shift to error, $(\Delta/\sigma)_{max}$, was 0.3 for C(1) and $(\Delta/\sigma)_{mean}$=0.07, maximum positive and maximum negative electron densities in final difference Fourier synthesis, $(\Delta\rho)_{max}$ and $(\Delta\rho)_{min}$, were 1.24 and −1.46e/Å^3, respectively.

$(Me_3NH)_2TeI_6$: Black, octahedral crystal used was 0.07×0.07×0.07 mm^3 in size; lattice parameters were refined by least-squares methods based on 12 2θ values (17°<2θ<22°, λ=0.71069 Å); ω scan technique, $2\theta_{max}$=55° ($0\leq h\leq 17$, $0\leq k\leq 17$, $0\leq l\leq 17$), 2800 measured reflections, 891 unique reflections, 628 unobserved [$|F_o|<7\sigma(F_o)$], 263 observed unique reflections used for the structure determination; R_{int}(based on F)=0.097, standard reflections 400, 040, 004, intensity variation less than 3.0%, absorption correction neglected because of small size of crystal; structure was solved by heavy atom method and refined by full-matrix least-squares on F with anisotropic thermal parameters for non-H atoms, $\sum w(|F_o|-|F_c|)^2$ minimized for 24 parameters, $w=[\sigma^2(F_o)]^{-1}$; R=0.057, R_w=0.040, S=2.04, $(\Delta/\sigma)_{max}$=0.01, $(\Delta\rho)_{max}$ and $(\Delta\rho)_{min}$ in final difference Fourier synthesis were 1.20 and −1.62 e/Å^3, respectively.

In both cases, neutral atom scattering factors and anomalous dispersion terms were taken from Internationl Tables for X-ray Crystallography[10] and *UNICS* Program System,[11] Finger Computing System[12] and their modifications used for calculations at the Computation Center of Osaka University and later at the Information Processing Center of Kobe University.

The crystal date are summarized in Table 1. The positional and thermal parameters of hexaiodo and heptaiodo complexes are listed in Tables 2 and 3, respectively.[13]

Results and Discussion

The Structure of Hexaiodo Complex, $(Me_3NH)_2TeI_6$. The crystal of hexaiodo complex consists of octahedral anions $[TeI_6]^{2-}$ and group cations $[(CH_3)_3NH]^+$ in an arrangement of the K_2PtCl_6 structure, as shown in Fig. 1. The length of six equivalent Te–I bonds is 2.952(2) Å, and the two I–Te–I bond angles are 89.90(7)° and 90.10(7)°, indicating that the coordination octahedra of Te^{IV} atoms are practically regular. The obtained value of 2.952 Å is more reliable than 2.93 Å found in K_2TeI_6[8] and can be compared to 2.947(2) Å corrected for thermal motion in Rb_2TeI_6.[14] The Me_3NH^+ cations occupy the eight tetrahedral holes at 1/4, 1/4, 1/4 etc. The C–N bond length 1.51(5) Å and the C–N–C bond angle 110(2)° are reasonable in comparison with those in the literature, cf. 1.466—1.487 Å, 110.2—112.1° for $(CH_3)_3NHCl$[15] and 1.478 Å and 111.6° for $(Me_3NH)_2SnCl_6$[16]. The threefold axis of each cation is aligned with the unit cell triad axis and its N–H bond approaches to one iodine triangle of the nearest octahedron with three symmetrical N···I distances of 3.87(3) Å. Then the H···I distance and the N–H–I angle were calculated to be 3.14 Å and 130°, respectively, by assuming the hydrogen position at a distance of 1.02 Å from its attached

Table 1. Crystal Data of Hexaiodo and Heptaiodo Complexes

Compound	$(Me_3NH)_2TeI_6$	$(Me_3NH)_2TeI_7$
Formula	$C_6H_{20}N_2TeI_6$	$C_6H_{20}N_2TeI_7$
Formula weight	1009.3	1136.2
Crystal system	cubic	tetragonal
Space group	*Pa*3	*P*4/*nmm*
a/Å	13.210(2)	13.921(3)
c/Å		6.224(2)
V/Å^3	2305.2(9)	1206.2(8)
D_m/Mg m^{-3}	2.93	3.19
D_x/Mg m^{-3}	2.91	3.13
Z	4	2
μ(Mo $K\alpha$)/mm^{-1}	9.24	10.1

Table 2. Fractional Coordinates and Equivalent Isotropic Thermal Parameters of non-H Atoms in $(Me_3NH)_2TeI_6$

Atom	*x*	*y*	*z*	B_{eq}/Å^2
Te	0	0	0	3.455(1)
I	0.0326(2)	−0.0281(2)	0.2193(2)	4.730(1)
N	0.2071(24)	0.2071(24)	0.2071(24)	6.150(1)
C	0.2184(25)	0.3094(24)	0.1576(27)	5.598(1)

$B_{eq}=(4/3)\sum_i\sum_j\beta_{ij}\boldsymbol{a}_i\cdot\boldsymbol{a}_j$.

Table 3. Fractional Coordinates (×10^4) and Thermal Parameters(Å^2) for $(Me_3NH)_2TeI_7$ with Their e.s.d.'s in Parentheses

Atom	*p*	*x*	*y*	*z*	B_{eq}/B
Te	1.0	2500	2500	0877(4)	3.009(1)*
I(1)	1.0	2500	4607(1)	0918(2)	5.404(2)*
I(2)	1.0	2500	2500	5896(5)	4.790(1)*
I(3)	1.0	7500	2500	2483(5)	6.424(2)*
N	0.5	4731(13)	4731(13)	4539(44)	3.9(6)
C(1)	0.25	4236(56)	5554(52)	5473(118)	6.8(19)
C(2)	0.25	5663(40)	5065(38)	3404(73)	4.3(12)
C(3)	0.25	5158(54)	3962(52)	5870(12)	5.7(17)

p: occupancy factor. *: $B_{eq}=(4/3)\sum_i\sum_j\beta_{ij}\boldsymbol{a}_i\cdot\boldsymbol{a}_j$.

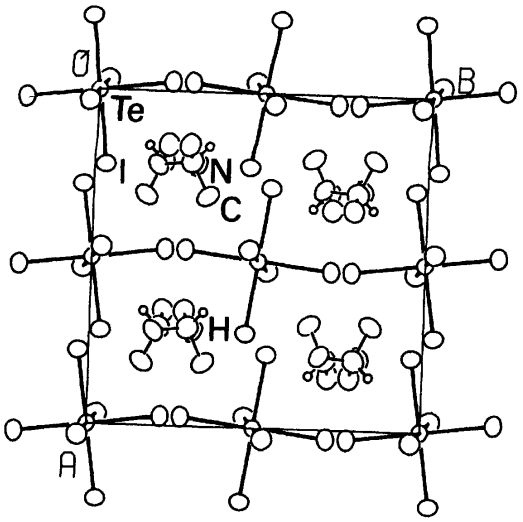

Fig. 1. Crystal structure of $(Me_3NH)_2TeI_6$ projected along [001].

nitrogen with sp^3 hybridization. The scheme of trifurcated hydrogen bonds, N-H···3I, is quite similar to that found in $(Me_3NH)_2TeCl_6$,[7] although H···I distance is only a little shorter than the normal van der Waals approach, 3.4 Å.[17] On the other hand, the CH_3 group is surrounded by five I(1) atoms with distances of 3.84—4.27 Å, less than or near the van der Waals distance 4.2 Å.

The Structure of Heptaiodo Complex, $(Me_3NH)_2TeI_7$. A projetion of the crystal structure along ***a*** with the numbering of atoms and a stereo pair of structure viewed along ***c*** are shown in Figs. 2 and 3, respectively. Selected interatomic distances and angles are listed in Table 4.

The Te atom is coordinated by six iodine atoms, 4I(1) and 2I(2), in an elongated octahedral arrangement. These octahedra are connected to each other by sharing two opposite vertices of each octahedron to form a linear trans chain running along ***c***. The bond length of Te to terminal I(1), 2.934(1) Å, is shorter than 2.952(2) Å found in cubic $(Me_3NH)_2TeI_6$ and agrees with 2.930(2) Å in Rb_2TeI_6, which is uncorrected for librational motion of $[TeI_6]^{2-}$ ion.[14] The central Te atom is at 0.026(3) Å below or above the coordination plane formed by 4I(1). The Te–I(2) bridging distances of 3.124(4) and 3.100(4) Å are longer than that for the terminal I(1) by 0.18 Å. The lengthening of a bond to a bridging halide ion is quite common: In $[MeAlCl_2]_2$ the Al–Cl distances are 2.25 and 2.05 Å for bridging and terminal chlorine atoms, respectively.[18] Another example is found in $BaFeF_5$, where the mean Fe–F distances are 1.90 Å for bridging atoms and 1.82 Å for terminal fluorine atoms within the linear trans $[FeF_5]_n^{2n-}$ chain.[19] Thus the formed polymeric chain is a previously unknown, newly found chemical species for halotellurate anions and can be described as $[TeI_5]_n^{n-}$.

Another striking feature of the structure is that extra

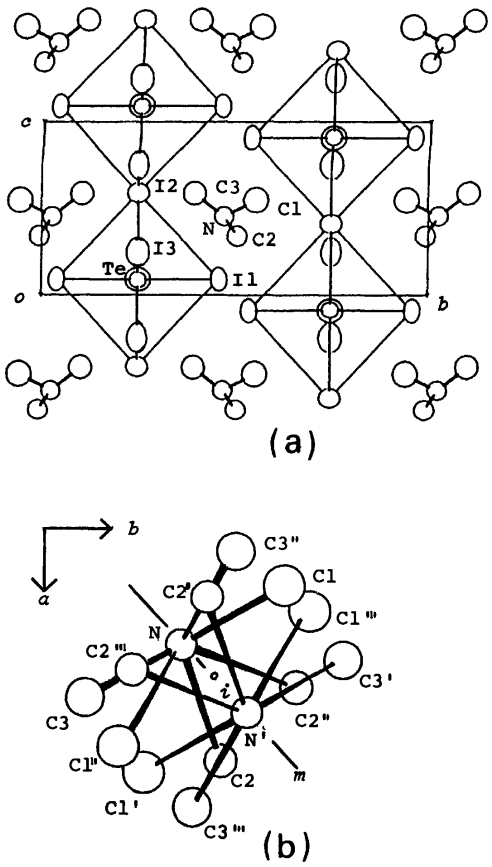

Fig. 2. Crystal structure of $(Me_3NH)_2TeI_7$. (a) The projection along [100], and (b) disordered configurations of the Me_3NH^+ cation. Symbols are: none, (x, y, z); $(')$, $(\bar{x}, \bar{y}, \bar{z})$; $('')$, (y, x, z); $(''')$, $(\bar{y}, \bar{x}, \bar{z})$.

iodine atoms, I(3)'s, are also stacked along ***c*** to form a linear polyiodide chain within the crystal lattice. More remarkable is the appearance of nearly equal I–I bond lengths with successive values of 3.091(6) and 3.133(6) Å. Both separations are larger than the I–I bond lengths of 2.715(6) Å in crystalline iodine and also of the mean 2.92(1) Å for seventeen compounds including linear, symmetric triiodide ions.[20,21] Such an approximately linear array of equally spaced iodine atoms was first proposed for some polyiodide compounds of starch and cyclodextrin, but later works proved that these results probably correspond to disordered structure.[22,23] On the other hand, recent studies on some metal complexes of α-cyclodextrin polyiodide and also on various stacked organometallic iodide compounds have shown that long polyiodide chains exclusively consist of I_2 and/or $[I_n]^-$ (n=1, 3, and 5) moieties.[24] Consequently, a linear and nearly equidistant array of iodine atoms was first realized in the heptaiodo complex, although its presence had been speculated so far only as an extreme model case or interpreted in terms of a statistical structure or disordered arrangements. In contrast with many other polyiodide compounds, no indication of diffuse scattering or superstructure appearance was disclosed on

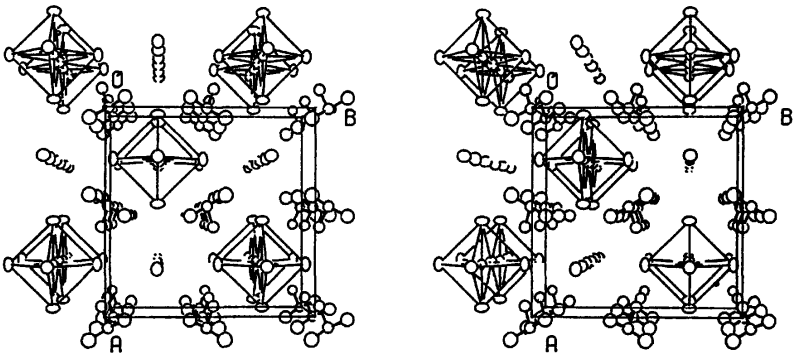

Fig. 3. Stereoscopic view of crystal structure of $(Me_3NH)_2TeI_7$ along the *c* axis. Thermal ellipsoids are shown at 50% probability level.

Table 4. Interatomic Distances (*l*/Å) and Angles (ϕ/°) in $(Me_3NH)_2TeI_7$

(i) $[TeI_5]^-$ anion			
Te-I(1)	2.934(1)	I(1)-Te-I(1)	179.0(1)
Te-I(2)	3.124(4)	I(1)-Te-I(2)	89.5(1)
Te-I(2′)	3.100(4)	I(1)-Te-I(2′)	90.5(1)
(ii) Polyiodide chain, $[I]^{n-}_{2n}$			
I(3)-I(3″)	3.133(6)	I(3)-I(3‴)	3.091(6)
(iii) $[(CH_3)_3NH]^+$ cation			
N-C(1)	1.46(8)	C(1)-N-C(2)	110(4)
N-C(2)	1.55(6)	C(1)-N-C(3)	122(4)
N-C(3)	1.48(8)	C(2)-N-C(3)	98(4)
(mean 1.50)		(mean 110)	

Symmetry code: none, (*x*, *y*, *z*); (′), (*x*, *y*, *z*−1); (″), (*x*, *y*, 1−*z*); (‴), (*x*, *y*, −*z*).

Weissenberg photographs of the heptaiodo complex. The thermal parameters of I(3) are, in fact, relatively large to those of I(1) and I(2) and more anisotropic with root-mean-square amplitudes of 0.34 Å (at most) parallel to the polyiodide chain and of 0.25 Å perpendicular to it, but there is no sufficient evidence for establishing disordered structure. The appearence of unique iodine array in the present complex may be associated with the fact that the length of repeating unit in $[I]^{n-}_{2n}$ chain is almost the same as that in $[TeI_5]^{n-}_n$ chain, which corresponds to the *c* spacing of the unit cell, 6.2 Å.[25]

The Me_3NH^+ cation is inserted between two $[TeI_5]^{n-}_n$ and two $[I]^{n-}_{2n}$ columns. The electron density map revealed a statistical arrangement of Me_3NH^+ ions. Four equivalent N atoms in the unit cell are distributed on the special position **8j** of the space group *P4/nmm* with a statistical weight of 0.5, while the methyl carbon atoms, C(1), C(2), and C(3), are located on each individual **16k** positions with a statistical weight of 0.25. Each Me_3NH^+ cation is therefore distributed over four configurations with the equal probability; any two of which are related by either the center of symmetry or the mirror plane as illustrated in Fig. 2(b). The mean C-N bond length of 1.50 Å and the mean C-N-C bond angle of 110° for the disordered Me_3NH^+ cations are comparable to those for the ordered one in the hexaiodide described earlier.

The NH hydrogen positions of cations were calculated on the basis of sp^3 N atoms with N-H distances of 1.02 Å as in hexaiodide. Weak, but significant hydrogen bonds are formed between NH and I atoms with distances of 3.84(2) Å for N···I and 2.90 Å for H···I, and with the angle N-H···I of 154°. The statistical distribution of Me_3NH^+ cation is probably associated with the formation of hydrogen bonds and packing restriction of molecular ions. Some intermolecular CH_3···I distances are less than the sum of the van der Waals radii of 4.2 Å, suggesting weak interaction due to C-H···I hydrogen bonds; their minimum distances are 3.85(7) Å for C(1)-I(3), 3.74(5) Å for C(2)-I(1) and 3.77(7) Å for C(3)-I(1).

In conclusion, the present X-ray analysis together with the neutralization principle of electric charges revealed that the chemical constitution of the newly prepared catena heptaiodo complex is $[(CH_3)_3NH]^{2n+}_{2n}[TeI_5]^{n-}_n[I]^{n-}_{2n}$. The presence of such a peculier polyiodide ion of $[I]^{n-}_{2n}$ is interesting in view of the chemical bond.

The authors wish to express their thanks to Lecturer Kichiro Koto of Osaka University for his guidance in part and to Dr. Yuriko Yamagata for her help during this work. The present work was partially supported by a Grant-in-Aid for Scientific Research No. 593700350 from the Ministry of Education, Science and Culture.

References

1) H. Ishida, R. Ikeda, and D. Nakamura, *Ber. Bunsenges. Phys. Chem.*, **88**, 546 (1984).

2) R. Ikeda, D. Nakamura, R. Kadel, and A. Weiss, *Ber. Bunsenges. Phys. Chem.*, **87**, 570 (1983).

3) Y. Furukawa, H. Kiriyama, and R. Ikeda, *Bull. Chem. Soc. Jpn.*, **50**, 1927 (1977).

4) K. Kitahama, H. Kiriyama, and Y. Baba, *Bull. Chem. Soc. Jpn.*, **52**, 324 (1979).

5) H. Kiriyama and T. Yamamoto, Molecular Structure Symposium of the Chemical Society of Japan, Sendai, September 1983, Abstr., No. 3P23.

6) K. Kitahama and H. Kiriyama, *Acta Crystallogr., Sect. A*, **34**, S302 (1978).
7) M. H. Ben Ghozlen and J. W. Bats, *Acta Crystallogr., Sect. B*, **38**, 1308 (1982).
8) S. Syoyama, K. Osaki, and S. Kusanagi, *Inorg. Nucl. Chem. Letters*, **8**, 181 (1972).
9) A. C. North, D. C. Phillips, and F. S. Mathews, *Acta Crystallogr., Sect. A*, **24**, 351 (1968).
10) "International Tables for X-Ray Crystallography," Birmingham (1974), Vol. IV, Knoch Press. (Present distributor D. Reidel, Dordrecht.)
11) *UNICS* (1967). Universal Crystallographic Computation Program System, edited by T. Sakurai, Tokyo; Crystallographic Society of Japan.
12) L. W. Finger, Carnegie Insitute Washington Yearb., **67**, 216 (1969).
13) Lists of structure factors and anisotropic thermal parameters are deposited as Document No.8617 at the office of the Editor of *Bull. Chem. Soc. Jpn.*
14) W. Abriel, *Mat. Res. Bull.*, **17**, 1341 (1982).
15) J. Lindgren and I. Olovsson, *Acta Crystallogr., Sect. B, 24*, 554 (1968).
16) O. Knop, J. S. Cameron, M. A. James, and M. Falk, *Can. J. Chem.*, **61**, 1620 (1983).
17) A. Bondi, *J. Phys. Chem.*, **68**, 441 (1964).
18) G. Allegra, G. Perego, and A. Immirzi, *Makromol. Chem.*, **61**, 69 (1963).
19) R. V. Muhll, S. Andersson, and J. Galy, *Acta Crystallogr., Sect. B*, **27**, 2345 (1971).
20) F. van Bolhuis, P. S. Koster, and T. MiGchelsen, *Acta Crystallogr.*, **23**, 90 (1967).
21) The files of the Cambridge Crystallographic Data Centre, Cambridge, England. F. H. Allen, S. Bellard, M. D. Brice, B. A. Cartwright, A. Doubleday, H. Higgs, T. Hummelink, B. G. Hummelink-Peters, O. Kennard, W. D. S. Motherwell, J. R. Rodgers, and D. G. Watson, *Acta Crystallogr., Sect. B*, **35**, 2331 (1979).
22) R. E. Rundle and E. C. Edwards, *J. Am. Chem. Soc.*, **65**, 2200 (1943); R. S. Stein and R. E. Rundle, *J. Chem. Phys.*, **16**, 195 (1948).
23) M. Noltemeyer and W. Saenger, *J. Am. Chem. Soc.*, **102**, 2710 (1980).
24) J. A. Ibers, L. J. Pace, J. Martinsen, and B. M. Hoffman, "Stacked Metal Complexes: Structures and Properties," in Structure and Bonding 50, Springer-Verlag Berlin Heidelberg (1982), pp. 1—55.
25) E. Rosshirt, F. Frey, H. Boysen, and H. Jagodzinski, *Acta Crystallogr., Sect. B*, **41**, 66 (1985).

 © 1986 The Chemical Society of Japan Bull. Chem. Soc. Jpn., 59, 587—591 (1986)

Effects of Bivalent Metal Cations on the Conformation and Aggregation of Poly(L-glutamic acid)

Hiroshi MAEDA,* Tsuyoshi HIRAMATSU, and Shoichi IKEDA
Department of Chemistry, Faculty of Science, Nagoya University, Chikusa-ku, Nagoya 464
(Received September 25, 1985)

In the solution of fully neutralized poly(L-glutamic acid) in the absence of supporting electrolytes, the α-helix was induced by the addition of five transition metal chlorides in the following order: $CuCl_2 \geq CdCl_2 > ZnCl_2 > NiCl_2 > CoCl_2$. The induction did not occur by the addition of $BaCl_2$, $CaCl_2$, or $MgCl_2$. The induction by transition metal cations was inhibited in the presence of a supporting electrolyte (NaCl). Distortion of circular dichroism (CD) spectra occurred as the induction of the α-helix proceeded, which was shown to be recognizable when apparent aggregation number m exceeded about 100. Conformation of the polypeptide in these aggregates was expected to be the α-helix based on the conformation in the precipitates obtained at these mixing ratios which gave distorted CD spectra, which was determined by infrared absorption spectra.

Induction of the secondary structures of fully neutralized anionic polypeptides was studied on poly(L-glutamic acid)(PGA)[1] and poly (*S*-carboxymethyl-L-cysteine)(poly[Cys(CH_2COOH)][2] by the addition of cationic surfactants of different head groups but of a common hydrocarbon tail. Different behaviors were observed between these two polypeptides. The induction of the α-helix of PGA occurred for three surfactants with small differences among their inducing powers,[1] while the induction of the β-structure of poly[Cys(CH_2COOH)] depended on the kind of head groups.[2] Furthermore, in the presence of 0.1 M NaCl, the induction of the α-helix of PGA was completely inhibited,[1] while that of the β-structure of poly[Cys(CH_2COOH)] was scarcely perturbed.[2]

It is interesting to examine whether such a definite difference exists between the inductions of the α-helix and the β-structure caused by the addition of bivalent metal cations. Effects of bivalent metal cations on the conformation of poly[Cys(CH_2COOH)][3] and its side chain homolog[4] were already examined. Interactions of bivalent metal cations with PGA has been extensively studied,[5–15] including the induction of the α-helix by Cu^{2+} and Cd^{2+} ions. Nevertheless, available data for the present purpose of comparison are not sufficient for PGA. Therefore, previous studies[3,4] are extended to the induction of the α-helix of PGA in the present study.

Another purpose of the present study is clarifying the origin of the distortion of the circular dichroism (CD) spectra of PGA. The distortion of CD has been attributed to the aggregation of α-helices,[16,17] or to the β-structure[15] without providing evidence for both aggregation and conformation. In the present study both the aggregation number and the conformation of the polypeptide in the aggregates are examined.

Experimental

Weight average molecular weight and the degree of polymerization of the used PGA sample were 6.3×10^4 and 480, respectively, as determined from light scattering. Reagent grade $CuCl_2\cdot2H_2O$, $CdCl_2\cdot(1/2)H_2O$, $NiCl_2\cdot6H_2O$, and $BaCl_2\cdot2H_2O$ were purchased from Nakarai Chemicals Ltd. (Kyoto). Reagent grade $ZnCl_2$ was from Wako Pure Chemicals or prepared by the reaction of Zn with HCl. $CaCl_2\cdot4H_2O$ (suprapur) and $CoCl_2\cdot6H_2O$ were from Merck. $MgCl_2\cdot6H_2O$ was from Baker.

Circular dichroism (CD) was measured with a Jasco J-40 A circular dichrograph using a cell of 1 mm light path at 25±0.1 °C. Light scattering was mesured on a Chromatix KMX-6 low-angle light-scattering photometer at ambient temperature (24±2°C). A 6—7° annulus was chosen to observe the scattered light which collected the light of about 4—5° scattering angle for aqueous solutions. A 0.2 mm field stop was selected which defined the scattering volume. Millipore membrane filters of 0.1, 0.22, and 0.30 μm pore size were used to filter the solutions containing aggregates of aggregation number smaller than 12, about 53 to 170, and greater than 250, respectively. Measurements of pH were carried out with an Iwaki M-225 pH meter. Infrared absorption spectra of precipitates in KBr pellets were taken with a Jasco IRA-2 spectrophotometer at 24±2°C. Precipitates of PGA-metal ion complexes were collected by centrifugation(ca. 1500 g), dried in a desicator over P_2O_5 for one or 2 d, and then mixed with dry KBr powder. The mixture was ground finely and kept in a desicator over P_2O_5 for several days. The mixture was pressed (6—7 t/cm^2) to a pellet for 3 min in vacuo. The pH of the solutions prior to the addition of a metal chloride was adjusted to be 6.7±0.2 by the addition of NaOH, if necessary. Then, various amounts of a metal chloride were added and the mixtures were incubated for 12—24 h at 24±2°C before the measurements. Concentrations of the polymer C_P and metals C_M are expressed in residue molarity and molarity M ($mol\,dm^{-3}$), respectively.

Results

Induction of the α-Helix. In Fig. 1 are shown the CD spectra of the solutions containing 1 mM PGA and various amounts of $NiCl_2$. On addition of $NiCl_2$, the α-helix was induced as indicated by a change of CD spectra. The helical content was about 75% at the mixing ratio C_M/C_P of 2.0. Further addition of $NiCl_2$ did not enhance the α-helix formation but distorted the CD spectra (curve f) and eventually led to the precipitation. No isodichroic point is seen in Fig. 1. The same behavior was observed on the addition of $CoCl_2$. On the contrary, an isodichroic point was found

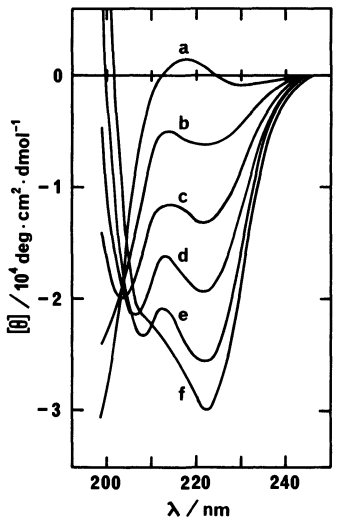

Fig. 1. CD spectra of PGA (C_P=1 mM) in the presence of various amounts of $NiCl_2$. Mixing ratio C_M/C_P. (a): 0, (b): 0.17, (c): 0.27, (d): 0.50, (e): 1.0, and (f): 6.0.

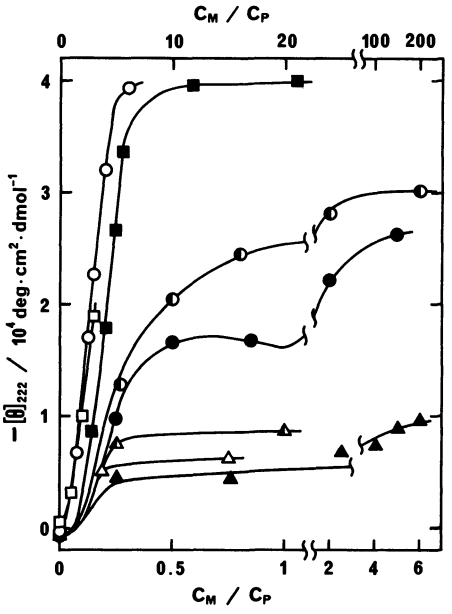

Fig. 2. Dependence of $[\theta]_{222}$ on the mixing ratio C_M/C_P. (○): $CuCl_2$, (□): $CdCl_2$, (■): $ZnCl_2$, (◐): $NiCl_2$, (●): $CoCl_2$, (△): $BaCl_2$, (▲): $CaCl_2$, and (▲): $MgCl_2$. Bottom and top scales of abscissae refer to transition metals and alkaline earth metals, respectively.

around 203—204 nm in the α-helix induction by $CuCl_2$ or $CdCl_2$. This behavior is consistent with the reported one.[11] Change of the CD spectra on the addition of $ZnCl_2$ was an intermediate one between these two types. Since a distortion of the CD spectra at high mixing ratios occurred around 210 nm, the residue ellipticity at 222 nm ($[\theta]_{222}$) was used as a measure of the helical content.

In Fig. 2, the residue ellipticities at 222 nm are plotted against the mixing ratio C_M/C_P for eight bivalent metal

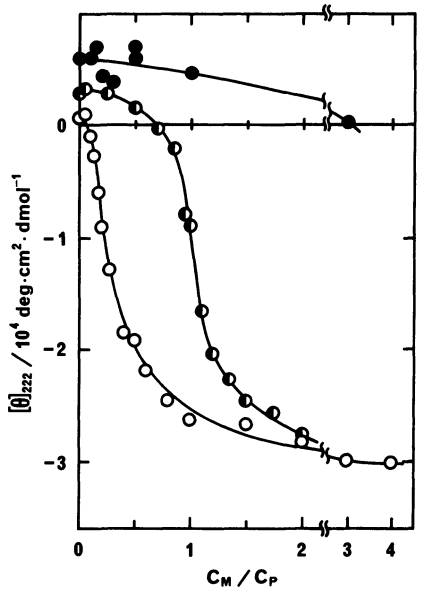

Fig. 3. Effects of NaCl on the induction of the α-helix by the addition of $NiCl_2$. C_P=1.0 mM. NaCl concentration (M). (○): 0, (◐): 0.010, and (●): 0.10.

chlorides. Induction of the α-helix occurred completely on the addition of $CuCl_2$ or $ZnCl_2$, while precipitation occurred before the induction was completed in the case of $CdCl_2$, $NiCl_2$, or $CoCl_2$. Contrary to these five transition metals, $BaCl_2$, $CaCl_2$, or $MgCl_2$ did not induce the α-helix. In the range of C_M/C_P below about 5, $[\theta]_{222}$ varied from nealy zero (or small positive) to −3000-−8000 for these three alkaline earth metals. No further change occurred, however, in the range of C_M/C_P greater than about 5. Consequently, the change of CD spectra can be ascribed to a kind of the reported effect of ionic strength[18] rather than to a partial conversion to the α-helix.

Precipitation of the polypeptide occurred in the range of C_M/C_P greater than about 30 in the case of $BaCl_2$ or $CaCl_2$, while precipitation did not occur at C_M/C_P=200 in the case of $MgCl_2$. The change of $[\theta]_{222}$ occurred in one step for every bivalent cation, although apparently two-step changes are seen in Figure 2 for Ni^{2+}, Co^{2+}, and Mg^{2+} simply because abscissa scales are changed.

Effect of Supporting Electrolyte. The effect of $NiCl_2$ on the conformation of PGA was also examined in 0.01 M and 0.1 M NaCl solutions. The result is shown in Fig. 3, together with the result in the absence of NaCl for the sake of comparison. In 0.01 M NaCl, the induction of the α-helix was hampered when C_M/C_P was smaller than about unity but became comparable with that in the absence of NaCl in the range of C_M/C_P between 1.5 and 2. Precipitation occurred when C_M/C_P was greater than about 2. In 0.1 M NaCl, the induction did not occur up to C_M/C_P=3 and precipitation occurred on further addition of $NiCl_2$. The inductive effect of $NiCl_2$ was thus largely suppressed in the

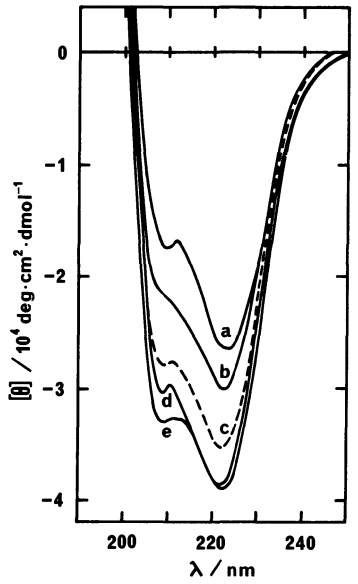

Fig. 4. CD spectra at the mixing ratios slightly smaller than those caused precipitation. Mixing ratios (C_M/C_P). (a): $CoCl_2$ 5.0, (b): $NiCl_2$ 6.0, (c): $CdCl_2$ 0.275, (d): $ZnCl_2$ 0.82, and (e): $CuCl_2$ 0.30. The CD curve (c) was obtained on turbid solutions.

presence of 0.1 M NaCl. This inhibitory action of ionic strength is similar to that found on the interaction of PGA with surfactants,[1] or other polyion-bivalent metal interactions.[19,20] This behavior is in contrary to the effect of ionic strength on the induction of β-structure of poly(*S*-carboxymethyl-L-cysteine) by bivalent metal cations.[3] Also, it is reported that interaction of $Cu(NO_3)_2$ with poly(methacrylic acid) was not affected by the presence of 0.1 M $NaNO_3$.[21]

Distortion of the CD Spectra. When a transition metal chloride was added to such an amount more than required to the maximum induction for that species, the CD spectra began to be distorted in a way that $[\theta]_{208}$ decreased in magnitude. The CD spectra obtained at the mixing ratio near but slightly smaller than that caused precipitation are shown in Fig. 4 for five transition metal chlorides. Distortion occurred only slightly in the case of $CuCl_2$. In the case of $CdCl_2$, the spectra were obtained on a turbid solution and hence represented by a dashed curve c. These spectra shown in Fig. 4 might be associated with the presence of the β-structure.

The distortion of the CD spectra can be clearly discriminated when the correlation between $[\theta]_{208}$ and $[\theta]_{222}$ is examined (Fig. 5) as proposed previously.[1] A straight line in Fig. 5 represents the induction of the α-helix, probably including the effect of ionic strength on the CD spectra. The data of $CdCl_2$ located in the range $-[\theta]_{222}>2\times10^4$ were taken on turbid solutions. Deviation from the straight line occurs at different helical contents for different species; the following order of the helical content is seen, $CoCl_2<NiCl_2<CdCl_2<ZnCl_2$. The deviation is not clear for $CuCl_2$.

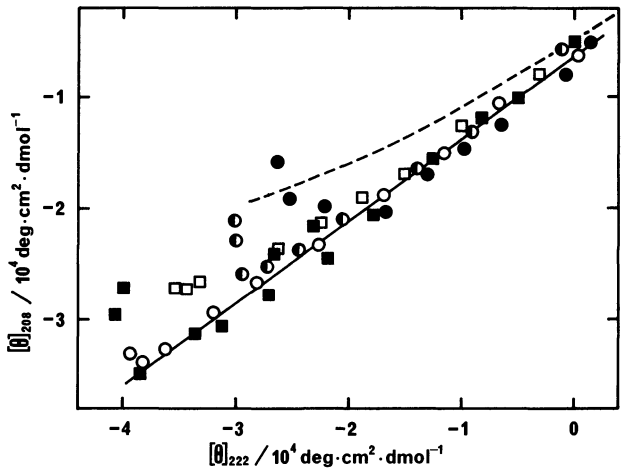

Fig. 5. Correlation between $[\theta]_{222}$ and $[\theta]_{208}$ in the presence of various amounts of a given metal chloride. The same symbols are used as in Figure 2 to represent different metal species. A dashed curve represents the result of the addition of $NiCl_2$ in 0.01 M NaCl.

A dashed line in Fig. 5 represents the result on the addition of $NiCl_2$ in 0.01 M NaCl. Distortion of the CD spectra also occurred in 0.01 M NaCl as shown by a non-zero curvature of the dashed line.

Aggregation of PGA in 0.01 M NaCl. Light scattering was measured on the 0.01 M NaCl solutions containing 1 mM PGA and various amounts of $NiCl_2$. Apparent aggregation number m was evaluated by Eq. 1.

$$m = \Delta R_\theta(C_M)/\Delta R_\theta(C_M=0) \quad (1)$$

In Eq. 1, ΔR_θ represents a difference of light intensities between a solution and a solvent at a scattering angle θ, which is very close to zero in the present study. Underlying assumptions leading to Eq. 1 are: (1) refractive index increment does not vary appreciably on addition of $NiCl_2$ and (2) the second virial coefficient can be ignored for any aggregates. (In the absence of $NiCl_2$, the contribution from the second virial coefficient did not exceed 5%) In spite of these approximations, the apparent aggregation number m is expected to be a useful measure for the extent of aggregation. When the dependence of m on the mixing ratio given in Fig. 6 is compared with that of $[\theta]_{222}$ given in Fig. 3, it is seen that aggregation occurs at small mixing ratios corresponding to low helical contents. For example, at $C_M/C_P=1.0$, $-[\theta]_{222}$ is smaller than 10^4, yet aggregation number already reaches 167. If every two carboxylate groups are assumed to bind to a Ni^{2+} ion, then m should be corrected to 136 instead of 167. This provides a rough estimate of the consequence of assumption (1).

As a measure of the extent of distortion of CD spectra, the slope of the dashed curve given in Fig. 5 was

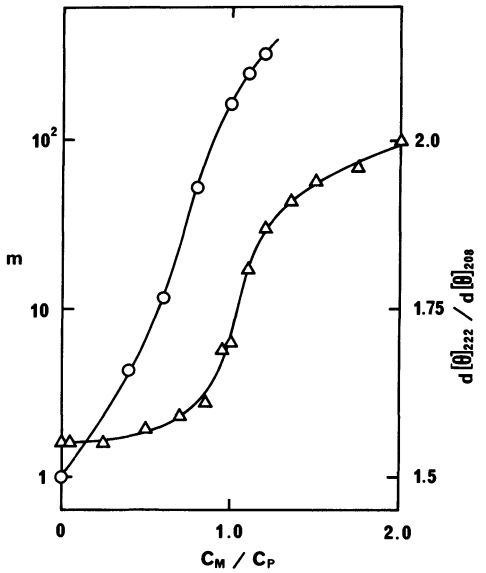

Fig. 6. Apparent aggregation number m and a measure of the distortion of the CD spectra, $d[\theta]_{222}/d[\theta]_{208}$, as functions of the mixing ratio (C_M/C_P) of $NiCl_2$ in 0.01 M NaCl. (○) m and (△) $d[\theta]_{222}/d[\theta]_{208}$ refer to the left and right ordinate scales, respectively.

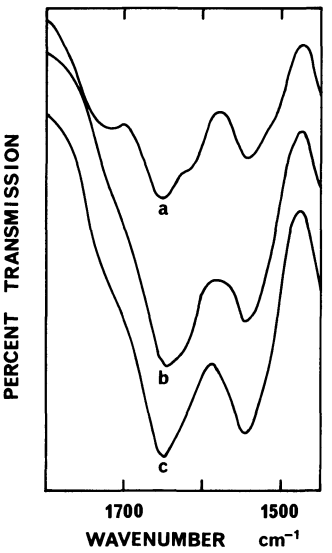

Fig. 7 Infrared absorption spectra of the precipitates in KBr disks consisting of PGA and (a): $CuCl_2$, (b): $NiCl_2$, or (c): $CoCl_2$.

tentatively employed which is represented by Eq. 2.

$$[\theta]_{208}/10^4 = 0.473([\theta]_{222}/10^4)^2 + 0.631([\theta]_{222}/10^4) - 0.050 \quad (2)$$

Equation 2 was obtained from the exeprimental points by the least square method. The slope, $d[\theta]_{222}/d[\theta]_{208}$ was evaluated by differentiating Eq. 2. The slope is 1.55—1.60 in the range well approximated by a straight line. When $C_M/C_P>1.0$, the slope increases sharply to 1.80 or greater. Consequently, it is concluded that the distortion of the CD spectra becomes first recognizable when m is larger than about 100.

Infrared (IR) Absorption Spectra of Precipitates. At the mixing ratio where the distorted CD spectra shown in Fig. 4 were obtained, precipitation occurred when the polypeptide concentration exceeded 1 mM. Consequently, conformation of the polypeptide in the precipitates rather than in solution was examined by infrared absorption spectra. The IR spectra of the precipitates are shown in Fig. 7 obtained from the solution of C_P=10 mM by the addition of $CuCl_2$, $NiCl_2$, or $CoCl_2$. Amide I, II, and V bands were found at 1650—1655 cm^{-1}, 1550 cm^{-1}, and 630 cm^{-1}, respectively, for these three complexes. These band positions indicated that the conformation of PGA was the α-helix.[22-24]

A band around 1620 cm^{-1} was observed in the complex with $CuCl_2$, which can be assigned to antisymmetric stretching of side chain carboxylato group covalently bound to a copper atom,[25,26] rather than to the amide I band in the β-structure. There is no room to expect the presence of the β-structure in the case of $CuCl_2$, since distortion of the CD spectra did not occur appreciably. Corresponding bands could not be resolved in the case of $NiCl_2$ or $CoCl_2$.

The β-structure is one of stable conformations of PGA in the solid state.[27-31] The presence of the β-structure of PGA in solution has not been confirmed until now. Furthermore, dissolution of the β-precipitates of PGA was reported to be very difficult.[30] Based on all these findings, it is quite unlikely that the conformation of the polypeptide changed from the β-structure to the α-helix during the precipitation in the present study. We can, therefore, conclude that the conformation of PGA in soluble aggregates is the α-helix.

Discussion

Induction of the α-Helix as Compared with That of the β-Structure. Induction of the α-helix of PGA in the media of no added salt occurred in the present study by the addition of transition metal chlorides in the order of $Cu^{2+} \gtrsim Cd^{2+} > Zn^{2+} > Ni^{2+} > Co^{2+}$. On the other hand, alkaline earth metals ($BaCl_2$, $CaCl_2$, $MgCl_2$) did not induce the α-helix. This result is in good agreement with that found on the induction of the β-structure of poly[Cys(CH_2COOH)].[3] Furthermore, the order of the inducing power of transition metal cations is also in good agreement with the interaction of poly(methacrylic acid) with these metal cations.[21] Contrary to the induction by cationic surfactants, where clearly different behaviors were found between the inductions of the α-helix[1] and the β-structure,[2] the induction of the secondary structures by bivalent metal cations is similar for both the α-helix. and the β-structure.[3]

The interaction of transition metal cations with these

two polypeptides, PGA and poly[Cys(CH_2COOH)], is much stronger than that of cationic surfactants. Difference of the stabilities between the α-helix and the β-structure escapes detection in the strong interaction with transition metal cations, while it is sensitively detected by the weak interaction with cationic surfactants.

However, clear difference between the interactions operating in the induction of the α-helix and the β-structure shows up when the effect of ionic strength is examined. The induction of the β-structure requires greater stabilization than that required for the α-helix induction. Hence the β-induction is scarcely affected by ionic strength of the environment, while the α-induction is effectively inhibited as the ionic strength increases.

Distortion of the CD Spectra. Distortion of CD spectra of the α-helix just as found in the present study has been often observed before.[1,16,17,32,33] Theoretical calculations show that the distortion occurs as a result of the aggregation of α-helices.[16,33,34] Comparison of the distorted CD spectra found in the present study with the calculated spectra[34] provides an estimate of the radius of assumed spherical aggregates to lie between 0.03 and 0.1 μm. On the other hand, the solution of C_M/C_P=1.0 could be filtered without trouble with a membrane of 0.22 μm pore size but not with a membrane with 0.1 μm pore size. Consequently, it is expected that the largest dimension of the aggregates in the solution exceeds 0.1 μm and that the aggregates have rather asymmetric shape but their optical properties are well approximated by spheres having a radius lying between 0.03 and 0.1 μm.

References

1) H. Maeda, H. Kato, and S. Ikeda, *Biopolymers*, **23**, 1333 (1984).
2) H. Maeda, M. Kimura, and S. Ikeda, *Macromolecules*, **18**, 2566 (1985).
3) H. Maeda, H. Nakajima, K. Oka, K. Ooi, and S. Ikeda, *Int. J. Biol. Macromol.*, **4**, 352 (1982).
4) K. Oka, H. Maeda, and S, Ikeda, *Int. J. Biol. Macromol.*, **5**, 342 (1983).
5) A. L. Jacobson, *Biopolymers*, **1**, 269 (1963).
6) A. L. Jacobson, *Biopolymers*, **2**, 207 (1964).
7) A. L. Jacobson, *Biopolymers*, **2**, 237 (1964).
8) H. Takesada, H. Yamazaki, and A. Wada, *Biopolymers*, **4**, 713 (1966).
9) N. Kono and A. Ikegami, *Biopolymers*, **4**, 823 (1966).
10) E. Bianchi, A. Bicchi, G. Conio, and A. Ciferri, *J. Macromol. Sci.*, **A1**, 909 (1967).
11) K. Yamaoka and T. Masujima, *Bull. Chem. Soc. Jpn.*, **52**, 1286 (1979).
12) T. Masujima and K. Yamaoka, *Biopolymers*, **19**, 477 (1980).
13) N. Imai and J. A. Marinsky, *Macromolecules*, **13**, 275 (1980).
14) S. Noji and K. Yamaoka, *Macromolecules*, **13**, 1114 (1980).
15) T. Kurotu and M. Kasagi, *Polymer J.*, **15**, 397 (1983).
16) D. W. Urry, "Spectroscopic Approaches to Biomolecular Conformation," ed by D. W. Urry, American Medical Association, Chicago (1970), Chap. III.
17) W. L. Mattice, R. McCord, and P. M. Shippey, *Biopolymers*, **18**, 723 (1979).
18) S. Krimm, J. E. Mark, and M. L. Tiffany, *Biopolymers*, **8**, 695 (1969).
19) Y. M. Joshi and J. C. T. Kwak, *Biophys. Chem.*, **13**, 65 (1981).
20) J. Mattal and J. C. T. Kwak, *J. Phys. Chem.*, **86**, 1026 (1982).
21) M. Mandel and J. C. Leyte, *J. Polymer Sci.*, **A2**, 2883 (1964).
22) T. Miyazawa and E. R. Blout, *J. Am. Chem. Soc.*, **83**, 712 (1961).
23) T. Miyazawa, *J. Chem. Phys.*, **32**, 1647 (1960).
24) T. Miyazawa, "Polyamino acids, Polypeptides and Proteins," ed by H. A. Stahmann, University of Wisconsin Press, Madison (1962), p. 201.
25) J. C. Leyte, L. H. Zuiderweg, and M. van Reisen, *J. Phys. Chem.*, **72**, 1127 (1968).
26) J. C. Leyte, "Polyelectrolytes," ed by E. Selegny, Reidel Publishing Co., Dordrecht, Holland (1974), p. 339.
27) H. Lenormant, A. Baudras, and E. R. Blout, *J. Am. Chem. Soc.*, **80**, 6191 (1958).
28) D. Keith, F. J. Padden, and G. Giannoni, *J. Mol. Biol.*, **43**, 423 (1969).
29) D. Keith, G. Giannoni, and F. J. Padden, *Biopolymers*, **7**, 775 (1969).
30) S. S. Zimmerman, J. C. Clark, and L. Mandelkern, *Biopolymers*, **14**, 585 (1975).
31) K. Itoh, B. M. Foxman, and G. D. Fasman, *Biopolymers*, **15**, 419 (1976).
32) S. S. Zimmermann, and L. Mandelkern, *Biopolymers*, **14**, 567 (1975).
33) A. S. Schneider, *Methods Enzymol.*, **27**, 751 (1973).
34) D. J. Gordon, *Biochemistry*, **11**, 413 (1972).

 © 1986 The Chemical Society of Japan Bull. Chem. Soc. Jpn., 59, 593—597 (1986)

Pulse Radiolysis Study of Positive-Charge Transfer in Freon-Mixture Matrix at 77 K

Akira KIRA,* Masashi IMAMURA, Seiichi TAGAWA,† and Yoneho TABATA††
The Institute of Physical and Chemical Research, Wako, Saitama 351-01
†Research Center for Nuclear Science and Technology, The University of Tokyo, Tokai-Mura, Ibaraki 319-11
††Nuclear Engineering Research Laboratory, The University of Tokyo, Tokai-Mura, Ibaraki 319-11
(Received September 30, 1985)

The pulse radiolysis of a Freon mixture (FM), an equivolume mixture of $CFCl_3$ and CF_2BrCF_2Br, at 77 K gave transient absorption bands with peaks at 360, 490, and 530 nm, whose decay was enhanced by cation scavengers: propylamine, triethylamine, *N,N'*-diethylaniline, and biphenyl. The degree of the enhancement was independent of the difference in the ionization potential between the matrix and the solute molecules. In the FM matrix, positive-charge transfer from biphenyl cations to some other solute molecules showed energy dependence similar to that observed in the *s*-butyl chloride matrix. The rate of inter-solute positive-charge transfer was faster in the FM matrix than in the *s*-butyl chloride matrix. These results were discussed in relation to current electron transfer theories.

An equivolume mixture of Freon 11 ($CFCl_3$) and Freon 114B2 (CF_2BrCF_2Br), which will be referred to as the Freon mixture or FM, provides an optically transparent glass at 77 K, which is used as an excellent matrix for preparation of radical cations by irradiation with ionizing rays.[1] The optical absorption spectra of (radical) cations of aromatic hydrocarbons and other compounds have been measured in the γ-irradiated FM matrix.[2-4] The formation of cations probably results from positive-charge (PC) transfer from trapped holes in the FM matrix produced by irradiation, as in the *s*-butyl chloride (*s*-BuCl) matrix;[5-8] however, no kinetic studies have been carried out concerning PC transfer in the FM matrix.

From the theoretical point of view, the vibrational mode of both matrix and solute molecules can affect the rate of electron or hole transfer.[9] The FM matrix which consists of carbon-halogen bonds differs in the vibrational mode from the *s*-BuCl matrix dominated by the carbon-hydrogen bond. Thus, the PC-transfer rate in FM may differ from that in *s*-BuCl, and comparative measurement of the same donor-acceptor pair in FM and in *s*-BuCl seemed to be the best feasible experiment to examine the effect of matrix vibrations.

This paper deals with a pulse radiolysis study on PC transfer in FM matrices at 77 K. Two types of PC transfer, matrix-to-solute and solute-to-solute, were studied. This study also revealed the presence of two or three types of holes or radiation-induced cationic entities in the FM matrix, although their nature is not yet elucidated. The compounds used as solutes and their ionization potentials in the gas phase are: biphenyl, 8.27 eV; pyrene, 7.55 eV; propylamine (PrA), 8.78 eV; triethylamine (TEA), 7.50 eV; *N,N*-dimethylaniline (DMA), 7.10 eV.

Experimental

A pulse radiolysis apparatus at Nuclear Engineering Research Laboratory, University of Tokyo, was used.[10] A 10-ns pulse of 35-MeV/1-A electron beam focused to a diameter of 2 mm was irradiated to a sample placed in a Dewer vessel filled with liquid nitrogen. The monitoring light passes through the sample to the opposite direction to the electron beam on the identical axis and is detected with a Hamamatsu-TV R-928 photomultiplier after monochromatized with a Ritsu MC-10 monochromator. The photoelectric signal was fed to a Riken-Denshi TCH-4000 transient digitizer whose time base was operated by a logarithmic time clock.[5] The shortest accessible time of this detection system was 1 μs, but measurememt was also made in the nanosecond region by the use of conventional detection devices.[10] The dosimetry was carried out by using hydrated electrons in water at room temperature on the basis of a value of 3.5 for *G*-value (molecules/100 eV) at 10 ns and 1.3×10^4 $M^{-1}cm^{-1}$ (1 M=1 mol dm^{-3}) for the molar absorption coefficient (ε) at 600 nm.[11]

Daifron S1 and 114B2 ($CFCl_3$ and CF_2BrCF_2Br, respectively) purchased from Daikin Ind. Co. were dried on Drierite. Other chemicals (Tokyo Kasei) were used as received. Samples were deaerated by the freezing-pumping method in early experiments but were aerated later, since aeration was found to cause no practical effects.

Results

Transient absorption spectra in the FM glass containing no solutes are exhibited in Fig. 1 and some decay curves are shown in Fig. 2. Although the shortest time indicated in Figs. 1 and 2 is 3 μs, no other transient bands were found before this time in the nanosecond measurement. As shown in Fig. 2, the transient absorptions at peaks of 360 and 490 nm decay with the logarithm of time but the absorption at 600 nm scarcely decays initially. This apparent constancy in the 600-nm absorption is probably ascribed to cancellation of the decrease in the 600-nm absorbing species by the increase due to its production from a transient with the 360-nm and/or the 490-nm band. In the spectrum at 10 ms, the 360-nm band is still alive but the 490-nm band has already been replaced by a broad band with a peak near 530 nm which will be called tentatively the 530-nm band, although this band can really be a composition of the 490-nm band and another band which may be a long-lived one with a peak near 560

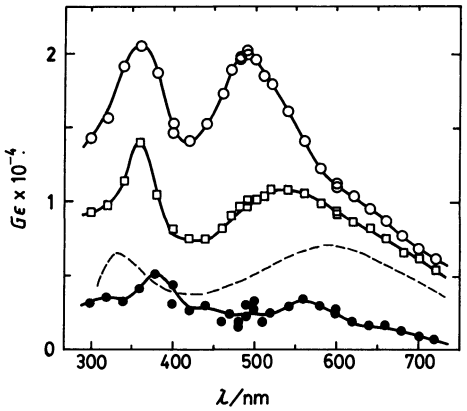

Fig. 1. Transient absorption spectra in an FM glass at 77 K at 3 μs ○, 10 ms □, and 3.7 s ● after the pulse. Thin dashed curve: the spectra taken after γ irradiation (Ref. 1).

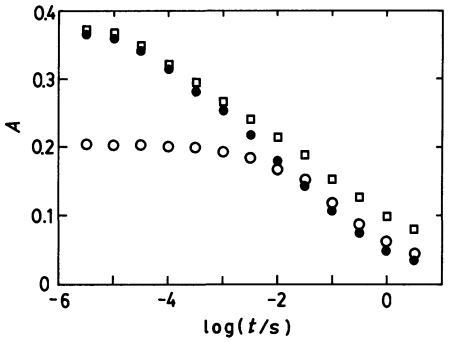

Fig. 2. The decay in the absorbances at 360 nm □, 490 nm ●, and 600 nm ○ in an FM glass plotted as a function of the logarithm of time.

nm.

The spectrum at 3.7 s differs from the one observed in steady-state measurement as shown in Fig. 1. Discrepancy between pulse and steady-state experiments also occurs in the absorption intensity: The $G\varepsilon$ at the 560-nm peak at the 3.7-s spectrum of the pulse radiolysis is 3.3×10^3 $M^{-1}cm^{-1}$, which is smaller than the values for a 585-nm peak in the γ-irradiated FM glass: $4.5\times10^3 M^{-1}cm^{-1}$ in measurement by Grimison and Simpson[1] and 7.1×10^3 $M^{-1}cm^{-1}$ in our re-measurement.[12] In the rather soft FM matrix, the rise in local temperature caused by the strongly focused electron beam in the pulse radiolysis may enhance charge recombination which removes these matrix transients. In fact, the fast decay of the matrix transients in FM glass as shown in Fig. 2 contrasts with the very slow decay of trapped electrons in the alkaline-ice[13] and the 2-methyltetrahydrofuran[14] matrices as well as of trapped holes in the *s*-BuCl matrix.[5-8] However, it should be remarked that the decay of the biphenyl cation in the FM matrix is as slow as its decay in the *s*-BuCl matrix, as will be shown later.

As shown in Figs. 3 and 4, the decay of these matrix transients was enhanced by addition of a solute like

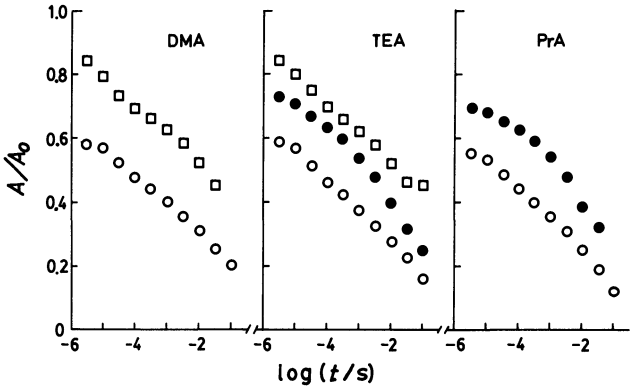

Fig. 3. Survival curves of trapped holes measured at 360 nm □, 490 nm ●, and 600 nm ○ in the presence of DMF, TEA, and PrA, each at 0.1 M.

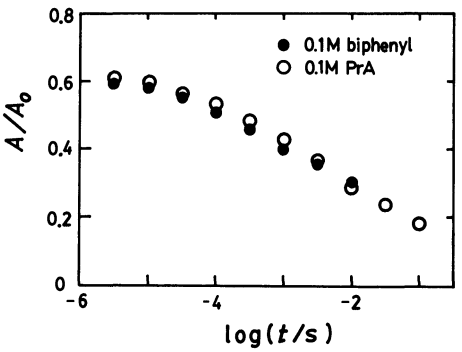

Fig. 4. Survival curves of the 490-nm hole band in the presence of biphenyl and PrA, each at 0.1 M.

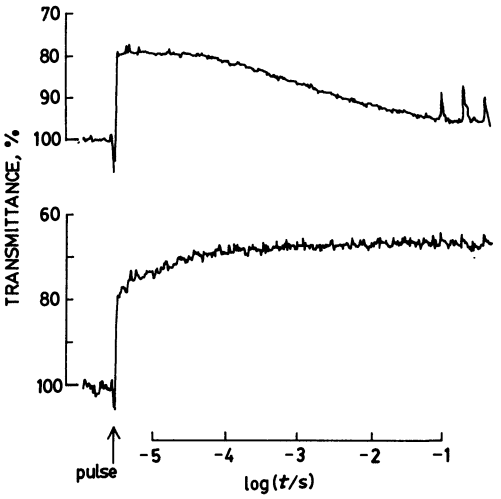

Fig. 5. The decay of the hole absorption at 490 nm and the corresponding growth of the biphenyl-cation absorption at 700 nm in an FM glass containing 0.03 M biphenyl.

triethylamine, propylamine, *N*,*N*-dimentylaniline, and biphenyl; the first three are typical cation scavengers that do not act on anionic species, and biphenyl scavenges both cationic and anionic species. Furthermore, the 490-nm absorption band of the DMA cation[4] and the 390- and 690-nm bands of the biphenyl

cation were oserved in these experiments (see also Fig. 5); cations of TEA and PrA were not detected simply because of their weak absorptions.[4] Thus, these matrix transients which are probably composed of a few entities can be regarded as cationic species originating in the matrix, and will be referred to the (trapped) holes in this paper, although some of them may not really be the hole but cationic fragment radicals of a solvent component or certain ion pairs.

In steady-state γ radiolysis at 77 K, absorption maxima appear at 330 and 585 nm in the FM matrix, at 310 and 535 nm in the $CFCl_3$ matrix, and at 360 nm in the CF_2BrCF_2Br matrix;[1] the last two matrices are opaque. Comparison of the wavelengths of these maxima suggests that the 360-nm transient band observed in the pulse radiolysis may be assigned to a cationic species originating in CF_2BrCF_2Br and the 530-nm transient to a cationic species from $CFCl_3$. Decisive assignment of these bands seems difficult; such assignment has been unsuccesful for transient bands of carbon tetrachloride on which extensive studies have been made.[15]

In Figs. 3 and 4, survival ratios, A/A_0, where A and A_0 denote the absorbances in the presence and in the absence of a solute, respectively, are plotted against the logarithm of time; the decay that proceeds with the logarithm of time is common to reactions in rigid matrices.[5-7] This type of plot is usually used for presentation of the kinetic data in rigid matrices, and is called a survival curve. No corrections in the absorbance were made for possible overlap of the bands, since the spectrum of each component could not be isolated. The absorbance for the broad 530-nm band was measured at 600 nm in order to avoid the influence of the tail of the 490-nm band. Cations of biphenyl and DMA possess intense absorption bands in the visible region as mentioned above; therefore, the change in the net hole absorption at such wavelengths could not be measured in systems containing these solutes. A survival curve for a single species is given by[16]

$$A/A_0 = \exp\left[-C\int_0^\infty \{1-\exp(-kt)\}4\pi R^2 dR\right] \quad (1)$$

where C is the solute (PC acceptor) concentration and k is the first-oder rate constant of PC transfer which depends on the donor-acceptor distance, R. Thus, if two survival curves measured for the same concentration of different solutes agree with each other, the rate constants of the PC transfer to these solutes are identical. Note that the parallel survival curves do not indicate the same rate constant.

In Fig. 3 the survival curves of the holes measured at different bands do not agree. This disagreement means that these bands should be assigned to different species, i.e., there are three kinds of holes or cationic species. The disagreement of these survival curves, however, may be due to an experimental reason that the absorbance could not be corrected for the overlap of other bands. The survival curves of the hole measured at the same wavelength agree with one another among glassy solutions containing different solutes, as shown in Fig. 3. This coincidence can be interpreted as that the rate is independent of the energy gap which is measured as the difference in the ionization potential between the matrix and the solute molecules. This independence contrasts with the previous result that the survival curve of trapped holes in the *s*-BuCl matrix shifts downward as the ionization potential of the solute compound decreases.[5]

A time profile of the absorption signal for the biphenyl-cation band at 700 nm is depicted in Fig. 5 in comparison with that of the 490 nm band of the hole. Monitoring of the holes at 360 and 600 nm was unable because of masking by the strong biphenyl-cation bands. The absorption at 700 nm already formed at the initial time can be attributed to the tail of the 530-nm band and also to a band of biphenyl cations produced within 1 μs. The growth of the biphenyl-cation band in parallel with the decay of the trapped hole absorbing at 490 nm suggests that the biphenyl cation is formed by PC transfer from this hole, although other holes may also contribute to the formation of biphenyl cations. The rather slow decay of biphenyl cations contrasts with the rapid decay of the holes in the neat FM glass. This contrast in decay suggests that the FM matrix is softer than the *s*-BuCl matrix so that small trapped holes can move to attain certain rearrangement but larger biphenyl cations cannot.

Positive-charge transfers from biphenyl cations to TEA, DMA, and pyrene molecules were also studied in FM matrices containing both 0.14 M biphenyl and 0.03 M of each of the acceptor solutes, where the positive charge is first trapped by excess biphenyl and then trasferred from biphenyl cations to acceptor molecules. The survival curves of these donor-acceptor pairs in FM are shown in Fig. 6. The curve shifts downward, i.e. the rate increases, with decreasing ionization potential of a PC acceptor. The similar dependence has also been observed in *s*-BuCl[5,6] and poly(methyl methacrylate) matrices[17] at 77 K. Thus such a dependence is normal, although it contrasts with the energy-gap-independent rate observed in PC transfer from the solvent holes. In Fig. 6 the curves in *s*-BuCl[5b] are also depicted for comparison. In each donor-acceptor pair, the curve for the FM matrix lies lower than that for the *s*-BuCl matrix. It should be noted, however, that this comparison is made under the conditions of different biphenyl concentrations: 0.2 M for *s*-BuCl and 0.14 M for FM, the latter being limited by solubility. As the biphenyl concentration decreases, the biphenyl cation yield may decrease owing to the competition with the acceptor which can also scavenge the hole. A decrease in the biphenyl cation yield was estimated at 5% for a biphenyl-pyrene system on the basis of previous results of steady-state experiments.[18] The magnitude of the observed shift is more than 15%; thus there seems to

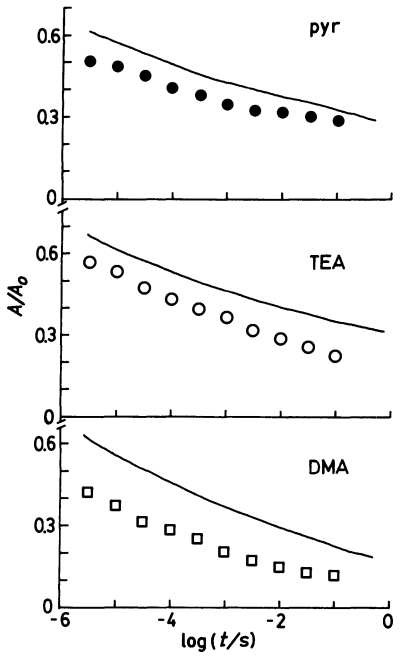

Fig. 6. Survival curves of biphenyl cations in the presence of PC acceptors at 0.03 M: pyrene, TEA, and DMA in FM (points) and in *s*-BuCl (lines) (Ref. 3).

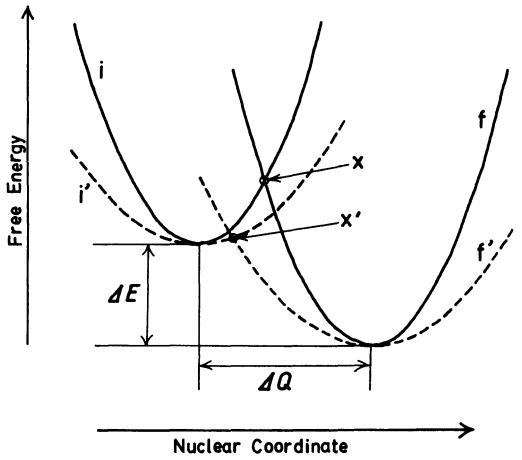

Fig. 7. Possible energy-surface diagrms of a donor-acceptor system in *s*-BuCl (solid curves) matrix and in FM matrix (dashed curves); *i* and *i'* indicate the initial states and *f* and *f'*, the final states.

be the shift of the survival curve with the change of matrix from *s*-BuCl to FM.

Discussion

Electron and hole transfers are explained on the basis of the Fermi golden rule, and the first-order rate constant is expressed as the product of a term associated with electronic interactions, ν, and the thermally-avaraged Franck-Condon factor, F:[5,6,9]

$$k = \nu F \qquad (2)$$

Early theories[19] predict that the (thermally-averaged) Franck-Condon factor first increases with the energy gap and then decreases. The regions where the Franck-Condon factor increases and decreases are called the normal and the inverted region, respectively. On the other hand, some experimental results[20] indicate that the rate reaches a plateau above a certain value of the energy gap in contrast to the theories. A new theoretical explanation has recently been presented for this plateau.[21]

Equation 2 indicates that the Franck-Condon factor can be estimated from the rate constant if the value of the electronic interaction term is known. However, its reliable evaluation is very difficult both experimentally and theoretically. In most data analyses, the electronic interaction has been regarded implicitly as being identical regardless of donors and acceptors. A modified assumption that it is identical for the same donor has also been adopted in analysis of long-range electron transfer.[5-7] In this paper, we assume that for donor-acceptor pairs containing a common PC donor electronic interactions are identical. i.e. the relative Franck-Condon factor is proportional to the observed rate.

A feature of PC transfer from the hole in the FM matrix is the lack of the energy dependence over a rather wide ΔE-range of 1.28 eV. The energy independent rate is known to occur actually if the energy gap of a systems is very large.[20] In other words, if a hole has such a high energy that the ΔE against a solute molecule becomes large enough, the rate will be almost constant irrespective of solute. In *s*-BuCl the rate of PC transfer from the hole to the same solute as that used in the present experiments increases with increasing energy gap. This fact indicates that the energy gap of the hole-acceptor pair in *s*-BuCl is as low as to correspond to the normal region. The ionization potential of FM is probably higher than that of *s*-BuCl (10.65 eV), since the ionization potentials of CF_2BrCF_2Br and $CFCl_3$ are 11.4[22] and 11.7 eV,[23] respectively. Thus, for PC transfer from a trapped hole, the energy difference of a system with the same solute will be larger in the FM matrix than in the *s*-BuCl matrix.

The results of the studies on carbon tetrachloride[15] suggest that the matrix transients in the FM glass may not be assigned to cations of solvent molecules but to other complicated species such as ion pairs similar to $CCl_3^+Cl^-$ proposed for carbon tetrachloride. If ion pairs are involved, the energetics of the system will be complicated, and the above simple consideration may not immediately apply.

The normal energy-gap dependence was observed for the positive-charge transfer from the biphenyl cation where energy gaps are not so large. The point of interest with this reaction is acceleration caused by change of a matrix from *s*-BuCl to FM. Freons and

their mixtures are characterized by poorer solvation abilities than *s*-BuCl. Major molecular vibrations in Freon are carbon-halogen vibrations whose frequency is lower than carbon-hydrogen vibrations dominating *s*-BuCl. These comparisons indicate that an energy surface for a donor-acceptor pair in the FM matrix is represented by a weaker function (or broader curve) than that for the same pair in the *s*-BuCl matrix. The energy diagram as illustrated in Fig. 7 can explain the faster rate in FM matrix in the normal energy-gap dependence region on the assumption that both energy gap (ΔE) and shift in nuclear coordinate (ΔQ) are unchanged. This diagram indicate that broadning of the energy surface lowers the crossing point from x to x' and reduces the activation energy to accelerate the reaction.

References

1) A. Grimison and G. A. Simpson, *J. Phys. Chem.*, **72**, 1776 (1968).
2) T. Shida and S. Iwata. *J. Am. Chem. Soc.*, **95**, 3473 (1973).
3) A. Kira and M. Imamura. *J. Phys. Chem.*, **83**, 2267 (1979).
4) T. Shida, Y. Nosaka, and T. Kato, *J. Phys. Chem.*, **82**, 695 (1979).
5) a) A. Kira, Y. Nosaka, and M. Imamura, *J. Phys. Chem.*, **83**, 2273 (1979); b) A. Kira, ibid., **85**, 3047 (1981).
6) J. R. Miller and J. V. Beitz, *J. Chem. Phys.*, **74**, 6746 (1981).
7) a) A. Namiki, T. Warashina, and T. Higashimura, *Chem. Phys. Lett.*, **85**, 136 (1982); b) A. Namiki, Y. Ito, and T. Higashimura, ibid. **88**, 492 (1982).
8) J. Cygler, G. G. Teather, and N. V. Klassen, *J. Phys. Chem.*, **87**, 455 (1983).
9) J. Ulstrup and J. Jortner, *J. Chem. Phys.*, **63**, 4358 (1975).
10) S. Tagawa, M. Washio, Y. Tabata, and H. Kobayashi, *Radiat. Phys. Chem.*, **19**, 277 (1982).
11) E. J. Har, and M. Anber, "The Hydrated Electron," Wiley-Interscience, New York (1972), p. 42.
12) T. Nakamura and A. Kira, unpublished results.
13) J. R. Miller, *J. Phys. Chem.*, **79**, 1079 (1975).
14) J. R. Miller, *J. Phys. Chem.*, **82**, 767 (1978).
15) R. E. Buehler, *Radiat. Phys. Chem.*, **21**, 139 (1983); T. Shida and Y. Takemura, ibid., **21**, 157 (1983); M. Washio, S. Tagawa and Y. Tabata, ibid., **21**, 239 (1983).
16) M. Inokuti and F. Hirayama, *J. Chem. Phys.*, **43**, 1978 (1965); M. Tachiya and A. Mozumder, *Chem. Phys. Lett.*, **28**, 87 (1974).
17) A. Kira and M. Imamura, *J. Phys. Chem.*, **88**, 1865 (1984).
18) A. Kira, T. Nakamura, and M. Imamura, *J. Phys. Chem.*, **82**, 1961 (1978).
19) R. A. Marcus, *Ann. Rev. Phys. Chem.*, **15**, 155 (1964); S. Efrima and M. Bixon, *Chem. Phys. Lett.*, **25**, 34 (1974).
20) D. Rehm and A. Weller, *Israel J. Chem.*, **8**, 259 (1970).
21) T. Kakitani and N. Mataga, *Chem. Phys.*, **93**, 381 (1985).
22) F. T. Chau and C. A. McDowell, *J. Phys. Chem.*, **80**, 2923 (1976).
23) T. Cvitas, H. Guesten, and L. Klasinc, *J. Chem. Phys.*, **67**, 2687 (1977).

Electrochemical Behavior of p-Type Indium Selenide Single Crystal Electrodes in Dark and under Illumination

Kohei UOSAKI,* Susumu KANEKO, Hideaki KITA, and A. CHEVY†
Department of Chemistry, Faculty of Science, Hokkaido University, Sapporo 060
†Physique des Milieux très Condensés, Université Pierre et Marie Curie-Paris VI, 75230 Paris Cedex 05, France
(Received September 30, 1985)

The electrochemical behaviors of van der Waals face of p-InSe single crystal electrodes in 0.5M H_2SO_4 and 1M NaOH (1M=1 mol dm^{-3}) with and without illumination have been thoroughly investigated. In 0.5M H_2SO_4, relatively large cathodic dark current was observed and the onset potentials for the current in dark and under illumination were ca. −0.8 V (vs. Ag/AgCl) and ca. −0.5 V, respectively, at as-prepared electrode. The current seemed to be mainly due to hydrogen evolution reaction. The dark current decreased significantly and the photocurrent increased by removing surface steps. These results and impedance analyses show that the surface steps create surface states which act as recombination centers and mediators for charge transfer. Both the dark- and photocurrent onset potentials in 1M NaOH were more negative than those in 0.5M H_2SO_4 by ca. 0.5 V. The dark current was quite large and the photocurrent was small in 1M NaOH even after removing surface steps. By depositing Pt on p-InSe, the photocurrent onset potential shifted towards positive by several hundred mV. The reaction mechanism of photoelectrochemical hydrogen evolution was discussed by considering the above results.

One of the major difficulties in the photoelectrochemical energy conversion is the lack of stability of the semiconductor electrodes under illumination.[1] Many attempts were made to stabilize the electrodes[2] and to seek new electrode materials.[3]

Layered compound semiconductors are expected to have high stability as photoelectrodes.[4] Also, because there is no dangling bond, which creates surface states, at cleaved surface of these materials,[5] the surface recombination probability should be low that leads to high conversion efficiency. Although the photoelectrochemical characteristics of transition metal chalcogenides have been studied very extensively,[6] those of III—VI compound semiconductors are not well known. Indium selenide (InSe) has an ideal energy gap (1.1—1.3 eV[7]) for solar energy conversion devices[8] but only a few reports are available for this application.[9] The photoelectrochemical behavior of InSe was first reported by McCann very briefly.[10] Recently, Levy-Clement et al. reported basic electrochemical characteristics of InSe relatively in detail.[11]

In this paper, we report the thorough study of (photo)electrochemical hydrogen evolution reaction at van der Waals face of p-InSe single crystal.

Experimental

InSe single crystals used in this study were grown by the Bridgman method.[12] p-InSe was doped with Zn by 0.1%. Cleaved surface was always used as an electrode. An ohmic contact was obtained by an In-Zn alloy. Because of weak mechanical strength of the material, Ti plate was used as a support. After the ohmic contact was insured, silver conducting paste (Fujikura Kasei Co. Ltd., Dotite D-550) was used to fix the back side of the electrode to a Ti plate to which Cu wire was connected by using the conducting paste. Except the front face, all other parts were covered with epoxy resin and the electrode was then placed in a glass tubing.

Electrolyte solutions were prepared by using reagnt grade chemicals and water purified by Milli-Q water purification system (Millipore Corp.).

An ordinary three compartment cell with a Pyrex window was used for the measurements. A counter and a reference electrode were a Pt wire and a Ag/AgCl electrode, respectively. The electrode potential was controlled by using a potentiostat (Hokuto Denko, HA-501).

A 500W Xe lamp (Ushio Electric Co. Ltd., UXL-500D-0) with an IR absorbing filter (Toshiba, IRA-20) or a monochromator (Ritsu Oyo Kogaku, MC-25NP) was used as a light source for photocurrent-potential and photocurrent-wavelength relation measurements. The photocurrent-wavelength measurements were carried out with a constant light intensity. A 20 mW He-Ne laser (NEC Corp., GLG5700) with ND filters was used as a light source for the light intensity-photocurrent relation measurements. The intensity of the light was monitored by means of a light power meter (Anritsu Electric Co. Ltd., ML-94A with an MA-97A detector).

Impedance measurements were carried out in dark by using the potentiostat and a frequency response analyzer (NF Electronic Co. Ltd., S-5720B) which was controlled by a personal computer (NEC Corp., PC-8801) via GP-IB interface. In these measurements, a large Pt foil was used as a counter electrode to minimize the impedance due to the counter electrode.

Platinization of the electrode was performed either by dipping the electrode in a H_2PtCl_6 solution (20 mM, pH=4) for 1 min or by the electodeposition in the same solution at 0 V (vs. Ag/AgCl). In the latter case, the amount of Pt deposited was estimated from the charge passed during the deposition.

XPS spectra and visible and near-IR absorption spectra were obtained by using an ESCA-3 (VG Scienticific Ltd.) and a photospectrometer (Shimadzu Ltd., UV-365), respectively.

All the electrochemical measurements were carried out at room temperature after the electrolyte solution was deaerated by passing a purified He gas for at least 20 min.

Results

Spectroscopic Characterization. Layers of InSe were removed by adhesive tape and visible and near-IR spectra of this sample were taken against the adhesive tape without InSe layers as a reference. Figure 1 shows

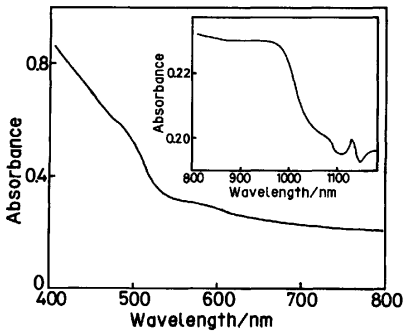

Fig. 1. Absorption spectra of InSe in visible region and in near IR region (inset).

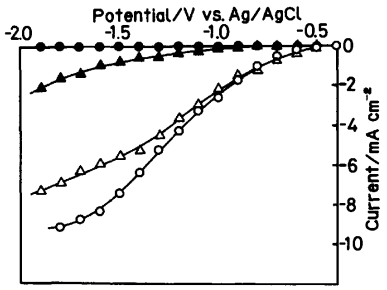

Fig. 2. The dark current (▲,●)- and photocurrent (△,○)-potential relations in 0.5 M H_2SO_4. ▲,△: As-prepared electrode. ●,○: Same electrode after removal of surface steps.

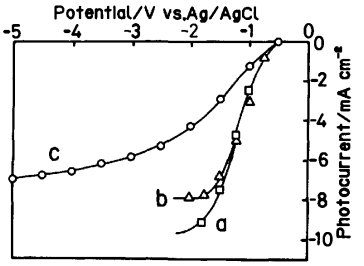

Fig. 3. The photocurrent-potential relations of three p-InSe samples in 0.5 M H_2SO_4. (a): Sample 1, (b): Sample 2, (c): Sample 3.

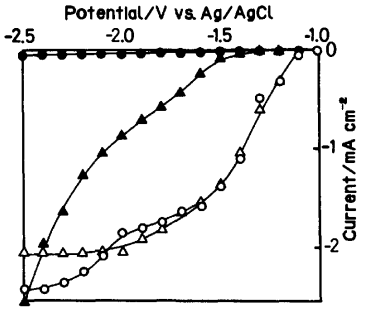

Fig. 4. The dark current (▲,●)- and photocurrent (△,○)-potential relations in 1 M NaOH. ▲,△: As-prepared electrode. ●,○: Same electrode after removal of surface steps.

the visible and near IR absorption spectra. The results were essentially in good agreement with those of Piccioli et al.[7b] with indirect absorption edge at ca. 1000 nm and direct absorption edge at ca. 500 nm. The peak around 1130 nm is considered to be due to exitons.[7b]

Peak energies of the XPS spectra of InSe surface due to In 3d peaks obtained without sputtering agree with those of In metal due to In 3d peaks with Ar^+ sputtering within experimental error, suggesting that indium exists as In(0) state and there is no noticeable indium oxide layer at InSe surface.

Current-Potential Relations with and without Illumination. Figure 2 shows typical current-potential relations of an as-prepared p-InSe electrode in 0.5M H_2SO_4 with and without illumination of light. Relatively large cathodic dark current was observed and while the dark current onset potential was ca. −0.8 V, the cathodic photocurrent was observed at potentials more negative than ca. −0.5 V. The current seemed to be mainly due to hydrogen evolution, since bubbles were observed at the electrode surface and no surface change was noticed after the measurements.

It has been known that the existence of steps at semiconductor electode surface, the van der Waals face of layered compounds in particular, affects the electrochemical behavior of the electrode both with and without illumination.[13] Although the electrode surface was prepared by removing steps with adhesive tape, there were still many steps on the as-prepared InSe clectrode. When the as-prepared electrode was anodically polarized, the dark anodic current due to the oxidation of the electrode was observed. The anodic dark current flowed preferentially through steps as regions near steps became red due to Se deposition.[14] After the Se deposition, the position of steps became more apparent and the removal of steps became easier. Thus, the most of the experiments reported in this work were carried out after the electrode was anodically polarized at 0.5 V (vs. Ag/AgCl) and the surface steps were removed as much as possible. Figure 2 also shows the current-potential relations of the same electrode but after the removal of steps. It is very clear from this figure that the dark current reduced significantly while the photocurrent increased by removing steps. The results reported by Levy-Clement et al. showed relatively large dark current, suggesting the existence of many surface steps.[11]

During the experiments, we noticed the electrochemical behavior differed from sample to sample quite significantly. Figure 3 shows the photocurrent-potential relations of three samples[15] used for the experiments. Although the photocurrents were observed at potentials more negative than ca. −0.5 V and saturated with the value of 8—10 mA cm^{-2} at all samples, the potentials at which the photocurrent showed saturation were different from sample to sample.

Figure 4 shows the current-potential relations in 1M

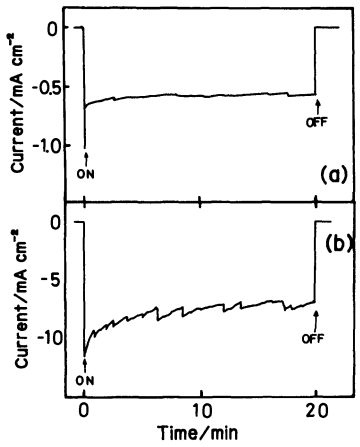

Fig. 5. Current-time relations of p-InSe in 0.5 M H_2SO_4 at (a) −1.0 V and (b) −2.0 V vs. Ag/AgCl. Current before illumination are taken as zero.

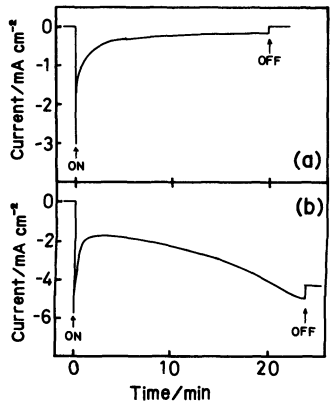

Fig. 6. Current-time relations of p-InSe in 1.0 M NaOH at (a) −1.5 V and (b) −2.5 V vs. Ag/AgCl. Current before illumination are taken as zero.

NaOH of the sample used in Fig. 2 with more and less surface steps. Both the dark and the photocurrent onset potential were more negative than those in 0.5M H_2SO_4 by ca. 0.5 V. These results contrast to the results of GaSe at which no pH dependence was observed.[16] In 1M NaOH, the dark current was quite large even with less surface steps and the photocurrent was small compared to the current in 0.5M H_2SO_4. After the measurements in 1M NaOH, white film was observed on the surface and the electrode swelled and was very easily broken.

Stability. The photocurrent was relatively constant and no significant change of the dark current was observed in 0.5M H_2SO_4 as shown in Fig. 5(a) and (b). The fluctuation of the current was mainly caused by hydrogen bubble which stack on and suddenly left from the electrode surface. On the other hand, in 1M NaOH the photocurrent decreased very quickly (Fig. 6(a) and (b)) and the dark current increased at strong negative bias (Fig. 6(b)). As was the case in the current-potential relation measurements, white film was formed and the electrode became mechanically very weak after the stability measurements in 1M NaOH.

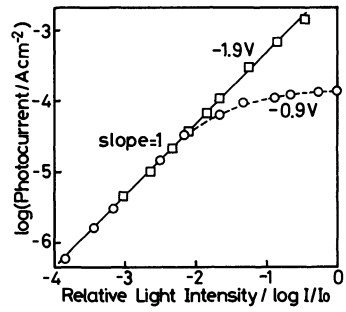

Fig. 7. Light intensity dependence of the photocurrent of p-InSe in 0.5 M H_2SO_4 at −0.9 V (○) and −1.9 V (□) vs. Ag/AgCl (I_o=1.41 mW cm^{-2}).

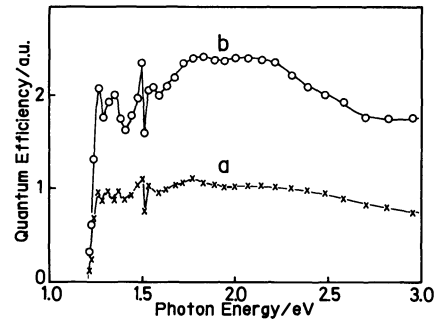

Fig. 8. The photocurrent action spectra of p-InSe in 0.5 M H_2SO_4. At −0.9 V (curve a) and −1.9 V (curve b) vs. Ag/AgCl.

Effect of Light Intensity on Photocurrent. Figure 7 shows the photocurrent-light intensity relations in 0.5M H_2SO_4 at −0.9 V and at −1.9 V. At −0.9 V at which the potential dependence of the photocurrent was large, the photocurrent increased linearly with light intensity as far as the intensity was not too strong but it tended to saturate at higher light intensity. On the other hand, at −1.9 V at which the photocurrent was almost independent of potential, the photocurrent increased lineary with the light intensity even at highest intensity employed in this study . Light intensity independent photocurent has been reported at various semiconductor electrodes.[17]

Quantum Efficiency Action Spectra. Since, as reported above, the quantum efficiency may be affected by light intensity, the quantum efficiency action spectra were obtained with constant light intensity for all measurements. Figure 8 shows the action spectra at −0.9 V and at −1.9 V. No significant shape difference between two spectra was observed. The bandgap energy obtained from these spectra (≈1.2 eV) is in good agreement with the absorption edge (cf Fig. 1).

Impedance Measurements. Figures 9 and 10 are the Cole-Cole plots of the impedance of p-InSe with many steps and with less steps, respectively, in 0.5M H_2SO_4. Although the real component increased with the decrease of the frequency in both cases, the frequency dependence of the imaginary component was

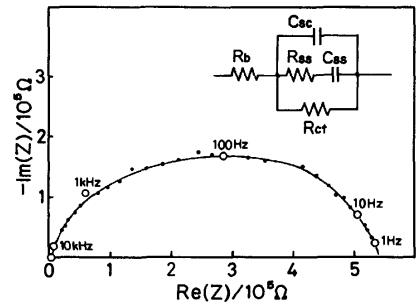

Fig. 9. Cole-Cole plot and the equivalent circuit of p-InSe electrode with many steps in 0.5 M H_2SO_4 without illumination of light. R_b and C_{sc} represent a bulk resistance and a space charge layer capacitance, respectively.

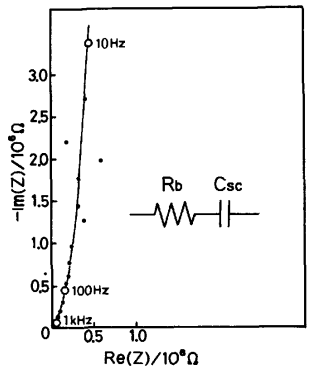

Fig. 10. Cole-Cole plot and the equivalent circuit of p-InSe electrode with many steps in 0.5 M H_2SO_4 without illumination of light. R_{ss} and C_{ss} are the resistance and capacitance of surface state, respectively, and R_{ct} is a charge transfer resistance.

quite different. While the absolute value of the imaginary component of p-InSe with many steps increased with the decrease of the frequency, reached the maximum at ca. 100 Hz and decreased with the decrease of the frequency, that of p-InSe with less steps increased monotonically with the decrease of the frequency.

The equivalent circuits for the former and the latter are also shown in Figs. 9 and 10, respectively.[18] Because of large dark current which leads to the sticking of hydrogen bubble on the electrode surface, the reproducibility of the impedance measurements was low and the potential dependence of the impedance was not determined at the electrode with many steps. The values of the space charge capacitance determined by analyzing the impedance results at various potentials in 0.5M H_2SO_4 with the equivalent circuit shown in Fig. 10 were used to obtain the Mott-Schottky plot of the electrode with less steps (Fig. 11). The flat band potential determined from the plot is +0.2 V (vs. Ag/AgCl). No reliable results were obtained in 1M NaOH due to continuous change of the electrode state.

Effect of Platinum Treatment. The photocurrent-potential relations in 0.5 M H_2SO_4 of p-InSe dip-treated in the H_2PtCl_6 solution and of p-InSe on which Pt was electrodeposited are shown in Fig. 12. In both cases, the photocurrent onset potential shifted towards positive by several hundred mV by Pt treatments. The saturated photocurrent was not affected by the treatments.

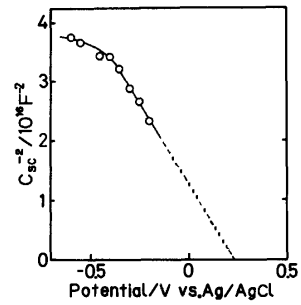

Fig. 11. The Mott-Schottky plot of p-InSe electrode with less steps in 0.5 M H_2SO_4.

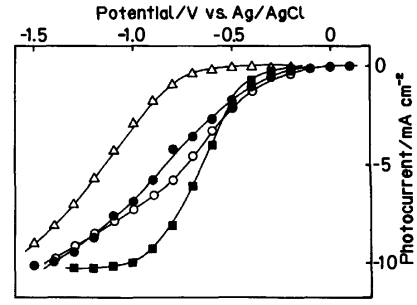

Fig. 12. The photocurrent-potential relations of p-InSe in 0.5 M H_2SO_4. △: Bare, ○: Dip-treated in 20 mM H_2PtCl_6 (pH=4) for 60 sec. ● and ■: Pt electrodeposited. Platinum was electrodeposited in 20 mM H_2PtCl_6 (pH=4) at 0 V vs. Ag/AgCl and the average thickness of Pt was estimated to be 2 Å (●) and 20 Å (■), respectively.

Discussion

pH-Potential Diagram (Pourbaix Diagram) and Stability. To examine the thermodynamic stability of InSe, the pH-potential diagram was constructed (Fig. 13). In Fig. 13, lines (1)—(10) represent the equilibrium reactions of the same numbers shown in Table 1. From the figure, it is confirmed that the red material deposited after the anodic polarization is Se. The white film observed on InSe surface after the (photo)-electrochcmical measurements in 1M NaOH solution must be indium, according to the figure. Although the stable region is wider in acidic solutions than in alkaline solutions, the big difference of the stability observed between these solutions experimentally cannot be explained simply by the thermodynamic data. Reaction (8) should be kinetically more favorable than reaction (6). There is also a possibility of intercalating reaction[22]

$$InSe + Na^+ + e^- \longrightarrow InSe(Na) \qquad (I)$$

Table 1. Equilibrium Reactions of InSe and the Corresponding Electrode Potentials

Reaction	Electrode Potential/V vs. NHE
(1) $In^{3+}+3/2H_2O=1/2In_2O_3+3H^+$	(pK=7.73)
(2) $In_2O_3+H_2O=2InO_2^-+2H^+$	(pK=−17.05)
(3) $In^{3+}+Se+3e^-=InSe$	E=0.233+0.0197 log[In^{3+}]
(4) $1/2In_2O_3+Se+3H^++3e^-=InSe+3/2H_2O$	E=0.386−0.0591 pH
(5) $InO_2^-+Se+4H^++3e^-=InSe+2H_2O$	E=0.721−0.0197 log[InO_2^-]−0.782pH
(6) $InSe+2H^++2e^-=In+H_2Se$	E=−0.987−0.0295 p_{H_2Se}−0.0591 pH
(7) $InSe+H^++2e^-=In+HSe^-$	E=−1.129−0.0295 log[HSe^-]−0.0295 pH
(8) $InSe+2e^-=In+Se^{2-}$	E=−1.546−0.0295 log[Se^{2-}]
(9) $H_2Se=H^++HSe^-$	(pK=4.77)
(10) $HSe^-=H^++Se^{2-}$	(pK=14.01)

The thermodynamic values used for calculation are all taken from Ref. 19 for indium compounds and from Ref. 20 for selenium compounds except for $\Delta G_f^\circ(InSe)$=129.26 kJ·mol^{-1} which is taken from Ref. 21.

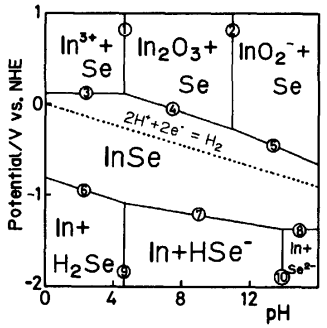

Fig. 13. The pH-potential diagram for the InSe-water system at 25 °C. Each line represents the equilibrium reaction of the same number shown in Table 1 with the following activity. For lines (1) and (3), [In^{3+}]=10^{-6}; for lines (2) and (5), [InO_2^-]=10^{-6}; for lines (6) and (9), p_{H_2Se}=10^{-6}; for lines (7), (9), and (10), [HSe^-]=10^{-6}; for lines (8) and (10), [Se^{2-}]=10^{-6}.

in 1M NaOH, as the mechanical strength of the electrode became very weak after the measurements.

The Reason for Irreproducible Current-Potential Relations. As shown in Fig. 3, the electrochemical behaviors were different from sample to sample. Particularly, the potentials at which the photocurrent showed saturation were different by as large as ≈3 V. In all cases, the photocurrent linearly increased with the potential at medium bias conditions and the resistances calculated from the linear portion by using ohmic law were 0.12 kΩ (sample 1), 0.13 kΩ (sample 2), and 0.50 kΩ (sample 3). The larger the resistance was, the more negative the potential at which the photocurrent saturated. The conductivity of InSe shows anisotropy and that perpendicular to the van der Waals face is relatively low.[23] Thus, the relatively large bulk resistance ⊥ the electrode surface causes large ohmic drop and the actual potential drop at the semiconductor/electrolyte interface (including within space charge layer) becomes low. The resistance difference among samples seemed to be due to the thickness difference.

Effect of Steps on the Electrochemical Behavior. As shown in Fig. 3, the dark current decreased significantly and the photocurrent increased by removing surface steps. The surface steps at which dangling bonds exist[24] certainly create surface states.[25] The results of current-potential relations can be explained by considering the existence of surface states at the electrode with many steps. Thus, the surface states act as recombination centers[26] and mediators for charge transfer,[27] resulting in smaller photocurrent and larger dark current at the electrode with many steps. The impedance analyses (Figs. 9 and 10) also support the above arguments. While the equivalent circuit for the electrode of less steps is simply a series combination of a bulk resistance, R_b, and a space charge capacitance, C_{sc}, the contribution of a surface state resistance, R_{ss}, a surface state capacitance, C_{ss}, and a charge transfer resistance, R_{ct}, should be taken into account in the case of the equivalent circuit for the electrode of many steps. Small R_{ct} is equivalent to a large dark current. By removing steps, the concentration of surface states becomes low and, therefore, C_{ss} becomes small and R_{ss} and R_{ct} become large, giving the equivalent circuit of the electrode of less steps.

The Mechanism for Photoelectrochemical Hydrogen Generation and Effect of Pt Modification. The photocurrent-potential and the photocurrent-light intensity relations at p-InSe in 0.5M H_2SO_4 provide information for the photoelectrochemical hydrogen generation mechanism. The hydrogen evolution reaction at p-type semiconductor under illumination proceeds by the following processes.[28]

(a) Bulk processes:

$$h\nu \longrightarrow p_v^+ + e_c^-, \quad (II)$$

$$e_c^- \longrightarrow (e_c^-)_s, \quad (III)$$

$$e_c^- + p_v^+ \longrightarrow \text{recombination}, \quad (IV)$$

where p_v^+ is the hole in the valence band and $(e_c^-)_s$ and e_c^- are the electrons in the conduction band at the surface and at other places, respectively.

(b) Surface processes:

$$(e_c^-)_s + H_3O^+ \longrightarrow H(a) + H_2O, \quad (V)$$

$$H(a) + (e_c^-)_s + H_3O^+ \longrightarrow H_2 + H_2O, \quad (VI)$$

$$H(a) + H(a) \longrightarrow H_2, \quad (VII)$$

$$(p_v^+)_s + H(a) + H_2O \longrightarrow H_3O^+, \quad (VIII)$$

$$(e_c^-)_s + (p_v^+)_s \longrightarrow \text{Surface recombination}, \quad (IX)$$

$$(e_c^-)_s + \square_{ss} \longrightarrow \boxed{e^-}_{ss}, \quad \boxed{e^-}_{ss} + (p_v^+) \longrightarrow \square_{ss}, \quad (X)$$

where H(a) represents hydrogen atom adsorbed on the semiconductor, $(p_v^+)_s$ is the hole in the valence band at the surface, $\boxed{e^-}_{ss}$ is the occupied surface state, and $\square_{ss}$ is the unoccupied surface state. The step expressed in Eq. (X) is the surface recombination via surface state. The combination of step (V) and step (VIII) could be called the surface recombination via adsorbed hydrogen state. The rate determining step for the hydrogen evolution reaction must be different at potentials more positive than ca. −1.8 V where the photocurrent incrcased with the increase of cathodic bias but became independent of light intensity at relatively high intensity from that at potentials more negative than ca. −1.8 V where the photocurrent was almost independent of the potential but increased linearly with light intensity. In the latter case, the generation of electron-hole pair (step (IV)) is the rate determining srep.[29] This was verified by the fact that the platinization did not affect the saturation photocurrent. On the other hand, in the former case, the rate seems to be controlled by the surface processes. The disagreement of the flat band potential (≈0.2 V) and the photocurrent onset potential (≈−0.5 V) is due to the fact that the reactions (V)—(VII) are slow compared to reactions (VIII)—(X). The significant increase of the photocurrent in this potential region and the positive shift of the photocurrent onset potential by the surface modification with Pt which is known to accelerate the hydrogen evolution reaction in dark[30] (steps (V)—(VII)) again support this mechanism. Although the photoelectrochemical characteristics of p-InSe is improved much by Pt modification, the photocurrent onset potential is still relatively negative and, thus, the efficiency is small. Further improvement is required to reach the efficiency level of other metal modified semiconductor electrodes, e.g. p-InP.[31]

Prof. T. Yokokawa is acknowledged for the encouragement during the course of this work.

References

1) a) H. Gerischer, *J. Electroanal. Chem.*, **58**, 263 (1975); b) M. S. Wrighton, *Acc. Chem. Res.*, **9**, 303 (1979); c) A. Heller, *Acc. Chem. Res.*, **14**, 154 (1981); d) B. Parkinson, *Acc. Chem. Res.*, **17**, 431 (1984).

2) a) Y. Nakato, T. Ohnishi, and H. Tsubomura, *Chem. Lett.*, **1975**, 883; b) J. O'M. Bockris and K. Uosaki, *Energy*, **1**, 76 (1976); c) R. Noufi, D. Tench, and L. F. Warren, *J. Electrochem. Soc.*, **128**, 2596 (1981); d) L. Fornarini, F. Stirpe, and B. Scrosati, *J. Electrochem. Soc.*, **130**, 2184 (1983).

3) a) G. Betz, H. Tributsch, and S. Fiechter, *J. Electrochem. Soc.*, **131**, 640 (1984); b) A. Katty, B. Fotouhi, and O. Gorochov, *J. Electrochem. Soc.*, **131**, 2806 (1984); c) S. H. Pawar, S. P. Tamhankar, and C. D. Lokhande, *J. Electrochem. Soc.*, **132**, 261 (1985).

4) a) J. Gobrecht, H. Gerischer, and H. Tributsch, *Ber. Bunsenges. Phys. Chem.*, **82**, 1331 (1978); b) H. Tributsch, *Ber. Bunsenges. Phys. Chem.*, **82**, 169 (1978); c) H. Tributsch, *J. Electrochem. Soc.*, **125**, 1086 (1978).

5) W. Kautek, J. Gobrecht, and H. Gerischer, *Ber. Bunsenges. Phys. Chem.*, **84**, 1034 (1980).

6) H. Tributsch, *Far. Diss. Chem. Soc.*, **70**, 189 (1980).

7) a) J. C. Merle, R. Bartiromo, E. Borsella, M. Piacentini, and A. Savoia, *Solid State Comm.*, **28**, 251 (1978); b) N. Piccioli, R. Le Toullec, F. Bertrand, and J. C. Chervin, *J. Phys.*, **42**, 1129 (1981).

8) G. H. Hewig and W. H. Bloss, *Thin Solid Films*, **45**, 1 (1977).

9) a) A. Segura, A. Chevy, J. P. Guesdon, and J. M. Besson, *Solar Energy Mater.*, **2**, 159 (1979/1980); b) A. Segura, J. P. Guesdon, J. M. Besson, and A. Chevy, *Rev. Phys. Appl.*, **14**, 253 (1979); c) A. Segura, J. P. Guesdon, J. M. Besson, and A. Chevy, *J. Appl. Phys.*, **54**, 876 (1983).

10) J. F. McCann and J. Pezy, *J. Electrochem. Soc.*, **128**, 1735 (1981).

11) a) C. Levy-Clement, N. Le Nagard, O. Gorochov, and A. Chevy, *J. Electrochem. Soc.*, **131**, 790 (1984); b) C. Levy-Clement and B. Theys, *J. Electrochem. Soc.*, **131**, 1300 (1984); c) R. Tenne, B. Theys, J. Rioux, and C. Levy-Clement, *J. Appl. Phys.*, **57**, 141 (1985).

12) A. Chevy, A. Kuhn, and M.-S. Martin, *J. Cryst. Growth*, **57**, 118 (1977).

13) a) H. J. Lewerenz, H. Gerischer, and M. Lübke, *J. Electrochem. Soc.*, **131**, 100 (1984); b) W. Kautek, H. Gerischer, and H. Tributsch, *Ber. Bunsenges. Phys. Chem.*, **83**, 1000 (1979).

14) See the pH-potential diagram in the discussion section.

15) All samples were taken from the same crystal.

16) H. Gerischer, J. Gobrecht, and J. Turner, *Ber. Bunsenges. Phys. Chem.*, **84**, 596 (1980).

17) a) K. Uosaki and H. Kita, *Solar Energy Mater.*, **7**, 421 (1983); b) K. Rajeshwar, *J. Electrochem. Soc.*, **129**, 1003 (1982).

18) M. Tomkiewicz, *J. Electrochem. Soc.*, **126**, 2220 (1976).

19) V. V. Losev and A. I. Molodov, "Encyclopedia of Electrochemistry of the Elements," ed by A. J. Bard, Marcel Dekker, New York (1975), Vol. VI, p. 2.

20) S. I. Zhdarov, "Encyclopedia of Electrochemistry of the Elements," ed by A. J. Bard, Marcel Dekker, New York (1975), Vol. IV, p. 362.

21) I. Barin and O. Knacke, "Thermochemical Properties of Inorganic Substances (Supplement)," Springer-Verlag, Berlin, Heidelberg and New York (1977), p. 312, p. 323, and p. 352.

22) H. Tributsch, *Appl. Phys.*, **23**, 61 (1980).

23) R. W. Damon and R. W. Redington, *Phys. Rev.*, **96**, 1498 (1954).

24) R. M. A. Lieth, "Physics and Chemistry of Materials

with Layered Structure," ed by R. M. A. Lieth, D. Reidel Pub. Co., Dordrecht-Holland (1977), Vol. I, p. 225.
25) R. H. Wilson, *J. Appl. Phys.*, **48**, 4292 (1977).
26) J. I. Pankove, "Optical Processes in Semiconductor," Dover Pub. Inc., New York (1971), p. 353.
27) P. Salvador and C. Gutierrez, *Surface Science*, **124**, 398 (1983).
28) K. Uosaki and H. Kita, *J. Electrochem. Soc.*, **128**, 2153 (1983).
29) a) J. A. Baglio, G. S. Calabrese, D. J. Harrison, E. Kamieniecki, A. J. Ricco, M. S. Wrighton, and G. D. Zoski, *J. Am. Chem. Soc.*, **105**, 2246 (1983); b) M. Gronet and N. S. Lewis, *J. Phys. Chem.*, **88**, 1310 (1984).
30) A. J. Appleby, M. Chemla, H. Kita, and G. Bronoël, "Encyclopedia of Electrochemistry of the Elements," ed by A. J. Bard, Marcel Dekker, New York (1982), Vol. IX, Part A, p. 383.
31) a) K. Uosaki and H. Kita, *Chem. Lett.*, **1984**, 301; b) A. Heller, E. Aharon-Shalom, W. A. Bonner, and B, Miller, *J. Am. Chem. Soc.*, **104**, 6942 (1982).

Preparation and Coercivity of Cobalt Ultrafine Particles by Reduction of Multilayered CoO-SiO Films

Yoshichika BANDO and Takahito TERASHIMA*
Institute for Chemical Research, Kyoto University, Uji, Kyoto 611
(Received April 27, 1985)

Films containing Co ultrafine particles were prepared by hydrogen reduction of periodically multilayered CoO–SiO films which were formed by alternating deposition of CoO and SiO. The films containing Co particles maintained the periodicity similar to the original films. Using samples of CoO single layer sandwiched between SiO layers, highly dispersed Co particles in the reduced sample were observed by transmission electron microscopy. The average size of the Co particles was almost as large as the thickness of CoO layer. The coercivities of the multilayered films containing Co particles were measured at room temperature and 77 K; they decreased with decreasing particle size from 20 nm to 3nm. Superparamagnetism was observed for the Co particles with average sizes below 4nm at room temperature. The formation and the magnetic property of the Co ultrafine particles in the Co–SiO system is dicussed.

Periodically multilayered films composed of two substances have been investigated as a means of producing materials having unusual properties.[1-4] Studies of multilayered films have been limited to their structure and physical properties such as their magnetic, electric and mechanical behavior. The present paper deals with chemical change of multilayered films of CoO–SiO. Silicon oxide ($SiO \sim SiO_2$) has been used as a coating for passivation of semiconductor devices and for coating ultrafine particles.

It has been reported that the coating of precursor particles, such as hydroxides and oxides with silicon compounds frequently has a great effect on the shape and size of metallic or oxide particles prepared by reduction or decomposition of the precursor.[5,6] The role of the silicon oxide in the reduction or decomposition process has not been made clear.

In multilayered CoO–SiO films, a CoO layer is coated with SiO layers. The reduction of the CoO layers in the multilayered film may therefore be similar to that of oxide precursor particles coated with silicon compounds which change into silicon oxide. Investigations of the reduction of multilayered CoO–SiO films contribute to the elucidation of the role of silicon oxide in the preparation of ultrafine particles.

SiO is readily evaporated and the deposited SiO is amorphous. SiO films have strong adhesion to various substrates, environmental stability, and superior mechanical properties. These properties improve the quality of the the multilayered films. Silicon oxide is oxidized during deposition process and its composition (SiO_{1+x}) depends on deposition parameters such as the evaporation rate, the substrate temperature and the degree of vacuum. Hereafter, SiO_{1+x} will be expressed as SiO. Since the thickness of the silicon oxide coating on the oxide or metal particles is considered to be below 2 nm, it is desirable that the SiO layer used in the present experiment be as thin as possible within the limits of a continuous films. We chose 1.5 nm as a suitable layer thickness of SiO.

Fine particles of Co are readily prepared by hydrogen reduction of CoO at a low temperature. Furthermore, Co ultrafine particles have many interesting properties as magnetic materials and catalysts. Therefore, CoO is the most suitable as a constituent of multilayered films for our purpose.

CoO ultrathin films can be prepared by reactive evaporation.[7] Periodically multilayered films may be prepared by alternating deposition of CoO and SiO.

Experimentals

SiO was deposited by evaporation of SiO in a vacuum of 10^{-4}Pa and CoO was reactively deposited by evaporation of Co metal in oxygen at a pressure of 5×10^{-2}Pa. The thickness and deposition rate of each layer were monitored by an oscillating quartz sensor. The deposition rates of both CoO and SiO were 0.1 nm s^{-1}. The thickness of the SiO layers was chosen to be at 1.5 nm and those of CoO layers were designed to be 1.5 to 20 nm. Glass plates and polyimide films were used as substrates (glass for X-ray diffraction and polyimide films for magnetic measurements). During deposition, the substrate was kept at room temperature by water cooling. Reduction of the multilayered films was achieved by heating them in a hydrogen atmosphere at 200°C for 1 h. The CoO–SiO films and the reduced films were examined by X-ray diffraction (RIGAKU ROTAFLEX RU-200) using Cu $K\alpha$ radiation and transmission electron microscopy (JEOL JEM-100CX and JEM-200CX). The magnetic properties of the reduced films were measured by a vibrating-sample magnetometer (TOEI VSM-3).

Results

Reduction of the Multilayered CoO–SiO Films.

The cobalt oxide layers in the as-deposited film were identified to be CoO by X-ray diffraction, as shown in Fig. 1(a). As-reduced films were black and lustrous. X-ray diffraction showed that there was mainly hcp Co metal in the reduced films as shown in Fig. 1(b). However, the existence of the fcc phase was confirmed by electron diffraction of the reduced film as shown in Fig. 1(c); this includes the (200) ring of fcc Co. These results of X-ray and electron diffractions thus showed that both hcp and fcc Co exist in the reduced films, but the amount of the fcc phase is small.

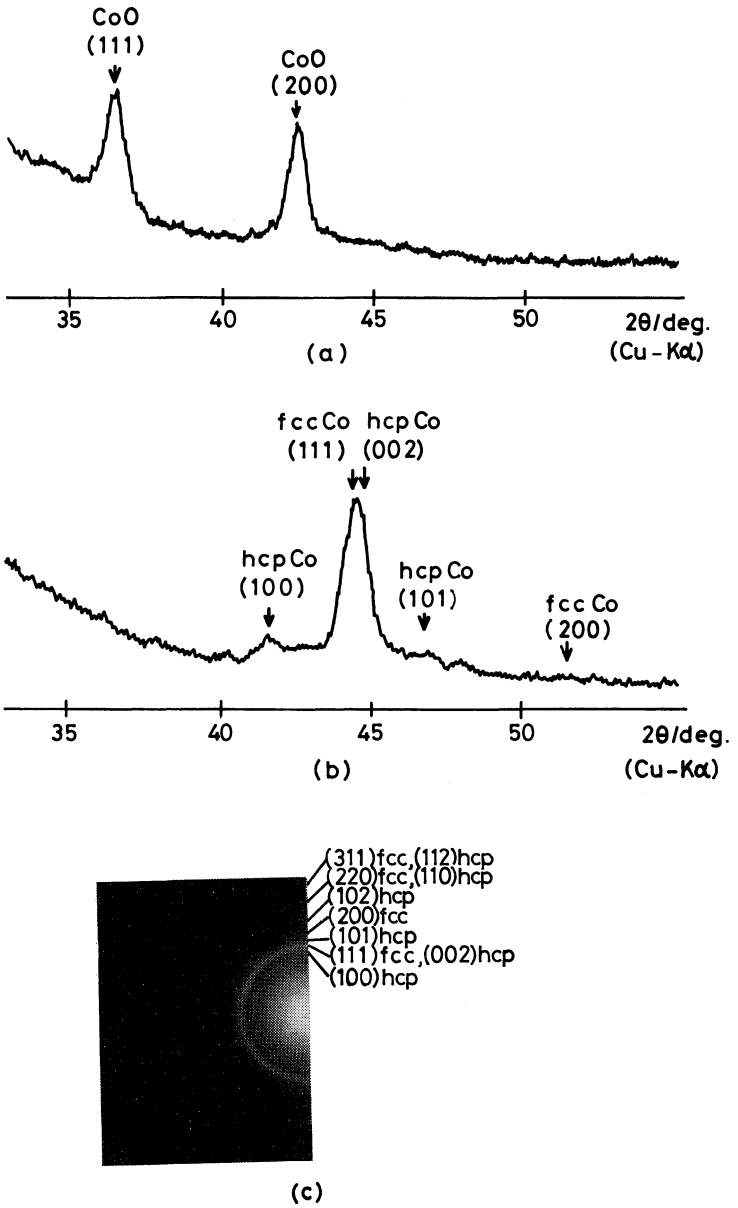

Fig. 1. (a) X-Ray diffraction pattern of the as-deposited [CoO-(13.5 nm)-SiO(1.5 nm)]×10. (b) X-Ray diffraction pattern of the reduced [CoO(13.5 nm)-SiO(1.5 nm)]×10. (c) Transmission electron diffraction pattern of the reduced [SiO(10 nm)-CoO(15 nm)-SiO(3 nm)].

Periodicity of the Multilayered Films Before and after Reduction. The periods of composition modulation in the multilayered films were determined by low angle X-ray diffraction. The 2nd and 3rd Bragg diffraction peaks for the as-deposited film were observed as shown in Fig. 2(a), and the period calculated from diffraction angles was in good agreement with the designed period.

As shown in Fig. 2(b), the value of period of the reduced film is almost the same as that of the as-deposited films. This means that the periodicity persists during reduction and the thickness of the Co layers is similar to that of CoO layers, as the thickness of SiO layer should be invariable.

Reduction of Single CoO Layer Sandwiched in between SiO Layers. The samples of single CoO layer sandwiched in between SiO were prepared as follows. The CoO layer was deposited on SiO support film on a mesh for electron microscopic observation and was coated by a SiO film. The single CoO layer was directly examined by TEM, as shown in Fig. 5. The electron diffraction pattern shows CoO and the micrograph shows a continuous film consisting of microcrystallites. Results of TEM examination for the sample after heated in H_2 at 200 °C are shown in Fig. 6. The diffraction pattern indicated metallic Co with the hcp and fcc structures; this is consistent with the pattern in Fig. 1(c). Co ultrafine particles with

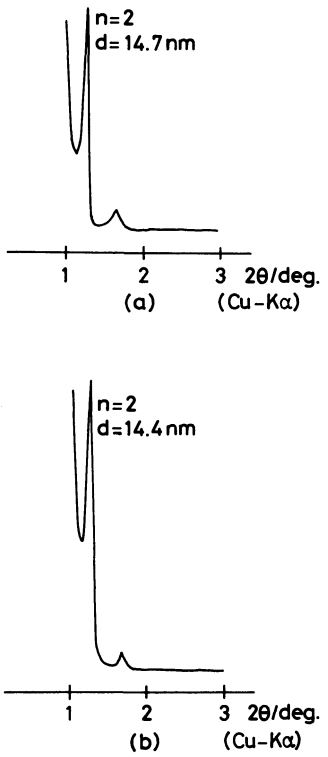

Fig. 2. (a) Low angle X-ray diffraction pattern of the as-deposited [CoO(13.5 nm)–SiO(1.5 nm)]×10. (b) Low angle X-ray diffraction pattern of the reduced [CoO(13.5 nm)–SiO(1.5 nm)]×10.

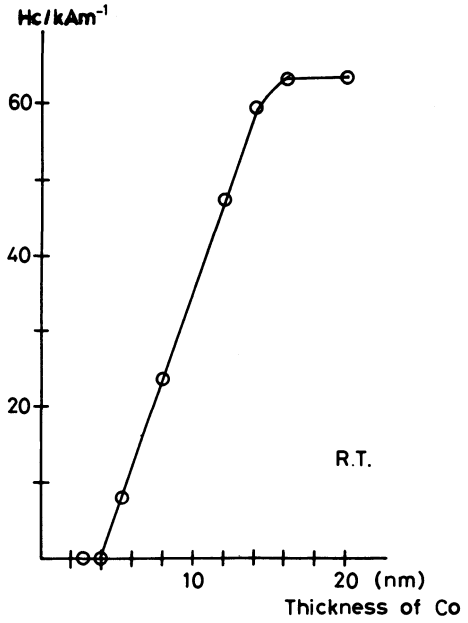

Fig. 3. Coercive force *Hc* measured at room temperature as a function of thickness of Co layer. Total thickness of Co layers in each film was fitted to be about 100 nm.

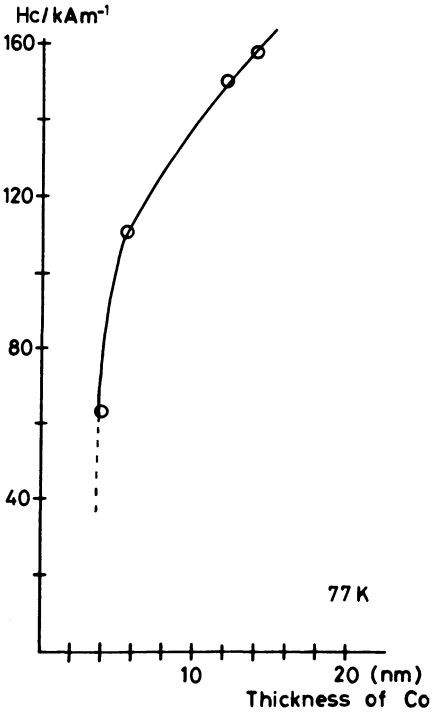

Fig. 4. Coercive force *Hc* measured at 77 K as a function of thickness of Co layer.

sizes ranging from 4 to 20 nm were clearly observed in microphotograph of a sample prepared by reducing the 9 nm thick CoO layer. For the 5 nm thick CoO layer, the size of the Co particles in the reduced sample ranged from 2.5 nm to 8 nm, as shown in Fig. 7(a). The average size of the Co particles is close to the value for the thickness of the original CoO layer. The lattice image of a Co particle shown in Fig. 7(b) indicates that the particle is a single crystal.

Magnetic Measurement of the Reduced Films. The reduced films showed ferromagnetism with typical hysteresis loops. Figure 3 shows the coercive force *Hc* measured at room temperature as a function of the thickness of Co layer. *Hc* decreased with decreasing Co layer thickness and became zero below 4 nm thick. The magnetic curves of films with 4 nm or less thick Co layers were superparamagnetic. When the magnetic curves were measured at 77 K, *Hc* for the film containing 4 nm thick Co layers was as high as 63 kA/m, as shown in Fig. 4. These magnetic data for the reduced films show that they contain metallic Co which is highly dispersed in ultrafine particles.

Discussion

It is clear from the experimental results that ultrafine Co particles are prepared by reducing the CoO–SiO multilayered film in H_2. Furthermore, it is surprising that the reduced films containing Co particles have the periodicity of composition modulation. This means that SiO layer as thin as 1.5 nm supports the multilayered structure during reduction, as shown in Fig. 8. The reduction of CoO to Co would not occur at once. When a CoO layer sandwiched between SiO

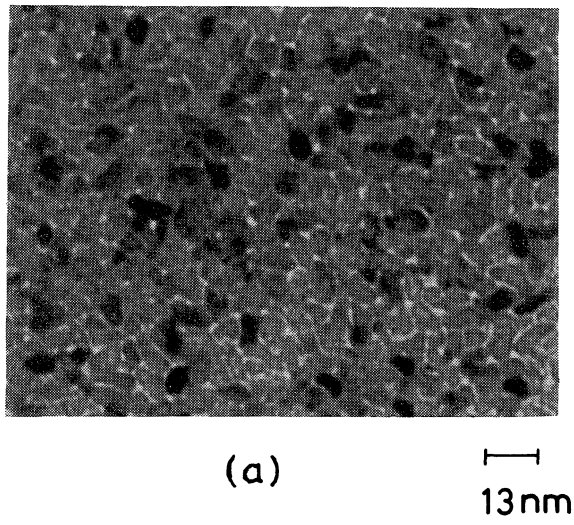

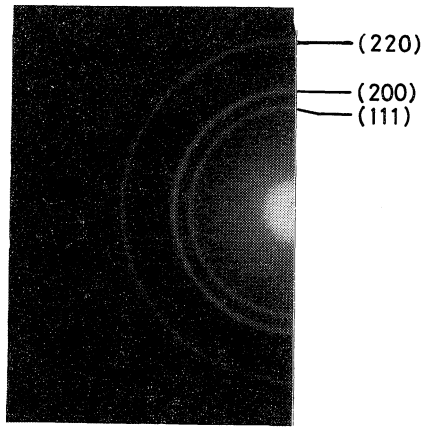

Fig. 5. (a) TEM image of the as-deposited [SiO(10 nm)–CoO(10 nm)–SiO(3 nm)]. (b) Transmission electron diffraction pattern of the same sample.

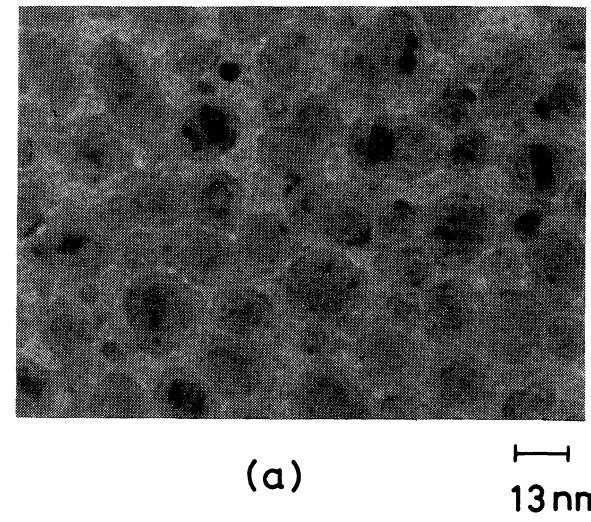

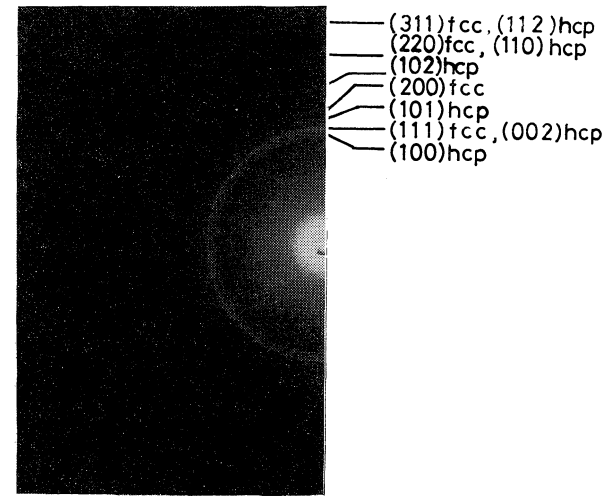

Fig. 6. (a) TEM image of [SiO(10 nm)–Co(10 nm)–SiO(3 nm)]. (b) Transmission electron diffraction pattern of the same sample.

films is reduced, some portions of the layer would remain as CoO and maintain the original SiO-SiO interlayer distance. When the remaining CoO is successively reduced, the Co particles already formed would maintain the interlayer distance. When CoO changes into Co, the volume reduces to about a half; this comes from the release of oxygen and an increase of the density from 6.3×10^3 kg m^{-3} for CoO to 8.9×10^3 kg m^{-3} for Co.

The formation of the highly dispersed ultrafine particles is caused by both of the constant SiO-SiO interlayer distance before and after reduction and of the volume decrease from CoO to Co. If the Co particles have the shape of columns with a diameter and a height equal to CoO layer thickness d and arrayed in a regular triangular lattice, as shown in Fig. 9, the distance between the nearest neighbor columns is calculated to be 1.35 d, showing formation of isolated particles.

The Co ultrafine particles less than 20 nm constitute a single magnetic domain. For an assembly of single domain particles with the easy axes oriented at random, in a non-ferromagnetic matrix, the value of Hc is expressed as follows:[8]

$$Hc = 0.48 \times 2K/Is \qquad (1)$$

where K is the magnetic anisotropy energy constant and Is is the saturation magnetization. Using Is=1.79 T[9] and $K=4.6\times10^5$ Jm^{-3}[10] for hcp Co, Hc would be about 247 kAm^{-1}. In Fig. 3, maximum coercivity of 63 kAm^{-1} is considerably lower compared with the calculated value. K value for fcc Co is considered to be as large as 2×10^4 Jm^{-3},[11] and Hc would be about 11 kAm^{-1}.

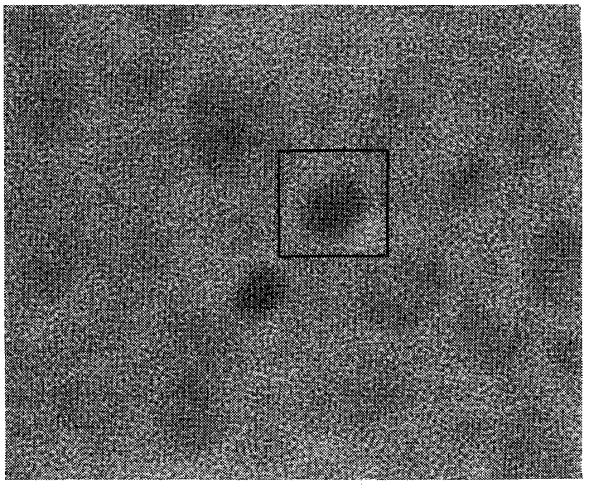

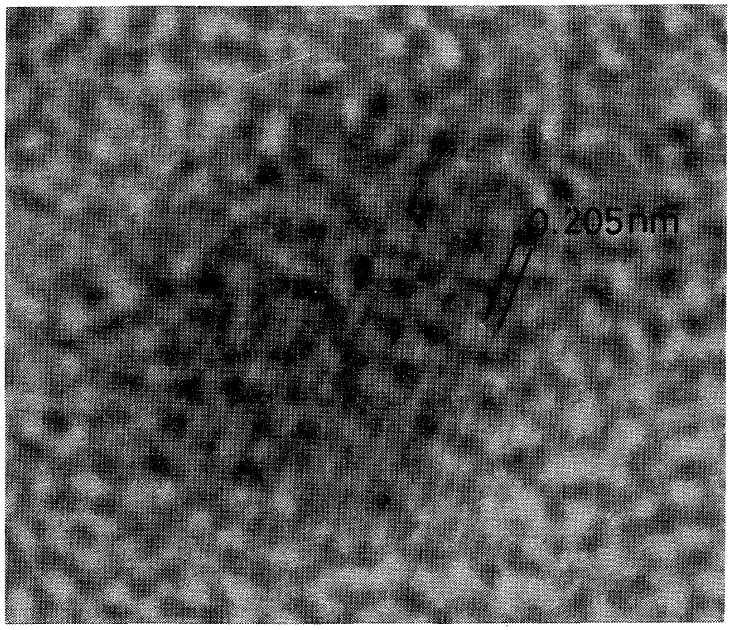

Fig. 7. (a) TEM image ot [SiO(10 nm)-Co(5 nm)-SiO(3 nm)].
(b) The lattice image of the particle indicated in (a).

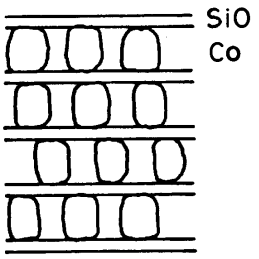

Fig. 8. Schematical illustration of the multilayered structure containing Co particles supported by continuous SiO layers.

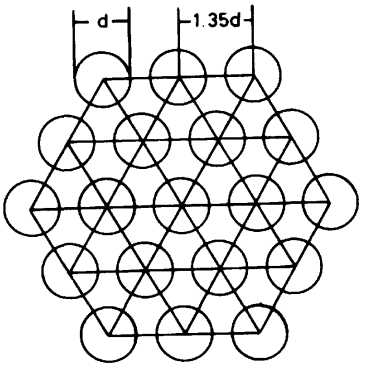

Fig. 9. Schematical illustration of the location and size of the reduced Co particles in film plane.

If the assembly of Co particles consists of both the fcc and the hcp particles, the low value of Hc obtained suggests that the amount of the fcc phase particles should be more than that of the hcp particles. However, the results of X-ray and electron diffraction measurements indicated only a small amount of the fcc phase. As the difference between the free energies of fcc and hcp in Co metal is small, a particle may frequently contain both phases; the fcc stacking may be regarded as stacking faults in the hcp phase.

Therefore, individual particles obtained may contain both phases. The existence of the fcc phase in the hcp Co may decrease the large uniaxial magnetic anisotropy energy due to hexagonal symmetry.

Using Is=1.79 T and Hc=63 kAm^{-1} of the experimental value, K would be 1.2×10^5 Jm^{-3}. Using this K value, we can calculate the critical size for superparamagnetism at room temperature by the expression,[11]

$$\tau = \tau_0 \times \exp(KV/kT) \quad (2)$$

where τ is the superparamagnetic relaxation time, τ_0 is the frequency factor, V is the magnetic volume of the particles, k is Boltzman's constant and T is the temperature. When the coercivity is zero for a static magnetic measurement, τ is of the order of 10^2 s. The blocking temperature T_B is defined as the temperature below which the particles show ferromagnetism, i.e., the temperature at which τ is of the order of 10^2 s. The critical size for superparamagnetism at room temperature is calculated by the relation KV/kT=25, assuming $\tau_0=10^{-9}$ s and $\tau=10^2$ s. The diameter calculated for column particles is 10.3 nm. In Fig. 6, the average size is 9 nm, but the sizes are distributed from 20 nm to 4 nm. The decrease in Hc for particle diameters below 1.6 nm in Fig. 3 is attributed to the presence of the superparamagnetic particles. With decreasing thickness, the ratio of the superparamagnetic particles increases and the value of Hc drops abruptly. It is reasonable that the particles with an average size of 9 nm have half the value of the maximum coercivity. At 77 K, the value of the anisotropy would be estimated to be 3.0×10^5 Jm^{-3} from maximum Hc=160 kAm^{-1}. The critical size for superparamagnetism is 4.8 nm; this is reasonable in consideration of the value of the coercivity of the Co particles with an average size of 5 nm.

So far, we have discussed the K value and the critical size for superparamagnetism on the assumption that the fcc phase exists within the hcp Co particles. The calculated values are in good agreement with the observed ones, which indicates that our assumption is reasonable.

The values of Is and Hc in the reduced films persisted over 1 year or longer. Therefore, SiO is a good protector to oxidation of Co ultrafine particles. On the other hand, SiO-coated CoO is readily reduced to Co at 200°C; accordingly oxygen atoms should be able to pass through SiO layer. Furthermore, it is clear that SiO has a function to support the original shape of the starting material such as the multilayered structure during reduction. It is concluded that these characteristics of SiO as a coating make it suitable for use in the preparation of metallic or oxide ultrafine particles for magnetic recording media and catalyst.

The authors thank Professors T. Takada and M. Takano of the Institute for Chemical Research, Kyoto University, and Prof. T. Shigematsu of Konan University for fruitful discussions. Thanks also due to Dr. N. Nakayama of the same Institute for the suggestion for the observation of TEM. This work was partially supported by a Grant-in-Aid for Scientific Research from the Ministry of Education.

References

1) I. K. Schuller, *Phys. Rev. Lett.*, **44**, 1597 (1980).
2) N. K. Flevaris, J. B. Ketterson, and J. E. Hilliard, *J. Appl. Phys.*, **53**, 11 (1982).
3) S. T. Ruggiero, T. W. Barbee, Jr., and M. R. Beasley, *Phys. Rev.*, **26**, 4894 (1982).
4) W. M. C. Yang, T. Tsakalakos, and J. E. Hilliard, *J. Appl. Phys.*, **48**, 876 (1977).
5) Y. Maeda, T. Manabe, K. Nagai, F. Yoshimura, and S. Hirono, "Ferrites: Proc. Inter. Conf.," ed by H. Watanabe et al., Center for Academic Pub., Japan (1981), p. 541.
6) Y. Tokuoka, R. Horimoto, T. Kobuke, and H. Morita, Ferrites:Proc. Inter. Conf.," ed by H Watanabe et al., Center for Academic Pub., Japan (1981), p. 553.
7) T. Terashima and Y. Bando, *J. Appl. Phys.*, **56**, 3445 (1984).
8) C. D. Mee and J. C. Jeschke, *J. Appl. Phys.*, **34**, 1271 (1963).
9) R. Bozorth, "Ferromagnetism," ed by D. van Nostrand, New York (1951), p. 867.
10) S. Chikazumi, T. Wakiyama, and K. Yoshida, Proc. of the Inter. Conf. on Magnetism, Nottingham (1964), p. 756.
11) L. Néel, *Ann. Geophys.*, **5**, 99 (1949).

 © 1986 The Chemical Society of Japan Bull. Chem. Soc. Jpn., 59, 613—616 (1986)

Kinetics and Mechanism of Replacement of Glycinate in Bis(glycinato)oxovanadium(IV) by Oxalate

Jung-Sung KIM,† Woo-Sik JUNG, Hiroshi TOMIYASU, and Hiroshi FUKUTOMI*
Research Laboratory for Nuclear Reactors, Tokyo Institute of Technology, O-okayama, Meguro-ku, Tokyo 152
(Received July 25, 1985)

The kinetics of formation of bis(oxalato)oxovanadate(IV) $[VO(ox)_2(H_2O)]^{2-}$ (hereafter water molecule will be omitted) from the reaction of bis(glycinato)oxovanadium(IV) $[VO(gly)_2]$ with oxalate has been studied by the stopped-flow method. The reaction was found to consist of two consecutive steps, a relatively slow step (k_1) and a fast one (k_2). The values of rate constants k_1 and k_2 were independent of the concentration of free oxalate and of the pH of solution ranging from 4.2 to 6.5. Similar behavior was also observed in the acid decomposition of $[VO(gly)_2]$. A mechanism passing through an intermediate, $[VO(ox)(gly)]^-$, was proposed.

The kinetics of ligand-substitution reactions for a variety of oxovanadium(IV) complexes has been studied extensively.[1-12] The study of ^{17}O NMR in $[VO(H_2O)_5]^{2+}$[2,3] revealed that the rate of water exchange at the axial position was extremely fast, but relatively slow at the basal positions, in which the rate constant was determined by the conventional NMR line-broadening method. Since then, much interest has been centered in the kinetic study of ligand substitutions in oxovanadium(IV) complexes to compare the rate constants of various ligand substitutions with those of water exchange.

The kinetic behavior of oxovanadium(IV) complexes appears to be quite interesting, for the rates of ligand substitutions differ as much as some hundreds according to substituting ligands and structures of complexes. In the case of formation of chelate complex, $[VO(gly)]^+$, from $[VO\text{-}gly]^+$, glycinate of which coordinates as a unidentate ligand, the rate constant was about 1/10 of that of water exchange at the basal positions.[6] Much slower rate was reported for the anation reaction in [VO(pmida)](pmida=*N*-(2-pyridylmethyl)iminodiacetate) by NCS^- and N_3^-.[9]

In this paper we report the kinetics of the replacement of glycinate in $[VO(gly)_2]$ by oxalate

$$[VO(gly)_2] + 2ox^{2-} \longrightarrow [VO(ox)_2]^{2-} + 2gly^- \qquad (1)$$

for a further understanding of substitution mechanisms in oxovanadium(IV) complexes.

Experimental

The preparation and analysis of the oxovanadium(IV) stock solution were described in a previous paper.[4] Analytical grade (Wako Pure Chemical Ind., Ltd.) perchloric acid, sodium oxalate and sodium perchlorate which was recrystallized twice from aqueous solution were used. The ionic strength was adjusted at 1.0 M (1 M=1 mol dm^{-3}) by using sodium perchlorate. A Union Giken RA-401 stopped-flow spectrophotometer was used for accumulated stopped-flow measurements, where accumulations were carried out at least ten times. Absorption spectra were measured by using a Shimadzu UV-365 spectrophotometer with 20 mm quartz cells.

Results and Discussion

The absorption spectra of $[VO(gly)_2]$ and $[VO(ox)_2]^{2-}$, whose assignment was reported in the earlier papers,[7,14] are shown in Fig. 1. It was found that the spectra of final products of the reaction between $[VO(gly)_2]$ and oxalate were consistent with that of $[VO(ox)_2]^{2-}$ indicating that the stoichiometry can be written by Eq. 1 under the conditions studied. The rate of the reaction was measured from the change in absorbance at 555 nm. A typical stopped-flow trace is shown in Fig. 2 together with a pseudo-first-order plot ($\log(A_t - A_f)$ vs. time), where A_t and A_f refer to the relative absorbances at times t and infinity, respectively. As is seen in Fig. 2, the pseudo-first-order plot deviates from a straight line in spite of excess sodium oxalate suggesting that the reaction consists of two consecutive steps. The results lead to the following reaction mechanism passing through an intermediate complex, (Int),

$$[VO(gly)_2] \xrightarrow{k_1} (Int) \xrightarrow{k_2} [VO(ox)_2]^{2-}, \qquad (2)$$

where k_1 and k_2 represent the first-order rate constants for each step. Based on the above reaction mechanism, the stopped-flow traces were analyzed by means of the nonlinear-least-squares method using k_1, k_2, and ε_{Int} (molar extinction coefficient of (Int)) as unknown parameters. The calculated values of absorbance with time agree remarkably with the observed data (Fig. 2), where ε_{Int} is taken to be 9.9 M^{-1}cm^{-1} at 555 nm. Since the consecutive first-order reaction similar to the present reaction admits of two mathematical solutions which are a set of alternative parameters, it is necessary to determine which is the correct set of parameters.[15] The alternative molar extinction coefficient, ε'_{Int}, is give by

$$\varepsilon'_{Int} = \varepsilon_{VO(gly)_2} + \frac{k_1(\varepsilon_{Int} - \varepsilon_{VO(gly)_2})}{k_2} \qquad (3)$$

and the value of ε'_{Int} is calculated at 13.2 M^{-1}cm^{-1} by using the values of $\varepsilon_{VO(gly)_2}$=16.0 M^{-1}cm^{-1} and ε_{Int}=

†Present address: Department of Chemistry, Taegu University, Taegu, Korea.

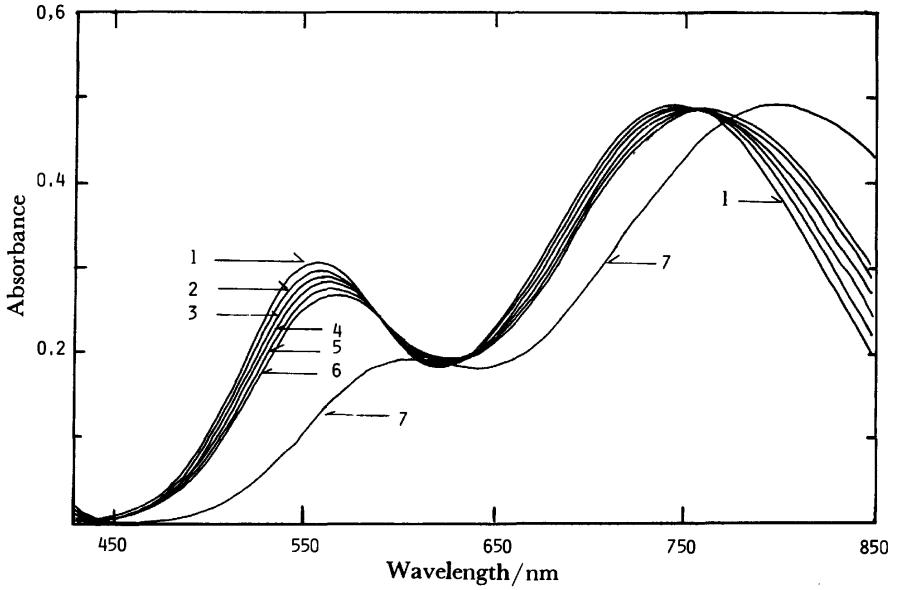

Fig. 1. Absorption spectra of $[VO(gly)_2]$ (1) and $[VO(ox)_2]^{2-}$ (7). Spectra (2—6) were obtained by the addition of small amounts of Na_2ox to the $[VO(gly)_2]$ solution. The conditions are as follow: [VO(IV)]=9.38×10^{-3} M, [glycine]= 2.00 M, pH=6.5 at 20°C. [Na_2ox]=0 (1), 1.24×10^{-3} (2), 2.49×10^{-3} (3), 4.98×10^{-3} (4), 7.46×10^{-3} (5), 9.95×10^{-3} M (6), and excess Na_2ox (7).

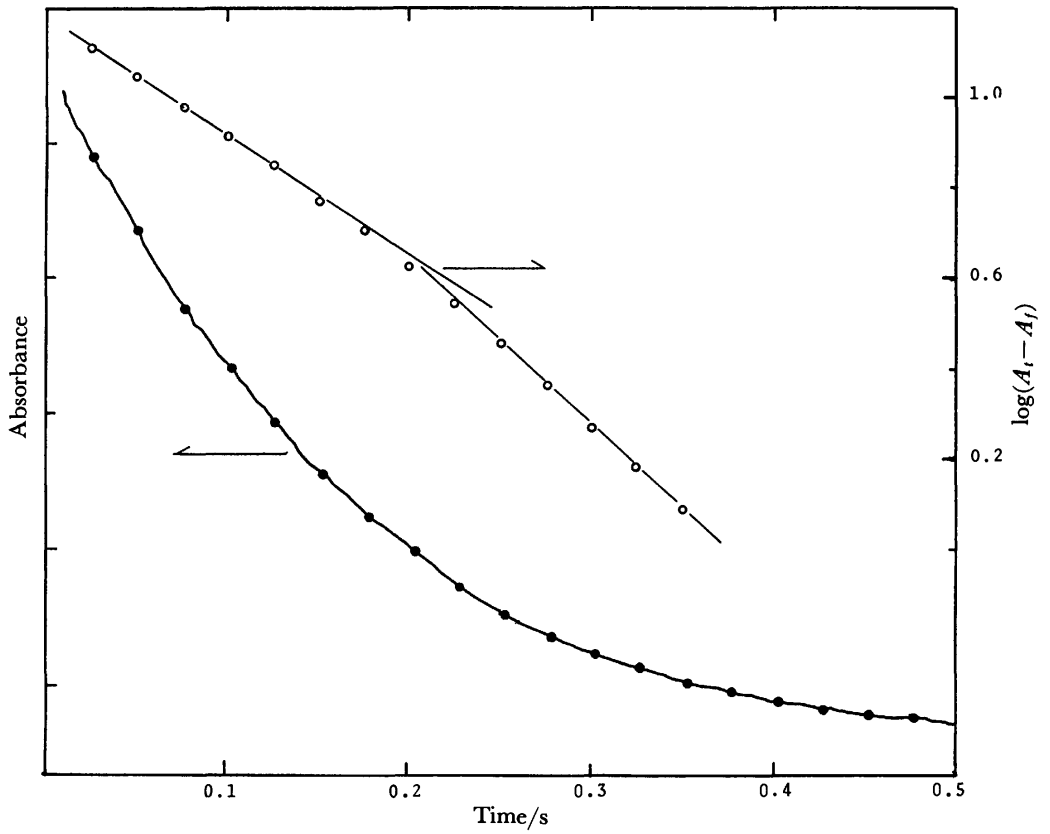

Fig. 2. Typical stopped-flow trace. $[VO(gly)_2]_o$=0.0116 M, $[Na_2ox]_o$=0.125 M, ionic strength= 1.0 M, pH=4.64 at 20°C.
○: Pseudo-first-order plot, ●: nonlinear-least-squares fits based on reaction mechansim (2).

Table 1. Values of k_1 and k_2 at 20 °C under Various Conditions

pH	$[Na_2ox]$ / M		k_1 / s^{-1}	k_2 / s^{-1}
4.64	0.125		6.95	17.5
4.93	0.100		7.76	14.8
5.74	0.075		7.96	16.1
6.57	0.050		8.81	17.8
4.67	0.075		7.45	14.5
4.23	0.050		7.07	19.3
		Average	7.67	16.7

$9.9\,M^{-1}cm^{-1}$ at 555 nm, $k_1=7.67\,s^{-1}$ and $k_2=16.7\,M^{-1}cm^{-1}$ at 20 °C in Table 1. Additional experiments were carried out to estimate the approximate value of molar extinction coefficient of (Int) and to choose between ε_{Int} and ε'_{Int}. A small amount of sodium oxalate was weighed and added to an aqueous solution at pH=6.5 containing $[VO(gly)_2]$ (9.38×10^{-3} M) and glycine (2.0 M), where a volume change due to the addition of Na_2ox was negligible. In Fig. 1, the absorbance at 555 nm decreases as the concentration of Na_2ox increases and the spectra have three isosbestic points at 585, 635, and 735 nm. Addition of excess Na_2ox gives the spectrum of $[VO(ox)_2]^{2-}$, which passes through neither of the above isosbestic points. It is clear that the addition of small amounts of Na_2ox results in the formation of an intermediate complex and it seems most likely that the intermediate is a mixed-ligand complex, $[VO(ox)(gly)]^-$. The value of ε_{Int} at 555 nm was determined to be $10.4\,M^{-1}cm^{-1}$ assuming that the absorbance change in Fig. 1 is based on the following equilibrium.

$$[VO(gly)_2] + ox^{2-} = [VO(ox)(gly)]^- + gly^- \qquad (4)$$

In conclusion, these results support the former solution for k_1 and k_2 with $\varepsilon_{Int}=9.9\,M^{-1}cm^{-1}$.

It can be seen in Table 1 that both k_1 and k_2 are independent of the initial concentrations of sodium oxalate and pH's within experimental errors. These results are particularly surprising in view of the fact that the substitution rates in oxovanadium(IV) complexes are usually affected by the species of substituting ligands and their concentrations.[4,5,9]

The rate of dissociation of glycinate from $[VO(gly)_2]$ by the addition of perchloric acid has been also measured by the stopped-flow method. Since the pH of the solution after mixing $[VO(gly)_2]$ and perchloric acid solutions was 3.0 and the major species in such a pH region of oxovanadium(IV)-glycine system was known to be $[VO(H_2O)_5]^{2+}$ and $[VO(Hgly)]^{2+}$ where glycine coordinated as a unidentate ligand,[14] the reaction can be written by

$$[VO(gly)_2] \xrightarrow{+H^+} [VO(H_2O)_5]^{2+} + [VO(Hgly)]^{2+}. \qquad (5)$$

The stopped-flow trace was very similar to that in Fig. 2 and showed again two components. Rate constants $k_{d(1)}$ and $k_{d(2)}$ for the initial and latter steps respectively were also determined by the nonlinear-least-squares method. The values of $k_{d(1)}$ and $k_{d(2)}$ in Table 2 were determined with the molar extinction coefficient of an intermediate, $\varepsilon_{d(Int)}=8.8\,M^{-1}cm^{-1}$, which was about the mean of those of $[VO(gly)_2]$ and $[VO(H_2O)_5]^{2+}$ at 555 nm, 16.0 and $2.2\,M^{-1}cm^{-1}$, respectively. In analogy with reaction (1), some uncertainty remains as to the reasonable sets of values of $k_{d(1)}$ and $k_{d(2)}$ in reaction (5). Since the molar extinction coefficient of $[VO(Hgly)]^{2+}$ has not been determined accurately, it is even more difficult to evaluate the molar extinction coefficient of the intermediate in reaction (5) than in reaction (1). Although the complete solution was not obtained at present, the fact that the reaction (5) proceeds via two steps might suggest a similarlity of mechanisms in both reactions. As the difference in rate constants $k_{d(1)}$ and $k_{d(2)}$ is not significant, the above suggestion as to the mechanistic similarity seems to be acceptable even when $k_{d(1)}$ and $k_{d(2)}$ are interchanged.

Considering the results in Tables 1 and 2, we propose a mechanism, in which the ring opening, i.e. the rupture of V-N bonds in $[VO(gly)_2]$, is the initiation step of the reaction as shown in Fig. 3. The bond rupture results in the formation of complex II, where one glycinate coordinates as a unidentate ligand. Complex II is attacked by ox^{2-} (Hox^-) and forms complex III, and then more stable complex IV. Complex IV corresponds to the (Int) in Eq. 2. If the initial ring opening is assumed to be rate determining, the oxalate specics, ox^{2-} and Hox^-, and their concentrations give no effect on the substitution rate, and k_1 should be the rate constant of the ring opening in $[VO(gly)_2]$. Similarly the k_2 step corresponds to the over-all process from IV to VI and k_2 refers to the rate constant of the ring opening in complex IV. Similar mechanism passing through an intermediate unis(glycinato)complex, $[VO(gly)]^+$, is proposed for the acid decomposition of $[VO(gly)_2]$. In the earlier study[7] dealing with the formation of $[VO(ox)_2]^{2-}$ from the aqua complex, the rate was dependent on the concentrations of ox^{2-} and Hox^-, and the second-order rate constants were determined to be 1.29×10^4 and $7.0\times10^2\,M^{-1}s^{-1}$ at 15 °C for ox^{2-} and Hox^-, respectively. These results clearly indicate that the rate of the over-all process from II to IV in Fig. 3 is at least hundred times faster than that of the initial ring opening under the present conditions.

It is interesting to compare the present reactions with the following reaction in unis(glycinato)oxovanadium(IV).[6]

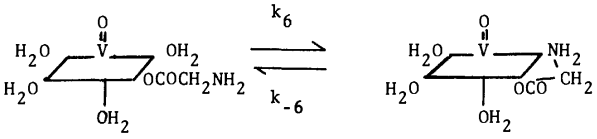

(6)

Table 2. Rate Constants and Activation Parameters in Ligand-Substitution Reactions in Oxovanadium(IV) Glycine Complexes

Reaction	Rate constant/s^{-1}		ΔH^*	ΔS^*
	20 °C	25 °C	kJ mol^{-1}	JK^{-1} mol^{-1}
$[VO(gly)_2]+ox^2 \longrightarrow [VO(ox)_2]^{2-}$				
k_1	7.67	11.3	51.2	−55
k_2	16.7	29.7	—	—
Acid decomposition of $[VO(gly)_2]$				
$k_{d(1)}$	7.47	—	—	—
$k_{d(2)}$	14.3	—	—	—
Ring closure of $[VO\text{-}gly]^+$	—	35	57.1	−24
Ring opening of $[VO(gly)]^+$	—	19	—	—

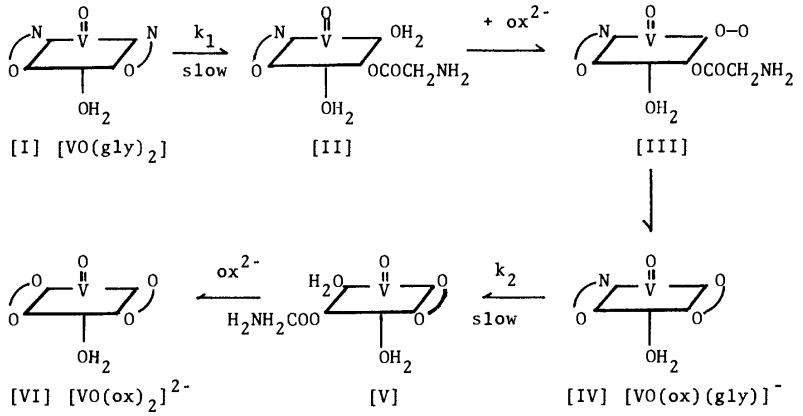

Fig. 3. Proposed reaction mechanism.

The values of rate constants k_6 and k_{-6} for the closing and opening of glycinate chelate ring, respectively, are listed with those of activation parameters in Table 2. The fact that the k_{-6} value (19 s^{-1} at 25 °C) is comparable to k_1 and k_2 values may support the proposed mechanism in Fig. 3.

In Table 1, the values of k_2 are nearly double the k_1 values under various conditions indicating that the amino group of glycine is more labile in $[VO(gly)(ox)]^-$ than in $[VO(gly)_2]$. This result can be accounted for by assuming that the oxalate at the basal positions in $[VO(gly)(ox)]^-$ has much stronger affinity for VO^{2+} than does glycinate and contributes to weakening the V-gly bond on the opposite side.

A mechanism in which the reaction is initiated by the rupture of V-N bonds at the basal positions can be ruled out because only $[VO\text{-}OCOCH_2NH_2]^+$ and $[VO\text{-}OCOCH_2NH_3]^{2+}$ complex ions have been known to be stable when glycine coordinates to the oxovanadium(IV) ion as a unidentate ligand.[13,14]

It may be concluded that there is little doubt of the mechanism in Fig. 3. However, it should be noted that this conclusion does not necessarily mean the dissociative mechanism. In oxovanadium(IV) ions water is a good ligand and said to be quite labile at the basal positions. The rate constant of water exchange was, in fact, reported to be 500 s^{-1} in $[VO(H_2O)_5]^{2+}$,[1,2] which is ten times larger in comparison with the time scale of the present study, and accordingly a water molecule might assist to initiate the ring opening.

References

1) J. Reuben and D. Fiat, *Inorg. Chem.*, **6**, 579 (1967).
2) K. Wüthrich and R. E. Connick, *Inorg. Chem.*, **6**, 583 (1967).
3) K. Wüthrich and R. E. Connick, *Inorg. Chem.*, **7**, 1377 (1968).
4) H. Tomiyasu, K. Dryer, and G. Gordon, *Inorg. Chem.*, **11**, 2409 (1972).
5) H. Tomiyasu, S. Itoh, and S. Tagami, *Bull. Chem. Soc. Jpn.*, **47**, 2843 (1974).
6) H. Tomiyasu and G. Gordon, *Inorg. Chem.*, **15**, 870 (1976).
7) O. Yokoyama, H. Tomiyasu, and G. Gordon, *Inorg. Chem.*, **21**, 1136 (1982).
8) M. Harada, Y. Ikeda, H. Tomiyasu, and H. Fukutomi, *Chem. Lett.*, **1984**, 1195.
9) M. Nishizawa and K. Saito, *Inorg. Chem.*, **17**, 3676 (1978).
10) M. Nishizawa and K. Saito, *Bull. Chem. Soc. Jpn.*, **51**, 483 (1978).
11) N. S. Angerman and R. B. Jordan, *Inorg. Chem.*, **8**, 65 (1969).
12) R. B. Jordan and N. S. Angerman, *J. Chem. Phys.*, **48**, 3983 (1968).
13) C. R. Johnson and R. E. Shepherd, *Bioinorg. Chem.*, **1**, 1 (1978).
14) H. Tomiyasu and G. Gordon, *J. Coord. Chem.*, **3**, 47 (1973).
15) J. H. Espenson, "Chemical Kinetics and Mechanisms," McGraw-Hill, New York (1981).

 © 1986 The Chemical Society of Japan Bull. Chem. Soc. Jpn., 59, 617—620 (1986)

Paramagnetic Cobalt(III) Complexes with Organic Ligands. IX.[1] The Preparation and Properties of Paramagnetic Tetraammine(5-nitrosalicylideneaminato)cobalt(III) Complexes

Yoshihisa YAMAMOTO* and Eiko TOYOTA
Faculty of Pharmaceutical Sciences, Higashi Nippon Gakuen University, Ishikari-Tobetsu, Hokkaido 061-02
(Received August 9, 1985)

The title paramagnetic cobalt(III) complexes, [Co(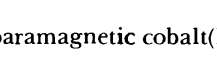)$(NH_3)_4$]X_3,(X_3: $Cl_2 \cdot NO_3$, $(NO_3)_3$), both green color, have been isolated and characterized by analytical, spectroscopic and magnetic methods. The effective magnetic moments are 1.7 BM, suggesting an unpaired spin. The ^1H NMR spectra indicate that the unpaired spin on the complexes is localized over the π-orbitals of the chelated ligand. In the XPS, the high binding energy area at 286—289 eV of the C 1s peak of both the complexe is larger than that for the corresponding diamagnetic cobalt(III) complex. The cobalt 2p peaks do not have satellites in the same manner as the usual diamagnetic cobalt(III) complexes. It can be concluded that an unpaired spin on complexes is not located on the cobalt atom, but is located over the π-orbitals of the chelated ligand of complexes.

Previously, we have been concerned with the preparation and properties of several green paramagnetic amine(5-nitrosalicylato)cobalt(III) complexes, [Co(5-NO_2sal)L]$^{2+}$ (L: $(NH_3)_4$,[2] en_2,[3] $(bpy)_2$,[4] quadridentate amine[4,5]). Their effective magnetic moments are 1.7—1.9 BM, suggesting an unpaired spin. Until now, the organic ligand in paramagnetic cobalt(III) complexes has been a 5-nitrosalicylato ligand. Therefore, very little is known regarding the isolation and physical properties of paramagnetic cobalt(III) complexes, in contrast to the information on diamagnetic cobalt(III) complexes with various organic ligands.[6—17] The isolation of a new paramagnetic cobalt(III) complex was tried with another organic ligand. As a result, a new paramagnetic cobalt(III) complex has been isolated with a 5-nitrosalicylideneaminato ligand, [Co(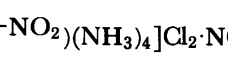)$(NH_3)_4$]$Cl_2 \cdot NO_3$. This paper deals with the preparation and properties of the paramagnetic cobalt(III) complex and with the electronic state of the unpaired spin.

Experimental

Measurements. The NMR spectra were recorded with an FX-60 apparatus (JEOL) for ^{13}C NMR and with an R-40 apparatus (Hitachi) or Varian XL-200 NMR spectrometer for ^1H NMR. The IR spectra were recorded on potassium bromide disks with an IR-27G apparatus (Shimadzu). The visible absorption spectra were recorded with a Shimadzu MPS-5000 recording spectrophotometer. The magnetic susceptibilities were measured by the Faraday's method using a magnetic balance (Shimadzu) between liq. N_2 and room temperature. The electric conductivities of aqueous solutions were determined by the use of a Shimadzu CM-30 conductometer at room temperature. For the XPS measurements, samples were placed on a gold mesh holder and dispersed with acetone. After evacuating to a vacuum better than 7×10^{-7} Pa(5×10^{-9} Torr), samples were cooled to 200 K and irradiated with Mg $K\alpha$ X rays (120 W). The instrument used was a VG ESCA 3-electron spectrometer. Analyzer energy was set so as to give the half width at half maximum [FWHM] of an Au $4f_{7/2}$ peak of 1.18 eV. The peak separation of N 1s or C 1s spectra was achieved using the Gauss-Newton least-squares method, where a mixed Gaussian-Lorentzian curve shape having a fixed FWHM was utilized. The binding energies of the electrons were calibrated by assigning 285.0 eV to the C 1s peak of the normal benzene-ring carbon.

Preparation of Complexes. Pramagnetic Tetraammine(5-nitrosalicylideneaminato)cobalt(III) Dichloride Nitrate (1a): Three cm^3 of 60% nitric acid were added to tetraammine(salicylideneaminato)cobalt(III) chloride hydrate (**2a**)[16] (2.0 g, 5.95 mmol) of russet color. The color of the complex changed to green. Further, 3 cm^3 of 60% nitric acid was added to the solution and stirred. The solution was filtered using a glass filter (G-4) and the filtrate was added to acetone. The precipitated green complex was filtered, washed with acetone, and dried. The obtained complex was dissolved in 3 cm^3 of 60% nitric acid, the solution was filtrated and the filtrate was added to acetone. A precipitated green complex was filtered, washed with acetone and dried. This process was repeated again. From an orange colored filtrate, the corresponding orange diamagnetic complexes **3** and **5** (see below) were isolated. Yield: 0.85 g (33.6%). Found: C, 19.55; H, 4.24; N, 22.62; Cl, 16.68%. Calcd for $CoC_7H_{17}N_7O_6Cl_2$ (MW 425.10) C, 19.78; H, 4.03; N, 23.06; Cl, 16.68%. Absorption spectrum: 363 nm (ε=5050), 450 nm (ε=2830), and 663 nm (ε=10060) in 60% nitric acid. IR spectrum: 1630 cm^{-1} ($C{=}N_{str.}$) and 830 cm^{-1} ($\rho_r(NH_3)_r$). Λ=371 S cm^2 $equiv^{-1}$ in water.

Paramagnetic Tetraammine(5-nitrosalicylideneaminato)cobalt(III) Trinitrate (1b): This complex was prepared from a reaction mixture of 60% nitric acid (6 cm^3) and tetraammine(salicylideneaminato)cobalt(III) nitrate (**2b**)[16] (2.0 g, 5.39 mmol) with the preparation method of **1a**. Yield: 0.93 g (36.1%). Found: C, 17.13; H, 3.85; N, 25.84%. Calcd for $CoC_7H_{17}N_9O_{12}$ (MW 478.21) C, 17.58; H, 3.58; N, 26.36%. Absorption spectrum: 360 nm (ε=4960), 455 nm (ε=3330) and 667 nm (ε=11000) in 60% nitric acid. IR spectrum: 1630 cm^{-1} ($C{=}N_{str.}$) and 830 cm^{-1} ($\rho_r(NH_3)_r$). Λ=363 S cm^2 $equiv^{-1}$ in water.

Tetraammine(5-nitrosalicylideneaminato)cobalt(III) Dinitrate (3): The orange colored acetone filtrate of **1a** or **1b** was concentrated. After 10 h, a precipitated orange complex was filtered and recrystallized from water. Yield: 0.32 g (12.9%).

Found: C, 19.80; H, 3.76; N, 26.70%. Calcd for $CoC_7H_{17}N_8O_9$ (MW 416.20) C, 20.20; H, 4.12; N, 26.92%. Absorption spectrum: 363 nm (ε=12600) and 480 nm (ε=210) in water. IR spectrum: 1635 cm^{-1} ($C{=}N_{str.}$) and 830 cm^{-1} ($\rho_r(NH_3)_r$). Λ= 226 S cm^2 $equiv^{-1}$ in water.

Tetraammine(3,5-dinitrosalicylideneaminato)cobalt(III) Dinitrate (5): The orange colored acetone filtrate of **1a** or **1b** was permitted to stand for at least 3 d, then, the solution was concentrated. Thus, precipitated complex **5** was filtered and recrystallized from water. Yield: 0.44 g (16.0%). Found: C, 18.59; H, 3.94; N, 26.78%. Calcd for $CoC_7H_{16}N_9O_{11}$ (MW 461.20) C, 18.23; H, 3.50; N, 27.33%. Absorption spectrum: 357 nm (ε=11900) and 480 nm (ε=210) in water. IR spectrum: 1635 cm^{-1} ($C{=}N_{str.}$) and 830 cm^{-1} ($\rho_r(NH_3)_r$). Λ=250 S cm^2 $equiv^{-1}$ in water. ^1H NMR spectrum δ=3.04 (s, 3H), 3.19 (s, 3H), 3.32 (s, 3H), 3.98 (s, 3H) for NH_3; δ=8.29 (d, 1H) for H_4, δ=8.44 (t, 1H) for H_6, δ=8.82 (dd, 1H) for CH=N and δ=10.58 (d, 1H) for C=NH in 1.8 mol dm^{-3} D_2SO_4 solution. The H_3 and H_5 proton signals disappeared by nitration at room temperature.

Solubility. Complexes **1a—b** are soluble in water, 60% nitric acid, DMSO, DMF, and 35% hydrochloric acid, and slightly soluble in methanol but insoluble in the common organic solvents. Complexes **3** and **5** are soluble in water, DMSO, DMF, and insoluble in the common organic solvents. Complex **3** is soluble in 60% nitric acid and 35% hydrochloric acid, but **5** is slightly soluble in 60% nitric acid and 35% hydrochloric aicd.

Results and Discussion

Paramagnetic tetraammine(5-nitrosalicylideneaminato)cobalt(III) complexes, $[Co(HN{=}HC\text{-}C_6H_3(NO_2)\text{-}O)(NH_3)_4]X_3$ (X_3:$Cl_2\cdot NO_3$ (**1a**) and $(NO_3)_3$ (**1b**)), have been isolated from reaction mixtures of diamagnetic tetraammine(salicylideneaminato)cobalt(III) complexes, $[Co(HN{=}HC\text{-}C_6H_4\text{-}O)(NH_3)_4]X_2\cdot nH_2O$ (X=Cl, n=1 (**2a**); X=NO_3, n=0 (**2b**)), 60% nitric acid and acetone. The electric conductivity in an aqueous solution was ca. 360 S cm^2 $equiv^{-1}$. The elemental analysis are in agreement with the theoretical values. The magnetic susceptibility obeyed the Curie-Weiss law with effective magnetic moments of 1.7 BM, suggesting the presence of one unpaired spin. The formula conforms to the quadrivalence of cobalt. The rocking frequency of ligand ammonia, however, was observed at 830 cm^{-1} in the IR spectra. This is the range for Co(III) ammine complexes.[18-20] The absorption spectra showed a characteristic strong peak at about 660 nm. In the XPS (Table 1), the nitrogen 1s peaks were separated into four peaks at ca. 399.6 for NH=, at 400.6 for NH_3, at 405.8 for NO_2, and at 407.4 eV for NO_3. The C 1s peaks were separated into four peaks at ca. 285.0, 286.1, 287.1, and 288.5 eV as is shown in Fig. 1. The peak at 285.0 eV is assigned to normal benzene-ring carbon atoms[21] and hydrocarbon contamination. Three peaks in the 286—289 eV region with high binding energies have been assigned to electron-poor carbon atoms, relative to normal ring carbon atoms. The spin orbit separation of Co 2p was 15.0 eV. The ^1H NMR spectra were measured in a 1.8 mol dm^{-3} D_2SO_4 solu-

Table 1. XPS and Magnetic Moments of Complexes

	XPS (eV) at 200 K						Magnetic moments	Curie-Weiss constants
	Co $2P_{3/2}$	Co $2p_{2/1}$	splitting	C 1s	N 1s	O 1s	μ_{eff}/BM	θ/K
1a	782.5	797.5	15.0	285.0(55)	399.6(1) =NH	532.4	1.7	+19
	FWHM 3.0			286.1(28)	400.6(4) NH_3			
	satellites no			287.1(11)	405.8(1) NO_2			
				288.5(6)	407.4(1) NO_3			
				FWHM 2.10	FWHM 2.25			
1b	782.6	797.5	15.1	285.0(51)	399.6(1) =NH	532.6	1.7	+20
	FWHM 2.4			286.5(29)	400.5(4) NH_3			
	satellites no			287.2(13)	405.9(1) NO_2			
				288.4(7)	407.1(3) NO_3			
				FWHM 1.82	FWHM 1.90			
3	782.2	797.1	15.1	285.0(61)	399.3(1) =NH	532.5	dia.	—
	FWHM 2.6			286.4(31)	400.3(4) NH_3			
	satellites no			288.4(8)	405.6(1) NO_2			
				FWHM 2.10	407.1(2) NO_3			
					FWHM 2.13			
4[a]	781.9	796.8	14.9	285.0(75)	399.9(4) NH_3	532.0	1.9	0
	FWHM 2.6			286.8(15)	405.3(1) NO_2			
	medium satellites			288.8(10)	406.6(1) NO_3			
				FWHM 1.82	FWHM 2.10			

a): Ref. 2 and 21. The values of XPS are slightly different from those reported previously,[21] as the data analysis has been carried out more precisely by using a computer and a different reference peak (cf. Experimental section).

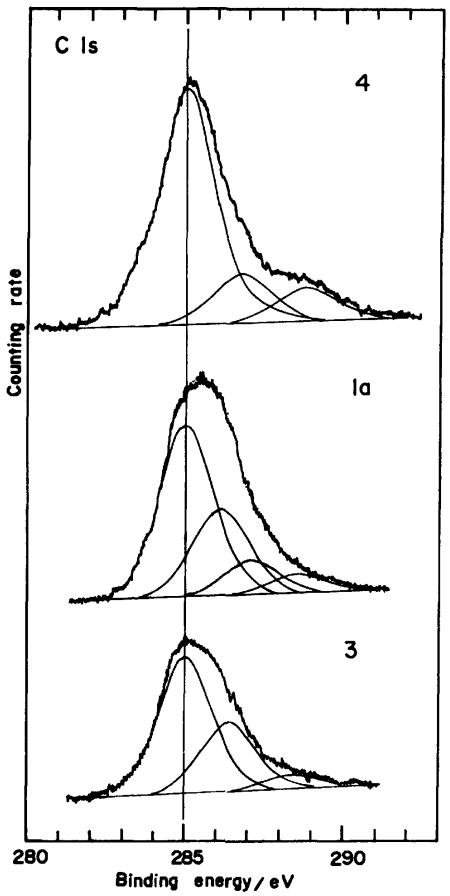

Fig. 1. The XPS in the C 1s region at 220 K of **1a**, **3**, and **4** complexes.

4 : $[Co(^{OOC}_{O}\langle\rangle\text{-}NO_2)(NH_3)_4]Cl\cdot NO_3\cdot H_2O$

1a : $[Co(^{HN=HC}_{O}\langle\rangle\text{-}NO_2)(NH_3)_4]Cl_2\cdot NO_3$

3 : $[Co(^{HN=HC}_{O}\langle\rangle\text{-}NO_2)(NH_3)_4](NO_3)_2$

tion but the ^{13}CNMR spectra did not show the expected signals due to of paramagnetism.

In the XPS results for **1a**, the peak of the high binding energy area of C 1s is larger than that of the corresponding orange diamagnetic cobalt(III) complex, $[Co(^{HN=HC}_{O}\langle\rangle\text{-}NO_2)(NH_3)_4](NO_3)_2$ (**3**) as is shown in Fig. 1. The peak area of the high binding energy region for **1a** is larger than that for the green paramagnetic tetraammine(5-nitrosalicylato)cobalt(III) complex,[21] $[Co(5\text{-}NO_2sal)(NH_3)_4]X_2$ (**4**). The total intensity ratio (carbon/nitrogen) between seven carbons and five nitrogens (NH_3+NH) is 1.47 for **1a** and 1.31 for **3**, and experimental scattering due to the contamination is about ±15%. The difference in the proportion between **1a** and **3**, however, is always clearly observed. Thus, the electronic state of the chelated ligand of **1a** is different from that of **3**. On the other hand, the Co $2p_{3/2}$ peak at 782.2 eV does not have satellites at 200 K. It is similar to that of diamagnetic cobalt(III) complexes[22,23] and paramagnetic cobalt(III) complexes, e.g., μ-amido-μ-hyperoxobis(ethylenediamine)cobalt(III) tetranitrate,[21] however, shows satellites at 200 K. Then, the unpaired spin on **1a** can be localized over the chelated ligand, but it can not be located on the cobalt atom.

In the ^{1}H NMR spectrum of **1a**, complex **1a** changed to **3** in 1.8 mol dm^{-3} D_2SO_4 solution at −20 °C,[1] the spectrum showing signals of both **1a** and **3**. An H_5 ring proton signal disappeared due to nitration. The signals at δ=7.28 (d), 7.90 (d), 8.20—8.46 (m) and 11.14 (d) were assigned to the H_3, H_4, H_6 and CH=N and C=NH protons, respectively. Their chemical shifts and coupling constants are very similar to those of **3** (Table 2). Thus, the σ-bonds which are formed from protons and carbon atoms (sp^2 configuration) of a chelated ligand resemble the σ-bond of **3**. The unpaired spin can not be located over the hydrogen of the chelated ligand.[1] Thus, an unpaired spin on **1a**

Table 2. ^{1}H NMR Spectra of Complexs **1a**, **2a**, and **3**

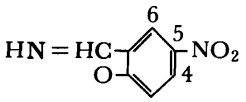

δ

Complex No.	H_3	H_4		H_5	H_6	CH=N	C=NH	NH_3 δ			Temp
	($^3J_{HCCH}$) Hz	($^3J_{HCCH}$) Hz	($^4J_{HCCCH}$) Hz	($^3J_{HCCH}$) Hz	($^4J_{HCCCH}$) Hz	($^3J_{HNCH}$) Hz					°C
1a	7.28 d (9.5)	7.90 d (9.5)	—	—	8.2—8.5 m	8.2—8.5 m	11.14 d	3.26(s)	3.50(s)	4.18(s)	−20
3	6.98 d (9.3)	7.94 dd (9.3)	(3.0)	—	8.30 d (3.0)	8.18 d (11.5)	10.47[a]	3.03(s, 3H)	3.15(s, 6H)	3.93(s, 3H)	+25
2a	7.00 d (8.5)	7.2—7.4 m		6.70 t (7.6)	7.2—7.4 m	8.05 d (11.5)	9.91[a]	3.01(s, 9H)		3.83(s, 3H)	+25

Solvent: 1.8 mol dm^{-3} D_2SO_4; Standard: internal DSS (δ=0). a): broad signal.

has been identified over the π-orbitals of the chelated ligand. Therefore, **1a** is a radical cobalt(III) complex;

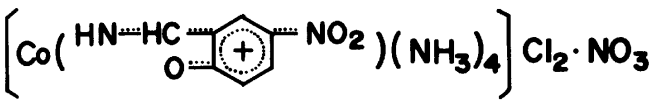

A clear distinction between **1a** and **4** was found regarding stability, the Curie-Weiss constant and the XPS of Co 2p. Complex **1a** is more unstable than **4** for ^{1}H NMR measurements. This might be due to a difference in the electronic state of the cobalt atom. The Curie-Weiss constant of **1a** indicates ferromagnetism and the Co 2p peak does not have any satellites.

The absorption spectra of **1a** and **4**[2] have characteristic strong peaks at about 660 nm ($\varepsilon \fallingdotseq 10000$). This strong peak was not observed for **2a** and **3**, the usual diamagnetic cobalt(III) complexes and paramagnetic μ-amido-μ-hyperoxo cobalt(III) complexes[24-26] ($\varepsilon \fallingdotseq 417$ at 687 nm) and the related complexes. Thus, the strong peak is due to the unpaired spin on the complex.

The results for **1b** are listed in Table 1. The results of orange diamagnetic tetraammine(3,5-dinitrosalicylideneaminato)cobalt(III) dinitrate, 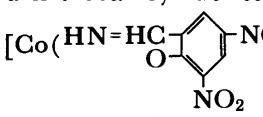 (**5**), are given in the experimental section.

The authors wish to express their gratitute to Dr. Hidetaka Konno of Hokkaido University for his discussion and XPS measurements.

References

1) Part VIII. Y. Yamamoto, S. Shimokawa, and E. Yamada, *Bull. Chem. Soc. Jpn.*, **57**, 1153 (1984).
2) Y. Yamamoto, K. Ito, H. Yoneda, and M. Mori, *Bull. Chem. Soc, Jpn.*, **40**, 2580 (1967).
3) Y. Yamamoto, M. Mori, H. Yoneda, S. Misumi, and K. Ito, *Bull. Chem. Soc. Jpn.*, **42**, 984 (1969).
4) Y. Yamamoto, E. Toyota, and N. Mitsudera, *Bull. Chem. Soc. Jpn.*, **53**, 3517 (1980).
5) Y. Yamamoto and H. Kudo, *Bull. Chem. Soc. Jpn.*, **57**, 287 (1984).
6) A. Ablov, *Bull. Soc. Chim. Fr.*, **53**, 234 (1933).
7) A. C. K. Poon and M. L. Tobe, *J. Chem. Soc., A*, 1968, 1549.
8) F. H. Burstall and R. S. Nyholm, *J. Chem. Soc.*, 1952, 3570.
9) A. Nakahara, *Bull. Chem. Soc. Jpn.*, **27**, 560 (1954).
10) B. Halpern, A. M. Sargeson, and K. R. Turnbull, *J. Am. Chem. Soc.*, **88**, 4630 (1966).
11) B. E. Douglas and S. Yamada, *Inorg. Chem.*, **4**, 1561 (1965).
12) L. J. Zompa, *Chem. Commun.*, 1969, 783.
13) S. Yamada, J. Hidaka, and B. E. Douglas, *Inorg. Chem*, **10**, 2187 (1971).
14) F. P. Dwyer, F. L. Garvan, *J. Am. Chem. Soc.*, **83**, 2610 (1961).
15) Y. Yamamoto and E. Toyota, *Bull. Chem. Soc. Jpn.*, **57**, 47 (1984).
16) Y. Yamamoto and E. Toyota, *Bull. Chem. Soc. Jpn.*, **57**, 2650 (1984).
17) Y. Yamamoto, E. Toyota, and S. Tsukuda, *Bull. Chem. Soc. Jpn.*, **58**, 1595 (1985).
18) G. F. Svatos, D. M. Sweeny, S. Mizushima, C. Curran, and J. V. Quagliano, *J. Am. Chem. Soc.*, **79**, 3313 (1957).
19) L. Sacconi, A. Sabatini, and P. Gans, *Inorg. Chem.*, **3**, 1772 (1964).
20) D. B. Powell and N. Sheppard, *J. Chem. Soc.*, **1956**, 3108.
21) Y. Yamamoto, M. Mori, and H. Konno, *Bull. Chem. Soc. Jpn.*, **54**, 1995 (1981).
22) D. C. Frost, C. A. Mcdowell, and I. S. Woolsey, *Molecular Physics*, **27**, 1473 (1974).
23) Y. Okamoto, H. Nakano, T. Imanaka, and S. Teranishi, *Bull. Chem. Soc. Jpn.*, **48**, 1163 (1975).
24) R. Davies and A. G. Sykes, *J. Chem. Soc., A*, **1968**, 2237.
25) R. Davies and A. G. Sykes, *J. Chem. Soc., A*, **1968**, 2831.
26) R. Davies, M. Mori, and A. G. Sykes, *Inorg. Syn.*, Vol. 12, 197.

 © 1986 The Chemical Society of Japan Bull. Chem. Soc. Jpn., 59, 621—626 (1986)

Solvent Effect on the Liquid-Liquid Partition Coefficients of Dimethyldithiocarbamic Acid and Its Copper(II) Chelate

Hisanori IMURA, Satoru MATSUMORA, and Nobuo SUZUKI*
Department of Chemistry, Faculty of Science, Tohoku University, Sendai 980
(Received August 16, 1985)

Partition coefficients of dimethyldithiocarbamic acid and its copper(II) chelate have been determined in various organic solvents –0.10 mol dm^{-3} aqueous perchlorate solution systems at 25 °C. The effects of inert organic solvents are explained with the aid of the regular solution theory. Also, a linear free-energy relationship between the partition coefficient of the copper(II) chelate and that of the reagent is demonstrated. The partition coefficient of the copper(II) chelate is compared with that of bis(2,4-pentanedionato)copper(II) and various factors governing the partition coefficients of these chelates are discussed with the aid of the scaled particle theory.

Dithiocarbamate derivatives are highly versatile chelating agents for the separation and determination of metals by solvent extraction, liquid chromatography, etc. In chelate extraction, the extractability of metal ions can be expressed by the partition coefficients of the reagent and the neutral metal chelate, the acid-dissociation constant of the reagent, and the stability constant of the chelate. The partition coefficients are strongly dependent on organic solvents and are the most important factors affecting the extractability of a metal ion. However, the partition for dithiocarbamate-group reagents and their metal chelates even for a diethyldithiocarbamate reagent which is most frequently used in extraction separation has been scarcely investigated. The effect of organic solvents has not been investigated at all.

In this research, the partition coefficients of dimethyldithiocarbamic acid(Hdmdtc), the most simple compound in the dithiocarbamate group, and its copper(II) chelate ($Cu(dmdtc)_2$) were determined in various organic solvent systems. Here, the relationship between the partition coefficient of the chelate and that of the reagent is theoretically explained. Such a relationship has been thoroughly studied regarding various β-diketone systems in this laboratory.[1-4] The solvent effect has been elucidated with the aid of the regular solution theory and the scaled particle theory. Some factors governing the partition coefficient of the metal chelate are discussed by comparing the partition coefficient of $Cu(dmdtc)_2$ with that of bis(2,4-pentanedionato)copper(II)($Cu(acac)_2$).[3]

Experimental

Reagents and Apparatus. Sodium dimethyldithiocarbamate dihydrate ($Nadmdtc \cdot 2H_2O$) was obtained from Tokyo Kasei Co., Ltd. and was purified by recrystallization from acetone-absolute ether. Bis(dimethyldithiocarbamato)copper(II) ($Cu(dmdtc)_2$) was obtained from Tokyo Kasei Co., Ltd. and purified by vacuum sublimation.

A carrier-free radioisotope, ^{67}Cu, was produced by a photonuclear reaction of $^{68}Zn(\gamma,p)^{67}Cu$. Radioactive copper(II) perchlorate solutions of the desired concentration were prepared as described in a previous paper.[3]

Organic solvents were purified by the usual chemical treatment and distillation. The ionic strength in the aqueous phase was adjusted to 0.10 M (1 M=1 mol dm^{-3}) by the use of sodium perchlorate. Other reagents and equipment were the same as those used previously.[3]

Measurements of Partition Coefficient (P_A) of Hdmdtc by a Kinetic Method. Dithiocarbamate group reagents have a strong tendency to decompose in acidic aqueous solutions. The partition coefficient of dimethyldithiocarbamic acid was determined by utilizing its decomposition reaction in the aqueous phase. The partition coefficient of Hdmdtc between carbon tetrachloride and 0.10—0.03 M perchloric acid solutions with an ionic strength of 0.10 was determined by measuring both the stripping rate of Hdmdtc from the organic to the aqueous phase and the decomposition rate in the aqueous phase. The organic solution of Hdmdtc was prepared by an extraction, as follows: A 1 cm^3 portion of a 0.06 M Nadmdtc aqueous solution was added to 9 cm^3 of 0.03 M perchloric acid and 10 cm^3 of carbon tetrachloride in a centrifuge tube with a ground-glass stopper. Immediately, the contents were shaken for 15 s and centrifuged for 30 s at 4000 rpm. The organic phase was taken out and diluted to about a 5×10^{-4} M Hdmdtc solution with carbon tetrachloride. This working solution of Hdmdtc was prepared just before the following kinetic stripping experiment. This Hdmdtc solution (5 cm^3) was vigorously shaken for various times between 10 and 150 s with an equal volume of 0.10 M or 0.03 M perchloric acid solution. The shaking speed was as high as 430 strokes per min in order to attain a rapid mass transfer of the organic-aqueous interface. Immediately after centrifuging for 30 s, the absorbance of Hdmdtc in the carbon tetrachloride phase was measured at 285 nm. The decomposition of Hdmdtc in the organic phase during the shaking within 150 s could be neglected. The stripping-rate constant of Hdmdtc was calculated from the absorbance measurement at various shaking time intervals.

The decomposition rate of Hdmdtc in an aqueous phase was separately measured by spectrophotometry. The decrease in absorbance at 270 nm was measured as a function of time after an injection of 0.01 cm^3 of a 0.06 M Nadmdtc aqueous solution into an optical cell containing 4 cm^3 of a 0.10 M or 0.03 M perchloric acid solution saturated with carbon tetrachloride. All experiments were carried out in a thermostated room at 25±1 °C.

Measurements of Distribution Ratio (D_A) of Hdmdtc. A 0.1 cm^3 portion of 0.1—0.4 M Nadmdtc in water was added to a centrifuge tube containig 5 cm^3 of an organic solvent, 1 cm^3 of 0.50 M sodium perchlorate, and 3.9 cm^3 of a 0.01

M phosphate buffer solution of pH 5.5—7.0. The contents were shaken for 30 s and centrifuged for 30 s. An aliquot of each phase was pipetted out. The aqueous phase was diluted with 0.1 M sodium hydroxide to about 100-fold and the absorbance was measured at 280 nm. In the alkali solution, dimethyldithiocarbamate was very stable and its molar absorption coefficient was 13800 $M^{-1}cm^{-1}$ at an absorption maximum of 280 nm due to the $dmdtc^-$ anion. To determine the Hdmdtc concentration distributed in the organic phase, the organic phase was shaken with an appropriate volume of a 0.1 M sodium hydroxide solution for 3 min. Dimethyldithiocarbamic acid was back-extracted into the alkaline aqueous solution and determined by measuring the absorbance at 280 nm. The distribution ratio of the dimethyldithiocarbamate was calculated from the concentration of each phase. The equilibrium pH value was measured with a glass electrode just after shaking.

Measurements of Partition Coefficient (P_M) of Cu(dmdtc)$_2$. A small portion (0.01 cm^3) of a 5×10^{-5}—5×10^{-2} M radioactive copper(II) solution was added to a 30 cm^3 centrifuge tube containing 5 cm^3 of an organic solvent and 5 cm^3 of a 1×10^{-4}—1×10^{-2} M Nadmdtc aqueous solution (pH 7—8). The contents were shaken for 15—60 min. After centrifuging, an aliquot (0.1—3 cm^3) was very carefully taken from each phase. The γ-activities of each phase were measured with a well-type NaI(Tl) scintillation counter and the partition coefficient of the copper(II) chelate was calculated. The equilibrium pH value was measured with a glass electrode.

A back extraction was performed as follows. An organic phase containing the radioactive copper(II) chelate which was prepared in the forward extraction (as just mentioned above) was shaken with the aqueous phase containing Nadmdtc at pH 7—8. The P_M value was determined by the same manner as that for the forward extraction.

Results

Partition Coefficient of Hdmdtc. Since dimethyldithiocarbamic acid very rapidly decomposes in an acidic aqueous solution, the partition coefficient was determined using the decomposition reation (decomposition rate) of Hdmdtc. When different organic solutions containing Hdmdtc were shaken with the aqueous solutions at pH 1—2, their concentrations in the organic phase decreased with an increase in the shaking time. This decrease was faster in accordance to the following order for organic solvents; benzene< carbon tetrachloride<heptane. This phenomenon seems to be due to the following reactions,

$$Hdmdtc_{org} \rightleftharpoons Hdmdtc \quad (1)$$

$$Hdmdtc \longrightarrow (CH_3)_2NH + CS_2, \quad (2)$$

where the subscript org denotes the species in the organic phase. The equilibrium constant for Eq. 1 corresponds to the partition coefficient of Hdmdtc and the rate constant for Eq. 2 is the decomposition-rate constant (k_d) in the aqueous phase. The decomposition rate of the aqueous phase in a sufficiently low pH region can be written as follows:[5,6]

$$-\frac{d[Hdmdtc]}{dt} = k_d[Hdmdtc]. \quad (3)$$

On the other hand, the decrease in the Hdmdtc concentration in the organic phase upon shaking is given by

$$-\frac{d[Hdmdtc]_{org}}{dt} = k_{st}[Hdmdtc]_{org}, \quad (4)$$

where k_{st} is the stripping-rate constant. From Eqs. 3 and 4, the following relation is obtained,

$$P_A = \frac{k_d}{k_{st}} - 1. \quad (5)$$

Respective first-order plots of Eqs. 3 and 4 gave good linear relationships from which the rate constants, k_d and k_{st}, were determined. The results for the carbon tetrachloride-perchloric acid system are shown in Table 1. The P_A values obtained at different perchloric acid concentrations are consistent within experimental error.

Table 1. Rate Constants for Stripping (k_{st}) and Decomposition (k_d) and Partition Coefficient (P_A) of Dimethyldithiocarbamic Acid in the Carbon Tetrachloride System at 25 °C

$[H^+]$	k_{st}	k_d [b]	P_A [c]
M	$10^{-3}s^{-1}$	$10^{-2}s^{-1}$	
0.10	4.62	6.42±0.22	12.9±0.5
0.030 [a]	3.85	5.49±0.14	13.3±0.4
0.030 [a]	3.78	5.49±0.14	13.5±0.4

Average value of P_A: 13.2±0.4.
a) I=0.10 by $NaClO_4$. b) Result for three measurements. c) Calculated from $P_A=k_d/k_{st}-1$.

The distribution ratio of dimethyldithiocarbamate is expressed by

$$D_A = \frac{[Hdmdtc]_{org}}{[Hdmdtc] + [dmdtc^-]}. \quad (6)$$

This can be written using P_A and the acid-dissociation constant, K_a,

$$D_A = \frac{P_A}{1 + K_a/[H^+]}. \quad (7)$$

If $[H^+]$ is much smaller than K_a,

$$D_A = \frac{P_A[H^+]}{K_a}. \quad (8)$$

Figure 1 shows plots of log D_A vs. pH for various organic solvent systems. Each plot is close to a straight line with a slope of −1; thus, Eq. 8 was found to hold in the pH regions as expected from the pK_a value of

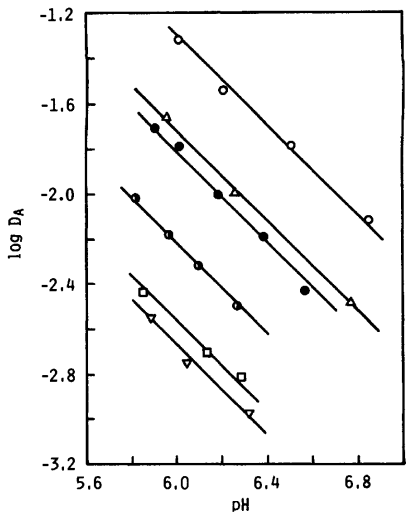

Fig. 1. Distribution ratio of dimethyldithiocarbamate as a function of pH in various organic solvent systems.
○: Benzene, △: isopropylbenzene, ●: carbon tetrachloride, ◑: dibutyl ether, □: heptane, ▽: hexane.

Hdmdtc shown below. The pK_a value of Hdmdtc can be obtained using the P_A value determined for the carbon tetrachloride system (Table 1). The value was determined to be 3.05±0.06 (the activity of hydrogen ions was used in place of the concentration in Eq. 8). This is in agreement with a value of 3.21 for an ionic strength of 0.01.[6] The partition coefficients of Hdmdtc in organic solvent systems other than carbon tetrachloride can be readily determined from Eq. 8 using the K_a value. These date are listed in Table 4.

Partition Coefficient of Cu(dmdtc)$_2$. The distribution ratio of copper(II) is expressed by

$$D_M = \frac{[Cu(dmdtc)_2]_{org}}{[Cu^{2+}] + [Cu(dmdtc)^+] + [Cu(dmdtc)_2] + \cdots} \quad (9)$$

and can be written using the partition coefficient of Cu(dmdtc)$_2$ and the overall stability constant (β_n) in the aqueous phase,

$$D_M = \frac{P_M\beta_2[dmdtc^-]^2}{1 + \beta_1[dmdtc^-] + \beta_2[dmdtc^-]^2 + \cdots}. \quad (10)$$

If the dimethyldithiocarbamate concentration in the aqueous phase is sufficiently high and the formation of such anionic complexes as $Cu(dmdtc)_3^-$ is negligible, the D_M values become independent of the ligand concentration and are consistent with P_M. To confirm this, P_M was determined at different ligand concentrations (Table 2). The obtained P_M values are thought to be constant within the experimental error when the ligand concentrations are altered by two orders of magnitude. The values obtained by forward extraction of copper(II) are in good agreement with those obtained by back extraction. This result demonstrates the complete attainment of the partition equilibrium of the copper(II) chelate.

Table 2. Partition Coefficient of Cu(dmdtc)$_2$ at Different Dimethyldithiocarbamate Concentration in the Heptane System at 25 °C

[dmdtc$^-$]/M	pH	log P_M
2.0×10^{-4}	6.37	2.238
2.0×10^{-4}	6.00	2.236[a]
2.0×10^{-3}	7.18	2.223
2.0×10^{-3}	6.09	2.217[a]
1.0×10^{-2}	7.65	2.196
1.0×10^{-2}	7.61	2.201[a]
2.0×10^{-2}	7.71	2.210

Concentration of copper(II): 1.0×10^{-7} M.
a) Obtained from back extraction.

Table 3. Partition Coefficient of Cu(dmdtc)$_2$ at Different Copper(II) Concentrations in the Carbon Tetrachloride System at 25 °C

[Cu(II)]/M	log P_M
5.0×10^{-7}	3.687
5.0×10^{-7}	3.736[a]
5.0×10^{-7}	3.669[a]
5.0×10^{-7}	3.787[a]
1.2×10^{-5}	3.690
1.2×10^{-5}	3.688[a]
1.2×10^{-5}	3.781[a]
1.2×10^{-5}	3.788[a]

Concentration of dmdtc$^-$: 1.0×10^{-2} M.
a) Obtained from back extraction.

The P_M value was measured at different copper(II) concentrations to ascertain the absence of a polymerized species of the chelate in the organic and aqueous phases. The results for the carbon tetrachloride system are shown in Table 3. A constant P_M was obtained within the experimental error when the copper(II) concentration was altered by more than an order of magnitude. The P_M values of Cu(dmdtc)$_2$ in various organic solvent systems are summarized in Table 4.

The partition coefficients of Cu(dmdtc)$_2$ were larger than those of Hdmdtc in all the solvents and the order of the solvents for each solute was the same, i.e., benzene>isopropylbenzene>carbon tetrachloride>dibutyl ether>heptane≈hexane.

Discussion

The partition coefficient of a molar fraction scale can be written using a modified equation based on the regular solution theory,[3]

$$\ln P_2^\circ = \frac{V_2}{RT}[C_{ww} - C_{oo} + 2(C_{o2} - C_{w2}')], \quad (11)$$

where V and C are the molar volume and the cohesive energy density, respectively. The subscripts (2, w, and o) denote the solute, water, and organic solvent, respectively. The parameter C_{w2}' expresses the interac-

Table 4. Partition Coefficients of Hdmdtc (P_A) and Its Copper(II) Chelate (P_M) at 25 °C

No.	Organic solvent	δ[b] / cal$^{1/2}$ cm$^{-3/2}$	μ[c] / D	log P_A	log P_M
1	Hexane	7.27	0	0.28±0.05	2.23±0.04
2	Heptane	7.43	0	0.38±0.04	2.21±0.02
3	Carbon tetrachloride	8.58	0	1.12±0.01	3.71±0.05
4	Isopropylbenzene	8.53	0.39	1.22±0.03	4.31±0.03
5	Benzene	9.16	0	1.65±0.04	4.57[a]
6	Dibutyl ether	7.62	1.18	0.73±0.02	3.42±0.02

a) Average of two measurements. b) Solubility parameter calculated from heat of vaporization at 25 °C.[18] c) Dipole moment (1D=3.333×10^{-30} Cm).

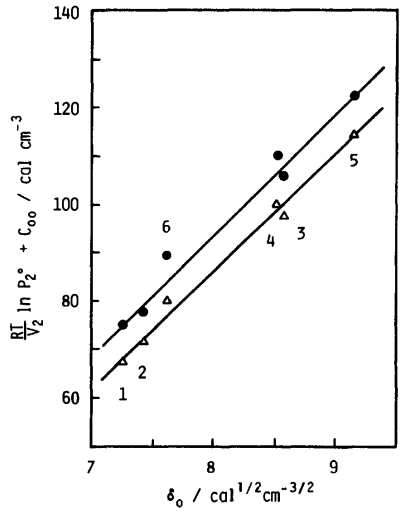

Fig. 2. Evaluation of the partition coefficients based on the regular solution theory. The numbers correspond to those in Table 4.
△: Hdmdtc, ●: Cu(dmdtc)$_2$.

tion between the solute and water involving a specific interaction such as hydrogen and coordination bonding. If a geometric mean approximation for C_{o2} with the solubility parameters, δ, is valid, Eq. 11 can be rewritten as follows,

$$\frac{RT}{V_2}\ln P_2^\circ + C_{oo} = 2\delta_2\delta_o + C_{ww} - 2C_{w2}'. \quad (12)$$

A linear relationship between the left hand side of Eq. 12 and δ_o is expected. An apparent solubility parameter of the solute(δ_2) and the interaction term with water ($C_{ww}-2C_{w2}'$) can be obtained from the slope and the intercept, respectively. Figure 2 shows plots for Hdmdtc and its copper(II) chelate, where their molar volumes were estimated as follows. The van der Waals volume[7] of Hdmdtc can be calculated to be 62.81 cm^3 mol^{-1} and is very close to that of enol of 2,4-pentanedione(acetylacetone, Hacac), 60.14 cm^3 mol^{-1}. Assuming that the ratio of the van der Waals volume to the molar volume of each chelating agent is the same in Hacac (the molar volume; 101.59 cm^3 mol^{-1}[18]) and Hdmdtc, the molar volume of Hdmdtc (106 cm^3 mol^{-1}) is obtained. The molar volume of Cu(dmdtc)$_2$ was estimated to be 190 cm^3 mol^{-1} using the relation between the molar volume of acetylacetone and that of its copper(II) chelate.[2] In the plots of Hdmdtc and its copper(II) chelate, good linear relationships are found for non-polar organic solvents, except for dibutyl ether (Fig. 2). It seems that the organic solutions of these solutes can be taken as apparently regular solutions and that the solvent effects can be interpreted according to Eq. 12. The apparent solubility parameters of Hdmdtc and Cu(dmdtc)$_2$ were calculated to be 12.2 and 12.7 cal$^{1/2}$cm$^{-3/2}$ (conversion factor: 1 cal$^{1/2}$cm$^{-3/2}$=2.0455 J$^{1/2}$cm$^{-3/2}$) respectively from the slope of the plots as described above. Since these values were obtained using a limited number of solvents (i.e., hexane and heptane in alkanes, carbon tetrachloride of haloalkanes and benzene and isopropylbenzene of phenyl compounds), it is difficult to precisely determine their magnitudes. However, the value for Cu(dmdtc)$_2$ is larger than those for copper(II) β-diketonates such as acetylacetonate (11.6 cal$^{1/2}$cm$^{-3/2}$), 1,1,1-trifluoro-2,4-pentanedionate (11.2 cal$^{1/2}$cm$^{-3/2}$), and 1-(2-thienyl)-4,4,4-trifluoro-1,3-butanedionate (11.0 cal$^{1/2}$cm$^{-3/2}$), which were determined by means of a similar technique.[4] This suggests a somewhat high polarity of the former. Metal dithiocarbamate chelates have lone-pair electrons at nitrogen atoms which are readily released from nitrogen to sulfur atoms.[9-12] This seems to be responsible for the polarity of the dimethyldithiocarbamate molecule and may cause interactions with a solvent having a large dipole moment, such as dibutyl ether. Hence, it follows that a positive deviation for dibutyl ether for Eq. 12 can be observed from Fig. 2.

The parameter, $C_{ww}-2C_{w2}'$, of Cu(dmdtc)$_2$, which indicates the interaction between the solute and water, is the same as that of the reagent, i.e., −110 cal cm^{-3} (convergion factor: 1 cal cm^{-3}=4.184 J cm^{-3}) was obtained from the plots for Eq. 12 (Fig. 2). This result means that Cu(dmdtc)$_2$ has no specific interaction with water (such as coordination bonding to the central metal) and is remarkably different from that in the acetylacetonate system.[3] In fact, the absorption spectrum of the dimethyldithiocarbamate chelate in donor solvents such as dibutyl ether and acetone was almost the same as that in carbon tetrachloride and benzene (the absorption peak was at 435 nm in

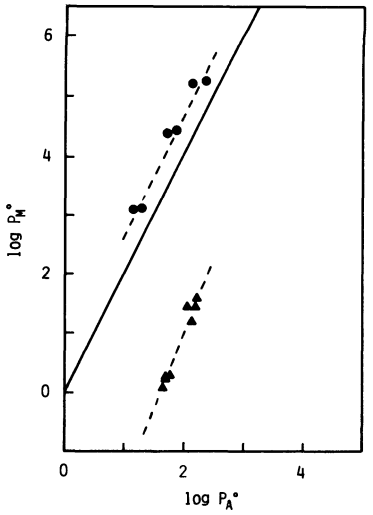

Fig. 3. Relationship between the partition coefficients of the copper(II) chelate and the reagent. ●: $Cu(dmdtc)_2$, ▲: $Cu(acac)_2$.[3]

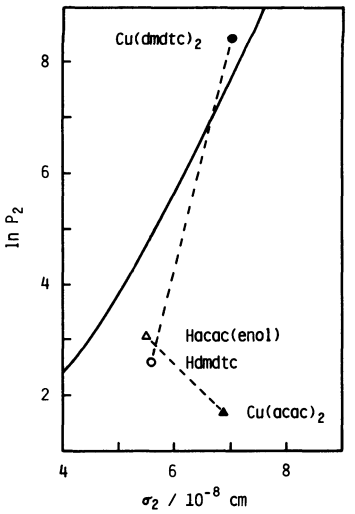

Fig. 4. Comparison of the partition coefficients of dimethyldithiocarbamates and acetylacetonates[3] with those of cavity calculated by the scaled particle theory in the carbon tetrachloride system. Solid line shows the calculated value of $(\bar{G}_{c,w}-\bar{G}_{c,o})/RT$.

these solvents) and the change in the absorption spectrum of the acetylacetonate chelate in dibutyl ether and water was observed.[3]

Since Eq. 12 holds for a chelate and a reagent, the following relation can be derived,

$$\log P_M^\circ = \frac{V_M}{V_A}\log P_A^\circ + \frac{2V_M}{2.30RT}(\delta_M-\delta_A)\delta_o + \frac{2V_M}{2.30RT}(C_{wA}'-C_{wM}'). \quad (13)$$

If the difference between δ_M and δ_A as well as between C_{wM}' and C_{wA}' is small, that is, solute-solvent interactions for the chelate are similar to those for the reagent, a plot of log P_M° vs. log P_A° is expected to be a straight line with a slope of two (V_M/V_A is approximately equal two) passing through the origin. Figure 3 shows plots for $Cu(dmdtc)_2$ together with those for $Cu(acac)_2$.[3,4] The plots of $Cu(dmdtc)_2$ are close to a straight line as expected from the preceding discussion; however, those of $Cu(acac)_2$ are in a much lower region. This suggests that the specific solute-water interactions are weak for the dimethyldithiocarbamate chelate but remarkably strong for the acetylacetonate chelate.

As described in a previous paper,[4] it is difficult to discuss the strict physical meaning of the solute-water interaction parameter based on the simple regular-solution concept, but it is worth evaluating a solute-water interaction with the aid of the scaled particle theory(SPT), which is applicable to an aqueous solution without any adjustable parameters.

The partition coefficient can be written using the Gibbs free energy for the cavity formation($\bar{G}_c$) and for an interaction ($\bar{G}_i$) in the organic and aqueous phases,[2,13]

$$\ln P_2 = \frac{\bar{G}_{c,w}-\bar{G}_{c,o}}{RT} + \frac{\bar{G}_{i,w}-\bar{G}_{i,o}}{RT}. \quad (14)$$

The cavity-formation energy can be calculated using the SPT;[14]

$$\bar{G}_c = -RT\ln(1-y) + RT\frac{3y}{1-y}\left(\frac{\sigma_2}{\sigma_1}\right) + RT\left[\frac{3y}{1-y}+\frac{9}{2}\left(\frac{y}{1-y}\right)^2\right]\left(\frac{\sigma_2}{\sigma_1}\right)^2 + \frac{N_A yp}{\rho}\left(\frac{\sigma_2}{\sigma_1}\right)^3 \quad (15)$$

where σ_1 and σ_2 are the molecular diameters of the solvent and solute, N_A is Avogadro's number, p is the pressure, ρ is the number density of the solvent and y is the packing fraction ($y=\pi\rho\sigma_1^3/6$). The molecular diameter of the solute was estimated using an empirical correlation[4] between the molecular diameter of various compounds determined by the SPT[14,15] and their molar volumes. The values for Hdmdtc and $Cu(dmdtc)_2$ are 5.59×10^{-8} and 6.98×10^{-8} cm, respectively. Figure 4 shows the partition coefficients of Hdmdtc, Hacac(enol) and respective copper(II) chelates as a function of the molecular diameter. The solid line indicates the hypothetical partition coefficient of the cavity, which may be considered to be of a solute where $\bar{G}_{i,w}=\bar{G}_{i,o}$. The plots for Hdmdtc and Hacac are similar, but those of both the copper(II) chelates are significantly different. The partition coefficients of Hdmdtc and $Cu(dmdtc)_2$ lie close to a solid line calculated according to the SPT, compared with that of $Cu(acac)_2$. This means that the difference in the interaction energies for solute-carbon tetrachloride and solute-water is not so great for $Cu(dmdtc)_2$ and Hdmdtc. Consequently, the partition coefficient in this system is mainly governed by the difference between the cavity-formation energy in the organic and aqueous phases. On the other hand, the partition coefficient of

$Cu(acac)_2$ is remarkably lower than that of $Cu(dmdtc)_2$ as well as the cavity. This suggests that interactions of $Cu(acac)_2$ with water molecules are much stronger than that with organic solvent molecules.

Such differences regarding dimethyldithiocarbamate and the acetylacetonate chelate in solute-solvent interactions may be ascribed to the nature of their coordination bonds. The dimethyldithiocarbamate chelate involving sulfur donor atoms has a larger effect on ligand field stabilization than the acetylacetonate chelate involving oxygen donor atoms. Hence, the copper(II)-sulfur bonding is more covalent.[16,17] This results in a greater electron transfer from the ligand to the metal. Consequently, in the dimethyldithiocarbamate chelate the ability of the further coordination to the central metal with donor solvents and of the hydrogen bonding to the donor atoms of the ligand is much lower than that in the acetylacetonate chelate.

In conclusion, the partition coefficient of $Cu(dmdtc)_2$ was close to that calculated from the difference of the cavity-formation energy between the organic and the aqueous phase. The partition coefficients of the chelating agents, Hdmdtc and Hacac(enol), did not deviate much from that calculated from the cavity-formation energy. This suggests that specific interactions with water are weak for those solutes, especially for $Cu(dmdtc)_2$. On the other hand, the partition coefficient of $Cu(acac)_2$ was remarkably lower than that calculated from the cavity-formation energy. This suggests that the specific interactions between $Cu(acac)_2$ and water, such as coordination and hydrogen bonding,[3] are strong.

References

1) T. Omori, T. Wakahayashi, S. Oki, and N. Suzuki, *J. Inorg. Nucl. Chem.*, **26**, 2265 (1964).
2) H. Watarai, H. Oshima, and N. Suzuki, *Quant. Struct. Act. Relat.*, **3**, 17 (1984).
3) H. Imura and N. Suzuki, *J. Radioanal. Nucl. Chem.*, **88**, 63 (1985).
4) H. Imura and N. Suzuki, *Talanta*, **32**, 785 (1985).
5) S. J. Joris, K. I. Aspila, and C. L. Chakrabarti, *J. Phys. Chem.*, **74**, 860 (1970).
6) K. I. Aspila, C. L. Chakrabarti, and V. S. Sastri, *Anal. Chem.*, **45**, 363 (1973).
7) A. Bondi, *J. Phys. Chem.*, **68**, 441 (1964).
8) M. Inoue, Y. Arai, S. Saito, and N. Suzuki, *J. Chem. Eng. Data*, **26**, 287 (1981).
9) D. Oktavec, E. Beinrohr, B. Siles, J. Stefanec, and J. Garaj, *Collection Czechoslov. Chem. Commun.*, **45**, 1495 (1980).
10) R. Kellner, *Anal. Chim. Acta*, **63**, 277 (1973).
11) B. B. Kaul and K. B. Pandeya, *J. Inorg. Nucl. Chem.*, **40**, 229 (1978).
12) M. L. Riekkola, T. Pakkanen, and L. Niinistö, *Acta Chem. Scand., Ser. A*, **37**, 807 (1983).
13) H. Watarai, M. Tanaka, and N. Suzuki, *Anal. Chem.*, **54**, 702 (1982).
14) R. A. Pierotti, *Chem. Rev.*, **76**, 717 (1976).
15) E. Wilhelm and R. Battino, *J. Chem. Phys.*, **55**, 4012 (1971).
16) T. R. Reddy and R. Srinivasan, *J. Chem. Phys.*, **43**, 1404 (1965).
17) A. K. Gregson and S. Mitra, *J. Chem. Phys.*, **49**, 3696 (1968).
18) J. A. Riddick and W. B. Bunger, "Organic Solvent," in "Techniques of Chemistry," Wiley-Interscience, New York (1970), Vol. 2.

New Multi-Sulfur 1,2-Dithiolene Complexes. Preparation, Structure, and Electrochemical Properties

Reizo KATO,* Hayao KOBAYASHI, Akiko KOBAYASHI,† and Yukiyoshi SASAKI†
Department of Chemistry, Faculty of Science, Toho University, Funabashi, Chiba 274
†Department of Chemistry, Faculty of Science, The University of Tokyo, Hongo, Tokyo 113
(Received September 2, 1985)

New multi-sulfur 1,2-dithiolene complexes in which the 1,2-dithiolene moiety is extended by incorporating heterorings have been prepared and characterized by IR spectroscopy, X-ray diffraction method, and cyclic voltammetry. Partial oxidation of these complexes are expected to provide the multi-dimensional molecular conductors. Electrochemical properties of these complexes are compared with those of the dmit-complexes (dmit=2-thioxo-1,3-dithiole-4,5-dithiolate).

Extensive works have been carried out to synthesize and study a large range of inorganic one-dimensional metals based on the partially oxidized platinum-atom chain (for example, KCP; $K_2Pt(CN)_4Br_{0.3}\cdot 3H_2O$).[1] Recent discoveries of the molecular conductors containing partially oxidized metal 1,2-dithiolene complexes have extended the range of materials for study.[2] In these compounds, the conduction pathway is formed by overlapping of ligand-centered π-system (predominantly the sulfur orbitals) and not principally of the metal orbitals. The dmit-complex (dmit=2-thioxo-1,3-dithiole-4,5-dithiolate), among others, has shown a special property, the multi-dimensional intermolecular S···S interaction, which originates from the 1,3-dithiole-2-thione rings incorporated to the 1,2-dithiolene moiety.[2] The dimensionality of the electronic structure is closely related to the stabilization of the metallic state. Although 1,2-dithiolene complexes extended by incorporating heterorings containing chalcogen atoms should be of special interest in view of the multi-dimensional molecular conductor, there was no well-characterized example except the dmit-complex and its isomer, the dmt-complex (dmt=3-thioxo-3*H*-1,2-dithiole-4,5-dithiolate).[3] In this paper, the preparation of new multi-sulfur 1,2-dithiolene ligands and their complex formation with nickel and platinum are reported.

Results and Discussion

Synthetic process is shown in the Scheme. For the preparation of the ligands, hydrolysis of 1,3-dithiole-2-thiones with base was used.[4] Hydrolysis of the 1,3-dithiole-2-thiones **1a—c** by hot ethanolic potassium hydroxide under argon provided air-sensitive dipotassium salts which were subsequently treated with $NiCl_2$ in methanol or K_2PtCl_4 in water at room temperature. After air-oxidation, addition of *n*-Bu_4NBr resulted in the precipitation of monoanionic species **2a—e**.

Infrared spectra (KBr disk, Table 1) of these complexes show the absorptions characteristic of the bis(1,2-dithiolene) metal complexes.[5]

The structure of the $Ni(C_4H_4S_5)_2^-$ anion is shown in Fig. 1. The Ni–S distances are comparable with those found in other monoanionic nickel dithiolene complexes.[5,6] The C–S bond distances in the dithiolene group vary from 1.707 to 1.728 Å and are thus close

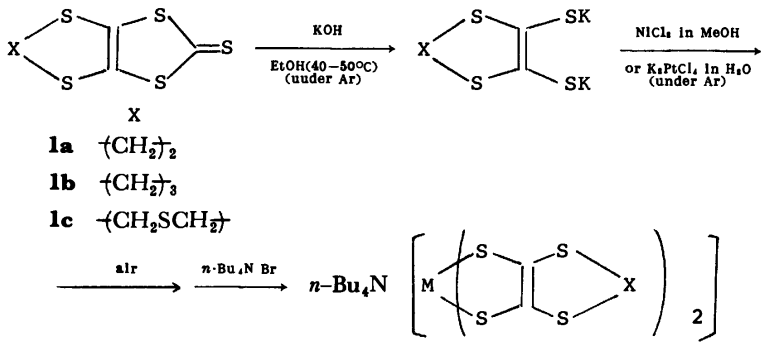

	X
1a	$-(CH_2)_2-$
1b	$-(CH_2)_3-$
1c	$-(CH_2SCH_2)-$

	M	X
2a	Ni	$-(CH_2)_2-$
2b	Pt	$-(CH_2)_2-$
2c	Ni	$-(CH_2)_3-$
2d	Pt	$-(CH_2)_3-$
2e	Ni	$-(CH_2SCH_2)-$

Scheme

Table 1. Infrared Spectra (cm^{-1}) of **2a—e**

	C=C	C=S	C—S	M—S
2a	1360 1280	·····	855	440
2b	1350 1280	·····	845	435
2c	1380 1270	990	860	460 395
2d	1360 1270	990	860	450
2e	1380 1210	·····	845	450

Table 2. Electrochemical Data of **2a—e** and $M(dmit)_2^-$ (M=Ni, Pt)[a]

Complex	E_1	E_2	$\Delta E(=E_1-E_2)$
2a	+0.06[b]	−0.69	0.75
2b	+0.06	−0.65	0.71
2c	+0.16	−0.71	0.87
2d	+0.15	−0.64	0.79
2e	+0.28[c]	−0.59	0.87
$Ni(dmit)_2^-$	+0.22[c]	−0.13	0.35
$Pt(dmit)_2^-$	+0.19[c]	−0.13	0.32

a) Measured at a glassy carbon electrode in CH_3CN, 0.1 mol dm^{-3} TBAP (volts vs. SCE); Temperature, 18 °C. b) Quasi-reversible. c) Irreversible; E_1 values were determined by differential pulse polarography, extrapolating the scan rate to 0 mV s^{-1}.

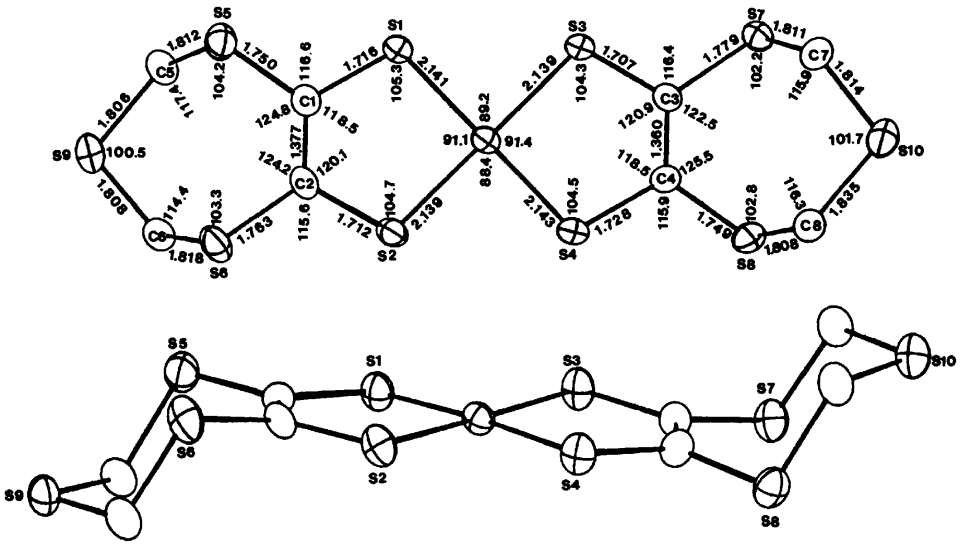

Fig. 1. Structure of $Ni(C_4H_4S_5)_2^-$. The standard deviations of the bond lengths and angles are 0.003—0.014 Å and 0.1—0.6° respectively.

Table 3. Final Atomic Coordinates (×10^4) with Estimated Standard Deviations in Parentheses for n-$Bu_4N[Ni(C_4H_4S_5)_2]$.

Atom	x	y	z	Atom	x	y	z
Ni	2000(1)	1345(1)	3427(1)	C(8)	481(8)	−1846(5)	1978(5)
S(1)	2893(2)	2539(1)	3523(1)	N	6749(6)	409(4)	3246(4)
S(2)	2175(2)	1506(1)	4531(1)	C(9)	6750(8)	1288(5)	3559(5)
S(3)	1851(2)	1168(1)	2331(1)	C(10)	5529(8)	1781(6)	3066(5)
S(4)	1007(2)	190(1)	3311(1)	C(11)	5735(10)	2739(7)	3305(7)
S(5)	4185(2)	3842(2)	4708(1)	C(12)	6663(8)	464(6)	2451(4)
S(6)	3534(3)	2638(2)	5850(1)	C(13)	7602(9)	1083(6)	2424(5)
S(7)	414(2)	50(1)	995(1)	C(14)	7417(10)	987(7)	1620(5)
S(8)	−453(2)	−1028(2)	2078(1)	C(15)	5632(8)	−134(6)	3100(5)
S(9)	3369(2)	4570(2)	5819(1)	C(16)	5437(9)	−224(6)	3808(5)
S(10)	433(2)	−1899(2)	1053(1)	C(17)	4282(9)	−782(6)	3555(6)
C(1)	3335(7)	2896(5)	4427(4)	C(18)	7974(7)	2(5)	3837(4)
C(2)	3032(7)	2415(5)	4883(4)	C(19)	8236(8)	−866(6)	3625(5)
C(3)	932(7)	291(5)	1969(4)	C(20)	9544(8)	−1143(6)	4303(5)
C(4)	552(7)	−156(5)	2396(4)	C(21)	4090(10)	−965(7)	4250(6)
C(5)	3206(8)	4566(6)	4876(5)	C(22)	8160(10)	1627(7)	1447(6)
C(6)	2634(8)	3572(6)	5802(5)	C(23)	6282(11)	2863(7)	4148(7)
C(7)	1233(8)	−929(5)	1066(5)	C(24)	9956(11)	−1987(7)	4143(6)

C(9)-C(24) are carbon atoms in tetrabutylammonium cation:

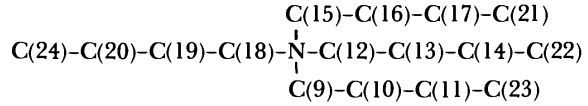

to the value 1.71 Å reported for C-S double bonds.[7] The "ethylenic" bond distances 1.360 and 1.377 Å are intermediate between double and single bond values. The external seven-membered heterorings take chair conformation, and C(5)-C(8), S(9), and S(10) largely deviate from the plane containing the rest of the anion. The C-S bond distances between the dithiolene ring and the external heteroring are slightly shorter than S(sp2)-C(sp2) distance 1.77 Å, and the remaining C-S bonds are single bonds since the usual value for a single bond is 1.81 Å.[7]

Electrochemical data of five new complexes **2a—e** and $(n\text{-Bu})_4N[M(dmit)_2]$ (M=Ni, Pt) are shown in Table 2. These complexes are reduced in one-electron step. This step is electrochemically reversible for all complexes. The reduction potential (E_2) values of the new complexes **2a—e** are comparable to those of alkyl-substituted arene-1,2-dithiolene complexes.[5] Fairly negative E_2 values explain the susceptibility to air-oxidation. The E_2 values of the dmit-complexes are less negative than those of **2a—e**, comparable to that of $Ni(S_2C_2(CF_3)_2)_2^-$.[5] In the 1,2-dithiolene complexes, the E_2 value is less negative when the substituted group is an electron-withdrawing group.[5] The above results suggest the electron-withdrawing property of the thioxo group in the dmit-complex. In all cases, the effect of the metal ion on the E_2 value is rather small.

In oxidation the cyclic voltammograms of **2b, c,** and **d** show a reversible oxidation to the neutral species at potentials (E_1) in the range of 0.06—0.28 V. At slow sweep rates (50 mV s^{-1}) the oxidation of **2a** is irreversible, at faster sweep rates becomes reversible (Fig. 2). At all sweep rates (50—200 mV s^{-1}), the oxidation of **2e** and $M(dmit)_2^-$ is irreversible (Fig. 2).

The $\Delta E(=E_1-E_2)$ values of the dmit-complex are ca. 0.3 V, while those for other 1,2-dithiolene complexes including **2a—e** are larger than 0.7 V.[5] This suggests that in the case of the dmit-complex the intermolecular Coulomb repulsion energy in the conducting state is smaller than that in other 1,2-dithiolene complexes.[8]

The ability of **2a—e** to form the conducting partially oxidized salt is suggested by the fact that the E_1 and E_2 values of **2a—e** are close to those of the unsubstituted 1,2-dithiolene complex $Ni(C_2H_2S_2)_2$ (E_1=0.09, E_2=−0.95 V vs. SCE) which provides the conducting compounds with the organic donors (TTF; Tetrathiafulvalene and TTT; Tetrathiotetracene(5, 6: 11,12-bis(epithio)naphthacene)).[9]

Experimental

1,3-Dithiole-2-thiones **1a—c** were synthesized from 4,5-bis(benzoylthio)-1,3-dithiole-2-thione and corresponding dibromoalkanes or bis(chloromethyl) sulfide.[10]

Preparation of Complexes. **n-$Bu_4N[Ni(C_4H_4S_4)_2]$ 2a:** A mixture of 20 ml of ethanol, 2.0 g (36 mmol) of potassium hydroxide, and 1.0 g (4.5 mmol) of 2,5,7,9-tetrathia-

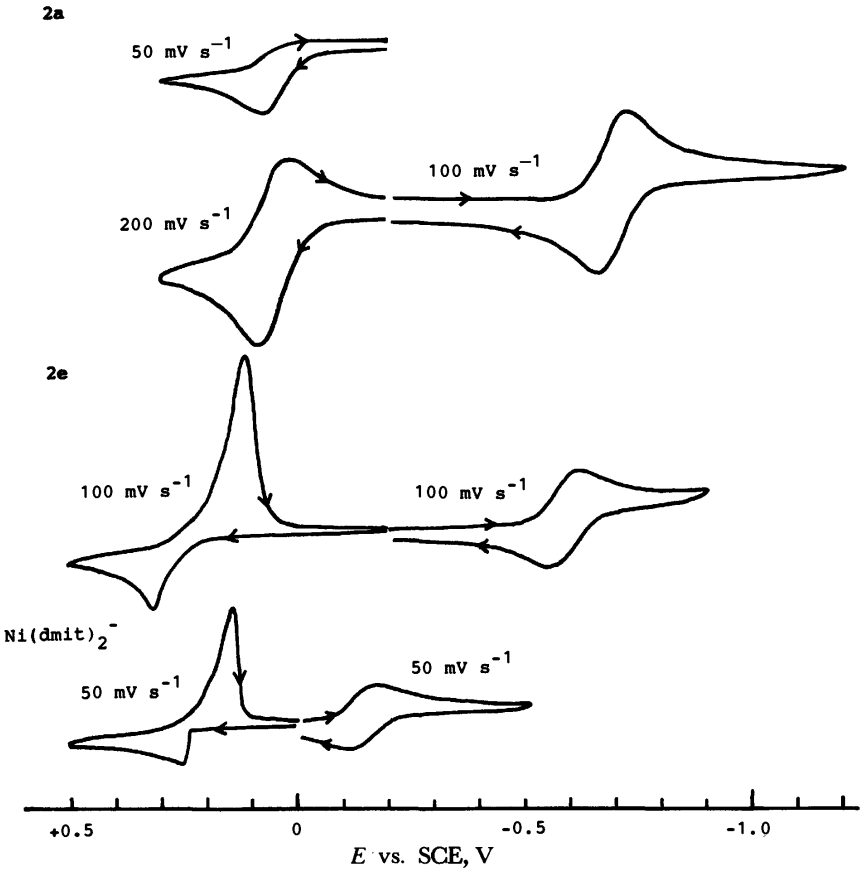

Fig. 2. Cyclic voltammograms of **2a**, **2e**, and $Ni(dmit)_2^-$.

bicyclo[4.3.0]non-1(6)-ene-8-thione **1a** was stirred for 1.5 h at 40—45 °C (water bath temperature) under argon. The resulting pale yellow micro crystals of the dipotassium salt were isolated by filtration, washed with a 4 ml portion of ethanol twice under argon, and dried in vacuo. The salt was dissolved in 20 ml of methanol and treated with 0.3 g (1.3 mmol) of $NiCl_2 \cdot 6H_2O$ in 20 ml of methanol. Stirring was continued overnight at room temperature under argon. Air was bubbled through the reaction mixture for 15 min. After filtration (yellow residue), to the dark green filtrate was added 2.0 g of tetrabutylammonium bromide. The dark green precipitate was isolated by filtration with suction, washed with methanol, and air-dried at room temperature. The crude complex was dissolved in 65 ml of acetone. After filtration, to the filtrate was added 65 ml of 2-propanol. Concentration of the solution with a rotary evaporator gave dark green crystals of **2a**, which were isolated by filtration, washed with methanol and ether, and dried in vacuo. Yield 0.45 g (54% based on Ni). Found: C, 43.39; H,7.13; N,2.00; S, 37.36%. Calcd for $C_{24}H_{44}NS_8Ni$: C, 43.55; H,6.70; N, 2.12; S, 38.76%.

Other complexes (**2b**, **2c**, **2d** and **2e**) were prepared analogously.

***n*-Bu_4N[Pt($C_4H_4S_4$)$_2$] 2b:** Yield 26% based on Pt. Found: C, 35.88; H, 5.83; N, 1.67; S, 31.91%. Calcd for $C_{24}H_{44}NS_8Pt$: C, 36.11; H, 5.56; N, 1.67; S, 31.91%.

***n*-Bu_4N[Ni($C_5H_6S_4$)$_2$] 2c:** Yield 34% based on Ni. Found: C, 44.98; H, 7.60; N, 1.90; S, 36.37%. Calcd for $C_{26}H_{48}NS_8Ni$: C, 45.27; H, 7.01; N, 2.03; S, 37.18%.

***n*-Bu_4N[Pt($C_5H_6S_4$)$_2$] 2d:** Yield 4% based on Pt. Found: C, 37.57; H, 6.23; N, 1.62; S, 31.07%. Calcd for $C_{25}H_{48}NS_8Pt$: C, 37.79; H, 5.85; N, 1.70; S, 31.04%.

***n*-Bu_4N[Ni($C_4H_4S_5$)$_2$] 2e:** Yield 46% based on Ni. Found: C, 39.72; H, 6.28; N, 1.69; S, 42.76%. Calcd for $C_{24}H_{44}NS_{10}Ni$: C, 39.71; H, 6.11; N, 1.93; S, 44.16%. To date, attempts to prepare *n*-Bu_4N[Pt($C_4H_4S_5$)$_2$] have been unsuccessful.

Infrared Spectra. Spectra of compounds pressed in KBr disks were recorded on a model 260-30 Hitachi infrared spectrophotometer over the range 400—4000 cm^{-1}.

Structural Study. The crystal of **2e** has been investigated by X-ray diffraction. The crystal data are: monoclinic, space group $P2_1/c$, a=12.374(3), b=15.748(4), c=20.127(5) Å, β=119.54(2)°, V=3412.2 Å^3, Z=4. A total of 4501 independent reflections ($2\theta \leq 60°$, $|F_o| > 3\sigma(|F_o|)$) were recorded on a Rigaku automatic four-circle diffractometer using Mo $K\alpha$ radiation. The intensity data were corrected for the Lorentz and the polarization effects, but not for absorption. The structure was solved by the direct method and refined by the block-diagonal least-squares method on a PANAFACOM U-1300 computer by the use of a local version of the UNICS-III programs.[11] Scattering factors were taken from Ref. 12. The weighting scheme, $w=1/(\sigma(F_o)^2+0.0001|F_o|^2)$ was employed. The final discrepancy factors were $R_1=\sum||F_o|-|F_c||/\sum|F_o|=0.067$ and $R_2=[\sum w(|F_o|-|F_c|)^2/\sum w|F_o|^2]^{1/2}=0.074$. The final atomic coordinates are listed in Table 3. A list of the final F_o-F_c table, and anisotropic temperature factors are deposited as Document No.8618 at the office of Bull. Chem. Soc. Jpn.

Electrochemical Study. Electrochemical measurements were performed with a YANACO polarographic analyzer P-1100 at 18 °C. Tetrabutylammonium perchlorate was used as a supporting electrolyte. A glassy carbon was employed as a working electrode. The counter electrode was a platinum wire which was immersed directly in the electrolysis solution. An aqueous saturated calomel electrode (SCE) was separated from the test solution by a fine-porosity glass frit and a salt bridge filled with the solution under study. All potentials are reported vs. an aqueous SCE.

References

1) J. S. Miller and A. J. Epstein, *Prog. Inorg. Chem.*, **20**, 1 (1976); A. E. Underhill and D. M. Watkins, *Chem. Soc. Rev.*, **9**, 429 (1980).

2) A. E. Underhill and M. M. Ahmad, *J. Chem. Soc., Chem. Commun.*, **1981**, 67; L. Valade, J. Bousseau, A. Gleizes, and P. Cassoux, ibid., **1983**, 110; R. Kato, T. Mori, A. Kobayashi, Y. Sasaki, and H. Kobayashi, *Chem. Lett.*, **1984**, 1; P. Cassoux, L. Valade, M. Bousseau, J-P. Legros, M. Garbauskas, and L. Interrante, *Mol. Cryst. Liq. Cryst.*, **120**, 377 (1985); R. Kato, H. Kobayashi, A. Kobayashi, and Y. Sasaki, *Chem. Lett.*, **1985**, 131; H. Kobayashi, R. Kato, A. Kobayashi, and Y. Sasaki, ibid., **1985**, 191, 535.

3) G. Steimecke, J. Sieler, R. Kirmse, W. Dietzsch, and E. Hoyer, *Phosphorus and Sulfur*, **12**, 237 (1982).

4) M. Mizuno, M. P. Cava, and A. F. Garito, *J. Org. Chem.*, **41**, 1484 (1976).

5) J. A. McCleverty, *Prog. Inorg. Chem.*, **10**, 49 (1968); R. P. Burns, and C. A. Mcauliffe, *Adv. Inorg. Radiochem.*, **22**, 303 (1979).

6) A. Kobayashi and Y. Sasaki, *Bull. Chem. Soc. Jpn.*, **50**, 2650 (1977).

7) "International Tables for X-ray Crystallography," Kynoch Press, Birmingham (1962), Vol. III, p. 276.

8) A. W. Addison, J. P. Barnier, V. Gujval, Y. Hoyano, S. Huizinga, and L. Weiler, "Molecular Metals," ed by W. E. Hatfield, Plenum Press, New York (1979), p. 15.

9) L. V. Interrante, K. W. Browall, H. R. Hart, Jr., I. S. Jacobs, G. D. Watkins, and S. H. Wee, *J. Am. Chem. Soc.*, **97**, 889 (1975); J. S. Kasper, L. V. Interrante, and C. A. Secaur, ibid., **97**, 890 (1975); J. W. Bray, H. R. Hart, Jr., L. V. Interrante, I. S. Jacobs, J. S. Kasper, P. A. Piacente, and G. D. Watkins, *Phys. Rev. B*, **16**, 6359 (1977).

10) G. Steimecke, H. Sieler, R. Kirmse, and E. Hoyer, *Phosphorus and Sulfur*, **7**, 49 (1979).

11) T. Sakurai and K. Kobayashi, *Rep. Inst. Phy. Chem. Res.*, **55**, 69 (1979).

12) "International Tables for X-Ray Crystallography," Kynoch Press, Birmingham (1974), Vol. IV.

Aftereffects of Nuclear Decay in $^{57}CoCl_2 \cdot nH_2O$ (n=2 and 6) Investigated by γ-X Ray Coincidence Mössbauer Spectroscopy

Takayuki KOBAYASHI*,† and Jean M. FRIEDT
Centre de Recherches Nucléaires, 67037 Strasbourg Cedex, France
(Received September 11, 1985)

The anomalous states produced by electron capture decay of ^{57}Co in $CoCl_2 \cdot 2H_2O$ and $CoCl_2 \cdot 6H_2O$ are investigated using conventional Mössbauer emission spectroscopy and a γ-X ray coincidence method which allows to isolate events with a reduced influence of the Auger electron self-irradiation. The formation of the anomalous electronic and structural configuration is assigned to the self-radiolysis of the water ligands. The mechanism involves both the nearest and the next nearest H_2O coordination shell according to the densities of these ligand molecules in the respective shells.

In insulating materials, doped or labelled with radioactive nuclei, anomalous valence or structural configurations of the decaying atoms are sometimes formed besides the normal state. This is called the aftereffect of nuclear decay which can be investigated very uniquely (in situ analysis on a time scale of the order of 100 ns after the decay) using Mössbauer emission spectroscopy.[1-6] One often invoked mechanism for these aftereffects considers that the chemical bonds in the immediate vicinity of the decaying atom are ruptured by the emitted photons and particles, e.g. the X-rays and Auger electrons emitted after the electron capture (EC) decay of ^{57}Co.[7] The resulting radicals hence formed around the atoms would play a determinant role in stabilizing the anomalous states. In the case of inorganic divalent compounds surrounded by water ligands it is considered that the formation of the anomalous trivalent Fe^{3+} arises mainly from free OH radicals produced by internal radiolysis of the H_2O ligands. This mechanism is simulated by γ-irradiation experiments of the Fe salt hydrates which for instance in the case of $FeSO_4 \cdot nH_2O$ (n=0,1,4,7) conclusively demonstrated the oxidation of Fe^{2+} by OH radicals:[8]

$$Fe^{2+} + OH \rightleftharpoons Fe^{3+} + OH^-. \quad (1)$$

However, the mechanisms of the aftereffects of nuclear decay are certainly more complicated than those of an external irradiation because of the superposition of primary excitations (direct ionization and excitation) and because of distribution in the particle flux and energy etc. In order to improve the understanding of those phenomena, it is desirable to modulate the conditions of the internal irradiation, i.e., to change the energy, intensity or the time involved in the processes. One possible approach relies on a γ-X ray coincidence technique, which allows to measure Mössbauer emission spectra corresponding to a reduced flux of Auger electrons after the EC decay of ^{57}Co. In this work we report a study, by using the γ-X ray coincidence technique, of the aftereffects in the hydrated compounds with water ligands; $CoCl_2 \cdot 2H_2O$ and $CoCl_2 \cdot 6H_2O$ labelled with ^{57}Co.

Experimental

Principle of the Experiment. After the EC decay of ^{57}Co, a K-X ray or K-Auger electron is emitted with the probability of approximately 30 or 60%, respectively.[9] The K-X ray emission causes one vacancy in the L or M shell, while two vacancies are produced in the L and/or M shells owing to the K-Auger effect. Each vacancy brings about the Auger cascade in the outer shells. Therefore, more (factor of $\approx$2) low-energy electrons are emitted during the Auger cascade after the K-Auger process than after the K-X ray emission. If a Mössbauer spectrum is observed, by the coincidence technique, i.e. only when K-X rays are emitted, the flux of the low-energy Auger electrons is reduced compared with that in the conventional Mössbauer emission method. By comparing the coincidence spectrum with the conventional one, it is expected to obtain new insights into the mechanisms of the aftereffects. This is the idea of the γ-X ray coincidence Mössbauer method, which is described elsewhere in more detail.[10,11]

Preparation of Samples. In order to avoid decomposition of the sample material during the measurements, very thin and little chemical compound ($CoCl_2 \cdot 2H_2O$ or $CoCl_2 \cdot 6H_2O$) labelled with ^{57}Co was surrounded with a large quantity of the same and unlabelled compound, and sealed between thin Mylar films. The intensity and specific activity of the sample source were approximately 10 μCi and 40 Ci mole^{-1}, respectively.

Measurements. The slow coincidence technique was used for the measurements, and the coincidence and conventional Mössbauer spectra were observed simultaneously at room temperature. The block diagram of the measuring system is shown in Fig. 1. The detectors used for 6.5 keV X-rays and 14.4 keV γ-rays were NaI(Tl) crystals with 1-inch diameter and 0.2-mm thickness. Since the resolving time of X-ray signals was approximately 4 μs, the universal coincidence unit was opened, for γ-rays, for sufficiently long time compared with the lifetime of the Mössbauer level and therefore the line-broadening due to the time effects[12,13] was considered to be negligible. In order to get a large geometrical efficiency, the sample source was placed just in front of the X-ray detector. The contribution of random coincidences was subtracted from the observed coincidence spectrum. The random coincidence counting rate was less than 20% of the total coincidence counting rate.

†Present address: Shiga University of Medical Science, Otsu, Shiga 520-21.

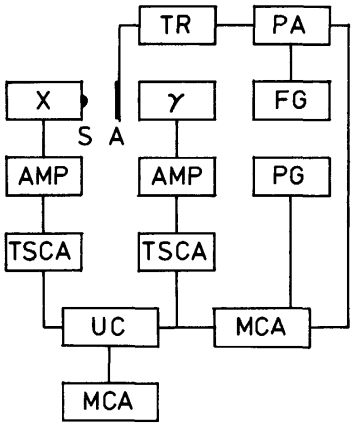

Fig. 1. Block diagram of the measuring system. S: sample source, A: absorber $Na_4Fe(CN)_6 \cdot 10H_2O$, X and γ:X- and γ-ray detectors, AMP: amplifier, TSCA: timing single channel analyzer, UC: universal coincidence, MCA: multichannel analyzer, TR: transducer, PA: power amplifier, FG: function generator, PG: pulse generator.

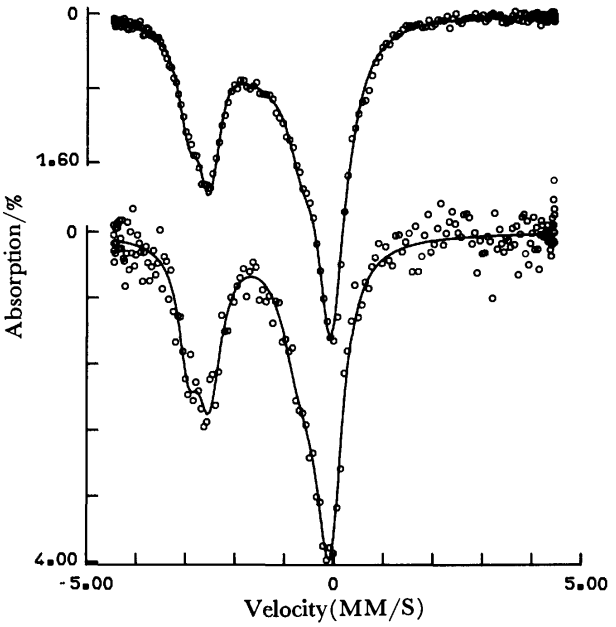

Fig. 2. Observed spectra of $CoCl_2 \cdot 2H_2O$. Upper and lower figures are the conventional and coincidence spectra with base-line counts of approximately 7.1×10^6 and 2.6×10^5, respectively.

Results

The observed spectra shown in Figs. 2 and 3 are composed of a large main peak and a small side peak, and were analyzed as a superposition of several Lorentzian lines. Rather good fits are obtained by assuming three symmetrical quadrupole doublets when the spectra are analyzed individually. However, in order to reach a consistent analysis of both the conventional and the coincidence data it appeared

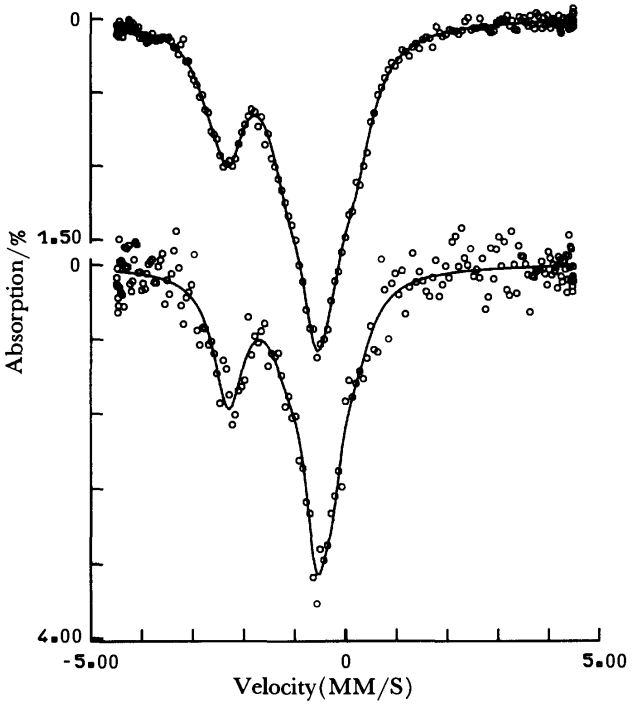

Fig. 3. Observed spectra of $CoCl_2 \cdot 6H_2O$. Upper and lower figures are the conventional and coincidence spectra with base-line counts of approximately 6.6×10^6 and 2.1×10^5, respectively.

necessary to introduce a number of conditions:

1) The hyperfine parameters of the several sites are equal in the coincidence and in the conventional spectra.

2) All the components in the coincidence spectrum must be found in the conventional spectrum, since the resonance absorption after X-ray emission contributes to the conventional spectrum as well as to the coincidence spectrum.

3) The line-width in the coincidence spectrum is equivalent to or less than the corresponding width in the conventional spectrum, because the defects of surroundings of ^{57}Fe after the decay of ^{57}Co under the coincidence conditions are expected to be reduced in comparison with the conventional measurements.

The good and simultaneous fits of the conventional and coincidence spectra are realized with the parameters in Table 1 which satisfy the above conditions.

In reference to the isomer shift (I.S.) and quadrupole splitting (Q.S.) of $FeCl_2 \cdot 2H_2O$[14] and $CoCl_2 \cdot 6H_2O$ doped with a small amount of Fe, the components Fe^{2+} (1) in Table 1 are attributed to the normal states in the lattice.

Discussion

The relative intensities of the components in the spectra are shown graphically in Fig. 4. The Fe^{2+}(1) contribution is greater in the coincidence spectrum than in the conventional one, reflecting the reduced influence of the low-energy electrons in the coincidence

Table 1. Mössbauer Parameters of the Conventional and Coincidence Spectra

State	I.S.	Q.S.	Conventional width	Conventional intensity	Coincidence width	Coincidence intensity
	mm s^{-1}	mm s^{-1}	mm s^{-1}	%	mm s^{-1}	%
			$CoCl_2 \cdot 2H_2O$			
$Fe^{2+}(1)$	−1.31±0.02	2.42±0.03	0.53±0.01	35.1	0.59±0.05	43.4
$Fe^{2+}(2)$	−1.48±0.11	2.93±0.22	0.53±0.01	21.4	0.47±0.07	23.4
$Fe^{2+}(3)$	−1.54±0.04	0.45±0.05	0.81±0.03	8.3	—	—
$Fe^{3+}(1)$	−0.52±0.03	0.41±0.09	0.79±0.11	13.1	0.79±0.11	33.1
$Fe^{3+}(2)$	−0.23±0.01	0.80±0.02	0.81±0.03	22.2	—	—
			$CoCl_2 \cdot 6H_2O$			
$Fe^{2+}(1)$	−1.43±0.03	1.75±0.02	0.73±0.04	31.1	0.72±0.07	47.9
$Fe^{2+}(2)$	−1.71±0.05	1.93±0.08	0.73±0.04	10.0	—	—
$Fe^{3+}(1)$	−0.42±0.13	0.32±0.13	0.68±0.08	23.6	0.52±0.08	27.1
$Fe^{3+}(2)$	−0.48±0.08	1.30±0.10	0.88±0.03	35.2	0.83±0.09	24.9

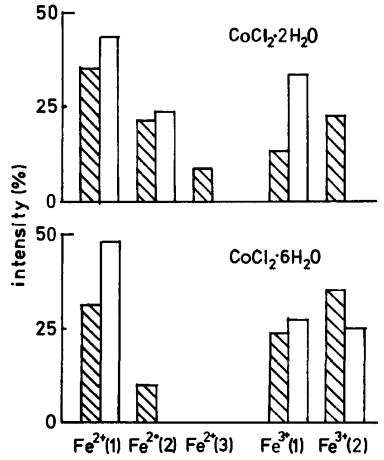

Fig. 4. Relative intensities of the components in the spectra. The slash marked and blank bars denote the results from the conventional and the coincidence spectra, respectively.

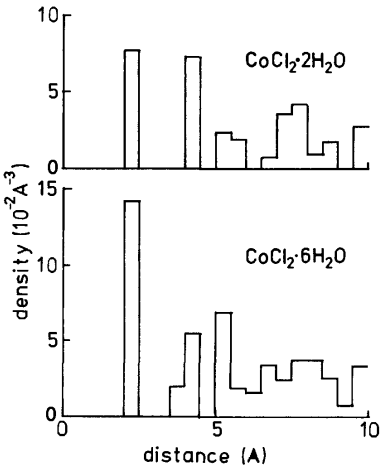

Fig. 5. Densities of H_2O molecules as a function of distance from a Co atom in $CoCl_2 \cdot 2H_2O$ and $CoCl_2 \cdot 6H_2O$.

spectrum. A mechanism for the appearance of the states other than $Fe^{2+}(1)$ is searched from consideration of the densities of H_2O molecules as a function of distance from a Co atom in the source materials (Fig. 5).

Many nearest neighbouring H_2O molecules exist in the hexahydrate. However, in the dihydrate the density of the second nearest neighbouring H_2O is equivalent to that of the nearest H_2O. Therefore, it is expected that the role of the second nearest H_2O in the aftereffects is relatively more important in the dihydrate than in the hexahydrate. The variety of the states in the dihydrate (Fig. 4) is assigned to the effect of these further H_2O molecules. Since the hypothesis that Fe^{3+} states are formed through oxidation of Fe^{2+} by OH radicals produced by radiolysis of H_2O in hydrated compounds (reaction (1)) is accepted widely, it is reasonably conjectured that one of $Fe^{3+}(1)$ and $Fe^{3+}(2)$ states corresponds to the effect of the nearest H_2O whereas the other is connected with the second nearest H_2O.

The nearest neighbouring H_2O exerts a greater influence on the electric field gradient (EFG) than the further H_2O. Therefore, the greater Q.S. of $Fe^{3+}(2)$ suggests the formation of $Fe^{3+}(2)$ due to radiolysis of the nearest H_2O and the $Fe^{3+}(1)$ states are the effect of the further H_2O. Some of the low-energy Auger electrons which have escaped from the nearest H_2O layer break a second nearest or further H_2O into H and OH radicals. However, contrary to the case of Fe^{2+}, an electron can hardly transfer to this OH radical from the Co^{2+} ion situated close to the OH through the reaction $Co^{2+}+OH \rightarrow Co^{3+}+OH^-$. Therefore, this OH radical oxidize the Fe^{2+} ion, which has emitted the Auger electrons, to form the $Fe^{3+}(1)$ state, or recombines with H after a while.

The energy of the Auger electrons determining the aftereffects is very low (less than a few hundred electron volts), and their range in the lattice is expected very short. Moreover, some of the electrons collide elastically with the H_2O molecules or Cl^- ions in the nearest H_2O layer (without breaking these molecules) and hence loose more energy. Therefore, it is expected

that the stopping power of the electrons is greater on the average in the second nearest or further layer than that in the nearest H_2O layer. Under the coincidence conditions, the number of the emitted Auger electrons is reduced to approximately a half,[10] and therefore the nearest H_2O in the dihydrate sustains hardly radiolysis. This might be the main reason why the $Fe^{3+}(2)$ component is not found in the coincidence spectrum of the dihydrate although the contribution of $Fe^{3+}(1)$ is rather great. In the hexahydrate, owing to the great density of the nearest H_2O, the probability of radiolysis in the nearest H_2O layer is fairly great even under the coincidence conditions. Consequently, both of the Fe^{3+} components appear in the conventional and coincidence spectra.

The appearence of the $Fe^{2+}(2)$ states can actually also be attributed to the effect of the second nearest H_2O. When a OH radical originated outside of the nearest H_2O layer oxidizes Fe^{2+}, it brings about the $Fe^{3+}(1)$ states as mentioned before. On the other hand, when the Fe^{2+} ion does not suffer oxidation by the OH radical in the second nearest H_2O layer, the $Fe^{2+}(2)$ state may appear. In the case that OH survives without recombination with H, the local symmetry around the Fe ion becomes lower and this results in an increase Q.S. value. In the other case that the OH recombines with H, the position of the produced H_2O may differ from its regular crystal site hence may increase the Q.S., as observed for $Fe^{2+}(2)$. Since the second nearest H_2O is less important in the hexahydrate than in the dihydrate, the relative intensity of $Fe^{2+}(2)$ is limited in the conventional spectrum of the hexahydrate. This state is not found in the coincidence spectrum due to the reduced number of the Auger electrons.

The $Fe^{2+}(3)$ state may appear by the effect of the further than second nearest H_2O. The absence of $Fe^{2+}(3)$ in the spectra of the hexahydrate supports this assumption. The unusually small Q.S. can arise from a fortuitous compensation between the lattice and orbital contributions to the EFG. Alternatively, thermal vibration of the localized lattice after the decay of ^{57}Co can conceivably reduce the EFG around Fe^{2+}.

In conclusion, the difference of the emission spectra observed in conventional and in γ-X ray coincidence Mössbauer spectroscopy confirms unambiguously the effectiveness of the Auger and conversion electron self-irradiation in determining the mechanism of stabilization of the anomalous configurations of the decayed atoms. A comparative analysis of the coincidence and regular data in the hydrates $CoCl_2 \cdot 6H_2O$ and $CoCl_2 \cdot 2H_2O$ suggests that the radical reactions involve mostly the nearest neighbour coordination shell in the hexahydrate. In the presence of a lower density of radiosensitive H_2O ligands, as found in the dihydrate, the second nearest coordination shell is also involved in the mechanism of stabilization of the anomalous configurations.

The authors wish to express their thanks to Richard Poinsot for his helpful cooperation.

References

1) R. Ingals, C. J. Coston, G. de Pasquali, H. G. Drickamer, and J. J. Pinajian, *J. Chem. Phys.*, **45**, 1057 (1966).
2) J. M. Friedt, G. K. Shenoy, G. Absteiter, and R. Poinsot, *J. Chem. Phys.*, **59**, 3831 (1973).
3) H. H. Wei, *J. Phys. (Paris), Colloq.*, **40**, C2-426 (1979).
4) J. Ladriére, J. C. Krack, and D. Apers, *J. Phys. (Paris), Colloq.*, **40**, C2-434 (1979).
5) Y. Sakai, K. Endo, and H. Sano, *Bull. Chem. Soc. Jpn.*, **54**, 3587 (1981).
6) D. L. Nagy, R. Doerfler, G. Ritter, J. Waigel, N. Zeman, and B. Molnár, *Phys. Lett.*, **95A**, 400 (1983).
7) J. M. Friedt and J. Danon, *Atom. Energy Rev.*, **18**, 893 (1981).
8) J. Mayer, J. Ladriére, M. Chavee and D. Apers, *J. Phys. (Paris), Colloq.*, **37**, C6-905 (1976).
9) W. Bambynek, B. Crasemann, R. W. Fink, H. U. Freund, H. Mark, C. W. Swift, R. E. Price, and P. V. Rao, *Rev. Mod. Phys.*, **44**, 716 (1972).
10) T. Kobayashi, K. Fukumura, and T. Kitahara, *Nucl. Instrum. Methods*, **166**, 257 (1979).
11) T. Kobayashi, *Radiochim. Acta*, **35**, 43 (1984).
12) F. J. Lynch, R. E. Holland, and M. Hamermesh, *Phys. Rev.*, **120**, 513 (1960).
13) T. Kobayashi and S. Shimizu, *Phys. Lett.*, **54A**, 311 (1975).
14) T. Tominaga and T. Sakai, *Radioisotopes*, **21**, 360 (1972).

 © 1986 The Chemical Society of Japan Bull. Chem. Soc. Jpn., 59, 635—638 (1986)

The Crystal and Molecular Structure of Δ-(8-Methyl-1,3,6,10,13,16,19-heptaazabicyclo[6.6.6]icosane)cobalt(III) Perchlorate Monohydrate

Ushio SAKAGUCHI* and Tasuku ITO†
Kumamoto University of Commerce, Ooe, 2-5-1, Kumamoto 862
†Institute for Molecular Science, Myodaiji, Okazaki 444
(Received October 2, 1985)

The structure of Δ-(8-methyl-1,3,6,10,13,16,19-heptaazabicyclo[6.6.6]icosane)cobalt(III) perchlorate monohydrate, Δ-[Co($C_{14}H_{33}N_7$)](ClO_4)$_3$·H_2O, has been determined by single crystal X-ray diffraction techniques. Crystal data are the following: space group $P2_12_12_1$, a=16.379(2) Å, b=16.388(2) Å, c=9.753(1) Å, V=2617.9(5) Å^3, Z=4, 3983 nonzero structure factors ($|F_o|>3\sigma(|F_o|)$), R=0.0447, and R_w=0.0491. The geometry of the cation can be approximated very closely by a composite of [Co(sen)]$^{3+}$ and [Co(sep)]$^{3+}$, where sen=1,1,1-tris(4-amino-2-azabutyl)ethane and sep=1,3,6,8,10,13,16,19-octaazabicyclo[6.6.6]icosane.

The macrotricyclic hexaamine cage complexes of cobalt(III), with a commom basic structure **I** in Fig. 1, have several interesting properties. We have recently reported that these complexes are 3 to 6 orders of magnitude more acidic than ordinary cobalt(III) amine complexes and exploited this property to show the dominance of double hydrogen bonding in the ion association of these complexes.[1] It was implicitly assumed there that for favorable double hydrogen bonding, the complexes all take the $(lel)_3$ conformation, where $(lel)_3$ refers to the C–C vectors of "ethylenediamine" (en) moieties parallel to the cap-to-cap axis of the molecule. In contrast to this, the [Co(diNOsar-H)]$^{2+}$ (I with X=Y=C–NO_2) ion has been reported[2] to have the $(ob)_3$ conformation, where diNOsar-H is the deprotonated form of 1,8-dinitro-3,6,10,13,16,19-hexaazabicyclo[6.6.6]icosane and $(ob)_3$ refers to the C–C vectors of "en" rings oblique to the cap-to-cap axis of the compound. Thus, it seemed to be interesting to investigate the conformation of [Co(azamesar)]$^{3+}$ (**I** with X=C–CH_3, Y=N), where azamesar=8-methyl-1,3,6,10,13,16,19-heptaazabicyclo[6.6.6]icosane. Further, we found that under some conditions, [Co(azamesar)]$^{3+}$ undergoes fragmentation reaction, which might result from steric strain.[3] Though the nature of this reaction is not clear as yet, steric strain has been shown to play an important role in determining spectroscopic[4] and chemical properties[5] as well as electron self-exchange rates in hexaamine cobalt(III) complexes. For example, complexes of type **I** exchange electron some 10^5-fold faster than the parent [Co(en)$_3$]$^{3+}$ ion[6] and Geselowitz[7] proposed a ligand strain as a mojor factor for this difference. Therefore, examination of ligand strain might be considered to contribute to the elucidation of these problems.

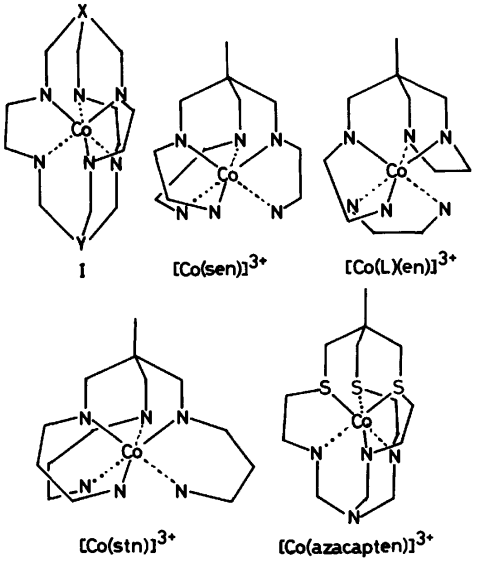

Fig. 1. Schematic illustration of complexes.

Experimental

Material. The compound was synthesized, according to the method of Creaser et al.,[8] by the reaction of aqueous ammonia and formaldehyde with Δ-[Co(sen)]$^{3+}$, which had been prepared[4] and optically resolved[9,10] by the methods reported previously, where sen=1,1,1-tris(4-amino-2-azabutyl)ethane. The crystals were grown by slow evaporation of an aqueous solution into orthorhombic blocks elongated along the c axis.

Crystal Data. A yellow crystal of [Co($C_{14}H_{33}N_7$)](ClO_4)$_3$·H_2O with dimensions of 0.32×0.24×0.20 mm was used for the data collection. The determination of cell constants and the collection of the intensity data were carried out at about 25 °C on a Rigaku AFC-5 automated four-circle diffractometer with Mo$K\alpha$ radiation made monochromatic by a graphite plate (λ=0.71073 Å). The cell constants, determined by a least-squares method using 50 independent reflections (25°<2θ<30°), were a=16.379(2) Å, b=16.388(2) Å, c=9.753(1) Å, and V=2617.9(5) Å^3. The space group was determined to be $P2_12_12_1$ (D_2^4, No. 19) from the systematic absences for $h00$ ($h=2n+1$), $0k0$ ($k=2n+1$), and $00l$ ($l=2n+1$). The measured density of 1.73 g cm^{-3} obtained by a flotation method agrees well with the calculated value of 1.712 g cm^{-3} for Z=4. The intensity data were collected for $+h$, $+k$, $+l$ and $-h$, $-k$, $-l$ by the θ—2θ scan technique to a maximum 2θ value of 60° at a scan rate of 3° min^{-1} (40 kV, 25 mA). Scan widths ($\Delta\theta$) were calculated from the formula $\Delta\theta=(1.1+0.5\tan\theta)°$. The intensity measurements were automatically repeated until $\sigma_c(|F_o|)/|F_o|$ became less than 0.05, where $\sigma_c(|F_o|)$ is a standard deviation calculated from counting statistics. The maximum

†Present address: Department of Chemistry, Faculty of Science, Tohoku University, Aoba, Aramaki, Sendai 980.

number of repetition was 3. Three reference reflections monitored after every cycle of 100 measurements showed no significant variation in intensity during the data collection. Out of 5632 independent reflections measured, 3983 reflections with $|F_o|>3\sigma(|F_o|)$ were used for the structure determination. They were corrected for Lorentz-polarization effects, but no absorption correction was applied since the linear absorption coefficient of $\mu(\mathrm{Mo}K\alpha)=10.65\,\mathrm{cm}^{-1}$ was low.

Structure Determination and Refinement. The structure was solved by standard heavy-atom techniques. The position of Co atom was determined from the three-dimensional Patterson map. The remaining atoms except hydrogen atoms were all revealed in subsequent Fourier syntheses. After all the non-hydrogen atoms were refined isotropically, a series of refinements using anisotropic thermal parameters for all non-hydrogen atoms reduced an R value, $\sum||F_o|-|F_c||/\sum|F_o|$, to 0.0614 and an R_w value, $[\sum w(|F_o|-|F_c|)^2/\sum w|F_o|^2]^{1/2}$, to 0.0724, where F_o and F_c are the observed and calculated structure factors, respectively. The weighting scheme used was $w=[\sigma_c^2+(0.015|F_o|)^2]^{-1}$. All the hydrogen atoms were located from subsequent difference Fourier maps. Further refinements, using anisotropic thermal parameters for all non-hydrogen atoms and isotropic thermal parameters for hydrogen atoms, reduced R to 0.0447 and R_w to 0.0491.

The absolute configuration was checked by reversing the signs of the $\Delta f''$ terms and repeating the final refinement sequence, to give significantly larger R of 0.0528 and R_w of 0.0597. In Table 1 are compared the observed and calculated intensity ratios of 12 Bijvoet pairs for which the observed reflection $|F(hkl)|$ and counter-reflection $|F(\bar{h}\bar{k}\bar{l})|$ differed by more than 14%.

The final difference Fourier map showed no peaks higher than 0.83 e/Å^3.

The atomic scattering factors for non-hydrogen atoms were taken from International Tables for X-ray Crystallography[11] and those for hydrogen atoms from Stewart, Davidson, and Simpson.[12] The anomalous dispersion coefficients[11] were used for non-hydrogen atoms in structure factor calculations. The final atomic coordinates for non-hydrogen atoms are given in Table 2,[13] according to the atom labels of Fig. 2. All the computations, including ORTEP[14] drawings were carried out by a HITAC M-200H computer at the Computer Center of the Institute for Molecular Science. The Universal Crystallographic Computation Program System, UNICS III,[15] was used.

Table 1. Determination of Absolute Configuration

h	k	l	$\lvert F_o\rvert$	$\lvert F_c\rvert$	$\dfrac{\lvert F_o(\bar{h}\bar{k}\bar{l})\rvert}{\lvert F_o(hkl)\rvert}$	$\dfrac{\lvert F_c(\bar{h}\bar{k}\bar{l})\rvert}{\lvert F_c(hkl)\rvert}$
2	9	1	20.90	20.07	1.24	1.24
$\bar{2}$	$\bar{9}$	$\bar{1}$	25.95	24.88		
11	6	2	18.41	17.72	1.16	1.16
$\bar{11}$	$\bar{6}$	$\bar{2}$	21.40	20.55		
4	2	3	24.29	26.57	0.85	0.78
$\bar{4}$	$\bar{2}$	$\bar{3}$	20.66	20.79		
1	6	3	38.30	38.06	1.14	1.12
$\bar{1}$	$\bar{6}$	$\bar{3}$	43.69	42.80		
6	10	3	29.72	29.00	1.14	1.08
$\bar{6}$	$\bar{10}$	$\bar{3}$	33.86	31.26		
3	4	4	26.06	25.16	1.14	1.07
$\bar{3}$	$\bar{4}$	$\bar{4}$	29.77	27.00		
7	4	5	23.09	23.17	1.14	1.09
$\bar{7}$	$\bar{4}$	$\bar{5}$	26.25	25.31		
4	9	5	26.96	26.82	1.15	1.08
$\bar{4}$	$\bar{9}$	$\bar{5}$	31.04	28.97		
9	5	6	20.02	21.23	1.14	1.08
$\bar{9}$	$\bar{5}$	$\bar{6}$	22.74	22.98		
2	3	7	17.82	18.40	1.28	1.19
$\bar{2}$	$\bar{3}$	$\bar{7}$	22.73	21.98		
1	2	8	26.75	26.82	1.14	1.06
$\bar{1}$	$\bar{2}$	$\bar{8}$	30.42	28.49		
5	2	8	28.61	28.33	1.16	1.09
$\bar{5}$	$\bar{2}$	$\bar{8}$	33.19	30.78		

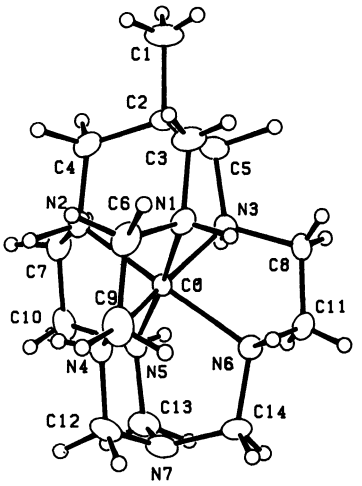

Fig. 2. Structure of the cation with atom labels. Thermal ellipsoids are drawn to include 30% of probability distribution.

Results and Discussion

The crystal structure as viewed down the c axis is shown in Fig. 3. The crystal may be considered to be made up of alternate layers of complex cations and anions, both extending in the bc plane. The cation hydrogen-bonds, via N-H groups, to water oxygens (N2···Ow=2.913(6) Å and N4···Ow=3.240(7) Å) and to perchlorate oxygens (N1···O(10)=3.038(6) Å, N1···O(11)=3.399(7) Å, N6···O(10)=3.057(6) Å, and N6···O(12)=3.317(10) Å). Interatomic distances and angles are given in Table 3.

The structure of Δ-[Co(azamesar)]$^{3+}$ cation, given in Fig. 2, has a pseudo-threefold axis of rotation and may be viewed as a composite of [Co(sen)]$^{3+}$ (Fig. 1) and [Co(sep)]$^{3+}$ (**I** with X=Y=N), where sep= 1,3,6,8,10,13,16,19-octaazabicyclo[6.6.6]icosane.[16] The absolute configuration of the cation that shows a positive circular dichroism peak in the first absorp-

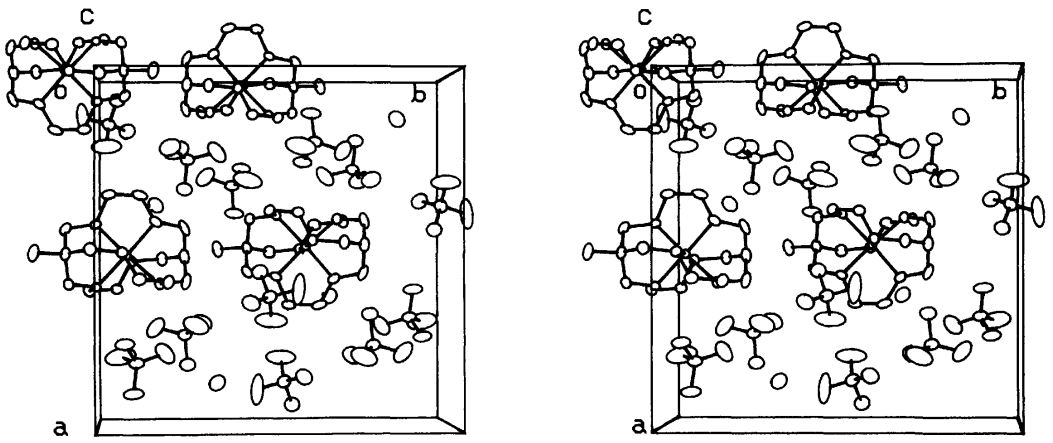

Fig. 3. Crystal packing.

Table 2. Atomic Coordinate. Positional Parameters are Multiplied by 10^5. Thermal Parameters are Given by the Equivalent Temperature factors (Å^2)

Atom	x	y	z	B_{eq}
Co	1165(3)	41387(3)	8080(6)	2.0
Cl(1)	30732(7)	38781(9)	7801(15)	4.4
Cl(2)	25958(8)	74594(9)	4443(14)	4.5
Cl(3)	−37368(8)	47288(9)	−2234(14)	4.3
O(1)	25364(22)	41883(32)	−2395(43)	6.4
O(2)	38888(22)	39653(31)	4098(45)	6.8
O(3)	29296(33)	43279(57)	19950(55)	13.4
O(4)	28170(41)	31025(41)	10621(111)	16.0
O(5)	29093(32)	79520(39)	14878(58)	9.5
O(6)	17502(26)	75464(28)	3917(55)	7.2
O(7)	27970(40)	66347(40)	5523(89)	12.7
O(8)	28887(36)	77706(46)	−8199(60)	11.3
O(9)	−35784(25)	41974(29)	8694(45)	6.9
O(10)	−44168(25)	44787(27)	−9787(53)	7.0
O(11)	−30743(30)	47876(58)	−11388(58)	13.4
O(12)	−39508(61)	55011(31)	2552(73)	14.1
N(1)	−7223(20)	49843(22)	10488(36)	2.6
N(2)	432(21)	42385(21)	−11980(33)	2.8
N(3)	9921(19)	49668(19)	8737(39)	2.4
N(4)	−7991(22)	33444(23)	8706(43)	3.3
N(5)	8937(22)	32430(21)	4727(38)	3.0
N(6)	2876(21)	40335(21)	28253(35)	2.8
N(7)	1529(30)	25629(22)	23300(43)	4.2
C(1)	536(43)	65863(30)	−15232(59)	5.4
C(2)	840(29)	57587(24)	−7283(46)	3.2
C(3)	−5944(29)	57804(30)	3118(54)	3.8
C(4)	−401(31)	50856(29)	−17748(46)	3.6
C(5)	9047(29)	56914(27)	−604(51)	3.3
C(6)	−15381(27)	46210(31)	7451(55)	3.9
C(7)	7487(30)	37844(32)	−18304(49)	3.6
C(8)	11236(27)	51965(27)	23386(46)	2.9
C(9)	−15359(31)	37841(37)	13953(59)	4.6
C(10)	8369(32)	30108(30)	−10018(56)	3.9
C(11)	10681(28)	44332(29)	31596(46)	3.0
C(12)	−6354(38)	25659(32)	16331(63)	4.9
C(13)	8398(39)	25209(31)	14481(57)	4.6
C(14)	2247(33)	31792(28)	33999(51)	3.8
Ow	36636(28)	16635(27)	23265(50)	7.1

tion band ($\Delta\varepsilon_{463}$=+3.10) has been determined to be Δ (see Table 1). This assignment is consistent with the deduction[16] made from the comparison of circular dichroism spectra of related complexes such as [Co(en)$_3$]$^{3+}$, [Co(sen)]$^{3+}$, and [Co(sep)]$^{3+}$.

Table 3. Bond Distances (l/Å) and Angles (ϕ/°) with E.S.D.'s

Co-N1	1.965(4)	Co-N2	1.967(3)
Co-N3	1.976(3)	Co-N4	1.987(4)
Co-N5	1.970(4)	Co-N6	1.995(4)
C1-C2	1.562(7)	C2-C3	1.505(7)
C2-C4	1.518(7)	C2-C5	1.497(7)
C6-C9	1.510(8)	C7-C10	1.510(8)
C8-C11	1.491(7)	N1-C3	1.505(7)
N1-C6	1.494(6)	N2-C4	1.505(6)
N2-C7	1.507(6)	N3-C5	1.504(6)
N3-C8	1.493(6)	N4-C9	1.496(7)
N4-C12	1.502(7)	N5-C10	1.490(7)
N5-C13	1.522(7)	N6-C11	1.473(6)
N6-C14	1.510(6)	N7-C12	1.463(8)
N7-C13	1.416(8)	N7-C14	1.457(7)
N1-Co-N4	86.0(2)	N1-Co-N5	175.3(2)
N2-Co-N5	86.3(2)	N2-Co-N6	175.4(2)
N3-Co-N6	85.8(2)	N3-Co-N4	175.7(2)
C1-C2-C3	106.8(4)	C2-C3-N1	113.8(4)
C1-C2-C4	107.1(4)	C2-C4-N2	114.0(4)
C1-C2-C5	107.9(4)	C2-C5-N3	114.0(4)
C3-N1-C6	112.0(4)	N1-C6-C9	106.0(4)
C4-N2-C7	111.8(4)	N2-C7-C10	105.5(4)
C5-N3-C8	113.3(3)	N3-C8-C11	107.0(4)
C9-N4-C12	112.6(4)	C12-N7-C14	113.7(4)
C10-N5-C13	113.7(4)	C13-N7-C14	113.9(5)
C11-N6-C14	112.8(4)	C12-N7-C13	114.8(5)
Co-N1-C3	117.3(3)	Co-N1-C6	108.7(3)
Co-N2-C4	117.0(3)	Co-N2-C7	108.7(3)
Co-N3-C5	117.0(3)	Co-N3-C8	108.0(3)
Co-N4-C9	107.7(3)	Co-N4-C12	116.0(3)
Co-N5-C10	108.1(3)	Co-N5-C13	116.0(3)
Co-N6-C11	107.6(3)	Co-N6-C14	112.5(4)

The coordination geometry around Co(III) appears to be typical for this type of complexes. The Co-N bond length and N-Co-N bond angle averaged over C_3 equivalents are 1.977(12)Å and 86.0(3)°. The corresponding values in [Co(sen)]$^{3+}$ are 1.971(6) Å and 86.1(2)°, respectively.[10] Further, other bond lengths and angles of the "[Co(sen)]$^{3+}$" moiety of [Co(azamesar)]$^{3+}$ are slso very similar to those of [Co(sen)]$^{3+}$. Thus, it may be concluded that the N(CH$_2$-)$_3$ capping takes place without affecting significantly the geometry of [Co(sen)]$^{3+}$.

The C1-C2 bond length (1.562(7)Å) appears to be

somewhat longer than normal. However, this may not be physically significant, because no such trend was observed in our previous structural studies on cobalt(III) complexes with ligands containing the $CH_3C(CH_2-)_3$ capping group, such as *Λ*-[Co(sen)]Cl·*d*-tart·$6H_2O$,[10] [Co(L)(en)]$(ClO_4)_3$,[4] and [Co(stn)]-$Cl_3\cdot 3.5H_2O$,[5] where tart=tartrate ion, L=6-methyl-6-(4-amino-2-azabutyl)-1,4-diazacycloheptane, and stn=1,1,1-tris(5-amino-2-azapentyl)ethane (see Fig. 1).

The C-N bond lengths alternate along the ligand strand from the capping nitrogen N7 to the first carbon atom of the "en" moiety; for example, the C-N bond lengths vary from 1.457(7) Å to 1.510(6) Å to 1.473(6) Å along the chain N7-C14-N6-C11, in this order. Concomitantly with the bond length alternation of this type, C(cap)-N(cap)-C(cap) angles open (the cap flattens) up to an average value of 114.1(6)°. Both of these tendencies are observed in other aza-capped complexes like $[Co(sep)]^{3+}$ and [Co(azacapten)]$^{3+}$ (azacapten=8-methyl-6,10,19-trithia-1,3,13,16-tetraazabicyclo[6.6.6]icosane; see Fig. 1),[16,17] and considered to be responsible for very reduced proton affinity of the capping nitrogens.[8]

The "en" rings of the cation adopt the $(lel)_3$ conformation. This is most clearly seen in Fig. 4. This $(lel)_3$ conformation has also been reported for *Λ*-[Co(sen)]Cl·*d*-tart·$6H_2O$[10] and *Λ*-[Co(sep)]$Cl_3\cdot H_2O$.[16] In this conformation, all the N-H hydrogens point approximately to the C_3 equatorial direction and therefore are more suitable for double hydrogen bonding proposed previously (between two N-H hydrogens of the cation and oxygen atoms of the associating anion) than in the $(ob)_3$ one. The energy difference between the $(lel)_3$ and $(ob)_3$ conformations in the cage complexes of cobalt(III) is estimated to be rather small.[2] Thus, it is probable that the $(lel)_3$ conformation may be stabilized by such double hydrogen bonding in aqueous solution; multiple hydrogen bonding is known to be capable of stabilizing one conformation selectively over the other.[18]

Deviations from the tetrahedral value are observed in C-C-N, C-N-C, and Co-N-C angles, as well as the previously noted C(cap)-N(cap)-C(cap) angles. The angles averaged over C_3 equivalents are, along the ligand strand from C2, C2-C(cap)-N(en)=113.9(1)°, C(cap)-N(en)-C(en)=112.4(8)°, C(en)-N(en)-C(cap)=113.0(6)°, and N(en)-C(cap)-N(cap)=112.8(7)°. The Co-N(en)-C(cap) angles similarly averaged are 115.9(22)° near the $CH_3C(CH_2-)_3$ cap and 116.0(1)° near the $N(CH_2-)_3$ cap. The torsional angles averaged similarly are, along the ligand strand from Cl to C2 to C(cap) and so on, Cl-C2-C(cap)-N(en)=173.7(12)°, C2-C(cap)-N(en)-C(en)=116.0(5)°, C(cap)-N(en)-C(en)-C(en)=171.8(8)°, N(en)-C(en)-C(en)-N(en)=53.4(5)°, C(en)-C(en)-N(en)-C(cap)=169.8(5)°, and C(en)-N(en)-C(cap)-N7=117.8(7)°. All these angles do not differ significantly from the corresponding angles of $[Co(sen)]^{2+}$ and $[Co(sep)]^{3+}$, suggesting that the ligand strain does not differ significantly.

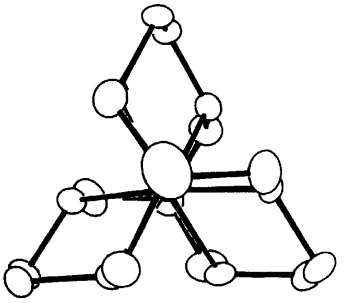

Fig. 4. Projection down the pseudo-threefold axis of rotation of the cation. Ellipsoids enclose 30% probabilities.

The authors are grateful to Dr. Haruko Ito, Aichi Kyoiku University, for technical assistance.

References

1) U. Sakaguchi, S. Tamaki, K. Tomioka, and H. Yoneda, *Inorg. Chem.*, **24**, 1624 (1985).
2) R. J. Geue, T. W. Hambley, J. M. Harrowfield, A. M. Sargeson, and M. R. Snow, *J. Am. Chem. Soc.*, **106**, 5478 (1984).
3) U. Sakaguchi, unpublished.
4) K. Tomioka, U. Sakaguchi, and H. Yoneda, *Inorg. Chem.*, **23**, 2863 (1984).
5) U. Sakaguchi, K. Tomioka, T. Kashihara, and H. Yoneda, *Inorg. Chem.*, **24**, 463 (1985).
6) I. I. Creaser, A. M. Sargeson, and A. W. Zanella, *Inorg. Chem.*, **22**, 4022 (1983).
7) D. Geselowitz, *Inorg. Chem.*, **20**, 4457 (1981).
8) I. I. Creaser, R. J. Geue, J. M. Harrowfield, A. J. Herlt, A. M. Sargeson, M. R. Snow, and J. Springborg, *J. Am. Chem. Soc.*, **104**, 6016 (1982).
9) J. E. Sarneski and F. L. Urbach, *J. Am. Chem. Soc.*, **93**, 884 (1971).
10) H. Okazaki, U. Sakaguchi, and H. Yoneda, *Inorg. Chem.*, **22**, 1539 (1983).
11) "International Tables for X-ray Crystallography," Kynoch Press, Birmingham, England (1974), Vol. IV.
12) R. F. Stewart, E. R. Davidson, and W. T. Simpson, *J. Chem. Phys.*, **42**, 3175 (1965).
13) Tables of positional parameters for hydrogen atoms, anisotropic thermal parameters for non-hydrogen atoms, and a list of the observed and calculated structure factors are kept in the office of the Chemical Society of Japan (Document No. 8619).
14) C. K. Johnson, *Rept. Oak Ridge Natl. Lab.* **1976**, ORNL-5138.
15) T. Sakurai and K. Kobayashi, *Rikagaku Kenkyusho Hokoku (Rept. Inst. Phys. Chem. Res.)*, **55**, 69 (1979).
16) I. I. Creaser, J. M. Harrowfield, A. J. Herlt, A. M. Sargeson, J. Springborg, R. J. Geue, and M. R. Snow, *J. Am. Chem. Soc.*, **99**, 3181 (1977).
17) R. J. Geue, T. W. Hambley, J. M. Harrowfield, A. M. Sargeson, and M. R. Snow, *J. Am. Chem. Soc.*, **106**, 5478 (1984).
18) J. L. Sudmeier, G. L. Blackmer, C. H. Bradley, and F. A. L. Anet, *J. Am. Chem. Soc.*, **94**, 757 (1972).

Parity Rule. Algorithmic Method for the Assignment of Chiral Centers

Mitsuharu KOTERA*
U. A. 464 Laboratoire de Chimie Organique, Faculté des Sciences et des Techniques de Rouen,
76130 Mont Saint Aignan, France
(Received July 30, 1985)

Synopsis. A simple new algorithm is presented for the assignment of *R/S* configuration of chiral centers described in any projection form.

The configuration *R* and *S* of a chiral center (such as carbon with four ligands) is generally determined by the sequence rule procedure:[1,2] This procedure involves, in the last step, a mental transfer of the molecule described in a two dimensional surface. Such a mental transfer can become more and more difficult with increasing molecular complexity and even experienced chemists may make mistakes in this step.

Here we wish to present a simple algorithm for the assignment of chiral center configuration. This method requires no transformation of the first projection described and is, furthermore, applicable to complex molecules.

The method is outlined as follows:

(1) Assign the priority numbers for each group surrounding the chiral center.

(2) Take the number of the group which is clearly directed forward, and then the three others in a clockwise manner. Thus a sequence of four numbers is obtained.[3]

(3) Then take each of the first three numbers in the sequence, and count *how many* smaller numbers follow each one from left to right. Take the sum of these counts.

(4) In the case of an *R*-configuration, the resulting sum will be even. For an *S*-configuration, the operation will yield an odd sum.[4]

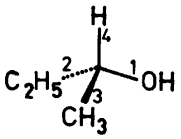

Fig. 1.

For example, consider the configuration of 2-butanol (Fig. 1). The number of the methyl group (No. 3) directed forward is taken first. Then the three other groups (No. 4, No. 1, No. 2) are taken in a clockwise manner. Thus the sequence 3-4-1-2 is obtained. After No. 3, TWO smaller numbers (No. 1 and No. 2) follow. After No. 4, TWO smaller numbers (No. 1 and No. 2) follow. After No. 1, NO smaller number follows. TWO+TWO+ZERO=FOUR, an even sum is obtained. This indicates that the configuration is *R*.

The Figs. 2—5 show the flexibility of this method for many different projection forms.

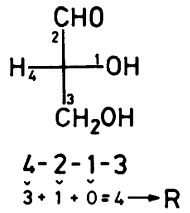

Fig. 2.

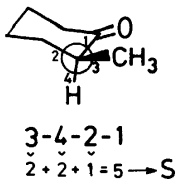

Fig. 3.

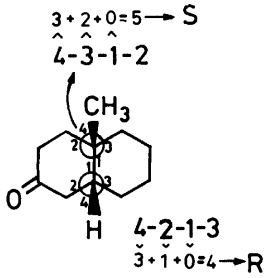

Fig. 4.

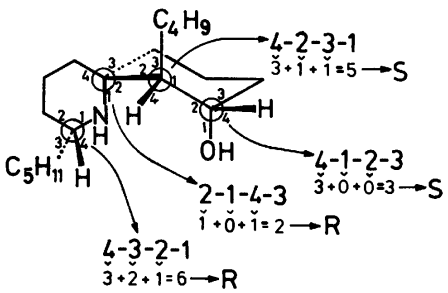

Fig. 5.

The rule will always give the correct answer provided the diagram is clearly drawn.[5] This method has advantages over the others,[6-10] in which many numbers or tables must be memorized. Here, the sequence to be remembered is simply "forward directed group first," "the three others in a clockwise manner," "how many smaller numbers follow" and "even=*R*." The rule will be particularly useful when there are many chiral centers to be assigned and verified.

The author thanks Dr. G. P. Moss for his helpful suggestion about the examples 7—10.

References

1) R. S. Cahn, C. K. Ingold, and V. Prelog, *Angew. Chem. Int. Ed.*, **5**, 385 (1966).

2) V. Prelog and G. Helmchen, *Angew. Chem. Int. Ed.*, **21**, 567 (1982).

3) Regardless of which number is taken in second place, the result is the same as long as the clockwise manner is respected.

4) This algorithm is based on the following facts.

1° The sequence 1-2-3-4 corresponds to the *R*-configuration.

2° When two numbers of a sequence are interchanged, the related configuration is inversed.

3° The sums of the number of smaller numbers following in the sequence correspond to the number of changes necessary to afford the series 1-2-3-4. For example, from the sequence 4-3-2-1, one can arrive at the sequence 1-2-3-4 with the six following exchanges:

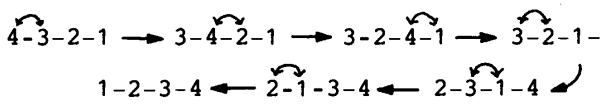

5) It must be noted that in some representations, it becomes difficult (Figs. 6—8) or even impossible (Figs. 9—10) to choose a forward directed group. In Fig. 6, only the backward directed group is indicated. In such cases, one must choose, as the forward directed group, one of the two neighbouring groups on either side of the backward directed group. In the case of Figs. 7—10, the problems are due to the representations themselves. The configuration of a chiral center represented as in Fig. 11 (a planar carbon) cannot be known without some further information. The true configuration of Fig. 11 must be either 12 or 14, and in each case, it is different. This ambiguous representation can be found in Figs. 7—10. In Figs. 7—8, we know what are intended here. But in the case of Fig. 9, we are not sure of the configuration of the carbon in question. The starred carbon in Fig. 10 which appeared in IUPAC E rule[11] is almost planar and it will be impossible to determine its configuration.

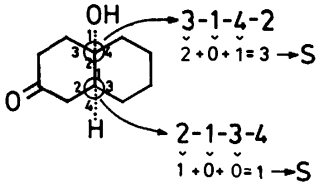

Fig. 6.

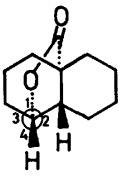
Fig. 7.

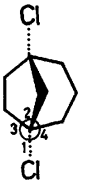
Fig. 8.

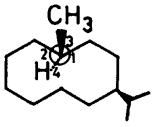
Fig. 9.

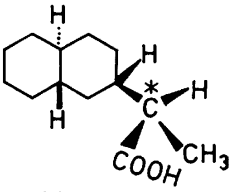
Fig. 10.

Fig. 11. Fig. 12. Fig. 13. Fig. 14. Fig. 15.

We wish to insist that the figures must be clearly drawn.

1° Generally, it is sufficient to indicate only one well chosen group directed forward or backward for each chiral center as in Fig. 13 and Fig. 15, and its configuration will be clear. (It is assumed that the Fisher type representation Fig. 12 or Fig. 14 is implicated in them)

2° If there are two groups directed respectively forward and backward on the opposite sides of one chiral center as in Fig. 11, its configuration is locally ambiguous.

Thus the configuration of encircled carbons in Fig. 7 and Fig. 8 will be clearer in Fig. 16 and Fig. 17. Figure 9 may be drawn as in Fig. 18, and Fig. 10 as in Fig. 19 or Fig. 20.

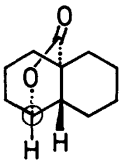
Fig. 16.

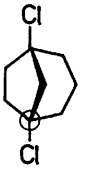
Fig 17.

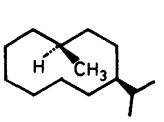
Fig. 18.

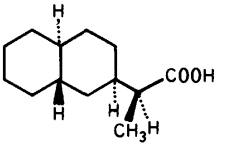
Fig. 19.

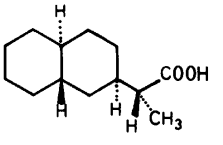
Fig. 20.

6) O. Cori, *J. Chem. Educ.*, **49**, 461 (1972).
7) R. A. Dietzel, *J. Chem. Educ.*, **56**, 451 (1979).
8) Y. Brun and P. Leblanc, *J. Chem. Educ.*, **60**, 403 (1983).
9) D. L. Mattern, *J. Chem. Educ.*, **62**, 191 (1985).
10) E. L. Eliel, *J. Chem. Educ.*, **62**, 223 (1985).
11) "IUPAC Tentative Rule for the Nomenclature of Organic Chemistry. Section E. Fundamental Stereochemistry," *J. Org. Chem.*, **35**, 2849 (1970).

^{35}Cl NQR and Ionicities of a Few *N*-Chloroimides

Yoshitaka NAGAO* and Shigeyoshi KATAGIRI
Department of Chemistry, Faculty of Science, Hirosaki University, Bunkyo-cho, Hirosaki 036
(Received July 26, 1985)

Synopsis. ^{35}Cl NQR frequencies were measured for *N*-chlorosuccinimide (NCS), *N*-chlorophthalimide (NCP), *N,N'*-dichlorobarbital (NDCB), sodium *N,N'*-dichloroisocyanurate dihydrate (Na-NDCI·2H$_2$O) and *N,N',N''*-trichloroisocyanuric acid (NTCI). The ionicities estimated by a ^{35}Cl NQR study increased in the following order; NCS<NCP <NDCB<Na-NDCI·2H$_2$O<NTCI. A linear relationship between the ionicities of chlorine atoms and the polarographic reduction potentials of N-Cl bonds was found. The ionicity was related to the reactivity.

Since the first report on a ^{35}Cl NQR study of the N-Cl bond by Segel et al.,[1] several papers about ^{35}Cl NQR studies of molecules with this bond have been published.[2-6] The ^{35}Cl NQR frequency is higher for a N-Cl bond than for a C-Cl bond because the electronegativity of chlorine is practically the same as that of nitrogen.

N-halogenoimides are effective reagents for the halogenation and the oxidation of olefins, alcohols and carbonyl compounds. In this paper, we report on the ^{35}Cl NQR frequencies for a few *N*-chloroimides and the reactivities of these compounds.

Experimental

The materials, except for *N,N'*-dichlorobarbital, were purified several times by the recrystallization of commercial products. *N,N'*-dichlorobarbital was prepared by a method described in the literrature[7] and purified by recrystallization. It was identified by its IR spectrum.

An NQR spectrometer of the type described by Dean[8] was used. The signals were either observed on a CRO or recorded on a chart. The resonance frequencies were measured on a CRO screen with the help of an RF-signal generator (Trio, Model SG-2) and a frequency counter (Anritsu, MF-55D).

Sample tubes of about 22-mm diameter were used. All measurements were made at liquid-nitrogen temperature.

Results and Discussion

The ^{35}Cl NQR frequencies of the *N*-chloroimides at liquid-nitrogen temperature are given in Table 1. For *N*-chlorosuccinimide (NCS) and *N*-chlorophthalimide (NCP), the observed frequencies agree with those found in the literature.[3] *N,N',N''*-trichloroisocyanuric acid† (NTCI) showed two resonance lines ν_1=58.902 MHz and ν_2=46.423 MHz. The latter agrees with the result of Fitzky et al.[4] The frequency ratio, ν_1/ν_2=1.2688, agrees with the isotope frequency ratio, $\nu(^{35}Cl)/\nu(^{37}Cl)$. Therefore, it was found that the result of Fitzky et al. corresponds to the ^{37}Cl NQR frequency of NTCI. According to Hart et al.,[3] all the nitrogen atoms of the compounds cited in Table 1 have $tr^1tr^1tr^1\pi^2$ hybridization states and their structures are either planar or near planar.[9] This conclusion is consistent with the IR and Raman spectra.[10,11]

Table 1. ^{35}Cl NQR Parameters of *N*-Chloroimides at Liquid Nitrogen Temperature

Compound	ν/MNz	e^2Qq/h / MHz	i
N-Chlorosuccinimide	54.095	108.2	−0.01
N-Chlorophthalimide	55.402	110.8	0.01
N,N'-Dichlorobarbital	57.036	114.1	0.03
Sodium *N,N'*-dichloroisocyanurate dihydrate	58.208	116.4	0.05
N,N',N''-Trichloroisocyanuric acid	ν_1=58.902 ν_2=46.423	117.8	0.06

The asymmetry of the field gradient in this case originates from the π-bond character of the N-Cl bond. From the possible resonance structures, the π character can be excluded. Therefore, the asymmetry parameter, η, must be negligibly small and the quadrupole coupling constant, e^2Qq/h, is twice the resonance frequency. We have calculated the quadrupole coupling constant (Table 1). The coupling constant of NCS is smaller and the values for other compounds are larger than that of the chlorine atom (109.74 MHz for ^{35}Cl[12]). This indicates that the chlorine atom of NCS has a negative charge and others are posivively charged. According to Townes and Dailey,[12] the coupling constant is given by

$$e^2Qq = (1+\alpha i)(e^2Qq)_{atom}$$

where i stands for the bond ionicity and $(e^2Qq)_{atom}$ denotes e^2Qq of the atomic chlorine. For a negative ionicty, α=−1 is used and for a positive ionicity α= 1.28. Here, the s and d characters of chlorine are neglected because the electronegativity of chlorine is practically the same as that of nitrogen and the d character is always less than 5% for the chlorine atom.[12] By the use of this relation, the ionic character of the N-Cl bonds were evaluated (Table 1). Sodium *N,N'*-dichloroisocyanurate†† dihydrate (Na-NDCI·2H$_2$O) has a lower ionicity than that of NTCI since the sodium ion decreases the inductive effect of the carbonyl group to the N-Cl bond. The ionicity increases in the following orde; NCS<NCP <NDCB<Na-NDCI·2H$_2$O<NTCI.

Figure 1 shows the relationship between the ionicity, i, and the polarographic reduction potential,[13] $E_{1/2}$, of *N*-chloroimides. The reduction of the N-Cl bond becomes easier when the polarity of the N-Cl bond increases. The result of a polarographic study shows

† Systematic name: 1,3,5-trichloro-1,3,5-triazine-2,4,6-(1*H*,3*H*,5*H*)-trione.

†† Systematic name: 1,3-trichloro-1,3,5-triazine-2,4,6-(1*H*,3*H*,5*H*)-trione sodium salt.

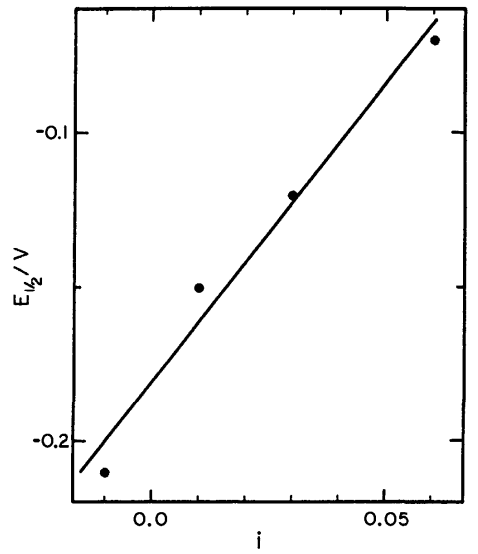

Fig. 1. The relationship between the ionic character, i, and reduction potential, $E_{1/2}$ of *N*-chloroimide.

that the polarity of *N*-chloroimide increases in the following order; NCS<NPC<NDCB<NTCI. This is in agreement with the results of our ^{35}Cl NQR study.

Reactions of NTCI and NCS with some metal alkyls and metal chlorides were studied by Leimeister et al.[14] Substitution reactions occur with NTCI, whereas NCS reacts only with $SnCl_5$, forming hexachloroantimonate. This fact shows that the chlorine atom of NTCI is more positive than that of NCS. Otsuji et al.[13] sudied the reactions of cyclohexanone with NTCI and NDCB. The results show that the N-Cl bond is more polar in NTCI than in NDCB. They also studied the chlorination of cyclohexene with NDCB and NCS and concluded that the polarity of the N-Cl bond increases from NCS to NDCB. These three facts explain why the polarity of the N-Cl bond increases in the following order; NCS<NDCB<NTCI. This agrees with the order of the ionicity evaluated in the present study. Thus, we conclude that the ionicity of *N*-chloroimides (as estimated by the ^{35}Cl NQR study) provides a good measure of the reactivities of the *N*-chloroimides.

References

1) S. L. Segel, R. G. Branes, and P. J. Bray, *J. Chem. Phys.*, **25**, 1286 (1956).
2) H. Kashiwagi, D. Nakamura, and M. Kubo, *Tetrahedron*, **21**, 1095 (1965).
3) R. M. Hart and M. A. Whitehead, *Trans. Faraday Soc.*, **67**, 1569 (1971).
4) H. G. Fitzky, D. Wendisch, and R. Holm, *Angew. Chem. Int. Ed. Eng.*, **11**, 979 (1972).
5) A. L. Fridman, L. O. Konshina, and S. A. Petukhov, *Zh. Org. Khim.*, **11**, 1187 (1975).
6) G. N. Delenko, A. V. Zibarev, S. A. Krupoder, L. N. Mazalov, O. Ch. Poleshchuk, G. G. Furin, G. F. Khudorozhko, and G. G. Yakobson, *J. Fluorine Chem.*, **17**, 1 (1981).
7) K. Ziegler, A. Späth, E. W. Schumann and E. Winkelmann, *Ann.*, **551**, 80 (1942).
8) C. Dean and M. Pollak, *Rev. Sci. Instrum.*, **29**, 630 (1958).
9) Brown indicated that *N*-chlorosuccinimide is significantly aplanar. N. R. Brown, *Acta Cryst.*, **14**, 711 (1961).
10) R. C. Petterson, U. Grzeskowiak, and L. H. Jules, *J. Org. Chem.*, **25**, 1595 (1960).
11) K. Dehnicke and H. Leimeister, *Z. Naturforsch., Teil B*, **26**, 1101 (1971).
12) T. P. Das and E. L. Hahn, "Nuclear Quadrupole Resonance Spectroscopy," Academic Press, New York, San Fracisco, London (1985), p. 142.
13) Y. Otsuji, T. Kuroda, and E. Imoto, *Bull. Chem. Soc. Jpn.*, **41**, 2124 (1968).
14) H. Leimeister and K. Dehnicke, *Z. Anorg. Allg. Chem.*, **415**, 115 (1975).

Activity Coefficients of Dimethyl-β-cyclodextrin in Aqueous Solutions

Koichiro MIYAJIMA,* Takayo MUKAI, Masayuki NAKAGAKI, Masaki OTAGIRI,† and Kaneto UEKAMA†
Faculty of Pharmaceutical Sciences, Kyoto University Yoshida-shimoadachi-cho, Sakyo-ku, Kyoto 606
†Faculty of Pharmaceutical Sciences, Kumamoto University 5-1, Oe-honmachi, Kumamoto 862
(Received August 1, 1985)

Synopsis. The activity coefficients of aqueous solutions of dimethyl-β-cyclodextrin were measured by vapor pressure osmometry at 25, 35, and 45±0.1 °C. The activity coefficient decreased with increase of concentration at each temperature. Both the excess enthalpy and the excess entropy were positive. The negative excess free energy originates from the large excess entropy term, indicating that dimethyl-β-cyclodextrin is a hydrophobic solute.

In a previous paper,[1] we determined the activity coefficients of α- and γ-cyclodextrins in aqueous solutions at 25 °C. In contrast with the concentration dependence of activity coefficients of aqueous solutions of D-glucose,[2] the activity coefficients of these cyclodextrins decreased with increase of concentration, implying that these solutes either associate or break the water structure.

Dimethyl-β-cyclodextrin(DM-β-CD) is heptakis(2,6-di-*O*-methyl)-β-cyclodextrin. The solubility of DM-β-CD in water is about ten times larger than that of β-CD and is soluble in organic solvents.[3] The complex formation and the properties of complexes are now being extensively studied.

From these points of view, we determined the temperature dependence of the activity coefficients of DM-β-CD in aqueous solutions to elucidate the solution property.

Experimental

Materials. DM-β-CD supplied from Toshin Chemicals was recrystallized from water. The purity was confirmed by HPLC and ^{1}H NMR. The compound was dried in vacuo at room temperature for several days before use. The melting point was 96 °C. Reagent grade sodium chloride obtained from Nakarai Chemical Co. Ltd. was used after drying in vacuo at 100 °C for 2 d. Aqueous solutions of these compounds were prepared with water purified by distillation and deionization.

Method. Vapor pressure over aqueous solution was measured at 25, 35, and 45±0.1 °C with an osmometer model 117 manufactured by Corona Electric Co. Ltd. To obtain the accurate results, osmotic pressures of DM-β-CD solution and NaCl solution (reference) of corresponding concentration were measured consecutively in every set of measurement. The experimental determination of osmotic coefficient was precise to ±0.02.

Results

The relations between the osmotic coefficients ϕ and the concentration m in $mol^{-1}kg$ at 25, 35, and 45 °C are shown in Fig. 1. The values of ϕ decrease with increase of concentration at each temperature. By the least-square fitting, the values of ϕ at the respective temperatures are expressed in terms of m as

$$\phi_{25} = 1 - 6.73\,m + 37.4\,m^2,$$

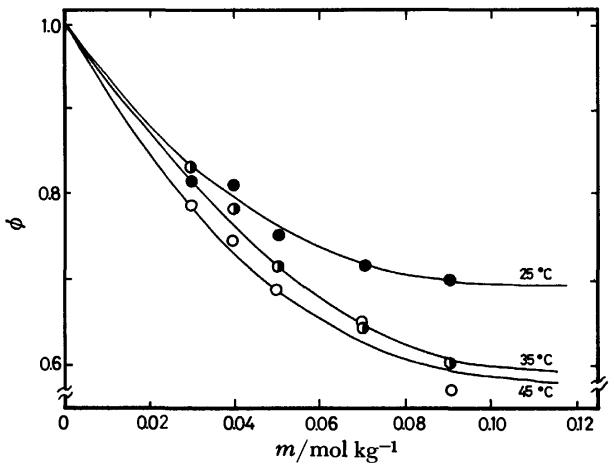

Fig. 1. Relation between osmotic coefficient and concentration for DM-β-CD at various temperatures.
●: 25 °C, ◑: 35 °C, ○: 45 °C.

$$\phi_{35} = 1 - 7.07\,m + 28.0\,m^2, \quad (1)$$

and

$$\phi_{45} = 1 - 8.49\,m + 44.4\,m^2.$$

The activity coefficient is calculated from Eq. 2.

$$\ln\gamma = (\phi - 1) + \int_0^m \frac{\phi - 1}{m}\,dm \quad (2)$$

Introducing Eq.1 into Eq. 2 and integrating, we obtain

$$\ln\gamma_{25} = -13.5\,m + 56.6\,m^2,$$

$$\ln\gamma_{35} = -14.1\,m + 42.0\,m^2, \quad (3)$$

and

$$\ln\gamma_{45} = -17.0\,m + 66.6\,m^2.$$

The activity coefficient vs. m curves are shown in Fig. 2.

The excess thermodynamic quantities are calculated from Eqs. 4, 5, and 6

$$G^{ex} = mRT(1 - \phi + \ln\gamma), \quad (4)$$

$$S^{ex} = -\left(\frac{\partial G^{ex}}{\partial T}\right)_p \quad (5)$$

and

$$H^{ex} = G^{ex} + TS^{ex}, \quad (6)$$

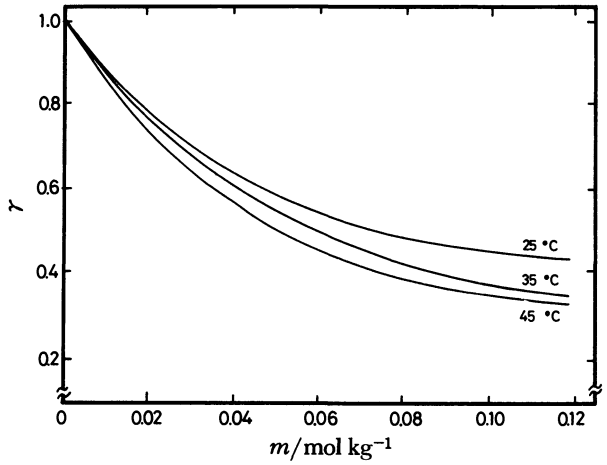

Fig. 2. Relation between activity coefficient and concentration at various temperatures.

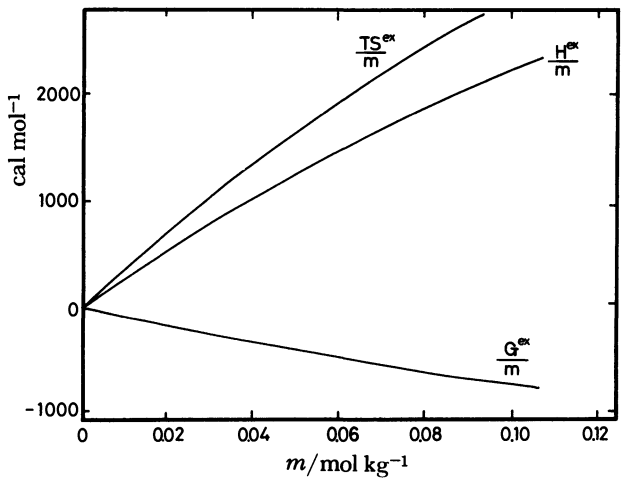

Fig. 3. Molar excess thermodynamic quantities vs. concentration curves at 35 °C. (1 cal=4.184 J)

where R and T are of usual meanings. The molar excess thermodynamic quantities are shown in Fig. 3 as a function of m.

Discussion

As shown in Figs. 1 and 2, the values of ϕ and γ decrease with increase of m. Similar trends were observed in aqueous solutions of α- and γ-CDs. But the decreasing tendency of activity coefficient with increase of m for DM-β-CD is more significant than those of α- and γ-CDs. In general, the decrease in activity coefficient with increase of m is interpreted in terms of two different effects, i.e. structure breaking effect and the association of the solutes. However, such a large decrease of activity coefficient in low concentration is more likely to take place as a results of the solute-solute interaction rather than the solute–solvent interaction. In contrast with the case of aqueous α-CD solution, the negative excess free

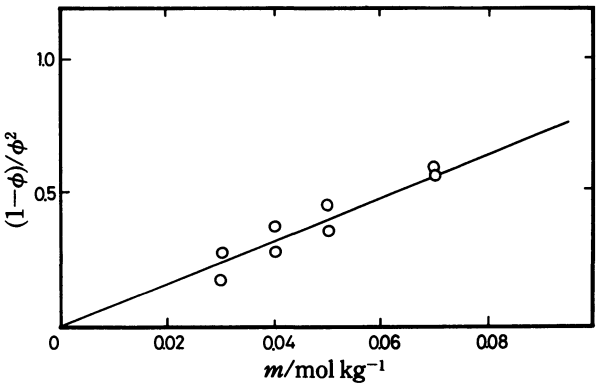

Fig. 4. $(1-\phi)/\phi^2$ vs. concentration curve at 25 °C.

energy of aqueous DM-β-CD solution originates from the predominance of positive entropy term over positive enthalpy as seen in Fig. 3, indicating that DM-β-CD is a hydrophobic solute like tetrabutylammonium salts.[5] The self salting-in effect based on the hydrophobic interaction among DM-β-CD molecules increase with concentration, resulting in the increase of excess entropy by the destruction of iceberg around DM-β-CD molecules. Positive enthalpy also increases with concentration because of the melting of iceberg. But the values of TS^{ex} is larger than that of H^{ex} for the hydrophobic solute. The hydrophobic nature of DM-β-CD should be attributed to the methyl groups which locate on the outer surface of the molecule.

By assuming that the large decrease of activity coefficient with increase of m is based on the dimer formation through hydrophobic interaction, we calculated the formation constant(K) at each temperature with Eq. 7.[6]

$$K = (1-\phi)/m\phi^2 \tag{7}$$

The relation between $(1-\phi)/\phi^2$ and m at 25 °C is shown in Fig. 4. From the slope of curve, 8.1, 11.4, and 12.5 $mol^{-1}kg$ were obtained as the K values at 25, 35, and 45 °C. The increase of K with temperature is consistent with the theoretical results of hydrophobic interaction between leucine and isoleucine in water.[7]

In conclusion, DM-β-CD is a hydrophobic solute in contrast with α- and γ-CDs which are hydrophilic.[1]

References

1) K. Miyajima, M. Sawada, and M. Nakagaki, *Bull. Chem. Soc. Jpn.*, **56**, 3556 (1983).
2) K. Miyajima, M. Sawada, and M. Nakagaki, *Bull. Chem. Soc. Jpn.*, **56**, 1954 (1983).
3) J. Szejtli, *J. Inclusion Phenom.* **1**, 135 (1983).
4) K. Uekama and M. Irie, *Seiyaku-kojyo*, **5**, 20 (1985).
5) S. Lindenbaum, *J. Phsy. Chem.*, **70**, 814 (1966).
6) P. O. P. T'so and S. I. Chan, *J. Am. Chem. Soc.*, **86**, 4176 (1964).
7) H. A. Sheraga and G. Nemethy, *J. Phys. Chem.*, **66**, 1773 (1962).

Thermal Diffusion of Prototropic Ions in Water

Naokata TAKEYAMA* and Kimie NAKASHIMA
Department of Industrial Chemistry, Faculty of Science and Engineering, Saga University, Saga 840
(Received August 5, 1985)

Synopsis. Regarding the Soret effect of prototropic ions of H^+ and OH^- in dilute aqueous solutions, it has been mentioned that heat-of-transport values for ions are in good agreement with those of the activation energies for ionic diffusion in the Arrhenius expression. The physicochemical significance of these facts is discussed in relation to the inclusion of thermal diffusion terms in Kramers' formula for ordinary diffusion flux.

The Soret effect regarding an aqueous ionic solution can be described with the Nernst-Hartley approximation in very dilute conditions by

$$J = -D^\circ \operatorname{grad} m - D'm \operatorname{grad} T \quad (1)$$

for ions under the Kohlrausch law which concerns the independent mobility of ions. J is the ionic diffusion flux, m the ionic molal concentration, D° the limiting ionic diffusion coefficient, D' the ionic thermal diffusion coefficient, and T the temperature which is dependent on the position coordinate.[1] At a Soret steady state of $J=0$, the Soret coefficient s° and the heat-of-transport Q^* are expressed[2] as

$$s^\circ = -d\ln m/dT = D'/D^\circ = Q^*/RT^2, \quad (2)$$

where R is the gas constant. The heats of transport for various ions are subject to the additivity rule for electrolytes in sufficiently dilute aqueous solutions.[2] Reversely, Q^* for ions should be derived from the observed heats of transport for various electrolytes. At present, there is no good method for dividing the heat of transport of an electrolyte into the heats of transport for constituent ions, except for a conventional method proposed by Snowdon and Turner[2] on the scale of $Q^*=0$ for Cl^- at 298 K and 0.01 mol kg^{-1}. It is obvious that the conventional values are not suitable for a physicochemical discussion. In this regard, the present authors have proposed a rational method for dividing the heats of transport for electrolytes into those for ions after the introduction of a reduction rule with reference to thermal diffusion coefficients of 1-1 electrolytes in aqueous solutions at 298 K and 0.01 mol kg^{-1}.[3] Although this method is quite different from the conventional method of Snowdon and Turner, the values of Q^* for H^+ and OH^- obtained from both methods are in good agreement.

On the other hand, as is well known, the Arrhenius expression for ionic diffusion coefficients shows a narrower applicability than for the reaction-rate constants.[4] An apparent activation energy E_a can still be introduced:

$$\partial \ln D^\circ/\partial T = E_a/RT^2 \quad (3)$$

for a certain temperature. However, E_a continues to be temperature dependent.[5,6]

Table 1. Ionic Quantities of Diffusion and Thermal Diffusion for H^+ and OH^- in Water at 298 K

Ion	D°	D'	Q^*	E_a
	$10^{-5}cm^2s^{-1}$	$10^{-8}cm^2s^{-1}K^{-1}$	kJ mol^{-1}	kJ mol^{-1}
H^+	9.31	161.1	12.8	12.8
OH^-	5.32	119.9	16.7	16.8

Here, we wish to discuss various relations between Q^* and E_a for H^+ and OH^- in water.

Table 1 summarizes the values of D°, D', Q^*, and E_a that were estimated for H^+ and OH^- at 298 K. The values of D° were obtained by the Nernst-Einstein relation from the limiting molar conductivities of H^+ and OH^-, of which the temperature dependences have been used to estimate the values of E_a according to Eq. 3.[6] The values of D' have been calculated from the values of Q^* using Eq. 2 with D° at 298 K.

It has been found that Q^* is equal to E_a for H^+ and OH^-, respectively. This relation is never valid for ions other than H^+ and OH^-. For example, referring to Li^+, there is a much larger difference between $Q^*=-0.01$ kJ mol^{-1} [3] and $E_a=18.9$ kJ mol^{-1}. These are obtained in a quite similar manner to the cases of H^+ and OH^-.

In order to understand this fact most simply for H^+ and OH^- in water, we use Kramers' formula for an isothermal diffusion flux[7]

$$J = -\exp(-U/RT) \operatorname{grad} D^\circ m \exp(U/RT). \quad (4)$$

The notation is the same as that mentioned above and U is an external potential which is dependent on the positions of the diffusing ions. For the present, we assume that D° is indirectly dependent on position through the position dependence of T, even in non-isothermal conditions. Thus, Eq. 4 can be expanded into

$$J = -D^\circ \operatorname{grad} m - (\partial D^\circ/\partial T)m \operatorname{grad} T + D^\circ m(U/RT^2) \operatorname{grad} T - (D^\circ m/RT) \operatorname{grad} U. \quad (4\cdot a)$$

The last term on the right side of Eq. 4.a is a drift term due to an external force. The second and third terms can be reduced to a thermal-diffusion term by taking the thermal-diffusion coefficient

$$D' = D^\circ(\partial \ln D^\circ/\partial T - U/RT^2). \quad (4\cdot b)$$

In the presence of U, using Eqs. 2 and 3, the heat of transport is

$$Q^* = E_a - U. \quad (4\cdot c)$$

In the absence of U, Eqs. 4.b and 4.c are simply

$$D' = \partial D^\circ/\partial T \quad (4\cdot d)$$

and

$$Q^* = E_a. \tag{4.e}$$

From Eqs. 2 and 3 it is easily seen that Eq. 4.d is equivalent to Eq. 4.e, and vice versa. Equation 4.e, which is independent of U, corresponds to cases of the thermal diffusion of H^+ and OH^- in water. Moreover, it can be mentioned that Eq. 4.d agrees with an earlier proposition by Wirtz.[8]

As an important consequence of Eq. 4.e and in harmony with the empirical fact that Q^* equals E_a for H^+ and OH^-, we can consider that the values of the heat of transport of H^+ and OH^- which we used are reasonable.

In this regard, it is a well known fact that in the case of superionic solid conductors the activation energies of ionic conduction are equal to the heats of transport derived from ionic thermoelectric power.[9] These conductors are composed of mobile superions and rigid lattice ions. These are dealt with theoretically by using a lattice gas model.[10] In comparison with these superionic conductors, it can be proposed that H^+ and OH^- behave like a superion in an immobile hydrogen bonded quasi-lattice in water due to the Grotthuss' mechanism.

References

1) D. D. Fitts, "Nonequilibrium Thermodynamics," McGraw-Hill, New York (1962), Chap. 9.

2) P. N. Snowdon and J. C. R. Turner, *Trans. Faraday Soc.*, **56**, 1409 (1960).

3) N. Takeyama and K. Nakashima, *J. Phys. Soc. Jpn.*, **52**, 2692, 2699 (1983).

4) H. J. V. Tyrrell and K. R. Harris, "Diffusion in Liquids," Butterworths, London (1984), p. 284.

5) In Ref. 4 the following equation is shown as the temperature dependence with rather more success:

$$D^\circ = AT^n \exp(-E/RT)$$

with constant A, n, and E within applicable temperature ranges.

For H^+, n and E are -13.7 and 46.9 kJ mol^{-1} from 273 to 329 K, and -3.31 and 18.5 kJ mol^{-1} from 329 to 373 K. For OH^- these are -27.7 and 85.4 kJ mol^{-1} from 273 to 308 K, and -5.41 and 27.5 kJ mol^{-1} from 308 to 373 K. As a reference, for Li^+ these are -17.2 and 61.6 kJ mol^{-1} from 273 to 310 K, and -8.12 and 38.1 kJ mol^{-1} from 310 to 373 K. The relationship to E_a is $E_a=E+nRT$ at a temperature T.

6) R. A. Robinson and R. H. Stokes, "Electrolyte Solutions," Butterworths, London (1959), p. 463. The results in Ref. 5 are also analyzed by the present authors from the data in this book.

7) H. A. Kramers, *Physica*, **7**, 284 (1940); S. Chandrasekhar, *Rev. Mod. Phys*, **15**, 1 (1943).

8) K. Wirtz, *Ann. Phys*, **36**, 295 (1939); *Phys. Z.*, **44**, 221 (1943).

9) T. Takahashi, O. Yamamoto, and E. Nomura, *Denki Kagaku*, **38**, 360 (1970); M. J. Rice and W. L. Roth, *J. Solid State Chem.*, **4**, 294 (1972).

10) G. D. Mahan, *Phys. Rev.*, **B14**, 780 (1976); M. Kobayashi and Y. Yamada, *J. Phys. Soc. Jpn.*, **44**, 259 (1978); K. Yonashiro, T. Tomoyose, and E. Sakai, *J. Phys. Soc. Jpn.*, **52**, 3837 (1983).

EXAFS Studies of the Behavior of $Rh_6(CO)_{16}$ Supported on γ-Al_2O_3 Surface

Kiyotaka ASAKURA, Yasuhiro IWASAWA,* and Haruo KURODA
Department of Chemistry, Faculty of Science, The University of Tokyo, Hongo, Tokyo 113
(Received August 13, 1985)

Synopsis. The structural change of $Rh_6(CO)_{16}$ supported on γ-Al_2O_3 surface during a decarbonylation-recarbonylation cycle was studied by means of EXAFS (extended X-ray absorption fine structure) spectroscopy. $Rh_6(CO)_{16}$ cluster framework was found to be decomposed into $Rh(CO)_2(OAl\lesssim)_2$ after the reaction with a mixture of O_2 and H_2O, and reversely regenerated by the subsequent treatment with a mixture of CO and H_2O.

Metal carbonyl clusters supported on inorganic oxides have been demonstrated to provide a new way of preparation of noble solid catalysts as well as new chemistry in the research boundary between homogeneous and heterogeneous catalytic systems. Smith et al. and Watters et al. suggested that $Rh_6(CO)_{16}$ physisorbed on Al_2O_3 surface was transformed to twin carbonyl Rh species by the treatment with a mixture of O_2 and H_2O, and reversely, the twin carbonyl Rh species was recarbonylated again to the original $Rh_6(CO)_{16}$ cluster by the subsequent treatment with a mixture of CO and H_2O from the results of IR spectroscopy.[1-3] Since the carbonyl stretching modes of Rh species give no direct information on the feature of Rh–Rh bonding, the details of the structural change of the metal framework of $Rh_6(CO)_{16}$ supported on Al_2O_3 surface still remaind to be solved.

In the present paper we report the EXAFS and XANES studies on a $Rh_6(CO)_{16}/\gamma$-Al_2O_3 system to obtain the information on structural changes of the Rh_6 framework.

Experimental

Supporting $Rh_6(CO)_{16}$ onto γ-Al_2O_3 was carried out by an impregnation method using a hexane or chloroform solution of $Rh_6(CO)_{16}$ under high purity Ar (99.9995%) atmosphere, followed by evacuation to remove the solvent. γ-Al_2O_3 was pretreated at 773 K for 2 h in a dry air in situ before use as a support. Hereinafter, the Al_2O_3 supported $Rh_6(CO)_{16}$ thus obtained is denoted as Sample 1. The sample was treated with a mixture of O_2 (26.6 kPa) and H_2O(2 kPa) at room temperature for 30 h in a closed-circulating system to which the cells for EXAFS measurements were connected. The treated sample is denoted as Sample 2. Sample 2 was further treated with a mixture of CO(26.6 kPa) and H_2O(2 kPa) at 323 k for 15 h, Sample 3 being thus obtained. After each treatment, the samples were transferred to EXAFS cells without contacting air. EXAFS measurements were conducted by use of synchrotron radiation at Photon Factory in National Laboratory for High Energy Physics (KEK-PF).[4] The analysis of EXAFS spectra was performed by a curve fitting technique employing theoretically derived phase shift and amplitude function.[5-7]

Results and Discussion

Figure 1 shows the EXAFS oscillations and Fourier transforms of the Rh K-edge EXAFS of $Rh_6(CO)_{16}$ powder, Samples 1, and 3, respectively. The Fourier

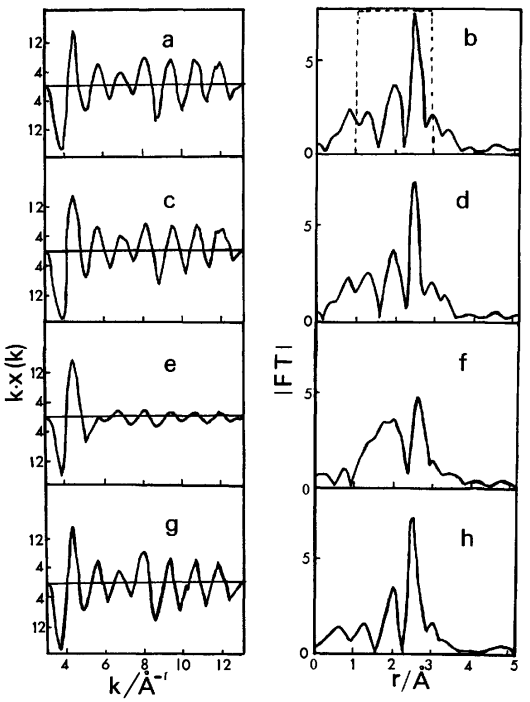

Fig. 1. k-Weighted EXAFS oscillations and Fourier transforms.
(a), (c), (e), and (g) are the k-weighted EXAFS oscillations of $Rh_6(CO)_{16}$ powder, Sample 1, Sample 2, and Sample 3, respectively. (b), (d), (f), and (h) are the Fourier transforms of $Rh_6(CO)_{16}$ powder, Sample 1, Sample 2, and Sample 3, respectively. The broken line in the Fig. 1b is the Fourier filtering window.

transform of $Rh_6(CO)_{16}$ showed a strong peak at 2.75 Å referred to the Rh–Rh bond in Fig. 1b. The contribution of back-scattering by Rh atoms to the Rh K-edge EXAFS oscillation was observed over a wide range of the wave number of ejected photoelectron(k) as shown in Fig. 1a. Thus the information obtained from the EXAFS analysis largely reflects the structure of Rh metal framework. The main peak in Fig. 1b was back-Fourier transformed in the range of 1—3 Å as shown in the Figure and four-shell curve fitting analyses were carried out considering Rh–C(terminal carbonyl group), Rh–C(triply bridged carbonyl group), Rh–O and Rh–Rh and the results were obtained to be given in Table 1. The Rh–Rh bond length (2.76Å) was in good agreement with the crystallographic data of $Rh_6(CO)_{16}$[8] (Rh–Rh=2.78 Å).

The EXAFS oscillation (Fig. 1c) and the Fourier transform (Fig. 1d) of Sample 1 were similar to those of $Rh_6(CO)_{16}$ cluster itself. The bond length and coordination number of each coordination shell around a Rh atom were found by the curve-fitting analysis to be about the same as those of $Rh_6(CO)_{16}$ as shown in Table 1. Thus, $Rh_6(CO)_{16}$ is concluded to be

Table 1. The Curve Fitting Results

Sample	Rh-C(term)[a]		Rh-C(bridge)[b]		Rh-O[c]		Rh-Rh[c]	
	N	r/Å	N	r/Å	N	r/Å	N	r/Å
$Rh_6(CO)_{16}$	(2)	1.93	(2)	2.27	(4)	2.99	(4)	2.76
Sample 1	2.2	1.93	2.2	2.26	4.0	2.97	4.1	2.75
Sample 2[d]							2.1	2.75
Sample 2[e]	2.1	1.94	2.3	2.20	4.2	2.98	2.0	2.74
Sample 3	2.0	1.94	2.0	2.25	3.9	2.96	3.8	2.74

a), b) C(term) and C(bridge) mean the carbon atoms of terminal and μ_3-bridged carbonyl ligands, respectively. c) Rh-O means the interaction between Rh and O in carbonyl ligand. d) 1-term curve fitting analysis of Rh-Rh. e) 4-term curve fitting analysis of Rh-C(term)+Rh-C(bridge)+Rh-O+Rh-Rh

supported on γ-Al_2O_3 retaining its cluster framework.

The EXAFS oscillation and Fourier transform of Sample 2 shown in Figs. 1e and 1f were much different from those of Sample 1. The decrease in the intensity of the main peak in the Fourier transform indicates the partial breaking of Rh–Rh bond of the cluster. Smith et al.[2] suggested by IR studies that $Rh_6(CO)_{16}$ supported on Al_2O_3 is decomposed to mononuclear $Rh^I(CO)_2$ species by O_2 treatments(more easily in the presence of moisture). The present EXAFS analysis also indicates the Rh–Rh bond breaking. However, in contrast to the almost complete decomposition of the Rh_6 framework by the IR studies,[2] the Rh–Rh bond was still observed at a distance of 2.75 Å similar to that found in $Rh_6(CO)_{16}$. The EXAFS data suggested that part of $Rh_6(CO)_{16}$ remained almost unchanged after O_2+H_2O treatment. The discrepancy between the IR observation[2] and the present EXAFS analysis is not clear at the present, but the generally known surface heterogeneity of Al_2O_3 employed may give an effect to the behaviors of Rh clusters.

The EXAFS oscillation and the Fourier transform of Sample 3 in Figs. 1g and 1h were identical to those of $Rh_6(CO)_{16}$ as well as Sample 1. The EXAFS analysis in Table 1 clearly reveals that the $Rh_6(CO)_{16}$ framework was completely regenerated on the γ-Al_2O_3 surface by the CO+H_2O treatment for 15 h.

The XANES spectra of Rh K-edge of Samples 1 and 3 given in Fig. 2b and Fig. 2d, respectively were similar to that of $Rh_6(CO)_{16}$ as shown in Fig. 2a, which is compatible with the EXAFS data. The relative intensity of peak A to peak B in the XANES region of Sample 2 changed as shown in Fig. 2c. In the EXAFS studies of a $Ru_3(CO)_{12}/Al_2O_3$ system, peak A near the Ru K-edge becomes stronger than peak B when the Ru_3 cluster was converted to a mononuclear $Ru(CO)_2(OAl\lesssim)_2$ species forming the chemical bonds between Ru atoms and surface oxygens.[9] The XANES spectra suggest the formation of the γ-Al_2O_3-attached species $Rh(CO)_2(OAl\lesssim)_2$ as previously proposed.

In summary, $Rh_6(CO)_{16}$ was physisorbed on the γ-Al_2O_3 surface without any structural change of the Rh_6 framework. $Rh_6(CO)_{16}$ was mostly decomposed into the mononuclear species $Rh(CO)_2(OAl\lesssim)_2$ by a mixture of O_2+H_2O treatment, but some of the cluster remain

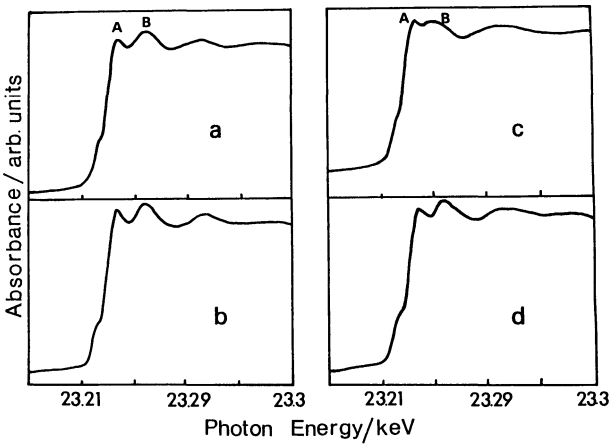

Fig. 2. XANES spectra of unsupported $Rh_6(CO)_{16}$ cluster (a), Sample 1 (b), Sample 2 (c), and Sample 3 (d).

ed in the form of $Rh_6(CO)_{16}$. After the subsequent treatment of the $Rh(CO)_2(OAl\lesssim)_2$ with a mixture of CO+H_2O, $Rh_6(CO)_{16}$ was found to be completely regenerated on the basis of the EXAFS and XANES spectra.

Reference

1) G. C. Smith, T. P. Chojnacki, S. R. Dasgupta, K. Iwatate, and K. L. Watters, *Inorg. Chem.*, **14**, 1419 (1975).
2) A. K. Smith, F. Hugues, A. Theolier, J. M. Basset, R. Ugo, G. M. Zanderighi, J. L. Bilhou, V. B. Bougnol, and W. F. Groydon, *Inorg, Chem.*, **28**, 3104 (1979).
3) K. L. Watters, R. F. Howe, T. P. Chojnacki, C. M. Fu, R. L. Schneider, and N. B. Wong, *J. Catal.*, **66**, 424 (1980).
4) H. Oyanagi, T. Matsushita, M. Ito, and H. Kuroda, *KEK Report* 8330, (1984).
5) B. K. Teo and P. A. Lee, *J. Am. Chem. Soc.*, **101**, 2815 (1979).
6) B. K. Teo, *J. Am. Chem. Soc.*, **104**, 3992 (1981).
7) N. Kosugi and H. Kuroda, Program EXAFS 1, Research Center for Spectrochemistry, the University of Tokyo (1985).
8) E. R. Corey, L. F. Dahl, and W. Beck, *J. Am. Chem.Soc.*, **85**, 1202 (1963).
9) K. Asakura, Y. Iwasawa, and H. Kuroda, *Chem. Lett.*, **1985** 551.

Crystal and Molecular Structure of a Potentially Five-Coordinate Palladium(II) Complex Containing 1,10-Phenanthroline. Chlorobis(triphenylphosphine)-(1,10-phenanthroline)palladium(II) Tetrafluoroborate

Zenei TAIRA† and Shinsaku YAMAZAKI*

†Department of Pharmaceutical Science, Tokushima Bunri University, 180 Nishihama Boji, Yamashiro-Cho, Tokushima 770
Chemistry Laboratory, Gakuen College Kochi, 292 Asahi Tenjin-Cho, Kochi 780

(Received July 15, 1985)

Synopsis. The X-ray crystal structure of a potentially five-coordinate palladium(II) complex containing 1,10-phenanthroline, $[PdCl(PPh_3)_2(phen)][BF_4]\cdot(CH_3)_2CO$ has been determined. The structure was solved by the heavy-atom method and refined to R=0.051.

Concerning intermediates in the rearrangement of square planar d^8 complexes, many five-coordinate platinum(II) complexes have hitherto been isolated.[1-9] The crystal structures of the platinum(II) complexes containing 1,10-phenanthroline[2,3] thus far studied are mostly distorted square pyramids. They do not display any dissociation processes in a solution, since ^{195}Pt satellites have been observed in the ^1H, ^{13}C NMR spectra.

On the other hand, palladium(II) analogues stabilized by potentially bidentate 1,10-phenanthroline are relatively rare, and their solution behaviour is still umbiguous.

The preparation and characterizations of potentially five-coordinate complexes of palladium(II) containing phen and its 2,9-dimethyl derivative have been described elsewhere by the present author.[10,11] Among them, $[PdCl(PPh_3)_2(phen)][BF_4]$ is especially interesting because, judging from some spectral evidence, the solution structure of this potentially five-coordinate complex seems to be rather close to a four-coordinate geometry with an unidentate phen.

This note will deal with the X-ray crystal and molecular structure of $[PdCl(PPh_3)_2(phen)][BF_4]\cdot(CH_3)_2CO$.

Structure Determination and Refinement

Large deep orange crystals of $[PdCl(PPh_3)_2(phen)][BF_4]\cdot(CH_3)_2CO$ were grown from an ethanol-acetone(1:1) mixed solution under natural vaporization at room temperature. A crystal with dimensions of 0.3×0.3×0.2 mm was mounted on a Rigaku AFC-6B four-circle diffractometer with graphite-monochromated Mo $K\alpha$ radiation. The crystal data are: space group *Pnma* with Z=4, a=19.915(5), b=14.833(2), and c=15.917(3) Å. V=4701.9 Å^3. μ(Mo $K\alpha$) 5.75 cm^{-1}. D_m= 1.406 g cm^{-3}(by flotation), D_x=1.401 g cm^{-3}. Within the range of $2\theta<50°$, 4139 independent reflections with $|F_o|>6\sigma_F$ were collected for background, Lorenz, and polarization factors, but absorption correction was not applied.

The position of the Pd atom was determined from a three-dimension Patterson map. The remaining non-hydrogen atoms were located by successive difference Fourier syntheses. The structure, in which Pd and Cl atoms and the phenanthroline occupy a mirror plane with y=1/4, was refined by the block-diagonal least-squares method with the anisotropic thermal parameters.

The hydrogen atoms included on the structure factor calculations were located from the difference map. The function minimized was $\sum w\Delta F^2$, where w=1.0.

The final R value was 0.051(R_w=0.056). The atomic scattering factors were taken from the International Tables for X-Ray Crystallography.[12] Lists of the anisotropic thermal parameters and the final positional parameters, tables of the bond distances and angles, and a table of the observed and calculated structure factors are preserved by the Chemical Society of Japan (Document No. 8609). The structure-analysis calculations were performed with a Rasa program (Rigaku) and X-STANP (Taira) using a PANAFACOM U-1400 computer system.

Results and Discussion

The crystal-structure view of the $[PdCl(PPh_3)_2(phen)][BF_4]\cdot(CH_3)_2CO$ is shown in Fig. 1. The inter-atomic distances and angles are shown in Table 1. The distances of the two nitrogen atoms of the phen from the palladium are unequal in that one nitrogen atom with a long Pd-N distance(2.68 Å) is at the apex of a distorted square pyramidal structure. The elonga-

Table 1. Bond Distances(l/Å) and Angles(ϕ/°) in the Coordination Sphere of $[PdCl(PPh_3)_2(phen)]^+$

Distances			
Pd-Cl	2.31(2)	Pd-P	2.34(2)
Pd-N(01)	2.09(5)	Pd-N(12)	2.68(4)
Angles			
Cl-Pd-P	88.0(3)	Cl-Pd-N(01)	166.5(1)
Cl-Pd-N(12)	123.3(1)	P-Pd-N(01)	92.3(4)
P-Pd-N(12)	90.0(6)	N(01)-Pd-N(12)	70.2(2)

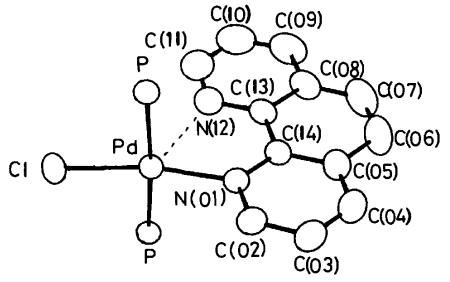

Fig. 1. Structural view of $[PdCl(PPh_3)_2(phen)]^+$. For the sake of clarity, phenyl rings of PPh_3 are omitted.

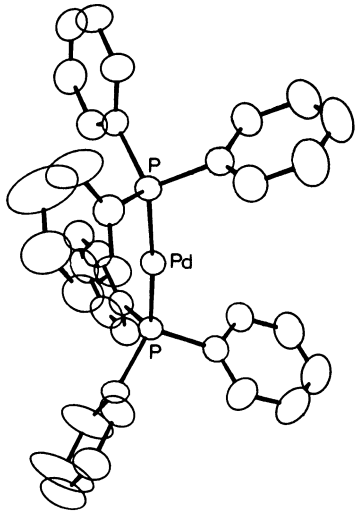

Fig. 2. Structural view of PPh_3 in $[PdCl(PPh_3)_2(phen)]^+$. For the sake of clarity, Cl atom and phenanthroline molecule are omitted.

tion of the apical M-N distance is in accordance with the observations previously reported for d^8 square pyramidal complexes.[2-4,8,9] It should be noticed that $[PdCl(PPh_3)_2(phen)]^+$ is so distorted as to approach a quasi-trigonal bipyramid. The phen plane, including the palladium and chlorine atoms, exactly coincides with a crystallographical mirror plane. The two angles of P-Pd-N(12) are both 90.03°, and those of P-Pd-N(01) are equivalent as well (92.3°). The bond lengths of P-Pd are 2.34Å, a value of which is comparable with those found in $[PdCl_2(PMe_2Ph)_3]$ (2.326 and 2.344Å for the basal bond lengths).[4]

Two phosphorous atoms in $[PdCl(PPh_3)_2(phen)]^+$ are displaced towards Cl and N(12), away from N(01) (P-Pd-P, 175.5°). The distortion is probably due to a steric crowding of the bulky phosphines,[4,8] and *N*-heterocyclic rings.

The distance of the non-bonding N···N bite of the phen molecule is 2.787 Å in $[PdCl(PPh_3)_2(phen)]^+$, slightly longer than the range (2.63—2.73 Å) cited in the bidentate phen.[13] The N(01)-Pd-N(12) angle, 70.2°, is, however, much smaller than that found in $[Pd(NO_3)_2(phen)]$ (83°).[13] In the five-coordinate platinum(II) complexes previously found, the corresponding N···N bite of the phen and the N-Pt-N angle are 2.81 Å, and 69.7° in $[PtCl(PEt_3)_2(phen)]^+$ (the two phosphines are mutually cis)[2] and 2.85 Å, and 68.2° in $[Pt(CN)(phen)_2]^+$[3] respectively. This preliminary information about the corresponding platinum(II) complexes may indicate that the bite of the phen in $[PdCl(PPh_3)_2(phen)]^+$ is more strengthened than those in $[Pt(CN)(phen)_2]^+$ and $[PtCl(PEt_3)_2(phen)]^+$. This effect may be seen in the C(07)-C(08)-C(09) angle whose deviation from 120° is 4.2°, while the deviations of the corresponding angle in $[PtCl(PEt_3)_2(phen)]^+$ and $[Pt(CN)(phen)_2]^+$ are within the range of 2.2—2.3°.[2,3]

The other bond distances and angles in the phen rings of $[PdCl(PPh_3)_2(phen)]^+$(Table preserved by the Chemical Society of Japan) do not differ significantly from those in the two platinum(II) complexes described above.

The cavities between cations are occupied by the

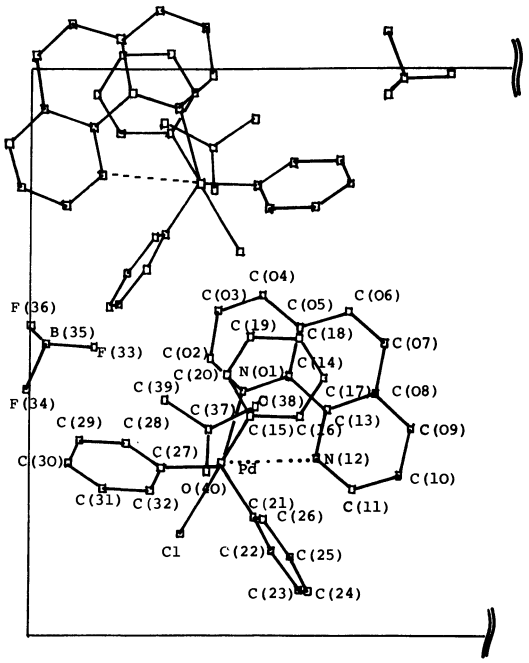

Fig. 3. The crystal structure of $[PdCl(PPh_3)_2(phen)][BF_4]\cdot(CH_3)_2CO$ viewed along b axis. For the sake of clarity, a half of the unit cell along b axis is omitted.

comparatively small solvation acetone, as is shown in Fig. 3. The BF_4^- anion is not bonded to the palladium, since the closest Pd-F distance is 4.83 Å.

Thus, the crystal structure of $[PdCl(PPh_3)_2(phen)]^+$ should be viewed either as a distorted square pyramidal complex in which there is a very weak apical metal-nitrogen interaction, or as a square planar complex involving a unidentate phen ligand, the second nitrogen being outside the coordination sphere of the metal.

References

1) P. Overbosch, G. van Koten, D. M. Grove, A. L. Spek, and A. J. M. Duisenberg, *Inorg. Chem.*, **21**, 3253 (1982).
2) G. W. Bushnell, K. R. Dixon, and M. A. Khan, *Can. J. Chem.*, **52**, 1367 (1974).
3) O. Wernberg and A. Hazell, *J. Chem. Soc., Dalton Trans.*, **1980**, 973.
4) W. J. Louw, D. J. A. de Waal, and G. J. Kruger, *J. Chem. Soc., Dalton Trans.*, **1976**, 2364.
5) P. F. Meier, A. E. Merbach, M. Dartiguenava, and Y. Dartiguenava, *Inorg. Chem.*, **18**, 610 (1979).
6) O. Meakin and J. P. Jesson, *J. Am. Chem. Soc.*, **96**, 5751 (1974).
7) J. J. MacDougall, J. H. Nelson, and F. Mathey, *Inorg. Chem.*, **20**, 1598 (1981).
8) R. Favez, R. Roulet, A. A. Pinkerton, and D. Schwarzenbach, *Inorg. Chem.*, **19**, 1356 (1980).
9) S. Okeya, T. Miyamoto, S. Ooi, Y. Nakamura, and S. Kawaguchi, *Bull. Chem. Soc. Jpn.*, **57**, 395 (1984).
10) S. Yamazaki, *Inorg. Chem.*, **21**, 1638 (1982).
11) S. Yamazaki, *Polyhedron*, **4**, 1915 (1985).
12) "International Tables for X-Ray Crystallography," The Kyonoch Press, Birmingham (1974), Vol. IV.
13) B. A. Frenz and J. A. Ibers, *Inorg. Chem.*, **11**, 1109 (1972). L. F. Power, *Inorg. Nucl. Chem. Lett.*, **6**, 791 (1970).
14) A. J. Deeming, I. P. Rothwell, M. B. Hursthouse, and L. New, *J. Chem. Soc., Dalton Trans.*, **1978**, 1490.

High-Resolution ^{13}C NMR Spectra of *trans*-[Co^{III}(2,3-Alkanedione dioximato)$_2$(pyridine)$_2$]I Complexes in the Solid State

Setsuko KINOSHITA,* Hisanobu WAKITA, and Isao MASUDA
Department of Chemistry, Faculty of Science, Fukuoka University, Nanakuma, Jonan-ku, Fukuoka 814-01
(Received July 30, 1985)

Synopsis. High-resolution ^{13}C NMR spectra of the title complexes showed two type signals based on the "packing effect" and the long-chain alkyl group of the dioximato ligand was found to be fixed near the axial pyridine ligand in the solid state.

To determine molecular structures in the solid state, X-ray crystal structure analyses are preferable. However, they are time consuming and are sometimes impossible because of the difficulty of making single crystals. Recently, high-resolution ^{13}C NMR techniques in the solid state (CP/MAS) have been developed, and attempts to apply these techniques are now being made.[1] The CP/MAS measurement can readily give some information about the molecular conformations and the molecular packings even for such compounds in the solid state.

In the previous paper, we reported that the pyridine liberation-anation reaction of the series of *trans*-[Co(R,CH_3-dioxH)$_2$(py)$_2$]I (R,CH_3-dioxH$_2$: CH_3-C(=NOH)-C(=NOH)-R; R=CH_3, C_2H_5, *n*-C_3H_7 and *n*-C_4H_9, py: pyridine) fitted well to the Taft's plot, indicating that the Co(III)-py bond is weakened not only by the electron-donating inductive effect of R but also by the steric effect of R.[2] Therefore, the long-chain alkyl group, R, was expected to be fixed near the axial pyridine ligand in the solid state. On the other hand, ^1H and ^{13}C NMR Spectra and T_1 measurements of the complexes indicated that the R group was moving segmentally in dimethyl-d_6 sulfoxide (DMSO-d_6) solution.[3]

In this paper, CP/MAS is applied to these complexes and the molecular structure and the molecular packing of the complexes are estimated in the solid state.

Experimental

A JEOL NM-SH 200 spectrometer (50 MHz for ^{13}C) was used for the CP/MAS measurement. The complexes used were fine needle crystals obtained by slow evaporation of a saturated solution in methanol. The spectral assignments were made using Opella's method[4] and in comparison with the spectra in DMSO-d_6 solution.[3]

Results and Discussion

As is shown in Fig. 1, the C^1 and C^2 resonances of the [Co(CH_3,CH_3-dioxH)$_2$(py)$_2$]I complex were separated into two peaks, respectively, though they appeared as a single peak in DMSO-d_6 solution. The [Co(C_2H_5,CH_3-dioxH)$_2$(py)$_2$]I complex showed a spectrum similar to that in DMSO-d_6 solution, but the [Co(*n*-C_3H_7,CH_3-dioxH)$_2$(py)$_2$]I showed a spectrum different from that in solution; the C^1 resonance was separated into two peaks, while the C^2 and C^3 resonances overlapped. The spectrum of [Co(*n*-C_4H_9, CH_3-dioxH)$_2$(py)$_2$]I complex was similar to that in solution. The numerical data for these spectra are summarized in Table 1.

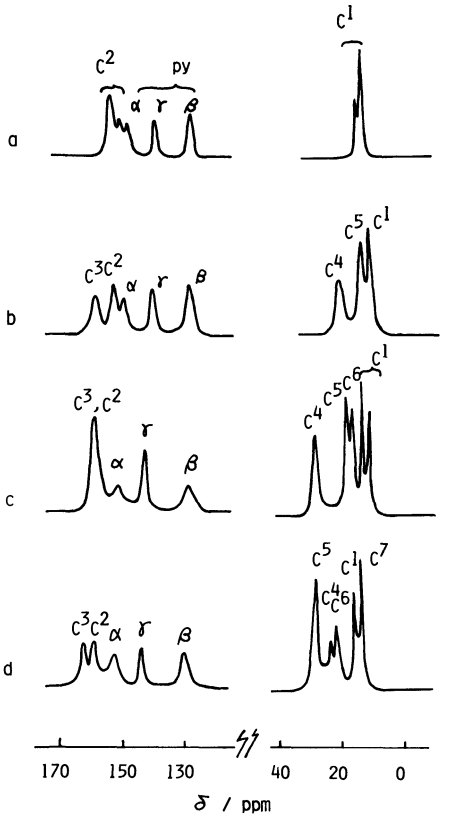

Fig. 1. High-resolution ^{13}CNMR spectra of [Co(R, CH_3-dioxH)$_2$(py)$_2$]I in the solid state.
a: R=CH_3, b: R=C_2H_5, c: R=*n*-C_3H_7, d: R=*n*-C_4H_9. Each carbon atom of the ligands is noted as a following example; C^1H_3-C^2(=NOH)-C^3(=NOH)-C^4H_2-C^5H_2-C^6H_2-C^7H_3.

The results obtained here are understandable if each carbon resonance of the complexes can show two type NMR signals, i.e., A type and B type, based on a "packing effect".[1] The observed signals were assigned as follows: C^1, 14.9 ppm (A type), 17.1 ppm (B type); C^2, 155.2 ppm (A type), 158.5 ppm (B type); C^3, 161.6 ppm (A type), 162.5 ppm (B type). The C^4, C^5, C^6, C^7, resonances showed no observable splittings between A type and B type. The [Co(C_2H_5,CH_3-dioxH)$_2$ (py)$_2$] I and [Co(*n*-C_4H_9,CH_3-dioxH)$_2$(py)$_2$]I complexes showed only A type or B type signal, respectively. While, [Co(CH_3,CH_3-dioxH)$_2$(py)$_2$]I and [Co(*n*-C_3H_7,CH_3-dioxH)$_2$(py)$_2$]I complexes showed both A type and B type signals. As for the [Co(*n*-C_3H_7,CH_3-dioxH)$_2$-(py)$_2$]I complex, four signals, i.e., C^2(A), C^2(B), C^3(A),

Table 1. High-Resolution ^{13}C NMR Data of $[Co(R,CH_3\text{-dioxH})_2(py)_2]I$ Complexes in the Solid State

R	δ/ppm									
	C^1		C^2		C^3		C^4	C^5	C^6	C^7
CH_3	15.6	17.5	155.0	158.0	—	—	—	—	—	—
C_2H_5	14.9	—	155.3	—	161.6	—	21.4	12.9	—	—
n-C_3H_7	14.2	17.0		159.6			29.1	19.4	12.2	—
n-C_4H_9	—	16.9	—	159.0	—	162.5	25.1	28.9	23.2	14.6

Each carbon atom of the ligands is noted as a following example;
C^1H_3-C^2(=NOH)-C^3(=NOH)-C^4H_2-C^5H_2-C^6H_2-C^7H_3.

C^3(B), were mixed up and appeared as a single peak at 159.6 ppm.

The splitting of an NMR signal based on a "packing effect" was also observed for $[Co(CH_3,CH_3\text{-dioxH})_2(NH_3)_2]NO_3$ complex: In D_2O solution, C^1 and C^2 appeared at 15.3 and 159.7 ppm, respectively, as a single peak, but, in the solid state, they appeared as a double peak, respectively. The X-ray structural analysis of the complex showed that two NH_3 ligands coordinate to Co(III) at trans positions and the space group is $P2_1/c$ with two molecules in the unit cell.[5] According to this X-ray structural analysis, there are two non-equivalent positions for the C^1 and C^2 carbons, respectively, which can cause the splitting of the NMR signals.

In DMSO solution, higher-field shifts were observed for both ^1H and ^{13}C resonances of the C^5, C^6, and C^7 groups on complex formation and the higher-field shifts of ^{13}C resonances were mainly attributable to the ring-current shielding of the axial pyridine ligand for these complexes.[3] In the solid state, the C^6 resonance of $[Co(n\text{-}C_3H_7,CH_3\text{-dioxH})_2(py)_2]I$ complex appears at 12.2 ppm, which is 4.0 ppm higher-field in comparison with that of free n-C_3H_7,CH_3-dioxH$_2$ ligand in the solid state. In DMSO solution, the corresponding peak shift was 1.3 ppm.[3] The amount of the shift caused by the above ring-current effect was the largest for C^6 carbon of $[Co(n\text{-}C_3H_7,CH_3\text{-dioxH})_2(py)_2]I$ complex of all the carbons in the series of the complexes. Judging from these facts, the long-chain alkyl group in the equatorial plane may be assumed to be fixed near the axial pyridine ligand in the solid state. Such a location of the R group is susceptible to ring-current shielding of the pyridine ligand and the chain length is most advantageous for the complex including R=n-C_3H_7 to experience the largest shielding effect. This location is also in accord with the expectation, based on the kinetic study, that the R group is fixed so as to weaken the Co(III)-py bonding.[2] In solution, the long-chain alkyl group is moving freely and the effect of the ring-current shielding is smaller than that in the solid state.

References

1) G. E. Balimann, C. J. Groombridge, R. K. Harris, K. J. Packer, B. J. Say, and S. F. Tanner, *Philos Trans. R. Soc. London A*, **299**, 643 (1981).
2) S. Kinoshita, H. Wakita, and I. Masuda, *Bull. Chem. Soc. Jpn.*, **57**, 1818 (1984).
3) S. Kinoshita and I. Masuda, *Polyhedron*, **4**, 1245 (1985).
4) S. J. Opella and M. H. Frey, *J. Am. Chem. Soc.*, **101**, 5854 (1979).
5) K. S. Viswanathan and N. R. Kunchur, *Acta Cryst.*, **14**, 675 (1961).

Estimation of Isomer Ratio of 2,3-Alkanedione Dioxime Using High-Resolution ^{13}C NMR in the Solid State

Setsuko KINOSHITA,* Hisanobu WAKITA, and Isao MASUDA
Department of Chemistry, Faculty of Science, Fukuoka University, Nanakuma, Jonan-ku, Fukuoka 814-01
(Received August 15, 1985)

Synopsis. High-resolution ^{13}C NMR spectra were measured for the CH_3-C(=NOH)-C(=NOH)-R (R=CH_3, C_2H_5, n-C_3H_7, and n-C_4H_9) series in the solid state. A commercially available powder, dimethylglyoxime (R=CH_3), produced two C^2 signals, indicating two isomers: i.e., *s-trans-(E,E)* and *s-cis-(E,E)*. The ratio of *trans*: *cis* was estimated to be 3:1.

Tanaka et al. reported that there are three possible structural isomers for dioximes.[1] Each isomer gave

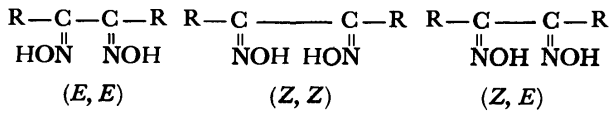

a different ^1H NMR signal for the NOH proton in DMSO-d_6 solution, and the ratio of the isomers was estimated from the ratio of the peak areas.[1]

On the other hand, a newly developed high-resolution ^{13}CNMR technique (CP/MAS) was applied for coal and oil shale and the aromatic-olefinic fraction was determined by an integration of the solid-state spectra.[2]

In this paper, CP/MAS spectra were measured for the 2,3-alkanedione dioxime (CH_3-C(=NOH)-C(=NOH)-R: R=CH_3, C_2H_5, n-C_3H_7, and n-C_4H_9) series in the solid state. The existence of *trans* and *cis* isomers was identified for a commercially available powder dimethylglyoxime (R=CH_3), and the ratio of the isomers was estimated from the ratio of the peak areas.

Experimental

A commercially available guaranteed reagent, dimethylglyoxime (Wako Pure Chemical Industries, LTD), was used for the measurement. Other 2,3-alkanedione dioximes were prepared as previously described[3] and recrystallized from methanol-chloroform (1:1). A JEOL NM-SH200 spectrometer (50 MHz for ^{13}C) was used for the measurements. All spectra were obtained using magic-angle spinning at room temperature. The spectra were generated from ca. 1000 scans at a rate of one scan per ten seconds. The methylen carbon of adamantane (29.5 ppm from TMS) was used as an external standard.

Results and Discussion

The high-resolution ^{13}CNMR (CP/MAS) spectra of 2,3-alkanedione dioximes are shown in Fig. 1. Also, numerical data are summerized in Table 1. Opella's method was used for the assignment of signals.[4] According to this method, only quarternary and methyl carbons appear as is exemplified for R=n-C_3H_7 dioxime in Fig. 2-a. In the case of R=C_2H_5, n-C_3H_7, n-C_4H_9 dioximes, the ^{13}CNMR spectra in the solid state were similar to those obtained in DMSO-d_6 solution

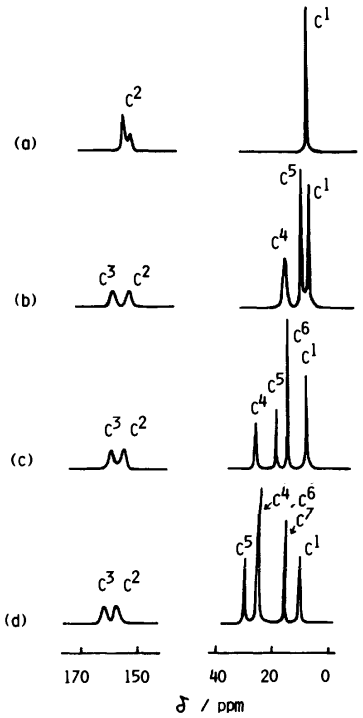

Fig. 1. High-resolution ^{13}CNMR spectra (CP/MAS spectra) of CH_3-C(=NOH)-C(=NOH)-R in the solid state.
(a): R=CH_3, (b): R=C_2H_5, (c): R=n-C_3H_7, (d): R=n-C_4H_9.
Each carbon atom is noted as a following example; C^1H_3-C^2(=NOH)-C^3(=NOH)-C^4H_2-C^5H_2-C^6H_2-C^7H_3.

Table 1. High-Resolution ^{13}C NMR Data of CH_3-C(=NOH)-C(=NOH)-R

R	δ/ppm						
	C^1	C^2	C^3	C^4	C^5	C^6	C^7
CH_3	9.5	155.9 153.6	—	—	—	—	—
C_2H_5	9.3	154.2	159.5	17.6	11.6	—	—
n-C_3H_7	9.6	155.1	159.0	27.5	20.2	16.2	—
n-C_4H_9	9.1	154.5	158.6	23.7	28.3	23.7	14.0

(Fig. 2-b, c). However, as for R=CH_3 dioxime, the C^2 resonance separated into two peaks in the solid state, though it appeared as a single peak in DMSO-d_6 solution (Fig. 3-b, c).

It was reported that carbons directly bonded to nitrogen atoms sometimes showed doublet patterns in CP/MAS spectra.[5] If this is also the case for the dioximes, the C^2 and C^3 resonances of R=C_2H_5, n-C_3H_7, and n-C_4H_9 dioximes should show similar splittings. However, such a phenomenon was not observed (Fig. 1).

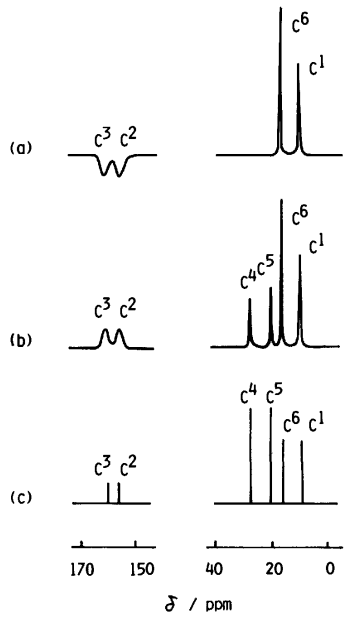

Fig. 2. ^{13}C NMR spectra of CH_3-C(=NOH)-C(=NOH)-CH_2-CH_2-CH_3.
(a): CP/MAS spectrum using Opella's method (in the solid state), (b): CP/MAS spectrum (in the solid state), (c): in DMSO-d_6 solution.

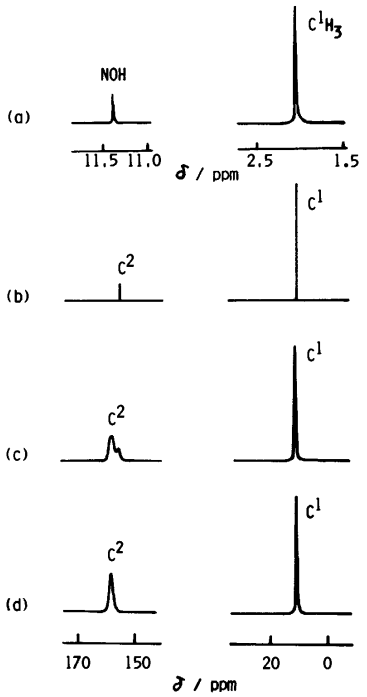

Fig. 3. ^1H and ^{13}C NMR spectra of CH_3-C(=NOH)-C(=NOH)-CH_3.
(a): ^1H NMR spectrum in DMSO-d_6 solution, (b): ^{13}C NMR spectrum in DMSO-d_6 solution, (c): CP/MAS spectrum of commercial powder compound, (d): CP/MAS spectrum of recrystallized crystal.

The ^1H NMR spectrum of the R=CH_3 dioxime showed only one NOH signal in DMSO-d_6 solution (Fig. 3-a), indicating that there are no isomers, such as the previously described *(E,E)*, *(Z,Z)*, and *(Z,E)*.[1] Since the rotation of a C=NOH double bond is inhibited, it is hardly expected that there are such isomers only in the solid state.

The CP/MAS resonance sometimes splits into two peaks based on the "packing effect."[6] According to an X-ray single crystal analysis of R=CH_3 dioxime (obtained by a slow evaporation of the solvent ethanol), the R=CH_3 dioxime has a *s-trans-(E,E)* conformation and the space group is $P\bar{1}$-C_i^1 with one molecule in the unit cell.[7] Therefore, the peak splitting based on the "packing effect" cannot be expected for the R=CH_3 dioxime. When commercially available dimethylglyoxime (R=CH_3) was recrystallized by a slow evaporation of solvent ethanol or methanol-chloroform (1:1), the splitting of the C^2 resonance was not observed, though the C^1 resonance showed a similar signal as that of the commercial powder compound (Fig. 3-d).

Considering these facts, it is concluded that there were two isomers, i.e., *s-trans-(E,E)* and *s-cis-(E,E)*, in the commercial powder dimethylglyoxime. In solution, these two isomers were indistinguishable since the (HON=)C-C(=NOH) single bond can rotate freely.

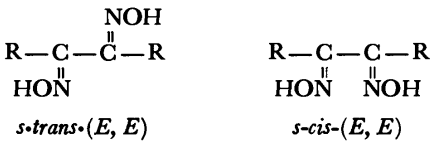

The molar fraction of the two isomers was estimated by an integration of the spectra. For a quantitative analysis, the contact time (CT) and the repetition time (RT) must be appropriately chosen.[2] In this study, the CP/MAS spectra were taken while choosing CT=2 ms and RT=10 s. Under these conditions, the dioximes (R=C_2H_5, n-C_3H_7 and n-C_4H_9) gave a peak ratio C^2:C^3=1:1 (Fig. 1), indicating the probability of the quantitative analysis. In the case of the commercial powder dimethylglyoxime (R=CH_3), it was estimated from an integration of the corresponding C^2 signals that the ratio *s-trans-(E,E)*: *s-cis-(E,E)* is 3:1. As for R=C_2H_5, n-C_3H_7 and n-C_4H_9 dioximes, these molecules are considered to exist only in *s-trans* or *s-cis* forms in the crystals.

References

1) M. Tanaka, T. Shono, and K. Shinra, *Anal. Chim. Acta*, **46**, 125 (1969).
2) G. E. Maciel, V. J. Bartuska, and F. P. Miknis, *Fuel*, **58**, 391 (1979); H. A. Resing, A. N. Garroway and R. N. Hazlett, *Fuel*, **57**, 450 (1978).
3) M. I, H. Wakita, and I. Masuda, *Bull. Chem. Soc. Jpn.*, **56**, 1627 (1983).
4) S. J. Opella and M. H. Frey, *J. Am. Chem. Soc.*, **101**, 5854 (1979).
5) G. E. Balimann, C. J. Groombridge, R. K. Harris, K. J. Packer, B. J. Say, and S. F. Tanner, *Phil. Trans. R. Soc. Lond. A*, **299**, 643 (1981).
6) S. Kinoshita, H. Wakita, and I. Masuda, *Bull. Chem. Soc. Jpn.*, **59**, 651 (1986).
7) W. C. Hamilton, *Acta Cryst.*, **14**, 95 (1961); L. L. Merritt, Jr. and E. Lanterman, *Acta Cryst.*, **5**, 811 (1952).

Total Synthesis of (±)-Zeylena

Seiichiro OGAWA* and Tohei TAKAGAKI
Department of Applied Chemistry, Faculty of Science and Technology, Keio University, Hiyoshi, Yokohama 223
(Received July 30, 1985)

Synopsis. Zeylena, isolated from the roots of *Uvaria zeylanica* L. (Annonaceae), has been synthesized as a racemic modification by an intramolecular cyclo-addition reaction of DL-*trans*-2,3-dihydroxy-1-(benzoyloxymethyl)cyclohexa-4,6-diene 3-(*E*)-cinnamate or its acetate.

Zeylena (**7**) was isolated from the methanol extract of the roots of *Uvaria zeylanica* L. (Annonaceae).[1] Although it was found to lack tumor inhibitory activity, its biogenetic relationship to other biologically active *Uvaria* constituents has stimulated much interest.[2]

In continuation to our study for highly-oxygenated cyclohexane compounds,[3] we now describe a synthesis of racemic zeylena starting from DL-*trans*-2,3-diacetoxy-1-(benzoyloxymethyl)-4,6-cyclohexadiene (**1**).[4]

Selective *O*-deacetylation of **1** with *p*-toluenesulfonic acid in methanol gave the 2-acetate (**2**) and the dihydroxy compound (**3**) in 29 and 51% yeild, respectively. The structures were assigned on the basis of the ^{1}H NMR spectra.[3]

The monoacetate **2** was treated with (*E*)-cinnamoyl chloride in dichloromethane and pyridine to give the 3-(*E*)-cinnamate (**4**) in 62% yield. Intramolecular Diels-Alder reaction of **4** was carried out in toluene in a sealed tube at 70 °C for 4 d to afford a 91% yield of crystalline (±)-zeylena acetate (**6**),[1] which was readily convertible into racemic **7** in 40% yield[5] by treatment with *p*-toluenesulfonic acid in methanol–dichloromethane. The ^{1}H NMR spectra data of **7** were shown to be superposable on those of an authentic sample.[1,6]

Alternatively, selective esterification of **3** with the acid chloride was attempted in dichloromethane and pyridine at −60 °C. A mixture of the products was separated on a silica-gel column to afford the desired 3-(*E*)-cinnmate (**5**) in 27% yield, the structure of which was confirmed by the ^{1}H NMR spectrum. The ester **5** was then subjected to similar cyclo-addition reaction conditions to afford racemic **7** in 98% yield.

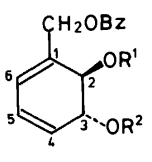

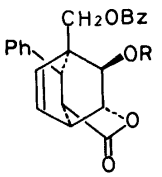

1 $R^1 = R^2 = Ac$
2 $R^1 = Ac$, $R^2 = H$
3 $R^1 = R^2 = H$
4 $R^1 = Ac$, $R^2 = COCH = CHPh$
5 $R^1 = H$, $R^2 = COCH = CHPh$

6 R = Ac
7 R = H

Fig. 1. The formulas depict only one of the respective enantiomers.

Experimental

Melting points were determined in a capillary in a MELTEMP melting point apparatus and are uncorrected. ^{1}H NMR spectra were recorded with a Varian EM-390 (90 MHz) spectrometer in chloroform-*d* solution with tetramethylsilane as an internal standard. Mass spectra were measured with a Hitachi M 80B spectrometer. The silica gel used for column chromatography was Wakogel C-300 (Wako Co., 300 mesh).

Selective *O*-Deacetylation of DL-*trans*-2,3-Diacetoxy-1-(benzoyloxymethyl)-4,6-cyclohexadiene (1).[4] Compound **1** (100 mg, 0.30 mmol) was treated with *p*-toluenesulfonic acid (25 mg) in methanol (5 ml) as described in the reaction of the optically active **1**.[3] The products were separated on a silica-gel column to give 25 mg (29%) of DL-*trans*-2-acetoxy-1-benzoyloxymethyl-4,6-cyclohexadien-3-ol (**2**) as a syrup and 38 mg (51%) of DL-*trans*-1-benzoyloxymethyl-4,6-cyclohexadiene-2,3-diol (**3**) as a syrup. Both compounds were assigned by comparison of their ^{1}H NMR spectra with those of the corresponding optically active compounds.[3] MS (70 eV) *m/z* (rel intensity), data for **2**, 288 (M^+; 2.8), 228 (12), 124 (8), and 105 (100); data for **3**, 246 (M^+; 2.7), 228 (11), 124 (86), and 105 (100).

DL-*trans*-2-Acetoxy-1-benzoyloxymethyl-3-[(*E*)-cinnamoyloxy]-4,6-cyclohexadiene (4). To a solution of **2** (67 mg, 0.23 mmol), dichloromethane (1.0 ml), and pyridine (0.2 ml) was added a solution of (*E*)-cinnamoyl chloride (83 mg, 0.50 mmol) in dichloromethane (0.5 ml) dropwise at −50 °C, and then the mixture was stirred at the same temperature for 10 min. The mixture was diluted with ethyl acetate (10 ml) and washed with 1 M† hydrochloric acid, saturated aqueous sodium hydrogencarbonate, and saturated aqueous sodium chloride, and then dried over anhydrous sodium sulfate. Removal of the solvent gave a syrup, which was chromatographed on a silica-gel column (8 g) with ethyl acetate–hexane (1:4) as an eluant to give mainly 60 mg (62%) of **4** as a syrup. ^{1}H NMR ($CDCl_3$, 90 MHz) δ=2.02 (3H, s, OAc), 4.93 (2H, s, CH_2OBz), 5.63 (1H, dd, $J_{2,3}$=6.2 Hz, $J_{3,4}$=3.3 Hz, H-3), 5.93 (1H, d, H-2), 6.00—6.33 (3H, m, H-4, 5, and 6), 6.37 (1H, d, J=15.5 Hz, COCH=CHPh), 7.33—7.57 (8H, m) and 7.80—8.03 (2H, m) (OBz and COCH=CHPh), 7.68 (1H, d, COCH=CHPh); MS (70 eV) *m/z* (rel intensity) 418 (M^+; 4.4), 376 (2.6), 228 (19), 131 (100), and 105 (60).

(±)-Zeylena Acetate (6). A solution of **4** (23 mg, 0.05 mmol) and toluene (1.0 ml) was heated in a sealed tube at 70 °C for 4 d. The mixture was concentrated and the residue was eluted from a column of silica gel (1 g) with ethyl acetate–hexane (2:5) to give 21 mg (91%) of **6** as plates; mp 150 °C (recrystallized from methanol–dichloromethane). ^{1}H NMR data ($CDCl_3$, 90 MHz) was identical with those reported for an optically active compound.[1]

Found: C, 71.60; H, 5.48%. Calcd for $C_{25}H_{22}O_6$: C, 71.77; H, 5.26%.

(±)-Zeylena (7). To a solution of **6** (39 mg, 0.09 mmol) in dichloromethane–methanol (1:6) (7 ml) was added *p*-toluenesulfonic acid (80 mg, 0.42 mmol) and the mixture was stirred at room temperature for 3 d. The mixture was then neutralized with sodium hydrogencarbonate and an insoluble material was removed by filtration. The filtrate was concentrated and the residue was chromatographed on a silica-gel column (2 g) with ethyl acetate–hexane (1:2) to give 14 mg (40%) of **7**; mp 173—174 °C (recrystallized from

† 1 M = 1 mol dm^{-3}.

dichloromethane–methanol). The ^{1}H NMR spectrum was superposable on that of an authentic sample.[1]

Found: C, 73.22; H, 5.51%. Calcd for $C_{23}H_{20}O_5$: C, 73.40; H, 5.32%.

DL-*trans*-1-Benzoyloxymethyl-3-[(*E*)-cinnamoyloxy]-4,6-cyclohexadien-2-ol (5). To a solution of **3** (193 mg, 0.78 mmol) in dichloromethane (2.0 ml) and pyridine (0.8 ml) was added at −60 °C a solution of (*E*)-cinnamoyl chloride (133 mg, 0.80 mmol) in dichloromethane (0.8 ml), and the mixture was stirred at 0 °C for 0.5 h. TLC [ethyl acetate–hexane (1:2)] showed three componets (R_f=0.53, 0.34, and 0.26) and a trace of **3**. The mixture was diluted with ethanol and the solution was concentrated. The residual products were processed as described in the preparation of **4**. Fractionation of the products on a silica-gel column with ethyl acetate–hexane (1:3) gave mainly 81 mg (27%) of **5**; mp 87—88 °C (recrystallized from ether). TLC, R_f=0.34. ^{1}H NMR ($CDCl_3$, 90 MHz) δ=3.09 (1H, br s, OH), 4.45 (1H, d, $J_{2,3}$=7 Hz, H-2), 5.04 (2H, narrow m, CH_2OBz), 5.67 (1H, dd, $J_{3,4}$=3 Hz, H-3), 5.82—6.14 (3H, m, H-4, 5, and 6), 6.41 (1H, d, J=15.5 Hz, CHCH=CHPh), 7.31—7.54 (8H, m) and 8.01—8.12 (2H, m) (OBz and COCH=CHPh), 7.70 (1H, d, COCH=CHPh).

Found: C, 73.54; H, 5.54%. Calcd for $C_{23}H_{20}O_5$: C, 73.40; H, 5.32%.

Intramolecular Diels-Alder Reaction of 5. A solution of **5** (60 mg, 0.16 mmol) and toluene (2.0 ml) was heated in a sealed tube at 70 °C for 4 d. The mixture was concentrated and the residue was purified on a silica-gel column to give 59 mg (98%) of **7**, mp 173—174 °C, identical with the compound obtained from **6** in all respects.

The authors wish to thank Mr. Saburo Nakada for his elemental analyses.

References

1) S. D. Joland, J. J. Hoffmann, K. H. Schram, J. R. Cole, M. S. Tempesta, and R. B. Bates, *J. Org. Chem.*, **46**, 4267 (1981).

2) M. Kodpinid, C. Sadavongvivad, C. Thebtaranonth, and Y. Thebtaranonth, *Tetrahedron Lett.*, **24**, 2019 (1983).

3) S. Ogawa and T. Takagaki, *J. Org. Chem.*, **50**, 2356 (1985).

4) S. Ogawa, T. Toyokuni, M. Ara, M. Suetsugu, and T. Suami, *Chem. Lett.*, **1980**, 379; *Bull. Chem. Soc. Jpn.*, **56**, 1710 (1983).

5) The reaction is not optimized. A considerable amount of the methyl ester has been shown to be formed under these conditions.

6) Comparison of the ^{1}H NMR spectrum with that of an authentic sample was kindly carried out by Professor Robert B. Bates (University of Arizona), to whom our thanks are due.

A Practical Synthesis of 1,3-Diene Using Allyltriphenylsilane and Titanium Tetraisopropoxide

Yoshihiko IKEDA and Hisashi YAMAMOTO*
Department of Applied Chemistry, Faculty of Engineering, Nagoya University, Chikusa-ku, Nagoya 464
(Received September 12, 1985)

Synopsis. A practical method for the stereoselective preparation of 1,3-dienes by the use of allyltriphenylsilane as a key reagent is described.

A Peterson reaction involves the addition of a stoichiometric quantity of an α-silyl carbanion to a carbonyl group.[1] Recently, the scope of this process has been extended significantly.[2] One problem which had not been resolved was the control of regio- and stereoselectivity in the reaction of α-silylallyl carbanions with aldehydes and ketones.[3] This problem has now been solved by converting carbanions into the corresponding organotitanium compounds. Thus, Reetz and Sato recently reported independently the regio- and stereochemistry in reactions of trimethylsilylallyl anions with aldehydes as being highly controlled via the corresponding titanium reagent.[4] We also described a similar synthesis of 1,3-dienes using phenyl 1-(trimethylsilyl)-2-propenyl sulfide and titanium tetraisopropoxide.[5] During the course of our work, we found that the triphenylsilyl group has excellent potential as a control element in Peterson olefination since the three phenyl groups provide strong steric screening, not only for the silicon to which they are attached but to the next atom and even beyond. Furthermore, and much more importantly, it was found to be that, because of the inductive effect of three phenyl groups, the proton-metal exchange reaction of triphenylsilyl derivatives using butyllithium is much easier compared to the more common trimethylsilyl derivatives.[6] In this note we illustrate the utility of allyltriphenylsilane[7] for the synthesis of 1,3-dienes.

Alylltriphenylsilane (**1**), mp 92—94°C, was readily prepared in 86% yield from allylmagnesium bromide and 1 equiv of chlorotriphenylsilane in ether at 0°C.[7] It undergoes clean metallation with butyllithium in tetrahydrofuran (THF) (0°C for 30 min) to form lithio derivative of **1**. In contrast to the metallation of allyltrimethylsilane, the reaction proceeded smoothly in the absence of *N,N,N',N'*-tetramethylethylenediamine (TMEDA) or hexamethylphosphoric triamide (HMPA).[6] The addition of titanium tetraisopropoxide to this solution at −78°C generated a solution of the titanium reagent **2** which is a highly useful reagent for the synthesis of either (*Z*)- or (*E*)-1,3-dienes. Thus, a reaction of **2** with an equivalent of aldehyde was completed in 1 h at −78°C. After the usual work-up, β-triphenylsilyl alcohols (**4**) were obtained. A treatment of **3** with potassium *t*-butoxide at room temperature for 10 min yielded (*Z*)-1,3-diene **4**, *E*/*Z*=<1:50. With sulfuric acid in THF for 16 h, followed by a similar work-up, **3** yielded (*E*)-1,3-diene **5**, *E*/*Z*=>50:1. The geometry was verified by a spectral comparison and/or gc analyses with alternatively prepared samples of 1,3-dienes using the conventional Wittig reactions.

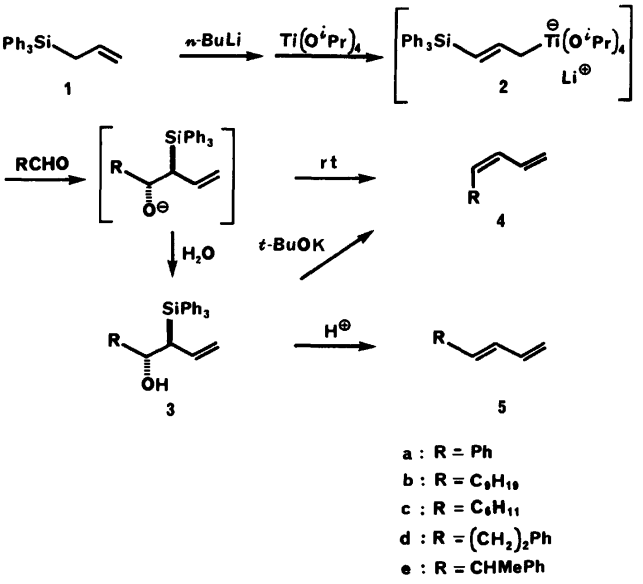

Experimental

The IR spectra were determined on a Hitachi 260-10 spectrometer in a CCl_4 solution unless otherwise stated. The NMR spectra were recorded on a JNM-PMX 60 spectrometer, using TMS (tetramethylsilane) as an internal standard. The analyses were performed at the Institute of Applied Organic Chemistry, Faculty of Engineering, Nagoya University. Tetrahydrofuran was distilled from benzophenone ketyl. All the experiments were carried out under an argon atmosphere. Purification of the product was carried out by column chromatography on silica gel Fuji BW-820.

1-Phenyl-2-triphenylsilyl-3-buten-1-ol (3a): To a solution of allyltriphenylsilane (901 mg, 3.0 mmol) in dry THF (6 ml) was added butyllithium (1.6 mol cm^{-3} hexane solution, 1.57 ml, 2.5 mmol) at 0°C. The resulting pale-yellow solution was stirred at 0°C for 1 h, turning redish brown, and cooled to −78°C. Titanium tetraisopropoxide (0.80 ml, 2.7 mmol) was added at −78°C and the mixture was stirred for 30 min at this temperature, during which period the color changed to bright yellow. Finally, a solution of benzaldehyde (211 mg, 2.0 mmol) in dry THF (2 ml) was added at −78°C, and the reaction mixture was then stirred for 1 h. The reaction was quenched by an addition of ice-cold aqueous hydrochloric acid. The product was extracted twice with hexane, dried over $MgSO_4$, concentrated in vacuo, and purified by column chromatography on silica gel to give the alcohol **3a** as colorless crystals (732 mg, 90% yield): Mp 135—137°C; IR (neat) 3550, 3030, 1425, 1100, 1040, 910, 735, and 695 cm^{-1}; ^{1}H NMR ($CDCl_3$) δ=1.87 (br, 1H, OH), 2.84 (dd, *J*=3 and 10 Hz, 1H), 4.68 (dd, *J*=2 and 17 Hz, 1H), 4.90 (dd, *J*=2 and 11 Hz, 1H), 5.13 (br, 1H), 6.05 (ddd, *J*=11, 17, and 10 Hz, 1H), 6.74—8.08 (m, 5H). Anal. ($C_{28}H_{26}OSi$) C, H.

3-Triphenylsilyl-1-tridecen-4-ol (3b) was obtained in 83%

yield as a colorless liquid: IR (CCl_4) 2880, 1410, and 990 cm^{-1}; ^1H NMR (CCl_4) δ=0.53—2.17 (br, 20H), 2.59 (dd, J=11 and 3 Hz, 1H), 3.85 (br, 1H), 4.70—5.20 (m, 2H), 5.95 (ddd, J=16, 11, and 11 Hz, 1H). Anal. ($C_{31}H_{40}OSi$) C, H.

(*Z*)-1-Phenyl-1,3-butadiene (4a): To a solution of the alcohol **3a** (296 mg, 0.73 mmol) in dry THF (3 ml) was added potassium *t*-butoxide (92 mg, 0.80 mmol) at room temperature. The mixture was stirred at room temperature for 10 min. TLC analyses showed the complete consumption of the starting alcohol. After the usual work-up, the crude product was purified by column chromatography on silica gel using pentane as an eluant to afford the diene **4a** as a clear liquid (95 mg, 100%): IR (neat) 3100, 3040, 2980, 2950, 1820, 1640, 1610, 1500, 1455, 1440, 1085, 1040, 1010, 955, 915, 870, 820, 790, 760, 700 cm^{-1}; ^1H NMR (CCl_4) δ=4.96—5.49 (br m, 2H), 5.93—7.49 (m, 8H). Anal. ($C_{10}H_{10}$) C, H.

A gc analysis of the product revealed an *E*/*Z* ratio of 1:50. An authentic mixture of the diene was prepared independently via allyl Wittig reagent and benzaldehyde.

Direct preparation of the (*Z*)-diene **4a**: After the addition of decanal, the reaction mixture was stirred at −78 °C for 1 h and at 30 °C for 3 h. After the usual work-up, (*Z*)-1,3-tridecadiene was obtained in 70% yield.

(*Z*)-1,3-Tridecadiene (4b) was similarly prepared in a quantitative yield as a colorless oil: IR (neat) 3100—2750, 1805, 1640, 1590, 1460, 1380, 970, 900, 780, 720 cm^{-1}; ^1H NMR (CCl_4) δ=0.67—2.50 (br, 19H), 4.86—5.60 (m, 3H), 5.88 (dd, J=11 and 11 Hz, 1H), 6.53 (ddd, J=11, 11, and 16 Hz); Anal. ($C_{13}H_{24}$) C, H.

(*Z*)-1-Cyclohexyl-1,3-butadiene (4c) was prepared in 69% yield as a colorless oil: IR (CCl_4) 3074, 2990, 1645, 1600, 1002, 967, 910 cm^{-1}; ^1H NMR (CCl_4) δ=0.66—2.35 (br. m, 10H), 2.41 (br. m, 1H), 4.85—5.44 (m, 3H), 5.79 (dd, J=11 and 11 Hz, 1H), 6.57 (ddd, J=11, 11 and 17 Hz, 1H); Anal. ($C_{10}H_{16}$) C, H.

(*Z*)-6-Phenyl-1,3-hexadiene (4d) was prepared in quantitative yield as a colorless oil:[8] IR (CCl_4) 3020, 2920, 1595, 1490, 1450, 1430, 990, 900 cm^{-1}; ^1H NMR (CCl_4) δ=2.20—2.90 (br. m, 4H), 4.83—5.62 (m, 3H), 5.91 (dd, J=11 and 11 Hz, 1H), 6.51 (ddd, J=11, 11 and 16 Hz, 1H), 7.07 (5H). Anal. ($C_{12}H_{14}$) C, H.

(*Z*)-5-Phenyl-1,3-hexadiene (4e) was prepared in 82% yield as a colorless oil: IR (CCl_4) 2970, 2930, 1600, 1490, 1450, 995, 905 cm^{-1}; ^1H NMR (CCl_4) δ=1.31 (d, J=7 Hz, 3H), 3.90 (dq, J=7 and 9 Hz, 1H), 4.94—5.58 (m, 3H), 5.87 (dd, J=10 and 10 Hz, 1H), 6.61 (ddd, J=10, 10, and 16 Hz, 1H), 7.06 (5H). Anal. ($C_{12}H_{14}$) C, H.

(*E*)-1-Phenyl-1,3-butadiene (5a): A mixture of the alcohol **3a** (217 mg, 0.53 mmol) and a catalytic amount of sulfuric acid (2 drops) in dry THF (10 ml) was stirred at room temperature for 16 h. The mixture was poured into water and the product was extracted with hexane, dried, and purified by column chromatography on silica gel to give the diene **5a** as an oil (57 mg, 82%): IR (CCl_4) 3070, 3005, 1795, 1625, 1593, 1480, 1440, 1155, 1065, 950, 890, 850 cm^{-1}; ^1H NMR (CCl_4) δ=4.92—5.49 (m, 2H), 6.07—6.89 (m, 3H), 6.89—7.59 (m, 5H). Anal. ($C_{10}H_{10}$) C, H.

(*E*)-1,3-Tridecadiene (5b): A mixture of the alcohol **3b** (220 mg, 0.48 mmol) and a catalytic amount of sulfuric acid (2 drops) in dry THF (6 ml) was stirred at reflux for 4 h. The mixture was poured into water and the product was extracted with hexane, dried, and purified by column chromatography on silica gel to give the diene **5b** as an oil (65 mg, 75%). IR (CCl_4) 3150—2800, 1870, 1660, 1610, 1560, 1480, 1390, 1265, 1130, 1050, 960, 905, 870 cm^{-1}; ^1H NMR (CCl_4) δ=0.63—2.47 (br, 19H), 4.70—6.53 (m, 5H). Anal. ($C_{10}H_{10}$) C, H.

References

1) P. F. Hudrlik and D. Peterson, *J. Am. Chem. Soc.*, **97**, 1464 (1975).

2) E. Colvin, "Silicon in Organic Synthesis," Butterworths, London (1981); W. P. Weber, "Silicon Reagents for Organic Synthesis," Springer-Verlag, New York (1983) and references cited therein.

3) P. W. K. Lau and T. H. Chan, *Tetrahedron Lett.*, **1978**, 2383; E. Ehlinger and P. Magnus, *J. Am. Chem. Soc.*, **102**, 5004 (1980).

4) a) F. Sato, Y. Suzuki, and M. Sato, *Tetrahedron Lett.*, **23**, 4589 (1982); b) M. T. Reetz and B. Wenderoth, *Tetrahedron Lett.*, **23**, 5259 (1982). See also Y. Yamamoto, Y. Saito, and K. Maruyama, *J. Chem. Soc., Chem. Commun.*, **1982**, 1326; D. J. S. Tsai and D. S. Matterson, *Tetrahedron Lett.*, **22**, 2751 (1981).

5) Y. Ikeda, K. Furuta, N. Meguriya, N. Ikeda, and H. Yamamoto, *J. Am. Chem. Soc.*, **104**, 7663 (1982); *Bull. Chem. Soc. Jpn.*, **57**, 2781 (1984); J. Ukai, Y. Ikeda, N. Ikeda, and H. Yamamoto, *Tetrahedron Lett.*, **25**, 5173 (1984); Y. Ikeda, J. Ukai, N. Ikeda, and H. Yamamoto, ibid., **25**, 5177 (1984).

6) The deprotonation of allyltrimethylsilane with butyllithium is very slow in the absence of HMPA and/or TMEDA. In the presence of HMPA and/or TMEDA, the titanium reaction turned out to be unsatisfactory.

7) H. Gilman and D. Aoki, *J. Organometal. Chem.*, **2**, 44 (1964); A. D. Petrov and L. L. Shchukovskaya, *Zhur. Obshei. Khim.*, **25**, 1083 (1955); D. Seyferth and M. A. Weiner, *J. Org. Chem.*, **26**, 4797 (1961).

8) Although the attempted separation of stereoisomers by gc was unsatisfactory, the NMR spectrum revealed the absence of the other isomer.

Stereoselective Synthesis of Allyl- or Alkynyl-Substituted (Z)-Vinylsilanes via Organoboranes

Masayuki HOSHI,* Yuzuru MASUDA, and Akira ARASE
Department of Industrial Chemistry, Kitami Institute of Technology, Kitami 090
(Received September 17, 1985)

Synopsis. Copper(I) iodide-catalyzed cross-coupling reactions of (Z)-(1-trimethylsilyl-1-alkenyl)dicyclohexylboranes with allyl bromide or 1-bromo-1-hexyne gave stereoselectively (Z)-1,4-dienes or conjugated (Z)-enynes having a trimethylsilyl group on the internal carbon atom of the double bond.

Vinylsilanes are versatile intermediate in organic synthesis.[1] There have been several approaches to the synthesis of these useful compounds. Uchida et al. reported a stereoselective synthesis of (Z)-vinylsilanes via (Z)-(1-trimethylsilyl-1-alkenyl)dicyclohexylboranes (**1**) starting from 1-trimethylsilyl-1-alkynes.[2] As depicted in Scheme 1, **1** were once transformed to the corresponding vinyllithium or vinylcopper(I) compounds before the cross-coupling reactions with organic halides while the reactions were carried out in situ. In the vinyllithium route, an excess amount of methyllithium, and in the vinylcopper(I) route, an excess amount of methyllithium and a small excess amount of copper(I) iodide were employed.

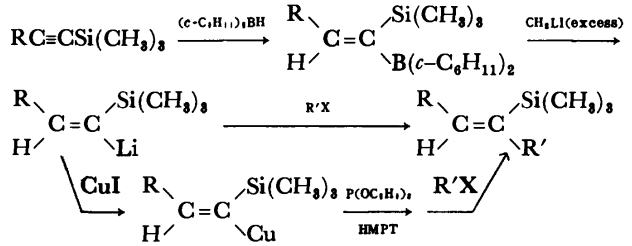

Scheme 1.

A similar cross-coupling reaction of (Z)-(1-trimethylsilyl-1-nonenyl)dicyclohexylborane with allyl bromide was performed by using stoichiometric amount of copper(I) bromide–methyl sulfide.[3]

On the other hand, the authors have found that a catalytic amount of bis(acetylacetonato)copper(II) catalyzed a stereoselective cross-coupling reactions of alkenyldialkylboranes with organic bromides including allyl bromide and 1-alkynyl bromides (Scheme 2).[4–6]

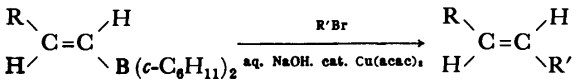

Scheme 2.

Above facts suggested that it was probable to transform 1-trimethylsilyl-1-alkenyldicyclohexylboranes (**1a**) directly to (Z)-vinylsilanes by using catalytic amount of bis(acetylacetonato)copper(II).

As was suggested, (Z)-4-(trimethylsilyl)-1,4-nonadiene (**2a**) was obtained in 84% yield, uncontaminated by *E* isomer, in the reaction of **1a** with allyl bromide in the presence of 5 molar% of bis(acetylacetonato)copper(II).

In further studies to increase the yield of **2a**, copper(I) iodide was found to be far more effective catalyst. Thus, **1a** was transformed to **2a** quantitatively in the presence of 10 molar% of copper(I) iodide (Scheme 3). The use of far less amount of copper(I) compound than in the reaction reported earlier seemed synthetically interesting.

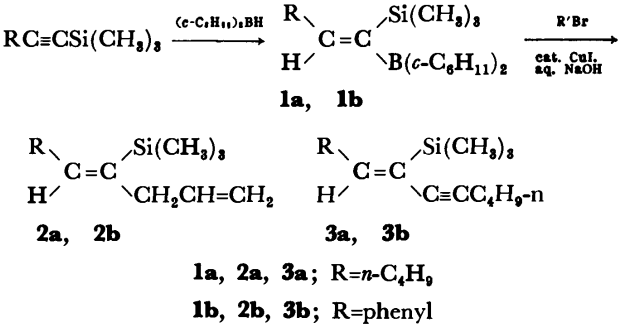

Scheme 3.

Copper(I) chloride and copper(I) bromide showed little catalytic effect and the yields of **2a** could not exceed 76 and 78% respectively even in the presence of stoichiometric amount of these copper compounds.[2,3]

Similarly, (Z)-1-phenyl-2-(trimethylsilyl)-1,4-pentadiene (**2b**) was afforded in 92% yield from (Z)-(1-trimethylsilyl-2-phenylvinyl)dicyclohexylborane (**1b**) and allyl bromide.

The present reaction could be applied also to the synthesis of trimethylsilyl-substituted conjugated enynes which were expected to be interesting intermediates because of the unique position of the trimethylsilyl group in the molecule. Thus, similar reactions of **1a** and **1b** with 1-bromo-1-hexyne afforded (Z)-6-(trimethylsilyl)-5-dodecen-7-yne (**3a**) and (Z)-1-phenyl-2-(trimethylsilyl)-1-octen-3-yne (**3b**) in moderate yields respectively.

Z-Configuration was assigned to these compounds by direct comparisons of IR and ^{1}H NMR spectra of 1,4-dienes and conjugated enynes, obtained by stereospecific desilylation of vinylsilanes[7] with those obtained by our previous work.[4]

These results are shown in Table 1.

All vinylsilanes obtained in the reactions were found to be isomerically pure by GLC using a glass capillary column and by ^{1}H NMR spectra.

Reactions of **1a** and **1b** with alkyl bromides failed to give satisfactory results under the present reaction conditions.

Experimental

Instruments. IR spectra (film) were recorded with a Hitachi 285 spectrometer. ^{1}H NMR (60 MHz) spectra (CCl_4,

Table 1. Yields of Substituted (*Z*)-Vinylsilanes

R	R′	Cu compd	mol %	Product	Yield/%[a] A	B
n-C_4H_9	$CH_2CH{=}CH_2$	Cu-$(acac)_2$	(5)	2a	47	
		CuCl	(100)	2a	76	
		CuBr	(100)	2a	78	
		CuI	(100)	2a	100	
		CuI	(10)	2a	100	91
		CuI	(5)	2a	93	
C_6H_5		CuI	(10)	2b	92	86
n-C_4H_9	$C{\equiv}CC_4H_9$-n	CuI	(10)	3a	75	66
C_6H_5		CuI	(10)	3b	78	70

a) The yields are based on 1-trimethylsilyl-1-alkynes. A; determined by GLC (5%-FFAP, supported on Diasolid M). B; isolated by column chromatography.

TMS) were run on a Hitachi R-20A spectrometer. Mass spectra were recorded with a Hitachi M-52 mass spectrometer.

Reagents. Cyclohexene and tetrahydrofuran (THF) were dried over lithium aluminium hydride and distilled under argon stream before use. 1-Trimethylsilyl-1-hexyne,[8] 1-phenyl-2-(trimethylsilyl)acetylene[8] and 1-bromo-1-hexyne[9] were prepared as described in the literatures. Allyl bromide was dried over molecular sieves-4A. Commercial copper(I) iodide was used without any purification. THF solution of BH_3 was prepared by the method described in the literature.[10]

Reaction Procedure. A 50-ml round bottomed flask, equipped with a gas inlet for argon, a sample inlet with a serum cap and a magnetic stirring bar, was flushed with argon. In the flask, 1-trimethylsilyl-1-alkyne (10 mmol) was added at 0 °C to the suspension of dicyclohexylborane (10 mmol) in THF, prepared by hydroboration of cyclohexene (20 mmol) with the THF solution of BH_3 (10 mmol) at 0 °C for 2 h, and then the reaction mixture was stirred at 0 °C for 1 h and then additional 1 h at room temperature in order to complete the reaction. Copper(I) iodide (1 mmol) and allyl bromide or 1-bromo-1-hexyne (10 mmol) were successively added to the solution at 0 °C and the solution was treated with 10 mmol of 3M[†]-NaOH at this temperature for 1 h. The residual boron compound was decomposed by oxidation with hydrogen peroxide. The reaction mixture was extracted three times with diethyl ether. The combined extracts were washed twice with NaCl-saturated water and dried over anhydrous sodium sulfate. After evaporation of the solvent, the residue was put on a column packed with silica gel (Wako-gel Q-50).

Spectral data of the products are as follows.

(*Z*)-4-Trimethylsilyl-1,4-nonadiene (2a). ^{1}H NMR δ=0.12 (s, 9H), 0.89 (m, 3H) 1.07—1.50 (m, 4H), 1.86—2.37 (m, 2H), 2.63—2.85 (m, 2H), 4.68—5.07 (m, 2H), and 5.40—6.07 (m, 2H). IR: 3075, 1640, 1615, 1250, 995, 910, 835, 760, and 685 cm^{-1}. MS: *m/z* 196 (M^+).

(*Z*)-1-Phenyl-2-trimethylsilyl-1,4-pentadiene (2b). ^{1}H NMR δ=0.15 (s, 9H), 3.03—3.24 (m, 2H), 5.00—5.40 (m, 2H), 5.68—6.39 (m, 1H), and 7.28 (s, 6H, one vinylic proton is contained). IR: 3075, 1645, 1595, 1495, 1440, 1260, 1000, 915, 840, 750, and 705 cm^{-1}. MS: *m/z* 216 (M^+).

(*Z*)-6-Trimethylsilyl-5-dodecen-7-yne (3a). ^{1}H NMR δ=0.12 (s, 9H), 0.83 (m, 6H), 1.06—1.55 (m, 8H), 1.84—2.34 (m, 4H), and 6.33 (t, *J*=7 Hz, 1H). IR: 1250, 840, and 755 cm^{-1}. MS: *m/z* 236 (M^+).

(*Z*)-1-Phenyl-2-trimethylsilyl-1-octen-3-yne (3b). ^{1}H NMR δ=0.13 (s, 9H), 0.99 (m, 3H), 1.18—1.76 (m, 4H), 2.23—2.60 (m, 2H), 7.23 (s, 5H), and 7.61 (s, 1H). IR: 1250, 840, 755, and 700 cm^{-1}. MS: *m/z* 256 (M^+).

† 1 M=1 mol dm^{-3}.

References

1) For example, see a) I. Fleming, "Comprehensive Organic Chemistry," ed by D. Barton and W. D. Ollis, Pergamon Press, Oxford (1979), Vol. 3, Chap. 13, p. 613. b) T. H. Chan, and I. Fleming, *Synthesis*, **1979**, 671.

2) K. Uchida, K. Utimoto, and H. Nozaki, *Tetrahedron*, **33**, 2987 (1977).

3) J. B. Campbell, Jr. and H. C. Brown, *J. Org. Chem.*, **45**, 550 (1980).

4) M. Hoshi, Y. Masuda, and A. Arase, *Bull. Chem. Soc. Jpn.*, **56**, 2855 (1983).

5) M. Hoshi, Y. Masuda, Y. Nunokawa, and A. Arase, *Chem. Lett.*, **1984**, 1029.

6) A. Arase, M. Hoshi, and Y. Masuda, *Chem. Lett.*, **1984**, 2093.

7) K. Utimoto, M. Kitai, and H. Nozaki, *Tetrahedron Lett.* **1975**, 2825.

8) G. Zweifel and S. J. Backlund, *J. Am. Chem. Soc.*, **99**, 3184 (1977).

9) K. E. Schulte and M. Goes, *Arch. Pharm.*, **290**, 118 (1959).

10) G. Zweifel and H. C. Brown, *Org. Reac.*, **13**, 1 (1963).

Amijitrienol and 14-Deoxyisoamijiol, Two New Diterpenoids from the Brown Seaweed *Dictyota linearis*

Masamitsu OCHI,* Kazuhiko ASAO, Hiyoshizo KOTSUKI, Iwao MIURA,† and Kozo SHIBATA††
Faculty of Science, Kochi University, Akebono-cho, Kochi 780
†Laboratories of Natural Products Chemistry, Otsuka Pharmaceutical Co. Ltd., Kawauchi-cho, Tokushima 771-01
††Faculty of Science, Osaka City University, Sugimoto, Sumiyoshi-ku, Osaka 558
(Received September 26, 1985)

Synopsis. The structures of amijitrienol and 14-deoxyisoamijiol, two new diterpenoids isolated from the brown seaweed *Dictyota linearis*, have been established as **1** and **2** on the basis of spectral and chemical evidence.

In previous papers, we have described the isolation of four diterpenoids of the dolastane class[1,2] and a unique member of the secodolastane class[3] from the brown seaweed *Dictyota linearis*. Our continuing search for the biologically active constituents of this alga has led to the isolation of two additional congeners, designated amijitrienol and 14-deoxyisoamijiol. In this note, a structural elucidation of these new compounds is presented. They were found to have a moderate antimicrobial activity against *Staphylococcus aureus* and *Mucor mucedo*.[4]

Amijitrienol (**1**), $C_{20}H_{30}O$, mp 129.0—129.5 °C, $[\alpha]_D^{18}$ +15.1° (*c* 0.09, EtOH), was isolated as fine needles in 0.0015% yield of fresh alga by conventional silica-gel column chromatography and preparative high-performance liquid chromatography. The IR, UV, and ^{1}H NMR spectra of **1** indicated the presence of one hydroxyl group [3440 cm^{-1}; δ=3.38 (1H, dd, *J*=3.0 and 3.0 Hz)], one conjugated diene [3080, 1640, and 890 cm^{-1}; 230 nm (ε=17000)], two tertiary methyl groups [δ=0.88 and 1.30 (3H each, s)], one isopropyl group [δ=0.93, 0.94 (3H each, d, *J*=6.8 Hz), and 2.64 (1H, qq, *J*=6.8 and 6.8 Hz)], and three olefinic protons [δ= 4.63 (1H, dd, *J*=2.6 and 2.6 Hz), 4.75 (1H, dd, *J*=2.6 and 2.1 Hz), and 5.81 (1H, s)]. In addition, the ^{13}C NMR data for **1** showed the presence of one fully-substituted double bond (δ=139.7 and 142.6), one tri-substituted double bond [δ=136.9 (s) and 138.8 (d)], and one exocyclic methylene group [δ=110.9 (t) and 150.5 (s)], together with two quaternary carbon atoms, one oxygen-bearing methine group, and six methylene groups. These facts suggested that **1** has a structure analogous to that of amijiol (**3**),[1] in which the allylic alcohol functionality in **3** is replaced by a C_{13}—C_{15} conjugated diene. This was confirmed by the chemical correlation of **1** with **3**. Thus, the acetylation of **1** with acetic anhydride and pyridine gave an acetate (**4**), which was found to be identical with the compound derived from **3** via the acetate (**5**)[1] by dehydration with phosphoryl chloride and pyridine.

14-Deoxyisoamijiol (**2**), $C_{20}H_{32}O$, mp 89.0—90.0 °C, $[\alpha]_D^{18}$—2.6° (*c* 0.09, EtOH), was obtained as fine needles in 0.0056% yield and displayed spectral data quite similar to that of 14-deoxyamijiol (**6**).[1] The 400 MHz ^{1}H NMR spectra of **2** and **6**, which were completely assigned by an extensive decoupling study and NOE measurements, were distinct from one another essentially only in the chemical shift of the methine proton on the oxygenated carbon atom [δ(**2**)—δ(**6**)=0.76 ppm]. This fact and the pertinent ^{13}C NMR data revealed that the hydroxyl group of **2** is attached to $C_{2\alpha}$ instead of $C_{4\alpha}$ in **6** and that the relationship of **6** to **2** corresponds to that of amijiol (**3**) to isoamijiol (**7**).[1] Consequently, 14-deoxyisoamijiol must be represented by structure **2**.

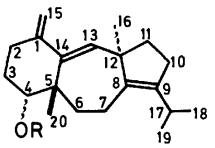

1 R=H
4 R=Ac

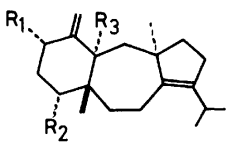

2 R_1=OH, R_2=R_3=H
3 R_1=H, R_2=R_3=OH
5 R_1=H, R_2=OAc, R_3=OH
6 R_1=R_3=H, R_2=OH
7 R_1=R_3=OH, R_2=H

Experimental

All the mps were determined on a Mitamura micromelting-point apparatus and are uncorrected. The IR and UV spectra were recorded on a JASCO model A-202 spectrophotometer and a Hitachi 340 spectrophotometer, respectively. The ^{1}H (400 MHz) and ^{13}C (100 MHz) NMR spectra were taken on a Bruker WH-400 instrument in $CDCl_3$ solutions, with TMS as the internal standard. Mass spectra were recorded at 70 eV on a Finnigan MAT 312. A Union Gikken apparatus, model PM-101, was used for a measurement of the rotations. High-performance liquid chromatographic separation was performed on a Waters Associates HPLC model 6000A, with a TSK-GEL LS-410KG (ODS) column.

Isolation. Fresh alga (3.9 kg), collected in the Bay of Tosa in July 1982, was chopped up and extracted with methanol (10 l) for one week. The methanol solution was concentrated up to about 1.5 l and extracted with dichloromethane (0.5 l×3). The dichloromethane layer was washed with water, dried over Na_2SO_4, and evaporated to dryness. Then, the residue (42 g) was subjected to chromatography over silicic acid (800 g), eluting with hexane–ethyl acetate mixtures, ethyl acetate increasing from 10 to 50%. Elution with 20% ethyl acetate in hexane gave a fraction (506 mg) which was further purified by high-performance liquid chromatography (TSK-GEL LS-410KG, 80% MeOH in water) to obtain amijitrienol (**1**) and 14-deoxyisoamijiol (**2**).

Amijitrienol (1). The crude material was recrystallized from hexane to give white needles (59 mg); mp 129.0—129.5 °C, $[\alpha]_D^{18}$ 15.1° (*c* 0.09, EtOH); IR (nujol) 3440, 3080, 1640, and 890 cm^{-1}; UV (EtOH) 230 nm (ε=17000); ^{1}H NMR ($CDCl_3$) δ=0.88 and 1.30 (3H each, s, 20- and 16-H_3), 0.93 and 0.94 (3H each, d, *J*=6.8 Hz, 18- and 19-H_3), 2.64 (1H, qq, *J*=6.8 and 6.8 Hz, 17-H), 3.38 (1H, dd, *J*=3.0and 3.0 Hz, 4-H), 4.63

(1H, dd, J=2.6 and 2.6 Hz, 15-Ha), 4.75 (1H, dd, J=2.6 and 2.1 Hz, 15-Hb), and 5.81 (1H, s, 13-H); ^{13}C NMR ($CDCl_3$) δ=150.5 (C_1), 142.6 (C_8), 139.7 (C_9), 138.8 (C_{13}), 136.9 (C_{14}), 110.9 (C_{15}), 78.3 (C_4), 52.3 (C_{12}), 44.8 (C_5), 42.5 (C_{11}), 33.4 (C_2), 29.2 (C_3), 28.6 (C_6), 27.3 (C_{10}), 27.1 (C_{17}), 27.0 (C_{16}), 21.9 (C_7), 21.3 (C_{18}), 20.9 (C_{19}), and 20.5 (C_{20}); MS (70 eV) m/z 286 (M^+), 271 (M^+-CH_3), 253 ($M^+-CH_3-H_2O$), 243 ($M^+-C_3H_7$), and 225 ($M^+-C_3H_7-H_2O$). Found: m/z 286.2326. Calcd for $C_{20}H_{30}O$: M, 286.2297.

14-Deoxyisoamijiol (2). The crude substance was recrystallized from hexane to yield white needles (217 mg); mp 89.0—90.0 °C, $[\alpha]_D^{18}$ −2.6° (c 0.09, EtOH); IR (nujol) 3260, 3080, 1640, and 890 cm^{-1}; ^{1}H NMR ($CDCl_3$) δ=0.64 and 1.11 (3H each, s, 20- and 16-H_3), 0.93 and 0.94 (3H each, d, J=7.0 Hz, 18- and 19-H_3), 1.08 (1H, ddd, J=13.1, 3.2, and 3.2 Hz, 4β-H), 1.33 (1H, ddd, J=14.6, 4.9, and 4.0 Hz, 6β-H), 1.45 (1H, dd, J=13.9 and 2.8 Hz, 13α-H), 1.54 (1H, dd, J=13.9 and 11.5 Hz, 13β-H), 1.58 (2H, m, 11-H_2), 1.75 (2H, m, 3-H_2), 1.86 (1H, ddd, J=14.6, 11.8, and 4.9 Hz, 6α-H), 1.91 (1H, ddd, J=13.1, 8.3, and 5.3 Hz, 4α-H), 2.13 (1H, ddddd, J=16.6, 4.9, 4.0, 1.5, and 1.5 Hz, 7α-H), 2.17 (2H, m, 10-H_2), 2.40 (1H, dddd, J=16.6, 11.8, 4.9, and 1.3 Hz, 7β-H), 2.61 (1H, qq, J=7.0 and 7.0 Hz, 17-H), 2.69 (1H, dddd, J=11.5, 2.8, 1.5, and 1.3 Hz, 14α-H), 4.28 (1H, dd, J=2.8 and 2.8 Hz, 2β-H), 4.67 (1H, dd, J=1.5 and 1.3 Hz, 15-Ha), and 4.97 (1H, dd, J=1.3 and 1.3 Hz, 15-Hb); ^{13}C NMR ($CDCl_3$) δ=153.8 (C_1), 140.2 (C_8), 139.0 (C_9), 109.8 (C_{15}), 74.3 (C_2), 50.1 (C_{12}), 42.1 (C_{13}), 41.2 (C_{11}), 41.1 (C_4), 40.5 (C_{14}), 39.4 (C_5), 36.6 (C_3), 30.2 (C_6), 27.4 (C_{10}), 26.8 (C_{17}), 24.1 (C_{16}), 21.9 (C_7), 21.1 (C_{18}), 20.9 (C_{19}), and 15.3 (C_{20}); MS (70 eV) m/z 288 (M^+), 273 (M^+-CH_3), 255 ($M^+-CH_3-H_2O$), 245 ($M^+-C_3H_7$), and 227 ($M^+-C_3H_7-H_2O$). Found: m/z 288.2459. Calcd for $C_{20}H_{32}O$: M, 288.2453.

Acetylation of 1. A solution of **1** (49 mg) in acetic anhydride (0.2 ml) and pyridine (0.8 ml) was allowed to stand at room temperature overnight and then worked up in the usual way. The product was subjected to chromatography using a Robar column (Merck, LiChroprep Si 60, size B) and 10% ether in hexane as the eluent to give an acetate (**4**) as a viscous oil (30 mg); IR ($CHCl_3$) 1738 and 1260 cm^{-1}; ^{1}H NMR ($CDCl_3$) δ=0.92 and 1.29 (3H each, s, 20- and 16-H_3), 0.92 and 0.94 (3H each, d, J=6.8 Hz, 18- and 19-H_3), 2.08 (3H, s, $COCH_3$), 2.63 (1H, qq, J=6.8 and 6.8 Hz, 17-H), 4.64 (1H, m, 15-Ha), 4.66 (1H, m, 15-Hb), 4.77 (1H, dd, J=3.0 and 2.0 Hz, 4-H), and 5.74 (1H, s, 13-H); ^{13}C NMR ($CDCl_3$) δ=170.9 ($\underline{C}OCH_3$), 150.3 (C_1), 142.7 (C_8), 139.7 (C_9), 137.1 (C_{13}), 136.7 (C_{14}), 111.0 (C_{15}), 80.1 (C_4), 52.2 (C_{12}), 43.3 (C_5), 42.5 (C_{11}), 32.8 (C_2), 29.8 (C_3), 29.4 (C_6), 27.2 (C_{10}), 27.0 (C_{17}), 26.9 (C_{16}), 21.8 (C_7), 21.4 ($CO\underline{C}H_3$ and C_{18}), 20.9 (C_{19}), and 20.5 (C_{20}); MS (70 eV) m/z 328 (M^+), 313 (M^+-CH_3), 285 ($M^+-C_3H_7$), 268 (M^+−AcOH), 253 (M^+-CH_3-AcOH), and 225 ($M^+-C_3H_7$-AcOH). Found: m/z 328.2404. Calcd for $C_{22}H_{32}O_2$: M, 328.2402.

Dehydration of 5. A mixture of **5** (80 mg) and $POCl_3$ (0.12 ml) in pyridine (0.6 ml) was stirred at room temperature for three days. The reaction mixture was worked up in the usual manner and the resulting product was chromatographed using a Robar column (LiChroprep Si 60, size B) and 10% ether in hexane as the solvent to yield a diene (30 mg) which was identified by TLC, IR, and ^{1}H NMR comparisons with **4**.

The present work was partially supported by a Grant-in-Aid for Co-operative Research from the Ministry of Education (No. 58340030).

References

1) M. Ochi, M. Watanabe, I. Miura, M. Taniguchi, and T. Tokoroyama, *Chem. Lett.*, **1980**, 1229.

2) M. Ochi, M. Watanabe, M. Kido, Y. Ichikawa, I. Miura, and T. Tokoroyama, *Chem. Lett.*, **1980**, 1233.

3) M. Ochi, I. Miura, and T. Tokoroyama, *J. Chem. Soc., Chem. Commun.*, **1981**, 100.

4) Amijitrienol (**1**) and 14-deoxyisoamijiol (**2**) inhibited the growth of both *S. aureus* and *M. mucedo* at the concentration of 0.5 and 1.0 mg/disc respectively.

An Improved Synthesis of *N*-Trifluoroacetyl-L-daunosamine

Yoshikazu KIMURA, Teruyo MATSUMOTO, Michiyo SUZUKI, and Shiro TERASHIMA*
Sagami Chemical Research Center, Nishi-Ohnuma, Sagamihara, Kanagawa 229
(Received July 18, 1985)

Synopsis. A process which can afford a large quantity of the title compound was explored by modifying the Horton's original route. The developed process features highly stereoselective reduction of the oxime with sodium dihydrobis(2-methoxyethanolato)aluminate(1-) and efficient dehydrobromination with 1,8-diazabicyclo[5.4.0]undec-7-ene.

L-Daunosamine (3-amino-2,3,6-trideoxy-L-*lyxo*-hexopyranose) (**1**) attracts much attention in recent years as an aminosugar component of natural and unnatural anthracycline antibiotics which show prominent anticancer properties.[1,2]

In connection with synthetic studies on optically active anthracyclines,[3] we required a large quantity of *N*-trifluoroacetyl-L-daunosamine (**2**) from which the substrate for glycosidation reaction, 1,4-bis(*O*-*p*-nitrobenzoyl)-3-*N*-trifluoroacetyl-L-daunosamine (**3**), can be readily prepared. It is well known that a trifluoroacetyl group is well suited for protecting the amino group of **1** during glycosidation reaction since it can be readily removed under mild alkaline conditions without cleavage of the formed glycoside linkage.[1-3] However, while **2** can be usually prepared from *N*-

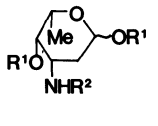

1: R^1= R^2= H
2: R^1= H, R^2= CF_3CO
3: R^1= p-$NO_2C_6H_4CO$, R^2= CF_3CO

acetyl- or *N*-benzoyl-L-daunosamine through **1**-hydrochloride by protective group exchange,[1,2,5] direct preparation method of **2** has never been explored.

In this note, we wish to describe a new synthesis of **2** which is developed by modifying the Horton's original synthetic scheme for *N-acetyl*-L-daunosamine.[4] The developed method includes the following advantages over the Horton's procedure. (1) Trifluoroacetyl group is introduced at the early stage of the synthetic process. This can exclude the above-mentioned tedious protective group exchange. (2) Highly stereoselective reduction of the oxime **5** can be accomplished with sodium dihydrobis(2-methoxyethanolato)aluminate(1-) (Vitride or Red-Al) in toluene in place of lithium aluminum hydride (LAH) in ether. The latter reported reduction which should be carried out using a Soxhlet extraction apparatus is clealy not applicable to a large scale synthesis. (3) Cheap 1,8-diazabicyclo-[5.4.0]undec-7-ene (DBU) can effect clean dehydrobromination in a similar manner to expensive silver fluoride. By employing these improved synthetic methods, we have succeeded in readily obtaining a large quantity of **2** from methyl α-D-mannopyranoside (**4**).

Thus, according to the reported method,[4] **5** was prepared in 52% overall yield starting from **4**. The reduction of **5** with Vitride in toluene was found to proceed more stereoselectively than with LAH, giving the trifluoroacetamide **6a** in 59% overall yield as a sole product after trifluoroacetylation. NMR analysis of **6a** definitely disclosed that the formation ratio of the desired *ribo*-isomer **6a** to the undesired *arabino*-isomer **6b** is more than 99:1. This result is clearly superior to the reported reduction of **3** with LAH in ether,[4] in which a mixture of the *ribo*- and *arabino*-isomers could be produced in a ratio of 88:12 by our hands. The highly stereoselective reduction observed for Vitride may be due to steric bulkiness of the reducing agent which carries two 2-methoxyethoxy groups.

Similarly to the original route,[4] treatment of **6a** with *N*-bromosuccinimide (NBS) gave the bromide **7** in 85% yield. Dehydrobromination of **7** with inexpensive DBU in benzene afforded **8** in 75% yield in a similar manner to that reported with silver fluoride. The unsaturated sugar **8** was elaborated to methyl *N*-trifluoroacetyl-L-daunosamine (**9**) in 53% yield, mp 155.5—156.5 °C, $[\alpha]_D^{20}$ −46.7° (methanol), by sequential transesterification with methanol and catalytic hydrogenation over palladium on carbon. Further hydrolysis of the methyl glycoside **9** with 20% acetic acid quantitatively produced **2**, mp 146—147 °C, $[\alpha]_D^{20}$ −127.2° (methanol).

Taking into account several novel aspects including high stereoselectivity, operational simplicity, and use of less expensive reagents, the explored synthetic scheme is expected to hold promise in a large scale preparation of **2**.

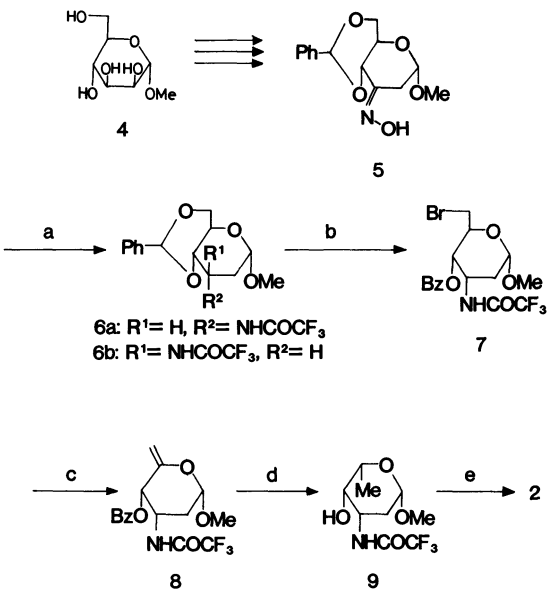

4 → 5

6a: R^1= H, R^2= $NHCOCF_3$
6b: R^1= $NHCOCF_3$, R^2= H

7 → 8 → 9 → 2

a: i) $NaAlH_2(OCH_2CH_2OMe)_2$—C_6H_5Me ii) $(CF_3CO)_2O$–Py,
b: NBS, c: DBU, d: i) NaOMe–MeOH ii) 5% Pd-C, H_2,
e: 20% AcOH

Scheme 1.

Experimental

Methyl 4,6-*O*-Benzylidene-2,3-dideoxy-3-trifluoroacetamido-α-D-ribo-hexopyranoside (6a). A 70% toluene solution of Vitride (95 mL, 333 mmol) was added to a solution of **5**[4] (mp 202 °C, $[\alpha]_D^{23}$ +203° (*c* 1.21, $CHCl_3$)) (lit,[4] mp 203 °C, $[\alpha]_D^{23}$ +202° (*c* 1.2, $CHCl_3$)) (20.0 g, 71.6 mmol) in toluene (350 mL) with stirring at −40 °C. After stirring at −40 °C for 0.5 h and at 25 °C for 4 h, the reduction was quenched by successively adding H_2O (7 mL), 15% NaOH (7 mL), and H_2O (21 mL) to the reaction mixture. The upper toluene layer was separated, dried over anhyd K_2CO_3, filtrated through a pad of Celite, then concentrated in vacuo, to afford crude methyl 3-amino-4,6-*O*-benzylidene-2,3-dideoxy-α-D-hexopyranoside as a pale yellow viscous oil.

Pyridine (24.1 g, 305 mmol) and trifluoroacetic anhydride (44.0 g, 210 mmol) were successively added to an ethereal solution (200 mL) of the oily amine with stirring at −40 °C. After stirring at 0 °C for 3 h, the ethereal mixture was filtered to remove insoluble materials and the solid collected was washed with ether. The ethereal filtrates and washings were combined, washed successively with satd $NaHCO_3$ and satd NaCl, then dried over anhyd $MgSO_4$. Filtration and concentration in vacuo, gave an oily residue, which was purified by column chromatography (benzene/EtOAc=10/1) to give pure **6a** as a colorless oil (15.1 g, 59%), $[\alpha]_D^{21}$ +8.6° (*c* 1.47, $CHCl_3$). IR (neat): 3410, 1735, 1540 cm^{-1}. ^1H NMR ($CDCl_3$) δ=1.93—2.10 (m, 2H, 2-H_2), 3.41 (s, 3H, OCH_3), 3.60—4.80 (m, 6H, 1-, 3-, 4-, 5-H_4+6-H_2), 5.57 (s, 1H, PhC<u>H</u>), 7.15—7.43 (m, 5H, Ph), 7.67 (d, *J*=9 Hz, 1H, NH). MS *m/z*: 361 (M^+).

Methyl 4-*O*-Benzoyl-6-bromo-2,3,6-trideoxy-3-trifluoroacetamido-α-D-ribo-hexopyranoside (7). Following to the reported method,[4] a suspension of **6a** ($[\alpha]_D^{21}$ +8.6° (*c* 1.47, $CHCl_3$)) (15.1 g, 41.9 mmol), NBS (9.03 g, 50.7 mmol), and $BaCO_3$ (12.0 g, 60.8 mmol) in anhyd CCl_4 (350 mL) was heated at reflux with stirring under irradiation with a 60W tungsten lamp. After 1.5 h reaction, the whole mixture was cooled and filtered to remove insoluble materials. The solid collected was washed with CH_2Cl_2 (10 mL×3). The organic phases were combined, washed successively with 5% $NaHSO_3$ and satd $NaHCO_3$, then dried over anhyd $MgSO_4$. Filtration and concentration in vacuo gave a residue, which was purified by column chromatography (benzene/EtOAc=20/1) to afford **7** as a pale yellow solid (16.3 g, 88%), mp 100—102 °C. This was recrystallized from a mixture of benzene and hexane to give an analytical sample of **7**, mp 111.5—112 °C, $[\alpha]_D^{20}$ +39.3° (*c* 1.07, $CHCl_3$). IR (KBr): 3400, 1730, 1545 cm^{-1}. ^1H NMR ($CDCl_3$) δ=1.83—2.40 (m, 2H, 2-H_2), 3.33—3.77 (m, 2H, 6-H_2), 3.35 (s, 3H, OCH_3), 4.02—4.30 (m, 1H, 5-H), 4.67—5.00 (m, 2H, 1-H+3-H). 5.10 (dd, *J*=10 and 5 Hz, 1H, 4-H). 7.23—8.07 (m, 6H, NH+Ph). MS *m/z*: 439 (M^+), 441 ($[M+2]^+$). Found: C, 43.83; H, 3.69; N, 3.14%. Calcd for $C_{16}H_{17}BrF_3NO_5$: C, 43.66; H, 3.89; N, 3.18%.

Methyl 4-*O*-Benzoyl-2,3,6-trideoxy-3-trifluoroacetamido-α-D-erythro-hex-5-enopyranoside (8). A mixture of **7** (mp 100—102 °C) (8.26 g, 18.8 mmol) and DBU (3.76 g, 24.7 mmol) in benzene (10.5 mL) was heated at reflux for 2.5 h with stirring. After cooling, the mixture was filtered and the solid collected was washed with benzene. The combined filtrates were concentrated in vacuo to give a dark brown oil, which was purified by column chromatography (benzene/EtOAc=20/1) to give pure **8** as a pale yellow oil (5.07 g, 75%), $[\alpha]_D^{20}$ +17.6° (*c* 0.67, $CHCl_3$). IR (neat): 3400, 1735, 1670, 1540, 1000 cm^{-1}. ^1H NMR ($CDCl_3$): δ=1.90—2.46 (m, 2H, 2-H_2), 3.47 (s, 3H, OCH_3), 4.61—4.98 (m, 4H, 1,3-H_2+6-H_2), 5.57—5.73 (m, 1H, 4-H), 7.20—8.10 (m, 6H, NH+Ph). MS *m/z*: 359 (M^+).

Methyl *N*-Trifluoroacetyl-L-daunosamine (9). A 1.0 M† solution of sodium methoxide in MeOH (0.7 mL, 0.7 mmol) was added to a solution of **8** ($[\alpha]_D^{20}$ +17.6° (*c* 0.67, $CHCl_3$)) (5.07 g, 14.1 mmol) in MeOH (15 mL), and the mixture was stirred at room temperature for 15 h. After acetic acid (0.05 mL) was added to the mixture, the methanolic solution was concentrated in vacuo. The residue was purified by filtration through a short silica-gel column (ether) to give crude methyl 3-trifluoroacetamido-2,3,6-trideoxy-α-D-*erythro*-hex-5-enopyranoside as a yellow oil (4.9 g, quantitative yield).

A mixture of the oily unsaturated sugar derivatives (4.9 g) and 5% Pd-C (505 mg) in MeOH (100 mL) was stirred under a hydrogen atmosphere at atmospheric pressure for 4 h. Filtration and concentration in vacuo gave a pale yellow solid, which was purified by column chromatography (benzene/EtOAc=4/1) to afford pure **9** as a colorless crystals (1.94 g, 53%), mp 143—145 °C. A part of this sample was recrystallized from a mixture of EtOAc and hexane to give an analytical sample of **9**, mp 155.5—156.5 °C, $[\alpha]_D^{20}$ −46.7° (*c* 0.10, CH_3OH). IR (KBr): 3475, 3300, 1750, 1588 cm^{-1}. ^1H NMR ($CDCl_3$) δ=1.30 (d, *J*=6.5 Hz, 3H, CH_3), 1.58 (dd, *J*=12 and 9 Hz, 1H, 2-*ax*-H), 2.05 (ddd, *J*=12, 4.5, and 2 Hz, 1H, 2-*eq*-H), 2.15 (d, *J*=10 Hz, 1H, OH), 3.48 (s, 3H, OCH_3), 3.38—3.70 (m, 2H, 4-, 5-H_2), 3.80—4.25 (m, 1H, 3-H), 4.35 (dd, *J*=9 and 2 Hz, 1H, 1-H), 6.75 (brs, 1H, NH). Found: C, 41.98; H, 5.64; N, 5.42%. Calcd for $C_9H_{14}F_3NO_4$: C, 42.03; H, 5.49; N, 5.45%.

***N*-Trifluoroacetyl-L-daunosamine (2).** A 20% acetic acid (10 ml) was added to **9** (mp 143—145 °C) (200 mg, 0.78 mmol) and the mixture was stirred at 100 °C for 2 h. After cooling, the mixture was concentrated in vacuo below 30 °C, and the residue was purified by filtration through a short silica-gel column (EtOAc) to give pure **2** as a pale yellow solid (187 mg, 100%), mp 140—141.5 °C. A part of this sample was recrystallized from EtOAc to give an analytical sample of **2**, mp 146—147 °C, $[\alpha]_D^{20}$ −127° (*c* 0.10, MeOH, *equil.*) (lit,[5] mp 146—147 °C). IR (KBr): 3460, 3350, 1710, 1550, 1170 cm^{-1}. ^1H NMR ($(CD_3)_2SO$) δ=1.08 (d, *J*=6 Hz, 3H, CH_3), 1.40—2.30 (m, 2H, 2-H_2), 3.30—4.50 (m, 3H, 3-, 4-, 5-H_3), 4.83 (d, *J*=5 Hz, 1H, OH), 5.00—5.27 (m, 1H, 1-H). 6.08 (d, *J*=3 Hz, 1H, OH), 9.00 (brd, *J*=9 Hz, 1H, NH). Found: C, 39.51; H, 5.50; N, 5.70%. Calcd for $C_8H_{12}F_3NO_4$: C, 39.51; H, 4.98; N, 5.76%.

References

1) F. Arcamone, *Lloydia*, **40**, 45 (1977); F. Arcamone, "Doxorubicin Anticancer Antibiotics," Academic Press, New York (1981).

2) S. Terashima, *Yuki Gosei Kagaku Kyokai Shi*, **40**, 20 (1982).

3) Y. Kimura, M. Suzuki, T. Matsumoto, R. Abe, and S. Terashima, *Chem. Lett.*, **1984**, 501; Y. Kimura, M. Suzuki, and S. Terashima, ibid., **1984**, 2113.

4) D. Horton and W. Weckerle, *Carbohydr. Res.*, **44**, 227 (1975).

5) T. H. Smith, A. N. Fujiwara, W. W. Lee, H. Y. Wu, and D. W. Henry, *J. Org. Chem.*, **42**, 3653 (1977).

† 1 M=1 mol dm^{-3}.

Reactions of Sodium Hydrogentelluride with α-Azido Ketones and α-Azido Bromides

Hitomi SUZUKI,* Takashi KAWAGUCHI, and Koji TAKAOKA
Department of Chemistry, Faculty of Science, Ehime University, Bunkyo-cho, Matsuyama 790
(Received August 15, 1985)

Synopsis. When treated with sodium hydrogentelluride in ethanol at room temperature, α-azido ketones are easily converted to pyrazines via the self-condensation of initially formed α-amino ketones followed by aerobic oxidation during work-up. On a similar treatment, activated α-azido bromide such as 1,2-diphenyl-1-azido-2-bromoethane suffers E2-type β-elimination to give the corresponding olefin as the sole product, while ordinary α-azido bromides afford complicated mixtures containing amino and olefinic compounds among other products.

On heating with an excess of sodium borohydride in ethanol under nitrogen, elemental tellurium is reduced to form sodium hydrogentelluride as a wine-colored

$$Te + NaBH_4 + 3C_2H_5OH \xrightarrow[N_2,\,\Delta]{} NaHTe + B(OC_2H_5)_3 + 3H_2$$

solution. This reagent was first introduced by Barton in 1975,[1] but, in spite of its versatility as a selective reagent for reduction of a variety of organic compounds,[2] it has received little attention until recently. In a recent paper,[3] we have reported that sodium hydrogentelluride has an excellent ability to reduce alkyl and aryl azides to the corresponding amines under mild conditions. The reaction proceeds rapidly to completion and products are usually obtained in high state of purity. As an extension of this work, we have examined the reactions of sodium hydrogentelluride with polyfunctional azides, α-azido ketones and α-azido bromides, with an intent to see if the reaction can be used as a means to construct some nitrogen-containing heterocycles under mild conditions.

α-Azido ketones (**2**), readily prepared from α-bromo ketones (**1**) by standard procedure, was reacted with sodium hydrogentelluride in ethanol under nitrogen. The reaction occurred with immediate liberation of nitrogen and precipitation of free tellurium. After a while, the reaction mixture was exposed to air, freed from insoluble matter by filtration over a thin layer of Celite, and evaporated under reduced pressure to afford pyrazines (**4**). Several substituted pyrazines prepared by utilizing this procedure are summarized in Table 1, together with spectral data of the products. Yields shown do not represent optimized values.

Although the present method worked quite well with ordinary secondary azido ketones, it is not of a general nature. Thus, treatment of some primary azido ketones

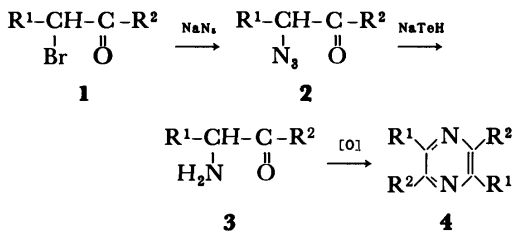

such as α-azidoacetophenone and azidoacetone with sodium hydrogentelluride led to complicated mixtures of unidentified products. Azido ketone activated by adjacent electron-withdrawing group also failed to yield pyrazine; ethyl α-azidoacetoacetate gave only polymeric materials.

Reported procedures for converting carbonyl compounds into pyrazines include the reaction of 1,2-diketones with 1,2-diamines[4,5] or α-amino amides,[6] ammonolysis of α-halo ketones,[7,8] oxidation of ketones with alkaline hexacyanoferrate(III),[9] reduction of α-azido ketones with hydrogen over catalyst[10] or triphenylphosphine,[11] and reaction of ketones with iodine azide.[12]

Conversion of azide to amine may be explained to occur via a pathway which involves the attachment of hydrogentelluride anion to the terminal nitrogen atom of the azido group, followed by the fragmentation of the resulting triazene-type adduct in a way as

Table 1. Preparation of Pyrazines **4** from α-Azido Ketones **2**

	Pyrazine **4**		Mp	Yield/%	IR (KBr)	^{1}H NMR ($CDCl_3$)
	R^1	R^2	θ_m/°C		ν/cm^{-1}	δ/ppm
a	$-(CH_2)_4-$		105—106	87	1455, 1440, 1420, 1335, 1190, 1130, 980, 875, 820	1.4—2.2 (br. 8H), 2.4—3.1 (br. 8H)
b	CH_3	CH_3	85—86	82	1460, 1410, 1220, 1200, 1180, 985, 800	2.45 (s, 12H)
c	CH_3	C_3H_7	oil	98	1460, 1410, 1195, 1160, 1050, 975	0.95 (t, 6H, J=7 Hz), 1.3—1.9 (m, 4H), 2.40 (s, 6H), 2.60 (t, 4H, J=7 H)
d	H	$(CH_3)_3C$	105—107	50	1485, 1360, 1320, 1165, 1140, 1030	1.42 (s, 18H), 8.54 (s, 2H)
e	CH_3	C_6H_5	122—124	40	1440, 1400, 1230, 1160, 1065, 1025, 965, 775, 750, 700	2.61 (s, 6H), 7.2—7.6 (m, 10H)

shown in Scheme 1. In a protic solvent such as ethanol, amide anion is protonated to give amine. It was therefore of interest for us to see if the amide anion generated from α-azido bromide might undergo an intramolecular nucleophilic displacement of bromine atom by adjacent negative nitrogen, leading to the nitrogen-containing cyclic system, i.e. aziridine. Thus, *erythro*-1-azido-2-bromo-1,2-diphenylethane (**6**) was prepared from *trans*-stilbene (**5**) and added to an ethanolic solution of sodium hydrogentelluride at room temperature. Tellurium immediately precipitated with effervescence and the original olefinic hydrocarbon **5** was obtained in nearly quantitative yield. The absence of amino compound in the product mixture and preservation of the original stereochemistry at carbon-carbon double bond suggest that this conversion involves the E2-type β-elimination as shown in Scheme 2.

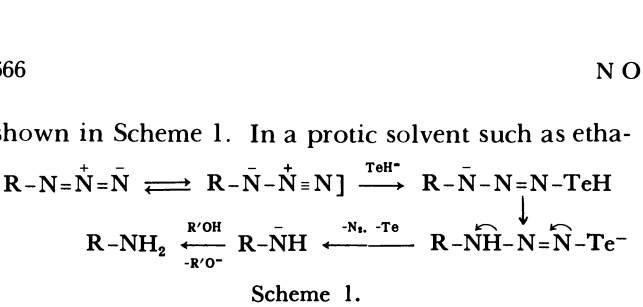

Scheme 1.

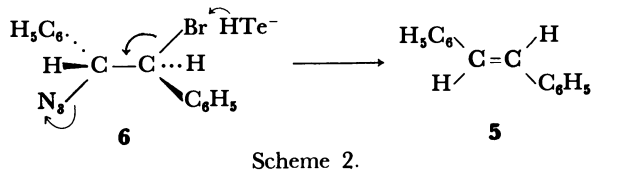

Scheme 2.

On a similar treatment, 3-azido-2-bromo-2-methylbutane and 1-azido-2-bromocyclohexane afforded complicated mixtures containing amino and olefinic compounds among other products, but the expected azacyclic compounds could not be detected.

Experimental

Melting points were determined on a hot stage apparatus and are not corrected. ^{1}H NMR spectra were obtained at 60 MHz on a JEOL model JMN-60 spectrometer for solutions in carbon tetrachloride. IR spectra were recorded as potassium bromide disks on a Hitachi EPI-3G spectrophotometer.

Powdered tellurium was a commercial product of 99.99% purity and used as received. Azido ketones were prepared from the corresponding bromo ketones by treatment with an excess of sodium azide in acetone. Bromo azides were obtained by treating olefins with bromine azide, generated in situ from bromine and sodium azide in dichloromethane/30% hydrochloric acid.[14] Products were identified by ^{1}H NMR, IR and mass spectra as well as by comparison with authentic specimens. All compounds obtained are known.

Conversion of α-Azido Ketones (2) to Pyrazines (4); Typical Procedure: Sodium hydrogentelluride was prepared by heating powdered tellurium (0.65 g, 5.1 mmol) and sodium borohydride (0.45 g, 11.9 mmol) in ethanol (20 ml) for 1 h under a nitrogen atmosphere. To the resulting dark red solution, 2-azidocyclohexanone (**2a**; 0.278 g, 2.0 mmol) in ethanol (5 ml) was added with stirring. The color instantly turned black and was followed by evolution of nitrogen. After stirring for a while, the mixture was left open to air to destroy excess reagent and oxidize a dihydropyrazine formed via self-condensation of α-amino ketone (**3a**). Removal of metallic tellurium by filtration over Celite followed by evaporation of solvent afforded crude 1,2,3,4,6,7,8,9-octahydrophenazine (**4a**) as a solid residue, which was purified by chromatography over silica gel or recrystallization from methanol. Yield, 0.164 g (87%). Mp 105—106 °C (lit,[15] 106—108 °C).

Reaction of *erythro*-1-Azido-2-bromo-1,2-diphenylethane (6) with Sodium Hydrogentelluride. To a solution of sodium hydrogentelluride, prepared from tellurium (0.26 g, 2.0 mmol), sodium borohydride (0.19 g, 5.0 mmol) and ethanol (20 ml), was added α-azido bromide **6** (0.60 g, 2.0 mmol) in ether (2 ml) under nitrogen and the resulting black mixture was stirred for 2 h at room temperature. Addition of water (20 ml) followed by extraction of the product with dichloromethane afforded *trans*-stilbene (0.35 g, 98%). Mp 122—124 °C (lit,[16] 123—124 °C).

References

1) D. H. R. Barton and S. W. McCombie, *J. Chem. Soc., Perkin Trans. 1*, **1975**, 1574.

2) Hydrogenation of conjugated double bond and imines. K. Ramasamy, S. K. Kalyanasundaram, and P. Shanmugam, *Synthesis*, **1978**, 545; M. Ramesh and P. Shanmugam, *Indian J. Chem. Sect. B*, **22B**, 617 (1983); M. Yamashita, T. Kato, and R. Suemitsu, *Chem. Lett.*, **1980**, 847; M. Yamashita, M. Kadokura, and R. Suemitsu, *Bull. Chem. Soc. Jpn.*, **57**, 3359 (1984). Debromination of *vic*-dibromides. K. Ramasamy, S. K. Kalyanasundaram, and P. Shanmugam, *Synthesis*, **1978**, 311. Hydrodehalogenation of halo ketones and *gem*-dibromo alkanes. A. Osuka and H. Suzuki, *Chem. Lett.*, **1983**, 119; A. Osuka, K. Takaoka, and H. Suzuki, *Bull. Chem. Soc. Jpn.*, **57**, 303 (1984). Hydrodenitration of tertiary nitro alkanes. H. Suzuki, K. Takaoka, and A. Osuka, *Bull. Chem. Soc. Jpn.*, **58**, 1067 (1985). Reduction of aromatic nitro compounds to azoxy compouds. A. Osuka, H. Shimizu, and H. Suzuki, *Chem. Lett.*, **1983**, 1373. Reductive opening of epoxide ring. A. Osuka, K. Takaoka, and H. Suzuki, *Chem. Lett.*, **1984**, 271. Formation of telluro esters from Vilsmeier salts. A. G. M. Barrett, D. H. R. Barton, and R. W. Read, *J. Chem. Soc., Chem. Commum.*, **1979**, 645; A. G. M. Barrett, R. W. Read, and D. H. R. Barton, *J. Chem. Soc., Perkin 1*, **1980**, 2191.

3) H. Suzuki and K. Takaoka, *Chem. Lett.*, **1984**, 1733.

4) E. Felder, D. Pitre, S. Boveri, and E. B. Grabitz, *Chem. Ber.*, **100**, 555 (1967).

5) J. P. Marion, *Chimia*, **21**, 510 (1967).

6) R. G. Jones, *J. Am. Chem. Soc.*, **71**, 78 (1949).

7) N. Vinot and J. Pinson, *Bull. Soc. Chim. Fr.*, **1968**, 4970.

8) M. Godchot and M. Mousseron, *Bull. Soc. Chim. Fr.*, **51**, 774 (1932).

9) D. G. Farnum and G. R. Carlson, *Synthesis*, **1972**, 191.

10) M. Nakajima, C. A. Loeschorn, W. E. Cimbrelo, and J. P. Anselme, *Org. Prep. Proced. Int.*, **12**, 265 (1980).

11) E. Zbiral and J. Stroh, *Justus Liebigs Ann. Chem.*, **727**, 231 (1969).

12) J. Fellman, S. H. Wilen, and C. A. Vander Werf, *J. Org. Chem.*, **21**, 713 (1956).

13) A. Hassner, G. J. Matthews, and F. W. Fowler, *J. Am. Chem. Soc.*, **91**, 5046 (1969).

14) A. Hassner and F. Boerwinkle, *J. Am. Chem. Soc.*, **90**, 216 (1968).

15) B. Mauer and G. Ohloff, *Helv. Chim. Acta*, **59**, 1169 (1976).

16) R. L. Shriner and A. Berger, *Org. Synth.* Coll. Vol. **3**, 786 (1955).

CD Spectra of Bis(2,4-dinitrophenyl) Derivatives of Acyclic Diamino Compounds Having Two Asymmetric Centers

Masao KAWAI,* Takahiro YAMAGISHI, Taketoshi MATSUURA,
Yasuo BUTSUGAN, and Ruka NAKASHIMA†
Department of Applied Chemistry, Nagoya Institute of Technology, Showa-ku, Nagoya 466
†Department of Industrial Chemistry, Faculty of Engineering, Tottori University, Tottori 680
(Received September 30, 1985)

Synopsis. Chiroptical properties of bis(2,4-dinitrophenyl) derivatives of acyclic diamino compounds were discussed. The derivatives of diamines in which the two NH_2-bearing carbons are asymmetric having the same chirality exhibited Cotton effects of much larger intensity than the corresponding diamine derivatives having only one asymmetric carbon atom. Relation between sign and magnitude of Cotton effect at the longest wavelength of bis(2,4-dinitrophenyl) derivatives and structure and stereochemistry of parent diamino compounds was summarized in a tabulated form.

Bis(2,4-dinitrophenyl) (di-Dnp) derivatives of α,ω-diamino acids exhibit characteristic pattern of CD spectra above 300 nm and sign of the Cotton effect at the longest wavelength was found to be negative for the diamino acid derivatives with L-configuration (**1**, n=1—4). The Cotton effect was assumed to be due to exciton coupling of the electric transition moments of 400 nm band of the two DnpNH chromophores. Direction of the transition moment was calculated to be oriented approximately parallel to the C-NHDnp

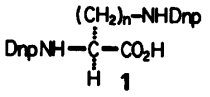

1

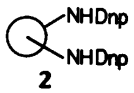

2

bond. Thus, conformers **2** having negative chirality of the two C-NHDnp bonds were assumed to be responsible for the characteristic negative Cotton effect at the longest wavelength, and a rule named di-Dnp chirality rule was proposed, which correlates sign of the Cotton effect around 400 nm with chirality of the two C-N bonds of the di-Dnp derivatives.[1]

CD spectrum of di-Dnp derivative of L-cystine (**3**, X=CH_2SSCH_2) was very similar to those of L-α,ω-diamino acid derivatives **1** exhibiting negative Cotton effect around 400 nm. Magnitude of the Cotton effect of the L-cystine derivative ($[\theta]_{412}$ −21100), however, was much larger than that of L-lysine derivative (**1**, n=4; $[\theta]_{427}$ −6400),[1] in spite of apparent larger separation of the two DnpNH chromophores by intervening six atoms in the former compound than in the latter which contains five intervening carbon atoms. Larger intensity of Cotton effects of the cystine derivative was assumed to be due to presence of additional chiral center, which restricts relative steric arrangement of the two chromophoric groups more effectively to interact with each other to give characteristic Cotton effects. Since the Cotton effects in concern are generated by electronic interaction of the two DnpNH chromophores, effect of presence and/or introduction of non-aromatic groups such as CO_2H upon the spectra can be considered essentially steric in nature.

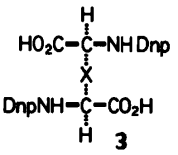

3

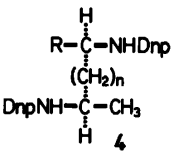

4

In order to ascertain the assumption di-Dnp derivatives of (2*S*,5*S*)-diaminoadipic and (2*S*,6*S*)-diaminopimelic acids [**3**, X=$(CH_2)_n$, n=2 and 3] were prepared, which correspond to derivatives of L-ornithine and L-lysine (**1**, n=3 and 4),[1] respectively, having an extra carboxyl group creating additional asymmetric center. As expected the di-Dnp derivatives **3** [X=$(CH_2)_n$, n=2 and 3] showed a similar pattern of CD spectra with the intensity two to three times as large as the corresponding **1** (n=3 and 4), respectively (Table 1).

Di-Dnp derivatives of alkanediamines (**4**, R=CH_3, n=0 and 1) were also synthesized and their CD spectra were recorded as summarized in Table 1. The (2*R*,3*R*)-butanediamine derivative (**4**, R=CH_3, n=0)[2] can be considered as an analog of (*R*)-1,2-propanediamine derivative (**4**, R=H, n=0)[1], whose methylene group is substituted by a methyl group generating an additional chiral center of the same chirality. Cotton effects of the butanediamine derivative were much larger than those of the propanediamine derivative, which also demonstrated the effect of introducing another chiral center. (2*R*,4*R*)-Pentanediamine derivative (**4**, R=CH_3, n=1) is an analog of the propanediamine derivative having an additional methyl group as well as an intervening methylene group between the two chromophore-bearing carbon atoms. While the additional chiral center is considered to restrict the two DnpNH groups in favorable conformation to give characteristic CD spectrum, the extra methylene group has an effect of spatially separating two chromophores and also giving more conformational freedom than the case of the propanediamine derivative. The two opposing effects seem to cancell each other to result in observed Cotton effects of comparable intensity.

From the results described above the sign and magnitude of Cotton effect around 400 nm of di-Dnp derivatives of chiral acyclic diamines can be summarized as given in Table 2. Positive and negative Cotton effects, respectively, are observed if absolute configuration of the asymmetric center corresponds to that of D- and L-α,ω-diamino acid derivatives. If the compound possesses two chiral centers of the same chirality larger Cotton effect is expected than that having only one chiral center, while chiral centers of different chirality evidently afford achiral meso compounds designated as 0 in Table 2 (entry c).

Table 1. CD Spectral Data of di-Dnp Derivatives of Acyclic Chiral Diamines[a)]

Compound	Molecular ellipticity ($[\theta]/10^2$) and wavelength (λ/nm) in parentheses
1, $n=3$[b)]	−210 (415), 0 (388), +516 (361), 0 (340), −186 (327), 0 (275), +75 (260)
1, $n=4$[b)]	− 64 (427), 0 (390), +125 (357), 0 (333), − 15 (320), 0 (290), +15 (262)
3, X=CH_2SSCH_2	−211 (412), 0 (378), +158 (361), 0 (342), − 90 (324), 0 (275)
3, X=$(CH_2)_2$	−490 (405), 0 (380), +1060 (356), 0 (336), −616 (319), 0 (274), +259 (259)
3, X=$(CH_2)_3$	−148 (405), 0 (377), +196 (354), 0 (332), − 45 (315), 0 (275), +20(260)
4, R=CH_3, $n=0$[c)]	−842 (420), 0 (382), +155 (356), 0 (329), −229 (318), 0 (300)
4, R=CH_3, $n=1$[c)]	−503 (427), 0 (379), +503 (357), 0 (325), − 13 (321), 0 (314), +238 (273)
4, R=H, $n=0$[b)]	−477 (423), 0 (386), +632 (357), 0 (325), − 77 (310), − 19 (282), − 49 (270)
5, R=CH_3	+111 (398), 0 (373), −176 (363), 0 (326), + 21 (317), 0 (310), −249 (270)
5, R=$CH(CH_3)_2$	+144 (398), 0 (365), − 90 (348), − 35 (310), −278 (274), −238 (263)

a) Recorded in methanol solution unless otherwise noted. b) Ref 1. c) Recorded in methanol–tetrahydrofuran (**1** : 1 v/v).

Table 2. Relation between Absolute Configuration and Sign of Cotton Effect at the Longest Wavelength of di-Dnp Derivatives of Acyclic Diamino Compounds

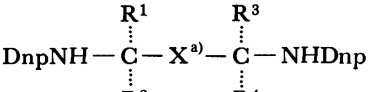

Entry	R^1	R^2	R^3	R^4	$[\theta]^{max}_{\approx 400}$
a	R[b)]	H	H	R	++[c)]
b	R	H	H	H	+
c	R	H	R	H	0[d)]
d	H	R	H	H	−
e	H	R	R	H	−−

a) X implies an achiral chain. b) R implies a non-aromatic group. c) ++ and −− mean that larger Coton effect is expected than + and − if comparisons are made among the compounds with the same or similar intervening group X. d) 0 means no chirality.

It is interesting that bis(Dnp-L-α-aminoacyl) derivatives **5** of ethanediamine correspond to general formula of entry a in Table 2 for which positive Cotton effect

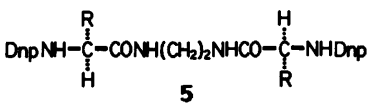

5

around 400 nm is expected in spite of L-configuration of the constituent amino acids. As expected the L-alanine derivative (**5**, R=CH_3) exhibited positive Cotton effect ($[\theta]_{398}$+11100) and a similar CD spectrum is observed also for the L-valine derivative (**5**, R=$CH(CH_3)_2$; $[\theta]_{398}$+14400).

Experimental

Melting points were measured on a Yanagimoto micro melting point apparatus and uncorrected. All the derivatives synthesized exhibited reasonable ^{1}H NMR spectra with a Varian XL-200 or a HITACHI R-24A spectrometer and gave satisfactory elemental analysis for C, H, and N (<±0.4%). CD spectra were recorded on a JASCO J-40C spectropolarimeter as summarized in Table 1.

(2*S*,5*S*)-Bis(2,4-dinitroanilino)hexanedioic Acid [3, X=$(CH_2)_2$]. (2*S*,5*S*)-Diaminoadipic acid[3] was 2,4-dinitrophenylated according to Sanger.[4] Yellow needles from ethyl acetate–benzene; mp 220—223 °C.

(2*S*,6*S*)-Bis(2,4-dinitroanilino)heptanedioic Acid [3, X=$(CH_2)_3$]. This compound was prepared similarly from (2*S*,6*S*)-diaminopimelic acid.[3,5] Yellow prisms from methanol; mp 114—118 °C.[6]

(2*R*,4*R*)-N^2,N^4-Bis(2,4-dinitrophenyl)-2,4-pentanediamine (4, R=CH_3, n=1). (2*R*,4*R*)-Pentanediamine (*R*,*R*)-di-*O*-benzoyltartrate[7] was dinitrophenylated with 1-fluoro-2,4-dinitrobenzene–$NaHCO_3$ in acetone–H_2O. Yellow prisms from acetone; mp 218—219 °C.

(2*S*,3*S*)-N^2,N^3-Bis(2,4-dinitrophenyl)-2,3-butanediamine (enantiomer of 4, R=CH_3, n=0). This compound was prepared from (2*S*,3*S*)-butanediamine *R*,*R*-tartrate.[8] Yellow prisms from acetone; mp 217—218 °C.

***N*,*N*'-Bis[*N*-(2,4-dinitrophenyl)-L-alanyl]ethanediamine 5 (R=CH_3).** This compound was synthesized by coupling of Dnp-L-alanine (153 mg, 0.6 mmol) and ethanediamine (15 mg, 0.25 mmol) in *N*,*N*-dimethylformamide(DMF)–tetrahydrofunan (2:1) using dicyclohexylcarbodiimide (124 mg, 0.6 mmol). Yellow powder (107 mg, 80%) from DMF–methanol; mp 277—280 °C.

***N*,*N*'-Bis[*N*-(2,4-dinitrophenyl)-L-valyl]ethanediamine 5 [R=$(CH_3)_2$CH].** This compound was synthesized from Dnp-L-valine similarly as above. Yellow powder; mp>300 °C.

We wish to thank Dr. Ukon Nagai of Mitsubishi-Kasei Institute of Life Sciences for helpful discussions.

References

1) M. Kawai, U. Nagai, and T. Kobayashi, *Tetrahedron Lett.* **1974**, 1881.

2) The compound actually synthesized was the enantiomer of **4** (R=CH_3, n=0) as described in experimental. For the purpose of making comparison easier, CD spectral data which are antipodal to those really observed are given in Table 1.

3) R. Nakashima, J. Matsumoto, Y. Shigemasa, and N. Ueda, to be published.

4) F. Sanger, *Biochem. J.*, **39**, 507 (1945).

5) Y. Izumi, *Nippon Kagaku Zasshi*, **75**, 1152 (1954).

6) Elemental analysis was consistent with dihydrated formula $C_{19}H_{18}N_6O_{12}\cdot 2H_2O$.

7) B. Bosnich and J. MacB. Harrowfield, *J. Am. Chem. Soc.*, **94**, 3425 (1972).

8) M. Gullotti, A. Pasini, P. Fantucci, R. Ugo, and R. D. Gillard, *Gazz. Chim. Ital.*, **102**, 855 (1972).

The Structure of Bis(dibenzyl sulfoxide)tris(*O,O'*-diethyl dithiophosphato)-lanthanum(III), $La\{(C_2H_5O)_2PS_2\}_3\{(C_6H_5CH_2)_2SO\}_2$

Takashi IMAI, Mamoru SHIMOI, and Akira OUCHI*
Department of Chemistry, College of Arts and Sciences, The University of Tokyo, Komaba, Meguro-ku, Tokyo 153
(Received August 21, 1985)

Synopsis. The crystal and molecular structure of the title complex has been determined by the use of the single-crystal X-ray diffraction method. The crystal of $LaC_{40}H_{58}O_8P_3S_8$, F.W.=1155.20, is triclinic; space group $P\bar{1}$, a=13.300(5), b=19.816(8), c=11.257(4) Å, α=92.79(4), β=114.92(3), γ=75.40(4)°, U=2598(2) Å^3, Z=2, D_m=1.48(3), D_x=1.48 g cm^{-3}, and μ(Mo $K\alpha$)=1.29 mm^{-1}. Each lanthanum(III) atom is octa-coordinated and is in a dodecahedral geometry. The oxygen atoms of dibenzyl sulfoxide molecules are ligated at both ends of the base of a trapezia, and the chelating *O,O'*-diethyl dithiophosphates span two m edges and one a edge.

Some stable *O,O'*-dialkyl dithiophosphate (R_2dtp)-Lewis base mixed complexes of lanthanoids(III), where the former ligands are ligated to the hard-metal atom through the soft sulfur atoms, have already been synthesized, and some of their structures have been elucidated.[1-6] In such mixed complexes, the same kind of the ligated atoms are apt to take contiguous positions;[3,7] the M(iPr_2dtp)$_3L_2$ complexes in the octa-coordinated dodecahedral geometry, where M=lanthanoid(III) metal, iPr=$(CH_3)_2CH$-, and L= dimethyl sulfoxide (dmso)[4] or *N,N*-dimethylacetamide (dma),[2] have the Lewis-base oxygen atoms at both ends of one m-edge; tentatively we have named these complexes the "mmm-type" after their chelating positions. However, even in the same type of complexes, when the Lewis-base ligands are relatively large in size, for example, in the cases of the triphenylphosphine oxide (Ph_3PO) and benzamide (bza) adducts, the base oxygen atoms ligate at both ends of the base of a trapezia; [1,3] tentatively we name these complexes the "mma-type." Although the steric hindrance of the ligands may be the main cause of this structure, the polarity of the Lewis base may affect the ligating position, too. Consequently, it is interesting to study the structures of some dialkyl sulfoxide adduct, where the base is more polar than acid amide, but is large. Therefore, we have investigated the structure of the title complex by means of the single-crystal X-ray diffraction method.

Experimental

Preparation of Bis(dibenzyl sulfoxide)tris(*O,O'*-diethyl dithiophosphato)lanthanum(III), and the Neodymium(III) Complex. Lanthanum(III) chloride heptahydrate (1.00 g, 2.7 mmol), Na(Et$_2$dtp) (Et=C_2H_5-) (2.24 g, 10.8 mmol), and dibenzyl sulfoxide (bzso) (1.36 g, 5.9 mmol) were dissolved in about 10 cm^3 of warm ethanol. After the residue has been filtered off, the solution was evaporated using a rotary vacuum evaporator at about 80 °C, and the resinous residue thus obtained was redissolved into warm benzene (about 10 cm^3). After the residue has then been cooled, it was allowed to stand in contact with the vapor of petroleum ether at the ambient temperature for several days. Crystals came out (about 2.2 g; 1.90 mmol; yield= 90%). The isomorphous neodymium(III) complex was obtained by almost the same process. Anal. ($MC_{40}H_{58}O_8P_3S_8$) M=La or Nd, C, H. Neither mmm-type complexes, such as [Nd(iPr_2dtp)$_3$(dmso)$_2$],[4] nor ionic ones, such as [Nd(iPr_2dtp)$_2$(dbso)$_3$][Nd(iPr_2dtp)$_4$] (where dbso=dibutyl sulfoxide),[6] were obtained by this process.

Single-Crystal X-Ray Analysis. A crystal with dimensions of 0.35×0.32×0.30 mm^3 was used for the measurement. All edges were ground off. The reflections within the range of $3°<2\theta<56°$ were collected on a Rigaku AFC-6A four-circle automated X-ray diffractometer with Mo $K\alpha$ radiation, employing the ω—2θ scan technique. Of the 12632 independent reflections, 9764 reflections with $|F_o|>3\sigma(|F_o|)$ were used for the refinement. The intensities were corrected for the Lorentz and polarization factors, but no correction was made for the absorption and extinction. All the calculations were carried out on a HITAC M-280H computer at the Computer Center of The University of Tokyo, using the local version of UNICS.[8] The scattering factors were taken from the tables.[9]

Structure Determination. The structure was solved by the heavy-atom method. All non-hydrogen atoms were found, and the positions of the phenyl hydrogen atoms were calculated from those of the neighboring carbon atoms, assuming that C-H=1.08 Å and that their B_{iso}=10.0. The final R value was 0.044,[10] applying anisotropic temperature factors for all non-hydrogen atoms.

Results and Discussion

Some selected bond lengths and angles are shown in Table 1.[11] A perspective drawing of the complex, with the numbering scheme, is shown in Fig. 1; the crystal packing diagram, in Fig. 2, and a schematic presentation of the bonding mode of the ligating atoms around the metal atom, in Fig. 3.

As is shown in the figures, the central metal atom is octa-coordinated and is in a dodecahedral geometry. Three Et$_2$dtp ligands are chelated through two corresponding sulfur atoms; two of them span m-edges, while the other one spans a-edge. Two bzso oxygen atoms ligate at both ends of the base of a trapezia. Therefore, this complex is of the mma-type; it was found that, even in the case of the adduct of polar dialkyl sulfoxides, the mma-type structure is more stable than the mmm-type structure when the steric effect is dominant.

The bond lengths of La-S are 2.992—3.091 Å (3.024 Å on the average); they are about the same as the sum of their ionic radii as presented by Shannon (3.00 Å).[12] On the other hand, the La-O bond lengths are 2.415 and 2.413 Å, shorter than the sum of the Shannon radii (2.51 Å); the phenomenon has previously been found in the other [La(R_2dtp)$_3L_2$]-type complexes, too.[1-4]

Respective complex molecules are independent in the crystal; no bridgings by the coordinated ligands or

Table 1. Bond Lengths and Bond Angles, with Estimated Standard Deviations in Parentheses

Bond length	(l/Å)	Bond length	(l/Å)	Bond length	(l/Å)
La-S(1)	3.023(2)	La-S(2)	2.992(2)	La-S(3)	3.018(3)
La-S(4)	3.008(2)	La-S(5)	3.013(2)	La-S(6)	3.091(2)
La-O(11)	2.415(3)	La-O(12)	2.413(3)	S(1)-P(1)	1.969(2)
S(2)-P(1)	1.959(2)	S(3)-P(2)	1.964(2)	S(4)-P(2)	1.961(2)
S(5)-P(3)	1.969(2)	S(6)-P(3)	1.955(2)	O(11)-S(11)	1.518(3)
O(12)-S(12)	1.504(3)				
Bond angle	**(ϕ/°)**	**Bond angle**	**(ϕ/°)**	**Bond angle**	**(ϕ/°)**
S(1)-La-S(2)	66.81(4)	S(3)-La-S(4)	65.71(3)	S(5)-La-S(6)	65.65(4)
S(1)-La-S(3)	124.76(3)	S(1)-La-S(5)	138.61(4)	S(2)-La-S(3)	88.38(4)
S(2)-La-S(5)	154.11(4)	S(3)-La-S(5)	78.97(4)	S(4)-La-S(5)	81.79(4)
O(11)-La-O(12)	151.27(10)	S(3)-La-O(11)	69.96(7)	S(4)-La-O(12)	72.53(7)
La-S(1)-P(1)	88.12(5)	La-S(2)-P(1)	89.20(6)	La-S(3)-P(2)	90.55(5)
La-S(4)-P(2)	90.90(5)	La-S(5)-P(3)	90.57(6)	La-S(6)-P(3)	88.58(5)
La-O(11)-S(11)	141.9(2)	La-O(12)-S(12)	158.6(2)		

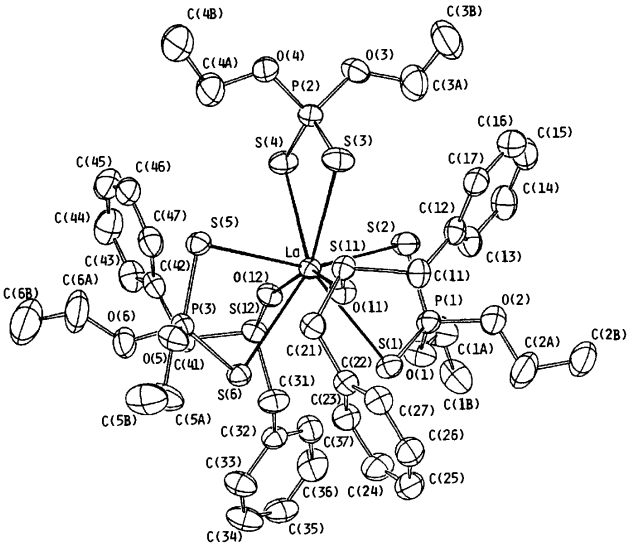

Fig. 1. A perspective drawing of the titled complex with the numbering scheme.

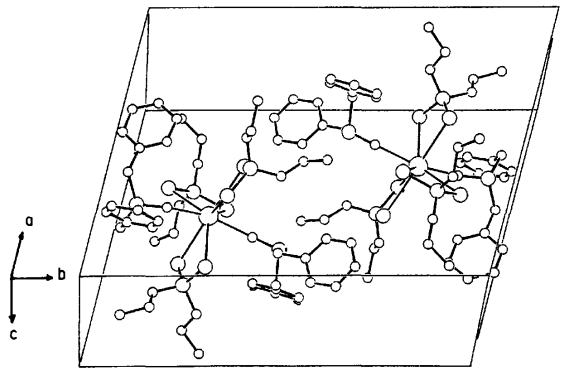

Fig. 2. The crystal packing diagram of the titled complex.

through the hydrogen bondings were found between them.

In the cases of the other Lewis-base adducts of lanthanoid *O,O'*-dialkyl dithiophosphates, it was found that the thermal parameters of some atoms,

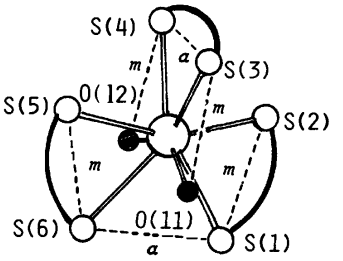

Fig. 3. A schematic presentation of the comprex around the central metal atom.

especially those of isopropyl carbon atoms, are very large.[3-6] In this complex, too, the temperature factors of the ethyl carbon atoms are large.

The authors are greatly obliged to the Shin-Etsu Chemical Ind. Co., Ltd., for presenting highly pure lanthanoid oxides.

References

1) A. A. Pinkerton and D. Schwarzenbach, *J. Chem Soc., Dalton Trans.*, **1976**, 2466.
2) K. Nagai, Y. Sato, S. Kondo, and A. Ouchi, *Bull. Chem. Soc. Jpn.*, **56**, 2605 (1983).
3) R. Nakamura, K. Nagai, M. Shimoi, and A. Ouchi, *Bull. Chem. Soc. Jpn.*, **57**, 2919 (1984).
4) M. Nakamura, K. Nagai, Y. Ohki, Y. Suzuki, M. Shimoi, and A. Ouchi, unpublished data.
5) K. Nagai, R. Nakamura, M. Shimoi, and A. Ouchi, *Bull. Chem. Soc. Jpn.*, **57**, 2725 (1984).
6) Y. Ohki, M. Nakamura, Y. Suzuki, K. Nagai, M. Shimoi, and A. Ouchi, *Bull. Chem. Soc. Jpn.*, **58**, 1593 (1985).
7) M. E. Silver, H. K. Chun, and R. C. Fay, *Inorg. Chem.*, **21**, 3765 (1982).
8) "The Universal Crystallographic Computation Program System (UNICS)," ed by T. Sakurai, Crystallographic Society of Japan, Tokyo (1967).
9) "International Tables for X-Ray Crystallography," Kynoch Press, Birmingham (1974), Vol. IV, pp. 72, 150.
10) $R=\sum||F_o|-|F_c||/\sum|F_o|$
11) The final positional and thermal parameters and the final F_o—F_c table are deposited as Document No. 8610 at the Office of the Editor of the Bull. Chem. Soc. Jpn.
12) R. D. Shannon, *Acta Crystallogr., Sect A*, **32**, 751 (1976).

The Nernst-Planck Type Equation in Nonequilibrium Thermodynamics

Hideo KIMIZUKA
Department of Chemistry, Faculty of Science, Kyushu University, Fukuoka 812
(Received September 27, 1985)

Synopsis. A single-term expression of the Nernst-Planck type equation conformable with nonequilibrium thermodynamics has been presented. The equation may be applicable to treat the electric properties of the multi-ionic system, although the individual ion flux is unobservable.

It is well known that the Nernst-Planck equation is a single-term expression and has been regarded as applicable to multi-ionic systems in classical transport theory.

On the other hand, in nonequilibrium thermodynamics, an isothermal ion flux in a multi-ionic system is expressed by a linear combination of the negative electrochemical potential gradients with the phenomenological coefficients, or the sum of Nernst-Planck type equations.[1] However, it is formidable to treat a multi-ionic system due to many phenomenological coefficients which must be experimentally determined, although nonequilibrium thermodynamics is known to be theoretically rigorous.

Thus, it is advantageous to determine the conditions for utilizing Nernst-Planck type equations in a way so as not to contradict nonequilibrium thermodynamics. This will greatly simplify the treatment of the transport process.

It has been shown in a preceding paper[2] that a Nernst-Planck type equation with a diffusion coefficient can express only ionic movements without an electric current in a binary electrolyte solution. It will be shown in the present paper that a Nernst-Planck type equation with a conductive absolute mobility is applicable to the transport process of a multi-ionic system, although the ion flux is unobservable.

Theory

The isothermal flux of an ion α, j_α, in a multi-ionic electrolyte solution may be written on the basis of nonequilibrium thermodynamics[1]

$$j_\alpha = -\sum_\beta l_{\alpha\beta}\nabla\bar{\mu}_\beta \tag{1}$$

where the subscript β refers to ion β; $l_{\alpha\beta}$ denotes the phenomenological coefficient, and $\nabla\bar{\mu}_\beta$ is the gradient of the electrochemical potential of ion β, $\bar{\mu}_\beta$.

For the sake of simplicity, it is assumed that the system is in a steady-state condition in which the fluxes, the concentration and the potential profiles are functions only of the coordinate and are independent of time.

Equation 1 leads to an equation for the electric current I as follows;

$$I = \sum_\alpha Z_\alpha F j_\alpha = -\sum_\alpha Z_\alpha F u_\alpha C_\alpha \nabla\bar{\mu}_\alpha \tag{2}$$

where Z_α denotes the charge, F the Faraday constant and C_α the concentration. u_α, the conductive absolute mobility, is related to $l_{\alpha\beta}$ by[1]

$$u_\alpha = \sum_\beta Z_\beta l_{\beta\alpha}/Z_\alpha C_\alpha . \tag{3}$$

Putting

$$j_\alpha^* = -u_\alpha C_\alpha \nabla\bar{\mu}_\alpha \tag{4}$$

and comparing Eq. 2 with Eqs. 1, 3 and 4, we find

$$I = \sum_\alpha Z_\alpha F j_\alpha = \sum_\alpha Z_\alpha F j_\alpha^*. \tag{5}$$

In Eq. 5, $Z_\alpha F j_\alpha^*$ denotes the part of the electrical ion current that is driven by the electrochemical potential gradient of ion α. Equation 4 is the same form as the Nernst-Planck equation with an absolute mobility. However, it should be noted that j_α^* is an unobservable flux and differs from the observable flux j_α as can be seen by comparing Eq. 1 with Eqs. 3 and 4. Nevertheless, Eq. 4 can be used to obtain an equation for the electric current, as can be seen from Eq. 5. When the system is in a steady state, j_α^* may also be regarded as a constant.

Equation 1 may also be written as[3]

$$j_\alpha = -\sum_\beta Z_\beta F l_{\alpha\beta}\nabla(\psi-\psi_\beta) \tag{6}$$

where ψ denotes the electric potential and ψ_β the equilibrium potential for ion β. Similarly, Eq. 4 leads to

$$j_\alpha^* = -Z_\alpha F C_\alpha u_\alpha \nabla(\psi-\psi_\alpha). \tag{7}$$

Equations 6 and 7 hold even in the absence of an electric current, where j_α, j_α^*, and ψ become j_α^0, j_α^{*0}, and ψ^0, respectively. When the electric current is small, it may be assumed that changes in the concentration profiles and phenomenological coefficients caused by an electric current can be ignored. This corresponds to an assumption of constant ψ_α's. In this case, we have from Eqs. 3, 6, and 7

$$j_\alpha - j_\alpha^0 = j_\alpha^* - j_\alpha^{*0} = -Z_\alpha F C_\alpha u_\alpha \nabla(\psi-\psi^0), \tag{8}$$

which is conformable with Eq. 5. It is evident from Eq. 8 that

$$j_\alpha = j_\alpha^* = -Z_\alpha F C_\alpha u_\alpha \nabla\psi, \tag{9}$$

when there is no concentration gradient.

For a membrane-aqueous electrolyte system with an isotropic membrane, the equations for isothermal fluxes relative to the membrane can be expressed by[4]

$$j_\alpha = -\sum_\beta l_{\alpha\beta}\nabla\tilde{\mu}_\beta - l_{\alpha w}\nabla\tilde{\mu}_w, \tag{10}$$

$$j_w = -\sum_\beta l_{w\beta}\nabla\tilde{\mu}_\beta - l_{ww}\nabla\tilde{\mu}_w, \tag{11}$$

where α and β refer to ions α and β, respectively, and w, water. The hydrodynamic electrochemical potential is given by

$$\tilde{\mu}_\gamma = \bar{\mu}_\gamma + P\bar{v}_\gamma, \quad (\gamma=\alpha, \beta, w) \tag{12}$$

where P denotes the pressure and $\bar{v}_\gamma$ the partial molar volume of species γ. For this system, the membrane current is given by

$$I = \sum_\alpha Z_\alpha F j_\alpha = \sum_\alpha Z_\alpha F j_\alpha^* + F j_w^*, \tag{13}$$

where

$$j_\gamma^* = -u_\gamma C_\gamma \nabla \tilde{\mu}_\gamma, \quad (\gamma = \alpha, \beta, w). \tag{14}$$

The conductive absolute mobility u_α for ion α is given by Eq. 3. Similarly, the equation for the electroosmotic water mobility is expressed by

$$u_w = \sum_\alpha Z_\alpha l_{\alpha w}/C_w. \tag{15}$$

Regarding flux, Eq. 8 also holds for all ionic species. For the observable flux of water, the equation for the electroosmotic water flow is

$$j_w - j_w^0 = -FC_w u_w \nabla(\psi - \psi^0). \tag{16}$$

For an unobservable flux,

$$j_w^* = j_w^{*0} \tag{17}$$

since there is no potential term in $\tilde{\mu}_w$.

Discussion

According to Eqs. 8 and 16, $C_\gamma u_\gamma$ ($\gamma = \alpha, \beta, w$) can be determined by measuring the fluxes and the potentials; hence, the electrical properties of the system, such as ion and electroosmotic conductances, the membrane conductance and the transport number can be evaluated from the $C_\gamma u_\gamma$'s. In addition, the unobservable fluxes (j_γ^* and j_γ^{*0}) can also be evaluated using Eq. 14. Thus, j_α can be calculated according to Eq. 8, provided j_α^0 is known. However, all the phenomenological coefficients should be determined in order to predict the diffusional flux j_α^0. Unfortunately, it seems to be hopeless to predict j_α^0 in a multi-ionic system having more than three kinds of ionic species. This is because there are too many phenomenological coefficients which must be experimentally determined.

For a binary electrolyte solution, the diffusional ion flux at zero electric current j_α^0 is given by a single-term expression[2]

$$j_\alpha^0 = -D_\alpha C_\alpha \nabla \bar{\mu}_\alpha / RT = -\omega_\alpha C_\alpha \nabla \tilde{\mu}_\alpha, \tag{18}$$

where D_α denotes the diffusion coefficient, ω_α ($=D_\alpha/RT$) the diffusional absolute mobility, R the gas constant, and T the absolute temperature. D_α and ω_α are related to the phenomenological coefficients as follows[2];

$$D_\alpha C_\alpha / RT = \omega_\alpha C_\alpha = Z_\beta (l_{\alpha\alpha} l_{\beta\beta} - l_{\alpha\beta}^2)/(Z_\alpha l_{\alpha\beta} + Z_\beta l_{\beta\beta}). \tag{19}$$

Comparing Eq. 18 with Eq. 4,

$$\frac{j_\alpha^0}{j_\alpha^{*0}} = \frac{\omega_\alpha}{u_\alpha} = 1 - \lambda_{\alpha\beta}\left(\frac{1}{\lambda_\alpha} + \frac{1}{\lambda_\beta}\right) = F(\lambda_{\alpha\beta}), \tag{20}$$

where λ_α and λ_β are the equivalent conductances of ions α and β, respectively. $\lambda_{\alpha\beta}$ is an element of the equivalent ion conductance matrix, given by the relation[2]

$$\lambda_{\alpha\beta} = Z_\alpha Z_\beta F^2 l_{\alpha\beta}/|Z_\alpha| C_\alpha. \tag{21}$$

Since the phenomenological coefficients or the elements of the conductance matrix for a binary electrolyte solution can be determined experimentally[1], j_α^0 can be evaluated according to Eq. 18. Hence, from Eqs. 8 and 20,

$$j_\alpha = j_\alpha^* - j_\alpha^{*0} + j_\alpha^0 = j_\alpha^* - j_\alpha^{*0}[1 - F(\lambda_{\alpha\beta})] \tag{22}$$

enabling us to evaluate j_α from j_α^*, j_α^{*0}, and $F(\lambda_{\alpha\beta})$.

Concerning $F(\lambda_{\alpha\beta})$, it has been shown in the preceding paper[2]

$$F(\lambda_{\alpha\beta}) = |Z_\alpha| F^2 D_\alpha / RT\lambda_\alpha \tag{23}$$

$$F(\lambda_{\alpha\beta}) = \nu_\alpha |Z_\alpha| D_s/(\nu_\alpha + \nu_\beta)\lambda t_\alpha t_\beta (1 + d \ln \gamma_s / d \ln C_s), \tag{24}$$

where the subscript s refers to salt. ν_α and ν_β denote the stoichiometric coefficients, D_s the diffusion coefficient, λ the equivalent conductance of salt, t_α and t_β the transport numbers, γ_s the activity coefficient and C_s, the salt concentration. The value of $F(\lambda_{\alpha\beta})$ decreases with a decrease in the electrolyte concentration and tends to unity as the concentration approaches zero[2] where $u_\alpha = \omega_\alpha$. This indicates that interionic interactions vanish at an infinite dilution and there is no distinction between Eqs. 1 and 4. When $F(\lambda_{\alpha\beta})$ is unity, Eqs. 23 and 24 lead to the Nernst–Einstein and Nernst–Hartley equations, respectively. These are derived on the basis of the Nernst–Planck equation. Thus, it may be said that the original Nernst–Planck equation is valid only at an infinite dilution where Eqs. 4 and 18 are identical.

Eqations 4 and 18 differ from each other at finite electrolyte concentrations (where $F(\lambda_{\alpha\beta})$ differs from unity) and should be used with the precautions described in the present paper. From this point of view, u_α and ω_α should be distinguished from each other and can be called the conductive absolute mobility and the diffusional absolute mobility, respectively. This is due to the process by which they are defined. Nevertheless, these equations are still being used in current papers without distinction. However, the Nernst–Planck type equations (4, 14, and 18) are single-term expressions and enable us to use the results from classical membrane theories based on the Nernst–Planck equation if those theories were formulated under reasonable assumptions and the proposed precautions are taken into account.

Thus, the use of single-term expressions is advantageous for an easier treatment of the transport process using nonequilibrium thermodynamics. Hence, these equations can be regarded as revised Nernst–Planck equations. A determination of all phenomenological coefficients is required in order to completely describe and characterize the transport process in a multi-ionic system. At present this process seems to be hopeless in systems having more than four

components. Further study is required in order to solve this problem.

This work was supported by a Grant-in-Aid for Scientific Research No. 58470007 from the Ministry of Education, Science and Culture.

References

1) A. Kachalsky and P. F. Curran, "Nonequilibrium Thermodynamics in Biophysics," Harvard University Press (1965).
2) E. Kumamoto and H. Kimizuka, *Bull. Chem. Soc. Jpn.*, **52**, 2145 (1979).
3) K. Nomura, A. Matsubara, and H. Kimizuka, *Bull. Chem. Soc. Jpn.*, **54**, 1324 (1981).
4) H. Kimizuka, Y. Nagata, and K. Kaibara, *Bull. Chem. Soc. Jpn.*, **56**, 2371 (1983).

New Application of Crown Ether. VII.[1] Synthesis and Complexation Behavior of Bis(crown ether)s Consisting of a Benzocrown Unit and a Monoazacrown Unit

Gong-Xin He, Akito Abe, Toshihiko Ikeda, Fumio Wada,
Kiyoshi Kikukawa, and Tsutomu Matsuda*
Department of Organic Synthesis, Faculty of Engineering, Kyushu University, Hakozaki, Higashi-ku, Fukuoka 812
(Received August 26, 1985)

Synopsis. New bis(crown ether)s **3** consisting of a benzocrown unit and a monoazacrown unit connected by an oxyethylene linkage were synthesized. Their complexation behavior proved to be analogous to that of lariat monoazacrown ethers rather than that of bis(benzocrown ether)s.

In our previous paper,[1] it was shown that the selectivity of bis(benzocrown ether)s in the complexation with alkali metal cations could be changed by varied combinations of two benzocrown units(ring size; 15, 18, 21), and the behavior was understood by the formation of an intramolecular sandwich complex. The results led us to investigate the complexation characteristics of a new type of bis(crown ether)s consisting of a benzocrown unit and a monoazacrown unit connected by an oxyethylene linkage. This paper describes their synthesis and relative contribution of the linking group and another crown unit in the complexation with alkali metal cations.

Experimental

Material. Benzocrown ethers, 4′-hydroxybenzocrown ethers **5**, monoazacrown ethers, *N*-[2-[2-(tosyloxy)ethoxy]-ethyl]substituted monoazacrown ethers **4** were prepared according to the published methods.[1-3] The guaranteed reagent of alkali metal chlorides, alkali metal hydroxide and picric acid were used without further purification except for drying.

Synthesis of Bis(crown ether)s 3. The tosylate **4** (3 mmol) in dioxane (15 cm³) was added dropwise to a mixture of 4′-hydroxybenzocrown ether **5** (3 mmol) and sodium hydroxide (10 mmol) in DMSO–dioxane (9:1, 15 cm³) under nitrogen over a period of 1 h at 80 °C, and then the solution was refluxed for 20 h. After cooling, the mixture was filtered and the filtrate was concentrated under reduced pressure. The residual oily product was chromatographed over an alumina column ($CHCl_3$ eluent) and then purified by a medium pressure liquid chromatography (Silica-gel/MeOH–$CHCl_3$, 2:98(v/v)). The lariat ethers **2** were prepared by a similar method and purified by Kugelrohr distillation.

2a: Colorless liquid, bp. 150—160 °C/1.3Pa Yield 30%. ^{1}H NMR($CDCl_3$) δ=2.6—3.0 (6H,t), 3.5—4.2 (22H, m), 6.8—7.4 (5H, m). Found: C, 62.25; H, 8.66; N, 3.42%, M^+, 383. Calcd for $C_{20}H_{33}NO_6$: C, 62.64; H, 8.67; N, 3.56%; Mol. wt, 383.

2b: Colorless liquid, bp. 135—139 °C/0.40Pa. Yield 30%. ^{1}H NMR ($CDCl_3$), δ=2.6—3.0 (6H, t), 3.5—4.2 (26H, m), 6.8—7.4 (5H, m). Found: C, 61.57; H, 8.75; N, 3.28%; M^+, 427. Calcd for $C_{22}H_{37}NO_7$: C, 61.80; H, 8.72; N, 3.27%; Mol.wt. 427. IR for **2a** and **2b** (neat): 2930, 2870, 1600, 1490, 1450, 1350, 1240, 1120 cm^{-1}.

3a: Yield 17%. ^{1}H NMR ($CDCl_3$) δ=2.6—3.0 (6H, t), 3.5—4.2 (38H, m), 6.3—6.9 (3H, m). Found: C, 58.42; H, 8.32; N, 2.47%; M^+, 573. Calcd for $C_{28}H_{47}NO_{11}$: C, 58.62; H, 8.26; N, 2.44%; Mol.wt. 573.

3b: Yield 22%. Found: C, 58.09; H, 8.30; N, 2.12%; M^+, 617.

3c: Yield 29%. ^{1}H NMR for **3b** and **3c** ($CDCl_3$) δ=2.6—3.0 (6H, t), 3.5—4.2 (42H, m), 6.3—6.9 (3H, m). Found: C, 58.00; H, 8.31; N, 2.32%; M^+. 617. Calcd for $C_{30}H_{51}NO_{12}$ (**3b** and **3c**): C, 58.30; H, 8.32; N, 2.26%, Mol.wt. 617.

3d: Yield 37%. ^{1}H NMR ($CDCl_3$) δ=2.6—3.0 (6H, t), 3.5—4.2 (46H, m), 6.3—6.9 (3H, m). Found: C, 57.34; H, 8.24; N,

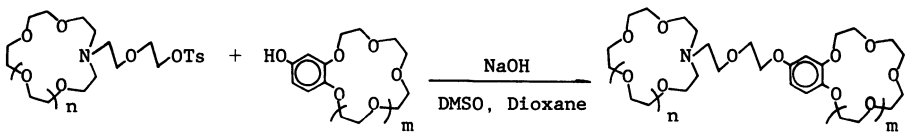

4a(n=1) 5a(m=1) 3a(n=1, m=1) 3c(n=2, m=1)
4b(n=2) 5b(m=2) 3b(n=1, m=2) 3d(n=2, m=2)

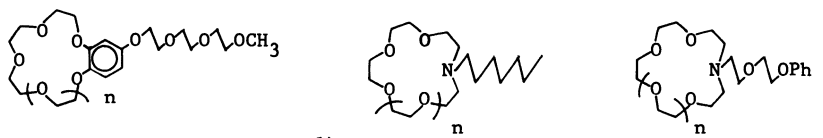

"lariat B15C5" (n=1)* [1] 1a(n=1) 2a(n=1)
"lariat B18C6" (n=2)* 1b(n=2) 2b(n=2)

* B15C5, benzo-15-crown-5; B18C6, benzo-18-crown-6.

Scheme 1.

2.06%; M^+, 661. Calcd for $C_{32}H_{55}NO_{13}$: C, 58.02; H, 8.34; N, 2.12%; Mol.wt. 661. **3a—d**: Pale yellow viscous liquid, IR (neat): 2930, 2870, 1600, 1510, 1460, 1360, 1220, 1120 cm^{-1}.

Solvent Extraction. The extraction experiment was carried out in a CH_2Cl_2-H_2O system at 25 °C, according to the Pedersen's procedure.[4] Extraction equilibria were measured under the same conditions, and four measurements were carried out at varied ligand concentrations in one system. The constants are defined as:

$$M^+_{aq} + A^-_{aq} + Cr_{org} \overset{K_e}{\rightleftharpoons} MCrA_{org}, \quad (1)$$

$$MCrA_{org} \overset{K_d}{\rightleftharpoons} MCr^+_{org} + A^-_{org}, \quad (2)$$

$$Cr_{org} \overset{P_e}{\rightleftharpoons} Cr_{aq}, \quad (3)$$

$$K_e = [MCrA]_{org}/[M^+]_{aq}[A^-]_{aq}[Cr]_{org}, \quad (4)$$

$$K_d = ([MCr^+]_{org}[A^-]_{org})/[MCrA]_{org}, \quad (5)$$

$$P_e = [Cr]_{aq}/[Cr]_{org}. \quad (6)$$

From Eqs. 4—6 we can get:[5]

$$K_e = \frac{(1+P_e)(2[A]+K_d-(K_d^2+4K_d[A])^{1/2})}{2f([M]_0-[A])([A]_0-[A])([Cr]_0-[A])} \quad (7)$$

where f is the single-ion activity coefficient of alkali metal cation in aqueous phase, [A] is the total concentration of the picrate anion in organic phase and $[M]_0$, $[A]_0$, and $[Cr]_0$ is the initial concentration of the cation, picrate anion and crown unit, respectively. Equation 8 is used for intermolecular sandwich complex, while Eq. 9 for intramolecular one.[6]

$$K_e = \frac{(1+P_e)^2(2[A]+K_d-(K_d^2+4K_d[A])^{1/2})}{2f([M]_0-[A])([A]_0-[A])([Cr]_0-2[A])^2} \quad (8)$$

$$K_e = \frac{(1+P_e)(2[A]+K_d-(K_d^2+4K_d[A])^{1/2})}{2f([M]_0-[A])([A]_0-[A])([Cr]_0-2[A])} \quad (9)$$

P_e can be obtained from the extraction in the absence of picrates. K_e was evaluated by a regression analysis with varied K_d to minimize the deviation among the calculated values for the measurements over the range of the concentration of crown unit (8.9×10^{-6}—1.4×10^{-3} mol dm^{-3}).

Stability Constants. The complex stability constants were determined on a mixture of ligand (0.30—0.60 mmol dm^{-3}) and MCl (0.4—2.0 mmol dm^{-3}) in 90% (w/w) aqueous MeOH at 25 °C. Emf was measured with the ion selective electrode (Na^+-ISE(TOA NA-15B) for Na^+ and monovalent cation electrode (Corning cat. No. 476220) for K^+, Cs^+ against a Ag/AgCl reference electrode by use of an Orion Research Model 701A digital "Ionalyzer." The details of the method of the measurement and calculation were described by H. K. Frensdorff[7a] and G. W. Gokel, et al.[7b] The results are shown in Table 3. The following equations were used in the calculation, Eqs. 10 and 11 for monocrown ethers and 12—16 for bis(crown ether)s.[1]

$$M^+ + Cr \overset{K_{m1}}{\rightleftharpoons} M^+Cr$$

$$K_{m1} = K_{obsd1} = [M^+Cr]/([M^+][Cr]) \quad (10)$$

$$M^+Cr + Cr \overset{K_{m2}}{\rightleftharpoons} CrM^+Cr$$

$$K_{m2} = K_{obsd2} = [CrM^+Cr]/([M^+Cr][Cr]) \quad (11)$$

$$\overset{\frown}{Cr}\ \overset{\frown}{Cr'} + M^+ \overset{K_{b1}}{\rightleftharpoons} \overset{\frown}{Cr}\ \overset{\frown}{Cr'}M^+$$

$$K_{b1} = [\overset{\frown}{Cr}\ \overset{\frown}{Cr'}M^+]/([\overset{\frown}{Cr}\ \overset{\frown}{Cr'}][M^+]) \quad (12)$$

$$\overset{\frown}{Cr}\ \overset{\frown}{Cr'}M^+ \overset{K_{b2}}{\rightleftharpoons} Cr\overset{\frown}{M^+}Cr'$$

$$K_{b2} = [Cr\overset{\frown}{M^+}Cr']/[\overset{\frown}{Cr}\ \overset{\frown}{Cr'}M^+] \quad (13)$$

$$\overset{\frown}{Cr}\ \overset{\frown}{Cr'}M^+ + M^+ \overset{K'_{b1}}{\rightleftharpoons} M^+\overset{\frown}{Cr}\ \overset{\frown}{Cr'}M^+$$

$$K'_{b1} = [M^+\overset{\frown}{Cr}\ \overset{\frown}{Cr'}M^+]/([\overset{\frown}{Cr}\ \overset{\frown}{Cr'}M^+][M^+]) \quad (14)$$

$$K_{obsd1} = K_{b1}(1+K_{b2}) \quad (15)$$

$$K_{obsd2} = K'_{b1}/(1+K_{b2}) \quad (16)$$

Results and Discussion

Presence of the lariat group markedly increased the extractability of monoazacrown ethers **2—3**, as described by M. Okahara, et al.[3,8] and the effect is in marked contrast to that of the similar group in benzocrown ethers as shown in Table 1.[1] The monoazacrown ethers bearing a lariat group showed a similar extractability with small cations. Li^+ and Na^+. For K^+, Rb^+, and Cs^+ the extraction behavior of the four bis(crown ether)s **3a—d** seems to be divided into two groups depending on the azacrown unit involved; i.e., **3a** and **3b** of lower extractability and **3c** and **3d** of higher one, which may be compared with **2a** and **2b**, respectively. The comparison between **2a** and **3a** (or between **2b** and **3c**) shows that the introduction of a terminal B15C5 group in place of a phenyl group does not exert any marked increase in the extractability, and the values in the parentheses obtained with the same concentration of the azacrown unit may be explained by a concomitant increase in concentration of B15C5 group. Considerable enhancement of the extractability of **3b** over **3a** and of **3d** over **3c** could be understood by the larger complexability of B18C6 than B15C5. It should be emphasized that none of these bis(crown

Table 1. Extraction of Alkali Metal Cations[a]

Crown Ether	Extracted Picrate Salts /%				
	Li^+	Na^+	K^+	Rb^+	Cs^+
1a	1.4	20.8	4.2	1.6	3.2
1b	4.0	17.0	79.0	53.5	25.9
2a	14.0	52.8	42.5	21.6	15.7
2b	10.0	58.4	95.9	90.0	65.4
3a	14.6	47.3	36.4	20.0	14.1
		(62.8)	(51.2)	(29.2)	(20.0)
3b	13.0	50.4	55.0	35.3	22.6
		(66.0)	(69.6)	(49.0)	(37.8)
3c	19.2	47.7	88.9	77.8	47.5
		(62.2)	(96.4)	(89.3)	(66.1)
3d	10.9	50.2	94.3	85.0	59.2

a) CH_2Cl_2=H_2O=10cm^3, Aqueous Phase: [Picric Acid]=7.0×10^{-5} mol dm^{-3}, [Metal Hydroxide]=0.01 mol dm^{-3}; Organic Phase: [Crown Unit]=3.5×10^{-4} mol dm^{-3}. The values in parentheses are for [Crown Unit]=7.0×10^{-4} mol dm^{-3}.
The data for benzocrown ethers with Na^+, K^+, Rb^+, and C^+s are;[1] B15C5: 2.6%, 14.2%, 11.2%, 7.7%; B18C6: 3.3%, 54.1%, 27.2%, 15.8%; lariat B15C5: 2.9%, 9.9%, 4.7%, 1.5%; lariat B18C6: 4.1%, 55.2%, 30.2%, 18.8%.

Table 2. Equilibrium Constants for Extraction of Alkali Metal Picrates[a,b,c]

Crown Ether	Na^+		K^+		Rb^+		Cs^+	
	K_e	K_d	K_e	K_d	K_e	K_d	K_e	K_d
2a	3.8×10^5	3.0×10^{-6}	2.0×10^5	7.3×10^{-6}	7.4×10^4	3.4×10^{-6}	1.2×10^4	4.9×10^{-5}
2b	2.2×10^5	4.6×10^{-5}	1.1×10^{12}	1.6×10^{-5}[d]	3.4×10^6	1.0×10^{-6}	3.2×10^5	4.1×10^{-5}
3a	2.7×10^5	6.0×10^{-6}	1.7×10^5	4.5×10^{-6}	4.0×10^4	1.2×10^{-5}	1.8×10^4	1.8×10^{-5}
3d	4.4×10^5	1.2×10^{-6}	1.8×10^{11}	2.4×10^{-5}[d]	1.5×10^6	1.0×10^{-6}	4.9×10^5	6.0×10^{-6}

a) The Conditions are the same as Table 1. [Crown Unit]=9.0×10^{-6}–7.0×10^{-4} mol dm^{-3}. K_e/dm^2 mol^{-2} and K_d/dm^{-1} mol were calculated with Eq. 7 unless noted otherwise. b) **2a**: P_e=0.17; **2b**: P_e=0.11; **3a**: P_e=0.25; **3d**: P_e=0.33. Mean activity coefficient for 0.01 mol dm^{-3} -cation f=0.889. c) Standard deviations were less than 10% except for **3d**-K^+(34%). d) K_e/dm^3 mol^{-3} and K_d/dm^{-1} mol were calculated with Eq. 8.

Table 3. Complexation Stability Constants in 90% Aqueous MeOH (w/w)

Crown Ether	Na^+		K^+		Cs^+	
	log K_{obsd1}	log K_{obsd2}	log K_{obsd1}	log K_{obsd2}	log K_{obsd1}	log K_{obsd2}
1a	2.76±0.04	*	2.29±0.03	*	2.71±0.01	*
1b	2.98±0.12	*	4.17±0.01	3.21±0.21	3.53±0.08	*
2a	3.43±0.03	*	3.64±0.03	3.34±0.10	3.15±0.09	*
2b	3.48±0.01	*	4.78±0.06	3.96±0.26	3.82±0.01	*
3a	3.10±0.01	*	3.16±0.01	*	3.23±0.05	*
3d	2.93±0.05	2.93±0.04	4.66±0.01	2.85±0.02	3.21±0.01	3.06±0.01

* No regression analysis was done for K_{obsd2}, since the standard deviation of K_{obsd1} was less than 10%.

ether)s **3a—d** shows any marked increase in extractability for cations larger than their hole size as is known in bis(benzo-15-crown-5)-K^+ or bis(benzo-18-crown-6)-Cs^+ system. These considerations lead us to the reasoning that the complexation behavior of the present bis(crown ether)s is principally governed by the effect of the lariat group and the benzocrown unit plays a minor role. The extraction equilibrium constants (Table 2) are almost consistent in tendency with the results in Table 1. The similarity in K_e of **2a** and **3a**, and of **2b** and **3d** again supports the absence of any extra effect of another crown unit in **3a—d** since the formation of the intramolecular sandwich complex is known to give rise to a definitive enhancement in K_e for bis(benzocrown ether)s.[1,9] In the cases of **2b**-K^+ and **3d**-K^+ the calculation with Eq. 7 or Eq. 9 gave larger deviation (>60%), while the recalculation with Eq. 8 gave a good result. The result suggests that the bis(crown ether) **3d**, as well as the lariat ether **2b**, can form an intermolecular sandwich complex in some cases.

Although the stability constants in a homogeneous system are not always parallel with the results from a two-phase equilibrium we can still get the following information from Table 3. The monoazacrown ether **1b** and the lariat ethers **2a**, **2b** can form 2:1 complex with K^+. If the bis(crown ether) **3a** or **3d** forms an intramolecular sandwich complex there must be an increase in K_{obsd1} due to the contribution of K_{b2} in Eq. 15, but **3a** and **3d** show K_{obsd1} comparable with the lariat ether **2a** and **2b**, respectively. The appearance of K_{obsd2} in **3d** means that there exists the complex in which both crown units hold two cations independently (Eq. 14).

The unique behavior of the bis(crown ether)s **3** should come from their special structures. For lariat ethers, e.g. *N*-(methoxyethyl)monoaza-18-crown-6, the X-ray analysis showed that the ring donor atoms take a chair conformation. A cation larger than the hole size is disposed above the ring plane, and the lariat group in the side arm is not cradling the cation between it and the macroring but rather is pushing the cation out.[10] This fact may explain why the lariat ether **2b** and the bis(crown ether)s **3c**, **3d** can hold K^+ as an intermolecular sandwich complex in the solvent extraction.

The present work was partly supported by a Grant-in-Aid for Scientific Research No. 56470077 from the Ministry of Education.

References

1) Part VI. in this series: K. Kikukawa, G-X. He, A. Abe, T. Goto, R. Arata, T. Ikeda, F. Wada, and T. Matsuda, submitted to *J. Chem. Soc., Perkin Trans. 2.*

2) M. Bourgoin, K. H. Wong, J. Y. Hui, and J. Smid, *J. Am. Chem. Soc.*, **97**, 3462 (1975); T. Ikeda, A. Abe, K. Kikukawa, and T. Matsuda, *Chem. Lett.*, **1983**, 369; K. Kimura, T. Maeda, H. Tamura, and T. Shono, *J. Electroanal. Chem.*, **95**, 91 (1979).

3) A. Masuyama, Y. Nakatsuji, I. Ikeda, and M. Okahara, *Tetrahedron Lett.*, **1981**, 4665.

4) C. J. Pedersen, *Fed. Pro., Fed. Am. Soc. Exp. Biol.*, **27**, 1305 (1968).

5) H. K. Frensdorff, *J. Am. Chem. Soc.*, **93**, 4686 (1971); S. Kopolow, T. E. Hogen Esch, and J. Smid, *Macromolecules*, **6**, 133 (1973).

6) T. Maeda, K. Kimura, and T. Shono, *Bull. Chem. Soc. Jpn.*, **55**, 3506 (1982).

7) a) H. K. Frensdorff, *J. Am. Chem. Soc.*, **93**, 600 (1971); b) G. W. Gokel, D. M. Goli, C. Minganti, and L. Echegoyen, ibid., **105**, 6786 (1983).

8) R. A. Schultz, D. M. Dishong, and G. W. Gokel, *J. Am. Chem. Soc.*, **104**, 625 (1982).

9) K. H. Wong, and H. L. NG, *J. Coord. Chem.*, **11**, 49 (1981).

10) F. R. Fronczek, V. J. Gatto, R. A. Schultz. S. J. Jungk, W. J. Colucci, R. D. Gandour, and G. W. Gokel, *J. Am. Chem. Soc.*, **105**, 6717 (1983).

Palladium-Catalyzed Coupling between Organic Halides and Organotin Compounds Involving C-N Unsaturated Bonds at the Reaction Centers

Masanori KOSUGI,* Mamoru KOSHIBA, Akira ATOH, Hiroshi SANO, and Toshihiko MIGITA*
Department of Chemistry, Faculty of Technology, Gunma University, Kiryu, Gunma 376
(Received September 19, 1985)

Synopsis. Imidoyl chlorides were good substrates which can react with a variety of organotin compounds to give ketimines in the presence of a catalytic amount of palladium complex. Under similar conditions, *C*-tributylstannyl imines did not give the products except with 2-(tributylstannyl)benzothiazole, -benzoxazole, and 1-methyl-2-(tributylstannyl)imidazole. And *N*-tributylstannyl imines could not be utilized.

The cross-coupling of organotin compounds with organic halides catalyzed by palladium complex is an important and versatile method of stereo- and regiospecific carbon–carbon bond formation.[1] Thus aryl and vinyl bromides are good substrates, and aryl- and vinyl-tin compounds are good reagents. From the structural analogy, imidoyl chlorides and stannyl imines are expected to be good substrates and reagents, respectively. This is further suggested by that imidoyl chloride undergoes the oxidative addition to the low valent palladium complex,[2] since such oxidative adducts are considered to be intermediates in the palladium-catalyzed coupling between organotins and halides. In this note, we report about possible utility of the following three types of reactions.

$$R^1CCl=NR^2 + n\text{-}Bu_3SnR^3 \xrightarrow{[Pd]} R^1R^3C=NR^2 + n\text{-}Bu_3SnCl$$

$$R^3X + n\text{-}Bu_3SnR^1C=NR^2 \xrightarrow{[Pd]} R^1R^3C=NR^2 + n\text{-}Bu_3SnX$$

$$R^3X + n\text{-}Bu_3SnN=CR^1R^2 \xrightarrow{[Pd]} R^3N=CR^1R^2 + n\text{-}Bu_3SnX$$

As for heterocycles containing C=N bonds, palladium-catalyzed couplings of 2-halobenzothiazole with organozinc compound are known.[3,4] We also applied the cross-coupling of tin compounds with halides to these heterocycle systems.

I. Palladium-Catalyzed Reaction of Imidoyl Chloride and Related Compound with Organotin Compounds. As is shown in Table 1, imidoyl chlorides were good substrates to give ketimines when treated with a variety of organotin compounds in the presence of a catalytic amount of palladium complex. Quite recently, we have found similar trials published.[5] The best yields were obtained when the reaction was carried out using a slightly excess amount of tin reagents and 1 mol% of dichlorobis(triphenylphosphine)-palladium at 120 °C for 20 h in xylene. Prolonged reaction time decreased the yield of the product. The reaction with acetonyltributyltin gave two products, that is, the acetonylated product (isomerized to conjugated enone) and the iso-propenylated one, though in relatively low yields.

In the reaction with tin enolate (α-stannyl ketone or enol stannyl ether), dichlorobis(tri-*o*-tolylphosphine)palladium was a better catalyst than dichlorobis(triphenylphosphine)palladium, as in the case of cross-coupling of tin enolate with other organic halides.[6]

In allylation of *N*-(α-chlorobenzylidene)aniline, the product was isomerized to the conjugated imine which was identical to the product derived from the reaction with 1-propenyltributyltin. Although the stereochemistry of the product was not fully characterized, GLC analysis showed the mixture of *E*- and *Z*-isomer being produced.

II. Palladium-Catalyzed Reaction of Bromobenzene with Tributylstannyl Imines. There are two types of stannyl imines, *C*-stannyl imine and *N*-stannyl imine. The results of trials for the cross-coupling reaction of these stannyl imines with bromobenzene were summarized in Table 2.

C-Stannyl heterocycles, such as 2-(tributylstannyl)benzothiazole, -benzoxazole, and 1-methyl-2-(tributylstannyl)imidazole were found to be good reagents, while acyclic *C*-stannyl imine, *N*-[α-(tributylstannyl)-benzylidene]aniline and *N*-[1-(tributylstannyl)pentylidene]-*t*-butylamine did not react.

On the other hand, *N*-tributylstannyl imines could hardly be utilized in this type of reaction.

Experimental

^1H NMR spectra were taken on a Varian EM-360 spectrometer. IR spectra were obtained on Jasco A-100 spectrometer. MS spectra were taken by using JMS-07. GLC analyses were carried out with Ohkura 802 instrument, using columns (1.5 m) packed with 10% Silicone SE-30 and SF-96 on Celite 545. Bp and mp are uncorrected values. (1 mmHg=133.322Pa).

Materials. *N*-(α-Chlorobenzylidene)aniline (bp 110—115 °C/0.3 mmHg, mp 41 °C; lit,[7] bp 174—176 °C/12 mmHg, mp 41 °C) and 2-chlorobenzothiazole (bp 83.5 °C/1.4 mmHg; lit,[8] bp 135—136 °C) were prepared by the treatment of benzophenone oxime and benzothiazole with phosphorus pentachloride, respectively. $Bu_3SnCH_2CH=CH_2$,[9] $Bu_3SnCH=CH_2$,[10] $Bu_3SnCH=CHCH_3$,[11] Bu_3SnPh,[12] $Bu_3SnCH_2COCH_3$,[13] 1-cyclohexenoxytributyltin,[13] $Bu_3SnN=C(CCl_3)(OMe)$,[14] $Bu_3SnN=CPh(NEt_2)$,[15] and $Bu_3SnN=C=NSnBu_3$[16] were prepared according to the methods described in the literatures. 1-Methyl-2-(tributylstannyl)imidazole (bp 123—130 °C/0.3 mmHg), 2-(tributylstannyl)benzoxazole (bp 135—140 °C/0.15 mmHg), and 2-(tributylstannyl)benzothiazole (bp 144—146 °C/0.15 mmHg) were prepared by the treatment of 1-methylimidazole, benzoxazole, and benzothiazole with butyl lithium, followed by the addi-

Table 1. Pd-Catalyzed Reaction of *N*-(α-Chlorobenzylidene)aniline and 2-Chlorobenzothiazole with Organotin Compounds

R-Cl	R′-SnBu$_3$	Cat.[a]	Solvent	Time / h	Temp / °C	Product R-R′	Yield / %[b]
PhN=CPh-	CH_2=$CHCH_2$-	none	PhH	10	120	I[c]	0
		A	PhH	10	120	I	86
		B	PhH	10	120	I	71
		C	PhH	10	120	I	33
		D	PhH	10	120	I	0
		E	PhH	10	120	I	0
		A	THF	10	120	I	52
		A	DMSO	10	120	I	0
		A	HMPA	10	120	I	trace
		A	DMP	10	120	I	trace
		A	Xylene	42	80	I	56
		A	Xylene	20	100	I	65
		A	Xylene	10	120	I	85
		A	Xylene	20	120	I	91 (67)
		A	Xylene	40	120	I	56
PhN=CPh-	CH_2=CH-	A	Xylene	10	120	II	(67)
PhN=CPh-	CH_3CH=CH-	A	Xtlene	20	120	I	(87)
PhN=CPh-	Ph-	A	Xylene	60	120	III	(78)
PhN=CPh-		C	Xylene	5	120	IV	74
PhN=CPh-	MeCOCH_2-	C	Xylene	5	120	V[d] VI[e]	9 25
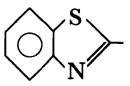	Ph-	A	Xylene	20	120	VII	(86)
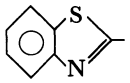	CH_3CH=CH-	A	Xylene	20	120	VIII	(88)

a) A: $PdCl_2(PPh_3)_2$, B: $Pd(PPh_3)_4$, C: $PdCl_2[P(o\text{-tolyl})_3]_2$, D: $PdCl_2$+2 $P(OEt)_3$, E: $PdCl_2(PhCN)_2$. b) GLC yield based on the halide, isolated yield in parentheses. c) PhN=CPh(CHCHMe). d) PhNHCPh=CH(COMe) e) PhN=CPh(OCMe=CH_2).

Table 2. Pd-Catalyzed Reaction of Bromobenzene with Tributylstannyl Imines[a]

Stannyl Imine	Product		Isolated Yield/%
Bu_3Sn-CPh=NPh	Ph_2C=NPh		0
Bu_3Sn-CBu^n=NBu^t	$PhBu^nC$=NBu^t		0
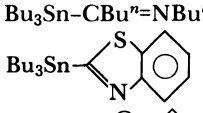	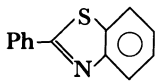	VII	56
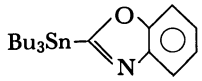	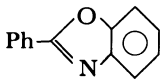	IX	75
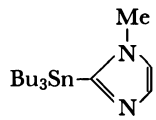	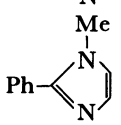	X	89
Bu_3Sn-N=C=N-$SnBu_3$	PhN=C=NPh		0
Bu_3Sn-N=CPh(NEt_2)	PhN=CPh(NEt_2)		0
Bu_3Sn-N=C(CCl_3)(OMe)	PhN=C(CCl_3)(OMe)		0

a) Reactions were carried out by using 1 mol% of $PdCl_2(PPh_3)_2$ in xylene at 120 °C for 20 h.

tion of tributyltin chloride, respectively. *N*-[1-(tributylstannyl)pentylidene]-*t*-butylamine (bp 120—122 °C/0.3 mmHg) was prepared by the insertion of butyl lithium into *t*-butyl isocyanide, then the addition of tributyltin chloride.[17] *N*-[α-(tributylstannyl)benzylidene]aniline (bp 148—155 °C/0.3 mmHg) was prepared by the reaction of *N*-(α-chlorobenzylidene)aniline with lithium tributylstannate(II). ^{1}H NMR spectra of these tin compounds showed reasonable structures of them which were used without further characterizations. Palladium complexes were already reported.[6]

Reaction Procedure. A mixture of halide (3.0 mmol), tin compound (3.6 mmol), and palladium complex (0.03 mmol) in xylene (6 ml) was heated under argon at 120 °C for 20 h. After washed with aqueous potassium fluoride to remove the tributyltin halide produced, organic layer was extracted with ether and dried over sodium sulfate. Then after evaporation of ether, the product was isolated by distillation or recrystallization.

Products. (I) Bp 110 °C/0.4 mmHg. ^{1}H NMR (CCl_4) δ=6.58—8.10 (m, 10H, phenyl), 5.52—6.35 (m, 2H, olefinic), 2.70 (d, *J*=7.0 Hz, 3H, methyl). IR (CCl_4) 1600 (C=N), 1650 and 1300 (C=C) cm^{-1}. MS *m/z* 221 (M^+). (II) Bp 95 °C/0.3 mmHg, mp 78—80 °C. ^{1}H NMR (CCl_4) δ=6.58—8.10 (m, 10H, phenyl) 5.24—6.65 (m, 3H, olefinic). IR (CCl_4) 1596 (C=N), 1630 (C=C) cm^{-1}. MS *m/z* 206 (M^+). (III) Mp 111—112 °C, lit,[18] 113 °C. ^{1}H NMR (CCl_4) δ=6.40—7.90 (m, phenyl). IR (KBr) 1598 (C=N) cm^{-1}. (IV) Bp 158 °C/0.4 mmHg. ^{1}H NMR (CCl_4) δ=6.11—8.38 (m, 10H, phenyl), 4.98 (s, 1H, olefinic), 0.68—2.67 (m, 8H, methylene). IR (CCl_4) 1600 (C=N), 1658 (C=C) cm^{-1}. MS *m/z* 278 (M^+). (V) GLC collection. ^{1}H NMR (CCl_4) δ=6.25—7.20 (m, 5H, *C*-phenyl), 7.30 (s, 5H, *N*-phenyl), 6.74 (s, 1H, olefinic), 2.12 (s, 3H, methyl), 5.29 (s, 1H, N-H). IR (CCl_4): 1620 (C=O), 1298(NH) cm^{-1}. (VI) GLC collection. ^{1}H NMR (CCl_4) δ=6.45—8.09 (m, 10H, phenyl), 1.82 (s, 3H, methyl), 4.10 (s, 2H, olefinic). IR (CCl_4) 1660 (C=N), 1640 (C=C) cm^{-1}. (VII) Mp 111—112 °C. Found: C 73.89, H 4.35, N 6.31%; Calcd for

$C_{13}H_9NS$: C 73.90, H 4.29, N 6.63%. (VIII) Mixtures of *E* and *Z*. *E* isomer: ^1H NMR (CCl_4) δ=6.91—8.08 (m, 4H, phenyl), 6.40—6.80 (m, 2H, olefinic), 1.92 (d, J=5 Hz, 3H, methyl). MS *m/z* 175 (M^+). *Z* isomer: ^1H NMR (CCl_4) δ=6.98—8.19 (m, 4H, phenyl), 5.72—6.43 (m, 2H, olefinic), 2.26 (d, J=6 Hz, 3H, methyl). MS *m/z* 175 (M^+). (IX) Mp 92—93 °C. ^1H NMR (CCl_4) δ=7.11—8.52 (m, phenyl). MS *m/z* 195 (M^+). Found: C 80.04, H 4.84, N 7.19%; Calcd for $C_{13}H_9ON$: C 79.98, H 4.65, N 7.17%. (X) bp 100 °C/0.35 mmHg. ^1H NMR (CCl_4) δ=7.09—7.60 (m, 5H, phenyl), 6.70 and 6.80 (s, 2H, olefinic), 3.51 (s, 3H, methyl). MS *m/z* 158 (M^+).

Financial support by Asahi Glass Foundation is gratefully acknowledged. We also thank Kohriyama Kasei Co. for a gift of tributyltin oxide.

Refefences

1) I. P. Beletskaya, *J. Organomet. Chem.*, **250**, 551 (1983) and references cited therein; W. F. Goure, M. E. Wright, P. D. Davis, S. S. Labadie, and J. K. Stille, *J. Am. Chem. Soc.*, **106**, 6417 (1984).
2) M. Tanaka and H. Alper, *J. Organomet. Chem.*, **168**, 97 (1979).
3) E. Negishi, "Current Trend in Organic Synthesis," ed by H. Nozaki, Pergamon Press (1983) p. 269.
4) H. Takei, M. Miura, H. Sugimura, and H. Okamura, *Chem. Lett.*, **1979**, 1447.
5) During preparing this manuscript, we have found similar trials published. T. Kobayashi, T. Sakakura, and M. Tanaka, *Tetrahedron Lett.*, **26**, 3463 (1985).
6) M. Kosugi, I. Hagiwara, T. Sumiya, and T. Migita, *Bull. Chem. Soc. Jpn.*, **57**, 242 (1984).
7) E. Beckman, *Ber.*, **19**, 989 (1886).
8) J. G. Grasselli and W. M. Ritehey, "Atlas of Spectral Data and Physical Constants for Organic Compounds," 2nd ed., CRC Press (1975).
9) D. Seyferth and M. A. Weiner, *J. Org. Chem.*, **24**, 1395 (1959).
10) D. Seyferth and F. G. A. Stone, *J. Am. Chem. Soc.*, **79**, 515 (1957).
11) D. Seyferth and L. G. Vaugan, *J. Organomet. Chem.*, **1**, 138 (1963).
12) M. Kosugi, T. Ishikawa, T. Nogami, and T. Migita, *Nippon Kagaku Kaishi*, **1985**, 520.
13) M. Pereyre, B. Bellegarde, J. Mendelsohn, and J. Valade, *J. Organomet. Chem.*, **11**, 97 (1968).
14) A. J. Bloodworth and A. G. Davis, *Proc. Chem. Soc.*, **1963**, 315; *Chem. Abstr.*, **60**, 2998f (1964).
15) K. Jones and M. F. Lappert, *Proc. Chem. Soc.*, **1964**, 22; *Chem. Abstr.*, **60**, 8054e (1964).
16) R. A. Cardona and E. J. Kupchik, *J. Organomet. Chem.*, **43**, 163 (1972).
17) P. Jutzi and U. Gilge, *J. Organomet. Chem.*, **146**, 163 (1983).
18) G. E. Niznik, W. H. Morison, and M. Waborsky, *J. Org. Chem.*, **39**, 600 (1974).

Platinum-Catalyzed Oxidation of Cholesterol

Toshihiro AKIHISA (ne ITOH),* Taro MATSUMOTO, Hiroshi SAKAMAKI,†
Masa-aki TAKE,† and Yoshiyuki ICHINOHE,*,†
College of Science and Technology, Nihon University, Surugadai Campus, Kanda Surugadai, Chiyoda-ku, Tokyo 101
†College of Science and Technology, Nihon University, Narashino Campus, Narashinodai, Funabashi, Chiba 274
(Received September 24, 1985)

Synopsis. Cholesterol was oxidized (12% conversion) with platinum and oxygen to give several 7-oxygenated products, cholest-5-en-3-one, and cholest-4-en-3-one accompanied with its further oxygenation products at C-6. The pathways and mechanisms of the catalytic oxidation are discussed.

Platinum-catalyzed oxidation[1] has been used successfully for the oxidation of saturated sterols including 5α-cholestan-3β-ol and its 3α-epimer by Sneeden and Turner.[2] The attempts at the oxidation of cholesterol (cholest-5-en-3β-ol, **1**) have, however, met with failure.[2] This paper describes our reinvestigation of the oxidation of **1** with platinum and oxygen, which demonstrated that **1** undergoes catalytic oxidation.

The oxidation of **1** was performed by oxygen over prereduced platinum in ethyl acetate at the ambient pressure and temperature to yield Δ^5- (**2**, **3**, **4**, and **5**) and Δ^4- (**6**, **7**, **8**, and **9**) oxidation products as summarized in Table 1, most of which are known to be autoxidation products of **1**.[3-6] The oxidation of the Δ^5-3-one **2** under the same conditions yielded the Δ^4-3-one **6** and the 6-oxygenated products, **7**, **8**, and **9**, whereas the oxidation of **6** yielded only the unaltered substrate. The controlled oxidation of **1** and **2** in the absence of the catalyst afforded only the unchanged starting material. From the above, it can be assumed that there are two pathways (**I** and **II**) for the catalytic oxidation of **1**, as is illustrated in Scheme 1.

The first, minor, one (**I**) is to form the allylic oxygenation products: **3**, **4**, and **5**. These 7-oxygenated products are well-known radical autoxidation products of **1** and have been established to be formed via the initial formation of the 7-hydroperoxides (**10** and **13**), followed by thermal decomposition.[3-5] Although these hydroperoxides were not detected in the present oxidation of **1**, we suppose that the initial formation of **10** and **13** is also involved in the catalytic oxidation

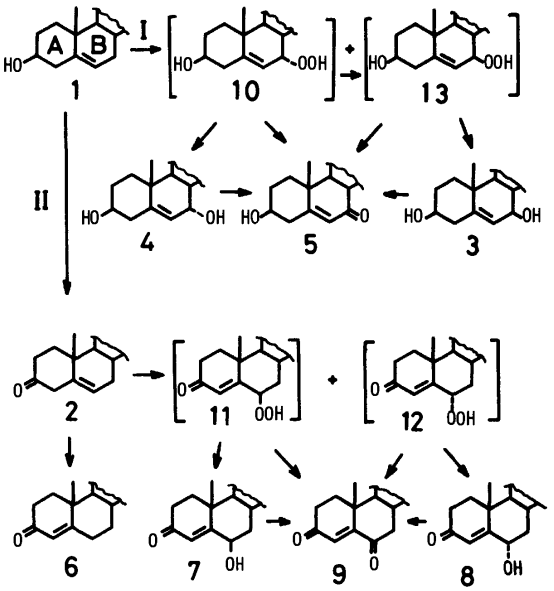

Scheme 1. Proposed pathways for the platinum-catalyzed oxidation of cholesterol (**1**).

of **1**, which might be, in situ, decomposed over the catalyst to afford the 7-ols **3** and **4** and the 7-ketone **5**. The attempted catalytic oxidation of the 7α-hydroperoxide **10** yielded **3**, **4**, and **5**, with no substrate being recovered, while **10** remained mostly unaltered upon controlled oxidation in the absence of the catalyst, thus suggesting the lability of hydroperoxide over the platinum catalyst. The 7β-ol **3** might arise from **10** through epimerization to the 7β-hydroperoxide **13**, followed by decomposition, the epimerization of which was previously observed in a solution of ethyl acetate and some other solvents.[3]

The second, major pathway (**II**) of the catalytic oxidation of **1** is that proceeding via the dehydrogena-

Table 1. Compositions (%) from the Platinum-Catalyzed Oxidation of Cholesterol and Some Other Steroids[a]

Substrate	Substrate reacted	Composition/% of the products								
		2	**3**	**4**	**5**	**6**	**7**	**8**	**9**	Others, unidentified
Cholesterol (**1**)	12.2	0.8	1.6	0.8	0.4	0.8	15.5	31.1	31.1	17.9
Cholest-5-en-3-one (**2**)	89.5					1.8	20.0	18.3	29.3	30.6
Cholest-5-ene-3β,7β-diol (**3**)	13.9				32.4					67.9
Cholest-5-ene-3β,7α-diol (**4**)	26.3				4.2					95.8
Cholest-4-en-3-one (**6**)	0									
6β-Hydroxycholest-4-en-3-one (**7**)	48.1								62.8	37.2
6α-Hydroxycholest-4-en-3-one (**8**)	20.1								58.7	41.3
7α-Hydroperoxycholest-5-en-3β-ol (**10**)	100		18.4	53.9	29.7					
6β-Hydroperoxycholest-4-en-3-one (**11**)	100						56.4		36.6	7.0
6α-Hydroperoxycholest-4-en-3-one (**12**)	100							62.9	29.1	8.0

a) **5**, 3β-Hydroxycholest-5-en-7-one; **9**, cholest-4-ene-3,6-dione.

Table 2. Melting Points, Chromatographic Data, and ^{1}H NMR Data of Some Steroids

Steroid	Mp θ_m/°C	RRT		^{1}H NMR data[b]					
		GLC[a]	HPLC	18-H_3(*s*)	19-H_3(*s*)	3α-H(*m*)	4-H	6-H	7-H
1	149—150	1.00	1.00	0.69	1.02	3.53(26)	—	5.35(m, 9)	—
2	130—131	1.92	0.80	0.71	1.19	—	—	5.33(m, 9)	—
3	170—174	1.19	0.18	0.70	1.04	3.53(25)	—	5.29(br. s)	3.86(m, 18)
4	178—182	0.82	0.17	0.69	1.01	3.50(25)	—	5.61(d, 4.8)	3.86(m,13)
5	168—170	2.49	0.29	0.68	1.20	3.63(26)	—	5.69(s)	—
6	80—82	1.92	0.64	0.71	1.18	—	5.72(s)	—	—
7	197—199	1.67	0.92	0.74	1.37	—	5.80(s)	4.35(m, 8)	—
8	161—164	2.41	0.20	0.71	1.18	—	6.17(d, 2)	4.33(m, 20)	—
9	123—125	3.30	0.22	0.72	1.16	—	6.17(s)	—	—
10	154—155	3.30	0.14	0.66	0.99	3.60(22)	—	5.73(d, 4.9)	4.16(m, 10)
11	176—178	3.30	0.23	0.71	1.33	—	5.88(s)	4.44(m, 7)	—
12	150—154	3.30	0.18	0.71	1.20	—	6.14(d, 2)	4.62(m, 22)	—

a) The RRTs of **2**, **6**, and **9** corresponded to the ketones, and those of the other steroids corresponded to the TMSE derivatives. The RRTs of **10**, **11**, and **12** were for GLC decomposition products. b) Gvien as δ values. Figures in parentheses denote *J* values (Hz) for doublet signals, whereas $W_{1/2}$ values (Hz) for multiplet signals. The signals at δ 0.87 (6H, *d*, *J*~6 Hz, 26-H_3, 27-H_3) and 0.92 (3H, *d*, *J*~5 Hz, 21-H_3) also were observed for all of the steroids. s: singlet, d: doublet, m: multiplet.

tion to afford the ketone **2** as the primary product. Upon isomerization, this yields conjugated ketone **6**, not further oxidized, and upon a second oxidation it yields the epimeric 6-hydroxy ketones **7** and **8**. These 6-ols are known to be formed from the ketone **2**, accompanied by the 6-hydroperoxides **11** and **12** and other products, by irradiation in air using ^{60}Co gamma radiation,[6] and by autoxidation in acetic acid.[7] Although we did not detect the 6-hydroperoxides **11** and **12** in the present oxidation of **1**, we consider the involvement of the 6-hydroperoxides in the catalytic oxidation to be as likely as in the autoxidation of **1**;[6] they may be involved as intermediates which might be decomposed, in situ, to form the epimeric 6-ols **7** and **8** and diketone **9**. The attempted oxidation of **11** and **12** in the presence of platinum yielded the 6-ols **7** and **8** respectively in addition to **9**, while no starting material was recovered. The formation of the ketones **6** and **9** is also known in the oxidation of **1** promoted by the Ni-Cr-O catalyst in xylene under reflux.[8]

Thus, **1** has undergone catalytic oxidation with platinum and oxygen under ambient pressure and temperature to yield several dehydrogenated and oxygenated products. The oxygenation of **1** in the catalytic oxidation is considered to proceed by means of a free-radical-type reaction promoted by platinum catalyst. Although saturated sterols have been oxidized successfully by the catalytic oxidation,[2] the reactivity of **1** in the catalytic oxidation was found to be extremely low (12% conversion) in this study. Such a low reactivity of **1** might be attributed to its 3β-hydroxy-Δ^5 structure since the other 3β-hydroxy-Δ^5-sterols **3** and **4**, which possess an additional hydroxyl group at C-7, also remained mostly unaltered by the catalytic oxidation. The oxidation has been found to proceed preferentially on the axial hydroxyl group rather than on the equatorial one as for the epimeric 6-hydroxy steroids **7** and **8** although the selectivity was not so clear cut as that of carbohydrates.[1] Table 2 showed the melting points, and chromatographic and ^{1}H NMR spectroscopic data of twelve steroids (**1**—**12**). The ^{1}H NMR spectroscopy has distinguished unequevocally between each of the double bond- and stereo-isomers of steroids. The ketone **2** was indistinguishable from conjugated ketone **6** in GLC which suggested the formation of **6** from **2** by thermal isomerization during GLC. The GLC peaks of the hydroperoxides **10**, **11**, and **12** were considered to be corresponded to the thermal decomposition products.[9]

Experimental

General Methods and Materials. The melting points are uncorrected. The HPLC was carried out on a Partisil 5 ODS-2 column (25 cm×10 mm i.d., two columns in series) using a UV detector (monitored at 212 nm) or a RI detector with MeOH as mobile phase. The GLC was performed with a SCOT OV-17 glass capillary column (30 m×0.3 mm i.d.) at 260 °C. The RRTs (relative retention times) in the HPLC and GLC were expressed relative to **1** and the trimethylsilyl ether (TMSE) derivative of **1**, respectively. The EI-MS spectra (70 eV) were taken by means of a probe injection. The ^{1}H NMR spectra (100 MHz) were obtained in a $CDCl_3$ solution, with Me_4Si as the internal standard. The thin-layer chromatography (TLC) was performed on plates of precoated silica gel. A commercial sample of **1** was purified through the dibromide by the method of Shoenheimer.[10,11] The other steroids were prepared from **1** as has previously been described.[12] All the steroid samples for the oxidation, which were identified on the basis of the mp, and the chromatographic and spectroscopic data, were recrystallized from MeOH or from MeOH-H_2O mixture several times and did not contain any detectable levels of autoxidation products.

Oxidation of Steroids and Analysis of the Oxidation Products. The oxidation was performed in a way similar to that described by Sneeden and Turner.[2] A suspension of PtO_2 (50 mg) in EtOAc (15 ml) was first reduced to Pt in an atmosphere of H_2, after which the H_2 was carefully replaced with air by repeated evacuation. The system was then filled with O_2, and the catalyst suspension was stirred until the uptake of O_2 ceased. The sample (50 mg) was added, the system was filled again with O_2, and the reaction was continued for 24 h at ambient pressure and temperature. The product was then passed through a short Florisil column in

order to remove the catalyst. A portion of the product was analyzed and fractionated by HPLC, while the other portion was analyzed by GLC as the TMSE derivatives. Steroid hydroperoxides were detected on TLC by spraying with *N,N*-dimethyl-*p*-phenylenediamine.[6] The oxidation products were identified on the basis of mp, and the chromatographic and spectroscopic data after isolation.

We wish to thank Kazuhisa Honma for his technical assistance.

References

1) a) K. Heyns and H. Paulsen, "Newer Methods of Preparative Organic Chemistry," ed by W. Roerst, Academic Press, Inc., New York (1963), Vol. 2, p. 303; b) J. Fried and J. A. Edwards, "Organic Reactions in Steroid Chemistry," Van Nostrand Reinhold Co., New York (1972), Vol. 1, p. 329.
2) R. P. A. Sneeden and R. B. Turner, *J. Am. Chem. Soc.*, **77**, 190 (1955).
3) J. I. Teng, M. J. Kulig, L. L. Smith, G. Kan, and J. E. van Lier, *J. Org. Chem.*, **38**, 119 (1973).
4) L. L. Smith, J. I. Teng, M. J. Kulig, and F. L. Hill, *J. Org. Chem.*, **38**, 1763 (1973).
5) N. Yanishlieva, H. Schiller, and E. Marinova, *Riv. Ital. Sostanze Grasse*, **57**, 572 (1980).
6) G. A. S. Ansari and L. L. Smith, *Chem. Phys. Lipids*, **22**, 55 (1978).
7) P. B. D. de la Mare and R. D. Wilson, *J. Chem. Soc., Perkin Trans. 2*, **1977**, 157.
8) M. Ishige, M. Shiota, and Y. Itoh, Abstracts of Papers, 23rd National Meeting of the Chemical Society of Japan, **1970**, p. 1716.
9) L. L. Smith, M. J. Kulig, and J. I. Teng, *Steroids*, **22**, 627 (1973).
10) R. Shoenheimer, *Z. Physiol. Chem.*, **192**, 86 (1930).
11) L. L. Engel and R. Brooks, *Steroids*, **17**, 531 (1971).
12) C. J. W. Brooks, "Rodd's Chemistry of Carbon Compounds, 2nd ed., ed by S. Coffey, Elsevier Publishing Co., Amsterdam (1970), Vol. IID p. 1, and the references cited therein.

 © 1986 The Chemical Society of Japan Bull. Chem. Soc. Jpn., 59, 683—687 (1986)

Preparation of Solid Catalysts for Vapor-Phase Decomposition of Carbonyl Sulfide

Masamichi AKIMOTO,* Hirotoshi SUTO, and Hiroo NIIYAMA
Department of Chemical Engineering, Tokyo Institute of Technology,
Ookayama, Meguro-ku, Tokyo 152
(Received May 31, 1985)

The vapor-phase catalytic decomposition of COS (COS→CO+1/xS$_x$ and 2COS→CO$_2$+CS$_2$) has been mechanistically investigated so as to prepare solid catalysts which are active and selective for the first reaction. The comparison of the catalytic activity and selectivity of a series of Al_2O_3 catalysts with their acid-base properties and the different behavior of these two catalytic decomposition reactions in the poisoning of an Al_2O_3 catalyst with SO_2 demonstrate that electron-donating sites catalyze the first reaction whereas Lewis acidic sites do so the second reaction. CaO catalysts are prepared by thermal decomposition of $CaCO_3$ at elevated temperatures and their catalytic activity is compared with their amount of electron-donating sites. The greatest catalytic activity and selectivity for the first reaction(yield of CO+S$_x$=21.4%, selectivity=80.2% at 873 K) are obtained over CaO catalyst prepared at 1123 K which has the greatest electron-donating ability. These values of the yield and selectivity to CO+S$_x$ are much greater than those obtained over Al_2O_3 catalysts.

The catalytic decomposition of COS to CO and elemental sulfur is of industrial importance in view of the recovery of hydrogen from H_2S and the oxidative dehydrogenation of hydrocarbons.

Fukuda and co-workers[1] proposed the following two-step closed cycle for the decomposition of H_2S.

$$H_2S + CO \longrightarrow H_2 + COS \quad (1)$$
$$COS \longrightarrow CO + 1/xS_x \quad (x=2,4,6,\cdots) \quad (2)$$

They reported that almost an equilibrium conversion of H_2 could be produced in the first reaction at 493—573 K with a cobalt sulfide catalyst.[2] In the second reaction, however, both CO_2 and CS_2 were always produced by the side reaction (Reaction 3) and in the

$$2COS \longrightarrow CO_2 + CS_2 \quad (3)$$

case of homogeneous decomposition reaction such an elevated temperature as 1103 K had to be used for the decomposition of COS to CO and elemental sulfur (S_x) with a selectivity of 95%.[2]

On the other hand, COS has been employed as a source of atomic sulfur in the catalytic oxidative dehydrogenation of lower paraffinic hydrocarbons and arylalkyl compounds.[3-6] In this oxidative dehydrogenation, COS is catalytically decomposed to CO and atomic sulfur which then abstracts hydrogen atoms from these hydrocarbons to give unsaturated hydrocarbons and H_2S. The most striking feature of this dehydrogenation is the ability to produce unsaturated hydrocarbons with high selectivity even over such catalysts SiO_2, Al_2O_3, MgO, and TiO_2 as have conventionally been used as carriers.

Although the catalytic decomposition of COS is thus industrially important, only a few papers have been published on the mechanism of the catalytic reaction and the preparation of active and selective catalysts.[5,7] In the present work, we have elucidated the nature of surface active sites responsible for the second and third reactions and have then tried to prepare active and selective catalysts for the second reaction by thermal decomposition of $CaCO_3$.

Experimental

Reaction and Catalyst. Vapor-phase catalytic decomposition of COS was carried out using a conventional flow fixed-bed reactor at atmospheric pressure (1 Torr=133.322 Pa). The reactor system comprised a 15-mm-i.d. quartz tube, 400 mm long, and a concentric thermowell. The reactor was heated with a cylindrical electric furnace. The catalysts employed are the referenced Al_2O_3 catalysts of the Catalysis Society of Japan (JRC-ALO-1, -2, -4, and -5) and CaO. CaO catalysts were prepared by thermal decomposition of $CaCO_3$ (Mallincrodt Inc., 99.95% purity) at elevated temperatures. Raschig rings (2×2 mm) were added above and below the catalyst bed. Purchased COS of greater than 97.5 vol% purity (Matheson Co., CO_2 1.4 vol%, N_2+CO 0.6 vol%, CS_2 0.19 vol%, O_2 0.10 vol%, and H_2O 0.01 vol%) was used without further purification. For convenience, helium (purity>99.99 vol%) was used as the diluent in the catalytic studies, and the total feed rate was always held at 200(NTP) cm^3 min^{-1}: the standard feed composition of COS was 5.0 vol%.

Analysis. The reaction products (COS, CO, CO_2, and CS_2) were analyzed by gas chromatography using Porapak R(0.8 m, 363 K) and Porapak S(0.6 m, 363 K) in series as the separating column and helium as the carrier gas. The ESR measurements were carried out with a JEOL JES-PE spectrometer operating in the X band, adopting a 100 kHz modulation frequency. The g values of paramagnetic species were determined by the use of Mn^{2+} dissolved in MgO, and radical concentrations were estimated by comparing with the standard solution of 2,2-diphenyl-1-picrylhydrazyl in benzene. Purchased SO_2 (Matheson Co., purity>99.98%) was used in the ESR studies after purification by freeze-pumping method.

Results

Nature of Active Sites. Table 1 summarizes the results of catalytic decomposition of COS at 873 K over the referenced Al_2O_3 catalysts of the Catalysis Society of Japan. Previous experiments indicated no effects of film and pore diffusions on the catalytic activity and selectivity in the decomposition of COS at 873 K (catalyst size=10—100 mesh, pore diameter=84—309 Å). Previous experiments also indicated the ratio of the yield of CO_2 to that of CS_2 to be unity in the catalytic decomposition of COS up to 923 K, and no significant change in the catalytic activity and selectivity with time was observed at 473—923 K.

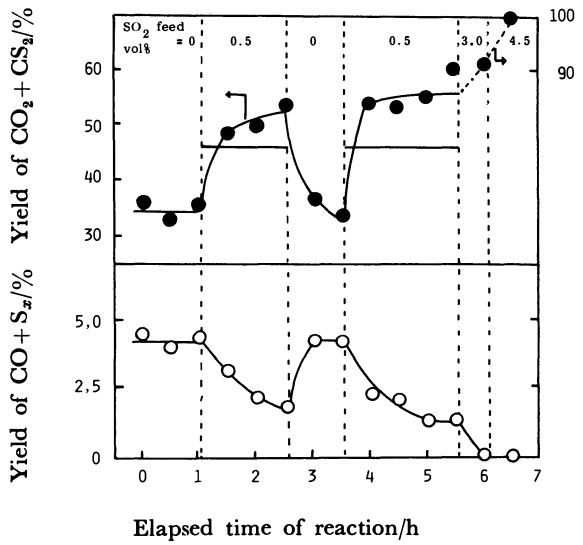

Fig. 1. Poisoning and promotional effects of SO_2 on the catalytic decomposition of COS at 763 K. Catalyst: JRC-ALO-4 Al_2O_3 1.0 g. COS+He: 200 (NTP)cm^3 min^{-1} (COS 10.0 vol%). The horizontal solid lines show the sum of the yield of CO_2+CS_2 in the absence of SO_2 (ca. 36%) and the yield of CO_2 calculated by assuming the complete consumption of introduced SO_2 due to Reaction 4(10.0%).

The yield of $CO+S_x$ was 14.3% over JRC-ALO-2 Al_2O_3, but it increased gradually with increasing the amount of basic sites and reached 16.9% over JRC-ALO-5 Al_2O_3. The selectivity to $CO+S_x$ also increased from 25.7% to 36.0% with such a change in the chemical properties of Al_2O_3 catalysts. In contrast, the yield of CO_2+CS_2 was the greatest, 41.3%, over the most acidic Al_2O_3 catalyst (JRC-ALO-2) and the selectivity to $CO+S_x$ was the lowest, 25.7%, over this catalyst.

The participation of electron-donating sites and acidic sites in the catalytic decomposition of COS was confirmed by the poisoning of JRC-ALO-4 Al_2O_3 catalyst with SO_2 at 763 K (Fig. 1). That is, the yield of $CO+S_x$ over JRC-ALO-4 Al_2O_3 decreased from 4.3% to 1.7% upon introduction of SO_2 into the reactant mixture (0.5 vol%) and the yield was nearly 0% when the concentration of SO_2 in the feed mixture was 3.0 and 4.5 vol%. When JRC-ALO-4 Al_2O_3 was degassed at 773 K for 1 h and then exposed to 20 Torr SO_2 at 673 K for 30 min, SO_2^- radicals with g values of $g_\perp$=2.002 and $g_{/\!/}$=2.008[9] were formed with an amount of ca. 10^{17} spins g^{-1}.

In contrast, the yield of CO_2+CS_2 increased upon introduction of SO_2 (Fig. 1). Here, a portion of SO_2 introduced reacted with COS to produce CO_2 and elemental sulfur according to Reaction 4.

$$SO_2 + 2COS \longrightarrow 2CO_2 + 3/xS_x \quad (4)$$

However, the yields of CO_2 observed in the presence of SO_2 were always greater than the sum (ca. 46%) of the yield of CO_2+CS_2 observed in the absence of SO_2 (ca. 36%) and that of CO_2 calculated by assuming the complete consumption of introduced SO_2 due to Reaction 4 (10.0%) (Fig. 1). This result is an evidence for the view that participation of acidic sites in the catalytic decomposition of COS to CO_2+CS_2 took place, as discussed later in this paper.

Preparation of CaO Catalysts. The results of Table 1 and Fig. 1 suggest that strongly basic and less acidic catalysts are superior for the catalytic decomposition of COS to $CO+S_x$. The preparation of

Table 1. Results of the Decomposition of COS over Al_2O_3 Catalysts at 873 K

Al_2O_3 catalysts	JRC-ALO-2	JRC-ALO-1	JRC-ALO-4	JRC-ALO-5
BET surface area/m^2 g^{-1}	298	176	174	253
Basic sites/10^{16} g^{-1}	3.42	3.52	3.89	4.43
Acidic sites/mmol g^{-1}	0.84	0.70	0.50	0.70
Conversion of COS/%	55.6	46.7	49.6	47.0
Yield of $CO+S_x$/%	14.3	15.6	16.7	16.9
Yield of CO_2+CS_2/%	41.3	31.1	32.9	30.1
Selectivity to $CO+S_x$/%	25.7	33.4	33.7	36.0

Catalyst: 1.0 g. COS+He:200(NTP) cm^3 min^{-1} (COS 5.0 vol%).
Data for the physicochemical properties of Al_2O_3 catalysts: Ref. 8.

strongly basic metal oxides by thermal decomposition of alkaline earth metal carbonates has been reported.[10] We have prepared CaO catalysts by thermal decomposition of $CaCO_3$ and then compared their catalytic activity and selectivity with their amount of electron-donating sites. Here, the amount of electron-donating sites was determined by the amount of SO_2^- radicals formed upon adsorption of SO_2 on CaO. Figure 2 shows the ESR spectrum of SO_2^- radicals formed on CaO. Figure 3 shows the variation of the amount of SO_2^- radicals formed on CaO prepared at different decomposition temperatures. $CaCO_3$ (0.178 g=CaO 0.10 g) was decomposed at various elevated temperatures for 5 h under 10^{-5} Torr. The obtained CaO was exposed to SO_2 at the pressure of 10 Torr at room temperature and was then heated at 473 K for 30 min in the presence of SO_2. The g values of SO_2^- radicals formed, g_1=2.008 and 2.009, g_2=2.004, and g_3=2.002 (Fig. 2), agree well with those reported.[10] The amount of SO_2^- radicals was negligibly small over CaO prepared at 873 K, but it increased with rising decomposition temperature to reach the maximum value (ca. 2×10^{17} spins g CaO^{-1}) at 1073—1123 K and then decreased with further rise (Fig. 3).

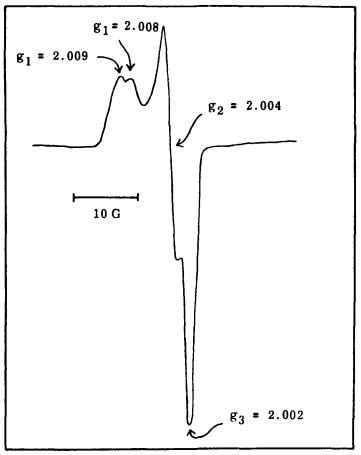

Fig. 2. ESR spectrum of SO_2^- radicals formed on CaO.
$CaCO_3$: 0.178 g (=CaO 0.10 g), decomposed at 1053 K for 5 h under 10^{-5} Torr. SO_2: 10 Torr, adsorbed at room temperature and then heated at 473 K for 30 min.

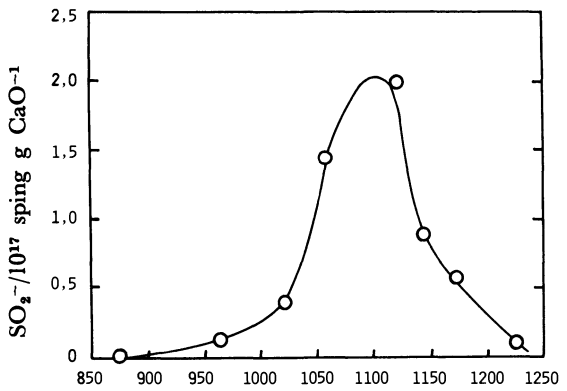

Fig. 3. Variation of the amount of SO_2^- radicals formed on CaO with rising decomposition temperature for thermal decomposition of $CaCO_3$.
$CaCO_3$: 0.178 g (=CaO 0.10 g), decomposed for 5 h under 10^{-5} Torr. The obtained CaO was exposed to SO_2 at the pressure of 10 Torr at room temperature and was then heated at 473 K for 30 min.

The rapid decrease in the amount of SO_2^- radicals above 1123 K is caused by the crystallization of CaO formed.[10] CaO catalyst prepared at a decomposition temperature of 1123 K had the greatest amount of electron-donating sites (Fig. 3).

Catalytic Decomposition of COS over CaO. Figure 4 shows the variation of the catalytic activity of CaO with rising decomposition temperature for $CaCO_3$. Here, $CaCO_3$ (0.89 g=CaO 0.50 g) was weighed into the catalytic reactor and was then decomposed for 5 h at various temperatures in flowing He(100(NTP) cm^3 min^{-1}). The obtained CaO was employed for catalytic studies without any exposure to air. These CaO catalysts also showed no significant change in the catalytic activity and selectivity with time during the decomposition of COS. The yield of $CO+S_x$ over CaO prepared at 923 K was 19.7% at 873 K, but it increased gradually with rising decomposition temperature to reach the

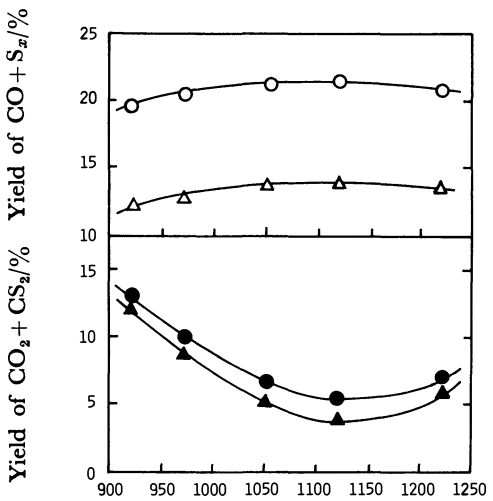

Fig. 4. Variation of the catalytic activity of CaO with rising decomposition temperature for $CaCO_3$.
$CaCO_3$: 0.89 g (=CaO 0.50 g), decomposed for 5 h in flowing helium (100(NTP)cm^3 min^{-1}) in the catalytic reactor. COS+He: 200 (NTP)cm^3 min^{-1} (COS 5.0 vol%). Reaction temperature: △,▲ —823 K, ○,● —873 K.

maximum value (21.4%) at a decomposition temperature of 1123 K and then decreased with further rise in decomposition temperature (Fig. 4). On the other hand, the yield of CO_2+CS_2 over CaO prepared at 923 K was 12.9% at 873 K, but it decreased with rising decomposition temperature to reach the minimum value (5.3%) at 1123 K and then increased with further rise. The selectivity to $CO+S_x$ at 873 K thus increased from 60.4% to 80.2% with rising decomposition temperature from 923 K to 1123 K and then decreased to 76.4% at 1223 K. A similar behavior of the catalytic activity and selectivity is seen at a reaction temperature of 823 K (Fig. 4). X-Ray diffraction analysis revealed no formation of calcium sulfide and calcium carbonate in these CaO catalysts during the catalytic decomposition of COS at 823 and 873 K. Thus, CaO catalyst prepared by thermal decomposition of $CaCO_3$ at 1123 K was the most active and selective one in the CaO prepared in the present work.

Effect of the Volume of Reactor. The observed relation of the yield of $CO+S_x$ with the temperature for thermal decomposition of $CaCO_3$ is fairly flat and the catalytic activity of CaO for the second reaction does not change so sharply as the amount of SO_2^- radicals formed (Figs. 3 and 4). A similar behavior can be seen between the yield of $CO+S_x$ over the referenced Al_2O_3 catalysts and their amount of basic sites (Table 1). These results suggest one possibility that a heterogeneously initiated homogeneous decomposition of COS to $CO+S_x$ also took place in the catalytic decomposition of COS at 823—873 K. This additional decomposition reaction must be of chain-reaction type. We have also studied the effect of volume of the reactor below catalyst bed on the catalytic activity and selectivity of JRC-ALO-4 Al_2O_3 at 873 K. As summarized in Table 2, the yields of $CO+S_x$ and CO_2+CS_2 and the selectivity to $CO+S_x$ were 16.9, 32.4, and 34.2%, respectively, when the volume of reactor below catalyst bed was 10 cm^3. Nearly the same values were obtained for the volume of 35 cm^3 (Table 2). Thus, no effect of the volume on the catalytic activity and selectivity was found.

Table 2. Effect of the Volume of Reactor below Catalyst Bed on the Catalytic Decomposition of COS at 873 K

Volume/cm^3	10	35
Conversion of COS/%	49.3	49.5
Yield of $CO+S_x$/%	16.9	16.5
Yield of CO_2+CS_2/%	32.4	33.0
Selectivity to $CO+S_x$/%	34.2	33.3

Catalyst: JRC-ALO-4 Al_2O_3 1.0 g. COS+He:200 (NTP) $cm^3\,min^{-1}$ (COS 5.0 vol%).

Discussion

The mechanism of the vapor-phase catalytic decomposition of COS was first investigated by Haas and Khalafala.[7] Since the degree of decomposition at a given temperature was approximately the same for such diverse catalysts as α-Al_2O_3, χ-Al_2O_3, Ti/χ-Al_2O_3, and silica gel regardless of their BET surface area and chemical composition, the catalytic decomposition of COS was believed to take place thermocatalytically.[7] In our previous studies on the catalytic oxidative dehydrogenation of hydrocarbons with COS over SiO_2, Al_2O_3, MgO, and TiO_2, however, it was demonstrated that the catalytic activity of these metal oxides for the decomposition of COS to $CO+S_x$ was great when the amount of electron-donating sites at the surface of these metal oxides was great.[6]

In the present work, the observed increase in the yield and selectivity to $CO+S_x$ with increasing the basicity of Al_2O_3 catalysts (Table 1) suggests that the participation of electron-donating sites in the catalytic decomposition of COS to $CO+S_x$ took place, as suggested previously.[6] On the other hand, the observation of the greatest yield of CO_2+CS_2 over the most acidic Al_2O_3 catalyst (JRC-ALO-2, Table 1) suggests the role of acidic sites (maybe Lewis acidic sites) in the catalytic decomposition of COS to CO_2+CS_2. These views are further supported by the results of poisoning of JRC-ALO-4 Al_2O_3 catalyst with SO_2 during the decomposition of COS, which resulted in the remarkable decrease in the yield of $CO+S_x$ (Fig. 1). Since COS^- radicals formed on the surface of MgO were readily decomposed to $CO+S_x$ even at low temperatures,[11] we believe that the catalytic decomposition of COS to $CO+S_x$ took place through the donation of electrons from the catalyst surface to adsorbed COS molecules.

$$\mathrm{COS} + * \rightarrow \overset{\mathrm{COS}^{\delta-}}{\underset{*}{\uparrow}}\mathrm{e} \rightarrow \mathrm{CO} + \mathrm{S} \rightarrow \mathrm{CO} + 1/x\mathrm{S}_x, \qquad (5)$$

where * is an electron-donating site at the surface of catalyst.

In contrast to the yield of $CO+S_x$, the yield of CO_2+CS_2 rather increased upon introduction of SO_2 (Fig. 1). It was reported that the catalytic activity of CaO–SiO_2 for the dehydrogenation of 1-butanol increased upon introduction of pyridine into the reactant mixture.[12] This promotional effect of pyridine was explained in terms of the high electron-donating ability of pyridine: The surface sites adjacent to adsorbed pyridines become rich in electron density and these sites act as basic sites.[12] In the present work, an acidic gas SO_2 was fed into the catalytic reactor and was adsorbed as SO_2^- at the

surface of Al_2O_3 catalyst. Hence it is probable that upon introduction of SO_2 the strength of Lewis acidic sites adjacent to adsorbed SO_2^- was greatly enhanced or that the surface sites adjacent to adsorbed SO_2^- became acidic sites. We believe that this inductive effect of SO_2 gave rise to increase in the catalytic activity of Al_2O_3 for the decomposition of COS to CO_2+CS_2. A concerted mechanism involving the participation of Lewis acidic sites and electron-donating sites is rejected for the reaction of COS to CO_2+CS_2 since the latter sites were poisoned by SO_2 (Fig. 1). We now believe that a COS molecule adsorbed on a Lewis acidic site reacts with a gaseous COS molecule to form a surface intermediate which then decomposes into CO_2+CS_2.

$$\begin{array}{l} \mathrm{COS} + * \rightarrow \underset{*}{\overset{\mathrm{COS}^{\delta+}}{\downarrow \mathrm{e}}} \quad + \mathrm{COS(g)} \\ \qquad\qquad\qquad\qquad \rightarrow \quad (\mathrm{intermediate})_{\mathrm{ads}} \\ \qquad\qquad\qquad\qquad\qquad \rightarrow \mathrm{CO_2} + \mathrm{CS_2} \end{array} \qquad (6)$$

where * is a Lewis acidic site.

Haag and Miale[5] proposed that the catalytic decomposition of COS to CO_2+CS_2 takes place through participation of surface sulfur atoms evolved by the decomposition of COS to CO+S. In the present work, however, the catalytic decomposition of COS to CO_2+CS_2 took place even at such low reaction temperatures as 473—573 K at which the catalytic decomposition of COS to CO+S_x did not take place (e.g., JRC-ALO-2 Al_2O_3, yield of CO_2+CS_2= 17.8% at 473 K and 23.4% at 573 K). This finding does not support the mechanism of CO_2+CS_2 formation proposed by Haag and Miale. Thus, in addition to the thermocatalytic mechanism proposed by Haas and Khalafala,[7] we propose the mechanism for the decomposition of COS involving the participation of surface electron-donating sites and Lewis acidic sites.

The above mechanistic finding made in the present work indicates that strongly basic catalysts are superior for the selective decomposition of COS to CO+S_x. CaO catalysts prepared by thermal decomposition of $CaCO_3$ have been well known as strongly basic catalysts. In the present work, CaO catalysts thus prepared showed very low catalytic activities for the decomposition of COS to CO_2+CS_2 compared with Al_2O_3 catalysts and the selectivity to CO+S_x was as high as 60—80% at 873 K (Table 1, Fig. 4). Particularly CaO catalyst prepared at 1123 K, which had the greatest electron-donating ability, showed the greatest values of the yield and selectivity to CO+S_x (21.4 and 80.2%) and at the same time the lowest yield of CO_2+CS_2 (5.3%) at 873 K (Figs. 3 and 4). This superiority of CaO catalyst prepared at 1123 K can be understood by comparing with the equilibrium conversion of COS at 873 K. That is, in the reaction conditions empolyed in Table 1 and Fig. 4 elemental sulfurs at equilibrium are of S_2 type[13] and the equilibrium conversions of COS to CO+S_2 and CO_2+CS_2 are 27.3 and 35.3%, respectively, the selectivity to CO+S_2 being 43.6%.[14] Although the surface acidity was not determined for these CaO catalysts, the observation of the greatest values of the yield and selectivity to CO+S_x and the lowest value of the yield of CO_2+CS_2 over CaO catalyst prepared at 1123 K (Fig. 4) is as expected.

On the other hand, the absenece of the effect of volume of the reactor below catalyst bed on the catalytic activity and selectivity of JRC-ALO-4 Al_2O_3 (Table 2) does not indicate the presence of a heterogeneously initiated chain reaction-type homogeneous decomposition of COS to CO+S_x in the catalytic decomposition of COS. At present, the reason for the lack of a close relation between the yield of CO+S_x and the amount of SO_2^- radicals (Figs. 3 and 4) is not known. At any rate, the above findings made in the present work suggest the possibility that we can further enhance the catalytic activity and selectivity for the decomposition of COS to CO+S_x by preparing much more strongly basic catalysts.

References

1) K. Fukuda, M. Dokiya, T. Kameyama, and Y. Kotera, *J. Catal.*, **49**, 379 (1977).

2) M. Dokiya, K. Fukuda, H. Yokokawa, and T. Kameyama, *Bull, Chem. Soc. Jpn*, **51**, 150 (1978).

3) D. E. Boswell, U. S. Patent 3399243 (1968), Mobil Oil Corporation.

4) W. O. Haag and J. N. Miale, U. S. Patent 3787517 (1974), 3821278 (1974), and 3875252 (1975), Mobil Oil Corporation.

5) W. O. Haag and J. N. Miale, "Proc. 6th Intern. Congr. Catal.," London (1976), Vol. 1, p. 397.

6) M. Akimoto, K. Yamagami, and E. Echigoya, *J. Catal.*, **86**, 205 (1984).

7) L. A. Haas and S. E. Khalafala, *J. Catal.*, **30**, 451 (1973).

8) *Shokubai (Catalyst)*, **22**, 115 (1980); Data for 5th Conference on Referenced Catalysts of the Catalysis Society of Japan, 1983, p. 56.

9) Y. Ono, H. Takagiwa, and S. Fukuzumi, *J. Catal.*, **50**, 181 (1977).

10) Y. Ono, H. Takagiwa, and S. Fukuzumi, *J. Chem. Soc., Faraday Trans. 1*, **75**, 1613 (1979).

11) M. J. Lin, D. P. Johnson, and J. H. Lunsford, *Chem. Phys. Lett.*, **15**, 412 (1972).

12) H. Niiyama and E. Echigoya, *Bull. Chem. Soc. Jpn*, **44**, 1739 (1971).

13) M. Wakihara, J. Nii, T. Uchida, and M. Taniguchi, *Chem. Lett.*, **1977** 621.

14) D. R. Stull, E. F. Westrum, Jr., G. C. Sinke, "The Chemical Thermodynamics of Organic Compounds," John Wiley & Sons Inc. (1969).

Catalysis by Transition-Metal Carbides. VII. Kinetic and XPS Studies of the Decomposition of Methanol on TiC, TaC, Mo_2C, WC, and W_2C

Masahiro ORITA, Isao KOJIMA, and Eizo MIYAZAKI*
Department of Chemistry, Tokyo Institute of Technology, Ookayama, Meguro-ku, Tokyo 152
(Received July 5, 1985)

The catalytic decomposition of methanol was investigated on a series of powdered transition-metal carbides, such as TiC, TaC, Mo_2C, WC, and W_2C, which had been catalytically activated by evacuation at high temperatures. WC was found to produce methyl formate ($HCOOCH_3$) with a high selectivity (above 80%), whereas CO and H_2 were mainly produced on clean TaC, Mo_2C, and W_2C surfaces. XPS measurements combined with an analysis of the peak intensities revealed that the catalytic activation of WC and TaC was attributable to the removal of surface oxygen and the subsequent formation of monocarbide surfaces. On the other hand, the minor activities leading to the formation of methyl formate on W_2C and Mo_2C were concluded to be due to the formation of oxycarbide surfaces. The deuterium distributions in the products during the reaction of CH_3OD suggest that the methyl formate is produced via the dimerization of the intermediate adspecies, CH_2O.

The transition metal carbides have been well investigated because of their unique physical properties, such as extremely high melting points, metal-like thermal and electronic conductivities, paramagnetism, and superconductivity.[1] In addition, they have recently been shown to form an interesting new group of catalysts;[2-7] the ordered incorporation of carbon atoms into a metal lattice makes chemisorptive and catalytic properties different from those of the parent metals. In order to characterize carbide catalysts, we have investigated the catalytic activities of the carbides of TaC, TiC, WC, and Mo_2C and have found that they exhibit high activities for the hydrogenation of benzene,[8] ethylene,[9,10] and carbon monoxide.[11] Further, detailed kinetic studies of the hydrogenation of carbon monoxide on powdered WC, W_2C, and W showed that the catalytic behavior of WC was in contrast with that of W_2C and W, that is, the activity depended on the carbon/metal ratio and on the lattice structure.[12]

On the other hand, the dehydrogenation of methanol to produce methyl formate with a high selectivity is currently an important problem in heterogeneous catalysis in relation to C_1 chemistry, and a great deal of research has been conducted into the catalysis of this reaction by metal and metal-oxide surfaces. In a previous paper,[13] it was found that WC was an excellent catalyst for producing methyl formate from the decomposition of methanol. In the present paper, we wish to report the detailed kinetic and XPS results for TiC, TaC, WC, W_2C, and Mo_2C.

Experimental

Two reaction systems were employed. One was a recirculation reactor, 520 ml in volume, which was directly connected with a gas chromatograph system equipped with two separation columns containing Porapak Q and Molecular sieve 5X. This system also had a U-tube connected to the gas circulation system to remove the condensable products from the reaction system during the course of the reaction by cooling them to a lower temperature. The other was a UHV batch reactor made of metal and glass. The analysis of the gas-phase composition was done by means of a quadrupole mass analyzer (ANELVA AGA 100). Most of the kinetic measurements were carried out using the former reactor. The distribution of D atoms contained in the products was, however, analyzed by the use of the latter batch reactor.

The reactants, CH_3OH(obtained from the Nakarai Kagaku Co., 99.6% pure) and CH_3OD(Merck, 98%), were subjected to vacuum distillation to remove any dissolved air prior to use for the reaction measurements. The powdered catalysts, TiC(99% purity), TaC(99%), WC(99%), W_2C(99%), and Mo_2C(99%), were obtained from Furu-uchi Kagaku or M. R. C., and they were catalytically activated as has been described previously[9,10] by heating in a vacuum at various high temperatures.

The surface analysis of the catalysts was performed on a Hewlett-Packard 5950A ESCA spectrometer, using monochromatic Al $K\alpha$ excited radiation. The samples, pressed into disks, were transferred into the preparation chamber of the spectrometer and subjected to in situ heat-treatment in a vacuum.

Results

Product Distributions. Table 1 shows the kinetic results and the product distributions at a 20% conversion of methanol on various carbide catalysts which had been pretreated at high temperatures in a vacuum. As has been reported previously on the hydrogenation of benzene[8] and ethylene,[9,10] the catalytic activities for methanol decomposition on TaC and WC were generated by evacuation at 1000 °C for TaC and 700 °C for WC and were almost unchanged up to 1200 °C. TaC produced mainly CO and H_2, plus a small amount of CO_2, and the product distribution did not depend on the temperature for the activation of the catalyst, whereas the activity gradually decreased with repeated use. WC produced methyl formate with a high selectivity (above 80%). On the other hand, the catalytic activities of Mo_2C were found to increase gradually

Table 1. The Kinetic Results and the Product Distributions on Various Carbides

Catalysts	Evacuation temperature / °C	Reaction temperature / °C	Initial rate[a] of CH_3OH consumption/(molecule s^{-1} g^{-1})	Distribution of carbon-containing products / %
TiC	1000	300	0	—
Tac	1100	190	3.1×10^{17}	CO(91), CO_2(9)
WC	900	200	1.5×10^{17}	HCO_2CH_3(81), CO(19)
W_2C	1200	220	3.5×10^{17}	CO(83), HCO_2CH_3(17)
Mo_2C	500	300	2.2×10^{17}	CH_4(84), CO(16)
	800	200	2.5×10^{17}	CO(59), HCO_2CH_3(41)
	1000	200	5.0×10^{17}	CO(100)

a) The initial pressure of methanol is 23 Torr (1 Torr=133.322 Pa).

with an increase in the evacuation temperature, and the distribution of products also varied with it; following the evacuation at 500 °C, the main products were CH_4, H_2O, H_2, CO_2, and CO, but at 800 °C they were CO, H_2, and methyl formate, and at 1000 °C they were only CO, and H_2. The activities of W_2C also increased with the increase in the evacuation temperatures, while the product distribution was unchanged. In the table, results at the highest activity are given for W_2C; the main products were CO, H_2, and methyl formate, while the selectivity for methyl formate was much lower than that of WC. The activity of TiC was negligible below 300 °C, whereas above 400 °C small amounts of CH_4 and H_2O were formed.

Kinetic Measurements. It is to be noted that, among the metal-carbide catalysts, only WC produced methyl formate with a high selectivity. The detailed kinetic measurements of WC were performed in order to compare the reaction mechanism with the previous results on the transition-metal and oxide catalysts on which the kinetics had already been established. Figure 1 shows the changes in the gas-phase components with the reaction time for the methanol decomposition at 200 °C. It may be seen that in the initial stage of the reaction, methyl formate appeared more rapidly than CO and reached almost a constant concentration after 30 min, while the CO concentration monotonously increased with the time. After 45 min, the U-tube connected to the reactor was cooled to −42 °C to reduce the methanol concentration and to allow the methyl formate to remain in the gas phase. However, the concentration of methyl formate gradually decreased, accompanied by almost twice as large an increase in CO, indicating that the methyl formate decomposed into CO. The selectivity for methyl formate on WC is plotted against the conversion at diferent reaction temperatures in Fig. 2. With the increase in the reaction temperature the selectivity apparently decreased, however it reaches nearly 100% when the line is extrapolated to zero conversion in each case.

The pressure and temperature dependences were

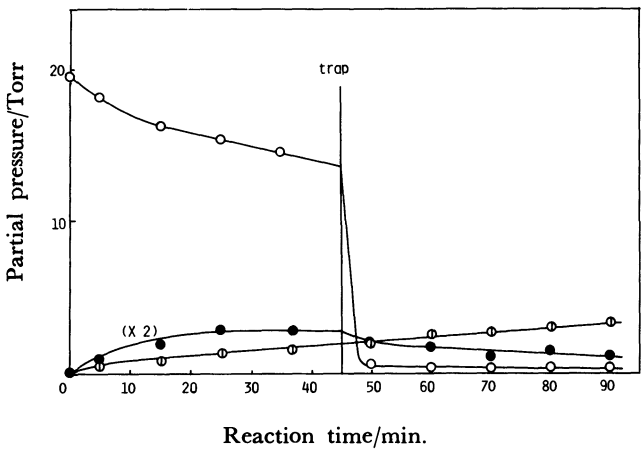

Fig. 1. The change in the gas phase components with the reaction time. After 45 min reaction, the U-tube was cooled down to −42°C. ○: Methanol, ⓘ: carbon monoxide, ●: methyl formate.

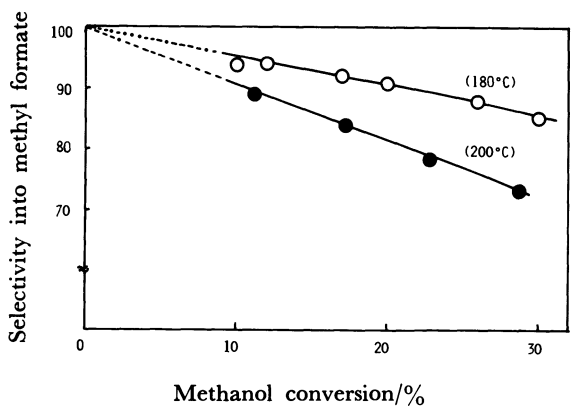

Fig. 2. The selectivity into methyl formate on WC as a function of the methanol conversion. The initial methanol pressure is 21.4 Torr. Reaction temperatures are 180 and 200 °C.

measured by changing the initial pressure of methanol and the reaction temperature respectively. It was found that the plots of the reciprocal of the reaction rate($1/r_0$) against the reciprocal of the initial pressure($1/p_0$) gave straight lines for a constant reaction temperatures, as is shown in Fig. 3. The

apparent activation energy was then estimated to be 6.2 kcal† mol^{-1}. The reaction of CH_3OD was also investigated using the batch-type reactor. Figure 4 shows the changes in the concentrations of deuterated methyl formate in the gas phase. The line was drawn using the mass peaks of m/z=59—64 and fragment patterns with a least-square approximation; d_0-methyl formate was predominantly formed in the initial stage of the reaction. The amount of d_1-species became appreciable with the passage of the time, but the d_2- to d_5-species produced by successive exchange reactions were negligible. Furthermore, among the molecules of H_2, HD, and D_2 produced during the decomposition, HD was predominant at the initial stage of the reaction.

The kinetic measurements were also carried out on Mo_2C, where the main products were CO and H_2. A linear relationship similar to that of WC was also obtained between $1/r_0$ and $1/p_0$. The reaction order and the apparent activation energy were found to be about 1.0 at 160 °C and 5.4 kcal mol^{-1} respectively.

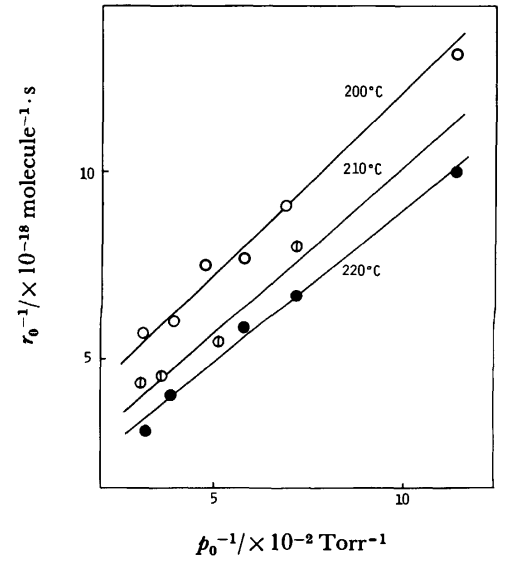

Fig. 3. Plots of the reciprocal of r_0 against the reciprocal of p_0. Reaction temperatures are 200°C, 210 °C, and 220°C.

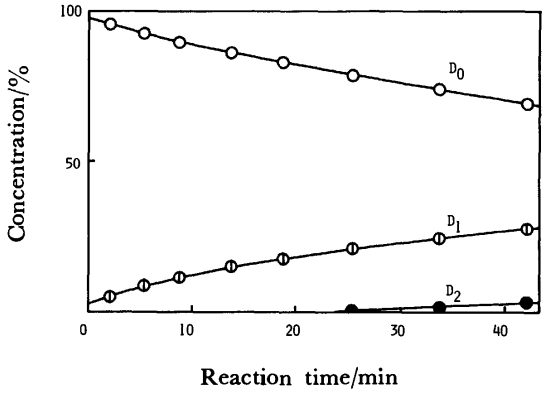

Fig. 4. Changes of concentration of deutrated-methyl formate during the decomposition of CH_3OD.

† 1 cal=4.184 J.

XPS Measurements. The XPS spectra were measured for all the catalysts employed. A part of the results have been published previously.[9,10] In Table 2 are summarized the atomic ratios of the surface concentration of the C or O atom to that of metal atoms of the catalysts which had been evacuated under conditions similar to those employed in the kinetic measurements. The ratios of the concentrations of the constituent atoms were estimated from the integrated peak area, upon taking into consideration the photoelectron cross section, the mean free path of electrons, and the apparatus function which is dependent on the kinetic energy of photoelectrons.[14] For the activated WC and TaC surfaces the ratio of C atoms to metals came out to be nearly unity. WC showed no traces of any contaminant oxygen, but TaC was slightly covered with oxygen. The values of the carbon/metal ratio for TiC and W_2C were lower than in the bulk composition, and their surfaces was found to be covered with oxygen. XPS measurements of Mo_2C were done for samples evacuated at room temperature, 550, 800, and 1050 °C since the catalytic behavior of Mo_2C changed with the evacuation temperature. Figure 5 shows the spectra of the Mo 3d, and the O ls regions for Mo_2C. Without any heat-treatment, the catalyst surface was mostly covered with oxygen and the Mo 3d states mainly consisted with highly oxidized states, as may be seen in Fig. 5(a) and (e). Following the evacuation at 550 °C, the peaks corresponding to Mo 3d shifted to the lower-binding-energy side, with a mixing of several states. Following the evacuation at 800 °C, two peaks due to the spin-orbit coupling of Mo 3d appeared, along with small shoulders on the higher-binding-energy side. At 1000 °C, they turned into two sharper peaks, and the peak due to O ls

Table 2. The Atomic Ratio of the Surface Concentration of C or O Atom to that of Total Metallic Species in the Catalysis

	Treatment temperature	Atomic ratio C/M	O/M
TiC	1100 °C	0.8	0.3
TaC	1130	1.1	0.1
WC	1080	0.94	0.0
W_2C	700[a]	0.33	0.3
Mo_2C	20	0.12	2.9[b]
	550	0.15	1.3
	800	0.13	0.8
	1050	0.18	0.1

a) The sample was reduced in the H_2 atmosphere at the temperature. b) Ratio of O to Mo(1) species.

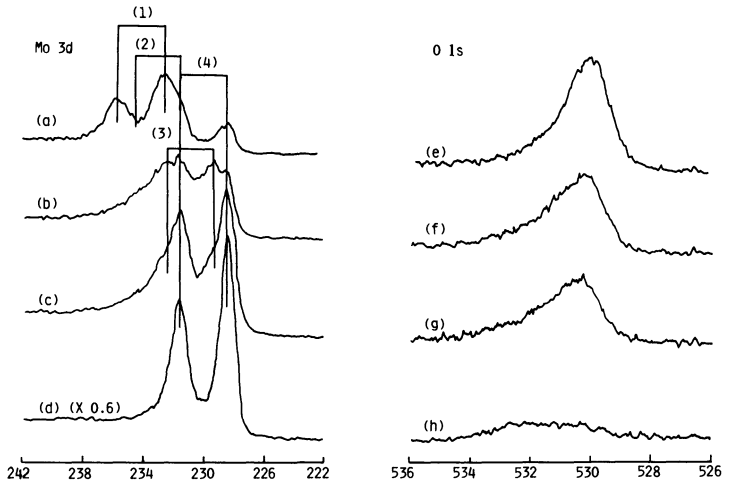

Fig. 5. The change of XPS spectra of Mo 3d and O 1 s regions for Mo_2C with pretreated temperatures. (a), (e); 20°C, (b), (f); 550°C, (c), (g); 800°C and (d), (h); 1050 °C.

almost disappeared. The various peaks in the Mo 3d regions described above can be classified into 4 different states, labeled from (1) to (4) in Fig. 5 (a—d). State 1, with the highest binding energy (232.6, 235.6 eV) observed mainly for the untreated surface, can be attributed to the Mo^{6+}-oxidized state, since the binding energies are almost identical to the values[15] reported for MoO_3 and the observed O/Mo ratio is also close to the ratio of the composition. State 2 (231.5, 234.6 eV) may be assigned to Mo^{5+} from the XPS results on the Mo/Al_2O_3 catalyst reported by Patterson et al.[15] Above the evacuation temperature of 800 °C, State 4 (228.3, 231.5 eV) becomes predominant, and the binding energies are larger than those of Mo metal, suggesting the formation of the carbide.[16] However, it is noteworthy that the C/Mo ratio is much smaller than that expected from the initial bulk composition. The sample evacuated at 800 °C is also interesting in the sense that it contains a slightly oxidized State 3 (229.4, 232.6 eV); this sample exhibited a special catalytic activity of producing methyl formate.

The XPS spectra of the valence regions are given in Fig. 6. The densities of states below E_f, which arise mainly from C 2p and metal d-electrons, are distinctive for the carbide catalysts: TiC and TaC have rock salt structure in which the electronic structures can be explained essentially in terms of a simple rigid-band model. The minimum of the density of states occurs at E_f for TiC; and thus, the extra electrons in Ta are induced to fill the higher-energy antibonding bands to increase the destabilization of TaC. This destabilization effect is compensated for by the lowering of the d-bands relative to the C 2p state for TaC. However, the additional filling of electrons which might occur for VIa-metal

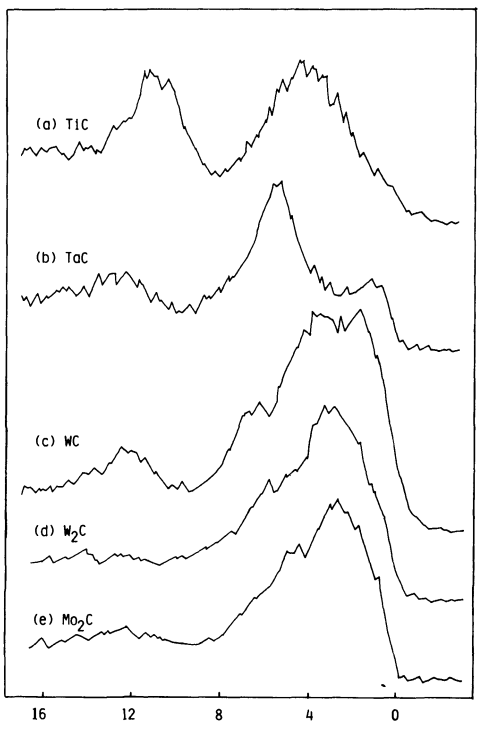

Fig. 6. The XPS valence band spectra of TiC, TaC, WC, W_2C, and Mo_2C.

elements, like W and Mo, change the crystal structure of their carbides into hcp; this results in a more extensive mixing of C 2p with metal d-electrons than in the rock salt structure. The peaks around 12 eV below the E_f correspond to C 2s bands. The difference in the intensities of the C 2s peaks relative to the density of the states near E_f is due to the difference in the photoelectron cross-section of d-

electrons in metal, which increase with an increase in the atomic number.[17] The present XPS spectra of WC and W_2C are generally consistent with those reported previously;[18] it is worth mentioning that the densities of the states of WC near E_f are higher than those of W_2C and Mo_2C. The lower intensities of the C 2s peaks of W_2C and Mo_2C, which are about one-half that of WC, suggest the accumulation of metallic species near the surface.

Discussion

Reaction Mechanism. So far, kinetic studies of the decomposition of methanol have been extensively carried out on various transition metals and their oxides.[19–22] Miyazaki et al. made detailed investigations of Cu[23] and Ni[24] catalysts and proposed two different reaction pathways for the decomposition of methanol. A recent review by Joyner also proposed two kinds of reaction mechanisms on the metallic catalysts;[25] one was a process to form methyl formate as given by Scheme 1, while the other was a process to decompose into CO and H_2 as is given by Scheme 2. The reaction mechanism by Scheme 1 is well known to occur on Cu and Ag catalysts, whereas Scheme 2 is for Pd, Rh, and Ni.

$$CH_3OH(g) \rightleftarrows CH_3OH(a) \quad (1a)$$
$$CH_3OH(a) \rightleftarrows CH_2O(a) + H_2(g) \quad (2a)$$
$$2CH_2O(a) \rightleftarrows HCOOCH_3(g) \quad (3a)$$

Scheme 1.

$$CH_3OH(g) \rightleftarrows CH_3O(a) + H(a) \quad (1b)$$
$$CH_3O(a) \rightleftarrows CH_2O(a) + H(a) \quad (2b)$$
$$CH_2O(a) \rightleftarrows CHO(a) + H(a) \quad (3b)$$
$$CHO(a) \rightleftarrows CO(a) + H(a) \quad (4b)$$
$$2H(a) \rightleftarrows H_2(g) \quad (5b)$$
$$CO(a) \rightleftarrows CO(g) \quad (6b)$$

Scheme 2.

The present results of methanol decomposition on the transition metal carbide catalysts may be interpreted within a similar framework; WC was found to produce methyl formate with a high selectivity, whereas the other carbides produced mainly CO and H_2. The one slight exception is on TiC and Mo_2C, where CH_4 and H_2O were produced. Since these products were generally formed on metal oxide catalysts[26] and since the XPS spectra showed presence of considerable oxygen on the catalysts, this distribution may safely be attributed to the oxide formation on the surfaces. The high selectivity for methyl formate on WC makes it easy to investigate the reaction mechanism. The linear relationship in Fig. 3 leads to the following rate equation in the initial stage of the reaction on WC

$$r_0 = a\,p_0/(1 + b\,p_0), \quad (1)$$

where a and b are constants. This rate Eq. 1 suggests that the decomposition of the adsorbed methanol into an intermediate adsorbate is the rate-determining step. As is shown in Fig. 4, the selective formation of d_0-methyl formate and HD from CH_3OD in the initial stage of the reaction strongly suggests that the reaction given by Step (2a) proceeds on the surface. These findings are quite similar to those observed on the Cu surface.[23]

Scheme 2 shows, on the other hand, that the decomposition into CO and H_2 is initiated by the dissociative adsorption of methanol into methoxide and H species. As no methyl formate was detected, the intermediate methoxide is considered to decompose directly via Steps (2b)—(4b) into CO. Further, the UPS results of NbC(111)[27] revealed the formation of methoxide after the admission of methanol, suggesting the involvement of a surface reaction like Step (2b) on W_2C, TaC, and clean Mo_2C, where the main products are carbon monoxide and hydrogen. The similar pressure dependence of the rate on Mo_2C to the rate equation (I) suggests that Step (2b) in Scheme 2 is the rate-determining step. Thus, the reaction Schemes (1 and 2) given above are also effective for the metal-carbide catalysts; the different product distributions among the carbide catalysts seem to result from the different stabilizations of intermediate species, $CH_3O(a)$ and $CH_2O(a)$.

Characteristics of Transition-Metal Carbides. (i) In the previous studies, the surface oxygen was found to play a dominant role in the catalytic activation of transition-metal carbides; the presence of oxygen strongly reduced the activity of the hydrogenation of benzene[8] and ethylene[9,10] on TaC. The present kinetic and XPS measurements also indicate that the removal of surface oxygen is necessary for the generation of the activity of methanol decomposition on TaC and WC. On the other hand, Mo_2C pretreated in vacuo at 800 °C yielded activities comparable to those of TaC and WC, even though its XPS spectra revealed the presence of a large amount of oxygen on the surface. Interestingly, on such a surface with oxygen, an appreciable amount of methyl formate is formed, whereas clean Mo_2C evacuated at 1100 °C, produced merely CO and H_2. This shows that the surface oxygen on Mo_2C forms an oxycarbide[3] like MoO_xC_y and that its electronic states are varied to be suitable for stabilizing the $CH_2O(a)$ adsorbate. The minor selectivity into methyl formate observed on W_2C may also be ascribed to the partial formation of oxycarbide. Thus, such oxycarbide-oxygen in dimetallic carbides of Mo_2C, and W_2C apperantly

behaves as "carbon" in the corresponding monocarbides, though MoC has not been obtained as a stable substance.

(ii) It is generally accepted that the electronic states near E_f have great importance for the chemical activity of a surface. Information about these states is available from the measurements using photoelectron spectroscopy. The few studies[18,28,29] which have been done following the first suggestion by Levy and Boudart[30] that the catalytic activity of WC is to be attributed to the density of states similar to Pt conflict as to the point whether or not the chemical activity can be directly related to the state densities of the valence regions. As is shown in Fig. 6, it seems to be sure that the onset of sharp peaks at E_f of TaC is responsible for the appearance of larger catalytic activity as compared with TiC and that the catalytic properties of WC can be related to the higher state density at E_f than at W_2C, although it is not clear in all cases that the higher density at E_f is related to the higher catalytic activity.

(iii) In the present work, the distinctive selectivity between WC and W_2C for methyl formate was shown. The improvement of selectivity for methyl formate by alloying into carbides was also reported by Ko et al.,[4,5] TPRS studies on Mo and W single crystals have shown that methyl formate is not formed from formaldehyde on the pure metal surfaces, but is apparently formed after the carburization of these crystals. Similar results were also obtained on powdered Ni catalysts at the reaction temperature of 30—80 °C.[31] The formation of carbide may result in the reduction of the chemical activity of the adsorbing gases and in suppression of the complete decomposition into C, O, and H atoms which occurs on the original pure metals.

(iv) It is likely that, for alloy systems with rigid crystal structures, like metal carbides, the surface arrangement of the constituent atoms plays a dominant role in the catalytic activity. According to recent calculations of the band structures of the bulk and surface of WC[32] by Mattheiss and Hamann, the metal-terminated W(1×1) surface of WC(0001) exhibits a distinctive surface-state density due to d-electrons at E_f. The work function of the metal-terminated surface is also much smaller than that of the carbon-terminated surface. Recently, surface spectroscopic studies of transition-metal carbides have been performed under uhv conditions using such single-crystal surfaces as TiC(100), TiC(111),[33,34] NbC(100), and NbC(111).[27] An important finding of these studies is that their cleaned (111) surfaces consist of metals on the topmost layer; thus they are chemically more active than the (100) surfaces which consist of a regular array of coexisting metal and carbon atoms. The previous comparative investigation of WC, W_2C, and W powdered catalysts for the hydrogenation of CO also showed that the catalytic behavior of WC is quite in contrast with those of W_2C and W; the metal-terminated surfaces are responsible for the catalysis, since the electronic states of the topmost metal layer of WC(0001) would preferably be modified by the second carbon underlayer to produce an active site for the hydrogenation of carbon monoxide, while, on the other hand, the influence of the third carbon layer on the topmost tungsten layer of W_2C would be small. These effects may contribute to the distinctive selectivity between WC and W_2C presently observed for the formation of methyl formate. Therefore, the complete carburization of W to form WC seems necessary for the appearance of a new catalytic feature to produce methyl formate on WC.

References

1) L. E. Toth, "Transition Metal Carbides and Nitrides," Academic Press, New York/London (1971).
2) S. T. Oyama and G. L. Haller, *Catalysis*, **3**, 333 (1982).
3) M. Boudart, S. T. Oyama, and L. Leclercq, "Proceeding of 7th Intern. Congr. Catalysis, Tokyo, 1980," Kodansha, Tokyo (1981), p. 578.
4) E. I. Ko and R. J. Madix, *Surf. Sci.*, **112**, 373 (1981).
5) E. I. Ko, J. B. Benziger, and R. J. Madix, *J. Catal.*, **64**, 132 (1980).
6) P. N. Ross, Jr., and P. Stonheart, *J. Catal.*, **39**, 298 (1975).
7) P. N. Ross, Jr., and P. Stonheart, *J. Catal.*, **48**, 42 (1977).
8) E. Miyazaki and K. Fuse, *Nippon Kagaku Kaishi*, **1972**, 815.
9) I. Kojima, E. Miyazaki, Y. Inoue, and I. Yasumori, *J. Catal.*, **59**, 472 (1979).
10) I. Kojima, E. Miyazaki, Y. Inoue, and I. Yasumori, *J. Catal.*, **73**, 128 (1982).
11) I. Kojima, E. Miyazaki, and I. Yasumori, *J. Chem. Soc., Chem. Commun.*, **1980**, 573.
12) I. Kojima, E. Miyazaki, Y. Inoue, and I. Yasumori, *Bull. Chem. Soc. Jpn.*, **58**, 611 (1985).
13) E. Miyazaki, I. Kojima, and M. Orita, *J. Chem. Soc. Chem., Commun.*, **1985**, 108.
14) M. Uda and K. Maeda, *Kinzoku Butsuri Seminar*, **3**, 11 (1975).
15) T. A. Patterson, J. C. Carver, P. E. Leyden, and D. M. Hercules, *J. Phys. Chem.*, **80**, 1700 (1976).
16) Yu. M. Shul'ga, A. P. Borisov, V. D. Makhaev, and A. P. Borisov, *J. Organomet. Chem.*, **164**, 47 (1979).
17) J. H. Scofield, *J. Electron Spectro. Relat. Phenom.*, **8**, 129 (1976).
18) R. J. Colton, J-T. J. Huang, and W. Rabalis, *Chem. Phys. Lett.*, **34**, 337 (1975).
19) B. A. Sexton, *Surf. Sci.*, **88**, 299 (1979).
20) S. R. Bare, J. A. Strocio, and W. Ho, *Surf. Sci.*, **140**, 415 (1984).
21) R. Ryberg, *J. Chem. Phys.*, **82**, 567 (1985).
22) W. Hirshwald and D. Hofmann, *Surf. Sci.*, **140**, 415 (1984).
23) E. Miyazaki and I. Yasumori, *Bull, Chem. Soc. Jpn.*, **40**, 2012 (1967).
24) I. Yasumori, T. Nakamura, and E. Miyazaki, *Bull.*

Chem. Soc. Jpn., **40**, 1372 (1967).
25) R. W. Joyner, *Catalysis*, **5**, 19 (1981).
26) F. Nozaki, *Hyomen(Surface)*, **21**, 194 (1983).
27) I. Kojima, M. Orita, and E. Miyazaki, *Surf. Sci.*, **160**, 153, (1985).
28) L. H. Bennett, J. R. Curthill, A. J. McAlister, N. E. Erickson, and R. E. Watson, *Science*, **184**, 563 (1973).
29) J. E. Houston, G. E. Laramore, and R. L. Park, *Science*, **185**, 258 (1974).
30) R. B. Levy and M. Boudart, *Science*, **181**, 547 (1973).
31) E. Miyazaki, *Proc. VIth Intern. Congr. on Catalysis*, **1**, 408 (1976).
32) L. F. Mattheiss and D. R. Hamann, *Phys. Rev. B* **30**, 1731 (1984).
33) C. Oshima, M. Aono, S. Zaiman, Y. Shibata, and S. Kawai, *J. Less- Common. Metals*, **82**, 69 (1981).
34) A. M. Bradshaw, J. F. van der Veen, F. J. Himpsel, and D. E. Eastman, *Solid State Commun.*, **37**, 37 (1980).

 © 1986 The Chemical Society of Japan Bull. Chem. Soc. Jpn., 59, 697—701 (1986)

Flocculation of Iron(III) Oxide Hydrate Sols Induced by α,ω-Type Surfactants

Kunio Esumi,* Kazuki Yamada, Toshie Sugawara, and Kenjiro Meguro
Department of Applied Chemistry, Institute of Colloid and Interface Science,
Science University of Tokyo, Kagurazaka, Shinjuku-ku, Tokyo 162
(Received July 23, 1985)

The interactions of disodium salt of bis(3-sulfopropyl) α,ω-alkanedicarboxylate(C10-α,ω and C12-α,ω) with monodispersed spherical particles of iron(III) oxide hydrate sols were studied by measuring the mean particle size, the zeta-potential and the amounts of adsorption. The sols were flocculated by the addition of small amounts of C10-α,ω and C12-α,ω. The flocks thus formed were redispersed by the further addition of these surfactants. The flocculation of sols upon the addition of α,ω-type surfactants occurred over a wider concentration range than upon the addition of an ordinary surfactant, such as sodium dodecyl sulfate(SDS). Furthermore, the mechanism of redispersion upon the addition of α,ω-type surfactants is different with the two-fold adsorption layer in SDS.

Studies of the interactions between surfactants and solid particles in an aqueous solution are very important from the point view of the dispersion stability of solids.[1-4] For this reason, the mechanism of the flocculation and redispersion of sol particles in the presence of surfactants[5,6] has been reported. However, the surfactants used in these works were ordinary ones which have a hydrophilic group at one end of the hydrophobic chain.

Recently, some reports on α,ω-type surfactants, which have a hydrophilic group at each end of a long hydrocarbon chain, have been published.[7-9] It seemed that it would be interesting to study the interactions of solid particles with α,ω-type surfactants, because α,ω-type surfactants could be expected to interact with solid particles differently from ordinary ones because of their structure.

In this work, the interactions between α,ω-type surfactants and monodispersed spherical particles of iron(III) oxide hydrate sols were investigated by measuring the mean particle size, the zeta-potential, and the amounts of adsorption. The results obtained were compared with those of an ordinary surfactant.

Experimental

Materials. (a) Surfactant: Disodium salt of bis(3-sulfopropyl)-α,ω-alkanedicarboxylate[7-9] was prepared from the corresponding dimethyl α,ω-alkanedicarboxylate, sodium hydroxide, and 1,3-propanesulfone, which had all been purified by vacuum distillation. The crude product was recrystallized three times from methanol and then further extracted for 100 h with acetone by means of a Soxhlets extractor.

The chemical formulae of the α,ω-type surfactants were as follows:

$$NaO_3S(CH_2)_3OOC(CH_2)_nCOO(CH_2)_3SO_3Na \quad (n=10,\ 12)$$

(b) Monodispersed Spherical Particles of Iron(III) Oxide Hydrate Sol: Hydro-sols consisting of spherical hematite particles with a narrow size distribution were prepared by essentially the same procedure as Matijevic et al.[10,11] described. 6.66 cm^3 of a 2.97 M† $FeCl_3$ solution was diluted to 1000 cm^3 with HCl(pH 3.1). Approximately 200 cm^3 of this solution was then passed through a 0.22 μm Nuclepore filter in order to equilibrate the membrane, after which the filtrate was discarded. The rest of the solution was filtered and distributed in 10 cm^3 screw-capped test-tubes, which were then aged for 24 h at 100 °C in an air-convection oven controlled at a constant temperature (Model DN-61, Yamato Science Co.). After cooling to room temperature, the collected particles were diluted with $HClO_4$ (pH 3.1) and then centrifuged at 8000 rpm for 30 min. The supernatant solution was discarded, and the particles were again diluted with the same $HClO_4$ solution and centrifuged. This procedure was repeated eight times. Upon the completion of the washing, the particles were redispersed in ion-exchanged water to be used as a stock sol. The washing process was repeated until no chloride or iron(III) ions could be detected in the supernatant solution. The final stock sol had a concentration of 1.31 mg cm^{-3}, as determined directly by dry-weight measurement, and was kept at pH 5.8.

The mean particle size was determined by the use of a particle analyzer(Autosizer Model 700, Malvern Co., Ltd.). The average diameter was 130 nm. X-ray diffraction measurements showed that the nearly spherical particles of α-Fe_2O_3 were paracrystalline; they consisted of very uniform globular crystallites.

Methods. The pH and the ionic strength of mixtures containing given amounts of ferric oxide sol and a surfactant were adjusted to make then suitable; then the mixture was agitated at a constant temperature(25 °C) for 2.5 h. In order to keep the ionic strength constant, all the measurements were carried out in 1×10^{-2} M sodium chloride: hydrochloric acid and sodium hydroxide were used to adjust the pH of these mixtures.

Measurements. (1) Zeta-Potential: The zeta-potential of the sols was measured at 20 °C by means of an electrophoresis apparatus, Laser-Zee meter Model-500(Pen Kem, Inc.). The zeta-potential values were calculated by using the Helmholtz-Smoluchowski

† 1 M=1 mol dm^{-3}.

equation:

$$\zeta = K\eta V/\varepsilon E,$$

where ζ is the zeta potential, K is a constant, η is the viscosity of the medium, V is the mobility, ε is the dielectric constant of the medium, and E is the electric field.

(2) Amount of Adsorption: Sixty cm^3 of the sol dispersion was mixed with the solution of the α,ω-type surfactant solutions of various concentrations, and the mixture was stirred for 2.5 h at 25 °C. After the adsorption was reached an equilibrium, the dispersion was separated by centrifugation at 10000 rpm for 30 min. A Methylene Blue acidic solution was added to the supernatant solution, and then the anionic surfactant–Methylene Blue complex thus formed was extracted in the chloroform phase.[12,13] The absorbance of the extract was measured at 652 nm by means of a double-beam spectrophotometer (220A, Hitachi Co.). The amount of adsorption was calculated from the difference in the absorbance before and after the adsorption.

(3) Stability Ratio: As soon as the sols had been mixed with the surfactant solution, the turbidity of the mixture was recorded and the initial slope of the optical density vs. time curve was obtained. The measurements were carried out at 25 °C and at a wavelength of 540 nm. The stability ratio(W) was calculated from the ratio of the rapid-coagulation rate(k_0) to the slow-coagulation rate(k) of sols:[14]

$$W = k_0/k$$

(4) Flushing: The sols flocculated by the addition of the surfactant solution were added to organic solvents, and then the mixture was shaken. The behavior of flushing for sols was observed with the naked eye.

Results and Discussion

In order to characterize the iron(III) oxide hydrate sol, the zeta-potential and the mean particle size of single sol were measured as a function of the pH. The isoelectric point of sol was estimated to be pH 7, which agreed fairly well with the literature value.[10]

On studying the interactions between iron(III) oxide hydrate sol and each surfactant, the values of the zeta-potential and the mean particle size of sols at various pH values were measured as a function of the concentration of each surfactant. Further, the amounts of surfactant adsorbed on sols were determined at two different pH values, i.e., pH 3.5 and pH 5.8. As it is considered that the interactions between the sol and anionic surfactant in an alkaline solution seem less significant because the surface of sol is negatively charged in alkaline solution, the pH values described above were employed.

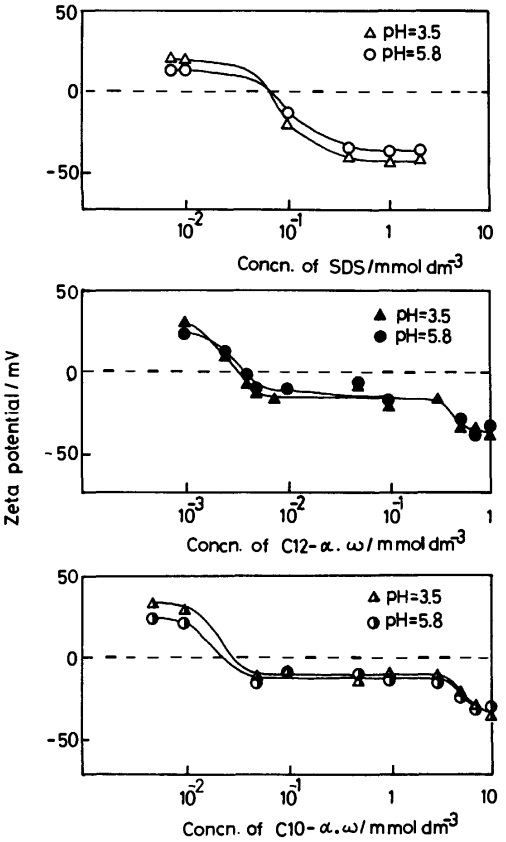

Fig. 1. The change in zeta-potential of sols as a function of concentration of surfactant.

Figure 1 shows the change in the zeta-potential of sols as a function of the concentration of the surfactant at pH 3.5 and pH 5.8. In the case of SDS, the surface of the sol charged positively at the initial stage became negative with an increase in the concentration of SDS, and the value of zeta-potential reached at a constant value, −40 mV. The results obtained for α,ω-type surfactants were similar to those of SDS. However, in the case of an α,ω-type surfactant, the zeta-potential was kept constant over a wide range of concentration at about −10 mV and then, with the further addition of an α,ω-type surfactant, decreased to about −40 mV for both α,ω-type surfactants.

Figure 2 shows the change in the mean particle size of the sols as a function of the concentration of the surfactant at pH 3.5 and pH 5.8. The particle size of the sols increased suddenly upon the addition of the surfactant, indicating that the sols were flocculated. Upon the further addition of the surfactant, the particle size of sols decreased again. Thus, the change in the mean particle size of the sols indicates that the dispersion-flocculation-redispersion of sols occurs by means of the surfactant. It is noteworthy that the flocculation of the sols upon the addition of

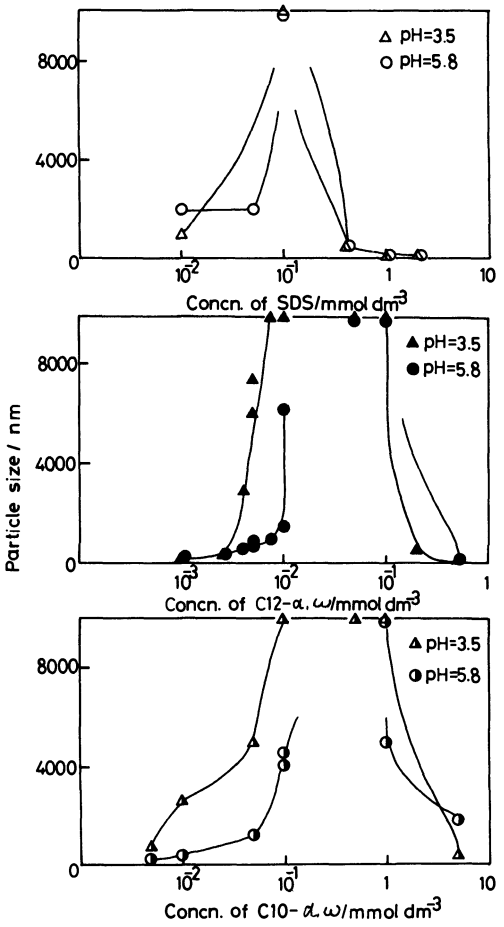

Fig. 2. The change in mean particle size of sols as a function of concentration of surfactant.

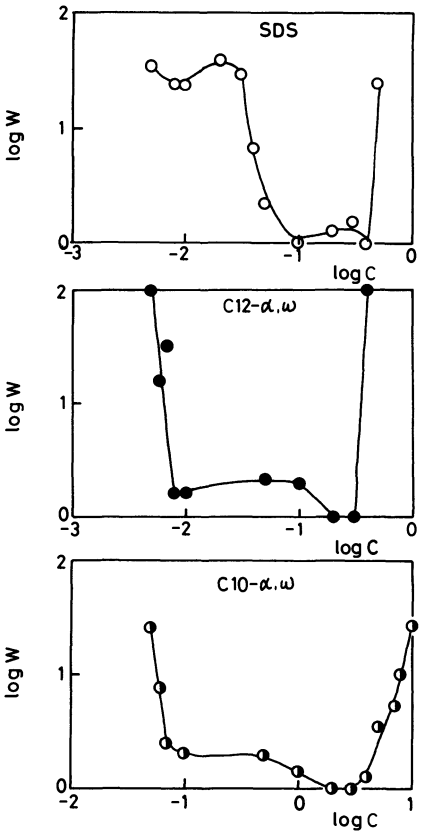

Fig. 3. Relationship between stability ratio of sols and concentration of surfactant at pH 5.8.

α,ω-type surfactants occurs over a wider range of surfactant concentrations than that in SDS.

To examine the flocculation region in detail, the stability ratio of the sols was measured. The change in the stability ratio of the sols as a function of the logarithm of the concentration of the surfactant at pH 5.8 is presented in Fig. 3. In the region of rapid coagulation, log W is nearly zero. From Fig. 3, it can be seen that the region of the flocculation of the sols upon the addition of SDS ranges from 0.1 mM to 0.4 mM. On the other hand, the region of the flocculation of the sols upon the addition of C12-α,ω ranges from 0.008 mM to 0.3 mM, and that of C10-α,ω, from 0.07 mM to 4 mM. Accordingly, it was found that the flocculation region upon the addition of an α,ω-type surfactant was much wider than that by SDS. The difference between the concentrations corresponding to the flocculation regions of C10-α,ω and C12-α,ω is mainly attributing to the difference in their surface activity: The surface activity of C12-α,ω is much higher than that of C10-α,ω.[7]

Figure 4 presents the adsorption isotherms at pH 3.5 and pH 5.8 where the adsorption density(mol m^{-2}) is given as a function of the equilibrium concentration of the surfactant. The adsorption density of SDS increased gradually and then became constant. A slight inflection point appeared at about 0.1 mM of SDS. The adsorption isotherms of the α,ω-type surfactants had a plateau over a wide range and then increased suddenly. Finally, the saturated amount of adsorption was obtained. It should be noted that the concentration ranges of these plateaus are in fairly good agreement with the flocculation region of the sols caused by the surfactants. From these results on the mean particle size, the zeta-potential, and the adsorption measurements, the interactions between the sols and the α,ω-type surfactant were found to be slightly stronger at pH 3.5 than at pH 5.8, probably because of the difference in the electric interactions between them.

The properties of the sol flocks formed by the addition of the α,ω-type surfactants and SDS were characterized by the flushing process. When the flocks of the sols formed by SDS were shaken with toluene, the flocks were transferred to the toluene phase; well-dispersed sols were obtained in the toluene phase. The reason for this transfer can be explained by the mechanism of forming a hydro-

phobic adsorption layer on the surface of the sol particles.[5] However, the flocks formed by the addition of the α,ω-type surfactants were dispersed in neither the water phase nor the toluene phase, but moved to the water/toluene interface.

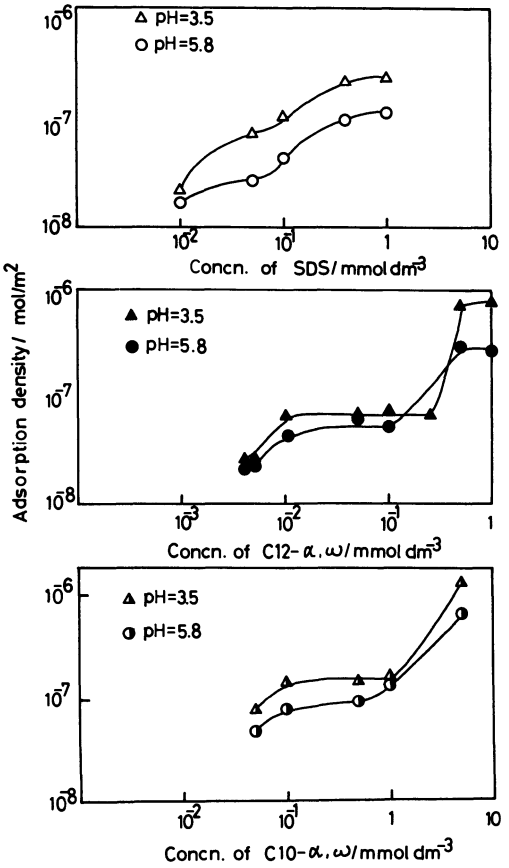

Fig. 4. Adsorption density of surfactant on sols as a function of concentration of surfactant.

Based on all the results obtained, the mechanisms of the flocculation and redispersion of sols occurring upon the addition of α,ω-type surfactants were discussed, and the results shown schematically in Fig. 5 were obtained. When low concentrations of α,ω-type surfactants are added to the sols, the surface charge of the sols is neutralized, resulting in the flocculation of the sols, much as in the case of SDS.[15] Two flocculation models by α,ω-type surfactants are proposed. The flocculation model of the left side seems unreasonable, however, because the surface of sols treated with α,ω-type surfactants does not exhibit the hydrophobic character usually obtained by flushing. On the other hand, the flocculation model of the right side indicates that α,ω-type surfactants act as bridging agents among the sols. The mechanism of bridge-forming among sols is a bimolecular process: the flocculation rate must be proportional to the product, $\theta(1-\theta)$, of the fractions covered(θ) and notcovered($1-\theta$) with the adsorbed α,ω-type surfactant. As can be seen in Fig. 3, the experimental points lie almost on a parabola, corroborating the bimolecular flocculation.[16] This bridging action renders the sols less hydrophobic than the surface of the sols flocculated by the addition of SDS. The flocculated sols thus obtained moved at the toluene/water interface and behaved like a film upon the flushing. This film-like behavior might be due to the penetration of toluene into the hydrocarbon chain of the α,ω-type surfactant, thus forming a bridge. On the further addition of an α,ω-type surfactant, the mean particle size of the sols decreased, as is shown in Fig. 2, since the redispersion of the sols was achieved. The mechanism of redispersion, which is schematically shown in Fig. 5, can be explained in terms of the monolayer

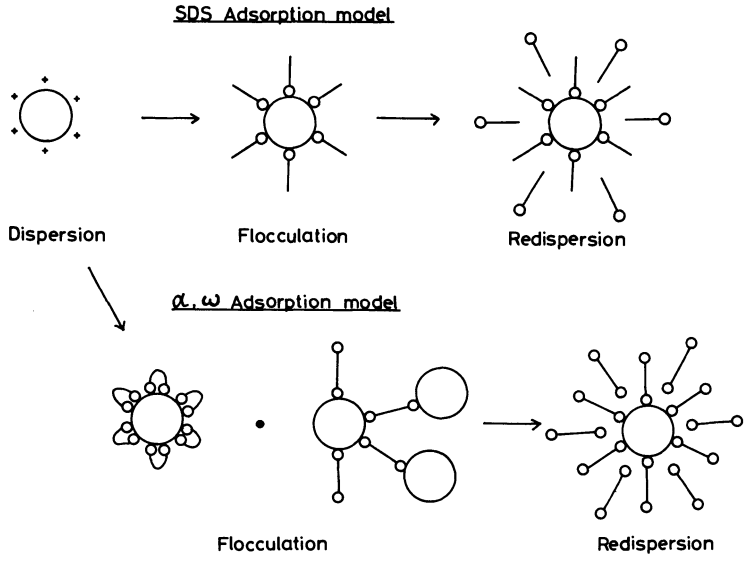

Fig. 5. A model for mechanism of flocculation and redispersion of sols by surfactant.

adsorption from the data of the zeta-potential and the amount of adsorption. Accordingly, the redispersion state of sols by α,w-type surfactants is different from the two-fold adsorption layer caused by SDS.

References

1) T. Suzuki, K. Esumi, and K. Meguro, *J. Colloid Interface Sci.*, **93**, 205 (1983).
2) H. Kuno and R. Abe, *Kolloid-Z.*, **181**, 70 (1964).
3) S. Kumagai and S. Fukushima, *J. Colloid Interface Sci.*, **56**, 227 (1976).
4) N. Moriyama, *Colloid Polymer Sci.*, **254**, 726 (1976).
5) K. Meguro, S. Tomioka, N. Kawashima, and K. Esumi, *Progr. Colloid Polymer Sci.*, **68**, 97 (1983).
6) K. Ogihara, S. Tomioka, K. Esumi, and K. Meguro, *Shikizai Kyokaishi*, **55**, 546 (1982).
7) M. Ueno, T. Hikota, T. Mitamura, and K. Meguro, *JAOCS*, **49**, 250 (1972).
8) M. Ueno, S. Yamamoto, and K. Meguro, *JAOCS*, **51**, 373 (1974).
9) Y. Gama and H. Suzuki, *Yukagaku*, **32**, 480 (1983).
10) E. Matijevic, R. S. Sapiensco, and J. B. Meville, *J. Colloid Interface Sci.*, **50**, 567 (1975).
11) E. Matijevic and R. Scheiner, *J. Colloid Interface Sci.*, **63**, 509 (1978).
12) S. G. Dick, D. W. Fuestenau, and T. W. Healy, *J. Colloid Interface Sci.*, **37**, 595 (1971).
13) S. Raghavan and D. W. Fuestenau, *J. Colloid Interface Sci.*, **50**, 319 (1975).
14) R. O. James, A. Homola, and T. W. Healy, *J. Chem. Soc., Faraday Trans. 1* **73**, 1436 (1977).
15) K, Meguro and T. Kondo, *Nippon Kagaku Zasshi*, **76**, 642 (1955).
16) K. Furusawa, H. Kakoki, and H. Matsumura, *Bull. Chem. Soc. Jpn.*, **57**, 3413 (1984).

The Electrical Properties of $La_{2-x}Sr_xNiO_4$ ($0 \leqq x \leqq 1$)

Kenji ISHIKAWA,* Shin-ichi KONDO, Yuichi SUZUKI, Shin-ichi TAKAYAMA, Kazuhiko SHIMADA, and Yasuo SUZUKI
Department of Industrial Chemistry, Faculty of Engineering, Meiji University, Higashi-mita, Tama-ku, Kawasaki 214
(Received July 27, 1985)

The electrical resistivities and Seebeck coefficients of mixed oxides, $La_{2-x}Sr_xNiO_4$, have been determined under an He atmosphere at 77.4—673.2 K. It has been shown that the temperature dependences of the Seebeck coefficients of the oxides were fairly well approximated by this equation: $S=AT+B+C/T$, where T is the thermodynamic temperature. The coefficients of the equation, A, B, and C, were given by the least-squares method. The metal-semiconductor ratios $\{\alpha \equiv (C/T)/(AT+C/T)\}$ were given to characterize the thermoelectrical properties of $La_{2-x}Sr_xNiO_4$. The maximal activation energies (E_a(resis.) and E_a(Seebeck)) and the maximal metal-semiconductor ratio (α) were obtained with the strontium concentration of $La_{2-x}Sr_xNiO_4$ at $x=0.5$. The lattice distortion of the oxides is responsible for the maxima of the activation energies and of the metal-semiconductor ratio at $x=0.5$.

The K_2NiF_4-type oxides are of great interest because of their unusual electrical properties. For example, La_2NiO_4 exhibits a gradual metal-semiconductor transition,[1-7] while $LaSrNiO_4$ is a metallic conductor[1,3,4] in the a axis direction of the tetragonal cell. The mixed oxides, La_2NiO_4 and $LaSrNiO_4$, form a continuous series of solid solutions,[3,4,8,9] $La_{2-x}Sr_xNiO_4$, which are also (tetragonal) K_2NiF_4-type oxides at $x=0$—1. Kononyuk et al.[3,4] have provided the resistivity and the thermoelectromotive force data of $La_{2-x}Sr_xNiO_4$. The measurements of the previous paper,[3,4] however, have been restricted to above room temperature; the data at temperatures below 300 K are not given.

In this paper, the electrical and transport properties of $La_{2-x}Sr_xNiO_4$ are reported in the range of 77.4—673 K, and the effects of lattice distortion on the electrical and transport properties are discussed.

Experimental

The mixed oxides, $La_{2-x}Sr_xNiO_4$, were prepared by heating a mixture of La_2O_3 (Shin-etsu Chem. Ind. Co., 99.9%), $SrCO_3$ (prepared from reagent grade $Sr(NO_3)_2$), and NiO (Koujundo Kagaku Co., 99.99%) in air at 1423 K for 20 h with intermittent grinding. The X-ray powder-diffraction method was employed for their identification.

Sintered specimens about 3 mm^2 in cross section and 10 mm long, which had been cut from pelletized samples 13 mm in diameter and 1 mm thick, were used for the electrical-resistivity and Seebeck-coefficient measurements.

Both four- and two-probe methods were employed for the resistivity measurements.

The Seebeck coefficients were determined by measuring the electric fields which were produced across a sintered bar of the specimen by the presence of temperature gradients. Two small copper blocks were employed for the potential leads. The temperature differences between the two potential leads were maintained within 15 K during the measurements.

The absolute Seebeck coefficients of the samples, S(abs.), were obtained by means of this equation:[10]

$$S(\text{abs.}) = S(\text{Cu}) - \Delta V/\Delta T, \quad (1)$$

where S(Cu) was the absolute Seebeck coefficient of copper[11] and where ΔV and ΔT were the potential and temperature differences between the two copper blocks respectively. All the resistivity and the Seebeck coefficient measurements were carried out under an He atmosphere.

Results and Discussion

The X-ray studies revealed that $La_{2-x}Sr_xNiO_4$ were tetragonal K_2NiF_4-type oxides over the entire range of x.[8]

The electrical resistivity measurements showed that all the sintered polycrystalline samples were semiconductors at room temperature (Fig. 1). In the series

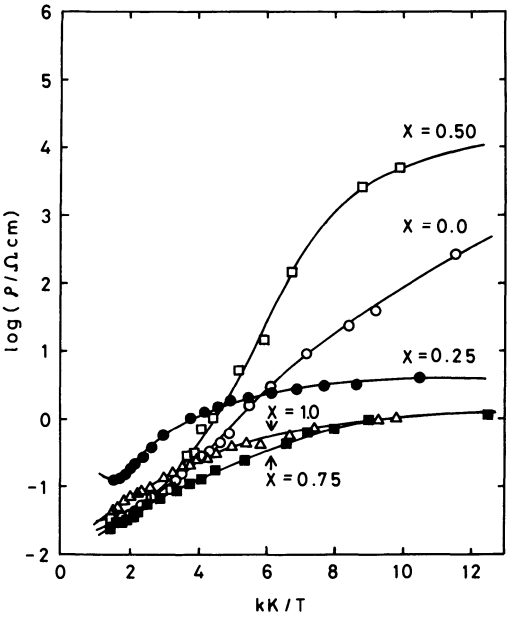

Fig. 1. Temperature dependence of electrical resistivity for $La_{2-x}Sr_xNiO_4$.

Table 1. Seebeck Coefficient and Activation Energy of $La_{2-x}Sr_xNiO_4$

x[a]	Temp range	Seebeck coefficient[b]			Activation energy[c]	
		A	B	C	E_a(resis.)	E_a(Seebeck)
	K	10^{-8} VK^{-2}	10^{-5} VK^{-1}	10^{-3} V	eV	eV
0.00	169—551	6.24	−4.80	8.91	0.081	0.009
0.25	146—619	2.93	−2.91	5.82	0.089	0.006
0.50	128—557	3.22	−5.22	11.2	0.097	0.011
0.75	110—506	−1.90	−0.93	1.78	0.052	0.002
1.00	91—607	−2.27	−0.19	0.56	0.072	<0.001

a) x in $La_{2-x}Sr_xNiO_4$. b) Seebeck coefficient at 300 K. $S=AT+B+C/T$. c) $\rho=\rho_0\exp(E_a(\text{resis.})/kT)$; $S=C/T=(k/e)(E_a(\text{Seebeck})/kT)$.

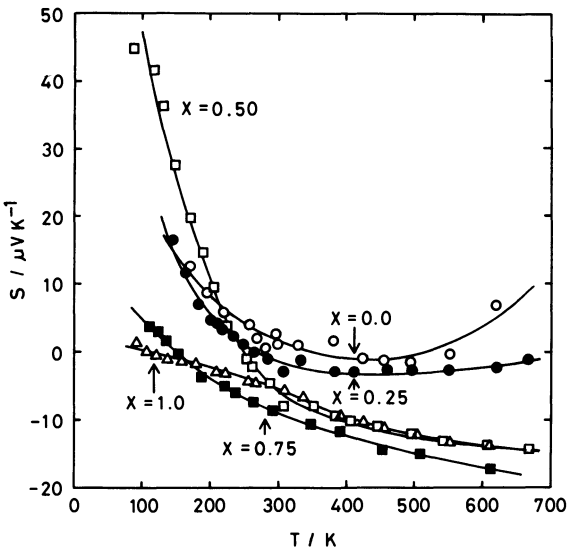

Fig. 2. Absolute Seebeck coefficients of $La_{2-x}Sr_xNiO_4$.

of $La_{2-x}Sr_xNiO_4$, a maximum value of the activation energy,

$$\rho=\rho_0\exp(E_a/kT), \quad (2)$$

was obtained from the slope of the resistivity curve of $La_{1.5}Sr_{0.5}NiO_4$[3,4] (Table 1). A gradual metal-semiconductor transition was found in the resistivity curves of La_2NiO_4 and $La_{1.75}Sr_{0.25}NiO_4$ around 500 K.[1-7,9]

The thermo-electromotive force data (Fig. 2) suggested that $LaSrNiO_4$ was a metallic conductor,[1,3,4] but the resistivity data (Fig. 1) indicated that $LaSrNiO_4$ was a semiconductor with small activation energy. Charge transport among the grains across the boundary is probably responsible for the semiconduction of the polycrystalline $LaSrNiO_4$.

Goodenough[5,6] has proposed a band model of La_2NiO_4 in which the conduction band, a narrow $\sigma^*_{x^2-y^2}$ band, is split into two bands by either electron correlations or a charge-density wave; the lower band of the two is fully occupied by electrons, whereas the higher one is empty. It is safe to assume that $La_{2-x}Sr_xNiO_4$ have essentially the same energy-band structure as that of La_2NiO_4, since the crystal structures of La_2NiO_4 and $La_{2-x}Sr_xNiO_4$ are identical.

The $La_{2-x}Sr_xNiO_4$ oxides contain x Ni^{3+} cations per formula. If $La_{2-x}Sr_xNiO_4$ have the same energy band as La_2NiO_4, $La_{2-x}Sr_xNiO_4$ must be metallic conductors at any x except at x=1, even at low temperatures, since x holes do exist in $La_{2-x}Sr_xNiO_4$. Metallic conduction, however, was not observed in the series of $La_{2-x}Sr_xNiO_4$ except for $LaSrNiO_4$ in either Kononyuk's[3,4] and the present work at room temperature. This phenomenon can be understood if the nickel 3d holes are trapped around Sr^{2+} and are in the collective state, because Sr^{2+} is more negative than La^{3+}. In $La_{2-x}Sr_xNiO_4$, many donors, that is, acceptors of holes, should exist in the lower band of La_2NiO_4, and the conduction band of La_2NiO_4 must be deformed by Sr^{2+}.

So many Sr^{2+} and Ni^{3+} should also influence the transport properties of $La_{2-x}Sr_xNiO_4$. Thermo-electromotive force measurements showed that the Seebeck coefficients of $La_{2-x}Sr_xNiO_4$, except for La_2NiO_4 and $La_{1.75}Sr_{0.25}NiO_4$, decreased with an increase in the temperature over the entire range of measurements (Fig. 2). The Seebeck coefficient curves of La_2NiO_4 and $La_{1.75}Sr_{0.25}NiO_4$, however, had minima at around 500 K, where metal-semiconductor transitions were observed. All oxides were p-type conductors at low temperatures, but they were n-type above moderate temperatures.

In general, the Seebeck coefficient of a metallic conductor can be represented by this relation:

$$S=AT+B, \quad (3)$$

where A and B are constants and where T is the thermodynamic temperature. On the other hand, the Seebeck coefficient of a semiconductor is expressed as:

$$S=C/T, \quad (4)$$

where C is a constant. In the case of an intrinsic semiconductor, Eq. 4 can be altered as:

$$S=(k/e)(E_a/kT), \tag{5}$$

where k is the Boltzmann constant, e is the electronic charge, and E_a is the activation energy.

The Seebeck coefficient curves of the sintered samples of $La_{2-x}Sr_xNiO_4$ (Fig. 2) were complicated and could not be expressed simply by either Eqs. 3 or 4. Since the oxides were electrically anisotropic and both La_2NiO_4 and $La_{1.75}Sr_{0.25}NiO_4$ exhibit a "gradual" metal-semiconductor transition (Fig. 1), we hypothetically assumed that the metallic conduction and the semiconduction parts of the thermo-electromotive force, viz., $AT+B$ and C/T, coexist in the polycrystalline samples of $La_{2-x}Sr_xNiO_4$ and that their Seebeck coefficient consists of the sum of the two parts. The Seebeck coefficient of $La_{2-x}Sr_xNiO_4$ can, then, be written as:

$$S=AT+B+C/T. \tag{6}$$

This equation can also be written in this form:

$$ST=AT^2+BT+C. \tag{7}$$

The coefficients A, B, and C were evaluated by fitting the experimental measurements to Eq. 7 with a digital computer, using the least-squares method.

In Fig. 3 the observed and calculated products, ST, are plotted as a function of the temperature. The solid lines represent the calculated values (ST(calcd)= AT^2+BT+C). The calculations by the least-squares method were employed to obtain the thermo-electromotive force data at high temperatures (Table 1). The calculated values were in fair agreement with the values found for most of the temperature region. However, large deviation of the observed ST values from the calculated lines, which were greater than the limits of experimental error (±2 mV), were found in the low-temperature p-type regions of La_2NiO_4, $La_{1.75}Sr_{0.25}NiO_4$, and $La_{1.5}Sr_{0.5}NiO_4$. Unfortunately, it was not elucidated from our experimental data why the ST values of the samples ($x\leqq0.5$) deviated from the calculated ST curves at low temperatures.

In Fig. 4 the A and C coefficients are plotted as a function of the strontium concentration, x. The A coefficient was positive at $x\leqq0.6$ and negative at $x>0.6$. On the other hand, the C coefficient was positive over the whole range of x and increased with an increase in x. Figure 4 shows that both holes ($A\geqq0$ at $x<0.6$) and electrons ($A<0$ at $x>0.6$) were involved in the metallic conduction and that the holes were responsible for the semiconduction ($C\geqq0$ at $x=0$—1).

We attempted to seek a parameter (or a function) which contained the thermo-electromotive force data,

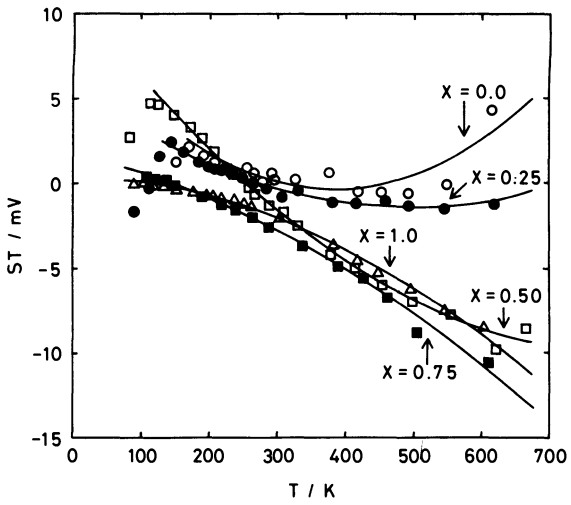

Fig. 3. ST vs. T plots of $La_{2-x}Sr_xNiO_4$. The solid lines indicate the calculated values.

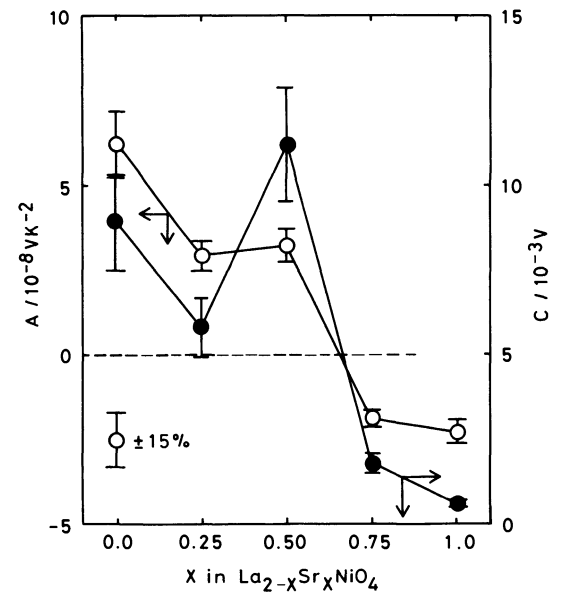

Fig. 4. The A and C values of $La_{2-x}Sr_xNiO_4$. $S=AT+B+C/T$

i.e., A, B, and C, and which was related to the resistivity data. As has been described previously, the A and B coefficients were correlated with the metallic conduction, while the C parameter was correlated with the semiconduction. The thermo-electromotive force, AT, and C/T were temperature-dependent, and their values were determined by the sign, the density, and the mobility of the charge carriers in the energy band, while the residual power, B, was temperature-independent and it was usually difficult to predict its value. It seemed inappropriate to compare the values of A and/or C with B, since the value of B was unpredictable. Therefore, the B coefficient was ignored in evaluating the parameter (or the fucncton) in this paper.

The paprameter (or the function) was conveniently

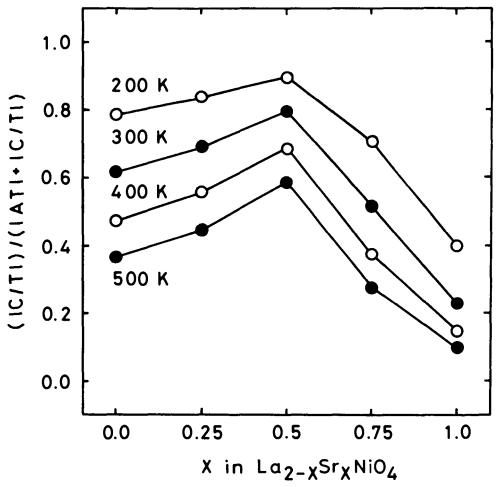

Fig. 5. The $(C/T)/(AT+C/T)$ values of $La_{2-x}Sr_xNiO_4$. $S=AT+B+C/T$

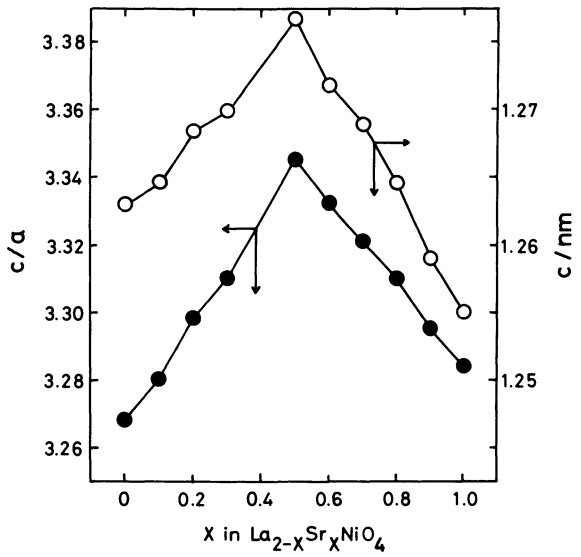

Fig. 6. Strontium concentration dependence of the c value and the c/a ratio of $La_{2-x}Sr_xNiO_4$ at 300 K. The lattice constants a and c were obtained from Gopalakrishnan et al.[8]

defined as the ratio of AT (metallic conductor) and C/T (semiconductor) as:

$$\alpha=\frac{C/T}{AT+C/T}\ . \tag{8}$$

The α parameter was named the metal-semiconductor ratio of the thermo-electromotive force.

In Fig. 5 the metal-semiconductor ratio of the oxides is plotted as a function of the strontium concentration. The metal-semiconductor ratio of the oxides decreased with an increase in the temperature. The ratio increased with x at $x<0.5$, but it decreased with x at $x\geqq 0.5$ at any temperature. Ganguly and Rao[1] and Kononyuk et al.[4] have reported that La_2NiO_4 showed a metal-semiconductor transition at 500 K and that $LaSrNiO_4$ was a metallic conductor. The metal-semiconductor ratio of La_2NiO_4 was 0.4 at 500 K, while that of $LaSrNiO_4$ was 0.2 at room temperature (Fig. 5). The metal-semiconductor transition seemed to occur at a critical value of $\alpha=0.3\pm0.1$. The $La_{1.5}Sr_{0.5}NiO_4$ oxide exhibited no metal-semiconductor transition because the metal-semiconductor ratio of the oxide was appreciably larger than the critical value in the temperature range measured.

In Fig. 6 the c/a and c values at room temperature of $La_{2-x}Sr_xNiO_4$, where a and c are the lattice constants of the tetragonal cell obtained from Gopalakrishnan et al.,[8] are plotted as a function of the strontium concentration. The shape of the metal-semiconductor ratio against the strontium-concentration curve in Fig. 5 very much more closely resembles the c vs. x curve than the c/a vs. x one.

In Table 1 the activation energies obtained from the resistivity data (E_a (resis.))(Eq. 2) and the activation energies calculated from the thermo-electromotive force data (E_a(Seebeck))(Eq. 5) are tabulated. The activation energies, E_a(Seebeck), are given merely as references, because the E_a(Seebeck) energies have some ambiguity which result from assuming that $La_{2-x}Sr_xNiO_4$ are intrinsic semiconductors. The activation energy (E_a(resis.)) and E_a(Seebeck) both had maxima at $x=0.5$. The activation energies must also be responsible for the crystal distortion.[5,6] The results in Figs. 5 and 6 and Table 1 indicate that the activation energy, as well as metal-semiconductor ratio of $La_{2-x}Sr_xNiO_4$, is correlated to the lattice distortion of the crystal.

References

1) P. Ganguly and C. N. R. Rao, *Mater. Res. Bull.*, **8**, 405 (1973).
2) J. B. Goodenough, *Mater. Res. Bull.*, **8**, 423 (1973).
3) L. F. Kononyuk, N. G. Surmach, and V. Maklnach, *Inorg. Mater.*, **18**, 1029 (1982).
4) I. F. Kononyuk, N. G. Surmach, and L. V. Makhnach, *Izv. Akad. Nauk SSSR, Neorg. Mater.*, **18**, 1222 (1982).
5) J. B. Goodenough and S. Ramasesha, *Mater. Res. Bull.*, **17**, 383 (1982).
6) K. K. Singh, P. Ganguly, and J. B. Goodenough, *J. Solid State Chem.*, **52**, 254 (1984).
7) C. N. R. Rao, D. J. Buttrey, N. Otsuka, P. Ganguly, H. R. Harrison, C. J. Sandberg, and J. M. Honig, *J. Solid State Chem.*, **51**, 266 (1984).
8) J. Gopalakrishnan, G. Colsmann, and B. Reuter, *J. Solid State Chem.*, **22**, 145 (1977).
9) P. Ganguly and C. N. R. Rao, *J. Solid State Chem.*, **53**, 193 (1984).
10) L. D. Muhlestein and G. C. Danielson, *Phys. Rev.*, **160**, 562 (1967).
11) N. Cusack and P. Kendall, *Proc. Phys. Soc.*, **72**, 898 (1958).

Precise Measurement of Ultrasonic Absorption in Micellar Solutions in the Frequency Range from 0.2 to 10 MHz

Shigeo KATO,* Hiroyasu NOMURA, Ryszard ZIELIŃSKI,†,†† and Shoichi IKEDA†
Department of Chemical Engineering, School of Engineering, Nagoya University, Chikusa-ku, Nagoya 464
†Department of Chemistry, Faculty of Science, Nagoya University, Chikusa-ku, Nagoya 464
(Received August 3, 1985)

A cylindrical resonator for the measurement of ultrasonic absorption has been designed. It was found that a newly designed resonator can determine the absolute value of the ultrasonic absorption coefficient of water at frequencies above 0.7 MHz. For aqueous solutions it has a sufficient resolution power down to 0.2 MHz by means of a reference measurement. Precise measurements of ultrasonic absorption were carried out for aqueous solutions of dodecyltrimethylammonium bromide using a newly designed resonator and two other previously reported resonators. The ultrasonic relaxation spectra show a single relaxation process within the investigated frequency range. The relaxation process can be ascribed to a "fast" relaxation related to the exchange of a surfactant between micelles and bulk solution. The kinetic parameters for the exchange process were estimated on the basis of Teubner's theory.

Precise measurements of the ultrasonic absorption below 10 MHz are very important for a variety of ultrasonic relaxation studies, such as the kinetics of micellar solutions,[1-5] the dynamics of segmental motions of polymer chains in a solution[6,7] and the dynamics of simple molecules.[8,9] For a kinetic study of micellar solutions, a precise measurement within this frequency range is inevitably required since it is well known that most micellar solutions show an ultrasonic relaxation phenomena within the frequency range 0.1 to 10 MHz.

For frequencies below 1 MHz, however, few measurements have been carried out and only an ultrasonic study has been reported for the typical micellar solutions of sodium dodecyl sulfate by Yasunaga et al.[4] using an ultrasonic reverberation method. Although the reverberation method has been an available technique for measuring ultrasonic absorption within this frequency range, it usually requires a great volume of a sample (several to ten liters).[10] Also, its accuracy is sometimes insufficient. Therefore, applications of this technique have been limited to the micellar solutions with high ultrasonic absorption coefficients.

On the other hand, a cylindrical resonator method which was originally developed by Eggers,[11] has proved to be a powerful technique for measuring the ultrasonic absorption coefficient of liquids and solutions at frequencies below 10 MHz. However, it is still difficult to make precise measurements using this method on samples with low ultrasonic absorption coefficients, such as water and dilute aqueous solutions at frequencies below 2.5 MHz. The main reason for the difficulty is that the mechanical loss of the cylindrical resonator sharply increases with a decreasing frequency. In order to reduce the mechanical loss, a few improvements have been made; for example, Eggers et al.[12,13] developed a pressure concave resonator and Choi et al.[14,15] proposed a plano-concave resonator and an optical detector using Raman-Nath light diffraction.

Recently, we have succeeded in reducing the mechanical loss of a cylindrical resonator without using a pressure concave resonator and without using an optical detector. Our improvement was simply in using a pair of X-cut quartz transducers with large diameters. It was found that a newly designed resonator can determine the absolute value of the ultrasonic absorption coefficient of water at frequencies above 0.7 MHz. For aqueous solutions it has a sufficient resolution down to 0.2 MHz, by means of a reference measurement.

In this paper we present a detailed description of the resonator and results regarding precise measurements of the ultrasonic absorption on aqueous solutions of a cationic surfactant, dodecyltrimethylammonium bromide, at frequencies from 0.2 to 10 MHz. The experimental results are discussed on the basis of a theory developed by Teubner.[16]

Experimental

Principle of the Resonator Method. Prior to a description of the resonator cell, the principle of the resonator method will be briefly presented. With this method, a resonator cell consists of a liquid column sealed by two X-cut quartz transducers. A frequency-variable oscillator drives the input transducer and produces a series of standing waves in the liquid column at resonance frequencies; then, sharp resonance peaks are detected by an output detector. At the n-th resonance frequency, f_n, the quality factor, Q, of the cell is given by

$$Q^{-1} = \Delta f_n / f_n, \quad (1)$$

where Δf_n is the half-power bandwidth (hereafter abbrevi-

†† Permanent Address; Academy of Economics, Department of General and Analytical Chemistry, Institute of Commodity Sciences, 60-957 Poznań, Poland.

ated as HPB) of the n-th resonance peak. For an ideal cylindrical resonator containing a liquid sample, the Q factor is given by

$$Q^{-1} = \alpha\lambda/\pi, \tag{2}$$

where α is the ultrasonic absorption coefficient of the sample and λ the ultrasound wavelength. In practice, Eq. 2 does not hold since there are several inherent factors called "mechanical" loss in the design of the cell. Therefore, Eq. 2 should be modified as follows:

$$Q^{-1} = \Delta f_n/f_n = \frac{\alpha\lambda}{\pi} + Q^{-1}_{mechanical}, \tag{3}$$

where $Q^{-1}_{mechanical}$ represents the mechanical loss of the cell. For a determination of the ultrasonic absorption coefficient of a sample, $Q^{-1}_{mechanical}$ should be eliminated by a reference measurement in the same cell at the same frequencies using a suitable liquid. Then, the excess absorption per wavelength $(\alpha\lambda)_{excess}$ in the liquid is obtained from Eq. 4.

$$(\alpha\lambda)_{excess} = \pi[(\Delta f_s - \Delta f_r)/f_n] \tag{4}$$

In Eq. 4, Δf_s and Δf_r represent the corresponding HPB values of the n-th resonance peak in the sample and the reference liquid, respectively.

Design of Resonator. The absolute value of the ultrasonic absorption coefficient can be determined using a resonator having a negligible mechanical loss compared with $\alpha\lambda/\pi$ of the liquid sample. Then, an accurate measurement can be easily performed. Therefore, a reduction of the mechanical loss is an essential point for the design of a resonator.

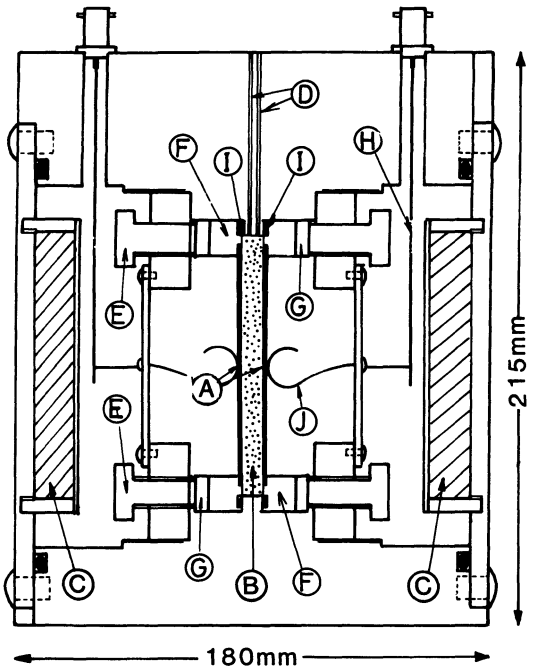

Fig. 1. Sectional view of the ultrasonic resonator, (A): X-cut quartz transducers, (B): cavity (sample room), (C): desiccant, (D): filling hole, (E): screw for parallelism adjustment, (F): supporter for transducer, (G): spacer, (H): lead, (I): O-ring, (J): electrode.

Figure 1 shows the resonator cell designed for this study. The dimensions of the cell are ca. 180 mm in width, 240 mm in length, and 215 mm in height, respectively. The acoustical path length is ca. 7 mm, and the liquid column has a total volume of ca. 50 ml, together with the dead space. The following improvements were carried out to reduce the mechanical loss as much as possible.

For the cell: (1) In order to separate the resonance frequency of the cavity from that of the total cell system, a sufficiently heavy cell (ca. 60 kg) was made of stainless steel (SUS 27). (2) Parallelism between transducers also contributes to the mechanical loss at the lower frequency region; thus, it was coarsely adjusted by measuring the distance between two transducers (with a precision of $\pm 1/100$ mm) using a dial indicator and was finally tuned by inspecting the pulse echo pattern on a synchroscope in a way similar to the usual pulse method. (3) Each transducer was supported only at its back surface with a holder to minimize the mechanical load on its surface. This makes the transducer vibrate better in thickness mode. (4) Two thin filling holes (1 mm in diam.) were drilled to minimize the disturbance of the resonance condition. (5) Desiccant (silica gel) was sealed within a cage attached to the wall of the cell since the mechanical loss of the resonator greatly depends on the humidity in the chamber behind the transducer.

For transducers: (1) In the frequency range below 2 MHz, the diffraction of sound makes a major contribution to the mechanical loss. The diffraction was suppressed by using a pair of quartz transducers with large diameters(90 mm). (2) A high quality factor of the transducers is also required in order to reduce the mechanical loss. For this purpose, the fundamental frequencies of the two transducers were matched within 0.05% (2.001 and 2.002 MHz, respectively) and their surfaces were polished to within optical grade. These transducers were purchased from Valpay-Fisher Co. Inc., U.S.A.

Measurement System and Temperature Control. Our apparatus for the resonator method consists simply of two frequency synthesizers (Rockland Model 5100, 0—2 MHz, John-Fluke Model 6039 A, above 2 MHz), a resonator cell and two detectors (Yokogawa Hewlett Packard Model 3400 RMS voltmeters). A detailed description of the apparatus has been published elsewhere.[17] Any temperature drift in a sample makes it difficult to obtain an accurate HPB reading since the resonance frequency is very sensitive to drift due to temperature fluctuations. The temperature of a water bath was controlled with an accuracy of $\pm 10^{-3}$ °C by means of a digital temperature-control system. The temperature drift in the sample could also be minimized using the sufficiently large heat capacity of the cell (due to its large size and weight).

Materials. Dodecyltrimethylammonium bromide (hereafter abbreviated as DTAB) and the other chemicals used in this study were purchased from Nakarai Chemicals Co. Ltd. and used without further purification. A chemical analysis of the DTAB was carried out at Prof. Tsuge's laboratory at our university and the purity of the sample was confirmed to be: C_{12}=99.9%, C_{10}=0.0%, and C_{14}=0.1%.

Ultrasonic Absorption and Sound Velocity Measurements. Three cylindrical resonators were used to measure the ultrasonic absorption in the frequency range

0.2—10 MHz: the resonator designed here (0.2—2 MHz); the other two reported previously,[17] one with 50 mm diameter crystals with a fundamental frequency of 2 MHz (0.8—3.2 MHz), and the other with a 30 mm diameter, 5 MHz crystals for the frequency range above 2.2 MHz. The ultrasonic absorption coefficients of aqueous solutions of DTAB were determined by the reference measurement on the basis of Eq. 4 using distilled, degased water as a reference liquid. The sound velocity was measured mostly with the cylindrical resonators and occasionally with an ultrasonic interferometer working at a fixed frequency 4.000 MHz.

Results and Discussion

Characteristic Properties of Resonator. Figure 2 shows the HPB values for water measured at 25 °C (using the designed resonator). For a comparison, the results using the other two resonators are also plotted. The HPB values of a resonator without a mechanical loss can be calculated using a modified form of Eq. 2:

$$\Delta f_n = \frac{\alpha}{f_n^2} \cdot \frac{u}{\pi} \cdot f_n^2, \tag{5}$$

where u is the sound velocity in the sample. Equation 5 shows that Δf_n should vary linearly with the square of the resonance frequency, f_n^2, in non-relaxing liquids. The solid line in the figure represents the HPB values of water calculated from Eq. 5. In that calculation, the ultrasonic absorption and sound velocity values for water at 25 °C were taken as $\alpha/f^2=22.6\times10^{-17}$ s^2 cm^{-1} and $u=1.497\times10^5$ cm s^{-1}, respectively. The deviation of the HPB data from a straight line represents the mechanical loss of the resonator at that frequency. If the obtained HPB values fall directly on a straight line, an absolute measurement of the ultrasonic absorption is possible using this resonator. It is readily seen from Fig. 2 that an absolute measurement for water is possible at frequencies above 0.7 MHz using a combination of these three resonators.

Figure 3 shows the resolution power of the designed resonator for measuring the ultrasonic absorption coefficient. Three lines represent the HPB values of water calculated from Eq. 5 at 15, 20, and 25 °C, respectively. The resonator can detect small differences (ca. 2.6×10^{-17} s^2 cm^{-1}) in α/f^2 of water at these temperatures. In the case of benzene having a higher ultrasonic absorption coefficient (860×10^{-17} s^2 cm^{-1} at 20 °C), the low-frequency limit of an absolute measurement goes down to ca. 0.5 MHz.

If the observed HPB values deviate from those

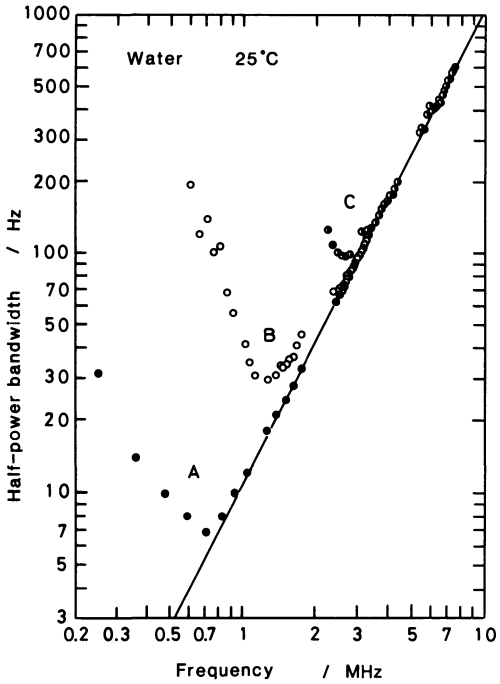

Fig. 2. The HPB values of resonance peaks for water at 25°C. A solid line represents the calculated HPB values of water from Eq. 5. For comparison, HPB values for the other two resonators used in this study are also plotted, (●): Resonator A (this work, 0.2—2 MHz), (○): resonator B (0.8–3.2 MHz), (◑): resonator C (2.2—8 MHz).

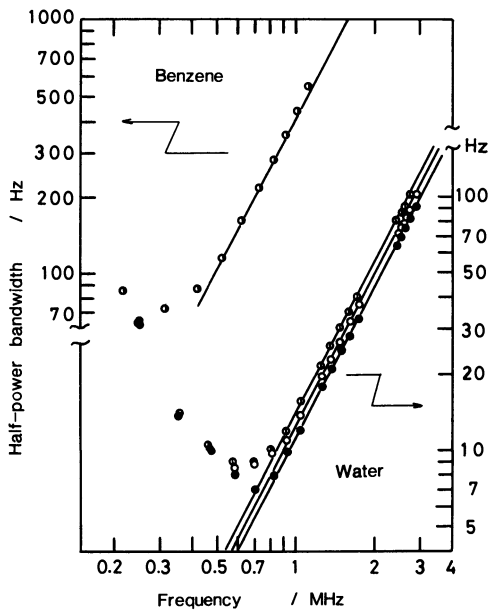

Fig. 3. The HPB values of resonance peaks observed in water at 15 (◫), 20 (○), and 25 °C (●) and in benzene (◑) at 20 °C. Solid lines represent the HPB values calculated from Eq. 5. Following data (except α/f^2 of benzene) are taken from literature[31] in the calculation, $\alpha/f^2=28.7\times10^{-17}$ s^2 cm^{-1}, $u=1.466\times10^5$ cm s^{-1} (water at 15°C), $\alpha/f^2=25.2\times10^{-17}$ s^2 cm^{-1}, $u=1.483\times10^5$ cm s^{-1} (water at 20°C), $\alpha/f^2=860\times10^{-17}$ s^2 cm^{-1}, $u=1.324\times10^5$ cm s^{-1} (benzene at 20°C).

calculated from Eq. 5, as is shown in Fig. 3 (for benzene at frequencies below 0.5 MHz and also for water below 0.7 MHz), the ultrasonic absorption coefficient can be determined by a reference measurement on the basis of the Eq. 4. Figure 4 shows the result of a reference measurement of the ultrasonic absorption of benzene at 20 °C. *o*-Xylene was used as a reference liquid because it has a similar acoustical impedance to that of benzene; also, no relaxation process in *o*-xylene was reported by Ohsawa[18] at the frequencies above 10 KHz. The ultrasonic absorption coefficient determined by the reference measurement is in good agreement with that determined by an absolute measurement using a pulse technique. This indicates that the designed resonator detects the reliable ultrasonic absorption coefficient at frequencies above 0.2 MHz.

Ultrasonic Absorption in Aqueous Solutions of DTAB. Figure 5 shows the result of ultrasonic absorption measurements for aqueous solutions of DTAB. The data are expressed as a plot of the absorption coefficient vs. the logarithmic frequency. An ultrasonic relaxation process can be observed within the frequency range investigated for all DTAB solutions. It is expressed well by the equation for a single relaxation

$$\frac{\alpha}{f^2} = \frac{A}{1+(f/f_r)^2} + B, \tag{6}$$

where f represents the measured frequency, f_r is the relaxation frequency, A the relaxation amplitude, and B the contribution to sound absorption from any other processes that may be occurring at higher frequencies beyond our frequency range. A linearlized least-square method was used to fit Eq. 6 to the ultrasonic absorption data and the relaxation parameters, A, B, and f_r, were determined. The solid lines in Fig. 5 represent the calculated ultrasonic relaxa-

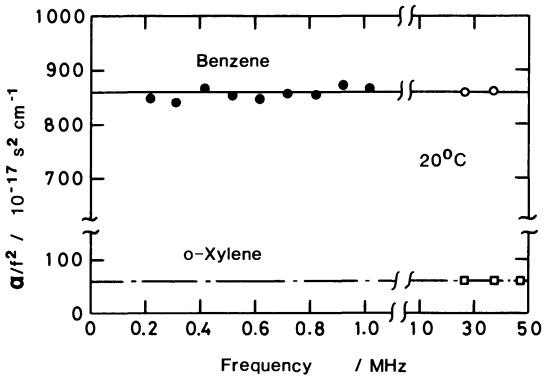

Fig. 4. Ultrasonic absorption coefficient of benzene determined by the reference measurement using the resonator (●) and that determined by pulse technique (○). Solid and chain lines show the average values of ultrasonic absorption coefficient determined by pulse technique for benzene (860×10^{-17} s^2 cm^{-1}) and *o*-xylene (61.2×10^{-17} s^2 cm^{-1}), respectively.

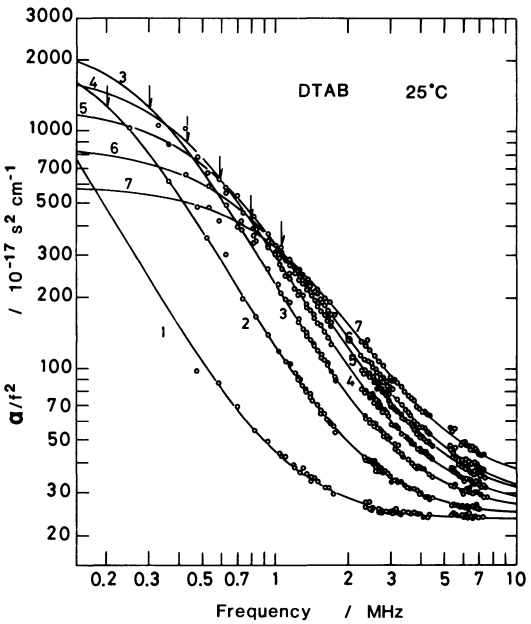

Fig. 5. Ultrasonic absorption as a function of frequency for aqueous solutions of DTAB at 25°C. The solid lines represent the calculated relaxation spectra from Eq. 6, and arrows show the location of relaxation frequencies. Numerical notations represent the concentration of solution, (1): 1.95×10^{-2} M, (2): 3.24×10^{-2} M, (3): 5.19×10^{-2} M, (4): 7.14×10^{-2} M, (5): 9.08×10^{-2} M, (6): 11.0×10^{-2} M, (7): 14.9×10^{-2} M.

Table 1. Ultrasonic Relaxation Parameters for Aqueous Solutions of DTAB at 25 °C

C	A	B	f_r	ρ	u	μ_{max}
10^{-2} M[b]	10^{-17} s^2 cm^{-1}	10^{-17} s^2 cm^{-1}	MHz	g cm^{-3}	10^5 cm s^{-1}	10^{-4}
1.95	3400	23.2	0.08_0	0.9974	1.500_3	2.04
3.24	2424	23.7	0.20_6	0.9975	1.501_1	3.75
5.19	2450	24.9	0.30_0	0.9978	1.501_4	5.52
7.14	1748	26.0	0.42_9	0.9978	1.501_5	5.63
9.08	1199	27.7	0.58_7	0.9983	1.501_7	5.28
11.0	800	27.4	0.79_0	0.9985[a]	1.502_1	4.75
14.9	551	32.3	1.0_6	0.9991[a]	1.502_6	4.39

a) Extrapolated values. b) M = mol dm^{-3}.

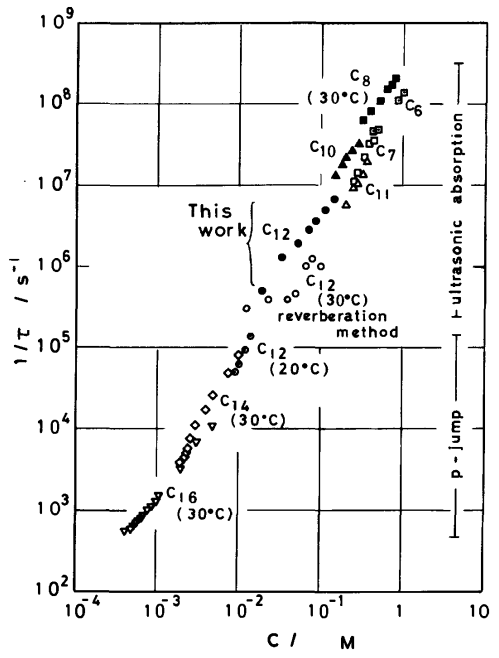

Fig. 6. Plot of reciprocal relaxation times vs. total concentration of surfactant. Filled symbols represent a series of alkyltrimethylammonium bromides: (●) this work C_{12}; (■) C_8[19]; (▲) C_{10}[2]. Open symbols represent a series of sodium alkyl sulfates: (◙): C_6[2], (□): C_7[2], (△): C_{11}[2], (○): C_{12}[4], (⊙): C_{12}[18], (◇): C_{14}[1], (▽): C_{16}[1]. Data without notation about temperature are for measurements at 25 °C.

tion spectra from Eq. 6 and the arrows indicate the location of the relaxation frequency. Table 1 summarizes the determined values of the relaxation parameters for aqueous solutions of DTAB. As can be seen in Fig. 5 and Table 1, the designed resonator can detect an ultrasonic relaxation process having a small relaxation amplitude. The relaxation amplitude observed here is about two orders smaller in magnitude than those of aqueous solutions of sodium dodecyl sulfate investigated by using the reverberation method.[4]

The reciprocal relaxation times can be calculated from the relaxation frequency as $1/\tau=2\pi f_r$ and are plotted as a function of the total concentration of DTAB in Fig. 6. For a comparison, the results of P-jump[1,19] and ultrasonic relaxation[2,4,20] studies on aqueous solutions of a series of sodium alkyl sulfates and those of alkyltrimethylammonium bromides are also plotted. The present results are consistent with those reported in the literature. Our data sufficiently completes the range from 10^5 to 10^7 s^{-1}, which has been a vacant zone since there are few available methods for ultrasonic absorption and P-jump measurements. It can also be seen from Fig. 6 that the reciprocal relaxation time of solutions that are a series of alkyltrimethylammonium bromides is always located at the higher frequency side in comparison with those solutions of sodium alkyl sulfates.

Estimation of Kinetic Parameters for Micellar Formation. Judging from the investigated frequency range and other information from the literature,[1-3] the relaxation process observed here should be ascribed to a "fast" relaxation process, due to an exchange process of a surfactant between micelles and a bulk solution. The kinetic parameters for this process can be estimated by applying some of the important relations derived from a general model of the micellar formation proposed recently.

Teubner[16] has derived the following expression for the relaxation time of the ultrasonic relaxation due to a surfactant exchange process between micelles and a bulk solution, using the approximations introduced by Aniansson and Wall.[21]

$$\frac{1}{\tau}=2\pi f_r=\frac{k_{-1}}{\sigma^2}+\frac{k_{-1}}{\bar{m}}\left(\frac{C}{C_1}-1\right), \tag{7}$$

where C and C_1 represent the total and monomer concentrations of surfactant, respectively, and usually C_1 is assumed to be equal to the critical micelle concentration. Notations $\bar{m}$ and σ represent the mean aggregation number and the variance of the size distribution on proper micelles, respectively, and k_{-1} is the mean of the dissociative rate constant. He has further derived an expression for absorption maxima per wavelength, μ_{max}, as follows[22]:

$$\mu_{max}=\frac{\pi\rho u^2(\Delta V_s)^2C_1\frac{\sigma^2}{\bar{m}}\left(\frac{C}{C_1}-1\right)}{2RT\left\{1+\frac{\sigma^2}{\bar{m}}\left(\frac{C}{C_1}-1\right)\right\}}, \tag{8}$$

where μ_{max} is defined as $\mu_{max}=A f_r u/2$. Here ΔV_s[23] represents the change in the molar volume due to the exchange process, ρ is the density of the solution, R is the gas constant and T is the temperature.

An examination of Eq. 7 indicates that a graph of $1/\tau$ vs. (C/C_1-1) should give a linear correlation with the intercept and slope of the line providing values for k_{-1}/σ^2 and $k_{-1}/\bar{m}$, respectively (Fig. 7 shows that a linear correlation).

If values of the critical micelle concentration and the micelle aggregation number are available, kinetic parameters k_{-1} and σ^2 can be estimated from the values of k_{-1}/σ^2 and $k_{-1}/\bar{m}$. The value of the associative rate constant k_1 is further estimated on the basis of the assumption, $k_1=k_{-1}/C_1$. Table 2 lists the values of the estimated kinetic parameters. Here, the following data were used: $C_1=1.46\times10^{-2}$ M (from experiment[24]); aggregation number $\bar{m}=49$ (average value in the literature[25-28]).

ΔV_s is estimated from an analysis of the relaxation amplitude. Figure 7 also shows the results of a relaxation amplitude analysis. As is seen in the figure, there is a small disagreement[29] between

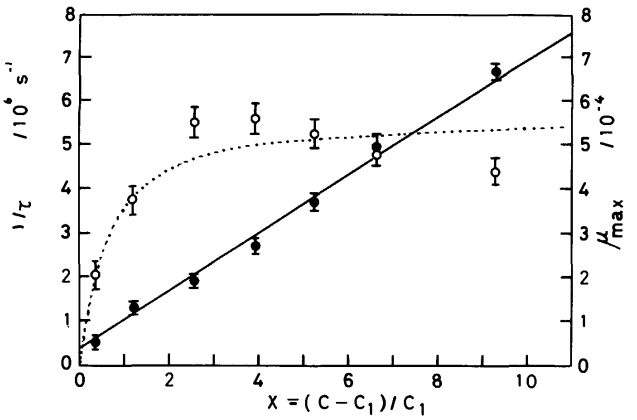

Fig. 7. Reciprocal relaxation times, $1/\tau$ (●), and absorption maxima per wavelength, μ_{max} (○), as a function of the ratio of micellar to monomer concentrations normalized with cmc, $X=(C-C_1)/C_1$. Solid and dotted lines represent values calculated from Eqs. 7 and 8, respectively.

Table 2. Kinetic Parameters for Aqueous Solutions of DTAB at 25 °C

k_1	k_{-1}	σ	$\sigma^2/\bar{m}$	ΔV_s
$M^{-1}s^{-1}$	s^{-1}	—	—	$cm^3\,mol^{-1}$
2.2×10^9	3.2×10^7	8.8	1.6	5.3

experiment and theory. The measured absorption maxima per wavelength, μ_{max}, at first, increases and reaches its maximum value, and then decreases with increasing concentration. On the other hand, a mathematical examination of Eq. 8 indicates that it should increase monotonically and never decrease with increasing concentration if $\sigma^2/\bar{m}$ and ΔV_s remain constant. A similar disagreement has been already reported by some investigators. Teubner[16] has pointed out that the disagreement may be due to a neglect of the activity coefficients and/or the monomer concentration decreasing with an increasing surfactant concentration above the critical micelle concentration. On the other hand, Gettins et al.[30] have pointed out that it may arise from a thermodynamical treatment in Teubner's theory. Though it is difficult, at this stage, to clarify the sources of the disagreement, the values of ΔV_s and kinetic parameters estimated here are quite reasonable if they are compared with those that have been reported in the literature.[1,16]

The authors would like to express their appreciation to Prof. Shin Tsuge of Nagoya University for chemical analysis of DTAB used in this study. The present work was supported in part by a Grant-in-Aid for Scientific Research (Special Research Project on Ultrasonic Spectroscopy and Its Application to Materials Science, No. 59220014) from the Ministry of Education, Science and Culture.

References

1) E. A. G. Aniansson, S. N. Wall, M. Almgren, H. Hoffmann, I. Kielman, W. Ulbricht, R. Zana, J. Lang, and C. Tondre, *J. Phys. Chem.*, **80**, 905 (1976).
2) J. Rassing, P. J. Sams, and E. Wyn-Jones, *J. Chem. Soc., Faraday Trans. 2*, **70**, 1247 (1974).
3) J. Lang, C. Tondre, R. Zana, R. Bauer, H. Hoffmann, and W. Ulbricht, *J. Phys. Chem.*, **79**, 276 (1975).
4) T. Yasunaga, H. Oguri, and M. Miura, *J. Colloid Interface Sci.*, **23**, 352 (1967).
5) J. Gormally, B. Szuba, E. Wyn-Jones, and D. G. Hall, *J. Chem. Soc., Faraday Trans. 2*, **81**, 395 (1985).
6) S. Kato, T. Suzuki, H. Nomura, and Y. Miyahara, *Macromolecules*, **13**, 889 (1980).
7) S. Kato, N. Yamauchi, H. Nomura, and Y. Miyahara, *Macromolecules*, **18**, 1496 (1985).
8) E. Wyn-Jones and W. J. Oriville-Thomas, *Trans. Faraday Soc.*, **64**, 2907 (1968).
9) L. W. Dickson, H. Nomura, R. E. Verrall, T. Suzuki, and S. Kato, *J. Phys. Chem.*, **85**, 2273 (1981).
10) T. Stuehr, "Ultrasonic Methods," in "Techniques of Chemistry," ed by G. G. Hammes, Wiley-Interscience, New York (1974) Vol. 6 Part 2, pp. 273—283.
11) F. Eggers, *Acustica*, **19**, 323 (1967).
12) F. Eggers and Th. Funck, *J. Acoust. Soc. Am.*, **57**, 331 (1975).
13) F. Eggers, Th. Funck, and K. H. Richmann, *Rev. Sci. Instrum.*, **47**, 361 (1976).
14) P. K. Choi, Y. Naito, and K. Takagi, *J. Acoust. Soc. Am.*, **74**, 1801 (1983).
15) Y. Naito, P. K. Choi, and K. Takagi, *J. Phys. E; Sci. Instrum.*, **18**, 13 (1985).
16) Teubner, *J. Phys. Chem.*, **83**, 2917 (1979).
17) S. Kato, H. Nomura, and Y. Miyahara, *Polymer J.*, **11**, 455 (1979).
18) T. Ohsawa, Ph. D. Thesis, The University of Tokyo, Tokyo (1969).
19) R. Folger, H. Hoffmann and W. Ulbricht, *Ber. Bunsenges. Phys. Chem.*, **78**, 986 (1974).
20) K. Takeda, J. Sci., *Hiroshima Univ. Ser. A*, **40**, 87 (1976).
21) E. A. G. Aniansson and S. N. Wall, *J. Phys. Chem.*, **78**, 1024 (1974).
22) It should be noted that the numerical factor of 2 is inserted in the denominator of Eq. 8 in order to make it compatible with the more practical definition of μ_{max} as previously defined in Ref. 32 and used in this study.
23) Note that ΔV in Teubner's theory represents the volume change of reaction per unit change of ordering parameter, ξ, at constant entropy and temperature (in our paper ΔV is expressed as ΔV_s). The ΔV is related to the volume change at constant pressure and temperature, $(\Delta V)_{P,T}$ as follows:

$$\Delta V = (\Delta V)_{P,T} - \frac{vT\theta^{\infty}}{C_p^{\infty}}\Delta S_P,$$

where ΔS_P represents the entropy change of reaction per unit change of ξ, and C_p, v, and θ are molar heat capacity at

constant pressure, molar volume, and expansivity, respectively. Superscript ∞ represents the instantaneous or "frozen" properties measured at fixed ξ.

24) R. Zieliński, S. Kato, H. Nomura, and S. Ikeda, to be published.

25) H. V. Tartar, *J. Colloid Sci.*, **14**, 115 (1959).

26) H. V. Tartar and A. L. Lelong, *J. Phys. Chem.*, **59**, 1185 (1956).

27) P. Debye and P. A. Smudski, cited in Ref. 25.

28) H. J. L. Trap and J. J. Hermans, *Proc. Koninkl. Ned. Akad. Wetenschap.* **B58**, 97 (1955).

29) Of course much better agreement will be obtained if we make the relaxation amplitude analysis, independently of the relaxation time analysis, as a few investigators[30] have done. However, ultrasonic relaxation spectra should be analysed in a selfconsistent way for both relaxation time and relaxation amplitude because the ultrasonic relaxation study does not provide a couple of information, relaxation time and amplitude, independently.

30) J. Gettins, P. L. Jobling, M. F. Walsh and E. Wyn-Jones, *J. Chem. Soc., Faraday Trans. 2*, **76**, 794 (1980).

31) O. Nomoto, "Cho-onpa Gijutsu Binran," ed by J. Saneyoshi et al., Nippon Kogyo Shinbunsha, Tokyo (1984) Part IV, pp. 1286.

32) R. Zana and S. Yiv., *Can. J. Chem.*, **58**, 1780 (1980).

 © 1986 The Chemical Society of Japan Bull. Chem. Soc. Jpn., 59, 715—720 (1986)

Studies of Collectors. VII.[1] Flotation of Heavy Metal Ions by Using Colored Surfactant

Yoshifumi KOIDE,* Shigekazu SATO, and Kimiho YAMADA
Department of Synthetic Chemistry, Faculty of Engineering, Kumamoto University, Kurokami, Kumamoto 860
(Received August 14, 1985)

Colored surfactants containing complex radicals(R-Bc, R-Bs, R-Sh, R-S, R-C, R-Ha, and R-Hb) were applied as ion-flotation collectors and foam-fractionation collectors. The extent of floatabilities for the colored complexing surfactants and metal ions was easily recognized by the degree of discoloration. R-Bc, R-Bs, and R-Sh with low HLB values formed floatable complexes in pH 6—9 with Cu^{2+}, Cd^{2+}, Hg^{2+}, Pb^{2+}, and Sr^{2+}. The residual concentrations of R-Sh, R-Bc, and R-Bs were below 0.1 ppm; however, these concentrations gradually increased after obtaining a minimum concentration of metal ions. Since R-C, R-Ha, and R-Hb had high HLB values, they easily floated Cu^{2+}, Pb^{2+}, and Cd^{2+} by foam fractionation. The concentrations of R-C, R-Ha, and R-Hb in foams or aqueous solutions were correlated to their foaming abilities.

Ion flotation is a method for separating trace amounts of metal ions from an aqueous solution.[2] The collector should be designed so as to effectively float specific metal ions, and the collector should not remain in the residual solution. In order to develop such a collector, the characteristics of surfactants containing complex radicals have been studied. In a previous paper, it was proved that complexing surfactants within an HLB range of 4—14 could very effectively remove metal ions during ion flotation. If their aqueous solutions produce a stable foam by bubbling air, such a complexing surfactant can be expected to be an excellent foam-fractionation collector. Therefore, such a complexing surfactant should be examined regarding applications both as an ion-flotation collector and a foam-fractionation collector. Thus far, its behavior in an aqueous solution and its characteristics during foam fractionation have not been sufficiently elucidated, e.g., as a residual collector, a mechanism of foam fractionation, etc.. In such studies, a simultaneous determination of metal ions and collectors is preferable. A colored surfactant can be easily detected by colorimetry. Moreover, the floatability of metal ions can also be estimated from the fading of a colored surfactant solution. In this study, seven easily prepared colored surfactants were applied as an ion-flotation collector and as a foam-fractionation collector. There have been some reports related to the removal of metal or dye ions using an ionic surfactant and a complexing agent.[2,4,5] However, no papers have been published on a comparative study of the metal-floating mechanism regarding ion flotation and foam fractionation using a colored complexing surfactant.

Experimental

Synthesis of Colored Surfactants. Diazotized *o*-aminobenzoic acid reacted at a pH of 4 with ethyl acetoacetate to form hydrazone. The hydrazone coupled at 0—3 °C with diazotized *p*-toluidine in an alkaline solution to form a 1,5-diphenyl-formazan compound(F).[6] Dyes containing carboxylic or sulfonic acid (R-Bc, M-Bc, R-Bs, and M-Bs, see Fig. 1) were obtained by the coupling of diazotized *p*-aminobenzoic acid and diazotized sulfanilic acid with *N*-dodecylaniline or with *N*-methylaniline, respectively,[7] The crude F, R-Bc, M-Bc, R-Bs, and M-Bs were purified by recrystallization from ethanol. Then, *p*-dodecylaniline was prepared by heating 1-dodecanol with aniline at 250 °C in the presence of zinc chloride (bp 185—191 °C/5 mmHg†).[8] The diazotized *p*-dodecylaniline coupled at pH 4 with 4,5-dihydroxy-1-naphthalene-sulfonic

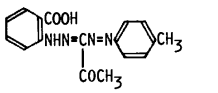

F

Abbr.	*n*	X
R-Bc	12	COOH
M-Bc	1	COOH
R-Bs	12	SO_3H
M-Bs	1	SO_3H

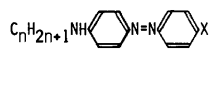

Abbr.	a	b	c	d	e
R-Sh	OH	H	H	SO_3Na	OH
R-S	NH_2	H	SO_3Na	H	OH
R-C	OH	SO_3Na	H	H	OH
R-Ha	OH	SO_3Na	H	H	NH_2
R-Hb	NH_2	SO_3Na	H	H	OH

Fig. 1. Formulas and abbreviations.

† 1 mmHg=133.322 Pa.

acid to form R-Sh, at pH 9 with 8-amino-1-naphthol,5-sulfonic acid to form R-S, at pH 5 with 4,5-dihydroxy-2,7-naphthalene-disulfonic acid to form R-C, or at pH 5 with 8-amino-1-naphthol-3,6-disulfonic acid to form R-Ha and at pH 9 to form R-Hb. The five crude dyes(disodium salts) were precipitated by salting techniques. The dyes were washed with acetone and then with small amount of cold water. The formulas and abbreviations are shown in Fig. 1.

Apparatus and Procedures. The flotation apparatus and procedures were the same as those previously reported.[3] The floatability(%) of a metal ion was calculated using:

$$f = \frac{a_0 - a_1}{a_0} \times 100,$$

where a_0 and a_1 denote the initial and the final metal concentrations. The metal ions were determined with an atomic absorption spectrophotometer (Hitachi 170—30) and the minimum values were determined by the decrease of the colored surfactant. The floatability of a colored surfactant was calculated using the same formula as that for metal ions. Its amount in an aqueous solution was determined by spectrophotometry (Hitachi model 101).

Results and Discussion

Colored Surfactant. The structures of colored surfactants were confirmed by means of their IR spectra (Shimadzu IR-408), chromatograms, elementary analyses (Yanaco CHN Corder MT-3), and a determination of an azo group using a titanium trichloride solution.[9] F: Mp 182.0—185.0 °C; IR (KBr) 1700 (carboxyl group $\nu_{C=O}$), 1600 ($\nu_{C=O}$), and 850 (phenylene δ_{C-H}) cm^{-1}; Found: C, 62.6; H, 4.8; N, 17.8%; Calcd for $C_{17}H_{16}N_4O_3$: C, 62.95; H, 4.97; N, 17.27%. R-Bc: Mp 199—202 °C; Found: C, 73.3; H, 8.4; N, 9.9%; Calcd for $C_{25}H_{35}N_3O_2$: C, 73.31; H, 8.61; N, 10.26%. R-Bs: Mp 225—228 °C; Found; C, 64.0; H, 8.0; N, 9.3%; Calcd for $C_{24}H_{35}N_3O_3S$: C, 64.68; H, 7.90; N, 9.43%. R-Sh: Yield 23%; Found: N, 4.96%; Calcd for $C_{28}H_{35}N_2O_5SNa$: N, 5.24%. R-S: Yield 37%; Found: N, 7.36%; Calcd for $C_{28}H_{36}N_3O_4SNa$: N, 7.87%. R-C: Yield 51%; Found: N, 4.28%; Calcd for $C_{28}H_{34}N_2O_8S_2Na_2$: N, 4.40%. R-Ha: Yield 44%; Found: N, 6.52%; Calcd for $C_{28}H_{35}N_3O_7S_2Na_2$: N, 6.61%. R-Hb: Yield 38%; Found: N, 6.57%; Calcd for $C_{28}H_{35}N_3O_7S_2Na_2$: N, 6.61%. The colors of these surfactants were orange or red. Table 1 shows their absorption spectra and surface activities. Their molar absorptivities were of the order 10^4, the same as that of a commercial dye. The absorption spectrum changed with pH. At pH 3, R-Sh and R-C showed a deep color (purple) and the others showed a slight color (R-Bc red, R-Bs red, R-Ha violet, and R-Hb red). The concentrations could be determined by absorbance measurements.

Surface tensions were measured on a Du Noüy surface-tension balance. The colored surfactants lowered the surface tension to 40—47 dyn cm^{-1} {above their critical micelle concentrations (cmc)}. However, M-Bc and M-Bs (having no long alkyl group) scarcely lowered the surface tension. The surface tension of an F solution was 53 dyn cm^{-1}. The cmc of colored surfactants were low, and that of R-S couldn't be measured because of a lower solubility. Their low solubility and low cmc might be caused by a hydrophobic property based on the naphthalene ring and on the hydrogen bridge between both hydroxyl groups or between hydroxyl and amino groups.

Table 1. Absorption Spectra and Surface Activities

Surfactant	Color[a]	Absorption spectrum[b] λ_{max} nm	ε $\times 10^4$	Surface activity[c] cmc wt%	γ dyn cm^{-1}
R-Bc	Orange	450	2.6	0.06	47
R-Bs	Yellow	330	1.2	0.07	43
R-Sh	Red	490	1.2	0.005	40
R-S	Violet[d]	540[d]	—	—	—
R-C	Red	515	2.9	0.05	47
R-Ha	Red	520	2.7	0.05	47
R-Hb	Purple	535	2.8	0.05	42
F	Red	440	1.9	—	53[e]

a) Color of the surfactant in alkaline soln (pH 11). b) Absorption spectrum at pH 11. c) cmc and surface tension(γ) at pH 11. d) Color and λ_{max} in ethanol. e) 0.1 wt% of F.

Ion Flotation. The determination method was at first examined using a colored precipitation reagent. An organic precipitation reagent usually has a slight ability to float metal ions[1] since its solution shows a weak surface activity. Cd^{2+} flotation using F was effective at pH 7, even from a solution of the Cd^{2+}–Ca^{2+} mixture (Fig. 2-left). The final concentration of Cd^{2+} was 2.2±0.1 ppm (initial: 10 ppm). The concentration was lowered a little by adding an excess of F. Dissolved metal and collector concentrations depend on their solubility product if the resulting complex is floatable. However, an excess additive is not effective. In order to easily detect final concentrations, reversed additives were examined, i.e., a small amount of Cd^{2+} was successively added to a colored F solution. Initially, the color scarcely changed. Then, it faded after Cd^{2+} was added (greater than 2.3±0.2 ppm) since the F formed a floatable Cd^{2+} complex. Figure 2-right shows the absorbance change of an F solution when metal ions (Cu^{2+}, Ni^{2+}, Cd^{2+}, Zn^{2+}, and Ca^{2+}) were successively added. The inflection point in the F concentration curve indicated the minimum metal concentration in the solution. The minimum concentration of Cd^{2+} (according to the inflection-

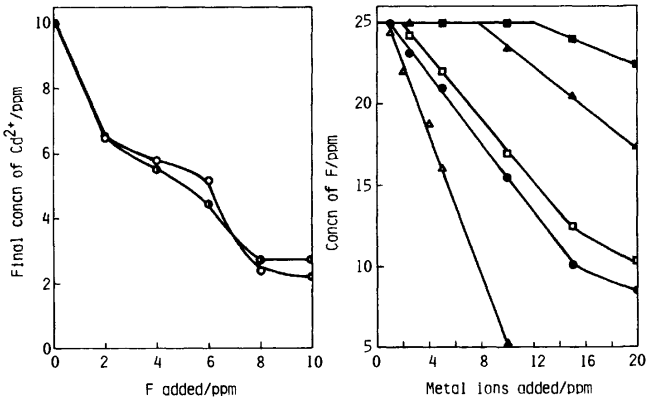

Fig. 2. Final concn of Cd^{2+} by usual determination and min metal concn according to inflection-point method.
Left usual determination. Right inflection-point method: inflection points in F concn curve suggest min metal concn. pH: 7.
○: Cd^{2+}, ◑: Cd^{2+} (+50 ppm Ca^{2+}).
△: Cu^{2+}, ●: Ni^{2+}, □: Cd^{2+}, ▲: Zn^{2+}, ■: Ca^{2+}.

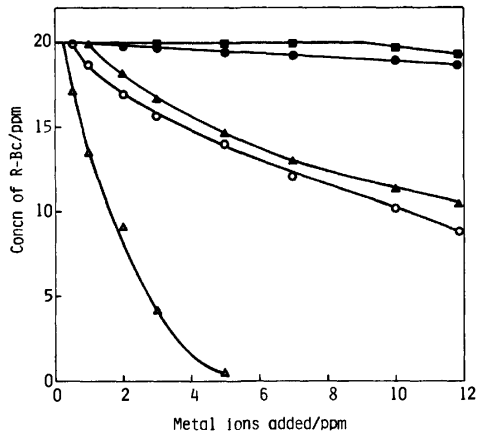

Fig. 3. Determination of min metal concn according to inflection point in R-Bc concn curve.
△: Cu^{2+}, ○: Cd^{2+}, ▲: Zn^{2+}, ●: Pb^{2+}, ■: Ca^{2+}.

point method) agreed with the final concentration of Cd^{2+} by the usual determination (Fig. 2-left). The minimum values from the F-concentration curve were Cu^{2+} 0.8 ppm<Ni^{2+} 1.5 ppm<Cd^{2+} 2.3 ppm<Zn^{2+} 9.3 ppm<Ca^{2+} 12 ppm. A selective removal of Cd^{2+} from the Ca^{2+} mixture can be seen by the inflection point in the F-concentration curve.

Then, the colored surfactants containing long alkyl groups (R-Bc, R-Bs, R-Sh, and R-S) were examined below their cmc as ion-flotation collectors. The floatabilities of these surfactants were easily determined by the discolored solution and the colored scum. The floatabilities of Cu^{2+}, Cd^{2+}, Zn^{2}, Pb^{2+}, and Ca^{2+} using R-Bc or R-Bs were high at pH 6—9. The minimum metal concentrations (from the inflection points of the R-Bc concentration curve) were Cu^{2+} below 0.5 ppm, Cd^{2+} 0.5 ppm, Zn^{2+} 1 ppm, Pb^{2+} 1.5 ppm (indistinct), Ca^{2+} 8 ppm (indistinct),

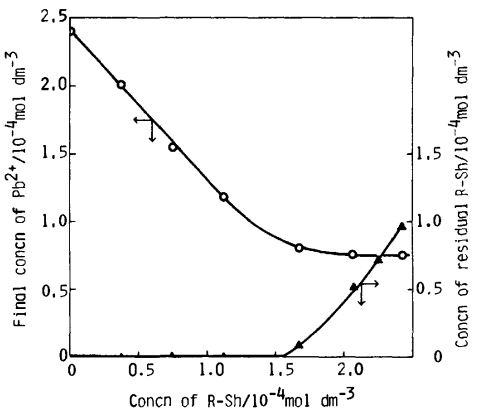

Fig. 4. Final concn of Pb^{2+} and concn of residual R-Sh.
Initial Pb^{2+} concn: 2.4×10^{-4} mol dm^{-3}; pH 6.0.
○: Pb^{2+}, ▲: R-Sh.

as shown in Fig. 3. Similarly, the values from an R-Bs concentration curve were all below 0.5 ppm. However, the inflection point of an M-Bc or M-Bs concentration curve was not observed in the metal-concentration range of 0—15 ppm (Cu^{2+}, Cd^{2+}, Zn^{2+}, Pb^{2+}, Ca^{2+}). Therefore, a long alkyl group is necessary to serve as an effective collector. Each minimum metal concentration according to R-Bc or R-Bs concentration curves (except Ca^{2+}) had similar values compared with that in F. The similar values suggest less selectivity. Their smaller selectivities were presumably caused by similar attractive electrostatic forces between the anionic collectors and the cationic metal ions. The removal of metal ions by ion flotation using sodium dodecanoate(SD) or sodium dodecyl sulfate(SDS) was also less selective,[10] but the minimum values were lower than those according to R-Bc or R-Bs concentration curves. The difference might be based on their HLB. The Cu^{2+} and Pb^{2+} floatabilities using the dihydroxy-type R-Sh were high at pH 4—8, and those using the hydroxy amino-type R-S were high at pH 7—10. The structures of floatable complexes were considered to be R-Sh$\langle_{O}^{O}\rangle$M(metal) and R-S$\langle_{NH_2}^{O}\rangle$MOH at an optimum pH, and those of unfloatable complexes would be cationic metal complexes at a lower pH and anion complexes with OH^- in higher pH. Thus, the flotation efficiency is affected by the HLB of a complex.[3] Figure 4 shows the relation between the additive, R-Sh, and its residual concentration in Pb^{2+} flotation. The Pb^{2+} concentration in an aqueous solution gradually decreased with an increase of R-Sh; then, it became constant (minimum value of Pb^{2+} concentration). The concentration of the residual R-Sh stayed close to zero (below 0.1 ppm) during while Pb^{2+} was decreasing. However, the R-Sh concentration gradually increased after an attainment of a minimum Pb^{2+} concentration. Similar

results were obtained using R-Bc and R-Bs. The increase in the collector concentration showed that the minimum concentration of a metal ion depended on their solubility product, and that the added collector was unfloatable. Therefore, an ion-flotation collector should be added carefully. Any addition must be stopped after an attainment of the minimum metal concentration. The removal slope of Pb^{2+} indicated that the molar ratio of the R-Sh–Pb complex was 1:1. The same ratio was obtained by an analysis of the scum and by a titration-curve measurement of 4,5-dihydroxy-2,7-naphthalene-disulfonic acid with Cu^{2+}, a similar chelate complex.[11] Furthermore, the potentiometric titration curves of R-Sh (with and without metal ions) were measured. The order of the stability constants was $Cu^{2+}>Pb^{2+}>Cd^{2+}>Ca^{2+}$. Therefore, Pb^{2+} could be selectively floated from a Pb^{2+}–Ca^{2+} mixture. The bonding forms of R-Sh, R-S, and F with metal ions differ from those of R-Bc and R-Bs. The minimum value using R-Sh, R-S, or F was inferior to that using R-Bc or R-Bs, since the solubilities of the complex salts (R-Bc and R-Bs) were lower than those of the chelate complexes (R-Sh, R-S, and F). However, the selectivities of the chelate complexes were superior to those of the complex salts.

Foam Fractionation. Disulfo-type R-C, R-Ha, and R-Hb with a large hydrophilic property were used below their cmc as foam-fractionation collectors after they showed a foaming ability. A separation was recognized by a discoloration of a solution and the appearance of a colored foam. Figure 5 shows a simple determination of the minimum metal concentration using R-Ha. The inflection point for the foam fractionation was not very clear since a colored surfactant also floated without the metal ions. However, the inflection points could be read from Fig. 5. The order of the selectivity was $Cd^{2+}>Ca^{2+}>Pb^{2+}>Cu^{2+}$, whereas the stability constants of R-Ha complexes were $Cu^{2+}>Hg^{2+}>Pb^{2+}>Cd^{2+}>Ca^{2+}$. These differences are probably caused by their foaming power, as described in the following section. Furthermore, 10^{-4} mol dm^{-3} of radioactive $^{90}Sr^{2+}$ was removed (80—87% in pH 4—11) using 2×10^{-4} mol dm^{-3} of R-Hb; the floatability was twice as high as that using SDS.

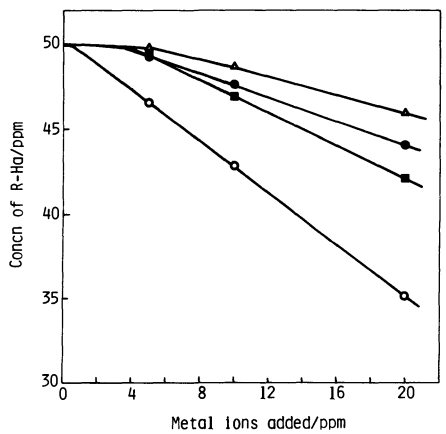

Fig. 5. Determination of min metal concn according to inflection point for foam fractionation.
○: Cd^{2+}, ■: Ca^{2+}, ●: Pb^{2+}, △: Cu^{2+}.

The foam fractionation for the floatabilities of four metal ions and these surfactants are shown in Table 2. The floatabilities using R-C were Cd^{2+} 97%, Cu^{2+} 68%, Pb^{2+} 65%, and Hg^{2+} 24%. The ratio of the metal-ion floatability to the R-C floatability was about 1(0.9—1.1) and the ratio to the R-Ha or R-Hb floatability was 0.7—1.0, except for that of Hg^{2+}. The order of the stability constants was $Cu^{2+}>Hg^{2+}>Pb^{2+}>Cd^{2+}>Ca^{2+}$. The stability constant of the 1,8-dihydroxylnaphthalene-3,6-disulfonic acid complex was log K_{CuL} 13.45,[11] while that of the metal hydroxide was log K_{HgOH} 11.51, log $K_{Hg(OH)_2}$ 11.15, and log K_{CuOH} 6.03.[12] Therefore, Hg^{2+} could be hydrolyzed at pH 7 and a ratio of the Hg^{2+} floatability to the colored surfactant of less than 0.6. Furthermore, the floatability was also affected by the foaming power. The relation between the foaming power and the concentration of the colored surfactant in a foam was measured at pH 3, 7, and 12 (Fig. 6). Such a foaming power (to rise to the top of a vessel) is required of a foam-fractionation collector. However, the formation of a rich foam lowered the surfactant concentration in the foam but not in an aqueous solution. A similar relation was observed in the presence of metal ions. The low foaming power was, consequently, excellent for the separation of the

Table 2. Foam Fractionation

Surfactant	Metal	Floatabilities[a]			Residual surfactant
		Metal	Surfactant	[M]/[Sur]	
		%	%	%/%	ppm
R-C	—	—	85	—	18
R-C	Cu	68	77	0.9	37
R-C	Hg	24	84	0.3	18
R-C	Pb	65	73	0.9	29
R-C	Cd	97	80	1.1	22
R-Ha	—	—	94	—	6
R-Ha	Cu	73	89	0.8	12
R-Ha	Hg	57	90	0.6	11
R-Ha	Pb	82	85	1.0	16
R-Ha	Cd	84	88	1.0	14
R-Hb	—	—	93	—	7
R-Hb	Cu	75	87	0.9	15
R-Hb	Hg	33	82	0.4	19
R-Hb	Pb	54	75	0.7	27
R-Hb	Cd	49	76	0.7	26

a) Initial concn of metal ions: 0.5×10^{-4} mol dm^{-3}; surfactant: 1.5×10^{-4} mol dm^{-3}; vol of soln: 50 cm^3; pH; 7.

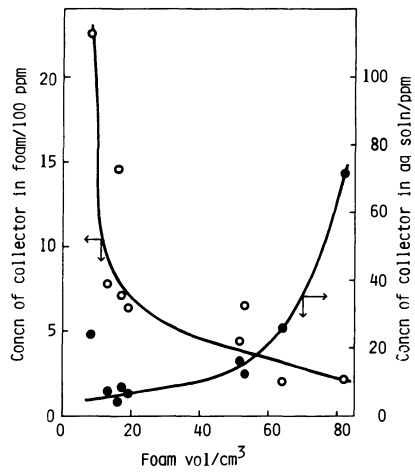

Fig. 6. Relation between foaming power and concn of surfactant in foam.
Foaming power: foam vol after shaking up the 100 cm^3 of measuring cylinder containing 20 cm^3 of 0.2 % surfactant soln for 20 times. Foam fractionation: 1.5×10^{-4} mol dm^{-3} of surfactant.
○: Surfactant in foam, ●: surfactant in aq soln.

complex. However, R-Bc, R-Bs, and R-Sh can't be used as a foam-fractionation collector because of the instability of the foam. The residual concentration of a colored surfactant in the presence of metal ions was higher than that in their absence; i.e., R-Ha 12 ppm (with Cu^{2+}), 11 ppm (with Hg^{2+}), 16 ppm (with Pb^{2+}), 14 ppm (with Cd^{2+}), 6 ppm (without). Contrary to ion flotation, an excess surfactant is necessary to float metal complexes by foam. Furthermore, the residual surfactant concentration is expected to become lower by increasing the bubbling rate.[2] However, its effect on foam fractionation was not examined.

HLB Character in Foam Fractionation. The minimum concentration for ion flotation depended on the solubility product when the resulting complex was floatable. The floatability was affected by the HLB. However, the minimum concentration and floatability in a foam fractionation depended on their complex formation and on their foaming abilities. Foaming ability was correlated to the residual concentration of a surfactant. The concentration became low when the solubility product of the complex was small. Then, the HLB values were also low. Therefore, the foaming power can be associated with their HLB value. The calculated HLB values of complexes, based on the Oda equation,[13] are shown in Table 3. The floatable species were thought to be surfactant-hydroxo-metal complexes (Sur-MOH). The suitable HLB value for ion flotation was considered to be 5—12 and the value for foam fractionation was considered to be 21. These HLB ion-flotation values are almost the same as the value (4—14) reported in a previous paper.[1] Also, the HLB values for a foam fractionation were found to be larger than those for ion flotation.

Table 3. HLB Values

	HLB values of complexes[a]			
	Sur-Na	$Sur\text{-}M^+$	Sur-MOH	$(Sur)_2$=M
Ion flotation				
F	25	16	10	—
R-Bc	16	9	5	4
R-Bs	18	11	7	6
R-Sh	19	15	12[b]	11
R-S	18	15	12	11
Foam fractionation				
R-C	32	24	21[b]	20
R-Ha	32	24	21	20
R-Hb	32	24	21	20
SDS	40	19	11	9

a) Calcd HLB based on the Oda equation.[13] b) Sur=M.

The results presented in this work provide an explanation for the character of a complexing surfactant during ion flotation and foam fractionation. A colored surfactant was well suited for a simultaneous determination of the collector and metal ions. The complexing surfactant remained slightly in an aqueous solution, but its ion-flotation concentration increased upon adding a collector after an attainment of the minimum metal concentration. The metal-floating mechanism in foam fractionation was explained using the HLB value. Thus, the characteristics of a complexing surfactant have become more apparent. In this experiment, the complex radicals which were used were less selective for specific metal ions. An excellent colored complexing collector can be obtained by a selection of a complex radical and the regulation of its HLB.

References

1) Y. Koide, S. Kitaoka, and K. Yamada, *Bull. Chem. Soc. Jpn.*, **58**, 2456 (1985).
2) F. Sebba, "Ion Flotation," Elserver Pub., London and New York (1962), pp. 120—122.
3) Y. Koide, H. Takamoto, K. Matsukawa, and K. Yamada, *Bull. Chem. Soc. Jpn.*, **56**, 3364 (1983).
4) R. Lemlich, "Adsorptive Bubble Separation Techniques," Academic Press, New York and London (1972), pp. 145—156.
5) K. Kobayashi, N. Watanabe, and T. Sasaki, *Bull. Chem. Soc. Jpn.*, **49**, 2701 (1976).
6) H. Iida, K. Ikeda, and T. Hidaka, *Kogyo Kagaku Zasshi*, **72**, 887 (1969).
7) K. Konishi, M. Kuroki, "Gosei-senryo no Kagaku," Maki-shoten, Tokyo (1965), p. 143.
8) O. Yoda, *Nippon Kagaku Zasshi*, **77**, 896 (1956).
9) S. Ueno, "Kagaku-jikkengaku, Dai-2bu Goseihen III," Kawaide, Tokyo (1943), p. 549.

10) K. Yamada and Y. Koide, Abstr. No. A-11. Nipponkagakukai-chugokushikokushibu-godotaikai, Hiroshima, Octorber 7—9, 1970.
11) R. Wake, H. Miyata, and K. Toei, *Bull Chem Soc Jpn*, **41**, 1452 (1968).
12) H. Freiser and Q. Fernando, "Ion-heiko", Kagakudojin, Kyoto (1970), p. 255.
13) R. Oda and K. Teramura, "Kaimen-kasseizai No Gosei To Sono-oyo" Makishoten, Tokyo (1962), p. 501.

Pulse Radiolysis Study of Reaction of OH Radicals with Triose Reductone

Hideo Horii,* Yasuo Abe, and Setsuo Taniguchi
Radiation Center of Osaka Prefecture, Shinke-cho, Sakai 593
(Received August 19, 1985)

The reaction between the hydroxyl radical (OH) and triose reductone (2,3-dihydroxy-2-propenal) in an aqueous solution has been studied by spectrophotometric pulse radiolysis. The OH radical adds to triose reductone (TRH_2) to form the transient OH adduct ($TRH(OH)^{-\cdot}$) with an absorption maximum at 398 nm, ε= 3150 $M^{-1}cm^{-1}$ (1 M=1 mol dm^{-3}) in a neutral solution. The OH adduct decays by second-order kinetics in the pH range 2—12. The rate constants for the reactions of the OH radical with dissociated and undissociated triose reductone are 1.4×10^{10} $M^{-1}s^{-1}$ and 9.9×10^{9} $M^{-1}s^{-1}$, respectively. The dependence of the transient absorption on the pH shows that the OH adduct has a pK_a value of 4.7.

The structure of triose reductone (2,3-dihydroxy-2-propenal) was determined to be CH(OH)=C(OH)-CHO by H. von Euler and C. Martius.[1] A very important characteristic of "reductone" is a strong reducing ability due to its enediol group, -C(OH)=C-(OH)-.[2] Well-known reductones, L-ascorbic acid,[3-5] adrenaline,[6] and dopamine[7] which play significant roles in biological systems, have been studied by pulse radiolysis. These reductones react with OH radicals to form OH adducts or one-electron oxidized radicals. The OH adducts can be converted to one-electron oxidized radicals by dehydration. Thus, the oxidation of the reductones has been shown to proceed through the intermediate radicals. Triose reductone is yielded in biological systems[1,8-10] and in the process of the browning reaction of milk.[11] In addition, it reacts with amino compounds to yield anil compounds[2] or causes a DNA-breaking action in the presence of Cu^{2+}.[12] The enzymatic oxidation of triose reductone has also been reported to produce a free radical in an ESR study.[13,14] It is useful to study the oxidation mechanism of triose reductone, as it is an important compound in biological systems[2] and is one of the simplest reductones. We have kinetically studied the oxidations of triose reductone using oxygen and hydrogen peroxide,[15] a peroxodisulfate ion,[16] and a hexacyanoferrate(III) ion,[17]. In our previous paper[18,19] it was found that triose reductone is oxidized by $X_2^{-\cdot}$ (X=SCN, Cl, Br, I) and $N_3\cdot$ to yield a one-electron oxidized radical. In the present research we studied the reaction of the OH radical with triose reductone kinetically and found a different transient species from the one-electron oxidized radical ($TR^{-\cdot}$).

Experimental

Pulse irradiation was accomplished using the 18 MeV linac (High Voltage Engineering Co.) of the Radiation Center of Osaka Prefecture at room temperature (about 20 °C). Details of the detection systems, dosimetry, and solution handling techniques were previously described.[19] All solutions were prepared from triply distilled water. Dinitrogen monoxide (Showa Denko Co., High Purity, upper limit of O_2 content: 10 ppm) was used after the deaeration of solutions by argon (Osaka Sanso Co., For Instrument Grade). The solutions were bubbled before irradiation for ≈60 min with Ar and N_2O. This procedure converts hydrated electrons into OH radicals. Triose reductone was prepared and purified by the method of Euler and Martius.[1] All other chemicals used were of analytical reagent grade. The pH of solutions was generally adjusted by an addition of the appropriate amounts of $HClO_4$ or NaOH.

Results and Discussion

Absorption Spectra of the Transient Intermediates Yielded by OH Radicals. A N_2O-saturated solution containing 300 μM of triose reductone at pH 7.8 was pulse-irradiated at a dose of about 500 rad per pulse. The spectrum of the transient intermediate immediately after a pulse at pH 7.8 is shown in Fig. 1. The transient absorption almost disappears upon the addition of 0.2 M *t*-BuOH, which scavenges OH

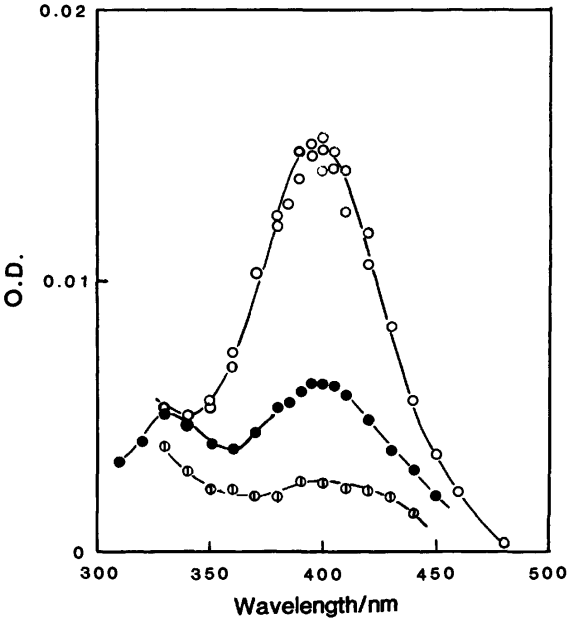

Fig. 1. Transient absorption spectra produced by pulse irradiation of N_2O saturated 3×10^{-4} M triose reductone solution. Normalized dose, 500 rad; pH 7.8 (○), pH 4.63 (●), pH 3.03 (Ⓓ).

radicals. The result indicates that a transient absorption is produced by a reaction of triose reductone with the OH radical. The absorption spectrum shows an almost symmetrical (Gaussian-type) band with a maximum at 398 nm and a width at half-maximum of 71 nm. The shape of this spectrum is similar to that[19] of the triose reductone radical ($TR^{-}\cdot$, λ_{max}=398 nm) yielded through the oxidation of triose reductone by the inorganic radicals ($N_3\cdot$, $(SCN)_2^{-}\cdot$, $Br_2^{-}\cdot$, etc). The absorption coefficient around a neutral pH was obtained to be 3150 $M^{-1}cm^{-1}$ at 398 nm from the linear slope of absorbance vs. pulse dose. This value is about half of that of the triose reductone radical (5500 $M^{-1}cm^{-1}$).[19] Analogous facts have been found through a pulse radiolysis of ascorbic acid.[3] The absorption coefficients of the spectra become smaller with a decrease in the pH. The spectra of the transients at pH 4.63 and 3.03 are also shown in Fig. 1. The absorption at 398 nm almost disappears at pH 3. The triose reductone radical ($TR^{-}\cdot$) has a pK_a of 1.4.[19] If this intermediate is the triose reductone radical, the absorbance around 400 nm should remain unchanged at a pH >3. From these facts, it is seen that this transient species is not the triose reductone radical. It should be the OH adduct of triose reductone, since the OH radical is easy to add to an unsaturated bond. Triose reductone has two dissociation constants[15] (pK_1=5.0, pK_2=13.0). Therefore, the reaction scheme can be described by the following equations.

$$H_2O \rightsquigarrow e_{aq}^{-},\ H,\ OH,\ H_2O_2,\ H_2 \qquad (1)$$

$$N_2O + e_{aq}^{-} \longrightarrow OH + OH^{-} + N_2 \qquad (2)$$

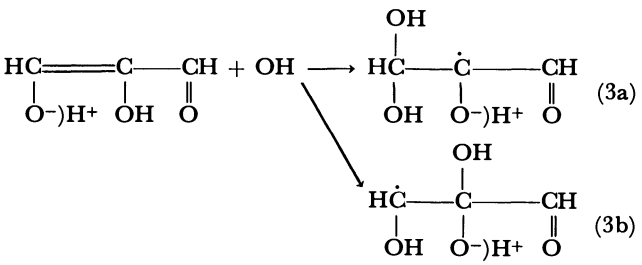

(3a)

(3b)

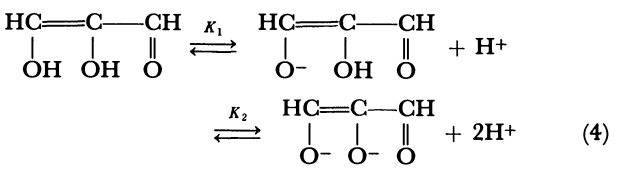

(4)

The electron density is greater on C2 than C3 from the results of ab initio MO calculations of triose reductone.[20] It is also presumed by electronic effects. Hence, an electrophilic attack of the OH radical is more likely to occur through reaction 3b than 3a. Ascorbic acid reacts with the OH radical to yield the OH adduct and the adduct loses H_2O (or OH^{-}) to form the ascorbic acid radical.[3] However, the conversion of the OH adduct of triose reductone into the $TR^{-}\cdot$ radical was not observed. This OH adduct should be rather stable and can not be converted into the $TR^{-}\cdot$ radical by dehydration as in the following reaction (5).

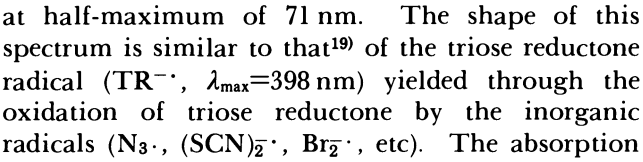

(5)

Rate Constants for the Reactions of Dissociated and Undissociated Triose Reductone with OH Radicals. The rate constant for the reaction of dissociated triose reductone with the OH radical was measured by the competition between TRH^{-} and *t*-BuOH with OH (Eqs. 3 and 6).

$$t\text{-BuOH} + OH \longrightarrow t\text{-BuOH radical} + H_2O \qquad (6)$$

From this competition it follows that

$$\frac{D_0}{D_s} = 1 + \frac{k_6[t\text{-BuOH}]}{k_3[TRH^{-}]}, \qquad (I)$$

where D_0 and D_s are the optical densities at 400 nm in the absence and presence of *t*-BuOH, respectively. *t*-Butyl alcohol is a well-known scavenger of OH redicals. A plot of D_0/D_s versus [*t*-BuOH]/[TRH^{-}] gives a straight line (Fig. 2a). From the slope, k_3 was determined to be 1.4×10^{10} $M^{-1}s^{-1}$, taking $k_6=5.2\times10^{8}$ $M^{-1}s^{-1}$.[21] Below a pH of 3.5, the transient absorption is very small above a wavelength of 310 nm. Therefore, the rate constant for a reaction of undissociated triose reductone with OH radicals was measured by the competition between TRH_2 and SCN^{-} with OH radicals. (Eqs. 3 and 7)

$$SCN^{-} + OH \longrightarrow \cdot SCN + OH^{-} \qquad (7)$$

The $\cdot SCN$ radical reacts with SCN^{-} to form $(SCN)_2^{-}\cdot$ which has an absorption maximum at 472 nm, according to the following reaction.

$$SCN^{-} + \cdot SCN \longrightarrow (SCN)_2^{-}\cdot \qquad (8)$$

From this competition it follows that

$$\frac{D_0}{D_s} = 1 + \frac{k_3[TRH_2]}{k_7[SCN^{-}]}, \qquad (II)$$

where D_0 and D_s are the optical densities at 472 nm, in the absence and presence of TRH_2, respectively. A plot of D_0/D_s versus [TRH_2]/[SCN^{-}] gives a straight line (Fig. 2b). From the slope, k_3 was determined to be 9.9×10^{9} $M^{-1}s^{-1}$, taking $k_7=1.1\times10^{10}$ $M^{-1}s^{-1}$,[22] which is most reliable in the competition method of thiocyanate. The rate constants of both the dissociated and the undissociated forms are summarized in Table 1. For the sake of a comparison, the data for L-ascorbic acid[3] (where 6×10^{9} $M^{-1}s^{-1}$ is used for k_7 and the recalculated data using $k_7=1.1\times10^{10}$

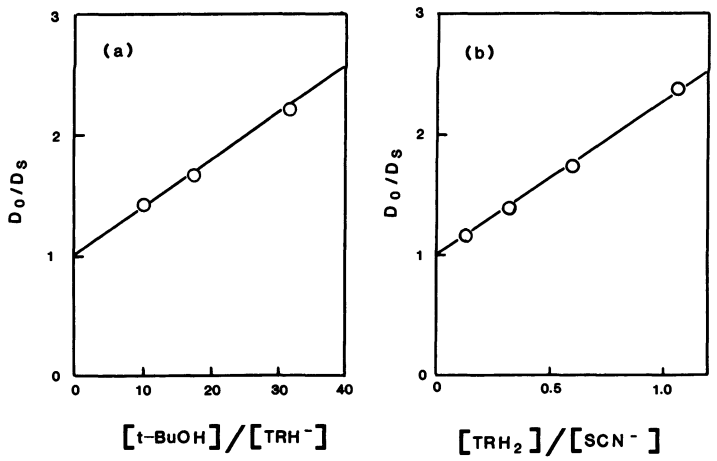

Fig. 2. Competition for OH by triose reductone and *t*-BuOH (or SCN^-). (a): N_2O saturated solution of 1×10^{-4} M triose reductone, pH 9.7, 1—3.2×10^{-3} M *t*-BuOH. (b): N_2O saturated solution of 4×10^{-4} M KSCN, pH 3.01, 0.5—4.3×10^{-4} M triose reductone.

Table 1. Rate Constants in $M^{-1}s^{-1}$ for the Reactions of Triose Reductone and Ascorbic Acid with OH Radicals

$k(TRH_2)$	$k(TRH^-)$	$k(AH_2)$	$k(AH^-)$
9.9×10^9	1.4×10^{10}	8.2×10^{9} a)	1.3×10^{10} a)
		4.5×10^{9} b)	7.0×10^{9} b)

TRH_2: triose reductone, TRH^-: monoanion of triose reductone, AH_2: ascorbic acid, AH^-: monoanion of ascorbic acid.
a: recalculated data from Ref. 3 using $k_6=1.1\times10^{10}$ $M^{-1}s^{-1}$.
b: Ref. 3.

$M^{-1}s^{-1}$) are also listed in Table 1. The rate constants for an addition of OH radicals with both reductones are almost diffusion controlled, but a little larger in dissociated forms than undissociated ones, respectively.

pK_a of the OH Adduct of Triose Reductone. The molar extinction coefficients (ε) of the OH adduct of triose reductone (determined at 400 nm as a function of pH) are shown in Fig. 3. The numerical values of ε were corrected for the transient species ($\varepsilon_{400\,nm}=300$ $M^{-1}cm^{-1}$)[19] produced by a reaction of triose reductone with the H radical. The smooth line in Fig. 3 was computed by assuming that the pH dependence of the extinction coefficient results from an acid-dissociation process, using $\varepsilon_{400\,nm}^{TRH_2(OH)\cdot}=250$ $M^{-1}cm^{-1}$, $\varepsilon_{400\,nm}^{TRH(OH)^{-}\cdot}=3150$ $M^{-1}cm^{-1}$. The acid-dissociation constant giving the best fit to the data was pK_a=4.7. The acid-base equilibrium is given as follows.

$$TRH_2(OH)\cdot \overset{pK_a=4.7}{\rightleftharpoons} TRH(OH)^{-}\cdot + H^+ \qquad (9)$$

The pK_a value of the OH adduct transient species is a little smaller than that of triose reductone (pK_1=5.0). This fact shows that the OH adduct radical is a little more acidic than triose reductone.

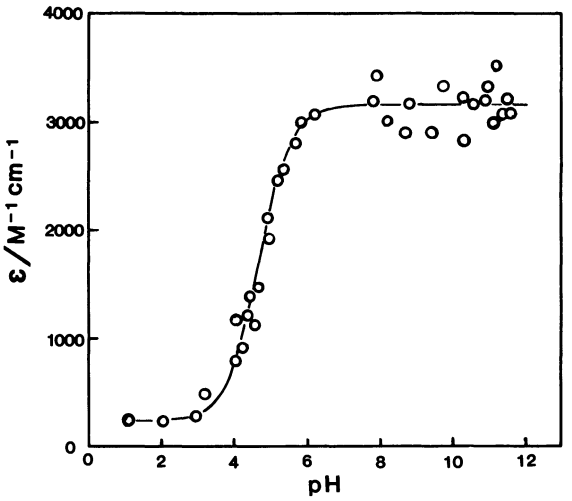

Fig. 3. Dependence of molar extinction coefficient(ε) at 400 nm, of the OH adduct of triose reductone on pH. N_2O saturated solutions of 1—5×10^{-4} M triose reductone.

Radical Decay Rate. The transient species yielded by a reaction of triose reductone with OH radicals decay by second-order kinetics over a wide pH range (pH 2—12). The reaction rate for two ions is dependent on the ionic strength (μ), as approximately given[23] by

$$\log k/k_0 = Z_AZ_B(1.02\mu^{1/2})/(1+\mu^{1/2}) = Z_AZ_Bm, \qquad (III)$$

where k_0 is the value of k at zero ionic strength, Z_A and Z_B are the charges of the two ions, and μ is the total ionic strength. The effect of the ionic strength on the decay rate of the OH adduct of triose reductone was studied at pH 9.4, where the radical was presumed to be dissociated from the value of pK_a (4.7), using sodium sulfate to vary μ. A plot of log $k_{obsd}/\varepsilon_{400}$ vs. m gave a straight line with a slope of

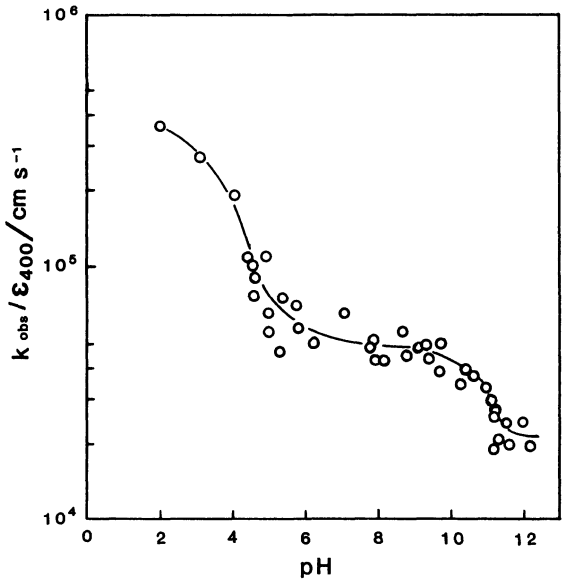

Fig. 4. Dependence of decay rate ($k_{obsd}/\varepsilon_{400}$) of the OH adduct of triose reductone radical corrected for ionic strength on pH.
N_2O saturated solutions of $1-5\times10^{-4}$ M triose reductone.

0.77. Hence, this intermediate probably has a unit negative charge and can be assigned to the one-dissociated OH adduct radical ($TRH(OH)^{-}\cdot$) in the pH range 5—10. Figure 4 shows the pH dependence of $k_{obsd}/\varepsilon_{400}$, where k_{obsd} is the observed second-order rate constants of the transients at 400 nm in triose reductone solutions saturated with N_2O. The rate constants were corrected for ionic strength. The values of k_{obsd} are almost constant in the pH range 5.5—9.5 ($k_{obsd}=1.5\times10^8$ M^{-1} s^{-1}). However, in the pH range 3—5.5, complex reactions as a result of the acid-base equilibrium of the intermediate occur according to the following equations.

$$TRH(OH)^{-}\cdot + TRH(OH)^{-}\cdot \longrightarrow \text{Products} \quad (10)$$

$$TRH_2(OH)\cdot + TRH(OH)^{-}\cdot \longrightarrow \text{Products} \quad (11)$$

$$TRH_2(OH)\cdot + TRH_2(OH)\cdot \longrightarrow \text{Products} \quad (12)$$

The effect of the H adduct of triose reductone seems to become greater around pH 2. The rate constant of k_{obsd} at pH 11.5 is 7×10^7 M^{-1} s^{-1}. The change of the rate constant around pH 11 is not yet well understood. This result might suggest the effect of a second dissociation of the OH adduct. However, since the data vary to a considerable extent, it is difficult to give a clean explanation.

The authors wish to thank the members of the linac group for operating the linac.

References

1) H. von Euler and C. Martius, *Liebigs. Ann. Chem.*, **505**, 73 (1933).
2) D. Nomura and H. Omura, "Chemistry of Reductone," Uchida Rokakuho Publishing Co., Ltd., Tokyo (1969).
3) M. Schöneshöfer, *Z. Naturforsh.*, **27b**, 649 (1972).
4) B. H. J. Bielski, D. A. Comstock, and R. A. Bowen, *J. Am. Chem. Soc.*, **93**, 5624 (1971).
5) B. H. J. Bielski, A. O. Allen, and H. A. Schwarz, *J. Am. Chem. Soc.*, **103**, 3516 (1981).
6) W. Bors, M. Saran, C. Michel, E. Lengfelder, C. Fuchs, and R. Spöttl, *Int. J. Radiat. Biol.*, **28**, 353 (1975).
7) H. W. Richter and W. H. Waddel, *J. Am. Chem. Soc.*, **105**, 5434 (1983).
8) G. Hesse and H. Schildknecht, *Angew. Chemie*, **68**, 75 (1956).
9) S. Adachi, *Nippon Nôgeikagaku Kaishi*, **30**, 713 (1956).
10) H. von Euler and E. Klussmann, *Z. Physiol. Chem.*, **217**, 167 (1933).
11) J. E. Hodge, *J. Agr. Food Chem.*, **1**, 928 (1953).
12) K. Shinohara, M. So, M. Nonaka, K. Nishiyama, H. Murakami, and H. Omura, *J. Nutr. Sci. Vitaminol.*, **29**, 481 (1983).
13) L. H. Piette, I. Yamazaki, and H. S. Mason, "Free Radicals in Biological Systems," M. S. Blois, Ed., Academic Press, p. 203 (1961).
14) I. Yamazaki and L. H. Piette, *Biochim. Biophys. Acta*, **77**, 47 (1963).
15) Y. Abe, H. Horii, S. Taniguchi, K. Kamai, and M. Takagi, *Bull. Chem. Soc. Jpn.*, **56**, 467 (1983).
16) Y. Abe, H. Horii, and S. Taniguchi, *Bull. Chem. Soc. Jpn.*, **57**, 222 (1984).
17) Y. Abe, T. Dohmaru, H. Horii, and S. Taniguchi, *Can. J. Chem.*, **63**, 1005 (1985).
18) H. Horii, Y. Abe, S. Taniguchi, S. Maeda, and T. Watanabe, *Chem. Lett.*, **1983**, 1313.
19) H. Horii, Y. Abe, and S. Taniguchi, *Bull. Chem. Soc. Jpn.*, **58**, 2751 (1985).
20) Y. Abe, H. Horii, S. Taniguchi, S. Yamabe, and T. Minato, *Can. J. Chem.*, in press.
21) R. L. Willson, C. L. Greenstock, G. E. Adams, R. Wageman, and L. M. Dorfman, *Int. J. Rad. Phys. Chem.*, **3**, 211 (1971).
22) L. M. Dorfman and G. E. Adams, *NSRDS-NBS* **46**, 57 (1973).
23) R. E. Weston, H. A. Schwarz, "Chemical Kinetics," Prentice-Hall, Inc., Englewood Cliffs, N. J., 169 (1972).

 © 1986 The Chemical Society of Japan Bull. Chem. Soc. Jpn., 59, 725—731 (1986)

Electrocatalysis in Metal Hydride Electrode. I. Hydrogen Electrode Reaction on Group-IB and VIII Metals Deposited on Palladium Substrates

Ken-ichi MACHIDA and Michio ENYO*
Research Institute for Catalysis, Hokkaido University, Sapporo 060
(Received September 2, 1985)

Hydrogen electrode reactions (HER) on thin-layer electrodes of group-IB and VIII metals (Cu, Ag, Au, Ni, and Pt) prepared by electro-deposition on Pd foil substrates were studied (together with the Pd foil itself) in 0.5 M H_2SO_4 and 1.0 M NaOH (M=mol dm^{-3}) at 303 K by a transient technique. The reactions on these metals were concluded to proceed via a Volmer-Tafel reaction route and the exchange current densities of the elementary steps, i_{oV} and i_{oT}, were then evaluated. The electrocatalytic activities towards the Volmer step were observed to be in the order Pt>Pd>Au>Ag>Cu in an acidic solution and Pt>Pd>Ni≧Ag≧Au≧Cu in an alkaline solution. The activities towards the Tafel step were Pt≧Pd>Au>Cu>Ag in an acidic solution and Pd>Pt>Au>Cu=Ag>Ni in an alkaline solution. The results were summarized in terms of the parameter m_o ($=i_{oV}/i_{oT}$). This parameter was used to describe the electrochemistry of the energy efficiency of a hydride-type hydrogen-storage electrode, when the metals were employed for the purpose of modifying the electrode surface. Pt and Ag (among the group-IB metals) in both acidic and alkaline solutions were revealed to be suitable electrocatalysts.

The entry of hydrogen into metal or alloy electrodes during the electrochemical evolution of hydrogen has been studied for a long time, mainly in connection with the problem of the hydrogen embrittlement of substrate metals.[1,2] On the other hand, the potential of hydrogen-absorbing metals or alloys as a means of energy storage has been noted during the last ten years.[3] Secondary batteries using hydrogen-storage matrices, such as alloys based on alkaline earth metals or lanthanoid metals, possess (in principle) larger capacitance per unit weight than lead-acid batteries. According to Videm,[4b] their theoretical energy densities are as follows: MgH_2/air; 1900, CaH_2/air; 680, and $LaNi_5H_6$/air; 458 Wh kg^{-1}, whereas the conventional lead-acid battery is 161 Wh kg^{-1}.

The construction of hydride cells using aqueous[4-7] electrolytes may be divided into two types: The direct type in which hydrogen-storage materials (metal hydrides) are directly immersed in the electrolyte,[4a,b,d] and the indirect type in which a hydrogen-permeable membrane (such as Pd foils) is employed as a hydrogen electrode at the same time as a container of metal hydrides.[4b,4c,5-7] The latter may also include a type in which hydrogen is stored outside the cell by means of, e.g. metal hydrides. While alkaline media might only be practical for the former type, both acid and alkaline solutions might be used in the latter.

The present discussion is not concerned with the latter indirect type since it is essentially a H_2/air fuel cell (with a combined operation as a water electrolyzer) equipped with a suitable device of H_2 storage. This type is probably suitable for a large-scale energy storage device. On the other hand, a more detailed analysis would be required regarding the former type. This is the topic of the present work.

Basic Concepts. In the direct-type electrochemical hydrogen energy storage system, hydrogen produced on the cathode is dissolved into the electrode material and then ionized during its use as a current generator. The efficiency of the energy conversion through charging and discharging processes may be lowered by various factors, such as hydrogen diffusion in the metal hydride. However, the most important factor concerning its electrochemistry is the overpotentials involved in those processes. In this respect, for a given metal-hydride system chosen for hydrogen storage, a surface modification with other (metallic) materials might be required in order to improve the efficiency.

Further, it is well known that many of the metal hydrides tend to pulverize during hydrogen charging/discharging cycles and, thus, introduce difficulties concerning practical devices. To prevent this, a microcapsulation technique involving the coating of a metal hydride powder with a ductile metal has been proposed.[8] This may completely change the electrocatalytic property of the hydride electrode; hence, one should know the surface modification effects of each candidate metal.

The majority of hydrogen-absorbing metals or alloys have a plateau region in the absorption isotherm, e.g. the α-β phase transition region in the Pd-H system. This provides the basic character of that hydrogen-storage system. Naturally, one should cover this region during operation in order to maximize the storage capacity.

The extent of hydrogen absorption into metals or alloys which are polarized in aqueous or other protonic environments is intimately related to the HER mechanism. If HER proceeds through the Volmer-Tafel reaction route:

Volmer step,

$$H^+B + e \rightleftharpoons H(a) + B \quad (B=H_2O, OH^-)$$

Tafel step,

$$2\,H(a) \rightleftharpoons H_2,$$

the overpotential components for these elementary steps (η_V and η_T) under steady-state polarization are given, respectively, by,[9]

$$\eta_V = \eta + \frac{RT}{F} \ln \gamma_H, \quad (1)$$

$$\eta_T = -\frac{RT}{F} \ln \gamma_H, \quad (2)$$

where $\gamma_H = a_H/a_{H,o}$, a_H is activity of the hydrogen adatom, H(a), established during the steady-state polarization. The subscript o indicates the equilibrium of the overall reaction. The overall overpotential, η, is related to the component overpotentials by $\eta = \eta_V + \eta_T$.[9]

If an electrode material with an extensive and rapid hydrogen absorption is used, a plateau region (in the time window of 10^{-3}—10^{0} seconds in the case of thin Pd foil) usually appears on the galvanostatic overpotential rise transient curves or on the overpotential decay transients after current interruption. The plateau overpotential value on the rise transient curve may be explained[9] as the overpotential component required for the Volmer step to proceed with the rate predetermined by the applied current. No overpotential component for the Tafel step should be required at the very beginning of the transient, provided that a_H is effectively equal to $a_{H,o}$, owing to high rate of dissolution of H(a) into the electrode and, hence, the insignificant growth of a_H during this very short period of time. Only after a prolonged polarization time does a growth of a_H take place and, hence, of η beyond this level. Accordingly, an extrapolation of the plateau to time zero yields the overpotential component, η_1. An analysis of η_1 readily provides the kinetic parameters of the Volmer step, e.g. i_{oV} and the symmetry factor, β, being separated from those of the Tafel step (see below, Fig. 3, etc.).

Likewise, an extrapolation of the plateau on the overpotential decay transient to time zero after a current interruption should divide η into two overpotential components: η_1' for the short time process and η_2' for the long time process, where $\eta = \eta_1' + \eta_2'$. As discussed elsewhere,[9] η_2' is related to γ_H, the activity level reached during a steady-state polarization as,

$$\frac{RT}{F} \ln \gamma_H = -\eta_2'. \quad (3)$$

Hence, we find, referring to Eq. 2,

$$\eta_2' = \eta_T. \quad (4)$$

Similarly,

$$\eta_1' = \eta - \eta_2' = \eta - \eta_T = \eta_V. \quad (5)$$

Equation 3 may be related to the equivalent hydrogen pressure/fugacity $\bar{P}_{H_2}$ of the plateau region of the metal hydride electrode, given as the ratio over the reference pressure $\bar{P}_{H_2,o}$ (usually the atmospheric pressure), by combining it with the Nernst equation for a concentration cell,

$$E = -\frac{RT}{2F} \ln (\bar{P}_{H_2}/\bar{P}_{H_2,o}) \quad (6)$$

and to the relation (in terms of chemical potentials concerning the hypothetical hydrogen adsorption equilibrium) $\mu_{H_2} = 2\mu_{H(a)}$. Thus, we find,[10]

$$\eta_2' = -\frac{RT}{2F} \ln (\bar{P}_{H_2}/\bar{P}_{H_2,o}). \quad (7)$$

This indicates that the value of η required to charge up an electrode with hydrogen should be such that it contains a magnitude of η_2' that at least satisfies Eq. 7. Since $\bar{P}_{H_2}$ should, in principle, be larger than the reference hydrogen pressure in the same system, η_2' must always be finite. Its magnitude is determined by the type of the hydride used and the operating conditions chosen.

On the other hand, η_1' is the overpotential component, or additional amount of energy which is required to produce hydrogen from water. Accordingly, the smaller the magnitude, the smaller will be the energy consumption during the charging (also discharging). Hence, the higher will be the efficiency of the energy storage. It may be said, therefore, that the surface modification electrocatalysts that have small η_1' values compared with η_2' should be employed in order to minimize the energy loss.

The ratio η_1'/η_2' (or η_V/η_T) is determined by the specific rates of the elementary reaction steps. A series of studies[11] on HER (by means of a deuterium tracer technique) have already revealed the rates of the Volmer and Tafel steps on several electrocatalysts (Rh, Ir, Ni, Pt, Ag, and Au). Also, in our recent studies,[12,13] details regarding HER characteristics on Pd, Cu, Ag, and Ni have been investigated by means of a galvanostatic overpotential transient analysis.

In the present work, the HER characteristics of group-IB and VIII metal catalysts, particularly the ratio of the rates of the Volmer and Tafel elementary steps, are reported and the use of these metals as surface modification electrocatalysts in metal-hydride type secondary batteries is discussed.

Experimental

Preparation of Electrodes. Pd foils (a rectangular form of 5×5 mm, 12.5 μm in thickness) were used as substrates of the electrodes, which provided the hydrogen storage characteristics needed to carry out the transient polarization analysis mentioned above. Pd foil electrodes coated with

one of the group-IB metals or with Pt were prepared by electro-deposition from 0.5 M H_2SO_4 solutions containing $CuSO_4 \cdot 5H_2O$, $AgNO_3$, $HAuCl_4 \cdot 4H_2O$, or $H_2PtCl_6 \cdot 6H_2O$, respectively. This was done up to a thickness corresponding to $2-5\times10^{-7}$ mol cm^{-2} (apparent) or of the order of 10^{-6} cm in thickness (as judged from the amount of electricity applied, assuming 100% current efficiency). A series of preliminary experiments indicated that these coatings were sufficient to give rise to their own electrodic characteristics and yet retain an acceptable level of hydrogen permeability into the Pd foil substrates. This is required for the present type of transient analysis.

Electrochemical Measurements. The galvanostatic and potentiostatic polarization experiments were carried out in 0.5 M H_2SO_4 and 1.0 M NaOH at 303 K by using a previously described technique.[14] The electrolytic solution was prepared from a special grade H_2SO_4 (Wako, Tokyo) and pro analysi grade NaOH (Merck Japan, Ltd.) with water obtained from a Millipore pure water system. The real surface areas of the test electrodes were evaluated from double-layer capacitance data obtained by a pulse technique, assuming a value of 18 μF cm^{-2} (true).

The amount of hydrogen stored in the electrode was determined by measuring the quantities of electricity needed for its potentiostatic anodic ionization at 400 mV (RHE). The measurements were carried out after a steady-state polarization for several hours which was set at a desired overpotential between $\eta=-20$ and 200 mV. The overpotential component η_2' was evaluated from short time decay transients taken during the steady-state polarization.

Results and Discussion

Overpotential Transients. For all the electrodes prepared in this work, the overpotential plateau in a short-time transient curve (several seconds) has been easily recognized. Thus, the electrodes are considered to have good hydrogen permeabilities. Typical long-time rise and decay transient curves observed on a Pd foil and Au- or Pt-coated Pd foils in acidic and alkaline solutions are shown in Figs. 1 and 2, respectively. Similar behaviors were also observed on the other electrodes. The ratio η_1'/η_2' was generally observed to be larger in an acidic than in an alkaline solution.

Palladium. This element has a high hydrogen permeability, allowing a detailed study of the HER characteristics by a previously reported transient technique.[9,10,12,14]

Typical "Tafel" plots of η_1 on a bare Pd foil electrode in both acidic and alkaline solutions are shown in Fig. 3. The polarization characteristics in these solutions were very similar to each other. The slope of the linear portions in their Tafel plots was usually close to 120 mV decade^{-1} (both in the anodic and cathodic sides). Thus, they are practically symmetric on the abscissa. This form well substantiates the view that η_1 originates from the Volmer step. The i_{oV} values were estimated from linear plots of η_1 vs. i near the reversible potential (the inset figures) by the relation[9] $i_{oV}=(RT/F)/(di/d\eta_1)_o$. These were in good agreement with those

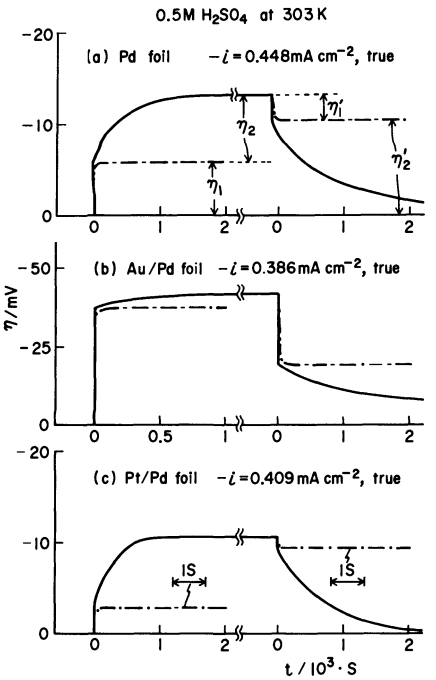

Fig. 1. Typical rise and decay transients of galvanostatic overpotentials on (a) Pd foil, (b) Au-deposited Pd foil, and (c) Pt-deposited Pd foil electrodes. 0.5 M H_2SO_4, 303 K.

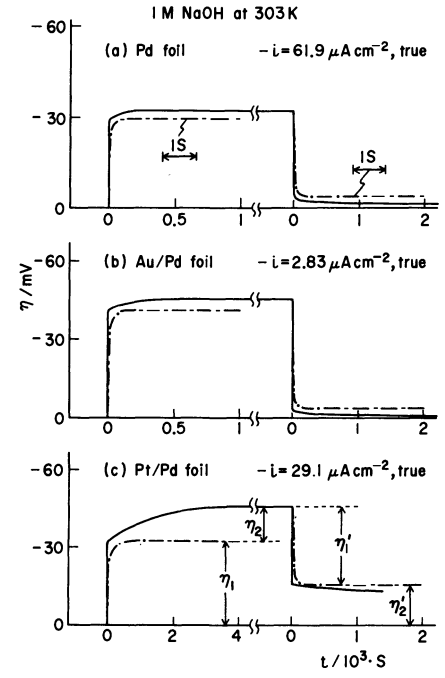

Fig. 2. Typical rise and decay transients of galvanostatic overpotentials on (a) Pd foil, (b) Au-deposited Pd foil, and (c) Pt-deposited Pd foil electrodes. 1.0 M NaOH, 303 K.

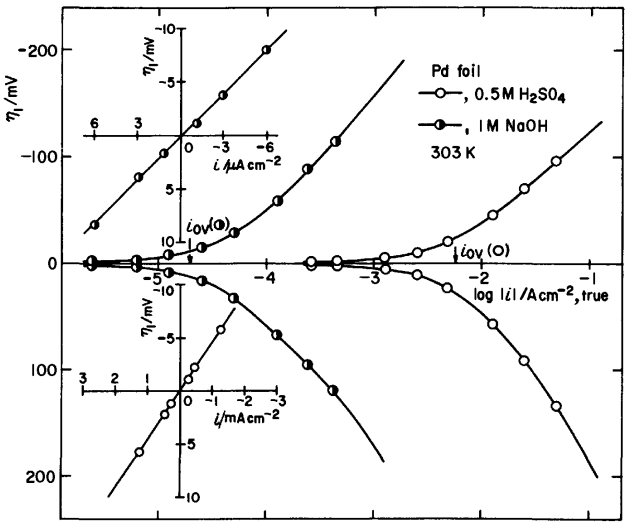

Fig. 3. Cathodic and anodic polarization behaviors of the rapidly rising overpotential component η_1 on a Pd foil. The arrows on the abscissa indicate i_{0V} evaluated from the linear plots (the inset figure) of η_1 vs. i near the reversible potentials.
0.5 M H_2SO_4 and 1.0 M NaOH, 303 K.

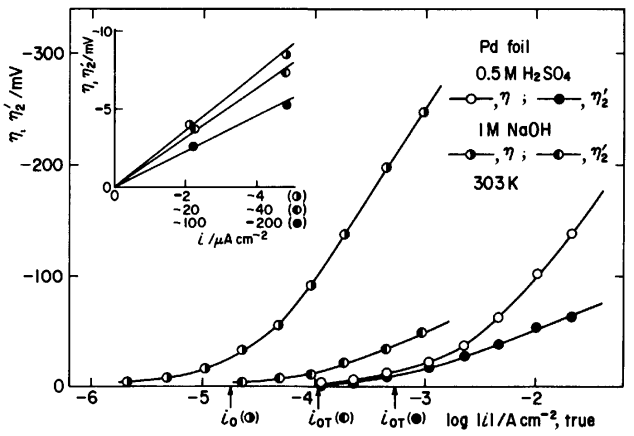

Fig. 4. Cathodic polarization behaviours of the total overpotential η and the slowly decaying overpotential component η_2' on a Pd foil electrode. The arrows on the abscissa indicate i_{0T} and i_0 obtained at low overpotentials (the inset figure).
0.5 M H_2SO_4 and 1.0 M NaOH, 303 K.

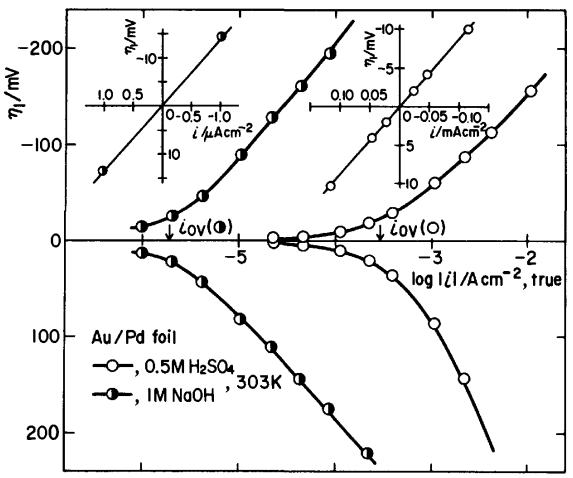

Fig. 5. Cathodic and anodic polarization behaviors of the rapidly rising overpotential component η_1 on Au-deposited Pd foils. The arrows indicate i_{0V} obtained at low overpotentials (the inset figure).
0.5 M H_2SO_4 and 1.0 M NaOH, 303 K.

anticipated from the Tafel plots, being about 5×10^{-3} and 2×10^{-5} A cm^{-2} (true) in the acidic and alkaline solutions, respectively.

The total overpotential, η, and the slowly decaying overpotential component, η_2', are shown in Fig. 4. Tafel plots of η and η_2' are seen to possess a linear portion with a slope of about 120—140 or 30—40 mV decade^{-1}, respectively. The latter value indicates that η_2' can be attributed to the Tafel step.[9] This again confirms the former conclusion that the HER on Pd proceeds via the Volmer-Tafel reaction route. The exchange current density of the Tafel step was evaluated by the relation[9] $i_{0T}=(RT/2F)/(\mathrm{d}i/\mathrm{d}\eta_2')_0$ to be about 5×10^{-4} and 1×10^{-4} A cm^{-2} (true) in the acidic and alkaline electrolyte, respectively.

In an alkaline solution, the rate of the overall HER was slower than in the acidic solution. In this case, the decrease in the rate was particularly significant for the Volmer step as compared with the Tafel step. As a consequence, the value of i_0 in the alkaline solution evaluated from the linear η vs. i plot (the reaction resistance) at low η by the relation[9] $i_0=(RT/F)/(\mathrm{d}i/\mathrm{d}\eta)_0$ (approximately valid when $i_{0V} \ll i_{0T}$) became fairly close to i_{0V} and smaller than i_{0T}. Thus, the HER kinetics were mostly dominated by the Volmer step. Correspondingly, the m_0 value became as small as 0.2. This is very small compared with that in an acidic solution (m_0=10). Accordingly, Pd in acidic solutions should yield a high energy storage efficiency if used by itself or to modify the surfaces of other hydrogen-storage electrode materials. However, that would not be the case in an alkaline solution.

Group-IB Metals. As is well known, the HER on these elements does not proceed as rapidly as on group-VIII metals. The i_0 values have been reported to be 10^{-5}—10^{-7} A cm^{-2} (true) both in acidic and alkaline solutions,[15,16] except that Au after anodic activation occasionally shows a very high activity.

The cathodic and anodic polarization behaviors of η_1 on an Au/Pd foil electrode are shown in Fig. 5. Like Pd, the polarization characteristics are quite acceptable as that of the Volmer step. The i_{0V} values were, however, scattered between 3×10^{-3} and 3×10^{-6} A cm^{-2} (true). Among them, the Volmer step on Au

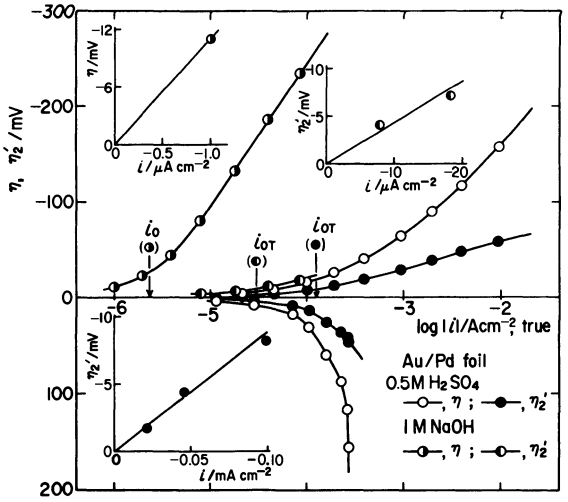

Fig. 6. Cathodic and anodic polarization behaviors of the total overpotential η and the slowly decaying overpotential component η_2' on Au-deposited Pd foils. The arrows indicate i_{oT} and i_o obtained at low overpotentials (the inset figure).
0.5 M H_2SO_4 and 1.0 M NaOH, 303 K.

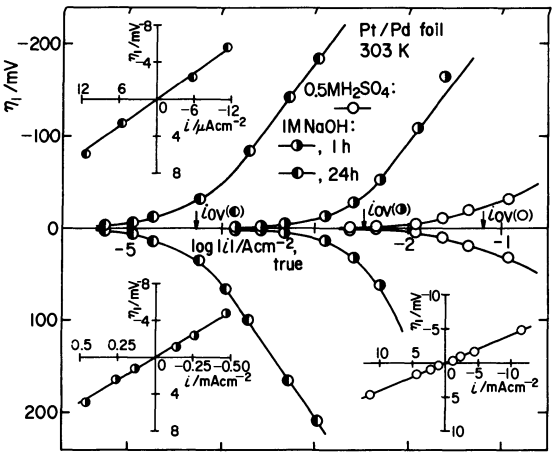

Fig. 7. Cathodic and anodic polarization behaviors of the rapidly rising overpotential component η_1 on Pt-deposited Pd foils. The arrows indicate i_{ov} obtained at low overpotentials (the inset figure).
0.5 M H_2SO_4 and 1.0 M NaOH, 303 K.

in an acidic solution only was very fast. On the other hand, the Tafel plots on η and η_2' (Fig. 6) had a slope of about 120 and 30 mV decade^{-1}, respectively. This was the same as for the previously observed values on Pd. The overpotential component η_2' was, hence, attributed to the Tafel step, yielding the i_{oT} values in the range 10^{-4} to 10^{-6} A cm^{-2} (true). These results on Cu and Ag in 0.5 M H_2SO_4 were in good agreement with those reported earlier.[12] The value of m_o was in the order Ag>Au>Cu in an acidic solution or Ag>Cu>Au in an alkaline solution (see Table 1 below). Among the group-IB metals, Ag was, thus, found to be an acceptable electrocatalyst in metal hydride secondary batteries in acidic (or alkaline) solutions.

Nickel. Details of HER on $LaNi_5$ film, Ni–Ti alloy films, amorphous Ni–Ti alloy ribbons, and Ni–V alloy ingots (all having a high hydrogen permeability) in 1.0 M NaOH were reported in previous papers.[13] The electrocatalytic characteristics on those alloys could essentially be attributed to the nickel on their surfaces. This idea was supported by SEM observations and XPS surface analyses.[13] The HER on these metals was also concluded to proceed via the Volmer-Tafel reaction mechanism with mixed rate-determining characteristics. Both the i_{ov} and i_{oT} values were estimated to be around 10^{-6} A cm^{-2} (true). Among these alloys in an alkaline solution, the m_o value on a $LaNi_5$ film was considerably larger (m_o=4) than the others (m_o=1—2.5). The scatter of the data among the alloys is not well understood. It may be due to an effect related to the different ways of preparation or to a synergistic effect due to the alloying component. The reasonably high values of m_o on Ni indicate that Ni may be an acceptable electrocatalyst in metal-hydride secondary batteries, or that a surface modification may not be required if Ni-based hydrogen storage materials are used without microcapsulation, etc.

Platinum. The exchange current density of HER on Pt is around 10^{-3} and 10^{-4} A cm^{-2} (true) in acidic and alkaline solutions, respectively.[15,16] However, in the latter media, the electrocatalytic activity of Pt is occasionally unstable and becomes considerably lower with time.

Figure 7 shows Tafel plots of η_1 in 0.5 M H_2SO_4 and 1.0 M NaOH. The polarization characteristics clearly show that η_1 originates from the Volmer step. As seen from the figure, the discharge process on Pt in an acidic solution was very rapid and i_{ov} was 6×10^{-2} A cm^{-2} (true). On the other hand, the activity in an alkaline solution was rather unstable and, after one day of standing, it became lower by nearly two orders of magnitude compared with the level immediately after the cell was set up. The i_{ov} values were 3.3×10^{-3} and 5.4×10^{-5} A cm^{-2} (true) for the former and the latter cases, respectively.

The cathodic and anodic polarization behaviors of η and η_2' are presented in Fig. 8. The slope of the Tafel plots of η_2' was about 30 mV decade^{-1}, indicating that this overpotential component was caused by the Tafel step (plus possibly a minor degree of contribution from the H_2 diffusion in the case of the acidic solution). The i_{oT} values on Pt (after one day of standing) were 5×10^{-4} and 1.3×10^{-5} A cm^{-2} (true) in acidic and alkaline solutions, respectively. Consequently, the m_o values were

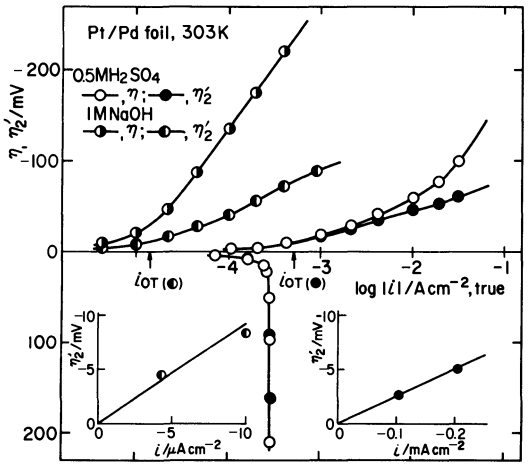

Fig. 8. Cathodic and anodic polarization behaviors of the total overpotential η and the slowly decaying overpotential component η_2' on Pt-deposited Pd foils. The arrows indicate i_{oT} and i_o obtained at low overpotentials (the inset figure.)
0.5 M H_2SO_4 and 1.0 M NaOH, 303 K.

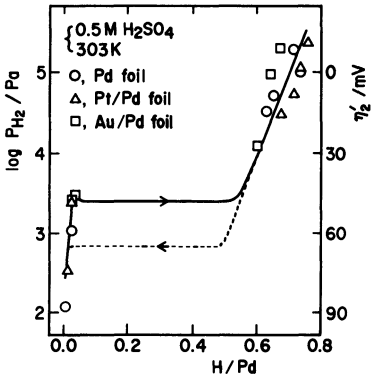

Fig. 9. Typical desorption isotherm (η_2' or $\log P_{H_2}$ vs. H/Pd) obtained on Pd and Au- or Pt-deposited Pd foil electrodes after polarizations between $\eta = -20$ and 200 mV at 303 K for several hours. The absorption/desorption isotherm[17] at ca. 300 K is shown for comparison.

evaluated to be 120 and 4 in the acidic and alkaline solutions, respectively. The value for an acidic solution is particulary large and, thus, Pt is an excellent electrocatalyst for a surface modification regarding this type of battery.

Amount of the Electrochemical Hydrogen Storage. The hydrogen absorbed into electrodes covered with Cu, Ag, Au, and Pt during hydrogen evolution is expected to obey Eq. 7, as the HER is concluded to proceed via the Volmer-Tafel reaction route, just as for the Pd or Ni electrodes.[12,13] In Fig. 9, the relationship between the hydrogen content and the overpotential component η_2' (and not η) observed on a bare Pd foil and a Pt- or Au-coated Pd foil electrodes are shown together with a typical absorption/desorption isotherm for Pd.[17] It can be seen that the experimental data are reasonably close to the isotherm curve in spite of the fact that the data were obtained on different metals with only the substrate being common (Pd). None of the data were found on the plateau region, presumably due to the sharp variation of the isotherm in this region. These observations substantiate the above analysis that the effective pressure of the electrochemically evolved hydrogen is determined by η_2' (Eq. 7) regardless of the type of electrode material as long as the HER obeys the Volmer-Tafel mechanism.

Comparison of Metals as Electrocatalysts. The obtained kinetic parameters are summarized in Table 1. In 0.5 M H_2SO_4, the Volmer step was generally more rapid than the Tafel step, or m_o was for the most part larger than unity. The order of the elementary step rates was Pt>Pd>Au>Ag>Cu for the Volmer step and Pt≧Pd>Au>Cu>Ag for the Tafel step, respectively. Consequently, that for m_o was Pt>Pd>Ag>Au>Cu. Hence, Pt was concluded to be the most suitable material for an electrode surface modification in the present context.

In 1.0 M NaOH, the rates of the Volmer step were considerably decreased (as a whole) compared with the Tafel step. Hence, the efficiency in question should be lowered. Their electrocatalytic activity was in the order Pt>Pd>Ni≧Ag≧Au≧Cu for the Volmer step and Pd>Pt>Au>Cu=Ag>Ni for the Tafel step. A relatively high m_o value was observed on Pt or Ni ($LaNi_5$ film), although the value for Ni was somewhat dispersed if Ti, Zr, or V was used instead of La as the alloying element. These are considered suitable for alkaline systems.

Conclusion

The HER on the electrodes of Cu, Ag, Pd, and Pt, was concluded to proceed via the Volmer-Tafel reaction route in both acidic and alkaline solutions, as well as on Ni in alkaline media. The relationship between the amount of hydrogen absorbed in the electrodes during a hydrogen evolution reaction and the overpotential component η_2' for the Tafel step, shows that this overpotential component is the quantity which determines the absorption conditions. On the other hand, η_1' represents the reaction affinity necessary for producing hydrogen from water. Thus, it entirely gives rise to a corresponding amount of energy consumption. The energy efficiency in the charge/discharge cycles of metal-hydride secondary batteries, therefore, dependes on the fraction of η_2' which shares in the overall

Table 1. Kinetic Parameters[a] of the Hydrogen Electrode Reaction on Group-IB and VIII Metals

	Electrode	0.5 M H_2SO_4			1.0 M NaOH		
		$\log i_{oV}$	$\log i_{oT}$	m_o	$\log i_{oV}$	$\log i_{oT}$	m_o
Cu	(Cu/Pd foil)	−5.15[b]	−4.5[b]	0.23[b]	−5.8	−5.2	0.25
Ag	(Ag/Pd foil)	−4.15[b]	−4.8[b]	4.2[b]	−5.5	−5.2	0.50
Au	(Au/Pd foil)	−3.53	−3.9	2.4	−5.6	−4.5	0.06
Ni	(amorphous Ni-Ti alloys)[c]				−5.1	−5.5	2.5
	(Ni-Ti alloy films)[d]				−5.6	−6.0	2.5
	($LaNi_5$ film)[d]				−5.5	−6.1	4.0
	(Ni-V alloys)[e]				−5.3	−5.3	1.0
Pd	(Pd foil)	−2.3	−3.3	10	−4.7	−4.0	0.20
Pt	(Pt/Pd foil)[f]	−1.2	−3.3	120	−4.3	−4.9	4.0

a) The i_o values are given per true unit surface area. b) Ref. 12. c) Ref. 13a. d) Ref. 13b. e) Ref. 13c. f) The i_{oT} value observed on this electrode (RF=ca. 5) was probably underestimated because of involvement in part of limiting rate of diffusion of H_2: The true value of m_o might hence be smaller than this value.

overpotential, η. This has been discussed here in terms of m_o. Among the metals studied, Pt in acidic solutions and Pt or Ni (or Ag among the group-IB metals) in alkaline solutions are considered to be suitable regarding the present purpose.

The present work is partly supported by Grants-in-Aid for Scientific Research No. 59045007 from the Ministry of Education, Science, and Culture.

References

1) M. A. V. Devanathan, Z. Stachurski, and W. Beck, *J. Electrochem. Soc.*, **110**, 886 (1963); M. A. V. Devanathan and Z. Stachurski, ibid., **111**, 619 (1964); C. D. Kim and B. E. Wilde, ibid., **118**, 202 (1971).

2) E. Gileadi, M. A. Fullenwider, and J. O'M. Bockris, *J. Electrochem. Soc.*, **113**, 926 (1966); J. O'M. Bockris and P. K. Subramanyan, ibid., **118**, 1114 (1971); J. O'M. Bockris, M. A. Genshaw, and M. Fullenwider, *Electrochim. Acta*, **15**, 47 (1970); J. O'M. Bockris and P. K. Subramanyan, ibid., **16**, 2169 (1971).

3) "Hydrides for Energy Storage," ed by A. F. Andressen and A. J. Maeland, Pergamon Press, New York (1978).

4) a) M. H. J. van Rijswick, "Metal Hydride Electrodes for Electrochemical Energy Storage," pp. 261—271 in Ref. 3; b) K. Videm, "Electrochemical Utilization of Metal Hydrides," pp. 463—477 in Ref. 3; c) F. A. Lewis, "Hydrogen Storage Electrode Systems," pp. 479—484 in Ref. 3; d) A. Percheron-Guegan, J. C. Achard, J. Sarrahin, and G. Bronoël, "Hydrogen Electrochemical Storage by Substituted $LaNi_5$ Compounds," pp. 485—490 in Ref. 3.

5) J. Ginder and J. D. Dunlop, *J. Electrochem. Soc.*, **122**, 4 (1975).

6) T. Shirogami, K. Murata, and H. Ogura, *Denki Kagaku*, **44**, 668 (1976).

7) G. L. Holleck, J. R. Driscoll, and B. E. Paul, *J. Less-Common Met.*, **74**, 379 (1980).

8) H. Ishikawa, K. Oguro, A. Kato, H. Suzuki, and E. Ishii, *J. Less-Common Met.*, **107**, 105 (1985).

9) M. Enyo and T. Maoka, *J. Electroanal. Chem.*, **108**, 277 (1980).

10) T. Maoka and M. Enyo, *Electrochim. Acta*, **26**, 607 (1981); T. Maoka and M. Enyo, ibid., **26**, 615 (1981).

11) a) M. Enyo, "Mechanism of the Hydrogen Electrode Reaction as Studied by Means of Deuterium as a Tracer," in "Modern Aspects of Electrochemistry," No. 11, ed by B. E. Conway and J. O'M. Bockris, Plenum, New York (1975), pp. 251—314; b) T. Matsushima and M. Enyo, *Electrochim. Acta*, **19**, 117 (1974); c) T. Matsushima and M. Enyo, ibid., **19**, 125 (1974); d) T. Matsushima and M. Enyo, ibid., **19**, 131 (1974).

12) M. Enyo, *J. Res. Inst. Catal., Hokkaido Univ.*, **30**, 11 (1982).

13) a) K. Machida, M. Enyo, I. Toyoshima, K. Miyahara, K. Kai, and K. Suzuki, *Bull. Chem. Soc. Jpn.*, **56**, 3393 (1983); b) K. Machida, M. Enyo, G. Adachi, and J. Shiokawa, *Electrochim. Acta*, **29**, 807 (1984); c) K. Machida, M. Enyo, K. Oguro, and M. Nakane, *Bull. Chem. Soc. Jpn.*, **57**, 2809 (1984).

14) M. Enyo, *J. Electroanal. Chem.*, **134**, 75 (1982).

15) H. Kita, *J. Electrochem. Soc.*, **113**, 1095 (1966); A. Belanger and A. K. Vijh, *Elektrokhim.*, **10**, 1854 (1974); A. J. Appleby, "Electrocatalysis," in "Modern Aspects of Electrochemistry," ed by B. E. Conway and J. O'M. Bockris, Plenum, New York (1974), No. 9. pp. 369—478; S. Trasatti, "The Work Function in Electrochemistry," in "Advances in Electrochemistry and Electrochemical Engineering," ed by H. Gerischer and C. W. Tobias, John Wiley & Sons, New York (1977), No. 10, pp. 213—321.

16) K. J. Vetter, "Electrochemical Kinetics-Theoretical and Experimental Aspects," Academic Press, New York (1967), p. 539.

17) F. A. Lewis, "The Palladium Hydrogen System," Academic Press, New York (1967), p. 33.

 © 1986 The Chemical Society of Japan Bull. Chem. Soc. Jpn., 59, 733—735 (1986)

Thermodynamic Study on Solvent Extraction of Alkali Metal Picrates with 18-Crown-6 into $CHCl_3$

Yasuyuki TAKEDA* and Akio TANAKA
Department of Chemistry, Faculty of Science, Chiba University, Yayoi-chō, Chiba 260
(Received October 11, 1985)

Enthalpy (ΔHex) and entropy changes (ΔSex) for overall extractions of alkali metal (Na, K, Rb, and Cs) picrates with 18-crown-6 (18C6), and those ($\Delta H_{D,L}$ and $\Delta S_{D,L}$) for distribution of 18C6 itself were determined between $CHCl_3$ and water, all the extracted complexes being 1:1:1 complexes. The ΔHex and ΔSex values of 18C6 for all the alkali metals are negative. The $\Delta H_{D,L}$ and $\Delta S_{D,L}$ values of 18C6 are both positive. Enthalpy (ΔHex′) and entropy changes (ΔSex′) for ion-pair extractions of 18C6-alkali metal ion complexes with picrate anions were calculated. All the ΔHex′ and ΔSex′ values are negative except for ΔSex′ value of Na (positive). The ion-pair extractions were discussed from the thermodynamic point of view.

In order to evaluate complexing power and selectivity of newly-synthesized crown compounds for metal ions, solvent extraction has been widely used. Numerous data have been reported for their extraction ability and selectivity toward metal ions. However, only a few thermodynamic parameters regarding solvent extraction with crown compounds have been presented.[1] Thermodynamic quantities provide very valuable information on extraction mechanisms on molecular grounds. Further investigation of extraction processes from the thermodynamic point of view is important for understanding in detail solute-solvent interactions of crown compounds and their complexes and for designing crown compounds with high extractability and selectivity.

In the present study, enthalpy and entropy changes for the overall extraction of alkali metal picrates with 18-crown-6 (18C6), and those for distribution of 18C6 have been determined between $CHCl_3$ and water. Extraction processes of alkali metal picrates with 18C6 were discussed from the standpoint of thermodynamics.

Experimental

18-Crown-6 (Nisso Co., Ltd.) was recrystallized from acetonitrile and, prior to use, dried at 80 °C in a vacuum. Chloroform, picric acid, NaOH, and KOH were analytical grade reagents. Rubidium and caesium hydroxides were reagent-grade. Chloroform was washed three times with distilled water. The other reagents were used without further purification.

The experimental procedures were almost the same as those described in previous papers.[2,3] Extractions were conducted at 15, 20, 25, 30, and 32±0.3 °C. Concentrations of 18C6, alkali metal hydroxides, and picric acid were 9.5×10^{-6}—6.3×10^{-3} M (1 M=1 mol dm^{-3}), 4.2×10^{-3}—1.8×10^{-2} M, and 2.1×10^{-4}—4.0×10^{-4} M, respectively. Extractions were carried out at pH 10.0—11.3.

The Distribution Coefficient of 18C6. Experimental procedures were similar to those in the previous paper.[2] The concentration range of 18C6 was from 2.0×10^{-3} M to 7.5×10^{-2} M. Experiments were carried out at 15, 20, 25, 30, and 32±0.3 °C. Each distribution coefficient value of 18C6 is the average of about ten measurements.

Results

In an equilibrium between a chloroform solution of a crown ether (L) and an aqueous solution of an alkali metal ion (M^+) and a picrate ion (A^-), the equilibrium constants are defined as

$$K\text{ex} = [MLA]_o/[M^+][L]_o[A^-], \quad (1)$$

$$K_{D,L} = [L]_o/[L], \quad (2)$$

$$K_{ML} = [ML^+]/[M^+][L], \quad (3)$$

$$K\text{ex}' = [MLA]_o/[ML^+][A^-], \quad (4)$$

where the subscript "o" and the lack of subscript denote the organic and aqueous phases, respectively. The overall extraction equilibrium constant (Kex) can be written as

$$K\text{ex} = K_{ML}K\text{ex}'K_{D,L}^{-1}. \quad (5)$$

The distribution ratio of the alkali metal is represented by

$$D = [MLA]_o/[M^+]. \quad (6)$$

Combination of Eqs. 1 and 6 leads to

$$D = K\text{ex}[L]_o[A^-]. \quad (7)$$

A plot of log ($D/[A^-]$) against log $[L]_o$ shows a straight line with a slope of 1 in every case, indicating that Kex can be described by Eq. 1. The values of $[L]_o$ and $[A^-]$ in Eq. 7 were calculated by

Table 1. Summary of Extraction Equilibrium Constants for 18C6 and Its Complexes with Alkali Metal Picrates between $CHCl_3$ and H_2O

Temp/°C	$K_{D,L}$	log Kex			
		Na	K	Rb	Cs
15	4.7_7	3.69	6.53	6.12	5.10
20	5.4_4	3.58	6.28	5.87	4.85
25	6.1_1	3.46	6.06	5.64	4.61
30	6.8_5	3.30	5.84	5.40	4.40
32	7.1_9	3.23	5.75	5.33	4.32

Table 2. Extraction Equilibrium Constants for 18C6 and Its Complexes with Alkali Metal Picrates at 25 °C

	$\log K_{D,L}$	$CHCl_3$ 0.78_6		C_6H_6[2] -1.19_8		CH_2Cl_2[4] 1.0	
	$\log K_{ML}$	$\log Kex$	$\log Kex'$	$\log Kex$	$\log Kex'$	$\log Kex$	$\log Kex'$
Na	0.80[5]	3.47	3.46	3.39	1.39	3.89	4.09
K	2.03[5,6]	6.07	4.83	5.97	2.74	6.20	5.17
Rb	1.56[5]	5.65	4.88	5.43	2.67	5.96	5.40
Cs	0.99[5]	4.62	4.42	4.38	2.19	5.17	5.18

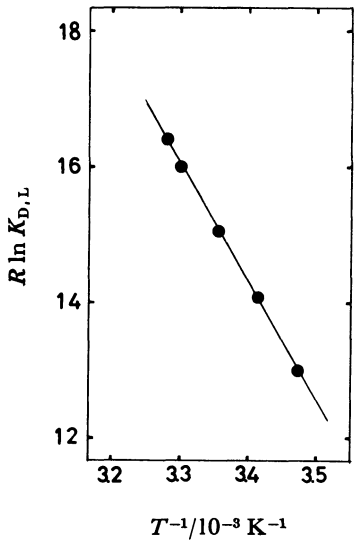

Fig. 1. $R \ln K_{D,L}$ vs. T^{-1} plots for 18C6 between $CHCl_3$ and water.

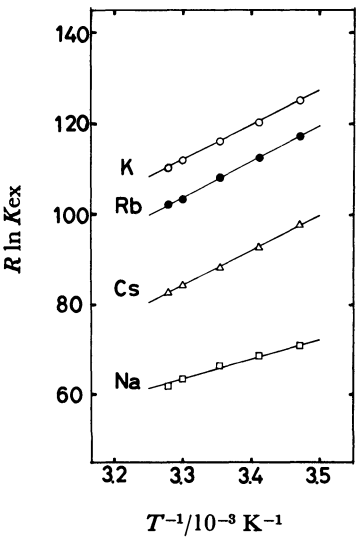

Fig. 2. $R \ln Kex$ vs. T^{-1} plots for 18C6-alkali metal picrate complexes between $CHCl_3$ and water.

$$[L]_o = ([L]_t - [MLA]_o)/(1 + K_{D,L}^{-1}), \quad (8)$$

$$[A^-] = [HA]_t - [MLA]_o, \quad (9)$$

where the subscript "t" refers to the total concentration. Equilibrium constants are summarized in Tables 1 and 2.

Table 3. Thermodynamic Quantities for Extraction of 18C6 and Its Complexes with Alkali Metal Picrates

	$\Delta H_{D,L}$/kJ mol^{-1} = 17.5	$T\Delta S_{D,L}$/kJ mol^{-1} = 22.0 (at 25 °C)	
	ΔH/kJ mol^{-1} [a]		
	ΔHex	ΔH_{ML}	$\Delta Hex'$
Na	−45.7	−9.41[5]	−18.8
K	−76.4	−25.01[6]	−33.9
Rb	−79.1	−16.0[5]	−45.6
Cs	−76.5	−15.9[5]	−43.1
	$T\Delta S$/kJ mol^{-1} (at 25 °C)[b]		
	$T\Delta Sex$	$T\Delta S_{ML}$	$T\Delta Sex'$
Na	−26.0	−4.6[5]	0.6
K	−41.8	−13.22[6]	−6.6
Rb	−46.9	−7.1[5]	−17.8
Cs	−50.1	−10[5]	−18.1

a) $\Delta Hex = -\Delta H_{D,L} + \Delta H_{ML} + \Delta Hex'$, b) $\Delta Sex = -\Delta S_{D,L} + \Delta S_{ML} + \Delta Sex'$, where subscripts "ex, D,L, ML, and ex'" refer to reactions represented by Eqs. 1—4, respectively.

From Figs. 1 and 2, $R \ln K_{D,L}$ vs. T^{-1} and $R \ln Kex$ vs. T^{-1} plots are found to be linear. Enthalpy change (ΔH) and entropy change (ΔS) for Eqs. 1 and 2 were calculated from these data. The thermodynamic parameters are listed in Table 3.

Discussion

Values of $\log K_{D,L}$ at 25 °C of 15-crown-5 (15C5) and benzo-15-crown-5 (B15C5) for $CHCl_3$/water system are 0.91[7] and 2.4[8a], respectively. The contribution of an ether oxygen atom to $\log K_{D,L}$ (π_0) at 25 °C for $CHCl_3$/water system can be calculated from $\log K_{D,L}$ values of 15C5 and 18C6 by using the contribution of a methylene group to extraction constants of ion-pairs (π_{CH_2}), π_{CH_2} being 0.47.[9] Values of π_0 are −0.76 for 15C5 and −0.81 for 18C6 (15C5: (0.91−0.47×10)÷5, 18C6: (0.786−0.47×12)÷6). The values are nearly identical. The π_0 value is −0.79 on the average. The contribution of a benzo group to $\log K_{D,L}$ ($\pi_{C_6H_4}$) can also be calculated from $\log K_{D,L}$ values of B15C5 and dibenzo-18-crown-6 (DB18C6) ($\log K_{D,L}$=3.9[8b] at 25 °C) by means of the values of π_{CH_2} and π_0. Values of $\pi_{C_6H_4}$ are 2.5$_9$ for B15C5 and 2.4$_4$ for DB18C6 (B15C5: 2.4−{0.47×8+(−0.79×5)},

DB18C6: [3.9−{0.47×8+(−0.79×6)}]÷2). They are nearly equal. The $\pi_{C_6H_4}$ value is 2.5[1] on the average. From these empirical parameters, log $K_{D,L}$ values at 25 °C between $CHCl_3$ and H_2O for several crown ethers can be estimated.

In the case of 18C6, the orders of log *K*ex and log *K*ex′ for $CHCl_3$ system and that of log K_{ML} are K>Rb>Cs>Na, Rb≧K>Cs>Na, and K>Rb>Cs>Na, respectively (Table 2). The extraction selectivity of 18C6 for alkali metal ions shows the size-fit correlation and is completely consistent with the selectivity in water, whereas it is not always in agreement with the ion-pair-extraction selectivity.

For 18C6, log *K*ex′ value sequences of a given alkali metal are CH_2Cl_2>$CHCl_3$>C_6H_6 (Table 2). This indicates that the extractability of the ion-pair, MLA, decreases with a decrease in dielectric constant (CH_2Cl_2 8.93,[10] $CHCl_3$ 4.9,[11] C_6H_6 2.3[11] at 25 °C).

It is interesting to compare the ion-pair extractability of K(18C6)A into $CHCl_3$ with that of tetrabutylammonium picrate (Bu_4NA). The log *K*ex′ value of K(18C6)A at 25 °C is about one order of magnitude smaller than the ion-pair extraction constant ($K_{ex,ip}$=$[Bu_4NA]_o/[Bu_4N^+][A^-]$=5.75[9] at 25 °C) of Bu_4NA, although the size of K(18C6)A is nearly identical with that of Bu_4NA.[12] From shapes and sizes of K(18C6)A and Bu_4NA, it seems that the difference in ion-association constants in water between them is not so large. Thus, the data indicate that solute-water interaction of $K(18C6)^+$ is much stronger than that of Bu_4N^+.

It is seen from Table 3 that $\Delta H_{D,L}$ and $\Delta S_{D,L}$ values of 18C6 are both positive and the $T\Delta S_{D,L}$ value at 25 °C is larger than the $\Delta H_{D,L}$ value. Consequently, the fact that 18C6 is more soluble in $CHCl_3$ than in water is completely due to entropy contribution. The explanation for the positive values of $\Delta H_{D,L}$ and $\Delta S_{D,L}$ of 18C6 is the same as that provided in the previous paper.[3]

The ΔHex and ΔSex values of 18C6 for all the alkali metals are negative. Tables 2 and 3 show that the second largest $-\Delta H$ex value of K is canceled by the second smallest $-T\Delta S$ex value, resulting in the greatest log *K*ex, and that the smallest $-\Delta H$ex and $-T\Delta S$ex values of Na balance each other, leading to the smallest log *K*ex. The ΔHex′ value plays a major role in determining the magnitude of ΔHex, whereas the $\Delta S_{D,L}$ value plays a major role in determining the magnitude of ΔSex.

The *K*ex′ value of 18C6 for the $CHCl_3$ system (at 25 °C) decreases in the order, Rb≈K>Cs>Na (Table 2). The largest ΔHex′ and ΔSex′ values of Na cancel each other, resulting in the lowest ion-pair extractability; the second greatest ΔHex′ and ΔSex′ values of K balance each other, leading to the highest ion-pair extractability (Table 3).

All the ΔHex′ and ΔSex′ values are negative except for the ΔSex′ value of Na. Although sizes of these 18C6-alkali metal ion complexes are much the same,[12] both ΔHex′ and ΔSex′ values vary with the alkali metal ion trapped in the 18C6 cavity. This reflects differences in chemical nature of the alkali metal ions in the cavity. The ΔHex′ and ΔSex′ values of Na are much larger than those of the other alkali metals. A possible explanation for the very large ΔHex′ and ΔSex′ values of Na is as follows. The 18C6-Na^+ complex may be most strongly hydrated in an aqueous phase due to the highest charge density of Na^+ and much smaller size of Na^+ compared to that of the 18C6 cavity. The strong interaction between Na^+ in cavities of 18C6 and its analog and solvent molecules was observed in the previous works.[12,13] When the Na^+ complex is extracted into $CHCl_3$ phase, a large amount of water molecules attached to the complex have to be released. This may be responsible for the very large ΔHex′ and ΔSex′ values fo Na.

References

1) Y. Takeda, "The Solvent Extraction of Metal Ions by Crown Compounds, Host Guest Complex Chemistry III," Springer-Verlag, Topics in Current Chemistry, Vol. 121, Berlin, Heidelberg, New York, Tokyo (1984), Chap. 1.

2) Y. Takeda and H. Gotō, *Bull. Chem. Soc. Jpn.*, **52**, 1920 (1979).

3) Y. Takeda, T. Namisaki, and S. Fujiwara, *Bull. Chem. Soc. Jpn.*, **57**, 1055 (1984).

4) M. Ouchi, Y. Inoue, T. Kanzaki, and T. Hakushi, *J. Org. Chem.*, **49**, 1408 (1984).

5) R. M. Izatt, R. E. Terry, B. L. Haymore, L. D. Hansen, N. K. Dalley, A. G. Avondet, and J. J. Christensen, *J. Am. Chem. Soc.*, **98**, 7620 (1976).

6) Y. Takeda and O. Arima, *Bull. Chem. Soc. Jpn.*, **58**, 3403 (1985).

7) Y. Takeda et al., unpublished data.

8) a) Y. Hasegawa, T. Nakano, Y. Odori, and Y. Ishikawa, *Bull. Chem. Soc. Jpn.*, **57**, 8 (1984); b) Y. Hasegawa, H. Wakabayashi, M. Sakuma, and T. Sekine, ibid., **54**, 2427 (1981).

9) H. Matsunaga and T. Yotsuyanagi, *Nippon Kagaku Kaishi*, **1982**, 785.

10) G. A. Barclay and R. J. W. Le Fèvre, *J. Chem. Soc.*, **1950**, 556.

11) J. A. Riddick and W. B. Bunger, "Organic Solvent," Wiley-Interscience (1970).

12) Y. Takeda, H. Yano, M. Ishibashi, and H. Isozumi, *Bull. Chem. Soc. Jpn.*, **53**, 72 (1980).

13) Y. Takeda, *Bull. Chem. Soc. Jpn.*, **58**, 1259 (1985).

 © 1986 The Chemical Society of Japan Bull. Chem. Soc. Jpn., 59, 737—740 (1986)

Behavior of the Cadmium Ion-Selective Electrode in Alcohol-Water Mixtures

Junko MOTONAKA,* Hiroshi KONISHI, Sanae IKEDA, and Nobuyuki TANAKA†
Technical College, The University of Tokushima, Minamijosanjima, Tokushima 770
†Nippon Jimuki Co., Ltd., 12, 3-Chome, Kanda Ogawa-cho, Chiyoda-ku, Tokyo 101
(Received April 12, 1985)

In an investigation on the behavior of a cadmium ion-selective electrode in methanol-water and ethanol-water mixtures, potential measurements were carried out with a digital pH/mV meter, a cadmium ion-selective indicator electrode and a silver-silver chloride reference electrode. The calibration curves, slopes of the response, response times, effects of temperature, relation between the potential and the pH-meter reading and selectivity of the electrode were discussed. The response of cadmium ions (electromotive force) was linear between 10^{-7}—10^{-2} mol dm^{-3} in water. However, the linear range became narrower with an increase in the alcohol content. The slopes in alcohol-water mixtures (27—33 mV/decade in methanol-water mixtures, 21—29 mV/decade in ethanol-water mixtures) were nearly equal to the Nernstian slope (29.6 mV/decade). The response times of the cadmium ion-selective electrode in 99 v/v% methanol and in 99 v/v% ethanol were somewhat long, but were still within 5 min for all solutions consisting of 10^{-5}—10^{-1} mol dm^{-3} of cadmium ions. The selectivity of the cadmium ion-selective electrode in various media was examined by the mixed-solution method using potassium, sodium, calcium and magnesium ions as the interfering ions. It was found that a cadmium ion-selective electrode could be used to determine cadmium ions in an alcohol-water solution, although the response time became longer and the linear range of the response became narrower with an increase in the alcohol content.

Ion-selective electrodes are used mainly for the determination of inorganic ions in aqueous solutions.[1,2] The behavior of ion-selective electrodes (halide ion-selective electrode,[3-6] copper ion-selective electrode,[7] lead ion-selective electrode[8] and so on) in nonaqueous solvents has already been reported. However, no study has been reported regarding the properties of a cadmium ion-selective electrode in organic solvents. When ion-selective electrodes are to be used in organic solvents, their properties (such as sensitivity, selectivity, and response time) might be expected to be strongly dependent on the solvents.[9] The effects of alcohol on the potentiometric chelatometric titration of cadmium ions with a cadmium ion-selective electrode was examined by the authors.[10]

This paper is concerned with the detailed behavior of a cadmium ion-selective electrode in methanol, ethanol, and their mixtures with water.

Experimental

Apparatus. A cadmium ion-selective electrode (Orion, Model 94-48A) was used in conjunction with a reference electrode (TOA, Model HS-205C) that was appropriate for the particular solvent used. In 99 v/v% methanol and ethanol solutions, a saturated aqueous potassium chloride solution in the reference electrode was replaced by a saturated solution of potassium chloride in methanol or ethanol.[11]

Reagent. Stock solutions (0.1 mol dm^{-3}) of cadmium chloride in water, in 25, 50, 75, and 99 v/v% methanol and in 25, 50, 75, and 99 v/v% ethanol were prepared and diluted as needed. Calcium nitrate tetrahydrate and magnesium sulfate heptahydrate were dehydrated by heating. All other reagents were analytical-reagent grade from Wako Pure Chemicals.

Procedure. All potentiometric measurements were carried out under constant stirring with a Teflon-covered stirring bar and a magnetic stirrer. The cell consisted of a 50-cm^3 glass beaker fitted with a rubber stopper, bored out for the insertion of electrodes and a thermometer. Successive runs were made by the immersion method in a series of cadmium-ion solutions (10^{-8}—10^{-1} mol dm^{-3}) in decade steps of increasing concentrations.

Results and Discussion

Calibration Curves. Calibration curves for the cadmium ion-selective electrode in water and in 25, 50, 75, and 99 v/v% methanol are shown in Fig. 1.

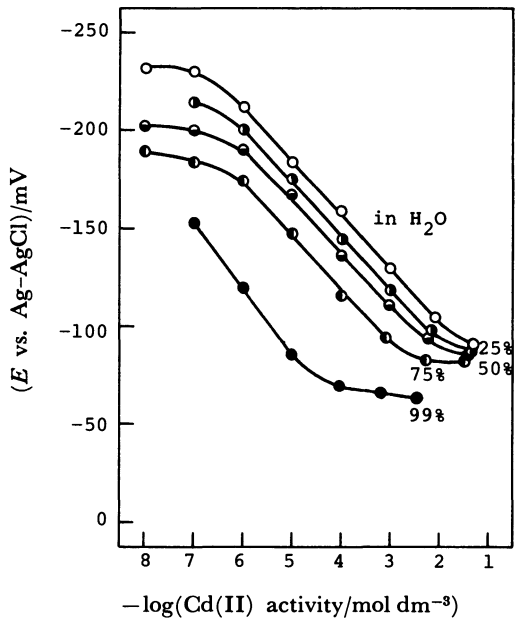

Fig. 1. Responses of the cadmium ion-selective electrode in methanol-water mixtures.

Cadmium-ion solutions of 10^{-8}—10^{-1} mol dm^{-3} are discussed. The logarithm of the cadmium ion activity, calculated by the Debye-Hückel approximation[12] (Eq. 1), was plotted along the X-axis.

$$\log \gamma_{\pm} = -\frac{A|Z_+Z_-|I^{1/2}}{1+BaI^{1/2}} \quad (1)$$

$\gamma_{\pm}$; Mean activity coefficient, Z; Electric charge, I; Ionic strength, A and B; Constants of the Debye-Hückel theory,[13] and a; Ion-size parameter.

The permittivities of alcohol-water mixed solutions (ε_{AW}) were obtained using the following equation;

$$\varepsilon_{AW} = \varepsilon_W - (\varepsilon_W - \varepsilon_A)X_A \quad (2)$$

ε_W; Permittivity of water, ε_A; Permittivity of alcohol, and X_A; Molar fraction of alcohol.

Curves shifted to more positive values with an increase in the alcohol content. The response was linear between 10^{-7}—10^{-2} mol dm^{-3} in water, but the range became narrower with an increase in alcohol content. Linearity was lost at higher cadmium-ion concentrations, presumably because ion pairs were formed by association in 50—99 v/v% methanol.

Figure 2 shows the calibration curves of the cadmium ion-selective electrode in water and in 25, 50, 75, and 99 v/v% ethanol. The results obtained in ethanolic solutions were similar to those in methanolic solutions.

The activity coefficients in alcohol-water mixed solutions were influenced by several factors compared with those in water. It was known that Eq. 1 could be used for aqueous solutions at ionic strengths of less than 0.1. However, in this work it was found that the activity coefficients could be calculated by the Debye-Hückel approximation within the following ranges; less than 10^{-2} mol dm^{-3} of cadmium ions in a 25 v/v% alcohol-water mixed solution, less than 10^{-3} mol dm^{-3} of cadmium ions in 50 and 75 v/v% alcohol-water mixed solutions and less than 10^{-5} mol dm^{-3} of cadmium ions in a 99 v/v% alcohol-water mixed solution.

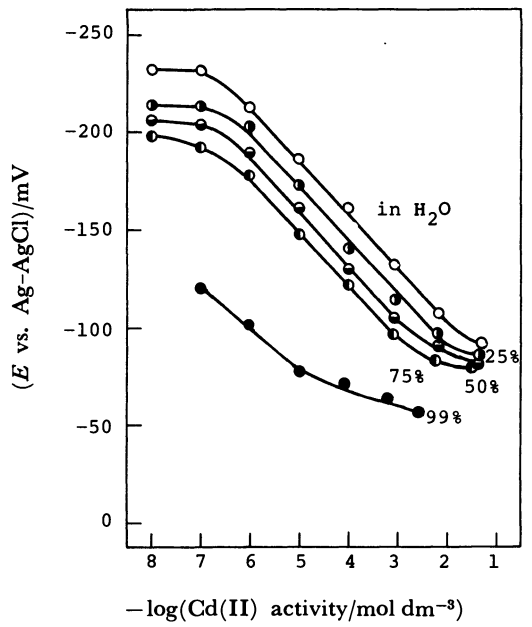

Fig. 2. Responses of the cadmium ion-selective electrode in ethanol-water mixtures.

Slopes of the Response. The slopes of the responses of the cadmium ion-selective electrode in various media are shown in Table 1. The slopes in alcohol-water mixtures (27—33 mV/decade in methanol-water mixtures and 21—29 mV/decade in ethanol-water mixtures) were similar to the Nernstian slope (29.6 mV/decade) and the correlation coefficient was nearly equal to 1. Good correlations were obtained between cadmium-ion activities and the observed potentials.

Response Time. The response times of the cadmium ion-selective electrode obtained in various media are shown in Table 2. The response time tended to decrease with an increase in the cadmium-ion concentration for all the solutions. The response times of the electrode in 99 v/v% methanol and in 99 v/v% ethanol were especially long, but the response times were less than 5 min in all solutions of 10^{-5}—10^{-1} mol dm^{-3} of cadmium ions.

Effects of Temperature. The effects of temperature on the slopes of the responses are shown in Table 3. Electrode potentials were measured between 0—50 °C. In all the solutions, the electrode potentials shifted to more positive values almost linearly with an increase in temperature. The theoretical slope calculated using the Nernst equation increased by ca. 1 mV per 10 °C rise in temperature. A similar tendency was observed in alcohol-water mixtures.

The Relation between the Potential and ΔpH. The relation between the electrode potential and the change in the reading of pH meter, ΔpH, upon an

Table 1. Slopes of the Response of the Cadmium Ion-Selective Electrode in Various Media

Solvent	Cd^{2+} Concn / mol dm^{-3}	Slope/mV	Coefficient of Correlation
99% MeOH	10^{-7}—10^{-5}	33.2	0.9999
75% MeOH	10^{-6}—10^{-3}	28.0	0.9991
50% MeOH	10^{-6}—10^{-3}	26.9	0.9969
25% MeOH	10^{-6}—10^{-2}	26.8	0.9976
99% EtOH	10^{-7}—10^{-5}	20.8	0.9982
75% EtOH	10^{-6}—10^{-3}	28.1	0.9995
50% EtOH	10^{-6}—10^{-3}	29.4	0.9993
25% EtOH	10^{-6}—10^{-2}	28.3	0.9960
H_2O	10^{-7}—10^{-2}	26.2	0.9978

Table 2. Response Times of the Cadmium Ion-Selective Electrode in Various Media

Cd^{2+} Concn mol dm^{-3}	Response time/min							
	Methanol in v/v%				Ethanol in v/v%			
	99	75	50	25	99	75	50	25
10^{-1}	—	0.0	2.5	1.0	—	3.0	0.0	0.0
10^{-2}	1.5	0.0	1.0	1.0	4.0	0.0	1.0	1.0
10^{-3}	4.0	0.0	1.0	1.0	3.0	0.0	1.0	0.0
10^{-4}	3.0	2.5	1.0	1.0	3.0	5.0	1.0	0.0
10^{-5}	1.0	4.0	1.0	1.0	1.5	1.0	2.5	1.0
10^{-6}	1.0	5.0	5.0	6.0	6.0	0.0	2.5	1.0
10^{-7}	5.0	6.0	8.0	6.0	8.0	7.0	11	7.0
10^{-8}	10	5.0	8.0	12	13	5.0	10	4.0

Table 3. Slopes of the Response of the Cadmium Ion-Selective Electrode at Various Temperature

Solvent	Cd^{2+} Concn mol dm^{-3}	Slope/mV					
		5 °C	10 °C	20 °C	30 °C	40 °C	50 °C
99% MeOH	10^{-7}—10^{-5}	33.7	33.2	33.2	34.5	35.7	36.3
75% MeOH	10^{-6}—10^{-3}	26.5	26.9	28.0	27.9	28.1	30.8
50% MeOH	10^{-6}—10^{-3}	24.5	25.5	26.9	28.1	30.4	31.0
25% MeOH	10^{-6}—10^{-2}	25.6	26.0	26.8	27.7	29.0	30.0
99% EtOH	10^{-7}—10^{-5}	17.8	19.6	20.8	22.6	25.3	28.4
75% EtOH	10^{-6}—10^{-3}	26.3	28.3	28.9	33.2	35.7	36.1
50% EtOH	10^{-6}—10^{-3}	29.8	29.6	29.4	29.5	32.5	35.0
25% EtOH	10^{-6}—10^{-2}	23.4	24.4	28.3	29.5	28.2	29.2
Nernstian slope		27.6	28.1	29.1	30.1	31.1	32.1

addition of acid was examined (Fig. 3). The pH meter was calibrated with a glass electrode, a saturated calomel electrode and a pH standard aqueous solution. The ΔpH values of samples were adjusted with acetic acid. The electrode potentials were constant at a ΔpH of 3.5—5.0 in alcohol-water mixtures. The deviation increased for a ΔpH below 3.5.

Selectivity of the Cadmium Ion-Selective Electrode. The selectivity of the cadmium ion-selective electrode in various media was examined using the mixed-solution method (Table 4). Interferences by potassium, sodium, calcium and magnesium were investigated. The selectivity coefficients for potassium ions in 25—99 v/v% methanol (7.2×10^{-3}—5.0×10^{-2}) and in ethanol (3.6×10^{-3}—4.2×10^{-3}) were greater than those reported in the literature for an aqueous solution (6.7×10^{-8}).[14] Similarly, those for sodium ions in 25—99 v/v% methanol (3.9×10^{-3}—8.4×10^{-2}) and in ethanol (2.4×10^{-3}—1.4×10^{-1}) were greater than those reported in the literature (3.2×10^{-8}).[14] The selectivity coefficients for calcium ions in 25—99 v/v% methanol (2.0×10^{-4}—3.6×10^{-4}) and in 25—99 v/v% ethanol (3.3×10^{-5}—2.1×10^{-4}), for magnesium ions in 25—75 v/v% methanol (5.2×10^{-4}—1.1×10^{-3}) and in 25—50 v/v% ethanol (1.9×10^{-4}—5.6×10^{-4}) were in fair agreement with those reported in the literature (2.2×10^{-4} and 1.6×10^{-4}),[14] respectively.

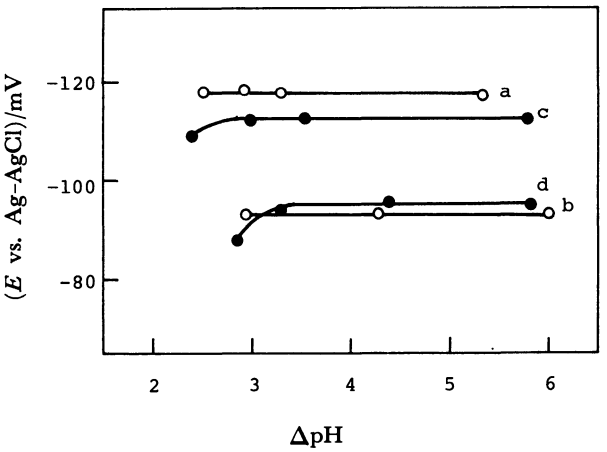

Fig. 3. The relation between the potential and ΔpH in methanol-water mixtures and ethanol-water mixtures: 10^{-3} mol dm^{-3} cadmium ion in (a) 25, (b) 75 v/v% methanol and in (c) 25, (d) 75 v/v% ethanol.

The cadmium ion-selective electrode could be used

Table 4. Selectivity Coefficient of the Cadmium Ion-Selective Electrode in Various Media

Solvent	Selectivity coefficient[a]			
	Interfering ion			
	K^+	Na^+	Ca^{2+}	Mg^{2+}
99% MeOH	5.0×10^{-2}	8.4×10^{-2}	2.7×10^{-4}	—
75% MeOH	7.2×10^{-3}	5.7×10^{-3}	2.2×10^{-4}	9.3×10^{-4}
50% MeOH	2.2×10^{-2}	3.9×10^{-3}	2.0×10^{-4}	5.2×10^{-4}
25% MeOH	7.2×10^{-3}	4.3×10^{-2}	3.6×10^{-4}	1.1×10^{-3}
99% EtOH	—	1.4×10^{-1}	2.1×10^{-4}	—
75% EtOH	4.0×10^{-3}	5.7×10^{-2}	1.0×10^{-4}	—
50% EtOH	3.6×10^{-3}	3.8×10^{-3}	9.9×10^{-5}	5.6×10^{-4}
25% EtOH	4.2×10^{-3}	2.4×10^{-3}	3.3×10^{-5}	1.9×10^{-4}
H_2O[b]	6.7×10^{-8}	3.2×10^{-8}	2.2×10^{-4}	1.6×10^{-4}

a) Mixed solution method. b) Literature value.

in alcohol–water solutions.

References

1) J. Motonaka, S. Ikeda, and N. Tanaka, *Anal. Chim. Acta*, **105**, 417 (1979).
2) W. S. Selig, *Ind. Eng. Chem., Prod. Res. Dev.*, **23**, 1, 140 (1984).
3) N. A. Kazarjan and E. Pungor, *Anal. Chim. Acta*, **51**, 213 (1970).
4) W. H. Ficklin and W. C. Gotschall, *Anal. Lett.*, **6**, 217 (1973).
5) G. J. Kakabadse, H. A. Maleila, M. N. Khayat, G. Tassopolos, and A. Vahdati, *Analyst*, **103**, 1046 (1978).
6) N. A. Kazarjan and E. Pungor, *Anal. Chim. Acta*, **60**, 193 (1972).
7) G. A. Rechnitz and N. C. Kenny, *Anal. Lett.*, **2**, 395 (1969).
8) G. A. Rechnitz and N. C. Kenny, *Anal. Lett.*, **3**, 259 (1970).
9) J. F. Coetzee and M. W. Martin, *Anal. Chem.*, **52**, 2421 (1980).
10) J. Motonaka, S. Ikeda, and N. Tanaka, *Bunseki Kagaku*, **33**, 551 (1984).
11) R. H. Cundiff and P. C. Markunas, *Anal. Chem.*, **28**, 792 (1956).
12) R. G. Bates, B. R. Staples, and R. A. Robinson, *Anal. Chem.*, **42**, 867 (1970).
13) R. A. Robinson and R. H. Stokes, "Electrolyte Solutions," 2nd ed., Butterworths, London (1959), Chap. 9.
14) M. J. Brand, J. Millitello, and G. A. Rechnitz, *Anal. Lett.*, **2**, 523 (1969).

 © 1986 The Chemical Society of Japan Bull. Chem. Soc. Jpn., 59, 741—745 (1986)

Spectrophotometric Determination of Micro Amounts of Thiocyanate via Permanganate Reaction

Yasuyuki MIURA* and Tomozo KOH
Department of Chemistry, Faculty of Science, Tokai University, 1117, Kitakaname, Hiratsuka, Kanagawa 259-12
(Received September 5, 1985)

A method has been developed for the determination of micro amounts of thiocyanate. It is based on the reaction of thiocyanate with a given amount of permanganate as an oxidizing agent in a dilute sulfuric acid medium and on the spectrophotometric measurement of iodine as triiodide, which is formed by the oxidation of iodide with an excess of permanganate for its reaction with thiocyanate. The conditions for the thiocyanate to be quantitatively oxidized were established by varying the temperature, reaction time, and amounts of sulfuric acid and permanganate. The present method can be successfully applied to the determination of thiocyanate in the range from 7×10^{-7} to 4×10^{-5} mol dm^{-3} (0.4—23.2 μg SCN^- in 10 cm^3). In eleven determinations for 10-cm^3 sample solutions containing 0.250 μmol of thiocyanate, the present method gave a mean value of 0.251 μmol, with a standard deviation of 0.0022 μmol and a relative standard deviation of 0.88%. Chloride, bromide, iodide, and cyanide did not interfere with the determination of 14.5 μg of thiocyanate in the presence of 1000 μg, 500 μg, 100 μg, and 50 μg, respectively.

Iron(III) reacts easily with thiocyanate to give a red iron(III)-thiocyanate complex in an acid medium. Therefore, iron(III)[1] is widely used for the photometric determination of small amounts of thiocyanate. However, in measuring thiocyanate at concentrations as low as the 10^{-5} mol dm^{-3} level, the iron(III) method is not considered useful because of its low sensitivity. For the sensitive spectrophotometric determination of thiocyanate, the pyridine-pyrazolone,[2,3] the pyridine–benzidine,[4,5] and the pyridine–barbituric acid[6] methods have been devised. Moreover, extraction methods using copper–pyridine,[7] tris(1,10-phenanthroline)iron(II),[8] Neutral Red,[9] mercury(II) Methylthymol Blue-zephiramine,[10] and mercury(II)–quinoline[11] reagents have been proposed. These methods[2-11] have, however, some disadvantages: pyridine is unpleasant and noxious, benzidine has a carcinogenic property, and solvent extraction is generally troublesome. Koh and Iwasaki[12] have previously reported a very sensitive method of determining thiocyanate (3×10^{-7}—1×10^{-5} mol dm^{-3}) based on the extraction of thiocyanate with Methylene Blue into 1,2-dichloroethane and the spectrophotometric measurement of the organic phase.

The purpose of this work, using the reaction of thiocyanate with permanganate, is to develop a method for the sensitive determination of thiocyanate without any solvent extractions or poisonous reagents. The optimal conditions under which thiocyanate can be oxidized by permanganate were established. The proposed method is based on the reaction of thiocyanate with a given amount of permanganate in an acidic medium[13] according to following Eq. 1, and then on the spectrophotometric measurement of the iodine thus formed, after converting the permanganate in excess for its reaction with thiocyanate into iodine[14] according to Eq. 2:

$$5SCN^- + 6MnO_4^- + 8H^+ \longrightarrow 6Mn^{2+} + 5SO_4^{2-} + 5CN^- + 4H_2O \quad (1)$$

$$2MnO_4^- + 10I^- + 16H^+ \longrightarrow 2Mn^{2+} + 5I_2 + 8H_2O \quad (2)$$

Experimental

Apparatus. All spectrophotometric measurements were made at 350 nm with a Shimadzu Model UV-240 recording spectrophotometer with 10-mm quartz cells. Desired temperatures were controlled by a Taiyo Coolnit Model CL-15 thermoregulator. Redistilled water used was freed from any permanganate-consuming impurities with a Nippon Millipore, Ltd., Model Milli-QII apparatus.

Reagents. All chemicals were of an analytical grade and were used without further purification.

Standard Thiocyanate Solution. A 0.1 mol dm^{-3} thiocyanate solution was prepared by dissolving potassium thiocyanate in redistilled water. The solution was standardized by Volhard's method. The working solutions were prepared by suitable dilution.

Standard Permanganate Solution.[15] A 0.02 mol dm^{-3} permanganage solution was prepared by heating the solution in which potassium permanganate had been dissolved to boiling, keeping it at a temperature slightly below the boiling point for 1 h, and then allowing it to stand for 3 d at room temperature. After the manganese dioxide thus obtained had been filtered off by suction with a sintered glass filter(3SG4), the filtrate was standardized by oxidation-reduction titration using standard sodium oxalate. The stock solution of 0.02 mol dm^{-3} standard permanganate proved to be stable; even after six months, no measurable change was found by the present method when it was stored at room temperature in dark. A working solution of the 2×10^{-4} mol dm^{-3} permanganate solution obtained by the appropriate dilution of the stock solution could be used for 2 d.

Standard Thiosulfate Solution. A 0.1 mol dm^{-3} thiosulfate solution was prepared by dissolving sodium

thiosulfate pentahydrate in freshly boiled and cooled redistilled water containing a small amount of sodium carbonate as a stabilizer. The thiosulfate solution was standardized by iodimetry a week after preparation. A 5×10^{-4} mol dm^{-3} thiosulfate solution was obtained by diluting the standardized thiosulfate exactly.

Iodide Solution. A 0.5 mol dm^{-3} iodide solution was prepared by dissolving 41.7 g of potassium iodide in redistilled water containing 200 mg of sodium carbonate as a stabilizer and by then diluting it to 500 cm^3.

Recommended Procedure. A 1.5 cm^3 of 0.8 mol dm^{-3} sulfuric acid and 4 cm^3 of a 2×10^{-4} mol dm^{-3} standard potassium permanganate solution were placed in a 25-cm^3 volumetric flask. To this mixture, 10-cm^3 of a sample solution containing thiocyanate up to 0.400 μmol were added. The mixture was then allowed to stand for 10 min in the temperature range from 15 to 40 °C to complete the oxidation of thiocyanate. Then, 1 cm^3 of 0.5 mol dm^{-3} potassium iodide was added to form iodine equivalent to the excess permanganate, and 3 cm^3 of 5×10^{-4} mol dm^{-3} sodium thiosulfate were added to decrease the absorbance of the iodine as triiodide to an appropriate value. The flask was filled to the mark with redistilled water. The absorbance of a solution of the triiodide complex thus formed was measured against distilled water at 350 nm in about 5 min after the dilution.

A permanganate-free reagent blank was prepared by placing 1.5 cm^3 of 0.8 mol dm^{-3} sulfuric acid, 14 cm^3 of redistilled water in place of both 4 cm^3 of 2×10^{-4} mol dm^{-3} permanganate and 10 cm^3 of a sample solution containing thiocyanate, and 1 cm^3 of 0.5 mol cm^{-3} iodide in a 25-cm^3 volumetric flask. After the flask had been filled to the mark with redistilled water, the absorbance was measured against distilled water at 350 nm in about 5 min. This absorbance value was subtracted from each of the absorbances for thiocyanate and the reagent blank, for iodide is susceptible to air-oxidation in an acid medium.

Results and Discussion

Calibration Plots. Figure 1 shows the calibration graphs obtained by treating a series of standard solutions of thiocyanate according to the recommended procedure and permanganate according to a procedure where 4 cm^3 of redistilled water were used instead of 4 cm^3 of 2×10^{-4} mol dm^{-3} permanganate. The graph for permanganate was prepared to confirm the stoichiometry and the completion of the reaction of thiocyanate with permanganate. According to Eq. 1, if 5 mol of thiocyanate react with 6 mol of permanganate completely and stoichiometrically, the graph for thiocyanate should coincide with that for permanganate (the expected graph) in excess amounts for the reaction with thiocyanate, when each of the molar concentration scales for thiocyanate and permanganate is drawn as in Fig. 1. Figure 1 proves that the reaction proceeded to stoichiometric completion under the conditions of Procedure.

The precision was estimated from 11 results for 10-cm^3 aliquots of a solution containing 0.250 μmol of thiocyanate. The present method gave a mean value of 0.251 μmol, with a standard deviation of 0.0022 μmol and a relative standard deviation of 0.88%. This method give a higher sensitivity than the copper(II) diethyldithiocarbamate-silver(I)[16] and the rhenium[17] methods without any need for solvent extractions or poisonous reagents.

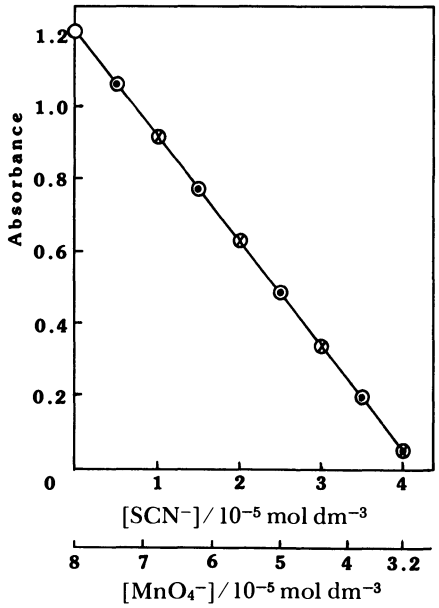

Fig. 1. Calibration plots.
○: Reagent blank, ⊙: SCN^-, ⊗: MnO_4^- (the expected value).

Table 1. Rate of Reaction of Thiocyanate with Permanganate at Various Temperatures

$\frac{t}{\text{min}}$	Absorbance			
	4×10^{-5} mol dm^{-3} SCN^-			
	10 °C	15 °C	25 °C	40 °C
	0.055[a]	0.053[a]	0.056[a]	0.055[a]
1	0.083	0.075	0.073	0.068
3	0.072	0.068	0.065	0.056
5	0.070	0.063	0.054	0.054
10	0.066	0.057	0.055	0.051
20	0.053	0.053	0.057	0.056
30	0.052	0.055	0.053	0.057

a) Absorbances for 3.2×10^{-5} mol dm^{-3} permanganate (the expected values).

Rate of Reaction of Thiocyanate with Permanganate. The reaction rate was investigated at temperatures ranging from 10 to 40 °C. The amount of the reagents and the addition order were as in the above procedure. The results are given in Table 1. The reaction was gradually accelerated by an increase in the temperature. The absorbances for

4×10^{-5} mol dm^{-3} thiocyanate reached those for 3.2×10^{-5} mol dm^{-3} permanganate, which are the expected values, in 20 min at 10 °C, in 10 min at 15 °C, in 5 min at 25 °C, and in 3 min at 40 °C, and then kept constant until 30 min had passed. These facts confirm that the reaction proceeds to completion as long as it is carried out for 10 min at temperatures from 15 to 40 °C. On the other hand, when thiocyanate was allowed to react with permanganate in a solution of a low acidity using 1.5 cm^3 of 0.3 mol dm^{-3} sulfuric acid, the reaction did not proceed to completion according to Eq. 1. Therefore, the effect of acidity was investigated at 20 °C. The results are shown in Table 2. The absorbances for 4×10^{-5} mol dm^{-3} thiocyanate coincided with the expected value in 10 min with 1.5 cm^3 of 0.6 mol dm^{-3} sulfuric acid, in 5 min with 1.5 cm^3 of each 0.8 and 1.0 mol dm^{-3} sulfuric acid, and in 3 min with 1.5 cm^3 of 1.5 mol dm^{-3} sulfuric acid. Consequently, 1.5 cm^3 of 0.8 mol dm^{-3} sulfuric acid was employed in this experiment.

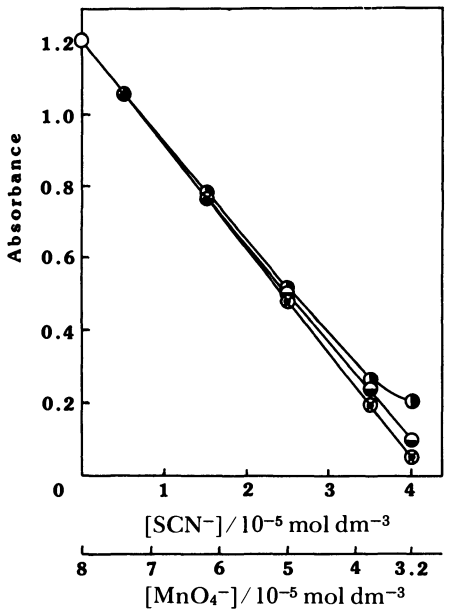

Fig. 2. Effect of amounts of permanganate on reaction with thiocyanate.
○: Reagent blank, ◑: SCN⁻ with 2.5 cm^3 of 2×10^{-4} mol dm^{-3} MnO_4^-, ◒: SCN⁻ with 3.0 cm^3 of 2×10^{-4} mol dm^{-3} MnO_4^-, ⊗: SCN⁻ with 3.5, 4.0, or 4.5 cm^3 of 2×10^{-4} mol dm^{-3} MnO_4^-, ⊙: SCN⁻ obtained under the conditions of Procedure.

Table 2. Effect of Amounts of Sulfuric Acid on Reaction of Thiocyanate with Permanganate at 20 °C

t / min	Absorbance: 4×10^{-5} mol dm^{-3} SCN⁻			
	0.6 mol dm^{-3} H_2SO_4	0.8 mol dm^{-3} H_2SO_4	1.0 mol dm^{-3} H_2SO_4	1.5 mol dm^{-3} H_2SO_4
	0.056[a)]	0.053[a)]	0.056[a)]	0.055[a)]
1	0.085	0.077	0.072	0.070
3	0.078	0.066	0.062	0.060
5	0.068	0.056	0.059	0.054
10	0.056	0.056	0.058	0.053
20	0.054	0.052	0.055	0.056
30	0.053	0.055	0.058	0.051

a) Absorbances for 3.2×10^{-5} mol dm^{-3} permanganate (the expected values). The volume of the sulfuric acids used was 1.5 cm^3.

Effect of Amounts of Permanganate. For measuring the effects of the amounts of permanganate, thiocyanate was allowed to react with various amounts of potassium permanganate for 10 min at 20 °C. In this experiment, the thiosulfate, which is used in order to reduce the absorbance, was not added. The absorbance, therefore, increased with the increase in the amounts of permanganate employed. The resulting graphs (given in Fig. 2) were normalized in such a way that each calibration graph for thiocyanate with various amounts of permanganate was permitted to shift in parallel fashion to cause each reagent blank to accord with that obtained under the conditions of Procedure. When 2.5 and 3.0 cm^3 of 2×10^{-4} mol dm^{-3} permanganate were used, the reaction did not go to completion because the amounts of permanganate were insufficient. However, when 3.5, 4.0, or 4.5 cm^3 of the permanganate solution were used, the graphs for thiocyanate formed a straight line and coincided completely with that obtained under the conditions

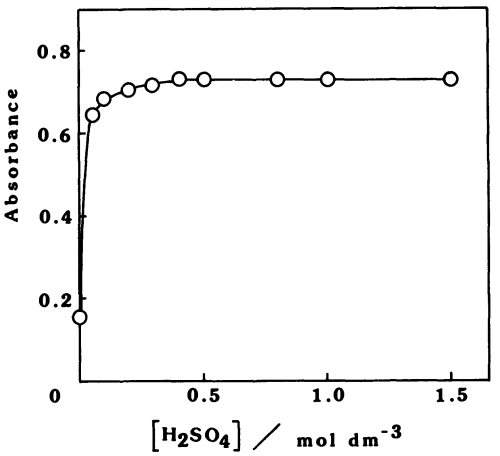

Fig. 3. Effect of amounts of sulfuric acid on liberation of iodine by oxidation with permanganate. A 10 cm^3 of 6×10^{-5} mol dm^{-3} permanganate was treated as in procedure, where 1.5 cm^3 sulfuric acid solution in various molar concentrations were used and 4 cm^3 of redistilled water were employed instead of 4 cm^3 of 2×10^{-4} mol dm^{-3} permanganate.

Table 3. Effect of Standing Time of Triiodide Solution

t / min	Absorbance	
	Reagent blank	4×10^{-5} mol dm^{-3} SCN^-
1	1.179	0.048
3	1.203	0.053
5	1.205	0.057
7	1.208	0.059
10	1.213	0.063
15	1.226	0.077
20	1.233	0.084

Table 4. Effect of Diverse Ions

Ion	Added as	Amount / μg	Amount of SCN^- found / μg	Error / %
None			14.5	
Na^+	Na_2SO_4	10000	14.5	0
K^+	K_2SO_4	10000	14.5	0
NH_4^+	$(NH_4)_2SO_4$	10000	14.5	0
Mg^{2+}	$Mg(NO_3)_2\cdot6H_2O$	10000	14.4	−0.7
Ca^{2+}	$Ca(NO_3)_2\cdot4H_2O$	10000	14.5	0
Zn^{2+}	$ZnSO_4\cdot7H_2O$	10000	14.6	+0.7
Cd^{2+}	$Cd(NO_3)_2\cdot4H_2O$	10000	14.5	0
Mn^{2+}	$MnSO_4\cdot5H_2O$	100	14.5	0
Co^{2+}	$CoSO_4\cdot7H_2O$	10000	14.5	0
Ni^{2+}	$NiSO_4(NH_4)_2SO_4\cdot6H_2O$	10000	14.5	0
Cu^{2+}	$CuSO_4\cdot5H_2O$	1000	14.4	−0.7
Pb^{2+}	$Pb(NO_3)_2$	1000	14.5	0
Fe^{2+}	$FeSO_4(NH_4)_2SO_4\cdot6H_2O$	1	14.4	−0.7
Fe^{3+}	$Fe(NO_3)_3\cdot9H_2O$	1	14.4	−0.7
		5000[a]	14.6	+0.7
Al^{3+}	$Al(NO_3)_3\cdot9H_2O$	10000	14.6	+0.7
F^-	NaF	30000	14.7	+1.4
Cl^-	NaCl	10000	14.5	0
Br^-	KBr	500	14.8	+2.1
I^-	KI	100	14.2	−2.1
CN^-	NaCN	50	14.6	+0.7
NO_3^-	KNO_3	10000	14.5	0
NO_2^-	KNO_2	1	14.6	+0.7
		1000[b]	14.5	0
S^{2-}	$Na_2S\cdot9H_2O$	0.5	14.8	+2.1
HSO_3^-	$NaHSO_3$	1	14.8	+2.1
CO_3^{2-}	Na_2CO_3	10000	14.5	0
$HAsO_4^{2-}$	$Na_2HAsO_4\cdot7H_2O$	10000	14.4	+0.7
$H_2PO_4^-$	$NaH_2PO_4\cdot2H_2O$	10000	14.5	0
Borate ion	H_3BO_3	10000	14.5	0

a) 3 cm^3 of 0.5 mol dm^{-3} NaF were added. b) 1 cm^3 of 0.05 mol dm^{-3} sulfamic acid was added.

of Procedure. Consequently, 4.0 cm^3 of 2×10^{-4} mol dm^{-3} permanganate were employed.

Effect of Amounts of Iodide. In order to estimate the optimal amount of iodide on the formation of iodine equivalent to excess amounts of permanganate for the reaction of Eq. 1, 1 cm^3 of 0.1, 0.3, 0.5, 0.7, or 1.0 mol dm^{-3} iodide solution was used in Procedure. In all cases, calibration graphs for thiocyanate gave straight lines with a good reproducibility, and the sensitivity increased with the increase in the amounts of iodide used. In the recommended procedure, 1 cm^3 of a 0.5 mol dm^{-3} iodide solution was used, for it gives the appropriate absorbance value for the reagent blank.

Effect of Amounts of Sulfuric Acid on Liberation of Iodine. For measuring the effects of the amounts of sulfuric acid on the oxidation of iodide by permanganate to iodine, 1.5 cm^3 of a sulfuric acid solution in various molar concentrations were employed in Procedure. As can be seen in Fig. 3, when 1.5 cm^3 of 0.4—1.5 mol dm^{-3} sulfuric acid were used, the absorbance reached the maximum value and subsequently remained constant. Therefore, 1.5 cm^3 of 0.8 mol dm^{-3} sulfuric acid were used in Procedure.

Stability of Triiodide Complex Solution. The absorbance of the triiodide complex solution increased progressively with time because iodine is formed by the air-oxidation of iodide in an acidic solution. The triiodide complex solution prepared according to Procedure was allowed to stand for various periods of time at room temperature. The results are given in Table 3. The absorbances for the reagent blank and 4×10^{-5} mol dm^{-3} thiocyanate gave nearly constant values over the range from 3 to 7 min. Therefore, all the absorbances were measured in about 5 min after the contents had been diluted to 25 cm^3 by the recommended procedure.

Effect of Diverse Ions. A 10-cm^3 portion of a solution containing 14.5 μg of thiocyanate and various amounts of diverse ions was treated exactly as in Procedure. Iron(II), nitrite, sulfide, and sulfite gave positive errors for the determination of thiocyanate, even when present in trace amounts, because they reduce permanganate. However, the interference of nitrite could be eliminated by decomposing it with sulfamic acid. Iron(III) gave a negative interference in the presence of 10 μg because it reacts with iodide to form iodine, but its interference was eliminated by masking with fluoride. For the determination of 14.5 μg of thiocyanate with an error of below 2.1% by the present method, foreign ions can be tolerated at the levels given in Table 4. Anions such as chloride, bromide, iodide, and cyanide, which interfere seriously in the conventional determination of thiocyanate are tolerated in amounts of 10000 μg, 500 μg, 100 μg, and 50 μg, respectively, in the present method.

References

1) F. D. Snell, "Photometric and Fluorometric Methods of Analysis, Nonmetals," Wiley Interscience, New York (1981), p. 477.
2) J. Epstein, *Anal. Chem.*, **19**, 272 (1947).
3) S. Nagashima, *Anal. Chem.*, **55**, 2086 (1983).
4) W. N. Aldridge, *Analyst*, **69**, 262 (1944).
5) W. N. Aldridge, *Analyst*, **70**, 474 (1945).
6) S. Nagashima, *Anal. Chem.*, **56**, 1944 (1984).
7) J. M. Kruse and M. G. Mellon, *Anal. Chem.*, **25**, 446 (1953).
8) Y. Yamamoto, T. Tarumoto, and Y. Hanamoto, *Bull. Chem. Soc. Jpn.*, **42**, 268 (1969).
9) M. Tsubouchi, *Anal. Chim. Acta*, **54**, 143 (1971).
10) T. Nomura, S. Takemura, T. Nakamura, and S. Komatsu, *Bunseki Kagaku*, **22**, 576 (1973).
11) H. Einaga, H. Ishii, and I. Iwasaki, *Talanta*, **20**, 1017 (1973).
12) T. Koh and I. Iwasaki, *Bull. Chem. Soc. Jpn.*, **40**, 569 (1967).
13) A. V. Hanley and F. W. Czech, "The Analytical Chemistry of Sulfur and Its Compounds," ed by J. H. Karchmer, Wiley Interscience, New York (1970), Part I, p. 395.
14) W. J. Williams, "Handbook of Anion Determination," Butterworths, London (1979), p. 163.
15) I. M. Kolthoff, E. B. Sandell, E. J. Meehan, and S. Bruckenstein, "Quantitative Chemical Analysis," 4th ed., Macmillan Company, London (1969), p. 825.
16) T. Nakamura, *Nippon Kagaku Kaishi*, **1972**, 1429.
17) R. E. Neas and J. C. Guyon, *Anal. Chem.*, **41**, 1470 (1969).

Stereoselectivity in the Synthesis of Enol Esters from Chloromercurio Aldehydes and Acyl Chlorides

Wakichi FUKUDA,* Hozumi SATO, and Hiroshi KAKIUCHI
Department of Applied Chemistry, Faculty of Engineering, Yokohama National University, Tokiwadai, Hodogaya-ku, Yokohama 240
(Received September 9, 1985)

Reactions of chloromercurio aldehydes with acyl chlorides gave a variety of (*Z*)- and (*E*)-enol esters. The *Z*/*E* ratio of the enol esters is dependent on the structure of chloromercurio aldehydes but independent of that of acyl chlorides. *Z*-Rich enol esters were prepared by acylation of 2-chloromercurio aldehydes derived from propanal, butanal, and 2-phenylethanal, while *E*-rich 1-acyloxy-1,3-butadiene was obtained by acylation of (*E*)-4-chloromercurio-2-butenal. Reaction mechanisms for the stereoselective formation of these enol esters are discussed together with the isomer composition of starting enol acetates from which the chloromercurio aldehydes were prepared.

Various methods are available for synthesis of enol esters. The most practical technique involves treatment of aldehydes or ketones with appropriate acid anhydrides or acid chlorides under either acidic or basic conditions.[1—10] Other major methods for preparing enol esters involve addition of carboxylic acids to alkynes[11—16] and palladium-catalyzed acyloxylation of olefins.[17]

Although limited in scope, organomercurials are used for preparing enol esters.[18] Halomercurio aldehydes or ketones can be *O*-acylated with acyl chlorides:[19,20]

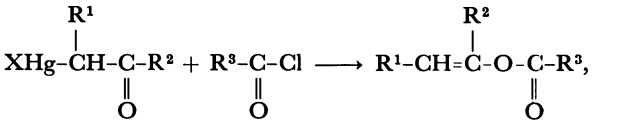

(1)

where R^1 and R^2 are each hydrogen, alkyl, or aryl, R^3 is alkyl or aryl, and X is halogen.

Reactions of vinylmercurials with mercury(II) carboxylates in the presence of a catalytic amount of palladium(II) acetate lead stereospecifically to formation of enol esters:[21]

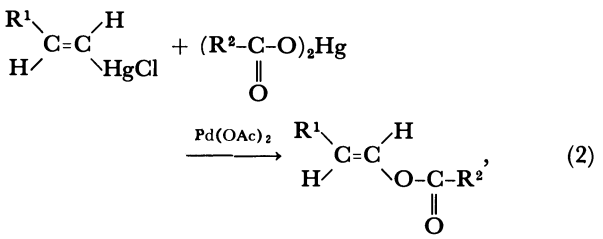

(2)

where R^1 is hydrogen, alkyl, or aryl, and R^2 is alkyl or aryl.

An attempt was made to prepare enol acrylate from propanal and acrylic anhydride or acryloyl chloride in the presence of quinoline or potassium acetate, but it was unsuccessful since polymers were formed easily. Under mild conditions, enol acrylates and methacrylates were prepared by reaction of chloromercurio aldehydes with acryloyl chloride or methacryloyl chloride according to the procedure by Nesmeyanov et al.[20] It was found with this reaction that enol esters prepared were stereoselective depending on the structure of chloromercurio aldehydes.

In this article, the stereoselectivity in the synthesis of enol esters from chloromercurio aldehydes and acyl chlorides is described, together with the effect of the isomer composition (*Z*/*E*) of starting enol acetates from which chloromercurio aldehydes are prepared.

Results and Discussion

Compositions of Geometric Isomers of Starting Enol Acetates. Enol acetates can be prepared by reactions of aldehydes either with acetic anhydride in the presence of potassium acetate (method A) or with 2-acetoxy-1-propene in the presence of *p*-toluenesulfonic acid (method B). Their yields were in the range from 12 to 73% (1-acetoxy-1-propene (**1a**)<1-acetoxy-1-butene (**2a**)<1-acetoxy-1,3-butadiene (**4a**)<1-acetoxy-2-(phenyl)ethene (**3a**)). This order may be interpreted in terms of the stability of enol forms. The enol/keto ratio for ethanal was less than 10^{-7} under conditions where the enol content of acetone was measurable.[22] On the other hand, aryl-substituted ethanals gave stable enols.[23]

All of the enol esters prepared were mixtures of (*Z*)- and (*E*)-isomers. The 1-acetoxy-1-propene (**1a**) obtained by method A was a *Z*/*E* mixture with a ratio of 51/49, which is consistent with the literature.[5,6] The *Z*/*E* ratio of 1-acetoxy-1-butene (**2a**) was 47/53, while those of 2-phenyl-1-(acetoxy)ethene (**3a**) and 1-acetoxy-1,3-butadiene (**4a**) were 35/65 and 38/62, respectively.

Scheme 1 shows the reaction process for method A where an ambident enolate anion may be formed as an intermediate. The geometry of the enol esters will be determined in the addition step of acyl residue to the enolates. The results for **1a** and **2a** suggest that methyl and ethyl substituents (R^1=CH_3, C_2H_5)

contribute little to the difference in stability and/or reactivity between (*Z*)- and (*E*)-enolates. Therefore, the *Z*/*E* ratios of **1a** and **2a** are almost 1/1.

When 2-substituent in the enolate is phenyl or vinyl, the *Z*/*E* ratios are less than 2/3. Heiszwolf and Kloosterziel[24] have reported an *O*-alkylation of ambident enolate anion obtained from 2-phenylethanal. The *Z*/*E* ratios of the enol ethers prepared in dimethyl sulfoxide and in liquid ammonia were 9/10 and 3/2, respectively, while those of the intermediate enolate anions were 3/2 in both solvents. Although the enolates prepared by method A are not so stable as those prepared in dimethyl sulfoxide and in liquid ammonia, the product determining step will be the reaction of the enolate with acetic anhydride. The result for **3a** suggests that the (*E*)-enolate of 2-phenylethanal reacts with acetic anhydride more rapidly than the (*Z*)-enolate. This may be interpreted in terms of steric and electronic effects of phenyl residue on the enolate anion. The reaction of 2-butenal with acetic anhydride may proceed along the same process as that of 2-phenylethanal. But the vinyl substituent will give little effect on both stability and reactivity of the enolates. Alternatively, the *Z*/*E* ratio of **4a** may rather be controlled by the concentrations of (*Z*)- and (*E*)-enolates since (*E*)-2-butenal is present mainly in *s-trans*-conformation[25,26] which leads to the formation of (*E*)-enolate.

The *Z*/*E* ratios of **2a** and **4a** prepared by method B were 65/35 and 17/83, respectively. Scheme 2 involves an intermediate cation in the reaction of butanal with 2-acetoxy-1-propene. The intermediate cation for (*E*)-isomer will be more stable than that for (*Z*)-isomer because of the steric interaction between acetoxy and ethyl residues. Both *anti*- and *syn*-elimination of proton from the intermediates will give *E*-rich enol ester. By contrast, the result suggests that the product determining step is not the elimination of proton but the addition of acetyl cation to butanal. It suggests a formation of the intermediate for (*Z*)-isomer in preference to that for (*E*)-isomer and no interconversion between the intermediates which was shown by Skell and Hall[27] for the E1 reaction of 3-deuteriobutyl-2-tosylate. The reason for the preferential formation of the intermediate for (*Z*)-isomer remains open.

Scheme 3 shows the reaction process of 2-butenal and 2-acetoxy-1-propene. The *Z*/*E* ratio of **4a** will be determined by the addition of acetyl cation to the carbonyl oxygen of 2-butenal, since the elimination of terminal methyl proton in the intermediate is of no effect on the geometry of the products. As the *O*-acetylations of *s-cis*- and *s-trans*-2-butenal give the intermediate cations of (*Z*)- and (*E*)-enol acetates, respectively, the *Z*/*E* ratio of **4a** may be controlled by the s-cis/s-trans ratio of 2-butenal. The result, the *Z*/*E* ratio of 17/83, is in agreement with the s-cis/s-trans ratio of the literature.[25,26]

Stereoselectivity in the Reaction of Chloromercurio Aldehydes with Acyl Chlorides. Reactions of four chloromercurio aldehydes with acyl chlorides were conducted to give respective enol esters. Table 1 shows that the reactions of 2-(chloromercurio)butanal (**2x**) with three acyl chlorides give the correspond-

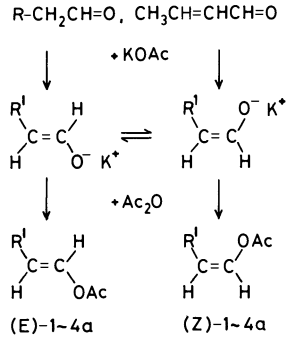

Scheme 1. Process of enol acetylation in the presence of potassium acetate.
R: CH_3, C_2H_5, C_6H_5.

Compound	**1a**	**2a**	**3a**	**4a**
R^1	CH_3	C_2H_5	C_6H_5	CH_2=CH

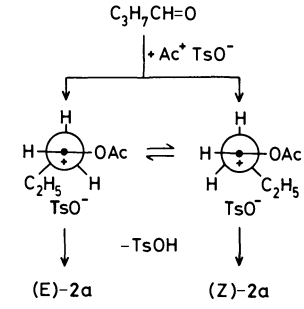

Scheme 2. Process for the acetylation of butanal with 2-aetoxy-1-propene in the presence of *p*-toluenesulfonic acid.

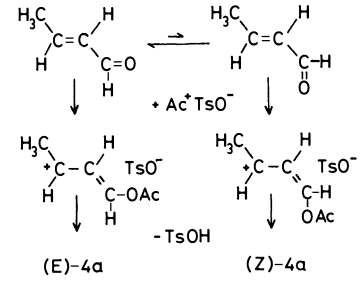

Scheme 3. Process for the acetylation of (*E*)-2-butenal with 2-acetoxy-1-propene in the presence of *p*-toluenesulfonic acid.

Table 1. Composition of Isomeric Enol Esters Prepared from Chloromercurio Aldehydes and Acyl Chlorides

Starting enol acetate		Substrate		Reaction conditions		Resulting enol ester		
	Z/*E* ratio[a]	-R in ClHg-R	R^2- in R^2-COCl		time / h		Isolated yield / %	*Z*/*E* ratio[a]
1a	51/49	-CHCH=O | CH_3 **1x**	CH_2=CH-	b)	6	**1b**	58	84/16(88/12)
2a	47/53	-CHCH=O	CH_2=CH-	c)	6	**2b**	38	87/13(83/17)
	47/53	|	C_6H_5-	c)	4	**2c**	70	85/15(83/17)
	47/53	C_2H_5	CH_3-	b)	6	**2a**	91	82/18(80/20)
	82/18	**2x**	CH_3-	b)	6	**2a**	88	86/14(82/18)
	(65/35)		CH_3-	e)	2	**2a**	77	(84/16)
3a	35/65	-CHCH=O | C_6H_5 **3x**	CH_2=CH-	c)	6	**3b**	51	74/26(76/24)
4a	38/62	$-CH_2CH$	CH_2=CH-	d)	3	**4b**	39	32/68(30/70)
	38/62	||	CH_2=C(CH_3)-	c)	6	**4c**	63	34/66
	17/83	CH	CH_2=C(CH_3)-	c)	6	**4c**	42	13/87
	17/83	|	CH_3-	e)	0.5	**4a**	—	(5/95)
	17/83	CH=O **4x**	CH_3-	e)	24	**4a**	—	(15/85)

a) Determined by ^{1}H NMR and by GLC (shown in parentheses). b) At 40—60 °C in tetralin. c) At 40—60 °C in benzene. d) At 30—50 °C in benzene. e) At ambient temperature in benzene.

ing enol esters of which the *Z*/*E* ratios are about 85/15. These ratios for the enol esters (**2a—c**) are independent of the acyl chlorides. The reactions of 2-(chloromercurio)propanal (**1x**) and 2-phenyl-2-(chloromercurio)ethanal (**3x**) with acryloyl chloride give 1-acryloyloxy-1-propene (**1b**) and 2-phenyl-1-(acryloyloxy)ethene (**3b**) having the *Z*/*E* ratios of 84/16 and 76/24, respectively.

Scheme 4 shows the reaction pathways of 2-substituted 2-chloromercurio aldehydes with acyl chlorides. Two stable conformations of the 2-chloromercurio aldehydes are suggested on the basis of torsional angle (98°) of Hg-C-C=O which was given by Halfpenny and Small.[28] Of the two conformations suggested, *syn*-1,2-dihydrogen form may be more stable than *anti*-1,2-dihydrogen form because of the steric interaction of 1-hydrogen with 2-substituent (R^1). 2-Chloromercurio aldehydes in each conformation will give stereoselectively (*Z*)- and (*E*)-enol esters. There are two reaction routes to be considered in each case. One of them is a spontaneous 1,3-displacement reaction of acyl cation with chloromercurio residue. The stereoselectivity of this route can be interpreted in terms of the formation of a six-membered intermediate between acyl chloride and 2-chloromercurio aldehyde

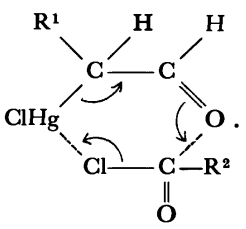

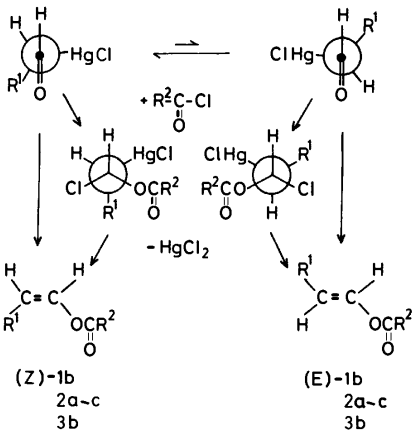

Scheme 4. Pathways for the formation of enol esters.

Compound	**1b**	**2a**	**2b**	**2c**	**3b**
R^1	CH_3	CH_3	C_2H_5	C_2H_5	C_6H_5
R^2	CH_2=CH	CH_3	CH_2=CH	C_6H_5	CH_2=CH

The other is an addition-elimination reaction between acyl chlorides and 2-chloromercurio aldehydes. The stereoselectivity will come from the *anti*-addition of chloride with respect to 2-chloromercurio residue and the *anti*-elimination of mercury(II) chloride from *threo*- and *erythro*-2-chloromercurio-1-acyloxy-1-chloro intermediates. Such compounds as 1-acyloxy-1-chloro derivatives were prepared by Kyburz et al.[29] through reaction of aldehydes or ketones with acyl chlorides in the presence of Lewis acid. The mechanism of *anti*-addition and *anti*-elimination was proposed by Larock and Bernhardt[30]

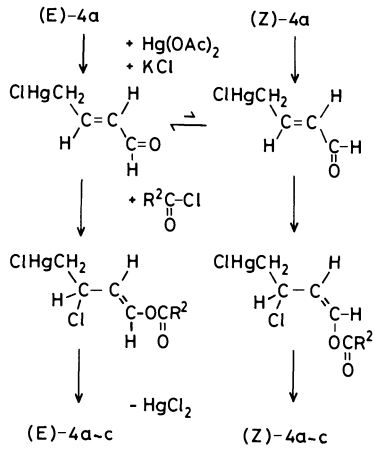

Scheme 5. Pathways for the formation of 1-acyloxy-1,3-butadienes.

Compound	4a	4b	4c
R^2	CH_3	CH_2=CH	CH_2=C(CH_3)

for the acylation of vinylmercurials.

In any cases the *syn*-1,2-dihydrogen conformation will lead to the formation of (*Z*)-enol ester. In conclusion, the stereoselectivity in the reactions of 2-chloromercurio aldehydes **1x—3x** with acyl chlorides may be controlled by the conformational structures of **1x—3x** when the reactions follow any one of the routes.

On the other hand, the reaction of 4-chloromercurio-2-butenal (**4x**) with acyl chlorides leads to the formation of *E*-rich 1-acyloxy-1,3-butadienes **4a—c** as shown in Table 1. Scheme 5 shows the reaction pathways for the stereoselective formations of *s-trans*- and *s-cis*-**4x** which react with acyl chlorides to give (*E*)- and (*Z*)-**4a—c**, respectively. The results suggest that conformational isomerization between *s-trans*- and *s-cis*-**4x** is difficult under reaction conditions where **4x** is slightly soluble and may associate together as verified on the basis of IR spectra. Another support for this suggestion is provided by the effect of reaction time on the *Z*/*E* ratio of product **4a** which was 5/95 at the beginning and 15/85 at the end for the reaction of **4x** with acetyl chloride. The *Z*/*E* ratio of the 1-acyloxy-1,3-butadiene prepared was almost equal to that of the starting enol acetate. The results also suggest that the product controlling step is the *O*-acylation of **4x**, since the elimination of a 4-chloromercurio residue from the *O*-acylated **4x** leads to the formation of a terminal vinylic double bond.

In conclusion, both the reaction of 1-acetoxy-1,3-butadiene with mercury(II) acetate and that with potassium chloride, as well as the reaction of the resultant (*E*)-4-chloromercurio-2-butenal with acyl chloride, can be carried out stereoselectively according to the structures of the substrates.

Experimental

General Method. Propanal, butanal, 2-phenylethanal, 2-butenal, 2-acetoxy-1-propene, acrylic acid, and methacrylic acid were commercial reagents and distilled before use. 2-Phenylethanal was supplied as a 50% solution in diethyl phthalate. Acryloyl chloride and methacryloyl chloride were prepared by the reaction of acrylic acid and methacrylic acid with benzoyl chloride, respectively. Solvents were purified in the usual way. The other reagents used were commercially available and used as they were.

Enol esters prepared were purified by distillation until their purities became higher than 99% as checked by GLC analyses on a 20% diethylene glycol succinate coated on Neopak 1A (Nishio Industry Co., Ltd.). They were identified by both IR and ^{1}H NMR spectra. GLC analyses were performed on a Shimadzu GC-4CPT gas chromatograph equipped with a thermal conductivity detector. ^{1}H NMR spectra were recorded on a JEOL-JNM C-60H spectrometer, and IR spectra were recorded on a Hitachi EPI-2 or a Shimadzu IR-400 spectrophotometer. The *Z*/*E* ratio of enol ester was determined by ^{1}H NMR spectrum and/or by GLC analysis. The peak of (*Z*)-olefinic proton in each ^{1}H NMR spectrum appeared at higher magnetic field than that of the (*E*)-olefinic proton. In the GLC analysis, the peak for the shorter retention time was assigned to the (*Z*)-isomer.

Preparation of Starting Enol Acetates. Method A: Enol acetylation with acetic anhydride in the presence of potassium acetate was conducted according to the procedure described in the literature.[2,3]

1-Acetoxy-1-propene (1a):[2] Propanal (1 mol), acetic anhydride (1.5 mol), and potassium acetate (0.125 mol) were refluxed for 8 h, the mixture was distilled, and the boiling fraction at 80—118 °C was washed with aqueous sodium carbonate and with distilled water and dried over sodium sulfate. Redistillation gave **1a**: Yield 12%; bp 103—106 °C; ^{1}H NMR δ=4.78 (0.51H, quintet, J=6.26 Hz, (*Z*)-2-H) and 5.30 (0.49H, quintet, J=6.24, 12.5 Hz, (*E*)-2-H); *Z*/*E* ratio 51/49 (lit,[5] 52.5/46.2; lit,[6] 48/52).

1-Acetoxy-1-butene (2a):[2] Similar treatment of butanal gave **2a**: Yield 37%; bp 122—124 °C; ^{1}H NMR δ=4.78 (0.47H, q, (*Z*)-2-H) and 5.36 (0.53H, sextet, (*E*)-2-H);[31,32] *Z*/*E* ratio 47/53.

1-Acetoxy-2-phenylethene (3a):[1] Similar treatment of 2-phenylethanal gave **3a**: Yield 73%; bp 73—74 °C/0.3 mmHg (1 mmHg=133.322 Pa); ^{1}H NMR δ=5.59 (0.35H, d, J=7.50 Hz, (*Z*)-2-H) and 6.32 (0.65H, d, J=13.05 Hz, (*E*)-2-H);[21,33] *Z*/*E* ratio 35/65.

1-Acetoxy-1,3-butadiene (4a):[3] 2-Butenal (1 mol) was added dropwise into a refluxing mixture of acetic anhydride (1.5 mol) and potassium acetate (1 mol). The mixture was refluxed further for half an hour. After cooling, it was washed successively with aqueous sodium carbonate, 20% sulfuric acid, and aqueous sodium carbonate and dried over sodium sulfate. Distillation under reduced pressure gave **4a**: Yield 57%; bp 56—58 °C/40 mmHg; ^{1}H NMR δ=7.05 (0.38H, d, (*Z*)-1-H) and 7.38 (0.62H, d, (*E*)-1-H); *Z*/*E* ratio 38/62.

Method B: Enol acetylation with 2-acetoxy-1-propene in the presence of *p*-toluenesulfonic acid and copper(II) acetate was carried out according to the literature.[4] Both **2a** and **4a** were prepared. **2a**: Yield 33%; bp 122—123 °C; *Z*/*E* ratio 65/35 by GLC. **4a**: Yield 70%; bp 51.0—52.5 °C/30 mmHg; *Z*/*E* ratio 17/83 by ^{1}H NMR.

Chloromercurio Aldehydes. 2-(Chloromercurio)propanal (1x): The preparative method for **1x** was a modification of that employed by Curtin and Hurwitz[2] as follows: Mercury(II) acetate (0.2 mole) was dissolved in 300 cm^3 of distilled water at ice-temperature. To this solution **1a** (0.2 mol) was added. When a homogeneous solution was obtained, 100 cm^3 of aqueous potassium chloride (0.2 mol) was added with vigorous stirring. It was agitated for several hours and allowed to stand overnight. The precipitate formed was separated on a suction funnel, washed with distilled water repeatedly, and dried in vacuo. **1x**: Yield 66%; mp 66—69 °C.

2-(Chloromercurio)butanal (2x):[2] Similarly, the reaction of **2a** with mercury(II) acetate and then with potassium chloride gave **2x**: Yield 83%; mp 90—94 °C; IR (benzene) 2700 (CO-H) and 1690 (C=O) and (Nujol mull) 2750 (CO-H) and 1630 cm^{-1} (C=O).

2-Chloromercurio-2-(phenyl)ethanal (3x): Similarly, the reaction of **3a** with mercury(II) acetate and then with potassium chloride gave **3x**: Yield 74%; mp 180 °C (decomp).

4-Chloromercurio-2-butenal (4x): The reaction of **4a** with mercury(II) acetate and then with potassium chloride gave **4x**: Yield 94%; mp 118—121 °C (decomp); IR (benzene) 1681 (C=O) and 1614 (C=C) and (Nujol mull) 1635 (C=O) and 1600 cm^{-1} (C=C). A comparison of the IR spectrum of **4x** with that of 2-butenal (1680 ((C=O) and 1640 cm^{-1} (C=C)) suggests that the chloromercurio group adds on 4-carbon rather than 2-carbon in **4x**. The lowering in wave number of the absorption band for the carbonyl stretching vibration has been observed by Susz[34] on a number of carbonyl compounds coordinated to Lewis acids; thus, coordination of mercury(II) chloride lowered 31 cm^{-1} the absorption band of the carbonyl in acetophenone.

The chloromercurio aldehydes (**1x**—**4x**) are slightly soluble in benzene, tetrahydrofuran, acetone, or tetrahydronaphthalene, and soluble in *N*,*N*-dimethylformamide.

Preparation of Enol Esters from Chloromercurio Aldehydes and Acyl Chlorides. The procedure employed was in general that employed by Nesmeyanov et al.[20]

1-Acryloyloxy-1-propene (1b): Acryloyl chloride (0.14 mol) was added to a tetrahydronaphthalene solution (150 cm^3) of **1x** (0.14 mol) and hydroquinone (0.5 g) at 40 °C under nitrogen stream. When the addition of acryloyl chloride was finished, the temperature was raised to 60 °C and the reaction was continued for 6 h. A few drops of quinoline were added to the reaction mixture. After the insoluble mercury(II) chloride was separated, the solution was distilled under reduced pressure. The low-boiling fraction was collected and redistillation gave **1b**: Yield 58%; bp 42.0—42.5/30 mmHg; n_D^{25} 1.4429; d_4^{25} 0.9409; IR (neat) 1730 (C=O), 1670 (enol C=C), and 1630 cm^{-1} (C=C); ^{1}H NMR δ=4.95 (0.84H, quintet, (*Z*)-2-H) and 5.33 (0.16H, sextet, (*E*)-2-H); *Z*/*E* ratio 84/16 and 88/12 by GLC.

1-Acryloyloxy-1-butene (2b): The reaction of **2x** with acryloyl chloride was carried out in benzene solution, the procedure employed being the same as that for **1b** except posttreatment: After removal of the insoluble mercury(II) salt, the benzene solution was evaporated off in a rotary evaporator. The residue was dissolved in diethyl ether, and the solution was washed with 10% aqueous sodium hydrogencarbonate and with distilled water, and then dried over sodium sulfate. Redistillation gave **2b**: Yield 38%; bp 47.5—48.0 °C/17 mmHg; n_D^{25} 1.4417; d_4^{25} 0.9260; IR (neat) 1730 (C=O), 1668 (enol C=C), and 1623 cm^{-1} (C=C); ^{1}H NMR δ=4.85 (0.87H, q, (*Z*)-2-H) and 5.45 (0.13H, sextet, (*E*)-2-H); *Z*/*E* ratio 87/13 and 83/17 by GLC.

1-Benzoyloxy-1-butene (2c): The reaction of **2x** with benzoyl chloride in a similar procedure with **2b** gave **2c**: Yield 70%; bp 66—70 °C/1.0 mmHg; IR (neat) 1724 (C=O) and 1663 cm^{-1} (enol C=C); ^{1}H NMR δ=4.91 (0.85H, q, (*Z*)-2-H) and 5.56 (0.15H, sextet, (*E*)-2-H); *Z*/*E* ratio 85/15 and 83/17 by GLC.

2-Phenyl-1-(acryloyloxy)ethene (3b): The reaction of **3x** with acryloyl chloride was carried out in a similar manner with **2b**. Redistillation gave **3b**: Yield 51%; bp 65—68 °C/0.15 mmHg; n_D^{25} 1.4480; d_4^{25} 1.0650; IR (neat) 1740 (C=O), 1660 (enol C=C), and 1630 cm^{-1} (C=C); ^{1}H NMR δ=7.96 (0.26H, d, (*E*)-1-H); *Z*/*E* ratio 74/26 and 76/24 by GLC.

1-Acryloyloxy-1,3-butadiene (4b): The reaction of **4x** with acryloyl chloride was carried out at 50 °C for 3 h because of a high polymerization tendency of **4b**. Redistillation gave **4b**: Yield 39%; bp 45.0—45.5 °C/5 mmHg; n_D^{25} 1.4956; d_4^{25} 0.9723; IR (neat) 1735 (C=O), 1660 (enol C=C), and 1631 cm^{-1} (C=C); ^{1}H NMR δ=7.10 (0.32H, d, (*Z*)-1-H) and 7.43 (0.68H, d, (*E*)-1-H); *Z*/*E* ratio 32/68 and 30/70 by GLC.

1-Methacryloyloxy-1,3-butadiene (4c): The reaction of **4x** with methacryloyl chloride was carried out in a similar manner to the preparation of **2b**. Redistillation gave **4c**: Yield 63%; bp 35.0—36.5 °C/1.5 mmHg; n_D^{25} 1.4897; d_4^{25} 0.9486; IR (neat) 1735 (C=O), 1660 (enol C=C), and 1637 cm^{-1} (C=C); ^{1}H NMR δ=7.14 (0.34H, d, (*Z*)-1-H) and 7.43 (0.66H, d, (*E*)-1-H); *Z*/*E* ratio 34/66.

References

1) P. Z. Bedoukian, *J. Am. Chem. Soc.*, **66**, 1325 (1944).
2) D. Y. Curtin and M. J. Hurwitz, *J. Am. Chem. Soc.*, **74**, 5381 (1952).
3) K. K. Georgieff and A. Dupre, *Can. J. Chem.*, **38**, 1070 (1960).
4) H. J. Hagemeyer, Jr. and D. C. Hull, *Ind. Eng. Chem.*, **41**, 2920 (1949).
5) D. J. Foster and E. Tobler, *J. Org. Chem.*, **27**, 834 (1962).
6) H. O. House and V. Kramar, *J. Org. Chem.*, **28**, 3362 (1963).
7) P. Z. Bedoukian, *J. Am. Chem. Soc.*, **67**, 1430 (1945).
8) W. M. Muir, P. D. Ritchie, and D. J. Lyman, *J. Org. Chem.*, **31**, 3790 (1966).
9) H. O. House, M. Gall, and H. O. Olmstead, *J. Org. Chem.*, **36**, 2361 (1971).

10) H. O. House and B. M. Trost, *J. Org. Chem.*, **30**, 2502 (1965).
11) W. Reppe, *Justus Liebigs Ann. Chem.*, **601**, 81 (1956).
12) R. F. Hudrlik and A. M. Hudrlik, *J. Org. Chem.*, **38**, 4254 (1973).
13) H. C. Haas, N. W. Schuler, and R. L. MacDonald, *J. Polym. Sci., Part A-1*, **7**, 3440 (1969).
14) H. Lemaire and H. J. Lucas, *J. Am. Chem. Soc.*, **77**, 939 (1955).
15) P. E. Peterson, R. J. Bopp, and M. M. Ajo, *J. Am. Chem. Soc.*, **92**, 2834 (1970).
16) R. H. Summerville and P. V. R. Schleyer, *J. Am. Chem. Soc.*, **96**, 1110 (1974).
17) W. Kitching, Z. Rappoport, S. Winstein, and W. G. Young, *J. Am. Chem. Soc.*, **88**, 2054 (1966).
18) R. C. Larock, *Tetrahedron*, **38**, 1713 (1982).
19) H. O. House, R. A. Auerbach, M. Gall, and N. P. Peet, *J. Org. Chem.*, **38**, 514 (1973).
20) A. N. Nesmeyanov, I. F. Lutsenko, and Z. M. Tumanova, *Izv. Akad. Nauk SSSR, Otd. Khim. Nauk*, **1949**, 601; *Chem. Abstr.*, **44**, 7225d (1950).
21) R. C. Larock, K. Oertle, and K. M. Beatty, *J. Am. Chem. Soc.*, **102**, 1966 (1980).
22) A. Gero, *J. Org. Chem.*, **19**, 469 (1954).
23) R. C. Fuson and T.-L. Tan, *J. Am. Chem. Soc.*, **70**, 602 (1948).
24) G. J. Heiszwolf and H. Kloosterziel, *Recl. Trav. Chim. Pays-Bas*, **86**, 1345 (1967); **89**, 1153 (1970).
25) M. Suzuki and K. Kozima, *Bull. Chem. Soc. Jpn.*, **42**, 2183 (1969).
26) G. Montaudo, V. Librando, S. Caccamese, and P. Maravigna, *J. Am. Chem. Soc.*, **95**, 6365 (1973).
27) P. S. Skell and W. L. Hall, *J. Am. Chem. Soc.*, **85**, 2851 (1963).
28) J. Halfpenny and R. W. H. Small, *Acta Crystallogr., Sect. B*, **35**, 1239 (1979).
29) R. Kyburz, H. Schaltegger, and M. Neuenschwander, *Helv. Chim. Acta*, **54**, 1037 (1971).
30) R. C. Larock and J. C. Bernhardt, *J. Org. Chem.*, **43**, 710 (1978).
31) D. B. Bigley and D. W. Paylin, *J. Chem. Soc.*, **1965**, 3977.
32) E. J. Panek, L. R. Kaiser, and G. M. Whitesides, *J. Am. Chem. Soc.*, **99**, 3708 (1977).
33) D. T. Witiak and B. B. Chaudhari, *J. Org. Chem.*, **30**, 1467 (1965).
34) B. P. Susz, *Bull. Soc. Chim. Fr.*, 2671 (1965).

Reaction Mechanism of Cathodic Crossed Coupling of Acetone with Unsaturated Compounds in Acidic Solution

Toshio KOIZUMI, Toshio FUCHIGAMI, Zaghloul El-Shahat KANDEEL,†
Norio SATO, and Tsutomu NONAKA*
Department of Electronic Chemistry, Tokyo Institute of Technology, 4259 Nagatsuta, Midori-ku, Yokohama 227
(Received June 10, 1985)

It was confirmed that the cathodic crossed coupling of acetone with unsaturated compounds in aqueous sulfuric acid could proceed smoothly, when the compounds which had radical-acceptable double bonds and were adsorbed on a mercury cathode were used. From this fact, it was concluded that the coupling occurs via the addition of a radical intermediate formed by the one-electron reduction of acetone to the double bonds on the cathode surface. Possibility of the addition of an anionic intermediate derived from acetone was excluded by no occurrence of the coupling of acetone with a polar acetylenic triple bond compound adsorbed on the cathode.

A number of electrochemical bimolecular reactions, e. g. dimerization, have been known and some of them have been used for purposes of syntheses in laboratories and industries. In previous works,[1-3] one (T. N.) of the authors reported a new type of crossed hydrocoupling reaction: When mixtures of acetone and activated olefins such as acrylic acid derivatives and maleic acid were reduced at a mercury cathode in aqueous sulfuric acid, their crossed hydrodimers were formed in good yields and current efficiencies. This reaction was successfully extended by using other aliphatic carbonyl compounds and C–N unsaturated compounds such as pyridines and amino nitriles instead of acetone and activated olefins, respectively.[4-13]

It should be generally important to clarify reaction mechanisms in order to design and optimize the reactions to be useful in a viewpoint of synthesis. A tentative mechanism (Scheme 1, path A, C=X–Y: CH_2=CH–CN) for the crossed hydrocoupling of acetone with acrylonitrile was first proposed by one(T. N.) of the authors. Afterward, Brown and Lister[14] also proposed another mechanism(Scheme 1, path B) on the basis of cyclic voltammetry of a mixture of acetone and acrylonitrile in aqueous sulfuric acid. However their mechanism was confuted by other investigators.[15]

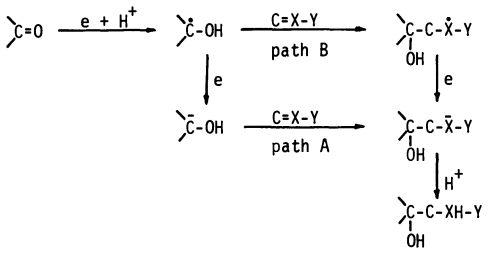

C=X-Y: Activated olefins(X: C, Y: Electron-withdrawing groups)
: Pyridines(X: N, Y: H^+)

Scheme 1.

† Present adress: Chemistry Department, Faculty of Science, Cairo University, Giza, Arabic Republic of Egypt.

More recently, Shono et al.[16,17] have reported that the intramolecular electroreductive cyclization of carbonyl compounds having inactive olefinic parts can occur in good yields in neutral solutions. Although they have briefly mentioned a mechanism equivalent to path B as the most plausible one, they have not given any obvious evidence and not verified the path B in comparison with path A.

In this study, we wish to clarify the reaction mechanism of which the key step has been still ambiguous and to indicate more clearly the scope, e. g. the possible extension and limitation, of this remarkable reaction.

Results and Discussion

Mixtures of acetone and various types of compounds having unsaturated carbon–carbon or carbon–nitrogen bonds were reduced at a mercury cathode in

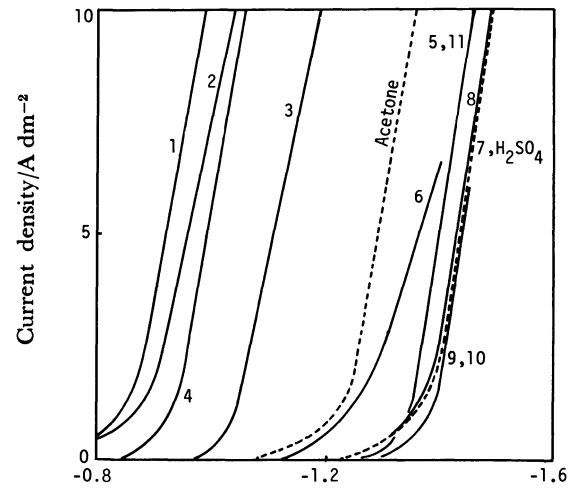

Fig. 1. Polarization curves of unsaturated compounds (**1**—**11**) and acetone at a mercury cathode in 20 wt% H_2SO_4. Concentration: **1**, **3**, and **8**, 0.1 mol dm^{-3}; **2**, **4**—**7**, and **9**—**10**, 0.4 mol dm^{-3}; **11**, saturated; acetone, 50 wt%.

aqueous sulfuric acid.

Polarization curves of acetone and the unsaturated compounds measured in aqueous sulfuric acid by a steady state method are shown in Fig. 1. By comparing the reduction potentials of the unsaturated compounds with that of acetone, the compounds were classified into two groups: One consists of the compounds which seem to be more easily reduced than acetone, while those in the other group are more difficultly or can not be reduced.

The compounds such as phenyl vinyl sulfoxide (**1**), methyl vinyl sulfone (**2**), *N*-vinylpyridinium bromide (**3**), and quinoline (**4**), which belong to the former group, were reduced at less negative potentials than acetone to give the corresponding non-crossed coupling products by their own reduction. When a mixture of **1** and acetone was electrolyzed by passing 2.0 F (1 F= 96480 C) mol^{-1} of charge, 1,2-bis(phenylthio)ethane was formed in 66% yield and 33% of the starting **1** were recovered. The reaction scheme of this reduction may be written down as in Scheme 2 on the basis of material and charge balances observed. According to this scheme, current efficiency for the reaction was estimated to be about 100%, though ethylene was not quantitatively analyzed. The reduction of **2** consumed coulometrically 2 F mol^{-1}, but any reduction products[18] were not separated. The reduction of **3** and **4** gave the corresponding dimeric hydropyridine and hydroquinoline, respectively, but their exact molecular structures could not be determined.

The unsaturated compounds having more negative reduction potentials than that of acetone could give the corresponding crossed coupling products with acetone as shown in Table 1. From a fact that considerable amounts of 2-propanol and 2,3-dimethyl-2,3-butanediol were formed as by-products in all the electrolyses, the occurrence of acetone reduction was confirmed.

It had been found that the addition of acetone to the 2-position of an *N*-unsubstituted pyridinium ring occurred exclusively.[4] However, though *N*-ethylpyridinium bromide (**5**) gave three crossed coupling products, their complete molecular structures (positions of 1-hydroxy-1-methylethyl groups and unsaturated bonds on the hydropyridine rings) could not be determined, as shown in Table 1. Isoquinoline (**6**) gave a sole crossed coupling product, though another isomeric one could be also expected to be formed as shown in Scheme 3. This result is rationalized as due to a more favorable limiting structure **6** than **6'** (in Scheme 3). Diethyl vinylphosphonate (**7**) behaved as a typical activated olefin to give the crossed coupling product with acetone as well as acrylonitrile.[2] The unsaturated bonds of **5**—**7** are highly polarized and they are so-called Michael acceptors[19] which should be able to accept a carbanion intermediate formed by the two-electron reduction of acetone. Therefore, the probability of path A in Scheme 1 can not be excluded.

Results described above are interesting but not very important to discuss the reaction mechanism in detail. The most important result for clarification of the mechanism was obtained in the reaction of trimethylvinylammonium bromide (**8**) with acetone.

Since a nitrogen atom has not d-orbital which can accept an electron, nitrogen ylids are generally very unstable and difficultly formed.[20] This is a reason for that vinylammoniums can not undergo Michael addition[21] which should proceed via nitrogen ylid intermediates, though their double bonds should be highly polarized. On the other hand, vinylsulfoniums and vinylphosphoniums can undergo the addition,[19,21] since both sulfur and phosphorus atoms have d-orbitals. As shown in Table 1, trimethylvinylammonium bromide (**8**) gave the corresponding crossed coupling product with acetone, though **8** is not a Michael acceptor but a polarized olefin. This fact should exclude path A and consequently supports path B.

A further evidence for path B was obtained by using inactive olefins such as allylamine (**9**) and allyl alcohol (**10**). The former and the latter gave the corresponding crossed coupling products in reasonable and much lower yields, respectively, in aqueous sulfuric acid. It was independently confirmed that the olefins themselves could not be reduced under electrolytic conditions. Since lifetimes of aliphatic radicals, except for allylic and benzylic ones, are generally very short, the addition of a radical intermediate derived from acetone to the olefins in

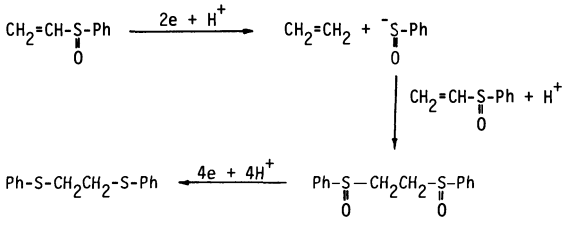

Scheme 2.

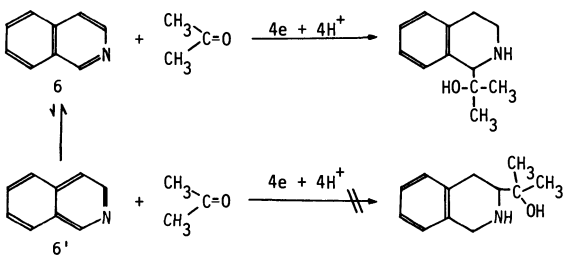

Scheme 3.

Table 1. Electrolytic Results of Mixtures of Unsaturated Compounds (**5**—**12**) and Acetone

Unsaturated compounds	Cathodic potential /V vs. SCE	Charge passed /F mol^{-1}	Crossed hydrocoupling products (Yield[a]/%)
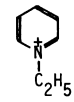 (**5**)	−1.30	4.0	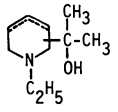 (22) 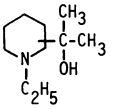 (11) 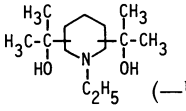 (—[b])
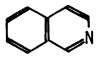 (**6**)	−1.30	4.0	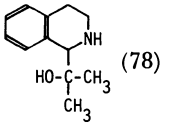 (78)
$CH_2{=}CHP(OC_2H_5)_2$ (**7**) ‖ O	−1.24	2.0	$CH_3{-}C(CH_3)(OH){-}CH_2CH_2P(OC_2H_5)_2$ (39) ‖ O
$CH_2{=}CH\overset{+}{N}(CH_3)_3$ (**8**)	−1.25	40.0	$CH_3{-}C(CH_3)(OH){-}CH_2CH_2\overset{+}{N}(CH_3)_3$ (54)
$CH_2{=}CHCH_2NH_2$ (**9**)	−1.24	2.0	$CH_3{-}C(CH_3){=}CHCH_2CH_2NH_2$ (26)
$CH_2{=}CHCH_2OH$ (**10**)	−1.24	2.0	$CH_3{-}C(CH_3)(OH){-}CH_2CH_2CH_2OH$ (1)
$CH_3{-}C{\equiv}C{-}COOCH_3$ (**11**)	−1.30	2.0	Recovered **11** (94)
$CH_3{-}CH{=}CH{-}COOCH_3$ (**12**)	—[c]	4.0	$CH_3{-}C(CH_3)_2(OH){-}CHCH_2{-}COOCH_3$[d] (38[e])

a) Based on the starting unsaturated compounds. b) Not estimated. c) Under galvanostatic conditions at 6 A dm^{-2} of current density. d) Isolated as a mixture of the corresponding cis and trans-lactones. e) Estimated from a result reported in previous work.[27]

path B should take place on surface or vicinity of cathode in competition with its own coupling to form 2,3-dimethyl-2,3-butanediol and its further reduction to form 2-propanol. On the basis of this consideration, the higher yield with **9** is rationalized as due to its higher concentration on the cathode surface. Such a higher concentration is achieved by adsorption of protonated **9** ($CH_2{=}CH{-}CH_2{-}NH_3^+$) which is electrostatically attracted to the negatively polarized cathode: It had been confirmed by electrode-interfacial capacity measurement and AC-polarography that acrylonitrile and pyridinium adsorb in aqueous sulfuric acid.[22] On the other hand, the protonation of **10** does not seem to be so sufficient that it can adsorb strongly and undergo easily the addition of the radical intermediate on the cathode surface.

In contrast, in the case of the intramolecular reductive cyclization of unsaturated carbonyl compounds,[16,17] high yields of the cyclized product should be reasonably expected, since the unsaturated part should exist in the vicinity of radical part formed: In this case, the high yields can be expected regardless of the adsorption. Recently, Little et al.[23] have reported that the intramolecular reductive cyclization of ketones having activated olefinic double bonds can proceed efficiently in not only acidic but also neutral media. More recently, Shono et al.[24] have reported an improved intermolecular reductive coupling of ketones with inactive olefins: They electrolyzed mixtures of aliphatic ketones and olefins in the presence of trimethylchlorosilane at a zinc cathode in DMF containing tetraethylammonium tetrafluoroborate to obtain the corresponding crossed coupling products in good yields but in low current efficiencies. They have shown a path B-like mechanism for this reaction. This method was also applicable to activated olefins and aldehydes.[25]

Regioselective addition of radicals in the intramolecular cyclization may be explained on the basis of ease and difficulty of formation of substituted ring systems in each case. However, regioselectivity observed in the intermolecular addition of radicals to polarized double bonds has not been rationalized yet. In this work, it was attempted to calculate reaction indexes for radical addition and collate with experimental results. The reaction indexes of acrylonitrile and pyridinium as typical sample molecules are given in Table 2. Table 2 shows that all the indexes indicate 3- and 2-positions in acrylonitrile and pyridinium, respectively, as the most favorable ones for the radical addition and in fact the addition took place at these positions. This coincidence may be one of evidences for path B.

It is generally known that acetylenes are less reactive than olefins towards free radicals while more reactive towards nucleophiles.[26] In fact, acetylenecarboxylic acid derivatives undergo Michael addition.[19] The reduction potential of methyl 2-butynoate (**11**) seemed more negative than that of acetone but it gave no crossed hydrocoupling product with acetone: The starting **11** was almost completely recovered. On the other hand, in a previous work[27] methyl crotonate (**12**) as an olefinic analogue of **11** had been found to give the corresponding crossed coupling product with acetone in a reasonable yield. In this work, it was also confirmed by the electrode-interfacial capacity measurement that the adsorption of **11** on a mercury cathode occurred similarly to that of **12**. These facts also exclude path A.

Path A might be also excluded to rationalize stereochemistry of the crossed hydrocoupling products of cyclohexenecarboxylic acid derivatives with acetone.[28]

It is known that the reduction of acetone in acidic solutions gives 2-propanol as a main product at a mercury cathode and propane as a sole product at other cathodes such as cadmium, aluminum, and zinc.[29] The formation of 2-propanol is obviously via the carbanion intermediate, while propane seems to be formed via the radical intermediate. In a previous work,[13] the cathodes other than mercury were also found to result in the formation of the crossed coupling product of acrylonitrile with acetone in considerable yields. This fact also may support path B.

Table 2. Reaction Indexes for Radical Addition to Acrylonitrile and Pyridinium

Reaction index	Positions				
	Acrylonitrile		Pyridinium		
	2	**3**[a]	**2**[a]	**3**	**4**
Free atomic valence	0.3678	0.8877	0.4094	0.3977	0.4051
Localization energy	2.5532	1.7136	2.5011	2.5413	2.5311
Frontier electron density	0.4061	0.7615	0.4094	0.2842	0.3052
Super delocalizability	0.8443	2.0210	0.8695	0.8336	0.8621

a) Position at which the addition occurred actually in electrolyses.

Conclusion

1) The crossed hydrocoupling of carbonyl compounds with unsaturated ones proceeds via the addition of radical intermediates genarated by the one-electrone reduction of the formers to the latters, as shown in path B, Scheme 1.

2) Radical-acceptable unsaturated bonds are available for the crossed coupling, regardless of their polarization.

3) Under conditions where concentration of the unsaturated compounds on the surface or vicinity of cathodes can be kept high by their adsorption, the crossed coupling can smoothly proceed: The composition of electrolytic solutions is not an essential factor, if they adsorb sufficiently.

4) In intramolecular coupling, so-called cyclization, the adsorption is not an important matter.

5) To obtain synthetically satisfactory results, it is required to use the unsaturated compounds reduced at more negative potentials than the carbonyl compounds.

Experimental

Materials. Methyl Vinyl Sulfone (2): To prepare **2**, methyl 2-hydroxyethyl sulfide was first synthesized from 2-chloroethanol and methanethiol by the modified method of Kirner and Richtery.[30] Yield 65%; bp 53—54 °C/8 Torr (1 Torr=133.322 Pa) (lit,[30] 68—70 °C/20 Torr). The sulfide obtained thus was converted into methyl 2-chloroethyl sulfide by treatment with thionyl chloride. Yield 67%; bp, 57—59 °C/12 Torr (lit,[31] 55—56 °C/30 Torr). This sulfide was oxidized to the corresponding sulfone with 30% hydrogen peroxide solution in acetic acid and then the reaction mixture was evaporated to dryness. The residual oily material was treated with triethylamine to convert it into the titled sulfone (**2**).[32] Yield 68%; bp 105—107 °C/17 Torr (lit,[32] 115—117 °C/19 Torr); IR (liquid film), 3030, 2950, 1300, 1140, and 960 cm^{-1}; ^{1}H-NMR ($CDCl_3$) δ=2.90 (s, 3H, $C\underline{H}_3$) and 6.7—7.0 (m, 3H, $C\underline{H}=C\underline{H}_2$).

***N*-Vinylpyridinium Bromide (3):** A mixture of pyridine (5.1 cm^3, 0.063 mol) and 1,2-dibromoethane (6.5 cm^3, 0.076 mol) was allowed to stand for 14 d at room temperature and then *N*-(2-bromoethyl)pyridinium bromide crystallized out was collected.[33] Yield, 65%. A mixture of the bromide thus obtained and potassium hydroxide in ethanol was stirred for 1.5 h at room temperature. The potassium bromide precipitated was filtered off and the filtrate was treated with

charcoal. The decolored ethanol solution was poured into ether, and then the titled compound (**3**) was collected and recrystallized from a mixture of ethanol and ether. Yield, 62%; mp 154—155 °C; ^{1}H-NMR (D_2O) δ=5.8—6.3 (m, 2H, CH=C$\underline{H}_2$), 7.3—7.8 (m, 1H, C$\underline{H}$=CH$_2$), and 8.0—9.1 (m, 5H, pyridine-$\underline{H}$).

***N*-Ethylpyridinium Bromide (5):** Pyridine (10.0 g, 0.13 mol) was reacted with ethyl bromide (14.5 g, 0.13 mol) for 2 d at room temperature and then precipitated **5** was collected and recrystallized from a mixture of ethanol and ether. Yield 81%; mp 120—121 °C; ^{1}H-NMR (D_2O) δ=1.78 (t, 3H, C$\underline{H}_3$), 4.80 (q, 2H, C$\underline{H}_2$), and 8.1—9.0 (m, 5H, pyridine-$\underline{H}$).

Other chemicals used were commercially supplied.

Electrolysis. An H-type divided cell with a sintered glass diaphragm was used. The cathode and anode were a mercury pool (7.1 cm^2) and a platinum plate, respectively.

Before electrolysis, polarization curves were measured by a steady state method. The electrolysis was carried out by a controlled potential method at 30 °C. The electrolytic solution was a mixture of acetone (30 g) and aqueous sulfuric acid (20 wt%, 30 g) containing substrates (**1—11**, 5—20 mmol).

Product Analysis. A general procedure was as follows. After the cathodic solution was neutralized (pH 1) with sodium hydroxide solution (20 wt%), it was extracted with organic solvents (mainly ether). When basic products were expected, the resulting aqueous layer was made strongly alkaline by addition of excess sodium hydroxide and then extracted again. All the extracts were dried over anhydrous sodium sulfate and analyzed by gas chromatography (PEG 20 M, 2 m, 190 °C for diethyl 3-hydroxy-3-methylbutylphosphonate; PEG 6000, 2 m, 70—170 °C for 2-propanol, 2,3-dimethyl-2,3-butanediol, 4-methyl-1,4-pentanediol, and methyl 3-methyl-2-butenyl sulfone; Tritone X305, 2 m, 170—180 °C or PEG-5% KOH, 1—2 m, 150—180 °C for 1-ethyl-2-(1-hydroxy-1-methylethyl)tetrahydropyridine, 1-ethyl-2-(1-hydroxy-1-methylethyl)piperidine, 1-ethyl-2,5-bis(1-hydroxy-1-methylethyl)piperidine, 4-methyl-3-pentenylamine, 2,2′-bi(1,2,3,4-tetrahydroquinoline), and 1-(1-hydroxy-1-methylethyl)-1,2,3,4-tetrahydroisoquinoline).

Reduction Product of Phenyl Vinyl Sulfoxide (1): 1,2-Bis(phenylthio)ethane crystallized out from the cathodic solution, when the solution was allowed to stand overnight. Mp 68—69 °C; IR (KBr), 1580, 1480, 1440, 740, and 690 cm^{-1}; MS (*m/z*), 246 (M$^+$). Found: C, 68.02; H, 5.71; S, 25.93%. Calcd for $C_{14}H_{14}S_2$: C, 68.25; H, 5.73; S, 26.03%.

Reduction Products of Methyl Vinyl Sulfone (2): The ethereal extract was evaporated and then the residual oil was distilled. The main fraction was methyl ethyl sulfone and also few drops of a higher boiling point fraction were obtained at ca. 120 °C/Torr. The high resolution mass spectrum indicated that the latter fraction would be methyl 3-methyl-2-butenyl sulfone which might be formed by dehydration of the original crossed hydrocoupling product (methyl 3-methyl-3-hydroxybutyl sulfone) with acetone. Found: *m/z* 148.0502. Calcd for $C_6H_{12}O_2S$: M 148.0556.

Reduction Product of *N*-Vinylpyridinium Bromide (3): A strongly basic product was separated by preparative gas chromatography. From the mass spectrum, it seemed to be 1,1′-divinyl-2,2′-bipiperidine or 1,4-bis(1-tetrahydropyridyl)butane. MS (*m/z*), 220 (M$^+$).

Reduction Product of Quinoline (4): A solid crystallized out from the cathodic solution made alkaline seemed to be a 2,2′-bi(1,2,3,4-tetrahydroquinoline). Mp 112—114 °C; MS (*m/z*), 262 (M$^+$); IR (KBr), 3360, 2940, 1605, 1490, 1260, 1120, and 750 cm^{-1}.

Crossed Hydrocoupling Products of *N*-Ethylpyridinium Bromide (5) with Acetone: Three fractions, which seemed to be isomeric mixtures, were separated by preparative gas chromatography, but the complete structures of products could not be determined by NMR study. 1-Ethyl-?-(1-hydroxy-1-methylethyl)-?,?,?,?-tetrahydropyridine. MS (*m/z*), 169 (M$^+$). 1-Ethyl-?-(1-hydroxy-1-methylethyl)piperidine. MS (*m/z*), 171 (M$^+$). Picrate: Mp, 156—157 °C. Found: C, 47.62; H, 6.00; N, 13.83%. Calcd for $C_{16}H_{24}N_4O_8$: C, 47.99; H, 6.04; N, 13.99%. 1-Ethyl-?,?-di(1-hydroxy-1-methylethyl)-piperidine. MS (*m/z*), 227 (M$^+$).

Crossed Hydrocoupling Product of Isoquinoline (6) with Acetone: 1-(1-Hydroxy-1-methylethyl)-1,2,3,4-tetrahydroisoquinoline was separated by preparative gas chromatography. Mp 82—83 °C; MS (*m/z*), 191 (M$^+$); IR (KBr), 3310, 3200, 2990, 2940, 2910, 1490, 1370, 1260, 1210, 1160, 1110, 970, 860, and 750 cm^{-1}; ^{1}H-NMR ($CDCl_3$) δ=1.04 (s, 3H, C$\underline{H}_3$), 1.32 (s, 3H, C$\underline{H}_3$), 2.6—3.4 (m combined, 6H, C$\underline{H}_2$C$\underline{H}_2$-N$\underline{H}$-C$\underline{H}$-C-O$\underline{H}$), 3.95 (s, 1H, C$\underline{H}$), and 7.1—7.3 ppm (m combined, 4H, benzo-$\underline{H}$). On adding D_2O, the total relative intensity of the complicatedly combined multiplets at δ 2.6—3.4 ppm decreased by one third and a singlet peak for HDO appeared. The IR and NMR spectra suggested an intermolecular hydrogen bonding between the hydroxyl and amino groups. Found: C, 75.23; H, 9.25; N, 7.32%. Calcd for $C_{12}H_{17}NO$: C, 75.12; H, 8.97; N, 7.32%.

Crossed Hydrocoupling Product of Diethyl Vinylphosphonate (7) with Acetone: Distillation of a chloroform extraction afforded diethyl 3-hydroxy-3-methylphosphonate. Bp 125 °C/6 Torr; IR (liquid film), 3370, 2990, 2950, 1220, 1030, and 960 cm^{-1}; MS (*m/z*), 224 (M$^+$); ^{1}H-NMR ($CDCl_3$) δ=1.2 (s, 6H, C$\underline{H}_3$-C-OH), 1.3 (t, 6H, C$\underline{H}_3$-CH$_2$-O), 1.7—2.2 (m, 4H, C$\underline{H}_2$-C$\underline{H}_2$), 3.0 (s, 1H, O$\underline{H}$), and 3.8—4.3 (overrapping m, 4H, C$\underline{H}_2$-O).

Crossed Hydrocoupling Product of Trimethylvinylammonium Bromide (8) with Acetone: The cathodic solution was neutralized (pH 6.0) and then extracted with ether. The aqueous layer was evaporated to dryness under reduced pressure and extracted with ethanol. The ethanolic extract was poured into ether, trimethyl(3-hydroxy-3-methylbutyl)ammonium bromide precipitated was collected, and recrystallized from a mixture of ethanol and ether. Mp 172—173 °C; MS (*m/z*), 94 and 96 (CH_3Br), 59 ($(CH_3)_2C$=OH$^+$), and 85 ($(CH_3)_2$N=CH$_2^+$); ^{1}H-NMR (CD_3OD) δ=1.30 (s, 6H, C$\underline{H}_3$), 1.8—2.1 (m, 2H, C$\underline{H}_2$-CH$_2$-N), 3.23 (s, 9H, (C$\underline{H}_3$)$_3$-N$^+$), and 3.4—3.7 (m, 2H, C$\underline{H}_2$-N). Found: C, 42.79; H, 9.35; N, 6.16%. Calcd for $C_8H_{20}NBrO$: C, 42.49; H, 8.91; N, 6.19%.

Crossed Hydrocoupling Product of Allyl Amine (9) with Acetone: 4-Methyl-3-pentenylamine, which corresponds to the dehydration product of 4-methyl-4-hydroxypentylamine, was separated by preparative gas chromatography. MS (*m/z*), 99 (M$^+$), 82 (M$^+$—NH$_3$), and 41 ($C_3H_5^+$).

Crossed Hydrocoupling Product of Allyl Alcohol (10) with Acetone: 4-Methyl-1,4-pentanediol was separated by distillation of the ethereal extract of the cathodic solution. Bp 100 °C/11 Torr. Identified with the authentic sample prepared from γ-butyrolactone and 2 equiv methylmagne-

sium iodide.

Electrode-Interfacial Capacity Measurement. The capacity was measured by an impedance-bridge method similar to that used in previous work.[22]

Calculation of Reaction Indexes. The indexes were calculated by a HMO method using a computing program given by Kikuchi.[34] Following HMO parameters concerning with nitrogen atom were used. Acrylonitrile: Coulomb integrations of N and C in the cyano group, 1.2 and 0.1, respectively; resonance integration of C≡N, 1.0. Pyridinium: Coulomb integrations of N^+ and C adjacent to the N^+, 0.6 and 0.3, respectively; resonance integration of $^+N{=}C$, 1.0.

We are grateful to the UNESCO and the Japanese Ministry of Education, Science, and Culture for making possible Dr. Kandeel's participation to this study.

References

1) K. Sugino and T. Nonaka, *J. Electrochem. Soc.*, **112**, 1241 (1965).
2) T. Nonaka and K. Sugino, *J. Electrochem. Soc. Jpn.*, **34**, 105 (1966).
3) K. Sugino and T. Nonaka, *Electrochim. Acta*, **13**, 613 (1968).
4) T. Nonaka and K. Sugino, *J. Electrochem. Soc.*, **116**, 616 (1969).
5) T. Nonaka and K. Sugino, *Nippon Kagaku Zasshi*, **90**, 686 (1969).
6) T. Nonaka and K. Sugino, *J. Electrochem. Soc. Jpn.*, **38**, 105 (1970).
7) T. Nonaka and K. Odo, *J. Electrochem. Soc. Jpn.*, **40**, 66 (1972).
8) T. Nonaka and K. Odo, *J. Electrochem. Soc. Jpn.*, **40**, 665 (1972).
9) T. Nonaka, S. Miyaji, and K. Odo, *J. Electrochem. Soc. Jpn.*, **41**, 142 (1973).
10) T. Nonaka and K. Odo, *J. Electrochem. Soc. Jpn.*, **41**, 662 (1973).
11) T. Nonaka, N. Yui, and K. Odo, *J. Electrochem. Soc. Jpn.*, **42**, 160 (1974).
12) T. Nonaka, A. Omura, T. Fuchigami, and K. Odo, *J. Electrochem. Soc. Jpn.*, **45**, 111 (1977).
13) T. Nonaka, T. Sekine, K. Odo, and K. Sugino, *Electrochim. Acta*, **22**, 271 (1977).
14) O. R. Brown and K. Lister, *Discuss. Faraday Soc.*, **45**, 106 (1968).
15) F. Beck and B. E. Conway, *Discuss. Faraday Soc.*, **45**, 118 (1968).
16) T. Shono and M. Mitani, *J. Am. Chem. Soc.*, **93**, 5285 (1971).
17) T. Shono, I. Nishiguchi, H. Ohmizu, and M. Mitani, *J. Am. Chem. Soc.*, **100**, 545 (1978).
18) A trace of a product which might be derived from the crossed hydrocoupling product with acetone was obtained.
19) E. D. Bergmann, D. Ginsburg, and R. Pappo, "Organic Reactions," John Wiley & Sons, New York (1959), Vol. 10, Chap. 3.
20) S. Kondo, "Gendai-no-Yukikagaku," ed by T. Goto, Hirokawa Shoten, Tokyo (1976), Chap. 2.
21) W. E. Doering and K. C. Achreiber, *J. Am. Chem. Soc.*, **77**, 514 (1955).
22) T. Nonaka and T. Sekine, *J. Electrochem. Soc. Jpn.*, **39**, 29 (1971).
23) R. D. Little, D. P. Fox, L. Móens, and M. M. Baizer, International Chemical Congress of Pacific Basin Societies, December 1984, Honolulu, Abstr. No. lOI21.
24) T. Shono, S. Kashimura, Y. Mori, and T. Hayashi, 50th National Meeting of the Chemical Society of Japan, April 1985, Tokyo, Abstr. No. 3S07.
25) T. Shono, H. Ohmizu, S. Kawakami, and H. Shigiyama, *Tetrahedron Lett.*, **21**, 5029 (1980).
26) Y. Aiel, "The Chemistry of Functional Groups, Supplement C," ed. by S. Patai and Z. Rapport, John-Wiley & Sons, New York (1983), Chap. 10.
27) H. Kanetsuna and T. Nonaka, *J. Electrochem. Soc. Jpn.*, **47**, 422 (1979).
28) H. Kanetsuna and T. Nonaka, *J. Electrochem. Soc. Jpn.*, **47**, 480 (1979).
29) T. Sekine, A. Yamura, and K. Sugino, *J. Electrochem. Soc.*, **112**, 439 (1965).
30) W. R. Kirner and G. H. Richtery, *J. Am. Chem. Soc.*, **51**, 3409 (1929).
31) W. R. Kirner and W. Windus, *Org. Synth.*, Coll. Vol. 2, 136 (1943).
32) G. D. Buckley, J. L. Charish, and J. D. Rose, *J. Chem. Soc.*, **1947**, 1515.
33) R. R. Renshaw and J. C. Ware, *J. Am. Chem. Soc.*, **47**, 2989 (1925).
34) O. Kikuchi, "Bunshi-Kido-Ho," Kodansha, Tokyo (1971), Chap. 2.

 © 1986 The Chemical Society of Japan Bull. Chem. Soc. Jpn., 59, 763—768 (1986)

Hydration of the Oxyethylene Chain. Hypersonic Velocities in Aqueous Solutions of α-Methyl-ω-methoxyoligo(oxyethylene)s and α-Methyl-ω-hydroxyoligo(oxyethylene)s as Studied by Brillouin Scattering

Hiroatsu MATSUURA* and Koichi FUKUHARA
Department of Chemistry, Faculty of Science, Hiroshima University,
Higashisenda-machi, Naka-ku, Hiroshima 730
(Received August 22, 1985)

Hydration of the oxyethylene chain was studied by a Brillouin-scattering method; hypersonic velocities in aqueous solutions of $CH_3(OCH_2CH_2)_mOCH_3$ with m=1—4 and $CH_3(OCH_2CH_2)_mOH$ with m=2 and 3 were measured. The concentration of the solution, at which the sound velocity gave a maximum value, led to the number of water molecules, at the highest hydration, per ether linkage in the oxyethylene chain. The experimental results showed that 1.8 water molecules take part in the hydration of each $-CH_2OCH_2-$ group and that the number of the water molecules is virtually constant independently of the oxyethylene-chain length as far as the number of the oxyethylene units is limited up to four. These findings indicate that a sort of hydration complex of approximately 1 $-OCH_2CH_2-$: 2 H_2O is formed in the aqueous solution. It is suggested that the stabilization of the *gauche* conformation for the OCH_2-CH_2O group in aqueous solution, as evidenced by Raman-spectroscopic observations, is promoted greatly by the hydrogen bond of water molecules which are bridged between the adjacent ether oxygens in the oxyethylene chain.

Properties and structures of nonionic surfactants having oxyethylene chain as a hydrophilic group have been studied extensively by various experimental methods.[1] One of the current interests in nonionic surfactant chemistry is the hydration of the oxyethylene chain,[2-9] since the hydration structure is closely related to the size and shape of the micelles[10,11] and the phase behavior.[12] In order to elucidate the hydration of the oxyethylene chain in the nonionic surfactants, investigation of hydration structure is first required for simple model compounds consisting of the oxyethylene units.

In the present work, we have studied hydration of the model compounds, α-methyl-ω-methoxyoligo(oxyethylene)s $CH_3(OCH_2CH_2)_mOCH_3$ (m=1—4) and α-methyl-ω-hydroxyoligo(oxyethylene)s $CH_3(OCH_2CH_2)_mOH$ (m=2 and 3), by measuring hypersonic velocities in aqueous solutions of these compounds by a Brillouin-scattering method. Brillouin scattering from liquid gives directly the velocity of sound propagating in the medium.[13] In the liquid medium, fluctuations of density arise from the presence of sound waves of various wavelengths associated with the thermal energy of the medium, and passing of a monochromatic light-beam through such a medium gives rise to a change of frequency in the scattered light owing to the density fluctuation, the frequency shift $\Delta\nu$ being given by[14]

$$\Delta\nu = \pm 2\nu_i(v/c)n\sin(\theta/2), \quad (1)$$

where ν_i is the frequency of the incident light, v is the velocity of sound in the medium, c is the velocity of light in vacuum, n is the refractive index of the medium, and θ is the angle of scattering. For usual Brillouin-scattering experiments, the sound velocities obtained are those in the hypersonic region with frequencies of 1—10 GHz.

The sound velocity is correlated with elasticity or, conversely, compressibility of the medium in which the sound propagates. Accordingly, knowledge of the sound velocity will provide useful information of the structure of liquid or solution. It is expected that, when some ordered close structure is formed in solution, the volume and the compressibility of the solution will in general change; this leads to a change in sound velocity in the medium. The composition of the solution, at which the sound velocity reaches the extreme, is often the stoichiometric composition of a complex formed between the components. We have, therefore, examined the variation of the sound velocity with concentration for the aqueous solutions of $CH_3(OCH_2CH_2)_mOCH_3$ (m=1—4) and $CH_3(OCH_2CH_2)_mOH$ (m=2 and 3). A similar procedure, by detecting the change in fluidity of solutions, has been used to investigate extent of hydration.[15]

Experimental

$CH_3(OCH_2CH_2)_mOCH_3$ (m=1—4) and $CH_3(OCH_2CH_2)_mOH$ (m=2 and 3) supplied by Tokyo Kasei Kogyo Co., Ltd. were purified by repeated distillation under reduced pressure. Water was carefully purified by distillation and filtration. Aqueous solutions of various mole fractions of these materials were prepared for the Brillouin-scattering measurements.

The experimental arrangement for the measurement of Brillouin scattering was essentially the same as that used in the previous studies.[16,17] The light source was a helium-neon gas laser (NEC GLG5800) operated in the fundamental transverse mode at 632.8 nm with an output of about 50 mW. The light scattered from the sample at 90°

away from the incident-beam direction (θ=90°) was analyzed by a pressure-scanned Fabry-Pérot interferometer of Mizojiri Kogaku Kogyo Co., Ltd. The spacer between the interferometer etalons had a thickness of 6.075 mm, which gave the free spectral range[18] of 24.674 GHz. The Brillouin-scattering measurements were made, at least five times for each of the solutions, at 298±0.5 K by using a thermostat apparatus.

Results and Discussion

Some typical Brillouin spectra measured in this work are shown in Fig. 1. For the determination of sound velocity from the frequency shift, refractive index is required for each of the solutions studied. The refractive indices of aqueous solutions of $CH_3OCH_2CH_2OCH_3$ and $CH_3(OCH_2CH_2)_2OCH_3$ at various concentrations are available in the literature.[19,20] Therefore, the refractive indices at desired concentrations for these compounds were obtained from these data. The sound velocity thus obtained as a function of mole fraction of the solute is shown in Fig. 2. Since precise refractive-index data are not available for aqueous solutions of $CH_3(OCH_2CH_2)_3OCH_3$, $CH_3(OCH_2CH_2)_4OCH_3$, $CH_3(OCH_2CH_2)_2OH$, and $CH_3(OCH_2CH_2)_3OH$, the refractive indices were assumed to be

$$n = x_1 n_1 + x_2 n_2, \tag{2}$$

where x_1 and x_2 are mole fractions of the solution components and n_1 and n_2 are the refractive indices for their neat liquids. The sound velocities thus derived for the four compounds given above are shown in Figs. 3 and 4. In order to ensure the assumption of Eq. 2, the sound velocities for $CH_3OCH_2CH_2OCH_3$ and $CH_3(OCH_2CH_2)_2OCH_3$ are plotted, as shown in Fig. 5, against the refractive indices evaluated through Eq. 2. The plots in Figs. 2 and 5 give in fact the same value, within experimental error, of the mole fraction x_m, at which the sound velocity gives a maximum value, for each of the two compounds.

Figures 2—4 show that the maximum value of the sound velocity is at the mole fractions of 0.100, 0.085, 0.074, and 0.065, respectively, for the aqueous solutions of the monomer, dimer, trimer, and tetramer of $CH_3(OCH_2CH_2)_mOCH_3$ and at the mole fractions of 0.126 and 0.103, respectively, for those of the dimer and trimer of $CH_3(OCH_2CH_2)_mOH$. At these mole fractions of x_m, the aqueous solutions of

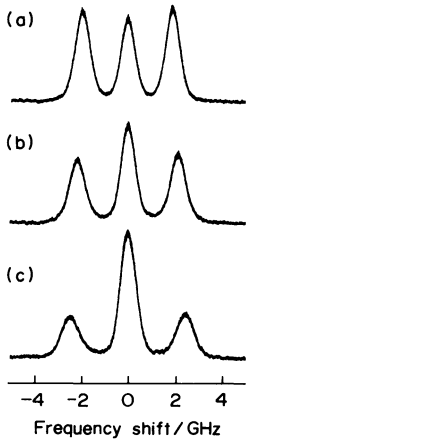

Fig. 1. Brillouin spectra of aqueous solutions of $CH_3OCH_2CH_2OCH_3$ with mole fractions of (a) 0.80, (b) 0.40, and (c) 0.125.

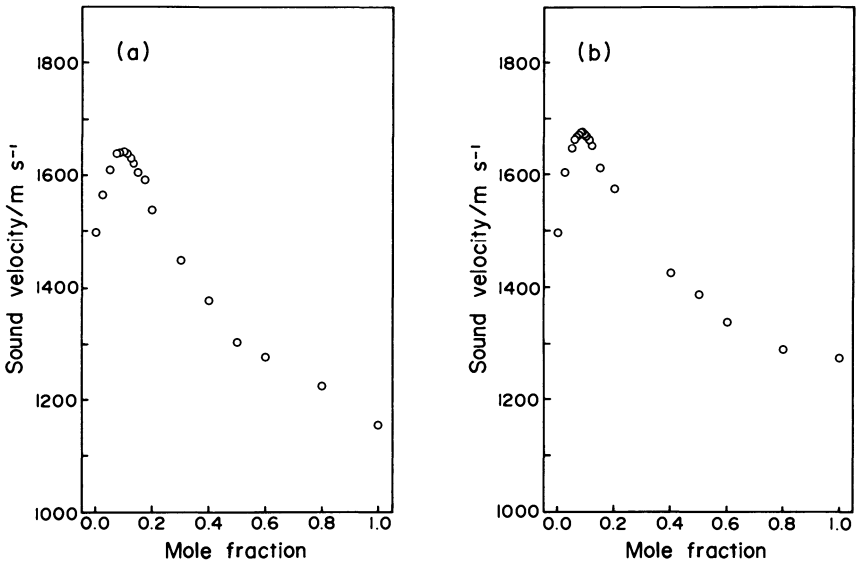

Fig. 2. Sound velocity vs. mole fraction of aqueous solutions of (a) $CH_3OCH_2CH_2OCH_3$ and (b) $CH_3(OCH_2CH_2)_2OCH_3$. Correct values for refractive index are employed.

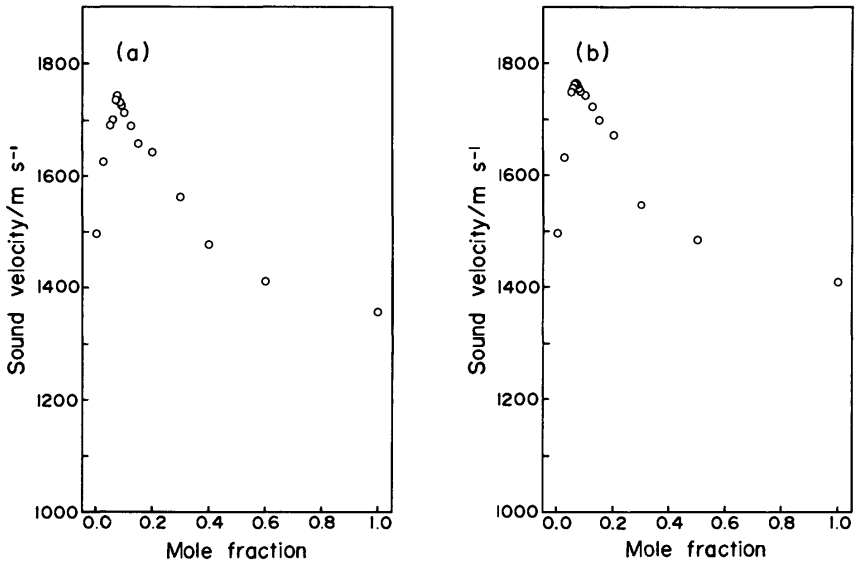

Fig. 3. Sound velocity vs. mole fraction of aqueous solutions of (a) $CH_3(OCH_2CH_2)_3OCH_3$ and (b) $CH_3(OCH_2CH_2)_4OCH_3$. A linear relation of refractive index with mole fraction is assumed.

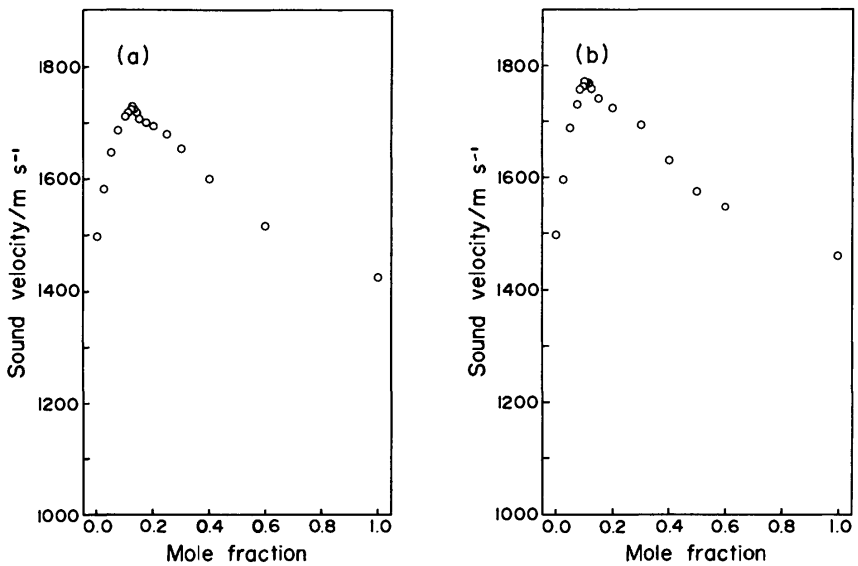

Fig. 4. Sound velocity vs. mole fraction of aqueous solutions of (a) $CH_3(OCH_2CH_2)_2OH$ and (b) $CH_3(OCH_2CH_2)_3OH$. A linear relation of refractive index with mole fraction is assumed.

the oligo(oxyethylene) compounds form the most compressed structure and all of the water molecules are expected to be involved in the hydration. For mole fractions of the solute larger than x_m, amount of water molecules is not enough to form the most close-packed solution structure; molecules of the oligo(oxyethylene) compounds themselves do not tend to form close structure as indicated by the fact that these molecules take rather disordered conformation in the neat liquid.[21] For mole fractions smaller than x_m, on the other hand, water molecules are more than enough for the highest hydration and the excess water molecules separate molecules of the oligo(oxyethylene) compounds from one another in solution, leading to less close solution structure.

The number of the water molecules, which are involved in the highest hydration, per each molecule of the oligo(oxyethylene) compounds is evaluated from their mole fractions x_m, at which the sound velocity is the maximum. The numbers obtained for

$CH_3(OCH_2CH_2)_mOCH_3$ with m=1, 2, 3, and 4 are 9.0_0, 10.7_6, 12.5_1, and 14.3_8, respectively, and those for $CH_3(OCH_2CH_2)_mOH$ with m=2 and 3 are 6.9_4 and 8.7_1, respectively. These results are summarized in Table 1.

The number of water molecules, at the highest hydration, per inner ether linkage $-CH_2OCH_2-$ in the molecular chain can be evaluated from the experimental results. If we assume that the corresponding number per terminal CH_3OCH_2- group is given by a half of the number of water molecules per molecule of $CH_3OCH_2CH_2OCH_3$. Thus, by using the number of 4.5 (=9.0/2) water molecules for the terminal CH_3OCH_2- part, the numbers of water molecules of hydration per $-CH_2OCH_2-$ group, $N_{CH_2OCH_2}$, are derived for the series of $CH_3(OCH_2CH_2)_mOCH_3$ compounds by the following equation:

$$N_{CH_2OCH_2} = (N_{mol} - 2\times 4.5)/n_{CH_2OCH_2}, \quad (3)$$

where N_{mol} is the number of water molecules, at the highest hydration, per molecule and $n_{CH_2OCH_2}$ is the number of the $-CH_2OCH_2-$ group in the molecule. The values obtained are 1.7_6, 1.7_6, and 1.7_9 for the compounds of m=2, 3, and 4, respectively, which contain one, two, and three $-CH_2OCH_2-$ groups in the molecule. For the series of $CH_3(OCH_2CH_2)_mOH$ compounds, the number of hydration water molecules per $-CH_2OCH_2-$, $N_{CH_2OCH_2}$, may be given as a difference between the numbers of water molecules per molecule of $CH_3(OCH_2CH_2)_3OH$ (8.7_1) and $CH_3(OCH_2CH_2)_2OH$ (6.9_4); the number derived is 1.7_7.

It is worthy to note that the number of water molecules per ether linkage in the inner part of the oxyethylene chain, when the highest hydration is attained, is essentially the same for all of the model compounds treated in the present work. This experimental finding indicates that extent of hydration of the oxyethylene chain is virtually constant independently of the chain length as far as the number of the oxyethylene unit is limited up to four. The composition of a maximum of 1.8 water molecules per inner ether linkage, or equivalently per inner oxyethylene group, determined in the present work indicates that a sort of hydration complex of

Table 1. Mole Fractions x_m[a] and Ratios of the Numbers of Molecules and/or Group at x_m for Aqueous Solutions of $CH_3(OCH_2CH_2)_mOCH_3$ (m=1—4) and $CH_3(OCH_2CH_2)_mOH$ (m=2 and 3)

m	x_m	Ratios of the numbers of molecules and/or group at x_m	
		Solute : H_2O	$-CH_2OCH_2-$: H_2O
$CH_3(OCH_2CH_2)_mOCH_3$			
1	0.100	1 : 9.0_0	—
2	0.085	1 : 10.7_6	1 : 1.7_6[b]
3	0.074	1 : 12.5_1	1 : 1.7_6[b]
4	0.065	1 : 14.3_8	1 : 1.7_9[b]
$CH_3(OCH_2CH_2)_mOH$			
2	0.126	1 : 6.9_4	—
3	0.103	1 : 8.7_1	1 : 1.7_7[b]

a) Mole fraction of the solute, $CH_3(OCH_2CH_2)_mOCH_3$ or $CH_3(OCH_2CH_2)_mOH$, at which the sound velocity gives a maximum value. b) For evaluation of the ratio, see text.

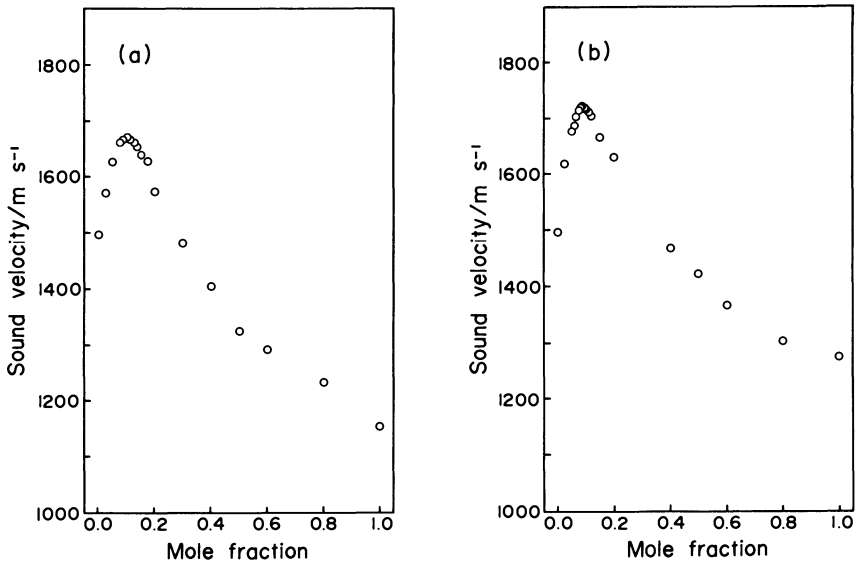

Fig. 5. Sound velocity vs. mole fraction of aqueous solutions of (a) $CH_3OCH_2CH_2OCH_3$ and (b) $CH_3(OCH_2CH_2)_2OCH_3$. A linear relation of refractive index with mole fraction is assumed.

approximately 1 $-OCH_2CH_2-$:2 H_2O is formed in the aqueous solution. The oxyethylene chain is incorporated with the water molecules in the formation of the structured hydration framework.

The present result of the extent of hydration appears to be consistent with the previous result, by means of the fluidity measurement, of 2.0 water molecules per ether linkage in $CH_3OCH_2CH_2OCH_3$ and $CH_3(OCH_2CH_2)_2OCH_3$.[15] The previous study[15] showed, however, that the extent of hydration was not different between the terminal CH_3OCH_2- group and the inner $-CH_2OCH_2-$ group. This inconsistency with the present result may be associated in part with the inherencies in the two different physical properties. It may be instructive to mention that the NMR measurements on α-hydro-ω-hydroxypoly(oxyethylene) with average molecular weight of 400, which corresponds to approximately nine oxyethylene units in the molecule, showed that three molecules of water were required for the hydration of each oxyethylene unit.[22]

The present observations show that more water molecules are involved in the hydration at the terminal CH_3OCH_2- group than at the inner $-CH_2OCH_2-$ group. This may be accounted for by possible existence of additional water molecules in the vicinity of the terminal methoxyl group. These water molecules will contribute, incorporated with the water molecules involved in the hydration at the inner ether linkages, to the formation of the structured hydration framework. This means that additional water molecules are necessary to close up an open end of the hydration framework at the CH_3O- terminal. For the compounds with the hydroxyl terminal, on the other hand, the $HOCH_2-$ group with hydrogen-bonding affinity can participate, in conjunction with the water molecules of hydration, in forming the hydration framework, and accordingly less water molecules of hydration will suffice for the terminal $HOCH_2-$ group. In fact, the results, shown in Table 1, on $CH_3(OCH_2CH_2)_mOH$ suggest that less than one water molecule is responsible for the hydration at the $HOCH_2-$ group.

The conformation of the oxyethylene chain in aqueous solution has been examined by a Raman-spectroscopic method[21,23,24]; further investigations are now in progress in our recent series of studies.[25,26] According to the analysis of Raman spectra,[21] the oxyethylene chain in aqueous solution becomes more ordered as the solution is diluted down to the mole fraction x_m, at which the hydration is completed. The dominant ordered structure is described by the *gauche* conformation of the OCH_2-OCH_2 group. On dilution with water, the *trans-gauche* conformation for the $O-CH_2-CH_2O$ group is most predominantly stabilized as compared with other possible conformations, and the *gauche-gauche* conformation follows the *trans-gauche*. The *gauche-trans* and *trans-trans* conformations are, however, much less stabilized than the above two, when the solution is diluted with water.[21]

These spectroscopic findings indicate that the stabilization of the *gauche* conformation for the OCH_2-CH_2O group is promoted greatly by the hydrogen bond formed between the ether oxygens and water molecules of hydration. Further speculation is possible that the water molecules are bridged between the immediately adjacent ether oxygens in the oxyethylene chain, in conformity with the stabilized *gauche* conformation of the OCH_2-CH_2O group. Various hydration models of the oxyethylene chain have been in fact proposed previously.[27–29] It seems, however, that further comprehensive experimental efforts are required for establishing more sophisticated hydration structures. The bridging hydrogen bonding mentioned above is nevertheless one of the most essential factors to maintain the *gauche* OCH_2-CH_2O structure in the oxyethylene chain.

It has been reported that the extent of hydration changes with increasing oxyethylene-chain length in α-n-alkyl-ω-hydroxypoly(oxyethylene)s, $CH_3(CH_2)_{n-1}(OCH_2CH_2)_mOH$, where the n-alkyl group is relatively long ($n>10$).[1] For these nonionic surfactant molecules, the effect of the alkyl chain seems to be significantly important in forming favorable hydration structures. The present result, obtained from the simpler model compounds, will be a basis for studying more complicated interactions between the hydrophilic moiety of the nonionic surfactants and water molecules.

The authors wish to express their thanks to Misses Noriko Soei and Tomoko Imabayashi for their assistance in the experimental work.

References

1) D. Attwood and A. T. Florence, "Surfactant Systems," Chapman and Hall, London (1983).
2) D. Attwood, *J. Phys. Chem.*, **72**, 339 (1968).
3) D. I. D. El Eini, B. W. Barry, and C. T. Rhodes, *J. Colloid Interface Sci.*, **54**, 348 (1976).
4) P. H. Elworthy and C. B. Macfarlane, *J. Chem. Soc.*, **1962**, 537.
5) J. M. Corkill, J. F. Goodman, and J. Wyer, *Trans. Faraday Soc.*, **65**, 9 (1969).
6) H. Schott, *J. Colloid Interface Sci.*, **24**, 193 (1967).
7) H. Schott, *J. Pharm. Sci.*, **58**, 1521 (1969).
8) T. Arnarson and P. H. Elworthy, *J. Pharm. Pharmacol.*, **33**, 141 (1981).
9) F. Podo, A. Ray, and G. Némethy, *J. Am. Chem. Soc.*, **95**, 6164 (1973).
10) P.-G. Nilsson, H. Wennerström, and B. Lindman, *J. Phys. Chem.*, **87**, 1377 (1983).
11) M. Zulauf and J. P. Rosenbusch, *J. Phys. Chem.*, **87**,

856 (1983).
12) D. J. Mitchell, G. J. T. Tiddy, L. Waring, T. Bostock, and M. P. McDonald, *J. Chem. Soc., Faraday Trans. 1*, **79**, 975 (1983).
13) I. L. Fabelinskii, "Molecular Scattering of Light," translated by R. T. Beyer, Plenum, New York (1968).
14) R. S. Krishnan, "Brillouin Scattering," in "The Raman Effect," ed by A. Anderson, Marcel Dekker, New York (1971), Vol. 1, Chap. 6, pp. 343—404.
15) H. Schott, *J. Chem. Eng. Data*, **11**, 417 (1966).
16) H. Matsuura and T. Miyazawa, *Bull. Chem. Soc. Jpn.*, **46**, 3031 (1973).
17) H. Matsuura and T. Miyazawa, *Bull. Chem. Soc. Jpn.*, **47**, 1143 (1974).
18) H. Matsuura, "Measurements of Brillouin Scattering," in "Shin-jikken Kagaku Koza," ed by T. Tachibana et al., Maruzen, Tokyo (1976), Vol. 4, pp. 697—725.
19) W. J. Wallace and A. L. Mathews, *J. Chem. Eng. Data*, **8**, 496 (1963).
20) W. J. Wallace and A. L. Mathews, *J. Chem. Eng. Data*, **9**, 267 (1964).
21) H. Matsuura and K. Fukuhara, *J. Mol. Struct.*, **126**, 251 (1985).
22) K.-J. Liu and J. L. Parsons, *Macromolecules*, **2**, 529 (1969).
23) J. L. Koenig and A. C. Angood, *J. Polym. Sci., Pt. A-2*, **8**, 1787 (1970).
24) J. Maxfield and I. W. Shepherd, *Polymer*, **16**, 505 (1975).
25) H. Matsuura, K. Fukuhara, and H. Tamaoki, *J. Sci. Hiroshima Univ., Ser. A*, **49**, 89 (1985).
26) H. Matsuura and K. Fukuhara, *J. Polym. Sci., Polym. Phys. Ed.*, to be published.
27) R. A. Horne, J. P. Almeida, A. F. Day, and N.-T. Yu, *J. Colloid Interface Sci.*, **35**, 77 (1971).
28) W. Luck, *Fortschr. Chem. Forsch.*, **4**, 653 (1964).
29) R. Kjellander and E. Florin, *J. Chem. Soc., Faraday Trans. 1*, **77**, 2053 (1981).

 © 1986 The Chemical Society of Japan Bull. Chem. Soc. Jpn., 59, 769—773 (1986)

Interaction of Poly[*S*-(2-carboxyethyl)-L-cysteine] with Cationic Surfactants

Hiroshi MAEDA,* Yoriko TANAKA, and Shoichi IKEDA
Department of Chemistry, Faculty of Science, Nagoya University, Chikusa-ku, Nagoya 464
(Received September 6, 1985)

The induction of the β-structure of fully ionized poly[*S*-(2-carboxyethyl)-L-cysteine] in solution markedly depended on the kind of head group of cationic surfactants; it occurred by the addition of dodecylammonium chloride (DAC) but not by the addition of dodecyldimethylammonium chloride (DDAC) or dodecyltrimethylammonium chloride (DTAC), as concluded based on circular dichroism spectra. The induction of the β-structure by DAC was not inhibited by raising ionic strength of the medium but was enhanced when the polypeptide concentration was increased. The polypeptide took the β-structure in the precipitates produced by the addition of any one of these three surfactants, as indicated by the infrared absorption (IR) spectra. Intensity of a characteristic absorption band of carboxylate group around 1570 cm^{-1} for the complex with DDAC was vanishingly weak, while those with DAC and DTAC were medium and strong, respectively. The precipitates were solubilized in the presence of excess amount of surfactants. In the solubilized solution, the β-structure was again found in the case of DAC, irrespective of the polypeptide concentration, but it was found only at high polypeptide concentrations in the case of DDAC.

Interaction of anionic polypeptides with cationic surfactants has been examined by monitoring the secondary structure of polypeptides.[1-3] Recently, we have examined the effect of different cationic surfactants on the induction of the secondary structures of anionic polypeptides.[4,5] Three surfactants used in these studies were dodecylammonium chloride (DAC), dodecyldimethylammonium chloride (DDAC), and dodecyltrimethylammonium chloride (DTAC). They have different ionic heads but a common hydrocarbon tail (dodecyl group).

Induction of the α-helix of poly(L-glutamic acid) (PGA) occurred by the addition of these three surfactants.[4] On the other hand, the β-structure of poly(*S*-carboxymethyl-L-cysteine) (poly[Cys(CH_2COOH)]) was induced by the addition of DAC but not by the addition of DDAC or DTAC.[5] PGA has been used as a standard model polypeptide for the α-helix.[6-10] Characterization of the β-structure of poly[Cys(CH_2COOH)] has been carried out recently.[11-13]

The observed marked difference between PGA and poly[Cys(CH_2COOH)] is expected to originate from different nature of the two secondary structures; α-helix and β-structure. Direct interaction sites in either polypeptide with surfactant ammonium groups are carboxylate groups. In the complexes of poly[Cys(CH_2COOH)] with DDAC or DAC, proton transfer to carboxylate groups from the ammonium head groups was indicated in the solid state.[5] The extent of proton transfer depends on the intrinsic dissociation constant K_0 of carboxyl group for a given surfactant head group. There is a great difference between the values of pK_0 of the two polypeptides; pK_0=4.4 for PGA[8] and pK_0=3.2 for poly[Cys(CH_2COOH)].[14] It is possible, therefore, that different nature of the interactions of these two polypeptides with the same surfactants partly originates from a consequence of the different values of pK_0. In the present study, the interaction of poly-[*S*-(2-carboxyethyl)-L-cysteine] (poly[Cys(CH_2CH_2COOH)]) with the three same cationic surfactants, DAC, DDAC, and DTAC, is examined by observing circular dichroism of solutions and infrared absorption spectra of precipitates. This polypeptide is a side-chain homolog of poly[Cys(CH_2COOH)] and carries carboxyl groups of pK_0=4.0.[14] Consequences of different values of pK_0 of carboxyl groups and different numbers of methylene groups are expected to show up in the interaction with the surfactants.

Experimental

Poly[*S*-(2-carboxyethyl)-L-cysteine] (poly[Cys(CH_2CH_2COOH)]) was synthesized as described previously[15] and its weight-average molecular weight and degree of polymerization were 3.5×10^4 and 200, respectively, as estimated from the viscosity-molecular weight relation on poly[Cys(CH_2COOH)].[16] Three surfactants used in the present study were the same lots as used in the previous studies.[4,5] Values of critical micelle concentration (cmc) in 0.01 M† NaCl are 1.23×10^{-2} M[17] and 1.14×10^{-2} M[18] for DAC and DDAC, respectively. Values of cmc for DTAC are 2.16×10^{-2} M (in water) and 1.59×10^{-2} M (in 0.02 M NaCl).[17] Concentrations of polypeptide C_P and surfactant C_D are expressed in residue molarity and molarity, mol dm^{-3} (M), respectively. Composition of the solutions is specified by C_P and the mixing ratio C_D/C_P. Circular dichroism (CD) spectra were taken on a Jasco J 40A circular dichrograph using cells of light paths of 1 and 10 mm. Four scans were averaged in most cases. Infrared absorption (IR) spectra of polypeptide-surfactant complexes in KBr discs were obtained on a Jasco IRA-2 spectrophotometer. Measurements of CD and IR were carried out at 24±2 °C.

Effects of different ways of preparing solutions were examined previously[5] and they were shown not to affect the obtained results significantly in so far as measurements were made on the solutions incubated more than 12 h. In

† 1 M=1 mol dm^{-3}.

the present study, solutions were prepared by adding small volumes of concentrated surfactant stock solutions to polypeptide solutions and incubated at 24±2 °C for 12 to 24 h.

Results

Interactions in 1×10^{-2} M Tris HCl (pH 7.4) in the absence of other supporting electrolytes were examined in the first place. In Fig. 1, CD spectra of solutions at a residue concentration C_P of 1×10^{-4} M are shown. In the absence of surfactants, the CD spectra (labeled a in Fig. 1A—C) of random coils are characterized by two negative bands, one around 200 nm and the other at 225 nm. On addition of DAC, the residue ellipticity, $[\theta]$, around 200 nm increased and became positive, while that at 225 nm became more negative. At the mixing ratio of 2.2, the spectrum (e) resembles that of typical β-structure (although incomplete) induced by protonation. On the other hand, no significant change occurred on addition of DDAC or DTAC. Effects of three surfactants can be compared clearly when values of residue ellipticities around band positions, $[\theta]_{205}$ and $[\theta]_{225}$, are plotted against the mixing ratio C_D/C_P (Fig. 2). The β-structure of poly[Cys(CH_2CH_2COOH)] was induced by the addition of DAC but not by DDAC or DTAC, similar to the previous result on poly[Cys(CH_2COOH)].[5] Further addition of the surfactants caused precipitation of the polypeptide. Precipitation occurred at the mixing ratios of about 3 for DAC, 15 for DDAC, and 20 for DTAC. When the mixing ratios exceeded 100, however, solubilization took place and the conformation of the polypeptide in the solubilized solutions was again the β structure in the case of DAC but random coils in the case of DDAC or DTAC.

The results at $C_P=1\times10^{-3}$ M are shown in Fig. 3. Induction of the β-structure by DAC was significantly enhanced when the polypeptide concentration was raised. Induction of the β-structure did not take place in the case of DDAC or DTAC even at this concentration. Precipitation occurred at the mixing ratios considerably smaller than those at $C_P=1\times10^{-4}$ M: about 0.8 for DAC, 1 for DDAC, and 3 for DTAC. Solubilization occurred for DAC when mixing ratios exceeded 100 and for DDAC ($C_D/C_P>400$) but not for DTAC up to $C_D/C_P=500$. In solubilized solutions, the β-structure was found for DAC and also for DDAC, although the extent of induction was not large for the latter.

Interaction in the presence of 0.1 M NaCl was examined at $C_P=1\times10^{-4}$ M (Fig. 4). As compared with the result on DAC in the absence of NaCl, increase in ionic strength slightly inhibited the induction of the β-structure by DAC. No induction by DDAC or DTAC was also found in the presence of 0.1 M NaCl. Solubility of the polypeptide decreased in 0.1 M NaCl, since precipitation of the polypeptide occurred at the mixing ratios (about 2, 6, and 12 for DAC, DDAC, and DTAC, respectively), which were smaller than those found in the absence of 0.1 M NaCl. Solubilization at high mixing ratios occurred only for DAC.

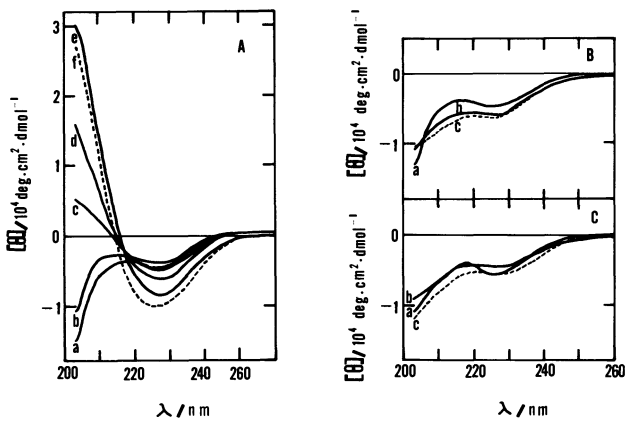

Fig. 1. CD spectra of poly[Cys(CH_2CH_2COOH)] in 1×10^{-2} M Tris HCl (pH 7.4) at $C_P=1\times10^{-4}$ M. (A) DAC. Mixing ratios (C_D/C_P): (a) 0, (b) 0.6, (c) 1.0, (d) 1.4, (e) 2.2, and (f) 100. (B) DDAC. Mixing ratios (C_D/C_P): (a) 0, (b) 6.2, and (c) 150. (C) DTAC. Mixing ratios (C_D/C_P): (a) 0, (b) 14, and (c) 100.

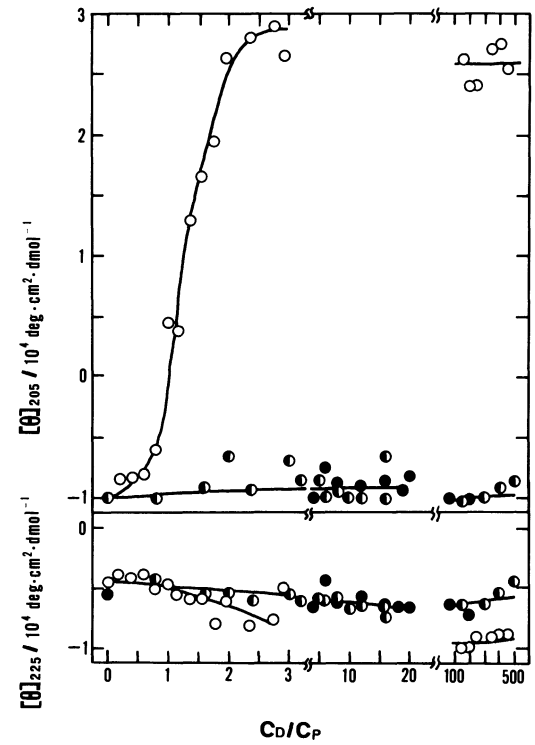

Fig. 2. Dependence of residue ellipticities $[\theta]_{205}$ and $[\theta]_{225}$ on the mixing ratio C_D/C_P in 1×10^{-2} M Tris HCl (pH 7.4) at $C_P=1\times10^{-4}$ M. (○) DAC, (◐) DDAC, and (●) DTAC.

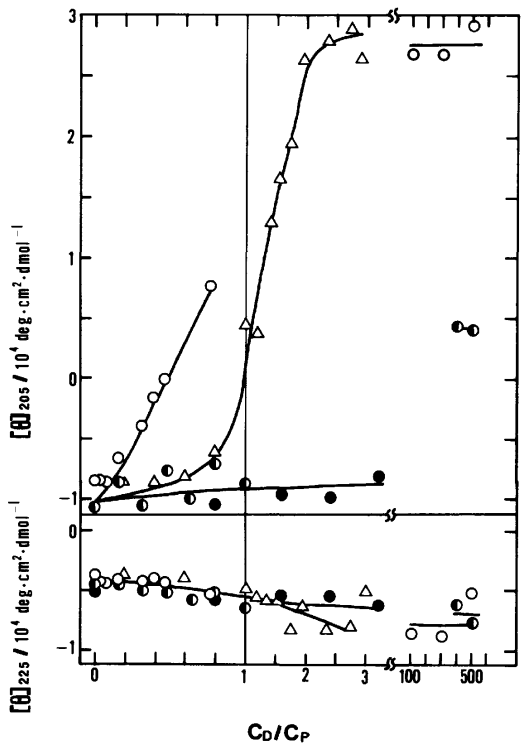

Fig. 3. Dependence of residue ellipticities $[\theta]_{205}$ and $[\theta]_{225}$ on the mixing ratio C_D/C_p in 1×10^{-2} M Tris HCl(pH 7.4) at $C_p=1\times10^{-3}$ M. (○) DAC, (◐) DDAC, and (●) DTAC. Data at $C_p=1\times10^{-4}$ M (△) in the case of DAC are also shown for comparison.

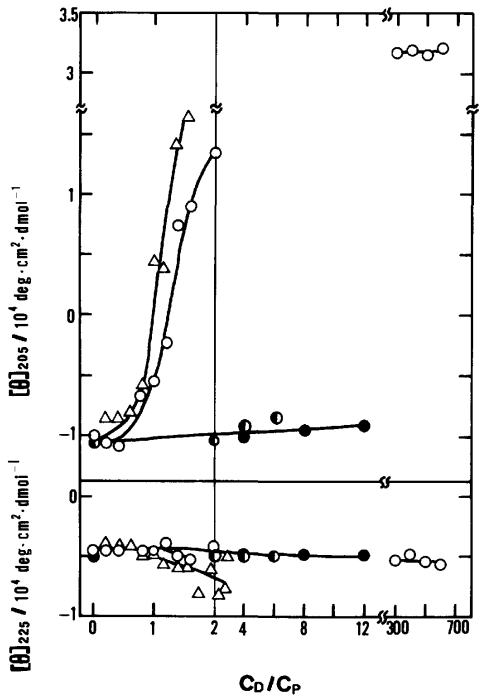

Fig. 4. Dependence of residue ellipticities $[\theta]_{205}$ and $[\theta]_{225}$ on the mixing ratio C_D/C_p in 1×10^{-2} M Tris HCl (pH 7.4) in 0.1 M NaCl at $C_p=1\times10^{-4}$ M. (○) DAC, (◐) DDAC, and (●) DTAC. Data for DAC in the absence of 0.1 M NaCl (△) are also shown for comparison.

In Fig. 5, correlation between two residue ellipticities of the polypeptide at 205 nm and 225 nm is shown. The data in the presence of DAC (open symbols) show two distinct regions; one corresponds to the induction of the β-structure at low mixing ratios and the other to solubilized solutions. The magnitude of the negative band around 225 nm, which is associated with n-π^* transition of the peptide chromophore, is greater in the solubilized solutions than in the solutions at low mixing ratios. This increased magnitude represents a decrease of the polarity around peptide chromophore in the solubilized state. This environmental effect on $[\theta]_{225}$ is very weak in solutions containing DTAC (filled symbols). In the presence of DDAC (half-filled symbols), however, the magnitude of $[\theta]_{225}$ increases considerably even for random coils at $C_p=1\times10^{-4}$ M, which is likely a preinduction stage of the β-structure at $C_p=1\times10^{-3}$ M in the solubilized solutions. Precipitation, solubilization and the conformation of the polypeptide in solution are summarized in Fig. 6. Three zones (A, B, C) for each surfactant represent, respectively, the results obtained at $C_p=1\times10^{-4}$ M, at $C_p=1\times10^{-3}$ M, and at $C_p=1\times10^{-4}$ M in 0.1 M NaCl. It is to be noted that 1×10^{-2} M Tris buffer (pH=7.4) was present in every case.

Infrared absorption (IR) spectra (Figure 7) of the complexes of poly[Cys(CH_2CH_2COOH)] with three surfactants were taken on the precipitates obtained at

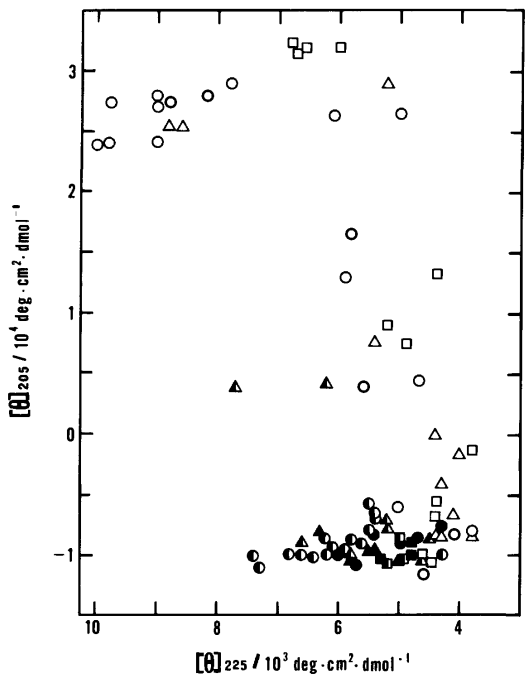

Fig. 5. Correlation between $[\theta]_{205}$ and $[\theta]_{225}$. Open, half-filled, and filled symbols represent the data on DAC, DDAC, and DTAC, respectively. Circles; $C_p=1\times10^{-4}$ M. Triangles; $C_p=1\times10^{-3}$ M. Squares; $C_p=1\times10^{-4}$ M in 0.1 M NaCl.

C_P=1×10^{-2} M and C_D/C_P=1. Amide I bands were observed at 1630 cm^{-1} [$\nu(\pi,0)$][19] and 1695 cm^{-1} [$\nu(0,\pi)$][19] and amide II bands were observed at 1525 cm^{-1} for three complexes, and hence antiparallel β-structure was confirmed as the conformation of the polypeptide. Proton transfer from ammonium head group to carboxylate was judged by measuring the intensity of antisymmetric streching mode of COO$^-$ groups found at 1570 cm^{-1}. The intensity was very weak, medium, and strong in the complexes with DDAC, DAC, and DTAC, respectively, if compared with the intensity of amide II band in each case. Thus, protonation of carboxylate groups was indicated in the complexes with DDAC and DAC.

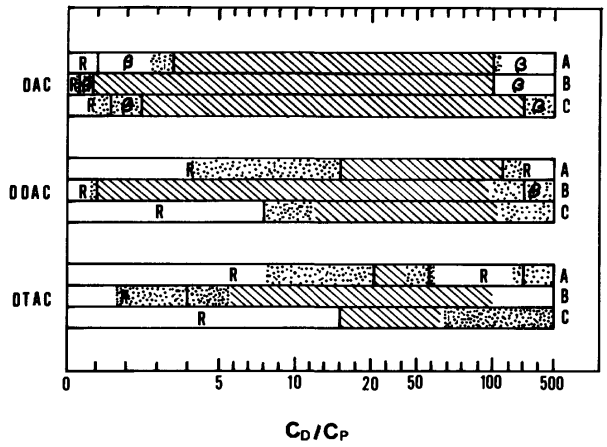

Fig. 6. Schematic phase diagram of a mixture of poly[Cys(CH_2CH_2COOH)] in the presence of a surfactant in 1×10^{-2} M Tris HCl (pH 7.4). Three zones A, B, and C correspond to the data at C_P=1×10^{-4} M, C_P=1×10^{-3} M, and C_P=1×10^{-4} M in 0.1 M NaCl, respectively. Blank region; solution. Dotted region; turbid solutions. Hatched region; precipitates. Conformations of the polypeptide in solutions are designated by R (random coils)or β(β-structure).

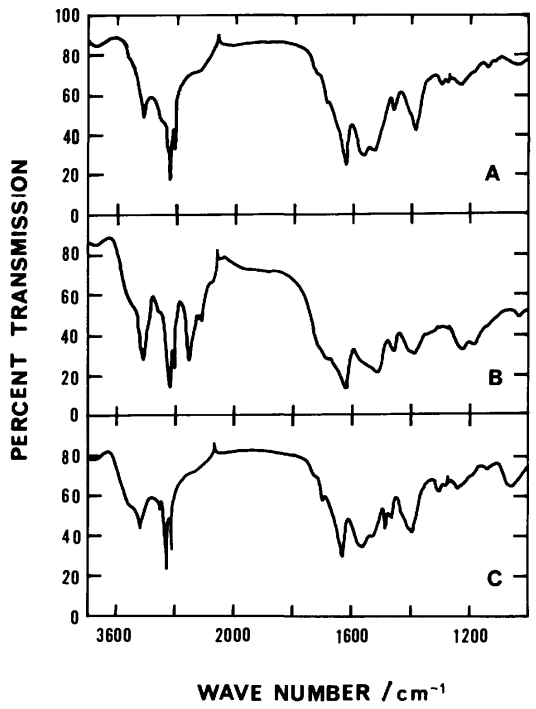

Fig. 7. Infrared absorption spectra of precipitates containing poly[Cys(CH_2CH_2COOH)] complexed with DAC (A), DDAC (B), and DTAC (C).

Discussion

Present results on poly[Cys(CH_2CH_2COOH)] and previous ones on poly[Cys(CH_2COOH)] are summarized in Table 1 and compared with each other. Very similar results are obtained between these two polypeptides with respect to the induction of the β-structure in solution as well as the effects of ionic strength and the polypeptide concentration on the induction. This comparison indicates that difference in acidities of the carboxyl groups between the two polypeptides scarcely affects their interaction with the cationic surfactants. It is concluded from this finding that the different interactions of the three surfactants with PGA[4] and poly[Cys(CH_2COOH)][5] essentially arise from different characters of the two secondary structures, α-helix and β-structure, and cannot be attributed much to different nature of the carboxyl groups of the two polypeptides. Therefore, present study confirms the validity of the previous discussion.[5]

On the other hand, there are several significant differences between the results on poly[Cys(CH_2COOH)] and poly[Cys(CH_2CH_2COOH)]. The addition of DDAC induced the β-structure of poly[Cys(CH_2CH_2COOH)] to some extent under a limited condition; solubilized solutions at high polypeptide concentrations. Induction of the β-structure of poly[Cys(CH_2COOH)] by the addition of DDAC did not occur under any condition examined. Conformations of the complexes with DTAC were random coil in the case of poly[Cys(CH_2COOH)] but the β-structure in the case of poly[Cys(CH_2CH_2COOH)]. Measurements of CD in solubilized solutions were hampered by the presence of (assumed) large aggregates in the case of the following combinations: DTAC-poly[Cys(CH_2CH_2-$COOH$)] and DDAC-poly[Cys(CH_2COOH)].

In addition to different values of pK_0 of side chain carboxyl groups, there is another important consequence of different side chains between these two polypeptides; different extents of hydrophobic nature of the side chains. Induction of the β-structure by DDAC in the solubilized solutions at C_P=1×10^{-3} M as well as the β-conformation of the complex with DTAC in the solid state can be ascribed to the enhanced stability of the β-structure of poly[Cys-(CH_2CH_2COOH)] due to increased nonpolar nature.[14,20]

Table 1. Comparison of Major Conformations of the Two Polypeptides in the Presence of Three Surfactants

	Solution		Precipitates		Solubilized solution	
Polypeptide[a)]	M	E	M	E	M	E
DAC	beta	beta	beta	beta	beta	beta
DDAC	coil	coil	beta	beta	x[b)]	beta (1 mM) coil (0.1 mM)
DTAC	coil	coil	coil	beta	coil	x[b)] (1 mM) coil (0.1 mM)

a) Poly[Cys(CH_2COOH)] and poly[Cys(CH_2CH_2COOH)] are abbreviated as M and E, respectively. b) Conformations could not be assessed from highly perturbed CD spectra.

References

1) W. L. Mattice, R. W. McCord, and P. M. Shippey, *Biopolymers*, **18**, 723 (1979).
2) K. Shirahama and J. T. Yang, *Int. J. Pept. Protein Res.*, **13**, 341 (1979).
3) I. Satake, T. Gondo, and H. Kimizuka, *Bull. Chem. Soc. Jpn.*, **52**, 361 (1979).
4) H. Maeda, H. Kato, and S. Ikeda, *Biopolymers*, **23**, 1333 (1984).
5) H. Maeda, M. Kimura, and S. Ikeda, *Macromolecules*, **18**, 2566 (1985).
6) P. Doty, A. Wada, J. T. Yang, and E. R. Blout, *J. Polymer Sci.*, **23**, 851 (1957).
7) A. Wada, *Mol. Phys.*, **3**, 409 (1960).
8) M. Nagasawa and A. Holtzer, *J. Am. Chem. Soc.*, **86**, 538 (1964).
9) J. Hermans, Jr., *J. Am. Chem. Soc.*, **88**, 2418 (1966).
10) D. S. Olander and A. Holtzer, *J. Am. Chem. Soc.*, **90**, 4549 (1968).
11) H. Maeda, K. Kadono, and S. Ikeda, *Macromolecules*, **15**, 822 (1982).
12) K. Saito, H. Maeda, and S. Ikeda, *Biophys. Chem.*, **16**, 67 (1982).
13) H. Maeda, Y. Gatto, and S. Ikeda, *Macromolecules*, **17**, 2031 (1984).
14) H. Maeda and S. Ikeda, *Biopolymers*, **14**, 1623 (1975).
15) H. Maeda and S. Ikeda, *Biopolymers*, **10**, 1635 (1971).
16) K. Kadono, A. Fukutome, H. Maeda, and S. Ikeda, *Rep. Prog. Polymer Phys. Japan*, **27**, 613 (1984).
17) L. M. Kushner, W. D. Hubbard, and R. A. Parker, *J. Res. Natl. Bur. Stand.*, **59**, 113 (1957).
18) S. Ozeki, M. Tsunoda, and S. Ikeda, *J. Colloid Interface Sci.*, **64**, 28 (1978).
19) T. Miyazawa and E. R. Blout, *J. Am. Chem. Soc.*, **83**, 712 (1961).
20) H. Maeda and S. Ikeda, *Biopolymers*, **10**, 2525 (1971).

 © 1986 The Chemical Society of Japan Bull. Chem. Soc. Jpn., 59, 775—779 (1986)

Optical and Magnetic Properties of $(DBTTF)_2(Cu_2Cl_6)$ and $(DBTTF)_2(Cu_2Br_6)$ Complexes

Masashi TANAKA
Department of Chemistry, College of General Education, Nagoya University, Chikusa-ku, Nagoya 464
(Received October 7, 1985)

Optical reflection and magnetic susceptibility measurements of $(DBTTF)_2(Cu_2Cl_6)$ and $(DBTTF)_2(Cu_2Br_6)$ complexes were carried out. The analysis of the reflection spectra of the single crystals of these complexes shows that the electronic structure of $DBTTF^+$ cation molecules is typical of the dimer type configuration. The magnetic susceptibilities of these complexes were measured over a temperature range of 2—300 K. The magnetic behavior conforms to a modified Bleaney-Bowers equation, indicating the existence of the spin coupling within the $Cu_2Cl_6^{2-}$ or $Cu_2Br_6^{2-}$ dimers and the antiferromagnetic spin interaction between $Cu_2Br_6^{2-}$ dimers.

There has been considerable interest recently in organic conductors which have highly anisotropic electrical, optical and magnetic properties. Tetrathiafulvalene-tetracyanoquinodimethane (TTF-TCNQ) is one of them which received the most detailed attention. After the discovery of the TTF-TCNQ complex, many compounds with fulvalene rings were synthesized to obtain the radical salts with highly electrical conductivity. Dibenzotetrathiafulvalene (DBTTF) is one of those compounds[1] and the direct oxidation of DBTTF by halogens and metal halides were reported to yield radical salts such as $(DBTTF)_2I_3$,[2] $(DBTTF)_8(SnCl_6)_3$,[3] and $(DBTTF)_3(SnBr_6)$.[3] Furthermore, we reported the crystal structure of $(DBTTF)_2(Cu_2Cl_6)$[4] and $(DBTTF)_2(Cu_2Br_6)$.[5] These complexes consist of the organic conducting stack and the inorganic magnetic stack and are supposed to have the interest properties of both the electrical conductivity and the magnetization. In the present paper, therefore, we report the optical and magnetic properties of $(DBTTF)_2(Cu_2Cl_6)$ and $(DBTTF)_2(Cu_2Br_6)$ complexes.

Experimental

The crystal of $(DBTTF)_2(Cu_2Cl_6)$ and $(DBTTF)_2(Cu_2Br_6)$ complexes was prepared by using the close system-evaporation crystallizer transfering DBTTF and $CuCl_2$ or $CuBr_2$ from solid sources to an acetonitrile solution.[6,7] The reflection spectra of the single crystal at the normal incidence were measured over the range of 5000—25000 cm^{-1} by means of a reflection spectrophotometer made in our laboratory and the temperature dependence of the magnetic susceptibility of the powder of the samples were recorded on a Oxford magnetic susceptibility instrument of the Instrument Center, Institute for Molecular Science, Okazaki. All calculations for the analysis of the experimental data were made on a FACOM M382 computer of Nagoya University.

Theoretical

For the dimer system of DBTTF cations, the Hamiltonian H can be written by the Hubbard approximation as follows,

$$H = -t\sum_{\sigma=\alpha,\beta}(a_{1,\sigma}^{+}a_{2,\sigma}+a_{2,\sigma}^{+}a_{1,\sigma}) + U\sum_{i=1,2}n_{i,\alpha}n_{i,\beta}, \quad (1)$$

where $a_{1,\sigma}$ and $a_{2,\sigma}$ are the annihilation operators of the π-electron occupying HOMO of the DBTTF molecule at the sites 1 and 2, σ represents the spin of π-electron, $n_{i,\sigma}=a_{i,\sigma}^{+}a_{i,\sigma}$, t is the electron transfer integral between the sites 1 and 2, and U is the intramolecular Coulomb integral. Then, the following ground and lower excited configuration functions are taken into account for the calculation of the electronic states of the dimer system.

$$\Phi_{T,1} = a_{1,\beta}a_{2,\beta}\Phi_{HF}, \quad (2)$$

$$\Phi_{T,0} = \frac{1}{\sqrt{2}}(a_{1,\beta}a_{2,\alpha}+a_{1,\alpha}a_{2,\beta})\Phi_{HF}, \quad (3)$$

$$\Phi_{T,-1} = a_{1,\alpha}a_{2,\alpha}\Phi_{HF}, \quad (4)$$

$$\Phi_{S,0} = \frac{1}{\sqrt{2}}(a_{1,\beta}a_{2,\alpha}-a_{1,\alpha}a_{2,\beta})\Phi_{HF}, \quad (5)$$

$$\Phi_{CT}(+) = \frac{1}{\sqrt{2}}(a_{1,\beta}a_{1,\alpha}+a_{2,\beta}a_{2,\alpha})\Phi_{HF}, \quad (6)$$

$$\Phi_{CT}(-) = \frac{1}{\sqrt{2}}(a_{1,\beta}a_{1,\alpha}-a_{2,\beta}a_{2,\alpha})\Phi_{HF}. \quad (7)$$

Here, Φ_{HF} means the Hartree-Fock wavefunction of the neutral dimer of DBTTF. Then, the secular equations are solved and the eigenfunctions and eigenvalues are obtained as follows, and the energy diagram of the cation dimer system is depicted in Fig. 1,

$$\left.\begin{aligned}\Psi_G &= c_1\Phi_{S,0}+c_2\Phi_{CT}(+),\\ E_G &= (U-\sqrt{U^2+16t^2})/2,\end{aligned}\right\} \quad (8)$$

$$\Psi_{T,i} = \Phi_{T,i}\ (i=-1,\ 0,\ 1), \quad E_{T,i} = 0, \quad (9)$$

$$\Psi_{CT}(-) = \Phi_{CT}(-), \quad E_{CT}(-) = U, \quad (10)$$

$$\left.\begin{aligned}\Psi_{CT}(+) &= c_2\Phi_{S,0}-c_1\Phi_{CT}(+),\\ E_{CT}(+) &= (U+\sqrt{U^2+16t^2})/2,\end{aligned}\right\} \quad (11)$$

where the parameters c_1 and c_2 are expressed by the next equations,

$$c_1 = \frac{2t}{\sqrt{E_G^2+4t^2}} \quad \text{and} \quad c_2 = \frac{-E_G}{\sqrt{E_G^2+4t^2}}. \tag{12}$$

The optically allowed transition from Ψ_G to $\Psi_{CT}(-)$ has the transition energy given by,

$$\Delta E_{CT} = E_{CT}(-) - E_G = (U+\sqrt{U^2+16t^2})/2, \tag{13}$$

and the oscillator strength of the CT band can be expressed as follows,

$$f = 3 \times 1.085 \times 10^{11}\Delta E_{CT}|\langle\Psi_G|r|\Psi_{CT}(-)\rangle|^2$$
$$= 3 \times 1.085 \times 10^{11}\frac{4t^2}{\sqrt{U^2+16t^2}}|R_{12}|^2, \tag{14}$$

where R_{12} is the distance between the DBTTF molecules.

The magnetic susceptibility X_{DBTTF} of the cation dimer system is given as follows,

$$X_{DBTTF} = \frac{N(g_1\beta)^2}{k_BT} \times \frac{1}{3+\exp(J_1/k_BT)}, \tag{15}$$

where $J_1=(\sqrt{U^2+16t^2}-U)/2$, g_1 is the magnetic field splitting factor, β the Bohr magneton, N the Avogadro number, k_B the Boltzman constant, and T the absolute temperature.

For the $Cu_2X_6^{2-}$ ion, the ground state of a free Cu^{2+} ion is $^2D_{5/2}$ corresponding to the electronic configuration of $(1s)^2(2s)^2(2p)^6(3s)^2(3p)^6(3d)^9$. The planar $Cu_2X_6^{2-}$ ion has D_{2h} symmetry and the symmetry orbitals can be obtained by group theoretical means from the 3d orbitals on the Cu^{2+} ion and the $np\sigma$ and $np\pi$ orbitals on the halogen ion X^-. For the 3d orbitals on the Cu^{2+} ion, the fivefold degeneracy of the d orbital is completely removed under the D_{2h} symmetry.[8] The d_{xy} level is the highest one occupied by an electron and the other levels (d_{z^2}, $d_{x^2-y^2}$, d_{xz}, d_{yz}) are occupied by two electrons. As the result, the d-d transitions are expected to be located in the 10000—15000 cm^{-1} region. The charge transfer bands from the ligand to the d orbital may occur over the higher wavenumber region. However, these transitions are very weak and can be neglected for the analysis of the reflection spectra of the complex. On the other hand, the pairs of Cu^{2+} ions interact through exchange forces and each pair forms a lower singlet and an upper triplet state as is shown in Fig. 1. The exchange energy J_2 corresponds to the magnitude of the splitting between the singlet and triplet states and the magnetic susceptibility $X_{Cu_2X_6}$ of the $Cu_2X_6^{2-}$ dimer system is given by the modified Bleaney-Bowers equation,[9]

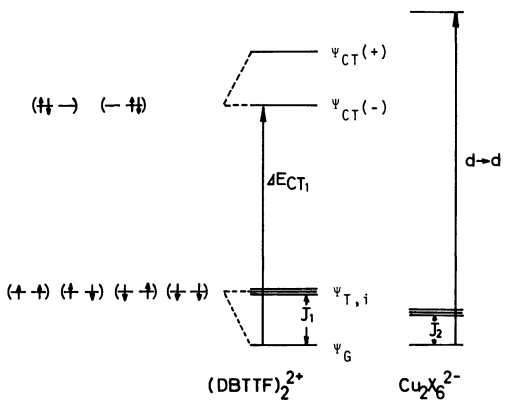

Fig. 1. Energy diagram of the complex $(DBTTF)_2$-(Cu_2X_6).

$$X_{Cu_2X_6} = \frac{N(g_2\beta)^2}{k_B(T-\Theta)} \times \frac{1}{3+\exp(J_2/k_BT)}, \tag{16}$$

where Θ is the Weiss constant that takes into account the spin interaction between the dimer ions.

The magnetic susceptibility $X(T)$ of the complex can be expressed by assuming that there is a separate contribution to the susceptibility from the DBTTF cation dimer, the $Cu_2X_6^{2-}$ anion dimer and the paramagnetic impurity,

$$X(T) = X_{DBTTF} + X_{Cu_2X_6} + \frac{N(g_3\beta)^2}{3k_BT}, \tag{17}$$

where the third term is the impurity term.

The optical reflectivity R can be expressed by the following equation,

$$R = \frac{1+|\varepsilon|-\sqrt{2(|\varepsilon|+\varepsilon_1)}}{1+|\varepsilon|+\sqrt{2(|\varepsilon|+\varepsilon_1)}}, \tag{18}$$

using the semiclassical Lorentz dielectric function,

$$\varepsilon(\omega) = \varepsilon_{core} + \sum_j \frac{\Omega_j^2}{\omega_j^2-\omega^2-i\omega\gamma_j}$$
$$= \varepsilon_1(\omega) + i\varepsilon_2(\omega), \tag{19}$$

where $\varepsilon_1(\omega)$ and $\varepsilon_2(\omega)$ are the real and imaginary parts of the dielectric function of the DBTTF cation dimers, and $|\varepsilon|=\sqrt{\varepsilon_1^2(\omega)+\varepsilon_2^2(\omega)}$. The oscillator strength f is determined by using the equation,

$$f = \frac{m_e}{4\pi N_0 e^2}\Omega_j^2. \tag{20}$$

Here, m_e is the electron mass, and N_0 is the number density of DBTTF molecule.

By fitting the above-mentioned equations of the reflectivity R and the magnetic susceptibility $X(T)$ to

the observed values, the optical and magnetic parameters of the complexes, $(DBTTF)_2(Cu_2X_6)$, can be obtained and their energy structure can be determined.

Results and Discussion

$(DBTTF)_2$-(Cu_2Cl_6) Complex. The crystal of $(DBTTF)_2$-(Cu_2Cl_6) complex crystallizes in the form of the dark reddish plates (0.35×0.008×0.60 mm) and has the natural developed plane of (010). The space group is monoclinic $C2/m$ and the unit cell dimensions are a=9.216, b=24.958, c=7.300 Å, and β=108.23°.[4,6] The projection of the complex onto the bc and ac planes are shown in Fig. 2. The stacking column of the cation molecules of DBTTF elongates along the c axis.

The reflection spectra were observed for the polarizations parallel and perpendicular to the c axis on the ac plane as is shown in Fig. 3. The 9000 cm^{-1} band in the c axis spectrum can be assigned to the CT_1 band of a dimer type system classified by Tanaka, et al.[10] and the dispersion around 20000 cm^{-1} in the $\perp$ c axis spectrum to the LE band of $DBTTF^+$ cation radical.[11] The best fit of Eq. 18 to the observed reflectivity is obtained and the calculated reflection spectra are depicted in Fig. 3 in order to compare with the observed ones. The obtained parameters (Ω_j, ω_j, γ_j, and ε_{core}) are shown in Table 1 together with the oscillator strength determined by Eq. 20. Then, the experimental data (ΔE_{CT_1}=8700 cm^{-1}, f=0.75, and R_{12}=3.65 Å) give U=6500 cm^{-1}, t=2200 cm^{-1}, and J_1=2200 cm^{-1} as the spectroscopic values. Accordingly, the crystal of the complex has the semiconductive property as the dielectric function can be well expressed by the Lorentz equation without the Drude equation.

The temperature dependence of the magnetic susceptibility of the powder of the complex were measured over a temperature range of 2—300 K as is shown in Fig. 4. The best fit of Eq. 17 to the observed one is obtained and the calculated susceptibility is depicted in Fig. 4. The obtained parameters are J_1>1000 cm^{-1}, J_2=95 cm^{-1}, g_2=2.65, Θ=0, g_3=0.89.

$(DBTTF)_2$-(Cu_2Br_6) Complex. The crystal of the $(DBTTF)_2$-(Cu_2Br_6) complex crystallizes in the form of the dark reddish plates (0.13×0.05×0.20 mm) and

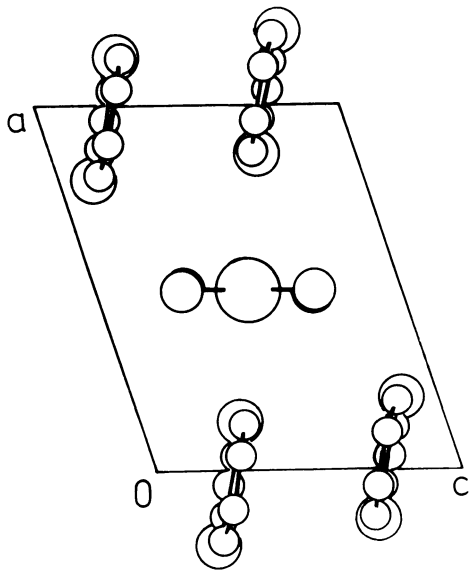

Fig. 2. The projection of the $(DBTTF)_2(Cu_2Cl_6)$ crystal onto the ac plane.

Table 1. Dielectric Parameters of the Lorentz Fits of Reflectivity Data for $(DBTTF)_2(Cu_2Cl_6)$

	// c spectrum	⊥ c spectrum	
ε_{core}	2.83	3.17	
Ω_j/cm^{-1}	13520	4000	90000
ω_j/cm^{-1}	8660	19000	30000
γ_j/cm^{-1}	2900	2500	2500
f	0.75	0.15	

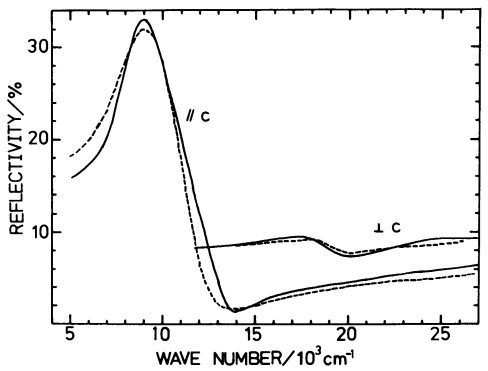

Fig. 3. The observed and calculated reflection spectra of the $(DBTTF)_2(Cu_2Cl_6)$ crystal. (——: Obsd, ----: Calcd)

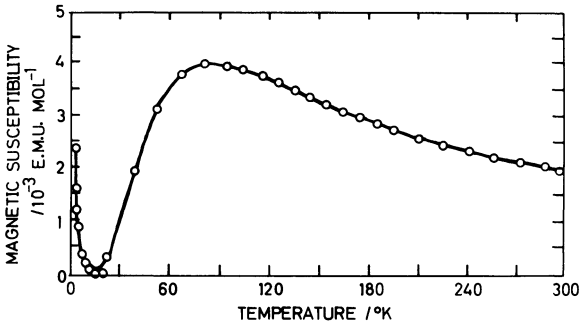

Fig. 4. The temperature dependence of the magnetic susceptibility of the powder of the complex $(DBTTF)_2$-(Cu_2Cl_6). (○○○○: Obsd, ——: Calcd)

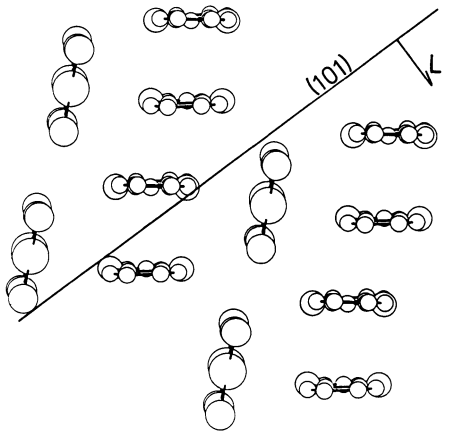

Fig. 5. The stacking of DBTTF molecules in the $(DBTTF)_2(Cu_2Br_6)$ crystal.

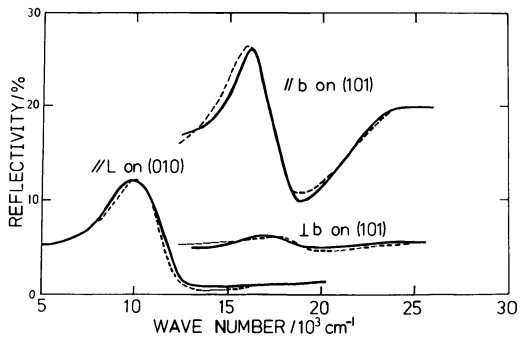

Fig. 6. The observed and calculated reflection spectra of the complex $(DBTTF)_2(Cu_2Br_6)$. (——: Obsd, ——: Calcd)

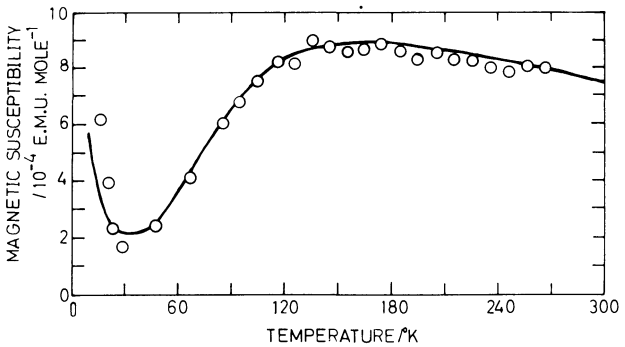

Fig. 7. The temperature dependence of the magnetic susceptibility of the powder of the complex $(DBTTF)_2(Cu_2Br_6)$. (oooo: Obsd, ——: Calcd)

has the natural developed planes of (010) and (101). The space group is triclinic, $P\bar{1}$ and the unit cell are dimensions a=9.982, b=12.122, c=7.893 Å, α=83.70, β=112.80, and γ=104.97°.[5,7] The stacking of DBTTF molecules is illustrated in Fig. 5. The stacking column of the $DBTTF^+$ cations elongates along the c axis with an interplanar distance of about 3.5 Å and two DBTTF molecules form the dimer system in the unit cell.

Table 2. Dielectric Parameters of the Lorentz Fits of Reflectivity Data for $(DBTTF)_2(Cu_2Br_6)$

	// L on (010)	// b on (101)		⊥ b on (101)	
ε_{core}	1.702	2.203		2.200	
Ω_j/cm^{-1}	7600	14600	23300	4600	14000
ω_j/cm^{-1}	9900	16000	23700	18500	30000
γ_j/cm^{-1}	2550	2500	6600	2800	9000
f	0.27	1.0		0.1	

The reflection spectra were observed for the polarization parallel and perpendicular to the b axis on the developed plane (101) and parallel to the L direction on the (010) plane as is shown in Fig. 6. The 10000 cm^{-1} band in the L axis spectrum can be assigned to the CT_1 band[11] and the 16000 and 18000 cm^{-1} bands in the spectra on the (101) plane to the LE bands of $DBTTF^+$ cation radical.[10] The best fit of Eq. 20 to the observed reflectivity is obtained and the calculated reflection spectra are depicted in Fig. 6 in order to compare with the observed ones. The obtained parameters (Ω_j, ω_j, γ_j, and ε_{core}) are shown in Table 2 together with the oscillator strength determined by Eq. 20. Then, the observed oscillator strength f_{obsd} on the (010) plane equals to the next equation,

$$f_{obsd} = f\cos^2\varphi. \tag{21}$$

Here f is given by Eq. 14 and φ=52° is the angle between the L direction shown in Fig. 5 and the stacking axis (c axis) of DBTTF molecule. The experimental data (ΔE_{CT_1}=9900 cm^{-1}, f_{obsd}=0.27, and R_{12}=3.5 Å) give U=7700 cm^{-1}, t=2300 cm^{-1}, and J_1=2150 cm^{-1} as the spectroscopic values. Accordingly, the crystal of the complex has the semiconductive property like $(DBTTF)_2$-(Cu_2Cl_6).

The temperature dependence of the magnetic susceptibility of the powder of the complex were measured over a temperature range of 2—260 K as is shown in Fig. 7. The best fit of Eq. 17 to the observed one is obtained and the calculated susceptibility is depicted in Fig. 7. The obtained parameters are J_1>1000 cm^{-1}, J_2=150 cm^{-1}, g_2=1.88, Θ=−83 K, g_3=1.23. The negative value for Θ indicates the presence of antiferromagnetic spin interaction between the anion dimers. Our result for J_2 and g_2 values is consistent with the conclusion observed in the majority of copper(II) complexes that the spin-exchange interaction is stronger through bromine ions than through chlorine ions.[9]

References

1) M. L. Khidekel and E. I. Zhilyaeva, *Synthetic Metal*, **4**, 1 (1981).

2) R. P. Shibaeva, L. P. Rozenberg, M. Z. Aldoshina, R. N. Lubovskaya, and M. L. Khidekel, *Zh. Strukt., Khim.*, **20**, 485 (1979).

3) R. P. Shibaeva, L. P. Rozenberg, and R. N. Lubovskaya, *Kristallografiya*, **25**, 507 (1980).

4) M. Honda, C. Katayama, J. Tanaka, and M. Tanaka, *Acta crystallogr., Sect. C.*, **41**, 197 (1985).

5) M. Honda, C. Katayama, J. Tanaka, and M. Tanaka, *Acta Crystallogr., Sect. C.*, **41**, 688 (1985).

6) M. Tanaka, M. Honda, C. Katayama, K. Kamiya, and J. Tanaka, *Chem. Lett.*, **1984**, 1355.

7) M. Tanaka, M. Honda, C. Katayama, H. Fujimoto, and J. Tanaka, *Chem. Lett.*, **1985**, 219.

8) R. D. Willet, and O. L. Liles, Jr., *Inorg. Chem.*, **6**, 1666 (1967).

9) M. Inoue, M. Kishita, and M. Kubo, *Inorg. Chem.*, **6**, 900 (1967).

10) J. Tanaka, M. Tanaka, T. Kawai, T. Takabe, and O. Maki, *Bull. Chem. Soc. Jpn.*, **49**, 2358 (1976).

11) C. Tanaka, J. Tanaka, K. Dietz, C. Katayama, and M. Tanaka, *Bull. Chem. Soc. Jpn.*, **56**, 405 (1983).

On the Mechanism of Transfer of Sodium Ion across the Nitrobenzene/Water Interface Facilitated by Dibenzo-18-crown-6

Tadaaki KAKUTANI, Yoshinori NISHIWAKI,† Toshiyuki OSAKAI,† and Mitsugi SENDA*,†
Research Center for Cell and Tissue Culture, Faculty of Agriculture, Kyoto University, Kyoto 606
†Department of Agricultural Chemistry, Faculty of Agriculture, Kyoto University, Kyoto 606
(Received November 1, 1985)

The question of the site of ionophore–ion complex formation, whether it is in the organic phase (EC), in the aqueous phase (CE), or at the interface (E), in the transfer facilitated by dibenzo-18-crown-6 of sodium ion across the nitrobenzene/water interface was studied by kinetic analysis of the ion transfer using a.c. polarographic method. The results indicate that the interface reaction mechanism (E) is the most probable of the three.

The transfer of alkali metal and alkaline earth metal ions across the organic solvent or oil(O)/water(W) interface facilitated by the presence of natural or synthetic ionophores, such as valinomycin, nonactin, and crown ethers in the organic phase, has been intensively studied by Koryta[1] and his group,[2–9] Wang and Pang[10] and Yoshida and Freiser[11] using various electrochemical techniques. Despite the great effort devoted to elucidate the mechanism of the ionophore-mediated ion transport, the central question about the site of the complex formation and its dissociation, whether it is in the organic phase (EC mechanism), in the aqueous phase (CE mechanism) or at the interface (E mechanism), has not been settled yet. Koryta et al.[6] came to the conclusion that the valinomycin-facilitated transfer of potassium ion across the nitrobenzene/water interface takes place via two mechanisms, the EC and E mechanisms in parallel. Experimental results suggesting the interface reaction mechanism (E mechanism) have also been presented.[12] By contrast, Yoshida and Freiser[11] have presented experimental evidence which they interpret as meaning that potassium ion reacts in the aqueous phase with valinomycin that has transferred from the nitrobenzene phase (that is, CE mechanism). Quite recently, Lin and Freiser[24] have presented further experimental results suggesting that the mechanism of the potassium ion transfer facilitated by dibenzo-18-crown-6 across the 1,2-dichloroethane/water interface may depend on the concentration of potassium ion in the aqueous phase. The facilitated transfer of the alkali metal ions at the O/W interface is a very rapid process and is diffusion-controlled when observed using electrochemical methods such as cyclic voltammetry,[1–9,12] chronopotentiometry,[10] and current-scan polarography with an electrolyte dropping electrode.[11] In our opinion, the answer about the mechanism can be obtained only by kinetic study of the formation and dissociation of the ion-ionophore complex at and near the interface.

In previous papers,[13,14] we have shown that the a.c. polarographic method is useful in studying the kinetics and mechanism of ion transfer across the O/W interface. In this study[15] we have applied the a.c. polarographic method to study the facilitated transfer of sodium ion across the nitrobenzene/water interface in the presence of dibenzo-18-crown-6 (DB18C6) in the nitrobenzene phase and attempted to elucidate its mechanism on the basis of the analysis of kinetic parameters obtained by this method.

Experimental

Chemicals. Tetrapentylammonium chloride (TPACl) and tetramethylammonium chloride (TMACl) were obtained commercially. Triply distilled water was used to prepare the aqueous electrolyte solution. An aqueous solution of TPACl was stirred with silver chloride overnight and the filtrate was used. The concentrations of TPACl and TMACl were determined by potentiometric titration with a standard silver nitrate solution. Tetrapentylammonium tetraphenylborate (TPATPB) was prepared by the equimolar addition of an ethanol solution of tetrapentylammonium iodide to an ethanol solution of sodium tetraphenylborate. The resulting precipitate was repeatedly washed with twice-distilled water and recrystallized several times from an ethanol–acetone (3:2) mixture. Commercial DB18C6 was twice recrystallized from benzene and was dried at 80 °C under reduced pressure. Analytical-grade nitrobenzene was purified by a method previously described.[13] The nitrobenzene solution of TPATPB was prepared in the dark just before use. The other chemicals of commercial analytical grade were used as received.

Electrochemical Measurements. The electrolytic cell used here was essentially the same as that described elsewhere.[13] A flat test interface with an area of 0.241 cm^2 was formed at the end of a glass tube, which was treated in advance with dimethyldichlorosilane as described before.[16] The test interface was renewed for each measurement of a single voltammogram or a single chronoamperometric current-time curve.

The electrochemical cell was:

$$\begin{array}{l} \qquad\qquad\qquad\

application of the potential step E and being corrected for the base current. The plot of the current, $I_{t=10\,s}$, against E gave well-defined current-potential curves, as shown in Fig. 3. The limiting current, $(I_{t=10\,s})_l$, was proportional to $^*C_L^o$. A plot of E against $\log\{(I_{t=10\,s})/[(I_{t=10\,s})_l-(I_{t=10\,s})]\}$ yielded a straight line with the slope of 58±2 mV over the $^*C_L^o$ range studied. The half-wave potential, $E_{1/2}$, coincided with the E_m of the corresponding cyclic voltammogram.

A.c. Polarography. In Fig. 4, curves a and a′ show the real (Y_t') and imaginary (Y_t'') components of the admittance plotted against the linear sweep voltage, that is, the applied d.c. potential, $E_{d.c.}$, for the transfer of Na^+ ion across the interface between a 0.1 mol dm^{-3} NaCl aqueous solution and a 0.1 mol dm^{-3} TPATPB nitrobenzene solution containing 0.5×10^{-3} mol dm^{-3} DB18C6. After correction for the base admittance (curves b and b′), these admittances give the real (Y_F') and imaginary (Y_F'') components of the facilitated transfer of Na^+ ion at the nitrobenzene/water interface. The summit potentials of the Y_F' vs. $E_{d.c.}$ and Y_F'' vs. $E_{d.c.}$ curves agreed well within experimental error with each other and with the midpoint potential of the corresponding cyclic voltammogram (Fig. 1). The ion-transfer admittance can be expressed by a series combination of an equivalent resistance, r_s, and an equivalent capacitance, c_s.[13] Figure 5 shows the plots of r_s and $1/\omega c_s$ at $E_{d.c.}=E_{1/2}=0.275$ V against $\omega^{-1/2}$ ($\omega=2\pi f$, f being the a.c. frequency) of the ion transfer across the same interface as that in curves a and a′ in Fig. 4. Both plots gave straight lines with a common slope. Similar linear plots of r_s and $1/\omega c_s$, each set with a common slope, σ, were obtained at several other d.c.

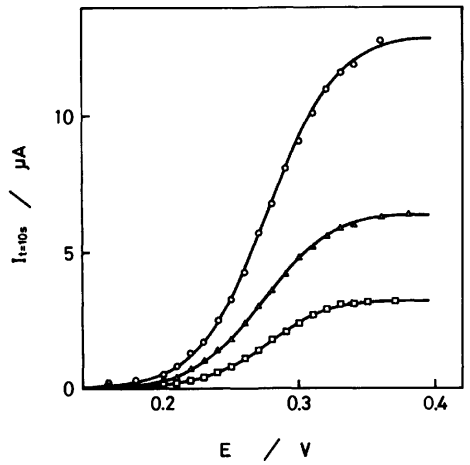

Fig. 3. Plot of $I_{t=10\,s}$, corrected for the base current, against E for the Na^+-ion transfer across the interface between a 0.1 mol dm^{-3} NaCl aqueous solution and a 0.1 mol dm^{-3} TPATPB nitrobenzene solution containing 0.5×10^{-3} (□), 1.0×10^{-3} (△), and 2.0×10^{-3} (○) mol dm^{-3} DB18C6.

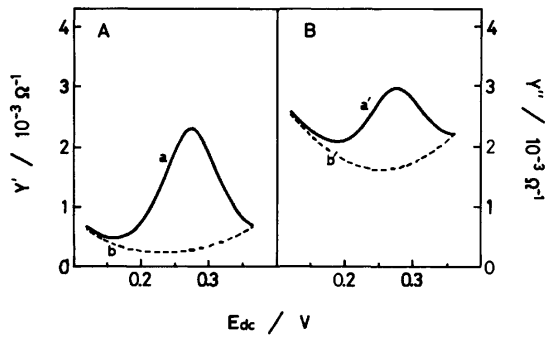

Fig. 4. Real (A) and imaginary (B) components of the admittance of the interface between a 0.1 mol dm^{-3} NaCl aqueous solution and a 0.1 mol dm^{-3} TPATPB nitrobenzene sotution, at $f=50$ Hz, in the presence (a and a′) and the absence (b and b′) of 0.5×10^{-3} mol dm^{-3} DB18C6 in the nitrobenzene phase.

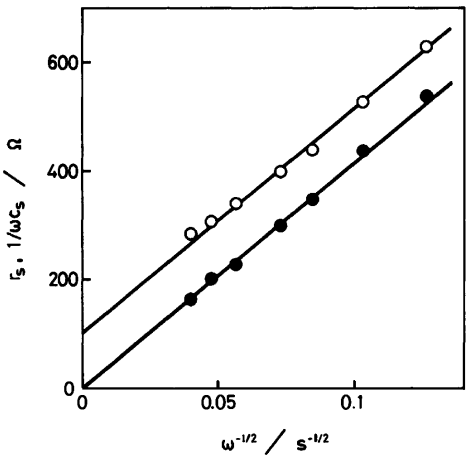

Fig. 5. Plots of the real (○) and imaginary (●) components of the ion transfer impedance at $E_{d.c.}=E_{1/2}^r=0.275$ V against $\omega^{-1/2}$, for the Na^+-ion transfer across the interface between a 0.1 mol dm^{-3} NaCl aqueous solution and a 0.1 mol dm^{-3} TPATPB nitrobenzene solution containing 0.5×10^{-3} mol dm^{-3} DB18C6.

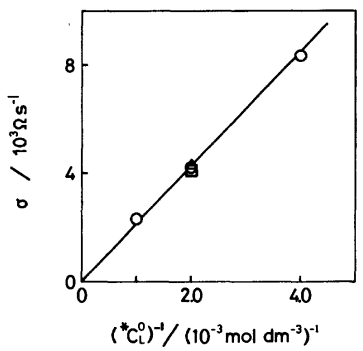

Fig. 6. Plot of σ at $E_{d.c.}=E_{1/2}^r$ against $(^*C_L^o)^{-1}$. $^*C_M^w$: (△) 0.05, (○) 0.1, and (□) 0.2 mol dm^{-3}.

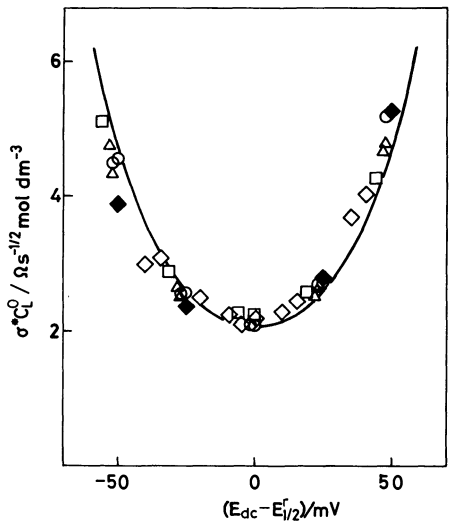

Fig. 7. Plot of $\sigma^*C_L^o$ against $(E_{d.c.}-E_{1/2}^r)$.
(○): $^*C_L^o=0.25\times10^{-3}$ and $^*C_M^w=0.1$ mol dm^{-3}, (△): $^*C_L^o=0.5\times10^{-3}$ mol dm^{-3} and $^*C_M^w=0.1$ mol dm^{-3}, (□): $^*C_L^o=1\times10^{-3}$ mol dm^{-3}, and $^*C_M^w=0.1$ mol dm^{-3}, (◇): $^*C_L^o=0.5\times10^{-3}$ mol dm^{-3} and $^*C_M^w=0.05$ mol dm^{-3}, (◆): $^*C_L^o=0.5\times10^{-3}$ mol dm^{-3} and $^*C_M^w=0.2$ mol dm^{-3}.
The solid line is the theoretical one drawn by Eq. 22 with $D_L^o=2.3\times10^{-6}$ cm^2 s^{-1}.

potentials in the range of $|E_{d.c.}-E_{1/2}|\leq0.05$ V for the interface between an aqueous solution of 0.05—0.2 mol dm^{-3} NaCl and a nitrobenzene solution of 2.5×10^{-4}—1×10^{-3} mol dm^{-3} DB18C6 containing 0.1 mol dm^{-3} TPATPB. Figure 6 shows a plot of σ obtained at $E_{d.c.}=E_{1/2}$ against $1/^*C_L^o$, indicating that σ was inversely proportional to $^*C_L^o$ but independent of $^*C_M^w$. The same dependence of σ on $^*C_L^o$ was observed at other $E_{d.c.}$'s at $|E_{d.c.}-E_{1/2}|\leq0.05$ V. Also, the σ values changed with $E_{d.c.}-E_{1/2}$ for a given set of $^*C_L^o$ and $^*C_M^w$ (see Fig. 7 below).

Discussion

When in the organic phase there is a lipophilic ligand, L, (usually belonging to the family of ionophores) that forms a lipophilic complex ML_n (n=1,2,...) with the transferring ion M^z (z=the number of charges), the transfer of M^z ion from the aqueous to the organic phase is facilitated; that is, it takes place at a less positive (if $z>0$) or at a less negative (if $z<0$) potential of the aqueous phase referred to that of the organic phase.[12] From a kinetic viewpoint, three kinds of the mechanisms of facilitated ion transfer may be postulated. In the following, we assume that the lipophilic ligand L is a neutral carrier.

(1) EC Mechanism. The ion M^z is transferred from the W to the O phase (Eq. 1a), followed by the formation of a complex ML_n with the ligand L (Eq. 1b) in the O phase:

$$M^z(W) \underset{\vec{k}_M(E)}{\overset{\vec{k}_M(E)}{\rightleftharpoons}} M^z(O), \tag{1a}$$

$$M^z(O) + nL(O) \underset{k_1^b}{\overset{k_1^f}{\rightleftharpoons}} ML_n^z(O) \quad K^o = k_1^f/k_1^b. \tag{1b}$$

(2) CE Mechanism. The ligand L is first transferred from the O to the W phase (Eq. 2a) and forms the complex ML_n with the ion M^z in the W phase (Eq. 2b); this is followed by the transfer of the complex from the W to the O phase (Eq. 2c):

$$L(O) \underset{k_L^b}{\overset{k_L^f}{\rightleftharpoons}} L(W) \qquad d_L = k_L^b/k_L^f, \tag{2a}$$

$$M^z(W) + nL(W) \underset{k_2^b}{\overset{k_2^f}{\rightleftharpoons}} ML_n^z(W) \quad K^w = k_2^f/k_2^b, \tag{2b}$$

$$ML_n^z(W) \underset{\vec{k}_{ML}(E)}{\overset{\vec{k}_{ML}(E)}{\rightleftharpoons}} ML_n^z(O). \tag{2c}$$

(3) E Mechanism. The complex ML_n is formed in a single step taking place at the O/W interface:

$$M^z(W) + nL(O) \underset{\vec{k}_{M/ML}(E)}{\overset{\vec{k}_{M/ML}(E)}{\rightleftharpoons}} ML_n^z(O). \tag{3}$$

Differential equations to express the diffusion coupled with complex formation of M, L, and ML_n in both organic and aqueous phases can easily be written and were solved, under appropriate conditions and assumptions, to give the theoretical equations of the polarographic (normal pulse polarographic) current-potential curves and also of the a.c. impedance of the ion transfer for each of these three mechanisms. Detailed results will be published elsewhere. Here only those important results relevant to discussion of the mechanism will be given.

Let us first assume (1) that the bulk concentration of M^z ion in the aqueous phase, $^*C_M^w$, is exceedingly large compared with that of L in the organic phase, $^*C_M^w \gg {}^*C_L^o$ (see Results), (2) that the partition coefficient of the carrier between the organic and aqueous phases, $d_L=C_L^o/C_L^w$, is so large ($d_L \gg 1$) that the presence of L in the bulk of the aqueous phase can be neglected, and (3) that the complex formation in the organic phase is largely shifted to the complex side ($K^oC_M^o \gg 1$) so that the presence of M^z ion in the organic phase can virtually be neglected. Then the reversible (*Nernstian*) normal pulse polarographic wave (I–E curve) of facilitated ion transfer can be expressed for the three mechanisms by the same equation:

$$E = E_M^\ddagger - (RT/zF)\ln K^o - (RT/zF)\ln {}^*C_M^w + (RT/zF)\ln[(\kappa_L^o)^n/\kappa_{ML}^o] + (RT/zF)\ln[I/(I_1-I)^n], \tag{4}$$

with

$$\kappa_L^\circ = (D_L^\circ/n^2\pi t)^{1/2} \quad \text{and} \quad \kappa_{ML}^\circ = (D_{ML}^\circ/\pi t)^{1/2} \tag{5}$$

where $E_M^\ominus$ is the standard ion transfer potential of Eq. 1a with respect to the reference electrode system (see Eq. 11 below) of Cell I and is related to the standard ion-transfer potentials of Eqs. 2c and 3, $E_{ML}^\ominus$ and $E_{M/ML}^\ominus$, respectively, both with respect to the same reference electrode system as above, by

$$E_M^\ominus - (RT/zF)\ln K^\circ = E_{ML}^\ominus - (RT/zF)\ln K^w + (RT/zF)\ln (d_L)^n \tag{6}$$

$$= E_{M/ML}^\ominus. \tag{7}$$

In these equations K° ($=k_1^f/k_1^b$) and K^w ($=k_2^f/k_2^b$) are the formation constants of Eqs. 1b and 2b, D_L° and D_{ML}° are the diffusion coefficients of L and ML_n in the organic phase, respectively, t is time measured from the voltage pulse rise, and I_l is the limiting diffusion current given by

$$I_l = zFA^*C_L^\circ(D_L^\circ/n^2\pi t)^{1/2}, \tag{8}$$

where A is the electrode surface area, and F, R, and T are used in their usual meanings.

Experimental results by cyclic voltammetry and potential-step chronoamperometry (normal pulse polarography) all indicate that the Na^+ ion transfer facilitated by DB18C6 at the nitrobenzene/water interface is d.c. reversible (*Nernstian*). That E_m and $E_{1/2}$ coincide with each other and are independent of $^*C_L^\circ$, and also that the log $[I/(I_l-I)]$ vs. E plot is linear with the reciprocal slope of 58±2 mV both indicate that n=1, that is, that there is formation of a 1:1 complex. Then Eq. 4 can be rewritten as Eq. 9 with the reversible half-wave potential $E_{1/2}^r$ defined by Eq. 10:

$$E = E_{1/2}^r + (RT/zF)\ln [I/(I_l-I)], \tag{9}$$

$$E_{1/2}^r = E_M^\ominus + (RT/2zF)\ln (D_L^\circ/D_{ML}^\circ) - (RT/zF)\ln K^\circ - (RT/zF)\ln {}^*C_M^w. \tag{10}$$

The observed dependence of $E_{1/2}(=E_m)$ on log $^*C_M^w$ (Fig. 2) was explained well by Eq. 10.

The potential E is usually expressed by

$$E = \Delta\phi + \Delta E_{ref}, \tag{11}$$

where $\Delta\phi$ is the potential difference between phases II and III in Cell I and ΔE_{ref} is the constant determined by the reference electrode system in Cell I, that is, RE1 and RE2 (see Experimental). In Cell I with 0.1 mol dm^{-3} TPATPB (NB, phase II)/0.1 mol dm^{-3} NaCl (W, phase III), ΔE_{ref} was determined to be 0.275 V from the reversible half-wave potential of tetramethylammonium (TMA^+) ion measured with the same reference electrode system as that used here and $\Delta\phi_{TMA}^\ominus$=0.035 V.[17] Then, $E_M^\ominus = E_{Na}^\ominus$ ($=\Delta\phi_{Na}^\ominus + \Delta E_{ref}$) was calculated to be 0.629 V using $\Delta\phi_{Na}^\ominus$=0.354 V.[17] Finally log K° was calculated to be 7.0 by Eq. 10 by assuming $D_L^\circ = D_{ML}^\circ$. Also, using the values from the literatures of d_L=2.3×10^4 [18] and K^w=14.6 mol^{-1} dm^3,[19] $E_{ML}^\ominus$ ($=\Delta\phi_{ML}^\ominus + \Delta E_{ref}$) was calculated by Eq. 6 (with n=1) to be 0.028 V, which gives $\Delta\phi_{ML}^\ominus$=−0.248 V. Similarly, $E_{M/ML}^\ominus$ was calculated by Eq. 7 to be 0.216 V, which gives $\Delta\phi_{M/ML}^\ominus$=−0.059 V.

In addition to the above assumptions (1)—(3), we further assume that the facilitated ion transfer processes are d.c. reversible. Then r_s and $1/\omega c_s$ of the facilitated ion transfer by 1:1 complex formation can be written[20] for each of the above three mechanisms, while assuming that $D_L^\circ = D_{ML}^\circ$, as follows.

(1) EC Mechanism:

$$r_s = \frac{RT}{z^2F^2A}\left[\frac{1}{\vec{k}_M(E_{d.c.})^*C_M^w} + \frac{K^\circ}{\rho_c}\cdot\left(\frac{1+\rho_c}{k_1^f D_L^\circ {}^*C_L^\circ}\right)^{1/2}\right] + \frac{RT}{z^2F^2A}\cdot\frac{1}{{}^*C_L^\circ\sqrt{2\omega D_L^\circ}}\cdot\frac{(1+\rho_c)^2}{\rho_c}, \tag{12}$$

$$1/\omega c_s = \frac{RT}{z^2F^2A}\cdot\frac{1}{{}^*C_L^\circ\sqrt{2\omega D_L^\circ}}\cdot\frac{(1+\rho_c)^2}{\rho_c}, \tag{13}$$

and

$$r_k \equiv (r_s - 1/\omega c_s) = \frac{RT}{z^2F^2A}\left[\frac{1}{\vec{k}_M(E_{d.c.})^*C_M^w} + \frac{K^\circ}{\rho_c}\left(\frac{1+\rho_c}{k_1^f D_L^\circ {}^*C_L^\circ}\right)^{1/2}\right] \tag{14}$$

with

$$\rho_c = \exp[zF(E_{d.c.} - E_{1/2}^r)/RT] \tag{15}$$

Here it is also assumed that the equilibrium and rate constants of the complex formation reaction in the organic plhase, K° and k_1^f, are so large that the conditions $K^\circ {}^*C_L^\circ \gg (\rho_c+1)^2$ and

$$\frac{k_1^f}{\omega}\left[\frac{K^\circ {}^*C_L^\circ + (1+\rho_c)^2}{K^\circ(1+\rho_c)}\right] \gg \left[\frac{K^\circ {}^*C_L^\circ}{\sqrt{2}(1+\rho_c)^2}\right]^{2/3}$$

are simultaneously satisfied.

(2) CE Mechanism:

$$r_s = \frac{RT}{z^2F^2A}\cdot\frac{(1+\rho_c)d_L}{K^w {}^*C_M^w {}^*C_L^\circ} \times\left[\frac{1}{\vec{k}_{ML}(E_{d.c.})} + \left(\frac{K^w(K^w {}^*C_M^w + 1)}{k_2^f D^w}\right)^{1/2}\right] + \frac{RT}{z^2F^2A}\cdot\frac{1}{{}^*C_L^\circ\sqrt{2\omega D_L^\circ}}\cdot\frac{(1+\rho_c)^2}{\rho_c} \tag{16}$$

$$1/\omega c_s = \frac{RT}{z^2F^2A}\cdot\frac{1}{{}^*C_L^\circ\sqrt{2\omega D_L^\circ}}\cdot\frac{(1+\rho_c)^2}{\rho_c} \tag{17}$$

and

$$r_k \equiv (r_s - 1/\omega c_s) = \frac{RT}{z^2F^2A}\cdot\frac{(1+\rho_c)d_L}{K^w {}^*C_M^w {}^*C_L^\circ} \times\left[\frac{1}{\vec{k}_{ML}(E_{d.c.})} + \left(\frac{K^w(K^w {}^*C_M^w + 1)}{k_2^f D^w}\right)^{1/2}\right]. \tag{18}$$

In Eqs. 16—18 the following three conditions are also assumed: (a) the rate constant of the transfer of L across the interface is large enough to satisfy $2k_L^f/\sqrt{2\omega D_L^\circ} \gg 1$, (b) the partition coefficient is large enough to satisfy both $d_L \gg (D^w/D_L^\circ)^{1/2}$ and $[(D^w/D_L^\circ)^{1/2}+d_L]/K^w{*}C_M^w \gg 1$ (where D^w is the common diffusion coefficient in the aqueous phase; $D^w=D_M^w=D_L^w=D_{ML}^w$), and (c) the rate constant of the complex formation in the aqueous phase is very large enough to satisfy $\xi=k_2^f(K^w{*}C_M^w+1)/\omega K^w \gg 1$ and $\xi \gg 2(K^w{*}C_M^w)^2$ simultaneously.

(3) E Mechanism:

$$r_s = \frac{RT}{z^2F^2A}\cdot\frac{(1+\rho_c)}{\vec{k}_{M/ML}(E_{d.c.}){*}C_M^w{*}C_L^\circ} + \frac{RT}{z^2F^2A}\cdot\frac{1}{{*}C_L^\circ\sqrt{2\omega D_L^\circ}}\cdot\frac{(1+\rho_c)^2}{\rho_c}, \quad (19)$$

$$1/\omega c_s = \frac{RT}{z^2F^2A}\cdot\frac{1}{{*}C_L^\circ\sqrt{2\omega D_L^\circ}}\cdot\frac{(1+\rho_c)^2}{\rho_c}, \quad (20)$$

and

$$r_k \equiv (r_s - 1/\omega c_s) = \frac{RT}{z^2F^2A}\cdot\frac{(1+\rho_c)}{\vec{k}_{M/ML}(E_{d.c.}){*}C_M^w{*}C_L^\circ}. \quad (21)$$

These theoretical equations predict that in either of the three mechanisms, the plot of r_s and $1/\omega c_s$ against $\omega^{-1/2}$ should yield straight lines with a common slope, σ, which is defined by

$$\sigma = \frac{RT}{z^2F^2A}\cdot\frac{1}{{*}C_L^\circ\sqrt{2D_L^\circ}}\cdot\frac{(1+\rho_c)^2}{\rho_c}. \quad (22)$$

The σ value should be inversely proportional to ${*}C_L^\circ$ but be independent of ${*}C_M^w$. These predictions agreed with the experimental results shown in Figs. 5 and 6. Figure 7 shows the plot of $\sigma{*}C_L^\circ$ against $E_{d.c.}$. The solid line in this figure is the theoretical line calculated by Eq. 22 using $D_L^\circ=2.3\times10^{-6}$ cm^2 s^{-1}. Thus the experimental dependence of r_s and $1/\omega c_s$ on $\omega^{-1/2}$ can be explained equally well by any of the mechanisms EC, CE, or E. On the other hand, the theoretical Eqs. 14, 18, and 21 predict that in the EC mechanism r_k ($\equiv(r_s-1/\omega c_s)$) should vary linearly with $({*}C_L^\circ)^{-1/2}$ (Eq. 14), whereas in the CE and E mechanisms r_k should be inversely proportional to ${*}C_L^\circ$ (Eqs. 18 and 21). In Figs. 8 and 9 r_k obtained at $E_{d.c.}=E_{1/2}^r$ for the case of ${*}C_M^w=0.1$ mol dm^{-3} is plotted against $({*}C_L^\circ)^{-1/2}$ or $({*}C_L^\circ)^{-1}$, respectively. The plot of r_k against $({*}C_L^\circ)^{-1/2}$ (Fig. 8) appears to be linear in the concentration range studied, but the intercept of the straight line at $({*}C_L^\circ)^{-1/2}=0$ was negative. This is inconsistent with the theoretical equation 14 (EC mechanism), which predicts a positive (or zero) intercept. Also, Eq. 14 predicts that the following inequality should hold in the EC mechanism:

$$(r_s - 1/\omega c_s) > \frac{RT}{z^2F^2A}\cdot\frac{K^\circ}{\rho_c}\left(\frac{1+\rho_c}{k_1^f D_L^\circ {*}C_L^\circ}\right)^{1/2}. \quad (23)$$

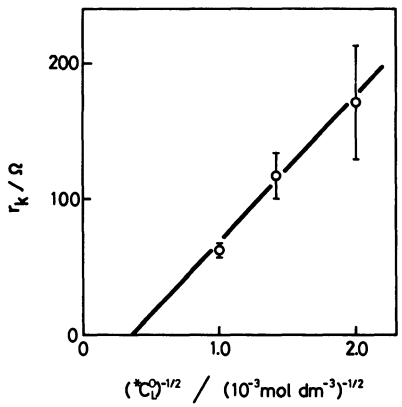

Fig. 8. Plot of $r_k(\equiv(r_s-1/\omega c))$ at $E_{d.c.}=E_{1/2}^r$ and ${*}C_M^w=0.1$ mol dm^{-3} against $({*}C_L^\circ)^{-1/2}$. The vertical bars indicate the standard deviations.

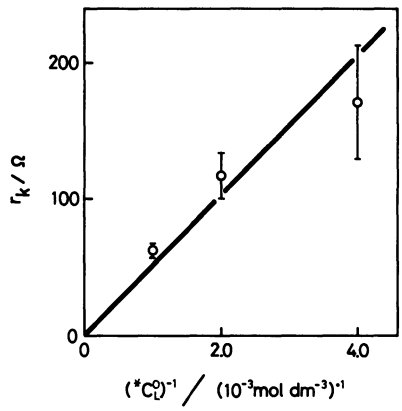

Fig. 9. Plot of $r_k(\equiv(r_s-1/\omega c_s))$ at $E_{d.c.}=E_{1/2}^r$ and ${*}C_M^w=0.1$ mol dm^{-3} against $({*}C_L^\circ)^{-1}$. The vertical bars indicate the standard deviations.

Application of this inequality to the result given in Fig. 5 with $K^\circ=9.8\times10^6$ mol^{-1} dm^3 and $D_L^\circ=2.3\times10^{-6}$ cm^2 s^{-1}, as determined in this paper, yielded the lowest limit of k_1^f to satisfy Eq. 14 as $k_1^f>1.5\times10^{13}$ mol^{-1} dm^3 s^{-1}. This value seems unreasonably high for a bimolecular reaction in solution. According to Debye,[21] the rate constant for a diffusion-controlled bimolecular reaction, k_D, is given by

$$k_D = 4\pi N_L(D_A+D_B)r_D, \quad (24)$$

where N_L is the Avogadro constant, D_A and D_B are the diffusion coefficients of the reactants A and B, and r_D is the reaction distance. Using $r_D=1.5\times10^{-7}$ cm and $(D_A+D_B)=10^{-5}$ cm^2 s^{-1}, we obtain $k_D=1.1\times10^{10}$ mol^{-1} dm^3 s^{-1}. These results indicate that the EC mechanism should be excluded from the present system. The plot shown in Fig. 9 indicates that r_k is inversely proportional to ${*}C_L^\circ$, suggesting that both the CE mechanism (Eq. 18) and the E mechanism (Eq. 21) are applicable to the present system. For the CE mechanism, the following inequality is predicted from Eq. 18:

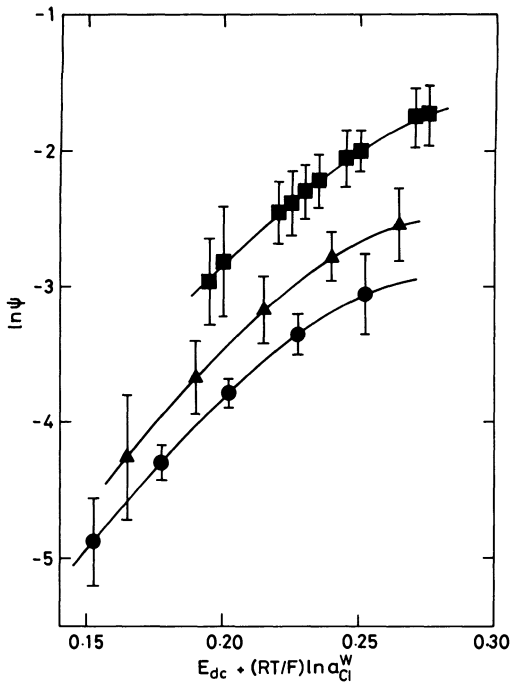

Fig. 10. Plot of $\ln\psi$ against $E_{d.c.}+(RT/F)\ln a^{W}_{Cl}$. $*C^{W}_{M}$: (■) 0.05; (▲) 0.1; (●) 0.2 mol dm^{-3}. The vertical bars indicate the standard deviations.

$$(r_s - 1/\omega c_s) > \frac{RT}{z^2F^2A}\cdot\frac{(1+\rho_c)d_L}{K^{W}*C^{W}_{M}*C^{\circ}_{L}}\left[\frac{K^{W}(K^{W}*C^{W}+1)}{k^{f}_{2}D^{W}}\right]^{1/2}. \quad (25)$$

Application of this inequality to the results shown in Fig. 5 with K^{w}=14.6 mol^{-1} dm^3,[19] d_L=2.3×10^4,[18] and D^{w}=10^{-5} cm^2 s^{-1} leads to the lowest limit of k^{f}_{2} to satisfy Eq. 18 as k^{f}_{2}>2.7×10^{12} mol^{-1} dm^3 s^{-1}. When another value of d_L=2×10^3, which is calculated from the solubility data of DB18C6 in water[22] and nitrobenzene,[23] is used, we obtain k^{f}_{2}>2×10^{10} mol^{-1} dm^3 s^{-1}. Either value suggests a very low probability of the CE mechanism, which leads us to the conclusion that the E mechanism is the most probable mechanism for the present system.

In Fig. 10 the logarithm of ψ defined by

$$\psi = \frac{RT}{z^2F^2A}\cdot\frac{(1+\rho_c)}{*C^{W}_{M}*C^{\circ}_{L}}\cdot\frac{1}{(r_s - 1/\omega C_s)} \quad (26)$$

is plotted against the corrected d.c. potential, $(E_{d.c.})_{corr}=E_{d.c.}+(RT/F)\ln a^{W}_{Cl}$ (see Results). In the E mechanism, ψ can be given from Eq. 21 by

$$\psi = \vec{k}_{M/ML}(E_{d.c.}). \quad (27)$$

Figure 10 shows that the rate constant of the interface reaction of the E mechanism (Eq. 3) $\vec{k}_{M/ML}(E_{d.c.})$ depends on the potential difference across the nitrobenzene/water interface, $\Delta\phi$, and that $\vec{k}_{M/ML}(E_{d.c.})$ increases with increasing positive $\Delta\phi$. This seems quite reasonable. Figure 10 also shows that the rate constant at a given potential difference increases with decreasing NaCl concentration in the aqueous phase. This result indicates that the rate constant of the interface reaction is highly dependent on the structure of the electric double layer at the interface.[13,14]

Equation 18 implies that, if the CE mechanism would be applicable to the present system, the dependence of the ψ values on the NaCl concentration ($*C^{W}_{M}$) could in part be explained by the second term in the square brackets on the right-hand side of Eq. 18. On the other hand, the dependence of ψ on $\Delta\phi$ in Fig. 10 implies that the first term in the square brackets is not negligible, which in turn implies that the value of the bimolecular-reaction rate constant k^{f}_{2} should be larger than a theoretically possible value of a bimolecular reaction in solution, as discussed above.

In conclusion, it can be stated that the a.c. polarographic behavior of the transfer of Na^+ ion facilitated by DB18C6 at the nitrobenzene/water interface is explained most reasonably by the interface reaction mechanism (E mechanism) of the three mechanisms that have been proposed.

References

1) J. Koryta, *Electrochim. Acta*, **24**, 293 (1979).
2) A. Hofmanova, L. Q. Hung, and W. Khalil, *J. Electroanal. Chem. Interfacial Electrochem.*, **135**, 257 (1982).
3) Z. Samec, D. Homolka, and V. Mareček, *J. Electroanal. Chem. Interfacial Electrochem.*, **135**, 265 (1982).
4) D. Homolka, K. Holub, and V. Mareček, *J. Electroanal. Chem. Interfacial Electrochem.*, **138**, 29 (1982).
5) E. Makrlik, L. Q. Hung, and A. Hofmanova, *Electrochim. Acta*, **28**, 847 (1983).
6) P. Vanýsek, W. Ruth, and J. Koryta, *J. Electroanal. Chem. Interfacial Electrochem.*, **148**, 117 (1983).
7) E. Makrlik and L. Q. Hung, *J. Electroanal. Chem. Interfacial Electrochem.*, **158**, 277 (1983).
8) E. Makrlik, *J. Colloid Interface. Sci.*, **97**, 595 (1984).
9) J. Koryta, G. Du, W. Ruth, and P. Vanýsek, *Faraday Discuss. Chem. Soc.*, **77**, 209 (1984).
10) Wang Erkang and Pang Zhicheng, *J. Electroanal. Chem. Interfacial Electrochem.*, **189**, 21 (1985).
11) Z. Yoshida and H. Freiser, *J. Electroanal. Chem. Interfacial Electrochem.*, **179**, 31 (1984).
12) J. Koryta, *Ion-selective Electrode Rev.*, **5**, 146 (1983).
13) T. Osakai, T. Kakutani, and M. Senda, *Bull. Chem. Soc. Jpn.*, **57**, 370 (1984).
14) T. Osakai, T. Kakutani, and M. Senda, *Bull. Chem. Soc. Jpn.*, **58**, 2626 (1985).
15) The main results of the present paper were presented at the 30th Annual Meeting on Polarography and Electroanalytical Chemistry, Oct. 12—13, 1984, Hiroshima; Abstract, T. Kakutani, Y. Nishiwaki, T. Osakai, and M. Senda, *Rev. Polarogr. (Kyoto)*, **30**, 30 (1984).
16) T. Kakutani, T. Osakai, and M. Senda, *Bull. Chem. Soc. Jpn.*, **56**, 991 (1983).

17) J. Rais, *Collect. Czech. Chem. Commun.*, **36**, 3235 (1971).
18) T. Iwachido, M. Minami, A. Sadakane, and K. Toei, *Chem. Lett.*, **1977**, 1511.
19) E. Shchori, N. Nae, and J. Jagur-Grodzinsky, *J. Chem. Soc. Dalton Trans.*, **1975**, 2381.
20) The present authors, in preparation.
21) P. Debye, *Trans. Electrochem. Soc.*, **82**, 265 (1942).
22) C. J. Pedersen, *J. Am. Chem. Soc.*, **89**, 7017 (1967).
23) Y. Marcus and L. E. Asher, *J. Phys. Chem.*, **82**, 1246 (1978).
24) Lin Sinru and H. Freiser, *J. Electroanal. Chem. Interfacial Electrochem.*, **191**, 437 (1985).

 © 1986 The Chemical Society of Japan Bull. Chem. Soc. Jpn., 59, 789—794 (1986)

Solvent Effects on Extraction of Aluminum(III), Gallium(III), and Indium(III) with Decanoic Acid

Hiromichi YAMADA,* Hisao HAYASHI, Yukio FUJII, and Masateru MIZUTA
Faculty of Engineering, Gifu University, 1-1 Yanagido, Gifu 501-11
(Received September 11, 1985)

Extraction of aluminum(III) and indium(III) with decanoic acid in 1-octanol was carried out at 25 °C and at an aqueous ionic strength of 0.1 mol dm^{-3} ($NaClO_4$). Monomeric and tetrameric aluminum(III) decanoates and monomeric indium(III) decanoate are responsible for the extraction. From a comparison of the present results with those obtained from the previous works,[1-4] the polymerization of the extracted species was found to be more extensive in benzene than in 1-octanol, and the metal decanoates were highly polymerized in the following order in both solvents: Al>Ga>In.

In the extraction of metal ions with carboxylic acids, polymerized metal carboxylates are sometimes found as an extracted species. In particular, trivalent aluminum, gallium, and indium are characterized to form up to hexameric decanoate in non-coordinating solvents such as benzene.[1-3] In the previous work which has described the results on the extraction of gallium(III) with decanoic acid in some inert solvents, it was noted that the more polar the solvent, the less polymerized were the extracted decanoates.[4] Subsequently, also in the extraction of copper(II) decanoate, the extracted species has been established to be only the dimeric copper(II) decanoate for the various inert solvents[5] but to be the monomeric and dimeric copper(II) decanoates for some alcohols[6,7] and ketones.[8]

The present paper deals with the extraction of aluminum(III) and indium(III) with decanoic acid in 1-octanol, and by comparison of the present results with those obtained from the previous papers,[1-4] it was found that the degree of polymerization of the metal decanoates decreased in the following order in both benzene and 1-octanol: Al>Ga>In, and the metal decanoates were more extensively polymerized in benzene than in 1-octanol.

Experimental

Reagents. Aluminum(III) perchlorate: Commercial aluminum(III) perchlorate nine hydrates (99.9%) was recrystallized from distilled water.

Indium(III) perchlorate was prepared in the same manner as presented previously.[3]

Sodium perchlorate, decanoic acid, and 1-octanol were purified by the method described previously.[6]

Reagent grade Xylenol Orange was used for the complexiметric titration of aluminum and indium as an indicator and for the spectrophotometric determination of lower concentration of aluminum.

All other reagents were of reagent grade and used without further purification.

Procedure. Partition was carried out in the same manner as was stated in the previous report.[4] Shaking for 17 h was found to be sufficient for complete equilibration in each extraction system. Total concentrations of metals and decanoic acid were 5×10^{-3} and 0.5—2.0 mol dm^{-3}, respectively. Ionic strength in the aqueous phase was adjusted to 0.1 mol dm^{-3} with sodium perchlorate. Hydrogen ion concentration in the aqueous phase was determined by the same method as presented previously.[4]

Apparatus. The apparatus were similar to those previously used.[4]

Results and Discussion

Extraction Equilibrium. When a j-merized metal decanoate of the composition $M_jA_aH_h(3j=a-h)$ is responsible for the extraction of a trivalent metal ion with decanoic acid, the extraction equilibrium is written as:

$$jM^{3+} + a(HA)_o \overset{K_{ex(jah)}}{\rightleftharpoons} (M_jA_aH_h)_o + 3jH^+$$

with $(HA)_o$ denoting the monomeric decanoic acid in the organic phase, and the extraction constant defined as

$$K_{ex(jah)} = \frac{[M_jA_aH_h]_o[H^+]^{3j}}{[M^{3+}]^j[HA]_o^a}, \quad (1)$$

where the subscript o refers to the organic phase and as described previously, the dimerization of decanoic acid does not occur to any appreciable extent in 1-octanol.[6] The total concentration of a metal in the organic phase, $C_{M,o}$ is represented by the following expression:

$$C_{M,o} = \sum_j\sum_a j[M_jA_aH_h]_o = \sum_j\sum_a jK_{ex(jah)}([M^{3+}][H^+]^{-3})^j[HA]_o^a. \quad (2)$$

When only $M_jA_aH_h$ is responsible for the extraction, the following equation is obtained under the conditions where any side reaction of a metal ion is not appreciable in the aqueous phase:

$$\log C_{M,o} = j(\log C_{M,w} - 3\log[H^+]) + a\log[HA]_o + \log j + \log K_{ex(jah)}. \quad (3)$$

According to Eq. 3, the degree of polymerization of the extracted species can be determined from the slope of the plot of log $C_{M,o}$ against (log $C_{M,w}$−3 log[H$^+$]) at constant [HA]$_o$. The results for aluminum(III) and indium(III) are shown in Figs. 1 and 2, respectively. From Fig. 1, it is expected that the monomeric and tetrameric aluminum(III) decanoates are preferentially extracted in 1-octanol. Then the following expression can be derived from Eq. 2:

$$\log C_{Al,o} - (\log C_{Al,w} - 3\log[H^+]) - a\log[HA]_o - \log K_{ex(1a,h)} = \log\left\{1 + \frac{4K_{ex(4a',h')}}{K_{ex(1a,h)}}[HA]_o^{(a'-a)}(C_{Al,w}[H^+]^{-3})^3\right\}, \quad (4)$$

where $K_{ex(1a,h)}$ and $K_{ex(4a',h')}$ denote the extraction constants of the monomeric and tetrameric aluminum(III) decanoates, respectively. It is expected that the plot of {log $C_{Al,o}$−(log $C_{Al,w}$−3 log[H$^+$])} against (log$C_{Al,w}$−3 log[H$^+$]) at constant [HA]$_o$ fits with the normalized curve, log(1+X^3) vs. log X. The results are depicted in Fig. 3. As shown in Fig. 3, it is confirmed that the monomeric and tetrameric species are responsible for the extraction. The plots deviate upward from the normalized curve at the middle region. This suggests that a small amount of the dimeric and/or trimeric species exists together with the main monomeric and tetrameric species.

As evident from Fig. 2, on the other hand, the monomeric indium(III) species is predominantly extracted. With decreasing concentration of decanoic acid in the organic phase and with increasing indium concentration in the organic phase, that is, with decreasing hydrogen ion concentration in the aqueous phase, the plots get to deviate from the straight line with a slope of 1.0. It seems most likely that these "deviations" are resulted from the hydrolysis of

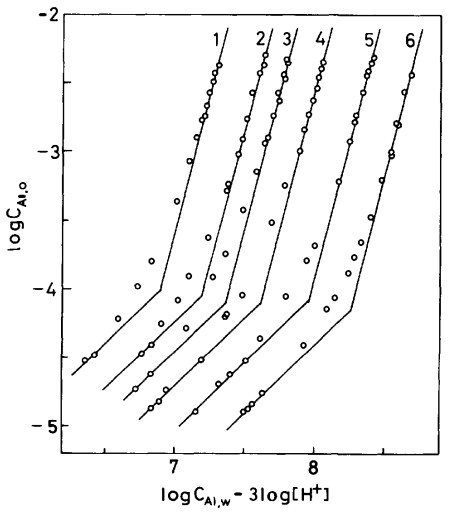

Fig. 1. Determination of the degree of polymerization of aluminum(III) decanoates.
C_{HA}; No. 1: 2.0, No. 2: 1.5, No. 3: 1.25, No. 4: 1.0, No. 5: 0.7, No. 6: 0.5 mol dm^{-3}. Solid lines are the straight lines with slopes of 1.0 and 4.0, respectively.

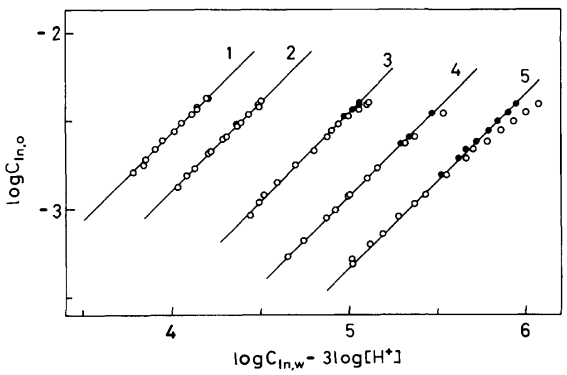

Fig. 2. Determination of the degree of polymerization of indium(III) decanoate.
C_{HA}; No. 1: 2.0, No. 2: 1.5, No. 3: 1.0, No. 4: 0.7, No. 5: 0.5 mol dm^{-3}. Solid lines are the straight lines with a slope of 1.0. Solid points are the corrected ones by considering the hydrolysis of indium(III) ion in the aqueous phase: log $C_{In,o}$, vs. log $C_{In,w}$ − 3 log [H$^+$] − log $\alpha_{In(OH)}$.

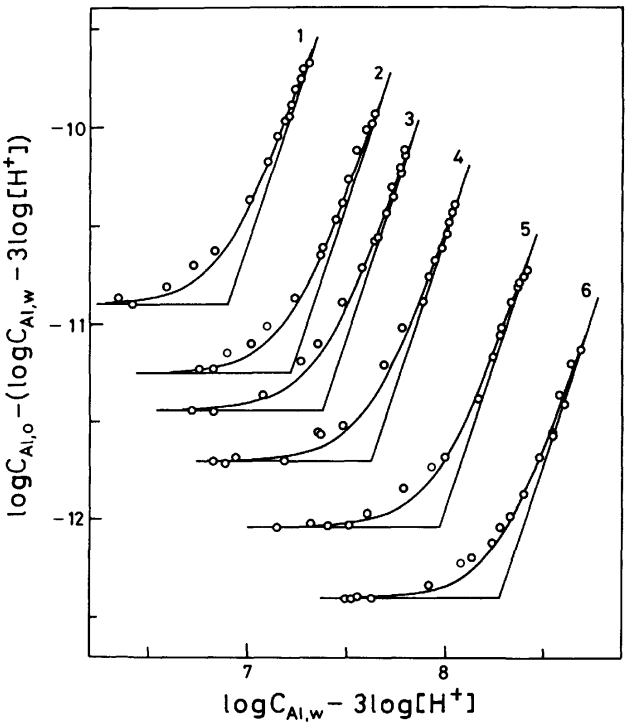

Fig. 3. The identification of the degree of polymerization of aluminum(III) decanoates.
Solid curves are the normalized curves, log(1+X^3) vs. log X. Solid lines are the asymptotes of the normalized curves. Numbers are the same as in Fig. 1.

indium(III) ion in the aqueous phase. Under the present experimental conditions, we can expect the following hydrolysis reactions of indium(III) ion in the aqueous phase:

$$In^{3+} + H_2O \rightleftharpoons In(OH)^{2+} + H_3O^+$$
$$In(OH)^{2+} + H_2O \rightleftharpoons In(OH)_2^+ + H_3O^+$$

with the hydrolysis constants,

$$K_1 = \frac{[In(OH)^{2+}][H_3O^+]}{[In^{3+}]}$$

and

$$K_2 = \frac{[In(OH)_2^+][H_3O^+]}{[In(OH)^{2+}]},$$

respectively. Taking into account these reactions, the following expression instead of Eq. 3 can be derived from Eq. 2:

$$\log C_{In,o} = \log C_{In,w} - 3\log[H^+] - \log \alpha_{In(OH^-)} + a\log[HA]_o + \log K_{ex(1ah)}, \quad (5)$$

where $\alpha_{In(OH^-)}$ denotes the side reaction coefficient of indium(III) ion in the aqueous phase:

$$\alpha_{In(OH^-)} = 1 + \frac{K_1}{[H_3O^+]} + \frac{K_1 \cdot K_2}{[H_3O^+]^2}. \quad (6)$$

Then in Fig. 2, the deviations of the observed points from the straight line with a slope of 1.0 refer to $\log \alpha_{In(OH^-)}$. According to Eq. 6, a plot of $(\alpha_{In(OH^-)}-1)[H^+]$ against $1/[H^+]$ for the markedly deviated points at C_{HA}=0.5 mol dm^{-3} (No. 5) in Fig. 2 is shown in Fig. 4. The plot is found to be linear and the following hydrolysis constants were calculated from the intercept and slope of the straight line by the least-squares method: $\log K_1$=−4.1 and $\log K_2$=−2.7. Various hydrolysis constants for indium(III) ion have been presented: $\log K_1$=−4.41 and $\log K_2$=−4.16 at 25 °C and at ionic strength of 3 mol dm^{-3} ($NaClO_4$),[9] $\log K_1$=−3.48, $\log K_2$=−4.19, and $\log K_3$=−5.08 at 25 °C and at ionic strength of 0.1 mol dm^{-3} ($NaClO_4$),[10] and $\log K_1$=−4.22 and $\log K_2$=−2.92 at 25 °C and at ionic strength of 3 mol dm^{-3} ($LiClO_4$).[11] As shown in Fig. 2, the solid points, which are corrected by considering the hydrolysis of indium(III) ion in the aqueous phase, fit well the straight line with a slope of 1.0 also at C_{HA}=1.0 and 0.7 mol dm^{-3}.

Subsequently, the number of decanoic acid molecules involved in the extracted species was determined in the following manner. In the region where the j-meric species prevails, the following expression is derived from Eq. 2:

$$\frac{1}{j}\log C_{M,o} - (\log C_{M,w} - 3\log[H^+]) = \frac{1}{j}\log \sum_a (K_{ex(jah)}[HA]_o^a) + \frac{1}{j}\log j. \quad (7)$$

According to Eq. 7, the total number of decanoic acid molecules involved in the j-mer can be determined from the slope of the plot of $\{\frac{1}{j}\log C_{M,o} - (\log C_{M,w} - 3\log[H^+])\}$ against $\log[HA]_o$. The results for both aluminum and indium are shown in Figs. 5 and 6, respectively. In the region where the monomeric aluminum decanoate prevails, the plot falls on the straight line with a slope of 3.0 at higher concentration of decanoic acid in the organic phase but deviates upward from the straight line at lower concentration of decanoic acid in the organic phase.

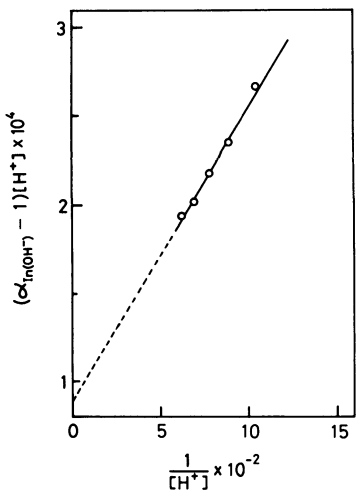

Fig. 4. Determination of the hydrolysis constants of indium(III) ion in the aqueous phase.
The intercept and slope of the straight line were calculated by the least-squares method.

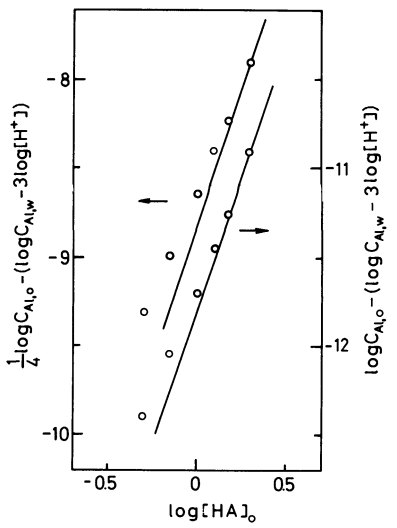

Fig. 5. Determination of the number of decanoic acid molecules involved in the monomeric and tetrameric aluminum(III) decanoates.
Solid lines are the straight lines with a slope of 3.0.

This result suggests that the two monomeric aluminum(III) decanoates are responsible for the extraction in the lower concentration of aluminum in 1-octanol: one of them is AlA_3 and the other $AlA_aH_h(a<3)$. Under these conditions the total concentration of aluminum in the organic phase can be written as:

$$\log C_{Al,o} - (\log C_{Al,w} - 3\log[H^+]) = 3\log[HA]_o + \log K_{ex(130)} + \log\left(1+\frac{K_{ex(1ah)}}{K_{ex(130)}}[HA]_o^{(a-3)}\right). \quad (8)$$

Comparing the plot of the left-hand side of Eq. 8 against $-\log[HA]_o$ with the normalized curves,

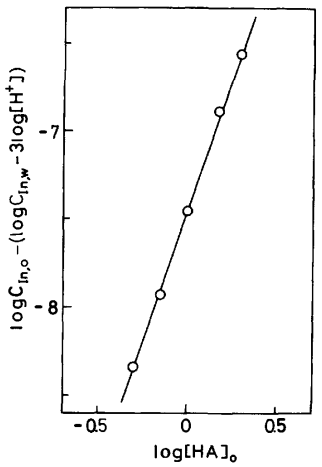

Fig. 6. Determination of the number of decanoic acid molecules involved in the monomeric indium(III) decanoate.
Solid line is the straight line with a slope of 3.0.

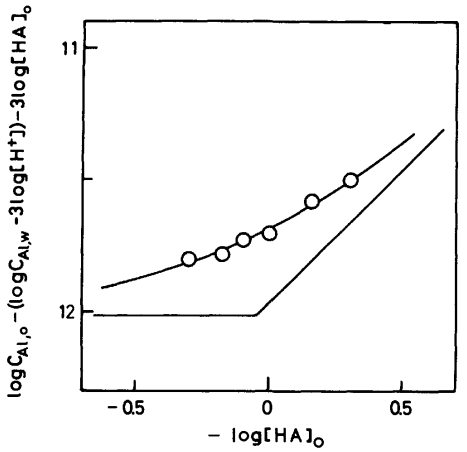

Fig. 7. Determination of the number of decanoic acid molecules involved in the monomeric aluminum(III) decanoates by the curve-fitting method.
Solid curve is the normalized curve, $\log(1+X)$ vs. $\log X$. Solid lines are the asymptotes of the normalized curve.

$\log(1+X^n)$ vs. $\log X$, we can determine another monomeric species. The result is shown in Fig. 7. The plot fits well the normalized curve: $\log(1+X)$ vs. $\log X$, that is, $n=3-a=1$ or $a=2$. From the electroneutrality of the extracted species, it can be noted that another monomeric species involves one hydroxyl group. From Fig. 7, we can also obtain the respective extraction constants, $K_{ex(130)}$ and $K_{ex(12-1)}$ by the curve-fitting method. The results obtained are summarized in Table 1 together with the other constants.

In the region where the tetrameric aluminum decanoate prevails, the slope of the plot of $\{\frac{1}{4}\log C_{Al,o} - (\log C_{Al,w} - 3\log[H^+])\}$ against $\log[HA]_o$ on the basis of Eq. 7 ($j=4$) gets steeper with the concentration of decanoic acid in the organic phase, and approaches 3.0. This result indicates the following species: Al_4A_{12} and $Al_4A_aH_h(a<12)$ as the tetrameric extracted species. Then the following relation can be derived:

$$\log C_{Al,o} - 4(\log C_{Al,w} - 3\log[H^+]) - 12\log[HA]_o = \log\left(1+\frac{K_{ex(4ah)}}{K_{ex(4120)}}[HA]_o^{(a-12)}\right) + \log 4 + \log K_{ex(4120)}. \quad (9)$$

The values of $\{\log C_{Al,o} - 4(\log C_{Al,w} - 3\log[H^+]) - 12\log[HA]_o\}$ are plotted against $-\log[HA]_o$ as depicted in Fig. 8. According to the curve-fitting method, in which the plot is compared with the normalized curves, $\log(1+X^n)$ vs. $\log X$, the number of decanoic acid molecules involved in another tetrameric species can be determined together with the extraction constants of the two tetrameric Al(III) decanoates. In Fig. 8, the plot fits the normalized curve, $\log(1+X^4)$ vs. $\log X$, that is, $n=12-a=4$, or $a=8$ and then h is equal to -4. In analogy with the monomer stated above, four hydroxide ions should

Table 1. Extracted Species and Extraction Constants[a] of Al(III)-, Ga(III)-, and In(III)-Decanoates

Metals	1-Octanol	Benzene
Al(III)	$AlA_3(-12.01)$ $AlA_2(OH)(-11.96)$ $Al_4A_{12}(-35.86)$ $Al_4A_8(OH)_4(-35.38)$	$Al_6A_{12}(OH)_6(-46.1)$[b]
Ga(III)	$GaA_2(OH)(-9.54)$[c] $Ga_2A_4(OH)_2(-14.92)$ $Ga_2A_6(-15.26)$	$Ga_6A_{12}(OH)_6(-35.8)$[d] $Ga_6A_{18}(H_2O)_6(-34.3)$ $Ga_jA_aH_h(j<6)$
In(III)	$InA_3(-7.45)$	$InA_3(HA)_3(-7.34)$[e] $In_3A_9(HA)_3(-18.6)$ $In_6A_{12}(OH)_6(-36.1)$

a) The respective extraction constants($\log K_{ex(jah)}$) are listed in parentheses. b) Ref. 1. c) Ref. 4. d) Ref. 2. e) Ref. 3.

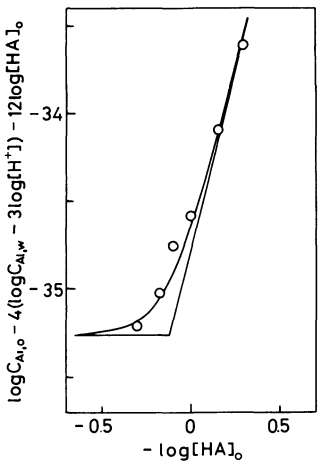

Fig. 8. Determination of the number of decanoic acid molecules involved in the tetrameric aluminum (III) decanoates by the curve-fitting method.
Solid curve is the normalized curve, $\log(1+X^4)$ vs. $\log X$. Solid lines are the asymptotes of the normalized curve.

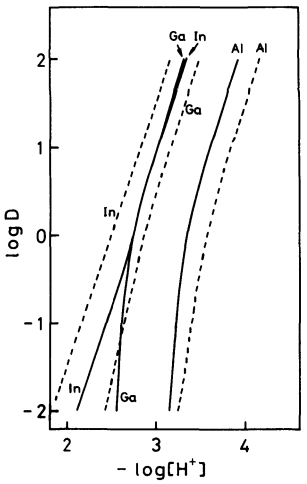

Fig. 9. Extraction curves calculated on the basis of the results obtained from the present and previous works.
$C_{M,tot}=5\times10^{-3}$ mol dm^{-3}. $C_{HA}=1.0$ mol dm^{-3}.
Solid and dotted curves correspond to benzene and 1-octanol, respectively.

be involved in another tetrameric aluminum(III) decanoate. The extraction constants $K_{ex(4120)}$ and $K_{ex(48-4)}$ determined by the curve-fitting method are given in Table 1. Consequently, AlA_3, $AlA_2(OH)$, Al_4A_{12}, and $Al_4A_8(OH)_4$ are responsible for the extraction with decanoic acid in 1-octanol.

In the case of indium(III), on the other hand, the plot of $\{\log C_{In,o}-(\log C_{In,w}-3\log[H^+])\}$ against $\log[HA]_o$ falls on the straight line with a slope of 3.0. Then only InA_3 is extracted with decanoic acid in 1-octanol. The extraction constant $K_{ex(130)}$ can be obtained from the intercept of the straight line in Fig. 6. The result is given in Table 1.

Consequently, the extraction equilibria for aluminum(III) and indium(III) are represented as follows:

Aluminum(III):

$$Al^{3+} + 3(HA)_o \overset{K_{ex(130)}}{\rightleftharpoons} (AlA_3)_o + 3H^+$$

$$Al^{3+} + 2(HA)_o + H_2O \overset{K_{ex(12-1)}}{\rightleftharpoons} (AlA_2(OH))_o + 3H^+$$

$$4Al^{3+} + 12(HA)_o \overset{K_{ex(4120)}}{\rightleftharpoons} (Al_4A_{12})_o + 12H^+$$

$$4Al^{3+} + 8(HA)_o + 4H_2O \overset{K_{ex(48-4)}}{\rightleftharpoons} (Al_4A_8(OH)_4)_o + 12H^+$$

Indium(III):

$$In^{3+} + 3(HA)_o \overset{K_{ex(130)}}{\rightleftharpoons} (InA_3)_o + 3H^+.$$

Solvent Effects. The previous results[1-4] are also listed in Table 1 for comparison. Table 1 suggests that the degree of polymerization of the extracted species for aluminum(III), gallium(III), and indium(III) is more extensive in benzene than in 1-octanol and increases in the following order in both solvents: Al>Ga>In. In 1-octanol the addition of a decanoic acid molecule to each metal decanoate did not occur to any appreciable extent. It is convenient to imagine that some octanol molecules are solvated to the extracted species. As shown in Table 1, the dimeric and tetrameric extracted species in benzene were not observed, while in 1-octanol the trimeric and hexameric ones were not detected. Then it can be expected that the polymerization of metal decanoates in benzene and 1-octanol proceeds through the different mechanism. Further, the difference in the composition of the monomeric indium(III) decanoates in benzene($InA_3(HA)_3$) and 1-octanol(InA_3) can be explained by a notion that in benzene decanoic acid behaves primarily as a dimer and, then a dimeric decanoate(HA_2^-) coordinates to indium ion as a bidentate ligand, whereas in 1-octanol decanoic acid exists only in a monomer form and, then a monomeric decanoate solvated by some octanol molecules binds to indium ion. As we have already reported, also in the extraction of copper(II) there was a remarkable difference in the extracted species between solvating[7,8] and nonsolvating[5] solvents.

The extraction curves calculated from the results given in Table 1 are illustrated in Fig. 9. As shown in Fig. 9, aluminum(III) and gallium(III) ions are extracted with decanoic acid in 1-octanol at the higher pH region than in benzene, while indium(III) decanoate is extracted in 1-octanol at the lower pH region than in benzene. Then it is expected that indium(III) is selectively extracted from a mixture of these three metal ions with decanoic acid by using 1-octanol as a diluent. Usually but not always, much

attention must be paid to the coextraction caused by the formation of mixed metal carboxylates in the extraction of polymerized metal carboxylates. Fortunately under the present experimental conditions, only the monomeric indium(III) decanoate is extracted with decanoic acid in 1-octanol. Therefore, there is scarcely a fear that aluminum(III) and gallium(III) are coextracted with indium(III) as a mixed metal decanoate.

Consequently, the selection of a solvent used in the extraction of metal carboxylates is one of the important considerations, and may occasionally results in the improvement of the selectivity.

References

1) M. Tanaka, N. Nakasuka, and H. Yamada, *J. Inorg. Nucl. Chem.*, **32**, 2791 (1970).
2) H. Yamada and M. Tanaka, *J. Inorg. Nucl. Chem.*, **35**, 3307 (1973).
3) M. Tanaka, N. Nakasuka, and H. Yamada, *J. Inorg. Nucl. Chem.*, **32**, 2759 (1970).
4) H. Yamada, S. Imai, and E. Takeuchi, *Bull. Chem. Soc. Jpn.*, **56**, 1401 (1983).
5) H. Yamada and M. Tanaka, *J. Inorg. Nucl. Chem.*, **38**, 1501 (1976).
6) H. Yamada, S. Suzuki, and M. Tanaka, *J. Inorg. Nucl. Chem.*, **43**, 1873 (1981).
7) H. Yamada, R. Kitazaki, and I. Kakimi, *Bull. Chem. Soc. Jpn.*, **56**, 3302 (1983).
8) H. Yamada, K. Takahashi, Y. Fujii, and M. Mizuta, *Bull. Chem. Soc. Jpn.*, **57**, 2847 (1984).
9) A. Aziz and S. J. Lyle, *J. Inorg. Nucl. Chem.*, **31**, 2431 (1969).
10) E. A. Biryuk, V. A. Nazarenko, and R. V. Ravitskaya, *Zh. Neorg. Khim.*, **14**, 965 (1969).
11) F. Ya. Kul'ba, Yu. B. Yakovlev, and D. A. Zenchenko, *Zh. Neorg. Khim.*, **19**, 923 (1974).

Formation of the *N,N*-Bidentate Chelates of 2-(2-Pyridylazo)-phenolic Ligands with Nickel(II) in Nonaqueous Solvents

Yoshihiro KUDO, Noboru YOSHIDA, and Masatoshi FUJIMOTO*
Department of Chemistry II, Faculty of Science, Hokkaido University, Sapporo 060
(Received September 17, 1985)

The formation of *N,N*-bidentate 1:2 complexes of nickel(II) with various *N,N,O*-terdentate 2-(2-pyridylazo)-phenolic ligands was detected spectrophotometrically in ethyl acetate and was examined with respect to the influences of Brønsted bases, the counter anions in the nickel(II) salts employed, solvent basicity, and the steric requirements around the donor nitrogen atoms in the ligand in the 1:2 complex. It is concluded that the stability of the *N,N*-bidentate complex species in solutions predominantly depends on the basicity of the counter anions X in NiX_2 and of the solvent. In the case of 1-(2-pyridylazo)-2-naphthol, owing to a high steric hindrance of the naphthalene ring, the formation of the *N,N*-bidentate complex was not observed even in the solvent of low basicity such as dioxane.

It is well known that in aqueous solutions nickel(II) ions react with *N,N,O*-terdentate 2-(2-pyridylazo)phenolic ligands such as 4-(2-pyridylazo)-resorcinol (PAR) to form *N,N,O*-terdentate complexes.[1] Recently, we first reported the formation of an *N,N*-bidentate complex of an *N,N,O*-terdentate ligand, 4-(4-methyl-2-pyridylazo)resorcinol (4-MePAR), with nickel(II) perchlorate in an aprotic solvent, 1,4-dioxane.[2] The *N,N*-bidentate complex was isolated from neat dioxane solution and identified to be in a distorted planar configuration in which four nitrogen atoms of the two ligand molecules are coordinated to the nickel(II) atom (Fig. 1). Upon addition of a Brønsted base such as imidazole to the dioxane solution of the *N,N*-bidentate species, an *N,N,O*-terdentate complex was formed.[2] This fact indicates that weak Brønsted bases can promote the release of the intramolecularly hydrogen-bonded proton, N···H–O, in the *N,N*-bidentate complex.

In the present paper, we discuss the conditions required for the formation of the *N,N*-bidentate complexes of *N,N,O*-terdentate 2-(2-pyridylazo)phenolic ligands with a number of nickel(II) salts in various nonaqueous solvents.

Experimental

Materials. Ethyl acetate (Wako) was dried with anhydrous magnesium sulfate (Nakarai) or Molecular Sieves 4A (Wako) and distilled under argon atmosphere immediately before use. Ethanol and pyridine were dried with Molecular Sieves 3A or 4A and distilled under argon atmosphere. 1,4-Dioxane was purified as reported in the previous paper.[2] The purified solvents were stored under argon atmosphere. Other solvents used here were of specially-prepared reagent grade (Nakarai) or of guaranteed reagent grade (Wako).

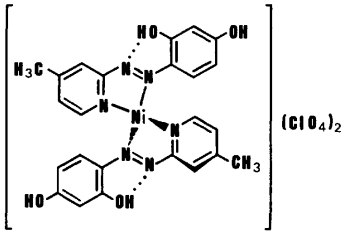

Fig. 1. Proposed configuration of the isolated *N,N*-bidentate chelate of nickel(II) perchlorate with 4-MePAR.[2]

Nickel(II) perchlorate dihydrate was prepared as described in the previous work.[2] Other nickel(II) salts were of reagent grade unless otherwise specified. The perchlorates of zinc(II), manganese(II), and lanthanum(III) were prepared by the same method as in the synthesis of nickel(II) perchlorate. The contents of water in the metal salts were determined by Karl-Fischer titration. Found: $Ni(ClO_4)_2 \cdot 2.4H_2O$ (dried by heating the hexahydrate in vacuo), $Ni(ClO_4)_2 \cdot 6.1H_2O$, $NiCl_2 \cdot 1.0H_2O$ (dried by heating the hexahydrate in vacuo), $NiCl_2 \cdot 5.7H_2O$ (Wako, $NiCl_2 \cdot 6H_2O$), $Zn(ClO_4)_2 \cdot 6.1H_2O$, $Mn(ClO_4)_2 \cdot 4.0H_2O$ (dried the hexahydrate in vacuo over P_2O_5 at room temperature).

The free ligands, 4-MePAR, 5-dimethylamino-2-(2-pyridylazo)phenol (DAPAP), and 4-(2-pyridylazo)phenol (*p*-PAP), were prepared as described in the previous paper.[2] Other ligands, PAR,[3] 4-(*x*-methyl-2-pyridylazo)-resorcinol (*x*-MePAR, *x*=3, 5, and 6),[4] 4-(2-pyridylazo)-orcinol (PAO),[5] and 2-(2-pyridylazo)-1-naphthol (α-PAN),[6] were prepared and purified according to the literature. 1-(2-Pyridylazo)-2-naphthol (β-PAN) was obtained from Dojindo Laboratories and used without further purification.

The *N,N,O*-terdentate complex of DAPAP employed here was synthesized as follows. The free ligand, DAPAP (172 mg, 0.71 mmol), was dissolved in 100 cm^3 of warm ethanol. Nickel(II) chloride (95 mg, 0.40 mmol) dissolved in 10 cm^3 of water was added to the deep red solution of DAPAP. A dark pink solution obtained was evaporated to ca. 2/3 volumes and allowed to stand for several days in the dark. The dark wine red crystals were filtered, washed with water, and dried overnight in vacuo over P_2O_5. Found: C, 57.64; H, 4.84; N, 20.74%. Calcd for $Ni(C_{13}H_{13}N_4O)_2$: C, 57.70; H, 4.84; N, 20.70%. The *N,N,O*-terdentate complexes of α- and β-PAN were obtained by the analogous method. Found: $[Ni(\alpha\text{-panH}_{-1})_2]^{0,\dagger}$: C, 64.67; H, 3.47; N, 13.47%.

† α-panH$_{-1}$ denotes the mono-deprotonated anionic form resulting from the dissociation of the *o*-hydroxyl proton of α-PAN.

$[Ni(\beta\text{-panH}_{-1})_2]^0$: C, 64.80; H, 3.73; N, 15.14%. Calcd for $Ni(C_{15}H_{10}N_3O)_2$: C, 64.90; H, 3.63; N, 15.14%.

Measurements. Electronic spectra and pH* (pH-meter readings) of the sample solutions at 25 °C were measured using the procedure reported previously.[2] Karl-Fischer titrations were performed with the 10—40 mg sample dissolved in 25 cm^3 of dried methanol (Dassui-Yozai ML, Mitsubishi) using a Mitsubishi Kasei Karl-Fischer titrator Model MS-2.

Results and Discussion

Formation of an *N,N*-Bidentate Complex of Nickel(II) Perchlorate with 4-MePAR in Ethyl Acetate. Figure 2 shows a spectral change for the complex formation of nickel(II) perchlorate dihydrate with 4-MePAR in ethyl acetate. The spectrum of the free ligand, 4-MePAR, possesses an absorption maximum at 381 nm ($\varepsilon_{max}=2.07\times10^4$ mol^{-1} dm^3 cm^{-1}) (Curve 1). In the low concentrations of nickel(II) perchlorate, an orange solution was formed (Curve 3). On further addition of nickel(II) perchlorate ($[Ni(II)]_t/[4\text{-MePAR}]_t>0.4$) to the orange solution, the absorbance around 450 nm decreased with the increase of that around 430 nm; the color of the solution was yellow. The spectrum of the yellow solution has a single absorption maximum at 428 nm ($\varepsilon_{max}=4.62\times10^4$ mol^{-1} dm^3 cm^{-1} at $[Ni(II)]_t/[4\text{-MePAR}]_t\simeq2$) (Curve 5). Two sets of isosbestic points were observed in the overall spectral change. Molar ratio method indicates that the metal to ligand ratio of the complex in the orange solution is 1:3. The metal to ligand ratio of the final complex in the yellow solution was found to be 1:2. The above reaction behavior in ethyl acetate was also reproduced by using a hexahydrate of nickel(II) perchlorate. This fact shows that the coordinated water in nickel(II) perchlorate specimen does not significantly affect the formation of the 1:2 complex of nickel(II) with 4-MePAR.[7]

Curve 1 in Fig. 3 shows a spectrum in ethyl acetate of an *N,N*-bidentate complex, $[Ni(4\text{-mepar})_2](ClO_4)_2$, which was isolated from dioxane solution.[2] The spectrum has a single absorption band at 431 nm ($\varepsilon_{max}=3.49\times10^4$ mol^{-1} dm^3 cm^{-1}).[8] The spectrum of the yellow ethyl acetate solution essentially coincides with that of the isolated bidentate complex. This fact indicates that the *N,N*-bidentate complex is also formed in ethyl acetate as in neat dioxane.

Reactions of the *N,N*-Bidentate Complex with Brønsted Bases in Ethyl Acetate. The color change from yellow to pink was observed upon addition of a Brønsted base such as *o*-chloroaniline, *m*-chloroaniline, 2,6-lutidine, and imidazole to the ethyl acetate solution of the isolated *N,N*-bidentate complex, $[Ni(4\text{-mepar})_2](ClO_4)_2$. The spectral change of the bidentate complex on addition of 2,6-lutidine is shown in Fig. 3. The spectral change shows two distinct isosbestic points at 481 nm for the first step and at 503 nm for the second step. This fact implies that the reaction proceeds in two steps. Molar ratio method indicates that the ratio of the bidentate complex to the base in the overall reaction is 1:2. The spectrum in ethyl acetate of the final complex with λ_{max}'s at 400 ($\varepsilon_{max}=3.5\times10^4$) and 546 nm ($\varepsilon_{max}=3.2\times10^4$ mol^{-1} dm^3 cm^{-1}) essentially coincides with that of an *N,N,O*-terdentate complex, $[Ni(4\text{-meparH}_{-1})_2]^0$, isolated from aqueous solution.[2] From these results, the spectral change of the reaction between the bidentate complex, $[Ni(4\text{-mepar})_2](ClO_4)_2$, and 2,6-lutidine is attributed to the formation of the *N,N,O*-terdentate complex, $[Ni(4\text{-meparH}_{-1})_2]^0$, indicating the deprotonation of the two *ortho*-hydroxyl groups of the ligands in the bidentate complex.

The behavior of the reactions in ethyl acetate of

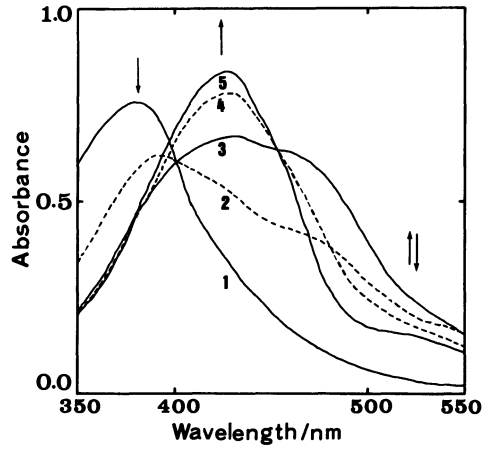

Fig. 2. Spectral change in the complex formation between nickel(II) perchlorate and 4-MePAR at 25 °C in ethyl acetate. $[4\text{-MePAR}]_t=3.57\times10^{-5}$ mol dm^{-3}. $[Ni(II)]_t=0.00$ (1), 0.75 (2), 1.31 (3), 3.00 (4), and 7.49×10^{-5} mol dm^{-3} (5).

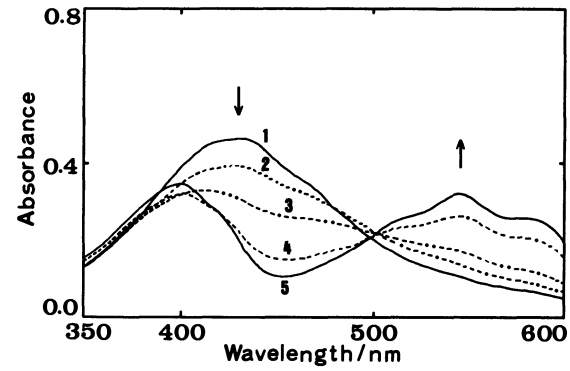

Fig. 3. Spectral change upon addition of 2,6-lutidine to the ethyl acetate solution of the isolated bidentate complex, $[Ni(4\text{-mepar})_2](ClO_4)_2$, at 25 °C. $[Ni\text{-}(4\text{-mepar})_2(ClO_4)_2]_t=9.89\times10^{-6}$ mol dm^{-3}. $[2,6\text{-Lutidine}]_t=0.00$ (1), 0.70 (2), 1.41 (3), 2.10 (4), and 4.66×10^{-5} mol dm^{-3} (5).

nickel(II) perchlorate with 4-MePAR and that of the bidentate complex with the base was identical with the behavior in neat dioxane.[2] This fact suggests that the effects of the solvation by ethyl acetate molecule on the reactions of $Ni(ClO_4)_2$ with 4-MePAR and of the Brønsted base with the bidentate complex are similar to the effects of the solvation by dioxane molecule.

Spectral Assignments of the Free Ligand 4-MePAR and Its Nickel(II) Complexes. In general, the bathochromic shift (red shift) of the absorption band in solution of azobenzene derivatives is caused by the following factors: Introduction of the auxochromic functional group such as OH and $N(CH_3)_2$ into the *para*-position of azo group, presence of the intramolecular hydrogen bond, N···H-O, bonding of cation such as proton to the azo nitrogens, and deprotonation of hydroxyl group.[9-13a,b] The absorption spectra of azobenzene derivatives with an auxochromic group have an absorption band in the range of 310—450 nm with relatively larger extinction coefficient ($\simeq 10^4$ mol^{-1} dm^3 cm^{-1}) in aqueous solutions and in organic solvents.[9-14] These bands are ascribed to the π-π^* (conjugation) transition of the azo chromophore.[9-12,15]

The absorption spectrum of 4-MePAR (Curve 1 in Fig. 2) is expected to show a large bathochromic shift compared with that of azobenzene, since 4-MePAR involves three functional groups, *p*-OH, *o*-OH, and CH_3, and the strong intramolecular hydrogen bonding. The main band of 4-MePAR shifted to longer wavelength (see below), owing to the interaction of transition dipole with highly polarizable solvents.[14] From the above results, the main band of the free ligand, 4-MePAR, could be assigned to that of π-π^* transition of the azo chromophore.

The *N,N*-bidentate chelate of nickel(II) with 4-MePAR has two five-membered chelate rings between nickel(II) and the two coordinated nitrogens in the ligand, namely, pyridyl and azo nitrogens (see Fig. 1). If the nickel(II) ions electrostatically act to the azo nitrogen in the same manner as proton, then the band of π-π^* transition of the free ligand should show a shift to longer wavelength by the formation of the Ni(II)-N(azo) bonds.[9,11] This assumption is consistent with the observed bathochromic shift of the *N,N*-bidentate complex. Thus, the main band at 431 nm of the *N,N*-bidentate chelate of nickel(II) (Curve 1 in Fig. 3) could probably be ascribed to a band of π-π^* transition. The absorption spectrum of the *N,N,O*-terdentate chelate of 4-MePAR in ethyl acetate (Curve 5 in Fig. 3) shows two characteristic bands at 400 and 546 nm with large molar extinction coefficients ($\simeq 3\times10^4$ mol^{-1} dm^3 cm^{-1}). The bands may be ascribed to those of π-π^* transition due to the deprotonation and/or the coordination of *o*-hydroxyl groups.[9]

The main bands of PAR, its methyl derivatives, and their nickel(II) complexes would also be assigned in a similar manner.

Spectral Features for Nickel(II) Complexes of 2-(2-Pyridylazo)phenolic Ligands. The absorption spectra of the free ligands generally show large red shifts by complex formation with metal ions in various solvent systems.[1,16,17] For example, Florence et al. have reported that in aqueous solution the *N,N,O*-terdentate complexes of M(II) ions with DAPAP derivatives have two absorption maxima in the range of 500 to 560 nm.[17] The similar spectral feature was observed in the complexes of other 2-(2-pyridylazo)-phenolic ligands.[1,16] Table 1 summarizes the value of the red shift, $\Delta\lambda_{max}=\lambda_{max}(\text{complex})-\lambda_{max}(\text{free ligand})$,[18] for the complexes of nickel(II) with 2-(2-pyridylazo)phenolic ligands in some nonaqueous solvents together with the color of the solution of the complexes. The complexes, $[Ni(pap)_2]^{2+}$,[19] and $[Ni(4\text{-mepar})_2]^{2+}$, have the *N,N*-bidentate structure both in dioxane[2] and in ethyl acetate. Other nickel(II) complexes, $[Ni(4\text{-meparH}_{-1})_2]^0$, $[Ni(\alpha\text{-panH}_{-1})_2]^0$, $[Ni(\beta\text{-panH}_{-1})_2]^0$, and $[Ni(\text{dapapH}_{-1})_2]^0$, which were isolated from aqueous solution, are in the *N,N,O*-terdentate structure.[1,2,17] The values of $\Delta\lambda_{max}$ for the *N,N*-bidentate and those for the *N,N,O*-terdentate complexes are remarkably different. The values of $\Delta\lambda_{max}$ for the *N,N*-bidentate complexes were in the range of 45 to 77 nm, while those for the *N,N,O*-terdentate complexes in the range of 102 to 165 nm regardless of the kind of solvent used here;

Table 1. The Values of Red Shift ($\Delta\lambda_{max}$) and the Color of the Solution of the *N,N*-Bidentate and the *N,N,O*-Terdentate Complexes of Nickel(II)

Species	$\Delta\lambda_{max}$[a]/nm	Color	Solvent[b]
$[Ni(pap)_2]^{2+}$[c]	77	Yellow	AcOEt
	73	Yellow	Dioxane[f]
$[Ni(4\text{-mepar})_2]^{2+}$[c]	48	Yellow	AcOEt
	49	Yellow	Dioxane[f]
$[Ni(4\text{-mepar})_2](ClO_4)_2$[e]	50[e]	Yellow	AcOEt
	45[e]	Yellow	Dioxane[f]
$[Ni(4\text{-meparH}_{-1})_2]^0$[c,d]	165	Pink	AcOEt
	161	Pink	Dioxane[f]
	134	Red	EtOH
	134[e]	Red	EtOH
	102, 122(sh)[e]	Red	DMF
$[Ni(\text{dapapH}_{-1})_2]^0$[c,d]	114	Pink	AcOEt
	>100[e]	Red	EtOH
$[Ni(\alpha\text{-panH}_{-1})_2]^0$[c,d]	118[e]	Purple	Dioxane
$[Ni(\beta\text{-panH}_{-1})_2]^0$[c,d]	111[e]	Pink	Dioxane

a) $\Delta\lambda_{max}=\lambda_{max}(\text{complex})-\lambda_{max}(\text{free ligand})$. b) AcOEt denotes ethyl acetate. c) *N,N*-Bidentate structure. d) *N,N,O*-Terdentate structure. e) Synthesized complex. f) Ref. 2.

the values of the red shifts for the formations of the *N,N,O*-terdentate complexes are much larger than those of the *N,N*-bidentate complexes.

These results suggest that the coordination mode of the ligand in nickel(II) complexes can be distinguished by the magnitude of the red shifts of the absorption bands in the complex formation. The colors of the complexes of nickel(II) with 2-(2-pyridylazo)phenolic ligands are also quite different depending on the coordination mode, namely, yellowish color of the solutions is ascribed to the *N,N*-bidentate species and reddish color to the *N,N,O*-terdentate species (Table 1).

Effects of the Counter Anions in Nickel(II) Salts on the Formation of the *N,N*-Bidentate Complex. The spectral data of the 4-MePAR complexes of various nickel(II) salts in dioxane and in ethyl acetate are listed in Table 2 together with the pK_a values of the corresponding conjugate acids of the counter anions in the nickel(II) salts, metal to ligand ratio in the complex, and the colors of the solutions of the complexes. From the values of $\Delta\lambda_{max}$ and the color of the solution, the formation of the *N,N*-bidentate complex is confirmed also in the reaction of nickel(II) bromide with 4-MePAR (Curve B in Fig. 4). The spectra for the complexes of 4-MePAR with other nickel(II) salts such as chloride, nitrate, and acetate do not show the single band characteristic of the *N,N*-bidentate complexes but show that of the *N,N,O*-terdentate complexes as depicted by the two characteristic bands in the visible region (Curve C in Fig. 4). The spectrum of the 4-MePAR complex of a nickel(II) salt with counter anions of higher pK_a value shows a larger red shift, indicating the formation of an *N,N,O*-terdentate complex. These results reveal that the counter anions, Cl^-, NO_3^-, and CH_3COO^-, act as an acceptor on the *o*-hydroxyl protons of the *N,N*-bidentate complex.[2]

Effects of Solvents on the Formation of the Bidentate Complex of Nickel(II) Perchlorate with 4-MePAR. Table 3 shows the absorption spectral data, metal to ligand ratios in the overall reaction, the color of the solution of the Ni(II)-4-MePAR complexes in thirteen solvents together with their properties, donor number (DN) and dielectric constants. The donor number is generally used as an empirical parameter of the solvent basicity; a high value of DN corresponds to the high basicity of solvent molecules.[20] The larger red shifts ($\Delta\lambda_{max}\simeq130$ nm) were observed for the reactions in the solvents of high DN, indicating only the formation of the *N,N,O*-terdentate complexes. In the solvents of lower DN such as nitromethane, the smaller red shifts, $\Delta\lambda_{max}$, were observed in the complex formation, showing the formation of the *N,N*-bidentate complexes. The addition of imidazole to the final

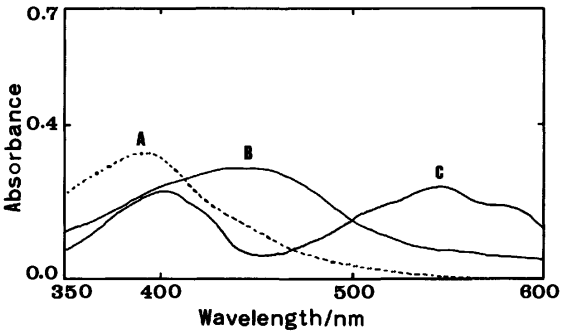

Fig. 4. Electronic spectra of the free ligand 4-MePAR, the *N,N*-bidentate, and the *N,N,O*-terdentate complexes at 25 °C in ethyl acetate. (A) Free ligand: $[4\text{-MePAR}]_t = 1.58\times10^{-5}$ mol dm^{-3}; (B) *N,N*-bidentate complex of nickel(II) bromide with 4-MePAR: $[4\text{-MePAR}]_t = 1.58\times10^{-5}$ mol dm^{-3}, $[Ni(II)]_t = 1.3\times10^{-5}$ mol dm^{-3}; (C) *N,N,O*-terdentate complex of nickel(II) nitrate with 4-MePAR: $[4\text{-MePAR}]_t = 1.35\times10^{-5}$ mol dm^{-3}, $[Ni(II)]_t = 1.0\times10^{-5}$ mol dm^{-3}.

Table 2. Spectral Data for the Complexes of Various Nickel(II) Salts with 4-MePAR

Nickel(II) salts	pK_a[a]	λ_{max}[b]/nm($\varepsilon_{max}/10^4$ mol^{-1} dm^3 cm^{-1})	M : L[c]	Color[d]
$Ni(OAc)_2\cdot4H_2O$	4.7[e]	402(1.68), 544(1.76)	1 : 1	Pink[g,h]
$Ni(NO_3)_2\cdot6H_2O$	−1.64[f]	403(3.36), 544(3.50)	1 : 2	Pink[i]
				Pink[g,h]
$NiCl_2\cdot H_2O$	−7,[f] −4[e]	406(3.2), 543(2.7)	1 : 2	Pink[g,h]
$NiCl_2\cdot6H_2O$				Pink[g]
$Ni(ClO_4)_2\cdot2.4H_2O$	−8[f]	428(4.62)	1 : 2	Yellow[i]
		426(3.90)[j]	1 : 2	Yellow[g,h]
$Ni(ClO_4)_2\cdot6.1H_2O$		429(4.69)	1 : 2	Yellow[i]
		430		Yellow[g]
$NiBr_2$	−9,[f] −7[e]	431(>3.6)	1 : 2	Yellow[i]

a) pK_a values of the conjugate acids of the counter anions in nickel(II) salts. b) At $[Ni(II)]_t/[4\text{-MePAR}]_t = 1-2$. c) Determined by molar ratio method. d) Color of the solution of the final complex. e) Ref. 23a. f) Ref. 23b. g) In neat dioxane. h) Ref. 2. i) In ethyl acetate. j) Synthesized complex.

Ni(II)-4-MePAR complex in nitromethane caused a further red shift of about 60 nm in the visible region. The color of the nitromethane solution was changed from orange to pink. These facts strongly support the conversion of the *N,N*-bidentate complex to the *N,N,O*-terdentate complex in nitromethane. The contribution of the dielectric effect of the solvents to the formation of the *N,N*-bidentate complex was not obvious (Table 3).

The above results indicate that the stability in the solution of the *N,N*-bidentate species is strongly influenced by the basicities of the solvents, the counter anions, and the bases, B, added.

The reaction behavior of the Ni(II)-4-MePAR system is summarized in Scheme 1, where the ligand 4-MePAR is represented by LHH*; H and H* denote the *ortho*- and the *para*-hydroxyl protons, respectively.

Reactions between Nickel(II) Perchlorate and Various 2-(2-Pyridylazo)phenolic Ligands in Dioxane and Ethyl Acetate. Table 4 shows the spectral data of various 2-(2-pyridylazo)phenolic ligands and their metal complexes in dioxane and in ethyl acetate. All ligands except for β-PAN reacted with nickel(II) perchlorate to form the *N,N*-bidentate complexes as deduced from the smaller values of the red shift, $\Delta\lambda_{max}$, and the color of the solution. Upon addition of a Brønsted base, the formation of the *N,N,O*-terdentate complexes was observed for all ligands except for *p*-PAP having no coordinating *o*-hydroxyl group.

The spectra of the yellow solutions of the Ni(II)-DAPAP complexes in dioxane and ethyl acetate showed negative $\Delta\lambda_{max}$. Upon addition of a Brønsted base to the yellow solution of the

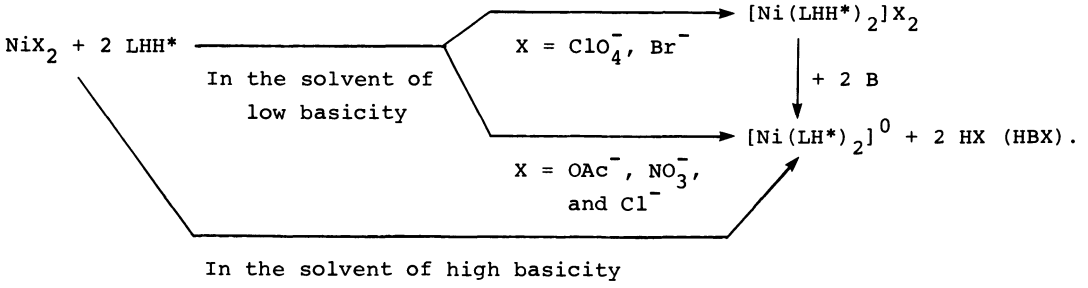

Scheme 1.

Table 3. Spectral Data for the Complex Formation of Nickel(II) Perchlorate with 4-MePAR in Various Solvents

Solvent	DN[a]	Dielectric constant[b]	λ_{max}/nm(ε_{max}/10^4 mol^{-1} dm^3 cm^{-1})		M : L[d]	Color[e]
			Ligand	Complex[c]		
$MeNO_2$	2.7	35.94	381 (1.92)	469 (1.60)	1 : 1	Orange
$PhNO_2$	4.4	34.82				Yellow
Dioxane	14.8	2.2	381 (2.10)	426 (3.90)[f]	1 : 2	Yellow[g]
Acetone	17.0	20.7				Pink
AcOEt	17.1	6.11 (20 °C)	381 (2.07)	428 (4.62)	1 : 2	Yellow
H_2O	18.0	78.54	389 (1.89)	401 (2.78), 511 (2.82)	1 : 2	Red[g,h]
MeOH	19	32.6				Red
EtOH	20	24.3	388 (2.24)	406 (2.74), 522 (3.15)	1 : 2	Red
DMF	26.6	36.71	398 (2.73)	513 (3.0)	1 : 1	Red
DMSO	29.8	46.6	390 (2.34)	405 (3.32), 537 (3.63)	1 : 2	Pink
Pyridine	33.1	12.01	391 (2.26)	413 (1.50), 528 (1.98)	1 : 1	Pink
$PhNH_2$		6.73				Pink
$CHCl_3$		4.724	386	440		Yellow

a) Donor number. b) The values at 25 °C. c) At $[Ni(II)]_t/[4\text{-MePAR}]_t \simeq 2$. d) Determined by molar ratio method. e) Color of the solution of the final complex. f) Synthesized complex. g) Ref. 2. h) In 10%(v/v) dioxane-water at pH* 4.2, I=0.1 mol dm^{-3} ($NaClO_4$).

Table 4. Spectral Data for the Complex Formation of Metal Perchlorates with Various 2-(2-Pyridylazo)phenolic Ligands

Species	λ_{max}/nm(ε_{max}/10^4 mol^{-1} dm^3 cm^{-1})	Color	Solvent
PAR	382(2.05)	Yellow	Dioxane
$[Ni(par)_2]^{2+}$	433(4.60)	Yellow	
$[Ni(parH_{-1})_2]^0$	407(3.41), 547(3.35)	Pink[a]	
3-MePAR	382(1.88)	Yellow	AcOEt
$[Ni(3\text{-}mepar)_2]^{2+}$	449(4.84)	Yellow	
$[Ni(3\text{-}meparH_{-1})_2]^0$	413(2.10), 529(4.50)	Pink[b]	
5-MePAR	384(2.23)	Yellow	AcOEt
$[Ni(5\text{-}mepar)_2]^{2+}$	437(4.84)	Yellow	
$[Ni(5\text{-}meparH_{-1})_2]^0$	407(2.18), 534(4.08)	Pink[b]	
6-MePAR	383(2.06)	Yellow	AcOEt
$[Ni(6\text{-}mepar)_2]^{2+}$	435(4.76)	Yellow	
$[Ni(6\text{-}meparH_{-1})_2]^0$	—	Pink[a]	
6-MePAR	384(2.03)	Yellow	Dioxane
$[Ni(6\text{-}mepar)_2]^{2+}$	439(4.32)	Yellow	
$[Ni(6\text{-}meparH_{-1})_2]^0$	—	Pink[a]	
PAO	378(2.43)	Yellow	AcOEt
$[Ni(pao)_2]^{2+}$	425(5.02)	Yellow	
$[Ni(paoH_{-1})_2]^0$	405(3—4), 548(2—3)	Pink[a]	
DAPAP	443(3.51—3.65)	Yellow	AcOEt
$[Ni(dapap)_2]^{2+}$	426(5.3)	Yellow	
$[Ni(dapapH_{-1})_2]^0$	529(sh, 7.10), 557(7.55)	Pink[a]	
DAPAP	444(3.46)	Yellow	Dioxane[c]
$[Ni(dapap)_2]^{2+}$	420(4.6)	Yellow	
$[Ni(dapapH_{-1})_2]^0$	511(9.10), 542(9.08)	Pink[d]	
p-PAP	347(2.34)	Yellow	AcOEt
$[Ni(pap)_2]^{2+}$	424(4.19)	Yellow	
p-PAP	347(2.18)	Yellow	Dioxane[c]
$[Ni(pap)_2]^{2+}$	420(3.7)	Yellow	
α-PAN	358(1.20), 485(1.91)	Orange	Dioxane
$[Ni(\alpha\text{-}pan)_2]^{2+}$	400(2.14), 512(3.24)	Red	
$[Ni(\alpha\text{-}panH_{-1})_2]^0$	561(2.9), 603(2.7)[e]	Purple	
β-PAN	463(1.82)	Yellow	Dioxane
$[Ni(\beta\text{-}panH_{-1})_2]^0$	396(1.6), 533(4.5), 574(5.3)[c]	Pink	
$[Zn(4\text{-}mepar)_2]^{2+}$	420(3.94)	Yellow	AcOEt
$[Zn(4\text{-}meparH_{-1})_2]^0$	—	Pink[a]	
$[Zn(6\text{-}mepar)_2]^{2+}$	440(4.52)	Yellow	
$[Zn(6\text{-}meparH_{-1})_2]^0$	—	Pink[a]	
$[La(6\text{-}mepar)]^{3+}$	392(1.6), 478(1.3)	Orange	
$[La(6\text{-}meparH_{-1})]^{2+}$	548—558(—)	Pink[a]	

a) Color of the solution after the addition of a small excess of imidazole to the solution of the *N,N*-bidentate complex. b) In 1%(v/v) 2,6-lutidine-AcOEt. c) Ref. 2. d) In 30%(v/v) dioxane-water, pH*=4.59, and I=0.1 mol dm^{-3} ($NaClO_4$). e) Synthesized complex.

Ni(II)-DAPAP complexes, the color of the solution turned pink, showing the formation of the *N,N,O*-terdentate complex. The complex in the yellow solution has been isolated as $[Ni(dapap)_2](ClO_4)_2 \cdot H_2O$[21] from the dioxane solution.[2] The amount of proton liberated in the reaction, $[Ni(dapap)_2]^{2+} + 2H_2O \rightarrow [Ni(dapapH_{-1})_2]^0 + 2H_3O^+$, was found to be almost twice that of the complex dissolved in 30%(v/v) dioxane-water.[2] The spectral feature of the *N,N*-bidentate complex in ethyl acetate was similar to that in dioxane. From these results, the Ni(II)-DAPAP complex, yellow in ethyl acetate, was confirmed to be in the *N,N*-bidentate structure.

α-PAN, an isomer of β-PAN, reacted with nickel(II) perchlorate to form the *N,N*-bidentate complex (Curves 1 and 2 in Fig. 5). Upon addition of imidazole in neat dioxane the bidentate complex converted to the *N,N,O*-terdentate complex (Curve 3 in Fig. 5). β-PAN, however, did not form the *N,N*-bidentate complex. The difference in the reaction behavior between α-PAN and β-PAN with nickel(II) may be due to a steric hindrance of the bulky naphthalene ring in β-PAN. The configuration of the *N,N*-bidentate complex, $[Ni(4\text{-}mepar)_2](ClO_4)_2$, isolated from dioxane solution, has been reported to be a distorted planar around the nickel(II) atom (see Fig. 1).[2,22] If the *N,N*-bidentate 1:2 nickel(II) complex of α-PAN and β-PAN in dioxane solution

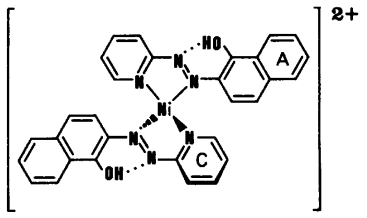

$[Ni(\alpha\text{-}pan)_2]^{2+}$

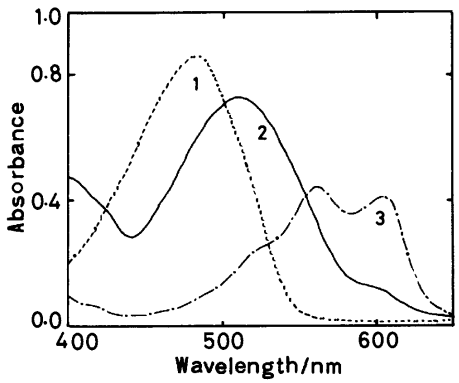

Fig. 5. Spectral features of the free ligand α-PAN and its nickel(II) complexes at 25 °C in neat dioxane. (1) Free ligand: $[\alpha\text{-PAN}]_t = 4.48 \times 10^{-5}$ mol dm^{-3}; (2) *N,N*-bidentate complex: $[\alpha\text{-PAN}]_t = 4.48 \times 10^{-5}$ mol dm^{-3}, $[Ni(II)]_t = 1.25 \times 10^{-4}$ mol dm^{-3}; (3) *N,N,O*-terdentate complex: $[\alpha\text{-PAN}]_t = 1.74 \times 10^{-5}$ mol dm^{-3}, $[Ni(II)]_t = 1.9 \times 10^{-5}$ mol dm^{-3}, and in the presence of an excess of imidazole.

are in the same configuration as that of the isolated bidentate complex, $[Ni(4\text{-mepar})_2](ClO_4)_2$, then the *N,N*-bidentate 1:2 nickel(II) complex of *β*-PAN is

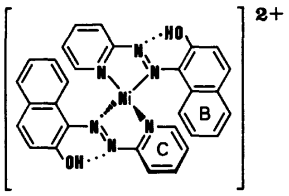

$[Ni(\beta\text{-pan})_2]^{2+}$

presumed to have a large steric hindrance caused by the pyridyl ring (Ring C) in one ligand molecule and the bulky naphthalene ring (Ring B) in another ligand molecule. The naphthalene ring in the isomer *α*-PAN is expected to show no steric hindrance on the coordination of the donor nitrogen atoms because the ring A in the bidentate complex of *α*-PAN should occupy an opposite position compared with the ring B in the possible *N,N*-bidentate complex of *β*-PAN. In the coordination of the donor nitrogens in the 1:2 complexes of nickel(II) with 6-MePAR or PAO, the steric hindrance of the *ortho*-methyl group in pyridine ring or benzene ring was not obviously observed, though the configuration of the *N,N*-bidentate 1:2 complexes of these ligands is considered to be highly strained.

Complex Formation of the Other Metal Ions with Methyl-PAR Derivatives. The reaction behavior of zinc(II) perchlorate with 4-MePAR or 6-MePAR in ethyl acetate suggests the formation of the similar *N,N*-bidentate complex to that of nickel(II) in ethyl acetate (Table 4). The same results were also obtained in the reactions of manganese(II) perchlorate or lanthanum(III) perchlorate with 6-MePAR in ethyl acetate (Table 4). The formation of the *N,N*-bidentate complex of cobalt(II) bromide with 4-MePAR was also detected spectrophotometrically in dioxane.

Enhanced Acidity of the *ortho*-Hydroxyl Group in the Ligand 4-MePAR as a Sequence of *N,N*-Coordination to Nickel(II). The pK_a values in aqueous solution of the conjugate acids of the Brønsted bases are increased in the orders of Br^-(−9)<ClO_4^-(−8)<Cl^-(−7)<NO_3^-(−1.64)<AcO^-(4.756) for the anionic bases[23b] and DMF(0.0)<*o*-chloroaniline(2.6)<*m*-chloroaniline(3.5)<aniline(4.6)<pyridine(5.2)<2,6-lutidine(6.75)<imidazole(7.4) for the neutral bases.[23c] In the solvents of lower basicity, the *N,N*-bidentate complex is formed in the reactions between 4-MePAR and nickel(II) salts, in which the counter anion of the nickel(II) is perchlorate or bromide. The other nickel(II) salts form only the *N,N,O*-terdentate complex. These facts indicate that the perchlorate and bromide ions behave as a weaker base than the other counter anions even in ethyl acetate and dioxane.

From the above results, an average pK_a value to be estimated in aqueous solution for the *ortho*-hydroxyl group of the ligand 4-MePAR in the *N,N*-bidentate nickel(II) complex may be evaluated to be ca. −7. The pK_a value of the *ortho*-hydroxyl group of the free ligand 4-MePAR in aqueous solution was reported to be ca. 11.[4] Namely, owing to the *N,N*-coordination to nickel(II), the *ortho*-hydroxyl group of the ligand 4-MePAR behaves as such a strong acid in aqueous media as HCl and $HClO_4$.

The authors are indebted to Dr. Taira Imamura for helpful discussion. They wish to thank Mr. Shoichi Kaihara for the syntheses and purifications of the free ligands, 3- and 5-MePAR.

References

1) S. Shibata, "2-Pyridylazo Compounds in Analytical Chemistry," in "Chelates in Analytical Chemistry," ed by H. A. Flaschka and A. J. Barnard, Jr., Vol. 4, Marcel Dekker, Inc., New York, N. Y. (1972), p. 1; H. Kawamoto, T. Takenouchi, and H. Akaiwa, *Nippon Kagaku Kaishi*, **1983**, 358; H. Hoshino and T. Yotsuyanagi, *Bull. Chem. Soc. Jpn.*, **58**, 1037 (1985).

2) Y. Kudo, N. Yoshida, T. Imamura, and M. Fujimoto, *Bull. Chem. Soc. Jpn.*, **57**, 3099 (1984).

3) F. H. Pollard, P. Hanson, and W. J. Geary, *Anal. Chim. Acta*, **20**, 26 (1959).

4) W. J. Geary and F. Bottomley, *Talanta*, **14**, 537 (1967).

5) M. Hniličková and L. Sommer, *Fresenius' Z. Anal. Chem.*, **177**, 425 (1960).

6) R. G. Anderson and G. Nickless, *Analyst*, **93**, 13 (1968).

7) In 3%(v/v) water-dioxane, only the formation of the *N,N,O*-terdentate complex was observed in the reaction of nickel(II) perchlorate with 4-MePAR.

8) Upon further addition of nickel(II) perchlorate to the ethyl acetate solution of the isolated *N,N*-bidentate complex, $[Ni(4\text{-mepar})_2](ClO_4)_2$, the absorbance around 430 nm increases by 10—15%. This result suggests that in the presence of a small excess of nickel(II) perchlorate ($[Ni(II)]_t/[4\text{-MePAR}]_t$=0.5—1.0) the reaction, Ni^{2+}+2 4-MePAR⇄$[Ni(4\text{-mepar})_2]^{2+}$, could not sufficiently proceed to the right.

9) J. P. Hart and W. F. Smyth, *Spectrochim. Acta, Part A*, **36**, 279 (1980).

10) S. Yamamoto, N. Nishimura, and S. Hasegawa, *Bull. Chem. Soc. Jpn.*, **44**, 2018 (1971).

11) F. Gerson and E. Heilbronner, *Helv. Chim. Acta*, **45**, 42 (1962).

12) I. M. Issa, R. M. Issa, M. R. Mahmoud, and Y. M. Temerik, *Z. Phys. Chem. (Leipzig)*, **253**, 289 (1973).

13) a) G. M. Badger and R. G. Buttery, *J. Chem. Soc.*, **1953**, 2156; b) W. R. Brode, J. H. Gould, and G. M. Wyman, *J. Am. Chem. Soc.*, **74**, 4641 (1952); c) N. Nishimura, T. Sueyoshi, H. Yamanaka, E. Imai, S. Yamamoto, and S. Hasegawa, *Bull. Chem. Soc. Jpn.*, **49**, 1381 (1976).

14) J. W. Sidman, *Chem. Rev.*, **58**, 689 (1958).

15) Since the intensity of *π*-*π** transitions of azobenzene derivatives is larger than that of n-*π** transitions by a factor

of about 100 under usual conditions,[9-12] we would not discuss the n-π^* transitions of 4-MePAR and its nickel(II) complexes.

16) S. Shibata, M. Furukawa, and K. Tôei, *Anal. Chim. Acta*, **66**, 397 (1973); K. Mochizuki and M. Fujimoto, *Bull. Chem. Soc. Jpn.*, **58**, 1520 (1985); K. Mochizuki, T. Imamura, T. Ito, and M. Fujimoto, ibid., **51**, 1743 (1978).

17) D. A. Johnson and T. M. Florence, *Talanta*, **22**, 253 (1975).

18) We adopt the value of the longest λ_{max}, when two or more absorption bands are observed in the visible region. Though the physical meaning of $\Delta\lambda_{max}$ is not yet clear, this value is useful for the discrimination of the *N,N*-bidentate and the *N,N,O*-terdentate species in solution.

19) The ligand *p*-PAP reacts with metal ions to form only the *N,N*-bidentate complexes in solution, since *p*-PAP possesses no coordinating *o*-hydroxyl group. See, R. G. Anderson and G. Nickless, *Anal. Chim. Acta*, **39**, 469 (1967); Ref. 2.

20) V. Gutmann, "The Donor-Acceptor Approach to Molecular Interactions," Plenum Press, New York, N. Y. (1978), p. 17.

21) The *N,N*-bidentate 1:2 complex of nickel(II) with DAPAP was identified to be a monohydrate (Found: 0.93H_2O) by Karl-Fischer titration. Found: C, 39.78; H, 3.62; N, 14.36; Cl, 9.20%. Calcd for $Ni(C_{13}H_{14}N_4O)_2(ClO_4)_2 \cdot H_2O$: C, 41.08; H, 3.98; N, 14.74; Cl, 9.33%.

22) In ethyl acetate, nickel(II) perchlorate hexahydrate was found to be in a six-coordinated structure with λ_{max} (ε_{max})=725 (2.2), 1163 (2.4), 1213 (2.5), 1450 (2.0), and 1938 nm (6.9 $mol^{-1}\,dm^3\,cm^{-1}$). It has been reported that in aqueous solution the spectrum of the $[Ni(H_2O)_6](ClO_4)_2$ has absorption maxima at 396 (ε_{max}=4.9), 663 (1.8), 729 (2.1), and 1176 nm (2.1 $mol^{-1}\,dm^3\,cm^{-1}$) (see, H. Ito, *Nippon Kagaku Zasshi*, **77**, 1383 (1956)). Since the wavelength for the d-d transition of the divalent nickel did not remarkably change upon addition of the free ligand 4-MePAR to the light green solution of nickel(II) perchlorate, the configuration of the bidentate nickel(II) complex in ethyl acetate solution may be considered to be an octahedral involving the coordination of water and/or solvent molecules.

23) a) F. Basolo and R. G. Pearson, "Mechanisms of Inorganic Reactions," 2nd ed, John Wiley & Sons, Inc., New York, N. Y. (1967), p. 140; b) A. Albert and E. P. Serjeant, "Ionization Constants of Acids and Bases. A Laboratory Manual," lst ed, Methuen & Co., Ltd., London (1962); c) M. Tanaka, "San to Enki (Acids and Bases)," 4th ed, Shōkabo, Tokyo (1977), p. 177.

Condensations of 1,4-Cyclohexanediones and Secondary Aromatic Amines. II. *N*-Phenylation of Diarylamines

Kazuo HAGA,* Katsumasa IWAYA, and Ryohei KANEKO
Department of Industrial Chemistry, Faculty of Engineering, Utsunomiya University, Ishii-machi, Utsunomiya 321
(Received April 15, 1985)

The condensations of 1,4-cyclohexanedione with several diphenylamines were investigated in order to determine the limit of the utility of this reaction for the *N*-phenylation of aromatic secondary amines. 4-Methoxy-, 4,4′-dimethyl-, and 4,4′-dibromodiphenylamines produced their *N*-phenylated compounds in fairly good yields, but 4-hydroxy-, 3-methoxy-, and 4,4′-bis(dimethylamino)diphenylamines produced poor yields. Nitro-substituted diphenylamines gave *N*-phenyl derivatives in low yields along with *N*-4-hydroxyphenyl derivatives. *N,N′*-Diphenyl-*p*-phenylenediamine and *N,N′*-diphenylbenzidine gave corresponding tetra-*N*-phenyl diamines in good yields. The condensation of *N*-phenyl-1-naphthylamine, *N*-phenyl-2-naphthylamine, di-2-pyridylamine, phenothiazine, and carbazole with 1,4-cyclohexanedione were also examined.

In a previous paper[1] the authors showed that the condensation of secondary aromatic amines with 1,4-cyclohexanedione(**1**) in the presence of *p*-toluenesulfonic acid gave *N*-phenyl derivatives. In the case of *N*-ethylaniline, a *p*-chloro or *p*-nitro substituent facilitated the reaction. Diphenylamine also reacted with the 1,4-dione to afford triphenylamine in good yield in spite of a low nucleophilicity. It would be interesting to know to what extent the *N*-phenylation of very low-nucleophilic amines proceeds since condensation with the 1,4-dione is expected to be useful for the *N*-phenylation of diarylamines under mild conditions. In this paper the condensation of several diphenylamines and some analogous amines with 1,4-cyclohexanedione are investigated, and the limit of the utility of this method for *N*-phenylation and solvent effects are discussed.

Results and Discussion

Condensation of Diphenylamines. The condensation of diphenylamines with 1,4-cyclohexanedione was carried out in the presence of *p*-toluenesulfonic acid in a manner similar to that discussed in the previous paper.[1] The results are shown in Table 1. The diphenylamines can be divided into three groups according to their reactivities. Most of diphenylamines (except nitro derivatives) gave only *N*-phenylated compounds (**3a—i**) as isolable products (Eq. 1). 4,4′-Dimethyl- and 4,4′-dibromodiphenylamines (**2g** and **2i**) gave the corresponding triphenylamines (**3g** and **3i**) in good yields, as did diphenylamine (**2h**).

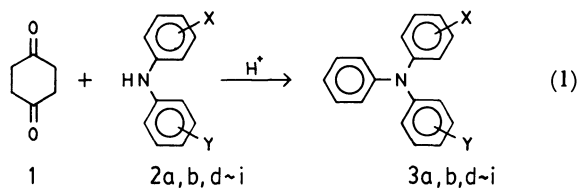

1 2a,b,d~i 3a,b,d~i (1)

Table 1. Condensation of Diphenylamines with 1,4-Cyclohexanedione[a]

Diphenylamine			Time[b]/h	Product (Yield/%)			
	X	Y		**3**(Z=H)		**4**(Z=OH)	
2a	*p*-$(CH_3)_2N$	*p*-$(CH_3)_2N$	18	**3a**	18	—	—
2b	H	*p*-HO	12	**3b**	14	—	—[c]
2c	*m*-HO	*m*-HO	12	—	—	—	—[c]
2d	H	*p*-C_2H_5O	12	**3d**	90	—	—
2e	H	*m*-C_2H_5O	11	**3e**	20	—	—[c]
2f	*m*-C_2H_5O	*m*-C_2H_5O	12	**3f**	2.8	—	—[c]
2g	*p*-CH_3	*p*-CH_3	12	**3g**	65	—	—
2h	H	H	12	**3h**	88	—	—
2i	*p*-Br	*p*-Br	12	**3i**	94	—	—
2j	H	*p*-NO_2	12	**3j**	43	**4j**	7.8
2k	*p*-NO_2	*p*-NO_2	18	**3k**	0.2	**4k**	4.2
2l	*m*-NO_2	*m*-NO_2	18	**3l**	23	**4l**	12

a) 1,4-Cyclohexanedione; 0.25 g (2.23 mmol). Diphenylamines; 2.23 mmol. *p*-Toluenesulfonic acid; 10 mg. b) The reaction was carried out in toluene (10 cm^3) at the refulux temperature. c) Resinous products were obtained.

On the other hand, strong electron-donating substituents seemed to be unfavorable for this type reaction, except for the *p*-ethoxyl group. 4-Hydroxy-, 3-ethoxy-, and 3,3′-diethoxydiphenylamines (**2b**, **2e**, and **2f**) produced triphenylamines in poor yields and 3,3′-dihydroxydiphenylamine (**2c**) gave no triphenylamine. The low yields of these *N*-phenyl derivatives may be similar to the results of the *N*-phenylation of *N*-ethylanilines. In the latter case, there was a tendency for electron-withdrawing substituents to facilitate the *N*-phenylation; *N*-ethylanilines substituted by electron-donating groups showed relatively low reactivity. These facts have been explained in terms of the acidity of the conjugate acids as the actual catalyst. However, 4-ethoxydiphenylamine

(**2d**) gave 4-ethoxytriphenylamine (**3d**) in good yield. This shows that the conjugate acid of **2d** is sufficiently acidic to catalyze the reaction. The basicity of diphenylamine, itself, is very weak. Therefore, the acidity of the conjugate acid of any diphenylamine must be strong even if it is substituted by an electron-donating group. Therefore, the low yields of the triphenylamines from **2b**, **2c**, **2e**, and **2f** must be due to side reactions. Actually, these diphenylamines produced some resinous by-products which could not be purified and remained unidentified. According to an infrared analysis, the by-products contained carbonyl groups. Also, the condensation of the secondary amines with the 1,4-dione seemed to occur at aromatic nuclei. In the case of the *p*-ethoxyl derivative (**2d**), the corresponding by-product was hardly produced. The difference between the reactivity of **2d** and that of **2e** is now under investigation. The condensation of 4,4′-bis(dimethylamino)diphenylamine (**2a**) with the 1,4-dione also gave triphenylamine **3a** in a low yield. In this case, 80% of the starting amine was recovered. The dimethylamino groups of **2a** are more basic than the inside diarylamino group; thus, protonation must occur on the dimethylamino group (the conjugate acid of **2a** is much more weak than that of diphenylamine). Therefore, the low reactivity of **2a** is due to the low activity of the conjugate acid.

The last group of diphenylamines (nitro-substituted diphenylamines) also showed a small reactivity and 4,4′-dinitrodiphenylamine (**2k**) could hardly give *N*-phenylated derivative. In these cases, by-products were isolated and identified to be 4-hydroxy-4′-nitrotriphenylamine (**4j**), 4-hydroxy-4′,4″-dinitrotriphenylamine (**4k**), and 4-hydroxy-3,3″-dinitrotriphenylamine (**4l**). The yields of these hydroxy

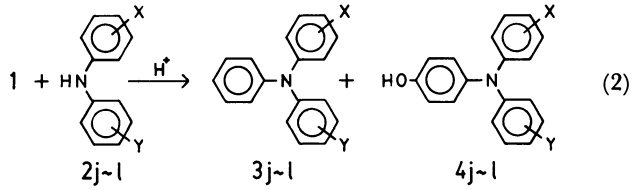

(2)

derivatives were also poor; therefore, the low yields of the triphenylamines must be due to the very low nucleophilicity of the amino groups. It is worth noting that the *p*-bromo substituent facilitated the reaction but the nitro substituent did not. That is to say, the effect of the bromo group on diphenylamines is parallel with that on *N*-ethylanilines, whereas the effect of the nitro group is opposite. This is because the decrease in the nucleophilicity of the nitro-substituted diphenylamines is more remarkable rather than an increase in the acidity of the conjugate acid.

These results indicate that the reaction depends on both the necleophilicity of the amine and the acidity of the conjugate acid. Since both factors can be assumed to have a reverse tendency for many amines, they must compensate for each other in the *N*-phenylation of most aniline derivatives. If either of the two factors decreases very much, *N*-phenylation proceeds with difficulty, for example, as in the case of aliphatic amines or the dinitrodiphenylamines. Consequently, this *N*-phenylation is applicable for an aromatic secondary amine which is more nucleophilic than 4-nitrodiphenylamine; however, it is necessary to take into account the side reaction for several diphenylamines substituted by electron-donating groups. The condensation of other secondary amines analogous to diphenylamine were examined in order to determine any further utility of this reaction.

The *N*-Phenylation of Other Secondary Amines. As analogies of diphenylamine, two aromatic diamines, three cyclic amines, di-2-pyridylamine, and *N*-phenyl naphthylamines were examined for the reactivity of the *N*-phenylation. The results are shown in Table 2. *N,N′*-Diphenyl-*p*-phenylenediamine (**5**) and *N,N′*-diphenylbenzidine (**7**) gave *N,N,N′,N′*-tetrapheny-*p*-phenylenediamine (**6**) and *N,N,N′,N′*-tetraphenylbenzidine (**8**), respectively, in good yields. In these reactions, *N,N,N′*-triphenylphenylenediamine (**9**) and *N,N,N′*-triphenylbenzidine (**10**) should be formed

Table 2. Condensation of Diarylamine Other than Diphenylamines[a)]

Diarylamine	Time/h	Product (yield/%)
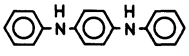 (**5**)	20	*N,N,N′,N′*-Tetraphenyl-*p*-phenylenediamine (**6**) (80)
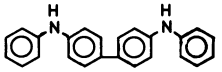 (**7**)	20	*N,N,N′,N′*-Tetraphenylbenzidine (**8**) (78)
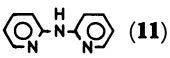 (**11**)	24	No product
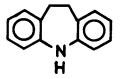 (**12**)	24	No product
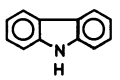 (**13**)	12	*N*-Phenylcarbazole (**14**) (6.6) 1-Phenylcarbazole (**15**) (12)
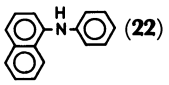 (**22**)	12	*N,N*-Diphenyl-1-naphthylamine (**23**) (19)
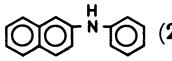 (**24**)	12	*N,N*-Diphenyl-2-naphthylamine (**25**) (28)
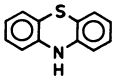 (**26**)	12	*N*-Phenylphenothiazine (**27**) (43)

a) The conditions were as same as that in Table 1.

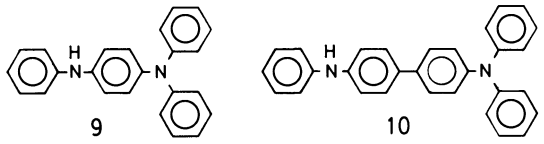

9 10

as intermediates. These compounds could not be isolated, but the formation of **6** and **8** showed that the intermediates also reacted easily with one further molecule of the 1,4-dione. On the other hand, di-2-pyridylamine (**11**) gave no tertiary amine and most of the starting materials were recovered. The facility of the *N*-phenylation of **5**, **7**, **9**, and **10** indicates that the *N*-phenylation of a polyamino aromatic compound proceeds if amino groups other than a reaction point are not more basic than the reaction point. In the case of **11**, however, both factors (nucleophilicity and acidity) which govern the reaction are under unfavorable situations. It is well known that 2- or 4-aminopyridine is more basic than aniline and that protonation occurs on the ring nitrogen,[2] and pyridine, itself, is much more basic than diphenylamine. Then, the conjugate acid of **11** is also less acidic than that of diphenylamine, but the exocyclic amino group is less nucleophilic because of the electron-withdrawing property of the pyridine ring.

Also, 10,11-dihydro-5*H*-dibenzo[*b*,*f*]azepine (**12**) did not give any phenylated compound and the starting amine was recovered. The differences between **12** and diphenylamine or carbazole must be due to a steric hindrance; that is, the ethylene linkage must inhibit the nitrogen from attacking the carbonyl of the 1,4-dione.

Carbazole (**13**) had been estimated to have a very low reactivity. Actually, about 80% of **13** was recovered upon condensation with the 1,4-dione. *N*-Phenylcarbazole (**14**), however, was obtained in low yield together with 1-phenylcarbazole (**15**). The fact that *C*-phenylation is easier than *N*-phenylation in carbazole can be explained by the mechanisms shown in Scheme 1. The formation of monoenamine **16** (an intermediate of *N*-phenylation) is a reversible reaction; but the formation of **19** is irreversible and **19** easily changes to **15** under the influence of a strong acid. Comparing the stability of **18** with that of **21**, the protonation of **20** is seen to be easier than that of **17**. *C*-Phenylation could not be observed for diphenylamines. Carbazole is a much weaker base than diphenylamine.[3] This suggests that the lone-pair electrons of the nitrogen atom of carbazole are more delocalized than those of diphenylamine. Therefore, the carbocyclic rings should be more active toward an electrophilic attack than the phenyl groups of diphenylamine. In the case of diphenylamines substituted with electron-donating groups, the substituents increase the activity of the phenyl group but also increase the nucleophilicity of the nitrogen. These reactions of carbazole are very interesting, but the low reactivity of the nitrogen of carbazole also shows the limit of the utility of this method for *N*-phenylation.

N-Phenyl-1-naphthylamine (**22**) and *N*-phenyl-2-naphthylamine (**24**) gave the corresponding *N*,*N*-diphenylnaphthylamines (**23** and **25**), respectively, but in low yields. Phenothiazine (**26**) produced *N*-phenylphenothiazine (**27**) in moderate yield. These results are less satisfactory, but still show that this *N*-phenylation method is applicable to secondary amines beyond aniline derivatives.

Solvent Effect. *N*-Phenylation reactions in several polar solvents were much slower than that in aromatic hydrocarbons. In the condensation of diphenylamine (**2h**) in dimethyl sulfoxide, triphenylamine was scarcely produced. The condensation of phenothiazine (**26**) in dioxane for 24h resulted in only a 13% yield of the *N*-phenyl derivative. Carbazole (**13**) in a mixture of xylene and nitrobenzene scarcely gave *N*-phenylcarbazole.

Diphenylamines substituted with nitro groups have poor reactivities, as described above. While the

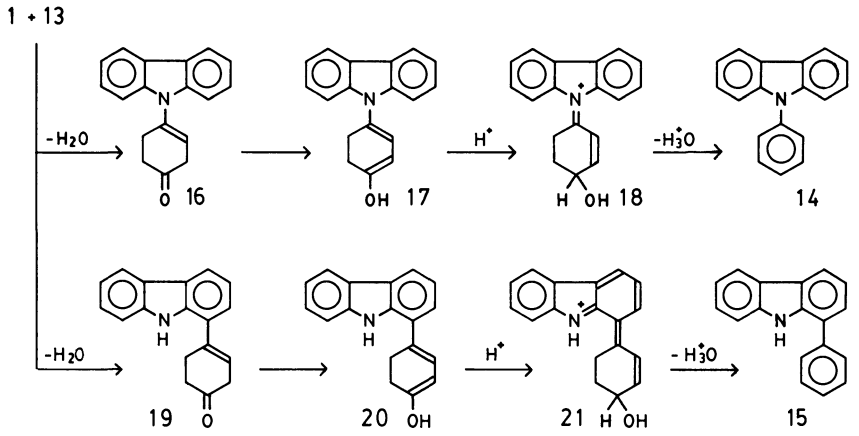

Scheme 1.

Table 3. Solvent Effect on the Condensation of 4,4′-Dinitrodiphenylamine with 1,4-Cyclohexanedione[a)]

Solvent	Catalyst /mg	Time /h	Product **3k**	(Yield/%) **4k**
Toluene	10	18	0.2	4.2
	40	18	0.6	4.6
	40	36	1.1	7.8
Toluene/DMSO	10	18	0.6	trace
(80/20)	40	18	1.9	trace
Dioxane	40	18	0.6	—
Xylene/Nitrobenzene (80/20)	40	18	—	13

a) The conditions were virtually identical with those shown in Table 1 except for the solvent and the amount of *p*-toluenesulfonic acid as the catalyst.

reactivity of **2k** is especially low, such a reaction of **2k** in high concentration could not be performed in toluene because of the poor solubility. Further, the formation of the 4-hydroxyphenyl derivatives suggests that the dehydrogenation of the monoenamines of the 1,4-dione is accompanied by their dehydration. The relative rates of these simultaneous reactions were expected to be affected by the polarity of solvent. The results of the condensation of **2k** carried out for several conditions are shown in Table 3. In toluene, an increase in the amount of the catalyst or the reaction period leads to an increase in the yields of both **3k** and **4k**; yet, their yields are very poor. In a mixture of toluene and dimethyl sulfoxide or in dioxane, **4k** was scarcely produced. In every solvent, the total yield of the two products was smaller than that in toluene. In a mixture of xylene and nitrobenzene, **3k** was not produced; however, the yield of **4k** increased. It can be said that nitrobenzene accelerated the dehydrogenation to afford **4k**, which resulted in inhibiting the formation of **3k**. This shows that an oxidizing action of a nitro group can occur in the reaction system. Therefore, dehydrogenation in the absence of nitrobenzene must be catalyzed by the nitro groups of 4,4′-dinitrodiphenylamine.

These results show that polar solvents are unfavorable and only the aromatic hydrocarbons are favorable as solvents for the condensation process.

Experimental

General. Melting points were uncorrected. ^{1}H-NMR spectra were recorded on a JNM-C-60HL spectrometer with $(CH_3)_4Si$ as an internal standard. IR spectra were taken on a JASCO Model IR-G spectrophotometer. Mass spectra were measured on a Hitachi M-80 mass spectrometer.

Materials. 4-Ethoxy-, 3-ethoxy-, and 3,3′-diethoxydiphenylamines were prepared from 4-hydroxy-, 3-hydroxy-, and 3,3′-dihydroxydiphenylamines, respectively. Ethylation was carried out using ethyl iodide in a 10% ethanolic potassium hydroxide solution. This was a modification of Houston's method[4)] for the preparation of 4-propoxydiphenylamine. 4-Ethoxydiphenylamine (**2d**) was prepared in 52% yield: Mp 71 °C. 3-Ethoxydiphenylamine (**2e**) was obtained in 80% yield: Bp 162 °C/1.5 Torr (1 Torr=133.322 Pa). 3,3′-Diethoxydiphenylamine (**2f**) was isolated by distillation and following column chromatography on silica gel: yield, 22%; bp 189 °C/1 Torr. *N*-Benzoyldiphenylamine was obtained by the usual method from diphenylamine and benzoyl chloride: Mp 175.5—176.5 °C (from ethanol). 4,4′-Dibromodiphenylamine (**2i**) was prepared by bromination of *N*-benzoyldiphenylamine in chloroform and following hydration in 3% ethanolic potassium hydroxide solution: Yield, 56%; mp 100—102 °C (lit,[5)] 105.5—107 °C). 3,3′-Dinitrodiphenylamine (**2l**) was prepared according to the method of Hodgson and Dodgson[6)]: Mp 186—187.5 °C (lit, 188 °C). 4-Nitrodiphenylamine (**2j**) was prepared from 4-bromonitrobenzene and acetanilide. The procedure was virtually identical with that of Hodgson and Dodgson for **2l** but the intermediate, *N*-acetyl-4-nitrodiphenylamine was hydrated in a 0.2% ethanolic potassium hydroxide solution since hydration in an acidic solution was difficult. Compound **2j** was obtained in 50% yield: Mp 131—132.5 °C; IR (KBr disk) 3320, 1595, 1475, 1295, 1105, 745, and 640 cm^{-1}. 4,4-Dinitrodiphenylamine (**2k**) was obtained from diphenylamine in a manner similar to that used by Chen et al.[5)]: Mp 216—218 °C (lit, 217—218 °C). All other diphenylamines and secondary amines in Table 2 were commercially available and were used after purification (if necessary).

Condensation of the Secondary Amines with 1,4-Cyclohexanedione (1). General Method: The procedure was virtually identical to that described in the previous paper.[1)] A two-necked flask was fitted with a reflux condenser and an inlet tube. In the flask, a filter paper thimble packed with $CaCl_2$ was hung under the condenser in order to dehydrate the refluxed solvent. A mixture of 0.25 g (2.23 mmol) of 1,4-cyclohexanedione, the amine (2.23 mmol) and 10 mg of *p*-toluenesulfonic acid in 10 cm^3 of toluene was refluxed. After 12 h, the solution was freed of solvent in vacuo and then the residue was separated by column chromatography on silica gel. The product was eluted with hexane-benzene.

Condensation of Diphenylamines (2a—i). The isolated products and the yields are shown in Table 1, and their properties are presented below.

4,4′-Bis(dimethylamino)triphenylamine (3a): Mp 151—152 °C (lit,[7)] 157 °C; ^{1}H NMR ($CDCl_3$) δ=2.88 (12H, broad s) and 7.30—6.52 (13H, m); IR (KBr disk) 1600, 1590, 1510, and 1490 cm^{-1}; MS (70 eV), *m/z* (rel intensity), 331 (M^+, 100), 316 (14), and 166 (11); High-resolution mass spectra (HR-MS), *m/z* 331.2105; Calcd for $C_{22}H_{25}N_3$: M, 331.2050.

4-Hydroxytriphenylamine (3b): Mp 125.5—126.5 °C; IR (KBr disk) 3550, 1580, 1510, and 1490 cm^{-1}; MS (70 eV), *m/z* (rel intensity), 262 (20), 261 (M^+, 100), 260 (17), 167 (6), and 77 (8); HR-MS, *m/z* 261.1117, Calcd for $C_{18}H_{15}NO$: M, 261.1154.

4-Ethoxytriphenylamine (3d): Mp 76—78 °C; NMR ($CDCl_3$), δ=1.46 (3H, t), 4.07 (2H, q), and 6.79—7.45 (14H, m); IR (KBr disk) 1580, 1485, and 1235 cm^{-1}; MS (70 eV), *m/z* (rel intensity), 289 (M^+, 94), 260 (100), and 77 (14); HR-MS, *m/z* 289.1511; Calcd for $C_{20}H_{17}NO_2$: M,

289.1466.

3-Ethoxytriphenylamine (3e): Colorless liquid; ^{1}H NMR ($CDCl_3$) δ=1.29 (3H, t), 3.89 (2H, q) and 6.38—7.38 (14H, m); IR (neat) 1580, 1490, and 1215 cm^{-1}; MS (70 eV), *m/z* (rel intensity), 289 (M^+, 100), 260 (35), 244 (18) and 77 (21); HR-MS, *m/z* 289.1513; Calcd for $C_{20}H_{17}NO_2$: M, 289.1466.

3,3′-Diethoxytriphenylamine (3f): Light blue liquid ^{1}H NMR ($CDCl_3$) δ=1.35 (6H, t), 3.91 (4H, q) and 6.42—7.33 (13H, m); IR (neat) 1580, 1480 and 1195 cm^{-1}; MS (70 eV), *m/z* (rel intensity), 333 (M^+, 100), 304 (6), and 276 (7); HR-MS, *m/z* 333.1634; Calcd for $C_{22}H_{23}NO_2$: M, 333.1727.

4,4′-Dimethyltriphenylamine (3g): Mp 107—108 °C; ^{1}H NMR ($CDCl_3$) δ=2.28 (6H, s) and 6.75—7.52 (13H, m); IR (KBr disk) 1593, 1507, 1490, 1320, 1290, and 1280 cm^{-1}; MS (70 eV), *m/z* (rel intensity), 273 (M^+, 100), 257 (6), and 180 (5); HR-MS, *m/z* 273.1539; Calcd for $C_{20}H_{19}N$: M, 273.1518.

4,4′-Dibromotriphenylamine (3i): Colorless viscous liquid; IR (neat) 1575, 1480, 1310, 820, and 505 cm^{-1}; MS (70 eV), *m/z* (rel intensity) 405 (51), 403 (100), and 401 (52); relative intensity of isotopic cluster calculated from $C_{18}H_{13}NBr_2$, 50.4:100:50.5 (M+4:M+2:M).

Condensation of Nitro Substituted Diphenylamines (2j, 2k, and 2l). The procedure was virtually identical with that described above. After **3j—l** were separated by column chromatography on silica gel eluted with hexane-benzene, hydroxy derivatives **4j—l** were eluted with benzene-ether. The latter compounds were further purified by chromatography on alumina. They were eluted with ethanol after elution with ether.

4-Nitrotriphenylamine (3j): Mp 138—139 °C; IR (KBr disk) 1575, 1490, 1320, and 1110 cm^{-1}; MS, *m/z* (rel intensity), 290 (M^+, 100), 244 (35), 243 (28), 242 (21), 167 (20), 166 (19), and 77 (19); HR-MS, *m/z* 290.1089; Calcd for $C_{18}H_{14}N_2O_2$: M, 290.1056.

4-Hydroxy-4′-nitrotriphenylamine (4j): Decomposed above 250 °C; IR (KBr disk) 3400, 1575, 1480, 1300, and 1110 cm^{-1}, MS, *m/z* (rel intensity), 306 (M^+, 100), 260 (23), 251 (26), and 83 (15); HR-MS, *m/z* 306.0988; Calcd for $C_{18}H_{14}N_2O_3$: M, 306.1002.

4,4′-Dinitrotriphenylamine (3k): Mp 206—207 °C; IR (KBr disk) 1585, 1575, 1500, and 1335 cm^{-1}; MS, *m/z* (rel intensity), 335 (M^+, 34), 259 (100), 223 (14), 167 (42), 166 (28), and 69 (51); HR-MS, *m/z* 335.0932, Calcd for $C_{18}H_{13}N_3O_4$: M, 335.0907.

4-Hydroxy-4′,4″-dinitrotriphenylamine (4k): Mp 243—245 °C; IR (KBr disk) 3500, 1575, 1490, 1305, and 1110 cm^{-1}; MS, *m/z* (rel intensity), 351 (M^+, 100), 259 (29), and 258 (16); HR-MS, *m/z* 351.0759; Calcd for $C_{18}H_{13}N_3O_5$: M, 351.0853.

3,3′-Dinitrotriphenylamine (3l): Mp 144.5—145.5 °C; IR (KBr disk) 1520, 1510, 1340, and 1270 cm^{-1}: MS, *m/z* (rel intensity), 335 (M^+, 100), 243 (39), 242 (39), and 241 (24); HR-MS, *m/z* 335.0929; Calcd for $C_{18}H_{13}N_3O_3$: M, 335.0907.

4-Hydroxy-3′,3″-dinitrotriphenylamine (4l): Mp 175—178.5 °C; IR (KBr disk) 3400, 1525, 1510, and 1345 cm^{-1}; MS, *m/z* (rel intensity), 351 (M^+, 100), 259 (39), 258 (26), and 257 (10); HR-MS, *m/z* 351.0915; Calcd for $C_{18}H_{13}N_3O_5$: M, 351.0854.

Condensation of Diamine 5 and 7. The procedure was virtually identical with the general method, but 1,4-cyclohexanedione was used by double molar quantity to 1 mol of the diamine.

***N,N,N′,N′*-Tetraphenyl-*p*-phenylenediamine (6):** Mp 197—198 °C; IR (KBr disk) 1590, 1505, 1493, and 1270 cm^{-1}; MS, *m/z* 412 (M^+).

***N,N,N′N′*-Tetraphenylbenzidine (8):** Mp 224—225 °C; IR (KBr disk) 1585, 1490, 1480, and 1275 cm^{-1}; MS, *m/z* 488 (M^+).

Condensation of Carbazole. The procedure was virtually identical with the general method but the column chromatograpy on silica gel with hexane was repeated several times to isolate products **14** and **15**.

***N*-Phenylcarbazole (14):** Mp 90—92 °C; Picrate, mp 127—128 °C; IR (KBr disk) 1590, 1500, 1445, and 1230 cm^{-1}; MS, *m/z* 243 (M^+).

1-Phenylcarbazole (15): Mp 129—130 °C (lit,[7] 133 °C); picrate, mp 150—151 °C (lit,[8] 151 °C); IR (KBr disk) 3320, 1620, 1590, 1500, 1410, 1320, and 1230 cm^{-1}; MS, *m/z* 243 (M^+).

Condensation of *N*-Phenyl-1-naphthylamine (22), *N*-Phenyl-2-naphthylamine (24) and Phenothiazine (26). These condensations were carried out by the general method.

***N,N*-Diphenyl-1-naphthylamine (23):** Mp, 137.5—138.5 °C; IR (KBr disk) 1590, 1490, 1390, 1290, and 1275 cm^{-1}; MS, *m/z* 295 (M^+).

***N,N*-Diphenyl-2-naphthylamine (24):** Mp, 120—121 °C; IR (KBr disk) 1620, 1590, 1490, 1275, and 755 cm^{-1}; MS, MS, *m/z* 295 (M^+).

***N*-Phenylphenothiazine (15):** Mp 93—94 °C; IR (KBr disk) 1580, 1485, 1455, and 1300 cm^{-1}; MS, *m/z* 243 (M^+).

The authors wish to thank Mr. Makoto Roppongi for his technical assistance in preparing some of amines.

References

1) K. Haga, M. Oohashi, and R. Kaneko, *Bull. Chem. Soc. Jpn.*, **57**, 1586 (1984).
2) E. Sppinner, *J. Chem. Soc.*, **1962**, 3119.
3) G. Berthier and B. Pullman, *C. R. Acad. Sci. Paris*, **226**, 1725 (1948).
4) D. F. Houston, *J. Am. Chem. Soc.*, **71**, 395 (1949).
5) M. M. Chen, A. F. Adamo and R. I. Walter, *J. Org. Chem.*, **26**, 2721 (1961).
6) H. H. Hodgson and D. P. Dodgson, *J. Chem. Soc.*, **1948**, 1004.
7) O. Neunhoeffer and P. Heitman, *Chem. Ber.*, **94**, 2511 (1961).
8) K. H. Pausacka, *J. Chem. Soc.*, **1950**, 612.

Electrochemical Reduction of Carbon Dioxide Using Iron-Sulfur Clusters as Catalyst Precursors

Makoto NAKAZAWA, Yasushi MIZOBE, Yoichi MATSUMOTO,† Yasuzo UCHIDA,†
Meguru TEZUKA,†† and Masanobu HIDAI*
Engineering Research Institute, Faculty of Engineering, The University of Tokyo,
Yayoi, Bunkyo-ku, Tokyo 113
†Department of Industrial Chemistry, Faculty of Engineering, The University of Tokyo,
Hongo, Bunkyo-ku, Tokyo 113
††The Saitama Institute of Technology, Okabe, Saitama 369-02
(Received, September 24, 1985)

The potential-current relationships of DMF solutions of a series of iron-sulfur compounds have revealed that in the presence of clusters $[Fe_4S_4(SR)_4]^{2-}$ (R=$PhCH_2$ or Bu^t) and $[M_2Fe_6S_8(SEt)_9]^{3-}$ (M=Mo or W) the electroreduction of CO_2 proceeds at the potential shifted by about 0.7 and 0.5 V, respectively, to the positive direction compared to the potential at which CO_2 is reduced without any catalyst. When controlled potential electrolysis of a DMF solution containing $[Fe_4S_4(SCH_2Ph)_4]^{2-}$ was carried out under CO_2 at −2.0 V vs. SCE, phenylacetate and formate were formed as the products resulting from CO_2 reduction. The cubane structure of this cluster collapsed rapidly under these conditions. However, when excess amount of $PhCH_2SH$ was added to the catholyte, the cluster structure was preserved during a relatively long period of electrolysis, and the yield of phenylacetate increased but that of formate decreased compared with the reaction in the absence of free $PhCH_2SH$.

Utilization of carbon dioxide has evoked much interest in relevance to the development of alternative carbon sources of fuels and chemicals. However, the fixation of CO_2, the stable carbon end product, inevitably necessitates considerable energy input. The electrochemical reduction of CO_2 is presumably one of the most potential methods for converting CO_2 into organic substances but the direct reduction requires the large overpotential.[1-4] Recently several transition metal complexes were reported as the catalysts to diminish the overvoltage. Among these are Co and Ni tetraazamacrocycles,[5-9] [Re(bipyridine)$(CO)_3Cl$][10] and [Rh(diphosphine)$_2$Cl].[11] From the former two catalytic systems, CO is produced in high current efficiencies, whereas the Rh complex catalyzes the formation of formate. In a previous communication, we reported that the iron-sulfur clusters $[Fe_4S_4(SR)_4]^{2-}$([2−]), first prepared by Holm and his coworkers as the ferredoxin model compounds,[12] remarkably diminish the overvoltage of CO_2 electroreduction.[13] From this reaction system, a substantial amount of formate is obtained together with a little CO. Here we wish to describe the detail of this reaction.

Results and Discussion

Current-Potential Relationships of DMF Solutions Containing Iron-Sulfur Clusters under CO_2. The direct electroreduction of CO_2 in nonaqueous media has been reported by several authors.[3,14] In every case the reduction proceeds only at extremely negative potentials. In fact, investigation of the reduction of CO_2 in a solution of 0.1 M $[Bu^n_4N][BF_4]$ (M= mol dm^{-3}) in DMF on mercury electrode has revealed that potentials more negative than −2.4 V vs. SCE are required for the reduction. However, addition of 2 mM $[Fe_4S_4(SR)_4]^{2-}$ (R=CH_2Ph or Bu^t) to the solution lowers the effective reduction potential by about 0.7 V. Figure 1 shows the current (I)-potential (E) relationship of a solution of $[Fe_4S_4(SCH_2Ph)_4]^{2-}$ (**1**) in DMF recorded on mercury pool cathode with 13.5 cm^2 surface area. Cluster **1** exhibits two succesive reduction waves corresponding to two redox processes [2−]/[3−] and [3−]/[4−] under N_2 (Fig. 1 c). When CO_2 gas was bubbled

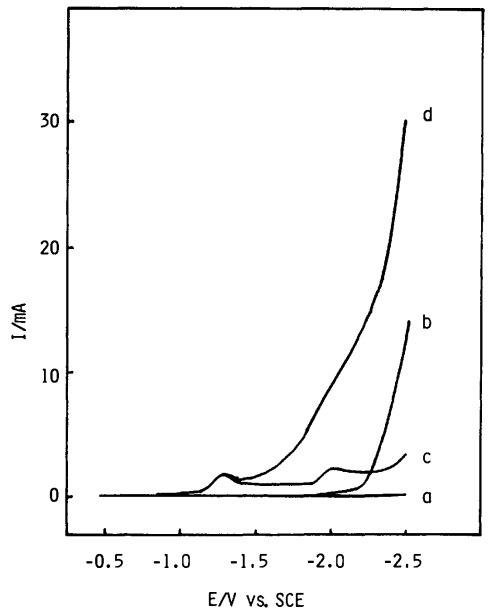

Fig. 1. I–E relationships of a solution of 0.1 M $[Bu^n_4N][BF_4]$ in DMF. (a): Without cluster under N_2, (b): Without cluster under CO_2, (c): In the presence of 2 mM cluster **1** under N_2, (d): In the presence of 2 mM cluster **1** under CO_2.

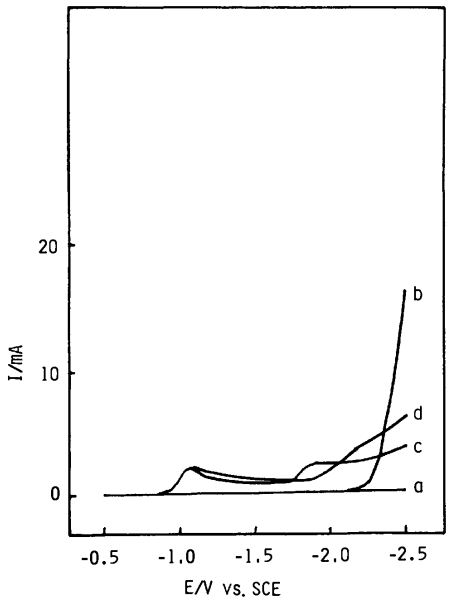

Fig. 2. *I–E* relationships of a solution of 0.1 M $[Bu^n_4N][BF_4]$ in DMF. (a): Without cluster under N_2, (b): Without cluster under CO_2, (c): In the presence of 2 mM cluster **3** under N_2, (d): In the presence of 2 mM cluster **3** under CO_2.

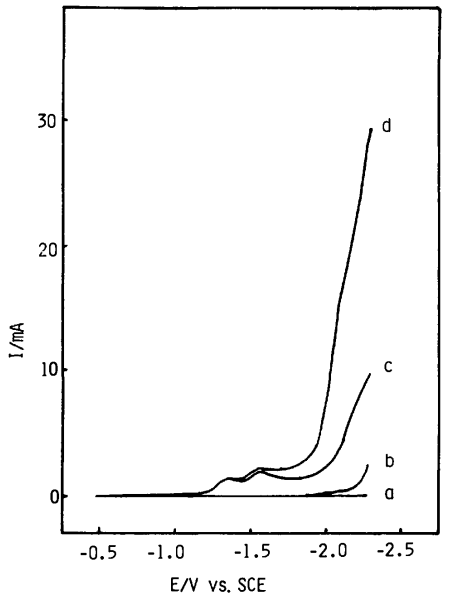

Fig. 3. *I–E* relationships of a solution of 0.1 M $[Bu^n_4N][BF_4]$ in DMF. (a): Without cluster under N_2, (b): Without cluster under CO_2, (c): In the presence of 2 mM cluster **4** under N_2, (d): In the presence of 2 mM cluster **4** under CO_2.

through the solution for several minutes, the reduction current of CO_2 increased remarkably at potentials more negative than −1.7 V (Fig. 1 d). The same trend is also observed in the case of $[Fe_4S_4(SBu^t)_4]^{2-}$ (**2**). In contrast with these compounds, the cluster $[Fe_4S_4(SPh)_4]^{2-}$ (**3**) does not have any effect on the electroreduction of CO_2 as shown in Fig. 2. Although cluster **3** is reduced to [3−] and then [4−] in the same manner as clusters **1** and **2**, the electron transfer from the reduced **3** to CO_2 does not occur substantially. When cluster **1** was reduced to [4−] under CO_2, it decomposed rapidly to generate in situ the other species which enhanced the electroreduction of CO_2 (vide infra). On the other hand, degradation of cluster **3** also proceeded substantially under the same conditions but the similar enhancement for reduction of CO_2 was not observed. It is interesting that the rate of the electroreduction of CO_2 depends very much upon the kind of thiolate ligands of cluster [2−].

We have also examined the potential-current relationships of DMF solutions of a series of other iron-sulfur compounds under N_2 and CO_2. The molybdenum-iron-sulfur cluster $[Mo_2Fe_6S_8(SEt)_9]^{3-}$ (**4**) is effective for the reduction of CO_2 (Fig. 3). The positive shift of the reduction potential amounts to about 0.5 V. The tungsten analogue $[W_2Fe_6S_8(SEt)_9]^{3-}$ also gives essentially the same results. However, the analogous clusters containing SPh ligands cannot facilitate the electroreduction of CO_2, as is also observed for cluster **3** (Fig. 4). The mononuclear

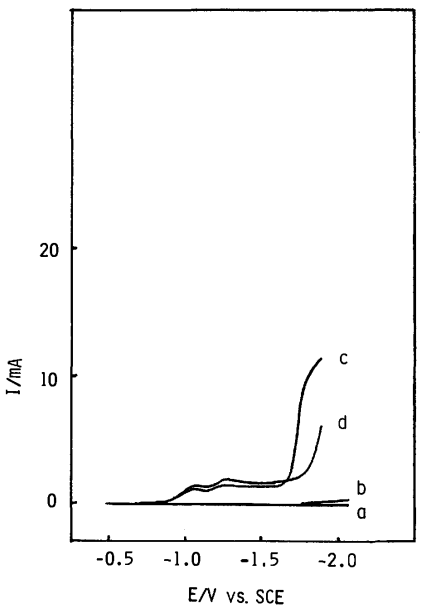

Fig. 4. *I–E* relationships of a solution of 0.1 M $[Bu^n_4N][BF_4]$ in DMF. (a): Without cluster under N_2, (b): Without cluster under CO_2, (c): In the presence of 2 mM cluster **5** under N_2, (d): In the presence of 2 mM cluster **5** under CO_2.

compound $[Fe(SEt)_4]^{2-}$ decomposed immediately in DMF to give an insoluble solid, when CO_2 was bubbled through the solution, and the *I–E* curve of this mixture under CO_2 is just the same as that of the direct noncatalyzed reduction. On the other hand,

the dinuclear compound $[Fe_2S_2(SEt)_4]^{2-}$ was rapidly converted to the cubane cluster with Fe_4S_4 core under the electrolytic condition.[15] Therefore, the *I–E* curve of a solution of this cluster in DMF becomes very close to that of cluster [2−].

Controlled Potential Electrolysis of a Solution of $[Fe_4S_4(SCH_2Ph)_4]^{2-}$ (1) or $[Mo_2Fe_6S_8(SEt)_9]^{3-}$ (4) in DMF Saturated with CO_2. Since a DMF solution of cluster **1** has demonstrated an excellent CO_2 fixing ability under the electroreductive conditions, the preparative controlled potential electrolysis was performed at the potential of −2.0 V vs. SCE by using $[Bu^n_4N][BF_4]$ as suporting electrolyte. Since CO was produced only with 1—2% current efficiency from the present system as reported already,[13] the analysis of the gaseous phase was omitted hereafter and CO_2 was bubbled through the catholyte during electrolysis to enhance the reaction rate.

To determine the lifetime of cluster **1** as catalyst, time-dependence of the concentration of cluster **1** during the electrolysis has been followed by measuring the cyclic voltammograms and the absorption spectra of the reaction solution, which are shown in Fig. 5. In the cyclic voltammograms, the reduction wave at the peak potential of about −1.4 V corresponding to the [2−]→[3−] process is observed clearly at the early stage of the electrolysis but it disappears when the electrolysis is furthermore continued. The absorption spectra of the catholyte also show a rapid decrease of the absorption band at 420 nm characteristic of cluster **1**. These findings indicate that the cubane structure of cluster **1** is preserved only for an initial period and CO_2 fixation catalyzed by cluster **1** occurs only at the early stage. However, it should be noted that the reduction current observed at potentials more negative than −1.5 V increases remarkably after the degradation of the cubane structure. This implies that other type(s) of catalysts may be generated in situ. Analogous rapid decomposition of the cubane structure is also observed when a DMF solution containing molybdenum-iron-sulfur cluster **4** is electrolyzed at −2.0 V under CO_2.

The products in the catholyte were analyzed by HPLC after removing the solid deposited by the addition of water to the electrolyte. A typical liquid chromatogram of the catholyte obtained from the electrolysis of the system containing cluster **1** is given in Fig. 6, which indicates the formation of six products (A—F). None of these peaks appeared in the chromatogram of the catholyte if the reduction was carried out at −2.0 V in the absence of cluster **1**. Formate corresponds to peak B. No oxalate was produced in this catalytic electrolysis. This is in sharp contrast to the predominant formation of oxalate in the electrolysis of CO_2 at −2.4 V in DMF without any catalyst. The product A isolated by preparative HPLC was identified as phenylacetate by its IR and NMR spectra. Isolation of the other products C, D, and E was also attempted. Since the IR spectra of these products in crude forms do not show C=O stretching bands, these compounds are

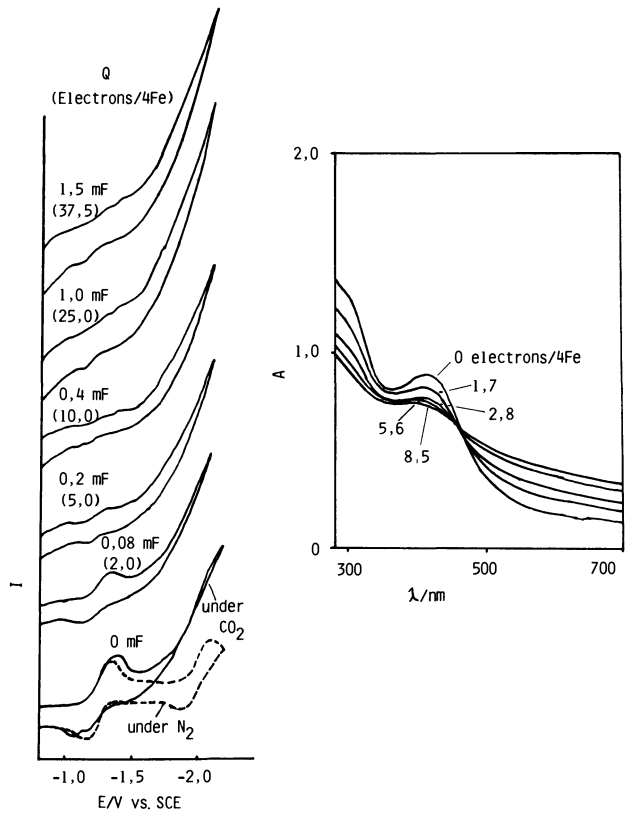

Fig. 5. Dependence of cyclic voltammograms (left) and absorption spectra (right) of a solution of 2 mM cluster 1 in DMF on the electricities passed.

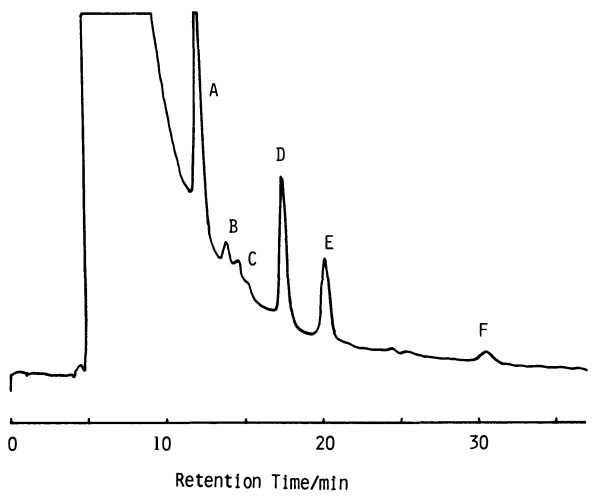

Fig. 6. Liquid chromatogram of the products after the electrolysis in the presence of 2 mM cluster **1** until 1.5 mF of electricities passed.

probably not derived from the electroreduction of CO_2. Thus, more effort to characterize these compounds was abandoned.

When the electrolysis of a DMF solution containing cluster **4** was performed at −2.0 V vs. SCE under CO_2, three products were detected by the HPLC analysis of the catholyte. One of them could be assigned to formate but the yield was quite low. The IR spectra of the other two components in crude forms indicate that these products may not be derived from CO_2. Neither propionate, which may be expected on the analogy of the formation of phenylacetate from the system containing **1**, nor oxalate was produced.

Table 1. Yields of Phenylacetate and Formate Formed by the Controlled Potential Electrolysis Using Cluster **1** as Catalyst Precursor[a)]

Q/mF	Phenylacetate Yield mol/4Fe atoms	Phenylacetate η %	Formate Yield mol/4Fe atoms	Formate η %
0.5	0.40	6.4	0.85	14
1.0	0.50	4.2	2.4	19
1.5	0.58	2.8	3.3	17
2.0	0.68	2.7	5.5	22
3.0	0.75	2.0	10	27
4.0	0.88	1.8	10	20
5.0	0.88	1.4	11	17

a) Cluster **1**: 2 mM; $[Bu^n_4N][BF_4]$: 0.1 M; At −2.0 V vs. SCE.

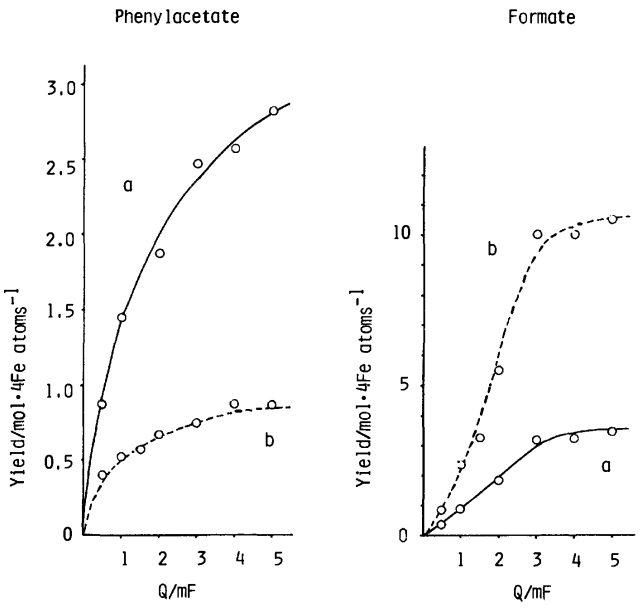

Fig. 7. Yields of phenylacetate and formate formed by the electrolysis of a solution of 2 mM cluster **1** in the presence (full line) or absence (broken line) of excess $PhCH_2SH$.

Formation of Phenylacetate and Formate by Controlled Potential Electrolysis Catalyzed by Cluster 1. In Table 1 are summarized the yields of phenylacetate and formate when the electroreduction of CO_2 in the presence of cluster **1** was continued until the prescribed electricities passed. Current efficiencies (η) are calculated by assuming that two electrons are required in the formations of each product ($H^+ + CO_2 + 2e^- \rightarrow HCOO^-$, $PhCH_2S^- + CO_2 + 2e^- \rightarrow PhCH_2COO^- + S^{2-}$).

The yields of these products are visuallized in Fig. 7 by broken lines. Production of both compounds nearly finished when about 3 mF of electricities passed. The ultimate yield of phenylacetate is close to 1 mol per mol of cluster **1** initially added to the catholyte before the electrolysis. This suggests that phenylacetate is produced from one thiolate ligand of each cubane. Degradation of the cubane structure, which is monitored by the change of cyclic voltammograms and absorption spectra of the reaction mixture, is probably initiated by the conversion of one $PhCH_2S$ ligand into phenylacetate. The final yield of formate amounts to about 10 mol per mol of cluster **1** in the catholyte for the electrolysis continued until 3 mF or more electricities have passed. The optimum current efficiency of 27% for production of formate is observed when 3.0 mF of electricities have passed. The hydrogen atom in formate, at least in part, seems to be derived from tetraalkylammonium ion of the supporting electrolyte or the cation of cluster **1**, since in the gas analysis after the electrolysis were detected considerable amounts of hydrocarbons, which were undetectable in such cases where oxalate was formed predominantly.

Since the conversion of $PhCH_2S$ ligands of cluster **1** into phenylacetate proceeds under this electrolytic conditions concurrent with the collapse of the cubane core, excess $PhCH_2SH$ was added to the catholyte to retain the cubane structure. Table 2 and the full line

Table 2. Yields of Phenylacetate and Formate Formed by the Electrolysis in the Presence of Excess $PhCH_2SH$[a)]

Q/mF	Phenylacetate Yield mol/4Fe atoms	Phenylacetate η %	Formate Yield mol/4Fe atoms	Formate η %
0.5	0.88	14	0.35	5.6
1.0	1.5	12	0.85	6.8
2.0	1.9	7.5	1.8	7.3
3.0	2.5	6.6	3.2	8.5
4.0	2.6	5.2	3.3	6.5
5.0	2.8	4.5	3.5	5.6

a) Cluster **1**: 2 mM; $[Bu^n_4N][BF_4]$: 0.1 M; $PhCH_2SH$: 21 mol/4Fe atoms; At −2.0 V vs. SCE.

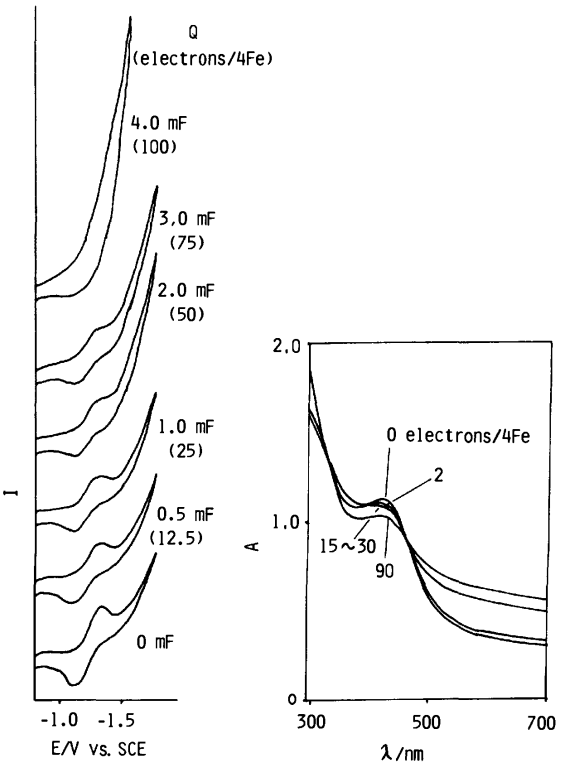

Fig. 8. Dependence of cyclic voltammograms (left) and absorption spectra (right) of a solution of 2 mM cluster **1** in DMF on the electricities passed in the presence of excess $PhCH_2SH$.

in Fig. 7 show the yields of phenylacetate and formate when the electrolysis was carried out in the presence of excess $PhCH_2SH$ (21 mol/mol of cluster **1**). The yield of phenylacetate is approximately tripled compared to that from the original system, whereas the formation of formate is remarkably supressed. Figure 8 illustrates time dependence of cyclic voltammograms and absorption spectra taken during the electrolysis, which definitely shows the retention of the redox wave and the absorption band characteristic of cluster **1**. This indicates that addition of excess $PhCH_2SH$ to the catholyte can prevent degradation of the cluster structure. Since the yield of formate decreases while the cluster structure is maintained, the species that catalyze the formation of formate are not the reduced cluster **1** but the other stuff generated in situ from cluster **1**.

Experimental

Materials. Iron-sulfur compounds, $[Et_4N]_2[Fe_4S_4(SCH_2Ph)_4]$(**1**),[12] $[Me_4N]_2[Fe_4S_4(SBu^t)_4]$(**2**),[12,16] $[Bu^n{}_4N]_2[Fe_4S_4(SPh)_4]$ (**3**),[12] $[Et_4N]_3[Mo_2Fe_6S_8(SEt)_9]$(**4**),[17,18] $[Bu^n{}_4N]_3[Mo_2Fe_6S_8(SPh)_9]$(**5**),[17] $[Et_4N]_3[W_2Fe_6S_8(SEt)_9]$,[17] $[Me_3NCH_2Ph]_2[Fe(SEt)_4]$,[19] and $[Me_3NCH_2Ph]_2[Fe_2S_2(SEt)_4]$[19] were prepared according to the published methods and handled under a nitrogen atmosphere. DMF was dried over CaH_2 and distilled under reduced pressure of N_2 before use.

Electrochemical Apparatus. A cylindrical cell with an anode compartment separated from a cathode by a glass frit and Hokuto Denko instrumentation (HA-501 Potentiostat, HF-201 Coulombmeter and HB-105 Function Generator) were used for the controlled potential electrolysis as well as the recording of current-potential curves and cyclic voltammograms of the catholyte. The mercury pool with 13.5 cm^2 surface area and a platinum plate were employed as working and counter electrodes, respectively, and the potential of the cathode was referred to SCE. The supporting electrolyte was 0.1 M $[Bu^n{}_4N][BF_4]$. Current-potential curves and cyclic voltammograms were recorded under N_2 or CO_2 with the scan rate of 2 and 200 mV s^{-1}, respectively.

Controlled Potential Electrolysis. A DMF solution containing 2 mM cluster **1** or **4** and 0.1 M $[Bu^n{}_4N][BF_4]$ was electrolyzed under CO_2 until the appropriate electricities passed, using the apparatus described above. CO_2 was continually bubbled through the catholyte (20 ml) during the electrolysis. Change in the cluster concentration with time was followed by recording the cyclic voltammograms of the catholyte directly and by measuring the absorption spectra of small portions of the catholyte diluted 4 times with DMF. Absorption spectra were recorded on a Shimadzu UV-240 spectrometer using a quartz cell with 1.0 mm path length connected to a Schlenk tube.

Analysis of the Product by HPLC. To the electrolyte was added water and then the solid precipitated was removed by filtration, which contains the supporting electrolyte and the compounds originated from clusters. The colorless filtrate was adjusted to 100 ml in volume with water and analyzed directly by Toyo Soda HLC-803 equipped with the column packed with a weakly basic anion exchange resin (Toyo Soda DEAE-2SW). The products were eluted at the flow rate of 0.7 ml min^{-1} by the phosphate buffer solution (pH 5.0) prepared by dissolving KH_2PO_4 (9.87 g) in distilled water/acetonitrile (725 ml/275 ml). To analyze oxalate pH of the eluant had to be neutralized up to 6.6. Chromatograms were recorded on a Toyo Soda UV-8 model II detector by monitoring the absorbance at 200 nm. A typical chromatogram is shown in Fig. 6. The amounts of formate and phenylacetate were determined from the calibration curve plotted separately.

Isolation and Characterization of the Products. As for the products formed by the electrolysis using cluster **1** and cluster **4**, an assignment by HPLC was not successful except for formate. Thus, isolation of four products from the former system (peaks A, C, D, and E in Fig. 6) and two from the latter was carried out. After the addition of water (about 200 ml) to the combined catholyte (about 350 ml) of the repeated electrolyses, the mixture was filtered. The filtrate was evaporated to nearly dryness in vacuo and the residue was extracted with water (100 ml×3). The extracts were combined, concentrated to about 50 ml and then fractionated by preparative HPLC. Since the phosphate buffer solution was used as the eluant, all fractions dried up contained KH_2PO_4 as the main component. So the residues were extracted with appropriate solvent by using Soxhlet extractor and the extracts were dried up carefully. The resulting solid or oil was characterized by recording its

IR and NMR spectra on Shimadzu IR-400 and JEOL GX-400 spectrometers, respectively.

The financial support of this research by the Ministry of Education, Science and Culture of Japan (Grant-in-Aid for Scientific Research 60119001) is greatly appreciated.

References

1) E. Lamy, L. Nadjo, and J. M. Savéant, *J. Electroanal. Chem. Interfacial Electrochem.*, **78**, 403 (1977).
2) L. V. Haynes and D. Sawyer, *Anal. Chem.*, **39**, 332 (1967).
3) J. C. Gressin, D. Michelet, L. Nadjo, and J. M. Saveant, *Nouv. J. Chim.*, **3**, 545 (1979).
4) P. G. Russel, N. Kovac, S. Srinivasan, and M. Steinberg, *J. Electrochem. Soc.*, **124**, 1329 (1977).
5) S. Meshitsuka, M. Ichikawa, and K. Tamaru, *J. Chem. Soc., Chem. Commun.*, **1974**, 158.
6) K. Hiratsuka, H. Sasaki, and S. Toshima, *Chem. Lett.*, **1977**, 1137.
7) K. Takahashi, K. Hiratsuka, H. Sasaki, and S. Toshima, *Chem. Lett.*, **1979**, 305.
8) B. Fisher and R. Eisenberg, *J. Am. Chem. Soc.*, **102**, 7361 (1980).
9) M. Beley, J.-P. Collin, R. Ruppert, and J.-P. Sauvage, *J. Chem. Soc., Chem. Commun.*, **1984**, 1315.
10) J. Hawecker, J.-M. Lehn, and R. Ziessel, *J. Chem. Soc., Chem. Commun.*, **1984**, 328.
11) S. Slater and J. H. Wagenknecht, *J. Am. Chem. Soc.*, **106**, 5367 (1984).
12) B. A. Averill, T. Herskovitz, R. H. Holm, and J. A. Ibers, *J. Am. Chem. Soc.*, **95**, 3524 (1973).
13) M. Tezuka, T. Yajima, A. Tsuchiya, Y. Matsumoto, Y. Uchida, and M. Hidai, *J. Am. Chem. Soc.*, **104**, 6834 (1982).
14) V. Kaiser and E. Heitz, *Ber. Bunsen. Gesell.*, **77**, 818 (1973).
15) J. Cambray, R. W. Lane, A. G. Wedd, R. W. Johnson, and R. H. Holm, *Inorg. Chem.*, **16**, 2565 (1977).
16) G. Christou and C. D. Garner, *J. Chem. Soc., Dalton Trans.*, **1979**, 1093.
17) G. Christou and C. D. Garner, *J. Chem. Soc., Dalton Trans.*, **1980**, 2354.
18) T. E. Wolff, J. M. Berg, K. O. Hodgson, R. B. Frankel, and R. H. Holm, *J. Am. Chem. Soc.*, **101**, 4140 (1979).
19) K. S. Hagen, A. D. Watson, and R. H. Holm, *J. Am. Chem. Soc.*, **105**, 3905 (1983).

 © 1986 The Chemical Society of Japan Bull. Chem. Soc. Jpn., 59, 815—818 (1986)

(*Z*)- and (*E*)-4,4-Dimethyl-5-oxo-2-pentenoic Acids and Their Derivatives

Kunio Ito and Shingo Miyajima*
Department of Applied Chemistry, Faculty of Engineering, Toyo University,
Kawagoe, Saitama 350
(Received October 21, 1985)

(*Z*)-4,4-Dimethyl-5-oxo-2-pentenoic acid (**1**) exists almost exclusively in the hydroxy lactone form, the tautomeric equilibrium constant (K=[Ring]/[Chain]) being 2.8×10^3 in water as estimated by the pK_a method. Several examples are described of preference for ring forms of derivatives of **1**, which are capable of exhibiting ring-chain tautomerism. (*E*)-4,4-Dimethyl-5-oxo-2-pentenoic acid (**7**) reacts with thionyl chloride to afford a trimeric chloro lactone, which on treatment with water or aniline gives the corresponding hydroxy or anilino lactone. Compound **1** or **7** reacts with a variety of phenylhydrazines to yield dihydropyrazole derivatives, except for 2,4-dinitrophenylhydrazine which on reaction with **1** gives a 2,4-dinitrophenylhydrazino lactone.

Recently (*Z*)-4,4-dimethyl-5-oxo-2-pentenoic acid (**1**) has been concluded to exist predominantly in the hydroxy lactone form (**1r**) on the basis of its IR and ^{1}H NMR spectra.[1,2] It seems of interest to examine this compound in more detail since six-membered hydroxy lactones have rarely been reported[1-3] and little is known about their ring-chain tautomerism or derivatives; five-membered ones have been extensively studied.[4] We report in this paper an investigation of the tautomerism and derivatives of **1**. We also report on the cyclic trimers of (*E*)-4,4-dimethyl-5-oxo-2-pentenoic acid (**7**) and its chloride and anilide.

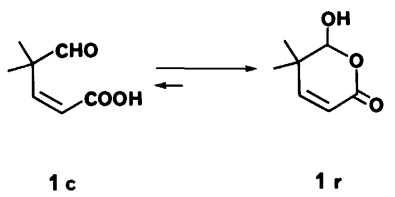

Fig. 1.

Although **1r** is the virtually sole detectable form, a rapid interconversion between **1r** and **1c** on the NMR time scale at ordinary temperature could be verified;[5] when less than one equivalent of *t*-butylamine as a base was added to **1** in water, the averaged resonances of **1r** and the *t*-butylammonium salt of **1c** appeared instead of the superposition of the individual ones.

The equilibrium constant, K, in water at 25 °C was estimated by the pK_a method. The observed pK_a value of **1** (7.63) can be related to p$K_{a,0}$ by Eq. 2[6]

$$K = [\mathbf{1r}]/[\mathbf{1c}], \quad (1)$$

$$pK_{a,0} = pK_a - \log(K+1), \quad (2)$$

where p$K_{a,0}$ denotes the hypothetical pK_a of **1c**. The p$K_{a,0}$ was estimated to be 4.18 from the pK_a of **7** (4.45) and the Hammett relations of the K_a values in (*Z*)- and (*E*)-3-substituted acrylic acids.[7] By applying Eq. 2 K was calculated to be 2.8×10^3. This strong preference of **1** for cyclization exhibits a marked contrast to the case of 5-oxoalkanoic acids which show no sign of cyclization.[4]

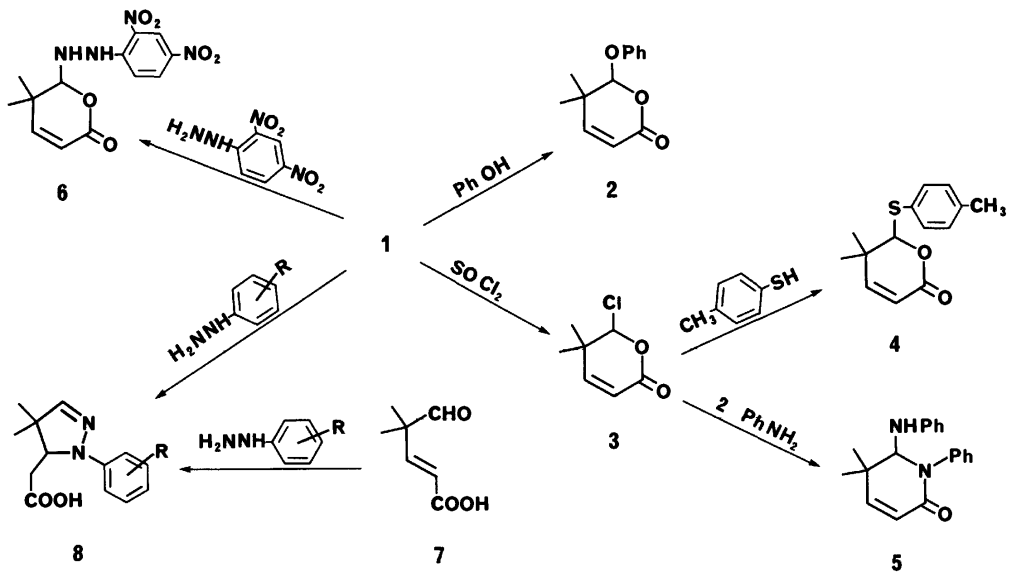

Fig. 2.

As described in our preceding paper,[2] methyl (*Z*)-4,4-dimethyl-5-oxo-2-pentenoate in methanol containing H_2SO_4 or sodium methoxide as a catalyst isomerizes almost completely to 6-methoxy-5,5-dimethyl-5,6-dihydro-2*H*-pyran-2-one. Further examples of preference for ring forms of the derivatives of **1**, which are capable of exhibiting ring-chain tautomerism, are described below. Compound **1** reacted with phenol in the presence of H_2SO_4–H_3BO_3 as a catalyst[8] to give the phenoxy lactone **2**. Treatment of **1** with thionyl chloride yielded the chloro lactone **3**. Compound **3** on reaction with *p*-toluenethiol or two equivalents of aniline afforded the *p*-tolylthio lactone **4** or the anilino lactam **5**.

Compound **1** or the (*E*)-isomer **7**, prepared by hydrolysis of methyl (*E*)-5-(*t*-butylimino)-4,4-dimethyl-2-pentenoate,[2] reacted with a variety of phenylhydrazines to afford the dihydropyrazoles **8** (Tables 1 and 2). Structural assignment was based primarily on their ^1H NMR spectra. The methylene protons in **8** are rendered non-equivalent by the adjacent chiral center and form part AB of pattern ABX. 2,4-Dinitrophenylhydrazine, on the other hand, on reaction with **1** gave the hydrazino lactone **6**. Presumably, the nucleophilicity of the –NH– nitrogen of the initially formed hydrazone is insufficient for addition to moiety –CH=CH–CO_2H.

It is interesting to note that, when **7** was allowed to react with thionyl chloride, the trimeric chloro lactone **9** was obtained in 48% yield. The trimeric

Table 1. Yields, Melting Points, and Analytical Data of **8**

R	Formyl acid	Method	Yield %	Mp θ_m/°C	Found/%			Calcd/%		
					C	H	N	C	H	N
H	1	A	82	124.0—124.8	67.19	6.84	11.99	67.22	6.94	12.06
H	7	A	80							
p-NO_2	1	A	83	195.8—196.5	56.56	5.52	15.14	56.31	5.42	15.15
p-NO_2	7	A	90							
p-Cl	1	B	87	131.0—131.7	58.78	5.58	10.34	58.54	5.67	10.50
p-Cl	7	B	82							
p-Br	7	B	84	139.8—140.4	50.14	4.75	8.96	50.18	4.86	9.00
p-Me	7	B	80	153.3—154.2	68.57	7.30	11.37	68.27	7.37	11.37
p-MeO	7	B	70	121.0—121.6	64.30	7.01	10.66	64.11	6.92	10.68
m-NO_2	1	B	86	140.3—140.8	56.21	5.25	15.23	56.31	5.45	15.15
m-NO_2	7	B	84							
m-Cl	7	B[a]	88	124.7—126.2	58.38	5.60	10.44	58.54	5.67	10.50
m-Me	7	B	78	125.5—126.2	68.09	7.41	11.19	68.27	7.37	11.37

a) *m*-Chlorophenylhydrazine sulfate was used.

Table 2. Spectral Data of **8**

R	IR(KBr)/cm^{-1} C=O	^1H NMR($CDCl_3$)[a]/δ(J/Hz)					
		$(CH_3)_2C$	CH_2	CH	CH=N	CO_2H	Others
H	1717	1.21 s and 1.23 s	2.50 dd and 2.75 dd (17, 9.5) (17, 4)	4.19 dd (9.5, 4)	6.51 s	11.40 br s	
p-NO_2	1698	1.23 s and 1.26 s	2.50 dd and 2.55 dd (17, 8) (17, 5)	4.34 dd (8, 5)	6.95 s	12.70 br s	
p-Cl	1704	1.25 s	2.53 dd and 2.66 dd (17, 9) (17, 4)	4.26 dd (9, 4)	6.56 s	11.35 br s	
p-Br	1704	1.24 s	2.53 dd and 2.66 dd (17, 9) (17, 4)	4.15 dd (9, 4)	6.54 s	10.80 br s	
p-Me	1698	1.20 s and 1.24 s	2.52 dd and 2.70 dd (17, 9.5) (17, 4)	4.13 dd (9.5, 4)	6.51 s	11.05 br s	2.25 s, $ArCH_3$
p-MeO	1712	1.17 s and 1.26 s	2.52 dd and 2.65 dd (17, 9) (17, 4.5)	3.97 dd (9, 4.5)	6.52 s	11.00 br s	3.74 s, OCH_3
m-NO_2	1698	1.29 s	2.56 dd and 2.69 dd (17, 8.5) (17, 5)	4.30 dd (8.5, 5)	6.61 s	10.30 br s	
m-Cl	1698	1.24 s	2.53 dd and 2.68 dd (17, 9) (17, 4)	4.20 dd (9, 4)	6.53 s	11.20 br s	
m-Me	1695	1.25 s	2.55 dd and 2.74 dd (17, 9) (17, 4)	4.20 dd (9, 4)	6.55 s	11.40 br s	2.32 s, $ArCH_3$

a) Aromatic protons are omitted. In the case of **8** (R=*p*-NO_2), $(CD_3)_2SO$ was used as a solvent.

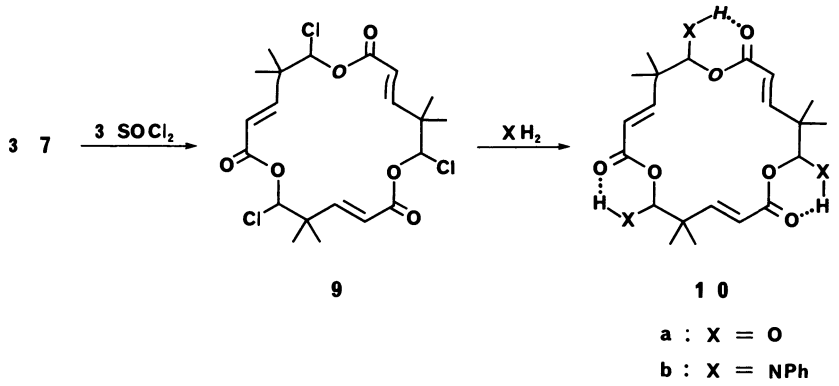

Fig. 3.

structure was confirmed by a relevant mass spectrum showing peaks at m/z 447 and 445 due to $(M-Cl)^+$ and further by vapor phase osmometry. With water or aniline **9** yielded the corresponding hydroxy (**10a**) [MS (CI) m/z 427 $(M+H)^+$] or anilino lactone (**10b**) [MS m/z 651 (M^+)]. In each of these crown-type compounds, the three methine protons occur as a single absorption in the ^1H NMR spectrum (δ 4.49—4.61). This suggests that these protons may have the cis configuration.

Experimental

All melting points and boiling points are uncorrected. IR spectra were recorded on a Hitachi 285 spectrometer. ^1H NMR data were obtained with a Hitachi R-24B spectrometer by using TMS or DSS as an internal standard. Mass spectra were measured with a Shimadzu GCMS-QP1000 spectrometer at 70 eV of ionization energy by use of a direct-inlet system. Microanalyses were performed at the Microanalysis Laboratory, Department of Chemistry, Faculty of Science, the University of Tokyo.

Observation of Progress of the Neutralization of 1 by ^1H NMR Spectroscopy. To a solution of **1** (30.0 mg, 0.211 mmol) in D_2O (0.50 ml) was added *t*-butylamine (15.6 mg, 0.213 mmol) in six portions. A typical signal of **1r** at δ 5.43 due to the methine proton shifted, on addition of the base, toward 9.34 due to an aldehyde proton proportionally to the amount of the base added.

pK_a Measurements. pK_a values were determined at 25±0.1 °C in N_2 by titration of acids in water (0.05 M, 1 M=1 mol dm^{-3}) with aq NaOH (0.05 M) under control by a pH meter with glass and calomel electrodes. The instrument was calibrated by using 0.05 M potassium hydrogen phthalate (pH 4.01 at 25 °C) and 0.01 M sodium tetraborate (pH 9.18 at 25 °C).

5,5-Dimethyl-6-phenoxy-5,6-dihydro-2*H*-pyran-2-one (2). A mixture of **1** (1.50 g, 10.6 mmol), phenol (15.0 g, 159 mmol), H_2SO_4 (20 mg, 0.20 mmol), H_3BO_3 (5 mg, 0.08 mmol), and toluene (25 ml) was refluxed under a water separator for 1 h. Water (60 ml) was added, and the aq layer was separated and extracted with ether (2×30 ml). The combined organic layers were dried (Na_2SO_4), concentrated, and distilled, giving 1.89 g of a fraction, bp 130.0—132.0 °C/0.35 mmHg (1 mmHg=133.322 Pa), which on standing crystallized (mp 65.0—74.0 °C). Recrystallization from ethyl acetate afforded 1.42 g (62%) of **2**: Mp 74.0—76.8 °C; mp 76.5—77.5 °C after further recrystallization; IR (KBr) 1727 cm^{-1} (C=O); ^1H NMR ($CDCl_3$) δ=1.22 (s, 6H, $C(CH_3)_2$), 5.49 (d, J=1 Hz, 1H, CH), 5.86 (d, J=9.5 Hz, 1H, CH=C<u>H</u>CO), 6.58 (dd, J=9.5, 1 Hz, 1H, C<u>H</u>=CHCO), and 6.9—7.4 (m, 5H, ArH). Found: C, 71.69; H, 6.47%. Calcd for $C_{13}H_{14}O_3$: C, 71.54; H, 6.47%.

6-Chloro-5,5-dimethyl-5,6-dihydro-2*H*-pyran-2-one (3). Thionyl chloride (7.00 g, 58.8 mmol) was added with stirring to **1** (7.11 g, 50.0 mmol) during 10 min. The mixture was allowed to stand at room temperature for 20 min and then heated at 65 °C for 20 min. Removal of the excess of thionyl chloride in vacuo and distillation gave 5.18 g (65%) of **3**: Bp 77.0—78.5 °C/0.55 mmHg; IR (neat) 1747 cm^{-1} (C=O); ^1H NMR ($CDCl_3$) δ=1.27 (s, 3H, CH_3), 1.32 (s, 3H, CH_3), 5.88 (d, J=9.5 Hz, 1H, CH=C<u>H</u>CO), 5.96 (d, J=1.5 Hz, 1H, CH), and 6.66 (dd, J=9.5, 1.5 Hz, 1H, C<u>H</u>=CHCO). Found: C, 52.17; H, 5.85%. Calcd for $C_7H_9ClO_2$: C, 52.35; H, 5.65%.

5,5-Dimethyl-6-(*p*-tolylthio)-5,6-dihydro-2*H*-pyran-2-one (4). A solution of **3** (1.50 g, 9.34 mmol) and *p*-toluenethiol (1.67 g, 13.4 mmol) in pyridine (8.0 ml) was refluxed for 5 h. Water (40 ml) was added and the mixture was extracted with ether (3×30 ml). The ethereal extract was dried (Na_2SO_4), concentrated, and distilled to give 1.93 g (83%) of **4**: Bp 141.0—143.0 °C/0.25 mmHg; mp 71.5—75.0 °C; mp 75.0—75.6 °C after recrystallization from cyclohexane; IR (KBr) 1720 cm^{-1} (C=O); ^1H NMR ($CDCl_3$) δ=1.22 (s, 3H, CH_3), 1.28 (s, 3H, CH_3), 2.26 (s, 3H, $ArCH_3$), 5.20 (s, 1H, CH), 5.74 (d, J=9.5 Hz, 1H, CH=C<u>H</u>CO), 6.51 (d, J=9.5 Hz, 1H, C<u>H</u>=CHCO), and 6.9—7.4 (m, 4H, ArH). Found: C, 67.74; H, 6.53%. Calcd for $C_{14}H_{16}O_2S$: C, 67.71; H, 6.49%.

6-Anilino-5,5-dimethyl-1-phenyl-5,6-dihydro-2(1*H*)-pyridinone (5). A mixture of **3** (0.287 g, 1.79 mmol) and aniline (1.01 g, 10.8 mmol) was heated at 100 °C for 2 h. Water (5 ml) was added, and the mixture was extracted with ether (3×5 ml). The ethereal extract was dried (Na_2SO_4) and concentrated. After removal of the excess of aniline in vacuo, the residual solid was recrystallized from benzene-hexane, giving 0.326 g (62%) of **5**: Mp 135.5—139.0 °C; mp 141.0—141.7 °C after further recrystallization; IR (KBr) 3305 (NH), 1655 (C=O), and 1610 cm^{-1} (sh, C=C); ^1H NMR ($CDCl_3$) δ=1.20 (s, 3H, CH_3), 1.42 (s, 3H, CH_3), 4.42 (br d, J=11 Hz, 1H, NH), 4.92 (br dd, J=11, 1.5 Hz, 1H, CH), 6.00 (d, J=10 Hz, 1H, CH=C<u>H</u>CO), 6.32 (dd, J=10, 1.5 Hz, 1H, C<u>H</u>=CHCO), and 6.2—7.4 (m, 10H, ArH). Addition of

D_2O resulted in loss of the signal at 4.42 and collapse of the signal at 4.92 to a doublet (J=1.5 Hz). Found: C, 78.35; H, 6.91; N, 9.29%. Calcd for $C_{19}H_{20}N_2O$: C, 78.05; H, 6.89; N, 9.58%.

6-(2,4-Dinitrophenylhydrazino)-5,5-dimethyl-5,6-dihydro-2*H*-pyran-2-one (6). To a hot solution of 2,4-dinitrophenylhydrazine (0.204 g, 1.03 mmol) in 0.1 M HCl (60 ml) was added **1** (0.141 g, 0.992 mmol) in water (2.0 ml). The mixture was heated under reflux for 8 h. The crude solid was collected, washed with water, dried, and recrystallized from ethyl acetate to afford 0.163 g (51%) of **6**: Mp 173.5—176.0 °C; mp 176.0—176.5 °C after an additional recrystallization from benzene; IR (KBr) 3370, 3348 (NH), 1670 (C=O), and 1614 cm^{-1} (C=C); ^1H NMR [$(CD_3)_2SO$] δ=1.19 (s, 3H, CH_3), 1.28 (s, 3H, CH_3), 4.81 (dd, J=5, 1 Hz, 1H, CH), 5.82 (d, J=9.5 Hz, 1H, CH=C<u>H</u>CO), 6.58 (dd, J=9.5, 1 Hz, 1H, C<u>H</u>=CHCO), 6.79 (br d, J=5 Hz, 1H, N<u>H</u>NHAr), 7.26—8.82 (m, 3H, ArH), and 9.97 (br s, 1H, NHN<u>H</u>Ar). Addition of D_2O resulted in loss of the signals at 6.79 and 9.97 and collapse of the signal at 4.81 to a doublet (J=1 Hz). Found: C, 48.25; H, 4.19; N, 17.24%. Calcd for $C_{13}H_{14}N_4O_6$: C, 48.45; H, 4.38; N, 17.38%.

(*E*)-4,4-Dimethyl-5-oxo-2-pentenoic Acid (7). A mixture of methyl (*E*)-5-(*t*-butylimino)-4,4-dimethyl-2-pentenoate[2] (21.2 g, 0.100 mol) and 4 M HCl (150 ml) was refluxed for 5 h. The reaction mixture was extracted with ether (3×50 ml). The ethereal extract was washed with water, dried (Na_2SO_4), concentrated, and distilled to give 10.6 g (75%) of **7**: Bp 115.0—117.0 °C/0.20 mmHg; mp 55.5—56.1 °C; IR (KBr) 3000 (OH), 2815, 2700 (CHO), 1720, 1682 (C=O), 1635 (C=C), and 988 cm^{-1} (H>C=C<H); ^1H NMR (CCl_4) δ=1.28 (s, 6H, $C(CH_3)_2$), 5.81 (d, J=16 Hz, 1H, CH=C<u>H</u>COOH), 7.00 (d, J=16 Hz, 1H, C<u>H</u>=CHCOOH), 9.37 (s, 1H, CHO), and 11.98 (br s, 1H, COOH). Found: C, 58.85; H, 7.16%. Calcd for $C_7H_{10}O_3$: C, 59.14; H, 7.09%.

1-Aryl-4,4-dimethyl-4,5-dihydro-1*H*-pyrazole-5-acetic Acids (8). Typical examples are as follows:

A: A solution of *p*-nitrophenylhydrazine (0.161 g, 1.05 mmol) in acetic acid-water (1:1, w/w) (3.0 ml) was refluxed with **1** (0.144 g, 1.01 mmol) for 3 h. Water (5.0 ml) was added and the mixture was cooled. The crystalline product was collected, washed with water, and dried, giving 0.234 g (83%) of **8** (R=*p*-NO_2), mp 195.3—196.3 °C. An analytical sample was prepared by recrystallization from ethanol-cyclohexane.

B: A solution of *p*-chlorophenylhydrazine hydrochloride (0.186 g, 1.04 mmol) and anhydrous sodium acetate (0.085 g, 1.04 mmol) in acetic acid-water (1:1, w/w) (3.0 ml) was refluxed with **7** (0.142 g, 1.00 mmol) for 3 h. Working up as described above gave 0.219 g (82%) of **8** (R=*p*-Cl), mp 128.0—130.0 °C. An analytical sample was prepared by recrystallization from ethanol-cyclohexane.

(3*E*,9*E*,15*E*)-6,12,18-Trichloro-5,5,11,11,17,17-hexamethyl-1,7,13-trioxacyclooctadeca-3,9,15-triene-2,8,14-trione (9). Thionyl chloride (8.85 g, 74.4 mmol) was added dropwise to **7** (10.0 g, 70.3 mmol) during 10 min. The mixture was allowed to stand overnight at room temperature. The resulting solid was recrystallized from chloroform to give 3.59 g of **9**, mp 153.5—156.7 °C. Further recrystallization from the mother liquor afforded an additional 1.87 g, mp 150.5—155.0 °C; overall yield 48%. The pure sample after additional recrystallizations had mp 156.8—157.5 °C: IR (KBr) 1754 (C=O), 1628 (C=C), and 987 cm^{-1} (H>C=C<H); ^1H NMR ($CDCl_3$) δ=1.15 (s, 18H, $6CH_3$), 4.61 (s, 3H, 3CH), 6.01 (d, J=15.5 Hz, 3H, 3CH=C<u>H</u>CO), and 7.18 (d, J=15.5 Hz, 3H, 3C<u>H</u>=CHCO); MS *m/z* (rel intensity) 447 (6), 446 (2), 445 (9), and 125 (100). Found: C, 52.48; H, 5.46; Cl, 22.04%; M, 480 (measured with a Corona 117 vapor pressure osmometer). Calcd for $C_{21}H_{27}Cl_3O_6$: C, 52.35; H, 5.65; Cl, 22.08%; M, 481.8.

Compound 10a. A solution of 0.483 g (1.00 mmol) of **9** in 50 ml of tetrahydrofuran containing 1.0 ml of water was kept at room temperature for 15 h. The solution was concentrated in vacuo to ca. 2 ml. Water (10 ml) was added and the mixture was extracted with chloroform (3×20 ml). The chloroform extract was dried (Na_2SO_4) and evaporated in vacuo. The residual solid was dried at 110 °C in vacuo for 3 h and recrystallized from chloroform to afford 0.378 g (88%) of **10a**: Mp 200.3—201.8 °C; IR (KBr) 3000 (OH), 1692 (C=O), 1649 (C=C), and 983 cm^{-1} (H>C=C<H); ^1H NMR ($CDCl_3$) δ=1.10 (s, 18H, $6CH_3$), 4.51 (s, 3H,3CH), 5.82 (d, J=16 Hz, 3H, 3CH=C<u>H</u>CO), 7.02 (d, J=16 Hz, 3H, 3C<u>H</u>=CHCO), and 11.8 (br s, 3H, 3OH); MS (CI) *m/z* 427 $(M+H)^+$. Found: C, 59.14; H, 6.99%. Calcd for $C_{21}H_{30}O_9$: C, 59.14; H, 7.09%.

Compound 10b. To a stirred solution of **9** (0.482 g, 1.00 mmol) in chloroform (20 ml) was added a solution of aniline (0.281 g, 3.02 mmol) and triethylamine (0.304 g, 3.00 mmol) in chloroform (5 ml) during 15 min. Stirring was continued for an additional 3 h. The mixture was washed with water (3×25 ml) and dried (Na_2SO_4). The solvent was removed in vacuo and the residual solid was recrystallized from chloroform, giving 0.546 g (84%) of **10b**: Mp 138.5—140.5 °C; mp 141.0—142.0 °C after further recrystallization; IR (KBr) 3270 (NH), 1663 (C=O), and 977 cm^{-1} (H>C=C<H); ^1H NMR ($CDCl_3$) δ=1.01 (br s, 18H, $6CH_3$), 4.49 (s, 3H, 3CH), 6.01 (d, J=15 Hz, 3H, 3CH=C<u>H</u>CO), 6.92 (d, J=15 Hz, 3H, 3C<u>H</u>=CHCO), 6.9—7.7 (m, 15H, ArH), and 8.45 (br s, 3H, 3NH); MS *m/z* 651 (M^+). Found: C, 71.59; H, 6.84; N, 6.39%. Calcd for $C_{39}H_{45}N_3O_6$: C, 71.87; H, 6.96; N, 6.45%.

References

1) A. A. Frimer, P. Gilinsky-Sharon, and G. Aljadeff, *Tetrahedron Lett.*, **23**, 1301 (1982).

2) S. Miyajima and K. Ito, *Bull. Chem. Soc. Jpn.*, **58**, 2659 (1985).

3) For six-membered hydroxy lactones in steroidal systems, see E. Caspi, W. Schmid, and B. T. Khan, *Tetrahedron*, **18**, 767 (1962); M. Kocór, A. Kurek, and J. Dabrowski, ibid., **25**, 4257 (1969).

4) See, e.g., "Rodd's Chemistry of Carbon Compounds," 2nd ed, ed by S. Coffey, Elsevier, New York, Vol. 1, Chap. 16 (1965) and Vol. 3, Chap. 17 (1974).

5) J. Kagan, *J. Org. Chem.*, **32**, 4060 (1967).

6) C. Pascual, D. Wegmann, U. Graf, R. Scheffold, P. F. Sommer, and W. Simon, *Helv. Chim. Acta*, **47**, 213 (1964).

7) K. Bowden, *Can. J. Chem.*, **43**, 3354 (1965).

8) W. W. Lowrance, Jr., *Tetrahedron Lett.*, **1971**, 3453.

Pseudo-Sugars. XIV. Synthesis of Sweet-Tasting Pseudo-β-DL-fructopyranose

Tetsuo SUAMI,* Seiichiro OGAWA, Makoto TAKATA, Kuninobu YASUDA, Kiyoshi TAKEI, and Atsuo SUGA
Department of Applied Chemistry, Faculty of Science and Technology, Keio University, Hiyoshi, Yokohama 223
(Received November 16, 1985)

Pseudo-β-DL-fructopyranose was synthesized from DL-1,2-di-*O*-acetyl-(1,3/2)-3-bromomethyl-5-cyclohexene-1,2-diol by a six steps reaction: Dehydrobromination, epoxidation, acetolysis, reduction, and deacetylation, in overall yield of 4.8%. Pseudo-β-DL-fructopyranose was found to be nearly as sweet as D-fructose which is the most sweet sugar known in naturally occurring carbohydrates.

In the preceding paper,[1] it was described that pseudo-β-DL-glucopyranose was equally as sweet as D-glucose. Therefore, a ring-oxygen in a pyranoid sugar plays no important role in an appearance of sweetness and a replacement of the ring-oxygen by a methylene group gives no detrimental effect on an intensity of its sweetness. This is not surprising, since a conformational feature of sweetness eliciting units, an AH (proton donor), a B (proton acceptor)[2-5] and a third hydrophobic component (γ),[6] of the pyranoid sugar with a distance of 0.30 (AH–B), 0.35 (AH–γ) and 0.55 nm (B–γ) is almost the same as those of the pseudo-hexopyranose.

While D-fructose is the most sweet sugar known in naturally occurring carbohydrates and its intense sweetness (1.8 times more sweet than sucrose) is attributable only to a β-D-fructopyranose form.[2,7,8] And it is anticipated that pseudo-β-D-fructopyranose must be fairly sweet. This expectation prompted us to synthesize pseudo-β-DL-fructopyranose (**1**) for an evaluation of its sweetness. A starting material used in the present synthesis is known DL-1,2-di-*O*-acetyl-(1,3/2)-3-bromomethyl-5-cyclohexene-1,2-diol[9] (**3**).

Results and Discussion

Dehydrobromination of **3** with 1,8-diazabicyclo-[5.4.0]undec-7-ene (DBU) in toluene afforded the aimed diene diacetate (**5**) as a major product in 56% yield, and the triacetate (**4**) as a minor by-product in 12% yield. The structure of **5** was elucidated by the ^{1}H NMR spectrum that exhibited the two broad singlets due to the methylene protons of the cyclic and exocyclic double bond at δ 3.00 (2H) and 5.05 (3H), respectively. Compound **4** is considered to be formed by a substitution of the bromo group in **3** with an acetate ion generated in situ by a partial deacetylation of **3**.

Preferential epoxidation of the exocyclic double bond in **5** with *m*-chloroperbenzoic acid (*m*CPBA) in the presence of phosphate buffered solution (pH 8) gave the epoxide (**6**) in 52% yield (based on **5** consumed) and a complex mixture which consisted

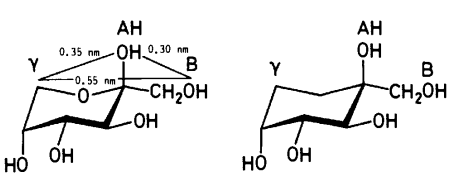

β-D-Fructopyranose Pseudo-β-D-fructopyranose

Scheme 1.

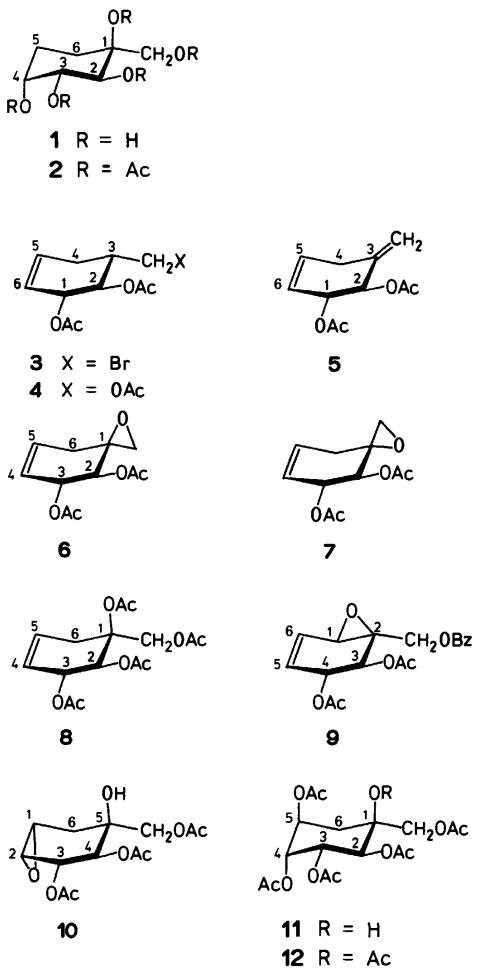

Formulas depict only one of the respective enantiomers.

Scheme 2.

mainly of another epoxide (**7**).[10] The structure of **6** was deduced from the following successive reactions.

Nucleophilic opening of the oxirane ring of **6** with an acetate ion, followed by acetylation with acetic anhydride and 4-dimethylaminopyridine (DMAP) gave the crystalline tetraacetate (**8**) as a sole product in 81% yield. The structure of **8** was elucidated by the fact that **8** was also obtained from known DL-3,4-di-*O*-acetyl-1,2-anhydro-(1,2,3/4)-2-*C*-benzoyloxymethyl-5-cyclohexene-1,2,3,4-tetrol[11] (**9**) by $LiAlH_4$ reduction, hydrolysis and subsequent acetylation.

Deacetylation of **8** in methanolic sodium methoxide and successive epoxidation with *m*CPBA in acetic acid for 6 d, followed by acetylation afforded the epoxide triacetate (**10**) in 59% yield, as well as the pentaacetate (**11**) in 12% yield. The structure of **10** was established by the ^1H NMR spectrum that showed a doublet of doublets at δ 3.50 (J=4.2 and 2.3 Hz), a doublet of doublets at δ 5.58 (J=9 and 2.3 Hz), and another doublet at δ 5.18 (J=9 Hz). These signals were attributable to H-2, H-3, and H-4, respectively. The structure of **11** was also assigned by the ^1H NMR spectrum that revealed four sharp singlets due to the five acetoxyl groups at δ 1.98 (3H), 2.07 (3H), 2.09 (6H), and 2.11 (3H). Furthermore, an exhaustive acetylation of **11** with acetic anhydride in the presence of DMAP gave the crystalline hexaacetate (**12**), which showed four sharp singlets ascribed to the six acetoxyl groups at δ 1.96 (3H), 2.04 (9H), 2.06 (3H), and 2.10 (3H) in its ^1H NMR spectrum.

Epoxidation of the double bond of the deacetylated **8** with *m*CPBA in acetic acid seemed to proceed stereoselectively with a cis-directing effect of the vicinal hydroxyl group on C-3[12] and **10** was obtained as a primary product, and a part of **10** was converted to **11** by hydrolysis during the prolonged reaction period of 6 d.

Reduction of **10** with $LiAlH_4$ in THF, followed by acetylation afforded the pentaacetate (**2**), mp 147—148 °C in 34% yield. The ^1H NMR spectrum of **2** revealed a doublet of doublets at δ 5.17 (J=10.5 and 3.3 Hz) which was due to an axial proton on C-3 coupled with an equatorial proton on C-4. The reaction seemed to proceed regioselectively through a reductive opening of the oxirane ring which was conducted by an existence of an axial tertiary hydroxyl group on C-5.[13]

Deacetylation of **2** in methanolic sodium methoxide gave pseudo-β-DL-fructopyranose **1** as a syrup in a quantitative yield. An evaluation of an intensity of its sweetness was carried out with six college personnel by a comparison with D-fructose, and **1** was found to be nearly as sweet as D-fructose.

Experimental

General. Melting points were determined on a Büchi 510 capillary melting point apparatus and are uncorrected. ^1H NMR spectra were taken on a Varian EM-390 (90 MHz) in chloroform-*d* with a reference to tetramethylsilane as an internal standard. TLC was performed on a plate coated with silica gel 60 F-254 (Merck, Darmstadt). The silica gel used for a column chromatography was Wakogel C-300 (Wako Co., Osaka). Organic solutions were dried over anhydrous sodium sulfate and concentrated below 45 °C under reduced pressure.

DL-(1,3/2)-1,2-Diacetoxy-3-acetoxymethyl-5-cyclohexene (4) and DL-*trans*-1,2-diacetoxy-3-methylene-5-cyclohexene (5). A mixture of DL-(1,3/2)-1,2-diacetoxy-3-bromomethyl-5-cyclohexene[9] (**3**) (22.3 g, 77 mmol), DBU (25 ml, 160 mmol) and toluene (250 ml) was stirred at 120 °C for 2.5 h. The cooled mixture was washed successively with 1 M hydrochloric acid(1 M=1 mol dm^{-3}), aqueous sodium hydrogencarbonate and water, dried, and concentrated, giving 15.8 g of a crude mixture of products. Chromatography on a silica-gel column (390 g) with ethyl acetate-toluene (1:20, v/v) as an eluant gave 9.1 g (56%) of **5** as a syrup: TLC, R_f=0.44 (ethyl acetate-toluene, 1:8); ^1H NMR ($CDCl_3$, 90 MHz) δ=2.04 (3H, s) and 2.10 (3H, s) (2 OAc), 2.87—3.03 (2H, m, H-4 and 4'), 5.00—5.10 (3H, m, H-1, 7, and 7'), 5.44 (1H, narrow m, H-2), 5.60 (1H, dq, $J_{5,6}$=10,5 Hz, $J_{1,5}$=$J_{4,5}$=$J_{4',5}$=2 Hz, H-5), 5.89 (1H, dt, $J_{1,6}$=$J_{4,6}$=3.4 Hz, H-6).

Found: C, 62.85; H, 6.71%. Calcd for $C_{11}H_{14}O_4$: C, 62.61; H, 6.67.

Another fraction gave 2.6 g (12%) of **4** as a syrup: TLC, R_f=0.20 (ethyl acetate-toluene, 1:8). ^1H NMR ($CDCl_3$, 90 MHz) δ=2.00 (6H, s) and 2.03 (3H, s) (3 OAc), 3.92 (1H, dd, $J_{3,7}$=5 Hz, J_{7gem}=11.3 Hz, H-7), 4.20 (1H, dd, $J_{3,7'}$=3.5 Hz, H-7'), 5.13 (1H, dd, $J_{1,2}$=7.5 Hz, $J_{2,3}$=11.5 Hz, H-2).

Found: C, 58.08; H, 6.72%. Calcd for $C_{13}H_{18}O_6$: C, 57.77; H, 6.71%.

DL-2,3-Di-*O*-acetyl-1,7-anhydro-(1,2/3)-1-*C*-hydroxymethyl-4-cyclohexene-1,2,3-triol (6). A mixture of **5** (2.1 g, 10 mmol), *m*CPBA (1.73 g, 10 mmol), 1,2-dichloroethane (60 ml), and 0.1 M phosphate buffer solution (pH 8) (30 ml) was stirred vigorously at 0—5 °C for 20 h. The mixture was washed with 10% aqueous sodium thiosulfate (10 ml), and the organic layer was dried and concentrated, giving 2.3 g of a syrup. Chromatography on silica-gel column (200 g) with 2-butanone-toluene (1:2, v/v) gave 0.75 g (52% yield based on **5** consumed) of **6** and 0.27 g of a mixture which consisted mainly of the isomeric epoxide (**7**), together with 0.92 g of **2** (recovered yield 44%). ^1H NMR ($CDCl_3$, 90 MHz) for **6**, δ=2.05 (3H, s) and 2.08 (3H, s) (2 OAc), 2.40 (2H, br s, H-6 and 6'), 2.70 (1H, d) and 2.08 (1H, d) ($J_{4,5}$=4.5 Hz, H-4 and 5), 5.06 (1H, d, $J_{2,3}$=6 Hz, H-2), 5.40—5.60 (1H, br d, H-3), 5.72 (1H, br dq, $J_{4,5}$=10.5 Hz, H-5), 5.95 (1H, dt, $J_{3,4}$=$J_{4,6}$=3.4 Hz, H-4), and for **7**, δ=2.56 (2H, d, J=6 Hz, H-6 and 6'), 2.82 (2H, br s, H-7 and 7'), 5.62 (1H, br d) and 5.91 (1H, br d) (J=12 Hz, H-4 and 5).

Found for **6**: C, 58.14; H, 6.26%. Calcd for $C_{11}H_{14}O_5$: C, 58.40; H, 6.24%.

DL-1,2,3-Tri-*O*-acetyl-(1,2/3)-1-*C*-acetoxymethyl-4-cyclohexene-1,2,3-triol (8). A mixture of **6** (0.44 g, 1.9 mmol), anhydrous sodium acetate (0.47 g, 5.7 mmol), and 90% aqueous 2-methoxyethanol (10 ml) was stirred at 75 °C for 2 h. The mixture was concentrated and the residue was treated with acetic anhydride (5 ml) and pyridine (5 ml) in the presence of DMAP (40 mg) at 75 °C for 14 h. The

product was purified by a silica-gel column with 2-butanone–toluene (1:10, v/v) as an eluant, giving crystals which were recrystallized from a small amount of water to yield 0.52 g (81%) of **8** as prisms; mp 76—77 °C. ^{1}H NMR ($CDCl_3$, 90 MHz) δ=2.00 (6H, s), 2.04 (3H, s), and 2.06 (3H, s) (4 OAc), 2.56 (1H, br dd, $J_{5,6}$=2.3 Hz, J_{6gem}=18.5 Hz, H-6), 3.19 (1H, dd, $J_{5,6'}$=3.5 Hz, H-6'), 4.52 (2H, s, C$\underline{H}_2$OAc), 5.36 (1H, d, $J_{2,3}$=7.5 Hz, H-2), 5.50—5.77 (3H, m, H-3, 4, and 5).

Found: C, 54.91; H, 6.03%. Calcd for $C_{15}H_{20}O_8$: C, 54.87; H, 6.03%.

Preparation of 8 from DL-3,4-Di-*O*-acetyl-1,2-anhydro-(1,2,3/4)-2-*C*-benzoyloxymethyl-5-cyclohexene-1,2,3,4-tetrol[11] (9). A mixture of **9** (0.10 g), $LiAlH_4$ (33 mg, 3 molar equiv), and THF (3 ml) was stirred at room temperature for 2 h. Excess reagent was decomposed by addition of ethyl acetate, the precipitates were filtered and the filtrate was concentrated. The residue was acetylated with acetic anhydride and pyridine at 60 °C for 28 h, and the product was purified by a silica-gel column, giving 23 mg (24%) of **8** as a syrup, the ^{1}H NMR spectrum of which was superposable on that of the compound obtained before.

DL-3,4-Di-*O*-acetyl-1,2-anhydro-(1,2,3/4,5)-5-*C*-acetoxymethyl-1,2,3,4,5-cyclohexanepentol (10) and DL-2,3,4,5-Tetra-*O*-acetyl-(1,2,5/3,4)-1-*C*-acetoxymethyl-1,2,3,4,5-cyclohexanepentol (11). To a solution of **8** (0.28 g, 0.85 mmol) in methanol (2 ml) was added 1 M methanolic sodium methoxide (0.15 ml), and the mixture was stirred at room temperature for 20 min. After neutrallization with Amberlite IR-120 (H^+) resin, the solution was concentrated. The residue was dissolved in acetic acid (2 ml) and treated with *m*CPBA (0.29 g, 1.7 mmol) at room temperature for 6 d. The mixture was processed in the usual way and the products were acetylated with acetic anhydride and pyridine. Fractionation of the crude products on a silica-gel column with ethyl acetate–hexane (2:3, v/v) as an eluant gave first 0.15 g (59%) of **10** as a syrup: ^{1}H NMR ($CDCl_3$, 90 MHz) δ=2.05 (3H, s), 2.07 (3H, s), and 2.10 (3H, s) (3 OAc), 2.65 (1H, br s, OH), 3.33 (1H, td, $J_{1,2}$=4.2 Hz, $J_{1,6}$=4 Hz, $J_{1,6'}$=ca. 1 Hz, H-1), 3.50 (1H, dd, $J_{2,3}$=2.3 Hz, H-2), 3.74 (1H, d) and 4.03 (1H, d) (J_{7gem}=11 Hz, C$\underline{H}_2$OAc), 5.18 (1H, d, $J_{3,4}$=9 Hz, H-4), 5.58 (1H, dd, H-3).

Found: C, 51.65; H, 5.84%. Calcd for $C_{13}H_{18}O_8$: C, 51.65; H, 6.00%.

The second fraction gave 0.04 g (12%) of **11** as a syrup: ^{1}H NMR ($CDCl_3$, 90 MHz) δ=1.98 (3H, s), 2.07 (3H, s), 2.09 (6H, s), and 2.11 (3H, s) (5 OAc), 3.87 (1H, d) and 4.07 (1H, d) (J_{7gem}=11.3 Hz, C$\underline{H}_2$OAc), 5.02 (1H, q, $J_{4,5}$=$J_{5,6}$=$J_{5,6'}$=*ca.* 4 Hz, H-5), 5.36 (1H, dd, $J_{3,4}$=3 Hz, H-4), 5.51 (1H, dd, $J_{2,3}$=9.8 Hz. H-3).

Compound **11** (22 mg, 0.05 mmol) was acetylated in the presence of DMPA, and the product was purified by a silica-gel column with 2-butanone–toluene (1:4, v/v) as an eluant to give the hexaacetate (**12**) (25 mg, 100%) as prisms; mp 135.5—136 °C. ^{1}H NMR ($CDCl_3$, 90 MHz) δ=1.96 (3H, s), 2.04 (9H, s), 2.06 (3H, s), and 2.10 (3H, s) (6 OAc), 4.40 (2H, s, C$\underline{H}_2$OAc), 5.09 (1H, q, $J_{4,5}$=$J_{5,6}$=$J_{5,6'}$=3 Hz, H-5), 5.29—5.59 (3H, m, H-2, 3, and 4).

Found: C, 50.88; H, 5.72%. Calcd for $C_{19}H_{26}O_{12}$: C, 51.12; H, 5.87%.

DL-1,2,3,4-Tetra-*O*-acetyl-(1,2/3,4)-1-*C*-acetoxymethyl-1,2,3,4-cyclohexanetetrol (2). To a solution of **10** (81 mg) in THF (10 ml) was added $LiAlH_4$ (52 mg, 5 molar equiv) and the mixture was refluxed for 0.5 h. After water had been added, an insoluble material was removed by filtration. The filtrate was concentrated and the residue was acetylated in the presence of DMAP. The product was purified by a silica-gel column with 2-butanone–toluene (1:10, v/v) as an eluant, giving 35 mg (34%) of **2** as prisms; mp 147—148 °C. ^{1}H NMR ($CDCl_3$, 90 MHz) δ=1.96 (3H, s), 2.05 (6H, s), and 2.13 (6H, s) (5 OAc), 4.48 (2H, s, C$\underline{H}_2$OAc), 5.17 (1H, dd, $J_{2,3}$=10.5 Hz, $J_{3,4}$=3.3 Hz, H-3), 5.45 (1H, d, H-2), 5.30—5.52 (2H, m, H-4 and 5).

Found: C, 52.58; H, 6.23%. Calcd for $C_{17}H_{24}O_{10}$: C, 52.81; H, 6.21%.

DL-(1,2/3,4)-1-*C*-Hydroxymethyl-1,2,3,4-cyclohexanetetrol (Pseudo-β-DL-fructopyranose) (1). A mixture of **2** (56 mg) and methanol (0.5 ml) containing 1 M methanolic sodium methoxide (15 μl) was stirred at room temperature for 2.5 h. The mixture was then passed through a short column of Amberlite IR-120 (H^+) resin and concentrated, giving 26 mg (100%) of **1** as a syrup.

Found: C, 47.43; H, 7.78%. Calcd for $C_7H_{14}O_5$: C, 47.19; H, 7.92%.

The authors wish to thank Mr. Saburo Nakada for his elementary analyses, and to Mr. Tohei Takagaki and Mr. Yasushi Shibata for their assistance in the preparative experiments.

References

1) T. Suami, S. Ogawa, M. Takata, K. Yasuda, A. Suga, K. Takei, and Y. Uematsu, *Chem. Lett.*, **1985**, 719.
2) R. S. Shallenberger, *Pure Appl. Chem.*, **50**, 1409 (1978).
3) R. S. Shallenberger, *J. Food Sci.*, **28**, 284 (1963).
4) R. S. Shallenberger and T. E. Acree, *Nature*, **216**, 480 (1967).
5) R. S. Shallenberger and T. E. Acree, *J. Agric. Food Chem.*, **17**, 701 (1969).
6) L. B. Kier, *J. Pharm. Sci.*, **61**, 1394 (1972).
7) M. G. Lindley and G. G. Birch, *J. Sci. Food Agric.*, **26**, 117 (1975).
8) O. R. Martin, S. K. Tommola, and W. A. Szareck, *Can. J. Chem.*, **60**, 1857 (1982).
9) S. Ogawa, T. Toyokuni, T. Kondoh, Y. Hattori, S. Iwasaki, M. Suetsugu, and T. Suami, *Bull. Chem. Soc. Jpn.*, **54**, 2739 (1981).
10) A fractionation of the mixture was rather difficult due to a contamination of diepoxides formed by further epoxidation of **6** and/or **7**.
11) S. Ogawa, T. Toyokuni, M. Ara, M. Suetsugu, and T. Suami, *Chem. Lett.*, **1980**, 379; *Bull. Chem. Soc. Jpn.*, **56**, 1710 (1983).
12) H. B. Henbest and R. A. L. Wilson, *J. Chem. Soc.*, **1957**, 1958; H. O. House, "Modern Synthetic Reactions," 2nd ed., Benjamin, Menlo Park, California (1972), p. 304.
13) J. G. Buchanan and H. Z. Sable, "Selective Organic Transformations," Vol. 2, ed by B. C. Thyagarajan, Wiley Interscience, New York (1972), pp. 40—43.

 © 1986 The Chemical Society of Japan Bull. Chem. Soc. Jpn., 59, 823—826 (1986)

The Hydrogenation of Benzil Catalyzed by Cobalt(II) Dimethylglyoxime Complex

Keisuke MITA
Osaka Municipal Technical Research Institute, Morinomiya, Joto-ku, Osaka 536
(Received May 21, 1985)

Kinetic studies on the catalytic hydrogenation of benzil to benzoin by bis(dimethylglyoximato)cobalt(II), $Co(Hdmg)_2$, were carried out by varying the concentration of $Co(Hdmg)_2$ and pyridine. The initial rate of the hydrogenation reaction was first order with respect to the overall cobalt concentration at a constant overall pyridine concentration. On the other hand, the rate passed through a peak as the overall pyridine concentration was increased at a constant overall cobalt concentration. The peak was observed at $[py]_T = 130\ mmol\ dm^{-3}$, where the square bracket denotes the concentration in the liquid phase. These results show that the initial reaction rate, V_{in}, can be expressed by the following rate equation,

$$V_{in} = k[Co(Hdmg)_2]\frac{58[py]_T}{1+58[py]_T},$$

where, $k=1.1\ min^{-1}$.

It has been known that bis(dimethylglyoximato)-cobalt(II), $Co(Hdmg)_2$, referred to as cobaloxime, shows a catalytic activity for the hydrogenation of certain unsaturated organic compounds in the presence of bases such as pyridine.[1] The influence of the concentration of cobalt and pyridine on the rate of hydrogenation has been studied by various researchers. Simandi and coworkers studied the hydrogenation of free dimethylglyoxime added in excess of the amount required for cobaloxime formation at a constant pyridine concentration.[2] Due to the influence of the cobalt concentration, they observed that the initial rate of the hydrogenation was second order with respect to the overall cobalt concentration. Yamakawa and coworkers studied the hydrogenation of benzil in the presence of 4,4′-trimethylenebis(pyridine) as a base at a constant ratio of the cobalt and the base.[3] They also found that the initial rate of hydrogenation was second order with respect to the overall cobalt concentration. In a previous paper, we reported that a plot of the reaction rate vs. the overall cobalt concentration gave a sigmoidal curve for benzil hydrogenation at a constant cobalt-pyridine ratio.[4]

Due to the influence of base concentrations, Yamakawa and coworkers reported that the initial reaction rate increased and remained constant as the concentration of base was increased.[3] Tylrik and coworkers studied the asymmetric hydrogenation of benzil in the presence of quinine or morpholine.[5] They also reported that the initial reaction rate increased and remained constant as the concentration of the base was increased.

The second-order dependence of the reaction rate on the cobalt concentration implies that two molecules of cobaloxime(II) are required to activate one molecule of H_2.[2] Although, due to the influence of the concentration of base, a mechanism in which excess base act as a proton acceptor and accelerate the H–H bond cleavage has been proposed,[2,6,8] no kinetic model that can quantitatively explain the dependency of the reaction rate on the base concentration has ever been proposed for catalytic hydrogenation by $Co(Hdmg)_2$.

In this work, kinetic studies on the catalytic hydrogenation of benzil to benzoin by $Co(Hdmg)_2$ were carried out. From the rate data obtained for various concentrations of $Co(Hdmg)_2$ and pyridine, it was found that the initial reaction rate was first order with respect to the overall cobalt concentration at a constant pyridine concentration and that the initial reaction rate passed through a peak as the pyridine concentration was increased at a constant overall cobalt concentration. These results could be successfully interpreted by a rate law which shows a first-order dependence on the concentration of $Co(Hdmg)_2py$ at a constant pyridine concentration. A kinetic model that can quantitatively explain the dependency of the reaction rate on the concentration of pyridine was also proposed.

Experimental

A 27 cm^3 methanol solution of $Co(Hdmg)_2$ was prepared by mixing $Co(NO_3)_2 \cdot 6H_2O$, dimethylglyoxime (H_2dmg), and NaOH in a ratio of 1:2:2 under a hydrogen atmosphere. The preliminary hydrogen uptake (H_2 uptake) was initiated by the injection of an appropriate amount of pyridine and a 1.5 cm^3 deoxygenated toluene solution of benzil to the reaction vessel under vigorous stirring. Just before the preliminary H_2 uptake was completed, 1.5 cm^3 of the methanol solution of benzil was again injected. The hydrogenation was carried out under an atmospheric pressure of hydrogen at 20 °C and was followed by measuring the volume of the H_2 uptake using a gas burette.

The H_2 uptake rate was almost constant at the first ca. 1—5 min and then droped. Therefore, the average volume of the H_2 uptake during the 2nd and 3rd minute was taken

as the initial reaction rate, V_{in}. This rate was found to increase and to saturate with increased stirring. The rate measurement was performed under conditions where the rate was independent of stirring. The reproducibility for measurements of the H_2 uptake rate was good. An analysis by gas chromatography showed that benzoin was the only product of the reaction.

Results

During this experiment, the same methanol solution of $Co(Hdmg)_2$ and pyridine was repeatedly used four times for the hydrogenation of 1.5, 1.5, 3.0, and 1.5 mmol benzil according to the method described in the Experimental section. After each incremental addition of benzil, the initial H_2 uptake rate was measured. As a typical example, Fig.1 shows that the initial rate increased after the first run and then became almost constant over the 2nd—4th runs. The results show that the initial rate of H_2 uptake was independent of the concentration of benzil, in agreement with results from the literature.[2,4] It can also be seen from Fig. 1 that the decomposition of $Co(Hdmg)_2$ or its pyridine adducts is negligible under the present experimental conditions. However, it is not clear why the rate of the lst run is lower compared with those of the other runs. Therefore, in all the experiments described here, the initial H_2 uptake rate of the 2nd run was taken as a measure of the catalytic activity in order to obtain a reproducible hydrogenation activity.

Figure 2 shows the dependence of the initial rate of H_2 uptake on $[Co]_T$ for the hydrogenation of benzil at a constant $[py]_T$, where $[Co]_T$ is the initial overall $Co(Hdmg)_2$ concentration and $[py]_T$ is the initial overall pyridine concentration. It can be seen from Fig. 2 that the initial rate of H_2 uptake (V_{in}) is first order with respect to $[Co]_T$,

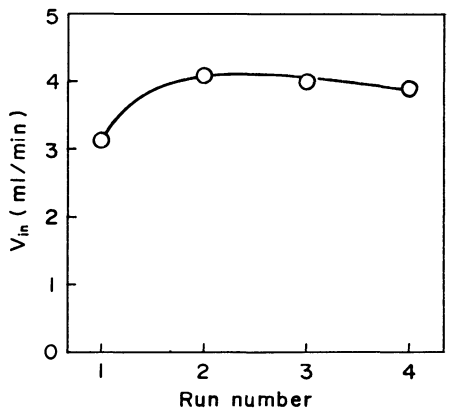

Fig. 1. Activity change of $Co(Hdmg)_2$–pyridine system for the hydrogenation of benzil.
$[Co]_T$: 13 mmol dm^{-3}, $[py]_T$: 330 mmol dm^{-3}, volume of catalytic solution: 30 cm^3, Temp: 20 °C, H_2 pressure: 1 atm, [benzil]: 25 mmol dm^{-3}.

$$V_{in} = k[Co]_T. \quad (1)$$

It can also be seen from Fig. 2 that the initial rate of H_2 uptake increases and then passes a peak as $[py]_T$ increases at a constant$[Co]_T$. The peak was observed at $[py]_T$=130 mmol dm^{-3}. As a typical example, the initial H_2 uptake rate at $[Co]_T$=13 mmol dm^{-3} was ploted against $[py]_T$ using the data in Fig. 2. This plot was indicated in Fig. 3 by a open circle.

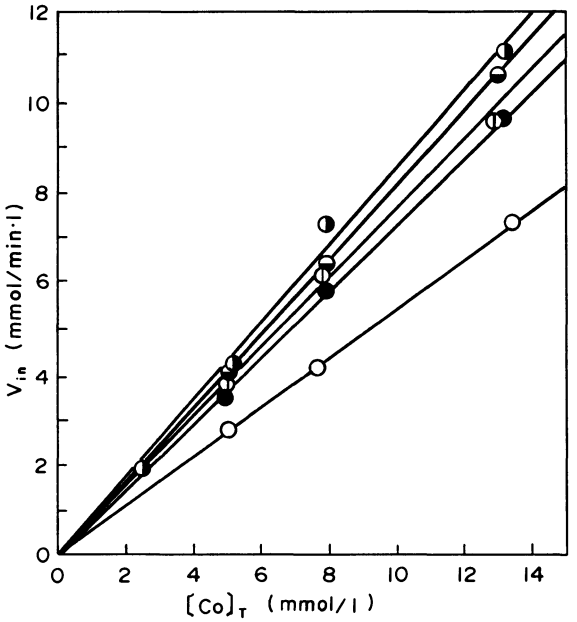

Fig. 2. Dependence of the initial rate of H_2 uptake (V_{in}) on $[Co]_T$.
$[py]_T$=33 (○), 66 (◑), 130 (◑), 330 (◒), and 530 mmol dm^{-3} (●).

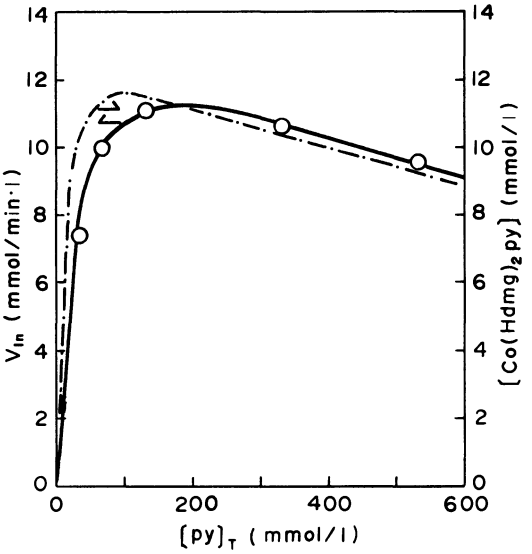

Fig. 3. Plots of V_{in} vs. $[py]_T$ (○: experimental, ——: calculated from Eq. 9) and plots of $[Co(Hdmg)_2py]$ vs. $[py]_T$ (----: calculated by using K_1=186 and K_2=0.75 dm^3 mol^{-1}). $[Co]_T$=13 mmol dm^{-3}.

Discussion

In a solution containing $Co(Hdmg)_2$ and pyridine, the following successive coordination equilibria are readily achieved.

$$Co(Hdmg)_2 + py \overset{K_1}{\rightleftharpoons} Co(Hdmg)_2py \quad (2)$$

$$Co(Hdmg)_2py + py \overset{K_2}{\rightleftharpoons} Co(Hdmg)_2py_2 \quad (3)$$

The stepwise stability constants (K_1 and K_2) were determined using the visible absorption spectra.[2] The calculated values are: K_1=186 and K_2=0.75 $dm^3\,mol^{-1}$.

According to the literature,[2,5,7] $Co(Hdmg)_2py_2$ dose not interact with molecular H_2. In the present experiment, the hydrogenation of benzil by $Co(Hdmg)_2$ did not occur in the absence of pyridine, indicating that $Co(Hdmg)_2$ shows no catalytic activity. Therefore, only $Co(Hdmg)_2py$ can be considered to be active for the hydrogenation of benzil.

The concentration of $Co(Hdmg)_2py$ can be calculated from $[Co]_T$ and $[py]_T$ by using the stepwise stability constants in Eqs. 2 and 3. Introducing the relation between $[Co]_T$ and $[Co(Hdmg)_2py]$, the plots of V_{in} vs. $[Co]_T$ in Fig. 2 were re-formed to the plots of V_{in} vs. $[Co(Hdmg)_2py]$. The plots are shown in Fig. 4. It can be seen from Fig. 4 that at a fixed pyridine concentration the initial H_2 uptake rate is linearly proportional to the concentration of $Co(Hdmg)_2py$ as is given by the following rate equation.

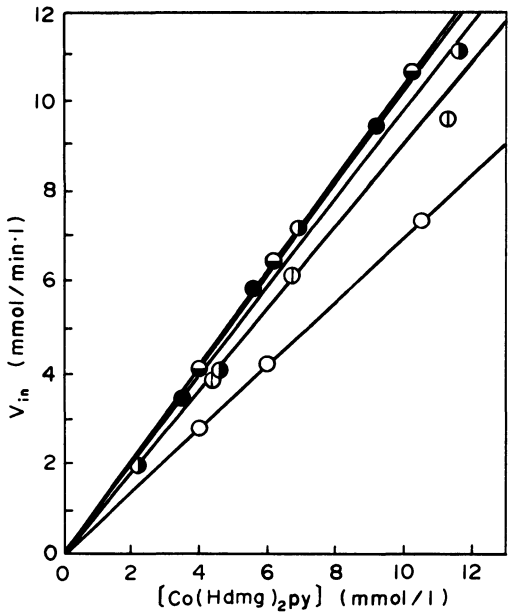

Fig. 4. Plot of V_{in} vs. $[Co(Hdmg)_2py]$.
$[py]_T$ (mmol dm^{-3})=33 (○), 66 (◑), 130 (◑), 330 (◒), and 530 (●).

$$V_{in} = k[Co(Hdmg)_2py] \quad (4)$$

The value of k, that is $V_{in}/[Co(Hdmg)_2py]$, was determined by the slope of the plot in Fig. 4 at each pyridine concentration and Fig. 5 shows the plot of $V_{in}/[Co(Hdmg)_2py]$ vs. $[py]_T$. As is shown in Fig. 5, the value of $V_{in}/[Co(Hdmg)_2py]$ increases and saturates upon increasing the pyridine concentration.

It has been proposed that excess pyridine acts as a proton acceptor and accelerates the H–H bond cleavage in the following manner.[5–7]

$$H_2 + Co(Hdmg)_2py + py \longrightarrow py\cdots H\cdots H\cdots Co(Hdmg)_2py \quad (5)$$

The plot in Fig. 5 also indicate that excess pyridine acts as catalysts together with $Co(Hdmg)_2py$ (in agreement with the literature). The simplest rate law which could be expected for the plot in Fig. 5 is given in Eq. 6.

$$k = k_1\frac{K[py]_T}{1+K[py]_T} \quad (6)$$

By uing Eq. 6, Eq. 4 leads to Eq. 7.

$$V_{in} = k_1[Co(Hdmg)_2py]\frac{K[py]_T}{1+K[py]_T} \quad (7)$$

Thus, the result shown in Fig. 5 was for an analysis according to Eq. 7. It is convenient to transform Eq. 7 into one that gives a straight-line plot. This can be done by taking the reciprocal of both side of Eq. 7 to give Eq. 8,

$$\frac{[Co(Hdmg)_2py]}{V_{in}} = \left(\frac{1}{k_1K}\right)\frac{1}{[py]_T} + \left(\frac{1}{k_1}\right), \quad (8)$$

where the quantities within the parentheses are constant. The plot of $V_{in}/[Co(Hdmg)_2py]$ vs. $[py]_T$ in Fig. 5 was transformed to a plot of $[Co(Hdmg)_2py]/V_{in}$ vs. $1/[py]_T$. As can be seen in Fig. 6, $[Co(Hdmg)_2py]/$

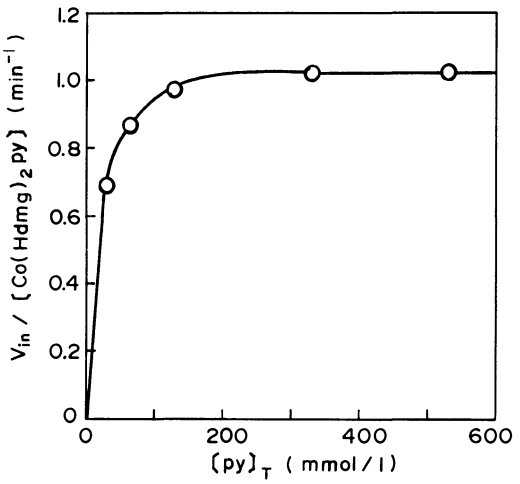

Fig. 5. Plot of $V_{in}/[Co(Hdmg)_2py]$ vs. $[py]_T$.

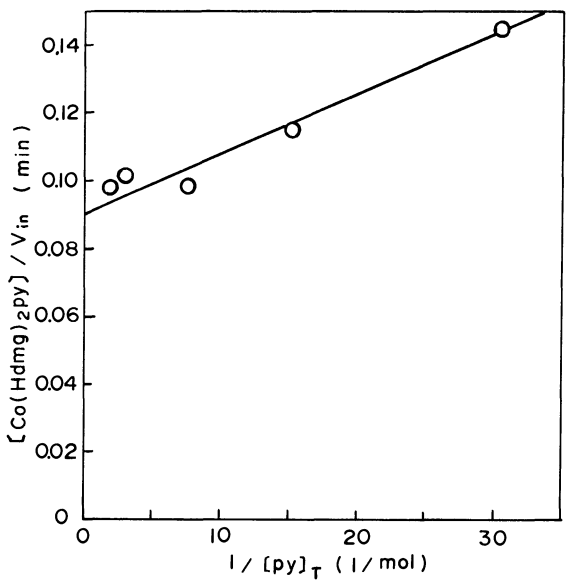

Fig. 6. Plot of $[Co(Hdmg)_2py]/V_{in}$ vs. $1/[py]_T$.

V_{in} is almost linearly proportional to $1/[py]_T$. This confirms the validity of the rate law.

The values of k_1 and K in Eq. 8 can be calculated from the slope and the intercept of the plot in Fig. 6. Finnally, the rate law was expressed as

$$V_{in} = 1.1(min^{-1})[Co(Hdmg)_2py]\frac{58[py]_T}{1+58[py]_T}. \quad (9)$$

The plot of $[Co(Hdmg)_2py]$ vs. $[py]_T$ at a constant $[Co]_T$ was calculated from $[Co]_T$ and $[py]_T$ using the stepwise stability constants in Eqs. 2—3. As a typical example, a plot at $[Co]_T=13$ mmol dm^{-3} is shown in Fig. 3 by a broken line. It can be seen from the plots that the concentration of $Co(Hdmg)_2py$ increased and passes a peak as the pyridine concentration increases. As is shown in Fig. 3, the concentration of pyridine at which the plot of $Co(Hdmg)_2py$ vs. $[py]_T$ shows a peak clearly deviates from that at which the plot of V_{in} vs. $[py]_T$ shows a peak. On the other hand, the V_{in} value which was calculated from Eq. 9 was ploted against $[py]_T$. This plot is shown in Fig. 3 by a real line. An excellent fit was observed between the calculated plot of V_{in} vs. $[py]_T$ and the experimental plot of V_{in} vs. $[py]_T$. This also suggest the validity of Eq. 9.

The value of V_{in} was calculated from Eq. 9 at a constant ratio of $[py]_T/[Co]_T$, and the values were ploted against $[Co]_T$. The plot showed a sigmoidal curves. This is the reason why the reaction rate is reported to be second order with respect to $[Co]_T$[3] or why the plot of V_{in} vs. $[Co]_T$ showed a sigmoidal curve[4] for the hydrogenation of benzil at a constant ratio of $[py]_T/[Co]_T$. However, the second-order dependence on $[Co]_T$ for the hydrogenation of dimethylglyoxime at a constant pyridine concentration[2] could not be interpreted by Eq. 9. The hydrogenation rate of dimethylglyoxime is much lower than that of benzil. Therefore, the mechanism of the hydrogenation of dimethylglyoxime may be different from that of benzil.

References

1) Y. Ohgo, S. Takeuchi, and J. Yoshimura, *Bull. Chem. Soc. Jpn.*, **44**, 283, 583, (1971).

2) L. I. Simandi, E. Budo-Zahonyi, Z. Szeverenyi, and S. Nemeth, *J. Chem. Soc., Dalton Trans.*, **1980**, 276.

3) S. Yamakawa, I. Yasumori, and E. Miyazaki, Preprint of 37th National Meeting of Chemical Society of Japan, April, 1978, Abstr. No. 2Q14.

4) K. Mita, K. Hotta, and S. Watanabe, *Nippon Kagaku Kaishi*, **1978**, 1583.

5) S. Tyrlik, M. M. Kucharska, and I. Wolochowicz, *J. Mol. Catal.*, **6**, 393, (1979).

6) T. Yamaguchi and R. Miyagawa, *Chem. Lett.*, **1978**, 89.

7) T. Yamaguchi and T. Tsumura, *Chem. Lett.*, **1973**, 409.

8) K. Mita, K. Hotta, and S. Watanabe, *Nippon Kagaku Kaishi*, **1979**, 1299.

 © 1986 The Chemical Society of Japan Bull. Chem. Soc. Jpn., 59, 827—832 (1986)

Dynamic Investigation of Aqueous Solutions of 2-*t*-Butoxyethanol and 3-Methoxy-3-methyl-1-butanol by Ultrasonic Methods

Sadakatsu NISHIKAWA,* Ryutaro SHINOHARA, and Goro TANAKA
Department of Chemistry, Faculty of Science and Engineering, Saga University, Saga 840
(Received September 17, 1985)

Ultrasonic absorption in the frequency range of 6.5 to 220 MHz has been measured in aqueous solutions of 3-methoxy-3-methyl-1-butanol and 2-*t*-butoxyethanol as a function of the concentration along with the measurement of sound velocity at 1.92 and 2.5 MHz at 25 °C. A single relaxational ultrasonic absorption has been found in both solutions and it is interpreted by a reaction kinetics associated with the interaction between solute and solvent, AB $\rightleftharpoons$ A+B where AB is the complex, A the solute and B the solvent. The forward and backward rate constants for the interaction have been determined from the concentration dependence of the relaxation frequencies to be $k_f=1.4\times10^8$ s^{-1} and $k_b=1.1\times10^8$ mol^{-1} dm^3 s^{-1} for 3-methoxy-3-methyl-1-butanol solution and $k_f=9.0\times10^7$ s^{-1} and $k_b=1.3\times10^8$ mol^{-1} dm^3 s^{-1} for 2-*t*-butoxyethanol solution. The water structure has also been estimated from the absorption data and it has been clarified for the water structure promoted by additions of such solutes. Correlations between the structures of the solutes and the ultrasonic properties of the solutions are discussed in terms of the hydrophobicity of the solutes.

The molecular structure of a self-associating liquid solvent is well known to be changed by the addition of solutes.[1] It is interesting and important to examine experimentally how much the change would be induced in relatively concentrated solutions. Ultrasonic techniques are very suitable to investigate such questions and they have been used extensively. They also give the dynamic information about the solutions and liquids. Rao and Verrall[2] have reported that in an aqueous micellar solution of 2-butoxyethanol (Butyl Cellosolve) the relaxation observed in the MHz frequency range is associated with the exchange reaction of the alcohol between the mixed micelles and the surrounding bulk solution. This has considerable interest in relation to microemulsions. However, clear relaxational absorptions are observed at concentrations below 1 mol dm^{-3} even if surfactant are not added.[3,4] Without some clarification of the mechanism, it is difficult to discuss such ternary systems. By means of ultrasonic absorption and velocity measurements, we have been studying the effects on water structure when non-electrolytes, e.g. alcohols or ethers, are added.[3-7] It has been found, so far, that the ultrasonic relaxations observed in the MHz frequency range are closely related to the balance of the hydrophobicity and hydrophilicity of the solute molecules.

To clarify the relation between the solute structures and the ultrasonic properties, we have chosen two isomeric solutes viz. 3-methoxy-3-methyl-1-butanol and 2-*t*-butoxyethanol. We consider that the structural effect of the solutes on the solvent water may shed light on the ultrasonic properties when they are examined in the solutions with isomeric solutes.

Experimental

The chemicals used were commercial samples obtained from Tokyo Kasei Co., Ltd. and distilled once under reduced pressure. Solvent water was doubly distilled. The desired concentrations of the solutions were made by weighing the solutes.

The ultrasonic absorption coefficient, α, was measured by the improved pulse apparatus in the frequency range from 6.5 MHz to 220 MHz; the principle and the detailed procedure of the measurement are described elsewhere.[4] The sound velocity was measured by an interferometer opperated at 2.5 MHz and a sing around meter at 1.92 MHz. The accuracy of both apparatuses is less than 1 m s^{-1}. The cells for the absorption and velocity measurements were immersed in a water bath which was controlled within ±0.005 °C and the measurements were performed at 25 °C.

The densities were measured at various temperatures by a standard pycnometer the volume of which was about 4.8 cm^3 and the thermal expansibility at 25 °C was determined. The viscosity coefficients of the solutions were measured by a Ubbelohde type viscometer at 25.0±0.1 °C.

Results and Interpretation

The quantity α/f^2 where f is the frequency has been found to be frequency dependent for aqueous solutions of 3-methoxy-3-methyl-1-butanol (from 2.2 mol dm^{-3} to 5.5 mol dm^{-3}) and 2-*t*-butoxyethanol (from 1.3 mol dm^{-3} to 5.0 mol dm^{-3}). The experimental values of α/f^2 for the 2-*t*-butoxyethanol solution are shown in Fig. 1 at various frequencies as a function of the analytical concentration, C_e. A peak sound absorption concentration has been observed though it is dependent on the measurement frequency. A similar dependence has also been observed for the 3-methoxy-3-methyl-1-butanol solution. No frequency dependence of α/f^2 is found in either liquid solutes.

In general, the frequency dependence of the sound absorption coefficient can be well described by the next equation if it is due to a single relaxation process.

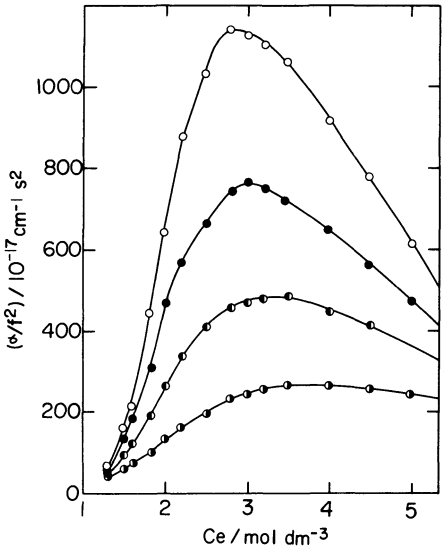

Fig. 1. The plots of α/f^2 vs. concentration for aqueous solution of 2-*t*-butoxyethanol at 25 °C. —○—: 15 MHz, —●—: 45 MHz, —◐—: 95 MHz, —◑—: 220 MHz.

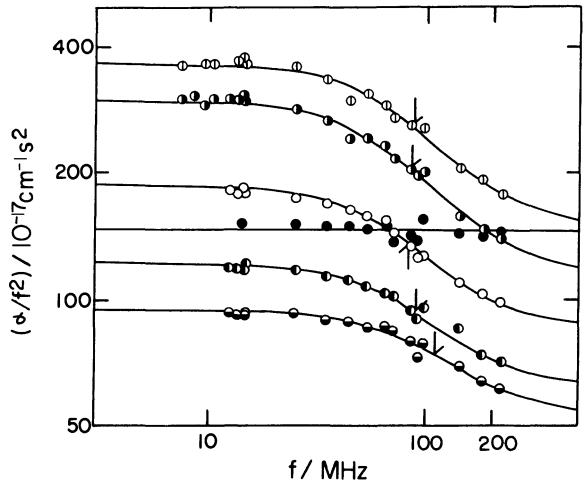

Fig. 2. The representative ultrasonic absorption spectra in aqueous solution of 3-methoxy-3-methyl-1-butanol at 25 °C. —◒—: 2.2 mol dm⁻³, —◐—: 2.4 mol dm⁻³, —○—: 2.8 mol dm⁻³, —◑—: 3.5 mol dm⁻³, —◔—: 4.5 mol dm⁻³, —●—: liquid solute.

$$\alpha/f^2 = A/[1+(f/f_r)^2] + B \quad (1)$$

or

$$\mu = (\alpha/f^2 - B)fc = Afc/[1+(f/f_r)^2], \quad (1')$$

where μ is the excess absorption per wavelength, A the amplitude of the excess absorption, B the back ground absorption, f_r the relaxation frequency and c the sound velocity. Figures 2 and 3 show the representative ultrasonic absorption spectra for both solutions and they are shown with different formula,

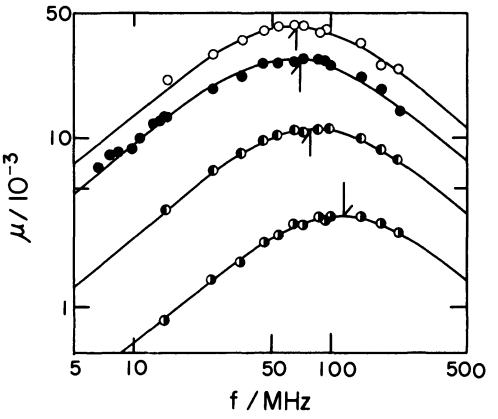

Fig. 3. The representaive ultrasonic absorption spectra in aqueous solution of 2-*t*-butoxyethanol at 25 °C. —◑—: 1.3 mol dm⁻³, —◐—: 1.6 mol dm⁻³, —●—: 2.0 mol dm⁻³, —○—: 3.0 mol dm⁻³.

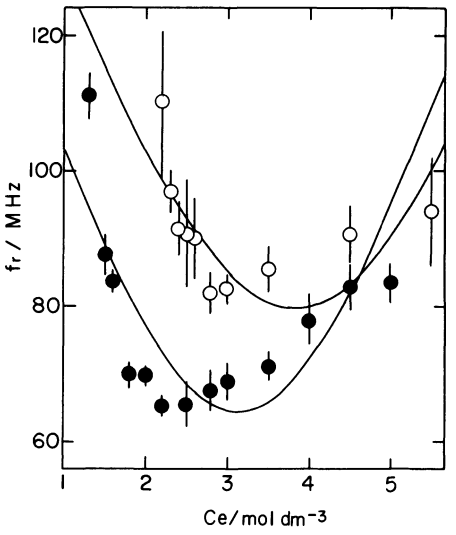

Fig. 4. The concentration dependence of the relaxation frequency for aqueous solutions of 3-methoxy-3-methyl-1-butanol(—○—) and 2-*t*-butoxyethanol (—●—) at 25 °C. The solid curves are the calculated ones.

that is, with Eq. 1 and Eq. 1′. The ultrasonic parameters, A, B, and f_r have been determined by a nonlinear least mean square method using microcomputer. The spectrum which is represented by both Eqs. 1 and 1′ can be seen on a computer display in order to check how the experimental data fit the theoretical curves. The ultrasonic results are listed in Table 1 along with some thermodynamic quantities. The solid curves in Figs. 2 and 3 are those calculated using these parameters. It is seen that a clear single relaxation process has been observed in both solutions. Figure 4 represents the concentration dependences of the relaxation frequencies and they

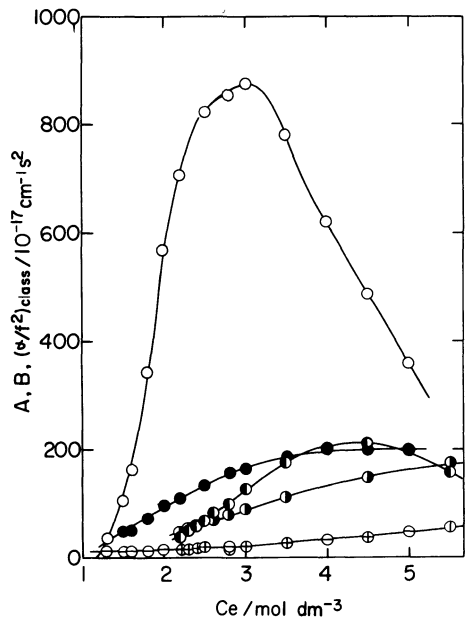

Fig. 5. The concentration dependences of the amplitude of the excess absorption. the background absorption and the classical absorption for aqueous solutions of 3-methoxy-3-methyl-1-butanol and 2-t-butoxyethanol. —◐—: A, —◑—: B and —ⓘ—: $(\alpha/f^2)_{class}$ for 3-methoxy-3-methyl-1-butanol, —○—: A, —●—: B and —⊖—: $(\alpha/f^2)_{class}$ for 2-t-butoxyethanol.

show a minimum. Figure 5 shows the dependence of the amplitude of the excess absorption and the back ground absorption. The classical absorption which is mainly due to shear viscosity is obtained by the next equation.[8]

$$(\alpha/f^2)_{class} = 8\pi^2\eta/3c^3\rho, \quad (2)$$

where η is the viscosity coefficient and ρ the solution density. The results for both solutions are also shown in Fig. 5 and are smaller than those of the back ground absorptions. This means that the observed relaxational absorptions are not due to the shear viscosity and another relaxation may be predicted at more than 200 MHz in both solutions which we will not consider further.

The sound velocity shows a maximum as is seen in Table 1. The adiabatic compressibility, κ_s, of the solution is obtained with the help of the next equation.

$$\kappa_s = (\rho c^2)^{-1} \quad (3)$$

The concentration dependences of the compressibility are shown in Fig. 6 along with some other solutions in order to compare where the concentra-

Table 1. Ultrasonic and Thermodynamic Parameters for Aqueous Solutions of 2-t-Butoxyethanol and 3-Methoxy-3-Methyl-1-Butanol at 25 °C

C_e / mol dm^{-3}	f_r / MHz	A	B	c	ρ	η	α_p°
		10^{-17} s^2 cm^{-1}		m s^{-1}	g cm^{-3}	10^{-2} g cm^{-1} s^{-1}	10^{-4} deg^{-1}
			(3-Methoxy-3-methyl-1-butanol)				
2.20	111	41.9	52.8	1622	0.9927	2.37	5.4
2.30	96.9	52.8	55.9	1623	0.9926	2.45	5.4
2.40	91.5	60.5	61.8	1624	0.9923	2.57	5.4
2.50	90.8	68.5	68.3	1625	0.9920	2.68	5.6
2.60	90.3	86.7	68.6	1625	0.9916	2.80	5.7
2.80	82.0	102	85.2	1629	0.9907	3.01	6.1
3.00	82.4	129	92.4	1624	0.9895	3.33	6.2
3.50	85.7	179	114	1615	0.9866	4.17	6.8
4.50	88.6	214	149	1586	0.9791	6.09	7.7
5.50	94.1	161	175	1546	0.9691	8.26	8.1
			(2-t-Butoxyethanol)				
1.30	114	38.2	35.3	1598	0.9953	1.61	4.4
1.50	87.4	112	48.8	1603	0.9943	1.77	4.6
1.60	83.8	166	52.1	1604	0.9938	1.84	—
1.80	69.5	346	72.5	1601	0.9929	2.02	5.4
2.01	69.2	531	90.6	1593	0.9916	2.24	6.1
2.20	65.1	708	110	1585	0.9901	2.39	6.5
2.50	65.3	824	135	1571	0.9878	2.79	6.8
2.80	67.5	856	166	1553	0.9845	2.99	7.1
3.00	68.8	876	163	1546	0.9827	3.14	7.6
3.50	71.3	784	189	1519	0.9758	3.76	7.6
4.00	77.9	618	201	1495	0.9694	4.31	7.9
4.50	83.2	485	198	1482	0.9623	4.86	8.3
5.00	83.4	359	198	1447	0.9546	5.49	8.7

tion is converted to the molar fraction, n_e.

These concentration dependences of the ultrasonic properties, e.g. peak sound absorption concentration and peak sound velocity concentration are characteristic of aqueous solutions of nonelectrolytes with hydroxyl groups. In order to analyze such dependences, various models have been proposed.[9,10] The present authors have also been studying such phenomena on the bases of the experimental facts and only one reasonable mechanism is possible.[3-7] This is expressed by the following reaction.

$$AB \underset{k_b}{\overset{k_f}{\rightleftharpoons}} A + B, \qquad (4)$$

where A is the solute, B the solvent and AB a solute solvent complex; k_f and k_b are the forward and backward rate constant respectively. In our model, it is assumed that the solvent water exists in hydrogen bonded and non-hydrogen bonded states, and the latter can participate in the above reaction. The model is similar to that proposed by Andreae et al. (model IV in Ref. 9). Under this assumption, the relation between the analytical concentrations and the relaxation frequency is derived as follows.[5]

$$2\pi f_r = k_b[(C_e - \beta C_w + K_{12})^2 + 4\beta C_w K_{12}]^{1/2}, \qquad (5)$$

where C_w the analytical concentration of the solvent, K_{12} the equilibrium constant defined as $K_{12}=k_f/k_b$ and β the molar fraction of the non-hydrogen bonded water. It is a good assumption that the parameters, k_b, K_{12}, and β are concentration independent and they are determined so as to obtain the best fit of the experimental relaxation frequencies to Eq. 5. The solid curves in Fig. 4 are those calculated using these parameters and they seem to fit reasonably for both solutions. The β parameter is a good measure to estimate the effect of the solute on water structure. These calculated rate and thermodynamic constants are tabulated in Table 2.

The excess absorption amplitude A is related to the volume and enthalpy change of the reaction by the next equation.[11]

$$\mu_{max} = Af_r c/2 = \pi(\rho c^2 \Gamma/2RT)(\Delta V - \alpha_p^\infty \Delta H/\rho C_p^\infty)^2 (C_p^\infty/C_p^\circ) \qquad (6)$$

where μ_{max} is the maximum excess absorption perwave length, R the gas constant, T the absolute temperature, ΔH the standard enthalpy change of the reaction, ΔV the standard volume change of the reaction, α_p^∞ the thermal expansibility at high frequency limit, C_p° the specific heat at low frequency, C_p^∞ that at high frequency limit and Γ the concentration term which is given by $\Gamma=(1/[AB]+1/[A]+1/[B]-1/[AB]+[A]+[B]))^{-1}$. The most effective terms to control the concentration dependence of the maximum excess absorption per wavelength may be $\rho c^2\Gamma$. Once the equilibrium constant, K_{12}, and the β value are determined, it is possible to calculate the concentration of the reactants and then the term is obtainable. In Fig. 7, the calculated values of $\rho c^2\Gamma$ for aqueous solution of 3-methoxy-3-methyl-1-butanol are plotted against the concentration along with the experimental results of the maximum excess absorption per wavelength. A similar dependence has also been observed in the solution of 2-*t*-butoxy-

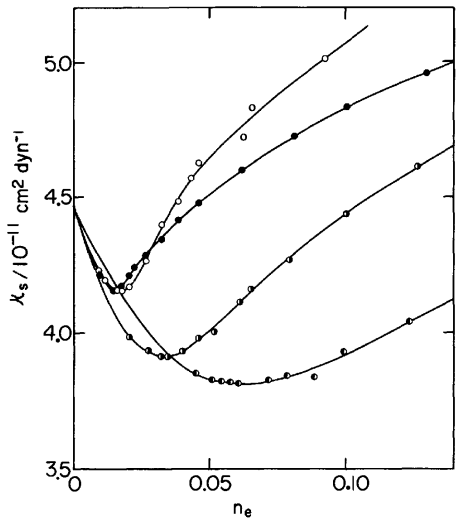

Fig. 6. The concentration dependence of the the adiabatic compressibility for four aqueous solutions. —●—: 2-butoxyethanol, —○—: 2-isobutoxyethanol, —◑—: 2-*t*-butoxyethanol, —○—: 3-methoxy-3-methyl-1-butanol.

Table 2. The Rate and Thermodynamic Constants for Aqueous Solutions of some Isomers at 25 °C

Solute	k_f / 10^8 s^{-1}	k_b / 10^8 dm^3 mol^{-1} s^{-1}	β	Ref.
$CH_3OC(CH_3)_2CH_2CH_2OH$	1.4 ±0.1	1.1±0.1	0.135	This work
$(CH_3)_3COCH_2CH_2OH$	0.90±0.09	1.3±0.1	0.0975	This work
$CH_3CH_2CH_2CH_2OCH_2CH_2OH$	1.1 ±0.1	2.0±0.2	0.0270	4
$(CH_3)_2CHCH_2OCH_2CH_2OH$	0.55±0.07	2.5±0.3	0.0428	6

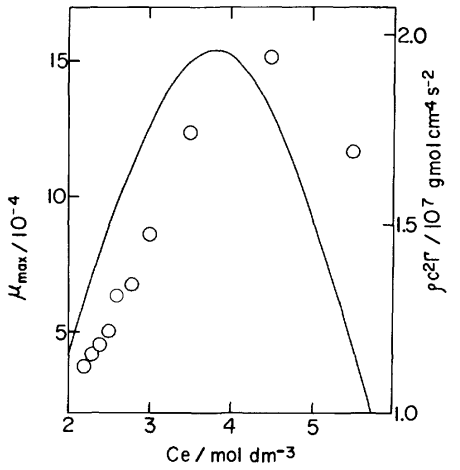

Fig. 7. The concentration dependences of the experimental maximum excess absorption per wave length (left scale) and the calculated $\rho c^2\Gamma$ (right scale) for aqueous solution of 3-methoxy-3-methyl-1-butanol.

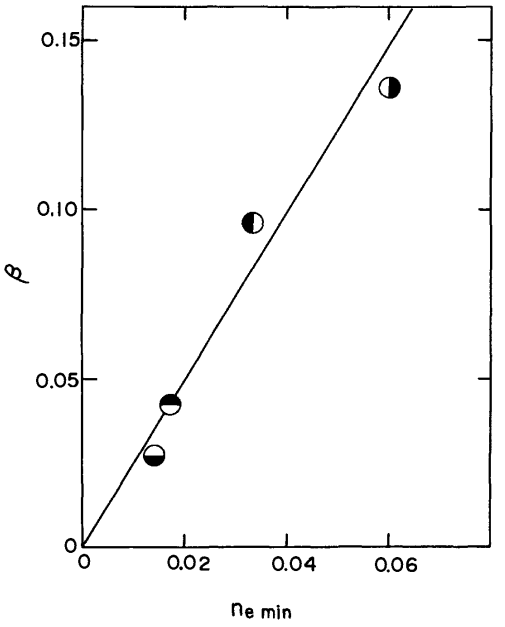

Fig. 8. The correlation between the β value and the concentration where the compressibility minimum appears. ◑: 2-butoxyethanol, ◐: 2-isobutoxyethanol, ◓: 2-*t*-butoxyethanol, ◒: 3-methoy-3-methyl-1-butanol.

ethanol.

Discussion

The observed ultrasonic absorption in aqueous solutions of 3-methoxy-3-methyl-1-butanol and 2-*t*-butoxyethanol are characteristic of a single relaxation in the frequency range from 6.5 to 220 MHz. However, in solutions of 2-butoxyethanol[3,4] and 2-isobutoxyethanol[6] which are also isomers, another relaxation has been observed at less than 10 MHz in addition to that observed from the range of 30 to 100 NHz. Such a process has also been predicted by Fanning and Kruus.[12] The slower relaxation has been attributed to the perturbation of the equilibrium associated with the molecular aggregates or microemulsions. Depending upon the structure of the solute or the property, which may be mainly due to the hydrophobicity, a single or double relaxations appear. This is the experimental fact obtained from the frequency dependence of the ultrasonic absorption.

It has been found that the β values which are introduced to interpret the observed relaxation process increase with decreasing hydrophobicity of the solute molecules.[13] The β values obtained increase in the series 2-butoxyethanol, 2-isobutoxyethanol, 2-*t*-butoxyethanol and 3-methoxy-3-methyl-1-butanol as is seen in Table 2. Therefore, this series is expected to indicate the order of the hydrophobicity of the solute. The β value indicates the fraction of water which can interact with solute molecules or the fraction of the less structured water. The lower this value, the higher the water structure is promoted. Comparing with the β value in liquid water,[14] the values obtained are still lower than that in liquid water. This means that the solutes used in this investigation act as the structure promoter to water within the seriese, 2-butyoxyethanol, 2-isobutoxyethanol, 2-*t*-butoxyethanol, 3-methyl-3-methoxy-1-butanol. This fact is also obtained from the analysis of the concentration dependence of the relaxation frequency.

The hydrophobicity of the solute may also influence the concentration dependence of the compressibility. As is seen in Fig. 6, κ_s goes through a minimum. The minimum occurs at the lower concentration and the curve is sharper the more hydrophobic the solute. This kind behavior is also seen in the concentration dependence of an apparent molar volume.[15] The series of the concentration where the compressibility shows a minimum or the series of the sharpness of the curve seems to be the same as that of the β values. This is the experimental fact obtained from the concentration dependences of the density and the sound velocity.

It is interesting to examine the correlation between these two independent results, that is, the value which is obtained from the absorption data and the behavior of the compressibility which is obtained from the velocity and density data. Figure 8 shows the plots of the β values vs. the molar fraction at which the compressibility of the solution indicates a minimum ($n_{e\,\min}$). A linear relationship seems to hold. Comparing the results of the 2-*t*-butoxyethanol

solution with that of 3-methoxy-3-methyl-1-butanol, it is seen that the position of the oxygen atom in the molecule may influence the hydrophobicity of the molecules because both the vertical and the horizontal values of the latter solution in Fig. 8 are lower than that of the former. This might be because the *t*-butyl group is bulky when the hydrophobic group of 3-methoxy-3-methyl-1-butanol is compared with that of 2-*t*-butoxyethanol. Murty and Subrahmanyan[16] have reported the structure enhancing efficiency of the isomeric butyl alcohols in the order, *t*-butyl>butyl alcohol from sound velocity studies. However, the present study indicated that 2-butoxyethanol has a more enhancing effect on water structure than 2-*t*-butoxyethanol. Lara and Desnoyers[17] have also investigated the solution properties of 2-butoxyethanol from the solution compressibility and they have found that microemulsions exist in the solution. Their result is consistent with ours which has been estimated from the ultrasonic absorption and velocity results. No previous reports of such a clear correlation between the results of the absorption and the compressibilities in the aqueous solutions are known to the authors.

It has been reported[4,7,13] that the standard volume and enthalpy changes of the reaction may be calculated using Eq. 6 on the assumption that $C_p^\infty/C_p^\circ \cong 1$ and $\alpha_p^\infty/\alpha_p^\circ \cong 1$. In order to estimate the reaction parameters, we have measured the thermal expansibility of both solutions and it is listed in Table 1. If such assumptions for the specific heat and the expansibility were satisfied, the plots of $(\mu_{max}/\rho c^2\Gamma)^{1/2}$ vs. $\alpha_p^\circ/\rho C_p^\circ$ might give a straight line. However, a linear plot has been obtained in a limited concentration range. We considered that the contribution of the relaxational specific heat, $\delta C_p = C_p^\circ - C_p^\infty$, may be important when the reaction parameters, ΔV and ΔH are determined simultaneously over such wide concentration ranges. However, it may be concluded that the dominant term which controls the concentration dependence of the maximum excess absorption is clearly $\rho c^2\Gamma$ as is seen in Fig. 6. In order to obtain the quantitative analysis of the concentration dependence of the maximum excess absorption per wavelength in the present two solutions, the experimental specific heat at a constant pressure is required but it is not available in our laboratory.

The effect of the second component, such as salts or surfactants, on the ultrasonic properties in aqueous solutions of nonelectrolytes are interesting in relation to the microemulsion in the solutions. They are now under investigation and the results will be reported in due course.

This work was partly supported by the Saneyoshi Fundation.

References

1) E. Grunwald, *J. Am. Chem. Soc.*, **106**, 5414 (1984).
2) N. P. Rao and R. E. Verrall, *J. Phys. Chem.*, **86**, 4777 (1982).
3) S. Nishikawa, M. Tanaka, and M. Mashima, *J. Phys. Chem.*, **85**, 686 (1981).
4) S. Nishikawa and K. Kotegawa, *J. Phys. Chem.*, **89**, 2896 (1985).
5) S. Nishikawa, M. Maekawa, M. Mashima, and T. Yasunaga, *Bull. Chem. Soc. Jpn.*, **48**, 2353 (1975).
6) S. Nishikawa and T. Uchida, *J. Soln. Chem.*, **12**, 771 (1983).
7) S. Nishikawa and R. Shinohara, *J. Soln. Chem.*, in press.
8) J. Lamb, "Physical Acoustics II part A," ed by W. P. Mason (1965), Academic Press.
9) J. H. Andreae, P. D. Edmonds, and J. F. McKellar, *Acustica*, **15**, 74 (1965).
10) G. Atkinson, S. Rajagopalan, and B. L. Atkinson, *J. Chem. Phys.*, **72**, 3511 (1980).
11) G. G. Hammes and W. Knoche, *J. Chem. Phys.*, **45**, 4041 (1966).
12) R. F. Fanning and P. Kruus, *Can. J. Chem.*, **48**, 2052 (1970).
13) S. Nishikawa and M. Shibata, *Bull. Chem. Soc. Jpn.*, **57**, 2357 (1984).
14) C. M. Davis. Jr. and J. Jarzynski, *Adv. Molecular Relax. Process*, **1**, 155 (1968).
15) G. Roux, G. Perron, and J. E. Desnoyers, *J. Soln. Chem.*, **7**, 639 (1978).
16) N. Manohama Murthy and S. V. Subrahmanyan, *Bull. Chem. Soc. Jpn.*, **50**, 2589 (1977).
17) Jaime Lara and J. E. Desnoyers, *J. Soln. Chem.*, **10**, 465 (1981).

 © 1986 The Chemical Society of Japan Bull. Chem. Soc. Jpn., 59, 833—837 (1986)

Hydrates of Organic Compounds. X. The Formation of Clathrate Hydrates of Tetrabutylammonium Alkanesulfonates

Haruo NAKAYAMA* and Hideyuki USUI
Department of Chemistry, Faculty of Engineering, Yokohama National University,
Tokiwadai, Hodogaya-ku, Yokohama 240
(Received September 25, 1985)

The solid–liquid phase diagrams of binary mixtures of water with tetrabutylammonium alkanesulfonate $(n\text{-}C_4H_9)_4NO_3SR$(R=$CH_3$–$C_5H_{11}$) and with tetrabutylammonium benzenesulfonate were examined in order to confirm the formation of clathrate-like hydrates. It has been found that (1) all the sulfonates examined can form clathrate-like hydrates with hydration numbers either around 30 or around 39; (2) these hydrates can be classified into three groups I, II, and III on the basis of the hydration numbers and melting points just as in the case of a series of tetrabutylammonium carboxylate hydrates; and (3) generally, the melting points of these sulfonate hydrates are lower than those of tetrabutylammonium carboxylate hydrates. The formation of clathrate-like hydrates of tetrabutylammonium hydrogensulfite and of tetrabutylammonium sulfite has also been reported and is discussed in an appendix.

In previous papers[1,2] the formation of a clathrate-like hydrate by a series of tetrabutylammonium carboxylates ($(n\text{-}C_4H_9)_4NOOCR$; R=H–$C_{10}H_{21}$ and unsaturated alkyl groups ranging from C_2H_3 to C_9H_{17}) was confirmed from the solid-liquid phase diagrams. These hydrates were classified into three groups, I, II, and III, on the basis of the melting points and hydration numbers.

The group I hydrates include the hydrates formed by salts with short alkyl groups such as R=H, CH_3, C_2H_5, $n\text{-}C_3H_7$, $i\text{-}C_3H_7$, $t\text{-}C_4H_9$, C_2H_3(acrylate), and C_3H_5(methacrylate, crotonate, and 3-butenoate). Two characteristic features of the group I hydrates are (a) the hydration number is around 30 and (b) most of the melting points are in the range 10—18 °C, i.e., they are very stable as compared with the group II and III hydrates mentioned below. From the fact that the hydration number is around 30, the crystal structure of the group I hydrates seem to be iso-structural with that of a well-known tetrabutylammonium fluoride hydrate.[3] However, high stability of the group I hydrates cannot be explained by a simple distortion effect of the anion on the hydrogen-bonded water framework within the hydrate.[4] Thus, it has been concluded that the alkyl group of the carboxylate anion is located in a pentagonal dodecahedron, which exists in a gap between the arrangement of large polyhedra (tetrakaidecahedron and/or pentakaidecahedron filled by one of the butyl groups of the tetrabutylammonium cation) and is believed to be either vacant or partially filled by a small molecule such as free water, oxygen, and nitrogen.

The group II hydrates are formed exclusively by all the carboxylates with R=C_4H_9, C_5H_{11}, C_4H_7, and C_5H_9 except for $t\text{-}C_4H_9$, and have hydration numbers around 39. The fact that the hydration number is around 39 indicates that the crystal structure of the group II hydrates are essentially similar to those of tetrabutylammonium benzoate hydrate, which has an ideal composition of $(n\text{-}C_4H_9)_4NOOCC_6H_5\cdot 39.5H_2O$,[5] in which the benzoate anion is surrounded by one more large cage of water. The melting points of these hydrates are not so high as those of the group I hydrates; they are at most about 12 °C.

The group III hydrates are formed by tetrabutylammonium carboxylates with long alkyl chains ranging from C_6 to C_{10} including unsaturated chains of C_7 and C_9. Although the hydration number of these hydrates is around 30 as in the case of the group I hydrate, the melting points are appreciably lower than those of the group I hydrates. From the fact that the hydration number is around 30 and such long alkyl chain cannot be accommodated within a single pentagonal dodecahedron, the possible crystal structure of these hydrates will be iso-structural with $(n\text{-}C_4H_9)_4NF$ hydrate but with the long alkyl chain of the carboxylate anion penetrating into two pentagonal dodecahedra which are facesharing with each other. The low stability of these hydrates, i.e., low melting point (around 5 °C or below), can be explained by a large distortion effect caused by the long alkyl chain of the carboxylate anion.

In this paper, from the solid–liquid phase diagrams for eight binary mixtures of tetrabutylammonium alkanesulfonate–water, the effect of the shape and/or length of the alkyl group of a sulfonate anion on the stability and the hydration numbers of their clathrate-like hydrates has been examined from a similar point of view. The formation of clathrate-like hydrates of tetrabutylammonium alkanesulfonates has not been reported previously.

In addition, the formation of clathrate-like hydrates of tetrabutylammonium salts containing either HSO_3^- ion or SO_3^{2-} ion, tetrabutylammonium hydrogensulfite and tetrabutylammonium sulfite, has also been reported and discussed.

Experimental

An aqueous solution of tetrabutylammonium alkanesulfonates, $(n\text{-}C_4H_9)_4NO_3SR$ (R=CH_3, C_2H_5, $n\text{-}C_3H_7$, i-

C_3H_7, n-C_4H_9, i-C_4H_9, and n-C_5H_{11}), and of tetrabutylammonium benzenesulfonate was prepared by neutralization of aqueous tetrabutylammonium hydroxide solution with an aqueous solution of either the corresponding alkanesulfonic acid or benzenesulfonic acid. The tetrabutylammonium hydroxide solution was obtained by treating tetrabutylammonium iodide with freshly prepared silver hydroxide in water followed by filtration of the AgI precipitate. Tetrabutylammonium iodide was prepared by precipitation from an aqueous solution of tetrabutylammonium bromide, which was purchased from Tokyo Kasei Kogyo Co. Ltd., with addition of potassium iodide, followed by washing with water and air-drying in a desiccator. The iodide was purified by repeated recrystallization from ethyl acetate–acetone mixture. Methanesulfonic acid and benzenesulfonic acid were purchased from Tokyo Kasei Kogyo Co. Ltd. and ethanesulfonic acid from Aldrich Chemical Co.. These acids were used without further purification. Aqueous solutions of n-$C_3H_7SO_3H$, i-$C_3H_7SO_3H$, n-$C_4H_9SO_3H$, i-$C_4H_9SO_3H$, and n-$C_5H_{11}SO_3H$ were obtained by passing each sodium salt solution through a column of cation exchange resin (Amberlite IR-120B) converted, in advance, into the acid form by about 2 M† hydrochloric acid solution. The sodium salts, except for n-$C_5H_{11}SO_3Na$ which was purchased from Tokyo Kasei Kogyo Co. Ltd., were synthesized by the Strecker reaction:[6] The corresponding alkyl iodide was refluxed for a few days with an aqueous sodium sulfite solution containing about twice the molar quantity of the iodide. After the water had been evaporated under reduced pressure, the reaction product was extracted with ethanol. The sodium salt was purified by repeated recrystallization from ethanol and was confirmed by its NMR spectra. Differential thermal analyses showed that melting points of all the sodium alkanesulfonates synthesized were higher than 350 °C.

The solid-liquid phase diagrams for the binary systems of water–tetrabutylammonium alkanesulfonate (or tetrabutylammonium benzensulfonate) were determined in the same manner as described in previous papers.[1,4] The concentration of each mother solution of tetrabutylammonium alkanesulfonate was determined by measuring the amount of tetrabutylammonium cation by titration with a sodium tetraphenylborate solution standardized by pure $(n\text{-}C_4H_9)_4NI$ solid.

Results and Discussion

The solid–liquid phase diagrams for tetrabutylammonium alkanesulfonate–water binary systems are shown in Figs. 1 and 2, as well as for a tetrabutylammonium benzenesulfonate–water system. In these figures the logarithm of the concentration of the tetrabutylammonium salt expressed as mole fraction (X) is plotted against the reciprocal of the absolute temperature. The temperature expressed in ordinary Celsius units is shown on the upper side of the figure.

In these figures the existence of the congruent melting points at $X\simeq0.033$ (Figs. 1 and 2) and at $X\simeq0.024$ (Fig. 2) clearly indicates that these sulfonates can form a clathrate-like hydrate. The former hydrate corresponds to the one with hydration numbers around 30 and the latter around 39. The presence of all the hydrates is confirmed in this study. As is seen in Fig. 2, phase diagrams of tetrabutylammonium 1-propanesulfonate–water and of tetrabutylammonium 1-butanesulfonate–water systems show

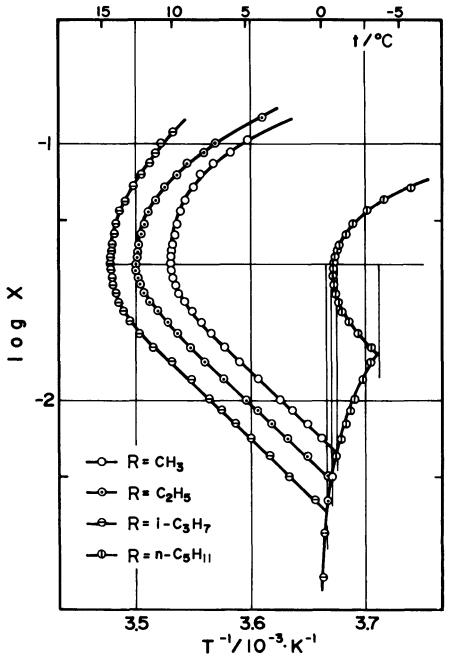

Fig. 1. Solid–liquid phase diagrams for the water–$(n\text{-}C_4H_9)_4NO_3SR$ systems.

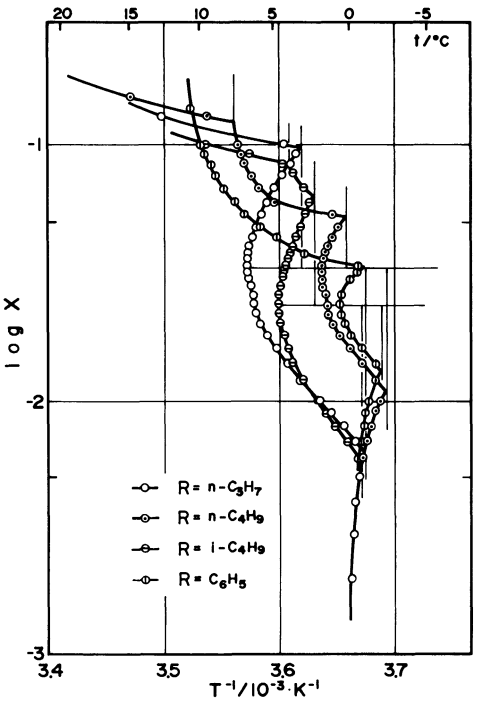

Fig. 2. Solid–liquid phase diagrams for the water–$(n\text{-}C_4H_9)_4NO_3SR$ systems.

† 1 M=1 mol dm^{-3}.

incongruent melting points at $X \simeq 0.025$. However, this temperature is almost the same as the dissolution temperature of the solution whose concentration is $X=0.024$; i.e., the $\log X$ vs. $1/T$ curve is virtually vertical around $X \simeq 0.024$. For this reason, and also for the other reason mentioned below, it can be concluded that in these systems two kinds of clathrate-like hydrates (with hydration numbers around 30 and 39) are formed simultaneously.

The other reason is the fact that in these two systems the slope $-\partial \log X/\partial(1/T)$ in dilute region, in the vicinity of $X \simeq 0.015$ for example, is about 1.20 times that of the hydrate having hydration numbers around 30 (Fig. 1) and is about 0.9 times that of the tetrabutylammonium 2-methyl-1-propanesulfonate system (Fig. 2) in which only one type of hydrate with hydration number around 39 is formed. It has been concluded in a previous paper[7] that a large portion of the molal heat of solution of a clathrate-like hydrate in water is the molal heat of fusion of the hydrate, which is approximately equal to the molal heat of fusion of ice I multiplied by the hydration number of the hydrate: i.e., the value of the slope $-\partial \log X/\partial(1/T)$ is roughly proportional to the hydration number of the hydrate. Thus, in the two systems noted above the mean hydration number is larger than 30 but smaller than 39. Since the possible structure of the hydrate is either the one with hydration number of around 30 or the one with around 39, this indicates that two types of the hydrates are present simultaneously.

All the melting points and the hydration numbers, determined from each congruent melting point and congruent composition, are summarized in Table 1. Although the curve shown in Figs. 1 and 2 has a fairly flat peak around a congruent composition, the hydration number of each hydrate can be determined within the limits of error indicated in Table 1 since, when the ampoules containing solutions of slightly different composition are warmed gradually, the ampoule which finally dissolves can easily be determined. In Fig. 3, the melting point of the hydrate is plotted against the number of carbon atoms in the main alkyl-chain of each sulfonate anion. The number attached to each point stands for the same sulfonate as the one listed in Table 1. The points corresponding to the hydrates of a series of normal alkanesulfonates are connected by a solid line. A filled circle indicates the hydrate with hydration number around 30 and an open circle indicates the one with a hydration number around 39. Similar to the carboxylate hydrates mentioned above, these hydrates can be classified into three groups; I, II, and III. They are also shown in Fig. 3.

The group I hydrates include the hydrates formed by sulfonates with R=CH_3, C_2H_5, and i-C_3H_7 (hydrates 1, 2, and 5 in Table 1) and have hydration numbers around 30. As mentioned in the introduction section, it can be concluded that these hydrates are iso-structural with $(n\text{-}C_4H_9)_4NF \cdot 30H_2O$ hydrate and that such alkyl chains as CH_3, C_2H_5, and i-C_3H_7 are accommodated within a vacant pentagonal dodecahedron. These hydrates are fairly stable as compared with the group II and III hydrates mentioned below. The most stable hydrate is that of tetrabutylammonium 3-methyl-1-butanesulfonate (14.4 °C, Table 1), indicating that the group i-C_3H_7 is most suitably fitted to a pentagonal dodecahedron. However, this melting point is relatively lower than that of the most stable carboxylate hydrates of group I: 18.0 °C for $(n\text{-}C_4H_9)_4NOOCC_2H_5$ hydrate.[1]

The group II hydrates which have hydration numbers around 39 are formed by sulfonates with

Table 1. Melting Points and Hydration Numbers of a Clathrate-Like Hydrate Formed by a Series of Tetrabutylammonium Alkanesulfonates and Tetrabutylammonium Benzenesulfonate $(n\text{-}C_4H_9)_4NO_3SR$

No	R	Mp θ_m/°C	Hydration number
1	CH_3	10.0	30±1
2	C_2H_5	12.5	30±1
3	n-C_3H_7	6.8	29±2
4*	n-C_3H_7	6.3	39±2
5	i-C_3H_7	14.4	28±2
6	n-C_4H_9	1.8	29±2
7*	n-C_4H_9	1.5	39±2
8	i-C_4H_9	4.6	39±2
9	n-C_5H_{11}	−0.8	30±2
10	C_6H_5	0.6	39±2

* See the text.

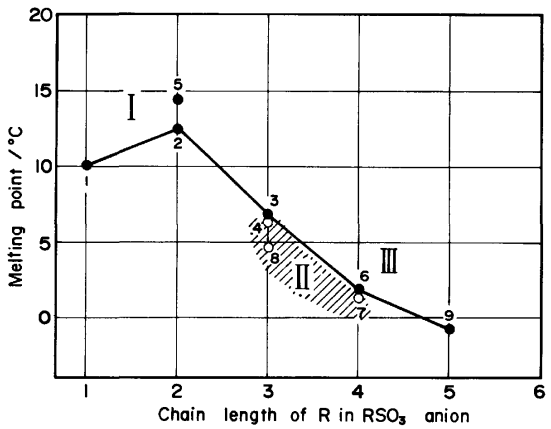

Fig. 3. Relationship between the melting points of the tetrabutylammonium alkanesulfonate, $(n\text{-}C_4H_9)_4NO_3SR$, hydrates and the chain length of R in the sulfonate anion. The number attached to each point indicates the same hydrate as the one listed in Table 1. Three groups shown by I, II, and III are explained in the text.

R=*n*-C_3H_7, *n*-C_4H_9, *i*-C_4H_9, and C_6H_5 (hydrates 4, 7, 8, and 10 in Table 1). Among them the most stable hydrate is the one with R=*n*-C_3H_7 (6.3 °C). As mentioned above, in these hydrates such alkyl groups as R=*n*-C_3H_7, *n*-C_4H_9, *i*-C_4H_9, and C_6H_5 seem to be surrounded by either a tetrakaidecahedron or a pentakaidecahedron as in the well-known (*n*-$C_4H_9)_4NOOCC_6H_5 \cdot 39.5H_2O$[5] hydrate.

Group III hydrates which have hydration numbers around 30, as in the case of the group I hydrates, are fairly unstable and are formed by sulfonates with R=*n*-C_3H_7, *n*-C_4H_9, and *n*-C_5H_{11} (hydrates 3, 6, and 9 in Table 1). These hydrates seem to be iso-structural with the (*n*-$C_4H_9)_4NF \cdot 30H_2O$ hydrate and such alkyl chains as *n*-C_3H_7, *n*-C_4H_9, and *n*-C_5H_{11} are supposed to be accommodated in a space where two face-sharing pentagonal dodecahedra are present. The hydrates 3 and 6, which have the same anion as the hydrate 4 and 7, respectively, are classified as group III hydrates instead of group I hydrates from the fact that their melting points are relatively low as compared with those of the hydrates 1, 2, and 5. Furthermore such anions as *n*-$C_3H_7SO_3^-$ and *n*-$C_4H_9SO_3^-$ are too large to form stable hydrates of group I as is mentioned below (Fig. 4). Although the reason why the sulfonates with R=*n*-C_3H_7 and *n*-C_4H_9 can form two kinds of hydrates is not clear; it is obvious that the stability of the two types of hydrates is almost the same since the difference in the melting points between hydrate 3 and 4, and between hydrate 6 and 7, is small as is shown in Table 1.

In Fig. 4 the melting points of a series of tetrabutylammonium alkanesulfonate hydrates are plotted against the conventional partial molal volume ($\overline{V}°_{conv}$) of the sulfonate anion at 25 °C. This figure includes similar plots for a series of tetrabutylammonium carboxylate hydrates reported earlier.[1] The conventional partial molal anionic volume is defined as a partial molal volume at infinite dilution on the assumption that partial molal volume of H^+ ion at infinite dilution is equal to zero.[14] These are used as an indication of the effective volume of the anion within a hydrate solid since the state in which an anion is surrounded by a hydrogen-bonded water cage will not be so different from the state in which the anion is surrounded by water molecules in an aqueous solution at infinite dilution. The conventional partial molal volume of each carboxylate and alkanesulfonate anion was obtained from the partial molal volume of each sodium salt[8-13] at infinite dilution using the relation that $\overline{V}°_{conv}$ for Na^+ ion is equal to $-1.21\ cm^3\ mol^{-1}$ at 25 °C.[14] Since the sulfonate anion is bulky as compared with carboxylate anion, the conventional partial molal volume of $C_nH_{2n+1}SO_3^-$ ion is nearly equal to that of $C_{n+1}H_{2n+3}COO^-$ ion. In Fig. 4, the domains of the group I, II, and III hydrates are also indicated. It is interesting to note that both the stability of the hydrate (i.e., the melting point) and the tendency toward which group of the hydrate can be formed are closely related to the anionic size in the two series of hydrates. However, for the same value of abscissa in Fig. 4 the melting points of a series tetrabutylammonium alkanesulfonate hydrates are lower than those of tetrabutylammonium carboxylate hydrates, indicating that the stability of the hydrates is dependent not only upon the anionic volume but also upon the chemical constitution of the anion. The distortion of the hydrogen-bonded water cage seems to be greater when it surrounds a SO_3 portion than when it surrounds a COO portion, due to the increased number of oxygen atoms in the former structure. The melting point of the tetrabutylammonium benzenesulfonate hydrate, 0.6 °C (Table 1), is also lower than that of tetrabutylammonium benzoate hydrate, which is reported to be about 6.0 °C.[5]

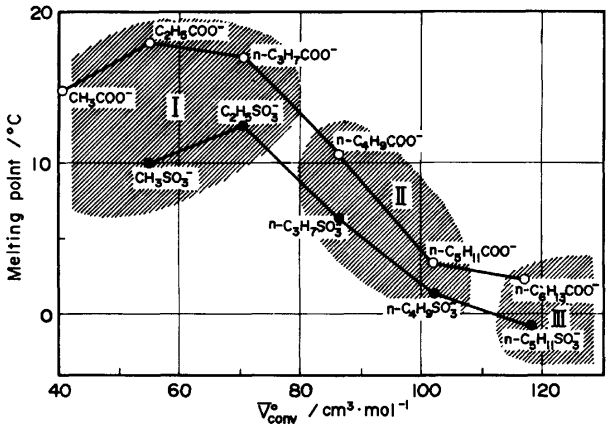

Fig. 4. Relationship between the melting points of the hydrates of either tetrabutylammonium alkanesulfonates or tetrabutylammonium carboxylates and the conventional partial molal anionic volumes. Anions are shown to each point. Three groups shown by I, II, and III are explained in the text.

Appendix

The formation of clathrate-like hydrates of two tetrabutylammonium salts whose anion is either HSO_3^- or SO_3^{2-}, tetrabutylammonium hydrogensulfite ((*n*-$C_4H_9)_4NHSO_3$) and tetrabutylammonium sulfite ([(*n*-$C_4H_9)_4N]_2SO_3$), has also been examined, although the electronic structure around the sulfur atom in these inorganic ions is different from that in an alkanesulfonate ion. The solid-liquid phase diagrams of two binary mixtures, (*n*-$C_4H_9)_4NHSO_3$-H_2O and [(*n*-$C_4H_9)_4N]_2SO_3$-H_2O, are shown in Fig. 5 in the same manner as in Figs. 1 and 2. Aqueous solutions of these two salts were obtained by neutralization of aqueous (*n*-$C_4H_9)_4NOH$ solution with an appropriate amount of sulfurous acid solution whose concentration was determined by iodometry.[15] Figure 5 clearly indicates that these

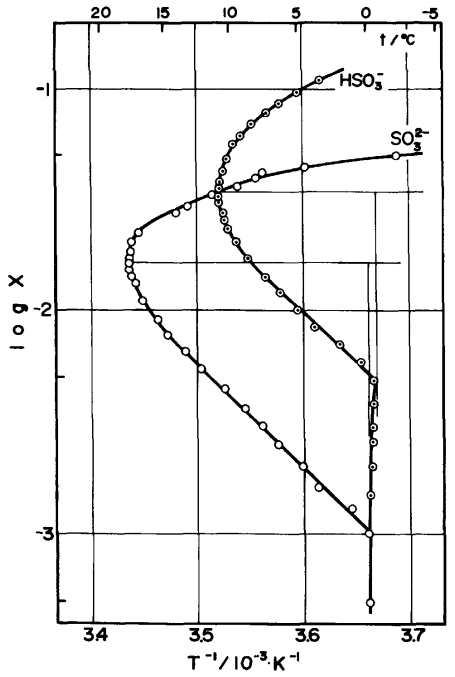

Fig. 5. Solid–liquid phase diagrams for the water–(n-$C_4H_9)_4NHSO_3$ and water–$[(n\text{-}C_4H_9)_4N]_2SO_3$ systems.

two salts can also form clathrate-like hydrates. This is confirmed in this experiment. The melting point and hydration number are 10.9 °C, 30±2 for the (n-$C_4H_9)_4NHSO_3$ hydrate and 17.8 °C, 62±4 for the $[(n\text{-}C_4H_9)_4N]_2SO_3$ hydrate, respectively. Like many other clathrate-like hydrates formed by tetrabutylammonium inorganic salts,[4] the crystal structure of both hydrates seems to be isostructural with the well-known (n-$C_4H_9)_4NF\cdot 30H_2O$ hydrate since the number of moles of water molecule per (n-$C_4H_9)_4N^+$ ion is about 30 in both hydrates.

The melting point of the $[(n\text{-}C_4H_9)_4N]_2SO_3$ hydrate is fairly high as has generally been found[4] in other hydrates of tetrabutylammonium salts having di-valent anions like CO_3^{2-} and WO_4^{2-}; 18.3 °C for the carbonate hydrate and 15.0 °C for the tungstate hydrate. The melting point of the (n-$C_4H_9)_4NHSO_3$ hydrate (10.9 °C) is somewhat higher (about 2 °C) than that expected from a linear relationship between the melting point of the hydrates and $\bar{V}°_{conv}$ of anions for a series of hydrates of tetrabutylammonium salts having mono-valent inorganic anions.[4] The value of $\bar{V}°_{conv}$ for HSO_3^- ion was estimated to be 25.68 $cm^3\ mol^{-1}$ at 25 °C from a density measurement for an aqueous solution of $NaHSO_3$ in the usual way.[13,16] The slightly elevated melting point of the (n-$C_4H_9)_4NHSO_3$ hydrate can be ascribed at least partly to the fact that a part of (n-$C_4H_9)_4NHSO_3$ is converted into $[(n\text{-}C_4H_9)_4N]_2SO_3$, which gives a more stable hydrate than (n-$C_4H_9)_4NHSO_3$, in aqueous solution since evolution of SO_2 gas is detected when concentrating a dilute solution of (n-$C_4H_9)_4NHSO_3$ by evaporation of water at reduced pressure. Thus, the aqueous solution of (n-$C_4H_9)_4NHSO_3$ is somewhat unstable especially in concentrated solution and the hydrate formed from this aqueous solution seems to be a mixed clathrate-like hydrate of (n-$C_4H_9)_4NHSO_3$ and $[(n\text{-}C_4H_9)_4N]_2SO_3$. Since both hydrates can be considered to be iso-structural with each other as mentioned above, the formation of a mixed clathrate hydrate of both salts is in principle possible. However, the amount of the $[(n\text{-}C_4H_9)_4N]_2SO_3$ salt within the mixed hydrate seems to be small because the observed melting point (10.9 °C) of the hydrate is about 7 °C as low as that of the $[(n\text{-}C_4H_9)_4N]_2SO_3$ hydrate (17.8 °C).

The present work was partially supported by a Grant-in-Aid for Scientific Research from the Ministry of Education, Science and Culture No. 60470006.

References

1) H. Nakayama and S. Torigata, *Bull. Chem. Soc. Jpn.*, **57**, 171 (1984).
2) H. Nakayama and H. Usui, *J. Inclusion Phenomena*, **2**, 249 (1984).
3) R. K. McMullan, M. Bonamico, and G. A. Jeffrey, *J. Chem. Phys.*, **39**, 3295 (1963).
4) H. Nakayama, *Bull. Chem. Soc. Jpn.*, **56**, 877 (1983).
5) M. Bonamico, G. A. Jeffrey, and R. K. McMullan *J. Chem. Phys.*, **37**, 2219 (1962).
6) R. M. Reed and H. V. Tartar, *J. Am. Chem. Soc.*, **57**, 570 (1935).
7) H. Nakayama, *Bull. Chem. Soc. Jpn.*, **55**, 389 (1982).
8) E. J. King, *J. Phys. Chem.*, **73**, 1220 (1969).
9) O. Redlich and L. E. Nielson, *J. Am. Chem. Soc.*, **64**, 761 (1942).
10) G. M. Watson and W. A. Felsing, *J. Am. Chem. Soc.*, **63**, 410 (1941).
11) M. Sakurai, *Bull. Chem. Soc. Jpn.*, **46**, 1596 (1973).
12) M. Sakurai, T. Komatsu, and T. Nakagawa, *Bull. Chem. Soc. Jpn.*, **48**, 3491 (1975).
13) K. Tamaki, Y. Ōhara, M. Inabe, T. Mori, and F. Murata, *Bull. Chem. Soc. Jpn.*, **56**, 1930 (1983).
14) F. J. Millero, "The Partial Molal Volumes of Electrolytes in Aqueous Solutions," in "Water and Aqueous Solutions," ed by R. A. Horne, Wiley-Interscience, London (1972), Chap. 13, pp. 519—595.
15) E. P. Treadwell and W. T. Hall, "Analytical Chemistry," John Wiley, New York (1963), Vol 2.
16) T. L. Broadwater and D. F. Evans, *J. Phys. Chem.*, **73**, 164 (1969).

Formation of NH($A^3\Pi$) by Electron-Impact Dissociation of Isothiocyanic Acid

Ikuo TOKUE and Yoshio ITO
Department of Chemistry, Faculty of Science, Niigata University, Niigata 950-21
(Received October 7, 1985)

Emission spectra of the fragments of Isothiocyanic acid (HNCS) produced by electron impact were studied. The onset for formation of NH($A^3\Pi$) is 9.2±0.5 eV. On the basis of the excitation function of the NH(A–X) band, NH(A) is shown to be formed via a spinforbidden process HNCS→NH($A^3\Pi$)+CS($X^3\Sigma^+$) near the onset. At higher energies, a spin-allowed process HNCS→NH(A)+CS($a^3\Pi$) seems to be predominant. The ratio of the formation rate of NH(c) to that of NH(A) is 0.18±0.03.

Isothiocyanic acid (HNCS) has 16 valence electrons and is isoelectronic with isocyanic acid (HNCO). The ground state of both molecules is known to have trans bent structure (C_s symmetry).[1,2] Emission spectra of the fragments from isocyanic acid (HNCO) and their formation mechanisms have been extensively investigated by photolysis[3–6] and electron-impact dissociation.[7,8] It was shown in a previous paper[8] that NH(A) near its onset is produced via a spin-forbidden excitation and that NH(A) at higher energies, NH(c), NCO(A), and NCO(B) are produced via a spin-allowed excitation. On the other hand, there has been only a little amount of information[9] about the dissociation mechanism of HNCS.

In the present study, the emission spectra of the fragments produced by electron-impact on HNCS have been analyzed for the first time. Dissociation processes for formation of NH(A) are assigned on the basis of the emission spectra and the excitation function. To sssist with the assignment, we have derived the excitation energy to the singlet and triplet states of HNCS by a semiempirical calculation (CNDO/S). In addition, the vibrational and rotational distributions of the NH(A) and NH(c) states are estimated on comparing the observed spectrum of the NH emission with synthetic envelopes.

Experimental

The apparatus and the experimental conditions have been described previously.[10] The pressure of the sample vapor in the collision region during the emission measurement was controlled to 2.7—6.7 mPa by a variable leak valve.

The HNCS was prepared by heating the mixture of dry, powdered samples of KSCN and $KHSO_4$ to 70 °C under vacuum.[11] The vapor generated was dried over P_2O_5 and trapped at liquid N_2 temperature. After being pumped several times at about −30 °C to remove volatile impurities, it was stored just before use in a gas reservoir at a pressure less than 3 Torr† measured by Pirani gauge to avoid deposition on the Pyrex wall.

A spectral band pass of 0.32 nm fwhm was used for the measurement of the excitation function. The energy scale for the impinging electron was calibrated by using the onset and the peak of the excitation function[12] for the (1,0) band of the $N_2(C^3\Pi_u–B^3\Pi_g)$ emission from N_2 mixed together in the sample gas.

Results and Discussion

Emission Spectra. Figure 1 shows the emission spectra in the region 250—500 nm obtained by electron impact on HNCS. These specta belong to the hydrogen Balmer lines, the CN($B^2\Sigma^+–X^2\Sigma^+$),

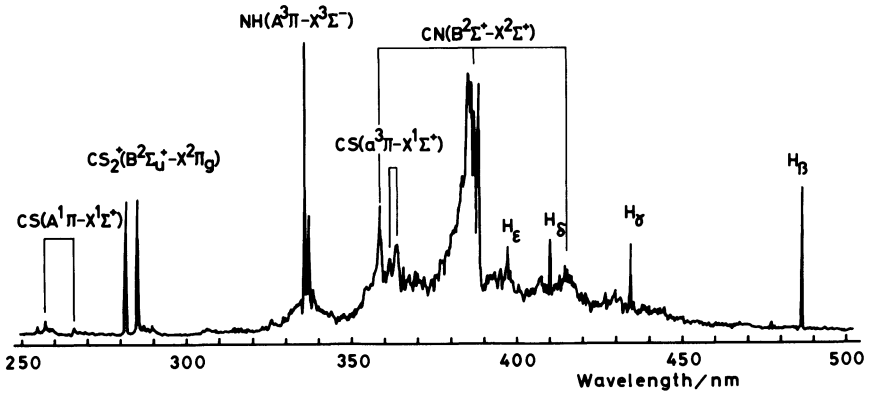

Fig. 1. Emission spectra produced by electron impact (150 V, 45 μA) on HNCS at 5.7 mPa.

† 1 Torr=133.322 Pa.

$CS(a^3\Pi-X^1\Sigma^+)$, $NH(A^3\Pi-X^3\Sigma^-)$, $CS(A^1\Pi-X^1\Sigma^+)$ bands.[13] The sharp emission near 280 nm is assigned to the $CS_2^+(B^2\Sigma_u^+-X^2\Pi_g)$ band from CS_2 impurity.[14] In addition, broad emission is observed between 340 and 470 nm. This is attributed to the NCS radical since the peaks observed near 370, 394, 396, 408, 430, 443 nm agree with those found in the literature.[15]

Although the CS_2^+(B–X) and $CS_2^+(A^2\Pi_u-X^2\Pi_g)$ band produced by electron impact on CS_2 are very strong,[16] the CS_2^+(A–X) band is not found between 450 and 530 nm as shown in Fig. 1. In a supplementary measurement, the CS(a–X) band is not observed by electron impact on CS_2 under the same conditions as for HNCS. It follows that the CS(a–X) band is produced from HNCS and that the CS(A–X) band includes a minor contribution from CS_2 impurity. On comparison with the emission produced from CS_2 under the same conditions, we concluded that the influence of CS_2 impurity in the emission spectrum is negligible except for the CS(A–X) band.

The ratio of the emission intensity of the NH(A–X) band to that of the CN(B–X) band was not reproducible. This indicates that the sample vapor includes HCN impurity since the CN(B–X) emission from HCN is generally known to be very strong. HCN is considered to be formed secondarily in the gas reservoir by the reaction[10] $3HNCS \rightarrow HCN + H_2C_2N_2S_3$. The influence of HCN impurity upon the CN(B–X) band is difficult to be estimated. In addition, the CS(a–X) band overlapped the CN(B–X) band. Hence, we did not measure the excitation function of the CS(a–X) band and did not attempt the population analysis about the CN(B–X) band. Neverthless, it is noteworthy that the appearance voltage of the CS(a–X) band is higher than the NH(A–X) band. This will be discussed in a later section.

Population Analysis of NH(A). The emission spectrum which covers the region 324—344 nm consists of two heavily overlapping bands corresponding to the (0,0) band of the NH(c–a) system and the (0,0) and (1,1) bands of the NH(a–X) system. The rotational structure can be resolved only partly due to the limited resolution. The observed spectrum is therefore compared with band envelopes simulated by a microcomputer. The procedure of the band-envelope analysis has been reported in detail.[17]

This analysis of the intensities of the NH emission bands provides information about the ratio of the formation rate of $NH(c^1\Pi)$ to that of $NH(A^3\Pi)$, P(c)/P(A), in the dissociative excitation. In addition, it provides the rotational distribution and the relative vibrational population, $N_v/N_{v=0}$, of the NH radical. In this analysis, the rotational distribution of the v level of the NH(A) or the NH(c) state is assumed to be represented by a Boltzmann temperature (T_v).

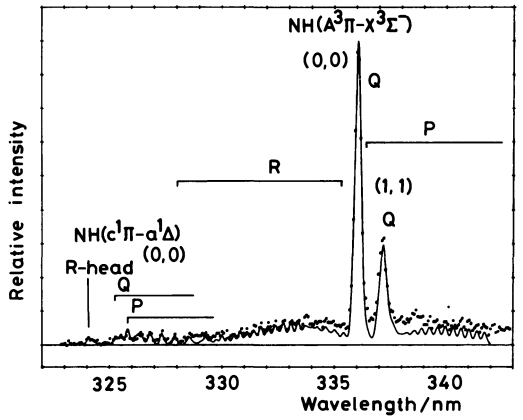

Fig. 2. The observed spectrum of NH (dots) at an impact energy of 30 eV with 0.17 nm fwhm resolution. The trace is the best-fit synthetic spectrum.

The observed spectrum at an impact energy of 30 eV is compared in Fig. 2 with synthetic envelopes. T_0 of NH(c) is fixed to be 1000 K. $P(c)/P(A)$ is derived to be 0.18±0.03 and is independent of the impact energy from the onset up to 80 eV. T_0 and N_1/N_0 of NH(A) are estimated to be ≃3000 K and 0.42±0.05, respectively. T_0 of NH(A) is nearly equal to that for HNCO, while N_1/N_0 of NH(A) is considerably larger than that for HNCO (0.24—0.30).

The disagreement between the observed spectra and the synthetic envelopes near 337 nm in Fig. 2 is attributable to the (2,2) band of the NH(A–X) transition which is not included in band envelopes. In addition, there is a tendency of synthetic envelopes to deviate from the observed spectrum at the wavelengths longer than 333 nm. This is probably caused by overlapping of the $NCS(A^2\Pi-X^2\Pi)$ and $NCS(B^2\Sigma^+-X^2\Pi)$ bands, since the NCS emission has been observed between 330 and 500 nm.[15]

Excitation Function of the NH(A–X) Band. Figure 3 shows the excitation function of the NH(A–X) band from HNCS. This is very similar in shape to that from HNCO.[8] The excitation function of the NH(c–a) band cannot be measured because of its weak intensity. The onset for formation of NH(A) is found to be 9.2±0.5 eV. In addition, the second rise in the plot appears near 20 eV.

The main dissociation processes leading to the formation of NH(A) and NH(c) from HNCS at low energy are as follows:

$$HNCS \rightarrow NH(A^3\Pi) + CS(X^1\Sigma^+), \quad \Delta H = 8.44\ \text{eV}, \quad (1)$$
$$HNCS \rightarrow NH(A^3\Pi) + CS(a^3\Pi), \quad \Delta H = 11.87\ \text{eV}, \quad (2)$$
$$HNCS \rightarrow NH(c^1\Pi) + CS(X^1\Sigma^+), \quad \Delta H = 10.17\ \text{eV}. \quad (3)$$

The ΔH values derived by using the electronic energy[13] and the enthalpy of formation[18] of HNCS and of the fragments, represent the enthalpy of

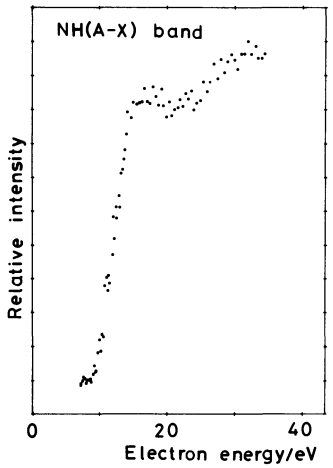

Fig. 3. NH(A-X) emission intensity at the head of the (0, 0) band versus electron energy.

dissociation. Process 1 is a spin-forbidden reaction, while Processes 2 and 3 are spin-allowed reactions. On comparing the observed onset with ΔH, it becomes evident that Process 1 is the main dissociation process leading to the formation of NH(A) near its onset. Process 2 seems to be the main dissociation process at higher energies on the following grounds. First, the excitation function of the NH(A-X) band rising linearly with the electron energy near the onset deviates from the straight line at 12 eV. This value is nearly equal to the ΔH for Process 2. Second, the excitation function above 20 eV increases monotonously with the electron energy. This implies that NH(A) is mainly produced via a spin-allowed excitation at higher energies. Third, the appearance voltage of the CS(a-X) band is higher than that of the NH(A-X) band. This indicates that CS(a) is not produced by the reaction HNCS→NH(X)+CS(a) with ΔH=8.45 eV.

In order to support the foregoing conclusion, we have carried out a semiempirical calculation (CNDO/S).[19] The excitation to the singlet and triplet HNCS states is estimated on the assumption that the Franck-Condon principle is valid. The structural parameters for the ground state of HNCS (trans bend) reported by Yamada et al.[1] are used for the calculation. The electronic configuration in the ground state of HNCS is $(1—4)a'^2 1a''^2 (5,6)a'^2 2a''^2$. This configuration agrees with the result by the HF/STO-3G calculation by using the GAUSSIAN 80 system.

Considering the accuracy of CNDO/S calculation, we can attempt only qualitative discussion. By resolving the species of NH($A^3\Pi$) and CS($X^1\Sigma^+$) into that of point group C_s, we obtain $^3A'+^3A''$ and $^1A'$, respectively. The product between these species yields the $^3A'$ and $^3A''$ states for non-linear HNCS. The observed onset for formation of NH(A) indicates that the precursor for the NH(A)+CS(X) products lies in the region 8.7—9.7 eV. Moreover, the NC bond of the precursor is expected to be weakened due to the promotion of an electron from the bonding orbital. Thus, the 6-$^3A'$ (at 8.0 eV) and 6-$^3A''$ (at 8.7 eV) states are considered to be most probable as the precursor. The former corresponds to the excitation out of the 5a′ MO into the 7a′ MO (in plane π_{NC}→in plane π_{NCS}*) and the latter corresponds to the excitation out of the 5a′ MO into the 3a″ MO (in plane π_{NC}→out-of-plane π_{NCS}*). The fact that the 6-$^3A'$ and 6-$^3A''$ states lie considerably lower than the next NH($a^1\Delta$)+CS($a^3\Pi$) state (9.74 eV) which can only correlate with the triplet HNCS states gives another ground for the above inference.

The authors thank the Computer Center, Institute for Molecular Science, for the use of the HITAC M-200H computer and the Library Program GAUSSIAN 80.

References

1) K. Yamada, M. Winnewisser, G. Winnewisser, L. B. Szalanski, and M. C. L. Gerry, *J. Mol. Spectrosc.*, **79**, 295 (1980).
2) L. Fusina and I. M. Mills, *J. Mol. Spectrosc.*, **86**, 488 (1981).
3) W. D. Woolley and R. A. Back, *Can. J. Chem.*, **46**, 295 (1968).
4) H. Okabe, *J. Chem. Phys.*, **53**, 3507 (1970).
5) W. S. Drozdoski, A. P. Baronavski, and J. R. McDonald, *Chem. Phys. Lett.*, **64**, 421 (1979).
6) G. T. Fujimoto, M. E. Umstead, and M. C. Lin, *Chem. Phys.*, **65**, 197 (1982).
7) K. Fukui, I. Fujita, and K. Kuwata, *J. Phys. Chem.*, **81**, 1252 (1977).
8) I. Tokue and Y. Ito, *Chem. Phys.*, **89**, 51 (1984).
9) C. R. Boxall and J. P. Simons, *J. Photochem.*, **1**, 363 (1972/73).
10) I. Tokue and M. Ikarashi, *Bull. Chem. Soc. Jpn.*, **54**, 2565 (1981); I. Tokue, M. Ikarashi, S. Takizawa, and Y. Ito, *Bull. Chem. Soc. Jpn.*, **56**, 583 (1983).
11) R. Kewley, K. V. L. Sastry, and M. Winnewisser, *J. Mol. Spectrosc.*, **10**, 418 (1963), and Ref. 2 in this paper.
12) T. G. Finn, J. F. M. Aarts, and J. P. Doering, *J. Chem. Phys.*, **56**, 5632 (1972).
13) K. P. Huber and G. Herzberg, "Constants of diatomic molecules," Van Nostrand, Princeton, (1979), and the related references there in.
14) L. C. Lee, D. L. Judge, and M. Ogawa, *Can. J. Phys.*, **53**, 1861 (1975).
15) P. D'amario, G. Di. Stefano, M. Lenzi, and A. Mele, *J. Chem. Soc., Faraday Trans. 1*, **68**, 940 (1972).
16) M. Toyoda, T. Ogawa, and N. Ishibashi, *Bull. Chem. Soc. Jpn.*, **47**, 95 (1974).
17) I. Tokue and M. Iwai, *Chem. Phys.*, **52**, 47 (1980).
18) D. D. Wagman, W. H. Evans, V. B. Parker, R. H.

Schumm, I. Halow, S. M. Bailey, K. L. Churney, and R. L. Nuttall, *J. Phys. Chem. Ref. Data*, **11**, (1982) suppl. No. 2.

19) The values of $1/2(I_s+A_s)$ and $1/2(I_p+A_p)$ for sulfur were not given in the original program. Hence, we used the values found in the book, J. A. Pople and D. L. Beveridge, "Approximate Molecular Orbital Theory," McGraw-Hill, New York, (1970). Orbital energies for COS molecule obtained by test run were reasonable.

 © 1986 The Chemical Society of Japan Bull. Chem. Soc. Jpn., 59, 843—851 (1986)

Electronic Spectra of Two Polymorphs of (5-Dimethylamino-2,4-pentadienylidene)dimethylammonium Perchlorate

Norimichi SANO and Jiro TANAKA*
Department of Chemistry, Faculty of Science, Nagoya University, Chikusa-ku, Nagoya 464
(Received October 28, 1985)

Reflection spectra were measured on two polymorphs of (5-dimethylamino-2,4-pentadienylidene)dimethylammonium perchlorate in order to determine the origin of the J band. One polymorph exhibited two bands with different polarization characteristics; one of them is explained by the molecular-exciton (MX) band of a $\pi\pi^*$ transition character and the other is an intermolecular charge-resonance (CR) band, the polarization being along the direction connecting the nitrogen atoms of the adjacent molecules. The other polymorph exhibited a quasi-metallic reflection due to the overlapping of the CR and MX bands.

Cyanine dyes have a characteristic structure with an odd polymethine chain and two terminal nitrogen

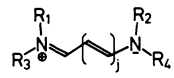

atoms. It has been well known that the aggregate of the cyanine dye exhibits peculiar spectral characteristics in the visible region. Especially, the aggregation behavior and the spectral sensitization of photographic silver halide emulsions have been investigated.[1-3]

From investigations of the spectra of some aggregates and those of crystals of cyanine dyes,[4-6] it has been shown that a J band appeared in the crystals when the molecular overlap was significant in laterally shifted dye stacks. In such a condition, the charge-resonance (CR) configuration strongly interacted with the molecular-exciton (MX) configuration, where the interaction was assisted by a strong π-electron overlap. In contrast with the case of the crystals of electron donor-acceptor complexes, the intermolecular CR absorption band of pure molecular crystals have eluded direct observation for years, especialy that of cyanine dyes, although electric field modulated spectra indicated the existence of intermolecular CR transition in 9,10-dichloroanthracene,[7] for which the anomalous absorption polarization had been reported.[8] The CR bands of anthracene,[9] naphthacene and pentacene[10] were also recently found.

In this paper, the reflection spectra and Kramers-Kronig (K-K) absorption spectra are presented on two polymorphs with space groups *Cc* (the yellow form)[11] and $P2_1/a$ (the orange form),[12] of (5-dimethylamino-2,4-pentadienylidene)dimethylammonium perchlorate (5-DMP, abbreviated to BDP in the literature).

Anex and Simpson[13] reported a quasi-metallic reflectivity in the spectra of the yellow form, and its origin has been investigated theoretically by Philpott[14] and Rimbey.[15] On the other hand, Dähne and his coworkers[16] have found the existence of an orange-colored crystal having the same constituent, and have noticed a difference in the reflection spectra. Although Sieber et al. had reported the molecular and crystal structures of the orange form,[17] a more precise X-ray analysis was performed by our group,[12] and the molecular geometry with a bond-alternated character on the conjugated system and the charge-density distribution were determined.

In this paper, we present evidence of an intermolecular CR band between cation molecules in crystals of the orange form. Investigations regarding two modifications of a crystal of 5-DMP and a comparison with the previous study for 3-DMP ((3-dimethylamino-2-propenylidene)dimethylammonium perchlorate)[18] are very illuminating for an assignment of the electronic transitions of the J-type band.

Experimental

Materials. 5-DMP was synthesized by the method of Malhotra and Whiting.[19] The product was purified with active charcoal and recrystallized several times from ethanol. Single crystals of the orange form were grown from methanol and those of the yellow form from ethanol. These were used for reflection measurements. Crystalline forms and faces were confirmed by taking X-ray photographs using the Weissenberg camera.[11,12,17]

Crystal Structures. The Orange Form:[12,17] Crystals of the orange form were prismatic (Fig. 1(a)) and were elongated along the *c* axis, showing the {100}, {110}, and {010} zone axes. Lattice parameters are given in Table 1. The molecular packing in the orange form is shown in Fig.

Table 1. Lattice Parameters for Polymorphs of 5-DMP

	Orange form	Yellow form
a/Å	13.671 (3)	12.27 (3)
b/Å	14.899 (2)	9.44 (2)
c/Å	6.186 (2)	12.42 (3)
β/°	97.27 (2)	114.80 (1)
V/Å^3	1249.9 (5)	1306
Z	4	4
Space group	$P2_1/a$	*Cc*
Reference	12	11

2 as a projection onto the (010) face (for clarity, only half of the molecules in a unit cell are illustrated). The nearest-neighbor molecules are related by a translational symmetry. Since the space group of the orange form is $P2_1/a$ (C_{2h}^5), the exciton wavefunction of the B_u symmetry is allowed for light polarized parallel with the *ac* plane and that of the A_u symmetry is active along the *b* axis.

The Yellow Form:[11] Crystals of the yellow form were transparent laths and elongated along the *c* axis. The prominent zone axes were {010} and {110} (Fig. 1(b)).

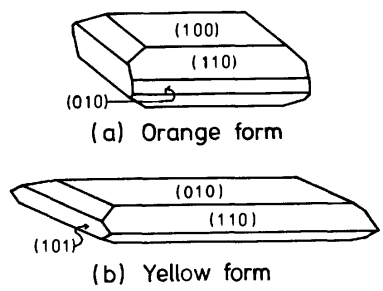

Fig. 1. Crystal morphology for (a) the orange form and (b) the yellow form.

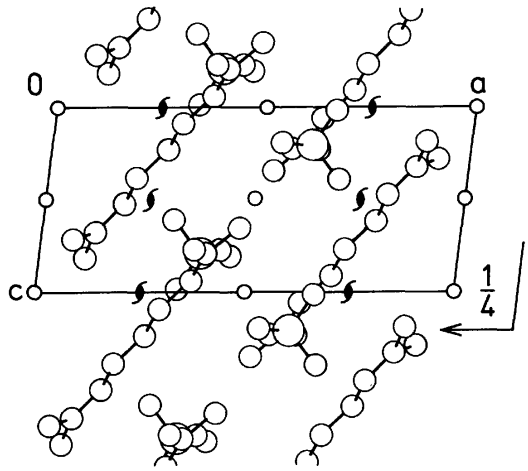

Fig. 2. Crystal structure of the orange form with symmetry symbols.

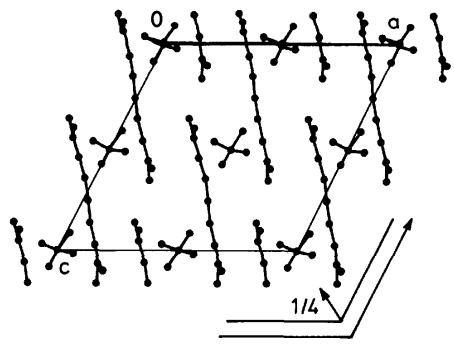

Fig. 3. Crystal structure of the yellow form with symmetry symbols.

Lattice parameters are shown in Table 1. The arrangement of the molecules in a crystal is shown in Fig. 3, where the molecules are stacked along the *c* axis. Since the space group of the yellow form is *Cc* (C_s^4), the exciton wavefunctions which have an *ac* component and a *b* component have A′ and A″ symmetries, respectively.

Measurements. Reflection spectra were measured on a microscopic spectrophotometer as reported previously.[5] The reflectivities were converted to molar absorption coefficients by a K-K transformation on a FACOM M-382 computer of the Nagoya University Computation Center. The computation program was based on the method of Ahrenkiel.[20] The absorption spectra of the monomer in solution were measured on a Hitachi 330 spectrophotometer.

Results

Solution Spectrum. The spectrum of a methanol solution at room temperature is shown in Fig. 4. Measurements of aqueous and chloroform solutions gave almost the same results. Although the absorption band has an asymmetric shape, vibrational structures are not clear. The oscillator strength is 1.08, and the transition-dipole length is estimated to be 2.02 Å.

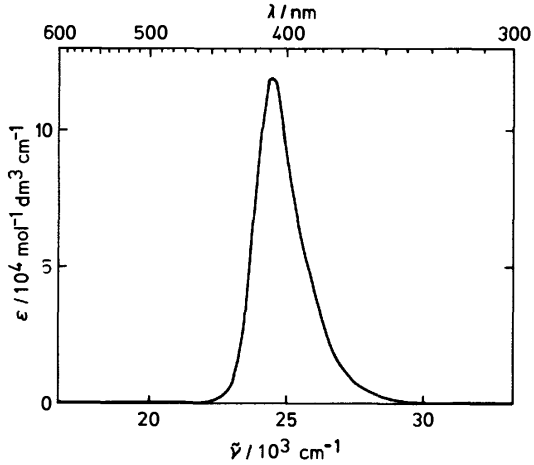

Fig. 4. Solution spectrum of 5-DMP at room temperature in methanol ($c=2\times10^{-5}$ mol dm^{-3}).

Crystalline Reflection Spectra. The Orange Form: Figure 5 shows the reflection spectra obtained for several polarization directions on the (010) face. Spectra **1** and **3**, respectively, are for parallel and perpendicular polarizations to the long axis of a cation molecule. It should be pointed out that a single reflection peak at 21500 cm^{-1} is found in the spectrum **3**. For the other polarization directions, there are at least two reflection peaks. One of them is apparently due to the $\pi\pi^*$ transition of the cation molecule, and the other in the 21500 cm^{-1} region is clearly due to an extra transition which appears only in a crystal through an intermolecular interaction.

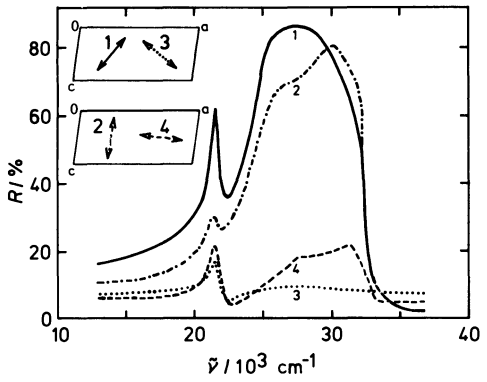

Fig. 5. Reflection spectra from the (010) face of the orange form.

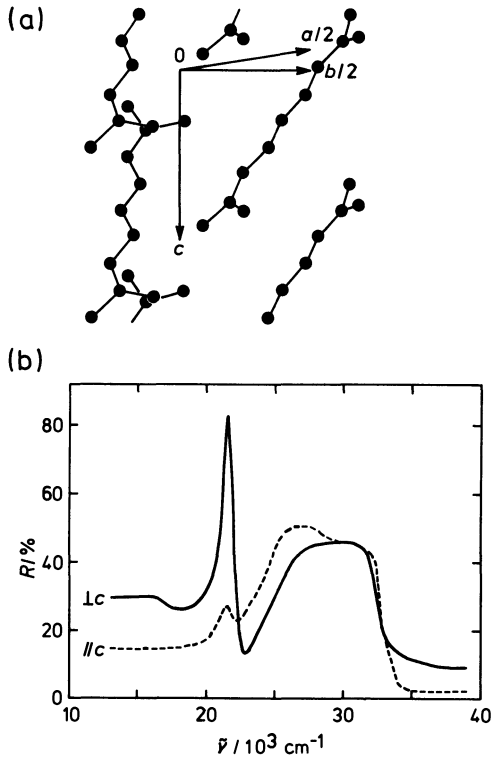

Fig. 6. (a) Projection onto the (1$\bar{1}$0) face of the orange form and (b) the reflection spectra from the (1$\bar{1}$0) face.

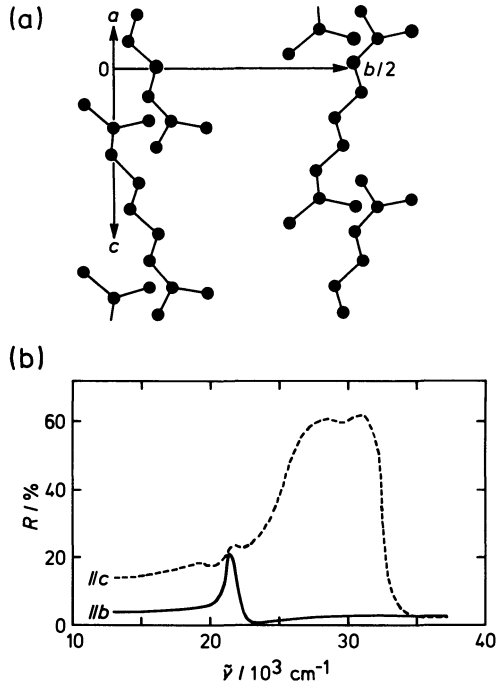

Fig. 7. (a) Projection onto the (100) face of the orange form and (b) the reflection spectra from the (100) face.

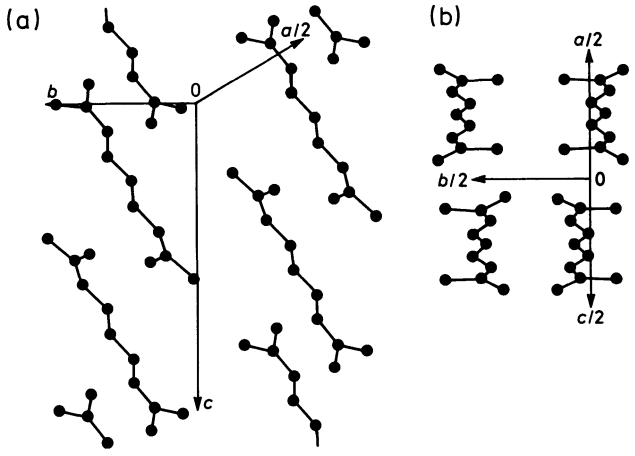

Fig. 8. (a) Projection onto the (110) and (101) faces of the yellow form.

The direction of the transition moment for the latter one is distinct from that of the $\pi\pi^*$ transition.

Figure 6(a) shows a projection onto the (1$\bar{1}$0) face. In this projection, two kinds of molecular orientations are shown, where the direction connecting the nitrogen atoms of the adjacent cation molecules is almost perpendicular to the c axis. The reflection spectra from the (1$\bar{1}$0) face is shown in Fig. 6(b). On this face, the intensity of the 21500 cm^{-1} band is maximum for the direction perpendicular to the c axis, and the B_u symmetry state of the $\pi\pi^*$ transition is greatly blue shifted in this direction. The apparent shift may be partly due to an interference effect by the 21500 cm^{-1} transition, since a sharp dip at 23000 cm^{-1} might influence the reflectance of the $\pi\pi^*$ transition at the lower edge.

In a projection onto the (100) face (Fig. 7(a)), the N···N direction is almost vertical to the developed face. Figure 7(b) shows the reflection spectra from the (100) face. In the c-axis spectrum, the 21500 cm^{-1} peak is observed very weakly and the $\pi\pi^*$ transition is largely blue shifted. In the b-axis spectrum, only a single band is found at 21500 cm^{-1}.

The Yellow Form: Figures 8(a) and (b) show projections onto the (110) and (101) faces. Figure 9 shows the reflection spectra from the (010), (110), and

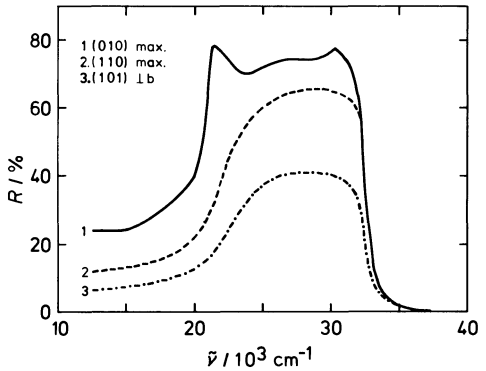

Fig. 9. Reflection spectra from the (010), (110), and (101) faces of the yellow form.

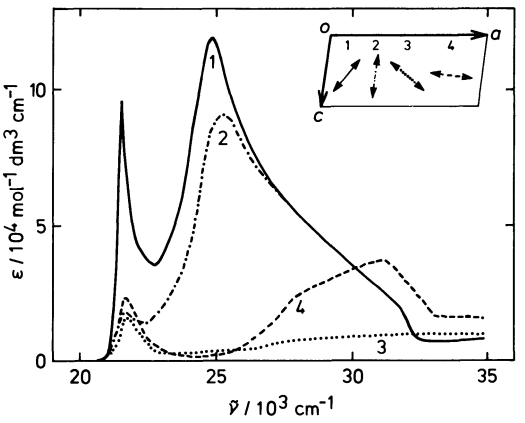

Fig. 10. Absorption spectra for the (010) face of the orange form.

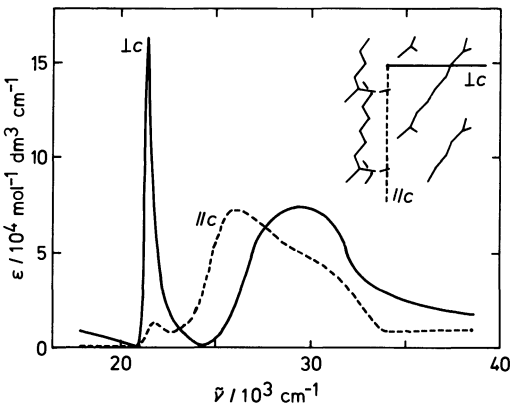

Fig. 11. Absorption spectra for the (1$\bar{1}$0) face of the orange form.

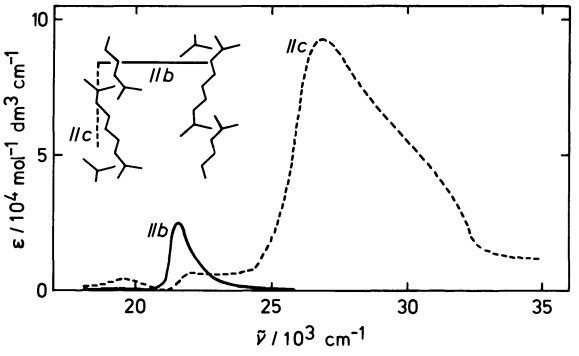

Fig. 12. Absorption spectra for the (100) face of the orange form.

(101) faces. The polarizations of light which gives the maximum reflectivities are almost parallel to the projections of the long axis of the cation molecules. This direction deviates by 5° from the long axis on the (010) face. On each face, the reflectivities with the polarization perpendicular to the maximum direction are less than 5%. Broad reflection bands are attributed mostly to the $\pi\pi^*$ transition on each face. On the (010) face, a high reflectance for a wide energy range of 1.5 eV ($\approx$12000 cm^{-1}) is shown; it exhibits a peak at the lower edge of 21200 cm^{-1}. This reflection band has been noticed as a typical quasi-metallic reflection band.[13,21,22]

K-K Transforms to Absorption Spectra. The Orange Form: The absorption spectra were obtained by a K-K transformation of the reflection spectra from the (010), (1$\bar{1}$0), and (100) faces (Figs. 10, 11, and 12). A remarkable feature of the absorption spectra is that the 21500 cm^{-1} peak shows a quite anomalous polarization behavior. As previously mentioned, the direction of the transition moment is different from that of the $\pi\pi^*$ transition on the (010) face, and the intensity is particularly strong on the (1$\bar{1}$0) face. Considering the dichroic ratio on these crystalline faces, the direction of the transition moment of the 21500 cm^{-1} band is deduced to be on the line connecting the N···N atoms; therefore, the character of this transition is assigned to the charge-resonance (CR) band between adjacent stacked molecules.

Another conspicuous characteristic of the spectra is that the peak positions of the $\pi\pi^*$ transition (MX band) are shifted to blue in many directions, presumably because the higher tail of the 21500 cm^{-1} band interferes with the rise of the reflection spectra due to the $\pi\pi^*$ transition. In the consideration of the energy levels of the MX band, this effect must be taken into account by assuming that the center of the MX band is blue shifted.

The absorption spectra of the (100) face along the *c* axis show weak peaks in the 21500 cm^{-1} region and a very strong band in the region 27000—32000 cm^{-1}. Along the *b* axis, the $\pi\pi^*$ transition shifts to red and overlaps with the CR band at 21500 cm^{-1}. These tendencies of the band shift and the splitting will be discussed in the next section.

The Yellow Form: The transformed absorption

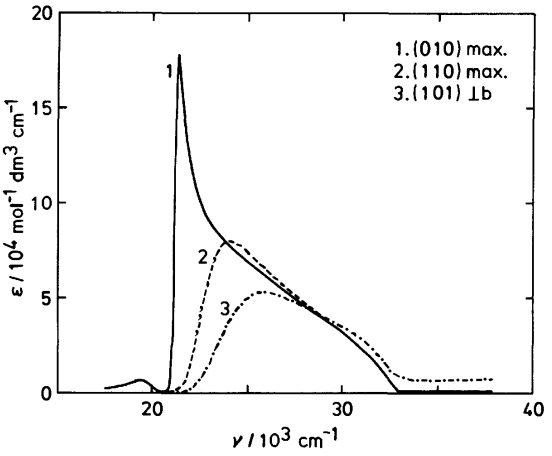

Fig. 13. Absorption spectra for the (010), (110), and (101) faces of the yellow form.

spectra for the yellow form are shown in Fig. 13. A very sharp peak at 21300 cm^{-1} and a broader peak near the 23000 cm^{-1} region were obtained on the (010) face. This is a characteristic feature of a strong metallic reflection band. The presence of two peaks was recognized in the earlier work of Fanconi et al.[21] The band feature may be due to the overlapping and mixing of the CR and MX configurations. Such a sharp peak is not found for the other faces, (110) and (101), although weak reflectivity humps are found in the 21500 cm^{-1} region. In this crystal, the effect of the CR interaction seems to appear only when the energy level of the MX configuration is close to that of the CR configuration.

Comparison with 3-DMP. In a previous study regarding the reflection spectra of 3-DMP,[18] we observed only an MX-type excited state; any token of the CR band was not detected. This is reasonable since the intermolecular overlap between cation molecules is not large and no specific interaction exists between nitrogen atoms of the adjacent molecules. In 5-DMP crystals, an additional transition is found which is due to an intermolecular electron exchange interaction due to a significant molecular overlap. The cause of such a contrast may be that 5-DMP has a longer conjugated system than 3-DMP; therefore, both the donor and the acceptor properties are enhanced in 5-DMP and the CR interaction is increased. The length of the conjugated chain in pentamethine may be optimum because a chain that is too long may reduce the charge density of the HOMO and the LUMO at the terminal nitrogen atoms.

Discussion

A criterion of the J band is a sharp and red-shifted absorption band, a characteristic of the aggregate; then, the 21500 cm^{-1} band of the orange form is a typical J band. Although the condition for the appearance of a J band is not yet clear, the present experimental result may provide a key for resolving this long-standing problem.

The 21500 cm^{-1} band is ascribed to a transition which is different from the $\pi\pi^*$ transition because the reflection spectra from the (010) face of the orange form (Fig. 5) show two strong peaks in the 21500 cm^{-1} and 27000 cm^{-1} regions. These are difficult to explain by an exciton-type band splitting of a single $\pi\pi^*$ transition. In the spectra on the (010) face, only the B_u state is observable using normally incident light. Also, a single transition should produce a single peak. Such a theoretical prediction has been confirmed from many experiments on various crystals. The direction of the transition moment of the 21500 cm^{-1} band should be determined from polarization measurements for all possible faces. However, the actual spectra are rather complicated because of the intensity borrowing or the mixing with the $\pi\pi^*$ transition.

In our previous studies on the spectra of cyanine dye crystals,[4,5] we have shown that the charge-resonance (CR) type band is strongly mixed with the molecular-exciton (MX) type band. Although the polarization of the charge-transfer (CT) band of the electron donor-acceptor complex is believed to lie along the direction connecting the centers of the HOMO of the donor and the LUMO of the acceptor molecules, the present CR band gives a different result. It shows that the transition moment is directed along the line connecting the N···N atoms of the adjacent dye molecules. This means that the nitrogen atoms of the cyanine dye may take on a canonical polar structure at the moment of a transition in which CR takes place between the $N\cdots N^+$ atoms. This argument is based on the fact that the intensity of the CR band arises from two sources; one is a genuine CR transition moment directed along the N···N direction, and the other comes from a mixing with the MX configuration.

By this assignment, the characteristic sharp band shape of the J band can be ascribed to the nitrogen π orbital since a sharp band feature is often found in the photoelectron spectra of the nonbonding orbital.[23] A sharp band shape is considered as an evidence of a small coupling with a molecular vibration; in other words, a nonbonding character of the nitrogen π orbital may give a small coupling with a molecular vibration in the CR spectra.

The present dye in solution exhibited a broad single absorption (Fig. 4). However, Gerhold observed two overlapping peaks in low temperature glass and estimated the vibrational interval at 1150 cm^{-1}.[14] The blue-shifted $\pi\pi^*$ bands are much

broader in the crystalline spectra than in the solution, but the 21500 cm^{-1} band is sharp without any vibrational progression.

Theoretical Consideration on the Electronic States in the Crystals. In order to discuss the interaction of the CR configuration with the MX configuration in the crystal, the effect of the intermolecular overlap interaction is considered here in detail. As previously mentioned, the interactions of the nearest-neighbor molecules extend along the c axis for both orange and yellow crystals. Therefore, we can restrict our treatment to a one-dimensional array of the molecules along the c axis.

An intense electronic absorption is found for the electronic transition between the HOMO (φ) and the LUMO (θ), and a charge transfer also occurs between the HOMO and the neighbor's LUMO. From the previous discussion regarding the direction of the CR band, an interaction between nitrogen atoms may be more important. However, in the following argument we consider interactions between molecular orbitals. The ground configuration of the system is given by

$$\Phi_G = |\cdots\varphi_{i-1}\bar{\varphi}_{i-1}\varphi_i\bar{\varphi}_i\varphi_{i+1}\bar{\varphi}_{i+1}\cdots|, \tag{1}$$

and the CR configuration is described by

$$\Phi^{\pm}_{CR} = \frac{1}{\sqrt{2N}}\sum_{i=1}^{N}(\Phi_{i\to i+1}\pm\Phi_{i+1\to i}), \tag{2}$$

where

$$\Phi_{i\to i+1} = \frac{1}{\sqrt{2}}(|\cdots\varphi_{i-1}\bar{\varphi}_{i-1}\theta_{i+1}\bar{\varphi}_i\varphi_{i+1}\bar{\varphi}_{i+1}\cdots| + |\cdots\varphi_{i-1}\bar{\varphi}_{i-1}\varphi_i\bar{\theta}_{i+1}\varphi_{i+1}\bar{\varphi}_{i+1}\cdots|) \tag{3a}$$

and

$$\Phi_{i+1\to i} = \frac{1}{\sqrt{2}}(|\cdots\varphi_{i-1}\bar{\varphi}_{i-1}\varphi_i\bar{\varphi}_i\theta_i\bar{\varphi}_{i+1}\cdots| + |\cdots\varphi_{i-1}\bar{\varphi}_{i-1}\varphi_i\bar{\varphi}_i\varphi_{i+1}\bar{\theta}_i\cdots|). \tag{3b}$$

The MX configuration can be represented for the translationally equivalent molecules by

$$\Phi_{MX} = \frac{1}{\sqrt{N}}\sum_{i=1}^{N}\Phi_i \tag{4}$$

where

$$\Phi_i = \frac{1}{\sqrt{2}}(|\cdots\varphi_{i-1}\bar{\varphi}_{i-1}\theta_i\bar{\varphi}_i\varphi_{i+1}\bar{\varphi}_{i+1}\cdots| + |\cdots\varphi_{i-1}\bar{\varphi}_{i-1}\varphi_i\bar{\theta}_i\varphi_{i+1}\bar{\varphi}_{i+1}\cdots|). \tag{5}$$

Now let us consider the matrix elements between these configurations by calculating the transfer integrals which are approximated as being propotional to the overlap integrals between the relevant molecular orbitals. The abbreviated formulae for the overlap integrals are given by

$$S_{11} = \langle\varphi_i|\varphi_{i+1}\rangle, \quad S_{12} = \langle\varphi_i|\theta_{i+1}\rangle, \quad S_{21} = \langle\theta_i|\varphi_{i+1}\rangle, \text{ and } S_{22} = \langle\theta_i|\theta_{i+1}\rangle. \tag{6}$$

An approximate formula for estimating the transfer integral is given by

$$t_{mn} = kS_{mn} \quad (m, n=1, 2). \tag{7}$$

The symmetries of the φ and θ orbitals in this system give a relation $S_{12}=-S_{21}$; hence, the matrix element between the Φ_G and the Φ^-_{CR} configurations is given by

$$\langle\Phi_G|\mathscr{H}|\Phi^-_{CR}\rangle = \frac{1}{\sqrt{N}}\sum_{i=1}^{N}(\langle\varphi_i|\mathscr{H}|\theta_{i+1}\rangle-\langle\theta_i|\mathscr{H}|\varphi_{i+1}\rangle) = \sqrt{N}k(S_{12}-S_{21}) = 2\sqrt{N}kS_{12}. \tag{8}$$

The Φ^+_{CR} configuration interacts with the Φ_{MX} configuration and the matrix element is calculated as

$$\langle\Phi^+_{CR}|\mathscr{H}|\Phi_{MX}\rangle = \frac{1}{\sqrt{2}}\cdot\frac{1}{N}\sum_{i=1}^{N}(\langle\Phi_{i\to i+1}|\mathscr{H}|\Phi_i\rangle + \langle\Phi_{i-1\to i}|\mathscr{H}|\Phi_i\rangle + \langle\Phi_{i+1\to i}|\mathscr{H}|\Phi_i\rangle + \langle\Phi_{i\to i-1}|\mathscr{H}|\Phi_i\rangle) = \sqrt{2}k(S_{22}-S_{11}). \tag{9}$$

The matrix element given in Eq. 8 is renormalized to evaluate the contribution of the Φ^-_{CR} configuration to the ground state per molecule. Then, the secular equation (including the Φ_G and the Φ^-_{CR} configurations) is given by

$$\begin{vmatrix} -E & 2kS_{12} \\ 2kS_{12} & E^-_{CR}-E \end{vmatrix} = 0. \tag{10}$$

The mixing of the Φ_{MX} and the Φ^+_{CR} configurations is calculated by solving the secular equation

$$\begin{vmatrix} E^+_{CR}-E & \sqrt{2}k(S_{22}-S_{11}) \\ \sqrt{2}k(S_{22}-S_{11}) & E_{MX}-E \end{vmatrix} = 0. \tag{11}$$

The calculation of the overlap integrals is performed by a previously reported method,[24] and obtained values are as shown in Table 2. The magnitudes of these integrals are fairly large for an intermolecular interaction and the transfer integrals are estimated by setting k=—15 eV in Eq. 7. This choice of k is reasonable in view of the Mulliken-

Table 2. Molecular Integrals between the MO's of Stacked Dye Molecules

Crystalline form	S_{mn} MO	φ_{i+1}	θ_{i+1}	$\langle\Phi_G\|\mathscr{H}\|\Phi_{CR}^-\rangle$ eV	$\langle\Phi_{CR}^+\|\mathscr{H}\|\Phi_{MX}\rangle$ eV
Orange	φ_i	0.00965	0.00872	−0.3105	0.3837
	θ_i	−0.01198	−0.00844		
Yellow	φ_i	0.00232	0.00477	−0.1362	0.1421
	θ_i	−0.00431	−0.00438		

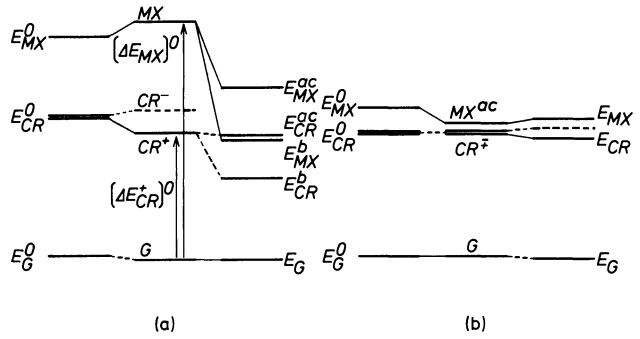

Fig. 14. Calculation procedures of the electronic states in the crystals; (a) for the orange form and (b) for the yellow form.

Wolfsberg-Helmholtz formula. It states that $k=KW$, since if we take the orbital energy of HOMO at $W=-10$ eV then $K=1.5$.[24]

The Orange Form: The calculation procedure is shown in Fig. 14(a), where the interaction of the Φ_{CR}^+ and the Φ_{MX} configurations is first considered; then, the exciton band splittings in the CR+ and the MX states are evaluated.

The initial diagonal energies for the orange form are set at $E_{CR}^0=22800\,cm^{-1}$ and $E_{MX}^0=29300\,cm^{-1}$, respectively. The blue shift of the MX state, compared to a solution spectra, is assumed to harmonize the calculated energy levels with the observed spectra. The transfer integrals of the orange form are apparently larger than those of the yellow form (Table 2). Accordingly, the mixing of the Φ_{CR}^+ configuration with the Φ_{MX} configuration is more impotant in the orange form than in the yellow form. After solving the secular equations, 10 and 11, the energy levels of the CR+ and the MX states were found at $(\Delta E_{CR}^+)^0=21900\,cm^{-1}$ and $(\Delta E_{EX})^0=30800\,cm^{-1}$, respectively, where the stabilization of the ground state was taken into account. These energy levels correspond to the center of the Davydov components. The transition moments were obtained as being a vector sum of the CR- and the MX-type moments multiplied by coefficients which were obtained by solving the secular equations. In this treatment, the CR-type moment was taken as the vector connecting the two nitrogen atoms of adjacent dye molecules. The transition length of the MX-type moment was set at 2.2 Å, larger by 10% than the solution's value. Such a bathochromism of the MX transition might exist due to the effect of the CR interaction.

In order to explain the splitting of the crystalline MX states, the exciton energy shifts were calculated for the measured faces by a dipole-dipole approximation.[5] The dipole sum was extended for molecules in a disc with a radius of 200 Å and a depth of 20 Å, placed in the crystalline surface. The wavefunctions for a MX state having A_u and B_u symmetries are given by

$$A_u : \Psi_b = \frac{1}{\sqrt{N}} \sum_{i=1}^{N} (\Psi_{1i} - \Psi_{2i} + \Psi_{3i} - \Psi_{4i}) e^{i\boldsymbol{k}\cdot\boldsymbol{R}_i} \quad (12a)$$

and

$$B_u : \Psi_{ac} = \frac{1}{\sqrt{N}} \sum_{i=1}^{N} (\Psi_{1i} - \Psi_{2i} - \Psi_{3i} + \Psi_{4i}) e^{i\boldsymbol{k}\cdot\boldsymbol{R}_i} \quad (12b)$$

where i is the numbering of the unit cell, and 1, 2, 3, and 4 designate the molecular sites. Ψ_{1i} means that the original site of the i-th cell is excited and others are in the ground state. Ψ_{2i}, Ψ_{3i}, and Ψ_{4i} are wavefunctions in which excitation occurs at sites related to the original site by the space group operators: center of symmetry, screw axis and glide plane, respectively.

The results of the calculation for the energy levels and intensities are shown in Table 3. Agreement between the observed and the calculated results is quite reasonable in spite of the complicated patterns of the spectra for the respective faces.

On the (010) face, only the B_u component is expected to appear and the observed band positions and intensities are well explained by the mixing of the Φ_{CR}^+ configuration with the Φ_{MX} configuration. The MX band for the $\perp c$ polarization was found at 28000—31000 cm^{-1} region, and such an unusual blue shift might be appeared by a decrease of the reflectivity at 26000 cm^{-1} region which is caused by the interference effect of the dip at 22500 cm^{-1}.

With the $(1\bar{1}0)$ face, the calculated spectrum for the $\|c$ direction is in good agreement with the observed spectrum. However the $\perp c$ component shows two discrepancies. First, the band intensity at the 21500 cm^{-1} region is much smaller than the observed

Table 3. Polarized Crystalline Spectra of the Orange Form

Face	pol. axis	CR ΔE_{CR}[a]/10^3 cm^{-1} Obsd	CR ΔE_{CR}[a]/10^3 cm^{-1} Calcd	CR f Obsd	CR f Calcd	MX ΔE_{MX}[a]/10^3 cm^{-1} Obsd	MX ΔE_{MX}[a]/10^3 cm^{-1} Calcd	MX f Obsd	MX f Calcd
(010)	$\parallel c$	21.6	21.1	0.12	0.28	25.2	24.2	2.90	2.81
	$\perp c$	21.6		0.21	0.43	31.0		1.30	0.78
	$\parallel$ L[b]	21.5		1.30	0.65	24.8		3.15	3.55
	$\perp$ L[b]	21.7		0.13	0.06	—		—	0.04
(1$\bar{1}$0)	$\parallel c$	21.7	21.8	0.21	0.28	26.0	25.4	3.30	2.81
	$\perp c$	21.4	21.8, 19.8	1.47	0.20, 0.07	29.0	25.4, 21.6	4.32	0.53, 0.14
(100)	$\parallel c$	22.0	23.5	0.12	0.28	26.8	28.0	3.52	2.81
	$\parallel b$	—	20.2	—	0.14	21.5	22.2	0.19	0.26

a) $\Delta E_{CR}=E_{CR}-E_G$ and $\Delta E_{MX}=E_{MX}-E_G$. b) Parallel and perpendicular to the molecular long axis.

Table 4. Polarized Crystalline Spectra of the Yellow Form

Face	pol. axis	CR ΔE_{CR}[a]/10^3 cm^{-1} Obsd	CR ΔE_{CR}[a]/10^3 cm^{-1} Calcd	CR f Obsd	CR f Calcd	MX E^{ac}_{MX}[b] 10^3 cm^{-1}	MX ΔE_{MX}[a]/10^3 cm^{-1} Obsd	MX ΔE_{MX}[a]/10^3 cm^{-1} Calcd	MX f Obsd	MX f Calcd
(010)	max.	24.6	22.2	1.10	1.26	21.7	21.3	21.4	4.09	2.24
	min.	—		—	0.00		—		—	0.05
(110)	max.	—	21.7	—	0.75	22.4	23.8	22.6	3.55	2.41
	min.	—		—	0.00		—		—	0.01
(101)	$\perp b$	—	21.9	—	0.04	26.1	25.7	26.2	2.25	0.70
	$\parallel b$	—		—	0.00		—		—	0.00

a) $\Delta E_{CR}=E_{CR}-E_G$ and $\Delta E_{MX}=E_{MX}-E_G$. b) The A′ level of the Φ_{MX} configuration.

value in spite of the fact that the CR$^+$- and the MX-A_u states were calculated to be in this region. The sum of these intensities were not sufficient to account for the prominent strong peak. Secondly, the MX level for the $\perp c$ direction was calculated at 25400 cm^{-1} while the observed value was 29000 cm^{-1}. This blue shift may have occurred due to an interference of the sharp peak at 21500 cm^{-1}.

On the (100) face, the spectrum for the *b*-axis polarization gives a single peak and the calculated energies for the CR and the MX states are close together in agreement with the experiment. The peak position for the *c* axis is well explained by the calculation. However, the calculated intensity for the 21500 cm^{-1} band is larger than the observed one. This may depend on the calculation method.

An alternative approach to the calculation of the energy level is that the splitting of the Φ_{MX} level is first calculated for each face; then, the interaction with the Φ^+_{CR} configuration is considered on each face (Fig. 14(b)). By this method, the mixing coefficient is varried on each face and an overly enhanced intensity for the CR band of the (100) face may be reduced.

The Yellow Form: The calculation of the yellow form follows the latter method, and the shift of the Φ_{MX} configuration is evaluated at first by taking E^0_{MX} at 23800 cm^{-1} with the transition dipole length of 2.2 Å. The dye molecule in the yellow form lies along its long axis perfectly perpendicular to the *b* axis; therefore, the A″ component is not expected. In fact, the observed spectra did not show any intensity of the A″ component.

Following the present calculation, the A′ level of the Φ_{MX} configuration was calculated at 21700 cm^{-1} for the (010) face; it was very close to the assumed CR level, E^0_{CR}=21900cm^{-1}. The coupling between these two configurations is very significant; therefore, the resultant states are regarded as completely mixed states of the Φ_{MX} and Φ^+_{CR} configurations. The observed intensity is much larger than the calculated one. This may be due to the effect of the CR interaction. The sharp pattern of the 21300 cm^{-1} band may be regarded as an example of the J band; this is reasonable because it has about 50% of the CR characteristics. However, it should also be mentioned that a metallic reflection band always gives a sharp peak at the lower edge.

On the (110) face, the MX band is predicted to be slightly red shifted, and the observed peak is so shifted. The calculated CR band was not found, presumably because it was burried under the tail of the strong peak situated at the higher-energy side.

The MX band for the (101) face is calculated to

shift to blue; this is in agreement with the observed tendency. The CR band is predicted to be very weak because of a small mixing with the Φ_{MX} configuration. No reflection peak was detected at the lower-energy side.

Concluding Remarks. The spectral features of the excited states of the orange and the yellow forms of 5-DMP crystals are well explained by a consideration of the CR excited configuration in the 22000 cm^{-1} region. The transition moment of this transition is directed along the N···N atoms of the adjacent dye molecules, suggesting that the CR occurs between molecules represented by a canonical structure of Me_2N-C=C-C=C-C=N^+Me_2. A large contribution of this structure to the molecular structure of the orange form is geometrically supported by a precise X-ray analysis.[12] The sharp envelope of the CR band may be associated with the mechanism of the appearance of the J band; a charge-transfer excitation in the nonbonding orbital of a nitrogen atom occurs in a rigid molecule. Although the J band has been considered to appear due to a red shift of the molecular $\pi\pi^*$ transition in the aggregates of laterally stacked dyes, the present analysis shows that the genuine origin of the J band is the existence of a new kind of excited configuration which appears in the N···N atoms at a short distance with a favorable molecular overlap in the stacking. A single and strong J-type band may appear when the CR configuration coexists and mixes with the MX configuration of a large transition moment in the same energy region. A separate and sharp J band is found when the CR configuration is situated away from the MX configuration. The spectrum of the (010) face of the yellow form corresponds to the former case, while the spectra of the orange form represent the latter situation. Thus, the spectral features of the aggregates and crystals of cyanine dye are characterized by a CR interaction between the moieties including the nitrogen atoms of the conjugated system of the cyanine dye; the interaction occurs in a specifically favorable molecular stacking. The appearance of the J band is thus explained to be a result of a peculiar intermolecular interaction between the cyanine dye molecules.

This reseach was supported by a grant in aid of the special research project on the properties of molecular assemblies (No. 60104002) from the Minitry of Education, Science and Culture.

References

1) H. Kobischke and S. Dähne, *Photogr, Sci. Eng.*, **16**, 173 (1972).
2) A. H. Herz, *Photogr. Sci. Eng.*, **18**, 323 (1974).
3) S. Dähne, *Photogr. Sci. Eng.*, **23**, 219 (1979).
4) J. Tanaka, M. Tanaka, and N. Kanamaru, "Relaxation of Elementary Excitations," ed by R. Kubo and E. Hanamura, Springer-Verlag Berlin Heidelberg (1980), Part IV, pp. 181—194.
5) J. Tanaka, M. Tanaka, and M. Hayakawa, *Bull Chem. Soc. Jpn.*, **53**, 3109 (1980).
6) S. Makio, N. Kanamaru, and J. Tanaka, *Bull. Chem. Soc. Jpn.*, **53**, 3120 (1980).
7) S. C. Abbi and D. M. Hanson, *J. Chem. Phys.*, **60**, 319 (1974).
8) J. Tanaka and M. Shibata, *Bull. Chem. Soc. Jpn.*, **41**, 34 (1968).
9) L. Sebastian, G. Weiser, G. Peter, and H. Bässler, *Chem. Phys.*, **75**, 103 (1983).
10) L. Sebastian, G. Weiser, and H. Bässler, *Chem. Phys.*, **61**, 125 (1981).
11) J. O. Selzer and B. W. Matthews, *J. Phys. Chem.*, **80**, 631 (1976).
12) M. Honda, C. Katayama, and J. Tanaka, *Acta Crystalogr., Sect. B.*, to be published.
13) B. G. Anex and W. T. Simpson, *Rev. Mod. Phys.*, **32**, 466 (1960).
14) M. R. Philpott, *J. Chem. Phys.*, **54**, 2120 (1971).
15) P. R. Rimbey, *J. Chem. Phys.*, **67**, 698 (1977).
16) S. Dähne, B. Bornowski, B. Grimm, S. Kulpe, D. Leupold, and M. Näther, *J. Signal* **AM5**, 277 (1977).
17) K. Sieber, L. Kutschabsky, and S. Kulpe, *Kristall und Technik*, **9**, 1111 (1974).
18) M. Otsu and J. Tanaka, *Bull. Chem. Soc. Jpn.*, **58**, 2468 (1985).
19) S. S. Malhotra and M. C. Whiting, *J. Chem. Soc. (London)*, **1960**, 3812.
20) R. K. Ahrenkiel, *J. Opt. Soc. Am.*, **61**, 1651 (1971).
21) B. M. Fanconi, G. A. Gerhold, and W. T. Simpson, *Mol. Cryst. Liq. Cryst.*, **6**, 41 (1969).
22) J. Merski and C. J. Eckhardt, *J. Chem. Phys.*, **75**, 3731 (1981).
23) K. Kimura, S. Katsumata, Y. Achiba, T. Yamazaki, and S. Iwata, "Handbook of HeI Photoelectron Spectra of Fundamental Organic Molecules," Japan Scientific Societies Press, Tokyo (1981).
24) J. Tanaka and C. Tanaka, *Mol. Cryst. Liq. Cryst.*, **126**, 121 (1985).

 © 1986 The Chemical Society of Japan Bull. Chem. Soc. Jpn., 59, 853—858 (1986)

Vibrational Correction for Methylamine and Determination of the Zero-Point Average Structure

Takao IIJIMA
Faculty of Science, Gakushuin University, Mejiro, Toshimaku, Tokyo 171
(Received November 2, 1985)

The method of vibrational corrections for a molecule which has a large amplitude intramolecular motion has been revised and applied to the determination of the zero-point average structure of methylamine. Necessity of torsional correction for this type of molecules has been pointed out and the method has been presented. A recent result of electron diffraction was jointly used with the effective moments of inertia obtained by microwave spectroscopy by Takagi and Kojima. The structural parameters in r_z and φ_z with the estimated limits of error in parentheses are: r(C–N)=1.471(3) Å, r(C–H)=1.101(3) Å, r(N–H)=1.019(6) Å, ∠HCH=108.4(5)°, ∠HNH=106.0(6)°, and ∠CNH=111.5(7)°. Deuterium isotope effects in the structural parameters were also determined.

Rotational constants obtained by molecular spectroscopy usually suffer complicated vibrational effects. Corrections for the effects have been successfully applied to the determination of molecular structures, especially in a joint analysis by means of a combined use of spectroscopic and diffraction data. The method is established in the small amplitude approximation for intramolecular motions.[1,2] The present author and coworker extended the method for the molecules which have a large amplitude torsional motion.[3,4] However, in an attempt to determine the structure of methylamine, it became apparent that the formulation given in the previous work[3] was not adequate for this molecule.

In Ref. 3 the formulation was based on the rigid top-rigid frame theory by Kilb, Lin, and Wilson,[5] in which the principal axes fixed to the frame were the reference axes of overall rotation of the molecule. This means that counter motion of the molecule to the internal rotation was neglected. This is an appropriate approximation for a molecule with a relatively heavy frame as compared with the top.

For CH_3NH_2, the frame NH_2 is lighter than the top CH_3, and the counter motion can not be neglected. The theory of rotation-torsion Hamiltonian of this molecule has been derived by many workers in the approximation of rigid semiasymmetric internal rotors.[6–9] Based on these works, especially on the one by Itoh[8], a revised method of vibrational corrections has been formulated in the present paper.

A correction has also been made to the expression of the n-matrix given in the appendix of Ref. 3. A transformation which projects the top-fixed coordinates onto the frame-fixed axes appears in the formulation. G and F matrices[10] are practically invariant under this transformation as assumed in Ref. 3, though it does not hold rigorously unless both the top and the frame have a common C_3 axis. However, the invariance of L matrix assumed at the same time is unacceptable.

Because of the near degeneracy of the E-type coordinates any L matrix obtained by an arbitrary rotation around the C_3 axis can be a set of eigenvectors of the vibrational equation. The assumed invariance of L means a choice among many equally valid sets.

In the calculation of n-matrix elements, evaluation of the derivative of l-matrix elements[11] with respect to the torsional angle is necessary. For this purpose the L matrix must be given as a function of the torsional angle. From the invariance of G and F alone, i.e. that of the vibrational secular equation, no answer to this question comes out. A more intuitive assumption has been introduced, and the formulation for calculating the n-matrix elements has been revised and described in the Appendix.

As a result, the method of the vibrational calculation employed in Ref. 3, in which the top and the frame were regarded as two independent molecules, has no special advantage. Therefore it has been abandoned and ordinary vibrational calculations of the GF matrix method has been employed.

The n-matrix has no effect on the vibrational corrections for the principal moments of inertia,[4] although the moments of inertia of the top around its axis are affected to a considerable extent. Most of the previously reported results of structure analyses are little affected by the present revision, because they have been obtained mainly from the principal moments of inertia.

Kinetic Energy and Vibrational Corrections

The motion of a methylamine-type molecule undergoing rotation and torsion is described by three angular velocities as discussed by Itoh.[8] The reference axes rotate by the angular velocity $\boldsymbol{\omega}$; the top, i.e. the methyl group, rotates around its C_3 axis by the angular velocity $\dot{\gamma}$, and the molecule as a whole rotates by the angular velocity $\boldsymbol{\omega}_1$ so that the angular momentum associated with $\dot{\gamma}$ may be canceled by the momentum of the counter motion which is associated with $\boldsymbol{\omega}_1$. The rotation of the reference axes is a constant of motion, and the

corresponding total angular momenta give a set of good quantum numbers. These axes may be called the molecule-fixed axes, but do not coincide with the principal axes of the moments of inertia which are fixed to the frame, i.e., the amino group, and rotate by the angular velocity $\boldsymbol{\omega}+\boldsymbol{\omega}_1$. Several of the notations in the present paper are different from those of Ref. 8. The comparisons are given in Table 1.

By considering vibrational motions as well, the velocity vector of each atom is now expressed as

$$\boldsymbol{V}_i = (\boldsymbol{\omega}\times\boldsymbol{r}_i) + (\boldsymbol{\omega}_1\times\boldsymbol{r}_i) + (\dot{\boldsymbol{\gamma}}\times\boldsymbol{\sigma}_i) + \boldsymbol{v}_i, \tag{1}$$

where

$$\boldsymbol{v}_i = \dot{\boldsymbol{\rho}} - (\boldsymbol{\omega}_1\times\boldsymbol{\rho}_i) - (\dot{\boldsymbol{\gamma}}\times\boldsymbol{\varepsilon}_i), \tag{2}$$

for the i-th atom of the top, and

$$\boldsymbol{V}_j = (\boldsymbol{\omega}\times\boldsymbol{r}_j) + (\boldsymbol{\omega}_1\times\boldsymbol{r}_j) + \boldsymbol{v}_j, \tag{3}$$

where

$$\boldsymbol{v}_j = \dot{\boldsymbol{\rho}}_j - (\boldsymbol{\omega}_1\times\boldsymbol{\rho}_j), \tag{4}$$

for the j-th atom of the frame. Equations 1 and 3 are the revised expression for Eqs. 4 and 6 of Ref. 3. In the present work, however, the term for the translation of the center of gravity of the molecule is omitted from the beginning. The definitions of various symbols are summarized in Table 2.

The requirement that the angular momentum associated with $\dot{\boldsymbol{\gamma}}$ is canceled by the momentum associated with $\boldsymbol{\omega}_1$ is expressed as

$$C_2^0\dot{\boldsymbol{\gamma}} = -\boldsymbol{I}^0\boldsymbol{\omega}_1, \tag{5}$$

and therefore,

$$\boldsymbol{\omega}_1 = -(\boldsymbol{I}^0)^{-1}C_2^0\dot{\boldsymbol{\gamma}}. \tag{6}$$

where C_2 is the moment of inertia of the top around its axis and $\boldsymbol{I}$ is the tensor of the moments of inertia of the whole molecule. The superscript 0 indicates the values at the equilibrium configuration. By introducing a unit vector $\boldsymbol{\lambda}$ along $\dot{\boldsymbol{\gamma}}$, we have

Table 1. Comparison of the Notations

	This work	Ref. 8
Angular velocity of the reference axes	$\boldsymbol{\omega}$	$\boldsymbol{\omega}_2$
Angular velocity of the frame-fixed axes	$\boldsymbol{\omega}+\boldsymbol{\omega}_1$	$\boldsymbol{\omega}$
Angular velocity of the top relative to the frame: scalar representation	$\dot{\gamma}$	$\dot{x}$
vector representation	$\dot{\boldsymbol{\gamma}}$	
Angular velocity of the counter motion of the whole molecule	$\boldsymbol{\omega}_1$	$\boldsymbol{\omega}_1$
Vector relating $\dot{\boldsymbol{\gamma}}$ to $\boldsymbol{\omega}_1$ (Eq. 7)	$\boldsymbol{\nu}$	$\boldsymbol{\lambda}$
Unit vector along the top axis	$\boldsymbol{\lambda}$	$\boldsymbol{c}/C_2$

$$\boldsymbol{\omega}_1 = -(\boldsymbol{I}^0)^{-1}C_2^0\boldsymbol{\lambda}\dot{\gamma} = \boldsymbol{\nu}\dot{\gamma}. \tag{7}$$

The mass-adjusted displacement vector can be expanded in terms of the vibrational normal coordinates Q_s by the use of the l-matrix[11] as

$$\sqrt{m_i}\boldsymbol{\rho}_i = \boldsymbol{l}_{is}Q_s, \tag{8}$$

where $\boldsymbol{l}_{is}$ is a vector with the components $(l_{is}^{(x)}, l_{is}^{(y)}, l_{is}^{(z)})$. The summation symbol over s is omitted by the convention that if a subscript appears only on one side of an equation twice or more in a term, the summation over it must be taken. Because of the possible dependence of $\boldsymbol{l}_{is}$ on Ω_1 and γ, the first term of Eq. 2 multiplied by $\sqrt{m_i}$, that is, the time derivative of Eq. 8 with respect to the reference axes, becomes

$$\sqrt{m_i}\dot{\boldsymbol{\rho}}_i = \boldsymbol{l}_{is}\dot{Q}_s + \frac{\mathrm{d}\boldsymbol{l}_{is}}{\mathrm{d}\Omega_1}\omega_1 Q_s + \frac{\mathrm{d}\boldsymbol{l}_{is}}{\mathrm{d}\gamma}\dot{\gamma}Q_s, \tag{9}$$

where Ω_1 is the virtual angle-variable corresponding to $\boldsymbol{\omega}_1$. It is easily conceived that

$$\frac{\mathrm{d}\boldsymbol{l}_{is}}{\mathrm{d}\Omega_1}\omega_1 = \boldsymbol{\omega}_1\times\boldsymbol{l}_{is}, \tag{10}$$

since the $\boldsymbol{l}_{is}$ vector changes only its direction when the whole molecule rotates by $\boldsymbol{\omega}_1$. From Eqs. 8 and 10 we have

$$\frac{\mathrm{d}\boldsymbol{l}_{is}}{\mathrm{d}\Omega_1}\omega_1 Q_s = \sqrt{m_i}(\boldsymbol{\omega}_1\times\boldsymbol{\rho}_i), \tag{11}$$

and this term divided by $\sqrt{m_i}$ is canceled by the second term of Eq. 2. For $(\mathrm{d}\boldsymbol{l}_{is}/\mathrm{d}\gamma)$, however, the situation is not so simple since the configuration of the molecule changes by the torsional motion.

The third term of Eq. 2 can be rewritten as

$$\dot{\boldsymbol{\gamma}}\times\boldsymbol{\varepsilon}_i = \dot{\boldsymbol{\gamma}}\times\boldsymbol{\rho}_i - \dot{\boldsymbol{\gamma}}\times\Delta\boldsymbol{g}, \tag{12}$$

where $\Delta\boldsymbol{g}$ is the displacement vector of the center of gravity of the top and is given in terms of the normal coordinates as

$$\Delta\boldsymbol{g} = M_T^{-1}\boldsymbol{L}_{Ts}Q_s, \tag{13}$$

Table 2. Definitions of Symbols

$\boldsymbol{r}_i$, $\boldsymbol{r}_j$	Instantaneous position vector of an atom; the origin is the center of gravity of the molecule.
$\boldsymbol{\rho}_i$, $\boldsymbol{\rho}_j$	Displacement vector: $\boldsymbol{r}_i-\boldsymbol{r}_i^0$, $\boldsymbol{r}_j-\boldsymbol{r}_j^0$ a)
$\boldsymbol{\sigma}_i$	Instantaneous position vector of an atom of the top; the origin is the center of gravity of the top.
$\boldsymbol{\varepsilon}_i$	Displacement vector: $\boldsymbol{\sigma}_i-\boldsymbol{\sigma}_i^0$ a)

a) The superscript 0 indicates the equilibrium values.

with M_T, the mass of the top, and

$$\boldsymbol{L}_{Ts} = \sqrt{m_i}\boldsymbol{l}_{is}. \tag{14}$$

By means of Eqs. 1, 2 and Equations derived so far, we have

$$\begin{aligned}\sqrt{m_i}\boldsymbol{V}_i &= \sqrt{m_i}(\boldsymbol{\omega}\times\boldsymbol{r}_i) + \sqrt{m_i}(\boldsymbol{\omega}_1\times\boldsymbol{r}_i) + \sqrt{m_i}(\dot{\gamma}\times\boldsymbol{\sigma}_i)\\ &\quad + \boldsymbol{l}_{is}\dot{Q}_s + \frac{d\boldsymbol{l}_{is}}{d\gamma}\dot{\gamma}Q_s - \dot{\gamma}\times\boldsymbol{l}_{is}Q_s\\ &\quad + \dot{\gamma}\times\boldsymbol{L}_{Ts}Q_s\sqrt{m_i}M_T^{-1}\\ &= \sqrt{m_i}(\boldsymbol{\omega}\times\boldsymbol{r}_i) + \sqrt{m_i}(\boldsymbol{\nu}\times\boldsymbol{r}_i)\dot{\gamma}\\ &\quad + \sqrt{m_i}(\boldsymbol{\lambda}\times\boldsymbol{\sigma}_i)\dot{\gamma} + \boldsymbol{l}_{is}\dot{Q}_s + \boldsymbol{n}_{is}\dot{\gamma}Q_s,\end{aligned} \tag{15}$$

for the i-th atom of the top, where

$$\boldsymbol{n}_{is} = \frac{d\boldsymbol{l}_{is}}{d\gamma} - \boldsymbol{\lambda}\times\boldsymbol{l}_{is} + \sqrt{m_i}M_T^{-1}\boldsymbol{\lambda}\times\boldsymbol{L}_{Ts}. \tag{16}$$

Similarly, Eq. 3 for the j-th atom of the frame is transformed to

$$\sqrt{m_j}\boldsymbol{V}_j = \sqrt{m_j}(\boldsymbol{\omega}\times\boldsymbol{r}_j) + \sqrt{m_j}(\boldsymbol{\nu}\times\boldsymbol{r}_j)\dot{\gamma} + \boldsymbol{l}_{js}\dot{Q}_s + \boldsymbol{n}_{js}Q_s\dot{\gamma}, \tag{17}$$

where

$$\boldsymbol{n}_{js} = \frac{d\boldsymbol{l}_{js}}{d\gamma}. \tag{18}$$

The expression for the kinetic energy T can now be obtained from Eqs. 15 and 17, and after simplification by Eckart's and Sayvetz's conditions,[12-14] as

$$\begin{aligned}2T &= (\sqrt{m_i}\boldsymbol{V}_i)^2 + (\sqrt{m_j}\boldsymbol{V}_j)^2\\ &= \boldsymbol{\omega}\boldsymbol{M}\boldsymbol{\omega} + 2\boldsymbol{\omega}\boldsymbol{\zeta}_{ss'}Q_s\dot{Q}_{s'} + \dot{Q}_s\dot{Q}_s.\end{aligned} \tag{19}$$

In Eq. 19 the vectors $\boldsymbol{\omega}$ and $\boldsymbol{\zeta}$ are extended to include $\dot{\gamma}$ and $\zeta_{ss'}^{(\gamma)}$ as the fourth component, i.e., $\boldsymbol{\omega}=(\omega_x, \omega_y, \omega_z, \dot{\gamma})$ and $\boldsymbol{\zeta}_{ss'}=(\zeta_{ss'}^{(x)}, \zeta_{ss'}^{(y)}, \zeta_{ss'}^{(z)}, \zeta_{ss'}^{(\gamma)})$. The expression is formally the same as that for the well known vibration-rotation energy of ordinary molecules,[10] except that the ordinary three-dimensional expression is extended to the four-dimensional one.

Among the components of the $\boldsymbol{M}$-tensor, $M_{\alpha\beta}(\alpha,\beta=x,y,z)$ are the ordinary instantaneous moments of inertia $\boldsymbol{I}$ with respect to the reference axes. The other components are,

$$\begin{aligned}M_{\gamma\gamma}(=U) &= \boldsymbol{\nu}\boldsymbol{I}\boldsymbol{\nu} + m_i\{\boldsymbol{\sigma}_i^2 - (\boldsymbol{\lambda}\cdot\boldsymbol{\sigma}_i)^2\}\\ &\quad + 2m_i\{(\boldsymbol{\lambda}\cdot\boldsymbol{\nu})\boldsymbol{\sigma}_i^2 - (\boldsymbol{\lambda}\cdot\boldsymbol{\sigma}_i)(\boldsymbol{\nu}\cdot\boldsymbol{\sigma}_i)\}\\ &\quad + 2\boldsymbol{\lambda}\cdot(\boldsymbol{\Lambda}_{is}\times\boldsymbol{n}_{is})Q_s^2 + 2\boldsymbol{\nu}\cdot(\boldsymbol{l}_{is}\times\boldsymbol{n}_{is})Q_s^2\\ &\quad + 2\boldsymbol{\nu}\cdot(\boldsymbol{l}_{js}\times\boldsymbol{n}_{js})Q_s^2 + \boldsymbol{n}_{is}^2Q_s^2\\ &\quad + \boldsymbol{n}_{js}^2Q_s^2 - 2\boldsymbol{\nu}\cdot(\boldsymbol{\lambda}\times\boldsymbol{L}_{Rs})Q_s,\end{aligned} \tag{20}$$

where

$$\boldsymbol{\Lambda}_{is} = \boldsymbol{l}_{is} - \sqrt{m_i}M_T^{-1}\boldsymbol{L}_{Ts}, \tag{21}$$

and

$$\boldsymbol{L}_{Rs} = \sqrt{m_i}(\boldsymbol{\sigma}_i^0\times\boldsymbol{\Lambda}_{is}). \tag{22}$$

And the cross terms are

$$\begin{aligned}M_{\alpha\gamma} &= m_i\{\nu_\alpha r_i^2 - (\boldsymbol{r}_i)_\alpha(\boldsymbol{\nu}\cdot\boldsymbol{r}_i)\} + m_i\{\lambda_\alpha\sigma_i^2 - (\boldsymbol{\sigma}_i)_\alpha(\boldsymbol{\lambda}\cdot\boldsymbol{\sigma}_i)\}\\ &\quad + m_j\{\nu_\alpha r_j^2 - (\boldsymbol{r}_j)_\alpha(\boldsymbol{\nu}\cdot\boldsymbol{r}_j)\}\\ &\quad + (\boldsymbol{l}_{is}\times\boldsymbol{n}_{is})_\alpha Q_s^2 + (\boldsymbol{l}_{js}\times\boldsymbol{n}_{js})_\alpha Q_s^2 - (\boldsymbol{\lambda}\times\boldsymbol{L}_{Rs})_\alpha Q_s.\end{aligned} \tag{23}$$

$(\alpha=x, y, z)$

In Eqs. 20 and 23 the terms of $Q_sQ_{s'}$ are omitted because they will vanish when the averaging over the vibrational state is performed. Note that for a vibrationless state (Q_s=0), Eq. 20 reduces to $C_2-\boldsymbol{\nu}\dot{\boldsymbol{I}}\boldsymbol{\nu}$ and Eq. 23 to 0, to become identical with the expression given by Eq. 7 of Ref. 8, $\boldsymbol{\omega}-\boldsymbol{\lambda}\dot{x}$ in Ref. 8 being replaced by the $\boldsymbol{\omega}$ in the present work.

The expression for $\zeta_{ss'}$ are,

$$\zeta_{ss'}^{(\alpha)} = (\boldsymbol{l}_{is}\times\boldsymbol{l}_{is'})_\alpha + (\boldsymbol{l}_{js}\times\boldsymbol{l}_{js'})_\alpha, \quad (\alpha=x, y, z) \tag{24}$$

and

$$\begin{aligned}\zeta_{ss'}^{(\gamma)} &= \boldsymbol{\lambda}\cdot(\boldsymbol{\Lambda}_{is}\times\boldsymbol{l}_{is'}) + \frac{1}{2}(\boldsymbol{n}_{is}\boldsymbol{l}_{is'} + \boldsymbol{n}_{is'}\boldsymbol{l}_{is})\\ &\quad + \frac{1}{2}(\boldsymbol{n}_{js}\boldsymbol{l}_{js'} + \boldsymbol{n}_{js'}\boldsymbol{l}_{js})\\ &\quad + \boldsymbol{\nu}\cdot(\boldsymbol{l}_{is}\times\boldsymbol{l}_{is'} + \boldsymbol{l}_{js}\times\boldsymbol{l}_{js'}).\end{aligned} \tag{25}$$

The procedure of transforming Eq. 19 to the quantum mechanical Hamiltonian and the method of numerical calculation to obtain vibrational corrections for $\boldsymbol{I}$ and U, are formally the same as given in Ref. 3, and are not reproduced here. Numerical values of the vibrational corrections for the configuration of γ=0 are listed in Table 3 as ΔI_{vib}. The force constants determined by Hamada et al.[15] were used in the numerical calculations.

Table 3. Vibrational and Torsional Corrections for the Moments of Inertia of CH_3NH_2 (in uÅ² units)

	$I^{(eff)}$ a)	ΔI_{tor}	ΔI_{vib}	$I^{(z)}$
A	22.331_6	-0.011_4	0.084_8	22.405_0
B	23.279_8	0.012_3	0.061_1	23.353_2
C	4.899_7	—	0.035_1	4.934_8
D	0.106_5	—	-0.001_3	0.105_2
U	1.114_7	—	0.006_6	1.121_3
$C_2(=I_\gamma)$	3.184_0 b)			3.211_3 b)

a) Effective values by Takagi and Kojima.[17] Conversion factor 505376 MHz·uÅ² was used. b) Obtained by solving Eq. 31.

Torsional Average

It seems that Itoh[8] did not pay much attention to the difference among the reference axes and the frame-fixed axes. His Hamiltonian (Eq. 11 of Ref. 8) is actually expressed in terms of the angular momentum conjugate to the angular velocity of the frame-fixed axes. In fact his expression for kinetic energy, the unnumbered equation before the Eq. 11, is easily shown to be equivalent to Eq. 3 by Hecht and Dennison.[6]

Itoh's skillful presentation succeeded in introducing the coupling between the torsional motion and the rotational quantum number K without a discussion on the boundary conditions for the wave function.[16] However his formulation did not include the additional rotation of the newly chosen axes around the axis in the direction of ω_1. This rotation would bring about the dependence of the rotational constants on the torsional angle γ, as is fully described by Hecht and Dennison.[6]

Because of the γ-dependence of the rotational constants, the effective values of the rotational constants determined by the analysis of microwave spectra, e.g. those by Takagi and Kojima[17], become slightly different from those values at $\gamma=0$. In the case of a methylamine-type molecule, this effect must be also corrected for in addition to the vibrational corrections.

The rotational constants tensor can be expressed as

$$\begin{pmatrix} b & 0 & 0 \\ 0 & c & d \\ 0 & d & a \end{pmatrix}, \tag{26}$$

with respect to the reference axes and for $\gamma=0$. The γ-dependence is derived by Hecht and Dennison[6] as

$$\begin{pmatrix} b\cos^2 \nu\gamma + c\sin^2 \nu\gamma & (b-c)\sin \nu\gamma \cos \nu\gamma & -d\sin \nu\gamma \\ (b-c)\sin \nu\gamma \cos \nu\gamma & b\sin^2 \nu\gamma + c\cos^2 \nu\gamma & d\cos \nu\gamma \\ -d\sin \nu\gamma & d\cos \nu\gamma & a \end{pmatrix}. \tag{27}$$

By expanding each element by γ to the order of γ^2 and taking average over γ, we find

$$\begin{aligned} b^{\mathrm{eff}} &= b - \Delta, \\ c^{\mathrm{eff}} &= c + \Delta, \end{aligned} \tag{28}$$

where

$$\Delta = (b-c)\nu^2\langle\gamma^2\rangle. \tag{29}$$

Corrections to other terms are minor.

The relation between b^{eff} and b (also c^{eff} and c) can be transferred to the relation between the moment of inertia A^{eff} and A (B^{eff} and B) with respect to the initially chosen conventional axes as

$$A = A^{\mathrm{eff}}\left(1-\frac{\Delta}{b}\right), \quad B = B^{\mathrm{eff}}\left(1+\frac{\Delta}{c}\right). \tag{30}$$

Numerical values for these torsional corrections are shown in Table 3 as ΔI_{tor}. The value of $\langle\gamma^2\rangle$ was estimated from the torsional frequency in the harmonic approximation.

The symbols A, B, C, etc. are usually used for rotational constants. However in the case of methylamine they are customarily used for the moments of inertia with respect to the conventional x, y, z axes; z axis is chosen parallel to the top axis and z-y plane is the symmetry plane of the molecule at $\gamma=0$. The components of the inertia tensor of this coordinate system are denoted as $I_{xx}=A$, $I_{yy}=B$, $I_{zz}=C$ and $I_{yz}=-D$. The rotational constants a, b, c, etc. are related to A, B, C, etc. as in Eq. 27 of Ref. 8 or in Table XII of Ref. 17.

Since the results of analysis of microwave spectra are reported in terms of A, B, C, etc., the vibrational and torsional corrections evaluated in the present work are reported in terms of the values applicable to A, B, C, etc. The observed effective values were first corrected for the torsional effect to yield the effective values for the configuration of $\gamma=0$. Then the vibrational corrections evaluated for $\gamma=0$ were applied, and the values of A, B, C, etc. corresponding to the zero-point average structure were obtained, as summarized in Table 3.

Zero-Point Average Structure

The moments of inertia for methylamine and its deuterated species CD_3ND_2 and CH_3ND_2 were reported by Takagi and Kojima.[17] The torsional and vibrational corrections as discussed in the preceding sections were applied to the reported values and the moments of inertia $I^{(z)}$ for the zero-point average structure were obtained as shown in Table 3 and 4. The zero-point moments of the methyl top around its axis, $C_2^{(z)}$ or $I_\gamma^{(z)}$, were also obtained from $U^{(z)}$ by solving the equation,

$$U^{(z)} = \frac{C_2^{(z)}[B^{(z)}(C^{(z)}-C_2^{(z)})-(D^{(z)})^2]}{B^{(z)}C^{(z)}-(D^{(z)})^2}. \tag{31}$$

The zero-point average structure, i.e. a set of structural parameters which give a best fit to $I^{(z)}$, was determined. The structural parameters are the

Table 4. Zero-Point Moments of Inertia for CD_3ND_2 and CH_3ND_2 (in uÅ^2 units)

	CD_3ND_2	CH_3ND_2
A	30.594_7	24.984_3
B	32.536_1	26.967_4
C	9.740_8	6.582_5
D	1.000	0.959_3
U	2.187_9	1.635_7
C_2	6.380_4	3.18—3.37

distances C–N, C–H, N–H, and the angles ∠HCH, ∠HNH, ∠CNH and the tilt of the methyl top. For the deuterated species, the parameters may be slightly different from those of the parent species. The difference (deuterated–parent) is called the isotope effect. The isotope effects in the C–N and C–H distances were fixed at the calculated values by assuming the Morse parameter a to be 2.0 Å^{-1}.[1,2] The isotope effects in N–D and ∠DND of CH_3ND_2 were assumed to be equal to those of CD_3ND_2. The isotope effects in ∠HCH and the tilt of CH_3ND_2 were assumed to be zero.

For the C–N distance, the result of electron diffraction[18] was transferred. Otherwise a rather wide range of structural parameters would have been permissible. The $r_g - r_z$ correction for the C–N distance was evaluated to be 0.0010 Å which includes the centrifugal distortion 0.0005 Å, by assuming the Morse parameter a to be 2.0 Å^{-1}.

The results are summarized in Table 5. The uncertainties in parentheses correspond to the uncertainty of the C–N distance, ±0.003 Å and the assumed uncertainties of $I^{(2)}$, ±0.01 uA^2. The C_2 of CH_3ND_2 was not used, because in this case the two solutions of the parabolic equation (Eq. 31) become very close and the uncertainties of B, C, and U are amplified and lead to a very uncertain value of C_2. It was attempted to adjust also the isotope effects in ∠DND and the tilt of CH_3ND_2. A better fit was obtained but the results were physically unacceptable because the values of the isotope effects were in contradiction to the naturally expected trend that the isotope effects for this species must be in between those of CD_3ND_2 and zero.

The determined N–H distance and its isotope effect are in agreement with those of ammonia by Morino et al.[19]; r_z 1.024(1) Å and δ(N–D) −0.002(2) Å. The HNH angle is smaller than that of ammonia 107.3(1)°. This result is examined as follows.

By considering the wagging-inversion potential determined by Tsuboi et al.[20] the zero-point average of the wagging-inversion normal coordinate Q_6 was estimated. From the L^{-1}-matrix elements it was found that major contribution to Q_6 came from the symmetry coordinates S_4, the C–N stretching, and S_6, the amino-wagging given by

$$S_6 = \frac{1}{\sqrt{3}}(\Delta\beta_1 + \Delta\beta_2 + \Delta\alpha), \tag{32}$$

where β_1 and β_2 are the two CNH angles and α is the HNH angle. The zero-point average of S_4 was estimated by the use of the mean square amplitude and the Morse parameter, and $\langle S_6\rangle_0$ was obtained from $\langle Q_6\rangle_0$. Then the zero-point average of $\Delta\beta_1+\Delta\beta_2+\Delta\alpha$ was evaluated to be 2.0°. The isotope effect for this sum of angles was then estimated to be −0.7°. The corresponding quantity from Table 5 becomes −1.2±0.8°, which is comparable to the estimated value from the wagging-inversion potential.

Table 5. Zero-Point Average Structure of Methylamine

	r_z, φ_z[a]	$\delta_{CD_3ND_2}$[b]	$\delta_{CH_3ND_2}$[b]
C–N	1.471(3)[c]	[−0.000$_4$][d]	[−0.000$_2$][d]
C–H	1.101(3)	[−0.002][d]	[0.0][e]
N–H	1.019(6)	−0.003(3)	[−0.003][e]
∠HCH	108.4(5)	−0.2(1)	[0.0][e]
∠HNH	106.0(6)	0.4(2)	[0.4][e]
∠CNH	111.5(7)	−0.8(3)	−0.6(3)
θ[f]	2.97(4)	0.00(3)	[0.00][e]

a) Distance in Å and angles in degrees units. 1Å=100 pm. Uncertainties in parentheses are the estimated limits of error. b) Isotope effects: deuterated−parent. c) The result of electron diffraction.[18] d) Calculated. e) Assumed. f) Tilt angle of the methyl group away from the hydrogen atoms of the amino group.

It is noted that the isotope effect for ∠CNH is negative while that for ∠HNH is positive. This suggests that the initial stage of the wagging-inversion motion is composed of a decrease in ∠HNH and an increase of ∠CNH, showing a repulsive effect of the methyl group. A slightly smaller value for the HNH angle of methylamine as compared with that for ammonia is consistent with this view of the repulsive interaction.

Appendix

n-Matrix Elements. In methylamine molecule each normal mode is well localized to the corresponding symmetry coordinate. Thus an assumption was made that the E-type symmetry coordinates change direction as the methyl group rotates relative to the frame, and the other types of symmetry coordinates are invariant. Then we have for the displacement vector of the i-th atom of the top,

$$\boldsymbol{\rho}_i = \begin{pmatrix} \mathcal{R}(\gamma) \\ & 1 \end{pmatrix} \{\boldsymbol{A}_{ir}L_{rs}Q_s + \boldsymbol{A}_{it}L_{ts}Q_s\} + \boldsymbol{A}_{iq}L_{qs}Q_s, \tag{A. 1}$$

where the notation follows Ref. 3. The γ-dependence of l_{is} is explicitly given by Eq. A.1, and the n-matrix elements are obtained by the definition given by Eq. 16 simply as

$$\boldsymbol{n}_{is} = -\sqrt{m_i}\boldsymbol{\lambda} \times \boldsymbol{A}_{iq}L_{qs} + \sqrt{m_i}M_T^{-1}\boldsymbol{\lambda} \times \boldsymbol{L}_{Ts}. \tag{A. 2}$$

Note that the γ-dependent terms in the first and the second term of Eq. 16 cancel each other.

Similarly for the j-th atom of the frame,

$$\boldsymbol{\rho}_j = \boldsymbol{A}_{jr}L_{rs}Q_s + \boldsymbol{A}_{jt}\mathcal{R}(\gamma)L_{ts}Q_s + \boldsymbol{A}_{jq}L_{qs}Q_s, \tag{A. 3}$$

and by Eq. 18 we have

$$\boldsymbol{n}_{js} = \sqrt{m_j}\boldsymbol{A}_{jt}\frac{d\mathcal{R}(\gamma)}{d\gamma}L_{ts}. \tag{A. 4}$$

The derivative is given as

$$\frac{d\mathcal{R}(\gamma)}{d\gamma} = \begin{pmatrix} -\sin\gamma & -\cos\gamma \\ \cos\gamma & -\sin\gamma \end{pmatrix}, \quad \text{(A. 5)}$$

and for the configuration at $\gamma=0$,

$$\left(\frac{d\mathcal{R}(\gamma)}{d\gamma}\right)_{\gamma=0} = \begin{pmatrix} 0 & -1 \\ 1 & 0 \end{pmatrix}. \quad \text{(A. 6)}$$

References

1) K. Kuchitsu, "MTP International Review of Science, Physical Chemistry Series One," Vol. 2, "Molecular Structure and Properties", ed by G. Allen, Ch. 6, Medical and Technical Publ. Co., Oxford (1972).

2) K. Kuchitsu and S. J. Cyvin, "Molecular Structures and Vibrations", ed by S. J. Cyvin, Ch. 12, Elsevier, Amsterdam (1972).

3) T. Iijima and S. Tsuchiya, *J. Mol. Spectrosc.*, **44**, 88 (1972).

4) T. Iijima, S. Tsuchiya, and M. Kimura, *Bull. Chem. Soc. Jpn.*, **50**, 2564 (1977).

5) R. W. Kilb, C. C. Lin, and E. B. Wilson, *J. Chem. Phys.*, **26**, 1695 (1957).

6) K. T. Hecht and D. M. Dennison, *J. Chem. Phys.*, **26**, 31 (1957).

7) K. Shimoda, T. Nishikawa, and T. Itoh, *J. Phys. Soc. Jpn.*, **9**, 974 (1954); *J. Chem. Phys.*, **22**, 1456 (1954).

8) T. Itoh, *J. Phys. Soc. Jpn.*, **11**, 264 (1956).

9) D. Kivelson and D. R. Lide, Jr., *J. Chem. Phys.*, **27**, 353 (1957).

10) E. B. Wilson, Jr., J. C. Decius, and P. C. Cross, "Molecular Vibrations," McGraw-Hill, New York (1955).

11) H. H. Nielsen, *Rev. Mod. Phys.*, **23**, 90 (1951).

12) C. Eckart, *Phys. Rev.*, **47**, 552 (1935).

13) A. Sayvetz, *J. Chem. Phys.*, **7**, 383 (1939).

14) B. Kirtman, *J. Chem. Phys.*, **37**, 2516 (1962); ibid., **41**, 775 (1964).

15) Y. Hamada, N. Tanaka, Y. Sugawara, A. Y. Hirakawa, M. Tsuboi, S. Kato, and K. Morokuma, *J. Mol. Spectrosc.*, **96**, 313 (1982).

16) J. S. Koehler and D. M. Dennison, *Phys. Rev.*, **57**, 1006 (1940).

17) K. Takagi and T. Kojima, *J. Phys.Soc. Jpn.*, **30**, 1145 (1971).

18) T. Iijima, H. Jimbo, and M. Taguchi, *J. Mol. Struct.*, in press.

19) Y. Morino, K. Kuchitsu, and S. Yamamoto, *Spectrochim. Acta*, **24A**, 335 (1967).

20) M. Tsuboi, A. Y. Hirakawa, and K. Tamagake, *Proceed. Jpn. Acad.*, **42**, 795 (1966).

 © 1986 The Chemical Society of Japan Bull. Chem. Soc. Jpn., 59, 859—863 (1986)

Absorption Spectra of Tetrahedral Co(II) in Single Crystals of $[N(CH_3)_4]_2[CoX_4]$ (X=Cl,Br)

Kazuo KOJIMA and Jiro MATSUDA*
Department of Chemistry, Faculty of Science and Engineering, Ritsumeikan University, Kita-ku, Kyoto 603
(Received July 18, 1985)

The optical absorption spectra of single crystals of $[N(CH_3)_4]_2[CoCl_4]$ and $[N(CH_3)_4]_2[CoBr_4]$ have been measured over the range of 4000—33000 cm^{-1} at the temperature of liquid nitrogen and at room temperature. The spectra have been analyzed using the crystal-field theory which includes spin-orbit coupling. Some discussion of the Racah parameter B and of the $^4T_1(^4F)$ and $^4T_1(^4P)$ states is presented.

The electronic spectra of tetrahalocobaltate(II) have been extensively studied[1-17] in two types of compounds, R_2CoX_4 and R_3CoX_5, but most reports have covered either the spin-allowed or the spin-forbidden transition regions. For example, Cotton et al.[4] have studied the spin-allowed transitions of R_2CoX_4, while Harada et al.[10,12,13] and Bird et al.[11] have analyzed in detail the spin-forbidden transitions in single crystals of Cs_3CoCl_5 and Cs_3CoBr_5. Exceptionally, Ferguson[5] has investigated the spectra of both the spin-allowed and spin-forbidden transitions in the mixed crystals of $R_2[Co_xZn_{1-x}Cl_4]$ at low temperatures.

In the present paper, the absorption spectra of $[CoX_4]^{2-}$ in single crystals of tetramethylammonium salts $[N(CH_3)_4]_2[CoX_4]$, where X is Cl or Br, are reported over the range of 4000—33000 cm^{-1}; this study was undertaken in order to investigate both the spin-allowed and the spin-forbidden d-d transitions in $[CoX_4]^{2-}$ and to compare the electronic transitions in the chloro complex with those in the bromo complex. Tetramethylammonium salts are chosen for the present study because the $[CoCl_4]^{2-}$ complex ion in this salt is known to show only a little deviation from regular tetrahedral symmetry, T_d, at room temperature.[16,18,19]

The spectra of $[N(CH_3)_4]_2[CoCl_4]$ have been studied in the infrared region by Quinn and Smith[9] and from the visible to the near-ultraviolet region by Hosoya et al.[17] as well as Ferguson.[5] The spectra of $[N(CH_3)_4]_2[CoBr_4]$ have never been reported in any region.

Other interesting studies have also been presented concerned with magnetic properties,[2,4,6,20-22] theoretical calculations[23,24] of energy levels, and the electron-spin density[25-28] of $[CoX_4]^{2-}$ complexes.

Experimental

Single crystals of $[N(CH_3)_4]_2[CoX_4]$ were obtained by the slow evaporation, at room temperature, of aqueous solutions containing a stoichiometric composition of $N(CH_3)_4X$ and CoX_2. Crystals of $[N(CH_3)_4]_2[CoCl_4]$ and $[N(CH_3)_4]_2[CoBr_4]$ are blue and greenish-blue prisms respectively. Mixed crystals of $[N(CH_3)_4]_2[Co_xZn_{1-x}X_4]$ were prepared from aqueous solutions of $N(CH_3)_4X$, CoX_2, and ZnX_2.

The spectra were recorded on a Shimadzu MPS-50L spectrophotometer at 77 K and on a Hitachi 340 instrument at room temperature. For measurements at 77 K, cut and polished specimens about 2×2 mm^2 and 0.2—1.0 mm thick were either immersed (visible and near-infrared regions) or not immersed (ultraviolet region) in liquid nitrogen in a glass Dewar apparatus. Filters of POLAROID HN-42T (visible region) and HR-INFRARED (near-infrared region) were used to measure the polarized spectra of $[N(CH_3)_4]_2[CoCl_4]$. The crystarographic c axis was determined by the X-ray oscillation method. For measurements in the spin-allowed bands at room temperature, small specimens about 1×1 mm^2 and 0.1—0.2 mm thick were used.

Results and Discussion

The unpolarized spectra are shown in Figs. 1 and 2, while their numerical data are summarized in Table 1. The overall features of the spectra are similar to the previous data.[1,5,11,16,17] Considerable differences can be found between the spectra of $[N(CH_3)_4]_2[CoCl_4]$ and $[N(CH_3)_4]_2[CoBr_4]$ in the III and IV bands in Fig. 2; the spectra in both these bands are, however, remarkably sharpened by the cooling of the crystals to 77 K. The low-energy absorption in the $^4T_1(^4F)$ band (near-infrared region) in $[N(CH_3)_4]_2[CoCl_4]$ is resolved at 77 K. A shoulder observed in the spectra of $[N(CH_3)_4]_2[CoBr_4]$ at room temperature appears as a peak of 30960 cm^{-1} at 77 K. Bird et al.[11] have reported the corresponding peak in Cs_3CoBr_5 at 4.2 K.

Since the spectra of the $^4T_1(^4P)$ bands are too intense to be resolved even at 77 K, those of the mixed crystals at room temperature are shown in Fig. 3. There are four structures in these bands, and their patterns are almost unchanged at 77 K.

The polarized spectra of $[N(CH_3)_4]_2[CoCl_4]$ are shown in Figs. 4 and 5. No significant difference between the polarized spectra for $\boldsymbol{E}//c$ and $\boldsymbol{E}\perp c$ can be found, and these results are similar to Ferguson's observations.[5]

The spectra of tetraethylammonium salt $[N(C_2H_5)_4]_2[CoCl_4]$ are also observed (not shown) and are similar to those of the tetramethylammonium salt

Table 1. Observed and Calculated Energies (in 10^{-3} cm^{-1})

$[N(CH_3)_4]_2[CoCl_4]$		$[N(CH_3)_4]_2[CoBr_4]$		$[N(CH_3)_4]_2[CoCl_4]$		$[N(CH_3)_4]_2[CoBr_4]$	
Observed[a]	Calculated[b]	Observed[a]	Calculated[b]	Observed[a]	Calculated[b]	Observed[a]	Calculated[b]
	49.37			17.96		17.89	
	49.34**			17.59[c]			
	48.79			17.31	17.44**		
			47.76				
			47.73**	16.90	16.92	16.86[c]	16.77**
			47.22		16.60*	16.53	
32.57	32.61*	33.03		16.26[c]			16.23
32.05[c]	32.46						15.98*
	31.74**			15.74			
	31.50		31.44*	15.61[c]		15.60	
31.25	31.19**		31.29		15.56		
		30.96			15.47*		
			30.68**		15.03 (d, e)		15.08
			30.44	14.93		14.97	
29.76		29.32	30.15**		14.89*		
		28.31			14.88		
26.64					14.88**	(d, e)	14.81*
26.34					14.63		
	25.39			14.44			14.41*
25.06		25.02					14.40
24.41			24.24			14.27	14.24
24.03							14.20**
	23.70						14.14
	23.29**	23.28				13.82	
23.07				8.61[d,f]			
		22.89		6.05	6.03		
			22.72		5.92**		
	22.59*					5.51	5.57
	22.46	22.22[c]	22.30**	5.42	5.40		
22.12							5.27**
21.93	21.70*	21.74		4.94	4.97*	4.94	4.92
			21.63*	4.67		4.61	
	21.58	21.23[c]	21.49			4.43	4.47*
		21.10		4.41			
20.87	20.96		20.81*	4.28 (f)		4.20	
			20.73	4.17		(f)	
		20.66		4.08		4.08	
20.00[c]	19.86*	19.91	20.17			3.95	
	19.68				3.41**		
19.36[c]	19.24**				3.33		
	19.15		19.17*				3.13**
18.93			19.03		3.07*		3.05
		18.52[c]	18.59**		2.92		2.78*
18.22			18.45				2.62

a) Observed at 77 K. b) Γ_6(*), Γ_7(**), and the others are Γ_8. c) Shoulder. d) Observed for mixed crystals. e) Observed at room temperature. f) Vibrational bands.

$[N(CH_3)_4]_2[CoCl_4]$, except that the spectra in the region of 17000—25000 cm^{-1} in the tetraethylammonium salt are shifted to wavenumbers lower by 150-300 cm^{-1} compared with the tetramethylammonium salt.

For $[N(CH_3)_4]_2[CoCl_4]$, the very weak peak of 8610 cm^{-1} observed distinctly at room temperature (Fig. 1) and the four peaks of 4410, 4280, 4170, and 4080 cm^{-1} may all be due to the vibrational transitions in $[CoCl_4]^{2-}$, accompanied by the $^4A_2 \rightarrow {}^4T_1(^4F)$ electronic transition. The spectra of these vibrations can not be assigned, although some

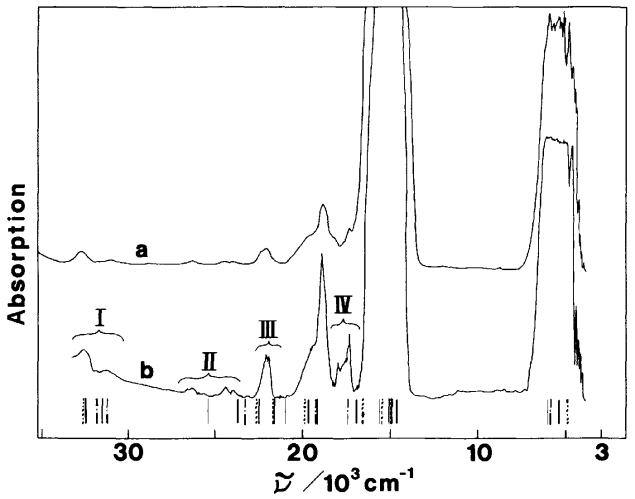

Fig. 1. Absorption spectra of $[N(CH_3)_4]_2[CoCl_4]$ at room temperature (a) and 77 K (b). Calculated energy levels are shown by vertical lines; Γ_8(——), Γ_7(– – –), and Γ_6(- - - -).

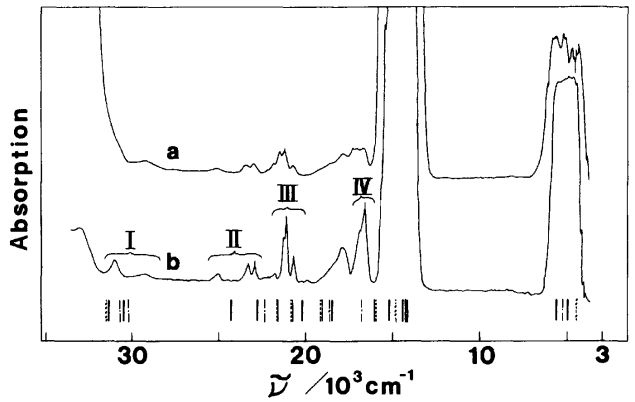

Fig. 2. Absorption spectra of $[N(CH_3)_4]_2[CoBr_4]$ at room temperature (a) and 77 K (b). Calculated energy levels are shown by vertical lines; Γ_8(——), Γ_7(– – –), and Γ_6(- - - -).

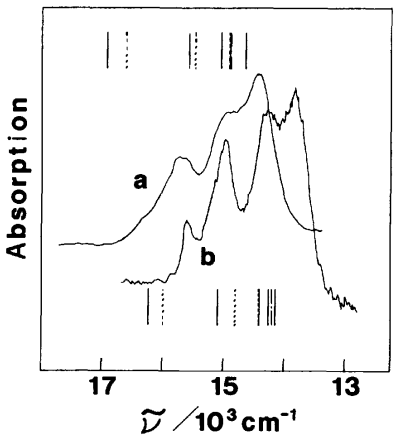

Fig. 3. The $^4A_2 \rightarrow {}^4T_1(^4P)$ absorption bands of mixed crystals $[N(CH_3)_4]_2[Co_xZn_{1-x}Cl_4]$ (a) and $[N(CH_3)_4]_2[Co_xZn_{1-x}Br_4]$ (b) at room temperature. Note that the scale of the ordinate for b is enlarged than that of a. Calculated energy levels are shown by vertical lines; Γ_8(——), Γ_7(– – –), Γ_6(- - - -).

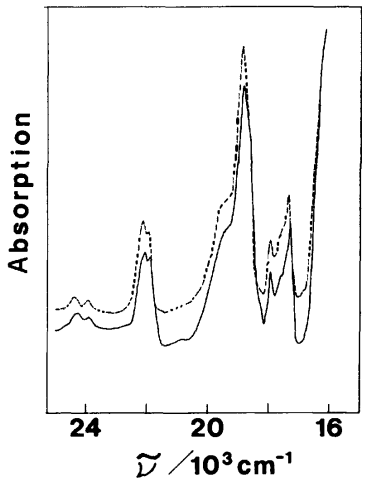

Fig. 4. The polarized spectra of the spin-forbidden bands in $[N(CH_3)_4]_2[CoCl_4]$ at 77 K; $\boldsymbol{E}_{\perp c}$ (——) and $\boldsymbol{E}_{//c}$ (- - - -).

vibrational bands in the $[CoCl_4]^{2-}$ complex have been reported.[13,16,29,30] For $[N(CH_3)_4]_2[CoBr_4]$, the corresponding bands are at 4200, 4080, and 3950 cm^{-1}, but those intensities are low relative to the bands of $[N(CH_3)_4]_2[CoCl_4]$.

In order to calculate the energy levels on the basis of the strong crystal-field theory, the symmetry of the $[CoX_4]^{2-}$ ion is assumed to be T_d, for little anisotropy is observed in the polarized spectra at 77 K (Figs. 4 and 5). Tanabe-Sugano energy matrices,[31] including spin-orbit ones,[32] are diagonalized, using a HITAC M-160H computer, for various values of the D_q, B, C, and ζ parameters, where D_q is the crystal-field strength, B and C are Racah parameters, and ζ is the spin-orbit coupling constant. The calculated energy levels are shown as vertical lines in Figs. 1—3 and in Table 1. Those levels are calculated with D_q=310 cm^{-1}, B=740 cm^{-1}, C=4.6B, and ζ=490 cm^{-1} for $[N(CH_3)_4]_2[CoCl_4]$ and D_q=280 cm^{-1}, B=720 cm^{-1}, C=4.6B, and ζ=500 cm^{-1} for $[N(CH_3)_4]_2[CoBr_4]$. From these calculations, it is shown that the bands of the regions of I and II are mainly due to the transitions of $^4A_2 \rightarrow {}^2T_1(^2F)$, $^2T_2(^2F)$, $^2A_2(^2F)$, and $^4A_2 \rightarrow {}^2E(^2D)$, $^2T_2(^2D)$ respectively. The other absorption bands in the regions of III and IV can be ascribed to the transitions to some components of the ^2P, ^2H, and ^2G terms.

The values calculated for the two complexes do not agree precisely with the observed data in the regions of II and III. If the higher energy states arising from the ^2D, ^2P, and ^2H terms were estimated with B over

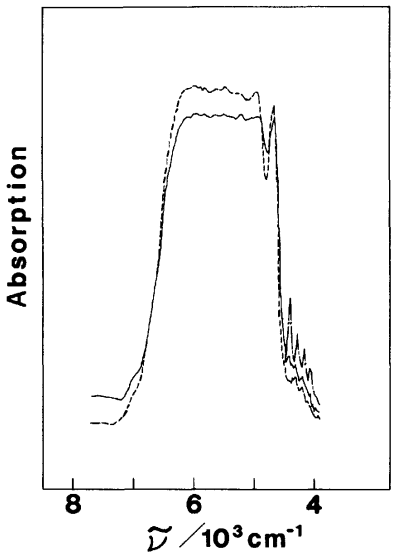

Fig. 5. The polarized spectra of the $^4T_1(^4F)$ band in $[N(CH_3)_4]_2[CoCl_4]$ at 77 K; $E \perp c$ (——), $E // c$ (– – –), and unpolarized (— — —).

740 cm^{-1}, the results of calculation should be in good agreement with the spectral regions of II and III. Hosoya et al.[17] have successfully estimated the energies only for the spin-forbidden transitions in $[N(CH_3)_4]_2[CoCl_4]$ with the large B value of 780 cm^{-1}. On the other hand, Ferguson[5] has obtained the small B value of 720 cm^{-1}. This may result from the disregard for the ≈26500 cm^{-1} band due to the ^2D term. Harada and Tsujikawa[12] have estimated the various values of B viz 740—840 cm^{-1} for Cs_3CoCl_5 and 710—798 cm^{-1} for Cs_3CoBr_5 in the regions of II and III. This can be explained by the fact that a different B value is necessary for each energy level, as in Ferguson's suggestion[5] that e orbitals differ from t_2 orbitals in the extent of expansion. There is a marked tendency for small B values and large B values to be obtained from the spectra for the spin-allowed and for the spin-forbidden transitions respectively.

Horrocks and Burlone[24] have obtained e_σ=2300 cm^{-1} and B=740 cm^{-1} for $[CoCl_4]^{2-}$ in both Cs_3CoCl_5 and Cs_2CoCl_4 by using the angular-overlap model for the spin-allowed transitions. This e_σ value corresponds to the D_q value of 307 cm^{-1}, which agrees with the D_q value in this study. The angular-overlap model is useful for the study of low-symmetry complexes and is a realistic model for metal-ligand covalent bonding, but the formalism is in the ligand-field theory. An analysis of the spectra due to the spin-forbidden transitions by the angular-overlap model is to be hoped for.

Hiller et al.[23] have obtained much valuable information on the cobalt-ligand bonding in $[CoCl_4]^{2-}$ by using the ab initio MO calculations only for the

Table 2. Main Contributions (%) of Electronic Configurations to the $^4T_1$ States of $[CoCl_4]^{2-}$ in $[N(CH_3)_4]_2[CoCl_4]$

State	Calculated energy 10^{-3} cm^{-1}	Configuration	
		$\|^4T_1t_2^4(^3T_1)e^3\rangle$	$\|^4T_1t_2^5e^2(^3A_2)\rangle$
$^4T_1(^4F)$			
Γ_6	4.97	29.5	67.8
Γ_8	5.40	29.5	65.6
Γ_7	5.92	32.0	66.7
Γ_8	6.03	30.6	64.1
$^4T_1(^4P)$			
Γ_7	14.88	67.2	32.5
Γ_8	14.88	65.0	30.5
Γ_8	15.03	53.2	25.4
Γ_6	15.47	67.9	28.0

$^4A_2$, $^4T_2$, and $^4T_1$, states. The calculated energies of 3450 cm^{-1} ($^4A_2 \rightarrow {}^4T_2(^4F)$), 6100 cm^{-1} ($^4A_2 \rightarrow {}^4T_1(^4F)$), and 21600 cm^{-1} ($^4A_2 \rightarrow {}^4T_1(^4P)$) do not seem to account successfully for the experimental data of 3000, 5500, and 15000 cm^{-1} respectively. Results for the spin-forbidden transitions are also desirable. Hiller et al. have described that the $^4T_1(^4P)$ and $^4T_1(^4F)$ states are composed mainly (≈60%) of the $e^3t_2^4$ and $e^2t_2^5$ configurations respectively and that these results disagree with the results of the simple crystal-field theory. This configuration has already been reported for CoO_4 complexes by Pappalardo et al.[33] Our results for the $^4T_1$ states for $[N(CH_3)_4]_2[CoCl_4]$ are shown in Table 2. A similar relation can be found in this study between the states of electronic configuration. The low-energy state of $^4T_1(^4F)$ is composed of the 64—68% $e^2t_2^5$ configuration, while the high-energy $^4T_1(^4P)$ state is composed of the 53—68% $e^3t_2^4$ configuration, where the e orbital has lower energies than the t_2 orbital in the T_d symmetry. On the contrary, Ferguson[5] has reported that $^4T_1(^4F)$ has the configurations of 66% $e^3t_2^4$ and 33% $e^2t_2^5$ and that $^4T_1(^4P)$ has 31% $e^3t_2^4$ and 69% $e^2t_2^5$. The reason for these inverse results can not be found in his report.

For $[N(CH_3)_4]_2[CoBr_4]$, the results are similar to those in Table 2 (not shown).

In the bands of I and $^4T_1(^4P)$, the computed energies agree less with the observed spectra in $[N(CH_3)_4]_2[CoBr_4]$ than with those of $[N(CH_3)_4]_2[CoCl_4]$; this may be due to the difference in the covalency of the Co-X bond between the two complexes.

The $^4A_2 \rightarrow {}^4T_2(^4F)$ transition may be expected to be in the infrared region, outside the spectral region in the present study. The computed energies of this transition for both the complexes are listed in Table 1. For $[N(CH_3)_4]_2[CoCl_4]$, those energies are predicted to be at 3410, 3330, 3070, and 2920 cm^{-1}; hence, the split width is 490 cm^{-1}. For the corresponding

transition, Quinn and Smith[9] have observed relatively sharp absorptions in the region of 3340—3540 cm^{-1} which lie at higher energies than our calculated ones. On the other hand, Stapele et al.[6] have reported this corresponding absorption band in the range of 2800—3500 cm^{-1} for $Cs_3Zn_{0.9}Co_{0.1}Cl_5$.

The present authors wish to thank Professor Naotake Nakamura of Ritsumeikan University for his kind help in the X-ray measurements.

References

1) L. I. Katzin, *J. Am. Chem. Soc.*, **76**, 3089 (1954).
2) R. H. Holm and F. A. Cotton, *J. Chem. Phys.*, **31**, 788 (1959).
3) N. S. Gill and R. S. Nyholm, *J. Chem. Soc.*, **1959**, 3997.
4) F. A. Cotton, D. M. L. Goodgame, and M. Goodgame, *J. Am. Chem. Soc.*, **83**, 4690 (1961).
5) J. Ferguson, *J. Chem. Phys.*, **39**, 116 (1963).
6) R. P. van Stapele, H. G. Beljers, P. F. Bongers, and H. Zijlstra, *J. Chem. Phys.*, **44**, 3719 (1966).
7) J. P. Jesson, *J. Chem. Phys.*, **48**, 161 (1968).
8) J. Ferguson, *Aust. J. Chem.*, **23**, 635 (1970).
9) M. B. Quinn and D. W. Smith, *J. Chem. Soc., A*, **1971**, 2496.
10) M. Harada, S. Sakatsume, and I. Tsujikawa, *J. Phys. Soc. Jpn.*, **35**, 1234 (1973); M. Harada, T. Murao, and I. Tsujikawa, ibid., **35**, 1243 (1973); M. Harada and I. Tsujikawa, ibid., **37**, 759 (1974).
11) B. D. Bird, E. A. Cooke, P. Day, and A. F. Orchard, *Philos. Trans. R. Soc. London, A*, **276**, 277 (1974).
12) M. Harada and I. Tsujikawa, *J. Phys. Soc. Jpn.*, **37**, 1367 (1974).
13) M. Harada and I. Tsujikawa, *J. Phys. Soc. Jpn.*, **37**, 1353 (1974); **37**, 1359 (1974); **40**, 513 (1976).
14) H. W. Smith and W. J. Stratton, *Inorg. Chem.*, **16**, 1640 (1977).
15) A. Saxena and N. K. Jha, *J. Inorg. Nucl. Chem.*, **40**, 1601 (1978).
16) L. Antolini, G. Marcotrigiano, L. Menabue, and G. C. Pellacani, *Inorg. Chem.*, **18**, 2652 (1979).
17) H. Hosoya, T. Yoshinari, and J. Aoyagi, 38th National Meeting of the Physical Society of Japan, Tokyo, March 1983, Abstr. No. 30aL8.
18) J. R. Wiesner, R. C. Srivastava, C. H. L. Kennard, M. Divaira, and E. C. Lingafelter, *Acta Crystallogr.*, **23**, 565 (1967).
19) The lattice parameters of the single crystal of $[N(CH_3)_4]_2[CoBr_4]$ are given in K. Gesi, *J. Phys. Soc. Jpn.*, **51**, 203 (1982), but the symmetry of the $[CoBr_4]^{2-}$ ion is not given there.
20) R. H. Holm and F. A. Cotton, *J. Chem. Phys.*, **32**, 1168 (1960).
21) B. N. Figgis, M. Gerloch, and R. Mason, *Proc. R. Soc. London, A*, **279**, 210 (1964).
22) M. Gerloch, J. Lewis, and R. Rickards, *J. Chem. Soc., Dalton Trans.*, **1972**, 980.
23) I. H. Hiller, J. Kendrick, F. E. Mabbs, and C. D. Garner, *J. Am. Chem. Soc.*, **98**, 395 (1976).
24) W. De W Horrocks, Jr., and D. A. Burlone, *J. Am. Chem. Soc.*, **98**, 6512 (1976).
25) G. S. Chandler and R. A. Phillips. *Chem. Phys. Lett.*, **75**, 363 (1980).
26) B. N. Figgis, P. A. Reynolds, G. A. Williams, R. Mason, A. R. P. Smith, and J. N. Varghese, *J. Chem. Soc., Dalton Trans.*, **1980**, 2333; B. N. Figgis, P. A. Reynolds, and G. A. Williams, ibid., **1980**, 2339.
27) G. S. Chandler, B. N. Figgis, R. A. Phillips, P. A. Reynolds, S. R. Mason, F. R. S., and G. A. Williams, *Proc. R. Soc. London, A*, **384**, 31 (1982).
28) L. A. Barnes, R. Glass, P. A. Reynolds, B. N. Figgis, and G. S. Chandler, *Acta Crystallogr., Sect. A*, **40**, 620 (1984).
29) R. J. H. Clark and T. M. Dunn, *J. Chem. Soc.*, **1963**, 1198; D. M. Adams, J. Chatt, J. M. Davidson, and J. Gerratt, ibid., **1963**, 2189; J. T. R. Dunsmuir and A. P. Lane, ibid., *A*, **1971**, 404.
30) A. Sabatini and L. Sacconi, *J. Am. Chem. Soc.*, **86**, 17 (1964).
31) Y. Tanabe and S. Sugano, *J. Phys. Soc. Jpn.*, **9**, 753 (1954).
32) W. A. Runciman and K. A. Schroeder, *Proc. R. Soc. London, A*, **265**, 489 (1962).
33) R. Pappalardo and R. E. Dietz, *Phys. Rev.*, **123**, 1188 (1961); R. Pappalardo, D. L. Wood, and R. C. Linares, Jr., *J. Chem. Phys.*, **35**, 2041 (1961).

The Separation and Concentration of Gallium(III) and/or Indium(III) Using Polystyrene Resins Functionalized with Complexane-Type Ligands

Toshishige M. SUZUKI,* Toshiro YOKOYAMA, Hideyuki MATSUNAGA, and Tetsuo KIMURA
Government Industrial Research Institute, Tohoku. 4-2-1 Nigatake, Sendai 983
(Received November 13, 1985)

Macroreticular styrene-divinylbenzene copolymers functionalized with iminodiacetic acid and diethylenetriamine-*N,N,N'',N''*-tetraacetic acid have been examined in order to apply them to the selective recovery of gallium(III) and/or indium(III) from acidic solutions. The equilibrium adsorption capacities, distribution coefficients, and metal-adsorption rates of the polymer resins for Group IIIb ions and other common metal ions have been studied. The selectivity sequence of the present resins are as follows: Fe(III)> In(III)>Ga(III)≈Cu(II)>Zn(II)>Al(III). The selective recovery of In(III) and/or Ga(III) from acidic solutions has been demonstrated using a column of the present resins.

In spite of the increasing requirement for gallium and indium in the electronic and semiconductor industries, the natural abundance of these metals is extremely small. Therefore, it is urgent to establish a process to recover gallium and indium selectively from low-grade ores or industrial scraps. For the recovery of less-common metals, there is a growing interest in the use of hydrometallurgical techniques which involve a leaching stage to dissolve the metals, followed by further stages to separate the metal ions of interest from other impurities. In 1976 a process based on solvent extraction was proposed to recover gallium from a sodium aluminate solution.[1] Chelating polymer resins containing a highly selective complexing group are one of the attractive candidates to apply to the metal separation procedure because of their operational flexibility and practical convenience.[2] Among the multidentate ligands, iminodiacetic acid (IDA) and ethylenediamine-*N,N,N',N'*-tetraacetic acid (EDTA) are known to form extremely stable complexes with Ga(III)[3] and In(III)[4], hence, the chelating resins with these types of functional groups seem promising for the recovery of the metal ions from the leaching solutions.

We have prepared cross-linked polystyrene resins with complexane-type ligands structurally analogous to IDA or EDTA (Fig. 1). It was found that these chelating resins can adsorb Ga(III) and In(III) selectively from an acidic solution; the preliminary results have previously been reported briefly.[5] This paper presents full, detailed description dealing with the adsorption characteristics of the chelating resins and their use in the column separation of Ga(III) and/or In(III) from other common-metal ions.

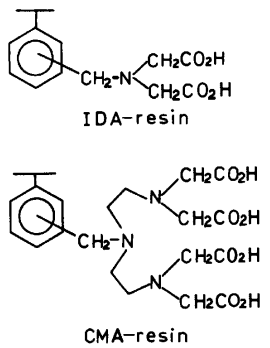

Fig. 1. Cross-linked polystyrene resins containing multidentate functional group.

Experimental

Materials. Reagent-grade $In(NO_3)_3 3H_2O$, $Ga(NO_3)_3 \cdot 3H_2O$, and metallic gallium (99.99% grade) were used for the preparation of the stock solution. Metallic gallium was dissolved with *aqua regia*, and this solution was used for the column feed. Chloromethylated polystyrene beads (Cl, 17.1%, 60—100 mesh) were kindly donated by the Mitsubishi Chemical Co., Ltd. The resin matrix was macroreticular (MR) type styrene-10%-divinylbenzene copolymer with a surface area and mean pore diameter of 7.3 $m^2 g^{-1}$ and 720 Å, respectively.

IDA Resin. A suspension of chloromethylated polystyrene beads (45 g) and diethyl iminodiacetate[6] (85.6 g) in 450 cm^3 of dioxane was refluxed for 72 h with continuous stirring. The solid beads were then transfered to a Soxhlet extractor, extracted with ethanol, and then dried in vacuo. Yield, 76 g. To the dry beads (75 g) we then added a sodium hydroxide solution (20 g in 500 cm^3 of ethanol); the mixture was refluxed for 24 h under stirring. The beads were filtered off and washed successively with water, 2 M HCl (M=mol dm^{-3}), water, and then ethanol. Following a final washing with ether, the beads were dried at 50 °C in vacuo. Yield, 54.4 g. The nitrogen content of the IDA resin thus obtained was 3.7%, which corresponds to a ligand content of 2.6 mmol per gram resin.

CMA Resin. Polystyrene beads were functionalized with bis[2-(salicylideneamino)ethyl]amine[7] by the reaction of chloromethylated polystyrene and the Schiff base.[8] The resulting resin was hydrolyzed by treating it with 6 M HCl, yielding the diethylenetriamine-bound resin.[8] The carboxymethylation of the diethylenetriamine resin using the following procedures afforded the CMA resin.

To a solution of bromoacetic acid (213.6 g in 600 cm^3 of water) we added a sodium hydroxide solution (133 g in 600 cm^3 of water) drop by drop keeping the temperature of the reaction solution below 5 °C. To this solution we then

added the diethylenetriamine resin (50 g), after which the mixture was gently shaken for 7 d at room temperature. The resin beads were collected, washed with water, and then treated with 2 M HCl. After having been washed successively with water, ethanol, and ether, the resin beads were dried in vacuo. Yield, 69.7 g. The nitrogen analysis of the resin (6.92%) indicates that the resin formally contains 1.65 mmol of the functional group per gram resin.

Determination of Adsorption Capacity. A batchwise technique was employed to determine the equilibrium adsorption capacity (amount of metal ion adsorbed on one gram of dry resin), with the metal ion always being in an excess over the ligand content. Typically, 500 mg of dry resin (H^+ form) was added to ca. 80 cm^3 of metal ion solution (0.02 M) of a certain pH, and the suspension was stirred at room temperature overnight. Then the mixture was transferred to a volumetric flask (100 cm^3) and finally diluted to the mark with water. The amount of the metal ion was determined with an atomic-absorption spectrometer. The capacity of the resins was calculated from the change in the metal concentration observed. The resin beads were placed in a glass column and washed thoroughly with water. The adsorbed metal ion was liberated from the resin beads by elution with 20 cm^3 of 2 M HCl, and the metal ion in the eluent was analyzed as has been described above. In most cases, a satisfactory material balance was observed between the metal ion liberated from the resin and that remaining in the solution.

Distribution Coefficients. The equilibrium distribution coefficients of the metal ions were determined by a batchwise procedure. A 500 mg portions of dry resin was immersed in 100 cm^3 of a metal ion solution (1 mM). The pH values from 3.0 to 5.0 were adjusted with an acetate buffer, while those below 3.0 were adjusted with perchloric acid. After shaking had continued for 5 d, the equilibrium pH and the amount of metal ion remain in the supernatant were determined. The results are expressed as the distribution coefficients, K_d=amount of metal adsorbed on one gram of the resin/amount of metal remaining in 1 cm^3 of the solution.

Adsorption Rate. The time-course of metal adsorption was monitored by measuring the change in the metal concentration in the solution. To a 1000 cm^3 portion of 1 mM metal solution (I=0.01, NaCl) at the given pH, we added 5 g of the chelating resin, which had been swollen with water in advance. While stirring, small portions of the metal solution were withdrawn at appropriate intervals and the change in the metal ion concentration was determined.

Column Separation of Metal Ion Mixture. A typical procedure is as follows: A 5-g sample of the CMA resin was swollen with water and poured onto a glass column (ϕ 1.2×10.2 cm). The metal ion solution containing Ga(III) (2.5 mM) and Al(III) (120 mM) was continuously passed through the column at a constant rate of 1.5 $cm^3\,min^{-1}$. The effluent was fractionated into 17 cm^3 portions, and the amount of the metal ion was determined. The Ga(III) in the feed solution was adsorbed quantitatively on the column up to 1600 cm^3, while Al(III) was leaked out of the column. The adsorbed Ga(III) was liberated from the column by elution with 2 M HCl. The resin was regenerated by this procedure and can be used in the successive column operations. In a similar manner, Ga(III) and/or In(III) was selectively adsorbed from the solution containing excess amounts of Al(III), Ca(II), and Zn(II).

For the actual leaching solution, which often contains Fe(III) and Cu(II), H_2S was bubbled in at pH 1.0 and the precipitate was removed prior to column operation.

Measurements. The metal-ion concentration was determined with a Shimadzu atomic absorption/flame photometer, Model AA-610S.

Results and Discussion

Chelating Resins. The IDA resin was prepared by the treatment of the chloromethylated polystyrene with diethyl iminodiacetate, followed by the hydrolysis of the ester with a sodium hydroxide solution. The CMA resin was obtained by the *N*-carboxymethylation of the diethylenetriamine-bound resin, in which the amine is linked to polystyrene uniquely through the secondary nitrogen.[8] The IDA resin contains tridentate iminodiacetic acid, whereas the functional group of the CMA resin formally involves two sets of IDA groups, by analogy with EDTA. The IDA and CMA resins contain approximately 2.6 and 1.7 mmol, respectively of the functional group per 1

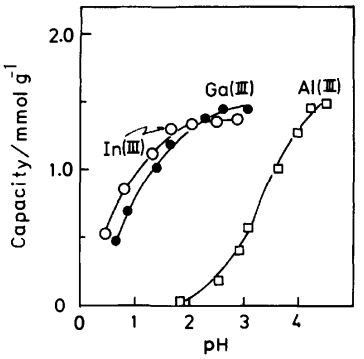

Fig. 2. Equilibrium adsorption capacity of the CMA resin for Al(III) (□), Ga(III) (●), and In(III) (○) as a function of pH.

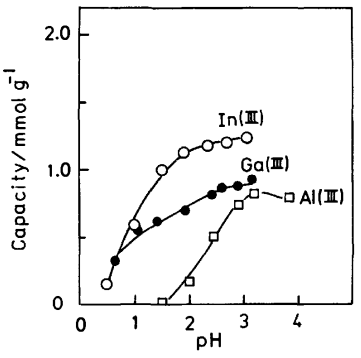

Fig. 3. Equilibrium adsorption capacity of the IDA resin for Al(III) (□), Ga(III) (●), and In(III) (○) as a function of pH.

Table 1. Maximum Adsorption Capacity of the Resins

Metal ion	Adsorption capacity/mmol metal g^{-1} (pH)	
	IDA resin	CMA resin
Al(III)	0.8 (4.0)	1.5 (4.2)
Ga(III)	0.9 (2.8)	1.5 (2.0)
In (III)	1.2 (2.0)	1.4 (1.8)
Fe(III)	0.7 (2.0)	1.5 (1.9)
Cu(II)	2.7 (4.0)	2.4 (4.0)
Zn(II)	2.3 (4.5)	2.2 (5.0)

gram of the resin.

Equilibrium Adsorption Capacity. The present resins readily adsorb various kinds of metal ions from an acidic solution. The profiles of the adsorption capacities as a function of the pH for Al(III), Ga(III), and In(III) are given in Figs 2 and 3. The maximum adsorption capacities, including other common metal ions, are listed in Table 1, along with the equilibrium pH. The capacities of the CMA resin for most of the trivalent metal ions are around 1.5 mmol g^{-1} resin; this value is comparable to the estimated ligand content, while those for the IDA resin are much lower than its ligand content. These results can be attributed to the difference in the dentate number of the functional groups. Each functional group in the CMA resin is expected to form 1:1 octahedral complexes in a fashion similar to those of EDTA complexes, whereas two sets of the IDA units are required for the IDA resin to form stable octahedral complexes. In contrast to homogeneous systems, such an opportunity must be considerably restricted when the IDA groups are fixed on a rigid polymer. For bivalent ions, such as Cu(II) and Zn(II), on the other hand, the adsorption capacities of the IDA resin are nearly equal to the ligand content, presumably because each IDA unit can form 1:1 complexes with these metal ions.

Distribution Coefficients. The distribution coefficients of the CMA resin for In(III), Ga(III), Fe(III), Cu(II), and Zn(II) were examined as a function of the pH; the results are given in Fig. 4. The slopes in the linear plots are approximately 3.0 for the adsorption of trivalent ions, whereas for Cu(II) and Zn(II) the slopes are close to 2.0. These results indicate that the adsorption of trivalent metal ions is accompanied by the release of three protons, while for bivalent ions two protons are liberated from the CMA resin. These observations are consistent with the expectation that each functional group in the CMA resin forms a 1:1 complex with trivalent metal ions.

Although the log K_d vs. pH profiles of the CMA and the IDA resins resemble each other, those of the CMA resin appear in a relatively lower pH region

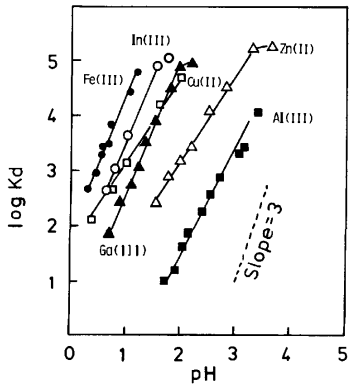

Fig. 4. Log K_d of the CMA resin for some metal ions as a function of pH.
Fe(III) (●), In(III) (○), Ga(III) (▲), Cu(II) (□), Zn(II) (△), Al(III) (■).

Table 2. Adsorption Rate of the Resins for Al(III), Ga(III), and In(III) ($t_{1/2}$, min)[a)]

Metal ion	pH	IDA Resin	CMA Resin
Al(III)	4.2	5	7
Ga(III)	2.0	30	25
In(III)	2.0	10	8

a) The time required to quench a half of the metal ion adsorbed at equilibrium. Metal ion concentration: 1 mM (1000 cm^3), I=0.01 (NaCl) Resin; 5 g.

than those of the IDA resin, irrespective of the metal ions examined. This demonstrates that the CMA resin can form much more stable complexes than the IDA resin due to the chelating effect of the functional group.

The selectivity sequence of the CMA resin is; Fe(III)>In(III)>Ga(III)≈Cu(II)>Zn(III)>Al(III), which coincides with the order of the formation constants of the EDTA complexes.[9] The apparent selectivity suggests the possibility of the column separation of Ga(III) and In(III) from the solution containing Zn(II) and Al(III). The K_d profile also suggests that Fe(III) and Cu(II) would greatly interfere with the adsorption of Ga(III) and In(III).

Adsorption Rate. Although the equilibrium capacity and the K_d values are of fundamental importance in characterizing the chelating resin, the rate of adsorption is extremely important from a practical point of view. The time-course of the adsorption of Al(III), Ga(III), and In(III) was examined at their optimal pH region by monitoring the metal ion concentration in the batch systems. The time required to adsorb a half of the metal ion adsorbed at the equilibrium ($t_{1/2}$) is listed in Table 2. The adsorption rates for these metal ions are, in any case, sufficiently rapid to allow a continuous column

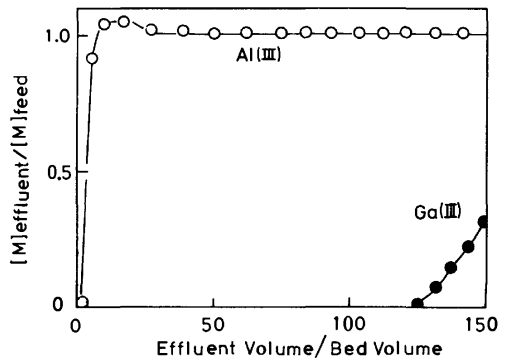

Fig. 5. Column breakthrough profile for the separation of Ga(III) and Al(III). Bed resin: CMA resin (5 g, 13 cm^3). pH: 1.8. $[M]_{feed}$: Al(III) (120 mM), Ga (III) (2.5 mM).

operation. The rate sequence is; Al(III)≳In(III)> Ga(III) under the present experimental conditions. The rate of adsorption has been claimed to be determined by the diffusion process inside the matrix in most of the ion-exchange systems.[10] On the basis of the electrophoresis experiments for the CMA resin, it was found that the resin beads are negatively charged at pH values higher than 2.0, where the carboxyl protons in the functional group may begin to dissociate.[11] The local charge density must be enriched inside the polymer beads with the sequential dissociation of protons; hence, the migration of positivily charged species into the polymer must be facilitated. The higher adsorption rate observed for Al(III) at pH 4.0 can be interpreted by this hypothesis. An opposed trend has been observed when the oxometalate anion (MoO_4^{2-}) was fed to the CMA resin and has been attributed to the charge repulsion between the resin and the incoming anion.[2e]

The observed rate sequence is almost independent of the nature of the anions present in the solution. Hence, provided that the chemical forms of Ga(III) and In(III) are not much different from each other under the given experimental conditions, the apparent difference in adsorption rate between them cannot be explained simply by the charge interaction mechanism. Although we have no clear explanation for the much slower rate for Ga(III) as compared to In(III), it should be noted that the rate sequence coincides with the order of lability of the metal ions.[12]

Column Separation. The apparent selectivity of the CMA resin suggests the possibility of the column separation of Ga(III) and In(III) from the solution of Al(III) or Zn(II). When a model solution (pH, 1.8) containing 2.5 mM of Ga(III) and 120 mM of Al(III) was passed through the column of the CMA resin, Ga(III) was quantitatively adsorbed on the resin, while Al(III) was found in the eluate, as is shown in Fig. 5. The amount of Ga(III) adsorbed on one gram of the resin at the breakthrough point (breakthrough capacity) was 0.95 mmol g^{-1}, approximately 65% of the equilibrium capacity. In a similar column operation using 1.7 mM of In(III) and 110 mM of Al(III), the breakthrough capacity for In(III) was found to be 0.8 mmol g^{-1}. The adsorbed Ga(III) or In(III) was liberated from the resin in a concentrated form on elution with 2 M HCl. Although a similar quantitative separation was achieved by using the IDA resin, the breakthrough capacity was much lower than in the case of the CMA resin, as is to be expected from the difference in their equilibrium capacities.

Among the metal ions commonly encountered in an acid-leaching solution of natural ores and industrial scraps, Fe(III) and Cu(II) compete most strongly in the adsorption of Ga(III) and In(III), as is to be expected from the K_d profiles. Therefore, it is preferable to remove these ions prior to the column operation. Interference from Cu(II) and Fe(III) can be considerably avoided by the treatment of the leaching solution with H_2S gas. By this procedure, Cu(II) can be eliminated from the solution as precipitate of CuS; at the same time, Fe(III) can be reduced to Fe(II), which has a much lower affinity for the present chelating resins than do In(III) and Ga(III).

References

1) J. Helgorsky and A. Leveque, French Patent, 2,307,047 (1976); *Chem. Abstr.*, 87, P42333n (1977).

2) a) R. G. Grinsted, *J. Metals*, **1979**, 13; b) F. Vernon, *Hydrometallurgy*, 4, 147 (1979); c) J. H. Hodgkin, *Chem. Ind. London*, **1979**, 153; d) Japan Kokai, 58-42737; *Chem. Abstr.*, **99**, 8873b (1983); e) M. Nishizawa, T. Yokoyama, T. Kimura, and T. M. Suzuki, *Bull. Chem. Soc. Jpn.*, **57**, 2859 (1984).

3) R. Motekaitis and A. E. Martel, *Inorg. Chem.*, **19**, 1646 (1980).

4) E. Bottari and G. Anderegg, *Helv. Chim. Acta*, **50**, 2349 (1967).

5) T. M. Suzuki, Toshiro Yokoyama, Hideyuki Matsunaga, and Tetsuo Kimura, *Chem. Lett.*, **1985**, 41.

6) A. Badinand, A. Boucherle, and C. Charbonier, *Bull. Soc. Chim. France*, **1958**, 1495.

7) W. M. Coleman and L. T. Taylor, *Inorg. Chem.*, **10**, 2195 (1971).

8) T. M. Suzuki and T. Yokoyama, *Polyhedron*, **2**, 127 (1983): T. M. Suzuki and T. Yokoyama, *Polyhedron*, **3**, 939 (1984).

9) G. Schwarzenabach, R. Gut, and G. Anderegg, *Helv. Chim. Acta*, **37**, 937 (1954).

10) F. Helfferich, "Ion Exchange," McGraw-Hill Book Co. New York (1962), p. 257.

11) G. Schwarzenbach and H. Ackermann, *Helv. Chim. Acta*, **30**, 1798 (1947).

12) F. Basolo and R. G. Pearson, "Mechanisms of Inorganic Reactions," John Wiley and Son, (1967), p. 145.

Studies on Nucleosides and Nucleotides. XII.[1] Carbon-Chain Extension at 5′-Position of Ribonucleosides

Junji KIMURA, Hideyuki KOBAYASHI, Osamu MIYAHARA, and Oyo MITSUNOBU*
Department of Chemistry, College of Science and Engineering, Aoyama Gakuin University, Chitosedai, Setagaya-ku, Tokyo 157
(Received September 19, 1985)

2,6-Di-*t*-butyl-4-nitrophenol reacted with O^2-methyluridine, N^3-methyluridine or 4-triazolyl-1-(β-D-ribofuranosyl)-2(1*H*)-pyrimidinone in the presence of diethyl azodicarboxylate and triphenylphosphine selectively at the 5′-position to give the corresponding 4-(nucleosid-5′-yl-*aci*-nitro)-2,6-di-*t*-butylcyclohexa-2,5-dienone (*aci*-nitro ester of nucleoside) in 39—72% yields along with varied amounts of 5′-deoxy-5′-[*N*,*N*′-bis(ethoxycarbonyl)-hydrazino]nucleosides. By comparison of the reactions of pyrimidine nucleosides having free 2′- and 3′-hydroxyl groups with those of their 2′,3′-*O*-isopropylidene derivatives, the ratio of *aci*-nitro ester to 5′-deoxy-5′-hydrazinonucleoside was affected by the protecting groups as well as the time required for the addition of diethyl azodicarboxylate to a solution of other reactants. Similarly, N^1,N^6,2′,3′-*O*-tetrabenzoyladenosine afforded the expected *aci*-nitro ester in 83% yield. The *aci*-nitro esters prepared were successfully reacted with stabilized phosphoranes such as (ethoxycarbonylmethylene)triphenylphosphorane or (acetylmethylene)triphenylphosphorane giving 1-[(*E*)-β-D-ribo-hept-5-enofuranosyl]- or 1-[(*E*)-β-D-ribo-oct-5-enofuranosyl]-pyrimidines and -purines. When the two stage reactions were carried out by one-pot procedure without isolation of *aci*-nitro esters, overall yields of alkenofuranosylpyrimidines were markedly improved.

Nucleoside antibiotics such as ezomycins, octosyl acids, and sinefungin have a common structural unit comprising higher-carbon sugars and pyrimidine or purine bases. For the synthesis of these antibiotics and their analogues from ribonucleosides, the creation of C–C bond at the 5′-position is required and nucleoside 5′-aldehyde has been generally chosen as a key intermediate. Thus, protection of 2′- and 3′-hydroxyl groups of a nucleoside, oxidation of 5′-hydroxyl group, and subsequent treatment of the resulting aldehyde with anionic species such as Wittig reagents affords the corresponding homologated nucleoside.[2,3] Because of instability of nucleoside 5′-aldehydes, however, only a limited number of oxidation process have been utilized.[2] Therefore, there are ongoing needs to develop a convenient procedure for carbon-chain extension of nucleosides.

Recently, we have reported the synthesis of *aci*-nitro esters by the reaction of alcohols with 2,6-di-*t*-butyl-4-nitrophenol (**1**), diethyl azodicarboxylate (**2**), and triphenylphosphine (**3**).[4] As a masked aldehyde, the *aci*-nitro ester prepared reacted with Wittig reagents giving the corresponding olefins.[5] The reaction would involve intermediacy of aldehyde or ketone which successively reacts with Wittig reagents. An advantage would thereby accrue to the preparation of olefins via unstable aldehydes. Further, it was found that improved yields were obtained when the sequence of reactions were carried out by one-pot procedure without isolation of *aci*-nitro ester. Application of this methodology to the synthesis of 1-[(*E*)-5-enofuranosyl]-uracils from uridine has also been shortly reported.[6]

In this paper, we wish to report the synthesis of 1-[(*E*)-5-enofuranosyl]-pyrimidine and -purine derivatives via *aci*-nitro esters.

Reactions of Uridine Derivatives. When 2′,3′-*O*-isopropylideneuridine was allowed to react with **1**, **2**, and **3**, intramolecular dehydration occurred giving 2′,3′-*O*-isopropylidene-O^2,5′-cyclouridine rather than expected *aci*-nitro ester. In order to prevent the cyclouridine formation, the uracil moiety was protected by methyl group. O^2-Methyl- or N^3-methyl-2′,3′-*O*-isopropylideneuridine (**4a**, **4c**) reacted smoothly with **1** in the presence of 1.5 molar amounts of **2** and **3** at room temperature overnight to give the corresponding *aci*-nitro ester (**5a** or **5c**) in 84 or 83% yield, respectively. We did not attempt to isolate 5′-deoxy-5′-hydrazinouridine derivative (**6a**, **6c**)(vide infra).

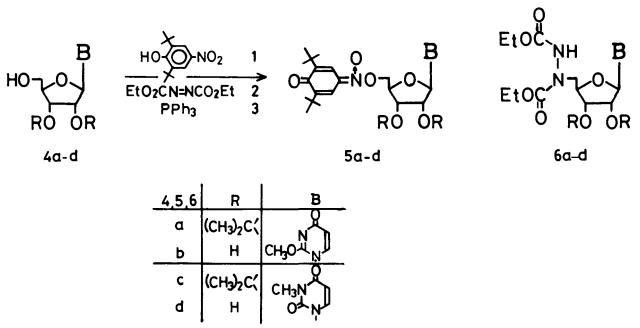

In view of the fact that the condensation of unprotected nucleosides with carboxylic acids using **2** and **3** selectively affords 5′-*O*-acylnucleosides,[7] high regioselectivity could also be expected in the formation of *aci*-nitro esters. Thus, O^2-methyluridine (**4b**) and N^3-methyluridine (**4d**) were used as nucleoside components. When **2** (3 equiv) was added dropwise over a period of 2 h to a solution of **1** (1.5 equiv), **3** (3 equiv), and **4b**, followed by being stirred overnight, *aci*-nitro ester (**5b**) was obtained in

72% yield accompanying a trace of 5′-deoxy-5′-hydrazinouridine derivative (**6b**). Under the same conditions, **4d** afforded *aci*-nitro ester (**5d**) and 5′-deoxy-5′-hydrazinouridine derivative (**6d**) in 39 and 41% yields, respectively. In both cases, the products derived from the reaction at 2′- and/or 3′-hydroxyl group could not be obtained.

In contrast to the preparation of *aci*-nitro esters of fully protected uridines (**4a**, **4c**),[8] more than two equivalents of **2** and **3** were required for the conversion of uridines having free 2′- and 3′-hydroxyl groups. In fact, when **4b** was treated with 1 molar amount each of **1**, **2**, and **3**, the corresponding *aci*-nitro ester (**5b**) was hardly formed as monitored by TLC of the reaction mixture. These results suggest that one-equivalents of **2** and **3** were consumed by the formation of 2′,3′-*O*-(triphenylphosphoranediyl) ring.[9] The data concerning to the reaction of uridine with **2**, **3**, and an acidic component support the initial formation of 5′-*O*-(triphenylphosphonio)uridine. Thus, when carboxylic acid or phosphoric diester was used as an acidic component the corresponding 5′-*O*-substituted uridine was exclusively formed. On the other hand, with weak nucleophile such as phthalimide, intramolecular process is favorable to give O^2,5′-cyclouridine.[9b] Since uracil moiety was protected in the present reactions, it would be rational to assume that phosphonio group migration predominated over the intermolecular displacement by *aci*-nitronate anion and 2′,3′-*O*-(triphenylphosphoranediyl)-O^2-methyl- or -N^3-methyluridine (**7**) was formed.[9]

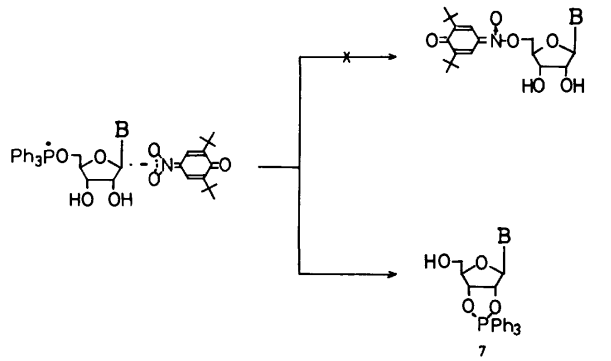

7

The formation of **6d** suggests that reaction mixture contains nucleoside phosphonium salts **8** and **9** in equilibrium. The reaction courses would therefore depend on the equilibrium constant and nucleophilicity of the counter anions comprising in **8** and **9**.

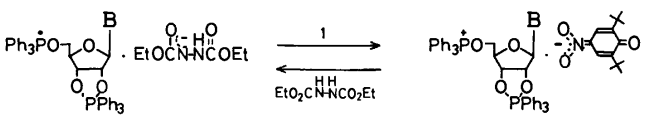

8 **9**

Although no kinetic data are available, the conversion of **9** to uridine 5′-*O*-*aci*-nitro ester would be rate-determining step because of low nucleophilicity of *aci*-nitronate anion. In order to suppress the formation of **6b** and **6d**, the concentration of diethyl hydrazinedicarboxylate must be minimized. This requirement could be satisfied at least at an early stage of the reaction by slow addition of **2** to a solution of other reactants.[10] In fact, when **2** was added dropwise within 0.5 h to a solution of **1**, **3**, and **4b**; **5b** and **6b** were obtained in 47 and 30% yields, respectively. When **4d** was used, the yield of **6d** was increased to 76%.

Next, the reaction of uridine 5′-*aci*-nitronates with Wittig reagents was examined. When *aci*-nitro ester (**5a** or **5c**) was treated with 2 molar amounts of (ethoxycarbonylmethylene)triphenylphosphorane (**10**) in benzene under reflux for 8 h, 1-[(*E*)-5,6-dideoxy-7-ethoxy-2,3-*O*-isopropylidene-β-D-ribo-hept-5-eno-1,4-furanosid-7-ulosyl]-O^2-methyl- or -3-methyluracil (**11a** or **12a**) was obtained in 81 or 70% yield, respectively. Under similar conditions, the reaction of *aci*-nitro ester (**5b** or **5d**) with (acetylmethylene)triphenylphosphorane (**13**) completed within 2 h to give 1-[(*E*)-5,6,8-trideoxy-β-D-ribo-oct-5-eno-1,4-furanosid-7-ulosyl]-O^2-methyl or -3-methyluracil (**11b** or **12b**) in 66 or

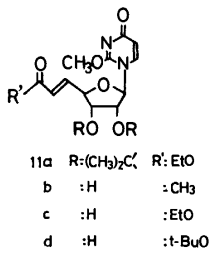

11a R:$(CH_3)_2C$, R′: EtO
b :H :CH_3
c :H :EtO
d :H :t-BuO

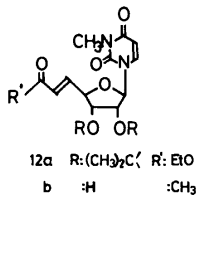

12a R:$(CH_3)_2C$, R′: EtO
b :H :CH_3

50% yield, respectively. ^{1}H-NMR spectroscopy showed that **11a** was pure *E*-isomer, $C_{5'}$H and $C_{6'}$H appearing as sharp double doublets at 7.06 and 6.03 ppm with $J_{5',6'}$=16.7 Hz, $J_{4',5'}$=5.5 Hz, and $J_{4',6'}$= 1.5 Hz. Similarly, the ^{1}H-NMR spectrum of **11b**, **12a**, and **12b** showed similar pattern of signals as shown in experimental section.

It was found that overall yields of enofuranosyluracils were improved by one-pot procedure without isolation of *aci*-nitro ester. Thus, to a solution of **4b**, **1**, and **3** in THF was added **2** in THF at room temperature for 2 h. The reaction mixture was stirred overnight and **13** in benzene was added. The resulting solution was successively refluxed for 2 h giving **11b** in 73% yield. By the same procedure, **4d** afforded **12b** in 43% yield. When **4b** was allowed to react with **1**, **2**, and **3**, followed by **10** or (*t*-butoxycarbonylmethylene)triphenylphosphorane by one-pot procedure, the second step completed in 3 h giving the expected 1-[(*E*)-β-D-ribo-hept-5-enofuranos-

yl]-uracils (**11c**, **11d**) in 70% yield.

Reactions of Cytidine Derivatives. Similar to the case of 2′,3′-*O*-isopropylideneuridine, the reaction of N^4-benzoyl-2′,3′-*O*-isopropylidenecytidine with **1**, **2**, and **3** quantitatively gave N^4-benzoyl-2′,3′-*O*-isopropylidene-O^2,5′-cyclocytidine. This result suggests that both hydrogen atoms of the amino group should be substituted to prevent undesirable cyclization. Thus, the cytosine moiety was protected by dimethylaminomethylene group. When N^4-dimethylaminomethylene-2′,3′-*O*-isopropylidenecytidine (**14a**) reacted with **1** by the use of 1.5 molar amounts of **2** and **3**, the corresponding *aci*-nitro ester (**15a**) was obtained in 54% yield. The reaction of N^4-dimethylaminomethylenecytidine (**14b**) with **1** (1.5 equiv), **2** (3 equiv), and **3** (3 equiv) afforded *aci*-nitroester (**15b**) in 32% yield accompanying with deprotected product (**16**; 14%).

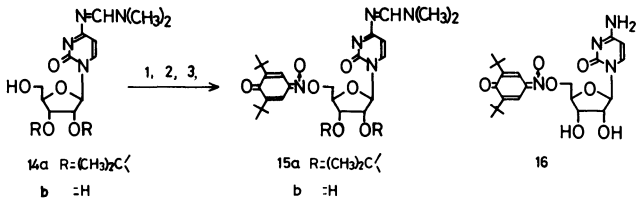

When **15a** was treated with **13** in THF under reflux for 6.5 h, no N^4-dimethylaminomethylene-1-[(*E*)-5,6,8-trideoxy-2,3-*O*-isopropylidene-β-D-ribo-oct-5-eno-1,4-furanosid-7-ulosyl]-2(1*H*)-pyrimidinone could be isolated but N^4-amino-1-[(*E*)-5,6,8-trideoxy-2,3-*O*-isopropylidene-β-D-ribo-oct-5-eno-1,4-furanosid-7-ulosyl]-2(1*H*)-pyrimidinone (**17**) was obtained in 18% yield. On the other hand, the reaction of **15b** with **13** gave N^4-dimethylaminomethylene-1-[(*E*)-5,6,8-trideoxy-β-D-ribo-oct-5-eno-1,4-furanosid-7-ulosyl]-2(1*H*)-pyrimidinone (**18**) in 31% yield. No deprotected product could be isolated.

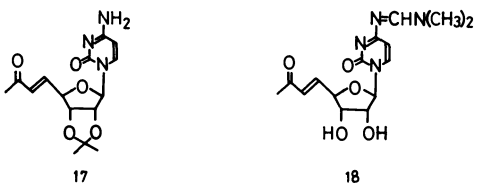

17 18

As the dimethylaminomethylene group was obviously inadequate for the present purpose because of instability, 4-triazolyl-1-(2,3-*O*-isopropylidene-β-D-ribofuranosyl)-2(1*H*)-pyrimidinone (**19a**) was used. Compound **19a** was readily prepared from 2′,3′-*O*-isopropylideneuridine by the modification of Reese's procedure.[11] The transformation of the triazolyl group into various functional groups involving amino group has been demonstrated.[12] Therefore, carbon-chain extension of **19a** is synthetically useful because a variety of pyrimidinenucleosides would be prepared from a single precursor. The reaction of **19a** with two equivalents of **1**, **2**, and **3** resulted in the formation of the corresponding *aci*-nitro ester (**20a**) and 5′-deoxy-5′-hydrazino derivative (**21a**) in 61 and 20% yields, respectively, while the reaction of 4-triazolyl-1-(β-D-ribofuranosyl)-2(1*H*)-pyrimidinone (**19b**) with two equivalents of **1**, **2**, and **3** exclusively gave *aci*-nitro ester (**20b**) in 71% yield without detectable formation of hydrazino derivative (**21b**).

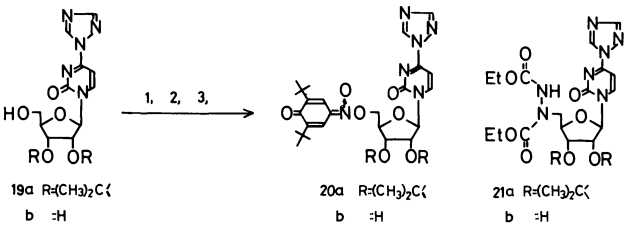

Similar to the case of uridine derivatives, the *aci*-nitro ester derived from the reaction at 2′- and/or 3′-hydroxyl group could not be detected.

The reaction of **13** with **20a** or **20b** afforded the corresponding (*E*)-olefins (**22a** or **22b**) in 61 or 77% yield, respectively. By a one-pot reaction, **19b** afforded **22b** in 68% yield.

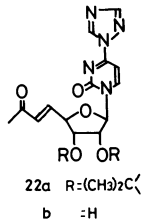

Reactions of Adenosine Derivatives. When N^6-dimethylaminomethylene-2′,3′-*O*-isopropylideneadenosine (**23**) was allowed to react with two equivalents of **1**, **2**, and **3**, expected *aci*-nitro ester could not be obtained. Examination of the crude reaction mixture by paper chromatography revealed the formation of a compound having UV_{max} (MeOH) 292 nm. Anzai has demonstrated that, by treatment with aqueous sodium hydroxide, 2′,3′-*O*-isopropylidene-N^3,5′-cycloadenosine (**24**; $X^- = CH_3SO_3^-$) converted into N^5,5′-anhydro-5-amino-4-amidino-1-(2,3-*O*-isopropylidene-β-D-ribofuranosyl)imidazole (**25**) which exhibits UV_{max} (MeOH) 290 nm.[13] Thus, the results obtained could be explained by assuming the initial formation of **24** (X^-=2,6-di-*t*-butyl-4-nitrophenoxide anion) which decomposed into **25** during manipuration. In order to prevent the undesirable cyclization, N^1,N^6,2′,3′-*O*-tetrabenzoyladenosine (**26**) was used where nucleophilicity of N^3-position was decreased by the electron-withdrawing group. When **26** was allowed to react with **1** in the presence of **2** and **3**, the corresponding *aci*-nitro ester (**27**) was obtained in 83% yield. When **27** was treated with **13** in THF

under reflux for 8 h, N^1,N^6-dibenzoyl-9-[(*E*)-2,3-di-*O*-benzoyl-β-D-ribo-oct-5-eno-1,4-furanosid-7-ulosyl]-adenine (**28a**) and N^6-benzoyl-9-[(*E*)-2,3-di-*O*-benzoyl-β-D-ribo-oct-5-eno-1,4-furanosid-7-ulosyl]-adenine (**28b**) were obtained in 19 and 36% yields, respectively.

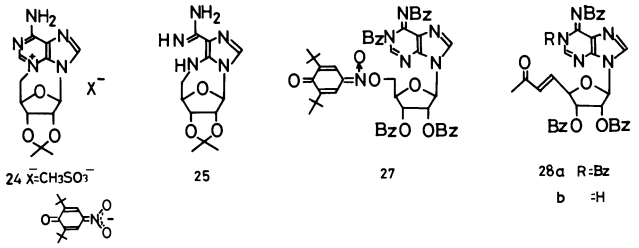

Conclusion. The reaction of nucleosides with **1**, **2**, and **3** resulted in the formation of the corresponding *aci*-nitro esters. The condensation selectively took place at 5′-hydroxyl group, no protection at 2′- and 3′-hydroxyl groups being required. A serious side reaction is the competitive formation of 5′-deoxy-5′-hydrazino nucleosides. However the formation of the side products could be partly suppressed by a slow addition of **2**. Although no explanation can be offered at the present stage of investigation, a comparison of reactions of nucleosides having free 2′- and 3′-hydroxyl groups with those of 2′,3′-*O*-isopropylidene nucleosides revealed that the protecting group might influence the reactivity of the intermediary phosphonium salts. Thus, the isopropylidene group of uridine derivatives (**4a**, **4c**) facilitated the *aci*-nitro ester formation, while the reverse was found for **19a**. The yield of 5′-deoxy-5′-hydrazinouridines was also affected by manner of protection of uracil moiety. Since *aci*-nitro esters can be utilized as masked aldehydes, the conversion of uridine, cytidine, and adenosine derivatives into *aci*-nitro esters and subsequent reaction with stabilized phosphoranes provides a convenient procedure for the preparation of the corresponding carbon-chain extended nucleosides.

Experimental

Methods. Preparative layer chromatography (PLC) was carried on 20 cm×30 cm glass coated with Merck silica gel PF_{254}. Kiesel-gel 60 (Merck, mesh 70—220) was used for column chromatography (5 cm×30 cm). ^{1}H-Nuclear magnetic resonance (NMR) spectra were measured on Hitachi R-20 (60 MHz) or JEOL GX-270 (270 MHz) spectrometer using tetramethylsilane as internal standard. Ultraviolet absorption spectra were obtained with a Hitachi EPS-3T recording spectrometer. Elemental analyses were obtained from Institute of Physical and Chemical Research, Wako, Saitama.

The nucleosidic starting materials, O^2-methyl-2′,3′-*O*-isopropylideneuridine (**4a**),[14] N^3-methyl-2′,3′-*O*-isopropylideneuridine (**4c**),[3b] O^2-methyluridine (**4b**),[8] N^3-methyluridine (**4d**),[3b] N^4-dimethylaminomethylene-2′,3′-*O*-isopropylidenecytidine (**14a**),[15] N^4-dimethylaminomethylenecytidine (**14b**),[15] 4-triazolyl-1-(2,3-*O*-isopropylidene-β-D-ribofuranosyl)-2(1*H*)-pyrimidinone (**19a**),[11] 4-triazolyl-1-(β-D-ribofuranosyl)-2(1*H*)-pyrimidinone (**19b**),[11] N^6-dimethylaminomethylene-2′,3′-*O*-isopropylideneadenosine (**23**),[15] and N^1,N^6,2′,3′-*O*-tetrabenzoyladenosine (**26**)[16] were prepared by known procedures or their modifications.

Preparations of *aci*-Nitro Ester. Preparations of 5a and 5c. A solution of **2** (261 mg, 1.5 mmol) in THF (1 ml) was added dropwise over a period of 1 h to a mixture of uridine derivative (**4a** or **4c**, 298 mg, 1 mmol), **1** (375 mg, 1.5 mmol), and **3** (393 mg, 1.5 mmol) in THF (3 ml). The solution gradually colored red-orange on addition of **2** and kept stirring at room temperature overnight. The **5a** was separated by PLC ($CHCl_3$:EtOAc: MeOH=10:5:1) in 84% yield: red-orange oily semisolid; ^{1}H-NMR ($CDCl_3$)[17] δ=1.29 and 1.30 (18H, s, *t*-Bu), 1.38 and 1.60 (6H, s, isopropylidene CH_3), 4.06 (3H, s, OCH_3), 4.37 (1H, dd, 4′-H), 4.58 and 4.67 (2H, dd, $J_{5'a,4'}$=4.3 Hz, $J_{5'b,4'}$=5.9 Hz, $J_{5'a,5'b}$=12.0 Hz, 5′-H), 4.82 (1H, dd, $J_{2',3'}$=6.6 Hz, $J_{3',4'}$=3.3 Hz, 3′-H), 4.89 (1H, dd, $J_{1',2'}$=2.3 Hz, 2′-H), 5.85 (1H, d, 1′-H), 5.99 (1H, d, $J_{5,6}$=7.6 Hz, 5-H), 7.41 (1H, d, 6-H), and 7.36 and 7.54 (2H, d, quinone H).

5c was isolated by PLC (benzene:EtOAc=10:1) in 83% yield: red-orange oil; ^{1}H-NMR ($CDCl_3$) δ=1.29 (18H, s, *t*-Bu), 1.36 and 1.56 (6H, s, isopropylidene CH_3), 3.31 (3H, s, NCH_3), 4.37 (1H, m, 4′-H), 4.62 and 4.63 (2H, d, $J_{4',5'}$=6.3 Hz, 5′-H), 4.95 (1H, dd, $J_{3',4'}$=4.0 Hz, $J_{2',3'}$=6.4 Hz, 3′-H), 5.12 (1H, dd, $J_{1',2'}$=1.6 Hz, 2′-H), 5.53 (1H, d, 1′-H), 5.77 (1H, d, $J_{5,6}$=7.9 Hz, 5-H), 7.20 (1H, d, 6-H), and 7.35 and 7.59 (2H, d, quinone H).

Preparations of 5b and 5d. A mixture of **1** (375 mg, 1.5 mmol), **3** (786 mg, 3 mmol), and uridine derivative (**4b** or **4d**, 256 mg, 1 mmol) in THF (3 ml) was stirred and a solution of **2** (261 mg, 1.5 mmol) in THF (1 ml) was added over a period of 1 h at room temperature. After 3 h, **2** (1.5 mmol) in THF (1 ml) was further added for 1 h. The nucleoside (**4b** or **4d**) dissolved on addition of **2** and the solution gradually colored red-orange. After the solution kept stirring overnight, the residue was evaporated under reduced pressure. The residue was purified by column chromatography ($CHCl_3$:MeOH=10:1) to afford **5b** or **5d** in 72 or 39% yield. **5b**: red-orange semisolid; ^{1}H-NMR (60 MHz, DMSO-d_6) δ=1.22 and 1.27 (18H, s, *t*-Bu), 3.91 (3H, s, OCH_3), 5.41 and 5.63 (2H, d, 2′-, 3′-OH), 5.79 (1H, d, $J_{1',2'}$=5.2 Hz, 1′-H), 5.90 (1H, d, $J_{5,6}$=8.4 Hz, 5-H), 7.30 and 7.58 (2H, d, quinone H), and 7.73 (1H, d, 6-H). **5d**: red-orange semisolid; ^{1}H-NMR (60 MHz, $CDCl_3$) δ=1.31 (18H, s, *t*-Bu), 3.31 (3H, s, NCH_3), 5.72 (1H, s, 1′-H), 5.80 (1H, d, $J_{5,6}$=7.6 Hz, 5-H), 7.45 (1H, d, 6-H), and 7.36 and 7.55 (2H, d, quinone H).

In the case of the preparation of **5d**, a side product (**6d**) was obtained in 41% yield (oil; UV_{max} (MeOH) 265 nm, UV_{min} 235 nm; ^{1}H-NMR (60 MHz, $CDCl_3$) δ=1.24 (6H, t, $-CH_2\underline{CH_3}$), 3.27 (3H, s, OCH_3), 5.70 (1H, d, 1′-H), 5.80 (1H, d, $J_{5,6}$=8.5 Hz, 5-H), 7.45 (1H, d, 6-H), and 7.63 (1H, br s, NH).

In a similar reaction, when **2** (3 mmol) was added to the THF solution of **1**, **3**, and **4b** or **4d** within 0.5 h, the undesirable products, 5′-deoxy-5′-hydrazino derivatives (**6b** or **6d**) was obtained in 30 or 76% yield, respectively. The **6b** was recrystallized from CH_3CN and melted at 147—149 °C (UV_{max} (MeOH) 235, 250 (sh) nm, UV_{min} 215 nm; ^{1}H-NMR (60 MHz, DMSO-d_6) δ=1.17 (6H, t, $-CH_2\underline{CH_3}$), 5.24 and

5.56 (2H, d, 2'-, 3'-OH), 5.70 (1H, d, $J_{1',2'}$=4.4 Hz, 1'-H), 5.88 (1H, d, $J_{5,6}$=7.8 Hz, 5-H), 7.75 (1H, d, 6-H), and 9.58 (1H, br s, NH)).

Preparation of 15a. By a similar procedure described in the preparation of **5a** and **5c**, **14a** (389 mg, 1.24 mmol) reacted with 1.5 equivalents of **1**, **2**, and **3**. The **15a** was isolated by the use of column chromatography ($CHCl_3$:EtOAc:MeOH=12:5:1) in 54% yield (orange oil; ^{1}H-NMR ($CDCl_3$) δ=1.27 and 1.29 (18H, s, *t*-Bu), 1.36 and 1.55 (6H, s, isopropylidene CH_3), 3.15 and 3.18 (6H, s, $-N(CH_3)_2$), 4.43 (1H, m, 4'-H), 4.68 and 4.79 (2H, dd, $J_{5'a,4'}$=7.2 Hz, $J_{5'b,4'}$=4.9 Hz, $J_{5'a,5'b}$=12.0 Hz, 5'-H), 5.06 (1H, dd, $J_{3',4'}$=3.3 Hz, $J_{2',3'}$=6.3 Hz, 3'-H), 5.27 (1H, d, 2'-H), 5.50 (1H, s, 1'-H), 6.04 (1H, d, $J_{5,6}$=7.3 Hz, 5-H), 7.39 (1H, d, 6-H), 7.36 and 7.59 (2H, d, quinone H), and 8.81 (1H, s, =CH-).

Preparations of 15b and 16. For the reaction of **14b** (420 mg, 1.53 mmol), 1.5 equivalents of **1** and 3 equivalents of **2** and **3** were used. **15b** and **16** were isolated by column chromatography ($CHCl_3$:MeOH=12:1) in 36 and 14% yields, respectively. **15b**: orange oil; ^{1}H-NMR ($CDCl_3$) δ=1.26 and 1.30 (18H, s, *t*-Bu), 3.13 and 3.20 (6H, s, $-N(CH_3)_2$), 4.1—4.3 (3H, m, 4'-H, 5'-H), 4.4—4.6 (2H, m, 2'-H, 3'-H), 4.74 and 4.79 (2H, d, 2'-, 3'-OH), 5.82 (1H, d, $J_{1',2'}$=3.3 Hz, 1'-H), 6.07 (1H, d, $J_{5,6}$=7.3 Hz, 5-H), 7.35 and 7.53 (2H, d, quinone H), 7.70 (1H, d, 6-H), and 8.73 (1H, s, =CH-).

Preparations of 20a and 20b. When **19a** (282 mg, 0.84 mmol) reacted with 2 equivalents of **1**, **2**, and **3**, **20a** and 5'-deoxy-5'-hydrazino derivative (**21a**) were isolated by the use of column chromatography ($CHCl_3$:MeOH=15:1) in 61 and 20% yields, respectively. **20a**: orange oil; ^{1}H-NMR (60 MHz, $CDCl_3$) 1.26 (18H, s, *t*-Bu), 1.36 and 1.60 (6H, s, isopropylidene CH_3), 5.68 (1H, s, 1'-H), 7.02 (1H, d, $J_{5,6}$=8.0 Hz, 5-H), 7.26 and 7.48 (2H, d, quinone H), 8.00 (1H, d, 6-H), and 8.06 and 9.15 (2H, s, triazole H). **21a**; oil; ^{1}H-NMR (60 MHz, CD_3OD) δ=1.23 (6H, t, $-CH_2\underline{CH_3}$), 1.32 and 1.52 (6H, s, isopropylidene CH_3), 5.83 (1H, s, 1'-H), 7.02 (1H, d, $J_{5,6}$=7.6 Hz, 5-H), 8.36 (1H, d, 6-H), and 8.26 and 9.30 (2H, s, triazole H).

Compound **19b** (210 mg, 0.71 mmol) was allowed to react with 2 equivalents of **1**, **2**, and **3** by the same procedure described in the preparation of **5b** and **5d**. The reaction mixture being stirred for 2 d, the residue obtained by the removal of THF was applied to a silica-gel column and eluted with a mixture of $CHCl_3$–EtOAc–MeOH (10:5:1) giving 71% yield of **20b**; orange oil; ^{1}H-NMR (60 MHz, $CDCl_3$) δ=1.33 (18H, s, *t*-Bu), 5.90 (1H, s, 1'-H), 7.05 (1H, d, $J_{5,6}$=7.0 Hz, 5-H), 7.30 and 7.58 (2H, d, quinone H), 8.30 (1H, d, 6-H), and 8.06 and 9.20 (2H, s, triazole H). A 20% of the starting material **19b** was recovered.

Preparation of 27. A solution of **2** (94 mg, 0.64 mmol) in THF (2 ml) was added dropwise over a period of 1 h to a mixture of **26** (203 mg, 0.3 mmol), **1** (149 mg, 0.6 mmol), and **3** (156 mg, 0.6 mmol) in THF (3 ml). The reaction mixture was kept stirring at room temperature for 2 d. After being evaporated, the residue was purified by PLC (benzene:EtOAc=10:1) giving **27** in 83% yield: orange oil; ^{1}H-NMR ($CDCl_3$) δ=1.24 and 1.27 (18H, s, *t*-Bu), 4.7—4.8 (2H, m, 5'-H), 4.94 (1H, m, 4'-H), 6.17—6.26 (2H, m, 2'-H, 3'-H), 6.39 (1H, d, $J_{1',2'}$=4.3 Hz, 1'-H), 7.2—8.0 (22H, m, aromatic and quinone H), and 8.25 and 8.67 (2H, s, purine H).

Reaction of *aci*-Nitro Esters with Wittig Reagents. Preparations of 11a and 12a. One mmol of **5a** or **5c** in benzene (10 ml) was treated with 2 molar amounts of **10** under reflux for 8 h and then evaporated. The **11a** and **12a** were isolated by the column chromatography using $CHCl_3$–MeOH (10:1) in 81 and 70% yields, respectively. **11a**: oil; ^{1}H-NMR (60 MHz, $CDCl_3$) δ=1.29 (3H, t, $-CH_2\underline{CH_3}$), 1.38 and 1.60 (6H, s, isopropylidene CH_3), 4.01 (3H, s, OCH_3), 6.00 (1H, d, $J_{5,6}$=8.0 Hz, 5-H), 6.05 (1H, d, 6'-H), 6.98 (1H, dd, $J_{5',6'}$=15.0 Hz, $J_{4',5'}$=4.8 Hz, 5'-H), and 7.36 (1H, d, 6-H). **12a**: oil; ^{1}H-NMR (60 MHz, $CDCl_3$) δ=1.29 (3H, t, $-CH_2\underline{CH_3}$), 1.38 and 1.59 (6H, s, isopropylidene CH_3), 3.31 (3H, s, NCH_3), 4.23 (2H, q, $-CH_2-$), 5.70 (1H, d, $J_{1',2'}$=1.5 Hz, 1'-H), 5.81 (1H, d, $J_{5,6}$=8.1 Hz, 5-H), 6.03 (1H, dd, $J_{4',6'}$=1.2 Hz, 6'-H), 7.06 (1H, dd, $J_{5',6'}$=16.7 Hz, $J_{4',5'}$=5.5 Hz, 5'-H), and 7.33 (1H, d, 6-H).

The **11a** was treated with 80% acetic acid under reflux for 2 h and then evaporated. The residue was purified by column chromatography (EtOAc) to quantitatively give 1-[(*E*)-5,6-dideoxy-7-ethoxy-β-D-ribo-hept-5-eno-1,4-furanosid-7-ulosyl]uracil; mp 163—165 °C; UV_{max} (MeOH) 263 nm, UV_{min} 241 nm; ^{1}H-NMR (60 MHz, CD_3OD) δ=1.28 (3H, t, $-CH_2\underline{CH_3}$), 5.75 (1H, d, $J_{5,6}$=7.6 Hz, 5-H), 5.83 (1H, d, $J_{1',2'}$=3.0 Hz, 1'-H), 6.10 (1H, dd, $J_{4',6'}$=1.2 Hz, 6'-H), 7.07 (1H, dd, $J_{5',6'}$=15.5 Hz, $J_{4',5'}$=5.2 Hz, 5'-H), and 7.58 (1H, d, 6-H); Found: C, 50.00; H, 5.16; N, 8.97%. Calcd for $C_{13}H_{16}N_2O_7$: C, 50.00; H, 5.16; N, 8.97%.[18]

Preparations of 11b and 12b. Similar to the case of preparations of **11a** and **12a**, **11b** and **12b** were obtained in 66 and 50% yields, respectively. The **11b** was recrystallized from EtOH, mp 189—190 °C; UV_{max} (H_2O) 228, 250 (sh) nm; ^{1}H-NMR (60 MHz, DMSO-d_6) δ=2.28 (3H, s, $COCH_3$), 3.92 (3H, s, OCH_3), 5.92 (1H, d, $J_{5,6}$=7.6 Hz, 5-H), 6.20 (1H, d, 6'-H), 7.00 (1H, dd, $J_{5',6'}$=16.0 Hz, $J_{4',5'}$=5.6 Hz, 5'-H), and 7.73 (1H, d, 6-H); Found: C, 52.28; H, 5.71%. Calcd for $C_{13}H_{16}N_2O_6$: C, 52.70; H, 5.44%. The **12b** was recrystallized from EtOH, mp 128—130 °C; UV_{max} (H_2O) 219, 260 nm, UV_{min} 250 nm; ^{1}H-NMR (60 MHz, $CDCl_3$) δ=2.30 (3H, s, $COCH_3$), 3.30 (3H, s, NCH_3), 5.83 (1H, d, $J_{5,6}$=8.0 Hz, 5-H), 6.35 (1H, d, 6'-H), 6.91 (1H, dd, $J_{5',6'}$=16.0 Hz, $J_{4',5'}$=4.5 Hz, 5'-H), and 7.38 (1H, d, 6-H); Found: C, 52.20; H, 5.44; N, 9.50%. Calcd for $C_{13}H_{16}N_2O_6$: C, 52.70; H, 5.44; N, 9.46%.

Preparation of 11b by One-Pot Reaction. To a solution of **4b** (256 mg, 1 mmol), **1** (377 mg, 1.5 mmol), and **3** (786 mg, 3 mmol) in THF (3 ml) was added **2** (261 mg, 1.5 mmol) in THF (1 ml) at room temperature for 1 h. The reaction mixture being stirred for 3 h, **2** (1.5 mmol) in THF (1 ml) was further added for 1 h. To the solution kept stirring overnight, **13** (636 mg, 2 mmol) in benzene (10 ml) was added. The resulting solution was refluxed for 3 h and evaporated under reduced pressure. The residue was purified by column chromatography ($CHCl_3$:MeOH=7:1) to give **11b** in 73% yield.

Preparations of 17 and 18. A THF solution of **15a** (437 mg, 0.80 mmol) and **13** (234 mg, 0.80 mmol) was refluxed for 7.5 h and then evaporated under reduced pressure. The residue was purified by PLC ($CHCl_3$:MeOH=9:1) to give **17** in 18% yield: oil; UV_{max} (MeOH) 271 nm; ^{1}H-NMR ($CDCl_3$) δ=1.35 and 1.57 (6H, s, isopropylidene CH_3), 2.26 (3H, s, $COCH_3$), 4.66 (1H, m, 4'-H), 4.98 (1H, m, 3'-H), 5.21 (1H, d, $J_{2',3'}$=6.0 Hz, 2'-H), 5.49 (1H, s, 1'-H), 5.88 (1H, d, $J_{5,6}$=7.3 Hz, 5-H), 6.24 (1H, d, 6'-H), 6.95 (1H, dd, $J_{5',6'}$=16.1 Hz, $J_{4',5'}$=6.4 Hz, 5'-H), and 7.30 (1H, d, 6-H).

The **15b** (209 mg, 0.38 mmol) in THF (8 ml) was treated with **13** (239 mg, 0.81 mmol) under reflux for 5 h and then evapotated. The **18** was isolated by column chromatography using $CHCl_3$–MeOH (8:1) in 31% yield; oil; UV_{max} (MeOH) 319 nm, UV_{min} 261 nm; ^{1}H-NMR ($CDCl_3$–CD_3OD) δ=2.35 (3H, s, $COCH_3$), 3.17 and 3.22 (6H, s, $N(CH_3)_2$), 3.94 (1H, m, 3′-H), 4.18 (1H, d, $J_{2',3'}$=5.4 Hz, 2′-H), 4.66 (1H, m, 4′-H), 5.82 (1H, s, 1′-H), 6.44 (1H, dd, $J_{4',6'}$=1.4 Hz, 6′-H), 6.18 (1H, d, $J_{5,6}$=7.2 Hz, 5-H), 6.95 (1H, dd, $J_{5',6'}$=16.3 Hz, $J_{4',5'}$=5.0 Hz, 5′-H), 7.71 (1H, d, 6-H), and 8.87 (1H, s, =CHN–).

Preparations of 22a and 22b. A solution of *aci*-nitro ester [**20a** (76 mg, 0.13 mmol) or **20b** (230 mg, 0.43 mmol)] and **13** (2 equiv) in THF (7 ml) was refluxed for 7 h. After the solvent was removed, the residue was purified by column chromatography. For the reaction of **20a**, elution with $CHCl_3$–MeOH (15:1) gave **22a** as an oil in 61% yield; UV_{max} (MeOH) 313 nm, UV_{min} 282 nm; ^{1}H-NMR ($CDCl_3$) δ=1.38 and 1.67 (6H, s, isopropylidene CH_3), 2.30 (3H, s, $COCH_3$), 4.78 (1H, m, 4′-H), 5.02 (1H, m, 3′-H), 5.23 (1H, d, $J_{2',3'}$=6.3 Hz, 2′-H), 5.74 (1H, s, 1′-H), 6.25 (1H, dd, $J_{4',6'}$=1.0 Hz, 6′-H), 6.94 (1H, dd, $J_{5',6'}$=16.2 Hz, $J_{4',5'}$=6.6 Hz, 5′-H), 7.09 (1H, d, $J_{5,6}$=7.3 Hz, 5-H), 7.96 (1H, d, 6-H), and 8.15 and 9.26 (2H, s, triazole H).

For the reaction of **20b**, elution with EtOAc–MeOH (8:1) afforded a 77% yield of **22b** which was recrystallized from $CHCl_3$–MeOH: mp 208—209 °C; UV_{max} (MeOH) 217, 251, 316 nm, UV_{min} 233, 280 nm; ^{1}H-NMR ($CDCl_3$) δ=2.32 (3H, s, $COCH_3$), 3.93 (1H, dd, $J_{3',4'}$=4.8 Hz, $J_{4',5'}$=7.7 Hz, 4′-H), 4.18 (1H, dd, $J_{2',3'}$=3.4 Hz, 2′-H), 4.57 (1H, dd, 3′-H), 5.85 (1H, d, $J_{1',2'}$=0.6 Hz, 1′-H), 7.03 (1H, d, $J_{5,6}$=7.7 Hz, 5-H), 6.29 (1H, d, 6′-H), 7.07 (1H, dd, $J_{5',6'}$=16.1 Hz, 5′-H), 8.41 (1H, d, 6-H), and 8.43 and 9.46 (2H, s, triazole H); Found; C, 49.90; H, 4.52; N, 20.73%. Calcd for $C_{14}H_{15}N_5O_5$: C, 50.45; H, 4.54; N, 21.01%.

Preparations of 28a and 28b. A THF (7 ml) solution of **27** (228 mg, 0.25 mmol) and **13** (148 mg, 0.5 mmol) was refluxed for 7.5 h and then evaporated. The residue was purified by PLC (benzene:EtOAc=5:1 and $CHCl_3$:MeOH=20:1) to give **28a** and **28b** in 19 and 36% yields, respectively. **28a**: mp 112—115 °C; UV_{max} (MeOH) 232, 277 nm, UV_{min} 219, 267 nm; ^{1}H-NMR ($CDCl_3$) δ=2.29 (3H, s, $COCH_3$), 5.03 (1H, dd, $J_{3',4'}$=5.9 Hz, $J_{4',5'}$=5.6 Hz, 4′-H), 6.04 (1H, dd, $J_{2',3'}$=5.6 Hz, 3′-H), 6.4—6.5 (2H, m, 1′-H, 2′-H), 6.38 (1H, d, 6′-H), 7.02 (1H, dd, $J_{5',6'}$=16.2 Hz, 5′-H), and 8.25 and 8.68 (2H, s, purine H). **28b**: oil; UV_{max} (MeOH) 232, 282 nm, UV_{min} 257 nm; ^{1}H-NMR ($CDCl_3$) δ=2.32 (3H, s, $COCH_3$), 5.08 (1H, dd, $J_{3',4'}$=5.3 Hz, $J_{4',5'}$=5.6 Hz, 4′-H), 6.09 (1H, dd, $J_{2',3'}$=5.6 Hz, 3′-H), 6.5—6.6 (2H, m, 1′-H, 2′-H), 6.57 (1H, d, 6′-H), 7.06 (1H, dd, $J_{5',6'}$=16.2 Hz, 5′-H), 8.31 and 8.84 (2H, s, purine H), and 9.29 (1H, br s, NH).

References

1) Part XI. J. Kimura, Y. Nishikubo, and O. Mitsunobu, *Bull. Chem. Soc. Jpn.*, **57**, 2017 (1984).

2) For the synthetic approach to ezomycins, octosyl acids, and sinefungin, see for example, a) K. S. Kim and W. A. Szarek, *Can. J. Chem.*, **59**, 878 (1981); b) G. A. Mock and J. G. Moffatt, *Nucleic Acid Res.*, **10**, 6223 (1982); c) J. W. Lyga and J. A. Secrist, III, *J. Org. Chem.*, **48**, 1982 (1983); d) M. Geze, P. Blanchard, J. L. Fourrey, and M. R. Gero, *J. Am. Chem. Soc.*, **105**, 7638 (1983); e) Y. Mizuno, K. Tsuchiya, and H. Tampo, *Chem. Pharm. Bull.*, **32**, 2915 (1984), f) for review of Higher-Carbon Carbohydrates, see Y. Fukuda and T. Suami, *Yuki Gosei Kagaku Kyokai Shi*, **43**, 836 (1985), and refs. therein.

3) An alternative approaches to these antibiotics has also been attempted where carbon skeletons of higher-carbon sugars constructed, followed by glycosidation. See for example, a) K. Anzai and T. Saita, *Bull. Chem. Soc. Jpn.*, **50**, 169 (1977); b) S. Hanessian, T. J. Liak, and D. M. Dixit, *Carbohydr. Res.*, **88**, C14 (1981); c) T. Suami, H. Sasai, and K. Masuno, *Chem. Lett.*, **1983**, 819.

4) J. Kimura, A. Kawashima, M. Sugizaki, N. Nemoto, and O. Mitsunobu, *J. Chem. Soc., Chem. Commun.*, **1979**, 303.

5) O. Mitsunobu, J. Kimura, T. Shimizu, and A. Kawashima, *Chem. Lett.*, **1980**, 927.

6) J. Kimura, T. Shimizu, and O. Mitsunobu, *Chem. Lett.*, **1981**, 1793.

7) S. Shimokawa, J. Kimura, and O. Mitsunobu, *Bull. Chem. Soc. Jpn.*, **49**, 3357 (1976).

8) For the condensation of uridine with carboxylic acid or phosphoric diesters, slight excess of **2** and **3** should also suffice to complete the reaction. J. Kimura, Y. Fujisawa, T. Yoshizawa, K. Fukuda, and O. Mitsunobu, *Bull. Chem. Soc. Jpn.*, **52**, 1191 (1979).

9) For the formation of phosphoranes by the reaction of di- and triols, see a) J. Kimura, K. Yagi, H. Suzuki, and O. Mitsunobu, *Bull. Chem. Soc. Jpn.*, **53**, 3670 (1980); b) O. Mitsunobu, *Synthesis*, **1981**, 1; c) H. H. Brandstetter and E. Zbiral, *Helv. Chim. Acta*, **61**, 1832 (1978); **63**, 327 (1980); d) E. Mark, E. Zbiral, and H. H. Brandstetter, *Monatsh. Chem.*, **111**, 289 (1980); e) R. D. Guthrie and I. D. Jenkins, *Aust. J. Chem.*, **34**, 1997 (1981); f) R. D. Guthrie, I. D. Jenkins, R. Yamazaki, B. W. Skelton, and A. H. White, *J. Chem. Soc., Perkin Trans. 1*, **1981**, 2328, and refs. therein.

10) An alternative procedure to suppress the formation of the hydrazinouridines is change the solvent (THF) to benzene or diethyl ether from which diethyl hydrazinedicarboxylate formed precipitates. Unfortunately however, these less polar solvents are not suitable for the present purpose because of low solubility of nucleoside derivatives.

11) C. B. Reese and A. Ubasawa, *Tetrahedron Lett.*, **21**, 2265 (1980).

12) W. L. Sung, *J. Org. Chem.*, **47**, 3623 (1982); *J. Chem. Soc., Chem. Commun.*, **1982**, 522.

13) K. Anzai, *Agr. Biol. Chem.*, **40**, 373 (1976). The product having UV_{max} 292 nm was treated with 0.2 M NaOH (1 M=mol dm^{-3}) giving N^3,5′-anhydro-5-amino-4-carbamoyl-1-(2,3-*O*-isopropylidene-β-D-ribofuranosyl) imidazole which exhibits UV_{max} 270 nm. K. Anzai and M. Matsui, *Agr. Biol. Chem.*, **37**, 301 (1973).

14) B. M. Brown, A. R. Todd, and S. Varadarajan, *J. Chem. Soc.*, **1957**, 868.

15) J. Zemlicka and A. Holy, *Collect. Czech. Chem. Commun.*, **32**, 3159 (1967).

16) M. Smith, D. H. Rammler, I. H. Goldberg, and H. G. Khorana, *J. Am. Chem. Soc.*, **84**, 430 (1962).

17) Unless otherwise stated, the data was obtained by JEOL GX-270.

18) The isopropylidene derivative of the product has already been prepared. J. M. Tronchet and M. J. Valero, *Helv. Chim. Acta*, **62**, 2788 (1979); J. A. Montgomery and H. J. Thomas, *J. Org. Chem.*, **46**, 594 (1981).

 © 1986 The Chemical Society of Japan Bull. Chem. Soc. Jpn., 59, 875—878 (1986)

Syntheses of Some 6-Oxa- and 2,8-Dioxabicyclo[3.2.1]octanes in Connection with the Daphniphyllum Alkaloids

Shigeru NISHIYAMA, Yoichi IKEDA, and Shosuke YAMAMURA*
Department of Chemistry, Faculty of Science and Technology, Keio University,
Hiyoshi, Kohoku-ku, Yokohama 223
(Received October 16, 1985)

In connection with the daphniphyllum alkaloids, some 6-oxa- and 2,8-dioxabicyclo[3.2.1]octanes, which are included as a partial structure of daphmacrine and codaphniphylline, have been synthesized starting from geraniol.

Previously, we could isolate a number of novel alkaloids from the plant *Daphniphyllaceae.*[1] From a structural point of view, these alkaloids, which are biosynthesized from six mevalonate via squalene, are classified into six types of nitrogen heterocyclic skeletons. Among them, remarkable variations in the remaining partial structure except for the main nitrogen heterocyclic skeleton are found in the group of daphniphylline-type alkaloids, in which codaphniphylline (**1**) and daphmacrine (**2**) are included. As a part of our synthetic study on these alkaloids, we wish to describe the syntheses of some 6-oxa- and 2,8-dioxabicyclo[3.2.1]octanes starting from geraniol.

The known monoacetate (**3**)[2] derived from geraniol in three steps was treated with PhCOCl–pyridine in dichloromethane (room temp, 3 h) in order to differentiate the two original allylic hydroxyl groups, giving rise to the corresponding benzoate (**4**), in quantitative yield, which was further converted into a desired cyclization product (**5**) in four steps, as follows.

The benzoate (**4**) was treated with $Hg(OCOCF_3)_2$ (1.5 equiv) in nitromethane under argon (−15 °C, 3 h) and then stirred with aqueous sodium chloride (room temp, 20 h) to give the corresponding organomercury chloride (**6**),[3] which was directly subjected to reductive demercuration with $NaBH_4$ in *N,N*-dimethylformamide with oxygen bubbling (0 °C, 30 min)[4] and then oxidized with pyridinium chlorochromate (PCC) in dichloromethane (room temp, 4 h) to afford the cyclohexanone derivative (**5**) in 60% overall yield from **4**. The ketone (**5**) was hydrolyzed with saturated methanolic ammonia (0 °C, 5 h) to afford a diol (**7**) in 89% yield, which was further oxidized with pyridinium dichromate (PDC) in *N,N*-dimethylformamide (0 °C, 1 h) to give an aldehyde (**8**) in 85% yield. The resulting aldehyde was treated with 1,2-ethanedithiol–BF_3 etherate to afford the corresponding thioacetal (**9**), which was hydrolyzed with K_2CO_3 in methanol (0 °C, 2 h) to give a dihydroxy compound (**10**), in 84% overall yield. Furthermore, the compound (**10**) was oxidized with PDC in *N,N*-dimethylformamide (room temp, 1 h) to give rise to a desired lactone (**11**) [mp 162—164 °C, IR (film) 1780 and 1715 cm^{-1}] in 54% yield. On $NaBH_4$ reduction in ethanol–dioxane (1:1) (0 °C, 2 h) followed by acetylation with Ac_2O–pyridine, the resulting lactone (**11**) was readily converted into an acetate (**12**), mp 146.5—147.5 °C, in 78% overall yield, in which the newly formed acetoxyl group must be in an axial configuration, as judged from its ^1H NMR spectrum [δ=4.91(1H, br s)].

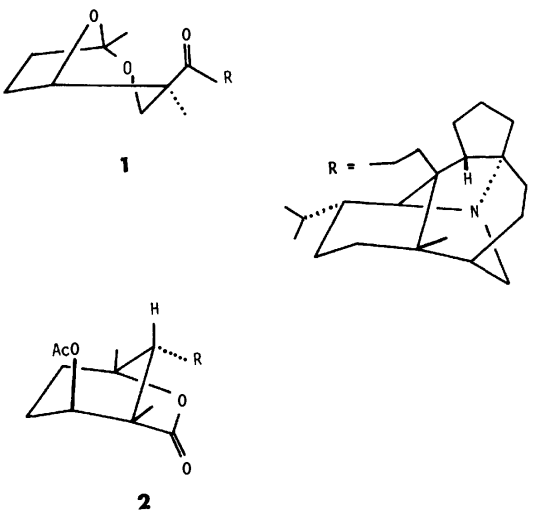

Fig. 1. Structures of codaphniphylline (**1**) and daphmacrine (**2**).

In the next step, the lactone (**12**) was successively treated with thallium trinitrate (TTN) (2.2 equiv) in chloroform–methanol (1:1) (room temp, 1 h),[5] trifluoroacetic acid (TFA) in chloroform containing a small amount of water (0 °C, 1 h), and SiO_2 (room temp, overnight) to afford an acid (**13**) which on methylation with MeI–K_2CO_3 in *N,N*-dimethylformamide (0 °C, 4 h) was converted into the corresponding ester (**14**) [IR (film) 1665 and 1625 cm^{-1}] in 48% overall yield from **12**. In the above procedure, the desired aldehyde (**15**) is too unstable to be separable and seems to be simultaneously converted into the α,β-unsaturated aldehyde (**13**), which has been also produced on exposure to K_2CO_3 in methanol. Finally, this ester (**14**) was successfully converted into the desired 2,8-dioxabicyclo[3.2.1]octane derivative (**16**) which has the same oxygen heterocyclic skeleton

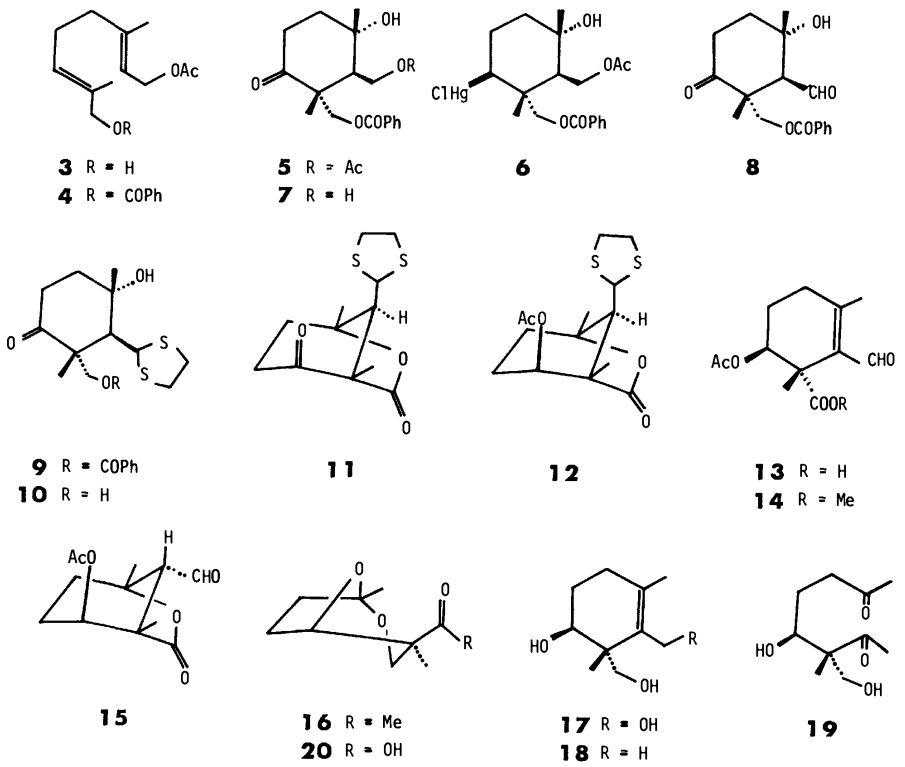

Fig. 2.

as that of codaphniphylline (**1**), as follows.

The ester (**14**) was reduced with excess $NaBH_4$ in ethanol (room temp, overnight) to afford a triol (**17**) and the acetate which on ammonolysis at 0 °C for 2 d afforded **17** in almost quantitative yield. Thus, the total yield of **17** from **14** was 69%. The triol so far obtained was subjected to hydrogenolysis using Pd-C in methanol (room temp, 1.5 h) to give a diol (**18**), mp 104—104.5 °C, in 87% yield. In the last step, on ozonization of **18** in methanol (−60 °C, 30 min) followed by reduction with excess Me_2S, the resulting diketone (**19**) was spontaneously cyclized to the desired acetal (**16**), in 72% yield, having the same oxygen heterocyclic skeleton as that of codaphniphylline (**1**), as judged from its ^1H NMR spectrum [δ=3.49 (1H, d, J=12 Hz), 4.27 (1H, dd, J=12, 2 Hz), and 4.68 (1H, m)], which was similar to that of the degradation product (**20**) of daphniphylline [δ=3.63 (1H, d, J=12 Hz), 4.30 (1H, dd, J=12, 2 Hz), and 4.77 (1H, m)].[6]

On the basis of biogenetic consideration of these daphniphyllum alkaloids, which are biosynthesized from squalene,[1] these two 6-oxa- and 2,8-dioxabicyclo-[3.2.1]octanes have been synthesized. Further synthetic study on the nitrogen heterocyclic moiety of these alkaloids are in progress.

Experimental

All the melting points were obtained on a Mitamura Riken melting point apparatus and uncorrected. IR spectra were recorded on a JASCO Model A-202 spectrophotometer. ^1H NMR spectra were obtained on a Varian EM-390 NMR spectrometer (90 MHz) using tetramethylsilane as an internal standard. Coupling constants are given in Hz (s, singlet; d, doublet; t, triplet; q, quartet; m, multiplet). High resolution mass spectra were obtained on a Hitachi M-80 GC-MS spectrometer operating with an ionization energy (70 eV). Preparative and analytical TLC were carried out on silica-gel plates (Kieselgel 60 F_{254}, E. Merck A. G. Germany) using UV light and/or 5% molbdophosphoric acid in ethanol for detection, unless otherwise stated.

Benzoylation of 3. A solution of **3** (3.0 g) and benzoyl chloride (3.5 ml) in CH_2Cl_2 (30 ml) containing pyridine (2.3 ml) was stirred at room temperature for 3 h. The resulted mixture was partitioned between EtOAc and water, and the organic layer was washed successively with 2M HCl (1 M=1 mol dm^{-3}) and aqueous $NaHCO_3$, and then dried over anhydrous Na_2SO_4. After evaporation of the solvent, the residue was chromatographed on silica gel (200 g) using hexane–EtOAc (5:1) as eluent to give the benzoyl derivative (**4**) as an oil (4.5 g): IR (film) 1730, 1720, 1600, and 1580 cm^{-1}; ^1H NMR ($CDCl_3$) δ=1.75 (6H, s), 2.07 (3H, s), 2.14 (4H, complex), 4.57 (2H, d, J=7 Hz), 4.71 (2H, s), 5.2—5.6 (2H, complex), 7.3—7.6 (3H, complex), and 7.95—8.15 (2H, complex); Found: m/z 316.1677. Calcd for $C_{19}H_{24}O_4$: M, 316.1673.

Cyclization of the Benzoate (4) to the Cyclohexanone Derivative (5). To a solution of $Hg(OCOCF_3)_2$ (4.0 g) in CH_3NO_2 (50 ml) at −20 °C under argon was added a solution of **4** (2.0 g) in CH_3NO_2 (10 ml). The mixture was stirred at approximate −15 °C for 3 h, and then excess

aqueous NaCl was added. After stirring at room temperature for 20 h, the reaction mixture was extracted with $CHCl_3$. The organic extract was dried over anhydrous Na_2SO_4, and concentrated under reduced pressure to leave an oil (3.9 g), which was dissolved in DMF (16 ml), and a 4 ml portion of the solution was gradually added to a solution of $NaBH_4$ (112 mg) in DMF (15 ml) with oxygen bubbling. After being reacted at 0 °C for 30 min, precipitated mercury was filtered off using Celite. The filtrate was partitioned between EtOAc and 2M HCl. The organic layer was washed with aqueous $NaHCO_3$ and dried over anhydrous Na_2SO_4, and then concentrated under reduced pressure. The remaining DMF solution was submitted to the same procedure as above. The combined product was dissloved in CH_2Cl_2 (50 ml), and oxidized with PCC (3.5 g) at room temperature for 4 h. The reaction mixture was filtered and the filtrate was concentrated under reduced pressure to give a brownish residue, which was chromatographed on silica gel (150 g) using $CHCl_3$-EtOAc (4:1) as eluent to afford **5** as an oil (1.3 g): IR (film) 3450, 1710br., 1595, and 1575 cm^{-1}; ^1H NMR ($CDCl_3$) δ=1.21 (3H, s), 1.42 (3H, s), 1.99 (3H, s), 2.0—3.0 (5H, complex), 4.16 (1H, dd, J=12, 5 Hz), 4.45 (1H, dd, J=12, 5 Hz), 4.50 (1H, d, J=11 Hz), 4.72 (1H, J=11 Hz), 7.3—7.6 (3H, complex), and 7.9—8.1 (2H, complex); Found: m/z 349.1627. Calcd for $C_{19}H_{25}O_6$: M+1, m/z 349.1649.

Hydrolysis of 5 to the Diol (7). The ketone (**5**) (0.17 g) was treated with saturated methanolic ammonia (10 ml) at 0 °C for 5 h, and then this mixture was concentrated under reduced pressure to leave an oil, which was purified by preparative TLC [hexane-EtOAc (1:1)] to give the desired diol (**7**) (0.11 g) and the starting material (**5**) (0.03 g). **7** as an oil: IR (film) 3450, 1705, 1595, and 1580 cm^{-1}; ^1H NMR ($CDCl_3$) δ=1.10 (3H, s), 1.52 (3H, s), 1.9—2.1 (2H, complex), 2.2—2.7 (3H, complex), 3.9—4.05 (2H, complex), 4.45 (2H, s), 7.3—7.6 (3H, complex), and 7.85—8.05 (2H, complex); Found: m/z 307.1534. Calcd for $C_{17}H_{23}O_5$: M+1, m/z 307.1543.

Oxidation of the Diol (7) with PDC. A mixture of **7** (36 mg) and PDC (89 mg) in DMF (1 ml) was stirred at 0 °C for 1 h. The reaction mixture was directly submitted to preparative TLC [hexane-EtOAc (1:1)] to yield the aldehyde (**8**) (11 mg) in addition to the starting material (**7**) (23 mg). **8** as an oil: IR (film) 3450, 1715, 1625, 1600, 1580, and 1550 cm^{-1}; ^1H NMR ($CDCl_3$) δ=1.22 (3H, s), 1.40 (3H, s), 2.0—2.7 (3H, complex), 2.8—3.2 (3H, complex), 4.53 (1H, d, J=11 Hz), 5.01 (1H, d, J=11 Hz), 7.3—7.6 (3H, complex), 7.9—8.1 (2H, complex), and 9.67 (1H, d, J=4 Hz); Found: m/z 305.1387. Calcd for $C_{17}H_{21}O_5$: M+1, m/z 305.1387.

Protection of the Aldehyde (8) with 1,2-Ethanedithiol. To a solution of **8** (41 mg) in CH_2Cl_2 (2 ml) were added 1,2-ethanedithiol (34 µl) and $BF_3 \cdot OEt_2$ (14 µl), and the mixture was stirred at 0 °C for 5.5 h. The resulting mixture was washed with aqueous $NaHCO_3$, and then dried over anhydrous Na_2SO_4, and concentrated under reduced pressure. The residue was purified by preparative TLC [hexane-EtOAc (1:1)] to give the thioacetal (**9**) (44 mg): Mp 125—127.5 °C (from hexane-EtOAc); IR (film) 3400, 1710, 1600, and 1580 cm^{-1}; ^1H NMR ($CDCl_3$) δ=1.25 (3H, s), 1.53 (3H, s), 1.5—2.2 (5H, complex), 3.0—3.4 (4H, complex), 4.25 (1H, d, J=12 Hz), 4.41 (1H, d, J=12 Hz), 4.52 (1H, d, J=12 Hz), 7.3—7.65 (3H, complex), and 8.0—8.15 (2H, complex); Found: m/z 381.1219. Calcd for $C_{19}H_{25}O_4S_2$: M+1, m/z 381.1193.

Hydrolysis of the Thioacetal (9). A solution of **9** (0.15 g) and K_2CO_3 (64 mg) in MeOH (7 ml) was stirred at 0 °C for 2 h. The reaction mixture was quenched with H_2O and worked up as usual to give a crude product, which was purified by preparative TLC using hexane-EtOAc (1:1) to give a diol (**10**) (0.1 g) as a crystalline solid: ca. 123 °C; IR (film) 3350 and 1695 cm^{-1}; ^1H NMR ($CDCl_3$+D_2O) δ=1.26 (3H, s), 1.56 (3H, s), 1.5—2.2 (5H, complex), 3.0—3.4 (4H, complex), 3.45 (1H, d, J=11 Hz), 3.91 (1H, d, J=11 Hz), and 4.41 (1H, d, J=12 Hz); Found: m/z 246.0734. Calcd for $C_{11}H_{18}O_2S_2$: M−CH_2O, m/z 246.0747.

Oxidation of the Diol (10) with PDC. A mixture of **10** (22 mg) and PDC (0.15 g) in DMF (1 ml) was stirred at room temperature for 1 h. The resulting brown solution was passed through a short silica-gel column [hexane-EtOAc (1:2)] and purified by preparative TLC [hexane-EtOAc (1:2)] to afford the lactone (**11**) (7.1 mg) and the starting diol (**10**) (8.7 mg). **11**: Mp 162—164 °C (from hexane-EtOAc); IR (film) 1780 and 1715 cm^{-1}; ^1H NMR ($CDCl_3$) δ=1.48 (3H, s), 1.77 (3H, s), 2.1—2.4 (2H, complex), 2.5—2.65 (2H, complex), 2.73 (1H, d, J=10 Hz), 3.0—3.4 (4H, complex), and 4.24 (1H, d, J=10 Hz); Found: m/z 272.0513. Calcd for $C_{12}H_{16}O_3S_2$: M, m/z 272.0539.

Reduction of the Lactone (11) Followed by Acetylation. A mixture of **11** (45 mg) and $NaBH_4$ (7 mg) in EtOH (1 ml) and dioxane (1 ml) was stirred at 0 °C for 1 h and then worked up as usual to give a hydroxy compound (38 mg): Mp 125.5—127 °C (from hexane); IR (film) 3450 and 1755 br. cm^{-1}; ^1H NMR ($CDCl_3$) δ=1.48 (3H, s), 1.63 (3H, s), 1.7—2.1 (4H, complex), 2.27 (1H, d, J=10 Hz), 3.0—3.3 (4H, complex), 3.37 (1H, br.s), and 5.23 (1H, d, J=10 Hz); Found: m/z 274.0694. Calcd for $C_{12}H_{18}O_3S_2$: M, m/z 274.0695.

This compound (28 mg) was dissolved in excess Ac_2O-pyridine and allowed to stand at room temperature overnight, and then worked up as usual to afford the acetate (**12**) (30 mg): Mp 146.5—147.5 °C (from hexane); IR (film) 1770 and 1735 cm^{-1}; ^1H NMR ($CDCl_3$) δ=1.40 (3H, s), 1.65 (3H, s), 1.6—2.1 (4H, complex), 2.14 (3H, s), 2.26 (1H, br.d, J=12 Hz), 3.1—3.4 (4H, complex), 4.94 (1H, br.s), and 5.02 (1H, d, J=12 Hz); Found: m/z 316.0813. Calcd for $C_{14}H_{20}O_4S_2$: M, m/z 316.0802.

Formation of the α,β-Unsaturated Aldehyde (14). A mixture of **12** (19 mg) and TTN (58 mg) in $CHCl_3$ (0.5 ml) and MeOH (0.5 ml) was stirred at room temperature for 1 h. After filtration of salt precipitated, the filtrate was partitioned between $CHCl_3$ and H_2O, and the organic layer was dried over anhydrous Na_2SO_4 and then concentrated under reduced pressure. The residue was treated with TFA (0.5 ml) in $CHCl_3$ (0.5 ml) containing small amount of H_2O at 0 °C for 1 h. The mixture was diluted with $CHCl_3$ and neutralized with aqueous $NaHCO_3$. The organic layer was dried over anhydrous Na_2SO_4 and then concentrated under reduced pressure to leave a syrup, which was charged on silica-gel plates and kept at room temperature overnight. Development of the plate using $CHCl_3$-MeOH (4:1) afforded a crude product, which on methylation with MeI (6 µl)-K_2CO_3 (11 mg) in DMF (0 °C, 4 h) led to the ester (**14**) (7.1 mg) as an oil: IR (film) 1730, 1665, and 1625 cm^{-1};

^{1}H NMR ($CDCl_3$) δ=1.35 (3H, s), 1.55—2.65 (4H, complex), 2.04 (3H, s), 2.18 (3H, S), 3.60 (3H, s), 5.19 (1H, m), and 10.00 (1H, s); Found: *m/z* 254.1114. Calcd for $C_{13}H_{18}O_5$: M, *m/z* 254.1152.

Formation of the Triol (17). To a solution of **14** (15 mg) in EtOH (1 ml) was added $NaBH_4$ (13 mg) at 0 °C, and then the reaction temperature was gradually elevated to room temperature. After being stirred at room temperature overnight, the mixture was neutralized with AcOH and then concentrated under reduced pressure to leave a syrup, which was passed through a short silica-gel column [hexane–acetone (3:1)] to give the triol (**17**) (4.4 mg) and the acetate (4.4 mg). The latter was directly treated with mathanolic ammonia at 0 °C for 2 d to afford **17** (3.3 mg) as a syrup: IR (film) 3380 cm^{-1}; ^{1}H NMR ($CDCl_3$+D_2O) δ=0.85 (3H, s), 1.77 (3H, s), 1.4—2.3 (4H, complex), 3.67 (2H, d, *J*=1.5 Hz), 4.02 (1H, d, *J*=12 Hz), ca. 4.0 (1H, overlapped with the doublet), and 4.29 (1H, d, *J*=12 Hz); Found: *m/z* 186.1261. Calcd for $C_{10}H_{18}O_3$: M, *m/z* 186.1255.

Hydrogenolysis of the Triol (17). The triol (**17**) (5.3 mg) in MeOH (1 ml) was hydrogenated over catalyst 10% Pd-C at room temperature for 1.5 h. After filtration of the catalyst, the filtrate was concentrated under reduced pressure and then directly separated by a short silica-gel column using hexane–acetone (5:1) to afford **18** (2.6 mg) and the unreacted **17** (2.0 mg). **18**: Mp 104–104.5 °C (from hexane–EtOAc); IR (film) 3400 cm^{-1}; ^{1}H NMR ($CDCl_3$) δ= 1.02 (3H, s), 1.61 (6H, s), 1.7—2.2 (4H, complex), 3.52 (1H, d, *J*=11 Hz), 3.74 (1H, d, *J*=11 Hz), and ca. 3.75 (1H, overlapped with the doublet); Found: *m/z* 170.1286. Calcd for $C_{10}H_{18}O_2$: M, *m/z* 170.1305.

Ozonization of the Diol (18). Ozone was passed through a solution of **18** (20 mg) in MeOH (5 ml) at −60 °C for 30 min. After excess ozone was purged with N_2, the reaction solution was treated with excess Me_2S as usual, and then concentrated under reduced pressure. The residue was purified by preparative TLC [hexane–EtOAc (1:1)] to give the acetal (**16**) (14 mg), and the starting material (2 mg) was recovered. **16** as an oil: IR (film) 1710 cm^{-1}; ^{1}H NMR ($CDCl_3$) δ=0.85 (3H, s), 1.48 (3H, s), 1.8—2.1 (4H, complex), 2.39 (3H, s), 3.49 (1H, *d*, *J*=12 Hz), 4.27 (1H, dd, *J*=2, 12 Hz), and 4.68 (1H, m); Found: *m/z* 184.1087. Calcd for $C_{10}H_{16}O_3$: M, *m/z* 184.1097.

This research has been supported in part by grants from the Ministry of Education, Science and Culture as well as from the Foundation for the Promotion of Research on Medicinal Resources, to which grateful acknowledgment is made.

References

1) S.Yamamura and Y. Hirata, "The Daphniphyllum Alkaloids" in "The Alkaloids, Chemistry and Physiology," ed by R. H. F. Manske, Academic Press., New York (1975), Vol. XV, p. 41; S. Yamamura and Y. Hirata, "Daphniphyllum Alkaloids" in "International Review fo Science, Organic Chemistry Series 2, Alkaloids," ed by K. Wiesner, Butterworths, London (1976), Vol. 9, p. 161; S. Yamamura, J. A. Lamberton, H. Irikawa, Y. Okumura, M. Toda, and Y. Hirata, *Bull. Chem. Soc. Jpn.*, **50**, 1836 (1977).

2) M. A. Umbreit and K. B. Sharpless, *J. Am. Chem. Soc.*, **99**, 5526 (1977).

3) T. R. Hoye, A. J. Caruso, and M. J. Kurth, *J. Org. Chem.*, **46**, 3550 (1981) and some references cited therein.

4) C. L. Hill and G. M. Whitesides, *J. Am. Chem. Soc.*, **96**, 870 (1974).

5) E. Fujita, Y. Nagao, and K. Kaneko, *Chem. Pharm. Bull.*, **26**, 3743 (1978).

6) H. Irikawa, N. Sakabe, S. Yamamura, and Y. Hirata, *Tetrahedron*, **24**, 5691 (1968).

 © 1986 The Chemical Society of Japan Bull. Chem. Soc. Jpn., 59, 879—884 (1986)

Polymer-Supported Diaryl Selenoxide and Telluroxide as Mild and Selective Oxidizing Agents

Nan Xing Hu, Yoshio Aso, Tetsuo Otsubo, and Fumio Ogura*
Department of Applied Chemistry, Faculty of Engineering, Hiroshima University,
Saijo, Higashi-Hiroshima 724
(Received October 18, 1985)

Polystyrene-bound diaryl selenoxide and telluroxide have been prepared, which behaved as mild oxidizing agents for thiols to disulfides, phosphines to phosphine oxides, hydroquinone and catechol to *p*- and *o*-benzoquinones, and thioketones to oxo compounds. The telluroxide completed these reactions in shorter periods or under milder conditions than the selenoxide. In addition, they effected novel solvent-dependent reactions of thioamides involving thioureas to 1,2,4-thiadiazoles or to nitriles. In nonacidic solvents, the dehydrosulfurization to nitriles occurred in preference to the oxidative dimerization to 1,2,4-thiadiazoles, but an acidic solvent such as acetic acid promoted the latter reaction.

Although organoseleniums[1] and telluriums[2] have recently received much attention as new synthetic reagents, most of their low-molecular species are extremely stinking and toxic. The immobilization of such reagents on polymer-resins would not only avoid the difficulties arising from volatility, but also provide some additional advantages including simplification of product work-up and recycle of the used reagents. There have been nevertheless known few examples of polymer-supported seleniums[3,4] and none of polymer-supported telluriums. Selenoxides[5–7] and telluroxides[8] have been recently recognized to have effective oxidizing abilities due to their weak chalcogen–oxygen bonds relative to sulfoxides. In particular, we and Barton et al. reported bis(*p*-methoxyphenyl) selenoxide **1a**[7] and telluroxide **1b**,[8] respectively, as new and versatile

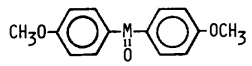

1a M=Se
1b M=Te

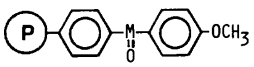

2a M=Se
2b M=Te

oxidizing agents. From the viewpoint of the practical use, we have designed the immobilization of these reagents on polymer-resins. Michels et al. already reported polymer-supported diphenyl selenoxide, but its reactivity has been revealed only for oxidation of 2-methylnaphthalene to 2-naphthaldehyde.[3] Here we report on the facile syntheses of polystyrene-bound diaryl selenoxide **2a** and telluroxide **2b** and on their reactivities toward various compounds as compared to monomeric counterparts **1a** and **1b**.[9]

Results and Discussion

Polystyrene-bound diaryl selenoxide **2a** and telluroxide **2b** were conveniently prepared as shown in Scheme 1. Poly(*p*-lithiostyrene) **3** was readily accessible from partial bromination of 1% cross-linked polystyrene resin, followed by halogen-metal exchange with butyllithium according to the method reported by Farrall and Fréchet.[10] Treatment of **3** with *p*-methoxyphenyl selenocyanate **4a**[11] gave a polymeric selenide **5a**, which was then converted via selenium dibromide **6a** into a light brown polymer of selenoxide **2a**. The infrared spectrum of **2a** closely resembled that of **5a**, but indicated a strong Se=O absorption at 820 cm^{-1}.[3] A polymeric telluroxide **2b** was similarly synthesized, starting from reaction of poly(*p*-lithiostyrene) **3** and *p*-methoxyphenyl tellurocyanate **4b**.[12] In contrast to well-defined Se=O absorptions, Te=O absorptions were obscure in the infrared spectrum of **2b**.

Both of the polymeric reagents **2a** and **2b**, like monomeric counterparts **1a** and **1b**, were inert to simple amines, amides, alcohols, and phenols, but readily oxidized thiols to disulfides, phosphine to phosphine oxides, and hydroquinone and catechol to *p*- and *o*-benzoquinones in dichloromethane, chloroform, or acetic acid as a swelling solvent at room temperature. In addition, **2a** converted sulfides into sulfoxides in acetic acid, while **2b** did not behave similarly.[13] These results are summarized in Table 1. The spent reagents could be recovered as the reduced species **5a** or **5b** by simple filtration and reused after

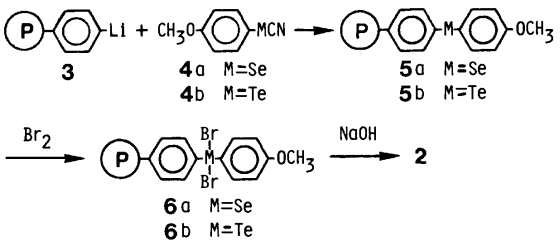

3 **4a** M=Se **4b** M=Te **5a** M=Se **5b** M=Te **6a** M=Se **6b** M=Te

Scheme 1.

Table 1. Oxidations of Thiols, Phosphines, Hydroquinones, and Sulfides with Polymer-Supported Selenoxide **2a** or Telluroxide **2b** at RT

Run	Substrate	Reagent	Solvent	Time/h	Product	Yield/%
1	C_6H_5SH	**2a**	CH_2Cl_2	1.5	$(C_6H_5S)_2$	95
		2b	CH_2Cl_2	0.6		95
2	*p*-$NH_2C_6H_4SH$	**2b**	CH_2Cl_2	3	(*p*-$NH_2C_6H_4S)_2$	89
3	$C_6H_5CH_2SH$	**2a**	CH_2Cl_2	1.5	$(C_6H_5CH_2S)_2$	93
		2b	CH_2Cl_2	0.5		92
4	*n*-$C_{16}H_{33}SH$	**2a**	CH_2Cl_2	3	(*n*-$C_{16}H_{33}S)_2$	97
5	$NH_2CH_2CH_2SH$	**2a**	CH_2Cl_2	1.5	$(NH_2CH_2CH_2S)_2$	100
		2b	CH_2Cl_2	0.6		98
6	$HOCH_2CH_2SH$	**2a**	CH_2Cl_2	1.5	$(HOCH_2CH_2S)_2$	97
		2b	CH_2Cl_2	0.6		98
7	$(C_6H_5)_3P$	**2a**	CH_2Cl_2	3.5	$(C_6H_5)_3PO$	87
		2b	AcOH	2		99
8	(*n*-$C_4H_9)_3P$	**2b**	$CHCl_3$	0.6	(*n*-$C_4H_9)_3PO$	89
9	Hydroquinone	**2a**	AcOH	12	*p*-Benzoquinone	63
10	3,5-Di-*t*-butylcatechol	**2a**	AcOH	4.5	3,5-Di-*t*-butyl-*o*-benzoquinone	96
		2b	$CHCl_3$	0.8		96
11	$(C_6H_5CH_2)_2S$	**2a**	AcOH	3.5	$(C_6H_5CH_2)_2SO$	98
12	(*n*-$C_4H_9)_2S$	**2a**	AcOH	3	(*n*-$C_4H_9)_2SO$	87

Table 2. Oxidations of Thiones and Thioesters with Polymer-Supported Selenoxide **2a** or Telluroxide **2b**

Run	Substrate	Reagent	Solvent	Temp	Time/h	Product	Yield/%
1	$C_6H_5CC_6H_5$ (S)	**2a**	$CHCl_3$	Reflux	6	$C_6H_5CC_6H_5$ (O)	30
		2b	$CHCl_3$	RT	1		98
2	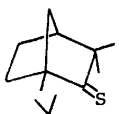	**2a**	$CHCl_3$	Reflux	20	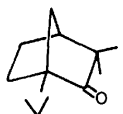	30
		2b	$CHCl_3$	RT	3		93
3	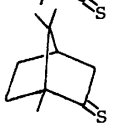	**2a**	$CHCl_3$	RT	20	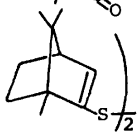	66
		2b	CH_2Cl_2	RT	3.5		44
4		**2a**	CH_2Cl_2	Reflux	8		71
		2b	CH_2Cl_2	Reflux	6		84
5	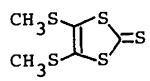	**2a**	$ClCH_2CH_2Cl$	Reflux	36	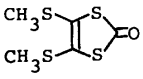	trace
		2b	$ClCH_2CH_2Cl$	Reflux	36		71
6	$C_6H_5COCH_3$ (S)	**2a**	$CHCl_3$	Reflux	12	$C_6H_5COCH_3$ (O)	0
		2b	CH_2Cl_2	RT	5		91

oxidation. The appreciable decrease of their activities was not observed even over ten recycles. Table 1 indicates that telluroxide **2b** completed reactions in shorter periods than selenoxide **2a**, reflecting the weaker Te=O bond relative to Se=O bond. The difference in reactivity between the two reagents became marked in the reactions toward thioketones. As shown in Table 2, telluroxide **2b** could smoothly convert thioketones and thioesters into the corresponding oxo compounds. As an exceptional case, thiocamphor was preferentially converted into a divinyl disulfide, being induced via enethiolization (Run 3). On the other hand, the selenoxide **2a** was less reactive toward most of the thioketones and failed to react with 4,5-bis(methylthio)-1,3-dithiole-2-thione (Run 5) and methyl thiobenzoate (Run 6) even under forced conditions.

It has become apparent that monomeric selenoxide

Table 3. Oxidations of Thioamides to Thiadiazoles with Polymer-Supported Selenoxide **2a** or Telluroxide **2b** in Acetic Acid

Run	Substrate	Reagent	Temp/°C	Time/h	Product	Yield/%
1	$C_6H_5CSNH_2$	**2a**	75	24	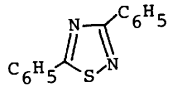	84
		2b	RT	12		53
2	p-$ClC_6H_4CSNH_2$	**2a**	75	6	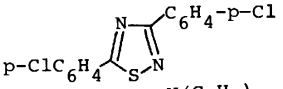	80
		2b	RT	5		31[a]
3	$(C_6H_5)_2NCSNH_2$	**2a**	75	24	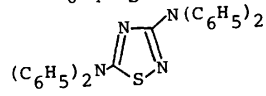	73
		2b	RT	5		0[b]
4	$C_6H_5NHCSNH_2$	**2b**	RT	12	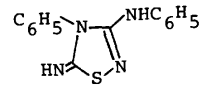	97

a) p-Chlorobenzonitrile was obtained in 47% yield as an acompanying product. b) Reaction at 75 °C resulted in dehydrosulfurization to give $(C_6H_5)_2NCN$ in 93% yield.

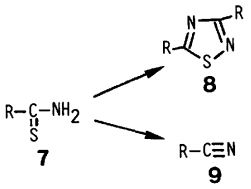

Scheme 2.

1a and telluroxide **1b** undergo different types of reactions toward thioamides involving thioureas as shown in Scheme 2. For example, reaction of thiobenzamide **7** (R=Ph) with **1a** in ethanol at room temperature gave 3,5-diphenyl-1,2,4-thiadiazole **8** (R=Ph) in 86% yield.[7] On the other hand, a similar treatment with **1b** gave benzonitrile **9** (R=Ph) in 78% yield. Polymeric selenoxide **2a**, unlike monomeric counterpart **1a**, hardly effected such oxidative dimerization, and permitted the formation of thiadiazole **8** in acetic acid at 75 °C. Some results are shown in Table 3. Treatments in usual solvents such as ethanol, acetonitrile, benzene, ethyl acetate, and 1,2-dichloroethane favored dehydrosulfurization to nitriles **9**. The best yield (84%) of benzonitrile from thiobenzamide was realized in refluxing ethanol. A wide variety of primary thioamides and thioureas were thus convertible into the corresponding nitriles in high yields as shown in Table 4. *N,N'*-Diphenylthiourea (Run 11) and tetramethylthiourea (Run 12), structurally incapable of forming nitriles, were smoothly oxidized to the corresponding ureas. The polymeric telluroxide **2b**, as a whole, behaved like the polymeric selenoxide **2a**, though the reaction conditions were much milder. Tables 3 and 4 also demonstrate the results of the oxidative dimerization and dehydrosulfurization, respectively, at room temperature. Table 3 shows that the oxidative dimerization with **2b** is not so effective and specific as that with **2a**. For example, treatment of p-chlorothiobenzamide with **2b** in acetic acid (Run 2) gave 3,5-bis(p-chlorophenyl)-1,2,4-thiadiazole (31%), together with p-chlorobenzonitrile (47%). Furthermore, *N,N*-diphenylthiourea did not undergo any oxidative dimerization on treatment with **2b** in acetic acid and rather favored dehydrosulfurization at an elevated temperature (Run 3).

Two mechanisms A and B, which can explain the formation of thiadiazole **8** and nitrile **9**, respectively, are proposed in Scheme 3.[14] Both mechanisms are initiated by addition of the reagent **2** to thioamide **7**, leading to an adduct **10**. A definite difference arises from whether the adduct **10** can react with another thioamide **7** to give a termolecular intermediate **11**, leading via a few steps to thiadiazole **8**, or degrade spontaneously to nitrile **9**. Monomeric selenoxide **1a** favors pathway A, while monomeric telluroxide **1b** favors pathway B. The difference is presumably related to their oxidizing abilities. On the other hand, both polymeric reagents **2a** and **2b** take pathway B in usual solvents, regardless of their oxidizing abilities and degree of swelling. The steric hindrance of the polymer lattice presumably prevents access of the reaction site of adduct **10** to another thioamide **7**, resulting in spontaneous degradation to nitrile **9**. The different reaction type in acetic acid is attributable to its acidity. The protonation of thioamide **7** to iminium **14** is expected to facilitate

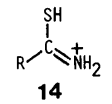

pathway A, because **14** is much more susceptible to nucleophilic attack of adduct **10** than **7**. This was supported by an additional experimental result that the dehydrosulfurization of thiobenzamide **7** (R=Ph) with polymeric selenoxide **2a** to benzonitrile **9** (R=Ph) in ethanol was depressed by addition of a

Table 4. Oxidations of Thioamides to Nitriles with Polymer-Supported Selenoxide **2a** or Telluroxide **2b**

Run	Substrate	Reagent	Solvent	Temp/°C	Time/h	Product	Yield/%
1	$C_6H_5CSNH_2$	**2a**	EtOH	Reflux	20	C_6H_5CN	84
		2a	MeCN	75	12		37
		2a	Benzene	75	12		82
		2a	AcOEt	75	12		50
		2a	$ClCH_2CH_2Cl$	75	12		33
		2b	CH_2Cl_2	RT	1		90
		2b	$CHCl_3$	RT	1		62
		2b	MeOH	Reflux	1		72
2	*p*-$CH_3OC_6H_4CSNH_2$	**2a**	EtOH	Reflux	24	*p*-$CH_3OC_6H_4CN$	96
		2b	CH_2Cl_2	RT	1		93
3	*p*-$ClC_6H_4CSNH_2$	**2a**	EtOH	Reflux	24	*p*-ClC_6H_4CN	88
		2b	CH_2Cl_2	RT	1		97
4	*o*-$ClC_6H_4CSNH_2$	**2a**	EtOH	Reflux	24	*o*-ClC_6H_4CN	95
		2b	CH_2Cl_2	RT	1		98
5	*p*-$NO_2C_6H_4CSNH_2$	**2a**	EtOH	Reflux	24	*p*-$NO_2C_6H_4CN$	98
		2b	CH_2Cl_2	RT	1		96
6	$C_6H_5CH_2CSNH_2$	**2a**	EtOH	Reflux	24	$C_6H_5CH_2CN$	69
		2b	CH_2Cl_2	RT	1		98
7	*n*-$C_{17}H_{35}CSNH_2$	**2a**	EtOH	Reflux	24	*n*-$C_{17}H_{35}CN$	94
		2b	CH_2Cl_2	RT	1		92
8	Thionicotinamide	**2a**	EtOH	Reflux	24	3-Cyanopyridine	88
9	$C_6H_5NHCSNH_2$	**2a**	MeOH	Reflux	24	C_6H_5NHCN	85[a]
10	$(C_6H_5)_2NCSNH_2$	**2a**	MeOH	Reflux	8	$(C_6H_5)_2NCN$	88
		2b	CH_2Cl_2	RT	24		95
11	$C_6H_5NHCSNHC_6H_5$	**2a**	MeOH-CH_2Cl_2	RT	12	$C_6H_5NHCONHC_6H_5$	82
		2b	CH_2Cl_2	RT	3.5		94
12	$(CH_3)_2NCSN(CH_3)_2$	**2a**	AcOH	RT	12	$(CH_3)_2NCON(CH_3)_2$	66

a) Yield contained that (42%) of 2,4,6-triimino-1,3,5-triphenyl-hexahydro-1,3,5-triazine which was formed by ready trimerization of phenylcyanamide; Ref. 22.

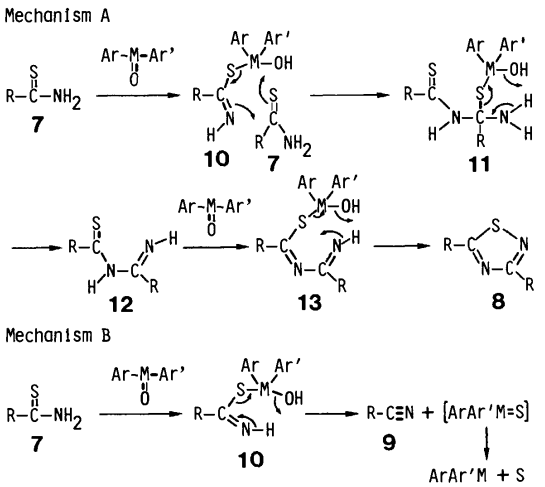

Scheme 3.

small amount of hydrochloric acid, forming instead 3,5-diphenyl-1,2,4-thiadiazole **8** (R=Ph) in 78% yield. In contrast, some of oxidative dimerizations with polymeric telluroxide **2b** in acetic acid competed with dehydrosulfurizations because of its relatively stronger oxidizing ability, indicating that the selectivity of either pathway A or B depends on a subtle balance of steric and electronic effects.

It has been thus understood that polymer-supported diaryl selenoxide **2a** and telluroxide **2b** like monomeric counterparts **1a** and **1b** behave as mild and selective oxidizing agents and complement each other owing to their different reactivities. In addition, they have turned out to effect novel solvent-dependent reactions of thioamides involving thioureas to 1,2,4-thiadiazoles or to nitriles. Although several methods for the oxidative dimerization of thioamides to 1,2,4-thiadiazoles[15] and for the dehydrosulfurization of thioamides to nitriles,[16] have so far been developed, they require relatively severe reaction conditions or highly reactive reagents which may affect other functional groups. The present methods using polymer-supported reagents **2a** and **2b** conveniently complement the preceding procedures, because of their wide applicability, high selectivity, and operational simplicity.

Experimental

Material. Polystyrene resin used in this research was 1% divinylbenzene-styrene copolymer, Bio-Beads S-Xl, purchased from Bio-Rad Laboratories. It was converted into poly(*p*-lithiostyrene) **3** according to the procedure of Farrall and Fréchet.[10] Most of the substrates examined in the oxidations with polymeric reagents **2a** and **2b** were commercially available. Thiobenzophenone, thiofenchone, thiocamphor, and methyl thiobenzoate (Runs **1**—3,6 of Table 2) were obtained from reactions of the corresponding ketones[17] and ester[18] with Lawesson's reagent, 2,4-bis(4-methoxyphenyl)-**1**,3-dithia-2,4-diphosphetane-2,4-disulfide. 4,5-Bis(methylthio)-**1**,3-dithiole-2-thione (Run 5 of Table 2) was accessible from reaction of carbon disulfide with sodium, followed by methyl iodide.[19] Substituted thiobenzamides, phenylethanethioamide, and octadecanethioamide (Runs 2—7 of Table 4) were obtained from reactions of the corresponding amides with phosphorus pentasulfide in dioxane.[16]

Preparation of Polymeric Selenide 5a. Poly(*p*-lithiostyrene) resin **3**, in situ prepared from 5.0 g of partially brominated polystyrene containing 3.0 mequiv of bromine per gram,[10] was swollen in 50 ml of dry THF in a nitrogen atmosphere. After a solution of *p*-methoxyphenyl selenocyanate **4a**[11] (5.1 g, 24 mmol) in 10 ml of dry THF was added, the slurry was stirred at room temperature for 30 min and then at 60 °C overnight. The resin was collected by filtration, and washed successively with THF, 1:1 THF-water, water, again THF, and finally MeOH. After dryness under reduced pressure at 60 °C, a light brown resin of selenide **5a** (5.69 g) was obtained. Elemental analysis for selenium revealed that the resin contained 1.5 mequiv of Se per gram.

Preparation of Polymeric Selenoxide 2a. A solution of bromine (1.92 g, 12 mmol) in 10 ml of CCl_4 was dropwise added into a suspension of the resin **5a** (5.0 g) swollen in 30 ml of CCl_4. The slurry was stirred at room temperature for 4.5 h. The resulting selenium dibromide **6a** was collected by filtration, and washed successively with CCl_4 and THF. It was then mixed with 50 ml of THF and 10 ml of 15% NaOH aq, and refluxed overnight. The resin was collected by filtration, and washed once with THF, repeatedly with 1:10 THF-water until the washings turned neutral, and finally with MeOH. After dryness under reduced pressure at 60 °C, a light brown resin of selenoxide **2a** (4.9 g) was obtained. IR (KBr disk); 820 cm^{-1} (Se=O).

Preparation of Polymeric Telluride 5b. In a similar manner as described for polymeric selenide **5b**, a reddish yellow resin of telluride **5b** (8.05 g) was obtained from reaction of poly(*p*-lithiostyrene) **3**, in situ generated from 8.0 g brominated polystyrene (3.0 mequiv of bromine per gram), and *p*-methoxyphenyl tellurocyanate **4b**[12] (8.0 g, 31 mmol). Elemental analysis for C (75.50%) and H (6.11%) indicated that the resin contained the degree of 1.3 mequiv functionalization per gram.

Preparation of Polymeric Telluroxide 2b. In the quite same way as described for the preparation of polymeric selenoxide **2a**, a brown resin of telluroxide **2b** (8.1 g) was obtained via tellurium dibromide **6b** from telluride **5b** (8.0 g).

General Procedure for Oxidations with Polymeric Selenoxide 2a or Telluroxide 2b. An oxidizable substrate (0.5 mmol) was mixed with 20% excess of polymeric reagent **2a** or **2b** swollen in 10 ml of a solvent specified for each reaction. The mixture was treated under such conditions as described in Tables 1, 2, 3, or 4. After the reaction was completed, the spent reagent was removed by suction filtration, and washed throughly with the same solvent as used in the reaction. The filtrate and washings were combined and concentrated in vacuo. The residue was subjected to short column chromatography on silica gel or gel permeation liquid chromatography to give the corresponding pure product. All the products were characterized by comparison of their melting points and spectral data with those of the authentic samples, which were commercially available except divinyl disulfide (Run 3 of Table 2),[8] 1,3-dithiolan-2-one (Run 4 of Table 2),[20] 4,5-bis(methylthio)-1,3-dithiol-2-one (Run 5 of Table 2),[21] 3,5-diphenyl-1,2,4-thiadiazole (Run **1** of Table 3),[7] 3,5-bis(*p*-chlorophenyl)-**1**,2,4-thiadiazole (Run 2 of Table 3),[21] 3,5-bis(diphenylamino)-**1**,2,4-thiadiazole (Run 3 of Table 3),[7] 5-imino-4-phenyl-3-phenylamino-4,5-dihydro-1,2,4-thiadiazole (Run 4 of Table 3),[7] phenylcyanamide (Run 9 of Table 4),[22] and diphenylcyanamide (Run 10 of Table 4).[23]

References

1) For excellent reviews on organoselenium chemistry, see D. L. J. Clive, *Tetrahedron*, **34**, 1049 (1978); H. J. Reich, *Acc. Chem. Res.*, **12**, 22 (1979); K. C. Nicolaou, *Tetrahedron*, **37**, 4097 (1981); J. V. Comasseto, *J. Organomet. Chem.*, **253**, 131 (1983); D. Liotta, *Acc. Chem. Res.*, **17**, 28 (1984).

2) For excellent reviews on organotellurium chemistry, see K. J. Irgolic, *J. Organomet. Chem.*, **103**, 91 (1975); ibid., **130**, 411 (1977); ibid., **158**, 235, 267 (1978); ibid., **189**, 65 (1980); ibid., **203**, 367 (1980).

3) R. Michels, M. Kato, and W. Heitz, *Makromol. Chem.*, **177**, 2311 (1976); M. Kato, R. Michels, and W. Heitz, *J. Polym. Sci., Polym. Lett. Ed.*, **14**, 413 (1976).

4) G. Zundel, *Angew. Chem., Int. Ed. Engl.*, **8**, 499 (1969); R. T. Taylor and L. A. Flood, *J. Org. Chem.*, **48**, 5160 (1983).

5) D. Barnard and D. T. Woodbridge, *Chem. Ind. (London)*, **1959**, 1603.

6) K. Balenović, R. Lazic, V. Polak, and P. Stern, *Bull. Sci., Cons. Acad. Sci. Arts RSF Yougoslavia Sect. A*, **17**, 147 (1972); N. Bregant, I. Perina, and K. Balenović, ibid., **17**, 148 (1972); K. Balenović, N. Bregant, and I. Perina, *Synthesis*, **1973**, 172; I. Perina, N. Bregant, and K. Balenović, *Bull. Sci., Cons. Acad. Sci. Arts RSF Yougoslavia Sect. A*, **18**, 3, 4 (1973); M. Poje and K. Balenović, ibid., **20**, 1 (1975); V. I. Naddaka, V. P. Gar'Kin, and V. I. Minkin, *Zh. Org. Khim.*, **12**, 2481 (1976); S. Tamagaki, I. Hatanaka, and S. Kozuka, *Bull. Chem. Soc. Jpn.*, **50**, 3421 (1977); M. Mikołajczyk and J. Łuczak, *J. Org. Chem.*, **43**, 2132 (1978); J. P. Marino and A. Schwartz, *Tetrahedron Lett.*, **1979**, 3253; A. G. Abatjoglou and D. R. Bryant, ibid., **22**, 2051 (1981); K. Takaki, M. Yasumura, and K. Negoro, *J. Org. Chem.*, **48**, 54 (1983); L. Syper and J. Młochowski, *Synthesis*, **1984**, 747.

7) F. Ogura, H. Yamaguchi, T. Otsubo, and T. Tanaka, *Bull. Chem. Soc. Jpn.*, **55**, 641 (1982); F. Ogura, T. Otsubo, K. Ariyoshi, and H. Yamaguchi, *Chem. Lett.*, **1983**, 1833; K. Ariyoshi, Y. Aso, T. Otsubo, and F. Ogura, *Chem. Lett.*,

1984, 891.

8) D. H. R. Barton, S. V. Ley, and C. A. Meerholz, *J. Chem. Soc., Chem. Commun.*, **1979**, 755; S. V. Ley, C. A. Meerholz, and D. H. R. Barton, *Tetrahedron Lett.*, **21**, 1785 (1980); *Tetrahedron*, **37**, 213 (1981).

9) A preliminary research on oxidations with polymeric selenoxide **2a** was presented in an earlier communication; N. X. Hu, Y. Aso, T. Otsubo, and F. Ogura, *Chem. Lett.*, **1985**, 603.

10) M. J. Farrall and J. M. J. Fréchet, *J. Org. Chem.*, **41**, 3877 (1976).

11) O. Behaghel and M. Rollmann, *J. Prakt. Chem.*, **123**, 336 (1929).

12) S. J. Falcone and M. P. Cava, *J. Org. Chem.*, **45**, 1044 (1980).

13) A. salt-like selenoxide-acetic acid complex $Ar_2\overset{+}{S}e\,OH\cdot\overline{O}Ac$ was considered to be an active reagent for the oxidations of sulfides to sulfoxides, because the reactions occurred only in acetic acid (Ref. 5). The inactivity of telluroxide for such reactions seems to be due to the rather higher stability of its acid complex.

14) F. Kurzer already reported that thiadiazole **8** could be formed by oxidation of an intermediate **12**; *J. Chem. Soc.*, **1955**, 1.

15) Y. Takikawa, K. Shimada, K. Sato, and S. Sato, *Bull. Chem. Soc. Jpn.*, **58**, 995 (1985) and references cited therein.

16) M. Lim, W. Ren, and R. S. Klein, *J. Org. Chem.*, **47**, 4594 (1982) and references cited therein.

17) B. S. Pedersen, S. Scheibye, N. H. Nilsson, and S. O. Lawesson, *Bull. Soc. Chim. Belg.*, **87**, 223 (1978).

18) S. L. Baxter and J. S. Bradshaw, *J. Org. Chem.*, **46**, 831 (1981).

19) G. Steinmecke, H. J. Sieler, R. Kiemese, and E. Hoyer, *Phosphorus Sulfur*, **7**, 49 (1979).

20) F. N. Jones and S. Andreades, *J. Org. Chem.*, **34**, 3011 (1969).

21) H. Klaus, K. Thomas, Q. Josef, and M. Rudolf, *Chem. Ber.*, **113**, 1898 (1980).

22) A. W. Hofmann, *Ber.*, **18**, 3217 (1885).

23) J. V. Braun, *Ber.*, **33**, 1438 (1900).

 © 1986 The Chemical Society of Japan Bull. Chem. Soc. Jpn., 59, 885—891 (1986)

2-Allylisourea as an Effective Agent for Direct α-Allylation of Ketone and Aldehyde Assisted by Palladium(0) under Neutral Conditions

Yoshio INOUE,* Masanori TOYOFUKU, Masaaki TAGUCHI, Shin-ichi OKADA, and Harukichi HASHIMOTO
Department of Applied Chemistry, Faculty of Engineering, Tohoku University, Aoba, Aramaki, Sendai 980
(Received October 23, 1985)

Direct α-allylation of a variety of ketones and aldehydes with 2-allylisourea took place in the presence of a catalytic amount of a palladium(0) complex under neutral and mild conditions. Scope and limitations of this novel method have been investigated.

The palladium-assisted allylation of active hydrogen compounds of pK_a's 10—17 is known to take place smoothly with a variety of allylic compounds,[1a] i.e., esters,[1b] ethers,[1b] alcohols,[1b] amines,[1b] sulfones,[1c] ammonium halides,[1d] sulfonium halides,[1d] nitro derivatives,[1e] and phosphates.[1f] The reaction pathway via π-allylpalladium intermediates is widely accepted.[1a] Usually the reaction is carried out under basic conditions to convert the active hydrogen compounds into their conjugate bases. However alkali metal enolates derived from ketones tend not to readily undergo this allylation.[2] Several improvement have been made including the change of the palladium catalyst[3] and metal enolates used.[4] Recently decarboxylative α-allylation of ketones under neutral conditions using allyl keto carboxylates and allyl enol carbonates have also been exploited.[5]

2-Alkylisourea can be used as the alkylating agent[6] for active hydrogen compounds such as hydrogen chloride, carboxylic acids, phenols, and imides. 2-Allylisourea is employed as an agent for the palladium-catalyzed allylation of imides[6f] and amides.[6g] Previously, we reported briefly that 2-allyl-1,3-dicyclohexylisourea (**1**) was an effective agent for

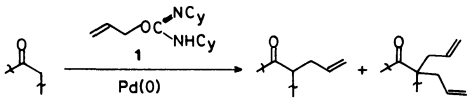

α-allylation of simple ketones.[7] That is the first example of the direct α-allylation of ketone assisted by palladium(0) under neutral conditions. A likely mechanism is as follows. The isourea **1** oxidatively adds to palladium(0) to afford a π-allylpalladium complex and the isourea anion. The anion thus formed is basic enough to abstract an α-proton of a ketone to produce the ketone enolate. Then the enolate attacks the π-allyl group on the palladium to afford the observed product.

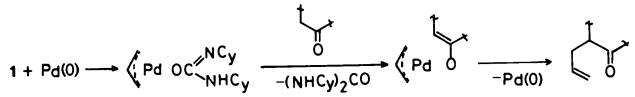

In this paper, we report the extension of this method to a variety of ketones and aldehydes and also describe the related reactions.

Results and Discussion

2-Allylic-substituted isoureas were prepared from allylic alcohols and dicyclohexylcarbodiimide (DCC) in the presence of a catalytic amount of copper(I) chloride.[8] The allylation reaction was carried out simply by mixing a substrate (1.0 equiv) and an allylic-substituted isourea (1.0 equiv) in the presence of a palladium(0) complex combined with PPh_3 or $Ph_2PCH_2CH_2PPh_2$ (dppe) as the catalyst.

α-Allylation of Ketone. Initially, several reaction parameters were examined using cyclohexanone as a probe for α-allylation with **1**. The results are shown in Table 1. Allylation occurred selectively toward monoallylation in tetrahydrofuran (THF), 1,4-dioxane, diethylene glycol dimethyl ether (diglyme), benzene, and acetonitrile, but the yields were modest. The reaction proceeded efficiently in dipolar, aprotic solvents, i.e., dimethyl sulfoxide (DMSO), hexamethylphosphoric triamide (HMPT), and *N*,*N*-dimethylformamide (DMF). Although monoallylation was main in these solvents, considerable diallylation also took place. This effect of solvent was similar to that observed usually in the alkylation of the metal enolate of a ketone.[9]

The effect of ligand was examined in DMF solvent. Tributylphosphine completely suppressed the reaction. A moderate yield toward monoallylation resulted with triphenylphosphine as ligand. The allylation took place efficiently by the use of ditertiary phosphines [$R_2P(CH_2)_nPR_2$; R=Ph (n= 2, 3, 4), R=Me (n=2)]. Substantial diallylation occurred at the same time. The diarsine ligand $Ph_2As(CH_2)_2AsPh_2$ afforded a catalytically less active species. The effectiveness of the bidentate phosphine ligand has been demonstrated in the palladium-catalyzed allylation.[5c,10] The effect is ascribed to its tendency to generate a cationic (π-allyl)palladium intermediate which is more active than the neutral

Table 1. Allylation of Cyclohexanone with **1**[a)]

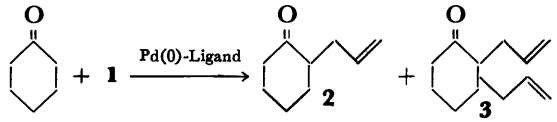

Solvent	Ligand	Temp °C	Time h	Product yield/%[b)] 2	3
THF	PPh_3	r.t.	5	13	0
	PPh_3	reflux	4 (2)[d)]	37 (56)[d)]	0 (5)[d)]
	dppe	reflux	3	41	3
1,4-Dioxane	PPh_3	reflux	2	20	0
Diglyme[c)]	PPh_3	60	1	13	0
Benzene	PPh_3	r.t.	48	9	0
Acetonitrile	PPh_3	r.t.	3	9	0
	PPh_3	60	5	37	10
	dppe	r.t.	3	15	0
HMPT	dppe	r.t.	1	56	42
DMSO	PPh_3	r.t.	4	78	22
	dppe	r.t.	0.25	65	35
DMF	PPh_3	r.t.	15	40	6
	PBu_3	60	3	0	0
	$Me_2P(CH_2)_2PMe$	r.t.	0.25	20	42
	$Ph_2P(CH_2)_nPPh_2$				
	$n=2$(dppe)	0	5	61	30
		r.t.	1	67	32
	$n=3$	r.t.	1	63	37
	$n=4$	r.t.	1	67	33
	$Ph_2As(CH_2)_2AsPh_2$	60	3	15	0

a) General procedure A. b) By GLC based on **1**. c) Diethylene glycol dimethyl ether. d) With addition of lithium acetate.

one toward nucleophilic reactions.[5c,11)]

Noteworthy is the inclination of THF as a solvent to afford a monoallylation product although the yield is unsatisfactory in general. In order to increase monoallylation, the effects of added inorganic salts, i.e., lithium acetate, sodium acetate, and lithium bromide, were examined with a [$Pd(PPh_3)_3$] catalyst. Addition of lithium acetate (0.16 equiv) afforded the monoallyl ketone in a significantly increasing yield. The formation of the diallyl ketone was only modest. In contrast, sodium acetate and lithium bromide did not gave influence respectably.

Enol trimethylsilyl ether from cyclohexanone also participated in the reaction involving 2-allylisourea. Somewhat slower reaction was observed compared to that of the original ketone with a slight increase in the mono/di ratio.

Table 2 shows the results of α-allylation of various ketones with **1** in DMF at ambient temperature in the presence of a palladium(0)-dppe catalyst. α,α-Diallylation predominated for acetone. Ethyl methyl ketone was allylated exclusively at the methylene carbon. These observations indicate that this allylation reaction involving **1** and ketone is controlled thermodynamically. Diethyl ketone afforded α-mono- and α,α'-diallylated products. Exclusive diallylation occurred for acetophenone. Propiophenone was selectively converted to the monoallylated product, whereas α-tetralone gave mainly the diallylation product. As a rule the allylation of simple ketones with **1** in DMF solvent by a palladium(0)-dppe catalyst afforded mainly or exclusively di- and trialkylated derivatives.

α,β-Unsaturated ketones, e.g., mesityl oxide and 2-cyclohexenone, reacted with **1** to produce α-allyl-β,γ-unsaturated ketones. Abstraction of the γ-hydrogen followed by allylation at the α-position will afford the observed products.

Usually α-alkylation of ketone with alkyl halide or sulfonate has been carried out using a strong base. Normally there are a number of obstacles; a) self-condensation; b) polyalkylation; c) non-regioselective alkylation for unsymmetrical ketones. The obstacle a) was completely eliminated by this neutral allylation means. Although palladium(0)-dppe was an effective catalyst in DMF solvent, polyallylation was usually accompanied. Effective monoallylation was accomplished only for propiophenone. A considerable improvement toward monoallylation of cyclohexanone was attained by the addition of

Table 2. Allylation of Ketone with **1**[a]

Ketone	Time/h	Product yield/%[b]
	5	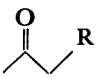 **4**: 8 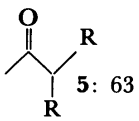 **5**: 63
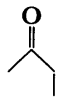	3	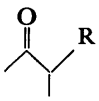 **6**: 51 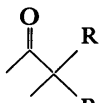 **7**: 33 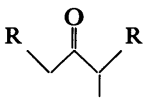 **8**: 7
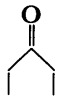	1	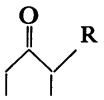 **9**: 37 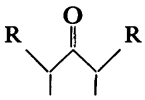 **10**: 43
	3	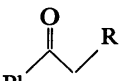 **11**: 4 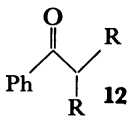 **12**: 96
	1	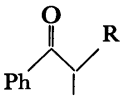 **13**: 90
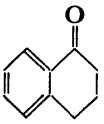	1	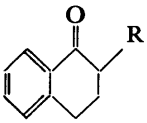 **14**: 17 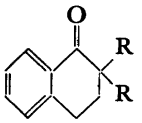 **15**: 67
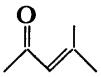	24	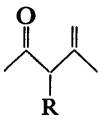 **16**: 45 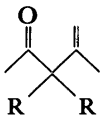 **17**: 22
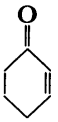	5	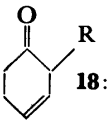 **18**: 31

a) General procedue B. R=allyl. b) Based on **1** by GLC.

Table 3. Allylation of Propiophenone with Allylic-Substituted Isourea[a]

Isourea	Temp °C	Yield %[b]	Product ratio %[c]
	r.t.	90[d]	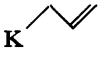 **13**: 100
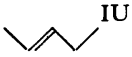	60	87	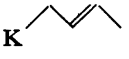 **19**: 60
			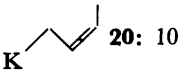 **20**: 10
			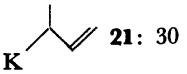 **21**: 30
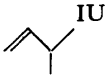	60	75	**19**: 62, **20**: 10, **21**: 28
	60	77	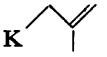 **22**: 100
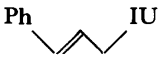	60	84	**23**: 78
			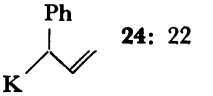 **24**: 22
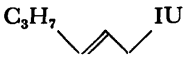	80	74	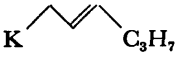 **25**: 93
			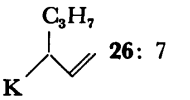 **26**: 7

a) General procedure C. IU=-OC(NHCy)(=NCy); Cy=cyclohexyl. K=PhCOCHCH$_3$. b) Isolated yield based on **1**. c) Determined by GLC. d) GLC yield.

lithium acetate with [Pd(PPh$_3$)$_3$] as the catalyst in THF solvent. Addition of lithium acetate was also effective to the other ketones. Thus, the monoallylation of diethyl ketone, acetophenone, and mesityl oxide increased from 5, 22, and 9% into 6, 34, and 20%, respectively (LiOAc, 0.2 equiv; [Pd(PPh$_3$)$_3$], THF, reflux, 2 h). As for the obstacle c), the regioselectivity of allylation is left to thermodynamic control.

Extension of this method was attempted intramolecularly to make a ring. The allylic isourea derived from 8-hydroxy-6-octen-2-one was submitted to the reaction at 100 °C for 2 h in DMF with a palladium(0)-dppe catalyst. However the only product isolated was 5,7-octadien-2-one (62% yield). Exclusive 1,4-elimination took place.

As propiophenone was selectively converted to the monoallylation product with 2-allylisourea, the regiochemistry with respect to the allylic group and the stereochemistry around the double bond were investigated with this ketone employing several 2-allylic-substituted isoureas. The results are summarized in Table 3. The less substituted site of the allylic system in the isourea reacted preferentially. The composition of the products from 2-(1-methyl-2-propenyl)isourea was analogous to that from (*E*)-2-butenylisourea. This indicates that the intermediate from each should be same. Initial (*E*)-geometry around the double bond was retained during the reaction except for the partial loss observed in the (*E*)-2-butenylisourea case. These results support the intermediacy of a π-allylpalladium species having the *syn*-configuration predoninantly.[12]

Unfortunately, the allylation involving γ,γ-disubstituted allylic system, i.e., prenyl and geranyl, did not occur by a palladium(0)-dppe catalyst. Instead 1,4-elimination of the isoureas proceeded exclusively to afford isoprene and myrcene/ocimene, respectively. Several papers dealt with 1,4-elimination of allylic compounds to dienes by palladium catalysts.[13] For comparison, we studied the 1,4-elimination of geranyl- and nerylisourea in the absence of ketone in some detail. Geranylisourea was converted to myrcene, (*E*)-, and (*Z*)-ocimene in the ratio 24:58:18 (DMF, 120 °C, 5 h; total yield 67%). Another experiment in THF afforded the same products in the ratio 67:21:12 (r.t., 48 h; total yield 99%). Nerylisourea gave the trienes in the ratio 77:16:7 (DMF, 120 °C, 5 h; total yield 58%). Thus the selectivity of the 1,4-elmination reaction involving allylic isourea was comparable to that involving allylic acetate,[13a] but was not to be compared with that involving allylic acetate and organozinc compounds.[13c]

Allylation of Aldehyde. Results are shown in Table 4. Generally direct alkylation of aldehydes with alkyl halide is not possible, because base treatment of aldehydes normally gives rapid aldol condensations. Only those aldehydes bearing one α-hydrogen have been alkylated in moderate yield by the use of a phase-transfer catalyst.[14] The present method enabled the effective allylation of cyclohexanecarbaldehyde having one α-hydrogen. Diallylation was predominant for butanal with a [$Pd(PPh_3)_3$] catalyst in DMF as solvent. The results obtained here were remarkable because aldol condensation was not observed. The reaction of butanal in THF solvent was very sluggish to afford monoallylation product in a low yield (<7%). With dppe as ligand, both α,α-diallylation and aldol-type condensation of butanal took place in DMF solvent. α,β-Unsaturated aldehyde, i.e., (*E*)-2-hexenal, was also α,α-diallylated giving a β,γ-unsaturated aldehyde.

In order to get the scope and the limitations of this neutral allylation method, various types of compounds were subjected to the reaction. Simple esters, nitriles, and 1-alkynes did not participate in this allylation under the standard reaction conditions (Pd(0)-dppe, DMF, r.t., 3 h), the pK_a values for which are higher than 24. In contrast, methyl phenylacetate and phenylacetonitrile were reactive to afford 2-phenyl-4-pentenoate (91%) and 2-phenyl-4-pentenenitrile (27%)/ 2-allyl-2-phenyl-4-pentenenitrile (34%)/ *N*-allylphenylethenimine (29%), respectively. Thus the introduction of a phenyl group facilitated the reaction. Indene (pK_a 20) and fluorene (pK_a 23) were reactive to yield 3-allyl-1*H*-indene (61%, monoallylation followed by the double bond isomerization)/ 1,1-diallyl-1*H*-indene (14%, diallylation) and 9-allyl-9*H*-fluorene (43%)/ 9,9-diallyl-9*H*-fluorene (51%), respectively. In the suggested scheme described earlier, the isourea anion generated in situ functions as a base to abstract a proton from the nucleophile. Although the exact pK_a value for the conjugate acid of the isourea anion is not available from current literatures, it seems probable that the generation of the conjugate anion is not sufficient for the compound of pK_a value higher than 24.

Table 4. Allylation of Aldehyde with **1**[a]

Aldehyde	Ligand	Time / h	Product yield / %[b]
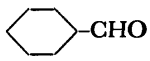	dppe	1	**27**: 92
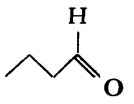	PPh_3	1	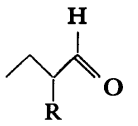 Trace
			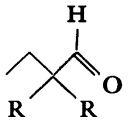 **28**: 41
	dppe	2	**28**: 29
			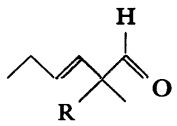 **29**: 41
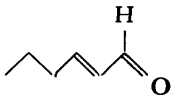	dppe	2	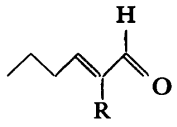 **30**: 15
			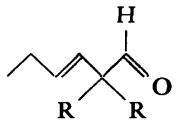 **31**: 61
	PPh_3	20	**30**: Trace, **31**: 63

a) General procedure D. R=allyl. b) GLC yield based on **1**.

Experimental

General. IR spectra were recorded on a Shimadzu IR 430 spectrometer. ^1H and ^{13}C NMR spectra were measured on a JEOL JNM-FX60Q and/or a Hitachi R-24A instrument using $CDCl_3$ as the solvent. The chemical shifts are expressed in parts per million downfield from the internal tetramethylsilane, and signal patterns are indicated as s, singlet; d, doublet; t, triplet; q, quartet; qu, quintet; m, multiplet. Mass spectra were recorded on a JEOL D-300 instrument. GLC analyses were performed on either Shimadzu GC-3AH, Shimadzu GC-6AM, or Hitachi 164 instrument, using the following columns: Column A, 20% Silicone DC-550, 3 m; Column B, 10% FFAP, 3 m; Column C, 20% Silicone GE SE-52, 2 m; Column D, 3% Silicone OV-1, 2 m.

Materials. 2-Allylic-substituted isoureas were prepared according to the published method.[8] An allylic alcohol (0.1 mol) and DCC (0.1 mol) were heated at 60—80 °C in the presence of a catalytic amount of copper(I) chloride (70 mg) till the absorptions of DCC disappeared in the IR spectrum. The reaction mixture was diluted with dicloromethane and filtered. The filtrate was washed with aqueous ammonia solution to remove the catalyst. The organic layer was washed with water, and dried over sodium sulfate. Although the isoureas thus obtained could be distilled under high vacuum (~10^{-4} mmHg*), they were sufficiently pure for the present allylation reactions.

General Procedure A for Allylation of Cyclohexanone with 1 (Table 1). Cyclohexanone (491 mg, 5 mmol) and **1** (1.32 g, 5 mmol) were reacted in a given solvent (10 cm^3) in the presence of a palladium catalyst under the conditions described in Table 1 under nitrogen. The palladium catalyst employed was $[Pd(PPh_3)_3]$[15] (89 mg, 0.1 mmol) or $[Pd(dba)_2]$[16] (58 mg, 0.1 mmol)-ligand (ligand/Pd=3 for the monodentate ones; ligand/Pd=1 for the bidentate ones). The reaction was analyzed by GLC (column A, 150 °C). Analytical samples were obtained by preparative GLC (column C, 140 °C).

2-Allyl-1-cyclohexanone (2): ^{1}H NMR δ=1.00—2.80 (m, 11H), 4.80—5.30 (m, 2H), 5.35—6.30 (m, 1H). ^{13}C NMR δ=212.17, 136.44, 116.11, 50.28, 42.02, 37.77, 33.37, 27.90, 24.94. IR (neat) 3080, 1710, 1640, 990, 910 cm^{-1}.

A Mixture of 2,2- and 2,6-Diallyl-1-cyclohexanone (3): ^{1}H NMR δ=1.08—2.65 (m, ca. 8H), 2.21—2.43 (m, ca. 4H), 4.70—5.18 (m, 4H), 5.36—6.18 (m, 2H). IR (neat) 3080, 1700, 1640, 990, 910 cm^{-1}.

Allylation of Cyclohexanone with 1 with Addition of Lithium Acetate. A mixture of the isourea **1** (5 mmol), cyclohexanone (5 mmol), $[Pd(PPh_3)_3]$ (0.1 mmol), and lithium acetate (53 mg, 0.8 mmol) was stirred for 2 h in refluxing THF (10 cm^3). GLC analysis (column A, 150 °C) showed that the yields of mono- and diallylcyclohexanone were 56 and 5%, respectively.

General Procedure B for Allylation of Ketones with 1 (Table 2). A DMF solution (10 cm^3) of a ketone (5 mmol) and **1** (1.32 g, 5 mmol) was stirred for 1—24 h at an ambient temperature in the presence of $[Pd(dba)_2]$ (58 mg, 0.1 mmol)-dppe (40 mg, 0.1 mmol) under nitrogen. The reaction was analyzed by GLC. Analytical samples were obtained by either preparative GLC (G) or column chromatography (C) on silica gel according to general procedure C. The products **4**,[17] **11**,[18] and **13**[18] were identified by the comparison of their ^{1}H NMR and IR spectra with those reported earlier.

3-Allyl-5-hexen-2-one (5): G (column A, 160 °C). ^{1}H NMR δ=2.18 (s, 3H), 2.20—2.40 (m, 4H), 2.40—2.92 (m, 1H), 4.80—5.18 (m, 4H), 5.38—6.02 (m, 2H). IR (neat) 1718, 1640, 990, 918 cm^{-1}.

3-Methyl-5-hexen-2-one (6): G (column A, 160 °C). ^{1}H NMR δ=1.07 (d, 3H), 2.09 (s, 3H), 1.93—3.00 (m, 3H), 4.80—5.45 (m, 2H), 5.39—6.09 (m, 1H). IR (neat) 3090, 1708, 1640, 985, 910 cm^{-1}.

3-Allyl-3-methyl-5-hexen-2-one (7): G (column A, 160 °C). ^{1}H NMR δ=1.08 (s, 3H), 2.06 (s, 3H), 2.20—2.35 (m, 4H), 4.80—5.18 (m, 4H), 5.36—6.07 (m, 2H). IR (neat) 3090, 1708, 1640, 990, 910 cm^{-1}.

4-Methyl-1,8-nonadien-5-one (8): G (column A, 160 °C). ^{1}H NMR δ=0.99 (d, 3H), 1.80—2.86 (m, 7H), 4.78—5.20 (m, 4H), 5.34—6.10 (m, 2H). IR (neat) 3080, 1708, 1640, 990, 910 cm^{-1}. MS (70 eV) *m/z* 152 (M^+), 109, 83, 69, 67, 55.

4-Methyl-6-hepten-3-one (9): G (column A, 150 °C). ^{1}H NMR δ=1.08 (d, 3H), 1.10 (t, 3H), 2.54 (q, 2H), 2.05—2.96 (m, 3H), 4.81—5.20 (m, 2H), 5.40—6.25 (m, 1H). ^{13}C NMR δ=214.17, 135.76, 116.56, 47.74, 34.45, 32.24, 16.17, 7.69. IR (neat) 3080, 1710, 1640, 990, 910 cm^{-1}.

4,6-Dimethyl-1,8-nonadien-5-one (10): G (column A, 150 °C). ^{1}H NMR δ=1.03 (dd, 6H), 1.56—2.58 (m, 6H), 4.80—5.16 (m, 4H), 5.32—6.03 (m, 2H). IR (neat) 3070, 1708, 1640, 990, 910 cm^{-1}.

1-Phenyl-2-allyl-4-penten-1-one (12): C (benzene). ^{1}H NMR δ=2.05—2.85 (m, 4H), 3.75 (qu, 1H), 4.77—5.20 (m, 4H), 5.30—6.07 (m, 2H), 7.19—8.00 (m, 5H). IR (neat) 3080, 1680, 1640, 1580, 1445, 990, 910 cm^{-1}.

2-Allyl-3,4-dihydro-1(2*H*)-naphthalenone (14): C (hexane/ethyl acetate=20). ^{1}H NMR δ=1.76—2.84 (m, 5H), 2.88—3.25 (dd, 2H), 4.89—5.41 (m, 2H), 5.49—6.20 (m, 1H), 7.10—8.23 (m, 4H). IR (neat) 3070, 1680, 1640, 990, 910 cm^{-1}.

2,2-Diallyl-1(2*H*, 3*H*, 4*H*)-naphthalenone (15): C (hexane/ethyl acetate=20). ^{1}H NMR δ=2.13 (t, 2H), 2.50 (t, 4H), 3.09 (t, 2H), 4.86—5.51 (m, 4H), 5.55—6.29 (m, 2H), 7.08—8.29 (m, 4H). IR (neat) 3070, 1675, 1640, 990, 910 cm^{-1}.

3-Isopropenyl-5-hexen-2-one (16): G (column C, 140 °C). ^{1}H NMR δ=1.64 (m, 3H), 2.10 (s, 3H), 2.40 (t, 2H), 3.18 (t, 1H), 4.76—5.18 (m, 4H), 5.36—6.08 (m, 1H). IR (neat) 3070, 1710, 1640, 990, 890 cm^{-1}. MS (70 eV) *m/z* 138 (M^+), 97, 95, 81, 67.

3-Allyl-3-isopropenyl-5-hexen-2-one (17): G (column C, 140 °C). ^{1}H NMR δ=1.64 (m, 3H), 2.02 (s, 3H), 2.43 (d, 4H), 4.74—5.40 (m, 6H), 5.44—6.08 (m, 2H). IR (neat) 1710, 1640, 990, 890 cm^{-1}. MS (70 eV) *m/z* 178 (M^+), 136, 93, 83, 81, 55.

2-Allyl-3-cyclohexen-1-one (18): G (column C, 140 °C). ^{1}H NMR δ=1.80—2.75 (m, 7H), 4.75—5.20 (m, 2H), 5.21—6.21 (m, 3H). IR (neat) 3090, 1710, 1640, 990, 912 cm^{-1}. MS (70 eV) *m/z* 136 (M^+), 108, 80, 79, 68.

General Procedure C for Allylation of Propiophenone with Allylic-Substituted Isourea (Table 3). A DMF solution (10 cm^3) of propiophenone (671 mg, 5 mmol) and an allylic-substituted isourea (5 mmol) was stirred for 1 h in the presence of $[Pd(dba)_2]$ (58 mg, 0.1 mmol)-dppe (40 mg, 0.1 mmol) at a given temperature under nitrogen. After being cooled to room temperature, the reaction mixture was diluted with diethyl ether and the *N,N'*-dicyclohexylurea that was formed was filtered off. The filtrate was washed with saturated NaCl solution. The organic layer was dried on $MgSO_4$ and the solvent was removed in vacuo. The products were isolated by column chromatography on silica gel (hexane/ethyl acetete=20). The isomer ratio was determined by GLC.

Reaction of Propiophenone with (*E*)-2-Butenylisourea: A Typical Procedure. Propiophenone (671 mg, 5 mmol) and (*E*)-2-butenylisourea (1.39 g, 5 mmol) were stirred in DMF (10 cm^3) at 60 °C for 1 h under nitrogen in the presence of

* 1 mmHg=133.322 Pa.

[Pd(dba)$_2$] (58 mg, 0.1 mmol)-dppe (40 mg, 0.1 mmol). The products were obtained according to the general procedure C after purification by column chromatography on silica gel eluting with hexane–ethyl acetate (20:1). Yield 818 mg (87%). Samples for spectroscopic analysis of the isomers **19**, **20**, and **21** were obtained by preparative GLC (column B, 160 °C).

(*E*)-2-Methyl-1-phenyl-4-hexen-1-one (19): G. ^{1}H NMR δ=1.16 (d, 3H), 1.60 (d, 3H), 1.90—2.70 (m, 2H), 3.10—3.80 (m, 1H), 5.20—5.60 (m, 2H), 7.26—8.00 (m, 5H). IR (neat) 1680, 965 cm^{-1}. MS *m/z* (70 eV) 188 (M$^+$), 173, 145, 134, 106, 105, 77.

(*Z*)-Isomer (20): G. This was isolated in an impure state, being contaminated by the (*E*)-isomer. ^{1}H NMR δ=1.20 (d, 3H), 1.60 (d, 3H), 2.12—2.56 (m, 2H), 3.20—3.72 (m, 1H), 5.24—5.56 (m, 2H), 7.17—8.04 (m, 5H). IR (neat) 1680 cm^{-1}. MS *m/z* (70 eV) 188 (M$^+$), 105, 77.

2,3-Dimethyl-1-phenyl-4-penten-1-one (21): G. ^{1}H NMR δ=1.00 (d, 3H), 1.12 (d, 3H), 2.28—2.96 (m, 1H), 3.04—3.80 (m, 1H), 4.76—5.16 (m, 2H), 5.40—6.12 (m, 1H), 7.18—8.05 (m, 5H). IR (neat) 1680, 990, 910 cm^{-1}. MS (70 eV) *m/z* 188 (M$^+$), 134, 106, 105, 77.

2,4-Dimethyl-1-phenyl-4-penten-1-one (22): C (hexane/ethyl acetate=20). ^{1}H NMR δ=1.16 (d, 3H), 1.72 (s, 3H), 2.03—2.80 (m, 2H), 3.17 (q, 1H), 4.71 (m, 2H), 7.25—8.03 (m, 5H). IR (neat) 1685, 1655, 890 cm^{-1}. MS (70 eV) *m/z* 188 (M$^+$), 106, 105, 83, 77.

(*E*)-2-Methyl-1,5-diphenyl-4-penten-1-one (23): G (column D, 200 °C). ^{1}H NMR δ=1.16 (d, 3H), 1.96—2.92 (m, 2H), 3.16—3.80 (m, 1H), 6.08 (dt, 1H), 6.36 (d, 1H), 6.92—8.04 (m, 10H). IR (neat) 1680, 960 cm^{-1}. MS *m/z* (70 eV) 250 (M$^+$), 235, 117, 115, 105.

2-Methyl-1,3-diphenyl-4-penten-1-one (24): G (column D, 200 °C). ^{1}H NMR δ=1.24 (d, 3H), 3.60—3.96 (m, 2H), 4.68—5.28 (m, 2H), 5.60—6.18 (m, 1H), 6.88—8.08 (m, 10H). IR (neat) 1680, 990, 910 cm^{-1}. MS (70 eV) *m/z* 250 (M$^+$), 235, 117, 105, 77.

(*E*)-2-Methyl-1-phenyl-4-octen-1-one (25): G (column D, 160 °C). ^{1}H NMR δ=0.84 (t, 3H), 1.20 (d, 3H), 1.10—1.60 (m, 2H), 1.68—2.76 (m, 4H), 3.16—3.80 (m, 1H), 5.20—5.55 (m, 2H), 7.25—8.08 (m, 5H). IR (neat) 1680, 965 cm^{-1}. MS *m/z* (70 eV) 216 (M$^+$), 173, 134, 106, 105, 77.

2-Methyl-1-phenyl-3-vinylhexan-1-one (26): G (column D, 160 °C). ^{1}H NMR δ=0.80 (t, 3H), 1.10 and 1.14 (d, 1.5H and d, 1.5H; due to the asymmetric carbon), 1.04—1.60 (m, 4H), 2.16—2.72 (m, 1H), 3.10—3.90 (m, 1H), 4.60—5.20 (m, 2H), 5.24—5.96 (m, 1H), 7.36—8.08 (m, 5H). IR (neat) 1680, 995, 910 cm^{-1}. MS (70 eV) *m/z* 216 (M$^+$), 173, 134, 105, 77.

General Procedure D for Allylation of Aldehydes with 1 (Table 4). A DMF solution (10 cm^3) of an aldehyde (5 mmol) and **1** (1.32 g, 5 mmol) was stirred for 1—20 h at an ambient temperature in the presence of [Pd(PPh$_3$)$_3$] (89 mg, 0.1 mmol) or [Pd(dba)$_2$] (58 mg, 0.1 mmol)-dppe (40 mg, 0.1 mmol) under nitrogen. The reaction was analyzed by GLC. Analytical samples were obtained by preparative GLC.

1-Allylcyclohexanecarbaldehyde (27): G (column C, 140 °C). ^{1}H NMR δ=1.10—2.01 (m, 8H), 2.15 (d, 2H), 4.80—5.22 (m, 2H), 5.26—6.07 (m, 1H), 9.44 (s, 1H). IR (neat) 3070, 1725, 1640, 990, 910 cm^{-1}.

2-Allyl-2-ethyl-4-pentenal (28): G (column C, 140 °C). ^{1}H NMR δ=0.85 (t, 3H), 1.58 (q, 2H), 2.27 (d, 4H), 4.85—5.33 (m, 4H), 5.35—6.14 (m, 2H), 9.42 (s, 1H). IR (neat) 3080, 1725, 1640, 990, 910 cm^{-1}.

(*E*)-2-Allyl-2-ethyl-3-hexenal (29): G (column C, 140 °C). ^{1}H NMR δ=0.82 (t, 3H), 0.98 (t, 3H), 1.65 (q, 2H), 1.81—2.31 (m, 2H), 2.37 (d, 2H), 4.81—5.26 (m, 2H), 5.30—6.07 (m, 3H), 9.30 (s, 1H). ^{13}C NMR δ=202.83, 135.70, 127.95, 118.38, 117.88, 36.79, 36.16, 26.19, 25.51, 13.72, 7.97. IR (neat) 3080, 1725, 1645, 990, 970, 910 cm^{-1}.

Reaction of (*E*)-2-Hexenal with 1: A Typical Procedure. (*E*)-2-Hexenal (491 mg, 5 mmol) and **1** (1.32 g, 5 mmol) were stirred for 2 h in DMF (10 cm^3) at an ambient temperature under nitrogen in the presence of [Pd(dba)$_2$] (58 mg, 0.1 mmol)-dppe (40 mg, 0.1 mmol). A mixture of the starting aldehyde, **30**, and **31** was obtained according to the general procedure C after chromatographic work-up on silica gel eluting with hexane–ethyl acetate (20:1). Samples for spectroscopic analysis of the product **30** and **31** were obtained by GLC (column C, 170 °C). Quantitative analyses were performed on GLC (column C, 170 °C).

(*E*)-2-Allyl-2-hexenal (30): ^{1}H NMR δ=0.95 (t, 3H), 1.22—1.87 (m, 2H), 2.45 (q, 2H), 3.00 (d, 2H), 4.73—5.21 (m, 2H), 5.32—6.19 (m, 1H), 6.53 (t, 1H), 9.36 (s, 1H). The chemical shift (δ=9.36) of the formyl proton indicated the presence of an (*E*)-double bond.[19] IR (neat) 3080, 1685, 1640, 990, 910 cm^{-1}. MS (70 eV) *m/z* 138 (M$^+$), 95, 81, 79, 67, 53.

(*E*)-2,2-Diallyl-3-hexenal (31): ^{1}H NMR δ=0.99 (t, 3H), 1.80—2.40 (m, 2H), 2.38 (d, 4H), 4.83—5.26 (m, 4H), 5.36—6.12 (m, 4H), 9.37 (s, 1H). IR (neat) 3080, 1725, 1640, 995, 975, 915 cm^{-1}. MS (70 eV) *m/z* 178 (M$^+$), 137, 93, 79, 67.

References

1) a) Reviews: B. M. Trost, *Tetrahedron*, **33**, 2615 (1977). J. Tsuji, "Organic Synthesis with Palladium Compounds," Springer Verlag, Heidelberg (1980), p. 125; b) K. E. Atkins, W. E. Walker, and R. M. Manyik, *Tetrahedron Lett.*, **1970**, 3821; c) B. M. Trost, N. R. Schmuff, and M. J. Miller, *J. Am. Chem. Soc.*, **102**, 5975 (1980); d) T. Hirano, N. Yamada, Y. Ohshiro, and T. Agawa, *J. Organomet. Chem.*, **236**, 409 (1982); e) R. Tamura and L. S. Hegedus, *J. Am. Chem. Soc.*, **104**, 3727 (1982); N. Ono, I. Hamamura, and A. Kaji, *J. Chem. Soc., Chem. Commun.*, **1982**, 820; f) Y. Tanigawa, K. Nishimura, A. Kawasaki, and S. Murahashi, *Tetrahedron Lett.*, **23**, 5549 (1982).

2) B. M. Trost, *Acc. Chem. Res.*, **13**, 385 (1980).

3) M. C. Fiaud and J. L. Malleron, *J. Chem. Soc., Chem. Commun.*, **1981**, 1159.

4) a) B. M. Trost and E. Keinan, *Tetrahedron Lett.*, **21**, 2591 (1980); b) E. Negishi, H. Matsushita, S. Chatterjee, and R. A. John, *J. Org. Chem.*, **47**, 3188 (1982). c) J. Tsuji, I. Minami, and I. Shimizu, *Chem. Lett.*, **1983**, 1325.

5) a) T. Tsuda, Y. Chujo, S. Nishi, K. Tawara, and T. Saegusa, *J. Am. Chem. Soc.*, **102**, 6384 (1980); b) J. Tsuji, I. Minami, and I. Shimizu, *Tetrahedron Lett.*, **24**, 1793 (1983); c) J. Tsuji, I. Shimizu, I. Minami, Y. Ohashi, T. Sugiura, and K. Takahashi, *J. Org. Chem.*, **50**, 1523 (1985), and references cited therein.

6) a) E. Dabritz, *Angew. Chem., Int. Ed. Engl.*, **5**, 470 (1960); b) F. B. Dains, *J. Am. Chem. Soc.*, **21**, 136 (1899); c) E. Vowinkel, *Angew. Chem.*, **75**, 377 (1963); d) K. Yamauchi and

M. Kinoshita, *J. Chem. Soc., Dalton Trans. 1*, **1973**, 391; e) Y. Inoue, M. Taguchi, and H. Hashimoto, *Synthesis*, in press; f) Y. Inoue, M. Taguchi, M. Toyofuku, and H. Hashimoto, *Bull. Chem. Soc. Jpn.*, **57**, 3021 (1984); g) Y. Inoue, M. Taguchi, and H. Hashimoto, *Bull. Chem. Soc. Jpn.*, **58**, 2721 (1985).

7) Y. Inoue, M. Toyofuku, and H. Hashimoto, *Chem. Lett.*, **1984**, 1227.

8) E. Vowinkel and I. Büthe, *Chem. Ber.*, **107**, 1353 (1974).

9) D. Caine, "Alkylation and Related Reactions of Ketones and Aldehydes via Metal Enolates," in "Carbon-Carbon Bond Formation," ed by R. L. Augustine, Marcel Dekker Inc., New York and Basel (1979), Vol. 1, Chap. 2, p. 102.

10) M. C. Fiaud and J. L. Malleron, *Tetrahedron Lett.*, **21**, 259 (1980).

11) B. M. Trost, L. Weber, P. E. Strege, T. J. Fullerton, and T. J. Dietsche, *J. Am. Chem. Soc.*, **100**, 3416 (1978), and references cited therein.

12) It has been reported that a ketone enolate produced in situ adds to the π-allyl ligand trans to the palladium; J. C. Fiaud and L. Aribi-Zouioueche, *Tetrahedron Lett.*, **23**, 2279 (1982). In order to obtain stereochemical information on this reaction, we submitted an optically active 2-allylic-substituted isourea derived from *l-cis*-carveol[20] to the reaction with propiophenone. Unfortunately the only product isolated was a triene, 2-methyl-5-isopropenyl-1,3-cyclohexadiene (73% yield). 1,4-Elimination took place predominantly.

13) a) J. Tsuji, T. Yamakawa, M. Kaito, and T. Mandai, *Tetrahedron Lett.*, **1978**, 2075; b) K. Yamamoto, S. Suzuki, and J. Tsuji, *Bull. Chem. Soc. Jpn.*, **54**, 2541 (1981); c) B. M. Trost, T. R. Verhoeven, and J. M. Fortunak, *Tetrahedron Lett.*, **1979**, 2301; d) T. Mandai, H. Yasuda, M. Kaito, J. Tsuji, R. Yamaoka, and H. Fukami, *Tetrahedron*, **35**, 309 (1979); e) H. Matsushita and E. Negishi, *J. Org. Chem.*, **47**, 4161 (1982).

14) a) H. K. Dietl and K. C. Brannock, *Tetrahedron Lett.*, **1973**, 1273; b) D. G. Oosterhoff and V. D. Gen, *Tetrahedron Lett.*, **1974**, 1653.

15) P. Giannocca, A. Sacco, and G. Vasapollo, *Inorg. Chim. Acta*, **37**, 455 (1979).

16) T. Ukai, H. Kawazura, Y. Ishii, J. J. Bonnet, and J. A. Ibers, *J. Organomet. Chem.*, **65**, 253 (1974).

17) Z. Brügel, *Electrochem.*, **64**, 1121 (1960).

18) E. N. Marvell and T. H.-C. Li, *J. Am. Chem. Soc.*, **100**, 883 (1978).

19) K. C. Chan, R. A. Jewel, W. H. Nutting, and H. Rapoport, *J. Org. Chem.*, **33**, 3382 (1968).

20) R. H. Reitsema, *J. Am. Chem. Soc.*, **75**, 1996 (1953).

 © 1986 The Chemical Society of Japan Bull. Chem. Soc. Jpn., 59, 893—895 (1986)

Asymmetric Addition of Hydrogen Cyanide to Substituted Benzaldehydes Catalyzed by a Synthetic Cyclic Peptide, *Cyclo*((*S*)-phenylalanyl-(*S*)-histidyl)

Yoshiyuki KOBAYASHI, Shoichi ASADA, Ichigen WATANABE, Hiroaki HAYASHI, Yoshiyuki MOTOO, and Shohei INOUE*

Department of Synthetic Chemistry, Faculty of Engineering, The University of Tokyo, Hongo, Bunkyo-ku, Tokyo 113

(Received November 8, 1985)

Using *cyclo*((*S*)-phenylalanyl-(*S*)-histidyl) as catalyst, optically active cyanohydrins from substituted benzaldehydes with *p*-methyl, *m*-methyl, *o*-methyl, *m*-methoxyl, or *m*-phenoxyl group were obtained with optical yield of 82—33%. For the asymmetric cyanohydrin synthesis, nonpolar solvent such as benzene or carbon tetrachloride was advantageous, while no asymmetric synthesis took place in methanol or dimethyl sulfoxide.

Enzymatic reactions are characterized by the high degree of specificity and high efficiency under mild conditions. In the application of natural enzyme as catalyst for synthetic reactions, possible shortcomings are the facts that natural enzymes are usually stable under rather limited conditions and that the product obtained is limited only to one of the possible optical isomers. In the asymmetric synthesis catalyzed by synthetic peptides, on the other hand, preferred configuration of the product of the catalyzed reaction can be selected as desired, by the selection of (*R*)- or (*S*)-amino acid in the synthesis of the catalytically active peptides. Therefore, the studies of asymmetric synthesis catalyzed by synthetic peptides are of much interest.

We have studied asymmetric cyanohydrin synthesis catalyzed by synthetic peptides.[1-4] Optically active cyanohydrin is a useful synthetic intermediate which can be readily transformed into optically active α-hydroxy carboxylic acid. More specifically, (*S*)-cyanohydrin of *m*-phenoxybenzaldehyde, for example, is an essential building block for the synthesis of a particularly effective insecticide.[5]

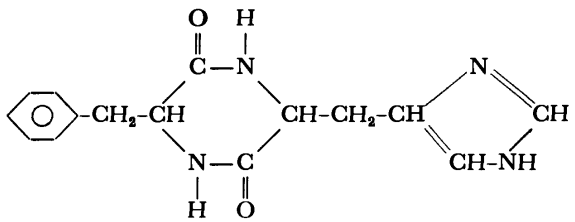

1

Since it is known that cyanohydrin synthesis is catalyzed by a base, we have used cyclic or linear dipeptides containing (*S*)-histidine as a base catalyst. Among the peptides we examined, *cyclo*((*S*)-phenylalanyl-(*S*)-histidyl) (**1**, *cyclo*(-(*S*)-Phe-(*S*)-His-)) was found to be an effective catalyst for the asymmetric cyanohydrin synthesis from benzaldehyde to give the highest optical yield ever reported (90%) under appropriate conditions.[2,3] This catalyst is applicable also to the asymmetric cyanohydrin synthesis from aliphatic aldehydes with optical yield of 30—40%.[4] In the present study, attempts were made to extend the application of *cyclo*(-(*S*)-Phe-(*S*)-His-) to asymmetric cyanohydrin synthesis from substituted benzaldehydes.

In the asymmetric cyanohydrin synthesis from benzaldehyde with *cyclo*(-(*S*)-Phe-(*S*)-His-) in benzene, the reaction mixture was heterogeneous at first but became homogeneous with the progress of the reaction, and the optical yield of the product was the highest in the early stage but decreased in prolonged reaction.[2,3] Since these phenomena are considered to be due, at least partly, to the change in the polarity of the system with the progress of the reaction by the formation of the product, the effect of the solvent on the reaction was investigated using benzaldehyde as substrate.

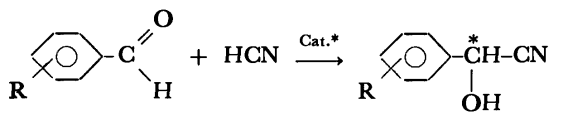

2 a-f **3 a-f**

2 a: R=*p*-CH_3- **3 a**: R=*p*-CH_3-
b: R=*m*-CH_3- **b**: R=*m*-CH_3-
c: R=*o*-CH_3- **c**: R=*o*-CH_3-
d: R=*m*-CH_3O- **d**: R=*m*-CH_3O-
e: R=*m*-C_6H_5O- **e**: R=*m*-C_6H_5O-
f: R=H- **f**: R=H-

Results and Discussion

Addition Reaction to Substituted Benzaldehyde. The results obtained in the addition of hydrogen cyanide to substituted benzaldehydes catalyzed by *cyclo*(-(*S*)-Phe-(*S*)-His-) are summarized in Table 1. The reaction conditions employed were the same as those that gave the highest optical yield for benzaldehyde; in benzene at 35 °C for 30 min. All the products obtained from the substituted benzaldehydes examined were of fairly high optical yields. These

Table 1. Asymmetric Addition of Hydrogen Cyanide to Substituted Benzaldehydes Catalyzed by *cyclo*(-(*S*)-Phe-(*S*)-His-)[a]

Run	Aldehyde Substituent	Conv. %	Optical yield of product/ e.e. %[b]	
			by *cyclo*(-(*S*)-Phe-(*S*)-His-)	by D-oxynitrilase[c]
1	*p*-Me (**2a**)	80	33	28
2	*m*-Me (**2b**)	83	82	60
3	*o*-Me (**2c**)	67	70	—
4	*m*-MeO (**2d**)	71	54	51
5	*m*-PhO (**2e**)	70	61[e]	—
6[d]	H (**2f**)	40	90[e]	100

a) Aldehyde: 25 mmol, hydrogen cyanide: 25 mmol, *cyclo*(-(*S*)-Phe-(*S*)-His-): 0.5 mmol, benzene: 10 cm^3, reaction time: 30 min, reaction temperature: 35 °C. b) E.e., enantiomeric excess. c) In 0.05 M† acetate buffer (H_2O:EtOH, 1:1; pH, 5.4); Conv., 94—100%.[6] d) Ref. 2), 3). e) Preferred configuration is *R*.

Table 2. Effect of Solvent on the Asymmetric Addition of Hydrogen Cyanide to Benzaldehyde Catalyzed by *cyclo*(-(*S*)-Phe-(*S*)-His-)[a]

Run	Solvent	React. Time min	Conv. %	Optical yield of product[b] e.e. %
1	Benzene[c]	30	40	90
		60	80	76
		960	90	21
2	Acetonitrile	30	73	30
		840	90	~0
3	Methanol	30	77	0
		660	85	0
4	Carbon Tetrachloride	30	80	58
5	Diethyl Ether	45	80	57
6	Chloroform	30	45	53
7	Dimethyl Sulfoxide	10 s	65	0

a) Benzaldehyde: 25 mmol, hydrogen cyanide: 25 mmol, *cyclo*(-(*S*)-Phe-(*S*)-His-): 0.5 mmol, solvent: 10 cm^3, reaction temperature: 35 °C. b) Preferred configuration is *R*. c) Ref. 2), 3).

optical yields were higher than those reported for D-oxynitrilase, which is a specific enzyme for the addition of hydrogen cyanide to benzaldehyde, although the reaction conditions are not indentical.[6] Using cinnamaldehyde as substrate under the same conditions, the optical yield of the product was 31% at 24% conversion. Thus, *cyclo*(-(*S*)-Phe-(*S*)-His-) is a better catalyst than natural enzyme for asymmetric cyanohydrin synthesis from some aldehydes.

Effect of Solvent on the Reaction of Benzaldehyde. As reported previously,[2] the reaction mixture in the addition of hydrogen cyanide to benzaldehyde in benzene catalyzed by *cyclo*(-(*S*)-Phe-(*S*)-His-) was heterogeneous in the early stage, and became homogeneous after about 30 min. This change from heterogeneity to homogeneity of the reaction mixture is considered to be due to the formation of the product, mandelonitrile. In fact, *cyclo*(-(*S*)-Phe-(*S*)-His-) (0.5 mmol) is soluble in a mixture of racemic mandelonitrile (25 mmol) and benzene (10 cm^3). We attempted to examine the influence of the product on the reaction by adding phenylacetonitrile or benzyl alcohol as the analog of the product to the reaction system. However, the addition of 5 cm^3 of the analog to the reaction mixture, consisting of benzaldehyde (50 mmol), hydrogen cyanide (50 mmol), *cyclo*(-(*S*)-Phe-(*S*)-His-) (1.0 mmol) and benzene (15 cm^3), did not dissolve the peptide, and the optical yield of the product in the asymmetric addition was not much affected. For example, upon addition of phenylacetonitrile the optical yield of the product was 72.5% after 30 min (conv. 60%) and 24.5% after 12 h (conv. 85%), respectively.

† 1 M=1 mol dm^{-3}.

The asymmetric benzaldehyde cyanohydrin synthesis catalyzed by *cyclo*(-(*S*)-Phe-(*S*)-His-) was examined in various solvents, as summarized in Table 2. The reaction in carbon tetrachloride was heterogeneous at first and then became homogeneous similarly to the reaction in benzene. The reaction in other solvents such as chloroform, diethyl ether, acetonitrile, and methanol was heterogeneous. On the other hand, dimethyl sulfoxide dissolved *cyclo*(-(*S*)-Phe-(*S*)-His-), and the reaction proceeded homogeneously and very rapidly to complete within a few minutes.

The reaction in nonpolar solvent such as benzene or carbon tetrachloride, or in solvent with lower polarity such as diethyl ether or chloroform, gave fairly high optical yield of the product. In the reaction using acetonitrile as solvent, the product had a moderate optical activity, while in methanol with almost the same dielectric constant the product exhibited no optical activity. No asymmetric reaction took place in strongly polar solvent such as dimethyl sulfoxide, although the reaction was stopped in a very short time in order to avoid possible decrease in the optical yield with reaction time.

Thus, nonpolar solvent is advantageous for this asymmetric cyanohydrin synthesis, while strongly polar solvent or protic solvent which is considered to weaken the interaction between catalyst and substrates is disadvantageous.

Experimental

Materials. Hydrogen cyanide was prepared from sodium cyanide and sulfuric acid as described previously.[4] All the aldehydes were distilled in nitrogen under reduced pressure. Carbon tetrachloride, diethyl ether, chloroform, and acetonitrile were distilled over calcium hydride in nitrogen. Methanol was distilled over magnesium in nitrogen. Dimethyl sulfoxide was distilled over calcium hydride in nitrogen under reduced pressure. Phenylacetonitrile and benzyl alcohol were distilled in nitrogen under reduced pressure. Commercially available racemic mandelonitrile was dried over Drierite. Other reagents and solvents were commercially purchased and used without futher purification.

Catalyst. *N*-Benzyloxycarbonyl-(*S*)-phenylalanyl-(*S*)-histidine methyl ester [Z-(*S*)-Phe-(*S*)-His-OMe] was prepared by the reaction of benzyloxycarbonyl-(*S*)-phenylalanine with (*S*)-histidine methyl ester as described previously.[4]

Cyclo[(*S*)-phenylalanyl-(*S*)-histidyl][*cyclo*(-(*S*)-Phe-(*S*)-His-)] was prepared from Z-(*S*)-Phe-(*S*)-His-OMe by the removal of benzyloxycarbonyl group by hydrogenation with palladium-black followed by cyclization in refluxing methanol according to the reported procedure.[2] The crude product was recrystallized from water and dried at room temperature under reduced pressure. This product was dissolved in hot ethanol and reprecipitated by adding the ethanol solution to five-fold amount of petroleum ether; mp 251—256 °C; $[\alpha]_D^{t.t.}=-62.1°$ (C=1.95 g/100 cm^3; acetic acid) (lit,[7] mp 267—268 °C; $[\alpha]_D^{20}=-72°$ (C=2.00 g/100 cm^3; acetic acid)).

Addition Reaction. *Cyclo*(-(*S*)-Phe-(*S*)-His-) (0.5 mmol) was placed in a 50 cm^3 round-bottomed flask equipped with a three-way cock, and the atmosphere of the flask was replaced with nitrogen. To this were added the solvent (10 cm^3) and aldehyde (25 mmol) with magnetic stirring, then 1 cm^3 of hydrogen cyanide was added with a chilled syringe. The conversion of aldehyde was determined by infrared spectrum of the reaction mixture using the absorption band due to ν_{C-H} of aldehydic hydrogen at 2735 cm^{-1}. The reaction was stopped by adding 0.5 cm^3 of 2 mol dm^{-3} HCl-CH_3OH. Unreacted hydrogen cyanide and solvent were removed from the reaction mixture through a trap containing aqueous alkali under reduced pressure. Ether was added to the residue, and the supernatant solution containing the product was separated. After washing the residue several times with ether, the combined ether solution and washings were filtered to remove the residual catalyst, then ether was removed under reduced pressure to leave a viscous liquid, which was confirmed to be a mixture of cyanohydrin and unreacted aldehyde by ^{1}H-NMR spectrum in $CDCl_3$. The mole fraction of cyanohydrin in this mixture was determined on the basis of ^{1}H-NMR signals due to C<u>H</u>(O<u>H</u>) (δ=5.5 and 4.5—5.0, respectively) of cyanohydrin and due to the aldehydic hydrogen (δ=9.9).

Determination of Optical Yield. For the determination of the optical purity of the product from *p*-tolualdehyde (**1a**), the product was reacted with (+)-perfluoro-2-propoxypropionyl chloride to give the corresponding ester quantitatively. ^{19}F-NMR spectrum of the ester was measured and the diastereomeric ratio of the ester was calculated from the signals of the trifluoromethyl group bonded to the chiral center.[8] As for *m*-phenoxybenzaldehyde and cinnamaldehyde, the optical purity of the product was calculated from the reported optical rotation of the product; for (*S*)-*m*-phenoxybenzaldehyde cyanohydrin ((*S*)-α-cyano-3-phenoxybenzyl alcohol), $[\alpha]_D^{25}=-24.8°$ (C=1.2 g/100 cm^3; $CHCl_3$)[9]; for (*R*)-cinnamaldehyde cyanohydrin, ((*R*)-α-cyanocinnamyl alcohol), $[\alpha]_D=+77°$ (C=8.4 g/100 cm^3; $CHCl_3$).[10] For the product from other aldehydes, the optical purity was determined by the high-pressure liquid chromatgraph using a chiral column Chiralcel OB (Daicel Chem. Ind., Ltd.); eluent, hexane/isopropyl alcohol (9/1); detecting wavelength, 254 nm.

Measurement. IR spectra were recorded on a Hitachi 260-30 spectrophotometer. NMR spectra were recorded on a Hitachi R-40 spectrometer. The optical rotations of the products at 589 nm were measured using Perkin-Elmer Polarimeter 241 or JASCO DIP-360 Digital Polarimeter. High pressure liquid chromatogram was recorded using Hitachi 638-30 High Pressure Liquid Chromatograph. Melting points were taken on a Yanagimoto Mel-Temp apparatus.

References

1) J. Oku, N. Ito, S. Inoue, *Makromol. Chem.*, **180**, 1089 (1979).
2) J. Oku, N. Ito, S. Inoue, *Makromol. Chem.*, **183**, 579 (1982).
3) J. Oku, S. Inoue, *J. Chem. Soc., Chem. Commun.*, **1981**, 229.
4) S. Asada, Y. Kobayashi, S. Inoue, *Makromol. Chem.* **186**, 1755 (1985).
5) M. Elliott, N. F. Janes, B. P. S. Khambay, D. A. Pulman, *Pestic. Sci.*, **14**, 182 (1983).
6) W. Becker, H. Freund, E. Pfeil, *Angew. Chem.*, **77**, 1139 (1965).
7) F. Schneider, *Hoppe-Seyler's Z. Physiol. Chem.*, **338**, 131 (1964).
8) H. Kawa, F. Yamaguchi, N. Ishikawa, *J. Fluor. Chem.*, **20**, 475 (1982).
9) H. Hirohara, S. Mitsuda, Jpn. Kokai Tokkyo Koho JP 58 94389 (1983); see also, *Chem. Abst.*, **99**, 86636r (1983).
10) V. Prelog, M. Wilhelm, *Helv. Chim. Acta*, **37**, 1634 (1954).

 © 1986 The Chemical Society of Japan Bull. Chem. Soc. Jpn., 59, 897—905 (1986)

Electron-Transfer-Initiated Photoreactions of 1-Methyl-2-phenyl-1-pyrrolinium Perchlorate with α-Heteroatom-Substituted Alkanoate Anions

Yoshiaki KURAUCHI, Hideo NOBUHARA, and Kazuya OHGA*
Department of Environmental Chemistry and Engineering, Faculty of Engineering, Oita University, Dannoharu, Oita 870-11
(Received September 20, 1985)

The irradiation of aqueous solutions of 1-methyl-2-phenyl-1-pyrrolinium perchlorate (**1**) in the presence of α-hydroxyalkanoate anions led to the formation of 2-(hydroxyalkyl)pyrrolidine adducts and a reduction product, 1-methyl-2-phenylpyrrolidine. Mechanistic studies demonstrated that photoaddition reactions were induced by one-electron transfers from the carboxylato groups of alkanoates to the excited singlet state of **1** ($\mathbf{1}^{S_1}$), followed by an efficient decarboxylation. Furthermore, the photoreaction of **1** with ethoxyacetate was found to give a 2-(ethoxymethyl)pyrrolidine adduct in preference to the reduction product. For photoreactions with 2-mercaptopropionate and α-amino acids, the reduction product was detected. *N*-Acetylglycinate gave a 2-(acetylaminomethyl)pyrrolidine adduct in fairly high yield (80%). The features of these photoreactions with α-heteroatom-substituted alkanoates are discussed in terms of fluorescence-quenching efficiencies and the properties of radicals formed through electron transfers to $\mathbf{1}^{S_1}$.

Carboxylic acids are known to undergo electron-transfer-initiated photodecarboxylations in the presence of such electron acceptors as heterocyclic[1] and carbonyl[2] compounds and 1-cyanonaphthalene.[3] The reactions are facile in the case of acetic acid derivatives of the type $RXCH_2CO_2H$(R=aryl, X=O, S, and NH). When aliphatic analogues (R=H or alkyl), except for the S compound, are employed as electron donors, however, electron transfers to the excited states of the acceptors were either not observed[2] or took place with a lower efficiency[1d] due to their higher ionization potentials. Consequently, few details are known about an electron-transfer-initiated photoreaction in which the α-heteroatom-substituted alkanoic acids participate.

On the other hand, various types of photoaddition reactions involving iminium cations have been systematically investigated by Mariano and his co-workers from mechanistic[4] and synthetic[5] points of view. A proposed mechanism involves one-electron transfers from a variety of donors to the excited singlet states of the cations as important primary steps. For example, 2-phenyl-1-pyrrolinium perchlorate and its *N*-methyl derivative (**1**) were converted into 2-pyrrolidinyl radicals by electron transfers. Then, cation radical intermediates derived from π- and *n*-electron donors (such as olefins, allylsilanes, alcohols, and ethers) were transformed into neutral radicals by nucleophilic capture, deprotonation, and desilylation. The coupling of resulting radical pairs afforded 2-substituted 2-phenylpyrrolidines.

Previously, we reported[6] on the decarboxylative photoaddition of a 3-butenoate anion to the pyrrolinium cation **1** in an aqueous solution. The photoaddition follows, on the whole, the above-mentioned mechanism. Moreover, fluorescence-quenching experiments and an estimation of the free-energy change have suggested that a mechamism which rationalizes this photoaddition involves electron-transfer processes from both the vinyl and carboxylato groups (Scheme 1). This implies that the carboxylato group possesses a reducing ability comparable to those of mono-substituted olefins and that the excited singlet state of the cation **1** ($\mathbf{1}^{S_1}$) behaves as an effective electron acceptor for the carboxylato group. In the present research, we employed this aqueous pyrrolinium-cation system in order to elucidate the chemical behavior of α-heteroatom-substituted alkanoic acids in an electron-transfer-initiated photoreaction.

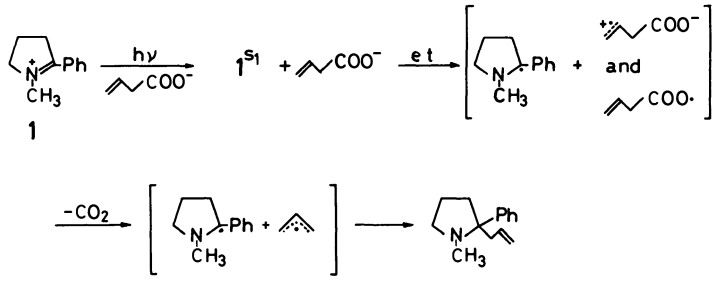

Scheme 1.

Results and Discussion

Fluorescence Quenching. The fluorescence of **1** was quenched by various aliphatic carboxylate anions (Table 1). All measurements were made on aqueous solutions with a pH of 6; thus, all the acids existed exclusively in carboxylate anionic forms. The solutions contained 0.5 M (1 M=1 mol dm^{-3}) $NaClO_4$ in order to minimize a salt effect (described later). Also, solutions containing **1** and the acids were stable while standing in the dark. The fluorescence and absorption spectra of **1** revealed an absence of the excited- or ground-state complex formation. Stern-Volmer plots yielded straight lines with intercepts equal to 1. The quenching constants ($k_q\tau$) obtained from the least-squares slopes of the plots are given in Table 1.

α-Hydroxyalkanoate anions, which can be seen in the first three rows, had quenching efficiencies similar to each other. On the other hand, no effective quenching was observed at a lower pH where the acids exist in undissociated forms. The oxidation potentials of aliphatic carboxylate anions in acetonitrile are normally lower (ca. 1.6 V vs. SCE)[7] than those of alcohols (ca. 2.5—3.8 V vs. SCE)[8] which are known to serve as quenchers for the fluorescence of the pyrrolinium cation **1**.[8] This leads us to infer that the fluorescence quenching by the hydroxyalkanoate anions is induced by electron transfers from the carboxylato groups to $\mathbf{1}^{S_1}$, although the Stern-Volmer quenching-rate constants (k_q, estimated to be ca. 6—8×10^8 M^{-1} s^{-1} using the singlet lifetime (τ=1 ns)[8] of **1** in 10% aqueous acetonitrile) are slightly less than a diffusion-controlled rate constant (6.64×10^9 M^{-1} s^{-1}).[9]

A more precise evaluation of the energetics of this electron transfer with the aid of Eq. 1 proposed by

$$\Delta G_{et}(\text{eV}) = E(D/D^+) - E(A^-/A) - e^2/\varepsilon\alpha - E_{0,0} \quad (1)$$

Rehm and Weller[10] requires knowledge of the electrochemical and spectroscopic data of **1** and the anions in an aqueous solution. The reduction potential, $E(A^-/A)$, and the singlet energy, $E_{0,0}$, of **1** were found to be −0.95 V (vs. SCE) and 3.9 eV, respectively. The oxidation potentials ($E(D/D^+)$) of the α-hydroxyalkanoates could not be obtained since discrete oxidation waves were difficult to observe in aqueous solutions;[11] thus, the critical potential of acetate (1.9 V vs. SCE)[12] was employed as the oxidation potential. The coulombic attraction term ($e^2/\varepsilon\alpha$) may be neglected since the two radical species generated by the one-electron transfer are neutral in the present systems. The free-energy change, ΔG_{et}, obtained in this way is −1.1 eV, and supports the idea that a one-electron transfer is energetically feasible. Furthermore, the $k_q\tau$ values for the anions were almost the same as those for acetate (0.57±0.03 M^{-1}) and propionate (0.62±0.02 M^{-1}) anions and the fluorescence of **1** was little quenched by 2-propanol ($k_q\tau$<0.04). These findings agree with the suggestion that electron transfers from the hydroxyl groups are not appreciably responsible for the quenching.

In the case of sulfur-substituted alkanoic acids, a more efficient quenching can be predicted by the high HOMO energies of analogous S compounds.[13] The quenching efficiency of 2-mercaptopropionate was high as shown in Table 1; the estimated k_q value

Table 1. Fluorescence Quenching Constants, Product Yields, and Quantum Yields for 1-Methyl-2-phenyl-1-pyrrolinium Cation **1**–Carboxylate Anion Systems

Carboxylate anion	$k_q\tau$[a]/M^{-1}	Product yields/%		Quantum yields[b]		
		Adduct	Reduction product **7**	ϕ_{dis}	ϕ_a	ϕ_r
$HOCH_2COO^-$	0.61±0.02	**2** 44	15	0.15	0.062±0.007	0.017
$HOCH(CH_3)COO^-$	0.59±0.02	**3** 31[c]	28		0.056[c]	
$HOC(CH_3)_2COO^-$	0.76±0.03	**4** 25	34	0.13	0.041	0.036
$C_2H_5OCH_2COO^-$	—[d]	**5** 42	<3		0.064	
$HSCH(CH_3)COO^-$	4.8±0.2	—[e]	37			
$H_3N^+CH_2COO^-$	<0.05	—[e]	5			
$H_3N^+C(CH_3)_2COO^-$	0.22±0.01	—[e]	8.5			
$CH_3CONHCH_2COO^-$	1.03±0.05	**6** 80[f]	Trace			

a) Obtained from Stern-Volmer plots at pH 6.0. b) ϕ_{dis}, ϕ_a, and ϕ_r are quantum yields for the **1** disappearance, the adduct formation, and the reduction product formation, respectively, and were obtained using aqueous solutions (pH 6.0) containing **1** of 1.00×10^{-3} M, carboxylate of 0.5 M, and $NaClO_4$ of 0.5 M. The quantum yields in blank spaces were not determined. c) Total yields of two diastereomers. d) It was difficult to purify this carboxylic acid up to a grade acceptable for quenching experiments. e) No major products other than the reduction product **7** were detected by means of GLC. f) Isolated yield. Other yields were determined by GLC analyses.

using the singlet lifetime of **1** was $4.8\times10^9\ M^{-1}\ s^{-1}$ and near the diffusion-controlled limit. Moreover, this efficiency was nearly equal to that of the free mercaptopropionic acid ($k_q\tau=4.33\pm0.09\ M^{-1}$), indicating a predominant electron transfer from the mercapto group. In conformity with these findings, the free acid and the carboxylate anion were found to have almost the same and much lower oxidation potentials: 0.79 V (vs. SCE) for the free acid, 0.66 V (vs. SCE) for the anion.

Glycine and α-aminoisobutyric acid exhibited less quenching-efficiencies than those of the α-hydroxyalkanoates and acetate since the α-amino acids exist as *N*-protonated forms at pH 6 and probably since the strongly electron-withdrawing NH_3^+ groups diminish an electron transfer from the carboxylato groups. Increasing the pH of the solution increased the efficiencies: e.g., a $k_q\tau$ value with glycine was $5.9\pm0.1\ M^{-1}$ at pH 12. This demonstrates an efficient electron transfer from the unprotonated amino group, as predicted by the generally recognized low ionization potentials of alkylamines.[14]

A *N*-acetylglycinate anion, not subject to *N*-protonation, afforded a somewhat large $k_q\tau$ value ($1.03\ M^{-1}$). Its free carboxylic acid also had a quenching ability, though the efficiency was fairly low ($k_q\tau=0.19\pm0.02\ M^{-1}$). This appears to imply that an electron transfer from the acetylamino group can take place to some extent in competition with that from the carboxylato.

Photoreactions of 1 in the Presence of Alkanoate Anions. The pyrrolinium cation **1** was irradiated in aqueous solutions adjusted to pH 6.0 with NaOH and contained carboxylic acids (0.08—0.69 M (listed in Table 1)) to give photoadducts **2—6** and a reduction product **7**. 2-Mercaptopropionic acid and two α-amino acids showed no formation of major

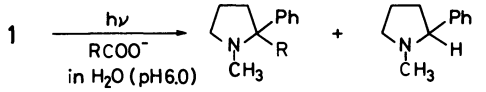

2—6 7

2, R = -CH_2OH
3, R = -$CH(CH_3)OH$
4, R = -$C(CH_3)_2OH$
5, R = -$CH_2OC_2H_5$
6, R = -CH_2NHCCH_3 (O)

products other than **7** in GLC analyses of the photolysates. The irradiations were carried out through a Pyrex glass permitting light absorption exclusively by **1** ($\lambda_{max}=258$ nm, $\varepsilon=12050$). The progress of a reaction was followed by the UV spectra. The irradiations were allowed to continue until ca. 90% of **1** disappeared. The products were isolated after being extracted with chloroform followed by either preparative TLC or preparative GLC.

The identification of the photoadduct **2** obtained from irradiation in the presence of glycolate was made by a direct comparison of the ^1H NMR and IR spectra with those of an authentic sample.[8] The other photoadducts were identified on the basis of comparisons of the characteristic spectroscopic properties of structurally related substances[4] and elemental analyses of 2,4,6-trinitroresorcinolate (styphnate) derivatives. The photoadduct **3** from lactate was a mixture (1 : 1.2) of two diastereomers, separable by silica-gel TLC. The structure of the reduction product **7** was verified by a direct spectroscopic comparison with an authentic sample.[15] The yields of the reduction product and photoadducts are summarized in Table 1 together with the quantum yields obtained for [carboxylates] of 0.5 M.

Mechanistic Studies. In order to unravel the mechanistic features of these photoreactions, the glycolic acid system was investigated in greater detail. Figure 1 shows that the quantum yields for the disappearance of **1** (ϕ_{dis}), for the formation of **2** (ϕ_a), and for the formation of **7** (ϕ_r) depend significantly on the concentration of $NaClO_4$. The quantum yields were reduced by an addition of $NaClO_4$, but exhibited no further decrease at $NaClO_4$ concentrations above ca. 0.4 M. A similar salt effect was observed regarding the fluorescence quenching. Thus, the fluorescence intensity of **1** in the presence of the quencher (glycolate) increased (namely, the quenching efficiency decreased) upon increasing the concentration of $NaClO_4$. The intensity remained unchanged in the $NaClO_4$ concentration range of 0.4 to 0.5 M, as shown in Fig. 2. Accordingly, the

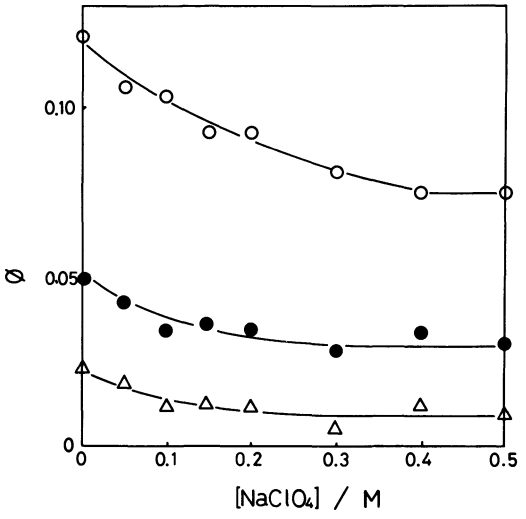

Fig. 1. Dependence of quantum yields, ϕ_{dis}(○), ϕ_a (●), and ϕ_r(△), on the concentration of $NaClO_4$ in a glycolate system (pH 6.0, [**1**]$=1.00\times10^{-3}$ M, [glycolate]$=0.2$ M).

mechanistic studies described in the present paper were made regarding aqueous solutions containing 0.5 M $NaClO_4$ (unless otherwise noted).

Figure 3 shows changes in the quantum yields as a function of the solution pH. ϕ_{dis} and ϕ_a increased steeply around pH 3.5 and remained, substantially, unchanged above pH 4.5. The pK_a of glycolic acid is 3.83; thus, Fig. 3 demonstrates that the disappearance of **1** and the formation of **2** took place more efficiently in the presence of the glycolate anion than in the presence of the free glycolic acid. This corresponds to the above-mentioned fact that the effective quenching of the fluorescence of **1** was observed with the anion, but not with the free acid. This suggests that the photoaddition reaction proceeds mainly via $\mathbf{1}^{S_1}$ by an electron transfer from the anion. Similar pH dependencies of the quantum yields were also observed in the case of an α-hydroxyisobutyric acid system (Fig. 4).

A plausible mechanism for the formation of the photoadduct **2** from the glycolate anion analogous to that for the 3-butenoate system[6] (as depicted in Scheme 2) involves the radical-pair intermediates **9** and **10**. **9** is formed by an electron transfer from the glycolate donor to $\mathbf{1}^{S_1}$ presumably through the intervention of an encounter complex **8** and is returned to the ground state of **1** and glycolate by a back electron transfer. The intermediate **10** is formed by the decarboxylation of **9** and is transformed into **2** by a radical coupling within the solvent cage. In addition, the formation processes of the reduction product **7** and other products, as yet unidentified, from **9** and **10** should be taken into consideration. The rate constants of these processes are appended in Scheme 2.

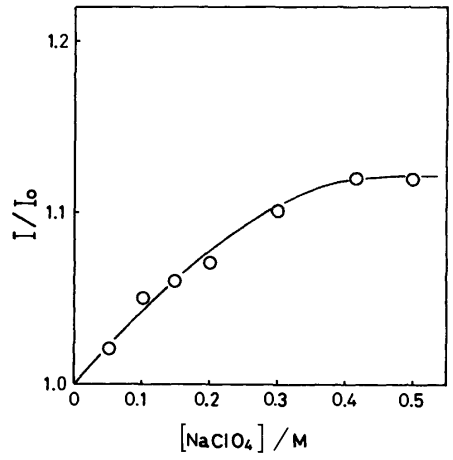

Fig. 2. Dependence of the fluorescence intensity of **1** (I) on the concentration of $NaClO_4$ in the presence of glycolate of 0.2 M. I_0 is the intensity in the absence of $NaClO_4$. The solution pH was 6.0 and [**1**] 1.00×10^{-3} M.

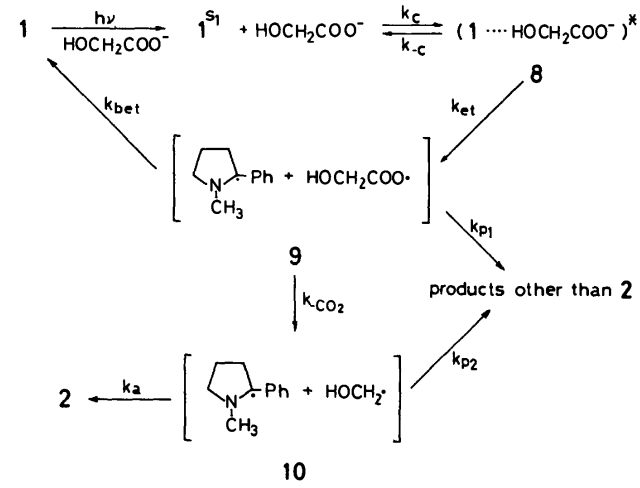

Scheme 2.

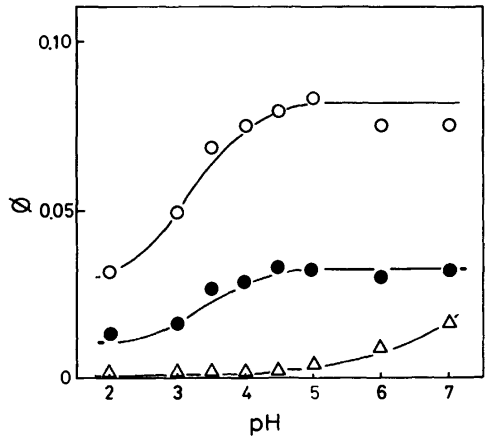

Fig. 3. Dependence of quantum yields, ϕ_{dis}(○), ϕ_a (●), and ϕ_r(△), on pH in a glycolic acid system([**1**]= 1.00×10^{-3} M, [glycolic acid]=0.2 M, [$NaClO_4$]= 0.5 M).

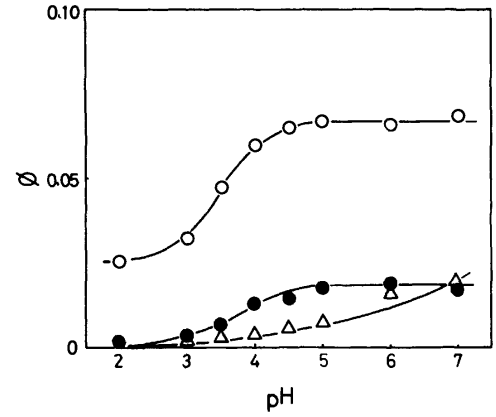

Fig. 4. Dependence of quantum yields, ϕ_{dis}(○), ϕ_a (●), and ϕ_r(△), on pH in an α-hydroxyisobutyric acid system([**1**]= 1.00×10^{-3} M, [$NaClO_4$]=0.5 M). In this case, ϕ_a represents a quantum yield for the formation of **4**.

A steady-state analysis of the sequence gives

$$\phi_a = \alpha_a k_q \tau[HA]/(1 + k_q\tau[HA]) \quad (2)$$

or

$$\phi_a^{-1} = \alpha_a^{-1} + (\alpha_a k_q \tau[HA])^{-1} \quad (3)$$

where [HA] and α_a represent the concentration of the glycolate anion and the limiting quantum yield (ϕ_a at [HA]$\rightarrow\infty$), $\{k_{-CO_2}/(k_{-CO_2}+k_{bet}+k_{p1})\}\{k_a/(k_a+k_{p2})\}$, respectively. k_q is mathematically equivalent to $k_c k_{et}/(k_{et}+k_{-c})$. The ratio ($k_q\tau$) of the intercept to the slope of a linear plot of ϕ_a^{-1} vs. $[HA]^{-1}$ (Fig. 5) was 0.66±0.27 M^{-1}. This value agreed with the $k_q\tau$ value (Table 1, 0.61 M^{-1}) obtained from the fluorescence quenching. This result also supports the idea that the photoaddition is an excited singlet-state process of **1**.

If, in this manner, both the reaction and the fluorescence-quenching processes can be considered together under a unified mechanism, the limiting quantum yield α_a can be estimated to be 0.27 (from Eq. 2) using $k_q\tau$ from the fluorescence quenching and the ϕ_a obtained at [HA] of 0.5 M. The limiting quantum yield α_{dis} ($=(k_{-CO_2}+k_{p1})/(k_{-CO_2}+k_{bet}+k_{p1})$) for the disappearance of **1** can also be calculated using the ϕ_{dis} denoted in Eq. 4 and is given in Table 2

$$\phi_{dis} = \alpha_{dis} k_q \tau[HA]/(1 + k_q\tau[HA]) \quad (4)$$

together with the limiting quantum yields estimated in a similar manner for the α-hydroxyisobutyrate system. The α_{dis} (0.64) for the glycolate system indicates that the fraction of the back electron transfer in the total disappearance pathways of **9** was 36%. Furthermore, the ratio ($=\{k_a/(k_a+k_{p2})\}\{k_{-CO_2}/(k_{-CO_2}+k_{p1})\}$) of α_a to α_{dis} implies that $k_{-CO_2}/(k_{-CO_2}+k_{p1})>0.42$. Thus, the decarboxylation of **9** takes place in a proportion of over 27% and the decarboxylation of the hydroxyacetoxyl radical partner in **9** is a sufficiently rapid pathway to compete with the back electron transfer.[16] This reflects the fact that the α_a and α_{dis} were fairly large; namely, the photoreaction of **1** in the presence of the glycolate anion was appreciably efficient.

Likewise, the fraction of decarboxylation for the α-hydroxyisobutyrate system can be estimated to be greater than 15%. However, it should be pointed out that a smaller α_a/α_{dis} value for this system, probably due to the formation of the reduction product **7** via the intermediate **10** in a higher quantum yield than that for the glycolate system (see Table 1), allowed us to underestimate k_{-CO_2}.

All the quantum yields, ϕ_{dis}, ϕ_a, and ϕ_r for the glycolate system were decreased by an addition of $NaClO_4$ (Fig. 1). Moreover, the degrees of the decreases were almost the same when considering at least two cases of ϕ_{dis} and ϕ_a: for example, ϕ_{dis} exhibited a 38% decrease at [$NaClO_4$] of 0.5 M; ϕ_a a 39% decrease. In addition, a decrease of the fluorescence-quenching efficiency upon an addition of the salt was also observed (Fig. 2). It is important to note that in the absence of the glycolate quencher, the salt did not affect the intensity of the fluorescence of **1**. This signifies that the singlet lifetime was not affected by the salt. Thus, it seems likely that the term k_q[HA], which is common to the two quantum yields (Eq. 2 and 4), and the fluorescence quantum

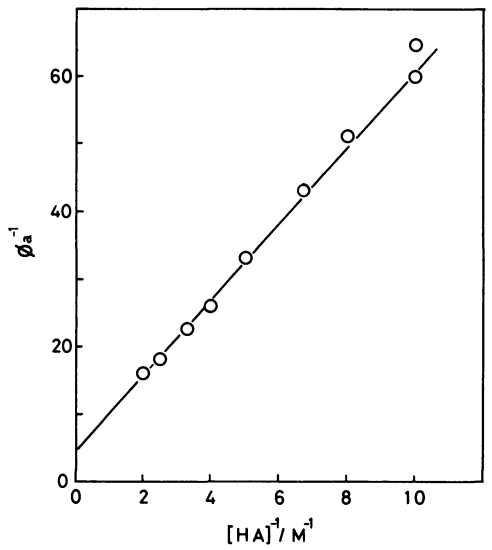

Fig. 5. Double reciprocal plot of the quantum yield for the formation of **2**(ϕ_a) vs. the concentration of glycolate([HA]).

Table 2. Limiting Quantum Yields for the **1** Disappearance(α_{dis}) and for the Photoadduct Formation(α_a) and Fractions of Pathways from the Intermediate **9**

Carboxylate anion (R-COO⁻) R-	α_{dis}	α_a	α_a/α_{dis}	Fractions of pathways		
				Back electron transfer	Decarboxylation	Formation of other products
$HOCH_2$-	0.64	0.27 (0.26)[a]	0.42	0.36	>0.27	<0.37
$HOC(CH_3)_2$-	0.47	0.15	0.32	0.53	>0.15	<0.32

a) Determined from the intercept(α_a^{-1}) of a linear plot shown in Fig. 5.

yield (ϕ_f) denoted in Eq. 5, was reduced by an addition of $NaClO_4$.

$$\phi_f = k_f\tau/(1 + k_q\tau[HA]), \quad (5)$$

where k_f is a rate constant for the fluorescence of **1**. Hence, the relationships between the increased rates of the quantum yields ($\phi/\phi^\circ - 1$) and the decreased rate of the fluorescence intensity in the presence of the quencher ($1 - I/I^\circ$), based on the quantum yields (ϕ°) and the intensity (I°) at [$NaClO_4$] of 0.5 M, can be expressed as

$$1 - I/I^\circ = k_q^\circ\tau[HA](\phi/\phi^\circ - 1). \quad (6)$$

Here, k_q° is the quenching-rate constant at a [$NaClO_4$] of 0.5 M.

Linear plots of $1 - I/I^\circ$ vs. $\phi_{dis}/\phi_{dis}^\circ - 1$ and $\phi_a/\phi_a^\circ - 1$ having slopes of $k_q^\circ\tau[HA]$ (Fig. 6) gave $k_q^\circ\tau = 0.87 \pm 0.07\ M^{-1}$ from a plot against $\phi_{dis}/\phi_{dis}^\circ - 1$ and $0.77 \pm 0.15\ M^{-1}$ from that against $\phi_a/\phi_a^\circ - 1$, respectively. These $k_q^\circ\tau$ values are in satisfactory agreement with the $k_q\tau$ ($0.61\ M^{-1}$) obtained from fluorescence-quenching experiments at a [$NaClO_4$] of 0.5 M, within the experimental limits of error. They verify the salt effect on the $k_q[HA]$ term. The addition of $NaClO_4$ probably causes an instability in the postulated encounter complex **8**, which is formed from a cation and an anion; thus, it is reasonable to assume that the salt effect involves (in part) a decrease in the k_q value.

It is again worth noting that a higher quantum yield for the formation of **7** was observed in the case of α-hydroxyisobutyrate compared to the case of glycolate (Table 1). This suggests that the α-hydrogen of the α-hydroxyalkanoate anions did not serve as a hydrogen source for the formation of **7**. On the other hand, ketyl radicals are known to be active reducing agents;[17] e.g., the radicals can transfer hydrogen atoms to aryl ketones.[17b] It thus seems reasonable to propose that a major pathway for the formation of **7** involves a disproportionation of the radical pairs formed after the decarboxylation (for the glycolate system, **10**), even though a mechanism for

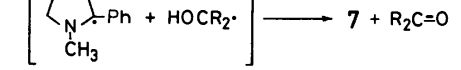

the formation was not investigated as thoroughly as that for the adduct formation. In particular, the reason why the yields of **7** increased with an increase in pH (Figs. 3 and 4) remains obscure. Formaldehyde (15%), acetaldehyde (18%), and acetone (32%) were formed in reasonable yields in the glycolate, lactate, and α-hydroxyisobutyrate systems, respectively. **7** was formed in a very low yield (<3%) for the case of an ethoxyacetate having no hydroxyl group. These findings support the idea of this disproportionation pathway. Furthermore, the results that a successive substitution of a methyl group at the α position induced a decrease in ϕ_a and, on the contrary, induced an increase in ϕ_r (Table 1) could be interpreted in terms of a simple steric hindrance of the methyl group during the radical pair combination which produced the photoadducts.

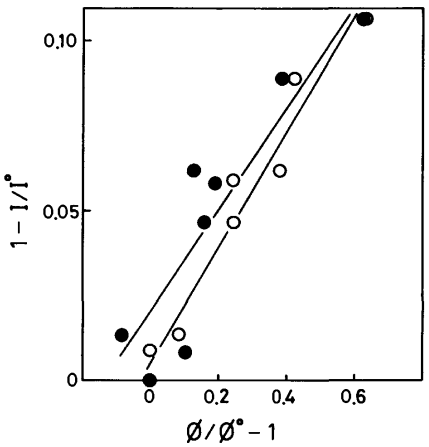

Fig. 6. Relationships between dependencies of the **1** fluorescence intensity(I) and the quantum yields, ϕ_{dis}(○) and ϕ_a(●), on the concentration of $NaClO_4$ in the presence of glycolate of 0.2 M. ϕ° and I° represent the quantum yields and the fluorescence intensity at [$NaClO_4$] of 0.5 M.

Photoreactions of 1 with Sulfur- and Nitrogen-Substituted Alkanoates. In the case of 2-mercaptopropionate, only the reduction product **7** was detected as a major product (Table 1). As described above, an electron transfer from 2-mercaptopropionate (predominantly from the mercapto group) to $\mathbf{1}^{S_1}$ takes place more efficiently than those from α-hydroxyalkanoates. Accordingly, a primary event for this photoreaction can be reasonably assumed to be an electron transfer leading to the formation of a 1-methyl-2-phenylpyrrolidinyl radical and the ensuing, predominant formation of a radical $H\overset{+}{S}\dot{C}H(CH_3)$-$COO^-$. On the other hand, S-H bonds possess relatively low dissociation energies and are, consequently, subject to a hydrogen-atom abstraction. Thus, **7** is quite likely to be formed through a hydrogen-atom abstraction of pyrrolidinyl radical within a solvent cage from $H\overset{+}{S}CH(CH_3)COO^-$ or a mercaptoalkyl radical $HS\dot{C}HCH_3$ resulting after decarboxylation, or through an out-of-cage hydrogen-atom abstraction from the mercaptopropionate anion, in preference to the formation of an adduct analogous to the photoadducts from the α-hydroxyalkanoates.

In cases of glycine and α-aminoisobutyric acid, **7** was also detected as a very low-yield product (Table 1). This is apparently due to a quite inefficient electron transfer at pH 6 (vide supra). A photolysis at

a higher pH (where the NH_3^+ groups of the α-amino acids are deprotonated) was impossible to perform since the higher pH brought about a thermal instability of **1**.[18]

On the other hand, *N*-acetylglycinate gave an adduct **6** in fairly high yield (80%, Table 1). A reasonably efficient electron transfer from the glycinate (vide supra) can induce the formation of an acetylaminoacetoxyl radical $CH_3CONHCH_2COO\cdot$ via an electron transfer from the carboxylato group and of a radical zwitterion $CH_3\overset{+}{C}\overset{\cdot}{N}HCH_2COO^-$ via an electron transfer from the acetylamino group. Both these radicals could be transformed into an acetylaminomethyl radical **11** via decarboxylation.

$$CH_3-\overset{O}{\overset{\|}{C}}-NHCH_2\cdot$$

11

This is rather efficiently induced since the methyl radical **11** is stabilized by a conjugation with the acetylamino group. Thus, the formation of **6** in high yield is understandable in terms of the formation of this stable radical as well as in terms of the efficient primary electron-transfer pathway.

Experimental

General. Melting points were determined with a Yanagimoto micro melting-point apparatus and are uncorrected. UV spectra were obtained with a Shimadzu UV-202 or JASCO UVIDEC-610A spectrophotometer. Fluorescence emission and IR spectra were recorded on a Shimadzu RF-510 spectrometer and a Hitachi 285 spectrophotometer, respectively. Mass spectra were taken with a JEOL JMS-01SG-2 spectrometer. ^1H NMR spectra were recorded on a Hitachi R-24B spectrometer with TMS as the internal standard. GLC (PEG-20M) was performed using a Shimadzu GC-3BF or a Hitachi 263-30 chromatograph with a flame-ionization detector. Preparative TLC was performed on silica-gel plates (Merck Kieselgel 60 PF_{254}).

Materials. **1** was prepared and purified according to a method from the literature:[8] mp 117.5—119.0 °C. *N*-Acetylglycine (Aldrich, 99%) was treated with an activated carbon, then recrystallized four times from methanol. The other reagents were all purchased from commercial sources and purified by recrystallization or vacuum distillation just before use.

Fluorescence Quenching Experiments. The relative intensities of the fluorescence at 380 nm of **1** (1.00×10^{-3} M) were measured at 25±1 °C. The excitation wavelength (at which the quenchers do not absorb light) was 305 nm. Aqueous solutions were adjusted to pH 6.0 with 4 M NaOH when carboxylate anions were used as quenchers. The slopes of Stern-Volmer plots were determined by a least-squares analysis of the obtained data for solutions containing 0.5 M $NaClO_4$. Concentrations of the quenchers were in the 0.05—0.5 M ranges.

Preparative Irradiations. Preparative irradiations were carried out using a 400 W high-pressure mercury lamp (Riko-Sha UVL-400HA) equipped with a Pyrex water jacket under an argon atmosphere. The lamp was immerged in the reaction solutions (200 cm^3, pH 6.0) and photolysates were acidified (pH 1) with HCl and then concentrated to 20 cm^3 in vacuo, unless otherwise noted. The acidic solutions were made basic (pH 10) with NaOH, saturated with NaCl, and extracted with three 40-cm^3 portions of chloroform. The extracts were dried over anhydrous Na_2SO_4 and then concentrated in vacuo to give oily residues. These were subjected to GLC analyses. Photoproducts were isolated by preparative GLC or TLC. Styphnate derivatives of the photoadducts and of reduction product **7** were separated out from equimolar solutions of the photoproducts and 2,4,6-trinitroresorcinol in ethanol, and recrystallized from ethanol.

The yields of the photoproducts were determined by GLC analyses (except for the *N*-acetylglycine photosystem) and are summarized in Table 1. The internal standards used were 9,10-dihydroanthracene for **2**, acenaphthene for **3**, **4**, and **5**, and naphthalene for **7**.

Photolysis of 1 with Glycolic Acid: An aqueous solution containing **1** (400 mg, 7.7 mM) and glycolic acid (10.5 g, 0.69 M) was irradiated for 120 min. Then, the photolysate was worked up by the above-mentioned method to give a crude oil (435 mg). A GLC analysis of the oil showed the formation of two major products: 1-methyl-2-hydroxymethyl-2-phenylpyrrolidine **2** and 1-methyl-2-phenylpyrrolidine **7**. These were isolated by preparative GLC. Spectral data for **2** and **7** were as follows and were identical with those of authentic samples.[8,15] **2**: ^1H NMR ($CDCl_3$) δ=1.65—3.4 (6H, m, ring methylenes), 2.11 (3H, s, N-CH_3), 2.85 (1H, s, OH), 3.77, 3.93 (2H, d and d, *J*=11 Hz, $C\underline{H}_2OH$), 7.1—7.6 (5H, m, ArH); IR (liquid film) 3390 (broad), 2940, 1600, 1445, 1060, 760, and 700 cm^{-1}. **7**: ^1H NMR ($CDCl_3$) δ=1.6—3.5 (7H, m, ring protons), 2.17 (3H, s, N-CH_3), 7.1—7.5 (5H, m, ArH).

The identification of **7** was confirmed by a direct comparison of the IR spectrum of a styphnate derivative from **7** with that from the authentic sample and by a melting-point value (184.5—185 °C) for a mixture of the derivatives. IR (KBr disk) of the styphnate derivative: 3425 (broad), 3030, 2760, 1650, 1590, 1540, 1460, 1380, 1345, 1300, 1200, 1090, 760, and 710 cm^{-1}.

Photolysis of 1 with Lactic Acid: The irradiation (190 min) of an aqueous solution of **1** (600 mg, 11.6 mM) containing lactic acid (5.41 g, 0.3 M) gave 760 mg of a crude oil. A GLC analysis of the oil showed the formation of three major products, **7** and two diastereomeric 1-methyl-2-(1-hydroxyethyl)-2-phenylpyrrolidines **3**. The diastereomers were separated by preparative TLC (hexane:diethyl ether=3:7, R_f=0.23 and 0.14).

3(R_f=0.23): ^1H NMR ($CDCl_3$) δ=1.05 (3H, d, *J*=6.4 Hz, CH($C\underline{H}_3$)OH), 1.90 (3H, s, N-CH_3), 1.0—3.2 (6H, m, ring methylenes), 3.84 (1H, s, OH), 4.42 (1H, q, *J*=6.4 Hz, $C\underline{H}$(CH_3)OH), 7.0—7.5 (5H, m, ArH); IR (liquid film) 3400 (broad), 2980, 1600, 1450, 1120, 765, and 705 cm^{-1}; MS (75 eV) *m/z* (rel intensity) 205 (M^+; 13), 204 (82), 160 (100).

This compound was further characterized as its styphnate derivative (mp 127.3—129.5 °C). Found: C, 50.76; H, 4.97; N, 12.72%. Calcd for $C_{19}H_{22}N_4O_9$: C, 50.67; H, 4.92; H, 12.44%.

3(R_f=0.14): ^1H NMR ($CDCl_3$) δ=0.92 (3H, d, *J*=6.4 Hz, CH($C\underline{H}_3$)OH), 2.14 (3H, s, N-CH_3), 0.85—3.3 (6H, m, ring methylenes), 3.45 (1H, s, OH), 4.06 (1H, q, *J*=6.4 Hz,

C<u>H</u>(CH$_3$)OH), 7.1—7.6 (5H, m, ArH); IR (liquid film) 3400 (broad), 2975, 1600, 1450, 1120, 765, and 705 cm^{-1}; MS (75 eV) *m/z* (rel intensity) 205 (M$^+$; 8.6), 204 (60), 160 (100).

The formation ratio of the isomers (R_f=0.23: R_f=0.14) was 1:1.2.

Photolysis of 1 with α-Hydroxyisobutyric Acid: The irradiation (180 min) of **1** (400 mg, 7.7 mM) in the presence of α-hydroxyisobutyric acid (4.16 g, 0.2 M) gave 374 mg of a crude oil. A GLC analysis of the oil showed the formation of **7** and 1-methyl-2-(1-methyl-1-hydroxyethyl)-2-phenylpyrrolidine **4**. The photoadduct **4** was isolated by preparative TLC (hexane:diethyl ether=3:7).

4: ^{1}H NMR ($CDCl_3$) δ=1.32, 1.44 (6H, s and s, C(C<u>H</u>$_3$)$_2$OH), 2.53 (3H, s, N-CH$_3$), 1.1—3.4 (6H, m, ring methylenes), 3.45 (1H, s, OH), 7.1—7.6 (5H, m, ArH); IR(liquid film) 3440 (broad), 2975, 1600, 1445, 1155, 760, and 705 cm^{-1}; MS (CI) *m/z* (rel intensity) 220 (M+H; 42), 160 (100).

An elemental analysis of the styphnate derivative of **4** (mp 130.8—133.5 °C) was as follows: Found: C, 51.79; H, 5.17; N, 12.23%. Calcd for $C_{20}H_{24}N_4O_9$: C, 51.72; H, 5.21; N, 12.06%.

Photolysis of 1 with Ethoxyacetic Acid: A GLC analysis of a crude oil (416 mg) obtained after the irradiation (120 min) of **1** (7.7 mM) in the presence of ethoxyacetic acid (0.2 M) showed the formation of 1-methyl-2-ethoxymethyl-2-phenylpyrrolidine **5** and a very small amount of **7** (<3%). The photoadduct **5** was isolated by preparative TLC (hexane:diethyl ether=3:7).

5: ^{1}H NMR ($CDCl_3$) δ=1.20 (3H, t, *J*=6.6 Hz, OCH$_2$C<u>H</u>$_3$), 1.7—2.6 (4H, m, methylenes at C-3 and C-4 of ring), 2.28 (3H, s, N-CH$_3$), 2.8—3.3 (2H, m, N-C<u>H</u>$_2$), 3.52 (2H, q, *J*=6.6 Hz, OC<u>H</u>$_2$CH$_3$), 3.6, 3.8 (2H, d and d, *J*=9.0 Hz, C<u>H</u>$_2$OCH$_2$CH$_3$), 7.1—7.7 (5H, m, ArH); IR (liquid film) 2975, 2865, 1600, 1445, 1115, 765, and 705 cm^{-1}; MS (75 eV) *m/z* (rel intensity) 219 (M$^+$, 3), 160 (100).

An elemental analysis of the styphnate derivative of **5** (mp 137.2—138.5 °C) was as follows: Found: C, 51.63; H, 5.16; N, 12.29%. Calcd for $C_{20}H_{24}N_4O_9$: C, 51.72; H, 5.21; N, 12.06%.

Photolysis of 1 with *N*-Acetylglycine: **1** (400 mg, 7.7 mM) was irradiated in the presence of *N*-acetylglycine (4.68 g, 0.2 M) for 240 min. The GLC analysis of an obtained oil (303 mg) revealed no distinct peak. 1-Methyl-2-(acetylaminomethyl)-2-phenylpyrrolidine **6** was isolated by preparative TLC (acetone) in a high yield (286 mg, 80%).

6: ^{1}H NMR ($CDCl_3$) δ=1.96 (3H, s, CH$_3$CO), 2.10 (3H, s, N-CH$_3$), 1.7—2.4 (4H, m, methylenes at C-3 and C-4 of ring), 2.6—3.2 (2H, m, methylene at C-5 of ring), 3.45, 3.93 (2H, dd and dd, *J*=13.4, 6.8, 3.4 Hz, C<u>H</u>$_2$NH), 6.05 (1H, broad s, NH), 7.1—7.5 (5H, m, ArH); IR (liquid film) 3300 (broad), 2960, 1650, 1540, 1440, 760, and 700 cm^{-1}; MS (75 eV) *m/z* (rel intensity) 232 (M$^+$; 0.16), 231 (100), 160 (63).

An elemental analysis of the styphnate derivative of **6** (mp 164.2—166.3 °C) was as follows: Found: C, 50.11; H, 5.00; N, 14.59%. Calcd for $C_{20}H_{23}N_5O_9$: C, 50.32; H, 4.86; N, 14.67%.

Photolysis of 1 with α-Amino Acids: A GLC analysis of a crude oil (250 mg), obtained after the irradiation (300 min) of **1** (400 mg, 7.7 mM) in the presence of α-aminoisobutyric acid (4.12 g, 0.2 M), showed the formation of **7**; other products were not identified.

When glycine was used as a carboxylic acid, **7** was also detected as a product.

Photolysis of 1 with 2-Mercaptopropionic Acid: An argon-purged aqueous solution (20 cm^3) containing **1** (40.0 mg, 7.7 mM) and 2-mercaptopropionic acid (0.425 g, 0.2 M) in a Pyrex glass tube was irradiated using a merry-go-round apparatus (described below) for 300 min. The photolysate was acidified (pH 1) with HCl and concentrated to ca. 2 cm^3 in vacuo. The concentrate was made basic (pH 10) with NaOH and then extracted with 6 cm^3 of chloroform. In this extract, only the reduction product **7** was detected as a major product by means of a GLC analysis.

Identification and Determination of Carbonyl Compounds: Aldehydes and acetone formed during photoreactions of the hydroxyalkanoate systems were isolated as their 2,4-dinitrophenylhydrazone derivatives which were identified by a direct comparison of the IR spectra and melting points with those of authentic samples. These derivatives were determined by means of HPLC (JASCO Familic-100, SC-01, 80% methanol).

Determination of Quantum Yields. The qantum yield for the formation of **2** was measured using a linear optical-bench system equipped with a 500 W super-high-pressure mercury lamp (Ushio USH-500D) at 25±1 °C. The beam of the 280 nm band was isolated with a monochromator (Jarrel Ash JE-25E) and was divided into two portions using a beam splitter tilted at 45° with respect to the beam. The transmitted light was used to irradiate an argon-purged aqueous solution (pH 6.0, [**1**]=1.00×10^{-3} M, [glycolate]=0.5 M, [$NaClO_4$]=0.5 M) in a cyclindrical cell (20×10 mm). It absorbed >96% of the light during photolysis runs. The diverted light (perpendicular to the transmitted light) was received by a UV radiometer (TOPCON UVR-254) in order to monitor the light output. The amount of transmitted light (1.54×10^{14} quanta s^{-1}) absorbed by the sample solution was determined by a calibration of the radiometer against the trioxalatoferrate-(III) actinometry (0.006 M potassium trioxalatoferrate-(III)).[19]

Product analyses were performed by GLC for the reaction mixtures. These were worked up in the same way as the preparative run using 9,10-dihydroanthracene as an internal standard: ϕ_a=0.057, 0.060, and 0.068 at 1.11, 1.08, and 0.878×10^{18} quanta of absorbed photons.

The quantum yields for the formation of the other photoadducts (**3**, **4**, and **5**), for the formation of reduction product, **7**, and for the disappearance of **1** were determined at 25±1 °C using a merry-go-round apparatus equipped with the same 400 W high-pressure mercury lamp that was employed for the preparative run. Aqueous solutions (20 cm^3) in Pyrex glass tubes containing **1** of 1.00×10^{-3} M, carboxylic acids of 0.5 M and $NaClO_4$ of 0.5 M were adjusted to pH 6.0. The glycolic acid solution employed for the determination of the quantum yield for the formation of **2** was used as an actinometer solution. Photolysates were subjected to a GLC analysis in the same manner as for the determination of the quantum yield of **2**. Internal standards were the same as those used for the determination of chemical yields in the preparative runs. The degrees (<10%) of the disappearance of **1** were obtained from the decrease of the absorbance at λ_{max} of 258 nm.

The relative quantum yields at different concentrations of glycolate and at different concentrations of $NaClO_4$ and

the pH dependencies of the quantum yields were also determined using the merry-go-round apparatus as described above.

Cyclic Voltammetry. The CV measurements were carried out using a Yanaco P8-ES unit and a Yanaco P8-PT potentiostat. The working electrode in a three-electrode cell was a platinum disk (3 mm diameter) sealed into a teflon tube and the counter electrode was a pool of mercury. SCE was used as a reference electrode. Current-voltage curves were recorded on a Yokogawa 3078 X-Y recorder. The reduction current of **1** was observed as a discernible shoulder on the large reduction wave of water when an aqueous solution containing **1** of 5.0×10^{-3} M and $NaClO_4$ of 0.1 M was used. The measured value (−0.95 V) was almost the same in magnitude as the value obtained in acetonitrile.[4] For a determination of the oxidation potentials of 2-mercaptopropionic acid and its carboxylate anion, aqueous solutions containing the acid of 4.0×10^{-3} M and $NaClO_4$ of 0.5 M were used. With the carboxylate anion, the pH of the aqueous solution was adjusted to 6.0 with NaOH.

The authors wish to express their thanks to Professor Patrick S. Mariano of the University of Maryland for his stimulating suggestions. We also would like to thank Professor Masashi Tashiro, the Research Institute of Industrial Science of Kyushu University, for elemental analyses and mass spectral measurements, and the staff of Oita Works of Sumitomo Chemical Co., Ltd. for CI-Mass measurements.

References

1) a) J. R. Barnett, A. S. Hopkins, and A. Ledwith, *J. Chem. Soc., Parkin Trans. 2*, **1973**, 80; b) D. R. G. Brimage, R. S. Davidson, and P. R. Steiner, *J. Chem. Soc., Perkin Trans. 1*, **1973**, 526; c) R. Noyori, M. Kato, M. Kawanishi, and H. Nozaki, *Tetrahedron*, **25**, 1125 (1969); d) I. Ahmad and G. Tollin, *Photochem. Photobiol.*, **34**, 441 (1981); e) M. Novak, A. Miller, T. C. Bruice, and G. Tollin, *J. Am. Chem. Soc.*, **102**, 1465 (1980).

2) R. S. Davidson and P. R. Steiner, *J. Chem. Soc., Perkin Trans. 2*, **1972**, 1357 and references therein.

3) J. Libman, *J. Am. Chem. Soc.*, **97**, 4139 (1975).

4) P. S. Mariano, *Acc. Chem. Res.*, **16**, 130 (1983) and references therein.

5) For example, F. T. Chiu, J. W. Ullrich, and P. S. Mariano, *J. Org. Chem.*, **49**, 228 (1984).

6) Y. Kurauchi, K. Ohga, H. Nobuhara, and S. Morita, *Bull. Chem. Soc. Jpn.*, **58**, 2711 (1985).

7) a) D. H. Geske, *J. Electroanal. Chem.*, **1**, 502 (1960); b) C. K. Mann and K. Barnes, "Electrochemical Reactions in Nonaqueous System," Mercel Dekker, New York (1970), Chap. 4.

8) a) P. S. Mariano, J. Stavinoha, and E. Bay, *Tetrahedron*, **37**, 3385 (1981); b) J. Stavinoha, E. Bay, A. Leone, and P. S. Mariano, *Tetrahedron Lett.*, **1980**, 3455.

9) The diffusion-controlled rate constant (k_{diff}) was calculated from the Debye equation, $k_{diff}=8RT/3000\eta(M^{-1}s^{-1})$. As a viscosity η was used a value (0.9845 cp) for an aqueous solution (pH 6.0) containing $NaClO_4$ of 0.5 M and glycolic acid of 0.5 M, which was measured with an Ostwald viscosimeter at 25.00±0.05 °C.

10) D. Rehm and A. Weller, *Isr. J. Chem.*, **8**, 259 (1970).

11) a) The anodic wave of acetate is also difficult to be observed in aqueous solutions;[11b] b) M. Hojo and Y. Imai, *Bull. Chem. Soc. Jpn.*, **56**, 1963 (1983).

12) L. Eberson, "Carboxylic Acids," in "Organic Electrochemistry," ed by M. M. Baizer, Marcel Dekker, New York (1973), Chap. XIII.

13) C. Nagata and T. Yamaguchi, *Radiat. Res.*, **73**, 430 (1978).

14) a) S. L. Murov, "Handbook of Photochemistry," Marcel Dekker, New York (1973), p. 197; b) Y. L. Chow, W. C. Danen, S. F. Nelsen, and D. H. Rosenblatt, *Chem. Rev.*, **78**, 243 (1978).

15) K. W. Blake, L. Gillies, and R. C. Denney, *J. Chem. Soc., Perkin Trans. 1*, **1981**, 700.

16) a) In fact, the decarboxylation of an acetoxyl radical is a rapid process and the half-life of the radical has been estimated to be of the order of 10^{-9}—10^{-10} s at 60 °C;[16b] b) W. Braun, L. Rojbenbach, and F. R. Eirich, *J. Phys. Chem.*, **66**, 1591 (1962); K. -O. Hiller, B. Masloch, M. Göbl, and K. -D. Asmus, *J. Am. Chem. Soc.*, **103**, 2734 (1981).

17) a) A. Padwa, *Chem. Rev.*, **77**, 37 (1977) and references therein; b) D. C. Neckers, "Mechanistic Organic Photochemistry," Reinhold, New York (1967), Chap. 7.

18) During the fluorescence quenching experiments, the instability was able to be neglected.

19) C. G. Hatchard and C. A. Parker, *Proc. R. Soc. London, Ser. A*, **235**, 518 (1956).

Photoionization Threshold Energies of Amine Solutions Studied by Photoelectron Emission by Solution

Iwao WATANABE,* Keiichi MAYA, Yoshiki YABUHARA, and Shigero IKEDA
Department of Chemistry, Faculty of Science, Osaka University,
Toyonaka, Osaka 560
(Received June 28, 1985)

The threshold energies E_t of photoelectron emission by solutions (PEES) were determined for several butylamines in acetonitrile and water. The correlations between E_t and gas-phase ionization potential I_P and oxidation potential E_{ox} were found to be linear. The difference between E_t and I_P originates from the electronic polarization energy of solvent molecules and the polarization energy was found to be inversely proportional to the solvation radius in accordance with the Born solvation free energy model. The E_t values were also compared with E_{ox} to discuss the reorientation relaxation of solvent molecules in the electron transfer process. The selective coverage of aqueous solution surface with amine molecule was indicated by the PEES technique.

The reactivity of an electron donor in solution is often estimated from its gas-phase ionization potential I_P or from the electrochemical oxidation potential E_{ox}. There are, however, many molecules which do not allow the measurement of I_P or E_{ox}. Low vapor pressure molecules of high molecular weight or ionic species present only in solvated state are almost out of the reach of the gas-phase UPS technique, while some molecules do not give clear oxidation wave owing to the limitations of availability of electrode material or supporting electrolytes, or to irreversible chemical reaction involved in the electron transfer reaction. The most controversial point on the use of I_P may be the complete neglect of solvation effects.

Although the UPS of solution samples have been measured for inorganic anions[1] and organic molecules,[2] the solvents used have been limited to the organic materials of the lowest vapor pressures.

The photoelectron emission by solution (PEES) experiment[3] is a new technique which has been used to determine the external ionization potential I_P(ext) of solvated organic[4] and inorganic anions[5] and metal cations[6] in aqueous solutions and it should be able to treat almost any solvent and any solvated species. The I_P(ext) can be obtained as the photoionization threshold energy E_t by using the PEES technique. The E_t for a molecule X corresponds to the energy change of the following reaction,

$$X(solv) \rightarrow X^+(solv) + e^-(vac). \qquad E_t \qquad (1)$$

The E_t is different from the internal ionization potential I_P(int) by the amount of V_0, the conduction band energy of the solvent referred to vacuum, and therefore, the reference level of the I_P(int) depends on the solvent while that of the E_t does not.

The I_P(int) corresponding to the following reaction,

$$X(solv) \rightarrow X^+(solv) + e^-(solv), \qquad I_P(int) \qquad (2)$$

has been determined either by measuring photoconductance[7] or by detecting solvated electron.[8] The photoconductance measurement can be performed only with low conductance organic solvents and the detection of solvated electron involves rather complicated experiments. On the other hand, the E_t measurement by PEES can treat not only low conductance organic solvent but also high conductance ionic aqueous solution and the concept of the experiment is rather simple.

This work reports the E_t values for primary, secondary, and tertiary butylamines in acetonitrile and water to be compared with gas-phase I_P and E_{ox} in solution. Both I_P and E_{ox} are available for these amines and the character of their HOMO is well understood.[9] The differences between E_t, I_P and E_{ox} will be interpreted in terms of their solvation radii and the reorientation of solvent molecules after the photoionization.

Experimental

The photoelectron emission spectra were obtained with a new instrument which is similar to the reported.[3a] In this paper, only the modification from the original will be described.

1. The VUV monochromater used is Model 302-VM (λ-Minuteman Lab., Acton, Mass., USA), focal length; 20 cm, grating; 1200 lines/mm. The slit width was 1 mm.

2. Photoelectron current was detected by using a charge integrator instead of a lock-in amplifier. The charge integrator is an Electrometer Operational Amplifier (Keithley Model 301) having a feedback capacitor of 100 pF and a mercury relay switch to discharge the capacitor. The integration and the discharge were synchronized to the rotation of a glass wheel covered with sample solution. The integration time was normally 1 s during which the wheel rotated exactly 4 times.

3. In order to monitor the photon intensity a part of the photon beam just after the exit slit was accepted by a sodium salicylate film on the end (cut at 45° and polished) of a quartz optical fiber (1 mm dia.) which guided the converted UV light to a photomultiplier (Hamamatsu,

R647). The current from the photomultiplier was fed to another integrator which worked exactly in the same manner as the one for the photoelectron current.

4. A beam shutter driven magnetically from outside the lamp housing was placed between the hydrogen lamp and the entrance slit of the monochromater. The shutter was open for 1 s to measure photoelectron current and close for the same period to measure "dark current."

In order to get high photon flux relatively wide slit width was used. Therefore, all the E_t values were corrected according to the resolution of the monochromater.

The spectra were taken at −30 °C for acetonitrile solutions and at 1 °C for aqueous solutions. In order to discriminate the photoionization of gaseous molecules from that of solution, the spectra at several different temperatures were also obtained for the acetonitrile solutions.

This technique is rather insensitive to impurity and needs a relatively high concentration solution, 0.1—1 mol dm^{-3}. However, the aqueous solution was extremely sensitive to the contamination from surface active species. Therefore, the spectrum for aqueous solution was always obtained after a run with pure water to evaluate the contribution from contaminations.

The water content in acetonitrile used was determined by Karl Fischer titration method. Though the content varied from 12 to 54 mmol dm^{-3}, it did not cause any change in the PEE spectra of amines.

The gas-phase He(I)-UPS had also been carried out in this laboratory.[10]

Results

In Fig. 1 are shown the PEE spectra of 0.1 mol dm^{-3} butylamine in acetonitrile at different temperatures. The PEE spectra show the quantum yield Y of photoelectron emission per incident exciting photon at the energy of the photon $h\nu$. The spectrum of acetonitrile (curve D) is included to show that the photoionization of the solvent was not detected. As the solution is cooled down, the yield at high energy region decreases, but that between 8 and 8.5 eV increases. The yield current at higher photon energy (>8.6 eV) is concluded to be originated from the photoionization of gaseous amine molecules present in the space between the exit window of the monochromater and the solution, since the rising point of the curve A is very close to the adiabatic I_P for butylamine (8.62 eV). At the lower temperature, viz. in the lower gas pressures of the amine and acetonitrile, the photoelectron from the solution increases. This is the result of the reduction of photoelectron collision with the gaseous molecules. The PEE spectra were taken at the lowest possible temperature, i.e. −30 °C for acetonitrile solutions, and only low energy region of the spectrum (lower than gas I_P) was used to determine the threshold energy.

The threshold energy E_t is determined by using the extrapolation method based on the following equation by Brodsky-Tsarevsky,[11]

$$Y = (h\nu - E_t)^n, \tag{3}$$

where $h\nu$ is the exciting photon energy. The PEES study on aqueous solutions has been done successfully by plotting $Y^{1/n}$ against photon energy with n value of 2 or 2.5 to determine E_t as follows,[3b,3c]

$$Y^{1/n} = h\nu - E_t. \tag{4}$$

In the present study on amines, n value of 2.5 gave better linear plot than 2 for all of the PEE spectra obtained. An example of the $Y^{0.4}$ plot to determine E_t is shown in Fig. 2 for the curve A, the same spectrum as C in Fig. 1.

Although it has recently been reported that the shape of the photoelectron emission yield against photon energy should be affected by dielectric dispersion of the solvent,[12] the difference on E_t resulted from the use of 2 or 2.5 for n value amounted 0.1 eV normally and the difference, therefore, does not affect the present discussion.

The quantum yield from butylamine in acetoni-

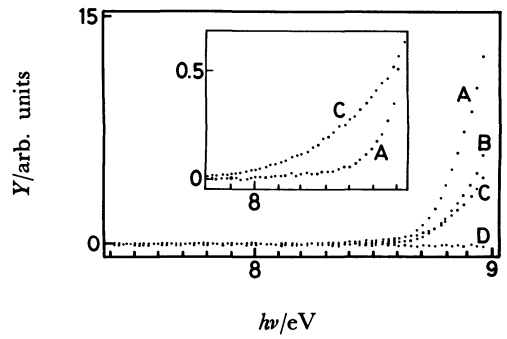

Fig. 1. PEE spectra of 0.1 mol dm^{-3} butylamine in acetonitrile taken at different temperatures. A: 1 °C, B: −10 °C, C: −30 °C, D: acetonitrile only at −30 °C.

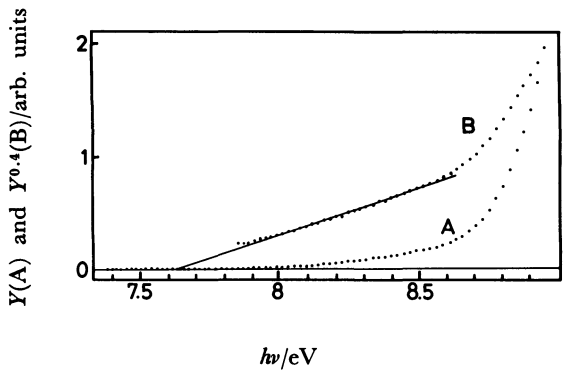

Fig. 2. PEE spectrum of 0.1 mol dm^{-3} butylamine in acetonitrile at −30 °C (A) and its $Y^{0.4}$ plot (B) to determine E_t.

trile solution is proportional to the concentration as shown in Figs. 3 and 4. In Fig. 3 are shown the yields at different photon energies, while the relation between the slope of the $Y^{0.4}$ plot and the concentration is shown in Fig. 4 by taking $(dY^{0.4}/dE)^{2.5}$ vs. concentration. In the figure are also included the E_t values determined at different concentrations. The yields for all the amines studied in acetonitrile were proportional to their concentrations, although the low solubility of tributylamine limited the highest yield at around 0.05 mol dm^{-3}.

Another example of PEE spectrum is shown in Fig. 5 for butylamine in water containing 10 mmol dm^{-3} KOH to suppress the protonation of the amine. It seems that the $Y^{0.4}$ plot is composed of two lines. One of them is drawn in the figure, which gives the E_t value of around 7.6 eV for the amine in water. The other corresponds to the ionization either of 10 mmol dm^{-3} OH^- ion whose E_t has been reported to be 8.45 eV,[13] or of gaseous amine. The yield from butylamine in aqueous solution is not proportional to the concentration as shown in Fig. 6. The 1 mmol dm^{-3} solution gave almost the same spectrum as the 0.1 mol dm^{-3} solution. This fact indicates that the surface of aqueous solution is covered with butylamine molecule and that this spectroscopic technique is sensitive only to the surface of the solution. The E_t obtained for butylamine in water (7.7 eV) is the same as that in acetonitrile. The PEE spectra of secondary and tertiary butylamines in water gave E_t values similar to the I_P values for the corresponding gas molecules, therefore, they will not be reported here.

The E_t values determined were corrected for the resolution of the monochromater and are collected in Table 1 together with I_P and E_{ox} values, by He(I)-UPS[9,10] and cyclic voltammetry,[14] respectively.

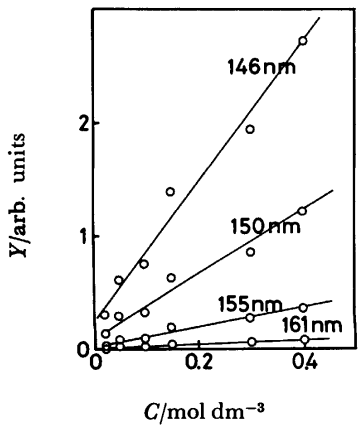

Fig. 3. Dependence of quantum yield Y on the concentration C of butylamine in acetonitrile at different exciting photon wave lengths. $T=-30$ °C.

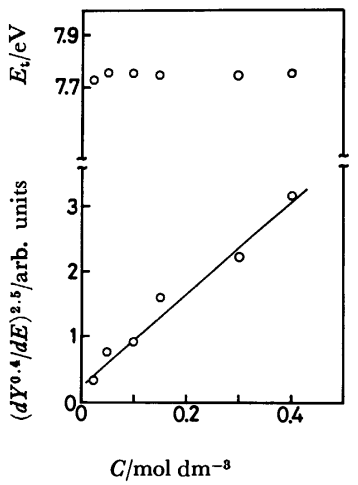

Fig. 4. Correlations between the slope of $Y^{0.4}$ plot and the concentration C shown as $(dY^{0.4}/dE)^{2.5}$ vs. C, and the threshold energy E_t and C for butylamine in acetonitrile. $T=-30$ °C.

Discussion

Correlation between E_t and I_P. The correlation

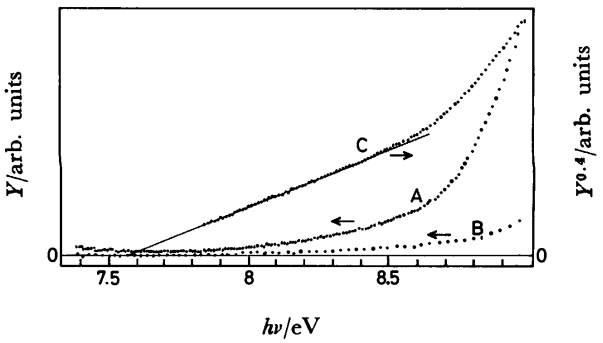

Fig. 5. PEE spectra of 0.1 mol dm^{-3} butylamine in 10 mmol dm^{-3} KOH aqueous solution (A) and 10 mmol dm^{-3} KOH aqueous solution (B). $Y^{0.4}$ plot for curve A is included (C). $T=1$ °C.

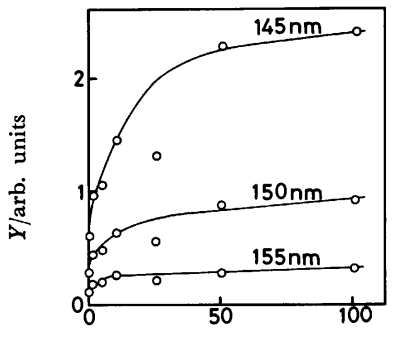

Fig. 6. Dependence of quantum yield Y for butylamine in 10 mmol dm^{-3} KOH aqueous solution at different exciting photon wave lengths upon the concentration C of the amine. $T=1$ °C.

Table 1. I_P, E_t and E_{ox} Values, and the Parameters Calculated for Acetonitrile Solutions

	I_{Pa}	I_{Pv}	E_t	$-P_+$	r	E_{ox}	$-R$[c]	$-R_{out}$
	eV	eV	eV	eV	nm	V	eV	eV
Butylamine	8.62	9.29	7.73	1.22	0.31[a] 0.27[b]	1.63	1.60	1.17
Isobutylamine	8.65	9.29	7.69	1.28	0.30[a] 0.27[b]	1.62	1.57	1.23
t-Butylamine	8.64	9.24	7.67	1.27	0.30[a] 0.27[b]	1.64	1.53	1.22
Dibutylamine	7.83	8.49	7.04	1.12	0.34[a] 0.32[b]	1.31	1.23	1.07
Diisobutylamine	7.77	8.47	7.04	1.08	0.35[a] 0.32[b]			
Tributylamine	7.20	7.88	6.68	0.86	0.44[a] 0.36[b]	1.02	1.16	0.82
Ethylenediamine	8.51	9.29	7.55	1.35	0.28[a] 0.23[b]			
Benzene	9.25	9.25	7.80	1.44	0.26[a] 0.26[b]			

a) Calculated from P_+. b) Calculated from densities at −30 °C. If the data are not available, they are estimated by extrapolating known values, Ref. 19. c) Calculated from E_t and E_{ox} ($-R=E_t-E_{ox}-4.5$). The 4.5 is to convert the value (vs. NHE) to the one referred to vacuum level.[26]

between E_t measured in acetonitrile and I_P in gas-phase was found to be linear,

$$E_t = 0.73 \times I_{Pa} + 1.40 \quad (5)$$

or

$$E_t = 0.74 \times I_{Pv} + 0.81, \quad (6)$$

where I_{Pa} and I_{Pv} are adiabatic or threshold and vertical ionization potentials for gaseous molecule, respectively. Therefore, the *photochemical* reactivity of the amine as an electron donor in acetonitrile can well be estimated from the gas-phase I_P values. The term *photochemical* is used here to distinguish vertical transition from adiabatic reaction process. Since I_P corresponds to the energy change of the following reaction,

$$X(vac) \rightarrow X^+(vac) + e^-(vac), \qquad I_P \quad (7)$$

the difference ($I_P - E_t$) comes from the difference between solvation energies $\Delta G(solv)$ of X and X^+,

$$X(vac) \rightarrow X(solv), \qquad \Delta G(solv) \quad (8)$$

$$X^+(vac) \rightarrow X^+(solv). \qquad \Delta G^+(solv) \quad (9)$$

$$I_P - E_t = \Delta G(solv) - \Delta G^+(solv). \quad (10)$$

It has been known that there exists the surface potential at a gas/solution interface (0.08±0.06 V for water[15] and −0.10±0.06 V for acetonitrile[16]). Though the values of E_t and $\Delta G^+(solv)$ include the surface potential, the effect of the potential is cancelled in Eq. 10, because the potential which accelerates the escaping photoelectron from solution to gas phase also accelerates the incoming cation from gas phase into solution by the same amount. In any case, the surface potential is considered to be small and will be neglected in the present study.

Note that the species $X^+(solv)$ which appears in Eqs. 1 and 9 is not completely solvated, because the photoionization leaves X^+ ion having the same solvation geometry as the neutral molecule X. Only the electronic polarization of the solvent molecules is induced by the photoionization of X. One, therefore, divides $\Delta G^+(solv)$ into $\Delta G(solv)$ and the polarization energy P_+,

$$\Delta G^+(solv) = \Delta G(solv) + P_+. \quad (11)$$

From Eqs. 10 and 11,

$$I_P - E_t = -P_+. \quad (12)$$

The polarization energy is frequently estimated by modifying the Born equation[17] for the electrostatic solvation energy of ion as follows,

$$P_+ = -(e^2/2r)(1 - \varepsilon_{op}^{-1}), \quad (13)$$

where r is the radius of the central ion, ε_{op} the optical dielectric constant of the solvent. Since, as already mentioned, the geometry of $X^+(solv)$ is quite the same as X(solv), r could be called the *radius of solvation sphere of the neutral molecule* X. Now we can obtain the r by using Eq. 13.

The problem one must answer for the use of Eq. 12 to obtain P_+ is whether the E_t value determined by the present method corresponds to adiabatic or vertical ionization process of the species in the solvent, or to somewhere else. We have obtained[18] a theoretical yield spectrum by use of Eq. 3 with an assumption that the density of states for amine molecules in solution is the same as that in gaseous phase, i.e. the Y was obtained by a convolution calculation of the gas-UPS band with Eq. 3. The UPS first band of butylamine pertaines to the ionization of nitrogen lone pair electron and is broad (0.83 eV in the half width). If the extrapolation to $Y^{0.4}=0$ on the theoretical yield curve is performed near to the threshold region, the E_t value comes close to I_{Pa}, while the extrapolation gives the value of I_{Pv} if the theoretical curve at far high energy region from I_{Pv} is used. In the higher energy region of the real PEE spectra there are other photoionization processes, e.g. the photoionizations of other species in the solution and the gaseous amine molecule. On the other hand, lower energy region is obscured by noise current. Therefore, the usable region for the extrapolation is limited to about 0.5 eV in the present study on amines. Our simulation calculation indicates that the extrapolation in the present study gives the E_t value corresponding to the midpoint of I_{Pa} and I_{Pv}. In the PEE studies by Delahay, the lenghth of the region for extrapolation used to determine E_t is almost 1 eV or even longer.[5] He considered the E_t obtained by his extrapolation method as the vertical ionization potential of the solute. In the present study we take the average of I_{Pa} and I_{Pv} as the I_P for gaseous amine to compare with E_t. Thus,

$$-P_+ = (I_{Pa} + I_{Pv})/2 - E_t. \quad (14)$$

The values of P_+ and r calculated by using Eq. 13 are included in Table 1. The ε_{op} in Eq. 13 is estimated to be 1.89[19] for acetonitrile at −30 °C.

The values of r should be used only to estimate the degree of solvation because of the following reason. Neither the geometrical shape nor the charge distribution on the amine cation is spherical. The density of the positive charge on the cation must be localized on the nitrogen atom, since the photoionization removes the nitrogen lone pair electron. The polarization energy is the function of the distance between charge center and solvent molecules, and the number of solvent molecules around the cation. We call the r most appropriately *effective* solvation radius.

The r of 0.25 nm is obtained for butylamine in water and is smaller than that in acetonitrile. The decrease of r in water could be interpreted in terms of the hydrogen bonds between the amine and water molecules. However, the fact that the amine molecule is deposited on the aqueous solution surface implies that such molecule must have smaller number of solvent molecules and thus larger effective solvation radius. We certainly need more knowledge of the solution structure of alkylamine to interpret the value of r.

Correlation between E_t and E_{ox}. Most of the butylamines studied in the present study can be oxidized electrochemically on a platinum electrode in acetonitrile. The oxidation potentials E_{ox} determined with cyclic voltammetry by Mann[14] are also included in Table 1. Since the cyclic voltammetry gives completely irreversible waves for the alkylamines, the E_{ox} values read at the peak position in the voltammograms are by no means equilibrium potentials thermodynamically meaningful and the values must depend on sweep rate and other experimental conditions.[25] In view of the present study, the E_{ox} values are considered to be the potentials at which the following one-electron oxidation reaction can take place at a rate comparable to that of diffusion process.

$$X(solv) \rightarrow X^+(solv) + e^-(electrode). \quad E_{ox} \quad (15)$$

If the E_{ox} were of an equilibrium oxidation potential, the difference between E_t and the E_{ox} both referred to the common vacuum level[26] should be the reorganization energy for the electron transfer reaction 15.[3c] That is because E_t is the energy difference between solvated molecule X and the cation X^+ with the same molecular and solvation structures as the neutral molecule X, while E_{ox} is the energy difference between the X and the X^+ with the most stable molecular and solvation structures. Therefore the energy states for the cations X^+ in Eqs. 1 and 15 are not the same.

Due to the irreversibility in the alkylamine case, however, the interpretation of the difference $(E_t - E_{ox})$ is not straightforward, but should be as follows. The difference is the relaxation energy from the photoionized state which corresponds to the ion having the same molecular and solvation geometries as the neutral molecule, to the partially relaxed ionic state as for the molecular (inner) and solvation (outer) geometries which corresponds to the transition state of the electron transfer. The plot of E_{ox} vs. E_t gives a line with a slope of 0.58 as shown in Fig. 7. The difference $(E_t - E_{ox})$, containing the relaxation energy R to the transition state, is greater for the smaller amine. Since the molecular relaxation energies R_{in} estimated from $(I_{Pa} - I_{Pv})$ are almost the same (0.60—0.68 eV) for the amines studied, the difference reflects the outer relaxation R_{out}. Therefore, the reorientation energy of acetonitrile molecules around the smaller amine cation is greater.

The R_{out} for metal complex has been calculated for the studies on the PEE of aqueous solutions[5,20,21] by

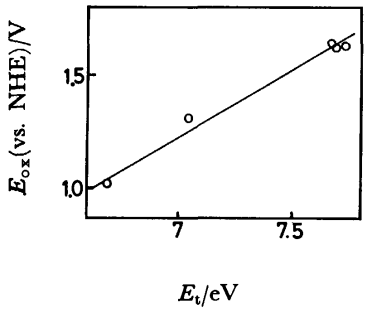

Fig. 7. Correlation between oxidation potential E_{ox} and threshold energy E_t of butylamines in acetonitrile. The data for E_{ox} are taken from Ref. 14.

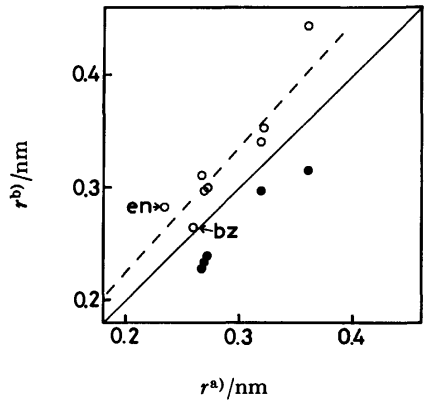

Fig. 8. Correlation between solvation radii determined from the densities of pure liquid $r^{a)}$ and PEE experiments $r^{b)}$; from polarization energy (○) and reorganization energy (●). The densities at −30 °C are estimated by extrapolating known values, Ref. 19. Solid line: slope=1, corresponding to k=0.5, broken line: the line corresponding to k=0.558, see the text. en: ethylenediamine, bz: benzene.

using the following equation,

$$R_{out} = -(e^2/2r)(\varepsilon_{op}^{-1} - \varepsilon_s^{-1}), \quad (16)$$

where ε_s is the static dielectric constant of solvent. The same equation has been used to calculate outer-sphere activation energy for electron exchange reactions.[22]

Since we already know the r value from polarization energy, the values of R_{out} can be calculated by using Eq. 16 and are listed in Table 1. The calculation concludes that most part of R comes from R_{out}.

Estimation of r. There are several different ways to estimate the value of r. Delahay[3c] calculated the r using the molecular density δ of pure material as follows,

$$r = k(m/\delta)^{1/3}, \quad (17)$$

where m is the molecular weight and k is $(3/4\pi)^{1/3}$ (=0.62). Inokuchi et al. have calculated the polarization energies for aromatic[23] and aliphatic[24] hydrocarbons using Eqs. 13 and 17 with k=0.5, and they obtained good agreement with experimental polarization energies for solid hydrocarbons. They also tried other r values but the agreement was poorer.

The r values determined from polarization energies and calculated by using Eq. 17 with k=0.5 are compared in Fig. 8. The result of Fig. 8 shows that the best linear relation between the r values is obtained at k=0.558. It was also found that the polarization energy obtained by taking I_P in Eq. 12 from I_{Pa} instead of $(I_{Pa}+I_{Pv})/2$ gave unreasonably large r values and, on the other hand, from I_{Pv} too small r. This fact is considered supporting our simulation calculation which indicates that the E_t values for amines are average ionization potentials for vertical and adiabatic processes.

Since the experimental value of $(E_t - E_{ox})$ seems to be almost equal to the outer relaxation energy, the estimation of r is attempted by taking $R_{out} = -(E_t - E_{ox})$ and by using Eq. 16 and the r values so obtained are plotted in Fig. 8. The agreement of the r values from the polarization and relaxation energies and from the densities implies that the Born approximation should be useful for a rough estimate of energetics of PEE process.

In the figure are added other experimental results for benzene and ethylenediamine. The added points lie on the same line as for amines. We have expected that these two molecules might behave in different way, because the butylamine cation has the electronic charge localized on the nitrogen atom, while the charge on benzene ion must be delocalized and two equivalent nitrogen atoms in ethylenediamine may contribute to the delocalization of cationic charge on the molecule. However, the experimental results show that the Born approximation could be applied to either of linear, plane or unsymmetrical molecule equally well. At the present stage, therefore, the PEES experiment can not predict how the charge produced by photoionization is distributed on the cation.

The present work was supported by a Grant-in-Aid for Developmental Scientific Research No. 56840002 and a Grant-in-Aid for Scientific Research No. 58540285 from the Ministry of Education, Science and Culture.

References

1) a) R. E. Ballard, J. Jones, and D. Hart, *J. Electron Spectrosc. Relat. Phenom.*, **26**, 31 (1982); b) R. E. Ballard, J. Jones, E. Sutherland, and Chun B. L., *Chem. Phys. Lett.*, **97**, 419 (1983); c) L. Nemec, B. Baron, and P. Delahay, ibid., **16**, 278 (1972); d) L. Nemec and P. Delahay, *J. Chem. Phys.*, **57**,

2135 (1972); e) L. Nemec, L. Chia, and P. Delahay, *J. Phys. Chem.*, **79**, 2935 (1975).

2) H. Aulich, L. Nemec, L. Chia, and P. Delahay, *J. Electron Spectrosc. Relat. Phenom.*, **8**, 271, (1976).

3) a) I. Watanabe, J. B. Flanagan, and P. Delahay, *J. Chem. Phys.*, **73**, 2057 (1980); b) P. Delahay, *Acc. Chem. Res.*, **15**, 40 (1982); c) P. Delahay, "Electron Spectroscopy: Theory, Techniques and Applications," ed by C. R. Brundle and A. D. Baker, Academic Press, London(1984), Vol. 5, pp. 124—196.

4) K. von Burg and P. Delahay, *Chem. Phys. Lett.*, **86**, 528 (1982).

5) K. von Burg and P. Delahay, *Chem. Phys. Lett.*, **78**, 287 (1981).

6) P. Delahay, K. von Burg, and A. Dziedzic, *Chem. Phys. Lett.*, **79**, 157 (1981).

7) J. Bullot and M. Gauthier, *Can. J. Chem.*, **55**, 1821 (1977).

8) A. Bernas, D. Grand, S. Hautecloque and A. Chambaudet, *J. Phys. Chem.*, **85**, 3684 (1981).

9) M. Takahashi, I. Watanabe, and S. Ikeda, *J. Phys. Chem.*, **87**, 5059 (1983).

10) M. Takahashi, I. Watanabe, and S. Ikeda, *J. Electron Spectrosc. Relat. Phenom.*, **37**, 275 (1985).

11) A. M. Brodsky and A. V. Tsarevsky, *J. Chem. Soc., Faraday Trans. 2*, **72**, 1781 (1976).

12) P. Delahay and A. Dziedzic, *J. Chem. Phys.*, **80**, 5381 (1984).

13) P. Delahay and K. von Burg, *Chem. Phys. Lett.*, **83**, 250 (1981).

14) C. K. Mann, *Anal. Chem.*, **36**, 2424 (1964).

15) J. E. B. Randles, *Phys. Chem. Liq.*, **7**, 107 (1977).

16) B. Case, N. S. Hush, R. Parsons, and M. E. Peover, *J. Electroanal. Chem.*, **10**, 360 (1965).

17) M. Born, *Z. Phys.*, **1**, 45 (1920).

18) K. Maya, I. Watanabe, and S. Ikeda, *J. Electron Spectrosc. Relat. Phenom.*, to be submitted.

19) "International Critical Tables of Numerical Data, Physics, Chemistry, and Technology," ed by E. W. Washburn, McGraw-Hill, New York (1926).

20) P. Delahay, *Chem. Phys. Lett.*, **87**, 607 (1982).

21) P. Delahay and A. Dziedzic, *J. Chem. Phys.*, **80**, 5793 (1984).

22) J. O'M. Bockris and S. U. M. Khan, "Quantum Electrochemistry," Plenum Press, New York (1979).

23) N. Sato, K. Seki, and H. Inokuchi, *J. Chem. Soc., Faraday Trans. 2*, **77**, 1621 (1981).

24) K. Seki and H. Inokuchi, *Bull. Chem. Soc. Jpn.*, **56**, 2212 (1983).

25) H. Matsuda and Y. Ayabe, *Z. Elektrochem.*, **59**, 494 (1955).

26) R. M. Noyes, *J. Am. Chem. Soc.*, **84**, 513 (1962).

^{1}H NMR Studies on the Reorientational Motions of Cations in Four Solid Phases of Methylammonium Iodide and the Self-Diffusion of Ions in Its Highest-Temperature Solid Phase

Hiroyuki Ishida, Ryuichi Ikeda, and Daiyu Nakamura*
Department of Chemistry, Faculty of Science, Nagoya University,
Chikusa-ku, Nagoya 464
(Received September 20, 1985)

Four solid phases of CH_3NH_3I named as α', β', δ, and ε were studied by the temperature dependence of ^{1}H spin-lattice relaxation time T_1 and ^{1}H spin-spin relaxation time T_2 (for ε) at several NMR frequencies, and of ^{1}H NMR second moment. Phase transitions were studied by means of differential thermal analysis and ^{1}H T_1. The X-ray powder patterns of the highest-temperature ε phase taken at ca. 440 K revealed that the crystal forms a CsCl-type cubic lattice. The measurements of differential scanning calorimetry gave unusually small entropy of melting indicating that the cations of the ε phase are in a state having the most part of their motional freedom. From ^{1}H NMR T_1 experiments, it was found that the transformation of the room-temperature α' phase to the low-temperature stable β' phase needed longer time than three months at Dry Ice temperature for samples carefully purified and dried for a long time under vacuum whereas it was completed within two weeks for roughly dried samples. The NMR results indicated that the cations are bound tightly in the β' phase whereas they are fairly free to reorient in the low-temperature substable δ phase. In the α' phase, the cations perform C_3 reorientations very rapidly about their C–N bond axis. The cations of the ε phase undergo overall rotation as well as self-diffusion which was confirmed by electrical conductivity measurements. The mechanism of the self-diffusion of the cations is discussed.

Methylammonium iodide (MAI) had been known for a long time to form two solid phases below room temperature from the temperature dependence study of infrared spectra.[1,2] The α' phase stable at room temperature has a tetragonal structure belonging to the space group $P4/nmm$, and is isomorphous with the room-temperature α' phase of CH_3NH_3Br.[3] The low-temperature δ phase of MAI has been thought to have the same crystal structure as the substable δ phase of the bromide, because the two phases showed very similar IR spectra.[1,2] Recently, the transition temperature T_{tr} between the α' and δ phases of MAI was determined to be 167 K from the ^{127}I NQR study.[4]

^{1}H NMR studies on the molecular motion of the cation[5,6] were reported for MAI and its partially deuterated analog CH_3ND_3I. Recently, we found the existence of a new high-temperature ε phase stable above 414 K for MAI and reported as a letter.[5] The new phase has a marked feature that the cations undergo self-diffusion as well as overall reorientation in the crystal. In view of the dynamical behavior of ions, this phase is thought to be analogous to the high-temperature phase of $CH_3NH_3NO_3$ ($MANO_3$), which is very close to the plastic phase found in various molecular crystals.[7,8]

Very recently, Yamamuro et al.[9] found the stable low-temperature phase named as β' from the calorimetric study of MAI crystals. This phase was obtained by annealing the sample at 205 K for ca. 5 d.

In the present investigation, we have carried out measurements on the 2nd moment M_2 of ^{1}H NMR absorptions, ^{1}H spin-lattice and spin-spin relaxation times T_1 and T_2, respectively, differential thermal analysis (DTA), differential scanning calorimetry (DSC), and X-ray powder diffraction of MAI, to obtain information about the nature of the liquid-like ε phase and also to compare the dynamical properties of the cation in the stable low-temperature β' phase with those in the α' and δ phases.

Experimental

Methylammonium iodide was synthesized by mixing an aqueous solution of methylamine with a nearly stoichiometrical amount of hydroiodic acid. The resulting solution was left to stand over phosphorus pentaoxide in a vacuum desiccator to evaporate water slowly. Pale yellow crystals separated were purified by recrystallizations three times from a mixed solvent of ethanol and chloroform. Colorless tabular crystals obtained were dried in a vacuum desiccator. The partially deuterated analog, CH_3ND_3I was prepared from purified MAI by performing successive crystallizations from heavy water. All the manipulations were carried out in a dry bag because the samples were hygroscopic. After the samples were ground and put in glass ampoules, they were again dried under vacuum at ca. 80 °C.

Temperature dependence measurements of wide-line ^{1}H NMR spectra were performed at a Larmor frequency of 40 MHz by means of JEOL-MW-40S spectrometer equipped with a temperature controller. ^{1}H T_1 observed at 11.5, 20, 31.5, and 42.5 MHz was measured by the inversion recovery method using two spectrometers described elsewhere.[10,11] ^{1}H T_2 was determined at 31.5 and 42.5 MHz by applying Hahn's spin-echo method.[12] Electrical conductivity and DTA measurements were carried out by use of homemade apparatus already reported.[8,13] A Perkin-Elmer DSC-1B apparatus was used to determine enthalpy changes at the solid-solid phase transition and melting temperatures abbreviated as T_{tr} and T_m, respectively. Observed transition enthalpies were calibrated by the melting enthalpy of

metallic indium[14] (purity: 99.99%). X-Ray powder diffraction photographs were taken for the ε phase with the sample sealed in a glass capillary, using a Weisenberg camera from Rigaku Denki Co.

Results

Structural information about the ε phase was obtained by taking X-ray powder photographs at ca. 440 K. The observed patterns were well explained with a CsCl-type cubic lattice having the lattice constant a=4.86 Å and Z=1. Table 1 shows the adequacy of the present analysis.

The DTA curves recorded in a temperature range of 80-520 K were shown in Fig. 1. When the sample was heated and cooled, a small heat anomaly accompanying a long tail on the low-temperature side was observed at the same peak-temperature of 167 K. As already reported for the phase transitions

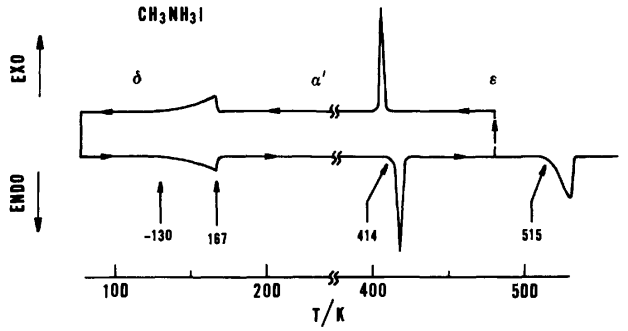

Fig. 1. Differential thermal analysis (DTA) curves of CH_3NH_3I crystals. Endothermic anomalies due to solid-solid phase transitions from the low-temperature substable δ to the room-temperature α' phase and from α' to the highest-temperature solid phase ε appear at 167 and 414 K, respectively. Heat anomaly due to phase transition between the low-temperature stable β' phase and α' is missing.

Table 1. Comparisons between Observed and Calculated 2θ Values of X-Ray Diffraction Patterns Taken at ca. 440 K for CH_3NH_3I, (Cubic, a=4.86 Å)

Index	2θ/degree	
hkl	Obsd	Calcd
100	18.4	18.3
110	26.0	25.9
111	31.9	31.9
200	37.0	37.0
210	41.5	41.6
211	45.5	45.7
220	53.2	53.3
300	56.6	56.8
310	60.0	60.2

taking place in some methylammonium salts[13,15,16] which showed small heat anomalies similar to the above one, the temperature of the DTA peak could be attributed to T_{tr} (167 K). This agrees well with T_{tr} determined for this salt from the temperature dependence study of ^{127}I NQR[4] and that (166.1 K) from the heat capacity study.[9]

When the sample was heated above room temperature, a large heat-absorption anomaly was recorded at 414 K. The enthalpy change at this phase transition was determined from DSC measurements as 6.1 kJ mol^{-1}. With increasing temperature furthermore, melting of the sample started at ca. 515 K together with gradual decomposition which was confirmed by observing the color change to yellow. The enthalpy of melting was roughly estimated to be ca. 7 kJ mol^{-1}.

In CH_3ND_3I, a heat anomaly was observed at the same temperature of 167 K as that of MAI, having almost the same shape as that of MAI recorded on the DTA measurements of both heating and cooling runs. On the other hand, the phase transition to the ε phase took place at 419 K which is higher by 5 K than that of MAI.

The samples used in the foregoing DTA experiments were dried by keeping the glass tubes at 80 °C for ca. 8 h under a high vacuum in order to remove an extremely small amount of water and other volatile impurities possibly included in them. These samples were only partly transformed in our experiments from α' into the low-temperature stable β' phase found by Yamamuro et al[9] although they were left to stand (annealed) for three months at the Dry Ice temperature (196 K). The existence ratio of β' to α' phase was determined at ca. 196 K by separating free induction decay signals of these phases which gave greatly different T_1 of 10 ms and 10 s, respectively. For the above samples repeatedly prepared several times, the β'-phase content was observed to be in a range of ca. 70—0% after the foregoing annealing treatment. These variations of the content values may be due to impurities included in the sample and/or the difference of the grain size of the pulverized crystals. On the other hand, the samples dried at room temperature for ca. 20 min under a high vacuum were transformed into the β' phase almost completely, even when they were annealed at the same temperature only for two weeks. Accordingly, the samples dried by the former method were employed for the ^1H NMR measurements of the α', δ, and ε phases and also for the DTA and DSC experiments, while those dried by the latter method were employed for the study of ^1H NMR only for the β' phase.

The temperature variation of M_2 observed for MAI between 77 and 430 K is shown in Fig. 2. An almost temperature independent M_2 of ca. 8.5 G^2 was

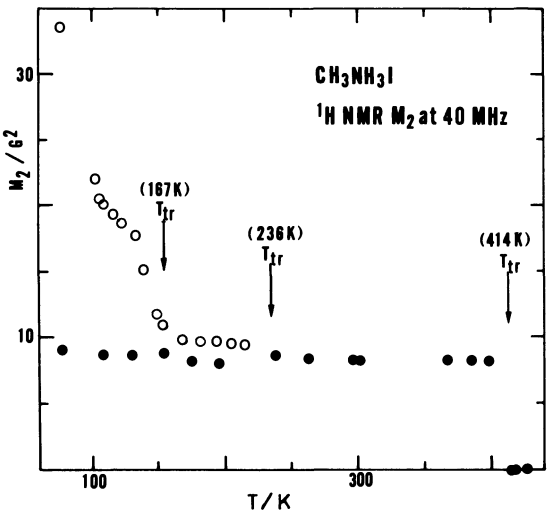

Fig. 2. Proton NMR second moment, M_2 observed at a Larmor frequency of 40 MHz for CH_3NH_3I crystals (○ for β': ● for α', δ, and ε). The transition temperature, T_{tr} from β' to α' was determined from ^1H T_1 experiments as 236 K while other T_{tr} values from DTA.

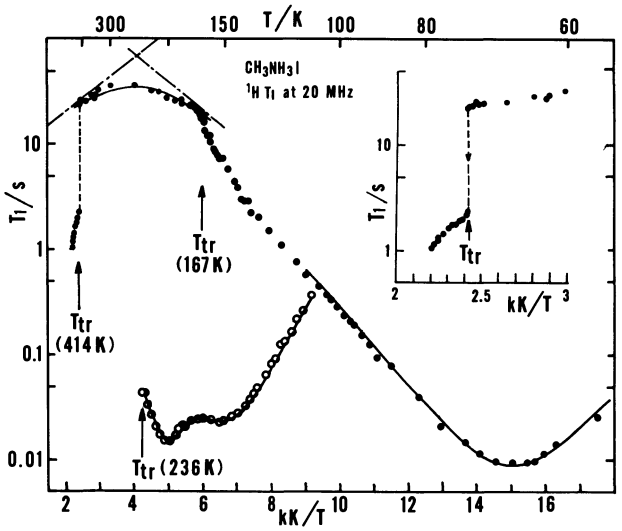

Fig. 3. Temperature dependences of ^1H T_1 observed at 20 MHz for CH_3NH_3I. T_1 data obtained for the α', δ, and ε phases are shown by dots while those of β' phase are plotted by open circles. The enlarged plots near T_{tr} from α' to ε are inserted. Solid curves indicate best fitted curves calculated by the least-squares method. Solid lines broken by dots given in the α' phase are the calculated log T_{1MA} and log T_{1SR} lines defined in the text.

obtained for the α' phase below ca. 410 K and also for the δ phase above 77 K. The M_2 values of 8.8 and 7.5 G^2 determined at 77 and 300 K, respectively, by Tsau and Gilson[17] are consistent with the present results. The large M_2 value of 34±3 G^2 was obtained at 77 K for the β' phase. With increasing temperature, M_2 of this phase decreased gradually and an almost constant value of 9.5±0.3 G^2 was observed between 170 and 220 K, above which temperature we could not definitely discriminate between the β' and α' phases because of the coexistence of both phases. When the sample was heated from room temperature, M_2 decreased discontinuously at T_{tr} to the ε phase and extraordinarily small M_2 values less than 0.01 G^2 were obtained for this phase.

The temperature dependences of ^1H T_1 in MAI and CH_3ND_3I determined in a temperature range of 57—455 K at 20 MHz are shown in Figs. 3 and 4, respectively.

The δ phase of MAI and CH_3ND_3I exhibited a single T_1 minimum the value of which was 9 and 12 ms, respectively, at approximately the same temperature of 67 K. With increasing temperature in this phase up to ca. 130 K, the log T_1 versus T^{-1} plot increased linearly. Above 130 K, the log T_1 value increased more steeply and deviated from a line obtained by extrapolation from the low-temperature side. Moreover, a small jump in the log T_1 curve could be found at 167 K. This temperature agrees well with T_{tr} determined by DTA. By referring to the anomalous DTA curve observed around T_{tr}, this transition is attributable to a second-order one.

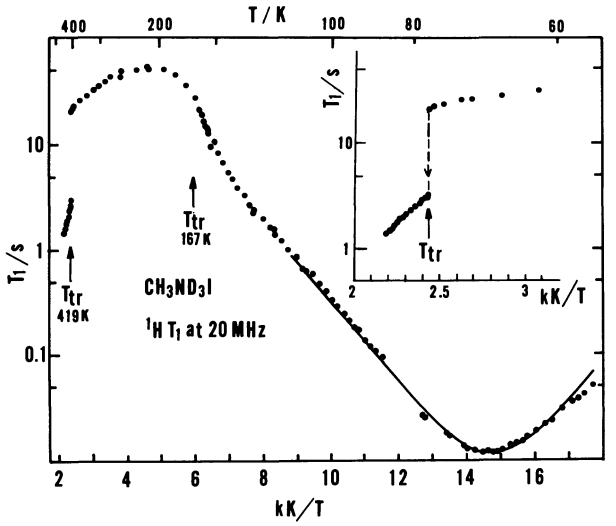

Fig. 4. Temperature dependences of ^1H T_1 observed at 20 MHz for CH_3ND_3I. Near T_{tr} from the α' to ε phase, the axis of abscissa is enlarged and an enlarged plot is inserted in the figure. The solid curve is the best-fitted theoretical curve.

However, a slight discontinuity in T_1 was observed at T_{tr} suggesting the presence of some first-order nature in this phase transition.

In the β' phase of MAI, two T_1 minima of 22 and 15 ms were located at 154 and 202 K, respectively. At 236 K, T_1 increased discontinuously by about two

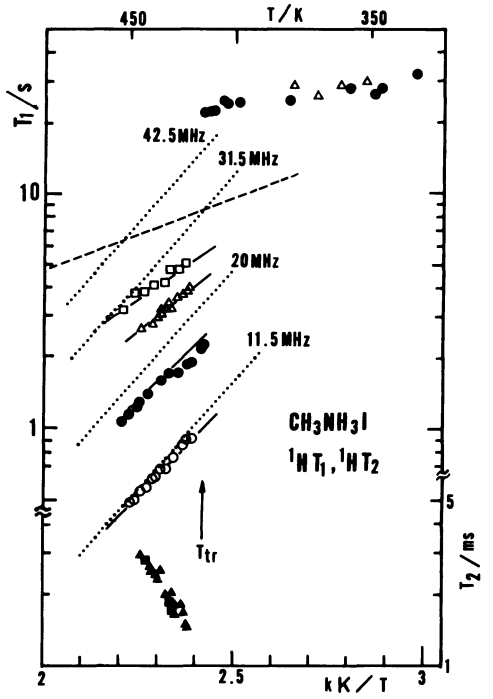

Fig. 5. Temperature dependences of ^1H T_1 observed at 11.5 (○) 20 (●), 31.5 (△), and 42.5 (□) MHz; and ^1H T_2 observed at 31.5 (▲) and 42.5 (■) MHz mainly for the ε phase of CH_3NH_3I. The frequency independent $\log T_{1I}$ estimated for the ε phase is shown by a broken line and frequency dependent $\log T_{1d}$ derived from each observed frequency is shown by dotted lines. Solid lines indicate the best fitted one to the observed values at each frequency.

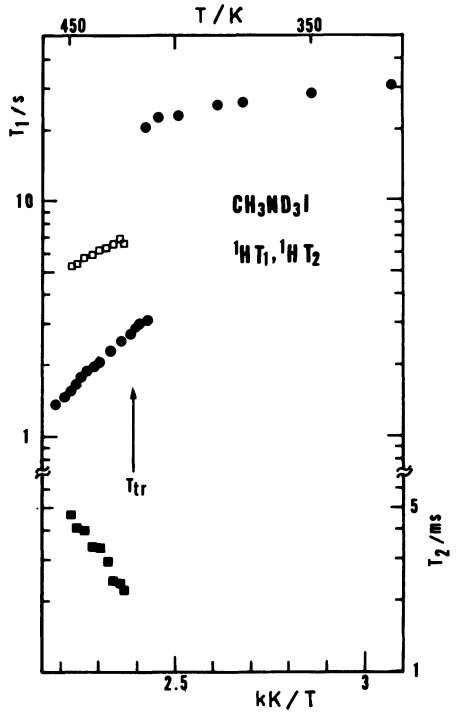

Fig. 6. Temperature dependences of ^1H T_1 observed at 20 (●) and 42.5 MHz (□); and ^1H T_2 observed at 42.5 MHz (■) mainly for the ε phase of CH_3ND_3I.

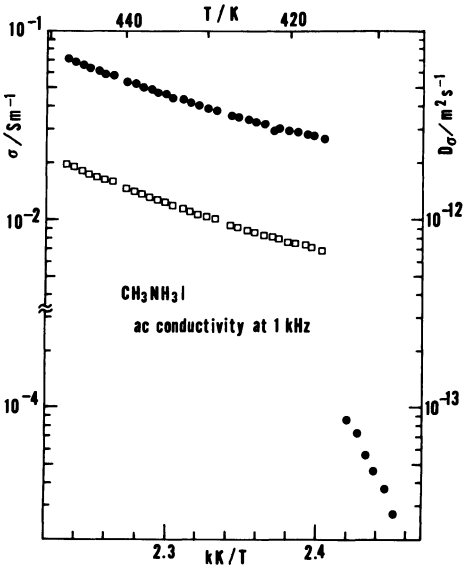

Fig. 7. Temperature dependences of electrical conductivity σ (●) values observed at 1 kHz and the diffusion constants D_σ (□) evaluated for CH_3NH_3I.

orders of magnitude, above which temperature the same T_1 values as those of the α' phase were observed. Accordingly, this discontinuity observed in T_1 can be assigned to the phase transformation from β' to α'. The transformation was completed with a reasonably fast rate at this temperature which is higher than T_{tr} of 220 K determined from the calorimetric study,[9] where superheating of β' by ca. 10 K was reported.

In the α' phase of MAI, a broad T_1 maximum (ca. 35 s) was observed at ca. 270 K. A similar maximum of ca. 40 s was also obtained at ca. 240 K for the α' phase of CH_3ND_3I. With increasing temperature, a sudden T_1 decrease was observed for the α' phase of MAI and CH_3ND_3I at 414 and 419 K, respectively. These temperatures agree well with T_{tr} to the ε phase already determined by DTA.

The temperature dependences of ^1H NMR relaxation times (T_1, T_2) determined for each ε phase of MAI and CH_3ND_3I are given in Figs. 5 and 6, respectively.

In each ε phase, plots of $\log T_1$ decreased linearly with decreasing T^{-1}, whereas those of $\log T_2$ increased linearly against T^{-1}.

Electrical conductivity measurements were performed for pulverized MAI crystals by use of 1 kHz ac electric field in a temperature range of 408—443 K and the results are shown in Fig. 7. When the sample was heated in the α' phase, the electrical conductivity σ increased steeply but continuously. However, it jumped at T_{tr} to the value of 2.7×10^{-2} S m^{-1}, which is larger by about three orders of magnitude than those obtained for the α' phase.

Discussion

Calculated Second Moments. Theoretical values of M_2 for a MA^+ ion in the following three motional states were evaluated by assuming the same geometry of the cation as that employed in our previous report on solid CH_3NH_3Br.[16] The M_2 values calculated for the cation, in the rigid lattice, performing the reorientation as a whole about the cationic C_3 axis, and undergoing the overall rotation about its center of gravity. They are 38, 11, and 1.1 G^2, respectively. ^1H-^1H and ^1H-^{127}I interionic contributions to M_2 were estimated by use of the crystal structure of the α' phase[3] for the calculations of the first two cationic motional states. For the ε phase revealed in the present investigation, M_2 was calculated for the last motional state because the cation should behave as an isotropic ion in the cubic ε phase.

Low-Temperature Substable δ Phase. The M_2 value of 8.5 G^2 observed for the δ phase is close to the value calculated for the cation in which both CH_3 and NH_3^+ groups perform C_3 reorientation about their symmetry axis. From this value, the averaged reorientational rates of both groups can be estimated to be faster than 10^5 Hz in the δ phase above 77 K.

The random C_3 reorientation of either CH_3 or NH_3^+ group gives rise to ^1H T_1 expressed by,[18]

$$T_1^{-1} = C\{\tau_R/(1+\omega_H^2\tau_R^2) + 4\tau_R/(1+4\omega_H^2\tau_R^2)\}, \quad (1)$$

where

$$C = (9/20)\gamma_H^4\hbar^2 r^{-6}. \quad (2)$$

In these equations, γ_H, r, ω_H, and τ_R are the gyromagnetic ratio of a proton, the interprotonic distance, the ^1H angular Larmor frequency, and the correlation time of either CH_3 or NH_3^+ C_3 reorientation, respectively. Taking into account only for each intragroup contribution to the relaxation, the spin-lattice relaxation rate, T_{1MA}^{-1} of the cations can be written as,

$$T_{1MA}^{-1} = (1/2)(T_{1CH_3}^{-1} + T_{1NH_3}^{-1}), \quad (3)$$

where T_{1CH_3} and T_{1NH_3} are given by Eq. 1.

The T_1 minima of 9 and 12 ms observed for the δ phase of MAI and CH_3ND_3I, respectively, agree well with the theoretical values of 9.9 and 11 ms in the same order. These values were calculated by use of Eqs. 1—3 for the C_3 reorientations of CH_3 and NH_3^+ groups in MAI crystals and for the C_3 reorientation of CH_3 groups in CH_3ND_3I crystals. In this calculation, we employed the same geometry of the cation as that used in the calculation of M_2.

Assuming an Arrhenius-type relationship between the activation energy, E_a for the C_3 reorientation and τ_R, we have

$$\tau_R = \tau_{RO}\exp(E_a/RT), \quad (4)$$

where τ_{RO} has the usual meaning. Fitting calculation of the ^1H T_1 data of MAI and CH_3ND_3I determined in the δ phase to Eqs. 1—4 was performed by the least-squares method using a program SALS[19] in the Computation Center of Nagoya University. The best fitted T_1 curves obtained are shown in Figs. 3 and 4 by solid lines. The optimum values of E_a, τ_{RO}, and C obtained through the calculation are given in Table 2.

The motional mode of the cation in the δ phase of MAI and CH_3ND_3I can be considered from the following discussion as the C_3 reorientation of the cation as a whole with keeping its rigid structure. This motional mode (correlated C_3 reorientation) of the cation has already been observed in some hexahalo metal complexes.[20,21] The presence of the correlated C_3 reorientation of the cation in the δ phase is explained by the facts that MAI gives a single T_1 minimum attributable to the C_3 reorientation of both CH_3 and NH_3^+ groups, and the E_a value of ca. 7 kJ mol^{-1} obtained for both salts is smaller than that of ca. 8 kJ mol^{-1} evaluated for the barrier to internal rotation of the cation.[20,21] The appearance of this motional mode indicates that the cations are considerably free to reorient about their C–N bond axes and, therefore, the δ phase forms loosely packed crystals.

Above 133 K, ^1H T_1 observed for MAI deviated gradually from the calculated curve. The deviation of T_1 from the normal BPP curve far below T_{tr} and the anomalous DTA curve recorded in the same temperature region have been also observed below T_{tr} from the δ to α' phase of CH_3NH_3Br crystals.[16] This T_1 deviation can be regarded as a significant feature of the second-order-like phase transition from the substable δ phase to the room-temperature α' phase. Therefore, it is expected that the correlation time of the C_3 reorientation of the cation in these crystals is shortened rapidly near T_{tr} with increasing temperature.

Low-Temperature Stable β' Phase. By comparing M_2 of 34±3 G^2 observed at 77 K in the β' phase with the theoretical value of 38 G^2 for the rigid lattice, the cations can be expected to be almost rigid in the crystal. This is in a marked contrast to the motional state of the cation in the δ phase described above and indicates that the cations in the β' phase are strongly hindered to reorient. Accordingly, one can conclude that the ions in the β' phase are more compactly packed in crystals than those of δ in accordance with the fact that the former phase rather than the latter is the stable one at low temperatures.[9]

The ^1H T_1 data of these phases are capable of a similar interpretation. A shallow T_1 minimum of

Table 2. Activation Energies (E_a), Pre-Exponential Factors (τ_{RO}), Motional Constants (C), and Motional Modes of Methylammonium Ions in Four Phases of Solid Methylammonium Iodide

	Phase	E_a/kJ mol^{-1}	$\tau_{RO}/10^{-14}$ s	$C/10^9$ s^{-2}	Motional Mode
CH_3NH_3I	δ	6.6±0.1	2.7	9.8	Correlated C_3 reorient.
	β'	11.2±0.1	73	7.3	C_3 reorient. of CH_3
		22.1±0.4	1.1	9.6	C_3 reorient. of NH_3^+
	α'	5±1			C_3 reorient. of CH_3 and NH_3^+
	ε	35±5 (48±3)*			Self-diffusion
CH_3ND_3I	δ	7.2±0.1	1.3	7.6	Correlated C_3 reorient.
	ε	(45±3)*			Self-diffusion

*Evaluated from T_2.

22 ms appearing at the lower temperature of 154 K in the β' phase of MAI can be assigned to the CH_3 C_3 reorientation, while the deep one (15 ms) at 202 K is attributable to the NH_3^+ C_3 reorientation in agreement with the temperature dependence of M_2 observed in this phase. These assignments of ^1H T_1 minima are acceptable because ^1H T_1 minima calculated for CH_3 and NH_3^+ groups performing the C_3 reorientation in the cation are 23 and 17 ms, respectively, at a Larmor frequency of 20 MHz.[20] The motional parameters and activation energies for the C_3 reorientation of both groups were evaluated in the same way as that described in the foregoing δ phase. The results are given in Table 2 and the calculated curve is shown in Fig. 3 by solid line. The E_a values obtained for the C_3 reorientation of both groups are larger in β' than in δ clearly indicating that the cations in the former phase are more tightly bound in the crystalline lattice in agreement with the foregoing discussion.

It is noteworthy that the β' crystal of MAI yields two ^1H T_1 minima while the δ only a single minimum. This indicates that the correlated C_3 reorientation of the cation is the easiest reorientational mode of the cation in the latter crystal, whereas the barrier of the CH_3 groups to reorient in the former, which is considerably higher than that of the internal rotation, is distinguishably lower enough than that of the NH_3^+ groups. The large E_a value derived for the NH_3^+ C_3 reorientation in β' suggests that this phase has a crystal structure efficiently to be formed by N–H···I type hydrogen bonds.

Room-Temperature α' Phase. In this phase, a ^1H T_1 maximum was observed for both MAI and CH_3ND_3I crystals, and it should be noted that no frequency dependence was observed in the hot side of the maximum. These experimental facts indicate that a new relaxation process other than the usual magnetic dipolar relaxation contributes to ^1H T_1 observed in this phase. The most feasible mechanism for the new motional process is spin-rotation relaxation originating from the uniaxial rotation of the CH_3 and NH_3^+ groups around each C–N bond axis of the cations. For the crystals of several ammonium salts,[22–24] where NH_4^+ ions are thought to be almost free to perform overall rotation, it is reported that ^1H T_1 can be interpreted in terms of this mechanism. Although the present cation performs uniaxial reorientation in the crystal, this process is still valid provided that the reorientation is rapid enough.

When both spin-rotation and magnetic dipolar interactions due to the uniaxial rotation of the cations contribute to ^1H T_1, the observed T_1 can be written by

$$T_1^{-1} = T_{1MA}^{-1} + T_{1SR}^{-1}, \tag{5}$$

where T_{1SR} indicates ^1H T_1 originating from the spin-rotation mechanism. Since the condition, $\omega_H\tau_R \ll 1$ is fulfilled for both CH_3 and NH_3^+ reorientations in the α' phase, T_{1MA} can be connected with the averaged C_3 reorientational correlation time $\bar{\tau}_R$ of these groups by,

$$T_{1MA}^{-1} = (5/2)(C_{CH_3} + C_{NH_3^+})\bar{\tau}_R, \tag{6}$$

where C_{CH_3} and $C_{NH_3^+}$ denote the motional constants for the CH_3 and NH_3^+ C_3 reorientations, respectively, as given in Eq. 2. Therefore, log T_{1MA} is expected to increase linearly with decreasing T^{-1} in this phase because $\bar{\tau}_R$ can be expressed by Eq. 4.

For T_{1SR}, a temperature dependence can be derived from a theoretical consideration that T_{1SR} is propor-

tional to $\bar{\tau}_R$ in the present system.[25] Under a condition that both $\log T_{1MA}$ and $\log T_{1SR}$ change linearly against T^{-1}, the T_1 data observed can be divided into two components by the least-squares method. The best fitted T_{1MA} and T_{1SR} straight lines thus obtained are shown in Fig. 3 using solid lines broken by dots. The gradient of the two lines having opposite signs yielded the same E_a of 5±1 kJ mol^{-1}. This result is compatible with our present assumptions that both T_{1MA}^{-1} and T_{1SR} are proportional to $\bar{\tau}_R$.

Since the present E_a obtained for the C_3 reorientation of the cation is comparable to the thermal energy at 300 K ($RT \approx 2.5$ kJ mol^{-1}), we can say that the cations perform the C_3 reorientation quite freely in this phase. This provides a strong support for the presence of the spin-rotation relaxation. Substituting the value of $(C_{CH_3}+C_{NH_3^+})$ calculated using Eq. 2 into Eq. 6, one obtains $\bar{\tau}_R$ to be 1.5×10^{-13} s at 300 K. This is extraordinarily short for usual solids and nearly the same order of magnitude as those usually observed for nonviscous liquids. For example, $\bar{\tau}_R$ for the C_3 rotation of CH_3 groups in liquid toluene is reported to be ca. 1×10^{-13} s at ca. 250 K,[26] and that for the overall rotation of molecules in liquid ammonia is ca. 2×10^{-13} s at 347 K.[27] ^{1}H T_1 observed for these compounds in their liquid state is reported to clearly involve the spin-rotation mechanism. Therefore, it may be concluded that the spin-rotation relaxation due to highly free uniaxial-rotation of the present cations plays an important role in ^{1}H T_1 observed at elevated temperatures.

High-Temperature ε Phase. The extremely small M_2 and unusually long T_2 values observed for this phase imply that the isotropic rotation of the cation about its center of gravity and also self-diffusion of the cations in the crystal take place rapidly. As reported previously for the highest-temperature solid phase of $CH_3NH_3NO_3$[7,8] the most effective relaxation mechanism in the ε phase of the present salt is expected to be the cationic self-diffusion.

In the present ε phase, MA^+ cations perform isotropic reorientations which are assumed to occur much more frequently than the translational jump of the cation through the lattice sites. This means that we can calculate average distances between protons belonging to different cations by simply regarding as that the all protons in a cation are fictitiously located at the center of gravity of the cation.

In our previous study,[8] we employed the monovacancy mechanism for the explanation of the cationic self-diffusion in crystals as a simple mechanism and could well explain the observed NMR data. According to Torrey and Sholl,[28,29] the ^{1}H spin-lattice relaxation rate, T_{1HH}^{-1} and the ^{1}H spin-spin relaxation rate, T_{2HH}^{-1} due to interionic ^{1}H dipolar interactions which are randomly modulated by self-diffusion can be written by,

$$T_{1HH}^{-1} = 2\alpha y[g(y) + 4g(2y)], \tag{7}$$

$$T_{2HH}^{-1} = \alpha y[3g(0) + 5g(y) + 2g(2y)], \tag{8}$$

where

$$\alpha = (3/20)\gamma_H^4\hbar^2 p a^{-6}\omega_H^{-1}, \tag{9}$$

$$y = (1/2)\omega_H\tau_H. \tag{10}$$

In the above equation, a, p, and τ_H are the lattice constant, the ratio of the number of the resonant protons to the number of the lattice sites in a unit sublattice, and the correlation time of the self-diffusion of the cations respectively. The detailed expression of $g(y)$ is given in Sholl's paper.[29]

Besides magnetic dipolar interactions operative between protons, interactions between protons and iodine nuclei also provide another relaxation process, because iodine nuclei having a large quadrupole moment are expected to have a shorter relaxation time than T_{1HH} due to appreciably fast quadrupolar relaxation even if the crystal has high symmetry such as cubic. In fact, the iodine nuclei in the crystals of the high-temperature phases of NH_4I having CsCl and NaCl type cubic structures are known to have the temperature independent T_1 of ca. 3.2 ms.[30] Under the assumption of shorter ^{127}I T_1, the relaxation times T_{1HI} and T_{2HI} can be expressed by,[18,29]

$$T_{1HI}^{-1} = 2\beta\tau_H[g'\{(\omega_H-\omega_I)\tau_H\} + 3g'(\omega_H\tau_H) + 6g'\{(\omega_H+\omega_I)\tau_H\}], \tag{11}$$

$$T_{2HI}^{-1} = \beta\tau_H[2g'(0) + g'\{(\omega_H-\omega_I)\tau_H\} + 3g'(\omega_H\tau_H) + 6g'(\omega_I\tau_H) + 6g'\{(\omega_H+\omega_I)\tau_H\}], \tag{12}$$

where

$$\beta = (7/12)\gamma_H^2\gamma_I^2\hbar^2 a^{-6}. \tag{13}$$

In these equations, γ_I and ω_I denote the gyromagnetic ratio and the angular resonance frequency of ^{127}I nuclei, respectively. The functional form of $g'(y)$ is the same as that of $g(y)$, where the positional vectors connecting protons are replaced by those connecting ^{1}H and ^{127}I nuclei for the former function.

As another relaxation mechanism between ^{1}H and ^{127}I nuclei, the dipolar relaxation of the second kind proposed by Norris et al.[31] is expected to contribute to ^{1}H T_1 because T_1 of the quadrupolar ^{127}I nuclei is considered to become very short as in the case reported for NH_4I.[30] Since no data of the relaxation times of ^{127}I in any phase of solid MAI are available, we roughly estimated the T_1 value of MAI due to this mechanism. The calculation was performed by use of the equation reported by Norris et al.[31]

assuming the same ^{127}I T_1 value as that of NH_4I described above. The T_1 value evaluated is longer by ca. 10^4 times than the values observed in this phase. This suggests that the contribution of ^{127}I T_1 to the observed T_1 through this mechanism can be neglected in the present discussion.

In Eqs. 11 and 12, the self-diffusion of iodide ions expected to be possibly excited was assumed to be much slower than that of the cations, namely, $\tau_H \ll \tau_I$ by considering their large mass. Here, τ_I indicates the diffusion correlation time of the anion. Eqs. 11 and 12 were proved to be still valid by substituting $(\tau_H^{-1}+\tau_I^{-1})$ for τ_H^{-1}, even if τ_I becomes comparable to τ_H. Since the observed T_1 of the ε phase decreased with increasing temperature, the condition of $\omega_H\tau_H \gg 1$ is reasonably assumed to be fulfilled over the whole temperature range of this phase. Therefore, Eqs. 7, 8, 11, and 12 can be rewritten as,

$$T_{1HH}^{-1} = 4\alpha(S_0 - S_1/\bar{Z})/y, \tag{14}$$

$$T_{2HH}^{-1} = 3\alpha y g(0), \tag{15}$$

$$T_{1HI}^{-1} = \beta[(S_0' - S_1'/\bar{Z})/(\omega_H - \omega_I)^2 + (S_0' - S_1'/\bar{Z})/\omega_H^2 + 2(S_0' - S_1'/\bar{Z})/(\omega_H + \omega_I)^2]1/2\tau_H, \tag{16}$$

$$T_{2HI}^{-1} = 2\beta\tau_H g'(0), \tag{17}$$

where $\bar{Z}$ denotes the number of the nearest neighbors of the simple cubic sublattice. S_i and S_i' are defined in Sholl's paper.[29] Accordingly, the total relaxation rates, $T_{1\varepsilon}^{-1}$ and $T_{2\varepsilon}^{-1}$ determined for the protons of this phase are given by $(T_{1HH}^{-1}+T_{1HI}^{-1})$ and $(T_{2HH}^{-1}+T_{2HI}^{-1})$, respectively.

In Eqs. 14 and 15, S_0, S_1, and $g(0)$ can be calculated by regarding as that the protonic system assumed to be concentrated at the center of gravity of the cation forms a simple cubic sublattice, because the crystal has the CsCl type bcc structure. According to the Sholl paper,[29] he obtained S_0=8.4019, S_1= 11.5739, and $g(0)$=18.21. Using the numerical values evaluated by Sholl[29] for the simple cubic and bcc lattices, S_0', S_1', and $g'(0)$ in Eqs. 16 and 17 applicable to the system involving ^1H-^{127}I interactions were calculated to be 20.644, −3.470, and 32.7, respectively. Employing the following values, a=4.86×10^{-10} m and $\bar{Z}$=6, the total relaxation rates can be obtained as,

$$T_{1\varepsilon}^{-1} = \tau_H^{-1}[20.1\omega_H^{-2} + 0.43(\omega_H - \omega_I)^{-2} + 1.28\omega_H^{-2} + 2.56(\omega_H + \omega_I)^{-2}] \times 10^8, \tag{18}$$

$$T_{2\varepsilon}^{-1} = 1.09 \times 10^9\tau_H. \tag{19}$$

Since ω_H/ω_I is approximately constant for the present case, it is evident from Eq. 18 that $T_{1\varepsilon}$ should be proportional to ω_H^2 at a constant temperature, and also the gradient of the log T_1 versus T^{-1} plot should be constant and independent of ω_H. However, the observed gradients of the log T_1 curves depend on ω_H employed and become gentle with increasing ω_H. Moreover, the ratio of ^1H T_1 observed at 20 and 42.5 MHz is T_1(20 MHz)/T_1(42.5 MHz)=0.36 in disagreement with the theoretical value of 0.22 derived from Eq. 18. These facts suggest that ^1H T_1 observed for the ε phase of MAI cannot be explained by the single relaxation mechanism of self-diffusion as dominantly concerned with.

Here, we introduce another assumption that two relaxation mechanisms appreciably contribute to ^1H T_1 of this phase and one of them involves ω_H whereas the other does not. For this case, the observed T_1 can be expressed by

$$T_1^{-1} = T_{1d}^{-1} + T_{1i}^{-1}, \tag{20}$$

where T_{1d} and T_{1i} represent ^1H T_1, which are proportional to ω_H^2 and independent of ω_H, respectively. Using Eq. 20, two components, T_{1d} and T_{1i}, were obtained from the observed T_1 values. The results are shown in Fig. 5. ^1H spin-rotation interaction already discussed in the α' phase can be proposed as the most probable relaxation mechanism for T_{1i} which decreases with increasing temperature. Because isotropic rotation of the cations is thought to be very rapid in this liquid-like ε phase, it will be the main origin of this mechanism.

The frequency dependent part T_{1d}, on the other hand, can be unequivocally assigned to the self-diffusion of the cations. The E_a value of 35 kJ mol^{-1} was obtained for this motional mode from the slope of the log T_{1d} curves of different ω_H. From the slope of the log T_2 versus T^{-1} curve, the same E_a value should be obtained as that derived above. However, a much larger E_a of ca. 48 kJ mol^{-1} was obtained from the log T_2 curve. Also for CH_3ND_3I, E_a derived from the log T_2 curve (45 kJ mol^{-1}) is much larger than that roughly evaluated from the log T_1 curve observed at 20 MHz (≈30 kJ mol^{-1}), although no accurate value could be determined because the T_1 data of CH_3ND_3I were obtained at only two ω_H.

In the preceding analysis of the relaxation times, we simply assumed that both T_{1d} and T_2 are determined through the same relaxation process. Referring to our T_1 and T_2 data observed in a fairly narrow temperature range without the location of T_1 minimum, the above assumption is not necessarily valid, because the origin of observed ^1H T_1 and T_2 cannot be definitely identified without the data in the temperature range where the condition $\omega_H\tau_H \leq 1$ is satisfied. The fact that the different E_a values were derived from T_{1d} and T_2 suggests the existence of at least two different relaxation processes of self-diffusion.

As one of the relaxation models involving two kinds of self-diffusion processes, it is conceivable for the present ε phase that both cations and anions perform self-diffusion with different correlation times. For this model, τ_H and τ_I can be calculated from the above T_{1d} and T_2 expressions by replacing τ_H^{-1} with $(\tau_H^{-1}+\tau_I^{-1})$. The τ_I values calculated in the whole temperature range observed were negative. This is unreasonable result and, therefore, the above model is unacceptable for the present case.

As another possible model, it is considered that the cations diffuse through the activation of two kinds of self-diffusion mechanisms, i.e., local translational jumps among the adjacent small number of vacancy sites and a long-range self-diffusion mode where the cations migrate to a long distance through many vacancies as already considered for simple ionic conductors.[32] It is expected that the former process gives a shorter τ_H and a smaller E_a than the corresponding values in the latter. By applying this model to the present ^1H relaxation data, we can derive a conclusion that the relaxation process of T_{1d} is thought to be caused by the short-range self-diffusion whereas that of ^1H T_2 is governed by the long-range process.

The observed values of σ shown in Fig. 7 increase discontinuously by three orders of magnitude at T_{tr} to the ε phase. The large value of σ in this phase is attributable to ionic conduction of the diffusible cations, the existence of which is verified by the present NMR study. From σ values observed, we can evaluate the diffusion constant D_σ of the cations using the Nernst-Einstein equation written by

$$D_\sigma = kT\lambda\sigma/(Ze)^2N, \tag{21}$$

where Ze, N, and λ are the charge of diffusing ions, their number in a unit volume, and the spacial correlation factor calculated to be λ=0.65331 for the simple cubic lattice,[33] respectively.

The conductivity measurements in the ε phase gave E_a of 51±3 kJ mol^{-1} which is larger than that derived from T_{1d}(31 kJ mol^{-1}) but close to that from ^1H T_2(48 kJ mol^{-1}). The fact that roughly the same value of E_a was obtained from σ and ^1H T_2 measurements suggests that the two different physical quantities are dominantly determined due to the same diffusion mechanism. In the present study, σ was measured by applying an ac electric field of 1 kHz. Since the transport distance, $\bar{r}_\sigma$ averaged in a time τ can be expressed by[34]

$$\bar{r}_\sigma = \sqrt{6D_0\tau}, \tag{22}$$

it can be shown that the long-range diffusion mainly contributes to σ, where ions migrate for longer distances than the order of 10^2 Å in a half cycle of 1 kHz. This gives a strong support for our previous conclusion about the process determing ^1H T_2.

The entropy changes at T_{tr}(414 K) and T_m of MAI crystals observed by DSC measurements were ΔS_{tr}=15 J K^{-1} mol^{-1} and $\Delta S_m \approx$14 J K^{-1}mol^{-1}, respectively. These values can be compared with ΔS_{tr}=28 J K^{-1} mol^{-1} and ΔS_m=12 J K^{-1} mol^{-1} obtained for $CH_3NH_3NO_3$ crystals,[8] because the highest-temperature solid phase of both crystals is the liquid-like solid one. The fact MAI has ΔS_{tr} smaller than $CH_3NH_3NO_3$ crystal is understandable by considering that spherical iodide ions have no orientational freedom. Although ΔS_{tr} and ΔS_m values in MAI are comparable, the latter is unusually small as compared with that of usual ionic crystals such as NaSCN, KSCN, and KN_3. These salts[35] have ΔS_m of 30—40 J K^{-1} mol^{-1}. Usual molecular plastic crystals[36] are known to have ΔS_m less than ca. 20 J K^{-1} mol^{-1}. Accordingly, it is concluded that the cations in the ε phase are in a state having the most part of their motional freedom in good agreement with the foregoing conclusion derived from the present NMR and X-ray studies, and the ε phase can be considered as a plastic phase. A similar state of molecule-like cations can be found in the highest-temperature solid phase of NH_4NO_3,[37] $CH_3NH_3NO_3$,[7,8] $CH_3NH_3ClO_4$,[7] $(CH_3NH_3)_2SO_4$,[38] and $[C(NH_2)_3]ClO_4$.[39]

The authors are grateful to Prof. S. Kawai and Dr. K. Kitahama of Osaka University and Dr. Y. Furukawa for their help in carrying out the measurements of X-ray diffraction. We also wish to thank Mr. K. Kawase and Dr. K. Toriyama in the Government Industrial Research Institute of Nagoya for help in the experiments of DSC.

References

1) A. Cabana and C. Sandorfy, *Spectrochim. Acta*, **18**, 843 (1962).
2) A. Théorêt and C. Sandorfy, *Spectrochim. Acta, Part A*, **23**, 519 (1967).
3) S. B. Hendricks, *Z. Kristallogr.*, **67**, 106 (1928).
4) G. Jugie and J. A. S. Smith, *J. Chem. Soc., Faraday Trans. 2*, **74**, 994 (1978).
5) H. Ishida, R. Ikeda, and D. Nakamura, *Phys. Stat. Sol. (a)* **70**, K151 (1982).
6) C. S. Sandaram and J. Ramakrishna, *Current Science*, **51**, 835 (1982).
7) H. Ishida, R. Ikeda, and D. Nakamura, *Chem. Lett.*, 1943 (1982).
8) H. Ishida, R. Ikeda, and D. Nakamura, *J. Chem. Soc., Faraday Trans. 2*, **81**, 963 (1985).
9) O. Yamamuro, M. Oguni, and H. Suga, to be published.
10) L. S. Prabhumirashi, R. Ikeda, and D. Nakamura, *Ber. Bunsenges. Phys. Chem.*, **85**, 1142 (1981).
11) S. Gima, Y. Furukawa, R. Ikeda, and D. Nakamura, *J. Mol. Struct.*, **111**, 189 (1983).

12) E. L. Hahn, *Phys. Rev.*, **80**, 580 (1950).
13) Y. Kume, R. Ikeda, and D. Nakamura, *J. Magn. Reson.*, **33**, 331 (1979).
14) F. D. Rossini, D. D. Wagman, W. H. Evans, S. Levine, and I. Jaffe, Selected Values of Chemical Thermodynamic Properties Part I. Tables, NBS Circular 500-Part I, U. S. Goverment Printing Office, Washington (1961).
15) Y. Kume, R. Ikeda, and D. Nakamura, *J. Phys. Chem.*, **82**, 1296 (1978).
16) H. Ishida, R. Ikeda, and D. Nakamura, *J. Phys. Chem.*, **86**, 1003 (1982).
17) J. Tsau and D. F. R. Gilson, *Can. J. Chem.*, **48**, 717 (1970).
18) A. Abragam, "The Principles of Nuclear Magnetism," Oxford Univ. Press, Oxford (1961).
19) T. Nakagawa and Y. Koyanagi, Program library in Computation Center of Nagoya University, code number 466.
20) R. Ikeda, Y. Kume, D. Nakamura, Y. Furukawa, and H. Kiriyama, *J. Magn. Reson.*, **24**, 9 (1976).
21) Y. Furukawa, H. Kiriyama, and R. Ikeda, *Bull. Chem. Soc. Jpn*, **54**, 103 (1981).
22) R. Ikeda and C. A. McDowell, *Chem. Phys. Lett.*, **14**, 389 (1972).
23) F. Köksal and S. Bahceli, *J. Chem. Soc., Faraday Trans. 2*, **74**, 1844 (1978).
24) K. Simomura, M. Yoshida, A. Sanjoh, and H. Negita, *Phys. Lett.*, **81A**, 189 (1981).
25) P. S. Hubbard, *Phys. Rev.*, **131**, 1155 (1963).
26) H. W. Spiess, D. Schweitzer, and U. Haeberlen, *J. Magn. Reson.*, **9**, 444 (1973).
27) D. W. G. Smith and J. G. Powles, *Mol. Physics*, **10**, 451 (1966).
28) H. C. Torrey, *Phys. Rev.*, **92**, 962 (1953).
29) C. A. Sholl, *J. Phys. C*, **7**, 3378 (1974); **8**, 1737 (1975).
30) A. R. Sharp and M. M. Pintar, *J. Chem. Phys.*, **75**, 2652 (1981).
31) M. O. Norris, J. H. Strange, J. G. Powles, M. Rhodes, K. Marsden, and K. Krynicki, *J. Phys. C* **1**, 422 (1968).
32) P. M. Richards, "Magnetic Resonance in Superionic Conductors," and T. Geisel, "Continuous Stochastic Models," in M. B. Salamon Ed., "Physics of Superionic Conductors," Springer-Verlag, Berlin, (1979), p. 141 and p. 202, respectively.
33) K. Compaan and Y. Haven, *Trans. Faraday Soc.*, **52**, 786 (1956); **54**, 1498 (1958).
34) J. M. Chezeau and J. H. Strange, *Phys. Rep.*, **53**, 1 (1979).
35) G. J. Janz, "Molten Salts Handbook," Academic Press, N. Y. (1967).
36) J. Timmermans, *J. Phys. Chem. Solids*, **18**, 1 (1961).
37) M. T. Riggin, R. R. Knispel, and M. M. Pintar, *J. Chem. Phys.*, **56**, 2911 (1972).
38) H. Ishida, T. Matsuhashi, R. Ikeda, and D. Nakamura, *Chem. Lett.*, **1985**, 1859.
39) S. Gima, Y. Furukawa, and D. Nakamura, *Ber. Bunsenges. Phys. Chem.*, **88**, 939 (1984).

Electrocatalysis in Metal Hydride Electrode. II. Hydrogen Electrode Reaction and Related Properties of Group-IB Metal-Coated $LaNi_5$ Electrodes

Ken-ichi MACHIDA, Michio ENYO,* Gin-ya ADACHI,† Hiroki SAKAGUCHI,† and Jiro SHIOKAWA†

Research Institute for Catalysis, Hokkaido University, Sapporo 060

†Department of Applied Chemistry, Faculty of Engineering, Osaka University, Yamadaoka, Suita, Osaka 565

(Received September 2, 1985)

Synopsis. Hydrogen storage type electrodes were fabricated from $LaNi_5$ powder after coating with group-IB metals by an electroless plating method, followed by press moulding. The hydrogen electrode reaction (HER) characteristics and mechanical stability during hydrogen charge/discharge cycles were then studied in 1.0 M (M= mol dm^{-3}) NaOH.

Storage type hydrogen/oxidant fuel cells using metal hydrides have been noted for their high energy storage capacities per unit weight.[1] There are, however, various problems to be solved before their realization, e.g. proper choice of systems with suitable pressure of the hydrogen charge/discharge cycles, prevention of pulverization of the hydrogen absorbing metals or alloys (metal hydrides) during use, etc. Ishikawa et al.[2] have reported recently that some hydrogen absorbing alloys can be "microcapsulated" with copper deposited by electroless plating so as to prevent the pulverization during repeated hydrogen charge/discharge cycles and that their hydrogen storage ability after the plating was maintained at the level comparable with those of the untreated alloys. We have reported elsewhere[3] that the electrocatalyst such as Pt or Ag, which possesses the greater rate of the Volmer over that of the Tafel step, namely the greater m_o ($=i_{ov}/i_{oT}$) value, is desirable as a surface modifier in the metal hydride electrode from the viewpoint of the energy efficiency in the charge/discharge cycles.

In this work, $LaNi_5$ powder was microcapsulated with a group-IB metal, and the electrochemical property in alkaline solution was investigated, together with their mechanical stability.

Experimental

Preparation of the Electrodes. $LaNi_5$ powder (particle size about 100 μm and the BET surface area 0.5 $m^2 g^{-1}$) was subjected to electroless plating of Cu or Ag from conventional solutions,[4] or of Au by immersion of the powder in 2.5×10^{-3} M tetrachloroauric (III) acid solution. Amount of the deposition in weight (mol) % was 12.5 (48.6) for Cu, 12.5 (36.4) or 25 (57.2) for Ag, and 25 (42.3) for Au, respectively.

The microcapsulated $LaNi_5$ powder was pelletized into discs (13 mm diameter×1 mm thickness) with use of Ni nets (200 mesh) as electric leads under a static pressure of 400 Kg cm^{-2} and then heated at 770 K in vacuo (5×10^{-4} Pa) for several hours. The $LaNi_5$ samples bound with PTFE [poly(tetrafluoroethylene)] emulsion were prepared according to the method described in the literature.[5] In some occasions, a small amount of Pt was further deposited electrochemically. The nickel nets were spot-welded to Ta wires which were in turn sealed into Pyrex glass tubings.

Electrochemical Measurements. Galvanostatic polarization studies[3] were carried out in 1.0 M NaOH at 303 K. Real surface area of the test electrode was evaluated from the double layer capacitance data assuming a value of 18 μF cm^{-2} (true).

Results and Discussion

HER Characteristics. A series of microcapsulated $LaNi_5$ electrodes showed stable electrochemical behaviors in a similar manner as bare $LaNi_5$ electrodes. Thus, a typical plateau region was clearly observed on their short time (a few seconds) galvanostatic overpotential rise or decay transient curves respectively before the attainment of the steady-state polarization or of equilibrium potential. Through these observations, the electrodes are judged to possess a good hydrogen absorbability. Hence, as discussed previously,[6-8] we could estimate two overpotential components, η_1 and η_2', for the water discharge step and the hydrogen adatom recombination step, respectively.

The Tafel plots of η_1 on these microcapsulated electrodes showed a basic symmetry between the anodic and cathodic branches and the slope of the linear portion was reasonably close to 120 mV $decade^{-1}$. This indicates that η_1 represents the component overpotential for an one electron transfer reaction, namely the Volmer step. Its exchange current density (i_{ov}) estimated from the linear plots of η_1 vs. i, the applied current, near the reversible HER potentials was as follows: Cu/$LaNi_5$ 5.9, Ag/$LaNi_5$; 9.8, and Au/$LaNi_5$; 3.7×10^{-6} A cm^{-2} (true).

On the other hand, the "Tafel lines" of η_2' in the cathodic region gave a slope of ca. 30 mV $decade^{-1}$, except in the region of very high current density where the slope became lower, and indicated that η_2' should be attributed to the Tafel step. The linear η_2' vs. i plots in the low overpotential region resulted in the following i_{oT} values: Cu/$LaNi_5$; 0.7, Ag/$LaNi_5$; 0.8, and Au/$LaNi_5$; 0.6×10^{-6} A cm^{-2} (true), which were roughly one order of magnitude smaller than the corresponding i_{ov} values. The values of i_{ov}, i_{oT}, and m_o ($=i_{ov}/i_{oT}$) estimated of the microcapsulated $LaNi_5$ electrodes are schematically summarized in Fig. 1, together with those observed on some Ni-based alloys[6-8] and PTFE-bound or Pt-modified $LaNi_5$ electrodes.

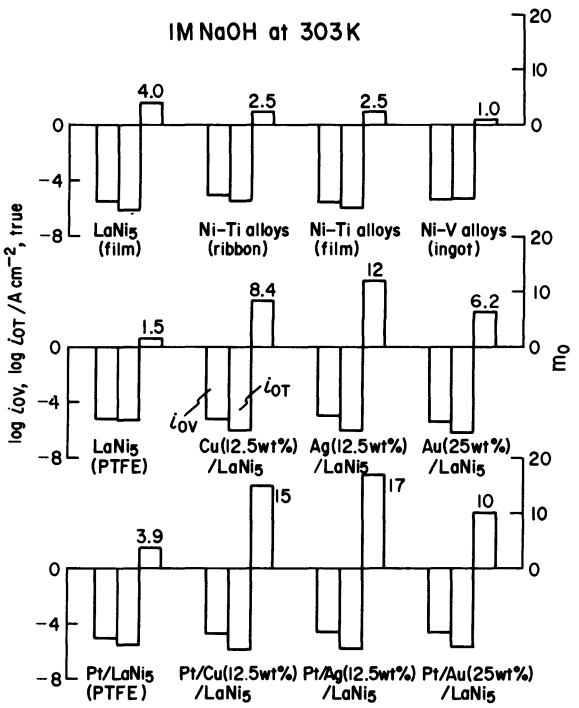

Fig. 1. Schematic diagram of the kinetic data obtained on Ni-based alloy ribbon or film electrodes, $LaNi_5$ electrodes coated with a series of group-IB metals, those further with Pt, and $LaNi_5$ electrodes bound with PTFE. 1.0 M NaOH, 303 K.

Table 1. Activation Energies for the Volmer and Tafel Steps and the Overall Reaction on Ni-Based Electrodes

Electrode	ΔE/kcal mol^{-1}		
	i_{ov}	i_{oT}	i_o
$Cu/LaNi_5$	9.0	4.5	4.6
$Ag/LaNi_5$	8.9	4.4	4.8
$Au/LaNi_5$	8.8	5.1	5.9

It was found that the microcapsulated $LaNi_5$ electrodes possessed much larger m_o values (6—12) than those (1—4) of the bare Ni-based alloys. Furthermore, they were considerably larger than those[3] observed on the group-IB metal electrocatalysts themselves. The larger m_o values were mainly caused by increased rates of the Volmer step and might indicate the existence of a synergistic effect between $LaNi_5$ and group-IB metals. A further increase up to m_o=17 was observed after a deposition of Pt on their surface. The PTFE-bound $LaNi_5$ electrode was mechanically very stable but the m_o value was relatively small (m_o=1.5): No polarization behaviors for HER could be studied with acceptable reliability, however, as hydrogen bubbles tightly adhered to the PTFE surface.

Mechanical Stability. The microcapsulated $LaNi_5$ electrodes prepared in this work were found to be stable even under polarizations up to η=−300 mV for a few ten hours. This was in agreement with the results reported on the hydrogen absorption/desorption cycles in gas phase[2] or in electrochemical system[9] of Cu-coated $LaNi_5$ specimens prepared in a similar manner as in this work. The electrodes were, however, damaged during polarizations over much longer durations even at potentials less than −300 mV.

Temperature Dependence. The activation heats evaluated from the Arrhenius plots of i_{ov}, i_{oT}, and i_o observed on the microcapsulated $LaNi_5$ electrodes are summarized in Table 1. The values were around 9 and 5 kcal† mol^{-1} for the Volmer and the Tafel step, respectively, and were in rough agreement with those observed on other Ni-based alloy electrodes.[6-8] Since the difference between the activation heats of two elementary reaction steps is appreciable (about 4 kcal mol^{-1}), m_o should significantly be increased at higher temperatures. This means that the energy efficiency may be improved if the hydrogen storage cells are operated at higher temperatures, but probably with the cost of decrease of the storage capacity.

The present work is partly supported by Grant-in-Aid for Scientific Research, No. 59045007, from the Ministry of Education, Science, and Culture.

References

1) "Hydrides for Energy Storage," ed by A. F. Andressen and A. J. Maeland, Pergamon Press, New York (1978).
2) H. Ishikawa, K. Oguro, A. Kato, H. Suzuki, and E. Ishii, *J. Less-Common Met.*, **107**, 105 (1985).
3) K. Machida and M. Enyo, *Bull. Chem. Soc. Jpn.*, the foregoing paper.
4) "Kagaku Binran, Oyohen (Handbook of Chemistry, Applications)," 3rd ed, ed by Chem. Soc. Jpn., Maruzen, Tokyo (1980), pp. 1159—1161.
5) N. Kaneki, H. Hara, K. Shimada, and Y. Jomoto, *Kagaku Kogaku Ronbunshu (Chemical Industry, Research Papers)*, **6**, 172 (1980).
6) K. Machida, M. Enyo, G. Adachi, and J. Shiokawa, *Electrochim. Acta*, **29**, 807 (1984).
7) K. Machida, M. Enyo, I. Toyoshima, K. Miyahara, K. Kai, and K. Suzuki, *Bull. Chem. Soc. Jpn.*, **56**, 3393 (1983).
8) K. Machida, M. Enyo, K. Oguro, and M. Nakane, *Bull. Chem. Soc. Jpn.*, **57**, 2809 (1984).
9) C. Iwakura, T. Asaoka, T. Sakai, H. Ishikawa, and K. Oguro, *Denki Kagaku*, **53**, 722 (1985).

† 1 cal=4.18 J.

Synthesis of 3-Substituted Indoles by a Palladium-Assisted Reaction

Akira KASAHARA,* Taeko IZUMI, Satoshi MURAKAMI, Hiroshi YANAI, and Masayuki TAKATORI†
Department of Applied Chemistry, Faculty of Engineering, Yamagata University, Yonezawa 992
†Department of Chemistry, Faculty of Education, Fukushima University, Fukushima 960-12
(Received October 3, 1985)

Synopsis. In the presence of palladium(II) chloride, 2-bromoanilines readily react with the methyl vinyl ketone and the ethyl acrylate to produce vinylogous arylamino ketones and esters. A palladium(0)-assisted cyclization of the arylamino ketones and the esters leads to a formation of 3-substituted indoles.

Beginning with the classical Fisher and Reissert methods, many reports on the synthesis of indoles have appeared from practical and theoretical points of view. Specifically, many 3-substituted indoles were well known to have a biological function, either as biochemical intermediates (aurin, tryptophan, tryptamine, serotonin) or as natural drugs (gramine, bufotenine, psilocine).

A variety of heterocyclic compounds can be synthesized using a palladium-catalyzed intramolecular functionalization of olefins as the ring-forming step.[1] Hegedus et al. have recently reported the synthesis of indoles from 2-allylanilines,[2] 2-vinylanilines,[2] and *N*-(3-bromo-2-vinylphenyl)-*p*-toluenesulfoamides[3] by a palladium-assisted cyclization reaction. Independent of their work, we present a new and efficient method for synthesizing 3-substituted indoles in two steps from 2-bromoanilines, based on a palladium-catalyzed reaction.

Bozell and Hegedus[4] reported previously that palladium(II) chloride catalyzed the reaction of anilines with methyl vinyl ketone and methyl acrylate to produce vinylogous arylamino ketones and esters. According to the method, 2-bromoaniline (**1a**), 2-bromo-5-methoxyaniline (**1b**), 2-bromo-3-methoxycarbonylaniline (**1c**), 2-bromo-4-methoxycarbonylaniline (**1d**), and 2-bromo-5-methoxycarbonylaniline (**1e**) reacted with conjugated olefins such as methyl vinyl ketone (**2a**) and ethyl acrylate (**2b**) to vinylogous arylamino ketones and esters (**3**) in good yield (Table 1). Nonconjugated olefins such as 1-hexene, styrene, and ethyl 2-acetamino-4-pentenoate, however, fail to undergo the amination. The structures of the products were determined on the basis of IR, ^{1}H-NMR, and mass spectral measurements and elemental analyses.

Table 1. The Reaction of 2-Bromoanilines and Olefins

2-Bromoaniline	Olefin	Product	Yield/%	Mp(θ_m/°C)
1a	**2a**	**3a**	76	46—47
1a	**2b**	**3b**	79	oil
1b	**2a**	**3c**	85	79—81
1b	**2b**	**3d**	78	67—68
1c	**2a**	**3e**	72	83—84
1c	**2b**	**3f**	74	80—81
1d	**2a**	**3g**	84	82—84
1d	**2b**	**3h**	68	113—114
1e	**2a**	**3i**	83	146—147
1e	**2b**	**3j**	85	112—113

A possible reaction course of **1** to **3** is shown in Eq 1. The catalytic palladium(II) species coordinates an olefin **2** which undergoes a nucleophilic attack by the amine to generate the σ-alkylpalladium complex. The σ-complex then decomposes by β-elimination to give an unstable palladium hydride complex and the observed product **3**. The palladium hydride complex ultimately forms palladium(0), which is reoxidized to palladium(II) by benzoquinone to complete the catalytic cycle.

In acetonitrile, the arylaminated olefins **3** were

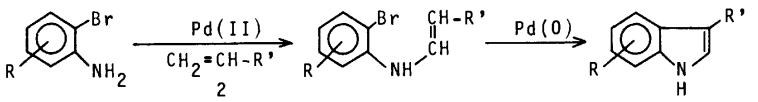

1 **3** **4**

2a: R′=COCH$_3$
2b: R′=COOEt

1a, 3a: R=H, R′=COCH$_3$
1b, 3b: R=H, R′=COOEt
1c, 3c: R=5-OMe, R′=COCH$_3$
1d, 3d: R=5-OMe, R′=COOEt
1e, 3e: R=3-COOMe, R′=COCH$_3$
1f, 3f: R=3-COOMe, R′=COOEt
1g, 3g: R=4-COOMe, R=COCH$_3$
1h, 3h: R=4-COOMe, R′=COOEt
1i, 3i: R=5-COOMe, R′=COCH$_3$
1j, 3j: R=5-COOMe, R′=COOEt

4a: R=H, R′=COCH$_3$
4b: R=H, R′=COOEt
4c: R=6-OMe, R=COCH$_3$
4d: R=6-OMe, R′=COOEt
4e: R=4-COOMe, R′=COCH$_3$
4f: R=4-COOMe, R′=COOEt
4g: R=5-COOMe, R′=COCH$_3$
4h: R=5-COOMe, R′=COOEt
4i: R=6-COOMe, R′=COCH$_3$
4j: R=6-COOMe, R′=COOEt

Scheme 1.

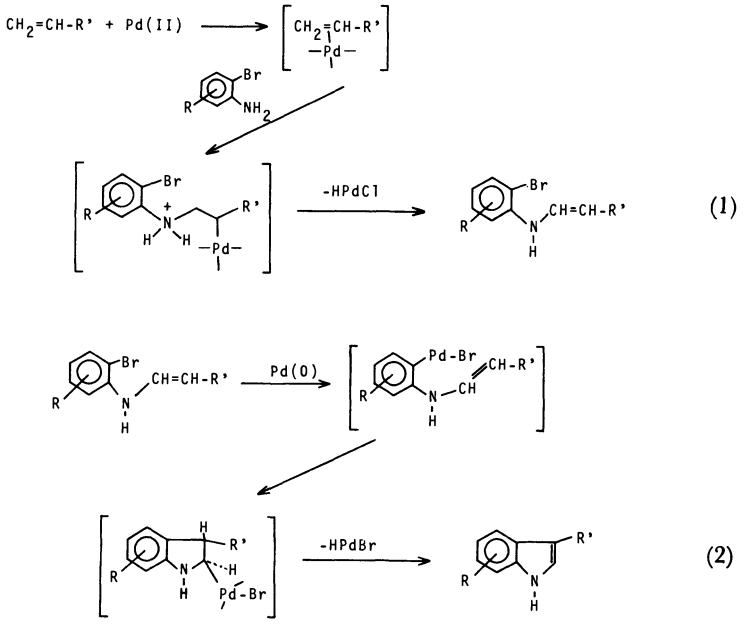

Table 2. The Palladium-Assisted Cyclization Reaction of the Arylaminated Olefins

Starting material	Product	Yield/%	Mp(θ_m/°C(lit. mp))
3a	**4a**	95	192—194(194[a])
3b	**4b**	96	118—119(118—119[b])
3c	**4c**	80	208—209
3d	**4d**	82	141—142(142—142.5[c])
3e	**4e**	95	143—144
3f	**4f**	93	93—94
3g	**4g**	84	223—224
3h	**4h**	85	186—188
3i	**4i**	86	213 (decomp)
3j	**4j**	90	160—161

a) J. W. Baker, *J. Chem. Soc.*, **1964**, 461. b) R. Majima, and M. Kotake, *Chem. Ber.*, **55**, 3865 (1922). c) Roussel-UCLAF, *Chem. Abst.*, **60**, 2899 (1964).

warmed with a catalytic amount of palladium(II) acetate and tri-*o*-tolylphosphine to afford the expected 3-substituted indoles (**4**) in high yield (Table 2). The reaction **3** to **4** is thought to proceed by an oxidative addition of an aromatic halide **3** to the palladium(0) complex, followed by an intramolecular olefin insertion and a β-hydride elimination (Eq 2).

Experimental

All melting points are uncorrected. The IR spectra were measured on KBr disks with a Hitachi 260-10 spectrometer and ^{1}H-NMR spectra were obtained using a Hitachi R-22 spectrometer in $CDCl_3$. TMS was used as internal standard. The mass spectra were obtained on a Hitachi RMU-6M mass spectrometer, using a direct-insertion probe at an ionization energy of 70 eV.

General Procedure for the Palladium-Catalyzed Reaction of 2-Bromoanilines (1) with Olefins (2). Dichlorobis-(acetonitrile)palladium(II) (778 mg, 3 mmol), benzoquinone (3.24 g, 30 mmol), lithium chloride (12.70 g, 300 mmol), and olefin 2 (30 mmol) were mixed in THF (100 cm^3) at room temperature. After stirring for 15 min, **1** (30 mmol) in THF (20 cm^3) was added. The resulting mixture was stirred for 24 h at room temperature and the solvent was removed under a reduced pressure. The residue was stirred with ether and filtered; the ether solution was repeatedly washed with 1 M sodium hydroxide(1 M=1 mol dm^{-3}) solution and water. The organic layer was dried over $MgSO_4$ and filtered and the solvent was removed to give the crude product which was purified by column chromatography using silica gel and hexane-benzene (2:1). The results are presented in Table 1.

General Procedure for the Palladium-Assisted Cyclization Reaction Vinylogous Arylamino Compounds (3) to Indoles (4). A mixture of **3** (14.9 mmol), palladium(II) acetate (0.167 g, 0.745 mmol), tri-*o*-tolylphosphine (0.906 g, 2.98 mmol), and triethylamine (1.88 g, 18.6 mmol) in acetonitrile (20 cm^3) was heated in a sealed tube flushed with nitrogen at 100 °C for 20 h. The cooled reaction mixture was diluted with ether and water. The ether layer was separated, washed with water, dried, and concentrated. The remaining residue was chromatographed on silica gel with benzene to give product **4**. The results are presented in Table 2.

The structures of the products were verified by elemental analyses, mass spectrometry, and by their ^{1}H-NMR and IR spectra. The complete ^{1}H-NMR, IR, and elemental analyses data are deposited at the Office of the Editor of the Bulletin of the Chemical Society of Japan (Document No. 8616).

References

1) J. Tsuji, "Organic Synthesis with Palladium Compounds," Berlin, Springer-Verlag, 1980, p. 13, 21, 33.

2) L. S. Hegedus, G. F. Allen, J. J. Bozell, and E. L. Waterman, *J. Am. Chem. Soc.*, **100**, 5800 (1978).

3) P. J. Harrington and L. S. Hegedus, *J. Org. Chem.*, **49**, 2657 (1984).

4) J. J. Bozell and L. S. Hegedus, *J. Org. Chem.*, **46**, 2561 (1981).

Generation of the Selenonium Ylide by the Carbenic Reaction. Formation of Cyclopropane Derivatives via Selenonium Ylide

Toshikazu IBATA* and Makoto KASHIUCHI
Institute of Chemistry, College of General Education, Osaka University,
Toyonaka, Osaka 560
(Received October 28, 1985)

Synopsis. The $Cu(acac)_2$-catalyzed decomposition of α-diazoacetophenones in the presence of bis(*p*-methoxyphenyl) selenide (**3**) did not give the corresponding selenonium ylide but gave *r*-1,*c*-2,*t*-3-tribenzoylcyclopropanes through the successive reaction of the intermediary selenonium ylide. On the other hand, the reaction of diazodimedone with **3** gave bis(*p*-methoxyphenyl)selenonium 4,4-dimethyl-2,6-dioxocyclohexylide.

The chemistry of the sulfonium ylide has extensively been studied in last two decades from the structural and synthetic interests.[1] Since the early work of Diekmann,[2] thermal and photolytic decomposition of diazo compounds in the presence of sulfides has been recognized as one of the general synthetic method of stable sulfonium ylide.[3] On the other hand, synthesis of the selenonium ylides have not so widely been studied.[4] As a continuation of our work on sulfonium ylide,[5] formation of selenonium ylide by the carbenic reaction was studied.

Results and Discussion

For the stabilization of selenonium ylide, decrease of positive charge induced on selenium atom seems to be effective. Therefore, diphenyl selenide attached by electron-releasing methoxyl groups on the para positions was used as a substrate of the reaction. The $Cu(acac)_2$-catalyzed decomposition of *p*-methoxy-α-diazoacetophenone (**1a**) in benzene solution at 80 °C in the presence of 3 molar amount of bis(*p*-methoxyphenyl) selenide (**3**) gave colorless crystals, mp 161 °C, besides the recovered selenide (**3**). The results of elemental analysis indicated that the product did not contain selenide moiety. The analytical values agreed with the calculated ones for the dimer or trimer of the corresponding carbene (**2**) generated from the diazoacetophenone (**1a**). The spectroscopic data showed that the product is *r*-1,*c*-2,*t*-3-tris(*p*-methoxybenzoyl)cyclopropane (**7a**). In its NMR spectrum the coupling pattern of methine proton signals, δ=3.62 (d, 2H) and 4.14 (t, 1H), revealed that the cyclopropane had trans configuration. Other substituted diazoacetophenones gave the corresponding cyclopropane derivatives in similar reactions in reasonable yields as is shown in Table 1.[6] In order to confirm the catalytic action of the selenide (**3**), the reactions were carried out using different amounts of **3**. When the amount of **3** was reduced to 1/3 of the amount to **1**, the yield of **7** decreased a little. However, 1/20 amount of **1** was still shown to be effective for promotion of the reaction (Table 2). Detailed inspection of these reaction mixtures by column chromatography indicated that neither *r*-1,*c*-2,*c*-3-triaroylcyclopropane nor 1,2-diaroylethylene (**8**) was detected, despite the 1,2-diaroylethylenes were obtained by the copper-catalyzed decomposition of **1** in the absence of sulfide or selenide (**3**).[7]

The reaction seems to be explained in the following Scheme. At the first stage of the reaction, the ketocarbene[8] generated by the $Cu(acac)_2$-catalyzed decomposition of diazoacetophenone reacts with selenide (**3**) to give bis(*p*-methoxyphenyl)selenonium aroylmethylide (**4**). Failure of the isolation of selenonium ylide (**4**) may be attributed to the high reactivity of **4** to give 1:2-betaine (**5**) by the further reaction with **1**. The betaine **5** reacts with another molecule of diazoacetophenone under the liberation of nitrogen affording 1:3-betaine (**6**) which gave the cyclopropane **7** by the cyclization via elimination of selenide (**3**). The elimination process of **3** from the betaine (**5**) to give 1,2-diaroylethylene (**8**) could be neglected because of absence even a trace amount of **8** in the reaction mixture. If the dimer (**8**) was formed,

Table 1. Yields and NMR Chemical Shift of *r*-1, *c*-2, *t*-3-Tribenzoylcyclopropanes

Run	Ar	Yield/%	Chemical shift of methine/δ	
a	*p*-$CH_3OC_6H_4$	55	3.63(d)	4.14(t)
b	*p*-$CH_3C_6H_4$	68	3.71(d)	4.20(t)
c	*m*-$CH_3C_6H_4$	54	3.74(d)	4.24(t)
d	C_6H_5	59	3.74(d)	4.19(t)
e	*p*-ClC_6H_4	54	3.67(d)	4.13(t)
f	*m*-ClC_6H_4	49	3.70(d)	4.14(t)
g	*p*-BrC_6H_4	48	3.67(d)	4.08(t)
h	*p*-NCC_6H_4	41	3.76(d)	4.16(t)

Table 2. The Effect of the Amount of **3** on the Yield of *r*-1, *c*-2, *t*-3-Tritoluoylcyclopropane (**7b**)[a]

Amount of **3**/g	Yield of **7b**/%
1.00	68
0.50	69
0.30 (1 mmol)	61
0.15	54
0.05	44

a) The reaction was carried out in benzene solution using 3 mmol of *p*-methyldiazoacetophenone and 0.050 g of $Cu(acac)_2$ at 80 °C.

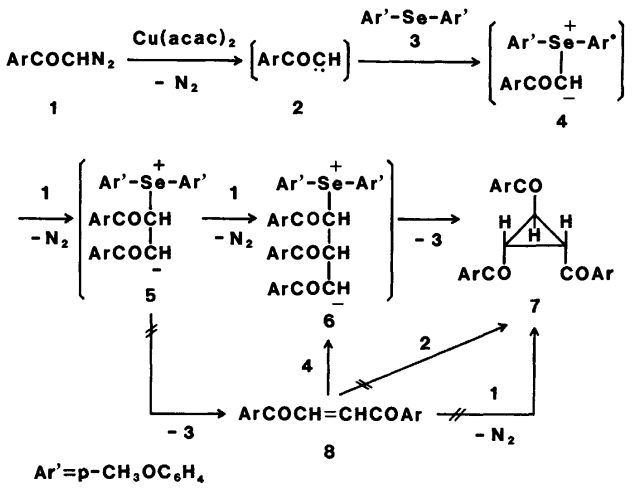

Scheme

the next steps to give cyclopropane (**7**) are: (a) reaction with **1** affording **7** and N_2 directly; (b) reaction with **1** to give **7** and N_2 via corresponding 1,3-dipolar cycloadduct; (c) reaction with the carbene (**2**) to give **7**; (d) reaction with **4** to give the 1:3-betaine (**6**).[10] The processes (a) and (b) are shown not to occur under the reaction conditions (1 atm., 70 °C), and the process (c) can be neglected from the previous observation.[7] The process (d) is possible deducing from the case of sulfonium ylide.[10] The preferential formation of the *trans*-isomer may be explained by the steric factor on the cyclization process.[6]

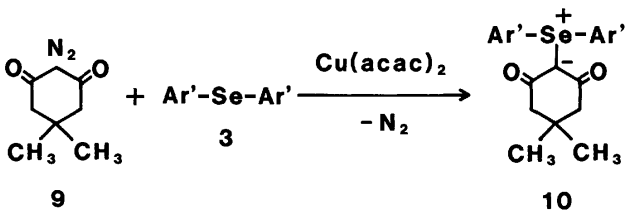

Another method to attain the stability of ylides is to attach electron-attracting groups on anionic carbon of the ylide. Therefore, the diazodimedone (**9**) was used as an example of diazodiacyl compound instead of diazoacetophenones. Decomposition of **9** in a similar manner in the presence of selenide (**3**) gave 40% yield of expected selenonium ylide (**10**), which was confirmed by the spectroscopic data showing singlet ^{1}H NMR signals of two methoxyl, two methyl, and two methylene groups at δ 1.10, 3.82, and 2.37 ppm, respectively together with those of aromatic protons. This indicates that the product includes both selenide and carbene components. The C=O absorption of the selenonium ylide (**10**) at 1580 cm^{-1} also supported the ylide structure **10** in comparison to that of dimethylsulfonium diacetylide at 1565 and 1595 cm^{-1}.[9]

Experimental

The IR spectra were recorded on Perkin-Elmer model 983 and the ^{1}H NMR spectra were measured in $CDCl_3$ solution at 90 MHz on a Varian Spectrometer model EM390 using TMS as an internal standard.

Materials. Substituted α-diazoacetophenones were synthesized by the reaction of corresponding acid chlorides with excess diazomethane according to the method of Newman.[11] Diazodimedone was prepared from dimedone via diazo group transfer reaction using tosyl azide and triethylamine.[12] Bis(*p*-methoxyphenyl) selenide was prepared by the reaction of *p*-methoxyphenyldiazonium chloride with potassium selenide.[13]

General Procedure of the Cu(acac)$_2$-Catalyzed Decomposition of α-Diazoacetophenones in the Presence of 3. A benzene solution of α-diazoacetophenone (3 mmol) and **3** (1.00 g, 3.4 mmol) was heated at 70 °C in the presence of 10 mg (0.04 mmol) of Cu(acac)$_2$ until the evolution of N_2 ceased. The reaction mixture was separated by silica-gel column chromatography.[14]

Decomposition of Diazodimedone in the Presence of 3. A benzene solution of diazodimedone (0.50 g, 3 mmol) and **3** (1.00 g, 3.4 mmol) was refluxed for 10 h in the presence of catalytic amount of Cu(acac)$_2$. Separation of the reaction mixture through silica-gel column chromatography gave white crystals; mp 194-6 °C, 0.52 g (40%). Found: C, 61.04; H, 5.72%. Calcd for $C_{22}H_{24}O_4Se$: C, 61.25; H, 5.61%.

References

1) B. M. Trost and L. S. Melvin, Jr. "Sulfur Ylides," Academic Press, New York (1975).
2) J. Diekmann, *J. Org. Chem.*, **30**, 2272 (1965).
3) W. Ando, T. Yagihara, S. Tozune, and T. Migita, *J. Am. Chem. Soc.*, **91**, 2786 (1969): W. Illger, A. Liedhegener, and M. Regitz, *Ann. Chem.*, **760**, 1 (1972).
4) D. Lloyd and M. I. C. Singer, *Chem. Commun.*, **1967** 390; S. Tamagaki and K. Sakai, *Chem. Lett.*, **1976**, 503.
5) M. Takebayashi, T. Kashiwada, M. Hamaguchi, and T. Ibata, *Chem. Lett.*, **1972**, 809.
6) Although Lotz and Gosselck reported the formation of *r*-1,*c*-2,*t*-3-tribenzoylcyclopropane in the decomposition of α-diazoacetophenone in the presence of dimethyl selenide, no experimental details were described; W. W. Lotz and J. Gosselck, *Tetrahedron*, **1973**, 917.
7) C. Grundmann, *Ann.*, **536**, 29 (1938): M. Takebayashi, T. Ibata, and K. Ueda, *Bull. Chem. Soc. Jpn.*, **43**, 1500 (1970).
8) The ketocarbene may probably react as a corresponding copper-carbenoid.
9) W. Ando, T. Yagihara, S. Tozune, I. Imai, J. Suzuki, T. Toyama, S. Nakaido, and T. Migita, *J. Org. Chem.*, **37**, 1721 (1972).
10) A. W. Johnson and R. T. Amel, *Tetrahedron Lett.*, **1966**, 819; F. Serratosa and J. Quintana, *Tetrahedron Lett.*, **1967**, 2245.
11) M. S. Newmann and P. F. Beal, *J. Am. Chem. Soc.*, **72**, 1506 (1949).
12) M. Regitz and D. Stadler, *Ann.*, **687**, 2314 (1965).
13) *Org. Synth.*, Coll. Vol 2, 238 (1948).
14) Cyclopropanes obtained were characterized by the spectroscopic and analytical data.

Improved Optical Resolution of (±)-1,2-Diphenylethylenediamine

Kazuhiko SAIGO,* Naomi KUBOTA, Shoko TAKEBAYASHI, and Masaki HASEGAWA
Department of Synthetic Chemistry, Faculty of Engineering, The University of Tokyo, Hongo, Bunkyo-ku, Tokyo 113
(Received November 11, 1985)

Synopsis. (±)-1,2-Diphenylethylenediamine (DPEDA) was efficiently resolved by the fractional crystallization of its diastereomeric salts with optically active mandelic acid. ^{1}H-NMR spectrum of *N*-monoacylated DPEDA with an optically active derivatizing agent showed that DPEDA thus obtained was optically pure.

(±)-Diphenylethylenediamine (DPEDA) having an interesing structure of C_2 symmetry has been frequently used as a unique ligand of several metal complexes.[1] Moreover, it can be an auxiliary in asymmetric induction and an optically active component for the synthesis of optically active polyamides. From the viewpoint of synthetic utilization of optically active DPEDA, it is very important to develop a highly efficient method for the optical resolution of (±)-DPEDA. For its optical resolution there has been reported only one method using optically active tartaric acid as a resolving agent.[2] However, this seems to have some operational problems since it is very hard to recrystallize the diastereomeric salt deposited from the reaction mixture of (±)-DPEDA with optically active tartaric acid. Additionally, (+)-DPEDA is difficult to obtain in pure state because nonnatural type (−)-tartaric acid is too expensive to obtain in a large quantity.

In the present paper, we describe an efficient optical resolution of (±)-DPEDA by fractional crystallization using optically active mandelic acid (MA) as a resolving agent, of which both enantiomers are industrially available. We also confirmed the specific rotation of optically pure DPEDA, for which various values have been reported previously.[2]

(±)-DPEDA was prepared from benzaldehyde via isoamarine according to the methods in the literatures,[1a,3] as shown in the following scheme. The

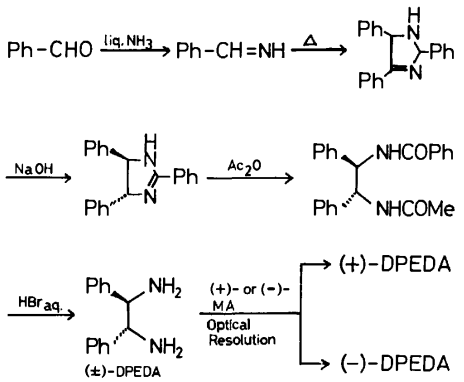

reaction of (±)-DPEDA with two molar amounts of (+)-MA gave a mixture of diastereomeric salts. Recrystallization of the mixture for two times from ethanol yielded (+)-DPEDA·(+)-MA (1:2) salt in 82% yield. (−)-Enriched DPEDA, recovered from the mother solution and the filtrates, was allowed to react with two molar amounts of (−)-MA, and the resulting salt was similarly recrystallized twice from ethanol to give (−)-DPEDA·(−)-MA (1:2) salt in 82% yield. Decomposition of each salt with aqueous sodium hydroxide solution gave (+)- and (−)-DPEDA in 72 and 79% total yields, respectively.

To determine the optical purity, (+)-DPEDA ($[\alpha]_D^{22}$ +106.5° (*c* 1.07, MeOH)) was acylated with (−)-(benzylmethylphenylsilyl)acetic acid (BMPSA),[4] giving monoacylated (+)-DPEDA. Its ^{1}H-NMR spectrum was compared with that of *N*-monoacylated (±)-DPEDA. On the basis of the area ratio of methyl protons of the (−)-BMPSA resudue in two diastereomeric monoamides, the optical purity of (+)-DPEDA was found to be 99.6%. Consequently, the specific rotations of optically pure DPEDA were determined as follows.

Table 1. The Specific Rotations of Optically Pure DPEDA

Solvent	[α] 589	577	546	435	405
MeOH[a]	106.9	109.8	126.3	243.7	290.5
Et_2O[b]	82.6	85.4	99.8	191.3	243.0

a) *c* 1.07 at 22 °C. b) *c* 0.97 at 18 °C.

Experimental

Melting points were measured by a laboratory devices MEL-TEMP apparatus and are uncorrected. IR spectra were recorded on a JASCO IR-810 Spectrophotometer. Optical rotations were masured by a JASCO DIP-360 Digital Polarimeter. ^{1}H-NMR spectra were recorded on a JEOL JMR GX 400 Spectrometer.

(±)-DPEDA was prepared by the methods reported in the literature,[1a,3] mp 76—77 °C (lit,[3] 83 °C).

Optical Resolution of (±)-DPEDA. (±)-DPEDA (1.70 g, 8 mmol) and (+)-MA (2.43 g, 16 mmol) were dissolved in ethanol (20 ml) on heating. After cooling to room temperature, the crystals deposited were collected by filtration and washed with two portions of ethanol (1.5 ml each). Recrystallization of the mixture of the diastereomeric salts for two times from ethanol (25 ml then 20 ml), followed by drying over P_2O_5 under reduced pressure, gave almost pure (+)-DPEDA·(+)-MA (1:2) salt (1.69 g, 82% based on the half amount of DPEDA used): Mp 164—165 °C; IR (KBr) 3450 (-OH), 3100 ($-\overset{+}{N}H_3$), and 1530 ($-CO_2^-$) cm^{-1}; $[\alpha]_{435}^{16}$ +278.8°, $[\alpha]_D^{16}$ +126.9° (*c* 1.51, MeOH).

Calcd for $C_{30}H_{32}N_2O_6$: C, 69.75; H, 6.24; N, 5.42%. Found: C, 69.49; H, 6.11; N, 5.30%.

The minus enriched DPEDA (0.96 g, 4.5 mmol), recovered from the mother liquor and the filtrates by treating with aqueous sodium hydroxide, was similarly reacted with (−)-MA (1.37 g, 9 mmol) in ethanol (20 ml) on heating.

Cooling the solution at room temperature gave almost pure (−)-DPEDA·(−)-MA (1:2) salt (1.70 g, 82% based on the half amount of DPEDA used) without any recrystallization: Mp 163—164 °C; IR (KBr) 3450 (-OH), 3100 ($-\overset{+}{N}H_3$), and 1530 ($-CO_2^-$) cm^{-1}; $[\alpha]_{435}^{20}$ −277.9°, $[\alpha]_D^{20}$ −126.5° (*c* 1.40, MeOH).

Calcd for $C_{30}H_{32}N_2O_6$: C, 69.75; H, 6.24; N, 5.42%. Found: C, 69.78, H, 6.31; N, 5.36%.

(+)-DPEDA·(+)-MA (1:2) salt (1.68 g, 3.3 mmol) was treated with 4 mol dm^{-3} sodium hydroxide solution (36 ml) and extacted with ether (3×40 ml). The extracts were combined, dried over sodium hydroxide pellets, and concentrated under reduced pressure. Recystallization of the remaining residue from hexane gave (+)-DPEDA (0.61 g, 72% based on the half amount of DPEDA used): Mp 85—86.5 °C (lit,[2c] 80 °C); IR (KBr) 3380 ($-NH_2$), 3360 ($-NH_2$), and 705 (-Ar) cm^{-1}; $[\alpha]_D^{22}$ +106.5° (*c* 1.09, MeOH).

Calcd for $C_{14}H_{16}N_2$: C, 79.21, H, 7.60, N, 13.20%. Found: C, 79.26; H, 7.40; N, 13.00%.

The enantiomeric excess of (+)-DPEDA thus obtained was determined as follows: The ^1H-spectrum of the diastereomeric N-monoacylated mixture, prepared from (±)-DPEDA and (−)-BMPSA according to the procedure in the literature,[4] showed two methyl proton signals at δ 0.216 and 0.247 ppm, which correspond to methyl proton signal of the (−)-BMPSA residue in each diastereomeric N-monoacylated DPEDA. The integral ratio of these signals was 1:1. The ^1H-NMR spectrum also showed two methyl proton signals, of which integral ratio was 249:1. Based on this integral ratio, the enantiomeric excess of (+)-DPEDA was established to be 99.6%.

Using the values of the specific rotation and the enantiomeric excess of (+)-DPEDA, the specific rotation of optically pure DPEDA was calculated as shown in the Table.

A similar alkaline treatment of (−)-DPEDA·(−)-MA (1:2) salt (1.70 g, 3.3 mmol) gave (−)-DPEDA (0.67 g, 79% based on the half amount of DPEDA used): mp 85.5—86 °C (lit,[2c] 85—90 °C); $[\alpha]_D^{16}$ −105.2° (*c*, 1.06, MeOH); 97.5% optical purity.

Calcd for $C_{14}H_{16}N_2$: C, 79.21; H, 7.60; N, 13.20%. Found: C, 79.25; H, 7.30; N, 13.16%.

Similar satisfactory results were obtained when the optical resolution was carried out in 0.1—0.05 mol scales.

The authors wish to express their thanks to Dr. Daiyo Terunuma of Saitama University for a gift of optically active BMPSA.

References

1) a) O. F. Williams and J. C. Bailer, Jr., *J. Am. Chem. Soc.*, **81**, 4464 (1959); b) Y. Kitani, Japan Patent 103192 (1981); *Chem. Abstr.*, **96**, 193435j (1982).

2) a) F. Feist, *Chem. Ber.*, **28**, 3167 (1895); b) P. Pfeiffer, W. Christeleit, Th. Hesse, H. Pfitzner, and H. Thielert, *J. Prakt. Chem.*, **150**, 261 (1938); c) M. Gullotti, A. Pasini, P. Fantucci, R. Ugo, and R. D. Gillard, *Gazz. Chim. Ital.*, **102**, 855 (1972); d) F. Vögtle and E. Goldschmitt, *Chem. Ber.*, **109**, 1 (1976).

3) I. Lifshitz and J. G. Bos, *Recl.Trav. Chim. Pays. Bas.*, **59**, 173 (1940).

4) D. Terunuma, M. Kato, M. Kamei, H. Uchida, and H. Nohira, *Chem. Lett.*, **1985**, 13.

Application of Electron Spectroscopy for Chemical Analysis to Studies of the Composition of Icosanoic Acid Monolayer

Koichi KOBAYASHI* and Kyo TAKAOKA
Laboratory of Chemistry, Musashi Institute of Technology, Setagaya-ku, Tokyo 158
(Received July 30, 1985)

Synopsis. Electron spectroscopy for chemical analysis (ESCA) was used to determine the composition of icosanoic acid (n-$C_{19}H_{39}COOH$) monolayer deposited on the microscope glass slide from the water surface containing Cd^{2+} at varying pH. It was found that the monolayers deposited from substrate at pH<4.6, pH>6.6, and pH=4.6—6.6 consist of icosanoic acid, cadmium icosanoate, and mixture of both substances, respectively.

A knowledge of the composition of a Langmuir-Blodgett film (L-B film) is important for understanding of its properties and structures. The compositions of L-B films have been studied by means of IR spectroscopy,[1,2] neutron activation analysis,[3] and photomeric measurements.[4]

Electron spectroscopy for chemical analysis (ESCA) has been attracting attention as a powerful method for determining structure and composition on the surface layer of materials. Few ESCA studies of Langmuir-Blodgett films, however, have been reported.[5,6]

In the present investigation, the attempt was made to determine the composition of icosanoic acid monolayer deposited on a microscope glass slide from cadmium substrate at various pHs by ESCA.

Experimental

Materials. Icosanoic acid (purity of 99%), cadmium chloride and potassium hydrogencarbonate were obtained from Sigma Chemical Co., Wako Pure Chemical Ind., and Kanto Kagaku Co., respectively and were used without further purification. Other chemicals used were of analytical reagent grade. Icosanoic acid was dissolved in purified chloroform to make a spreading solution of 3×10^{-4} mol dm^{-3}. The pH of the solution in the trough was adjusted by the addition of aqueous solutions of NaOH and HCl.

The water used was distilled three times after refluxing ordinary distilled water with acid permanganate, and then distilling it from an alkaline permanganate solution.

Apparatus. The substrates for film deposition were commercially available microscope glass slides (24 mm×50 mm×0.5 mm). The surfaces of the microscope slides were cleaned in the following manner: they were first sonicated with distilled water, subsequently soaked in a cleaning solution of concentrated acid permanganate overnight, rinsed repeatedly with distilled water, and then dried in a desiccator. The monolayer was prepared in a Langmuir trough (40 mm×385 mm×7 mm) with a well of a water depth of 37 mm and was deposited on the microscope glass slide by lifting the previously immersed glass slide at a velocity of 7 mm min^{-1} at constant surface pressure of 29.5 mN m^{-1}, which was given by the use of piston oil (*cis*-9-octadecenoic acid).

The solution in the trough was 3×10^{-4} mol dm^{-3} $CdCl_2$ and 5×10^{-4} mol dm^{-3} $KHCO_3$ with varying pH. Under these conditions, no visible drops of water occurred on the microscope slides. The deposition ratio was monitored by comparing the geometric area of the microscope slide to the change in the monolayer area during the deposition process at constant surface pressure. Only monolayer films whose deposition ratio was maintained within 100±1% were used in this experiment.

ESCA measurements were made with a JEOL JESCA-4 spectrometer using Mg $K\alpha$ X-ray source (1253.6 eV). The samples were mounted to give a take-off angle of 45°. The peak areas of the C_{1s} and Cd_{3d} bands of the samples were measured to calculate the composition of the cadmium icosanoate monolayer.

All the experiments were carried out at about 20 °C.

Results and Discussion

It is important to know the escape depth of photoelectrons in the case of quantitative analysis using ESCA. Brundle et al.[7] reported that the escape depth of photoelectrons from gold, silver, and indium substrates through cadmium icosanoate (2.68 nm thick) was 3.6—4.1 nm. In our study, the escape depth for photoelectrons emitted from Cd through the icosanoate moiety is generally expected to be larger than that determined for cadmium icosanoate. In addition, recent studies[8-10] on the structure of L-B film indicate that the orientation of molecules to the substrate surface is perpendicular in the first layer of the deposited monolayers either of long chain fatty acids or their salts. Therefore, the peak areas of the Cd_{3d} and C_{1s} bands observed are assumed to be proportional to the amount of Cd and C in the monolayer films, respectively.

The vacuum stability of the monolayer film deposited at pH 7.4 were studied. Figure 1 shows the effect of time on the peak areas of C_{1s} and Cd_{3d} bands under a pressure of about $(2—4)\times10^{-8}$ mmHg (1 mmHg=133.322 Pa). As can be seen in Fig. 1, the peak areas of C_{1s} bands decrease linearly with increasing time, while the peak areas of Cd_{3d} bands are almost invariable within experimental error. The investigations of the vacuum stability of deposited films of cobalt octadecanoate[11] and cadmium icosanoate[12] show that the salts of these fatty acids are stable even under high vacuum. Thus, the decrease in peak area of C_{1s} band is considered to be caused by the breaking of the hydrocarbon chain in cadmium icosanoate under the X-ray radiation. Accordingly, all subsequent ESCA experiments were performed over a time period during which the damage to the hydrocarbon chain was negligible.

Figure 2 shows typical C_{1s} and Cd_{3d} photoelectron spectra obtained from the deposited monolayer at pHs' 4.7, 5.8, and 7.6. In Fig. 2, we can see the photoelectron signals for C_{1s} at 288.0 eV, which correspond to the carbon (284.3 eV) of the ordinary hydrocarbon chain. The shift in the C_{1s} peak occurs by the electrical insulating properties of the monolayer and glass. In addition, it is evident from Fig. 2,

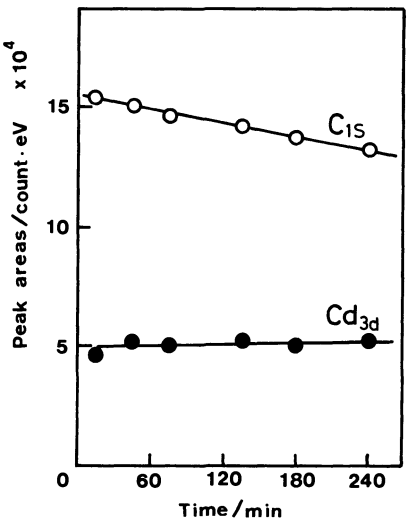

Fig. 1. Vacuum stability of cadmium icosanoate monolayer. The monolayers were deposited from cadmium substrate with pH=7.4.

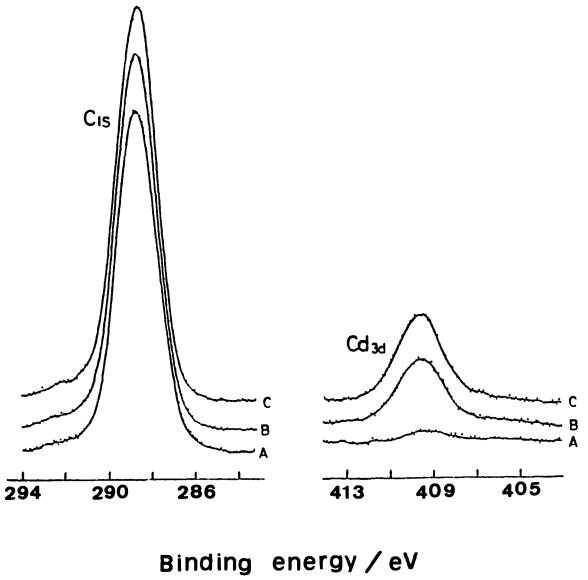

Fig. 2. C_{1s} and Cd_{3d} peaks for monolayer deposited from cadmium substrate with varying pH.
A: pH 4.7, B: pH 5.8, C: pH 7.6

that the carboxylic carbon band appears as a shoulder on the high energy side.[13] Also, we observed that the peak area of Cd_{3d} band was nearer to 0 in the lower pH region than about 4.6 and showed a constant value in the higher pH region than about 6.6. The near zero value at lower pH indicates no formation of cadmium icosanoate([Cd/RCOOH]=0), while the constant value at higher pH indicates the formation of cadmium icosanoate([Cd/RCOOH]=0.5), considering the pK_s value of 5.6. In order to calculate the [Cd/RCOOH] ratio at various pH, we assumed a linear relationship between the peak area of the Cd_{3d} band and the pH. The Cd_{3d}/C_{1s} peak area ratio calculated from the peak area of Fig. 2 and the [Cd/RCOOH] ratio were plotted against pH. The results are shown in Fig. 3. In this figure, the Cd_{3d}/C_{1s} peak area ratio or the [Cd/RCOOH] ratio

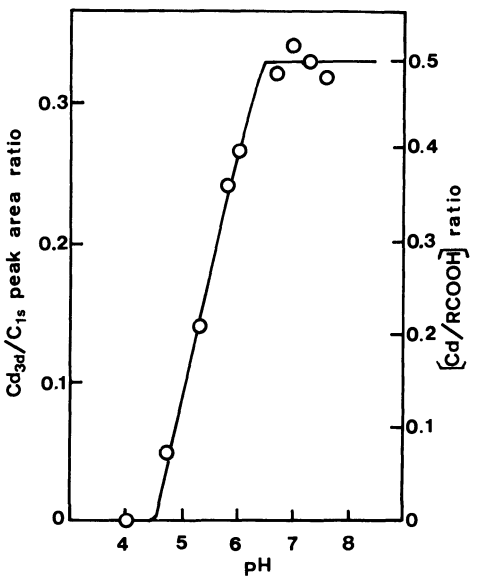

Fig. 3. Dependence of Cd_{3d}/C_{1s} peak area ratio or [Cd/RCOOH] ratio on pH.

increases from about pH 4.6 and reaches a plateau above about pH 6.6. In the lower pH region, the value of [Cd/RCOOH] is 0 which means the absence of cadmium ions. In the higher pH region, the value of [Cd/RCOOH] is about 0.5 which corresponds to the equivalent proportion of one bivalent cation to two fatty acids. Therefore, the monolayer deposited from solutions with pH<4.6 and pH>6.6 consist of icosanoic acid and cadmium icosanoate, respectively, and the monolayer deposited from solutions with pH=4.6—6.6 consist of the mixture of free acid and cadmium salt. Our experimental results are in good agreement with the observations of Petrov et al.,[3] using a combination of Langmuir-Blodgett technique and neutron activation analysis.

References

1) J. W. Ellis and J. L. Pauley, *J. Colloid Interface Sci.*, **19**, 755 (1964).
2) J. Bagg, M. B. Abramson, M. Fichman, M. D. Haber, and H. P. Gregor, *J. Am. Chem. Soc.*, **86**, 2759 (1964).
3) J. G. Petrov, I. Kuleff, and D. Platikanov, *J. Colloid Interface Sci.*, **88**, 29 (1982).
4) J. G. Petrov, H. Kuhn, and D. Möbius, *J. Colloid Interface Sci.*, **73**, 66 (1980).
5) K. Larsson, M. Lundquist, S. Stallberg-Stenhagen, and E. Stenhagen, *J. Colloid Interface Sci.*, **29**, 268 (1969).
6) T. Ohnishi, A. Ishitani, H. Ishida, N. Yamamoto, and H. Tsubomura, *J. Phys. Chem.*, **82**, 1989 (1978).
7) C. R. Brundle, H. Hospter and J. D. Swallen, *J. Chem. Phys.*, **70**, 5190 (1979).
8) J. F. Rabolt, F. C. Burns, N. E. Schlotter, and J. D. Swallen, *J. Chem. Phys.*, **78**, 15 (1983).
9) J. B. Baterman and E. J. Conunington, *J. Colloid Interface Sci.*, **16**, 531 (1961).
10) F. Kimura, J. Umemura, and T. Takenaka, *Langmuir*, in press.
11) M. Mizuno, C. Mori, and T. Watanabe, *Ohyobutsuri*, **45**, 514 (1976).
12) M. Iwahashi, F. Naito, N. Watanabe, and T. Seimiya, *Chem. Lett.*, **1985**, 187.
13) D. Briggs, *J. Adhesion*, **13**, 287 (1982).

Influence of Higher Alcohols on Acid-Catalyzed Hydrolysis of Sodium Dodecyl Sulfate. Effect of Complex Formation

Masayuki NAKAGAKI and Shoko YOKOYAMA*
Faculty of Pharmaceutical Sciences, Kyoto University, Yoshida-Shimoadachi-cho, Sakyo-ku, Kyoto 606
(Received September 20, 1985)

Synopsis. The order of effectiveness of 1-alkanols for increasing the rate of acid-catalyzed hydrolysis of sodium dodecyl sulfate is 1-dodecanol>1-tetradecanol ≫ 1-decanol. The effect of 1-alkanols on this hydrolysis is discussed from the viewpoint of formation of complexes composed of SDS and 1-alkanol.

In our preceding paper,[1] we reported the influence of 1-dodecanol ($C_{12}OH$) on the acid-catalyzed hydrolysis of sodium dodecyl sulfate (SDS) at concentrations above and below the critical micelle concentration (cmc). The hydrolysis of SDS at a concentration below the cmc is accelerated by addition of $C_{12}OH$ due to formation of a complex (SDS:$C_{12}OH$=2:1), and at concentrations above the cmc is initially suppressed by addition of $C_{12}OH$ due to reduction in surface charge density of the SDS micelle.

On the other hand, it has been known that complexes are formed not only between $C_{12}OH$[2-6] and SDS but also between other 1-alkanols[7,8] and SDS.

In this paper, therefore, we will deal with the influence of higher alcohols on the acid-catalyzed hydrolysis of SDS at concentrations below the cmc from the viewpoint of complex formation.

Experimental

Normal higher alcohols, 1-octanol (C_8OH), 1-decanol ($C_{10}OH$), 1-dodecanol ($C_{12}OH$), and 1-tetradecanol ($C_{14}OH$) obtained from Nakarai Chemicals Co. were of guaranteed reagent grade and used without further purification. Sodium dodecyl sulfate (SDS) was the same as that specified in our preceding paper.[1] Solutions were prepared by adding 1-alkanol to an aqueous 0.5 mmol dm^{-3} solution of SDS, followed by stirring for 20 h at 25 °C. The hydrolysis of SDS was carried out at pH 3.22±0.01 and 25±0.2 °C, and second-order rate constants were estimated as previously described.[1]

Results and Discussion

Effects of C_8OH, $C_{10}OH$, $C_{12}OH$, and $C_{14}OH$ on the Hydrolysis of SDS. Figure 1 shows rate constants for the hydrolysis of SDS against concentrations of 1-alkanols (or mole ratios of 1-alkanol to SDS). The relationship between $C_{12}OH$ and SDS which has been given in the preceding paper[1] is also included in Fig. 1. When the solution contains only premicellar SDS, the rate constant for the hydrolysis is very small but is increased markedly by addition of $C_{12}OH$ or $C_{14}OH$. Above mole ratio 0.5 of 1-alkanol to SDS, the rate constant is independent of the 1-alkanol concentration, which suggests formation of a complex of SDS with $C_{12}OH$[5,6] or $C_{14}OH$.[7]

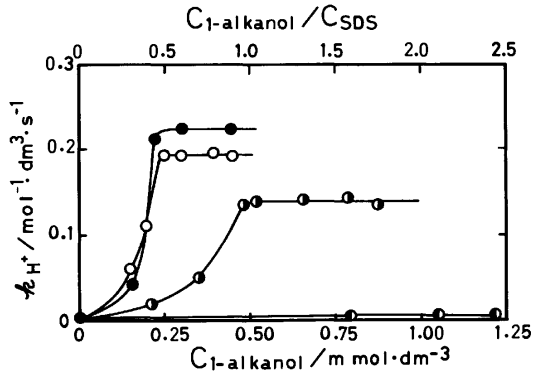

Fig. 1. Effect of 1-alkanols on the rate constant for hydrolysis of SDS at a concentration below the cmc
1-alkanol: ◐ C_8OH, ◑ $C_{10}OH$, ● $C_{12}OH$, ○ $C_{14}OH$
C_{SDS}: 0.50 mmol dm^{-3}
pH: 3.22

In the case of $C_{10}OH$, the rate constant increases with increasing concentration of $C_{10}OH$ and assumes a constant value at mole ratios of $C_{10}OH$ to SDS above 1.0. This tendency is consistent with formation of a 1:1 complex of SDS with $C_{10}OH$.[8]

The rate constants in the presence and absence of C_8OH do not so much differ from each other, even if C_8OH is added above mole ratio 2.0 to SDS. This suggest that there is no characteristic interaction between SDS and C_8OH. It has been reported[9] that a liquid crystal is formed in the C_8OH–SDS–water ternary system at a SDS concentration of 40 w/v%. We used too low a concentration of SDS for the formation of micelle (cmc values of SDS in the presence of 1-alkanols have been reported[8]). Therefore, it may be concluded that neither liquid crystal nor surfactant-alcohol complex is formed in this C_8OH system.

Regarding the relationship between the formation of liquid crystal and the rate constant for the hydrolysis of SDS, Barry and Schotten[10] reported that the rate constant was increased by an addition of 1-hexadecanol ($C_{16}OH$) due to formation of a liquid crystal in the $C_{16}OH$–SDS–water ternary system.

Effect of Complex Formation on Rate Constant. It has been suggested[4,6,7] that these complexes are formed by hydrogen bonding between the oxygen atom of sulfate and the OH group of alcohols. Therefore, the faster hydrolysis of SDS in the complexed state than in the noncomplexed state may be considered due to a proton being supplied by hydrogen bonding from $C_{12}OH$ to SDS in the first step of the hydrolysis mechanism:[11,12]

First step

$$C_{12}H_{25}OSO_3^- + H^+ \longrightarrow C_{12}H_{25}OSO_3H,$$

Second step

$$C_{12}H_{25}OSO_3H + H_2O \longrightarrow C_{12}H_{25}OH + HSO_4^- + H^+.$$

Moroi et al.[6] suggested that alkyl alcohol is more strongly bound to alkyl sulfate in a complex with alcohol to sulfate mole ratio 0.5 than in one with mole ratio 1.0. It is, therefore, considered that the complex with mole ratio 0.5 is more easily supplied with a proton in the first step of the hydrolysis than the one with mole ratio 1.0, which facility leads to the order of rate constants of hydrolysis: $k_c(C_{10}OH) < k_c(C_{12}OH)$, $k_c(C_{14}OH)$. In addition, the smaller k_c of the $C_{14}OH$-SDS complex than that of the $C_{12}OH$-SDS complex is considered due mainly to the steric effect. It is further considered that the aggregation of $C_{14}OH$ with SDS is more difficult than that of $C_{12}OH$ with SDS, because the two carbon atoms of $C_{14}OH$ protrude from the alkyl chain of SDS. This is consistent with the fact[4] that the complex between alkyl sulfate and 2-alkanol cannot be formed because of a difficulty of the aggregation.

Conclusion

The rate constant for the hydrolysis of SDS is increased by addition of $C_{10}OH$, $C_{12}OH$, or $C_{14}OH$ due to formation of complex (SDS:$C_{10}OH$=1:1), (SDS:$C_{12}OH$=2:1), or (SDS:$C_{14}OH$=2:1), respectively. Furthermore, the order of effectiveness of 1-alkanols for increasing the rate constant is $C_{12}OH > C_{14}OH > C_{10}OH$. This is due to the strength of hydrogen bonding between SDS and 1-alkanols and the steric effect of the complex.

In conclusion, we call attention to the difference in the effects of 1-alkanols on the hydrolysis of SDS (with respect to the formation of complex between SDS and 1-alkanols, and the rate constant for the complexed state), in contrast to the suggestion of Barry and Schotten[10] that $C_{16}OH$ and $C_{12}OH$ have a similar effect on the hydrolysis.

References

1) M. Nakagaki and S. Yokoyama, *J. Pharm. Sci.*, **74**, 1047 (1985).
2) M. B. Epstein, A. Wilson, C. W. Jakob, L. E. Conroy, and J. Ross, *J. Phys. Chem.*, **58**, 860 (1954).
3) J. N. Phillips and K. J. Mysels, *J. Phys. Chem.*, **59**, 325 (1955).
4) H. C. Kung and E. D. Goddard, *J. Colloid Sci.*, **20**, 766 (1965).
5) M. Abe and K. Ogino, *J. Colloid Interface Sci.*, **80**, 146 (1981).
6) Y. Moroi, K. Motomura, and R. Matuura, *Bull. Chem. Soc. Jpn.*, **44**, 2078 (1971).
7) H. C. Kung and E. D. Goddard, *J. Phys. Chem.*, **67**, 1965 (1963).
8) K. Ogino, M. Abe, and N. Takesita, *Bull. Chem. Soc. Jpn.*, **49**, 3679 (1976).
9) Y. Kasai and M. Nakagaki, *Nippon Kagaku Zasshi*, **91**, 19 (1970).
10) B. W. Barry and E. Schotten, *J. Pharm. Pharmacol.*, **19**, 785 (1967).
11) R. L. Bullwell, *J. Am. Chem. Soc.*, **74**, 1462 (1952).
12) J. H. Fendler and E. J. Fendler, "Catalysis in Micellar and Macromolecular Systems," Academic Press, New York (1975), p. 131.

Effective Rotational Temperatures of N_2^+ (X) Produced by Electron-Impact Ionization on N_2

Hirofumi KAWAZUMI, Tuneaki UCHIDA, and Teiichiro OGAWA*
Department of Molecular Science and Technology, Kyushu University, Kasuga, Fukuoka 816
(Received September 21, 1985)

Synopsis. The laser-induced fluorescence of molecular ions, N_2^+ (X, $^2\Sigma_g^+$), was measured under the controlled electron-impact ionization of N_2 in the thermal gas jet. The effective rotational temperature of N_2^+ (X) increased from 320±5 K to 367±15 K for the incident electron energy from 750 eV to 17 eV.

The rotational distribution of ions should be a valuable probe of the dynamics of the ionization process. Nitrogen molecule is suitable for this purpose. The ionization process to the B state of N_2^+ has been studied upon the electron-impact ionization-excitation.[1,2] At high electron energies, $\Delta|J|=1$ is obeyed; at low electron energies (<100 eV), however, $\Delta|J|\geq 3$ transitions occur through multipole transitions.[2]

The rotational distribution has been measured on the X state of N_2^+ produced by controlled electron impact in the thermal gas flow[3,4] and the supersonic beam[5,6] using laser-induced fluorescence (LIF) technique. The incident electron energies previously used, however, were only 60[3] and 100[3,4] eV in the former and 50,[5] 80,[5] and 300[6] eV in the latter.

In this study, we measured the rotational distribution of N_2^+ (X) in the thermal gas jet at the wide electron energy range of 17—750 eV, and determined the effective rotational temperature (T_R) of N_2^+(X) in order to discuss the ionization process.

Experimental

The apparatus has been described in detail previously.[4] In brief, the sample gas was jetted into a collision chamber through a multicapillary array and was crossed perpendicularly with an electron beam. The excitation light was produced by a N_2 laser pumped tunable dye laser (Molectron UV24+DL14). The signal was accumulated using gated detection electronics with a boxcar integrator or a 100 MHz photoncounter. We calculated the number density of ions to be about 10^8 ions cm^{-3} from the electron-beam current (500 μA), the sample gas pressure (0.13 Pa), the ionization cross section (1.0×10^{-16} cm^{-2}),[7] and the fly-out rate coefficient from the laser-irradiation region (1.4×10^6 s^{-1}). There are comparable number of ions in the ion trap techniques.[8,9] About 0.2 counts of the LIF signal per laser pulse were necessary to obtain a good spectrum with a signal to noise ratio of 15 in several hours of accumulation; the typical intensity of scattering light from the laser was 0.04 counts.

Results and Discussion

A typical excitation spectrum of the B($v'=0$)—X($v''=0$) of N_2^+ (X) produced by controlled electron impact on N_2 at the incident electron energy of 28 eV is shown in Fig. 1. The relative rotational line intensities, $\ln\{I_{N',N''}/(N'+N''+1)\}$, were plotted versus

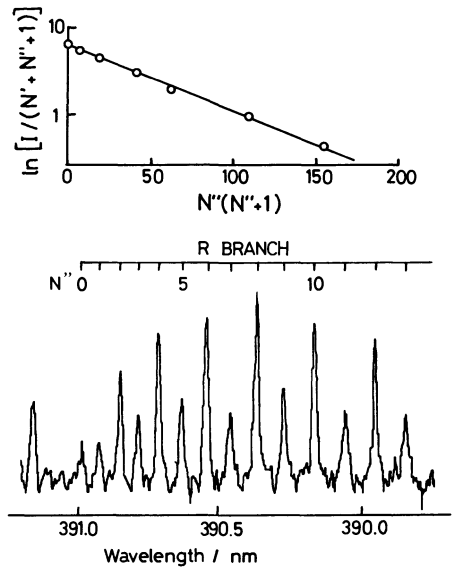

Fig. 1. Excitation spectrum of N_2^+ (X) (lower) and the rotational line intensity plot of even N'' lines of R branch (upper). Electron energy was 28 eV and N_2 pressure was 0.13 Pa.

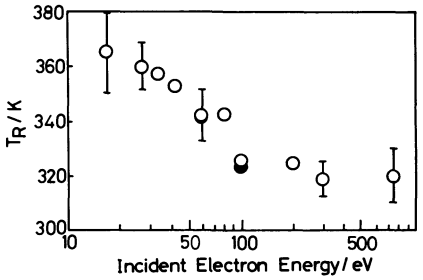

Fig. 2. The electron energy dependence of the effective rotational temperature (T_R) of N_2^+(X) produced by electron-impact ionization on N_2.
●: Allison et al., ○: this work.

$N''(N''+1)$, where N' and N'' are the upper and lower rotational quantum numbers of the transition, as also shown in Fig. 1. The plots were linear at all incident electron energies and gave the effective rotational temperature (T_R) of N_2^+ (X).

The electron energy dependence (17—750 eV) of T_R is shown in Fig. 2. The results obtained at 60 and 100 eV agree with the previous values[3] within experimental uncertainties. T_R was constant above 100 eV, and increased below 100 eV up to 367±15 K at 17 eV; T_R at 17 eV was higher by about 50 K than T_R at 750 eV.

In order to estimate effects of collisional relaxation, fly-out rate of the ions from the laser-irradiation

region has been measured through the intensity changes of the LIF signal at various delay times (0—2 μs) of the laser after the end of the pulsed electron beam. The LIF signal decayed exponentilly. The first-order decay analysis leads to a fly-out rate coefficient of 1.4×10^6 s^{-1} and a characteristic fly-out time of 0.71 μs. These values agree with the free diffusion rate estimated from the gas dynamics; a nitrogen molecular ion with the root-mean-square velocity of 511 m/s at 20 °C flies across the laser beam with the radius of 0.5 mm in about 1 μs. The characteristic collisional time at a pressure of 0.13 Pa is about 100 μs. These findings indicate that the observed spectrum was not disturbed by collisional relaxation. Cascade contributions are unimportant as the radiative lifetime of the A state (10 μs) is longer than the characteristic fly-out time and the ionization-excitation cross section to the B state is small[7]

In the ionization process for a homonuclear diatomic molecule such as H_2 and N_2, the selection rule of a rotational transition indicates ΔN to be an even number, e.g., $N''=N$, $N''=N\pm2$, and $N''=N\pm4$, where N and N'' are the rotational quantum number of N_2 and N_2^+ (X).[10,11] Change of the rotational quantum numbers between neutral and ionic molecules balances the angular momentum of the ejected electron, since the total angular momentum is conserved. In the photoionization of H_2, $\Delta N=0$ and $\Delta N=2$ transitions were observed with rotationally resolved photoelectron spectroscopy and $\Delta N=2$ transition was accounted for coupling between the p and f photoelectron waves.[11] The electron-impact ionization may be accompanied by an ejected electron with the large angular momentum through the multipole transition.[12] Therefore, the increase of T_R at lower electron energies is due to the increase of larger N transitions. At higher electron energies, $\Delta N=0$ transition is predominant and T_R of N_2^+ (X) do not change from that of N_2.

The electron energy dependence of T_R of N_2^+ (X) in this paper is considerably different from that of N_2^+ (B) previously reported.[13] This may be caused by the fact that the molecular orbital of the ejected electron for N_2^+ (X) is σ_g 2p, while that for N_2^+ (B) is σ_u 2s. The detailed analysis requires an experimental determination of the partial cross-section for each ΔN transition from a single rotational level.

The authors thank Professor Tamotsu Kondow of the University of Tokyo for his comments. The present study was partially supported by a Grant-in-Aid for Scientific Research from the Ministry of Education, Science and Culture (56470014).

References

1) B. M. DeKoven, D. H. Levy, H. H. Harris, B. R. Zegarski, and T. A. Miller, *J. Chem. Phys.*, **74**, 5659 (1981).
2) S. P. Hernandez, P. J. Dagdigian, and J. P. Doering, *J. Chem. Phys.*, **77**, 6021 (1982).
3) J. Allison, T. Kondow, and R. N. Zare, *Chem. Phys. Lett.*, **64**, 202 (1979).
4) H. Kawazumi, T. Uchida, and T. Ogawa, *Eng. Sci. Repts. Kyushu Univ.*, **6**, 171 (1985).
5) M. I. Lester, B. R. Zegarski, and T. A. Miller, *J. Phys. Chem.*, **87**, 5228 (1983).
6) H. Helvajian, B. M. DeKoven, and A. P. Baronavski, *Chem. Phys.*, **90**, 175 (1984).
7) St. Halas and B. Adamczyk, *Int. J. Mass Spectrom. Ion Phys.*, **10**, 157 (1972/73).
8) B. H. Mahan and A. O'Keefe, *J. Chem. Phys.*, **74**, 5606 (1981).
9) J. Danon, G. Mauclaire, T. R. Govers, and R. Marx, *J. Chem. Phys.*, **76**, 1255 (1982).
10) D. Dill, *Phys. Rev.*, **A6**, 160 (1972).
11) J. E. Pollard, D. J. Trevor, J. E. Reutt, Y. T. Lee, and D. A. Shirley, *Chem. Phys. Lett.*, **88**, 434 (1982).
12) R. J. Van Brunt, *J. Chem. Phys.*, **60**, 3064 (1974).
13) G. Culp and A. T. Stair, Jr., *J. Chim. Phys. Phys. Chim. Biol.*, **64**, 57 (1967).

Kinetic Studies of Fast Equilibrium by Means of High-Performance Liquid Chromatography. XIII.[1] Separation of Rotamers of *N*-Alkyl-Substituted Amides

Masataka MORIYASU,* Atsushi KATO, and Yohei HASHIMOTO
Kobe Women's College of Pharmacy, Motoyamakita-machi, Higashinada-ku, Kobe 658
(Received September 26, 1985)

Synopsis. Rotamers of *N*-alkyl-substituted amides have been separated by means of high-performance liquid chromatography(HPLC) at low column temperatures. The ratios of the *E*-rotamers have been found to increase in the following order: propionamides<acetamides<formamides.

We have already reported[1-3] the separation of rotamers of anilides by means of HPLC at low column temperatures. A similar separation seems to be possible for aliphatic amides. This report deals with the separation of rotamers of *N*-alkyl-substituted amides. The separation is found to be rather

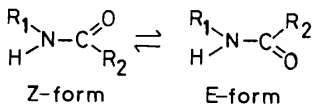

Chart

difficult for the following reasons, although the energy barriers of the bond rotation about the carbonyl-nitrogen bonds for aliphatic amides are higher than those for anilides.[4] (1) Since aliphatic amides usally have only weak UV absorption in the range shorter than 230 nm, their detection is not easy when the amount is low. Furthermore, the solvent systems usable in HPLC is seriously restricted. (2) Aliphatic amides, especially their low molecular weight analogues such as *N*-methylformamide and *N*-methylacetamide, are adsorbed strongly on the surface of silica gel, and therefore broad and tailing peaks appear on the chromatograms.

Experimental

N-Methylformamide, *N*-methylacetamide, *N*-ethylacetamide, *N*-benzylformamide, and *N*-benzylacetamide were obtained commercially. *N*-Ethylformamide, *N*-propylformamide, and *N*-isopropylformamide were prepared from trichloroacetaldehyde (chloral) and the corresponding aliphatic amines.[5] *N*-Propylacetamide, *N*-isopropylacetamide, *N*-methylpropionamide, *N*-ethylpropionamide, and *N*-propylpropionamide were prepared by the reaction of acetamide (or propionamide) with hydrochlorides of aliphatic amines.[6] These synthesized amides were all purified by distillation. Several silica gel packings with different adsorptive activity (LiChrosorb SI 60, LiChrosorb SI 100, LiChrosphere SI 1000, and LiChrosphere SI 4000) were tried, and the least active among them (LiChrosphere SI 4000) gave the best results. Other experimental conditions were detailed elswhere.[1-3]

Results and Discussion

We first attempted the separation of rotamers of *N*-benzylformamide because this aliphatic amide has relatively strong absorption in the UV by dint of the benzyl substituent and the presence of both *E*-and *Z*-rotamers had been confirmed by NMR study.[7] The solvent system of hexane and 1-propanol containing a small amount of acetic acid, which had been successfully applied for the separation of rotamers of acetanilides,[3] did not give the separation of rotamers at different column temperatures (25 to −50 °C). The replacement of 1-propanol by other alcohols also did not give satisfactory results. The addition of acetic acid to the eluent had a significant effect on the peak shape and very broad and tailing peaks were obtained in the complete absence of acid. The increase of the acetic acid content suppressed tailing, but the two rotamers were still not separated. Addition of too much acetic acid is not suitable for UV detection due to the UV absorption of acetic acid. The activity of silica gel packings also had significant effects on the peak shape and the less active packings gave the better results. Other various solvent systems were tested for the separation of the rotamers of *N*-benzylformamide. The solvent system of hexane and ethyl acetate containing a small amount of acetic acid[2] achieved the separation of the rotamers at 0 °C, but this solvent system could not be used for other aliphatic amides due to the UV absorption of ethyl acetate. The use of other various common solvents including esters, ketones, and alkyl halides, was also impossible. The only solvent system which separated the rotamers was a mixture of hexane and diethyl ether containing a very small amount of acetic acid. Under this solvent system rotamers of *N*-alkyl-substituted amides including *N*-benzylformamide were separated as is exemplified in Fig. 1. The separation of formamides was achieved near 0 °C, while for the separation of acetamides a lower column temperature (−20 °C) was required. With the increase of the column temperature the two peaks

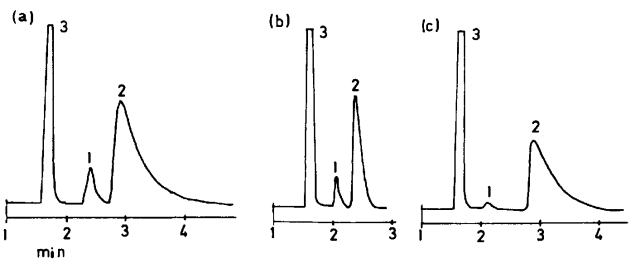

Fig. 1. Separation of rotamers of formamides and acetamides. Column: LiChrosphere SI 4000 (10 μm, 4.6 mm × 15 cm). Eluent : hexane : diethyl ethyl : acetic acid = 100 : 50 : 0.5, 2.5 cm^3 min^{-1}. Detector: UV 228 nm. Column temperature: (a) and (b) 0 °C, (c) −20 °C. (a): 0.2 mol dm^{-3} *N*-methylformamide, (b): 0.2 mol dm^{-3} *N*-benzylformamide, (c): 0.2 mol dm^{-3} *N*-ethylacetamide.
1: *E*-form, 2: *Z*-form, 3: solvent ($CHCl_3$).

Table 1. Percentages of Formamides and Acetamides Existing as *E*-Form

Amides	*E*-form/%			
	This work[a] (HPLC)	Other works		
		(NMR)	Experimental conditions	Ref.
N-Methylformamide	11	8	35 °C, pure liquid?[b]	8
N-Ethylformamide	19	12	35 °C, pure liquid?[b]	8
N-Propylformamide	22			
N-Isopropylformamide	21	12	35 °C, pure liquid?[b]	8
N-Benzylformamide	14	10	room temperature, 16.7% in molar ratio in benzene	7
N-Methylacetamide	2.0			
N-Ethylacetamide	2.1			
N-Propylacetamide	3.9			
N-Isopropylacetamide	2.0			
N-Benzylacetamide	1.1			

a) 25 °C, 0.2 mol dm^{-3}. b) Experimental conditions were not well documented.

coalesced gradually and at room temperature only one peak appeared. As shown in Fig. 1 the HPLC conditions are far from ideal due to tailing. Further addition of acetic acid would alleviate tailing, but this was impossible for the UV detection. Contrary to formamides and acetamides, *E*-rotamers of propionamides were not detected even at very low column temperatures (−60 °C), which suggests that either the content of the *E*-rotamers is very low (<0.5%) or retention times of the two rotamers are close to each other. We consider that the former explanation is more probable. Table 1 indicates the percentages of *E*-rotamers in chloroform. The identification of the peak was carried out by comparing the HPLC results with the data obtained by ^{1}H-NMR for formamides.[8] The presence of *E*-rotamers of acetamides had not hitherto been reported by NMR studies,[4] but the presence of a few percent of *E*-rotamers was confirmed by HPLC. The following sequence of increasing percentages of *E*-rotamers (propionamides<acetamides<formamides) is explained in terms of the difference in steric hindrance between R_1 and R_2 in the *E*-forms.

The ratios of rotamers should also be affected by various conditions such as concentration, temperature, and solvent composition in which the amides are dissolved. *N*-Methylformamide was dissolved in several solvents (0.2 mol dm^{-3}, 25 °C) and the percentages of *E*-rotamers were determined which were as follows; 11% (carbon tetrachloride), 11% (chloroform), 10% (benzene), 9.0% (tetrahydrofuran), 8.2% (ethyl acetate), 8.2% (acetonitrile), 7.0% (diethyl ether), 6.3% (ethanol), and 5.8% (methanol). The effect of the concentration was also examined for *N*-methylformamide in chloroform, and the percentages of the *E*-rotamer were as follows; 13% (0.13 mol dm^{-3}), 11% (0.67 mol dm^{-3}), and 7.8% (6.7 mol dm^{-3}). The population ratios were relatively insensitive to the solvent composition and concentration, although some tendency was observed for the content of the *E*-rotamer to be slightly higher in nonpolar solvents and in dilute solutions. Similar behavior was also observed for other formamides such as *N*-ethylformamide and *N*-benzylformamide. This behavior is different from that of formanilides because the population ratios of formanilides are sensitive to the solvent composition as well as to the concentration[2] due to ring dimer formation.[9] The population ratios of formamides have more resemblance to those of *o*-substituted acetanilides.[3] These results suggest that ring dimer formation does not play an important role in the case of formamides. The population ratios of acetamides, on the other hand, resemble those of *o*-unsubstituted acetanilides.

The attempt to determine the rotational energy barriers by means of HPLC[1] was not carried out due to tailing. It can however, be safely concluded that the energy barriers for aliphatic amides are larger than those for anilides, because the separation of the rotamers of aliphatic amides was possible at relatively higher column temperatures. It can also be concluded that the energy barriers to the bond rotation of formamides are higher than those of acetamides.

References

1) M. Moriyasu, K. Kawanishi, A. Kato, Y. Hashimoto, M. Sugiura, and T. Sai, *Bull. Chem. Soc. Jpn.*, **58**, 3351 (1985).

2) M. Moriyasu, K. Kawanishi, A. Kato, and Y. Hashimoto, *Bull. Chem. Soc. Jpn.*, **57**, 1766 (1984).

3) M. Moriyasu, K. Kawanishi, A. Kato, Y. Hashimoto, and M. Sugiura, *Bull. Chem. Soc. Jpn.*, **58**, 2581 (1985).

4) For the NMR study of the restricted bond rotation of various amides, see the following review and the references cited therein: W. E. Stewart and T. H. Siddall. III., *Chem. Rev.*, **70**, 517 (1970).

5) F. F. Blicke and C. Lu, *J. Am. Chem. Soc.*, **74**, 3933 (1952).

6) A. Galat and G. Elion, *J. Am. Chem. Soc.*, **65**, 1566 (1943).

7) W. Walter and G. Maerten, *Liebigs Ann. Chem.*, **712**, 58 (1968).

8) L. A. LaPlanche and M. T. Rogers, *J. Am. Chem. Soc.*, **86**, 337 (1964).

9) A. J. R. Bourn, D. G. Gillies, and E. W. Randall, *Tetrhedron*, **20**, 1811 (1964).

Spectrophotometric Determination of Nickel with Sarcosinexylenol Blue

Joichi UEDA,* Yukiko FUKAZAWA, and Yuu KOIZUMI
Department of Chemistry, Faculty of Education, Kanazawa University,
Marunouchi, Kanazawa 920
(Received October 11, 1985)

Synopsis. Sarcosinexylenol Blue (SXB) was synthesized and the possibility of using SXB as a spectrophotometric reagent was examined. The fundamental conditions for the photometric determination of nickel which gave relatively strong coloration with SXB were studied. The simultaneous determination of nickel and zinc was also studied.

In a series of sulfophthalein derivatives, there are many useful compounds utilized as the spectrophotometric reagents for various metal ions.[1,2] The authors have newly synthesized Sarcosinexylenol Blue, 3,3′-bis[*N*-(carboxymethyl)methylaminomethyl]-*p*-xylenolsulfophthalein, as sulfophthalein derivative and examined its color reactions with metal ions. It was found that this reagent generally does not react as sensitively as Xylenol Oragne[1] which is a representative sulfophthalein reagent. However it gives relatively strong colors with some metal ions such as nickel, cobalt, cadmium, and iron(III), and there is a possibility to use this reagent as the photometric reagent for those ions. Nickel gave the strongest color, and we have studied in detail the best conditions for its use for the photometric determination of this ion and for the simultaneous determination of nickel and zinc. The usefulness of SXB in comparison with Glycinethymol Blue, Glycinecresol Red, and Methylthymol Blue[3] has been established, these have a similar structure to that of SXB, but SXB is more sensitive than those reagents. It also has relatively good selectivity for the diverse ions. The results obtained are shown below.

Experimental

Reagents. Standard Metal Solutions: A solution containing about 1 mg cm^{-3} of nickel or zinc was prepared by dissolving guaranteed reagent grade metal nitrate in a small amount of nitric acid and diluted with distilled water. The solutions were standardized by complexometric titration.

SXB Solution: A 0.05% SXB solution was prepared by dissolving in distilled water a weighed amount of SXB. The SXB was synthesized from Paraxylenol Blue, sarcosine, and formaldehyde by the Mannich condensation,[1] and separated from the reaction mixture on a cellulose column by 1-butanol saturated with 10% acetic acid. Then, the SXB was passed through a column of cation-exchange resins to convert it to the free acid form. The SXB, obtained as on orange compound has mp 137—140 °C. The result of the elemental analysis was as follows. Found: C, 56.52; H, 6.33; N, 4.12; S, 5.15%. Calcd for $C_{31}H_{36}O_9N_2S \cdot 2H_2O$: C, 57.41; H, 6.17; N, 4.32; S, 4.94%.

Buffer Solution: The pH was adjusted with 0.1 mol dm^{-3} borax-0.1 mol dm^{-3} hydrochloric acid and 0.1 mol dm^{-3} borax-0.1 mol dm^{-3} sodium hydroxide.

All the other reagents used were of guaranteed reagent grade.

Results and Discussion

Absorption Curves of SXB. The absorption spectra of 6.2×10^{-5} mol dm^{-3} SXB solution at various pH are shown in Fig. 1. The SXB solution colors reddish-orange in 4 mol dm^{-3} nitric acid. The color of the solution changes to yellow with increasing pH, but, over the pH range from 1.8 to 5.0, there is no color change and the solutions show almost the same absorption curves having an absorption maximum at 439—443 nm. On increase of the pH, however, the color of the solution changes again, and it becomes yellow-green at pH 6.0, blue-violet at pH 10.8, violet at pH 11.7, and blue at 13.4. With these color changes, the absorption maximum at 439—443 nm decreases, accompanied by an increase of that at 599—602 nm. At pH 13.4, the absorption maximum of the solution shifts to 611—614 nm.

Complexes of SXB and Metal Ions. The color reactions between SXB and metal ions were investigated. The results are summarized in Table 1, nickel, cobalt, cadmium, and iron(III) gave relatively strong colors whose molar absorptivities are $1—2\times10^4$. The chemical formula of the nickel complex obtained by mole ratio method is $Ni(SXB)_2$. In the case of zinc, there are two complexes, $Zn(SXB)_2$ at 650 nm and $Zn(SXB)_3$ at 580 nm. Cobalt forms $Co(SXB)_2$. Concerning the compositions of the cadmium and iron(III) complexes, no clear results could be obtained.

Determination of Nickel. Standard Procedure: A sample solution containing up to 60 μg of nickel is

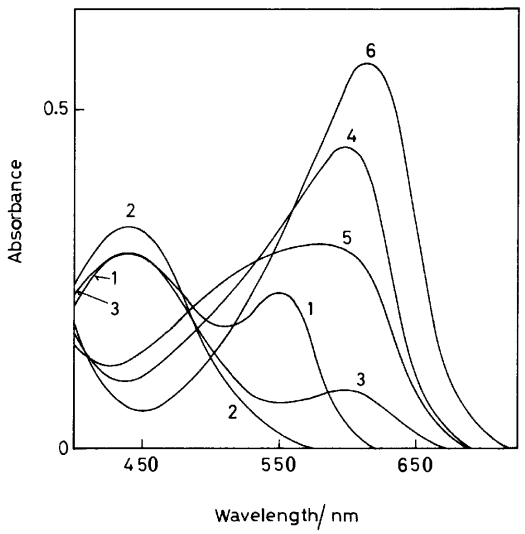

Fig. 1. Absorption curves of SXB.
[SXB]$=6.2\times10^{-5}$ mol dm^{-3}, reference: water, 1 : 4 mol dm^{-3} HNO_3, 2: pH 1.8—5.0, 3: pH 6.0, 4: pH 10.8, 5: pH 11.7, 6: pH 13.4.

Table 1. Reactions of SXB with Metal Ions

Ion	pH	Color of complex	Wavelength nm	Molar absorptivity	Composition (M:SXB)
Al^{3+}	5.9	Reddish brown*			
Ga^{3+}	5.9	Reddish brown	517—521	8.5×10^3	
In^{3+}	5.9	Reddish brown	513—518	7.3×10^3	
Sn^{4+}	10.1	Reddish violet*			
Pb^{2+}	10.1	Blue violet*			
Cu^{2+}	5.3	Blue violet	554—564	5.2×10^3	
Zn^{2+}	10.1	Blue	649—651	9.1×10^3	1:2
	10.1	Blue	579—582	7.2×10^3	1:3
Cd^{2+}	10.7	Blue	573—575	1.9×10^4	
	10.7	Blue	640	5.6×10^3	
Hg^{2+}	10.1	Blue*			
Cr^{3+}	5.0	Reddish brown*			
Mn^{2+}	10.1	Violet*			
Fe^{3+}	5.3	Reddish violet	524—529	1.4×10^4	
Co^{2+}	9.8	Blue	649—650	1.6×10^4	1:2
Ni^{2+}	10.1	Blue	640—642	2.2×10^4	1:2

Alkali metals, alkaline earth metals, bismuth(III), scandium, yttrium, thorium, zirconium, molybdenum(VI), and tungsten(VI) did not react with SXB. * Weak color.

placed in a 25 cm^3 volumetric flask. Then, 10 cm^3 of buffer solution and 5 cm^3 of 0.05% SXB solution are added. After making up the volume to 25 cm^3 (the final pH: 10.1), the absorbance is measured at 641 nm against a reagent blank.

Absorption Curves of Nickel Complex: The colored solution of the nickel complex has an absorption maximum at 640—642 nm which is nearly constant at pH 10.0—10.5.

The Effect of the Amount of SXB: The maximum and almost constant absorbance was obtained by adding from 3 to 7 cm^3 of 0.05% SXB solution for 20 μg of nickel.

Calibration Curves: Beer's law is observed up to 2.4 μg cm^{-3} of nickel. The relative standard deviation for five determinations was 0.91%.

Simultaneous Determination of Nickel and Zinc: The colored solution of the zinc complex has two absorption maxima at 579—582 and 649—651 nm. On the other hand, that of the nickel complex has only one absorption maximum at 640—642 nm. As a result, the absorbance at 649—651 nm of the zinc complex is affected by the absorbance of the nickel complex, but the absorbance at 579—582 nm of the zinc complex is not affected by that of nickel complex. Utilizing these facts, the simultaneous determination of these two elements has been investigated. Satisfactory results were obtained for a solution containing 5—25 μg of nickel and 20—50 μg of zinc. The procedure is as follows. The sample solution containing nickel and zinc is placed in a 50 cm^3 Erlenmeyer's flask. Then, 10 cm^3 buffer solution and 6 cm^3 of 0.05% SXB solution are added. After being kept for a few minutes in about 50 °C water bath, the solution is cooled with running water, transferred to a 25 cm^3 volumetric flask, and diluted to the mark with distilled water (the final pH: 10.1). The absorbance is measured at 580 and 650 nm within 15 min against a reagent blank. Zinc is determined from the absorbance at 580 nm, then, nickel is determined by subtracting the absorbance due to zinc from the total absorbance at 650 nm.

The Effect of Diverse Ions: The effect of thirty-seven diverse ions on the determination of 20 μg of nickel and 50 μg of zinc has been examined. Concerning anions, the presence of 10 mg each of oxalate, citrate, tartrate, phosphate, and sulfate, and 1 mg of fluoride does not interfere with either the nickel or the zinc determinations. For cations, nickel can be determined within 5% error in the presence of 500 μg each of alkali metals, alkaline earth metals, aluminium, gallium, gold, scandium, yttrium, lanthanoids, thorium, molybdenum(VI), and tungsten(VI), 100 μg each of indium, antimony(III), and manganese(II), and 20 μg each of bismuth(III), mercury(II), and palladium. But beryllium, tin(IV), lead, copper, zinc, cadmium, chromium(III), iron(III), and cobalt interfere with the determination. For the zinc determination, the presence of 500 μg each of alkali metals, alkaline earth metals, aluminium, gallium, bismuth(III), gold, scandium, yttrium, lanthanoids, thorium, molybdenum(VI), tungsten(VI), and palladium, 100 μg each of indium, antimony(III), and manganese(II), and 50 μg of mercury(II) does not interfere with the determination. Beryllium, tin(IV), lead, copper, cadmium, chromium(III), iron(III), cobalt, and nickel interfere when the measurements are carried out at 650 nm, but the interference from cobalt and nickel can be eliminated by the measurements at 580 nm.

References

1) M. Otomo, *Bunseki Kagaku*, **21**, 436 (1972).
2) V. N. Tikhonov, *Zh. Anal. Khim.*, **32**, 1435 (1977).
3) O. A. Tataev, S. A. Akhmedov, and B. A. Magomedova, *Zh. Anal. Khim.*, **25**, 1229 (1970).

A Molecular Orbital Approach to the Effect of Acid and Base on Mutarotation of D-Glucose

Akira IMAMURA,* Toshiya OKAJIMA, and Katsuya KANDA
Department of Chemistry, Faculty of Science, Hiroshima University,
Higashisenda-machi 1-1-89, Naka-ku Hiroshima 730
(Received November 15, 1985)

Synopsis. Molecular orbital calculations were performed for the study of the mechanism of the mutarotation of D-glucose (in Fig. 1) by the CNDO/2 method. The calculated results for a proposed mechanism are in good agreement with the experimental results in relation to the effect of the acid and the base, suggesting the validity of the proposed mechanism of mutarotation.

The mutarotation of D-glucose in solution is caused by the interconversion between α- and β-anomers. The mutarotation has been reported to be accelerated by acid or base, but this reaction is accelerated by the combination of both acid and base.[1,2] The proposed mechanisms of the acid, the base or the acid-base catalysis are shown in Fig. 1. All the three mechanisms include the formation of a chain intermediate by the cutting of the C_1–O_α bond. If we assume that the formation of this chain intermediate is the rate-determining step, it follows that if the acid or the base accelerates the breaking of the C_1–O_α bond, the reaction rate of the mutarotation should become faster on the whole. To investigate the validity of this interpretation, we performed a molecular orbital calculation by the CNDO/2 approximation,[3] and tried to inquire into the effect of the acid or the base.

Results and Discussion

The molecular structures of α- and β-D-glucose were determined by the energy gradient method in the CNDO/2 approximation using the program package GEOMIN.[4] The molecular structures thus obtained reproduced fairly well those obtained by the X-ray diffraction method.[5] In order to examine the effect of the acid and the base, we built models for the three mechanisms shown in Fig. 1. We chose H_3O^+ for the acid and H_2O, NH_3, OH^- for the base. The structures of the acid and the bases were optimized fully by the energy gradient method. H_3O^+ was set on the equatrial position of the ether oxygen(O_α) and the distance between the ether oxygen and the proton of H_3O^+ is 1.5 Å. The distance between the central atom of the bases and the proton of the anomeric OH group is also 1.5 Å. The central atom of the bases and this OH group were on a straight line. The conformation of the bases are as follows; the dihedral angle of C_1–O_β–O(base)–H′ equals to 90 degrees for H_2O and that of C_1–O_β–N(base)–H′ 180 degrees for NH_3. H′ stands for a proton of the bases. For OH^-, the proton of OH^- ion was set linearly. The position of the proton of the bases was determined so as to reduce the steric hindrance. We selected the arrangement of all atoms of the bases in this manner.

Furthermore, we define the symbols for special species; isolated glucose molecule is glucose^0, glucose interacting with H_3O^+ at the ether oxygen is glucose$^+$ and glucose^0 and glucose$^+$ interacting with the bases at the anomeric OH group are glucose^0-"base" and glucose$^+$-"base", respectively.

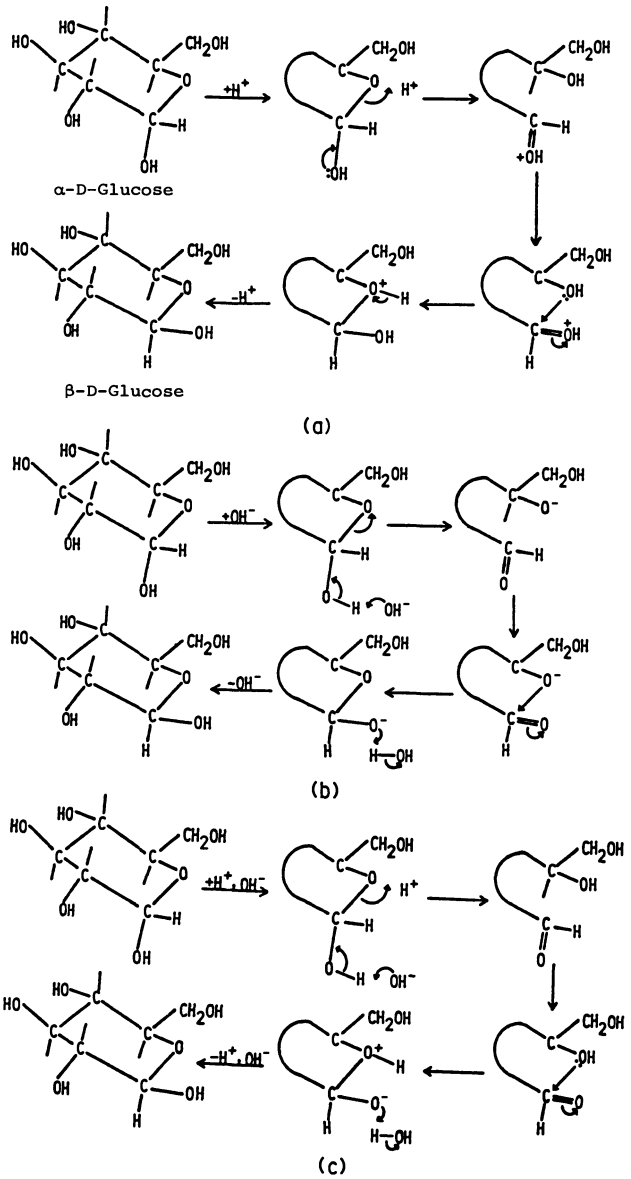

Fig. 1. (a) Acid catalyzed mechanism of mutarotation. (b) Base catalyzed mechanism of mutarotation. (c) Acid and base catalyzed mechanism of mutarotation.

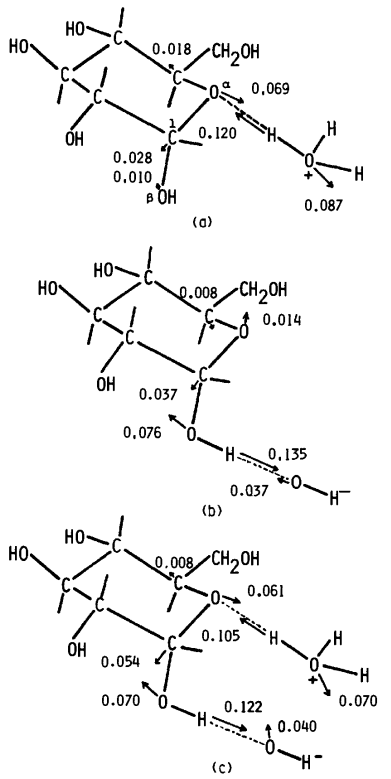

Fig. 2. Force on each atom for glucose$^+$ (a), glucose -OH$^-$ (b), and glucose$^+$ -OH$^-$ (c). Arrows in the figure represent the directions of forces, and numbers represent the magnitude of the forces in hartree/bohr.

For these models, the forces acting on the atoms were calculated by the energy gradient method. The results are shown in Fig. 2 for α-D-glucose. The common feature for the acid catalysis (a)(c) is that the force on the proton of H_3O^+ and that on the ether oxygen acts so as to attract each other and form a new O-H bond. As for the base catalysis (b)(c), the force on the proton of the anomeric OH group acts to elongate this O-H bond. Moreover it is noteworthy that the force to lengthen the C_1-O_α bond acts on both atoms and the C_1-O_β bond tends to shorten for all systems. These results are common to H_2O and NH_3. Needless to say glucose^0 has no component of force on each atom since its molecular structure was determined to be the equilibrium one by the energy gradient method.

In all model systems, the C_1-O_α bond was weakened by the interaction between glucose^0 and the acid or the base. The effects of the acid and the base were quantitatively evaluated by using the energy partition technique in the CNDO/2 method. The total energy (E) in the CNDO/2 method is represented in following form,

$$E = \sum_A E_A + \sum_{A<B}\sum E_{AB}$$

where E_A denotes the monoatomic contribution to the total energy of atom A, and E_{AB} the diatomic contribution of atoms A and B. The terms involved in E_A and E_{AB} were already evaluated in the literature[6] and hence are omitted here. The effects of the acid and the base were quantitatively evaluated by using the value of $E_{C_1\text{-}O_\alpha}$. That is, E_{AB} was regarded as a measure for the bond energy. In Table 1, the values of $E_{C_1\text{-}O_\alpha}$ are listed for α-D-glucose. This indicates that the C_1-O_α bond energy decreases in both glucose$^+$ and glucose^0-"base", and decreases much more in glucose$^+$-"base". These are in good agreement with the magnitude and the directions of the forces shown in Fig. 2. From these results, it is expected that the acid and the base increase the reaction rate for the mutarotation and the combination of the acid and the base increases the rate much more.

Next, on the supposition that the base abstracts the anomeric hydroxyl proton, $E_{C_1\text{-}O_\alpha}$ was calculated at

Table 1. The Changes of Two Center Energies (E_{AB}) of C_1-O_α Bond (in kcal mol^{-1}) (α-form)

Species	E_{AB}	ΔE_{AB}[a]
Isolated form		
Glucose^0	−655.2	—
Acid catalysis		
Glucose$^+$	−640.3	15.0
Base catalysis		
Glucose^0-OH_2	−653.0	2.2
Glucose^0-NH_3	−652.3	2.9
Glucose^0-OH^-	−645.2	10.1
Acid-base catalysis		
Glucose$^+$-OH_2	−636.9	18.3
Glucose$^+$-NH_3	−635.7	19.5
Glucose$^+$-OH^-	−629.9	25.4

a) $\Delta E_{AB} = E_{AB}(\text{Species}) - E_{AB}(\text{Glucose}^0)$.

Table 2. The Changes of Two Center Energies (E_{AB}) of C_1-O_α Bond when Anomeric Hydroxyl Proton is Extracted by Bases H_2O, NH_3, and OH^- (in kcal mol^{-1}) (α-form)

O-H bond length(Å)	H_2O	NH_3	OH^-
Glucose^0-"base" system[a,c]			
r_e	2.23	2.93	10.06
$r_e+0.1$	2.71	3.69	11.49
$r_e+0.2$	3.21	4.50	13.15
$r_e+0.3$	3.72	5.57	15.14
Glucose$^+$-"base" system[b,c]			
r_e	3.38	4.51	10.40
$r_e+0.1$	3.98	5.68	12.47
$r_e+0.2$	4.80	6.88	14.94
$r_e+0.3$	5.53	8.23	17.77

a) $\Delta E_{AB} = E_{AB}(\text{Glucose}^0\text{-"base"}) - E_{AB}(\text{Glucose}^0)$. b) $\Delta E_{AB} = E_{AB}(\text{Glucose}^+\text{-"base"}) - E_{AB}(\text{Glucose}^+)$. c) Optimized anomeric O_β-H bond length (r_e) is 1.032(Å).

three bond lengths of the O–H group. The differences in $E_{C_1\text{-}O_\alpha}$ between glucose^0 and glucose^0-"base" or between glucose$^+$ and glucose$^+$-"base" are respectively listed in Table 2 for α-D-glucose, indicating that the C_1–O_α bond energy decreases as the bond length of the O–H group increases. Moreover, the extent of the weakening of the C_1–O_α bond has relation to the strength of the base; OH^- remarkably decreases $E_{C_1\text{-}O_\alpha}$ followed by NH_3 and H_2O. The same results were obtained in β-D-glucose. That is, when the acid and the base interact with β-D-glucose, the forces on the atoms and the changes of the C_1–O_α bond energy have the same tendency as α-D-glucose.

Conclusion

We studied the effect of the acid or the base for the formation of a chain intermediate by analysis of both force and the C_1–O_α bond energy. From the results, we propose that the acid or the base facilitates the cleavage of the C_1–O_α bond and therefore speeds up the mutarotation as the whole. We also conclude that the acid-base catalysis increases the reaction rate more than the acid or the base catalysis alone and that the stronger the base the greater is the effect. Consequently, we can explain the experimental result by the present calculation and therefore suggest that the mechanism of the acid and the base catalysis in Fig. 1 is valid.

This work was supported in part by a Grant-in-Aid for Scientific Research from the Ministry of Education. We are also grateful to the Information Processing Center of Hiroshima University for generous permission to use HITAC M-200H.

References

1) C. G. Swain and J. F. Brown. Jr, *Biochem. Z.*, **74**, 2534 (1952).
2) T. M. Lowry and G. F. Smith, *J. Chem. Soc.*, **1927**, 2539.
3) J. A. Pople and D. L. Bevieridge, "Approximate Molecular Orbital Theory," McGraw-Hill, New York (1970).
4) GEOMIN, "Quantum Chemistry Program Exchange, No. 312".
5) G. M. Brown and H. A. Levy, *Acta. Cryst.*, **B35**, 656 (1979).
6) J. A. Pople and G. A. Segal, *J. Chem. Phys.*, **44**, 3289 (1966).

α,β-Epoxy Sulfoxides as Useful Intermediates in Organic Synthesis. IV.[1] A Novel Synthesis of α-Acetoxy Ketones from α,β-Epoxy Sulfoxides

Tsuyoshi SATOH, Shigeyasu MOTOHASHI, and Koji YAMAKAWA*
Faculty of Pharmaceutical Sciences, Science University of Tokyo,
Ichigaya-funagawara-machi, Shinjuku-ku, Tokyo 162
(Received September 21, 1985)

Synopsis. The treatment of α,β-epoxy sulfoxides, prepared from 1-chloroalkyl phenyl sulfoxides with ketones or aldehydes, with cesium acetate in dimethyl sulfoxide in the presence of lead tetraacetate afforded α-acetoxy ketones in moderate to good yields.

α-Oxygenated ketones are useful intermediates in synthetic organic chemistry. Recent years have seen a dramatic development in the synthetic procedures for α-hydroxy ketones and their derivatives. Among them, the acyloin condensation method[2] is one of the most well-known. The addition of acyl anion equivalents, such as lithium aldimines,[3] α-methoxyvinyllithium,[4] or carbanion of dithioacetal[5] to carbonyl compounds is a convenient procedure for constructing α-hydroxy ketones. The reaction of enol silyl ethers or enol acetates with *m*-chloroperbenzoic acid followed by hydrolysis,[6] acetoxylation of ketones with lead tetraacetate,[7] or direct oxidation of enolates with oxidants[8] are other good methods for the preparation of α-hydroxy ketones and their derivatives.

Recently, we reported[9] a new and versatile procedure for synthesizing α-substituted carbonyl compounds from α,β-epoxy sulfoxides (**1**). In the course of studies on the synthesis of α-substituted carbonyl compounds from α,β-epoxy sulfoxides (**1**), a new and efficient procedure was found which has a very different methodology from those mentioned above for the synthesis of α-acetoxy ketones (**2**). Such a procedure is given in Scheme 1.

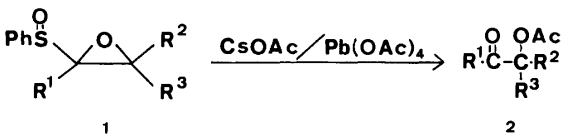

Scheme 1.

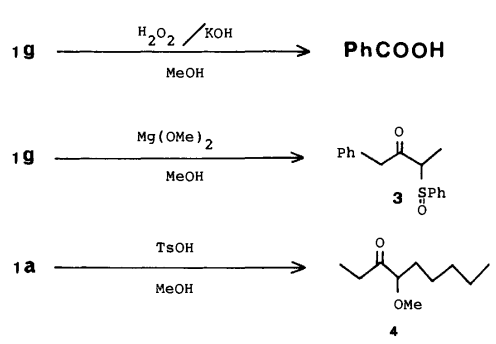

Scheme 2.

It has already been reported[9] that the β-carbon of α,β-epoxy sulfoxides is highly reactive with various kinds of nucleophiles (including selenolates, thiolates, and amines) to afford carbonyl, α-sulfenylated carbonyl, and α-amino carbonyl compounds, respectively, in good yields. On the other hand, oxygen nucleophiles are known to have fewer nucleophilic properties than those of sulfur and nitrogen. In fact, alcoholates and potassium acetate were found to show almost no reactivity toward α,β-epoxy sulfoxides (**1**) in alcohol or in dimethyl sulfoxide (DMSO) at a temperature below 50 °C (within 30 min). On the other hand, a treatment of **1g** with alkaline hydrogen peroxide in methanol gave benzoic acid in 58% yield. A treatment of **1g** with magnesium methoxide in refluxing methanol yielded a rearranged product, 1-phenyl-3-phenylsulfinyl-2-butanone (**3**), in 63% yield. An acidic opening of the epoxy group of **1a** with *p*-toluenesulfonic acid in methanol gave the desired 4-methoxy-3-nonanone (**4**); however the yield was not sufficient. After much work, we at last found that the treatment of **1** with cesium acetate[10] in DMSO (in the presence of lead tetraacetate) afforded the desired α-acetoxy ketones in good yield. The results are summarized in Table 1.

In reactions in the absence of lead tetraacetate, the yields of the α-acetoxy ketones (**2**) were always less than 50% and α-phenylthio ketones[9a,11] were observed. To prevent the formation of this by-product, some oxidants were added to the reaction mixture and it was found that two equivalents of lead tetraacetate[12] worked well. Further, lead tetraacetate was found to show no reactivity toward α,β-epoxy sulfoxides in DMSO, namely the treatment of the sulfoxide (**1g**) with lead tetraacetate (2 equiv) in DMSO at 70 °C for 30 min afforded only the starting material in almost quantitative yield.

In entries 1—4, and 6—8 the α,β-epoxy sulfoxides have two diastereomers, expressed as L and P.[9b] These isomers show almost the same reactivity toward cesium acetate to afford the desired α-acetoxy ketones (**2**). It is worthwhile noting that regeioselectively acetoxylated products without their isomers are afforded in moderate to good yields (entries 1, 2, 4, and 5). Entry 5 shows that the α,β-epoxy sulfoxide having two alkyl groups on β-carbon exhibits much less reactivity than those having one alkyl group. The epoxy sulfoxide having a benzyl group in R^1 gave low yields of α-acetoxy ketones. This may be interpreted that lead tetraacetate oxidized benzyl group of the product **2g** (entry 7).[13] Entry 8 shows that an α-acetoxy ketone having

Table 1. α-Acetoxy Ketones from α,β-Epoxy Sulfoxides with Cesium Acetate

Entry	α,β-Epoxy sulfoxide (1)				Conditions	α-Acetoxy ketone	Yield[a] %
	R^1	R^2	R^3				
1	**1a** C_2H_5	$CH_3(CH_2)_4$	H	L	100 °C, 45 min	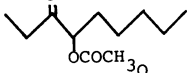 **2a**	84
				P	100 °C, 45 min		73
2	**1b** $CH_3(CH_2)_5$	CH_3	H	L	100 °C, 45 min	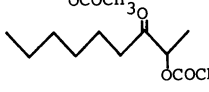 **2b**	65
				P	100 °C, 45 min		71
3	**1c** $CH_3(CH_2)_5$	$CH_3(CH_2)_4$	H	L	100 °C, 1 h	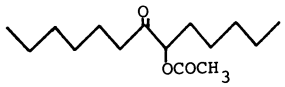 **2c**	64
				P	100 °C, 1 h		78
4	**1d** $(CH_3)_2CH$	$CH_3(CH_2)_4$	H	L	100 °C, 1 h	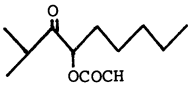 **2d**	78
				P	100 °C, 2 h		74
5	**1e** $CH_3(CH_2)_5$	CH_3	CH_3		100 °C, 9 h	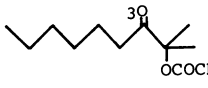 **2e**	48
6	**1f**	$CH_3(CH_2)_4$	H	L	100 °C, 2 h	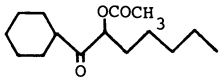 **2f**	81
				P	100 °C, 5 h		70
7	**1g** $PhCH_2$	CH_3	H	L	70 °C, 1.5 h	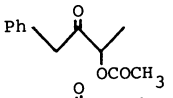 **2g**	48
				P	70 °C, 45 min		29
8	**1h** $CH_3(CH_2)_5$	Ph	H	P	70 °C, 1.5 h	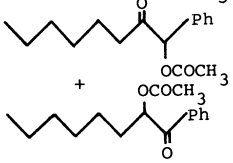 **2h** **2i**	70[b]

a) Isolated yields after silica-gel column chromatography. b) The yield of a mixture of **2h** and **2i**. The ratio of **2h** : **2i** is 5 : 4, which was determined by ^{1}H-NMR.

highly acidic hydrogens (**2h**) afforded **2i** through acyl migration.

Experimental

General. Infrared (IR) spectra were measured directly on a NaCl plate with a Hitachi 215 spectrometer. ^{1}H NMR spectra were measured in a $CDCl_3$ solution with a JEOL-FX-100 pulse Fourier-transform spectrometer using Me_4Si as an internal standard. All α,β-epoxy sulfoxides (**1**) used in this study are given in Refs. 9b and 11.

Treatment of 1g with Alkaline Hydrogen Peroxide. To a solution of **1g** (54 mg) in MeOH (3 ml) was added 10% KOH (1 ml) and 40% H_2O_2 (0.2 ml) and the solution was stirred at room temperature for 4 d. The MeOH was evaporated and the residue was extracted with benzene. The water layer was acidified and extracted with benzene. The usual work-up gave 14.2 mg (58%) of benzoic acid as colorless crystals.

1-Phenyl-3-phenylsulfinyl-2-butanone (3). A solution of $Mg(OMe)_2$ was prepared from dry MeOH (2 ml) and Mg (24.3 mg; 1 mmol) in a dry flask. To this was added a solution of **1g** (54.4 mg; 0.2 mmol) in MeOH; then the reaction mixture was refluxed under N_2 for 2 h. After the usual work-up, the product was purified by silica-gel column chromatography to afford 34 mg (63%) of **3** (diastereomeric mixture) as colorless oil. IR (neat): 1710 (CO), 1045 (SO) cm^{-1}; ^{1}H NMR δ=1.20, 1.34 (each d, J=7 Hz), 3.68—4.20 (m), 7.00—7.74 (m); MS m/z (%): 272 (M^+, trace), 147 (75), 125 (30), 91 (100); Found: m/z 272.0881. Calcd for $C_{16}H_{16}O_2S$: M, 272.0870.

4-Methoxy-3-nonanone (4). A solution of **1a** (53 mg; 0.2 mmol) in MeOH (1 ml) was added to a solution of $TsOH \cdot H_2O$ (190 mg; 1 mmol) in MeOH (1 ml) and the reaction mixture was refluxed under N_2 for 20 h. The MeOH was evaporated and the residue was extracted with benzene. After the usual work-up, the product was purified by silica-gel chromatography to give 9.4 mg (27%) of **4** as colorless oil. IR (neat): 1720 (CO) cm^{-1}; ^{1}H NMR δ=0.88 (3H, t, J=7 Hz), 1.07 (3H, t, J=7 Hz), 1.16—1.78 (8H, m), 2.56 (2H, q, J=7 Hz), 3.38 (3H, s), 3.62 (1H, t, J=6 Hz); MS m/z (%): 172 (M^+, 8), 115 (100).

General Procedure for the Preparation of α-Acetoxy Ketones (2) from α,β-Epoxy Sulfoxides (1). A typical procedure is described for the synthesis of 4-acetoxy-3-nonanone (**2a**). A solution of 3,4-epoxy-3-phenylsulfinylnonane (**1a**; 270 mg; 1 mmol) in DMSO (2.5 ml) was added to a mixture of CeOAc (1.92 g; 10 mmol) and $Pb(OAc)_4$ (985 mg; 2 mmol) in DMSO (2.5 ml). The reaction mixture was stirred at 100 °C under N_2 for 45 min. To the reaction mixture was added 10 ml of 10%-HCl and the whole was extracted with ether. Then the ether layer was washed with sat. aq $NaHCO_3$ followed by brine. The product was purified by silica-gel column chromatography to afford 170.7 mg (84%) of **2a** as a colorless oil. IR (neat): 1745, 1730 (CO) cm^{-1}; ^{1}H NMR δ=0.90 (3H, t, J=7 Hz), 1.08 (3H, t, J=7 Hz), 1.18—1.92 (8H, m), 2.18 (3H, s), 2.50 (2H, m), 5.04

(1H, dd, J=5, 6 Hz); MS m/z (%): 200 (M^+, trace), 157 (3), 130 (5), 83 (6), 43 (100).

2-Acetoxy-3-nonanone (2b). Colorless oil; IR (neat): 1745, 1730 (CO) cm^{-1}; ^1H NMR δ=0.89 (3H, t, J=7 Hz), 1.00—1.72 (8H, m), 1.40 (3H, d, J=7 Hz), 2.15 (3H, s), 2.50 (2H, m), 5.11 (1H, q, J=7 Hz); MS m/z (%): 200 (M^+, trace), 113 (80), 87 (17), 43 (100).

6-Acetoxy-7-tridecanone (2c). Colorless oil; IR (neat): 1745, 1730 (CO) cm^{-1}; ^1H NMR δ=0.89 (6H, t, J=6 Hz), 1.08—1.90 (16H, m), 2.16 (3H, s), 2.46 (2H, m), 5.05 (1H, dd, J=5, 7 Hz); MS m/z (%): 256 (M^+, trace), 113 (78), 85 (10), 43 (100); Found: m/z 256.2033. Calcd for $C_{15}H_{28}O_3$: M, 256.2036.

4-Acetoxy-2-methyl-3-nonanone (2d). Colorless oil; IR (neat): 1745, 1730 (CO) cm^{-1}; ^1H NMR δ=0.90 (3H, t, J=7 Hz), 1.00—1.90 (8H, m), 1.10, 1.16 (each 3H, d, J=8 Hz), 2.15 (3H, s), 2.60—3.00 (1H, m), 5.15 (1H, dd, J=5, 7 Hz); MS m/z (%): 214 (M^+, 1), 171 (4), 71 (45), 43 (100).

2-Acetoxy-2-methyl-3-nonanone (2e). Colorless oil; IR (neat): 1735, 1720 (CO) cm^{-1}; ^1H NMR δ=0.89 (3H t, J=6 Hz), 1.08—1.76 (8H, m), 1.48 (6H, s), 2.09 (3H, s), 2.46 (2H, t, J=7 Hz); MS m/z (%): 214 (M^+, 1), 171 (11), 113 (65), 85 (11), 43 (100).

2-Acetoxy-1-cyclohexyl-1-heptanone (2f). Colorless oil; IR (neat): 1750, 1730 (CO) cm^{-1}; ^1H NMR δ=0.90 (3H, t, J=6 Hz), 1.00—2.08 (18H, m), 2.15 (3H, s), 2.20—2.72 (1H, m), 5.14 (1H, dd, J=5, 7 Hz); MS m/z (%): 254 (M^+, 1), 184 (5), 111 (60), 83 (100), 43 (70); Found: m/z 254.1872. Calcd for $C_{15}H_{26}O_3$: M, 254.1880.

3-Acetoxy-1-phenyl-2-butanone (2g). Colorless oil; IR (neat): 1740, 1725 (CO) cm^{-1}; ^1H NMR δ=1.28 (3H, d, J=7 Hz), 2.14 (3H, s), 3.84 (2H, s), 5.20 (1H, q, J=7 Hz), 7.08—7.52 (5H, m); MS m/z (%): 206 (M^+, 3), 91 (48), 87 (18), 43 (100).

A Mixture of 1-Acetoxy-1-phenyl-2-octanone (2h) and 2-Acetoxy-1-phenyl-1-octanone (2i). Colorless oil; IR (neat): 1745, 1730 (CO) cm^{-1}; ^1H NMR δ=0.84 (t, J=7 Hz), 0.88 (t, J=6 Hz), 1.00—2.00 (m), 2.18, 2.20 (each s), 2.24—2.56 (m), 5.90 (dd, J=6, 7 Hz), 6.00 (s), 7.12—7.72 (m); MS m/z (%): 262 (M^+, 1), 149 (40), 113 (35), 107 (61), 105 (92), 43 (100).

References

1) α,β-Epoxy sulfoxides as useful intermediates in organic synthesis. III. T. Satoh, Y. Kaneko, K. Sakata, and K. Yamakawa, *Bull. Chem. Soc. Jpn.* **59**, 457 (1986).

2) J. J. Blomfield, D. C. Owsley, and J. M. Nelke, *Org. React.*, **23**, 259 (1976).

3) G. E. Niznik, W. H. Morrison, and H. M. Walborsky, *J. Org. Chem.*, **39**, 600 (1974); H. Hirowatari and H. M. Walborsky, ibid., **39**, 604 (1974).

4) J. E. Baldwin, G. A. Höfle, and O. W. Lever, Jr., *J. Am. Chem. Soc.*, **96**, 7125 (1974).

5) J. C. Stowell, "Carbanions in Organic Synthesis" John Wiley and Sons, New York (1979), pp. 103—110.

6) H. Minato and T. Nagasaki, *J. Chem. Soc., (c)*, **1968**, 621; G. M. Rubottom, M. A. Vazquez, and D. R. Pelegrina, *Tetrahedron Lett.*, **1974**, 4319; A. Hassner, R. H. Reuss, and H. W. Pinnick, *J. Org. Chem.*, **40**, 3427 (1975); G. M. Rubottom and J. M. Gruber, ibid., **43**, 1599 (1978).

7) G. R. Pettit, C. L. Herald, and J. P. Yardley, *J. Org. Chem.*, **35**, 1389 (1970).

8) J. N. Gardner, F. E. Carlon, and O. Gnoj, *J. Org. Chem.*, **33**, 3294 (1968); E. Vedejs, D. A. Engler, and J. E. Telschow, ibid., **43**, 188 (1978); K. Yamakawa, T. Satoh, N. Ohba, R. Sakaguchi, S. Takita, and N. Tamura, *Tetrahedron*, **37**, 473 (1981); S. J. Daum, *Tetrahedron Lett.*, **25**, 4725 (1984); N. K. Dunlap, M. R. Sabol, and D. S. Watt, ibid. **25**, 5839 (1984).

9) a) T. Satoh, Y. Kaneko, T. Kumagawa, T. Izawa, K. Sakata, and K. Yamakawa *Chem. Lett.*, **1984**, 1957; b) T. Satoh, Y. Kaneko, T. Izawa, K. Sakata, and K. Yamakawa, *Bull. Chem. Soc. Jpn.*, **58**, 1983 (1985); c) T. Satoh, Y. Kaneko, K. Sakata, and K. Yamakawa, *Chem. Lett.*, **1985**, 585.

10) W. H. Kruizinga, B. Strijtveen, and R. M. Kellogg, *J. Org. Chem.*, **46**, 4321 (1981); J. W. Huffman and R. C. Desai, *Synth. Commun.*, **13**, 553 (1983); Y. Torisawa, H. Okabe, and S. Ikegami, *Chem. Lett.*, **1984**, 1555.

11) T. Satoh, T. Kumagawa, and K. Yamakawa, *Bull. Chem. Soc. Jpn.*, **58**, 2849 (1985).

12) L. Field and J. E. Lawson, *J. Am. Chem. Soc.*, **80**, 838 (1958).

13) S. Moon and H. Bohm, *J. Org. Chem.*, **37**, 4338 (1972).

X-Ray Crystal Structures of 2,4-Dimethyl-4,4a-dihydro-1*H*-[1,3,5]-triazino[1,2-*a*]quinoline-1,3,6(2*H*,5*H*)-trione and Its Dehydrogenated Derivative. Bond Length and EI Mass Fragmentation

Masami SAWADA,* Takanori TANAKA, Yoshio TAKAI, Yoshiro FURUKAWA, Terukiyo HANAFUSA, and Soichi MISUMI

Material Analysis Center, The Institute of Scientific and Industrial Research, Osaka University, 8-1, Mihogaoka, Ibaraki, Osaka 567

(Received October 5, 1985)

Synopsis. The crystal structures of the cyclic adduct **1** of 4-quinolinone with methyl isocyanate and its dehydrogenated derivative **2** have been determined by X-ray crystal structure analysis. Both crystal structure data of the C–N bond lengths in the triazinedione-ring skeleton suggest which bonds are broken in the initial EI mass fragmentation followed by the subsequent loss of a neutral MeNCO moiety.

Reactions and reactivities of pyridine derivatives have received continuous interest from organic chemists.[1] We recently reported on the preparation of some fused ring 1,3-dialkyl-1,3,5-triazine-2,4-(1*H*,3*H*)-dione derivatives and their mechanisms for the reactions of 4-pyridinone or 4-pyrimidinone with various alkyl isocyanates.[2] Here, we describe the X-ray structures of the parent cyclic adduct, 2,4-dimethyl-4,4a-dihydro-1*H*-[1,3,5]triazino[1,2-*a*]quinoline-1,3,6(2*H*,5*H*)-trione (**1**) and the corresponding dehydrogenated compound (**2**). The crystal structure data may allow to estimate the C–N bond which is broken in the initial EI mass fragmentation followed by the subsequent loss of a neutral molecule.[3]

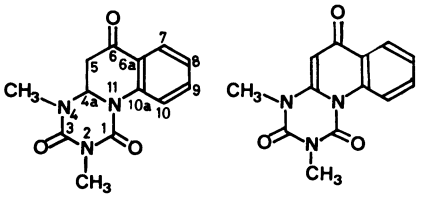

1 **2**

Experimental

Colorless crystals of **1** and **2** were obtained by ordinary recrystallization procedures from a hexane/$CHCl_3$ solution and an acetonitrile solution, respectively.[2,3] A single crystal was selected or cut to an appropriate size for each X-ray study. Crystal data and experimental conditions for both **1** and **2** are summarized in Table 1. For the measurements of the unit-cell dimensions and integrated intensities at room temperature, a Rigaku computer-controlled four-circle diffractometer was employed with graphite-monochromatized Mo $K\alpha$ radiation (a rotating anode type, 60 KV, 200 mA; AFC 5FOS). The cell constants were determined by the least squares method from 10—12 reflections. Three standard reflections were checked every 55 reflections during the course of the intensity-data collection and no intensity decrease was observed. The intensities were corrected for the usual Lorentz and polarization effects.

The crystal structures were solved by the direct method with the MULTAN 78 program.[4] The refinements of the structures were performed by the block-diagonal least squares method using the HBLS-V program.[5] Several cycles of refinement, including anisotropic temperature factors and all the hydrogen atoms, reduced the R values for both cases (Table 1): the hydrogen atoms of the molecules were found from the difference Fourier maps and

Table 1. Crystal and Experimental Data

Compound	**1**	**2**
Formula	$C_{13}H_{13}N_3O_3$	$C_{13}H_{11}N_3O_3$
Molecular Weight	259.16	257.16
Crystal System	Monoclinic	Orthorhombic
Space Group	$P2_1/c$	$P2_12_12_1$
Lattice Constants		
a	14.411(2) Å	14.850(5) Å
b	7.593(3)	10.618(3)
c	10.709(3)	7.066(3)
β	96.34(3)°	
V	1164.6(7) Å^3	1114.2(5) Å^3
Z	4	4
D_c	1.479 gcm^{-3}	1.534 gcm^{-3}
μ(Mo $K\alpha$)	1.164 cm^{-1}	1.212 cm^{-1}
Crystal Size	0.3×0.3×0.25 mm	0.4×0.3×0.25 mm
Scan Method	θ—2θ	θ—2θ
Scan Range $\Delta(2\theta)$	2.0°+0.70° tan θ	2.0°+0.70° tan θ
Scan Speed in 2θ	16°/min	16°/min
$2\theta_{max}$(Mo $K\alpha$)	55°	55°
Background	2×5.5 s	2×2.0 s
No. of Reflections		
Measured	4715	4550
Independent	2681	1531
Used for refinement[a]	2233	1233
R_{sym}[b]	0.016	0.048
Final R	0.0426	0.0612
Final R_w	0.0759	0.0758
a[c]	0.01615	−0.08771
b[c]	0.00039	0.00577

a) $F_o > 3\sigma(F_o)$. b) $R_{sym} = \Sigma(|F_o| - \langle|F_o|\rangle)/\Sigma\langle|F_o|\rangle$. $\langle|F_o|\rangle$: averaged values for symmetry-equivalent reflections. c) See Text.

Table 2. Atomic Positional and Thermal Parameters for 1[a]

Atom	x	y	z	B_{eq}/Å^2 [b]
C(1)	0.6598(16)	0.5358(18)	0.7175(16)	2.56
C(2)	0.624(2)	0.625(3)	0.5009(19)	3.48
C(3)	0.7771(17)	0.4967(19)	0.5692(16)	2.84
C(4)	0.929(3)	0.377(3)	0.639(3)	4.72
C(4A)	0.8220(16)	0.4422(18)	0.7956(16)	2.63
C(5)	0.8767(18)	0.586(3)	0.8694(19)	3.30
C(6)	0.8587(19)	0.5817(19)	1.0054(18)	3.06
C(6A)	0.7691(17)	0.5036(18)	1.0322(16)	2.74
C(7)	0.749(3)	0.488(2)	1.1567(18)	3.40
C(8)	0.665(3)	0.424(3)	1.1834(18)	3.72
C(9)	0.599(3)	0.371(3)	1.0868(19)	3.49
C(10)	0.6169(18)	0.3814(19)	0.9625(17)	2.98
C(10A)	0.7017(17)	0.4497(17)	0.9351(16)	2.47
N(2)	0.6913(14)	0.5551(15)	0.6011(13)	2.71
N(4)	0.8374(15)	0.4376(17)	0.6650(14)	3.06
N(11)	0.7228(14)	0.4635(15)	0.8090(13)	2.55
O(1)	0.5814(13)	0.5782(16)	0.7356(14)	3.82
O(3)	0.7950(15)	0.4993(18)	0.4609(13)	4.32
O(6)	0.9147(16)	0.6400(17)	1.0878(15)	4.50

a) Standard deviations in parentheses refer to the least significant digits. b) Equivalent isotopic temperature factors.[11]

Table 3. Atomic Positional and Thermal Parameters for 2[a]

Atom	x	y	z	B_{eq}/Å^2 [b]
C(1)	0.224(5)	0.184(4)	0.829(5)	3.04
C(2)	0.269(6)	0.401(5)	0.811(7)	5.47
C(3)	0.382(5)	0.240(4)	0.870(5)	3.00
C(4)	0.496(4)	0.078(5)	0.909(6)	3.92
C(4A)	0.338(4)	0.020(4)	0.864(4)	2.28
C(5)	0.362(4)	−0.102(4)	0.843(5)	3.00
C(6)	0.298(5)	−0.201(4)	0.820(6)	3.36
C(6A)	0.203(4)	−0.163(4)	0.843(5)	2.70
C(7)	0.137(5)	−0.257(5)	0.845(5)	3.64
C(8)	0.049(5)	−0.227(5)	0.875(5)	4.18
C(9)	0.026(5)	−0.104(6)	0.911(6)	4.16
C(10)	0.089(4)	−0.009(5)	0.910(5)	3.36
C(10A)	0.179(4)	−0.038(4)	0.870(4)	2.39
N(11)	0.247(3)	0.057(3)	0.864(4)	2.32
N(4)	0.293(4)	0.268(4)	0.841(4)	3.28
N(2)	0.401(3)	0.114(4)	0.885(4)	2.88
O(1)	0.149(3)	0.217(3)	0.791(5)	4.89
O(3)	0.439(4)	0.320(3)	0.884(4)	4.46
O(6)	0.319(4)	−0.310(4)	0.788(5)	5.87

a) Standard deviations in parentheses refer to the least significant digits. b) Equivalent isotopic temperature factors.[11]

they were refined with isotropic thermal parameters. The function minimized was $\sum w(|F_o|-|F_c|)^2$ with the following weighting scheme: $\omega=1/(\sigma^2(F_o)+a|F_o|+b|F_o|^2)$ for $|F_o|>0$ and $w=0$ for $|F_o|=0$. All the atomic scattering factors of C, N, O were taken from the "International Tables for X-Ray Crystallography".[6] The computations

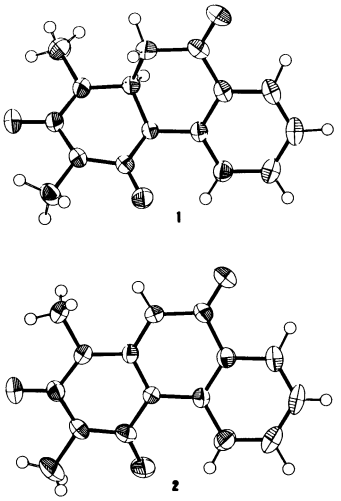

Fig. 1. ORTEP views of the compound **1** and **2**. The nonhydrogen atoms were drawn at the 50% probability level and the hydrogen atoms at an arbitrary diameter.

were carried out on an ACOS-850 computer at the Crystallographic Research Center, Institute for Protein Research, Osaka University. The final atomic positional and thermal parameters of **1** and **2** are listed in Tables 2 and 3, respectively. The tables of F_o and F_c, and anisotropic thermal parameters of the non-hydrogen atoms are deposited at the Chemical Society of Japan (Document No. 8620).

Results and Discussion

Figure 1 is a computer generated perspective (ORTEP)[7] view of these structures. The structures which had been previously determined by NMR and other spectral correlations[2] were confirmed. The bond lengths and the bond angles are given in Fig. 2 and Fig. 3, respectively, together with the atomic numberings. Neither abnormal bond lengths nor bond angles were found in these structures.

EI mass fragmentations of the compound **1** and **2** are reported,[3] where it is considered that the initial fragmentation of **1** mainly proceeds to the loss of a neutral MeNCO dimer via C(4A)–N(4) bond cleavage, yielding the *M/Z* 145 ion, and that of **2** proceeds to the loss of a neutral MeNCO monomer via C(1)–N(11) cleavage, yielding the *M/Z* 200 ion (Fig. 4).

In the present triazinedione ring, there are five C–N bonds directly concerned with the possible cleavage which is followed by the subsequent loss of the neutral molecule: i.e., C(4A)–N(4)–C(3)–N(2)–C(1)–N(11). The crystal data of the bond lengths in Fig. 2 show that the C(1)–N(11) bond for **2** is the longest among the five C(sp^2)–N bonds: on the other hand, the C(4A)–N(4) bond for **1** is the longest because of the C(sp^3)–N constituent. Therefore, although the comparison is restricted, the longest C–N bond among the five bonds seems to identify the C–N bond to be broken in the initial EI mass fragmentation giving the subsequent loss of the neutral *n*MeNCO moiety (*n*=1 or 2). A similar

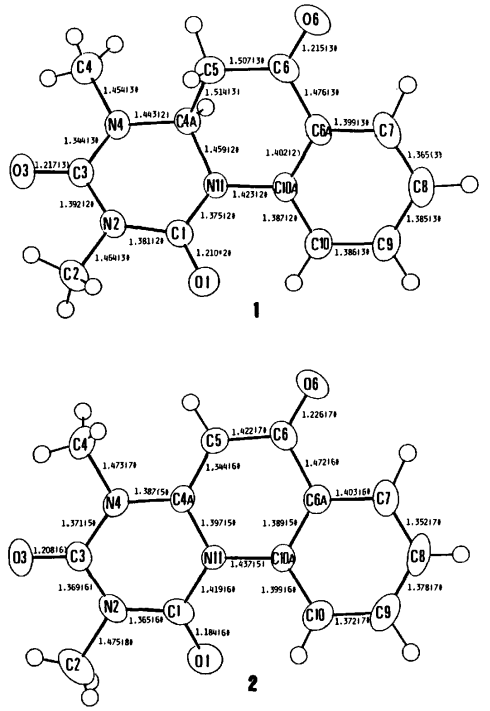

Fig. 2. Bond lengths (l/Å) of the compound **1** and **2**. Standard deviations in parentheses refer to the least significant digit.

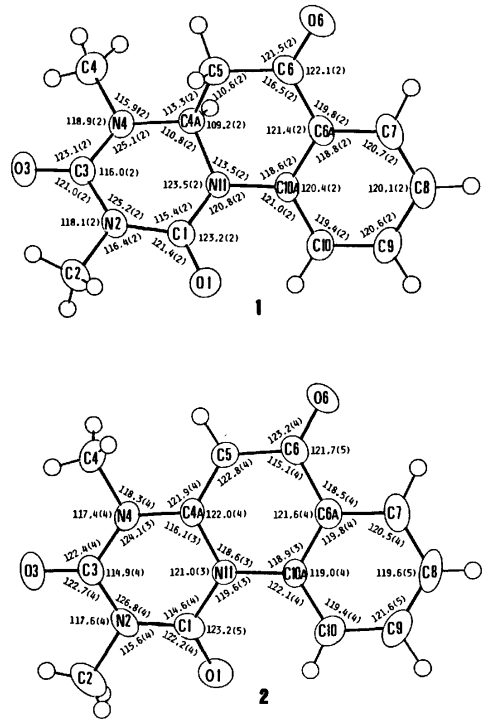

Fig. 3. Bond angles (ϕ/°) of the compound **1** and **2**. Standard deviations in parentheses refer to the least significant digit.

situation is also observed between the C(sp^2)–N bond length and the initial EI mass fragmentation in the related structure of caffein.[8,9] This feature suggests that detailed information about bond lengths in crystals is important for mechanistic studies of reactions,[10] including initial EI mass fragmentation in a gas phase.

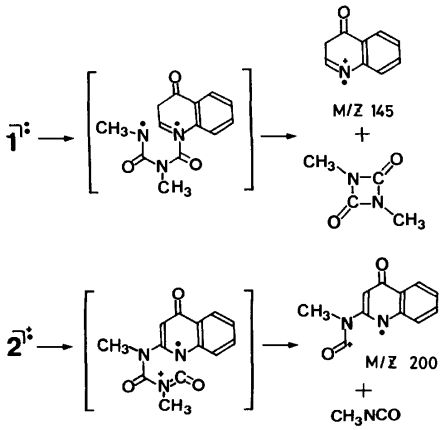

Fig. 4. Main initial EI mass fragmentations of the compound **1** and **2**.

The authors wish to express their sincere thanks to Drs. Hiroyuki Kageyama and Kunio Miki, and Profs. Nobutami Kasai and Noritake Yasuoka, and emeritus Professor Toshiyasu Ishimaru for their kind introductions, discussions and encouragement about X-ray crystal structure analysis.

Referenes

1) D. M. Smith, "Comprehensive Organic Chemistry," Vol. 4, ed. by P. G. Sammes, Pergamon Press (1979), Chap. 16.

2) M. Sawada, M. Ichihara, Y. Furukawa, Y. Takai, T. Ando, and T. Hanafusa, *Tetrahedron Lett.*, **23**, 3181 (1982); M. Sawada, Y. Furukawa, Y. Takai, and T. Hanafusa, *Synthesis*, **1983**, 593; *Heterocycles*, **22**, 501 (1984).

3) M. Sawada, H. Yamada, Y. Furukawa, C. Chong, F. Fukuda, T. Tanaka, Y. Takai, T. Hanafusa, and S. Misumi, *Nippon Kagaku Kaishi*, in press, No. 4 (1986).

4) P. Main, S. E. Hull, L. Lessinger, G. Germain, J-P. Declercq, M. H. Woolfson, "A System of Computer Programs for the Automatic Solution of the Crystal Structures from X-Ray Diffraction Data, MULTAN 78," University of York (1978).

5) T. Ashida, "The Universal Crystallographic Computing System-Osaka, HBLS-V," The Computation Center, Osaka University (1979), p. 53.

6) "International Tables for X-Ray Crystallography," Kynoch Press, Birmingham (1974), Vol. 4, p. 71.

7) C. K. Johnson, "ORTEP-II: A FORTRAN Thermal-Ellipsoid Plot Program for Crystal-structure Illustrations, ORNL-5138," March, 1976, Oak Ridge National Laboratory.

8) H. Budzikiewicz, C. Djerassi, and D. H. Williams, "Structure Elucidation of Natural Products by Mass Spectrometry," Vol. 1, Holden-Day (1964), p. 214.

9) "Kagaku Binran," Chemical Society of Japan, Maruzen (1984), Vol. 2, p. 673.

10) F. H. Allen and A. J. Kirby, *J. Am. Chem, Soc.*, **106**, 6197 (1984).

11) As a general expression, $B_{eq}=4/3[a^2B(1,1)+b^2B(2,2)+c^2B(3,3)+ab(\cos\gamma)B(1,2)+ac(\cos\beta)B(1,3)+bc(\cos\alpha)B(2,3)]$.

Preparation of Arylimidobis(sulfates)[1]

Fujio KANETANI
Department of Applied Chemistry, Faculty of Engineering, Hiroshima University,
Saijo, Higashi-Hiroshima 724
(Received October 18, 1985)

Synopsis. Seven arylimidobis(sulfates), six of which are new compounds, have been prepared by the *N*-sulfonation of the corresponding primary aromatic amines with 2-methylpyridine-sulfur trioxide in 60—92% yields.

In our previous work[1] we isolated (2,4,6-trimethylphenylimido)bis(sulfate) from the thermal reaction of 2,4,6-trimethylanilinium butylamidosulfate. Mechanistic consideration of this reaction led us to the successful preparation of this imidobis(sulfate) by fusion of an equimolar mixture of butylamidosulfuric acid and butylammonium (2,4,6-trimethylphenylamido)sulfate. Recently, considerable attention has been given to the mechanism of the sulfonation of aniline with excess concentrated and fuming sulfuric acid,[2,3] and the intermediacy of phenylimidobis(sulfuric) acid[4] as well as (2- and 4-sulfophenylamido)sulfuric acid,[2,5] has been suggested. In this context, we have become interested in the chemistry of arylimidobis(sulfuric) acids and their salts. In this paper we report the preparation of arylimidobis(sulfates).

Results and Discussion

The standard method for the preparation of unsubstituted imidobis(sulfate) on a laboratory scale involves the fusion of ammonium amidosulfate itself[6] or the fusion of an equimolar mixture of ammonium amidosulfate and amidosulfuric acid.[7]

$$2\,NH_2SO_3NH_4 \xrightarrow[290-305\,^\circ C]{\Delta} HN(SO_3NH_4)_2 + NH_3$$

$$NH_2SO_3NH_4 + NH_3{}^+SO_3{}^- \xrightarrow[145-150\,^\circ C]{\Delta} HN(SO_3NH_4)_2$$

This method, however, cannot be applied to the synthesis of arylimidobis(sulfates) except (2,4,6-trimethylphenylimido)bis(sulfate), because their *N*-sulfonate group tends to thermally migrate to position(s) ortho and/or para relative to the amino group. In fact, the fusion of an intimate mixture of butylammonium (3,5-dimethylphenylamido)sulfate and butylamidosulfuric acid gave, in a 69% yield, (3,5-dimethyl-2-sulfonatophenylamido)sulfate instead of the desired (3,5-dimethylphenylimido)bis(sulfate) (see Experimental section).

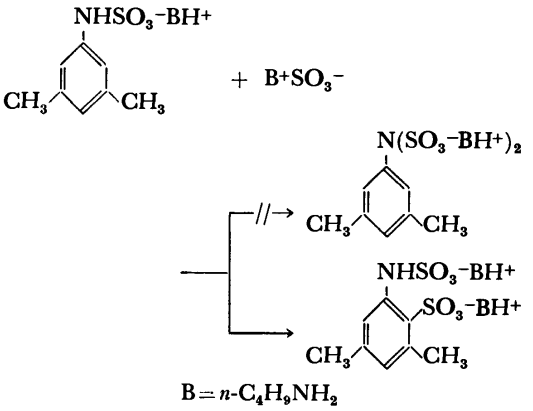

Previously,[8] we reported a one-step method for the preparation of *N*-substituted imidobis(sulfates). This method involving the *N*-sulfonation of an appropriate amine with triethylamine-sulfur trioxide works well with aliphatic and alicyclic amines, but with aromatic amines gives only poor yields (see Ref. 8 and Table 1).

Vrba and Allan[9] have prepared disodium phenylimidobis(sulfate) by the *N*-sulfonation of aniline with 2-methylpyridine-sulfur trioxide. Unfortunately, this work was limited to the preparation of phenylimidobis(sulfate) itself and published only in a short communication. In addition, the yield of the isolated product was not given (presumably much less than 50%). Accordingly, we examined this reaction in some detail and found optimal conditions giving arylimidobis(sulfates) in good yields (Table 1).

Table 1. Preparation of Phenylimidobis(sulfate)[a]
$C_6H_5NH_2 + 2B\cdot SO_3 \longrightarrow C_6H_5N(SO_3{}^-BH^+)_2$

B	Mr[b]	Solv.	Reaction temp/°C	Reaction time/h	Yield/%[c]
$(C_2H_5)_3N$	2.19	2-MePy	25—30	71	17[e]
$(C_2H_5)_3N$	2.06	2-MePy	88—91	8	7
2-MePy[d]	2.42	2-MePy	17—18	71	84
2-MePy	2.34	2-MePy	88—92	1	78[f]

a) The imidobis(sulfate) was isolated as a sodium salt. b) Molar ratio of $B\cdot SO_3$ to aniline. c) Yields refer to the yield of isolated product based on aniline. d) 2-Methylpyridine. e) Data cited from: F. Kanetani and H. Yamaguchi, *Bull. Chem. Soc. Jpn.*, **47**, 2713 (1974). f) Isolated as the potassium salt.

Thus the *N*-sulfonation of aniline with a slight excess of 2-methylpyridine-sulfur trioxide at room temperature for 71 h gave phenylimidobis(sulfate) in a 84% yield, together with a small amount of phenylamidosulfate. The use of higher temperature accelerated the reaction without significant lowering of the yield; i.e., the reaction at 88—91 °C for 1 h produced the imidobis(sulfate) in a 77% yield. TLC analysis of the reaction mixture revealed the formation of (4-sulfonatophenylamido)sulfate[1] as a by-product. This compound may arise either from the para sulfonation of the phenylamidosulfate or from the thermal rearrangement of phenylimidobis(sulfate) formed.

Table 2. Preparation of Arylimidobis(sulfates)[a]
$ArNH_2 + 2(2\text{-}MePy \cdot SO_3$[b]$) \longrightarrow ArN(SO_3^- \ 2\text{-}MePyH^+)_2$

$ArNH_2$	Mr[c]	Reaction temp/°C	Reaction time/h	Yield/%[d]
2-Methyl-aniline	2.14	89—91	2	67
3-Methyl-aniline	2.09	20—21	71	71
		88—92	2	trace[e]
4-Methyl-aniline	2.16	89—91	2	63
2-Chloro-aniline	1.99	22—23	142	60
3-Chloro-aniline	2.08	21—22	71	70
4-Chloro-aniline	2.05	22—23	120	92

a) All imidobis(sulfates) were isolated as potassium salts and characterized by IR spectroscopy and elemental analysis. b) 2-Methylpyridine-sulfur trioxide addition compound. c) Molar ratio of 2-MePy·SO_3 to substrate amine. d) Yields refer to the yield of isolated product based on amine. e) TLC analysis revealed the formation of (3-methylphenylimido)bis(sulfate) but in a trace; the chief product was (3-methyl-4-sulfonatophenylamido)sulfate.

Table 2 summarizes the results of the *N*-sulfonation of some other primary aromatic amines with 2-methylpyridine-sulfur trioxide. As can be seen from the table, the reaction at room temperature for 2—6 d or at 90 °C for 1—2 h gives arylimidobis(sulfates) in yields of 60—92%. 3-Methylaniline provided an exception; thus the reaction at 88—92 °C for 2 h failed to yield (3-methylphenylimido)bis(sulfate) and resulted in the formation of a new compound, which is identified as (3-methyl-4-sulfonatophenylamido)sulfate.[10] On the contrary, at room temperature the reaction proceeded in an expected manner to afford (3-methylphenylimido)bis(sulfate) in a 71% yield. Our results suggest that the use of the reaction conditions of Vrba and Allan (0 °C, 1 h) would lead to much lower yields of arylimidobis(sulfates).

The IR spectra of all the arylimidobis(sulfates) prepared, as well as alkylimidobis(sulfates),[11] showed two to four strong absorption peaks in the range of 1220—1298 cm^{-1}, and two strong peaks at 1029±3 and 1080±4 cm^{-1}. The former peaks are attributable to antisymmetric and the latter to symmetric vibrations of the SO_3^- groups. The imidobis(sulfates) were soluble in water, sparingly soluble in methanol, and insoluble in other ordinary organic solvents. All the arylimidobis(sulfates) are very liable to acid hydrolysis, which leads to the formation of sulfate ion by way of the corresponding arylamidosulfate ions.

$$ArN(SO_3^-)_2 \longrightarrow ArNHSO_3^- + HSO_4^-$$
$$\longrightarrow ArNH_3^+ + 2HSO_4^-$$

Experimental

Pyridine, 2-methylpyridine and triethylamine were dried

Table 3. Analytical Data for Arylimidobis(sulfates)

Ar	Formula	C(%) (Calcd)	H(%) (Calcd)	N(%) (Calcd)	IR spectra ($\tilde{\nu}$/cm^{-1})			
					$\nu_{as}SO_3^-$		$\nu_sSO_3^-$	Other prominent peaks
C_6H_5	$C_6H_5NO_6S_2Na_2$ (297.21)	24.18	1.58	4.70	1287	1250	1081	952 902 756 714 700
		(24.25)	(1.70)	(4.71)	1229	1193	1029	
2-$CH_3C_6H_4$	$C_7H_7NO_6S_2K_2$ (343.46)	24.20	2.13	4.01	1284	1250	1081	956 912 862 171 704
		(24.48)	(2.05)	(4.08)	1219		1029	
3-$CH_3C_6H_4$	$C_7H_7NO_6S_2K_2$ (343.46)	24.40	2.08	4.13	1285		1076	947 895 817 790 705
		(24.48)	(2.05)	(4.08)	1230	1195	1026	695
4-$CH_3C_6H_4$	$C_7H_7NO_6S_2K_2$ (343.46)	24.32	2.01	4.08	1298	1255	1078	956 917 816 685
		(24.48)	(2.05)	(4.08)	1245	1193	1027	
2-ClC_6H_4	$C_6H_4NClO_6S_2K_2$ (363.88)	19.50	1.03	3.81	1277		1084	971 937 867 757 735
		(19.80)	(1.11)	(3.85)	1225		1029	718 682
3-ClC_6H_4	$C_6H_4NClO_6S_2K_2$ (363.88)	19.69	1.20	3.73	1291	1256	1078	966 945 903 880 796
		(19.80)	(1.11)	(3.85)	1236	1197	1030	759 695 680
4-ClC_6H_4	$C_6H_4NClO_6S_2K_2$ (363.88)	19.82	1.17	3.82	1287	1260	1078	960 928 824 745 713
		(19.80)	(1.11)	(3.85)	1235	1205	1032	670

over KOH pellets, distilled, and stored over molecular sieves 4A. 1,2-Dichloroethane was dried over $CaCl_2$, distilled and stored over molecular sieves 4A. Sulfur trioxide was obtained by distillation of 60% fuming sulfuric acid. IR spectra were recorded on a JASCO IR-S spectrophotometer. Thin-layer chromatography was performed on 0.25 mm-thick cellulose plates (Cellulose Mikrokristallin, E. Merck). Compounds were visualized by UV fluorescence or by placing the plates in a container filled with nitrous gases, followed by spraying with sodium 1-naphthol-4-sulfonate and subsequent exposure to ammonia gas. All the reactions were carried out under anhydrous conditions.

General Procedure for the Preparation of Arylimidobis(sulfates). Sulfur trioxide was distilled into 10 ml of cooled (5—10 °C) 1,2-dichloroethane. To this solution was added 30 ml of 2-methylpyridine drop by drop. After stirring for 10 min at 10 °C, a substrate amine in 10 ml of 2-methylpyridine was added and the mixture was then stirred at room temperature or at 90 °C. After the reaction had been complete, the solvent was removed in vacuo at a bath temperature below 30 °C. The residue was dissolved in aqueous potassium hydroxide. The solution was warmed for 30 min at 50 °C while its pH being kept at 8—9. The mixture was then treated with a 5% barium acetate solution until no more precipitate was formed. The filtered solution was concentrated to about 5 ml. To this solution was added a few drops of 10% aqueous KOH and 100 ml of hot ethanol. The mixture was allowed to stand overnight. The crystals were collected by filtration, washed with 90% ethanol, and dried in a vacuum desiccator.

Reaction of Butylammonium (3,5-Dimethylphenylamido)sulfate with Butylamidosulfuric Acid. An intimate mixture of butylammonium (3,5-dimethylphenylamido)sulfate (0.548 g, 2.00 mmol) and butylamidosulfuric acid (0.303 g, 1.98 mmol) was heated at 120 °C for 4 h. After cooling to room temperature, the glass-like product was dissolved in 10% aqueous KOH and the solution was evaporated to dryness. The residual solid was dissolved in a little hot water. This solution was then added, with vigorous stirring, to hot ethanol (90 ml) containing a few drops of 10% aqueous KOH. The mixture was allowed to cool to room temperature to give colorless crystals (0.491 g). Recrystallization gave the pure dipotassium N, 2-disulfonate; IR (KBr) 3280 (NH), 1201 (SO_3^-), 1149, 1086, 1050 (SO_3^-), 1015, 874, 856 (1H), and 755 cm^{-1}. This disulfonate furnished 2-amino-4,6-dimethylbenzenesulfonic acid when heated with dil. HCl.[10]

The author thanks Professor Richard N. Butler and Dr. William J. Spillane for the laboratory facilities during his stay at University College, Galway (Republic of Ireland) on sabbatical leave.

References

1) Studies of Reactions of Amines with Sulfur Trioxide. Part 7. Part 6: F. Kanetani and H. Yamaguchi, *Bull. Chem. Soc. Jpn.*, **54**, 3048 (1981).
2) P. K. Maarsen and H. Cerfontain, *J. Chem. Soc., Perkin Trans. 2*, **1977**, 1008 and references cited therein.
3) R. N. Khelevin, *Zhur. Org. Khim.*, **20**, 124 (1984).
4) Z. Vrba and Z. J. Allan, *Tetrahedron Lett.*, **1968**, 4507.
5) E. R. Alexander, *J. Am. Chem. Soc.*, **69**, 1599 (1947).
6) H. H. Sisler and L. F. Audrieth, *Inorg. Synth.*, Vol. 2, 179 (1946).
7) P. Baumgarten, *Ber.*, **69**, 1929 (1936).
8) F. Kanetani and H. Yamaguchi, *Bull. Chem. Soc. Jpn.*, **47**, 2713 (1974).
9) Z. Vrba and Z. J. Allan, *Collect. Czech. Chem. Commun.*, **32**, 2035 (1967).
10) The structure of this compound was established by IR spectroscopic analysis and chemical conversion to known 4-amino-2-methylbenzenesulfonic acid.
11) F. Kanetani and H. Yamaguchi, *Yuki Gosei Kagaku Kyokai Shi*, **32**, 460 (1974).

Color Reaction among Pyrogallol Red, Thorium(IV) and Samarium(III), and Its Application to the Determination of These Metals

Itsuo MORI,* Yoshikazu FUJITA, Kinuko FUJITA, Shoko KITANO, Itsuko OGAWA, Hiroshi KAWABE, Yozo KOSHIYAMA, and Takeshi TANAKA

Osaka College of Pharmaceutical Sciences, 2-10-65, Kawai, Matsubara, Osaka 580

(Received July 1, 1985)

Synopsis. The color reactions between Pyrogallol Red(PR) and thorium(IV), and also those among PR, thorium(IV) and samarium(III) were studied. Simple and sensitive spectrophotometric determinations of these ions were newly carried out in the range for 1—22 μg/10 cm³ of thorium (IV) and 0.5—10 μg/10 cm³ of samarium(III) at 635 nm by using the PR-Th-Sm ternary complex.

Although Pyrogallol Red(PR) has already been used for chelatometric titration and spectrophotometric determination of various metal ions,[1-5] the studies on the color reactions between PR and thorium(IV) or PR and rare earth elements such as samarium(III), lanthanum(III), etc. were comparatively few. We have found that the color reaction between PR and thorium(IV) or PR and samarium(III) was catalyzed by the coexistence of small amounts of samarium(III) or thorium(IV), respectively, and that the color was caused by a ternary complex system.

In this paper, the color reaction among PR, thorium(IV) and samarium(III) in the presence of a nonionic surfactant was studied, and the spectrophotometric determination of these ions using the PR-Th-Sm ternary complex was proposed.

Experimental

Apparatus and Reagents. Spectrophotometric determination was done on Shimadzu model UV-240 and 260 recording spectrophotometers with 1.0-cm fused quartz cells. The Hitachi-Horiba M-5 and F-7AD glass electrode pH meters were used for the pH measurements.

A 1.0×10^{-3} mol dm^{-3} solution of PR was prepared by dissolving PR (Tokyo Kasei Kogyo Co., Ltd.) in methanol. A stock solution (1.0×10^{-2} mol dm^{-3}) of thorium(IV) was prepared by dissolving of thorium nitrate in water. A stock solution (1.0×10^{-2} mol dm^{-3}) of samarium(III) was prepared by dissolving 360 mg of Sm_2O_3 in 3 cm³ of concd. hydrochloric acid, and it was diluted to 100 cm³ with water. The concentrations of the stock solutions of thorium(IV) and samarium(III) were determined by chelatometric titration,[4] and then the working solutions (5.0×10^{-4} mol dm^{-3}) were prepared by dilution of these stock solutions. A 1.0% of poly(vinyl alcohol) (PVA) solution was prepared by dissolving PVA (n=2000) in water. A 2.0×10^{-1} mol dm^{-3} sodium acetate-acetic acid buffer solution (Walpole buffer) was used for the pH adjustment. All the other reagents and materials were of analytical grade. Doubly-distilled water was used.

Determination of Thorium(IV): To a solution containing 1—22 μg thorium(IV) in a 10 cm³ volumetric flask were added 2.0 cm³ of a Walpole buffer solution (pH 4.5), 2.0 cm³ of a 1.0% PVA solution, 1.0 cm³ of a 1.0×10^{-4} mol dm^{-3} samarium(III) solution, and 1.5 cm³ of 1.0×10^{-3} mol dm^{-3} PR solution. The mixture was diluted to 10 cm³ with water, and the solution was kept at 60 °C for 30 min. After the mixture was cooled in water for 10 min, the absorbance of the PR-Sm-Th solution (Solution D) was measured at 635 nm against the PR-Sm solution (Solution C).

Determination of Samarium(III): A solution containing 0.5—10 μg samarium(III) was placed in a 10 cm³ volumetric flask. To this solution 2.0 cm³ of 1.0% PVA and buffer solutions, 1.0 cm³ of a 5.0×10^{-4} mol dm^{-3} thorium(IV) solution, and 1.5 cm³ of 1.0×10^{-3} mol dm^{-3} PR solution were added. The mixture was diluted to the mark with water, and heated at 60 °C for 30 min. After the mixture was cooled in water for 10 min, the absorbance of Solution D was measured at 635 nm against the PR-Th solution (Solution B).

Results and Discussion

Figure 1 shows the absorption spectra of PR solution (Solution A), PR-Th solution (Solution B), PR-Sm solution (Solution C) and PR-Th-Sm complex solution (Solution D) in the presence of PVA, respectively. Solution D gave a larger absorbance

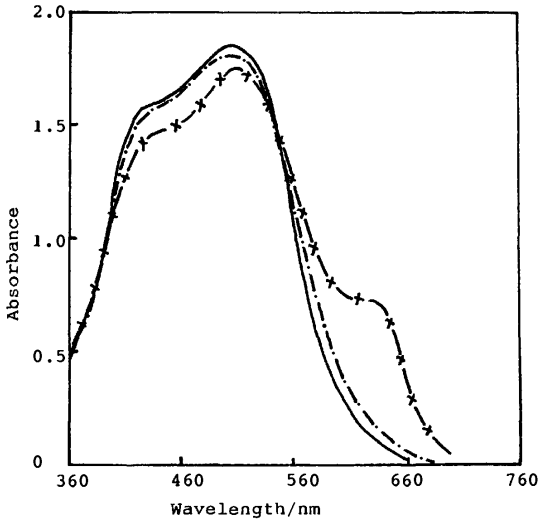

Fig. 1. Absorption spectra of PR-Th-Sm solution, PR-Th solution, PR-Sm solution and PR solution at pH 4.5 in the presence of PVA.
Thorium(IV): 5.0×10^{-6} mol dm^{-3}; Samarium(III): 1.0×10^{-5} mol dm^{-3}; PR: 1.5×10^{-4} mol dm^{-3}; PVA: 2.0 cm³ of 1.0% PVA solution/10 cm³; Reference: water.
—×—: PR-Th-Sm solution=Solution D, —·—: PR-Th solution=Solution B, ——: PR-Sm solution=Solution C and PR solution=Solution A.

Application of Xanthene Derivatives for Analytical Chemistry, Part LII. Part LI. I. Mori, Y. Fujita, H. Kawabe, K. Fujita, S. Kitano, and Y. Koshiyama: *Chem. Pharm. Bull.*, **33**, 4629 (1985).

Table 1. Effects of Some Surfactants

Surfactants		Absorbance at max λ nm	
PVA,	Poly(vinyl alcohol)		
(2000)		0.470	635
(500)		0.450	635
PVP,	Poly(*N*-vinyl-2-pyrrolidone)	0.328	620
Tween 20			
	Poly(oxyethylene) sorbitan monolaurate	0.338	620
HTAC,	Hexadecyltrimethyl-ammonium chloride	0.126	630
SDS	Sodium dodecyl sulfate	0.272	625

PR, 1.5×10^{-4} mol dm^{-3}; Thorium(IV), 5.0×10^{-6} mol dm^{-3}; Samarium(III), 1.0×10^{-5} mol dm^{-3}; Surfactant, 2.0 cm^3 of 1.0% surfactant/10 cm^3; pH 4.5; Reference, PR-Sm solution=Solution C

and was more stable than Solution B or C, and its absorbance was proportional to the concentration of thorium(IV) or samarium(III). The similar phenomena were observed in this reaction system, when rare earth elements such as lanthanum(III) were used instead of samarium(III), and hafnium(IV) or zirconium(IV) instead of thorium(IV).

The effect of pH on the reaction systems was examined. The maximum and constant absorbance was obtained in the pH range of 4.2 to 5.2 with 2.0 cm^3 of 2.0×10^{-1} mol dm^{-3} buffer solution. The reproducibilities of color development of Solutions B, C, and D without a surfactant were poor. As a dispersion agent, PVA was the most effective one among nonionic surfactants and these solutions gave the stable and the highest sensitivity as shown in Table 1.

The use of samarium(III) among the various rare earth elements tested-lanthanum(III), cerium(III), praseodymium(III), gadolinium(III), dysprosium(III), etc. was the most effective in terms of sensitivity.

The maximum and almost constant absorbance was obtained by using of $0.8—1.4\times10^{-5}$ mol dm^{-3} samarium(III) for the determination of thorium(IV), and $3.75—7.5\times10^{-5}$ mol dm^{-3} thorium(IV) solution for the determination of samarium(III) in the final concentration, respectively. The recommended volume of PR was 1.5 cm^3 of a 1.0×10^{-3} mol dm^{-3} solution in the final 10 cm^3.

Consequently, all further work was carried out with 1.0×10^{-5} mol dm^{-3} samarium(III) and 1.5×10^{-4} mol dm^{-3} PR solution for thorium(IV), and 1.5×10^{-4} mol dm^{-3} PR and 5.0×10^{-5} mol dm^{-3} thorium(IV) in the final concentration for the determination of samarium(III), respectively. A nearly constant absorbance of Solution D against Solution B or C was obtained after aging for 5 h at room temperature, or after 30 min at 60 °C. The absorbance was almost constant for at least 32 h at room temperature.

The calibration curves covered the range of 1—22 μg/10 cm^3 thorium(IV) and 0.5—10 μg/10 cm^3 samarium(III). The sensitivities of Sandell's scale were 0.0028 μg cm^{-2} for thorium(IV) and 0.0015 μg cm^{-2} for samarium(III), and the apparent molar absorption coefficients were 8.2×10^4 dm^3 mol^{-1} cm^{-1} for thorium(IV) and 1.0×10^5 dm^3 mol^{-1} cm^{-1} for samarium(III), respectively. The reproducibilities for thorium(IV)(11.6 μg) and samarium(III)(5 μg) were 1.4% and 1.5% (8 experiments).

Table 2. Effects of Foreign Ions for the Determination of Thorium(IV)

Foreign ion	Added as	Added μg/10 cm^3	Absorbance at 635 nm	Tolerance molar ratio*
—	—	—	0.470	—
Bi(III)	Nitrate	0.03	0.369	1/400
Zr(IV)	Nitrate	68.4	0.694	5
Sn(IV)	Sulfate	0.4	0.400	1/100
Al(III)	Nitrate	1.4	0.533	1/20
Fe(III)	Sulfate	0.6	0.519	1/10
Ni(II)	Nitrate	596.9	0.430	50
Cu(II)	Nitrate	47.7	0.693	10
Cd(II)	Nitrate	112.4	0.503	10
Zn(II)	Nitrate	16.3	0.512	20
Co(II)	Nitrate	294.7	0.500	10
Mg(II)	Nitrate	243.1	0.470	300
Tartrate	Acid	370.2	0.398	25
Citrate	Acid	9.5	0.402	1/2
Oxalate	Sodium	7.1	0.402	1
Sulfite	Sodium	9.6	0.491	10
Sulfide	Sodium	15.0	0.355	10
TEA	—	4.9	0.470	1
NTA	Sodium	225.0	0.405	10

Thorium(IV) taken, 11.6 μg/10 cm^3; PR, 1.5×10^{-4} mol dm^{-3}; Samarium(III), 1.0×10^{-5} mol dm^{-3}; pH, 4.5; PVA, 2.0 cm^3 of 1.0% PVA solution/10 cm^3; Reference, PR-Sm solution=Solution C

* foreign ion/thorium(IV)

The effects of foreign ions on the determination of thorium(IV) and samarium(III) were examined. The coexistence of sulfate, chloride, nitrate, nitrite, nickel(II), magnesium(II), calcium(II), etc. did not interfere in 100—200 fold mole excess over thorium-(IV) or samarium(III), and thiosulfate, sulfite, triethanolamine(TEA), L-ascorbic acid, copper(II), iron(III), zinc(II), cadmium(II), etc. in 2—10 fold mole excess over thorium(IV) or samarium(III). The tolerance limits were taken as the amount causing 2% error in the absorbance. Meanwhile, the coexistence of bismuth(III), tin(IV), etc. seriously interfered, and these interfering ions must be separated by suitable procedures. Interference by copper(II), iron(III) or zinc(II) can be prevented by addition of a sodium thiosulfate, TEA or L-ascorbic acid solution. The results for the determination of thorium(IV) are shown in Table 2.

The molar ratios of thorium(IV) to PR in the presence of large amounts of samarium(III), and those of samarium(III) to PR in the presence of thorium(IV) were estimated by the molar-ratio and continuous-variation methods, and these molar ratios

were found to be 1:2. On the other hand, the molar ratio of thorium(IV) to PR in the absence of samarium(III) was 2:3. Although further investigation is necessary, the coloring formed among PR, thorium(IV) and samarium(III) in the presence of PVA as a nonionic surfactant may be regarded as the ternary complex system.

In conclusion, the color reactions among PR, thorium(IV) and samarium(III) in the presence of PVA as a nonionic surfactant were discussed. The ternary complex system, PR-Th-rare earth elements such as samarium(III), was more stable and gave higher absorbance than the PR-Th system or PR-Sm system (Slution C)(=PR solution). Thus, simple, rapid and sensitive spectrophotometric determinations for thorium(IV) and samarium(III) by using the ternary complex (thorium(IV) 1:samarium(III) 1:PR 2) were established. The present method was 2—10 fold more sensitive than other methods[1-9] utilizing xanthene dyes (for example, Xylenol Orange(XO), Methylthymol Blue(MTB), PR) alone, and it was simple and rapid.

Although further investigation is necessary, the color reaction among various xanthene dyes (for example, gallein, XO, MTB, etc.), thorium(IV) and rare earth elements such as samarium(III) may be used as a new color reaction system in analytical chemistry like the reactions reported previously[10].

Presented at the 45th Symposium of the Society of the Analytical Chemistry of Japan, in Muroran, July, 1984.

References

1) A. Jenickova, V. Suk, and M. Malat, *Chem. Listy*, **50**, 760 (1956); *Anal. Abstr.*, **4**, 1106 (1957).
2) A. Jenickova, M. Malat, and V. Suk, *Chem. Listy*, **50**, 1113 (1956); *Anal. Abstr.*, **4**, 1487 (1957).
3) T. Tanaka, Y. Nakagawa, and S. Senda, *Bunseki Kagaku*, **10**, 1148 (1961).
4) K. Ueno, "Chelatometry," p. 386 (1972), Nankodo Publ. Co. Tokyo (in Japanese).
5) V. Suk, *Collect. Czech. Chem. Commum.*, **31**, 3127 (1966).
6) S. B. Sabin and Yu. M. Dedkov, *Zhur. Anal. Khim.*, **19**, 21 (1964).
7) M. Ohtomo and Y. Wakamatsu, *Nippon Kagaku Zasshi*, **89**, 1087 (1968).
8) J. Adam and R. Pribill, *Talanta*, **16**, 1596 (1969).
9) "Muki Ooyo Hisyoku Bunseki (Inorganic Applied Colorimetric Analysis)," Kyoritsu Publ. Co. Tokyo (1976), Vol. 5, p. 232.
10) I. Mori, Y. Fujita, and K. Sakaguchi, *Bunseki Kagaku*, **31**, 99 (1982).

Color Reaction between Indium(III) and *o*-Hydroxyhydroquinonephthalein, and Its Application

Itsuo MORI,* Yoshikazu FUJITA, Kinuko FUJITA, Yozo KOSHIYAMA, Hiroshi KAWABE, Takeshi TANAKA, and Reiko MUNAKATA
Osaka College of Pharmaceutical Sciences, 2-10-65, Kawai, Matsubara, Osaka 580
(Received July 15, 1985)

Synopsis. Color reaction between indium(III) and *o*-hydroxyhyroquinonephthalein(Qnph) in the presence of a cationic surfactant was studied, and its application for the spectrophotometry and photometric titration of indium(III) was discussed. The color reaction between Qnph and indium(III) in the presence of hexadecyltrimethylammonium chloride(HTAC) was stable in weakly acidic media. The calibration curve was rectilinear in the range of 0—10 μg/10 cm³ of indium(III) at 560 nm, and the apparent molar absorption coefficient was 1.3×10^5 dm³ mol^{-1} cm^{-1}. The Sandell sensitivity was 0.0008 μg/cm² for indium(III).

For the detection and determination of indium(III) various methods using oxine, dithizone, Xylenol Orange(XO), Methylthymol Blue(MTB), Pyrocatechol Violet(PV), etc. have been reported.[1-11] However, most of these methods are complicated and/or not sufficiently sensitive. The color formation between *o*-hydroxyhydroquinonephthalein(Qnph) and indium(III) in the presence of hexadecyltrimethylammonium chloride(HTAC) as a cationic surfactant was sharp, stable and gave a larger absorbance than the color reaction without surfactant.

In this paper, the color reaction between Qnph and indium(III) was discussed, and then a simple, rapid and sensitive spectrophotometric method for the determination of indium(III) was established.

Experimental

Apparatus and Reagents. Spectrophotometric measurements were carried out on Shimadzu Model UV—200, UV-240 and Hitachi Model 150-20 recording spectrophotometers with 1.0-cm fused silica cells. A Shimadzu Model QV-50 spectrophotometer and its attachments were used for photometric titration of indium(III). Hitachi-Horiba Model F-7AD and M-5 glass electrode pH meters were used for the pH measurements.

A 1.0×10^{-3} mol dm^{-3} solution of Qnph was prepared according to the previous report.[12] The working solutions (5.0×10^{-4} mol dm^{-3}) of indium(III) and a 1.0×10^{-2} mol dm^{-3} EDTA solutions were prepared according to the previous reports,[9] respectively. A 2.0×10^{-2} mol dm^{-3} HTAC solution was prepared by dissolving HTAC in water, and a 2.0×10^{-1} mol dm^{-3} sodium acetate–acetic acid buffer solution was used for the pH adjustments. All the other reagents and materials were of analytical grade and were used without further purification. Doubly distilled water was used.

Standard Procedure. Spectrophotometric determination of indium(III): To a solution containing up to 10 μg indium(III) in a 10 cm³ volumetric flask were added 1.0 cm³ of a 2.0×10^{-2} mol dm^{-3} HTAC solution, 1.5 cm³ of a 1.0×10^{-3} mol dm^{-3} Qnph solution, and 2.0 cm³ of a 2.0×10^{-1} mol dm^{-3} acetate buffer solution(pH 5.4). The mixture was diluted to 10 cm³ with water(Solution B), and the solution was mixed well, and kept at room temperature for 10 min. The absorbance of Solution B was measured at 560 nm against the reagent blank(Solution A).

Photometric titration of indium(III): A solution containing less than 900 μg of indium(III) was placed in a tall beaker (40×90 mm); to this solution 5.0 cm³ of a 2.0×10^{-3} mol dm^{-3} HTAC solution and 1.5 cm³ of a 1.0×10^{-3} mol dm^{-3} Qnph solution were added. The pH of the solution was adjusted to about 3.5 with a 2.0×10^{-1} mol dm^{-3} sodium acetate-hydrochloric acid solution, was diluted to 30 cm³ with water, and was heated at 60—70 °C for 10 min. Then the mixed solution was titrated by a 1.0×10^{-2} mol dm^{-3} EDTA solution by measuring the absorbance at 560 nm or 520 nm. The concentrations of indium(III) were calculated from the relationship between the absorbance at 560 nm or 520 nm and the amounts used of a 1.0×10^{-2} mol dm^{-3} EDTA solution.

Results and Discussion

Color Reaction and Absorption Spectra. The color reaction between Qnph and indium(III) was studied in weakly acidic media with or without various kinds of surfactants——poly(oxyethylene)-sorbitan monolaurate (Tween 20) as a nonionic, HTAC as a cationic or sodium dodecyl sulfate(SDS) as an anionic surfactant. The Qnph–indium(III) complex solution in the presence of HTAC showed a considerable bathochromic shift with two times larger and more stable absorbance than the complex in the presence of Tween 20 or SDS.

Effects of pH and Surfactants. The maximum and constant absorbance was obtained in the pH range from 5.2 to 6.2 for indium(III) by addition of 2.0 cm³ of a 2.0×10^{-1} mol dm^{-3} Walpole acetate buffer solution in the final volume of 10 cm³. Among various surfactants, HTAC, hexadecylpyridinium chloride(HPC), zephiramine, HTAC, a cationic surfactant, was found to be the best as a dispersion agent. The maximum and constant absorbance could be obtained over the range of 0.5 to 2.0 cm³ of a 2.0×10^{-2} mol dm^{-3} HTAC solution to the final volume of 10 cm³. Subsequent measurement was carried out by addition of 2.0 cm³ of the buffer solution(pH 5.4) and 1.0 cm³ of a 2.0×10^{-2} mol dm^{-3} HTAC solution in the final volume of 10 cm³.

Effects of Qnph Concentration and Stability. The recommended concentration of Qnph was 1.5×10^{-4} mol dm^{-3} in the final solution. Under the conditions of the standard procedure, the maximum and almost constant absorbance was obtained by keeping the Qnph–indium(III) solution at room temperature for

---

Application of Xanthene Derivatives for Analytical Chemistry, Part LIII. Part LII. I. Mori, Y. Fujita, K. Fujita, S. Kitano, I. Ogawa, H. Kawabe, Y. Koshiyama, and T. Tanaka, *Bull. Chem. Soc. Jpn.*, **59**, 955 (1986).

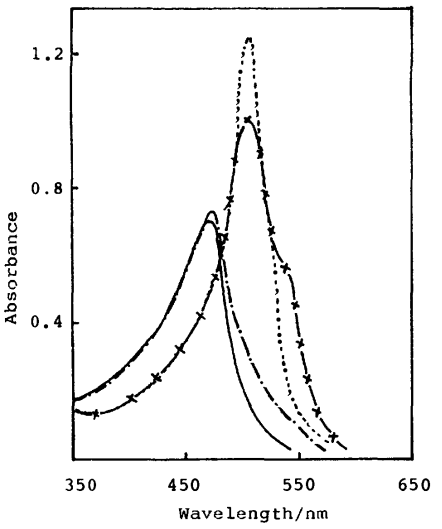

Fig. 1. Absorption spectra of Qnph and Qnph-indium(III) complex solutions in the presence of Tween 20 or HTAC at pH 5.4.
Indium(III): 4.0×10^{-6} mol dm^{-3}; Qnph: 4.0×10^{-5} mol dm^{-3}; HTAC: 2.0×10^{-3} mol dm^{-3}; Tewen 20 : 1.0 cm^3 of a 1.0% Tween 20 solution/10 cm^3; Reference : water.
——: Qnph-Tween 20 solution, —·—: Qnph-Tween 20-indium(III) solution, ----: Qnph-HTAC solution, —×—: Qnph-HTAC-indium(III) solution.

Table 1. Effects of Foreign Ions

Foreign ions	Added as	Added μg/10 cm^3	Absorbance at 560 nm
—	—	—	0.776
Bi(III)	Nitrate	1.6	0.980
Th(IV)	Nitrate	1.5	0.824
Al(III)	Nitrate	2.7	0.830
Fe(III)	Sulfate	1.5	0.850
Co(II)	Nitrate	1.6	0.845
Ni(II)	Nitrate	12.0	0.750
Cu(II)	Nitrate	1.6	0.820
Zn(II)	Nitrate	11.0	0.845
Ce(III)	Chloride	0.2	0.776
MoO_4^{2-}	Sodium	0.5	0.776
SCN^-	Ammonium	0.5	0.750
NO_2^-	Potassium	58.0	0.750
CN^-	Potassium	126.0	0.780
$C_2O_4^{2-}$	Sodium	180.0	0.750
Cl^-	Sodium	443.0	0.776
F^-	Sodium	23.7	0.776
$S_2O_3^{2-}$	Sodium	114.5	0.776
Citrate	Sodium	190.0	0.685
Tartrate	Sodium	15000.0	0.695

Indium(III) taken: 7.2 μg/10 cm^3; Qnph: 1.5×10^{-4} mol dm^{-3}; pH: 5.4; HTAC: 2.0×10^{-3} mol dm^{-3}: Reference: Reagent blank.

longer than 10 min. The absorbance was almost constant at least for 90 min.

Calibration Curve and Repeatability. The calibration curve for indium(III) was constracted according to the standard procedure. Beer's law held in the concentration range of 0—10 μg of indium(III) in the final volume of 10 cm^3. The apparent molar absorption coefficient was estimated to be 1.3×10^5 dm^3 mol^{-1} cm^{-1} at 560 nm, and the Sandell sensitivity was calculated to be 0.0008 μg cm^{-2} for indium(III). The coefficient of variation(n=5) for 7.2 μg indium(III) was 1.5%.

Effects of Foreign Ions. The tolerance limits were taken as the amount causing 2% error in the absorbance. The coexistence of small amounts of copper(II), iron(III), aluminum(III), bismuth(III), etc. showed positive errors because of the formation of a colored complex with Qnph. In 2—30 fold molar excess of indium(III), the interference of copper(II), aluminum(III), and iron(III) could be overcome to some extent by addition of sodium thiosulfate, nitrilotriacetic acid(NTA) or sodium fluoride and potassium cyanide or sodium fluoride solutions, respectively. Also, the interference of bismuth(III) could be overcome by addition of NTA in a 50-fold excess. Although the coexistence of large amounts of tartrate, citrate and oxalate ions, etc. interfered, the presence of most anions scarcely interfered in the 100—200 fold molar excess of indium(III). The results are summarized in Table 1.

The Composition of the Complex. The molar ratio of Qnph to indium(III) in the presence of HTAC was estimated to be 2:1 by the molar-ratio and the continuous-variation methods. On the other hand, the molar ratio of Qnph to indium(III) in the coexistence of Tween 20 without HTAC was 3:2 by the molar-ratio method. The molar ratio of HTAC to the indium(III)-Qnph solution was found to be 2:1 in the presence of nonionic surfactants.

Photometric Titration. At the end point of the photometric titration of indium(III) by using Qnph as a metal indicator at around pH 3—5 in the coexistence of HTAC the color changed from orange red to yellow. In the photometric titration of indium(III), the difference of absorbance at 560 or 520 nm of the Qnph-indium(III) solution and that of the Qnph solution was measured. The proposed method was well suitable for differential titration of the mixed metal ion solution (for example, indium(III)-bismuth(III), indium(III)-thorium(IV), indium(III)-aluminum(III)-cobalt(II), etc.).

The recovery of indium(III) added to a waste water involving of copper(II), cadmium(II), lead(II), zinc(II), aluminum(III), iron(III), bismuth(III), etc. was examined, and the results were satisfactory (98.5—103.0%).

In conclusion, the color reactions between indium(III) and Qnph in the presence of various surfactants were studied, and a simple, rapid and sensitive spectrophotometric determination of indium(III) was established by using the color reaction between Qnph and indium(III) in the presence of HTAC in weakly acidic media. The calibration curve was linear in the concentration range of 0—10 μg/10 cm^3 for indium(III). The apparent molar absorption coefficient was estimated to be 1.3×10^5 dm^3 mol^{-1} cm^{-1}. The sensi-

tivity of this method was about 9 times greater than the oxine or MTB method,[3] and 3—4 fold greater than 1-(2-pyridylazo)-2-naphthol(PAN)[2] or previously reported method.[9] The effects of foreign ions were relatively smaller than the previous method.[9]

Though further investigation is necessary, the proposed method may be useful for the determination of indium(III) in alloys, iron ores, semiconductors, etc.

Presented at the 45th Symposium Society of the Analytical Chemistry of Japan, in Muroran, July, 1984.

References

1) S. Shibata, *Anal. Chim. Acta*, **23**, 434 (1960).
2) K. L. Cheng and B. L. Goydish, *Anal. Chim. Acta*, **34**, 154 (1966).
3) E. B. Snell and C. T. Snell, *Colorimetric Method for Analysis*, **1**, 1221 (1947).
4) B. Evtimova and D. Norova, *Anal. Chim. Acta*, **67**, 107 (1973).
5) K. Akatsuka, *Bunseki Kagaku*, **21**, 1372 (1972).
6) Y. Shijo and T. Takeuchi, *Bunseki Kagaku*, **14**, 115 (1965).
7) F. Jarslav and V. Jaromir, *Sb. Vys. Sk. Chem.-Technol. Praze., Anal. Chem.*, H15, 171 (1980); *Anal. Abstr.*, **43**, 1B133 (1982).
8) Z. T. Chan and E. L. Glushchenko, *Tezisy Resp. Nauchn. Konf. Molodykh. Uch-Khim. Azeeb*, **1974**, 20; *Chem. Abstr.*, **87**, 15463y (1977).
9) I. Mori, Y. Fujita, M. Ida, and T. Enoki, *Bunseki Kagaku*, **25**, 239 (1976).
10) V. N. Tikhonov and V. V. Bakhtina, *Zhur. Anal. Khim.*, **39**, 169 (1985).
11) V. N. Tikhnov and O. K. Palvlova, *Zhur. Anal. Khim.*, **37**, 1402 (1983).
12) I. Mori, Y. Fujita, K. Sakaguchi, and S. Kitano, *Bunseki Kagaku*, **31**, E239 (1982).

Excited-State Reactions of Coumarins in Aqueous Solutions. III. The Fluorescence Quenching of 7-Ethoxycoumarins by the Chloride Ion in Acidic Solutions

Tetsuo MORIYA
Electrotechnical Laboratory, 1-1-4 Umezono, Sakura-mura, Niihari-gun, Ibaraki 305
(Received July 31, 1985)

The fluorescence yield of 7-ethoxycoumarins in acidic aqueous solutions becomes reduced with an increase in the chloride-ion concentration. In acidic solutions, two types of excited molecules, a neutral molecule and a protonated molecule with a positive charge, are generated by a UV light illumination. Only the excited state of a protonated molecule is quenched by a chloride ion; the quenching reaction proceeds via both a diffusional and a static process. The rate constant for the diffusional process is $(3.7—5.8)\times10^9$ mol^{-1} dm^3 s^{-1}. The static quenching component can be approximately described by the $V[Q]$ expression and the static quenching constant, V, is 1.2—1.7 mol^{-1} dm^3. One possible physical interpretation of the quenching mechanism is discussed in relation to the charge of colliding species and the electron transfers between them.

In a previous paper[1] interactions between 7-ethoxycoumarins and halide ions in a neutral aqueous solution were discussed. It has been revealed that bromide and iodide ions cause a very pronounced quenching effect on the fluorescence of 7-ethoxycoumarins. On the other hand, chloride ions show no indication of quenching, even at considerably high quencher concentrations. This has been explained in terms of the oder of the quenching ability of the halide ions, i.e., $I^- > Br^- \gg Cl^-$.

When a solution is changed from neutral to acidic, 7-ethoxycoumarins can take two forms of the photo-excited state, neutral and protonated. It was recently found that in an acidic solution, even chloride ions have a remarkable quenching effect on the fluorescence of the two molecular species.

To quantitatively analyze this phenomena, chloride ions were chosen as the quencher. Then, the fluorescence intensities of 7-ethoxycoumarin (**1**) and 7-ethoxy-4-methylcoumarin (**2**) in acidic aqueous solutions were measured in detail as a function of the quencher concentration. In this paper a reasonable scheme for the reaction kinetics is proposed and several reaction-rate constants are derived by means of the obtained data. The quenching mechanism is discussed while taking account of the ionic nature of the interacting species.

Experimental

Material. High-purity grade reagents of 7-ethoxycoumarin (**1**) and 7-ethoxy-4-methylcoumarin (**2**) were obtained from Molecular Probes Inc. and used as purchased. Their melting points were determined by means of DTA:[2] **1**, mp 84.8°; **2**, mp 115.5°. Sodium chloride, hydrochloric acid, and perchloric acid were of pure-quality from Wako Pure Chemical Ind. Water was permeated and distilled.

Methods. The UV absorption spectra were obtained on a Hitachi 323 spectrophotometer and fluorescence intensity measurements were made on a Hitachi MPF 4 spectrofluorometer with an S-5 type photomultiplier tube. Spectral measurements were performed at 20°C unless otherwise mentioned. For fluorescence measurements, the wavelengths of the excitation light were chosen to be 324 nm for **1** and 321 nm for **2**, corresponding to the absorption maximum of the respective compounds. The concentrations of the fluorescent molecules in a solution were $\approx5\times10^{-5}$ mol dm^{-3} for **1** and $\approx4\times10^{-5}$ mol dm^{-3} for **2**. These provided for the most reliable recordings of the fluorescence intensity using the spectrofluorometer.[3] The pH or H_0 value[4] of the solution was controlled with $HClO_4$ and HCl. In the quenching experiment, the fluorescence of a series of samples containing a constant amount of a fluorescent compound and a graduated amount of quencher was measured. Fluorescence lifetime measurements were performed by means of a time-correlated single-photon-counting fluorometer, similar to the one described in Ref. 5. When the lifetime was close to the decay time of repetitive short-pulsed light at 337 nm from an air-flash lamp, the deconvolution procedure was performed assuming the exponential decay of the fluorescence intensity. The resulting accuracy was within ±0.05 ns.

Results and Discussion

pH Dependence of Absorption and Fluorescence Spectra. In the electronically ground state of 7-ethoxycoumarins, only one molecular species was spectroscopically detectable in an aqueous solution of neutral and acidic regions (pH 7 to H_0 −3) where fluorescence-quenching measurements have been carried out. In the excited state, a neutral molecule, $\overset{*}{N}$ and a protonated molecule, $\overset{*}{C}^+$ appear.[6] The interconversion of these species can be described by the reaction:

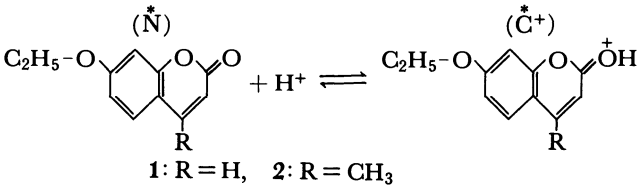

1: R = H, **2**: R = CH_3

Figure 1 shows the UV absorption spectrum and the visible fluorescence spectra of 7-ethoxycoumarin (**1**). The absorption maxima of **1** and **2** in the neutral solution were 324 and 321 nm respectively. These absorption spectra did not vary over the wide pH range

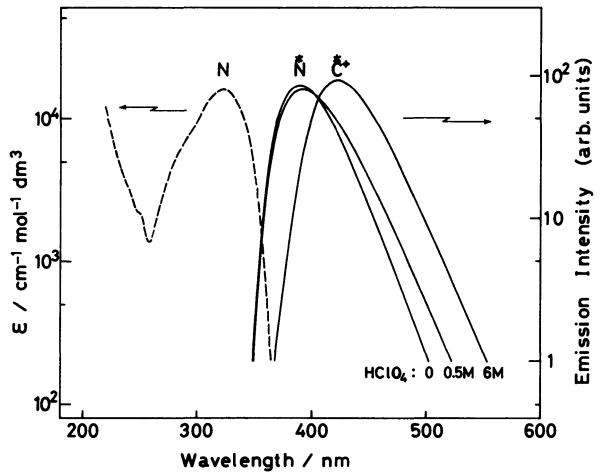

Fig. 1. Absorption and fluorescence spectra of 7-ethoxycoumarin (**1**) in aqueous solutions. N indicates the absorption spectrum of the neutral molecule. $\overset{*}{N}$ and $\overset{*}{C}^{+}$ are the fluorescence spectra from the excited state of the neutral and the protonated molecules respectively; the typical fluorescence spectra for the neutral solution and for the solution with 0.5 and 6 mol dm^{-3} $HClO_4$ added are shown.

of interest (H_0>−3). The new absorption band of a protonated molecule barely appeared in a solution of concentrated sulfric acid (H_0<−6) at longer wavelengths. Such absorption bands have been observed by others for similar coumarin derivatives;[18,19] the peaks are at 362 and 353 nm for **1** and **2**, respectively. In contrast, the fluorescence spectra began to change in shape and wavelength position for moderately acidic solutions. The fluorescence peak at 390 nm of Compound **1** in a neutral solution shifted to at last 423 nm at H_0≈−3; in the case of Compound **2**, these peaks were at 382 and 412 nm, respectively. The fluorescence peaks of these compounds at shorter wavelengths correspond to a neutral molecule in an excited state. The peaks at longer wavelengths correspond to a protonated molecule in an excited state.[6]

In moderately acidic solutions, these two types of fluorescence bands overlapped each other; therefore, it is necessary to separate the spectral bands in order to obtain a quantitative value for the relative fluorescence intensities of the two molecular species. For this procedure, it is very convenient to plot the emission intensity of the fluorescence spectrum with a logarithmic scale (Fig. 1). This is done because the contribution from each molecular species is readily recognized by adding the respective spectral bands and reconstructing the data in the graph at a given pH.

Fluorescence Quenching by Halide Ions. The fluorescence quenching by halide ions in a neutral aqueous solution was fully investigated in a previous paper and the quenching process was clarified.[1] From the experimentally obtained results, it has been concluded that chloride ions have no effect on the fluorescence intensity of a neutral molecule. Figure 2 shows plots of I_0/I vs. [Cl^-], where I_0 and I are the fluorescence intensities in the absence and in the presence of chloride ions. At pH≈7, a neutral molecule is the only species both in ground and excited states and Cl^- has no effect on the fluorescence intensity for [Cl^-]≲0.5 mol dm^{-3}.

Fluorescence Quenching by Chloride Ions in a Strongly Acidc Solution. When 6 mol dm^{-3} of $HClO_4$ was added beforehand to the solution (H_0=−2.84), protonated molecules became the unique species in the excited state and fluorescence was considerably quenched by the Cl^- (contained as a controlled amount of NaCl up to 0.25 mol dm^{-3}). In Fig. 2 data are shown for an aqueous solution with 6 mol dm^{-3} $HClO_4$ added; it can be seen from the figure that I_0/I depends linearly on [Cl^-]. In such case, the Stern-Volmer relationship derived under steady state conditions is apllicable:[7]

$$\frac{I_0}{I} = 1 + K_{sv}[Q]. \quad (1)$$

K_{sv} is the collisional quenching constant and [Q] is the quencher concentration. The data in Fig. 2 show the linear dependence of I_0/I on the concentration of chloride ions; the quenching constant, K_{sv}, of a protonated molecule (due to Cl^-) is estimated to be 6.80 mol^{-1} dm^3 for **1** and 4.21 mol^{-1} dm^3 for **2**. Using the rate constant, k_q, and the lifetime of the excited state of a protonated molecule, τ', the quenching constant is given by $K_{sv}=k_q\tau'$. The k_q values were estimated to be 1.39×10^9 mol^{-1} dm^3 s^{-1} for **1** and 8.77×10^8 mol^{-1} dm^3 s^{-1} for **2**, respectively, with the lifetimes shown in Table 2. The occurrence of this quenching effect is attributable to an increase in the interaction between positively charged molecules and negatively charged chloride ions through an attractive electrostatic force in comparison with the interaction between a neutral molecule and an ion.

Fluorescence Quenching by Chloride Ions in a Moderately Acidic Solution. When the same quenching experiment was performed in a moderately acidic solution, the dependence of I_0/I (for neutral and protonated molecules) on the Cl^- concentration did not obey the usual Stern-Volmer relationship, as can be clearly seen in Fig. 2 (a plot of I_0/I vs. [Cl^-]). The curve for the fluorescence of the neutral molecule curved downward away from a linear dependence; the curve for the protonated molecule curved upward. Since the sum of the concentrations of $HClO_4$ and HCl was made to be constant at 0.5 mol dm^{-3}, the ionic concentration,[8] Γ, and the acidity strength,[4] H_0, did not change for various concentrations of [Cl^-] (Γ=1 mol dm^{-3} and H_0=0.20). $\Gamma=\sum_i c_i z_i^2$, where c_i and z_i are the molar concentration and the valence of the ions in a solution. Thus, the unexpected behavior (mentioned above) cannot be related to a change in these values.

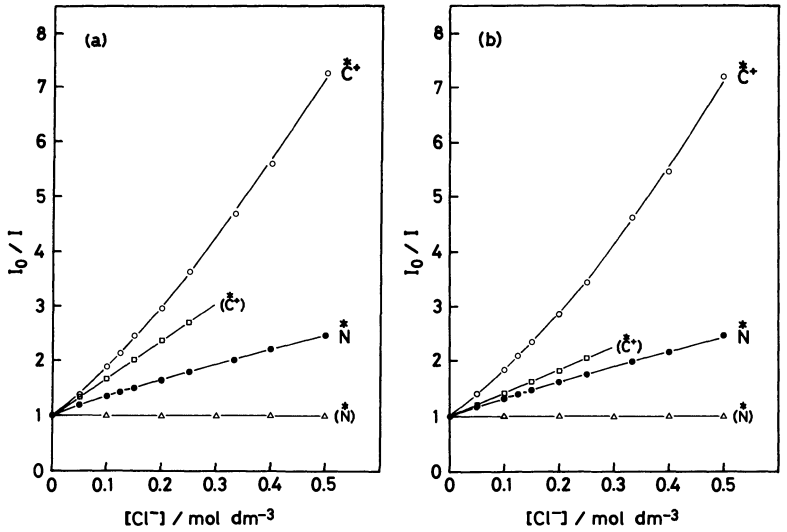

Fig. 2. Dependence of I_0/I on the concentration of the chloride ion in the neutral (△), the moderately acidic (○; ●), and the strongly acidic (□) solutions. (a), 7-ethoxycoumarin (**1**); (b), 7-ethoxy-4-methylcoumarin (**2**).

In order to analyze such phenomena from a general point of view, the following scheme for the chemical reaction and the fluorescence-quenching process is given:

$$N + h\nu_A \xrightarrow{G_{abs}} \overset{*}{N}, \tag{2}$$

$$\begin{array}{ccc} \overset{*}{N} + H^+ & \underset{k_2}{\overset{k_1}{\rightleftharpoons}} & \overset{*}{C}^+ \\ {\scriptstyle n_1}\swarrow\ \searrow{\scriptstyle n_2} & & {\scriptstyle n_1'}\swarrow\ \searrow{\scriptstyle n_2'} \\ N + h\nu_F \quad N & & C^+ + h\nu_F' \quad C^+ \end{array}, \tag{3}$$

$$W: \overset{*}{C}^+ + Q \underset{k_2'}{\overset{k_1'}{\rightleftharpoons}} (C^+Q)^* \xrightarrow{k_3'} C^+ + Q, \tag{4}$$

$$1 - W: \overset{*}{C}^+ + Q \longrightarrow C^+ + Q. \tag{5}$$

Here, N and C^+ represent neutral and protonated molecules, respectively. $\overset{*}{N}$ and $\overset{*}{C}^+$ are their excited states and Q and $h\nu$ represent the quencher and the light quantum. $(C^+Q)^*$ is the excited state of the encounter complex between $\overset{*}{C}^+$ and the quencher. G_{abs} is the generation rate of $\overset{*}{N}$; the k's and n's are the reaction-rate constants and the transition probabilities, respectively. Equation 3 describes an excited-state reaction of neutral molecules with protons which generates a protonated molecule. n_1 and n_1' are the radiative-transition probabilities that cause the fluorescence; n_2 and n_2' are the nonradiative-transition probabilities toward the electronic ground state. Equation 4 shows that the fraction, W, of $\overset{*}{C}^+$ obeys a collisional quenching process in which the encounter complex, $(C^+Q)^*$, decays nonradiatively to C^+ and Q with a rate of k_3'; Equation 5 shows that a fraction, $1-W$, of $\overset{*}{C}^+$ obeys the instantaneous deactivation process discussed in Ref. 1.

It is an essential idea for the explanation of experimental data that only a certain fraction, W, of the excited states is actually quenched by the collisional mechanism. The remaining fraction, $1-W$, is deactivated almost instantaneously after being formed since a quencher is accidentally positioned in the proximity of the molecule at the time of light-absorption and interacts very strongly with the molecule. Generally, this additional factor, W (a function of the quencher concentration, [Q]), can be approximated by $\exp(-V[Q])$, where V is the static quenching constant. If the model of Frank and Vavilov[9] is adopted for the instantaneous or "static" quenching process, an instantaneous quenching results when a quencher happens to reside within a "sphere of action" having a volume of V/N', where N' is the Avogadro's number per millimole.[10]

Since illuminating light is absorbed solely by neutral molecules under experimental conditions and the fraction, $1-W$, of the protonated molecule in the excited state is immediately quenched, the effective generation rate of neutral molecules in the excited state, $\tilde{G}(Q)$, is as a first approximation:

$$\begin{aligned} \tilde{G}(Q) &= G_{abs} - \{1 - W(Q)\} G_{abs} \frac{k_1[H^+]}{n_1 + n_2 + k_1[H^+]} \\ &= G_{abs} \frac{n_1 + n_2 + W(Q) k_1[H^+]}{n_1 + n_2 + k_1[H^+]}, \end{aligned} \tag{6}$$

where

$$W(Q) = \exp(-V[Q]) \text{ and } W(0) = 1. \tag{7}$$

The rate equations for each molecular species, therefore, become:

$$\frac{d[\overset{*}{N}]}{dt} = \tilde{G} - (n_1 + n_2 + k_1[H^+])[\overset{*}{N}] + k_2[\overset{*}{C}^+], \tag{8}$$

$$\frac{d[\overset{*}{C}^+]}{dt} = k_1[H^+][\overset{*}{N}] - (n_1'+n_2'+k_1'[Q]+k_2)[\overset{*}{C}^+] + k_2'[(C^+Q)^*], \quad (9)$$

$$\frac{d[(C^+Q)^*]}{dt} = k_1'[Q][\overset{*}{C}^+] - (k_2'+k_3')[(C^+Q)^*]. \quad (10)$$

If the steady-state condition is satisfied, we may obtain the densities of the excited molecules by letting the left-hand side of Eqs. 8—10 be zero. Then, the densities of $\overset{*}{N}$ and $\overset{*}{C}^+$ are:

$$[\overset{*}{N}] = \tilde{G}\tau / \left(1+\frac{1+k_q\tau'[Q]}{1+k_2\tau'+k_q\tau'[Q]}k_1\tau[H^+]\right), \quad (11)$$

$$[\overset{*}{C}^+] = \left(\tilde{G}\tau'\frac{k_1\tau[H^+]}{1+k_2\tau'+k_q\tau'[Q]}\right) \Big/ \left(1+\frac{1+k_q\tau'[Q]}{1+k_2\tau'+k_q\tau'[Q]}k_1\tau[H^+]\right), \quad (12)$$

where

$$\tau = \frac{1}{n_1+n_2} \text{ and } \tau' = \frac{1}{n_1'+n_2'}, \quad (13)$$

$$k_q = \gamma k_1' = \frac{k_3'}{k_2'+k_3'}k_1'. \quad (14)$$

τ and τ' correspond to the lifetimes of neutral and protonated molecules. k_q and γ are the apparent rate constant for the collisional quenching process and the efficiency of the quenching reaction, respectively. The total fluorescence intensities from $\overset{*}{N}$ and $\overset{*}{C}^+$ are defined by:

$$I^N = n_1[\overset{*}{N}] \text{ and } I^C = n_1'[\overset{*}{C}^+]. \quad (15)$$

Since the value of $\tilde{G}$ at [Q]=0 is G_{abs}, the fluorescence intensities at [Q]=0 for $\overset{*}{N}$ and $\overset{*}{C}^+$, i.e., I_0^N and I_0^C, are written as:

$$I_0^N = G_{abs}n_1\tau / \left(1+\frac{k_1\tau[H^+]}{1+k_2\tau'}\right) \text{ and} \quad (16)$$

$$I_0^C = \left(G_{abs}n_1'\tau'\frac{k_1\tau[H^+]}{1+k_2\tau'}\right) \Big/ \left(1+\frac{k_1\tau[H^+]}{1+k_2\tau'}\right). \quad (17)$$

Then, the relative fluorescence intensities, in comparison with the intensity at [Q]=0, of each excited molecule are given by:

$$\frac{I_0^N}{I^N} = \left\{\left(1+\frac{1+k_q\tau'[Q]}{1+k_2\tau'+k_q\tau'[Q]}k_1\tau[H^+]\right) \Big/ \left(1+\frac{k_1\tau[H^+]}{1+k_2\tau'}\right)\right\}\frac{1+k_1\tau[H^+]}{1+W(Q)k_1\tau[H^+]}, \quad (18)$$

$$\frac{I_0^C}{I^C} = \frac{I_0^N}{I^N}\frac{1+k_2\tau'+k_q\tau'[Q]}{1+k_2\tau'}. \quad (19)$$

From Eqs. 18 and 19, it is easily shown that $I_0^N/I^N \to 1$ and $I_0^C/I^C \to 1$ if $[Q] \to 0$, and $I_0^C/I^C > I_0^N/I^N > 1$ for $[Q] > 0$. These results can reasonably explain, in principle, the dependence of I_0/I on the concentration of the quencher. The experimental data in Fig. 2 show that I_0^C/I^C is always larger than I_0^N/I^N.

Tabel 1. Typical Values of I_0^N/I^N Shown in Fig. 2

Substance	[Cl⁻]			
	0	0.05 mol dm^{-3}	0.1 mol dm^{-3}	0.125 mol dm^{-3}
1	1	1.19_3	1.34_7	1.42_2
2	1	1.17_0	1.32_3	1.39_4

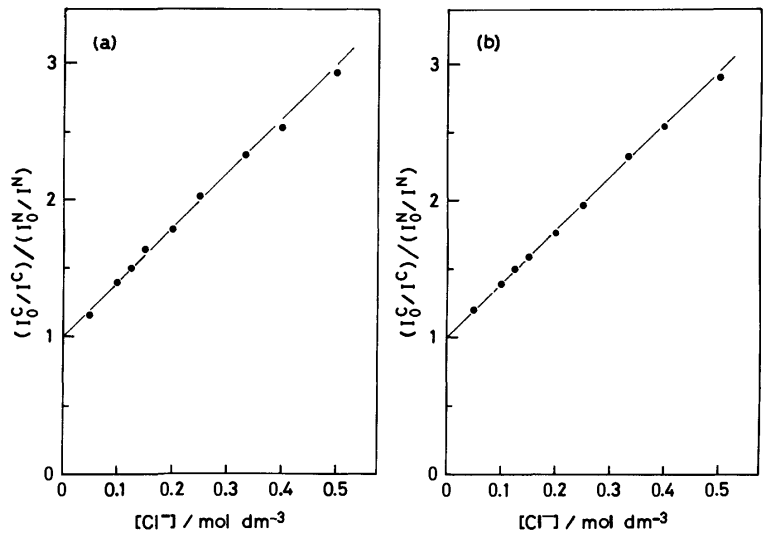

Fig. 3. Plots of $(I_0^C/I^C)/(I_0^N/I^N)$ vs. [Cl⁻]. (a), 1; (b), 2.

Table 2. Lifetimes of the Two Molecular Species, τ and τ', and Values of $k_q\tau'/(1+k_2\tau')$ and $k_1\tau[H^+]/(1+k_2\tau')$

Substance	τ/ns[a]	τ'/ns[a]	$k_q\tau'/(1+k_2\tau')$/mol^{-1}dm^3	$k_1\tau[H^+]/(1+k_2\tau')$[b]
1	2.0_0	4.9_0	4.0_0	0.17_6
2	2.2_5	4.8_0	3.9_2	0.26_1

a) The lifetime was measured at a suitably chosen pH value where only one molecular species was detectable. b) The value at $[H^+]=0.5$ mol dm^{-3}.

Table 3. Rate Constants Obtained for the Excited-State Reactions and for the Collisional Quenching Process, Collisonal Quenching Constants, Static Quenching Constants, and Radii of the Sphere of Action in the Aqueous Solution with $[H^+]=0.5$ mol dm^{-3} and $I=1$ mol dm^{-3}

Substance	$k_1\times10^{-9}$	$k_2\times10^{-9}$	$k_q\times10^{-9}$	K_{sv}	V	r
	mol^{-1}dm^{3}s^{-1}	s^{-1}	mol^{-1}dm^{3}s^{-1}	mol^{-1}dm^3	mol^{-1}dm^3	Å
1	1.2_5	1.2_4	5.8_0	28.4	1.2	7.7
2	1.0_4	0.72_1	3.6_5	17.5	1.7	8.8

Reaction-Rate Constants for the Quenching Process. To quantitatively analyze the quenching process in an acidic solution, we can derive from Eq. 19:

$$\frac{I_0^C/I^C}{I_0^N/I^N}=1+\frac{k_q\tau'}{1+k_2\tau'}[Q]. \tag{20}$$

This relationship predicts the linear dependence of $(I_0^C/I^C)/(I_0^N/I^N)$ on the concentration of the quencher; its slope gives the value of $k_q\tau'/(1+k_2\tau')$. The experimental data of $(I_0^C/I^C)/(I_0^N/I^N)$ vs. $[Cl^-]$ are plotted in Fig. 3. The dependence is a linear function of $[Cl^-]$ and the values of $k_q\tau'/(1+k_2\tau')$ are 4.00 mol^{-1}dm^3 for **1** and 3.92 mol^{-1}dm^3 for **2**, respectively.

It is helpful, at this stage, to define the fluorescence intensity of excited molecules at both $[Q]=0$ and $k_1\tau[H^+]\ll1$ by $\bar{I}_0^N$. From Eq. 16 we obtain $\bar{I}_0^N=G_{abs}n_1\tau$, and

$$\frac{\bar{I}_0^N}{I_0^N}=1+\frac{k_1\tau[H^+]}{1+k_2\tau'}. \tag{21}$$

The values of $\bar{I}_0^N/I_0^N$ and, of course, $k_1\tau[H^+]/(1+k_2\tau')$ are obtainable from the fluorescence data of a neutral solution and an acidic solution with $[H^+]=0.5$ mol dm^{-3}. The resulting values of $k_1\tau[H^+]/(1+k_2\tau')$ at $[H^+]=0.5$ mol dm^{-3} are 0.176 for **1** and 0.261 for **2**, respectively. Since the original form of $W(Q)$ as an exponential function of $[Q]$ is not tractable for an analytical calculation, the same approximation as was adopted in the former work[1] may be used again for a relatively low quencher concentration:

$$W(Q)\approx1-V[Q]. \tag{22}$$

Here, V is the static quenching constant. It is noted that this approximation has meaning only for $V[Q]<0.15$ when estimating the unknown parameter. Thus, the numerical values of I_0^N/I^N for the low concentration region of $[Cl^-]$ are cited in Table 1.

By using Tables 1 and 2 as well as the approximation given by Eq. 22, values of $k_q\tau'(=K_{sv})$ and V can be obtained from a best-fit analysis of the data points and the theoretical prediction. Then, K_{sv}, V, k_1, k_2, and k_q are given as cited in Table 3. Incidentally, the radius of the sphere-of-action for the quenching process, r, is estimated and cited in the same table, with the relation, $V/N'=4\pi r^3/3$, where N' is Avogadro's number per millimole. Qualitatively speaking, it is shown with the theoretical prediction that both I_0^N/I^N and I_0^C/I^C increase monotonically with an increase in the quencher concentration. The increase in I_0^N/I^N saturates at the higher concentration range and the value of I_0^N/I^N reaches asymptotically to $(1+k_2\tau')(1+k_1\tau[H^+])^2/(1+k_2\tau'+k_1\tau[H^+])$. The increase in I_0^C/I^C becomes linear with a slope of $(1+k_1\tau[H^+])^2k_q\tau'/(1+k_2\tau'+k_1\tau[H^+])$ in the higher concentration range. In general, I_0^N/I^N and I_0^C/I^C change in a complicated manner; thus, an analytical treatment has been possible only in the low concentration range where Eq. 22 is valid.

Equilibrium Constants in the Excited State. Since we know the values of k_1 and k_2, the reaction kinetics of Eq. 3 can be dealt with quantitatively. If equilibrium is reached in the excited state, analogous to the case in the ground state, the equilibrium constant for the conjugate acid of the neutral molecule, $\overset{*}{C}{}^+$, is described by $\overset{*}{K}_{C^+}=\overset{*}{a}_N a_{H^+}/\overset{*}{a}_{C^+}$. $\overset{*}{a}_N$ and $\overset{*}{a}_{C^+}$ are the activities of the neutral and protonated molecules in excited states, and a_{H^+} is the activity of a hydrogen ion. By using the difinition of the acidity function,[4] $H_0=-\log(a_{H^+}\overset{*}{f}_N/\overset{*}{f}_{C^+})$, where $\overset{*}{f}_N$ and $\overset{*}{f}_{C^+}$ are the activity coefficients of $\overset{*}{N}$ and $\overset{*}{C}{}^+$, and by assuming the relation, $k_1[\overset{*}{N}][H^+]=k_2[\overset{*}{C}{}^+]$, the following relation is obtainable for the $p\overset{*}{K}$ value:

$$p\overset{*}{K}_{C^+}=-\log\overset{*}{K}_{C^+}=-\log\frac{k_2}{k_1[H^+]}+H_0. \tag{23}$$

With the aid of Eq. 23, the $p\overset{*}{K}_{C^+}$ values were determined to be -0.10 for **1** and 0.06 for **2**, respectively.

Table 4. Comparison between the Collisional Quenching-Rate Constants and the Static Quenching Constants under Various Conditions

Substance	Quencher-Species	Condition	$k_q \times 10^{-9}$ / $mol^{-1}\,dm^3\,s^{-1}$	V / $mol^{-1}\,dm^3$
1	I^-–$\overset{*}{N}$	Neutral	10.2	1.6_2
	Br^-–$\overset{*}{N}$	Neutral	4.3_0	0.0_8
	Cl^-–$\overset{*}{C}^+$	$HClO_4$+HCl, 0.5M[a)]	5.8_0	1.2
	Cl^-–$\overset{*}{C}^+$	$HClO_4$, 6M	1.3_9	0
2	I^-–$\overset{*}{N}$	Neutral	9.6_5	1.8_1
	Br^-–$\overset{*}{N}$	Neutral	3.7_6	0.0_4
	Cl^-–$\overset{*}{C}^+$	$HClO_4$–HCl, 0.5M	3.6_5	1.7
	Cl^-–$\overset{*}{C}^+$	$HClO_4$, 6M	0.87_7	0

a) 1 M=1 mol dm^{-3}.

This shows that the forward and backward reactions described by Eq. 3 become competitive when the acidity function of a solution is in the proximity of zero.

Efficiency of the Collisional Quenching Process and Static Quenching Constant. The rate constant for the generation of the encounter complex, $(C^+Q)^*$, in Eq. 4 can be roughly estimated by the relation, $k_1' \approx 4\pi N' RD$. Here, R is the encounter distance between the reactants and D is the sum of the individual diffusion coefficients of the reactants.[11,12] If the values of R and D are reasonably assigned as 7 Å and 1.5×10^{-5} $cm^2\,s^{-1}$ (based on molecular and ionic volumes and the Stokes-Einstein relation[7]), the diffusion-limited value of the quenching-rate constant, k_1', is estimated to be about 8×10^9 $mol^{-1}\,dm^3\,s^{-1}$. The apparent rate constants for the collisional quenching, k_q, under various conditions are given in Table 4, together with the static quenching constants, V. k_q and k_1' are related by Eq. 14 and different by a factor, γ, representing the efficiency of the collisional quenching process.

Since k_q with $\overset{*}{N}$ quenched by iodide ions are comparable or slightly greater than 8×10^9 $mol^{-1}\,dm^3\,s^{-1}$, the efficiency of collisional quenching is supposed to be nearly unity, as has been concluded in previous work.[1] Such an effective collisional quenching has been attributed to a charge-transfer interaction between $\overset{*}{N}$ and I^- since the lower ionization energy of I^- (compared to other halide ions) increases the probability of a transfer of an electron from I^- to $\overset{*}{N}$.[13,14] However, the external heavy-atom effect through a spin-orbit coupling in the encounter complex between $\overset{*}{N}$ and I^- might also play a role in the collisional quenching process.[15] From the static quenching constant, V, for an interaction between $\overset{*}{N}$ and I^-, the radius of the sphere-of-action was calculated to be 8—9 Å. This is slightly larger than the value (6—7 Å) estimated as the sum of the radii of the coumarin and an iodide ion. Excited molecules generated very near to or in contact with iodide ions are subjected to an instantaneous deactivation toward the ground state due to the very strong interaction among the reactants.

When Br^- is used as a quencher, the efficiency of the collisional quenching process in a neutral solution becomes lower and, consequently, k_q decreases. This phenomenon is attributable to an increased ionization energy of Br^-, compared with I^-. This leads to a decrease in the strength of the charge-transfer interaction. Of course, a decrease in the heavy-atom effect of bromide ions might explain a part of this phenomenon. In parallel with this tendency, the static quenching constant, V in Table 4, decreases drastically and the encounter distance, R, for the collisional process is effectively shortened to γR. Thus, the radius of the sphere-of-action, being a measure of the interaction strength, is also considered to be shortened by the same order of magnitude as represented by the small value of V. Incidentally, Cl^- has no effect on fluorescence quenching for an excited neutral molecule, $\overset{*}{N}$, over the examined range of the quencher concentration.

In addition to the above-mentioned usual type of fluorescence quenching, we have recently found that $\overset{*}{C}^+$ is also quenched, even by the chloride ions in a moderately acidic solution, where $[H^+]=0.5$ mol dm^{-3}, while $\overset{*}{N}$ does not suffer quenching to any extent; k_q becomes $3.7—5.8\times10^9$ $mol^{-1}\,dm^3\,s^{-1}$, comparable in magnitude to the value for Br^- in a neutral solution. Since the heavy-atom effect of chloride ions is negligibly small compared to that from iodide and bromide ions, the occurrence of such intermediate quenching of $\overset{*}{C}^+$ by Cl^- (examined here) can be attributed to the existence of an attractive coulomb interaction between the reactants. Since $\overset{*}{N}$ does not have any charge on it, the interaction between $\overset{*}{N}$ and halide ions will be a contact interaction (a hard-core type interaction) in nature. Interactions between $\overset{*}{C}^+$ and Cl^-, on the other hand, are based on a long-ranged coulomb force, as long as the ionic concentration is low. However, the high concentration of dissolved ions tends to screen the interaction force. This attractive coulomb interaction will increase the probability of an electron being transferred from Cl^- to $\overset{*}{C}^+$ in the encounter complex, and, consequently, deactivating the complex to C^+ and Cl^- (Eq. 4). k_q is less than 8×10^9 $mol^{-1}\,dm^3\,s^{-1}$. One reason for

this may be that the efficiency of the collisional-quenching process becomes less than unity; then, every encounter event with Cl^- does not lead to a nonradiative decay of the excited protonated molecule. The other one is that k_i' may be affected by the ionic concentration, Γ, the effect of which would not be negligible under the experimental conditions. It is well known that the rate constant of a chemical reaction between particles with opposite charges becomes smaller if the ionic concentration of the solution would increase.[16] It has been very difficult to decide from only the data obtained here which factor for the collisional quenching process is essential to cause a smaller k_q value compared with the diffusion-limited value.

The static quenching constants, V (Table 4), for the quenching of $\overset{*}{C}^+$ by Cl^- in a moderately acidic solution is close to that for the quenching of $\overset{*}{N}$ by I^- in a neutral solution. The accuracy of V is not as high as that of k_q because of the approximation used here. However, it is sufficient for a qualitative discussion of the static quenching process. The estimated radius of the sphere-of-action for static quenching by Cl^- is 8—9 Å. This is, again, slightly larger than 6—7 Å that was estimated as the sum of the radii of the coumarin and a chloride ion. It may be considered strange that the interaction between $\overset{*}{N}$ and Br^- and the interaction between $\overset{*}{C}^+$ and Cl^- have similar k_q values but very different V values. The interaction between $\overset{*}{C}^+$ and Cl^- originates from an attractive coulomb force and extends rather widely over the solvent media; that between $\overset{*}{N}$ and Br^- is a contact interaction. This situation determines the great difference in V for the two cases.

Moreover, solvation effects and ion-pair generation[17] are considered to be important in a static-quenching event. The drastic decrease in V from I^- to Br^- (mentioned above) might be partly due to the strength of solvation ordering: $I^- < Br^- < Cl^-$. The solvation by water molecules will intervenes with the contact interaction and the static quenching of Br^- decreases in consequence. This point could not be checked for Cl^- since it shows no sign of a quenching effect in a neutral solution. Ion-pair generation is expected in the case of an interaction between $\overset{*}{C}^+$ and Cl^- if the both ionic species reside accidentally very near each other at the time the excited state of the protonated molecule is generated. There are, in general, two types of ion-pairs: the solvent-separated ion-pair and the contact-type ion-pair. The former is so loosely coupled that the electronic character of the species is almost the same as that of free ions. Considering the unchanged shape of the fluorescence spectrum of $\overset{*}{C}^+$ for a high concentration of Cl^- and the estimated sphere-of-action value, a solvent-separated ion-pair may be formed. This leads to the occurrence of an effective static quenching. In conclusion, static quenching may be effectively initiated in an atmosphere where reactants are caged by surrounding solvated water molecules. Ion-pair formation will strongly increase the probability of a deactivation of excited molecules.

Effect of the Ionic Concentration on the Rate Constant. When the ionic concentration, Γ, is 1 mol dm^{-3}, the Debye's screening length[8] is 4.3 Å. This is comparable to the mean radius of a molecule. The coulomb force between $\overset{*}{C}^+$ and Cl^-, being extended over the molecular dimension, is effective for static quenching. In the case of a solution with 6 mol dm^{-3} $HClO_4$ added, the Γ is almost determined by the amount of $HClO_4$ and $\Gamma \approx 12$ mol dm^{-3}. In this case, Debye's screening length becomes 1.2 Å and the electrostatic attraction is strongly screened by the ionic atomosphere. Thus, the interaction is limited to a region near the surface of the ionic species and the static quenching constant, V, becomes effectively zero, being inferred by the fact that the usual Stern-Volmer relation is apllicable to a plot of I_0/I vs. $[Cl^-]$.

As can be seen from Table 4, k_q for an interaction between $\overset{*}{C}^+$ and Cl^- in a solution of $[H^+]=0.5$ mol dm^{-3} is about four times larger than for a solution with an added 6 mol dm^{-3} $HClO_4$. As mentioned earlier, the reaction rate between particles with opposite charges becomes smaller if the ionic concentration is increased. Because of the very high value of the ionic concentration, the Debye-Hückel theory does not hold in its fundamental form, while the tendency of the change in the rate constant in ionic solutions is qualitatively correct from the point of view of a more detailed analysis.[16] The qenching effect of I^- and Br^- for $\overset{*}{C}^+$ in a solution containing 6 mol dm^{-3} $HClO_4$ was very large and the fluorescence was almost completely quenched in spite of the high ionic concentration. A quantitative experiment could not be performed in these cases.

The author wishes to thank Dr. Hiroyuki Anzai of this laboratory for his helpful advice and stimulating discussions during the course of this work.

References

1) T. Moriya, *Bull. Chem. Soc. Jpn.*, **57**, 1723 (1984).
2) T. Moriya and H. Anzai, *Bull. Electrotech. Lab.*, **46**, 431 (1982).
3) T. Moriya, *Bull. Electrotech. Lab.*, **47**, 81 (1983).
4) M. A. Paul and F. A. Long, *Chem. Rev.*, **57**, 1 (1957).
5) C. Lewis, W. R. Ware, L. J. Doemeny, and T. L. Nemzek, *Rev. Sci. Instrum.*, **44**, 107 (1973).
6) T. Moriya, *Bull. Chem. Soc. Jpn.*, **56**, 6 (1983).
7) A. H. Alwattar, M. D. Lumb, and J. B. Birks, "Organic Molecular Photophysics," ed by J. B. Birks, Wiley, New York (1973), Vol. 1, p. 403.
8) H. S. Harned and B. B. Owen, "The Physical Chemistry of Electrolytic Solutions," Reinhold, New York (1957).
9) J. M. Frank and S. J. Vavilov, *Z. Phys.*, **69**, 100 (1931).

10) M. R. Eftink and C. A. Ghiron, *J. Phys. Chem.*, **80**, 486 (1976).
11) A. Weller, *Z. Phys. Chem. N. F.*, **13**, 335 (1957).
12) W. R. Ware and J. S. Novros, *J. Phys. Chem.*, **70**, 3246 (1966).
13) A. R. Watkins, *J. Phys. Chem.*, **78**, 2555 (1974).
14) R. Beer, K. M. C. Davis, and R. Hodgson, *J. Chem. Soc., Chem. Commun.*, **1970**, 840.
15) M. Kasha, *J. Chem. Phys.*, **20**, 71 (1952).
16) S. Glasstone, K. J. Laidler, and H. Eyring, "The Theory of Rate Process," McGraw-Hill, New York and London (1941).
17) L. P. Hammett, "Physical Organic Chemistry," 2nd ed., McGraw-Hill, New York and London (1970).
18) G. J. Yakatan, R. J. Juneau, and S. G. Schulman, *Anal. Chem.*, **44**, 1044 (1972).
19) A. Dienes, C. V. Shank, and R. L. Kohn, *IEEE J. Quantum Electron.*, **QE-9**, 833 (1973).

The Solvent-Mode Effect on the Resonance Raman Excitation Profiles of Lycopene

Mineo SAITO and Yasushi MIKAMI*
Department of Chemistry, Faculty of Science, Tohoku University, Sendai 980
(Received August 6, 1985)

The solvent-induced broadening mechanisms are considered in the calculation of resonance Raman excitation profiles (RREP) for the ν_1 and ν_2 vibrational modes of lycopene. The broadening mechanisms are classified into two groups: Inhomogeneous broadening due to a distribution of the 0-0 transition energies and solvent-induced homogeneous broadening due to coupling with low-frequency solvent-solute interactions. The conventional sum-over-states formula for RREP is transformed to a formally equivalent expression in the time domain. The results show that the homogeneous broadening dominates the RREP of lycopene.

Recently, Cotting et al.[1] have analyzed the Raman lines of lycopene by using a model including both homogeneous and inhomogeneous broadening mechanisms as well as the multi-mode theory. They have assumed that each broadening is characterized by a Lorentzian distribution with a line width, either Γ (homogeneous) or Γ_{inh} (inhomogeneous). They have calculated the resonance Raman excitation profiles (RREP) for the ν_1, ν_2, and ν_3 Raman lines using various values of Γ and Γ_{inh}, holding the total width Γ_{tot} ($=\Gamma+\Gamma_{\text{inh}}$) constant at a value determined from the absorption spectra. At the values of Γ_{tot} ranging from 450 cm^{-1} to 500 cm^{-1}, with about a 75% (350 cm^{-1}) contribution from Γ, the theoretical excitation profiles are in good agreement with the experimental data measured in ethyl alcohol, toluene, and carbon disulfide solvents. These results are more informative than those calculated by Hokins[2] with only homogeneous broadening. Cotting et al.[1] do not explicitly refer to the origin of homogeneous broadening. However, 350 cm^{-1} seems to be too large for a realistic damping constant.

In this context, it is worthwhile to see how the interpretations of the damping constant in the RREP for β-carotene analogous to lycopene have changed in the last several years. Since Inagaki et al.[3] reported the experimental RREP of β-carotene, their broad band shapes have been questioned by many investigators. In earlier work, the phenomenological damping constant was used in explaining the broadness of the RREP. Siebrand et al.[4] took a value larger than 200 cm^{-1} as a damping constant to reproduce the experimental data. However, Kodama et al.[5] have pointed out that the large value is due not to the damping effect but mainly to the solvent (-solute) low-frequency modes, which are not Raman active. Ho et al.[6] have found the pure damping constant to be of the order of 50 cm^{-1}, considering both the damping and the low-frequency-mode effects. Further, Chan et al.[7] emphasized that low-frequency modes provide a Gaussian type of broadening.

We can expect that the damping constant in lycopene is similar to that of β-carotene. Thus, the low-frequency-mode effect should be included in analyzing the RREP of lycopene. In this article, we will investigate the RREP of lycopene by considering the low-frequency-mode effect as well as the homogeneous broadening with a rather small damping constant. Inhomogeneous broadening is also taken into account. This broadening is static in nature, reflecting the spread in molecular transition frequencies. Thus, the statistical distribution provides a Gaussian-type broadening, in contrast with the Lorentzian shape taken by Cotting et al.[1]

Theory

In order to analyze the band shapes of the absorption spectra and the RREP of lycopene, we make the following assumptions:

(a) The Condon approximation is used, since the π-π^* transition is strongly allowed.

(b) Only one component of the electronic-transition moments is nonzero.

(c) The displaced harmonic oscillator model is used for both intramolecular modes and solvent (-solute) low-frequency modes.

(d) The Einstein model is assumed for the solvent modes. Thus, these modes are reduced to one collective mode, whose frequency and displacement are given by $\omega_s=N^{-1}\sum\omega_k$ and $\Delta_s^2=N^{-1}\sum\Delta_k^2$ respectively, were N is the total number of the solvent modes and where k refers to an individual solvent mode.

(e) The distribution of 0-0 transition frequencies is responsible for the inhomogeneous broadening and has a Gaussian form, i.e.:

$$\rho_{\text{inh}}(\omega)=(\sqrt{\ln 2})/\sqrt{\pi\Gamma_{\text{inh}}^2}\,\exp\left[-(\omega-\omega_{0'0})^2\ln 2/\Gamma_{\text{inh}}^2\right], \quad (1)$$

where $\omega_{0'0}$ is the mean value of the 0-0 transition frequencies and where Γ_{inh} is the inhomogeneous width.

The band-shape function of the absorption spectra of the system with inhomogeneous broadening is given by:

$$I(\omega_I)=\int d\omega\rho_{\text{inh}}(\omega+\omega_I)I_h(\omega), \quad (2)$$

where ω_I is the frequency of the incident light and where $I_h(\omega)$ is the band-shape function without inhomogeneous broadening. Within the Condon approximation, we can separate $I_h(\omega)$ into the high-frequency part, $I_0(\omega)$, and the low-frequency part, $\rho_{\text{low}}(\omega)$. Thus,

$$I_h(\omega)=|M_{ge}|^2\int d\omega' \rho_{low}(\omega')I_0(\omega'+\omega), \quad (3)$$

where M_{ge} is the electronic transition moment between the ground state (g) and the excited state (e). The high-frequency part, $I_0(\omega)$, represents the contribution from the optical modes which determine the intensity of the vibronic band. We can assume that the thermal excitation of the high-frequency modes can be neglected. Thus, the high-frequency part, $I_0(\omega)$, is given by:

$$\begin{aligned} I_0(\Omega) &= \frac{1}{\pi}\mathrm{Re}\sum_{v_1'=0}^{\infty}\cdots\sum_{v_n'=0}^{\infty}\prod_{j=1}^{n}|\langle 0|v_j'\rangle|^2\int_0^{\infty}dt\exp \\ &\quad [i(\Omega+\sum_{j=1}^{n}v_j'\omega_j)t-\Gamma t] \\ &= \frac{1}{\pi}\mathrm{Re}\int_0^{\infty}dt\prod_{j=1}^{n}\exp\left(-\frac{\Delta_j^2}{2}(1-e^{i\omega_j t})\right)\exp(i\Omega t-\Gamma t), \end{aligned} \quad (4)$$

where ω_j and v_j' are the vibrational frequency and the vibrational quantum number of the j-th mode in the excited state, and where Γ is the damping constant whose depenence on a vibrational level is neglected. The low-frequency part, $\rho_{low}(\omega')$, forms the band-shape function for the optical modes and is given by:

$$\rho_{low}(\omega')=\sum_{v_s=0}^{\infty}\sum_{v_s'=0}^{\infty}P_{v_s}|\langle v_s|v_s'\rangle|^2(v_s\omega_s-v_s'\omega_s-\omega') \quad (5)$$

where ω_s is a common vibrational frequency in the ground state and the excited state and where P_{v_s} the Boltzmann-distribution function of the v_s-th vibrational level in the ground state. $\rho_{low}(\omega')$ is also given by the following time integration:

$$\begin{aligned} \rho_{low}(\omega') &= \frac{1}{2\pi}\int_{-\infty}^{\infty}dt\exp\left(\frac{1}{2}\Delta_s^2(\langle n_s\rangle+1)e^{i\omega_s t}\right. \\ &\quad \left.+\frac{1}{2}\Delta_s^2\langle n_s\rangle e^{-i\omega_s t}-\frac{1}{2}\Delta_s^2(2\langle n_s\rangle+1)-i\omega' t\right) \end{aligned} \quad (6)$$

where $\langle n_s\rangle=(e^{h\omega_S/kT}-1)^{-1}$ is the thermal-average quantum number. We are concerned with the strong coupling case, i.e., $(1/2)\Delta_s^2(2\langle n_s\rangle+1)\gg 1$, in which the short time approximation used by Chan et al.[7] is valid. Thus, we can approximate $\rho_{low}(\omega')$ in this form:

$$\begin{aligned} \rho_{low}(\omega') &= \frac{1}{2\pi}\int_{-\infty}^{\infty}dt\exp\left(-it\left(-\frac{1}{2}\Delta_s^2\omega_s+\omega'\right)\right. \\ &\quad \left.-\frac{1}{4}\Delta_s^2(2\langle n_s\rangle+1)\omega_s^2 t^2\right) \\ &= (\sqrt{\ln 2}/\sqrt{\pi\Gamma_{low}^2})\exp[-(\omega'-\omega_{low})^2\ln 2/\Gamma_{low}^2], \end{aligned} \quad (7)$$

where $\omega_{low}=(1/2)\Delta_s^2\omega_s$ and where

$$\Gamma_{low}=\sqrt{\ln 2}\Delta_s\omega_s(2\langle n_s\rangle+1)^{1/2}. \quad (8)$$

Equation 7 indicates that the low-frequency mode induces a homogeneous broadening with a Gaussian shape with the width Γ_{low} and that the bodies of the absorption spectra are blue-shifted by ω_{low}. We call this broadening a "solvent-induced broadening."

By inserting Eq. 3 into Eq. 1, we obtain:

$$I(\omega_I)=|M_{ge}|^2\int d\omega\int d\omega'\rho_{inh}(\omega+\omega_I)\rho_{low}(\omega')I_0(\omega+\omega'). \quad (9)$$

Since both $\rho_{inh}(\omega+\omega_I)$, and $\rho_{low}(\omega')$ are Gaussian functions, their convolution is given by a Gaussian function:

$$I(\omega_I)=|M_{ge}|^2\int d\omega_a\rho_{tot}(\omega_a+\omega_I)I_0(\omega_a), \quad (10)$$

where:

$$\rho_{tot}(\Omega)=(\sqrt{\ln 2}/\sqrt{\pi\Gamma_{tot}^2})\exp[-(\Omega-\omega_{0'0}-\omega_{low})^2\ln 2/\Gamma_{tot}^2]$$

with $\Gamma_{tot}=\sqrt{\Gamma_{inh}^2+\Gamma_{low}^2}$. Only the total width, Γ_{tot}, can be obtained from the band shapes of the absorption spectra, so we cannot distinguish between inhomogeneous and solvent-induced homogeneous broadening. On the other hand, each broadening mechanism has a different influence on the band shapes of the RREP, as will be shown below.

The resonance Raman intensity of a fundamental line is given by:

$$S(\omega_I)\propto\omega_p^3\omega_I\int d\omega_a\rho_{inh}(\omega_a+\omega_I)\sum_{v_s=0}^{\infty}P_{v_s}|\alpha_{v_s}(\omega_a)|^2, \quad (11)$$

where ω_p is the frequency of the scattered light and where $\alpha_{v_s}(\omega_a)$ is the Raman tensor:

$$\begin{aligned} \alpha_{v_s}(\omega_a) &= -i(M_{ge})^2\sum_{v_1'=0}^{\infty}\cdots\sum_{v_1'=0}^{\infty}\int_0^{\infty}dt\langle 0|v_1'\rangle\langle v_1'|1\rangle e^{iv_1'\omega_1 t} \\ &\quad \times\prod_{j=2}^{n}|\langle 0|v_j\rangle|^2 e^{iv_j'\omega_j t}|\langle v_s|v_s'\rangle|^2 e^{i(v_s'-v_s)\omega_s t}e^{i\omega_a t-\Gamma t}. \end{aligned} \quad (12)$$

We can convert Eq. 12 into the analytic form, using the following relations:

$$\langle 0|v_j'\rangle\langle v_j'|1\rangle=\frac{\Delta_1}{\sqrt{2}}(1-e^{i\omega_1 t})\exp\left[-\frac{\Delta_1^2}{2}(1-e^{i\omega_1 t})\right], \quad (13)$$

$$|\langle 0|v_j'\rangle|^2 e^{iv_j'\omega_j t}=\exp\left[-\frac{\Delta_1^2}{2}(1-e^{i\omega_j t})\right] \quad (14)$$

and:

$$\begin{aligned} |\langle v_s|v_s'\rangle|^2 e^{i(v_s'-v_s)\omega_s t} &= \exp\left[-\frac{\Delta_s^2}{2}(1-e^{i\omega_s t})\right] \\ &\quad \times\sum_{p=0}^{v_s}\frac{v_s!\,e^{i(p-v_s)\omega_s t}}{p![(v_s-p)!]^2}\left(\frac{\Delta_s}{\sqrt{2}}(1-e^{i\omega_s t}-1)\right)^{2(v_s-p)}, \end{aligned} \quad (15)$$

where Δ_α (α=1, j, s) is the displacement of the α-th mode.

The lower-frequency part, Eq. 15, in Eq. 12 cannot be separated from the others, as in the case of absorption spectra, because the Boltzmann distribution factor, P_{v_s}, operates after $\alpha_{v_s}(\omega)$ is squared. The solvent-induced line-width, Γ_{low}, is related to the displacement, Δ_s, and the frequency, ω_s, of the low-frequency mode through Eq. 8. Thus, the solvent-induced line-broadening indirectly affects the RREP, though Γ_{low} does not explicitly appear in the formula. Fur-

ther, the RREP calculation clearly differentiates between the inhomogeneous broadening and the homogeneous broadening effects.

The time integrations in Eq. 4 and Eq. 12 can now be evaluated by the use of the time-dependent method proposed by Tannor and Heller.[9] In this article, the actual numerical integration is performed with the normalizing frequency, which has already been used in the calculation of radiationless transition rates in large molecules.[10,11] We now introduce the normalizing frequency, ω_N, which defines the integers:

$$\tilde{\omega}_j = \omega_j/\omega_N \text{ and } \tilde{\omega}_a = \omega_a/\omega_N.$$

Furthermore, the following quantities are defined:

$$\gamma = \Gamma/\omega_N \text{ and } x = \omega_N t.$$

Thus, we can write $I_0(\omega_a)$ in Eq. 9 as follows (see Eq. 4):

$$I_0(\omega_a) = \frac{1}{\pi\omega_N}\mathrm{Re}\sum_{v_1'=0}^{\infty}\cdots\sum_{v_n'=0}^{\infty}\prod_{j=1}^{n}|\langle 0|v_j'\rangle|^2 \times\int_0^{\infty}dx\exp(i\tilde{\omega}_a x+\sum_{j=1}^{n}iv_j'\tilde{\omega}_j x-\gamma x) \quad (16)$$

The time-integration in Eq. 16 leads to:

$$\int_0^{\infty}dx\exp(i\tilde{\omega}_a x+\sum_{j=1}^{n}iv_j'\tilde{\omega}_j x-\gamma x)=\frac{i}{\tilde{\omega}_a+\sum_{j=1}^{n}v_j'\tilde{\omega}_j+i\gamma} \quad (17)$$

On the other hand, we can easily obtain this relation:

$$\int_0^{2\pi}dx\exp\left(i\tilde{\omega}_a x+\sum_{j=1}^{n}v_j'\tilde{\omega}_j x-\gamma x\right)=\frac{i(1-e^{-2\pi\gamma})}{\tilde{\omega}_a+\sum_{j=1}^{n}v_j'\tilde{\omega}_j+i\gamma}. \quad (18)$$

because ω_j and ω_a are integers. Thus, we obtain:

$$I_0(\omega_a)=\frac{1}{\pi\omega_N(1-e^{-2\pi\gamma})}\sum_{v_1'=0}^{\infty}\cdots\sum_{v_n'=0}^{\infty}\prod_{j=1}^{n}|\langle 0|v_j\rangle|^2 \times\int_0^{2\pi}dx\exp(i\tilde{\omega}_a x+\sum_{j=1}^{n}iv_j'\omega_j x-\gamma x) =\frac{1}{\pi\omega_N(1-e^{-2\pi\gamma})}\int_0^{2\pi}dx\prod_{j=1}^{n}\exp\left[-\frac{\Delta_j^2}{2}(1-e^{i\tilde{\omega}_j x})\right]e^{i\tilde{\omega}_a x-\gamma x}. \quad (19)$$

Furthermore, we can replace the integration over the frequency in Eq. 10 by the following sum:

$$I(\omega_I)=\sum_{m=-\infty}^{\infty}\int_{m\omega_N}^{(m+1)\omega_N}d\omega_a\rho_{tot}(\omega_a+\omega_I)I_0(\omega_a) =\omega_N\sum_{m=-\infty}^{\infty}\rho_{tot}(m\omega_N+\omega_I)I_0(m\omega_N), \quad (20)$$

where we neglect the variation of the integrand in the $m\omega_N<\omega_a<(m+1)\omega_N$ region. A similar procedure leads to the following expressions for the resonance Raman intensity:

$$\alpha_{v_s}(\omega_a)=\frac{i}{\pi\omega(1-e^{-2\pi\gamma})}\int_0^{2\pi}dx\frac{1}{\sqrt{2}}(1-e^{i\omega_1 x}) \times\exp\left[-\frac{\Delta_1^2}{2}(1-e^{i\omega_1 x})\right] \times\prod_{j=2}^{n}\exp\left[-\frac{\Delta_1^2}{2}(1-e^{i\omega_j x})\right]\exp\left[-\frac{\Delta_s^2}{2}(1-e^{i\omega_s x})\right] \times\sum_{p=0}^{v_s}\frac{v_s!\,e^{i(p-v_s)\omega_s x}}{p![(v-p)!]^2}\left[\frac{\Delta_s^2}{2}(e^{i\omega_s x}-1)\right]^{2(v_s-p)} \quad (21)$$

and:

$$S(\omega_I)\propto\omega_p^3\omega_I\omega_N\sum_{m=-\infty}^{\infty}\rho_{inh}(m\omega_N+\omega_I)\sum_{v_s=0}^{\infty}P_{v_s}|\alpha_{v_s}(m\omega_N)|^2. \quad (22)$$

Results and Discussion

We will now analyze the band-shapes of the absorption spectrum and the RREP of lycopene in toluene solvents. The damping constant, Γ, is assumed to be $50\,cm^{-1}$ according to the case of β-carotene[6]; this corresponds to a picosecond relaxation process and seems to be realistic. This value has only a minor effect on the band-shapes of the absorption spectrum and the RREP, in the presense of inhomogeneous and solvent-induced homogeneous broadening mechanisms due to low-frequency modes.

The frequencies of the three Franck-Condon active modes, ν_1, ν_2, and ν_3, of lycopene are taken to be $\omega_1=1516\,cm^{-1}$, $\omega_2=1154\,cm^{-1}$, and $\omega_3=1005\,cm^{-1}$ respectively. The frequency, ω_s, and the displacement, Δ_s, of the solvent mode are related to the homogeneous line-width, Γ_{low}, through Eq. 8. In the following calculations, we first estimate the homogeneous line-width, Γ_{low}, from the absorption spectra. Thus, we do not need to provide ω_s and Δ_s independently. We prefer to give ω_s. Further, ω_s and Δ_s are somewhat arbitrary because only their combined quantity, i.e., Γ_{low}, is determined. Therefore, we can assume a round value of $50\,cm^{-1}$ as ω_s; this seems to be reasonable for an approximate frequency of the solvent mode. Let us now refer to the normalizing frequency, ω_N. For a given set of ω_j, a large number of ω_N values may give a value identical to those in Eqs. 19 and 21 because of the periodicity of the integrands. It is sufficient, however, to consider only their maximum- the largest common integer divider in the set. The value of ω_N should be, at most, $1\,cm^{-1}$ for our three ω_j values. However, even if some larger ω_N is used, the relative values of $\tilde{\omega}_j$ are not very largely altered, provided that each $\tilde{\omega}_j$ is redefined as the integer nearest to ω_j/ω_N. Therefore, we are allowed to adopt a larger ω_N than the largest common integer divider, disregarding a small rounding error. Thus, we take $25\,cm^{-1}$ as a value of ω_N. This value also satisfies the condition under which we can replace the integration into the sum in Eqs. 20 or 22, because the linewidth of lycopene is very large.

We adopt the same displacements of the three Franck-Condon active modes as those Cotting et al.[1] have used. Thus, we have $\Delta_1=1.1$, $\Delta_2=1.0$, and $\Delta_3=0.5$. Using these values of the displacements and varying the total width, Γ_{tot}, we calculate the absorp-

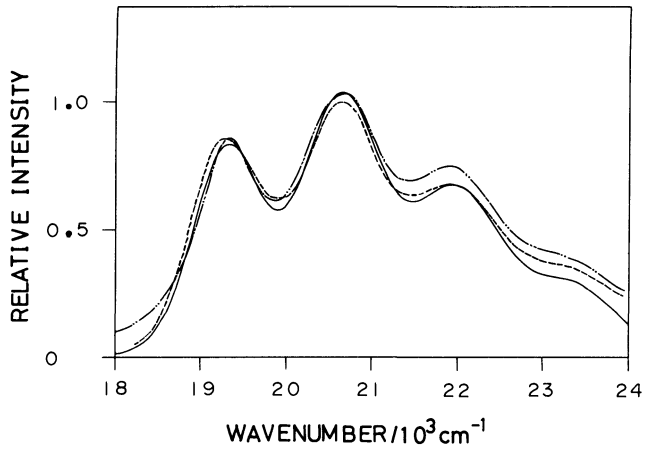

Fig. 1. Optical absorption line shapes for lycopene in toluene at 300 K. The measured absorption line shape (dashed line) is that of Ref. 1. The best fitted theoretical line shape (solid line) was obtained using Γ=50 cm^{-1} and Γ_{tot}=450 cm^{-1}, together with A_1=1.1, A_2=1.0, A_3=0.5 and $\omega_{0'0}+\omega_{low}$=19310 cm^{-1}. The (---) line is the another theoretical line shape with Γ=450 cm^{-1} and Γ_{tot}=0 cm^{-1}.

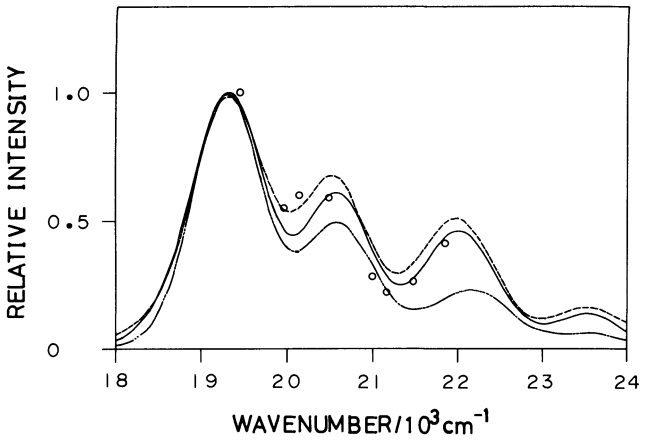

Fig. 2. Resonance Raman excitation profile line shapes of the ν_1 mode for lycopene in toluene at 300 K. The circles give a measured profile line shape of Ref. 1. The three theoretical curves are shown. The solid line is for Γ_{inh}=300 cm^{-1} and Γ_{low}=335 cm^{-1} the dashed line for Γ_{inh}=0 cm^{-1}, and Γ_{low}=450 cm^{-1} and the (---) line for Γ_{inh}=450 cm^{-1} and Γ_{low}=0 cm^{-1}. The other parameters used are the same as those in Fig. 1.

tion spectra and seek the curve best-fitting the experimental value. Figure 1 shows that the best fit is obtained at Γ_{tot}=450 cm^{-1} and $\omega_{0'0}+\omega_{low}$=19310 cm^{-1}. We also stress the good agreement in the lower-frequency region of the 0-0 band; this is in contrast to the result of Cotting et al. The disagreement may be due to a Lorentzian shape of the broadening. This fact is suggested by the following hypothetical calculations. We assume that only a pure damping effect contributes to the absorption band-width. That is to say, we take 450 cm^{-1} as the damping constant, Γ, and reduce Γ_{tot} to zero. The calculated absorbance comes to be higher than the one observed in the tail of the 0-0 band and resembles the result of Cotting et al. These results suggest that the main broadening mechanism is not related to the damping constant, Γ, giving a Lorentzian-type broadening, but to the width of inhomogeneous broadening, Γ_{inh}, and/or the width of the solvent-mode-induced broadening, Γ_{low}, both of which provide a Gaussian-type broadening.

In our model, Γ_{inh} and Γ_{low} cannot be distinguished in the analysis of the absorption spectra. On the other hand, the RREP calculation clearly differentiates between these effects, as has been shown in the previous section. First, we calculate the RREP for the two extreme cases. Figure 2 shows the RREP for the ν_1 vibrational mode of lycopene when only an inhomogeneous broadening exists and another extreme case in which only a homogeneous broadening mechanism is operative. The agreement between the theory and the experiment is better for the full homogeneous case than for the full inhomogeneous one. This fact suggests that the presence of low-frequency modes essentially determine the observed features of the RREP, in the case of the realistic damping constant, Γ, of 50 cm^{-1}. Further, a fairly large value (300 cm^{-1}) of inhomogeneous broadening Γ_{inh} only partly improves the RREP. This is intimately related to the Gaussian shape of homogeneous and inhomogeneous broadening. The total line-width for our Gaussian broadening is the same as that Cotting et al.[1] obtained by using the Lorentzian broadening mechanism. In the Lorentzian case, the total line-width, Γ_{tot}, is a sum of the inhomogeneous broadening, Γ_{inh}, and a damping constant, Γ. Since Γ_{tot} is determined to be constant from the absorption spectra, a large value of Γ_{inh} considerably reduces Γ. Cotting et al.[1] have already suggested that values of Γ_{inh} larger than 300 cm^{-1} may cause the major effect in the RREP. In our Gaussian case, however, the total line-width, Γ_{tot}, equals $\sqrt{\Gamma_{inh}^2+\Gamma_{low}^2}$. This relation leads to a still larger Γ_{low} (335 cm^{-1}), even at the large Γ_{inh} (300 cm^{-1}). The features of the RREP calculated with this Γ_{low} are similar to that of the full homogeneous case (Γ_{low}=450 cm^{-1}). In the presence of a large homogeneous broadening, an inhomogeneous broadening itself may little affect the RREP. A similar tendency is also shown for the ν_2 vibrational mode, as we can see in Fig. 3.

In conclusion, a reasonable damping constant, which is also similar to that of β-carotene, can be assumed for the case of lycopene if we take into account the solvent-induced broadening mechanisms. The full inhomogeneous broadening mechanism provides a rather large discrepancy between theory and experiment for the RREP. The experimental data are roughly consistent with the full homogeneous broadening mechanism. The effect of inhomogeneous

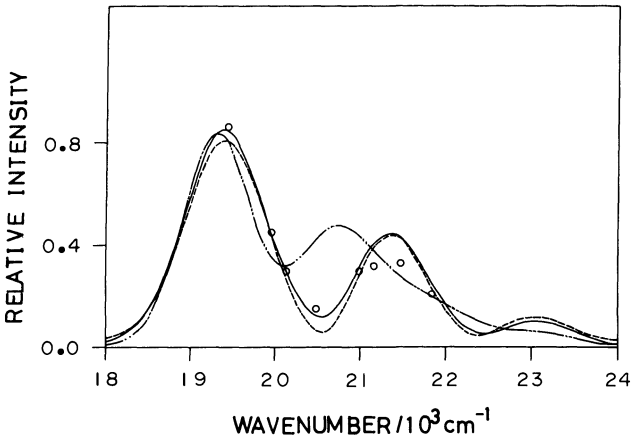

Fig. 3. Resonance Raman excitation profile line shapes of the ν_2 mode for lycopene in toluene at 300 K. The circles give a measured profile line shape of Ref. 1. The three theoretical curves are shown: The solid line is for $\Gamma_{inh}=300\,cm^{-1}$ and $\Gamma_{low}=335\,cm^{-1}$, the dashed line for $\Gamma_{inh}=0\,cm^{-1}$, and $\Gamma_{low}=450\,cm^{-1}$, and the (---) line for $\Gamma_{inh}=450\,cm^{-1}$ and $\Gamma_{low}=0\,cm^{-1}$. The other parameters used are the same as those in Fig. 1.

broadening partly improve the results, though the RREP values for the ν_1 and ν_2 vibrational modes of lycopene are insensitive to the large variation in Γ_{inh}.

The authors would like to thank Professor Takeshi Nakajima for his guidance and encouragement.

References

1) J. E. Cotting, L. C. Hoskins, and M. E. Levan, *J. Chem. Phys.*, **77**, 1081 (1982).
2) L. C. Hoskins, *J. Chem. Phys.*, **74**, 882 (1981).
3) F. Inagaki, M. Tasumi, and T. Miyazawa, *J. Mol. Spectrosc.*, **50**, 286 (1974).
4) W. Siebrand and M. Zgierski, *J. Chem. Phys.*, **71**, 3561 (1979).
5) K. Kodama and A. D. Bandrauk, *Chem. Phys. Lett.*, **80**, 248 (1981).
6) Z. Z. Ho, R. C. Hanson, and S. H. Lin, *J. Chem. Phys.*, **77**, 3414 (1982).
7) C. K. Chan and J. B. Page, *J. Chem. Phys.*, **79**, 5234 (1983).
8) Y. Toyozawa, "Dynamical Processes in Solid State Optics," R. Kubo and H. Kamimura, Benjamin, New York (1967), p. 90.
9) D. J. Tannor and E. J. Heller, *J. Chem. Phys.*, **77**, 202 (1982).
10) A. Nitzan and J. Jortner, *Theor. Chim. Acta*, **30**, 217 (1973).
11) Y. Mikami, *J. Chem. Phys.*, **73**, 3314 (1980).

 © 1986 The Chemical Society of Japan Bull. Chem. Soc. Jpn., 59, 975—980 (1986)

The Independent Electrochemical Detection of H_2O_2 and O_2 in Aqueous Alkaline Solutions on an Alkylsilanized Gold Electrode

Masamichi FUJIHIRA,* Hiroji MURAKI, and Shigeru AOYAGUI
Department of Chemical Engineering, Tokyo Institute of Technology, Ohokayama, Meguro-ku, Tokyo 152
(Received August 27, 1985)

The cyclic voltammetric studies of H_2O_2 and O_2 in aqueous alkaline solutions were carried out on stationary gold electrodes unmodified and modified chemically with dodecyltriethoxysilane. Although two cathodic waves were observed for both H_2O_2 and O_2 on the unmodified electrode, only the second wave was observed for H_2O_2 on the modified electrode. Since the first cathodic wave of H_2O_2 overlaps that of O_2 on the unmodified electrode, the disappearance of the first wave of H_2O_2 makes it possible to distinguish O_2 from H_2O_2 on the modified electrode. The effect of alkylsilanization on the diminution and evolution of H_2O_2 or O_2 on gold electrodes was also confirmed by employing rotating ring-disk gold electrodes unmodified and modified similarly with dodecyltriethoxysilane. Furthermore, the reduction mechanism of H_2O_2 and the application of the independent electrochemical detection of H_2O_2 and O_2 are discussed.

In the last decade, the chemical modification of electrode surfaces has been intensively investigated as a means of making various functional electrodes.[1] In relation to the electrocatalysis of the modified electrodes for fuel cells, most researchers have been involved in the pursuit of a novel molecular design to accelerate electrochemical reactions.[2-4] However, for analytical purposes or mechanistic studies, we very often require the suppression of some undesirable electrode reactions to avoid the overlapping of a wave of interest with these unwanted ones. In the present paper, we demonstrate a novel electrode with a chemically modified surface for the independent detection of H_2O_2 and O_2 in aqueous alkaline solutions.

The analysis of H_2O_2 and O_2 in solutions is of great importance in the studies of fuel cells,[5-13] photocatalytic water splitting,[14-18] bioelectrochemistry,[19,20] etc. It has been difficult so far, however, to detect H_2O_2 and O_2 independently in their mixed system by electrochemical methods or by the conventional methods employed in the fields mentioned above, such as mass spectrometry and gas chromatography, since the waves of H_2O_2 and O_2 overlap each other on the electrodes and H_2O_2 is easily decomposed into O_2 and H_2O in the mass spectrometric and chromatographic apparatuses. The experimental findings described in the present paper show that the surface catalytic reduction of H_2O_2 on a polycrystalline gold electrode in aqueous alkaline solutions can be greatly suppressed by the chemical modification of the electrode surface with dodecyltriethoxysilane, while neither the reduction of O_2 nor the oxidation of H_2O_2 is affected appreciably. Namely, it is possible to detect H_2O_2 and O_2 on the electrode at different potentials without the overlapping of their waves. Recently we succeeded in finding evidence for the photolytic formation of H_2O_2 in TiO_2[21] and in $[Ru(bpy)_3]^{2+}$-modified TiO_2 aqueous suspensions by applying the present method. The present paper will describe the basis of the method in detail. The reduction mechanism of H_2O_2 will also be discussed on the basis of the new insight given by such a chemical modification.

Experimental

A gold plate and a gold ring-disk electrode were chemically modified with dodecyltriethoxysilane.[22] The chemical modification was carried out as follows. An unmodified gold plate, which had been thoroughly washed as has been described previously,[23] was immersed in a 10% silane coupling reagent solution, after which the solution was refluxed for 24 h. The reagent solution was prepared by the addition of dodecyltriethoxysilane to dry toluene. After silanization, the electrode was washed thoroughly with dry toluene. A gold ring-disk electrode was also chemically modified by the same procedure except that the ring-disk electrode was dipped in the coupling reagent solution in a desiccator at room temperature without reflux for 3 d. A gold plate or a chemically modified gold plate was used as a stationary working electrode. Electrochemical measurements with a homemade potentiostat were performed in a glass cell using, in addition, a gold plate and a saturated calomel electrode as a counter electrode and a reference electrode, respectively. Voltammetry with a gold ring-disk electrode or a chemically modified one was carried out with a Nikko Keisoku rotating ring-disk electrode system consisting of an RRDE-1 rotating ring-disk electrode drive with an SC-5 speed controller and a DPGS-1 dual potentiogalvanostat. A deaerated 0.3 mM H_2O_2 or an air-saturated aqueous solution, both containing 10 mM NaOH and 0.1 M KCl, was employed as the sample solution (1 M=1 mol dm^{-3}). All the solutions were prepared with doubly distilled water and G. R. -grade reagents. All the electrochemical measurements were performed at 25 °C.

Results and Discussion

Reduction and Oxidation of H_2O_2 on Unmodified and Chemically Modified Gold Electrodes. Figure 1A shows the cyclic voltammogram of the deaerated H_2O_2 solution on the unmodified gold electrode. On the negative sweep, starting at the rest potential of −0.13 V, two cathodic waves were observed with peak potentials of −0.2 and −0.8 V, respectively. Three mechanistic

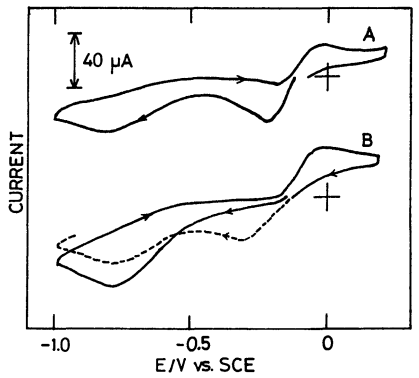

Fig. 1. Cyclic voltammograms of deaerated H_2O_2 aqueous solution on (A) an unmodified Au electrode and (B) a chemically modified Au electrode. NaOH (10 mM); KCl (0.1 M); H_2O_2 (ca. 0.3 mM); N_2 purged; sweep rate (40 mV s^{-1}); electrode area (0.79 cm^2).

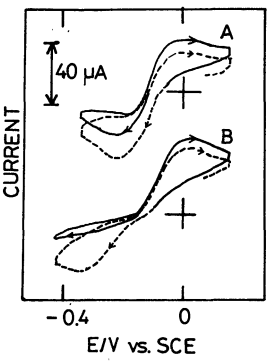

Fig. 2. Cyclic voltammograms of deaerated H_2O_2 aqueous solution on (A) an unmodified Au electrode and (B) a chemically modified Au electrode in the narrower potential range. Experimental conditions are the same as in Fig. 1.

interpretations of the first cathodic wave, with the peak potential of −0.2 V, have been presented. The first one is the surface catalytic reduction of H_2O_2, which proceeds via the adsorption of H_2O_2 on the surface of gold in the form of OH:[6,8]

$$HO_2^- + H_2O \longrightarrow 2OH(ads) + OH^- \quad (1)$$

$$2OH(ads) + 2e^- \longrightarrow 2OH^- \quad (2)$$

The second one is the surface catalytic reduction of H_2O_2, which proceeds via the adsorption of H_2O_2 on the surface in the form of O:[9]

$$HO_2^- \longrightarrow O(ads) + OH^- \quad (3)$$

$$O(ads) + e^- + H_2O \longrightarrow OH(ads) + OH^- \quad (4)$$

$$OH(ads) + e^- \longrightarrow OH^- \quad (5)$$

The third one is the reduction of O_2 generated by the chemical decomposition of H_2O_2 on the surface:[6,10]

$$2HO_2^- \longrightarrow O_2 + 2OH^- \quad (6)$$

$$O_2 + 2e^- + H_2O \longrightarrow HO_2^- + OH^- \quad (7)$$

However, the third mechanism can be ruled out because the peak potential of the first cathodic wave of H_2O_2 reduction is ca. 100 mV more positive than that of the O_2 reduction, as will be shown below. The second wave, with a peak potential of −0.8 V, may be due to the direct reduction of H_2O_2 on the gold surface:

$$HO_2^- + 2e^- + H_2O \longrightarrow 3OH^- \quad (8)$$

On the reverse scan, the cathodic current increased again in the potential region between −0.4 and −0.2 V. This indicates that the reduction shown by the first cathodic wave is limited within the narrow potential region.[6] Following the increase in the cathodic current, an anodic wave started at −0.15 V. This wave can be assigned to the oxidation of H_2O_2:[6,8]

$$HO_2^- + OH^- \longrightarrow O_2 + H_2O + 2e^- \quad (9)$$

Figure 1B shows the cyclic voltammogram of the deaerated H_2O_2 solution on the chemically modified gold electrode. In contrast with the current observed on the unmodified electrode, only one cathodic wave, with a peak potential of ca. −0.8 V, was observed. This wave can be ascribed to the direct reduction of H_2O_2 described above. The pronounced suppression of the first wave on the modified surface may result from the blocking of the catalytic sites which bind H_2O_2 in the form of OH or O. On the reverse scan, an anodic wave with an onset potential of −0.15 V was observed. This indicates that neither the oxidation of H_2O_2 to O_2 nor the direct reduction of H_2O_2 to H_2O is appreciably affected by alkylsilanization. On the second negative scan, a new wave starting at −0.1 V appeared. The peak potential of this new wave was −0.3 V which coincided with the peak potential of the first wave of the O_2 reduction, as will be shown below. This wave, therefore, can reasonably be assigned to the reduction of the O_2 which was generated on the preceding positive sweep.

Figure 2A shows the cyclic voltammogram of the deaerated H_2O_2 solution on the unmodified gold electrode recorded in a narrower potential region than that shown in Fig. 1A. All the waves can be assigned in the same way as those in Fig. 1A.

Figure 2B shows the cyclic voltammogram of the deaerated H_2O_2 solution on the chemically modified gold electrode, also recorded in a narrower potential region than that shown in Fig. 1B. On the first negative sweep, very little current flowed. On the reverse scan, consequently, a higher anodic current for the oxidation of H_2O_2 (Eq. 9) than that in Fig. 2A appeared because the irreversible transformation of H_2O_2 to H_2O was suppressed. On the second negative scan, a cathodic wave with a peak potential of −0.3 V was observed. This peak potential coincided with that of the first wave of O_2 reduction, as will be shown below. On the second

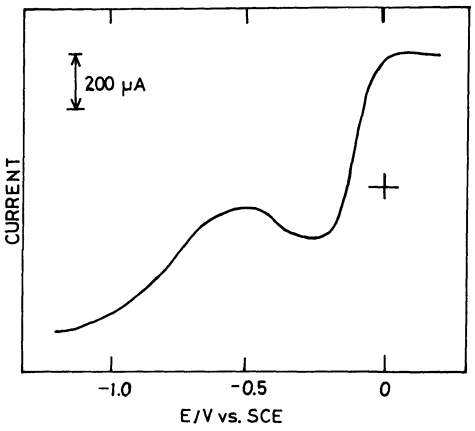

Fig. 3. Voltammetric curve of deaerated H_2O_2 aqueous solution on a rotating unmodified Au disk electrode. Sweep rate (20 mV s^{-1}); rotation speed (3600 rpm). Solution conditions are the same as in Fig. 1.

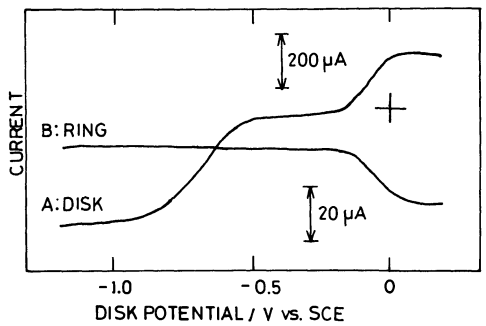

Fig. 4. (A) Current on a rotating chemically modified Au disk electrode and (B) current on a rotating chemically modified Au ring electrode for deaerated H_2O_2 aqueous solution as a function of the disk potential. Sweep rate (20 mV s^{-1}); rotation speed (3600 rpm); ring potential (−0.45 V vs. SCE). Solution conditions are the same as in Fig. 1.

positive sweep, the anodic wave height decreased a little, but the height was still much higher than that in Fig. 2A.

Figure 3 shows the current-potential curve for the deaerated H_2O_2 solution on an unmodified rotating disk electrode. This curve indicates that the oxidation wave height at anodic potentials is equal to the cathodic one at the potentials more negative than −1.0 V. This result is reasonable because both reactions, i.e., oxidation to O_2 and reduction to H_2O, are two-electron processes from H_2O_2. The dependence of these currents on the rotational speed confirmed that both currents are mass-transfer-limited. A maximal value of catalytic current was observed around −0.25 V. This also indicates that the surface catalytic reduction of H_2O_2 is limited within this potential region.

Figure 4A shows the current-potential curve for the deaerated H_2O_2 solution on a chemically modified rotating disk electrode. It is remarkable that the increase in the cathodic current between −0.15 and

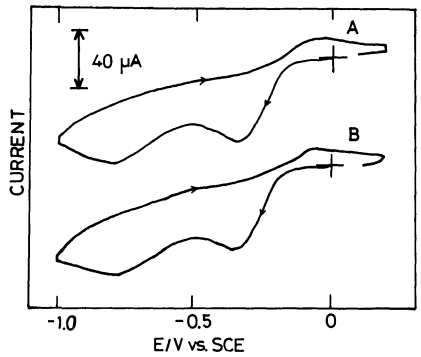

Fig. 5. Cyclic voltammograms of air-saturated aqueous solution on (A) an unmodified Au electrode and (B) a chemically modified Au electrode. Air-saturated. Other experimental conditions are the same as in Fig. 1.

−0.4 V shown in Fig. 3 was completely suppressed and that very little current flowed in the potential region. This suppression of the cathodic current corresponds to that observed on the stationary chemically modified gold electrode shown in Figs. 1B and 2B. The suppresion of the wave indicates that the chemical modification of the surface may block the catalytic sites of the gold surface. It is also seen in Fig. 4A that the magnitude of the H_2O_2 oxidation current at the potentials more positive than 0 V was smaller than that of H_2O_2 reduction current at the potentials more negative than −1.0 V. This may come from the contamination of the gold surface with impurities in the solution, which inhibits the oxidation of H_2O_2 more than the reduction of H_2O_2, since the cleaning of the gold surface by applying a more positive potential than +0.5 V, that was used for the unmodified electrode, had to be avoided for the maintenance of the modified surface.

Reduction of O_2 on Unmodified and Chemically Modified Gold Electrodes. Figure 5A shows the cyclic voltammogram of the air-saturated solution on the unmodified gold electrode. Two cathodic waves, with peak potentials of −0.3 and −0.8 V, respectively, were observed. The first wave corresponds to the reduction of O_2:[6,8-11]

$$O_2 + 2e^- + H_2O \longrightarrow HO_2^- + OH^- \qquad (10)$$

By comparing the results shown in Figs. 1—4 and 5A, we assigned the second wave to the direct reduction of H_2O_2 (Eq. 8) which had been generated by the O_2 reduction at the first cathodic wave (Eq. 10). On the reverse scan, an anodic wave starting at −0.15 V was observed. This was not observed when the sweep started first in the positive direction. The comparison of Figs. 1—4 and 5A also reveals that this anodic wave corresponds to the oxidation of H_2O_2.

Figure 5B shows the cyclic voltammogram of the air-saturated solution on the chemically modified gold electrode. The voltammogram is similar to that

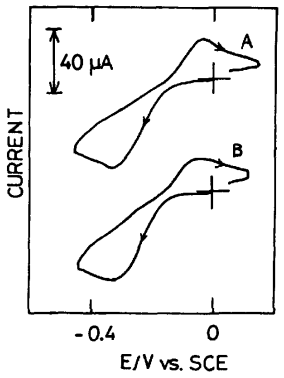

Fig. 6. Cyclic voltammograms of air-saturated aqueous solution on (A) an unmodified Au electrode and (B) a chemically modified Au electrode in the narrower potential range. Experimental conditions are the same as in Fig. 1.

recorded on the unmodified gold electrode shown in Fig. 5A. However, the ratio of the peak current of the first cathodic wave to that of the second cathodic wave, i_{p1}/i_{p2}, was slightly smaller on the chemically modified electrode shown in Fig. 5B than the ratio obtained on the unmodified one shown in Fig. 5A. On the unmodified gold electrode, the H_2O_2 generated by the O_2 reduction in the first cathodic wave (Eq. 10) was partially reduced further to H_2O by the succeeding reactions shown by the first cathodic wave in Fig. 1A (Eqs. 1, 2 or 3—5). On the other hand, since the further reactions were suppressed on the chemically modified electrode, the value of i_{p1}/i_{p2} became smaller than that on the unmodified one.

Figures 6A and 6B show the cyclic voltammograms of the air-saturated solution on the unmodified and chemically modified gold electrodes, respectively, recorded in a narrower potential region than those in Figs. 5A and 5B. The cathodic waves with a peak potential of −0.3 V indicate the reduction of O_2 to H_2O_2. On the reverse scan, the anodic waves with larger peak current than those shown in Figs. 5A and 5B were observed, since the H_2O_2 generated by the O_2 reduction at the cathodic waves (Eq. 10) was not consumed in the succeeding irreversible cathodic reaction, as is shown in Figs. 5A and 5B (Eq. 8). When the sweep started first in the positive direction, though not shown in the figures, these anodic waves were not observed on either electrode.

Figure 7 shows the disk and ring currents as a function of the disk potential for the air-saturated solution on an unmodified rotating gold ring-disk electrode. The ring potential was set at +0.16 V, where the H_2O_2 oxidation had been shown to be diffusion controlled by prior CV measurements. The current-potential curves clearly indicate that O_2 is reduced to H_2O_2 between −0.4 and −0.7 V and that O_2 is further reduced to H_2O under totally mass-transfer-limited conditions at potentials more negative than −1.0 V. A comparison of Figs. 3 and 7

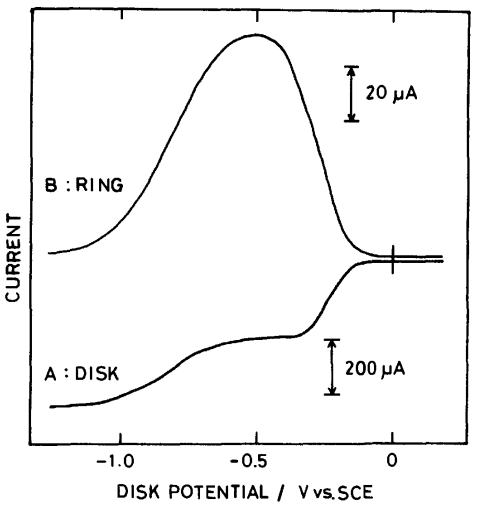

Fig. 7. (A) Current on a rotating unmodified Au disk electrode and (B) current on a rotating unmodified Au ring electrode for air-saturated aqueous solution as a function of the disk potential. Sweep rate (20 mV s^{-1}); rotation speed (3600 rpm); ring potential (0.16 V vs. SCE). Solution conditions are the same as in Fig. 1.

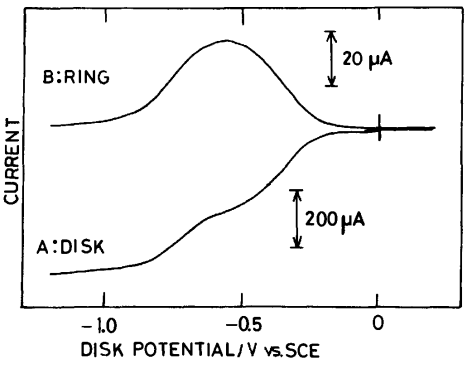

Fig. 8. (A) Current on a rotating chemically modified Au disk electrode and (B) current on a rotating chemically modified Au ring electrode for air-saturated aqueous solution as a function of the disk potential. Sweep rate (20 mV s^{-1}); rotation speed (3600 rpm); ring potential (0.10 V vs. SCE). Solution conditions are the same as in Fig. 1.

clearly shows that the potential where the H_2O_2 reduction starts is more positive than the potential where the O_2 reduction starts. This also supports the above interpretation that the intermediate of the H_2O_2 reduction between −0.2 and −0.4 V is not O_2, but adsorbed OH or O.

Figure 8 shows the disk and ring currents as a function of the disk potential for the air-saturated solution on a rotating electrode whose disk and ring electrodes had both been chemically modified. The ring potential was set at +0.1 V where the ring current reaches a plateau. In a qualitative sense, however, there was no significant difference from the result obtained on an unmodified rotating ring-disk electrode (shown in Fig. 7).

Independent Detection of H_2O_2 and O_2 on the Chemically Modified Gold Electrode. The experimental findings presented above lead to the conclusion that, on an alkylsilanized gold electrode, only oxygen can be reduced at around −0.3 V; therefore, the independent electrochemical detection of H_2O_2 and O_2 in their mixture is possible. More specifically, the concentration of H_2O_2 can be determined by its anodic or cathodic currents, and that of O_2 by its cathodic currents. Frumkin and his co-workers obtained two separate two-electron reduction waves for O_2 and H_2O_2 on an amalgamated gold electrode,[24] just as on mercury.[25] However, the use of amalgamated and other foreign-metal-adatom-modified electrodes[26] in positive potentials is limited by the dissolution of the foreign metals. In addition, the amalgamation is not suitable for modifying an optically transparent gold electrode for photoelectrochemical studies, for the stability of gold films decreases upon the amalgamation.

Figure 4B shows the ring current as a function of the disk potential for the deaerated H_2O_2 solution on a chemically modified rotating ring-disk electrode. The ring potential is set at −0.45 V, where O_2 can, but H_2O_2 cannot be reduced on the chemically modified gold electrode, as has been described above. The abrupt increase in the ring current from the residual current indicates that H_2O_2 is oxidized to O_2 at potentials more positive than −0.15 V. It should be noted that this observation is possible only on the chemically modified electrode, since, on the unmodified one, O_2 and also H_2O_2 are reduced at the potential of −0.45 V. This independent detection of O_2 is one of the most effective applications of the chemically modified electrode. In the experimental procedure of the chemical modification of the ring-disk electrode, however, the coupling solution could not be refluxed to avoid the contamination of the gold surface. The lack of refluxing sometimes causes an incomplete coverage of the electrode surface with the modifying molecules. The residual current observed at the potentials more negative than −0.15 V in Fig. 4B results from such an incompleteness, which permits the partial reduction of H_2O_2.

The present work was partially supported by a Grant-in-Aid for Scientific Research No. 60040051 from the Ministry of Education, Science, and Culture.

References

1) R. W. Murray, "Electroanalytical Chemistry," ed by A. J. Bard, Marcel Dekker, New York (1984), Vol. 13, p. 191.

2) J. P. Collman, M. Marrocco, P. Denisevich, C. Koval, and F. C. Anson, *J. Electroanal. Chem.*, **101**, 117 (1979); J. P. Collman, P. Denisevich, Y. Konai, M. Marrocco, C. Koval, and F. C. Anson, *J. Am. Chem. Soc.*, **102**, 6027 (1980).

3) T. Kuwana, M. Fujihira, K. Sunakawa, and T. Osa, *J. Electroanal. Chem.*, **88**, 299 (1978); N. Kobayashi, M. Fujihira, K. Sunakawa, and T. Osa, *ibid.*, **101**, 269 (1979); N. Kobayashi, T. Matsue, M. Fujihira, and T. Osa, *ibid.*, **103**, 427 (1979).

4) R. Jasinski, *J. Electrochem. Soc.*, **112**, 526 (1965); A. J. Appleby and M. Savy, *Electrochim. Acta*, **21**, 567 (1976); J. Zagal, R. K. Sen, and E. Yeager, *J. Electroanal. Chem.*, **83**, 207 (1977); H. Meier, U. Tschirwitz, E. Zimmerhackl, W. Albrecht, and G. J. Zeitler, *J. Phys. Chem.*, **81**, 712 (1977); B. Z. Nikolic, R. R. Adzic, and E. B. Yeager, *J. Electroanal. Chem.*, **103**, 281 (1979); R. Kotz and E. Yeager, *ibid.*, **113**, 113 (1980).

5) D. J. Shiffrin, "The Electrochemistry of Oxygen," in "Electrochemistry," The Royal Society of Chemistry, London (1980), p. 126.

6) R. R. Adzic, N. M. Markovic, and V. B. Vesovic, *J. Electroanal. Chem.*, **165**, 105 (1984); N. M. Markovic, R. R. Adzic, and V. B. Vesovic, *ibid.*, **165**, 121 (1984).

7) R. R. Adzic and A. R. Depic, *Z. Phys. Chem.*, **1975**, 95; R. R. Adzic, A. V. Tripkovic, and N. M. Markovic, *J. Electroanal. Chem.*, **114**, 37 (1980); M. Alvarez-Rizatti and K. Juttner, *ibid.*, **144**, 351 (1983); G. Kokkinidis and D. Jannakoudakis, *ibid.*, **162**, 163 (1984).

8) R. W. Zurilla, R. K. Sen, and E. Yeager, *J. Electrochem. Soc.*, **125**, 1103 (1978).

9) A. Damjanovic, M. A. Genshaw, and J. O'M. Bockris, *J. Electroanal. Chem.*, **15**, 173 (1967).

10) F. van den Brink, E. Barendrecht, and W. Visscher, *J. Electrochem. Soc.*, **127**, 2003 (1980).

11) H. S. Wroblowa, Y. C. Pan, and G. Razumney, *J. Electroanal. Chem.*, **69**, 195 (1976).

12) P. Fischer and J. Heitbaum, *J. Electroanal. Chem.*, **112**, 231 (1980).

13) A. J. Appleby and M. Savy, *J. Electroanal. Chem.*, **92**, 15 (1978); K.-L. Hsueh and D. -T. Chin, *ibid.*, **153**, 79 (1983).

14) M. S. Wrighton, D. S. Ginley, P. T. Wolczansky, A. B. Ellis, D. L. Morse, and A. Linz, *Proc. Natl. Acad. Sci. U. S. A*, **72**, 1518 (1975); M. S. Wrighton, A. B. Ellis, P. T. Wolczanski, D. L. Morse, H. B. Abrahamson, and D. S. Ginley, *J. Am. Chem. Soc.*, **98**, 2774 (1976).

15) K. Hirano and A. J. Bard, *J. Electrochem. Soc.*, **127**, 1056 (1980); R. I. Bickley and V. Vishwanathan, *Nature*, **280**, 306 (1979); H. V. Damme and W. K. Hall, *J. Am. Chem. Soc.*, **101**, 4373 (1979); P. Salvador and C. Gutierrez, *J. Phys. Chem.*, **88**, 3696 (1984); P. Salvador and F. Decker, *ibid.*, **88**, 6116 (1984).

16) C. Creutz and N. Sutin, *Proc. Natl. Acad. Sci. U. S. A*, **72**, 2858 (1975); P. K. Ghosh, B. S. Brunschwig, M. Chou, C. Creutz, and N. Sutin, *J. Am. Chem. Soc.*, **106**, 4772 (1984).

17) A. Mills, A. Harriman, and G. Porter, *Anal. Chem.*, **53**, 1254 (1981); M. Fujihira, *J. Electroanal. Chem.*, **130**, 351 (1981); **138**, 89 (1982); **138**, 99 (1982).

18) W. W. Dunn, Y. Aikawa, and A. J. Bard, *J. Electrochem. Soc.*, **128**, 222 (1981); W. W. Dunn, Y. Aikawa, and A. J. Bard, *J. Am. Chem. Soc.*, **103**, 3456 (1981); M. D. Ward and A. J. Bard, *J. Phys. Chem.*, **86**, 3599 (1982); M. D. Ward, J. R. White, and A. J. Bard, *J. Am. Chem. Soc.*, **105**, 27 (1983).

19) "Electrochemical Studies of Biological Systems," ed by D. T. Sawyer, ACS Symposium Series 38, American Chemical Society, Washington (1977).

20) "Electrochemical and Spectrochemical Studies of Biological Redox Components," ed by K. M. Kadish, Advances in Chemistry Series 201, American Chemical Society, Washington (1982).

21) H. Muraki, T. Saji, M. Fujihira, and S. Aoyagui, *J. Electroanal. Chem.*, **169**, 319 (1984).
22) P. R. Moses, L. Wier, and R. W. Murray, *Anal. Chem.*, **47**, 1882 (1975).
23) M. Fujihira, M. Fukui, and T. Osa, *J. Electroanal. Chem.*, **106**, 413 (1980).
24) A. Frumkin, L. Nekrasov, B. Levich, and Ju. Ivanov, *J. Electroanal. Chem.*, **1**, 84 (1959/60).
25) A. J. Bard and L. R. Faulkner, "Electrochemical Methods," John Wiley and Sons, New York (1980), p. 173.
26) R. R. Adzic in "Advances in Electrochemistry and Electrochemical Engineering," John Wiley and Sons, New York (1984), Vol. 13, p. 159.

 © 1986 The Chemical Society of Japan Bull. Chem. Soc. Jpn., 59, 981—986 (1986)

^{129}I Mössbauer Spectroscopic Study of Several n-σ Charge-Transfer Complexes of Iodine with Thioethers

Hiroshi SAKAI,* Tomochika MATSUYAMA, and Yutaka MAEDA
Research Reactor Institute, Kyoto University, Kumatori-cho, Sennan-gun, Osaka 590-04
(Received September 24, 1985)

^{129}I Mössbauer studies have been made of n-σ charge-transfer complexes of iodine with thioethers, such as thiane, 1,4-oxathiane, and 1,4-dithiane. The spectra of these complexes consist of two sets of quadrupole octets, corresponding to the bridging and terminal iodine atoms. The transferred charges from the thioethers are localized on the terminal iodine atoms, and the bridging iodine atoms have slightly positive charges. This result can be well explained in terms of a covalent bond between the sulfur and bridging iodine atoms or the MO treatment of a delocalized three-center four-electron bonding. The contributions of the dative structure to the ground state are estimated to be 36, 28, and 24% for thiane-iodine, 1,4-oxathiane-iodine, and 1,4-dithiane-iodine respectively. The nature of the charge-transfer bond is discussed in comparison with amine-iodine complexes.

The Mössbauer spectroscopy of ^{129}I is a powerful tool for the study of charge-transfer (CT) complexes containing iodine as an electron acceptor. The electronic structure of iodine is directly derived from the Mössbauer spectroscopy parameters, such as the quadrupole coupling constant (e^2Qq) and its sign, the asymmetry parameter (η), and the isomer shift (δ). Actually, many investigations of CT complexes of iodine have been reported to date using ^{129}I Mössbauer spectroscopy.[1-10] However, these investigations have been mostly concerned with nitrogen-containing compounds (amines) and with aromatic compounds as the electron donors.

Sulfur-containing compounds (thioethers) also act as electron donors and form n-σ type CT complexes with iodine in the same way as do amines. The crystal and molecular structures for some of these complexes (1,4-dithiane–iodine,[11] dibenzyl sulfide–iodine,[12] and 1,5-dithiocane–iodine[13]) have been determined by the X-ray diffraction method. In these complexes, the iodine molecule is bonded to the sulfur atom to give a linear S···I–I arrangement. The intramolecular I–I bond distance is longer than that of the free iodine molecule, whereas the intermolecular S···I bond distance is shorter than the sum of the respective van der Waals radii. Hendra and Sadasivan[14] measured the far-infrared spectrum of the 1,4-dithiane-iodine complex and found the I–I stretching frequency at 158 cm^{-1}, lower than that of free iodine molecules at 213 cm^{-1}.[15]

The properties of the CT complexes have been interpreted on the basis of the CT theory developed by Mulliken.[16] As is well known, the CT interaction between an electron donor (D) and an electron acceptor (A) is to be described in terms of the electronic-wave function of the ground state in this form;

$$\Psi_g = a\phi_0(\mathrm{D,A}) + b\phi_1(\mathrm{D^+-A^-}), \quad (1)$$

where ϕ_0 represents the wave function for a non-bond structure and ϕ_1, that for a dative structure in which one electron has been completely transferred from the donor to the acceptor molecule. The ground state, Ψ_g, stabilized by a resonance between the non-bond and dative structures. When A is the iodine molecule, the transferred electron may occupy the antibonding molecular orbital (σ_u*) of the iodine molecule. Therefore, the contribution of ϕ_1 to Ψ_g gives rise to an increase in the I–I bond distance and a decrease in the stretching frequency of the I–I bond. It is, therefore, important and interesting to estimate the contribution of the dative structure in order to understand the properties of the CT complexes in the electronic ground state.

In this paper we wish to report an ^{129}I Mössbauer spectroscopic study of the crystalline n-σ CT complexes between iodine and thioethers, such as thiane (tetrahydrothiopyrane)–iodine (1:1), 1,4-oxathiane–iodine (1:1), and 1,4-dithiane–iodine (1:2). The charge density and the charge distribution on each iodine atom are determined for these complexes, and the nature of the CT bond is discussed in comparison with amine–iodine complexes.

Experimental

Materials. The ^{129}I-labeled complexes were prepared on a small scale by mixing approximately stoichiometric amounts of the components in appropriate solvents. The radioisotope ^{129}I was purchased from the New England Nuclear Corporation in the standard form of Na^{129}I in a Na_2SO_3 solution. Molecular iodine ($^{129}I_2$), obtained by oxidizing Na^{129}I with 3 mol dm^{-3} H_2SO_4 and 10% H_2O_2, was extracted with chloroform, hexane, or carbon tetrachloride. Each iodine solution was thoroughly washed with water and passed through a Teflon filter to eliminate any slight amount of water.

The thiane–iodine complex was prepared by adding a stoichiometric amount of thiane to the iodine solution of chloroform. A dark-brown crystalline product was obtained by the subsequent concentration and cooling of the solution. The orange-red 1,4-oxathiane–iodine complex was prepared in hexane in the same manner as the thiane–iodine complex. The purple crystalline complex of 1,4-dithiane–iodine was obtained by adding a saturated iodine solution of carbon tetrachloride to a dithiane solution of the same solvent. Since those complexes slowly decompose in air, the samples obtained were immediately mounted in Teflon sample holders and kept in liq. N_2 until ready for the Mössbauer

measurements. The mole ratio of each component for these complexes was checked on nonradioactive (natural iodine) preparation samples by means of iodometry and elemental analysis. The thioether: I_2 ratios determined for the thiane-iodine, 1,4-oxathiane-iodine, and 1,4-dithiane-iodine complexes were 1:1, 1:1, and 1:2 respectively. The thichnesses of the absorbers were in the range of 20 to 30 mg $^{129}I/cm^2$.

^{129}I Mössbauer Effect Measurement. The $^{66}Zn^{129}Te$ source ($t_{1/2}$=70 min) was prepared by the irradiation of 150 mg $^{66}Zn^{128}Te$ at a thermal neutron flux of 2×10^{13} n cm^{-2} s^{-1} for 1 h in the Kyoto University Reactor (KUR). The source activity produced was initially about 10 mCi, which was sufficient to obtain a reasonable spectrum in 3—4 h of data collection. The 27.8 keV Mössbauer γ-ray was detected with a 1 mm-thick NaI(Tl) scintillation counter, and a 100 μm In foil was inserted between the absorber and the detector in order to selectively absorb 29.8 keV X-ray, resulting in the conversion of 39.6 keV Xe γ-ray. The Mössbauer measurement was performed in the transmission geometry by cooling the source and the absorber to 16 K with a closed-cycle helium refrigerator, "Cryodyne 1020." The Mössbauer spectrometer was calibrated using an iron spectrum.

Results and Discussion

In Figs. 1 and 2 the ^{129}I Mössbauer spectra at 16 K of the thiane-iodine, 1,4-oxathiane-iodine, and 1,4-dithiane-iodine complexes are presented. These spectra consist of a superposition of two quadrupole octets, as is to be expected from the molecular structure of the 1,4-dithiane-iodine complex. The spectra were analyzed by the least-squares method using a double set of the fitting parameters, e^2Qq, η, δ, full-width at half-maximum (2Γ), each peak intensity, and a single base line. The solid lines and the stick diagrams in the figures represent the best-fitted Lorentzian curves and the peak positions respectively. The Mössbauer parameters computed are given in Table 1, together with the results for some amine-iodine complexes published elsewhere. The e^2Qq value was converted to that of the ^{127}I nucleus by using the ground-state quadrupole moment ratio, $^{129}Q/^{127}Q=+0.70121$.[17]

The crystallographic data for the 1,4-dithiane-iodine complex suggest that only one atom of the iodine molecule is bonded to the sulfur atom, resulting in a linear S···I–I arrangement (Fig. 3).[11] The Mössbauer spectra shown in Figs. 1 and 2 are similar to each other. The similarity of these spectra suggests that iodine molecules are also bonded equatorially to the sulfur atoms of thiane and 1,4-oxathiane in the thiane-iodine and 1,4-oxathiane-iodine complexes. Since the values of e^2Qq, η, and δ for the 1,4-oxathiane-iodine complex are close to those for the other complexes, the iodine molecule may not interact with the oxygen atom of the 1,4-oxathiane molecule. In the 1,4-oxaselenane-iodine complex, the oxygen atom is also not involved in the intermolecular bonding.[18] These spectra are similar to those of the amine-iodine complexes. By analogy with the pyridine-iodine complex,[3,8] it is appropriate to assign the iodine with the larger quadrupole splitting (I_A) to the iodine atom coordinated to the sulfur atom (the bridging iodine atom), whereas the I_B should be assigned to the terminal iodine atom.

The values of e^2Qq, η, and δ are closely related to the charge distribution and the charge density on the iodine atom. As is shown in Table 1, these values for the I_A atoms are very close to each other in these complexes, suggesting that they are also similar in S···I_A bond

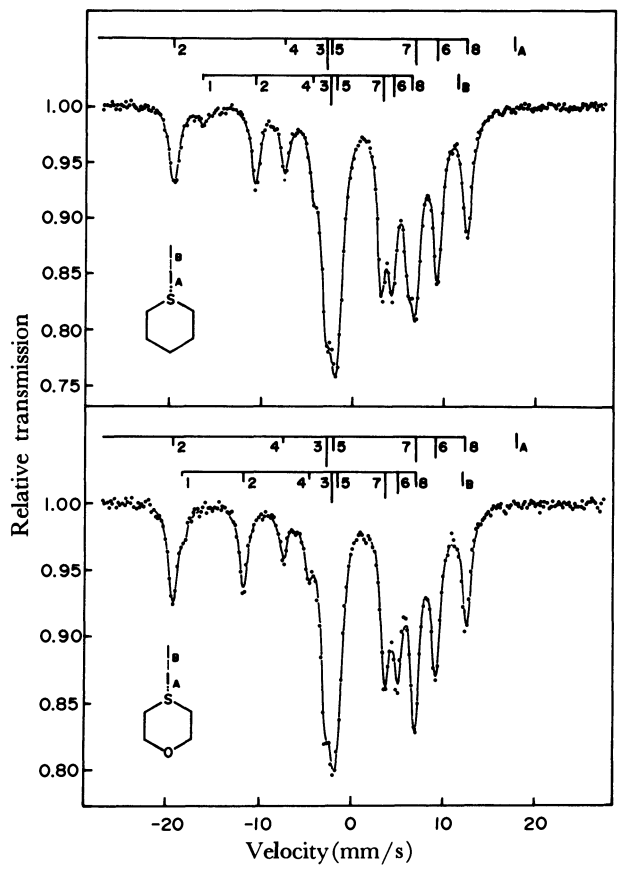

Fig. 1. ^{129}I Mössbauer spectra at 16 K of the thiane-iodine (top) and 1,4-oxathiane-iodine (bottom) complexes.

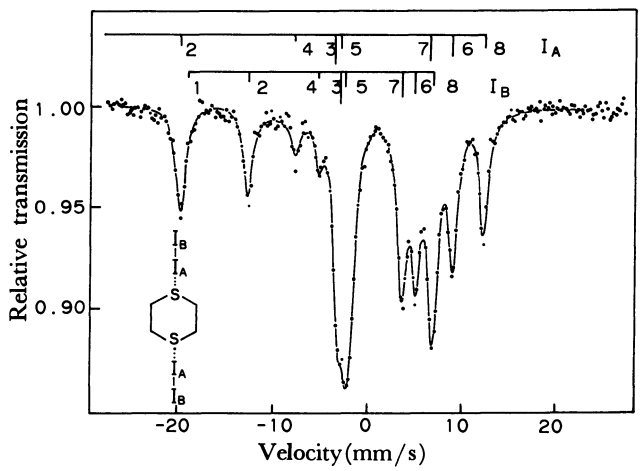

Fig. 2. ^{129}I Mössbauer spectrum at 16 K of the 1,4-dithiane-iodine complex.

Table 1. Values of the Quadrupole Coupling Constant (e^2Qq), the Asymmetry Parameter (η), the Isomer Shift (δ), the Full-Width at Half-Maximum (2Γ), the Relative Intensity, the Unbalanced p-Electron (U_p), and the 5p-Electron Hole (h_p) for the Thioether-Iodine and Amine-Iodine Complexes

		e^2Qq[a] MHz	η	δ[b] mm s^{-1}	2Γ mm s^{-1}	Relative[c] intensity	U_p[d]	h_p[e]	Ref.
Thiane-I_2	I_A	−2513±13	0.02±0.04	1.54±0.04	1.27±0.03	1.23	1.10	1.39	
	I_B	−1310±13	0.02±0.04	0.32±0.04	1.22±0.03	1.00	0.57	0.57	
1,4-Oxathiane-I_2	I_A	−2512±13	0.04±0.04	1.47±0.04	1.20±0.03	1.05	1.10	1.34	
	I_B	−1475±13	0.09±0.04	0.43±0.04	1.26±0.03	1.00	0.63	0.65	
1,4-Dithiane-$2I_2$	I_A	−2526±13	0.02±0.04	1.47±0.04	1.11±0.03	1.04	1.10	1.34	
	I_B	−1553±13	0.06±0.04	0.50±0.04	1.16±0.03	1.00	0.68	0.69	
Hexamethylene-tetramine-I_2	I_A	−2582±20	0.19	1.51±0.02	—	—	1.13	1.37	(2)
	I_B	−1272±20	0.06	0.28±0.02	—	—	0.55	0.55	
Pyridine-I_2 in pyridine	I_A	−2600±30	—	1.40±0.07	—	—	1.13	1.29	(3)
	I_B	−1300±15	—	0.28±0.05	—	—	0.57	0.55	
Pyridine-I_2 in CS_2	I_A	−2631±20	0.10	1.82±0.04	—	—	1.15	1.57	(8)
	I_B	−1439±20	—	0.39±0.04	—	—	0.63	0.62	
Triethylamine-I_2 in CS_2	I_A	−2604±20	—	1.56±0.05	—	—	1.14	1.40	(8)
	I_B	−1261±20	0.09	0.40±0.05	—	—	0.55	0.62	

a) The e^2Qq values are converted to those of the ^{127}I nucleus by using the $^{129}Q/^{127}Q$=0.70121 ratio. b) The δ values are relative to the ZnTe source. c) The relative intensities are normalized with respect to the I_B atom. d) $U_p=-e^2Qq_{obsd}/e^2Qq_{atom}$, e^2Qq_{atom}=2292.7 MHz. e) $\delta=1.5\,h_p-0.54$ (mm/s).

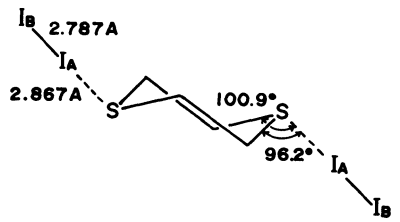

Fig. 3. The structure of the 1,4-dithiane-iodine complex (Ref. 11).

character. The small η values for I_A are consistent with the axially symmetric linear S···I_A–I_B orientation. On the other hand, the values of e^2Qq and δ for the I_B atoms increase in the order: thiane<1,4-oxathiane<1,4-dithiane. Since an increase in e^2Qq and δ corresponds to a decrease in the p-electrons charge density on the iodine atom, the extent of CT, i.e., the contribution of the dative structure to the ground state, increases in the order of : thiane>1,4-oxathiane>1,4-dithiane in these complexes.

The quantitative treatment of e^2Qq, η, and δ has been developed by Townes and Dailey[19] and Hafemeister et al.,[20] and an additional discussion of the ^{129}I Mössbauer parameters has been given in reviews.[21,22] According to those reviews, the observed e^2Qq, η, and δ values are related to the population of the 5p-electrons and the number of 5p-electron holes in the iodine atom as follows:

$$U_p = -e^2Qq_{obs}/e^2Qq_{atom} = -N_z + (N_x+N_y)/2 \quad (2)$$

$$\eta = 3(N_x-N_y)/2U_p \quad (3)$$

$$\delta = 1.5h_p - 0.54 \quad \text{(mm/s, for ZnTe source)} \quad (4)$$

where U_p is the number of unbalanced p-electrons and e^2Qq_{atom}, the atomic iodine quadrupole coupling constant, is equal to 2292.7 MHz for ^{127}I. N_x, N_y, and N_z are the populations of the 5p-electrons in the x, y, and z orbitals respectively, and $h_p=6-(N_x+N_y+N_z)$ is the number of p-electron holes in the $5p^6$ shell.

The U_p and h_p values obtained for the I_A and I_B atoms of the thioether-iodine complexes are presented in Table 1, together with those for some amine-iodine complexes. It can be observed that all the h_p values are larger than the U_p values for the I_A atoms. The same tendency is found in the I_A atoms of the amine-iodine complexes. This phenomenon has been successfully interpreted in terms of the contribution of $4d_\sigma$-electrons to the CT-bond formation.[8] That is, the S···I–I or N···I–I bonding can be described as a mixture of two extreme bonding schemes, i.e., a delocalized three-center four-electron bond using only the valence p-electrons and covalent σ bonds of two $d_\sigma p_\sigma$ hybrid orbitals of the center atom (I_A) with the two terminal atoms (S or N and I_B), as was first pointed out by Lucken.[23] The effect of the $4d_\sigma$ hybridization leads to an increase in the effective s-electron density and therefore markedly increases the δ value because of the large shielding coefficient, 0.85, for 4d-electrons compared to the value 0.35 for 5p-electrons.[8] On the contrary, if 5s-electrons take part in the CT-bond

formation ($sp\sigma$ hybridization), the δ value decreases greatly. Using Eqs. 4 and 5 in Ref. 8, the number of the $4d\sigma$-electron promotion to the 5p orbital can be easily estimated from the δ and e^2Qq values. The average values of δ and e^2Qq for the I_A atoms lead to 0.19 for h_d (the number of 4d-electron defects) and 0.88 for h_p. The contribution of the $d\sigma p\sigma$ hybridization to the S···I–I bond formation is estimated to be 19%, which is close to the value for the triethylamine–iodine complex. The promotion energy of the $4d\sigma$-electron may be compensated for by the stabilization of the CT-bond formation. Consequently, the bridging iodine atom is positively charged by 0.07(=0.19+0.88−1) in the present complexes.

On the other hand, Table 1 shows that the h_p values are in good agreement with the U_p values for the terminal iodine atoms (I_B). In the amine–iodine complexes, the h_p values are also close to U_p for the I_B atoms. This agreement implies that the bonding of the I_B atom is mainly due to $5p\sigma$-electrons. Therefore, the charge density of the I_B atom can be described with $1-h_p$. From the h_p values in Table 1, the I_B atoms for the thiane–iodine, 1,4-oxathiane–iodine, and 1,4-dithiane–iodine complexes are evaluated to be negatively charged by 0.43, 0.35, and 0.31 respectively.

The experimental fact that the transferred electron is not equally distributed on both I_A and I_B, but is strongly localized on I_B in the electronic ground state, can be qualitatively explained in terms of a covalent bond between the sulfur and I_A atoms. The distance of the intermolecular S···I_A bond is only 2.867 A for the 1,4-dithiane–iodine complex,[11] compared with the sum of the van der Waals radii of the sulfur and iodine atoms (4.0 A) or the sum of each covalent bond radius (2.37 A). This bond distance strongly suggests that a relatively strong covalent bond exists between the S and I_A atoms. For such strong CT complexes, Eq. 1, used for the weak interaction between a donor and an acceptor, is no longer applicable. Equation 1 may, then, be rewritten as follows:

$$\Psi_g = a\psi_0(>S,I_2) + b\psi_1(>S,I_A^+I_B^-) + c\psi_2(>S^+-I_AI_B^-), \quad (5)$$

where the first and second terms refer to the non-bond structures, and the third term, to the dative structure.. The fact that the I_A atom has slightly positive charges introduces the second term to the ground-state wave function. Fleming and Hanna[24] pointed out the importance of the second term because the electric field from lone pairs would give rise to an induced dipole in I_2 and would polarize partly to I^+I^-. Although the dative structure is usually described in terms of $\psi(>S^+-I_2^-)$, in which the two iodine atoms are equivalent, it is reasonable, in the case of strong complexes, to rewrite the dative structure as the third term because of the strong covalent bond between S^+ and I_A. The positive charge on the thioether is likely to be largely localized on the sulfur atom. Since S^+ presumably has a greater electron affinity than I_A in the intermolecular S^+–I_A bond, some positive charges may also be localized on I_A, resulting in the structure of $>S\ I_A^+\ I_B^-$. This structure is the same as that of the second term. Therefore, we include the effect of the ionic character on the second term, which is called "the ionic structure." The contribution of each structure to the ground-state wave function can be evaluated by means of the charge densities on the I_A and I_B atoms obtained from the Mössbauer spectrum, neglecting the overlap between ψ_0 and ψ_1, or between ψ_0 and ψ_2, as follows. Since the I_A atom is positively charged by 0.07, the contribution of the second term, in which I_A is a monocation, is found to be 7%. In both the second and third terms, the I_B atom exists as a monoanion. Therefore, the −0.43 charge localized on the I_B of the thiane complex leads to 43% for the contributions of the second and third terms. We obtain 36% for the contribution of the third term alone. The results for the thioether–iodine complexes are given in Table 2, together with those for some amine–iodine complexes.

Table 2. Contributions of the Non-Bond (a^2), Ionic (b^2), and Dative Structures (c^2) to the Ground-State Wave Function for the Thioether–Iodine and Amine–Iodine Complexes

	a^2/%	b^2/%	c^2/%	Ref.
Thiane–I_2	57	7	36	
1,4-Oxathiane–I_2	65	7	28	
1,4-Dithiane–$2I_2$	69	7	24	
Hexamethylene-tetramine–I_2	55	11	34	(2)
Pyridine–I_2 in CS_2	62	11	27	(8)
Triethylamine–I_2 in CS_2	59	11	30	(8)

As is shown in Table 2, there is no great difference in the contribution of the dative structure (c^2) between the thioether and amine complexes. However, it is obvious that the amount of the ionic structure (b^2) for the thioether complexes is less than that for the amine complexes. This result is quite reasonable, for amine cations (N^+) have a larger electron affinity than thioether cations (S^+) and, therefore, attract more electrons from the bridging iodine atom (I_A) than do S^+.

It is interesting to interpret the charge densities on the I_A and I_B atoms and the nature of the CT bond on the basis of the simple LCAO-MO theory. The MO treatment of the delocalized three-center four-electron bond has been successfully applied to the halogen NQR results for amine–halogen or –interhalogen complexes.[25] Therefore, we have also applied the same procedure to our thioether–iodine complexes and compared the results with those for the amine–iodine complexes. According to Bowmaker and Hacobian,[25] the secular equation for the S···I_A–I_B configuration can be written as:

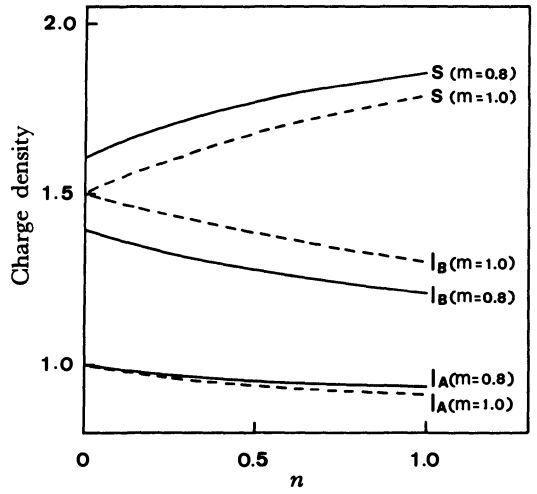

Fig. 4. Charge densities on the sulfur (S), bridging iodine (I_A), and terminal iodine (I_B) atoms as a function of the Coulomb parameter n.

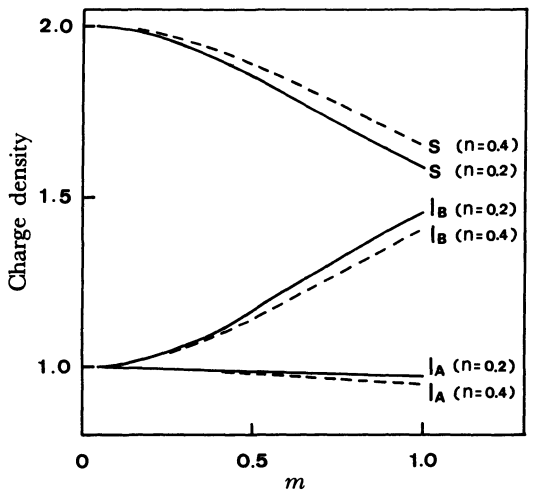

Fig. 5. Charge densities on the sulfur (S), bridging iodine (I_A), and terminal iodine (I_B) atoms as a function of the resonance integral parameter m.

$$\begin{vmatrix} \alpha + n\beta - E & m\beta & 0 \\ m\beta & \alpha - E & \beta \\ 0 & \beta & \alpha - E \end{vmatrix} = 0$$

where α is the Coulomb integral for the valence p_z orbital of iodine and β, the resonance integral between two valence p_z orbitals of iodine; n refers to the Coulomb parameter of sulfur and m, to the resonance integral parameter for the S···I_A bond.

The charge densities on each atom calculated are shown in Fig. 4 as a function of n in the cases of 0.8 (—) and 1.0 (----) for m. The charge density on the sulfur atom increases with an increase in the n value, which depends on the difference in electronegativity between the donor (sulfur) and iodine atoms. In the amine-iodine complexes, the n value for nitrogen is estimated to be 0.9 from the charge densities on the bridging and terminal iodine atoms.[25] Since the electronegativity of sulfur is smaller than that of nitrogen, a smaller n value for sulfur is required. When the n values are taken to be 0.2 (—) and 0.4 (---), the charge densities calculated as a function of m are shown in Fig. 5. It is found that an increase in the m value causes a decrease in the charge density on sulfur. The transferred charges from sulfur are localized on the terminal iodine atom (I_B), and the bridging iodine atom (I_A) has slightly positive charges. Judging from the charge densities on the I_B atoms obtained from the Mössbauer results, the appropriate value of the Coulomb parameter n seems to be about 0.2 for the sulfur atoms in the thioethers. This value seems reasonable, because the electronegativity of sulfur is only slightly larger than that of iodine. In the range of 0.75 to 0.95 for the m value, the charge densities on the I_B atoms calculated are in good agreement with those obtained experimentally. The appropriate m value is estimated to be 0.9 for the amine–iodine complexes.[25] When the n and m values are 0.2 and 0.9 respectively, the charge density on the I_A atom is calculated to be 0.97 (positively charged by 0.03). Considering that the simple LCAO-MO calculation is used for these complexes, the n and m values which seem chemically reasonable give a good agreement between the calculated and experimentally observed charge densities on each atom. Therefore, the S···I–I bonding is described mainly in terms of the delocalized three-center four-electron bond in the electronic ground state, such as the bonding in the triiodide anion. The quantity of the transferred charges depends strongly on the Coulomb integral of the donor atom and the resonance integral of the bond between the donor and the bridging iodine atoms.

We are very grateful to Professors Takenobu Higashimura and Hitoshi Yamaoka (Research Reactor Institute, Kyoto University) for their useful discussions and encouragement.

References

1) C. I. Wynter, J. Hill, W. Bledsoe, G. K. Shenoy, and S. L. Ruby, *J. Chem. Phys.*, **50**, 3872 (1969).
2) S. Ichiba, H. Sakai, H. Negita, and Y. Maeda, *J. Chem. Phys.*, **54**, 1627 (1971).
3) S. Bukshpan, C. Goldstein, T. Sonnino, L. May, and M. Pasternak, *J. Chem. Phys.*, **62**, 2606 (1975).
4) S. Bukshpan, M. Pasternak, and T. Sonnino, *J. Chem. Phys.*, **62**, 2916 (1975).
5) C. H. W. Jones, *J. Chem. Phys.*, **62**, 4343 (1975).
6) R. C. Teitelbaum, S. L. Ruby, and T. J. Marks, *J. Am. Chem. Soc.*, **101**, 7568 (1979).
7) C. I. Wynter, Y. W. Chow, and A. Mukerji, *J. Chem. Phys.*, **72**, 5412 (1980).
8) H. Sakai, Y. Maeda, S. Ichiba, and H. Negita, *J. Chem. Phys.*, **72**, 6192 (1980).
9) H. Sakai, T. Matsuyama, Y. Maeda, and H. Yamaoka, *J. Chem. Phys.*, **75**, 5155 (1981).

10) H. Sakai, T. Matsuyama, H. Yamaoka, and Y. Maeda, *Bull. Chem. Soc. Jpn.*, **56**, 1016 (1983).
11) G. Y. Chao and J. D. McCullough, *Acta Cryst.*, **13**, 727 (1960).
12) Chr. Romming, *Acta Chem. Scand.*, **14**, 2145 (1960).
13) H. Hope and B. G. Nichols, *Acta Cryst.*, **B37**, 158 (1981).
14) P. J. Hendra and N. Sadasivan, *Spectrochim. Acta*, **21**, 1127 (1965).
15) H. Rosen, Y. R. Shen, and F. Stenman, *Mol. Phys.*, **22**, 33 (1971).
16) R. S. Mulliken and W. B. Person, "Molecular Complexes," Wiley, New York (1969).
17) R. Livingston and H. Zeldes, *Phys. Rev.*, **90**, 609 (1953).
18) H. Maddox and J. D. McCullough, *Inorg. Chem.*, **5**, 522 (1966).
19) C. H. Townes and B. P. Dailey, *J. Chem. Phys.*, **17**, 782 (1949); **20**, 35 (1952).
20) D. W. Hafemeister, G. DePasquali, and H. DeWaard, *Phys. Rev.*, **B135**, 1089 (1964).
21) N. N. Greenwood and T. C. Gibb, "Mössbauer Spectroscopy," Chapman and Hall, London (1971), Chap. 15.
22) S. L. Ruby and G. K. Shenoy, "Mössbauer Isomer Shifts," ed by G. K. Shenoy and F. E. Wagner, North-Holland, Amsterdam (1978), Chap. 9.
23) E. A. C. Lucken, "Nuclear Quadrupole Coupling Constants," Academic, London (1969), p. 290.
24) H. C. Fleming and M. W. Hanna, *J. Am. Chem. Soc.*, **93**, 5030 (1971).
25) G. A. Bowmaker and S. Hacobian, *Aust. J. Chem.*, **22**, 2047 (1969).

The Crystal and Molecular Structures of 4-Ethyl-3,5-bis(phenylimino)-1,2,4-dithiazolidine and 2-Ethyl-4-phenyl-5-phenylimino-1,2,4-thiadiazolidin-3-thione

Mineo KURIYAMA, Noritake YASUOKA,† Nobutami KASAI,* Mitsuo KOMATSU, Yoshiki OHSHIRO, and Toshio AGAWA

Department of Applied Chemistry, Faculty of Engineering, Osaka University, Yamadaoka, Suita, Osaka 565

(Received October 30, 1985)

The molecular structures of title compounds, two of the three isomeric products in the reaction of 2-ethyl-3-phenyloxaziridine with phenyl isothiocyanate, have been determined by means of X-ray diffraction. 4-Ethyl-3,5-bis(phenylimino)-1,2,4-dithiazolidine (**6b**), orthorhombic, space group *Pcab*, a=27.171(1), b=10.213(2), c=11.421(1) Å, Z=8; 2-Ethyl-4-phenyl-5-phenylimino-1,2,4-thiadiazolidin-3-thione (**8b**), monoclinic, space group $P2_1/n$, a=9.278(1), b=27.525(3), c=5.826(1) Å, β=92.74(1)°, Z=4. Both structures were solved by the heavy atom method, and refined anisotropically by the block-diagonal least-squares procedure (R=0.066 and 0.060, respectively). The results corrected the reaction scheme proposed for the reaction of *N*-alkyloxaziridine with phenyl isothiacyanate.

It has been reported that the reaction of *N*-alkyloxaziridine (**1**) with phenyl isothiocyanate (**2**) gave heterocyclic compounds with incorporation of alkylnitrene.[1] However, stimulated by extensive studies by L'Abbé and co-workers on similar reactions of alkyl azides with isothiocyanates,[2,3] the structures of the cyclic adducts (R≠*t*-Bu) were reexamined by ^{13}CNMR. It indicated that the former assignment for **3** and **4** structures was not correct. In order to obtain the exact information on the molecular structures of the cyclic products, **6b** and **8b** (previously assigned as **3b** and **4b**), have been determined by means of X-ray diffraction.

Experimental

Crystal Data. **6b**, $C_{16}H_{15}N_3S_2$, M 313.3, orthorhombic, space group *Pcab* (No. 61, absent reflections, $0kl$: l=2n+1, $h0l$: h=2n+1, $hk0$:k=2n+1), a=27.171(1), b=10.213(2), c=11.421(1)Å, D_m=1.30 g cm^{-3}, D_c=1.31 g cm^{-3} for Z=8, μ(Mo $K\alpha$)=3.3 cm^{-1}; **8b**, $C_{16}H_{15}N_3S_2$, M 313.3, monoclinic, space group $P2_1/n$ (No. 14, absent reflections, $h0l$:h+l=2n+1, $0k0$:k=2n+1), a=9.278(1), b=27.525(3), c=5.826(1)Å, β=92.74(1)°, D_m=1.33 g cm^{-3}, D_c=1.34 g cm^{-3} for Z=4, μ(Cu $K\alpha$)=29.6 cm^{-1}.

A Rigaku automated, four-circle diffractometer equipped with graphite monochromator was used for X-ray experiments. The crystals used had approximate dimensions of 0.2×0.2×0.2 (**6b**) and 0.2×0.2×0.3 mm (**8b**). Unit-cell dimensions of both crystals were determined by the least-squares fit of 2θ values of higher order reflections. Integrated intensities were measured on the diffractometer by the θ-2θ scan technique at a 2θ rate of 4° min^{-1}. Scan width for **6b** was $\Delta 2\theta$=(2.0+0.7tanθ)° for Mo $K\alpha$ radiation (λ=0.71069Å) and for **8b** $\Delta 2\theta$=(2.0+0.3tanθ)° for Cu $K\alpha$ (λ=1.5418Å). Backgrounds were counted for 7.5 s at both ends of a scan. Three standard reflections were measured after every 60 reflections, which showed no intensity decrease during intensity measurements on both crystals. Totals of 3470 and 2342 reflections were measured, of which 1292 and 2044 were observed ($|F_o|>3\sigma(F_o)$) for **6b** and **8b**, respectively. The usual Lorentz and polarization corrections were applied ignoring absorption correction. Densities were measured by flotation method in carbon tetrachloride-hexane mixed solutions.

Structure Solution and Refinement

Both structures were solved by the heavy atom method, and refined anisotropically by the block-diagonal least-squares procedure minimizing $\sum w(\Delta F)^2$ (*HBLS* V).[4] All hydrogen atoms were located on the difference Fourier map, which were refined isotropically. Three

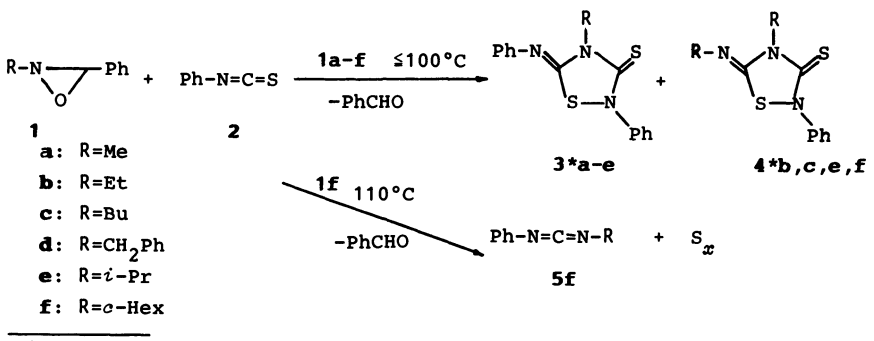

†Present address: Himeji Institute of Technology, Shosha, Himeji, Hyogo 671-22.

reflections (020, 002, and 302), which were considered affected by the extinction largely, were excluded at the final stage. Final R values are 0.066 and 0.060 for **6b** and **8b**, respectively. Unit weights were employed only at the early stage of the refinement and the weighting schemes used at the final cycles were $w=\{\sigma^2(F_o)-1.1709|F_o|+0.0518|F_o|^2\}^{-1}$ for **6b** and $w=\{\sigma^2(F_o)-0.0762|F_o|+0.0095|F_o|^2\}^{-1}$ for **8b**, where σ is the standard deviation obtained by the counting statistics. Atomic scattering factors used were taken from International Tables for X-Ray Crystallography[5] for non-hydrogen atoms and from Stewart and coworkers[6] for hydrogen atoms. Final atomic coordinates are given in Table 1.††

Computations were done on an ACOS 850 computer at the Crystallographic Research Center, Institute for Protein Research Center, Osaka University.

Results and Discussion

Reaction Scheme. The conclusive evidence for the structure of the molecules formerly assigned as **3** and **4** has been obtained by the present X-ray crystal structure analysis. As is clearly seen in Fig. 1, the molecule assigned as **3b** (R=Et) is found to be 4-ethyl-3,5-bis(phenylimino)-1,2,4-dithiazolidine (**6b**) and that as **4b** (R=Et) is 2-ethyl-4-phenyl-5-phenylimino-1,2,4-thiadiazolidin-3-thione (**8b**). Therefore, the reaction scheme proposed formerly[1] should be corrected as follows.[8]

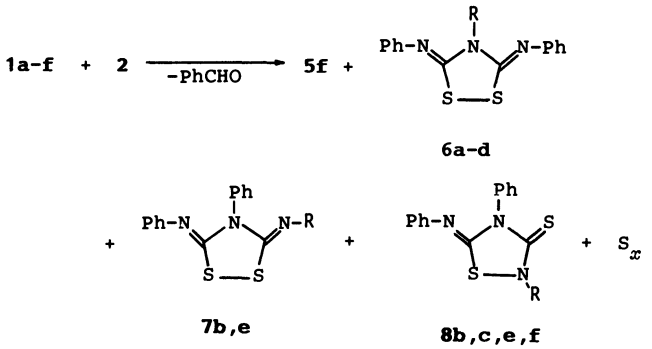

Table 1. Final Atomic Coordinatesof Non-Hydrogen Atoms with Estimated Standard Deviation in Parentheses

	Atom	x	y	z	B_{eq}[7]/Å^2
6b	S(1)	0.40347(4)	0.20928(12)	0.59890(12)	4.6
	S(2)	0.47677(4)	0.22428(12)	0.55385(13)	4.9
	C(3)	0.46558(12)	0.2698(4)	0.4063(5)	3.2
	N(4)	0.41605(10)	0.2740(3)	0.3767(3)	3.2
	C(5)	0.38041(13)	0.2420(4)	0.4594(4)	3.3
	N(6)	0.33527(10)	0.2377(3)	0.4320(4)	4.2
	N(7)	0.49907(10)	0.2958(3)	0.3338(4)	4.1
	C(41)	0.40279(12)	0.3081(4)	0.2559(5)	4.5
	C(42)	0.40261(15)	0.4533(5)	0.2342(6)	7.3
	C(61)	0.30124(12)	0.1999(4)	0.5209(4)	3.6
	C(62)	0.27841(13)	0.0781(4)	0.5107(5)	3.9
	C(63)	0.24395(13)	0.0415(4)	0.5943(5)	4.6
	C(64)	0.23200(13)	0.1214(5)	0.6850(5)	5.4
	C(65)	0.25397(13)	0.2419(5)	0.6946(6)	6.0
	C(66)	0.28896(14)	0.2820(4)	0.6123(5)	5.0
	C(71)	0.54859(12)	0.2853(4)	0.3730(5)	3.8
	C(72)	0.57224(13)	0.1657(4)	0.3692(5)	4.9
	C(73)	0.62135(15)	0.1585(4)	0.4009(5)	6.0
	C(74)	0.64716(14)	0.2685(5)	0.4359(5)	6.0
	C(75)	0.62319(15)	0.3852(5)	0.4392(5)	6.9
	C(76)	0.57381(14)	0.3960(4)	0.4067(5)	5.8
8b	S(1)	0.14872(9)	0.19651(3)	0.31987(16)	3.9
	N(2)	0.0284(3)	0.21323(9)	0.1112(5)	4.2
	C(3)	−0.0520(4)	0.17739(12)	0.0252(6)	3.7
	N(4)	−0.0173(3)	0.13411(9)	0.1341(5)	3.5
	C(5)	0.0952(3)	0.13538(11)	0.2911(6)	3.3
	N(6)	0.1496(3)	0.09826(10)	0.3840(5)	3.6
	S(7)	−0.17358(10)	0.18346(4)	−0.18110(19)	5.2
	C(21)	0.0161(4)	0.26509(12)	0.0466(7)	5.3
	C(22)	0.1004(6)	0.27888(17)	−0.1456(8)	7.7
	C(41)	−0.0916(3)	0.08958(11)	0.0895(5)	3.1
	C(42)	−0.1796(4)	0.07389(13)	0.2528(7)	4.6
	C(43)	−0.2499(5)	0.03070(14)	0.2137(7)	5.4
	C(44)	−0.2313(4)	0.00474(13)	0.0167(7)	4.9
	C(45)	−0.1452(4)	0.02043(12)	−0.1436(6)	4.5
	C(46)	−0.0734(4)	0.06388(12)	−0.1091(6)	4.0
	C(61)	0.2641(4)	0.10519(11)	0.5412(6)	3.5
	C(62)	0.3835(4)	0.07940(14)	0.5032(6)	4.6
	C(63)	0.4965(4)	0.08360(16)	0.6570(7)	5.6
	C(64)	0.4900(4)	0.11249(15)	0.8507(6)	5.0
	C(65)	0.3713(4)	0.13734(14)	0.8881(6)	4.9
	C(66)	0.2589(4)	0.13370(13)	0.7347(6)	4.2

Table 2. Selected Bond Lengths and Bond Angles in **6b** and **8b** with Estimated Standard Deviations in Parentheses

6b		**8b**	
Bond length [l/Å]			
S(1)-S(2)	2.063(2)	S(1)-N(2)	1.711(3)
S(1)-C(5)	1.744(4)	S(1)-C(5)	1.767(3)
S(2)-C(3)	1.775(5)	S(7)-C(3)	1.654(3)
C(3)-N(4)	1.388(5)	C(3)-N(2)	1.341(4)
C(5)-N(4)	1.392(5)	C(3)-N(4)	1.384(4)
C(3)-N(7)	1.258(6)	C(5)-N(4)	1.393(4)
C(5)-N(6)	1.267(6)	C(5)-N(6)	1.261(4)
Bond angles [ϕ/°]			
S(2)-S(1)-C(5)	96.1(2)	N(2)-S(1)-C(5)	90.0(2)
S(1)-S(2)-C(3)	95.2(2)	S(1)-N(2)-C(3)	115.8(3)
S(2)-C(3)-N(4)	113.9(4)	N(2)-C(3)-N(4)	109.7(3)
S(2)-(3)-N(7)	123.8(4)	N(2)-C(3)-S(7)	125.5(3)
N(4)-C(3)-N(7)	112.3(5)	N(4)-C(3)-S(7)	124.8(3)
S(1)-C(5)-N(4)	114.5(3)	S(1)-C(5)-N(4)	107.8(3)
S(1)-C(5)-N(6)	124.6(4)	S(1)-C(5)-N(6)	128.0(3)
N(4)-C(5)-N(6)	120.9(4)	N(4)-C(5)-N(6)	124.2(3)
C(3)-N(4)-C(5)	120.1(4)	C(3)-N(4)-C(5)	116.5(3)

††Tables of anisotropic thermal parameters, coordinates of hydrogen atoms and tables of observed and calculated structure factors are kept at the Chemical Society of Japan, Document No. 8624.

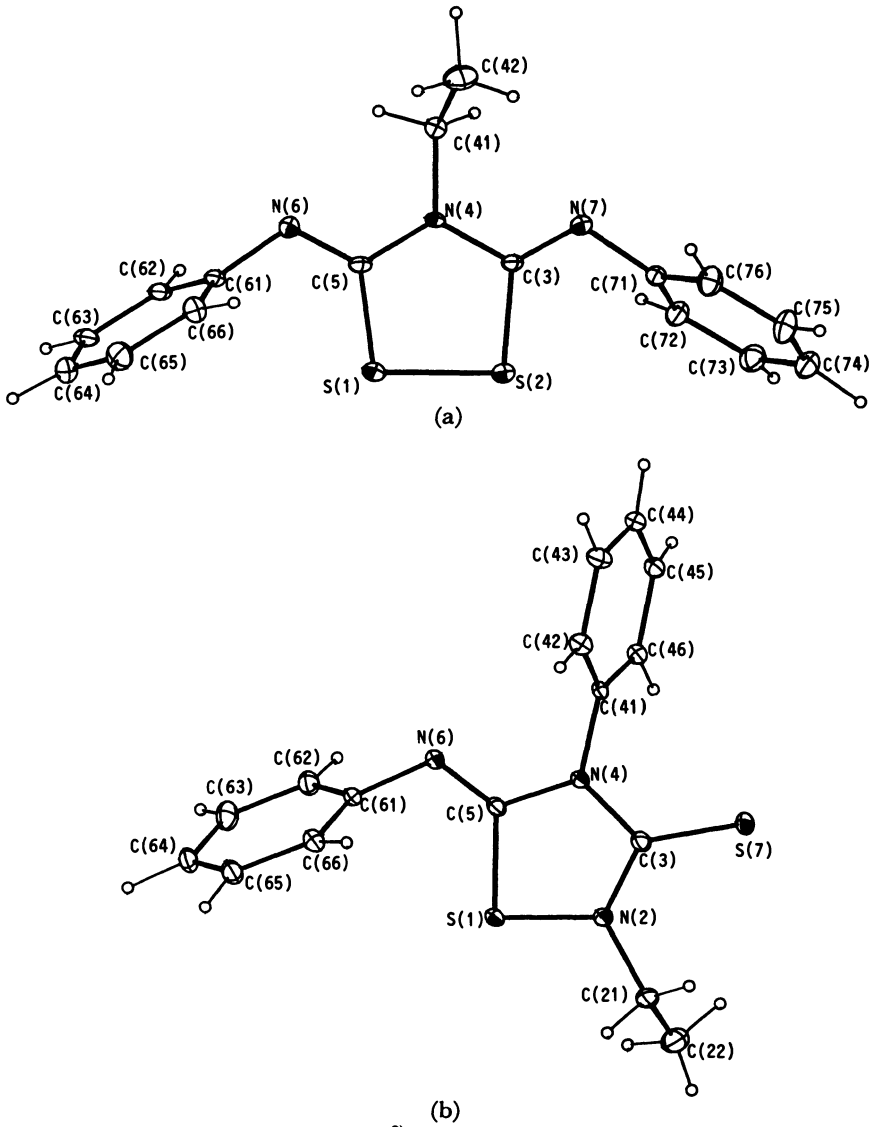

Fig. 1. Molecular structures.[9]
Non-hydrogen atoms are expressed as thermal ellipsoids with 10% probability level and hydrogen atoms as spheres with B=1.0 Å^2.
(a) **6b**, (b) **8b**.

Molecular Structure. Selected bond lengths and bond angles in the **6b** and **8b** molecules are given in Table 2.

The symmetrical **6b** molecule has an approximate two-fold axis except the ethyl group attached to the N(4) atom. 1,2,4-Dithiazolidine ring is planar, the maximum deviation of the atoms from the plane being 0.033 Å at the C(5) atom. In the ring, the S–S bond has a single bond length, 2.063(2) Å. Two C–N bonds are equal in length [1.388(5) and 1.392(5) Å], however, the S(1)–C(5) bond [1.744(4) Å] is slightly shorter than the S(2)–C(3) bond [1.775(5) Å]. Two S–S–C [96.1(2) and 95.5(2)°] and two S–C–N [114.5(3) and 113.9(4)°] bond angles are equal to each other. This structural feature is very similar to that of the dithiazolidine ring in 4-benzyl-3,5-bis(phenylimino)-1,2,4-dithiazolidine[10] except for the S(1)–C(5) bond length, but differs from those of the 1,2,4-dithiazolidines containing four colinear sulfur atoms.[11,12] In the phenylimino groups attached to the dithiazolidine ring of **6b**, two C=N bond lengths [1.267(6) and 1.258(6) Å] and C=N–C(Ph) angles [117.4(4) and 117.5(4)°] are respectively equal. Two phenyl groups make different angles of 106.1 and 94.8° with the dithiazolidine ring.

The 1,2,4-thiadiazolidine ring of **8b** is also planar, maximum deviation of the atom from the plane being 0.030 Å at C(5). The S(1)–N(2) bond length is 1.711(3) Å, which seems to be an intermediate value among those in 1,2,4-thiadiazolidines[13–15] and 2,4-dimethyl-1,2,4-thidiazolidin-3,5-dithione.[16] This bond length is comparable with those in 2,3,3,5-tetraphenyl-1,2,5-thiadiazolidin-4-one [1.726(11) and 1.701(9) Å][17] and also to one of the S–N bonds in 2-diphenylmethylene-3,5,7,7-tetraphenyl-2,3,6,7-tetrahydro-5H-1,4,3,5-

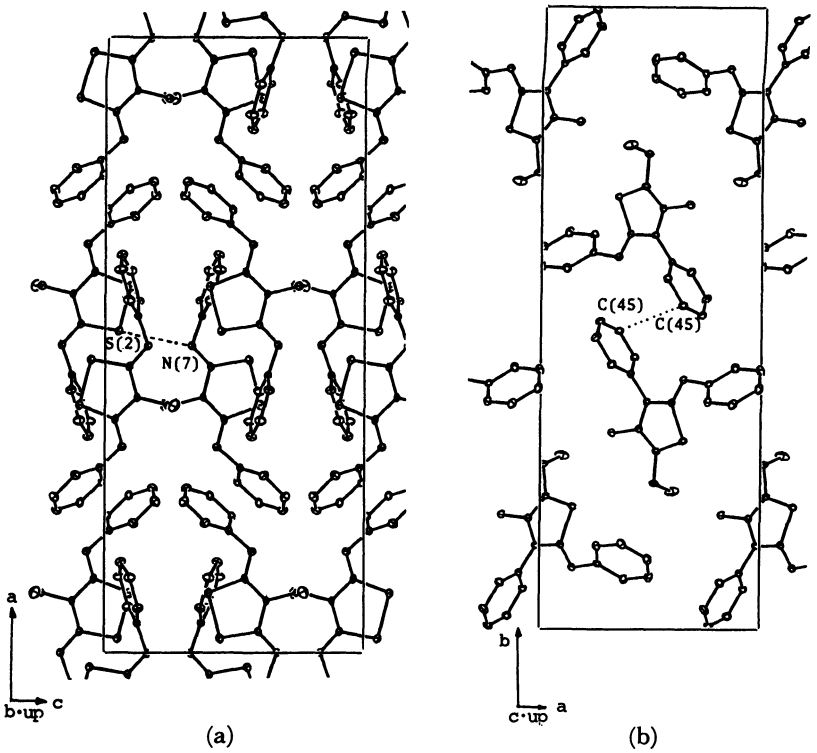

Fig. 2. Crystal structures.[9]
Non-hydrogen atoms are expressed as thermal ellipsoids with 10% probability level. Hydrogen atoms are omitted for clarity.
(a) **6b**, projected along the *b* axis, (b) **8b**, projected along the *c* axis

oxathiadiazepin-6-one [1.718(8)Å].[18] The S(1)–C(5) bond length of 1.767(3)Å is equal to those in the 1,2,4-thiadiazolidines and also equal to the S(2)–C(3) length in **6b**. Of the three C–N bonds in the ring, the C(3)–N(4) and C(5)–N(4) bonds have equal lengths [1.384(4) and 1.393(4)Å], which can be compared with the corresponding lengths in **6b**. The C(3)–N(2) [1.341(4)Å] and the C(3)=S(7) [1.654(3)Å] lengths are respectively equal to those in the 1,2,4-thiadiazolidin-3,5-dithione [1.347(5) and 1.655(4)Å]. The N(2)–S(1)–C(5) angle [90.0(2)°] is smaller than those in the 1,2,4-thiadiazolidines and the 1,2,4-thiadiazolidin-3,5-dithione. Bond angles around the N(2) and C(3) atoms are respectively equal to the corresponding angles in the 1,2,4-thiadiazolidin-3,5-dithione, and those around the N(4) and C(5) are equal to the corresponding angles in the 1,2,4-thiadiazolidines.

Crystal Structure. The packing modes of molecules in both crystals are shown in Fig. 2. In the **6b** crystal molecules are packed rather tightly (Fig. 2a), the closest intermolecular contact between non-hydrogen atoms being 3.272(4)Å(N(7)(x, y, z)···S(2)(1−x, 0.5−y, −0.5+z)). The loose packing of molecules are observed in the **8b** crystal (Fig. 2b), the shortest contact being 3.405Å between the C(45)(x, y, z) and C(45)($\bar{x}$, $\bar{y}$, $\bar{z}$) atoms (Table 3).

Table 3. Close Intermolecular Atomic Contact [l/Å] Less than 3.6Å with Estimated Standard Deviation in Parentheses

6b		
N(7)···S(2)[a]	3.272(4)	key: a, 1−x, 0.5−y, −0.5+z;
C(71)···S(1)[a]	3.391(5)	key: b, 0.5−x, y, 0.5+z;
C(72)···S(1)[a]	3.406(5)	key: c, x, 0.5+y, 0.5+z.
C(64)···N(6)[b]	3.566(6)	
C(42)···N(4)[c]	3.531(7)	
8b		
C(44)···C(46)[a]	3.534(5)	key: a, −x, −y, −z;
C(45)···C(45)[a]	3.405(7)	key: b, 0.5+x, 0.5−y, −0.5+z.
C(45)···C(46)[a]	3.432(5)	
N(6)···C(45)[a]	3.554(4)	
C(22)···S(7)[b]	3.560(5)	

The authors wish to express their deep thanks to Miss Nobuko Kanehisa for the computations at the final stage and the *ORTEP* drawings.

References

1) M. Komatsu, Y. Ohshiro, K. Yasuda, S. Ichijima, and T. Agawa, *J. Org. Chem.*, **39**, 957 (1974).
2) G. L'Abbé, *Tetrahedron*, **38**, 3537 (1982); *J. Heterocycl. Chem.*, **21**, 627 (1984), and references cited therein.
3) G. L'Abbé, E. van Loock, G. Verhelst, and S. Toppet, *J. Org. Chem.*, **40**, 607 (1975); G. L'Abbé, G. Verhelst, and S. Toppet, *ibid.*, **42**, 1159 (1977).
4) T. Ashida, *HBLS* V, "The Universal Crystallographic

Computing System-Osaka," The Computation Center, Osaka Univ., 1973, p. 55.
5) International Tables for X-Ray Crystallography, Vol. IV, Kynoch Press, Birmingham (1974), p. 71.
6) R. F. Stewart, E. R. Davidson, and T. Simpson, *J. Chem. Phys.*, **42**, 3175 (1965).
7) W. C. Hamilton, *Acta Crystallogr.*, **12**, 609 (1959).
8) M. Komatsu, Y. Ohshiro, T. Agawa, M. Kuriyama, N. Yasuoka, and N. Kasai, *J. Org. Chem.*, **51**, 407 (1986).
9) C. K. Johnson, *ORTEP* II, Report ORNL-5138, Oak Ridge National Laboratory, Tennessee (1976).
10) M. J. Begley, T. J. King, and D. B. Sowerby, *Cryst. Struct. Commun.*, **8**, 319 (1979).
11) J. L. Flippen, *J. Am. Chem. Soc.*, **95**, 6073 (1973).
12) J. Sletten and O. C. Lφkke, *Acta Chem. Scand.*, **A31**, 271 and 423 (1975).
13) C. Christophersen, T. Øttersen, K. Seff, and S. Treppendahl, *J. Am. Chem. Soc.*, **97**, 5237 (1975).
14) T. Kinoshita, S. Sato, and C. Tamura, *Bull. Chem. Soc. Jpn.*, **49**, 2236 (1976).
15) S. Sato, T. Kinoshita, T. Hata, and C. Tamura, *Acta Crystallogr., Sect. B.*, **33**, 550 (1977) and **36**, 2703 (1980).
16) C. L. Raston, A. H. White, and A. C. Willis, *J. Chem. Soc., Perkin Trans. 2*, **1974**, 1096.
17) N. Yasuoka, N. Kasai, T. Minami, Y. Ohshiro, T. Agawa, and M. Kakudo, *Bull. Chem. Soc. Jpn.*, **43**, 1905 (1970).
18) T. Minami, K. Yamataka, Y. Ohshiro, T. Agawa, N. Yasuoka, and N. Kasai, *J. Org. Chem.*, **37**, 3810 (1972).

 © 1986 The Chemical Society of Japan Bull. Chem. Soc. Jpn., 59, 993—996 (1986)

Fluorescence Quenching of Perfluoronaphthalene by Triethylamine

Koji KANO,* Masaru YANAGIMOTO, Hisashi URAKI, Bin ZHOU, and Shizunobu HASHIMOTO
Department of Applied Chemistry, Faculty of Engineering, Doshisha University, Kamikyo-ku, Kyoto 602
(Received November 8, 1985)

The relatively fast fluorescence quenching of perfluoronaphthalene by triethylamine as well as the lack of the exciplex emission of this system has been interpreted in terms of the electron transfer from triethylamine to photoexcited perfluoronaphthalene, where the electron donor-acceptor pair takes a loose geometric configuration.

Some hydrocarbons have been known to yield exciplexes through a charge-transfer interaction with aromatic or aliphatic amines.[1] In some cases, the exciplexes show broad fluorescence bands at longer wavelengths in nonpolar solvents.[2] The possibility of a direct electron transfer which yields a solvent-separated ion pair has been accounted for the absence of exciplex emission in strongly polar solvents.[3] The exciplex formation is also affected by the structures of amines as electron donors. Although aromatic amines such as *N,N*-dimethyl- and *N,N*-diethylanilines form the exciplexes with hydrocarbons with diffusion-controlled rates,[4] the rates of exciplex formation for aliphatic amines are smaller by one order of magnitude.[5] The conformational change of aliphatic amine from pyramidal to planar is required for exciplex formation. Such geometric requirement causes larger activation energy for exciplex formation.[5] Some hydrocarbons such as pyrene and naphthalene are known to form the fluorescent exciplexes with aliphatic amines.[5,6]

The present study deals with the effects of the fluorine substituents attached to the naphthalene ring on photoinduced electron transfer and exciplex formation. The results suggest an electron transfer from triethylamine (TEA) to perfluorinated naphthalene in the excited state prior to exciplex formation.

Experimental

Materials. Octafluoronaphthalene (perfluoronaphthalene, PFN, Tokyo Kasei) was recrystallized from cyclohexane. Naphthalene (Nakarai) was purified by sublimation. 1-Fluoronaphthalene (1-FN, Tokyo Kasei), triethylamine (TEA, Nakarai), and perfluorohexane (PFH, PCR Research Chemicals) were purchased and used without further purification. All solvents used were analytical or reagent grades.

Measurements. The absorption spectra were taken on a Shimadzu UV-200S spectrophotometer. The fluorescence emission and excitation spectra were measured on a Shimadzu RF-540 or a Hitachi 650-60 spectrofluorometers whose cell compartments were thermostated at 298 K. The phosphorescence spectra were taken on a Hitachi 650-60 spectrofluorometer using an attachment 650-0175 for phosphorescence measurement at 77 K. The fluorescence spectra at 77 K were measured on a Shimadzu RF-540 spectrofluorometer using a Dewar vessel described previously.[7] The fluorescence lifetimes were determined by using an Ortec-PRA single-photon counting appratus.[8] The fluorescence quantum yields were determined by measuring the corrected fluorescence spectra on a Hitachi 650-60 spectrofluorometer and using quinine sulfate as a standard.[9]

Results and Discussion

Absorption and Fluorescence Spectra. Introduction of the fluorine substituents into the naphthalene ring causes red shifts of the ^1L_a and ^1L_b bands, broadening of the vibronic structures of these bands, and increase in the intensities of the ^1L_b bands. The extinction coefficients of the 0–0 bands of naphthalene, 1-FN, and PFN in cyclohexane are 274 $M^{-1}cm^{-1}$ at 311.5 nm, 631 $M^{-1}cm^{-1}$ at 317 nm, and 2367 $M^{-1}cm^{-1}$ at 323 nm, respectively.

The fluorescence maxima in hexane are 313(sh), 323, 332(sh), 336, and 344(sh) nm for naphthalene, 317, 321(sh), 332, 336(sh), and 348 nm for 1-FN, and 348 nm for PFN. PFN shows a structureless fluorescence in solutions at 25 °C. The fluorescence quantum yield (Φ_f) of 1-FN determined in degassed hexane (0.23±0.010) is the same as that of naphthalene (0.22±0.010) and Φ_f of PFN (0.10±0.015) is about half of those of naphthalene and 1-FN. The fluorine substituents introduced to the naphthalene ring markedly reduce the fluorescence lifetimes (τ_f), the τ_f values of naphthalene, 1-FN, and PFN being 120, 42.5, and 3.1 ns, respectively. The rate constants for the emission process ($k_f=\Phi_f/\tau_f$) increased in the order of naphthalene ($1.8\times10^6\,s^{-1}$), 1-FN ($5.4\times10^6\,s^{-1}$), and PFN ($3.2\times10^7\,s^{-1}$). The S_0–S_1 transition of naphthalene is orbital symmetry forbidden. For PFN, however, this transition may be partially allowed.

Fluorescence Quenching. The fluorescence of naphthalene, 1-FN, and PFN were quenched by TEA and the data could be treated by a simple Stern-Volmer equation. The rate constants for fluorescence quenching (k_q) determined from the plots of I_0/I vs. [TEA] are listed in Table 1, where I_0 and I are the fluorescence intensities in the absence and presence of quencher, respectively.

As the TEA concentration increased, the broad exciplex emissions appeared at longer wavelengths in the cases of naphthalene and 1-FN when ethyl acetate, cyclohexane, hexane, and PFH were used as the solvents. The emission maxima of the exciplexes are shown in Table 1. Of course, no exciplex emission was observed in polar solvents such as ethanol and

Table 1. Rate Constants for Fluorescence Quenching (10^{-9} k_q, $mol^{-1}dm^3s^{-1}$) of Naphthalene, 1-FN, and PFN by TEA and Fluorescence Maxima (λ_{max}, nm) of Exciplexes of These Naphthalene Derivatives and TEA in Various Solvents at 298 K

Solvent	Naphthalene		1-FN		PFN	
	k_q	λ_{max}	k_q	λ_{max}	k_q	λ_{max}
Acetonitrile	5.5	a	8.7	a	10.8	a
Ethanol	1.0	a	1.5	a	3.5	a
Ethyl acetate	4.9	473	6.9	482	10.8	a
Cyclohexane	3.4	413	4.8	417	10.1	a
Hexane	1.0	413	5.8	418	14.3	a
Perfluorohexane	5.7	402	7.6	417	19.0	a

a) No exciplex emission was observed.

acetonitrile. Interestingly, PFN did not show the exciplex emission in any solvents used in spite of the quenching of the monomer fluorescence by TEA. Van and Hammond reported the dipole moment of the naphthalene–TEA exciplex to be 11.1 D,[6] which has been determined from a plot of energies of exciplex emission maxima vs. solvent polarity parameters ($f(\varepsilon,n)$).[10] The same plot provided a dipole moment of an exciplex of 1-FN and TEA to be 11.6 D. Since an electron transfers almost completely from donor to acceptor in the exciplex system, no effect of a fluorine substituent of the acceptor molecule seems to be observed.

As Table 1 shows, the fluorine substituents introduced to the naphthalene ring enhanced the fluorescence quenching. In agreement with the results obtained by Van and Hammond,[6] the rate of fluorescence quenching of naphthalene by TEA in each nonpolar solvent was smaller than the diffusion-controlled rate, which may be attributed to the higher activation energy for forming exciplexes because of a conformational change of aliphatic amines to form exciplexes.[5] By the way, relatively large k_q values were obtained for the quenching in acetonitrile. In strongly polar solvents, electron transfer is known to occur from loose electron donor–acceptor pairs prior to exciplex formation.[3] A major factor which dominates the k_q values in strongly polar solvents including acetonitrile, therefore, may be the diffusion rates of both donor and acceptor molecules. The fluorescence quenching of 1-FN by TEA occurred more efficiently than that of naphthalene. Extremely fast fluorescence quenching proceeded in the case of PFN where the k_q value in each solvent is very close to the diffusion-controlled rate constant. In the system where an exciplex needs forming upon fluorescence quenching, the quenching should be accelerated by substituent(s) if the substituent(s) can stabilize the exciplex state. This may be the case for the fluorescence quenching of 1-FN in nonpolar solvents. A fluorine substituent, a strongly electronegative substituent, should stabilize an anionic form of the naphthalene moiety in the exciplex leading to lowering of the activation energy for exciplex formation. The situation of PFN seems to be different from those of naphthalene and 1-FN because no exciplex emission was detected in this system. No ground-state interaction between donor and acceptor molecules was suggested for all cases by means of the absorption spectroscopy.

Irreversible photoreactions of PFN (1×10^{-4} mol dm^{-3}) took place in both hexane and acetonitrile solutions containing TEA (1×10^{-3} mol dm^{-3}) under anaerobic conditions. Upon irradiation with an Hg lamp, a photoproduct having absorption maximum at around 380 nm was generated. Although we did not determine the reaction product(s) in the present study, the radical ion pairs of PFN and TEA should be generated as the intermediates. Dehalogenation is the most plausible photoreactions.[11]

Fluorescence at 77 K. In methylcyclohexane matrices at 77 K, the relative fluorescence intensity of the naphthalene derivatives decreased in the order of 1-FN, naphthalene, and PFN and weak phosphorescence emissions of these naphthalene derivatives were observed at longer wavelengths (Fig. 1). The difference in the fluorescence and phosphorescence yields between these naphthalene derivatives is appreciable, but not very large.

In glassy TEA at 77 K, the relatively strong monomer fluorescence emissions of naphthalene and 1-FN were observed along with the weak exciplex fluorescence and monomer phosphorescence emissions (Fig. 2). The monomer fluorescence of PFN, however, was quenched almost completely and very weak exciplex emission centered at 420 nm was observed in neat TEA at 77 K. The exciplex emissions of naphthalene and 1-FN in the TEA matrices decayed multiexponentially without rise (the data are not shown), suggesting that several exciplex states are formed immediately upon photoexcitation. Some of the naphthalene and 1-FN molecules may make pairs with TEA molecules which have preferable geometric configurations for exciplex formation. Large amounts of the naphthalene and 1-FN molecules seem to exist without any interaction with surrounding TEA molecules. In the case of PFN, however, most of the PFN molecules were quenched by surrounding TEA molecules, whose mobility was strictly restricted. It is reasonable, therefore, to assume a

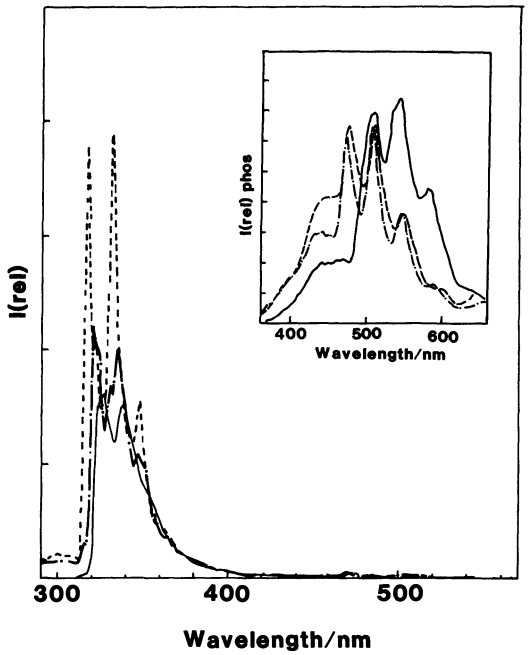

Fig. 1. Fluorescence and phosphorescence spectra of naphthalene (—·—), 1-FN (---), and PFN (——) in methylcyclohexane at 77 K. Naphthalene, 1-FN, and PFN (1×10^{-5} mol dm^{-3}) were excited at 278, 281, and 290 nm, respectively. The insert shows the phosphorescence spectra.

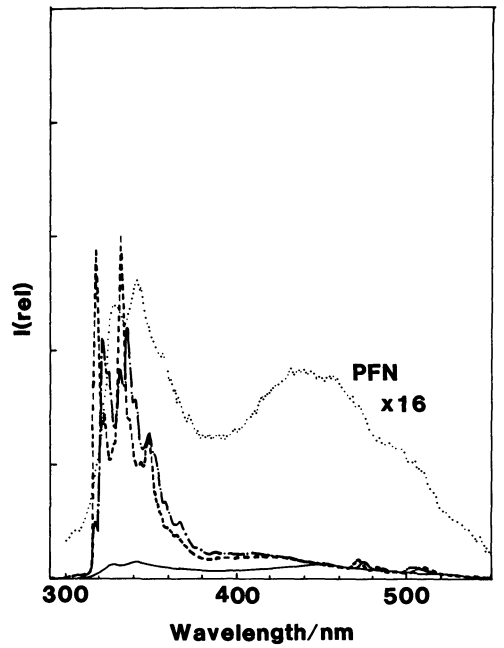

Fig. 2. Fluorescence spectra of naphthalene (—·—), 1-FN (---), and PFN (——) in TEA at 77 K. Naphthalene, 1-FN, and PFN (1×10^{-5} mol dm^{-3}) were excited at 279, 282, and 290 nm, respectively.

long-distance interaction between PFN and TEA. It is noteworthy that the exciplex emission for the PFN–TEA system is observed only in the TEA matrix. PFN can form a fluorescent exciplex with TEA if these two molecules take an appropriate configuration

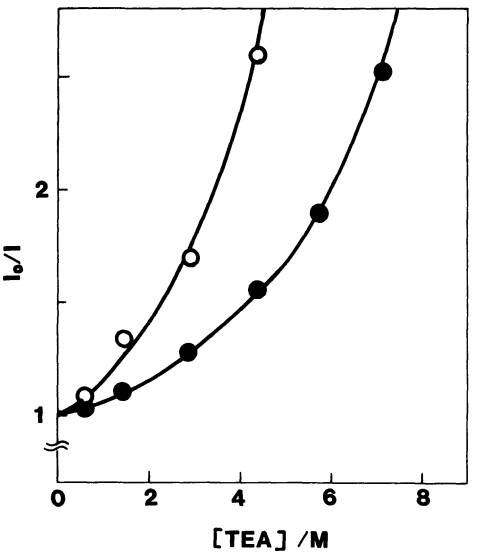

Fig. 3. Plots of I_0/I vs. [TEA] for the fluorescence quenching of naphthalene (●) and PFN (○) in EPA at 77 K.

for forming an exciplex. In fluid organic solvents, however, no exciplex emission of this donor-acceptor pair was observed at any TEA concentrations. These observations strongly suggest the fluorescence quenching of PFN by TEA prior to the exciplex formation.

Figure 3 shows the plots of I_0/I vs. [TEA] for the fluorescence quenching of naphthalene and PFN in the EPA (diethyl ether:isopentane:ethanol=5:5:2) matrices at 77 K. Although a Stern-Volmer linear relationship was observed in fluid media, the plots were deviated upward from the straight lines for the fluorescence quenching in the rigid matrices. Since both fluorescer and quencher molecules cannot move freely in glassy EPA, only donor-acceptor pairs within an interaction radius can participate in fluorescence quenching. The fluorescent state of PFN was quenched more efficiently than that of naphthalene at each quencher concentration in rigid medium. This clearly indicates that an interaction radius for the PFN–TEA system is larger than that for the naphthalene–TEA system. The data shown in Fig. 3, therefore, support a long-distance electron transfer via a loose donor-acceptor pair in the PFN–TEA system.

This work was supported by Grant-in-Aid for Scientific Research No. 59550560 from the Ministry of Education, Science and Culture.

References

1) For reviews, see: "The Exciplex," ed by M. Gordon and W. R. Ware, Academic Press, New York (1975); N. Mataga and M. Ottolengi, "Molecular Association," ed by R. Foster, Academic Press, London (1979), Vol. 2, Chap. 1; H. Masuhara and N. Mataga, *Acc. Chem. Res.*, **14**, 312 (1981).

2) H. Leonhardt and A. Weller, *Ber. Bunsenges. Phys. Chem.*, **67**, 791 (1963); N. Mataga, T. Okada, and K. Ezumi, *J.*

Mol. Phys., **10**, 201 (1966).

3) H. Knibbe, K. Röllig, F. P. Schäfer, and A. Weller, *J. Chem. Phys.*, **47**, 1184 (1967); Y. Taniguchi, Y. Nishina, and N. Mataga, *Bull. Chem. Soc. Jpn.*, **45**, 764 (1972).

4) W. R. Ware and H. P. Richter, *J. Chem. Phys.*, **48**, 1595 (1968); K. Yoshihara, T. Kasuya, A. Inoue, and S. Nagakura, *Chem. Phys. Lett.*, **9**, 469 (1971); M. -H. Hui and W. R. Ware, *J. Am. Chem. Soc.*, **98**, 4718 (1976).

5) N. Nakashima, N. Mataga, F. Ushio, and C. Yamanaka, *Z. Phys. Chem. (Frankfurt am Main)*, **79**, 150 (1972); N. Nakashima, N. Mataga, and C. Yamanaka, *Int. J. Chem. Kinet.*, **5**, 833 (1973); A. Nakajima, *Bull. Chem. Soc. Jpn.*, **42**, 3409 (1969).

6) S. -P. Van and G. S. Hammond, *J. Am. Chem. Soc.*, **100**, 3895 (1978).

7) K. Kano, B. Zhou, and S. Hashimoto, *J. Phys. Chem.*, **89**, 3748 (1985).

8) K. Kano, Y. Ueno, K. Umakoshi, S. Hashimoto, T. Ishibashi, and T. Ogawa, *J. Phys. Chem.*, **88**, 5087 (1984).

9) J. N. Demas and G. A. Crosby, *J. Phys. Chem.*, **75**, 991 (1971).

10) Y. Ooshika, *J. Phys. Soc. Jpn.*, **9**, 594 (1954); E. G. McRae, *J. Phys. Chem.*, **61**, 562 (1957).

11) K. Hamanoue, S. Tai, T. Hidaka, T. Nakayama, M. Kimoto, and H. Teranishi, *J. Phys. Chem.*, **88**, 4380 (1984).

 © 1986 The Chemical Society of Japan Bull. Chem. Soc. Jpn., 59, 997—1000 (1986)

Ion-Chromatographic Determination of Valproic Acid

Hisaaki ITOH,* Yoshio SHINBORI, and Norihiro TAMURA†
Faculty of Pharmaceutical Sciences, Josai University, Sakado, Saitama 350-02
†Josai Dental University, Sakado, Saitama 350-02
(Received October 15, 1985)

A new direct chromatographic assay method of valproic acid (2-propylpentanoic acid) using a carbonic acid solution as the eluent and conductivity detection was developed and applied to its determination in Depakene tablets and human plasma. The analytical recovery and the coefficients of variation of the method obtained by the use of drug-free plasma samples spiked with various amounts of valproic acid were ranged from 96.5 to 104% and from 3.2% at 12.4μg cm^{-3} to 0.8% at 124μg cm^{-3}, respectively. No interference from the plasma constituents or from other anticonvulsants was observed. The procedure is simple, fast, specific, and precise. The plasma levels of valproic acid obtained from patients receiving sodium valproate together with other anticonvulsants are indicated.

Valproic acid is the free-acid form of the drug marketed under the names of Valerin, Depakene and Sodium Valproate; it is clinically used as an anticonvulsant in the treatment of epilepsy.

Recently, several methods have been described in the literature for the analysis of valproic acid in plasma. These include gas chromatography (GC),[1-7] high-performance liquid chromatograpny (HPLC),[8-13] and enzyme immunoassay (EMIT).[14-17] Although a number of methods have been reported, certain problems still remain such as the assay being time-consuming, expensive, nonspecific, and/or insensitive. Three major characteristics of valproic acid which have restricted the development of an analytical method are its poor ultraviolet absorbance, its high volatility as a free acid, and its relatively high adsorptive power onto the GC column packings.[1,5] Because of this poor ultraviolet absorption, a direct sensitive assay of valproic acid by HPLC is difficult. In order to overcome this problem, derivatization to a chromophoric species, such as phenacyl,[10,13] 4-bromophenacyl[12] and 2-naphthylcarbonylmethyl esters,[11] has been necessary.

On the other hand, the GC methods are usable for the direct analysis of carboxylic acids. However, these methods are mostly limited to short-chain fatty acids. In order to improve the separation characteristics and the detection sensitivity of valproic acid, many efforts have been made.[2,5,7] More recently, Rege et al.[6] have reported that, for the GC method, the derivatization of valproic acid to the phenacyl ester was effective in its determination in plasma, although the method required extraction and evaporation steps.

The EMIT method is simple and fast, but requires some expensive reagents. However, a critical comparision of the GC and EMIT methods has been reported recently showing that, although the two methods produced no statistical differences in control samples, there was a highly significant proportional error of 26% when the same patient sample was split and analyzed by both methods.[17] The higher EMIT values for patients' samples than those with GC were probably due to the cross-reactivity of some unsaturated metabolites of valproic acid, which may interfere with the enzyme immunoassay.

In this paper, we describe a novel method for the analysis of valproic acid in drug and human plasma. Having noticed that valproic acid is a fatty acid and has the pK_a of 2.5,[18] we examined its determination by the ion-exclusion technique using a carbonic acid solution as the eluent and conductivity detection.[19] The procedure is simple, fast, specific, and precise.

Experimental

Materials. The sodium valproate was obtained from Kyowa Hakko (Tokyo, Japan). The depakene tablets were from commercial sources. All the other chemicals were of an analytical grade. A stock solution of sodium valproate was prepared by dissolving the salt in distilled and deionized water. Plasma samples were stored at −20°C.

Chromatographic System. Analyses were performed using a Dionex M-10 Ion Chromatograph equipped with a conductivity detector. The details of the modification of the system, except for a guard and a separator column, have been described in a previous paper.[19] The guard column was made by packing the Aminex Q-150S resin, which is a high-capacity cation exchanger, into a glass column(3 mm i.d.×50 mm). On the other hand, the separator column was made by repacking the Dionex ICE separator resin[19] as a slurry into a glass column(6 mm i.d.×65 mm). The column conditioning was performed as follows. At the flow rate of 0.7 cm^3 min^{-1}, both columns were first rinsed with deionized water for 60 min, then with a 0.5 mol dm^{-3} sulfuric acid solution for 40 min, and again with deionized water for 40 min, and then finally they were equilibrated with an eluent solution.

Procedures. Drug Sample: A tablet of Depakene (200 mg as sodium valproate) was dissolved in deionized water in a volumetric flask(500 cm^3). 5 cm^3 of the solution was diluted to 100 cm^3 with deionized water. This diluted solution was injected onto the chromatograph through the filter(0.42 μm).

Plasma Sample: A plasma sample was mixed with an equivolume of a 0.1 mol dm^{-3} sodium hydroxide solution and then with eight volumes of acetonitrile by means of a Voltex-type mixer. After centrifugation for 5 min at 3000 rpm, the supernatant was diluted with an equivolume of deionized water. An aliquot of the solution was then injected onto the

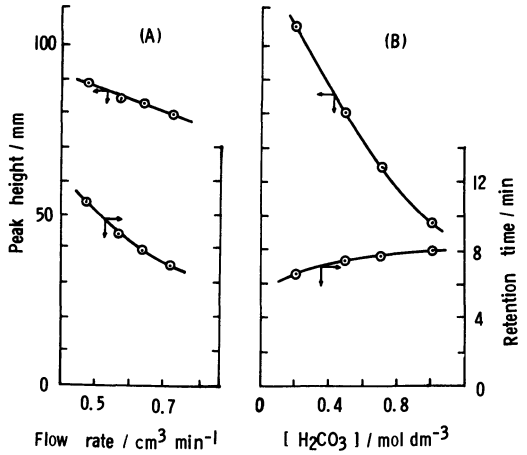

Fig. 1. Variations in the retention time and in the peak height of valproic acid with the flow rate(A) and with the concentration of carbonic acid in the eluent. All chromatographic conditions are the same as shown in Table 1 except for the flow rate(A) and the concentration of carbonic acid in eluent(B). Valproic acid: 10.0 μg cm^{-3}.

chromatograph.

Results and Discussion

1. Elution Behavior of Valproic Acid. At first, as a separator, we tried to use a Dionex ICE separator column(9 mm i.d.×200 mm), which has been used for the separation of low-molecular-weight organic acids.[19,20] However, in this case, using a 0.5 mmol dm^{-3} H_2CO_3 eluent at a flow rate of 0.7 cm^3 min^{-1}, valproic acid was eluted as a broad peak at about 60 min. After considerable exploratory experiments directed at faster elution and a more sensitive detection of valproic acid, we found that the small column described above was fit for our purposes. By the use of this small column, the elution characteristics of valproic acid were investigated. Figure 1 shows the variations in the retention time and in the peak height of valproic acid with the flow rate(A) and with the concentration of carbonic acid in the eluent(B). With the increase in the concentration of carbonic acid in the eluent, — that is, with the decrease in the pH of the eluent[19] accompanied by an increase in the background conductivity, the variation in the retention time is not very much, but the decrease in the peak height, that is, the detector response, is quite large. On the other hand, the increase in the flow rate does not appreciably affect the peak height, but makes the retention time decrease sharply. In other words, the use of a low concentration of carbonic acid in the eluent is effective for the more sensitive detection of, and the higher flow rate is effective for the faster elution of, valproic acid. Thus, the chromatographic conditions were set as shown in Table 1.

2. Valproic Acid in Drugs. The calibration curve constructed by the use of the peak height of a standard solution was linear from 0.2 to 25 μg cm^{-3}. The detection limit of the assay was 50 ng cm^{-3} of valproic acid in the sample solution. Figure 2 shows a typical chromatogram obtained from the analysis of valproic acid in a Depakene® sample solution.

Table 1. Chromatographic Conditions

Eluent	:	0.5 mmol dm^{-3} H_2CO_3
Guard column	:	3 mm i.d.×50 mm Aminex Q-150S resin column
Separator	:	6 mm i.d.×65 mm Dionex ICE separator resin column
Flow rate	:	0.7 cm^{-3} min^{-1}
Sample loop	:	50 mm^3
Meter setting	:	1 μS

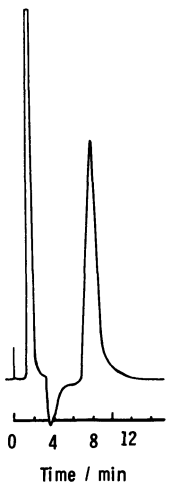

Fig. 2. Chromatogram of valproic acid in Depakene® tablet sample solution.
All chromatographic conditions are the same as shown in Table 1.

The precision and accuracy of the method were examined by analyzing valproic acid in Depakene® tablets. Against the calculated value (17.35 μg cm^{-3}) from the appended content table, the assay for three sample solutions prepared by following the procedure indicated 17.37—17.44 μg cm^{-3}. Furthermore three Depakene® sample solutions spiked with valproic acid (5 μg cm^{-3}) were also analyzed. Recoveries ranging from 99.4% to 100.2% was obtained. It was thus proven that the method was satisfactorily precise and accurate.

3. Valproic Acid in Plasma. In analyzing biological samples by the chromatographic method, it is always a great problem how to carry out deproteinization while retaining an adequate recovery of the material of interest. In order to ascertain the optimal conditions for deproteinization, a study using a drug-free plasma sample spiked with valproic acid (40 μg) was performed.

Optimization of Deproteinization Conditions. Afer considerable exploratory experiments by the use of such solutions as methanol, acetonitrile, hydrochloric

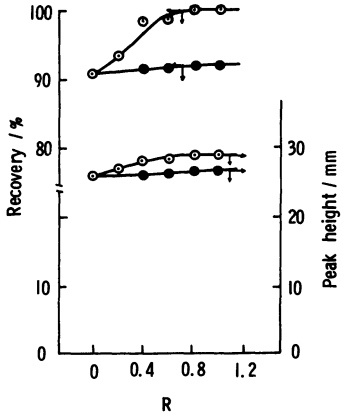

Fig. 3. Effect of acid and base on valproic acid recovery in deproteinization step.
All chromatographic conditions are the same as shown in Table 1. R: the volume ratio denoted in 0.1 mol dm^{-3} hydrochloric acid (●) and/or sodium hydroxide solution (⊙) to plasma.

Table 2. Analytical Recovery and Precision Data of Valproic Acid in Human Plasma

Sample No.	Added	Found	C.V.	Recovery
	μg cm^{-3}	μg cm^{-3} Mean±s.d.	%	%
1	12.4	12.6±0.4	3.2	102
2	17.3	16.7±0.5	3.0	96.5
3	24.8	24.3±0.4	1.6	98.0
4	34.6	34.6±0.6	1.7	100
5	52.0	54.1±0.5	0.9	104
6	86.8	87.7±0.8	0.9	101
7	121	120 ±1	0.8	99.2
8	124	126 ±1	0.8	102

acid, and sodium hydroxide and/or SEP-PAK® C_{18} cartridges (Waters Associates, Massachusetts), it was found that the complete recovery of valproic acid could be obtained by the addition of 0.1 mol dm^{-3} of a sodium hydroxide solution with a volume ratio of 0.8 or more(sodium hydroxide solution to plasma) prior to the addition of acetonitrile, as is shown in Fig. 3. In this case, the valproic acid recovery was calculated by comparing the peak height of the valproic acid obtained from the sample solution prepared by spiking with valproic acid before and after the deproteinization treatment.

Calibration Curve. The calibration curve was constructed by the use of a drug-free plasma spiked with valproic acid. The curve using the peak height was linear over the concentration range of 5—200 μg of valproic acid in 1.0 cm^3 of plasma. The detection limit of the plasma assay was 2 μg cm^{-3} of valproic acid.

Analytical Recovery and Precision. The analytical recovery and precision of the method were determined by analyzing plasma samples spiked with various known amounts of valproic acid. The results are shown in Table 2. The recovery of valproic acid was in the range from 96.5% to 104%. The coefficients of variation ranged from 3.2% at 12.4 μg cm^{-3} to 0.8% at 124 μg cm^{-3}. The procedure was found to be satisfactorily reproducible and precise.

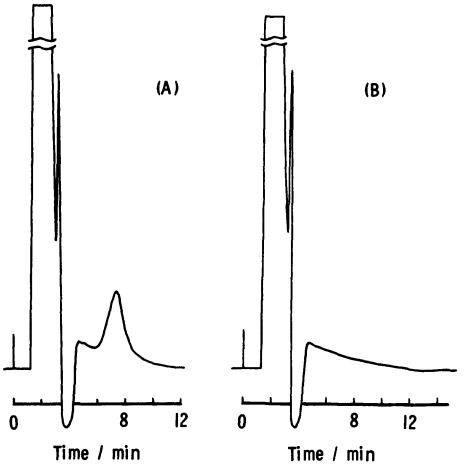

Fig. 4. Chromatograms of valproic acid in human plasma.
All chromatographic conditions are the same as shown in Table 1. (A): plasma from a patient receiving treatment with sodium valproate together with other anticonvulsants. (B): plasma from a patient receiving treatment with some anticonvulsants other than sodium valproate.

Figure 4(A) shows a typical chromatogram obtained from the analysis of valproic acid in a plasma sample containing other anticonvulsants(primidone, ethotoin, clonazepam, and acetazolamide). Figure 4(B) also shows a chromatogram obtained by means of a plasma sample from a patient receiving treatment with primidone, ethotoin, sulthiame, and clonazepam. No interference from the plasma constituents or other anticonvulsants was observed.

Valproic-Acid Levels in Patient Plasma. The assay was performed on plasma from patients receiving sodium valproate together with various anticonvulsants, such as primidone, sulthiame, ethotoin, phenytoin, clonazepam, diazepam, acetazolamide, and carbamazepine. The results are shown in Table 3. These data indicated that the plasma levels of valproic acid were in the range of 24—74 mg dm^{-3} when daily medication was between 10—91 mg kg^{-1}. There were, however, marked variations among different patients in the relationship between drug dose and plasma level.

The authors wish to express their thanks to Mr. Toshio Nishida of the Shimoshizu Byoin National Sanatorium, and Professor Naosi Maeshiro, Department of Psychiatry, Saitama Medical University, for kindly supplying the plasma samples. We also would like to thank Professor Shigero Ikeda of Osaka University for his helpful suggestions.

Table 3. Plasma Levels of Valproic Acid from Patients Receiving Sodium Valproate

Patient	Weight	Daily medication		Time after administration	Plasma level
	kg	mg	mg kg^{-1}	h	mg dm^{-3}
1	23	2100	91	2.0	68
				15.0	39
2	21	1800	86	2.0	54
				15.0	36
3	22	1500	68	2.0	63
				15.0	51
4	37	2400	65	2.0	71
				15.0	31
5	50	1200	24	2.5	74
6	52	1200	23	4.2	60
7	54	800	15	4.0	24
8	56	800	14	4.0	24
9	57	800	14	3.5	70
10	59	600	10	3.0	34

References

1) L. J. Dusci and L. P. Hackett, *J. Chromatogr.*, **132**, 145 (1977).
2) R. N. Gupta, F. Eng, and M. L. Gupta, *Clin. Chem.*, **25**, 1303 (1979).
3) F. M. Runci and G. Segre, *Farmaco, Ed. Pract.*, **34**, 261 (1979).
4) G. A. Peyton, S. C. Harris, and J. E. Wallace, *J. Anal. Toxicol.*, **3**, 108 (1979).
5) M. I. Arranz Pena, *J. Chromatogr.*, **225**, 459 (1981).
6) A. B. Rege, J. J. L. Lertora, L. E. White, and W. J. George, *J. Chromatogr.*, **309**, 397 (1984).
7) F. Andreolini, C. Borra, A. Di Corcia, and R. Saperi, *J. Chromatogr.*, **310**, 208 (1984).
8) G. J. Shmidt and W. Slavin, *Chromatogr. Newslett.*, **6**, 22 (1978).
9) R. Farinotti, M. C. Pfaff, and G. Mahuzier, *Ann. Biol. Clin.*, **36**, 347 (1978).
10) R. N. Gupta, P. M. Keane, and M. L. Gupta, *Clin. Chem.*, **25**, 1984 (1979).
11) R. Alric, M. Cociglo, J. P. Blayac, and R. Puech, *J. Chromatogr.*, **224**, 289 (1981).
12) H. Cisse, R. Farionotti, S. Kirkiacharian, and A. Dauphin, *J. Chromatogr.*, **225**, 509 (1981).
13) M. Nakamura, K. Kondo, R. Nishioka, and S. Kawai, *J. Chromatogr.*, **310**, 450 (1984).
14) H. Miura, K. Minagawa, T. Kaneko, and Y. Sudo, *Kitazato Igaku*, **10**, 570 (1980).
15) Y. Kohda, K. Nishihara, Y. Saito, F. Nakagawa, and Z. Tamura, *Igaku no Ayumi*, **115**, 813 (1980).
16) S. L. Braun, A. Tausch, W. Vogt, K. Jacob, and M. Knedel, *Clin. Chem.*, **27**, 169 (1981).
17) A. H. Kumps, B. Kumps-Grandjean, and Y. Mardens, *Clin. Chem.*, **27**, 1788 (1981).
18) "Dictionary of Organic Compounds," ed by J. R. A. Pollock, R. Stevens, Eyre & Spottiswoode Publishers, London (1965), Vol. 5, p. 2799.
19) H. Itoh and Y. Shinbori, *Chem. Lett.*, **1982**, 2001; *Bull. Chem. Soc. Jpn.*, **58**, 3244 (1985).
20) W. R. Rich, E. Johnson, L. Lois, B. E. Stafford, P. M. Kabara, and L. J. Marton, "Liquid Chromatography in Clinical Analysis," ed by L. J. Marton and P. M. Kabara, The Humana Press, New Jersey (1981), Chap. 17, pp. 393—407.

Preparation and Stereochemistry of Cobalt(III) Complexes Containing 2,11-Diphenyl-5,8-diaza-2,11-diphosphadodecane or (4*S*,9*S*)-4,9-Dimethyl-2,11-diphenyl-5,8-diaza-2,11-diphosphadodecane, $(C_6H_5)(CH_3)PCH_2CHRNHCH_2CH_2NHCHRCH_2P(CH_3)(C_6H_5)$ (R=H or CH_3)

Masamichi Atoh, Kazuo Kashiwabara, and Junnosuke Fujita*
Department of Chemistry, Faculty of Science, Nagoya University, Chikusa-ku, Nagoya 464
(Received November 5, 1985)

New quadridentate ligands having two chiral phosphorus donor atoms, 2,11-diphenyl-5,8-diaza-2,11-diphosphadodecane (mp-PNNP) and (4*S*,9*S*)-4,9-dimethyl-2,11-diphenyl-5,8-diaza-2,11-diphosphadodecane (*SS*(C)-mp-PNNP), and their cobalt(III) complexes, *trans*-$[CoCl_2$(mp- or *SS*(C)-mp-PNNP)$]^+$ and *cis*β-[Co(acac)(mp- or *SS*(C)-mp-PNNP)$]^{2+}$ (acac=2,4-pentanedionate ion) were prepared and characterized. For both mp- and *SS*(C)-mp-PNNP, the dichloro and acac complexes formed three and four isomers, respectively, which were separated by column chromatography or fractional crystallization. No *cis*α-acac complex was yielded. The acac complexes of *SS*(C)-mp-PNNP formed a Λ-isomer stereoselectively. The absolute configurations of the phosphorus donor atoms in the *SS*(C)-mp-PNNP complexes were assigned on the basis of the ^1H NMR and CD spectra. It was shown that the phosphorus donor atoms at chemically unequivalent coordination positions in *cis*β-[Co(acac)(*SS*(C)-mp-PNNP)$]^{2+}$ give remarkably different vicinal effects on the CD spectra.

In previous papers, we have reported preparation and stereochemistry of octahedral cobalt(III) complexes containing new quadridentate phosphine ligands of the PNNP type, $(R_2PCH_2CH_2NHCH_2-)_2$ (R=CH_3: mm-PNNP, R=C_6H_5: pp-PNNP),[1] and the optically active methyl-substituted derivatives, $(R_2PCH_2CH(CH_3)NHCH_2-)_2$ (R=CH_3: *SS*(C)-mm-PNNP, R=C_6H_5: *SS*(C)-pp-PNNP).[2] These PNNP complexes formed selectively particular geometrical or optical isomers. Introduction of asymmetric phosphorus donor atoms into the PNNP-type ligands will cause new stereoselectivity in the complex formation, and will give useful information for studying chiral phosphine complexes, which have little been studied.[3] This paper concerns preparation and stereochemistry of two new chiral phosphine ligands, 2,11-diphenyl-5,8-diaza-2,11-diphosphadodecane (mp-PNNP) and (4*S*,9*S*)-4,9-dimethyl-2,11-diphenyl-5,8-diaza-2,11-diphosphadodecane (*SS*(C)-mp-PNNP), and their cobalt(III) complexes, *trans*-$[CoCl_2$(mp- or *SS*(C)-mp-PNNP)$]^+$ and *cis*β-[Co(acac)(mp- or *SS*(C)-mp-PNNP)$]^{2+}$ (acac=2,4-pentanedionate ion).

Experimental

Phosphine ligands, mp-PNNP and *SS*(C)-mp-PNNP were prepared and handled under an atmosphere of nitrogen until they formed cobalt(III) complexes. All solvents used for the preparation were made oxygen-free by bubbling nitrogen for 20 min immediately before use. Absorption, circular dichroism (CD) and ^1H NMR spectra were recorded on a Hitachi 323 spectrometer, a Jasco J-40CS spectropolarimeter and a Jeol JNM PMX-60 spectrometer, respectively.

Preparation of Ligands. 2,11-Diphenyl-5,8-diaza-2,11-diphosphadodecane (*RS*(P)- and *RR,SS*(P)-mp-PNNP). To liquid ammonia (200 cm^3) in a 500 cm^3 three-necked, round-bottom flask with a mechanical stirrer and a nitrogen inlet was added metallic sodium (1.33 g, 49.1 mmol) with stirring at −78 °C. After 1 h $PH(CH_3)(C_6H_5)$[4] (1.33 g, 49.1 mmol) was added dropwise and the mixture was stirred for 20 min. To the resulting yellow solution of $NaP(CH_3)(C_6H_5)$ was added $(ClCH_2CH_2NHCH_2-)_2\cdot 2HCl$[5] (3.16 g, 12.3 mmol) in small portions with stirring. Stirring was continued for 2.5 h, and then liquid ammonia was evaporated. Water (30 cm^3) and then diethyl ether (40 cm^3) were added to the residue with stirring. The ethereal layer was separated from the aqueous layer and dried over $MgSO_4$ (1.5 g). The solvent and unreacted $PH(CH_3)(C_6H_5)$ were removed by distillation (83 °C, 1300 Pa). The colorless oily residue (3.71 g) thus obtained was a mixture of *RS*(P)- and *RR,SS*(P)-mp-PNNP and used for preparing the cobalt(III) complexes without further purification and separation of the isomers.

(4*S*,9*S*)-4,9-Dimethyl-2,11-diphenyl-5,8-diaza-2,11-diphosphadodecane (*RS*(P)-, *RR*(P)-, and *SS*(P)-*SS*(C)-mp-PNNP). This ligand was obtained as oily substance by the same method as that for mp-PNNP in a yield of 2.70 g, using liquid ammonia (150 cm^3), metallic sodium (0.83 g, 36 mmol), $PH(CH_3)(C_6H_5)$ (4.5 g, 36 mmol), and (2*S*,7*S*)-2,7-dimethyl-1,8-dichloro-3,6-diazaoctane dihydrochloride[2] (2.95 g, 9.05 mmol).

Preparation of Complexes. *trans*-$[CoCl_2$(*RS*(P)-mp-PNNP)$]ClO_4$ (F-1), *trans*-$[CoCl_2$(*RR,SS*(P)-mp-PNNP)$]ClO_4$ (F-2), and *trans*-$[CoCl_2$(*RR,SS*(P)-mp-PNNP)$]ClO_4\cdot 1.5H_2O$ (F-3).[6] To *cis*-$[CoCl_2(en)_2]Cl$[7] (0.96 g, 3.36 mmol) (en: ethylenediamine) in methanol (50 cm^3) was added a mixture of *RS*(P)- and *RR,SS*(P)-mp-PNNP (1.0 g, 2.77 mmol) with stirring at room temperature. After 15 min concd HCl (1 cm^3) was added and the solution was stirred overnight at room temperature. The resulting solution was filtered to remove $[Co(en)_3]Cl_3$ precipitated. The filtrate was mixed with water (300 cm^3) and the unreacted phosphine ligand was extracted with diethyl ether (ca. 50 cm^3). The green aqueous layer was mixed with $NaClO_4\cdot H_2O$ (10 g) and the green complex was extracted twice with CH_2Cl_2 (50 cm^3×2). The extract was evaporated to dryness under reduced pressure and the residue was dissolved in methanol (100 cm^3). The solution was diluted with water (1 dm^3) and applied on a column (φ2.5 cm×120 cm) of SP-Sephadex C-25. The adsorbed product was eluted with 0.05 mol dm^{-3} HCl, giving three green bands F-1, F-2, and F-3. The eluate

containing each green band was collected, $NaClO_4 \cdot H_2O$ (5 g) was added to it, and the complex was extracted with CH_2Cl_2 (50 cm^3). The extract was evaporated to dryness under reduced pressure and the residue was dissolved again in a small amount of methanol. On addition of excess $NaClO_4 \cdot H_2O$ the solution gave green crystals, which were filtered, washed with water and air-dried. The complex obtained from the first band (F-1) was a racemic pair of $[CoCl_2(RS(P)\text{-mp-PNNP})]^+$ (*RR*(N)*RS*(P) and *SS*(N)*SR*(P) isomers), and those from the second (F-2) and the third (F-3) bands are two racemic pairs of $[CoCl_2(RR,SS(P)\text{-mp-PNNP})]^+$ (*RR*(N)*SS*(P) and *SS*(N)*RR*(P), and (*RR*(N)-*RR*(P) and *SS*(N)*SS*(P) isomers) (vide infra). Yield (F-1): 245 mg. Found: C, 40.87; H, 5.19; N, 4.39%. Calcd for $C_{20}H_{30}N_2Cl_3CoO_4P_2$: C, 40.74; H, 5.13; N, 4.75%. Yield (F-2): 100 mg. Found: C, 40.67; H, 5.05; N, 4.40%. Calcd for $C_{20}H_{30}N_2Cl_3CoO_4P_2$: C, 40.74; H, 5.13; N, 4.75%. Yield (F-3): 95 mg. Found: C, 38.98; H, 5.16; N, 4.23%. Calcd for $C_{20}H_{33}N_2Cl_3CoO_{5.5}P_2$: C, 38.95; H, 5.39; N, 4.54%. All the complexes are soluble in methanol, acetone and dichloromethane, slightly in water, but not in diethyl ether and benzene.

Λ[*RS*(P)]Δ[*SR*(P)]-*cis*β-[Co(acac)(*RS*(P)-mp-PNNP)](ClO$_4$)$_2$ and Λ[*SR*(P)]Δ[*RS*(P)]-*cis*β-[Co(acac)(*RS*(P)-mp-PNNP)](ClO$_4$)$_2$·1.5H$_2$O (see Fig. 5). A methanol solution (30 cm^3) containing *trans*-$[CoCl_2(RS(P)\text{-mp-PNNP})]ClO_4$ (100 mg, 0.17 mmol) and Li(acac) (60 mg, 0.57 mmol) was stirred for 12 h at room temperature. The resulting red solution was diluted with water (200 cm^3) and applied on a column (ϕ2.5 cm×100 cm) of SP-Sephadex C-25. The adsorbed product was eluted with 0.2 mol dm^{-3} NaCl, giving two red bands. The eluate containing each band was collected, evaporated to dryness under reduced pressure, and the complex in the residue was extracted with ethanol (50 cm^3). The extract was evaporated to dryness, and the residue was dissolved in water (10 cm^3). On addition of $NaClO_4 \cdot H_2O$ (ca. 1.0 g) the solution gave a red precipitate, which was filtered, washed with a small amount of cold water, and dried in vacuo. The complex obtained from the first band is the Λ[*RS*(P)]Δ[*SR*(P)] isomer and that from the second band the Λ[*SR*(P)]Δ[*RS*(P)] isomer (see Fig. 5). Yield (the Λ[*RS*(P)]Δ-[*SR*(P)] isomer): 11 mg. Found: C, 42.03; H, 5.18; N, 4.11%. Calcd for $C_{25}H_{37}N_2Cl_2CoO_{10}P_2$: C, 41.85; H, 5.20; N, 3.91%. Yield (the Λ[*SR*(P)]Δ[*RS*(P)] isomer): 40 mg. Found: C, 40.18; H, 5.31; N, 3.55%. Calcd for $C_{25}H_{40}N_2Cl_2CoO_{11.5}P_2$: C, 40.34; H, 5.42; N, 3.76%.

Λ[*SS*(P)]Δ[*RR*(P)]-*cis*β-[Co(acac)(*RR,SS*(P)-mp-PNNP)](ClO$_4$)$_2$ and Λ[*RR*(P)]Δ[*SS*(P)]-*cis*β-[Co(acac)(*RR,SS*(P)-mp-PNNP)](ClO$_4$)$_2$·0.5H$_2$O. These complexes were obtained from *trans*-$[CoCl_2(RR,SS(P)\text{-mp-PNNP})]ClO_4$ (F-2) (95 mg, 0.161 mmol) or *trans*-$[CoCl_2(RR,SS(P)\text{-mp-PNNP})]ClO_4 \cdot 1.5H_2O$ (F-3) (100 mg, 0.162 mmol) and Li(acac) (60 mg, 0.57 mmol) by the same method as that for the corresponding *RS*(P)-mp-PNNP complex. The complex obtained from the first band is the Λ[*SS*(P)]Δ[*RR*(P)] isomer and that from the second band the Λ[*RR*(P)]Δ[*SS*(P)] isomer. Yield (the Λ[*SS*(P)]Δ[*RR*(P)] isomer): 17 mg. Found: C, 41.71; H, 5.41; N, 3.85%. Calcd for $C_{25}H_{37}N_2Cl_2CoO_{10}P_2$: C, 41.85; H, 5.20; N, 3.91%. Yield (the Λ[*RR*(P)]Δ[*SS*(P)] isomer): 36 mg. Found: C, 41.36; H, 5.24; N, 3.89%. Calcd for $C_{25}H_{38}N_2Cl_2CoO_{10.5}P_2$: C, 41.34; H, 5.27; N 3.86%. All the $[Co(acac)(mp\text{-}PNNP)]^{2+}$ complexes are soluble in water, methanol, acetone and dichloromethane, but not in diethyl ether and benzene.

***trans*-[CoCl$_2$(*RS*(P)-*SS*(C)-mp-PNNP)]ClO$_4$·NaClO$_4$·H$_2$O and a Pseudo Racemate of *trans*-[CoCl$_2$(*RR,SS*(P)-*SS*(C)-mp-PNNP)]ClO$_4$·H$_2$O.** To *cis*-$[CoCl_2(en)_2]Cl$ (220 mg, 0.77 mmol) in methanol (150 cm^3) was added a mixture of *RS*(P)-, *RR*(P)- and *SS*(P)-*SS*(C)-mp-PNNP (300 mg, 0.77 mmol) with stirring at room temperature. After 30 min concd HCl (2 cm^3) was added to the resulting green solution, and the mixture was stirred overnight at room temperature. The solution was filtered, and the filtrate was concentrated to 50 cm^3 under reduced pressure. To the concentrate were added $NaClO_4 \cdot H_2O$ (6.0 g) and water (200 cm^3), and the complex was extracted twice with CH_2Cl_2 (30 cm^3×2). The green extract was evaporated to dryness under reduced pressure, and the residue was dissolved in hot methanol (20 cm^3, 60 °C). To the solution was added $NaClO_4 \cdot H_2O$ (2.0 g), and the mixture was allowed to stand at room temperature to yield a green precipitate, which was filtered, washed with water and air-dried. The filtrate was preserved because it contains the other isomer. Yield: 138 mg. Found: C, 41.80; H, 5.88; N, 4.15%. Calcd for $C_{22}H_{36}N_2Cl_3CoO_5P_2$: C, 41.56; H, 5.71; N, 4.41%. This complex was assigned to a pseudo racemate of *trans*-$[CoCl_2(RR,SS(P)\text{-}SS(C)\text{-mp-PNNP})]^+$ from the ^1H NMR spectrum. From the filtrate green crystals were formed by addition of a large excess of diethyl ether (ca. 80 cm^3), filtered, washed with water and air-dried. Yield: 100 mg. Found: C, 34.74; H, 4.56; N, 3.48%. Calcd for $C_{22}H_{36}N_2Cl_4CoNaO_9P_2$: C, 34.85; H, 4.79; N, 3.69%. This complex was assigned to the *trans*-$[CoCl_2(RS(P)\text{-}SS(C)\text{-mp-PNNP})]^+$ isomer from the ^1H NMR spectrum. Both dichloro complexes are soluble in methanol and dichloromethane, slightly in water, but not in diethyl ether.

***trans*-[CoCl$_2$(*SS*(P)-*SS*(C)-mp-PNNP)]ClO$_4$ and *trans*-[CoCl$_2$(*RR*(P)-*SS*(C)-mp-PNNP)]ClO$_4$·0.5H$_2$O.** A pseudo racemate of *trans*-$[CoCl_2(RR,SS(P)\text{-}SS(C)\text{-mp-PNNP})]ClO_4 \cdot H_2O$ (340 mg, 0.540 mmol) obtained above was converted into the chloride by stirring with Dowex 1X8 (Cl^- form, 6 g) in methanol (50 cm^3) for 6 h at room temperature. The mixture was filtered, the filtrate was diluted with water (500 cm^3), and the solution was applied on a column (ϕ2.5 cm×100 cm) of SP-Sephadex C-25. By elution with 0.05 mol dm^{-3} HCl, two green bands appeared. The eluate containing each band was collected, mixed with $NaClO_4 \cdot H_2O$ (ca. 10 g), and the complex was extracted with CH_2Cl_2. The green extract was evaporated to dryness under reduced pressure. The residue was dissolved in methanol (20 cm^3), and $NaClO_4 \cdot H_2O$ (2 g) was added to the solution. On standing at room temperature, the solution obtained from the first band yielded green crystals of *trans*-$[CoCl_2(SS(P)\text{-}SS(C)\text{-mp-PNNP})]ClO_4$, which were filtered, washed with water and air-dried. Yield: 80 mg. Found: C, 42.35; H, 5.45; N, 4.48%. Calcd for $C_{22}H_{34}N_2Cl_3CoO_4P_2$: C, 42.77; H, 5.55; N, 4.53%. The methanol solution containing $NaClO_4 \cdot H_2O$ obtained from the second band gave a green precipitate by addition of water. It was filtered, washed with water and air-dried. Yield: 65 mg. Found: C, 41.93; H, 5.33; N, 4.37%. Calcd for $C_{22}H_{35}N_2Cl_3CoO_{4.5}P_2$: C, 42.16; H, 5.63; N, 4.47%. The pruduct is *trans*-$[CoCl_2(RR(P)\text{-}SS(C)\text{-mp-PNNP})]ClO_4 \cdot 0.5H_2O$.

Λ-*cis*β-[Co(acac)(*SS*(P)-*SS*(C)-mp-PNNP)](ClO$_4$)$_2$·1.5H$_2$O and Λ-*cis*β-[Co(acac)(*RR*(P)-*SS*(C)-mp-PNNP)](ClO$_4$)$_2$·H$_2$O. A methanol solution (30 cm^3) containing a pseudo racemate of *trans*-$[CoCl_2(RR,SS(P)\text{-}SS(C)\text{-mp-PNNP})]ClO_4 \cdot H_2O$ (200 mg, 0.314 mmol) and Li(acac) (100 mg, 0.945 mmol)

was stirred for 8 h at room temperature. The resulting red solution was diluted with water (1 dm^3) and the solution applied on a column (ϕ2.5 cm×25 cm) of SE-Toyopearl. By elution with 0.1 mol dm^{-3} Na_2SO_4, two red bands appeared. The eluate of each band was collected, concentrated to nearly dryness under reduced pressure, and the complex was extracted with ethanol (50 cm^3). The extract was evaporated to dryness under reduced pressure, and the residue was dissolved in water (10 cm^3). On addition of $NaClO_4 \cdot H_2O$ (1.5 g) in water (5 cm^3), the solution gave a red precipitate, which was filtered, washed with a small amount of cold water and air-dried. The complex obtained from the first band is *Λ-cisβ*-[Co(acac)(*SS*(P)-*SS*(C)-mp-PNNP)]$(ClO_4)_2 \cdot 1.5H_2O$ and that from the second band *Λ-cisβ*-[Co(acac)-(*RR*(P)-*SS*(C)-mp-PNNP)]$(ClO_4)_2 \cdot H_2O$. These complexes were also prepared separately from trans-dichloro complexes of *SS*(P)- and *RR*(P)-*SS*(C)-mp-PNNP. Yield (the *SS*(P)-isomer): 59 mg. Found: C, 42.15; H, 6.05; N, 3.66%. Calcd for $C_{27}H_{44}N_2Cl_2CoO_{11.5}P_2$: C, 41.98; H, 5.74; N, 3.63%. Yield (the *RR*(P)-isomer): 45 mg. Found: C, 42.48; H, 6.04; N, 3.69%. Calcd for $C_{27}H_{43}N_2Cl_2CoO_{11}P_2$: C, 42.48; H, 5.68; N, 3.67%. The complexes are soluble in water, methanol and dichloromethane, but not in diethyl ether and benzene.

***Λ*[*RS*(P)]-*cisβ*-[Co(acac)(*RS*(P)-*SS*(C)-mp-PNNP)](ClO$_4$)$_2$ and *Λ*[*SR*(P)]-*cisβ*-[Co(acac)(*RS*(P)-*SS*(C)-mp-PNNP)](ClO$_4$)$_2 \cdot 1.5H_2O$ (see Fig. 5).** These complexes were prepared from *trans*-[$CoCl_2$(*RS*(P)-*SS*(C)-mp-PNNP)]$ClO_4 \cdot NaClO_4 \cdot H_2O$ (285 mg, 0.376 mmol) and Li(acac) (40 mg, 0.377 mmol) according to a method similar to that for the corresponding *RR*(P)- and *SS*(P)-*SS*(C)-mp-PNNP complexes. In column chromatography, the *Λ*[*RS*(P)]-isomer was eluted faster than the *Λ*[*SR*(P)]-isomer. Yield (the *Λ*[*RS*(P)]-isomer): 31 mg. Found: C, 43.76; H, 5.73; N, 3.80%. Calcd for $C_{27}H_{41}N_2Cl_2CoO_{10}P_2$: C, 43.51; H, 5.54; N, 3.76%. Yield (the *Λ*[*SR*(P)]-isomer): 20 mg. Found: C, 42.00; H, 5.75; N, 4.16%. Calcd for $C_{27}H_{44}N_2Cl_2CoO_{11.5}P_2$: C, 41.98; H, 5.74; N, 3.63%. The complexes are soluble in water, methanol and dichloromethane, but not in diethyl ether and benzene.

Results and Discussion

Quadridentate ligands having chiral phosphorus donor atoms, mp-PNNP and *SS*(C)-mp-PNNP were prepared according to methods similar to those for 1,1,10,10-tetraphenyl-4,7-diaza-1,10-diphosphadecane (pp-PNNP)[1] and (3*S*,8*S*)-3,8-dimethyl-1,1,10,10-tetraphenyl-4,7-diaza-1,10-diphosphadecane (*SS*(C)-pp-PNNP),[2] respectively (Scheme). The ligands have two chiral phosphorus atoms. The mp-PNNP ligand exists in two diastereomers, *RR*,*SS*(P) (racemic) and

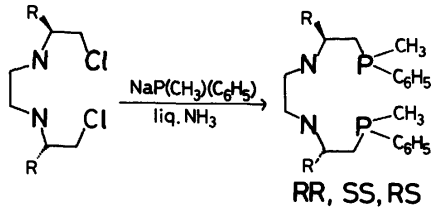

R = H : mp-PNNP

R = CH_3: SS(C)-mp-PNNP

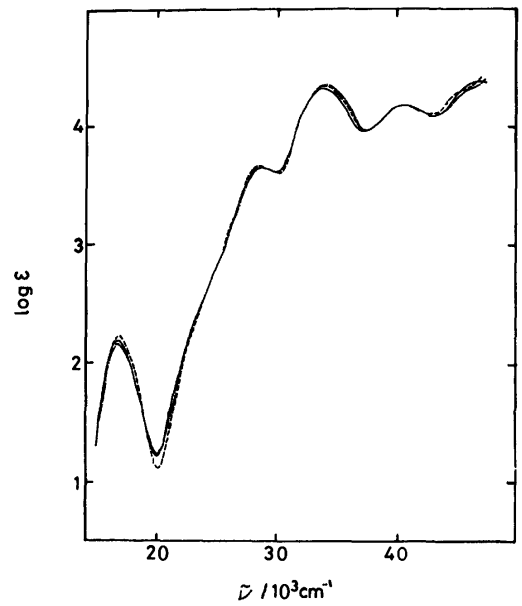

Fig. 1. Absorption spectra of *trans*-[$CoCl_2$(*RS*(P)-mp-PNNP)]$^+$ (F-1) (——), *trans*-[$CoCl_2$(*RR*,*SS*(P)-mp-PNNP)]$^+$ (F-2) (—·—·—), and *trans*-[$CoCl_2$(*RR*,*SS*-(P)-mp-PNNP)]$^+$ (F-3) (– – –).

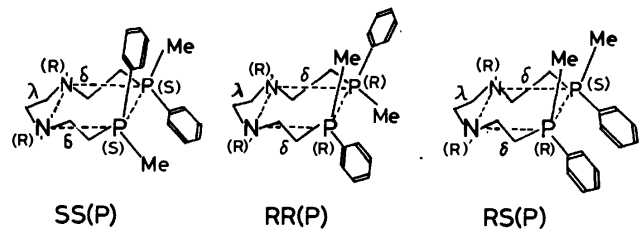

trans-RR(N)-[$CoCl_2$(mp-PNNP)]$^+$

Fig. 2. Three possible diastereomers of *trans*-[$CoCl_2$(mp- or *SS*(C)-mp-PNNP)]$^+$.

RS(P) (meso), and the *SS*(C)-mp-PNNP ligand in three optically active diastereomers, *RR*(P)-*SS*(C), *SS*(P)-*SS*(C), and *RS*(P)-*SS*(C). The separation of these diastereomers was not attempted for the free lignds because they are easily oxidized in the air, but done successfully through complexation with Co(III). The Co(III) complexes with these chiral phosphine ligands were prepared by methods similar to those for the previous PNNP complexes.[1,2]

The [$CoCl_2$(mp-PNNP)]$^+$ complex was separated into three green isomers, F-1, F-2, and F-3 by SP-Sephadex C-25 column chromatography. Figure 1 shows absorption spectra of these isomers. The spectra are essentially the same and show a pattern characteristic of the *trans*(Cl,Cl), *cis*(P,P)-[$CoCl_2N_2P_2$]-type complex.[8,9] Thus all of the isomers can be assigned to have the *trans*(Cl,Cl) configuration. For *trans*-[$CoCl_2$(mp-PNNP)]$^+$, there are three possible isomers as shown in Fig. 2. All the isomers exist in a pair of enantiomers, in which the two chiral nitrogen

atoms have the same absolute configutation (*RR* or *SS*) and all the chelate rings take a gauche conformation (δ or λ). The *RS*(N) isomers, in which the N–N chelate ring takes an envelop (ε) conformation as found for 3,6-diazaoctane-1,8-diamine (trien) complex,[10] are also probable. However, they can be excluded by considering stereoisomers of the trans-dichloro complexes of *SS*(C)-mp-PNNP and of the acac complexes derived from the *trans*-dichloro complexes (vide infra). In ^{1}H NMR spectra, isomer F-1 shows a P-CH_3 signal at 1.92(t) ppm, while isomers F-2 and F-3 give the signals at a remarkably high field, 1.37(t) and 1.32(t) ppm, respectively. As shown in Fig. 2, the methyl groups of the two isomers containing *RR*,*SS*(P)-mp-PNNP are disposed to the same direction as the phenyl group on the other P atom to face with each other. The high field shift of the mehtyl groups of isomers F-2 and F-3 will be attributable to the shielding effect of this phenyl group. The isomer containing *RS*(P)-mp-PNNP has no such a shielded methyl group. Thus isomers F-2 and F-3 can be assigned to the complexes containing *RR*,*SS*(P)-mp-PNNP, and isomer F-1, which shows the P-CH_3 signal at a lower field, to the complex containing *RS*(P)-mp-PNNP. Grocott and Wild[11] assigned the configurations of donor atoms of *o*-phenylenebis(methylphenylarsine) and its phosphorus analogue in Ru(II) complexes on the basis of similar high field shifts of the methyl group. All of the isomers do not show optical activity. Thus isomer F-1 is assigned to a racemate of the *RR*(N)-*RS*(P)- and *SS*(N)-*SR*(P)-mp-PNNP complexes. Assignment of the *RR*(N)-*SS*(P)-, *SS*(N)-*RR*(P)-mp-PNNP, and the *RR*(N)-*RR*(P)-, *SS*(N)-*SS*(P)-mp-PNNP complexes in Fig. 2 to the two isomers, F-2 and F-3 can not be made at present. Both isomers were obtained in nearly the same yield. There will be little difference in stability between them. To assign the isomers, the circular dichroism (CD) spectra will be needed. Attempts to resolve the isomers were unsuccessfull.

The $[CoCl_2$(*SS*(C)-mp-PNNP)$]^+$ complex also yielded three green isomers. These isomers will correspond to the above three isomers of *trans*-$[CoCl_2$(mp-PNNP)$]^+$, since the absorption spectra of six isomers are very similar (Fig. 3). The chelate ring of the N–P moiety of *SS*(C)-mp-PNNP will be stabilized in a δ-gauche conformation with the equatorial methyl group, and the ligand will form a $\delta\lambda\delta$ conformation preferentially. Hence all of the isomers are expected to be optically pure and the structures should be those given in Fig. 2.

The three isomers of *trans*-$[CoCl_2$(*SS*(C)-mp-PNNP$)]^+$ were separated by fractional crystallization and column chromatography. A pseudo racemate of the *RR*(P)-*SS*(C)- and *SS*(P)-*SS*(C)-mp-PNNP complexes was precipitated from a methanol solution containing the three isomers by the addition of excess $NaClO_4 \cdot H_2O$. The precipitate gives the P-CH_3 signal at a higher field (around 1.30(m) ppm). From the methanol solution filtered off the precipitate, the *RS*(P)-*SS*(C)-mp-PNNP complex was obtained by adding large excess diethyl ether. The product shows the P-CH_3 signal at 1.84(t) ppm. Thus the complexes containing *RR*(P)-*SS*(C)- and *SS*(P)-*SS*(C)-mp-PNNP, and *RS*(P)-*SS*(C)-mp-PNNP can be easily separated by the solubility difference in methanol. The separation of the *RR*(P)-*SS*(C)- and *SS*(P)-*SS*(C)-mp-PNNP complexes was achieved by SP-Sephadex C-25 column chromatography using 0.05 mol dm^{-3} HCl as an eluent; the *SS*(P)-*SS*(C)-mp-PNNP complex was eluted faster than the other complex. The absolute configurations of the two isomers were assigned from the CD spectra described below. The P-CH_3 signals of the *RR*(P)-*SS*(C)- and *SS*(P)-*SS*(C)-mp-PNNP complexes were observed at 1.30(t) and 1.38(t) ppm, respectively.

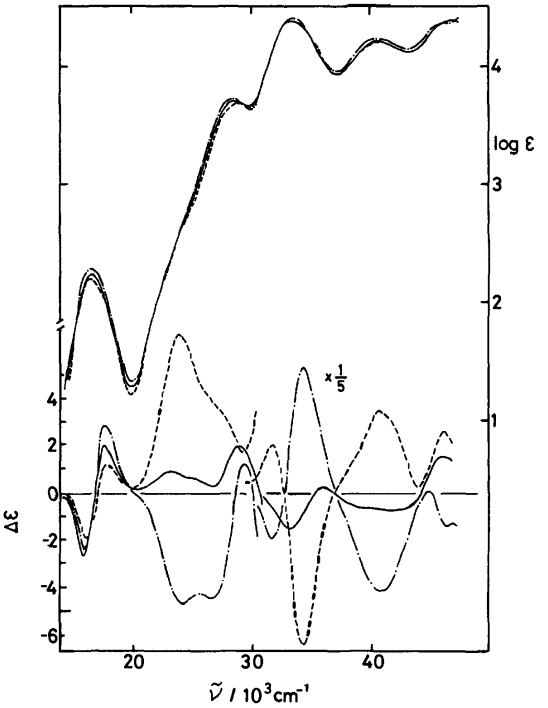

Fig. 3. Absorption and CD spectra of *trans*-$[CoCl_2$(*RS*(P)-*SS*(C)-mp-PNNP$)]^+$ (——), *trans*-$[CoCl_2$(*SS*(P)-*SS*(C)-mp-PNNP$)]^+$ (----), and *trans*-$[CoCl_2$(*RR*(P)-*SS*(C)-mp-PNNP$)]^+$ (-·—·-).

Figure 3 compares CD spectra of the three isomers of *trans*-$[CoCl_2$(*SS*(C)-mp-PNNP$)]^+$. The spectra show similar patterns in the region of 15000 to 20000 cm^{-1} (Ia absorption band region[2]). In the higher energy region, however, the *RR*(P)-*SS*(C)- and *SS*(P)-*SS*(C)-mp-PNNP complexes exhibit fairly strong CD nearly enantiomeric to each other, while the *RS*(P)-*SS*(C)-mp-PNNP complex shows rather weak CD. The similarity in the three spectra in the Ia band region indicates that these dichroisms arise mainly from the vicinal effects of the (*R*,*R*)-nitrogen donor atoms and the $\delta\lambda\delta$ conformation which are common chiralities among the three complexes. Figure 4 shows the CD spectrum of

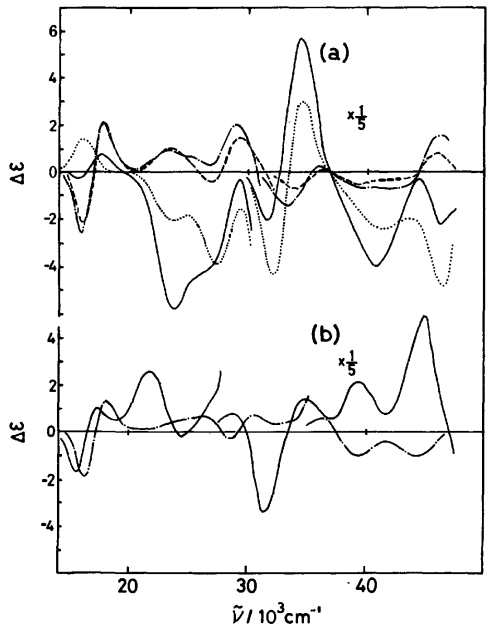

Fig. 4. a) Calculated vicinal effects of asymmetric phosphorus donors, Δε[*RR*(P)] (——) and Δε[*RR*(N),*SS*(C),*δλδ*] (– – –), and CD spectra of *trans*-[$CoCl_2$(*R*-ebpp)$_2$]$^+$ (·····) and *trans*-[$CoCl_2$(*RS*(P)-*SS*(C)-mp-PNNP)]$^+$ (–·—·–). b) CD spectra of *trans*-[$CoCl_2$(*SS*(C)-pp-PNNP)]$^+$ (——) and *trans*-[$CoCl_2$-(*SS*(C)-mm-PNNP)]$^+$ (–·—·–).

trans(Cl,Cl), *cis*(P,P)-[$CoCl_2$(*R*-ebpp)$_2$]$^+$ (*R*-ebpp=(*R*)-(2-aminoethyl)butylphenylphosphine) whose absolute configuration was determined by the X-ray method.[8] The complex exhibits rather strong negative bands in the region of 22000 to 28000 cm^{-1} and strong bands with opposite signs in the region of 30000 to 37000 cm^{-1}. The CD patterns of the *RR*(P)-*SS*(C)- and *SS*(P)-*SS*(C)-mp-PNNP complexes are similar and enantiomeric to that of the *R*-ebpp complex in these regions, respectively. From a comparison of these spectra, the isomer which was eluted faster in column chromatography is assigned to the *SS*(P)-*SS*(C)-mp-PNNP complex, and the other to the *RR*(P)-*SS*(C)-mp-PNNP complex.

When the additivity of the vicinal effects due to the chiral P, C, and N atoms and the chiral chelate conformation is assumed, the effect of the two chiral P atoms can be estimated by the equation, Δε[*RR*(P)]= 1/2{Δε[*RR*(N), *RR*(P), *SS*(C), *δλδ*-isomer]−Δε[*RR*(N), *SS*(P), *SS*(C), *δλδ*-isomer]} (1), and the effect of the sum of the chiral two N and two C atoms and the *δλδ* conformation by the equation, Δε[*RR*(N), *SS*(C), *δλδ*]=1/2{Δε[*RR*(N), *RR*(P), *SS*(C), *δλδ*-isomer]+ Δε[*RR*(N), *SS*(P), *SS*(C), *δλδ*-isomer]} (2). The calculated curves of effects (1) and (2) are given in Fig. 4. The curve of effect (1) (Δε[*RR*(P)]) is similar in pattern to the spectrum of *trans*(Cl,Cl), *cis*(P,P)-[$CoCl_2$(*R*-ebpp)$_2$]$^+$, in which the chiral source is only at the P atom, since the chiral conformational effect seems to be very small.[8] The curve of effect (2) (Δε[*RR*(N), *SS*(C),*δλδ*]) is nearly the same as the spectrum of *trans*-[$CoCl_2$(*RS*(P)-*SS*(C)-mp-PNNP)]$^+$ in which the effect of the chiral P atoms should be cancelled. The curve is also very similar to those of *trans*-[$CoCl_2$(*SS*(C)-mm-PNNP or *SS*(C)-pp-PNNP)]$^+$ [2] which have the same chiralities (*RR*(N), *SS*(C), *δλδ*).[2] The results indicate that the additivity of the vicinal effects due to various chiral sources holds in CD spectra of these trans-dichloro-phosphine complexes.

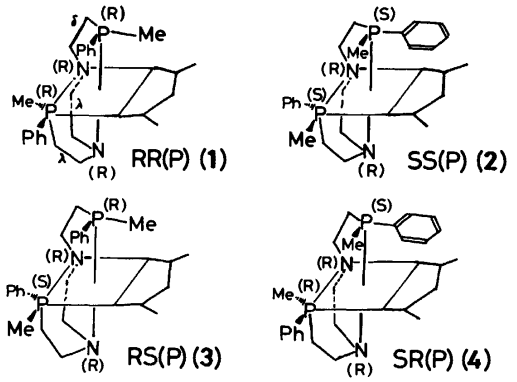

Fig. 5. Four diastereomers of *cisβ*-[Co(acac)(mp- or *SS*(C)-mp-PNNP)]$^{2+}$.

The [Co(acac)(mp-PNNP or *SS*(C)-mp-PNNP)]$^{2+}$ complexes were obtained from the corresponding trans-dichloro complexes and Li(acac). All of the acac complexes can be assigned to the *cisβ*-isomer from the ^{1}H NMR and absorption spectra (Table 1). The *cisα*-isomer which has two mutually trans P donor atoms will be unstable because of the strong trans influence of the phosphine ligand.[1,2,12]

The *cisβ*-[Co(acac)(mp-PNNP)]$^{2+}$ complex has four possible isomers as shown in Fig. 5. All the isomers have their antipodes. The notation *RS*(P) and *SR*(P) are used for two isomers of the *RS*(P)-mp-PNNP (meso) complex; the first symbol *R* or *S* denotes the absolute configuration of the P atom at the apical coordination position with respect to the acac ligand. Each of *trans*-[$CoCl_2$(*RS*(P)-mp-PNNP)]$^+$ (F-1) and *trans*-[$CoCl_2$(*RR*,*SS*(P)-mp-PNNP)]$^+$ (F-2 and F-3) yielded two isomers by reaction with Li(acac), and the isomers were separated by SP-Sephadex C-25 column chromatography. Of these isomers, one *RS*(P)-mp-PNNP and one *RR*,*SS*(P)-mp-PNNP complexes show the methine proton signal of acac at a remarkably high field, *δ* 5.00 and 5.08, respectively, while the other *RS*(P)-mp-PNNP and *RR*,*SS*(P)-mp-PNNP complexes give the signal at *δ* 5.90 and 5.97, respectively. As seen in Fig. 5, in the *Λ*[*SR*(P)](*Δ*[*RS*(P)]) and *Λ*[*SS*(P)]-(*Δ*[*RR*(P)]) isomers, one of the two phenyl groups is disposed over the acac ring and will shield the methine proton to make its signal shift to a high field. Thus the isomers whose methine proton signals show the high field shift can be assigned to the *Λ*[*SR*(P)](*Δ*[*RS*(P)]) and *Λ*[*SS*(P)](*Δ*[*RR*(P)]) configurations, and the other

Table 1. Absorption Spectral Data in the Visible to Near Ultraviolet Region (Solvent: CH_3OH, at 298K)

Complex	$\tilde{\nu}/10^3 cm^{-1}$ (log ε)			
trans-[$CoCl_2$(*RS*(P)-mp-PNNP)]$^+$ (F-1)	16.64(2.18),	28.78(3.67),	33.73(4.34),	40.57(4.19)
trans-[$CoCl_2$(*RR*,*SS*(P)-mp-PNNP)]$^+$ (F-2)	16.81(2.17),	28.99(3.67),	33.96(4.36),	40.65(4.19)
trans-[$CoCl_2$(*RR*,*SS*(P)-mp-PNNP)]$^+$ (F-3)	16.75(2.22),	28.65(3.67),	33.90(4.36),	40.65(4.20)
Λ[*RS*(P)]*Δ*[*SR*(P)]-*cisβ*-[Co(acac)(*RS*(P)-mp-PNNP)]$^{2+}$	20.50(2.83),	26(2.9)*,	29(3.8)*,	33.50(4.40)
Λ[*SR*(P)]*Δ*[*RS*(P)]-*cisβ*-[Co(acac)(*RS*(P)-mp-PNNP)]$^{2+}$	21.07(2.89),	26(2.9)*,	29(3.6)*,	33.44(4.39)
Λ[*RR*(P)]*Δ*[*SS*(P)]-*cisβ*-[Co(acac)(*RR*,*SS*(P)-mp-PNNP)]$^{2+}$	20.75(2.82),	26(2.9)*,	29(3.7)*,	33.50(4.37)
Λ[*SS*(P)]*Δ*[*RR*(P)]-*cisβ*-[Co(acac)(*RR*,*SS*(P)-mp-PNNP)]$^{2+}$	20.70(2.90),	26(2.9)*,	28.5(3.7)*,	33.22(4.41)
trans-[$CoCl_2$(*RS*(P)-*SS*(C)-mp-PNNP)]$^+$	16.56(2.23),	28.57(3.69),	33.39(4.37),	40.65(4.19)
***trans*-[$CoCl_2$(*SS*(P)-*SS*(C)-mp-PNNP)]$^+$**	16.67(2.19),	28.78(3.68),	33.61(4.39),	40.73(4.19)
trans-[$CoCl_2$(*RR*(P)-*SS*(C)-mp-PNNP)]$^+$	16.60(2.27),	28.45(3.72),	33.54(4.39),	40.57(4.22)
Λ-cisβ-[Co(acac)(*SS*(P)-*SS*(C)-mp-PNNP)]$^{2+}$	20.50(2.85),	25.5(2.9)*,	33.3(4.36)	
Λ-cisβ-[Co(acac)(*RR*(P)-*SS*(C)-mp-PNNP)]$^{2+}$	21.00(2.70),	29(3.6)*,	33.5(4.30)	
Λ[*RS*(P)]-*cisβ*-[Co(acac)(*RS*(P)-*SS*(C)-mp-PNNP)]$^{2+}$	20.3(2.78),	29.5(3.8)*,	33.8(4.39)	
Λ[*SR*(P)]-*cisβ*-[Co(acac)(*RS*(P)-*SS*(C)-mp-PNNP)]$^{2+}$	20.92(2.39),	25.5(2.9)*,	33.5(4.32)	

* Shoulder.

Table 2. CD Spectral Data in the Visible to Near Ultraviolet Region (Solvent: CH_3OH, at 298K)

Complex	$\tilde{\nu}/10^3 cm^{-1}$ ($\Delta\varepsilon$)		
trans-[$CoCl_2$(*RS*(P)-*SS*(C)-mp-PNNP)]$^+$	16.0(−2.84), 29.5(+1.97),	17.8(+2.01), 33.3(−7.79)	23.9(+0.83),
trans-[$CoCl_2$(*SS*(P)-*SS*(C)-mp-PNNP)]$^+$	16.3(−2.01), 31.8(+9.83),	18.0(+1.15), 34.5(−32.5)	24.0(+6.58),
trans-[$CoCl_2$(*RR*(P)-*SS*(C)-mp-PNNP)]$^+$	16.0(−2.37), 26.7(−4.57),	17.8(+2.85), 29.5(+1.25),	24.3(−4.81), 31.8(+10.1)
Λ-cisβ-[Co(acac)(SS(P)-SS(C)-mp-PNNP)]$^{2+}$	19.5(+9.04), 32.6(+15.5)	22.5(−2.6),	29.3(−19.7),
Λ-cisβ-[Co(acac)(*RR*(P)-*SS*(C)-mp-PNNP)]$^{2+}$	19.0(+4.05), 32.5(+19.4)	21.8(−2.87),	28.8(−16.9),
Λ-[*RS*(P)]-*cisβ*-[Co(acac)(*RS*(P)-*SS*(C)-mp-PNNP)]$^{2+}$	19.3(+3.77), 29.1(−13.4),	21.6(−2.48), 32.9(+25.8)	24.5(+2.34),
Λ-[*SR*(P)]-*cisβ*-[Co(acac)(*RS*(P)-*SS*(C)-mp-PNNP)]$^{2+}$	19.3(+9.28), 32.5(+22.8)	21.5(−1.3)*,	29.0(−20.1)

* Shoulder.

isomers to the *Λ*[*RS*(P)](*Δ*[*SR*(P)]) and *Λ*[*RR*(P)](*Δ*-[*SS*(P)]) configurations which have a methyl group over the acac ring. Similar high field shifts of the methine proton of acac have been reported for several phenyl-substituted phosphine-acac complexes.[9,13] Attempts to resolve the isomers by SP-Sephadex C-25 column chromatography with $Na_2[Sb_2(d\text{-tartrate})_2]$ were unsuccessfull, although the *Λ*[*RR*(P)]*Δ*[*SS*(P)] and *Λ*[*SR*(P)]*Δ*[*RS*(P)] isomers were partially resolved.

Each of *trans*-[$CoCl_2$(*RR*,*SS*(P)-*SS*(C)-mp-PNNP)]$^+$ (a pseudo racemate) and *trans*-[$CoCl_2$(*RS*(P)-*SS*(C)-mp-PNNP)]$^+$ yielded two isomers of the acac complex by reaction with Li(acac). The isomers were separated by SE-Toyopearl column chromatography. The two isomers, the *RR*(P)- and *SS*(P)-SS(C)-mp-PNNP complexes were also prepared separately from the trans-dichloro-*RR*(P)-*SS*(C)-mp-PNNP and -*SS*(P)-*SS*(C)-mp-PNNP complexes, respectively. All the isomers are optically pure and show a large positive and a small negative CD bands in the first absorption band region, indicating the *Λ* configuration (vide infra). The ^1H NMR spectra show all the isomers to have the cis*β* structure. The selective formation of the *Λ*-cis*β* isomers was also observed for analogous acac complexes of *SS*(C)-mm-PNNP and *SS*(C)-pp-PNNP.[2] The X-ray structure analysis on [Co(acac)(*SS*(C)-mm-PNNP)]$^{2+}$ revealed that the complex has the *Λ*-cis*β*, *RR*(N), *SS*(C) configuration, distorted gauche ($\delta\lambda\lambda$) conformations for the three chelate rings formed by PNNP, and the axial methyl group on carbon of the *λ*-(P–N) chelate ring.[2] The skeletal structures of all the isomers of [Co(acac)(*SS*(C)-mp-PNNP)]$^{2+}$ will be the same as those found in this *SS*(C)-mm-PNNP complex.

The *SS*(P)-*SS*(C)-mp-PNNP complex and one of two isomers of the *RS*(P)-mp-PNNP complex exhibit the methine proton signal of acac at a high field, *δ* 5.20 and 5.00, respectively. The methine protons in these isomers should be shielded by the phenyl group disposed over the acac chelate ring. The methine protons of the *RR*(P)-*SS*(C)-mp-PNNP complex (*δ* 5.85) and of the other isomer of the *RS*(P)-*SS*(C)-mp-PNNP complex (*δ* 5.93) do not show such a high field shift. The results confirm that the configurational structures of the four isomers are those given in Fig. 5. Each absorption spectrum of the isomers given in Fig. 6 is very similar to that of the corresponding isomer of the

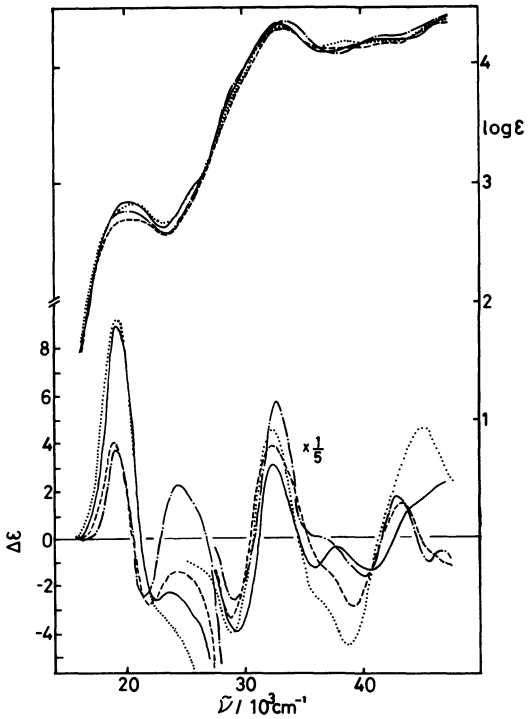

Fig. 6. Absorption and CD spectra of *Λ-cisβ*-[Co(acac)(*SS*(C)-mp-PNNP)]$^{2+}$: *SS*(P)-isomer (——), *RR*(P)-isomer (----), *SR*(P)-isomer (·····), and *RS*(P)-isomer (-·—·-).

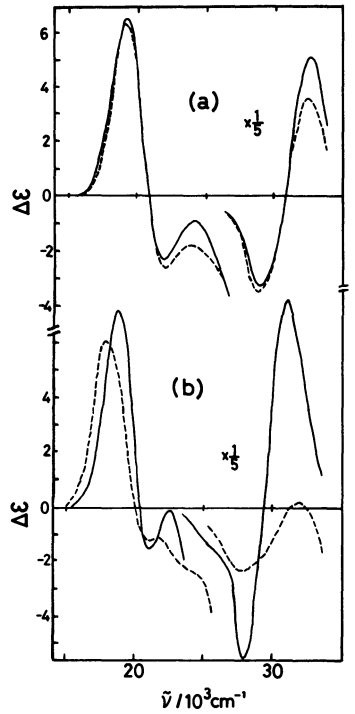

Fig. 7. a) Calculated curves for the effect of the sum, *Λ*, *SS*(C), *RR*(N), and *δλλ* (Δε[*Λ*,*SS*(C),*RR*(N), *δλλ*]): 1/2{Δε[isomer(**3**)]+Δε[isomer(**4**)]} (——) and 1/2{Δε[isomer(**1**)]+Δε[isomer(**2**)]} (----). b) CD spectra of *Λ-cisβ*-[Co(acac)(*SS*(C)-pp-PNNP)]$^{2+}$ (——) and *Λ-cisβ*-[Co(acac)(*SS*(C)-mm-PNNP)]$^{2+}$ (----).

mp-PNNP complex, especially in the first absorption band region, where the spectral patterns are fairly different among the isomers.

Figure 6 shows the CD spectra of four isomers of the *SS*(C)-mp-PNNP complex. The spectra have similar patterns and show a large positive and a small negative bands in the first absorption band region. Thus all the isomers will have the same skeletal configuration, *Λ-cisβ*. However, the positive CD bands of the *SS*(P)- and *SR*(P)-*SS*(C)-mp-PNNP complexes are much larger than those of the *RR*(P)- and *RS*(P)-*SS*(C)-mp-PNNP complexes. The former two complexes have a phenyl group disposed over the acac chelate ring, whereas the latter two complexes a methyl group in place of the phenyl group. The *SR*(P)- and *RS*(P)-*SS*(C)-mp-PNNP complexes show the positive CD band largely different in strength. These results indicate that the magnitude of the vicinal effect of the chiral P atom at one coordination position is remarkably different from that at the other chemically unequivalent coordination position. When the two effects are similar, the *SR*(P)-and *RS*(P)-*SS*(C)-mp-PNNP complexes will give similar CD spectra by cancellation of the effects due to the (*S*)- and (*R*)-P atoms.

Isomers (**1**) to (**4**) in Fig. 5 have common chiralities, *Λ*, *SS*(C), *RR*(N) and *δλλ*, and the following chiralities for the P atoms; (**1**) *R*(P_a), *R*(P_p), (**2**) *S*(P_a), *S*(P_p), (**3**) *R*(P_a), *S*(P_p), and (**4**) *S*(P_a), *R*(P_p), where P_a and P_p denote

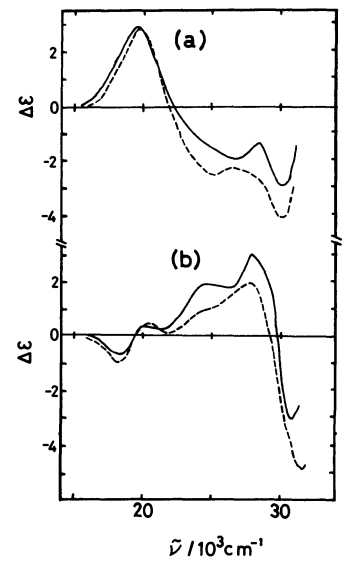

Fig. 8. a) Calculated vicinal effects of (*S*)-P atom at the apical position (Δε[*S*(P_a)]): 1/2{Δε[isomer(**4**)]−Δε[isomer(**1**)]} (——) and 1/2{Δε[isomer(**2**)]−Δε[isomer(**3**)]} (----). b) Calculated vicinal effect of (*S*)-P atom at the planar position (Δε[*S*(P_p)]): 1/2{Δε[isomer(**3**)]−Δε[isomer(**1**)]} (——) and 1/2{Δε-[isomer(**2**)]−Δε[isomer(**4**)]} (----).

P atoms at the apical and planar coordination positions, respectively with respect to the acac ligand. The effect of the sum of common chiralities, *Λ*, *SS*(C),

RR(N) and $\delta\lambda\lambda$ can be estimated by $\Delta\varepsilon[\Lambda, SS(C), RR(N), \delta\lambda\lambda]=1/2\{\Delta\varepsilon[\text{isomer}(\mathbf{1})]+\Delta\varepsilon[\text{isomer}(\mathbf{2})]\}$ (3a) or $\Delta\varepsilon[\Lambda, SS(C), RR(N), \delta\lambda\lambda]=1/2\{\Delta\varepsilon[\text{isomer}(\mathbf{3})]+\Delta\varepsilon[\text{isomer}(\mathbf{4})]\}$ (3b). Figure 7(a) shows two curves of $\Delta\varepsilon[\Lambda, SS(C), RR(N), \delta\lambda\lambda]$ calculated from (3a) and (3b). The vicinal effect of the apical (*S*)-P atom can be estimated by $\Delta\varepsilon[S(P_a)]=1/2\{\Delta\varepsilon[\text{isomer}(\mathbf{2})]-\Delta\varepsilon[\text{isomer}(\mathbf{3})]\}$ (4a) or $\Delta\varepsilon[S(P_a)]=1/2\{\Delta\varepsilon[\text{isomer}(\mathbf{4})]-\Delta\varepsilon[\text{isomer}(\mathbf{1})]\}$ (4b), and the effect of the planar (*S*)-P atom by $\Delta\varepsilon[S(P_p)]=1/2\{\Delta\varepsilon[\text{isomer}(\mathbf{3})]-\Delta\varepsilon[\text{isomer}(\mathbf{1})]\}$ (5a) or $\Delta\varepsilon[S(P_p)]=1/2\{\Delta\varepsilon[\text{isomer}(\mathbf{2})]-\Delta\varepsilon[\text{isomer}(\mathbf{4})]\}$ (5b). The curves of $\Delta\varepsilon[S(P_a)]$ calculated from (4a) and (4b) are given in Fig. 8(a), and those of $\Delta\varepsilon[S(P_p)]$ from (5a) and (5b) in Fig. 8(b). The two curves for each chiral effect are very similar, and the results indicate that the additivity of the three effects, $\Delta\varepsilon[\Lambda, SS(C), RR(N), \delta\lambda\lambda]$, $\Delta\varepsilon[S(P_a)]$ and $\Delta\varepsilon[S(P_p)]$ holds for the CD spectra of four isomers of $[Co(acac)(SS(C)\text{-mp-PNNP})]^{2+}$.

The $\Delta\varepsilon[\Lambda, SS(C), RR(N), \delta\lambda\lambda]$ curve in Fig. 7(a) shows a large positive and a small negative bands in the first absorption band region. This pattern has been observed for a number of Λ-complexes of Co(III). Thus it is suggested that the effects of *SS*(C), *RR*(N) and $\delta\lambda\lambda$ are fairly small compared with the Λ configurational effect. Figure 7(b) shows CD spectra of Λ-*cis*β-$[Co(acac)(L)]^{2+}$ (L=*SS*(C)-mm-PNNP, *SS*(C)-pp-PNNP).[2] The spectra are very similar to the $\Delta\varepsilon[\Lambda, SS(C), RR(N), \delta\lambda\lambda]$ curve, although the *SS*(C)-mm-PNNP complex shows a somewhat different spectrum in the high energy region. The difference will be attributable to the difference in substituent on the P atom, methyl or phenyl. The absolute configuration (Λ, Λ) of the $[Co(acac)(PNNP)]^{2+}$-type complex can be safely assigned from the CD sign in the first absorption band region.

The curves of $\Delta\varepsilon[S(P_a)]$ and $\Delta\varepsilon[S(P_p)]$ in Fig. 8(a) and 8(b) are those for chiral donor P atoms with the same *S* configuration. However, the curves are quite different and almost enantiomeric to each other. In the first absorption band region, the $\Delta\varepsilon[S(P_a)]$ curve shows a band much larger than that in the $\Delta\varepsilon[S(P_p)]$ curve. The vicinal effect of the chiral P donor atom depends largely on its coordination position in $[Co(acac)((SS(C)\text{-mp-PNNP})]^{2+}$. To our knowledge, there has been no report on such a coordination position dependence for the vicinal effect of a chiral donor atom. Care must be taken when the absolute configuration of a chiral donor atom is assigned by CD spectroscopy.

The authors wish to thank the Ministry of Education for Scientific Research Grant-in-Aid No. 60470046.

References

1) M. Atoh, K. Kashiwabara, and J. Fujita, *Bull. Chem. Soc. Jpn.*, **58**, 2793 (1985).

2) M. Atoh, K. Kashiwabara, and J. Fujita, *Bull. Chem. Soc. Jpn.*, **58**, 3492 (1985).

3) For examples, J. W. L. Martin, J. A. L. Palmer, and S. B. Wild, *Inorg. Chem.*, **23**, 2664 (1984), and references cited therein.

4) N. K. Roberts and S. B. Wild, *J. Am. Chem. Soc.*, **101**, 6254 (1979).

5) L. Valgha, L. Toldy, Ö. Fehér, and S. Lendrai, *J. Chem. Soc.*, **1957**, 805.

6) The symbols, *RS*, *RR*, etc, denote the absolute configurations of asymmetric phosphorus atoms. The notation of the absolute configurations, *R* and *S*, for a chiral phosphorus atom of a free ligand is reversed upon coordination. However, to avoid confusion, we use the same notation for a coordinated ligand as that when it is free. Refer to Figs. 2 and 5.

7) *Inorg. Synth.*, **2**, 223 (1946).

8) I. Kinoshita, Y. Yokota, K. Matsumoto, S. Ooi, K. Kashiwabara, and J. Fujita, *Bull. Chem. Soc. Jpn.*, **56**, 1067 (1983).

9) M. Atoh, I. Kinoshita, K. Kashiwabara, and J. Fujita, *Bull. Chem. Soc. Jpn.*, **55**, 3179 (1982).

10) S. Utsuno, Y. Sakai, Y. Yoshikawa, and H. Yamatera, *J. Am. Chem. Soc.*, **102**, 6903 (1980).

11) S. C. Grocott and S. B. Wild, *Inorg. Chem.*, **21**, 3526 (1982).

12) K. Katoh, H. Sugiura, K. Kashiwabara, and J. Fujita, *Bull. Chem. Soc. Jpn.*, **57**, 3580 (1984).

13) K. Kashiwabara, I. Kinoshita, T. Ito, and J. Fujita, *Bull. Chem. Soc. Jpn.*, **54**, 725 (1981).

 © 1986 The Chemical Society of Japan Bull. Chem. Soc. Jpn., 59, 1009—1014 (1986)

Calorimetric and Raman Spectroscopic Studies on Formation of Cadmium(II) Thiocyanato Complexes in Aqueous Solution

Shin-ichi ISHIGURO, Kiyoshi YAMAMOTO, and Hitoshi OHTAKI*
Department of Electronic Chemistry, Tokyo Institute of Technology at Nagatsuta,
4259, Nagatsuta-cho, Midori-ku, Yokohama 227
(Received November 8, 1985)

Complex formation equilibria between cadmium(II) and thiocyanate ions have been calorimetrically studied at 25 °C in aqueous solution containing $NaClO_4$ in order to keep 3 mol dm^{-3} ionic strength in the test solutions. Calorimetric titration curves thus obtained were well explained in terms of formation of dinuclear $[Cd_2X]^{3+}$ (X=SCN) and mononuclear $[CdX_n]^{(2-n)+}$ (n=1—4) complexes, and their formation constants, enthalpies and entropies were determined. The stepwise enthalpy and entropy values at the third consecutive step were largely positive, indicating that water molecules solvating Cd(II) ion were extensivelyl liberated at this step. It was thus suggested that the coordination symmetry around Cd(II) ion changed from octahedral to tetrahedral at the formation of $[CdX_3]^-$. Raman spectra of the C-S and C-N stretching vibrations of SCN^- ion were measured in cadmium(II) thiocyanate solutions with varying molar ratios of the metal to ligand ions. It was shown that SCN^- ion coordinated to Cd(II) ion through the N atom at the first step of the complex formation, and the S atom at the second, N at the third and then S at the last. The suggested bonding type of SCN^- ion with Cd(II) ion within each cadmium(II) thiocyanato complex was supported by the thermodynamic data.

In a previous paper,[1] we elucidated the structures of the tetrathiocyanato complexes of the Group 2B metal ions, Zn(II), Cd(II), and Hg(II), in aqueous solutions by X-ray scattering, Raman and ^{13}C- and ^{14}N-NMR measurements.

Thiocyanate (SCN^-) ion binds with metal ions through either the sulfur or nitrogen atom depending on the softness or hardness of metal ions. Relatively hard zinc(II) and soft mercury(II) ions are coordinated with the N and S atoms, respectively, of SCN^- ions within $[Zn(NCS)_4]^{2-}$ and $[Hg(SCN)_4]^{2-}$.

On the other hand, cadmium(II) ion shows an intermediate character between Zn(II) and Hg(II) ions. Then, it has been indicated that, within the tetrathiocyanatocadmate(II) ion, cadmium(II) ion is linked to two N and two S atoms of SCN^- ions to form $[Cd(SCN)_2(NCS)_2]^{2-}$ in aqueous solution.

Raman and infrared spectroscopic measurements so far carried out for various cadmium(II) thiocyanate solutions provided evidence of formation of mono- and polynuclear complexes of Cd(II) having different types of bonding of SCN^- ion.[2-6] Recently, Antić-Jovanović et al.[7] reported Raman spectra of the cadmium(II) thiocyanate aqueous solutions and assigned the band at 2132 cm^{-1} to the C-N stretching vibration within $[Cd(SCN)]^+$ and the bands at 2102 and 784 cm^{-1} to the C-N and C-S stretching vibrations within the higher $[Cd(NCS)_n]^{(2-n)+}$ (n>2) complexes.

Enthalpies and entropies of formation of thiocyanato complexes of metal ions also afford us useful information on the coordination structures of the complexes. Ahrland and Kullberg[8] indicated that SCN^- ion coordinated to Zn(II) ion through the N atom and to Hg(II) ion through the S atom. However, as to the thiocyanato complexes of Cd(II) in aqueous solution, no reliable data for enthalpies and entropies of formation of the complexes have been obtained yet.

In this study, therefore, we aimed at obtaining thermodynamic quantities of formation of thiocyanato complexes of Cd(II) in aqueous solution by calorimetry at 25 °C. A computer-controlled on-line system for calorimetry was employed.[9] Raman spectral measurements were also carried out in cadmium(II) thiocyanate aqueous solutions with varying ratios of the metal to ligand ions. The coordination structure within each thiocyanato complex of cadmium(II) ion is discussed on the basis of the thermodynamic and Raman spectroscopic data obtained.

Experimetal

Reagents. All chemicals used were of reagent grade. *Cadmium(II) perchlorate* was prepared by dissolving cadmium oxide into perchloric acid of super special grade and recrystallized twice from water. *Sodium thiocyanate* was recrystallized twice from ethanol. *Sodium perchlorate* was purified by the method described elsewhere.[10]

The concentration of metal ions in the cadmium(II) perchlorate stock solution was determined by titration with EDTA.

Calorimetric Measurements. Calorimetric measurements were carried out in a thermostated bath controlled at (25.000±0.007) °C placed in a room at (25.0±0.2) °C.

Cadmium(II) perchlorate solutions with varying concentrations of the metal ion in the range 10—400 mmol dm^{-3} were prepared, all the solutions containing 3 mol dm^{-3} $NaClO_4$ as a constant ionic medium. A 1 mol dm^{-3} NaSCN solution containing 2 mol dm^{-3} $NaClO_4$ as an ionic medium was used as a titrant solution. 100 cm^3 of a cadmium(II) perchlorate solution was placed in a Dewar vessel, and then, was titrated with the 1 mol dm^{-3} NaSCN titrant solution.

Back titration procedures were also employed. Four NaSCN solutions of 1.0, 1.5, 2.0, and 3.0 mol dm^{-3} were prepared, each solution containing $NaClO_4$ in order to adjust its ionic strength to 3 mol dm^{-3}. A 0.25 mol dm^{-3} $Cd(ClO_4)_2$ solution containing 3 mol dm^{-3} $NaClO_4$ was employed as a titrant solution.

Heats of dilution were determined by titrating a 3 mol dm^{-3} $NaClO_4$ solution with each titrant solution used. In each case, heat of dilution at the addition of an aliquot (δv cm^3) of the titrant solution slightly varied with the total volume (v cm^3) of the titrant added. Thus, the heat of dilution was represented as a function of v and δv as follows:

$$q_{dil} = \int_{v}^{v+\delta v} (a_0 + a_1 u)\mathrm{d}u, \quad (1)$$

where a_0 and a_1 denote constants, which were evaluated by the least-squares method to be -0.365 J cm^{-3} and 2.68×10^{-3} J cm^{-6}, respectively, for the NaSCN titrant solution and -0.317 J cm^{-3} and 1.85×10^{-3} J cm^{-6}, respectively, for the $Cd(ClO_4)_2$ titrant solution.

Heat evolved q_{obsd} at each titration point was thus corrected by knowing the q_{dil} value as follows:

$$q_{corr} = q_{obsd} - q_{dil}, \quad (2)$$

and the q_{corr} values thus obtained were used for the evaluation of formation constants and enthalpies of formation of cadmium(II) thiocyanato complexes in aqueous solution.

The specific heat C_p and the heat transfer coefficient λ of the test solutions, which were used for analyzing a set of temperature changes at each titration point, slightly varied with volumes of the test solution during the titrations, and thus, the C_p and λ values were determined at the addition of every 10 cm^3 of the titrant. The volume of an aliquot of the titrant solution added at each titration point was changed in the range 1—5 cm^3 depending on the extent of heat evolved during the titrations. The whole titration procedure was carried out by using a fully automatic on-line system for calorimetry as described elsewhere.[9]

Raman Spectral Measurements. Raman spectral measurements were carried out in cadmium(II) thiocyanate solutions with varying ratios of the metal to ligand ions as summarized in Table 1. Raman spectra were recorded on a JEOL JRS-S1 spectrometer using 514.5 nm line of NEC GLG-3200 argon ion Laser in a room at (25.0±0.2) °C.

Analysis of Colorimetric Data. The analytical method used for the calorimetric data obtained was similar to that used in a previous paper.[9] However, since titration curves obtained in the present work were not explainable in terms of formation of a series of mononuclear complexes, the formation of polynuclear thiocyanato complexes of Cd(II) was also taken into account.

Results and Discussion

Calorimetric titration curves obtained by titrating cadmium(II) perchlorate solutions having different concentrations of the metal ion with the NaSCN titrant solution are depicted in Fig. 1. Enthalpies $\Delta H°$ calculated by $\Delta H° = -q_{corr}/(\delta v C_{X,tit})$, where δv and $C_{X,tit}$ denote the volume of an aliquot of the titrant added and the concentration of NaSCN in the titrant solution, respectively, were plotted against the ratio C_X/C_M in the test solution at each titration point, where C_X and C_M stand for total concentations of SCN^- and Cd(II) ions, respectively, in a solution.

Table 1. Total Concentrations C_M and C_X of Cd^{2+} and SCN^- Ions, Respectively, in Cadmium(II) Thiocyanate Aqueous Solutions Used for Raman Spectroscopic Measurements

Solution	C_M/mol dm^{-3}	C_X/mol dm^{-3}	C_X/C_M
1	0.126	0.590	4.68
2	0.267	0.585	2.19
3	0.357	0.590	1.65
4	0.462	0.587	1.27
5	0.565	0.586	1.04
6	0.897	0.582	0.65
7	0.913	0.0727	0.08
8	2.090	0.0716	0.034

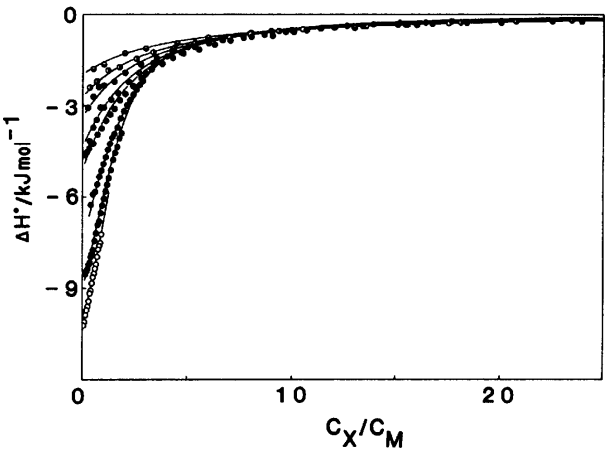

Fig. 1. Calorimetric titration curves of cadmium(II) thiocyanate solutions containing 3 mol dm^{-3} $NaClO_4$ at 25 °C. Initial concentrations of cadmium(II) perchlorate (C_M/mmol dm^{-3}): 10.04(◒), 14.93(◑), 20.02(⊕), 29.96(◘), 39.96(◉), 100.1(◎), 200.1(●), and 400.1(○). The solid lines show the curves calculated by using the constants of case 2 in Table 2.

The calorimetric data thus obtained were first analyzed by assuming the only formation of mononuclear $[CdX_n]^{(2-n)+}$ (X=SCN and n=1—4) complexes. The formation constants of the third and fourth complexes estimated from the data were rather uncertain. However, as seen in Fig. 2 where the titration curves in Fig. 1 are expanded over the range C_X/C_M= 0—4, we see some deviation of the experimental points from the theoretical curves (the broken lines) calculated by assuming the only formation of $[CdX]^+$ and $[CdX_2]$ at relatively higher concentrations of the metal ion in the range $C_X/C_M<1$. The deviation suggested the formation of polynuclear thiocyanato complexes of Cd(II) in aqueous solution.

Since the formation of $[CdX_3]^-$ and $[CdX_4]^{2-}$ was not conclusive from the data in Fig. 1, titrations of sodium thiocyanate solutions with the 0.25 mol dm^{-3} $Cd(ClO_4)_2$ solution were carried out, where the $[CdX_3]^-$ and $[CdX_4]^{2-}$ complexes were expected to form at the initial stage of the titrations. Calorimetric titration curves thus obtained are illustrated in Fig. 3, in which enthalpies $\Delta H°$ ($=-q_{corr}/(\delta v C_{M,tit})$ where

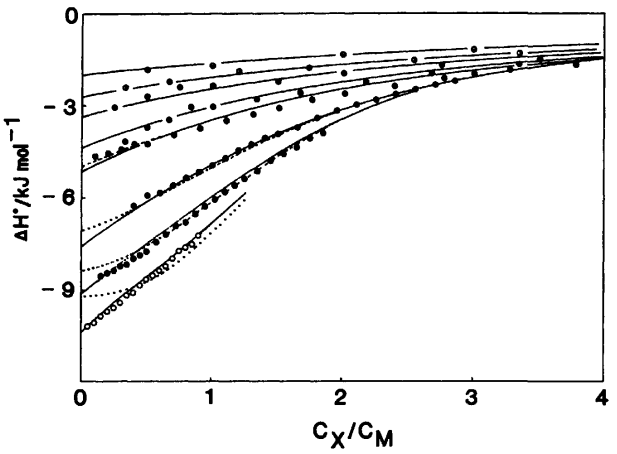

Fig. 2. Calorimetric titration curves of cadmium(II) thiocyanate solution expanded over the range C_X/C_M=0—4. Symbols used are the same as those in Fig. 1. The solid lines show the curves calculated by using the constants of case 2 in Table 2. The broken lines show the curves calculated by assuming the formation of the only mononuclear complexes.

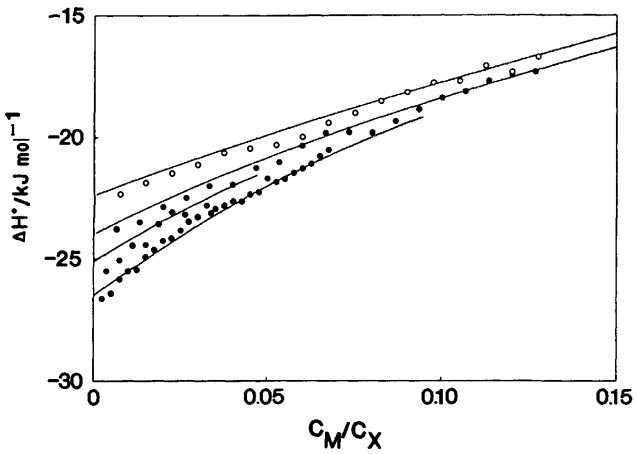

Fig. 3. Calorimetric titration curves obtained by titrating NaSCN solutions with $Cd(ClO_4)_2$ solution. Initial concentrations of sodium thiocyanate (C_X/mol dm^{-3}): 1.0(○), 1.5(●), 2.0(◎), and 3.0(◉). The solid lines show the curves calculated by using the constants of case 2 in Table 2.

$C_{M,tit}$ denotes the concentration of Cd(II) ion in the titrant), were plotted against the ratio C_M/C_X in the test solution at each titration point.

All the calorimetric data thus obtained were simultaneously analyzed by assuming the formation of mono- and polynuclear thiocyanato complexes of Cd(II) and their formation constants and enthalpies were obtained by the least-squares method. Among various cases examined by assuming the formation of different sets of complexes, two cases gave relatively small error-square sums. The results are summarized in Table 2, in which we assumed the formation of $[Cd_2X]^{3+}$ and $[CdX_n]^{(2-n)+}$ (n=1,2 and 4) in case 1, and the formation of $[Cd_2X]^{3+}$ and $[CdX_n]^{(2-n)+}$ (n=1—4)

Table 2. The Least-Squares Refinement of Formation Constants, β_{pq}/mol$^{-(p+q-1)}$ dm$^{3(p+q-1)}$, and Enthalpies, $\Delta H^\circ_{\beta pq}$/kJ mol^{-1}, of the Reaction, $qCd^{2+}+pX^-=[Cd_qX_p]^{(2q-p)+}$ (X=SCN), in Aqueous Solution Containing 3 mol dm^{-3} $NaClO_4$ as a Constant Ionic Medium at 25 °C

	Case 1	Case 2
β_{11}	23.66±0.01	23.48±0.01
β_{21}	79.26±0.01	58.52±0.01
β_{31}	—	65.97±0.01
β_{41}	11.00±0.02	100 ±4
β_{12}	9.4 ±0.9	17.83±0.01
$\Delta H^\circ_{\beta 11}$	−10.39±0.09	−10.19±0.06
$\Delta H^\circ_{\beta 21}$	−24.80±0.07	−30.3 ±0.3
$\Delta H^\circ_{\beta 31}$	—	−7.7 ±0.6
$\Delta H^\circ_{\beta 41}$	−29.6 ±0.2	−30.5 ±0.2
$\Delta H^\circ_{\beta 12}$	−17 ±2	−14.8 ±0.4
NP	241	241
U	8.88	5.67

Uncertainties refer to standard deviations. NP refers to the number of calorimetric data points.

Table 3. Formation Constants $\log(K_n$/mol dm$^{-3})$ for the Stepwise Reaction, $[MX_{n-1}]^{(3-n)+}+X^-=[MX_n]^{(2-n)+}$ (M=Zn or Cd, X=SCN and n=1—4) in Water and in Dimethyl Sulfoxide at 25 °C

	Cd(II)		Zn(II)	
	Water[a] 3 mol dm^{-3} $NaClO_4$	DMSO[b] 1 mol dm^{-3} NH_4ClO_4	Water[c] 5 mol dm^{-3} $NaClO_4$	DMSO[d] 1 mol dm^{-3} NH_4ClO_4
$\log K_1$	1.378	1.81	0.917	1.38
$\log K_2$	0.396	0.91	0.673	1.40
$\log K_3$	0.052	0.20	0.577	2.43
$\log K_4$	0.180	—	0.347	1.65

a) This work. b) Ref. 11. c) Ref. 9. d) Ref. 12.

in case 2. Theoretical curves calculated by using the constants of case 2 in Table 2 are drawn by the solid lines in Figs. 1—3, which well reproduced the experimental points over the whole range of C_X/C_M and C_M/C_X examined here. On the other hand, although the error-square sum U of case 1 was not too large compared with that of case 2, theoretical curves calculated by using the constants of case 1 did not well reproduce the experimental points in Fig. 3. Therefore, we concluded that the formation of $[CdX_3]^-$ should not be neglected even if the complex was not significantly formed under the present experimental conditions.

The stepwise formation constants $\log(K_n$/mol^{-1} dm$^3)$ of formation of $[CdX_n]^{(2-n)+}$ (X=SCN and n=1—4) thus obtained are summarized in Table 3, together with those of $[ZnX_n]^{(2-n)+}$ in water,[9] and $[CdX_n]^{(2-n)+}$ and $[ZnX_n]^{(2-n)+}$ in DMSO[11,12] for comparison. The formation constants of $[CdX_n]^{(2-n)+}$ have also been reported by Gerding[13-15] in aqueous solution containing various ionic media, and the log K_n values in 3 mol dm^{-3} $NaClO_4$ ionic medium are 1.41, 0.83, 0.24, and 0.0 for n=1, 2, 3, and 4, respectively. The log

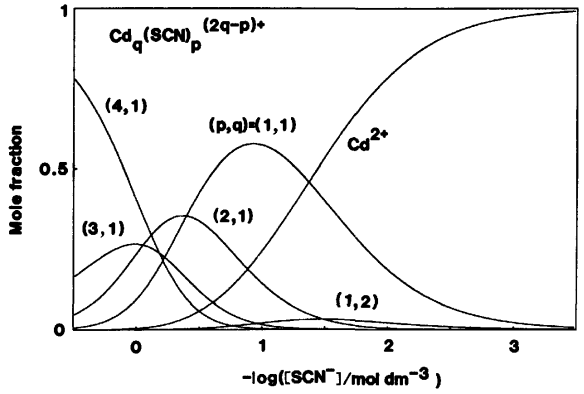

Fig. 4. Distribution of cadmium(II) thiocyanato complexes in 3 mol dm^{-3} $NaClO_4$ aqueous solution containing 0.1 mol dm^{-3} Cd(II) ion at 25 °C. (p, q) represents the number of ions within the $[Cd_qX_p]^{(2q-p)+}$ (X=SCN) complex.

K_1 value is in good agreement with ours, but the log K_n (n=2—4) values are appreciably different from the results of the present work. Particularly, the value of log K_2 according to Gerding is remarkably large compared to that obtained in our work.

In Table 3, one finds that the log K_1 value of $[CdX]^+$ is larger than that of $[ZnX]^+$ but stepwise formation constants of the other $[CdX_n]^{(2-n)+}$ complexes were smaller than those of the corresponding zinc(II) complex in water and in DMSO.

We also found the formation of dinuclear $[Cd_2X]^{3+}$ complex in solutions of relatively high concentrations of the metal ion at $C_X/C_M<1$. The log K value for the reaction, $Cd^{2+}+[CdX]^+=[Cd_2X]^{3+}$, was −0.12 and the corresponding $\Delta G°$, $\Delta H°$, and $\Delta S°$ values for the reaction being 0.7 and −4.6 kJ mol^{-1} and −18 J K^{-1} mol^{-1}, respectively.

Distribution of species in cadmium(II) thiocyanate solutions containing 0.1 mol dm^{-3} Cd(II) ions is illustrated in Fig. 4.

Raman Spectra of Cadmium(II) Thiocyanate Solutions. Raman spectra of the C-N and C-S stretching vibrations of SCN^- ion measured in cadmium(II) thiocyanate aqueous solutions with varying ratios of C_X/C_M are shown in Figs. 5 and 6, respectively. The Raman bands observed were assigned by taking into account the distribution of species in each cadmium(II) thiocyanate solution.

The Raman spectra in Fig. 5 show three peaks at ca. 2070, 2105, and 2130 cm^{-1}, the first band being ascribed to the vibration of free SCN^- ion. It was expected from the result of the formation constants obtained that $[CdX]^+$ and $[Cd_2X]^{3+}$ (X=SCN) were formed in cadmium(II) thiocyanate solutions at $C_X/C_M<1$ and the $[Cd_2X]^{3+}$ complex predominated in the solutions with lowering ratio of C_X/C_M and with increasing C_M as examined here. Two peaks at 2105 and 2130 cm^{-1} were observed in the solution of C_X/C_M=0.08, while the former peak disappeared in the solution

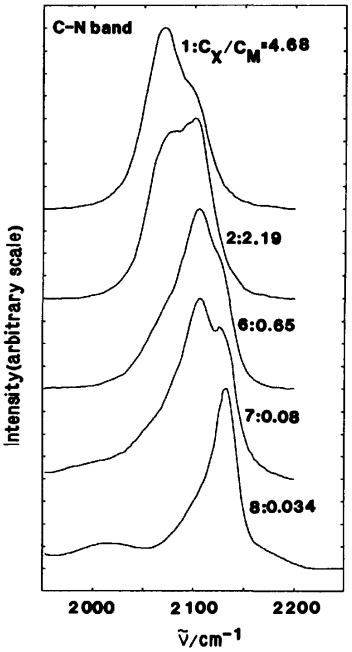

Fig. 5 Raman spectra of the C-N stretching vibration of SCN^- ion measured in various cadmium(II) thiocyanate solutions.

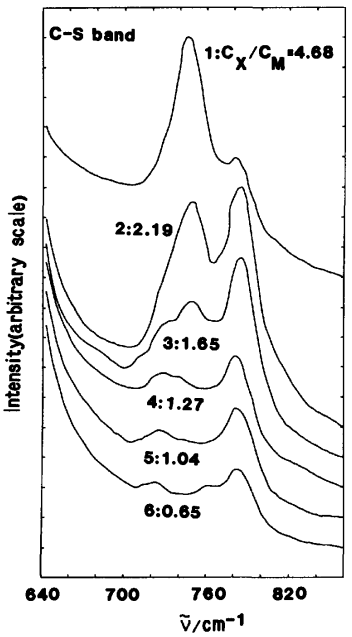

Fig. 6. Raman spectra of the C-S stretching vibration of SCN^- ion measured in various cadmium(II) thiocyanate solutions.

of C_X/C_M=0.034. Thus the 2105 and 2130 cm^{-1} bands were assigned to the C-N vibration within $[CdX]^+$ and $[Cd_2X]^{3+}$, respectively.

The Raman spectra in Fig. 6 show predominant peaks at ca. 720, 740, and 780 cm^{-1}, the second band being attributable to the vibration of free SCN^- ion. In the solutions of C_X/C_M=0.65—2.19 examined, the intensity of the 780 cm^{-1} band relative to that of the

Table 4. Thermodynamic Quantities, $\log(\beta_{41}/\text{mol}^{-1}\,\text{dm}^3)$, $\Delta G^\circ_{\beta41}/\text{kJ mol}^{-1}$, $\Delta H^\circ_{\beta41}/\text{kJ mol}^{-1}$, and $\Delta S^\circ_{\beta41}/\text{J K}^{-1}\,\text{mol}^{-1}$, for the Overall Reaction, $M^{2+}+4X^-=[MX_4]^{2-}$ (X=SCN and M=Zn, Cd and Hg) in Aqueous Solutions at 25 °C

	Zn(II)[a]	Cd(II)	Hg(II)[b]
$\log\beta_{41}$	2.51	2.00	21.67
$\Delta G^\circ_{\beta41}$	−14.3	−11.4	−123.7
$\Delta H^\circ_{\beta41}$	−12.8	−30.5	−141.5
$\Delta S^\circ_{\beta41}$	5	−64	−60

a) Ref. 12. b) Ref. 18.

720 cm^{-1} band increased with increasing ratios of C_X/C_M, and thus, these two bands should be assigned to the vibrations of, at least, two different species. Since it was indicated from the distribution of the cadmium(II) thiocyanato complexes in the solutions that $[CdX]^+$ was present as the main species and the concentration of the complex increased with increasing ratios of C_X/C_M in the range 0.65—1.65, the 780 cm^{-1} band was assigned to the C-N stretching vibration within $[CdX]^+$. Since it was indicated from the thermodynamic data that the $[Cd_2X]^{3+}$ complex was appreciably formed in the solutions of C_X/C_M=0.65—1.04 and the $[CdX_2]$ complex in the solutions of C_X/C_M=1.27—2.19, a weak band at 720 cm^{-1} may be ascribed to the C-S stretching vibration of the $[Cd_2X]^{3+}$ and $[CdX_2]$ species.

Thermodynamic Quantities of Formation of Thiocyanato Complexes of Cd(II). Thermodynamic quantities of formation of the tetrathiocyanato complexes of Zn(II), Cd(II), and Hg(II) are summarized in Table 4. The overall formation constant $\log\beta_{41}$ varied in the sequence Zn(II)>Cd(II)<Hg(II), and thus, the formation of $[CdX_4]^{2-}$ (X=SCN) is the least favorable within the metal complex in aqueous solution. The corresponding $\Delta H^\circ_{\beta41}$ and $\Delta S^\circ_{\beta41}$ values vary in the sequence, Zn(II)>Cd(II)$\gg$Hg(II) and Zn(II)$\gg$Cd(II)$\approx$Hg(II), respectively. The less favorable formation of $[CdX_4]^{2-}$ than that of $[ZnX_4]^{2-}$ is thus ascribed to the small entropy term, i.e., the $\Delta S^\circ_{\beta41}$ value of the former complex is largely negative compared to that of the latter.

Among tetrahalogeno complexes of Cd(II) in aqueous solution, $\Delta H^\circ_{\beta41}$ becomes negative in the only case of the complex with soft iodide ions (−29 kJ mol^{-1}).[16] The fact that the $\Delta H^\circ_{\beta41}$ value of the tetrathiocyanatocadmate(II) complex was also negative in aqueous solution, therefore, suggests that cadmium(II) ion has some bonds with the soft *S* atoms within the ligating SCN^- ions. However, the $\Delta S^\circ_{\beta41}$ value of the tetraiodocadmate(II) complex is much more positive (26 J $\text{K}^{-1}\,\text{mol}^{-1}$)[16] than that of the corresponding thiocyanato complex in aqueous solution. The larger difference in the entropy values may mainly be ascribed to the loss of vibrational and rotational freedoms of triatomic SCN^- ion on coordination to Cd(II) ion. Such a difference in the entropies of formation of the halogeno and thiocyanato complexes of Cd(II) has also been observed in DMSO.[11]

Table 5. Thermodynamic Quantities, $\Delta G^\circ_n/\text{kJ mol}^{-1}$, $\Delta H^\circ_n/\text{kJ mol}^{-1}$, and $\Delta S^\circ_n/\text{J K}^{-1}\,\text{mol}^{-1}$, for the Stepwise Reaction, $[MX_{n-1}]^{(3-n)+}+X^-=[MXn]^{(2-n)+}$ (M=Zn or Cd, X=SCN and n=1—4), in Water and in Dimethyl Sulfoxide at 25 °C

	Cd(II)		Zn(II)	
	Water[a] 3 mol dm^{-3} $NaClO_4$	DMSO[b] 1 mol dm^{-3} NH_4ClO_4	Water[c] 5 mol dm^{-3} $NaClO_4$	DMSO[d] 1 mol dm^{-3} NH_4ClO_4
ΔG°_1	−7.8	−10.3	−5.2	−7.9
ΔG°_2	−2.3	−5.2	−3.8	−8.1
ΔG°_3	−0.3	−1.2	−3.3	−13.7
ΔG°_4	−1.0	—	−2.0	−9.4
ΔH°_1	−10.2	−3.0	−5.0	5.5
ΔH°_2	−20.1	−2.8	2.9	23.5
ΔH°_3	22.6	4.2	−6.3	−17.8
ΔH°_4	−22.8	—	−4.4	−10.7
ΔS°_1	−8	25	1	45
ΔS°_2	−60	8	23	105
ΔS°_3	77	18	−10	−13
ΔS°_4	−73	—	−8	−4

a) This work. b) Ref. 11. c) Ref. 9. d) Ref. 12.

Coordination Structures of $[Cd_2X]^{3+}$ and $[CdX_n]^{(2-n)+}$ (X=SCN). It has been known that the C-S stretching vibration of SCN^- ion shifts toward the higher and lower frequencies, respectively, within metal complexes than that of the free ion as the result of the coordination of SCN^- ion to a matal ion through the N and S atoms.[2-7] The Raman bands observed at ca. 720 and 780 cm^{-1} thus indicated the formation of the complexes having the Cd-S and Cd-N bonds.

Thermodynamic quantities, $\Delta G^\circ_n/\text{kJ mol}^{-1}$, $\Delta H^\circ_n/\text{kJ mol}^{-1}$ and $\Delta S^\circ_n/\text{J K}^{-1}\,\text{mol}^{-1}$, for the stepwise reaction, $[MX_{n-1}]^{(3-n)+}+X^-=[MX_n]^{(2-n)+}$ (M=Zn and Cd, X=SCN and n=1—4), in aqueous solutions are summarized in Table 5, together with those in DMSO for comparison.[11,12] The ΔH°_n and ΔS°_n values for the $[CdX_n]^{(2-n)+}$ complexes in aqueous solution irregularly varied with n and they mostly compensated each other to result in rather smooth changes in ΔG°_n. The irregularities of ΔH°_n and ΔS°_n with n might be correlated to the bonding type of SCN^- ions with Cd(II) ion as well as a structural change in the cadmium(II) thiocyanato complexes in aqueous solution.

$[Cd(SCN)Cd]^{3+}$. It is expected that two cadmium(II) ions are bridged by an SCN^- ion within the dinuclear complex. A similar bridged structure -[Cd-SCN-Cd]- is found in $Cd(SCN)_2$ crystal. The $[Cd(SCN)Cd]^{3+}$ complex has both Cd-S and Cd-N bonds, and thus, showed the C-S vibrational band at 720 cm^{-1} which is an indicative of the Cd-S bond formation within the complex.

$[Cd(NCS)]^+$. Since the 780 cm^{-1} band is assigned to the C-S stretching vibration within the monothiocyanatocadmium(II) complex predominantly formed in the solutions of C_X/C_M=0.65—2.19 in Fig. 6, the coordination structure $[Cd(NCS)]^+$ is suggested

for the complex. The ΔS_1° value for the formation of the monothiocyanatocadmium(II) complex is comparable with that of $[Zn(NCS)]^+$ in aqueous solution. The result may also support the formation of $[Cd(NCS)]^+$, instead of $[Cd(SCN)]^+$.

$[Cd(SCN)(NCS)]$. In the cadmium(II) thiocyanate solutions of C_X/C_M=1.27—2.19, the mono- and dithiocyanatocadmium(II) complexes are formed but the formation of the dinuclear complex is negligible. Therefore, the 720 cm^{-1} band still observed in the solutions may arise from the formation of the Cd-S bond within the dithiocyanatocadmium(II) complex. Consequently, the structure $[Cd(SCN)(NCS)]$ having both Cd-S and Cd-N bonds is suggested. The stepwise ΔH_2° and ΔS_2° values for the reaction, $[Cd(NCS)]^+ + SCN^- = [Cd(SCN)(NCS)]$, are largely negative, which is probably due to the formation of a covalent-type bond between moderately soft Cd(II) ion and the soft S atom of SCN^- ion.

$[Cd(SCN)(NCS)_2]^-$. Although there is no evidence on the coordination structure of the trithiocyanatocadmate(II) complex from Raman spectroscopic data, the structure $[Cd(SCN)(NCS)_2]^-$ is suggested, because the tetrathiocyanatocadmate(II) complex may be formed from the trithiocyanato complex with an SCN^- ion by bonding through the S atom as discussed below.

$[Cd(SCN)_2(NCS)_2]^{2-}$. The coordination structure of the tetrathiocyanatocadmate(II) complex has been elucidated by a previous X-ray scattering measurement to be $[Cd(SCN)_2(NCS)_2]^{2-}$. The ΔH_4° and ΔS_4° values were similar to the ΔH_2° and ΔS_2° values, respectively, the result indicating that the Cd-S bond may form at the formation of the tetrathiocyanatocadmate(II) complex in aqueous solution. From this result we concluded that the third complex is $[Cd(SCN)(NCS)_2]^-$, from which an additional Cd-S bond is formed to produce $[Cd(SCN)_2(NCS)_2]^{2-}$.

Change in the Coordination Symmetry around Cd(II). Relatively largely positive ΔH_3° and ΔS_3° values observed at the third consecutive step of formation of $[Cd(SCN)(NCS)_2]^-$ suggest the change in the coordination symmetry around Cd(II) ion from octahedral to tetrahedral.

It is known that cadmium(II) ion is tetrahedrally coordinated with four SCN^- ions and no solvent molecules in the first coordination sphere within the tetrathiocyanatocadmate(II) complex in aqueous solution.[1] On the other hand, aquàcadmium(II) ion is octahedrally coordinated with six water molecules in aqueous solution.[17] Thus, the coordination symmetry around Cd(II) ion changes at a certain step of formation of the thiocyanato complexes of the metal ion. When the symmetry changes from octahedral to tetrahedral, more than one (three in this case) water molecules should be replaced to an entering SCN^- ion. Such an extensive dehydration process should be accompanied with a relatively large entropy gain. At the same time, a large absorption of heat should result due to the rupture of many metal-solvent bonds. As seen in Table 5, the same trend in the variation of ΔH_n° has been observed in the formation of the thiocyanto complexes of Cd(II) in DMSO.[11]

It is noted that the ΔH_2° and ΔS_2° values are largely positive in the complex formation reaction of the zinc(II) thiocyante system in both water[9] and DMSO,[12] and the result suggests that the coordination symmetry around zinc(II) ion may be changed at the second step of the complex formation. The structure change occurring at a different stage of the complex formation in the zinc(II) thiocyanate system from that in the cadmium(II) system may be due to a smaller ionic size of zinc(II) ion than that of cadmium(II) ion.

The work has been supported by the Grant-in-Aid for Scientific Research No. 59540386 from the Ministry of Education, Science and Culture.

References

1) T. Yamaguchi, K. Yamamoto, and H. Ohtaki, *Bull. Chem. Soc. Jpn.*, **58**, 3235 (1985).
2) A. Tramer, *J. Chim. Phys.*, **59**, 232 (1962).
3) S. Fronaeous and R. Larsson, *Acta Chem. Scand.*, **16**, 1447 (1962).
4) K. A. Taylor, T. V. Long II, and R. A. Plane, *J. Chem. Phys.*, **47**, 138 (1967).
5) R. E. Hester and K. Krishnan, *J. Chem. Phys.*, **48**, 825 (1968).
6) D. P. Strommen and R. A. Plane, *J. Chem, Phys.*, **60**, 2643 (1974).
7) A. Antić-Jovanović, M. Jemeric, and D. A. Long, *J. Raman Spectrosc.*, **12**, 91 (1982).
8) S. Ahrland and L. Kullberg, *Acta Chem. Scand.*, **25**, 3692 (1971).
9) S. Ishiguro, K. Yamamoto, and H. Ohtaki, *Anal. Sci.*, **1**, 263 (1985).
10) H. Ohtaki, *Denki Kagaku*, **44**, 151 (1976).
11) S. Ahrland and N-O. Björk, *Acta Chem. Scand., Ser. A*, **30**, 257 (1976).
12) S. Ahrland and N-O. Björk, and R. Portanova, *Acta Chem. Scand., Ser. A*, **30**, 270 (1976).
13) P. Gerding, *Acta Chem. Scand.*, **20**, 2771 (1966).
14) P. Gerding, *Acta Chem. Scand.*, **22**, 1283 (1968).
15) P. Gerding and B. Johansson, *Acta Chem.Scand.*, **22**, 2255 (1968).
16) I. Leden, "Potentiometrisk undersökning av några kadmiumsalters komplexitet," Dissertation of University of Lund, (1943).
17) H. Ohtaki, M. Maeda, and S. Itoh, *Bull. Chem. Soc. Jpn.*, **47**, 2217 (1974).
18) S. Ahrland, I. Persson, and R. Portanova, *Acta Chem. Scand., Ser. A*, **35**, 49 (1981).

 © 1986 The Chemical Society of Japan Bull. Chem. Soc. Jpn., 59, 1015—1019 (1986)

The Crystal and Molecular Structure of Tetrakis(μ-1-hydroxy-2-naphthoato)-bis{aqua(ethanol)(1-hydroxy-2-naphthoato)neodymium(III)}-Water-Ethanol (1/2/2), $[\{Nd[C_{10}H_6(OH)(COO)]_3(H_2O)(C_2H_6O)\}_2]\cdot 2H_2O\cdot 2C_2H_6O$

Yoshiyuki Ohki,† Yasuo Suzuki,† Toshio Takeuchi,†† Mamoru Shimoi, and Akira Ouchi*
Department of Chemistry, College of Arts and Sciences, The University of Tokyo, Komaba, Meguro-ku, Tokyo 153
†Department of Industrial Chemistry, Faculty of Engineering, Meiji University, Higashi-Mita, Tama-ku, Kawasaki, Kanagawa 214
††Department of Natural Sciences, Faculty of Science and Technology, Sophia University, Kioi, Chiyoda-ku, Tokyo 102
(Received November 18, 1985)

The structure of the title complex was determined by the single-crystal X-ray-diffraction method. It is triclinic, with the space group $P\bar{1}$; the cell constants were a=12.529(2), b=15.044(4), c=10.063(1) Å, α=104.15(2), β=98.73(1), and γ=87.16(2)°; Z=1, and the final R value was 0.053. The central metal atom is in a tricapped trigonal-prism geometry and is ennea-coordinated with seven oxygen atoms of the carboxylate ligands and with each oxygen atom of one water and one ethanol molecule. The complex is dimeric and the metal atoms are bridged with four carboxylate ions; two of them act as bidentates, and the other two, as tridentates, where one oxygen atom is coordinated to both metal atoms. The other carboxylate ion makes a chelate ring with each metal atom. The dimer is connected through hydrogen bondings to the atoms on both sides along the c-axis.

It has already been reported by several authors that carboxylate complexes of lanthanoids(III) take many kinds of geometries.[1-5] In cases of the aromatic carboxylates,[1,3] as well as of some nicotinates and isonicotinates,[4,6] the central metal is in a square-antiprism geometry and is octa-coordinated, where the squares of the complex molecules are parallel and are lined up along one axis. They are dimeric or linear polymeric bridged by the carboxylate ligands. On the other hand, acetates of some heavy lanthanoids[5] and cerium(III) *m*-hydroxybenzoate,[7] for example, take the tricapped trigonal prism geometry, and the central metal atoms are ennea-coordinated. The geometries of the complexes are thought to depend on the size of the ligand compared with that of the metal atom, as well as on the substituted groups of the carboxylate ions, which affect the mutual interaction of the ligand molecules. In a previous paper, we have reported about the interesting structures of some lanthanoid 2-naphthalenesulfonates, where the hydrophobic layer of the naphthalene rings makes a sheet between the hydrophilic metal complex cores, which form network layers bridged by hydrogen bondings via water molecules.[8] Along this line of research, we have tried to determine the structure of the title complex, where the ligand molecule has a naphthalene ring as well as a carboxyl group, using the single-crystal X-ray-diffraction method.

Experimental

Synthesis of Tetrakis(μ-1-hydroxy-2-naphthoato)-bis{aqua(ethanol)(1-hydroxy-2-naphthoato)neodymium(III)}-water-ethanol (1/2/2) (1). Neodymium(III) chloride hexahydrate (0.72 g, 2.0 mmol) was dissolved in water, and an excess of sodium hydroxide (in an aqueous solution) was added. The hydroxide thus precipitated was filtered off, washed with water, and warmed (60 °C) in 20 cm³ of an ethanol–water mixture (2:1=v/v), together with 1-hydroxy-2-naphthoic acid (1.13 g, 6.0 mmol), for 30 min: The solution obtained was then filtered off. The filtrate was left standing for several days at ambient temperature, thus precipitating the crystals. The crystals thus obtained effloresced in a few min when they were separated from their mother liquor; however, they are stable for several weeks if they are not dried. By the same way of synthesis, praseodymium, samarium, dysprosium, and erbium complexes were obtained in a crystalline state, but all of them effloresce rapidly, too. Especially the crystals of the erbium complex cleave even when they are left in pure ethanol, water, or a mixture of them. The elemental analysis of the complex after it has dried for 24 h on a vacuum silica-gel desiccator shows it to be the dihydrate; all the ethanol is removed. Found: Nd, 19.80: C, 53.58: H, 3.29%. Calcd for $NdC_{33}H_{25}O_{11}$: Nd, 19.44: C, 53.43: H, 3.40%. The mass-loss of the rapidly washed and dried sample after it has been left standing on the vacuum silica-gel desiccator for 24 h: Found: 11.11%. Calcd for the difference between $NdC_{37}H_{37}O_{13}$ and $NdC_{33}H_{25}O_{11}$ (corresponding to two ethanols per neodymium) : 11.05%.

Thermal Analysis. Simultaneous thermogravimetric (TG) and differential thermal analyses (DTA) were carried out with a Rigaku-Denki "Thermoflex" M-8075, using a sample of about 10 mg in each run, with reference to Al_2O_3, at the heating rate of 10 K min^{-1}.

Single-Crystal X-Ray Analysis. A crystal 0.45×0.30×0.20 mm³ in size was used as the sample. It was sealed in a glass capillary immediately after having been picked out from the mother liquor. Crystallographic data: $Nd_2C_{74}H_{74}O_{26}$, F.W. 1667.86, triclinic, space group $P\bar{1}$, a=12.529(2), b=15.044(4), c=10.063(1) Å, α=104.15(2), β=98.73(1), γ=87.16(2)°, U=1817.7(6) Å³, Z=1, D_x=1.52, D_m=1.52(3) Mg m^{-3} by floatation in a CH_2BrCH_2Br–CCl_4 mixture, μ(Mo $K\alpha$)=1.51 mm^{-1}. The reflections were collected on a Rigaku AFC-6A automated four-circle diffractometer with graphite-monochromated Mo $K\alpha$ radiation (0.7107 Å), in the range of $3°<2\theta<65°$, the ω—2θ scan technique being employed (scan speed: 4° min^{-1} (θ): scan width: $(1.25+0.5\tan\theta)°$). Of the 13315 independent reflections observed, 10370 $|F_o|>3\sigma(|F_o|)$ reflections were used for the refinement. The intensities were corrected for

the Lorentz and polarization factors, but no correction was made for absorption or extinction.

Structure Determination. The structure was solved by the heavy-atom method. The positions of the metal and some oxygen atoms were deduced from the three-dimensional Patterson map. The positional and thermal parameters were refined successively by the repeated block-diagonal least-squares method and by Fourier syntheses. At the end, all the non-hydrogen atoms were found. An uncoordinated water molecule was found to be disordered and to have been divided into two: The occupancy factors of O(W2A) and O(W2B) were determined to be 0.66 and 0.34, respectively. The atoms of one ethanol molecule, O(E2), C(E3), and C(E4), are fixed assuming their isotropic temperature parameters to be 8.0. The positions of the naphthalene hydrogen atoms were calculated by assuming the C-H bond length to be 1.08 Å; their B_{iso}'s were assumed to be 6.0. The parameters of the hydrogen atoms were also fixed in the refinement. The final R value was 0.053, R_w=0.065, and S=4.07.[9]

All the calculations were carried out on a HITAC M-280H apparatus at the Computer Center of The University of Tokyo, using the local version of the UNICS program.[10] The atomic-scattering factors were taken from Ref. 11.

Infrared-Absorption-Spectrum Measurement. The infrared-absorption spectra were obtained by means of a JASCO A202 grating infrared spectrophotometer, using Nujol and hexachloro-1,3-butadiene mull.

Results and Discussion

The final atomic parameters are listed in Table 1, while some bond lengths and bond angles, as well as some interatomic distances which are thought to be the hydrogen-bonding ones, are tabulated in Table 2. The projection of the unit-cell along the a-axis, the perspective drawing along the metal–metal axis, and the schematic presentation of the coordination geometry around the central metal atom are shown in Figs. 1, 2, and 3.[12]

The complex is dimeric, with a center of inversion between the metal atoms, bridged by four carboxylate ligands. As is depicted in Fig. 3, the metal atom is ennea-coordinated and is in a deformed tricapped trigonal prism geometry, where seven oxygen atoms of five carboxylate ligands and two oxygen atoms of ethanol and water molecules are bound to the metal atom.

A pair of carboxylates span two neodymium atoms through both oxygen atoms of each carboxyl group. As is shown in Table 1, the C–O and Nd–O bond lengths of two oxygen atoms of this type of ligand are not equal. The longer C–O bonding has the longer Nd–O bond; therefore, the double-bonding oxygen atom, not the single-bonding oxygen atom, of the carboxyl group bonds with the metal atom more strongly. The other pair of carboxylate ligands act as a "tridentate" bridge: one of the oxygen atoms is bridging two metal atoms, and the other oxygen atom is coordinating to one of the metal atoms to form a chelate ring at the same time.

Table 1. Final Atomic Coordinates (×10⁴), with Estimated Standard Deviations in Parentheses, and Their Equivalent Isotropic Temperature Factors (B_{eq}/Å²)

Atom	x	y	z	B_{eq}/Å²[a]	Atom	x	y	z	B_{eq}/Å²[a]
Nd	4586.5(2)	4543.3(2)	2906.3(3)	2.38	C(12)	6257(4)	2508(3)	122(5)	3.04
O(1)	6755(3)	4361(2)	6076(4)	3.48	C(13)	7128(5)	2725(4)	−471(7)	4.88
O(2)	6319(3)	3997(3)	3775(4)	3.92	C(14)	7881(6)	2089(5)	−883(8)	5.86
O(3)	4764(3)	3024(3)	1314(4)	3.55	C(15)	7815(5)	1182(4)	−732(6)	4.05
O(4)	5688(3)	4066(2)	833(4)	3.80	C(16)	8640(6)	510(5)	−1071(8)	5.66
O(5)	5411(3)	5966(2)	2793(4)	3.61	C(17)	8577(6)	−344(5)	−885(8)	5.96
O(6)	5530(3)	5896(2)	4947(4)	3.43	C(18)	7674(6)	−588(4)	−377(7)	5.24
O(W1)	3521(3)	5011(3)	870(4)	3.74	C(19)	6866(5)	30(4)	−56(6)	4.13
O(E1)	2843(3)	3696(3)	2326(4)	3.98	C(20)	6940(4)	937(3)	−201(5)	3.16
O(C1)	8398(3)	3610(3)	7184(4)	4.13	C(21)	5965(4)	7827(3)	3526(5)	2.96
O(C11)	5324(4)	1354(3)	741(5)	4.51	C(22)	5795(4)	7347(3)	4492(5)	2.94
O(C21)	5932(4)	7410(3)	2173(4)	4.04	C(23)	5831(5)	7832(4)	5905(5)	4.01
C(C1)	6883(4)	3893(4)	4854(5)	3.06	C(24)	6034(5)	8735(4)	6319(5)	4.06
C(C2)	5531(4)	3237(3)	747(5)	3.00	C(25)	6223(4)	9231(3)	5363(5)	3.24
C(C3)	5574(4)	6356(3)	4066(5)	2.89	C(26)	6455(5)	10179(4)	5779(6)	4.00
C(1)	8455(4)	3071(3)	5899(5)	3.05	C(27)	6623(5)	10649(4)	4837(7)	4.36
C(2)	7755(4)	3187(3)	4754(5)	3.01	C(28)	6558(6)	10208(4)	3434(7)	4.73
C(3)	7858(5)	2599(4)	3445(6)	4.14	C(29)	6334(5)	9284(4)	2978(6)	4.03
C(4)	8630(5)	1934(4)	3294(7)	4.81	C(30)	6178(4)	8778(3)	3940(5)	2.98
C(5)	9358(4)	1814(4)	4452(6)	3.83	C(E1)	1894(7)	3786(6)	2990(11)	7.91
C(6)	10166(5)	1119(4)	4316(8)	5.18	C(E2)	1288(9)	2965(8)	2673(15)	11.28
C(7)	10871(5)	1018(5)	5442(9)	5.77	O(W2A)	7594(7)	7151(6)	404(8)	6.29
C(8)	10800(5)	1581(5)	6755(8)	5.68	O(W2B)	7698(12)	6636(10)	524(15)	5.62
C(9)	10022(5)	2259(4)	6919(7)	4.51	O(E2)	8309	5499	1001	(8.0)
C(10)	9278(4)	2387(4)	5764(6)	3.40	C(E3)	8002	5207	2194	(8.0)
C(11)	6150(4)	1614(3)	214(5)	3.01	C(E4)	8901	5205	3296	(8.0)

a) The equivalent isotropic temperature factors were computed using the following equation:

$$B_{eq}=4/3(B_{11}a^2+B_{22}b^2+B_{33}c^2+B_{12}ab\cos\gamma+B_{13}ac\cos\beta+B_{23}bc\cos\alpha).$$

The B_{ij}'s are defined by:

$$T=\exp[-(h^2B_{11}+k^2B_{22}+l^2B_{33}+2klB_{23}+2hlB_{13}+2hkB_{12})].$$

Table 2. Selected Interatomic Distances and Bond Angles of the Complex

Bond length	(l/Å)	Bond length	(l/Å)	Bond length	(l/Å)
Nd-O(1^{i})	2.452(4)	Nd-O(2)	2.398(4)	Nd-O(3)	2.471(4)
Nd-O(4)	2.611(4)	Nd-O(5)	2.457(4)	Nd-O(6)	2.685(3)
Nd-O(W1)	2.501(4)	Nd-O(E1)	2.503(4)	Nd-O(6^{i})	2.435(5)
O(1)-C(C1)	1.288(7)	O(2)-C(C1)	1.241(7)	C(C1)-C(2)	1.482(7)
O(3)-C(C2)	1.280(7)	O(4)-C(C2)	1.252(6)	C(C2)-C(12)	1.471(7)
O(5)-C(C3)	1.262(6)	O(6)-C(C3)	1.261(8)	C(C3)-C(22)	1.474(7)
O(W1)···O(4^{ii})	2.769(7)	O(W1)···O(E2^{ii})	2.747(4)	O(E2)···O(W2A)	2.773(9)
O(W2A)···O(C21)	2.893(11)	Nd···Nd^{i}	4.087(1)	Nd···Nd^{ii}	6.564(1)
Bond angle	**(ϕ/°)**	**Bond angle**	**(ϕ/°)**	**Bond angle**	**(ϕ/°)**
O(1^{i})-Nd-O(6)	68.61(11)	O(1^{i})-Nd-O(6^{i})	77.62(14)	O(1^{i})-Nd-O(E1)	74.47(12)
O(1^{i})-Nd-O(5)	81.37(13)	O(6)-Nd-O(6^{i})	74.18(13)	O(6)-Nd-O(2)	71.88(12)
O(6)-Nd-O(5)	49.89(12)	O(6^{i})-Nd-O(2)	70.66(14)	O(6^{i})-Nd-O(E1)	78.05(14)
O(E1)-Nd-O(5)	142.71(13)	O(2)-Nd-O(5)	90.10(13)	O(2)-Nd-O(E1)	127.03(13)
O(W1)-Nd-O(3)	86.16(13)	O(W1)-Nd-O(4)	71.91(14)	O(W1)-Nd-O(5)	74.48(14)
O(W1)-Nd-O(E1)	72.43(13)	O(3)-Nd-O(4)	50.70(13)	O(3)-Nd-O(E1)	68.56(12)
O(3)-Nd-O(2)	76.64(12)	O(4)-Nd-O(2)	72.66(13)	O(4)-Nd-O(5)	75.02(14)
O(1^{i})-Nd-O(W1)	76.11(13)	O(6)-Nd-O(4)	112.43(12)	O(6^{i})-Nd-O(3)	100.89(14)
C(C1)-O(1)-Nd^{i}	136.4(3)	C(C1)-O(2)-Nd	142.6(4)	O(1)-C(C1)-O(2)	123.9(5)
C(C2)-O(3)-Nd	96.4(3)	C(C2)-O(4)-Nd	90.5(3)	O(3)-C(C2)-O(4)	118.9(5)
C(C3)-O(5)-Nd	99.7(3)	C(C3)-O(6)-Nd^{i}	163.0(4)	C(C3)-O(6)-Nd	88.9(3)
O(5)-C(C3)-O(6)	119.4(5)	Nd-O(6)-Nd^{i}	105.82(14)		

Keys to the symmetric operations: i, 1−x, 1−y, 1−z, ii, 1−x, 1−y, −z.

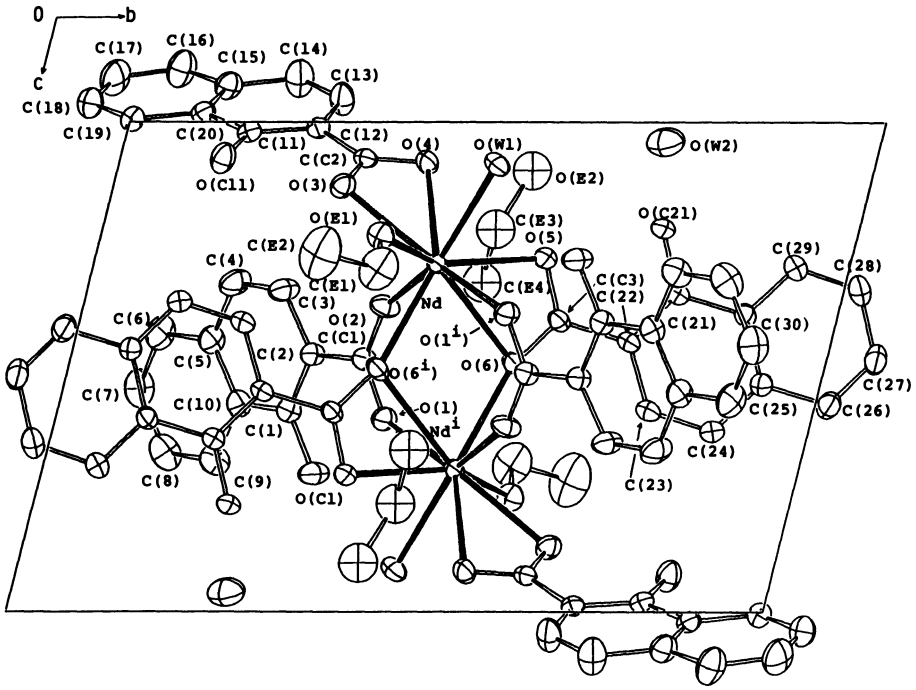

Fig. 1. The projection ot the unit cell along a-axis with the numbering scheme. (O(W2B) is neglected. Key to the symmetry operation: i, 1−x, 1−y, 1−z).

Its C-O bond lengths, as well as the bridging Nd-O lengths of the respective oxygen atoms, are almost the same; however, the third Nd-O bond, Nd-O(6), is longer than the other two.

The other carboxylate ligand chelates to the metal atom, forming a four-membered ring. The two C-O bond lengths of the ligand are not equal, and the oxygen atom of the longer C-O bond has the shorter Nd-O bond; this shows that its C=O double bond is localized. The chelate spans one edge of the bottom triangle of the prism; although the structures of some lanthanoid carboxylates taking the tricapped trigonal prism geometry have been reported, the chelating carboxylate is apt to span an apex of the prism and the cap position; therefore, the spanning position of this complex is exceptional.

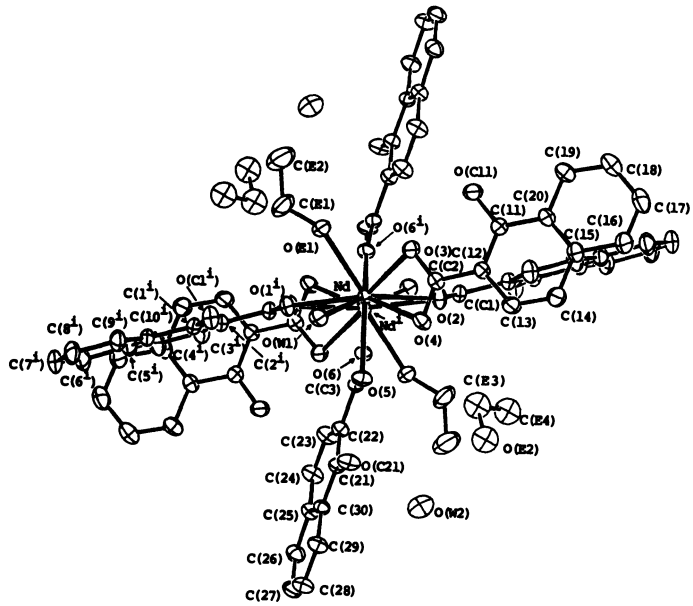

Fig. 2. The perspective of the complex along Nd-Nd^{i} axis.

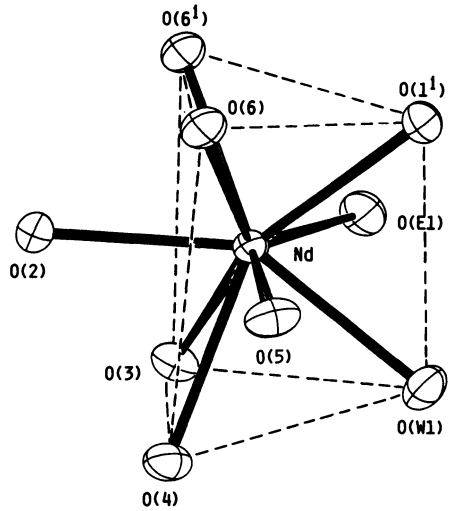

Fig. 3. The schematic presentation of the coordination geometry of the central metal atom.

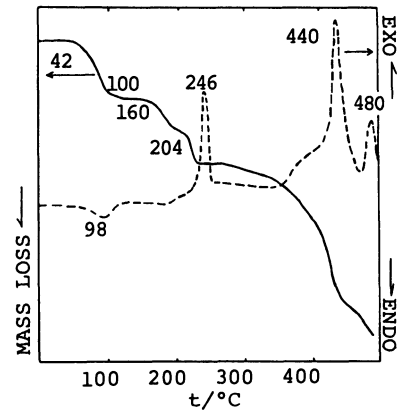

Fig. 4. TG(——) and DTA(---) curves of the complex. Mass loss of TG was taken downwards, and the exothermal change of DTA was taken upwards.

As is depicted in Fig. 2, the naphthylene group of the bridging carboxylates are arrayed radially from the line of the metal atoms. The dihedral angle between the planes of C(1)···C(10) and C(21^{i})···C(30^{i}) is 62.6° The C(11)···C(20) naphthalene ring is lying over the C(1)···C(10) ring, with a dihedral angle of 81.6°.

The Nd-O bond length to the water oxygen atom is almost the same as that to the ethanol oxygen atom; 2.501(4) and 2.503(4) Å, respectively. The distances are almost the same as the average Nd-O bond length to the seven carboxyl oxygen atoms (2.501 Å). Generally, the water molecules are bound more strongly to lanthanoid metal atoms than are those of ethanol; therefore, it is necessary to use an anhydrous medium to synthesize their alcohol complexes. This is the first case in which water and alcohol are coordinated at the same time to one lanthanoid atom, although the ethanol is quite easily removed in open air. As is shown in Fig. 2, the ethanol ligands are surrounded by the naphthalene rings. Probably the large naphthylene group of the carboxylates around the core of the complex makes the moiety more feasible for the ethanol molecule to be kept between them.

As is shown in Table 2, the coordinating water molecule forms a hydrogen bond with the carboxyl oxygen atom of the neighboring complex along the c-axis. The crystals contain uncoordinated ethanol and water molecules. These are bound to the complex through hydrogen bonds with the coordinated water molecule and the hydroxyl group of the naphthalene ring, as is shown in Table 2. The water molecule was found to be disordered, and the position of ethanol is nebulous. Furthermore, the interatomic distance of

O(E2)···O(W2B) is too short (1.976(15) Å). This phenomenon may be due to the only partial occupancy of ethanol, a result of the efflorescence of the crystal.

The results of thermogravimetric (TG), and differential thermal analyses (DTA) simultaneous measurements are depicted in Fig. 4. The TG curve shows that, when the complex is heated, the ethanol and also all of the water molecules seem to be removed in the first step, from 42 °C to about 100 °C. The anhydrous salt thus formed is stable up to about 160 °C; then the decomposition of the ligand starts to occur.

The ν_{as}(COO) band as well as the ν_{s}(COO) band in the infrared spectrum of the title complex is split. The former is split into three peaks: 1632(m), 1580(s), and 1550(sh) cm^{-1}. The relatively low-wavenumber bands may correspond to the bridging carboxyl groups. The latter band is also split into three peaks: 1470(m), 1440(s), and 1412(s) cm^{-1}.

The authors wish to thank heartily the Shin-Etsu Chemical Ind. Co., Ltd., for presenting the highly pure lanthanoid oxides.

References

1) Y. Koizumi, H. Sawase, Y. Suzuki, T. Takeuchi, M. Shimoi, and A. Ouchi, *Bull. Chem. Soc. Jpn.*, **57**, 1809 (1984).

2) G. C. Sadikov, G. A. Kukina, and M. A. Porai-Koshits, *Zh. Strukt. Khim.*, **12**, 859 (1971).

3) M. S. Khiyalov, I. R. Amiraslanov, Kh. S. Mamedov, and E. M. Movsumov, *Koord. Khim.*, **7**, 445 (1981).

4) L. A. Aslanov, I. K. Abdul'minev, and M. A. Porai-Koshits, *Zh. Strukt. Khim.*, **13**, 468 (1972).

5) H. Sawase, Y. Koizumi, Y. Suzuki, M. Shimoi, and A. Ouchi, *Bull. Chem. Soc. Jpn.*, **57**, 2730 (1984).

6) I. K. Abdul'minev, L. A. Aslanov, M. A. Porai-Koshits, and R. A. Chupakhina, *Zh. Strukt. Khim.*, **14**, 383 (1973).

7) Y. Koizumi, H. Sawase, Y. Suzuki, M. Shimoi, and A. Ouchi, *Bull. Chem. Soc. Jpn.*, **57**, 1677 (1984).

8) Y. Ohki, Y. Suzuki, M. Nakamura, M. Shimoi, and A. Ouchi, *Bull. Chem. Soc. Jpn.*, **58**, 2968 (1985).

9) $R=\sum||F_o|-|F_c||/\sum|F_o|$; $R_w=[\sum w(|F_o|-|F_c|)^2/\sum wF_o^2]^{1/2}$ where $w=1/[\{\sigma(|F_o|)\}^2+(F_{wt}\times F_o)^2]$, $F_{wt}=0.015$; $S=[\sum w(|F_o|-|F_c|)^2/(N_o-N_p)]^{1/2}$, where N_o=number of reflections and N_p number of parameters.

10) "Universal Crystallographic Computation Program System (UNICS)," ed by T. Sakurai, Crystallographic Society of Japan, Tokyo (1967).

11) "International Tables for X-Ray Crystallography," Kynoch Press, Birmingham (1974), Vol. IV, pp. 72, 150.

12) Some additional bond-length and bond-angle data, the positions of the hydrogen atoms, the final anisotropic thermal parameters, and the F_o-F_c tables are deposited as Document No. 8623 at the Office of the Editor of the *Bull. Chem. Soc. Jpn.*

 © 1986 The Chemical Society of Japan Bull. Chem. Soc. Jpn., 59, 1021—1026 (1986)

Transformation of 3-(2,2-Dichloroethenyl)-2,2-dimethylcyclopropanecarboxylates to the Corresponding 2,2-Dibromoethenyl Analogs by Halogen Exchange Reaction[1)]

Kiyohide MATSUI,* Akemi SAITO, and Kiyosi KONDO
Sagami Chemical Research Center, Nishi-Ohnuma 4-4-1, Sagamihara, Kanagawa 229
(Received October 3, 1985)

The title transformation is effected with aluminium tribromide or related reagents in over 80% yields without cis-trans isomerization or epimerization. Efficient removal of hydrogen bromide is essential for optimum yields of the desired products. Use of boron tribromide instead of aluminium tribromide results in opening of the cyclopropane ring with no halogen exchange.

A new artificial pyrethroid having 2,2-dichloroethenyl substituent, i.e., permethrin (**1**),[2)] is now one of the common agricultural insecticides thanks to its moderate stability and high insecticidal activity. Its dibromoethenyl analog, decamethrin (**2**), is found by Elliott et al.[3)] and revealed to be more than ten times as active as permethrin.

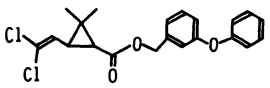

permethrin (**1**)
(cis-, trans- and racemic mixture)

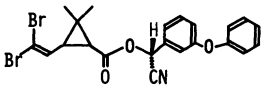

decamethrin (**2**)
(ester of (1*R*)-cis acid)

To the synthesis of permethrin, we developed a convenient process, which involved the addition of carbon tetrachloride to 3,3-dimethyl-4-pentenoates (**3**) and successive dehydrochlorination and cyclization of 4,6,6,6-tetrachloro-3,3-dimethylhexanoates (**4**) with a base to afford 3-(2,2-dichloroethenyl)-2,2-dimethylcyclopropanecarboxylates (**5**).[4)]

In the case of decamethrin synthesis, the method was applied with less synthetic value because of the following drawbacks: (a) The addition of carbon tetrabromide to **3** was relatively inefficient; (b) Trans-rich 3-(2,2-dibromoethenyl)-2,2-dimethylcyclopropanecarboxylates (**6**) was usually produced upon base-treatment of the resulting adduct.[4)]

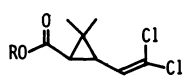

5

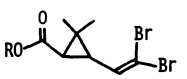

6

a: R=Et, b: R=Me, c: R=H

The processes developed so far by other groups also involve such serious disadvantages as low product yields, high cost and/or tedious operations.[3,5)]

This paper details the conversion of dichloroethenyl compounds **5** to the corresponding dibromoethenyl analogs **6** by halogen exchange which provides a convenient route to decamethrin.

Exchange of the halogen of haloethenes has been usually performed with copper(I) halides in dipolar aprotic solvents.[6)] We first attempted the reaction of **5a** with copper(I) bromide under various conditions and obtained a mixture of dichloro-, bromochloro-, and dibromoethenylcyclopropanecarboxylates (**5a**, **7a**, and **6a**, respectively). For example, treatment of **5a** with copper(I) bromide (8 equiv) in DMF at 150 °C for 8 h afforded a mixture of **5a** (77%), **7a** (16%), and **6a** (1%). The prolonged treatment usually induced the decomposition of the products and the total recovery of **5a**, **6a**, and **7a** diminished. Use of a large excess of copper(I) bromide gave no significant change in product distribution.

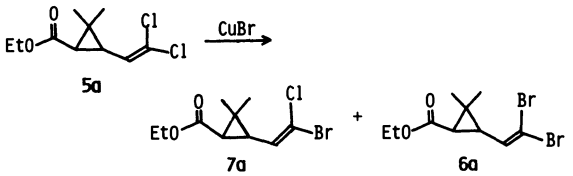

5a **7a** **6a**

Aluminium tribromide and boron tribromide are also capable of halogen exchange.[7)] They are active for the halogen exchange of relatively stable compounds such as simple alkyl halides,[8)] gem-polyhalogenated compounds,[9)] bridgehead-halogenated bicyclic compounds,[10)] and a few haloethenes.[11)]

We found aluminium tribromide did promote the halogen exchange of **5a** without affecting the ester group or cyclopropane ring as follows: Treatment of **5a** with commercial aluminium tribromide in 1,2-dibromoethane under ice-water cooling afforded **6a** (area % on GLPC=88%) and **7a** (5%) along with a by-product (6%). The structure of this by-product was assigned to 2,2,2-tibromoethyl compound **8a** by the GLPC-MS data and by its conversion to **6a** with DBU. A 76% yield of **6a** with 95% purity was attained by transforming the concomitant **8a** into **6a**.

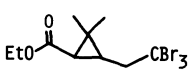

8a

The formation of **8a** suggests the possibility that the halogen exchange is initiated by the addition of hydrogen bromide to the dichloroethenyl moiety of **5a**.[12)] This hypothesis prompted us to study the halogen exchange of 2,2,2-trichloroethyl compound **9a** with aluminium tribromide. The reaction in fact pro-

Table 1. Direct Conversion of **9a** and **5a** to **6a** Using HBr Scavenger

Substrate	HBr scavenger	Time	Yield (GLPC)/%		
		h	**6a**	**8a**	**7a**
9a	Al metal	7.5	23.4	15.5	0.8
9a	Pyridine	4.5	49.3	33.1	4.7
9a	Na_2CO_3	7.0	56.7	26.5	4.1
9a	Argon[a]	6.0	82.9	11.8	3.7
9a	Argon, red. press.[b]	3.0	95.6	4.2	—
5a	Argon, red. press.[b]	4.0	91.0	1.8	1.7

a) Argon=The reaction mixture was bubbled with argon gas under ice-water cooling. b) Argon, red. press.=The reaction mixture was bubbled with argon gas under reduced pressure (≈20 mmHg) under ice-water cooling.

ceeded smoothly in dibromomethane, and tribromoethyl compound **8a** was produced in 62% yield accompanied by ca. 30% of dibromoethenyl compound **6a**.

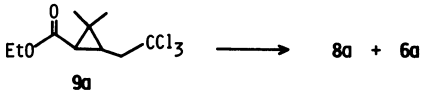

9a

The formation of **6a** suggests that the aluminium trihalides promotes also the dehydrobromination of the tribromoethyl moiety.

Therefore, we then studied the conversion of **9a** into **6a** and the complete transformation of **5a** into **6a**. Such hydrogen bromide scavenger as aluminium metal, pyridine or sodium carbonate turned out ineffective in the transformation of **9a** into **6a** (Table 1). In order to purge the hydrogen bromide, the reaction mixture was bubbled by an argon gas with promising results. Finally, argon bubbling under reduced pressure was found to be most effective, and the contaminating **8a** was reduced to below 5% (Table 1). By using this technique, **9a** and **5a** were successfully transformed into **6a** as shown in Table 1.

The reagent generated from aluminium metal and 1,2-dibromoethane (or bromine, or hydrogen bromide) was found also effective for the transformation of **5a** to **6a**. Furthermore, aluminium trichloride could be used instead of aluminium tribromide when hydrogen bromide was introduced during the reaction. In practical view point, the aluminium metal-hydrogen bromide reagent (91% yield, 95% purity) and aluminium trichloride-hydrogen bromide reagent (92% yield, 91% purity) were most useful. Other metal bromides, e.g., $ZnBr_2$, $FeBr_3$, $CuBr_2$, $BiBr_3$, $SbBr_3$, $HgBr_2$, $TiBr_4$, were almost ineffective for this halogen exchange.

Brominated hydrocarbon, e.g., dibromomethane, or 1,2-dibromoethane, was the most appropriate solvent and the use of aromatic halides and carbon disulfide gave comparable results. In dichloromethane, the halogen exchange was not so effective as in the case of dibromomethane. The optimum amount of the aluminium reagent was found to be ca. 1.5 molar equivalents of the substrate in view of the product yield and the purity. The halogen exchange did not occur with less than one molar equivalent of the reagent. The product yield decreased with a large excess reagent.

These findings may suggest the reaction mechanism for the halogen exchange reaction as illustrated in Scheme 1: (1) Addition of hydrogen bromide to the dichloroethenyl moiety.[13] (2) Halogen exchange of the trihaloethyl intermediates (**10a**, **11a**, and **8a**). (3) Dehydrobromination of these intermediates. The aluminium reagents should have played an important role in the above every step.

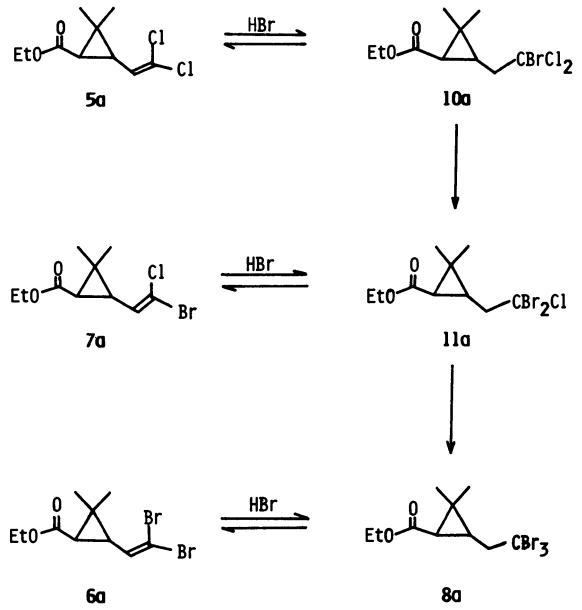

Scheme 1.

The chlorine-bromine exchange reaction is applicable as well to the methyl ester **5b** or free acid **5c**. The yields of the corresponding dibromoethenyl compound **6b** or **6c** were also satisfactory. The exchange reaction of the free acid **5c** proceeded faster than that of the corresponding esters. Actually, the halogen exchange of **5c** almost finished when the addition of the substrate to aluminium tribromide was completed. In this acid case, the formation of tribromoethyl acid **8c** was remarkable as compared with the ester cases (**6c**/**8c**=1/2). The rapid halogen exchange and the presence of a larger amount of **8c** is attributed to the hydrogen bromide generated by the initial contact of the starting acid **5c** with the aluminium reagent. Efficient removal of hydrogen bromide from the reaction mixture by argon bubbling was, therefore, necessary for optimum yield of dibromoethenyl acid **6c** (90—95%).

In order to apply this halogen exchange to the preparation of the acid part of decamethrin, it is essential that cis-trans isomerization or epimerization should not take place during the reaction.

Table 2. Stereochemistry in Transformation of **5** to **6**

5	(cis/trans)	Reagent	6 Yield/%	6 cis/trans	6 Purity/%[a]
5a	(77/23)	Al-HBr	92	77/23	95
5b	(99/1)	Al-HBr	90	99/1	92
5c	(0/100)	$AlBr_3$	93	0/100	96
5c	(100/0)	$AlBr_3$	94	100/0	96
5c	(0/100)[b]	$AlBr_3$	93	0/100[c]	96

a) Based on GLPC area %. b) $[\alpha]_D$=−36.3° ($CHCl_3$). c) $[\alpha]_D$=−37.2° ($CHCl_3$).

The halogen exchange upon the dichloroethenyl compounds **5a—c** of various cis/trans ratio showed complete preservation of the original stereochemistry as shown in Table 2.

For example, 100% *trans*-dibromoethenyl acid **6c** was obtained by the treatment of 100% *trans*-dichloroethenyl acid **5c** with aluminium tribromide. Similarly, 100% *cis*-**5c** was stereospecifically converted into 100% *cis*-**6c** in an excellent yield. The retention of the stereochemistry was also verified in the last example. Acid *trans*-**5c** with ca. 98% optical purity was transformed into **6c** having over 90% optical purity.[14]

Boron tribromide is also known to be capable of halogen exchange.[11] When dichloroethenyl compound **5a** was treated with boron tribromide in dibromomethane at room temperature, **5a** disappeared completely after stirring overnight. Acidification of the reaction mixture followed by usual work-up afforded only a carboxylic acid which was readily transformed into a neutral compound by treating with aqueous sodium hydrogencarbonate. The former carboxylic acid was assigned to ring-opened acid **12** and the neutral compound to **13** (Scheme 2). The yields of the two products were 65 and 63%, respectively, based on **5a**. When the reaction mixture was quenched with dry ethanol, the ester **14** was obtained in 89% yield. Scheme 2 shows possible routes to these products. The coordination of boron tribromide to the ester carbonyl followed by the ring opening and the transfer of bromide ion to the cationic carbon produces intermediary ethenyl borate **15**.[18] Hydrolysis or ethanolysis of **15** affords **12** or **14** as the final product. No halogen exchange was observed during this reaction. The stronger Lewis acidity of boron tribromide than aluminium tribromide would account for the observed different reactivity between them.

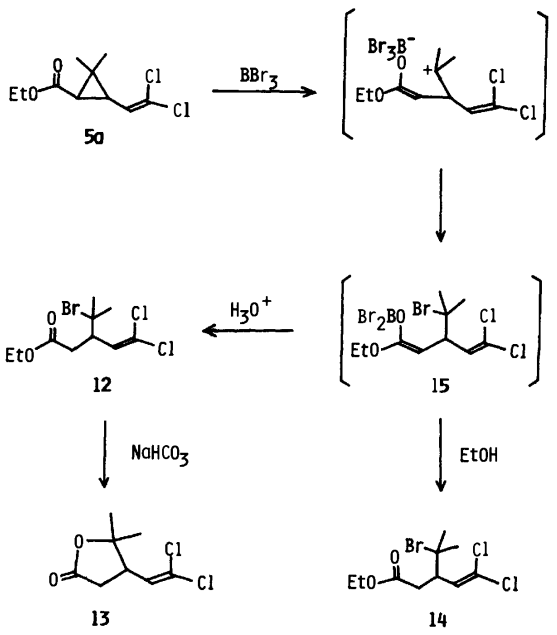

Scheme 2.

Experimental

General. All the melting points and boiling points are uncorrected. IR spectra were recoreded on a Hitachi EPI-G3 grating spectrophotometer. ^1H NMR spectra were measured with Varian HA-100 spectrometer and Hitach-Perkin-Elmer R-20B using TMS as an internal standard. Mass spectra were recoreded on Hitachi RMU-6E mass spectrometer (70 eV). Analytical determinations by GLPC were performed on a Hitachi 163 gas chromatograph (5 mm o.d.×1 m, 2% EGA on Uniport B or diasolid ZS).

Attempted Halogen Exchange of Ethyl 3-(2,2-Dichloroethenyl)-2,2-dimethylcyclopropanecarboxylate (5a) with CuBr. A solution (DMF or DMSO) of **5a** (0.47 g, 2.0 mmol) was added to a mixture of CuBr (16—40 mmol) in the same solvent (total 5 ml). The resulting mixture was heated at 130—150 °C for 8—55.5 h under an argon atmosphere. The composition of the reaction mixture was checked by GLPC at intervals.

Halogen Exchange of 5a with $AlBr_3$ in 1,2-Dibromoethane and Succesive Dehydrobromination with DBU. A solution of $AlBr_3$ (Kishida Kagaku, GR) (25 g, 94 mmol) in 1,2-dibromoethane (20 ml) was added dropwise to a solution of **5a** (15 g, 63 mmol) in 1,2-dibromoethane (30 ml) under ice-water cooling. After 4.5 h the reaction mixture was poured into ice-water and extracted with ether. The ethereal layer was washed with water, aq $NaHCO_3$, and finally with brine, and dried ($MgSO_4$). GLPC analysis of the crude product showed mainly three products whose area % were 5, 88, and 6% in the order of the retention time.

The solvent was evaporated and the residue dissolved in DMF (30 ml) was treated with DBU (1.5 g, 10 mmol) under ice-water cooling. After having been stirred for 3.5 h the reaction mixture was poured into ice-cooled dil HCl and extracted with ether. The ethereal layer was worked up as described above. Distillation gave 16 g of ethyl 3-(2,2-dibromoethenyl)-2,2-dimethylcyclopropanecarboxylate (**6a**)[4] (95% purity based on IR, ^1H NMR, GLPC, and GLPC-MS analyses). Bp 104—105 °C/0.28 mmHg (1 mmHg= 133.322Pa). The minor product (6%) with the latest retention time was converted to **6a** by the DBU treatment being attributed to ethyl 2,2-dimethyl-3-(2,2,2-tribromoethyl)cyclopropanecarboxylate (**8a**). Its retention time on GLPC and GLPC-MS data were coincident with those of an authentic sample.[4] Another minor component (5%) with fastest retention time isolated by GLPC separation was assigned to ethyl 3-(2-bromo-2-chloroethenyl)-2,2-dimethylcyclopropanecarboxylate (**7a**). ^1H NMR (CCl_4) δ=6.38 (dd), 5.73 (dd)(total 1H), 4.03 (q, 2H), 2.3—1.5 (m, 2H), 1.4—1.1 (m, 9H). MS *m/z* 281

(M+), 41 (base). Found: C, 42.43; H, 4.96%. Calcd for $C_{10}H_{14}BrClO_2$: C, 42.66; H, 5.01%.

Halogen Exchange of Ethyl 2,2-Dimethyl-3-(2,2,2-trichloroethyl)cyclopropanecarboxylate (9a).[15] To a solution of **9a** (0.55 g, 2.0 mmol) in dibromomethane (3 ml) was added a solution of $AlBr_3$ (0.53 g, 2.0 mmol) in dibromomethane (1 ml) under ice-water cooling. The composition of the reaction mixture was analysed by GLPC (diasolid ZS) at appropriate time intervals. The products (area %) formed after 45 min were **8a** (62%) and **6a** (29%).

Examination of the Effect of HBr Scavenger. a) Addition of Al Metal: A solution of $AlBr_3$ (0.80 g, 3.0 mmol) in dibromomethane (2 ml) was added to a solution of **9a** (0.55 g, 2 mmol) in dibromomethane under ice-water cooling. Small pieces of Al foil (ca. 50 mg) was added to the reaction mixture. After having been stirred for 7.5 h the reaction mixture was poured into ice-water and extracted with ether. Usual work-up, followed by GLPC (diasolid ZS) assay (octadecane (0.25 g) as an internal standard) gave the results cited in Table 1.

b) Bubbling with Argon Gas at Atmospheric Pressure: After the halogen exchange of **9a** was carried out in a similar manner as described above, argon gas was introduced to the reaction mixture. After 6 h the product yields were determined by GLPC.

c) Bubbling with Argon Gas under Reduced Pressure: The reaction was carried out in a similar manner as described in section b. After argon gas was introduced for 15 min the pressure of the reaction system was gradually reduced to 20 mmHg. The flow of argon gas was controlled so as to maintain moderate bubbling under ice-water cooling. After 3 h the reaction mixture was worked up.

Direct Conversion of Dichloroethenyl Compound 5a to 6a. To a solution of **5a** (0.48 g) in dibromomethane (2 ml) was added dropwise a solution of $AlBr_3$ (0.80 g, 3.0 mmol) in dibromomethane (3 ml) under ice-water cooling. After 1.5 h the pressure of reaction system was reduced to 20 mmHg under moderate argon bubbling for 4 h.

General Procedure for the Reaction of 5a with Various Metal Bromides. A solution of **5a** (0.47 g, 2.0 mmol) in dibromomethane (2 ml) was added dropwise to a mixture of a metal bromide (3.0 mmol) in dibromomethane (3 ml) under ice-water cooling. When no change of the composition of the reaction mixture was observed on GLPC analysis, the reaction temperature was raised to room temperature, 60 °C, and finally to the refluxing temperature. The composition of the mixture was analyzed by GLPC at every temperature.

Halogen Exchange of 5a with Aluminium Compound Other than Commercial $AlBr_3$. a) Al-$BrCH_2CH_2Br$ Method: A small amount of bromine (ca. 40 mg) was added to two pieces (ca. 30 mg) of Al foil (Showa Aluminium Co., cut into small pieces) in 1,2-dibromoethane (5 ml) and the mixture was heated by open flame until an exothermic reaction started. After the reaction had started, remaining Al foil (total 0.41 g, 15 mmol) was added one by one. After all Al foil had been dissolved, the resulting black mixture was transferred into a dropping funnel which was attached to a second flask in which a solution of **5a** (2.4 g, 10 mmol) in 1,2-dibromoethane (10 ml) was placed. After the addition of the complex prepared above under ice-water cooling, the reaction mixture was allowed to warm to 20 °C. The reaction mixture was stirred for 9.5 h and then poured into ice-water and worked up as usual. Distillation of the crude product gave 2.7 g of a pale yellow oil which was composed of **6a** (89%), **7a** (3%), and **8a** (5%), bp 101—106.5 °C/0.27 mmHg.

b) Al-Br_2 Method: Bromine (2.6 g, 16 mmol) was added to one piece of Al foil suspended in dibromomethane (8 ml) and the mixture was heated by open flame until an exothermic reaction started. Then, remaining Al foil (total 0.43 g, 16 mmol) was added one by one. After all Al foil had been dissolved, the resulting black solution was transferred into a syringe and was added dropwise to a solution of **5a** (2.4 g, 10 mmol) in dibromomethane under ice-water cooling. After the addition was completed, the reaction mixture was allowed to warm to 10 °C. Then, the reaction mixture was stirred overnight at room temperature. GLPC analysis showed that the reaction mixture was composed of **6a** (47%) and **8a** (35%) along with a small amount of **7a**.

c) Al-HBr Method: To a mixture of Al metal [Al ribbon (Merck, GR) was cut into small pieces] (0.40 g, 15 mmol) in dibromomethane (10 ml) was introduced HBr gas through gas inlet tube at 30 °C (water bath). After 5 min an exothermic reaction started and brown solids formed gradually. After all Al metal had disappeared, the resulting brown suspension was heated until the reaction mixture became a brown clear solution. Then, the mixture was cooled with ice-water and a solution of **5a** (2.4 g, 10 mmol) in dibromomethane (10 ml) was added dropwise to the cooled mixture. The introduction of HBr was continued until the color of the reaction mixture changed to reddish black (ca. 10 min after the addition of the substrate). After the completion of the reaction was confirmed by GLPC (2 h after the addition of the substrate), the pressure of the reaction system was reduced to 20 mmHg, argon gas being gently introduced. After 2.5 h (GLPC check) the reaction mixture was worked up. Distillation afforded 2.8 g (86%) of **6a**, bp 108—110 °C/0.3 mmHg (purity 96%).

d) $AlCl_3$-HBr Method: To a suspension of $AlCl_3$ (Kishida Kagaku, GR) (0.99 g, 7.5 mmol) in dibromomethane (6 ml) was introduced HBr gas at 30 °C. After 30 min a solution of **5a** (1.2 g, 5.1 mmol) in dibromomethane (4 ml) was added dropwise to the resulting suspension under ice-water cooling. The introduction of HBr was continued until the color of the reaction mixture changed to reddish black (ca. 1.5 h after the addition of the substrate). After the completion of the reaction was confirmed by GLPC (4 h after the addition of the substrate), the pressure of the reaction system was reduced to 20 mmHg under argon bubbling. After 3.5 h, the reaction mixture was worked up. Distillation afforded 1.5 g (90%) of **6a**, bp 105—109 °C/0.25 mmHg (purity 95%).

Methyl 3-(2,2-Dibromoethenyl)-2,2-dimethylcyclopropanecarboxylate (6b). This reaction was carried out as described above (Al-HBr method), starting from methyl 3-(2,2-dichloroethenyl)-2,2-dimethylcyclopropanecarboxylate (**5b**) (2.2 g, 10 mmol) and Al metal (0.40 g, 15 mmol). Distillation of crude product afforded 2.8 g (90%) of **6b**, bp 101—103 °C/0.26 mmHg (purity 96%). The structure was confirmed by the comparison with an authentic sample.[15]

3-(2,2-Dibromoethenyl)-2,2-dimethylcyclopropanecarboxylic Acid (6c). a) $AlBr_3$ Method: A solution of 3-(2,2-dichloroethenyl)-2,2-dimethylcyclopropanecarboxylic acid (**5c**) (trans 100%)[15] (4.2 g, 20 mmol) in dibromomethane (20 ml) was added dropwise to a solution of $AlBr_3$ (8.0 g, 30 mmol) in dibromomethane (20 ml) over a period of 15 min under ice-water cooling. After the addition was completed, argon gas was introduced to the reaction mixture through syringe needle for 15 min. The pressure of the reaction system was then gradually reduced to 20 mmHg under argon bubbling.

After 2.5 h the reaction mixture was poured into ice-water. Then, dil HCl was added and the resulting mixture was extracted with ether-AcOEt (ca. 4:1). The organic layer was washed with dil HCl and brine, and then dried ($MgSO_4$). After removal of the solvents, the crude product was extracted with hot hexane and insoluble parts were filtered off. Removal of the solvent afforded 5.5 g (93%) of yellow solids assigned to **6c** by the comparison of the spectral data with those of authentic sample.[5a,15] Purity was 96%, and isomeric purity was 100% trans based on GLPC analysis after esterification with CH_2N_2. Mp 118—120 °C (hexane). lit,[5a] 117—118 °C (ethanol-water). Similarly, 5.6 g (94%) of *cis*-**6c** (purity 96%, 100% cis) was obtained starting from 4.2 g of 100% *cis*-**5c**. The isomeric purity was also checked by GLPC analysis. Mp 108—111 °C (hexane). lit,[15] 112—114 °C (hexane). Halogen exchange of (−)-*trans*-**5c** was similarly carried out, starting from 2.0 g (9.5 mmol) of (−)-*trans*-**5c** ($[\alpha]_D$=−36.3° ($CHCl_3$), lit,[17] $[\alpha]_D$=−36.6° ($CHCl_3$)) by means of $AlBr_3$ (3.8 g, 14 mmol). After extraction with hot hexane, removal of the solvent afforded 2.6 g (93%) of yellow solids. GLPC analysis of the product after esterification by CH_2N_2 showed that the product obtained was composed of 96% of **6c** (trans 100%). $[\alpha]_D$=−37.5° ($CHCl_3$). lit,[5b] $[\alpha]_D$=−40.5° ($CHCl_3$).

b) Al-HBr Method: An aliquot of Al ribbon cut into small pieces (5.1 g in total, 0.19 mmol) in dibromomethane (125 ml) was warmed to 30 °C and HBr gas was introduced. When an exothermic reaction started, the rest of Al metal was added portionwise to maintain the reaction temperature between 60—65 °C. After all Al metal had dissolved (ca. 1.5 h), the gas inlet tube was replaced by a dropping funnel through which a solution of *cis*-**5c** (26 g, 0.13 mol) in dibromomethane (100 ml) was added dropwise at 5—7 °C. When the completion of the halogen exchange was confirmed by GLPC (ca. 2 h from the start of the addition), the pressure in the reaction flask was reduced to 20 mmHg under usual argon bubbling (ice-water bath). After 4.5 h (GLPC check) the reaction mixture was worked up. Removal of the solvent afforded 33 g (89%) of *cis*-**6c** as brown solids, whose purity was 93% on GLPC, mp 105—108 °C (hexane).

3-(1-Bromo-1-methylethyl)-5,5-dichloro-4-pentenoic Acid (12). A solution of BBr_3 (0.6 ml) in dibromomethane (4 ml) was added dropwise to a solution of **5a** (0.95 g, 4.0 mmol) in dibromomethane under ice-water cooling. After the addition was completed, the reaction mixture was allowed to warm to room temperature and stirred overnight. The mixture was poured into cold dil HCl and extracted with ether-AcOEt (4:1). The organic layer was washed with water (twice) and brine, and dried ($MgSO_4$). Recrystallization (hexane) gave 0.75 g (65%) of **12** as slightly brown crystals, (needles), mp 81—82 °C. IR (KBr disk): 3200—2600, 1700, 1620, 1310, 875 cm^{-1}. ^1H NMR (CCl_4) δ=5.94 (d, 1H), 3.25—2.8 (m, 2H), 2.48 (dd, 1H), 1.84 (s, 3H), 1.77 (s, 3H). MS *m/z* 288 (M^+), 122 (base). Found: C, 33.32; H, 3.79%. Calcd for $C_8H_{11}BrCl_2O_2$: C, 33.14; H, 3.82%.

3-(2,2-Dichloroethenyl)-4-methyl-4-pentanolide (13). The reaction of **5a** (4.7 g, 20 mmol) with BBr_3 (3.0 ml) in dibromomethane was carried out as described above. The reaction mixture after having been stirred overnight was poured into ice-water and extracted with ether. The ethereal layer was washed with brine and aq $NaHCO_3$ (three times). The aqueous layer was extracted with ether and the combined ethereal layer was washed with brine (twice) and dried ($MgSO_4$). Recrystallization (hexane : AcOEt=5:1) afforded 2.6 g (63%) of **13**, mp 118—119 °C (lit,[14] 115—117 °C). IR (neat): 1770, 1625, 1280, 1260, 1100, 890 cm^{-1}. ^1H NMR (CCl_4) δ=5.89 (d, 1H), 3.36 (m, 1H), 2.95—2.3 (m, 2H), 1.52 (s, 3H), 1.35 (s, 3H). MS *m/z* 208 (M^+), 122 (base).

Ethyl 3-(1-Bromo-1-methylethyl)-5,5-dichloro-4-pentenoate (14). After the overnight reaction of **5a** (2.4 g, 10 mmol) with BBr_3 (1.5 ml) the reaction mixture was concentrated in vacuo. The residue was dissolved in 3 ml of dry ethanol. After 30 min the resulting mixture was diluted with ether, washed with water (twice) and brine, and dried ($MgSO_4$). Distillation of the crude product afforded 2.8 g (88%) of **14**, bp 93—94 °C/0.17 mmHg. IR (neat): 1740, 1620, 1255, 1175, 1115, 880 cm^{-1}. ^1H NMR (CCl_4) δ=5.89 (d, 1H), 4.12 (q, 2H), 3.15—2.65 (m, 2H), 2.35 (dd, 1H), 1.82 (s, 3H), 1.77 (s, 3H), 1.26 (t, 3H). MS *m/z* 317 (M^+), 237 (base). Found: C, 37.89; H, 4.66%. Calcd for $C_{10}H_{15}BrCl_2O_2$: C, 37.77; H, 4.75%.

References

1) Preliminary account: K. Kondo, T. Takashima, A. Negishi, K. Matsui, T. Fujimoto, K. Sugimoto, C. E. Hatch III, and J. S. Baum, *Pestic. Sci.*, **11**, 180 (1980).

2) M. Elliott, A. W. Farnham, N. F. Janes, P. H. Needham, D. A. Pulman, and J. H. Stevenson, *Nature (London)*, **246**, 169 (1973).

3) M. Elliott, A. W. Farnham, N. F. Janes, P. H. Needham, and D. A. Pulman, *Nature (London)*, **248**, 710 (1974).

4) K. Kondo, K. Matsui, and A. Negishi, ACS Symposium Series No. 42, "Synthetic Pyrethroids," ed by M. Elliott, 1977, p. 128.

5) a) D. G. Brown, O. F. Bodenstein, and S. J. Norton, *J. Agric. Biol. Chem.*, **21**, 767 (1973); b) M. Elliott, A. W. Farnham, N. F. Janes, P. H. Needham, and D. A. Pulman, *Pestic. Sci.*, **6**, 537 (1975); c) C. E. Hatch III, J. S. Baum, T. Takashima, and K. Kondo, *J. Org. Chem.*, **45**, 3281 (1980).

6) a) R. G. R. Bacon and H. A. O. Hill, *J. Chem. Soc.*, **1964**, 1097; b) R. Lapouyade, M. Daney, M. Lapenne, and H. Bouas-Laurent, *Bull. Soc. Chim. Fr.*, **1973**, 720.

7) The halogen exchange with these reagents was first observed in the mechanistic study of the Friedel-Crafts reaction: a) H. C. Brown, and W. J. Wallace, *J. Am. Chem. Soc.*, **75**, 6279 (1953); b) H. C. Brown and M. Grayson, *ibid.*, **75**, 6285 (1953).

8) P. J. Trotter, *J. Org. Chem.*, **28**, 2093 (1963).

9) W. T. Smith, Jr., H. H. Chen, and J. M. Patterson, *J. Org. Chem.*, **26**, 4713 (1961).

10) J. W. McKinley, R. E. Pincock, and W. B. Scott, *J. Am. Chem. Soc.*, **95**, 2031 (1973).

11) a) S. W. Tobey and F. West, *J. Am. Chem. Soc.*, **88**, 2481 (1966); b) R. West and P. T. Kwitowsky, ibid., **90**, 4097 (1968).

12) The hydrogen bromide is considered to be generated by the decomposition of the aluminium tribromide used.

13) The addition of hydrogen bromide to dichloroethenyl compound **5a** did not occur in the absence of the aluminium ion. Thus, coordination of alminium trihalide most probably to carbonyl oxygen first occurred and then assisted the addition of HBr. The coordinated aluminium trihalide would be inactive for halogen exchange.

14) Exact optical purity was not determined. However, purified product (purity 99% on GLPC) by repeated

recrystallization had specific rotation of −40.3° which was almost equal to the one of pure (−)-*trans*-**6c**.

15) K. Matsui, A. Negishi, Y. Takahatake, K. Sugimoto, T. Fujimoto, T. Takashima, and K. Kondo, *Bull. Chem. Soc. Jpn.*, **59**, 221 (1986).

16) B. D. Clemensen, H. Andersen, and H. B. Madson, Jpn. Kokai Tokkyo Koho, 52-144654 (1977).

17) T. Honda, N. Itaya, F. Horiuchi, O. Magara, and T. Mizutani, Jpn. Kokai Tokkyo Koho, 50-131953 (1975).

18) Authors wish to express their thanks to the referee for his valuable suggestions on the intermediate of the reaction of **5a** with boron tribromide.

Synthesis of Aspartyl Pentapeptide Esters in Relation to Structural Features of Sweet Peptides

Yasuo ARIYOSHI
Central Research Laboratories, Ajinomoto Co., Inc. Suzuki-cho, Kawasaki-ku, Kawasaki 210
(Received November 13, 1985)

A series of seven analogues of aspartyl pentapeptides has been synthesized in relation to the structural features of sweet peptides. The rule in the structure-taste relationships of di-, tri-, and tetrapeptides is inapplicable to the pentapeptides. All the pentapeptides were devoid of sweetness, though they satisfied the requirements for sweet peptides. The result indicates that oligopeptides can not fit a deep receptor pocket. The mode of interactions between sweet peptides and the receptor is drawn schematically.

In a previous paper,[1] the tastes of aspartyl dipeptide esters have been rationalized through Fischer projection formulas. Recently, in order to deduce the mode of interactions between the sweet peptides and the receptor site, various aspartyl tri- and tetrapeptide esters have been synthesized.[2,3] In the structures (Ia, II, and III), a small alkyl group (S or R^2) has been considered to participate in binding with the receptor through a hydrophobic interaction. Another hydrophobic interaction at R^4 with the receptor has also been suggested.[2] The carboxyl and amino groups serve as a proton acceptor and a proton donor, respectively, in the hydrogen bonding with the receptor. Another hydrogen bonding at the peptide bond with the receptor has also been suggested by the fact that any modification of the peptide bond resulted in a complete loss of sweetness.[4,5] The shape and size of a molecule are important, since the receptor site is considered to be in the shape of a deep pocket[6] or a narrow cleft.[7] Another important factor, common to all sweet compounds, is the hydrophilic-hydrophobic balance in a molecule. In this paper, a series of seven analogues of aspartyl pentapeptides was synthesized in order to obtain further information about the mode of interactions between the sweet peptides and the receptor site.

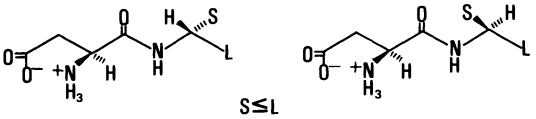

Fig. 1. General structure for sweet aspartyl dipeptide esters: S=small hydrophobic group (1—4 atoms); L=larger hydrophobic group (3—6 atoms).[1,2]

Synthesis

Syntheses of Boc-tripeptide esters and the removal of the Boc group were carried out according to the method described in a previous paper.[3] The protected tetrapeptides in Table 1 were prepared by condensation of the appropriate tripeptide ester with a Boc-amino

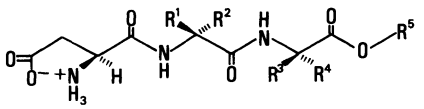

II

Fig. 2. L-α-Aspartyl tripeptide esters.

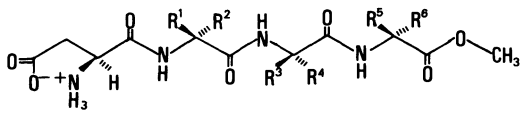

III

Fig. 3. L-α-Aspartyl tetrapeptide esters.

Table 1. Protected Tetrapeptides

No.	Compound[a]	Yield %	Mp θ_m/°C	Recrys. solvent[b]	Appearance[c]	$[\alpha]_D^{25}$ Degree[d]	Formula[e]
1	Boc-D-Ala-L-Ala-L-Ala-L-Ala-OMe	59.8	196—197	E	N	−38.7	$C_{18}H_{32}O_7N_4$
2	Boc-D-Ala-L-Ala-L-Val-L-Ala-OMe	79.6	213—214	C	N	−52.9	$C_{20}H_{36}O_7N_4$
3	Boc-D-Ala-L-Val-L-Ala-L-Ala-OMe	59.6	230—231	E	N	−42.2	$C_{20}H_{36}O_7N_4$
4	Boc-D-Ala-L-Val-L-Val-L-Ala-OMe	87.8	219—220	E	N	−47.2	$C_{22}H_{40}O_7N_4$
5	Boc-D-Ala-L-Val-L-Ala-L-Leu-OMe	84.9	214—215	E	N	−40.4	$C_{23}H_{42}O_7N_4$
6	Boc-D-Val-L-Ala-L-Val-L-Ala-OMe	84.4	232—233	E	P	−55.4[f]	$C_{22}H_{40}O_7N_4$
7	Boc-L-Ala-L-Val-L-Val-L-Ala-OMe	79.4	231—232	E	N	−98.5	$C_{22}H_{40}O_7N_4$

a) Abbreviations follow the recommendations of the IUPAC-IUB Commission on Biochemical Nomenclature in *Eur. J. Biochem.*, **138**, 9 (1984). b) Recrystallization solvent: C, Chloroform; E, Ethyl acetate. c) Appearance: N, Needles; P, Powder. d) In methanol, c=1.0%. e) All compounds were analyzed for C, H, and N, and the results were within ±0.3% of the theoretical values. Complete analytical data for all compounds have been deposited at the office of the Chemical Society of Japan (Document No. 8622). f) c=0.5%.

Table 2. Protected Pentapeptides, Z-L-Asp(OBzl)-X

Compd No.	X	Yield %	Mp θ_m/°C	Recrys. solvent[a]	$[\alpha]_D^{25}$ Degree[b]	Formula[c]
8	D-Ala-L-Ala-L-Ala-L-Ala-OMe	76.6	222—223	D-W	−27.5	$C_{32}H_{41}O_{10}N_5$
9	D-Ala-L-Ala-L-Val-L-Ala-OMe	80.3	213—215	D-W	−26.9	$C_{34}H_{45}O_{10}N_5$
10	D-Ala-L-Val-L-Ala-L-Ala-OMe	87.1	236—237	E	−27.7	$C_{34}H_{45}O_{10}N_5$
11	D-Ala-L-Val-L-Val-L-Ala-OMe	89.4	239—240	D-W	−24.1	$C_{36}H_{49}O_{10}N_5$
12	D-Ala-L-Val-L-Ala-L-Leu-OMe	67.2	224—225	D-W	−25.8	$C_{37}H_{51}O_{10}N_5$
13	D-Val-L-Ala-L-Val-L-Ala-OMe	80.4	240—241	D-W	−32.5	$C_{36}H_{49}O_{10}N_5$
14	L-Ala-L-Val-L-Val-L-Ala-OMe	85.5	251—252	D-W	−17.1	$C_{36}H_{49}O_{10}N_5$

a) Recrystallization solvent: D, *N,N*-Dimethylformamide; W, Water; E, Ethyl acetate. b) In *N,N*-dimethylformamide, c=1.0%. c) All compounds were analyzed for C, H, and N, and the results were within ±0.3% of the theoretical values. Complete analytical data for all compounds have been deposited at the office of the Chemical Society of Japan (Document No. 8622).

Table 3. Pentapeptide Esters, L-α-Asp-X

Compd No.	X	Yield %	R_f[a]	Mp θ_m/°C	Recrys. solvent[b]	Appearance[c]	$[\alpha]_D^{25}$ Degree	Formula[d]
15	D-Ala-L-Ala-L-Ala-L-Ala-OMe	71.9	0.27	202—203 dec	W-A	P	−62.5[e]	$C_{17}H_{29}O_8N_5 \cdot 1.25H_2O$
16	D-Ala-L-Ala-L-Val-L-Ala-OMe	86.5	0.38	219—220	W-A	N	−54.7[e]	$C_{19}H_{33}O_8N_5 \cdot 1.75H_2O$
17	D-Ala-L-Val-L-Ala-L-Ala-OMe	69.6	0.38	205—206 dec	W-A	P	−57.4[e]	$C_{19}H_{33}O_8N_5 \cdot 1.75H_2O$
18	D-Ala-L-Val-L-Val-L-Ala-OMe	64.5	0.48	>245	W	P	−31.6[f]	$C_{21}H_{37}O_8N_5 \cdot 1.5H_2O$
19	D-Ala-L-Val-L-Ala-L-Leu-OMe	61.8	0.49	206—207 dec	W	N	−31.6[f]	$C_{22}H_{39}O_8N_5 \cdot 2H_2O$
20	D-Val-L-Ala-L-Val-L-Ala-OMe	65.2	0.52	>245	W-AA	N	−33.2[g]	$C_{21}H_{37}O_8N_5 \cdot 2.5H_2O$
21	L-Ala-L-Val-L-Val-L-Ala-OMe	40.1	0.44	>245	W	P	−70.6[f]	$C_{21}H_{37}O_8N_5 \cdot 2H_2O$

a) *n*-BuOH:AcOH:H_2O=4:1:1 (v/v). b) Recrystallization solvent: W, Water; A, Acetone; AA, Acetic acid. c) Appearance: P, Powder; N, Needles. d) All compounds were analyzed for C, H, and N, and the results were within ±0.3% of the theoretical values. Complete analytical data for all compounds have been deposited at the office of the Chemical Society of Japan (Document No. 8622). e) In water, c=1.0%. f) In acetic acid, c=0.5%. g) In acetic acid, c=0.25%.

acid *N*-hydroxysuccinimide ester. The Boc group of the tetrapeptide esters was removed with *p*-toluenesulfonic acid (TosOH) in methanol.[8] The protected pentapeptide esters in Table 2 were prepared by condensation of *N*-benzyloxycarbonyl-L-aspartic acid β-benzyl α-succinimide ester (Z-L-Asp(OBzl)-ONSu)[2] with the appropriate tetrapeptide ester. The desired pentapeptide esters in Table 3 were obtained by deprotection of the benzyloxycarbonyl and benzyl groups from the protected pentapeptides in Table 2 by hydrogenation over palladium on charcoal.

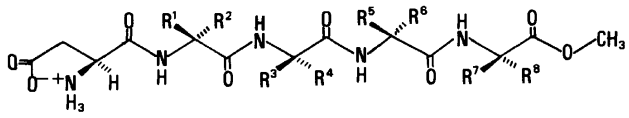

IV

Fig. 4. L-α-Aspartyl pentapeptide esters.

Results and Discussion

In order for aspartyl tri- and tetrapeptides to be sweet, the second amino acid must have a D-configuration and a small alkyl side chain.[2,3] Therefore, a small alkyl group was introduced at R^2 so as to meet the sweet structure (II). In structural variation, a pentapeptide (**21**) with an opposite configuration at the chiral center was also synthesized. An L-antipode was introduced for the third amino acid, because the modification of tripeptides (II) showed that an L-configuration at the third amino acid was required for a potent sweet taste.

Most of the pentapeptides were predicted not to be sweet, since aspartyl peptides while elongating their peptide bonds significantly decrease their sweetness potencies and in some cases lose their sweet tastes. As expected, all the pentapeptides synthesized here were essentially tasteless or faintly bitter (Table 4).

The rule in the structure-taste relationships of di-, tri-, and tetrapeptides is inapplicable to pentapeptides. With increasing the length of a peptide, it becomes difficult to fit the narrow receptor pocket. This may be a major reason that some of the tetrapeptides and all of the pentapeptides were not sweet but bitter or tasteless, though they satisfied the requirements for sweet peptides. As a typical case, a series of L-α-aspartyl oligoalanine esters is illustrated in Table 5, in which the sweetness potencies suddenly fall off when the peptide bond is elongated. The taste of aspartyl peptides while elongating their peptide bonds tends to follow Ney's rule[9] for bitter peptides, in which peptides can be classified as bitter or nonbitter, depending upon the magnitude of the hydrophobicity of their side chains.[9] Accordingly, the results obtained for the pentapeptides, in conjunction with the results of di-, tri-, and tetrapeptides, have further supported the previous idea that the receptor site is

Table 4. Taste of Pentapeptides (L-α-Asp-X)[a]

Compd No.	X	R^1	R^2	R^3	R^4	R^5	R^6	R^7	R^8	Taste[b]
15	D-Ala-L-Ala-L-Ala-L-Ala-OMe	H	Me	H	Me	Me	H	H	Me	0
16	D-Ala-L-Ala-L-Val-L-Ala-OMe	H	Me	H	Me	*i*-Pr	H	H	Me	0
17	D-Ala-L-Val-L-Ala-L-Ala-OMe	H	Me	H	*i*-Pr	Me	H	H	Me	—
18	D-Ala-L-Val-L-Val-L-Ala-OMe	H	Me	H	*i*-Pr	*i*-Pr	H	H	Me	0
19	D-Ala-L-Val-L-Ala-L-Leu-OMe	H	Me	H	*i*-Pr	Me	H	H	*i*-Bu	0
20	D-Val-L-Ala-L-Val-L-Ala-OMe	H	*i*-Pr	H	Me	*i*-Pr	H	H	Me	0
21	L-Ala-L-Val-L-Val-L-Ala-OMe	Me	H	H	*i*-Pr	*i*-Pr	H	H	Me	0

a) For structure, see Fig. 4. b) 0=tasteless; —=faintly bitter.

Table 5. Taste of Aspartyl Oligoalanine Esters

Compound	Sweetness value[a]
L-α-Asp-D-Ala-OMe	25[10]
L-α-Asp-D-Ala-OEt	80[10]
L-α-Asp-D-Ala-OPr	125
L-α-Asp-D-Ala-L-Ala-OMe	50
L-α-Asp-D-Ala-L-Ala-L-Ala-OMe	0.5
L-α-Asp-D-Ala-L-Ala-L-Ala-L-Ala-OMe	0

a) Times sucrose (weight basis, sucrose=1).

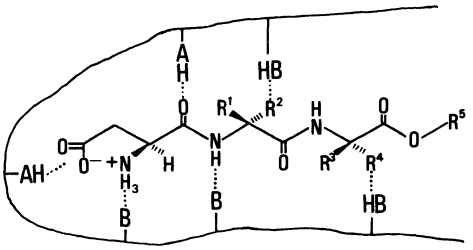

Fig. 5. Schematic drawing of interactions between the sweet peptides and the receptor.
R^1=R^3=H; R^2=R^4=small alkyl group.
AH, Proton donor; B, Proton acceptor; HB, Hydrophobic binding group.

in the shape of a deep pocket with the binding sites inside. The mode of interactions between the sweet peptides and the receptor is illustrated in Fig. 5; here, the case of tripeptides is shown. In the case of Aspartame (L-α-Asp-L-Phe-OMe), the methyl ester group corresponds to R^2 and will interact with the receptor through a hydrophobic interaction, and the phenyl moiety will interact with the receptor at the partner of R^4 through a hydrophobic interaction. These hydrophobic interactions increased the sweetness potency.[1-3] As mentioned above, by increasing the length of a sweet peptide, it becomes difficult to fit the deep receptor. The decrease in its binding ability to the receptor reduces or loses the sweetness potency.

Experimental

All the melting points were taken on a Yanagimoto capillary melting point apparatus Model MP-21 and are uncorrected. Optical rotations were measured on a JASCO DIP-140 digital polarimeter with a 10 cm water-jacketed cell at 25 °C and a 1% concentration. Thin-layer chromatography (TLC) was performed on precoated silica gel $60F_{254}$ plates (E. Merck) and spots were detected with ninhydrin. All compounds were homogeneous on TLC. All of the pentapeptides were almost tasteless or faintly bitter. Therefore, it was judged only whether a peptide was sweet, bitter, or tasteless by tasting crystals of each pentapeptide.

Materials. Boc-amino acids were purchased from Peptide Institute Inc. Esters of L-Ala and L-Leu, and Z-L-Asp(OBzl)-OH were purchased from Kokusan Chemical Works Ltd.

Protected Tetrapeptides (1—7). A typical run (**3** in Table 1) was as follows: To a solution of Boc-L-Val-L-Ala-L-Ala-OMe (2.05 g, 5.5 mmol) in 15 ml of methanol was added TosOH·H_2O (1.26 g, 6.6 mmol). The mixture was stirred at 35 °C for 5 h. The solvent was evaporated under reduced pressure at a bath temperature of 50 °C to give H-L-Val-L-Ala-L-Ala-OMe·TosOH as a semisolid residue. The residue was dissolved in chloroform and the solvent was evaporated under reduced pressure to leave a semisolid residue. The residue was dissolved in 40 ml of chloroform and cooled in an ice-bath. To this solution was added triethylamine (Et_3N, 0.67 g, 6.6 mmol), followed by Boc-D-Ala-ONSu (1.43 g, 5 mmol) with stirring. The mixture was stirred at room temperature for 3 h and then kept standing overnight. The reaction mixture was washed successively with water, a 10% citric acid solution, a 5% sodium hydrogencarbonate solution, and water, and then concentrated under reduced pressure to leave Boc-D-Ala-L-Val-L-Ala-L-Ala-OMe (**3**) as a solid. The solid was crystallized from ethyl acetate–hexane to give **3** as needles. Recrystallization was carried out from ethyl acetate. The data are given in Table 1.

Protected Pentapeptide Esters (8—14). A typical run (**10** in Table 2) was as follows: To a solution of Boc-D-Ala-L-Val-L-Ala-L-Ala-OMe (**3**, 1.10 g, 2.5 mmol) in 20 ml of methanol was added TosOH·H_2O (1.00 g, 5.3 mmol). The mixture was stirred at 40 °C for 4 h. The solvent was evaporated under reduced pressure at a bath temperature of 50 °C to give H-D-Ala-L-Val-L-Ala-L-Ala-OMe·TosOH as an oily residue. The residue was dissolved in chloroform and the solvent was evaporated under reduced pressure. The procedure was repeated twice. The crystalline residue, thus obtained, was suspended in 50 ml of chloroform at room temperature. To this suspension was added Et_3N (0.54 g, 5.3 mmol), followed by Z-L-Asp(OBzl)-ONSu[2] (1.10 g, 2.4 mmol) with stirring. The mixture was stirred for 3 h and then kept standing overnight. A geratinous material appeared was dissolved by

adding 100 ml of chloroform with warming. The reaction mixture was washed successively with water, 1 M HCl (1 M=1 mol dm^{-3}), a 5% sodium hydrogencarbonate solution, and water, and then concentrated under reduced pressure to leave a solid residue. The residue was triturated with ethyl acetate and collected by filtration. The residue was recrystallized from ethyl acetate. The data are given in Table 2.

Pentapeptide Esters (15—21). A typical run (**17** in Table 3) was as follows: Z-L-Asp(OBzl)-D-Ala-L-Val-L-Ala-L-Ala-OMe (**10**, 1.20 g) was dissolved in a mixture of acetic acid (45 ml) and water (10 ml), and hydrogenated in the presence of 5% Pd/C (0.50 g) with stirring at atmospheric pressure and 35°C for 5 h. The reaction mixture was filtered and the filtrate was concentrated to dryness under reduced pressure. The residue was dissolved in water and the solvent was evaporated under reduced pressure to remove the trace amount of remaining acetic acid. The procedure was repeated three times. The residue was recrystallized from water-acetone. The data are given in Table 3.

References

1) Y. Ariyoshi, *Agric. Biol. Chem.*, **40**, 983 (1976).
2) Y. Ariyoshi, *Bull. Chem. Soc. Jpn.*, **57**, 3197 (1984).
3) Y. Ariyoshi, *Bull. Chem. Soc. Jpn.*, **58**, 1727 (1985).
4) S. A. MacDonald, C. G. Willson, M. Chorev, F. S. Vernacchia, and M. Goodman, *J. Med. Chem.*, **23**, 413 (1980).
5) Y. Ariyoshi, unpublished result. L-α-Asp-Gly-OMe was 8 times sweeter than sucrose,[1] whereas its *N*-methylated analogue, L-α-Asp-Sar-OMe, was devoid of sweetness.
6) Y. Ariyoshi, *Agric. Biol. Chem.*, **44**, 943 (1980).
7) F. Lelj, T. Tancredi, P. A. Temussi, and C. Toniolo, *J. Am. Chem. Soc.*, **98**, 6669 (1976).
8) J. Goodacre, R. J. Ponsford, and I. Stirling, *Tetrahedron Lett.*, **1975**, 3609.
9) K. H. Ney, *Z. Lebensm., Unters.-Forsch.*, **147**, 64 (1971).
10) R. H. Mazur, J. A. Reuter, K. A. Swiatek, and J. M. Schlatter, *J. Med. Chem.*, **16**, 1284 (1973).

Synthesis and Characterization of Macrocyclic Polyaza(2,5)pyridinophanes Possessing Vitamin B_6 Functionality

Masaaki IWATA* and Hiroyoshi KUZUHARA
Riken (The Institute of Physical and Chemical Research), Wako, Saitama 351-01
(Received November 14, 1985)

Series of macrocyclic polyaza[*m*](2,5)pyridinophanes (poly=tri, tetra, penta; *m*=9, 12, 15)(**8—10**) and polyaza[*m*]paracyclophanes (**11—13**) were synthesized in excellent yields by the reaction of dichloropyridoxine derivatives (**4**) and α,α'-dibromo-*p*-xylene (**5**), respectively, with a series of 1,2-ethanediamine derivatives (**1—3**). These phanes were characterized on the basis of ^{1}H NMR spectra. The methyl group at C_6 of the pyridoxine moiety (a-series) revealed restricted rotation for all bridge sizes (*m*=9—15). In **8—10** without the methyl group (b-series), *m*=12 was the boundary between restricted and free rotation. In series **11—13**, only **11** (*m*=9) showed restricted rotation. Atomic group equivalence was discussed in terms of boundary restricted rotation and an empirical rule for the prediction of the relationship between the bridge size and restricted rotation was proposed.

Along the line of our continuing interest in chemical congeners for coenzyme-B_6, dithia(2,5)pyridinophanes[1] and diaza(2,5)pyridinophanes[2] have been prepared and characterized. Their properties have been compared with those of coemzyme-B_6. These artificial coenzymes feature outstanding stability and efficiency in comparison with natural coenzyme, with excellent stereoselectivity for specific amino acids. By functionalizing the bridge moiety, we have designed new artificial coenzymes with additional sites for complexation in consideration of host-guest complexation.[3] In terms of the previously reported relationship between restricted rotation and the length of the bridge chain[2b] and predictable synthetic feasibility owing to molecular symmetry, we selected 1,2-ethanediamine derivatives (**1—3**) as the bridge moiety. In the present report, we would like to describe the details of synthesis and properties of macrocyclic polyaza(2,5)pyridinophanes and -paracyclophanes.

Results and Discussion

Preparation of 1,2-Ethanediamine Derivatives (1—3). It was expected that chain elongation of the 1,2-ethanediamine could be achieved by iterative reaction of *N*-(2-bromoethyl)tosylamide (**6**) with *N,N'*-ditosyl-1,2-ethanediamine (**7**). It was difficult, however, to prepare pure *N,N*-bis[2-(tosylamino)ethyl]tosylamide (**1**), since further alkylation occurred to give the higher homologues, **2** and **3**. Thus, **1—3** were obtained by chromatographic separation of the reaction mixture. ^{1}H NMR spectral data of **1—3** are summarized in Fig. 1.

6 **7**

Scheme. 1. Synthesis of poly(*N*-tosyl-1,2-ethanediamine) derivatives (**1—3**).

Synthesis of Polyaza[*m*](2,5)pyridinophanes (8—10) and Polyaza[*m*]paracyclophanes (11—13) (*m*=9, 12, 15).[4] The synthetic procedure was based on a previously reported method[2] except that the reaction temperature was lowered to room temperature and the sulfonamide was not metallated before the reaction but reacted directly in the presence of excess potassium carbonate. Therefore, 1,2-ethanediamine derivatives (**1—3**) reacted independently in DMF with protected dichloropyridoxine hydrochloride (**4**) at room temperature to give polyaza[*m*](2,5)pyridinophanes (**8—10**) (*m*=9, 12, 15). Work-up was just the same as in the preceding report.[2b] Likewise, **1—3** reacted with α,α'-dibromo-*p*-xylene (**5**) to afford polyaza[*m*]pracyclophanes (**11—13**) (*m*=9, 12, 15). The results obtained are summarized in Table 1.

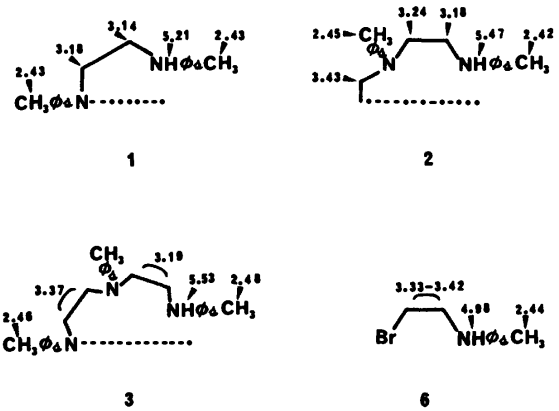

Fig. 1. ^{1}H NMR spectral data of open chain *p*-tosylamides **1**, **2**, **3**, and **6** (δ, in $CDCl_3$); the structure shown is a half part of the molecule due to its molecular symmetry for **1**, **2**, and **3**.

Although the reaction conditions were not optimized, product yields were unexpectedly excellent. The compounds, **11** and **12**, were incidentally purified by one recrystallization of the reaction mixture after work-up without the necessity of silica-gel chromatography.

Properties. Referred to the present design, it is of special importance to characterize the property with regard to relationship between induced restricted rotation and miximum numbers of nitrogen atoms included on the bridge chain. The presence of restricted rotation has been judged by the simple criteria based on

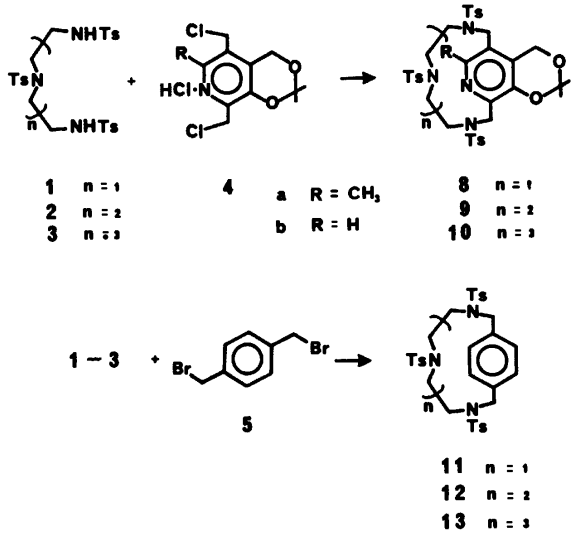

Scheme 2. Preparation of polyaza[m](2,5)pyridinophanes (**8**—**10**) and polyaza[m]paracyclophanes (**11**—**13**) (poly=tri, tetra, penta).

Table 1. Preparation of Polyaza[m](2,5)pyridinophanes and Polyaza[m]paracyclophanes

Compd	Yield[a] %	Mp θ_m/°C	Rotation[b]	Bridge size[c]/m	Included N atom
8a	94	230[d]	R	9	3
9a	70	126—128	R	12	4
10a	47	155—157	R	15	5
8b	95	230—232[d]	R	9	3
9b	98	247—249[d]	B	12	4
10b	68	133—135	F	15	5
11	96	274—275	B	9	3
12	96	282—284	F	12	4
13	72	131—133	F	15	5

a) Isolated yield after purification. b) Represents the presence or the absence of molecular rotation judged from ^{1}H NMR spectral signal (see Table 2). c) Numbers of the disposed atoms on the bridge chain. d) Decomposed.

^{1}H NMR spectral analysis.[1a,g,2b] The methyl protons in the isopropylidene group are informative as well for the judgment of restricted rotation. They appear as two separate sharp singlets if restricted rotation is induced. They become broadening to be one singlet signal if the bridge is in the boundary length. A sharp singlet signal is detected if free rotation is allowed. On the basis of these empirical criteria, rotational properties of the polyaza[m](2,5)pyridinophanes (**8**—**10**) and polyaza[m]paracyclophanes (**11**—**13**) are clearly determined. In Figs. 2, 3, and 4, parts of ^{1}H NMR spectra are depicted in the region δ 2.5—5.5. These signals are assignable to the methylene protons attached to the aromatic ring and to the methylene protons in the bridge. In Fig. 2, it is common feature that the methylene protons contiguous to the pyridine ring are split into AB quartet patterns though the methylene protons contiguous to the oxygen atom appear as incidental singlet (spectrum a) at δ 4.78 and signal overlapping

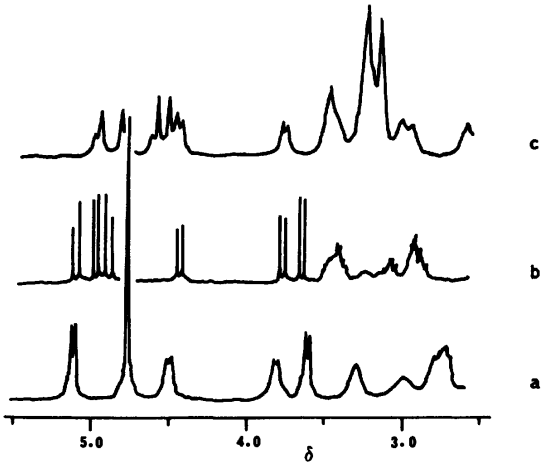

Fig. 2. ^{1}H NMR spectra of methyl-polyaza[m](2,5)-pyridinophanes (a-series) in the region δ=2.5—5.5; **a** for **8a** (m=9), **b** for **9a** (m=12), and **c** for **10a** (m=15) ($CDCl_3$, 18°C).

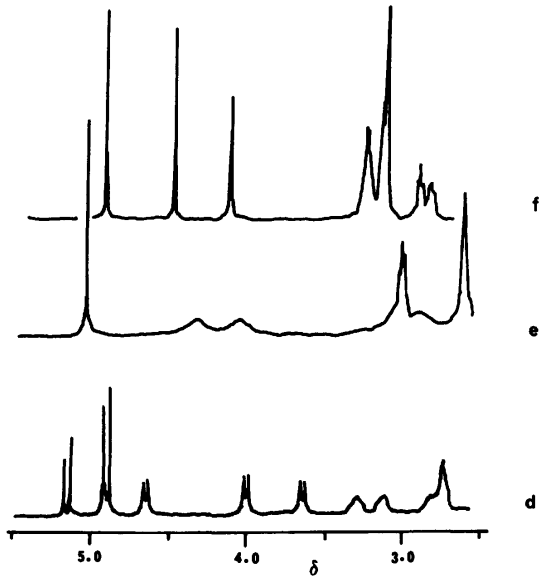

Fig. 3. ^{1}H NMR spectra of polyaza[m](2,5)pyridinophanes (b-series) in the region δ=2.5—5.5; **d** for **8b** (m=9), **e** for **9b** (m=12), and **f** for **10b** (m=15) ($CDCl_3$, 18°C).

is observable (spectrum c). In Fig. 3, three typical patterns of restricted rotation (spectrum d), boundary (spectrum e), and free rotation (spectrum f) are incidentally demonstrated. Since polyaza[m]paracyclophanes (**11**—**13**) have symmetry element in each case, it would not be chiral in any case. However, restricted rotation resulting in line-broadening are detectable in **11** (spectrum g in Fig. 4).

Relationship between restricted rotation and bridge chain length for all series of (2,5)pyridinophanes so far investigated is summarized in Table 2. This presents information about practical spherical bulk of atomic groups, S, N, and CH_2, and about prediction rule for restricted rotation of unsynthesized congeners. In comparison of dithiapyridinophanes (S-series)[1a,b,g]

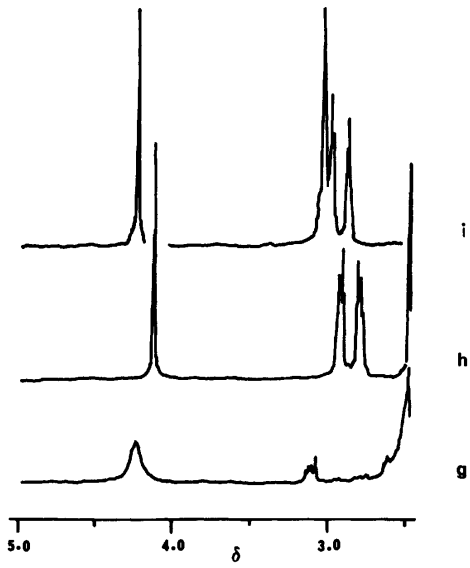

Fig. 4. ^{1}H NMR spectra of polyaza[m]paracyclophanes in the region δ=2.5—5.0; **g** for **11** (m=9), **h** for **12** (m=12), and **i** for **13** (m=15) ($CDCl_3$, 18°C).

with diazapyridinophanes (N-series),[2b] it is found that spherical bulk of two sulfur atoms is correlated nearly to that of two nitrogen atoms plus one methylene group. Equivalence of spherical bulk of one nitrogen atom to that of one methylene group could be seen when diazapyridinophanes (N-series)[2b] and polyazapyridinophanes (N-pAz-series), or methyl-diazapyridinophanes (Me-N-series)[2b] and methyl-polyazapyridinophanes (Me-N-pAz-series) are compared. Furthermore, it is seen that introduction of the methyl group into the pyridine ring at C_6-position provides expansion of the bridge chain required for restricted rotation by three to four methylene units (compare N-series with methyl-diazapyridinophanes (Me-N-series)[2b] or N-pAz-series with Me-N-pAz-series). Therefore, it is predictable that methyl-dithiapyridinophanes (Me-S-series), in which complete set of comparable series of congeners has not been synthesized, would show boundary bridge size at m=14 for restricted rotation. In addition, empirical conclusion drawn from the consideration of spherical bulk of atomic groups is well coincident with theoretical result calculated from covalent radii for individual atoms as has been previously pointed out.[2b]

It is of special significance that methyl-pentaaza[15]-(2,5)pyridinophane (**10a**) still retains restricted rotation since this contains five nitrogen atoms on the bridge probably enough to incorporate a guest in a mechanism of peripheral complexation proposed for catecholamine-macrocyclic polyamine complex.[3b] Since appropriate guests should be a matter of choice, polyaza[m]paracyclophanes (**11**—**13**) would contribute to provide informations about selection of guest molecules and mechanism of complexation.

Table 2. Relationship between Restricted Rotation and Bridge Chain Length in [m](2,5)Pyridinophanes Based on ^{1}H NMR Spectra
(F; free rotation, R; restricted rotation, B; boundary)

$(CH_2)_n$ n	Bridge Size/m	Compound Types[a]					
		S	Me-S	*N*	Me-N	N-pAz	Me-N-pAz
4	8	R					
5	9	R		R	R	R	R
6	10	R		R	R		
7	11	B[b]		R	R		
8	12	F	R	B	R	B	R
9	13		R[b]	F	R		
10	14		B[b]	F	R		
11	15		F[b]		B[b]	F	R
12	16			F	F		

a) S and N stand for pyridinophane with sulfur and nitrogen atoms at juncture point. Prefix Me- represents the presence of the methyl substituent on pyridoxine moiety at C_6-position. Suffix -pAz shows polyaza-containing bridge repeated by the iminoethylene group. See actual structures in Ref. 1a, b, g) for S, in Ref. 2b) for Me-S, N, and Me-N, and in the present report for N-pAz (**8a**—**10a**) and Me-N-pAz (**8b**—**10b**). b) Based on the empirical rule for the prediction of spherical bulk of the atomic group.

Experimental

The ^{1}H NMR spectra ware recorded in $CDCl_3$ on a JEOL JNM-GX 400 (400 MHz) spectrometer with Me_4Si as the internal standard; chemical shifts (δ) and coupling constants (J) are in parts per million and Herz, respectively. Infrared spectra (IR) were obtained as KBr disks on a Shimadzu IR-27G spectrophotometer. Mass spectra (MS, rel intensity) were obtained on a Hitachi RMU 6-MG spectrometer by using a direct-inlet method, an ionizing potential of 20 eV, and sample and chamber temperatures of 230°C. Merck silica gel 60 (Art. 7734, 0.063—0.20) was used for column chromatography, and Merck precoated silica gel 60 F_{254} plates (Art. 5715, 20×20 cm) were used for thin-layer chromatography (TLC). Two solvent systems were used for column chromatography and TLC unless otherwise mentioned; benzene-acetone 9:1 v/v (solvent A) and chloroform-acetone 93:7 v/v (solvent B). Product spots on TLC were detected either with a UV-lamp or in an iodine vapor bath. *N,N*-Dimethylformamide (DMF) was dried over molecular sieves (Type A), and the supernate was used directly for the reaction. The uncorrected melting points were measured with a micro melting point apparatus (Yanagimoto Seisakusho, Serial No. 2647). *N,N'*-Ditosyl-1,2-ethanediamine (**7**) was prepared from 1,2-ethanediamine according to a method previously reported.[5] 5'-Deoxy-2',5'-dichloro-3,4'-*O*-isopropylidene-6-methylpyridoxine hydrochloride (**4a**)[6] and 5'-deoxy-2',5'-dichloro-3,4'-*O*-isopropylidenepyridoxine (**4b**)[2b] were prepared immediately preceding the coupling reaction to sulfonamides from the corresponding dihydroxypyridoxine derivatives.

***N*-(2-Bromoethyl)-*p*-toluenesulfonamide (6).**[7] To a stirred solution of 2-bromoethylamine hydrobromide (40.0 g, 0.195 mol) in 320 ml of pyridine at 0—5°C, *p*-toluenesulfonyl chloride (48.38 g, 0.245 mol; 1.3 equiv) was added at once. The reaction was monitored by TLC (solvent B) every ten

min. When the absence of HBr-free 2-bromoethylamine was detected by spraying ninhydrin at R_f=0 (3 h), the mixture was poured into 2.6 l of water containing NaCl and stirred for ca. 1 h. The precipitate was collected by filtration and recrystallized from chloroform–cyclohexane to give 49.13 g of **6** (91%) as colorless leaflets: mp 93.5—94.5 °C (lit,[7] mp 88—90 °C); Calcd for $C_9H_{12}O_2NSBr$: C, 38.86; H, 4.35; N, 5.04; S, 11.53; Br, 28.73. Found: C, 38.99; H, 4.36; N, 5.01; S, 11.45; Br, 28.60. The yield of **6** was dependent on reaction temperature and time; at ambient temperature, the reaction mixture included considerable amounts of the corresponding dimer, *N*-(2-bromoethyl)-*N,N'*-ditosyl-1,2-ethanediamine. It was difficult to separate this from **6**, either on TLC or by recrystallization. Thus, the purity marker of **6** was elemental analyses and ^{1}H NMR. ^{1}H NMR data are shown in Fig. 1.

1,2-Ethanediamine Derivatives (1—3). Method A. To a suspended mixture of disodium *N,N'*-ditosyl-1,2-ethanediamine in DMF (55 ml) which was prepared by the reaction of *N,N'*-ditosyl-1,2-ethanediamine (2.0 g) with sodium metal (0.29 g, 2.3 equiv) in ethanol (30 ml) (refluxed for 1.5 h) followed by evaporation of ethanol, *N*-(2-bromoethyl)-*p*-toluenesulfonamide (**6**) (3.02 g, 2 equiv) in 20 ml of DMF was added dropwise at ca. 80 °C and then stirred until **6** disappeared. The reaction mixture was poured into 200 ml of water and the precipitate was collected by filtration. Silica-gel chromatography eluting with benzene–ethyl acetate (4:1 v/v) provided 1.26 g (63%) of the starting *N,N'*-ditosyl-1,2-ethanediamine, 0.47 g (15%) (R_f=0.3) of **1**, and 0.9 g (22%) (R_f=0.4) of **2** were isolated. Recrystallization of **1** from ethanol gave colorless crystals; mp 164—166 °C. Calcd for $C_{25}H_{31}O_6N_3S_3$: C, 53.07; H, 5.52; N, 7.43; S, 17.00. Found: C, 52.87; H, 5.58; N, 7.37; S, 16.96. MS: *m/z* 410 (the highest peak, 1.2%, M^+−155(Ts)) and 184 (100%, CH_2NHTs). IR: 3290(NH), and 1325 and 1150(SO_2) cm^{-1}. ^{1}H NMR spectral data are shown in Fig. 1. Recrystallization of **2** from ethanol gave colorless crystals; mp 193—195 °C. Calcd for $C_{34}H_{42}O_8N_4S_4$: C, 53.52; H, 5.55; N, 7.34; S, 16.81. Found: C, 53.57; H, 5.53; N, 7.20; S, 16.45. IR: 3290(NH), and 1325 and 1155(SO_2) cm^{-1}. ^{1}H NMR spectral data are shown in Fig. 1.

Method B. (a) A mixture of *N,N'*-ditosyl-1,2-ethanediamine (7.00 g), *N*-(2-bromoethyl)-*p*-toluenesulfonamide (5.813 g, 1.1 equiv) and 7.88 g (3 equiv) of anhydrous potassium carbonate in 250 ml of DMF was stirred at room temperature for 16 h. The reaction mixture was poured into 2.5 l of water and the precipitate was collected by filtration. Chromatography on silica gel eluting with chloroform–acetone (15:1 to 12:1 to 10:1 to 85:15 v/v) gave **1**, **2**, and **3** in the ratio 5:4:1. Recrystallization of **3** from chloroform–metahnol gave colorless crystals; mp 166—167 °C. Calcd for $C_{43}H_{53}O_{10}N_5S_5$: C, 53.78; H, 5.56; N, 7.29; S, 16.70. Found: C, 53.64; H, 5.53; N, 7.29; S, 16.58. IR: 3280(NH), and 1340 and 1155(SO_2) cm^{-1}. ^{1}H NMR spectral data are shown in Fig. 1.

(b) A mixture of **1** (2.03 g), *N*-(2-bromoethyl)-*p*-toluenesulfonamide (1.098 g, 1.1 equiv) and 0.99 g (2 equiv) of anhydrous potassium carbonate in 50 ml of DMF was stirred at room temperature for 53 h. After work-up as before, the residue was chromatographed on silica gel eluting with chloroform–acetone (10:1 to 9:1 v/v) to give recovered **1** (0.5 g), **2** (1.7 g), and **3** (0.4 g).

General Preparation Method of Polyaza(2,5)pyridinophanes and Polyazaparacyclophanes. To a stirred mixture of *N*-tosylated 1,2-ethanediamine derivatives (**1—3**) and excess anhydrous potassium carbonate (14 equiv mol to **1—3**) in DMF (1.5 g of **1—3**/150 ml of DMF) at room temperature, dichloropyridoxine (**4a,b**) (1 equiv) dissolved in DMF (0.5 g of **4a,b**/15 ml of DMF) was added dropwise (1 h). The stirring was continued for 12 h. The reaction mixture was poured into water containing NaCl. The resulting precipitate was collected by filtration followed by purification with silica-gel chromatography, unless otherwise noted. The product yield and mp are listed in Table 1. Line shapes of their ^{1}H NMR spectra are depicted comparatively in Figs. 2, 3, and 4 at δ 2.5=5.5. IR spectra of **8a—10a, 8b—10b,** and **11—13** are commonly characterized by bands at ca. 1600, 1340, and 1155(SO_2), and ca. 1380($C(CH_3)_2$) cm^{-1}. Specifically reported IR data are limited to the bands in the region 900—500 cm^{-1}.

N^2,N^5,N^8-Tritosyl-14-hydroxy-15-hydroxymethyl-14,15'-*O*-isopropylidene-11-methyl-2,5,8-triaza[9](2,5)pyridinophane (8a). Starting from **1** (1.186 g) and **4a** prepared from the corresponding dihydroxy-6-methylpyridoxine derivative (0.52 g, 1.04 equiv) in the presence of anhydrous potassium carbonate (4.056 g, 14 equiv) in 50 ml of DMF, 1.51 g (94%) of **8a** was obtained. Recrystallization from ethanol gave colorless crystals; Calcd for $C_{37}H_{44}O_8N_4S_3$: C, 57.53; H, 6.10; N, 6.95; S, 11.94. Found: C, 57.33; H, 5.96; N, 6.74; S, 12.13. R_f=0.73 (chloroform–acetone 85:15 v/v). IR: 812, 745, 656, 582, 570, 560, and 545 cm^{-1}. ^{1}H NMR: 1.50 and 1.58 (3H each, s, $C(C\underline{H}_3)_2$), 1.87 (1H, m, H-C-$\underline{H}$), 2.27 (3H, m, $C\underline{H}_2$), 2.73 (2H, m, $C\underline{H}_2$), 3.0 (1H, m, $C\underline{H}_2$), 3.31 (1H, m, $C\underline{H}_2$), 3.62 and 5.13 (1H each, AB-q, J=11.47, py-$C_{(5')}\underline{H}_2$-N), 3.84 and 4.50 (1H each, AB-q, J=12.16, py-$C_{(2')}\underline{H}_2$-N), 4.78 (2H, s, py-$C_{(4')}\underline{H}_2$-O), 2.44, 2.64, 2.47, and 2.49 (3H each, s, Ar-$C\underline{H}_3$), 7.31 (4H, m, aromatic protons) and 7.37, 7.63, 7.67, and 7.70 (2H each, d, J=8.05, aromatic protons). MS *m/z* 613 (31%, M^+−155(Ts); the highest peak).

N^2,N^5,N^8,N^{11}-Tetratosyl-17-hydroxy-18-hydroxymethyl-17,18'-*O*-isopropylidene-14-methyl-2,5,8,11-tetraaza[12](2,5)-pyridinophane (9a). Starting from **2** (2.326 g) and **4a** prepared from the corresponding dihydroxy-6-methylpyridoxine derivative (0.765 g, 1.04 equiv) in the presence of anhydrous potassium carbonate (5.90 g, 14 equiv) in 200 ml of DMF, 2.065 g (70.1%) of **9a** was isolated. Recrystallization from ethanol gave colorless crystals; Calcd for $C_{46}H_{55}O_{10}N_5S_4$: C, 57.18; H, 5.74; N, 7.25; S, 13.28. Found: C, 56.92; H, 5.70; N, 7.17; S, 13.32. R_f=0.50 (solvent A). IR: 810, 760, 734, 650, 572, 565, and 545 cm^{-1}. ^{1}H NMR: 1.45 and 1.53 (3H each, s, $C(C\underline{H}_3)_2$), 2.33 (3H, s, py-$C\underline{H}_3$), 2.46, 2.45, and 2.48 (3H, 6H, 3H each, s, $SO_2C_6H_4$-$C\underline{H}_3$), 2.05 (1H, m, $C\underline{H}_2$), 2.25 (1H, m, $C\underline{H}_2$), 2.35 (1H, m, $C\underline{H}_2$), 2.50 (1H, m, $C\underline{H}_2$), 2.93 (3H, m, $C\underline{H}_2$), 3.07 (2H, m, $C\underline{H}_2$), 3.40 (3H, m, $C\underline{H}_2$), 3.65 and 4.97 (1H each, AB-q, J=12.33, py-$C_{(2')}\underline{H}$-N), 3.77 and 4.43 (1H each, AB-q, J=13.31, py-$C_{(5')}\underline{H}_2$-N), 4.89 and 5.09 (1H each, AB-q, J=17.34, py-$C_{(4')}\underline{H}_2$-O), 7.33 (4H, m, aromatic protons), and 7.35, 7.42, 7.67, 7.71, 7.77, and 7.80 (2H each, d, J=8.30, aromatic protons). MS *m/z* 606 (0.1%, M^+−155(Ts)-205; the highest peak).

N^2,N^5,N^8,N^{11},N^{14}-Pentatosyl-20-hydroxy-21-hydroxymethyl-20,21'-*O*-isopropylidene-17-methyl-2,5,8,11,14-pentaaza[15](2,5)pyridinophane (10a). Starting from **3** (2.80 g) and **4a** prepared from the corresponding dihydroxy-6-methylpyridoxine derivative (0.698 g, 1.04 equiv) in the presence of anhydrous potassium carbonate (5.64 g, 14 equiv) in 200 ml of DMF, 1.58 g (46.6%) of **10a** was isolated. Recrystallization from benzene–ethanol gave colorless crystals. Calcd for

$C_{55}H_{66}O_{12}N_6S_5$: C, 56.78; H, 5.72; N, 7.22; S, 13.78. Found: C, 56.91; H, 5.72; N, 7.15; S, 13.66. R_f=0.63 (chloroform–acetone 95:5 v/v). IR: 810, 740, 712, 690, 655, 572, and 546 cm^{-1}. ^{1}H NMR: 1.25 and 14.9 (3H each, b-s, C(CH_3)$_2$), 2.06 (3H, s, py-CH_3), 2.36, 2.38, 2.44, 2.45, and 2.50 (3H each, s, $SO_2C_6H_4$-CH_3), 2.00, 2.40, 2.60, 3.00, and 3.46 (1H, 1H, 1H, 2H, 3H each, m, N-CH_2CH_2-N), 3.14 and 3.23 (8H total, m, N-CH_2CH_2-N), 3.76 and 4.44 (1H each, AB-q, J=12.45, py-C$_{(5')}H_2$-N), 4.49 and 4.59 (1H each, AB-q, J=14.16, py-C$_{(2')}H_2$-N), 4.79 and 4.96 (1H each, AB-q, J=15.75, py-C$_{(4')}H_2$-O), MS m/z 578 (0.1%; the highest peak).

N^2,N^5,N^8-Tritosyl-14-hydroxy-15-hydroxymethyl-14,15′-*O*-isopropylidene-2,5,8-triaza[9](2,5)pyridinophane (8b). Starting from **1** (0.89 g) and **4b** prepared from the corresponding dihydroxypyridoxine derivative (0.48 g, 1.35 equiv) in the presence of anhydrous potassium carbonate (4.1 g, 14 equiv) in 150 ml of DMF, 1.125 g (95%) of **8b** was obtained. Recrystallization from acetone–ethanol gave colorless crystals. Calcd for $C_{36}H_{42}O_8N_4S_3$: C, 57.27; H, 5.61; N, 7.42; S, 12.74. Found: C, 57.37; H, 5.61; N, 7.32; S, 12.75. R_f=0.55 (solvent B). IR: 810, 765, 755, 740, 655, 585, 575, and 545 cm^{-1}. ^{1}H NMR: 1.54 and 1.56 (3H each, s, C(CH_3)$_2$), 1.75, 2.34, 2.40, 2.80, 3.12, and 3.30 (1H each, m, N-CH_2CH_2-N), 2.72 (2H, m, N-CH_2CH_2-N), 2.45 and 2.47 (6H and 3H, s, $SO_2C_6H_4$-CH_3), 3.64 and 4.64 (1H each, AB-q, J=12.45, py-C$_{(5')}H_2$-N), 4.00 and 4.89 (1H each, AB-q, J=11.23, py-C$_{(2')}H_2$-N), 4.90 and 5.14 (1H each, AB-q, J=16.84, py-C$_{(4')}H_2$-O), and 8.00 (1H, s, py-H).

N^2,N^5,N^8,N^{11}-Tetratosyl-17-hydroxy-18-hydroxymethyl-17,18′-*O*-isopropylidene-2,5,8,11-tetraaza[12](2,5)pyridinophane (9b). Starting from **2** (1.526 g) and **4b** prepared from the corresponding dihydroxypyridoxine derivative (0.600 g, 1.33 equiv) in the presence of anhydrous potassium carbonate (3.87 g, 14 equiv) in 150 ml of DMF, 1.86 g (98%) of **9b** was isolated. Recrystallization from chloroform–ethanol gave colorless crystals. Calcd for $C_{45}H_{53}O_{10}N_5S_4$: C, 56.76; H, 5.61; N, 7.36; S, 13.47. Found: C, 56.66; H, 5.56; N, 7.33; S, 13.42. R_f=0.65 (solvent B). IR: 815, 740, 657, 573, and 549 cm^{-1}. ^{1}H NMR: 1.52 (6H, s, C(CH_3)$_2$), 2.45 and 2.47 (four 3H, s, $SO_2C_6H_4$-CH_3), 2.62 (5H, b-s, N-CH_2CH_2-N), 2.90 (2H, b-m, N-CH_2CH_2-N), 3.01 (5H, m, N-CH_2CH_2-N), 4.07 (2H, b-s, py-C$_{(5')}H_2$-N), 4.33 (2H, b-s, py-C$_{(2')}H_2$-N), 5.04 (2H, s, py-C$_{(4')}H_2$-O), and 7.82 (1H, s, py-H).

N^2,N^5,N^8,N^{11},N^{14}-Pentatosyl-20-hydroxy-21-hydroxymethyl-20,21′-*O*-isopropylidene-2,5,8,11,14-pentaaza[15](2,5)pyridinophane (10b). Starting from **3** (0.500 g) and **4b** prepared from the corresponding dihydroxypyridoxine derivative (0.152 g, 1.3 equiv) in the presence of anhydrous potassium carbonate (1.00 g, 14 equiv) in 50 ml of DMF, 0.408 g (68%) of **10b** was isolated. Recrystallization from chloroform–ethanol gave colorless crystals. Calcd for $C_{54}H_{64}O_{12}N_6S_5$: C, 56.42; H, 5.61; N, 7.31; S, 13.95. Found: C, 56.36; H, 5.57; N, 7.20; S, 13.88. R_f=0.70 (solvent B). IR: 813, 739, 715, 696, 657, 571, and 547 cm^{-1}. ^{1}H NMR: 1.46 (6H, s, C(CH_3)$_2$), 2.40, 2.41, 2.44, and 2.48 (3H, 3H, 6H, 3H, respectively, s, $SO_2C_6H_4$-CH_3), 2.83, and 2.90 (2H, each, b-t, CH_2-N^8-CH_2), 3.12 and 3.16 (8H, m, N^2-CH_2CH_2-N^5 and N^{11}-CH_2CH_2-N^{15}), 3.25 (4H, m, N^5-CH_2 and CH_2-N^{11}), and 7.78 (1H, s, py-H).

N^2,N^5,N^8-Tritosyl-2,5,8-triaza[9]paracyclophane (11). By the reaction of **1** (1.130 g) with **5** (0.549 g, 1.04 equiv) in the presence of anhydrous potassium carbonate (1.93 g, 7 equiv) in 80 ml of DMF, 1.274 g (96%) of **11** was isolated through direct recrystallization of the reaction mixture from chloroform–ethanol as colorless crystals. Calcd for $C_{33}H_{37}O_6N_3S_3$: C, 59.34; H, 5.59; N, 6.29; S, 14.40. Found: C, 59.24; H, 5.51; N, 6.17; S, 14.36. R_f=0.85 (solvent A). IR: 815, 785, 759, 742, 729, 653, 580, 560, and 545 cm^{-1}. ^{1}H NMR: 2.50, 2.60, and 3.10 (6H, 1H, and 1H, respectively, m, N-CH_2CH_2-N), 2.45 and 2.46 (3H and 6H, s, $SO_2C_6H_4$-CH_3), 4.24 (4H, b-s, CH_2-C_6H_4-CH_2), 7.34 and 7.67 (4H each, d, J=7.81, N^2- and N^8-aromatic protons), 7.29 and 7.65 (2H each, d, J=7.81, N^5-aromatic protons), and 7.40 (4H, s, C-C_6H_4-C). MS m/z 513 (19%, M$^+$−155(Ts); the highest peak) and 133 (base peak).

N^2,N^5,N^8,N^{11}-Tetratosyl-2,5,8,11-tetraaza[12]paracyclophane (12). By the reaction of **2** (1.50 g) with **5** (0.54 g, 1.04 equiv) in the presence of anhydrous potassium carbonate (1.90 g, 7 equiv) in 80 ml of DMF, 1.627 g (96%) of **12** was obtained by direct recrystallization of the reaction mixture from chloroform–ethanol as colorless crystals. Calcd for $C_{42}H_{48}O_8N_4S_4$: C, 58.31; H, 5.59; N, 6.49; S, 14.83. Found: C, 58.12; H, 5.52; N, 6.41; S, 14.80. R_f=0.50 (solvent B). IR: 810, 746, 732, 656, 571, 564, and 546 cm^{-1}. ^{1}H NMR: 2.45 (6H, s, N^5- and N^8-$SO_2C_6H_4$-CH_3), 2.47 (6H, s, N^2- and N^{11}-$SO_2C_6H_4$-CH_3), 2.50 (4H, s, N^5-CH_2CH_2-N^8) 2.83 and 2.94 (4H each, A_2B_2-m, N^2-CH_2CH_2-N^5) 4.14 (4H, s, CH_2-C_6H_4-CH_2), 7.33 (4H, s, C-C_6H_4-C), 7.32 and 7.68 (4H each, d, J=8.30, N^5- and N^8-aromatic protons), and 7.37 and 7.78 (4H each, d, J=8.30, N^2- and N^{11}-aromatic protons).

N^2,N^5,N^8,N^{11},N^{14}-Pentatosyl-2,5,8,11,14-pentaaza[15]paracyclophane (13). By the reaction of **3** (0.400 g) with **5** (0.132 g, 1.2 equiv) in the presence of anhydrous potassium carbonate (0.400 g, 7 equiv) in 40 ml of DMF, 0.318 g (72%) of **13** was isolated by chromatography. Recrystallization from acetone–ethanol gave colorless crystals; Calcd for $C_{51}H_{59}O_{10}N_5S_5$: C, 57.66; H, 5.60; N, 6.60; S, 15.09. Found: C, 57.42; H, 5.55; N, 6.45; S, 15.05. R_f=0.8 (solvent B) and 0.4 (benzene–ethyl acetate 9:1 v/v). IR: 813, 740, 715, 695, 657, 568, 546, and 540 cm^{-1}. ^{1}H NMR: 2.44 (3H, s, N^8-$SO_2C_6H_4$-CH_3), 2.45 (6H, s, N^5- and N^{11}-$SO_2C_6H_4$-CH_3), 2.47 (6H, s, N^2- and N^{14}-$SO_2C_6H_4$-CH_3), 2.91 and 3.02 (two 2H each, t, J=6.59, N^5-CH_2CH_2-N^8 and N^8-CH_2CH_2-N^{11}), 3.07 (two 4H, b-s, N^2-CH_2CH_2-N^5 and N^{11}-CH_2CH_2-N^{14}), 4.26 (4H, s, CH_2-C_6H_4-CH_2), 7.32 and 7.59 (2H each, d, J=8.30, N^8-aromatic protons), 7.34 and 7.71 (four 2h each, d, J=8.30, N^5- and N^{11}-aromatic protons), 7.35 and 7.75 (four 2H each, d, J=8.30, N^2- and N^{14}-aromatic protons), and 7.19 (4H, s, C-C_6H_4-C).

We are indebted to Dr. Haruo Homma and his staff in Riken for performing elemental analyses and to Dr. Jun Uzawa and Mrs. Tamiko Chijimatsu in Riken for measurement of ^{1}H NMR spectra.

References

1) a) M. Iwata, H. Kuzuhara, and S. Emoto, *Chem. Lett.*, **1976**, 983; b) H. Kuzuhara, M. Iwata, and S. Emoto, *J. Am. Chem. Soc.*, **99**, 4173 (1977); c) H. Kuzuhara, T. Komatsu, and S. Emoto, *Tetrahedron Lett.*, **1978**, 3563; d) M. Iwata and H. Kuzuhara, *Chem. Lett.*, **1981**, 5; e) Y. Tachibana, M. Ando, and H. Kuzuhara, *Chem. Lett.*, **1982**, 1765 and 1769; f) M. Ando, Y. Tachibana, and H. Kuzuhara, *Bull. Chem. Soc. Jpn.*, **55**, 829 (1982), **56**, 2263 and 3652 (1983); **57**, 237 (1984); g) M. Iwata and H. Kuzuhara, *Bull. Chem. Soc. Jpn.*, **58**, 2502 (1985).

2) a) M. Iwata and H. Kuzuhara, *Chem. Lett.*, **1981**, 1749; b) M. Iwata and H. Kuzuhara, *J. Org. Chem.*, **48**, 1282 (1983).

3) a) I. Tabushi, Y. Kimura, and K. Yamakura, *J. Am. Chem. Soc.*, **103**, 6486 (1981); b) E. Kimura, A. Watanabe, and M. Kodama, *ibid.*, **105**, 2063 (1983); c) H. Tsukube, *J. Chem. Soc., Chem. Commun.*, **1983**, 970.

4) See for phane-nomenclature, F. Voegtle and P. Neumann, *Tetrahedron*, **26**, 5847 (1970).

5) M. Iwata and H. Kuzuhara, *Bull. Chem. Soc. Jpn.*, **55**, 2153 (1982).

6) M. Iwata and H. Kuzuhara, *Bull. Chem. Soc. Jpn.*, **55**, 2295 (1982).

7) D. H. Peacock and U. C. Dutta, *J. Chem. Soc.*, **1934**, 1303.

The Wet Oxidation Treatment of Wastewater from SO_x Removal Facilities

Takatoshi YOSHIDA,* Hiroshi OHTA,† Kimihiko SUGIMOTO,†† Jiro BANNO,†† and Kan-ichi HASEGAWA†††
Junior College Division of Chukyo Women's University, Nadakayama, Yokone-cho, Ohbu 474
†Enviromental Research Center, Aichi Institute of Technology, Yagusa, Toyota 470-03
††Tokai Gijutsu Center, Unagihazama, Inokoshi, Idaka-cho, Meito-ku, Nagoya 465
†††Nagoya University of Arts, Shikatsu-cho, Nishikasugai-gun 481
(Received October 9, 1985)

The wet oxidation of sodium dithionate was carried out at an elevated temperature between 100 and 300 °C. The decomposition of the dithionate solution proceeded rapidly at 150—170 °C and (approximately) a complete decomposition occurred at temperatures greater than 200 °C within 30 min. The removed percentage of the dithionate under a large excess of air was independent of the concentration. The addition of iron(II) sulfate and hydrogen peroxide accelerated the decomposition. Wet oxidation was effective for the disposal of wastewater containing dithionates.

Sulfoxylates, except for sulfate in wastewater arising from wet SO_x removal facilities for exhaust gas, are refractory components for COD (chemical oxygen demand) removal (because of their reducing powers). In particular, dithionates comprise 60—85% of total sulfur compounds but are decomposed by oxidizing agents such as chlorine and ozone to an extent which varies from only several % to 40%, in spite of chemical reducing substances.[1,2] Therefore, it has been proposed to treat them by means of ion-exchange, electro-dialysis, and reverse-osmosis methods as well as coagulation and biological disposals.[3,4] However, problems regarding the great quantities of chemicals used and the waste products remained unsolved in those treatments.[3,4]

On the other hand, wet oxidation that is valid for resistant organic matter at an elevated temperature (150—350°C) and under a high pressure (3—25 MPa), has been put to practical use as a Zimmerman process in the field of wastewater treatment.[5-12] Wet oxidation is especially effective for the treatment of refractory substances for biological decompositions and is capable of recovering inorganic compounds. Furthermore, it is easy to recover energy on the basis of a heat exchange and there are few problems regarding inorganic salts in comparison with the pyrocombution method.

Lack of investigations regarding materials and corrosion for the facilities, however, retarded the application to a wide range of wastewater treatment.[13] Therefore, there have been several studies[14-17] on wet oxidation with catalysts, in order to enhance the decomposition rate or to reduce temperature and pressure used. Wet oxidation using Fenton's reagent[18,19] for refractory organic compounds and its reaction mechanism[20,21] were reported.

This paper deals with the wet oxidation of sodium dithionate as a model experiment for the wastewater treatment of SO_x removal facilities, including refractory dithionates. For practical use, the additive and temperature effects of Fenton's reagent and the protection of apparatus from corrosion due to by-product sulfuric acid have also been examined.

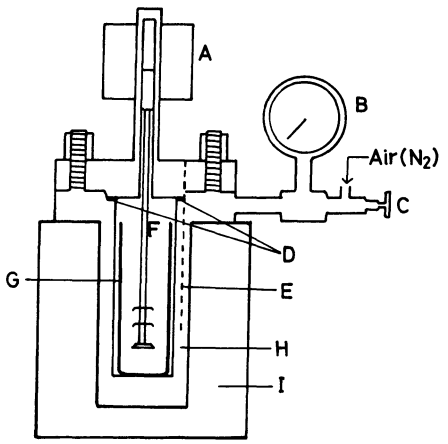

Fig. 1. Apparatus for wet oxidation: A, magnetic coil; B, pressure gauge; C, valve; D, copper packing; E, thermocouples; F, magnet drive rotating axis; G, glass tube; H, reactor; I, electric furnace. The glass tube was used only in Table 6.

Experimental

Apparatus. Wet oxidation and decomposition were carried out in a 200-ml Sakashita SE stainless autoclave equipped with a magnetic stirrer (Fig. 1).

Reagents. Commercial sodium dithionate (Extra Pure) and other chemicals (Guaranteed Reagent) were used without further purification.

Procedures. In the case of wet oxidation, the reaction vessel was charged with a 100-ml aqueous solution of sodium dithionate containing dithionate ion of 3500—35000 mg l^{-1} (or COD_{Mn} of 100—1000 mg l^{-1}) and, subsequently, an initial air pressure of 0.10—8.21 Mpa. Then, the solution was heated to a prescribed temperature between 100 and 300°C without stirring for 30 min. Finally, the temperature was maintained with stirring for 30 min. Wet decomposition was carried out in the same way as described above, except for an initial nitrogen pressure of 2.13 Mpa. Immediately after the required reaction time, the resulting sulfur dioxide was fixed by connecting three-jointed impingers (sodium hydroxide 1 wt/v % 20 ml×3) during reduced pressure. Sulfuric and sulfurous acids produced in the wet oxidation and decomposition were converted to sodium sulfate and sulfite by pouring an aqueous solution of sodium hydroxide into the autoclave, respectively. They

Table 1. Effect of Temperature on the Wet Oxidation of Sodium Dithionate under an Excess of Air[a)]

Temp	Pressure/MPa		COD_{Mn}[b)]/mg l^{-1}	Removed
°C	t=0[c)]	t=30[c)]	After oxidn.	%
100	2.7	2.8	95.8	0.6
140	2.8	3.5	62.7	35.0
145	3.0	3.6	49.3	48.9
150	3.0	3.9	31.6	67.2
155	3.0	3.9	14.9	84.5
170	3.2	4.0	4.5	95.3
200	3.6	4.4	2.3	97.6
250	4.5	6.2	1.8	98.1
300	6.4	9.1	0.8	99.2

a) Sample of 100 ml containing dithionate ion of 3500 mg l^{-1} was decomposed during promotion time 30 min and reaction time 30 min. The initial pressure of air at 20 °C was 2.13 MPa. b) The COD_{Mn} value for the sample prepared before the oxidation was 96.4 mg l^{-1}. c) The symbols of t=0 and t=30 stand for the reaction at time 0 and 30 min, respectively.

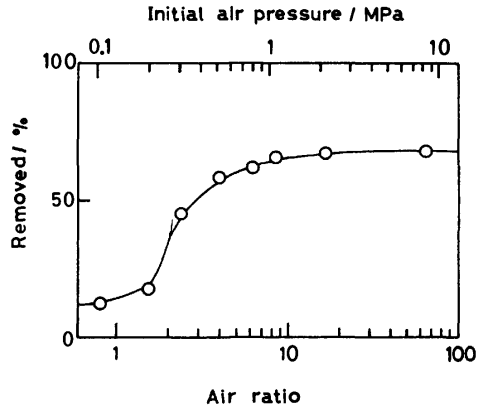

Fig. 2. Correlation of the removed percentage of sodium dithionate with the air ratio or the initial air pressure measured at 20 °C for the wet oxidation of the dithionate at 150 °C under air whose volume was 100 ml. Sample of 100 ml containing dithionate ion of 3500 mg l^{-1} was charged in the reactor.

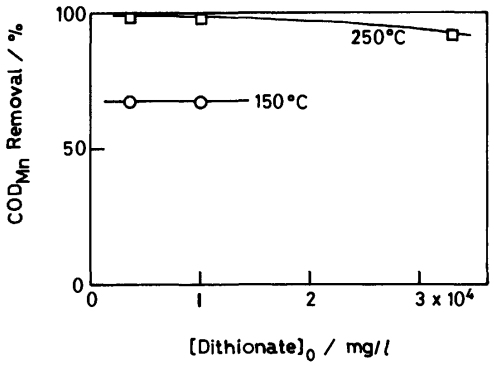

Fig. 3. Correlation of the initial concentration of dithionate with its removed percentage for the wet oxidation of sodium dithionate. The initial pressure of air at 20 °C was 2.1 MPa.

were then subjected to the chemical analyses described below.

Analyses. COD_{Mn} was determined on the basis of the oxygen demand by means of potassium permanganate at 100 °C (JIS K 0102(1981) 17). In the case of coexisting iron(II) ions and/or hydrogen peroxide, the solution was oxidized at room temperature by potassium permanganate; then, the COD_{Mn} was determined as described above. The dithionate concentration was determined from the oxygen demand during the potassium dichromate method (JIS K 0102, 20); its concentration in the presence of sulfite was obtained by subtracting the concentration of sulfite based on the iodine back titration method (JIS K 0102, 40) from the concentration of the both ($S_2O_6^{2-}$+SO_3^{2-}) by the dichromate method. The sulfate concentration was determined by means of the barium chromate method (JIS K 0102, 40-1); in the case of coexisting sulfite, the sulfate concentration was obtained by the subtraction of the sulfite concentration, estimated as described above, from the total concentration of the solution which was oxidized by ozone and then boiled, on the basis of the barium chromate method. The composition of red mud was determined by a fluorescent X-ray analysis of glass beads sintered at 1000 °C within 30 min. The amounts of components involved were: Na_2O, 7.42; K_2O, 0.19; MgO, 0.45; CaO, 1.70; Al_2O_3, 19.97; Fe_2O_3, 28.73; TiO_2, 3.52; SiO_2, 21.97; others, 4.55; Ig loss of carbonate and organic matters, 11.50%.

Results and Discussion

The Wet Oxidation of Sodium Dithionate. Table 1 lists the effect of temperature (100—300 °C) on the wet oxidation of an aqueous solution containing dithionate ions of 3500 mg l^{-1} at an initial air pressure of 2.13 MPa within 30 min. The decomposition of a sodium dithionate solution hardly proceeded at a temperature lower than 100 °C; however, it proceeded rapidly between 150 and 170 °C, at which a dithionate of 95% was removed. An approximately complete decomposition occurred at a temperature higher than 200 °C within 30 min. The change of promotion time, reaching a required reaction temperature, from 15 to 200 min without stirring, scarcely affected the removed percentage of sodium dithionate under stirring conditions.

If the wet oxidation of sodium dithionate proceeded according to Eq. 1, the theoretical pressure of air, P MPa, necessary to complete the decomposition of the dithionate ions (A mg) at t °C is approximately given by Eq. 2.

$$2S_2O_6^{2-} + O_2 + 2H_2O \longrightarrow 2SO_4^{2-} + 2H_2SO_4 \quad (1)$$

$$P = 1.208 \times 10^{-7}(273.15+t)A/V \quad (2)$$

Here, V denotes the volume of air expressed in liters. The air ratio is defined as the ratio of the initial air pressure charged to the theoretical air pressure.

Figure 2 shows the effect of the air ratio on the wet oxidation of sodium dithionate. The removed percentage of dithionate increased remarkably until

Table 2. Effect of Temperature on the Wet Decomposition of Sodium Dithionate under a Nitrogen Atmosphere[a)]

Temp	Pressure/MPa		Dithionate/mg		Sulfite/mg	Sulfate/mg	Total	Removed
°C	t=0[c)]	t=30[c)]	t=0	t=30	t=30	t=30	Sulfate[b)]/mg	%
130	2.8	2.8	339(407)[d)]	333(400)	2.2(2.6)	5.0	408	1.6
140	2.9	3.0	341(409)	326(391)	5.3(6.3)	13.7	411	4.6
150	3.2	3.3	336(403)	308(370)	9.1(10.9)	26.1	407	8.1
180	3.4	3.8	338(406)	150(180)	67(81)	144	405	55.6
200	4.0	4.3	340(408)	43.1(51.7)	114(137)	218	407	87.3
250	5.2	6.0	338(405)	21.3(25.5)	115(138)	242	406	93.7
270	5.7	6.9	342(410)	20.5(24.6)	114(137)	248	410	94.0
300	7.2	8.2	338(405)	6.1(7.3)	120(144)	256	407	98.2

a) Sample of 100 ml containing dithionate of ca. 3400 mg l^{-1} was decomposed during promotion time 30 min and reaction time 30 min. The initial pressure of nitrogen at 20 °C was 2.1 MPa. Various components before and after the reaction are listed in mg in the sample of 100 ml. b) Sum of the resulting sulfate and sulfate equivalent. c) The symbols of t=0 and t=30 represent the reaction at time 0 and 30 min, respectively. d) The amount of sulfate equivalent to that of the corresponding ion is shown in parenthesis.

the air ratio reached ca. 4 and was almost unchanged at an air ratio of more than 10. In general, organic compounds are completely oxidized with a theoretical amount of air under suitable temperatures and pressure conditions. In the wet oxidation of sodium dithionate, however, dissolved oxygen attacks not only the starting dithionate but also the intermediate sulfurous acid to form sulfuric acid. Therefore, the effect of air on the wet oxidation of dithionate became weaker in comparison with that of general organic compounds.

Figure 3 shows a correlation of the dithionate concentration with its removed percentage. In the case of a constant temperature, the removed percentage of the dithionate was independent of its concentration if the air ratio was more than 6. These results are consistent with the fact that the decomposition rate of dithionic acid was proportional to its concentration.[22-27] When the initial concentration of the dithionate was 33000 mg l^{-1}, the decreased removed percentage could be ascribed to a low air ratio of 1.8, as is clear from Fig. 2.

The Wet Decomposition of Sodium Dithionate. In order to clarify the action of oxygen, the wet decomposition of sodium dithionate was examined under an inert gas: in this case, a nitrogen atmosphere. Table 2 lists the respective components before and after the wet decomposition of the dithionate aqueous solution containing dithionate ion of 3400 mg l^{-1} under a nitrogen atmosphere. Since the sum of the respective components calculated in the sulfate equivalent after the reaction was almost equal to the amount of dithionate in the sulfate equivalent before the reaction, the decomposition of the dithionate solution under a nitrogen atmosphere is

$$S_2O_6^{2-} + H_2O \longrightarrow SO_4^{2-} + H_2SO_3. \quad (3)$$

The removed percentage of dithionate increased considerably at temperatures higher than 180°C; its percentage in the wet decomposition under an inert gas was of the same order as that in wet oxidation at a lower temperature (by 30—50°C).

The Mechanism of the Wet Oxidation of Sodium Dithionate. In the case of a neutral aqueous solution, the first step consists of a decomposition of dithionate into sulfate and sulfur dioxide.[22] The resulting sulfur dioxide in an aqueous solution is in equilibrium with the sulfurous acid. When an excess of air is present, sulfurous acid is oxidized to sulfuric acid. Therefore,

$$SO_2 + H_2O + 1/2O_2 = H_2SO_4. \quad (4)$$

The overall reaction is expressed by

$$S_2O_6^{2-} \xrightarrow{k_1} SO_4^{2-} + SO_2 \xrightarrow[+H_2O,\,O_2]{k_2} SO_4^{2-} + H_2SO_4, \quad (5)$$

where k_1 and k_2 are the rate constants.

The decomposition rate of dithionic acid into sulfuric and sulfurous acids in the presence of hydrochloric or perchloric acid was proportional to the concentrations of dithionic acid and of the hydrogen ion.[22-26] The activation energy estimated from the decomposition rate in the presence of hydrochloric acid was reported to be 29.8 kcal mol^{-1} (1 cal=4.184 J); similarly, in an alkaline solution the activation energy was evaluated to be 25 kcal mol^{-1}.[25]

From Arrhenius plots between the rate constants calculated on the basis of the first-order reaction of the dithionate concentration, i.e., $k_1 \ll k_2$ in Eq. 5, and the absolute temperature, the activation energy of the decomposition over the range 100—155°C (Table 1) was evaluated to be 32.5 kcal mol^{-1}.[28] The decomposition percentage at a temperature of 170 °C or greater was lower than that estimated from the activation energy. Although the magnitude of the evaluated activation energy was the same as that for the decomposition of dithionic acid,[25] an extreme assumption may be insufficient for our system, probably because an accumulation of the resulting sulfuric acid accelerates the decomposition of the dithionate. The pH for an aqueous solution contain-

Table 3. Effect of Catalyst Concentration on the Wet Oxidation of Sodium Dithionate at 150°C[a)]

$[S_2O_6^{2-}]_0$	$[H_2O_2]_0$/COD-O	$[FeSO_4]_0/[H_2O_2]_0$	Removed/%
mg l^{-1}	oxygen ratio	molar ratio	estimated by COD_{Mn}
3500	None	None	67.2
3500	0.5	0.2	67.2
3500	1.0	0.2	73.6
3500	1.5	0.2	59.5
3500	2.0	0.2	56.4
3500	1.0	1.0	95.6
3500	1.0	0.3	74.8
3500	1.0	0.1	66.6
10000	None	None	67.1
10000	1.0	None	84.0
10000	None	0.2	96.5
10000	1.0	0.2	95.6

a) Sample volume, promotion time, reaction time, and the initial pressure of air are the same values as described in Table 1.

Table 4. Effect of Temperature on the Wet Oxidation of Sodium Dithionate in the Presence of Fenton's Reagent[a)]

Temp	Pressure/MPa		pH		COD_{Mn}/mg l^{-1}		Removed
°C	t=0[b)]	t=30[b)]	Before oxidn.	After oxidn.	Before oxidn.	After oxidn.	%
100	2.7	2.9	2.5	2.2	112	102	8.8
120	2.8	3.0	2.5	1.7	114	62.0	45.6
135	3.0	3.1	2.5	1.6	108	30.9	71.2
150	3.1	3.2	2.5	1.4	103	4.5	95.6
180	3.4	3.7	2.5	1.4	114	1.3	98.9

a) Sample of 100 ml containing dithionate ion of ca. 3500 mg l^{-1} was decomposed during promotion time 30 min and reaction time 30 min. The initial pressure of air at 20°C was 2.1 MPa; $[H_2O_2]_0$/COD-O oxygen ratio=1.0, $[FeSO_4]_0/[H_2O_2]_0$ molar ratio=1.0. b) The symbols of t=0 and t=30 indicate the reaction at 0 and 30 min, respectively.

ing dithionate ions (3500 mg l^{-1} at 20°C) varied from 5.8 (before decomposition) to 1.5 (after complete decomposition). The fact that the decomposition percentage of the dithionate increased with an increasing air ratio can be ascribed to the increased concentration of the resulting hydrogen ions.

Since the accumulating sulfuric acid in a wet oxidation is a stronger acid than the sulfurous acid produced in a wet decomposition, it is reasonable from a comparison of the hydrogen ion concentration that the decomposition rate of the dithionate at the same temperature was higher in the former than in the latter. In other words, the wet oxidation of sodium dithionate under an excess of air proceeds at a lower temperature than does wet decomposition under a nitrogen atmosphere.

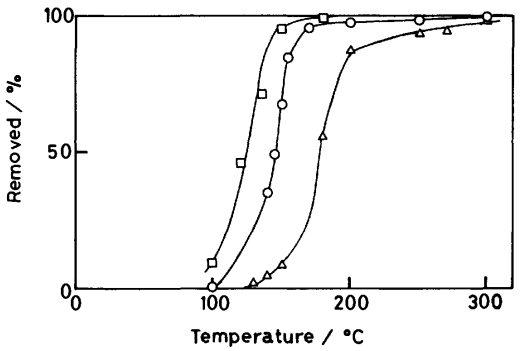

Fig. 4. Effect of temperature on the removed percentage of sodium dithionate for the wet oxidation and decomposition: □, in the presence of Fenton's reagent; ○, under air; △, under nitrogen atmosphere.

The Wet Catalytic Oxidation of Sodium Dithionate Using Fenton's Reagent. Fenton's reagent has a strong oxidation power on the basis of an electron acceptor of the hydroxyl radical produced from hydrogen peroxide in the presence of iron(II) salts. The resulting iron(III) ions are reduced to the starting iron(II) ions by use of hydrogen peroxide and/or a reducing radical produced during the oxidation-reduction process. Most transition metals can be applied as redox catalysts because of their valence transformation abilities. However, it is only the iron(II) ions among the transition metals that do not cause problems during an after treatment.

Table 3 lists the additive effect of catalysts such as hydrogen peroxide and iron(II) sulfate on the removed percentage of the dithionate. The addition of both hydrogen peroxide and iron(II) sulfate brought about a considerably higher decomposition of the dithionate than that in the absence of the additives at the same temperature. The optimum molar ratio of $[FeSO_4]_0$/

Table 5. Additive Effect of Neutralizer on the Wet Oxidation of Sodium Dithionate at 200 °C[a]

Neutralizer	Additive ratio[b]	Pressure/MPa		pH[d]	COD_{Mn}/mg l^{-1}		Removed
		t=0[c]	t=30[c]	After oxidn.	Before oxidn.	After oxidn.	%
$CaCO_3$	0.5	3.1	3.8	8.2	303	227	25.1
Red mud (Fe_2O_3)	0.5	3.2	4.0	8.1	305	220	27.8
Red mud (Fe_2O_3)	0.25	3.1	3.6	8.0	305	204	33.1
Red mud (Fe_2O_3)	0.05	3.1	3.6	1.5	303	7.9	97.4

a) Run conditions except for dithionate of ca. 10000 mg l^{-1} are the same as shown in Table 1. b) Molar ratio of neutralizer to the theoretical amount of sulfuric acid produced by complete decomposition. c) t=0 and t=30 indicate the reaction at time 0 and 30 min, respectively. d) The pH value before oxidation was 5.5.

Table 6. The Wet Oxidation of Sodium Dithionate in a Glass Tube[a]

Run No.	Sample ml	Air ratio	Temp °C	Gap[b]	COD_{Mn}/mg l^{-1}		Removed
					Before oxidn.	After oxidn.	%
1	100	15.9	150	None	100	33.0	67.0
2	80	13.0	150	Air	108	87.2	19.3
3	80	15.7	150	Air	108	81.3	24.7
4	80	9.1	150	Water	108	71.7	33.6
5	80	15.8	150	Water	108	69.4	35.7
6	50	15.3	160	Air	104	36.6	64.8
7	50	15.8	160	Water	108	24.1	77.7
8	50	15.8	180	Water	108	5.1	95.3

a) Sample containing dithionate ion of ca. 3500 mg l^{-1} was decomposed during promotion time 30 min and reaction time 30 min. Run 1 and the other Runs were carried out without and with a glass tube, respectively. b) Between the glass tube and the high pressure vessel shown in Fig. 1.

$[H_2O_2]_0$ was 1.0 for this system although its value was reported to be 0.2 for the decomposition of organic compounds.[20]

The temperature effect on decomposition was examined under the optimum conditions (Table 4). Figure 4 shows the temperature dependence of the removed percentages on the wet catalytic oxidation using Fenton's reagent, on the wet oxidation under air, and on the wet decomposition under a nitrogen atmosphere. Figure 4 suggests that the decomposition of the dithionate using Fenton's reagent proceeded at a lower temperature (by ca. 20 °C) compared to that of the wet oxidation without a catalyst.

Treatment of By-Product Sulfuric Acid. The wet oxidation of sodium dithionate resulted in equimolecular amounts of sulfuric acid and sodium sulfate. In the case of the complete decomposition of the aqueous solution containing dithionate ions (3500 mg l^{-1}), the concentration of the resulting sulfuric acid became 0.022 mol l^{-1}. In order to neutralize the acid, the additive effect of bases (such as calcium carbonate and red mud) on the wet oxidation of the dithionate was investigated (Table 5). When a solution after a reaction was weakly basic (pH 8.0—8.2), the decomposition proceeded only by 25.1—33.1%. More acidic conditions for a system after reaction (with the addition of a smaller amount of a base) favor a decomposition.

Protection of Apparatus from Corrosion with a Combined Glass Tube. In the case of purge water drained from S-removal circuit lines for coke-oven gas, titanium containing 0.2% of palladium has been used for the main equipment due to the resulting sulfuric acid and ammonium sulfate.[13] We examined the wet oxidation using a glass tube in an autoclave (Table 6). The magnitude of the removed percentage of dithionate in a glass tube at 150 °C was less than half of that in an autoclave at the same temperature. However, the former (used at 160 °C) produced almost the same results as the latter at 150 °C. Since the removal difference can be ascribed to a lowering of the thermal conductivity, based on the gap between the glass tube and the high pressure vessel, the removed percentage was improved by filling the gap with water (see in Fig. 1). Corrosion of the autoclave due to the resulting sulfuric acid was not observed during repeated experiments using the glass tube.

Table 7. The Wet Oxidation of Wastewater Involving Dithionate at 180 °C[a]

Water	pH	COD_{Mn}/mg l^{-1}	Removed/%
Wastewater	5.4	475	
Treated water	0.2	15	96.8

a) The initial pressure of air at 20 °C=2.1 MPa, reaction time=60 min.

The Wet Oxidation Treatment of Wastewater from SO_x Removal Facilities. In light of the above investigations, the wet oxidation of actual wastewater was examined. As Table 7 shows, an almost complete decomposition (97%) occurred. The COD_{Mn} value (475 mg l^{-1}) of the wastewater suggests that the concentration of the dithionate ion was ca. 16600 mg l^{-1}.[29]

A higher temperature enhances the decomposition percentage and makes it possible to obtain a treated-water COD_{Mn} of less than 10 mg l^{-1}.

Conclusions

The wet oxidation of sodium dithionate, as a model of wastewater involving dithionates from SO_x removal facilities, is summarized as follows.

1. The wet oxidation of an aqueous dithionate solution depends remarkably on the temperature. The wet oxidation did not proceed at a temperature lower than 100°C, even after long time. However, it rapidly proceeded at 150—170°C. Approximately a complete decomposition was observed at temperatures higher than 200°C.
2. The promotion time (15—120 min) reaching a required temperature did not affect the removed percentage of the dithionate unless the solution was stirred during the time.
3. The decomposition percentage of the dithionate under a large excess of air was independent of its concentration.
4. Wet decomposition of the dithionate under a nitrogen atmosphere produced sulfurous acid and wet oxidation under an excess of air produced sulfuric acid. The latter oxidation proceeded at a lower temperature than the former decomposition because of the accelerating effect of the resulting hydrogen ions.
5. Sodium dithionate in aqueous solution was easily decomposed at lower temperatures by using Fenton's reagent. The optimum molar ratio of iron(II) sulfate to hydrogen peroxide was 1.0.
6. The neutralization of the by-product sulfuric acid by using a solid base, resulted in the lowering of the decomposition percentage. A combined glass tube was useful in protecting the reaction vessel from corrosion due to sulfuric acid.
7. In the wet oxidation of actual wastewater at 180°C, a decomposition percentage of 97% was obtained. It is possible to obtain a treated-water COD_{Mn} of less than 10 mg l^{-1}.

Grateful acknowledgement is made to several students of Aichi Institute of Technology, Noriyuki SAKAI, Toshio TAMURA, Akira IDA, and Hidenori KAWAMURA for their collaboration.

References

1) Y. Isohata, *Thermal and Nuclear Power*, **23**, 960 (1977).
2) S. Tsuda, *Fuel and Combution Engineering*, **49**, 123 (1982).
3) S. Tsuda, *Ebara Infilco Times*, No. 88, 2 (1983).
4) A. Nishino, Japan Kokai 109152 (1976); K. Okayasu, *ibid.* 132181 (1976); H. Arimitsu, *ibid.* 133961 (1976).
5) T. Yoshida, Y. Ueno, K. Hasebe, and A. Minami, *J. Japan Sewage Works Association*, **9** No. 11, 1 (1972); T. Yoshida, Y. Ueno, M. Katayama, and K. Nagai, *ibid.*, **11** No. 8, 1 (1974).
6) S. Imamura, Y. Tonomura, N. Kawabata, and T. Kitao, *Bull. Chem. Soc. Jpn.*, **54**, 1548 (1981); S. Imamura, H. Kinunaka, and N. Kawabata, *ibid.*, **55**, 3679 (1982).
7) S. Imamura, *Water Purification and Liquid Wastes Treatment*, **24**, 93 (1983).
8) J. Koshitani, T. Kado, Y. Ueno, and T. Yoshida, *Bull. Chem. Soc. Jpn.*, **55**, 1931 (1982).
9) R. A. Miller and R. D. Fox, *Am. Chem. Soc. Natl. Meet. Div. Environ. Chem.*, **21**, 96 (1981).
10) R. G. W. Laughlin, T. Gallo, and H. Robey, *Proc. 2nd World Congress Chemical Engineering*, **6**, 62 (1981).
11) H. Perkow, R. Steiner, and H. Voblmüller, *Chem. Ind. Tech.*, **52**, 943 (1980).
12) D. T. Schaefer, *Hydrocarbon Processing*, **60**, 100 (1981).
13) K. Murakami, *Kagaku Kôzyô*, **26** No. 3, 85 (1982).
14) Y. Ohba, H. Nakamura, and T. Kirihara, *J. Japan Sewage Works Association*, **22**, 69 (1985).
15) J. Kimoto, Y. Harada, T. Ueda, and K. Katagiri, *J. Japan Aromatic Industry Association*, **36**, 161 (1984).
16) T. Sato, K. Kubo, M. Takashima, and M. Tsuyuguchi, *J. Water and Waste*, **25**, 471 (1983).
17) H. Yamada, J. Kimoto, T. Kawakatsu, Y. Harada, and T. Ueda, *Dyeing Research*, **26**, 77 (1982).
18) K. Hagiwara, Y. Murakami, K. Higashi, T. Saito, and S. Honda, *Ind. Pollution*, **32**, 456 (1984); K. Hagiwara, Y. Murakami, T. Saito, S. Honda, and Y. Ozakai, *Environ. Tech.*, **11**, 293 (1982); K. Hagiwara, Y. Murakami, K. Higashi, T. Saito, and S. Honda, *PPM*, 1983/2, 36 (1983).
19) Y. Murakami, K. Hagiwara, K. Higashi, T. Saito, Y. Ozakai, and S. Honda, *Water Purification and Liquid Wastes Treatment*, **23**, 1031 (1982).
20) T. Mizumaru, N. Jaksirinont, and T. Kitao, *J. Japan Sewage Works Association*, **18** No. 8, 20 (1981).
21) T. Kitao, Y. Kiso, and R. Yabashi, *Water Purification and Liquid Wastes Treatment*, **23**, 1019 (1982).
22) For reviews,"Gmerins Handbuch der Anorganishen Chemie **8**B2 Schwefel," Verlag Chemie, GmbH., Weinheim/Bergstrasse (1960); "Comprehensive Treatise on Inorganic and Theoretical Chemistry," J. W. Mellor Ed., Vol. X, Longmans, Green and Co., London (1930).
23) D. M. Yost and R. Pomeroy, *J. Am. Chem. Soc.*, **49**, 703 (1927).
24) J. Meyer, *Z. Anorg. Chem.*, **222**, 337 (1935).
25) P. Goldfinger and H. D. Graf von Schweinitz, *Z. Phys. Chem.*, **B22**, 117 (1933).
26) H. Bassett and A. J. Henry, *J. Chem. Soc.*, 914, (1935).
27) F. Ishikawa and H. Hagisawa, *Sci. Rep. Tohoku I*, **21**, 484 (1932).
28) The general equation of the first-order reaction is given by $\ln(a/(a-x))=-\ln(1-r)=kt$ where r denotes the decomposition fraction. The rate constant $k\times10^5$ (s^{-1}) obtained are as follows; 0.33(100°), 23.9(140°), 37.3(145°), 61.9(150°), 103.6(155°), 169.9(170°).
29) From the correlation of the concentration of dithionate with its COD_{Mn} value, the following equation was obtained (correlation coefficient r=0.9973; the oxidation of dithionate, 29.07%): $S_2O_6^{2-}$ (mg l^{-1})=$-5.3+35.0\times COD_{Mn}$ (mg l^{-1}).

 © 1986 The Chemical Society of Japan Bull. Chem. Soc. Jpn., 59, 1043—1049 (1986)

Active Carbon-Supported Aluminium Copper(I) Chloride as Solid Carbon Monoxide Adsorbent

Hidefumi HIRAI,* Keiichiro WADA, and Makoto KOMIYAMA
Department of Industrial Chemistry, Faculty of Engineering, The University of Tokyo, Hongo, Bunkyo-ku, Tokyo 113
(Received October 21, 1985)

Active carbon-supported aluminium copper(I) chloride ($AlCuCl_4$) is prepared by mixing active carbon with toluene solution of $AlCuCl_4$, followed by the removal of the liquid phase at 6 mmHg, 100 °C. The active carbon-supported $AlCuCl_4$ rapidly adsorbs carbon monoxide (CO) at 20 °C under 1 atm from 9:1 CO-N_2 mixture and the equilibrium molar ratio of adsorbed CO to $AlCuCl_4$ is 1.03. Adsorbed CO is desorbed either by reducing pressure or by elevating temperature. In the second adsorption, which is carried out after the desorption at 6 mmHg, 20 °C for 10 min, the molar ratio of adsorbed CO to $AlCuCl_4$ is 0.51. The molar ratios are constant at 0.51 in the third and later adsorptions. The CO adsorbing ability of the active carbon-supported $AlCuCl_4$ remains virtually unchanged on repeated contacts with nitrogen gas containing 9000 ppm of water.

Carbon monoxide (CO), a valuable raw material in chemical industry,[1] is produced in large scale by partial oxidation and water gas reaction of petroleum or coal.[2] In addition, considerable amounts of CO are present in exhausted gases from various chemical plants. Since all of these sources of CO are gas mixtures with methane, hydrogen, nitrogen, carbon dioxide, and water, separation and purification of CO from gas mixtures are necessary.[2,3]

Many liquid absorbents for CO have been proposed.[2-8] The toluene solution of polystyrene-aluminium copper(I) chloride ($AlCuCl_4$) complex, devised by the present authors,[7,8] has reversibly absorbed CO under mild conditions. $AlCuCl_4$, which is highly reactive with water vapor, is protected from water vapor by the polystyrene in the polymer-metal complex, and thus separation of CO from gas mixtures containing water vapor is successfully achieved with the absorbent.

In contrast to a number of proposals on liquid CO absorbents, reports on solid adsorbents for CO are scanty. Although Y zeolite-supported Cu(I) ion adsorbed CO, the adsorption was so strong that adsorbed CO did not effectively desorb even at 10^{-4} mmHg (1.0 mmHg=1.33×10^2 Pa).[9] In the case of the adsorbents composed of Cu(I) ion and zeolites having high SiO_2/Al_2O_3 molar ratios,[10] the amounts of Cu(I) ion, and thus the amounts of adsorbed CO, per 1 g adsorbents were small due to small ion-exchange capacities of the zeolites.

In preliminary communications, the authors reported solid CO adsorbents composed of $AlCuCl_4$ and active carbon[11] or polystyrene resin.[12] These adsorbents exhibited reversible adsorptions of CO under mild conditions and were stable against water in gas mixtures.

In this paper, CO adsorbing and desorbing abilities of adsorbents composed of $AlCuCl_4$ and active carbon as well as their water-resistance are reported in detail. The selectivity of the adsorbents for the adsorption of CO with respect to the adsorptions of other gases is shown. Furthermore, results of measurements of pore size distributions both for the adsorbents and for the original active carbon are presented. The mechanism of the water-resistance of the present adsorbents is discussed in terms of these results.

Experimental

Materials. Active carbon, prepared from petroleum pitch, was obtained from Kureha Chemical Industry Co. (BAC G-70R, Lot No. 810117, average diameter ca. 0.7 mm), and was subjected to a reduced pressure (6 mmHg) at 200 °C immediately before use.

Aluminium chloride (Kishida Chemical Co., guaranteed grade) was purified by sublimation. Copper(I) chloride (Koso Chemical Co., guaranteed grade) was reprecipitated from concentrated hydrochloric acid solution by the addition of water, followed by washing successively with ethanol and diethyl ether, and then was dried in vacuo.[13] Toluene was dried over metallic sodium and was distilled.

Carbon monoxide gas and nitrogen gas, which had purities of 99.95 and 99.999%, respectively, were passed through the columns of molecular sieve 3 A immediately before use.

Preparation of Adsorbent. 20.0 mmol of aluminium chloride and 20.0 mmol of copper(I) chloride were magnetically stirred in 20 cm^3 of toluene at 50 °C for 4 h under dry nitrogen. The resultant homogeneous dark-colored toluene solution of $AlCuCl_4$ was added to 10 g of active carbon, kept in an evacuated 100 cm^3 vessel, avoiding contamination of air with the use of a dropping funnel. The mixture was stirred with a magnetic stirrer for 1 h, and then the liquid phase was thoroughly removed at 6 mmHg, 100 °C for 1 h. The adsorbents were obtained as black to grey beads.

Solid of $AlCuCl_4$ without active carbon was prepared as described above except for the absence of active carbon. The solid was white to grey aggregates.

Determination of the Amount of Metal Salt in the Adsorbent. The adsorbent was thoroughly washed by stirring for 6 h in three portions of aqueous hydrochloric acid solution (3 mol dm^{-3}, total volume 1500 cm^3). The total amounts of copper atoms in the solution were evaluated by atomic absorption spectroscopy (Shimadzu Co., model AA-646).

Measurement of BET Surface Area and Pore Size Distribution. BET surface area was calculated from desorption isotherm of nitrogen at 77 K. Pore size distribution was determined also from the isotherm by the method of Dollimore.[14] The method takes advantage of capillary condensation theory and is based on the assumption of cylindrical pores with

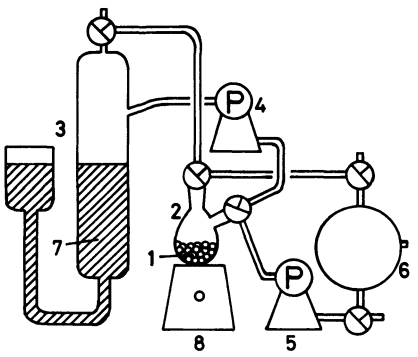

Fig. 1. Apparatus for measuring the amount of CO adsorbed by the adsorbents or desorbed from them; **1**: adsorbent; **2**: flask; **3**: gas burette; **4**: gas pump A; **5**: gas pump B; **6**: gas reservoir for nitrogen containing water; **7**: leveling liquid (toluene); **8**: magnetic stirrer.

radius r. The value $\Delta v/\Delta r$ is obtained as a function of r, where Δv is sum of volume for the pores having radii between r and $r+\Delta r$. Desorption isotherm of nitrogen at 77 K was measured on a Calroerba Co. Sorptomatic Series 1800.

Measurement of CO Adsorption and Desorption. The adsorptions of CO from CO-N_2 mixtures by the adsorbents were carried out at 20 °C under the atmospheric pressure using the apparatus depicted in Fig. 1. Uptake of CO was followed by a gas burette (3) using toluene as leveling liquid (7). The flask (2) containing the adsorbent (1) under nitrogen was connected with CO or CO-N_2 mixtures, and the adsorption was initiated by circulating the gas with the use of gas pump A (4). The circulation was effected for the first 10 min at a rate of 30 $cm^3 s^{-1}$ in order to mix the gas phase sufficiently.

The desorption of the adsorbed CO was carried out either by reducing the total pressure in the flask at 20 °C for 10 min or by elevating temperature from 20 °C to a predetermined temperature.

Contacts of the Adsorbent with Water Vapor. The contact of the adsorbent with water vapor was effected by circulating 5000 cm^3 of nitrogen gas, which had total pressure of 1 atm and contained 2.0 mmol of water (water content 9000 ppm), for 10 min on the magnetically stirred adsorbent with the use of a gas pump B (5). The nitrogen-water mixture was prepared by the introduction of water into an evacuated 5000 cm^3 vessel ((6) in Fig. 1) using a microsyringe, followed by the addition of dry nitrogen gas in an amount required to make the total pressure atmospheric.

Results

Preparation of Active Carbon-Supported $AlCuCl_4$. Toluene solutions of $AlCuCl_4$ were obtained as homogeneous dark-colored solutions by heating aluminium chloride and copper(I) chloride at charged molar ratio unity in toluene. On the addition of the toluene solution of $AlCuCl_4$ to active carbon, the color of the liquid phase rapidly decolorized. This result shows specific interactions between active carbon and $AlCuCl_4$. On removal of the liquid phase, active carbon-supported $AlCuCl_4$ was obtained as black to grey beads.

Table 1. BET Surface Areas of Adsorbents

Adsorbent	BET surface area / $m^2 g^{-1}$
Active carbon-supported $AlCuCl_4$[a)]	870
Original active carbon	1230

a) The adsorbent was prepared from 20.0 mmol of $AlCuCl_4$ and 10 g /of active carbon, and contained 17.2 mmol of $AlCuCl_4$.

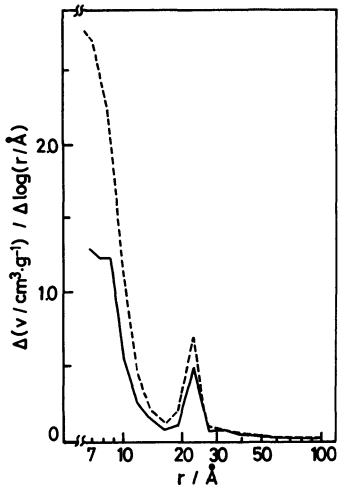

Fig. 2. Pore size distributions in the active carbon-supported $AlCuCl_4$ (——) and original active carbon (---): Δv is sum of volume for the pores having radii between r and $r+\Delta r$.

The atomic absorption spectroscopy showed that 17.2 mmol of $AlCuCl_4$ was supported to 10 g of active carbon, when 20.0 mmol of $AlCuCl_4$ in 20 cm^3 of toluene was treated with the active carbon. Thus, 86% of the charged $AlCuCl_4$ was supported to the active carbon under these conditions.

Table 1 shows the results on the measurement of BET surface area. The surface area (870 $m^2 g^{-1}$) for the adsorbent is about 70% of the value (1230 $m^2 g^{-1}$) for the original active carbon.

Figure 2 depicts pore size distribution either in the present adsorbent (the solid line) or in the original active carbon (the dotted line). The ordinate ($\Delta v/\Delta r$) approximately corresponds to number of pores. The number of pores with radii smaller than 15 Å for the present adsorbent is significantly smaller than the value for the original active carbon. In contrast, the number of pores with radii larger than 15 Å is almost identical with the value for the original active carbon. This result shows that small BET surface area (870 $m^2 g^{-1}$) of the present adsorbent, compared with the value (1230 $m^2 g^{-1}$) of the original active carbon, is almost totally attributable to decrease in the number of pores with radii smaller than 15 Å.

Adsorption and Desorption of CO by the Active Carbon-Supported $AlCuCl_4$. As shown by the open

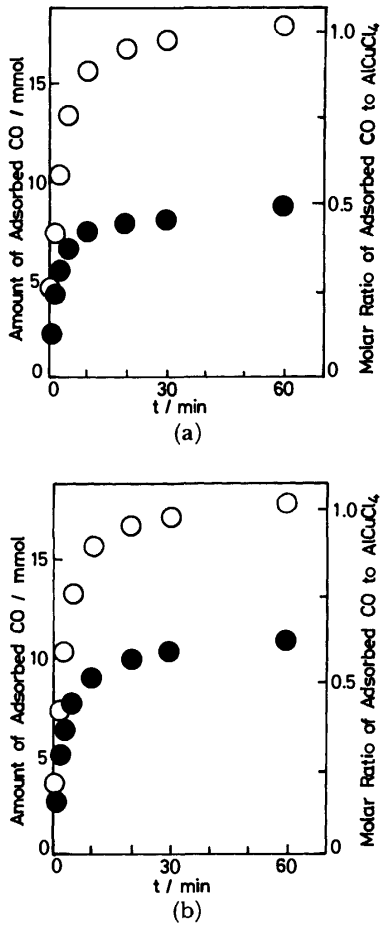

Fig. 3. Adsorption of CO by the active carbon-supported $AlCuCl_4$ at 20°C under 1 atm: the desorption conditions were 6 mmHg at 20°C for 10 min for (a), and 100°C, 1 atm for (b); the first adsorption by a virgin adsorbent (○); the second adsorption by the adsorbent which was subjected to the desorption conditions after the first adsorption (●); the adsorbent was prepared from 20.0 mmol of $AlCuCl_4$ and 10 g of active carbon, and contained 17.2 mmol of $AlCuCl_4$; the initial volume of gas mixture was 1500 cm^3 and the initial partial pressures of CO and N_2 were 0.9 and 0.1 atm, respectively.

circles in Fig. 3(a), the adsorbent rapidly adsorbs CO on the contact with 9:1 CO–N_2 mixture at 20°C under 1 atm. After 10 min, the amount of adsorbed CO is 15.6 mmol, which is 88% of the equilibrium value (17.7 mmol) determined after 60 min. The equilibrium molar ratio of adsorbed CO to the $AlCuCl_4$ supported to active carbon is 1.03; the amount of the supported $AlCuCl_4$ is 17.2 mmol.

After being subjected to a reduced pressure (6 mmHg) at 20°C for 10 min, the adsorbent was again contacted with 9:1 CO–N_2 mixture. The adsorbent showed a rapid adsorption and the equilibrium value of adsorbed CO was 8.8 mmol (● in Fig. 3(a)). The equilibrium value for the third adsorption by the adsorbent, which was subjected to a reduced pressure (6 mmHg) at 20°C for 10 min after the second adsorption, was

Table 2. Effect of CO Partial Pressure on the Amount of CO Adsorbed by the Active Carbon-Supported $AlCuCl_4$ at 20°C[a)]

CO partial pressure / mmHg	Molar ratio of CO adsorbed in 60 min to $AlCuCl_4$
152	0.13
380	0.36
684	1.03
760	1.05

a) $AlCuCl_4$, 17.2 mmol; active carbon, 10 g.

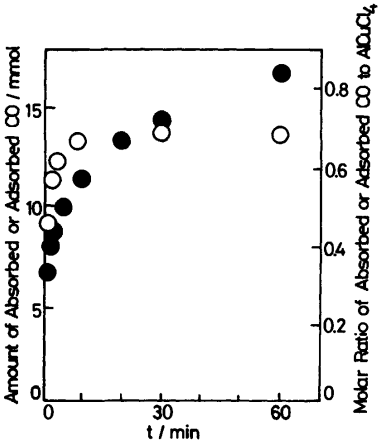

Fig. 4. Absorption or adsorption of CO by a toluene solution of $AlCuCl_4$ (○) or by a solid of $AlCuCl_4$ (●) at 20°C under 1 atm: the initial partial pressure of CO for the absorption by the toluene solution was 0.8 atm, whereas that for the adsorption by the solid was 0.9 atm; the amount of $AlCuCl_4$, 20.0 mmol.

also 8.8 mmol. The CO adsorption-desorption cycle, composed of the adsorption of 8.8 mmol of CO at 760 mmHg and the desorption of almost the identical amount of CO at 6 mmHg, was repeated five (the maximum number examined) times without measurable deterioration.

The adsorbed CO was also desorbed by elevating temperature (Fig. 3(b)). The active carbon-supported $AlCuCl_4$, which was prepared separately, adsorbed 17.7 mmol of CO on the first contact with 9:1 CO–N_2 mixture at 20°C (the open circles). On the elevation of temperature from 20 to 100°C under 1 atm, the adsorbent rapidly desorbed 11.0 mmol of CO. In the following adsorption, the equilibrium value of the adsorbed CO was 11.0 mmol (the closed circles in Fig. 3(b)). The cycle involving the adsorption of 11.0 mmol of CO at 20°C, followed by the desorption of 11.0 mmol of CO at 100°C, was repeated five times without deterioration.

Table 2 shows the dependence of the amount of CO adsorbed by the active carbon-supported $AlCuCl_4$ on the partial pressure of CO in CO–N_2 mixtures. The molar ratio of the adsorbed CO to $AlCuCl_4$, supported to active carbon, decreases with decreasing partial

Table 3. Adsorbing Capacities of the CO Adsorbents and Absorbent[a)]

Adsorbent or absorbent	CO adsorbed in 60 min	
	Amount/mmol	Molar ratio to $AlCuCl_4$
Active carbon-supported $AlCuCl_4$[b,c)]	17.7	1.03
Solid of $AlCuCl_4$[b)]	14.6[d)]	0.85
Toluene solution of $AlCuCl_4$[b)]	14.4	0.84
Original active carbon[c)]	3.3[e)]	—

a) At 20°C; initial volume of gas mixture 1500 cm^3; initial partial pressures of CO and N_2, respectively, were 0.9 and 0.1 atm. b) $AlCuCl_4$, 17.2 mmol. c) Active carbon, 10 g. d) This value was estimated from the result in Fig. 4, using the fact that the amount of adsorbed CO was proportional to the amount of $AlCuCl_4$. e) The measurement was carried out using helium, in place of nitrogen, as balance, since the magnitudes of adsorptions of CO and N_2 to active carbon were comparable with each other, and adsorption of helium was negligibly small (Table 5).

pressure from 1.05 at 760 mmHg to 0.13 at 152 mmHg.

For the purpose of comparison, the time course of the CO absorption by a toluene solution of $AlCuCl_4$ (○) and the time course of the adsorption by a solid of $AlCuCl_4$ (●) without active carbon are depicted in Fig. 4. The toluene solution of 20.0 mmol of $AlCuCl_4$ in 20 cm^3 of toluene rapidly absorbs CO from 8:2 CO–N_2 mixture. The equilibrium amount of absorbed CO, determined after 60 min, is 14.0 mmol ($CO/AlCuCl_4$= 0.70). The solid of 20.0 mmol of $AlCuCl_4$ also adsorbs CO on the contact with 9:1 CO–N_2 mixture. The rate of adsorption, however, is much smaller than the value for the active carbon-supported $AlCuCl_4$ adsorbent, and the adsorption does not attain an equilibrium even after 6 h.

Table 3 lists the amounts of CO adsorbed or absorbed for 60 min by the three types of the adsorbents and absorbent as well as the value for the original active carbon. The active carbon-supported $AlCuCl_4$ adsorbs CO about equimolar to $AlCuCl_4$, and shows larger adsorbing capacity either than the toluene solution of $AlCuCl_4$ or than the solid of $AlCuCl_4$. The CO adsorbing ability of the original active carbon itself is small under these conditions.

Desorption of Adsorbed CO under Various Desorption Conditions. The effect of desorption conditions on the degree of desorption of adsorbed CO from the adsorbent is shown in Table 4. Here, the degrees of desorption under the specified conditions are expressed in terms of the ratios of the amounts of desorbed CO to the capacities of the adsorbent (the amounts of CO adsorbed in the first adsorption by a virgin adsorbent). The first adsorption and the second one by the adsorbent, which was subjected to the specified desorption conditions after the first adsorption, were carried out, keeping the adsorption conditions constant: 20°C and the initial CO pressure 0.9 atm. The amount of the CO desorbed under the desorption conditions was evaluated from the amount of CO adsorbed in the second adsorption.

When the desorption conditions are 20°C, 6.0 mmHg, the amount of adsorbed CO in the second and later adsorptions is 8.8 mmol, as depicted in Fig. 3(a). Thus, 50% of CO with respect to the amount (17.7 mmol) adsorbed in the first adsorption is desorbed under the above conditions.

Table 4. Dependence of the Amount of Desorbed CO on the Desorption Conditions for the Active Carbon-Supported $AlCuCl_4$[a)]

Desorption conditions		Ratio of amount of desorbed CO to adsorbing capacity[b)]
T/°C	Pressure/mmHg	
20	6.0	0.50
20	0.4	0.61
100	0.4	0.91
180	0.4	0.99
180	760.0	0.72
100	760.0	0.62

a) $AlCuCl_4$, 17.2 mmol; active carbon, 10 g. b) The ratio of the amount of desorbed CO under specified conditions to the amount of CO adsorbed in the first adsorption by a virgin adsorbent.

Table 5. Adsorbing Capacities of the Active Carbon-Supported $AlCuCl_4$ and the Original Active Carbon for Various Kinds of Gases[a)]

Gas	Amount of gas adsorbed by 1 g of Adsorbent/$cm^3\,g^{-1}$	
	Active carbon-supported $AlCuCl_4$	Original active carbon
H_2	0.0	0.0
He	0.0	0.0
N_2	0.8	7.2
Ar	0.9	6.3
CH_4	4.2	21.5
CO	24.1	9.5

a) Gas pressure 1 atm, 20°C.

Almost all of the adsorbed CO is desorbed at a reduced pressure and a high temperature: 0.4 mmHg and 180°C. When these desorption conditions are used, 17.7 mmol of CO is separated by each of adsorption-desorption cycles.

Selectivity of CO Adsorption for the Active Carbon-Supported $AlCuCl_4$. Table 5 shows adsorbing capacities on various gases for the active carbon-supported $AlCuCl_4$. The adsorbent exhibits no measurable ad-

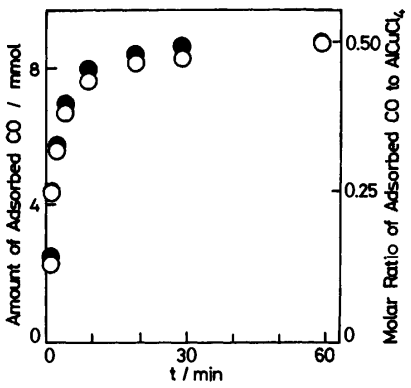

Fig. 5. CO adsorbing capacity of the active carbon-supported $AlCuCl_4$ before (○) and after (●) the contact of the adsorbent with 5000 cm^3 nitrogen gas containing 2.0 mmol of water (water content 9000 ppm) for 10 min: The adsorptions of CO were carried out by the contacts with 9:1 $CO-N_2$ gas mixtures at 20 °C, 1 atm; the desorptions of CO were achieved at 20 °C, 6 mmHg for 10 min.

sorption of hydrogen or helium at 1 atm, 20 °C. Adsorption of nitrogen or argon is not significant either. The amount of methane adsorbed is only 17% of the value of CO.

In contrast, the amount of methane adsorbed by the original active carbon is more than two times as large as the value of CO. The active carbon also shows considerable adsorptions on nitrogen and argon, although the adsorptions of hydrogen and helium are minimal.

Water-Resistivity of the Active Carbon-Supported $AlCuCl_4$. The open circles in Fig. 5 exhibit the adsorption of CO by the active carbon-supported $AlCuCl_4$, which has adsorbed 17.7 mmol of CO on the first contact with 9:1 $CO-N_2$ mixture (see Fig. 3), and then has been subjected to a reduced pressure (6 mmHg) at 20 °C for 10 min. Without contacts of the adsorbent with water vapor, almost identical time courses were obtained for repeated CO adsorptions (Fig. 3(a)).

The closed circles in Fig. 5, which are for the adsorption after the contact of the adsorbent with nitrogen containing 2.0 mmol of water (water content 9000 ppm) for 10 min, almost perfectly superimpose the open circles for the adsorption prior to the contact. Thus, water vapor has no measurable effects on the activity of the active carbon-supported $AlCuCl_4$ with respect to both the rate of CO adsorption and the adsorbed amount. Even after the contacts of the adsorbent with nitrogen gas containing 2.0 mmol of water, prepared separately for each contact, are repeated five times (total period of the contact is 50 min and total amount of water is 10 mmol), both the rate of adsorption and the equilibrium value of adsorbed CO are also identical with the values prior to the contacts (Table 6).

In contrast, the CO adsorbing activity of solid of $AlCuCl_4$ without active carbon largely decreases on the contacts with water vapor, as also shown in Table 6.

Table 6. Water Resistivities of the Adsorbents[a)]

Number of repeated contacts of the adsorbents with water vapor	Relative adsorbing capacity[b)]	
	Active carbon-supported $AlCuCl_4$[c)]	$AlCuCl_4$ solid[d)]
0	100	100
1	102	59
2	103	54
3	99	—
4	101	—
5	100	—

a) Adsorbents were contacted with 5000 cm^3 of N_2 gas containing 2.0 mmol of water (water content: 9000 ppm) at 20 °C for 10 min. b)The ratios in percent of the amounts of CO adsorbed after the contacts with water vapor to the value for the adsorbent without the contacts. c) $AlCuCl_4$, 17.2 mmol; active carbon 10 g. d) $AlCuCl_4$, 20.0 mmol.

Discussion

Preparation of Active Carbon-Supported $AlCuCl_4$. Significant decrease (360 $m^2 g^{-1}$) of the BET surface area of active carbon on the formation of the adsorbent from active carbon and $AlCuCl_4$ (Table 1) shows that the double salt is supported on the surface of the pores in the active carbon. $AlCuCl_4$ largely exists in the pores with radii smaller than 15 Å, as clearly seen by the decrease of number of these small pores on the formation of the adsorbent (Fig. 2). Thus, the double salts in the adsorbents are mostly in their monomeric or dimeric forms. A possibility of formation of large aggregates of the salts is ruled out, since they are too large to be accommodated in these small pores.

Rough estimation, based on the decrease (360 $m^2 g^{-1}$) of the BET surface area and the amount (17.2 mmol) of $AlCuCl_4$ supported to 10 g of active carbon, indicates that one molecule of the double salt occupies around 35 $Å^2$ of the surface area of the active carbon. The double salts are separated from each other by about 6 Å on the surface.

Presence of $AlCuCl_4$ in such a close proximity without mutual aggregation is attributable to specific and strong interactions between the double salt and the condensed aromatic rings of active carbon. $AlCuCl_4$ forms charge-transfer complexes with various aromatic compounds such as benzene,[15] toluene,[16] and mesitylene,[16] and thus easily dissolves in these aromatic solvents.

Adsorption and Desorption of CO by the Active Carbon-Supported $AlCuCl_4$. The adsorption of CO by the adsorbent is ascribed to complex formation of $AlCuCl_4$ with CO. Active carbon alone exhibits a small adsorption of CO (Table 3). Physical adsorption of CO by the adsorbent is ruled out, since the adsorptions of gases other than CO, e.g. methane, nitrogen, and argon, by the present adsorbent are, in con-

trast with promotion of CO adsorption, less efficient than the adsorptions by the original active carbon (Table 5).

High selectivity of CO adsorption for the present adsorbent (Table 5) is attributable to effective coverage of the surface of active carbon by $AlCuCl_4$. CO is sufficiently adsorbed by coordination to the double salt (vide infra), whereas physical adsorptions of other gases by the active carbon is suppressed by the $AlCuCl_4$.

The rate of adsorption of CO by the present adsorbent is almost identical with the value for the toluene solution of $AlCuCl_4$ (Figs. 3 and 4). This is ascribed to high and virtually molecular dispersion of $AlCuCl_4$ on the surface of the active carbon. In addition, CO can effectively diffuse to the double metal salt through the pores in the active carbon. The adsorption by solid $AlCuCl_4$ (Fig. 4), which has not a high dispersion, is much slower than that by the active carbon-supported $AlCuCl_4$.

Larger amount of the adsorbed CO for the active carbon-supported $AlCuCl_4$ (103 mol% with respect to $AlCuCl_4$: Table 3) than that (84 mol%) for the toluene solution of $AlCuCl_4$ is associated with absence of competition between CO and toluene in the complex formation with $AlCuCl_4$. On the CO absorption by the toluene solution, CO coordinates to $AlCuCl_4$ by replacing a toluene molecule which is originally complexing with the double salt.[16]

The adsorption of CO by the adsorbent takes place by the coordination of CO to the vacant coordination site at copper(I) ion in $AlCuCl_4$. The vacant coordination site is produced during the process of the preparation of the adsorbent. Here, $AlCuCl_4$, in which the copper(I) ion is complexing with toluene, is first supported on the surface of the active carbon, and then the toluene is removed by evaporation. By the coordination of CO to the vacant site, the copper(I) ion takes the most stable tetrahedral and four-coordinate state.[17]

Desorption of the adsorbed CO is accompanied by the structural change of the copper(I) ion from the stable four-coordinate state to less stable three-coordinate state. This process requires a considerable activation energy and thus rather severe conditions (180 °C, 0.4 mmHg) are required to desorb all the adsorbed CO during the desorption period 10 min employed in the present study (Table 4). The amount (50 mol% with respect to $AlCuCl_4$) of CO desorbed at 20 °C, 6 mmHg for 10 min (Table 4) is considerably smaller than the value (90 mol%) estimated for milder desorption conditions (20 °C, 152 mmHg) under the assumption that an equilibrium is attained in 10 min for desorption. If this assumption were valid, the desorbed amount at 20 °C, 152 mmHg should be the difference (90 mol%) between the amount (103 mol%) adsorbed at 20 °C, 684 mmHg (the CO partial pressure in 9:1 $CO-N_2$ mixture at 1 atm) and the value (13 mol%) adsorbed at 20 °C, 152 mmHg (see Table 2).

A prolonged desorption (3 h) at 20 °C, 6 mmHg increased the amount of desorbed CO from the value (50 mol%) for the 10 min desorption to 57 mol%.

With the present solid adsorbent, pressure-swing separation, which takes advantage of change in partial pressure of CO and is not possible with the use of liquid absorbents, is successfully carried out (Fig. 3 (a)) in addition to thermal-swing separation using change in temperature (Fig. 3 (b)). By use of adsorption-desorption cycles composed of the adsorption at 20 °C, 1 atm from 9:1 $CO-N_2$ mixture and the desorption at 20 °C, 6 mmHg, 8.8 mmol of CO is separated. Each of the cycles involving the adsorption at 20 °C, 1 atm and the desorption at 180 °C, 0.4 mmHg separates 17.7 mmol of CO (Table 4).

Water-Resistivity of Active Carbon-Supported $AlCuCl_4$. Stability of the present adsorbent against water vapor, clearly shown in Fig. 5 and Table 6, is attributable to protection of the double metal salt by active carbon, since the solid of $AlCuCl_4$ without active carbon is rapidly deactivated with water vapor (Table 6). Toluene solutions of $AlCuCl_4$ are also easily deactivated by water vapor.[5-8] In the present adsorbent, $AlCuCl_4$ is almost molecularly dispersed and is located in the micropores with radii smaller than 15 Å (Fig. 2). The inside of the micropores is rather hydrophobic, since the pores are surrounded by the walls of fused aromatic rings. Thus, $AlCuCl_4$ can be shielded from water vapor in the micropores. In addition, diffusion of water vapor to the inside of quite small micropores through hydrophobic pores should be less efficient, which is also favorable for the stability of the double metal salt.

The argument is consistent with the previous result[12] that cross-linked polystyrene-supported $AlCuCl_4$ is also a water-resistant CO adsorbent. There, $AlCuCl_4$ is located in the micropores of the polystyrene resin, and is protected by the hydrophobic aromatic rings.

Water-resistivity of the present adsorbent is quite important from the viewpoints of practical applications, since the sources of CO in industry are usually saturated with water. With this adsorbent, separation of CO from the gas mixtures containing water can be achieved without severe dehydration of the feed gases by pretreatments.

The authors would like to thank Dr. Toshio Osawa at the University of Tokyo for his assistance in the measurements of the BET surface area and pore size distribution.

References

1) "New Syntheses with Carbon Monoxide," ed by J. Falbe, Springer-Verlag, Berlin (1980).

2) "Kirk-Othmer Encyclopedia of Chemical Technology," 3rd ed, ed by H. F. Mark, D. F. Othmer, C. G. Overberger, and G. T. Seaborg, John-Wiley & Sons, New York (1978), p. 772.

3) L. Kohl and F. C. Riesenfeld, "Gas Purification," 3rd ed., Gulf Publishing Co., Houston (1979).
4) A. T. Larson and C. S. Teitsworth, *J. Am. Chem. Soc.*, **44**, 2878 (1922).
5) D. J. Haase and D. G. Walker, *Chem. Eng. Prog.*, **70**, 74 (1974).
6) D. J. Haase, *Chem. Eng.*, August 4, 52 (1975).
7) H. Hirai, M. Komiyama, and S. Hara, *Makromol. Chem., Rapid Commun.*, **2**, 495 (1981).
8) H. Hirai, M. Komiyama, and S. Hara, *Chem. Lett.*, **1981**, 1447.
9) Y.-Y. Huang, *J. Catal.*, **30**, 187 (1973).
10) J. A. Rabo, J. N. Francis, and C. L. Angell, U. S. Patent 4019879 (1977).
11) H. Hirai, M. Komiyama, and K. Wada, *Chem. Lett.*, **1982**, 1025.
12) H. Hirai, M. Komiyama, and S. Hara, *Chem. Lett.*, **1982**, 1685.
13) D. D. Perrin, W. L. F. Armarego, and D. R. Perrin, "Purification of Laboratory Chemicals," 2nd ed., Pergamon Press (1980), p. 486.
14) D. Dollimore and G. R. Heal, *J. Appl. Chem. (London)*, **14**, 109 (1964).
15) R. W. Turner and E. L. Amma, *J. Am. Chem. Soc.*, **88**, 1877 (1966).
16) H. Hirai, M. Nakamura, and M. Komiyama, *Bull. Chem. Soc. Jpn.*, **56**, 2519 (1983).
17) F. A. Cotton and G. Wilkinson,"Advanced Inorganic Chemistry," 4th ed., John Wiley & Sons, New York (1980), p. 804.

Polymer-Protected Metal Complex for Gas Separation. II. Cross-Linked Polystyrene-Supported Aluminium Copper(I) Halide as Solid Carbon Monoxide Adsorbent

Hidefumi HIRAI,* Susumu HARA, and Makoto KOMIYAMA
Department of Industrial Chemistry, Faculty of Engineering, The University of Tokyo, Hongo, Bunkyo-ku, Tokyo 113
(Received December 9, 1985)

Macroreticular (MR) type cross-linked polystyrene-supported aluminium copper(I) chloride is prepared by refluxing MR type polystyrene (divinylbenzene content 20%), aluminium chloride, and copper(I) chloride in benzene, toluene, carbon disulfide, or dichloromethane, followed by evaporation of the liquid phase. All the polystyrene-supported aluminium copper(I) chloride exhibit rapid and reversible adsorptions of carbon monoxide (CO). For the adsorbent prepared by using toluene as solvent, the equilibrium molar ratio of adsorbed CO to the charged copper(I) chloride is 0.83 at 20 °C under 1 atm (initial partial pressure of CO: 0.90 atm). Desorption of CO is carried out at 7 mmHg, 20 °C for 10 min. The equilibrium molar ratio of adsorbed CO to the charged copper(I) chloride in the second adsorption is 0.56. In the following adsorptions, the equilibrium molar ratios are virtually constant at 0.56. Usage of either gel type cross-linked polystyrenes or a linear polystyrene in place of the MR type cross-linked polystyrene results in CO adsorbents having poor abilities with respect to both adsorption rates and capacities. The adsorbing capacities of the CO adsorbents prepared from aluminium halide, copper(I) halide, and the MR type cross-linked polystyrene decrease as follows: $AlCl_3$-CuCl system > $AlBr_3$-CuBr system $\gg$ AlI_3-CuI system $\approx$ $AlCl_3$-CuI system $\approx$ AlI_3-CuCl system ≈ 0.

Carbon monoxide (CO), which is one of the important raw materials in chemical industry,[1] is usually obtained as gas mixtures.[2] Thus, separation of CO from gas mixtures is required for effective utilization of CO.

Previously,[3,4] the authors reported on CO absorbents composed of linear polystyrene, aluminium chloride ($AlCl_3$), copper(I) chloride (CuCl), and toluene. The absorbents reversibly absorbed CO under mild conditions, and were stable against water vapor due to protection of water-sensitive aluminium copper(I) chloride ($AlCuCl_4$), a double salt formed from $AlCl_3$ and CuCl, by the polystyrene. Separation of CO from gas mixtures containing water vapor was successfully achieved with the use of the absorbents.

In spite of many proposals on liquid CO absorbents,[2-5] informations on solid adsorbents of CO are rather scanty. Although Y zeolite-supported copper(I) ions adsorbed CO, the adsorption was so strong that the adsorbed CO was not sufficiently released even at 10^{-4} mmHg (1 mmHg=133.3 Pa).[6] A patent[7] claimed that copper(I) ions supported on zeolites having high SiO_2/Al_2O_3 molar ratios adsorbed CO. The equilibrium amount of CO adsorbed by 1 g of the adsorbent at 50 °C was 16 cm^3 (standard temperature and pressure), which was almost independent of partial pressure of CO at the partial pressure 100 mmHg or larger.

In preliminary communications,[8,9] the authors showed that the macroreticular (MR) type cross-linked polystyrene-supported $AlCuCl_4$ adsorbed and desorbed CO under mild conditions.

This paper describes the results of detailed studies on the MR type cross-linked polystyrene-supported $AlCuCl_4$. Dependences of CO adsorbing capacities of the adsorbents either on adsorbing temperature, on partial pressure of CO, or on the preparation solvent are described. The adsorbing and desorbing abilities of the adsorbents are compared with those for the adsorbents prepared by use of gel type cross-linked polystyrene or linear polystyrene in place of MR type cross-linked polystyrene. Furthermore, the adsorbing capacities of the adsorbents prepared from various aluminium halides, copper(I) halides, and MR type cross-linked polystyrene are shown.

Experimental

Materials. A macroreticular (MR) type cross-linked polystyrene (styrene-divinylbenzene (DVB) copolymer, divinylbenzene content 20%; 20—50 mesh; diameter, 296—740 μm; average pore diameter, 9 nm; surface area, 300 m^2/g)[10] was obtained from Bio-Rad Laboratories (Bio-Beads SM-2). A cross-linked (DVB 12%) gel type polystyrene (200—400 mesh; diameter, 37—74 μm) and a cross-linked (DVB 1%) gel type polystyrene (200—400 mesh; diameter, 37—74 μm) were purchased also from Bio-Rad Laboratories (Bio-Beads S-X12 and Bio-Beads S-X1, respectively). They were purified by stirring successively in the following solvents under the specified conditions: aqueous hydrochloric acid solution, 4 mol dm^{-3}, 55 °C, 2 h; aqueous sodium hydroxide solution, 2 mol dm^{-3}, 55 °C, 2 h; distilled water, 55 °C, 2 h; methanol, room temperature, 1 h; dichloromethane, room temperature, 1 h. The resins were dried in vacuo at 80 °C for 12 h.

Linear polystyrene, purchased from Wako Pure Chemical Co., was reprecipitated using the chloroform–methanol system and was dried in vacuo at 60 °C for 12 h. The number-averaged molecular weight and the weight-averaged molecular weight were 4.4×10^4 and 1.5×10^5, respectively, as determined by the gel permeation chromatography using columns of TSK-GEL, G5000H+G3000H, Toyo Soda Manufacturing Co.

Aluminium chloride (Kishida Chemical Co.) was purified by sublimation. Copper(I) chloride (Koso Chemical Co.) was reprecipitated from an aqueous concentrated hydrochloric

acid solution by the addition of distilled water, followed by washing successively with ethanol and diethyl ether, and then was dried overnight in vacuo at 100 °C. Aluminium bromide, copper(I) bromide, aluminium iodide, and copper(I) iodide were commercially obtained (guaranteed grades) and were used without further purification.

Carbon disulfide and dichloromethane were dried over diphosphorus pentaoxide and were distilled. Toluene and benzene were distilled after being dried over metallic sodium.

Carbon monoxide gas and nitrogen gas, which had purities of 99.95 and 99.999%, respectively, were passed through columns of molecular sieve 3A immediately before use.

Preparation of CO Adsorbents. Preparation of the solid CO adsorbent was carried out as follows. Aluminium halide, copper(I) halide, and the macroreticular type polystyrene resin were refluxed in various solvents under dry nitrogen for 4—6 h, during which the mixture was magnetically stirred. Then, the solvent was thoroughly removed from the mixture by evaporation at 4 mmHg for several hours. Evaporation temperature was gradually elevated from room temperature to 60 °C, as the evaporation proceeded.

Charged molar ratio of aluminium halide to copper(I) halide was 1.0 unless otherwise noted and the ratio of phenyl residue in the polystyrene resin to copper(I) halide was 1.2—2.0.

Adsorption and Desorption of CO. Adsorption of CO by the adsorbent (1), continuously stirred by use of a magnetic stirrer (3), from atmospheric CO or CO-N_2 mixtures (total pressure: 1 atm) was carried out under 1 atm, using the apparatus depicted in Fig. 1. The amount of adsorbed CO was determined by a gas burette (4) using liquid paraffin as leveling liquid (5). Adsorption from atmospheric CO was initiated by introduction of CO to a flask containing the adsorbent. The flask was evacuated to 7 mmHg prior to the introduction. In case of adsorption from CO-N_2 mixtures, the gas mixtures were made to flow over the adsorbent by use of a gas-circulating pump (6) for the first 10 min in the adsorption.

Desorption of CO from the adsorbent was carried out at 7 mmHg for 10 min at room temperature or prescribed temperatures.

Fourier Transfer Infrared (FT-IR) Spectroscopy. FT-IR spectra were taken at room temperature with a JEOL FT-IR model 10 spectrometer at various CO pressures. Specimen was prepared from 2.05 g (15.4 mmol) of $AlCl_3$, 1.52 g (15.4 mmol) of CuCl, and 3.35 g (30.7 mequiv in phenyl residue) of the macroreticular type cross-linked polystyrene by use of 10 cm^3 of carbon disulfide as solvent. The adsorbent was mixed with silica gel (Cab-O-Sil, Wako Pure Chemical Co.) after being thoroughly ground. The content of copper atom in disk was 2.5 wt%.

Results

Preparation of Macroreticular Type Polystyrene-Supported $AlCuCl_4$. When $AlCl_3$, CuCl, and the macroreticular type polystyrene resin (DVB 20%) were refluxed in toluene or benzene for 6 h, both the polystyrene beads and the liquid phase turned dark brown. Solid adsorbents were obtained as yellowish green beads by evaporating the solvents thoroughly at 4 mmHg from the mixtures.

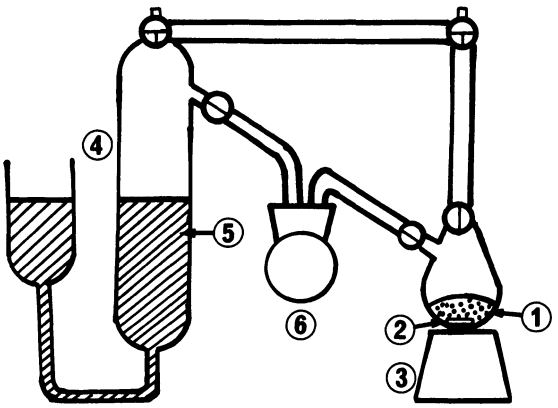

Fig. 1. Apparatus for measuring the amounts of carbon monoxide adsorbed by the adsorbents; 1: CO adsorbent, 2: rotor, 3: magnetic stirrer, 4: gas burette, 5: leveling liquid (liquid paraffin), 6: gas-circulating pump.

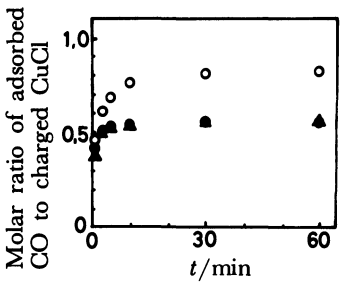

Fig. 2. Adsorption of carbon monoxide from 9:1 CO-N_2 mixture at 20 °C under 1 atm by the macroreticular (MR) type polystyrene-supported aluminium copper(I) chloride prepared by use of toluene as solvent: The first adsorption (○), the second adsorption (●), and the third adsorption (▲); the desorption of CO was carried out at 7 mmHg for 10 min; the adsorbent was prepared from 5.21 g (39.1 mmol) of $AlCl_3$, 3.87 g (39.1 mmol) of CuCl, and 7.04 g (64.6 mequiv in phenyl residue) of the MR type polystyrene with the use of 20 cm^3 of toluene; the initial volume of the gas mixture was 2000 cm^3 with initial pressures of CO and N_2, 0.9 and 0.1 atm, respectively.

On the refluxing of $AlCl_3$, CuCl, and the polystyrene resin in carbon disulfide or dichloromethane, however, only the polystyrene beads turned dark brown after refluxing. The liquid phase was almost transparent with quite a faint dark orange color. The adsorbents obtained after evaporation of the solvent were reddish brown beads.

Depositions of metal salts on the inside walls of the flasks, used for the preparation of the adsorbents, were hardly observed in any of these cases. These results show that almost all of the charged metal salts are incorporated to the adsorbents.

CO Adsorbing and Desorbing Abilities of Macroreticular Type Polystyrene-Supported $AlCuCl_4$. Figure 2 depicts the adsorption of CO at 20 °C from 9:1 CO-N_2 mixture (initial partial pressure of CO: 0.9 atm) under 1 atm by the adsorbent prepared from 5.21

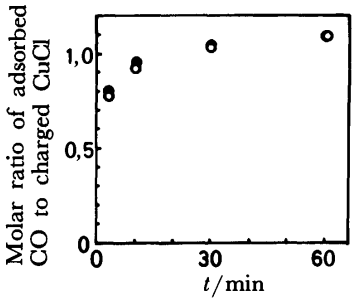

Fig. 3. Adsorption of carbon monoxide from atmospheric CO at 20°C under 1 atm by the macroreticular (MR) type polystyrene-supported aluminium copper(I) chloride prepared by use of toluene as solvent: The first adsorption (○), and the second adsorption (●); the desorption of CO was carried out at 7 mmHg, 90°C for 30 min after the first adsorption; the adsorbent was prepared from 2.75 g (20.6 mmol) of $AlCl_3$, 2.04 g (20.6 mmol) of CuCl, and 2.58 g (23.7 mequiv in phenyl residue) of the MR type polystyrene using 10 cm^3 of toluene.

g (39.1 mmol) of $AlCl_3$, 3.87 g (39.1 mmol) of CuCl, and 7.04 g (64.6 mequiv in phenyl residue) of the macroreticular type polystyrene resin with the use of 20 cm^3 of toluene. As shown by the open circles, the adsorbent rapidly adsorbs CO and the equilibrium molar ratio of the adsorbed CO to the charged CuCl is 0.83 (45 cm^3 (standard temperature and pressure) of CO per 1 g of the adsorbent).

Desorption of adsorbed CO is carried out at 7 mmHg, 20°C for 10 min. On the second contact with 9:1 CO–N_2 mixture, the adsorbent rapidly adsorbs CO and the equilibrium molar ratio of adsorbed CO to the charged CuCl is 0.56 (31 cm^3 (standard temperature and pressure) of CO per 1 g of the adsorbent; solid circles in Fig. 2).

The third adsorption of CO by the adsorbent, which is subjected to a reduced pressure (7 mmHg) at 20°C for 10 min after the second adsorption, from 9:1 CO–N_2 mixture is also rapid and the equilibrium molar ratio of adsorbed CO to the charged CuCl is 0.57 (solid triangles in Fig. 2). This molar ratio is identical with the value (0.56) in the second adsorption within experimental error.

The open circles in Fig. 3 depict CO adsorption by the adsorbent, prepared separately using toluene as solvent, from atmospheric CO at 20°C. The adsorption is rapid and the equilibrium molar ratio of adsorbed CO to the charged CuCl is 1.10 (69 cm^3 (standard temperature and pressure) of CO per 1 g of the adsorbent). The adsorbed CO is desorbed by heating the adsorbent at 90°C under 7 mmHg for 30 min. In the second adsorption, shown by the closed circles, the equilibrium molar ratio of adsorbed CO to the charged CuCl is 1.10, which is identical with the value for the first adsorption.

Effect of Preparation Solvent on CO Adsorbing Capacity of Macroreticular Type Polystyrene-Supported $AlCuCl_4$. Table 1 shows the equilibrium molar ratios of adsorbed CO to the charged CuCl for the polystyrene-supported $AlCuCl_4$ prepared by using various solvents. All the adsorbents, except for the one prepared by use of tetrachloromethane as solvent, adsorb CO around equimolar to the charged CuCl in the first adsorptions. The equilibrium amounts of the adsorbed CO in the second adsorptions are about one half to one third of the values in the first adsorptions. The desorptions are carried out at 7 mmHg, room temperature for 10 min.

Table 1. CO Adsorbing Capacities of the Macroreticular Type Polystyrene-Supported Aluminium Copper(I) Chloride Prepared by Use of Various Solvents[a)]

Preparation solvent	Molar ratio[b)]	
	1st[c)]	2nd[d)]
Toluene	1.05	0.55
Benzene	1.03	0.43
Carbon disulfide	1.07	0.54
Dichloromethane	1.11	0.35
Tetrachloromethane	0.55	0.23

a) Charged molar ratios of $AlCl_3$ and phenyl residue in the cross-linked polystyrene to CuCl are 1.0 and 1.2, respectively. b) Equilibrium molar ratios of adsorbed CO to the charged CuCl at room temperature under 1 atm of CO. c) The value in the first adsorption by a virgin adsorbent. d) The value in the second adsorption by the adsorbent which has been subjected to a reduced pressure (7 mmHg) for 10 min at room temperature after the first adsorption.

When the desorptions were achieved at 7 mmHg, 90°C for 30 min, the amount of adsorbed CO in the second adsorption for the adsorbent prepared by use of carbon disulfide as solvent was 67% of the value in the first adsorption.

On the usage of tetrachloromethane as solvent, liquid phase gradually turned black on refluxing and gray precipitates were formed. The adsorbent, obtained as black beads after evaporation, showed considerably smaller CO adsorbing capacity than the adsorbents prepared by use of toluene, benzene, carbon disulfide, and dichloromethane (Table 1).

Effects of Adsorbing Temperature and CO Partial Pressure on Adsorbing Capacity of Macroreticular Type Polystyrene-Supported $AlCuCl_4$. Open circles in Fig. 4 show the plot of the equilibrium molar ratio of adsorbed CO to the charged CuCl vs. adsorption temperature for the adsorbent prepared by using dichloromethane. Below 50°C, the molar ratio is larger than unity. The adsorbing capacity markedly decreases with increasing temperature above 70°C and the amount of adsorbed CO at 145°C is nearly zero.

Solid circles in Fig. 4 are for the second adsorptions by the adsorbent which desorbs CO at 7 mmHg for 10 min after the first adsorptions. The desorptions are carried out at the same temperatures as the first adsorptions are achieved. The amounts of CO adsorbed in the second adsorptions are almost identical with

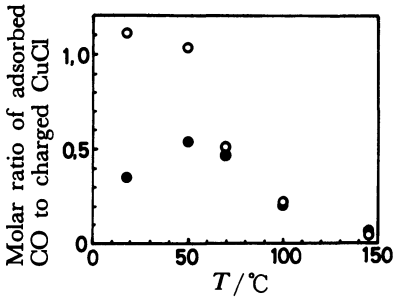

Fig. 4. Temperature dependence of the adsorbing capacity for the macroreticular (MR) type polystyrene-supported aluminium copper(I) chloride prepared by use of dichloromethane as solvent: The first adsorption at a prescribed temperature under 1 atm (○) and the second adsorption at the same temperature (●); prior to the second adsorption, the adsorbed CO was desorbed at 7 mmHg for 10 min at the temperature that was employed for the first and the second adsorptions; the charged molar ratios of $AlCl_3$ and phenyl residues in the polystyrene to CuCl were 1.0 and 1.2, respectively.

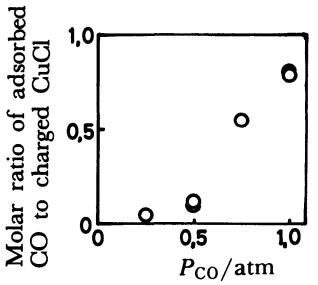

Fig. 5. Effect of partial pressure (P_{CO}) of carbon monoxide on the carbon monoxide adsorption at room temperature by the MR type polystyrene-supported aluminium copper(I) chloride prepared using dichloromethane as solvent: The adsorbent was subjected to a reduced pressure (7 mmHg) at 90 °C for 60 min after a CO adsorption in order to desorb virtually all of the adsorbed CO, and was then used for the following adsorption at a different partial pressure of carbon monoxide; the adsorbent was prepared from 1.35 g (10.1 mmol) of $AlCl_3$, 1.00 g (10.1 mmol) of CuCl, and 1.05 g (9.6 mequiv in phenyl residue) of the MR type polystyrene with the use of 10 cm^3 of dichloromethane.

those in the first adsorptions, when the desorption temperatures are 70 °C or higher. This result shows that almost all of the adsorbed CO is desorbed at 7 mmHg at a temperature higher than 70 °C.

Figure 5 depicts dependence of the equilibrium molar ratio of adsorbed CO to the charged CuCl on CO partial pressure. The amount of adsorbed CO gradually decreases with decreasing CO partial pressure. Decrease in CO partial pressure during CO adsorption was at most 0.02 atm.

CO Adsorbing Abilities of Adsorbents Prepared from Macroreticular Type Polystyrene, Various Aluminium Halides, and Various Copper(I) Halides. The adsorbent, prepared from 11.8 g (44.2 mmol) of aluminium bromide, 6.35 g (44.3 mmol) of copper(I) bromide, and 4.60 g (42.2 mequiv in phenyl residue) of the macroreticular (MR) type polystyrene resin using 20 cm^3 of toluene as solvent, adsorbs CO from 9:1 CO-N_2 mixture (partial pressure of CO: 0.9 atm) at 30 °C, as shown in Fig. 6. The equilibrium molar ratio of the adsorbed CO to the charged copper(I) ion is 0.38, which is smaller than that (0.83) of the MR type polystyrene-supported $AlCuCl_4$. The adsorption of CO by the MR type polystyrene-supported $AlCuBr_4$ is considerably slower than that by the MR type polystyrene-supported $AlCuCl_4$.

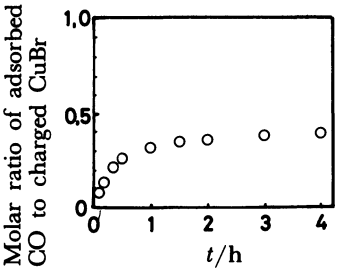

Fig. 6. Adsorption of carbon monoxide from 9:1 CO-N_2 mixture at 30 °C under 1 atm by the macroreticular (MR) type polystyrene-supported aluminium copper(I) bromide prepared by use of toluene as solvent: The adsorbent was prepared from 11.80 g (44.2 mmol) of $AlBr_3$, 6.35 g (44.3 mmol) of CuBr, and 4.60 g (42.2 mequiv in phenyl residue) of the MR type polystyrene using 20 cm^3 of toluene.

The adsorbent, prepared from aluminium iodide, copper(I) iodide, and the MR type polystyrene resin using carbon disulfide as solvent, showed quite a small capacity of CO adsorption : The molar ratio of the CO adsorbed in 3 h to the charged copper(I) iodide was 0.01. Either the adsorbent prepared from aluminium iodide, copper(I) chloride, and the resin or the one from aluminium chloride, copper(I) iodide, and the resin exhibited no measurable CO adsorption.

FT-IR Spectra of CO Adsorbed by Macroreticular Type Cross-Linked Polystyrene-Supported $AlCuCl_4$. A peak appeared at 2121 cm^{-1} on the contact of the adsorbent with 20 mmHg of CO (Fig. 7 (a)). The peak completely disappeared when CO was pumped off from the adsorbent at 10^{-4} mmHg, as shown in Fig. 7 (b). The height of the peak increased with increasing pressure of CO: (d, 760 mmHg)>(c, 300 mmHg)>(a, 20 mmHg)>(b, 10^{-4} mmHg)=0. This signal is definitely attributable to stretching vibration of CO, which is adsorbed by the adsorbent.

The bands in the 1600—2050 cm^{-1} region are assignable to the vibrations for the MR type polystyrene backbone.

Effect of Molar Ratio of $AlCl_3$ to CuCl on CO Adsorbing Ability. The CO adsorbent, prepared as white beads from CuCl and the macroreticular type polystyrene resin in the absence of $AlCl_3$ using carbon

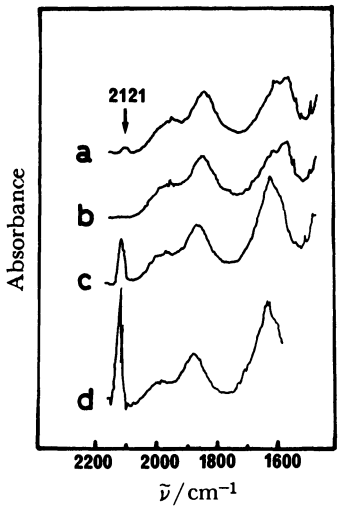

Fig. 7. Partial FT-IR spectra of the macroreticular type polystyrene-supported aluminium copper(I) chloride at various partial pressures of CO: Partial pressures of CO were 20 mmHg (a), 10^{-4} mmHg (b), 300 mmHg (c), and 760 mmHg (d); the spectra were measured in the order of a, b, c, and d.

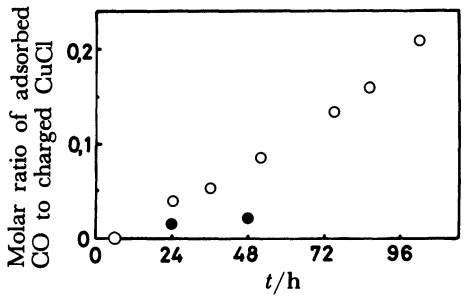

Fig. 8. Adsorption of carbon monoxide at room temperature under 1 atm by the macroreticular (MR) type polystyrene-supported copper(I) chloride prepared in the absence of aluminium chloride by use of carbon disulfide (○) or concentrated hydrochloric acid solution (●) as solvent: The adsorbents were prepared from 2.00 g (20.2 mmol) of CuCl and 2.58 g (23.7 mequiv in phenyl residue) of the MR type polystyrene, using 13 cm^3 of carbon disulfide and 40 cm^3 of concentrated hydrochloric acid solution, respectively, as solvents.

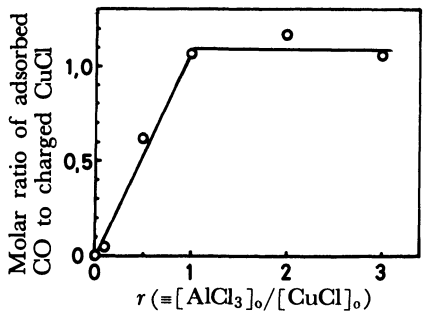

Fig. 9. Plot of the molar ratio of adsorbed carbon monoxide to the charged copper(I) chloride vs. the charged molar ratio (r) of AlCl$_3$ to CuCl for the macroreticular (MR) type polystyrene-supported AlCuCl$_4$: The adsorption at 25 °C under 1 atm for 60 min by the adsorbent prepared from the MR type polystyrene, AlCl$_3$, and CuCl using carbon disulfide; the charged molar ratio of phenyl residue in the polystyrene to CuCl was 1.2.

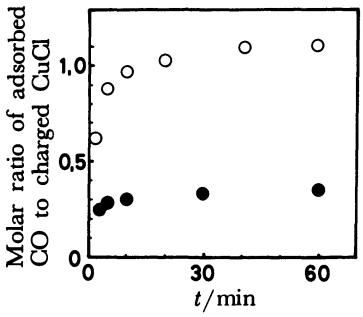

Fig. 10. Adsorption of carbon monoxide at 18 °C under 1 atm by the adsorbent prepared from the macroreticular (MR) type (DVB 20%) polystyrene, AlCl$_3$, and CuCl by use of dichloromethane as solvent: The first adsorption (○) and the second adsorption (●); the desorption of CO was carried out at 18 °C for 10 min under 7 mmHg after the first adsorption; the adsorbent was prepared from 2.47 g (18.5 mmol) of AlCl$_3$, 1.83 g (18.5 mmol) of CuCl, and 2.31 g (21.2 mequiv in phenyl residue) of the MR type polystyrene with the use of 10 cm^3 of dichloromethane.

disulfide (open circles) or concentrated hydrochloric acid (solid circles) as solvent, exhibited very small adsorbing ability (Fig. 8). The molar ratios of the CO adsorbed in 24 h to the charged CuCl were 0.04 and 0.02, respectively.

Figure 9 shows the plot of the molar ratio of the adsorbed CO to the charged CuCl as a function of the charged molar ratio (r) of AlCl$_3$ to CuCl for the adsorbents composed of AlCl$_3$, CuCl, and the macroreticular type polystyrene resin. Here, the charged amount of AlCl$_3$ is changed, keeping the amounts of CuCl and the polystyrene resin constant. The amount of adsorbed CO proportionally increases with increasing ratio r in the range of r value from 0.0 to 1.0. At the r value larger than 1.0, however, the amount is almost independent of r.

Adsorbing Abilities of CO Adsorbents Prepared from AlCl$_3$, CuCl, and Various Polystyrenes. Figure 10 depicts the adsorption of CO by the reddish brown adsorbent prepared from AlCl$_3$, CuCl, and the macroreticular (MR) type polystyrene by use of dichloromethane as solvent.

Yellowish brown beads were obtained as CO adsorbents, when AlCl$_3$, CuCl, and gel type polystyrene resins (divinylbenzene (DVB) contents; 1 and 12%) were refluxed in dichloromethane for 6 h and then the liquid phase was removed by evaporation. Figures 11 and 12 show the adsorptions of CO by these adsorbents. The adsorptions are much slower than that (Fig. 10) for the adsorbent prepared from the macroreticular (MR) type polystyrene resin as support.

Table 2. CO Adsorbing Capacities of Adsorbents Prepared from Various Types of Polystyrenes, $AlCl_3$, and CuCl[a)]

Polystyrene		Preparation solvent	Molar ratio of adsorbed CO to charged CuCl[b)]	
Type	DVB content / %		at 10 min	at 60 min
MR	20	Carbon disulfide	0.99	1.07
Gel	1		0.60	0.77
Gel	12		0.55	0.64
None	—		0.63	0.79
MR	20	Toluene	0.92	1.05
Gel	1		0.30	0.71
Gel	12		0.58	0.76
None	—		0.44	0.76
MR	20	Dichloromethane	0.97	1.11
Gel	1		0.52	0.64
Gel	12		0.51	0.63
Linear	0		0.02	0.02
None	—		0.66	0.78

a) Charged molar ratios of $AlCl_3$ and phenyl residue in polystyrene to CuCl are 1.0 and 1.2, respectively. b) The first adsorption of CO by a virgin adsorbent at room temperature under 1 atm.

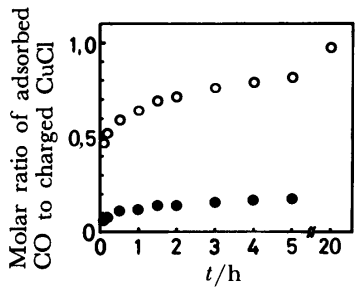

Fig. 11. Adsorption of carbon monoxide at 25°C under 1 atm by the adsorbent prepared from the gel type (DVB 1%) polystyrene, $AlCl_3$, and CuCl by use of dichloromethane as solvent: The first adsorption (○) and the second adsorption (●); the desorption of CO was carried out at 25°C for 10 min under 7 mmHg after the first adsorption; the adsorbent was prepared from 3.96 g (29.7 mmol) of $AlCl_3$, 2.94 g (29.7 mmol) of CuCl, and 3.71 g (35.5 mequiv in phenyl residue) of the gel type (DVB 1%) polystyrene with the use of 40 cm^3 of dichloromethane.

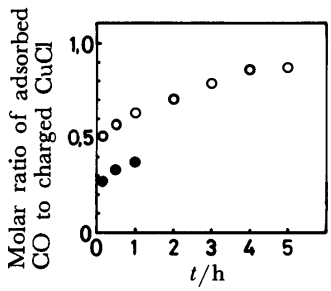

Fig. 12. Adsorption of carbon monoxide at 25°C under 1 atm by the adsorbent prepared from the gel type (DVB 12%) polystyrene, $AlCl_3$, and CuCl by use of dichloromethane as solvent: The first adsorption (○) and the second adsorption (●); the desorption of CO was carried out at 25°C for 10 min under 7 mmHg after the first adsorption; the adsorbent was prepared from 3.50 g (26.3 mmol) of $AlCl_3$, 2.60 g (26.3 mmol) of CuCl, and 3.28 g (30.9 mequiv in phenyl residue) of the gel type (DVB 12%) polystyrene with the use of 20 cm^3 of dichloromethane.

On the refluxing of linear polystyrene, $AlCl_3$, and CuCl in dichloromethane, dark orange precipitates were formed under a yellow solution after refluxing. On the evaporation of dichloromethane, dark yellow aggregates were produced. The aggregates, however, did not show measurable adsorption of CO.

When $AlCl_3$ and CuCl were refluxed in dichloromethane in the absence of polystyrene and the liquid phase was evaporated, solid of $AlCuCl_4$ was obtained as a dark yellowish green powder. The solid without polystyrene support showed only a slow adsorption of CO (Fig. 13).

Table 2 lists the molar ratios of the CO adsorbed in 10 and 60 min to the charged CuCl for the adsorbents prepared from various types of polystyrenes. All the molar ratios for the MR type polystyrene-supported $AlCuCl_4$, prepared by use of either carbon disulfide, toluene, or dichloromethane, are significantly larger than the corresponding values both for the adsorbents prepared from gel type polystyrenes or linear polystyrene and for the adsorbents prepared in the absence of polystyrene. The adsorptions by the MR type polystyrene-supported $AlCuCl_4$ are much faster than those by the other adsorbents. Here, the rates of adsorption are evaluated from the ratio of the value at 10 min to that at 60 min.

A film, prepared by evaporation of the solvent from a toluene solution of linear polystyrene-protected

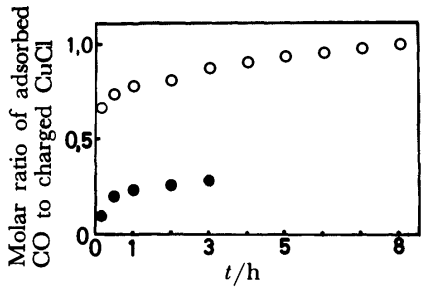

Fig. 13. Adsorption of carbon monoxide at 25 °C under 1 atm by the adsorbent prepared from $AlCl_3$ and CuCl in the absence of polystyrene by use of dichloromethane as solvent: The first adsorption (○) and the second adsorption (●); the desorption of CO was carried out at 25 °C for 10 min under 7 mmHg after the first adsorption; the adsorbent was prepared from 3.32 g (24.9 mmol) of $AlCl_3$ and 2.46 g (24.9 mmol) of CuCl with the use of 15 cm^3 of dichloromethane.

$AlCuCl_4$, did not adsorb CO.

Discussion

Preparation of CO Adsorbents. Carbon disulfide and dichloromethane are good solvents for macroreticular (MR) type polystyrene resin, whereas they are poor solvents for $AlCuCl_4$. When $AlCl_3$, CuCl, and the MR type polystyrene resin are refluxed in these solvents, the metal salts are effectively incorporated into the resin during refluxing. Thus, almost transparent liquid phase, which does not contain the metal salts any more, is obtained after refluxing, prior to evaporation of the liquid phase. $AlCuCl_4$ promptly penetrates into the polystyrene beads, since it favorably interacts with aromatic rings of the polystyrene due to formation of molecular complexes. $AlCuCl_4$ forms molecular complexes with various aromatic compounds such as benzene,[11,12] toluene,[12] and mesitylene.[12] The color of the adsorbents, reddish brown, is in accord with the position of the charge transfer absorption band (λ_{max}: 460 nm)[13] for the molecular complex between $AlCuCl_4$ and linear polystyrene in toluene solutions.

On the usage of toluene or benzene as preparation solvent, however, both the polystyrene beads and the solution part were colored after refluxing. Here, a considerable portion of the $AlCuCl_4$ remains in the liquid phase and only the rest penetrates into the polystyrene resin, since both toluene and benzene are quite good solvents for $AlCuCl_4$. On evaporation of the solvents, the $AlCuCl_4$ in the liquid phase deposits at the surface of the beads.

These arguments are confirmed by the results of a scanning electron microscopy and an energy dispersive X-ray microanalysis.[14,15] For the polystyrene-supported $AlCuCl_4$, prepared by use of carbon disulfide as solvent, $AlCuCl_4$ uniformly distributes in the beads of the adsorbent. For the polystyrene-supported $AlCuCl_4$ prepared with toluene, however, distribution of the double salt in the beads is not uniform and considerable amounts of $AlCuCl_4$ are located on the surface of the beads.

In the present adsorbents with the charged molar ratio unity of $AlCl_3$ to CuCl, most of the charged CuCl and $AlCl_3$ form a double salt $AlCuCl_4$. If only small part of the charged metal salts were forming $AlCuCl_4$ and large part were present as the single salts, the adsorbing capacity at the charged molar ratio 1.0 should be significantly smaller than the values at the charged molar ratios larger than 1.0, due to smaller amount of $AlCuCl_4$, the active species for adsorption (vide infra). Obviously, it is not the case (see Fig. 9).

Adsorption of CO. The plot of the adsorbing capacity vs. the charged molar ratio (r) of $AlCl_3$ to CuCl (Fig. 9), which involves linear increase of the capacity with increasing r below r=1 and virtually constant capacity irrespective of r above r=1, shows that the active component in the polystyrene-supported $AlCuCl_4$ is the double salt $AlCuCl_4$, composed of CuCl and $AlCl_3$ in a molar ratio 1:1. On the CO adsorption by the adsorbent, CO forms a complex with $AlCuCl_4$, where CO coordinates to the copper(I) ion.

Terminal coordination of CO to $AlCuCl_4$ in the polystyrene-supported $AlCuCl_4$ is supported by the fact that the frequency (2121 cm^{-1}) of the stretching vibration of the adsorbed CO (Fig. 7) is smaller than the value (2143 cm^{-1}) for free CO.[16] This decrease in frequency is mainly attributable to back donation from the copper(I) ion in $AlCuCl_4$ to the CO, which decreases bond order of the C–O bond. The frequency for the CO adsorbed by the present adsorbent is slightly smaller than the value (2135 cm^{-1}) for the CO absorbed by toluene solution of linear polystyrene-protected $AlCuCl_4$.[4]

Formation of a bridging CO from CO and two $AlCuCl_4$ molecules in the adsorbents is ruled out by the stretching frequency (2121 cm^{-1}) of the adsorbed CO. Bridging CO should exhibit stretching vibration mode around 1800 cm^{-1}.[16]

In the macroreticular (MR) type polystyrene-supported $AlCuCl_4$, high dispersion of $AlCuCl_4$ in the beads of the polystyrene, due to formation of molecular complexes of the double salt with the aromatic rings, promotes adsorption of CO. In the absence of $AlCl_3$, however, dispersion of CuCl in the polystyrene beads is not sufficient, resulting in an adsorbent with poor ability (Fig. 8). Furthermore, effective adsorption of CO by the MR type polystyrene-supported $AlCuCl_4$ is associated with decrease of electron density on the copper(I) ion by the formation of the double salt. The decrease of electron density enhances electron donation from CO to the copper(I) ion. On the complex formation of CO with $AlCuCl_4$, contribution of donation from CO to the copper(I) ion is larger than that of back donation from the ion to CO.[4]

The amounts (103—111 mol% with respect to the charged CuCl: Table 1) of CO adsorbed by the macro-

reticular type polystyrene-supported $AlCuCl_4$, prepared using benzene, toluene, carbon disulfide, or dichloromethane, are larger than the amount (85 mol%) of CO absorbed by toluene solution of linear polystyrene-protected $AlCuCl_4$.[4] This is ascribed to absence of competition between CO and toluene in the coordination to $AlCuCl_4$ for the solid adsorbents. In the CO absorption by the toluene solutions, CO coordinates to $AlCuCl_4$ by replacing a toluene molecule which originally coordinates to the $AlCuCl_4$.[12]

The macroreticular type polystyrene-supported $AlCuCl_4$ prepared using carbon disulfide adsorbs 67 cm^3 (standard temperature and pressure) of CO per 1 g of the adsorbent under 1 atm of CO at 25 °C. When the cycles involving adsorption of CO at 760 mmHg, 25 °C and desorption at 7 mmHg, 25 °C are repeated using the adsorbent, 34 cm^3 (standard temperature and pressure) of CO is separated for each of the cycles per 1 g of the adsorbent.

The order in the adsorbing capacities of various adsorbents, prepared from the macroreticular type cross-linked polystyrene, aluminium halides, and copper(I) halides, is as follows: $AlCl_3$–CuCl system > $AlBr_3$–CuBr system $\gg$ AlI_3–CuI system ≈ 0. This order is identical with that in the absorbing capacities for toluene solutions of linear polystyrene-protected aluminium copper(I) halide.[4]

Effect of Polystyrene Support on CO Adsorbing and Desorbing Abilities. Efficient adsorption and desorption of CO for the macroreticular (MR) type polystyrene-supported $AlCuCl_4$ (Figs. 2, 3, and 10 and Table 2) are attributable to the presence of macroporosity and microporosity in the MR type resin.[17] Through the porosities, $AlCuCl_4$ is effectively introduced into the polystyrene beads in preparation of the adsorbent. The porosities are also important for prompt diffusion of CO either to the metal salt on CO adsorption or from the metal salt on CO desorption. Furthermore, $AlCuCl_4$ is highly dispersed in the adsorbent due to large surface area (300 m^2/g) of the MR type polystyrene, providing sufficient contact of the double salt with CO.

These arguments are confirmed by quite slow adsorptions of the gel type polystyrene-supported $AlCuCl_4$ (Figs. 11 and 12). Here, $AlCuCl_4$ is poorly dispersed in the gel type polystyrene beads having so small surface area. CO can not promptly diffuse to the $AlCuCl_4$ in the adsorbent due to absence of porosity, since porosity of the gel type resin exists only in swollen states in good solvents.[17,18] Absence of porosity is also responsible for inefficient desorption of adsorbed CO.

Either the adsorbent, prepared from the linear polystyrene, $AlCl_3$, and CuCl or the film of linear polystyrene–$AlCuCl_4$ complex, prepared by evaporating toluene solution of linear polystyrene-protected $AlCuCl_4$,[3,4] which has no porosity, exhibits no measurable adsorbing capacity. The CO adsorption by $AlCuCl_4$ solid without polystyrene (Fig. 13) is much slower than that by the MR type polystyrene-supported $AlCuCl_4$ (Fig. 10).

In conclusion, usage of macroreticular type cross-linked polystyrene as support is essential for the preparation of CO adsorbents having large abilities both in adsorption and desorption.

The authors wish to express their thanks to Professor Makoto Misono and Dr. Toshio Okuhara at the University of Tokyo for their kind assistance in the FT-IR spectroscopy.

References

1) "New Syntheses with Carbon Monoxide," ed by J. Falbe, Springer-Verlag, Berlin (1980).
2) A. L. Kohl and F. C. Riesenfeld, "Gas Purification," 3rd ed, Gulf Publishing Co., Houston (1979).
3) H. Hirai, M. Komiyama, and S. Hara, *Makromol. Chem., Rapid Commun.*, **2**, 495 (1981).
4) H. Hirai, S. Hara, and M. Komiyama, *Bull. Chem. Soc. Jpn.*, **59**, 109 (1986).
5) D. J. Haase and D. G. Walker, *Chem. Eng. Prog.*, **70**, 74 (1974).
6) Y.-Y. Huang, *J. Catal.*, **30**, 187 (1973).
7) J. A. Rabo, J. N. Francis, and C. L. Angell, U. S. Patent, 4019879 (1977).
8) H. Hirai, M. Komiyama, and S. Hara, *Makromol. Chem., Rapid Commun.*, **3**, 95 (1982).
9) H. Hirai, S. Hara, and M. Komiyama, *Chem. Lett*, **1982**, 1685.
10) "Materials, Equipment and Systems for Chromatography Electrophoresis Immunochemistry and HPLC," Catalog G, Bio-Rad Laboratories Ltd. (1981), p. 28.
11) R. W. Turner and E. L. Amma, *J. Am. Chem. Soc.*, **88**, 1877 (1966).
12) H. Hirai, M. Nakamura, and M. Komiyama, *Bull. Chem. Soc. Jpn.*, **56**, 2519 (1983).
13) H. Hirai, K. Kanaka, and M. Komiyama, *Polymer Preprints Japan*, **34**, 484 (1985).
14) H. Hirai, S. Hara, and M. Komiyama, *Polymer Preprints, Japan*, **31**, 2013 (1982).
15) S. Hara, M. Komiyama, and H. Hirai, *Polymer Preprints, Japan*, **32**, 1807 (1983).
16) F. A. Cotton and G. Wilkinson, "Advanced Inorganic Chemistry," 4th ed, John Wiley and Sons, Inc., New York (1980), p. 85, 1072.
17) W. L. Sederel, G. J. Dejang, *J. Appl. Polymer Sci.*, **17**, 2815 (1973).
18) V. K. Sarin, S. B. H. Kent, and R. B. Merrifield, *J. Am. Chem. Soc.*, **102**, 5463 (1980).

 © 1986 The Chemical Society of Japan Bull. Chem. Soc. Jpn., 59, 1059—1065 (1986)

Study of Short Hydrogen Bonds. I. Structures of 4-Methylpiperidinium Hydrogen Bis(*p*-methylbenzoate) and Piperidinium Hydrogen Bis(*p*-methylbenzoate)

Shintaro MISAKI, Setsuo KASHINO,* and Masao HAISA
Department of Chemistry, Faculty of Science, Okayama University, Tsushima, Okayama 700
(Received October 17, 1985)

The crystal structures of 4-methylpiperidinium hydrogen bis(*p*-methylbenzoate) **1** and piperidinium hydrogen bis(*p*-methylbenzoate) **2** have been determined by X-ray diffraction method. Crystal data: **1**, monoclinic, $P2_1/n$ (No. 14), $a=19.260(2)$, $b=8.0061(5)$, $c=14.065(1)$ Å, $\beta=94.391(7)°$, $V=2162.5(3)$ Å^3, $Z=4$, $D_x=1.141$ g cm^{-3}; **2**, orthorhombic, *Pcan* (No. 60), $a=10.292(1)$, $b=25.248(4)$, $c=7.763(2)$ Å, $V=2017.2(5)$ Å^3, $Z=4$, $D_x=1.177$ g cm^{-3}. Final R values for **1** and **2** are 0.088 and 0.065 for 3446 and 1510 unique reflections, respectively. In both crystals the piperidinium cations and the hydrogen bis(benzoate) anions are held together by two kinds of N-H···O hydrogen bonds. The structure of **2** is disordered around a two-fold axis. Two benzoate residues in the anions are linked by the very short O-H···O hydrogen bonds; in **1** asymmetric [O···O 2.505(3), O-H 1.07(5), H···O 1.48(5) Å, O-H···O 158(5)°]; in **2** crystallographically symmetric [O···O related by the two-fold axis 2.473(4), O···H 1.25(5) Å, O···H···O 163(5)°]. The short hydrogen bonds in hydrogen bis(carboxylate) anions are discussed with reference to the crystal structures of **1** and **2**.

Very short hydrogen bonds with O···O distances between 2.4 and 2.5 Å are of interest in connection with the nature of hydrogen bonding.[1] In general, hydrogen bis(carboxylate) anions tend to form the very short hydrogen bonds in the crystals.[1-29] In many cases the anions have crystallographic symmetry $\bar{1}$ or 2,[1-19] but it is difficult to determine whether the hydrogen atoms participating in the hydrogen bonds are situated at the midpoint of the two oxygen atoms or not, because either ordered or disordered structure involving the hydrogen atoms makes possible to account for the observations. The genuine symmetry has been proposed for some crystallographically symmetric hydrogen bonds,[7,9,13] but the range of the O···O distances can not be differentiated from those found in crystallographically asymmetric hydrogen bonds. Therefore, it is desirable to examine more thoroughly the geometric details of the symmetric hydrogen bonds and the asymmetric ones. In the present work crystals of **1** and **2**, which contain the same anions but have different symmetry, have been studied.

Experimental

Experimental details for **1** and **2** are listed in Table 1. The compounds were prepared by the same procedure as reported previously.[30] Systematic absences were determined from the Weissenberg photographs. The intensities were collected on a Rigaku AFC-5 four-circle diffractometer equipped with rotating anode using Ni filtered Cu $K\alpha$ ($\lambda=1.5418$ Å) with ω—2θ scan method [scan speed 4° min^{-1} in ω, scan range $\Delta 2\theta=1.2°+0.15°\tan\theta$]. Background was measured for 4 s on either side of peak. Three standard reflections were recorded after every 57 reflections; their fluctuation was within 3% in F. Lorentz and polarization correction were applied,

Table 1. Crystal Data and Experimental Details

	1	**2**
Chemical formula	$C_6H_{14}N^+\cdot C_{16}H_{15}O_4^-$	$C_5H_{12}N^+\cdot C_{16}H_{15}O_4^-$
Formula weight	371.48	357.45
Mp(θ_m/°C)	95—98 decomposed	111—113 decomposed
Morphology	Prismatic **b**	Prismatic **c**
Solvent for crystallization	Toluene	Benzene
Space group	$P2_1/n$ (No. 14)	*Pcan* (No. 60)
Systematic absences	$h+l$ odd for $h0l$ k odd for $0k0$	l odd for $0kl$ h odd for $h0l$ $h+k$ odd for $hk0$
a/Å	19.260(2)	10.292(1)
b/Å	8.0061(5)	25.248(4)
c/Å	14.065(1)	7.763(2)
β/°	94.391(7)	
V/Å^3	2162.5(3)	2017.2(5)
Z	4	4
D_x/g cm^{-3}	1.141	1.177
$F(000)$	800	768
Size of specimen/mm	0.30×0.25×0.25	0.30×0.20×0.40
μ(Cu $K\alpha$)/mm^{-1}	0.59	0.62
$2\theta_{max}$/°	125	120
No. of unique reflections	3446	1510
No. of reflections with $\lvert F_o\rvert>1.0\sigma(F_o)$	3008	1387

but no absorption correction.

Structure Determination and Refinement

The structure of **1** was solved by *MULTAN* 78, and refined by block-diagonal least-squares method. All the unique reflections within $2\theta_{max}$ were used for the refinement. The value minimized was $\sum w(|F_o|-|F_c|)^2$, where $w=1/[\sigma(F_o)^2+0.0006|F_o|+0.0040|F_o|^2]$ for $|F_o|>0$, and $w=0.608$ for $|F_o|=0$. All the hydrogen atoms were located on a difference Fourier map. The non-hydrogen atoms were refined anisotropically and the hydrogen atoms isotropically. Correction for the secondary extinction was applied for the strongest 26 reflections according to the equation: $I_{corr}=I_o(1+gI_c)$, where $g=2.74\times10^{-5}$. Final R was 0.088 for 3446 unique reflections. In the final difference Fourier map $\Delta\rho_{max}$ and $\Delta\rho_{min}$ were +0.20 and −0.23 eÅ^{-3}, respectively.

For **2**, orientation and position of the anion were found from a three-dimensional Patterson map. The non-hydrogen atoms of the cation were found by successive application of Fourier and difference Fourier syntheses. Since the space group is *Pcan* and $Z=4$, a twist form having a two-fold symmetry was assumed for the cation at first. After refinement by block-diagonal least-squares method, a difference Fourier map showed some peaks in the region of the cation, which could not be explained as those of the hydrogen atoms. Thus, the conformation of the cation was changed to a chair form, and a disordered structure around a two-fold axis was assumed. All the hydrogen atoms were located on a difference Fourier map. Full-matrix least-squares calculations were performed, the N-C, C-C, and N-H lengths of the cation being restrained to 1.51, 1.53, and 1.00 Å, respectively. The positional parameters of the hydrogen atoms attached to the carbon atoms of the cation were fixed. The other hydrogen atoms were refined isotropically and the non-hydrogen atoms anisotropically using 1428 non-zero reflections. The $\sum w(|F_o|-|F_c|)^2$ was minimized, where $w=1/\sigma(F_o)^2$. The extinction correction was applied with $g=2.49\times10^{-5}$ for the strongest 12 reflections. Final R was 0.065 for 1510 unique reflections. The $\Delta\rho_{max}$ and $\Delta\rho_{min}$ were +0.23 and −0.30, respectively.

The atomic scattering factors were taken from International Tables for X-Ray Crystallography.[31] Programs used were *MULTAN* 78,[32] *RSSFR*-5,[33] *HBLS*-V,[34] *FMLS*,[34] modified version of *CRLS*,[35] *DAPH*,[34] *MOLCON*,[36] and *ORTEP*.[37] Computations were carried out at Okayama University Computer Center.

Results and Discussion

The final atomic parameters for **1** and **2** are listed in Table 2.[38] The thermal ellipsoids of the molecules are shown in Fig. 1 with numbering of the atoms, and the stereo views of the crystal structures in Fig. 2. Bond lengths and angles are listed in Table 3. The geometries of the hydrogen bonds are summarized in Table 4.

Crystal Structure. In the crystal of **1**, the O(10) and O(20) atoms of the hydrogen bis(carboxylate) anion are linked together by an asymmetric O-H···O hydrogen bond. The O(19) of the anion accepts two hydrogen bonds from N(21) and N(21^{ii}) to form a

Table 2. Final Atomic Parameters (Positional ×10^4) of the Non-Hydrogen Atoms with e.s.d.'s in Parentheses

	x	y	z	B_{eq}/Å^2		x	y	z	B_{eq}/Å^2
4-Methylpiperidinium hydrogen bis(p-methylbenzoate) (**1**)					C(23)	2064(2)	5107(5)	232(2)	7.4(2)
C(1)	4857(1)	5571(4)	2856(2)	5.6(1)	C(24)	1285(2)	5229(5)	270(3)	7.2(2)
C(2)	5386(1)	4970(5)	3501(2)	6.2(1)	C(25)	1112(2)	6519(5)	1019(3)	7.5(2)
C(3)	6024(1)	4594(6)	3173(3)	7.2(2)	C(26)	1481(2)	6145(5)	1972(2)	6.6(2)
C(4)	6164(2)	4808(6)	2242(3)	7.6(2)	C(27)	911(3)	5609(8)	−717(4)	12.0(3)
C(5)	5636(2)	5409(6)	1607(3)	8.0(2)					
C(6)	4986(2)	5779(5)	1920(3)	7.3(2)	Piperidinium hydrogen bis(*p*-methylbenzoate) (**2**)				
C(7)	4159(1)	5995(4)	3172(2)	5.5(1)	C(1)	1549(2)	1320.3(8)	2605(2)	4.67(9)
C(8)	6863(2)	4377(8)	1899(4)	10.9(3)	C(2)	2510(2)	1553.1(8)	3602(3)	5.4(1)
O(9)	3686(1)	6484(4)	2616(2)	7.9(1)	C(3)	2474(2)	2086.5(8)	3961(3)	5.8(1)
O(10)	4090(1)	5812(3)	4080(1)	6.1(1)	C(4)	1492(2)	2407.2(8)	3362(2)	5.5(1)
C(11)	1836(1)	4762(4)	5008(2)	5.3(1)	C(5)	525(2)	2174.5(9)	2372(3)	5.7(1)
C(12)	1809(2)	5608(5)	5854(2)	6.6(2)	C(6)	557(2)	1639.8(9)	1989(2)	5.3(1)
C(13)	1246(2)	5393(5)	6417(2)	7.3(2)	C(7)	1568(2)	745.7(9)	2182(3)	5.5(1)
C(14)	709(2)	4326(5)	6124(2)	6.5(2)	C(8)	1473(3)	2992.6(9)	3741(4)	7.8(1)
C(15)	741(2)	3501(5)	5267(2)	6.9(2)	O(9)	734(1)	550.7(6)	1237(2)	6.86(8)
C(16)	1295(2)	3706(5)	4707(2)	6.2(1)	O(10)	2503(1)	478.4(6)	2841(2)	7.34(9)
C(17)	2436(1)	5016(4)	4404(2)	5.2(1)	N(11)[a]	−1536(3)	−4(3)	1941(4)	6.2(2)
C(18)	97(2)	4068(6)	6724(3)	8.8(2)	C(12)[b]	−2194(3)	−500(1)	2589(4)	8.4(2)
O(19)	2443(1)	4267(3)	3616(1)	5.75(9)	C(13)[a]	−3635(5)	−509(2)	2103(8)	8.9(3)
O(20)	2914(1)	5991(3)	4721(2)	6.7(1)	C(14)[a]	−4236(4)	−12(14)	2899(20)	8.7(6)
N(21)	2241(1)	6020(3)	1902(2)	5.8(1)	C(15)[a]	−3563(5)	463(2)	2058(7)	7.7(3)
C(22)	2424(2)	4743(5)	1181(2)	6.5(2)	C(16)[b]	−2194(3)	500(1)	2411(4)	8.4(2)

a) Occupancy factor was assumed to be 0.5. b) C(12) and C(16) were related with each other by the two-fold axis, and the refinement was made as a single atom at the position of C(12).

Table 3. Bond Lengths (l/Å) and Bond Angles (ϕ/°) with e.s.d.'s in Parentheses

4-Methylpiperidinium hydrogen bis(*p*-methylbenzoate) (**1**)				C(1)-C(7)-O(10)	115.5(3)	C(22)-C(23)-C(24)	112.2(3)
C(1)-C(2)	1.397(5)	C(15)-C(16)	1.384(6)	O(9)-C(7)-O(10)	122.5(3)	C(23)-C(24)-C(25)	109.7(3)
C(2)-C(3)	1.378(6)	C(11)-C(16)	1.383(5)	C(16)-C(11)-C(12)	119.3(3)	C(24)-C(25)-C(26)	111.6(3)
C(3)-C(4)	1.368(6)	C(11)-C(17)	1.500(4)	C(11)-C(12)-C(13)	120.7(4)	N(21)-C(26)-C(25)	111.0(3)
C(4)-C(5)	1.387(6)	C(14)-C(18)	1.515(6)	C(12)-C(13)-C(14)	120.1(4)	C(23)-C(24)-C(27)	112.2(4)
C(5)-C(6)	1.390(6)	C(17)-O(19)	1.261(4)	C(13)-C(14)-C(15)	118.3(4)	C(25)-C(24)-C(27)	112.0(4)
C(1)-C(6)	1.368(5)	C(17)-O(20)	1.262(4)				
C(1)-C(7)	1.487(4)	N(21)-C(22)	1.501(5)	Piperidinium hydrogen bis(*p*-methylbenzoate) (**2**)			
C(4)-C(8)	1.505(8)	C(22)-C(23)	1.485(6)	C(1)-C(2)	1.387(3)	C(7)-O(9)	1.232(3)
C(7)-O(9)	1.219(4)	C(23)-C(24)	1.509(6)	C(2)-C(3)	1.376(3)	C(7)-O(10)	1.282(3)
C(7)-O(10)	1.302(4)	C(24)-C(25)	1.530(6)	C(3)-C(4)	1.376(3)	N(11)-C(12)	1.510(8)
C(11)-C(12)	1.374(5)	C(25)-C(26)	1.499(6)	C(4)-C(5)	1.388(3)	C(12)-C(13)	1.530(7)
C(12)-C(13)	1.401(6)	N(21)-C(26)	1.478(5)	C(5)-C(6)	1.383(3)	C(13)-C(14)	1.53(4)
C(13)-C(14)	1.380(6)	C(24)-C(27)	1.544(7)	C(1)-C(6)	1.386(3)	C(14)-C(15)	1.53(4)
C(14)-C(15)	1.380(6)			C(1)-C(7)	1.488(3)	C(15)-C(16)	1.438(6)
C(6)-C(1)-C(2)	119.3(3)	C(14)-C(15)-C(16)	121.9(4)	C(4)-C(8)	1.507(4)	N(11)-C(16)	1.487(8)
C(1)-C(2)-C(3)	118.8(4)	C(11)-C(16)-C(15)	119.6(4)	C(6)-C(1)-C(2)	118.1(2)	C(1)-C(7)-O(9)	120.8(2)
C(2)-C(3)-C(4)	122.6(4)	C(12)-C(11)-C(17)	120.4(3)	C(1)-C(2)-C(3)	120.6(2)	C(1)-C(7)-O(10)	115.8(2)
C(3)-C(4)-C(5)	118.1(4)	C(16)-C(11)-C(17)	120.3(3)	C(2)-C(3)-C(4)	121.8(2)	O(9)-C(7)-O(10)	123.4(2)
C(4)-C(5)-C(6)	120.2(4)	C(13)-C(14)-C(18)	121.0(4)	C(3)-C(4)-C(5)	117.7(2)	C(16)-N(11)-C(12)	115.1(5)
C(1)-C(6)-C(5)	120.9(4)	C(15)-C(14)-C(18)	120.7(4)	C(4)-C(5)-C(6)	121.0(2)	N(11)-C(12)-C(13)	111.4(4)
C(2)-C(1)-C(7)	121.0(3)	C(11)-C(17)-O(19)	119.6(3)	C(1)-C(6)-C(5)	120.8(2)	C(12)-C(13)-C(14)	106(2)
C(6)-C(1)-C(7)	119.6(3)	C(11)-C(17)-O(20)	117.2(3)	C(2)-C(1)-C(7)	121.8(2)	C(13)-C(14)-C(15)	107(2)
C(3)-C(4)-C(8)	121.7(4)	O(19)-C(17)-O(20)	123.2(3)	C(6)-C(1)-C(7)	120.1(2)	C(14)-C(15)-C(16)	114(2)
C(5)-C(4)-C(8)	120.2(4)	C(26)-N(21)-C(22)	112.1(3)	C(3)-C(4)-C(8)	121.4(2)	N(11)-C(16)-C(15)	110.1(4)
C(1)-C(7)-O(9)	122.0(3)	N(21)-C(22)-C(23)	110.9(3)	C(5)-C(4)-C(8)	120.9(2)		

Table 4. Geometries of Hydrogen Bonds in **1** and **2**[a] (l/Å, ϕ/°)

4-Methylpiperidinium hydrogen bis(*p*-methylbenzoate) (**1**)			Piperidinium hydrogen bis(*p*-methylbenzoate) (**2**)		
(I)	O(10)···O(20)	2.505(3)	(I)	O(10)···O(10^{ii})	2.473(4)
	O(10)-H(10)	1.07(5)		O(10)···H(10)	1.25(5)
	H(10)···O(20)	1.48(5)		O(10)···H(10)···O(10^{ii})	163(5)
	O(10)-H(10)···O(20)	158(5)			
(II)	N(21)···O(19)	2.791(4)	(II)	N(11)···O(9^{ii})	3.060(7)
	N(21)-H(21B)	1.13(4)		N(11)-H(11A)	1.00(6)
	H(21B)···O(19)	1.71(4)		H(11A)···O(9^{ii})	2.09(6)
	N(21)-H(21B)···O(19)	159(3)		N(11)-H(11A)···O(9^{ii})	162(5)
(III)	N(21^{ii})···O(19)	2.780(4)	(III)	N(11^{iv})···O(9)	2.945(7)
	N(21^{ii})-H($21A^{ii}$)	0.91(4)		N(11^{iv})-H($11B^{iv}$)	1.00(7)
	H($21A^{ii}$)···O(19)	1.88(4)		H($11B^{iv}$)···O(9)	2.19(7)
	N(21^{ii})-H($21A^{ii}$)···O(19)	174(4)		N(11^{iv})-H($11B^{iv}$)···O(9)	131(5)

a) Symmetry code: for **1**, (i) x, y, z; (ii) $1/2-x$, $-1/2+y$, $1/2-z$; for **2**, (i) x, y, z; (ii) x, $-y$, $1/2-z$; (iii) $-x$, y, $1/2+z$; (iv) $-x$, $-y$, $-z$.

ribbon along a two-fold screw axis. The ribbons related by a center of symmetry form a sheet along the [101] by van der Waals interactions. The sheets related by an n glide plane are stacked along the [10$\bar{1}$] to form the $P2_1/n$ structure. Crystals of many acid salts[9,21,22,24,28] with the asymmetric hydrogen bond adopt this space group.

The structure of **2** is disordered around a two-fold axis. This disordered structure adopts the same space group as potassium hydrogen bis(*p*-methoxybenzoate)[5] [*Pcan*, Z=4, a=7.05(7), b=35.77(10), c=6.16(6), O···O 2.48(2) Å]. The O···O distances in them are equal to within the experimental errors. The disordered structure may be split into two fundamental structures: types *A* and *B*, by eliminating the two-fold axis, resulting in two possible N-H···O hydrogen-bond systems as shown in Fig. 3. The center of symmetry is retained in the type *A*, while the c glide plane is retained in the type *B*. This means that the elimination of the two-fold axis gives rise to the descent of the space group to its maximal subgroups, $P2_1/a$ for the type *A* and $Pca2_1$ or $Pc2_1n$ for the type *B*. In both cases the environments of the O(9) and O(9^{ii}) are different. For the type *A*, the O(9) and O(9^{ii}) accept hydrogen bonds from N(11^{iv}) and N(11), respectively, in the different way. For the type *B*, only the O(9^{ii}) accepts two kinds of hydrogen bonds from N(11) and N(11^{iii}). Thus, the hydrogen bond O(10)···H(10)···O(10^{ii}) is not the "centered,"[1] but the disordered. In fact, though H(10) was found on the two-fold axis, the peak in the difference Fourier map was as low as 0.21 eÅ^{-3}. The O···O distance is significantly shorter than that in **1**, probably depending on their crystallographic symmetry, because the same trend is also seen in ammonium hydrogen bis(acetate)[6] [2.474(6) Å for $\bar{1}$, 2.517(4) Å for asymmetric] and in potassium hydrogen

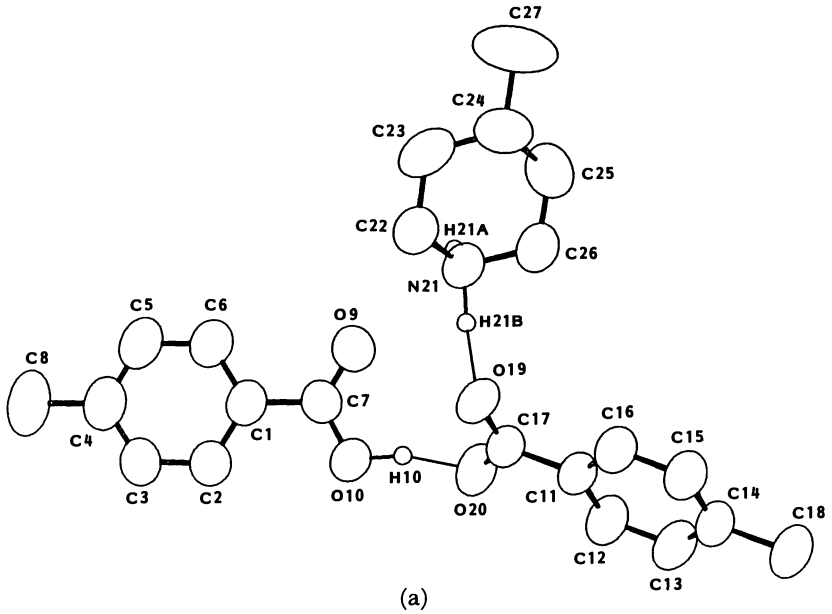

(a)

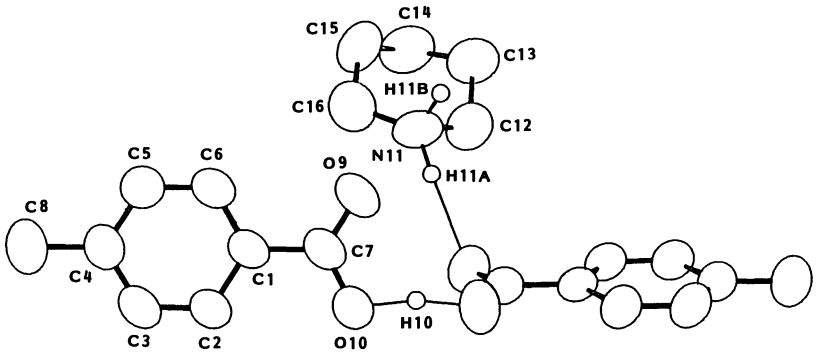

(b)

Fig. 1. Views of the molecules **1** (a) and **2** (b) with numbering of the atoms. The hydrogen atoms attached to the carbon atoms are omitted. Ellipsoids of 50% probability are used for the non-hydrogen atoms; the hydrogen atoms are represented as spheres equivalent to B=1.0 Å^2. The hydrogen bonds are shown by thin lines.

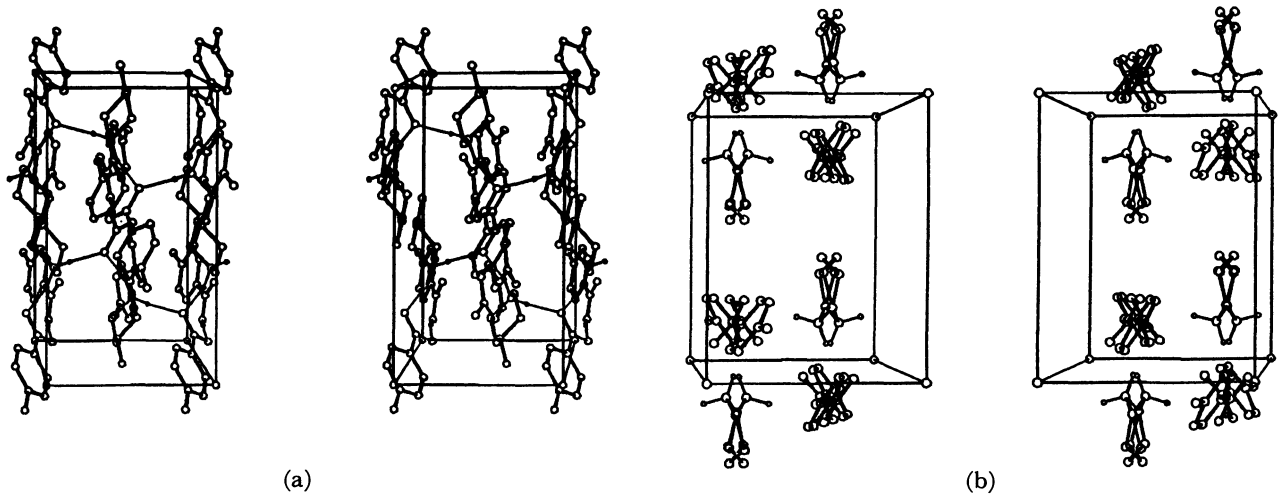

(a) (b)

Fig. 2. Stereo views of molecular packing. (a) For **1**, the **a** axis points onto the plane of the paper, the **b** axis left to right, and the **c** axis upwards. The hydrogen bonds are shown by thin lines. (b) The disordered structure for **2**. The **a** axis points upwards, the **b** axis onto the plane of the paper, and the **c** axis left to right. Only the molecular arrangement around the two-fold axes at y=0 is shown. See Fig. 3 for the hydrogen bonds.

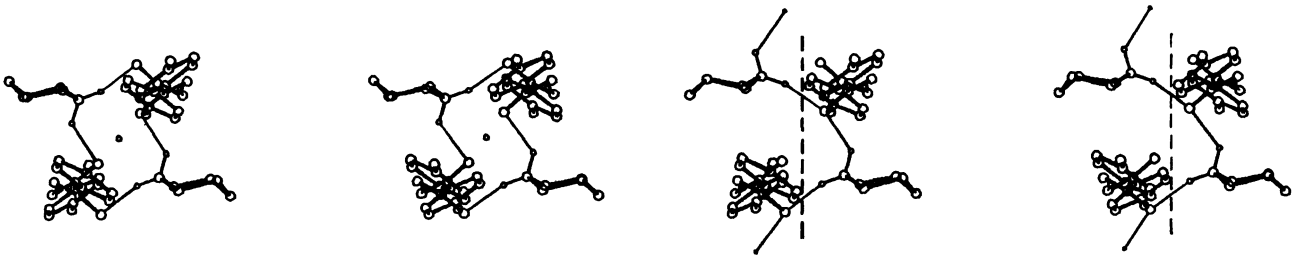

(a) (b)

Fig. 3. Two possible N-H···O hydrogen-bond systems in **2**. The hydrogen bonds are shown by thin lines. (a) Type *A* with the center of symmetry; (b) type *B* with the glide plane.

Table 5. The O···O Distances in Crystallographically Symmetric Hydrogen Bonds

Compound	Space group	Symmetry of anion	Radiation[a)]	O···O (*l*/Å)
$KH(C_6H_5COO)_2$[3)]	*C*2/*c*	$\bar{1}$	X	2.51(4)
$NH_4H[CH_2(COO)_2]$[12)]	*C*2/*c*	$\bar{1}$	X	2.488(3)
		2		2.476(3)
$KH(p\text{-}MeOC_6H_4COO)_2$[5)]	*Pbcn*	2	X	2.48(2)
$NaH(CH_3COO)_2$[11)]	*Ia*3	2	N	2.48(1)
$NH_4H(CH_3COO)_2$[6)]	$P\bar{1}$	$\bar{1}$	X	2.474(6)
$KH(CHOHCOO)_2$[13)]	$P\bar{1}$	$\bar{1}$	N	2.474(8)
				2.440(8)
$C_5H_{10}NH_2H(p\text{-}MeC_6H_4COO)_2$[b)]	*Pcan*	2	X	2.473(4)
$KHS(CH_3COO)_2$[15)]	*P*2/*c*	$\bar{1}$	X	2.47(1)
$RbHS(CH_3COO)_2$[15)]	*P*2/*c*	$\bar{1}$	X	2.46(2)
$KH(CCl_3COO)_2$[10)]	$I\bar{4}2d$	2	X	2.46(2)
$NH_4H(C_6H_5COO)_2$[16)]	*C*2/*c*	$\bar{1}$	X	2.46(1)
$KH(p\text{-}FC_6H_4COO)_2$[19)]	*C*2/*c*	$\bar{1}$	X	2.460(4)
$KH(p\text{-}HOC_6H_4COO)_2$[4)]	*P*2/*c*	$\bar{1}$	X	2.458(6)
$NH_4H(CCl_3COO)_2$[14)]	$I\bar{4}2d$	2	X	2.454(6)
$RbHO(CH_2COO)_2$[9)]	$I\bar{4}2d$	2	N	2.449(3)
$KH(CHBr_2COO)_2$[17)]	*Pbcn*	$\bar{1}$	X	2.44(3)
$KH(CF_3COO)_2$[7)]	*I*2/*a*	$\bar{1}$	N	2.437(4)
$KH(m\text{-}ClC_6H_4COO)_2$[8)]	*C*2/*c*	$\bar{1}$	X	2.437(6)
$RbH(CHBr_2COO)_2$[18)]	$P2_1/n$	$\bar{1}$	X	2.43(2)

a) X denotes X-Ray and N neutron. b) This work.

meso-tartrate[13)] [2.440(8) and 2.474(8) Å for $\bar{1}$, 2.521(5) Å for asymmetric].

Molecular Structure. For **1** the anion is composed of ionized and neutral residues. The C-O and C=O bond lengths of the neutral residue are close to those in some benzoic acids,[39,40)] which display no disorder in the carboxyl groups. The C(17)-O(19) bond in the ionized residue is longer than 1.22—1.25 Å found in acidic salts of alkaline metals in which the corresponding O atoms accept no hydrogen bond. The piperidinium ring takes a chair conformation as in piperidinium benzoates:[41,42)] N(21) and C(24) deviate by −0.644 and 0.661 Å from the plane through C(22), C(23), C(25), and C(26). The methyl group is equatorially bonded to the ring: the torsion angle C(22)-C(23)-C(24)-C(27)=180.0 (4)° and C(26)-C(25)-C(24)-C(27)=−179.6(4)°.

For **2** the bond lengths of C(7)-O(9) and C(7)-O(10) correspond to the average for the ionized and neutral residues because of disordering. The piperidinium ring takes a chair conformation as in **1**.

The Short Hydrogen Bonds of Hydrogen Bis(carboxylate) Anions. The O···O distances for crystallographically symmetric hydrogen bonds are listed in Table 5, where the H···O distances and the O···H···O angles are not given, because the hydrogen atom is assumed to lie on $\bar{1}$ or 2 in most of the structure analyses. The geometries of the hydrogen bonds for some asymmetric hydrogen bonds are shown in Table 6. It is seen from Tables 5 and 6 that (i) the intermolecular O···O distances range from 2.51 to 2.43 Å and 2.57 to 2.44 Å for the symmetric and asymmetric hydrogen bonds, respectively, (ii) the lower limit of the O···O distances is expected to be about 2.4 Å for both the symmetric and asymmetric bonds as shown for general O-H···O hydrogen bonds,[43)] and (iii) for the ionized residues the C(17)-O(20) bond participating in the hydrogen bond is longer than C(17)-O(19). The effects of a decrease in the O···O distance can be confirmed from Table 6: (i) the O-H distance is increased, while the H···O distance is decreased,[43,44)] (ii) the C(7)-O(10) length in the neutral residue is decreased while the C(7)=O(9) length is increased, and (iii) difference in the bond lengths of C(7)-O(10) and C(17)-O(20) is

Table 6. Geometries of Asymmetric Hydrogen Bonds[a] (l/Å, ϕ/°)

Compound	Space group	Radiation	O···O	O–H	H···O	O–H···O	C(7)=O(9)	C(7)–O(10)	C(17)–O(19)	C(17)–O(20)
(I)	$P\bar{1}$	N(295K)	2.571(1)	1.036(1)	1.537(1)	176.2(1)	1.210(1)	1.307(1)	1.245(1)	1.249(1)
		N(120K)	2.566(2)	1.036(2)	1.531(2)	176.8(2)	1.215(1)	1.308(1)	1.247(1)	1.253(1)
(II)	$P2_1/n$	X	2.563(2)	0.97(3)	1.61(3)	167(3)	1.203(2)	1.304(2)	1.237(2)	1.260(2)
(III)	$P\bar{1}$	N	2.521(5)	1.019(8)	1.514(8)	168.7(7)	1.206(5)	1.315(5)	1.256(5)	1.260(5)
(IV)	$P2_1/n$	X	2.505(3)	1.07(5)	1.48(5)	158(5)	1.219(4)	1.302(4)	1.261(4)	1.262(4)
(V)	$P2_1/c$	N	2.498(3)	1.107(4)	1.392(4)	177.6(3)	1.207(2)	1.291(2)	1.226(3)	1.275(3)
(VI)	$P2_1/c$	X	2.486(2)	1.04(3)	1.47(3)	166(3)	1.233(2)	1.290(2)	1.231(2)	1.289(2)
(VII)	Cc	X	2.482(2)	1.25(2)	1.31(2)	152(2)	1.220(2)	1.297(2)	1.219(2)	1.280(2)
(VIII)	$P2_1/c$	N	2.476(2)	1.152(3)	1.328(3)	174.2(3)	1.221(2)	1.294(2)	1.230(2)	1.275(2)
(IX)	$P2_1/c$	X	2.462(3)	1.01(5)	1.47(5)	165(5)	1.223(4)	1.286(4)	1.235(4)	1.277(4)
(X)	$I2/c$	X	2.450(2)	1.13(3)	1.33(3)	171(3)	1.226(2)	1.285(2)	1.217(2)	1.290(2)
(XI)	$Pbca$	N(295K)	2.444(2)	1.163(3)	1.281(3)	179.4(3)	1.217(1)	1.260(2)	1.229(1)	1.260(2)
		N(120K)	2.437(1)	1.167(1)	1.270(1)	179.3(1)	1.226(1)	1.276(1)	1.235(1)	1.276(1)

a) The numbering of the atoms corresponds to that of **1**. (I) $NaHC_2O_4 \cdot H_2O$.[23,29] (II) $LiHO(CH_2COO)_2$.[22] (III) $KH(CHOHCOO)_2$.[13] (IV) $CH_3C_5H_9\,NH_2H(p\text{-}MeC_6H_4COO)_2$ (This work). (V) $KH(CHCl_2COO)_2$.[24] (VI) $LiH[C_4H_8(COO)_2]$.[28] (VII) $KH(OOCCH_2CHOHCOO) \cdot H_2O$[26] (VIII) $KHO(CH_2COO)_2$.[9] (IX) $NaHO(CH_2COO)_2$.[21] (X) $NH_4HO(CH_2COO)_2$.[25] (XI) $KH(HCOO)_2$.[27]

decreased, as for the lengths of C(7)–O(9) and C(17)–O(19). These tendencies show that with a decrease in the O···O distance, the hydrogen atom comes closer to the midpoint.[43,44] However, the "asymmetric-centered"[1] hydrogen bond has never been reported. Even at the O···O distance of 2.388(4) Å the intramolecular hydrogen bond in lithium hydrogen phthalate is the "asymmetric-noncentered."[45] Thus, the bond symmetry should be introduced by a crystallographic symmetry.[46]

For the symmetric hydrogen bonds in the compounds with alkaline metals as cations, it has been impossible to distinguish the disordered symmetry from genuine one by diffraction methods, but the present study of **2** with the piperidinium cation makes it possible to conclude that the hydrogen bond in the crystals of **2** is disordered and still not the "symmetric-centered."[1]

The authors thank the Crystallographic Research Center, Institute for Protein Research, Osaka University, for the use of the diffractometer.

References

1) I. Olovsson and P.-G. Jönsson, "X-Ray and Neutron Diffraction Studies of Hydrogen Bonded Systems," in "The Hydrogen Bond, Recent Developments in Theory and Experiments," ed by P. Schuster, G. Zundel, and C. Sandorfy, North-Holland, Amsterdam, New York, Oxford (1976). Vol. II, Part B, Chap. 8, pp. 426—433.

2) J. C. Speakman, *Nature (London)*, **162**, 695 (1948).

3) J. M. Skinner, G. M. D. Stewart, and J. C. Speakman, *J. Chem. Soc.*, **1954**, 180.

4) L. Manojlović, *Acta Crystallogr., Sect. B*, **24**, 326 (1968).

5) D. R. McGregor and J. C. Speakman, *J. Chem. Soc. (A)*, **1968**, 2106.

6) I. Nahringbauer, *Acta Chem. Scand.*, **23**, 1653 (1969).

7) A. L. Macdonald, J. C. Speakman, and D. Hadži, *J. Chem. Soc., Perkin Trans. 2*, **1972**, 825.

8) A. L. Macdonald and J. C. Speakman, *J. Chem. Soc., Perkin Trans. 2*, **1972**, 1564.

9) J. Albertsson and I. Grenthe, *Acta Crystallogr., Sect. B*, **29**, 2751 (1973).

10) L. Golič and F. Lazarini, *Cryst. Struct. Commun.*, **3**, 645 (1974).

11) M. J. Barrow, M. Currie, K. W. Muir, J. C. Speakman, and D. N. J. White, *J. Chem. Soc., Perkin Trans. 2*, **1975**, 15.

12) G. Chapuis, A. Zalkin, and D. H. Templeton, *J. Chem. Phys.*, **62**, 4919 (1975).

13) M. Currie, J. C. Speakman, J. A. Kanters, and J. Kroon, *J. Chem. Soc., Perkin Trans. 2*, **1975**, 1549.

14) L. Golič and F. Lazarini, *Cryst. Struct. Commun.*, **4**, 487 (1975).

15) H. Herbertsson, *Acta Crystallogr., Sect. B*, **32**, 3107 (1976).

16) I. A. Oxton, T. S. Cameron, O. Knop, and A. W. McCulloch, *Can. J. Chem.*, **55**, 3831 (1977).

17) J. Baran, V. Videnova, T. Glowiak, and H. Ratajczak, *Acta Crystallogr., Sect. B*, **35**, 2722 (1979).

18) V. Videnova, J. Baran, T. Glowiak, and Ratajczak, *Acta Crystallogr., Sect. B*, **36**, 459 (1980).

19) J. Longo and M. F. Richardson, *Acta Crystallogr., Sect. B*, **38**, 2482 (1982).

20) M. Currie, *J. Chem. Soc., Perkin Trans. 2*, **1972**, 832.

21) J. Albertsson, I. Grenthe, and H. Herbertsson, *Acta Crystallogr., Sect. B*, **29**, 1855 (1973).

22) H. Herbertsson, *Acta Crystallogr., Sect. B*, **32**, 2381 (1976).

23) R. Tellgren, J. O. Thomas, and I. Olovsson, *Acta Crystallogr., Sect. B*, **33**, 3500 (1977).

24) D. Hadži, I. Leban, B. Orel, M. Iwata, and J. M. Williams, *J. Cryst. Mol. Struct.*, **9**, 117 (1979).

25) H. Herbertsson and B. Hedman, *Acta Crystallogr., Sect. B*, **38**, 320 (1982).

26) H. J. Geise, J. F. J. Van Loock, and A. T. H. Lenstra, *Acta Crystallogr., Sect. C*, **39**, 69 (1983).

27) K. Hermansson, R. Tellgren, and M. S. Lehmann, *Acta Crystallogr., Sect. C*, **39**, 1507 (1983).

28) X. He and B. M. Craven, *Acta Crystallogr., Sect. C*, **40**, 1157 (1984).

29) R. G. Delaplane, R. Tellgren, and I. Olovsson, *Acta Crystallogr., Sect. C*, **40**, 1800 (1984).
30) S. Kashino, K. Kanei, and S. Hasegawa, *Bull. Chem. Soc. Jpn.*, **45**, 1247 (1972).
31) "International Tables for X-Ray Crystallography," Kynoch Press, Birmingham (1974), Vol. IV, pp. 72—98.
32) P. Main, S. E. Hull, L. Lessinger, G. Germain, J.-P. Declercq, and M. M. Woolfson, "*MULTAN* 78, A System of Computer Programs for the Automatic Solution of Crystal Structures from X-Ray Diffraction Data," Univs. of York, England, and Louvain, Belgium (1978).
33) T. Sakurai, "*RSSFR*-5. The Universal Crystallographic Computing System (I)," The Crystallographic Society of Japan (1967).
34) T. Ashida, "*HBLS*-V, *FMLS* and *DAPH*. The Universal Crystallographic Computing System-Osaka," The Computation Center, Osaka Univ. (1973).
35) F. Takusagawa, "*CRLS*. Technical Report, ICR-1982-0001-0002-001," The Institute for Cancer Research, Philadelphia (1982).
36) S. Fujii, "*MOLCON*, The Universal Crystallographic Computing System-Osaka," The Computation Center, Osaka Univ. (1979).
37) C. K. Johnson, "*ORTEP*. Report ORNL-3794," Oak Ridge National Laboratory, Tennessee (1965).
38) Tables of anisotropic thermal parameters, atomic parameters for hydrogen atoms, bond lengths and angles involving hydrogen atoms, and structure factors have been deposited as Document No. 8625 at the Office of the Chemical Society of Japan.
39) K. Ohkura, S. Kashino, and M. Haisa, *Bull. Chem. Soc. Jpn.*, **45**, 2651 (1972).
40) M. Colapietro and A. Domenicano, *Acta Crystallogr., Sect. B*, **33**, 2240 (1977).
41) S. Kashino, Y. Sumida, and M. Haisa, *Acta Crystallogr., Sect. B*, **28**, 1374 (1972).
42) S. Kashino, *Acta Crystallogr., Sect. B*, **29**, 1836 (1973).
43) M. Ichikawa, *Acta Crystallogr., Sect. B*, **34**, 2074 (1978).
44) W. Joswig and H. Fuess, *Acta Crystallogr., Sect. B*, **38**, 2798 (1982).
45) H. Küppers, Å. Kvick, and I. Olovsson, *Acta Crystallogr., Sect. B*, **37**, 1203 (1981).
46) M. Catti and G. Ferraris, *Acta Crystallogr., Sect. B*, **32**, 2754 (1976).

 © 1986 The Chemical Society of Japan Bull. Chem. Soc. Jpn., 59, 1067—1071 (1986)

Electronic Properties of Black Phosphorus Single Crystals and Intercalation Compounds

Yusei MARUYAMA,* Setsuko SUZUKI,† Tomoko OSAKI,† Hizuru YAMAGUCHI,† Sumiko SAKAI,† Kyoko NAGASATO,† and Ichimin SHIROTANI††
Institute for Molecular Science, Myodaiji, Okazaki 444
†Department of Chemistry, Ochanomizu University, Otsuka, Bunkyo-ku, Tokyo 112
††Applied Science for Energy, Muroran Institute of Technology, Mizumoto, Muroran 050
(Received October 17, 1985)

Actual procedures for the preparation of black phosphorus single crystals by a bismuth flux method have been explored and the details are described. The anisotropy and the temperature dependence of the electrical conductivity and the Raman scattering spectra of the crystals obtained by the above-method have been measured. The reflection spectra of crystals which were prepared by a high pressure technique have also been observed and compared with the calculated data. Several preliminary attempts for synthesizing black phosphorus intercalation compounds have been carried out for the first time. Evidence for the intercalation by an X-ray analysis is presented.

Some interesting properties of black phosphorus (BP) single crystals have been extensively explored after the recent success of single-crystal preparation.[1,2] During the first stage of the present study, we started to prepare BP single crystals by the bismuth flux method and measured the electrical and optical properties of these crystals.[1] After that, Shirotani succeeded in the preparation of larger BP crystals by the use of the melt-growth technique under high pressure.[2] Narita's group followed and developed the Shirotani's method,[3] and has revealed the fundamental quantities regarding charge-carrier transport (such as Hall mobilities and effective masses) and structural and transport behaviors under the high pressure of a large BP single crystal.[4,5] It is easier to handle a large crystal; thus, the successful preparation of such large crystals has motivated further studies of BP crystals. Large crystals have showed, not only qualitatively but also quantitatively in some cases, similar behaviors to small crystals prepared by the bismuth flux method. However, some details regarding the properties of these two kinds of the crystals, e.g. temperature-dependence details of the electrical conductivities or the crystal qualities, might not necessarily coincide with each other.

BP is one modification of the phosphorus polymorphs and the BP phase was discovered by Bridgman under high pressure.[6] Some electrical and optical properties of polycrystalline BP were studied by Keys[7] and Warschauer[8] and the crystal structure was reported by Brown and Rundqvist.[9] It crystallizes in orthorhombic form and takes on an infinite puckered-layer structure in which every layer overlaps the next layer and is shifted by a/2 units (Fig. 1).

Crystalline BP is known to undergo phase transitions from the orthorhombic form (semiconducting) to the rhombohedral form (semi-metallic) at ≈60 kbar and, finally, to the simple cubic form (metallic) at ≈110 kbar,[10] in which superconductivity (T_c=6 K) was observed.[11,12] Very recently, a more precise measurement of the pressure dependence of electrical properties revealed that a semiconductor-to-semimetal transition occurs at 17 kbar,[13] and T_c for superconduction increases up to 13 K at 300 Kbar for quenched samples.[14]

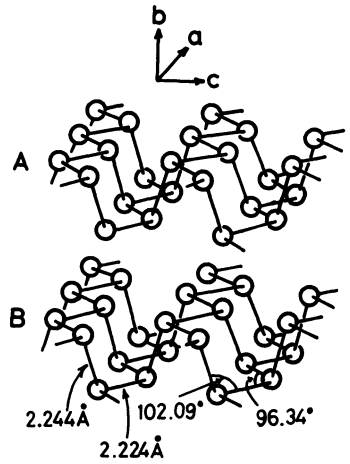

Fig. 1. Layer structure of black phosphorus crystal. B layer is shifted by 1/2 unit along the a axis relative to A layer.

Moreover, electrical transport properties of BP single crystals, such as the temperature dependence of the conductivities, magnetoresistance,[1] charge-carrier mobilities by Hall effect,[4] effective masses by cyclotron resonance method,[5] and 2-dimensional Anderson localization at low temperature[15] have been reported. The elaborate theoretical calculations for the electron band structure,[16] and the frequencies and the dispersion relations of the phonon modes[17] of BP have been carried out by Morita et al.

In this paper, we report on the actual procedures for single-crystal preparation by the bismuth flux method, the anisotropic properties in the electrical conductivities, and the optical reflection spectra and microscope Raman spectra of BP single crystals. Preliminary results of attempts to synthesize the intercalation compounds of BP are also described.

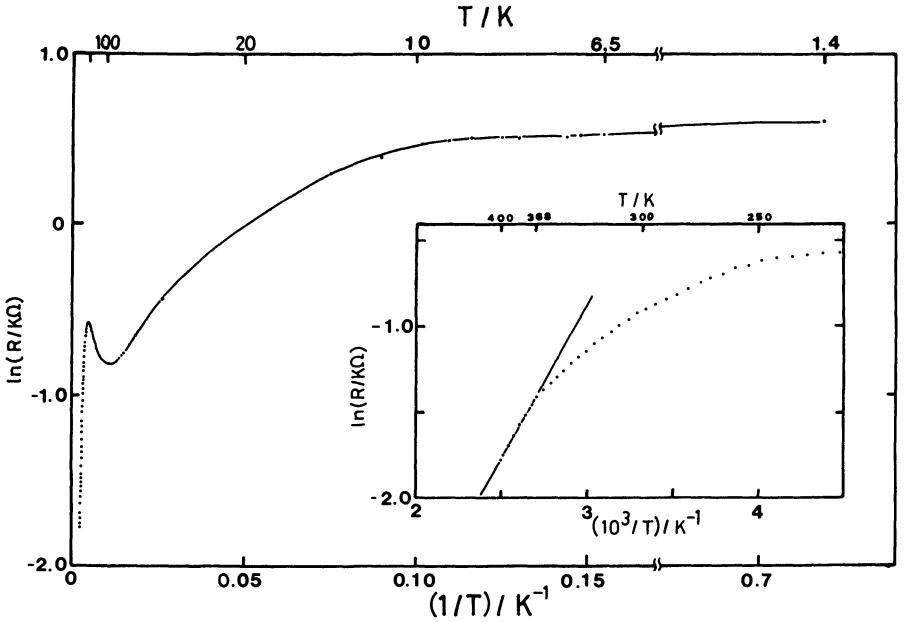

Fig. 2. Temperature dependence of the electrical resistance (a-direction) of a black phosphorus single crystal prepared by the bismuth flux method.

Experimental

In the course of this experiment, we used two kinds of single crystals; one was grown in melted bismuth[1] and the other was melt-grown under high pressure.[2] The former was obtained in rather thin rod or needle form, 10X0.2X0.05 mm^3 and the latter was in a block form, the size of which was determined by the size of the high-pressure cell. The typical size of the latter single crystal was 5X5X0.5 mm^3.

The details of the preparation procedure from bismuth solution are as follows : Amorphous or polycrystalline BP, 0.25 g, obtained by the conversion of red phosphorus under high pressure, was mixed with high-purity bismuth (37 g) in a Pyrex tube filled with 1/2 atm helium gas (atomic ratio of Bi to P is ≈22). It was kept at 400 °C for 44 h and then gradually cooled to room temperature at the rate of 0.2 °C min^{-1}. The crystals, obtained as a residue after dissolving the bismuth matrix with 30% nitric acid, were generally needle shaped with the needle axis coincident with the crystallographic a-axis. Even in melt-grown crystals, such a crystal habit is often recognizable on the cleaved ac-plane. One can determine the a- and c-axes of a crystal by carefully observing the fine stripes near the edges of the surface. Purified white phosphorus was also used as a starting material instead of BP powder.

We measured the anisotropy of the electrical conductivities for the thin rod crystals. Silver paste was used as electrodes. For the measurement along the a-axis only a four-probe method could be applied. The anisotropy of the melt-grown crystals has already been reported by Shirotani,[2] and Akahama et al.[4]

Polarized reflection spectra of a melt-grown crystal were observed in the 400—2000 nm wavelength region using an OLYMPUS MMSP microscope reflectophotometer. Polarized Raman spectra were also observed using the High-Resolution Microscope Raman Scattering Measuring System of Prof. Tominaga's laboratory in Ochanomizu University. The 5145 Å line of an Ar^+ laser (NEC GLG 3200) was used as the exciting light.

As an attempt to chemically modify the BP, intercalations with cesium, lithium, and iodine were tried. In the case of cesium or iodine, a vapor-phase reaction was carried out. The electrolytic method was employed for lithium intercalation. The cathode and anode were a BP crystal and lithium metal, respectively, and a 0.2 mol l^{-1} THF solution of $LiClO_4$ was used for the electrolyte. Electrolysis was carried out under an argon atmosphere in a dry box. Intercalated specimens were directly transferred to a measurement vessel (a cryostat) without being exposed to air.

Thin-rod crystals which were reacted with cesium vapor were analyzed using an X-ray diffraction oscillation camera method. Weak but definitely new spots were recognized and ascribed to a change of the lattice constant for the interlayer direction, b.

Results and Discussion

1. Electrical Conduction. The temperature dependence of the electrical resistance in the a-direction is shown in Fig. 2. The overall behavior of the curve was just like a typical impurity semiconductor[18] and the intrinsic band gap was estimated to be 0.34 eV from the slope of plots of ln R vs. $1/T$ in the high-temperature region (see the inset of Fig. 2).

The anisotropy of electrical conductivities at room temperature is shown in Table 1 for our thin-rod crystals and large melt-grown crystals under high pressure. The large anisotropy between the a- and b-directions (which was observed for our crystals) could not be found for the crystals of Narita's group. They have measured Hall mobilities and effective masses (Table 1). Morita et al. recently showed that the anomalous relationships in the anisotropies of the mobilities and the effective masses along the a- and b-axes, which

Table 1. Anisotropy in the Electrical Properties (Holes)

Crystal axes	a	b	c
Conductivities/S cm^{-1}	0.2×0.1	10^{-3}—10^{-2}	1×0.5[a]
	0.7	0.4	2.5[b]
	10	10^{-3}—10^{-2}	1[c]
Hall mobilities/cm^2 v^{-1} s^{-1} (200K)	1300	540	3300[b]
Relative effective masses, m/m_0 (observed)	0.66	0.28	0.075[d]
Relative effective masses, m/m_0 (calculated)	0.81	0.36	0.09[e]

a) This study. b) Ref. 4. c) Ref. 2. d) Ref. 5. e) Ref. 16.

had not been well understood, could be explained by a theoretical calculation involving an electron-phonon interaction in the regime of a deformation potential model.[19] However, the large difference in the conductivities along the b axis (interlayer direction, see Fig. 1) between our crystals and the crystals of Narita's group has not yet been elucidated. The possible interpretations are defect effects, interlayer misfits, difficulties to obtain proper electrode contacts, and so on. Anyhow, the reliability of the observed values in the interlayer direction may be lower than other directions because of the inapplicability of the four-probe method to measurements in this direction. The needle-like crystals prepared by the bismuth flux method has a two-dimensional Anderson localization character at low temperature, as reported by Iwasaki et al.[15] On the contrary, the temperature dependence of the a-axis conductivity of a Narita crystal does not fit a logarithmic temperature dependence in the corresponding temperature region (below 10 K) which should be observed in the two-dimensional Anderson localization regime.

2. Reflection Spectra. Polarized reflection spectra were measured for a cleaved flake of a melt-grown crystal. The observed results are shown in Fig. 3 and are compared with the calculated curves by Asahina and Morita.[20] The absolute values of the reflectances do not coincide with each other, but the overall qualitative features correspond well, except for the low-energy region of the a-polarized reflectance. According to Asahina and Morita,[20] an optical transition around this region may occur through the effect of an interlayer interaction. Thus, the rising reflectance in this region might be caused by a phonon-assisted indirect transition. We measured the temperature dependence of the reflectance down to 40 K and revealed that an enhancement with temperature is more significant in the a-polarized spectra than in the c-polarized spectra (Fig. 4).

3. Raman Spectra. A microscope Raman-scattering technique was applied for the thin-rod crystals in order to detect Raman-active lattice phonons of BP. The obtained results are almost coincident with those reported by Sugai et al.[21] The 442 cm^{-1} band was

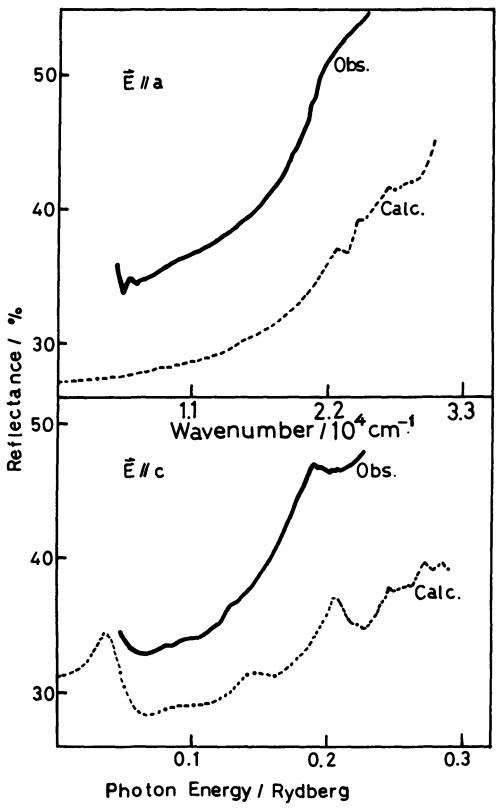

Fig. 3. Polarized reflectances of the ac plane of a black phosphorus single crystal.

assigned to the B_{2g} mode by Sugai et al,[21] however, recent calculations have shown that there could be two closely located bands, 439 and 441 cm^{-1}. They should be assigned to B_{2g} and B_{3g}, respectively.[17] These two bands could not be separated in our experiment since the microscope optical path reduced the polarization of the scattered light. The origin of the lower band (below 100 cm^{-1}) has not yet been determined.

4. Intercalation Compounds. A single crystal obtained by the bismuth flux method was set in a very thin glass capillary and fully exposed to a cesium vapor at 150°C for 14 d. In the photographs taken by an X-ray diffraction oscillation camera, the weak spots which correspond neither to BP nor cesium metal were

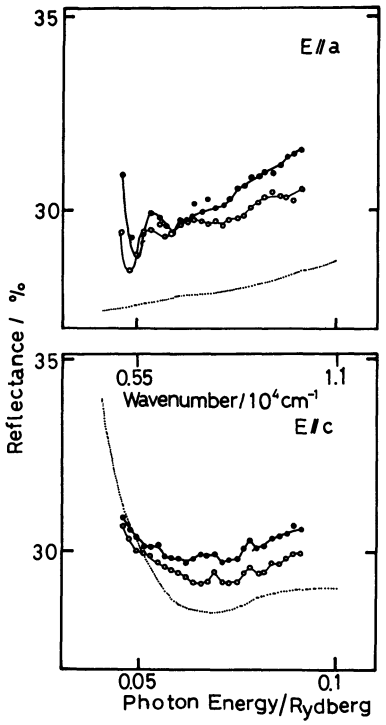

Fig. 4. Temperature dependence of the polarized reflectances.
●: At room temperature, O: at 40 K, ····: calculated spectra.

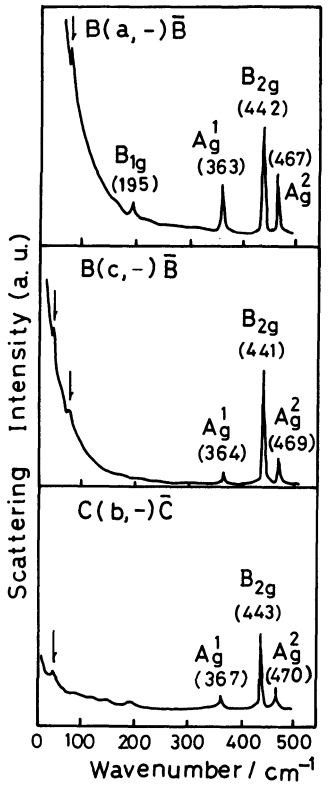

Fig. 5. Raman spectra of a black phosphorus single crystal.

recognized. The cesium vapor was introduced mostly through the cross section of one end of the crystal.

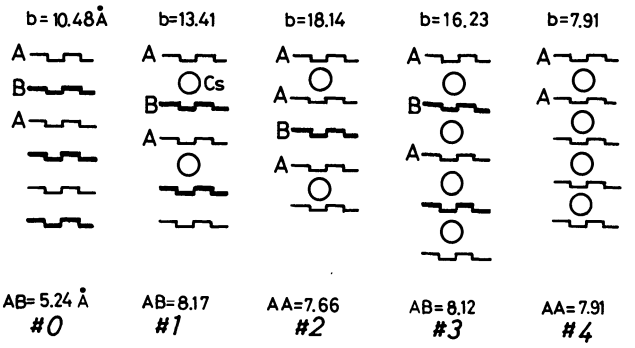

Fig. 6. Possible intercalated structures of various stages for Cs-black phosphorus.

Cesium diffusion was so slow that the other end of the crystal was still unchanged after a long exposure to cesium vapor (until the front end changed to an amorphous structure by the complete reaction). Successive X-ray analyses of the crystal (from one end to the other) revealed corresponding layer structures (illustrated in Fig. 6).

The alternately piled up structure (AB type) of a genuine BP crystal (#0) is transformed to a simple overlap structure (AA type) by the highest degree introduction of cesium atoms (or ions) (#4) similar to the first-stage structure (AA type) of graphite intercalation compounds. Other possible structures are also shown in this figure. In the next rank of an intercalation (#3), an AB-type piling is retained, even after a full intercalation of cesium. The interlayer spacing is a little larger than the AA type. In this experiment, four different b-lattice constants were identified in one piece of crystal together with the original b-axis length of a BP crystal.

Further investigations regarding homogeneous intercalation are now being undertaken. The effect of a cesium intercalation on the electrical conductivity of BP was also examined. The best reaction conditions have not yet been established for a cesium intercalation; therefore, we only present typical examples in Fig. 7. The reaction proceeded under the homogeneous heating of a sample tube in which cesium metal and a BP crystal were present. In the case of Fig. 7 (a), the reaction started at the upper-right (point A). With a raising temperature, the resistance decreased remarkably. It should be noted that both the effect of the reaction and the intrinsic change in the BP resistance due to heating are involved in this process.

On the other hand, the process from B to C corresponds to the intrinsic temperature dependence of the resistance of the cesium-intercalated BP crystal. The sample resistance showed almost no change within this temperature range (C–B). This means that this compound has almost a metallic character. However, only two samples showed this type behavior during several attempts. Another example is shown in Fig. 7 (b). In this case, the net change due to a cesium reaction was rather small. The conditions for obtaining a

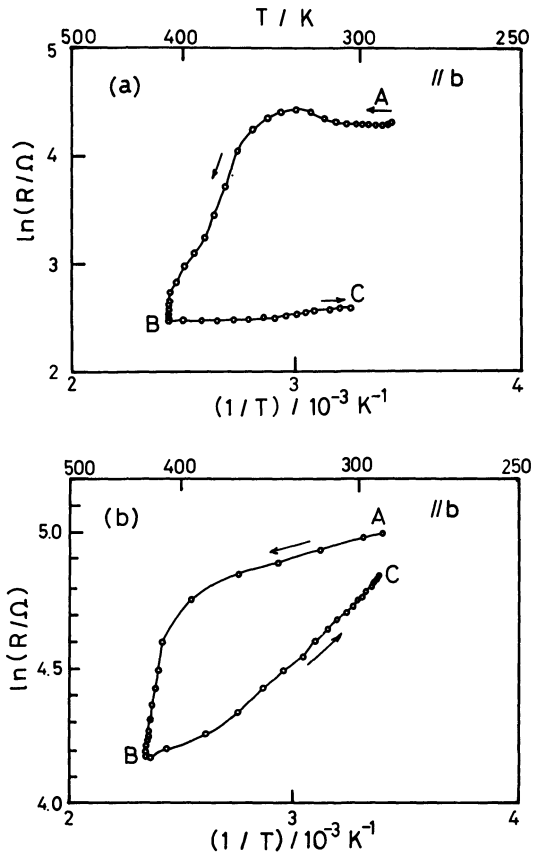

Fig. 7. Temperature dependence of $\ln(R/\Omega)$ of Cs-black phosphorus.

reproducible result are now being pursued.

To introduce lithium into BP, we empolyed two kinds of electrolytic methods. In the first method, a hexane solution of butyllithium was used as the electrolyte solution; the electrodes were a BP single crystal and a platinum plate. The second type cell consisted of a BP crystal and a lithium metal rod for the electrodes and a $LiClO_4$–THF solution for the electrolyte. In both cases, a swelling of the crystal was observed. The resistances decreased at first to 80—90% and then increased to the values that were higher than the original ones. The latter effect may be due to the partial breakdown of the crystal or the contacts between the crystal and the lead wires. A further investigation is also required to establish the intercalation conditions for the case of lithium. We have also tried to introduce iodine, pyridine, or ammonia into BP. About 20% decreases in the resistance were observed in these cases. Further study is going on, especially for an iodine intercalation.

In summary, we have prepared black phosphorus single crystals from a black or white phosphorus bismuth solution, and have observed electrical and optical properties of these crystals. We have also used crystals prepared under high pressure. We have tried to synthesize novel intercalation compounds between black phosphorus and cesium, lithium, iodine, pyridine, or ammonia. Homogeneous and stable intercalation compounds have not yet been obtained, but evidence for intercalation has been acquired by an X-ray diffraction method. Some increases in the electrical conductivities and the their different temperature dependecies in these intercalation compounds have been observed. Further investigation regarding the characterization of the intercalation compounds of black phosphorus and measurements of their physical properties are now under way.

We are very grateful to Prof. A. Morita for his important theoretical discussion. We thank to Prof. Y. Sasada and Prof. Y. Ohashi for their kind cooperation in the X-ray diffraction measurement, to Prof. H. Yakushi for the optical reflection measurement, and to Prof. Y. Tominaga for the Raman spectra measurement. This work was partly supported by the Grant-in-Aid for the Special Research on the Property of Molecular Assemblies (No. 59212044) from the ministry of Education, Science and Culture.

References

1) Y. Maruyama, S. Suzuki, K. Kobayashi, and S. Tanuma, *Physica*, **105B**, 99 (1981).
2) I. Shirotani, *Mol. Cryst. Liq. Cryst.*, **86**, 1943 (1982).
3) S. Endo, Y. Akahama, S. Terada, and S. Narita, *Japan. J. Appl. Phys.*, **21**, L482 (1982).
4) Y. Akahama, S. Endo, and S. Narita, *J. Phys. Soc. Jpn.*, **52**, 2148 (1983).
5) S. Narita, S. Terada, S. Mori, M. Muro, Y. Akahama, and S. Endo, *J. Phys. Soc. Jpn.*, **52**, 3544 (1983).
6) P. W. Bridgman, *J. Am. Chem. Soc.*, **36**, 1344 (1914).
7) R. W. Key, *Phys. Rev.*, **92**, 580 (1953).
8) D. Warschauer, *J. Appl. Phys.*, **34**, 1853 (1963).
9) A. Brown and S. Rundqvist, *Acta Crystallogr.*, **19**, 684 (1965).
10) J. C. Jamieson, *Science*, **139**, 129 (1963).
11) J. Wittig and B. T. Matthias, *Science*, **160**, 994 (1968).
12) I. V. Berman and N. B. Brandt, *JETP Lett.*, **7**, 323 (1968).
13) M. Okajima, S. Endo, Y. Akahama, and S. Narita, *Japan. J. Appl. Phys.*, **23**, 15 (1984).
14) H. Kawamura, I. Shirotani, and K. Tachikawa, *Solid State Commun.*, **49**, 879 (1984).
15) N. Iwasaki, Y. Maruyama, S. Kurihara, I. Shirotani, and M. Kinoshita, *Chem. Lett.*, **1985**, 119.
16) H. Asahina, K. Shindo, and A. Morita, *J. Phys. Soc. Jpn.*, **51**, 1193 (1982).
17) A. Morita, C. Kaneta, and H. Katayama-Yoshida, *Physica*, **117B**, **118B**, 517 (1983).
18) P. P. Debye and E. M. Conwell, *Phys. Rev.*, **93**, 693 (1954).
19) A. Morita, H. Asahina, C. Kaneta, and T. Sakai, "Proc. of 17th Int. Conf. Phys. on Semicond.," San Francisco (1984).
20) H. Asahina and A. Morita, *J. Phys. c: Solid State Phys.*, **17**, 1839 (1984).
21) S. Sugai, T. Ueda, and K. Murase, *J. Phys. Soc. Jpn.*, **50**, 3356 (1981).

A Calorimetric Study on the Formation of $[CuCl_n]^{(2-n)+}$ (n=1—4) in Acetonitrile-*N,N*-Dimethylformamide Mixtures

Shin-ichi ISHIGURO, Bojana G. JELIAZKOVA,† and Hitoshi OHTAKI*
Department of Electronic Chemistry, Tokyo Institute of Technology at Nagatsuta, 4259, Nagatsuta-cho, Midori-ku, Yokohama 227
†Department of Analytical Chemistry, Sofia University, Anton Ivanov 1, Sofia, Bulgaria
(Received August 29, 1985)

Complex formation equilibria between copper(II) and chloride ions have been studied by calorimetry in various acetonitrile(AN)-*N,N*-dimethylformamide(DMF) mixtures containing 0.2 mol dm^{-3} $(C_2H_5)_4NClO_4$ as a constant ionic medium at 25 °C. Calorimetric titration curves in each AN-DMF mixture examined were well explained in terms of formation of $[CuCl_n]^{(2-n)+}$ (n=1—4), and their formation constants, enthalpies, and entropies were determined. The overall enthalpy $\Delta H^\circ_{\beta 4}$ in any mixture, even in the acetonitrile-rich 0.025 mole fraction DMF mixture, was practically the same as that (19.2 kJ mol^{-1}) in pure DMF, but largely different from that (−54.5 kJ mol^{-1}) in pure AN. The result indicated that copper(II) ion was markedly preferentially solvated with DMF molecules in AN-DMF mixtures. On the other hand, the overall entropy value $\Delta S^\circ_{\beta 4}$ in any AN-DMF mixture was significantly larger than the values in both pure solvents. As to thermodynamic quantities of stepwise formation of $[CuCl_n]^{(2-n)+}$ (n=1—4), a remarkable change was found at the second step with varying solvent compositions. The stepwise enthalpy and entropy values of formation of $[CuCl_2]$ became more positive as the DMF content of the mixture decreased. Enthalpies of solution of anhydrous $CuCl_2$ crystals were also measured in the same AN-DMF mixtures. The enthalpy $\Delta H^\circ_s(CuCl_2)$ of solution of the neutral $[CuCl_2]$ complex largely changed depending on the solvent composition, while $\Delta H^\circ_s(Cu^{2+}, 2Cl^-)$, which is the sum of enthalpies of solution of relevant ions, remained practically unchanged. The result for the $[CuCl_2]$ complex indicated that the complex was not strongly preferentially solvated with DMF molecules in contrast to copper(II) ion in the AN-DMF mixtures.

In both acetonitrile (AN) and *N,N*-dimethylformamide (DMF), copper(II) ion forms a series of four mononuclear complexes with chloride ions, although the formation of the complex is more favorable in the former solvent than in the latter.[1-4]

The donor property of AN (the donor number (D_N)= 14.1) is much weaker than that of DMF (D_N=26.6), while the acceptor property is similar in both solvents (the acceptor number (A_N)=19.3 and 16.0 for AN and DMF, respectively).[5] Consequently, copper(II) ion is more strongly solvated with DMF than with AN. On the other hand, since the enthalpy of transfer of the chloride ion from AN to DMF is close to zero,[6] the extent of solvation of the ion may not largely differ in these solvents. Therefore, more favorable formation of the copper(II) chloro complexes in AN than in DMF is mainly ascribed to a weaker solvation of copper(II) ion in the former solvent than in the latter.

Copper(II) ion is strongly coordinated with four DMF molecules in its first coordination sphere to form the $[Cu(dmf)_4]^{2+}$ solvate even in acetonitrile-rich AN-DMF mixtures.[7]

Copper(II) ion within its chloro complexes except for $[CuCl_4]^{2-}$ may be also solvated with solvent molecules in the first solvation sphere of the metal ion in AN-DMF mixtures. The metal ion prefers DMF owing to a stronger donicity of DMF than that of AN. However, the electron acceptor ability of copper(II) ion decreases with increasing number of chloride ions within the complexes due to the electron donation from the ligands to the metal ion. Thus, the strength of the metal-DMF bonds is weakened with increasing number of chloride ions within the $[CuCl_n]^{(2-n)+}$ complex.[8]

In the present work, complex formation equilibria between copper(II) and chloride ions have been calorimetrically studied in various AN-DMF mixtures. Heats of solution of anhydrous $CuCl_2$ crystals have also been measured in the AN-DMF mixtures. Thermodynamic behavior of formation of $[CuCl_n]^{(2-n)+}$ (n=1—4) in the AN-DMF mixtures will be discussed in connection with the change in solvation of the metal ion and the complexes with varying solvent compositions.

Experimental

Reagent. All chemicals used were of reagent grade. Methods of preparation and purification of the chemicals were the same as those described in previous papers.[1,2]

Measurements. Calorimetric measurements were carried out in a thermostated bath controlled at (25.000±0.007)°C placed in a room thermostated at (25.0±0.2)°C.

All solutions used for calorimetric measurements contained 0.2 mol dm^{-3} $(C_2H_5)_4NClO_4$ as a constant ionic medium. In each calorimetric measurement, 100 cm^3 of a copper(II) perchlorate solution of a given solvent composition was placed in a Dewar vessel filled with nitrogen gas and prevented from moisture with a P_2O_5 guard-tube, and then, was titrated with a 0.2 mol dm^{-3} $(C_2H_5)_4NCl$ solution of the same solvent composition. Concentrations of copper(II) perchlorate in initial test solutions were varied in the range 5—30 mmol dm^{-3}. Heat evolved at each titration point was measured in the range −5—5 J with a certainty ±0.05 J. Since heats of dilution of chloride ions in any AN-DMF mixture examined were found to be negligible by separate experiments, they were neglected in the course of the data treatments of heats measured.

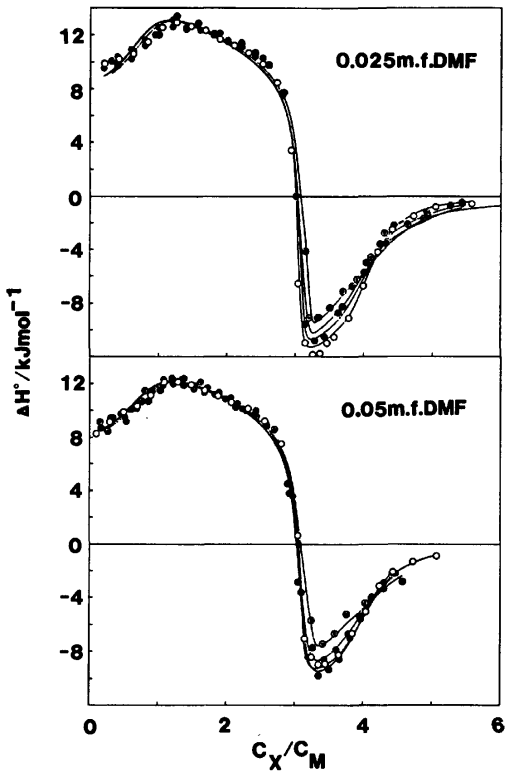

Fig. 1. Calorimetric titration curves of copper(II) chloride solutions in the AN-DMF mixtures of 0.025 and 0.05 mole fraction DMF containing 0.2 mol dm^{-3} $(C_2N_5)_4NClO_4$. Initial concentrations of copper(II) perchlorate (C_M/mol dm^{-3}): 4.55 (⊙), 7.14 (◎), 10.19 (●), and 19.25 (○) in the 0.025 mole fraction DMF mixture, and 6.05 (⊙), 11.83 (●), 20.48 (○), and 26.37 (◎), in the 0.05 mole fraction DMF mixture.

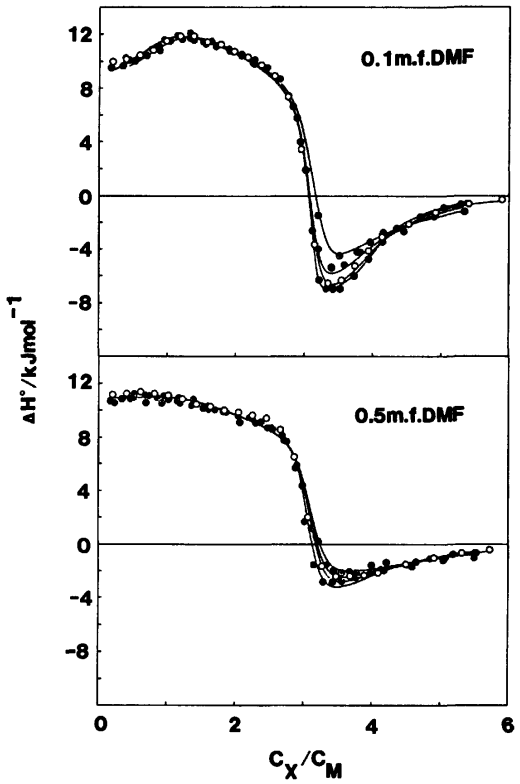

Fig. 2. Calorimetric titration curves of copper(II) chloride solutions in the AN-DMF mixtures of 0.1 and 0.5 mole fraction DMF containing 0.2 mol dm^{-3} $(C_2N_5)_4NClO_4$. Initial concentrations of copper(II) perchlorate (C_M/mol dm^{-3}): 4.59 (⊙), 10.69 (◎), 20.50 (○), and 29.23 (●) in the 0.1 mole fraction DMF mixture and 8.87 (⊙), 13.75 (◎), 19.81 (○), and 29.94 (●) in the 0.5 mole fraction DMF mixture.

Heats of solution of anhydrous $CuCl_2$ crystals were measured in the same AN-DMF mixtures as those used for the calorimetric titrations, but the mixtures involved no ionic medium, and the enthalpies $\Delta H_s^\circ(Cu^{2+},2Cl^-)$ and $\Delta H_s^\circ(CuCl_2)$ for the reactions, $CuCl_2(c)=Cu^{2+}(s)+2Cl^-(s)$ and $CuCl_2(c)=CuCl_2(s)$, respectively, were evaluated, where c and s stand for the crystalline and solution states, respectively.

Both titration and solution calorimetric measurements were carried out by using fully automatic on-line systems developed in our laboratory.[9-11]

Analysis of Calorimetric Data. The analytical method used for the calorimetric titration data was the same as that described in previous papers.[1,2]

The enthalpy of solution $\Delta H_{s,obsd}^\circ$ ($=-q_s/m$, where q_s and m denote the heat of solution measured and the number of moles of $CuCl_2$ dissolved, respectively) varied with the salt concentration in a solvent mixture because of the complex formation equilibria between copper(II) and chloride ions in the solvent. Therefore, the enthalpies $\Delta H_s^\circ(Cu^{2+},2Cl^-)$ and $\Delta H_s^\circ(CuCl_2)$ of solution were obtained by using the measured enthalpy of solution $\Delta H_{s,obsd}^\circ$ and the formation constants and enthalpies of formation of $[CuCl_n]^{(2-n)+}$ in each AN-DMF mixture as follows:

$$\Delta H_s^\circ(Cu^{2+},2Cl^-) = \Delta H_{s,obsd}^\circ - \sum_n \alpha_n \Delta H_{\beta n}^\circ, \quad (1)$$

$$\Delta H_s^\circ(CuCl_2) = \Delta H_s^\circ(Cu^{2+},2Cl^-) + \Delta H_{\beta 2}^\circ, \quad (2)$$

where α_n denotes the mole fraction of the $[CuCl_n]^{(2-n)+}$ complex. The α_n (n=1—4) values in a given solvent mixture were calculated in each measurement by knowing the formation constants of the $[CuCl_n]^{(2-n)+}$ (n=1—4) complexes and the total concentration of $CuCl_2$ dissolved in the solvent mixture.

Results and Discussion

Calorimetric titration curves in AN-DMF mixtures of 0.025, 0.05, 0.1, and 0.5 mole fraction DMF examined are illustrated in Figs. 1 and 2. In each solvent mixture, enthalpies ΔH° ($=-q/(vC_{X,tit})$ where v and $C_{X,tit}$ stand for the volume of an aliquot of the titrant added and the concentration of chloride ion in the titrant, respectively) were plotted against the ratio C_X/C_M in the test solution at each titration point.

As seen in Figs. 1 and 2, the ΔH° value was positive in the range $C_X/C_M<3$ but was turned to negative in the range $C_X/C_M>3$ in all the AN-DMF mixtures examined. The trend in the variation of ΔH° is similar to that in pure DMF, but different from that in pure AN where the ΔH° value is negative over the whole range of C_X/C_M.[2] Calorimetric titration curves in the 0.5 mole fraction DMF mixture were essentially the same as

Table 1. The Least-Squares Refinement of Formation Constants, β_n/mol^{-n}dm^{3n}, and Enthalpies, $\Delta H^\circ_{\beta n}$/kJ mol^{-1}, of Formation of Copper(II) Chloro Complexes in Acetonitrile-*N*,*N*-Dimethylformamide Mixtures Containing 0.2 mol dm^{-3} $(C_2H_5)_4NClO_4$ as a Constant Ionic Medium at 25 °C

	DMF content/mole fraction			
	0.025	0.05	0.1	0.5
log β_1	6.7(0.4)	6.2(0.2)	5.9(0.1)	6.0(0.1)
log β_2	12.2(0.7)	11.4(0.4)	10.8(0.3)	10.9(0.1)
log β_3	18.4(1.2)	16.9(0.5)	15.8(0.4)	15.2(0.4)
log β_4	21.4(1.2)	19.7(0.5)	18.4(0.4)	17.3(0.4)
$\Delta H^\circ_{\beta 1}$	8.7(0.3)	8.3(0.2)	9.2(0.1)	10.9(0.1)
$\Delta H^\circ_{\beta 2}$	37.1(5)	29.9(2)	26.7(1)	22.2(0.2)
$\Delta H^\circ_{\beta 3}$	31.2(0.2)	29.9(0.2)	30.2(0.1)	30.0(0.2)
$\Delta H^\circ_{\beta 4}$	18.7(0.3)	18.8(0.2)	20.9(0.2)	23.5(0.2)
NP[a]	95	99	94	94
U[b]	1.67	1.29	0.84	1.51

Values in parentheses refer to standard deviations. a) The number of data points. b) The error-square sum.

those in pure DMF.[1] However, the titration curve noticeably changed with further decreasing the DMF content, i.e., the ΔH° values became more positive in the range C_X/C_M=1—2, but more negative in the range C_X/C_M=3—4 in the AN-DMF mixtures of lower DMF contents.

Calorimetric data in any AN-DMF mixture examined, as well as those in pure AN and DMF, were well explained in terms of the formation of $[CuCl_n]^{(2-n)+}$ (n=1—4). The formation constants and enthalpies of formation of the complexes obtained in each mixture are summarized in Table 1. As illustrated by the solid lines in Figs. 1 and 2, theoretical curves calculated by using the constants in Table 1 well reproduced the experimental points in each AN-DMF mixture examined.

Formation of the $[CuCl_4]^{2-}$ Complex. The $[CuCl_4]^{2-}$ complex is not solvated in the first solvation sphere of the metal ion in AN and in DMF.[1,2,8] The solvation energy of chloride ion in AN does not significantly differ from that in DMF because these solvents have a relatively poor acceptor property.[5] Consequently, the energy of formation of $[CuCl_4]^{2-}$ mainly depends on the solvation energy of the metal ion, especially in its first solvation sphere, in these solvents.

Thermodynamic quantities for the overall reaction, $Cu^{2+}+4Cl^-=[CuCl_4]^{2-}$, in the AN-DMF mixtures are summarized in Table 2, together with those in AN and in DMF for comparison. As seen in Table 2, the $\Delta G^\circ_{\beta 4}$, $\Delta H^\circ_{\beta 4}$, and $\Delta S^\circ_{\beta 4}$ values even in the acetonitrile-rich AN-DMF mixtures, such as the 0.025 mole fraction DMF mixture, were remarkably different from those in AN. Particularly, the $\Delta H^\circ_{\beta 4}$ value drastically changed from negative in pure AN to positive in the mixtures. Besides, the $\Delta S^\circ_{\beta 4}$ values in all the AN-DMF mixtures examined were much larger than those in AN and in DMF.

Table 2. Thermodynamic Quantities, $\Delta G^\circ_{\beta 4}$/kJ mol^{-1}, $\Delta H^\circ_{\beta 4}$/kJ mol^{-1}, and $\Delta S^\circ_{\beta 4}$/J K^{-1} mol^{-1}, for the Overall Reaction, $Cu^{2+}+4Cl^-=[CuCl_4]^{2-}$, in Acetonitrile, in *N*,*N*-Dimethylformamide and in Their Mixtures Containing 0.2 mol dm^{-3} $(C_2H_5)_4NClO_4$ as a Constant Ionic Medium at 25 °C

	DMF content/mole fraction					
	0.0[a]	0.025	0.05	0.1	0.5	1.0[b]
$\Delta G^\circ_{\beta 4}$	−144.1	−122.1	−112.5	−105.3	−98.8	−96.2
$\Delta H^\circ_{\beta 4}$	−54.5	18.7	18.8	20.9	23.5	19.2
$\Delta S^\circ_{\beta 4}$	300	473	441	423	410	387

a) 0.1 mol dm^{-3} $(C_2H_5)_4NClO_4$ ionic medium, Ref. 2. b) Ref. 1.

Table 3. Thermodynamic Quantities, log(K_n/mol^{-1}dm^3), ΔG°_n/kJ mol^{-1}, ΔH°_n/kJ mol^{-1}, and ΔS°_n/J K^{-1} mol^{-1}, for the Stepwise Reaction, $[CuCl_{n-1}]^{(3-n)+}+Cl^-=[CuCl_n]^{(2-n)+}$ (n=1—4), in Acetonitrile-*N*,*N*-Dimethylformamide Mixtures Containing 0.2 mol dm^{-3} $(C_2H_5)_4NClO_4$ as a Constant Ionic Medium at 25 °C

	DMF content/mole fraction					
	0.0[a]	0.025	0.05	0.1	0.5	1.0[b]
log K_1	9.7	6.7	6.2	5.9	6.0	6.8
log K_2	8.0	5.5	5.2	4.9	4.9	4.5
log K_3	4.9	6.1	5.5	5.0	4.3	4.0
log K_4	2.9	3.0	2.9	2.6	2.2	1.5
ΔG°_1	−55.3	−38.3	−35.5	−33.8	−34.5	−38.8
ΔG°_2	−45.4	−31.5	−29.5	−28.1	−27.8	−25.9
ΔG°_3	−28.2	−35.0	−31.3	−28.5	−24.3	−22.8
ΔG°_4	−16.3	−17.3	−16.4	−14.9	−12.3	−8.8
ΔH°_1	−11.7	8.8	8.3	9.2	10.9	10.3
ΔH°_2	−5.0	28.4	21.6	17.5	11.3	9.7
ΔH°_3	−4.4	−5.9	0.0	3.5	7.8	7.3
ΔH°_4	−34.3	−12.5	−11.1	−9.3	−6.5	−8.1
ΔS°_1	147	158	147	144	152	165
ΔS°_2	135	201	171	153	131	120
ΔS°_3	80	98	105	107	107	101
ΔS°_4	−61	16	18	19	20	2

a) 0.1 mol dm^{-3} $(C_2H_5)_4NClO_4$ ionic medium, Ref. 2. b) Ref. 1.

The thermodynamic quantities for the reaction, $[Cu(dmf)_4]^{2+}+4Cl^-=[CuCl_4]^{2-}+4dmf$, in AN can be calculated by combining those for two reactions, $Cu^{2+}+4Cl^-=[CuCl_4]^{2-}$ and $Cu^{2+}+4dmf=[Cu(dmf)_4]^{2+}$,[7] in the solvent. The enthalpy $\Delta H^{\circ *}_{\beta 4}$ and entropy $\Delta S^{\circ *}_{\beta 4}$ values thus calculated are 19.1 kJ mol^{-1} and 409 J K^{-1} mol^{-1}, respectively, which may be compared with the $\Delta H^\circ_{\beta 4}$ and $\Delta S^\circ_{\beta 4}$ values in the AN-DMF mixtures. The result indicates that a large difference of the $\Delta H^\circ_{\beta 4}$ and $\Delta S^\circ_{\beta 4}$ values found in the AN-DMF mixtures from those in pure AN may mainly be interpreted in terms of the preferential solvation of copper(II) ion with four DMF molecules in the mixtures.

Stepwise Formation of $[CuCl_n]^{(2-n)+}$ (n=1—4). Thermodynamic quantities, log(K_n/mol^{-1}dm^3), ΔG°_n/kJ mol^{-1}, ΔH°_n/kJ mol^{-1}, and ΔS°_n/J K^{-1} mol^{-1}, for the stepwise reaction, $[CuCl_{n-1}]^{(3-n)+}+Cl^-=[CuCl_n]^{(2-n)+}$ (n=1—4), are summarized in Table 3. Distribution of species

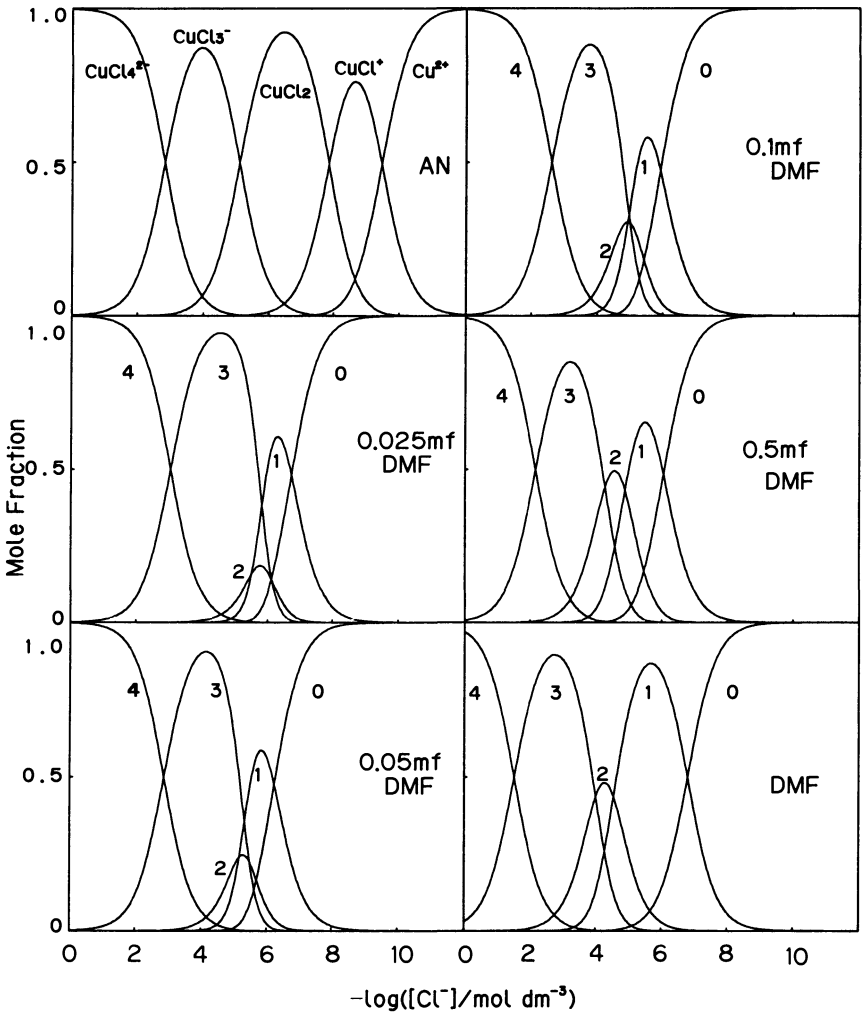

Fig. 3. Distribution curves of the copper(II) chloro complexes in various AN-DMF mixtures containing 0.2 mol dm^{-3} $(C_2N_5)_4NClO_4$ at 25 °C.

calculated by using the formation constants in each AN–DMF mixture examined is depicted in Fig. 3, together with those in the pure solvents for comparison.

The ΔH_1° and ΔS_1° values were both positive and practically kept constant in all the mixtures examined. The ΔH_1° value in any mixture was more positive by ca. 20 kJ mol^{-1} than that in pure AN, the magnitude is about one fourth of the overall enthalpy of formation of $[Cu(dmf)_4]^{2+}$ in AN.[7] It is thus plausible that one DMF molecule within $[Cu(dmf)_4]^{2+}$ is replaced with a chloride ion and $[CuCl(dmf)_3]^+$ is formed.

The ΔH_2° and ΔS_2° values became markedly positive in the AN-DMF mixtures of low DMF contents. The result indicates that the desolvation of DMF molecules from $[CuCl(dmf)_3]^+$ takes place in a different manner in each mixture depending on the solvent composition. On the other hand, the ΔH_3° value became less positive with lowering DMF contents in the mixtures and the $(\Delta H_2^\circ+\Delta H_3^\circ)$ value was practically independent of the solvent composition. The result indicates that total number of DMF molecules desolvating at the second and third steps may be kept constant in all the mixtures examined. As discussed later, the $[CuCl_3(dmf)]^-$ species is expected to be present in all the AN–DMF mixtures examined. Therefore, two DMF molecules may be liberated at the second and third consecutive steps, but the desolvating scheme depends on the solvent composition in the mixtures. We propose:

$$[CuCl(dmf)_3]^+ + Cl^- = [CuCl_2(dmf)_2] + dmf, \quad (3)$$

$$[CuCl_2(dmf)_2] + Cl^- = [CuCl_3(dmf)]^- + dmf, \quad (4)$$

in a mixture of a high DMF content, while in a mixture of a relatively low DMF content,

$$[CuCl(dmf)_3]^+ + Cl^- = [CuCl_2(dmf)] + 2dmf, \quad (5)$$

$$[CuCl_2(dmf)] + Cl^- = [CuCl_3(dmf)]^-. \quad (6)$$

Accordingly, the dichlorocopper(II) complex may be solvated with one or two DMF molecules in the first coordination sphere of the metal ion, and thus, an equilibrium as represented by reaction 7 is established between the two solvate species of the dichloro

Table 4. Enthalpies of Solution, ΔH_s°/kJ mol^{-1}, of Anhydrous Copper(II) Chloride Salt in Various Acetonitrile-*N*,*N*-Dimethylformamide Mixtures at 25 °C

DMF content / mole fraction	$\Delta H_{s,obsd}^\circ$	$\Delta H_s^\circ(CuCl_2)$	$\Delta H_s^\circ(Cu^{2+}, 2Cl^-)$
0.0	−15.9	−15.9	0.6
0.025	−38.0	−24.3	−61.3
0.05	−41.9	−34.2	−64.1
0.1	−42.5	−37.0	−63.7
0.5	−51.5	−50.5	−72.7
1.0	−55.3	−54.7	−74.6

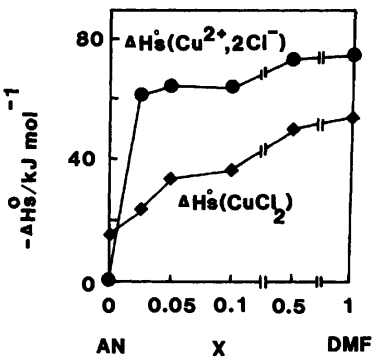

Fig. 4. Variations of $\Delta H_s^\circ(Cu^{2+}, 2Cl^-)$ and $\Delta H_s^\circ(CuCl_2)$ with mole fraction x of DMF in the AN-DMF mixtures.

complex,

$$[CuCl_2(dmf)] + dmf = [CuCl_2(dmf)_2], \quad (7)$$

and the equilibrium shifts depending on the DMF content in the AN-DMF mixtures.

The ΔH_4° value was negative in any AN-DMF mixture examined and became slightly more negative with lowering DMF contents in the mixtures, but it remained much less negative than that in pure AN. The ΔS_4° value was positive and was practically independent of the solvent composition in all the mixtures examined, while the ΔS_4° value in AN was largely negative. The result suggests that one DMF molecule still coordinates to copper(II) ion within the trichlorocuprate(II) complex and $[CuCl_3(dmf)]^-$ is formed in all the mixtures.

Enthalpies of Solution of Anhydrous $CuCl_2$ Crystal. Copper(II) chloride dissolved in an AN-DMF mixture is mostly associated to form various chloro complexes of Cu(II), the distribution of which can be calculated by knowing the formation constants of the complexes and the total concentration of $CuCl_2$ dissolved in a solution. Therefore, by using the procedure described in the Experimental section, the enthalpies $\Delta H_s^\circ(Cu^{2+}, 2Cl^-)$ and $\Delta H_s^\circ(CuCl_2)$ of solution have been determined in various AN-DMF mixtures, the former being the sum of enthalpies of solution of relevant ions and the latter the enthalpy of the neutral complex. The results are summarized in Table 4 and also depicted in Fig. 4.

Although the enthalpies of transfer of both copper(II) and chloride ions from AN to any AN-DMF mixture have not been known, the change in $\Delta H_s^\circ(Cu^{2+}, 2Cl^-)$ with varying solvent compositions may mainly reflect the change in enthalpy of solvation of copper(II) ion because the acceptor properties (the property of solvating anions) of AN and DMF are weak and not appreciably different.

As seen in Table 4, the $\Delta H_s^\circ(Cu^{2+},2Cl^-)$ values in all the mixtures examined were largely negative. They are compared with the value in pure DMF, but are very different from the value in pure AN. This also indicates that copper(II) ion is preferentially solvated with DMF molecules in a wide range of the solvent composition of the AN-DMF mixtures.

The $\Delta H_s^\circ(CuCl_2)$ value in the 0.025 mole fraction DMF mixture was close to the value in pure AN, but the value in the 0.5 mole fraction DMF mixture was close to that in pure DMF as seen in Table 4. The values in the 0.05 and 0.1 mole fraction DMF mixture were laid just in the middle of the values in AN and in DMF. The variation of $\Delta H_s^\circ(CuCl_2)$ with solvent composition indicates that solvation of $[CuCl_2]$ with DMF molecules markedly weakens in an AN-DMF mixture of a low DMF content. Therefore, we concluded that the $[CuCl_2]$ complex was not markedly preferentially solvated with DMF molecules in contrast to copper(II) ion in the AN-DMF mixtures. This is not unexpected, considering that an electron donation from the ligands to the central metal ion within $[CuCl_2]$ may reduce the acceptor ability of copper(II) ion to lead to a weakened interaction of the metal ion with DMF molecules. The conclusion obtained here is also consistent with the result obtained in a preceding section that the ΔH_2° value of stepwise formation of $[CuCl_2]$ became more positive with lowering DMF contents in the AN-DMF mixtures.

The work has been supported by the Grant-in-Aid for Scientific Research No. 59540386 from the Ministry of Education, Science and Culture.

References

1) S. Ishiguro, B. G. Jeliazkova, and H. Ohtaki, *Bull. Chem. Soc. Jpn.*, **58**, 1143 (1985).

2) S. Ishiguro, B. G. Jeliazkova, and H. Ohtaki, *Bull. Chem. Soc. Jpn.*, **58**, 1749 (1985).

3) M. Elleb, J. Meullemeestre, M. J. Schwing-Weil, and F. Vierling, *Inorg. Chem.*, **19**, 2699 (1980).

4) S. E. Manahan and R. T. Iwamoto, *Inorg. Chem.*, **4**, 1409 (1965).

5) V. Gutmann, "The Donor-Acceptor Approach to Molecular Interactions," Prenum, New York (1978).

6) Y. Marcus, *Pure Appl. Chem.*, **57**, 1103 (1985).

7) S. Ishiguro, B. G. Jeliazkova, and H. Ohtaki, unpublished data by calorimetric measurements. The $\Delta G_{\beta 4}^\circ$, $\Delta H_{\beta 4}^\circ$, and $\Delta S_{\beta 4}^\circ$ values for the reaction, $Cu^{2+}+4dmf=[Cu(dmf)_4]^{2+}$ in acetonitrile containing 0.1 mol dm^{-3} $C_2H_5)_4NClO_4$

as a constant ionic medium at 25 °C were −41.2, −73.6 kJ mol^{-1}, and −109 J K^{-1} mol^{-1}, respectively.

8) K. Ozutsumi, S. Ishiguro, and H. Ohtaki, unpublished data by X-ray diffraction measurement for the structures of $[Cu(dmf)_6]^{2+}$, $[CuCl_3]^-$, and $[CuCl_4]^{2-}$ in DMF and of $[Cu(dmf)_4]^{2+}$ in the AN-DMF mixture of 0.1 mole fraction DMF.

9) S. Ishiguro and H. Ohtaki, *Bull. Chem. Soc. Jpn.*, **57**, 2622 (1984).

10) S. Ishiguro, Y. Oka, and H. Ohtaki, *Bull. Chem. Soc. Jpn.*, **56**, 2426 (1983).

11) S. Ishiguro, K. Yamamoto, and H. Ohtaki, *Anal. Sci.*, **1**, 263 (1985).

ESR and Mössbauer Studies of Crystallization Process of Iron Phosphate Glass

Katsuhisa TANAKA, Naohiro SOGA,* Rikuo OTA, and Kazuyuki HIRAO
Department of Industrial Chemistry, Faculty of Engineering, Kyoto University, Yoshida, Sakyo-ku, Kyoto 606
(Received November 11, 1985)

$0.7Fe_2O_3$-$0.3P_2O_5$ glass was prepared by using a twin-roller method and the crystallization process of this glass was followed by means of ESR and Mössbauer spectroscopy in order to understand the state and the behavior of iron ions in the glass. The ESR line shape of the quenched $0.7Fe_2O_3$-$0.3P_2O_5$ glass was much broader than that of the crystallized glass heat-treated at 710 °C for 5 h. Moreover, the linewidth of Mössbauer spectra decreased monotonously through the crystallization process. These facts indicated that there existed a distribution of ligand fields around iron ions in the glass. The Mössbauer parameters, that is the isomer shift and the quadrupole splitting, of the $0.7Fe_2O_3$-$0.3P_2O_5$ glass showed that Fe^{3+} ions in this glass were laid on distorted octahedral ligand fields. The magnetic interaction working in the $0.7Fe_2O_3$-$0.3P_2O_5$ glass at room temperature was dipole-dipole interaction. Besides, the Mössbauer spectrum of the glass exhibited no internal field line at room temperature. Hence, the glass is considered paramagnetic at room temperature. At the first stage of crystallization process, the α-Fe_2O_3 particles precipitated were sufficiently small and so the specimen was superparamagnetic, as revealed from the ESR and Mössbauer spectra of heat-treated specimens.

Spin glass behavior of oxide glasses containing large amounts of iron(III) or iron(II) ions has attracted much attention recently as a number of attempts have been made to characterize their magnetic properties as well as the state of iron ions in these glasses. Although most of the studies carried out so far indicate that these glasses exhibit antiferromagnetic properties at low temperatures,[1-10] several papers[7-9] report that well below the freezing temperature, individual spins are frozen in random directions and a new magnetic phase, which shows speromagnetism,[11,12] appears. Thus, the magnetic structure of iron-containing oxide glass has not been completely clarified. More detailed informations about the state of iron ions in these glasses are needed to comprehend the characteristics of their magnetic properties. One approach is to use such a method as ESR or Mössbauer spectroscopy, which is sensitive to the local change around iron ions and to follow the change occurring during the crystallization process of iron-containing glasses.[13]

In the present work, Fe_2O_3-P_2O_5 binary glasses containing a much larger amount of iron oxide than that in the previously studied glasses were prepared by using a rapid quenching method. The choice of phosphate glass comes from the fact that P_2O_5 forms glass most easily with transition metal oxides. The ESR and Mössbauer spectra of these glasses were obtained to find out a glass structure having no trace of microcrystals. Then, the glass was subjected to heat treatment and the change in the state of iron ions was followed in detail by means of ESR and Mössbauer effect measurements in order to discuss the structure of glass containing a very large amount of iron oxide.

Experimental

The glass samples were prepared by using reagent-grade Fe_2O_3 and $FePO_4$ hydrate as starting materials. $FePO_4$ hydrate was kept in an electric furnace at 400 °C for several hours for the purpose of excluding water, and then it was mixed thoroughly with Fe_2O_3 in suitable proportions (Table 1) and sintered at 800—900 °C for 3 h in air. The resultant material was melted by heating it in an image furnace with a xenon lamp and the melt was rapidly quenched by falling it on a twin-roller rotating at 3000 rpm. The cooling rate of this method is about 10^5 K s^{-1}. The specimen obtained was a thin film of about 20 μm thickness. X-Ray diffraction measurements were employed to determine whether the specimen was amorphous or not.

Table 1. Compositions of Fe_2O_3-P_2O_5 Binary System and Results of X-Ray Diffraction Analysis

Composition/mol%		Results of X-ray diffraction
Fe_2O_3	P_2O_5	
50	50	Amorphous
60	40	Amorphous
70	30	Amorphous
75	25	Amorphous
76	24	Amorphous
77	23	Fe_3O_4 precipitated
80	20	Fe_3O_4 precipitated

For the heat treatment experiments, the $0.7Fe_2O_3$-$0.3P_2O_5$ glass was used. The heat treatment was carried out in an electric furnace at various temperatures from 220 to 710 °C for 5 h in air. The crystals precipitated in the heat treatment process were ascertained by X-ray diffraction analysis.

The ESR measurements were made using a JEOL PE-2X spectrometer operating at X-band frequency (ν=9.4 GHz) with 1.0×10^{-4} T magnetic modulation width at room temperature. Reference signals of Mn^{2+} ions in MgO were used as the standards for the linewidth and effective g-value.

The Mössbauer effect measurements were carried out at room temperature. As the γ-ray source, a 10 mCi ^{57}Co in metallic rhodium was used. The velocity calibration and the calculation of the isomer shift were made from the spectra of pure iron foil.

Results

Glass Forming Limit. The compositions of the specimens prepared to select a glass having no trace

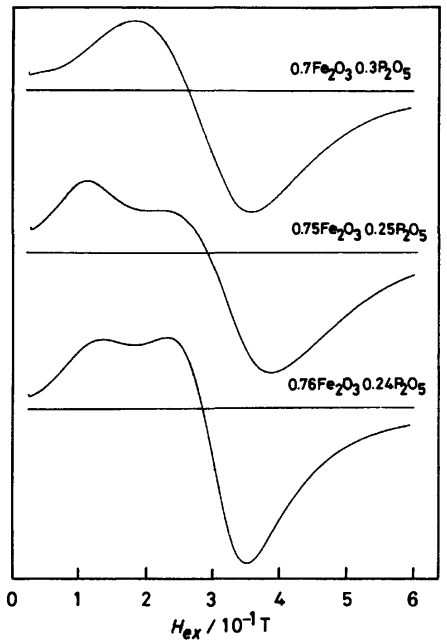

Fig. 1. ESR spectra of $0.7Fe_2O_3$–$0.3P_2O_5$, $0.75Fe_2O_3$–$0.25P_2O_5$, and $0.76Fe_2O_3$–$0.24P_2O_5$.

Table 2. ESR Linewidth and Effective g-Value of $0.7Fe_2O_3$–$0.3P_2O_5$, $0.75Fe_2O_3$–$0.25P_2O_5$, and $0.76Fe_2O_3$–$0.24P_2O_5$

Composition/mol%		ΔH	g_{eff}
Fe_2O_3	P_2O_5	10^{-1}T	
70	30	1.78	2.38
75	25	1.61	2.18
		0.46	4.29
76	24	1.23	2.18
		0.51	4.28

of microcrystals are summarized in Table 1 along with the results of X-ray diffraction analysis. The X-ray diffraction pattern of the specimen exhibited an amorphous state until the concentration of Fe_2O_3 reached up to 76 mol% and showed the appearance of Fe_3O_4 when the content of Fe_2O_3 exceeded 77 mol%. However, in the X-ray diffraction patterns of $0.75Fe_2O_3$–$0.25P_2O_5$ and $0.76Fe_2O_3$–$0.24P_2O_5$ one very weak peak was noticed in the halo pattern. The existence of a minute amount of some microcrystalline phase was confirmed by employing ESR and Mössbauer effect measurements on the three specimens, $0.7Fe_2O_3$–$0.3P_2O_5$, $0.75Fe_2O_3$–$0.25P_2O_5$, and $0.76Fe_2O_3$–$0.24P_2O_5$.

ESR spectra of these specimens are shown in Fig. 1. The linewidth and effective g-value obtained from these spectra are summarized in Table 2. As seen in Fig. 1, the spectra of $0.75Fe_2O_3$–$0.25P_2O_5$ and $0.76Fe_2O_3$–$0.24P_2O_5$ were different from that of $0.7Fe_2O_3$–$0.3P_2O_5$. The latter consisted of only one broad peak centered at g=2.0, but the former spectra were composed of two

Table 3. Results of Mössbauer Effect Measurements of $0.7Fe_2O_3$–$0.3P_2O_5$, $0.75Fe_2O_3$–$0.25P_2O_5$, and $0.76Fe_2O_3$–$0.24P_2O_5$

Composition/mol%		I.S.	Q.S.
Fe_2O_3	P_2O_5	mm s^{-1}	mm s^{-1}
70	30	Fe^{3+} 0.43	Fe^{3+} 1.18
		Fe^{2+} 1.06	Fe^{2+} 2.45
75	25	Fe^{3+} 0.41	Fe^{3+} 0.79
		Fe^{2+} 1.22	Fe^{2+} 2.41
76	24	Fe^{3+} 0.36	Fe^{3+} 0.78
		Fe^{2+} 1.10	Fe^{2+} 2.26

Table 4. Precipitated Crystals through the Crystallization Process of $0.7Fe_2O_3$–$0.3P_2O_5$ Glass

T_A [a]	t_A [a]	Results of X-ray diffraction
°C	h	
300	5	Amorphous
400	5	Amorphous
420	5	α-Fe_2O_3
500	5	α-Fe_2O_3, $Fe(PO_3)_2$
600	5	α-Fe_2O_3, $Fe(PO_3)_2$
710	5	α-Fe_2O_3, $FePO_4$, Fe_3PO_7

a) T_A and t_A mean heat treatment temperature and heat treatment time, respectively.

peaks at g=4.3 and 2.0. These peaks are attributable to the resonance of Fe^{3+} ion whose spin state is $^6S_{5/2}$.

Table 3 shows the results of Mössbauer effect measurements. Fe^{2+} ions, which were not detectable in the ESR spectra, were detected in all the specimens. It is apparent from this table that the values of the quadrupole splitting of Fe^{3+} ions in both $0.75Fe_2O_3$–$0.25P_2O_5$ and $0.76Fe_2O_3$–$0.24P_2O_5$ are significantly smaller than that in $0.7Fe_2O_3$–$0.3P_2O_5$. This fact means that the symmetry of Fe^{3+} ion sites is more distorted in $0.7Fe_2O_3$–$0.3P_2O_5$ than in $0.75Fe_2O_3$–$0.25P_2O_5$ or $0.76Fe_2O_3$–$0.24P_2O_5$, because the quadrupole splitting is a measure of the symmetry of the environment around an iron ion. This result of Mössbauer effect measurements indicates the precipitation of some microcrystals in both $0.75Fe_2O_3$–$0.25P_2O_5$ and $0.76Fe_2O_3$–$0.24P_2O_5$, while no crystalline phase existed in the $0.7Fe_2O_3$–$0.3P_2O_5$ specimen. Thus, this composition was used for the following heat treatment experiments.

Change of ESR and Mössbauer Spectra upon Heat Treatment. The kinds of crystals, precipitated in the $0.7Fe_2O_3$–$0.3P_2O_5$ specimen during the crystallization process are summarized in Table 4. As seen in this table, α-Fe_2O_3 precipitated at 420 °C, and at 500 °C Fe^{2+} ions formed iron metaphosphate $Fe(PO_3)_2$.

Figure 2 shows the ESR spectra of the quenched $0.7Fe_2O_3$–$0.3P_2O_5$ glass and the specimen heat-treated at 710 °C. The former is apparently much broader than the latter.

The change in linewidth of ESR spectra appearing

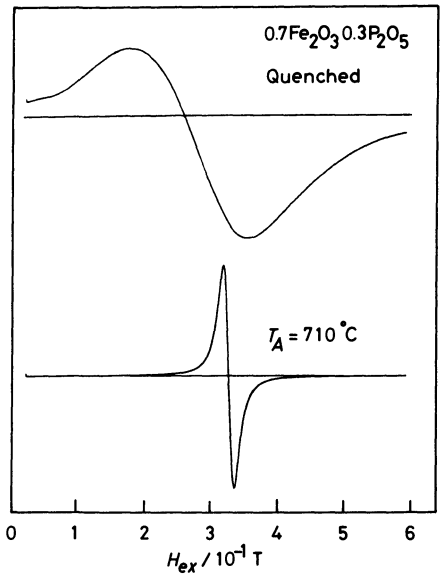

Fig. 2. ESR spectra of $0.7Fe_2O_3$-$0.3P_2O_5$ quenched glass and heat-treated at 710°C. T_A means the heat treatment temperature.

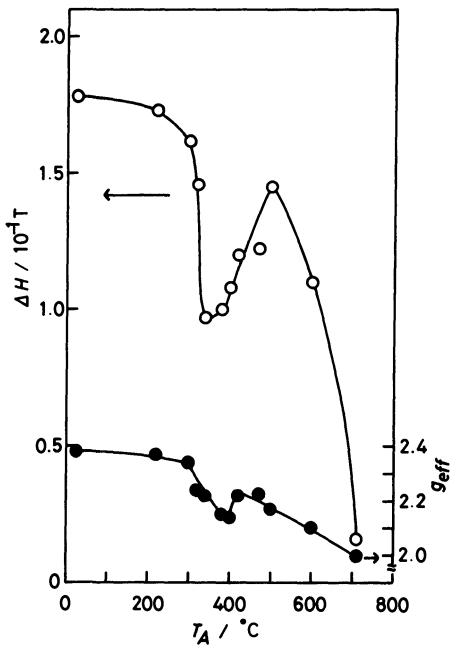

Fig. 3. Change on linewidth and effective g-value of ESR spectrum through the crystallization process of $0.7Fe_2O_3$-$0.3P_2O_5$ glass.

during the heat treatment process is shown in Fig. 3, along with the change of effective g-value. The linewidth started to decrease at about 300°C and took a minimum at about 340°C, beyond which it increased. When the heat treatment temperature exceeded 500°C, it decreased again rapidly. A similar tendency was seen on the change of effective g-value.

The change in linewidth of Mössbauer spectra appearing during the heat treatment process is shown in Fig. 4. The linewidth of Fe^{3+} did not change until

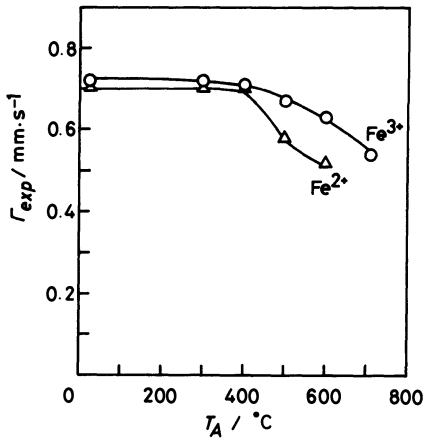

Fig. 4. Change on linewidth of Mössbauer spectra through the crystallization process.

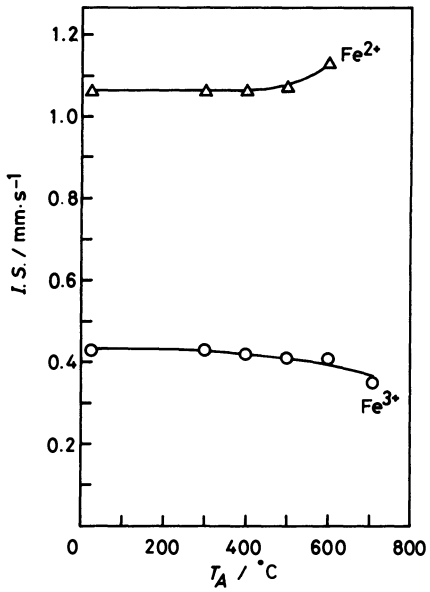

Fig. 5. Change on isomer shift of Fe^{3+} and Fe^{2+} through the crystallization process.

the heat treatment temperature reached up to 300°C and decreased monotonously when the heat treatment temperature exceeded 400°C, at which α-Fe_2O_3 microcrystals started to precipitate according to the X-ray diffraction measurements. The linewidth of Fe^{2+} also decreased at 400°C.

The change of isomer shift is shown in Fig. 5. The isomer shift of Fe^{3+} in the quenched $0.7Fe_2O_3$-$0.3P_2O_5$ glass was 0.43 mm s^{-1} when referred to pure iron. The isomer shift of Fe^{3+} decreased slowly through the crystallization process. On the contrary, the isomer shift of Fe^{2+} increased with increasing heat treatment temperature.

The change of quadrupole splitting, which is a measure of symmetry of the shape of electron clouds around an iron ion, is shown in Fig. 6. The quadrupole splitting of Fe^{2+} decreased at first and then increased as $Fe(PO_3)_2$ crystal grew. This change corresponds to

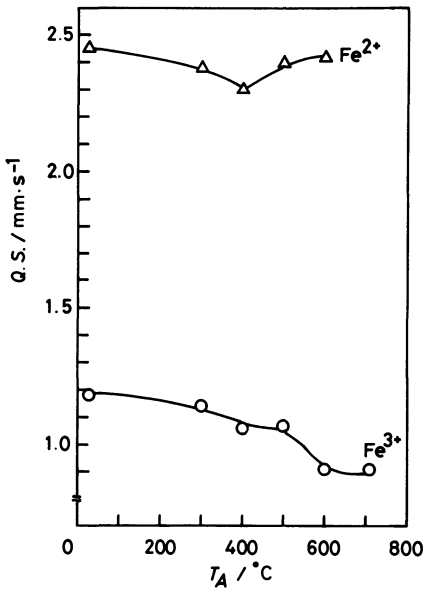

Fig. 6. Change on quadrupole splitting of Fe^{3+} and Fe^{2+} through the crystallization process.

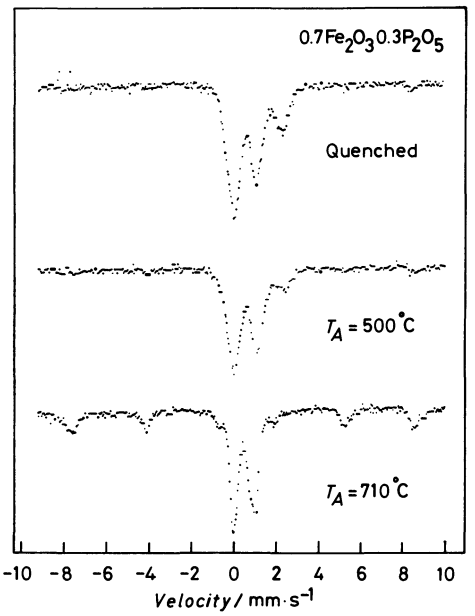

Fig. 7. Mössbauer spectra of quenched, heat-treated at 500°C, and heat-treated at 710°C, $0.7Fe_2O_3$–$0.3P_2O_5$ glass.

the change of isomer shift.

Discussion

ESR Spectra and Structural Change. The quenched glass showed much broader ESR spectra than the heat-treated specimen (Fig. 2). This fact indicates that the ligand field around Fe^{3+} fluctuates in $0.7Fe_2O_3$–$0.3P_2O_5$ glass. Generally, Hamiltonian yielding the energy levels of spin is written as follows:

$$H = g\beta HS + D\left\{S_z^2 - \frac{1}{3}S(S+1)\right\} + E(S_x^2 - S_y^2) + \frac{1}{6}a\left\{S_x^4 + S_y^4 + S_z^4 - \frac{1}{5}S(S+1)(3S^2+3S-1)\right\} + H_{ss} + H_{hf} + H_Q. \quad (1)$$

The first term is Zeeman energy and the second and the third terms are ligand field energies. The fourth term is fourth dimensional one of spin peculiar to Fe^{3+}, spin quantum number of which is larger than 2. H_{ss}, H_{hf}, and H_Q correspond to Hamiltonian representing spin–spin interaction, hyperfine interaction, and quadrupole interaction of nucleus, respectively. If there exists a variation of ligand fields, the crystal field parameters D and E are not uniform but fluctuate. So, Hamiltonian must be affected by the fluctuation, and the eigenvalue of Hamiltonian, that is the energy level of spin, should have a distribution. Therefore, the ESR spectrum of $0.7Fe_2O_3$–$0.3P_2O_5$ glass is expected to exhibit a very broad tail as observed in Fig. 2.

The linewidth of the quenched $0.7Fe_2O_3$–$0.3P_2O_5$ glass was 1.78×10^{-1} T, which is much larger than that of the specimen heat-treated at 710°C (1.60×10^{-2} T). The latter is attributable to the parasitic ferromagnetism of α-Fe_2O_3,[14,15] which causes a strong superexchange interaction at room temperature. According to the Anderson-Weiss theory,[16] the observed linewidth is represented as follows:

$$\Delta H = \frac{\frac{10}{3}(\Delta H_p)^2 + (\Delta H_H)^2}{\Delta H_e}, \quad (2)$$

where ΔH_p, ΔH_e, and ΔH_H represent the linewidth due to dipole–dipole interaction, exchange (superexchange) interaction, and fine structure field, respectively. Therefore, the linewidth of the specimen heat-treated at 710 °C should become very narrow due to the precipitation of α-Fe_2O_3. On the other hand, dipole–dipole interaction governs the magnetic interaction between iron ions in the quenched glass. Consequently, the linewidth of the quenched glass becomes broadened as indicated in Eq. 2.

A complicated change of linewidth with heat treatment temperature shown in Fig. 3 requires another mechanism of line narrowing than the superexchange interaction in the precipitated α-Fe_2O_3. According to Néel,[17] α-Fe_2O_3 is also known as a compound which shows superparamagnetism when the size of the particles is sufficiently small.

The smallness of the size of α-Fe_2O_3 precipitated in this temperature range can be demonstrated by the result of Mössbauer effect measurements. The Mössbauer spectrum of the specimen heat-treated at 500°C is drawn in Fig. 7 along with the spectra of the quenched glass as well as the specimen heat-treated at 710°C. Although α-Fe_2O_3 has already precipitated in

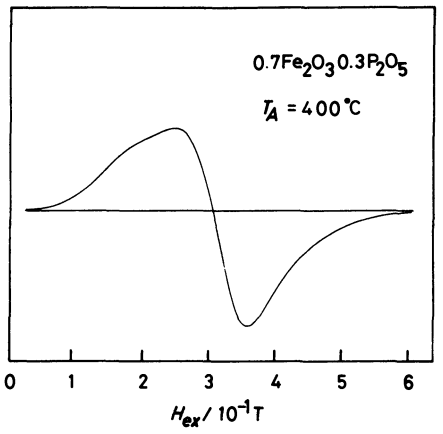

Fig. 8. ESR spectrum of $0.7Fe_2O_3$-$0.3P_2O_5$ glass heat-treated at 400°C.

the specimen heat-treated at 500°C as ascertained by X-ray diffraction analysis shown in Table 4, the sextet peak due to the internal field in α-Fe_2O_3 did not appear in this specimen. This fact indicates that α-Fe_2O_3 in this specimen is small and shows superparamagnetic. The existence of superparamagnetism can be seen in the ESR spectrum of the specimen heat-treated at 400°C shown in Fig. 8. The shoulder at about 1.8×10^{-1} T is attributable to Fe^{3+} ions which still exist in the glassy state in this specimen, and the peak at the higher field is due to Fe^{3+} ions in the superparamagnetic α-Fe_2O_3 particle. This ESR spectrum is very similar to that of ultrafine particles of Fe_3O_4 in various liquid observed by Sharma and Waldner.[18]

The line narrowing due to superparamagnetism was observed by Sharma and Waldner,[18] who investigated ultrafine particles of Fe_3O_4 in various ferrofluids by means of X-band ESR measurements. They defined the superparamagnetic narrowing factor f as follows:

$$f = \tau_{sp}/\tau_L = M_S V/\gamma k T \tau_L, \quad (3)$$

where τ_{sp} and τ_L are the superparamagnetic relaxation time and Larmor precession time, respectively, M_S is the saturation magnetization, V is the volume of the superparamagnetic particle, and γ is the gyromagnetic ratio. The proportional relation between the superparamagnetic narrowing linewidth and the volume of the particle was demonstrated by the data measured by Aharoni and Litt.[19] The increase in linewidth with increasing heat treatment temperature from 340 to 500°C observed in the present study is attributable to the growth of α-Fe_2O_3 crystallites.

When the heat treatment temperature exceeded 500°C, the linewidth decreased sharply. As described above, this narrowing is assigned to superexchange interaction owing to Fe^{3+} in α-Fe_2O_3 particles, the size of which is large enough not to show superparamagnetism. This interpretation agrees with the Mössbauer spectrum of the specimen heat-treated at 710°C in Fig. 7, which exhibited internal field lines. The internal field of α-Fe_2O_3 in this specimen is estimated to be 506 kOe (1kOe=$10^6/4\pi$ A m^{-1}).

As for the effective g-value, it was 2.00 for the specimen heat-treated at 710°C. This value is reasonable for Fe^{3+} ions because the spin state of Fe^{3+} is $^6S_{5/2}$ and its orbital angular momentum is zero. The effective g-value of the quenched $0.7Fe_2O_3$-$0.3P_2O_5$ glass was 2.38, larger than 2.00. This deviation from g=2.00 is ascribed to the contribution of orbital angular momentum to the g-value. The fraction of the orbital angular momentum in the total angular momentum, which is the sum of orbital angular momentum and spin angular momentum, is represented by the following relation:[20,21]

$$\varepsilon = \frac{1}{2}g - 1. \quad (4)$$

In the case of $0.7Fe_2O_3$-$0.3P_2O_5$ glass, ε=0.19. As described above, however, the orbital angular momentum quantum number of Fe^{3+} is zero, so that ε should be zero. The reason why ε was not zero in the $0.7Fe_2O_3$-$0.3P_2O_5$ glass is not clear at present, but might be related to the existence of Fe^{2+} ions in this glass. Fe^{2+} is known as an ion which is magnetically extremely anisotropic. The spin state of Fe^{2+} is S=2, L=2, indicating that the orbital angular momentum remains. In a general crystal such as an ionic crystal, this orbital angular momentum is quenched because of strong orbital-lattice interaction. Since there is a distribution of ligand field in this glass as described above, it is predictable that quenching of orbital angular momentum is not complete. Moreover, it may be presumed that there exists a resonance structure in this glass like the next one:

$$Fe^{2+}\text{-}O^{2-}\text{-}Fe^{3+} \rightleftarrows Fe^{3+}\text{-}O^{2-}\text{-}Fe^{2+}. \quad (5)$$

It is considered that Fe^{2+} has an effect on Fe^{3+} by way of such a resonance. As a result, the effective g-value becomes significantly larger than 2.00.

Mössbauer Parameters and State of Iron Ions. The linewidth of Mössbauer spectrum of $0.7Fe_2O_3$-$0.3P_2O_5$ glass was broader than that of the crystallized specimen (Fig. 4). This demonstrates a distribution of electric field gradient around both Fe^{3+} and Fe^{2+} ions in this glass. Eibschütz et al.[22] studied vitreous yttrium iron garnet by Mössbauer effect measurements and succeeded in fitting the computed absorption line to the experimental spectrum by assuming an asymmetric non-Gaussian distribution of electric field gradient. The existence of distribution of electric field gradient, that is a fluctuation of ligand field around Fe^{3+} ions, is ascertained by the shape of ESR spectra as described above.

The isomer shift of Fe^{3+} in the quenched $0.7Fe_2O_3$-$0.3P_2O_5$ glass (0.43 mm s^{-1}) shows that Fe^{3+} ions in this glass are coordinated by six O^{2-} ions as indi-

cated by Kurkjian and Sigety.[23] The change of isomer shift reflects the change in distance between an iron ion and an O^{2-} ion.[24] A smaller value of isomer shift shows a higher density of 4s-electrons around an iron ion, indicating the shorter distance between an iron ion and an O^{2-} ion. Therefore, the decrease of isomer shift of Fe^{3+} exhibits the decrease of the distance between Fe^{3+} and O^{2-} ions through the crystallization process and the increase of isomer shift of Fe^{2+} shows that the distance between Fe^{2+} and O^{2-} ions in $0.7Fe_2O_3$–$0.3P_2O_5$ glass is smaller than that in $Fe(PO_3)_2$ polycrystal.

The quadrupole splitting of Fe^{3+} directly reflects the geometrical symmetry of the coordination state of O^{2-} ions, because the 3d-orbitals of Fe^{3+} is half filled and the electric field gradient caused by 3d-electrons is tetrahedrally symmetrical. Hence, the decrease of quadrupole splitting of Fe^{3+} through the crystallization process reveals that the coordination state of O^{2-} ions around Fe^{3+} in $0.7Fe_2O_3$–$0.3P_2O_5$ glass is more asymmetrical than that in α-Fe_2O_3.

The increase of isomer shift of Fe^{2+} after $Fe(PO_3)_2$ precipitated may be explained by the decrease of 4s-electron density of Fe^{2+} as described above. Because of the decrease of 4s-electron density, the nucleus of iron in Fe^{2+} interacts more easily with 3d-electrons. Since five 3d-orbitals of Fe^{2+} is filled with six electrons, the electric field gradient induced by 3d-electrons of Fe^{2+} is significantly asymmetrical. So, the quadrupole splitting of Fe^{2+} increases with decreasing 4s-electron density as $Fe(PO_3)_2$ crystals grow.

Structure of $0.7Fe_2O_3$–$0.3P_2O_5$ Glass. The structure and magnetic properties of $0.44Fe_2O_3$–$0.56P_2O_5$ glass were investigated by Egami et al.[2] using susceptibility measurements and neutron diffraction analysis, and by Wedgwood and Wright[3] using neutron diffraction analysis. Although Egami et al. suggested that it is microcrystalline, Wedgwood and Wright gave a different interpretation and proposed that the glass is composed of two phases, one of which is a silica-like network containing alternate FeO_4 and PO_4 tetrahedra and another is chains of PO_4.

For $0.7Fe_2O_3$–$0.3P_2O_5$ glass studied in the present paper, the glass structure of a silica-like network composed of alternate FeO_4 and PO_4 tetrahedra is not suitable, because the coordination number of O^{2-} ion around Fe^{3+} is 6 as shown by the Mössbauer effect measurements. The glass consists of FeO_6 octahedra instead of FeO_4 tetrahedra.

Furthermore, no microcrystalline phase was detected in the present $0.7Fe_2O_3$–$0.3P_2O_5$ glass. As shown by the broader line shape of ESR spectrum and the broader linewidth of Mössbauer spectrum for $0.7Fe_2O_3$–$0.3P_2O_5$ glass, there is a distribution of ligand fields around iron ions in the glass. Moreover, the coordination state around iron ions in the glass is more unsymmetrical than that in the precipitated crystal. These facts show that $0.7Fe_2O_3$–$0.3P_2O_5$ glass is not microcrystalline but has a disordered state.

Besides, the magnetic interaction between iron ions working in $0.7Fe_2O_3$–$0.3P_2O_5$ glass at room temperature was dipole-dipole interaction, indicating that this glass is paramagnetic at room temperature. This fact also ruled out the existence of microcrystals in this glass. If microcrystals were to exist and the glass were superparamagnetic at room temperature, the superparamagnetic line of ESR spectrum would have been detected in this glass and its linewidth would have been narrow as observed at the first stage of precipitation of α-Fe_2O_3 in the crystallization process.

At the present moment it is considered that $0.7Fe_2O_3$–$0.3P_2O_5$ glass contains an assemblage of Fe^{3+} and Fe^{2+} which definitely has a magnetic anisotropy. Although it is still uncertain whether such assemblage is possible in a completely random state or not, it seems easier to make a resonance structure of Fe^{3+} and Fe^{2+} from a slightly disordered state, or *pseudo*-microcrystal or *quasi*-microcrystal structure (like monodomains proposed by Verhelst et al.[25]), which fluctuates a little in the glass.

The authors express their great thanks to Dr. Yasuhito Isozumi at the Kyoto University Radioisotope Research Center for the Mössbauer effect measurements and his kind advice on the discussion.

References

1) A. W. Simpson and J. M. Lucas, *J. Appl. Phys.*, **42**, 2181 (1971).
2) T. Egami, O. A. Sacli, A. W. Simpson, A. L. Terry, and F. A. Wedgwood, *J. Phys. C: Solid State Phys.*, **5**, L261 (1972).
3) F. A. Wedgwood and A. C. Wright, *J. Non-Cryst. Solids*, **21**, 95 (1976).
4) E. J. Friebele, L. K. Wilson, A. W. Dozier, and D. L. Kinser, *Phys. Status. Solidi B*, **45**, 323 (1971).
5) E. M. Gyorgy, K. Nassau, M. Eibschütz, J. V. Waszczak, C. A. Wang, and J. C. Shelton, *J. Appl. Phys.*, **50**, 2883 (1979).
6) H. Laville and J. C. Bernier, *J. Mater. Sci.*, **15**, 73 (1980).
7) O. Horie, Y. Syono, Y. Nakagawa, A. Ito, K. Okamura, and S. Yajima, *Solid State Commun.*, **25**, 423 (1978).
8) Y. Syono, A. Ito, and O. Horie, *J. Phys. Soc. Jpn.*, **46**, 493 (1979).
9) J. P. Sanchez, J. M. Friedt, R. Horne, and A. J. van Duyneveldt, *J. Phys. C: Solid State Phys.*, **17**, 127 (1984).
10) S. K. Mendiratta, R. Horne, and A. J. van Duyneveldt, *Solid State Commun.*, **52**, 371 (1984).
11) J. M. D. Coey, *J. Phys. (Paris), Colloq.*, **35**, C6-89 (1974).
12) J. M. D. Coey, *J. Appl. Phys.*, **49**, 1646 (1978).
13) T. Komatsu and N. Soga, *J. Chem. Phys.*, **72**, 1781 (1980).
14) I. Dzyaloshinsky, *J. Phys. Chem. Solids*, **4**, 241 (1958).
15) T. Moriya, *Phys. Rev. Lett.*, **4**, 228 (1960).
16) P. W. Anderson and P. R. Weiss, *Rev. Mod. Phys.*, **25**, 269 (1953).

17) L. Néel, *Rev. Mod. Phys.*, **25**, 293 (1953).
18) V. K. Sharma and F. Waldner, *J. Appl. Phys.*, **48**, 4298 (1977).
19) S. M. Aharoni and M. H. Litt, *J. Appl. Phys.*, **42**, 352 (1971).
20) C. Kittel, *Phys. Rev.*, **76**, 743 (1946).
21) J. H. Van Vleck, *Phys. Rev.*, **78**, 266 (1950).
22) M. Eibschütz, M. E. Lines, and K. Nassau, *Phys. Rev. B*, **21**, 3767 (1980).
23) C. R. Kurkjian and E. A. Sigety, *Phys. Chem. Glasses*, **9**, 73 (1968).
24) T. Komatsu and N. Soga, *J. Appl. Phys.*, **51**, 601 (1980).
25) R. A. Verhelst, R. W. Kline, A. M. de Graaf, and H. O. Hooper, *Phys. Rev. B*, **11**, 4427 (1975).

 © 1986 The Chemical Society of Japan Bull. Chem. Soc. Jpn., 59, 1087—1094 (1986)

Synthesis of Stable 1,2-Diazocines, 4,7-Disubstituted 3,8-Diaryl-1,2-diazacycloocta-2,4,6,8-tetraenes, and Their Thermolysis

Seiichi YOGI,* Kozo HOKAMA, Kazunori UENO,† and Otohiko TSUGE†,*
Department of Chemistry, Faculty of Science, Ryukyu University, Nishihara, Nakagami-gun, Okinawa 901-24
†Research Institute of Industrial Science, Kyushu University, Kasugakoen, Kasuga 816
(Received November 16, 1985)

Stable 1,2-diazocines, 3,8-diaryl-4,6-dichloro-1,2-diazacycloocta-2,4,6,8-tetraenes, were prepared via a chlorination-dehydrochlorination sequence starting from readily-available 3,8-diaryl-1,2-diazacycloocta-2,8-dienes. When reacted with metal carboxylates in benzene under reflux, the dichloro-1,2-diazocines were converted into stable 4-acyloxy- and/or 4,7-bis(acyloxy)-1,2-diazocines. On the thermolysis in toluene under reflux, all the diazocines gave only pyridine derivatives with extrusion of the corresponding benzonitriles. The thermal behavior of the diazocines are also discussed.

In contrast to the rich chemistry of cyclooctatetraenes,[1] 1,2-diazacycloocta-2,4,6,8-tetraenes (1,2-diazocines) have not attracted much attention. Dibenzo[*c*,*g*][1,2]diazocine[2] and substituted dibenzo[*d*,*f*]-[1,2]diazocines[3] have been prepared and found to be stable, but 1,2-diazocines free of benzo groups were not known until Trost et al.[4] succeeded in an elegant synthesis of the parent 1,2-diazocine **1**, which decomposes slowly in solution at room temperature and rapidly neat, by irradiation of a polycyclic azoalkane (Eq. 1). On the other hand, an attempt to isolate substituted 1,2-diazocines by thermal valence tautomerization of diazabicyclooctatrienes was unsuccessful, but instead substituted benzenes were obtained with the elimination of nitrogen[5] (Eq. 2). Thus, substituted monocyclic 1,2-diazocines have not been prepared up to date.

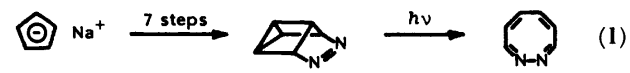

(1)

1

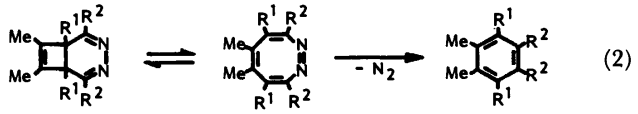

(2)

R¹=H, R²=Ph; R¹=Me, R²=Ph; R¹=R²=Me

As part of the investigation of halogenation-dehydrohalogenations of cyclic azines,[6-8] we have investigated the chlorination–dehydrochlorination of readily-available 3,8-diaryl-1,2-diazacycloocta-2,8-dienes, and it has been found that this classical reaction sequence provided a convenient method for the preparation of chlorinated monocyclic 1,2-diazocines. This is in contrast to an unsuccessful attempt to prepare **1** via a halogenation–dehydrohalogenation sequence through 1,2-bis(*t*-butoxycarbonyl)-1,2-diazacyclooct-5-ene.[9]

This paper describes the preparation of 4,7-dichloro-3,8-diaryl-1,2-diazocines and the conversion of the 4,7-dichloride into acyloxy 1,2-diazocines. In addition. thermolysis of 4,7-disubstituted 1,2-diazocines obtained above is also presented.[10]

Results and Discussion

Preparation of 4,7-Dichloro-3,8-diaryl-1,2-diazocines. Eight-membered cyclic azines, 3,8-diaryl-1,2-diazacycloocta-2,8-dienes, **3a—f**, were prepared by the reaction of 1,4-diaroylbutanes, **2a—f**, with hydrazine hydrate. After several attempted chlorinations under various conditions, it was found that the corresponding 4,4,7,7-tetrachlorides, **4a—f**, were obtained by the chlorination of **3** with sulfuryl chloride (4 equiv) in dichloromethane at room temperature for 1 h.

Dehydrochlorinations of the tetrachloride **4a** were next investigated using various bases. Treatment of **4a** with sodium hydroxide, sodium ethoxide, DBU or ethyl sodiomalonate (each 4 equiv) in refluxing ethanol gave 4,7-dichloro-3,8-diphenyl-1,2-diazocine **5a** as yellow prisms in 76, 79, 61, or 81% yield, respectively. On similar treatment with triethylamine, however, **4a** was unchanged. When treated with ethyl sodiomalonate which was the most effective reagent for the dehydrochlorination of **4a**, other tetrachlorides, **4b—f**, afforded the corresponding stable 1,2-diazocines, **5b—f** (Scheme 1).

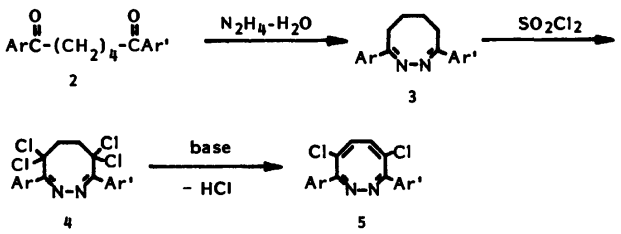

2 3 4 5

a: Ar=Ar'=Ph; b: Ar=Ar'=p-MeC$_6$H$_4$; c: Ar=Ar'=p-ClC$_6$H$_4$;
d: Ar=Ph, Ar'=p-MeC$_6$H$_4$; e: Ar=Ph, Ar'=p-ClC$_6$H$_4$;
f: Ar=p-MeC$_6$H$_4$, Ar'=p-ClC$_6$H$_4$

Scheme 1.

Structural elucidation of the tetrachlorides, **4a—f**, and 1,2-diazocines, **5a—f**, was accomplished on the basis of spectral data. The yields, physical and analytical data of **4** and **5** are summarized in Tables 1 and 2, respectively.

Conversion of 4,7-Dichloro-3,8-diphenyl-1,2-diazo-

Table 1. 3,8-Diaryl-4,4,7,7-tetrachloro-1,2-diazacycloocta-2,8-dienes **4**

	Compd[a]		Yield	Mp	^{1}H-NMR ($CDCl_3$)	Calcd (Found) (%)			M$^+$
	Ar	Ar′	%	θ_m/°C	δ	C	H	N	*m/z*
4a	Ph	Ph	83	150—151	3.14 (4H, s), 7.3—7.8 (10H, m)	54.03 (54.26)	3.53 (3.78)	7.00 (6.90)	398, 400, 402, 404
4b	*p*-MeC_6H_4	*p*-MeC_6H_4	57	167—168	2.46 (6H, s), 3.12 (4H, s), 7.0—7.7 (8H, m)	56.10 (56.11)	4.24 (4.50)	6.54 (6.25)	426, 428, 430, 432
4c	*p*-ClC_6H_4	*p*-ClC_6H_4	50	159—160	3.10 (4H, s), 7.2—7.7 (8H, m)	46.09 (46.35)	2.58 (2.70)	5.97 (6.06)	466, 468, 470, 472, 474
4d	Ph	*p*-MeC_6H_4	48	175—176	2.38 (3H, s), 3.12 (4H, s) 7.1—7.8 (9H, m)	55.10 (55.32)	3.89 (4.05)	6.76 (6.54)	412, 414, 416, 418
4e	Ph	*p*-ClC_6H_4	37	161—162	3.10 (4H, s), 7.2—7.7 (9H, m)	49.74 (49.52)	3.02 (3.12)	6.45 (6.17)	432, 434, 436, 438
4f	*p*-MeC_6H_4	*p*-ClC_6H_4	39	156—157	2.39 (3H, s), 3.08 (4H, s), 7.1—7.7 (8H, m)	50.87 (50.89)	3.37 (3.08)	6.25 (5.95)	446, 448, 450, 452, 454

a) All the tetrachlorides **4** are colorless prisms.

Table 2. 3,8-Diaryl-4,7-dichloro-1,2-diazocines **5**

	Compd[a]		Yield	Mp[b]	^{1}H-NMR ($CDCl_3$)	Calcd (Found) (%)			M$^+$
	Ar	Ar′	%	θ_m/°C	δ	C	H	N	*m/z*
5a[c]	Ph	Ph	81	158—159	6.53 (2H, s, =C**H**), 7.2—7.9 (10H, m)	66.07 (66.09)	3.70 (3.93)	8.56 (8.35)	326, 328, 330,
5b	*p*-MeC_6H_4	*p*-MeC_6H_4	70	180—181	2.41 (6H, s), 6.50 (2H, =C**H**), 7.1—7.8 (8H, m)	67.61 (67.41)	4.54 (4.64)	7.89 (7.89)	354, 356, 358,
5c	*p*-ClC_6H_4	*p*-ClC_6H_4	68	168—170	6.50 (2H, s, =C**H**),7.2—7.8 (8H, m)	54.58 (54.57)	2.55 (2.70)	7.07 (6.83)	394, 396, 398, 400
5d	Ph	*p*-MeC_6H_4	74	158—159	2.39 (3H, s), 6.50 (2H, s =C**H**), 7.1—7.9 (9H, m)	66.87 (66.66)	4.14 (4.08)	8.21 (7.99)	340, 342, 344,
5e	Ph	*p*-ClC_6H_4	35	154—155	6.51 (2H, s, =C**H**),7.1—7.8 (9H, m)	59.78 (60.01)	3.07 (3.33)	7.75 (7.63)	360, 362, 364,
5f	*p*-MeC_6H_4	*p*-ClC_6H_4	47	164—165	2.40 (3H, s), 6.52 (2H, s, =C**H**), 7.1—7.8 (8H, m)	60.74 (60.58)	3.49 (3.78)	7.46 (7.20)	374, 376, 378, 380

a) All the 1,2-diazocines are yellow prisms. b) Melted with decomposition. c) ^{13}C-NMR ($CDCl_3$) δ=127.92 (d), 128.52 (d), 128.83 (s), 130.56 (d), 131.63 (d), 132.72 (s), 150.45 (s, **C**=N).

cine into Acyloxy-Substituted 1,2-Diazocines. In contrast to the parent 1,2-diazocine **1**, 4,7-dichloro-1,2-diazocines **5** obtained above were stable even in benzene under reflux. When heated with excess metal acetate in refluxing benzene, however, **5a** was converted into a mixture of 4-acetoxy-7-chloro-3,8-diphenyl- **6a** and 4,7-di(acetoxy)-3,8-diphenyl-1,2-diazocine **7a**. Similarly, **5a** afforded a mixture of the corresponding mono-acyloxy-, **6b—e**, and bis(acyloxy)-1,2-diazocines, **7b—e**, respectively, when heated with silver isobutyrate, pivalate, benzoate, and cinnamate (Scheme 2). The results are given in Table 3.

When 4-acetoxy-7-chloro-1,2-diazocine **6a** was heated with silver isobutyrate in benzene under reflux, 4-acetoxy-7-isobutyryloxy-1,2-diazocine **8** was isolated

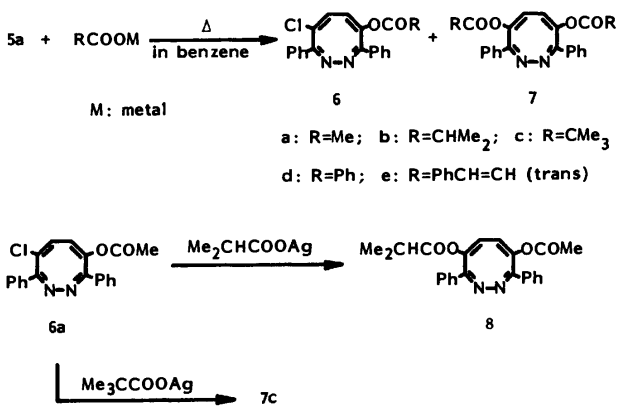

Scheme 2.

Table 3. Reactions of 1,2-Diazocine **5a** with Metal Carboxylates[a)]

RCOOM	5a/RCOOM mol/mol	Reaction time/h	Products yield/%	Recovered 5a/%
MeCOOAg	1/6	3	**6a** 12 **7a** 18	35
MeCOOAg	1/6	6	**6a** 5 **7a** 61	0[b)]
$(MeCOO)_2Pb$	1/4	3	**6a** 10 **7a** 20	30
$(MeCOO)_2Pb$	1/4	6	**6a** 7 **7a** 69	0[b)]
$Me_2CHCOOAg$	1/6	3	**6b** 15 **7b** 17	30
$Me_2CHCOOAg$	1/6	6	**6b** 11 **7b** 43	0[b)]
$Me_3CCOOAg$	1/6	3	**6c** 20 **7c** 17	21
$Me_3CCOOAg$	1/6	6	**6c** 9 **7c** 60	0[b)]
PhCOOAg	1/6	3	**6d** 13 **7d** 15	40
PhCOOAg	1/6	6	**6d** 15 **7d** 52	0[b)]
PhCH=CHCOOAg	1/6	3	**6e** 11 **7e** 30	16

a) The reactions were carried out in benzene under reflux. b) Unidentified viscous products were formed.

Table 4. Thermolysis of Dichloro-1,2-diazocines **5**[a)]

1,2-Diazocine	Products/%[b)] Pyridine **9**	Benzonitrile **10**
5a (Ar=Ar'=Ph)	**9a** (Ar=Ar'=Ph) 88	**10a** (Ar=Ar'=Ph) 71
5b (Ar=Ar'=*p*-MeC_6H_4)	**9b** (Ar=Ar'=*p*-MeC_6H_4) 41	**10b** (Ar=Ar'=*p*-MeC_6H_4) 39
5c (Ar=Ar'=*p*-ClC_6H_4)	**9c** (Ar=Ar'=*p*-ClC_6H_4) 78	**10c** (Ar=Ar'=*p*-ClC_6H_4) 63
5d (Ar=Ph, Ar'=*p*-MeC_6H_4)	**9a** 12, **9b** 19.5	**10a** 14, **10b** 10
5e (Ar=Ph, Ar'=*p*-ClC_6H_4)	**9a** 9.5, **9c** 23.5	**10a** 40, **10c** 19
5f (Ar=*p*-MeC_6H_4, Ar'=*p*-ClC_6H_4)	**9b** 17, **9c** 21	**10b** 16.5, **10c** 13

a) The 1,2-diazocine **5** was heated in dry toluene under reflux for 4 h. b) Analyses of the pyridine(s) and benzonitrile(s) were conducted by vapor-phase chromatography and mass fragmentgraphy, respectively.

in 25% yield, together with bis(isobutyryloxy)-1,2-diazocine **7b** and unchanged **6a**. In the reaction of **6a** with silver pivalate, however, bis(pivaloyloxy)-1,2-diazocine **7c** was obtained as the sole isolated product in 60% yield.

The reaction pathway for the nucleophilic substitution with a carboxylate anion will be described later.

Structural elucidation of **6—8** was accomplished on the basis of spectral data.

Thermolysis of 1,2-Diazocines. Trost et al.[4] reported that the parent 1,2-diazocine **1** thermally decomposed to benzene and pyridine with comparable rates. Thus, we have investigated thermolysis of stable 1,2-diazocines, **5—7**, in order to compare with the thermal behavior of **1**.

We have first investigated thermolysis of 4,7-dichloro-1,2-diazocines **5**. When **5a** was heated without solvent at 160—165 °C (bath temp) for 15 min, 3,6-dichloro-2-phenylpyridine **9a** and benzonitrile **10a** were isolated in 82 and 64% yields, respectively. Although **5a** was stable in refluxing benzene, it decomposed in dry toluene under reflux to give the pyridine **9a** and nitrile **10a**. Similarly, other dichloro-1,2-diazocines, **5b—f**, decomposed to give the corresponding pyridine(s) **9** and benzonitrile(s) **10** under the same conditions (Scheme 3). As shown in Table 4, two pyridines **9** and two benzonitriles **10** were formed in the thermolysis of unsymmetrical 1,2-diazocines, **5d—f**.

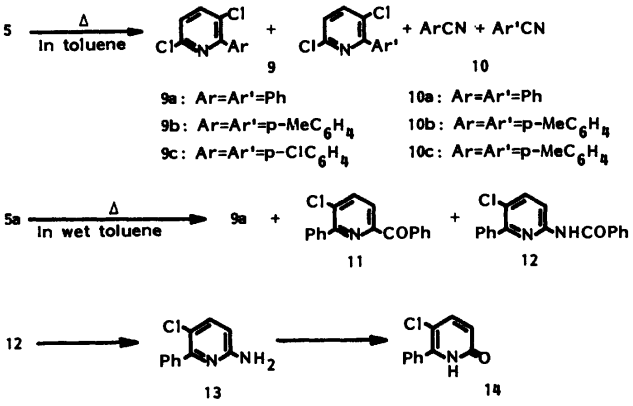

Scheme 3.

It should be emphasized that in contrast with **1** thermolysis of **5** exclusively gave the pyridine **9** with the extrusion of the benzonitrile **10**, and no benzene derivative (terphenyl) was detected in all cases.

On the other hand, when heated in wet toluene under reflux for 2 h, **5a** afforded **9a**, 6-benzoyl-3-chloro-2-phenylpyridine **11**, and 6-benzoylamino-3-chloro-2-phenylpyridine **12** in 16, 25, and 6% yields, respectively, together with the nitrile **10a** (7%) and unidentified oily products. Hydrolysis of **12** with an ethanolic alkali solution gave 6-amino-3-chloro-2-phenylpyridine **13** which was then converted, by diazotization, into 5-chloro-6-phenyl-2-pyridone **14**. The formation of **11** and **12** provides a significant information for the ring-contraction of **5a**.

Next, thermal decomposition of mono(acyloxy)-

and bis(acyloxy)-1,2-diazocines was investigated. In dry toluene under reflux for 6 h, 4-acetoxy-7-chloro-1,2-diazocine **6a** gave the nitrile **10a** (5%) and 3-acetoxy-6-benzoyl-2-phenylpyridine **16** (27%), together with a trace amount of 3-acetoxy-6-chloro-2-phenylpyridine **15**. The pyridine **16** was also obtained in 63% yield in the thermolysis of **6a** in wet toluene under reflux. Reduction of **15** with zinc dust in acetic acid gave 3-acetoxy-2-phenylpyridine **18**, which was identical with an authentic sample prepared from 2-phenyl-3-pyridinol **17**.[11] Hydrolysis of **16** with an ethanolic potassium hydroxide solution under reflux gave 6-benzoyl-2-phenyl-3-pyridinol **19** (Scheme 4).

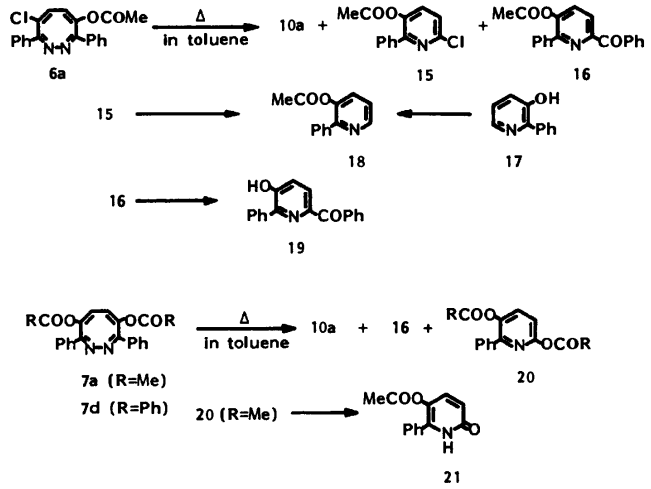

Scheme 4.

Thermolysis of di(acetoxy)-1,2-diazocine **7a** in dry toluene under reflux afforded the nitrile **10a**, benzoylpyridine **16**, and 3,6-di(acetoxy)-2-phenylpyridine **20** (R=Me) in 18, 9, and 30% yields, respectively. Under similar conditions, bis(benzoyloxy)-1,2-diazocine **7a** gave a 43% yield of 3,6-bis(benzoyloxy)-2-phenylpyridine **20** (R=Ph) as the sole isolated product. Hydrolysis of **20** (R=Me) with an ethanolic alkali solution gave 5-acetoxy-6-phenyl-2-pyridone **21** (Scheme 4).

In contrast to the reaction with silver or lead acetate, heating dichloro-1,2-diazocine **5a** with copper(II) acetate in benzene under reflux gave three pyridine derivatives, **11**, **16**, and 3-acetoxy-6-(*N*-chlorobenzimidoyl)-2-phenylpyridine **22**, besides **6a** (Scheme 5). It is evident that the pyridine **11** arises from the thermolysis of **5a** itself, and the pyridines **16** and **22** are the pyrolysates of mono(acyloxy)-1,2-diazocine **6a**. In this case di(acetoxy)-1,2-diazocine **7a** was not formed. The above

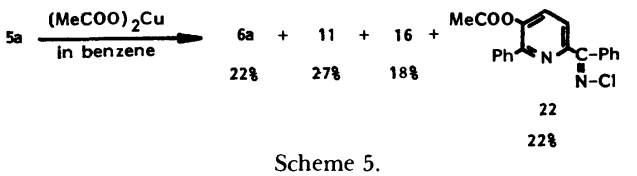

Scheme 5.

results indicate that **5a** and **6a** are pyrolyzed in the presence of copper(II) acetate even in benzene under reflux.

Structural elucidation of products, **9** and **11**—**22**, was accomplished on the basis of spectral data and/or chemical conversion. The pathway for the formation of various pyridines from 1,2-diazocines, **5**—**7**, will be discussed below.

Pathways for the Thermal Reactions of 1,2-Diazocines. On the basis of the above results, it is reasonable to conclude that the thermal reactions of 1,2-diazocines, **5**—**7**, proceed via valence isomers, 1,8-diazabicyclo[4.2.0]octatrienes.

The pathways for the thermal reactions of **5a** are illustrated as the representative example (Scheme 6). 1,2-Diazocine **5a** is thermally isomerized into its valence isomer, diazabicyclooctatriene **A**. The diazabicyclooctatriene **A** decomposes by two routes: One is the formation of the pyridine **9a** with the extrusion of benzonitrile **10a**, and the other the ring opening to an imidoylpyridine **C** (X=Cl or OH) via the azonia intermediate **B**. The benzoyl- **11** and benzoylaminopyridine **12** which were obtained in thermolysis in wet toluene, correspond to the hydrolytic compound of **C** and to the Beckmann rearrangement product of oxime **C** (X=OH), respectively. In addition, the isolation of *N*-(chlorobenzimidoyl)pyridine **22** (Scheme 5) strongly supports the intervension of **A** and **B**.

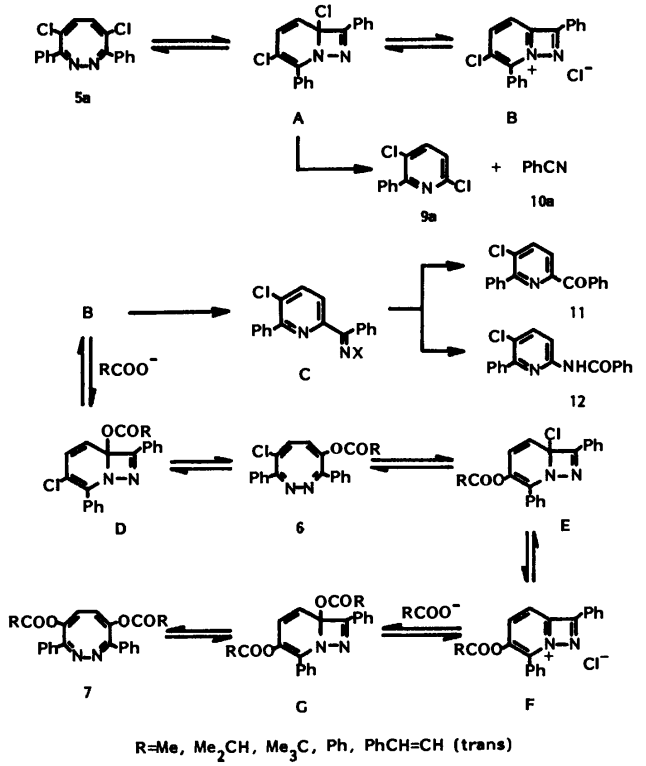

Scheme 6.

The formation of acyloxy-substituted 1,2-diazocines **6** and **7** from **5a** is readily understood by the processes, **5a**→**B**→**D**→**6** and **6**→**E**→**F**→**G**→**7**, respectively. Diazabicyclooctatrienes **D**, **E**, and **G**, and azonia

compound **F** are intervened in these processes.[12]

Experimental

IR spectra were obtained on a JASCO A-302 spectrometer. ^{1}H-NMR spectra were recorded on a Hitachi R-24 or a JEOL FX-100 instrument, and ^{13}C-NMR spectra were measured on a JEOL FX-100 spectrometer at 25.05 MHz. Chemical Shifts are expressed in parts per million downfield from tetramethylsilane. Mass spectra were taken with a Hitachi RMU-6L spectrometer at 70 eV ionization energy. Elemental analyses were performed on a Yanaco MT 2 CHN corder instrument.

Materials. 5-Benzoyl-, 5-(*p*-toluoyl)-, and 5-(*p*-chlorobenzoyl)valeric acids were prepared from the Friedel-Crafts acylation of the corresponding benzene with 5-(ethoxycarbonyl)valeroyl chloride[13] according to the reported method[14] for the preparation of benzoyl derivative. 5-Benzoylvaleric acid: Mp 70—71 °C (lit,[14] mp 71 °C); colorless prisms. 5-(*p*-Toluoyl)valeric acid: Mp 155—156 °C; colorless prisms; IR (KBr) 1734, 1668 cm^{-1}. Found: C, 70.61; H, 7.34%. Calcd for $C_{13}H_{16}O_3$: C, 70.89; H, 7.32%. 5-(*p*-Chlorobenzoyl)valeric acid: Mp 138—139 °C; colorless prisms; IR (KBr) 1719, 1669 cm^{-1}. Found: C 60.13; H, 5.59%. Calcd for $C_{12}H_{13}O_3Cl$: C, 59.88; H, 5.45%. Metal carboxylates were commercially available.

Symmetrical 1,4-Diaroylbutanes. 1,4-Dibenzoyl- **2a**, 1,4-di-(*p*-toluoyl)- **2b**, and 1,4-bis(*p*-chlorobenzoyl)butane **2c** were prepared by the Friedel-Crafts acylation of the corresponding benzene with adipoyl dichloride according to the procedure that was employed by Fuson and Walker[15] for **2a**. **2a**: Mp 106—107 °C (lit,[15] mp 106—107 °C); colorless prisms. **2b**: Mp 133—134 °C; colorless prisms; IR (KBr) 1669 cm^{-1}. Found: C, 81.63; H, 7.45%. Calcd for $C_{20}H_{22}O_2$: C, 81.60; H, 7.53%. **2c**: Mp 175—176 °C; colorless prisms; IR (KBr) 1676 cm^{-1}. Found: C, 64.25; H, 4.70%. Calcd for $C_{18}H_{16}O_2Cl_2$: C, 64.48; H, 4.81%.

Unsymmetrical 1,4-Diaroylbutanes. Typical run is illustrated for the preparation of 1-benzoyl-4-(*p*-toluoyl)-butane **2d**. A solution of 5-(*p*-toluoyl)valeric acid (10 g, 45 mmol) in dry benzene (100 ml) was stirred with phosphorus pentachloride (12 g, 50 mmol) at room temperature for 3 h, and the solution was degassed with dry nitrogen. The above solution of the valeroyl chloride was added over a 30 min period to a stirred mixture of aluminum chloride (20 g, 150 mmol) in benzene (50 ml) at 0—5 °C. Stirring was continued at room temperature for 2 h, and the mixture was then poured onto a mixture of ice and hydrochloric acid. The benzene layer was washed with a 10% aqueous sodium carbonate solution, then with water, and dried over magnesium sulfate. The benzene solution was concentrated in vacuo, and the residue was recrystallized from ethanol to give 7.76 g (62%) of **2d** as colorless prisms: Mp 120—121 °C; IR (KBr) 1673 cm^{-1}. Found: C, 81.19; H, 6.98%. Calcd for $C_{19}H_{20}O_2$: C, 81.39; H, 7.19%.

1-Benzoyl-4-(*p*-chlorobenzoyl)butane **2e** and 1-(*p*-chlorobenzoyl)-4-(*p*-toluoyl)butane **2f** were prepared from the reactions of 5-(*p*-chlorobenzoyl)valeroyl chloride with benzene, and of 5-(*p*-toluoyl)valeroyl chloride with chlorobenzene, respectively.

2e: Yield 73%; mp 125—126 °C; colorless prisms; IR (KBr) 1676 cm^{-1}. Found: C, 71.81; H, 5.52%. Calcd for $C_{18}H_{17}O_2Cl$: C, 71.87; H, 5.70%.

2f: Yield 41%; mp 148—149 °C; colorless prisms; IR (KBr) 1671 cm^{-1}. Found: C, 72.22; H, 6.28%. Calcd for $C_{19}H_{19}O_2Cl$: C, 72.49; H, 6.08%.

3,8-Diaryl-1,2-diazacycloocta-2,8-dienes. Typical run is illustrated for the preparation of 3,8-diphenyl-1,2-diazacycloocta-2,8-diene **3a**. After a solution of 1,4-dibenzoylbutane **2a** (10.6 g, 40 mmol) and hydrazine hydrate (2.0 g, 40 mmol) in dry ethanol (150 ml) was refluxed with concd hydrochloric acid (0.8 ml) for 4 h, the solution was poured into ice water. The slightly yellow-colored solid was collected, and recrystallized from acetone to give 9.1 g (87%) of pure **3a** as colorless prisms: Mp 135—136 °C (lit, [16] mp 136—137 °C).

3,8-Diaryl-1,2-diazacycloocta-2,8-dienes, **3b—f**, were prepared from the reaction of the corresponding 1,4-diaroylbutanes, **2b—f**, with hydrazine hydrate under similar conditions.

3,8-Di(*p*-tolyl)diazacyclooctadiene 3b: Yield 70%; mp 173—174 °C; colorless prisms; MS *m/z* 290 (M$^+$). Found: C, 82.99; H, 7.65; N, 9.62%. Calcd for $C_{20}H_{22}N_2$: C, 82.72; H, 7.64; N, 9.65%.

3,8-Bis(*p*-chlorophenyl)diazacyclooctadiene 3c: Yield 85%; mp 186—187 °C; colorless prisms; MS *m/z* 334, 332, 330 (M$^+$). Found: C, 64.98; H, 5.01; N, 8.26%. Calcd for $C_{18}H_{16}N_2Cl_2$: C, 65.26; H, 4.87; N, 8.46%.

3-Phenyl-8-(*p*-tolyl)diazacyclooctadiene 3d: Yield 75%; mp 124—125 °C; pale yellow prisms; MS *m/z* 276 (M$^+$). Found: C, 82.29; H, 7.38; N, 10.35%. Calcd for $C_{19}H_{20}N_2$: C, 82.57; H, 7.29; N, 10.14%.

3-Phenyl-8-(*p*-chlorophenyl)diazacyclooctadiene 3e: Yield 80%; mp 144—145 °C; pale yellow prisms; MS *m/z* 298, 296 (M$^+$). Found: C, 72.56; H, 5.70; N, 9.15%. Calcd for $C_{18}H_{17}N_2Cl$: C, 72.84; H, 5.77; N, 9.44%.

3-(*p*-Chlorophenyl)-8-(*p*-tolyl)diazacyclooctadiene 3f: Yield 56%; mp 170—171 °C; pale yellow prisms; MS *m/z* 312, 310 (M$^+$). Found: C, 73.57; H, 6.37; N, 9.21%. Calcd for $C_{19}H_{19}N_2Cl$: C, 73.42; H, 6.16; N, 9.01%.

3,8-Diaryl-4,4,7,7-tetrachloro-1,2-diazacycloocta-2,8-dienes 4. A solution of 3,8-diphenyl-1,2-diazacyclooctadiene **3a** (1.3 g, 5 mmol) in dichloromethane (40 ml) was stirred with sulfuryl chloride (2,6 g, 20 mmol) at room temperature for 1 h. The reaction mixture was concentrated in vacuo, and the residue was recrystallized from acetone to give 1.65 g (83%) of 4,4,7,7-tetrachloride **4a**.

Chlorinations of other 3,8-diaryl-1,2-diazacyclooctadienes, **3b—f**, with sulfuryl chloride under similar conditions gave the corresponding tetrachlorides, **4b—f**. The yields, physical and analytical data of tetrachlorides, **4a—f**, are summarized in Table 1.

Dehydrochlorination of Tetrachlorides 4. A solution of tetrachloride **4a** (1.99 g, 5 mmol) in benzene (50 ml) was added into a solution of ethyl sodiomalonate, which was prepared from metallic sodium (0.46 g, 0.02 atom) and diethyl malonate (3.2 g, 20 mmol) in dry ethanol (30 ml), and the resultant mixture was refluxed for 2 h. The mixture was poured into water, and then extracted with benzene (50 ml×2). The benzene extract was dried over magnesium sulfate and concentrated in vacuo. Recrystallization of the residue from ethanol gave 1.3 g (81%) of 4,7-dichloro-3,8-diphenyldiazacyclooctatetraene **5a**.

Dehydrochlorinations of other tetrachlorides, **4b—f**, under similar conditions afforded the corresponding dichlorodiazacyclooctatetraenes, **5b—f**. The yields, physi-

cal and analytical data of dichlorides, **5a—f**, are listed in Table 2.

Reaction of Dichlorodiazacyclooctatetraene 5a with Metal Carboxylates. i) With Silver Acetate. A solution of **5a** (0.65 g, 2 mmol) in benzene (40 ml) was refluxed with silver acetate (2.0 g, 12 mmol) for 6 h. The reaction mixture was filtered, and the precipitate was washed with benzene (50 ml). The combined benzene solution was concentrated in vacuo, and the residue was chromatographed on silica gel to give 0.04 g (5%) of monoacetoxydiazocine **6a** (from benzene elution) and 0.46 g (61%) of diacetoxydiazocine **7a** (from chloroform elution), together with unidentified reddish resinous materials.

6a: Mp 138—139°C (decomp); colorless prisms; IR (KBr) 1760 cm^{-1}; ^{1}H-NMR ($CDCl_3$) δ=1.96 (3H, s, CH_3), 6.20, 6.54 (each 1H, d, =CH, J=4.2 Hz), 7.3—7.5 (6H, m), 7.6—7.8 (4H, m); MS m/z 352, 350 (M^+). Found: C, 68.17; H, 4.38; N, 7.74%. Calcd for $C_{20}H_{15}N_2O_2Cl$: C, 68.47; H, 4.31; N, 4.31%.

7a: Mp 186—188°C (decomp); colorless prisms; IR (KBr) 1760 cm^{-1}; ^{1}H-NMR ($CDCl_3$) δ=1.96 (6H, s, CH_3), 6.23 (2H, s, =CH), 7.2—7.5 (6H, m), 7.6—7.8 (4H, m); ^{13}C-NMR ($CDCl_3$) δ=20.5 (q, CH_3), 118.3 (d, 5- and 6-C), 127.8, 128.4, 130.0 (each d), 133.5 (s), 145.1 (s, 4- and 7-C), 149.0 (s, C=N), 166.9 (s, C=O); MS m/z 374 (M^+). Found: C, 70.36; H, 4.82, N, 7.32%. Calcd for $C_{22}H_{18}N_2O_4$: C, 70.58; H, 4.85; N, 7.48%.

ii) With Lead Acetate. A solution of **5a** (0.32 g, 1 mmol) in benzene (20 ml) was refluxed with lead acetate (1.3 g, 4 mmol) for 6 h. Similar work-up of the reaction mixture gave 25 mg (7%) of **6a** and 258 mg (69%) of **7a**. The result of the reaction for 3 h is shown in Table 3.

iii) With Silver Isobutyrate. A solution of **5a** (0.65 g, 2 mmol) and silver isobutyrate (2.4 g, 12 mmol) in benzene (40 ml) was refluxed for 6 h. Similar work-up gave 80 mg (11%) of mono(isobutyryloxy)diazocine **6b** and 0.37 g (43%) of bis(isobutyryloxy)diazocine **7b**.

6b: Mp 135—136°C (decomp); colorless prisms; IR (KBr) 1744 cm^{-1}; ^{1}H-NMR ($CDCl_3$) δ=0.85, 0.94 (each 3H, d, CH_3, J=7.6 Hz), 2.40 (1H, m, CH), 6.18, 6.53 (each 1H, d, =CH, J=4.2 Hz), 7.2—7.5 (6H, m), 7.5—7.9 (4H, m); MS m/z 380, 378 (M^+). Found: C, 69.53; H, 5.09; N, 7.06%. Calcd for $C_{22}H_{19}N_2O_2Cl$: C, 69.74; H, 5.06; N, 7.40%.

7b: Mp 160—162°C (decomp); colorless needles; IR (KBr) 1757 cm^{-1}; ^{1}H-NMR ($CDCl_3$) δ=0.89, 0.99 (each 6H, d, CH_3, J=7.6 Hz), 2.46 (2H, m, CH), 6.23 (2H, s, =CH), 7.2—7.5 (6H, m), 7.5—7.9 (4H, m); MS m/z 430 (M^+). Found: C, 72.55; H, 6.37; N, 6.60%. Calcd for $C_{26}H_{26}N_2O_4$: C, 72.54; H, 6.09; N, 6.51%.

The result of the reaction for 3 h is shown in Table 3.

iv) With Silver Pivalate. A mixture of **5a** (0.65 g, 2 mmol) and silver pivalate (2.5 g, 12 mmol) in benzene (40 ml) was refluxed for 6 h. Similar work-up afforded 70 mg (9%) of mono(pivaloyloxy)diazocine **6c** and 0.55 g (60%) of bis(pivaloyloxy)diazocine **7c**.

6c: Mp 154—156°C (decomp); colorless needles; IR (KBr) 1743 cm^{-1}; ^{1}H-NMR ($CDCl_3$) δ=0.97 (9H, s, CH_3), 6.13, 6.55 (each 1H, d, =CH, J=4.8 Hz), 7.3—7.5 (6H, m), 7.5—7.9 (4H, m); MS m/z 394, 392 (M^+). Found: C, 70.06; H, 5.41; N, 6.92%. Calcd for $C_{23}H_{21}N_2O_2Cl$: C, 70.31; H, 5.39; N, 7.13%.

7c: Mp 186—188°C (decomp); colorless needles; IR (KBr) 1753 cm^{-1}; ^{1}H-NMR ($CDCl_3$) δ=0.97 (18H, s, CH_3), 6.22 (2H, s, =CH), 7.2—7.5 (6H, m), 7.6—7.9 (4H, m); MS m/z 458 (M^+). Found: C, 73.07; H, 6.87; N, 6.01%. Calcd for $C_{28}H_{30}N_2O_4$: C, 73.34; H, 6.59; N, 6.11%.

The result of the reaction for 3 h is given in Table 3.

v) With Silver Benzoate. The similar reaction of **5a** (0.65 g, 2 mmol) with silver benzoate (2.7 g, 12 mmol) in benzene (40 ml) under reflux for 6 h afforded 0.12 g (15%) of mono(benzoyloxy)diazocine **6d** and 0.51 g (52%) of bis(benzoyloxy)diazocine **7d**.

6d: Mp 151—152°C (decomp); colorless needles; IR (KBr) 1735 cm^{-1}; ^{1}H-NMR ($CDCl_3$) δ=6.42, 6.63 (each 1H, d, =CH, J=4.2 Hz), 7.2—7.6 (9H, m), 7.6—8.1 (6H, m); MS m/z 414, 412 (M^+). Found: C, 72.43; H, 4.21; N, 6.54%. Calcd for $C_{25}H_{17}N_2O_2Cl$: C, 72.72; H, 4.15, N, 6.79%.

7d: Mp 207—208°C; colorless needles; IR (KBr) 1730 cm^{-1}; ^{1}H-NMR ($CDCl_3$) δ=6.20 (2H, s, =CH), 7.2—7.5 (12H, m), 7.6—8.1 (8H, m); MS m/z 498 (M^+). Found: 76.93; H, 4.59; N, 5.49%. Calcd for $C_{32}H_{22}N_2O_4$: C, 77.09; H, 4.45; N, 5.62%.

The result of the reaction for 3 h is shown in Table 3.

vi) With Silver Cinnamate. The similar reaction of **5a** (0.32 g, 1 mmol) with silver cinnamate (1.53 g, 6 mmol) in benzene (20 ml) under reflux for 3 h gave 48 mg (11%) of mono(cinnamoyloxy)diazocine **6e** and 166 mg (30%) of bis(cinnamoyloxy)diazocine **7e**, together with recovery of 51 mg (16%) of **5a**.

6e: Mp 153—155°C (decomp); colorless needles; IR (KBr) 1730 cm^{-1}; ^{1}H-NMR ($CDCl_3$) δ=6.23 (1H, d, CH=CHCO, J=15.0 Hz), 6.30, 6.56 (each 1H, d, =CH, J=4.8 Hz), 7.70 (1H, d, CH=CHCO, J=15.0 Hz), 7.2—7.5 (16H, m), 7.6—7.9 (4H, m); MS m/z 440, 438 (M^+). Found: C, 73.77; H, 4.62; N, 6.25%. Calcd for $C_{27}H_{19}N_2O_2Cl$: C, 73.89; H, 4.36; N, 6.38%.

7e: Mp 196—197°C (decomp); colorless needles; IR (KBr) 1730 cm^{-1}; ^{1}H-NMR ($CDCl_3$) δ=6.25 (1H, d, CH=CHCO, J=15.0 Hz), 6.41 (2H, s, =CH), 7.62 (1H, d, CH=CHCO, J=15.0 Hz), 7.2—7.5 (16H, m), 7.6—7.9 (4H, m); MS m/z 550 (M^+). Found: C, 78.77; H, 5.03; N, 4.92%. Calcd for $C_{36}H_{26}N_2O_4$: C, 78.53; H, 4.76; N, 5.09%.

Reaction of Monoacetoxydiazocine 6a with Silver Isobutyrate. A solution of **6a** (0.22 g, 0.6 mmol) in benzene (20 ml) was refluxed with silver isobutyrate (1.0 g, 5 mmol) for 3 h. The reaction mixture was filtered, and the precipitate was washed with benzene (50 ml). The combined benzene solution was concentrated in vacuo, and the residue was recrystallized from benzene-petr. ether (1:1) to give 60 mg (25%) of 4-acetoxy-7-(isobutyryloxy)diazocine **8**. The mother liquor contained unchanged **6a** and bis(isobutyryloxy)diazocine **7b**, but further purification was not carried out.

8: Mp 173—175°C (decomp); colorless needles; IR (KBr) 1760, 1752 cm^{-1}; ^{1}H-NMR ($CDCl_3$) δ=0.89, 1.10 (each 3H, d, CH_3), 1.96 (3H, s, $COCH_3$), 2.43 (1H, m, CH), 6.22 (2H, s, =CH), 7.3—7.6 (6H, m), 7.6—8.0 (4H, m); MS m/z 402 (M^+). Found: C, 71.59; H, 5.46; N, 6.74%. Calcd for $C_{24}H_{22}N_2O_4$: C, 71.62; H, 5.51; N, 6.96%.

Similar reaction of **6a** (0.35 g, 1 mmol) with silver pivalate (1.0 g, 4.8 mmol) in benzene (20 ml) gave 0.28 g (60%) of bis(pivaloyloxy)diazocine **7c**.

Thermolysis of Dichlorodiazocine 5a. i) Without Solvent. Dichlorodiazocine **5a** (1.0 g, 3 mmol) in a test tube was heated at 160—165°C (bath temp) for 15 min. The pyrolysate was chromatographed on alumina (benzene) to give 0.5 g (82%) of 3,6-dichloro-2-phenylpyridine **9a** and 0.2 g (64%) of benzonitrile **10a**.

9a: Mp 100—101 °C; colorless needles; ^{1}H-NMR ($CDCl_3$) δ=7.10, 7.59 (each 1H, d, pyridine ring **H**, J=8.0 Hz), 7.3—7.8 (5H, m); MS m/z 227, 225, 223 (M^+). Found: C, 59.17; H, 3.33; N, 6.17%. Calcd for $C_{11}H_7NCl_2$: C, 58.95; H, 3.15; N, 6.25%.

ii) In Dry Toluene. A solution of **5a** (1.0 g) in dry toluene (20 ml) was refluxed for 3 h. The reaction mixture was concentrated in vacuo, and the residue was chromatographed on alumina to give **10a** (0.18 g, 57%) and the pyridine **9a** (0.48 g, 70%) (from benzene elution), and unidentified viscous materials (0.2 g).

iii) In Wet Toluene. A solution of **5a** (3.0 g) in toluene (30 ml) containing 3 drops of water was refluxed for 3 h. Chromatography (Al_2O_3) of the residue gave **10a** (0.07 g, 7%), **9a** (0.43 g, 16%), 6-benzoyl-3-chloro-2-phenylpyridine **11** (0.52 g, 25%) from benzene elution, and 6-benzoylamino-3-chloro-2-phenylpyridine **12** (0.16 g, 6%) from chloroform elution.

11: Mp 119—120 °C; colorless needles; IR (KBr) 1650 cm^{-1}; ^{1}H-NMR ($CDCl_3$) δ=7.2—8.2 (10H, m), 7.98 (2H, s, pyridine ring **H**); ^{13}C-NMR ($CDCl_3$) δ=123.76, 127.97, 129.05, 129.45, 131.04 (each d), 132.86, 135.86, 137.32 (each s), 139.08 (d), 152.76, 154.76, 192.04 (each s); MS m/z 295, 293 (M^+). Found: C, 73.51; H, 4.30; N, 4.68%. Calcd for $C_{18}H_{12}NOCl$: C, 73.60; H, 4.12; N, 4.77%.

12: Mp 135—136 °C; yellow prisms; IR (KBr) 3320, 1665 cm^{-1}; ^{1}H-NMR ($CDCl_3$) δ=7.76, 8.27 (each 1H, d, pyridine ring **H**, J=8.4 Hz), 7.3—8.0 (10H, m), 8.70 (1H, broad s, N**H**); MS m/z 310, 308 (M^+). Found: C, 69.97; H, 4.13; N, 8.91%. Calcd for $C_{18}H_{13}ON_2Cl$: C, 70.02; H, 4.24; N, 9.07%.

Conversion of the Pyridine 12 into 5-Chloro-6-phenyl-2-pyridone 14. A solution of **12** (0.1 g) in ethanol (30 ml) containing potassium hydroxide (0.2 g) was refluxed for 4 h. The reaction mixture was concentrated in vacuo, and water (10 ml) was added to the residue which was extracted with chloroform (30 ml). The extract was concentrated in vacuo, and the residue was chromatographed on silica gel to give 40 mg (67%) of 6-amino-3-chloro-2-phenylpyridine **13** from the chloroform elution.

13: Mp 94—95 °C; yellow needles; IR (KBr) 3460 cm^{-1}; ^{1}H-NMR ($CDCl_3$) δ=4.60 (2H, broad s, N**H**$_2$), 6.34, 7.42 (each 1H, d, pyridine ring **H**, J=8.4 Hz), 7.24—7.74 (5H, m); MS m/z 206, 204 (M^+). Found: C, 64.56; H, 4.35; N, 13.87%. Calcd for $C_{11}H_9N_2Cl$: C, 64.46; H, 4.43; N, 13.69%.

After diazotization of the pyridine **13** (40 mg) with sodium nitrite in aqueous sulfuric acid (concd H_2SO_4 (1 ml) and H_2O (5 ml)) at 0—5 °C, the reaction mixture was heated at 50—60 °C for 1 h. The mixture was extracted with chloroform (20 ml×2) and the extract was concentrated in vacuo to leave 13 mg (32%) of 5-chloro-6-phenyl-2-pyridone **14**.

14: Mp 204—206 °C; colorless needles; IR (KBr) 2700—3100, 1660, 1635 cm^{-1}; ^{1}H-NMR ($CDCl_3$) δ=6.42, 7.35 (each 1H, d, pyridine ring **H**, J=9.0 Hz), 7.48 (5H, m). Found: C, 63.99; H, 4.05; N, 6.81%. Calcd for $C_{11}H_8NOCl$: C, 64.24; H, 3.92; N, 6.81%.

Thermolysis of Dichlorodiazocine 5b. A solution of **5b** (0.5 g, 1.4 mmol) in dry toluene (10 ml) was refluxed for 4 h. A similar work-up and chromatography (Al_2O_3) of the pyrolysate gave 30 mg (18%) of tolunitrile **10b** and 0.11 g (41.5%) of 3,6-dichloro-2-(*p*-tolyl)pyridine **9b** (from benzene elution) and unidentified viscous materials (0.25 g).

9b: Mp 63—64 °C; colorless needles; ^{1}H-NMR ($CDCl_3$) δ=2.42 (3H, s), 7.19, 7.65 (each 1H, d, pyridine ring **H**, J=8.1 Hz), 7.1—7.8 (4H, m); MS m/z 241, 240, 239, 238, 237 (M^+). Found: C, 60.66; H, 4.08; N, 5.70%. Calcd for $C_{12}H_9NCl_2$: C, 60.53; H, 3.81; N, 5.88%.

Tolunitrile **10b** was identified by comparison of an authentic sample.

Thermolysis of Dichlorodiazocine 5c. A solution of **5c** (0.5 g, 1.3 mmol) in dry toluene (10 ml) was refluxed for 4 h. By the similar work-up *p*-chlorobenzonitrile **10c** (90 mg, 52%) and 3,6-dichloro-2-(*p*-chlorophenyl)pyridine **9c** (0.23 g, 70%) were obtained together with unidentified viscous materials (0.1 g).

9c: Mp 125—126 °C; yellow needles; ^{1}H-NMR (CCl_4) δ=7.12, 7.62 (each 1H, d, pyridine ring **H**, J=8.1 Hz), 7.2—7.8 (4H, m); MS m/z 263, 261, 259, 257 (M^+). Found: C, 50.89; H, 2.08; N, 5.47%. Calcd for $C_{12}H_6NCl_3$: C, 51.10; H, 2.38; N, 5.42%.

p-Chlorobenzonitrile **10c** was identified by comparison of an authentic sample.

Thermolysis of unsymmetrical diazocines, **5d—f**, was performed in toluene under the similar conditions, and the pyrolysates were analyzed using gas chromatography. The results are shown in Table 4.

Thermolysis of 4-Acetoxy-7-chlorodiazocine 6a. i) In Dry Toluene. A solution of **6a** (0.73 g, 2.1 mmol) in dry toluene (20 ml) was refluxed for 6 h. The similar work-up of the pyrolysate gave 10 mg (ca. 5%) of benzonitrile **10a**, a trace amount of 3-acetoxy-6-chloro-2-phenylpyridine **15**, and 0.22 g (27%) of 3-acetoxy-6-benzoyl-2-phenylpyridine **16**, together with intractable materials.

ii) In Wet Toluene. A solution of **6a** (0.35 g) in toluene (10 ml) containing 2 drops of water was refluxed for 6 h. By the similar work-up 0.25 g (63%) of the pyridine **16** was only isolated.

15: Oil; IR (neat) 1770 cm^{-1}; ^{1}H-NMR ($CDCl_3$) δ=2.10 (3H, s), 7.15—7.95 (7H, m); MS m/z 249, 247 (M^+).

16: Mp 60—61 °C; pale yellow needles; IR (KBr) 1760, 1670 cm^{-1}; ^{1}H-NMR ($CDCl_3$) δ=2.20 (3H, s), 7.25—8.3 (12H, m); MS m/z 317 (M^+). Found: C, 75.92; H, 4.84; N, 4.54%. Calcd for $C_{20}H_{15}NO_3$: C, 75.69; H, 4.76; N, 4.41%.

3-Acetoxy-2-phenylpyridine 18. A solution of the pyridine **15** (0.16 g) in acetic acid (20 ml) was refluxed with zinc dust for 5 h. After filtration, the filtrate was poured into water, and extracted with benzene. The benzene extract was washed with water, dried over magnesium sulfate, and then concentrated in vacuo. The residue was chromatographed on silica gel to give 0.05 g (36%) of **18** from the chloroform elution. The compound **18** was identical with an authentic sample prepared from the acetylation of 2-phenyl-3-pyridinol **17**[11]: Oil; ^{1}H-NMR ($CDCl_3$) δ=2.15 (3H, s), 6.98—7.85 (7H, m), 8.52 (1H, dd, pyridine ring **H**, J=2.2, 4.4 Hz); MS m/z 213 (M^+).

Hydolysis of the Pyridine 16. A solution of **16** (0.2 g) in ethanol (10 ml) containing potassium hydroxide (0.1 g) was refluxed for 2 h. The reaction mixture was poured into water, and extracted with benzene. The benzene extract was concentrated in vacuo, and recrystallization of the residue from ethanol gave 0.1 g (73%) of 6-benzoyl-2-phenyl-3-pyridinol **19**.

19: Mp 172—173 °C; colorless prisms; IR (KBr) 3100, 1625 cm^{-1}; ^{1}H-NMR ($CDCl_3$) δ=4.50 (1H, br, O**H**), 7.25—8.25 (12H, m); ^{13}C-NMR ($CDCl_3$) δ=124.60, 126.13, 128.13, 128.25, 128.72, 129.19, 131.86, 132.89 (each d), 136.25, 136.95, 145.13, 145.54, 154.29, 193.54 (each s); MS m/z 275 (M^+).

Found: C, 78.83; H, 4.65; N, 5.09%. Calcd for $C_{18}H_{13}NO_2$: C, 78.53; H, 4.76; N, 5.09%.

Thermolysis of 4,7-Di(acetoxy)diazocine 7a. A solution of **7a** (0.61 g, 1.6 mmol) in dry toluene (20 ml) was refluxed for 6 h. By the similar work-up 0.13 g (30%) of 3,6-di-(acetoxy)-2-phenylpyridine **20** (R=Me) was isolated together with benzonitrile **10a** (30 mg, 18%) and the benzoylpyridine **16** (50 mg, 9%).

Hydrolysis of **20** (R=Me, 0.2 g) with an ethanolic alkali solution (0.2 g $NaHCO_3$ in 20 ml EtOH) under reflux gave 0.11 g (65%) of 5-acetoxy-6-phenyl-2-pyridone **21**.

20 (R=Me): Oil; IR (neat) 1755, 1710 cm^{-1}; ^{1}H-NMR ($CDCl_3$) δ=2.11, 2.28 (each 3H, s), 7.03, 7.53 (each 1H, d, pyridine ring **H**, J=7.8 Hz), 7.25—7.8 (5H, m).

21: Mp 176—177 °C; colorless needles; IR (KBr) 2900, 2832, 1757, 1658, 1640 cm^{-1}; ^{1}H-NMR ($CDCl_3$) δ=2.07 (3H, s), 6.41, 7.23 (each 1H, d, pyridine ring **H**, J=10.8 Hz), 7.41 (5H, m); MS m/z 229 (M^+). Found: C, 68.31; H, 5.00; N, 6.33%. Calcd for $C_{13}H_{11}NO_3$: C, 68.11; H, 4.84; N, 6.11%.

Thermolysis of 4,7-Bis(benzoyloxy)diazocine 7d. A solution of **7d** (0.3 g, 0.6 mmol) in dry toluene (20 ml) was refluxed for 6 h. The similar work-up afforded 0.1 g (43%) of 3,6-bis(benzoyloxy)-2-phenylpyridine **20** (R=Ph) as the sole isolated product: Mp 175—176 °C; colorless needles; IR (KBr) 1733 cm^{-1}. Found: C, 75.83; H, 4.06; N, 3.44%. Calcd for $C_{25}H_{17}NO_4$: C, 75.94; H, 4.33; N, 3.54%.

Reaction of Dichlorodiazocine 5a with Copper(II) Acetate. A solution of **5a** (0.32 g, 1 mmol) in benzene (20 ml) was refluxed with copper(II) acetate (0.72 g, 4 mmol) for 6 h. The reaction mixture was filtered, and the precipitate was washed with benzene (30 ml). The combined benzene solution was dried over magnesium sulfate, and concentrated in vacuo. The residue was chromatographed on silica gel using benzene as an eluent to give 80 mg (27%) of 6-benzoyl-3-chloro-2-phenylpyridine **11**, 60 mg (18%) of 3-acetyl-6-benzoyl-2-phenylpyridine **16**, 80 mg (22%) of 4-acetoxy-6-chloro-3,7-diphenylidiazocine **6a**, and 70 mg (22%) of 3-acetoxy-6-(*N*-chlorobenzimidoyl)-2-phenylpyridine **22**. The compound **22** was readily hydrolyzed into a mixture of **16** and **19**.

22: Mp 139—141 °C; pale yellow needles; IR (KBr) 1755 cm^{-1}; ^{1}H-NMR ($CDCl_3$) δ=2.13 (3H, s), 7.2—7.5 (10H, m), 7.43, 8.00 (each 1H, d, pyridine ring **H**, J=8.0 Hz). Found: C, 68.18; H, 4.40; N, 8.01%. Calcd for $C_{20}H_{15}N_2O_2Cl$: C, 68.47; H, 4.31; N, 7.99%.

References

1) L. A. Paquette, *Tetrahedron*, **31**, 2855 (1975).

2) W. W. Paudler and A. G. Zeiler, *J. Org. Chem.*, **34**, 3237 (1969). However, they gave the erroneous nomenclature, dibenzo[*b*,*f*][1,2]diazocine, for dibenzo[*c*,*g*][1,2]diazocine.

3) D. M. Hall, J. E. Ladburg, M. S. Lesslie, and E. E. Turner, *J. Chem. Soc.*, **1956**, 3475; R. G. R. Bacon and W. S. Lindsay, *ibid.*, **1958**, 1382.

4) B. M. Trost and R. M. Cory, *J. Am. Chem. Soc.*, **93**, 5573 (1971); B. M. Trost, P. H. Schudder, R. M. Cory, N. J. Turro, V. Ramamurthy, and T. J. Katz, *J. Org. Chem.*, **44**, 1264 (1979).

5) G. Maier, V. Heep, M. Wieβler, and S. Straβer, *Chem. Ber.*, **102**, 1928 (1969).

6) O. Tsuge and K. Kamata, *Heterocycles*, **3**, 15 (1975).

7) O. Tsuge and K. Kamata, *Heterocycles*, **3**, 547 (1975).

8) O. Tsuge, K. Kamata, and S. Yogi, *Bull. Chem. Soc. Jpn.*, **50**, 2153 (1977).

9) L. A. Carpino and J. P. Masaracchia, *J. Org. Chem.*, **37**, 1851 (1972).

10) A part of these results has been already reported as a preliminary communication: S. Yogi, K. Hokama, and O. Tsuge, *Chem. Lett.*, **1982**, 1579.

11) H. Leditschke, *Chem. Ber.*, **85**, 202 (1952).

12) Although the intervension of homoazirinium salts like **B'** was proposed in the previous communication,[10]

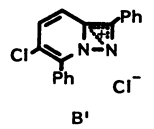

B'

we wish to correct the intervension of homoazirinium salts to that of such azonia compounds as **B** and **F**. Two diazabicyclooctatrienes, **E** and **H**, are possible for valence isomers of **6**. In the thermolysis of **6a**, however, no products arisen from **H** were isolated (Scheme 4). On the other hand, the data in Table 4 indicate that unsymmetrical 1,2-diazocines, **5d—f**, are isomerized into two diazacyclooctatrienes **I** and **J**.

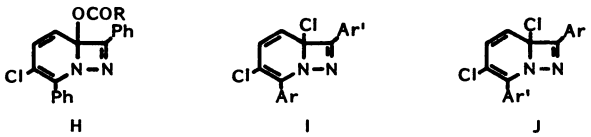

H I J

13) E. E. Blaise and A. Koehler, *Bull. Soc. Chim. France*, **7**, 219 (1910).

14) D. Papa, E. Schwenk, and H. Hankin, *J. Am. Chem. Soc.*, **69**, 3018 (1947).

15) R. C. Fuson and J. T. Walker, *Org. Syn.*, Coll. II, 169 (1943).

16) C. G. Overberger and I. Tashlick, *J. Am. Chem. Soc.*, **81**, 217 (1959).

Anthracene Derivatives as Acceptors of the Reaction Intermediate Generated by the Decomposition of Tropone Tosylhydrazone Sodium Salt. Regioselective Cycloaddition Reactions of Cycloheptatrienylidene or 1,2,4,6-Cycloheptatetraene with 9-Substituted Anthracene Derivatives

Katsuhiro SAITO* and Hiraku ISHIHARA
Department of Chemistry, Nagoya Institute of Technology, Gokiso-cho, Showa-ku, Nagoya 466
(Received July 25, 1985)

The rearrangement of the carbene, cycloheptatrienylidene, to the allene, 1,2,4,6-cycloheptatetraene, was investigated. Tropone tosylhydrazone sodium salt, the precursor of cycloheptatrienylidene was decomposed in the presence of various kinds of 9-substituted anthracene derivatives to afford cycloaddition products, whose structures show that the carbenic carbon atom or the allenic carbon atom of the carbene or the allene attacks the carbon atoms at the 10-position of the anthracenes. It is obvious that the electronic natures of the substituents on the anthracenes have no effect on the regioselectivity of the addition reaction, suggesting that the reaction proceeds via 1,2,4,6-cycloheptatetraene, which is derived from the cycloheptatrienylidene initially generated from the tosylhydrazone.

The structure of the nucleophilic singlet carbene, cycloheptatrienylidene (**2**), is considered to be the 6π-electron aromatic structure (**2a**) bearing the divalent carbenic carbon atom of sp^2 hybridization (**2b**).[1] The experimental facts that **2** adds to maleonitrile and fumaronitrile with stereospecificity[1b,c] and that the relative rate constants of the addition reaction of **2** with styrene derivatives correlate well with the Hammet equation ($\rho=+1.05$)[1d] prove the singlet and the nucleophilic natures of **2** respectively.

Recently, the possibility of interconversion between **2** and the allene, 1,2,4,6-cycloheptatetraene (**4**), which has a twisted structure bearing the sp hybridized allenic carbon atom (**4a**), has attracted the attention of chemists, and a number of papers have been published.[2] One of them says that **2** does not represent an energy minimum; instead, it is the transition state for the interconversion of enantiometric allenes.[2d,g,h] Previously, the present authors reported an example of the rearrangement of **2** to **4**, in connection with the [4+2]-type cycloaddition reactions of **2** with a variety of enophiles.[2c,e,f] We have now examined the reaction of **2** with various kinds of 9-substituted anthracene derivatives in order to get additional evidence on the rearrangement with the expectation that, if the reaction proceeds via the nucleophilic carbene **2**, the introduction of the electron-donating or the electron-attracting substituents on anthracene will affect the regioselectivity or the product yields of the reaction. Here the result of these reactions will be reported.

Results and Discussion

When tropone tosylhydrazone sodium salt (**1**) was decomposed at 125 °C for 15 min in anhydrous diglyme in the presence of one molar equivalent of the anthracene derivatives (**5a—g**), the respective adducts (**6a—g**) were obtained together with quantitative amounts of nitrogen gas and sodium *p*-toluenesulfinate (**3**). The yields, the chemical shifts, and the coupling constants in the NMR spectra of the adducts are summarized in the table.

The structures of the adducts were determined on the basis of their physical properties and confirmed by a comparison of the spectral properties, especially the NMR spectral properties, with those of the analogous compounds.[2e,3] The singlet signals due to the methine proton (H_a) in the NMR spectra definitely show the arrangement of the double bonds in the cycloheptatriene moiety of the adducts, showing the regioselectivity of the reaction.

These structures of the adducts show that the carbenic carbon atom of **2** or the allenic carbon atom of **4** selectively attacks the carbon atoms at the 10-position of the anthracene derivatives.

Two possible mechanisms may be thought of for

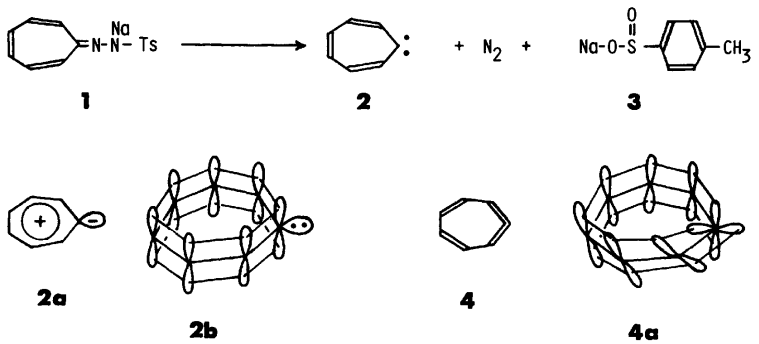

Fig. 1.

the reaction. Pathway A includes the carbene intermediate **2**, which reacts with **5** to afford the tropylium cation intermediate (**7**). Subsequent cyclization reaction of the intermediate leads to the formation of **6**. Closer examination into Pathway A, however, reveals that it does not adequately explain the observed products. That the intermediate **2** is proved to be a nucleophilic carbene; therefore, it seems reasonable that the carbenic carbon atom of **2** attacks the electron-deficient carbon atoms at the 10-position of **5b—g**, which have electron-withdrawing groups, to give the observed adducts, **6b—g**, via the intermediates **7b—g**. However, as for the other substance, anthracene **5a**, which has the electron-donating group, the carbenic carbon atom of **2** should attack the carbon atom at the 9-position to give the imaginary adducts **8a**, for in this anthracene the electron density at the 9-position is less than that at the 10-position. The experimental result shows that the attacking positions are the same at the 10-position for all of the **5**, without distinction of the electronic natures of the substituents. The lack of any obvious effect on the product yields by the electronic natures of the substituents also seems to suggest that the reaction does not proceed via **2**.

Table 1. Yields and NMR Spectral Data of the Adducts

No	6a	6b	6c	6d	6e	6f	6g
X	CH_3	Ph	Cl	Br	$COCH_3$	CN	NO_2
Yield	15%	4%	8%	12%	14%	8%	25%
NMR spectral data*							
H_a (s)	4.82	4.90	4.82	4.82	4.82	4.83	4.83
H_b (d) J_{bc}=5	1.95	2.64	2.55	2.61	2.67	2.59	2.97
H_c (dd) J_{bc}=5, J_{cd}=10	4.52	4.53	4.79	4.76	4.48	4.68	4.57
H_d (d) J_{cd}=10	5.90	5.91	5.96	5.96	5.94	5.81	5.91
H_e H_f (m) H_g	6.25	6.24	6.24	6.24	6.31	6.10	6.25
CH_3 (s)	2.03				2.60		
Ph (m)	6.9—7.5 (8H)	6.9—7.5 (13H)	7.0—7.8 (8H)	7.0—7.8 (8H)	7.0—7.5 (8H)	6.9—7.8 (8H)	7.0—7.5 (8H)

* Chemical shifts in δppm and coupling constants in Hz.

Pathway B involves the rearrangement of **2** to the allene intermediate **4**. Allenes are known to proceed radical-type reactions.[4] The radical-type attack of the allenic carbon atom of **4** on the carbon atom at the 10-position of **5** gives the diradical intermediate **9**, which then cyclizes to form **6**. When the allenic carbon atom attacks the 9-position carbon of **5**, the imaginary adduct **8** might be formed via the diradical intermediate **10**. It is, however, obvious that the diradical intermediate **9** is more stable than **10**; therefore the preferential product should be **6**.

The facts that some carbenes are known to rearrange to the corresponding allenes,[5] and that anthracenes are active acceptors in addition reactions with allenes,[6] seem also to support the estimation that these reac-

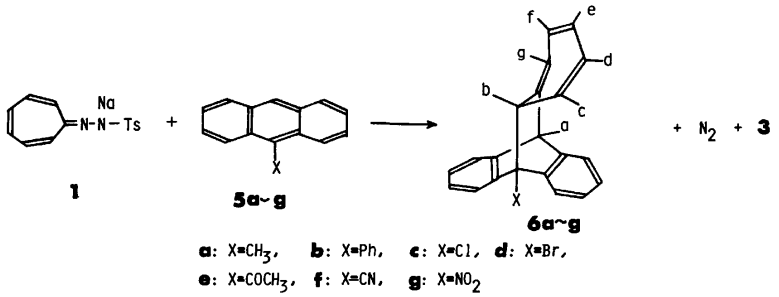

Fig. 2.

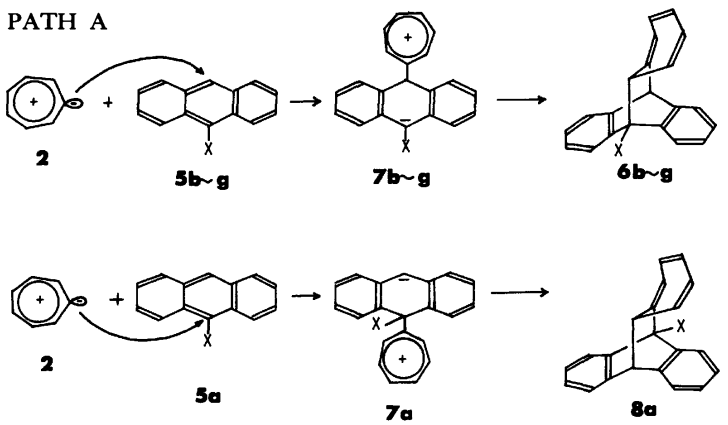

Fig. 3.

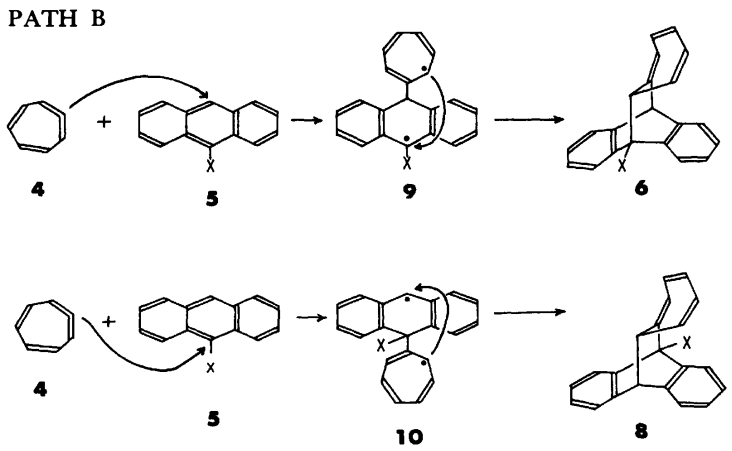

Fig. 4.

tions are addition reactions between the anthracene derivatives and the allene intermediate **4**.[7]

Experimental

All the melting and boiling points are uncorrected. The NMR spectra were measured with a Hitachi R-20B or a Varian XL 200 spectrometer, with tetramethylsilane as the internal standard. The mass spectra were recorded with a Hitachi M-52 or a JMS-DX300 spectrometer. The UV and IR spectra were measured with Hitachi 220A and DS-701G spectrometers respectively. Wako gel C-200 and Wako gel B5-F were used for the column and thin-layer chromatography respectively. The diglyme was dried over Molecular Sieves 3A 1/16.

Reaction of 1 with 5a. A mixture of 1 (14.80 g, 50 mmol), **5a** (9.60 g, 50 mmol), and anhydrous diglyme (100 ml) was heated at 120 °C for 15 min. After the evolution of a quantitative amount of nitrogen gas had ceased (1.1 l), a quantitative amount of a brown powder of **3** (8.85 g) was removed by filtration. The filtrate was diluted with ether, washed several times with water and brine, and dried over anhydrous sodium sulfate. After filtration, the solvent was removed on a rotary evaporator to give a tarry material, which was chromatographed on silica gel to give crystals of the recovered **5a** (7.44 g) when pet ether was used and yellow crystals **6a** (1.65 g, 12%) by the use of pet ether–benzene (9:1). Recrystallization from benzene gave pure **6a**.

6a: Mp 134—135 °C. Found: *m/z* 283.1404. Calcd for $C_{22}H_{18}$: 283.1417. Mass *m/z* (rel intensity): 283 (M^+, 96), 267 (52), 192 (100). IR (KBr): 3020, 2950, 1460, 1380 cm^{-1}. UV (EtOH): 273 nm (log ε, 3.70).

Reaction of 1 with 5b. A mixture of 1 (14.80 g, 50 mmol), **5b** (12.70 g, 50 mmol), and anhydrous diglyme (100 ml) was heated at 120 °C for 15 min to evolve a quantitative amount of nitrogen gas (1.1 l). After the removal of **3** (8.60 g, 97%) by filtration, the filtrate was treated as usual to give a mixture of crystals and an oil. The crystals of the recovered **5b** (11.13 g) were removed by filtration, and the filtrate was chromatographed on silica gel to yield a pale yellow oil **6b** (0.67 g, 4%) by the use of pet ether–benzene (8:2). The oil **6b** was further purified by thin-layer chromatography on silica gel, using pet ether–benzene (9:1) as the developing solvent (R_f=0.75).

6b: Found: *m/z* 344.1568. Calcd for $C_{27}H_{24}$: 344.1564. Mass (rel intensity): 344 (M^+, 100), 268 (13), 253 (60). IR (oil): 3020, 2950, 1160, 1460 cm^{-1}. UV (EtOH): 253 nm (log ε, 3.66).

Reaction of 1 with 5c. A mixture of 1 (14.80 g, 50 mmol), **5c** (10.65 g, 50 mmol), and anhydrous diglyme (100 ml) was heated at 120 °C for 15 min to evolve a quantitative amount of nitrogen gas (1.1 l). After the separation of **3** (8.13 g, 91%) by filtration, the filtrate was treated as usual to give a mixture of crystals and an oil. The crystals of the recovered **5c** (2.81 g) were removed by filtration, and the filtrate was chromatographed on silica gel to give crystals of the recovered **5c** (6.46 g) when pet ether was used and a pale yellow oil **6c** (1.17 g, 8%) when pet ether–benzene (9:1) was used. The oil **6c** was further purified by thin-layer chromatography, using pet ether–benzene (9:1) as the developing solvent (R_f=0.40).

6c: Found: *m/z* 302.0839. Calcd for $C_{21}H_{15}Cl$: 302.0861. Mass *m/z* (rel intensity): 302 (M^+, 55), 267 (90), 252 (36), 212 (100). IR (oil): 3040, 2950, 1460 cm^{-1}. UV (EtOH): 275 nm (log ε, 3.91).

Reaction of 1 with 5d. A mixture of 1 (14.80 g, 50 mmol), **5d** (12.90 g, 50 mmol), and anhydrous diglyme (100 ml) was heated at 120 °C for 15 min to evolve a quantitative amount of nitrogen gas (1.1 l). After the separation of **3** (8.85 g, 99%) by filtration, the filtrate was treated as usual to give a mixture of crystals and an oil. The crystals of the recovered **5d** (7.30 g) were removed by filtration, and the filtrate was chromatographed on silica gel to give crystals of the recovered **5d** (4.10 g) when pet ether was used and a yellow oil **6d** (2.15 g, 13%) when pet ether–benzene (8:2) was used. The oil **6d** was further purified by thin-layer chromatography on silica gel, using pet ether–benzene (8:2) as the developing solvent (R_f=0.60).

6d: Found: *m/z* 346.0355. Calcd for $C_{21}H_{15}Br$: 346.0375. Mass *m/z* (rel intensity): 348 (M^+, ^{81}Br, 65), 346 (M^+, ^{79}Br, 69), 268 (100), 259 (43), 257 (43). IR (oil): 3030, 2960, 1450 cm^{-1}. UV (EtOH): 273 nm (log ε, 3.84).

Reaction of 1 with 5e. A mixture of 1 (14.80 g, 50 mmol), **5e** (11.00 g, 50 mmol), and anhydrous diglyme (100 ml) was heated at 120 °C for 15 min to evolve a quantitative amount of nitrogen gas (1.1 l). After the separation of a quantitative amount of **3** (8.90 g) by filtration, the filtrate was treated as usual to give a tarry material, which was then chromatographed on silica gel to give a yellow oil **6e** (2.11 g, 14%) when pet ether–benzene (7:3) was used and crystals of the recovered **5e** (6.91 g) when pet ether–benzene (6:4) was used. The oil **6e** was further purified by

thin-layer chromatography, using pet ether–benzene (7:3) as the developing solvent (R_f=0.60).

6e: Found: *m/z* 310.1350. Calcd for $C_{23}H_{18}O$: 310.1356. Mass *m/z* (rel intensity): 310 (M^+, 31), 267 (100), 220 (28), 205 (52). IR (oil): 3030, 2950, 1710, 1455 cm^{-1}. UV (EtOH): 246 nm (log ε, 4.41).

Reaction of 1 with 5f. A mixture of **1** (5.92 g, 20 mmol), **5f** (4.06 g, 20 mmol), and anhydrous diglyme (50 ml) was heated at 120 °C for 15 min to evolve a quantitative amount of nitrogen gas (0.45 l). After the separation of a quantitative amount of **3** (3.55 g), the filtrate was treated as usual to give a mixture of crystals and an oil. The crystals of the recovered **5f** (1.85 g) were removed by filtration, and the filtrate was chromatographed on silica gel to give a pale yellow oil **6f** (480 mg, 8%) when pet ether–benzene (5:5) was used and crystals of the recovered **5f** (1.65 g) when pet ether–benzene (4:6) was used. The oil **6f** was further purified by thin-layer chromatography, using pet ether–benzene (5:5) as the developing solvent.

6f: Found: *m/z* 293.1194. Calcd for $C_{22}H_{15}N$: 239.1204. Mass *m/z* (rel intensity): 293 (M^+, 81), 265 (7), 203 (43), 117 (100). IR (oil): 3030, 2950, 2220, 1460 cm^{-1}. UV (EtOH): 273 nm (log ε, 4.16).

Reaction of 1 with 5g. A mixture of **1** (14.80 g, 50 mmol), **5g** (11.20 g, 50 mmol), and anhydrous diglyme (100 ml) was heated at 120 °C for 15 min to evolve a quantitative amount of nitrogen gas (1.1 l). After the separation of a quantitative amount of **3** (3.55 g) by filtration, the filtrate was treated as usual to give a tarry material, which was then chromatographed on silica gel to yield crystals **6g** (3.84 g, 25%) when pet ether–benzene (7:3) was used and crystals of the recovered **5g** (6.98 g) when pet ether–benzene (6:4) was used. Recrystallization from benzene gave pure **6g**.

6g: Mp 105—106 °C. Found: *m/z* 313.1083. Calcd for $C_{21}H_{15}NO_2$: 313.1103. Mass *m/z* (rel intensity): 313 (M^+, 100), 267 (75), 253 (12), 208 (10). IR (KBr): 3030, 2960, 1540, 1460 cm^{-1}. UV (EtOH): 273 nm (log ε, 3.52).

The authors are indebted to Professor Toshio Mukai of Tohoku University, Professor Takashi Toda of Utsunomiya University, and Professor Tomoo Nakazawa of the Medical University of Yamanashi for their fruitful suggestions.

References

1) a) T. Mukai, T. Nakazawa, and K. Isobe, *Tetrahedron Lett.*, **1968**, 565; b) W. M. Jones and C. L. Ennis, *J. Am. Chem. Soc.*, **91**, 6391 (1969); c) W. M. Jones, B. N. Hamon, R. C. Joins, and C. L. Ennis, *Tetrahedron Lett.*, **1969**, 3909; d) L. W. Christensen, E. E. Waali, and W. M. Jones, *J. Am. Chem. Soc.*, **94**, 2118 (1972); e) T. Mitsuhashi and W. M. Jones, *J. Chem. Soc., Chem. Commun.*, **1974**, 103.

2) a) K. Untch, International Symposium on the Chemistry of Non-Benzenoid Aromatic Compounds, Sendai, Japan, 1970; b) C. Mayor and W. M. Jones, *Tetrahedron Lett.*, **1977**, 3855; c) K. Saito, Y. Omura, and T. Mukai, *Chem. Lett.*, **1980**, 349; d) J. W. Harris and W. M. Jones, *J. Am. Chem. Soc.*, **104**, 7329 (1982); e) K. Saito, Y. Omura, and T. Mukai, *Bull. Chem. Soc. Jpn.*, **58**, 1663 (1985); f) K. Saito and H. Ishihara, *ibid.*, **58**, 2664 (1985); g) R. W. Alder, J. C. Petts, and T. Clark, *Tetrahedron Lett.*, **26**, 1585 (1985); h) R. O. Angus, Jr., M. W. Schmidt, and R. P. Johnson, *J. Am. Chem. Soc.*, **107**, 532 (1985).

3) C. H. Jutz, I. Rommel, I. Lengyel, and J. Feeney, *Tetrahedron*, **22**, 1809 (1966); A. S. Kende, *Tetrahedron Lett.*, **1967**, 2661. T. Toda, K. Saito, and T. Mukai, *ibid.*, **1972**, 1981; T. Sasaki, K. Kanematsu, H. Hayakawa, and M. Sugiura, *J. Am. Chem. Soc.*, **97**, 355 (1975).

4) D. J. Pasto and S. E. Warren, *J. Am. Chem. Soc.*, **104**, 3670 and 3676 (1982).

5) F. T. Bond and D. E. Bradway, *J. Am. Chem. Soc.*, **87**, 4977 (1965); W. M. Jones and D. L. Klayse, *ibid.*, **93**, 551 (1971); O. L. Chapmann, P. W. Wajtkowski, W. Adam, O. Rodriguez, and R. Rucktascel, *ibid.*, **94**, 1365 (1972); M. Oda, Y. Ito, and Y. Kitahara, *Tetrahedron Lett.*, **1975**, 2587.

6) L. Friedman and F. M. Logullo, *J. Am. Chem. Soc.*, **85**, 1549 (1963); H. D. Scharf, *Angew. Chem. Int. Ed.*, **13**, 520 (1974). M. Oda, N. Fukazawa, and Y. Kitahara, *Tetrahedron Lett.*, **1977**, 3277.

7) A referee has pointed out the possibility of the secondary formation of **6** via 1,5-hydrogen shifts or Berson-Willcott rearrangements in the tropylidene moiety of **8**, which, in this case, should be the initial addition product. According to the literature,[8] the quantitative proceedings of these rearrangements usually need the reaction conditions of heating at a higher temperature for longer periods than those of our reaction conditions (for example, the rearrangement of 1,3,6-triphenyltropylidene to 2,5,7-triphenyltropylidene is not completed even after heating at 121 °C for 70 h[8c]). Because of the mild reaction conditions (120 °C, 15 min) and because we detected no adduct of the **8** type, we consider **6** to be the initial addition product. We are indebted to the referee for his sugestion.

8) a) J. A. Berson and M. R. Willcott, III, *J. Am. Chem. Soc.*, **88**, 2494 (1966); b) E. Ciganek, *ibid.*, **89**, 1458 (1967); c) T. Mukai, H. Kubota, and T. Toda, *Tetrahedron Lett.*, **1967**, 3581; d) T. Toda, *Yuki Gosei Kagaku, Kyokai Shi* **30**, 412 (1972).

Quantitative Analysis of Effects of Substituted Phenols on Membrane Characteristics of Lecithin Liposomes

Hideto MIYOSHI, Takaaki NISHIOKA, and Toshio FUJITA*
Department of Agricultural Chemistry, Faculty of Agriculture, Kyoto University, Sakyo-ku, Kyoto 606
(Received November 1, 1985)

The partition coefficient of a series of substituted phenols in a lecithin liposome/water system, P(L/W), and the effects of these compounds on the perturbation of liposomal membranes were quantitatively investigated using physicochemical molecular parameters. Partition behavior is primarily governed by hydrophobicity, represented in terms of the 1-octanol/water partition coefficient. Steric and electronic characters also were of significance. Potency in perturbation of liposomal membranes was governed by the degree of partitioning to the membrane and the steric bulkiness of the phenol. This kind of quantitative procedure was very helpful in investigating the effects of organic molecules on membrane characteristics.

A variety of medicinal and agricultural chemicals interact with cell membranes as a part of their pharmacological or physiological effects. Thus, characterization of such interactions is important for understanding their overall mechanisms of action. Substituted phenols have fungicidal activity due to their causing an abnormal release of intracellular substances during their incorporation into the cell membranes.[1-3] The relationship between their fungicidal activity index and a hydrophobicity parameter derived from their partition coefficient in organic solvent/water systems is linear.[4-6] These studies suggest that the hydrophobicity of substituted phenols is most important, but the effect of other factors such as steric bulk and electronic property on the interaction with cell membranes should not be overlooked.

Here, we selected the lecithin liposome as a model of the cell membrane, since the effect of solutes is easily analyzed physicochemically with this system, the components of which are chemically uniform. We measured the partition coefficient of a number of substituted phenols between the lecithin liposome and an external aqueous phase. The substituents were chosen so that their steric and electronic characters would be as different as possible under experimental conditions. We also evaluated the degree of perturbation of the liposomal membrane by phenols, in terms of the change in the membrane permeability to glucose. Using physicochemical parameters of substituents and regression analysis, we first examined factors influencing their partitioning into the lecithin liposome. Then we analyzed the degree of liposomal membrane perturbation in terms of the liposome–aqueous phase partition coefficient, along with other parameters.

Experimental

Materials. Lecithin was prepared from fresh egg yolk and purified by the method of Singleton.[7] Phenols were purchased from the Nakarai Chemical Co. and purified before use. Hexokinase (EC 2.7.1.1), glucose 6-phosphate dehydrogenase (EC 1.1.1.49), and ADP were obtained from the Oriental Yeast Co. *N*-Dansylhexadecylamine (DSHA) was bought from the Sigma Chemical Co.

Preparation of Bilayered Liposome. Lecithin, 100 mg, was dissolved in 1 ml of $CHCl_3$ and placed in a 30 ml flask under Ar gas. The solvent was removed in vacuo. The lipid film was suspended in 20 ml of pH 7.2 Tris buffer (10 mM Tris-HCl, 50 mM NaCl (1 M=1 mol dm^{-3}), 0.2 mM EDTA) and sonicated with a Type 4280 sonicator (Kaijodenki Co.) in an ice-cooled bath under Ar gas to avoid oxidation of lecithin. Bilayered liposome was separated from the undispersed lecithin by centrifugation of the suspension at 15000 rpm for 30 min, and from multilayered liposome by gel filtration on Sepharose 4B at 4 °C.[8] The amount of lecithin was calculated from that of phosphorus by a modification of the Bartlett method.[9] The resultant solution of liposome contained about 1 mg lecithin/ml. Electron microscopy (JME-100C) was used to study the liposome negatively stained with 2% sodium tungstophosphate.

Measurement of Partition Coefficient. The partition coefficient, P(L/W), of substituted phenols between the liposome and the external aqueous phase was measured by equilibrium dialysis.[10] The solution of phenols was prepared with the same pH 7.2 Tris-HCl buffer as for the liposome solution. For phenols other than those that were alkyl-substituted, the pH of the buffer was adjusted by addition of dilute HCl so that they would exist as the nonionized form, except for 2,4-$(NO_2)_2$ and 2-*s*-Bu-4,6-$(NO_2)_2$ derivatives, which ionize by 3—10% even at pH 3.0. The concentration of the phenol in the buffer was 10^{-5} to 10^{-4} M. The pH of the liposome solution was adjusted to that of the phenol solution. Using an equilibrium dialysis cell (10×1 ml chambers, Sanko Plastic Co.), we equilibrated the liposome suspension (1 ml) with the phenol solution (1 ml) through a cellophane dialysis membrane at 25 °C for 12 h. The partition coefficient, P(L/W), was calculated by Eq. 1,

$$P(\mathrm{L/W}) = \frac{2(C_o - C)}{C \times C_L}\left[\frac{\text{mol phenol/kg lecithin}}{\text{mol phenol/l external solution}}\right], \quad (1)$$

where C is the concentration of phenol in a liposome-free chamber at equilibrium, C_o is that of phenol in a control experiment in which the phenol solution was equilibrated with the Tris buffer without liposome, and C_L is the concentration of lecithin (kg l^{-1}) in the liposome suspension. The total amount of lecithin in 1 ml of the liposome suspension was about 1 mg. The concentration of the phenol was measured spectrophotometrically on a Shimadzu UV-360

spectrophotometer. The P(L/W) value was calculated at least three times with different initial phenol concentrations, and the log P(L/W) values were averaged. For 2,4-dinitro- and 2-*s*-butyl-4,6-dinitrophenols, the partition coefficient is an apparent value for a mixture of ionized and nonionized species in the aqueous phase. For these two derivatives, the effect of variation in pH was examined.

Measurement of Glucose Permeability. The permeability of the liposomal membrane to glucose was calculated as the rate of release of glucose from the internal aqueous phase to the external aqueous phase at 25°C. Liposome enclosing glucose internally (glucose-liposome) was prepared by sonication of lecithin in pH 7.2 Tris buffer (10 mM Tris-HCl, 0.2 mM EDTA) containing 0.15 M glucose, and then separated with Sepharose 4B gel filtration. Glucose, which remained in the outer phase, was quickly removed with further gel filtration using Sephadex G25. An enzyme mixture for the glucose-assay was prepared in a quartz cell for fluorescence measurement.[11] The mixture consisted of 2.5 ml of pH 7.2 buffer (10 mM Tris-HCl, 0.2 mM EDTA, and 0.15 M NaCl), 0.2 ml of 0.02 M magnesium acetate, 0.1 ml of 0.02 M ATP, 0.1 ml of 0.01 M $NADP^+$, and 20 µl of aqueous solution containing 100 IU of hexokinase and 250 IU of glucose 6-phosphate dehydrogenase. After the addition of 80—130 µl of a stock solution in which various amounts of a phenol was dissolved in pH 7.2 Tris buffer, 0.5 ml (about 0.1 mg of lecithin) of the glucose-liposome suspension was quickly added to the cell. The final pH of the reaction mixture was 5.3. The amount of the phenol stock solution to be added was decided so as to cover the lower concentration region for highly effective compounds and the higher region for less effective compounds, in a range of final concentrations between 0.08 and 17 mM. The concentration of glucose in the outer phase was assayed at intervals with gentle stirring from the fluorescence intensity at 460 nm (ex. at 340 nm) arising from the NADPH produced from $NADP^+$ with glucose 6-phosphate dehydrogenase in the presence of the glucose 6-phosphate that is in turn derived from glucose with hexokinase and ATP. Fluorescence was recorded on a Shimadzu RF-503A spectrofluorophotometer. At 30 min after the start of the reaction, 10% Triton-X100 aqueous solution (300 µl) was added to the reaction mixture, and the glucose-liposome was completely disrupted to release the enclosed glucose. The fluorescence intensity after the disruption corresponded to the total amount of glucose. The course over time for the 4-*t*-Bu derivative is shown in Fig. 1 as an example. The total volume of the internal aqueous phase of liposome was calculated from the total amount of glucose in the entire reaction mixture and from the initial concentration of glucose (0.15 M) enclosed in the glucose-liposome. The pH of the external solution where the enzymatic reaction proceeds did not vary in this experimental period. Phenols used here are mostly not ionized at the final pH of 5.3 except for the 2-*s*-Bu-4,6-$(NO_2)_2$ derivative.

Estimation of Polarity of the Liposomal Membrane Surface. The variations in the polarity of membrane surface were estimated as the change of the λ_{max} of the emission spectrum of DSHA at 25°C. A chloroform solution of DSHA was added to lecithin at the molar ratio of 1:50 for DSHA to lecithin.[12] Chloroform was removed in vacuo and liposome (DSHA-liposome) was prepared in a similar way. The λ_{max} of the DSHA-liposome was recorded with excitation at 330 nm.

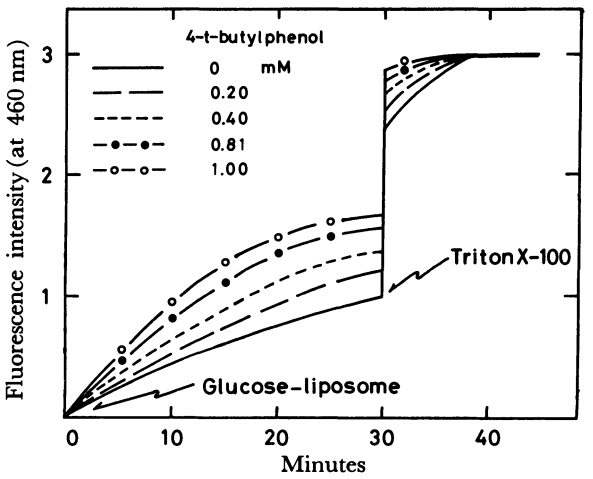

Fig. 1. Spectrofluorophotometric assay for glucose released from liposome in the presence of 4-*t*-butylphenol. Glucose-liposomes were added to experimental (+$NADP^+$) and control (−$NADP^+$) cuvettes at time zero. Triton X-100 (300 µl) to give the final concentration of 1% was added to the cuvettes at 30 min. Fluorescence intensity values were corrected for dilution following the addition of Triton X-100.

Table 1. log P(L/W) of 2,4-$(NO_2)_2$ Derivatives at Different pH

pH	2,4-$(NO_2)_2$ [pK_A=4.09]		2-*s*-Bu-4,6-$(NO_2)_2$ [pK_A=4.40]	
	% ionized	log P(L/W)	% ionized	log P(L/W)
7.2	99.9	1.90	99.8	2.95
5.3	94.2	2.00	88.8	3.16
3.0	7.5	2.42	3.8	3.33
Neutral		2.46[a]		3.35[a]

a) Estimated by correcting log P(L/W) at pH 3.0 according to the pH-partitioning model by adding $\log\{(K_A+[H^+])/[H^+]\}$, where K_A is the dissociation constant and $[H^+]$ is the hydrogen ion concentration.

Results

Characterization of Liposome. Electron microscopy showed that liposomes prepared in this way did indeed have an internal space surrounded by a spherical bilayered membrane. The diameter of the liposomes was between 150 and 300 Å, which agrees with that reported in the literature.[13] The volume of the internal cavity of the liposomes estimated from the total volume for the glucose-liposomes was 2.6 (±0.3)× 10^{-4} cm^3 μmol^{-1} lecithin, which is close to the 3.1×10^{-4} cm^3 μmol^{-1} lecithin obtained by Brunner.[14]

Partition Coefficient. The partition coefficient, P(L/W), of some representative phenols was measured with different initial concentrations in the external aqueous phase from 5×10^{-6} to 10^{-3} M under conditions where they exist as the nonionized form. For the 4-Cl and 4-*t*-Bu derivatives, the log P(L/W) values were

Table 2. log P(1-octanol/water) and log P(liposome/water) of Substituted Phenols

Substituent	log P(O/W)[a]	Δlog K_A[b]	ΔV_w(m, p)[c]	ΔV_w(di-ortho)[c]	log P(L/W)	
			$\times 10$ cm^3 mol^{-1}	$\times 10$ cm^3 mol^{-1}	Obsd[d]	Calcd[e]
H	1.46	0	0	0	1.81(0.05)	1.90
2-Me	1.97	−0.30	0	0	2.25(0.04)	2.32
3-Me	2.02	−0.10	1.12	0	2.10(0.04)	2.30
4-Me	1.94	−0.16	1.12	0	2.17(0.03)	2.22
4-Et	2.58	−0.23[f]	2.14	0	2.68(0.06)	2.70
4-n-Pr	3.06[g]	−0.23[h]	3.07	0	3.09(0.02)	3.05
2-t-Bu	3.31	−1.18[f]	0	0	3.44(0.03)	3.43
3-t-Bu	3.31[g]	−0.14[f]	4.09	0	3.18(0.06)	3.20
4-t-Bu	3.31	−0.25[f]	4.09	0	3.21(0.05)	3.19
2-s-Bu	3.27	−0.36[f,i]	0	0	3.40(0.03)	3.45
2-Ph	3.09	0.01	0	0	3.50(0.02)	3.32
4-Ph	3.20	0.43	4.33	0	3.16(0.03)	3.12
4-t-Pent	3.87[g]	−0.25[j]	5.20	0	3.53(0.04)	3.59
2,6-(Me)$_2$	2.30[k]	−0.64[l]	0	2.24	2.52(0.02)	2.34
2,6-(Et)$_2$	3.03[k]	−0.59[l]	0	4.28	2.83(0.01)	2.75
2-Cl	2.15	1.50	0	0	2.47(0.04)	2.60
3-Cl	2.50	0.96	0.95	0	2.81(0.06)	2.80
4-Cl	2.39	0.60	0.95	0	2.80(0.03)	2.68
2,4-Cl$_2$	3.06	2.09[f]	0.95	0	3.42(0.01)	3.36
2,6-Cl$_2$	2.75[k]	3.19[l]	0	1.90	2.80(0.02)	3.02
3-Me-4-Cl	3.10	0.43[f]	2.07	0	3.15(0.01)	3.20
3-NO$_2$	2.00	1.58	1.43	0	2.52(0.02)	2.36
4-SO$_2$Me	0.58[m]	2.15	3.80	0	0.95(0.02)	0.99
2,4-(NO$_2$)$_2$	1.54	5.89[f]	1.43	0	2.42(0.03)	2.24
2,4,6-Cl$_3$	3.69	3.99[f]	0.95	1.90	3.75(0.01)	3.82
2-s-Bu-4,6-(NO$_2$)$_2$	3.56[k]	5.58[k]	1.43	5.52	3.33(0.02)	3.37

a) Unless otherwise noted, from T. Fujita, *Prog. Phys. Org. Chem.*, **14**, 75 (1983) and log P data bank compiled by Pomona College Medicinal Project, Claremont, California, U. S. A., 1983. b) Unless otherwise noted, from A. Albert and E. P. Serjeant, "Ionization Constants of Acid and Base," Methuen, London (1962), p. 130 c) From A. Bondi, *J. Phys. Chem.*, **68**, 441 (1964). d) For the nonionized form, see text. The figures in parentheses are the standard deviation. e) By Eq. 3. f) From "Tables of Rate and Equilibrium Constants of Heterolytic Organic Reactions," ed by V. A. Palm, Tartu State University, 1975, Vol. 1. g) Estimated from the value of closely related compounds. h) Taken as the same as that of 4-ethylphenol. i) Taken as the same as that of 2-isopropylphenol. j) Taken as the same as that of 4-t-butylphenol. k) Newly found. l) From G. J. Bijiloo and R. F. Rekker, *Quant. Struc.-Act. Relat.*, **3**, 91 (1984) or estimated according to a procedure presented there. m) Estimated according to a procedure published in T. Fujita, *Prog. Phys. Org. Chem.*, **14**, 75 (1983), assuming that $\rho_{SO_2Me}=\rho_{NO_2}$ (=−0.14).

almost constant regardless of the initial concentration in the aqueous phase, varying only slightly from 2.75 to 2.81 for the 4-Cl and from 3.19 to 3.28 for the 4-t-Bu compounds. For the 2,4-dinitrophenols, the P(L/W) value was measured at pH 7.2, 5.3, and 3.0. As shown in Table 1, these phenols were partitioned into the liposome membrane even from the aqueous phase where they exist almost always in the ionized form. Judging from the difference in log P(L/W) value between higher pH and a pH of 3.0, the partition of the phenolate ions is lower than that of the neutral phenols, but the difference does not seem to be very large. Although the partitioning system with liposomes seems to work according to a simple partition model as far as the nonionized species are concerned, it does not obey the pH-partition model.[15] The log P(L/W) value of 2,4-dinitro- and 2-s-butyl-4,6-dinitrophenols at pH 3.0 was "corrected" for the ionization according to the pH-partition model, since the "corrected" valus is thought to be the highest estimate for the valus for the nonionized neutral molecule. The log P(L/W) valus found at pH 3.0 did not differ much from the corrected value shown in Table 1 and was used without correction along with those for other compounds for further analyses, as an approximate value for the neutral form.

The log P(L/W) value was listed in Table 2. The total volume of the internal cavity of vesicles is very small compared with that of the external aqueous phase. Even the partition into the cavity for the least hydrophobic phenols used here having the log P(L/W) value at about 1.00 can be neglected. The log P value measured with the 1-octanol/water system, log P(O/W), has been widely used as a standard for the hydrophobic parameter of the molecule.[16] We plotted the log P(L/W) value against the log P(O/W) for each phenol in Fig. 2, for which Eq. 2 was derived by regression analysis.

$$\log P(\mathrm{L/W}) = \underset{(\pm 0.102)}{0.767} \log P(\mathrm{O/W}) + \underset{(\pm 0.283)}{0.781} \quad (2)$$

$$(n = 26,\ s = 0.195,\ r = 0.953)$$

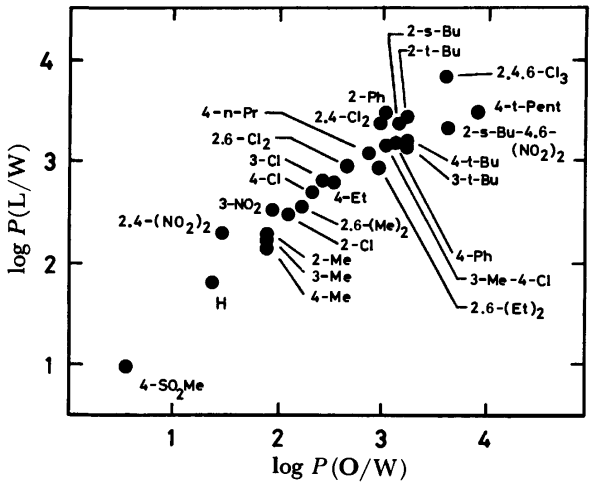

Fig. 2. Plot of log P(liposome/water) vs. log P(1-octanol/water) of substituted phenols.

In this and the following equations, n is the number of substituted phenols, s is the standard deviation, and r is the correlation coefficient. The figures in parentheses are the 95% confidence interval.

Although Eq. 2 seems to show reasonable correlation, slight negative deviations were observed for meta and para isomers. The deviations suggest contributions from factors other than the hydrophobicity of the molecule. Regression analysis was repeated using additional terms for steric and electronic factors of substituents. As the steric parameter, the van der Waals volume of substituents, ΔV_w (V_w relative to that of H and multiplied by 0.1 in order to make it equiscalar with other parameters), was found to delineate the effects best among steric parameters such as STERIMOL, E_s, and E_s^c.[17] The $\Delta\log K_A$ value ($\log K_A$ relative to that of the unsubstituted phenol) was used as the electronic parameter of substituents. Eq. 3 had the best correlation.

$$\log P(\mathrm{L/W}) = \underset{(\pm 0.070)}{0.870}\log P(\mathrm{O/W}) - \underset{(\pm 0.042)}{0.111}\,\Delta V_w(\text{di-ortho}) - \underset{(\pm 0.033)}{0.074}\,\Delta V_w(\mathrm{m,p}) + \underset{(\pm 0.029)}{0.064}\,\Delta\log K_A + \underset{(\pm 0.182)}{0.629} \quad (3)$$

$$(n = 26,\ s = 0.117,\ r = 0.986)$$

ΔV_w(di-ortho) is the sum of the parameters of both ortho substituents for di-ortho-substituted phenols. ΔV_w(m,p) is for the meta and para substituents. The addition of each of the ΔV_w and $\Delta\log K_A$ terms to Eq. 2 was justified at a level higher than 99.5%. The addition of the ΔV_w value for the mono-ortho-substituted compounds was not statistically significant. The coefficient of the log P(O/W) term in Eq. 3 is closer to 1 than that in Eq. 2. This is reasonable, since the degree of desolvation during partitioning from the aqueous to the organic phase is thought to be similar between the two partitioning systems. In the liposome/aqueous system, however, additional factors are significant. The ΔV_w terms suggest that the partitioning into liposomal membrane is slightly but significantly lowered by the bulkiness of substituents and that the effect is dependent upon the substitution patterns. From the regression coefficients, it appears that the effect of two ortho substituents is about double that of meta and para substituents. Interestingly enough, the single ortho substituent in monosubstituted compounds does not have this type of steric effect. The significance of the electronic term means that electron withdrawal from substituents favors partitioning. It should be noted that the electronic effect is not related to that on ionization, since the partition coefficient is that for the nonionized form. The electronic effect of substituents probably reflects a difference in the hydrogen bonding factor of the nonionized OH group with sites that can accept hydrogen between 1-octanol and lecithin.

Glucose Permeability. The rate of glucose release from liposome depends on the concentration of glucose in the internal aqueous phase. It follows first-order kinetics, as in Eq. 4.[14]

$$\text{Rate of glucose release} = k_p[\text{glucose}]_t^i, \quad (4)$$

where $[\text{glucose}]_t^i$ is the internal concentration of glucose at time t and k_p is the first-order rate constant. The integrated form of this equation cover the time t is shown as Eq. 5.

$$\ln\{[\text{glucose}]_{t=0}^i/[\text{glucose}]_t^i\} = k_p \cdot t. \quad (5)$$

Glucose released to the outer aqueous phase is converted into glucose 6-phosphate, which produces NADPH. Since the conversion is also a rate process, and since the glucose concentration of the outer phase is also governed by both permeation and the enzymatic reaction, the concentration of NADPH that is found experimentally does not correspond with that of the glucose in the outer phase. If the overall enzymatic reaction of the glucose assay system is approximated to follow first order kinetics, the [NADPH] at time t is formulated as Eq. 6:

$$[\text{NADPH}]_t = [\text{glucose}]_t^o\{1 - \exp(-k_e \cdot t)\}, \quad (6)$$

where $[\text{glucose}]_t^o$ is the concentration of glucose in the external medium at time t and k_e is the rate constant of the enzymatic reactions. Since $[\text{glucose}]_t^i$ is related to $[\text{glucose}]_t^o$ by Eq. 7,

$$[\text{glucose}]_t^i = [\text{glucose}]_{t=0}^i - [\text{glucose}]_t^o \cdot (V_o/V_i). \quad (7)$$

Eq. 8 is derived by substituting Eq. 7 into Eq. 5, where V_o and V_i are the volume of the external and internal liposome, respectively.

$$\ln \frac{[\text{glucose}]_{t=0}^i}{[\text{glucose}]_{t=0}^i - [\text{NADPH}]_t\{1-\exp(-k_e \cdot t)\}^{-1}(V_o/V_i)} = k_p \cdot t \quad (8)$$

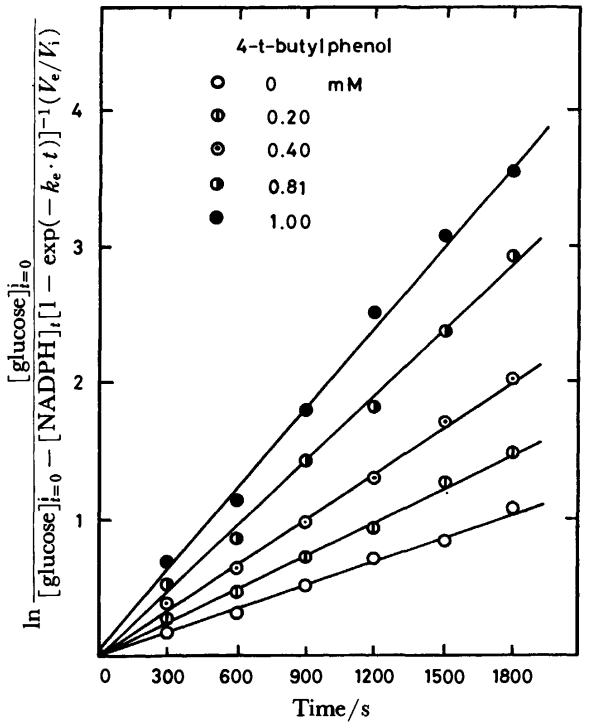

Fig. 3. Release kinetics of glucose. Data were plotted using Eq. 8.

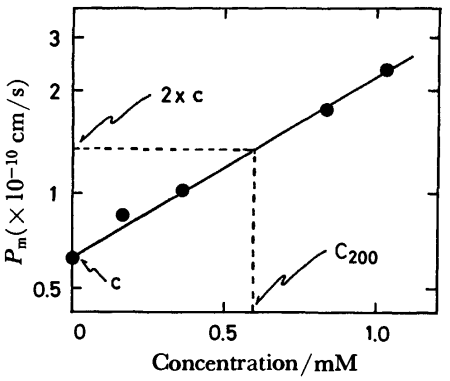

Fig. 4. Plot of the permeability coefficient of glucose vs. the concentration of 4-*t*-butylphenol. Data were analyzed by the least squares method using Eq. 10.

The k_e value might be as a constant regardless of the phenols used. In fact, it varies depending upon the structure of the phenols, since the enzymatic reaction is more or less inhibited by individual phenols. The k_e value was determined under the same experimental conditions as the glucose release assay for different concentrations of each phenol in the presence of 1.5×10^{-5}M glucose without glucose-liposome. It ranged between 5×10^{-4}s^{-1} and 3×10^{-3}s^{-1} (data not shown). The plot of the left side of Eq. 8 against time t was linear, as shown in Fig. 3 for 4-*t*-butylphenol. When we neglected the effect of the enzymatic rate process by using $k_e \gg k_p$, the denominator of the ln term in Eq. 8 reduced to $[\text{glucose}]^{i}_{t=0}-[\text{NADPH}]_t$ (V_o/V_i). The plot with this modification against t was not linear. This means that the approximation made for Eq. 6 was in fact appropriate.

The permeability coefficient, P_m, is defined by Eq. 9, where A is the surface area of liposome and k_p is evaluated according to Eq. 8.

$$P_m = k_p \cdot V_i/A \tag{9}$$

The average surface area of liposome was calculated to be 2.0×10^3cm^{2}μmol^{-1} lecithin from the average diameter of vesicles, estimated by electron microscopy. The mean value of the P_m of glucose, from 30 runs, was $6.6\pm1.3\times10^{-11}$cm s^{-1}. This value is close to the $3.0\pm2.0\times10^{-11}$ cm s^{-1} observed by Brunner.[15]

The P_m value of glucose increases with successive additions of phenols in the outer phase, as shown in Table 3. We defined a parameter, C_{200}, for each phenol to represent potency of accelerating the release of glucose to twice that of the control in terms of the initial external concentration. For some phenols, the C_{200} concentration could not be found because of their limited solubility. In that case, we estimated this concentration by an empirical relationship such as that of Eq. 10 between P_m and the initial external concentrations of each phenol (C).

$$\log P_m = aC + c \tag{10}$$

Equation 10 holds for the 18 phenols used here with a correlation coefficient higher than 0.96 and a standard deviation smaller than 0.06. An example of the relationship is shown in Fig. 4. This relationship can be understood if we consider that the free energy of activation for the permeation process of glucose decreases linearly with the amount of each phenol partitioned into the liposomal membrane that is proportional to the external concentration. The a and c values in Eq. 10 were estimated by the least squares method and the quality of the correlation is shown in Table 4. The C_{200} value was calculated as $(\log 2)/a$ and listed in Table 4 as the logarithm.

The partitioning of organic solutes with a liposome/aqueous system reaches an equilibrium within a few minutes.[19] Since glucose release in this study obeys first-order kinetics very well, the effect of the conditions before equilibrium could be neglected. Release proceeds mostly under equilibrated conditions with respect to the partition of phenols. In fact, the C_{200} value (in log form) is almost identical to the value corrected for the partition equilibrium for each phenol. As an index for potency in perturbing the liposome membrane structure, it was suitable to use $\log(1/C_{200})$.

At pH 5.3, the phenols used here, except for 2-*s*-butyl-4,6-dinitrophenol, exist almost entirely as the neutral form. The $\log 1/C_{200}$ value of phenols other than this exception had a good linear relationship with log P(O/W) for the nonionized phenols, that of as Eq. 11.

$$\log 1/C_{200} = 0.912 \log P(\text{O/W}) + 0.162 \tag{11}$$
$$(\pm0.170) \qquad (\pm0.480)$$
$$(n = 17, s = 0.192, r = 0.947)$$

Table 3. Permeability Coefficient of Glucose for Substituted Phenols

Substituent	External Concd/mM	P_m $\times 10^{-11}$ cm/s	Substituent	External Concd/mM	P_m $\times 10^{-11}$ cm s^{-1}
2-Me	0	4.19	4-Ph	0	5.11
	3.57	5.36		0.098	6.77
	7.14	5.71		0.204	7.05
	14.30	9.66		0.253	8.06
	17.10	15.50		0.326	8.34
3-Me	0	6.15	4-*t*-Pent	0	8.08
	3.56	6.74		0.084	9.09
	6.91	8.59		0.166	11.10
	11.10	8.78		0.277	11.90
	13.80	10.80		0.356	18.10
4-Me	0	6.96	2-Cl	0	5.41
	3.17	8.05		1.73	5.95
	6.37	9.58		2.59	7.09
	7.91	10.50		4.17	8.61
	8.52	11.63		5.18	9.94
4-Et	0	9.15	3-Cl	0	7.23
	1.61	11.60		1.09	8.28
	2.07	11.50		1.77	8.84
	3.22	18.00		2.20	9.83
	6.23	21.70		2.83	10.90
4-*n*-Pr	0	5.88	4-Cl	0	7.31
	0.486	7.23		2.72	9.22
	0.770	8.73		3.45	10.00
	1.28	13.80		4.30	11.70
	1.59	17.10		6.88	18.80
2-*t*-Bu	0	5.43	2,4-Cl_2	0	6.04
	0.152	5.81		0.669	8.58
	0.228	7.51		1.62	16.10
	0.360	7.78		1.80	18.50
	0.746	15.79		2.01	23.00
3-*t*-Bu	0	5.80	3-Me-4-Cl	0	6.62
	0.220	6.57		0.560	7.48
	0.272	7.18		0.720	7.91
	0.454	8.14		1.12	10.30
	0.585	8.82		1.87	16.50
4-*t*-Bu	0	6.28	3-NO_2	0	2.94
	0.199	8.19		3.06	3.91
	0.399	9.32		6.12	7.21
	0.805	14.90		8.20	9.20
	0.999	16.70		12.20	11.30
2-Ph	0	5.05	2-*s*-Bu-4,6-(NO_2)$_2$	0	8.55
	0.118	6.26		0.166	9.77
	0.153	6.75		0.225	11.90
	0.354	10.10		0.268	12.90
	0.456	11.30		0.333	14.40

Table 4. log $1/C_{200}$ Value Estimated from Eq. 10 and Substituent Parameters[a)]

Substituent	a[b)]	c[b)]	s[c)]	r[d)]	log $1/C_{200}$[e)]	C_{200}^m[f)] mol/Kg lipids	V_w[g)] $\times 10$ cm^3 mol
2-Me	0.031[h)] (0.014)	−10.404 (0.148)	0.063	0.971	1.97	1.94	6.51
3-Me	0.017[h)] (0.008)	−10.214 (0.070)	0.028	0.968	1.75	1.67	6.51
4-Me	0.022 (0.004)	−10.160 (0.019)	0.005	0.999	1.88	1.67	6.51
4-Et	0.063[i)] (0.038)	−10.031 (0.127)	0.055	0.951	2.29	1.96	7.53
4-*n*-Pr	0.304 (0.079)	−10.262 (0.079)	0.031	0.990	2.99	1.19	8.46
2-*t*-Bu	0.637 (0.234)	−10.297 (0.091)	0.042	0.981	3.32	1.21	9.48
3-*t*-Bu	0.320 (0.068)	−10.239 (0.025)	0.010	0.993	3.02	1.34	9.48

Table 4. (Continued)

Substituent	a[b]	c[b]	s[c]	r[d]	log $1/C_{200}$[e]	C_{200}^{m}[f] mol/Kg lipids	V_w[g] ×10 cm³ mol
4-*t*-Bu	0.428 (0.075)	−10.191 (0.046)	0.020	0.995	3.15	1.06	9.48
2-Ph	0.791 (0.114)	−10.294 (0.031)	0.013	0.997	3.30	1.11	9.72
4-Ph	0.624 (0.364)	−10.267 (0.077)	0.029	0.953	3.42	0.655	9.72
4-*t*-Pent	0.897[i] (0.522)	−10.109 (0.114)	0.047	0.953	3.44	0.752	10.59
2-Cl	0.053 (0.017)	−10.287 (0.055)	0.021	0.986	2.20	1.83	6.34
3-Cl	0.062 (0.017)	−10.148 (0.032)	0.012	0.989	2.39	2.53	6.34
4-Cl	0.060 (0.025)	−10.173 (0.103)	0.039	0.975	2.30	2.48	6.34
2,4-Cl_2	0.287 (0.080)	−10.237 (0.107)	0.029	0.996	3.00	2.28	7.29
3-Me-4-Cl	0.217[h] (0.102)	−10.226 (0.108)	0.045	0.969	2.87	1.81	7.46
3-NO_2	0.050[i] (0.031)	−10.522 (0.215)	0.064	0.980	2.21	2.13	6.82
2-*s*-Bu-4,6-$(NO_2)_2$	0.700 (0.338)	−10.085 (0.077)	0.027	0.967	3.37	0.621	12.34

a) log P(L/W) and log P(O/W) values at pH 5.3 used in Eqs. 11 and 12 are equal to values for the neutral form listed in Table 2 except for 2-*s*-Bu-4,6-$(NO_2)_2$. log P(L/W) value at pH 5.3 of 2-*s*-Bu-4,6-$(NO_2)_2$ is 3.16. b) Slope and intercept in Eq. 10. Unless otherwise noted, the correlation was justified above the 99.5% level; figures in parentheses are the 95% confidence interval. c) Standard deviation of the correlation according to Eq. 10. d) Coefficient of correlation accoding to Eq. 10. e) The C_{200} value was calculated as (log 2)/a from Eq. 10. f) The concentration of phenols in the liposomal membrane equilibrated with C_{200}. g) The van der Waals volume of compounds estimated according to A. Bondi, *J. Phys. Chem*, **68**, 441 (1964). h) Justified at the 99% level. i) Justified at the 97.5% level.

This equation means that the potency of membrane perturbation is linearly dependent on the hydrophobicity of phenols in terms of log P(O/W). The addition of other parameters does not further improve the correlation. To incorporate 2-*s*-butyl-4,6-dinitrophenol into the analysis, the log P(L/W) value found at pH 5.3 was used as the independent variable, since the partitioning occurring during the glucose release is better simulated by the P(L/W) value. For 2-*s*-butyl-4,6-dinitrophenol, log P(L/W) is the value for the ionization equilibrium mixture, since the liposome can incorporate both species. Equation 12 was derived for perturbation potency.

$$\log 1/C_{200} = 0.868 \log P(\mathrm{L/W}) + 0.119\, V_w - 0.794 \quad (12)$$
$$(\pm 0.136) \qquad (\pm 0.035) \quad (\pm 0.280)$$
$$(n = 18,\ s = 0.086,\ r = 0.991)$$

In Eq. 12, the term of steric parameter V_w for the entire molecular volume is also significant, which indicates that perturbation potency is governed not only by partitioning into liposome but also by the steric bulkiness of the phenols. Although the collinearity between log P(L/W) and V_w is rather high (r^2=0.514) in this set of compounds, the addition of the V_w term is significant at a level higher than 99.5%.

Polarity of the Liposomal Membrane Surface. The fluorescent probe DSHA is thought to be buried in the lecithin bilayer in such a way that its polar dansyl group is directed toward the surface and the hydrophobic long alkyl chain is arranged along the alkyl chain of lecithin.[12] The emission maximum of DSHA has been used as an indicator of the surface polarity of liposomal membranes.[12] It was observed at 520 nm for the liposome suspension here. The maximum in methanol was at 518 nm and that in the 2:1 methanol-water mixture at 522 nm. Therefore, the surface region of liposomal membrane is probably more polar than methanol and less polar than 2:1 methanol-water. In this study, we examined the effect of the 2-*t*-butyl-, 4-methyl-, 4-propyl- and 4-*t*-butylphenols on the emission maximum. As shown in Fig. 5 for the 4-*t*-Bu derivative, the maximum was shifted to the polar side by the addition of substituted phenols. When the concentration increased, it approached to 528—529 nm, which corresponds to that of 1:1 methanol-water. The concentration range where the maximum shift was observed varied depending upon the structure of the phenol (data not shown). In terms of the concentration in the membrane phase, however, it was located in the range of 1.5—2.5 mol kg^{-1} lecithin.

Discussion

Several studies examined the partition behavior of

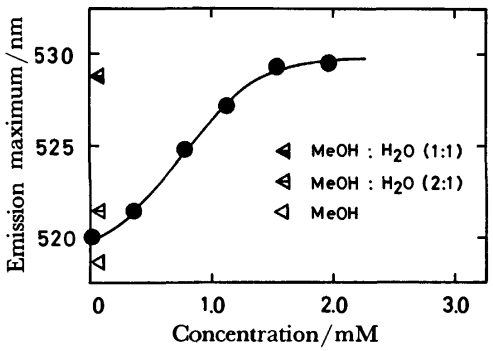

Fig. 5. Position of the fluorescence emission maximum of DSHA incorporated in liposomal membrane in the presence of 4-*t*-butylphenol. Emission maximum of DSHA in 1:1 MeOH-H_2O, in 2:1 MeOH-H_2O, and in MeOH are shown for reference.

various organic solutes in the liposome/water system as a model of biological membranes. Diamond and Katz[18] and Jain and his coworkers[19] found that the effects of the substituents and the substructural features such as chain-branching on the liposome/water partition coefficient are qualitatively similar to those observed for organic solvent/water partition systems. They also noticed that the effect of chain-branching in aliphatic alcohols in lowering the partition coefficient is greater in a liposome/water system than in systems with organic solvents such as olive oil and 1-octanol. They stated that this difference is due to steric repulsion on the more or less parallel arrangement of hydrocarbon tails in the interior of liposomal membranes. There seemed to be an extra steric effect when partition coefficients of liposome/water and organic solvent/water systems were compared.

The quantitative result formulated for substituted phenols in Eq. 3 seems to conform to these previous general findings. Phenol molecules are dehydrated in the lecithin membrane to a degree close to that occurring in the 1-octanol/water partitioning process. However, the steric bulkiness of substituents in terms of the group van der Waals volume lowers the partitioning into liposome more than into the octanol phase. The effect of ortho substituents is most important when they occupy both ortho positions, but not significant in mono-ortho-substituted derivatives, so that the bulkiest substituents, such 2-*t*-Bu, 2-*s*-Bu, and 2-Ph, alone have no significant steric effect. The effect of meta and para substituents is significant but less important than that of di-ortho substitution. From these positional specificities in the steric effect, the following model for the orientation of phenols in the liposomal membrane can be proposed. The substituted phenols are buried from the side of the substituted benzene ring holding the polar OH group toward the external aqueous phase. In this situation, meta and para substituents have an unfavorable effect on packing of the lecithin molecules, in proportion to their volume. For ortho-substituted derivatives, the OH and the single ortho substituent would be located together close to the outside of the membrane where the lecithin polar head groups are loosely packed, having no significant steric effect on the packing structure of the membrane. This kind of orientation would no longer be possible for di-ortho-substituted derivatives. In such compounds, interaction of the OH group with the polar head substituents of lecithin could be hindered. Since the di-ortho-substituted derivatives could behave as less polar molecules than the other substituted phenols, they tend to be buried deeper in the membrane structure. Thus, the steric effect of two ortho substituents acting as a wedge against the parallel arrangement of lecithin molecules is significant. As shown in Eq. 3, electron-withdrawing substituents are more favorable to the partitioning into liposome than into the 1-octanol phase. This could be rationalized by the fact that the basicity of the hydrogen-bond acceptor in liposome (perhaps phosphate anion) is higher than that of the oxygen of 1-octanol.

This orientation model is consistent with information from surface polarity measurements. The marked increase in the surface polarity of the membrane caused by substituted phenols shows that the interactions between polar head groups are weakened due to disorder of the membrane structure near the surface where phenols are buried, and the hydration around the head groups increases greatly. These results seems to be in accord with those obtained earlier,[20] where substituted phenols such as BHT (2,6-di-*t*-butyl-4-methylphenol) and its analogs disturbed molecular packing primarily near the polar head-group region of the lecithin bilayer.

Liposomal membrane perturbation caused by phenols, studied in terms of the increase in passive glucose permeability, was affected by partitioning into the membrane phase and steric bulkiness. The higher the partition coefficient and the steric bulkiness, the higher the degree of perturbation, leading to higher glucose permeability. Lipid-soluble drug molecules generally stabilize the membrane structure, to decrease permeability to permeants.[20-22] This stabilization is thought to be the origin of the antihemolytic activity on erythrocytes of various organic compounds, including anesthetics and tranquilizers. This kind of effects, however, was observed in concentration ranges that had a threshold, and high concentrations of organic molecules irreversibly disordered the membrane structure to increase permeability, as in haemolysis.[23] In this study, glucose permeability did not decrease in the lower range of phenol concentrations. The experimental system could inherently be such that no membrane stabilization was observable, requiring concentrations higher than the "threshold" to cause membrane perturbation.

Steric bulkiness increases the perturbation of the liposomal membrane, as shown in Eq. 12. We ex-

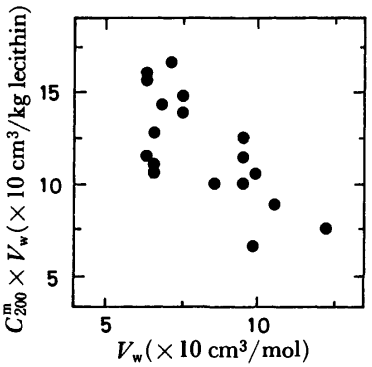

Fig. 6. Plot of the occupying volume in liposomal membrane vs. van der Waals volume of phenols. The scale of V_w was multiplied by 0.1.

amined the nature of this steric effect in terms of the occupying volume of substituted phenols in the membrane phase, and derived Eq. 13, where C^m_{200} is the concentration of phenols in the liposomal membrane (mol phenol/kg lecithin) equilibrated at the C_{200} concentration estimated from the log P(L/W) value, and where V_w is the molecular van der Waals volume of compounds.

$$C^m_{200} \cdot V_w = -1.133\, V_w + 21.141 \quad (13)$$
$$(\pm 0.626) \qquad (\pm 5.229)$$
$$(n = 18,\ s = 2.193,\ r = 0.692)$$

Although the correlation coefficient is not very high, the V_w term is significant above the 99.5% confidence level. As shown in Fig. 6, there is a clear trend in which the larger the steric bulk of the molecule, the smaller is the occupying volume with the equivalent degree of membrane perturbation potency. This may mean that the effect of steric bulk is caused not by the bulk itself, but that the effect is enhanced proportionally to the bulk.

This study indicates that the separation of various effects is very helpful to understand the mechanisms of membrane phase partitioning and the membrane structure perturbation of organic compounds. Understanding can be achieved only by quantitative analysis using physicochemical molecular parameters. The effect of substituted phenols on these membrane characteristics can be separated in terms of the hydrophobicity and the steric bulk relative to these for appropriate reference systems. Work in progress in this laboratory indicates that a procedure of this sort can be used in analysis of the effect of the same series of compounds on the proton permeability across the lecithin bilayer, simulating the inner mitochondrial membrane.

The calculations were performed with a FACOM M382 computer at the Data Processing Center of this University. We thank Professor Hiroshi Terada, the Faculty of Pharmaceutical Sciences, Tokushima University for his invaluable discussions.

Reference

1) Y. Uesugi and K. Fukunaga, *Ann. Phytopath. Soc. Jpn.*, **33**, 168 (1967).
2) P. Maurice, *Proc. Soc. Appl. Bacteriol.*, **15**, 144 (1952).
3) J. Tomcsik, *Proc. Soc. Exp. Biol. Med.*, **89**, 459 (1955).
4) T. Fujita, *J. Med. Chem.*, **9**, 797 (1966).
5) E. J. Lien, C. Hansch, and J. M. Anderson, *J. Med. Chem.*, 11, 430 (1968).
6) A. E. Beezer, W. H. Hunter, and D. E. Storey, *J. Pharm. Pharmacol.*, **32**, 815 (1980); **35**, 406 (1983).
7) S. Singleton, M. S. Gray, M. L. Brown, and J. L. White, *J. Am. Oil. Chem. Soc.*, **42**, 53 (1965).
8) C. H. Huang, *Biochem.*, **8**, 344 (1969).
9) I. Shibuya, H. Honda, and B. Maruo, *Agr. Biol. Chem.*, **31**, 111 (1967).
10) P. T. Englund, J. A. Huberman, T. M. Jovin, and A. Kornberg, *J. Biol. Chem.*, **244**, 3038 (1969).
11) S. C. Kinsky, J. Haxby, C. B. Kinsky, and R. A. Demel, *Biochem. Biophys. Acta.*, **152**, 174 (1968).
12) A. S. Waggoner and L. Stryer, *Proc. Nat. Acad. Sci.*, **67**, 579 (1970).
13) I. Tabushi, T. Nishiya, M. Shimomura, T. Kunitake, H. Inokuchi, and T. Yagi, *J. Am. Chem. Soc.*, **106**, 219 (1984).
14) J. Brunner, D. E. Graham, H. Hauser, and G. Semenza, *J. Membrane Biol.*, **57**, 133 (1980).
15) H. Terada, K. Kitagawa, Y. Yoshikawa, and F. Kametani, *Chem. Pharm. Bull.*, **29**, 7 (1981).
16) C. Hansch and A. Leo, "Substituent Constants for Correlation Analysis in Chemistry and Biology," Wiley, New York (1979), p. 13.
17) T. Fujita and H. Iwamura, *Topics Curr. Chem.*, **114**, 119 (1984).
18) Y. Katz and J. M. Diamond, *J. Membrane Biol.*, **17**, 69, 87, 101, 121 (1974).
19) M. K. Jain and L. V. Wray, *Biochem. Pharmacol.*, **27**, 1294 (1978).
20) M. Singer and J. Wan, *Biochem. Pharmacol.*, **26**, 2259 (1977).
21) P. Seeman, W. O. Kwant, M. Goldberg, and M. Chau-Wong, *Biochem. Biophys. Acta.*, **241**, 349 (1971).
22) K. Tanaka and Y. Iizuka, *Biochem. Pharmacol.*, **17**, 2023 (1968).
23) P. Seeman, *Pharmacol. Rev.*, **24**, 583 (1972).

Synthetic Photochemistry. XXXIV.[1] Synthetic Strategy of 5-8-5-Membered Tricyclic Higher Terpenoids Based on the Condensation of Two Optically-Active Iridoids, C_{10}-Synthons Obtained from Photo-Cycloadduct of Methyl 2,4-Dioxopentanoate-Isoprene, and Its Application to a Synthesis of the Basic Carbon Skeleton of Fusicoccane[2]

Nobuo KATO, Kohji NAKANISHI,† and Hitoshi TAKESHITA*
Research Institute of Industrial Science, 86, Kyushu University, Kasuga-koen, Kasuga, Fukuoka 816
†Graduate School of Engineering Sciences, 39, Kyushu University, Kasuga-koen, Kasuga, Fukuoka 816
(Received October 22, 1985)

One of the photocycloadducts obtained during methyl 2,4-dioxopentanoate to isoprene was converted to optically active iridoids. Using a $CrCl_2$ reductive-coupling reaction, proper combinations of two kinds of enantiomeric iridoids, 1-iriden-7-al and 9-benzyloxy-7-chloro-1-iridene, produced versatile intermediates for various types of 5-8-5-membered tricyclic natural products. From one such product, fusicocca-2,8,10(14)-triene (**1**) was synthesized by sequential transformations.

There are several higher terpenoids that have 5-8-5-membered tricyclic frameworks e.g, fusicoccins (**A**) and cotylenins (**B**),[3] ophiobolins (**C**),[4] ceroplastols (**D**),[5] and several other recently found derivatives.[6,7] From their stereochemical characteristics, one can say that i) these tricyclic skeletons can be divided into two iridoid blocks, and ii) depending on their origins, these natural products possess different stereochemistries involving a basic carbon skeleton. Therefore, a synthetic strategy based on the dimerization of iridoid synthons to natural products, many of which possess heavy oxygenated functions, and are reported to be physiologically or biologically active, should be attractive. In addition, there are related tricyclic derivatives, e.g., marine metabolites, 6-7-5-membered tricyclo compounds, clavularenes (**E**) isolated from *Clavularia inflata*.[8] Their total synthesis might also be achieved by a slight modification of this method. Recently, we developed a facile preparation of iridoid synthons from the photoadduct of methyl 2,4-dioxopentanoate (**F**) to isoprene (**G**)[9] via titanium(II) chloride-mediated retro-ozonolysis.[10]

In this paper, the first synthesis of fusicocca-2,8,10(14)-triene (**1**) is described.[11] It is thought to be the missing link in the biogenesis of natural fusicoccins,[2] all of which possess the trans-8β,9α-diol function.[3]

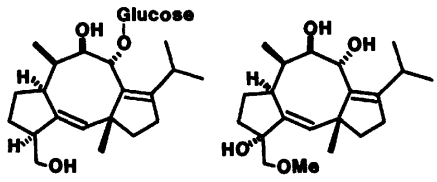

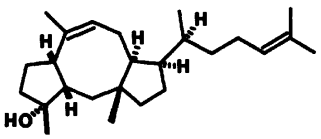

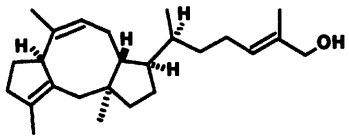

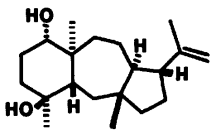

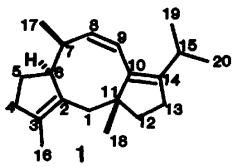

Scheme 1.

Results and Discussion

Optical Resolution. As previously described,[13] Mukaiyama's titanium(II) chloride-mediated reductive cyclization of photoadduct (**2**) from **F** to **G** gave three 1,2-diol derivatives (**3**, **H**, and **J**), among which the major product, **3**, was convertible to the olefin (**4**) in good yield. Since diols are appropriate for introducing an optically active segment for the resolution, we first investigated the optical resolution of these iridoids to minimize the number of isomers of the dimeric condensates in the subsequent steps. The **3** was treated with trimethoxymethane (**5**) and pyridinium *p*-toluenesulfonate (PPTS) in benzene and with potassium salt of *l*-menthol (**6**) followed by aqueous acetic acid-hydrolysis to form, via an orthoester, *l*-menthyl 1,2-dihydroxy-8-iriden-7-oates (**7a** and **7b**).[14]

Fractional recrystallization of **7a** and **7b** easily enabled the resolution; the isomer with a higher-melting point, mp 97—97.5 °C, showed $[\alpha]_D=-57.1°$, while the isomer with a lower-melting point, mp 81.5—82 °C, showed $[\alpha]_D=-40.8°$. The former was (3*S*)-**7b** and the latter was (3*R*)-**7a** based on the following transformations. The (3*S*)-**7b** was consecutively treated with **5** and PPTS and then with acetic anhydride under reflux[15] to give *l*-menthyl (3*S*)-1,8-iridadien-7-oate ((3*S*)-**8b**). This was, according to a known procedure, transformed to (3*S*)-1,8-iridadien-7-ol ((3*S*)-**9**) by diisobutylaluminum hydride (DIBAH)-reduction and (3*S*)-1,8-iridadien-7-al ((3*S*)-**10**) by manganese(IV) oxide-oxidation.[16] Previously, enantiomeric **10** was prepared and the absolute stereochemistry clarified.[16] For the preparation of **10** from **9**, a Collins oxidation produced a poor result due to the formation of a byproduct, (3*S*)-1,2-epoxy-8-iriden-7-ol (**11**). A catalytic reduction of (3*S*)-**7b** gave a dihydro derivative, *l*-menthyl (1*R*,2*S*,3*S*)-1,2-dihydroxyiridan-7-oate (**12b**), which, upon similar treatment with **5** and PPTS, followed by thermolytic deoxygenation, DIBAH-reduction and oxidation, formed *l*-menthyl (3*S*)-1-iriden-7-oate ((3*S*)-**13b**), (3*S*)-1-iriden-7-ol ((3*S*)-**14**), and (3*S*)-1-iriden-7-al ((3*S*)-**15**). The same transformations starting from (3*R*)-**7a** were carried out.

Chromium(II) Chloride-Mediated Coupling of Two Iridoids and the Stereochemistry. For the chromium(II) chloride-mediated coupling reaction, the required (3*S*)-9-benzyloxy-7-chloro-1-iridene ((3*S*)-**16**) was prepared by (3*S*)-**10** by treating 1,2-ethanediol to give an acetal (**17**), stereoselective hydroboration[9] to (3*S*,8*R*)-7,7-ethylenedioxy-1-iriden-9-ol (**18**), benzylation to 9-benzyloxy derivative (**19**), hydrolysis to 9-benzyloxy-1-iriden-7-al (**20**), reduction to 9-benzyloxy-1-iriden-7-ol (**21**), and treatment with oxalyl dichloride and dimethyl sulfoxide (DMSO)[17] to (3*S*)-**16**.

When (3*S*)-**15** and (3*S*)-**16** were treated with chromi-

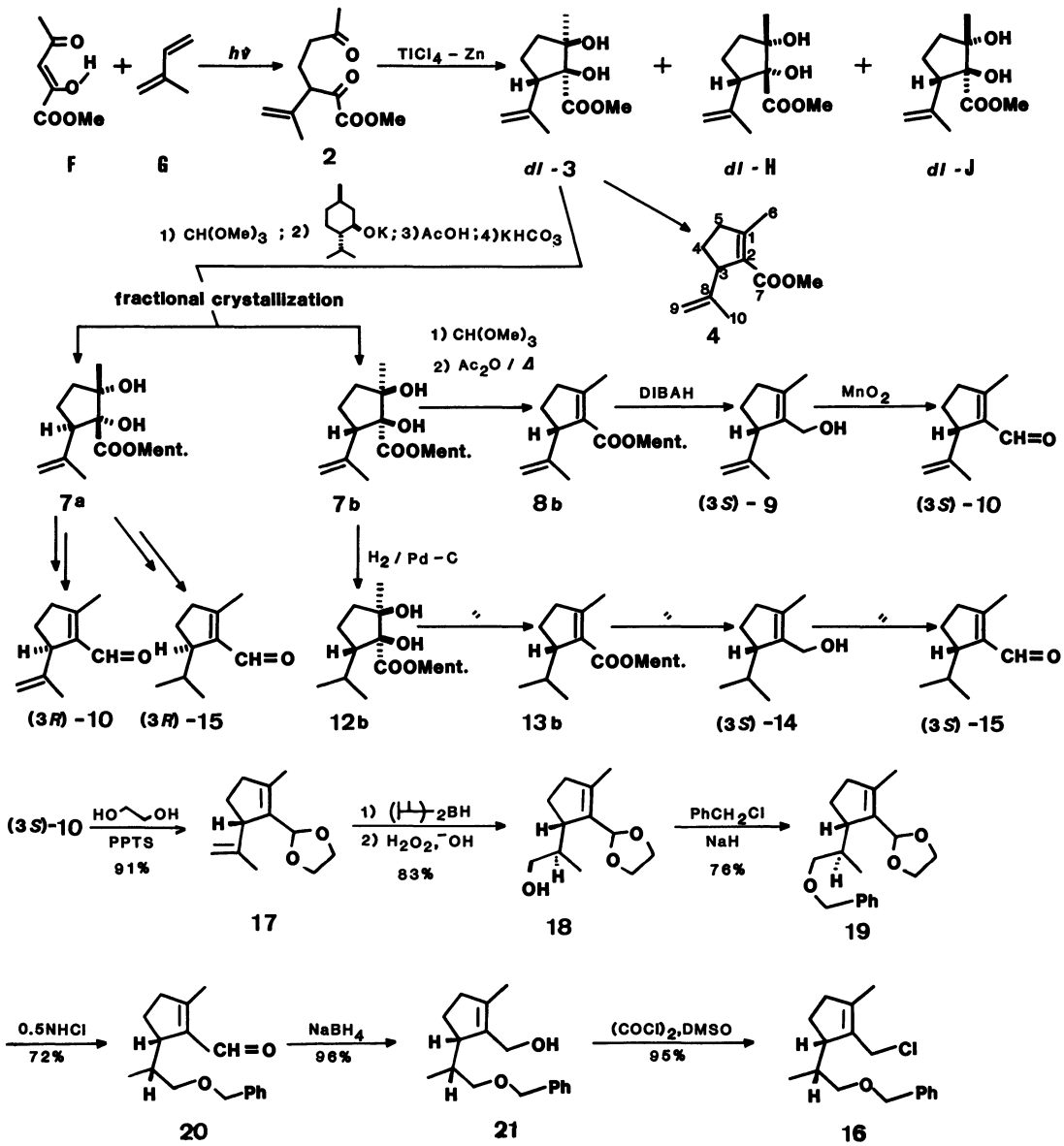

Scheme 2.

um(II) chloride in *N*,*N*-dimethylformamide (DMF), two condensates (**22** and **23**) were obtained in 82% yield with a ratio of 7:2. Collins oxidation of **22** gave a dehydro ketone (**24**), and its lithium aluminum hydride (LAH)-reduction in tetrahydrofuran (THF) reproduced **22** and **23** in a ratio of 3:4. Therefore, **22** and **23** are epimeric. In parallel, (3*R*)-**15** and (3*S*)-**16** also gave two condensates (**25** and **26**) in 20:1, and by Collins oxidation, the former, **25**, yielded another dehydro ketone (**27**) which was reduced to **25** and **26** by LAH.

Nevertheless, in both cases the chromium(II) chloride condensation yielded only a pair of epimers. The observed product distributions might indicate the stereochemistry of the C–C bonding site as being an attack of carboanion from the less hindered side to produce a cis-relationship for the quaternary methyl and isopropyl groups.

This has been verified unambiguously as follows. The four condensates (**22**, **23**, **25**, and **26**) were easily debenzylated by a Birch reduction to give 1,2-diols (**28**, **29**, **30**, and **31**) in good yields. When the Birch reduction of **26** was carried out in ethylamine, the products were **31** and its bond-migrated isomer (**32**) with two tetrasubstituted double bonds. This was also the case when **23** was reduced in ethyl amine; the debenzylated products were **29** and the isomeric diene (**33**), the major product (66% yield). All of these (**28** to **31**) formed iodine-free bis-ether derivatives (**34**, **35**, **36**, and **37**). Since these are triply fused five-membered ring systems, their ring junctures should all be cis. From this requirement, quaternary methyl and isopropyl groups are cis, as depicted. The stereochemistry of the secondary hydroxyl groups were determined by the nuclear Overhauser effect between each singlet methyl signal and the proton signal from the carbinyl carbon. The observed enhancement of carbinyl proton signals upon irradiation with radio frequencies corresponding to the chemical shifts ascribable to the quaternary methyl singlets were shown to be 1% for **34**, 13% for **35**, 7% for **36**, and 19% for **37**, respectively. Thus, **35** and **37** possessed a cis-configuration, while their counterparts, **34** and **36**, showed a trans-relationship. The original stereochemistry of **22**, **23**, **25**, and **26** was established as shown.

Cope Rearrangement and the Singlet-Oxygen Oxidation. At first, the recently developed anionic *oxy*-Cope rearrangement[19] was attempted, but gave an inferior result. For instance, the thermolysis of the oxy anion species derived from a potassium hydride treatment of **25** in anhydrous THF caused the fragmentation to two iridoids ((3*R*)-**15** and **38**) and only a small amount of the products (**39a** and **39b**) were obtained as a mixture. The ^{1}H NMR spectra of **38** and **39** revealed that their structures are in agreement with those predicted from the reaction mechanism. On the other hand, the Cope rearrangement was dramatically improved when the secondary hydroxyl was protected by the trimethylsilyl (TMS) group. In this case, the TMS derivative (**40**, **42**, or **43**) prepared from **22**, **25**, or **26**, at 190 °C in a sealed tube, a single thermolysate (**44**, **45**, or **46**) was produced each time. However, in the case of **41**, for the TMS derivative of **23**, it was necessary to heat above 200 °C for 4 d to produce two products (**47** and **48**). This stereochemical behavior is attributable to the

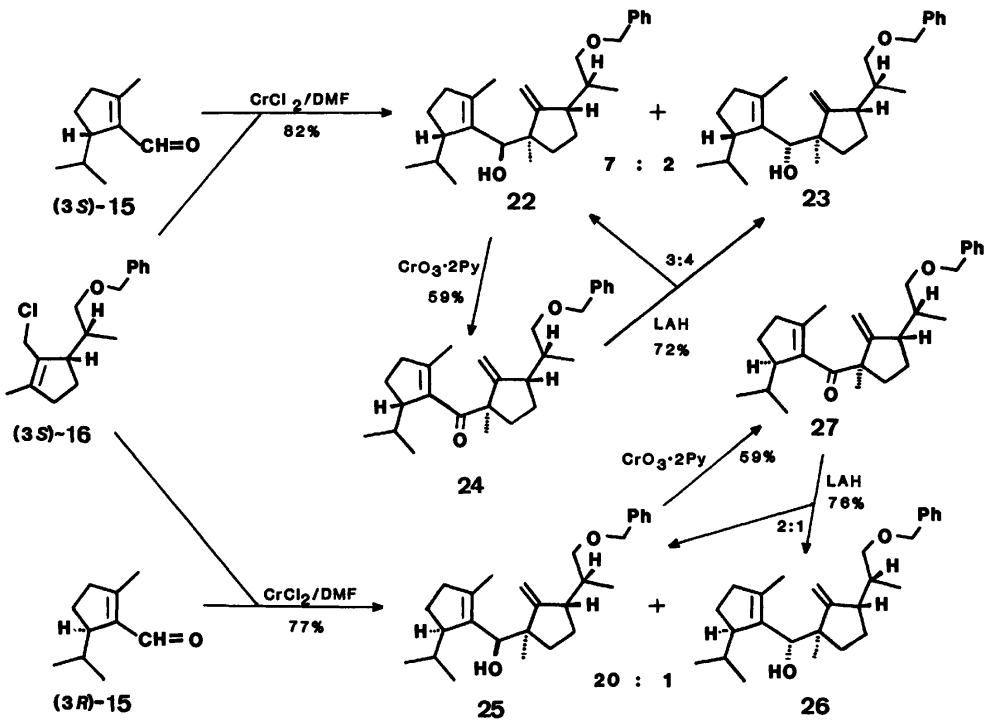

Scheme 3.

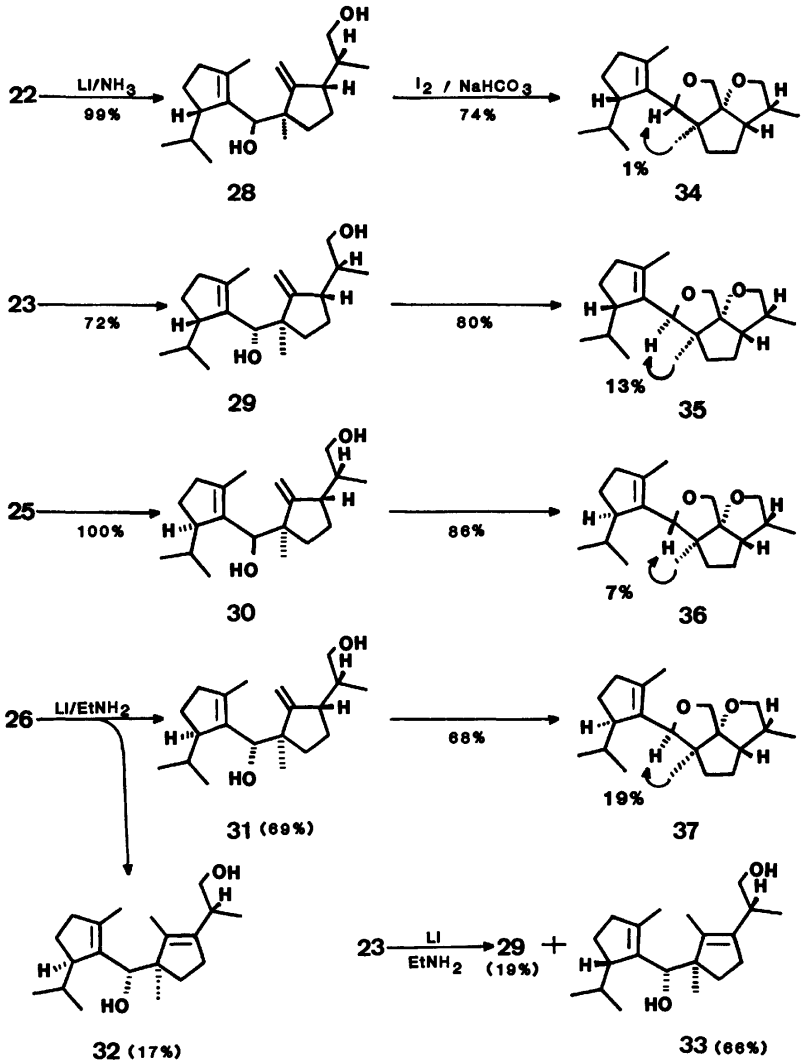

Scheme 4.

geometry of the transition state in the rearrangement, a concerted [3,3] sigmatropy.

According to a study using molecular models, it is certain that the predominant conformers in the transition state of the rearrangement should be chair-like for **42** and **43**, respectively (Scheme 6). Alternative boat-like conformers suffer heavy nonbonding interactions. On the other hand, the chair-like conformers for **40** and **41** suffer nonbonding interactions and, furthermore, in the boat-like conformer of **41** a considerable interaction also exists between the newly-formed quaternary methyl group and the trimethylsiloxy (TMSO) group due to a 1,3-diaxial mode. As a result, both conformations which are required for an electrocyclic reaction are more unstable than any other extended conformers. Indeed, the thermolysis of **41** required more severe conditions than others and gave two thermolysates, **47** and **48**, via the different transition states.

Although the reaction conditions were different and reflected the geometries of the transition states of

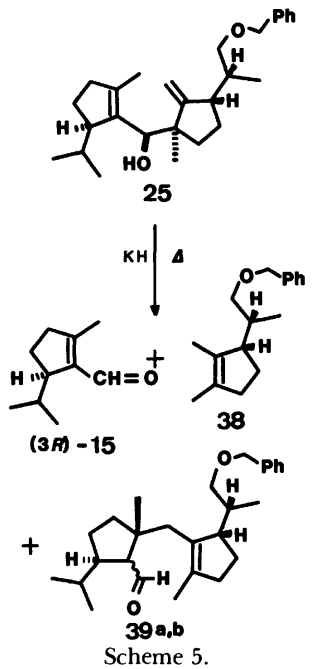

Scheme 5.

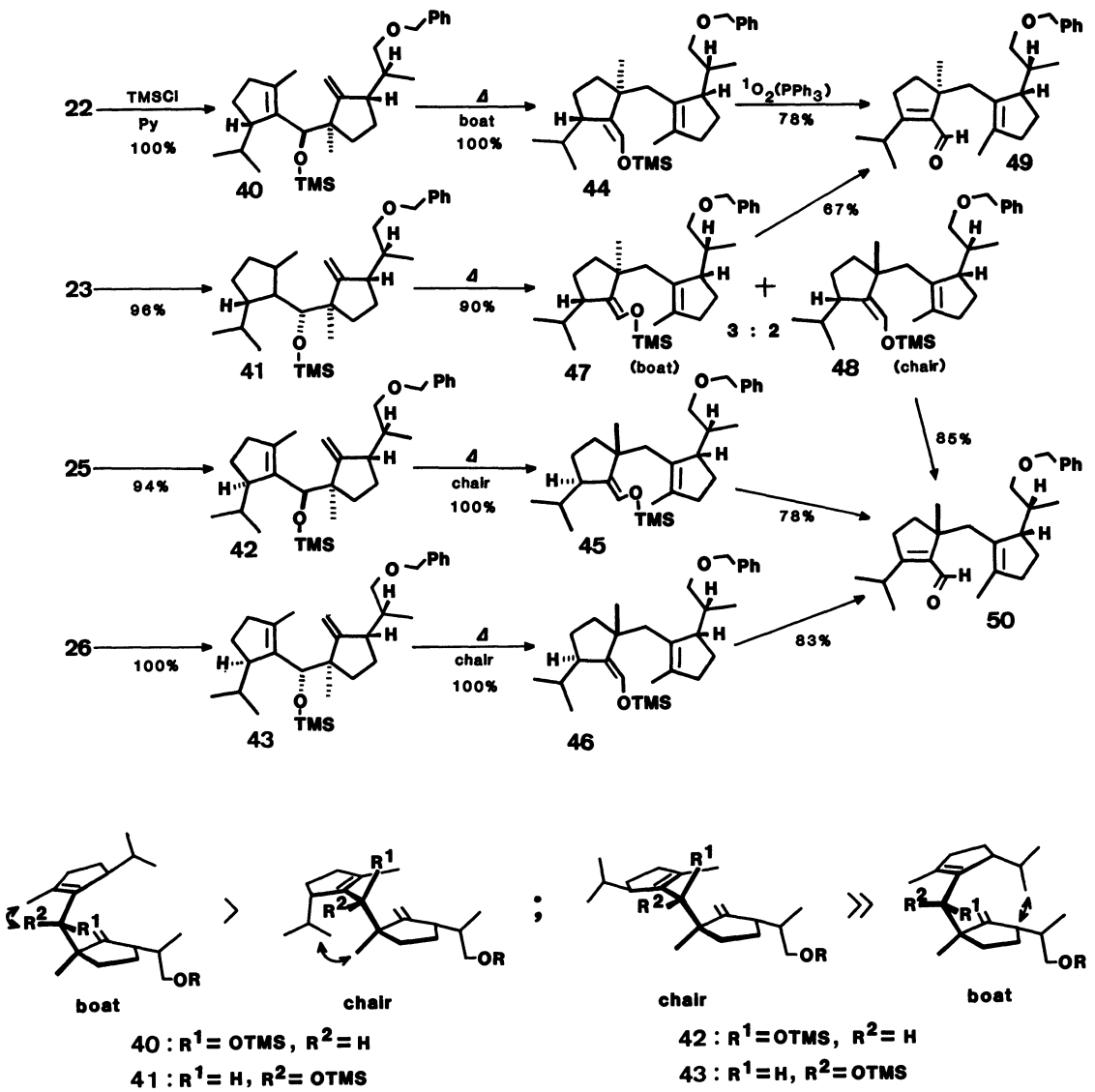

Scheme 6.

the compounds, the reaction mixture remained clean and neat, and the yields of the thermolysates were satisfactory.

Thus, Cope rearrangement worked to not only transfer an oxygen function to the required position for subsequent cyclization, but also worked to adjust the stereochemistry of fused tricyclic frameworks. This means one can synthesize various stereoisomers with or without a Cope rearrangement. In view of the oxidation state around the ring C of fusicoccane derivatives and for the sake of a convenient structural analysis, thermolysates were oxidized to α,β-unsaturated aldehydes (**49** and **50**). For this purpose either singlet oxygen ($^1O_2$)-oxidation[19] or palladium(II) acetate-oxidation[20] might be suitable. The former gave the better result. It is particularly advantageous that, at least for a preparative purpose, the separation of $CrCl_2$-induced condensation products was not necessary. The subsequent transformation of **25** and **26** resulted in the formation of the same compounds, while the thermolysis conditions of **22** and **23** were greatly different.

Dialdehyde Formation. Based on the establishment of a stereoelectronic course for the Cope rearrangement, we then investigated the thermolysis with more suitable reactants than the benzyloxy derivatives (**40**, **41**, **42**, and **43**): The bis-TMS derivatives (**51** and **52**) derived from **28** and **30**. Indeed, a clean stereospecific rearrangement occurred forming **53** and **54**. In parallel to **40**, and **42**, **53**, and **54** were each oxidized with $^1O_2$ to α,β-unsaturated aldehydes (**55** and **56**) which, by the advantage of TMS derivatives, generated the primary hydroxyl groups during the workup. An alternative palladium(II) acetate oxidation gave **56** from **54** in fair yield, but gave no **55** from **53**.

The Swern oxidation[17] of **55** and **56** gave the desired dialdehydes (**57** and **58**) in good yields. From its stereostructure, **58** should be a precursor of diterpenoids such as cotylenins or fusicoccins while **57** should be a good precursor for sesterterpenoids such as ophio-

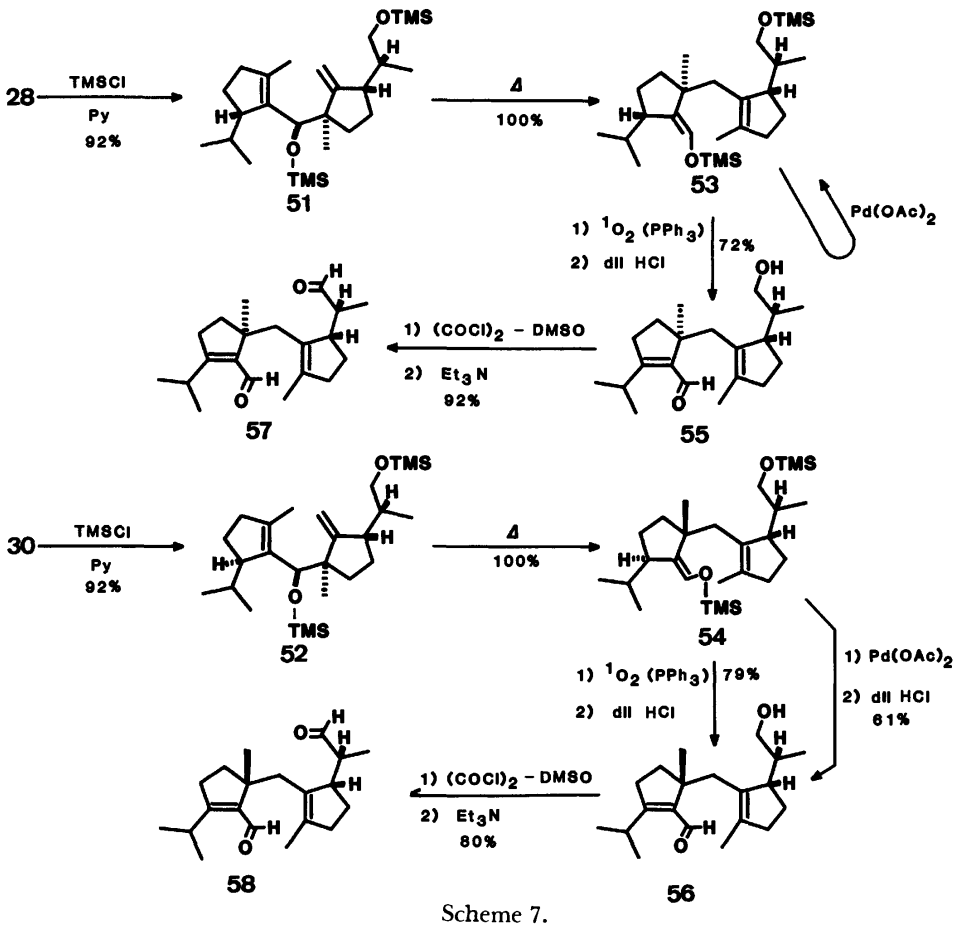

Scheme 7.

bolanes or ceroplastanes. This is true even though further transformations are required to furnish the correct stereochemistry on the side chains. Recently, several diterpenoids with a "sesterterpenoid-like" ring systems have been isolated.[7]

Titanium(II) Chloride-Mediated Reductive Cyclization. When **57** was reduced with titanium(II) chloride (generated in THF by Mukaiyama's method),[10] three cyclisates (**59**, **60**, and **61**) were formed (5:5:3) with a combined yield of 68%. However, it required high-dilution conditions to prevent an intermolecular condensation. Although the central eight-membered B-ring might be conformationally flexible, a careful inspection of the ^{1}H NMR spectra showed their stereostructures. Both **60** and **61** revealed large vicinal couplings (J=9 Hz) between the protons on the carbons of 1,2-diol functions, making them to be trans-diols. The **59** revealed a small coupling constant (J=4 Hz), indicating a cis-diol structure. Moreover, **59** and **61** exhibited relatively lower signals which were ascribable to the quaternary methyl singlets at δ=1.20, while the signal of the corresponding methyl of **60** was at 0.98. Accordingly, the quaternary methyl and C-9 hydroxyl of **59** and **61** are in cis-direction, and, thus, have a 1,3-diaxial relationship. From these facts, **59**, **60**, and **61** must be 8α,9α-diol, 8α,9β-diol, and 8β,9α-diol, respectively. The chemical shifts of their secondary methyl groups at C-7, were 0.93 for **59**, 0.96 for **60**, and 0.98 for **61**. These were also explainable in terms of an anisotropic effect due to adjacent C-8 hydroxyl groups.

On the other hand, the titanium(II) chloride-induced cyclization of **58** was much superior with respect to product distributions; it gave almost one product (**62**) in a yield greater than 80%. Although a byproduct (**63**) could not be isolated as diol, its formation was confirmed after silica-gel column chromatography of the monoacetates (**64** and **65**) prepared from a mixture of the cyclisates. Its yield was estimated to be ca. 11%. A diacetate (**66**) was obtained by the acetylation of **62** with acetic anhydride and 4-(dimethylamino)pyridine (DMAP) together with some amount of **64**. The removal of the acetyl group of **65** by LAH-reduction resulted in a solvolytic rearrangement; the major product was indeed **63** whose ^{1}H NMR spectrum had a close resemblance to that of **65**. The byproduct (**67**) showed the signal for the quaternary methyl group at relatively low-field to indicate an epimerization of C-9 hydroxyl to form 8α,9β-diol. It is certain that the original mixture did not contain **67**. A smooth sodium periodate-oxidation of **62** afforded **58**; therefore, the original configuration was retained during the cyclization. The structure of **62** resembles that of the natural fusicoccins; only the differences are orientation

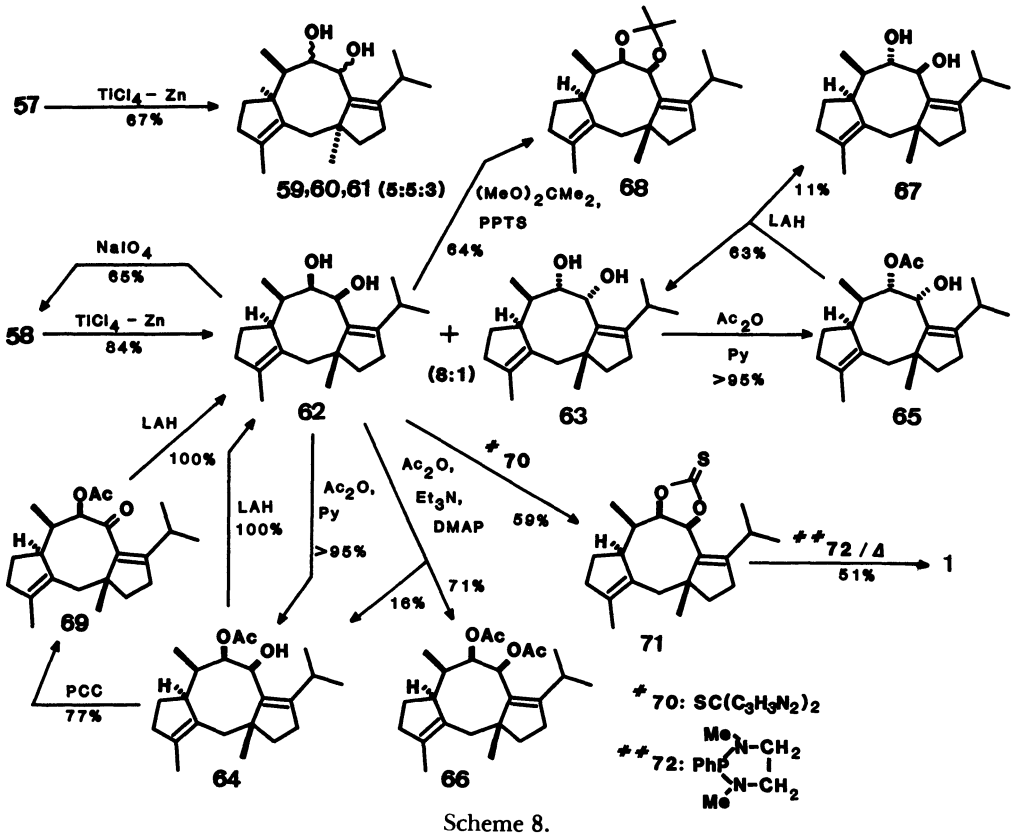

Scheme 8.

of C-9 hydroxyl and the position of the double bond in the A/B rings. The stereochemistry of the 1,2-diol function of **62** was further confirmed by the formation of an acetonide (**68**) which could be prepared by a PPTS-treatment of **62** and 2,2-dimethoxypropane. The central eight-membered ring of **68** became rigid and showed sharp ^{1}H NMR signals which revealed the coupling patterns of the methine protons, i.e., the signals at δ=4.20 and 5.17 mutually coupled with 9 Hz to clarify the cis relationship. Also the former signal showed an additional coupling (1 Hz) to the vicinal methine proton at a carbon bearing the secondary methyl group. We tried hard to invert the hydroxyl group at C-9; for example, when the keto acetate (**69**), prepared from **64** by pyridinium chlorochromate (PCC)-oxidation, was reduced by LAH. The isolable product was only regenerated **62**. We are still studying this matter.[21]

Synthesis of Fusicoccatriene. According to the biogenetic concept, the C-8 and C-9 positions of these terpenoids correspond to one of the head-to-tail junctures of the isoprene units.[22] Therefore, in the original precursors (geranylgeraniol or geranylfarnesol) they were the sp^3-carbons. This means that the 1,2-diol function was derived via a dehydrogenation followed by epoxidation and hydrolysis. Consequently, the reductive elimination of the 1,2-diol to an olefin (**1**) should constitute a synthesis of a common intermediate during biogenesis. Following Corey's procedure,[23] **62** was converted by 1,1'-(thiocarbonyl)bis[diimidazole] (**70**) to a thiocarbonate (**71**). After several unsuccessful attempts, **71** was finally converted to **1**. Its heating in benzene to reflux with a thiophile, 1,3-dimethyl-2-phenyl-1,3,2-diazaphospholidine (**72**),[24] afforded a hydrocarbon whose NMR features and molecular weight (by mass spectrometry) were fully consistent with the structure of **1**.

Up to now, several synthetic studies regarding these tricyclic higher terpenoids have been reported, but most of the current effort seems to be concerned with the construction of model system.[25-27]

Experimental

All mps (measured by means of a Yanagimoto Micro-mp Apparatus) are uncorrected. Elemental analyses were performed by Miss S. Hirashima of Research Institute of Industrial Science, Kyushu University. The purity of the each analytical specimen was checked by high-pressure liquid chromatography (HPLC) on a Nippon Waters ALC 244 Model apparatus with a prepacked Micropolasil column (stainless steel, diameter; 7.8 mm, and length; 300 mm). Gas-liquid chromatography (GLC) was carried out by means of a Yanagimoto Model G 80 apparatus with a thermal-conductivity detector. Optical rotations were measured by means of a Union Model PM-101 apparatus. The NMR spectra were measured using a JEOL FX 100 Spectrometer with a $CDCl_3$ solutions. Chemical shifts measured were expressed in δ units from the internal Me_4Si. The mass spectra were measured by means of a JEOL 01SG-2 Spectrometer. The IR spectra were taken in either as KBr disks or as liquid film (NaCl plates) using a JASCO

IR-A 102 Spectrometer.

Optical Resolution of 3. A mixture of **3** (1.54g), **4** (15 cm³), and PPTS (100 mg) was kept room temperature for 16 h. Then, the mixture was partitioned between a 1:1-mixture of hexane and AcOEt and aqueous $NaHCO_3$. The organic layer was washed with brine, dried on $MgSO_4$ and chromatographed on a silica-gel column with AcOEt–hexane (1:8) to give a colorless oil (1.80 g; 98%). To a THF solution (25 cm³) containing potassium salt of **6** (prepared from **6** (7.5 g) and potassium (500 mg)), a THF solution (18 cm³) of the above oily product was added and refluxed under an N_2 atmosphere for 20 min with the gradual removal of THF (18 cm³). Subsequently, aqueous NH_4Cl was added to the cooled mixture and extracted with AcOEt and hexane (1:5). The organic extract was washed with aqueous $NaHCO_3$, water and brine and dried on $MgSO_4$. The evaporation of the solvent left a pale-yellow oil which was chromatographed on a silica-gel column to remove an excess of **6** from a diastereomeric mixture of *l*-menthyl ester (2.50 g; 94%).

This was dissolved in a mixture (40 cm³) of AcOH, THF, and water (2:2:1) and refluxed for 2 h. After dilution with water, K_2CO_3 was introduced to neutralize AcOH in the mixture. The mixture was then extracted with AcOEt and heated in vacuo to give a yellow-oily diastereomeric mixture of formates, which was further treated with saturated aqueous $KHCO_3$ (5 cm³) in MeOH (30 cm³) at room temperature for 45 min. After removal of MeOH in vacuo. The residue was diluted with water and extracted with AcOEt. A yellow oil from the extract was chromatographed on a silica-gel column to give a mixture of a *l*-menthyl ester of 1,2-dihydroxy-8-iriden-7-oate, **7a** and **7b** (2.125 g). Fractional recrystallizations from hexane by alternate seeding of **7a** and **7b** afforded, after repeating the operation several times, (3*S*)-**7b** [colorless prisms, mp 97—97.5°C, 1.007 g; 95%. Found: C, 71.21; H, 10.24%. Calcd for $C_{20}H_{34}O_4$: C, 70.97; H, 10.12%. $[\alpha]_D=-57.1°$ (*c* 2.10, $CHCl_3$). ^1H NMR δ=0.74 (3H, d, *J*=7 Hz), 0.91 (6H, d, *J*=7 Hz), 1.25 (3H, s), 1.73 (3H, br s), 3.02 (1H, br s, OH), 3.18 (1H, br m), 3.56 (1H, s, OH), 4.73 (1H, td, *J*=10, 4 Hz), 4.79 (1H, m), and 4.87 (1H, m). ^{13}C NMR δ=15.6, 20.8, 22.0, 22.5, 22.9, 24.7, 25.5, 25.8, 31.4, 34.2, 38.8, 40.6, 46.8, 51.4, 76.5, 81.2, 85.0, 112.8, 143.7, and 173.8. IR ν: 3425, 2970, 2940, 2880, 1720, 1638, 1448, 1377, 1290, 1254, 1128, 1023, and 884 cm^{-1}] and (3*R*)-**7a** [colorless plates, mp 81.5—82°C, 1.020 g; 96%. Found: C, 71.23; H, 10.18%. $[\alpha]_D=-40.8°$ (*c* 2.11, $CHCl_3$). ^1H NMR δ=0.74 (3H, d, *J*=7 Hz), 0.91 (6H, d, *J*=7 Hz), 1.25 (3H, s), 1.71 (3H, br s), 3.10 (1H, br m), 3.13 (1H, br s, OH), 3.71 (1H, s, OH), 4.77 (1H, td, *J*=10, 4 Hz), 4.78 (1H, m), and 4.85 (1H, m). ^{13}C NMR δ=15.5, 20.9, 22.0, 22.5, 22.8, 24.5, 25.7, 25.8, 31.4, 34.1, 38.8, 40.6, 47.0, 51.5, 76.7, 81.3, 84.6, 112.5, 143.7, and 174.3. IR ν: 3555, 3495, 2955, 2930, 2870, 1710, 1640, 1448, 1354, 1248, 1110, 970; and 898 cm^{-1}].

Reductive Elimination of (1*R*,2*S*,3*S*)-7b to *l*-Menthyl (3*S*)-1,8-Iridadien-7-oate ((3*S*)-8b). A mixture of (3*S*)-**7b** (249 mg), **5** (3 cm³) and PPTS (30 mg) was stirred at room temperature for 15 h. The resultant dioxolane derivative (after the usual workup) was heated in Ac_2O (3 cm³) for 3 h. The mixture was poured into aqueous $NaHCO_3$ and stirred an additional 1 h at room temperature and extracted with a mixture of hexane and ether. The organic extract was, after removing the solvent, chromatographed on a silica-gel column with hexane–ether (15:1) to give (3*S*)-**8b** [a colorless oil, 222 mg; 99%. Found: C, 79.12; H, 10.59%. Calcd for $C_{20}H_{32}O_2$: C, 78.90; H, 10.59%. $[\alpha]_D=-28.5°$ (*c* 1.86, $CHCl_3$). ^1H NMR δ=0.76 (3H, d, *J*=7 Hz), 0.88 (6H, d, *J*=7 Hz), 1.67 (3H, br s), 2.11 (3H, br s), 3.57 (1H, br m), 4.62 (2H, m), and 4.67 (1H, td, *J*=10, 4 Hz). ^{13}C NMR δ=16.2, 16.6, 20.4, 20.8, 22.1, 23.7, 26.5, 28.6, 31.4, 34.4, 39.3, 40.8, 47.2, 53.5, 73.3, 109.2, 130.1, 148.0, 155.2, and 165.6. IR ν: 2955, 1705, 1648, 1454, 1372, 1274, 1220, 1123, 1052, and 894 cm^{-1}].

Reductive Elimination of (1*S*,2*R*,3*R*)-7a to *l*-Menthyl (3*R*)-1,8-Iridadien-7-oate ((3*R*)-8a). Similarly, (3*R*)-**7a** (268 mg) was converted to (3*R*)-**8a** [a colorless oil, 239 mg; 99%. Found: C, 79.02; H, 10.65%. $[\alpha]_D=-112.9°$ (*c* 2.17, $CHCl_3$). ^1H NMR δ=0.69 (3H, d, *J*=7 Hz), 0.85 (3H, d, *J*=7 Hz), 0.89 (3H, d, *J*=7 Hz), 1.68 (3H, br s), 2.13 (3H, br s), 3.57 (1H, br m), 4.62 (2H, m), and 4.68 (1H, td, *J*=10, 4 Hz). ^{13}C NMR δ=15.7, 16.2, 20.8, 21.0, 22.1, 23.0, 25.4, 28.7, 31.5, 34.4, 39.2, 41.3, 47.3, 53.3, 73.2, 109.1, 130.1, 148.2, 155.8, and 165.6. IR ν: 2955, 1705, 1649, 1455, 1372, 1273, 1223, 1127, 1051, and 885 cm^{-1}].

DIBAH-Reduction of (3*S*)-8b to (3*S*)-9. Following the method described by Paquette,[16] (3*S*)-**8b** (122 mg) was reduced with a toluene solution (1 cm³) of DIBAH (1.5 M) in anhydrous ether (8 cm³) at −78°C to (3*S*)-**9** [a colorless oil, 55 mg; 90%. $[\alpha]_D=+193.6°$ (*c* 1.40, $CHCl_3$ (lit,[16] +143.9°)). ^1H NMR δ=1.64 (3H, br s), 1.72 (3H, br s), 3.97 (1H, d, *J*=12 Hz), 4.20 (1H, d, *J*=12 Hz), and 4.75 (2H, m). IR ν: 3550, 2900, 1370, and 890 cm^{-1}].

MnO_2 Oxidation of (3*S*)-9 to (3*S*)-10. (3*S*)-**9** (1.00 g) was treated with MnO_2 (10 g) in CH_2Cl_2 (40 cm³) for 2 d to give, after chromatographic purification, (3*S*)-**10** [a colorless oil, 675 mg; 68%. $[\alpha]_D=+45.8°$ (*c* 1.40, $CHCl_3$ (lit,[16] +56.1°; lit,[28] +61.5°, EtOH)). ^1H NMR δ=1.68 (3H, br s), 2.18 (3H, br s), 3.60 (1H, br m), 4.64 (2H, m), and 9.91 (1H, s). ^{13}C NMR δ=14.5, 20.5, 28.6, 39.4, 50.8, 109.6, 139.1, 146.8, 163.4, and 187.8. IR ν: 3010, 2950, 2850, 2740, 1660, 1437, 1378, and 890 cm^{-1}].

Collins Oxidation of (3*S*)-9 to (3*S*)-10. To a CH_2Cl_2 solution (25 cm³) of (3*S*)-**9** (119 mg), Collins reagent (1.20 g) was added and stirred at room temperature for 45 h. The mixture was then diluted with hexane–AcOEt (1:1) and filtered on a short silica-gel column to remove the reagent. The organic filtrate was distilled in vacuo and further fractionated through a silica-gel column to give (3*S*)-**10** (62 mg; 53%) together with **11** [a colorless oil, 14.9 mg; 11%. Found: M.W., 168.1155. Calcd for $C_{10}H_{16}O_2$: 168.1150. ^1H NMR δ=1.44 (3H, s), 1.68 (3H, s), 2.97 (1H, br d, *J*=7 Hz), 3.58 (1H, d, *J*=12 Hz), 3.98 (1H, d, *J*=12 Hz), and 4.74 (2H, m). ^{13}C NMR δ=15.5, 20.9, 25.7, 32.7, 48.4, 60.1, 70.2, 72.4, 112.3, and 145.7. IR ν: 3450, 2950, 1450, 1380, 1030, 893, and 755 cm^{-1}].

Conversion of (3*R*)-8a to (3*R*)-10 via (3*R*)-9. Similarly, (3*R*)-**8a** was converted to (3*R*)-**9** [a colorless oil, 95%. $[\alpha]_D=-195.0°$ (*c* 0.80, $CHCl_3$)] which was then oxidized into (3*R*)-**10** [a colorless oil, 91%. $[\alpha]_D=-45.1°$ (*c* 3.66, $CHCl_3$)].

Catalytic Reduction of (3*S*)-7b to (3*S*)-12b. (3*S*)-**7b** (181 mg) was hydrogenated with Pd/carbon (5%, 15 mg) in MeOH (5 cm³) to give (3*S*)-**12b** [colorless prisms, mp 141—142°C, 182 mg; 100%. Found: C, 70.61; H, 10.76%. Calcd for $C_{20}H_{36}O_4$: C, 70.55; H, 10.66%. $[\alpha]_D=-40.0°$ (*c* 2.80, $CHCl_3$). ^1H NMR δ=0.72 (3H, d, *J*=7 Hz), 0.83 (3H, d, *J*=7 Hz), 0.88 (3H, d, *J*=7 Hz), 0.90 (6H, d, *J*=7 Hz), 1.20 (3H, s), 2.74 (1H, br s, OH), 3.62 (1H, br s, OH), and 4.73 (1H, td, *J*=10.5, 4 Hz). IR ν: 3420, 2955, 2870, 1725, 1378,

1250, 1117, and 1016 cm^{-1}].

Catalytic Reduction of (3*R*)-7a to (3*R*)-12a. Similarly, (3*R*)-**7a** (178 mg) was converted to (3*R*)-**12a** [colorless needles, mp 115—116°C, 179 mg; 100%. Found: C, 70.61; H, 10.76%. $[\alpha]_D=-65.4°$ (*c* 1.99, $CHCl_3$). ^1H NMR δ=0.74 (3H, d, *J*=7 Hz), 0.81 (6H, d, *J*=7 Hz), 0.91 (3H, d, *J*=7 Hz), 0.93 (3H, d, *J*=6 Hz), 1.22 (3H, s), 2.96 (1H, s, OH), 3.74 (1H, s, OH), and 4.74 (1H, td, *J*=10.5, 4 Hz). IR ν: 3565, 3510, 2960, 2870, 1717, 1353, 1250, 1138, and 1104 cm^{-1}].

Reductive Elimination of (3*S*)-12b to (3*S*)-13b. Similar to the case of **7** to **8**, (3*S*)-**12b** (173 mg) was treated with **5** (3 cm^3) and PPTS (30 mg) to yield a dioxolane derivative which was then heated in Ac_2O (3 cm^3) to give (3*S*)-**13b** [a colorless oil, 152 mg; 98%. Found: C, 78.43; H, 11.23%. Calcd for $C_{20}H_{34}O_2$: C, 78.38; H, 11.18%. $[\alpha]_D=-64.5°$ (*c* 2.20, $CHCl_3$). ^1H NMR δ=0.69 (3H, d, *J*=7 Hz), 0.77 (3H, d, *J*=7 Hz), 0.88 (6H, d, *J*=7 Hz), 0.91 (3H, d, *J*=6 Hz), 2.03 (3H, br s), 2.98 (1H, br m), and 4.74 (1H, td, *J*=10.5, 4 Hz). IR ν: 2955, 2930, 2870, 1706, 1646, 1468, 1369, 1240, 1220, 1108, and 1052 cm^{-1}].

Conversion of (3*R*)-12a to (3*R*)-13a. Similarly, (3*R*)-**12a** (170 mg) gave (3*R*)-**13a** [a colorless oil, 147 mg; 96%. Found: C, 78.36; H, 11.24%. $[\alpha]_D=-58.5°$ (*c* 1.95, $CHCl_3$). ^1H NMR δ=0.69 (3H, d, *J*=7 Hz), 0.76 (3H, d, *J*=7 Hz), 0.88 (9H, d, *J*=7 Hz), 2.03 (3H, br s), 2.98 (1H, br m), and 4.76 (1H, td, *J*=10.5, 4 Hz). IR ν: 2955, 2920, 2865, 1702, 1643, 1468, 1368, 1238, 1218, 1099, and 1050 cm^{-1}].

DIBAH-Reduction of (3*S*)-13b to (3*S*)-14. Similar to the case of **8** to **9**, (3*S*)-**13b** (132 mg) was treated with DIBAH to give (3*S*)-**14** [a colorless oil, 61 mg; 92%. Found: M. W., 154.1367. Calcd for $C_{10}H_{18}O$: 154.1357. $[\alpha]_D=+17.6°$ (*c* 3.76, $CHCl_3$). ^1H NMR δ=0.67 (3H, d, *J*=7 Hz), 0.92 (3H, d, *J*=7 Hz), 1.70 (3H, br s), 2.82 (1H, br m), 3.99 (1H, d, *J*=12 Hz), and 4.26 (1H, d, *J*=12 Hz). ^{13}C NMR δ=13.9, 15.9, 21.4, 21.8, 28.7, 38.0, 51.8, 57.3, 136.4, and 137.0. IR ν: 3350, 2900, 1470, 1380, 1360, and 1000 cm^{-1}].

MnO_2 Oxidation of (3*S*)-14 to (3*S*)-1-Iriden-7-al ((3*S*)-15). Similar to the case of **9** to **10**, (3*S*)-**14** (1.00 g) was oxidized with MnO_2 (10 g) in CH_2Cl_2 (40 cm^3) to (3*S*)-**15**[29] [a colorless oil, 893 mg; 90%. Found: M.W., 152.1199. Calcd for $C_{10}H_{16}O$: 152.1200. $[\alpha]_D=-5.5°$ (*c* 5.47, $CHCl_3$). ^1H NMR δ=0.65 (3H, d, *J*=7 Hz), 0.88 (3H, d, *J*=7 Hz), 2.14 (3H, s), 3.00 (1H, br m), and 9.97 (1H, s). ^{13}C NMR δ=14.3, 16.4, 21.3, 22.1, 28.9, 40.1, 50.0, 140.0, 163.1, and 188.2. IR ν: 2980, 1670, and 760 cm^{-1}].

Conversion of (3*R*)-13a to (3*R*)-15 via (3*R*)-14. Similarly, (3*R*)-**13a** was converted to (3*R*)-**14** [a colorless oil, 95%. $[\alpha]_D=-17.9°$ (*c* 2.79, $CHCl_3$)], which was then oxidized to (3*R*)-**15**[30] [a colorless oil, 70%. $[\alpha]_D=+6.9°$ (*c* 3.77, $CHCl_3$)].

Preparation of Ethylenedioxy Acetal of 1,8-Iridadien-7-al (17). An anhydrous benzene solution (330 cm^3) of (3*S*)-**10** (23.5 g) and 1,2-ethanediol (50 cm^3) was refluxed in the presence of PPTS (3.2 g) for 9 h along with the removal of liberated water by means of a Dean-Stark apparatus. To the mixture, aqueous $NaHCO_3$ was added and extracted with benzene. The organic extract was dried on K_2CO_3 and evaporated to leave a brown oil which was purified by distillation in vacuo (bp 60—70°C/2 mmHg) to give **17** [a colorless oil, 27.7 g; 91%. Found: M.W., 194.1315. Calcd for $C_{12}H_{18}O_2$: 194.1306. ^1H NMR δ=1.64 (3H, br s), 1.81 (3H, br s), 3.50 (1H, br m), 3.72—4.08 (4H, m), 4.58 (1H, br s), 4.67 (1H, br s), and 5.49 (1H, s). ^{13}C NMR δ=14.1, 18.7, 28.7, 38.6, 53.5, 64.8, 65.3, 100.3, 109.4, 132.9, 142.5, and 149.1. IR ν: 3070, 2945, 2890, 1677, 1642, 1437, 1390, 1185, 1100, 1055, 943, and 881 cm^{-1}].

Hydroboration of 17. To an anhydrous diethylene glycol dimethyl ether solution (40 cm^3) containing $NaBH_4$ (1.62 g), 2-methyl-2-butene (13.0 cm^3) was introduced at 0°C. Subsequently, BF_3-etherate (5.9 cm^3) was added dropwise and stirred at 0°C for 2 h. After this, an anhydrous diglyme solution (10 cm^3) of **17** (5.34 g) was added dropwise within a 20-min period. After keeping 0°C for another 30 min, the mixture was warmed to room temperature with stirring for 2 h. Then, the mixture was cooled again to below 0°C, aqueous 3M[†] NaOH (28 cm^3) was introduced, 30% H_2O_2 (25 cm^3) was also introduced within a 40-min period at 50°C, and further stirred for 1 h. The mixture was then extracted with ether, dried on K_2CO_3 and distilled by means of a Kugelrohr apparatus in vacuo to give **18** [a colorless oil, 4.86 g; 83%]. The sample obtained by this workup was suitable for subsequent reaction, but the analytical sample [Found: M.W., 212.1416. Calcd for $C_{12}H_{20}O_3$: 212.1411. ^1H NMR δ=0.88 (3H, d, *J*=7 Hz), 1.76 (3H, br s), 2.63 (1H, br, OH), 3.01 (1H, br m), 3.2—3.7 (2H, m) which changed to 3.31 (1H, dd, *J*=10.9, 7.8 Hz), and 3.54 (1H, dd, *J*=10.9, 5.9 Hz) by addition of D_2O, 3.8—4.2 (4H, m), and 5.51 (1H, s). ^{13}C NMR δ=13.8, 15.9, 23.2, 38.0, 38.2, 48.4, 63.9, 64.4, 64.6, 100.2, 131.1, and 143.3. IR ν: 3440, 2880, 1675, 1460, 1438, 1397, 1380, 1195, 1092, 1048, 980, and 943 cm^{-1}] was obtained by alumina column chromatography.

Preparation of 9-Benzyloxy-1-iriden-7-al (20) via Its Ethylenedioxy Acetal (19). To an anhydrous DMF solution (280 cm^3) of NaH (1.4 g), a DMF solution (20 cm^3) of **18** (4.45 g) was added and stirred for 1 h. Then, benzyl chloride (4.0 cm^3) was added and stirred at room temperature for 96 h. Ether extraction of the mixture yielded **19** [a colorless oil, 4.82 g; 76%. ^1H NMR δ=1.02 (3H, d, *J*=7 Hz), 1.75 (3H, br s), 3.00 (1H, br m), 3.19 (1H, t, *J*=9 Hz), 3.49 (1H, dd, *J*=9, 4 Hz), 3.7—4.0 (4H, m), 4.39 (1H, d, *J*=12 Hz), 4.47 (1H, d, *J*=12 Hz), 5.47 (1H, s), and 7.27 (5H, br s). ^{13}C NMR δ=14.2, 16.6, 23.9, 35.8, 38.3, 49.4, 64.4, 64.9, 72.7, 72.8, 100.6, 127.1, 127.3 (2C), 128.1 (2C), 131.6, 139.1, and 143.0. IR ν: 2955, 2880, 1677, 1498, 1455, 1095, 943, 735, and 696 cm^{-1}], which was without purification, treated with 0.5 M HCl (80 cm^3) in ether (150 cm^3) for 4 h. Subsequently, the mixture was treated with 10%-$NaHCO_3$, extracted with ether, chromatographed on a silica-gel column to give **20** [colorless needles, mp 53—53.5°C, 3.10 g; 72%. Found: C, 78.74; H, 8.76%. Calcd for $C_{17}H_{22}O_2$: C, 79.03; H, 8.58%. $[\alpha]_D=-12.2°$ (*c* 5.72, $CHCl_3$). ^1H NMR δ=0.95 (3H, d, *J*=7 Hz), 2.07 (3H, br s), 3.14 (1H, br m), 3.20 (1H, dd, *J*=9, 7 Hz), 3.34 (1H, dd, *J*=9, 5.5 Hz), 4.39 (2H, br s), 7.24 (5H, br s), and 9.92 (1H, s). ^{13}C NMR δ=14.3, 16.0, 24.2, 35.2, 39.6, 47.1, 72.7, 73.0, 127.2 (3C), 128.1 (2C), 138.7, 139.3, 163.4, and 188.1. IR ν: 2950, 2850, 2730, 1655, 1618, 1493, 1450, 1425, 1365, 1210, 1088, 990, 758, and 700 cm^{-1}].

Preparation of 9-Benzyloxy-1-iriden-7-ol (21). An MeOH solution (130 cm^3) of **20** (5.07 g) was reduced with $NaBH_4$ (750 mg) to give **21** [colorless liquid, 4.947 g; 96.5%. Found: C, 78.45; H, 9.32%. Calcd for $C_{17}H_{24}O_2$: C, 78.42; H, 9.29%. ^1H NMR δ=0.91 (3H, d, *J*=7 Hz), 1.68 (3H, br s), 2.70 (1H, dd, *J*=7, 6 Hz, OH), 2.84 (1H, br m), 3.25 (1H, dd, *J*=9, 6 Hz), 3.36 (1H, dd, *J*=9, 7 Hz), 4.08 (2H, br m), 4.36 (1H, d, *J*=12 Hz), 4.45 (1H, d, *J*=12 Hz), and 7.25 (5H, br s). ^{13}C NMR δ=14.0, 16.6, 23.3, 35.5, 37.6, 50.6, 57.7, 72.9, 73.2, 127.5, 127.6 (2C),

[†] 1 M=1 mol dm^{-3}.

128.7 (2C), 136.1, 137.1, and 138.1. IR ν: 3410, 2960, 1677, 1498, 1457, 1096, 1005, 736, and 698 cm^{-1}].

Preparation of 9-Benzyloxy-7-chloro-1-iridene (16). To an anhydrous CH_2Cl_2 solution (30 cm^3) of $(COCl)_2$ (0.8 cm^3), anhydrous DMSO (1.3 cm^3) was added at −60 °C with stirring. After 5 min, an anhydrous CH_2Cl_2 solution (2 cm^3) of **21** (1.984 g) was added dropwise during a 15-min period. The mixture was then gradually warmed to 0 °C within 1 h, extracted with ether, dried on $MgSO_4$, and distilled in vacuo to remove the solvent to leave **16** [pale yellow oil, 2.01 g; 95%. ^1H NMR δ=1.02 (3H, d, J=7 Hz), 1.71 (3H, br s), 2.93 (1H, br m), 3.20 (1H, dd, J=9, 7 Hz), 3.34 (1H, dd, J=9, 5 Hz), 4.05 (1H, br d, J=12 Hz), 4.20 (1H, d, J=12 Hz), 4.41 (2H, br s), and 7.25 (5H, br s)], which was very sensitive towards the acidic species that it prevented a further purification.

$CrCl_2$-Mediated Condensation of (3*S*)-16 and (3*S*)-15. To an anhydrous THF suspension (30 cm^3) of $CrCl_3$ (3.76 g) under an N_2 atmosphere at 0 °C, LAH (440 mg) was added to form $CrCl_2$. After 30 min, the medium was changed, in vacuo, from THF to anhydrous DMF (40 cm^3) by transfer. Subsequently, a DMF solution (5 cm^3) of (3*S*)-**15** (1.80 g) and a DMF solution (5 cm^3) of (3*S*)-**16** (2.02 g) was added consecutively at 0 °C. After 5 h under stirring, the mixture was treated with water, and extracted with ether. The organic extract was dried on K_2CO_3 and the solvent removed in vacuo, treated with $NaBH_4$ in MeOH to reduce any excess amount of (3*S*)-**15**, and chromatographed on a silica-gel column to give **22** [a colorless oil, 1.92 g; 64%. Found: C, 82.06; H, 10.36%. Calcd for $C_{27}H_{40}O_2$: C, 81.77; H, 10.17%. ^1H NMR δ=0.73 (3H, d, J=7 Hz), 0.90 (3H, d, J=7 Hz), 1.11 (3H, d, J=7 Hz), 1.15 (3H, s), 1.68 (3H, br s), 2.82 (1H, br m), 3.20 (1H, dd, J=9, 8 Hz), 3.45 (1H, dd, J=9, 4 Hz), 4.31 (1H, br s), 4.45 (2H, br s), 4.93 (1H, d, J=2.5 Hz), 5.03 (1H, d, J=3 Hz), and 7.28 (5H, br s). ^{13}C NMR δ=15.0, 15.7, 17.1, 21.5, 21.9, 22.1, 24.9, 30.4, 35.2, 35.7, 38.0, 47.6, 51.9, 53.4, 72.6, 73.0 (2C), 106.0, 127.3, 127.4 (2C), 128.2 (2C), 135.9, 138.7, 138.8, and 162.1. IR ν: 3545, 2955, 1642, 1498, 1467, 1456, 1367, 1099, 1012, 895, 733, and 697 cm^{-1}], and **23** [a colorless oil, 1.35 g; 18%. Found: C, 81.87; H, 10.32%. ^1H NMR δ= 0.75 (3H, d, J=7 Hz), 0.92 (3H, s), 0.93 (3H, d, J=7 Hz), 1.11 (3H, d, J=7 Hz), 1.88 (3H, br s), 2.48 (2H, br m), 3.21 (1H, dd, J=9, 8.5 Hz), 3.46 (1H, dd, J=9, 4 Hz), 4.26 (1H, br s), 4.41 (1H, d, J=12 Hz), 4.48 (1H, d, J=12 Hz), 4.93 (1H, d, J= 3 Hz), 4.96 (1H, d, J=2.5 Hz), and 7.28 (5H, br s). ^{13}C NMR δ=16.2, 16.8, 17.0, 21.7, 22.5, 24.9, 25.1, 29.4, 32.6, 34.6, 39.3, 49.6, 54.0, 56.5, 72.6, 72.9, 75.1, 104.4, 127.2, 127.3 (2C), 128.1 (2C), 136.3, 138.7, and 160.4. IR ν: 3570, 3500, 2955, 2875, 1642, 1498, 1465, 1457, 1368, 1100, 1029, 886, 735, and 698 cm^{-1}].

Collins Oxidation of 22 to 24. To an anhydrous CH_2Cl_2 solution (2 cm^3) containing CrO_3 (150 mg) and pyridine (245 mg), CH_2Cl_2 solution (2 cm^3) of **22** (95 mg) was added and stirred at room temperature for 1 h. The mixture was then diluted with ether, and passed through a Florisil column to remove inorganic material. The removal of the solvent in vacuo left a colorless oil, which was purified by a silica-gel column chromatography to yield **24** [a colorless oil, 56 mg; 59%. Found: C, 82.18; H, 9.80%. Calcd for $C_{27}H_{38}O_2$: C, 82.18; H, 9.71%. ^1H NMR δ=0.72 (3H, d, J=7 Hz), 0.84 (3H, d, J=7 Hz), 1.09 (3H, d, J=7 Hz), 1.21 (3H, s), 1.60 (3H, br s), 2.45 (1H, br m), 2.92 (1H, br m), 3.21 (1H, dd, J=9, 8 Hz), 3.45 (1H, dd, J=9, 4 Hz), 4.41 (1H, d, J=12 Hz), 4.46 (1H, d, J=12 Hz), 4.96 (1H, d, J=2.5 Hz), 4.99 (1H, d, J=3 Hz), and 7.26 (5H, br s). ^{13}C NMR δ=15.4, 16.5, 17.1, 21.3, 23.4, 25.3, 25.7, 30.8, 34.9, 35.7, 37.8, 48.4, 55.5, 59.5, 72.7, 73.0, 108.1, 127.4 (3C), 128.2 (2C), 138.7, 139.8, 141.4, 156.2, and 211.3. IR ν: 2960, 2875, 1677, 1455, 1368, 1098, 895, 735, and 696 cm^{-1}].

LAH-Reduction of 24. An anhydrous THF solution (2 cm^3) of **24** (50 mg) was reduced with LAH (10 mg) in THF (1 cm^3) at room temperature for 50 min. An ordinary work up of the mixture yielded **22** (15 mg; 30%) and **23** (21 mg; 42%), whose identity with the authentic samples were confirmed by direct comparisons.

$CrCl_2$-Mediated Condensation of (3*S*)-16 and (3*R*)-15. Similarly, (3*R*)-**15** (5.11 g) and (3*S*)-**16** (6.39 g) were condensed with $CrCl_2$, prepared from $CrCl_3$ (10.64 g), in DMF (80 cm^3) to form **25** [a colorless oil, 7.02 g; 73%. Found: C, 82.01; H, 10.25%. ^1H NMR δ=0.70 (3H, d, J=7 Hz), 0.85 (3H, d, J=7 Hz), 1.09 (3H, s), 1.10 (3H, d, J=7 Hz), 1.90 (3H, br s), 2.45 (2H, br s), 3.18 (1H, dd, J=9, 8 Hz), 3.45 (1H, dd, J=9, 4 Hz), 4.04 (1H, br s), 4.42 (1H, d, J=12 Hz), 4.47 (1H, d, J=12 Hz), 4.91 (1H, d, J=2.5 Hz), 4.99 (1H, d, J=3 Hz), and 7.27 (5H, br s). ^{13}C NMR δ=15.8, 16.9, 17.3, 21.7, 22.2, 23.5, 25.4, 28.9, 34.4, 35.2, 39.2, 48.4, 52.7, 55.8, 72.7, 72.9, 74.9, 105.9, 127.4 (3C), 128.2 (2C), 136.6, 137.4, 138.7, and 160.5. IR ν: 3510, 2955, 1643, 1599, 1455, 1367, 1098, 1028, 734, and 695 cm^{-1}], and **26** [a colorless oil, 0.37 g; 4%. Found: C, 81.98; H, 10.41%. ^1H NMR δ=0.71 (3H, d, J=7 Hz), 0.77 (3H, s), 0.87 (3H, d, J=7 Hz), 1.11 (3H, d, J=7 Hz), 1.73 (3H, br s), 2.72 (1H, br m), 3.21 (1H, t, J=9 Hz), 3.47 (1H, dd, J=9, 4 Hz), 4.42 (1H, d, J=12 Hz), 4.47 (1H, d, J=12 Hz), 4.65 (1H, br s), 4.96 (1H, d, J=2.5 Hz), 4.99 (1H, d, J=3 Hz), and 7.27 (5H, br s). ^{13}C NMR δ=15.0, 15.7, 17.2, 22.0, 22.1, 25.4 (2C), 30.4, 32.2, 38.0, 49.8, 52.5, 53.1, 72.7, 73.0, 75.2, 104.0, 127.4 (3C), 128.2 (2C), 135.4, 138.7, 139.1, and 161.4. IR ν: 3575, 3510, 2875, 1642, 1498, 1455, 1366, 1098, 1018, 882, 732, and 695 cm^{-1}].

Collins Oxidation of 25 to 27. Similarly, **25** (1.00 g) was oxidized with CrO_3 (1.5 g) and pyridine (245 mg) in CH_2Cl_2 (30 cm^3) to form **27** [a colorless oil, 585 mg; 59%. Found: C, 81.91; H, 9.68%. ^1H NMR δ=0.71 (3H, d, J=7 Hz), 0.80 (3H, d, J=7 Hz), 1.12 (3H, d, J=7 Hz), 1.17 (3H, s), 1.60 (3H, br s), 2.57 (1H, br m), 2.80 (1H, br m), 3.24 (1H, dd, J=9, 8 Hz), 3.46 (1H, dd, J=9, 4 Hz), 4.41 (1H, d, J=12 Hz), 4.46 (1H, d, J=12 Hz), 4.87 (1H, d, J=3 Hz), 4.92 (1H, d, J=2.5 Hz), and 7.27 (5H, br s). ^{13}C NMR δ=15.2, 15.9, 17.0, 21.5, 22.8, 24.7, 26.2, 30.1, 34.6, 35.9, 37.9, 48.8, 55.1, 59.5, 72.6, 72.9, 107.7, 127.3 (3C), 128.1 (2C), 138.6, 140.4, 141.0, 156.5, and 209.5. IR ν: 2960, 1677, 1455, 1368, 1098, 895, 735, and 696 cm^{-1}].

LAH-Reduction of 27 to 25 and 26. Similarly, **27** (315 mg) was treated in THF (5 cm^3) with LAH (100 mg) in THF (5 cm^3) to give **25** (167 mg; 53%) and **26** (72 mg; 23%). Their identities with the authentic samples were confirmed by direct comparisons.

Birch Reduction of 22 to 28. To liquid NH_3 (30 cm^3) containing lithium (50 mg), an anhydrous ether solution (2 cm^3) of **22** (780 mg) was added dropwise and refluxed for 2 h. The mixture was then treated with NH_4Cl and water, and almost all of NH_3 was allowed to evaporate. The residue was extracted with ether and dried on K_2CO_3. Silica-gel column chromatography of the mixture yielded, beside recovered **22** (30 mg; 3.8%), **28** [a colorless oil, 598 mg; 99.5%. Found: C, 78.48; H, 11.24%. Calcd for $C_{20}H_{34}O_2$: C, 78.38; H, 11.18%. ^1H NMR δ=0.71 (3H, d, J=7 Hz), 0.88 (3H, d, J=7 Hz), 1.05 (3H, d, J=7 Hz), 1.17 (3H, s), 1.67 (3H, br s), 2.82 (1H, br m),

3.36 (1H, dd, J=10, 8 Hz), 3.64 (1H, dd, J=10, 5 Hz), 4.31 (1H, br s), 4.97 (1H, d, J=2.5 Hz), and 5.07 (1H, d, J=3 HZ). ^{13}C NMR δ=14.9, 15.7, 16.6, 21.9 (2C), 22.1, 24.6, 30.4, 35.2, 37.9, 38.0, 47.6, 51.8, 53.3, 64.6, 73.2, 106.0, 136.1, 138.6, and 162.3. IR ν: 3410, 2960, 1645, 1470, 1385, 1370, 1020, and 900 cm^{-1}].

Birch Reduction of 23 to 29. Similarly, **23** (286 mg) was reduced to **29** [a colorless oil, 160 mg; 72%. Found: C, 78.21; H, 11.39%. ^{1}H NMR δ=0.76 (3H, d, J=7 Hz), 0.93 (3H, d, J=7 Hz), 0.96 (3H, s), 1.07 (3H, d, J=7 Hz), 1.90 (3H, br s), 2.51 (2H, br m), 3.40 (1H, dd, J=10, 8 Hz), 3.68 (1H, dd, J=10, 5 Hz), 4.28 (1H, br s), 4.98 (1H, d, J=3 Hz), and 5.03 (1H, d, J=2.5 Hz). ^{13}C NMR δ=16.2, 16.5, 16.8, 21.8, 22.6, 24.6, 25.2, 29.4, 32.6, 36.7, 39.4, 49.5, 54.0, 56.6, 64.9, 75.1, 104.5, 136.3, 136.9, and 160.8. IR ν: 3410, 2955, 1643, 1467, 1369, 1032, and 884 cm^{-1}].

Birch Reduction of 25 to 30. Similarly, **25** (7.39 g) was reduced with lithium (390 mg) in liquid NH_3 (250 cm^3) to give **30** [a colorless oil, 5.12 g; 100%. Found: C, 78.24; H, 11.24%. ^{1}H NMR δ=0.71 (3H, d, J=7 Hz), 0.87 (3H, d, J=7 Hz), 1.06 (3H, d, J=7 Hz), 1.12 (3H, s), 1.91 (3H, br s), 3.33 (1H, dd, J=10, 8 Hz), 3.64 (1H, dd, J=10, 5 Hz), 4.07 (1H, br s), 4.97 (1H, d, J=2.5 Hz), and 5.04 (1H, d, J=3 Hz). ^{13}C NMR δ=15.9, 16.8, 16.9, 21.7, 22.3, 23.5, 25.0, 29.0, 34.5, 37.4, 39.2, 48.4, 52.8, 55.9, 65.1, 74.9, 106.0, 136.6, 137.5, and 161.1. IR ν: 3410, 2960, 2880, 1644, 1465, 1368, 1024, and 893 cm^{-1}] together with the recovered **25** (866 mg; 12%).

Birch Reduction of 26 to 31 and 32. To an anhydrous $EtNH_2$ solution (8 cm^3) of lithium (100 mg), an anhydrous ether solution (2 cm^3) of **26** (85 mg) was added and stirred at 0 °C for 2 h. The usual work up yielded a C=C bond-migrated diol (**32**) [a colorless oil, 11 mg; 17%. ^{1}H NMR δ=0.72 (3H, d, J=7 Hz), 0.84 (3H, d, J=7 Hz), 0.89 (3H, d, J=7 Hz), 0.99 (3H, s) 1.64 (3H, t, J=1 Hz), 1.70 (3H, br s), 2.78 (1H, br m), 2.81 (1H, sext, J=7 Hz), 3.45 (2H, br s), and 4.61 (1H, br s)], and **31** [a colorless oil, 45 mg; 69%. Found: C, 78.25; H, 11.32%. ^{1}H NMR δ=0.70 (3H, d, J=7 Hz), 0.81 (3H, s), 0.87 (3H, d, J=7 Hz), 1.06 (3H, d, J=7 Hz), 1.73 (3H, br s), 3.36 (1H, dd, J=10, 8 Hz), 3.68 (1H, dd, J=10, 5 Hz), 4.68 (1H, br s), and 5.03 (2H, br d, J=2.5 Hz). ^{13}C NMR δ=15.0, 15.7, 16.7, 22.0, 22.2, 25.0, 25.6, 30.5, 32.1, 36.3, 38.1, 49.8, 52.5, 53.1, 65.2, 75.3, 104.1, 135.3, 139.4, and 162.2. IR ν: 3400, 2950, 1645, 1470, 1025, and 885 cm^{-1}] was obtained.

The Birch Reduction of 23 in Ethylamine. Formation of 29 and Its Isomer, 33. Similar to this, the reduction of **23** (67 mg) in $EtNH_2$ (10 cm^3) with lithium (25 mg) afforded **29** (a colorless oil, 10 mg; 19%) and **33** [colorless prisms, mp 119.5—120 °C, 34 mg; 66%. Found: C, 78.52; H, 11.29%. ^{1}H NMR δ=0.74 (3H, d, J=7 Hz), 0.91 (3H, d, J=7 Hz), 0.98 (3H, d, J=7 Hz), 1.03 (3H, s), 1.63 (3H, t, J=1 Hz), 1.92 (3H, br s), 2.45 (1H, br m), 2.71 (1H, sext, J=7 Hz), 3.45 (2H, br m), and 4.16 (1H, br s). ^{13}C NMR δ=10.3, 15.2, 16.1, 16.5, 21.7, 22.5, 22.9, 29.0, 29.5, 32.3, 35.7, 39.4, 56.0, 57.9, 66.0, 73.2, 136.5, 137.2, 138.7, and 138.9. IR ν: 3300, 2950, 1667, 1465, 1452, 1366, 1020, 1000, and 765 cm^{-1}].

Bis-Etherification of 28 to 34 with I_2 and a Base. To an ether solution (10 cm^3) of **28** (240 mg), saturated $NaHCO_3$ (20 cm^3) and an excess of I_2 were added and kept room temperature for 3 h. The mixture was then treated with $NaHSO_3$ and saturated K_2CO_3 and extracted with ether. Silica-gel column chromatography of the extract afforded **34** [a colorless oil, 192 mg; 74%. Found: C, 78.98; H, 10.71%. Calcd for $C_{20}H_{32}O_2$: C, 78.90; H, 10.59%. ^{1}H NMR δ=0.69 (3H, d, J=7 Hz), 0.83 (3H, s), 0.88 (3H, d, J=7 Hz), 0.95 (3H, d, J=7 Hz), 1.65 (3H, br s), 2.68 (1H, br m), 3.23 (1H, dd, J=10, 8 Hz), 3.71 (1H, d, J=9 Hz), 3.80 (1H, d, J=9 Hz), 3.88 (1H, dd, J=8, 7 Hz), and 4.64 (1H, br s). ^{13}C NMR δ=11.2, 14.9, 15.8, 16.4, 22.3, 22.7, 24.9, 30.5, 36.2, 38.1, 40.3, 53.4, 53.8, 57.7, 74.1, 76.8, 86.4, 102.2, 135.8, and 136.3. IR ν: 2960, 2880, 1470, 1455, 1380, and 1053 cm^{-1}].

Bis-Etherification of 29 to 35 with I_2 and a Base. A similar treatment of **29** (40 mg) with I_2 (55 mg) and saturated $NaHCO_3$ solution (4 cm^3) yielded **35** [a colorless oil, 35 mg; 80%. Found: C, 79.04; H, 10.70%. ^{1}H NMR δ=0.71 (3H, d, J=7 Hz), 0.87 (3H, d, J=7 Hz), 0.94 (3H, d, J=7 Hz), 1.01 (3H, s), 1.89 (3H, br s), 2.60 (1H, br m), 3.28 (1H, dd, J=10, 8 Hz), 3.31 (1H, d, J=9 Hz), 3.81 (1H, d, J=9 Hz), 3.86 (1H, dd, J=8, 7 Hz), and 4.00 (1H, br s). ^{13}C NMR δ=10.8, 15.3, 15.7, 18.8, 21.6, 21.9, 24.6, 28.6, 35.3, 35.5, 39.4, 53.6, 55.6, 55.8, 73.2, 76.1, 87.7, 101.1, 132.0, and 136.0. IR ν: 2960, 2845, 1465, 1379, 1063, and 995 cm^{-1}].

Bis-Etherification of 30 to 36 with I_2 and a Base. Similarly, **30** (60 mg) was converted to **36** [a colorless oil, 51 mg; 86%. Found: C, 78.98; H, 10.82%. ^{1}H NMR δ=0.73 (3H, d, J=7 Hz), 0.87 (3H, s), 0.89 (3H, d, J=7 Hz), 0.96 (3H, d, J=7 Hz), 1.85 (3H, br s), 3.25 (1H, dd, J=10, 8 Hz), 3.67 (1H, d, J=9 Hz), 3.90 (1H, dd, J=8, 7 Hz), 3.93 (1H, d, J=9 Hz), and 4.21 (1H, br s). IR ν: 2955, 2875, 1466, 1455, 1378, and 1050 cm^{-1}].

Bis-Etherification of 31 to 37 with I_2 and a Base. Similarly, **31** (22 mg) was converted to **37** [colorless needles, mp 69.5—70 °C, 15 mg, 68%. Found: C, 79.02; H, 10.81%. ^{1}H NMR δ=0.67 (3H, d, J=7 Hz), 0.85 (3H, d, J=7 Hz), 0.88 (3H, s), 0.94 (3H, d, J=7 Hz), 1.68 (3H, br s), 2.70 (1H, br m), 3.23 (1H, dd, J=10.5, 8 Hz), 3.37 (1H, d, J=9 Hz), 3.83 (1H, d, J=9 Hz), 3.85 (1H, dd, J=8, 7 Hz), and 4.23 (1H, br s). IR ν: 2960, 2840, 1460, 1373, and 1051 cm^{-1}].

Attempted Anionic Oxy-Cope Rearrangement with 25. To an anhydrous THF suspension (3 cm^3) of KH (35% in a mineral oil, 100 mg), **25** (55 mg) was added under ice-cooling. After standing at room temperature for 20 h, the mixture was treated with aqueous ether and extracted. HPLC with AcOEt–hexane eluted **38** [a colorless oil, 3 mg; 11%. ^{1}H NMR δ=1.01 (3H, d, J=7 Hz), 1.56 (6H, br s), 2.56 (1H, br m), 3.16 (1H, t, J=10 Hz), 3.30 (1H, dd, J=10, 4 Hz), 4.42 (2H, br s), and 7.30 (5H, br s)], a colorless-oily mixture of **39a** and **39b** (1:1) [10 mg; 23%. ^{1}H NMR δ=0.82 (1.5H, d, J=7 Hz), 0.83 (1.5H, d, J=7 Hz), 0.87 (1.5H, d, J=7 Hz), 0.92 (1.5H, d, J=7 Hz), 0.97 (1.5H, s), 1.01 (1.5H, s), 1.02 (3H, d, J=7 Hz), 1.58 (3H, br s), 3.07 (0.5H, t, J=9.5 Hz), 3.09 (0.5H, t, J=9.5 Hz), 3.22 (0.5H, dd, J=9.5, 4.5 Hz), 3.24 (0.5H, dd, J=9.5, 4.5 Hz), 4.40 (2H, br s), 7.27 (5H, br s), 9.65 (0.5H, d, J=7 Hz), and 9.66 (0.5H, d, J=4 Hz)], (3*R*)-**15** (1 mg; 6%), and the recovered **25** (11 mg; 20%), which were identified by direct comparisons.

Preparation of the TMS Derivative (40) from 22. To a pyridine solution (1 cm^3) of **22** (15 mg), trimethylsilyl chloride (TMSCl, 200 mg) was added and stirred at 15—25 °C for 24 h. The mixture was then treated with aqueous $NaHCO_3$, extracted with hexane–ether, dried on K_2CO_3, and chromatographed on a silica-gel column to give colorless oily **40** [18 mg; 100%. Found: C, 76.83; H, 10.44%. Calcd for $C_{30}H_{48}O_2Si$: C, 76.86; H, 10.32%. ^{1}H NMR δ=0.04 (9H, s), 0.67 (3H, d, J=7 Hz), 0.86 (3H, d, J=7 Hz), 1.09 (3H, d, J=7 Hz), 1.11 (3H, s), 1.64 (3H, br s), 2.77 (1H, br m), 3.17 (1H, t, J=9 Hz), 3.46 (1H, dd, J=9, 4 Hz), 4.30 (1H, s), 4.40 (1H, d, J=12 Hz), 4.48 (1H, d, J=12 Hz), 4.80 (2H, br d, J=2.5 Hz), and 7.28 (5H, br s). ^{13}C NMR δ=0.7 (3C), 15.1, 16.1, 17.3, 21.9,

22.4, 23.9, 25.0, 29.5, 34.9, 35.3, 37.8, 47.9, 51.2, 53.1, 72.9 (2C), 74.5, 106.0, 127.2, 127.4 (2C), 128.2 (2C), 136.8, 136.9, 138.8, and 160.2. IR ν: 2960, 2875, 1645, 1455, 1250, 1062, 880, 837, and 695 cm^{-1}].

Preparation of the TMS Derivative (41) from 23. Similarly, **23** (29 mg) was converted to **41** [a colorless oil, 33 mg; 96%. Found: C, 77.08; H, 10.34%. ^1H NMR δ=0.03 (9H, s), 0.75 (3H, d, J=7 Hz), 0.92 (3H, d, J=7 Hz), 0.92 (3H, s), 1.11 (3H, d, J=7 Hz), 1.84 (3H, br s), 3.21 (1H, dd, J=9, 8 Hz), 3.48 (1H, dd, J=9, 4 Hz), 4.24 (1H, br s), 4.43 (1H, d, J=12 Hz), 4.45 (1H, d, J=12 Hz), 4.82 (2H, br d, J=2.5 Hz), and 7.28 (5H, br s). ^{13}C NMR δ=0.4 (3C), 16.3, 16.5, 17.3, 22.4 (2C), 25.0, 25.5, 29.5, 33.4, 34.8, 39.6, 49.8, 54.0, 56.2, 73.0, 73.2, 77.1, 103.8, 127.3, 127.4 (2C), 128.2 (2C), 136.5, 137.7, 139.1, and 161.5. IR ν: 2955, 2865, 1645, 1366, 1246, 1077, 876, 835, 745, 730, and 694 cm^{-1}].

Preparation of the TMS Derivative (42) from 25. Similarly, **25** (77 mg) was treated with TMSCl (200 mg) to give **42** [a colorless oil, 85 mg; 94%. Found: C, 76.89; H, 10.36%. ^1H NMR δ=0.08 (9H, s), 0.71 (3H, d, J=7 Hz), 0.82 (3H, d, J=7 Hz), 1.01 (3H, s), 1.08 (3H, d, J=7 Hz), 1.84 (3H, br s), 3.18 (1H, dd, J=9, 8 Hz), 3.47 (1H, dd, J=9, 4 Hz), 4.12 (1H, br s), 4.40 (1H, d, J=12 Hz), 4.48 (1H, d, J=12 Hz), 4.81 (1H, d, J=2 Hz), 4.87 (1H, d, J=3 Hz), and 7.28 (5H, br s). ^{13}C NMR δ=0.3 (3C), 15.9, 16.8, 17.3, 22.1, 22.3, 25.7, 26.7, 28.8, 33.1, 34.7, 39.3, 49.5, 52.6, 55.4, 72.9, 73.1, 77.8, 105.4, 127.3, 127.4 (2C), 128.2 (2C), 136.9, 137.0, 138.8, and 160.2. IR ν: 2960, 2880, 1645, 1456, 1250, 1066, 880, 835, and 695 cm^{-1}].

Preparation of the TMS Derivative (43) from 26. Similarly, **26** (24 mg) was converted to **43** [colorless prisms, mp 67—67.5 °C, 29 mg; 100%. Found: C, 76.71; H, 10.26%. ^1H NMR δ=0.01 (9H, s), 0.66 (3H, d, J=7 Hz), 0.72 (3H, s), 0.84 (1H, d, J=7 Hz), 1.11 (3H, d, J=7 Hz), 1.60 (3H, br s), 2.64 (1H, br s), 3.19 (1H, dd, J=8.8, 8.5 Hz), 3.49 (dd, J=8.8, 3.5 Hz), 4.42 (1H, d, J=12 Hz), 4.49 (1H, d, J=12 Hz), 4.54 (1H, s), 4.83 (1H, d, J=2.5 Hz), 4.89 (1H, d, J=3 Hz), and 7.27 (5H, br s). ^{13}C NMR δ=0.5 (3C), 14.7, 16.1, 17.6, 22.1, 26.1 (2C), 29.7, 32.3, 33.7, 37.9, 50.3, 51.2, 52.7, 72.9 (2C), 136.7, 136.9, 138.8, and 162.7. IR ν: 2955, 2865, 1644, 1453, 1368, 1246, 1101, 1064, 878, 833, 745, and 696 cm^{-1}].

Cope Rearrangement of 40 to 44. An anhydrous oxygen-free toluene solution (5 cm^3) of **40** (18 mg) was sealed and heated in an autoclave at 190 °C for 12 h. The mixture was then distilled in vacuo to remove the solvent. The residue was practically pure thermolysate, **44** [a colorless oil, 18 mg; 100%. ^1H NMR δ=0.16 (9H, s), 0.74 (3H, d, J=7 Hz), 0.89 (3H, d, J=7 Hz), 1.03 (3H, d, J=7 Hz), 1.04 (3H, s), 1.58 (3H, br s), 2.75 (2H, br m), 3.08 (1H, dd, J=9, 8 Hz), 3.27 (1H, dd, J=9, 4 Hz), 4.39 (1H, d, J=12 Hz), 4.44 (1H, d, J=12 Hz), 6.03 (1H, d, J=2 Hz), and 7.25 (5H, br s)].

Cope Rearrangmement of 42. Formation of 45. Similarly, a toluene solution (5 cm^3) of **42** (82 mg) was heated in an autoclave at 190 °C for 8 h to give **45** [a colorless oil, 82 mg; 100%. ^1H NMR δ=0.19 (9H, s), 0.81 (3H, d, J=7 Hz), 1.02 (3H, d, J=7 Hz), 1.05 (3H, s), 1.62 (3H, br s), 2.68 (1H, d, J=14 Hz), 2.74 (1H, br m), 3.10 (1H, t, J=9 Hz), 3.27 (1H, dd, J=9, 4 Hz), 4.36 (1H, d, J=12 Hz), 4.46 (1H, d, J=12 Hz), 5.93 (1H, d, J=2 Hz), and 7.26 (5H, br s)].

Cope Rearrangement of 43. Formation 46. Similarly, a toluene solution of **43** (29 mg) was heated at 190 °C for 8 h in an autoclave to give **46** [a colorless oil, 29 mg; 100%. ^1H NMR δ=0.16 (9H, s), 0.75 (3H, d, J=7 Hz), 0.88 (3H, d, J=7 Hz), 0.94 (3H, s), 1.00 (3H, d, J=7 Hz), 1.58 (3H, br s), 3.08 (1H, t, J=9 Hz), 3.26 (1H, dd, J=9, 4 Hz), 4.36 (1H, d, J=12 Hz), 4.45 (1H, d, J=12 Hz), 6.08 (1H, d, J=2 Hz), and 7.24 (5H, br s)].

Cope Rearrangement of 41. Formation of 47 and 48. A toluene solution of **41** (74 mg) was heated at 200 °C for 4 d in an autoclave to give a mixture of **47** and **48** (3:2, 67 mg; 90%), which was separated by GLC (SE 30 column, 300 cm in length; column temperature, 285 °C; and He-flow, 25 $cm^3 min^{-1}$) to obtain **47** [a colorless oil. ^1H NMR δ=0.16 (9H, s), 0.80 (3H, d, J=7 Hz), 0.90 (3H, d, J=7 Hz), 1.03 (3H, d, J=7 Hz), 1.17 (3H, s), 1.56 (3H, br s), 2.78 (1H, br m), 3.10 (1H, t, J=9 Hz), 3.28 (1H, dd, J=9, 4 Hz), 4.33 (1H, d, J=12 Hz), 4.46 (1H, d, J=12 Hz), 5.97 (1H, d, J=2 Hz), and 7.24 (5H, br s)] and **48** [a colorless oil. ^1H NMR δ=0.16 (9H, s), 0.81 (3H, d, J=7 Hz), 0.89 (3H, d, J=7 Hz), 0.93 (3H, s), 1.02 (3H, d, J=7 Hz), 1.60 (3H, br s), 3.08 (1H, t, J=9 Hz), 3.25 (1H, dd, J=9, 4 Hz), 4.36 (1H, d, J=12 Hz), 4.43 (1H, d, J=12 Hz), 6.10 (1H, d, J=2 Hz), 7.25 (5H, br s)].

The $^1O_2$-Oxidation of 44. Formation of 49. An anhydrous toluene solution (5 cm^3) of **44** (82 mg), pyridine (0.03 cm^3), *meso*-5,10,15,20-tetraphenylporphine (TPP, 2 mg) was externally irradiated by means of a 500-W tungsten lamp with an O_2-stream under ice-cooling for 50 min. The mixture was then treated with PPh_3 to neutralize peroxy derivatives, solvent removed in vacuo, and chromatographed on a silica-gel column to give **49** [a colorless oil, 54 mg; 78%. Found: C, 82.38; H, 9.96%. Calcd for $C_{27}H_{38}O_2$: C, 82.18; H, 9.71%. ^1H NMR δ=1.01 (3H, d, J=7 Hz), 1.03 (3H, d, J=7 Hz), 1.10 (3H, d, J=7 Hz), 1.29 (3H, s), 1.47 (3H, br s), 2.68 (1H, br m), 3.09 (1H, t, J=9 Hz), 3.24 (1H, dd, J=9, 4.5 Hz), 3.38 (1H, sept, J=7 Hz), 4.37 (1H, d, J=12 Hz), 4.44 (1H, d, J=12 Hz), 7.25 (5H, br s), and 9.95 (1H, s). ^{13}C NMR δ=15.2, 16.9, 21.2, 21.5, 23.8, 26.7, 27.3, 30.0, 35.0 (2C), 36.3, 37.2, 51.1, 52.8, 72.2, 127.2, 127.4 (2C), 128.2 (2C), 134.6, 135.8, 138.8, 141.4, 171.8, and 188.2. IR ν: 2970, 2940, 2875, 2745, 1670, 1615, 1456, 1373, 1100, 732, and 695 cm^{-1}].

The $^1O_2$-Oxidation of 45. Formation of 50. Similarly, an anhydrous benzene solution (5 cm^3) of **45** (82 mg) and pyridine (0.03 cm^3) was irradiated 50 min under an O_2 atmosphere; after PPh_3-treatment, the mixture was chromatographed on a silica-gel column to give **50** [a colorless oil, 54 mg; 78%. Found: C, 82.42; H, 9.94%. ^1H NMR δ=0.87 (3H, d, J=7 Hz), 1.08 (6H, d, J=7 Hz), 1.18 (3H, s), 1.62 (3H, br s), 3.07 (1H, dd, J=9, 8 Hz), 3.21 (1H, dd, J=9, 4 Hz), 3.40 (1H, sept, J=7 Hz), 4.34 (1H, d, J=12 Hz), 4.42 (1H, d, J=12 Hz), 7.25 (5H, br s), 9.96 (1H, s). ^{13}C NMR δ=14.8, 17.0, 21.1, 21.5, 23.2, 26.2, 26.7, 30.1, 34.3 (2C), 36.2, 37.0, 50.7, 52.0, 72.1, 72.9, 127.1, 127.3 (2C), 128.1 (2C), 134.8, 135.4, 138.9, 141.7, 171.4, 188.1. IR ν: 2960, 2740, 1670, 1455, 1100, 735, 696 cm^{-1}].

The $^1O_2$-Oxidation of 46. Formation of 50. Similarly, **46** (29 mg) was converted to **50** (20 mg; 83%).

The $^1O_2$-Oxidation of 47. Formation of 49. Similarly, **47** (7.0 mg) was oxidized with $^1O_2$ by irradiation for 5 min to give **49** (a colorless oil, 4.0 mg; 67%).

The $^1O_2$-Oxidation of 48. Formation of 50. Similarly, **48** (7.0 mg) was converted to **50** (5.0 mg; 85%).

Preparation of the TMS Derivative (51) from 28. To an anhydrous pyridine solution (5 cm^3) of **28** (298 mg), TMSCl (0.7 cm^3) was added dropwise at room temperature. After being stirred for 12 h, the mixture was then diluted with water, extracted with hexane-ether (1:1), dried on K_2CO_3, and distilled in vacuo to remove the solvent. The residue was chromatographed quickly on a silica-gel column to give

51 [a colorless oil, 405 mg; 92%. Found: C, 69.38; H, 11.27%. Calcd for $C_{26}H_{50}O_2Si_2$: C, 69.27; H, 11.18%. ^{1}H NMR δ= 0.04 (9H, s), 0.09 (9H, s), 0.86 (3H, d, J=7 Hz), 1.03 (3H, d, J=7 Hz), 1.13 (3H, s), 1.65 (3H, br s), 2.80 (2H, br m), 3.21 (1H, t, J=9.5 Hz), 3.59 (1H, dd, J=9.5, 4 Hz), 4.31 (1H, s), and 4.82 (2H, br d, J=2.5 Hz). ^{13}C NMR δ=−0.4 (3C), 0.7 (3C), 15.1, 16.1, 16.8, 21.9, 22.4, 23.9, 24.8, 29.5, 35.0, 37.6, 37.8, 47.7, 51.3, 53.1, 64.6, 74.4, 106.0, 136.8, 137.0, and 160.3. IR ν: 2955, 1647, 1468, 1250, 1087, 1066, 879, and 746 cm^{-1}].

Preparation of the TMS Derivative (52) from 30. Similarly, **30** (5.123 g) in pyridine (35 cm^3) was treated with TMSCl (7.5 cm^3) to give **52** [a colorless oil, 6.913 g; 92%. Found: C, 69.56; H, 11.23%. ^{1}H NMR δ=0.09 (18H, s), 0.71 (3H, d, J=7 Hz), 0.82 (3H, d, J=7 Hz), 1.02 (3H, d, J=7 Hz), 1.04 (3H, s), 1.84 (3H, br s), 3.22 (1H, t, J=9.5 Hz), 3.60 (1H, dd, J=9.5, 4 Hz), 4.12 (1H, br s), 4.82 (1H, d, J=2 Hz), and 4.88 (1H, d, J=2.5 Hz). ^{13}C NMR δ=−0.4 (3C), 0.3 (3C), 15.9, 16.8 (2C), 22.1, 22.3, 25.6, 26.8, 28.9, 33.3, 37.1, 39.4, 49.4, 52.7, 55.5, 64.9, 77.9, 105.5, 137.2, 137.3, and 160.6. IR ν: 2955, 2875, 1643, 1250, 1068, 878, and 836 cm^{-1}].

Cope Rearrangement of 51 to 53. An anhydrous toluene solution (5 cm^3) of **51** (857 mg) was placed in a sealed tube and heated in an autoclave at 190 °C for 12 h. The mixture was then heated in vacuo to remove the solvent to give **53** [a colorless oil, 857 mg; 100%. Found: C, 69.33; H, 11.19%. ^{1}H NMR δ=0.08 (9H, s), 0.16 (9H, s), 0.75 (3H, d, J=7 Hz), 0.88 (3H, d, J=7 Hz), 0.95 (3H, d, J=7 Hz), 1.04 (3H, s), 1.60 (3H, br s), 2.74 (2H, br m), 3.15 (1H, t, J=10 Hz), 3.38 (1H, dd, J=10, 4 Hz), and 6.05 (1H, d, J=2.5 Hz). ^{13}C NMR δ=−0.4(6C), 15.1, 16.6, 18.0, 21.8, 23.4, 23.9, 27.9, 28.4, 37.0, 37.4, 38.4, 38.6, 46.2, 47.9, 52.7, 64.1, 132.7, 134.9, and 135.5 (2C). IR ν: 2955, 2875, 1667, 1252, 1154, 1081, 873, 838, and 748 cm^{-1}].

Cope Rearrangement of 52 to 54. Similarly, a toluene solution of **52** (238 mg) was heated in an autoclave to give **54** [a colorless oil, 238 mg; 100%. Found: C, 69.02; H, 11.09%. ^{1}H NMR δ=0.06 (9H, s), 0.18 (9H, s), 0.79 (3H, d, J=7 Hz), 0.92 (6H, d, J=7 Hz), 1.04 (3H, s), 1.63 (3H, br s), 2.70 (1H, br m), 2.66 (1H, d, J=14 Hz), 3.12 (1H, t, J=10 Hz), 3.37 (1H, dd, J=10, 4 Hz), and 5.91 (1H, d, J=2 Hz). ^{13}C NMR δ=−0.5 (3C), −0.4 (3C), 14.8, 16.8 (2C), 22.0, 23.2, 24.8, 24.9, 28.7, 34.5, 36.6, 37.2, 38.5, 46.4, 49.4, 51.9, 63.9, 132.2, 132.5, 134.3, and 136.1. IR ν: 2960, 2875, 1668, 1252, 1160, 1082, 872, 840, and 748 cm^{-1}].

Conversion of 53 to Unsaturated Aldehyde (55). An anhydrous toluene solution (25 cm^3) of **53** (857 mg), TPP (9 mg), and pyridine (0.05 cm^3) was irradiated with a 500-W tungsten lamp under an O_2 atmosphere at −70 °C for 30 min. The mixture was then treated with PPh_3 and extracted with ether. The ether extract was hydrolyzed with dil HCl and chromatographed on a silica-gel column, from benzene–hexane (2:1) to hexane–AcOEt (5:1), to give **55** [a colorless oil, 417 mg; 72%. Found: C, 78.95; H, 10.68%. Calcd for $C_{20}H_{32}O_2$: C, 78.90; H, 10.60%. ^{1}H NMR δ=0.97 (3H, d, J=7 Hz), 1.08 (3H, d, J=7 Hz), 1.13 (3H, d, J=7 Hz), 1.32 (3H, s), 1.53 (3H, br s), 2.73 (1H, br m), 3.26 (1H, dd, J=11, 7.5 Hz), 3.41 (1H, sept, J=7 Hz), 3.50 (1H, dd, J=11, 6 Hz), and 9.97 (1H, s). ^{13}C NMR δ=14.9, 16.2, 21.0, 21.2, 23.2, 26.4, 26.9, 29.8, 34.7, 36.0, 37.0 (2C), 50.8, 52.5, 64.0, 134.7, 135.6, 141.1, 172.0, and 188.0. IR ν: 3430, 2950, 1670, 1613, 1460, and 1025 cm^{-1}].

Conversion of 54 to Unsaturated Aldehyde (56). a) Similarly, **54** (223 mg) was oxidized with $^1O_2$ and hydrolyzed with dil HCl to give **56** [a colorless oil, 119 mg; 79%. Found: C, 78.77; H, 10.77%. ^{1}H NMR δ=0.84 (3H, d, J=7 Hz), 1.09 (6H, d, J=7 Hz), 1.20 (3H, s), 1.62 (3H, br s), 3.21 (1H, dd, J=10.5, 7 Hz), 3.40 (1H, sept, J=7 Hz), 3.46 (1H, dd, J=10.5, 6 Hz), and 9.97 (1H, s). ^{13}C NMR δ=14.8, 16.5, 21.1, 21.5, 22.9, 26.6, 26.7, 30.2, 34.3, 35.9, 36.7, 37.1, 50.7, 51.9, 64.7, 135.6, 135.7, 141.6, 171.9, and 188.3. IR ν: 3440, 2960, 2870, 1670, 1610, 1465, 1455, and 1025 cm^{-1}].

b) An acetonitrile solution (10 cm^3) of **54** (778 mg) was mixed with $Pd(OAc)_2$ (420 mg) and maintained at room temperature for 72 h. The mixture was then extracted with ether, hydrolyzed with dil HCl in aqueous ether, washed with water and dried on K_2CO_3. Silica-gel column chromatography of the organic extract gave **56** (322 mg; 61%).

The Oxidation of 55 to a Dialdehyde (57). To an anhydrous CH_2Cl_2 solution (10 cm^3) of $(COCl)_2$ (72 mg), DMSO (122 mg) was added at −70 °C, and stirred for 5 min. Then CH_2Cl_2 solution (2 cm^3) of **55** (202 mg) was introduced to the mixture. After stirring for another 20 min at this temperature it was further stirred with NEt_3 (650 mg) added. The reaction mixture was warmed to room temperature, extracted with ether, and chromatographed on a silica-gel column to give **57** [a colorless oil, 186 mg; 92%. Found: M.W., 302.2247. Calcd for $C_{20}H_{30}O_2$: 302.2244. ^{1}H NMR δ=1.03 (3H, d, J= 7 Hz), 1.08 (3H, d, J=7 Hz), 1.13 (3H, d, J=7 Hz), 1.31 (3H, s), 1.55 (3H, br s), 2.98 (1H, br m), 3.41 (1H, sept, J=7 Hz), 9.53 (1H, d, J=1 Hz), and 9.96 (1H, s). ^{13}C NMR δ=12.0, 15.1, 21.3, 21.5, 25.0, 26.7, 26.8, 29.9, 34.9, 36.3, 37.0, 47.8, 51.3, 52.1, 133.5, 137.5, 141.7, 172.0, 188.2, and 206.0. IR ν: 2970, 2940, 2875, 2840, 2740, 1722, 1668, 1612, and 1460 cm^{-1}].

The Oxidation of 56 to a Dialdehyde (58). Similarly, **56** (119 mg) was oxidized with $(COCl)_2$ (40 mg) and DMSO (70 mg) to give **58** [a colorless oil, 80 mg; 80%. Found: M.W., 302.2245. ^{1}H NMR δ=0.93 (3H, d, J=7 Hz), 1.05 (6H, d, J=7 Hz), 1.22 (3H, s), 1.62 (3H, br s), 3.41 (1H, sept, J= 7 Hz), 9.48 (1H, br s), and 10.00 (1H, s). ^{13}C NMR δ=12.3, 14.8, 21.3, 21.5, 24.3, 26.8 (2C), 30.2, 34.5, 35.7, 38.8, 47.1, 50.8, 51.3, 133.9, 137.0, 141.4, 172.3, 188.2, and 206.4. IR ν: 2970, 2750, 1725, 1668, 1613, and 1460 cm^{-1}].

$TiCl_2$-Mediated Cyclization of 57. To an anhydrous THF solution (60 cm^3) of $TiCl_4$ (1 cm^3) prepared at 0 °C, pyridine (0.5 cm^3) and powdered Zn (1.3 g) were added in portions, and stirred for 30 min. Then, a THF solution (15 cm^3) of **57** (184 mg) was slowly introduced over a 2-h period to maintain high-dilution conditions, and stirred for another 40 min. The mixture was then treated with aqueous K_2CO_3, extracted with ether and dried on K_2CO_3. Silica-gel column chromatography and further HPLC of the extract afforded **59** [a colorless oil, 47 mg; 25%. Found: C, 78.76; H, 10.73%. Calcd for $C_{20}H_{32}O_2$: C, 78.90; H, 10.60%. ^{1}H NMR δ=0.92 (3H, d, J=7 Hz), 0.93 (6H, d, J=7 Hz), 1.20 (3H, s), 1.64 (3H, br s), 2.61 (1H, sept, J=7 Hz), 2.98 (1H, br), 3.53 (1H, dd, J=6, 4 Hz), and 4.97 (1H, d, J=4 Hz). IR ν: 3450, 2950, 1470, 1382, and 1105 cm^{-1}], **60** [colorless prisms, mp 146.5—148 °C, 53 mg; 28%. Found: C, 78.93; H, 10.67%. ^{1}H NMR δ=0.86 (3H, d, J=7 Hz), 0.96 (6H, d, J=7 Hz), 0.98 (3H, s), 1.64 (3H, br s), 2.85 (2H, br), 3.04 (1H, sept, J=7 Hz), 3.76 (1H, dd, J=9, 2 Hz), and 4.10 (1H, d, J=9 Hz). IR ν: 3420, 2950, 1465, 1450, 1375, 1200, 1013, and 983 cm^{-1}], and **61** [a colorless oil, 27 mg; 14%. Found: M.W., 304.2388. Calcd for $C_{20}H_{32}O_2$: 304.2401. ^{1}H NMR δ=0.76 (3H, d, J=7 Hz), 0.95 (3H, d, J=7 Hz), 0.98 (3H, d, J=7 Hz), 1.20 (3H, s), 1.64 (3H, br s), 2.80 (1H, br), 2.82 (1H, sept, J=7 Hz), 4.18 (1H, d, J=9 Hz), and 4.49 (1H, d, J=9 Hz). IR ν: 3610, 3570, 2960, 2930, 1463, 1370, and 996 cm^{-1}].

$TiCl_2$-Mediated Cyclization of 58. To an anhydrous THF

solution (5 cm³) of $TiCl_4$ (106 mg) prepared carefully at 0 °C, pyridine (51 mg) and powdered Zn (126 mg) were added, and stirred for 30 min. Then, the THF solution (2 cm³) of **58** (97 mg) was introduced dropwise under stirring for 1 h. After being diluted with aqueous K_2CO_3, the mixture was extracted with ether and chromatographed on a silica-gel column to give **62** [a colorless oil, 82 mg; 84%. Found: M.W., 304.2404. ^1H NMR δ=0.94 (3H, d, J=7 Hz), 0.97 (3H, d, J=7 Hz), 1.14 (3H, d, J=7 Hz), 1.24 (3H, s), 1.67 (3H, br s), 3.54 (1H, br t, J=5 Hz), and 4.87 (1H, br). IR ν: 3350, 2950, 2880, 1460, 1385, 1370, and 1030 cm^{-1}].

Acetylation of a Mixture of 62 and 63. A pyridine solution (4 cm³) of the whole product (485 mg) was mixed with Ac_2O (0.5 cm³) and kept at room temperature for 16 h. The mixture was then diluted with water, extracted with hexane–ether (9:1) and chromatographed on a silica-gel column to give **64** [a colorless oil, 461 mg; 84%. Found: M.W., 346.2515. Calcd for $C_{22}H_{34}O_3$: 346.2506. ^1H NMR δ=0.92 (3H, d, J=7 Hz), 1.02 (6H, d, J=7 Hz), 1.21 (3H, s), 1.62 (3H, br s), 2.11 (3H, s), 2.64 (1H, sept, J=7 Hz), 4.76 (1H, br t, J=5 Hz), and 5.04 (1H, br). IR ν: 3550, 2950, 2870, 1745, 1720, 1465, 1384, 1370, 1242, 1028, and 964 cm^{-1}], and **65** [colorless needles, mp 117—120 °C, 72 mg; 13%. Found: M.W., 346.2510. ^1H NMR δ=0.93 (3H, d, J=7 Hz), 0.98 (3H, d, J=7 Hz), 1.01 (3H, d, J=7 Hz), 1.07 (3H, s), 1.60 (3H, br s), 2.10 (3H, s), 3.18 (1H, sept, J=7 Hz), 4.29 (1H, d, J=11 Hz), and 5.28 (1H, br). IR ν: 3490, 2950, 1725, 1452, 1377, 1260, and 1030 cm^{-1}].

Hydrolysis of 65. An anhydrous ether solution (3 cm³) of **65** (20 mg) was treated with LAH (10 mg) at room temperature for 1 h, after which the mixture was extracted with ether. Silica-gel column chromatography of the extract gave **63** [a colorless oil, 11 mg; 63%. Found: M.W., 304.2388. ^1H NMR δ=0.97 (9H, br d, J=7 Hz), 1.06 (3H, br s), 1.62 (3H, br s), 3.18 (1H, br), 3.90 (1H, br), and 4.23 (1H, br)] and an isomer, **67** [a colorless oil, 2 mg; 11%. Found: M.W., 304.2404. ^1H NMR δ=0.96 (6H, d, J=7 Hz), 1.02 (3H, d, J=7 Hz), 1.16 (3H, s), 1.61 (3H, br s), 2.59 (1H, br), 2.88 (1H, sept, J=7 Hz), 2.97 (1H, br), 3.97 (1H, dd, J=10, 8 Hz), and 4.38 (1H, d, J=10 Hz). IR ν: 3630, 3600, 2960, 2880, 1460, 1380, 1240, 1015 cm^{-1}].

Acetylation of 62 to a Diacetate (66). An anhydrous CH_2Cl_2 solution (3 cm³) of **62** (246 mg), DMAP (20 mg), Ac_2O (300 mg) and Et_3N (100 mg) was kept at room temperature for 16 h. The mixture was then diluted with water, extracted with ether, and chromatographed on a silica-gel column to give **64** (46 mg; 16%) and **66** [a colorless oil, 223 mg; 71%. Found: C, 74.14; H, 9.36%. Calcd for $C_{24}H_{36}O_4$: C, 74.19; H, 9.34%. ^1H NMR δ=0.92 (3H, d, J=7 Hz), 1.00 (3H, s), 1.04 (3H, d, J=7 Hz), 1.07 (3H, d, J=7 Hz), 1.60 (3H, br s), 2.01 (3H, s), 2.08 (3H, s), 2.78 (1H, br), 2.84 (1H, sept, J=7 Hz), 4.80 (1H, dd, J=5.5, 3 Hz), and 6.30 (1H, br). IR ν: 2950, 2870, 1750, 1460, 1370, 1245, 1230, and 1030 cm^{-1}].

Hydrolysis of 64. Similarly, **64** (20 mg) was reduced with LAH in ether to give **62** (19 mg; 100%).

Formation of Dimethyl Acetal, 68, from 62. To an anhydrous benzene solution (4 cm³) of **62** (46 mg), $Me_2C(OMe)_2$ (1 cm³) was added and stirred with PPTS (3 mg) at room temperature for 72 h. The mixture was then treated with aqueous K_2CO_3 and extracted with ether. Silica-gel column chromatography of the extract yielded **68** [a colorless oil, 33 mg; 64%. Found: M.W., 344.2716. Calcd for $C_{23}H_{36}O_2$: 344.2713. ^1H NMR δ=0.94 (3H, d, J=7 Hz), 1.00 (3H, d, J=7 Hz), 1.11 (3H, d, J=7 Hz), 1.24 (3H, s), 1.28 (3H, s), 1.37 (3H, s), 1.60 (3H, br s), 2.52 (1H, sept, J=7 Hz), 2.59 (1H, br), 4.20 (1H, dd, J=9, 1 Hz), and 5.17 (1H, br d, J=9 Hz). IR ν: 2950, 1460, 1380, 1205, 1042, and 886 cm^{-1}].

$NaIO_4$-Cleavage of 62. Formation of 58. A THF solution (2 cm³) of **62** (29 mg) was treated with $NaIO_4$ (40 mg) dissolved in water (2 cm³) at room temperature for 12 h. The mixture was then, diluted with water and extracted with ether. Silica-gel column chromatography of the extract afforded **58** (19 mg; 65%), which was identical with the authentic sample in every respect.

PCC-Oxidation of 64 to 69. To an anhydrous CH_2Cl_2 suspension (2 cm³) of PCC (64 mg), NaOAc (9 mg), and Celite (40 mg), a CH_2Cl_2 solution of **64** (5 mg) was added dropwise. After 3 h, the mixture was diluted with ether and filtered on a short Florisil column to give **69** [a colorless oil, 33 mg; 77%. Found: M.W., 344.2353. Calcd for $C_{22}H_{32}O_3$: 344.2350. ^1H NMR δ=0.96 (6H, d, J=7 Hz), 1.06 (3H, d, J=7 Hz), 1.16 (3H, s), 1.60 (3H, br s), 2.15 (3H, s), 2.80 (1H, br), 3.10 (1H, br), and 5.25 (1H, d, J=5 Hz). IR ν: 2950, 1753, 1705, 1460, 1372, 1240, 1045, and 808 cm^{-1}].

LAH-Reduction of 69 to 62. An anhydrous ether solution of **69** (5.0 mg) was treated with LAH (5 mg) to give **62** (4.5 mg; 100%), whose identity as the authentic sample was confirmed by direct comparisons.

Conversion of 62 to Fusicoccatriene (1) via Elimination of Cyclic Thiocarbonate (71). To an anhydrous toluene solution (4 cm³) of **62** (277 mg), 1,1′-(thiocarbonyl)bis[imidazole] (**70**, 540 mg; 90%) was added and refluxed for 5 h. The mixture was then diluted with ether, passed through a short silica-gel filter, heated in vacuo to remove the solvent, and chromatographed to obtain **71** [a colorless oil, 185 mg; 59%. Found: M.W., 346.1963. Calcd for $C_{21}H_{30}O_2S$: 346.1965. ^1H NMR δ=0.95 (3H, d, J=7 Hz), 1.01 (3H, d, J=7 Hz), 1.16 (3H, d, J=7 Hz), 1.27 (3H, s), 1.66 (3H, br s), 4.91 (1H, dd, J=10, 1 Hz), and 5.82 (1H, d, J=10 Hz)]. Without further purification, **71** (174 mg) was dissolved together with 1,3-dimethyl-2-phenyl-1,3,2-diazaphospholidine (**72**, 1 cm³) in benzene (1.5 cm³), and refluxed for 9 h. After dilution with ether, the extract was passed through a short silica-gel column to obtain **1** [a colorless oil, 65 mg; 51%. Found: M.W., 270.2347. Calcd for $C_{20}H_{30}$: 270.2346. ^1H NMR δ=0.92 (6H, d, J=7 Hz), 0.95 (3H, s), 0.96 (3H, d, J=7 Hz), 1.58 (3H, br s), 2.51 (1H, sept, J=7 Hz), 2.60 (1H, br), 5.40 (1H, br dd, J=11, 7 Hz), and 5.79 (1H, br d, J=11 Hz). IR ν: 2960, 2880, 1460, 1370, 1110, and 1025 cm^{-1}], together with the recovered **71** (46 mg; 26%).

The authors are grateful to the Ministry of Education, Science and Culture for financial assistance through a Grant-in-Aid for the Scientific Research, No. 59740260 (to N. K.) and No. 59104006 (to H. T.), by which, part of the expenses were defrayed.

References

1) Part XXXIII: A. Mori and H. Takeshita, *Kyushu Daigaku Seisan Kagaku Kenkyusho Hokoku*, in press (1985).

2) A part of this study was published in a preliminary form: H. Takeshita, N. Kato, K. Nakanishi, H. Tagoshi, and T. Hatsui, *Chem. Lett.*, **1984**, 1495.

3) T. Sassa, *Nippon Nogei Kagaku Kaishi*, **49**, R35 (1975); A. Ballio, M. Brufani, C. G. Casinovi, S. Cerrini, W. Fedeli, R. Pellicciari, B. Santurbano, and A. Vaciago, *Experientia*, **24**, 631 (1968); K. D. Barrow, D. H. R. Barton, E. B. Chain, U. F.

W. Ohnsorge, and R. Thomas, *Chem. Commun.*, **1968**, 1198.

4) S. Nozoe, M. Morisaki, K. Tsuda, Y. Iitaka, N. Takahashi, S. Tamura, K. Ishibashi, and M. Shirasaka, *J. Am. Chem. Soc.*, **87**, 4968 (1965).

5) Y. Iitaka, I. Watanabe, I. T. Harrison, and S. Harrison, *J. Am. Chem. Soc.*, **90**, 1092 (1968).

6) S. Huneck, G. Baxter, A. F. Cameron, J. D. Connolly, and D. S. Rycroft, *Tetrahedron Lett.*, **24**, 3787 (1983); N. Enoki, A. Furusaki, K. Suehiro, R. Ishida, and T. Matsumoto, *ibid.*, **24**, 4341 (1983).

7) A. A. Adesomoju, J. I. Okogun, M. P. Cava, and P. J. Carroll, *Phytochemistry*, **22**, 2535 (1983); A. A. Adesomoju, and J. I. Okogun, *J. Natural Prod.*, **47**, 308 (1984); J. I. Okogun, A. A. Adesomoju, G. A. Adesida, H. J. Lindner, and G. Habermehl, *Z. Naturforsch.*, **37c**, 558 (1982).

8) J. C. Braekman, D. Daloze, R. Schubert, M. Albericci, B. Tursch, and R. Karlsson, *Tetrahedron*, **34**, 1551 (1978). See also W. Fenical, H. L. Sleeper, V. J. Paul, M. O. Stallard, and H. H. Sun, *Pure Appl. Chem.*, **51**, 1865 (1979); G. R. Pettit, R. H. Ode, C. L. Herald, R. B. von Dreele, and C. Michel, *J. Am. Chem. Soc.*, **98**, 4677 (1976).

9) H. Takeshita, T. Hatsui, N. Kato, T. Masuda, and H. Tagoshi, *Chem. Lett.*, **1982**, 1153.

10) T. Mukaiyama, T. Sato, and J. Hanna,. *Chem. Lett.*, **1973**, 1041; J. E. McMurry and M. P. Fleming, *J. Am. Chem. Soc.*, **96**, 4708 (1974); H. Takeshita, T. Hatsui, and O. Jinnai, *Chem. Lett.*, **1976**, 1059.

11) The numbering of the fusicoccane system was adopted to that of the cyclized geranylgeraniol based on the biogenetic concept.

12) Y. Okude, S. Hirano, T. Hiyama, and H. Nozaki, *J. Am. Chem. Soc.*, **99**, 3179 (1977).

13) N. Kato and H. Takeshita, *Bull. Chem. Soc. Jpn.*, **58**, 1574 (1985).

14) For the 3-isopropyl-1,2-dimethylcyclopentane, the name, "iridane" with the numbering as shown, was adopted throughout this text.

15) M. Ando, K. Wada, and K. Takase, *Tetrahedron Lett.*, **26**, 235 (1985); F. W. Eastwood, K. J. Harrington, J. S. Josan, and J. L. Pura, *Tetrahedron Lett.*, **1970**, 5223; S. Hanessian, A. Bargiotti, and M. LaRue, *Tetrahedron Lett.*, **1978**, 737.

16) R. A. Roberts, V. Schull, and L. A. Paquette, *J. Org. Chem.*, **48**, 2076 (1983).

17) A. J. Mancuso, S.-L. Huang, and D. Swern, *J. Org. Chem.*, **43**, 2480 (1978).

18) D. A. Evans, D. J. Baillargeon, J. V. Nelson, *J. Am. Chem. Soc.*, **100**, 2242 (1978).

19) G. Rousseau, P. Le Parchec, and J. M. Conia, *Synthesis*, **1978**, 67.

20) Y. Ito, T. Hirao, and T. Saegusa, *J. Org. Chem.*, **43**, 1011 (1978).

21) Some of the results on this matter will be reported elsewhere.

22) K. D. Barrow, R. B. Jones, P. W. Pemberton, and L. Phillips, *J. Chem. Soc., Perkin Trans 1*, **1975**, 1405; A. Banerji, R. Hunter, G. Mellows, K.-y Sim, and D. H. R. Barton, *J. Chem. Soc., Chem. Commun.*, **1978**, 843.

23) E. J. Corey and R. A. E. Winter, *J. Am. Chem. Soc.*, **85**, 2677 (1963); L. A. Paquette, I. Itoh, and W. B. Farnham, *J. Am. Chem. Soc.*, **97**, 7280 (1975).

24) E. J. Corey and P. B. Hopkins, *Tetrahedron Lett.*, **23**, 1979 (1982).

25) W. G. Dauben and D. J. Hart, *J. Org. Chem.*, **42**, 922 (1977); R. K. Boeckman, Jr., J. P. Bershas, J. Clardy, and B. Salheim, *ibid.*, **42**, 3630 (1977); T. K. Das, P. C. Dutta, G. Kartha, and J. M. Bernassau, *J. Chem. Soc., Perkin Trans. 1*, **1977**, 1287.

26) L. A. Paquette, D. R. Andrews, and J. P. Springer, *J. Org. Chem.*, **48**, 1147 (1983); L. A. Paquette, J. A. Colapret, and D. R. Andrews, *ibid.*, **50**, 201 (1985).

27) D. H. Grayson and J. R. H. Wilson, *J. Chem. Soc., Chem. Commun.*, **1984**, 1695.

28) J. Wolinski, M. R. Slabaugh, and T. Gibson, *J. Org. Chem.*, **29**, 3740 (1964).

29) J. F. Ruppert, M. A. Avery, and J. D. White, *J. Chem. Soc., Chem. Commun.*, **1976**, 978.

30) E. E. van Tamelen, G. M. Milne, M. I. Suffness, M. C. R. Chauvin, R. J. Anderson, and R. J. Achini, *J. Am. Chem. Soc.*, **92**, 7202 (1970).

Synthesis of 3-Arylmethyl-*p*-tropoquinones from 5-Alkoxy-2-(arylmethoxy)-tropones via Homolytic Rearrangement and Oxidation

Hitoshi TAKESHITA,* Akira MORI, and Yasutomo GOTO†
Research Institute of Industrial Science, 86, Kyushu University, Kasuga-koen, Kasuga, Fukuoka 816
†Graduate School of Engineering Sciences, 39, Kyushu University, Kasuga-koen, Kasuga, Fukuoka 816
(Received November 11, 1985)

The 3-(arylmethyl)-*p*-tropoquinones were synthesized by starting from the homolytic thermal rearrangement of 2-(arylmethoxy)-5-methoxytropones or 2,5-bis(arylmethoxy)tropones, followed by hydrolysis and oxidation. The half-wave potentials of these tropoquinones were determined by cyclic voltammetry. A remote substituent effect was observed for 3-(4-hydroxybenzyl)-*p*-tropoquinone, which may be attributable to intermolecular hydrogen bonding.

Recently, we have synthesized several halo-, alkyl-, and alkenyl-substituted *p*-tropoquinones,[1] and have measured their reduction potentials by cyclic voltammetry (CV)[2] to show the typical quinone character of *p*-tropoquinones; indeed, tropoquinones revealed stronger oxidizing ability than the benzoquinone derivatives carrying similar substituents.[3] However, an additional oxidation wave appeared around zero V together with two pairs of reduction-oxidation waves. The appearance of these new waves was more or less common to *p*-tropoquinones, and relatively intense waves were observed in 3-substituted derivatives. We have now synthesized another group of derivatives, 3-(arylmethyl)-*p*-tropoquinones, by application of the recently-found homolytic rearrangement of 2-(arylmethoxy)tropones to 3-(arylmethyl)tropolones.[4] The CV measurement of these 3-(arylmethyl)tropoquinones disclosed intense waves in that region. The findings will be described herein.

Synthesis of 3-(Arylmethyl)-*p*-tropoquinones. 2-(Arylmethoxy)-5-methoxytropones (**1**) were prepared in good yields from 5-methoxytropolone (**2**) and appropriate arylmethanols (**3**) by the dicyclohexylcarbodiimide (DCC)-condensation[5] or by condensation of **2** and arylmethyl chloride (**4**) in the presence of sodium hydride in hexamethylphosphoric triamide (HMPA).[4] Thermolysis of **1** proceeded in a manner similar to that of 2-(arylmethoxy)tropones,[4] or in even better yields; the only by-product identified was the debenzylated tropolone, **2**. The structures of the products (**5**) were obviously 3-(arylmethyl)-5-methoxytropolones from the known reaction mechanism, and characterized by their ^{1}H- and ^{13}C NMR spectra. Particularly, there is a distinct long-range coupling between the protons on the C-4 and C-6 of each product and a regular change of the ^{13}C chemical shift from the parent **2** in the vicinity of the substituents.

In view of the specificity of the homolytic rearrangement for 2-benzyloxy group, 2,5-bis(arylmethoxy)-tropone (**6**) prepared directly from 5-hydroxytropolone (**7**), could also be used for the present purpose. However, for the preparation of the 3-(4-methoxybenzyl) derivative, lc was better than 2,5-bis(4-methoxybenzyloxy)tropone (**6c**), from which, the major product was the debenzylated 5-(4-methoxybenzyloxy)-tropolone (**8c**); the desired 3-(4-methoxybenzyl)-5-(4-methoxybenzyloxy)tropolone (**9c**) was obtained only in a 10% yield. The yield of rearrangement products from the other two pairs of reactants (**1a** vs. **6a** and **1b** vs. **6b**) were not significantly different. Subsequently, the hydrolysis of **5** or **9** with hydrobromic acid in acetic acid afforded the desired 3-(arylmethyl)-5-hydroxytropolone (**10**) in good yields. In the case of **5c**, the methoxyl group on the benzene ring was

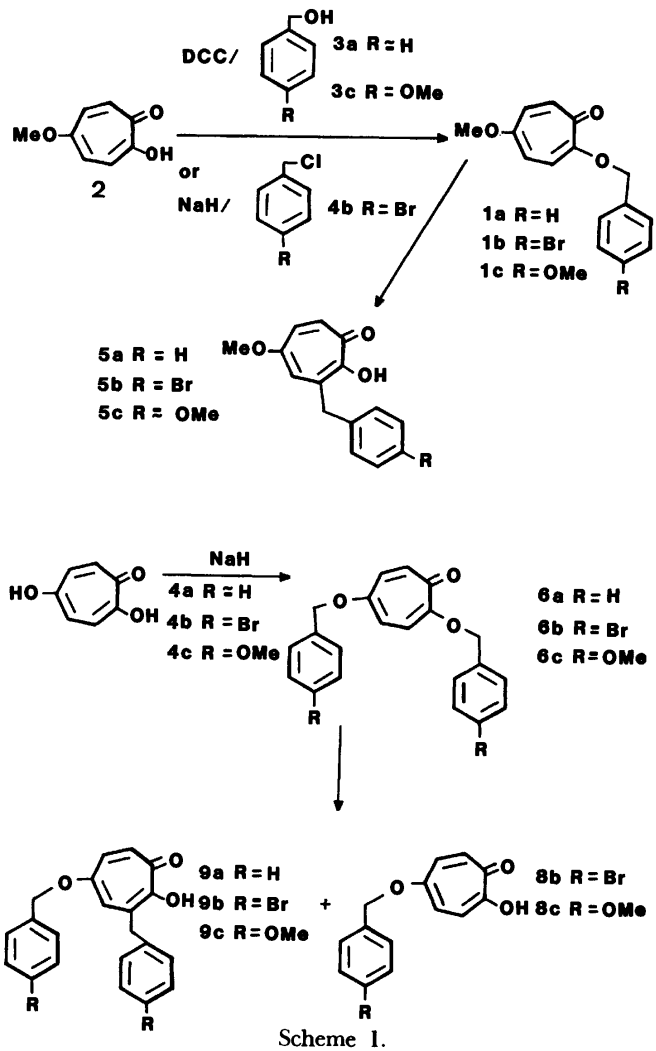

Scheme 1.

Table 1. Half-Wave Potentials of **11**[a] and Reference *p*-Tropoquinones

	E_1	E_2	$\Sigma(E_1+E_2)$	$\Delta(E_1-E_2)$
11a	−0.26	−1.04	−1.30	+0.78
11b	−0.24	−0.80	−1.04	+0.56
11d	−0.19	−0.72	−0.91	+0.53
12	−0.21	−1.10	−1.31	+0.89
13	−0.28	−1.15	−1.43	+0.87

a) CV measurements were carried out at the concentrations of 1.09×10^{-3} mmol cm^{-3} for **11a**, 1.03×10^{-3} mmol cm^{-3} for **11b**, and 8.18×10^{-4} mmol cm^{-3} for **11d**.

simultaneously demethylated to form 5-hydroxy-3-(4-hydroxybenzyl)tropolone (**10d**). By the DDQ (2,3-dichloro-5,6-dicyano-*p*-benzoquinone)-oxidation, **10** yielded corresponding quinones (**11**).

Measurement of the Cyclic Voltammetry. The half-wave potentials were determined by the CV and are summarized in Table 1 together with those of *p*-tropoquinone (**12**) and 4-methyl-*p*-tropoquinone (**13**).[2] The values were corrected with an internal standard for the redox potential of ferrocenium/ferrocene couple, +0.465 V vs. Ag/AgCl. Similar to other 3-substituted tropoquinones,[2] the CV of all **11** disclosed oxidation waves around +0.11 to +0.135 V. The intensities of these waves, which indicated an electrochemical formation of a different species, were as large as that of 3,6-diallyl-*p*-tropoquinone (**14**)[1b] and were even comparable to their first oxidation waves. The responsibility of the anion radical species (**A**) for these waves was verified by scanning between +0.3 to −0.5 V for CV of **11d**. It is likely that the species responsible for the waves are coupling products derived from **A**. As previously reported, treatment of 5-hydroxy-2-methoxytropones or 5-hydroxytropolones with a one-electron oxidation agent, such as cerium(IV) ammonium nitrate or silver acetate, led to a facile formation of several dimerization products.[2,6,7] For elucidation of the structures of the coupling products, preparative electrolytic study is being undertaken.

As in the benzoquinones,[8] a hydroxyl group of **11d** at a remote position caused an enhancement of the reduction potential. Although the mesomeric electron transmission through the benzene ring was blocked by the methylene group as has been indicated by the similar first reduction potentials of **11a**, **11b**, and **13**,[1b] the potential of **11d** exceeded the value not only of **11a** but also of unsubstituted **12**. Since intramolecular hydrogen bonding was sterically prohibited, this enhancement of the reduction potential may be attributed to intermolecular hydrogen bonding[8] to increase the electron affinity of the quinonoid carbonyl groups.

In conclusion, since the *p*-tropoquinones are stronger oxidizing agents than benzoquinones, it is interesting to prepare *p*-tropoquinone derivatives having stronger oxidizing ability than DDQ. In this respect, the present observations on the substituent effects suggested an approach. Furthermore, this easy method for the synthesis of benzyl-*p*-tropoquinones should be applicable to preparation of the polymer-supported tropoquinones, which is our current interest.

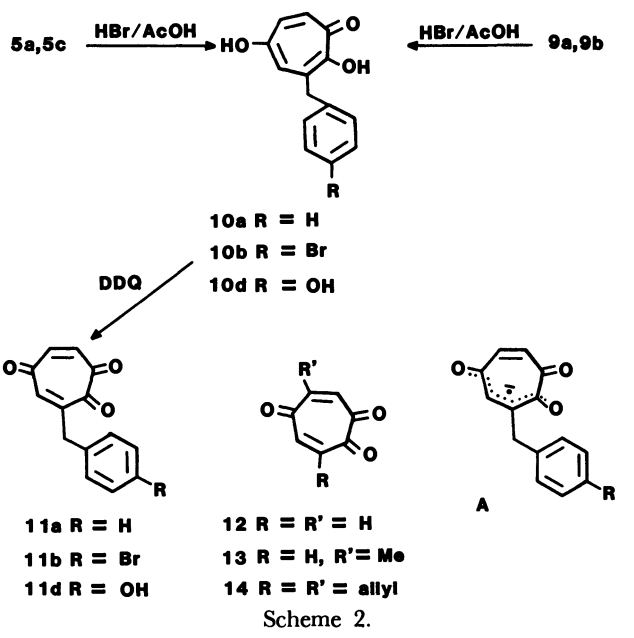

Scheme 2.

Experimental

All the mps, measured with a Yanagimoto Micro-mp apparatus, are uncorrected. Elemental analyses were performed by Miss S. Hirashima of the Research Institute of Industrial Science, Kyushu University. The CV were measured by Yanaco Polarographic Analyzer Model P-1100 apparatus in a standard three-electrode cell with a standard Ag/AgCl reference electrode in anhydrous *N,N*-dimethylformamide (DMF) solutions in the presence of 0.1 M[†] Bu_4NBF_4 under N_2. The scan rate was 100 mV/s at 22—23 °C. The NMR spectra were measured by means of a JEOL FX 100 Spectrometer in $CDCl_3$ solutions unless otherwise specified, and the chemical shifts were expressed in δ units from the internal Me_4Si. The mass spectra were measured by means of a JEOL OlSG-2 Spectrometer.

2-Benzyloxy-5-methoxytropone (1a). A mixture of **3a** (0.3 cm^3) and DCC (663 mg) was kept at 60 °C for 14 h with CuCl (5 mg). Then, a benzene solution (0.5 cm^3) of **2** (301 mg) was added and kept at 60 °C for 16 h. After removal of the precipitates, the mixture was chromatographed on a silica-gel column with AcOEt–benzene (1:5) to give **1a** [yellow crystals, mp 102—103 °C, 441.5 mg; 92%. Found: C, 74.46; H, 5.90%. Calcd for $C_{15}H_{14}O_3$: C, 74.36; H, 5.83%. ^{1}H NMR δ=3.68 (3H, s), 5.16 (2H, s), 6.18 (1H, dd, J=11, 2.5 Hz), 6.99 (1H, dd, J=13.5, 2.5 Hz), 7.18 (1H, d, J=13.5 Hz), and 7.25—7.5 (6H, m). ^{13}C NMR δ=55.5, 71.0, 107.1, 117.6, 127.2 (2C), 128.0, 128.5 (2C), 132.6, 136.2, 137.8, 158.6, 159.7, and 179.7. IR ν: 1570 and 1202 cm^{-1}. UV λ_{max}^{MeOH}: 227 nm (ε=24000), 252 (7500, sh), 328 (11200), 347 (10200), 361 (9300, sh), and 376 (6400, sh)].

2-(4-Bromobenzyloxy)-5-methoxytropone (1b). To an

† 1 M=1 mol dm^{-3}.

HMPA solution (3 cm³) of **2** (203 mg) and NaH (50%, 81 mg), **4b** (341 mg) was added at 60 °C. The mixture was kept at 60 °C for further 13 h, the reaction mixture was poured into water to precipitate **1b** [yellow crystals, mp 157—159 °C, 329 mg; 77%. Found: C, 55.80; H, 4.06%. Calcd for $C_{15}H_{13}O_3Br$: C, 56.09; H, 4.08%. ^1H NMR δ=3.72 (3H, s), 5.10 (2H, s), 6.18 (1H, dd, J=11, 2.5 Hz), 6.78 (1H, d, J=11 Hz), 7.06 (1H, dd, J=13, 2.5 Hz), 7.18 (1H, d, J=13 Hz), 7.26 (2H, d, J=8.5 Hz), and 7.46 (2H, d, J=8.5 Hz). ^{13}C NMR δ=55.5, 70.3, 106.8, 118.3, 121.9, 128.9 (2C), 131.7 (2C), 132.7, 135.3, 138.1, 158.3, 160.0, and 179.7. IR ν: 1570 and 1200 cm^{-1}. UV λ_{max}^{MeOH}: 227 nm (ε=16500), 252 (4100, sh), 327 (5900), 332 (5900), 341 (5600), 362 (4800, sh), and 376 (3400, sh)].

2-(4-Methoxybenzyloxy)-5-methoxytropone (1c). To a mixture prepared from **3c** (380 mg), DCC (615 mg), and CuCl (5 mg) by warming at 60 °C for 10 h a benzene solution (0.5 cm³) of **2** (297 mg) was added. After standing at 60 °C for 30 min, the precipitates were removed by filtration, the filtrate was heated in vacuo to remove the volatile material, and the residue was recrystallized from a mixture of benzene and hexane (2:1) to give **1c** [yellow needles, mp 157—158.5 °C, 527 mg; 99%. Found: M. W., 272.1033. Calcd for $C_{16}H_{16}O_4$: 272.1048. ^1H NMR δ=3.72 (3H, s), 3.78 (3H, s), 5.12 (2H, s), 6.20 (1H, dd, J=11, 2.8 Hz), 6.82 (1H, d, J=11 Hz), 6.86 (2H, d, J=9 Hz), 7.00 (1H, dd, J=13, 2.8 Hz), 7.18 (1H, d, J=13 Hz), and 7.52 (2H, d, J=9 Hz). ^{13}C NMR δ=55.3, 55.5, 70.8, 107.3, 114.0 (2C), 118.1, 128.2, 129.0 (2C), 132.6, 137.8, 158.7, 159.5, 159.8, and 179.8. IR ν: 1610, 1573, 1520, 1237, 1200, 1108, and 825 cm^{-1}. UV λ_{max}^{MeOH}: 229 nm (ε=15200), 252 (4200, sh), 274 (1300), 282 (1500), 327 (5400), 332 (5400), 348 (4900), 362 (4200, sh), and 378 (3100, sh)].

2,5-Bis(benzyloxy)tropone (6a). To an HMPA solution (12 cm³) prepared from **7** (500 mg) and NaH (392 mg) by warming at 60 °C for 3 h, **4a** (1.2 cm³) was added. After 13 h, the mixture was poured into water, and the resultant precipitates were collected by filtration. Recrystallizations from a mixed solution of benzene and hexane yielded **6a** [yellow crystals, mp 114—115 °C, 915 mg; 80%. Found: C, 79.30; H, 5.67%. Calcd for $C_{21}H_{18}O_3$: C, 79.22; H, 5.70%. ^1H NMR δ=4.95 (2H, s), 5.18 (2H, s), 6.30 (1H, ddd, J=11, 2, 1 Hz), 6.78 (1H, d, J=11 Hz), 7.07 (1H, dd, J=13, 2 Hz), 7.25 (1H, dd, J=13, 1 Hz), and 7.35 (10H, br s). ^{13}C NMR δ=70.4, 71.0, 108.7, 117.3, 127.2 (2C), 127.4 (2C), 128.0, 128.4, 128.6 (2C), 128.7 (2C), 132.8, 135.4, 136.1, 137.9, 158.8 (2C), and 179.7. IR ν: 1601, 1566, 1233, 1193, 1126, 849, and 759 cm^{-1}. UV λ_{max}^{MeOH}: 227 nm (ε=13300), 253 (5200, sh), 327 (6300), 332 (6300), 344 (5700), 360 (4900, sh), and 370 (3400, sh)].

2,5-Bis(4-bromobenzyloxy)tropone (6b). Similarly, **7** (276 mg) in HMPA (4 cm³) with NaH (218 mg) was treated with **4b** (1070 mg) in HMPA (4 cm³) to give **6b** [yellow crystals, mp 142—143 °C, 903 mg; 95%. Found: C, 52.87; H, 3.44%. Calcd for $C_{21}H_{16}O_3Br_2$: C, 52.97; H, 3.39%. ^1H NMR δ=4.88 (2H, s), 5.08 (2H, s), 6.24 (1H, d, J=11 Hz), 6.72 (1H, d, J=11 Hz), 7.12 (2H, s), 7.20 (2H, d, J=9 Hz), 7.22 (2H, d, J=9 Hz), 7.42 (2H, d, J=9 Hz), and 7.44 (2H, d, J=9 Hz). ^{13}C NMR δ=69.6, 70.2, 108.6, 117.6, 122.0, 122.4, 129.0 (4C), 131.7 (2C), 131.8 (2C), 132.8, 134.4, 135.1, 138.1, 158.7 (2C), and 179.6. IR ν: 1630, 1595, 1570, 1516, 1245, 1190, and 1010 cm^{-1}. UV λ_{max}^{MeOH}: 228 nm (ε=38700), 254 (9600, sh), 327 (11700), 346 (10300, sh), 360 (8900, sh), and 376 (5900, sh)].

2,5-Bis(4-methoxybenzyloxy)tropone (6c). In a similar manner to **6b**, **7** (411 mg) was converted to **6c** [yellow needles, mp 145—148 °C, 1060 mg; 94%. Found: C, 73.02; H, 5.85%. Calcd for $C_{23}H_{22}O_5$: C, 73.00; H, 5.86%. ^1H NMR δ=3.76 (3H, s), 3.78 (3H, s), 4.86 (2H, s), 5.10 (2H, s), 6.30 (1H, ddd, J=11, 2.5, 1 Hz), 6.78 (1H, d, J=11 Hz), 6.84 (2H, d, J=9 Hz), 6.88 (2H, d, J=9 Hz), 7.04 (1H, dd, J=13, 2.5 Hz), 7.20 (1H, dd, J=13, 1 Hz), 7.26 (2H, d, J=9 Hz), and 7.30 (2H, d, J=9 Hz). ^{13}C NMR δ=55.3 (2C), 70.3, 70.8, 108.7, 114.0 (2C), 114.1 (2C), 117.7, 124.1, 127.4, 128.9 (2C), 129.2 (2C), 132.8, 137.9, 158.9, 159.4, 159.7, 168.3, and 179.8. IR ν: 1612, 1518, 1252, 1232, 1185, and 1175 cm^{-1}. UV λ_{max}^{MeOH}: 229 nm (ε=41200), 253 (10700, sh), 330 (12200), and 382 (6100, sh)].

3-Benzyl-5-methoxytropolone (5a). A decalin solution (9 cm³) of **1a** (225 mg) was refluxed for 4.5 h. The mixture was then chromatographed on a silica-gel column to give **5a** [yellow needles, mp 86—88 °C, 98 mg; 44%. Found: C, 74.46; H, 5.64%. Calcd for $C_{15}H_{14}O_3$: C, 74.36; H, 5.83%. ^1H NMR δ=3.70 (3H, s), 4.13 (2H, s), 6.70 (1H, dd, J=11, 2.5 Hz), 7.09 (1H, d, J=2.5 Hz), 7.24 (5H, s), and 7.26 (1H, d, J=11 Hz). ^{13}C NMR δ=40.8, 55.8, 117.4, 120.3, 126.8, 128.8 (2C), 129.4 (2C), 129.5, 139.2, 141.7, 158.7, 162.9, and 171.3. IR ν: 1608, 1529, and 1210 cm^{-1}. UV λ_{max}^{MeOH}: 227 nm (ε=11900), 253 (7500), 322 (3400), 372 (2900), and 386 (2800)] and **2** (16.7 mg; 12%).

3-(4-Bromobenzyloxy)-5-methoxytropolone (5b). Similarly, **1b** (148 mg) was converted to **5b** [yellow crystals, mp 109—111 °C, 84.5 mg; 57%. Found: M.W., 319.9975 and 322.0017. Calcd for $C_{15}H_{13}O_3Br$: 320.0028 and 322.0048. ^1H NMR δ=3.73 (3H, s), 4.08 (2H, s), 6.70 (1H, dd, J=11.5, 3 Hz), 7.08 (1H, d, J=3 Hz), 7.18 (2H, d, J=9 Hz), 7.26 (1H, d, J=11.5 Hz), and 7.38 (2H, d, J=9 Hz). ^{13}C NMR δ=40.5, 55.8, 116.7, 119.8, 129.9, 130.9 (2C), 131.6 (2C), 135.0, 138.0, 141.1, 158.5, 162.2, and 171.4. IR ν: 1609, 1515, 1484, 1450, 1400, and 1207 cm^{-1}. UV λ_{max}^{MeOH}: 228 nm (ε=21100), 241 (21100), 271 (6700, sh), 330 (7600), 370 (5400), and 384 (4800, sh)]. In this case, **2** could not be isolated.

3-(4-Methoxybenzyloxy)-5-methoxytropolone (5c). Similarly, **1c** (54 mg) was converted to **5c** [yellow crystals, mp 78—80 °C, 30 mg; 56%. Found: C, 70.80; H, 6.08%. Calcd for $C_{16}H_{16}O_4$: C, 70.57; H, 5.92%. ^1H NMR δ=3.72 (3H, s), 3.78 (3H, s), 4.10 (2H, s), 6.72 (1H, dd, J=11, 3 Hz), 6.82 (2H, d, J=8.5 Hz), 7.10 (1H, d, J=3 Hz), 7.18 (2H, d, J=8.5 Hz), and 7.28 (1H, d, J=11 Hz). ^{13}C NMR δ=40.0, 55.2, 55.7, 114.0 (2C), 116.9, 119.9, 129.3, 130.2 (2C), 130.8, 142.0, 158.3, 158.5, 162.4, and 171.1. IR ν: 1605, 1508, 1453, 1397, 1247, 1040, and 740 cm^{-1}. UV λ_{max}^{MeOH}: 227 nm (ε=24300), 240 (21200, sh), 251 (14900, sh), 276 (4200), 330 (7300), 371 (6100), and 387 (6100)] and **2** (5.4 mg; 18%).

3-Benzyl-5-benzyloxytropolone (9a). Similarly, **6a** (727 mg) was converted to **9a** [pale yellow crystals, mp 79—80 °C, 361 mg; 50%. Found: C, 79.38; H, 5.71%. Calcd for $C_{21}H_{18}O_3$: C, 79.22; H, 5.70%. ^1H NMR δ=4.12 (2H, s), 4.94 (2H, s), 6.83 (1H, dd, J=11.5, 3 Hz), 7.23 (6H, br s), 7.24 (1H, d, J=11.5 Hz), and 7.30 (5H, s). ^{13}C NMR δ=40.8, 70.8, 120.1, 121.0, 126.7, 127.6 (2C), 128.4, 128.7 (2C), 128.8 (2C), 129.2 (2C), 129.5, 135.6, 139.0, 141.1, 157.8, 163.9, and 170.3. IR ν: 1608, 1548, 1458, 1400, and 1192 cm^{-1}. UV λ_{max}^{MeOH}: 237 nm (ε=22600), 250 (18800, sh), 332 (8600), 370 (6100), and 387 (5900)].

Thermolysis of 6b to 3-(4-Bromobenzyl)-5-(4-bromobenzyloxy)-tropolone (9b) and 5-(4-Bromobenzyloxy)tropolone (8b). Similarly, **6b** (80.6 mg) was heated. Silica-gel column chromatography of the mixture yielded **9b** [yellow crystals, mp 62 °C, 32.8 mg; 41%. Found: M.W., 473.9484, 475.9440, and 477.9440. Calcd for $C_{21}H_{16}O_3Br_2$: 473.9466, 475.9447, and 477.9427. ^1H NMR δ=4.04 (2H, s), 4.90 (2H, s), 6.80

(1H, dd, J=11, 3 Hz), 7.06 (2H, d, J=9 Hz), 7.12 (1H, d, J=3 Hz), 7.17 (2H, d, J=9 Hz), 7.22 (1H, d, J=11 Hz), 7.35 (2H, d, J=9 Hz), and 7.47 (2H, d, J=9 Hz). ^{13}C NMR δ=40.4, 70.2, 119.4, 120.4, 120.7, 122.6, 129.2 (2C), 130.0, 131.0 (2C), 131.8 (2C), 132.1 (2C), 134.7, 138.1, 140.8, 157.4, 163.5, and 171.1. IR ν: 1608, 1555, 1488, 1456, 1398, 1367, 1259, 1015, 1188, and 804 cm^{-1}. UV λ_{max}^{MeOH}: 227 nm (ε=29300), 241 (24100, sh), 250 (19700, sh), 332 (8300), 370 (5800), 387 (5600), and 422 (1400)] and **8b** [yellow crystals, mp 121—123 °C. 8.7 mg; 11%. Found: M.W., 305.9878 and 307.9871. Calcd for $C_{14}H_{11}O_3Br$: 305.9889 and 307.9871. ^{1}H NMR δ=4.98 (2H, s), 7.00 (2H, d, J=12 Hz), 7.24 (2H, d, J=9 Hz), 7.28 (2H, d, J=12 Hz), and 7.52 (2H, d, J=9 Hz)].

Thermolysis of 6c to 3-(4-Methoxybenzyl)-5-(4-methoxybenzyloxy)tropolone (9c) and 5-(4-Methoxybenzyloxy)-tropolone (8c). Similarly, **6c** (549.5 mg) was converted to **9c** [a yellow oil, 55.6 mg; 10%. Found: M.W., 378.1462. Calcd for $C_{23}H_{22}O_5$: 378.1464. ^{1}H NMR δ=3.74 (3H, s), 3.80 (3H, s), 4.06 (2H, s), 4.88 (2H, s), 6.7—7.0 (6H, m), and 7.05—7.3 (5H, m). ^{13}C NMR δ=40.4, 55.2 (2C), 70.7, 113.7, 114.0 (2C), 114.1 (2C), 119.5, 120.5, 127.6, 129.3 (2C), 129.6, 130.2 (2C), 130.9, 141.4, 157.7, 158.3, 163.5, and 170.5] and **8c** [colorless crystals, mp 181.5 °C (decomp), 274.5 mg; 73%. Found: C, 69.86; H, 5.47%. Calcd for $C_{15}H_{14}O_4$: C, 69.75; H, 5.46%. ^{1}H NMR δ=3.80 (3H, s), 4.94 (2H, s), 6.90 (2H, d, J=9 Hz), 7.00 (2H, d, J=12 Hz), 7.26 (2H, d, J=12 Hz), and 7.30 (2H, d, J=9 Hz). ^{13}C NMR δ=40.0, 55.3, 114.1 (2C), 124.1 (2C), 124.2 (2C), 127.4, 129.3 (2C), 158.8, 159.7, and 168.3 (2C). IR ν: 1618, 1547, 1454, 1269, 1254, 1190, and 1173 cm^{-1}].

Demethylation of 5a to 3-Benzyl-5-hydroxytropolone (10a). A 1:1-mixture of conc HBr–AcOH (1.2 cm^3) and **5a** (30.6 mg) were heated. The product mixture was then poured into water, and extracted with AcOEt. Recrystallizations from a mixed solution of acetone and ether yielded **10a** [yellow crystals, mp 192 °C (decomp), 12 mg; 42%. Found: M.W., 228.0787. Calcd for $C_{14}H_{12}O_3$: 228.0787. ^{1}H NMR (DMF-d_7) δ=4.11 (2H, s), 6.96 (1H, dd, J=11, 3 Hz), 7.23 (1H, d, J=3 Hz), and 7.28 (6H, br s). ^{13}C NMR δ=40.9, 120.3, 121.2, 126.9, 129.0 (2C), 129.8 (2C), 130.3, 140.6, 143.6, 158.2, 159.4, and 171.3. IR ν: 1605, 1376, 1277, 1215, and 962 cm^{-1}. UV λ_{max}^{MeOH}: 239 nm (ε=21200), 270 (3900, sh), 342 (8700), 380 (7300, sh), 393 (7700), and 422 (2600, sh)].

Debenzylation of 9a to 10a. Similarly, **9a** (48.3 mg) was hydrolyzed to **10a** (25.2 mg; 73%).

Debenzylation of 9b to 10b. Similarly, **9b** (284 mg) was converted to **10b** [yellow needles, mp 161 °C (decomp), 78 mg; 42%. Found: C, 54.51; H, 3.76%. Calcd for $C_{14}H_{11}O_3Br$: C, 54.75; H, 3.61%. ^{1}H NMR (CD_3OD) δ=4.07 (2H, s), 6.94 (1H, dd, J=11, 2.5 Hz), 7.15 (2H, d, J=8.5 Hz), 7.16 (1H, d, J=2.5 Hz), 7.28 (1H, d, J=11 Hz), and 7.39 (2H, d, J=8.5 Hz). ^{13}C NMR δ=41.0, 121.2, 123.9, 124.8, 129.8, 132.0 (2C), 132.6 (2C), 140.0, 142.5, 159.3, 166.1, and 169.6. IR ν: 1605, 1370, 1277, and 1214 cm^{-1}. UV λ_{max}^{MeOH}: 230 nm (ε=23700, sh), 237 (23800), 336 (8100), 379 (7200), and 394 (7400)].

Demethylation of 5c to 10d. Similarly, **5c** (110 mg) was converted to **10d** [yellow crystals, mp 191 °C (decomp), 54.4 mg; 55%. Found: M.W., 244.0733. Calcd for $C_{14}H_{12}O_4$: 244.0733. ^{1}H NMR (CD_3OD) δ=4.01 (2H, s), 6.70 (2H, d, J=9 Hz), 6.94 (1H, dd, J=11.5, 3 Hz), 7.05 (2H, d, J=9 Hz), 7.12 (1H, d, J=3 Hz), and 7.24 (1H, d, J=11.5 Hz). ^{13}C NMR δ=40.7, 116.6 (2C), 124.0, 125.2, 129.7, 131.5 (3C), 144.3, 157.3, 159.7, 166.4, and 169.7. IR ν: 1610, 1518, 1373, 1214, and 1201 cm^{-1}. UV λ_{max}^{MeOH}: 229 nm (ε=21000), 239 (20800), 280 (3900, sh), 344 (8500), 395 (6800), and 422 (3100, sh)].

3-Benzyl-*p*-tropoquinone (11a). An acetone solution (10 cm^3) of **10a** (104.5 mg) was treated with DDQ (121 mg) at 20—25 °C for 2 to 5 h. Silica-gel column chromatography of the mixture afforded **11a** [a yellow oil, 93.8 mg; 91%. Found: M.W., 226.0630. Calcd for $C_{14}H_{10}O_3$: 226.0630. ^{1}H NMR δ=3.84 (2H, d, J=1.5 Hz), 6.57 (1H, br s), 6.77 (2H, s), and 7.0—7.4 (5H, m). ^{13}C NMR δ=38.8, 127.3, 129.0 (2C), 129.3 (2C), 133.6, 135.6, 136.9, 139.5, 147.7, 187.7, 189.1, and 189.9. IR ν: 1680, 1644, and 1615 cm^{-1}. UV $\lambda_{max}^{CHCl_3}$: 252 nm (ε=12600) and 272 (7600)].

3-(4-Bromobenzyl)-*p*-tropoquinone (11b). Similarly, **10b** (101.7 mg) was oxidized to **11b** [yellow crystals, mp 97.5—99.5 °C, 76.7 mg; 76%. Found: M.W., 303.9758 and 305.9729. Calcd for $C_{14}H_9O_3Br$: 303.9735 and 305.9715. ^{1}H NMR δ=3.80 (2H, d, J=1.5 Hz), 6.57 (1H, q, J=1.5 Hz), 6.80 (2H, s), 7.03 (2H, d, J=9 Hz), and 7.42 (2H, d, J=9 Hz). ^{13}C NMR δ=38.3, 121.4, 131.0 (2C), 132.2 (2C), 133.7, 134.7, 137.1, 139.4, 147.0, 187.5, 188.7, and 189.4. IR ν: 1665, 1630, and 1600 cm^{-1}. UV $\lambda_{max}^{CHCl_3}$: 253 nm (ε=19200), 258 (19800), 265 (19200), and 271 (16700)].

3-(4-Hydroxybenzyl)-*p*-tropoquinone (11d). Similarly, **10d** (37.4 mg) was oxidized with DDQ (39.7 mg) to give **11d** [a yellow oil, 35.2 mg; 95%. Found: C, 68.12; H, 4.68%.[9] Calcd for $C_{14}H_{10}O_4 \cdot C_{14}H_{12}O_4 + 1/3H_2O$: C, 68.29; H, 4.61%. m/z, 278 (M^++36), 244 (M^++2), and 242 (M^+). ^{1}H NMR δ=3.78 (2H, d, J=1.5 Hz), 6.57 (1H, q, J=1.5 Hz), 6.74 (2H, d, J=9 Hz), 6.80 (2H, s), and 7.01 (2H, d, J=9 Hz). ^{13}C NMR δ=38.1, 116.0 (2C), 127.5, 130.6 (2C), 133.6, 136.7, 139.7, 148.2, 154.9, 187.9, 189.2, and 190.0. IR ν: 1680, 1640, 1615, and 1515 cm^{-1}].

The authors thank the Ministry of Education, Culture, and Science for a financial support with the Grant-in-Aid for Scientific Research to A. M. (No. 60470025).

References

1) a) H. Takeshita, T. Kusaba, and A. Mori, *Bull. Chem. Soc. Jpn.*, **55**, 1659 (1982); b) A. Mori, Y. Isayama, T. Kusaba, and H. Takeshita, *Kyushu Daigaku Sogo Rikogaku Kenkyuka Hokoku*, **6**, 185 (1985).

2) A. Mori, T. Kusaba, Y. Isayama, and H. Takeshita, *Chem. Lett.*, **1986**, 155.

3) The redox potentials of **12** have been determined by polarographic measurement. Cf., S. Itô, Y. Shoji, H. Takeshita, M. Hirama, and K. Takahashi, *Tetrahedron Lett.*, **1975**, 1075. A related study was also reported. See A. Kawamata, Y. Fukazawa, Y. Fujise, and S. Itô, *ibid.*, **1982**, 1083.

4) H. Takeshita, H. Mametsuka, and N. Matsuo, *Chem. Lett.*, **1981**, 73; H. Takeshita and H. Mametsuka, *Heterocycles*, **22**, 663 (1984).

5) E. Vowinckel, *Chem. Ber.*, **99**, 1479 (1966).

6) A. Mori, Y. Isayama, and H. Takeshita, *Bull. Chem. Soc. Jpn.*, **59**, 511 (1986).

7) According to the CV study, 2,10-dihydroxydicyclohepta[*b*]-furan-3,9-diones were different to the species responsible to the wave around zero V.

8) M. E. Peover, *J. Chem. Soc.*, **1962**, 4540.

9) These figures are reproducible within experimental error after repeated attempts of combustion analysis for this sample. This could be due to an instability of the quinone.

NMR Study on Inclusion Complexes of L-Phenylalanine and Aspartame with Cyclodextrins in Aqueous Solution

Shin-ichiro TAKAHASHI,* Ei-ichiro SUZUKI, and Nobuya NAGASHIMA
Central Research Laboratories, Ajinomoto Co., Inc., Suzuki-cho, Kawasaki-ku, Kawasaki 210
(Received November 22, 1985)

The interactions of Phenylalanine and Aspartame (*N*-L-α-Aspartyl-L-phenylalaninel-methyl ester, APM) with α- and β-cyclodextrins (CD) in aqueous solutions were investigated by ^{1}H and ^{15}N NMR techniques. The changes in chemical shift of CD protons on going from free CD to the mixture with phenylalanine and APM indicate that the phenyl ring is included in the cavity of CD in the complex states. The changes in the chemical shift of the β-protons of phenylalanine and APM following the binding to α- and β-CD indicate that the simple association constants (K_a) are not applicable to these systems except for the case of APM/β-CD (K_a=90), and that the large changes of the rotamer fractional population of APM side-chain occur for APM/β-CD system. The analysis with Asp-Phe(^{15}N)-OMe suggests that the torsional angles of the main chain of APM are unchanged on the formation of the inclusion complex. The low-field shifts of amide proton and its nitrogen resonances of Asp-Phe(^{15}N)-OMe in the complex formation suggest that the amide part of APM is hydrogen-bonded to the C2 or C3 hydroxyl group of β-CD.

APM (*N*-L-α-Aspartyl-L-phenylalaninel-methyl ester) is a well-known dipeptide used as a sweetner. We have obtained a crystal of the equimolar inclusion compound of APM with β-CD, and examined the crystal by Raman and solid-state ^{13}C NMR spectroscopy.[1] In the crystal state the phenyl ring of APM was found to be included in the cavity of β-CD. Also in aqueous solution the relatively hydrophobic environment of CD cavity seems to be favorable for the inclusion of the phenyl ring of phenylalanine and APM. We tried to elucidate the intermolecular interaction in aqueous solution by ^{1}H and ^{15}N NMR. In the past a number of papers investigated about the guest/CD interaction in solution by NMR examination.[2-10] Most of them pay attention to the conformational changes of CD molecule with which guests are included. In the present paper we report mainly on the conformational change of APM molecule which is included with β-CD as studied by the use of NMR techniques.

Experimental

Materials. Phenylalanine and APM were prepared in our laboratories. CD were purchased from Sanraku-Ocean CO., LTD. Asp-Phe(^{15}N)-OMe synthesized in the previous study[1] was used.

Apparatus. ^{1}H and ^{15}N NMR spectra were recorded on a JEOL GX-400 spectrometer operating at 399.55 MHz for ^{1}H and 40.40 MHz for ^{15}N. The proton chemical shifts were referenced to internal sodium 2,2-dimethyl-2-silapentane-5-sulfonate (DSS) and the nitrogen chemical shifts were to external 5 M† ammonium nitrate.

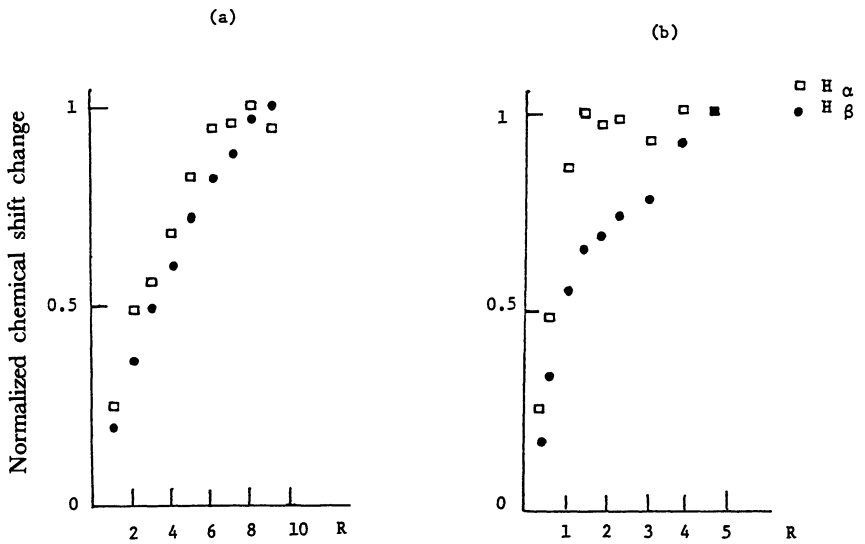

Fig. 1. CD-induced shifts of the chemical shifts of β-protons of Phe (a: α-CD, b: β-CD) in an aqueous solution at pH 6.0. R is [CD]:[Phe] molar ratio. The chemical shift changes are normalized with that at the highest molar ratio [CD]/[Phe].

† 1 M=1 mol dm^{-3}.

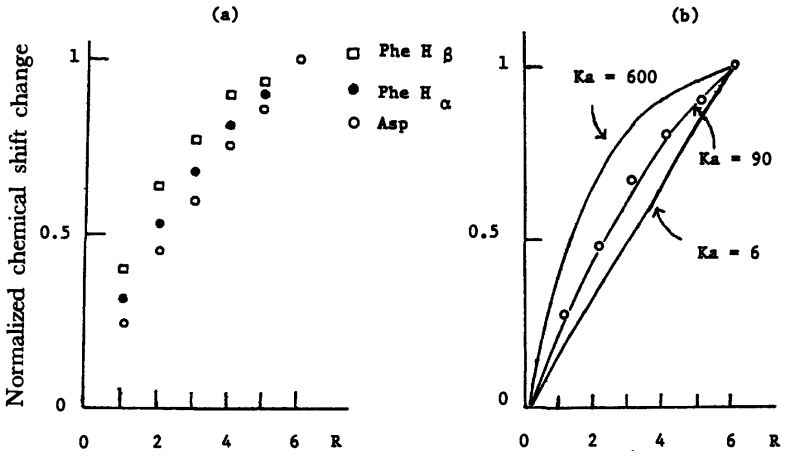

Fig. 2. CD-induced shifts of the chemical shifts of β-protons of Asp and Phe residues of APM (a: α-CD, b: β-CD) pH 6.0 in an aqueous solution. Solid lines in Fig. 2 b show variation of chemical shift changes with R for three association constants, calculated assuming a 1:1 adduct stoichiometry.

Results

(a) Binding of Phenylalanine and APM to CD. Figure 1 shows the chemical shift of β-protons of phenylalanine as a function of [α-CD]/[Phe] (Fig. 1(a)) and [β-CD]/[Phe] (Fig. 1(b)). The changes in the chemical shift are normalized to the values obtained at the highest molar ratio [CD]/[Phe]. The values for the two β-protons do not lie on the same line for α- and β-CD indicating that the simple association constant (K_a) for the complexation with CD is not applicable to these models. Figure 2 shows the chemical shift of methylene protons of Asp and Phe residues of APM as a function of [α-CD]/[APM] (Fig. 2(a)) and [β-CD]/[APM] (b). It is seen from Fig. 2(a) that the curves for four protons in [α-CD]/[APM] system are different and do not give the simple association constant while in Fig. 2(b) it is seen that in [β-CD]/[APM] the data points lie on the same curve so that the description on one association constant applies to [β-CD]/[APM] system. In Fig. 2(b) the curves corresponding to three K_a values (K_a=6, 90, 600 M^{-1}) are also shown. From those the value K_a=90 is obtained as a best fit.

(b) Depth of Inclusion of APM in the Cavity of β-CD. Figure 3 shows the changes of the ^1H NMR spectrum of β-CD on the complexation with APM in D_2O solution at pH 6.0. The upfield shifts of H3 and H5 located in the inner surface of β-CD were observed. We interprete that the shifts are due to the phenyl ring current and that the phenyl ring of APM is included in the cavity of β-CD. Then the most probable position of APM in the β-CD cavity in an aqueous solution can be determined from the Johnson-Bovey equation[11] when the intrinsic chemical shifts (δ_{int}) of H3 and H5 as defined as $\delta_b-\delta_o$ with δ_b and δ_o being the chemical shifts in fully

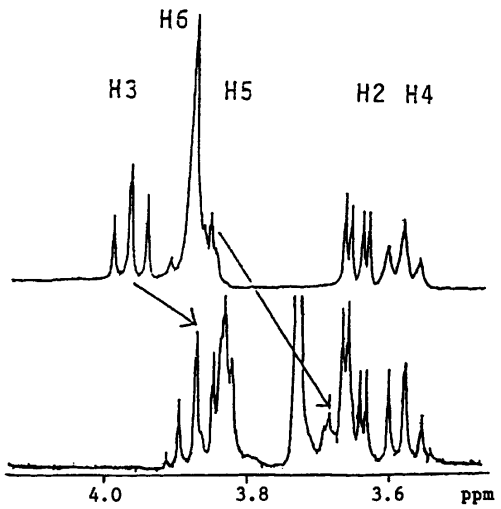

Fig. 3. 400 MHz ^1H NMR spectra of β-CD (top) and β-CD plus APM (bottom:molar ratio 1:20=CD:APM, [β-CD] 1.7 mM) in D_2O.

complexed and free state, respectively, are known. The values of δ_b and thus δ_{int} were estimated from the chemical shifts at known concentration of β-CD and APM with the aid of K_a value determined in section (a). Thus the estimated distance between the center of the phenyl ring and the plane containing seven H3 of β-CD is +1.7 Å. (the positive sign corresponds to the direction H3→H5 plane.) (Fig. 4)

(c) The Change of the Side-Chain and Backbone of APM in Complex Formation with β-CD. Table 1 summarized the vicinal coupling constants of the side-chain and the fractional populations of the rotamer in the free and complexed states in an aqueous solution. The fractional populations of three rotamers, PI, PII, and PIII were calculated using the following equations:

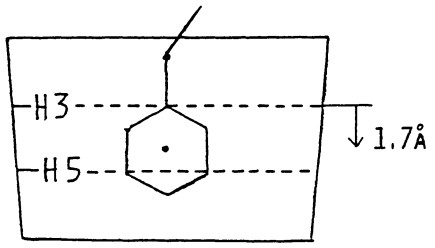

Fig. 4. Time-averaged conformation of the inclusion complex of APM with β-CD in an aqueous solution.

Table 1. Vicinal Coupling Constants (Hz) and Rotamer Fractional Populations for APM at pH 5.2

		Free	Complex
	J_{AX}	4.6	6.6
	J_{BX}	8.7	7.2
Asp	PI	0.56	0.43
	PII	0.19	0.36
	PIII	0.25	0.21
	J_{AX}	5.6	8.0
	J_{BX}	9.0	7.8
Phe	PI	0.59	0.47
	PII	0.27	0.49
	PIII	0.14	0.04

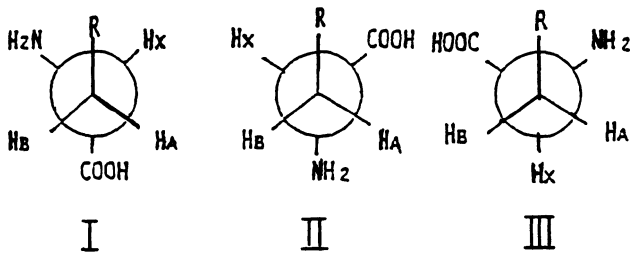

I II III

$$PI = (J_{BX}-J_g)/(J_t-J_g),$$

$$PII = (J_{AX}-J_g)/(J_t-J_g),$$

$$PIII = 1 - PI - PII,$$

where J_t=13.6 Hz, J_g=2.56 Hz.[12] The coupling constants and therefore the fractional population of the rotamer change on forming the inclusion with β-CD. In Table 2 are compared the three coupling constants $^1J15_{NH}$, $^3J15_{NCCH}$, and $^3J_H15_{NCH}$ of Asp-Phe(^{15}N)-OMe in the free and complexed state to indicate the effect of the backbone dihedral angles. The three coupling constants do not change on the complex formation. It suggests that the backbone dihedral angles of APM do not vary in the complex. Table 2 also shows the chemical shifts of amide proton and amide nitrogen of Asp-Phe(^{15}N)-OMe in the free and complexed states in H_2O. The low-field shifts in the complex formation were observed suggesting that the amide part of APM is hydrogen-bonded to the C2 or C3 hydroxyl group of β-CD in the complex.

Table 2. ^{1}H Coupling Constants (Hz) and Amide Proton and Nitrogen Chemical Shifts (ppm) for Asp-Phe(^{15}N)-OMe at pH 4.3

	Free	Complex with β-CD
$J15_{NH}$	93.1	93.1
J_H15_{NCH}	7.6	7.6
$J15_{NCCH}$	<0.2	<0.2
δ_{NH}	8.76	9.12
$\delta15_N$	119.6	120.0

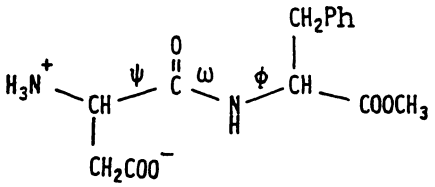

Fig. 5. The torsion angles of APM molucule.

Discussion

A number of papers on the investigation of the host/CD interaction by NMR examination have been published.[2-10] Komiyama and Hirai estimated time-averaged position of phenol derivatives in the cavity of β-CD in aqueous solution with the Johnson-Bovey equation.[8] The estimated distance between the center of the aromatic ring of phenol and the plane containing the seven H-3 atoms of β-CD is 1.8 Å. The value is very close to the present result of 1.7 Å. A number of papers about the association constants of guest molecules with β-CD with ^{1}H and ^{13}C NMR[2-7] are published. The reported values range between 100 and 1000 and our result is within this range. The molecular size of the guest molecules examined in the past on complexation with β-CD is comparatively small. On the other hand the guest molecule now in question is a large-sized dipeptide and so we have the problem of the conformational change of the guest molecule on complexation with β-CD. ^{15}N labeling of the amide nitrogen is useful technique for the examination of the conformation of dipeptides. The study of the preferred conformation of APM in an aqueous solution by using the same method as that described in this paper was reported.[13] The torsional angles of ψ and ϕ, (Fig. 5) in the free state are −150° and −90°, respectively. The results differed from those by F. Lelj et al, which were derived from the potential energy calculations.[14] The present results (section c) suggest that the torsional angles ϕ, ψ, and ω of APM do not change on the complexation with β-CD. On the other hand the rotamer fractional populations of both Phe and Asp residues do change in the complex formation. Figure 6 shows the conformation of APM in the various states. The upper figure shows the preferred conformation in the free state and the middle one is the preferred conformation in the complex and the lower one is the least preferred conformation in the complex. The

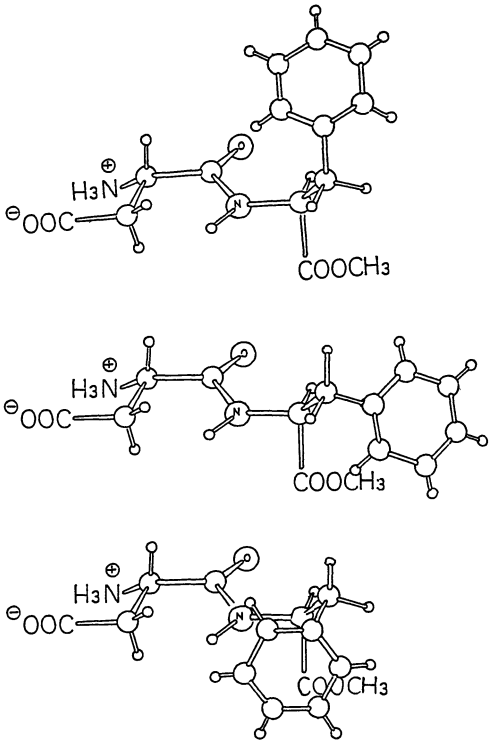

Fig. 6. The conformations of APM molucule in an aqueous solution, (upper) the preferred one in the free state (middle) the preferred one in the complexed state with β-CD (bottom) the least preferred one in the complexed state with β-CD.

preferred conformation in the complex is seen to be rod like and is suitable for the inclusion in the cavity of β-CD. The stereo model of this conformer based on Fig. 6 shows that the amide part of APM is so close to the C2 or C3 hydroxyl group that the hydrogen bonding is possible between them. The least preferred conformer in the complex formation is also reasonable because the phenyl ring is so close to the backbone of APM in this conformer that APM can not be included within β-CD.

In conclusion

(1) The phenyl ring of APM is included with β-CD with the association constant K_a=90 in an aqueous solution.

(2) The estimated distance between the center of the phenyl ring of APM and the plane containing seven H-3 of β-CD is 1.7 Å.

(3) The backbone conformation of APM is not varied in the complexed formation with β-CD.

(4) The side chain of APM is changed to the extented conformation in the complexed formation with β-CD.

References

1) S. Takahashi, E. Suzuki, N. Nagashima, Y. Nishimura, and M. Tsuboi, *Bull. Chem. Soc. Jpn.*, **59**, 93 (1986).

2) D. J. Wood, F. E. Hruska, and W. Saenger, *J. Am. Chem. Soc.*, **99**, 1735 (1977).

3) J. P. Behr and J. M. Lehn, *J. Am. Chem. Soc.*, **98**, 1743 (1976).

4) R. I. Gelb, L. M. Schwartz, B. Cardelino, H. S. Fuhrman, R. F. Johnson, and D. A. Laufer, *J. Am. Chem. Soc.*, **103**, 1750 (1981).

5) K. Uekama and F. Hirayama, *Chem. Pharm. Bull.*, **26**, 1195 (1978).

6) H. Ueda and T. Nagai, *Chem. Pharm. Bull.*, **28**, 1415 (1980).

7) M. Suzuki and Y. Sasaki, *Chem. Pham. Bull.*, **32**, 832 (1984).

8) M. Komiyama and H. Hirai, *Chem. Lett.*, **1980**, 32.

9) Y. Inoue, T. Okuda, Y. Miyata, and R. Chujo, *Carbohydr. Res.*, **125**, 65 (1984).

10) S. G. Frank and D.R. Kavaliunas, *J. Phar. Sci.*, **72**, 1215 (1983).

11) C. E. Johnson and F. A. Bovey, *J. Chem. Phys.*, **29**, 1012 (1958).

12) K. G. R. Pachler, *Spectrochim. Acta.*, **20**, 581 (1964).

13) A. Murai, K. Ajisaka, N. Nagashima, Y. Takeuchi, M. Kamisaku, and M. Kainosho, "The 13th Symposium on Peptide Chemistry" 1975, p. 52.

14) F. Lelj, T. Tancredi, P. A. Temussi, and C. Toniolo, *J. Am. Chem. Soc.*, **98**, 6669 (1976).

Photochemical Reactions of Aromatic Compounds. XLII.[1] Photosensitized Reactions of Some Selected Diarylcyclobutanes by Aromatic Nitriles and Chloranil. Implications of Charge-Transfer Contributions on Exciplex Reactivities

Chyongjin PAC,* Tomohito OHTSUKI, Yozo SHIOTA, Shozo YANAGIDA, and Hiroshi SAKURAI
Department of Chemical Process Engineering, Faculty of Engineering, Osaka University, Suita, Osaka 565
(Received December 9, 1985)

Photosensitized reactions of *cis*- and *trans*-1,2-diphenylcyclobutane and *cis-transoid-cis*-cyclobuta[1,2-*a*:4,3-*a'*]diindene by 1-cyanonaphthalene, 9,10-dicyanoanthrancene, 1,4-dicyanonaphthalene, and chloranil, which mainly give the ring-splitting product (styrene or indene), have been investigated to explore steric and electronic requirements of the reactions associated with charge-transfer and excitation-resonance contributions of exciplex intermediates. The reaction efficiencies increase with an increase in the electron-accepting power of the sensitizers irrespective of the spin states. The formation of 1-phenyltetralin in the photosensitized reactions of the diphenylcyclobutanes occurs from the polar singlet exciplex with the dicyanoarenes but not at all from the less polar exciplex with 1-cyanonaphthalene nor from the triplet chloranil exciplex of high charge-transfer nature. Exciplex reactivities are discussed in terms of roles of charge-transfer contributions in exciplex decay channels as well as in terms of configurational and conformational effects on orbital interactions in the cyclobutanes.

Splitting of the cyclobutane ring is a typical prototype for theoretical predictions of chemical reaction courses.[2] More importantly this reaction can provide an excellent probe to explore chemical and dynamic behaviors of reactive states and/or intermediates as well as to manifest steric and electronic factors operating reaction courses.[1,3-12] Recently we reported the redox-photosensitized ring-splitting reactions of some diarylcyclobutanes,[7a-c] a novel type of photosensitization that is initiated by photochemical electron transfer from an aromatic hydrocarbon (ArH) to an electron acceptor, typically *p*-dicyanobenzene (DCNB).[7a-c,13] A key mechanistic pathway is the formation of a π complex between a cyclobutane (CB) and the cation radical of ArH, by which a positive charge is populated on CB to effect the cleavage of the cyclobutane ring in cases where the both ends of a ring sigma bond bear π or *n*-electron systems as substituents.

$$\mathrm{ArH + DCNB} \xrightarrow{h\nu} {}^1\mathrm{ArH^*ArH^* + DCNB} \longrightarrow \mathrm{ArH^{+\cdot} + DCNB^{-\cdot}}$$

$$\mathrm{ArH^{+\cdot} + CB} \longrightarrow \mathrm{[ArH \cdot CB]^{+\cdot}} \longrightarrow \mathrm{ArH^{+\cdot} + Products}$$

Likewise the population of a positive charge on CB can be achieved by the exciplex formation with an electron-accepting molecule, thus resulting in a ring-splitting reaction of CB depending on charge-transfer (CT) contributions.[7d,8c] Since exciplexes are electronically excited species unlike the π complexes, however, chemical behaviors should be different between them. In other words exciplex decays are associated with exciplex reactivities that may be controlled by electronic properties of exciplexes, i.e., CT and excitation-resonance (ER) contributions, as has been discussed for the exciplex isomerization of quadricyclane to norbornadiene.[11-12a]

$$\mathrm{S + CB} \xrightarrow{h\nu} \mathrm{S^* + CB} \longrightarrow \mathrm{[S \cdot CB]^*} \longrightarrow \mathrm{S + Products}$$

(S=electron acceptors and CB=cyclobutanes.)

$$\mathrm{[S \cdot CB]^* \equiv S^*CB \longleftrightarrow S \cdot CB^* \longleftrightarrow S^-CB^+} \quad (1)$$

Table 1. Excitation Energies and Reduction Potentials of the Sensitizers

S[a]	τ[b]/ns	E^*[c]/eV	$-E_{1/2}^{red}$[d]/V	E_{red}^*[e]/V
CNN	12.3	3.75[f]	2.33	1.42
DCN	10.5	3.45[f]	1.05	2.40
DCA	12.4	2.88[f]	1.12	1.76
CHL		2.83[g]	0.28	2.55

a) CNN=1-cyanonaphthalene, DCN=1,4-dicyanonaphthalene, DCA=9,10-dicyanoanthracene, and CHL=chloranil. b) Fluorescence lifetimes. c) Excitation energies of the excited-singlet aromatic nitriles and triplet chloranil. d) Half-wave reduction potentials vs. $Ag/AgNO_3$ in acetonitrile. e) Reduction potentials of the excited states calculated from E^* plus $E_{1/2}^{red}$. f) S. L. Mattes and S. Farid, *Org. Photochem.*, **6**, 233 (1983). g) M. Kasha, *Chem. Rev.*, **47**, 401 (1947).

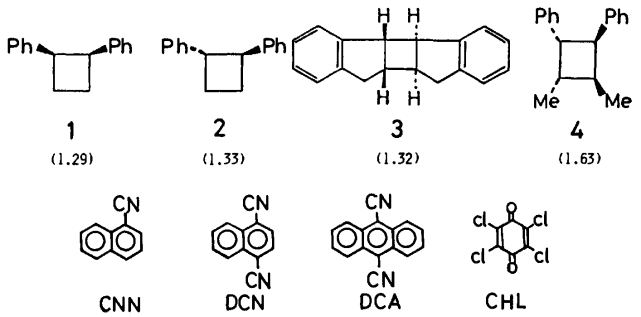

Fig. 1. Structures of the diarylcyclobutanes and the sensitizers. In parentheses are oxidation potentials of the cyclobutanes vs. Ag/Ag^+ in acetonitrile.

From this point of view, we attempted photosensitized reactions of some diarylcyclobutanes (CB; **1**—**4**) by 1-cyanonaphthalene (CNN), 1,4-dicyanonaphthalene (DCN), 9,10-dicyanoanthracene (DCA), and chloranil (CHL); these sensitizers (S) are typical electron acceptors which have different excitation energies (E^*) and reduction potentials in the ground and excited states ($E_{1/2}^{red}$ and E_{red}^*) (Table 1). Figure 1 shows the structures of S and CB together with the observed

oxidation potentials of CB. Major aims of the present investigation are focussed on (1) relative importance of CT and ER contributions of putative exciplex intermediates in bond-cleavage reactions of CB, (2) spin effects on the photoreactions, and (3) relationships of reactivities with structures of CB in the exciplex chemistry.

Results

Photoproducts. Photoreactions were carried out by irradiation of benzene solution at 313 nm for the CNN and DCN runs or at 366 nm for the DCA and CHL runs, and the progress of the photoreactions was followed by gas chromatography. The photoproducts are shown in Scheme 1.

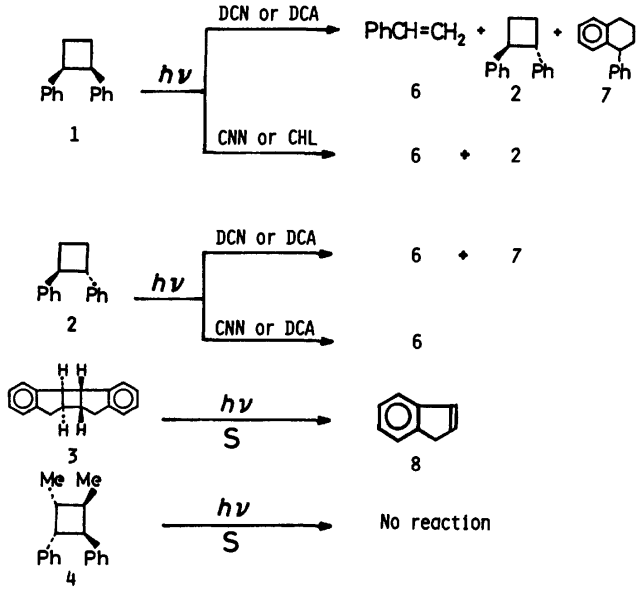

Scheme 1.

Styrene (**6**) was mainly formed by the photosensitized reactions of either **1** or **2**. All the photosensitizers (S) commonly effected the photoisomerization of **1** to **2** but not at all the reverse isomerization, whereas the rearrangement of either **1** or **2** to 1-phenyltetralin (**7**) occurred with DCN or DCA but not at all with CNN or CHL. In the case of **3**, all the sensitizers effected the ring-splitting reaction to give indene (**8**) as the sole product. At low conversions (<10%), material balances were better than 90% without any consumption of the sensitizers, though other unreclaimed reactions increasingly occurred at higher conversions. Interestingly, **4** remained virtually unchanged even upon extensive irradiation in the presence of any of the sensitizers, a puzzling observation that is hardly expected from the configurational similarity to **2** and **3**.

Quantum Yields. Limiting quantum yields that are significant for discussions of exciplex reactivities were determined for the olefin formation from **1** or **3** by usual double-reciprocal plots of quantum yield vs. concentration of CB (Fig. 2) in the case of CHL and in cases where fluorescence quenching is inefficient (vide infra). Such plots were not taken for the formation of **2** and **7** from **1** as well as for the photosensitized reactions of **2** because of poor reproducibilities of data, particularly at low concentrations of CB due to low quantum efficiencies. In the case of the DCN-**1** or **3** pair, the observed quantum yield at [**1**] or [**3**]= 0.3 M† was used in place of the limiting quantum yield, since the fluorescence quenching was complete at [CB]≥0.2 M. Table 2 lists the intercepts (I) and the intercept-to-slope ratios (I/S) of the plots in Fig. 2 together with the limiting quantum yields for the olefin formation (ϕ_{ol}^{∞}). In Table 3 are shown the observed quantum yields of the products in the photosensitized reactions of **1** at [**1**]=0.3 M.

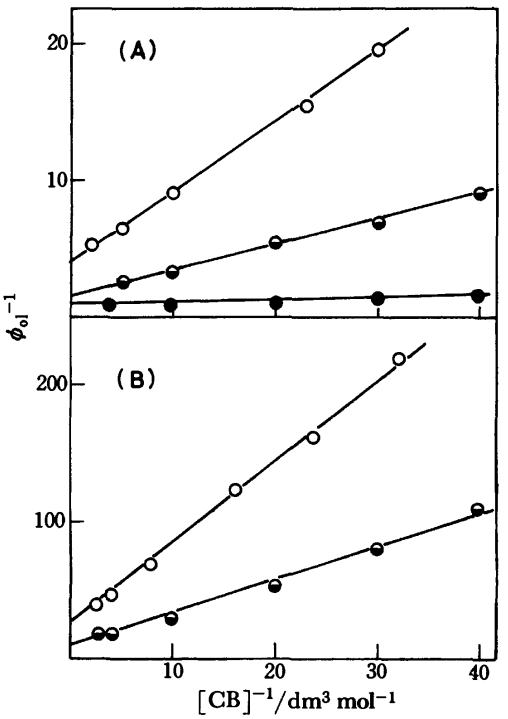

Fig. 2. Double-reciprocal plots of quantum yield for the olefin formation vs. concentration of CB: (A) CNN-**3** (—○—), DCA-**3** (—◒—), and CHL-**1** (—●—) pairs; (B) CNN-**1** (—○—) and DCA-**1** (—◒—) pairs.

Fluorescence Quenching. The fluorescence of the aromatic nitriles was quenched by CB following linear Stern-Volmer relationships. Table 2 includes the Stern-Volmer constants (K_{SV}) and the fluorescence-quenching rate constants (k_e) calculated from K_{SV} and the fluorescence lifetimes (τ). It is of mechanistic significance to note that the quenching of the CNN fluorescence by either **1** or **2** is accompanied by the appearance of weak exciplex emission at longer wavelength as is shown in Fig. 3A. A very weak exciplex

† 1 M = 1 mol dm^{-3}.

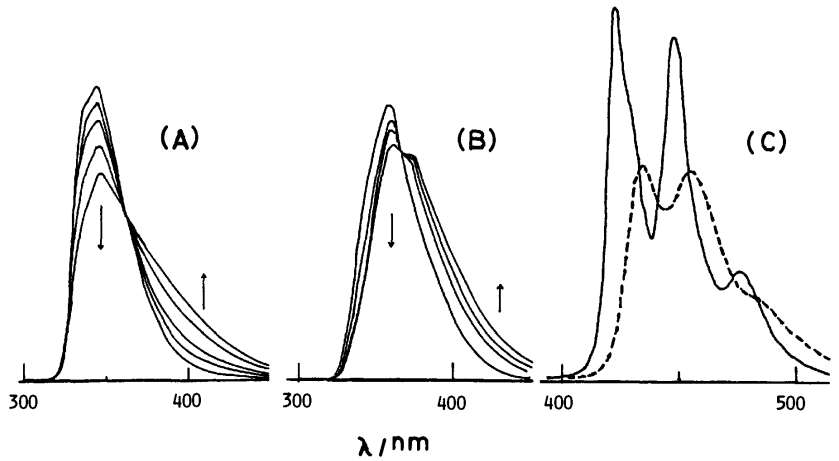

Fig. 3. Fluorescence spectra of the aromatic nitriles. (A) The CNN fluorescence in benzene at [1]=0.0, 1×10^{-2}, 4×10^{-2}, 9×10^{-2}, and 1.2×10^{-1} M. (B) The DCN fluorescence in cyclohexane at [4]=0.0, 5×10^{-3}, 1×10^{-2}, 1.5×10^{-2}, and 2×10^{-2} M. (C) The DCA fluorescence in cyclohexane in the presence of 1 (0.2 M) (dashed line) and in its absence (solid line).

Table 2. Limiting Quantum Yields for the Olefin Formation (ϕ_{ol}^{∞}) and Fluorescence-Quenching Rate Constants (k_e)

CB[a]	S[a]	I[b]	I/S[c]/dm^3 mol^{-1}	ϕ_{ol}^{∞}	K_{SV}/dm^3 mol^{-1}	k_e/dm^3 mol^{-1} s^{-1}
1	CNN	12	4.0	0.083	3	2.4×10^8
	DCA	4.0	3.3	0.25	5	4.0×10^8
	DCN			0.90	46	4.4×10^9
	CHL	1.0	≳100	1.0		
3	CNN	4.0	7.0	0.25	5	4.0×10^8
	DCA	1.3	7.0	0.77	9	7.3×10^8
	DCN			1.3	42	4.0×10^9

a) For abbreviations see Table 1 and Fig. 1. b) The intercepts of the plots in Fig. 2. c) The intercept-to-slope ratios of the plots in Fig. 2.

Table 3. Quantum Yields of the Photosensitized Reactions of 1[a]

S[b]	ϕ_6[c]	ϕ_2	ϕ_7	ϕ_6/ϕ_2
CNN	0.05	0.007[d]	$<10^{-4}$	7.0
DCA	0.11	0.01[d]	0.007[d]	10
DCN	0.90	0.10[c]	0.025[d]	9.0
CHL	1.0	0.18[c]	$<10^{-4}$	5.6

a) Mean values for 3—5 runs at [1]=0.3 mol dm^{-3}. b) For abbreviations see Table 1 and Fig. 1. c) ≤±10%. d) ≤±30%.

emission was also detected in the case of the DCA-1 pair. Interestingly, the quenching of the DCN fluorescence by the unreactive cyclobutane, 4, was accompanied by a relatively strong exciplex emission (Fig. 3B), though no exciplex emission was detected in the quenching of the DCN fluorescence by the reactive cyclobutanes. Moreover, it should be noted that the fluorescence quenching by 3 revealed no exciplex emission at all in any case.

Discussion

Mechanism. It is no doubt that the photosensitization by the aromatic nitriles proceeds via the excited-singlet state, since the fluorescence of DCN is quenched by either 1 or 3 near a diffusion-controlled limit and since the intercept-to-slope ratios obtained from quantum-yield measurements for the CNN and DCA-1 or 3 pairs show reasonable agreements with the K_{SV} values for the fluorescence quenching. Moreover, the appearance of exciplex emissions strongly suggests that singlet exciplexes are involved as the intermediates of the photoreactions. In this regard, it should be noted that relatively strong exciplex emissions were detected with the unreactive DCN-4 pair and also with the least reactive CNN-1 pair, whereas the more reactive DCA-1 pair shows a much weaker exciplex emission. In contrast, no exciplex emission was detected at all with the very reactive DCN-1 pair as well as in the fluorescence quenching by 3 which is more reactive than 1. These opposite behaviors be-

tween exciplex-emission efficiencies and reactivities suggest that the chemical reaction of CB occurs as a nonradiative decay of the sensitizer-CB exciplexes in competition with the emission pathway.

On the basis of these arguments, essential mechanistic pathways for the photosensitized reactions of CB by the aromatic nitriles are shown in Scheme 2. A usual kinetic treatment gives Eqs. 2—4.

$$S \xrightarrow{h\nu} {}^1S^*$$

$${}^1S^* \xrightarrow{\tau^{-1}} S$$

$${}^1S^* + CB \xrightarrow{k_e} {}^1[S\cdot CB]^*$$

$${}^1[S\cdot CB]^* \xrightarrow{k_{o1}} S + 2\ \text{Olefin}\ (\mathbf{6}\ \text{or}\ \mathbf{8})$$

$${}^1[S\cdot CB]^* \xrightarrow[(CB=1)]{k_1} S + \mathbf{2} + \mathbf{7}$$

$${}^1[S\cdot CB]^* \xrightarrow{k_f} S + CB + h\nu'$$

$${}^1[S\cdot CB]^* \xrightarrow{k_d} S + CB$$

(S = CNN, DCA, and DCN.)

Scheme 2.

$$\frac{1}{\phi_{o1}} = \frac{1}{\phi_{o1}^{\infty}}\left(1+\frac{1}{k_e\tau[CB]}\right) \tag{2}$$

$$\phi_{o1}^{\infty} = \frac{2k_{o1}}{k_{o1}+k_1+k_d+k_f} \tag{3}$$

$$I_F^0/I_F = 1 + K_{SV}[CB] = 1 + k_e\tau[CB] \tag{4}$$

On the other hand, a triplet mechanism should operate in the CHL-photosensitized reaction of **1**, since the intersystem crossing of excited-singlet CHL to the triplet is extremely fast ($>10^{10}\,s^{-1}$).[14] However, classical excitation transfer from triplet CHL to **1** is unlikely to occur, since no photoreaction of **1** was effected at all by the photosensitization using acetophenone which has a much higher triplet energy (309 kJ mol^{-1})[15] than CHL (261 kJ mol^{-1}).[16] Consequently, a triplet exciplex mechanism seems to be a reasonable choice. The high reduction potential of triplet CHL may give a benefit to the formation of an exciplex. Scheme 3 shows a possible mechanism for the CHL-photosensitized reaction of **1**, which is very similar to Scheme 2 except for the spin state.

$$CHL \xrightarrow{h\nu} {}^1CHL^* \xrightarrow{>10^{10}\,s^{-1}} {}^3CHL^*$$

$${}^3CHL^* \xrightarrow{\tau_T^{-1}} CHL$$

$${}^3CHL^* + \mathbf{1} \xrightarrow{k_e} {}^3[CHL\cdot\mathbf{1}]^*$$

$${}^3[CHL\cdot\mathbf{1}]^* \xrightarrow{k_{o1}} CHL + 2\ \mathbf{6}$$

$${}^3[CHL\cdot\mathbf{1}]^* \xrightarrow{k_1} CHL + \mathbf{2}$$

$${}^3[CHL\cdot\mathbf{1}]^* \xrightarrow{k_d} CHL + \mathbf{1}$$

Scheme 3.

$$\frac{1}{\phi_{o1}} = \frac{1}{\phi_{o1}^{\infty}}\left(1+\frac{1}{k_e\tau_T[CB]}\right) \tag{5}$$

$$\phi_{o1}^{\infty} = \frac{2k_{o1}}{k_{o1}+k_1+k_d} \tag{6}$$

Electronic Properties and Reactivities of Exciplexes. Electronic properties of exciplexes are approximately described by Eq. 1, in which CT and ER contributions can be qualitatively estimated by E_{red}^* and E^* respectively. Since the excitation energies of excited-singlet CB are commonly ≈440 kJ mol^{-1} (105 kcal mol^{-1} (1 cal=4.184 J)) as determined by the fluorescence spectra,[17] differences of excited-singlet excitation energy between CB and S are ≈66 kJ mol^{-1} for the CNN–CB pairs, ≈100 kJ mol^{-1} for the DCN–CB pairs, and ≈160 kJ mol^{-1} for the DCA–CB pairs. Since the energy differences for the DCA–CB pairs are too large to allow significant ER, the binding origin of the DCA exciplexes should exclusively come from CT contributions. For the DCN exciplexes, CT contributions are certainly dominant because of the high E_{red}^* value of DCN, whereas the CNN exciplexes have higher ER contributions but less CT contributions compared with the other exciplexes. Although the CHL-**1** exciplex appears to be of dominant CT nature, a significant ER contribution might be indicated by a relatively small energy difference between the triplets of CHL and **1** (37—62 kJ mol^{-1}).[18]

As shown in Tables 2 and 3, the quantum yields strongly depend on E_{red}^* but not significantly on E^*, thus demonstrating that reactivities of the exciplexes are mainly controlled by CT contributions irrespective of the spin states. Moreover, the formation of **7** occurs from the more polar exciplexes of DCN and DCA but not at all from the CNN exciplex of a less CT contribution. Interestingly, **7** is not formed again from the triplet CHL-**1** exciplex of polar nature. Presumably, the rearrangement to **7** would proceed via a very polar state on singlet hypersurface in a way different from the decay pathways for the formation of **6** and **2**, while no decay channel for the formation of **7** is available in the triplet state.

Comparisons of the exciplex chemistry with other types of photoreactions of CB may be diagnostic for discussing decay channels of the exciplexes which should depend on CT contributions. The redox-photosensitized reaction of **1** gives only **7** without any formation of **6** and **2**,[19] revealing behaviors different from the exciplex chemistry. This difference appears to reflect different reaction surfaces since key chemical events in the former reaction occur in the ground state. On the other hand, the ratios of ϕ_6 to ϕ_2 in the photosensitized reactions of **1** by the aromatic nitriles are similar to that of the direct photolysis (7.2)[18b] but still higher than those of the acetone-photosensitized reaction (2.6) and the thermal reaction (2.0).[18b] It is

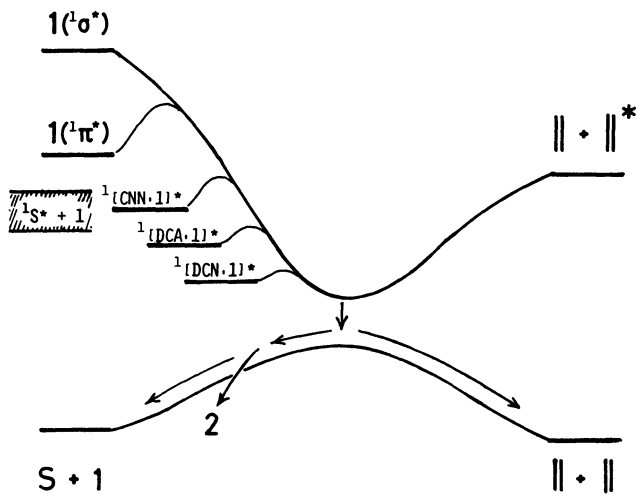

Fig. 4. A schematic potential hypersurface diagram for singlet photochemistry of **1**.

therefore suggested that the singlet exciplexes cross to the reaction surface involved in the direct photolysis to reach a common pericyclic minimum.

Figure 4 shows hypothetical reaction hypersurfaces for the singlet photochemistry of **1**, which are qualitatively illustrated on the basis of the Michl's prediction concerning [2+2] cycloaddition and cycloreversion.[20] The exciplex formation should lead to the population of a positive charge on **1** by CT contributions. As is shown in Scheme 4, this positive

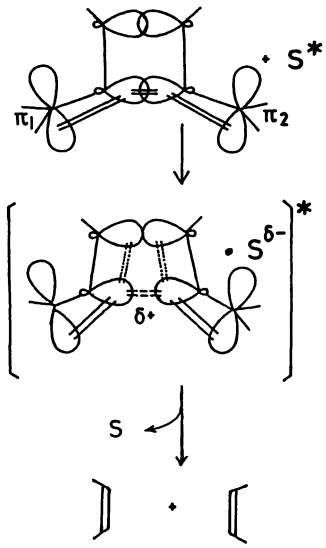

Scheme 4.

charge on CB is delocalized mostly on the π_1–C–C–π_2 orbital array since the π_1 and π_2-electron systems interact with each other through the ring C–C sigma orbitals.[7,21] This means that the ring sigma bond should be weakened by a decrease of electron density depending on CT contributions. As a result, an exciplex state of higher CT nature might be located closer to the reaction surface, and activation barriers for the crossing to the reaction surface would be decreased with an increase of CT contributions.

On the other hand, it is of interest to note that the direct photoexcitation of **1** is much less effective to cause the reaction than the exciplex formation; $\phi_6+\phi_2\cong0.02$ in the direct photolysis.[18b] Since the UV-absorption and fluorescence spectra of **1** and the other cyclobutanes are essentially identical with those of simple alkylbenzenes,[17] the electronic excitation of **1** in the spectroscopic state is almost localized on the isolated π-electron chromophore. In other words, little perturbation of the ring C–C bond might occur in the spectroscopic state, thus implying that crossing to the reaction surface perhaps requires a high activation barrier because of the extremely high σ^* level compared with the π^* level. This may also give a rationale to interpret minor roles of ER contributions in the exciplex chemistry.

On the other hand, the decay channels of the triplet CHL-**1** exciplex can not be straightforwardly interpreted, since the ϕ_6/ϕ_2 value is substantially greater than that of the acetone-photosensitized reaction and since **7** is not formed regardless of the polar nature of the exciplex. Although the triplet exciplex can efficiently go into reactive states, the decay pathways are not the same as those of the triplet state of **1**. A plausible interpretation is that the triplet exciplex would competitively cross to both singlet and triplet reaction surfaces. The former crossing requires a prior spin flip, which may be facilitated by high CT interactions[22] and/or by a considerable distortion of the cyclobutane ring in the exciplex state.[23]

Relationships of Exciplex Reactivities with Structures of CB. In previous papers,[7a–c] we demonstrated that through-bond interactions between vicinally substituted π or n-electron systems are essential to determine reactivities of cyclobutanes in the redox-photosensitized ring-splitting reactions. For example, **3** is very reactive because of the head-to-head structure favorable for efficient through-bond interactions, while no photosensitized reaction occurs at all with the head-to-tail isomer of **3** for which such interactions are configurationally forbidden. Interestingly, however, the complete lack of any reaction of **4** in the exciplex chemistry would apparently disagree with this concept, since this cyclobutane has a head-to-head structure. Actually, the methyl substituents sterically inhibit the phenyl groups from taking conformations favorable for through-bond interactions.[21] In other words, through-bond interactions are conformationally disallowed, a conclusion supported by the oxidation potential of **4** (1.63 V) which is considerably higher than those of the reactive cyclobutanes. Therefore, the through-bond-interaction concept is valid to interpret reactivities of CB in the exciplex chemistry as well.

Another significant feature in structure-reactivity relationships is that **3** is much more reactive than **1** and **2**, though they have similar oxidation potentials and fluorescence-quenching capabilities. Apparently,

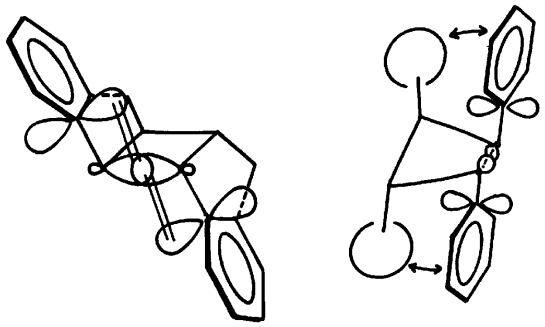

this difference arises from the rigid tricyclic structure of **3** compared with the more flexible monocyclic structure of **1** and **2**, since free rotation around the C–Ph bond is certainly unfavorable for through-bond interactions. Moreover, conformational rigidity of **3** is again favorable for orbital interactions between the Cl(C2) and C4(C3) sigma orbitals which are required for splitting of the cyclobutane ring to occur. In cases of **1** and **2**, on the other hand, the cyclobutane ring may be distorted unfavorably for such orbital interactions as the C1–C2 bond is elongated by the exciplex formation; the isomerization reactions of **1** and **2** perhaps occur as the consequences of ring distortion. As a result, the exciplexes of **3** can cross to the reaction surface with lower activation barriers than the exciplexes of **1** or **2** can do. This would also interpret why the CNN and DCA-**1** exciplexes can emit even in low efficiencies and why the exciplexes of **3** can not at all.

Conclusions

It is suggested that the photosensitized reactions of **1**—**3** proceed via the singlet exciplexes of the aromatic nitriles or the triplet CHL exciplex. CT contributions are essential to control the exciplex chemistry as the consequences of the population of a positive charge on the π_1–Clσ–C2σ–π_2 orbital array which weakens the ring C–C bond. It is speculated that such bond-weakening effects lower activation barriers for the crossing from the singlet-exciplex state to a reaction hypersurface involved in the direct photolysis, whereas the decay channels of the triplet chloranil exciplex are not the same as those of the triplet state of CB. On the other hand, a different pathway is indicated for the formation of **7** from the singlet exciplexes of **1** or **2**, involving a very polar state which is not realized from the triplet CHL exciplex.

The lack of any reaction of **4** by the exciplex formation is attributed to conformations unfavorable for through-bond interactions between the two π-electron systems. Higher reactivities of **3** compared with **1** and **2** are associated with the rigid tricyclic structure that facilitates orbital overlaps between the Cl(C2)–C4(C3) sigma orbitals in the progress of the reaction.

Experimental

Instruments. Gas chromatography was performed on a Shimadzu GC-7A gas chromatograph using a 2-m column of 25% PEG 20M on Shimalite NAW for analyses of **6** and **8** and a 2-m column of 2% OV-17 on Chromosorb W for analyses of **7** and the cyclobutanes. Oxidation and reduction potentials were determined by cyclic voltammetry vs. $Ag/AgNO_3$ in acetonitrile using tetraethylammonium tetrafluoroborate as the supporting electrolyte; the instrument and methods are the same as those reported previously.[7a] IR, UV, and ^1H NMR spectra were obtained on Hitachi 260-10, Hitachi 220-A, and JEOL JNM-PMX60 spectrometers, respectively. A Hitachi MPF-4 spectrofluorometer equipped with a data processor (612-0085) was used for fluorescence measurements; all the fluorescence spectra were recorded after the correction of spectral responses of the instrument.

Materials. Commercial 1-cyanonaphthalene (Tokyo Kasei) was thoroughly purified by the method described in a previous paper.[24] Both chloranil and 9,10-dicyanoanthracene (Tokyo Kasei) were purified by repeated recrystallization from benzene followed by vacuum sublimation. 1,4-Dicyanonaphthalene was prepared according to the literature method[25] and was purified by repeated recrystallization from benzene followed by vacuum sublimation. The indene dimer (**3**)[26] and the diphenylcyclobutanes (**1** and **2**)[27] were prepared according to the literature methods. The purification of **1** and **3** was performed by repeated recrystallization from methanol.

***r*-1,*t*-2-Dimethyl-*t*-3,*c*-4-diphenylcyclobutane (4).** Dimethyl *t*-3,*c*-4-diphenyl-*r*-1,*t*-2-cyclobutanedicarboxylate (dimethyl μ-truxinate), which had been prepared by the photoaddition of dimethyl fumarate to *trans*-stilbene,[28] was reduced by an excess of $LiAlH_4$ in tetrahydrofuran to give *r*-1,*t*-2-bis(hydroxymethyl)-*t*-3,*c*-4-diphenylcyclobutane (mp 130—132 °C from a benzene–hexane mixture); ^1H NMR δ=1.6 (t, 2H, OH×2), 2.6 (m, 2H, H-1 and H-2), 3.5 (d-d, 4H, CH_2×2), 4.2 (m, 2H, H-3 and H-4), 8.2 (m, 10H, C_6H_5×2). This dialcohol was converted to the ditosylate, which was then reduced by an excess of $LiAlH_4$ in tetrahydrofuran to give the dimethyldiphenylcyclobutane in a 60% yield based on the truxinate (bp 108—110°C/0.15 Torr†); ^1H NMR δ=0.9 (d, 6H, CH_3×2), 2.3 (m, 2H, H-1 and H-2), 4.1 (m, 2H, H-3 and H-4), 7.2 (m, 10H, C_6H_5×2).

Found: C, 91.14; H, 8.63%. Calcd for $C_{18}H_{20}$: C, 91.47; H, 8.53%.

Photoreactions and Determination of Quantum Yields. Photoirradiation was carried out with an Eikosha PIH-300 high-pressure Hg lamp under cooling with water using appropriate light filters and a "merry-go-round" turntable. A pottassium chromate solution (0.2 g dm^{-3}, 10-mm path length) was used to isolate the 313-nm light, whereas the 366-nm light was obtained by the passage through an uranyl glass and a solution (10-mm path length) obtained by the dissolution of $CoCl_2 \cdot 6H_2O$ (45.2 g), $NiCl_2 \cdot 6H_2O$ (22.7 g), and a concentrated hydrochloric acid (15 cm^3) in a mixture of ethanol (52.5 cm^3), acetone (37.5 cm^3), and water (60 cm^3).[29] A 2-hexanone actinometer[30] and a benzophenone–benzhydrol actinometer[31] were used for the determination of quan-

† 1 Torr≈133.322 Pa.

tum yields at 313 nm for the CNN and DCN-photosensitized reactions and at 366 nm for the DCA and CHL runs respectively. Concentrations of the aromatic nitriles and CHL were set in 5×10^{-4}—10^{-3} M and $\approx10^{-2}$ M, respectively, which were confirmed to be high enough for the complete absorption of the incident light under photoreaction conditions. Pyrex tubes (8 mm i.d.) were used as the common vessels for the photoreactions and for the actinometry. Benzene solutions of the reactants (3 cm^3) and actinometer solutions (3 cm^3) were irradiated, and the progress of the photoreactions was followed by gas chromatography.

This work was partially supported by Grant-in-Aid for Scientific Research (No. 60045071) from the Ministry of Education, Science and Culture.

References

1) Part XLI: C. Pac, T. Ohtsuki, T. Fukunaga, S. Yanagida, and H. Sakurai, *Chem. Lett.*, **1985**, 1855. Part XL: M. Yasuda, T. Matsumoto, K. Shima, and C. Pac, *J. Org. Chem.*, **50**, 3667 (1985).

2) R. B. Woodward and R. Hoffmann, "The Conservation of Orbital Symmetry," Verlag Chemie, GmbH, Weinheim/Bergstr., 1970; R. Hoffmann, S. Swaminathan, B. G. Odell, and R. Gleiter, *J. Am. Chem. Soc.*, **92**, 7091 (1970); G. A. Segal, *ibid.*, **96**, 7892 (1974).

3) E. Shauman and R. Ketcham, *Angew. Chem., Int. Ed. Engl.*, **21**, 225 (1982).

4) G. Kaupp and M. Stark, *Chem. Ber.*, **110**, 3084 (1977).

5) C. Pac and H. Sakurai, *Bull. Chem. Soc. Jpn.*, **51**, 329 (1978).

6) S. Takamuku and W. Schnabel, *Chem. Phys. Lett.*, **69**, 399 (1980); H. Kobashi, H. Ikawa, R. Kondo, and T. Morita, *Bull. Chem. Soc. Jpn.*, **55**, 3013 (1982); D. H. R. Barton, B. Charpiot, L. J. Johnson, W. B. Motherwell, J. C. Scaiano, and S. Stanforth, *J. Am. Chem. Soc.*, **107**, 3607 (1985).

7) a) T. Majima, C. Pac, and H. Sakurai, *J. Am. Chem. Soc.*, **102**, 5265 (1980); b) *J. Chem. Soc., Perkin Trans. 1*, **1980**, 2705; c) C. Pac, J. Kubo, T. Majima, and H. Sakurai, *Photochem. Photobiol.*, **36**, 273 (1982); d) C. Pac, T. Fukunaga, T. Ohtsuki, and H. Sakurai, *Chem. Lett.*, **1984**, 1847.

8) a) T. Mukai, K. Sato, and Y. Yamashita, *J. Am. Chem. Soc.*, **103**, 7210 (1981); b) H. D. Roth, M. L. M. Schilling, T. Mukai, and T. Miyashi, *Tetrahedron Lett.*, **24**, 5815 (1983); c) E. Hasegawa, K. Okada, and T. Mukai, *J. Am. Chem. Soc.*, **106**, 6852 (1984).

9) a) H. Sakurai, S. Takamuku, and S. Toki, *Mem. Insti. Sci. Ind. Res., Osaka Univ.*, **39**, 55 (1982); b) S. Takamuku, T. Kuroda, and H. Sakurai, *Chem. Lett.*, **1982**, 377.

10) a) L. M. Stephenson and G. S. Hammond, *Pure Appl. Chem.*, **16**, 125 (1968); b) D. A. Labianca, G. N. Tailor, and G. S. Hammond, *J. Am. Chem. Soc.*, **94**, 3679 (1972); c) G. N. Tailor and G. S. Hammond, *ibid.*, **94**, 3684 and 3687 (1972).

11) B. S. Solomon, C. S. Steel, and A. Weller, *Chem. Commun.*, **1972**, 927.

12) a) G. Jones, II, S.-H. Chiang, W. G. Becker, and D. P. Greenberg, *J. Chem. Soc., Chem. Commun.*, **1980**, 681; b) G. Jones, II, S. -H. Chiang, W. G. Becker, and J. A. Welch, *J. Phys. Chem.*, **86**, 2805 (1982).

13) T. Majima, C. Pac, A. Nakasone, and H. Sakurai, *J. Am. Chem. Soc.*, **103**, 4499 (1981).

14) E. F. Hilinski, S. V. Milton, and P. M. Rentzepis, *J. Am. Chem. Soc.*, **105**, 5193 (1983).

15) S. L. Murov, "Handbook of Photochemistry," Marcel Dekker, New York (1973).

16) M. Kasha, *Chem. Rev.*, **47**, 401 (1947).

17) C. Pac, K. Goan, S. Yanagida, and H. Sakurai, unpublished results.

18) a) The triplet excitation energy of **1** can be estimated to be 298—323 kJ mol^{-1} since the triplet-photosensitized reaction of **1** is effected by acetone but not at all by propiophenone.[17,18b] b) G. Jones, II and V. L. Chow, *J. Org. Chem.*, **39**, 1447 (1974).

19) T. Gotoh, M. Kato, M. Yamamoto, and Y. Nishijima, *J. Chem. Soc., Chem. Commun.*, **1981**, 90.

20) W. Gerhartz, R. D. Poshuta, and J. Michl, *J. Am. Chem. Soc.*, **98**, 6427 (1976); J. Michl, *Photochem. Photobiol.*, **25**, 141 (1977).

21) C. Pac, Y. Shiota, M. Yasuda, K. Imada, and K. Shima, manuscript in preparation.

22) T. Okada, I. Karaki, and N. Mataga, *J. Am. Chem. Soc.*, **104**, 7191 (1982) and references cited therein.

23) N. J. Turro, "Modern Molecular Photochemistry," The Benjamin/Cummings, Menlo Park, Chapter 6 (1978).

24) C. Pac, M. Yasuda, K. Shima, and H. Sakurai, *Bull. Chem. Soc. Jpn.*, **55**, 1605 (1982).

25) L. Heiss, E. F. Paulus, and H. Lehling, *Justus Liebigs Ann. Chem.*, **1980**, 1583.

26) W. Metzner and D. Wendisch, *Justus Liebigs Ann. Chem.*, **730**, 111 (1969).

27) R. M. Dodson and A. G. Zielsske, *J. Org. Chem.*, **32**, 28 (1967).

28) B. S. Green and M. Rejto, *J. Org. Chem.*, **39**, 3384 (1974).

29) W. W. Wladimiroff, *Photochem. Photobiol.*, **5**, 243 (1966).

30) D. R. Coulson and N. C. Yang, *J. Am. Chem. Soc.*, **88**, 4511 (1968).

31) W. M. Moore and M. Ketchum, *J. Am. Chem. Soc.*, **84**, 1388 (1962).

Molecular Motions in Plastic Phase of 2-Methyl-2-nitropropane, $(CH_3)_3CNO_2$, by Pressure and Temperature Dependences of ^1H-NMR Spin-Lattice Relaxation

Tooru HASEBE* and Hideaki CHIHARA†
Department of Chemistry, Faculty of Education, Fukushima University, Matsukawa-machi, Fukushima 960-12
†Department of Chemistry, Faculty of Science, Osaka University, Toyonaka, Osaka 560
(Received November 15, 1985)

Proton NMR spin-lattice relaxation time, T_1, in the plastic phase of 2-methyl-2-nitropropane $(CH_3)_3CNO_2$ was measured at 10 MHz up to 150 MPa between 262 and 320 K. The overall molecular reorientation with an activation enthalpy of ΔH^*_r=6.8±1.0 kJ mol^{-1} and an activation volume of ΔV^*_r= (0.07±0.02)V_m did not show significant pressure dependence up to 140 MPa, where V_m is the molar volume of $(CH_3)_3CNO_2$ at 273.2 K. The self-diffusion, which was treated by the Torrey's isotropic diffusion model, showed large pressure dependence; the activation enthalpy, ΔH^*_d, changed from 46±4 kJ mol^{-1} under saturated vapor pressure of the sample to 95±8 kJ mol^{-1} under 100 MPa and the activation volume, ΔV^*_d, changed from V_m at 278.0 K to 0.8V_m at 320.0 K. These results strongly suggest monovacancy mechanism for self-diffusion. The phase diagram of liquid-plastic and plastic-brittle phase transitions is also given.

The study of NMR spin-lattice relaxation time, T_1, brings us valuable information of structure and dynamics of molecules. The method is particularly useful in plastic crystals for studying both reorientational and translational molecular motions. Solids, of which the constituent molecules have a globular shape, generally form a plastic crystalline phase before melting. The plastic phase, in which the motion of overall molecular reorientation is already excited, has a cubic or hexagonal close-packed structure in a majority of cases and is mainly characterized by a low entropy of fusion ($\Delta S \lesssim 20$ J K^{-1} mol^{-1}). 2-Methyl-2-nitropropane is one of such globular molecules, but its plastic phase belongs to the orthorhombic system (a=0.612 nm, b=0.617 nm, and c=0.879 nm, $a \cong b \cong c/\sqrt{2}$) with two molecules in the unit cell.[1] This phase exists between 260.1 K and the melting point (299.2 K) with the entropy of fusion, 8.66 J K^{-1} mol^{-1}.

The molecular motions in this phase have been studied by a number of experimental methods. Dielectric relaxation study reported the potential barrier hindering rotation of the molecular electric dipole (3.77 D* at 299 K)[2] as 6.78±0.84 kJ mol^{-1} [3] and its correlation time (from 8.7×10^{-12} s at the melting point to $\approx 5\times10^{-12}$ s near the transition point).[4] On the other hand, far infrared absorption study[5] reported that the residence time of a librator in the potential well was 10×10^{-12} s at 294 K.

Recently we reported the NMR study[6] of molecular motions in solid $(CH_3)_3CNO_2$. In our previous study[6] we obtained the values of the activation parameters, E_a=46.5±0.9 kJ mol^{-1} and $\tau_0=(4.6\pm1.8)\times10^{-15}$ s for self-diffusion and the mean jump time (6×10^{-7} s) of the molecule at the melting point; however, we did not get enough information on the molecular reorientation and mechanism of self-diffusion in the plastic phase.

To get such information we measured temperature- and pressure-dependence of spin-lattice relaxation time in the plastic phase. In this paper we report on the molecular motions and their roles in the spin-lattice relaxation in the plastic phase, and on the phase diagram of 2-methyl-2-nitropropane.

*1D=3.33×10^{-30} C m.

Experimental

2-Methyl-2-nitropropane (Aldrich Chemicals Co., Inc.) was purified by a preparative gas chromatograph. The purity of this specimen was estimated to be higher than 99.87 mol per cent by a gas chromatographic analysis. Furthermore the specimen was subjucted to dehydration using Molecular Sieve 4A, vacuum distillation, and degassing by the conventional freeze-pump-thaw technique and then transferred into the NMR pressure vessel via a specially designed adapter which was already reported.[7]

Proton spin-lattice relaxation time was measured using $(\pi/2)_{satn}$-τ-$\pi/2$ pulse sequences with an operating frequency of 10.0 MHz. The working pressure and temperature ranges over which T_1 was measured were between the saturated vapor pressure of the sample and 150 MPa and between 262.0 K and 320.0 K, respectively. The pressure was measured with a manganin gauge.[7] The uncertainty of the pressure value in the present study was estimated to be within 1.4 MPa. The temperature was controlled to within 0.1 K and measured with a Chromel-P/Constantan thermocouple attached to the NMR pressure vessel.

Results and Discussion

Molecular Motions. The results of experimental determination of T_1 under various pressures are given in Fig. 1. The upper and lower bounds of the existence of the plastic phase of 2-methyl-2-nitropropane are indicated by vertical dotted lines. The T_1 curves in Fig. 1 do not directly correspond to the results of a continuous run under a given pressure, except the one at the saturated vapor pressure of the sample, because the pressure inside the vessel changed when the temperature of the sample changed. Therefore, the primary results were rearranged to show the temperature dependence of T_1 under a constant pressure

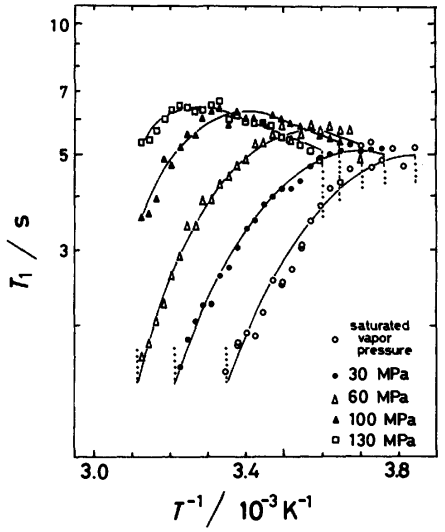

Fig. 1. Temperature dependence of T_1 under various pressures in plastic 2-methyl-2-nitropropane. The upper and lower bounds of the existence of the plastic phase of $(CH_3)_3CNO_2$ are indicated by vertical dotted lines.

in Fig. 1.

It is seen from Fig. 1 that the T_1 at a constant pressure of larger than 60 MPa has a maximum; it indicates that a change occurs in the molecular motion that is responsible for the relaxation on either side of the maximum. It is interpreted to be a change from overall molecular reorientation to translational self-diffusion as reported in our previous NMR study.[6] When such two different relaxation mechanisms contribute to the observed T_1 and if we can treat the motions independently, the relaxation rate, $T_1(\text{obsd})^{-1}$, can be expressed by the sum of the two relaxation rates as follows:

$$T_1(\text{obsd})^{-1} = T_{1r}^{-1} + T_{1d}^{-1}, \tag{1}$$

where the subscripts, r and d, denote overall molecular reorientation and molecular translational self-diffusion, respectively. At this stage it is necessary to separate T_{1r} and T_{1d} from $T_1(\text{obsd})$. Here the value of T_{1r} may be estimated by extrapolating from the T_1 data at 130 MPa from the low temperature side of the maximum, since the pressure dependence of the temperature coefficient of T_1 on the lower temperature side of the T_1 maximum was not large at pressure values below 140 MPa. The T_{1r} is related to the correlation time τ_r associated with overall molecular reorientation as follows:

$$T_{1r}^{-1} \propto \tau_r \ (\omega\tau_r \ll 1). \tag{2}$$

On the other hand, the T_{1d} (in this case, $\omega\tau_d \gg 1$) is given by Torrey's isotropic diffusion model[8,9] as follows:

$$T_{1d}^{-1} = 2.67\,\gamma^2 \langle \Delta M_2 \rangle / (\omega^2 \tau_d), \tag{3}$$

where γ is the gyromagnetic ratio of proton, $\langle \Delta M_2 \rangle$ is the part of the second moment (in Gauss unit**) that is modulated by translational self-diffusion, and τ_d is the mean diffusional jump time of molecules. Boden et al.[10] reported that Torrey's isotropic diffusion model was a good model especially for organic plastic crystals with a low value of the entropy of fusion; the entropy of fusion of $(CH_3)_3CNO_2$ is only 8.66 J K^{-1} mol^{-1}.[11]

For thermally activated motions, the correlation time τ should obey the relation of Arrhenius type,

$$\tau = \tau_0 \exp(\Delta G^*/RT), \tag{4}$$

where ΔG^*, the Gibbs energy of activation, is defined by

$$\Delta G^* = \Delta H^* - T\Delta S^*. \tag{5}$$

According to thermodynamics, the activation volume is defined by

$$\Delta V^* = (\partial \Delta G^*/\partial P)_T, \tag{6}$$

so that, if one assumes that the pressure dependence of τ_0 is negligible,[11] the values of τ derived by fitting the experimental data to Eqs. 2 and 3 may be used to obtain ΔV^* and ΔH^* through the relation,

$$\Delta V^* = RT(\partial \ln \tau/\partial P)_T, \tag{7}$$

and

$$\Delta H^* = R\{\partial \ln \tau/\partial(1/T)\}_P. \tag{8}$$

The volume of the plastic phase decreased linearly with increasing pressure up to ≈73 MPa at 291 K, and it was described by a constant isothermal compressibility $(7.1\pm0.8)\times10^{-4}$ MPa^{-1}, which was determined from the distance of the piston plunger traveled into the pressure vessel upon compression.

When one attempts to calculate the value of τ_d under various pressures using Eq. 3, one should consider a change of $\langle \Delta M_2 \rangle$ by the pressure. Because the second moment $\langle \Delta M_2 \rangle$ is inversely proportional to the square of the volume of the unit cell, one expects the value of $\langle \Delta M_2 \rangle$ to increase with increasing pressure. This would be the case only if the effect of pressure is such as to decrease the intermolecular distance rather than to decrease the number of vacancies that exist in plastic crystals, e.g. in solid argon and krypton[12] or even in solid chlorine.[13] Actually, as is seen from Fig. 1, the T_{1d} increases with pressure at a constant temperature, which fact, together with the large value of compressibility, suggests that the second moment is not significantly affected by the application of pressure. An approximate estimate indicates that the T_{1d} at 73 MPa would be 10% smaller than the T_{1d} under the

**1G=10^{-4} T.

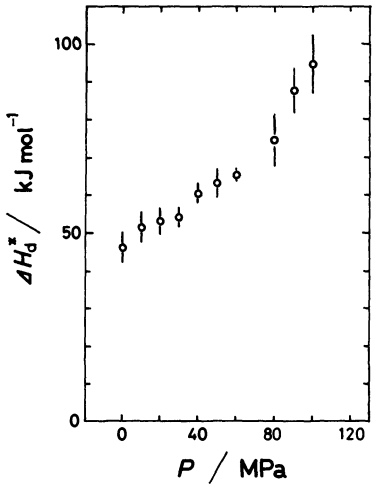

Fig. 2. Pressure dependence of activation enthalpy, ΔH_d^*, for the molecular self-diffusion in plastic $(CH_3)_3CNO_2$.

saturated vapor pressure if the pressure compressed the intermolecular distance. We now use the value of $\langle \Delta M_2 \rangle = 1.0\,G^2$ ($0.01\,mT^2$) calculated from $T_{1\rho}$ minimum value[6] under saturated vapor pressure of the sample, in calculating τ_d using T_1 data and Eq. 3.

The activation enthalpy of self-diffusion (ΔH_d^*) obtained in this study shows remarkable pressure dependence from 46±4 kJ mol^{-1} under saturated vapor pressure to 95±8 kJ mol^{-1} under 100 MPa as shown in Fig. 2; These can be compared with the cases of 2,2,3,3-tetramethylbutane (from 70 kJ mol^{-1} to 90 kJ mol^{-1}) and hexamethyldisilane (from 40 kJ mol^{-1} to 50 kJ mol^{-1}) in the same pressure range. The value of ΔV_d^* decreased gradually from 101±35 cm^3 mol^{-1} at 278 K {this value of ΔV_d^* is equal to V_m (=101 cm^3 mol^{-1}) which is the molar volume at 273.2 K} to 77±6 cm^3 mol^{-1} ($\approx 0.8 V_m$) at 320.0 K with increasing temperature. This tendency is very similar to the case of plastic phases of 2,2,3,3-tetramethylbutane and hexamethyldisilane,[14] and thus these values of the activation volume strongly suggest the monovacancy mechanism for self-diffusion.[14] Figure 3 shows the calculated correlation time, τ_d, of the molecular self-diffusion at the melting point and at the plastic-brittle phase transition point under various pressures. In contranst to the behavior of the values of τ_d at the melting point, which is almost constant ($\approx 9\times10^{-7}$ s), the values at the plastic-brittle phase transition increase as the transition point moves to higher temperatures (from 1.5×10^{-5} s under the saturated vapor pressure to 2×10^{-4} s under 80 MPa). These results suggest that the self-diffusion is the direct trigger of the fusion phenomenon but it is not a direct trigger of the plastic-brittle phase transition.

On the other hand, the activation enthalpy for overall molecular reorientation, ΔH_r^*, was obtained to be 6.8±1.0 kJ mol^{-1} which did not show remarkable pressure dependence up to 140 MPa. The activation

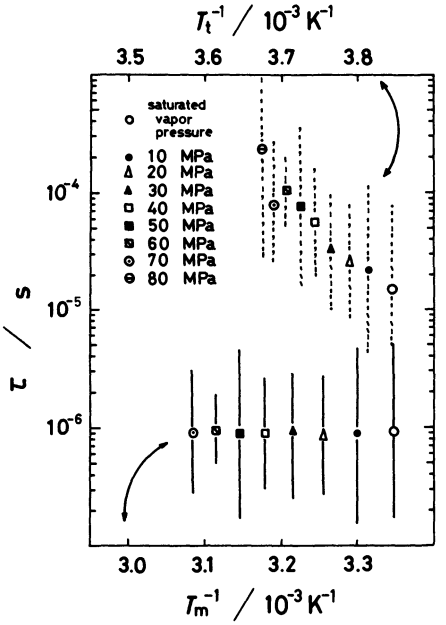

Fig. 3. The correlation time of molecular self-diffusion at the melting points (T_m) and the plastic-brittle phase transition points (T_t) under different pressures in $(CH_3)_3CNO_2$.

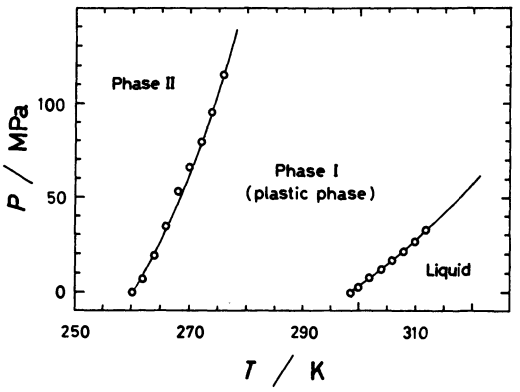

Fig. 4. Phase diagram of 2-methyl-2-nitropropane.

volume of the overall molecular reorientation, ΔV_r^*, increased slightly with increasing temperature from 7±2 cm^3 mol^{-1} at 274.0 K to 8±1 cm^3 mol^{-1} at 320.0 K. However, the ratio of ΔV_r^* to the molar volume V_m is expected to be a constant value of 0.07±0.02, because the value of V_m, which depends on the lattice spacing, would also be expected to increase with increasing temperature. The value of the ratio, 0.065, is in good agreement with results on overall molecular reorientation in other plastic crystals; in cases[7,11] of norbornane, cyclohexane, 2,2,3,3-tetramethylbutane, and 2-methylpropanoic acid, the ratios are 0.04, 0.07, 0.07—0.09, and 0.12, respectively.

Phase Diagram. The phase diagram is shown in Fig. 4, which was obtained by determining the temperature of phase changes from the jumps of the T_1 values. Figure 4 shows that the two curves become further separated as the pressure increases, and this

separation is more remarkable than in the case of $(CH_3)_3CCOOH$.[7] The average slopes of the boundary curves are

$$\frac{dP}{dT} = 7.65 \text{ MPa K}^{-1} \text{ (on the plastic-brittle phase transition curve: } \Delta S = 17.9 \text{ J K}^{-1} \text{ mol}^{-1})$$
$$= 2.5 \text{ MPa K}^{-1} \text{ (on the melting curve: } \Delta S = 8.66 \text{ J K}^{-1} \text{ mol}^{-1}).$$

The average slope for the melting in $(CH_3)_3CNO_2$ is very similar to the slope (2.22 MPa K^{-1}) in $(CH_3)_3CCOOH$ but the slope for the plastic-brittle phase transition is about twice as large as that (3.26 MPa K^{-1}) of $(CH_3)_3CCOOH$. The volume changes at these transition points were calculated by the use of the Clapeyron-Clausius equation from the entropy changes; they were 2.34 $cm^3 mol^{-1}$ for the plastic-brittle phase transition and 3.46 $cm^3 mol^{-1}$ for the melting. It is interesting to note that an application of external pressure displaces the region of the existence of the plastic crystal phase to a higher and a wider temperature, and that the volume changes of $(CH_3)_3CNO_2$ and $(CH_3)_3CCOOH$ at their melting points are not so different from each other but their volume changes at the respective plastic-brittle phase transition points are very different. Different crystal conditions of the two brittle crystal phases are reflected in the latter difference of the volume change. By comparison of $(CH_3)_3CNO_2$ with $(CH_3)_3CCl$ and $(CH_3)_3CBr$, it is also interesting to note that the temperature region (ΔT) of existence of their plastic phase relates to the entropy of fusion, i.e. ΔT=24.7 K and ΔS_m=7.53 J K^{-1} mol^{-1} for $(CH_3)_3CBr$, ΔT=29.0 K and ΔS_m=7.99 J K^{-1} mol^{-1} for $(CH_3)_3CCl$, and ΔT=39.1 K and ΔS_m=8.66 J K^{-1} mol^{-1} for $(CH_3)_3CNO_2$, respectively.

References

1) S. Urban, Z. Tomkowicz, J. Mayer, and T. Waluga, *Acta Phys. Pol.*, **A48**, 61 (1975).
2) P. Freundlich, J. Kalenik, E. Narewski, and L. Sobczyk, *Acta Phys. Pol.*, **A48**, 701 (1975).
3) S. Urban, *Acta Phys. Pol.*, **A49**, 741 (1976).
4) C. Clemett and M. Davies, *Trans. Faraday Soc.*, **58**, 1705 (1962).
5) R. Haffmans and I. W. Larkin, *J. Chem. Soc., Faraday Trans. 2*, **68**, 1729 (1972).
6) T. Hasebe, N. Nakamura, and H. Chihara, *Bull. Chem. Soc. Jpn.*, **57**, 179 (1984).
7) T. Hasebe, G. Soda, and H. Chihara, *Bull. Chem. Soc. Jpn.*, **54**, 2583 (1981).
8) H. C. Torrey, *Phys. Rev.*, **92**, 962 (1953).
9) J. M. Chezea and J. H. Strange, *Physics Reports*, **53**, 1 (1979).
10) N. Boden, J. Cohen, and R. T. Squires, *Mol. Phys.*, **31**, 1813 (1976).
11) R. Folland, S. M. Ross, and J. H. Strange, *Mol. Phys.*, **26**, 27 (1973).
12) R. H. Beaumont, H. Chihara, and J. A. Morrison, *Proc. Phys. Soc. (London)*, **A74**, 1462 (1961).
13) N. Nakamura and H. Chihara, *J. Phys. Soc. Jpn.*, **22**, 201 (1967).
14) S. M. Ross and J. H. Strange, *J. Chem. Phys.*, **68**, 3078 (1978).

 © 1986 The Chemical Society of Japan Bull. Chem. Soc. Jpn., 59, 1145—1150 (1986)

Preparation and Spectral Properties of Cobalt(III) Complexes with *S,S'*-Ethylenebis(L-homocysteinate) and *S,S'*-Trimethylenebis(L-homocysteinate)

Mikako KANESAKA,* Ken-ichi OKAMOTO, and Jinsai HIDAKA
Department of Chemistry, University of Tsukuba, Sakura, Ibaraki 305
(Received November 14, 1985)

Three cobalt(III) complexes of [Co(sexidentate-N_2,S_2,O_2)] and [Co(terdentate-$N,S,O)_2$] types were prepared; where sexidentate-N_2,S_2,O_2 denotes *S,S'*-ethylenebis(L-homocysteinate) (L,L-ebhc) and *S,S'*-trimethylenebis(L-homocysteinate) (L,L-tbhc), and terdentate-*N,S,O* denotes L-ethioninate (L-eth). Each of the L,L-ebhc and L,L-tbhc complexes was chromatographically separated into two isomers, *trans(O)* and *trans(N)*, and the L-eth complex was separated into three isomers, *trans(O)*, *trans(N)*, and *trans(S)*. These isomers were characterized by their electronic absorption, CD, and ^{13}C NMR spectra. The stereoselectivity in the formation of each geometrical isomer for the L,L-ebhc and L,L-tbhc complexes is discussed in relation to the flexibilities of the *S,S*-bridged backbone chelate ring and the L-homocysteinate moiety.

Cobalt(III) complexes with sexidentate-N_2,S_2,O_2 ligands such as *S,S'*-ethylenebis(L-cysteinate) (L,L-ebc), *S,S'*-trimethylenebis(L-cysteinate) (L,L-tbc), *N,N'*-ethylenebis(*S*-methyl-L-cysteinate) (L,L-ebsmc), *N,N'*-trimethylenebis(*S*-methyl-L-cysteinate) (L,L-tbsmc), and *N,N'*-ethylenebis(L-methioninate) (L,L-ebm) exhibit an extreme *trans(O)* selectivity concerning the formation of the geometrical isomers,[1-3] where the expectant isomers are *trans(O)* and *trans(N)* for the *S,S*-bridge complexes, and *trans(O)* and *trans(S)* for the *N,N*-bridge ones.[4] Of these complexes the *N,N*-bridge L,L-tbsmc one revealed the formation of the *trans(S)* isomer which isomerized rapidly to the *trans(O)* one.[1] This stereoselective behavior seems to relate not only to the flexibility of the bridged ethylene or trimethylene backbone chelate ring of the sexidentate-N_2,S_2,O_2 ligand but also to that of the L-cysteinate or L-homocysteinate moiety of the ligand. The present work was undertaken in continuation of the previous work[1] in order to investigate the stereoselectivity in the formation of the geometrical isomers.

In the present paper, the cobalt(III) complexes with sexidentate-N_2,S_2,O_2 ligands, *S,S'*-ethylenebis(L-homocysteinate) (L,L-ebhc) and *S,S'*-trimethylenebis(L-homocysteinate) (L,L-tbhc), $[Co(L,L\text{-ebhc})]^+$ and $[Co(L,L\text{-tbhc})]^+$, were prepared and chromatographically separated into two geometrical isomers, *trans(O)* and *trans(N)*, respectively. All isomers were characterized by their electronic absorption, CD, and ^{13}C NMR spectra, and their stereochemical and spectrochemical features are discussed. Bis(L-ethioninato)cobalt(III) complex, $[Co(L\text{-eth})_2]^+$, which corresponds to the non-bridge type of the above *S,S*-bridge complexes, was also prepared and separated into the *trans(O)*, *trans(N)*, and *trans(S)* isomers. Their spectral behaviors are compared with those of the three isomers of $[Co(L\text{-met})_2]^+$ [5] in order to investigate the influence due to the change of the substituent on the sulfur donor atom in the L-terdentate-*N,S,O* ligand.

Experimental

Preparation of Ligands. 1) *S,S'*-Ethylenebis(L-homocysteine) was prepared by a procedure modified from that used for the preparation of *S*-(carboxymethyl)-L-homocysteinate,[6,7] using 1,2-dibromoethane instead of chloroacetic acid. L-Methionine (30 g) and 1,2-dibromoethane (8.6 cm^3) were dissolved in 400 cm^3 of concentrated hydrochloric acid and the solution was refluxed for 24 h. The solution was concentrated with a rotary evaporator until it became syrupy and then neutralized with 28% aqueous ammonia. The resultant crystalline product was filtered, washed well with water, and dried in a vacuum desiccator. Yield; 9.5 g (32%). Found: C, 40.28; H, 6.80; N, 9.42%. Calcd for L,L-H_2ebhc=$C_{10}H_{20}N_2O_4S_2$: C, 40.28; H, 6.76; N, 9.39%.

2) *S,S'*-Trimethylenebis(L-homocysteine) was prepared by the same procedure as in 1), using 1,3-dibromopropane instead of 1,2-dibromoethane. Found: C, 30.68; H, 8.08; N, 6.40%. Calcd for L,L-H_2tbhc·6.5H_2O=$C_{11}H_{35}N_2O_{10.5}S_2$: C, 30.90; H, 8.26; N, 6.55%.

Preparation of Complexes. 3) [*S,S'*-Ethylenebis(L-homocysteinato)]cobalt(III) Bromide and Perchlorate: [Co(L,L-ebhc)]X; X=Br^- and ClO_4^-. A suspension containing 4.0 g of L,L-H_2ebhc in 50 cm^3 of water was adjusted to pH 9 with a 1 mol dm^{-3} aqueous solution of NaOH. To this were added a solution containing 4.0 g of $CoCl_2·6H_2O$ in 10 cm^3 of water, 2.0 g of PbO_2, and 0.2 g of activated charcoal. The mixture was stirred at ca. 60 °C for 30 min and then filtered. The filtrate was poured onto a column of SP-Sephadex C-25 (Na^+ form, 5 cm×43 cm). After sweeping the column with water, the adsorbed band was eluted with a 0.1 mol dm^{-3} aqueous solution of KBr. Two colored bands, brown (A-1) and violet (A-2), were eluted in this order. It was found from the absorption and CD spectral measurements that the eluates A-1 and A-2 contained *trans(N)*- and *trans(O)*-$[Co(L,L\text{-ebhc})]^+$, respectively. The formation ratio of the isomers, *trans(N)*:*trans(O)*, was about 1:1. Each of the eluates A-1 and A-2 was concentrated to a small volume with a rotary evaporator below 25 °C and the deposited KBr was filtered off. Each filtrate was passed through a column of Sephadex G-10 (3 cm×53 cm), and eluted with water in order to eliminate KBr. Each eluate was concentrated to a small volume. To the eluate A-1 was added a small amount of ethanol and the solution was kept in a refrigerator for several days. The resultant violet crystals were

collected by filtration. To the eluate A-2 an excess amount of aqueous solution of $NaClO_4$ was added and then a small amount of acetone. The solution was kept in a refrigerator for 4 d. The brown crystals which appeared were collected by filtration and obtained as perchlorate salt. Found for A-1: C, 22.74; H, 4.32; N, 5.36%. Calcd for $[Co(L,L\text{-ebhc})]Br \cdot 0.4KBr \cdot 2.5H_2O = CoC_{10}H_{18}N_2O_4S_2Br \cdot 0.4KBr \cdot 2.5H_2O$: C, 22.84; H, 4.41; N, 5.33%. Found for A-2: C, 25.49; H, 4.29; N, 5.94%. Calcd for $[Co(L,L\text{-ebhc})]ClO_4 \cdot H_2O$: C, 25.51; H, 4.28; N, 5.95%.

4) [*S,S'*-Trimethylenebis(L-homocysteinato)]cobalt(III) Perchlorate: [Co(L,L-tbhc)]ClO$_4$. This complex was prepared and chromatographed by the same procedure as in **3)**, using L,L-H_2tbhc instead of L,L-H_2ebhc. Two colored bands, brown (B-1) and violet (B-2), were eluted in this order. It was found from the absorption and CD spectral measurements that the eluates B-1 and B-2 contained *trans(N)*- and *trans(O)*-$[Co(L,L\text{-tbhc})]^+$, respectively. The formation ratio of the isomers, *trans(N)* and *trans(O)*, was about 1:14. The B-1 isomer could not be isolated as a solid, because the fast-moving band (B-1) contained a very small amount. Therefore, the concentration of the B-1 isomer was measured by a plasma emission spectral analysis. The eluate B-2 was converted into the perchlorate salt by use of an anion-exchange column (ClO_4^- form). Found for B-2: C, 26.46; H, 4.53; N, 5.59%. Calcd for $[Co(L,L\text{-tbhc})]ClO_4 \cdot 1.5H_2O = CoC_{11}H_{20}N_2O_8S_2Cl \cdot 1.5H_2O$: C, 26.75; H, 4.70; N, 5.67%.

5) Bis(L-ethioninato)cobalt(III) Bromide: [Co(L-eth)$_2$]Br. This complex was prepared by the same procedure as that used for $[Co(L\text{-met})_2]Br$,[5] using L-Heth instead of L-Hmet. The reaction mixture was poured onto a column of Dowex 50W-X8 (200—400 mesh, NH_4^+ form, 3.5 cm×40 cm). After sweeping the column with water, the adsorbed band was eluted with a 0.1 mol dm^{-3} aqueous solution of NH_4Br. Three colored bands, dark-red (C-1), brown-red (C-2), and red-violet (C-3), were eluted in this order. The eluates C-1, C-2, and C-3 contained *trans(S)*-, *trans(N)*-, and *trans-(O)*-$[Co(L\text{-eth})_2]^+$, respectively. Each of the three eluates was separately concentrated with a rotary evaporator below 30°C. The deposited NH_4Br was filtered off and a large amount of ethanol was added to the filtrate. The crude isomers, C-1, C-2, and C-3, were recrystallized from as little water as possible by adding ethanol, respectively. Found for C-1:

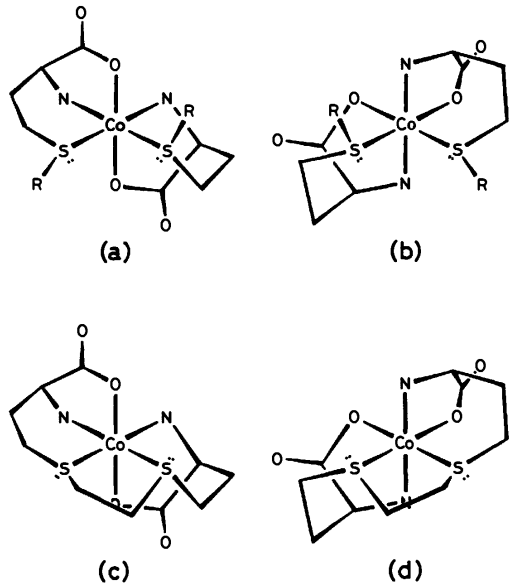

Fig. 1. Probable configurations of *trans(O)* and *trans(N)* for $[Co(L\text{-eth})_2]^+$ (R=C_2H_5): (a) *trans(O)*-*R(S),R(S)* and (b) *trans(N)*-*S(S),S(S)*, and for $[Co(L,L\text{-ebhc})]^+$: (c) *trans(O)*-*R(S),R(S)* and (d) *trans(N)*-*S(S),S(S)*.

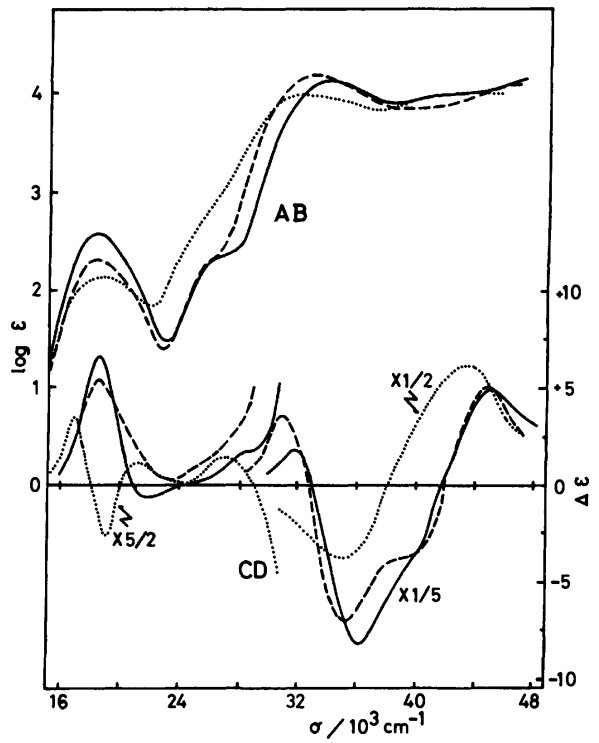

Fig. 2. Absorption and CD spectra of the *trans(O)* isomer for $[Co(L,L\text{-ebhc})]^+$ (——), $[Co(L,L\text{-tbhc})]^+$ (-----), and $[Co(L\text{-eth})_2]^+$ (·····).

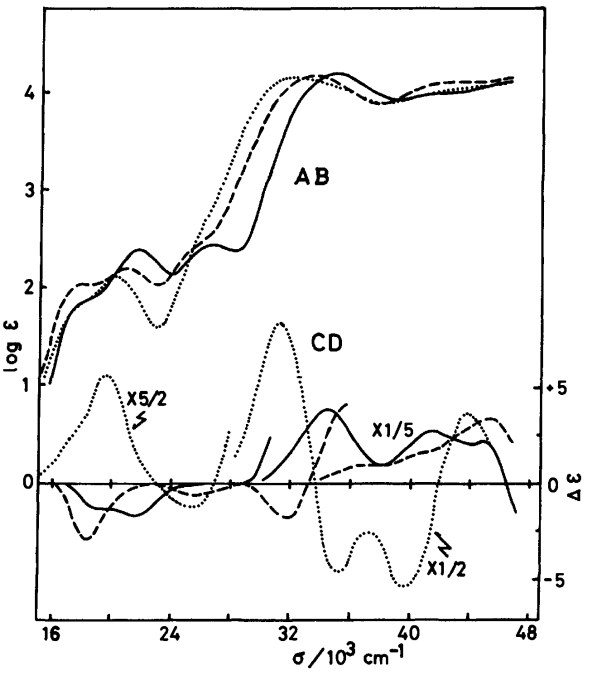

Fig. 3. Absorption and CD spectra of the *trans(N)* isomer for $[Co(L,L\text{-ebhc})]^+$ (——), $[Co(L,L\text{-tbhc})]^+$ (-----), and $[Co(L\text{-eth})_2]^+$ (·····).

C, 31.62; H, 5.42; N, 5.90%. Calcd for [Co(L-eth)$_2$]Br·0.25C_2H_5OH=$CoC_{12}H_{24}N_2O_4S_2Br$·0.25$C_2H_5OH$: C, 31.40; H, 5.79; N, 5.89%. Found for C-2: C, 27.86; H, 5.80; N, 5.42%. Calcd for [Co(L-eth)$_2$]Br·3H_2O: C, 27.84; H, 5.86; N, 5.43%. Found for C-3: C, 28.64; H, 5.51; N, 5.63%. Calcd for [Co(L-eth)$_2$]Br·2H_2O: C, 28.87; H, 5.61; N, 5.61%.

Measurements. The electronic absorption spectra were recorded with JASCO UVIDEC-1 and UVIDEC-610 spectrophotometers and the CD spectra with a JASCO J-20 spectropolarimeter. All measurements were carried out in aqueous solution at room temperature. The concentration of *trans(N)*-[Co(L,L-tbhc)]$^+$ was measured with a Jarrel-Ash Model 96—975 Plasma Atom Co. The ^{13}C NMR spectra were recorded in deuterium oxide on a JEOL JNM-FX-100 NMR spectrometer at the probe temperature. Sodium 2,2-dimethyl-2-silapentate-5-sulfonate (DSS) was used as an internal reference.

Results and Discussion

Structural Assignments. *S,S*-Bridge (L,L-sexidentate-N_2,S_2,O_2) Type Complexes. For each of the *S,S*-bridge complexes, [Co(L,L-ebhc)]$^+$ and [Co(L,L-tbhc)]$^+$, two geometrical isomers, *trans(O)* and *trans(N)*, are expected (Fig. 1). The absorption and CD spectra of the A-1, A-2, B-1, and B-2 isomers are shown in Figs. 2 and 3, and their data are summarized in Tables 1 and 2 together with those of *trans(O)*-, *trans(N)*-, and *trans(S)*-[Co(L-eth)$_2$]$^+$. Four isomers of the *S,S*-bridge complexes exhibit commonly the sulfur-to-metal charge transfer bands in the region of 33—35×10^3 cm^{-1}, indicating that all isomers have a *cis(S)* configuration.[1,8-13] In the first d-d absorption band

Table 1. Absorption Spectral Data of [Co(sexidentate-N_2,S_2,O_2)]$^+$ and [Co(terdentate-N,S,O)$_2$]$^+$ Type Complexes

Complex	First band	Second band	Charge transfer band
trans(O)-[Co(L,L-ebhc)]$^+$	18.42 (2.58)	26.67 (2.34 sh)	34.25 (4.13)
trans(N)-[Co(L,L-ebhc)]$^+$	17.86 (1.85 sh)	26.74 (2.43)	34.72 (4.21)
	21.51 (2.39)		
trans(O)-[Co(L,L-tbhc)]$^+$	18.45 (2.30)	25.80 (2.27 sh)	33.33 (4.19)
trans(N)-[Co(L,L-tbhc)]$^+$	17.92 (2.02)		33.11 (4.17)
	20.75 (2.20)		47.62 (4.11)
trans(S)-[Co(L-eth)$_2$]$^+$	18.40 (2.01)		28.17 (4.05)
trans(O)-[Co(L-eth)$_2$]$^+$	19.00 (2.11)	26.67 (2.89 sh)	32.80 (3.98)
trans(N)-[Co(L-eth)$_2$]$^+$	17.54 (1.80 sh)		32.36 (4.14)
	20.00 (2.11)		

Wavenumbers and $\Delta\varepsilon$ values (in parentheses) are given in 10^{3}cm^{-1} and mol^{-1}dm^{3}cm^{-1}, respectively. sh denotes a shoulder.

Table 2. CD Spectral Data [Co(sexidentate-N_2,S_2,O_2)]$^+$ and [Co(terdentate-N,S,O)$_2$]$^+$ Type Complexes

Complex	First band region	Second band region	Charge transfer band region
trans(O)-[Co(L,L-ebhc)]$^+$	18.69 (+6.66)	28.17 (+1.61 sh)	31.95 (+9.23)
	21.74 (−0.64)		36.10 (−40.93)
			40.00 (−17.9 sh)
			44.84 (+24.48)
trans(N)-[Co(L,L-ebhc)]$^+$	19.23 (−1.31 sh)	28.17 (−0.10)	34.48 (+18.93)
	21.56 (−1.63)		41.67 (+13.36)
			44.84 (+11.14)
trans(O)-[Co(L,L-tbhc)]$^+$	18.69 (+5.45)		31.25 (+17.99)
			35.34 (−34.78)
			40.00 (−18.0 sh)
			44.84 (+25.19)
trans(N)-[Co(L,L-tbhc)]$^+$	18.32 (−2.95)	25.51 (−0.69)	31.85 (−1.82)
			36.23 (+4.42 sh)
			45.25 (+16.74)
trans(S)-[Co(L-eth)$_2$]$^+$	15.87 (+0.44)	25.97 (−0.21)	28.57 (+0.59)
	17.30 (−0.55)		35.09 (−1.89)
	19.20 (+0.34)		40.80 (+3.40)
trans(O)-[Co(L-eth)$_2$]$^+$	16.95 (+1.44)	27.03 (+0.62)	35.09 (−7.55)
	18.69 (−0.57)		43.48 (+12.40)
	20.83 (+0.53)		
trans(N)-[Co(L-eth)$_2$]$^+$	19.61 (+2.26)	25.32 (−0.51)	31.25 (+17.00)
			35.09 (−8.87)
			40.00 (−10.20)
			43.48 (+7.22)

Wavenumbers and $\Delta\varepsilon$ values (in parentheses) are given in 10^{3}cm^{-1} and mol^{-1}dm^{3}cm^{-1}, respectively. sh denotes a shoulder.

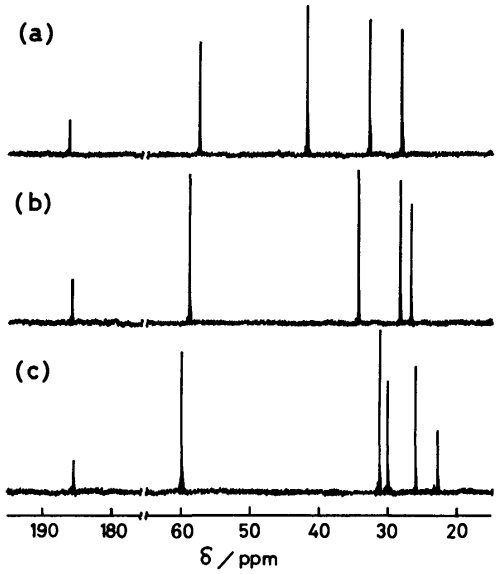

Fig. 4. ^{13}CNMR spectra of [Co(sexidentate-N_2,S_2,O_2)]$^+$: (a) *trans(N)* L,L-ebhc, (b) *trans(O)* L,L-ebhc, and (c) *trans(O)* L,L-tbhc.

region of [Co(L,L-ebhc)]$^+$, the A-1 isomer exhibits a band with an explicit shoulder on the lower energy side of the major peak and the A-2 one a broad band with a vague shoulder on the higher energy side (Figs. 2 and 3). These splittings of the first d-d absorption bands indicate that the A-1 and A-2 isomers are *trans(N)* and *trans(O)*, respectively.[1,13] The same relationship in absorption spectrum as the L,L-ebhc isomers is also observed for the B-1 and B-2 isomers of [Co(L,L-tbhc)]$^+$ (Figs. 2 and 3, and Table 1). Accordingly, the B-1 isomer can be assigned to *trans(N)* and the B-2 one to *trans(O)*.

The ^{13}CNMR spectra of the *S,S*-bridge complexes were measured in order to estimate the configuration, *R(S)* or *S(S)*, of the sulfur donor atom (Fig. 4). *trans(N)*- and *trans(O)*-[Co(L,L-ebhc)]$^+$ exhibit five resonance lines for ten carbon atoms (Fig. 4 (a) and (b)), and *trans(O)*-[Co(L,L-tbhc)]$^+$ exhibits six lines for eleven carbon ones (Fig. 4 (c)). These facts indicate that all isomers have C_2 symmetry, namely, the conformation of the *S,S*-bridged backbone chelate ring takes a gauche form for the ethylene bridge in the L,L-ebhc complex and a skew form for the trimethylene bridge in the L,L-tbhc one. It is considered, therefore, that each of the four isomers takes either the *R(S)*,-*R(S)* or *S(S)*,*S(S)* configuration with respect to the two asymmetric sulfur donor atoms. The model constructions reveal that the two sulfur donor atoms of the *trans(N)* L,L-ebhc or *trans(N)* L,L-tbhc isomer take the *S(S)*,*S(S)* configuration. On the other hand, the two *trans(O)* isomers are possible to take both of the *R(S)*,-*R(S)* and *S(S)*,*S(S)* configurations, however, the *R(S)*,-*R(S)* one is more preferable than the other because there is less strain of the *S,S*-bridged backbone chelate ring.

Bis(L-ethioninato) Complexes. In order to investigate the spectral behavior due to the change of the substituent on the sulfur donor atom of the ligand, *trans(N)*-, *trans(S)*-, and *trans(O)*-[Co(L-eth)$_2$]$^+$ were prepared. Their absorption and CD data are summarized in Tables 1 and 2. Splittings of the first d-d absorption bands and the maximum positions (28—33×10^3 cm^{-1}) of the sulfur-to-metal charge transfer bands of the three isomers agree well with those of the corresponding three isomers of [Co(L-met)$_2$]$^+$, respectively.[5] The behavior of these absorption spectra confirms that the C-1, C-2, and C-3 isomers are *trans(S)*, *trans(N)*, and *trans(O)*, respectively.[14] Each of the three isomers exhibits a similar CD spectrum to that of the corresponding isomer of [Co(L-met)$_2$]$^+$,[5] suggesting that the CD contribution due to the change of the substituent on the two sulfur donor atoms is inconspicuous.

The ^{13}CNMR spectrum of *trans(S)*-[Co(L-eth)$_2$]$^+$ exhibits six resonance lines (13.00, 27.90, 30.45, 32.61, 58.40, and 186.03 ppm) for twelve carbon atoms, the *trans(N)* isomer fourteen lines (13.27, 14.30, 25.73, 26.06, 26.55, 27.79, 28.06, 28.98, 31.75, 32.56, 59.10, 60.78, 185.49, and 186.58 ppm), and the *trans(O)* isomer eight lines (14.36, 25.79, 26.98, 27.20, 28.66, 57.70, 187.44, and 187.93 ppm). Taking the configuration, *R(S)* or *S(S)*, of the sulfur donor atom into consideration, the ^{13}C NMR spectrum of the *R(S)*,*R(S)* or *S(S)*,*S(S)* isomer having a twofold axis can be expected to exhibit six resonance lines, while the *R(S)*,-*S(S)* isomer to exhibit twelve. The present results suggest that the *trans(S)* isomer is either *S(S)*,*S(S)* or *R(S)*,*R(S)* and the other two isomers are a mixture of *R(S)*,*S(S)*, *R(S)*,*R(S)*, and/or *S(S)*,*S(S)*. These trends are in accord with those of the [Co(L-met)$_2$]$^+$ isomers.[5] Accordingly, taking the model constructions and the similarity in CD spectrum with the [Co(L-met)$_2$]$^+$ isomers into consideration, the *trans(S)* isomer prefers the *S(S)*,*S(S)* configuration, the *trans(N)* isomer a mixture of the *R(S)*,*S(S)* and *S(S)*,*S(S)* ones, and the *trans(O)* isomer takes a mixture of the *R(S)*,*R(S)*, *R(S)*,-*S(S)*, and *S(S)*,*S(S)* ones, as in the case of [Co(L-met)$_2$]$^+$.[5] These results seem to support that the CD spectra of the three isomers of [Co(L-eth)$_2$]$^+$ resemble the corresponding isomers of [Co(L-met)$_2$]$^+$, respectively.

Formation of Isomers. The *trans(O)* and *trans(N)* isomers were formed for each [Co(L,L-ebhc)]$^+$ and [Co(L,L-tbhc)]$^+$ in this work, though the *trans(N)* L,L-tbhc isomer could not be isolated as a solid because of the very small amount. Contrary to the L,L-ebhc and L,L-tbhc complexes, only the *trans(O)* isomer was selectively formed for each of [Co(L,L-ebc)]$^+$ and [Co(L,L-tbc)]$^+$.[1] These results are probably related to the difference in flexibility between the N-S chelate rings of the L,L-ebhc or L,L-tbhc complex and the L,L-ebc or L,L-tbc one. For [Co(L,L-ebhc)]$^+$ and [Co(L,L-tbhc)]$^+$, namely, the ethylene and trimethylene bridges span the two sulfur donor atoms of the rather flexible six-membered N-S rings of the L-homocysteinate

moieties, while the bridges in [Co(L,L-ebc)]$^+$ and [Co(L,L-tbc)]$^+$ span the sulfur donor atoms of the rigid five-membered N–S rings of the L-cysteinate moieties. In the case of the *N,N*-bridge L,L-sexidentate-N_2,S_2,O_2 type complexes,[1-3] on the other hand, of the expectant *trans(O)* and *trans(S)* isomers only the *trans(O)* one was selectively formed for the ethylene bridge complexes, [Co(L,L-ebsmc)]$^+$ and [Co(L,L-ebm)]$^+$, while the two geometrical isomers were formed for the trimethylene bridge complex, [Co(L,L-tbsmc)]$^+$, though the *trans(S)* isomer could not be isolated because of the isomerization to the *trans(O)* species during the procedure after elution.[1] These results are obviously caused by the difference in flexibility between the ethylene and trimethylene bridges, because both of the bridges span the nitrogen donor atoms of the rigid five-membered N–O rings of the ligands. From these results, it can be deduced that the selective formation of the isomers for the *S,S*-bridge complexes depends mainly on the flexibility of the N–S chelate rings of the ligand and the difference between the ethylene and trimethylene backbone bridges is a minor factor for the selective formation of the isomers.

Absorption and CD Spectra. The three geometrical isomers of [Co(L-eth)$_2$]$^+$ exhibit similar absorption and CD spectral behaviors to the corresponding isomers of [Co(L-met)$_2$]$^+$,[5] over the whole region, indicating that their spectra hardly change with the substitution of ethyl group for methyl one on the sulfur donor atoms (Tables 1 and 2). The CD spectra of the *trans(O)* and *trans(N)* isomers of [Co(L,L-ebhc)]$^+$ and [Co(L,L-tbhc)]$^+$ deviate significantly from those of the corresponding isomers of [Co(L-eth)$_2$]$^+$, respectively, although the absorption spectral patterns of the former isomers are similar to those of the latter, respectively, as shown in Figs. 2 and 3.

The absorption maxima of the sulfur-to-metal charge transfer bands (32—35×10^3 cm^{-1} for the *cis(S)* isomers) are shifted to lower energy in the order of L,L-ebhc>L,L-tbhc>non-bridge complex in either of the *trans(O)* and *trans(N)* isomers (Figs. 2 and 3). This order coincides with that for the *cis*·*cis*·*cis*-[Co(*R,S*-ebp)]$^+$, -[Co(*R,S*-tbp)]$^+$, -[Co(*R,S*-tetp)]$^+$, and -[Co(*R*-smp) (*S*-smp)]$^+$.[15] This behavior reflects the order of the rigidities of the *S,S*-bridged backbone chelate rings. The first d-d absorption bands of the present *S,S*-bridge *trans(O)* isomers are almost unchanged from that of *trans(O)*-[Co(L-eth)$_2$]$^+$ as in the case of *trans(O)*-[Co(L,L-ebc)]$^+$, -[Co(L,L-tbc)]$^+$, and -[Co(L-smc)$_2$]$^+$, where L-smc denotes *S*-methyl-L-cysteinate.[1] However, the first absorption bands of the *S,S*-bridge *trans(N)* isomers significantly change from that of the *trans(N)* L-eth isomer, namely, the absorption components in the higher energy side are shifted to lower energy in accordance with the absorption spectral behavior of the sulfur-to-metal charge transfer bands mentioned above, though the components (ca. 17.9×10^3 cm^{-1}) in the lower energy side remain unchanged.

The deviation in CD spectrum between the *trans(O)* L,L-ebhc or L,L-tbhc isomer and *trans(O)*-[Co(L-eth)$_2$]$^+$ is quite similar to that between the *trans(O)* L,L-ebc or L,L-tbc isomer and *trans(O)*-[Co(L-smc)$_2$]$^+$ which possess a rigid L-cysteinate framework.[1] Accordingly, this deviation is attributed to the CD contribution due to the fixation of two sulfur donor atoms located in the cis position. In contrast to the *trans(O)* isomers, the CD spectra of the *S,S*-bridge *trans(N)* isomers change drastically from that of *trans(N)*-[Co(L-eth)$_2$]$^+$ (Fig. 3 and Table 2). In the first d-d absorption band region, *trans(N)*-[Co(L-eth)$_2$]$^+$ exhibits a positive CD band (19.61×10^3 cm^{-1}) with a shoulder in the lower energy side, while the *S,S*-bridge *trans(N)* isomers exhibit negative CD bands (19.2 sh and 21.56×10^3 cm^{-1} for the L,L-ebhc isomer and 18.32×10^3 cm^{-1} for the L,L-tbhc one) which correspond to the two absorption components. In the ligand band region (36—48×10^3 cm^{-1}) where the bridge L,L-isomer usually exhibits a similar CD pattern to that of the non-bridge L-isomer,[1,2] the *trans(N)* L,L-ebhc and L,L-tbhc isomers exhibit a reversed CD pattern to that of *trans(N)*-[Co(L-eth)$_2$]$^+$ (Fig. 3). Considered from another viewpoint, the CD spectra of the *S,S*-bridge *trans(N)* isomers seem roughly enantiomeric to those of the *S,S*-bridge *trans(O)* ones. These CD spectral changes of the *trans(N)* isomers seem to indicate an additional CD contribution besides that due to the fixation of the two sulfur donor atoms in the cis position. On this viewpoint, the present results may be considered as follows. When the two sulfur donor atoms of the non-bridge isomer are spanned by ethylene or trimethylene, the *S,S*-bridge *trans(O)* isomers retain the net configurational chirality of the non-bridge *trans(O)* one. While, the *S,S*-bridge *trans(N)* isomers obtain a configurational chirality of the L,L-sexidentate type which is quasi-enantiomeric geometrical isomers to the *S,S*-bridge *trans(O)* ones, though *trans(N)*-[Co(L-eth)$_2$]$^+$ is not quasi-enantiomeric to the *trans(O)* isomer. As a result, the *S,S*-bridge *trans(N)* isomers exhibit approximately enantiomeric CD spectra to the *S,S*-bridge *trans(O)* ones. The CD spectral behavior of the *trans(N)* isomers in this work suggest that care must be taken in relating the CD spectra to the absolute configurations of the complexes with sulfur-containing terdentate amino carboxylates and their sexidentate derivatives.

The authors wish to express thanks to Miss Shino Takahashi and Mrs. Yoko Koizumi for their aid in the experiment. This work was supported by a Grant-in-Aid for Scientific Research No. 60470043 from the ministry of Education, Science and Culture.

References

1) T. Konno, K. Okamoto, and J. Hidaka, *Bull. Chem. Soc. Jpn.*, **56**, 2631 (1983).

2) R. J. Magee, W. Mazurec, M. J. O'Conner, and A. T. Phillip, *Aust. J. Chem.*, **27**, 1629 (1974).

3) K. Okamoto, T. Isago, M. Ohmasa, and J. Hidaka, *Bull. Chem. Soc. Jpn.*, **55**, 1077 (1982).

4) The *S,S*-bridge denotes that two sulfur donor atoms in the ligand are bridged by ethylene or trimethylene, and the *N,N*-bridge denotes that two nitrogen donor atoms are bridged.

5) J. Hidaka, S. Yamada, and Y. Shimura, *Chem. Lett.*, **1974**, 1487.

6) M. D. Armstrong and J. D. Lewis, *J. Org. Chem.*, **16**, 749 (1951).

7) K. Okamoto, M. Suzuki, H. Einaga, and J. Hidaka, *Bull. Chem. Soc. Jpn.*, **58**, 1807 (1985).

8) K. Kanamori, T. Sudani, and K. Kawai, *Bull. Chem. Soc. Jpn.*, **49**, 2739 (1976).

9) P. de Meester and D. J. Hodgson, *J. Chem. Soc., Dalton Trans.*, **1976**, 618.

10) H. M. Helis, P. de Meester, and D. J. Hodgson, *J. Am. Chem. Soc.*, **99**, 3309 (1977).

11) K. Yamanari, N. Takeshita, and Y. Shimura, *Bull. Chem. Soc. Jpn.*, **57**, 1227, 2852 (1984).

12) K. Yamanari, N. Takeshita, T. Komorita, and Y. Shimura, *Chem. Lett.*, **1981**, 861.

13) K. Okamoto, K. Wakayama, H. Einaga, S. Yamada, and J. Hidaka, *Bull. Chem. Soc. Jpn.*, **56**, 165 (1983).

14) H. Yamatera, *Bull. Chem. Soc. Jpn.*, **31**, 95 (1958).

15) M. Kanesaka, K. Okamoto, M. Nomoto, and J. Hidaka, *Bull. Chem. Soc. Jpn.*, **57**, 3111 (1984). The abbreviations of the ligands are as follows: *R,S*-ebp=(2*R*,9*S*)-2,9-diamino-3,3,8,8-tetramethyl-4,7-dithia-1,10-decanedioate, *R,S*-tbp=(2*R*,10*S*)-2,10-diamino-3,3,9,9-tetramethyl-4,8-dithia-1,11-undecanedioate, *R,S*-tetp=(2*R*,11*S*)-2,11-diamino-3,3,10,10-tetramethyl-4,9-dithia-1,12-dodecanedioate, and *R*- or *S*-smp=*S*-methyl-L- or -D-penicillaminate.

 © 1986 The Chemical Society of Japan Bull. Chem. Soc. Jpn., 59, 1151—1153 (1986)

Voltammetric Determination of Dialkylammonium Ion in the Presence of Monoalkylammonium Ion by Addition of 18-Crown-6

Tomokazu MATSUE, Uichi AKIBA, and Tetsuo OSA*
Pharmaceutical Institute, Tohoku University, Aobayama, Sendai 980
(Received December 9, 1985)

The addition of 18-crown-6 to the electrolyte solution discriminated the reduction current peak for dialkylammonium ions from that for monoalkylammonium homologues, which made it possible to determine voltammetrically the dialkylammonium ions in the presence of the monoalkylammonium ions.

Voltammetry has been widely used as an effective method for determination of a specific electroactive species in the presence of others. Reliable results for such a system have been obtained when the reduction (or oxidation) potential of the species to be determined differs from those of others by $\gtrsim$0.1 V. If the separation in the potentials is unsatisfactory, one should use a procedure to diminish the undesired influences of the interfering species. This may be accomplished by use of a potential-shifting additive[1] which affects chemical reactions prior to and/or following electron transfer. If the interfering species are structually and chemically similar to the species to be determined, a high recognition ability of substrate is required for the potential-shifting additive. In this paper, we wish to report the voltammetric determination of dialkylammonium (secondary ammonium) ions in the presence of monoalkylammonium (primary ammonium) ions by taking advantage of the recognition ability of 18-crown-6 (18CR6) for ammonium cations. Although crown ethers have been used for ion-selective electrodes aimed at determining a specific alkali metal ion,[2] this potentiometric method is essentially unsuitable for detection of secondary ammonium ions. Amperometric method can be used for the purpose but coexistence of primary ammonium ions reduces the reliability since reduction current for the primary ions overlaps that for the secondary ions. In such a case, the addition of crown ethers, especially 18CR6 derivatives, to the electrolyte solution discriminates the two reduction currents and makes it possible to determine the secondary ammonium ion even though the primary homologues are present in the solution.

Experimental

Differential pulse voltammetry was carried out using a Yanaco voltammetric analyzer model P-1000 at room temperature. Cyclic voltammetry was also performed with conventional instruments. The working electrode was a 3 mm diameter Pt disk sealed into a soft glass tube and it was polished finally with 0.3 μm alumina powder (Buehler Co.) to give a mirror-like surface. The reference electrode was an Ag wire immersed in 0.10 mol dm^{-3} tetraethylammonium perchlorate (TEAP)/0.010 mol dm^{-3} $AgNO_3$ in acetonitrile and a Pt wire was used as the counter electrode. All chemicals (GR grade) were obtained commercially and used without further purification.

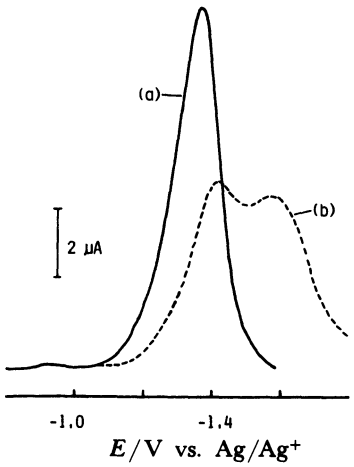

Fig. 1. Differential pulse voltammograms of a mixture of 1.0 mmol dm^{-3} $Me_2NH_2^+Cl^-$ and 1.0 mmol dm^{-3} $EtNH_3^+Cl^-$ in the absence (a) and presence (b) of 40 mmol dm^{-3} 18CR6.
Scan rate: 5 mV s^{-1}. Modulation amplitude: 50 mV. Pulse interval: 1.0 s. Electrode: Pt disk. Electrolyte: 0.1 mol dm^{-3} TEAP/acetonitrile.

Results and Discussion

Figure 1 shows differential pulse voltammograms of a mixture of 1.0 mmol dm^{-3} dimethylammonium chloride ($Me_2NH_2^+Cl^-$) and its structual isomer, 1.0 mmol dm^{-3} ethylammonium chloride ($EtNH_3^+Cl^-$). The reduction potentials of the two ions are close each other, so only single wave was observed on the voltammogram. However, the addition of 18CR6 to the electrolyte solution changes the sole peak to the splitting two peaks. The reduction peak at −1.42 V is originated from the electrochemical reduction of $Me_2NH_2^+$ and the other peak from the reduction of $EtNH_3^+$. The large shift in the reduction potential for $EtNH_3^+$ is resulted from its strong complexation with 18CR6. Only a few reports[3] have been published on the effect of crown ethers on the electroreduction of NH_4^+. From these results, the following mechanism can be deduced for the electrochemical reduction of $EtNH_3^+$ in the presence of 18CR6:

$$EtNH_3^+ + CR \rightleftharpoons EtNH_3^+ \cdot CR \quad (1)$$

$$EtNH_3^+ + e^- \longrightarrow EtNH_2 + 1/2\,H_2. \quad (2)$$

Since the preceding reaction (1) exists before the electron-transfer process (2) (so-called CE mechanism), the apparant half-wave potential for the reduction shifts to the negative direction as the concentration of 18CR6 in the electrolyte solution increases. The formation constant for the CR complex can be determined by these potential shifts[4] and the value was roughly estimated to be $\gtrsim$2000 $dm^3 mol^{-1}$ assuming fast chemical reaction and irreversible electron-transfer step (C_rE_i mechanism). Thus almost all $EtNH_3^+$ exists as the complexed form under the present conditions. The addition of 18CR6 also caused a decrease of the reduction peak current on the voltammogram because the effective diffusion coefficient is reduced by the complexation[5] of $EtNH_3^+$ with large 18CR6 molecule. This phenomenon also plays an important role on the clear appearance of the reduction wave for $Me_2NH_2^+$ on the voltammogram. On the other hand, the effect of the added 18CR6 on the reduction of $Me_2NH_2^+$ was small. The shift in the reduction potential was only 0.03 V (cyclic voltammetry) by the addition of 40 mmol dm^{-3} 18CR6. The consideration with the CPK molecular model shows that $Me_2NH_2^+$ forms no clear complex but only sits on the ether ring.

Figure 2 shows the relationship between the current at -1.42 V and the concentration of $Me_2NH_2^+$ in the presence of 1.0 mmol dm^{-3} $EtNH_3^+$ and 40 mmol dm^{-3} 18CR6. A good linearity over the concentration range measured indicates that the concentration of $Me_2NH_2^+$ can be determined by addition of 18CR6 to the electrolyte solution even though the sample contains $EtNH_3^+$ ion. A small current at the intercept of the current axis is due to the residual reduction of $EtNH_3^+$. When the concentration of $Me_2NH_2^+$ is largely excess over that of $EtNH_3^+$, the undesired influence from the residual current is negligible. Although the contribution of the residual current becomes large as the concentration of $EtNH_3^+$ increases, it can be estimated by $0.18i_p$ where i_p is the peak current for the reduction of $EtNH_3^+$ at -1.58 V. Thus, the concentration of $Me_2NH_2^+$ can be determined by considering this residual effect. The present analysis will give reliable results if the concentration of $Me_2NH_2^+$ is larger than one-tenth that of $EtNH_3^+$.

Table 1 shows the shifts of the peak potential caused by the addition of crown ethers in cyclic voltammetry. All crown ethers used had a remarkable ability for shifting the peak potentials of the primary ammonium ions in acetonitrile. However, the shifts observed in dimethylformamide (DMF) were relatively small, reflecting low binding ability of the crown ethers in this solvent. It is also notable that the shift in the peak potential, i.e., binding ability, depends greatly on the structure of the crown ether. The tendency observed here is in accord with those reported previously.[6,7] The complexation of ammonium ions is stabilized by forming tetrahedral conformation via three hydrogen bondings between ammonium hydrogens and ether

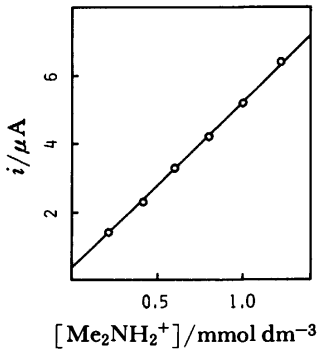

Fig. 2. Relationship between the current at -1.42 V and the concentration of $Me_2NH_2^+Cl^-$ in the presence of 1.0 mmol dm^{-3} $EtNH_3^+Cl^-$ and 40 mmol dm^{-3} 18CR6. The current was measured by the differential pulse voltammetry under the same experimental conditions described in Fig. 1.

Table 1. The Shifts in the Peak Potential (V) Induced by the Addition of 20 mmol dm^{-3} Crown Ethers in Cyclic Voltammetry[a]

CR	$R-NH_3^+$ R=	Solvent	
		acetonitrile	DMF
18CR6	Me	0.21	0.09
	Et	0.20	0.08
	Pr	0.20	0.08
B18CR6[b]	Me	0.20	0.09
DB18CR6[c]	Me	0.10	0.09
	Et	0.11	
	Pr	0.14	
15CR5[d]	Me	0.08	

a) Scan rate: 0.1 V s^{-1}. Concentration of substrate: 1.0 mmol dm^{-3}. Other conditions are same as those in Fig. 1. b) Benzo-18-crown-6. c) Dibenzo-18-crown-6. d) 15-crown-5.

oxygens.[6] Thus, 15CR5 is obviously inferior to 18CR6 derivatives in binding ability since only two hydrogen bondings are operative in the 15CR5 complexes. Another important factor governing the binding strength is electron density on the oxygen atoms in the ether rings. Replacement of ethylene groups by aryl groups reduces the binding ability[7] due to slight delocalization of the aryl oxygen electron into the aryl π system.

These effects of crown ethers are very small for the electroreduction of secondary ammonium ions. The largest influence of 18CR6 was observed on the reduction of $Me_2NH_2^+$ and it decreased rapidly with length of the alkyl chains. 18CR6 had only negligible effect on the reduction of $Et_2NH_2^+$ in terms of the peak potential and peak current. The above results indicate that there are pronounced difference[8] in the formation constants for primary and secondary ammonium ions. However, it is difficult to determine the exact values of these constants by the shifts in the peak potential induced by the complexation since the detailed mechanism of this electrochemical reaction

is unclear. For the present purpose to determine secondary ammonium ion, it is not essential to obtain the formation constants. If the peak separation is unsatisfactory, further addition of crown ethers will provide a better resolution. This procedure is applicable to the determination of other secondary ammonium ions in the presence of primary homologues, and can be extended to the analysis of tertiary ammonium (trialkylammonium) ions.

References

1) T. Matsue, M. Fujihira, and T. Osa, *Anal. Chem.*, **53**, 722 (1981).

2) K. Kimura, A. Ishikawa, H. Tamura, and T. Shono, *J. Chem. Soc., Perkin Trans. 2*, **1984**, 447; K. Kimura, H. Tamura, and T. Shono, *J. Chem. Soc., Chem. Commun.*, **1983**, 492; and references therein.

3) K. Angelis, M. Brezina, and J. Koryta, *J. Electroanal. Chem.*, **45**, 504 (1973); C. Boudon, M. Gross, and F. Peter, ibid., **145**, 181 (1983).

4) T. Matsue, T. Osa, and D. H. Evans, *J. Inclus. Phenom.*, **2**, 547 (1984); T. Matsue, D. H. Evans, T. Osa, and N. Kobayashi, *J. Am. Chem. Soc.*, **107**, 3411 (1985); T. Matsue, U. Akiba, K. Suzufuji, and T. Osa, *Denki Kagaku*, **53**, 508 (1985).

5) V. Kachna and L. Matousek, *Collec. Czech. Chem. Commun.*, **18**, 294 (1953); Z. Zabaransky, *ibid.*, **24**, 3075 (1959); T. Osa, T. Matsue, and M. Fujihira, *Heterocycles*, **6**, 1833 (1977).

6) J. M. Timko, R. C. Halgeson, M. Newcomb, G. W. Gokel, and D. J. Cram, *J. Am. Chem. Soc.*, **96**, 7097 (1974); F. De Jong, D. N. Reinhoudt, and R. Huis, *Tetrahedron Lett.*, **1977**, 3985.

7) J. M. Timko, S. S. Moore, D. M. Walba, P. C. Hiberty, and D. J. Cram, *J. Am. Chem. Soc.*, **99**, 4207 (1977).

8) M. Schroder-Nielsen, *Acta Pharm. Suec.*, **13**, 190 (1976).

An X-Ray Diffraction Investigation of the Coordination Structure of Mn(II) Ions in Highly Concentrated Aqueous $MnBr_2$ and $MnCl_2$ Solutions

Yoshichika TAJIRI, Mitsuyoshi ICHIHASHI,† Takeharu MIBUCHI,†† and Hisanobu WAKITA*
Department of Chemistry, Faculty of Science, Fukuoka University, Nanakuma, Jonan-ku, Fukuoka 814-01
(Received August 15, 1985)

The solute structures of highly concentrated aqueous 5.087 and 2.744 mol dm^{-3} $MnBr_2$, and 4.744 and 2.732 mol dm^{-3} $MnCl_2$ solutions were determined by the analysis of the radial-distribution function curves of X-ray diffraction experiments. Mixed-ligand aquahalogenomanganese(II) complexes were found to be present in these solutions, holding a distorted octahedral geometry. The interatomic distances of the aquabromo complex are 2.178—2.184 Å for Mn-OH_2 and 2.596—2.643 Å for Mn-Br; those of the aquachloro complex are 2.183—2.185 Å for Mn-OH_2 and 2.492—2.496 Å for Mn-Cl. The interatomic distances of Mn-OH_2 are shorter than those of the $MnBr_2 \cdot 4H_2O$ and $MnCl_2 \cdot 4H_2O$ crystals and are consistent with those of the $Mn(OH_2)_6(NO_3)_2$ crystal. The length of the Mn-Cl bond here determined is practically the same as that within the $MnCl_2 \cdot 4H_2O$ crystal, but the Mn-Br bond found is shorter than that within the $MnBr_2 \cdot 4H_2O$ crystal. The average coordination number of the Mn-Br contact per Mn(II) increased from 1.104 to 1.212 with an increase in the Br/Mn ratio from 2.076 to 3.269, while the number of the Mn-Cl contact per Mn(II) increased from 1.259 to 1.501 with an increase in the Cl/Mn ratio from 2.000 to 3.352. In all solutions, the aquamonohalogeno and aquadihalogeno complexes exist as the main species, but the aquadihalogeno complex is more dominant in the $MnCl_2$ solution than in the $MnBr_2$ solution.

The aquahalogenomanganese(II) complex in octahedral environments has a very characteristic visible spectrum which gives rise only to spin-forbidden d-d transitions. As its most striking feature is the extreme weakness of the bands, spectroscopic investigations of solution equilibria must be done in highly concentrated solutions, although the solutions may be more or less contaminated by impurities.[1,2] Therefore, the equilibrium constants, e.g., K_1, range from 0.14—3.89 $mol^{-1}\,dm^3$ for the aqueous ca. 1 mol dm^{-3} $MnCl_2$ solution and from 0.08—1.86 $mol^{-1}\,dm^3$ for the aqueous ca. 1 mol dm^{-3} $MnBr_2$ solution.[5] Thus, a "hard" element, manganese, is placed at different positions in the order of hardness by different investigations.[6]

The results of the X-ray crystal structural analysis of $MnCl_2 \cdot 4H_2O$ and $MnBr_2 \cdot 4H_2O$ show that manganese(II) in the crystals exists as a *cis*-dihalogenotetraaqua complex. In this paper, in oder to determine the structures of aquahalogeno complexes of the manganese(II) ion and the coordination number of manganese(II), and also in order to show the difference in the structures with different bases, such as Br and Cl, an X-ray diffraction investigation has been carried out in highly concentrated aqueous $MnBr_2$ and $MnCl_2$ solutions.

Experimental

All the reagents were of a reagent-grade and were obtained from Wako Pure Chemical Industries.

Aqueous Manganese(II) Bromide Solutions. Manganese(II) bromide was prepared by crystallizing the Mn(II) bromide obtained by dissolving $MnCO_3$ with a purified aqueous hydrobromic acid solution. The Br-1 sample solution was prepared by dissolving the manganese(II) bromide in degasified distilled water. The Br-2 sample solution was prepared by dissolving the manganese(II) bromide in a purified aqueous hydrobromic acid solution and by then diluting the solution with degasified distilled water.

Table 1. Solution Composition (mol dm^{-3}) and the Stoichiometric Volume V per Manganese Atom in Solutions

Solution	Br-1	Br-2	Cl-1	Cl-2
Mn	5.087	2.744	4.744	2.732
X	10.56	8.971	9.488	9.157
H_2O	42.19	44.52	46.08	46.64
ρ/g cm^{-3}	1.859	1.673	1.445	1.319
μ/cm^{-1}	76.68	63.40	13.90	9.923
V/Å^3	326.4	605.2	350.0	607.9

ρ: Density; μ: linear absorption coefficient of the solutions for Mo $K\alpha$ radiation.

Aqueous Manganese(II) Chloride Solutions. The Cl-1 and Cl-2 sample solutions were prepared in ways similar to those described in the preceding section.

The results obtained in the manganese(II) bromide system were compared with those of Fe(II) and Co(II) systems reported in our previous paper.[9] Furthermore, Br-1 and Cl-1 solutions are saturated solutions; thus, the coordination structures of the Mn(II) complexes in the solution may be compared with those in the $MnBr_2 \cdot 4H_2O$ and $MnCl_2 \cdot 4H_2O$ crystals respectively.

The concentrations of manganese(II) and halide ions in the solutions were determined by EDTA titration and the Volhard method respectively. The composition of the sample solutions is shown in Table 1.

X-Ray Diffraction Measurements and Data Treatments. X-Ray diffraction measurements were carried out under an N_2 atmosphere; the N_2 gas was purified by passing it through an alkaline pyrogallol.[9] The scattered intensities were measured at every 0.5° from θ=70° to 36°, at every

†Present address: Yokohama Laboratory, Fine Chemicals Division, Chisso Corporation, 2 Kamariya-cho, Kanazawa-ku, Yokohama 236.
††Present address: Central Institute, Idemitsu Kosan Co., Ltd., Kamiizumi, Sodegaura-machi, Kimitsu-gun, Chiba 292-01.

0.25° from 36° to 18°, and at every 0.1° from 18° to 0.5°; 2θ was the scattering angle. The time required for accumulating 40000 counts was recorded for the Br-2 and Cl-2 solutions, and that for accumulating 80000 counts, for the Br-1 and Cl-1 solutions. The measurements and the treatment of the diffraction intensity data were carried out in the same way described in a previous paper.[10]

The radial distribution function $D(r)$ is given in Eq. 1;

$$D(r) = 4\pi r^2\rho_0 + \frac{2r}{\pi}\int_0^{15} s\cdot i(s)\cdot M(s)\cdot\sin(r\cdot s)\cdot ds, \qquad (1)$$

where ρ_0 is the average scattering density of the sample solution and is given in the electron unit, and where s is equal to $4\pi\sin\theta/\lambda(\lambda=0.7107\text{ Å})$. The modification function, $M(s)$, was the same as that employed previously. The intensities due to the interatomic interactions were:

$$i(s)_{\text{calcd}} = \sum_i^{i\neq j}\sum_j n_{ij}\cdot f_i(s)\cdot f_j(s)\frac{\sin(r_{ij}\cdot s)}{r_{ij}\cdot s}\exp(-b_{ij}\cdot s^2), \qquad (2)$$

where $f_i(s)$ and $f_j(s)$ are the atomic scattering factors of the i and j atoms; n_{ij}, r_{ij}, and b_{ij} are, respectively, the frequency factor, the distance, and the temperature factor of the interaction between the i and j atoms.

In order to attain more precisely the structure parameter values, the above parameter values were refined by the least-squares refinement so as to minimize the difference between $i(s)_{\text{calcd}}$ and observed $i(s)$.

Results

Aqueous Manganese(II) Bromide Solutions. The radial-distribution function curves, $D(r)$ and $D(r)-4\pi r^2\rho_0$ of the Br-1 and Br-2 solutions are shown in Figs. 1 and 2. The radial distribution curve of the Br-1 solution and that of each atom-pair in it are depicted in Fig. 3. Four peaks are seen in the curves at ca. 1.0, 2.2, 2.7, and 3.5 Å; these are probably closely connected with intra- and inter-molecular atomic interactions of the solute complex and solvent H_2O molecules. The distance of the first peak at 1.0 Å is consistent with that of the O–H bond in water molecules.[11] The second peak at 2.2 Å can be ascribed to the Mn–O interaction in the solute complexes, the distance having been reported in the aqueous solution of 2.612 mol dm^{-3} $Mn(ClO_4)_2$.[12] The peak at 2.7 Å may be attributed to the Mn–Br interaction, because the distance is very close to the sum of the ionic radii of Mn^{2+} and Br^-, i.e., 2.79 Å {=0.970 Å(Mn^{2+})+1.82 Å(Br^-)};[13] the distance is also close to the values of 2.802 and 2.913 Å in the $MnBr_2\cdot 4H_2O$ crystal.[8]

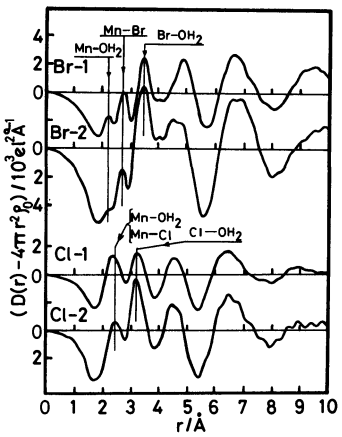

Fig. 2. The $D(r)-4\pi r^2\rho_0$ curves of Br-1, Br-2, Cl-1, and Cl-2 solutions.

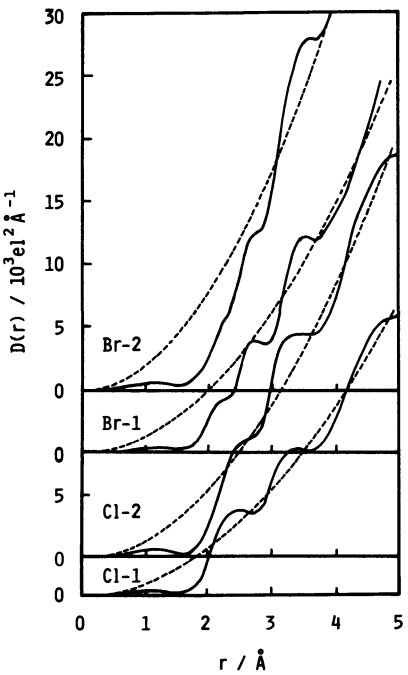

Fig. 1. The radial distribution curves, $D(r)$, for Br-1, Br-2, Cl-1, and Cl-2 solutions. The curves of $4\pi r^2\rho_0$ are shown by dashed lines.

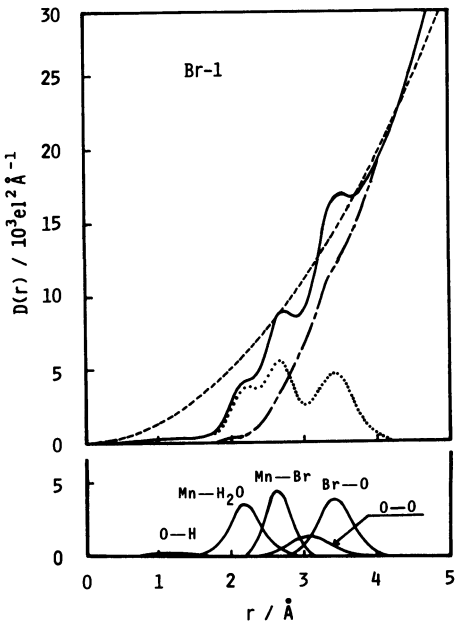

Fig. 3. The residual (——) $D(r)$ curves obtained by subtracting calculated $D(r)$ curves (……) from observed $D(r)$ curve (——) for solution Br-1.

The peak at 3.5 Å can be attributed to the Br–OH_2 interaction, because no comparable peak in this region on the radial-distribution curves is observed for the aqueous 2.612 mol dm^{-3} $Mn(ClO_4)_2$ solution, while a clear peak due to the Br–OH_2 interaction is observed at 3.4 Å for the aqueous 2.5 mol kg^{-1} LiBr solution.[14]

Aqueous Manganese(II) Chloride Solutions. The radial-distribution function curves, $D(r)$ and $D(r)-4\pi r^2\rho_0$, of the Cl-1 and Cl-2 solutions are shown in Figs. 1 and 2. The radial-distribution curve of the Cl-1 solution and that of each atom-pair are shown in Fig. 4. Three peaks are seen in these curves at ca. 1.0, 2.5, and 3.3 Å. The first peak is also consistent with that of the O–H bond in water molecules.[11] The second peak at 2.5 Å may include the Mn–OH_2 and Mn–Cl interactions, because this peak shifted to longer distance with an increase in the concentration of chloride ions, and the position of this peak is close to the sum of the ionic radii of Mn^{2+} and Cl^-, i.e., 2.64 Å{=0.97 Å(Mn^{2+})+1.67 Å(Cl^-)},[13] and it is close to the values of 2.475 and 2.500 Å of Mn–Cl in the $MnCl_2\cdot 4H_2O$ crystal.[7] The Mn–OH_2 interaction observed in the aqueous 2.612 mol dm^{-3} $Mn(ClO_4)_2$ solution at 2.20 Å[12] also appears in the $MnCl_2\cdot 4H_2O$ crystal at 2.22—2.19 Å. Therefore, the peak at 2.5 Å may tentatively be ascribed to the sum of those of the Mn–Cl and Mn–OH_2 interactions.

The peak at 3.3 Å can be ascribed to the Cl–OH_2 interaction, because no comparable peak in this region on the $D(r)$ curve is observed for the aqueous 2.612 mol dm^{-3} $Mn(ClO_4)_2$ solution,[12] but a clear peak due to the Cl–OH_2 interaction is observed at 3.2 Å for the aqueous LiCl solution (mole ratio H_2O: LiCl=3).[15]

From the above considerations, the parameter values on the interatomic distances and frequency and temperature factors of these interactions have been refined. The final parameters are listed in Table 2.

Discussion

Figures 5 and 6 show that the $s\cdot i(s)$ curves calculated from these final data are in good agreement with the observed $s\cdot i(s)$ curves in the region above $s>5$ Å^{-1}. Calculations for the $s\cdot i(s)$ curves made by taking into consideration the Br(Cl)–Br(Cl) or Br(Cl)–H_2O interactions within the *cis*- or *trans*-dihalogeno complexes of manganese(II) did not appreciably improve the results. However, the final data for intramolecular interactions are, we believe, reliable enough, because we obtained smooth background curves in the radial-distribution curves of Br-1 and Cl-1 in the $r<3$ Å region; the disagreement found in the $s\cdot i(s)$ curves of the sample solutions at $s<5$ Å^{-1} is, therefore, due to long-range interactions which we did not take into account in the present calculation.

Aqueous Manganese(II) Bromide Solutions. Since the frequency factors, that is, the mean coordination numbers, n, of Br^- to Mn(II) for Br-1 and Br-2 solutions of Table 2 are 1.104 and 1.212 respectively, not only the monobromoaqua complex but also higher-

Table 2. Results of the Least-Squares Refinement of Solutions

Interaction	Parameter	Br-1	Br-2	Cl-1	Cl-2
Mn–O	r	2.178	2.184	2.185	2.183
	b	0.0045	0.0051	0.0049	0.0047
	n	4.986	4.809	4.654	4.444
Mn–X	r	2.643	2.596	2.492	2.496
	b	0.0050	0.0055	0.0052	0.0049
	n	1.104	1.212	1.259	1.501

X: Br, Cl; r: bond distance, Å; b: temperature factor, Å^2; n: frequency factor.

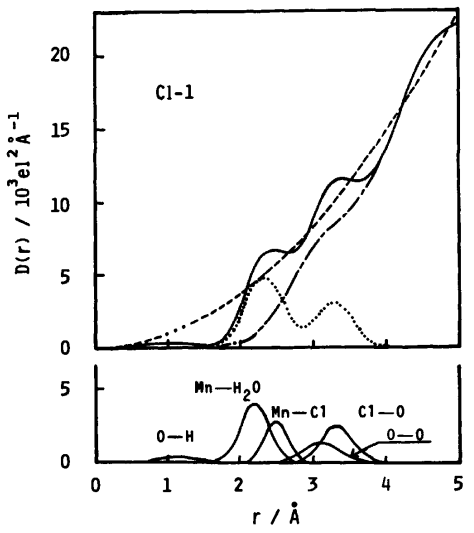

Fig. 4. The residual (——) $D(r)$ curve obtained by subtracting calculated $D(r)$ curve (·····) from observed $D(r)$ curve (——) for solution Cl-1.

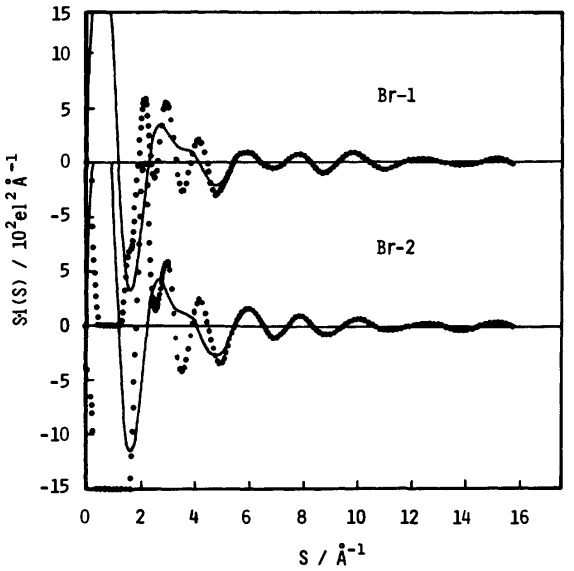

Fig. 5. Observed (°°°°°°) and calculated (——) $s\cdot i(s)$ curves for solutions Br-1 and Br-2.

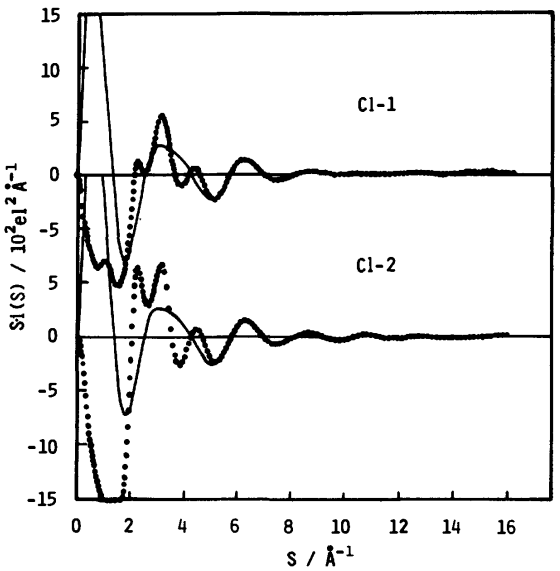

Fig. 6. Observed (○○○○○○) and calculated (——) $s \cdot i(s)$ curves for solutions Cl-1 and Cl-2.

bromoaqua complexes should be formed in these solutions. From a visible-spectrum investigation of the aqueous 4.5 mol dm^{-3} $MnBr_2$ solution, Ito[2] determined the equilibrium constants, K_1 and K_2, to be $K_1=K_2=$ 1.1 mol^{-1} dm^3. Libuś et al.[3,4] also reported the formation constant, K_1, of an aqueous 3.0 mol kg^{-1} $MnBr_2$ solution to be 0.19 mol^{-1} kg. If the K_3 and K_4 of our Br-1 solution are equal to zero, the mean coordination number is calculated as n=1.46 from these constant values;[2] this is close to the value obtained for the bromide solution by the X-ray diffraction experiment, if we take into consideration the different experimental conditions. From the present n value, we can conclude that the monobromoaqua complex is the predominant one in the solution, but that a small amount of the dibromoaqua complex may coexist. Little of the tri- and tetrabromo complexes presumably exist. The coordination numbers of the manganese(II) bromide solutions and those of the iron(II), cobalt(II), nickel(II), and copper(II) bromide solutions[9] suggest that the tendency of metal ions to form bromo complexes is in this order; Cu(II)>Mn(II)>Fe(II)>Co(II)>Ni(II).

Aqueous Manganese(II) Chloride Solutions. Since the mean coordination numbers, n, of Mn(II) with Cl^- in Cl-1 and Cl-2 solutions given in Table 2 are 1.259 and 1.501 respectively, some higher-chloroaqua complexes should exist besides the monochloroaqua complex in these solutions. The equilibrium constants of Mn(II) and Cl^- were determined by Ito[2] to be K_1=3.6 mol^{-1} dm^3 and K_2=2.4 mol^{-1} dm^3. The average coordination number in the Cl-1 solution calculated from these constants is 1.96, which is not too greatly different from the value obtained by the X-ray diffraction experiment. From the n-value results, the predominant solute species in the chloride solutions can be said to be the monochloroaqua complex, as a small amount of the dichloroaqua complex is also present. The concentrations of the tri- and tetrachloro complexes are presumably negligible in these solutions.

X-Ray diffraction measurements at different concentrations of solutions showed that the average coordination number of the Mn–X (X=Br,Cl) contact per Mn(II) increased slightly with an increase in the X/Mn ratios.

Since we could not prepare appropriate solutions for the structural analysis of the dihalogeno complexes because of the lack of reliable stability constants, we employed two saturated solutions, Br-1 and Cl-1, in order to determine the structure of the dihalogeno complexes in these solutions. However, we could not conclude whether the structure of the dihalogeno complexes in the solutions has a *cis*- or *trans*-geometry for the configuration of halogen, since calculated $s \cdot i(s)$ curves from both models of the *cis*- and *trans*-geometries of halogen agreed with the observed curves over the same s regions.

The Mn–OH_2 bond distances are 2.178 and 2.184 Å for the Br-1 and Br-2 solutions respectively, and 2.185 and 2.183 Å for the Cl-1 and Cl-2 solutions respectively. They are well consistent with those within the $Mn(H_2O)_6(NO_3)_2$ crystal[16] (2.157—2.211 Å) (average, 2.181 Å), and are shorter than those of the $MnBr_2 \cdot 4H_2O$ crystal[8] (2.221—2.475 Å) and the $MnCl_2 \cdot 4H_2O$ crystal[7] (2.185—2.224 Å) (average, 2.206 Å). The shortening of the Mn–OH_2 bond distances in these solutions may be understood by the explanation that the water molecules of the Mn–OH_2 bonds are attracted by other water molecules or halide ions less strongly in the solutions than in $MnX_2 \cdot 4H_2O$ crystals. The Mn–X bond distances are 2.643 and 2.596 Å for the Br-1 and Br-2 solutions respectively, and 2.492 and 2.496 Å for the Cl-1 and Cl-2 solutions respectively. The Mn–Cl bond distances are well consistent with those of the $MnCl_2 \cdot 4H_2O$ crystal, 2.475 and 2.500 Å. However, the Mn–Br bond in solution is appreciably shorter than those in the $MnBr_2 \cdot 4H_2O$ crystal (2.802 and 2.913 Å). The shortening of the Mn–Br bond distances in $MnBr_2$ solutions may also be understood by the explanation that the attraction between the bromine atoms of the Mn–Br bonds and water molecules coordinated to other Mn(II) bonds is less strong in the solutions than in the $MnBr_2 \cdot 4H_2O$ crystal, but in the case of the chlorine atoms of the Mn–Cl bonds, the analogous attractions in $MnCl_2$ solutions and in the $MnCl_2 \cdot 4H_2O$ crystal are nearly equal in strength.

References

1) F. A. Cotton and G. Wilkinson, "Advanced Inorganic Chemistry," 2nd ed., Interscience Publishers, New York (1966), p. 840.

2) H. Ito, *J. Sci. Univ. Tokushima*, **14**, 61 (1981).

3) Z. Libuś and H. Tialowska, *J. Solution Chem.*, **4**, 1011 (1975).

4) Z. Libuś and G. Kowalewska, *Pol. J. Chem.*, **52**, 709 (1978).
5) L. G. Sillén and A. E. Martell, "Stability Constants," The Chemical Society, London (1964), Spec. Publ. No. 17, p. 279; Spec. Publ. No. 25, p. 202.
6) K. Saito, *Kagaku to Kogyo*, **26**, 189 (1973).
7) A. Zalkin, J. D. Forrester, and D. H. Templeton, *Inorg. Chem.*, **3**, 529 (1964).
8) K. Sudarsanan, *Acta Crystallogr., Sect. B*, **31**, 2720 (1975).
9) M. Ichihashi, H. Wakita, and I. Masuda, *J. Solution Chem.*, **13**, 505 (1984).
10) H. Wakita, M. Ichihashi, T. Mibuchi, and I. Masuda, *Bull. Chem. Soc. Jpn.*, **55**, 817 (1982).
11) A. H. Narten, "X-Ray Diffraction Data on Liquid Water in the Temperature Range 4—200°C," ORNL-4578 (1970).
12) H. Ohtaki, T. Yamaguchi, and M. Maeda, *Bull. Chem. Soc. Jpn.*, **49**, 701 (1976).
13) R. D. Shannon, *Acta Crystallogr., Sect. A*, **32**, 751 (1976).
14) R. M. Lawrence and R. F. Kruh, *J. Chem. Phys.*, **47**, 4758 (1969).
15) A. H. Narten, F. Vaslow, and H. A. Levy, *J. Chem. Phys.*, **58**, 5017 (1973).
16) B. Ribár, D. Petrović, S. Djurić, and I. Krstanović, *Z. Krist.*, **144**, 334 (1976).

Solution Properties of Phycoerythrin. I. Characterization of Phycoerythrin

Haruo MIZUNO,* Naomichi ISO, Takahide SAITO, Fumiaki OHZEKI,† Hiroo OGAWA,†† and Zao WANG†††
Department of Food Science and Technology, Tokyo University of Fisheries, Minato-ku, Tokyo 108
(Received July 29, 1985)

Phycoerythrin, one of the chromoproteins, from the red alga *Porphyra yezoensis* has been characterized by physicochemical measurement. The value of the sedimentation constant was 12s and it did not change with the change in pH from 5.4 to 6.8. This was assumed from the fact that the phycoerythrin did not undergo reversible dissociation-association reaction under these conditions. The weight average molecular weight of phycoerythrin was determined to be 2.2×10^5, and the intrinsic viscosity of phycoerythrin was determined to be 2.29×10^{-2} (10^{-1} dm^3/g). From these values, the molecular shape of phycoerythrin was inferred to be globular based on the Scheraga-Mandelkern equation. The SDS-polyacrylamide gel electrophoresis of phycoerythrin showed that the phycoerythrin consisted of two subunits with molecular weights of 3.8×10^4 and 2.3×10^4. The sedimentation behavior of phycoerythrin suggested that the phycoerythrin solution was multicomponent. The phycoerythrin dissociated into two molecular species on treatment with sodium dodecyl sulfate. Their sedimentation constants were 12s and 2s. The 2s species was supposed to be phycoerythrin monomer.

Phycoerythrin, which is found widely in red and blue-green algae, is one of the photosynthetic accessory chromoproteins similar to phycocyanin. The function of phycoerythrin in the algal cell is to harvest the light energy during photosynthesis. The properties of the chromoproteins isolated from various algae have been studied extensively by several researchers in various fields of science.[1-4]

We have reported previously on the physicochemical properties, such as the molecular weight, molecular shape and size, dissociation-association behavior, and on the sedimentation and viscosity behavior of phycocyanin isolated from *Porphyra tenera* or *Porphyra yezoensis*.[5-10] Compared with phycocyanin, the physicochemical properties of phycoerythrin from *Porphyra tenera* or *Porphyra yezoensis* have not been studied as extensively, therefore, some points still remain to be clarified.

In this study, we investigated several characteristic properties of phycoerythrin isolated from *Porphyra yezoensis* based on absoption spectra measurement, sedimentation transportation and equilibrium measurements, viscosity measurements, electrophoresis measurements, and amino acid composition analysis.

Experimental

Sample Preparation. The phycoerythrin used in this study was isolated from the dried red alga, *Porphyra yezoensis*, by repeated precipitation with ammonium sulfate. The procedure was essentially the same as that used for the purification of phycocyanin.[5] The ultraviolet and visible absorption spectra of purified phycoerythrin exhibited characteristic peaks at 280, 497, and 565 nm, as shown in Fig. 1, which was the typical spectrum of phycoerythrin.[11] The ratio of the optical density at 565 nm to that at 280 nm has been used to judge the purity of phycoerythrin: The phycoerythrin which had a ratio of more than 5.0 was considered sufficiently pure.[12] The ratio was 5.0 or greater for the phycoerythrin used in this study. The purified sample was stored in a refrigerator at 5 °C as a precipitate with 40% saturated ammonium sulfate. Prior to use, the sample of phycoerythrin was dissolved in water and dialyzed against a phosphate or acetate buffer at 5 °C. Dialysis was continued for at least 48 h, with an occasional change of the external solution.

Ultracentrifugation. The sedimentation velocity measurements were performed on a Hitachi 282 ultracentrifuge. Double sectorial cells were used for all measurements. The rotor speed was set at 47000 rpm, and the temperature was maintained at 25 °C. Schlieren optics was used for the sedimentation velocity measurement. The Schlieren pattern was taken as a photograph on Fuji medical imaging film type FX. The position of the peak in the Schlieren pattern was measured using a Sinko-12 Projector. The sedimentation constant was calculated by the usual method. Phosphate buffer, pH 6.8 and I(ionic strength) 0.1, and acetate buffer, pH 5.4 and I 0.1, were used as solvents. The sedimentation equilibrium experiments were performed on the same ultracentrifuge apparatus as for the sedimentation velocity measurements. All measurements were made at a given speed for approximately 20 h, so as to ensure that an equilibrium was established in a liquid column of about 3 mm. The rotor speeds were set at approximately 9000—12000 rpm, and a temperature of 25 °C was maintained. Interference optics were used for the sedimentation equilibrium measurement. The interference pattern was taken as a photograph on the same film as was used for photographing the Schlieren pattern. The concentration at a radial distance in the cell was calculated from the concentration difference by the use of the formula

$$\Delta c = \Delta J/K$$

where Δc is the concentration difference, ΔJ the number of fringe counted from the meniscus, K the apparatus constant. The number of fringes were measured using the projector. The value of K was determined from the interference pattern of a phycoerythrin solution of known concentration. The weight average molecular weights were calculated by the usual method. The partial specific volume of phycoerythrin, $\bar{v}$, was calculated after ascertaining the

Present address:
†Tobishi Pharmaceutical Co., Ltd., Koganei Research Laboratory, Koganei, Tokyo 184.
††Yamamoto Nori Research Laboratory, Oota-ku, Tokyo 143.
†††Shanghai Fisheries College, 334 Jun Gong Lu, Shanghai, China.

amino acid composition by the Cohn and Edsall method;[13] it was also calculated from the density of the phycoerythrin solutions which were measured by using the Sibayama Model SS-D-200-EXT precision densimeter at various concentrations of phycoerythrin. The value of 0.73 $cm^3 g^{-1}$ was obtained for the partial specific volume from the amino acid composition as shown in Table 1, and the value of 0.72 $cm^3 g^{-1}$ as the partial specific volume was obtained from the density measurement. These values are similar to the value of 0.73 $cm^3 g^{-1}$ reported by MacColl et al.[12] The value of 0.73 $cm^3 g^{-1}$ was used for the calculation of the molecular weight.

Determination of Concentration. The protein concentrations were determined by weighing the substances which were obtained from the aliquots of protein solution by drying at 105 °C until a constant weight. They were also determined by the semi-micro-Kjeldahl method.

Viscosity Measurement. Viscosity measurements were made for phycoerythrin in phosphate buffer solutions of pH 6.8 and I 0.1, at 25 °C. An Ubbelohde dilution type viscometer with a flow time for water ca. 120 s was used for the measurements.

Acrylamide Disc Gel Electrophoresis. Disc electrophoresis of native phycoerythrin was performed according to the method of Davis.[14] A 0.005 mol dm^{-3} Tris-0.0038 mol dm^{-3} glycine system adjusted to pH 8.3 was used for the running buffer solution. The phycoerythrin sample was applied to 4.5 to 7.0% acrylamide gels with the constant ratio of *N,N'*-methylenebis[acrylamide] to acryamide contents. The gel was calibrated by using the following reference proteins: bovine albumin (molecular weight, M_w, 6.8×10^4), catalase (M_w, 2.4×10^5), and ferritin (M_w, 4.5×10^5).

SDS-Polyacrylamide Gel Electrophoresis. The SDS-polyacrylamide gel electrophoresis procedure of Weber and Osborn[15] was employed to measure the molecular weight of the phycoerythrin subunit. The phycoerythrin sample was incubated overnight at room temperature in a 0.01 mol dm^{-3} phosphate buffer solution with 1% 2-mercaptoethanol. The following proteins were used as molecular weight calibration markers: cytochrome c (M_w, 1.25×10^4), chymotrypsinogen (M_w, 2.5×10^4), trypsin inhibitor (M_w, 2.8×10^4), egg albumin (M_w, 4.5×10^4), bovine serum albumin (M_w, 6.8×10^4).

Amino Acid Analysis. The amino acid analysis of phycoerythrin was performed on a JEOL JLC-6AS amino acid analyzer with a Hokusin Laboratory recorder R140-O-D.

Results and Discussion

The sedimentation velocity pattern of phycoerythrin obtained by using Schlieren optics showed a single boundary in phosphate and acetate buffer solutions, respectively. The plot of the sedimentation coefficient versus the concentration of protein was linear over the concentration region of 0.025—0.44 g/10^{-1} dm^3 as shown in Fig. 2. As is seen in this figure, the sedimentation coefficient did not significantly change despite the change in pH of the solution. The concentration dependence of the sedimentation coefficient was not observed at any of the concentrations that were studied. The sedimentation constant of this protein was determined to be 12.2 s at pH 6.8 and 11.9 s at pH 5.4, respectively. These values were

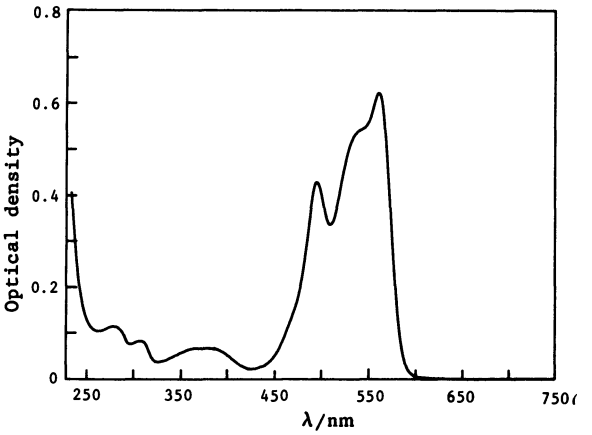

Fig. 1. Typical absorption spectrum of phycoerythrin solution at pH 6.8 and I 0.1.

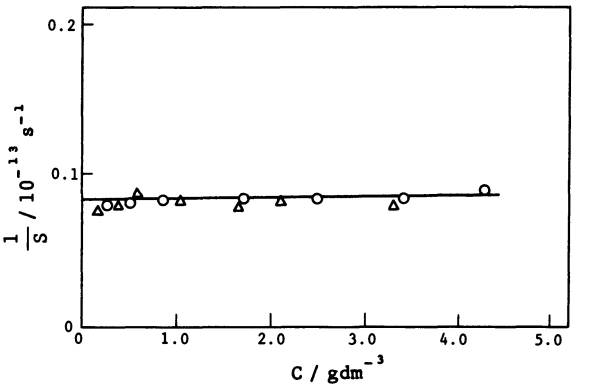

Fig. 2. Plot of the reciprocal of sedimentation coefficients versus concentration in phosphate and acetate buffer solutions.
△: phosphate buffer solution, pH 6.8 and I, 0.1,
○: acetate buffer solution, pH 5.4 and I 0.1.

considered to be almost the same and were in good agreement with the value of 10.8 s for phycocyanin in acetate buffer solutions at pH 5.4 and I 0.1.[5] It is well known that the sedimentation constant of phycocyanin changes with the change in pH of the solution because of the self-dissociation-association reaction.[5,16] Namely, the phycocyanin existed predominantly in the form of a hexamer at pH 5.4, and predominantly in the form of a trimer or tetramer at pH 6.8. The sedimentation constant of the hexamer is 11.3 s, and that of the trimer or tetramer is 6.3 s.[5] Therefore, it seems from the result of this study that the phycoerythrin solution is a single component solution over the pH range of 5.4 to 6.8. The phycoerythrin does not undergo any reversible self-dissociation-association reactions under these pH conditions.

Figure 3 shows the plot of the logarithm of concentration of the protein versus the square of the radial distance in the sedimentation equilibrium cell. It was drawn from the analysis of the sedimentation equilibrium pattern for the phycoerythrin at pH 5.4 and I 0.1. As is clearly seen from the figure, the plot

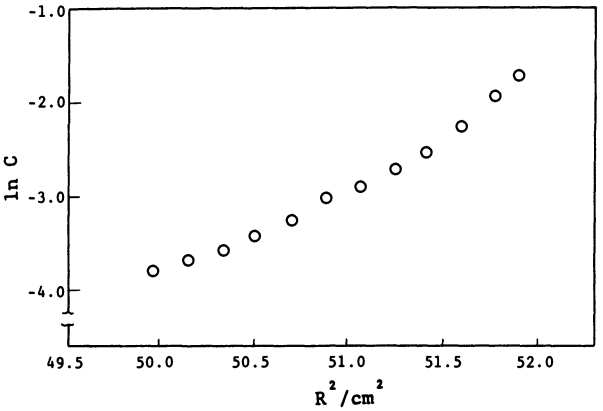

Fig. 3. Plot of the logarithm of concentration versus the square of radial distance in sedimentation equilibrium cell.

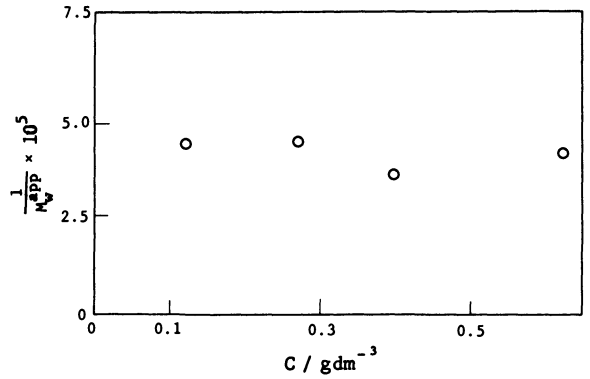

Fig. 4. Plot of the reciprocal of apparent weight average molecular weight versus concentration.

has a curvature. This sedimentation equilibrium behavior means that the phycoerythrin solution is a multicomponent solution at pH 5.4 and I 0.1. This result is inconsistent with that from the sedimentation velocity measurements. It may be reasonable to consider that the minor components in the phycoerythrin solution, probably phycoerythrin monomer and its associated species, were not found in the Schlieren pattern under our experimental conditions because the concentration of these minor components is very low.

Figure 4 shows the plot of the reciprocal of the apparent weight average molecular weight of phycoerythrin, $1/M_w^{app}$, versus concentration. The weight-average molecular weight of phycoerythrin was determined to be 2.2×10^5 from the plot. This value agrees with that reported by Svedberg et al.[1] The second virial coefficient, A_2, was estimated to be 1.1×10^{-5} ($cm^3 mol/g^2$). Therefore, the phycoerythrin solution may be considered to be a pseudo-ideal solution similar to a phycocyanin solution. This property is characteristic of globular proteins.

Figure 5 shows the result of the viscosity measurements for phycoerythrin performed at pH 6.8 and I 0.1. The intrinsic viscosity of phycoerythrin was found

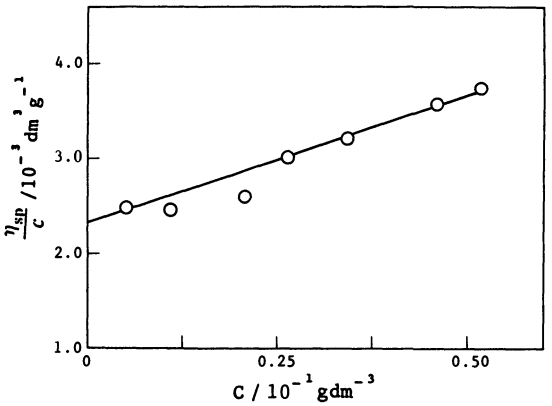

Fig. 5. Plot of the reduced viscosity of phycoerythrin in phosphate buffer versus concentration.

to be 2.29×10^{-2} ($10^{-1} dm^3/g$). Tanford has stated that the values of the intrinsic viscosity of globular proteins lie between 3.3×10^{-2} ($10^{-1} dm^3/g$) and 4.0×10^{-2} ($10^{-1} dm^3/g$) regardless of the molecular weight of the protein.[17] The value of the intrinsic viscosity of phycoerythrin did not differ greatly from that of the globular proteins.

Scheraga and Mandelkern derived the following equation for a revolutional ellipsoid:[18]

$$s_0[\eta]^{1/3} = \frac{M^{2/3}(1-\bar{v}\rho)\beta}{N_A\eta_0}, \quad (1)$$

where s_0 is the sedimentation constant, $[\eta]$ the intrinsic viscosity, M the molecular weight, $\bar{v}$ the partial specific volume of the solute, ρ the density of the solvent, N_A Avogadro's number and η_0 the viscosity of the solvent. The quantity β is a function of the axial ratio of ellipsoid, and has a value of $2.12—2.20\times10^6$ for a prolate ellipsoid when the axial ratio is less than 5.

The β value for the phycoerythrin was calculated to be 2.16×10^6 using Eq. 1. Therefore, it is reasonable to assume from the values of A_2, $[\eta]$, and β, that the phycoerythrin is a globular protein.

Disc gel electrophoresis for phycoerythrin exhibited two bands. The molecular weight of each band was calculated to be 2.3×10^5 and 2.4×10^5 from the calibration plot as shown in Fig. 6. Although the values of the molecular weights of the two bands are nearly the same, the result suggests that the phycoerythrin solution is a multicomponent solution. Also, the result corresponds to the sedimentation equilibrium behavior observed for phycoerythrin in this study. It may be assumed that the appearance of two bands is due to some denaturation occurred during the disc electrophoresis or some difference in their structure. However, these points are not clear.

SDS-polyacrylamide gel electrophoresis for phycoerythrin exhibited two bands, with the molecular weights of 3.8×10^4 and 2.3×10^4 as is shown in Fig. 7. Those molecular weights might correspond to

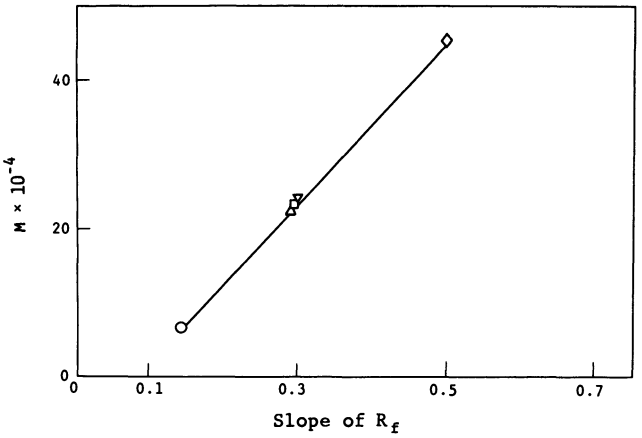

Fig. 6. Molecular weight determination of native phycoerythrin by disc electrophoresis. Three marker proteins used were, bovine serum albumin, catalase and ferritin. All proteins were run on various different concentrations of gel, and the slope (axis of abscissa) was obtained from the plot of the R_f-value versus concentration.
○: Bovine serum albumin, □: catalase, ◇: ferritin, △ and ▽: phycoerythrin.

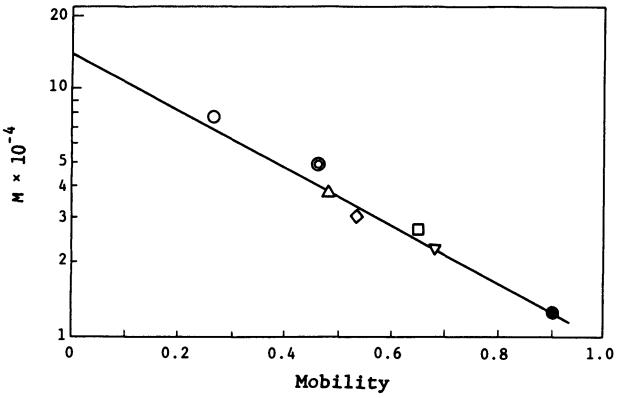

Fig. 7. Determination of molecular weight of denatured phycoerythrin by SDS-polyacrylamide gel electrophoresis. The mobilities on 10% gel were plotted against the known molecular weight expressed on a semi-logarithmic scale. The five proteins used as the marker.
●: Cytochrome c, □: chymotrypsinogen, ◇: trypsin inhibitor, ◎: egg albumin, ○: bovine serum albumin, △ and ▽: phycoerythrin.

the subunits which have been reported for phycoerythrin from *Porphyridium cruentum* by Glazer et al.[3] O'Carra and Killilea have observed two polypeptides for phycoerythrin from *Phormidium persicinum* by polyacrylamide gel electrophoresis in SDS solution. They suggested that the phycoerythrin existed as a polypeptide dimer composed of two different types of chain with a molecular weight of 1.97×10^4 and 2.20×10^4.[19] MacColl et al. have proposed that the phycoerythrin from *Rhodomonas lens* was composed of two pairs of subunits ($\alpha_2\beta_2$), and the molecular weights of α and β are 9.8×10^3 and 1.7×10^4, respectively.[12] It may be said that the phycoerythrin

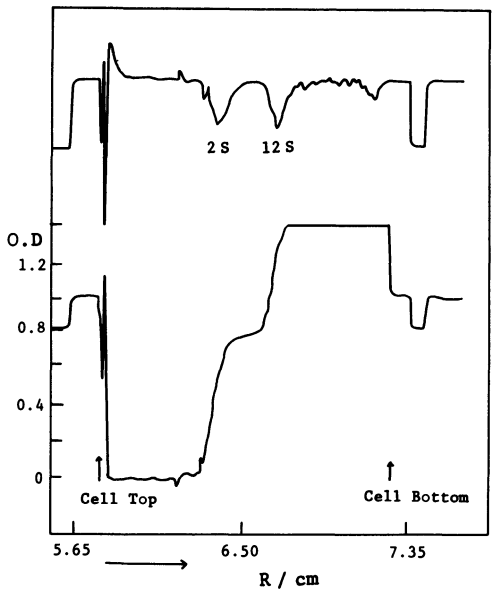

Fig. 8. Absorbance distribution and absorbance gradient distribution corresponding to the concentration distribution in the sedimentation velocity measurement for the denatured phycoerythrin. The curve in the under side and in the upper side represents the absorbance distribution and absorbance gradient distribution, respectively. The abscissa represents the radial distance, R, in the ultracentrifuge cell.

from *Porphyra yezoensis* is composed of two subunits similar to the other phycoerythrin from various different algae.

Figure 8 represents the result of the sedimentation velocity measurement for the denatured phycoerythrin treated with sodium dodecyl sulfate at a concentration of 0.005 mol dm^{-3}. The curves of absorbance distribution (under side) and of its differentiation (upper side) in the ultracentrifuge cell were drawn by the recorder connected with the absorption scanner. In this figure, two boundaries with a sedimentation coefficient of approximately 12 and 2 s were observed for the denatured phycoerythrin. The value of 12 s is close to that of phycoerythrin in the phosphate and acetate buffers obtained in this study. It is supposed that the 12 s component is probably a native phycoerythrin which was not affected by the sodium dodecyl sulfate treatment. It is also supposed that the appearance of the 2 s component can be attributed to the dissociation of the phycoerythrin. The 12 s component may correspond to the band in the disc electrophoresis. Hattori et al. have reported the value of 3.2 s for the phycocyanin monomer.[16] Although the value of 2 s is somewhat lower than that of the phycocyanin monomer, it may be said that the 2 s component corresponds to the phycoerythrin monomer composed of two subunits which appeared in the SDS electrophoresis observed in this study. The 2 s component may expand a little by interaction with the sodium dodecyl sulfate so that the sedimentation velocity decreases.

Thus, it is likely that the phycoerythrin from *Porphyra yezoensis* is a globular protein and its solution is a multicomponent solution although the concentration of the minor component is very low. Phycoerythrin seems to be stable compared with phycocyanin in solution over the pH range of 5.4 to 6.8. Unlike phycocyanin, there is no evidence that phycoerythrin undergoes a reversible self-associating reaction with change of pH from 5.4 to 6.8.

References

1) T. Svedberg and T. Katsurai, *J. Am. Chem. Soc.*, **51**, 3573 (1929).
2) E. Gantt and C. A. Lipschulitz, *Biochemistry*, **13**, 2960 (1974).
3) A. N. Glazer and C. S. Hixon, *J. Biol. Chem.*, **252**, 32 (1977).
4) R. Kikuchi, K. Ashida, and S. Hirao, *Bull. Japan. Soc. Sci. Fish.*, **45**, 1461 (1979).
5) T. Saito, N. Iso, and H. Mizuno, *Bull. Chem. Soc. Jpn.*, **47**, 1375 (1974).
6) A. Kotera, T. Saito, N. Iso, H. Mizuno, and N. Taki, *Bull. Chem. Soc. Jpn.*, **48**, 1176 (1975).
7) H. Mizuno, T. Saito, and N. Iso, *Bull. Chem. Soc. Jpn.*, **48**, 3496 (1975).
8) N. Iso, H. Mizuno, T. Saito, N. Nitta, and K. Yoshizaki, *Bull. Chem. Soc. Jpn.*, **50**, 2892 (1977).
9) T. Saito, N. Iso, H. Mizuno, and I. Kitamura, *Bull. Chem. Soc. Jpn.*, **51**, 3471 (1978).
10) T. Saito, N. Iso, H. Mizuno, F. Ozeki, and Y. Matsui, *Bull. Chem. Soc. Jpn.*, **53**, 599 (1980).
11) A. Hattori and Y. Fujita, *J. Biochem.*, **46**, 663 (1959).
12) R. MacColl, D. S. Berns, and O. Gibbons, *Arch. Biochem. Biophys.*, **177**, 265 (1976).
13) E. J. Cohn and J. T. Edsall, "Proteins, Amino Acids, and Peptides," Reinhold, New York (1943), p. 372.
14) B. J. Davis, *Ann. N. Y. Acad. Sci.*, **121**, 404 (1964).
15) K. Weber and M. Osborn, *J. Biol. Chem.*, **244**, 4406 (1969).
16) A. Hattori, H. L. Crespi, and J. J. Katz, *Biochemistry*, **41**, 1225 (1965).
17) C. Tanford, "Physical Chemistry of Macromolecules," John Wiley and Sons, Inc., New York and London (1961), p. 394.
18) H. A. Scheraga and L. Mandelkern, *J. Am. Chem. Soc.*, **75**, 179 (1953).
19) O. O'Carra and S. D. Killilea, *Biochem. Biophys, Res. Commun.*, **45**, 1192 (1971).

An Electric-Field-Pulse Relaxation Study of the Electron-Donor-Acceptor Complex Formation Involving 7,7,8,8-Tetracyanoquinodimethane Solubilized at the Surfactant Bilayer/Magnetite Particle Interface

Tetsuya IKEDA,* Shoji HARADA, and Tatsuya YASUNAGA
Department of Chemistry, Faculty of Science, Hiroshima University, Higashisenda-machi, Naka-ku, Hiroshima 730
(Received October 11, 1985)

Ultrafine magnetite particle (Fe_3O_4) which adsorbed the 7,7,8,8-tetracyanoquinodimethane (TCNQ)-dioctadecyldimethylammonium bromide (DODAB) bilayer on the surface were prepared in an aqueous solution by sonication. A single relaxation was found by using the electric-field-pulse method and was attributed to the association-dissociation process of the electron-donor-acceptor complexes involving TCNQ solubilized at the DODAB bilayer/magnetite particle interface.

In a previous paper,[1] we have shown that tungstic acid particles incorporated with a dioctadecyldimethylammonium bromide (DODAB) bilayer exhibit unique properties. Surfactants can solubilize various organic materials in the lamellar layer.[2] The kinetic studies of various reactions in the lamellar layer of the vesicles have made a significant contribution to various research fields, e.g., colloid chemistry and photochemistry.[2-5] The surfactants sonicated with the ultrafine particles form a rigid lamellar layer on the dispersed particle surface. In order to understand the dynamic behavior of solubilized molecules and electrons in the lamellar layer of the surfactant, one must study the kinetics of various reactions in the lamellar layer around the ultrafine particles. The ultrafine magnetite particle we chose for such a study is a suitable material, for it has monodispersity and easily adsorbs the surfactant bilayer onto the particle surface.

In this paper, we present our findings on the electric-field-pulse relaxation kinetics of the electron-donor-acceptor complex formation involving TCNQ solubilized at the DODAB bilayer/magnetite particle interface.

Experimental

The 7,7,8,8-tetracyanoquinodimethane (TCNQ) and dioctadecyldimethylammonium bromide (DODAB) were purchased from the Kodak Co.

The ultrafine magnetite particles (Fe_3O_4) were prepared from an aqueous solution containing 1.51 g $FeCl_3$ and 0.64 g $FeCl_2$.[6] During stirring, the pH of the solution was kept in the range of 10—11 by the drop-by-drop addition of 7.5% NH_4OH; the solution was then heated to about 60 °C in a water bath for 15 min. The precipitate was washed several times with distilled water by using the centrifugation of 10000 g for 10 min and was then dispersed in an aqueous solution. The large particles which aggregated were removed by using a membrane filter (pore size, 0.2 μm).

The magnetite particles which adsorbed TCNQ-containing DODAB were prepared as follows. DODAB of 10 mg and the required amount of TCNQ were dispersed in chloroform. After the evaporation of the chloroform, the residue was dispersed in distilled water (10 ml). The turbid suspension was added to the magnetite suspension and was sonicated by a horn-type ultrasonic homogenizer (28 kHz, Choonpa Co.) for 20 min at a temperature of about 60 °C. The magnetite particles are stabilized for a few days by the adsorption of the surfactant bilayer onto the solid surface. The size of the ultrafine magnetite particle studied here is less than 0.2 μm. The values of the pH after the preparation were in the range of 6.5—7. The details of the electric-field-pulse apparatus have been described elsewhere.[7] The transient optical-transmittance change caused by the applied electric field was recorded with a transient recorder. The strength and the length of the electric-square pulse were 20 kV/cm and 25 μs respectively.

The ζ-potential of the magnetite particles incorporating the DODAB bilayer was measured by means of microelectrophoresis method.

The temperature of all the kinetic and spectral experiments was controlled at 25 °C.

Results and Discussion

To make clear the surface character of the present materials, microelectrophoretic measurements were carried out. It was found that the DODAB/magnetite particles which appeared in the microscope field moved toward the negative electrode in the pH range of 3—11. The values of the ζ-potential of the DODAB/magnetite particle system solubilized TCNQ were determined to be 70±3 mV in this pH range. This experimental result shows that no negatively charged particles exist in the basic region. Taking into account the fact that the pH_{zpc} value of the magnetite particle in an aqueous solution is nearly 7, one can see that the negative charge due to the surface functional groups of the magnetite particle is counteracted by the positive DODAB molecule of the bilayer under the present experimental conditions. Furthermore, it is seen that the surface charge may originate from only the DODAB molecule of the bilayer adsorbed on the particle surface or entrapping the particle in the vesicle.

Figure 1 shows the absorption spectrum of the TCNQ–DODAB system incorporating the magnetite particles. In this figure, three absorption bands appear at the wavelengths of 680, 750, and 850 nm, in agreement with those of the anion radical of TCNQ

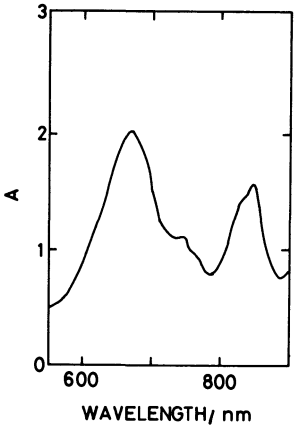

Fig. 1. Electronic absorption spectrum of the DODAB bilayer/magnetite particle system solubilized TCNQ. [TCNQ]=2.95×10^{-5} mol dm^{-3}, [DODAB]=2.54×10^{-3} mol dm^{-3}, particle concentration=0.36 g dm^{-3}, path length=1 cm.

Table 1. Kinetic Data of the Electric-Field Pulse Experiment in the TCNQ-DODAB/Magnetite System at 25 °C[a)]

[TCNQ]	[DODAB]	C_p	τ^{-1}
10^{-5} mol dm^{-3}	10^{-3} mol dm^{-3}	g dm^{-3}	10^4 s^{-1}
0.74	0.63	0.91	9.5±0.5
1.23	0.63	0.91	9.8±0.4
1.23	1.59	2.28	9.2±0.4
1.72	0.63	0.91	10.8±0.1
1.85	1.59	2.28	10.7±0.7
1.97	2.54	3.64	10.2±0.2
2.95	2.54	3.64	9.5±0.7
3.08	1.59	2.28	9.8±0.5
4.31	1.59	2.28	11.0±0.5
4.92	2.54	3.64	9.9±0.3
6.89	2.54	3.64	11.1±0.1

a) Each point is the mean value of the five lowest individual determinations. The experimental error stands for the standard deviation.

which have been reported by Melby et al.[8] However, the TCNQ-DODAB system without particles and the TCNQ/magnetite particle system in chloroform do not show the absorption peak at 850 nm. Since TCNQ is insoluble in an aqueous solution, and since the steric hindrance of the DODAB molecule is too large to form an electron-donor-acceptor complex of DODAB with TCNQ in the DODAB bilayer solubilized TCNQ, an electron donor in this system may be the magnetite particles. Thus, one can see that an electron transfer from the magnetite particle to the solubilized TCNQ molecule takes place in the DODAB bilayer adsorbed on the magnetite-particle surface. In this reaction, the DODAB bilayer is not related to the complex formation, but provides only the reaction field.

A single relaxation was observed in the TCNQ-DODAB/magnetite system at the wavelength of 630—650 nm by using the electric-field-pulse method, in which the relaxation signal indicates an increase in the transmittance of the sample solution during the application of the electric field. No relaxation was observed in the aqueous solutions of DODAB-solubilized TCNQ or in the aqueous suspensions of only the DODAB/magnetite system. The value of the relaxation time, τ, in the presence of the electric field is equal to that in the absence of the electric field. The dependences of τ^{-1} on the concentrations of TCNQ and DODAB are given in Table 1. As can be seen from this table, the value of τ^{-1} increases slightly with an increase in concentration of TCNQ. In view of the lack of relaxation in both the DODAB/magnetite and the TCNQ-DODAB systems, it may be suggested that the single relaxation observed relates to an interfacial process at the DODAB bilayer/magnetite particle interface.

The formation of the electron-donor-acceptor complex at the bilayer/particle interface can be written schematically as:

$$(\mathrm{TCNQ})_{\mathrm{bilayer}} + \mathrm{Fe_3O_4} \overset{K}{\rightleftharpoons} (\mathrm{TCNQ^{\cdot-}\cdots Fe_3O_4^{+}})_{\mathrm{bilayer}}, \quad [\mathrm{I}]$$

with:

$$K = \frac{[(\mathrm{TCNQ^{\cdot-}\cdots Fe_3O_4^{+}})_{\mathrm{bilayer}}]}{[\mathrm{Fe_3O_4}][(\mathrm{TCNQ})_{\mathrm{bilayer}}]}, \quad (1)$$

where ( )$_{\mathrm{bilayer}}$ stands for "in the bilayer." TCNQ$^{\cdot-}$ is the anion radical of TCNQ, and K is the equilibrium constant. For the condition $C_P \gg C_{TCNQ}$, one can obtain the following equation:

$$\frac{C_{\mathrm{TCNQ}}}{A_{850}} = \frac{1}{\varepsilon_{850}}\left\{\frac{1}{KC_p}+1\right\}, \quad (2)$$

where C_{TCNQ}, C_P, A_{850}, and ε_{850} are the total concentration of TCNQ, the total concentration of the magnetite particle, the absorbance, and the molar extinction coefficient of the anion radical of TCNQ at the wavelength of 850 nm respectively. The plot of C_{TCNQ}/A_{850} vs. $1/C_P$ yields a straight line, as is shown in Fig. 2a. From the intercept of the straight line, the value of ε_{850} was obtained as 44000. This value is in good agreement with that of 43300 reported by Melby et al.[8] The value of the slope in this plot is close to zero, indicating a very high value for K. Thus, all of the TCNQ molecules form an electron-donor-acceptor complex with magnetite at the interface of the DODAB bilayer.

For the reaction at the interface (Mechanism II),

$$2(\mathrm{TCNQ^{\cdot-}\cdots Fe_3O_4^{+}})_{\mathrm{bilayer}} \underset{k_b}{\overset{k_f}{\rightleftharpoons}} (\mathrm{TCNQ^{\cdot-}\cdots Fe_3O_4^{+}})_{\mathrm{bilayer},2} \quad [\mathrm{II}]$$

the reciprocal relaxation time is written as:

$$(\tau^{-1})^2 = 8k_fk_bC_{\mathrm{TCNQ}} + (k_b)^2. \quad (3)$$

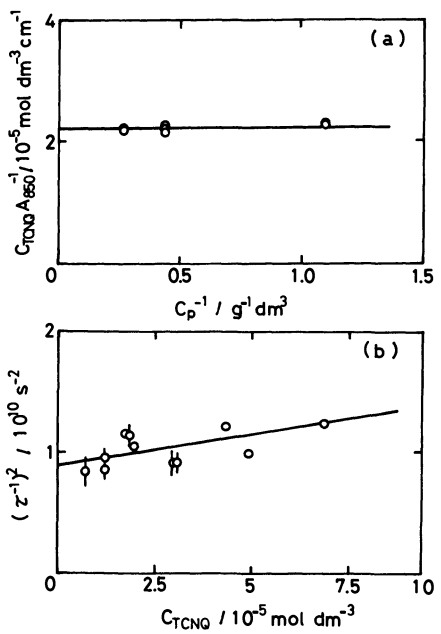

Fig. 2. (a) Plot of C_{TCNQ}/A_{850} vs. $1/C_p$ in Eq. 2. (b) Plot of $(\tau^{-1})^2$ vs. C_{TCNQ} in Eq. 3.

The plot of $(\tau^{-1})^2$ vs. C_{TCNQ}, shown in Fig. 2b, yields a straight line. This linearity leads to the conclusion that the single relaxation phenomenon observed may be attributed to Mechanism II. The values of the rate constants, k_f and k_b, obtained from the values of the slope and the intercept of the straight line in Fig. 2b are as follows: $k_f=6.6\times10^7$ mol^{-1} dm^{3}s^{-1}; $k_b=9.5\times10^4$ s^{-1}. The anion radical of the TCNQ molecule, which has the absorption peak at 850 nm, could not be found in the TCNQ–DODAB system. This fact indicates that it is too hard to form an electron-donor-acceptor complex in the bilayer because of the lack of an electron donor. Since the DODAB bilayer/magnetite particle interface was made by incorporating the particle, we are led to the conclusion that the interface may act as a reaction field for the electron-donor-acceptor complex formation between the magnetite particle and the TCNQ molecule.

The authors are grateful to Professor Z. A. Schelly in the University of Texas at Arlington for his critical reading of the manuscript and for his helpful discussion.

References

1) T. Ikeda and T. Yasunaga, *J. Phys. Chem.*, in press.
2) J. H. Fendler and E. J. Fendler, "Catalysis in Micellar and Macromolecular Systems," Academic Press, N. Y. (1975).
3) S. Harada and Z. A. Schelly, *J. Phys. Chem.*, **86**, 2098 (1982).
4) S. Harada, Y. Takada, and T. Yasunaga, *J. Colloid Interface Sci.*, **101**, 524 (1984).
5) Yves-M. Tricot and J. H. Fendler, *J. Am. Chem. Soc.*, **106**, 2475 (1984).
6) R. S. Molday and D. J. Mackenzie, *J. Immunol. Methods*, **52**, 353 (1982).
7) Y. Tsuji, T. Yasunaga, T. Sano, and H. Ushio, *J. Am. Chem. Soc.*, **98**, 813 (1976).
8) L. R. Melby, R. J. Harder, W. R. Hertler, W. Mahler, R. E. Benson, and W. E. Mochel, *J. Am. Chem. Soc.*, **84**, 3374 (1962).

 © 1986 The Chemical Society of Japan Bull. Chem. Soc. Jpn., 59, 1171—1173 (1986)

Molecular Motion in $GeCl_4$ as Studied by ^{35}Cl Nuclear Quadrupole Resonance

Hirokazu NAKAYAMA, Nobuo NAKAMURA, and Hideaki CHIHARA*
Department of Chemistry, Faculty of Science, Osaka University, Toyonaka, Osaka 560
(Received November 12, 1985)

Temperature dependence of ^{35}Cl nuclear quadrupole resonance frequencies and quadrupole relaxation time was measured of $GeCl_4$ in the metastable phase. Above 160 K, molecular reorientation is seen active; its activation energy is 63.5 kJ mol^{-1}. This energy probably prevents $GeCl_4$ from undergoing a rotational phase transition.

Although a series of molecules MCl_4 (M=C, Si, Ge, Sn) are nearly globular assuming Td symmetry in gas phase, they do not solidify into plastic crystal except CCl_4[1] nor undergo any solid-solid phase transitions.[2-4]

In a series of works on the dynamical properties and the stability of plastic crystals, we recognized that $GeCl_4$ shows an interesting thermal behavior: This material was reported to crystallize into two phases, stable and metastable, although the condition of the preparation of each phase has not been established. The stable phase melts at 223.7 K and the metastable phase melts at 221.4 K.[5] In the heat capacity measurements[6] of the so-called metastable phase of this compound an exothermic phenomenon was observed near its melting point which appeared to be a kind of relaxation. This thermal effect may be a manifestation of some phase properties similar to the case of carbon tetrachloride[7] where the metastable cubic phase is transformed into the stable rhombohedral phase spontaneously. Such consideration led us to study of the temperature dependence of the NQR frequencies and of the spin-lattice relaxation times in $GeCl_4$.

Experimental

Commercially available specimen of $GeCl_4$ (Soekawa Chemical Co., Ltd, stated purity 99.999999%) was vacuum distilled and sealed in a glass ampoule with 13 Pa He gas. This sample is of the same origin as that used for the previous heat capacity measurements.[6]

All the measurements were made using a MATEC pulsed spectrometer system by the FT method to determine the frequencies of three closely spaced resonance lines, the error being ±0.2 kHz. The nuclear quadrupolar spin-lattice relaxation time T_1 was measured with the $\pi/2-\tau-\pi/2$ method with an estimated error of ±10 percent.

The temperature dependence was determined by using a simple cryostat with liquid nitrogen as the refrigerant. The temperature was kept constant within ±0.1 K during the measurement and measured with Chromel-P vs. Constantan thermocouples, calibrated against the standard platinum resistance thermometer.

Results and Discussion

In our experiment only one of the two phases reported so far could be obtained by both rapid quenching and slow cooling. The solid samples prepared by different cooling rates gave the same NQR spectrum and their melting points were 221.6 K. Therefore, we identified our specimen as the "metastable phase."

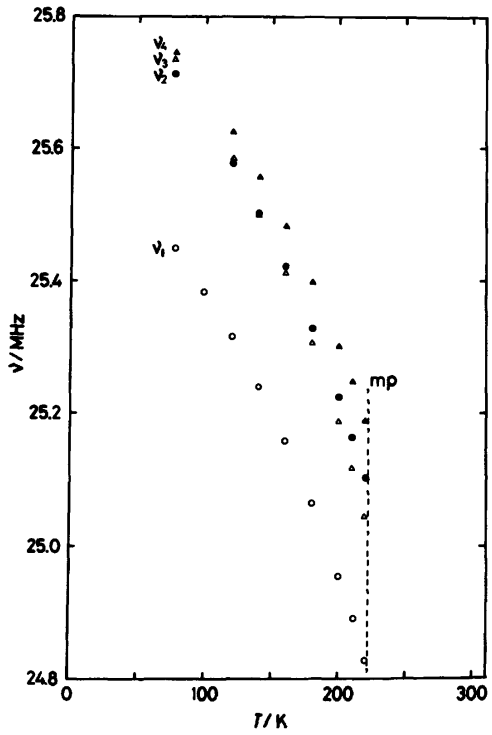

Fig. 1. Temperature dependence of ^{35}Cl NQR frequencies in $GeCl_4$.

Four ^{35}Cl nuclear quadrupole resonance lines were observed at 77 K and their frequencies (ν_1=25.4491 MHz, ν_2=25.7131 MHz, ν_3=25.7356 MHz, ν_4=25.7463 MHz) agree with those reported by S. Sengupta et al.[8] within ±0.2 kHz. Temperature dependence of the resonance frequencies is shown in Fig. 1.

At around 120 K only three resonance signals are observed because of accidental overlap of two of the resonance lines. The NQR signals broadened above 210 K and disappeared just below the melting point. This broadening is induced by the molecular reorientation as will be discussed later.

Because the upper three resonance lines (ν_2, ν_3, and ν_4) occurred in a very narrow frequency range, their spin-lattice relaxation times could not be measured accurately. The temperature dependence of the spin-lattice relaxation time for the lowest resonance line

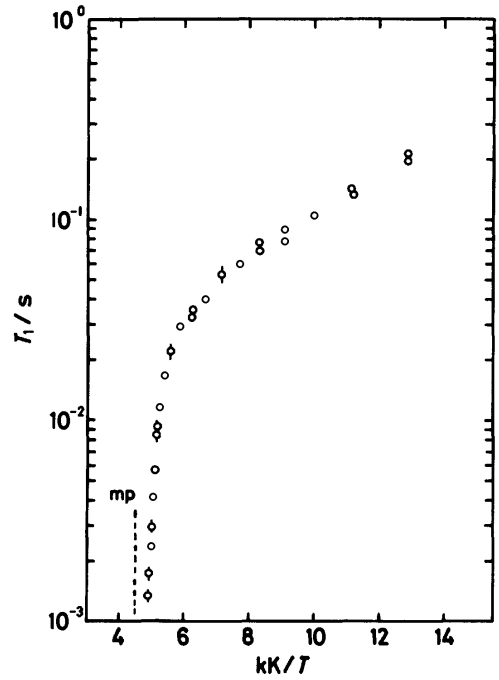

Fig. 2. Temperature dependence of ^{35}Cl spin-lattice relaxation time for the line ν_1 in $GeCl_4$.

(ν_1) is shown in Fig. 2. The plot of the relaxation rate T_1^{-1} vs. T^2 gives a straight line below 160 K, suggesting that the librational motion[9] of $GeCl_4$ molecules governs the spin-lattice relaxation below 160 K. Above 160 K a sharp decrease in the spin-lattice relaxation time was observed due to molecular reorientational motion.[10] The spin-lattice relaxation time T_1 can be reproduced by the expression

$$T_1^{-1}/s^{-1} = 9.77 \cdot 10^{-4} \cdot (T/K)^2 + 1.30 \cdot 10^{19} \exp(-63.5\ kJ\ mol^{-1}/RT). \quad (1)$$

The first term is the contribution of librational motion of the molecule, which is dominant below 160 K. The second term is brought about by the molecular reorientation with the activation energy of 63.5 kJ mol^{-1} and is dominant above 160 K. The correlation time, τ_c, can be related to T_1 by assuming an isotropic sudden jump process between four nearly tetrahedral sites as[10]

$$\tau_c \simeq (3/4) T_1. \quad (2)$$

The τ_c thus obtained is plotted in Fig. 3 as a function of the reciprocal temperature; it gives the pre-exponential factor τ_0 a value of $5.76 \cdot 10^{-20}$ s. The correlation time, τ_c, at the melting point is $5.4 \cdot 10^{-5}$ s.

In globular molecules having tetrahedral or octahedral symmetry, which show plastic phases, the correlation time of the molecular overall reorientation at the brittle-plastic phase transition lies usually in the range between $7 \cdot 10^{-9}$ and 10^{-11} s,[11-14] whereas, τ_c for $GeCl_4$ is as long as 10^{-5} s even at the melting

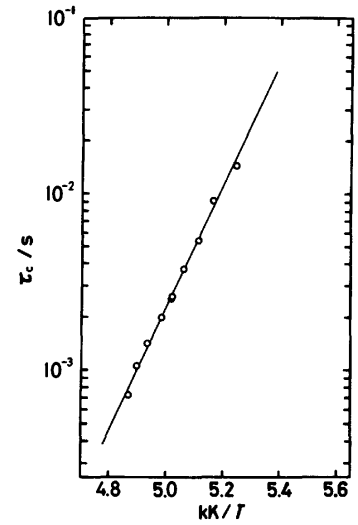

Fig. 3. Temperature dependence of the correlation time for the overall rotation in $GeCl_4$.

point. This fact shows that in $GeCl_4$ the molecular reorientation is not so sufficiently excited that the crystal undergoes a rotational transition to a plastic phase even at the melting point. If we use the empirical relation[15] $E_r = \alpha \cdot R \cdot T_c$ to derive the hypothetical rotational transition point T_c from the rotational activation energy E_r, the rotational transition would not occur until about 1000 K is reached, using $\alpha = 7.5$ for the brittle phase.[15] Although the origin of the very high E_r is not known at the present stage, it prevents the $GeCl_4$ crystal from undergoing a rotational transition despite the fact that the each molecule is globular.

As mentioned in the introduction, an interesting thermal relaxation was observed above 190 K during the heat capacity measurements.[6] Thus, a small but distinct exothermic phenomenon occurs with a time constant of 40 min at 190 K, 2 h at 200 K and 10 h at 210 K. Hence we attempted to detect some effect of such a thermal relaxation phenomenon on the NQR parameters. Because of the very long (≈700 μs) free induction signal and short T_1 (≈1 ms) it was not possible to measure T_1 above 205 K. We, therefore, searched for a possible change of the ^{35}Cl NQR line shape with time: At 200, 205, 210, and 212 K, any variation of the line shape was not detected during twice the thermal time constant in each temperature. The reason why NQR did not see the corresponding anomaly is not apparent at present.

Among MX_4 compounds (M=Si, Ge, Sn; X=halogen), $SnCl_4$[16] and $SnBr_4$[17] show $P2_1/c$ structures with $Z=4$. The unit cell contains four crystallographically inequivalent halogen atoms. These two compounds as well as most of other tetrahalo compounds including $GeCl_4$ give similar NQR spectra, i.e., there are four NQR lines[18,19] of which three higher frequency lines are closely spaced and the lowest frequency line is far removed from the three upper lines. Thus, the NQR

Table 1. Values of the Ratio of Atomic Radii

	F	Cl	Br	I
C	0.24	0.17	0.16	0.14
Si	0.34	0.24	0.22	0.19
Ge	0.45	0.32	0.29	0.26
Sn	0.58	0.41	0.38	0.33

spectrum of $GeCl_4$ suggests strongly that the crystal assumes the crystal structure isomorphous with $SnCl_4$ and $SnBr_4$, i.e., $P2_1/c$. A recent Zeeman NQR study of $GeCl_4$[7] claimed that the metastable phase is orthorhombic with *mmm* or D_{2h} symmetry. Close examination of the result of their Zeeman effect study reveals, however, that the direction cosines of the twelve principal Z axes of the EFG (electric field gradient) could be classified into two sets: The angles between the principal Z axes of equivalent chlorines were calculated to be 124, 140, and 121°, for each set, corresponding to those in $SnBr_4$[16] and $SnCl_4$,[15] i.e., 125, 140, and 125° according to the X-ray structure data. The Zeeman effect data may well be interpreted by the $P2_1/c$ structure if the single crystal used in their experiment happened to have a twin texture.

It is interesting to try to understand why some of the MX_4 molecules form a plastic crystal while others do not. Detailed molecular dynamical calculation will be able to disclose the overall picture but we have discovered an interesting relation between the molecular shape and the crystal structure such as the one that exists among alkali halide crystals.

Table 1 shows values of the ratio of atomic radii[20] $r(M)/r(X)$. The dotted line across the Table separates the regions of the existence of a plastic phase. The limiting radius ratio below which the atom M can fit into the cavity formed by a close-packed tetrahedron of four X atoms is 0.23. Table 1 suggests that if the ratio is larger than 0.24, the molecule does not form a plastic crystal; it is presumably because the interaction between molecular octupoles, which is the lowest possible electric multipole for such a tetrahedral molecule,[21] is then so large that reorientation of molecules can not average the directional character of interaction. Carbon tetrafluoride is an exception to this rule but it is very close to the limiting case. It will be interesting to examine germanium iodide for existence of a plastic phase since it also lies close to the borderline.

References

1) B. Post, *Acta Crystallogr.*, **12**, 349 (1959).
2) F. J. Bartoli and T. A. Litovitz, *J. Chem. Phys.*, **56**, 413 (1972).
3) J. P. Badiali, J. Bruneaux-Poulle, and A. Defrain, *J. Chim. Phys.*, **73**, 113 (1976).
4) W. M. Latimer, *J. Am. Chem. Soc.*, **44**, 90 (1922).
5) H. H. Sisler, W. J. Wilson, B. J. Gibbins, H. H. Batey, B. Pfahler, and R. Mattair, *J. Am. Chem. Soc.*, **70**, 3818 (1948).
6) H. Kawaji, T. Atake, and H. Chihara, to be published.
7) R. Rudman and B. Post, *Science*, **154**, 1009 (1966).
8) S. Sengupta, G. Litzistorf, and E. A. C. Lucken, *J. Magn. Reson.*, **42**, 45 (1981).
9) J. Van Kranendonk and M. Walker, *Phys. Rev. Lett.*, **18**, 70 (1967).
10) S. Alexander and A. Tzalmona, *Phys. Rev.*, *A***138**, 845 (1965).
11) H. A. Rasing, *Mol. Cryst. Liq. Cryst.*, **9**, 101 (1969).
12) H. W. Spiess, R. Grosescu, and U. Haeberlen, *Chem. Phys.*, **6**, 226 (1974).
13) J.Virlet and P. Rigny, *Chem. Phys. Lett.*, **4**, 501 (1970).
14) H. Chihara and N. Nakamura, *Mol. Cryst. Liq. Cryst.*, **41**, (Letters), 21 (1977).
15) H. Chihara and Y. Koga, *Bull. Chem. Soc. Jpn.*, **44**, 2681 (1971).
16) V. P. Brand and H. Sackmann, *Z. Anorg. Allg. Chem.*, **321**, 262 (1963).
17) V. P. Brand and H. Sackmann, *Acta Crystallogr.*, **16**, 446 (1963).
18) D. Biedenkapp and A. Weiss, *Z. Naturforsch.*, **19a**, 1518 (1964).
19) A. L. Shawlow, *J. Chem. Phys.*, **22**, 1211 (1954).
20) R. D. Shannon and C. T. Prewitt, *Acta Crystallogr., Sect. B*, **25**, 925 (1969).
21) H. M. James and T. A. Keeman, *J. Chem. Phys.*, **31**, 12 (1959).

The Effect of the Pressure on Proton Jumps in Ethanol-Water Mixtures at 25 °C

Masakatsu UENO,* Kazunori ITO, Noriaki TSUCHIHASHI, and Kiyoshi SHIMIZU
Department of Applied Chemistry, Faculty of Engineering, Doshisha University,
Karasuma Imadegawa, Kamigyo-ku, Kyoto 602
(Received November 13, 1985)

The limiting molar conductances of hydrochloric acid in 0, 5, 10, 20, 30, and 80 mol% ethanol-water mixtures, and those of potassium chloride in 80 mol% of ethanol, were determined at 25 °C as a function of the pressure up to 2000 kgf cm^{-2} (1 kgf cm^{-2}=0.9807×10^5 Pa) from the conductances measured in a dilute concentration range. In each solvent except for 80 mol% of ethanol, the limiting molar conductances of the proton, $\lambda^\circ(H^+)$, are about four to six times larger than those of the potassium ion, $\lambda^\circ(K^+)$, at all the pressures studied; in 80 mol% of ethanol, the value of $\lambda^\circ(H^+)$ is very close to that of $\lambda^\circ(K^+)$ at atmospheric pressure. The results suggest that the proton-jump mechanism acts in the water-rich region, but not in the ethanol-rich region. The excess proton conductances at an infinite dilution, λ°_E, as estimated by $[\lambda^\circ_E=\lambda^\circ(H^+)-\lambda^\circ(K^+)]$, were found to increase with an increase in the pressure. The pressure dependence of the excess proton conductances normalized to their values at 1 atm, $\lambda^\circ_E{}^{(P)}/\lambda^\circ_E{}^{(1)}$, is most prominent in 5 mol% of ethanol; its magnitude decreases in this order; 5>0>10≫20≫30 mol% of ethanol. These results are discussed in relation to the effect of ethanol molecules on the water structure in the mixtures; a small addition of ethanol to water stabilizes the three-dimensional networks of water, while a further addition of ethanol makes it difficult to form them.

The proton is a much better probe than any other usual ion for a study of the solvent structure in hydrogen-bonded solvents, since protons are transferred through the hydrogen-bonded networks in addition to the hydrodynamic migration. In a previous paper,[1] the conductances of HCl and KCl in water were measured at 0 °C as a function of the pressure, and it was found that the excess proton conductance, λ°_E, increases with an increase in the pressure and that the rate of the increase in λ°_E becomes larger with a decrease in the temperature. The lower the temperature, the more significant the water structure. Therefore, the pressure dependence of λ°_E is considered to be closely related to the structural stability of water at atmospheric pressure. The structure of water is dominated by the directional attractive intermolecular potential and is sensitive to any change in pressure or temperature. Another way to change the structure is the introduction of organic molecules into the water. Alcohol-water mixtures have, in particular, attracted many researchers since structural effects appear to be significant in the water-rich region of these mixtures.[2,3] Recently computer experiments on these systems (5 mol% of methanol[4] and 3 mol% of *t*-butyl alcohol[5]) have been carried out, and structural promotion of water has been observed in radial-distribution functions. Accordingly, it seemed that it would be interesting to study the excess proton conductance in compressed alcohol-water mixtures in order to elucidate the influence of alcohol molecules on the water structure. Here, ethanol-water mixtures are used since the physical properties of the mixtures can be used for the analysis of the data on the conductances at high pressures.

Experimental

Chemicals and Solutions. The purification of the water and the ethanol, and the preparation of dilute KCl solutions, were the same as have been described in the previous papers.[6,7] Hydrochloric acid of an ultrapure grade was supplied by Merck. All the dilute solutions of HCl were prepared gravimetrically in a dry box under a nitrogen atmosphere by diluting an aqueous stock solution of HCl [ca. 1×10^{-2} M (1 M=1 mol dm^{-3})] with conductivity water and ethanol. The concentration of the stock solution was determined by measuring the conductance of the solution and by using the empirical equation proposed by Shedlovsky.[8] The concentrations of the dilute HCl soluti ns at each pressure were calculated by using the density of the stock solution at atmospheric pressure and assuming that the

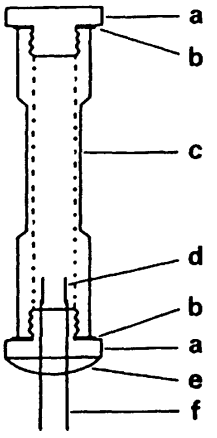

Fig. 1. Conductance cell of Teflon.
a: Teflon plug, b: rubber packing, c: Teflon capsule, d: platinum electrode, e: Araldite, f: platinum lead.

Table 1. Correction Fractors, $f^{(P)}$, for the Cell Constant of the Teflon Cell

P/kgf cm^{-2}	$f^{(P)}$	$f^{(P)}$[a]
500	0.9926	0.9946
1000	0.9861	0.9893
1500	0.9814	0.9863
2000	0.9775	0.9836

a) These values were estimated from the compression data of Ref. 10.

Table 2. Physical Properties of Ethanol-Water Mixtures at High Pressures and at 25 °C

P/kgf cm^{-2}	ρ/g cm^{-3}	ε	η/cP	P/kgf cm^{-2}	ρ/g cm^{-3}	ε	η/cP
	Water				20 mol% of Ethanol		
1	0.9970	78.5	0.8937	1	0.9336	55.8	2.453
500	1.0181	80.2	0.8865	500	0.9539	57.5	2.663
1000	1.0372	81.9	0.8897	1000	0.9717	59.1	2.880
1500	1.0546	83.5	0.9034	1500	0.9877	60.5	3.080
2000	1.0707	85.0	0.9232	2000	1.0023	61.8	3.280
	5 mol% of Ethanol				30 mol% of Ethanol		
1	0.9772	71.7	1.426	1	0.9043	47.7	2.467
500	0.9951	73.3	1.396	500	0.9232	49.4	2.800
1000	1.0133	74.9	1.386	1000	0.9418	50.8	3.157
1500	1.0300	76.2	1.392	1500	0.9590	52.2	3.510
2000	1.0449	77.5	1.405	2000	0.9739	53.5	3.880
	10 mol% of Ethanol				80 mol% of Ethanol		
1	0.9626	66.1	1.973	1	0.8088	28.0	1.438
500	0.9816	67.8	1.996	500	0.8421	29.5	1.810
1000	0.9991	69.3	2.035	1000	0.8699	30.7	2.164
1500	1.0142	70.7	2.065	1500	0.8902	31.7	2.534
2000	1.0284	71.9	2.098	2000	0.9085	32.6	2.968

densities of the dilute HCl solutions were equal to that of the solvent. To examine the validity of this assumption, the densities of the aqueous HCl solutions, ρ(HCl), were measured as a function of the concentration at 25 °C and at atmospheric pressure by means of a digital vibrating densimeter (SS-D-200 twin-type) manufactured by the Shibayama Scientific Co., Ltd. The following empirical equation was obtained:

$$\rho(\mathrm{HCl}) = 0.9970_6 + 0.018_1 c, \quad (1)$$

where ρ(HCl) is in g cm^{-3} and where c is the concentration of solution in M. The use of the density of water instead of those of the solutions leads to an increase in the conductances of the dilute HCl solutions of only about 0.02%, indicating that the assumption is not unreasonable.

Apparatus. An acid-proof Teflon cell (capacity, 12 cm^3) with unplatinized electrodes and the glass cell (capacity, 10 cm^3) described in the previous paper[7] were employed, respectively, for the conductance measurements of HCl and KCl aqueous mixtures. As is shown in Fig. 1, the Teflon cell has a membrane thin enough to transmit the oil pressure to the solution in the cell. The cell constants at atmospheric pressure were determined with an accuracy of ±0.03% by using 6×10^{-4}, 1×10^{-3}, 5×10^{-3}, and 1×10^{-2} M aqueous KCl solutions;[9] their values were 0.5592 cm^{-1} for the Teflon cell and 0.3872 cm^{-1} for the glass cell. The cell constant of the glass cell was assumed to be invariant with the pressure. On the other hand, Teflon is compressible, and so the cell constant varies with pressure. Since it is somewhat ambiguous to estimate corrections to the cell constant from the interpolation of the compression data on Teflon,[10] as the phase transition occurs below 2000 kgf cm^{-2} at 25 °C,[11] correction factors as a function of the pressure were determined by comparing the conductances of 2×10^{-3} and 1×10^{-2} M aqueous KCl solutions obtained with the Teflon and glass cells. Table 1 shows the correction factors, $f^{(P)}=K^{(P)}/K^{(1)}$, in which $K^{(P)}$ and $K^{(1)}$ are the cell constant at pressure P and at atmospheric pressure respectively. The values of $f^{(P)}$ determined by this method are smaller than those estimated from the compression data[10] by about 0.5%.

The details of the experimental apparatus and procedure were described in a previous paper.[7]

Results and Discussion

The physical properties of the various solvent mixtures, such as the density, ρ;[12,13] the dielectric constant, ε,[14,15] and the viscosity, η,[16,13,17] used in the present work are collected in Table 2. The molar conductances, Λ, of HCl and KCl in ethanol-water mixtures were determined in the concentration range of (0.6—6)×10^{-3} M for HCl and (2—8)×10^{-4} M for KCl after solvent corrections. The conductance data obtained had a maximum deviation of ±0.1%. The data on the Λ of HCl summarized in Table 3 were analyzed by the Fuoss-Onsager conductance equation for unassociated electrolytes,[18,19] which is expressed thus:

$$\Lambda = \Lambda^\circ - Sc^{1/2} + Ec\log c + Jc, \quad (2)$$

where Λ° is the limiting molar conductance, c is the molar concentration (M), and S, E, and J have the usual meanings. On the other hand, it has been found that KCl is slightly associated in ethanol-water mixtures above 15 mol% of ethanol.[7] Therefore, the Shedlovsky equation:[20]

$$1/\Lambda S(z) = 1/\Lambda^\circ + K_\Lambda c\Lambda S(z) f_\pm^2/\Lambda^{\circ 2}, \quad (3)$$

where:

$$S(z) = \{z/2 + [1+(z/2)^2]^{1/2}\}^2, \quad (4)$$

$$z = [8.204\times 10^5 \Lambda^\circ/(\varepsilon T)^{3/2} + 82.5/\eta(\varepsilon T)^{1/2}] \times (c\Lambda/\Lambda^{\circ 3})^{1/2}, \quad (5)$$

Table 3. Molar Conductances (Λ/S cm^2 mol^{-1}) at Various Concentrations, Limiting Molar Conductances ($\Lambda°$/S cm^2 mol^{-1}), Ion-Size Parameters ($\mathring{a}$/Å), and Standard Deviations of Λ (σ_Λ/S cm^2 mol^{-1}) of HCl in Ethanol–Water Mixtures as a Function of the Pressure at 25°C

P/kgf cm^{-2}	Λ								$\Lambda°$	$\mathring{a}$	σ_Λ
				Water							
	0.6656[a]	0.9381[a]	1.514[a]	1.926[a]	2.244[a]	2.781[a]	3.188[a]				
1	422.1	421.4	420.2	419.5	419.0	418.2	417.7		426.2	4.0	0.03
500	434.3	433.6	432.4	431.8	431.4	430.6	430.2		438.3	4.8	0.05
1000	442.7	442.1	441.0	440.4	439.9	439.2	438.8		446.7	5.2	0.05
1500	449.2	448.5	447.4	446.9	446.5	445.8	445.6		453.0	6.0	0.07
2000	453.2	452.4	451.6	451.2	450.8	450.4	450.2		456.7	8.2	0.08
				5 mol% of Ethanol							
	0.6674[a]	0.9049[a]	1.171[a]	1.777[a]	2.556[a]	3.401[a]	4.639[a]	5.923[a]			
1	308.0	307.5	307.1	306.2	305.4	304.8	304.0	303.3	311.0	5.1	0.04
500	316.6	316.4	315.9	315.3	314.4	314.0	313.1	312.3	319.9	5.7	0.17
1000	322.6	322.4	322.1	321.5	320.8	320.4	319.6	318.9	325.9	6.6	0.21
1500	327.5	327.2	327.1	326.5	326.0	325.6	324.9	324.3	330.7	7.5	0.24
2000	331.1	330.9	330.7	330.4	330.0	329.6	329.0	328.6	334.2	8.7	0.28
				10 mol% of Ethanol							
	0.9460[a]	1.262[a]	1.893[a]	2.705[a]	3.311[a]	3.988[a]	4.940[a]	5.973[a]			
1	231.9	231.6	231.1	230.5	230.2	229.9	229.6	229.3	234.8	6.5	0.05
500	235.9	235.6	235.0	234.5	234.1	233.8	233.5	232.9	238.9	5.8	0.11
1000	238.6	238.2	237.9	237.5	237.0	236.8	236.6	235.9	241.5	6.5	0.19
1500	241.3	241.2	240.8	240.4	240.0	239.8	239.6	239.0	244.2	6.9	0.19
2000	243.2	243.0	242.7	242.4	242.1	241.9	241.8	241.3	246.0	7.9	0.18
				20 mol% of Ethanol							
	0.8099[a]	1.256[a]	1.643[a]	2.054[a]	2.620[a]	3.492[a]	4.392[a]	5.651[a]			
1	153.1	152.5	152.2	151.8	151.4	150.9	150.5	150.1	155.5	5.0	0.03
500	150.5	150.0	149.7	149.4	149.1	148.7	148.4	148.1	152.7	5.9	0.01
1000	148.1	147.8	147.4	147.2	146.9	146.6	146.3	146.0	150.2	6.2	0.05
1500	145.9	145.7	145.5	145.4	145.1	144.8	144.5	144.4	148.0	7.1	0.11
2000	144.0	143.8	143.7	143.5	143.3	143.1	142.8	142.6	146.0	7.3	0.12
				30 mol% of Ethanol							
	0.6241[a]	0.9405[a]	1.327[a]	1.844[a]	2.354[a]	2.953[a]	3.538[a]	4.282[a]			
1	115.6	115.1	114.6	114.0	113.6	113.1	112.8	112.4	117.8	4.0	0.04
500	111.4	111.1	110.4	110.0	109.6	109.2	108.9	108.3	113.5	3.7	0.09
1000	107.5	107.2	106.5	106.2	105.8	105.5	105.2	104.7	109.4	3.9	0.10
1500	103.8	103.5	103.0	102.7	102.4	102.1	101.8	101.5	105.5	4.5	0.05
2000	100.5	100.3	99.8	99.5	99.3	98.9	98.7	98.5	102.1	4.7	0.07
				80 mol% of Ethanol							
	0.5938[a]	0.9960[a]	1.494[a]	1.984[a]	2.477[a]	2.975[a]	3.461[a]	4.045[a]			
1	47.82	46.90	46.02	45.29	44.64	44.02	43.49	42.88	51.02	2.5	0.04
500	42.27	41.54	40.93	40.34	39.77	39.28	38.92	38.43	44.86	2.7	0.06
1000	38.20	37.58	37.06	36.56	36.12	35.69	35.39	34.95	40.38	2.7	0.05
1500	35.04	34.48	34.03	33.61	33.26	32.87	32.60	32.23	36.91	2.8	0.04
2000	32.35	31.91	31.50	31.13	30.86	30.51	30.26	29.96	34.00	3.0	0.04

a) Concentrations (10^{-3} M) at atmospheric pressure.

and:

$$-\ln f_\pm^2 = 3.649 \times 10^6 [c\Lambda S(z)/\Lambda°]^{1/2}/(\varepsilon T)^{3/2}, \quad (6)$$

was employed to obtain $\Lambda°$ and the association constant, K_A, from the data on the Λ of KCl in 80 mol% of ethanol shown in Table 4. Here, $f_\pm$ is the mean activity coefficient as determined by the Debye-Hückel limiting law, and T is the absolute temperature.

The limiting molar conductances, $\Lambda°$(HCl) and $\Lambda°$(KCl), thus obtained are also listed in Tables 3 and 4 respectively, together with their related quantities, the ion-size parameter, $\mathring{a}$; the association constant, K_A, and the standard deviation of Λ, σ_Λ. The present values of $\Lambda°$(HCl) in various aqueous mixtures at 1 atm (426.2, 311.1, 234.8, 155.5, and 117.8 in 0, 5, 10, 20, and 30 mol% of ethanol respectively) are in good agreement with those obtained from the interpolation of the literature data[21] (426.6, 311, 235, 156, and 118 in 0, 5, 10, 20, and 30 mol% of ethanol respectively). In 80 mol% of ethanol, the value of $\Lambda°$(HCl) at 1 atm is not available in the literature, but the value of $\Lambda°$(KCl), 45.60, is

Table 4. Molar Conductances (Λ/S cm^2 mol^{-1}) at Various Concentrations, Limiting Molar Conductances ($\Lambda°$/S cm^2 mol^{-1}), Association Constants (K_A/mol^{-1} dm^3), and Standard Deviations of Λ (σ_Λ/S cm^2 mol^{-1}) of KCl in 80 mol% Ethanol-Water Mixtures as a Function of the Pressure at 25 °C

P/kgf cm^{-2}	Λ						$\Lambda°$	K_A	σ_Λ
	2.000[a]	3.000[a]	4.000[a]	5.000[a]	6.000[a]	8.000[a]			
1	43.49	42.91	42.40	41.97	41.56	40.84	45.60	80.8	0.01
500	36.52	36.08	35.74	35.42	35.13	34.58	38.09	57.3	0.01
1000	31.57	31.24	30.91	30.68	30.43	29.98	32.87	50.8	0.02
1500	27.76	27.45	27.21	27.01	26.81	26.45	28.82	42.3	0.02
2000	24.72	24.45	24.25	24.10	23.92	23.60	25.62	38.1	0.02

a) Concentrations (10^{-4} M) at atmospheric pressure.

Table 5. Limiting Ionic Molar Conductances ($\lambda°$/S cm^2 mol^{-1}) and Excess Proton Conductances ($\lambda°_E$/S cm^2 mol^{-1}) in Compressed Ethanol-Water Mixtures at 25 °C

P/kgf cm^{-2}	$\lambda°$			$\lambda°_E$	P/kgf cm^{-2}	$\lambda°$			$\lambda°_E$
	K^+	Cl^-	H^+			K^+	Cl^-	H^+	
	Water					20 mol% of Ethanol			
1	73.6	76.4	349.8	276.2	1	28.9	28.9	126.6	97.7
500	73.9	77.9	360.4	286.5	500	26.8	26.9	125.8	99.0
1000	73.3	78.9	367.8	294.5	1000	25.0	25.2	125.0	100.0
1500	72.6	78.8	374.2	301.6	1500	23.4	23.6	124.4	100.9
2000	71.2	78.0	378.7	307.4	2000	22.1	22.4	123.6	101.5
	5 mol% of Ethanol					30 mol% of Ethanol			
1	51.9	51.4	259.6	207.7	1	24.4	25.7	92.1	67.8
500	51.7	52.0	267.9	216.2	500	22.2	23.3	90.2	68.0
1000	51.2	52.2	273.7	222.5	1000	20.2	21.2	88.2	68.0
1500	50.5	52.1	278.6	228.1	1500	18.4	19.2	86.3	67.9
2000	49.7	51.7	282.5	232.8	2000	16.8	17.5	84.6	67.8
	10 mol% of Ethanol					80 mol% of Ethanol			
1	39.2	38.3	196.5	157.3	1	22.9	22.7	28.3	5.4
500	38.3	37.8	201.1	162.8	500				6.8
1000	37.6	37.3	204.2	166.6	1000				7.5
1500	36.8	36.8	207.4	170.6	1500				8.1
2000	36.2	36.4	209.6	173.4	2000				8.4

somewhat larger than the literature one,[22] 44.6. The pressure dependence of $\Lambda°$(HCl) in water agrees well with the literature values[23,24] within ±0.1% up to 1500 kgf cm^{-2}, but at 2000 kgf cm^{-2} our value is smaller by (0.3—0.4)% than theirs. No high-pressure data are available for comparison in ethanol-water mixtures, however. As is shown in Table 3, $\Lambda°$(HCl) increases monotonously with an increase in the pressure in 0, 5, and 10 mol% of ethanol, irrespective of the pressure dependence of the solvent viscosity, but in 20 mol% of ethanol and above, $\Lambda°$(HCl) diminishes with an increase in the pressure. The variation in $\Lambda°$(HCl) in each solvent with the pressure is mainly to be ascribed to the pressure dependence of the limiting molar conductance of the proton, as is shown below.

The limiting ionic molar conductances, $\lambda°$, of the proton under the various conditions were determined by using $\Lambda°$(HCl), $\Lambda°$(KCl),[7] and the limiting cation-transference number for KCl, $t°(K^+)$,[6,7] as follows:

$$\lambda°(K^+) = \Lambda°(KCl)t°(K^+), \quad (7)$$

$$\lambda°(Cl^-) = \Lambda°(KCl) - \lambda°(K^+), \quad (8)$$

and:

$$\lambda°(H^+) = \Lambda°(HCl) - \lambda°(Cl^-). \quad (9)$$

The values of $\lambda°(H^+)$ thus obtained are listed in Table 5, together with those of $\lambda°(K^+)$ and $\lambda°(Cl^-)$, in which the values of $\lambda°(K^+)$ and $\lambda°(Cl^-)$ at 2000 kgf cm^{-2} in the mixtures below 30 mol% of ethanol were obtained by expressing the data on $\Lambda°$(KCl) and $t°(K^+)$ up to 1500 kgf cm^{-2} [7] as quadratic equations of pressure. The standard deviations of the empirical equations were (0.01—0.06) conductance units for $\Lambda°$(KCl) and (1—7)×10^{-4} for $t°(K^+)$. No data are available for $t°(K^+)$ in 80 mol% of ethanol except at atmospheric pressure.[25] As is shown in Table 5, the values of $\lambda°(H^+)$ are about four to six times larger than those of $\lambda°(K^+)$ in 5, 10, 20, and 30 mol% of ethanol as well as in water, indicating that the proton-jump mechanism works well in these mixtures and that it dominates the conductance of the proton. However, the value of $\lambda°(H^+)$ is very close to that of $\lambda°(K^+)$ in 80 mol% of ethanol.

The excess proton conductance due to the proton jump, $\lambda°_E$, was estimated thus:

$$\lambda^\circ_E = \lambda^\circ(H^+) - \lambda^\circ(K^+) = \Lambda^\circ(HCl) - \Lambda^\circ(KCl), \quad (10)$$

where the translational mobility of the proton, i.e., the oxonium ion, H_3O^+, is approximated by that of the K^+ ion because of their similarity in size. The values of λ°_E are also shown in Table 5. Here, one problem is whether the protons are present as the oxonium ions in ethanol–water mixtures. The distribution of the protons between water and ethanol molecules for this reaction:

$$C_2H_5OH + H_3O^+ \rightleftharpoons C_2H_5OH_2^+ + H_2O, \quad (11)$$

has been investigated in the ethanol-rich region by the conductivity method[26,27] and by the use of an acid-base indicator[28] at 25 °C and at atmospheric pressure. The equilibrium constant for the reaction, $K=c(EtOH_2^+)c(H_2O)/c(H_3O^+)$, in which c(i) is the concentration of the species i in M, is in the range of (0.052—0.059) M, which indicates that the protons are present almost entirely as H_3O^+ under the experimental conditions studied here; even in 80 mol% of ethanol, the percentage of protons present as $C_2H_5OH_2^+$ is estimated to be below 1.5%. Therefore, it seems reasonable to consider that almost all the protons are transferred from the H_3O^+ ions to water molecules, and that the excess proton conductances reflect the variation in the hydrogen bonds between water molecules with the ethanol content and/or the pressure.

It has been proved that the rotation of hydrogen-bonded water molecules near the H_3O^+ ion is the rate-determining step in the proton-jump mechanism.[29] This mechanism of the proton jump has been confirmed[23] by comparing the pressure dependence of the excess proton conductance with that of the reorientational relaxation time of water molecules derived approximately from the NMR spin-lattice relaxation time;[30] the increase in the excess proton conductance with the pressure has been ascribed to the distortion and weakness of the hydrogen bonds between water molecules caused by the pressure.[1] As is shown in Table 5, λ°_E increases with an increase in the pressure, especially in the water-rich region. Therefore, it can be said that the reorientation of water molecules is promoted by the pressure in the ethanol–water mixtures as well as in water until it becomes retarded by an increase in the number of nearest neighbors.

The values of λ°_E themselves decrease markedly with an increase in the ethanol content at each pressure. Factors responsible for that would be: (i) the reorientation of water molecules becomes slower with an increase in the ethanol content, as is suggested by the dielectric relaxation time measured at atmospheric pressure,[31] and (ii) the fraction of water molecules adjacent to the H_3O^+ ion decreases with an increase in the ethanol content, and consequently the frequency of the proton transfer from the H_3O^+ ion to the water

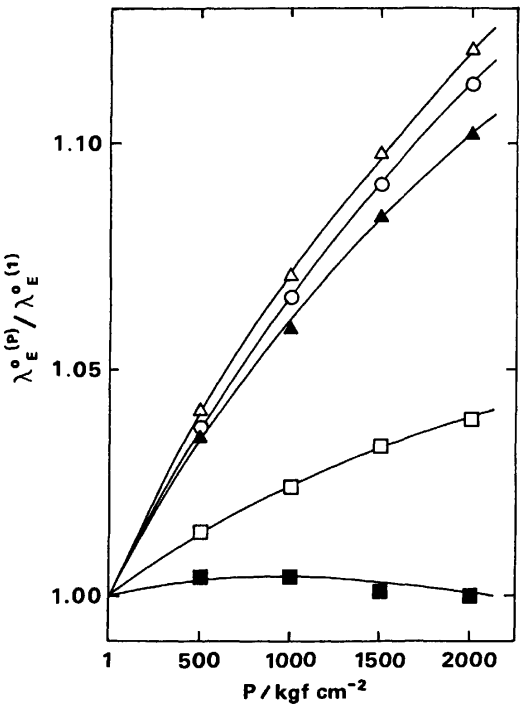

Fig. 2. Excess proton conductances normalized to their values at 1 atm as a function of the pressure. ○: Water, △: 5 mol%, ▲: 10 mol%, □: 20 mol%, ■: 30 mol% of ethanol.

molecules diminishes with an increase in the ethanol content. Thus, the excess proton conductances, normalized to their values at 1 atm, $\lambda^\circ_{E(P)}/\lambda^\circ_{E(1)}$, were calculated in each solvent; they are shown in Fig. 2 as a function of the pressure as a step toward determining the pressure effect on the excess proton conductance for one rotator, i.e., one water molecule adjacent to the H_3O^+ ion. Figure 2 shows that the pressure dependence of $\lambda^\circ_{E(P)}/\lambda^\circ_{E(1)}$ is most prominent in 5 mol% of ethanol and that its magnitude decreases in this order; 5>0>10≫20≫30 mol% of ethanol. It has been found in pure water that the pressure dependence of $\lambda^\circ_{E(P)}/\lambda^\circ_{E(1)}$ becomes larger with a decrease in the temperature.[1,23] Since the hydrogen bonds between water molecules become more stable and are strengthened at lower temperatures because of the weaker thermal motion of water molecules, the water structure is more stabilized and enhanced at lower temperatures. Therefore, it is reasonable to consider that the pressure effect on $\lambda^\circ_{E(P)}/\lambda^\circ_{E(1)}$ is closely related to the structural stability of water: The more stable the hydrogen bonds between water molecules at atmospheric pressure, the more prominent the pressure effect on $\lambda^\circ_{E(P)}/\lambda^\circ_{E(1)}$. If this finding is applied to the results in ethanol–water mixtures, the fact that the pressure dependence of $\lambda^\circ_{E(P)}/\lambda^\circ_{E(1)}$ is larger in 5 mol% of ethanol than in water will confirm the viewpoint that a small addition of ethanol to water stabilizes the three-dimensional networks of water, mainly because of the hydrophobic hydration around the ethyl group.

With an increase in the ethanol content, it seems to become difficult to form stable bonds, as may be seen in 30 mol% of ethanol in Fig. 2. Furthermore, in 80 mol% of ethanol the value of $\lambda^\circ(H^+)$ is close to that of $\lambda^\circ(K^+)$, as has been mentioned above. In this case, the contribution of the proton jump may be very small, and that of the hydrodynamic migration may be dominant. Thus, the increase in the Walden product, $\Lambda^\circ\eta$, of HCl and KCl with the pressure may be explained qualitatively in terms of the dielectric friction theory,[32] described in a previous paper.[7]

References

1) M. Ueno, M. Nakahara, and J. Osugi, *J. Solution Chem.*, **8**, 881 (1979).
2) F. Franks and D. J. G. Ives, *Quart. Rev. London*, **20**, 1 (1966).
3) "Water, A Comprehensive Treatise," ed by F. Franks, Plenum Press, New York (1973), Vols. 2 and 3.
4) S. Okazaki, H. Touhara, and K. Nakanishi, *J. Chem. Phys.*, **81**, 890 (1984).
5) H. Tanaka, K. Nakanishi, and H. Touhara, *J. Chem. Phys.*, **81**, 4065 (1984).
6) M. Ueno, S. I, and K. Shimizu, *Bull. Chem. Soc. Jpn.*, **56**, 846 (1983).
7) M. Ueno, N. Tsuchihashi, and K. Shimizu, *Bull. Chem. Soc. Jpn.*, **58**, 2929 (1985).
8) T. Shedlovsky, *J. Am. Chem. Soc.*, **54**, 1141 (1932).
9) G. C. Benson and A. R. Gordon, *J. Chem. Phys.*, **13**, 473 (1945).
10) C. E. Weir, *J. Res. N. B. S.*, **53**, 245 (1954).
11) C. E. Weir, *J. Res. N. B. S.*, **50**, 95 (1953).
12) C. T. Chen, R. A. Fine, and F. J. Millero, *J. Chem. Phys.*, **66**, 2142 (1977).
13) M. Yusa, G. P. Mathur, and R. A. Stager, *J. Chem. Eng. Data*, **22**, 32 (1977).
14) K. R. Srinivasan and R. L. Kay, *J. Chem. Phys.*, **60**, 3645 (1974).
15) T. Moriyoshi, T. Ishii, and S. Takahashi, 20th High Press. Conf. Jpn., 1979, Abstr., p. 199; T. Moriyoshi, private communication.
16) J. B. Cappi, Ph. D. Thesis, London University, 1964; K. E. Bett and J. B. Cappi, *Nature*, **207**, 620 (1965).
17) The viscosities of 5 mol% of ethanol at high pressures have been estimated by smoothing the data of Ref. 13.
18) R. M. Fuoss and F. Accascina, "Electrolytic Conductance," Interscience Pub., New York (1959), Chap. 15.
19) P. C. Carman, *J. Phys. Chem.*, **74**, 1653 (1970).
20) T. Shedlovsky, *J. Franklin Inst.*, **225**, 739 (1938); R. M. Fuoss and T. Shedlovsky, *J. Am. Chem. Soc.*, **71**, 1496 (1949).
21) H. O. Spivey and T. Shedlovsky, *J. Phys. Chem.*, **71**, 2165 (1967).
22) R. L. Kay and T. L. Broadwater, *J. Solution Chem.*, **5**, 57 (1976).
23) M. Nakahara and J. Osugi, *Rev. Phys. Chem. Jpn.*, **47**, 1 (1977).
24) A. Fischer, B. R. Mann, and J. Vaughan, *J. Chem. Soc.*, **1961**, 1093.
25) A. Fratiello and R. L. Kay, *J. Solution Chem.*, **3**, 857 (1974).
26) I. I. Bezman and F. H. Verhoek, *J. Am. Chem. Soc.*, **67**, 1330 (1945).
27) H. Goldschmidt, *Z. Physik. Chem.*, **89**, 129 (1914).
28) L. S. Guss and I. M. Kolthoff, *J. Am. Chem. Soc.*, **62**, 1494 (1940).
29) B. E. Conway, J. O'M. Bockris, and H. Linton, *J. Chem. Phys.*, **24**, 834 (1956).
30) J. Jonas, T. DeFries, and D. J. Wilber, *J. Chem. Phys.*, **65**, 582 (1976).
31) D. E. Buck, *U. S. Govt. Res. Develop. Rept.*, **40**, 59 (1965).
32) R. Zwanzig, *J. Chem. Phys.*, **52**, 3625 (1970).

The Solvent Effects on the Optical Rotatory Properties of 1,7-Diaryl-5-hydroxy-3-heptanones and Related Compounds

Shinji OHTA
Department of Chemistry, Faculty of Science, Hiroshima University, Higashisenda-machi, Naka-ku, Hiroshima 730
(Received September 17, 1985)

The ORD and CD curves of (*S*)-1,7-diphenyl-5-hydroxy-3-heptanone, (*S*)-1,7-bis(3,4-dimethoxyphenyl)-5-hydroxy-3-heptanone, and the related model compounds were obtained in selected solvents with different polarity. Causing the 1,7-diaryl-5-hydroxy-3-heptanones dextro-rotatory in chloroform was attributed to the formation of the intramolecular hydrogen bond between the C-3 carbonyl and C-5 hydroxyl groups, regardless of the presence of the phenyl groups. On the other hand, causing the compounds levo-rotatory in methanol was proved to necessitate simultaneously the breaking of the intramolecular hydrogen bond followed by solvation to the carbonyl and/or hydroxyl groups, as well as the presence of the phenyl groups. The ca. 30% of the solvent effect on the optical rotation was based on the change in the rotational strength associated with the $n\rightarrow\pi^*$ transition of the carbonyl group as changing a solvent. The residual 70% was based on the change in the rotational strength associated with the electronic transitions at around 200 nm of the carbonyl and/or hydroxyl groups.

Previously, the absolute structures of five diarylheptanoids isolated from *Alnus serrulatoides* Call.[1,2] and one isolated from *A. sieboldiana* Matsum.[3] were elucidated. In the course of the determination of their absolute configuration, the reversal in the sense of the optical rotation was observed for 1,7-diaryl-5-hydroxy-3-heptanones, such as (*S*)-1,7-diphenyl-5-hydroxy-3-heptanone (**1**)[3] and (*S*)-1,7-bis(3,4-dimethoxyphenyl)-5-hydroxy-3-heptanone (**2**),[1,2] when their optical rotations were measured in the selected solvents, such as chloroform and methanol, with different polarity. The reversal in the sense of the optical rotation is also reported for some natural compounds.[4,5] However, causes for this phenomenon have not been solved yet. In this paper, the author wishes to describe the solvent effects on the optical rotatory properties of the 1,7-diaryl-5-hydroxy-3-heptanones and related compounds. The results are in part outlined in the form of a preliminary communication.[6]

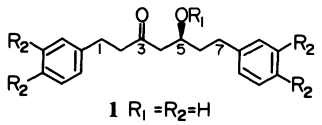

1 $R_1=R_2=H$
2 $R_1=H$, $R_2=OMe$
3 $R_1=Ac$, $R_2=H$
4 $R_1=Ac$, $R_2=OMe$

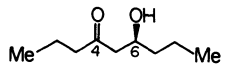

5

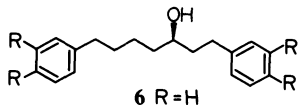

6 R=H
7 R=OMe

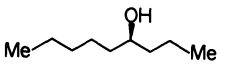

8

Results and Discussion

The compounds **1** and **2** were dextro-rotatory in chloroform and levo-rotatory in methanol, while their acetates **3** and **4** were dextro-rotatory in both of the solvents (Table 1). These observations suggest that the interaction between the solvent and the β-ketol moiety of the compounds **1** and **2** is responsible for the reversal in the sense of their optical rotations.

The Relationships between the Molecular Rotations

Table 1. Optical Rotations of **1**—**4**

Compound	$[\alpha]_D^{25}$/°	
	Chloroform	Methanol
1	+14.0±0.6	−2.7±0.6
2	+12.0±0.1	−2.3±0.1
3	+3.6±0.3	+4.1±0.3
4	+3.5±0.5	+2.9±0.5

Table 2. Molecular Rotations of **1**, **2** and ^{13}C Chemical Shifts at C-3 of **1**—**4**

Solvent	$[M]_D^{25}$[a]/°		δ_{C-3}[b]			
	1	**2**	**1**	**2**	**3**	**4**
a Carbon tetrachloride	+48.8	+52.1	27.7	27.6	23.5	23.1
b Chloroform	+39.6	+48.2	29.7	29.1	25.3	25.0
c Dichloromethane	+44.6	+46.0	29.3	29.3	25.2	24.8
d Benzene	+39.6	+48.1	27.7	27.4	23.3	23.1
e Toluene	+34.5	+42.0	27.9	27.3	23.1	22.8
f Diethyl ether	+29.6	+25.7	25.9	c)	22.3	23.3
g Dioxane	+13.5	+19.6	26.9	26.5	24.3	23.9
h Ethyl acetate	+6.7	+9.6	27.0	26.8	23.9	23.7
i Acetone	−2.5	−2.8	27.0	26.7	24.2	24.0
j Acetonitrile	−7.6	−7.2	28.1	27.8	25.3	25.0
k Methanol	−7.6	−9.2	28.3	28.0	26.2	25.7
l Ethanol	−5.1	−6.0	27.9	27.7	25.6	25.2
m 2-Propanol	−3.4	−3.2	28.0	27.8	25.3	25.0

a) 0.025 mol dm^{-3}. b) Ppm with respect to an external reference of $CH_3{}^{13}CO_2Na$. c) It was impossible to measure the spectrum of **2** because of its poor solubility in diethyl ether.

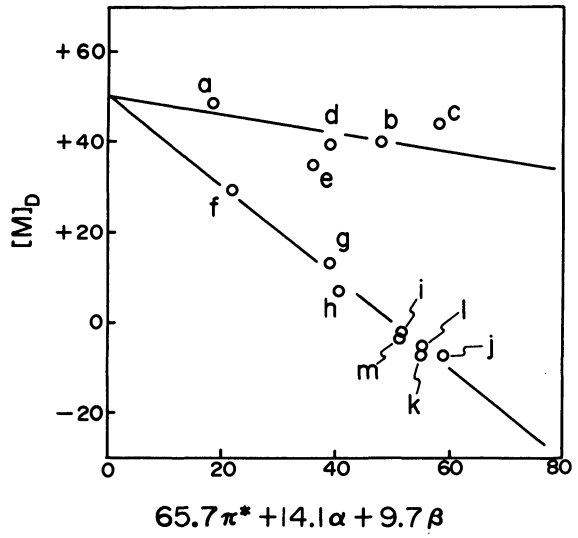

Fig. 1. A plot of $[M]_D$ of **1** vs. $65.7\pi^*+14.1\alpha+9.7\beta$. For the symbols of the data points, see Table 2.

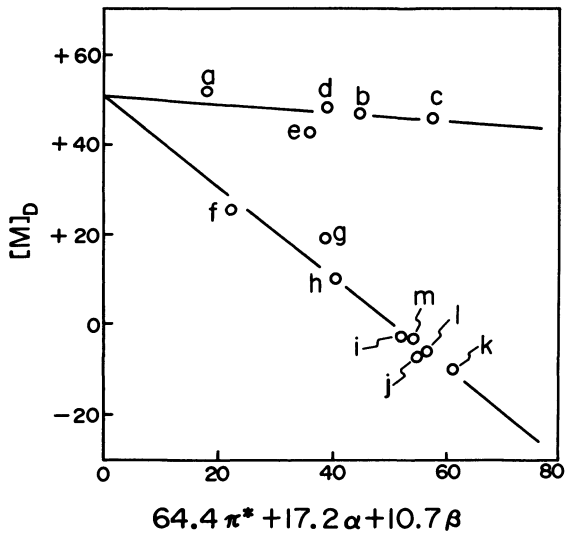

Fig. 2. A plot of $[M]_D$ of **2** vs. $64.4\pi^*+17.2\alpha+10.7\beta$. For the symbols of the data points, see Table 2.

of the Compounds 1 and 2 and Solvatochromic Parameters. The effect of the solvents on the optical rotation of the compounds **1** and **2** were examined by a solvatochromic comparison method[7] with the solvents (a)—(m) given in Table 2. The molecular rotations $[M]_D$ of the compounds **1** and **2** in these solvents were independent of the concentration (0.005—0.1 mol dm^{-3}) and truly constant. The relationship between the $[M]_D$ of the compound **1** (Table 2) and the solvatochromic parameters π^*, α, and β[†] was represented by the following least-squares regression equation,

$$[M]_D=49.6-k_1(65.7\pi^*+14.1\alpha+9.7\beta).$$

A plot of $[M]_D$ vs. $65.7\pi^*+14.1\alpha+9.7\beta$ is shown in Fig. 1, and the constant k_1 was 0.2 for the solvents (a)—(e) and 1.0 for the solvents (f)—(m). Separate correlation lines were observed for the individual solvent families. The similar facts were observed for the compound **2**. The relationship between the $[M]_D$ of the compound **2** (Table 2) and the solvatochromic parameters was represented by the following equation,

$$[M]_D=50.9-k_2(64.4\pi^*+17.2\alpha+10.7\beta).$$

A plot of $[M]_D$ vs. $64.4\pi^*+17.2\alpha+10.7\beta$ is shown in Fig. 2, and the constant k_2 was 0.1 for the solvents (a)—(e) and 1.0 for the solvents (f)—(m). The $[M]_D$ of the both compounds was dextro-rotatory in the solvents (a)—(e). The β values are very small (0—0.11)[7] for the solvents (a)—(e). Thus, the ability of the solvents to accept the proton from the C-5 hydroxyl group of the compounds **1** and **2** is so small that there is a fair chance of the formation of the intramolecular hydrogen bond between the C-3 carbonyl and C-5 hydroxyl groups in such solvents. On the other hand, the $[M]_D$ obtained in the solvents (f)—(m) changed from dextro-rotatory to levo-rotatory with the change in the values of the solvatochromic parameters. The β values for the solvents (f)—(m) are 0.31—0.95[7] and higher than those for the solvents (a)—(e). In the solvents (f)—(m), therefore, the proton of the C-5 hydroxyl group of the compounds **1** and **2** is strongly attracted to the solvent molecules. Accordingly, there is a fair possibility of the breaking of the intramolecular hydrogen bond in the solvents (f)—(m). Therefore, the variation in the $[M]_D$ of the compounds **1** and **2** in the solvents (f)—(m) can be attributed to the solvation to the β-ketol moiety. The relative contribution of each solvent property to the $[M]_D$ of the compounds **1** and **2** was estimated by the method described in the literature.[8] The relative contributions of the π^*, α, and β were 67, 20, and 13%, respectively, for the compound **1**, and 65, 22, and 13%, respectively, for the compound **2**. The superiority of the contribution of the π^* indicates a great contribution of the ability of the solvents to stabilize the dipole[7] of the compounds **1** and **2** to the variation in the $[M]_D$ of the compounds in the solvents (f)—(m). So, the fact that the compounds **1** and **2** were dextro-rotatory in the solvents (f), (g), and (h) could be rationalized in terms of the very weak interaction of these solvents to the β-ketol moiety of the compounds **1** and **2**. Such a solute/solvent interaction is weakened by the formation of the intramolecular hydrogen bond between the carbonyl and hydroxyl groups. Thus, the variation in the $[M]_D$ of the compounds **1** and **2** is minimized in the solvents (a)—(e).

The Formation and Breaking of the Intramolecular Hydrogen Bond. A more definite study for demonstrating the formation and breaking of the intramo-

[†] π^*, α, and β are a measure of solvent dipolarity/polarizability, that of solvent hydrogen bond donor acidity, and that of solvent hydrogen bond acceptor basicity, respectively.[7]

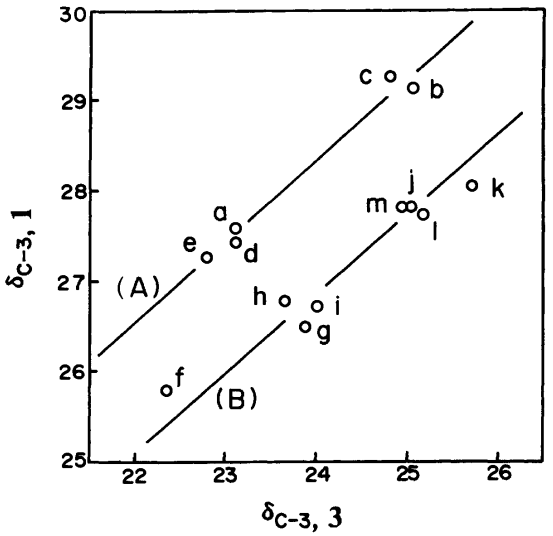

Fig. 3. A plot of δ_{C-3} for 1 vs. δ_{C-3} for **3** in the selected solvents (ppm with respect to an external reference of $CH_3{}^{13}CO_2Na$). For the symbols of the data points, see Table 2.

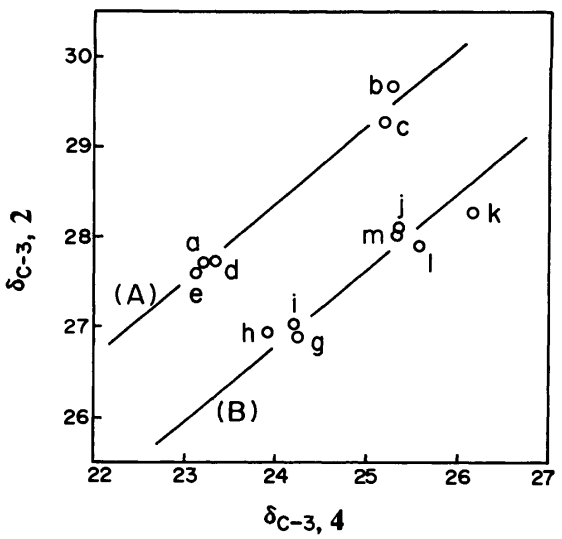

Fig. 4. A plot of δ_{C-3} for **2** vs. δ_{C-3} for **4** in the selected solvents (ppm with respect to an external reference of $CH_3{}^{13}CO_2Na$). For the symbols of the data points, see Table 2.

lecular hydrogen bond in the compounds **1** and **2** was carried out by a combination of IR and ^{13}CNMR spectroscopies. The IR spectra of the compounds **1** and **2** in carbon tetrachloride exhibited the presence of an intramolecular hydrogen-bonded OH absorption band at 3556 and 3563 cm^{-1}, respectively, which were independent of the concentration (0.005—0.1 mol dm^{-3}). Figure 3 shows the relation of the ^{13}CNMR chemical shift (Table 2) between the C-3 carbonyl carbons of the compound **1** and its acetate (**3**) in the solvents (a)—(m). The data points for the solvents (a)—(e) and the solvents (f)—(m) are situated along by lines (A) and (B), respectively. The line (A) is shifted by ca. 1.5 ppm to a lower field, compared with the line (B). The similar relation was also found for the compound **2** and its acetate (**4**) as shown in Fig. 4. These lower-field shifts[9] indicate clearly the formation of the intramolecular hydrogen bond between the C-3 carbonyl and C-5 hydroxyl groups in the solvents (a)—(e) and the formation of the intermolecular hydrogen bond between the solvent and the β-ketol group in the solvents (f)—(m). It was thus confirmed that the formation of the intramolecular hydrogen bond between the C-3 carbonyl and C-5 hydroxyl groups causes the compounds **1** and **2** dextro-rotatory in the solvents (a)—(e), while the breaking of the intramolecular hydrogen bond followed by the solvation to the β-ketol moiety causes the compounds **1** and **2** levo-rotatory in the solvents (i)—(m).

The Roles of the β-Ketol Moiety and the Phenyl Groups. The participation of the β-ketol moiety and the phenyl groups in determining the sense of the optical rotation cannot be ignored, and this was examined with the model compounds, such as (*S*)-6-hydroxy-4-nonanone (**5**), (*R*)-1,7-diphenyl-3-heptanol (**6**), (*R*)-1,7-bis(3,4-dimethoxyphenyl)-3-heptanol (**7**), and (*S*)-4-nonanol (**8**) by means of ORD measurements. Figure 5 shows the ORD curves of the compounds **1**, **2**, and **5**—**8** in chloroform and methanol. The ORD curves of the compounds **1**, **2**, and **5** showed the solvent dependence, whereas the curves of the compounds **6**—**8** were not the case. This finding indicates the indispensability of the β-ketol moiety for occurrence of the solvent effect on the optical rotation. On the other hand, the compounds **6** and **7** were levo-rotatory in 400—600 nm in chloroform and methanol, while the compound **8** was dextro-rotatory in these solvents. This fact indicates unambiguously that, in addition to the breaking of the hydrogen bond followed by the solvation, the presence of the phenyl groups in the molecules of the compounds **1**, **2**, **6**, and **7** is essential for the appearance of levo-rotation.

The Conformational Analysis in the β-Ketol Moiety. The variations in the optical rotation are presumably caused by the conformational changes in the β-ketol moiety; the conformational changes are associated with the formation and breaking of the intramolecular hydrogen bond and with the solvational effect. Such conformational changes should be effectively analyzed by means of CD measurement. The CD curves of the compound **1** in the selected solvents were shown in Fig. 6. These CD curves are complicated, because of the overlapping of the CD bands associated with the electronic transitions of the carbonyl and phenyl groups. So, the CD spectra of the model compounds **5** and **6** were examined and shown in Fig. 6. The CD curves of the compound **5** showed remarkable changes as changing the solvent, while the compound **6** showed solvent independent, negative CD maxima at 263—265 and 257—259 nm. These observations indicate that the CD maxima at 263—

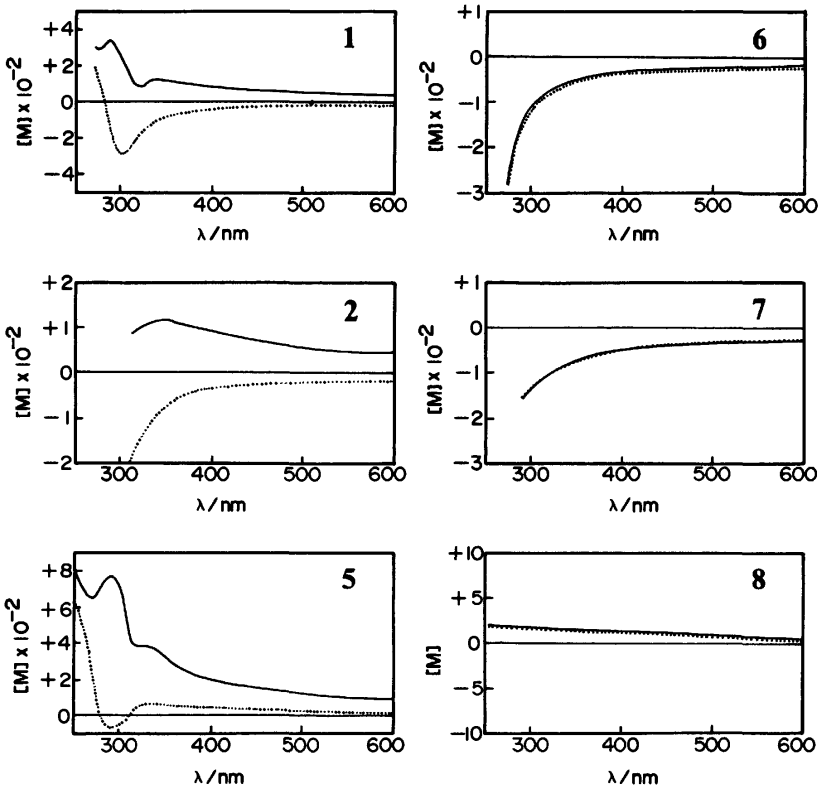

Fig. 5. ORD curves of 1, 2, and 5—8: —— in chloroform, ------ in methanol.

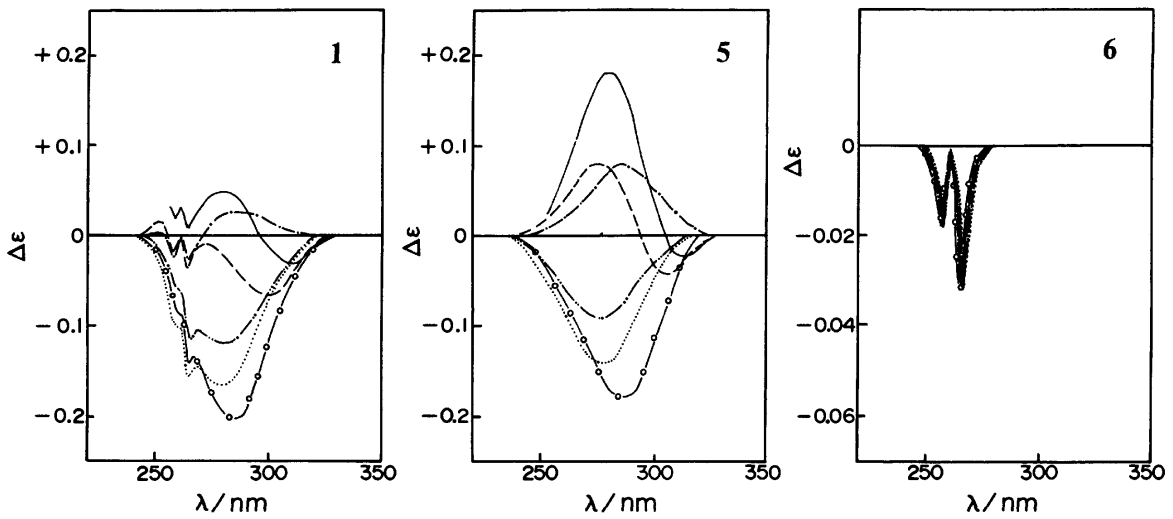

Fig. 6. CD curves of 1, 5, and 6: — in carbon tetrachloride (a), —— in chloroform (b), —·—· in diethyl ether (f), —··—·· in dioxane (g), —o—o in acetonitrile (j), ····· in methanol (k).

265 and 257—259 nm in the compound **1** are associated with the phenyl $\pi \rightarrow \pi^*$ transition and the other CD maxima with the carbonyl $n \rightarrow \pi^*$ transition, only the latter CD maxima vary as changing the solvent. This indication was supported by the good fit between the CD curve of the compound **5** and the CD curve obtained by subtracting the CD curve of the compound **6** from that of the compound **1** in each solvent.

So, the conformational analysis was performed for the compound **5** as follows. The formation of the intramolecular hydrogen bond in the solvents (a) and (b) and the breaking in the solvents (f), (g), (j), and (k) were confirmed by a combination of the IR and ^{13}CNMR spectroscopies. The values for conformational energy differences in the compound **5** were estimated by a semiempirical molecular orbital calculation based upon the CNDO/2 approximation. When the intramolecular hydrogen bond is broken, this compound seems to prefer the eclipsed conformation of the carbonyl and α-alkyl groups. Such a conformation is known to be a predominant one for acyclic carbonyl compounds.[10,11] Thus, three confor-

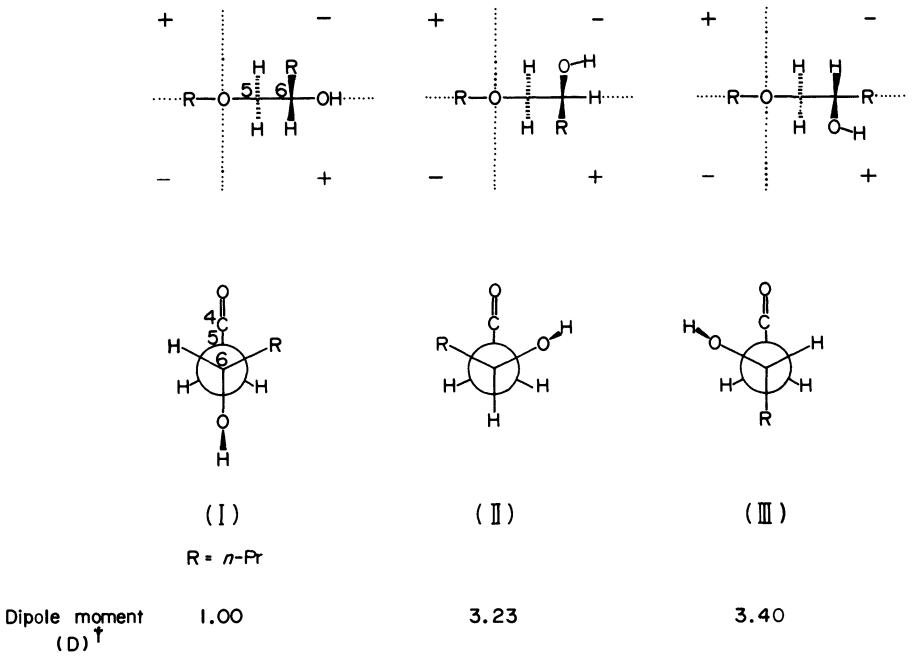

Fig. 7. Conformational isomers of **5** in the case that the intramolecular hydrogen bond is broken.
† 1 D=3.335×10^{-30} C m.

mational isomers(I)—(III) with respect to the C(5)–C(6) bond could be considered as stable ones, as illustrated in Fig. 7. The conformer(I) having the hydroxyl group in the trans position with respect to the carbonyl bond is 0.4 and 0.7 kcal mol^{-1}†† more stable than the conformers(II) and (III) having the gauche hydroxyl group, respectively. The signs for the Cotton effect of the conformers(I) and (III) can be predicted to be positive and negative, respectively, by assuming that the alkyl group R in the conformer(I) and the hydroxyl group in the conformer(III) fall into the front octants as shown in Fig. 7. For the conformer(II), its Cotton effect is predicted to be nearly nil. Hence, the Cotton effect of the compound **5** should be positive in the isolated state when the intramolecular hydrogen bond is broken. This predicted sign for the Cotton effect is in agreement with the sign observed in the solvent (f) as shown in Fig. 6. So, the positive CD band observed in the solvent (f) can be attributed to the conformer(I). However, the negative Cotton effect was observed in the solvents (g), (j), and (k). Since the conformers(II) and (III) are more dipolar than the conformer(I) as shown in Fig. 7, the relative stabilities of the conformers(II) and (III) are predicted to be enhanced by the strong solvational effect in solution.[12] Therefore, the negative CD band is expected to be attributed to the conformer(III) stabilized by the solvational energies. On the other hand, the conformer(IV) is the most predominant one in the case that the intramolecular hydrogen bond between the carbonyl and hydroxyl groups is formed as shown in Fig. 8. The conformer(IV) is 3.9 kcal mol^{-1} more

†† 1 cal=4.184 J.

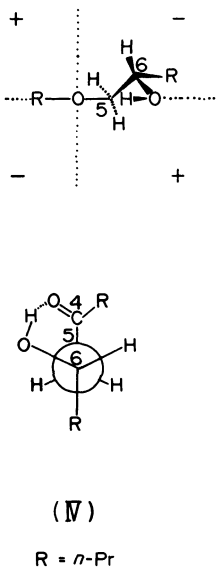

Fig. 8. The most stable conformation of **5** in the case that the intramolecular hydrogen bond is formed.

stable than the conformer(I). In the conformer(IV), the hydroxyl group is coplanar to the carbonyl one. The positive CD band at shorter wavelength in the solvents (a) and (b) can be attributed to the conformer(IV), while the negative one at longer wavelength is presumably attributed to the conformer(III) which is stabilized by the large solvational energies.

Accordingly, there is the conformational equilibrium between the intramolecularly hydrogen-bonded and solvated forms in the solvents (a) and (b), and the former hydrogen-bonded form is predominant. On the other hand, there is the conformational equi-

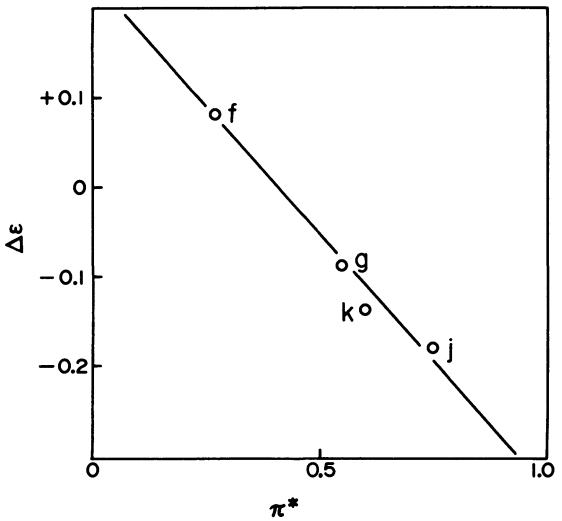

Fig. 9. A plot of CD maximum ($\Delta\varepsilon$) for **5** vs. π^* in the selected solvents. For the symbols of the data points, see Table 2.

librium among the three solvated forms in the solvents (f), (g), (j), and (k). This conformational equilibrium is dominated by the solvational effect, which is supported by the existence of a good correlation between the CD maximum ($\Delta\varepsilon$) and the solvatochromic parameter π^* as shown in Fig. 9. These results were also the case for the compound **1**.

The Contribution of the Carbonyl n→π* Cotton Effect to the Molecular Rotation. The contribution of the Cotton effect associated with the n→π* transition of a carbonyl chromophore to the molecular rotation was calculated by a simplified Kronig-Kramer's equation.[13,14] When a CD band of the compound **1** overlapped with a benzenoid band of the phenyl group, Gaussian band associated with an only n→π* transition of the carbonyl group was obtained by a graphic method. The relationships between the contribution to the molecular rotation, $[M]_D$(n→π* component), and the observed molecular rotation, $[M]_D$(obsd), were obtained for the compounds **1** and **5** in the selected solvents (a), (b), (f), (g), (j), and (k). As shown in Fig. 10, the $[M]_D$(n→π* component) was correlated with the $[M]_D$(obsd) for both the compounds. The slope of the correlation line represents the contribution of the solvent effect on the Cotton effect to the solvent effect on the molecular rotation. Both the slopes for the compounds **1** and **5** were ca. 0.3. Accordingly, ca. 30% of the solvent effect on the molecular rotations of these β-hydroxy ketones is found to be based on the solvent effect on the Cotton effect associated with the n→π* transition of the carbonyl group. The residual 70% of the solvent effect on the molecular rotation was probably based on the solvent effect on the Cotton effect at shorter wavelength (below 230 nm) associated with the electronic transitions of the carbonyl and/or hydroxyl groups. Here, it is noted that the deviation in the correlation is too large to be ignored, as shown in Fig. 10. This deviation might be

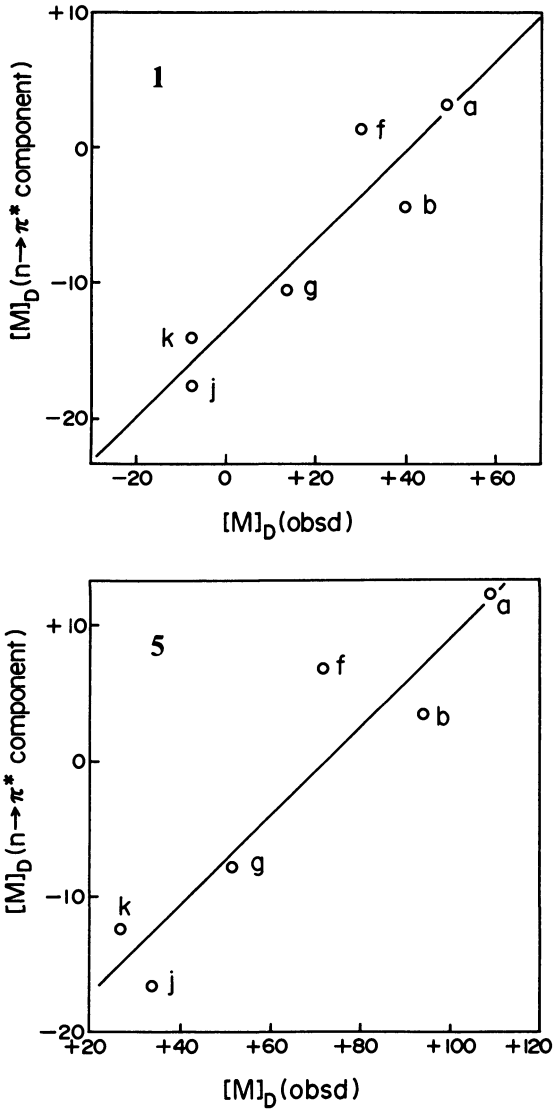

Fig. 10. A plot of $[M]_D$(n→π* component) vs. $[M]_D$(obsd) for **1** and **5**. For the symbols of the data points, see Table 2.

due to the difference in the nature between the solvent effect on the Cotton effect at 280 nm and that on the Cotton effect below 230 nm.

The Wavelength of the Cotton Effect below 230 nm. Since there is a good correlation between the $[M]_D$ of the compound **1** and that of the compound **5** in the selected solvents (a), (b), (f), (g), (j), and (k), the Cotton effect below 230 nm was examined for the compound **5** free of the phenyl group, instead of the compound **1**. The wavelength (λc) of the Cotton effect below 230 nm was calculated by use of a one-term Drude equation[15] as follows. The ORD data, [M(λ)](dif), used in the Drude analysis were derived from the difference between the observed ORD data, [M(λ)](obsd), and the contribution of the carbonyl n→π* Cotton effect to the molecular rotation, [M(λ)](n→π* component), in both chloroform and methanol. The [M(λ)](n→π* component) were calculated by use of the simplified Kronig-Kramer's equation described above. The [M(λ)]-

(dif) in the wavelength region of 340 to 600 nm were used for the calculation, because the compound **5** showed a plain ORD curve in the region in both the solvents. When the λc was assumed to be 200±10 nm, the [M(λ)](dif) from 340 to 600 nm fit the one-term Drude equation well in both chloroform and methanol. This suggests that a strong Cotton effect presents at around 200 nm, and the solvent effect on the Cotton effect largely affects the solvent effect on the optical rotation at sodium-D line. This CD band will probably correspond to carbonyl and/or hydroxyl CD bands at 185—200 nm.[16,17] The similar results is expected for the compound **1**, because there is the good correlation between $[M]_D$ of the compound **1** and that of the compound **5** as mentioned above.

In conclusion, it was found that causing the 1,7-diaryl-5-hydroxy-3-heptanones dextro-rotatory in chloroform was attributed to the formation of the intramolecular hydrogen bond between the C-3 carbonyl and C-5 hydroxyl groups in the molecules, and the presence of the phenyl groups did not affect the determination of the sense of their optical rotations. On the other hand, causing the compounds levo-rotatory in methanol was proved to be attributed to the breaking of the intramolecular hydrogen bond followed by solvation to the carbonyl and/or hydroxyl groups, as well as the presence of the phenyl groups. The ca. 30% of the solvent effect on the optical rotation is based on the change in the rotational strength associated with the $n\rightarrow\pi^*$ transition of the carbonyl group as changing a solvent. This change is caused by the conformational equilibrium. The formation and breaking of the intramolecular hydrogen bond is dominated by the ability of the solvents to accept the proton from the C-5 hydroxyl group of the compounds. When the intramolecular hydrogen bond is broken, the conformation of the compounds is dominated by the dielectric effect of the solvents. The residual 70% of the solvent effect on the optical rotation is based on the change in the rotational strength associated with the electronic transitions at around 200 nm of the carbonyl and/or hydroxyl groups.

Experimental

General. The ^{1}H NMR spectra were obtained on a Hitachi R-600 FT NMR (60 MHz) spectrometer using TMS as an internal standard. The ^{13}C NMR spectra were obtained on a Hitachi R-42 FT NMR (22.6 MHz) spectrometer. Tris[3-(2,2,2-trifluoro-1-hydroxyethylidene)-*d*-camphorato]europium [Eu(tfc)$_3$] was obtained from Merck. The mass spectra were obtained on a Shimadzu QP-1000 spectrometer with an EI ion source at 70 eV and a CI ion source with isobutane. The analytical GLC was carried out with a Shimadzu GC-6A gas chromatograph using a glass column (3 mm×2 m) packed with 2% OV-17 on Chromosorb W (AW-DMCS; 80—100 mesh). The optical rotation was measured with a JASCO DIP-360 digital polarimeter, using a 1.0-dm cell. The CD spectra were recorded on a JASCO J-40 spectropolarimeter. The ORD curves were recorded on a JASCO ORD/UV-5 spectropolarimeter at 25 °C in a quartz cell of 1.0-cm path length. The UV spectra were obtained on a Shimadzu UV-240 spectrometer. Solvents were either spectrophotometric grade or distilled immediately before use.

(*S*)-6-Hydroxy-4-nonanone (5). Into a slurry of pyridinium chlorochromate (710 mg) in 10 cm^3 of dry dichloromethane, (4*S*,6*S*)-4,6-nonanediol (506 mg) (see below) dissolved in 10 cm^3 of dry dichloromethane was added all at once, after which the mixture was kept for 3 h with stirring at room temperature. The reaction mixture was then added to dry diethyl ether (30 cm^3), and the resulting slurry was kept for another hour under stirring. The slurry was then passed through a column packed with 20 g of Florisil, and the eluate was concentrated under a reduced pressure at room temperature. The condensate was purified on a silica-gel column with diethyl ether–hexane (1:4) and then distilled at 88 °C (bath temperature) at 5 Torr (1 Torr=133.322 Pa) through a short-path distillation apparatus to afford **5** (313 mg, 63%) as colorless oil: $[\alpha]_D^{25}$ +59.3±0.5° (*c* 0.39, chloroform); $[\alpha]_D^{25}$ +16.9±0.5° (*c* 0.40, methanol); IR (neat) 3420 (OH) and 1705 cm^{-1} (C=O); ^{1}H NMR ($CDCl_3$) δ=0.92 (6H, t, *J*=7 Hz, Me×2), 1.23—1.90 (6H, m, >CH_2×3), 2.29—2.57 (4H, m, >CH_2×2), 3.04 (1H, brs, OH), and 4.04 (1H, m, >C<u>H</u>OH); EI-MS *m/z* (rel intensity) 140 (2, M^+-H_2O), 115 (14), 97 (10), 71 (65), and 43 (100); CI-MS *m/z* (rel intensity) 159 (62, M^++H) and 141 (100, M^+-H_2O+H). The GLC (90 °C) showed a single peak (retention time 16 min). The optical purity of **5** was determined by measuring the ^{1}H NMR with a soln of its acetate (5 mg) and Eu(tfc)$_3$ (3 molar equivalents to the acetate) in $CDCl_3$ (0.4 cm^3). The acetate showed no detectable signal of the enantiomer.

Preparation of (4*S*,6*S*)-4,6-Nonanediol. 4,6-Nonanedione (5.96 g), prepared from methyl butyrate and 2-pentanone by the method previously reported,[18] was hydrogenated with an asymmetrically modified Raney nickel [(*S*,*S*)-TA-NaBr-MRNi][19,20] followed by crystallization from hexane to afford (4*S*,6*S*)-4,6-nonanediol (1.04 g, 17%) as colorless needles: mp 52—53 °C (lit,[20] 58—59 °C); $[\alpha]_D^{25}$ +20.5±0.2° (*c* 10, ethanol) (lit,[20] $[\alpha]_D^{20}$ +21.2°); IR (KBr) 3340 cm^{-1} (OH); ^{1}H NMR ($CDCl_3$) δ=0.74—1.12 (6H, m, Me×2), 1.18—1.68 (10H, m, >CH_2×5), 2.50—2.67 (2H, br, OH×2), 3.93 (2H, m, >C<u>H</u>OH×2); EI-MS *m/z* (rel intensity) 117 (16, M^+-43), 99 (35), 81 (83), and 73 (100); CI-MS *m/z* (rel intensity) 161 (17, M^++H), 160 (14, M^+), 143 (27, M^+-H_2O+H), and 125 (100, M^+-2H_2O+H). Found: C, 67.65; H, 12.76%. Calcd for $C_9H_{20}O_2$: C, 67.45; H, 12.58%. The GLC (120 °C) showed a single peak (retention time 8 min).

(*R*)-1,7-Diphenyl-3-heptanol (6). A solution of *p*-toluenesulfonyl chloride (220 mg) in dry pyridine (3 cm^3) was added to a solution of (3*S*,5*S*)-1,7-diphenyl-3,5-heptanediol (300 mg), prepared as shown below, in dry pyridine at 0 °C. The solution was allowed to stand at 4 °C for 3 d, poured into ice-cold 5% HCl, and then extracted with diethyl ether. The solution was washed with cold 5% HCl, 5% $NaHCO_3$, and saturated NaCl solutions, successively, and then dried over Na_2SO_4 followed by concentration in vacuo. The tosylate obtained was used for the next preparation without further purification. A solution of the optically active tosylate in dry THF (20 cm^3) was added to a slurry of $LiAlH_4$ (0.5 g) in dry THF (10 cm^3). The mixture was then heated under reflux for 5 h. An excess of $LiAlH_4$ was decomposed with a solution of methanol in diethyl ether and then 5% HCl.

The mixture was extracted with diethyl ether. The diethyl ether solution was washed with 5% HCl and saturated NaCl solutions, successively, and then dried (Na_2SO_4) followed by concentration in vacuo. The residue was purified on a silica-gel column with a mixture of ethyl acetate and hexane (1:4) to afford **6** (170 mg, 60%) as colorless needles: mp 60—61 °C; $[\alpha]_D^{25}$ −5.8±0.1° (*c* 1.70, chloroform) (lit,[21] $[\alpha]_D^{25}$ −4.3±2.9° (*c* 0.14, chloroform)); $[\alpha]_D^{25}$ −7.3±0.1° (*c* 1.70, methanol); UV (ethanol) 268 (log ε 2.51), 261 (2.64), 255 (2.57), 248 (2.44), and 243 nm (2.29); IR (KBr) 3340 (OH), 1598 and 1492 cm^{-1} (aromatic ring); ^1H NMR (CCl_4) δ= 1.06 (1H, brs, OH), 1.30—1.84 (8H, m, $>CH_2$×4), 2.45—2.81 (4H, m, $>CH_2$×2), 3.48 (1H, m, >CHOH), 7.13 (10H, m, aromatic H); EI-MS *m/z* (rel intensity) 250 (62, M^+-H_2O), 159 (10), 145 (8), 131 (9), 117 (31), 104 (57), and 91 (100); CI-MS *m/z* (rel intensity) 267 (65, M^+-H) and 251 (100, M^+-H_2O+H). Found: C, 85.25; H, 9.21%. Calcd for $C_{19}H_{24}O$: C, 85.02; H, 9.01%. The optical purity of **6** was determined by the same method as described for the determination of the optical purity of **5**. The acetate derived from **6** showed no detectable signal of the enantiomer.

Preparation of (3*S*,5*S*)-1,7-Diphenyl-3,5-heptanediol. 1,7-Diphenyl-3,5-heptanedione (2.70 g) prepared with the method previously reported[22] was hydrogenated with the asymmetrically modified Raney nickel described for the preparation of (4*S*,6*S*)-4,6-nonanediol followed by crystallization from hexane to afford (3*S*,5*S*)-1,7-diphenyl-3,5-heptanediol (1.10 g, 40%) as colorless needles: mp 89.5—90.5 °C; $[\alpha]_D^{25}$ −11.1±0.2° (*c* 1.06, ethanol); UV (ethanol) 268 (log ε 2.50), 261 (2.63), 255 (2.55), 249 (2.39), 243 nm (2.16); IR (KBr) 3350 (OH), 1600 and 1490 cm^{-1} (aromatic ring); ^1H NMR (CCl_4) δ=1.45—1.88 (6H, m, $>CH_2$×3), 2.52—2.81 (6H, m, $>CH_2$×2 and OH×2), 3.87 (2H, m, >CHOH×2), 7.13 (10H, m, aromatic H); EI-MS *m/z* (rel intensity) 266 (9, M^+-H_2O), 248 (17, M^+-2H_2O), and 91 (100); CI-MS *m/z* (rel intensity) 285 (50, M^++H), 267 (72, M^+-H_2O+H), and 249 (100, M^+-2H_2O+H). Found: C, 80.41; H, 8.77%. Calcd for $C_{19}H_{24}O_2$: C, 80.24; H, 8.51%. The optical purity of this diol was determined by measuring the ^1H NMR with a soln of its diacetate (5 mg) and Eu(tfc)$_3$ (3 molar equivalents to the diacetate) in $CDCl_3$ (0.4 cm^3). The diacetate showed no detectable signal of the enantiomer.

(*R*)-1,7-Bis(3,4-dimethoxyphenyl)-3-heptanol (7). Compound **7** was prepared following the previously reported method.[21] The reduction of the carbonyl group of the compound **2** (69 mg) with $TsNHNH_2$ (35 mg) and $NaBH_4$ (300 mg) in methanol gave **7** (51 mg, 77%): mp 67—69 °C; $[\alpha]_D^{25}$ −4.7±0.4° (*c* 0.51, chloroform); $[\alpha]_D^{25}$ −5.5±0.4° (*c* 0.51, methanol); UV (ethanol) 280 (log ε 3.70), 229 nm (4.13); IR (KBr) 3430 (OH), 1587 and 1515 cm^{-1} (aromatic ring); ^1H NMR ($CDCl_3$) δ=1.25—1.90 (8H, m, $>CH_2$×4), 1.70 (1H, brs, OH), 2.38—2.81 (4H, m, $>CH_2$×2), 3.60 (1H, m, >CHOH), 3.84 and 3.85 (12H, each s, OMe×4), 6.68—6.82 (6H, m, aromatic H); EI-MS *m/z* (rel intensity) 388 (32, M^+), 370 (2, M^+-H_2O), 177 (8), 164 (7), and 151 (100). Found: C, 71.14; H, 8.29%. Calcd for $C_{23}H_{32}O_5$: C, 71.10; H, 8.30%.

(*S*)-4-Nonanol (8). The tosylation of (4*S*,6*S*)-4,6-nonanediol (465 mg), prepared as shown above, followed by the reduction with $LiAlH_4$ was carried out in the same manner described for the preparation of **6**. The distillation of the product at 68 °C (bath temperature) at 4 Torr through a short-path distillation apparatus afforded **8** (191 mg, 46%) as colorless oil: $[\alpha]_D^{25}$ +0.6±0.2° (*c* 2.25, chloroform); $[\alpha]_D^{25}$ +0.5±0.2° (*c* 2.25, methanol) (lit,[23] $[\alpha]_D^{25}$ +0.57°); IR (neat) 3350 cm^{-1} (OH); ^1H NMR ($CDCl_3$) δ=0.70—1.04 (6H, m, Me×2), 1.16—1.53 (12H, m, $>CH_2$×6), 1.73 (1H, brs, OH), 3.61 (1H, m, >CHOH); EI-MS *m/z* (rel intensity) 126 (1, M^+-H_2O), 101 (9), 83 (34), 73 (40), and 55 (100); CI-MS *m/z* (rel intensity) 143 (11, M^+-H) and 127 (100, M^+-H_2O+H). The GLC (90 °C) showed a single peak at 6 min of retention time.

The author wishes to express his hearty gratitude to Professor Takayuki Suga of Hiroshima University for his continual guidance and encouragement throughout the course of this work and to Dr. Toshifumi Hirata of Hiroshima University and Dr. Tadashi Aoki of Suzugamine Women's College for their valuable discussions.

References

1) T. Suga, S. Ohta, T. Hirata, and T. Aoki, *Chem. Lett.*, **1982**, 895.
2) S. Ohta, T. Aoki, T. Hirata, and T. Suga, *J. Chem. Soc., Perkin Trans. 1*, **1984**, 1635.
3) T. Suga, S. Ohta, T. Aoki, and T. Hirata, *Bull. Chem. Soc. Jpn.*, **56**, 3353 (1983).
4) K. Mori, N. Mizumachi, and M. Matsui, *Agric. Biol. Chem.*, **40**, 1611 (1976).
5) H. Ishii, F. Sekiguchi, and T. Ishikawa, *Tetrahedron*, **37**, 285 (1981).
6) T. Suga, S. Ohta, T. Aoki, and T. Hirata, *Chem. Lett.*, **1985**, 1331.
7) M. J. Kamlet, J.-L. M. Abboud, M. H. Abraham, and R. W. Taft, *J. Org. Chem.*, **48**, 2877 (1983).
8) T. M. Krygowski and W. R. Fawcett, *J. Am. Chem. Soc.*, **97**, 2143 (1975).
9) G. E. Maciel and G. B. Savitsky, *J. Phys. Chem.*, **68**, 437 (1964).
10) M. Abe, K. Kuchitsu, and T. Shimanouchi, *J. Mol. Struct.*, **4**, 245 (1969).
11) T. Shimanouchi, Y. Abe, and M. Mikami, *Spectrochim. Acta, Part A*, **24**, 1037 (1968).
12) M. F. Ruiz-Lopez and D. Rinaldi, *J. Mol. Struct.*, **93**, 277 (1983).
13) W. Moffitt and A. Moscowitz, *J. Chem. Phys.*, **30**, 648 (1959).
14) C. Djerassi, "Optical Rotatory Dispersion: Applications to Organic Chemistry," McGraw-Hill, New York (1960), pp. 155—167.
15) E. Iizuka and J. T. Yang, *Biochemistry*, **3**, 1519 (1964).
16) D. N. Kirk, *J. Chem. Soc., Perkin Trans. 1*, **1980**, 787.
17) D. N. Kirk, W. P. Mose, and P. M. Scopes, *J. Chem. Soc., Chem. Commun.*, **1972**, 81.
18) J. T. Adams and C. R. Hauser, *J. Am. Chem. Soc.*, **66**, 1220 (1944).
19) T. Harada and Y. Izumi, *Chem. Lett.*, **1978**, 1195.
20) K. Ito, T. Harada, and A. Tai, *Bull. Chem. Soc. Jpn.*, **53**, 3367 (1980).
21) S. Ohta, M. Koyama, T. Aoki, and T. Suga, *Bull. Chem. Soc. Jpn.*, **58**, 2423 (1985).
22) Y. Asakawa, *Bull. Chem. Soc. Jpn.*, **45**, 1794 (1972).
23) P. A. Levene and M. Kuna, *J. Biol. Chem.*, **140**, 259 (1941).

 © 1986 The Chemical Society of Japan Bull. Chem. Soc. Jpn., 59, 1189—1194 (1986)

Molecular Complexes of *N,N,N',N'*-Tetraisopropyloxamide. Crystal Structures of Its 1:1 Adduct with *m*-Cresol, and Its 1:1 and 1:2 Adducts with *p*-Cresol

Fumio Toda,* Yasunori Tagami, and Thomas C. W. Mak*,†

Department of Industrial Chemistry, Faculty of Engineering, Ehime University, Matsuyama 790

†Department of Chemistry, The Chinese University of Hong Kong, Shatin, New Territories, Hong Kong

(Received October 2, 1985)

The crystal structures of a 1:1 complex (I) of *N,N,N',N'*-tetraisopropyloxamide with *m*-cresol, a 1:1 complex (**II**) with *p*-cresol, and a 1:2 complex (**III**) with *p*-cresol have been determined by X-ray crystallography. The crystal data are: **I**, $C_{21}H_{36}N_2O_3$, $P2_1/c$, a=12.104(4), b=6.860(3) c=27.186(8) Å, β=93.46(2)°, Z=4, and R_F=0.093 for 1661 observed Mo$K\alpha$ data; **II**, $C_{21}H_{36}N_2O_3$, $P2_1/n$, a=7.825(2), b=11.379(4), c=25.39(1) Å, β=91.01(2)°, Z=4, and R_F=0.105 for 1326 data; **III**, $C_{28}H_{44}N_2O_4$, $C2/c$, a=11.744(3), b=10.658(2), c=23.576(4) Å, β=102.07(2)°, Z=4, R_F=0.045 for 1382 data. The stoichiometric formulas faithfully represent the structures of all three complexes, with each phenolic OH group forming a donor hydrogen bond to an O atom of the oxamide host molecule.

Recently we reported that *N,N,N',N'*-tetraisopropyloxamide (**1**) forms crystalline inclusion compounds of 1:1 stoichiometry with a variety of aromatic guest molecules such as benzene, *m*- and *p*-xylenes, phenol, *m*- and *p*-cresols, naphthalene, 1- and 2-methylnaphthalenes, and 1- and 2-naphthols.[1] X-Ray analysis of its 1:1 complex (**IV**) with 1-methylnaphthalene showed that the aromatic molecules are accommodated in channels, with no significant interaction between host and guest components other than dispersion forces.[1] For a better understanding of the inclusion properties of **1**, we have carried out crystal structure determinations of its 1:1 complexes (**I** and **II** respectively) with *m*- and *p*-cresols, with anticipation of hydrogen bonding but uncertainty as to whether host-guest or guest-guest association would be the dominating factor. In the course of our studies we further isolated a 1:2 crystalline adduct (**III**) of **1** with *p*-cresol, whose structure is also reported in the present paper.

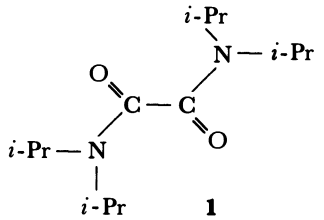

1

Experimental

Diamide **1** (mp 102—103°C) was synthesized from oxalyl dichloride and diisopropylamine according to a literature method.[2] Complexes **I—III** were obtained as colorless prisms from slow evaporation of a solution of **1** and the appropriate cresol in hexane. Complexes **II** and **III** were prepared separately by using different stoichiometric amounts of *p*-cresol, and crystals of **II** ($\nu_{C=O}$ 1615, 1648 cm^{-1}) are generally bigger and better formed than those of **III** ($\nu_{C=O}$ 1625 cm^{-1}).

X-Ray Data Collection. All three complexes quickly turned milky upon exposure to air, and each selected crystal was therefore enclosed inside an 0.5 mm Lindemann glass capillary. Intensity measurement[3] was performed on a Nicolet R3m four-circle diffractometer[4] using graphite-monochromatized Mo$K\alpha$ radiation (λ=0.71069 Å). Accurate unit-cell parameters were derived from a least-squares fit of the angular settings for 25 reflections in the range $14° < 2\theta < 18°$. Reflection intensities were recorded at an ambient laboratory temperature of 22°C, and three standards monitored every 50 data measurements showed only random fluctuations within ±2% of their mean values. The raw intensities were processed with the learnt-profile procedure.[5] No absorption correction was applied. The crystal data and processing parameters for **I—III** are summarized in Table 1.

Structure Determination and Refinement

For each complex the statistical distributions of the normalized structure factors strongly favoured a centrosymmetric space group, and structure solution was achieved by direct phase determination based on negative quartets.[6]

The structures of **I** and **II** were refined in the same manner. The N, O, and methyl C atoms were varied anisotropically, and the remaining C atoms isotropically. In view of the unfavorable data-to-parameter ratio,[7] the phenyl ring was treated as a rigid group (regular hexagon of side 1.395 Å). All H atoms were generated geometrically (C–H=0.96 Å) and included in structure factor calculations with fixed isotropic temperature factors.

In complex **III**, the oxamide molecule **1** is located on a crystallographic diad. All non-hydrogen atoms in the asymmetric unit (half of an oxamide molecule and one *p*-cresol) were refined anisotropically. A difference Fourier map revealed the proton belonging to the phenolic group at a reasonable location, and all H atoms were included with assigned isotropic thermal parameters in subsequent refinement.

Computations were performed on a Data General Corporation Nova 3/12 minicomputer using the SHELXTL program package.[8] Analytic expressions of atomic scattering factors were employed, and anomalous dispersion corrections were incorporated.[9] Blocked-cascade least-squares refinement[10] converged to the R indices and parameters listed in Table 1.

Table 1. Data Collection and Processing Parameters

Complex	I	II	III
Molecular formula	$C_{14}H_{28}N_2O_2 \cdot C_7H_8O$	$C_{14}H_{28}N_2O_2 \cdot C_7H_8O$	$C_{14}H_{28}N_2O_2 \cdot 2C_7H_8O$
Molecular weight	364.52	364.52	472.66
Cell constants	a=12.104(4)Å β=93.46(2)°	a=7.825(2)Å β=91.01(2)°	a=11.744(3)Å β=102.07(2)°
	b=6.860(3) V=2253(1)Å^3	b=11.379(4) V=2260(1)Å^3	b=10.658(2) V=2886(1)Å^3
	c=27.186(8) Z=4	c=25.39(1) Z=4	c=23.576(4) Z=4
Density (calcd)	1.075 g cm^{-3}	1.071 g cm^{-3}	1.088 g cm^{-3}
Space Group	$P2_1/c$	$P2_1/n$	$C2/c$
Absorption coefficent	0.66 cm^{-1}	0.66 cm^{-1}	0.67 cm^{-1}
Crystal size	0.40×0.36×0.36 mm	0.42×0.40×0.28 mm	0.44×0.40×0.40 mm
Scan type and speed		ω–2θ; 2.02—8.37 deg min^{-1}	
Scan range		1° below $K\alpha_1$ to 1° above $K\alpha_2$	
Background counting	stationary counts for one-half of scan time at each end of scan		
Collection range	h, k, $\pm l$; $2\theta_{max}$=42°	h, k, $\pm l$; $2\theta_{max}$=40°	h, k, $\pm l$; $2\theta_{max}$=45°
Unique data measured	2034	1635	1616
Observed data with $\lvert F_o\rvert > 3\sigma(\lvert F_o\rvert)$, n	1661	1326	1382
Number of variables, p	190	190	169
$R_F=\sum\lvert\lvert F_o\rvert-\lvert F_c\rvert\rvert/\sum\lvert F_o\rvert$	0.093	0.105	0.045
Constant g in weighting scheme $w=[\sigma^2(F_o)+g\lvert F_o\rvert^2]^{-1}$	0.0020	0.0020	0.0015
$R_G=[\sum w(\lvert F_o\rvert-\lvert F_c\rvert)^2/\sum w\lvert F_o\rvert^2]^{1/2}$	0.140	0.140	0.063
$S=[\sum w(\lvert F_o\rvert-\lvert F_c\rvert)^2/(n-p)]^{1/2}$	2.454	2.410	1.250
Residual extrema in final difference map	+0.48 to −0.30 e Å^{-3}	+0.36 to −0.41 e Å^{-3}	+0.13 to −0.13 e Å^{-3}

Table 2. Atomic Coordinates (×10^4) and Thermal Parameters[a] (Å^2×10^3) for Complexes I and II

Atom	I				II			
	x	y	z	U/U_{eq}	x	y	z	U/U_{eq}
Host Molecule								
O(1)	3769(3)	5467(6)	3430(1)	69(2)*	4620(8)	5052(5)	1760(3)	66(3)*
O(2)	1510(3)	5695(6)	3899(2)	67(2)*	8384(8)	4293(6)	1580(3)	69(3)*
N(1)	2553(3)	3299(7)	3082(2)	48(2)*	5395(8)	3553(6)	2286(3)	45(3)*
N(2)	2653(3)	3503(7)	4312(2)	50(2)*	6578(9)	3257(6)	1040(3)	49(3)*
C(1)	2942(4)	4391(8)	3450(2)	50(1)	5563(10)	4182(8)	1854(4)	42(2)
C(2)	1579(4)	2003(9)	3134(2)	58(2)	6565(12)	2498(7)	2381(4)	54(3)
C(3)	1874(6)	−111(10)	3026(3)	90(3)*	5505(15)	1383(9)	2459(5)	83(5)*
C(4)	586(5)	2721(12)	2821(3)	84(3)*	7767(15)	2707(10)	2827(5)	93(6)*
C(5)	3049(4)	3352(9)	2601(2)	60(2)	4225(11)	3842(8)	2701(4)	54(3)
C(6)	4209(5)	2554(13)	2633(3)	89(3)*	2348(13)	3689(10)	2506(5)	93(5)*
C(7)	2939(6)	5366(11)	2368(3)	84(3)*	4487(16)	5021(9)	2941(5)	85(5)*
C(8)	2290(4)	4541(9)	3908(2)	51(2)	6942(10)	3893(7)	1472(3)	45(2)
C(9)	3566(4)	2059(9)	4285(2)	63(2)	4813(12)	2863(8)	928(4)	61(3)
C(10)	3181(6)	48(10)	4415(3)	88(3)*	4747(16)	1534(8)	846(5)	89(5)*
C(11)	4587(5)	2737(14)	4600(3)	95(3)*	4045(14)	3508(10)	465(5)	89(5)*
C(12)	2102(5)	3691(10)	4778(2)	66(2)	7902(12)	3015(8)	643(4)	57(3)
C(13)	934(5)	2964(13)	4733(3)	93(3)*	9285(14)	2221(10)	884(5)	85(5)*
C(14)	2196(6)	5743(10)	4989(3)	82(3)*	8630(14)	4116(9)	410(4)	77(5)*
Guest Molecule								
O(3)	5310(4)	7804(10)	3878(2)	135(3)*	4702(8)	6813(6)	1065(3)	82(3)*
C(15)	6389(3)	7216(8)	3813(2)	89(2)	3113(5)	7249(5)	966(2)	55(3)
C(16)	6634(3)	5389(8)	3622(2)	101(3)	2952(5)	8354(5)	732(2)	58(3)
C(17)	7731(3)	4874(8)	3557(2)	109(3)	1334(5)	8816(5)	622(2)	62(3)
C(18)	8582(3)	6186(8)	3683(2)	106(3)	−124(5)	8172(5)	744(2)	54(3)
C(19)	8337(3)	8014(8)	3873(2)	96(2)	38(5)	7066(5)	977(2)	54(3)
C(20)	7240(3)	8529(8)	3938(2)	94(2)	1656(5)	6605(5)	1088(2)	56(3)
C(21)	9265(10)	9321(19)	3987(4)	186(7)*	−1876(14)	8693(10)	625(5)	87(5)*

a) Asterisk indicates equivalent isotropic temperature factor U_{eq} defined as 1/3 of the trace of the orthogonalised U matrix. The exponent of the isotropic temperature factor takes the form $-8\pi^2 U \sin^2\theta/\lambda^2$.

Table 3. Atomic Coordinates ($\times 10^4$) and Equivalent Thermal Parameters[a] ($Å^2 \times 10^3$) for Complex **III**

Atom	*x*	*y*	*z*	U_{eq}	Atom	*x*	*y*	*z*	U_{eq}
Host Molecule					Guest Molecule				
O(1)	3870(2)	5136(2)	2712(1)	64(1)	O(2)	4083(2)	6103(2)	3792(1)	76(1)
N	3753(2)	3675(2)	2014(1)	46(1)	C(8)	4911(2)	6975(2)	4017(1)	58(1)
C(1)	4336(2)	4398(2)	2437(1)	47(1)	C(9)	4849(3)	7514(3)	4540(1)	78(1)
C(2)	4350(2)	2768(2)	1703(1)	58(1)	C(10)	5668(3)	8388(3)	4786(1)	83(1)
C(3)	4218(3)	3125(3)	1068(1)	90(1)	C(11)	6549(3)	8762(3)	4521(1)	72(1)
C(4)	3939(3)	1426(2)	1778(1)	78(1)	C(12)	6590(2)	8224(3)	3997(1)	72(1)
C(5)	2462(2)	3744(2)	1850(1)	52(1)	C(13)	5781(2)	7341(2)	3744(1)	65(1)
C(6)	2037(3)	5000(2)	1578(1)	70(1)	C(14)	7455(4)	9701(3)	4804(2)	102(2)
C(7)	1891(3)	3376(3)	2344(1)	70(1)					

a) U_{eq} defined as 1/3 of the trace of the orthogonalised U matrix.

Table 4. Bond Distances (*l*/Å) and Angles for Complexes **I** and **II**

	I	**II**		**I**	**II**
O(1)-C(1)	1.248(7)	1.256(11)	O(2)-C(8)	1.231(7)	1.243(10)
N(1)-C(1)	1.314(7)	1.318(11)	N(1)-C(2)	1.490(7)	1.527(11)
N(1)-C(5)	1.472(7)	1.446(11)	N(2)-C(8)	1.359(7)	1.340(11)
N(2)-C(9)	1.489(7)	1.475(12)	N(2)-C(12)	1.473(8)	1.484(12)
C(1)-C)8)	1.518(8)	1.500(12)	C(2)-C(3)	1.526(9)	1.530(14)
C(2)-C(4)	1.513(8)	1.479(16)	C(5)-C(6)	1.504(8)	1.552(14)
C(5)-C(7)	1.522(9)	1.487(14)	C(9)-C(10)	1.504(9)	1.528(13)
C(9)-C(11)	1.532(9)	1.502(15)	C(12)-C(13)	1.498(9)	1.529(15)
C(12)-C(14)	1.521(9)	1.503(14)	O(3)-C(15)	1.388(7)	1.357(8)
C(19)-C(21)	1.456(13)		C(18)-C(21)		1.519(12)
C(1)-N(1)-C(2)	121.5(5)	119.3(7)	C(1)-N(1)-C(5)	121.1(4)	123.8(7)
C(2)-N(1)-C(5)	117.8(4)	116.7(7)	C(8)-N(2)-C(9)	120.9(5)	120.5(7)
C(8)-N(2)-C(12)	120.5(5)	121.0(7)	C(9)-N(2)-C(12)	118.4(4)	118.3(7)
O(1)-C(1)-N(1)	123.7(5)	121.4(8)	O(1)-C(1)-C(8)	117.0(5)	118.4(8)
N(1)-C(1)-C(8)	118.9(5)	120.2(7)	N(1)-C(2)-C(3)	110.7(5)	110.3(8)
N(1)-C(2)-C(4)	111.0(5)	111.4(8)	C(3)-C(2)-C(4)	112.8(6)	111.9(9)
N(1)-C(5)-C(6)	111.6(5)	110.5(8)	N(1)-C(5)-C(7)	111.2(5)	114.8(8)
C(6)-C(5)-C(7)	114.3(6)	110.8(8)	O(2)-C(8)-N(2)	124.3(5)	123.8(8)
O(2)-C(8)-C(1)	117.5(5)	116.0(7)	N(2)-C(8)-C(1)	118.0(5)	120.2(7)
N(2)-C(9)-C(10)	110.9(5)	110.9(8)	N(2)-C(9)-C(11)	110.3(5)	111.3(8)
C(10)-C(9)-C(11)	113.5(6)	111.5(9)	N(2)-C(12)-C(13)	112.0(5)	109.6(8)
N(2)-C(12)-C(14)	112.2(5)	112.8(8)	C(13)-C(12)-C(14)	112.8(6)	112.3(8)
O(3)-C(15)-C(16)	122.1(4)	118.9(4)	O(3)-C(15)-C(20)	117.9(4)	121.1(4)
C(18)-C(19)-C(21)	117.0(5)		C(17)-C(18)-C(21)		119.3(5)
C(20)-C(19)-C(21)	123.0(5)		C(19)-C(18)-C(21)		120.7(5)

Results and Discussion

Perspective views, each with atom labelling, of the asymmetric units in complexes **I** and **III** are shown in Figs. 1 and 2, respectively. Figure 1 is also applicable to complex **II**, except that C(21) is bonded to C(18) instead of C(19). The final atomic parameters are listed in Table 2 and 3,[11,12] and molecular dimensions tabulated in Tables 4 and 5.

The crystal structures of **I**—**III** are illustrated in Fig. 3—5, respectively. A common feature is the exclusive occurrence of host-guest, rather than guest-guest,* hydrogen bonding, giving rise to discrete molecular aggregates which are dimeric in **I** and **II** and trimeric [two-fold axis passing through the center of the C(1)-C(1)' bond] in **III**. In the two 1:1 com-

*Hydrogen bonding involving cresol molecules exclusively might be expected to yield a zigzag polymeric arrangement which fits the chennel structure of **IV**.

Table 5. Bond Distances (*l*/Å) and Angles for Complex **III**[a]

O(1)-C(1)	1.238(3)	N-C(1)	1.330(3)
N-C(2)	1.477(3)	N-C(5)	1.487(3)
C(1)-C(1)'	1.525(5)	C(2)-C(3)	1.519(4)
C(2)-C(4)	1.532(4)	C(5)-C(6)	1.522(3)
C(5)-C(7)	1.512(4)	O(2)-C(8)	1.369(3)
C(8)-C(9)	1.377(4)	C(8)-C(13)	1.373(4)
C(9)-C(10)	1.377(4)	C(10)-C(11)	1.375(5)
C(11)-C(12)	1.374(4)	C(11)-C(14)	1.510(4)
C(12)-C(13)	1.380(4)		
C(1)-N-C(2)	121.8(2)	C(1)-N-C(5)	120.2(2)
C(2)-N-C(5)	117.9(2)	O(1)-C(1)-N	123.9(2)
O(1)-C(1)-C(1)'	116.3(2)	N-C(1)-C(1)'	119.5(2)
N-C(2)-C(3)	111.3(2)	N-C(2)-C(4)	111.1(2)
C(3)-C(2)-C(4)	112.2(2)	N-C(5)-C(6)	112.3(2)
N-C(5)-C(7)	112.3(2)	C(6)-C(5)-C(7)	113.2(2)
O(2)-C(8)-C(9)	117.7(3)	O(2)-C(8)-C(13)	123.3(2)
C(9)-C(8)-C(13)	119.0(2)	C(8)-C(9)-C(10)	119.8(3)
C(9)-C(10)-C(11)	122.0(3)	C(10)-C(11)-C(12)	117.3(3)
C(10)-C(11)-C(14)	121.3(3)	C(12)-C(11)-C(14)	121.3(3)
C(11)-C(12)-C(13)	121.5(3)	C(8)-C(13)-C(12)	120.3(2)

a) Symmetry transformation for generating the primed atom: $1-x$, y, $1/2-z$.

plexes, only one of the two amido groups of **1** is involved in acceptor hydrogen bonding [O(1)···O(3)= 2.694(8) and 2.67(1)Å, respectively], whereas both amide groups of the C_2 host molecule in **III** interact with the phenolic groups of a pair of *p*-cresol molecules [O(1)···O(2)=2.699(4)Å]. These modes of hydrogen bonding provide a rationale for the observed stoichiometries and infrared absorption spectra in the inclusion of *p*-cresol by **1**.

The oxamide host **1** adopts very similar configurations and molecular dimensions in this series of complexes, a planar bond configuration being found about each N atom (Tables 4 and 5). The O-C-C-O torsion angles take the values 91.8(6), 95.3(10) and −85.4(2)° for **I**—**III**, respectively, so that the two planar amide moieties of each host molecule behave as separate π systems with negligible conjugation across the central C-C single bond [1.518(8), 1.50(1), and 1.525(5) Å, respectively]. It is also noted that the involvement of either one or two amido groups in acceptor hydrogen bonding, as in complexes **II** and **III**, corresponds to a difference of about 10° (absolute value) in the O-C-C-O torsion angle.

Comparison of the present structures with that of the 1:1 complex (**IV**) of **1** with 1-methylnaphthalene (see Fig. 1 of Ref. 1) leads to the conclusion that the host system **1** adapts itself readily to the nature of the guest species present, forming crystalline lattices which are determined primarily by the bonding characteristics and steric requirement of the latter.

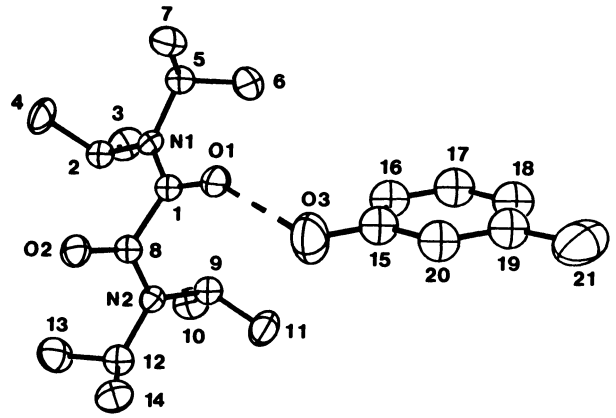

Fig. 1. Perspective view and atom labelling of the asymmetric unit in the 1:1 complex (**I**) of **1** with *m*-cresol. The atoms are represented as 30% thermal ellipsoids, and the hydrogen bond by a broken line. This figure also applies to the 1:1 complex (**II**) of **1** with *p*-cresol, with the modification that C(21) now bonds to C(18).

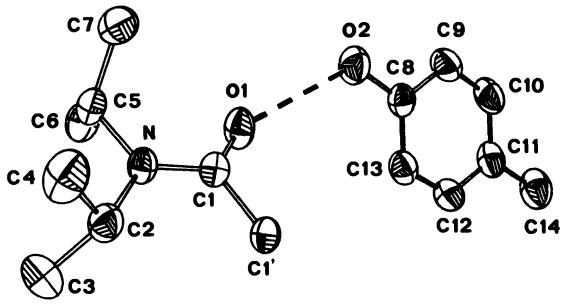

Fig. 2. Perspective view and atom labelling of the asymmetric unit in the 1:2 complex (**III**) of **1** with *p*-cresol. The atoms are represented as 35% thermal ellipsoids, and the hydrogen bond by a broken line. The primed atom is related to the unprimed one by the symmetry transformation $1-x$, y, $1/2-z$.

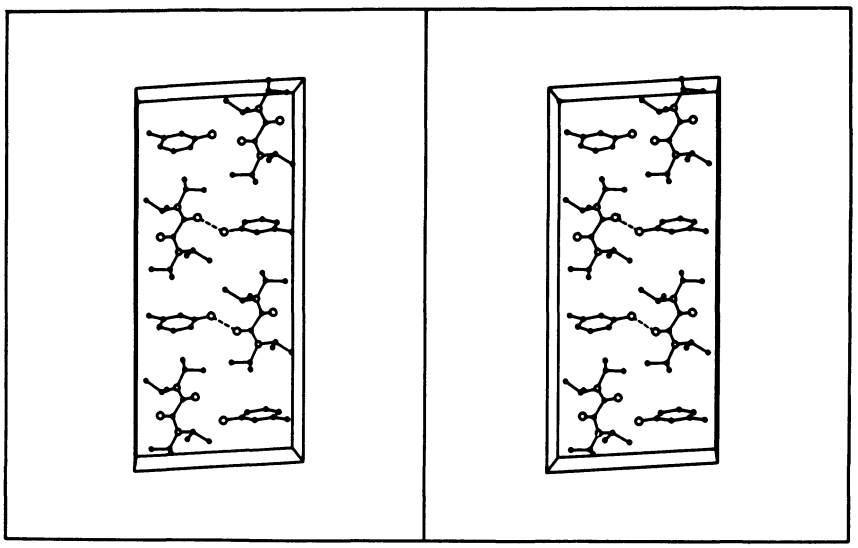

Fig. 3. Stereo view of the crystal structure of **1**·*m*-cresol, **I**. The origin of the unit cell lies at the upper left corner, with a pointing from left to right, b towards the reader, and c downwards. Hydrogen bonds are indicated by broken lines.

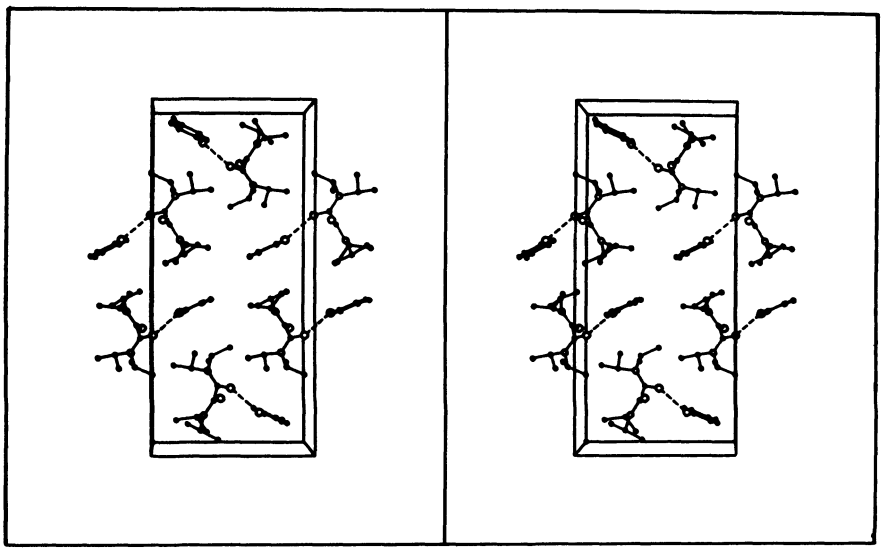

Fig. 4. Stereo view of the crystal structure of **1**·*p*-cresol, **II**. The origin of the unit cell lies at the lower left corner, with a pointing towards the reader, b from left to right, and c upwards. Hydrogen bonds are indicated by broken lines.

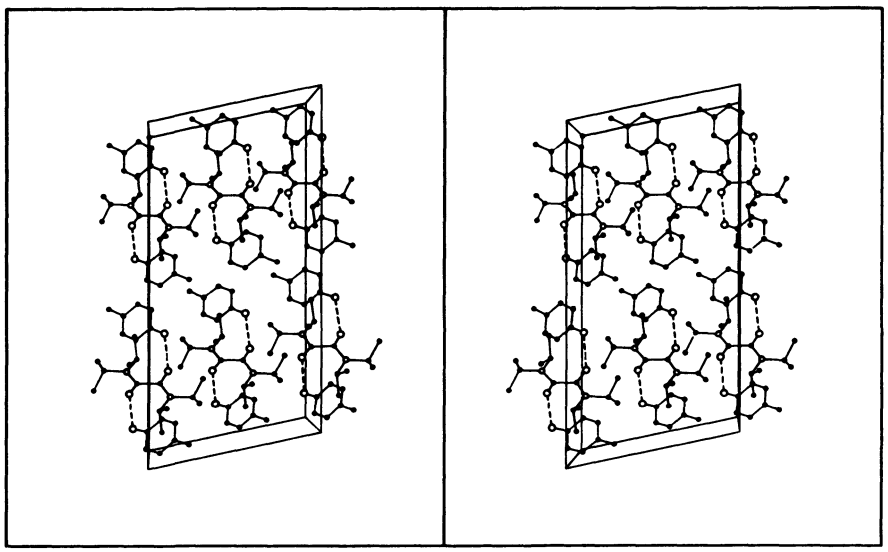

Fig. 5. Stereo view of the crystal structure of **1**·2*p*-cresol, **III**. The origin of the unit cell lies at the upper left corner, with a pointing from left to right, b towards the reader, and c downwards. Hydrogen bonds are indicated by broken lines.

References

1) F. Toda, K. Tanaka, Y. Tagami, and T. C. W. Mak, *Chem. Lett.*, **1985**, 195.

2) R. Adams, H. B. Bramlet, and F. H. Tendick, *J. Am. Chem. Soc.*, **42**, 2369 (1920).

3) The intensities declined rapidly with increasing Bragg angle, such that reflections with $2\theta_{max}>40$—42° were not detectable.

4) R. A. Sparks, "Crystallographic Computing Techniques," ed by F. R. Ahmed, Munksgaard, Copenhagen (1976), pp. 452—467.

5) R. Diamond, *Acta Crystallogr., Sect. A*, **25**, 43 (1969).

6) G. T. DeTitta, J. W. Edmonds, D. A. Langs, and H. Hauptman, *Acta Crystallogr., Sect. A*, **31**, 472 (1975).

7) The unfavorable data-to-parameter ratio precluded the use of anisotropic refinement of all non-hydrogen atoms. The phenyl ring was refined as a rigid group in order to restrict the number of variables.

8) G. M. Sheldrick, "Computational Crystallography," ed by D. Sayre, Oxford University Press, New York (1982), pp. 506—514.

9) "International Tables for X-Ray Crystallography," Kynoch Press, Birmingham (1974), Vol. IV, pp. 55—60, 99—101, 149—150.

10) J. W. Schilling, "Crystallographic Computing," ed by F. R. Ahmed, Munksgaard, Copenhagen (1970), pp. 201—204.

11) Tables of anisotropic thermal parameters, atomic parameters for hydrogen atoms, and structure factors have been deposited as Document No. 8626 at the Office of the Chemical Society of Japan.

12) The refined thermal parameters gave no evidence of non-stoichiometric ratio or disorder.

Photochemical Hydroxymethylation of Alicyclic and Aliphatic Alkenes Induced by a Eu^{III}/Eu^{II} Photoredox System in Methanol

Akito ISHIDA,* Shinya YAMASHITA, Susumu TOKI, and Setsuo TAKAMUKU
The Institute of Scientific and Industrial Research, Osaka University, Ibaraki, Osaka 567
(Received November 1, 1985)

The photoirradiation of a methanol solution of $EuCl_3$ and alkenes such as cyclohexene, cyclooctene, cyclododecene, and tetramethylethylene afforded (hydroxymethyl) alkane. The dihydro dimer of alkene, hydrogen, and ethylene glycol are also formed. Reactions proceed via a radical mechanism induced by hydrogen atoms and hydroxymethyl radicals, which are produced by a photoredox reaction of Eu^{III}/Eu^{II} in methanol.

Transition-metal organometallic chemistry has become important, principally due to the usefulness of members of this class of compounds for catalyzing or assisting in the transformation of organic substrates. However, photochemistry related to this field seems to be restricted to classical coordination compounds in aqueous solutions.[1] In recent years much attention has been paid to the decomposition of water into hydrogen and oxygen using metal catalysts from the viewpoint of the utilization of solar energy.[2] A few photochemical studies have been conducted on the metal compounds or metal complexes which can lead to catalytically and synthetically useful transformations of organic compounds.[3,4] The photochemistry of lanthanoids such as cerium, europium, or samarium has almost been restricted to spectroscopic investigations in aqueous systems,[5] there are a few applications regarding organic syntheses.

We have investigated the photoredox reactions of a Eu^{III}/Eu^{II} system in alcohols in the presence of some organic substrates in order to apply such a redox system of metal ions to organic photochemical reactions. Recently, we reported the formation of a dihydro dimer and a 2:1 styrene–methanol adduct via a radical mechanism when styrene and its derivatives are used as the substrate.[6] On the other hand, when uracil and its derivatives are used, a regioselective hydroxymethylation took place via an electron-transfer mechanism.[7] Here, we report on a photoreaction of europium chloride in the presence of alicyclic or aliphatic alkenes in methanol as a series which shows the scope and limitations for this reaction.

Results and Discussion

Photoreaction of $EuCl_3$ in Methanol. $EuCl_3$ does not absorb light of a longer wavelength than 250 nm in an aqueous solution, but has an absorption band around 280 nm in methanol. This might be due to a solvent-to-metal charge transfer. Upon irradiation of a methanol solution of $EuCl_3$ with a high-pressure mercury lamp through a Pyrex filter, a new absorption band appeared at 320 nm and was assigned to Eu^{II} on the basis of spectroscopic data.[6] Figure 1 shows the absorption spectra before and after irradiation. Hydrogen gas and ethylene glycol were formed

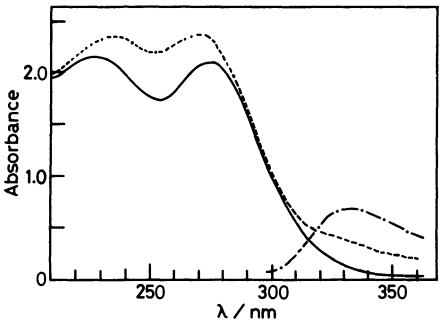

Fig. 1. Absorption spectra of a methanol solution of $EuCl_3$ before and after irradiation. $EuCl_3\,6H_2O$ 5 mmol dm^{-3} in methanol.
——: Before, -----: atfer 8 h irradiation. -·-·-·-: differential spectrum enlarged by a factor of 3.

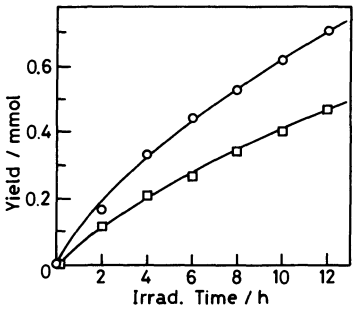

Fig. 2. Yields of hydrogen (—○—) and ethylene glycol (—□—) vs. time plot for the photoreaction of 5 mmol dm^{-3} solution of $EuCl_3$ 5 mL of methanol.

monotonously with the irradiation time. The yield of ethylene glycol was less than that of hydrogen (Fig. 2). The formation of formaldehyde was also detected upon the addition of 2,4-dinitrophenylhydrazine to the reaction mixture. After irradiation for 10 h, the yields of these products (based on the $EuCl_3$ used) reached 2000 and 1500%, respectively. This indicates that $EuCl_3$ operated catalytically. Taking the reaction mechanism in an aqueous solution into consideration,[5d] the following reaction scheme is suggested for the present system.

$$Eu^{3+} - CH_3OH \xrightarrow{h\nu} Eu^{2+} + CH_3O\cdot + H^+ \quad (1)$$

$$Eu^{2+} \xrightarrow{h\nu} Eu^{2+*} \quad (2)$$

$$Eu^{2+*} + H^+ \longrightarrow Eu^{3+} + H \quad (3)$$

$$CH_3O\cdot + CH_3OH \longrightarrow CH_3OH + \cdot CH_2OH \quad (4)$$

$$H + CH_3OH \longrightarrow H_2 + \cdot CH_2OH \quad (5)$$

$$2\cdot CH_2OH \longrightarrow HO(CH_2)_2OH \quad (6)$$

$$Eu^{3+} + \cdot CH_2OH \longrightarrow Eu^{2+} + HCHO + H^+ \quad (7)$$

The methoxyl radical formed in Reaction 1 is very reactive because of the large O–H bond-dissociation energy of methanol (435 kJ mol^{-1} [8]) and promptly abstracts H atoms from methanol to give hydroxymethyl radicals (Reaction 4). In the Eu^{III}/Eu^{II} photoredox systems, therefore, it is clear that H atoms and hydroxymethyl radicals are effectively formed. Hydrogen atoms and hydroxymethyl radicals formed by the reactions (Reactions 1—6) should afford equimolecular amounts of hydrogen and ethylene glycol. The hydroxymethyl radical, however, probably reacts with the Eu^{III} ion and decomposes into protons and formaldehyde.

Photoreaction of $EuCl_3$ in the Presence of Alkene in Methanol. The present photoredox system of Eu^{III}/Eu^{II} in methanol was applied to the reaction of alkene. A methanol solution of alkene (**1a—d**: 100 mmol dm^{-3}) and $EuCl_3$ (5 mmol dm^{-3}) was irradiated under an argon atmosphere at λ>300 nm. The methanol adduct of **1** (**2**) and the dihydro dimer of **1** (**3**) were obtained as the main products along with a large amount of hydrogen gas and ethylene glycol. In the absence of $EuCl_3$, the alkene was recovered unchanged from methanol after irradiation for 8 h.

$$R^1R^2C{=}CR^1R^2 \xrightarrow[EuCl_3,\,CH_3OH,\,8h]{h\nu,\,\lambda>300\,nm} R^1R^2CHCR^1R^2CH_2OH + (R^1R^2CHCR^1R^2-)_2$$

1 → **2** + **3**

a : $R^1 = H$ $R^2\text{-}R^2 = -(CH_2)_4-$

b : $R^1 = H$ $R^2\text{-}R^2 = -(CH_2)_6-$

c : $R^1 = H$ $R^2\text{-}R^2 = -(CH_2)_{10}-$

d : $R^1 = R^2 = CH_3$

The results are shown in Table 1. **4a**, **5a**, and **6a** from cyclohexene (**1a**) were obtained as minor products. In the case of tetramethylethylene (**1d**), **7d** was formed as one of the main products.

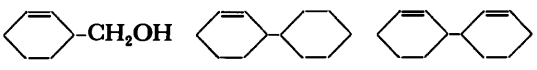

4a **5a** **6a**

$(CH_3)_2CHCH(CH_3)_2$

7d

The formation of these main products (**2** and **3**) can be reasonably explained as the results of the efficient trapping of primarily formed radicals from methanol (H and $\cdot CH_2OH$) by the added alkene (Reactions 8—10).

Table 1. The Photoreaction of Eu^{III} and Alkene in Methanol[a]

Alkene	Concn/ mmol dm^{-3}	Conv/%	Product yield/%[b]			
			2	**3**	H_2	$(CH_2OH)_2$
1a[c]	100	71	49	22	197	40
1a[d]	500	49	3	7	12	0
1b	100	78	52	25	128	23
1b	500	50	8	31	12	—[g]
1c	100	64	42	36	250	—
1c	300	43	7	61	55	—
1d[e]	100	81	37	4	44	—
1d[f]	500	50	13	7	3	—

a) $EuCl_3\,6H_2O$ 5 mmol dm^{-3}, methanol 5 mL, 8 h irrad. b) The yields are based on 1 consumed. c) Yields of minor products **4a**: 1, **5a**: 16, **6a**: 2%. d) **4a**: 2, **5a**: 15, **6a**: 15%. e) **7d**: 26%. f) **7d**: 25%. g) Not determined.

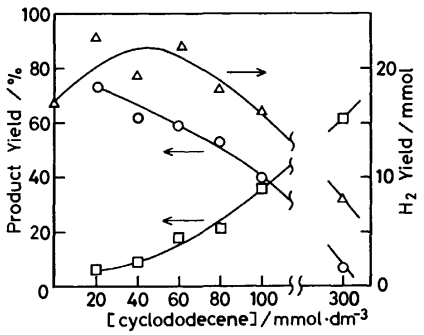

Fig. 3. Dependence of yields of hydrogen (—△—), **2c** (—○—), **3c** (—□—) on the concentration of cyclododecence for the photoreaction of $EuCl_3\,6H_2O$ (5 mmol dm^{-3}) in methanol (5 mL) for 8 h.

$$H + \mathbf{1} \longrightarrow \cdot RH \quad (8)$$

$$\cdot CH_2OH + \mathbf{1} \longrightarrow \cdot R\text{-}CH_2OH \quad (9)$$

$$2\cdot RH \longrightarrow RH\text{-}RH\ (\mathbf{3}) \quad (10)$$

$$\cdot R\text{-}CH_2OH \xrightarrow{[H]} H\text{-}R\text{-}CH_2OH\ (\mathbf{2}) \quad (11)$$

The addition of a H atom to alkene (Reaction 8) competes with the abstraction of a H atom from methanol (Reaction 5). These competitive processes depend on the concentration of the alkene used, The product ratio (**2**:**3**) was found to be very sensitive to the concentration of the alkene (Fig. 3). At a low alkene concentration, hydrogen mainly abstracts the hydrogen from methanol, producing hydrogen molecules and hydroxymethyl radicals. Thus, the main reaction becomes the hydroxymethylation of the alkene. With an increase in the concentration of alkene, the addition of a hydrogen atom to alkene becomes competitive and the yield of the dihydro dimer (**3**) increases to 61% at 0.3 mol dm^{-3} in the case of cyclododecene (**1c**). These reulsts are also consistent with the estimation on the basis of the kinetic data reported.[9]

The unsaturated products, **4a—6a** formed consider-

Table 2. Deuterium Isotope Effects in Photoreaction of $EuCl_3$ and Cyclododecene in Isotopic Methanols[a)]

Solvent	Concn	Product yield/%[b)]		Product Ratio	
	1c/mmol dm^{-3}	2c	3c	2c/3c	H_2/mL
CH_3OH	60	59	19	3.1	17
CH_3OD	60	58	16	3.6	16
CD_3OH	60	21	28	0.75	14

a) $EuCl_3$ $6H_2O$ 5 mmol dm^{-3}, Solvent 2 mL, 8 h irrad. b) Based on 1c consumed.

ably in the case of cyclohexene. It has been known that the allylic hydrogens of cyclohexene are much more reactive toward abstraction than those of other alkenes. This fact had been explained by the coplanarity of the cyclohexenyl radical and was substantiated by results reported by Mayo et al.[10] The ratios of k_{ab} (rate of H atom abstraction from alkene) to k_{ad} (rate of addition to alkene) were 16, 0.4, 1.5, and 1.2 for cyclohexene, cyclooctene, cyclododecene, and tetramethylethylene, respectively. The unsaturated products (**4a**, **5a**, and **6a**) might have been formed via the cyclohexenyl radicals. In the case of tetramethylethylene, the reduction of **1d** took place to afford 2,3-dimethylbutane (**7d**). The radical **8d** formed by the addition of a hydrogen atom to **1d** was a tertiary alkyl radical. The steric repulsion by an isopropyl and two methyl groups was anticipated as making the coupling reaction difficult. For a *t*-butyl radical (similar to **8d**), the disproportionation prevailed over the coupling in solution, whereas for alicyclic alkyl radicals, the former was interior to the latter.[11] These facts suggest that the hydrogenation of alkene occurs mainly in tetramethylethylene and are consistent with the experimental results.

$(CH_3)_2\dot{C}CH(CH_3)_2$

8d

In order to obtain an insight into this reaction, experiments were carried out using deuterium-labelled compounds. The results are summarized in Table 2.

The europium chloride used contained 6 gram-equivalent H_2O as the water of crystallization. However, its quantity was less than 0.1 wt% of the methanol and the effects of the water are presumed to be negligible. The yields of **2c** and **3c** did not differ greatly in CH_3OH and CH_3OD. When CD_3OH was used, however, **2c** decreased significantly with an increase of **3c**. The evolution of hydrogen gas was also reduced in the case of CD_3OH. The initial processes (Reactions 1—3) were regarded as not being influenced by the deuterium labelling. A reaction for which deuterium-isotope effects are expected is the hydrogen atom abstraction from methanol by hydrogen atom (Reaction 5) among the initial processes. The retardation of Reaction 5 in CD_3OH leads to a decrease in the yields of the hydroxymethyl radical as well as the hydrogen evolution with corresponding increases in the yields of the cyclododecyl radical. These explanations are in accord with the experimental results given in Table 2.

Concerning the hydrogen source for the formation of **2c** from the 2-(hydroxymethyl)cyclododecyl radical (**9c**) (Reaction 11), there are three possibilities: (1) recombination with a hydrogen atom, (2) disproportionation with other radicals, and (3) the abstraction of hydrogen from methanol. The first case seems to be not so important because the concentrations of hydrogen atoms and the radical **9c** are very low. The second and the third cases are of some importance for the present reaction conditions. Especially, considering the dissociation energies of the C–H bond in cyclohexane (402 kJ mol^{-1})[12] and the C–H bond in methanol (394 kJ mol^{-1}),[13] hydrogen abstraction from methanol becomes more exothermic than that from cyclohexane by 8 kJ mol^{-1}. Therefore, for this process, the effects of deuterium isotopes might be important. This interpretation is in accord with the fact that in the case of styrene, a 2:1 styrene–methanol adduct and a dihydro dimer were obtained as the main products, however, a 1:1 adduct was not detected. The benzyl-type radical derived from styrenes can not abstract H atom from methanol because the C–H bond energy of the benzylic C–H bond is low, 356 kJ mol^{-1}.[13] Therefore, the benzyl radical can only terminate by coupling with another benzyl radical.

An example of photochemical hydroxymethylation is known for norbornene in which hydroxymethylation proceeds by a xylene-sensitization in methanol via a radical mechanism.[14] On the contrary, cyclohexene and cycloheptene undergo a dipolar addition of methanol to give methoxy products.[14] The reactions are selective for cyclic six- and seven-membered rings. The present photoreactions of Eu-alkene systems in methnol are able to efficiently transform aliphatic and alicyclic alkenes to (hydroxymethyl) alkanes, in which europium ions act as an efficient sensitizer. The photoreaction of Eu(III) and alkene in methanol is useful as a general synthetic method for the hydroxymethylation of alkenes.

Experimental

Instruments. GLC analyses were carried out on a Shimadzu GC-7A gas chromatograph with OV-17 (2 m) for cyclohexene, cyclooctene, and cyclododecene, with a Porapak-

type QS (40 cm) or a Porapak-type T (40 cm) for tetramethylethylene and ethylene glycol. ^1H and ^{13}C NMR spectra were recorded in a $CDCl_3$ solution on a Bruker WM-360 spectrometer using TMS as an internal standard. The mass spectra were run on a JEOL JMS-DX300 (Gas chromatograph-Mass spectrometer) using the same columns as for the GC analysis. UV-spectra were recorded on a Hitachi 323 spectrophotometer.

Materials. Cyclohexene, cyclooctene, cyclododecene, and tetramethylethylene (Nakarai) were distilled over sodium prior to use and $EuCl_3\ 6H_2O$ (Nakarai) was used without further purification. Methanol was distilled over CaH_2. Isotopically labelled methanols (Merck) were used without further purification.

Spectral Change for the Eu^{III}–Methanol System by Irradiation. A methanol solution of $EuCl_3$ (2 mmol dm^{-3}) was irradiated under an argon atmosphere through a Pyrex filter with a 350-W high-pressure mercury lamp at running-water temperature. Absorption spectra were measured before irradiation and subsequently at regular time intervals. During the irradiation evolution of hydrogen gas was observed.

General Procedure. Photoreaction of a Methanol Solution of Eu^{III} and Alkenes. A methanol solution of alkene (**1**: 100 mmol dm^{-3}) and $EuCl_3$ (5 mmol dm^{-3}) was placed in a Pyrex cell connected to a gas syringe through a capillary tube to collect evolved hydrogen gas and irradiated under an argon atmosphere with a 350-W high-pressure mercury lamp for 8 h. After irradiation, the solution was concentrated under reduced pressure. The identification of products was carried out by a direct comparison of GLC and MS with those of available authentic samples. The following products were isolated by means of preparative gas chromatography (OV-17, 2 m) or the column chromatography on silica gel with hexane and benzene and were identified by spectral data.

Hydroxymethylcyclohexane (2a): Viscous oil; MS *m/z* (rel intensity) 96 (M^+-18, 7%), 83(16), 81(13), 67(28), 55(63), 41(100), 39(96), 31(66).

3-Hydroxymethylcyclohexene (4a): Viscous oil; **4a** was transformed into **2a** by hydrogenation of the reaction solution mixture by palladium-carbon. MS *m/z* (rel intensity) 94 (M^+-18, 2%), 81(11), 79(21), 66(5), 53(11), 41(12), 39(32), 31(100).

Bicyclohexyl (3a), 2-Cyclohexyl-cyclohexene (5a), 3,3'-Bicyclohexene (6a): **6a** was obtained by a photoreaction of **1a** and benzophenone, and hydrogenated by palladium-carbon to give new peaks coinciding with **3a** and **5a** at an early stage and concentrated at one peak after the end of the reaction.

3a: Viscous oil; MS *m/z* (rel intensity) 166 (M^+, 45%), 109(19), 96(29), 83(97), 82(100), 67(90), 53(39).

5a: MS *m/z* (rel intensity) 164(M^+, 2%), 91(13), 82(22), 81(54), 79(72), 77(35), 67(24), 55(100), 53(54), 41(94), 39(81).

6a: MS *m/z* (rel intensity) 162(M^+, 1%), 91(11), 82(7), 81(100), 79(89), 77(43), 66(20), 55(22), 53(51), 41(92), 39(69).

Hydroxymethylcyclooctane (2b): ^1H NMR ($CDCl_3$) δ= 1.33 (m, 14H), 1.83 (m, 1H), 2.47 (bs, 1H), 3.42 (d, J=6 Hz, 2H), 2,4-dinitrobenzoate of **2b**: mp 63—64 °C; MS *m/z* (rel intensity) 336(M^+, vw), 306(3), 195(12), 149(13), 124(15), 111(21), 96(100).

Bicyclooctyl (3b): Colorless needles; mp 46—47 °C; MS *m/z* (rel intensity) 222(M^+, vw), 111(100), 110(40), 82(36), 69(98), 55(42), 41(22); ^1H NMR ($CDCl_3$) δ=1.26—1.72(m); ^{13}C NMR ($CDCl_3$, off-resonance) δ=44.5(d), 30.9(t), 27.0(t).

Hydroxymethylcyclododecane (2c): Viscous oil; ^1H NMR ($CDCl_3$) δ=1.32 (m, 22H), 1.63 (t, J=6 Hz, 1H), 1.90 (bs, 1H), 3.47 (d, J=6 Hz, 2H); MS *m/z* (rel intensity) 198(M^+, vw), 180(7), 166(6), 152(6), 137(6), 123(11), 111(37), 97(70), 83(87), 69(73), 55(100). ^{13}C NMR ($CDCl_3$, off-resonance) δ=69.27(t), 40.67(d), 30.04(t), 29.73(t), 27.36(t), 26.88(t), 25.99(t).

Bicyclododecyl (3c): Needles; mp 117—118 °C; MS *m/z* (rel intensity) 334(M^+, 30), 166(100), 111(26), 97(48), 96(37), 83(43), 82(30), 69(30), 55(41); ^{13}C NMR ($CDCl_3$, off-resonance) δ=33.46(d), 26.26(t), 24.14(t), 23.93(t), 23.74(t), 22.92(t), 22.86(t); Found: C, 86.14; H, 13.86%. Calcd for $C_{24}H_{46}$: C, 86.13; H, 13.62%.

2,3-Dimethylbutane (7d) and 2,3,3,4,4,5-Hexamethylhexane (3d): **4d** was identified by the comparion of GC and MS with those of authentic sample obtained by a hydrogenation of tetramethylethylene. **3d** was identified based on GC-Mass data.

2,2,3-Trimethyl-1-butanol (2d): Viscous oil; ^1H NMR ($CDCl_3$) δ=0.82 (s, 6H), 0.85 (d, J=7 Hz, 6H), 1.64 (q, J= 7 Hz, 1H), 1.90 (bs, 1H), 3.37 (s, 2H); ^{13}C NMR ($CDCl_3$, off-resonance) δ=17.40(q), 30.00(q), 32.65(d), 37.36(s), 70.92(t).

The authors wish to thank the members of Material Analysis Center in the Institute of Scientific and Industrial Research, Osaka University, for the NMR and mass-spectra measurements and the elemental analyses.

References

1) V. Balzani and V. Carassiti, "Photochemistry of Coordination Compounds," Academic Press, New York (1970).

2) M. Graetzel, *Acc. Chem. Res.*, **14**, 376 (1981), and references cited therein; D. G. Whitten, *Acc. Chem. Res.*, **13**, 83 (1980).

3) G. L. Geoffroy and M. S. Wrighton, "Organometallic Photochemistry," Academic Press, New York (1979), Chap. 3.

4) T. Sato, H. Kaneko, and S. Yamaguchi, *J. Org. Chem.*, **45**, 3778 (1980); E. Murayama, A. Kohda, and T. Sato, *J. Chem. Soc., Perkin Trans. 1*, **1980**, 947; A. Kohda, K. Ueda, and T. Sato, *J. Org. Chem.*, **46**, 509 (1981).

5) a) P. C. Ford, R. E. Hinze, and J. D. Peterson, "Concepts of Inorganic Photochemistry," ed by A. W. Adamson and P. D. Fleischauer, Wiley (Interscience), New York (1974), p. 203; b) G. Adachi, K. Tomokiyo, K. Sorita, and J. Shiokawa, *J. Chem. Soc., Chem. Commun.*, **1980**, 914; G. Adachi, K. Sorita, K. Kawata, K. Tomokiyo, and J. Shiokawa, *J. Less-Common Met.*, **93**, 81 (1983); c) Y. Hass, G. Stein, and M. Tomkiewicz, *J. Phys. Chem.*, **74**, 2558 (1970); d) M. Brandys and G. Stein, *J. Phys. Chem.*, **82**, 852 (1978); e) N. Azuma, A. Matsumoto, and J. Shiokawa, *Polyhedron*, **2**, 63 (1983).

6) A. Ishida, S. Toki, and S. Takamuku, *Chem. Lett.*, **1985**, 893.

7) A. Ishida, S. Toki, and S. Takamuku, *J. Chem. Soc., Chem. Commun.*, **1985**, 1481.

8) G. Baker, J. H. Littlefair, R. Shaw, and J. C. Thynne, *J. Chem. Soc.*, **1965**, 6970.

9) Rate of addition of H atom to ethylene is 3.2×10^9 $mol^{-1}\,dm^3\,s^{-1}$ [J. K. Thomas, *J. Phys. Chem.*, **71**, 1919 (1967)] and one of abstraction of H atom from methanol by H atom is 2.9×10^6 $mol^{-1}\,dm^3\,s^{-1}$ [P. Neta, G. R. Holdren, and R. H.

Schuler, *J. Phys. Chem.*, **75**, 449 (1971)]. When the olefin is ca 0.02 mol dm^{-3} the reactions of addition and abstraction are suggested to be comparable.

10) F. R. Mayo, *Acc. Chem. Res.*, **1**, 193 (1968); D. E. Van Sickle, F. R. Mayo, and R. M. Arluck, *J. Am. Chem. Soc.*, **87**, 4824 (1965).

11) M. J. Gibian, R. C. Corley, *Chem. Rev.*, **73**, 441 (1973); R. A. Scheldon and J. K. Kochi, *J. Am. Chem. Soc.*, **92**, 4395 (1970).

12) K. C. Ferguson and E. Whittle, *Trans. Faraday Soc.*, **67**, 2618 (1976).

13) D. M. Golden, and S. W. Benson, *Chem. Rev.*, **69**, 125 (1969).

14) P. J. Kropp, *J. Am. Chem. Soc.*, **91**, 5783 (1969).

Syntheses of Cyclic Decapeptides with Four Ornithyl Residues Related to Gramicidin S[1)]

Setsuko ANDO,* Hiroshi NISHIKAWA, Hideo TAKIGUCHI, and Nobuo IZUMIYA†
Department of Chemistry, Faculty of Science, Fukuoka University, Jonan-ku, Fukuoka 814-01
†Laboratory of Chemistry, Kurume Institute of Technology, Kamitsu-machi, Kurume 830
(Received December 7, 1985)

Three cyclic decapeptides with four L-ornithyl residues related to gramicidin S (GS), *cyclo*(-Orn-Leu-Orn-D-Phe-Pro-)$_2$ (**D-L-12**), *cyclo*(-Orn-Leu-Orn-Phe-Pro-)$_2$ (**L-L-12**), and *cyclo*(-Orn-Leu-Orn-Phe-D-Pro-)$_2$ (**L-D-12**), were synthesized to investigate the contribution of increase of the basic amino acid residues and of configurations of phenylalanyl and prolyl residues toward antibacterial activity. These GS-like analogs were synthesized by the solution method of peptide synthesis. Protected cyclic decapeptides were synthesized through a cyclization reaction of linear decapeptide azide in pyridine. Hydrogenolysis of the protected cyclic decapeptides afforded crystalline tetrahydrochlorides of the desired analogs. In the experiment of circular dichroism, **D-L-12** gave a curve similar to that of GS, while **L-L-12** and **L-D-12** gave different curves. Antibacterial assays showed **L-L-12** exhibited substantial activities against Gram-negative bacteria, whereas **D-L-12** and **L-D-12** negligible activity.

Gramicidin S (Fig. 1) is a cyclic decapeptide antibiotic, and exhibits the activity against Gram-positive bacteria. Its decapeptide backbone holds a rigid β-sheet structure stabilized with four hydrogen bonds as shown in Fig. 2. In the previous paper, we reported new function of a GS analog; [D-Dap$^{4,4'}$]GS exhibited the activity against Gram-negative bacteria such as Escherichia coli and Salmonella typhosa, whereas GS shows no activity for these bacteria (Table 1).[2,3)] We also observed that GS-like cyclic tetradecapeptide, *cyclo*(-Leu-Orn-Leu-Orn-Leu-D-Phe-Pro-)$_2$ (**LOP**), exhibited the activity against Gram-negative bacteria.[4)] [D-Dap$^{4,4'}$]GS and LOP contain four basic amino acid residues and hold the β-sheet conformation similar to that of GS. It would be noteworthy that [D-Dap-(β-*Z*)$^{4,4'}$]GS, which contains two ornithyl residues and holds GS-like conformation, exhibited no activity against Gram-negative bacteria, but the activity against Gram-positive ones.[3)]

In the course of studies on the new function of GS analogs, we designed a GS-like analog containing four L-ornithyl residues, *cyclo*(-Orn-Leu-Orn-D-Phe-Pro-)$_2$ (**D-L-12** in Fig. 1). We assumed that **D-L-12** with D-Phe-L-Pro sequence holds GS-like conformation as shown in Fig. 2, then **D-L-12** possesses the activity against Gram-negative bacteria as [D-Dap$^{4,4'}$]GS or **LOP**. Additionally, we planned to synthesize two optical diastereomers of **D-L-12**, namely **L-L-12** with L-Phe-L-Pro and **L-D-12** with L-Phe-D-Pro sequence (Fig. 1); we were interested in examining possible activity for Gram-negative or positive bacteria though we could not speculate on the conformation for two GS-like analogs.

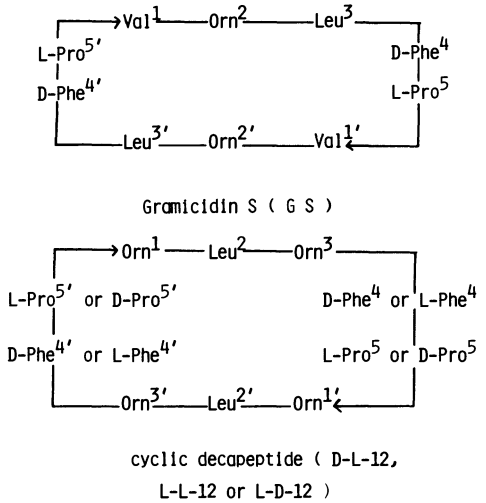

Fig. 1. Structures of GS and GS-like analogs. **D-L-12**, **L-L-12**, and **L-D-12** contain D-Phe-L-Pro, L-Phe-L-Pro, and L-Phe-D-Pro sequences, respectively.

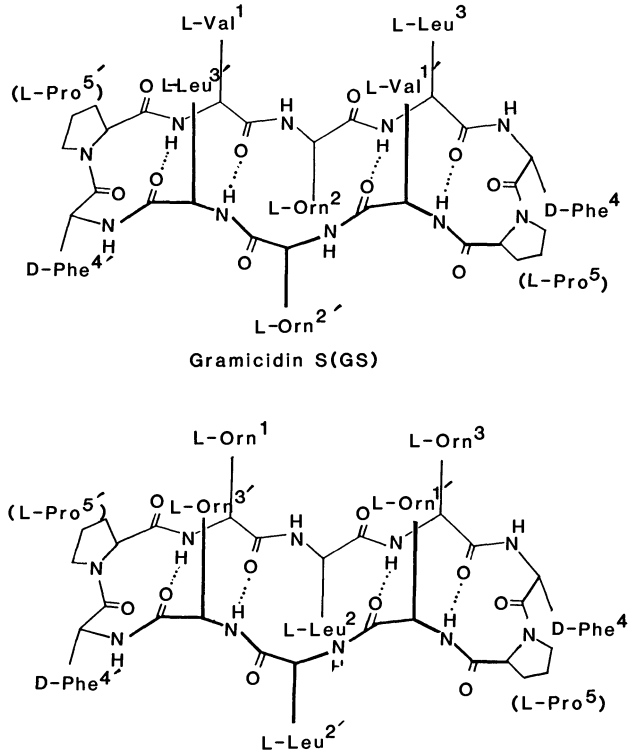

Fig. 2. Conformation of GS and assumed one of **D-L-12**.

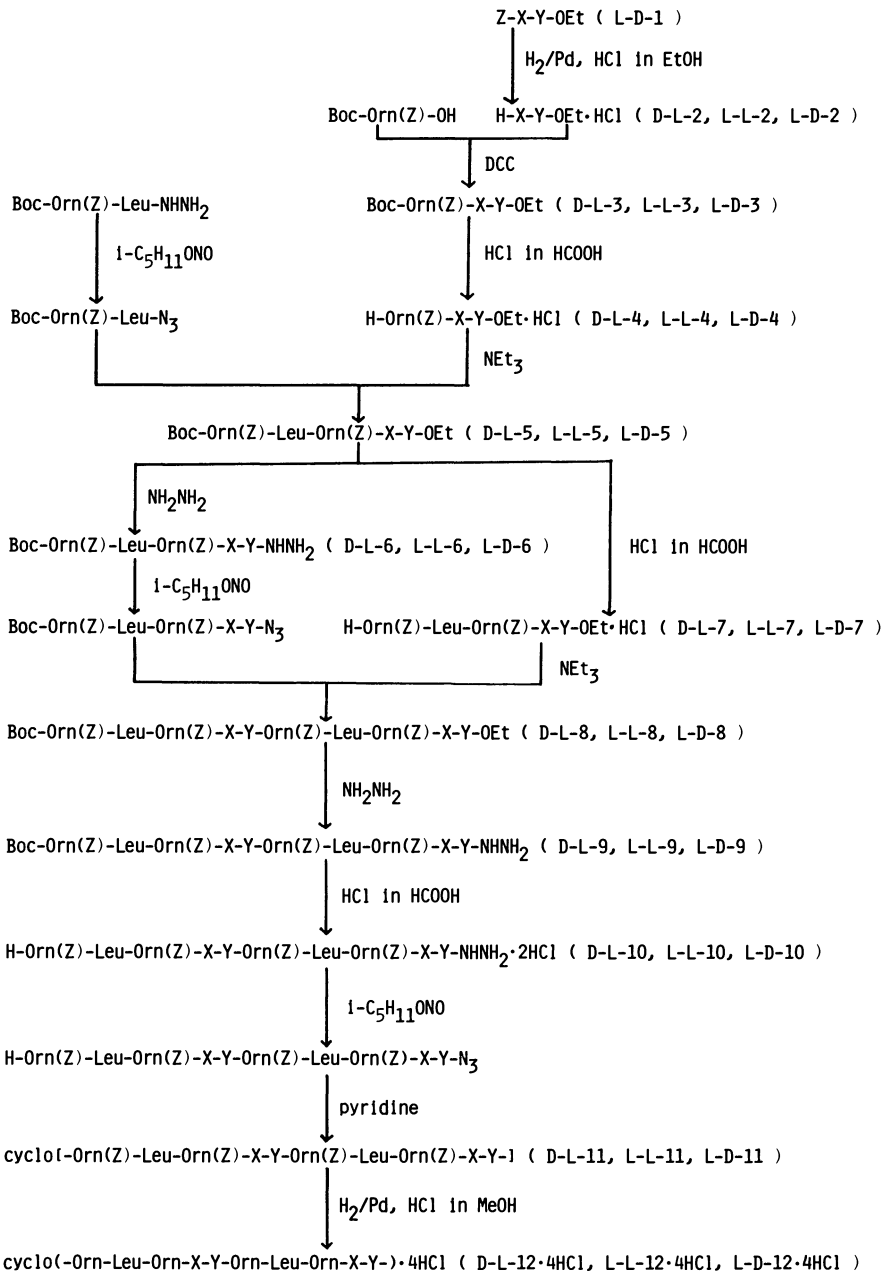

Fig. 3. Syntheses of GS-like analogs. **D-L**-series; X=D-Phe, Y=L-Pro. **L-L**-series; X=L-Phe, Y=L-Pro. **L-D**-series; X=L-Phe, Y=D-Pro.

Syntheses of tetrahydrochlorides of three analogs are outlined in Fig. 3. Boc-pentapeptide ester (**5**) was prepared by the coupling of Boc-dipeptide azide with H-tripeptide ester (**4**). A part of **5** was converted into Boc-pentapeptide hydrazide (**6**), and **6** was changed to the corresponding azide. Coupling of the azide and H-pentapeptide ester (**7**) afforded Boc-decapeptide ester (**8**) which was converted to the corresponding hydrazide (**9**). The Boc-hydrazide **9** was converted to H-decapeptide hydrazide (**10**), and **10** was changed to H-decapeptide azide. Then, the azide was subjected to cyclization in pyridine, and the protected cyclic decapeptide (**11**) was obtained in 49% yield for **D-L-11**, 45% **L-L-11** or 55% **L-D-11**. It should be noted that we could obtain pure cyclic decapeptide (**L-L-11**) with all L-amino acid residues in a good yield (45%) from the cyclization product of H-decapeptide azide though several investigators only isolated cyclic decapeptide in poor yield by the cyclization of H-peptide active ester with all L-amino acid residues.[5] Desired crystalline **D-L-12·4HCl**, **L-L-12·4HCl** or **L-D-12·4HCl** was obtained by hydrogenolysis of each **11** in methanol containing hydrogen chloride.

The homogeneity of **11** and **12·4HCl** was ascertained by several analytical experiments such as TLC, paper electrophoresis and amino acid analysis. The fact that **11** and then **12·4HCl** are a cyclic monomer was confirmed by determination of molecular weight

Table 1. Antibacterial Activities of GS Analogs[a)]

Organism	D-L-12	L-L-12	L-D-12	[D-Dap$^{4,4'}$]GS[b)]	LOP[c)]	GS
Staphylococcus aureus FDA 209P	>100	50	>100	100	12.5	3.13
Bacillus subtilis PCI 219	50	12.5	12.5	12.5	6.25	3.13
Escherichia coli NIHJ JC-2	>100	50	>100	25	12.5	100
Salmonella typhosa Boxhill 58	>100	25	100	25	25	>100
Shigella flexneri EW-10	50	6.25	50	25	6.25	6.25
Shigella sonnei EW-33	100	25	>100	50	12.5	100
Klebsiella pneumoniae DT	100	25	>100	50	12.5	12.5

a) Numerals show the minimum inhibitory concentration ($\mu g\,cm^{-3}$). b) Data are cited from the literature.[3)] c) Data are cited from the literature.[4)] **LOP** represents *cyclo*(-Leu-Orn-Leu-Orn-Leu-D-Phe-Pro-)$_2$.

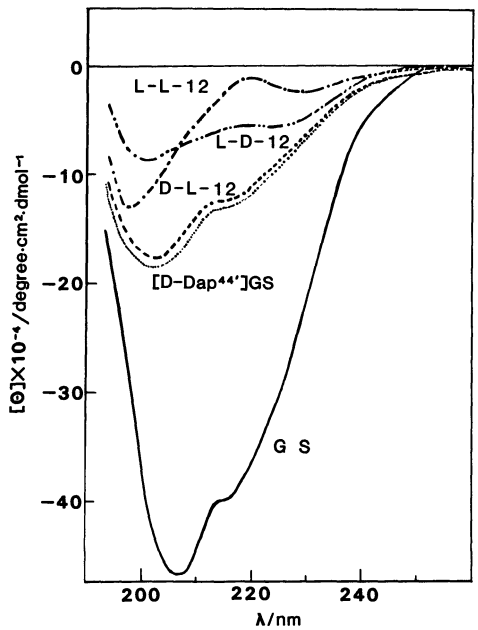

Fig. 4. CD spectra of GS-like analogs and GS in MeOH at 25 °C. Curve of [D-Dap$^{4,4'}$]GS is cited from the literature.[3)]

by an osmometer for **11**, and by a fast atom bombardment (FAB) mass spectroscopy for **12**·4HCl.

Figure 4 shows CD curves of synthesized analogs and GS. The analog **D-L-12** exhibited the similar pattern for GS as expected, though the troughs (203 and 216 nm) were shallower than those of GS; the result suggested that the conformation of peptide-backbone is not changed significantly by the presence of L-Orn-L-Leu-L-Orn instead of L-Val-L-Orn-L-Leu sequence in GS. The CD curve of **D-L-12** is very similar to that of [D-Dap$^{4,4'}$]GS (Fig. 4).[3)] Other analogs, **L-L-12** and **L-D-12**, exhibited the CD curves different from that of GS; the result suggests that the changes in conformation are due to presence of L-Phe-L-Pro and L-Phe-D-Pro sequence.

Results of the antibacterial assay are shown in Table 1. Unexpectedly, **D-L-12** showed negligible activity against Gram-negative bacteria such as Escherichia coli and Salmonella typhosa and also against Gram-positive bacteria such as Staphylococcus aureus and Bacillus subtilis. On the other hand, **L-L-12** showed substantial activity against several Gram-negative bacteria, and even some activity for Gram-positive bacteria. Level of the activities for Gram-negative and -positive bacteria by **L-L-12** is similar to those by [D-Dap$^{4,4'}$]GS. Analog **L-D-12** showed weak activity against a Gram-positive bacteria, Bacillus subtilis PCI 219.

In the previous papers, we reported that [D-Dap$^{4,4'}$]GS and LOP containing four basic amino acid residues possess the activity against Gram-negative bacteria and hold GS-like conformation.[3,4)] However, present cyclic decapeptide **D-L-12** satisfying two requirements (four basic amino acid residues and GS-like conformation) should no activity against Gram-negative bacteria. Whereas, the **L-L-12** holding a certain conformation other than that of GS exhibited the activity. At present, we can not give definite explanation why **D-L-12** shows no activity while **L-L-12** the activity. In this connection, it would be noteworthy that cyclic polymyxins, known for their activity against Gram-negative bacteria, contain six basic amino acid residues of all L-configuration out of ten component amino acid residues.[6)]

Experimental

All melting points are uncorrected. Prior to analysis, compounds were dried over P_2O_5 at 80 °C and 2 mmHg†. Linear and cyclic decapeptide derivatives were dried over P_2O_5 at 25 °C in a desiccator. TLC was carried out on Merck silica gel G with following solvent system: R_f 1-butanol-acetic acid-pyridine-water (4:1:1:2, v/v).

Z-Phe-D-Pro-OEt (L-D-1). To a solution of Z-Phe-OH (14.93 g, 50 mmol) in chloroform (70 cm^3) was added DCC (11.57 g, 55 mmol) at −5 °C. After several min, H-D-Pro-OEt·TsOH (15.77 g, 50 mmol) and triethylamine (7 cm^3, 50 mmol) in chloroform (70 cm^3) was added to the solution. After the mixture was stirred for 45 h at 5 °C, resulting *N,N'*-dicyclohexylurea was filtered off and the filtrate was evaporated to dryness in vacuo. Oily residue was dissolved in ethyl acetate (200 cm^3), and the solution was washed successively with 4% $NaHCO_3$, 2% HCl, water, and dried (Na_2SO_4). The filtrate from the salt was evaporated, and product was obtained as an oil; yield, 19.24 g (90%); R_f=0.97.

H-Phe-Pro-OEt·HCl (L-L-2). Z-Phe-Pro-OEt[7)] (16.88 g, 40 mmol) in 1.7 M†† HCl in ethanol (34 cm^3) was hydrogenated in the presence of Pd black. The filtrate was

† 1 mmHg≈133.322 Pa.
†† 1 M=1 mol dm^{-3}.

evaporated, and the resulting crystals were collected by filtration with the aid of ether; yield, 10.3 g (87%); mp 153—154 °C; $[\alpha]_D^{25}$ −22° (*c* 1, DMF); R_f=0.78.

Found: C, 58.01; H, 7.39; N, 8.35%. Calcd for $C_{16}H_{23}O_3N_2Cl \cdot 1/4H_2O$: C, 58.00; H, 7.15; N, 8.45%.

H-Phe-D-Pro-OEt·HCl (L-D-2). This compound was prepared from **L-D-1** (19.24 g, 45 mmol) as described for the preparation of **L-L-2**. Product was obtained as an oil; yield, 14.71 g (100%); R_f=0.77.

Boc-Orn(Z)-D-Phe-Pro-OEt (D-L-3). To a solution of Boc-Orn(*Z*)-OH (13.0 g, 35.5 mmol) in chloroform (60 cm³) was added DCC (7.21 g, 35.5 mmol) at −5 °C. After several min, **D-L-2**[8] (12.9 g, 35.5 mmol) and triethylamine (4.97 cm³, 35.5 mmol) in chloroform (60 cm³) was added to the solution. The mixture was stirred for 3 d at 5 °C, the filtrate from *N,N'*-dicyclohexylurea was evaporated, and oily residue was dissolved in ethyl acetate (150 cm³). The solution was washed successively with 4% $NaHCO_3$, 0.5 M citric acid, water, and dried (Na_2SO_4). The filtrate was evaporated and product was obtained as an oil; yield, 17.2 g (76%); R_f= 0.97.

Boc-Orn(Z)-Phe-Pro-OEt (L-L-3). This compound was obtained from Boc-Orn(*Z*)-OH (10.5 g, 28.7 mmol) and **L-L-2** (10.4 g, 28.7 mmol) as described for the preparation of **D-L-3**; yield of an oil, 17.4 g (95%); R_f=0.93.

Boc-Orn(Z)-Phe-D-Pro-OEt (L-D-3). This compound was obtained from Boc-Orn(*Z*)-OH (11.0 g, 30 mmol) and **L-D-2** (9.93 g, 30 mmol) as an oil; yield, 17.4 g (90%); R_f=0.95.

H-Orn(Z)-D-Phe-Pro-OEt·HCl (D-L-4). Compound **D-L-3** (17.3 g, 26.9 mmol) was dissolved in 0.183 M HCl in formic acid (177 cm³). After standing at room temperature for 20 min, the solution was evaporated to dryness. Product was obtained as an oil; yield, 15.5 g (100%); R_f=0.81.

H-Orn(Z)-Phe-Pro-OEt·HCl (L-L-4). This compound was obtained from **L-L-3** (16.9 g, 25.0 mmol) as described for the preparation of **D-L-4**. Product was obtained as an oil; yield, 13.7 g (90%); R_f=0.85.

H-Orn(Z)-Phe-D-Pro-OEt·HCl (L-D-4). This compound was obtained from **L-D-3** (17.4 g, 27.0 mmol) as an oil; yield, 15.5 g (100%); R_f=0.84.

Boc-Orn(Z)-Leu-Orn(Z)-D-Phe-Pro-OEt (D-L-5). To a solution of Boc-Orn(*Z*)-Leu-$NHNH_2$[9] (11.3 g, 22.9 mmol) in DMF (70 cm³) at −20 °C were added 2.02 M HCl in dioxane (34 cm³) and isopentyl nitrite (3.44 cm³, 25.2 mmol). After 5 min, the solution was neutralized with *N*-methylmorpholine (7.56 cm³, 68.7 mmol). To this solution was added a chilled solution of **D-L-4** (14.0 g, 22.9 mmol) and *N*-methylmorpholine (2.77 cm³, 25.2 mmol) in DMF (70 cm³). The mixture was stirred at 0 °C for 7 d and evaporated in vacuo. Residual solid was dissolved in ethyl acetate (150 cm³), and the solution was washed successively with 0.5 M citric acid, 4% $NaHCO_3$, water, and dried (Na_2SO_4). The filtrate was evaporated and oily residue solidified upon the addition of ether. Product was obtained as crystalline solid; yield, 15.9 g (71%); mp 108—110 °C; $[\alpha]_D^{25}$ −64° (*c* 0.1, MeOH); R_f=0.98.

Found: C, 63.59; H, 7.58; N, 9.71%. Calcd for $C_{53}H_{73}O_{12}N_7$: C, 63.65; N, 7.36; N, 9.80%.

Boc-Orn(Z)-Leu-Orn(Z)-Phe-Pro-OEt (L-L-5). Azide derived from Boc-Orn(*Z*)-Leu-$NHNH_2$[9] (9.87 g, 20 mmol) was coupled with **L-L-4** (13.7 g, 22.4 mmol) as described for the preparation of **D-L-5**. Product was recrystallized from ethyl acetate-ether-petroleum ether; yield, 14.1 g (68%); mp 98—99 °C; $[\alpha]_D^{25}$ −68° (*c* 0.2, MeOH); R_f=0.93.

Found: C, 62.96; H, 7.65; N, 9.55%. Calcd for $C_{53}H_{73}O_{12}N_7 \cdot 1/2H_2O$: C, 63.08; H, 7.39; N, 9.72%.

Boc-Orn(Z)-Leu-Orn(Z)-Phe-D-Pro-OEt (L-D-5). Azide derived from Boc-Orn(*Z*)-Leu-$NHNH_2$[9] (6.18 g, 12.6 mmol) was coupled with **L-D-4** (7.67 g, 12.6 mmol) as described for the preparation of **D-L-5**. Product was obtained as crystalline solid; yield, 12.2 g (97%); mp 107—108 °C; $[\alpha]_D^{25}$ −3.58° (*c* 0.2, DMF); R_f=0.93.

Found: C, 62.87; H, 7.55; N, 10.06%. Calcd for $C_{53}H_{73}O_{12}N_7$: C, 63.65; H, 7.36; N, 9.80%.

Boc-Orn(Z)-Leu-Orn(Z)-D-Phe-Pro-$NHNH_2$ (D-L-6). A solution of **D-L-5** (8.29 g, 8.3 mmol) and hydrazine hydrate (16.1 cm³, 332 mmol) in DMF (40 cm³) was allowed to stand at room temperature for 7 d. Excess hydrazine was evaporated in vacuo, and water (60 cm³) was added to the residue. Resulting solid was collected by filtration; yield, 7.93 g (97%); mp 136—138 °C; $[\alpha]_D^{25}$ −45° (*c* 0.3, AcOH); R_f=0.97.

Found: C, 61.77; H, 7.50; N, 12.83%. Calcd for $C_{51}H_{71}O_{11}N_9$: C, 62.11; H, 7.26; N, 12.78%.

Boc-Orn(Z)-Leu-Orn(Z)-Phe-Pro-$NHNH_2$ (L-L-6). This hydrazide was obtained from **L-L-5** (10.4 g, 10 mmol) as described for the preparation of **D-L-6**; yield, 6.38 g (95%); mp 111—112 °C; $[\alpha]_D^{25}$ −47° (*c* 0.5, AcOH); R_f=0.93.

Found: C, 61.37; H, 7.55; N, 12.61%. Calcd for $C_{51}H_{71}O_{11}N_9 \cdot 1/2H_2O$: C, 61.66; H, 7.29; N, 12.67%.

Boc-Orn(Z)-Leu-Orn(Z)-Phe-D-Pro-$NHNH_2$ (L-D-6). This hydrazide was obtained from **L-D-5** (8.24 g, 8.24 mmol); yield, 7.92 g (96%); mp 119—120 °C; $[\alpha]_D^{25}$ −19.7° (*c* 0.5, AcOH); R_f=0.93.

Found: C, 60.07; H, 7.07; N, 12.63%. Calcd for $C_{51}H_{71}O_{11}N_9 \cdot 3/2H_2O$: C, 60.46; H, 7.33; N, 12.44%.

H-Orn(Z)-Leu-Orn(Z)-D-Phe-Pro-OEt·HCl (D-L-7). This compound was obtained from **D-L-5** (5.18 g, 5 mmol) as described for the preparation of **D-L-4**; yield of an oil, 4.68 g (100%); R_f=0.83.

H-Orn(Z)-Leu-Orn(Z)-Phe-Pro-OEt·HCl (L-L-7). This compound was obtained from **L-L-5** (5.11 g, 5 mmol); yield of an oil; 4.68 g (100%); R_f=0.83.

H-Orn(Z)-Leu-Orn(Z)-Phe-D-Pro-OEt·HCl (L-D-7). This compound was obtained from **L-D-5** (3.80 g, 3.8 mmol); yield of an oil; 3.50 g (100%); R_f=0.83.

Boc[-Orn(Z)-Leu-Orn(Z)-D-Phe-Pro-]$_2$OEt (D-L-8). Azide derived from **D-L-6** (5.11 g, 5 mmol) was coupled with **D-L-7** (4.88 g, 5 mmol) as described for the preparation of **D-L-5**. Product was recrystallized from ethyl acetate-ether; yield, 5.78 g (62%); mp 139—142 °C; $[\alpha]_D^{25}$ −33° (*c* 0.2, MeOH); R_f= 0.95.

Found: C, 63.61; H, 7.42; N, 10.26%. Calcd for $C_{99}H_{132}O_{21}N_{14} \cdot 3/2H_2O$: C, 63.61; H, 7.15; N, 10.31%.

Boc[-Orn(Z)-Leu-Orn(Z)-Phe-Pro-]$_2$OEt (L-L-8). Azide derived from **L-L-6** (5.11 g, 5 mmol) was coupled with **L-L-7** (4.88 g, 5 mmol). Product was obtained as crystalline solid; yield, 6.60 g (70%); mp 151—154 °C; $[\alpha]_D^{25}$ −53° (*c* 0.2, MeOH); R_f=0.98.

Found: C, 62.87; H, 7.40; N, 10.39%. Calcd for $C_{99}H_{132}O_{21}N_{14} \cdot 3H_2O$: C,62.72; H, 7.21; N, 10.16%.

Boc[-Orn(Z)-Leu-Orn(Z)-Phe-D-Pro-]$_2$OEt (L-D-8). Azide derived from **L-D-6** (2.76 g, 2.8 mmol) was coupled with **L-D-7** (2.62 g, 2.8 mmol); yield of crystalline solid, 4.34 g (82%); mp 129—132 °C; $[\alpha]_D^{25}$ −8.36° (*c* 0.2, MeOH); R_f=0.97.

Found: C, 63.32; H, 7.47; N, 10.42%. Calcd for $C_{99}H_{132}O_{21}N_{14} \cdot 2H_2O$: C, 63.31; H, 7.17; N, 10.26%.

Boc[-Orn(Z)-Leu-Orn(Z)-D-Phe-Pro-]$_2$NHNH$_2$ (D-L-9). This compound was obtained from **D-L-8** (5.58 g, 2.98 mmol) as described for the preparation of **D-L-6**. Product was recrystallized from ethyl acetate-ether; yield, 4.94 g (90%); mp 107—110 °C; $[\alpha]_D^{25}$ −46° (*c* 0.5, AcOH); R_f=0.98.

Found: C, 61.54; H, 7.49; N, 12.13%. Calcd for $C_{97}H_{130}O_{20}N_{16}\cdot 3H_2O$: C, 61.51; H, 7.24; N, 11.83%.

Boc[-Orn(Z)-Leu-Orn(Z)-Phe-Pro-]$_2$NHNH$_2$ (L-L-9). This hydrazide was obtained from **L-L-8** (3.72 g, 2.0 mmol); yield, 3.65 g (99%); mp 145—147 °C; $[\alpha]_D^{25}$ −49° (*c* 0.5, AcOH); R_f=0.98.

Found: C, 61.49; H, 7.18; N, 12.04%. Calcd for $C_{97}H_{130}O_{20}N_{16}\cdot 3H_2O$: C, 61.51; H, 7.24; N, 11.83%.

Boc[-Orn(Z)-Leu-Orn(Z)-Phe-D-Pro-]$_2$NHNH$_2$ (L-D-9). This hydrazide was obtained from **L-D-8** (3.72 g, 2.0 mmol); yield, 3.39 g (80%); mp 139—142 °C; $[\alpha]_D^{25}$ −10.8° (*c* 0.5, AcOH); R_f=0.98.

Found: C, 61.53; H, 7.38; N, 12.76%. Calcd for $C_{97}H_{130}O_{20}N_{16}\cdot 3H_2O$: C, 61.51; H, 7.24; N, 11.83%.

H[-Orn(Z)-Leu-Orn(Z)-D-Phe-Pro-]$_2$NHNH$_2\cdot$2HCl (D-L-10). This compound was obtained from **D-L-9** (1.84 g, 1 mmol) as described for the preparation of **D-L-4**; yield of an oil, 1.81 g (100%); R_f=0.82.

H[-Orn(Z)-Leu-Orn(Z)-Phe-Pro-]$_2$NHNH$_2\cdot$2HCl (L-L-10). This compound was obtained from **L-L-9** (1.81 g, 1.0 mmol); yield of an oil, 1.81 g (100%); R_f=0.82.

H[-Orn(Z)-Leu-Orn(Z)-Phe-D-Pro-]$_2$NHNH$_2\cdot$2HCl (L-D-10). This compound was obtained from **L-D-9** (1.10 g, 0.6 mmol); yield of an oil, 1.10 g (100%); R_f=0.82.

***cyclo*[-Orn(Z)-Leu-Orn(Z)-D-Phe-Pro-]$_2$ (D-L-11).** To a solution of **D-L-10** (1.81 g, 1 mmol) in DMF (30 cm^3) at −20 °C, were added 1.71 M HCl in dioxane (1.75 cm^3) and isopentyl nitrite (0.15 cm^3, 1.1 mmol). After stirred at −20 °C until a hydrazine test became negative, this solution was added dropwise into pyridine (500 cm^3) at 0 °C for 5 min, and stirring was continued for 2 h at 0 °C and for 65 h at 5 °C. After the solvent was removed, the residue was dissolved in a mixture (280 cm^3, 6:1 v/v) of methanol and water, the solution was passed through the columns of Dowex 1 (OH^- form) and 50 (H^+ form). The columns were washed with the same solvent (560 cm^3), and effluent was evaporated to dryness. The residue was collected by filtration with the aid of water. For purification, solution of the crude product (1.02 g) in DMF (6 cm^3) was applied to a column (25×845 mm) with Sephadex LH-20, and development continued with DMF. Elution was carried out at room temperature at flow rate of 20 cm^3/h; a 3 cm^3 fraction was collected in each test tube. Peptide content in the fractions was determined with LKB 2138 Uvicord S at 245 nm. Fractions 55—65 containing **D-L-11** were evaporated, and product was collected by filtration with the aid of water; yield, 837 mg (49%); mp 107—109 °C; $[\alpha]_D^{25}$ −71° (*c* 0.1, MeOH); R_f=0.98.

Found: C, 61.15; H, 7.03; N, 11.27%. Calcd for $C_{92}H_{118}O_{18}N_{14}\cdot 5H_2O$: C, 61.45; H, 7.18; N, 10.91%.

***cyclo*[-Orn(Z)-Leu-Orn(Z)-Phe-Pro-]$_2$ (L-L-11).** This compound was prepared from **L-L-10** (1.81 g, 1 mmol) as described for the preparation of **D-L-11**. Product was collected by filtration with the aid of water; yield, 775 mg (45%); mp 135—140 °C; $[\alpha]_D^{25}$ −43° (*c* 0.1, MeOH); R_f=0.97.

Found: C, 64.80; H, 7.22; N, 11.18%. Calcd for $C_{92}H_{118}O_{18}N_{14}$: C, 64.49; H, 7.22; N, 11.48%.

***cyclo*[-Orn(Z)-Leu-Orn(Z)-Phe-D-Pro-]$_2$ (L-D-11).** This compound was prepared from **L-D-10** (1.09 g, 0.6 mmol); yield, 568 mg (55%); mp 139—141 °C; $[\alpha]_D^{25}$ −37.5° (*c* 0.1, MeOH); R_f=0.98.

Found: C, 62.16; H, 6.99; N, 11.32%. Calcd for $C_{92}H_{118}O_{18}N_{14}\cdot 4H_2O$: C, 62.08; H, 7.13; N, 11.02%.

***cyclo*(-Orn-Leu-Orn-D-Phe-Pro-)$_2\cdot$4HCl (D-L-12·4HCl).** Compound **D-L-11** (200 mg, 0.12 mmol) in 0.094 M HCl in methanol (6.2 cm^3) was hydrogenated in presence of Pd black. The filtrate was evaporated and resulting crystals were collected by filtration with the aid of ether. Product was recrystallized from methanol-ether; yield, 129 mg (82%); mp 209—211 °C; $[\alpha]_D^{25}$ −68° (*c* 0.1, MeOH); R_f=0.78. Amino acid ratios: Orn, 1.98; Leu, 1.04; Phe, 1.00; Pro, 0.97.

Found: C, 48.40; H, 7.72; N, 12.90%. Calcd for $C_{60}H_{98}O_{10}N_{14}Cl_4\cdot 10H_2O$: C, 48.12; H, 7.94; N, 13.09%.

***cyclo*(-Orn-Leu-Orn-Phe-Pro-)$_2\cdot$4HCl (L-L-12·4HCl).** This compound was prepared from **L-L-11** (200 mg, 0.12 mmol); yield, 101 mg (65%); mp 192—194 °C; $[\alpha]_D^{25}$ −46° (*c* 0.1, MeOH); R_f=0.75. Amino acid ratios: Orn, 1.96; Leu, 1.06; Phe, 1.00; Pro, 0.99.

Found: C, 50.66; H, 7.88, N, 13.50%. Calcd for $C_{60}H_{98}O_{10}N_{14}Cl_4\cdot 6H_2O$: C, 50.56; H,7.78; N, 13.76%.

***cyclo*(-Orn-Leu-Orn-Phe-D-Pro-)$_2\cdot$4HCl (L-D-12·4HCl).** This compound was prepared from **L-D-11** (200 mg, 0.12 mmol); yield, 104 mg (68%); mp 194—196 °C; $[\alpha]_D^{25}$ −30° (*c* 0.1, MeOH); R_f=0.73. Amino acid ratios: Orn, 2.03; Leu, 0.98; Phe, 1.00; Pro, 0.96.

Found: C, 50.64; H, 7.83; N, 13.60%. Calcd for $C_{60}H_{98}O_{10}N_{14}Cl_4\cdot 6H_2O$: C, 50.56; H, 7.78; N, 13.76%.

Molecular Weight Determination. Molecular weight (MW) of *Z*-substituted cyclic decapeptides was determined by the use of CORONA osmometer type 117 in DMF as a solvent. The values of MW for three analogs (**D-L-11**, **L-L-11**, and **L-D-11**) were 1788, 1698, and 1720, respectively, whereas the calculated value is 1708. FAB mass spectra of three analogs were obtained by the use of JEOL JMS-DX300. The values of *m/z* 1172 were observed, whereas the calculated value as [$C_{60}H_{95}O_{10}N_{14}$ (M+H)$^+$] is 1172.

Amino Acid Analysis. Analyses were carried out using JASCO HPLC amino acid analysis system, after hydrolysis of the peptides in 6 M HCl at 110 °C for 24 h.

Electrophoresis. Electrophoresis on Toyo Roshi No. 52 paper was carried out with the solvent system, formic acid-acetic acid-methanol-water (1:3:6:10, v/v; pH 1.8), for 2 h at 500 V/30 cm. Each of three analogs gave single spot. Ratios of mobility of **D-L-12**, **L-L-12**, and **L-D-12** toward GS were 1.43, 1.44, and 1.44, respectively.

CD Measurement. Measurement of CD spectra was performed with JASCO Model J-40 over a wavelength range of 190 to 260 nm in methanol as a solvent at 25 °C. Cell of 0.01 and 0.1 cm path length was used. In Fig. 5 are shown CD spectra of the analogs and GS.

Antibacterial Assays. Minimum amount of peptides necessary for the complete inhibition of growth was determined by a dilution method with Bouillon agar medium. Results are shown in Table 1.

Authors thank the staffs of Takeda Chemical Industries, Ltd. for the antibacterial assays. Authors are indebted to Assoc. Prof. Norikazu Nishino of Kyushu Institute of Technology for measurement of FAB mass spectra. Present work was partially supported by a grant from Central Research Institute of Fukuoka

University.

References

1) A part of this work has been communicated: S. Ando, H. Nishikawa, H. Takiguchi, and N. Izumiya, "Peptide Chemistry 1984," ed by N. Izumiya, Protein Research Foundation (1985), p. 355.

2) Abbreviations: Z, benzyloxycarbonyl; Boc, *t*-butoxycarbonyl; DCC, dicyclohexylcarbodiimide; TsOH, *p*-toluenesulfonic acid; DMF, *N,N*-dimethylformamide; Dap, 2,3-diaminopropionic acid; Dap(*β*-*Z*), 3-benzyloxycarbonyl-2,3-diaminopropionic acid. Amino acid symbols except D-Phe and D-Pro denote the L-configuration.

3) S. Ando, H. Aoyagi, S. Shinagawa, N. Nishino, M. Waki, T. Kato, and N. Izumiya, *FEBS Lett.*, **161**, 89 (1983).

4) S. Ando, H. Takiguchi, and N. Izumiya, *Bull. Chem. Soc. Jpn.*, **56**, 3781 (1983).

5) M. Kawai and U. Nagai, "Peptide Chemistry 1975," ed by S. Yamada, Protein Research Foundation (1976), p. 130. M. Roth and F. Eisenbeiss, *Angew. Chem.*, **80**, 907 (1968); M. Kawai and U. Nagai, *Biopolymers*, **17**, 1549 (1978).

6) T. Suzuki, K. Hayashi, K. Fujikawa, and K. Tsukamoto, *J. Biochem.*, **54**, 555 (1963).

7) T. Kato, M. Ohno, S. Makisumi, and N. Izumiya, *Nippon Kagaku Zasshi*, **87**, 493 (1966).

8) M. Ohno, T. Kato, S. Makisumi, and N. Izumiya, *Bull. Chem. Soc. Jpn.*, **39**, 1738 (1966).

9) H. Abe, K. Sato, T. Kato, and N. Izumiya, *Bull. Chem. Soc. Jpn.*, **49**, 3113 (1976).

Basic Study on Lithium Recovery from Lithium Containing Solution

Tetsutaro YOSHINAGA,* Kentaro KAWANO, and Hirotsugu IMOTO†
Department of Environmental Science, Faculty of Engineering, Kyushu Institute of Technology, Sensuicho, Tobata-ku, Kitakyushu 804
(Received September 12, 1985)

Basic study of Li recovery using high purity sodium aluminate solution as coprecipitating agent has been made. Al concentration, pH and temperature greatly affect the Li recovery, and in this study the temperature was maintained constant (25 °C). For reference lithium solution, the optimum (initial) pH obtained increased with an increase in Al concentration. Optimum pH=11.0—12.5 for [Al]=50—1000 mg dm^{-3}. The optimum pH values obtained were lower than those in the previous work by about one pH unit. The following relationship was found between the Al concentration C_{Al} (mg dm^{-3}) and the optimum pH; Opt. $pH^{exp}=8.23+1.5 \log C_{Al}$. Furthermore, these experimental pH values were in fair agreement with the pH values calculated from the solubility product of aluminium hydroxide, $K_{sp}(HAlO_2)=[H^+][AlO_2^-]=10^{-13.2}$, i.e., $pH^{calcd}=9.5+\log C_{Al}$. Effects of coexistent ions on Li recovery were examined. Sodium and potassium ions did not interfere, while calcium, magnesium, and monosilicate ions did. However, the interference from Ba^{2+} ions was small. Especially, interference by calcium and monosilicate ions were significant. Bubbling of CO_2 gas into the Li solution with proper Al concentration made a remarkable improvement on Li recovery. Accordingly, the influence of water soluble carbonates on Li recovery was investigated. The carbonates (Na_2CO_3, K_2CO_3, $(NH_4)_2CO_3$) used were found to be very effective for Li recovery. The addition of sodium aluminate solution (500 mg dm^{-3}) to untreated geothermal water showed around 70% of Li recovery at the best. This incomplete recovery of lithium is due to the matrix effect of geothermal water. For reference Li solution with Al concentration of 500 mg dm^{-3}, optimum pH was 12.5, while for Ca, SiO_2-free geothermal water the same pH gave very low Li recovery. However, when a pH value of 11.5 is chosen, a remarkable increase in Li recovery was obtained (98—99%). The silica component in geothermal water interfered with the Li recovery, but the influence was relatively small. The silica in the geothermal water in this case, was polymerized and showed some buffering action, such as prevention of interference from calcium ions. This is the significant difference between poly and monosilicate ions which do not show any buffering action. The addition of sodium carbonate to the Ca,SiO_2-free geothermal water caused a remarkable acceleration of the Li recovery, similar to that for the reference Li solution.

Lithium has been widely used in recent years in batteries, glass, ceramics, aluminium refinning and other industries. A world wide increase in demand is expected in future. In addition to these commercial uses, lithium is also anticipated to be the fuel for nuclear fusion and a blanket material in fusion reactors[1] in the 21 century. The estimated lithium resources are not enough when the increase in future demand is taken into account. Lithium recovery from geothermal water using a coprecipitation method has been studied as a part of the basic investigation of lithium extraction from brines.[2] The results have taught us that among the coprecipitating agents used in the previous work, aluminium salts showed the best performance. The appropriate pH for Li recovery is in the high pH region of 10—13. Thus, from the operational point of view, the use of $NaAlO_2$ seemed better than that of $AlCl_3$. In the previous work, the $NaAlO_2$ addition method was partly applied. However, the salt was added in a powdered form and the data obtained showed some scatter, although the trends were probably real. Commercially obtained $NaAlO_2$ was used as the coprecipitating agent in the form of a highly alkaline solution.[3] Provided the same lot number of $NaAlO_2$ is used, the data showed relatively good reproducibility, but the data obtained from different lots showed large discrepancies. The reason could be: (1) a difference in the ratio of Al to NaOH, for example Al/NaOH=0.76—0.82, (2) the presence of impurities. In this study, a $NaAlO_2$ solution of high purity, except for NaOH, was prepared as coprecipitating agent for lithium recovery.

Experimental

Reagents. The special grade LiCl, NaCl, KCl, $CaCl_2 \cdot 2H_2O$, $MgCl_2 \cdot 6H_2O$, $BaCl_2 \cdot 2H_2O$, Na_2CO_3, K_2CO_3, $(NH_4)_2CO_3$ were obtained from Wako Pure Chemical Industries, Ltd. Al plates (99.99%) and $Na_2SiO_3 \cdot 9H_2O$ were obtained from Wako pure Chemical Industries, Ltd. All other reagents used were also obtained from Wako Pure Chemical Industries, Ltd.

Measurements and Apparatus. The concentration of lithium, sodium, potassium, calcium and magnesium were measured on a Japan-Jarrel Ash AA-8200 atomic absorption spectrophotometer. Silica was measured on a Shimadzu UV-200 double beam spectrophotometer, according to the JIS method.[4] pHs of solutions containing lithium were measured with an Instrument Co.Ltd., digital pH meter, DP-1400. An Ikeda Rika six-series magnetic stirrer was used to stir solutions.

Sample Solutions. a) Li Solution: The proper amount of LiCl was dissolved in distilled water, and adjusted to a Li concentration of 10 mg dm^{-3} ($[Li^+]_0$=10 mg dm^{-3}).

b) Geothermal Water: Geothermal water was sampled from a reservoir pond at mixed wells at the Hatchobaru power plant in Ohita prefecture, in January, 1983. Geothermal water was used in the laboratory six months after sampling.

Coprecipitating Agent. Prior to the preparation of the

† Present address: Division of Magnetic Recording Material, Toda Kogyo Corporation, Shinmachi, Yokokawa, Hiroshima 733.

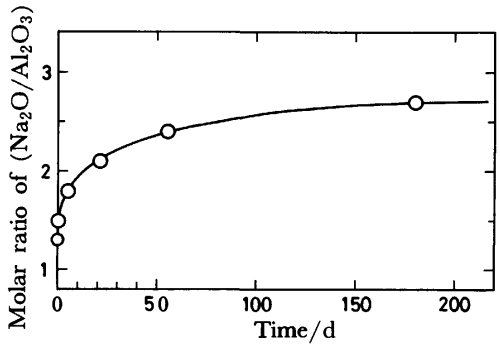

Fig. 1. Spontaneous decomposition of sodium aluminate solution with various (Na_2O/Al_2O_3) molar ratios at room temperature. [Na_2O]: 150 (g dm^{-3}).

$NaAlO_2$ coprecipitating agent, a preliminary test was made to examine the stability of the $NaAlO_2$ solution. The $NaAlO_2$ solution is said to be unstable at an Na_2O concentration of less than 90 g dm^{-3} and molar ratio of Na_2O to Al_2O_3 less than 1.3 at 25—50 °C, but when the ratio of $(Na_2O/Al_2O_3)_{mol}$ is set between 1.5—2.5, it is relatively stable at room temperature.[5] In the present work, the Na_2O concentration was fixed at 150 g dm^{-3}, and the value of $(Na_2O/Al_2O_3)_{mol}$ was changed between 1.3—2.7 taking into account the results obtained by Shimizu et al.[5] The stability of the sodium aluminate solution prepared as described above was examined at room temperature (around 25 °C) as shown in Fig. 1. It was found that the relationship between the spontaneous decomposition time, t (in day) and the molar ratio, R[=$(Na_2O/Al_2O_3)_{mol}$] was given by:

$$\log t = 1.78R - 2.504$$

Thus, the $NaAlO_2$ stock solution was adjusted to be; [NaOH]=200 g dm^{-3}, [Al]=50 g dm^{-3} and $(Na_2O/Al_2O_3)_{mol}$=2.7.

High grade Al plates were washed with acetone and water, dipped in alkaline solution(1 M*-NaOH), washed with water, dipped in acidic solution (1M-HCl), washed with water, and finally washed with acetone and/or ether. The plates were then stored in a desiccator. Al (25g) was taken into the solution in which 100 g of NaOH was dissolved with 400 ml of distilled water, and the solution was stirred. After the complete dissolution of the aluminium plates, the solution was filtrated with a sintered-glass filter (G-4), washed and transfered to a 500 ml volumetric flask to be diluted to the mark.

Procedure. The similar experimental procedure on Li recovery was used as was described in the previous work.[2] In the present study, the Li containing solutions were placed in a thermostat (25 °C) to be free from temperature effect. The initial pH was adjusted using 1 M-HCl solution. Carbonates were added after the addition of coprecipitating agents to examine their effects. The pHs were then adjusted. When the influence of coexistent ions was being examined, the ions were just added to the Li solution. Subsequently the same procedure was followed as for the solution which were free from coexistent ions.

Treatment of Geothermal Water. Geothermal water was treated in the same way as that described above.[2] Ca-free geothermal water was prepared as follows; 30 ml of saturated $Na_2C_2O_4$ solution was added to the 1 liter of geothermal water, stirred for 2 h; the CaC_2O_4 precipitate that formed was filtrated with a glass filter (G-4). Silicate-free geothermal water was prepared as follows; $FeCl_3$ was added to be Fe concentration of 1000 mg dm^{-3}, and pH was adjusted (pH=9.5) with 5 M-NaOH solution. After being stirred for 2 h, the precipitate formed was filtered with filter paper (No. 131). Ca,SiO_2-free geothermal water was prepared by combining the above procedures, that is, by first removing calcium ions, and then silicate ions. The main components of the geothermal water are shown in Table 1.

Table 1. Li, Ca, and SiO_2 Concentrations in Hatchobaru Geothermal Water (Nontreated and Treated) in (mg dm^{-3})

Geoth. Water	Li	Ca	Total SiO_2
Nontreated G.W.	10.56	12.9	870
G4-filtreated G.W.[a)]	10.56	12.9	434
Ca free-G.W.	10.21	0.2	788
SiO_2 free-G.W.	9.63	6.2	4
Ca, SiO_2 free-G.W.	9.33	0.2	4

a) G4: Glass filter G4, G.W.: Geothermal Water.

Results and Discussion

The Relationship betweem Al Concentration and Optimum pH on Li Recovery for Li Solution. pH dependence on Li recovery at various Al concentrations (50—1000 mg dm^{-3}) was examined. Figure 2 (1) shows the data for Al concentration of 300 mg dm^{-3} as an example. In the upper half of the left side of the figure(a) are given the residual Li concentrations as a function of time elapsed at various pHs. In the lower half of the left side of the figure(b) are given the time traces of pHs for the Li containing solutions with six initial pHs. Those solutions with initial pHs of 10—11.5 show rapid increase in pHs at the beginning, while those with initial pHs of 12—12.5 change slowly. The relationship between the initial pH and the percent recovery of lithium is shown in the right side of the figure(c). After 3 h, the curve with initial pH of 12 shows the maximum percent recovery of lithium among those with several pHs. At pH 12, around 86% of lithium was recovered after 6 h, while after 24 h, 100% was recovered. The data for other Al concentrations are shown in Fig.2 (2). The relationship between the Al concentration and the optimum pH for Li recovery thus obtained are shown as a solid line in Fig. 3, where at the appropriate pH if maximum recovery of lithium is obtained we designate that the optimum pH. For a Li solution, as the figure shows, the optimum initial pH obtained increases continuously with increase in Al concentration, where the optimum pH is 11.0—12.5 for [Al]= 50—1000 mg dm^{-3}. The optimum pH values obtained were lower than those obtained in the previous work[2] by about one pH unit. The following empirical formula

* 1 M=1 mol dm^{-3}.

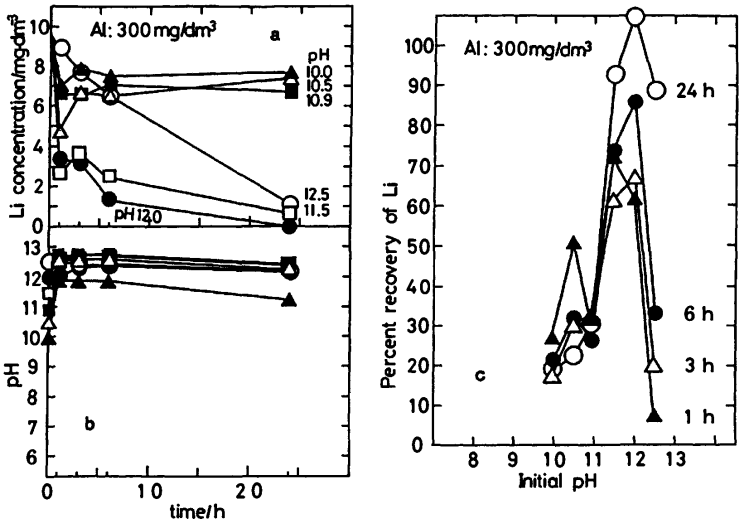

Fig. 2.(1) Initial pH dependence on Li recovery at Al concentration of 300 mg dm^{-3} at 25°C. a) Time course of [Li^+], b) Time course of pH, c) The relation of initial pH and percent recovery of lithium.

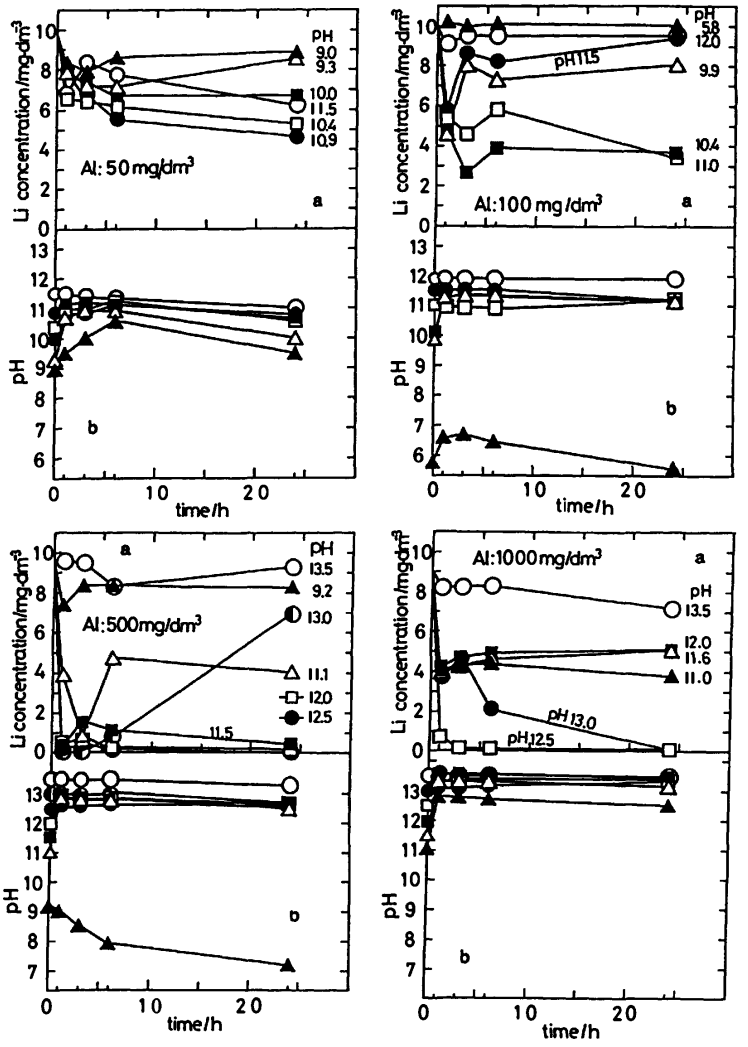

Fig. 2.(2) Initial pH dependence on Li recovery at various Al concentrations at 25°C.

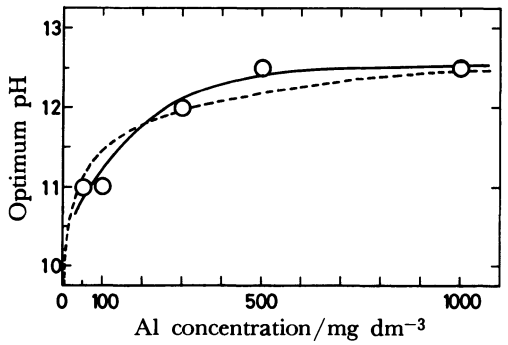

Fig. 3. The relationship between Al concentration and optimum initial pH for Li concentration of 10 (mg dm^{-3}) solution at 25°C. ——: Experimental curve, -----: Theoretical curve obtained using solubility product of aluminium hydroxide $\{K_{sp}(HAlO_2)=[H^+][AlO_2^-]=10^{-13.2}\}$.

was found between the Al concentration C_{Al}(mg dm^{-3}) and the optimum pH;

$$pH_{opt}^{exp}([Li]_0 = 10\ mg\ dm^{-3}:25°C) = 8.23 + 1.5 \log C_{Al}$$

These experimental optimum pH values were in fair agreement with the pH values calculated from the solubility product of aluminium hydroxide, $K_{sp}(HAlO_2)=[H^+][AlO_2^-]=10^{-13.2}$ that is, $pH^{calcd}=9.5+\log C_{Al}$. The broken line in Fig. 3 was plotted using these calculated values. This characteristic correspondence suggests that the optimum pH for Li recovery using the coprecipitation method will have some relation to the solubility product of aluminium hydroxide.

Influence of Coexistent Ions. Ca^{2+} and Mg^{2+} ions were known to interfere with the precipitation of lithium ions as aluminate.[6] The influence of Na^+, (K^+), Ca^{2+}, Mg^{2+}, (Ba^{2+}), and monosilicate ions on the Li recovery was investigated using freshly prepared high purity $NaAlO_2$ solution. The results are shown in Fig. 4. Sodium ions seem to behave differently in comparison with the Li solution. However, after 24 h, nearly the same percent recovery was obtained. Potassium ions seemed not to have any influence on Li recovery although its concentration is low, about two orders comparing with sodium ions. Alkaline earth metal ions, Ca^{2+} and Mg^{2+} ions interfere

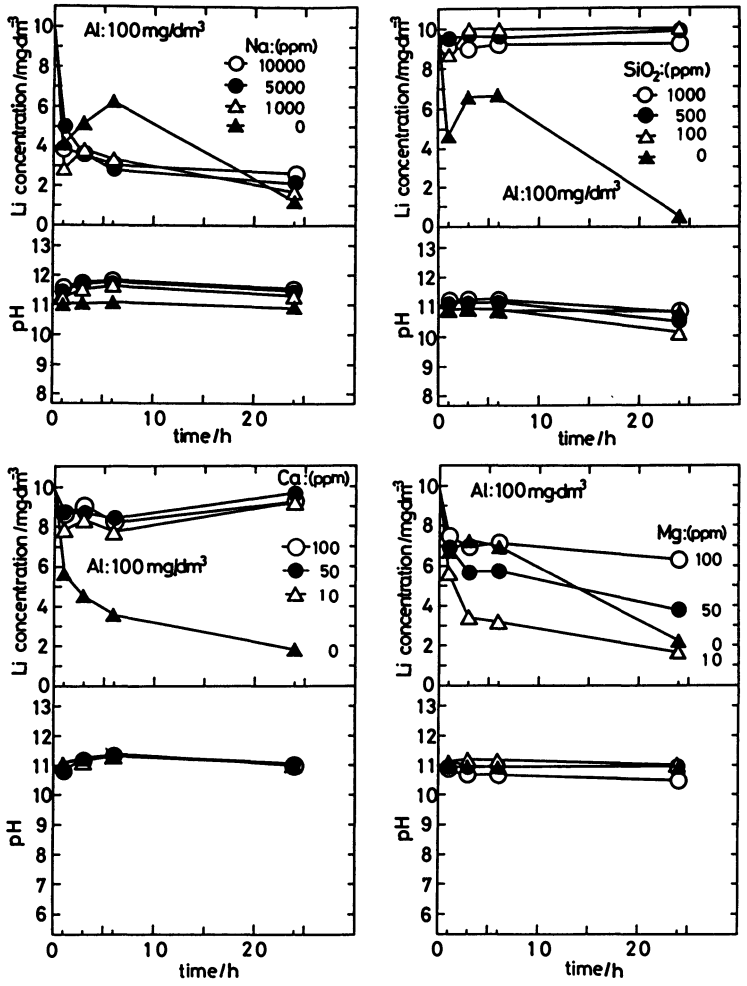

Fig. 4. Influence of coexistent ions on Li recovery at 25°C. Interference ions illustrated were; [Na^+], [Ca^{2+}], [Mg^{2+}], [SiO_3^{2-}]. Counter ions used were Cl^- for cations, Na^+ for anions.

with the Li recovery as is shown in the figure. Especially, Ca^{2+} ions give large interference. Even a Ca concentration as low as 10 mg dm^{-3}, prevented the recovery of lithium. To examine the uptake of Ca ions into aluminate precipitates in detail, the residual Ca concentration in the Li containing solutions was measured. Figure 5 shows the results. For the solution with an initial Ca concentration of 10 mg dm^{-3}, the maximal uptake was 99%, while for Ca concentrations of 50 and 100 mg dm^{-3}, it was 94 and 70%, respectively. If Ca^{2+} ions were taken up into the precipitate in the form of $Ca(AlO_2)_2$, the total calcium content which corresponds to 74 mg Ca dm^{-3} will be incorporated into the precipitates, assuming that the calcium aluminate is completely insoluble. Considering these results, when a Ca salt is added to a Ca concentration of 10 mg dm^{-3}, there should remain enough room for the aluminate ions to react with lithium ions. In practice, however, very little lithium was recovered. The reason is not clear at present. But one possible explanation is that the calcium aluminate precipitated accelerates the formation of aluminium hydroxide, and the aluminate covers the surface of hydroxide. Interference from Mg^{2+} ions is not so large as is easily recognized in Fig. 4. Even for a Mg concentration of 50 mg dm^{-3}, a Li recovery of 60% (24 h) was obtained, and for 100 mg dm^{-3}, 36% (24 h). If Mg^{2+} ions were precipitated completely as $Mg(AlO_2)_2$, magnesium corresponding to a Mg concentration of up to 45 mg dm^{-3} would be taken up completely for 100 mg dm^{-3} of Al. Therefore, it seems that Ca $(AlO_2)_2$ is only slightly soluble in water, while $Mg(AlO_2)_2$ is more soluble than Ca $(AlO_2)_2$. Nevertheless, the residual Mg concentration in the solution became zero within 1 h at any initial Mg concentration. This phenomenon might be interpreted by the occulusion of magnesium ions into magnesium and/or lithium aluminate precipitates and by adsorption on aluminium hydroxide. Interference from Ba^{2+} ions was also studied but no meaningful influence was found. The influence of addition of monosilicate ions is also shown in Fig. 4. Monosilicate ions differ greatly from the polysilicate ions in geothermal water as is described later. This difference will be attributed to the reactivities of silicate ions with aluminate ions.

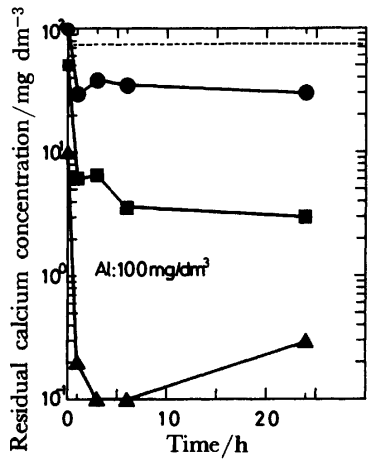

Fig. 5. Uptake of calcium ions into aluminate precipitates at 25°C. $[Al]_0$=100(mg dm^{-3}), $[Li]_0$=10(mg dm^{-3}).
—▲—: $[Ca]_0$=10(mg dm^{-3}), —■—: $[Ca]_0$=50(mg dm^{-3}), —●—: $[Ca]_0$=100(mg dm^{-3}).

Effects of Carbonate Ions. We found that the blowing of CO_2 gas into the Li solution with appropriate Al concentration raised the Li recovery remarkably. Thus, three kind of water soluble carbonates were used to examine whether carbonate ions are effective or not on Li recovery. Concentrations of carbonates were chosen to be 0.2, 0.6, 1.0, and 2.0 g dm^{-3}. Figure 6 illustrates the effects of carbonates. The figure evidently shows the effectiveness of carbonate addition; the more carbonate, the better the Li recovery. The effects of potassium and ammonium salts seems to be superior to sodium salt although the

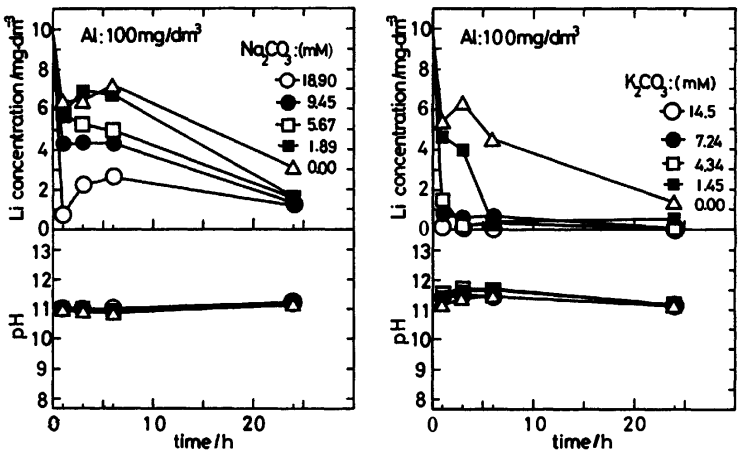

Fig. 6. Effects of addition of carbonates on Li recovery at 25°C.
Concentrations of carbonates:
—△—: 0.0 (g dm^{-3}), —■—: 0.2 (g dm^{-3}), —□—: 0.6 (g dm^{-3}),
—●—: 1.0 (g dm^{-3}), —○—: 2.0 (g dm^{-3}).

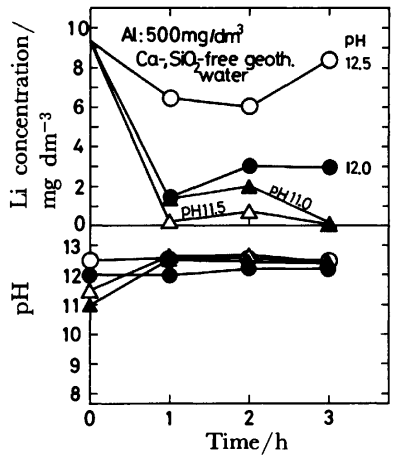

Fig. 7. pH dependence on Li recovery for Ca,SiO_2-free geothermal water at 25 °C. $[Al]_0$=300 (mg dm^{-3}). —▲—: pH 11.0, —△—: pH 11.5, —●—: pH 12.0, —○—: pH 12.5.

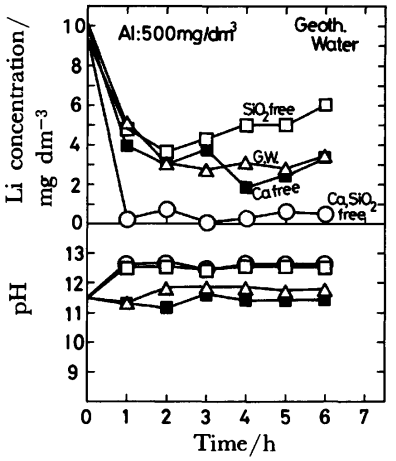

Fig. 8. Time courses of Li recovery for non-treated, Ca-free, SiO_2-free, and Ca,SiO_2-free geothermal waters at pH 11.5 at 25 °C. $[Al]_0$=500 (mg dm^{-3}). —△—: Non-treated geothermal water, —■—: Ca-free geothermal water, —□—: SiO_2-free geothermal water, —○—: Ca,SiO_2-free geothermal water.

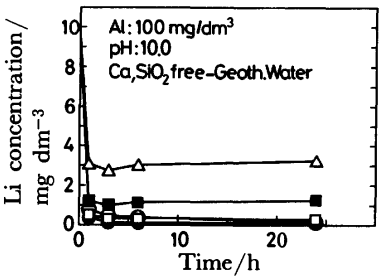

Fig. 9. Effects of Na_2CO_3 addition on Li recovery for Ca,SiO_2-free geothermal water at pH 10.0 at 25 °C.
—△—: $[Na_2CO_3]$=0.0 (g dm^{-3}), —■—: $[Na_2CO_3]$= 0.25(g dm^{-3}) (=2.36×10^{-3} M), —□—: $[Na_2CO_3]$=0.50 (g dm^{-3}) (=4.72×10^{-3} M), —●—: $[Na_2CO_3]$=1.0 (g dm^{-3}) (=9.44×10^{-3} M), —○—: $[Na_2CO_3]$=2.0 (g dm^{-3}) (=18.9×10^{-3} M).

results of ammonium salt was not shown here. However, the difference in univalent (alkaline) cations seems not to have any appreciable influence on Li recovery, as is already stated above. The effects of carbonate addition on Li recovery is significant but the reason is not clear. Three reasons are considered as follows: First, carbonate ions affect the surface conditions of aluminium hydroxide which is simultaneously formed with lithium aluminate to raise the adsorption capacity for lithium uptake (i.e., amorphous aluminium hydroxide which is very effective on Li adsorption[7] will be stably maintained). Second, the addition of carbonates lowers the solubility of the lithium aluminate formed. Thirdly, the optimum pH might be maintained by a pH buffer action due to the carbonate ions.

Mechanism. A mechanism for the Li recovery using the coprecipitation method was proposed in the previous paper.[2] That is, lithium is recovered by the formation of lithium aluminate and by adsorption on aluminium hydroxide. However, it seems that all the properties found in the study will not be explained satisfactorily by this mechanism. More detail discussion will be made in the following paper.

Lithium Recovery from Geothermal Water. The results of pH dependence on Li recovery from geothermal waters (nontreated and treated) is shown in Fig. 7. For an Li solution, optimum pH value for an Al concentration of 500 mg dm^{-3} was 12.5. However, for Ca,SiO_2-free geothermal water, the same pH gave only low recovery of 32—12% after 1—3 h from the beginning of Al salt addition. In this Ca,SiO_2-free geothermal water, the optimum pH was 11.5 which is lower than that of Li solution by one pH unit, and a high percent recovery of 98—99% was obtained after 1—3 h. The results for Ca-free, SiO_2-free, Ca,SiO_2-free and nontreated geothermal waters at an initial pH of 11.5 are shown in Fig. 8. The figure shows that there is little difference between nontreated and Ca-free geothermal waters. That is to say, the influence of polymerized silica is not large on Li recovery. However, for SiO_2-free geothermal water, the percent recovery of lithium is poorer compared with non-treated geothermal water because of the presence of calcium ions. The reason is that as the polysilicate ions have a buffer action, silicate ions prevent the interference from Ca ions to form calcium silicate although the polymerized silica itself exhibits some interference on Li recovery.

Effects of Carbonate Addition on Ca,SiO_2-free Geothermal Water. Sodium aluminate was added to generate an Al concentration of 100 mg dm^{-3} in Ca,SiO_2-free geothermal water in order to examine the effectiveness of Na_2CO_3 addition on Li recovery. As the optimum pH for the Li solution with an Al concentration of 100 mg dm^{-3} is 11.0, an initial pH of 10.0 was chosen for this solution. As Fig. 9 shows, the

effect of the Na_2CO_3 addition is clearly recognized. The reason for the improvement in Li recovery found on Ca,SiO_2-free geothermal water will be the same as that for the Li solution.

The authors would like to express their thanks to Dr. Kenjiro Yanagase for help with the sampling of the geothermal water.

References

1) a) J. A. Epstein, E. M. Feist, J. Zmora, and Y. Marcus, *Hydrometallurgy*, **6**, 269 (1981); b) H. Hayashi and A. Shimoyama, *Nippon Kogyo Kaishi*, **97**, 221 (1981); c) H. Ohmachi, *Japan Society of Energy and Rescorces*, **2**, 205 (1981); d) "U. S. Bureau of Mines, Minerals Yearbook 1980." (Vol **1**. Metals and Minerals); e) "Kisho Kinzoku to Sentan Gijutsu," ed. by the Ministry of International Trade and Industry, Nikkan Kogyo Shinbun, Tokyo (1982), p. 136.

2) K. Yanagase, T. Yoshinaga, K. Kawano, and T. Matsuoka, *Bull. Chem. Soc. Jpn.*, **56**, 2490 (1983).

3) T. Yoshinaga, K. Kawano, K. Yanagase, and A. Shiga, *Bull. Kyushu Institute of Technology*, **51**, 99 (1985).

4) JIS K0101-1979 (Japanese Industrial Standard) Published by Japanese Standard Association.

5) a) T. G. Pearson, "Chemical Back Ground of the Aluminium Industry," London (1956); b) Y. Shimizu, N. Mitsui, and K. Funaki, *Kogyo Kagaku Zasshi*, **70**, 425 (1967).

6) R. D. Goodenough, U. S. Patent 2,964,381 (1960).

7) T. Kitamura and H. Wada, *Nippon Kaisui Gakkaishi*, **32**, 78 (1978).

 © 1986 The Chemical Society of Japan Bull. Chem. Soc. Jpn., 59, 1215—1222 (1986)

The Studies on the Hydration Energy and Water Structures in Dilute Aqueous Solution

Myung Jun MOON and Mu Shik JHON*
Department of Chemistry, Korea Advanced Institute of Science and Technology,
P. O. Box 150, Cheongyangni, Seoul, Korea
(Received May 10, 1985)

Thermodynamic properties of dilute aqueous solutions are influenced by the interactions between ions and water molecules as well as the change of the water structure around the ion. To obtain hydration energies of monoatomic ions and local water structures around the ions, we make use of the discrete-continuum method. The calculated values for the hydration energies of ions are in good agreement with experimental values. The hydration energies of monoatomic cations can be qualitatively correlated with the sum of the successive ionization potentials from its atomic state to the ionic state. From their correlations, we can classify various ions as three groups. It is also found that the main factors which determine the stability of water structures around the ions are the charges and dimensions of ions.

The properties of aqueous electrolyte solution in chemical processes are strongly influenced by ions and their surrounding water molecules.[1-3] In particular, we would like to chemically classify various ions into three groups by correlating the hydration energies of ions with the sum of successive ionization potentials from its atomic state to ionic state[4] and into two groups by comparing the intermolecular interaction energies among water molecules in aqueous solution with those in pure water.[5-7]

Recent progresses in the ab initio quantum mechanical method,[8-11] statistical thermodynamics,[12,13] and the simulation using computer technology[14-17] have given the remarkable information for local water structures around ions.

In order to understand the local water structures around ions, we have calculated hydration energies of ions using the empirical potential function.[18-22] Earlier theoretical approaches calculating thermodynamic properties of aqueous solution can be divided into the discrete[23-25] and continuum methods.[10,14,15] Since it is possible to make accurate studies of solvation effects using relatively small clusters[16] and it takes much computing time to include all water molecules in calculation, we make use of the discrete-continuum method.[13,18] In this method, the water molecules interacting strongly with an ion are discretely treated, while the remaining water molecules are considered as a polarizable dielectric continuum.

Especially, if the interaction energies of water molecules oriented by the electric field of an ion are compared with those of pure water molecules, the enhancement of the water structure around the ion can be quantitatively known. The foci of our studies are to understand the experimental observation on aqueous ionic solution according to the characteristics of ions.

Model System. I) Hydration Scheme: According to the idea presented by Frank and Wen,[5] the environment of a dissolved ion is divided into three regions. As shown in Fig. 1, the ion is discretely surrounded by several water molecules within the first hydration shell, the second hydration shell water and bulk water are treated as the dielectric continuum. Dielectric saturation is assumed to occur in the secondary hydration shell water, but the dielectric constant of bulk water is equal to that of pure water.

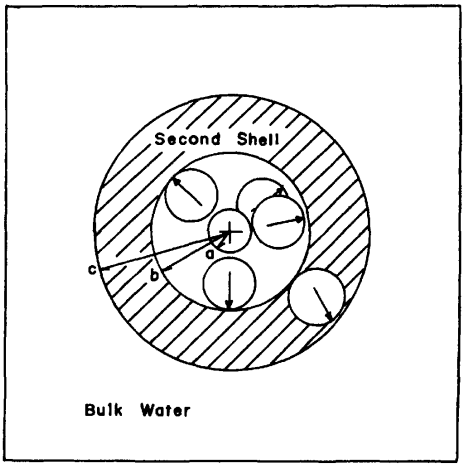

Fig. 1. Schematic diagram to indicate that an ion is enveloped by the first hydration shell (b), the second hydration shell (c), and the bulk water which is equivalent to pure water.

One of the arrangements of water molecules in the first hydration shell can be assumed to be either one of the tetrahedral, trigonal bipyramidal, and octahedral structure, which have been shown by ab initio calculations.[10] As the water molecules are discretely added outside the first hydration shell according to the hydration number, geometrical features could be recognized by the results of Monte Carlo simulations[17] for aqueous solutions of alkali metal and halide ions.

The hydration schemes of water molecules in the first hydration shell around the ion are determined by the given hydration number and can be defined by the variables θ_w and Φ_w which are shown in Fig. 2.

II) Water Molecule. The water molecule is taken to be isotropic polarizable sphere which ignores the detailed charge distribution and has the permanent off-centered dipole.[20] Multipoles higher than the di-

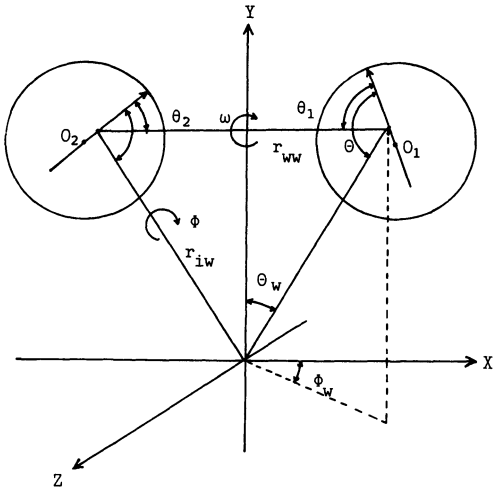

Fig. 2. Geometric features for the water dipole around the point charge. The distance between O_1 and O_2 is equal to the distance between oxygens of water molecules.

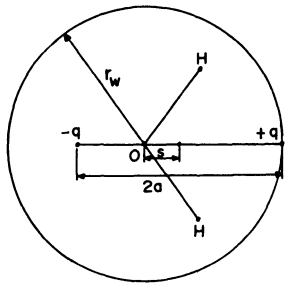

r_w = 1.45 Å
2a = 2.00 Å
S = 0.45 Å

Fig. 3. Permanent electrostatic distribution in water from gas phase calibration data (since μ=1.85×10^{-18} esu cm, $q=\mu/2a$=0.1926e).

pole are not considered in this work, because its inclusion for potential functions is arbitrary and the use of multipoles would not alter the final results significantly. The model of water molecule[20] is described by estimating three parameters, namely the length of the off-centered dipole (2a), the amount by which the dipole is off-centered(s) and the van der Waals radius of water molecule (r_w).

The water model and the values of the parameters used in this work are shown in Fig. 3. The parameters are empirically obtained by fitting the oxygen–oxygen distance and the energy of water dimer.[26-28] The computed results are −21.25 kJ mol^{-1} and 2.77 Å for the dimerization energy and oxygen–oxygen distance, respectively.

The value of the permanent dipole moment of water molecule is used as 1.85D (1D = 3.325×10^{-30} Cm) which is experimentally determined.[29]

For the polarizability of water, there are important contributions to the static polarizability, α_w, from intra- and intermolecular motions. It should be noted that we have used the value of α_w which includes the electronic polarizability of water (=1.44×10^{-24} cm^3) as well as the small increment of 0.16×10^{-24} cm^3 according to the effect of intramolecular motions.[26,30]

III) Ion. The ions in solution are taken to be charged conducting spheres. The choice of X-ray crystallographic radii for ions brings out a good approximation to the respective radii of the bare ions in solution.[21] Since ion–solvent interaction energies in a strong polar solvent are similar to those between cations and anions in crystals, it is reasonable that the ion in the solution may be compressed to its crystallographic radius.[31] We have used the effective ionic radii which are measured according to the coordination number of ion.[32] The coordination number of ion corresponds to the number of water molecules in the first hydration shell of ion. The hydration numbers in our work are taken from the X-ray diffraction data on structures of metal complexes in solution.[33] The hydration numbers of ions not included in Ref.33 are decided by fitting the hydration energies of ion.

Potential Function.[34-36] The energies of the dipole–dipole interaction, E_{dd}, and the dipole-induced dipole interaction, E_{did}, will be calculated by using Eqs. 1 and 2.

$$E_{dd} = -\frac{\mu^2}{Dr_{ww}^3}(2\cos\theta_1\cos\theta_2 - \sin\theta_1\sin\theta_2\cos\omega), \quad (1)$$

$$E_{did} = -\frac{1}{2}\frac{\mu^2\alpha_w}{Dr_{ww}^6}(3\cos^2\theta_1 + 1). \quad (2)$$

Geometrical parameters for the dipole–dipole interaction are shown in Fig. 2, D is the dielectric constant, α_w is the polarizability, and μ is the permanent dipole moment of water molecule. The energies of the ion-dipole interaction, E_{id}, and the ion-induced dipole interaction, E_{iid} will be calculated by using Eqs. 3 and 4.

$$E_{id} = -\frac{q\mu}{Dr_{iw}^2}\cos\theta, \quad (3)$$

$$E_{iid} = -\frac{q^2\alpha_w}{2Dr_{iw}^4}, \quad (4)$$

where q is the ionic charge, r_{iw} is the distance between the ion and the dipole.

The dielectric constant is represented by Eq. 5.[34]

$$D = \left(\frac{\varepsilon_0-\varepsilon_1}{c-a}\right)r_{iw} + \varepsilon_1 - \left(\frac{\varepsilon_0-\varepsilon_1}{c-a}\right)a, \quad (5)$$

where D means the dielectric constant at the distance separated from the ion, ε_1 and ε_0 denote the dielectric constant at the surface of ion, and that of bulk water, respectively. a and c are the radius of ion and the distance from a point charge to bulk water, respectively.

The nonbonded interaction energies, E_{nb}, between

Table 1. The Radii, the Sum of True Ionization Potentials, and Polarizabilities for the Water Molecule and the Ions

Specie	R/Å[a]	$\sum I$/eV[b]	α/Å^3[c]	Specie	R/Å[a]	$\sum I$/eV[b]	α/Å^3[c]
H_2O	1.45	12.59	1.60	Zn^{2+}	0.88	67.08	0.94
Li^+	0.93	80.93	0.03	Mn^{2+}	0.97	46.38	1.30
Na^+	1.17	52.42	0.21	Fe^{2+}	0.92	54.70	1.00
K^+	1.49	35.97	0.87	Co^{2+}	0.89	58.41	1.10
Rb^+	1.64	31.47	1.98	Ni^{2+}	0.83	60.97	1.00
Cs^+	1.83	27.01	3.34	Cu^{2+}	0.87	64.86	1.00
Be^{2+}	0.59	181.43	0.01	Ag^+	1.29	29.07	2.25
Mg^{2+}	0.86	102.82	0.12	Tl^+	1.64	26.53	4.30
Ca^{2+}	1.14	68.89	0.90	Hg^{2+}	1.16	63.39	5.20
Sr^{2+}	1.32	60.35	1.42	Pb^{2+}	1.33	44.02	4.20
Ba^{2+}	1.49	50.72	2.40	Al^{3+}	0.68	173.25	0.07
F^-	1.19	3.34	0.95	Sc^{3+}	0.89	117.57	1.10
Cl^-	1.67	3.62	3.48	Y^{3+}	1.04	100.91	1.50
Br^-	1.82	3.37	4.82	La^{3+}	1.18	85.77	2.40
I^-	2.06	3.06	7.22	Fe^{3+}	0.79	109.52	2.20

a) From Ref. 32. b) From Ref. 41. c) From Ref. 39.

ion and water and between water molecules are calculated by using the familiar Lennard-Jones 6-12 potential and are given by Eq. 6.

$$E_{nb} = -K_6(i,j)/Z_{ij}^6(1-0.5/Z_{ij}^6) \quad (6)$$

where $k_6(i,j)=C(i,j)/r_{ij}^{06}$ and $Z_{ij}=r_{ij}/r_{ij}^0$, r_{ij}^0 is the sum of the van der Waals radii of the interacting molecules and $C(i,j)$ is calculated by using London-Margenau formulas.[38]

The values of effective ionization potential used in the nonbonded energy term could be obtained by multiplying the true ionization potential by a suitable coefficient.[40] In this work, we obtained new coefficients in the process of fitting the dimerization energy of water molecule and the heat of hydration of all ions. The correction coefficients which would be used in this calculation are 4.5 for the water molecule and 3.0 for all ions.

The radii, true ionization potentials, and polarizabilities for the water molecule and all ions are summarized in Table 1.

The polarization energy for the continuous medium outside the first hydration shell is given by Eq. 7[12,24,25]

$$E_{pol} = \frac{1}{2}\left\{\left(\frac{1-\varepsilon_b'}{\varepsilon_b'}\right)\frac{q^2}{b} + \left(\frac{1-\varepsilon_0}{\varepsilon_0}\right)\frac{q^2}{c}\right\}, \quad (7)$$

where

$$\varepsilon_b' = \varepsilon_b\left(\frac{(1-\varepsilon_b)(1-\varepsilon_c)}{\varepsilon_c}\frac{b}{c}+1\right)^{-1}$$

and

$$\varepsilon_b = \varepsilon_m/\varepsilon_1$$
$$\varepsilon_c = \varepsilon_0/\varepsilon_m.$$

The first hydration shell of radius b is surrounded by a water layer of thickness $(c-b)$, which is immersed in the bulk water of dielectric constant ε_0. The relative permittivity ε_m between $\varepsilon_1=1$ and $\varepsilon_0=78.5$ is calculated by using Eq. 5. The thickness of the secondary layer $(c-b)$ was taken as the diameter of water molecule.

Hydration Energy Analysis.[14,20] The energy for the process of transferring an ion from vacuum into a position inside the liquid water, ΔE_{hyd}, can be obtained from the energies of intermolecular interaction in pure water and dilute aqueous solution. The thermodynamic cycle of this process is shown in Fig. 4.[20] The total energy of solution is composed of the ion-water interaction, E_{iw}, the water-water interaction in aqueous solution, E_{ww}, and that of the pure water, E_{ww}°. The energy of hydration is given by[14,42]

$$\Delta E_{hyd} = E_{iw} + E_{ww} - E_{ww}^\circ. \quad (8)$$

The ion-water interaction energy, E_{iw}, can be divided into the contributions exclusively arising from the first shell water molecules, E_{fw}, and from the polarization of the water molecules outside the first hydration shell, E_{pol}.

$$E_{iw} = E_{fw} + E_{pol}. \quad (9)$$

Also, the water-water interaction can be considered as being composed of three components representing the first hydration shell-first hydration shell interaction, E_{ff}, the first hydration shell-remaining water interaction, E_{fr}, and the remaining water-remaining water interaction, E_{rr}.

$$E_{ww} = E_{ff} + E_{fr} + E_{rr}. \quad (10)$$

As the reference system, the pure water was also considered as a dilute solution containing a water solute.[14,15,42] Since the average number of hydrogen bonds per a water molecule in pure water is about 4,[44] we considered that the water solute is surrounded with four water molecules in a tetrahedral configuration and this water cluster may be successively surrounded

by the other water molecules.

The total intermolecular interaction energy in pure water is expressed as

$$E^{\circ}_{ww} = E^{\circ}_{fw} + E^{\circ}_{ff} + E^{\circ}_{fr} + E^{\circ}_{rr}, \quad (11)$$

where E°_{fw} is the interaction energy for the water solute-surrounding water molecules, E°_{ff} for the first hydration shell-first hydration shell, E°_{fr} for the first hydration shell-remaining water, and E°_{rr} for the remaining water-remaining water.

E°_{fw} is the sum of the energies of separating $n+1$ water molecules from pure water to make a room for the ion of which the hydration number is n. This value is equal to the dissociation energy in the gas phase.

$$E^{\circ}_{fw} = nE^{\circ}_{1}, \quad (12)$$

where $E_1{}^{\circ}$ is the average hydrogen bond energy which is calculated from the water cluster with the ice-like structure. The calculated value of $E_1{}^{\circ}$ in this work is -18.24 kJ mol^{-1}.

E°_{ff} is the sum of the interaction energies between the first hydration water molecules around the water solute, which is the same as the sum of the interaction energies between the secondary neighbor water molecules in the water cluster. The interaction energy between the secondary neighbor water molecules in pure water is -1.84 kJ mol^{-1}.

E°_{fr} is the interaction energy between the water molecules in the first hydration shell and the remaining water, which is the energy forming a cavity in the supermolecule-approach.[20] E°_{fr} in Eq. 11 arises from some changes of the water structure at the second hydration shell in transferring the solvated ion into the cavity inside the bulk water. Since the nature and extent of the second hydration shell is not well understood at this time, it is very difficult to calculate the energies of E°_{fr} and E_{fr} quantitatively. If E°_{fr} in pure water is compared with E_{fr} in the ionic solution, the difference of these energies is qualitatively estimated to be about 41.84 kJ mol^{-1}.[13,20] Therefore, we can assume that the water structure in the second hydration shell is not variant in transferring of ion from vacuum into pure water.

Finally, one water molecule in vacuum has to be returned to the aqueous solution to complete the cycle by checking the thermodynamic cycle in Fig. 4. The exchange of energy involved in this process is equal to the work of condensation, ΔH_{con}. This value can be taken from the latent heat of condensation to be about 44.76 kJ mol^{-1}.[20] Thus, the total hydration energy, ΔE_{hyd}, is represented as

$$\begin{aligned}\Delta E_{hyd} &= E_{fw} + E_{pol} - E^{\circ}_{fw} + E_{ff} - E^{\circ}_{ff} + \Delta H_{con} \\ &= E_{fw} + E_{pol} - E^{\circ}_{fw} + \Delta E_{ww} + \Delta H_{con}, \end{aligned} \quad (13)$$

where

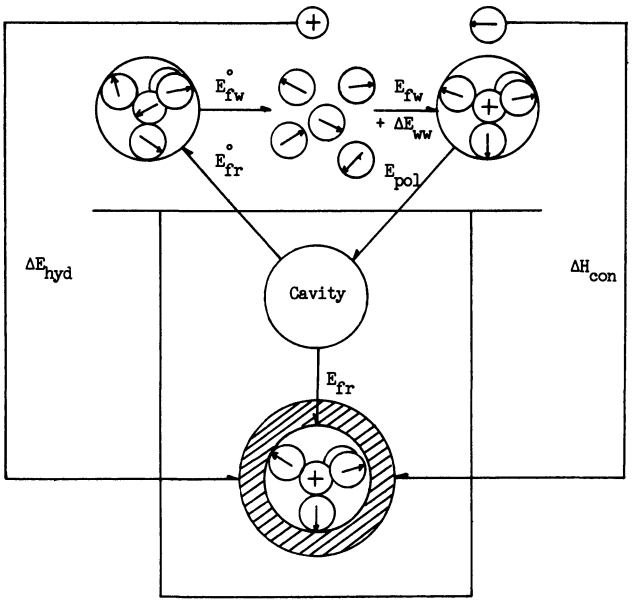

Fig. 4. The total hydration energy of ion (ΔE_{hyd}) separated into the various steps.

$$\Delta E_{ww} = E_{ff} - E^{\circ}_{ff}. \quad (14)$$

ΔE_{ww} is the energy which indicates the change of local water structures around the ion. Therefore, the phenomena of structure making and breaking of ions can be explained by the quantity of these values.

Free Energy Analysis.[3] The free energy of hydration of an ion at constant volume and pressure is given by

$$\Delta F_{hyd} \simeq \Delta E_{hyd} + T\Delta S_{hyd}. \quad (15)$$

The entropy of hydration for the ion is given by

$$\Delta S_{hyd} = \Delta S_f + S_{pol}, \quad (16)$$

where ΔS_f is the contribution from the water molecules in the first hydration shell and estimated by Frank and Evans.[45,46] The second term is the contribution from the water molecules outside the first hydration shell and is given by[12,25]

$$S_{pol} = -\frac{q^2}{2}\left\{\frac{(b-c)}{bc}\frac{1}{\varepsilon_m^2}\left(\frac{\partial \varepsilon_m}{\partial T}\right)_p - \frac{1}{c}\frac{1}{\varepsilon_0^2}\left(\frac{\partial \varepsilon_0}{\partial T}\right)_p\right\}, \quad (17)$$

where q is the ionic charge, $(\partial\varepsilon_m/\partial T)_p$ is the temperature variation of the local relative permittivity and $(\partial\varepsilon_0/\partial T)_p$ is that of the bulk dielectric constant. Of the parameters, the values of $(\partial\varepsilon_m/\partial T)_p$ and $(\partial\varepsilon_0/\partial T)_p$ for water are -0.00160 K^{-1} and -0.3595 K^{-1}, respectively.[25]

Results and Discussion

The hydration energies of ions are obtained by one by one optimizing r_{iw},θ, and ϕ which indicate the position of water molecules around the ion. The calcu-

Table 2. The Hydration Energies and the Free Energies of Ions[a)]

Ion	n	R_{i-o}[b)]	$-E_{iw}$	$-E_{pol}$	$-\Delta E_{ww}$	$-\Delta E_{hyd}$	$-\Delta F_{hyd}$	$-\Delta H_{exp}$[c)]
Li^+	4	1.80	514.2	132.6	27.2	623.8	584.1	558.6
Na^+	4	2.21	351.9	123.0	3.3	427.6	397.1	443.9
K^+	5	2.61	335.1	114.6	−3.8	372.0	351.5	360.2
Rb^+	5	2.90	312.5	109.2	−6.3	341.8	325.1	338.9
Cs^+	5	3.06	284.5	106.7	−8.8	308.4	292.0	314.6
Ag^+	6	2.59	515.9	115.1	4.2	537.2	504.6	513.4
Tl^+	5	2.94	348.5	108.8	−7.1	376.6	356.9	364.0
Be^{2+}	4	1.49	2257.7	564.4	−184.5	2587.8	2470.2	2563.1
Mg^{2+}	5	1.85	1603.3	525.5	−8.8	2046.4	1961.5	1998.3
Ca^{2+}	6	2.27	1262.7	486.2	32.2	1683.6	1615.0	1668.6
Sr^{2+}	6	2.45	1082.0	471.1	10.5	1466.1	1399.1	1520.9
Ba^{2+}	6	2.63	946.8	457.3	1.3	1307.9	1255.2	1378.6
Zn^{2+}	6	2.10	1592.8	501.7	50.6	2047.6	1962.3	2046.0
Mn^{2+}	6	2.19	1466.5	493.3	42.3	1904.1	1822.1	1841.0
Fe^{2+}	6	2.13	1532.2	498.7	48.5	1981.5	1898.3	1946.0
Co^{2+}	6	2.13	1586.2	498.7	48.5	2035.9	1943.9	1996.2
Ni^{2+}	6	2.09	1686.2	502.5	51.0	2141.8	2046.8	2105.0
Cu^{2+}	6	2.11	1615.4	500.8	49.8	2068.6	1984.5	2100.0
Hg^{2+}	6	2.51	1492.0	466.5	10.9	1872.3	1806.2	1823.8
Pb^{2+}	6	2.57	1133.4	461.9	5.9	1503.3	1451.0	1480.7
Al^{3+}	5	1.67	3960.6	1224.7	−313.4	4798.2	4659.3	4665.2
Sc^{3+}	6	2.07	2844.3	1134.7	51.9	3933.0	3810.0	3897.0
Y^{3+}	6	2.20	2439.7	1108.3	41.0	3491.1	3368.6	3583.2
La^{3+}	6	2.34	2122.5	1080.7	23.0	3128.8	3022.1	3296.2
Fe^{3+}	6	2.07	3220.4	1134.7	51.9	4309.5	4168.5	4430.0

a) All energies have units of kilojoule per mol. b) R_{i-o} is the calculated distance between ion and oxygen and has unit of Å. c) The experimental results are taken from the compilation of Rosseinsky[47] and Smith.[48]

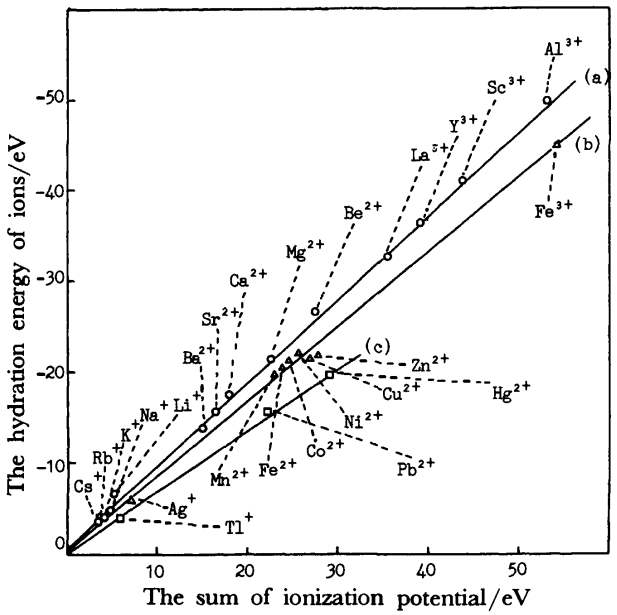

Fig. 5. The relation between ΔE_{hyd} and $\sum I$ at 25 °C.

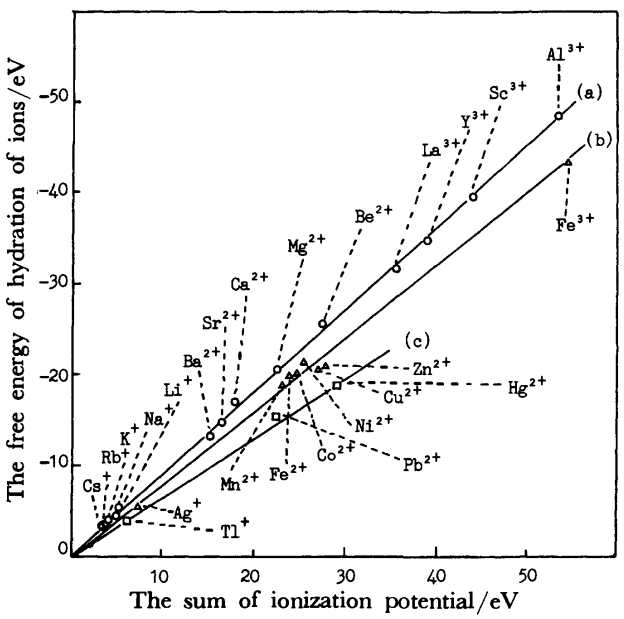

Fig. 6. The relation between ΔF_{hyd} and $\sum I$ at 25 °C.

lated hydration energies and free energies of ions are summarized in Table 2. Comparing the calculated hydration energy with the experimental data, ΔH_{exp}, the difference of energies may be about ±42 kJ mol^{-1}. From the calculated results, the hydration energies of monoatomic cations can be qualitatively correlated with the sum of the successive ionization energies from its atomic state to the ionic state.[4] From inspecting the plots in Figs. 5 and 6, we classify the cations into three groups in terms of the hydration energy and free energy of ion, respectively. In Table 3, since the correlation coefficients for linearity of the plots in Figs. 5 and 6 are about 1.0, the present classification can be proven.[49]

The cationic species are classified as group(a) belonging to IA-IIIA groups including Al^{3+} in IIIB group, group(b) belonging to VIA-IIB groups, and group(c) belonging to IIB-IVB groups in the periodic table. This classification is in good agreement with

the result obtained by Matsuda and Notoya.[4]

It is interesting to empirically investigate the chemical characteristics of each group. The present classification of cationic species originates from the consideration of the different shape of nonbonded energy curve between ion and water. The contributive components for interaction between ion and water molecule are given in Table 4. In the same charge ions, it is found that the nonbonded term in the potential energy plays an essential role in classifying the ionic species. The variations of the nonbonded energy term between ion and one water molecule depending on the ion-oxygen distance are minutely represented in Fig. 7. The ions of group(c) have the stronger nonbonded energy than those of groups(a) and (b). It is mainly due to the low ionization potential of two electrons in 6s configuration. The lower ionization potential and larger polarizability the ion has, the larger nonbonded energy the ion has. The ions of group(c) have been considered as soft acids in the principle of hard and soft acids and bases.[50]

In the case of the ions of group(b), their 3d electrons are distributed among 3d orbitals. For Mn^{2+} with five 3d electrons and Zn^{2+} with a completely filled 3d shell, the hydration energies mainly depend on the electrostatic energy term in the potential energy, since their polarizabilities and radii are small.

Since the ions of group(a) have no 3d electrons and are small in size and low in the polarizability (relatively large core charges, less shielded nucleus), the ions have the large electrostatic energies and low nonbonded energies (see Fig. 7). From the above results, the ions of group(a) have been recognized as the hard acids in the principle of hard and soft acids and bases.

The interaction energies among water molecules around an ion are expressed as ΔE_{ww} in Tables 4 and 5. Since the water molecule in our model is an isotropically polarizable sphere including only dipole, the geometric approach[15] for a hydrogen bonding is not reasonable. Therefore, comparison of the interaction energies among water molecules around the ion with those around the water solute in pure water gives the information about enhancement of the structures of water molecules in the first hydration shell. The intermolecular interaction energy changes due to the

Table 3. The Slopes and Interceptions for Each Group

	Group	a[a]	b[a]	σ^2[b]	ρ[b]
ΔE_{hyd}	a	0.93	0.06	0.49	1.00
	b	0.82	0.06	1.22	1.00
	c	0.68	−0.11	0.30	1.00
ΔF_{hyd}	a	0.90	−0.13	0.42	1.00
	b	0.80	−0.38	1.26	0.98
	c	0.66	−0.18	0.35	1.00

a) The slopes a and interceptions b for each group are calculated by the least square method. b) σ^2 and ρ represent the variance of the fit and the correlation coefficient, respectively.

Table 4. The Contributive Components for Interactions between Ion and Water Molecules and between the Water Molecules[a]

Group[b]	Ion	$-E_{id}$	$-E_{iid}$	E_{ni}[c]	E_{dd}	$-E_{did}$	$-E_{nw}$[c]	$-E_{iw}$	ΔE_{ww}
a	Li^+	422.6	173.2	81.6	20.9	2.5	56.5	514.2	−27.2
	Na^+	302.5	88.7	39.3	12.6	0.8	25.9	351.9	−3.3
	K^+	285.8	63.2	13.8	15.1	0.8	26.8	335.1	3.8
	Rb^+	238.1	43.9	−30.5	8.8	0.4	13.0	312.5	6.3
	Cs^+	217.1	36.4	−30.5	7.5	0.4	9.6	284.5	8.8
	Be^{2+}	1136.8	1254.4	133.5	32.2	5.9	−146.9	2257.7	184.5
	Mg^{2+}	1010.9	793.7	201.3	37.7	5.0	41.8	1603.3	8.8
	Ca^{2+}	867.3	487.0	91.6	36.4	3.3	92.9	1262.7	−32.2
	Sr^{2+}	763.2	377.0	58.2	30.1	2.1	66.1	1082.0	−10.5
	Ba^{2+}	676.6	296.2	25.5	22.6	1.3	44.4	946.8	−1.3
	Al^{3+}	1784.9	2474.0	298.3	48.1	8.4	−255.6	3960.6	313.4
	Sc^{3+}	1515.9	1487.0	158.6	45.6	5.0	120.0	2844.3	−51.9
	Y^{3+}	1370.7	1216.3	147.3	39.3	3.8	103.3	2439.7	−41.0
	La^{3+}	1236.8	989.9	104.2	33.9	2.9	81.6	2122.5	−23.0
b	Ag^+	347.3	77.8	−90.4	23.4	1.7	48.1	515.9	−4.2
	Zn^{2+}	987.0	630.5	24.3	44.4	4.6	117.6	1592.8	−50.6
	Mn^{2+}	920.9	548.5	3.3	39.7	3.8	105.4	1466.5	−42.3
	Fe^{2+}	964.0	601.7	33.5	42.7	4.6	114.2	1532.2	−48.5
	Co^{2+}	964.0	601.7	−20.5	42.7	4.6	114.2	1586.2	−48.5
	Ni^{2+}	994.5	640.6	−51.0	44.8	5.0	118.4	1686.2	−51.0
	Cu^{2+}	979.1	620.5	−15.9	43.5	4.6	116.3	1615.9	−49.8
	Fe^{3+}	1515.9	1487.0	−217.6	45.6	5.0	120.1	3220.4	−51.9
c	Tl^+	232.6	41.8	−74.1	8.4	0.4	12.1	348.5	7.1
	Hg^{2+}	732.6	347.3	−412.5	25.1	1.7	56.5	1492.0	−10.9
	Pb^{2+}	703.7	320.5	−109.2	23.8	1.7	49.8	1133.4	−5.9

a) All energies have units of kilojoule per mol. b) a, b, and c mean the groups of ions. c) E_{ni} and E_{nw} represent the nonbonded energies between ion and water molecules and between the water molecules, respectively.

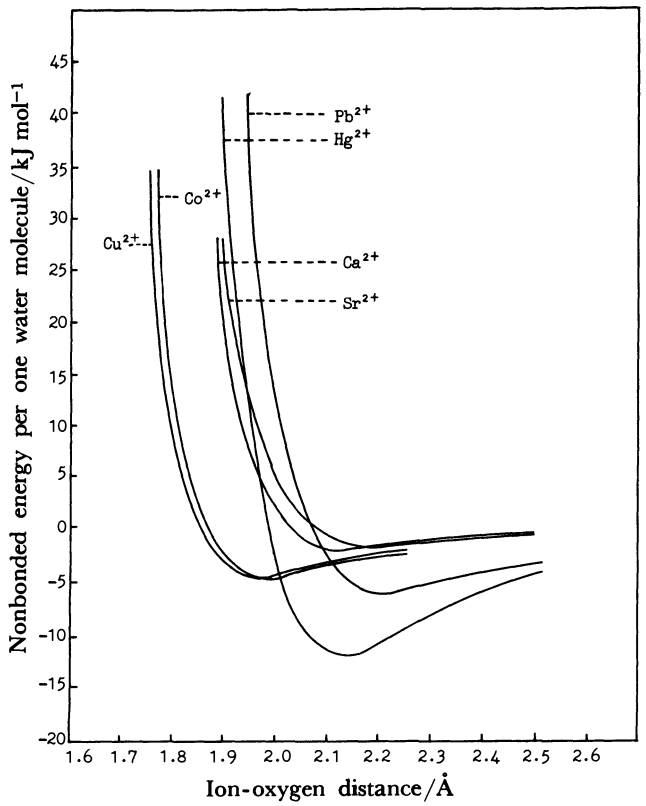

Fig. 7. The nonbonded energy term between ion and one water molecule according to the ion–oxygen distance.

Table 5. The Hydration Energies of Anions[a)]

Ion	n	R_{i-o}[b)]	$-E_{iw}$	$-E_{pol}$	ΔE_{ww}	$-\Delta E_{hyd}$
F^-	5	2.99	420.9	125.5	18.0	454.8
Cl^-	6	3.57	354.8	113.4	7.5	363.6
Br^-	6	3.60	322.6	113.0	7.5	330.5
I^-	6	3.78	274.1	109.6	7.9	278.2

a) All energies have units of kilojoule per mol. b) R_{i-o} is the calculated distance between ion and oxygen and has unit of Å.

structure making and breaking ions are represented as the negative and positive values from Eq.14, respectively.

In alkali metal ions, Li^+ and Na^+ are the structure making ions of which the surrounding water molecules are more stable than the pure water. On the other hand, K^+, Rb^+, and Cs^+ are the structure breaking ions. Here, it is found that the water structure around the ion was gradually broken according to the increment of the ionic radius. This result correspondes to the tendency of the B-coefficient of the Jones-Dole equation in electrolyte solution.[51)] Compared with the alkali metal ions, the halide ions have the structure breaking effect which arises from the expansion of the first hydration shell due to the change of the direction of dipole.

Since multiple charged ions, such as Zn^{2+}, Ni^{2+}, and Fe^{3+}, strongly attract the surrounding water molecules, the distances among water molecules in the first hydration are shorter than that in pure water and the water structure around these ions are enhanced. Therefore, these ions are structure making ions.

On the other hand, since Be^{2+}, Mg^{2+}, and Al^{3+} are very small ions and the interactions between ion and water molecules are very strong, the ion and surrounding water molecules are close to the aquo complex compounds. In these ions, it is difficult to explain the structure enhancement by only water molecules in the first hydration shell.

Jorgensen's Monte Carlo calculation suggested that structure makers may not be explained by a pronounced increase in solvent-solvent hydrogen bonding.[14)] The structure making effect in our method can be explained not by the increment of hydrogen bonding but by the comparison of average energy in the first hydration shell of an ion in aqueous solution with those of pure water. Although the formation of the first hydration shell represents a significant change in water structure, the contribution to the total hydration energy of the ion is not remarkable.

Our calculation leads to conclusions that the classification of ions into three groups is accomplished by the values of the nonbonded energy which involves the sum of ionization potential and polarizability of the ions. And the main factors which determine whether the ions will be structure makers or structure breakers in aqueous solution are the interaction energy of the ions with water molecules in the first hydration shell and the dimension of the ions characterized by the polarizability.

We thank Dr. A. Matsuda and Dr. R. Notoya, Hokkaido University for providing us the experimental data.

References

1) B. E. Conway and R. G. Barradas, Ed., "Chemical Physics of Ionic Solutions," John Wiley, New York (1966).
2) "Ionic Processes in Solution," ed by R. W. Gurney Dover Publ. Co., New York (1962).
3) F. Franks, "Water. A Comprehensive Treatise," Plenum Press, New York (1973). Vol. 3.
4) A. Matsuda and R. Notoya, "Thermodynamical Empirical Rules for Solvation of Monoatomic Cations," Research Institute for Catalysis, Hokkaido University (1982).
5) H. S. Frank and W. Y. Wen, *Discuss. Faraday Soc.*, **24**, 133 (1957).
6) M. Kaminsky, *Discuss. Faraday Soc.*, **24**, 171 (1957).
7) O. Y. Samoilov, *Discuss. Faraday Soc.*, **24**, 141 (1957).
8) B. M. Rode, R. Fujikura, and S. Fujiwara, *Bull. Chem. Soc. Jpn.*, **53**, 1965 (1980).
9) E. Clementi, H. Kistenmacher, W. Kolos, and S. Romano, *Theor. Chim. Acta*, **55**, 257 (1980).
10) H. Kistenmacher, H. Popkie, and E. Clementi, *J. Chem. Phys.*, **61**, 799 (1974).
11) S. Fujiwara and R. M. Rode, *Bull. Chem. Soc. Jpn.*, **52**, 3221 (1979).
12) D. L. Beveridge and G. W. Schnuelle, *J. Phys. Chem.*, **78**, 2064 (1974).

13) G. W. Schnuelle and D. L. Beveridge, *J. Phys. Chem.*, **79**, 2566 (1975).
14) J. Chandrasekhar, D. C. Spellmeyer, and W. L. Jorgensen, *J. Am. Chem. Soc.*, **106**, 903 (1984).
15) M. Mezei and D. L. Beveridge, *J. Chem. Phys.*, **74**, 622 (1981).
16) M. Rao and B. J. Berne, *J. Phys. Chem.*, **85**, 1498 (1981).
17) F. T. Marchese and D. L. Beveridge, *J. Am. Chem. Soc.*, **106**, 3713 (1984).
18) A. D. Buckingham, *Discuss. Faraday Soc.*, **24**, 151 (1957).
19) B. T. Gowda and S. W. Benson, *J. Phys. Chem.*, **86**, 847 (1982).
20) J. O' M. Bockris and A. K. N. Reddy, "Modern Electrochemistry," Plenum Press, New York (1970), Vol. 1, p. 45.
21) S. Goldman and R. G. Bates, *J. Am. Chem. Soc.*, **94**, 1476 (1972).
22) I. Eliezer and P. Krindel, *J. Chem. Phys.*, **57**, 1884 (1972).
23) K. J. Laidler and J. S. Muirhead-Gould, *Discuss. Faraday Soc.*, **40**, 953 (1965).
24) M. H. Abraham and J. Liszi, *J. Chem. Soc., Faraday Trans. 1*, **74**, 1604 (1978).
25) M. H. Abraham, J. Liszi, and L. Mészáros, *J. Chem. Phys.*, **70**, 2491 (1979).
26) J. C. Owicki, L. L. Shipman, and H. A. Scheraga, *J. Phys. Chem.*, **79**, 1794 (1975).
27) O. Matsuoka, E. Clementi, and M. Yoshimine, *J. Chem. Phys.*, **64**, 1351 (1976).
28) T. R. Dyke, K. M. Mack, and J. S. Muenter, *J. Chem. Phys.*, **66**, 498 (1977).
29) S. A. Clough, Y. Beers, G. P. Klein, and L. S. Rothman, *J. Chem. Phys.*, **59**, 2254 (1973).
30) S. Nir, S. Adams, and R. Rein, *J. Chem. Phys.*, **59**, 3341 (1973).
31) B. E. Conway, *J. Solution Chem.*, **7**, 721 (1978).
32) R. D. Shannon, *Acta Crystallogr., Sect. A*, **32**, 751 (1976).
33) H. Ohtaki, "X-ray Diffraction Studies on the Structures of Metal Complexes in Solution," Tokyo Institute of Technology, Nagatsuta (1981).
34) A. D. Buckingham, "Intermolecular Interactions: From Diatomics to Biopolymers," ed by B. Pullman, John Wiley, New York (1978), p. 1.
35) A. J. Hopfinger, "Conformational Properties of Macromolecules," Academic Press, New York (1973), p. 38.
36) J. O. Hirshfelder and W. J. Meath, "Intermolecular Forces," ed by J. O. Hirshfelder, John Wiley, New York (1967), p. 3.
37) M. J. Moon, M. S. Jhon, and Y. K. Kang, *Bull. Korean Chem. Soc.*, **4**, 133 (1983).
38) T. M. Reed and K. E. Gubbins, "Applied Statistical Mechanics," McGraw-Hill, New York (1973), p. 138.
39) J. R. Tessman and A. H. Kahn, *Phys. Rev.*, **92**, 890 (1953).
40) K. S. Pitzer, *Advan. Chem. Phys.*, **2**, 59 (1959).
41) J. E. Huheey, "Inorganic Chemistry, "Haper and Row, New York (1978), p. 40.
42) A. Warshel, *Chem. Phys. Lett.*, **55**, 454 (1978).
43) W. L. Jorgensen, *J. Am. Chem. Soc.*, **103**, 335 (1981).
44) F. H. Stillinger, *Science*, **209**, 451 (1980).
45) H. S. Frank, *J. Chem. Phys.*, **13**, 493 (1945).
46) H. S. Frank and M. W. Evans, *J. Chem. Phys.*, **13**, 507 (1945).
47) D. R. Rosseinsky, *Chem. Rev.*, **65**, 467 (1965).
48) D. W. Smith, *J. Chem. Educ.*, **54**, 540 (1977).
49) K. J. Johnson, "Numerical Methods in Chemistry," Marcel Dekker, New York (1980), p. 241.
50) R. F. Nalewajski, *J. Am. Chem. Soc.*, **106**, 944 (1984).
51) E. R. Neightingale, Jr., "Chemical Physics of Ionic Solution," ed by B. E. Conway, and R. G. Barradas, John Wiley, New York (1966), p. 87.

 © 1986 The Chemical Society of Japan Bull. Chem. Soc. Jpn., 59, 1223—1227 (1986)

Spectrophotometric Determination of Micro-Amounts of Ruthenium(III) and Platinum(IV) with Acenaphthenequinone Mono(thiosemicarbazone)

Shailendra Kumar SINGH, Rakesh Kumar SHARMA, and Sharwan Kumar SINDHWANI*
Department of Chemistry, University of Delhi, Delhi-110007, India
(Received February 19, 1985)

Ruthenium(III) and platinum(IV) form 1:2 (metal:ligand) complexes with acenaphthenequinone mono(thiosemicarbazone) (AQTS). The complexes are soluble in 70% *N*,*N*-dimethylformamide (DMF). The reagent has been used for the spectrophotometric determination of Ru(III) and Pt(IV). The optimum ranges of concentration for the determination of Ru(III) and Pt(IV) are 2.02—7.09 and 2.83—11.6 ppm over the pH range 5.3—6.8 and 1.9—4.1, respectively. The Sandell sensitivities for the determination of Ru(III) and Pt(IV) are 0.01 and 0.016 μg cm^{-2}, respectively. The determination has also been carried out in the presence of foreign ions.

When the solution of acenaphthenequinone mono (thiosemicarbazone) was added to Ru(III) or Pt(IV) solution, a yellowish green or yellowish orange colored complex was formed. The present study was undertaken to investigate the possibility of the use of AQTS as a reagent for spectrophotometric determination of ruthenium or platinum. Optimum conditions for maximum color development, composition of the complex and possibility of determination of ruthenium(III) or platinum(IV) alone or in the presence of diverse ions have also been investigated. Further, attempts to increase the selectivity by the use of masking agents have been made. To ascertain the selectivity of the reagent the method was successfully used for the determination in alloys.

Experimental

Reagents and Apparatus. Preparation of acenaphthenequinone mono(thiosemicarbazone) (AQTS) has been reported earlier.[1] The 3.2×10^{-3}M (1M=1 mol dm^{-3}) solution of AQTS was prepared in *N*, *N*-dimethylformamide.

In the pH range 3.42—5.89, walpole buffers[2] prepared by mixing 0.2 M acetic acid and 0.2 M sodium acetate in various proportions, were used. Below and above these pH values, dilute solutions of acetic acid, hydrochloric acid, or sodium hydroxide were added for pH variations.

Standard Ruthenium(III) Solution. A required amount of ruthenium(III) chloride (Johnson Matthey, London) was dissolved in doubly distilled water, containing sufficient hydrochloric acid to give the final concentration of 1M HCl. Since the ruthenium(III) has a tendency to burn dark brown on keeping due to oxidation, the stock solution was obtained by refluxing for 3—5 h with hydrochloric acid and ethanol. The ruthenium content was determined gravimetrically by precipitating ruthenium as the hydrated oxide, followed by careful ignition in the air. The oxide was reduced to the metal in the presence of hydrogen and by cooling in an atmosphere of carbon dioxide. Subsequent dilutions were made from the stock solution according to requirements. In no case, the solutions older than 10 d were used.

Standard Platinum(IV) Solution. One gram of grade I platinum thermocouple wire (99.99%) was dissolved in aqua regia. The resultant solution was evaporated almost to dryness and a small amount of hydrochloric acid was added. The solution was again evaporated to dryness. This treatment was repeated 3 or 4 times in order to distroy any nitroso complexes. After the final evaporation, 5 cm^3 of hydrochloric acid was added and the solution was made upto 100 cm^3 with doubly distilled water. More dilute solutions, as required, were prepared by diluting the stock solution. Two standard platinum solutions prepared by exactly the same procedure were found to give the same spectrophotometric readings.

Reagent grade chemicals were used in the study of interferences. Doubly distilled water was used throughout the work. A Unicam, SP 600, spectrophotometer, with a tungsten filament lamp and matched glass cells of 10-mm light path, were used for absorbance measurements. An ECIL expanded scale pH-meter, PH821A, was used for pH adjustment.

Absorption Spectra and Effect of pH. Both ruthenium and platinum show maximum absorption at 655 and 515 nm, respectively (Figs. 1 and 2). Subsequent studies have carried out at these wavelengths. A plot of absorbance vs. pH shows that the absrobances remain constant in the pH range 5.3—6.8 and 1.9—4.1 for Ru(III) and Pt(IV), respectively. Further studies have been carried out at pH 6.1 and 2.8 for ruthenium and platinum, respectively.

Rate of Color Development and Stability of the Complexes. The rate of reaction between metal and AQTS is slow at room temperature. The color intensity was found to increase when the solutions containing a fixed amount of Ru(III) or Pt(IV) and excess of reagents were heated on a water bath for various intervals of time and absorbance was measured at 655 or 515 nm for Ru or Pt, respectively. Results of this study show that complete complex formation takes place on heating the contents for about 2.5 h and 40 min for ruthenium and platinum, respectively.

Effect of DMF Concentration. The complexes were found to be soluble in *N*, *N*-dimethylformamide. Increasing volumes of DMF added it was observed that complete dissolution of precipitate takes place in 70% DMF medium. Higher percentage of DMF had no effect on the absorbance. In subsequent work, the percentage of DMF was maintained at 70.

Effect of Reagent Concentration. A plot of absorbance vs. moles of ligand shows that at least five and seven times molar excess of the reagent is required for maximum complex formation for ruthenium and platinum, respectively (Figs. 3 and 4). In further studies ten times molar excess of the reagent was used for both metals.

Adherence to Beer's Law, Optimum Range and Sensitivity. Beer's law is obeyed upto 9.39 and 13.58 ppm (1 ppm=

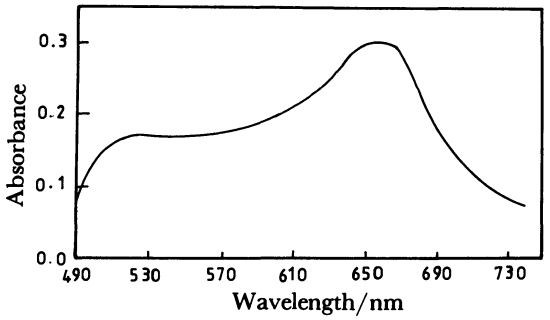

Fig. 1. Absorption spectra of ruthenium(III) complex vs. reagent.
Ru(III): 3.2×10^{-5} M, AQTS: 3.2×10^{-4} M, pH: 5.9.

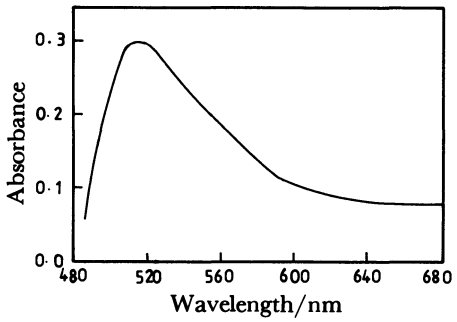

Fig. 2. Absorption spectra of platinum(IV) complex vs. reagent.
Pt(IV): 2.5×10^{-5} M, AQTS: 2.5×10^{-4} M, pH: 2.7.

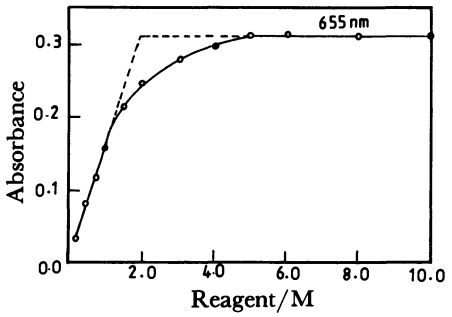

Fig. 3. Effect of reagent concentration.
Ru(III): 3.2×10^{-5} M.

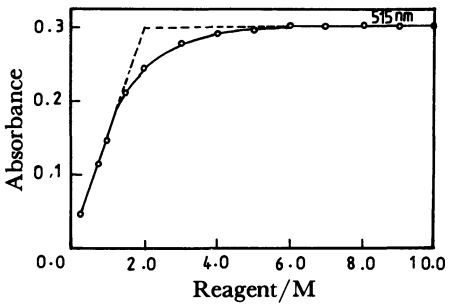

Fig. 4. Effect of reagent concentration.
Pt(IV): 2.5×10^{-5} M.

1 $\mu g\,cm^{-1}$) while the optimum concentration ranges for accurate determination, as deduced from Ringbom plot (Figs. 5 and 6), are 2.01—7.09 ppm and 2.83—11.6 ppm for

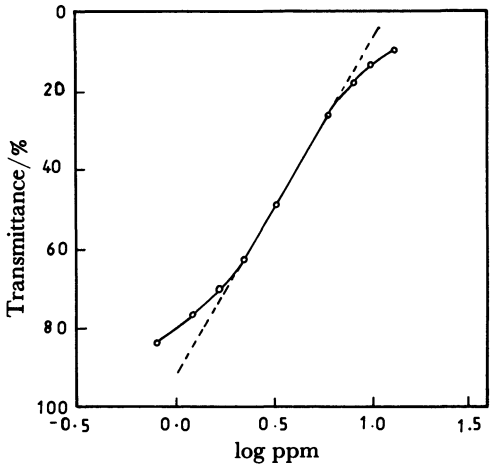

Fig. 5. Ringbom plot for Ru(III)-AQTS complex.

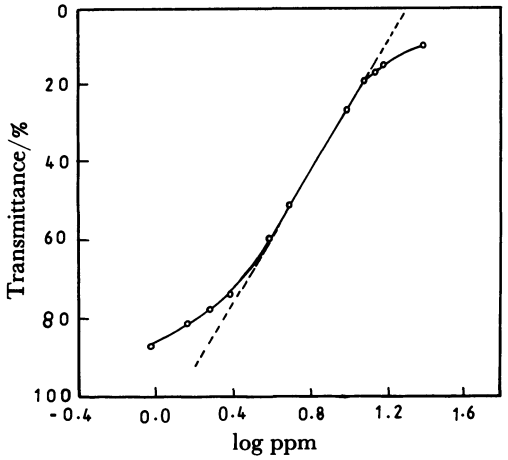

Fig. 6. Ringbom plot for Pt(IV)-AQTS complex.

ruthenium and platinum, respectively. The sensitivity in terms of Sandell's definition is 0.01 μg Ru/cm^2 and 0.01 μg Pt/cm^2 for log I_o/I=0.001 with molar absorptivity 9843.9 and 12000 $mol^{-1}cm^2$, respectively.

Recommended Procedure. To a suitable aliquot containing 50.25—177.25 μg of Ru(III) or 70.8—290 μg of Pt(IV) is added to ten times molar excess of reagent. The pH is adjusted between 5.3—6.8 for ruthenium and 1.9—4.1 for platinum with acetate buffer and dilute solution of sodium hydroxide. The mixture is heated on a boiling water-bath for 2.5 h and 40 min respectively for ruthenium and platinum, and it is cooled to room temperature (30±0.5 °C). The total volume is raised to 25 cm^3 with doubly distilled water, keeping 70% *N,N*-dimethylformamide concentration. The absorbance of the solution is measured at 655 nm for ruthenium and 515 nm for platinum against reagent blank prepared under similar conditions. The amount of ruthenium and platinum is deduced from the calibration curve.

Molar Composition of the Complexes. The composition of the complexes were determined by Job's method of continuous variations[3,4] (Figs. 7 and 8) and mole ratio method[5] (Figs. 3 and 4). Both of these methods show that the stoichiometric ratio of metal to AQTS in the (Ru: AQTS) and (Pt: AQTS) complex is 1:2.

Absorbance Deviations. The precision of the procedure was checked by measuring absorbance of eight samples, each

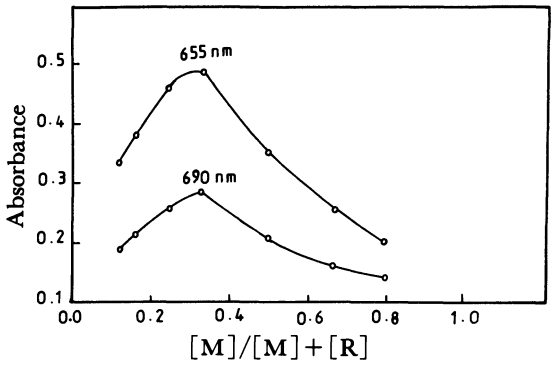

Fig. 7. Composition of Ru(III)-AQTS complex by Job's method.
Total molarity: 2.4×10^{-4} M.

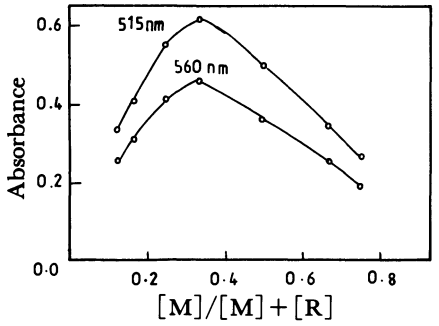

Fig. 8. Composition of Pt(IV)-AQTS complex by Job's method.
Total molarity: 3.2×10^{-4} M.

containing 3.37 ppm of ruthenium. The average relative deviation was found to be 0.33% with standard deviation of 3.6×10^{-3}. In case of platinum eight samples each containing 4.89 ppm of platinum gave average relative deviation 0.53% with standard deviation of 4.18×10^{-3}.

Effect of Diverse Ions. The effect of diverse ions was studied in the determination of ruthenium and platinum following the recommended procedure. The amounts (in ppm) of ions which do not cause any interference with 3.37 ppm of ruthenium(III) are summarized in Table 1. However nitrite, copper(II) and rhodium(III) interfere seriously.

Platinum(IV) has been determined in synthetic solution, each containing 4.89 ppm of platinum and varying amounts of foreign ions. The amounts of different ions tolerated are shown in Table 2. Among anions, iodide and thiourea interfere seriously and among cations copper(II), rhodium(III) and palladium(II) could not be masked. Masking agents were used wherever necessary.

Table 1. Effect of Diverse Ions in the Determination of Ruthenium(III)
Ruthenium Taken=3.37 ppm

Diverse ion added	Amount tolerated (in ppm)	Diverse ion added	Amount tolerated (in ppm)
Chloride	550	Calcium(II)	65
Bromide	350	Barium(II)	65
Nitrate	350	Magnesium(II)	65
Sulfate	350	Iron(II)[a]	15
Iodide	250	Cobalt(II)[b]	2
Oxalate	250	Nickel(II)[b]	4
Fluoride	40	Silver(I)[c]	15
Tartrate	40	Zinc(II)[b]	2
Cyanide	40	Cadmium(II)[b]	2
Borate	150	Osmium(VIII)[b]	5
Phosphate	80	Iridium(III)[d]	10
Thiocyanate	300	Platinum(IV)[e]	4
EDTA	30	Manganese(II)	15
Thiosulfate	25	Uranyl(II)	65
		Aluminium(III)	5
		Vanadium(V)	5
		Lead(II)[e]	5

a) Masked with phosphate. b) Masked with cyanide.
c) Masked with chloride. d) Masked with thiocyanate.
e) Masked with iodide.

Table 2. Effect of Diverse Ions in the Determination of Platinum(IV)
Platinum Taken=4.89 ppm

Diverse ion added	Amount tolerated (in ppm)	Diverse ion added	Amount tolerated (in ppm)
Chloride	700	Magnesium(II)	100
Bromide	700	Calcium(II)	100
Fluoride	700	Strontium(II)	100
Nitrate	600	Barium(II)	100
Nitrite	40	Iron(II)	20
Borate	55	Cobalt(II)	5
Thiosulfate	50	Mercury(II)	20
Tartrate	250	Nickel(II)	20
Phosphate	250	Silver(I)[a]	50
EDTA	100	Zinc(II)	40
Thiocyanate	40	Cadmium(II)	40
Citrate	175	Tungsten(IV)	80
Oxalate	30	Ruthenium(III)	6
Sulfite	200	Osmium(VIII)[b]	2
		Iridium(III)[c]	5
		Tin(II)	20
		Vanadium(V)	50
		Manganese(II)	20
		Uranyl(II)	80
		Aluminium(III)	60

a) Masked with chloride. b) Masked with cyanide.
c) Masked with thiocyanate.

Discussion

Many organic reagents have been employed for the spectrophotometric determination of ruthenium(III) and platinum(IV), but most of them lack in selectivity or sensitivity or both, and there are objectionable interferences from many of the bases and noble metals. The most sensitive method yet reported is a catalytic method,[6] but this method is lengthy and offers no special advantage over others except for its sensitivity. Thiocyanate,[7] 2,4,6-tri(2-pyridyl)-1,3,5-triazine,[8] and 2,3-diaminopyridine[9] have been suggested for the determination of ruthenium, but they require controlled parameters and the selectivity of these methods is not very high. Thiocyanate method has the disadvantage that the determination of ruthenium

Table 3. Comparison of the Sensitivities of Reagents for Ru and Pt Determination

Reagent	Sensitivity μg Ru/cm²	Reagent	Sensitivity μg Pt/cm²
Anthranilic acid	0.024/620 nm	*N,N*-Dimethyl-*p*-nitrosoaniline	0.0029/525 nm
4-Hydroxy-2*H*-1-benzopyran-2-one oxime	0.014/520 nm	Anthranilic acid	0.068/500 nm
		Tin(II) chloride	0.024/405 nm
Dithiooxamide	0.020/630 nm	Thiotropolone	0.012/600 nm
	0.010/650 nm	4-Hydroxy-2*H*-1-benzopyran-2-one oxime	0.138/490 nm
N,N-Dimethyl-*p*-nitrosoaniline	0.0028/610 nm		
2,3-Diaminopyridine	0.0084/572 nm	Acenaphthenequinone monoxime	0.021/390 nm
		Benzil α-monoxime	0.29/440 nm
Thiocyanate/CCl_4	0.0071/590 nm	Acenaphthenequinone mono(thiosemicarbazone) (Present method)	0.016/515 nm
Acetylacetone	2.5/505 nm		
1,4-Diphenylthiosemicarbazide	0.010/565 nm		
Acenaphthenequinone mono(thiosemicarbazone) (Present method)	0.01/655 nm		

Table 4. Determination of Pt(IV) in Synthetic Solutions

Mixture	Pt taken	Metal ion added/ppm		Pt found	Error/%
	ppm	Ni	W	ppm	
Pt-Ni alloy	(I) 6.0	4.0		5.97	−0.50
	(II) 4.5	5.5		4.48	−0.44
	(III) 3.0	2.0		3.01	+0.33
Pt-W alloy	(I) 2.0		0.09	2.00	0.00
	(II) 3.0		0.14	3.00	0.00
	(III) 5.0		0.23	5.02	+0.40

has to be carried out after the extraction of its tetraoxide in carbon tetrachloride. Oxidation of ruthenium to tetraoxide is a critical step in this method. 4-Hydroxy-2*H*-1-benzopyran-2-one oxime[10] has low sensitivity. 4-Hydroxyimino-4-phenyl-2-butanone[11] has low sensitivity (0.018 μg cm^{-2}/470 nm) and iron, platinum, and palladium interfere. 4-Hydroxyimino-2-pentanone,[12] phenothiazine,[13] and 2-thiophenecarbaldehyde oxime[14] methods have low sensitivity. As for the 3-(4-dimethylaminophenyl)-3-hydroxy-1-phenyltriazene[15] method, pH range is narrow (7.7—7.8). Tin(II) chloride[16] method is not selective, Pd(II), Rh(III), Ir(IV), Fe(III), Cu(II), Co(II), and SO_4^{2-}, NO_3^-, PO_4^{3-} interfere seriously. In furil α-dioxime[17] method other platinum metals and iron interfere.

For the determination of platinum with *N,N*-dimethyl-*p*-nitrosoaniline,[18] time of heating, pH changes and amount of buffer used are critical factors. Most of the associated metals interfere. Potassium iodide[18] is a useful reagent for platinum but it is less selective. Anthranilic acid[19] is not sensitive and large amount of reagent result in decrease of absorbance. In *o*-phenylenediamine[18] associated base metals and platinum metals interfere and also the complex is stable only for 1 h. In case of 4-hydroxy-2*H*-1-benzopyran-2-one oxime,[20] sensitivity is poor. Os, Pd, and Ru must be removed initially in 3,4-diaminobenzoic acid.[21]

The present method, using acenaphthenequinone mono(thiosemicarbazone) involves simple technique. The method is quite sensitive and the complexes formed are stable for many hours. Other factors such as heating time, pH, effect of buffer, and amount of reagent do not have any effect on the absorbance. Most of the associated metals do not interfere. The sensitivity is comparable (Table 3) with other methods known for the purpose.

Determination of Platinum in Synthetic Mixtures. To ascertain the selectivity of the reagent the method was successfully used for the determination of platinum in alloys. Analyzed sample of platinum–nickel and platinum–tungsten alloy were not available. Synthetic solutions similar to these alloys of platinum were prepared and the amount of platinum was determined following the recommended procedure. The results are summarised in Table 4.

One of the authors (S. K. Singh) thanks the University Grants Commission, New Delhi, for financial assistance.

References

1) P. T. Sah Peter and T. C. Daniels, *Rec. Trav. Chim. Pays-Bas*, **69**, 1545 (1950).
2) H. T. S. Briton, "Hydrogen Ions," Chapman and Hall Ltd., London (1955), Vol. 1, p. 357.
3) P. Job, *Ann. Chim.*, **9**, 113 (1928).
4) H. Irving and T. B. Pierce, *J. Chem. Soc.*, **1959**, 2565.
5) J. H. Yoe and A. L. Jones, *Ind. Eng. Chem. Anal. Ed.*, **16**, 111 (1944).
6) C. Surasiti and E. B. Sandell, *Anal. Chim. Acta*, **22**, 261 (1960).
7) F. E. Beamish, "Analytical Chemistry of Platinum

Metals," Pergamon, London (1966), p. 366.
8) W. A. Embry and G. H. Ayres, *Anal. Chem.*, **40**, 1499 (1968).
9) G. H. Ayres and D. T. Eastes, *Anal. Chim. Acta*, **44**, 67 (1969).
10) G. S. Manku, A. N. Bhat, and B. D. Jain, *Talanta*, **14**, 1229 (1967).
11) B. J. Desai and V. M. Shinde, *Z. Anal. Chem.*, **295**, 412 (1979).
12) V. V. Yeole and V. M. Shinde, *Z. Anal. Chem.*, **286**, 251 (1977).
13) B. Keshavan and H. Sanke Gowda, *Indian J. Chem.*, **17**, 315 (1979).
14) N. M. Pradhan and D. N. Patkar, *Natl. Acad. Sci. Lett.*, **3**, 83 (1980).
15) D. N. Purohit, Nizamuddin, and J. S. Noriega Rodriguez, *Z. Anal. Chem.*, **298**, 160 (1979).
16) E. Halmos and A. Vizi, *Mogy. Kem. Foly.*, **88**, 238 (1982).
17) V. I. Lazareva and A. I. Lazarev, *Zavod. Lab.*, **49**, 11 (1983).
18) F. E. Beamish, *Talanta*, **12**, 743 (1965).
19) A. K. Majumdar and J. G. Sengupta, *Z. Anal. Chem.*, **177**, 265 (1960).
20) G. S. Manku, A. N. Bhat, and B. D. Jain, *Talanta*, **16**, 1421 (1969).
21) C. D. Johnson and G. H. Ayres, *Anal. Chem.*, **38**, 1218 (1966).

1,1′-Bis(thiocyanatomercurio)ferrocene as Ligand towards $M(NCS)_2$[M=Mn(II), Co(II), Ni(II), Cu(II), Zn(II)]

Pashupati Prasad SINGH* and Meena SINGH
Chemistry Department, M. L. K. College, Balrampur-271 201, India
(Received February 28, 1985)

Complexes having three different metal atoms have been prepared by reacting 1,1′-bis(thiocyanatomercurio)-ferrocene with $M(NCS)_2$ [M=Mn(II), Co(II), Ni(II), Cu(II), Zn(II)]. The complexes have been referred to as Lewis acid and have molecular formula $Fe(C_5H_4HgSCN)_2M(NCS)_2$. They have unsaturation at M, hence have been reacted with nicotinamide and 2,2′-bipyridyl and adducts of molecular formula $Fe(C_5H_4HgSCN)_2M(NCS)_2L_x$ [x=2 when nicotinamide and 1 when bipyridyl] have been isolated. The Lewis acids and the adducts have been characterized by elemental analysis, molar conductance, magnetic moment, infrared and electronic spectral studies. These studies reveal that the coordination geometry of M is tetrahedral in the Lewis acids of cobalt, zinc, and manganese. The geometry around M in the Lewis acids of nickel and copper is octahedral through axial bonding. The adducts have a bridged structure and the geometry around M is octahedral. Quantitative softness parameters have also been applied to derive certain information.

Complexes having two different metals have recently been reported.[1-3] Attempts have also been made[4,5] to prepare trimetallic complexes but no systematic studies could be made. In this paper, a new class of complexes having three different metals have been prepared and studied for the first time.

Experimental

Reagent grade solvents were purified before use. $M(NCS)_2 \cdot 2nia$ [M=Mn(II), Co(II), Ni(II), Cu(II), Zn(II) nia=nicotinamide] were prepared by direct reaction of nicotinamide and $M(NCS)_2$ in ethanol. 2,2′-Bipyridyl (bpy) was used from fresh bottle. 1,1′-Bis(thiocyanatomercurio)-ferrocene (FBMT) was prepared as given below.

Preparation of 1,1′-Bis(thiocyanatomercurio)ferrocene. 9.2 g (0.25 mole) ferrocene was dissolved in 50 ml of benzene in a two necked flask. A homogenesous suspension of 16 g (0.25 mole) of mercury(II) acetate in 200 ml of methanol was separately prepared. This suspension was very slowly added to the solution of ferrocene through a dropping funnel, with continuous stirring. A dark brown clear solution was obtained. To this, a solution of 4.8 g (0.25 mole) KSCN in 10 ml of water was added, and stirred for 30 min. A yellow precipitate was formed which was filtered on büchner funnel and washed with petroleum ether. This yellow compound was a mixture of (thiocyanatomercurio) ferrocene and 1,1′-bis-(thiocyanatomercurio)ferrocene.

Separation of Mono and Bis Derivatives. The yellow mass was placed in upper disc of the Soxhlet apparatus and the flask was filled with 25 ml of 1,2-dichloroethane and extracted for 30 min. A portion of yellow mass dissolved in 1,2-dichloroethane and its color became yellow. The yellow solution was collected and fresh 25 ml of pure 1,2-dichloroethane was added and again extracted for 30 min. The process was continued till there was no change in the color of 1,2-dichloroethane. On evaporation of the yellow extract impure (thiocyanatomercurio)ferrocene was obtained. The undissolved yellow residue was FBMT. This compound was purified by dissolving in dimethylsulfoxide (DMSO) and isolating the pure compound by addition of water. The analytical data of the bis derivative are; mp 145 °C (decomp), sulfur calcd. 9.14%, found 8.85%, nitrogen calcd. 4% found 3.72%, mercury calcd. 57.14% found 56.01%.

Preparation of Lewis Acids: "$Fe(C_5H_4HgSCN)_2M(NCS)_2$" [M=Mn(II), Co(II), Ni(II), Cu(II), and Zn(II)]. FBMT was dissolved in a small quantity of DMSO and diluted to 200 ml by acetone. $M(NCS)_2$ were similarly dissolved either in acetone or DMSO-acetone mixture separately. $Mn(NCS)_2$ was however, dissolved in ethyl acetate. The solutions of FBMT and $M(NCS)_2$ were mixed in 1:1 molar ratio and stirred for 24 h. Precipitate appeared in each case. When the quantity of DMSO became more the precipitates were obtained by addition of ethanol. The precipitates were filtered, washed with ethanol, and dried in vacuum. The compounds were recrystallized from acetone-ethanol mixture.

Preparation of Adducts: $Fe(C_5H_4HgSCN)_2M(NCS)_2L_x$[$x$=2 when L is nia and 1 when bpy]. The adducts were prepared by two methods. (1) A suspension or solution of the Lewis acids was prepared in acetone-ethanol mixture and mixed with an ethanol solution of nicotinamide in 1:2 molar ratio or with 2,2′-bipyridyl in 1:1 molar ratio and stirred for 24 h. In each case precipitate was formed, filtered, washed with ethanol, and dried in vacuum. The compounds were recrystallized from acetone-ethanol mixture. (2) $M(NCS)_2 \cdot 2nia$ was dissolved in acetone. The corresponding manganese compound was dissolved in ethyl acetate. FBMT was dissolved in DMSO-acetone mixture. The solutions of $M(NCS)_2 \cdot 2nia$ and FBMT were mixed in 1:1 molar ratio and stirred for 48 h. Precipitate was formed in each case which was filtered, washed with ethanol, and dried in vacuum. Recrystallized from acetone-ethanol mixture. The copper analog could not be prepared by this method.

Analysis of the Complexes. The complexes were analyzed for cobalt as anthranilate, and for nickel as dimethylglyoximate. Sulfur as sulfate and mercury as sulfide. Nitrogen was estimated by semimicro Kjeldahl's method. Analytical results along with melting points are presented in Table 1.

Physical Measurements. The molar conductance of the complexes were measured in DMSO using a Philip conductivity bridge model PR-9500. The molecular weights were determined in DMSO solution by cryoscopic method. The magnetic susceptibility measurements were made at room temperature by Gouy's method using $CoHg(SCN)_4$ as standard. The diamagnetic corrections were made using Pascal's constants. Infrared spectra of the complexes were recorded as nujol mulls or as KBr pellets on a Pye Unicam sp 3-300 spectrophotometer in the range 4000—200 cm^{-1}. Elec-

Table 1. Analytical Data of the Complexes

Complex	Color	Mp θ_m/°C	Sulfur %		Mercury %		Metal %		Nitrogen %		Molecular wt.		Molar Conductance cm^{-1} mhos/mol M/1024
			Calcd	Found	Calcd	Found	Calcd	Found	Calcd	Found	Calcd	Found	
$Fe(C_6H_4HgSCN)_2Ni(NCS)_2$	Light green	240(d)	14.65	14.12	45.71	45.43	6.62	6.71	6.40	6.16	875	—	70.34
$Fe(C_6H_4HgSCN)_2Co(NCS)_2$	Blue	230(d)	14.65	14.16	45.71	45.27	6.62	6.80	6.40	6.21	875	—	58.62
$Fe(C_6H_4HgSCN)_2Cu(NCS)_2$	Light green	185(d)	14.54	14.26	45.45	45.12	7.15	7.82	6.36	6.19	880	—	30.58
$Fe(C_6H_4HgSCN)_2Zn(NCS)_2$	Light brown	178(d)	14.51	14.32	45.35	45.03	7.36	7.40	6.34	6.23	882	—	48.38
$Fe(C_6H_4HgSCN)_2Mn(NCS)_2$	Grey	164(d)	14.71	14.30	45.97	45.07	6.20	6.73	6.43	6.21	870	—	48.02
$Fe(C_6H_4HgSCN)_2Ni(NCS)_2(bpy)$	Mustard	210(d)	12.42	12.33	38.83	38.21	5.63	5.82	5.43	5.31	1030	842	73.45
$Fe(C_6H_4HgSCN)_2Ni(NCS)_2(nia)_2$	Brown	200(d)	11.44	12.20	35.77	35.13	5.18	5.29	5.00	4.94	1118	975	62.75
$Fe(C_6H_4HgSCN)_2Co(NCS)_2(bpy)$	Dirty pink	190(d)	12.42	12.13	38.83	38.36	5.63	5.50	5.43	5.22	1030	872	70.29
$Fe(C_6H_4HgSCN)_2Co(NCS)_2(nia)_2$	Dirty pink	195(d)	11.44	11.22	35.77	35.46	5.18	5.12	5.00	4.85	1118	913	60.23
$Fe(C_6H_4HgSCN)_2Cu(NCS)_2(bpy)$	Mustard	175(d)	12.36	11.13	38.68	38.12	6.28	6.18	5.41	5.32	1035	924	50.44
$Fe(C_6H_4HgSCN)_2Cu(NCS)_2(nia)_2$	Green	190(d)	11.39	11.01	35.60	35.32	5.60	5.70	4.98	4.79	1123	914	50.25
$Fe(C_6H_4HgSCN)_2Zn(NCS)_2(bpy)$	Dirty white	162(d)	12.34	12.03	38.57	38.42	6.26	6.41	5.40	5.23	1037	842	43.28
$Fe(C_6H_4HgSCN)_2Zn(NCS)_2(nia)_2$	Dirty white	185(d)	11.37	11.12	35.55	35.12	5.77	5.82	4.97	4.82	1125	932	43.08
$Fe(C_6H_4HgSCN)_2Mn(NCS)_2(bpy)$	Light brown	180(d)	12.45	12.04	38.91	38.82	5.25	5.33	5.44	5.12	1028	—	43.13
$Fe(C_6H_4HgSCN)_2Mn(NCS)_2(nia)_2$	Grey	170(d)	11.46	11.20	35.84	35.01	4.83	4.18	5.01	4.82	1116	—	43.00

(d) = decomp.

tronic spectra in the range 200—990 nm were recorded on Pye Unicam sp 5-500. The thermodynamics stability constant (log K), has been determined by spectrophotometric method.

Results and Discussion

The spectra of FBMT were recorded in solid and solution phase. The solid phase spectra show the presence of three bands at 2190, 2120, and 2100 cm^{-1} in ν(CN) region, two bands at 730 and 720 cm^{-1} in ν(CS) region and two bands at 460 and 410 cm^{-1} in δ(NCS) region. The band at 2190 cm^{-1} disappears in solution. This shows that FBMT exists as dimer in solid phase like CH_3HgSCN[6] as shown below.

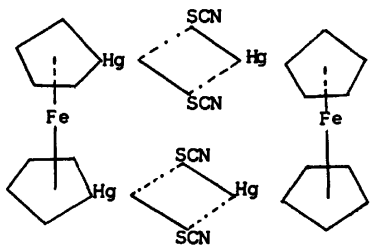

(Dimer in solid)

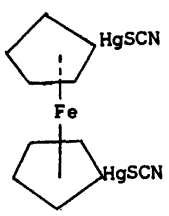

(Monomer in solution)

In solution phase the thiocyanato bridge is broken and this becomes a monomer. The solution spectra have therefore, been taken for the purpose of comparison. The band at about 2120 cm^{-1} in ν(CN) region, at about 740 cm^{-1} in ν(CS) region and at about 450 cm^{-1} in δ(NCS) indicate the presence of S-bonded thiocyanate in FBMT.

Lewis acids: $Fe(C_5H_4HgSCN)_2M(NCS)_2$[M = Mn(II), Co(II), Ni(II), Cu(II), Zn(II)].

The FBMT has been used as ligand and reacted with $M(NCS)_2$. This results in the formation of a complex of general formula $Fe(C_5H_4HgSCN)_2M(NCS)_2$. These compounds have been referred to as Lewis acids. Comparison of the infrared spectra of the FBMT with the Lewis acids shows that the position of ν(CN), ν(CS), and δ(NCS) bands are changed. The ν(CN) band moves to about 2190 cm^{-1}, ν(CS) band to about 790 cm^{-1} and δ(NCS) band to about 480 cm^{-1}. The positions of these bands are indicative of the presence of thiocyanato bridge.[7] A band is also observed in 2070 cm^{-1} to 2010 cm^{-1} region. Band in this region is assigned to N-bonded terminal thiocyanate arising from ν(M-NCS).[8]

The electronic spectra of the Lewis acid where M is Co(II), show the presence of two intense bands in the region 17450 cm^{-1} and 10640 cm^{-1} which are assigned to $^4A_2 \rightarrow {}^4T_2(F)$ (ν_3) and $^4A_2 \rightarrow {}^4T_1(P)$ (ν_2) transitions, respectively (Table 2). The D_q value derived from ν_3 and ν_2 bands is 541 cm^{-1}. The positions of these bands and the magnetic moment values show that the cobalt is in tetrahedral geometry. The compound is nonconducting in nature. On the basis of these results the following structure (Fig. 1) can be proposed for this Lewis acid.

The infrared spectra of the Lewis acids where M is Zn(II) or Mn(II) are similar to the Lewis acid where M is cobalt(II). It can, therefore, be presumed that the structure of these Lewis acids is also similar to that in Fig. 1. The electronic spectra of Lewis acid where M is Ni(II) show the presence of three bands in the region 27790, 16650, and 10400 cm^{-1} which are assigned to $^3A_{2g} \rightarrow {}^3T_{1g}(P)(\nu_3)$, $^3A_{2g} \rightarrow {}^3T_{1g}(F)(\nu_2)$, and $^3A_{2g} \rightarrow {}^3T_{2g}(F)(\nu_1)$, respectively. The D_q value derived from ν_2 and ν_3 bands is 1020 cm^{-1} (Table 2). The spectra and magnetic moment values indicate the

Table 2. Infrared Spectral and Electronic Spectral Bands with Spectral Parameters

Complex	ν(CN) cm^{-1}	ν(CS) cm^{-1}	δ(NCS) cm^{-1}	ν(M-NCS) cm^{-1}	ν_3 cm^{-1}	ν_2 cm^{-1}	ν_1 cm^{-1}	Dq cm^{-1}	B' cm^{-1}	β	μ_{eff} (BM)
$Fe(C_5H_4HgSCN)_2$ (solid)	2190(w), 2120(s), 2100(s)	730(s), 720(m)	460(s), 410(sh)	—	—	—	—	—	—	—	—
$Fe(C_5H_4HgSCN)_2$ (solution)	2120(s), 2070(m)	740(s), 720(w)	450(s), 420(m)	—	—	—	—	—	—	—	—
Lewis acid											
$Fe(C_5H_4HgSCN)_2Ni(NCS)_2$	2170(w), 2100(s)	780(s), 760(s)	470(s), 450(s)	260(s), 240(sh)	27790	16650	10400	1020	906	0.87	3.07
$Fe(C_5H_4HgSCN)_2Co(NCS)_2$	2190(s), 2120(s)	790(s), 760(w)	480(sh), 460(s)	320(s), 295(s)	17540	10640	—	541	796	0.77	4.24
$Fe(C_5H_4HgSCN)_2Cu(NCS)_2$	2180(s), 2100(m)	760(s), 740(w)	480(w), 440(s)	265(s), 245(m)	—	—	—	—	—	—	1.92
$Fe(C_5H_4HgSCN)_2Zn(NCS)_2$	2160(sh), 2100(s)	770(m), 740(s)	470(s), 450(s)	325(s), 280(m)	—	—	—	—	—	—	—
$Fe(C_5H_4HgSCN)_2Mn(NCS)_2$	2180(s), 2110(w)	750(w), 720(s)	460(m), 450(s)	315(m), 285(s)	—	—	—	—	—	—	6.40
Adduct											
$Fe(C_5H_4HgSCN)_2Ni(NCS)_2(bpy)$	2170(s), 2090(sh)	770(s), 740(s)	480(s), 420(s)	270(s), 220(sh)	28500	16650	10300	1003	1004	0.97	3.21
$Fe(C_5H_4HgSCN)_2Ni(NCS)_2(nia)_2$	2180(sh), 2100(s)	760(s), 730(sh)	480(m), 420(s)	265(s), 215(m)	26900	16450	10200	1010	866	0.84	3.17
$Fe(C_5H_4HgSCN)_2Co(NCS)_2(bpy)$	2160(s), 2090(s)	760(s), 730(m)	470(w), 430(s)	235(s), 210(w)	20850	16400	—	855	910	0.93	5.10
$Fe(C_5H_4HgSCN)_2Co(NCS)_2(nia)_2$	2180(s), 2090(sh)	760(s), 730(w)	480(s), 420(m)	215(s), 205(w)	21105	17110	—	862	857	0.88	5.24
$Fe(C_5H_4HgSCN)_2Cu(NCS)_2(bpy)$	2150(s), 2080(sh)	750(s), 720(sh)	470(w), 410(s)	260(m), 210(w)	—	—	—	—	—	—	2.03
$Fe(C_5H_4HgSCN)_2Cu(NCS)_2(nia)_2$	2140(s), 2080(s)	750(m), 720(s)	470(w), 420(s)	265(s), 240(w)	—	—	—	—	—	—	2.16
$Fe(C_5H_4HgSCN)_2Zn(NCS)_2(bpy)$	2130(s), 2090(s)	780(s), 735(m)	460(m), 410(s)	225(s), 210(sh)	—	—	—	—	—	—	
$Fe(C_5H_4HgSCN)_2Zn(NCS)_2(nia)_2$	2140(s), 2080(s)	760(m), 740(s)	465(s), 430(m)	220(s)	—	—	—	—	—	—	
$Fe(C_5H_4HgSCN)_2Mn(NCS)_2(bpy)$	2120(s), 2010(m)	780(s), 735(s)	470(s), 440(m)	210(s)	—	—	—	—	—	—	6.23
$Fe(C_5H_4HgSCN)_2Mn(NCS)_2(nia)_2$	2135(w), 2100(s)	770(w), 720(s)	460(m), 400(s)	215(s)	—	—	—	—	—	—	6.60

s=strong, sh=shoulder, m=medium, w=weak.

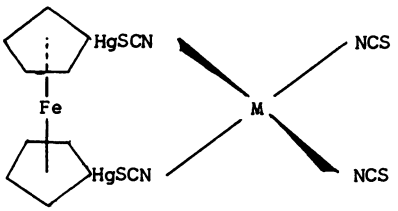

where M=Co(II), Zn(II), Mn(II).

Fig. 1.

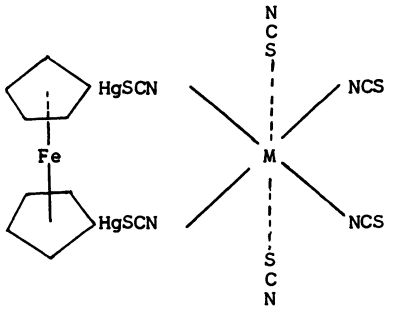

where M=Ni(II), Cu(II).

Fig. 2.

presence of octahedral coordination geometry around nickel. The electronic spectra and the magnetic moment values where M is Cu(II) are also indicative of the presence of octahedral coordination geometry around Cu(II). Both these metal ions acquire octahedral geometry through axial coordination.[9] These complexes are nonconducting in dimethyl sulfoxide. On the basis of these results the structure as shown in Fig. 2 can be proposed.

Adducts: $Fe(C_5H_4HgSCN)_2M(NCS)_2L_x$($x$=2 when L is nia and 1 when bpy). The coordination number of M in the Lewis acid where M is Co(II), Zn(II), or Mn(II) is four against the maximum of six. Due to this unsaturation at M, they have been named as Lewis acid. Where M is Ni(II) or Cu(II) the coordination number six has been achieved through weak axial bonding which can easily be replaced by ligands. Accordingly both types of Lewis acids have been reacted with nicotinamide and 2,2-bipyridyl and adducts of general formula $Fe(C_5H_4HgSCN)_2M(NCS)_2L_x$ have been prepared.

The infrared spectra of the adducts where M is Ni(II) or Cu(II) show that there is no significant change in the positions of ν(CN), ν(CS), δ(NCS), and ν(M-NCS) bands. This shows that the bridging nature of thiocyanate and octahedral coordination geometry around M are retained. The infrared spectra of the adducts where M is Co(II), Zn(II) or Mn(II) also show that the

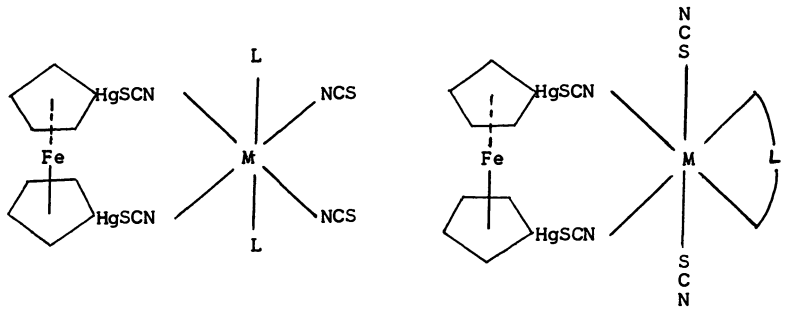

Fig. 3.

Table 3. $\Delta E^{\ddagger}_{nm}$ Derived from $E^{\ddagger}_{n(eff)}$ of M in $M(NCS)_2$ and $E^{\ddagger}_{m(eff)}$ of FBMT in the Formation of Lewis Acids

S.No.	Lewis Acid	$E^{\ddagger}_{n(eff)}$ of M in $M(NCS)_2$	$E^{\ddagger}_{m(eff)}$ of FBMT	$\Delta E^{\ddagger}_{nm}$	CFSE	Matching Constant $\Delta E^{\ddagger}_{nm}$+CFSE
1.	$Fe(C_5H_4HgSCN)_2Ni(NCS)_2$	−3.10	−11.16	8.06	6.66	15.72
2.	$Fe(C_5H_4HgSCN)_2Co(NCS)_2$	−3.56	−11.16	7.60	4.55	12.15
3.	$Fe(C_5H_4HgSCN)_2Zn(NCS)_2$	−4.92	−11.16	6.24	—	6.24
4.	$Fe(C_5H_4HgSCN)_2Mn(NCS)_2$	−9.01	−11.16	2.15	—	2.15

bridging nature of the thiocyanate is retained but a negative shift is observed in ν(M–NCS) band. This negative shift is on account of change in tetrahedral geometry around M to octahedral.[8,10] Such a change is not observed where M is Ni(II) or Cu(II), because the geometry around M, in these cases, remains octahedral in the Lewis acid and the adducts as well. The electronic spectral data of all adducts, their assignments, various spectral parameters, and magnetic moment values, as presented in Table 2, indicate that the coordination geometry around M is octahedral. All the adducts are nonconducting in nature. On the basis of these results the structure as shown in Fig. 3 can be proposed for the adducts.

Comparison with the Complexes of RHgSCN: (R=*p*-tolyl, *p*-naphthyl, phenyl, ethoxy, methoxy, *p*-chlorophenyl). RHgSCN have been reported to act as Lewis bases towards $M(NCS)_2$. The base strength of RHgSCN changes on change of R. The following sequence of base strength on the basis of various physicochemical studies has been established.[11]

p-tolyl > *p*-naphthyl > phenyl > ethoxy > methoxy > *p*-chlorophenyl

The FBMT also acts as a base towards $M(NCS)_2$. This base has two thiocyanato groups as donor sites, and consequently the complexes formed by this base are more stable. The D_q values of Co(II) and Ni(II) Lewis acids are 541 cm^{-1} and 1020 cm^{-1}. These values are higher than the D_q values of the corresponding complexes of the RHgSCN. This fact is also demonstrated experimentally. The thiocyanato bridge between Hg(II) and M(II) in the Lewis acids of RHgSCN is ruptured on reaction with 2,2′-bipyridyl, resulting in the formation of cationic-anionic complexes of general formula $[M(bpy)_3][RHg(SCN)_2]_2$. The Lewis acids of the present series, however, form adducts on such a reaction, and the thiocyanato bridge between M(II) and Hg(II) is retained. This shows that the base strength of this compound is higher than any of the RHgSCN.

Quantitative Softness Parameters: The effective softness $E^{\ddagger}_{n(eff)}$ value of M in $Fe(C_5H_4HgSCN)_2M(NCS)_2$, $E^{\ddagger}_{m(eff)}$ value of N-end of nicotinamide and 2,2′-bipyridyl and of N-end of FBMT have been evaluated by the method described elsewhere,[12] and the results are included in Table 3. The FBMT reacts with $M(NCS)_2$ and forms Lewis acid of general formula $Fe(C_5H_4HgSCN)_2M(NCS)_2$. The difference ($\Delta E^{\ddagger}_{nm}$) between $E^{\ddagger}_{m(eff)}$ of N-end of FBMT and $E^{\ddagger}_{n(eff)}$ of M in $M(NCS)_2$ have been evaluated by the following equation:

$$\Delta E^{+}_{nm} = \left| E^{+}_{n(eff)} - E^{+}_{m(eff)} \right|$$

The $\Delta E^{\ddagger}_{nm}$ value is the highest when M is Ni(II) and the lowest when Mn(II). The $\Delta E^{\ddagger}_{nm}$ between $E^{\ddagger}_{n(eff)}$ of M in Lewis acids and $E^{\ddagger}_{m(eff)}$ of nicotinamide and 2,2′-bipyridyl and the matching constant values have been derived in order to find out which out of the two ligands forms more stable bond with M and which out of the various M forms more stable bond with nicotinamide or bipyridyl. The results are included in Table 3. The $\Delta E^{\ddagger}_{nm}$ values show that bipyridyl forms more stable M–L bond than nicotinamide which is in concurrence with the established fact. $\Delta E^{\ddagger}_{nm}$ values are the highest when M=Ni(II) and the lowest when M=Mn(II). The sequence with other M is as follows:

Nickel > Cobalt > Zinc > Manganese.

Table 4. $\Delta E^{\ddagger}_{nm}$ Derived from $E^{\ddagger}_{n(eff)}$ of M in $Fe(C_5H_4HgSCN)_2M(NCS)_2$ and $E^{\ddagger}_{m(eff)}$ of the Ligand in the Formation of Adducts

Complex	$E^{\ddagger}_{n(eff)}$ of M in Lewis Acid	$E^{\ddagger}_{m(eff)}$ of nia	$\Delta E^{\ddagger}_{nm}$	CFSE	Matching Constant	log K
$Fe(C_5H_4HgSCN)_2Ni(NCS)_2(nia)_2$	−2.28	−11.47	11.49	6.42	17.91	5.16
$Fe(C_5H_4HgSCN)_2Co(NCS)_2(nia)_2$	−2.83	−11.47	10.94	4.29	15.23	5.09
$Fe(C_5H_4HgSCN)_2Zn(NCS)_2(nia)_2$	−4.11	−11.47	9.66	—	9.66	4.92
$Fe(C_5H_4HgSCN)_2Mn(NCS)_2(nia)_2$	−8.90	−11.47	4.87	—	4.87	4.43

nia = nicotinamide.

The stability of metal ligand bond in case of transition metal ions has been expressed in terms of matching constant, by adopting the following relation:

$$\text{Matching constant} = \Delta E^{\ddagger}_{nm} + \text{CFSE}$$

The matching constant values are presented in Table 4, along with thermodynamic stability constant (log K). Both the values indicate that most stable M–L bond is formed where M is Ni(II) and sequence is as follows:

Nickel(II), Cobalt(II), Zinc(II), and Manganese(II).

The authors gratefully acknowledge the financial support received from University Grants Commission, New Delhi.

References

1) R. C. Agrawal, N. Singh, and S. Singh, *Ind. J. Chem.* **21A**, 268 (1982).
2) B. S. Biradar, B. R. Patil, and V. H. Kulkarni, *J. Inorg. Nucl. Chem.*, **37**, 1901 (1975).
3) P. P. Singh, *Coord. Chem. Rev.*, **32**, 33 (1980).
4) D. E. Scaife, *Inorg. Chem.*, **6**, 625 (1967).
5) P. P. Singh and N. Singh, *J. Coord. Chem.*, **9**, 197 (1979).
6) K. Dehnicks, *J. Organomet. Chem.*, **9**, 11 (1967).
7) S. M. Nelson and T. M. Shepherd, *J. Inorg. Nucl. Chem.*, **27**, 2123 (1965).
8) R. J. H. Clark and C. S. Williams, *Spectrochim. Acta.* **22**, 1081 (1966).
9) D. Forster and D. M. L. Goodgame, *Inorg. Chem.*, **4**, 715 (1965).
10) R. Makhija, L. Pazdernik, and R. Rivest, *Can. J. Chem.*, **51**, 2987 (1973).
11) P. P. Singh, S. P. Yadav, and D. Singh, *Ind. J. Chem.*, **23A**, 853 (1984).
12) P. P. Singh, S. K. Srivastava, and A. K. Srivastava, *J. Inorg. Nucl. Chem.*, **42**, 521 (1980).

 © 1986 The Chemical Society of Japan Bull. Chem. Soc. Jpn., 59, 1235—1238 (1986)

Novel Synthesis of Furo[2,3-*b*]indole Derivatives

Fathy Faheem Abd El-Latif,† Abd El-Kareem Mohammed Nasr Gohar,† Atiat Mohammed Fahmy,† and Mahmoud Zarif Amin Badr*

†Chemistry Department, Faculty of Science, El-Minia University, Egypt
Chemistry Department, Faculty of Science, Assiut University, Assiut, Egypt

(Received September 1, 1984)

Isatin reacted with diethyl 3-amino-2-cyano-2-pentenedioate in ethanol and in presence of Et_3N to give 3-(1-amino-2-cyano-2-ethoxycarbonylethenyl-2*H*-furo[2,3-*b*]indol-2-one. The reaction of (2-oxo-3-indolinylidene)-malononitrile (**3a**) with the diethyl ester gave a mixture of diethyl 3-amino-4-(2-amino-3-cyano-4-quinolyl-carbonyl)-2-cyano-2-pentenedioate (80%) and diethyl 3-amino-4-(2-amino-3-cyano-3a*H*-furo[2,3-*b*]indol-3a-yl)-2-cyano-2-pentanedioate (20%). Treatment of **3a** and 3-[cyano(ethoxycarbonyl)]methylene-2-indolinone (**3b**) with 2-(ethoxycarbonylmethyl)-2-thiazolin-4-one gave the corresponding two pyrano[4′,5′-*c*] and furo[2″,3″-*b*]indole compounds, respectively. When **3a** and **3b** also reacted, with 3-methyl-2-pyrazolin-5-one or 3-methyl-1-phenyl-2-pyrazolin-5-one, the corresponding four spiro indoline-3,4′-(1′*H*)-pyrano[2, 3-*c*]pyrazol products were obtained. The reaction of **3b** with benzoylacetonitrile gave ethyl 2-amino-3a-[benzoyl(cyano)methyl]-3a*H*-furo[2,3-*b*]indole-3-carboxylate.

It is well known that indole itself and some of its derivatives are known to induce leuckaemia in rodents.[1] Polynuclear indoles are used as potential carcinogenic and/or leuckaemogenic.[2]

The present paper constitutes a study on a novel synthesis of these compounds involving condensation of nucleophiles with isatin or its ylidene derivatives. Treatment of isatin (**1**) with diethyl 3-amino-2-cyano-2-pentenedioate in the presence of triethylamine (Et_3N) as basic catalyst gave the corresponding 3-(1-amino-2-cyano-2-ethoxycarbonylethenyl)-2*H*-furo[2,3-*b*]indol-2-one (**2**) (through Knoevenagel condensation followed by cyclization).

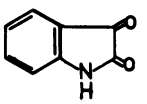

1

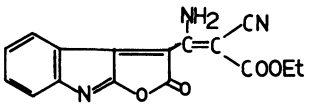

The structure of compound **2** has been confirmed by its IR absorption spectrum which showed broad band extending at 3300—3150 cm^{-1} (NH_2), at 2205 cm^{-1} (C≡N), at 1710, 1750 cm^{-1} (C=O of the ester and ring) and broad band extending at 3020—2900 cm^{-1} (CH_2, CH_3 stretches). The ^{1}H-NMR spectrum revealed the following signals: multiplet extending at δ 7.6—8.3 (m, 4H; aromatic protons), triplet at δ 2.2 (t, 3H, ester CH_3), quartet at δ 4.1 (q, 2H, ester CH_2), and singlet at δ 3.7 (s, 2H, NH_2). Similarly, treatment of (2-oxo-3-indolinylidene)malononitrile[3] (**3a**) with the diethyl ester in the presence of Et_3N produced a mixture of diethyl 3-amino-4-(2-amino-3-cyano-4-quinolylcarbonyl)-2-cyano-2-pentenedioate (**4**) (yield 80%) and diethyl 3-amino-4-(2-amino-3-cyano-3a*H*-furo[2,3-*b*]indol-3a-yl)-2-cyano-2-pentenedioate (**5**) (20% yield), respectively.

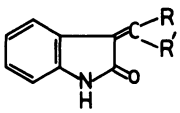

3a, R = R′ = CN
b, R = CN, R′ = COOEt

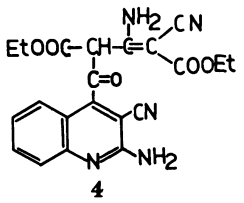

4

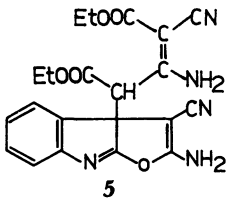

5

Formation of the quinoline derivative (**4**) may be rationalized in terms of a carbanion attack at the carbonyl carbon of (2-oxo-3-indolinylidene)malononitrile followed by ring opening and recyclization affording the structure **4** according to the mechanism discussed in a previous paper.[4] Compound **5** was suggested to be formed by the carbanion attack at the olefinic carbon of the ylidene followed by cyclization producing the final product (Scheme 1).

The assigned structure of compound **4** was based on its IR spectrum which showed broad band at 3300—3150 cm^{-1} (NH_2), 2250, 2200 cm^{-1} (C≡N), broad band extending at 1740—1700 cm^{-1} (C=O), and 3000—2950 cm^{-1} (CH_2, CH_3 stretches). Moreover, ^{1}H-NMR spectrum of compound **4** revealed singlet at δ 3.7 (s, 2H, NH_2), quartet at δ 4—4.4 (q, 4H for 2 ester CH_2), triplet at δ 1.2 (t, 3H ester CH_3); triplet at δ 1.5 (t, 3H, CH_3 of the other ester group), and multiplet extending at δ 6.9—7.5 (m, 5H, 4H aromatic protons and CH proton.[5] Further proof for the suggested structure was derived from its electronic spectrum which exhibits characteristic quinoline maxima at λ_{max}360 nm (log ε 4.88), 285 (5.32), and 235 (5.30),[6] although with some bathochromic shift due to substituent effects.

The assigned structure of compound **5** was inferred from its IR spectrum which showed broad band at 3300—3150 cm^{-1} for NH_2, at 2210 cm^{-1} for C≡N, a broad band at 1750—1710 cm^{-1} for C=O, and a broad band extending at 3010—2950 cm^{-1} for CH_2, CH_3 stretches. It may be suggested that the final separated product formed should be through the suggested intermediate structure **A** (Scheme 1). However, probable formation of **9** from **A** is excluded on bases of analytical data reported.

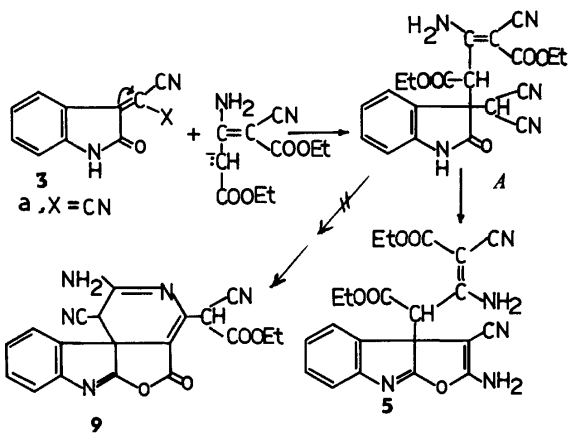

Scheme 1.

In the same manner, when **3a** and **3b** reacted with 2-(ethoxycarbonylmethyl)-2-thiazolin-4-one gave the corresponding compounds **6a** and **6b**, respectively. The formation of compounds **6a, b** was assumed to proceed via the attack of the carbanion nucleophile on the olefinic carbon of the ylidene, followed by the cycloaddition of highly acidic thiazole (OH) on the cyano group to form the suggested intermediate spiro compound (**B**) (Step a) followed by cycloaddition of the less acidic indole (OH) on the second cyano or the ester group to form the final isolated products, ethyl 5,6-diimino-thiazolo[4,5-*b*]pyrano[4′, 5′-*c*]furo[2″,3″-*b*]indole-2-acetate (**6a**) and ethyl 5-imino-thiazolo[4, 5-*b*]pyrano[4′,5′-*c*]furo[2″,3″-*b*]indole-6-one-2-acetate (**6b**), respectively (Step b) (Sheme 2). The suggested preliminary formation of intermediate spiro compound (**B**) although not separated in such mechanism had been proved through the separation of their analogues (**7a—d**) when cyclization proceeded in the absence of Et_3N which is discussed later.

The structure of compound **6a** agrees with its IR spectrum which showed broad band at 3200—3100 cm^{-1} NH), 3000—2900 cm^{-1} (CH_2, CH_3 stretches), 1700 cm^{-1} (C=O), and 1660 cm^{-1} (C=N–). Moreover, its ^{1}H-NMR spectrum in DMSO gives a clue for the assigned structure showing the following signals: triplet at δ 1.3 (t, 3H, ester CH_3), singlet at δ 2.8 (s, 2H, CH_2 group), quartet at δ 4—4.3 (q, 2H ester CH_2), singlet at δ 5.7 (s, 1H, CH proton), multiplet at δ 6.9—7.4 (m, 4H, aromatic protons), and two singlet at δ 8.1 and 9 (s, 2H, 2NH protons). The UV spectrum of **6a** in ethanol showed absorption bands at λ_{max} 425 nm (log ε 4.91), 270 (4.58), and 258 (3.76).

The IR spectrum of compound **6b** agrees well with the assigned structure which showed characteristic absorption bands at 3300, 3346 cm^{-1} (NH), 3000—2900 cm^{-1} (CH_2, CH_3 stretches), 1730, 1700 cm^{-1} (C=O ring and ester), and 1660 cm^{-1} (C=N). Its ^{1}H-NMR spectrum showed the following signals: triplet at δ 0.9 (t, 3H, ester CH_3), singlet at δ 2.7 (s, 2H, CH_2), quartet at δ 4.00 (q, 2H, ester CH_2), multiplet at δ 6.7—7.4 (m, 5H, CH proton and 4 aromatic protons), and singlet at δ 9.1 (s, 1H, NH proton). The UV spectrum of **6b** showed the following bands at λ_{max} 414 nm (log ε 5.76), 279 (5.396), and 262 (5.98).

When **3a** or **3b** was treated with 3-methyl-2-pyrazolin-5-one or 3-methyl-1-phenyl-2-pyrazolin-5-one in ethanol or dioxane and in the absence of Et_3N, it gave the corresponding spiro products, namely, 6′-amino-5′-cyano-3′-methylspiro[indoline-3,4′(1′*H*)-pyrono[2,3-*c*]pyrazol]-2-one (**7a**); ethyl 6′-amino-3′-methyl-2-oxospiro[indoline-3, 4′(1′*H*)-pyrano[2,3-*c*]-pyrazole]-5′-carboxylate (**7b**), 6′-amino-5′-cyano-3′-methyl-1′-phenylspiro[indoline-3, 4′(1′*H*)-pyrano[2,3-*c*]-pyrazol]-2-one (**7c**), and ethyl 6′-amino-3′-methyl-2-oxo-1′-phenylspiro[indoline-3,4′(1′*H*)-pyrano[2,3-*c*]-pyrazole]-5′-carboxylate (**7d**) which is rationalized in terms of the addition of active methylene group on the olefinic double bond followed by cyclization on the same bases as in (Step a) of Scheme 2.

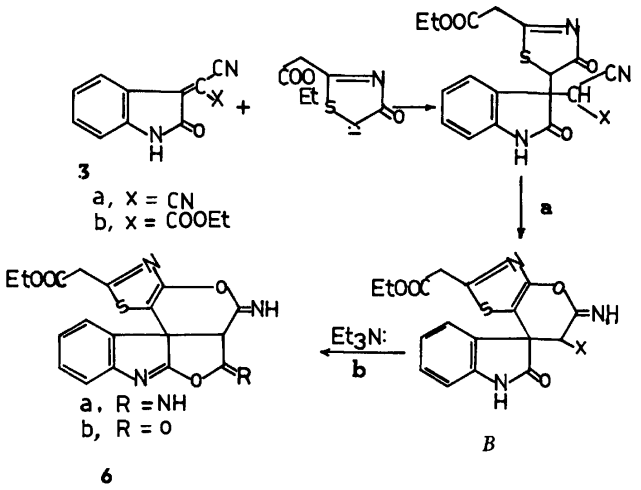

Scheme 2.

The structure of compound **7a** was confirmed by its IR spectrum which showed absorption bands at 3400, 3150 cm^{-1} (NH and NH_2), 2205 cm^{-1} (C≡N), at 1720 cm^{-1} (C=O), and 1650 cm^{-1} (C=N). Moreover, its ^{1}H-NMR spectrum in DMSO gave further confirmation which showed the following signals: singlet at δ 1.6 (s, 3H, CH_3 group), multiplet at δ 6.9—7.5 (m, 6H, 4H aromatic protons and NH_2 protons) and two singlets at δ 10.6 and 12.2 (s, 2H, 2NH proton) (Table 1). Similarly, ^{1}H-NMR spectra of **7b—d**, Table 1 showed the corresponding characteristic signals confirming its assigned structures.

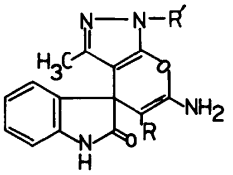

7 a, R = CN; R′ = H
b, R = COOEt; R′ = H
c, R = CN; R′ = Ph
d, R = COOEt; R′ = Ph

Table 1. UV, IR, and ^{1}H-NMR Spectral Measurements for the Compounds **7a—c**

Compound	UV spectra[a] λ_{max}/nm (log ε)	IR (KBr) ν/cm^{-1}	^{1}H-NMR (DMSO)[b,c] δ/ppm
7a	253 (4.18)	3400, 3150(NH, NH_2), 2205(C≡N), 1720(C=O), 1650(-C=N)	1.6(s, 3H, CH_3), 6.9—7.5(m, 6H, 4 aromatic protons, NH_2), 10.6, 12.2(s, 2H, 2NH)
7b	248.5(4.23)	3450, 3300(NH, NH_2), 1750, 1720 (C=O), 1630 (-C=N)	0.9(t, 3H, ester CH_3), 1.2(s, 3H, pyrazole CH_3), 4.0(q, 2H, ester CH_2), 6.9—7.8(m, 6H, 4 aromatic protons and NH_2), 10.8 (s, 2H, 2NH)
7c	246 (4.94)	3440, 3280, 3140(NH, NH_2), 2150 (C≡N), 1695(ring C=O), 1650(-C=N)	1.6(s, 3H, CH_3), 6.8—7.8(m, 11H aromatic and NH_2), 11(s, 1H, NH)
7d	248 (4.91)	3350, 3150(NH, NH_2), br 1720—1690 (ester and ring carbonyl)	1.1(t, 3H, ester CH_3), 1.6(s, 3H, CH_3), 4.1(q, 2H, CH_2), 6.9—7.8(m, 11H, aromatic and NH_2), 11(s, 1H, NH)

a) In absolute ethanol solvent. b) Dimethyl sulfoxide-d_6 solvent. c) s=Singlet, m=multiplet; q=quartet, t=triplet.

Treatment of **3b** with benzoylacetonitrile in ethanol and in the absence of Et_3N to give ethyl 2-amino-3a-[benzoyl(cyano)methyl]-3a*H*-furo[2,3-*b*]indole-3-carboxylate (**8**) (through an addition and cyclization mechanism on the same bases as that suggested in Scheme 1.

The structure of compound **8** was elucidated by its IR spectrum which showed broad band at 3500—3000 cm^{-1} for NH_2 group, 2205 cm^{-1} for CN, and 1740, 1710 cm^{-1} for C=O groups of ester and of ketone, respectively.

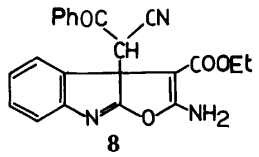

8

The biological activity of the new compounds thus obtained is still under study and will be published elsewhere.

Experimental

Melting points are uncorrected. IR spectrum (KBr) were recorded on Shimadzu 408 Spectrophotometer. ^{1}H-NMR spectra were recorded on EM-390, 90 MHz and A-60, 60 MHz Spectrometer.

General Procedure. Isatin (0.1 mol) or its derivatives was treated under reflux in ethanol (40 ml) with 0.1 mol of the reagent in the presence of two drops of Et_3N/ and in the absence of Et_3N for 1 h, left to cool then filtered. The solid thus obtained was crystallized from the proper solvent.

3-(1-Amino-2-cyano-2-ethoxycarbonylethenyl)-2*H*-furo(2,3-*b*)-indol-2-one (2). It is obtained as red crystals from DMF, mp 270 °C; yield is ca. 60%. Found: C, 62.2; H, 3.5; N, 13.8%. Calcd for $C_{16}H_{11}N_3O_4$: C, 62.13; H, 3.55; N, 13.59%.

Diethyl 3-Amino-4-(2-amino-3-cyano-4-quinolylcarbonyl)-2-cyano-2-pentenedioate (4). It is formed as yellow crystals from acetone mp 258 °C; yield is ca; 80%. Found: C, 59.9; H, 4.4; N, 16.5%. Calcd for $C_{21}H_{19}N_5O_5$: C, 59.8; H, 4.5; N, 16.6%.

Diethyl 3-Amino-4-(2-amino-3-cyano-3a*H*-furo[2,3-*b*]indol-3a-yl)-2-cyano-2-pentenedioate (5). It is obtained by evaporation of the acetone mother liquor of the product **4** crystallization, then poured onto water to give a solid product which crystallized from dilute ethanol as brown crystals, mp 160 °C; yield is ca. 20%. Found: C, 59.80; H, 4.5; N, 16.4%. Calcd for $C_{21}H_{19}N_5O_5$: C, 59.85; H, 4.51; N, 16.6%.

Ethyl 5,6-Diimino-thiazolo[4,5-*b*]pyrano[4′,5′-*c*]furo[2″,3″-*b*]indole-2-acetate (6a). It is isolated as red crystals from DMF-H_2O, mp 300 °C, yield is ca. 80%. Found: C, 56.29; H, 3.5; N, 14.5%. Calcd for $C_{18}H_{14}N_4O_4S$: C, 56.51; H, 3.66; N, 14.65%.

Ethyl 5-Imino-thiazolo[4,5-*b*]pyrano[4′,5′-*c*]furo[2″,3″-*b*]indole-6-one-2-acetate (6b). It is formed as red crystals of mp 280 °C from DMF-H_2O, yield is ca. 70%. Found: C, 56.5; H, 3.5; N, 10.8%. Calcd for $C_{18}H_{13}N_3O_5S$: C, 56.39; H, 3.39; N, 10.96%.

6′-Amino-5′-cyano-3′-methylspiro[indoline-3,4′(1′*H*)-pyrano-[2,3-*c*]pyrazol]-2-one (7a). It is formed as colorless crystals from acetone, mp 275 °C; yield is ca. 70%. Found: C, 61.8; H, 4.0; N, 23.85%. Calcd for $C_{15}H_{11}N_5O_2$: C, 61.6; H, 3.75; N, 23.89%.

Ethyl 6′-Amino-3′-methyl-2-oxospiro[indoline-3,4′(1′*H*)-pyrano[2,3-*c*]pyrazole]-5′-carboxylate (7b). It is obtained from acetone as colorless crystals of mp 212 °C; yield is ca. 72%. Found: C, 60.3; H, 4.6; N, 16.7%. Calcd for $C_{17}H_{16}N_4O_4$: C, 60.0; H, 4.7; N, 16.5%.

6′-Amino-5′-cyano-3′-methyl-1′-phenylspiro[indoline-3,4′(1′*H*)-pyrano[2,3-*c*]pyrazole]-2-one (7c). Obtained as colorless crystals from acetone, mp 220 °C, yield 70%. Found: C, 68.1; H, 3.9; N, 18.88%. Calcd for $C_{21}H_{15}N_5O_2$: C, 68.29; H, 4.06; N, 18.96%.

Ethyl 6′-Amino-3′-methyl-2-oxo-1′-phenylspiro[indoline-3,4′-(1′*H*)-pyrano[2,3-*c*]pyrazole]-5′-carboxylate (7d). It is isolated as pale yellow crystals from acetone, mp 205 °C; yield is ca. 83%. Found: C, 66.6; H, 5.0; N, 13.4%. Calcd for $C_{23}H_{20}N_4O_4$: C, 66.34; H, 4.8; N, 13.46%.

Ethyl 2-Amino-3a[benzoyl(cyano)methyl]-3a*H*-furo[2,3-*b*]indole-3-carboxylate (8). It is obtained as brown crystals from acetone, mp 218 °C, yield is 67%. Found: C, 68.6; H, 4.3; N, 10.69%. Calcd for $C_{22}H_{17}N_3O_4$: C, 68.2; H, 4.3; N, 10.8%.

Thanks are due to Professor Dr. Y. S. Mohammed, Department of Chemistry, Faculty of Science, El-Minia University, for his valuable discussions.

References

1) A. Lacassagne, N. P. Buu-Hoi, F. Zajdela, and N. D. Xuong, *Bull. Cancer*, **42**, 3 (1955).

2) P. Bigot, G. Saint-Ruf, and N. P. Buu-Hoi, *J. Chem. Soc., Perkin Trans. 1*, **1972**, 2573.

3) P. W. Walter, *Chem. Ber.*, **34**, 1320 (1902).

4) A. M. Fahmy, M. Z. A. Badr, Y. S. Mohammed, and F. F. Abdel-Latif, *J. Heterocycl. Chem.*, **21**, 1233 (1984).

5) D. H. Williams and I. Fleming, "Spectroscopic Methods in Organic Chemistry," 2nd ed (1973), p. 136.

6) R. Silverstein, "Spectroscopic Identification of Organic Compounds," John Wiley and Sons, London (1963), p. 168.

 © 1986 The Chemical Society of Japan Bull. Chem. Soc. Jpn., 59, 1239—1243 (1986)

Reaction of Azomethine *N*-Oxides. III.[1] Reactions of Some Azomethine *N*-Oxides with Fluoranil, Phenyl Vinyl Sulfone, and β-Nitrostyrene

Ahmed Moukhtar Nour El-Din
Chemistry Department, Faculty of Science, El-Minia University, El-Minia, Egypt
(Received December 22, 1984)

Isomerization of 3*H*-indole 1-oxides in the presence of tetrafluoro-2,5-cyclohexadiene-1,4-dione (fluoranil) to the thermodynamically more stable lactams was found to proceed via formation of charge-transfer complexes. However, addition of fluoranil to some open chain nitrones did not give the corresponding amides. Both electron-deficient β-nitrostyrene and phenyl vinyl sulfone did not form charge-transfer complexes with nitrones, but instead they undergo 1,3-dipolar cycloaddition giving 4- or 5-substituted isoxazolidines.

Döpp et al.[2,3] have shown that electron-deficient nitriles, ethentetracarbonitrile (TCNE) or oxiranetetracarbonitrile (TCNO) accelerate isomerization of the 3*H*-indole 1-oxide (**1a**) into the lactam (**3a**). Two reaction pathways for this isomerization were postulated.[2,3] The first is the cycloaddition of the nitrone (**1a**) with the cyano group of TCNE or TCNO, followed by fission of the cycloadduct and 1, 2-oxygen migration. The second is the complexation of the 3*H*-indole 1-oxide (**1a**) with the electron-deficient compounds followed by oxygen and hydrogen atoms shifts.[3]

We have recently reported[4–6] that nitrones form charge-transfer complexes with various electron-deficient compounds such as TCNE and 2,3-dichloro-5,6-dicyano-*p*-benzoquinone (DDQ). This result has urged us to investigate[2,3] about formation and chemical behavior of the complexes between the 3*H*-indole 1-oxides (**1a,b**) and the electron-deficient fluoranil (**2**), together with some analogous reaction systems.

Additions of **1a** and **1b** to equimolar quantities of fluoranil (**2**) in dichloromethane at room temperature have given rise to greenish orange colored solutions, which show two absorption shoulders in the visible region at λ_{max} 490 and 505 nm for **1a** and **1b**, respectively (Table 1). These two absorptions are due to complexation[4–6] between each of the 3*H*-indole 1-oxides (**1a**·or **1b**), and the electron-deficient fluoranil. The decomposition of the charge-transfer complexes by heating has led to the thermodynamically more stable lactams (**3a,b**).[7,8] The structures of the lactams (**3a,b**) were varified by both the relevant physical and spectrometric data given in Tables 1 and 2. This result implies that the formation of the charge-transfer complexes between each of 3*H*-indole 1-oxides (**1a,b**) and fluoranil is the first step in the isomerization of **1a** and **1b** to the lactams (**3a,b**). Since the fluoranil does not contain any cyano group, the suggestion[2,3] of the cycloaddition of the 3*H*-indole 1-oxides (**1a,b**) with cyano group in the electron-deficient nitrile compounds can be ruled out. Instead, the too fast isomerization[2] of the 3*H*-indole 1-oxide (**1a**) into the lactam (**3a**) in the presence of TCNE can be attributed to the higher electron affinity of the TCNE compared with that of fluoranil.[9]

The formation of the lactams (**3a,b**) are likely to take place via formation of charge-transfer complexes (**4a,b**) and removal of one electron out of the highest occupied molecular orbital (HOMO) of the 3*H*-indole 1-oxides (**1a,b**). Such an electron transfer facilitates the migration of the oxygen atom from the nitrogen atom to the α-carbon atom, which is followed by an 1,2-hydrogen shift and additional bond reorganization (Fig. 1).

On addition of equimolar quantity of the pyrrole 1-oxide (**12**) to fluoranil in dichloromethane, a pale yellow color developed, and no band for charge-transfer complex was observed in the spectra of the pale yellow solution obtained. Heating of this mixture did not lead to the formation of the corresponding lactam, instead the starting compounds **12** and **2** were recovered. This result reinforces the suggestion that, the rearrangement of the indole 1-oxides (**1a,b**) to lactams (**3a,b**) proceeds via charge-transfer complex formation.

Table 1. Maximum Absorption Wavelengths λ_{max}/nm of Change-Transfer Complexes Formed between the Nitrones (**1a**, **b**; **8a**, **b**, **c**, **d**) and Tetrafluoro-2,5-cyclohexadiene-1,4-dione (**2**) in Dichloromethane at 25 °C

Nitrone	UV-VIS absorption band λ/nm
5,7-Di-*t*-butyl-3,3-dimethyl-3*H*-indole 1-Oxide (**1a**)	490 sh
3,3-Dimethyl-6-*t*-butyl-3*H*-indole 1-Oxide (**1b**)	505 sh
N-(2-Methylbenzylidene)aniline *N*-Oxide (**8a**)	482 sh
N-(3-Methylbenzylidene)aniline *N*-Oxide (**8b**)	475 sh
N-(2,4-Dimethoxybenzylidene)aniline *N*-Oxide (**8d**)	498
N-(3,4-Dimethoxybenzylidene)aniline *N*-Oxide (**8e**)	491

Table 2. Physical and Analytical Data of the Reaction Products of Nitrones (**1a, b**), (**8a—c**), and (**12**) with Tetrafluoro-2,5-cyclohexadiene-1,4-dione, β-Nitrostyrene and Phenyl Vinyl Sulfone

Compound	Yield %	Mp (θ_m/°C) (Recryst. from)	Mol formula	Found (Calcd) (%) C	H	N
5,7-Di-*t*-butyl-3,3-dimethyl-2-indolinone (**3a**)[7]	88	240—241 (Ethanol)	$C_{18}H_{27}NO$	79.18 (79.07	9.90 9.95	5.26 5.12)
3,3-Dimethyl-6-*t*-butyl-2-indolinone (**3b**)[8]	72	195—196 (Cyclohexane)	$C_{14}H_{19}NO$	77.51 (77.38	8.87 8.81	6.40 6.45)
N-(2,4-Dimethoxybenzylidene)aniline *N*-Oxide (**8d**)	69	84—86 (Benzene-hexane)	$C_{15}H_{15}NO_3$	70.21 (70.02	5.75 5.88	5.31 5.45)
N-(3,4-Dimetoxybenzylidene)aniline *N*-Oxide (**8e**)	62	74—76 (Ethanol-hexane)	$C_{15}H_{15}NO_3$	70.12 (70.02	5.76 5.88	5.34 5.45)
2,5-Diphenyl-3-(2-methylphenyl)-4-nitroisoxazolidine (**10a**)	85	75—76 (Ethanol)	$C_{22}H_{20}N_2O_3$	73.20 (73.31	5.51 5.59	7.62 7.77)
2,5-Diphenyl-3-(3-methylphenyl)-4-nitroisoxazolidine (**10b**)	91	90—92 (Ethanol)	$C_{22}H_{20}N_2O_3$	73.22 (73.31	5.48 5.59	7.64 7.77)
3-(4,4-Dimethylaminophenyl)-2,5-diphenyl-4-nitroisoxazolidine (**10c**)	78	103—105 (Benzene-hexane)	$C_{23}H_{23}N_3O_3$	70.88 (70.93	5.89 5.95	12.21 12.32)
3-(2-Methylphenyl)-2-phenyl-4-(phenylsulfonyl)isoxazolidine (**14a**)	89	112—114 (Ethanol-hexane)	$C_{22}H_{21}NSO_3$	69.55 (69.63	5.47 5.58	3.51 3.69)
3-(3-Methylphenyl)-2-phenyl-4-(phenylsulfonyl)isoxazolidine (**14b**)	82	87—89 (Ethanol-hexane)	$C_{22}H_{21}NSO_3$	69.58 (69.63	5.52 5.58	3.54 3.69)
6,6-Dimethyl-2,3,3a,4,5,6-hexahydro-5-phenyl-2-(phenylsulfonyl)pyrrolo-[1,2-*b*]isoxazole (**15**)	87	173—174 (Ethanol-hexane)	$C_{20}H_{23}NSO_3$	67.16 (67.21	6.39 6.48	3.80 3.92)

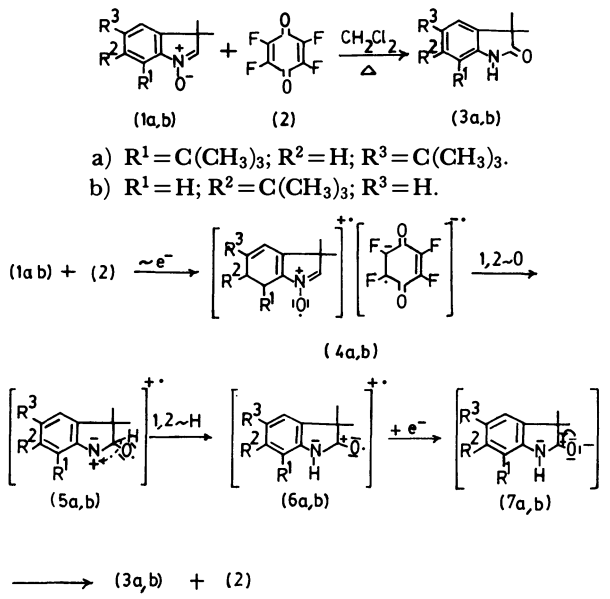

Fig. 1.

A new broad band in the visible spectrum, 475—498 nm, was observed immediately on mixing equimolar solutions of the fluoranil with each of the open chain nitrones (**8a,b,d,e**) in dichloromethatne (Table 1). These absorptions were ascribed to the charge-transfer complexes formation, since neither the fluoranil nor the nitrones (**8a,b,d,e**) alone absorb in this region (Table 1). However, the separation of the mixtures by preparative layer chromatography (PLC) did not give the corresponding amides even after prolonged heating, but the starting materials were recovered. Attempts to isolate these nitrone-fluoranil complexes in crystalline form were failed. These results may suggest that the charge-transfer interaction between the open chain nitrones and fluoranil are weak[9] to undergo rearrangement of **8a—c** to their corresponding amides.

On addition of the electron-deficient β-nitrostyrene (**9**) to each of the nitrones (**8a—c**) in dichloromethane at room temperature, pale yellow colored solutions were obtained, which gave no characteristic absorption band for charge-transfer complexes. This behavior can be ascribed to the relatively low electron affinity of the β-nitrostyrene.[9-11] After heating of the mixture of each of nitrones (**8a—c**) with β-nitrostyrene in toluene, only stable 4-nitroisoxazolidines (**10a—c**) were obtained, regiospecifically. This result is consistent with the

Table 3. Spectroscopic Data of Products Listed in Table 2

Compound	IR $\tilde{\nu}$/cm^{-1} (selected bands)	^{1}H-NMR δ	MS *m/z* (Rel intensity)
3a[7]	3120 (NH), 1711 (CO)	($CDCl_3$): 1.35 (9H, s, $C(CH_3)_3$), 1.40 (15H, s, $C(CH_3)_3$ and $C(CH_3)_2$), 7.15 (2H, dd, *J*=2Hz, phenyl protons), 8.6 (1H, s, NH)	273 (29, M^+), 258 (100), 230 (6)
3b[8]	3177 (NH), 1704 (CO)	($CDCl_3$): 1.31 (9H, s, $C(CH_3)_3$), 1.42(6H, s, $C(CH_3)_2$), 7.06 (3H, m, phenyl protons), 9.8 (1H, s, NH)	217 (60, M^+), 202 (100)
8d	1208 (NO), 1600 (C=N)	($CDCl_3$): 3.85 (6H, s, $2CH_3O$), 6.4—6.7 (1H, m, phenyl proton), 7.2—8.15 (2H, m, phenyl protons), 8.3 (1H, s, CH=N)	257 (50, M^+), 251 (5), 226 (100), 210 (8)
8e	1209 (NO), 1598 (C=N)	($CDCl_3$): 3.95 (3H, s, CH_3O), 3.97 (3H, s, CH_3O), 6.81 (1H, d, *J*=4Hz, phenyl proton), 7.1—7.81 (1H, m, phenyl proton), 7.82 (1H, s, CH=N), 8.85 (1H, d, *J*=1.5Hz, phenyl proton)	257 (5, M^+), 251 (50), 226 (100)
10a	1549 (NO_2)	(C_6D_6): 2.26 (3H, s, CH_3), 3.05 (1H, t, *J*=4Hz, H-4), 3.6 (1H, d, *J*=5Hz, H-3), 3.95 (1H, d, *J*=4Hz, H-5), 6.5—7.9 (14H, m, phenyl protons) ($CDCl_3$): 2.32 (3H, s, CH_3), 5.25 (1H, t, *J*=5Hz, H-4), 5.72 (2H, m, H-3 and H-5), 6.55—7.95 (14H, m, phenyl protons)	360 (42, M^+), 314 (10), 106 (26), 77 (100)
10b	1550 (NO_2)[a]	($CDCl_3$): 2.35 (3H, s, CH_3), 5.35 (1H, t, *J*=5Hz, H-4), 5.58 (1H, d, *J*=4Hz, H-3), 5.75 (1H, d, *J*=6Hz, H-5), 6.65—7.95 (14H, m, phenyl protons)	360 (26, M^+), 314 (9), 106 (22), 77 (100)
10c	1757 (NO_2)	($CDCl_3$): 2.28 (6H, s, $N(CH_3)_2$), 4.0 (1H, t, *J*=8Hz, H-4), 4.82 (1H, d, *J*=9Hz, H-3), 5.25 (1H, d, *J*=8Hz, H-5), 6.85—7.5 (14H, m, phenyl protons)	389 (5, M^+), 283 (10), 240 (10), 106 (20), 77 (100)
14a	1312, 1151 (SO_2)[a]	(C_6D_6): 2.35 (3H, s, CH_3), 3.85 (CH_2, dd, *J*=4 and 8Hz, H-5), 4.35 (1H, dd, *J*=4 and 8Hz, H-4), 5.35 (1H, d, *J*=4Hz, H-3), 6.24—8.05 (14H, m, phenyl protons)	379 (10, M^+), 363 (3), 141 (29), 77 (100)
14b	1305, 1145 (SO_2)	($CDCl_3$): 2.25 (3H, s, CH_3), 4.22 (CH_2, dd, *J*=4 and 7Hz, H-5), 4.41 (1H, dd, *J*=7 and 4Hz, H-4), 4.9 (1H, d, *J*=4Hz, H-3), 6.68—7.95 (14H, m, phenyl protons)	379 (12, M^+), 363 (5), 141 (32), 77 (100)
15	1308, 1142 (SO_2)	($CDCl_3$): 0.75 (3H, s, CH_3), 1.1 (3H, s, CH_3), 1.8—2.8 (3H, m, CH_2-3 and H-4), 3.05—3.6 (2H, m, H-4 and H-5), 3.75—4.45 (1H, m, H-3a), 5.25 (1H, dd, *J*=3 and 9Hz, H-2), 6.95—8.11 (10H, m, phenyl protons)	357 (6, M^+), 341 (2), 187 (29), 170 (17), 141 (35), 77 (100)

interaction between the frontier orbitals of the nitrones and the frontier orbitals of the electron-deficient dipolarophiles.[10,11] The observation of the methine proton signal of the 5-H at δ 5.25—5.75 for the cycloadducts (**10a—c**) respectively (Table 3) is indicative of the methine group being located between an oxygen atom and a nitro group.[10] Moreover, besides the molecular ions at *m/z* 360, 360, and 389 for the products (**10a—c**) respectively, an interesting fragment *m/z* 106 (20—26%), probably for the C_6H_5CHO structure (Table 3) was observed in their mass spectroscopic data. This is another strong evidence confirming the structure of the products, 4-nitroisoxazolidine isomers (**10a—c**).

Treatment of the nitrones **8a,b**, and **12** with phenyl vinyl sulfone (**13**) did not form charge-transfer

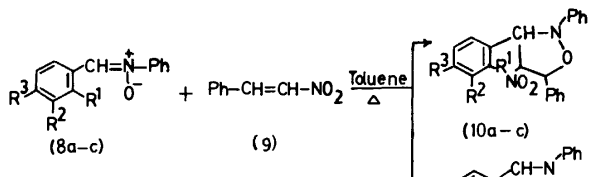

a) $R^1=CH_3$; $R^2=R^3=H$.
b) $R^1=H$; $R^2=CH_3$; $R^3=H$.
c) $R^1=R^2=H$; $R^3=(CH_3)_2N$.
d) $R^1=OCH_3$; $R^2=H$; $R^3=OCH_3$.
e) $R^1=H$; $R^2=OCH_3$; $R^3=OCH_3$.

Fig. 2.

complexes, but instead they undergo 1,3-dipolar cycloaddition reactions giving the cycloadducts (**14a,** b), and (**15**). This behavior can also be attributed to the lower electron affinity of the phenyl vinyl

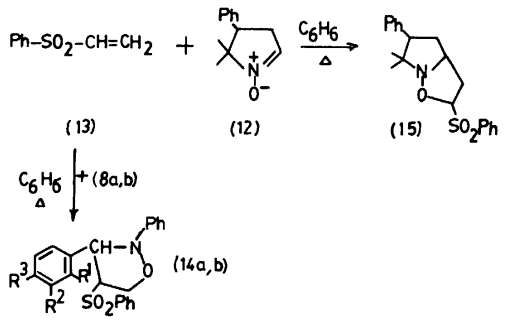

Fig. 3.

sulfone (0.8 eV) than that of fluoranil (0.97 eV).[9,10]

While the reaction of the electron-deficient **13** with the nitrones (**8a,b**) afforded the 4-(phenylsulfonyl)-isoxazolidines (**14a,b**), a dipole highest occupied–dipolarophile lowest unoccupied controlled product, 5-(phenylsulfonyl)isoxazolidine (**15**), a dipole lowest unoccupied–dipolarophile highest occupied controlled product was obtained from the addition reaction of **13** to the nitrone **12**. The reversal of the regioselectivity in the case of the open chain nitrones may be ascribed to their high orbital energies, which favor of the 4-substituted isomers.[10]

The distinction between the 4- and 5-(phenylsulfonyl)isoxazolidines (**14a,b**, and **15**, respectively), was provided by the chemical shift[10] of the methylene protons. The signal for the CH_2 protons of the 4-(phenylsulfonyl)isoxazolidines (**14a,b**) appears at relatively low magnetic field δ 3.85 and 4.22, respectively, while the corresponding signal for the 5-(phenylsulfonyl)isoxazolidine (**15**) occurs at δ 1.18—2.80 (Table 3).

When each of the electron-deficient dipolarophiles (**9** and **13**) was added to the indole 1-oxides (**1a,b**) in dichloromethane (equimolar ratio), the solution turned pale yellow in color. Such solution gave no broad band for charge-transfer complexes. It is plausible to suggest that the results can be ascribed to the low electron affinity of the electron-deficient dipolarophiles (**9** and **13**). Heating of the solutions gave yellow unstable products, which could not be obtained in a pure form.

Experimental

All melting points are uncorrected. IR spectra were recorded (KBr) on a Perkin-Elmer 283 spectrophotometer. UV and visible spectra were measured with a Beckman spectrophotometer model 26. ^{1}H-NMR spectra were recorded on Varian EM-360 (60 MHz) NMR spectrometer using TMS as the standard. Mass spectra were obtained on a MAT 311A spectrometer operating at 70 eV. Elemental analysis were performed by the Microanalytical Unit of Cairo University. The nitrones **1a,b**,[7,12] **8a—e**[13], and **12**[14] were prepared according to literature procedures.

Reaction of Nitrones (1a,b) with Tetrafluoro-2,5-cyclohexadiene-1,4-dione (2). General Procedure: To a solution of **1a** or **1b** (1 mmol) in 5 ml dry dichloromethane, 180 mg (1 mmol) fluoranil was added. The mixture was refluxed for 3 h and then the solvent was evaporated. The residue was chromatographed on a preparative layer chromatography (PLC) of silica gel, using a mixture of benzene–ethyl acetate (9:1) as eluent, to give one zone. Extraction with acetone and recrystallization from the appropriate solvent (Table 2) gave **3a** or **3b**.

Reaction of 5,5-Dimethyl-4-phenyl-Δ^1-pyrroline 1-Oxide (12) with 2. To a stirred solution of 100 mg (0.53 mmol) of **12** in 5 ml dry dichloromethane, 95 mg (0.53 mmol) of **2** in 2 ml of dichloromethane was added. The reaction mixture was refluxed for 12 h and then the solvent was evaporated. The residue was separated on PLC of silica gel, using a mixture of benzene–ethyl acetate (10:1) as eluent, to give two zones. Extraction with acetone and recrystallization from ethanol–hexane gave the starting materials **12** and **2**.

Charge-Transfer Complexes of Nitrones (8a,b,d,e) with 2. To a stirred solution of each of nitrones (**8a,b,d,e**) (0.5 mmol) in dry dichloromethane, 0.5 mmol of **2** in dichloromethane was added. A greenish-orange color appeared. The colored solution was refluxed for 12 h. The solvent was evaporated and the residue was chromatographed on PLC (benzene–ethyl acetate, (10:1). The starting materials, nitrones (**8a,b,d,e**) as well as fluoranil (**2**) were recovered.

Reaction of Nitrones (8a—c) with β-Nitrostyrene (9). Mixture of nitrone (**8a—c**) (1 mmol), β-nitrostyrene (**9**) (1 mmol) and dry toluene (10 ml) was heated to reflux for 12 h. The solvent was evaporated and the residue was separated on PLC (benzene). Extraction with acetone and recrystallization from the proper solvent (Table 2) afforded the products (**10a—c**).

Reaction of Nitrones (8a,b) and (12) with Phenyl Vinyl Sulfone (13). To a solution of each of nitrones (**8a,b**) and **12** (1 mmol) in 10 ml dry benzene, 168 mg (1 mmol) of phenyl vinyl sulfone was added. The reaction mixture was refluxed for 8 h and then the solvent was evaporated. The residue was separated on PLC (benzene) to give one zone. Extraction with acetone and recrystallization from a proper solvent gave the cycloadducts (**14a,b**, and **15**).

Reaction of Nitrones (1a,b) with 9. General Procedure: A solution of **1a** or **1b** (1 mmol) in 4 ml dichloromethane was added to a solution of **9** (1 mmol) in 4 ml dichloromethane. The resulting mixture was refluxed for 24 h. Evaporation of the solvent under reduced presure with rotary evaporator and chromatography of the residue on PLC of silica gel, using a mixture of benzene–ethyl acetate (10:1) as eluent, gave yellow unstable products, which could not be obtained in pure form.

Reaction of Nitrones (1a,b) with 13. Applying the same reaction conditons used for the reaction **1a,b** with **9**, the addition of **1a** or **1b** (1 mmol) to **13** (1 mmol) in dichloromethane gave also unstable products, which could not be identified.

References

1) Part 2. A. M. Nour El-Din, *J. Chem. Res.*, **1984**, 3019.

2) D. Döpp and A. M. Nour El-Din, *Chem. Ber.*, 111, 3952 (1978).

3) D. Döpp, H. Kretz, A. M. Nour El-Din, A. P. Schaap, and S. Anderson, 3rd International Symposium on Organic Free Radicals, Freiburg (1981).

4) A. M. Nour El-Din and A. E. Mourad, *Bull. Soc. Chim. Belg.*, **91**, 539 (1982).
5) A. M. Nour El-Din and A. E. Mourad, *Monatsh. Chem.*, **114**, 211 (1983).
6) A. M. Nour El-Din and A. E. Mourad, *J. Prakt. Chem.*, **325**, 908 (1983).
7) D. Döpp and K. H. Sailer, *Chem. Ber.*, **108**, 301 (1975).
8) D. Döpp, *Chem. Ber.*, **104**, 1043 (1971).
9) R. Foster, "Organic Charge Transfer Complexes," Academic Press, London (1969).
10) J. Sims and K. N. Houk, *J. Am. Chem. Soc.*, **95**, 5798 (1973).
11) K. N. Houk, A. Bimanand, D. Mukherjee, J. Sims, Y. M. Chang, D. C. Kaufman, and L. N. Domelsmith, *Heterocycles*, **7**, 293 (1977).
12) D. Döpp, *Chem. Ber.*, **109**, 3849 (1976).
13) W. Rundel, "Methoden der Organischen Chemie (Houben-Weyl-Müller)," Thieme, Stuttgart (1968) X14, p, 309.
14) J. P. Bapat and D. St. C. Black, *Aust. J. Chem.*, **21**, 2483 (1968).

Synthesis of 2-(Alkyl and Aryl)thiazolo[4,5-*b*]quinoxaline Derivatives and Study of Their Fluorescent Properties

Ravindra Chintaman PHADKE and Dinesh Wamanrao RANGNEKAR*
Dyes Research Laboratory, Department of Chemical Technology,
University of Bombay, Matunga, Bombay-400 019, India
(Received March 18, 1985)

Synthesis of 2-(alkyl and aryl)thiazolo[4,5-*b*]quinoxaline derivatives has been achieved by reacting 2, 3-dichloroquinoxaline derivatives with various thiocarboxylic acid amides. The resulting compounds have been studied for their fluorescent properties. Some of these compounds have been applied as fluorescent dyes on polyester fiber having fair dyeing properties.

In the recent years newer heterocyclic compounds are being synthesised and investigated as dyes and fluorescent brighteners. Quinoxaline derivatives have been described in literature as useful reactive dyes,[1] cyanine dyes,[2] azo dyes,[3] fluorescent dyes,[4,5] and pigments.[6] With the exception of a report of application of 1,4-oxazino[2,3-*b*]quinoxaline as fluorescent brighteners described,[7] there has been no investigation of quioxaline derivatives in the field of fluorescent brighteners.

We report here the synthesis of 2-(alkyl and aryl)-thiazolo[4,5-*b*]quinoxaline derivatives and the study of their fluorescent properties. The 2-(alkyl and aryl)-thiazolo[4,5-*b*]quinoxaline derivatives were synthesized by the reaction of 2,3-dichloroquinoxaline derivative with appropriate thiocarboxylic acid amides in refluxing *N*,*N*-dimethylformamide. The compounds **IIIa** and **IIIb** were obtained from thioacetamide and 4-methoxythiobenzamide, respectively. The products obtained were characterized by elemental anlyses and superimposable infrared spectra. The compound **IIIa** was further confirmed by recording its mass spectrum which showed molecular ion peak (*m/z*) at 201 corresponding to the molecular weight of **IIIa**. The compound **IIIb** was further confirmed by recording its ^{1}H NMR in trifluoroacetic acid: singlet at δ 3.95 (3H) corresponding to $-OCH_3$ group and multiplet δ 7.6—8.05 (4H) corresponding to all the aromatic protons.

The compounds **IIIa** and **IIIb** did not possess strong fluorescence. In order to obtain compounds which have stronger fluorescence, it was intended to prepare derivatives of **IIIa** and **IIIb** and observe the changes in the fluorescence properties. It is known that incorporation of certain groups in a given compound increases its possibility of enhancing fluorescence. An amino group in appropriate position is many a times helpful. It was, therefore, proposed to synthesise compounds with an amino group at the 7-position of the thiazolo[4,5-*b*]quinoxaline.

The 7-amino derivatives of **IIIa** and **IIIb** were prepared via its 7-nitro derivatives. The 7-nitro derivatives **IIIc** and **IIId** were prepared by reaction of 2,3-dichloro-6-nitroquinoxaline with thioacetamide and 4-methoxythiobenzamide, respectively, in refluxing *N*,*N*-dimethylformamide. The nitro derivatives were characterized by their elemental

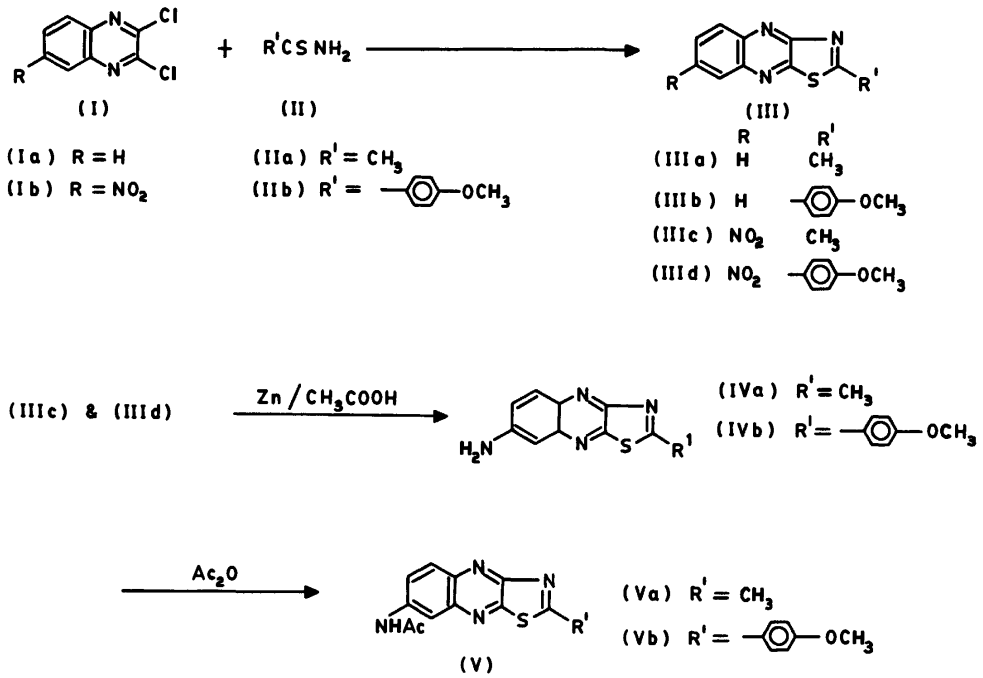

Table 1. Physical Data of 2-(Alkyl and Aryl)thiazolo[4,5-*b*]quinoxaline Derivatives

Compound No.	Yield %	Mp θ_m/°C	Recrystallization Solvent	λ_{max}/nm Absorption	log ε	λ_{max}/nm Emission	Elemental Analysis	C	H	N	S
IIIa	75	355	DMF	384	4.1535	448	Calcd	59.70	3.50	20.90	15.90
							Found	59.95	3.31	21.12	15.79
IIIb	72	357	DMF	385	4.3038	443	Calcd	65.50	3.70	14.30	10.90
							Found	65.39	3.62	14.51	10.73
IIIc	71	220—221	DMF	405	4.1703	471	Calcd	48.80	2.40	22.80	13.00
							Found	49.00	2.27	22.96	13.15
IIId	69	292	DMF	412	4.3102	469	Calcd	56.80	2.90	16.50	9.50
							Found	57.01	2.79	16.63	9.38
IVa	67	336	DMF	376	4.05	447	Calcd	55.60	3.70	25.90	14.80
							Found	55.38	3.63	25.79	14.70
IVb	65	343	DMF	380	4.2945	459	Calcd	62.30	3.90	18.20	10.40
							Found	62.57	3.78	18.06	10.23
Va	78	>360	DMF	368	4.0351	439	Calcd	51.30	4.30	23.90	13.70
							Found	51.12	4.18	23.80	13.56
Vb	73	>360	DMF	359	4.2630	442	Calcd	61.70	4.00	16.00	9.10
							Found	61.56	4.10	16.09	8.96

analyses and their superimposable infrared spectra. The nitro derivatives **IIIc** and **IIId** were subsequently reduced by zinc dust and acetic acid to yield the 7-amino derivatives **IVa** and **IVb**. The compounds **IVa** and **IVb** were characterised by their elemental analyses and infrared spectra (two peaks at 3280 and 3220 cm^{-1} corresponding to the amino group). The absorption maxima showed a shift to the lower wavelength (see Table 1). In order to shift the fluorescent towards the blue region which is desired in the case of fluorescent brighteners, the amino derivatives **IVa** and **IVb** were converted to the *N*-acetyl derivatives **Va** and **Vb** by refluxing in acetic anhydride. The compounds **Va** and **Vb** were characterized by their elemental analyses and infrared spectra (absence of two peaks corresponding to amino group, presence of a peak at 3300 cm^{-1} corresponding to -NH group, and a peak at 1720 cm^{-1} corresponding to the carbonyl group). The emission maxima of these derivatives shifted towards the blue region(see Table 1).

All the compounds synthesised in general showed fluorescence in greenish blue region (439 to 471 nm) (see Table 1). As the compounds were coloured, some of these were applied on polyester fibers as fluorescent dyes. The compounds **IIIc** dyed the fiber in orange red shade whereas **IIIb** and **Va** gave light greenish yellow and pale yellow shades with fair dyeing properties.

Experimental

All melting points are uncorrected. The IR sprctra were recorded on Perkin Elmer-397 spectrophotometer in Nujol mull. The UV and fluorescence spectra were recorded on Beckman Model-25 spectrophotometer and Aminco Bowman spectrophotofluorometer, respectively. The ^1H NMR spectra was recorded on Varian-60 MHz.

2,3-Dichloroquinoxaline,[8] 2,3-dichloro-6-nitroquinoxaline,[9] and 4-methoxythiobenzamide[10] were prepared by the methods reported.

General Procedure of Synthesising Thiazolo[4,5-*b*]-quinoxaline Derivatives (IIIa and IIIb). In a 50ml R.B. flask were placed 2,3-dichloroquinoxaline derivatives (**Ia** and **Ib**) (0.005mol), appropriate thiocarboxylic acid amides (**IIa** and **IIb**) (0.005mol), and *N*,*N*-dimethylformamide (5—7ml). The reaction mixture was refluxed till the reaction was complete (4—5h) (checked by TLC). The reaction mixture was slowly added to ice water mixture when the product precipitated. The yield, mp, and recrystallization solvents are given in the Table 1.

General Procedure of Synthesising 7-Aminothiazolo[4,5-*b*]-quinoxaline Derivatives (IVa and IVb). In a 50ml R.B. flask was placed 7-nitrothiazolo[4,5-*b*]quinoxaline (**IIIa** and **IIIb**) (0.005mol). Acetic acid (10ml) and concentrated hydrochloric acid (0.5—1ml) were subsequently added. The reaction mixture was stirred and slowly heated so that the temperature was 80°C. To this hot reaction mixture, zinc dust (0.006mol) was added in portions over a period of 30—45 min. At the end of the addition the contents were refluxed (115—112°C) under stirring for 3—4h, till the reaction was complete (checked by TLC). The reaction mixture was then filtered hot and after cooling the filtrate was slowly added to a stirred ice-water mixture. The product was filtered, washed thoroughly with water, and dried. The yield, mp, and recrystallization solvents are given in the Table 1.

General Procedure of 7-Acetamidothiazolo[4,5-*b*]quinoxaline Derivatives (Va and Vb). The 7-aminothiazolo[4,5-*b*]-quinoxaline (**IVa** and **IVb**) (0.005mol) was placed in a R.B. flask, and to this acetic anhydride (2—3ml) and acetic acid (1—2ml) were added. The reaction mixture was heated in an oil bath so that it gently refluxed. The reaction mixture was refluxed for 3—4h till the reaction was complete (checked by TLC). On cooling the reaction mixture was slowly poured over ice-water mixtuer with continuous stirring when product precipitated. The compound was filtered, washed with water, and dried. The yield, mp, and recrystallization solvents are given in Table 1.

One of us (R.C.P) is thankful to C.S.I.R., New Delhi for the award of a junior research fellowship and senior research fellowship.

References

1) A. Schweizer, (Sandoz Ltd.), Swiss, 537446, *Chem. Abstr.* **80**, 4905 (1974).

2) C. H. Eldredge and J. D. Mee, (Eastman Kodak Co.), U. S. Patent, 3674782, *Chem. Abstr.*, **77**, 128093 (1972).

3) W. Sauer, A. Seifert, and H. J. Binte, Ger. (East), 101910, *Chem. Abstr.*, **83**, 61643 (1975).

4) U. Eckstein, and H. Theidel, (Bayer A-G), Ger. Offen., 2730644, *Chem. Abstr.*, **90**, 153494 (1979).

5) H.H.Credner, and W. Pneschel, (Agfa-Geveart, A. G.), Ger. Offen., 2109455, *Chem. Abstr.*, **78**, 5406 (1973).

6) L. Wojciechowski, (IPO) Pol., 64713, *Chem. Abstr.*, **79**, 6780 (1973).

7) S. Taihei, and O. Ryohei, *Kogyo Kagaku Zasshi*, **67**, 576 (1964), *Chem. Abstr.* **61**, 9605 (1964).

8) G. W. H. Cheeseman, *J. Chem. Soc.*, **1955**, 1804.

9) J. K. Landquist, *J. Chem. Soc.*, **1953**, 2816.

10) E. C. Taylor, and J. A. Zoltewicz, *J. Am. Chem. Soc.*, **82**, 2656 (1960).

Ab Initio MO Theoretical Studies on Direct Fragmentation of Organic Ions Produced by Electron-Bombardment

Hiroshi ICHIKAWA* and Atsushi SHIGIHARA
Hoshi College of Pharmacy, Shinagawa, Tokyo 142
(Received November 8, 1985)

Synopsis. The possibility of bond-scission within a single vibration (direct fragmentation) in a molecular ion produced by electron-bombardment has been studied. MP2/6-31G* calculations have shown that a direct fragmentation in the ground-state ion is possible for the C–H bonds of hydrocarbons.

So far, fragmentations which are caused by vibrational excitations have been well-studied from both theoretical and experimental standpoints. Much knowledge about such fragmentations has been accumulated and it is recognized that most fragmentations take place in the ground electronic state, consuming a lot of time (more than 10^{-13} s).[1] However, we do not have any information on fragmentation within a single vibration, termed direct fragmentation. It is uncertain whether direct fragmentation actually occurs. However, an apparent difference in the mass spectra between lower and higher ionization energies suggests the existence of direct fragmentations. Such a difference is not a proof.

The electron-impact (EI) ionization takes place by a resonance between the wave of an electron in a molecule and that of an impinging electron; those electrons are indistinguishable. Therefore, any kind of excited state can possibly take place during electron-bombardment. Two types of direct fragmentation are possible according to the Franck-Condon principle: A direct fragmentation at the ground electronic state and that due to antibonding states (Fig. 1). We examined the former case using the second order Mϕller-Plesset perturbation method[2] based on the 6-31G* basis set[3] (MP2/6-31G*).[4]

Previous work on intramolecular rearrangements in smaller systems has indicated that relative energies (including up to third order of Mϕller-Plesset perturbation (MP3)) are in good agreement (less than 5 kJ mol^{-1}) with the results of a full coupled-cluster calculation.[5] We estimate a similar error for a MP2/6-31G* calculation, since it is shown that the difference of the effect of electron correlation between MP2 and MP3 are almost the same.[6]

The investigation method for the ground-state process is rather straightforward since it is sufficient to consider the potential energies referring to the potential energy curves of the molecule and the ions in the ground state, whatever the process is (see Fig. 1).

Most molecules are in the ν_0 state (the ground vibrational state) while maintaining a near-equilibrium distance (r_0). Vertical ionization reaches the point p_0 of the ground-state potential-energy curve of the molecular ions. If the potential energy at $p_0(V_0)$ is higher than that after dissociation (V_∞), i.e. ΔV ($=V_0-V_\infty$) is positive, ions can possibly undergo ground state direct fragmentation; if ΔV is negative,

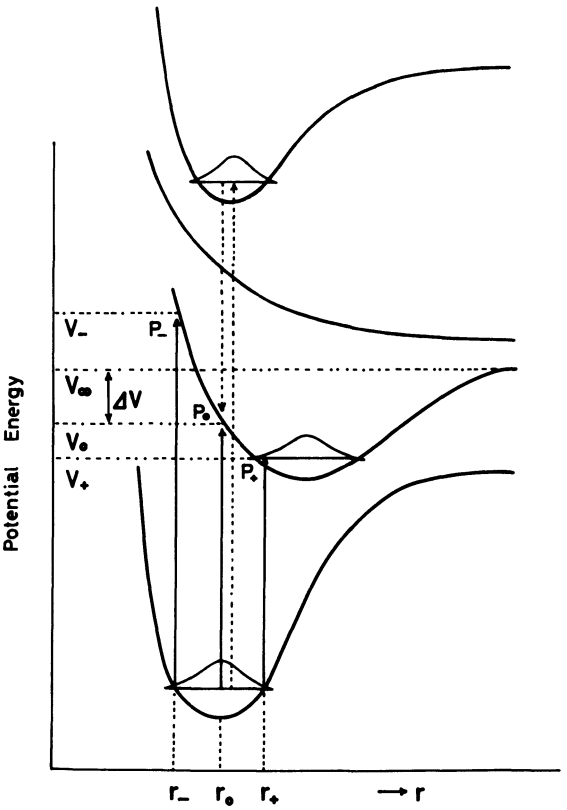

Fig. 1. The Franck-Condon principle of vertical ionization of molecule.

direct fragmentation can not take place. However, the latter case does not always mean that direct fragmentation never occurs. Although it is a small possibility, there is a chance that a molecule can be ionized at a shorter distance. If the potential energy at $p-$ ($V-$) is higher than V_∞, direct fragmentation can occur.

Figure 2 shows the results for hydrogen fluoride. The equilibrium distance of the ground-state ion is increased by about 0.1 Å from that of the molecular state. The vertical ionization at the equilibrium distance reaches a PE of −99.610387 au; this is lower than the energy after dissociation (−99.487271 au). Therefore, it may be concluded that ground-state direct fragmentation does not take place.

Figure 3 shows the case for methane. The PE curve for the ion is that of a C_{3v} adiabatic fragmentation, the lowest for a CH cleavage. It has a potential minimum at a very long distance (1.3280 Å).[7] Ionization at the equilibrium distance of the molecule gives a PE (−39.816667 au) which is higher than that after dissociation (−39.823607 au). Therefore, direct fragmentation is possible by ionization. It should be, however, stressed that this does not always mean that

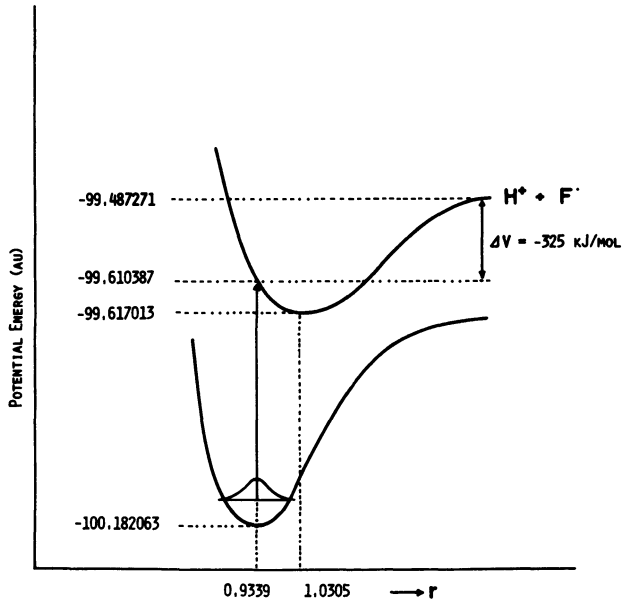

Fig. 2. Potential energy curves of the hydrogen fluoride ion and molecule by MP2/6-31G*.

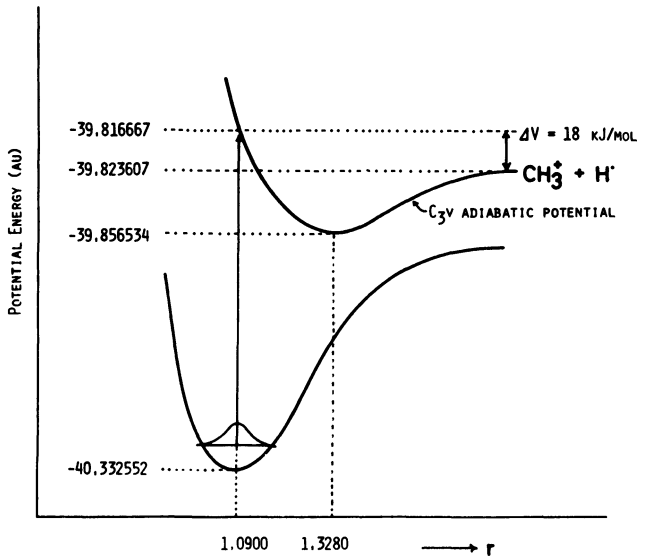

Fig. 3. Potential energy curves of the methane ion and molecule by MP2/6-31G*.

the appearance potential of a methyl cation is lower than that of a methane ion.[8]

Table 1. The ΔV Values and Appearance Potentials by MP2/6-31G*

Compound	ΔV	$Ap^{calcd\ a)}$	$Ap^{expl\ b)}$
	kJ/mol	(eV)	(eV)
$H\text{-}C_2H_5$	73	12.1	12.7
$CH_3\text{-}CH_3$	−76	13.6	13.5
$H\text{-}CH_2OH$	−15	11.0	11.7
$H\text{-}CH_2NH_2$	−13	9.5	10.3
$C_2H_5\text{-}NH_2$	−254	11.7	13.5
$CH_3\text{-}CH_2NH_2$	−30	9.4	9.7

a)Zero-point energies are not corrected. b)Appearance potentials are taken from Ref. 9.

In a similar way, we obtained results for some other compounds (summarized in Table 1). As references, the calculated and experimental[9] appearance potentials are listed in addition to the ΔV values. The positive ΔV values suggest a possible direct fragmentation. It is well known that the C–C bond in an ethylamine ion is easily broken under the EI condition; however, the present results show that such a cleavage is not a direct fragmentation. Consequently, it can be said that a direct fragmentation in the ground electronic state is possible in the CH bonds of hydrocarbons.

References

1) The works of Mass spectrometry have been periodically reviewed and recorded in "Mass Spectrometry," Vol. 1—7, The Chemical Society, London.

2) C. Møller and M. S. Plesset, *Phys. Rev.*, **46**, 618 (1934).

3) P. C. Hariharan and J. A. Pople, *Theoret. Chim. Acta*, **28**, 213, (1973).

4) We have used the GAUSSIAN-80H program (Hitac version of GAUSSIAN-80 (QCPE 437, 1982)) at the Computation Center of the University of Tokyo. Geometry optimization has been carried out by the Fletcher-Powell procedure (R. Fletcher and M. J. D. Powell, *Comput. J.*, **6**, 163 (1963)). The thresholds of bond-length and angle are 0.0003 Hartree/Bohr or radian in terms of force.

5) J. A. Pople, R. Krishnan, H. B. Schlegel, and J. S. Binkley, *Int. J. Quantum Chem.*, **14**, 545 (1978).

6) R. H. Nobes, W. R. Rodwell, W. J. Bouma, and L. Radom, *J. Am. Chem. Soc.*, **103**, 1913 (1981).

7) The bond length of the three equivalent C–H bonds is determined as 1.0965 Å.

8) The appearance potentials of CH_4^+ and CH_3^+ are observed at 12.7 eV and 14.3 eV, respectively.

9) H. M. Rosenstock, K. Draxl. B. W. Steiner, and J. T. Herron, *J. Phys. Chem. Ref. Data*, **6**, Suppl. 1 (1977).

Synthesis and Properties of Manganese(III) Complex of Salen-Analog Containing Phenolic Pendant Group

Wakako KANDA
Laboratory of Chemistry, Kyushu Institute of Design, 4-9-1 Shiobaru, Minami-ku, Fukuoka 815
(Received October 8, 1985)

Synopsis. A manganese(III) complex, [Mn(sal-pen)], with *N,N'*-disalicylidene-2-methyl-4-(2-hydroxy-5-methylphenyl)-1,2-butanediaminate trianion (sal-pen^{3-}) has been synthesized and characterized. The complex was shown to have a square-pyramidal structure with a pendant phenolate group at the apex. The electronic spectral and electrochemical properties of the complex are discussed in terms of an axial coordination of the phenolate group.

The salen-analog, composed of a planar N_2O_2-donating system and a pendant phenolic group, *N,N'*-disalicylidene-2-methyl-4-(2-hydroxy-5-methylphenyl)-1,2-butanediamine (H_2(sal-Hpen), Fig. 1), functions as a pentadentate ligand to yield iron(III) and cobalt(III) complexes, [M(sal-pen)], with a deprotonated pendant phenolic oxygen at the apical position.[1] In general, iron(III) and cobalt(III) complexes with unidentate phenolic ligands readily undergo dissociations of the phenolate groups. On the other hand, it has been shown that [Co(sal-pen)] is very stable in nondonating solvents[2] and [Fe(sal-pen)] is stable even in alcohols.[3] The stabilities of these complexes in solutions are probably due to a chelating effect of the pendant phenolate group combined at the ethylene backbone of the salen skelton.

In this study, a manganese(III) complex of H_2(sal-Hpen) was prepared and its chemical properties were examined in view of the axial coordination of the pendant phenolic group.

The synthesis of [Mn(sal-pen)] was as follows: an ethanolic solution (10 cm^3) of manganese(II) acetate tetrahydrate (0.3 g) was added to an ethanolic solution (10 cm^3) of H_2(sal-Hpen)[1] (0.5 g) and sodium hydroxide (0.1 g) under a nitrogen atmosphere. The resulting pale-orange solution was then stirred for 3 h in the open air. The color of the solution immediately changed from orange to brown. Then, the solvent was evaporated at room temperature to give brown prisms, which were recrystallized from dichloromethane. The yeild was ca. 0.2 g.

Found: C, 62.35; H, 5.52; N, 5.09%. Calcd for $C_{26}H_{25}N_2O_3Mn \cdot 2H_2O$: C, 61.90; H, 5.79; N, 5.55%.

[Mn(salen)Cl] and [Mn(salen)OAc] were prepared by methods described in the literature.[4,5]

The effective magnetic moment of [Mn(sal-pen)] is 4.7 BM at room temperature; this corresponds to the value of high-spin manganese(III) complexes (4.7—5.0 BM).[6] A small temperature dependance of the moment in the range 80—300 K suggests a monomeric structure for the complex.

[Mn(sal-pen)] exhibits no IR band which can be attributed to an O–H vibration around 3200—3300 cm^{-1}. However, H_2(sal-Hpen), [Cu(sal-Hpen)], and [Ni(sal-Hpen)] show an O–H vibration in this region.[1] This suggests that the phenolic O–H in the pendant

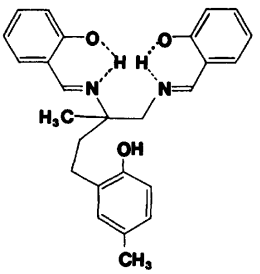

Fig. 1. The chemical structure of H_2(sal-Hpen).

group becomes deprotonated and coordinated to the metal. By an analogy of the IR spectrum with those of [Fe(sal-pen)] and [Co(sal-pen)], which possess a pentacoordinate structure with an N_2O_2-donating system at the equatorial plane and a phenolic oxygen at the apical site, [Mn(sal-pen)] is presumed to have a square-pyramidal structure with a phenolic oxygen at the apex.

The electronic spectrum of [Mn(sal-pen)] in dichloromethane (1×10^{-3} mol dm^{-3}) exhibits absorption bands at 20.6×10^3 (ε 1450), 25.0×10^3 (3850), 32.3×10^3 (16400), 35.7×10^3 (19200), and 43.5×10^3 (40300) cm^{-1}. The spectrum resembles those of pentacoordinate [Mn(salen)Cl] and [Mn(salen)OAc] with a chloride ion or an acetate ion at the apical site.[7] Molar conductivity measurements revealed these Mn complexes to be nonelectrolyte in dichloromethane. Thus, [Mn(sal-pen)] is presumed to have a square-pyramid geometry with a pendant phenolic group at the apex. According to these results, the lowest energy band (20.6×10^3 cm^{-1}) of [Mn(sal-pen)] can be assigned to the d-d band and the absorption at 25.0×10^3 cm^{-1} to the charge-transfer band.[7,8] The electronic spectrum of [Mn(sal-pen)] in methanol differs markedly from that in dichloromethane. This suggests a dissociation of the pendant group in polar methanol.[4]

The electrochemical properties of [Mn(sal-pen)] were investigated in comparison with those of [Mn(salen)Cl] and [Mn(salen)OAc] by means of polarography and cyclic voltammetry in dichloromethane. A three-electrode cell with a glassy carbon electrode as the working electrode, a platinum coil as the auxiliary electrode, and a saturated calomel electrode as the reference electrode was used for measurements. Tetrabutylammonium perchlorate was used as the supporting electrolyte. All the potentials were normalized using ferrocene as the internal standard (V vs. F_c/F_c^+).[9] The electrochemical results are shown in Fig. 2.

[Mn(sal-pen)] exhibits an irreversible wave at +0.32 V and a quasi-reversible wave at −0.76 V. Similar results were obtained for [Mn(salen)Cl] and [Mn(salen)OAc] in this study.[10] The redox wave around

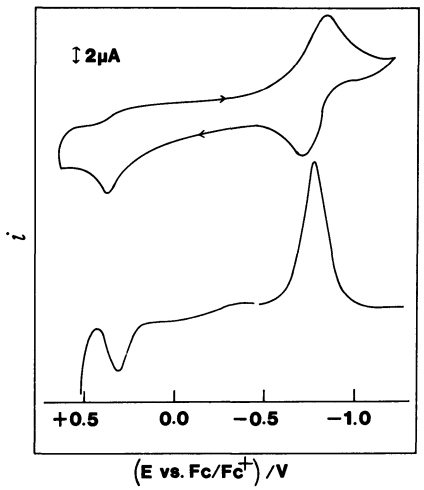

Fig. 2. Cyclic voltammogram (above) and differential pulse polarogram (below) of Mn(sal-pen) in dichloromethane.

−0.7 V was assigned to the Mn(II)/Mn(III) process while the irreversible oxidation at a positive potential was assigned to the Mn(III)/Mn(IV) process.[11–13] There was a slight difference in the Mn(III)/Mn(II) reduction potential among these complexes. The reduction potentials seem to be independant of the axial ligand. This is probably due to the fact that this process is associated with an electron acceptance on the $d_{x^2-y^2}$ orbital and, thus, not substantially influenced by a change in the axial ligand. On the contrary, the Mn(III)/Mn(IV) oxidation potentials are highly dependant upon the axial ligand. This is reasonable since the process involves the release of an electron from the d_{z^2} orbital. This must be much influenced by the charge of the axial ligand. The oxidation of [Mn(sal-pen)] occurred at a considerably lower potential relative to those of [Mn(salen)Cl] and [Mn(salen)OAc]. This suggests that the axial phenolate ligand in [Mn(sal-pen)] donates more strongly than a chloride ion or an acetate ion does.

Manganese(III) complexes with a unidentate phenolate ligand are generally difficult to synthesize because of the high lability of phenolate ligands. The present study reveals that a phenolatomanganese(III) complex can be readily isolated by incorporating a phenolate group into the tetradentate salen moiety.

The author wishes to express her thanks to Associate Professor Hisashi Ōkawa and Professor Shigeo Kida of the University of Kyushu for the magnetic measurement and the helpful discussions.

References

1) W. Kanda, H. Ōkawa, and S. Kida, *Bull. Chem. Soc. Jpn.*, **56**, 3268 (1983).
2) H. Ōkawa, W. Kanda, S. Kida, and K. Nakamoto, *Inorg. Chim. Acta.*, **104**, 77 (1985).
3) W. Kanda, H. Ōkawa, and S. Kida, *Bull. Chem. Soc. Jpn.*, **57**, 1159 (1984).
4) C. P. Prabhakaran and C. C. Patel, *J. Inorg. Nucl. Chem.*, **31**, 3316 (1969).
5) A. Earnshaw, E. A. King, and L. F. Larkworthy, *J. Chem. Soc., (A)*, **1968**, 1048.
6) F. E. Mabbs and D. J. Marchin, "Magnetism and Transition Metal Complexes," Chapman and Hall., London (1973), p. 178.
7) L. J. Boucher and M. O. Farrell, *J. Inorg. Nucl. Chem.*, **35**, 3731 (1973).
8) C. Bellitto, A. A. G. Tomlinson, and C. Furlani, *J. Chem. Soc., (A)*, **1971**, 3267.
9) H. M. Koepp, H. Wendt, and H. Strehlow, *Z. Electrochem.*, **64**, 483 (1960).
10) Redox potentials for [Mn(salen)Cl]: +0.55, −0.69; for [Mn(salen)OAc]: +0.59, −0.72 (V vs. F_c/F_c^+).
11) W. M. Coleman, R. K. Boggess, J. W. Hughes, and L. T. Taylor, *Inorg. Chem.*, **20**, 1253 (1981).
12) T. Matsushita, H. Kono, and T. Shono, *Bull. Chem. Soc. Jpn.*, **54**, 2646 (1981).
13) T. Matsushita and T. Shono, *Bull. Chem. Soc. Jpn.*, **54**, 3743 (1981).

The Structure of Diaquatetrakis(thiocyanato)cobalt(II)mercury(II)-*N*-Methyl-2-pyrrolidone(1/2), $CoHg(SCN)_4(H_2O)_2 \cdot 2(C_3H_6CONCH_3)$

Hisashi KINOSHITA,* Mamoru SHIMOI,† and Akira OUCHI†
Department of Chemistry, Faculty of Liberal Arts, Shizuoka University, Ohya, Shizuoka 422
†Department of Chemistry, College of Arts and Sciences, The University of Tokyo, Komaba, Meguro-ku, Tokyo 153
(Received October 21, 1985)

Synopsis. The crystal and molecular structure of the title complex was determined using the single-crystal X-ray diffraction method. A crystal of $CoHgC_{14}H_{22}N_6O_4S_4$, F.W. 726.15, is tetragonal with a space group $P\bar{4}$, a=12.082(3), c=8.097(2) Å, U=1182.0(5) Å^3, Z=2, D_x=2.04 Mg m^{-3}, and μ(Mo $K\alpha$)=7.72 mm^{-1}. Tetrahedral mercury(II) coordinated with four sulfur atoms and octahedral cobalt(II) coordinated with four nitrogen atoms of SCN^- (equatorially) and two oxygen atoms of H_2O (axially) are linked by thiocyanate bridges to form planar networks parallel to (001). The planes are connected by *N*-methyl-2-pyrrolidone (mpd) molecules through the hydrogen bonds with two coordinated water molecules at both side networks. The structure resembles that of the *N*,*N*-dimethylacetamide (dma) adduct, $CoHg(SCN)_4(H_2O)_2 \cdot 2$dma. These are new types of inclusion compounds.

Cobalt(II), mercury(II), thiocyanate (**1**),[1] and its Lewis-base adducts[2–5] are known to exist in a variety of polymeric structures. Among them, the previously reported *N*,*N*-dimethylacetamide (dma) adduct, $CoHg(SCN)_4(H_2O)_2 \cdot 2$dma (**2**),[5] was regarded as a kind of inclusion compound because dma molecules are maintained between the metal–thiocyanate networks by only the hydrogen bonds to the two ligating water molecules of both planes. The dma molecules are not easily removed, even when they are left standing for a long time in the air.

During the course of our further investigation we synthesized the *N*-methyl-2-pyrrolidone (mpd) adduct shown in the title (**3**). The structure has been determined by an X-ray diffraction analysis using its single crystal.

Experimental

Single-Crystal X-Ray Analysis. Crystals of **3** were obtained as follows: **1** (1.0 g, 2.0 mmol) was dissolved into 20 cm^3 of mpd. To the blue solution, an equal volume of water was added; the color of the solution turned red. After the solution was left standing overnight, precipitated **3** (red-brown in color) was separated. The yield was 1.1 g (74%). Anal. ($CoHgC_{14}H_{22}N_6O_4S_4$) Co, C, H, N.

The crystal was shaped into a sphere (ϕ=0.22 mm). Reflections within the range $3° < 2\theta < 70°$ were studied with a Rigaku AFC-6A automated four-cirle diffractometer using graphite-monochromated Mo $K\alpha$ radiation and the ω—2θ scan technique (scan speed 4° min^{-1}, scan width, 1.35+0.5 tanθ°). The intensities were corrected for Lorentz and polarization factors as well as for absorption. Of the 3082 independent reflections collected, 1751 reflections with $|F_o| > 3\sigma(|F_o|)$ were used for a structure determination. All the calculations were carried out on a HITAC M-280H computer at the Computer Center of the University of Tokyo using the local version of UNICS.[6] The scattering factors were taken from Ref. 7. The final R value[8] for all non-hydrogen atoms (applying the anisotropic temperature parameters) was 0.052. (The R value was 0.053 for the structure with an inverse chirality.)

Results and Discussion

Figures 1 and 2 show projections of the structures of **3** and **2**[5,a] (along the c axis) together with the numbering scheme of the atoms. Perspective drawings around the mpd bridge are given in Fig. 3. The select-

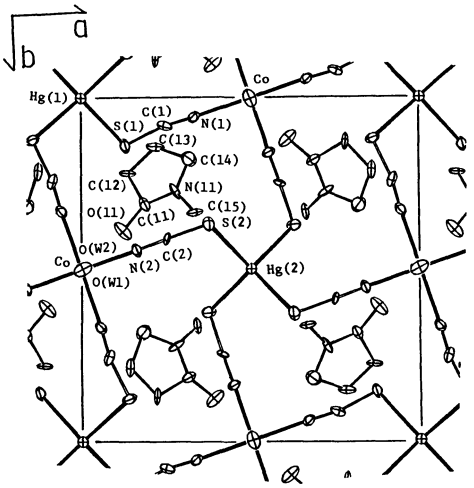

Fig. 1. The projection of the unit cell of **3** along c-axis.

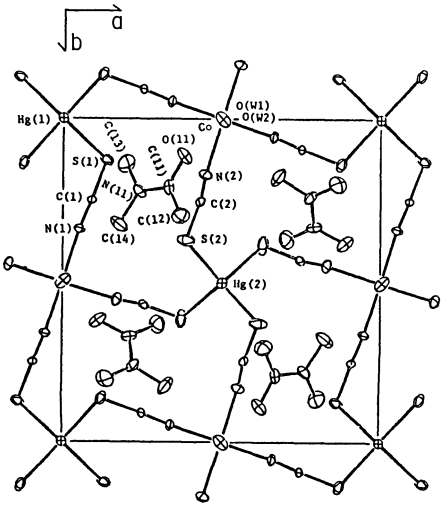

Fig. 2. The projection of the unit cell of **2** along c-axis.[5]

a) For the convenience to compare the respective structures of **2** and **3**, the numbering of some atoms in **2** shown in Ref. **5** is modified.

Table 1. Selected Bond Lengths and Bond Angles with Estimated Standard Deviations in Parentheses

Bond length	l/Å	Bond length	l/Å	Bond length	l/Å
Hg(1)-S(1)	2.535(3)	Co-O(W1)	2.110(9)	C(1)-N(1)	1.115(16)
Hg(2)-S(2)	2.536(4)	Co-O(W2)	2.107(9)	C(2)-N(2)	1.196(14)
Co-N(1)	2.151(10)	S(1)-C(1)	1.634(12)	O(W1)···O(11)	2.694(13)
Co-N(2)	2.068(9)	S(2)-C(2)	1.665(11)	O(W2^{i})···O(11)	2.799(13)
Bond angle	ϕ/°	**Bond angle**	ϕ/°	**Bond angle**	ϕ/°
S(1)-Hg(1)-S(1^{vi})	100.7(1)	N(1^{vi})-Co-N(2)	90.3(4)	Co-N(2)-C(2)	164.0(9)
S(1)-Hg(1)-S(1^{ii})	128.8(1)	N(2)-Co-O(W1)	88.7(4)	S(1)-C(1)-N(1)	170.0(11)
S(2)-Hg(2)-S(2^{iii})	105.5(1)	N(2)-Co-O(W2)	91.3(4)	S(2)-C(2)-N(2)	178.0(10)
S(2)-Hg(2)-S(2^{iv})	117.6(1)	Hg-S(1)-C(1)	101.8(2)	O(W1)···O(11)···O(W2^{i})	89.9(4)
N(1^{vi})-Co-N(1^{iii})	174.1(4)	Hg(2)-S(2)-C(2)	100.4(2)	O(11)···O(W1)···O(11^{v})	92.3(4)
N(2)-Co-N(2^{v})	177.4(4)	Co-N(1^{vi})-C(1^{vi})	170.8(9)	O(11)···O(W2^{i})···O(11^{v})	87.9(4)

Key to the symmetry operations: i, x, y, 1+z; ii, $-x$, $-y$, z,; iii, y, 1$-x$, $-z$; iv, 1$-x$, 1$-y$, z; v, $-x$, 1$-y$, z; vi, $-y$, x, $-z$

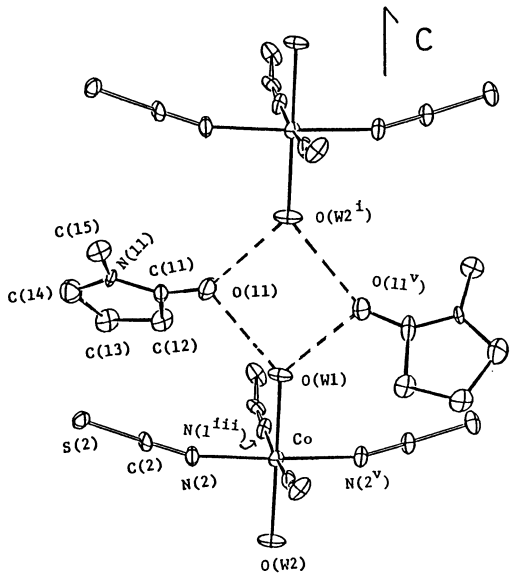

Fig. 3. A perspective drawing of the complex around a cobalt atom and the hydrogen bridging.

ed interatomic distances and bond angles are shown in Table 1.[9] The general feature of the thiocyanate network, as well as the hydrogen-bond bridging, is quite similar to that of **2**. The Hg(1) and Hg(2) atoms are tetrahedrally coordinated by four thiocyanate sulfur atoms, while the cobalt(II) atom is coordinated octahedrally with four thiocyanate nitrogen atoms (equatorially) and two water oxygen atoms (axially). The mpd molecules of **3** are maintained between two thiocyanate networks by only the hydrogen bonds. Thus, we can add **3** as the second member of the **2**-type inclusion compound. The interatomic distances and bond angles of the thiocyanate network, as well as those of the hydrogen-bridging part, are about the same as the corresponding values in **2**, respectively.

The volume of a unit cell of **3** is larger than that of **2** by 13 Å^3.[5] This is because an mpd molecule is larger than a dma molecule. Comparing Figs. 1 and 2, the corresponding position of the carbonyl oxygen atoms of dma and mpd in **2** and **3** are about the same; however, the positions of the other atoms are different, probably to pack dma or mpd molecules into the spaces most effectively. The angles around O(11), the carbonyl oxygen atom, in **2** and **3** are different from each other: O(W1)···O(11)-C(11), O(W1)···O(11)···O(W2^{i}), and O(W2^{i})···O(11)-C(11) are 122.2(9), 89,9(4), and 147.3(10) in **3**, and are 138.9(9), 86.1(4), and 127.7(7)° in **2**,[5] respectively. (The key to the symmetry operation; i,x,y, 1+z.) The Lewis base molecules in **2** or **3** are considered to occupy this space in order to pack the cage of the thiocyanate network well.

Our attempts to obtain the same type of complexes using *N*,*N*-diethylacetamide, *N*,*N*-dimethylpropionamide, *N*-ethyl-2-pyrrolidone, *N*,*N*-dimethylformamide, and *N*-methylformamide as the guests have not yet been successful. To be a guest of this type complex, of course, the formation of the effective hydrogen bonds to bridge it to the network-oxygen atoms is indispensable. Also, there may be some restrictions regarding the shape and the size of the guest molecule to be included into the vacancy of a host.

References

1) J. W. Jeffery and K. M. Rose, *Acta Crystallogr., Sect B*, **24**, 653 (1968).

2) H. Kinoshita, M. Shimoi, and A. Ouchi, *Bull. Chem. Soc. Jpn.*, **58**, 1304 (1985).

3) A. L. Beauchamp, L. Pazdernik, and R. Rivest, *Acta Crystallogr., Sect B*, **32**, 650 (1976).

4) M. R. Udupa and B. Krebs, *Inorg. Chim. Acta*, **42**, 37 (1980).

5) H. Kinoshita, M. Shimoi, A. Ouchi, and S. Sato, *Bull. Chem. Soc.Jpn.*, **58**, 2782 (1985).

6) "The Universal Crystallographic Computation Program-System (UNICS)," ed by T. Sakurai, Crystallographic Society of Japan, Tokyo (1967).

7) "International Tables for X-ray Crystallography," Kynoch Press, Birmingham (1974) Vol. IV, pp. 72, 150.

8) $R=\sum||F_o|-|F_c||/\sum|F_o|$

9) The final atomic and thermal parameters, the final F_o-F_c table and additional data of bond lengths and bond angles are deposited as Document No. 8621 at the Office of the editor of Bull. Chem. Soc. Jpn.

Acid Dissociation Constants of Dialkyldithiocarbamic Acids and *O,O'*-Dialkyl *S*-Hydrogen Dithiophosphates and Formation Constants of Their Complexes with Cadmium(II), Zinc(II), and Lead(II) in 1:1 v/v Water-DMF Medium

Kenjiro HAYASHI,* Yoshiaki SASAKI, Shoji TAGASHIRA, and Takagimi YANAGIDANI
Department of Chemistry, Faculty of Science, Yamaguchi University, Yoshida, Yamaguchi 753
(Received October 23, 1985)

Synopsis. The log values of β_3, the formation constants of metal complexes with dialkyldithiocarbamates and *O,O'*-dialkyl dithiophosphates, were determined by polarography. The pK_a values, the acid-dissociation constants of these ligands, were also determined kinetically. A linear relationship exists between these two variables for each metal and straight parallel lines were obtained.

Dithio-acids such as alkylxanthic acids (*O*-alkyl hydrogen dithiocarbonates, HRxan), dialkyldithiocarbamic acids (HR_2dtc), and *O,O'*-dialkyl *S*-hydrogen dithiophosphates (HR_2dtp) are chelating reagents which coordinate to metal ions through two sulfur atoms and have been used for the solvent extraction of metal ions.[1-3]

The present authors have been studying the thermodynamical stability of metal dithioato complexes using a solvent-extraction method.[4,5] Furthermore, in a preceding paper[6] the formation constants of metal-Rxan complexes in a 1:1 v/v water-*N,N*-dimethylformamide (DMF) medium were determined by polarography.

Following the previous research, the formation constants of metal-R_2dtc and -R_2dtp complexes in a water-DMF medium were determined. The stabilities of these complexes are discussed on the basis of the basicity of the ligands.

Experimental

Reagents. KR_2dtp and NaR_2dtc were synthesized and purified according to methods described in the literature.[7,8] Aqueous solutions of KR_2dtp were freshly prepared and those of NaR_2dtc were prepared immediately before use due to the instability of their solutions.

Stock solutions of cadmium(II), zinc(II), and lead(II) were prepared by dissolving each nitrate salt in 0.1 mol dm^{-3} of nitric acid, respectively. These solutions were volumetrically standardized with EDTA.

Apparatus and Procedures. The decomposition rate of R_2dtc^- was spectrophotometrically measured at 285 nm according to a previously described procedure.[6]

Direct-current polarographic waves were recorded with the same apparatus and under the same conditions as previously described.[6]

Results and Discussion

Acid Dissociation Constant of HR_2dtc. The decomposition rate of R_2dtc^- depended on the pH of the test solution. Hence, the decomposition rate (k_3) and the acid-dissociation (K_a) constants of HR_2dtc were determined using similar equations to those of the preceding paper:[6]

$$-\frac{d\ln([R_2dtc^-]+[HR_2dtc])}{dt} = \frac{k_3}{1+K_a[H^+]} \equiv \kappa$$

$$\log\frac{Abs_1}{Abs_2} = \frac{\kappa}{2.303}(t_2-t_1)$$

where Abs_1 and Abs_2 denote the absorbances at time t_1 and t_2, respectively. The obtained constants are given in Table 1.

On the other hand, HR_2dtp were too stable for determining the constants by a method based on the decomposition rate.

Figure 1 shows plots of the pK_a value in an aqueous medium vs. that in a water-DMF medium. The data used in Fig. 1, except that determined in this paper, are quoted from the preceding paper[6] and others.[9-11] Obviously, a linear relationship exists between the

Table 1. Acid Dissociation (K_a) and Decomposition Rate (k_3) Constants of HR_2dtc

	R			
	Methyl	Ethyl	Propyl	Butyl
pK_a	4.25	4.62	4.72	4.80
k_3/min^{-1}	11.2	21.4	15.6	15.9

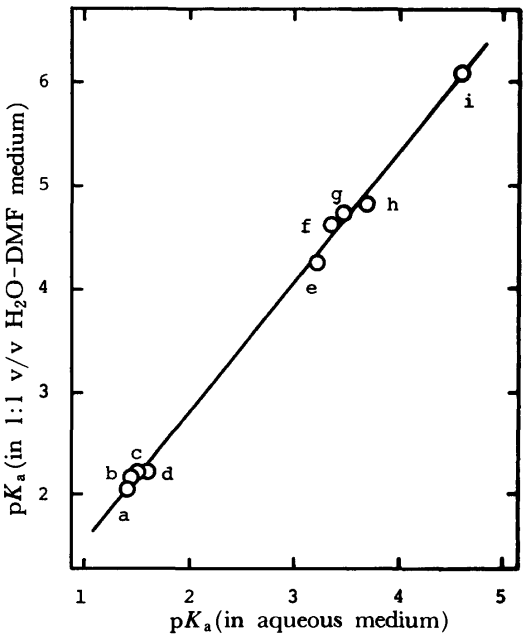

Fig. 1. Relationship between the pK_a-values in aqueous medium and in 1:1 v/v water-DMF medium.
a: HMexan, b: HEtxan, c: HPrxan, d: HBuxan, e: HMe_2dtc, f: HEt_2dtc, g: HPr_2dtc, h: HBu_2dtc, i: acetic acid.

two variables. Therefore, the unknown pK_a values of HEt_2dtp and HBu_2dtp in the water–DMF medium can be estimated from the values for the aqueous medium[12] by means of a straight-line relationship. Thus, their values were obtained as 0.18 and 0.58, respectively.

Formation Constants of Metal–R_2dtc and –R_2dtp Complexes. The direct-current polarographic waves, which were all cathodic and quasi-reversible waves for the two-electrons reduction of metal ions, were analyzed in the same manner as described previously[6]

Table 2. Formation constants (β_j) of Metal-R_2dtc and -R_2dtp Complexes

			R			
			Methyl	Ethyl	Propyl	Butyl
R_2dtc	Cd	log β_3	19.12	19.83	20.03	20.30
		log β_2	4.70	5.96	5.92	—
	Cd	log β_3	6.33	7.82	7.82	8.83
		log β_4	7.01	8.76	8.76	9.95
R_2dtp	Zn	log β_3	—	2.47	2.57	—
		log β_2	5.85	7.38	—	—
	Pb	log β_3	8.02	9.64	9.71	10.66
		log β_4	8.76	10.44	10.86	11.84

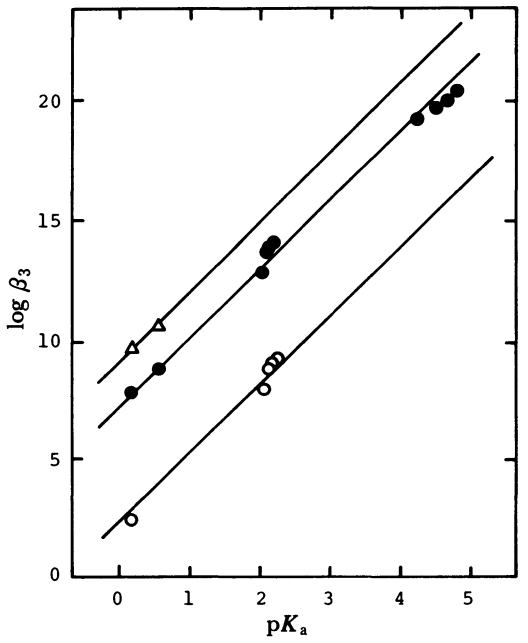

Fig. 2. Plots of log β_3 for metal complex vs. pK_a for ligand.
△: lead(II) complex, ●: cadmium(II) complex, ○: zinc(II) complex.

and the overall formation constants, β_j, of the complexes were obtained (Table 2).

It was observed that the β_j value for each metal increased upon increasing the pK_a value, i.e., the basicity of the ligand. This tendency was confirmed for β_3, including the results for metal–Rxan complexes[6] (Fig. 2). The individually observed points for each metal lie well along straight parallel lines. This is one instance of a "linear free-energy relationship",[13] indicating that R_2dtc^-, R_2dtp^-, and $Rxan^-$ have similar charactaristics regarding the formation of a metal complex. The difference in the complex-forming abilities of these ligands might be due to a difference in the electron density on the sulfur atoms in the ligand molecules.[14]

The β_3 values of the lead- and zinc–R_2dtc complexes could not be determined because of the difficulty in finding the pH region in which neither the hydrolysis of the metal ion nor the acid decomposition of the ligand occurred. However, these values can be estimated, respectively, by reading off a point on the line in Fig. 2.

References

1) E. M. Donaldson, *Talanta*, **23**, 417 (1976).
2) J. Stary, "The Solvent Extraction of Metal Chelates," Pergamon Press, London (1964), pp. 155—168.
3) H. Bode and W. Arnswald, *Fresenius' Z. Anal. Chem.*, **185**, 13 (1962).
4) Y. Sasaki, *Bunseki Kagaku*, **31**, E107 (1982).
5) K. Hayashi, Y. Sasaki, S. Tagashira, and M. Nakashima, *Anal. Sci.*, **1**, 51 (1985).
6) K. Hayashi, Y. Sasaki, S. Inomata, and T. Yanagidani, *Bull. Chem. Soc. Jpn.*, **57**, 3074 (1984).
7) K. Hayashi, Y. Sasaki, S. Tagashira, S. Inomata, J. Rikitake, Y. Hisatomi, and M. Suzuki, *Bunseki Kagaku*, **33**, 247 (1984).
8) D. Oktavec, J. Štefanec, B. Síleš, V. Konečný, and J. Garaj, *Collect. Czech. Chem. Commun.*, **44**, 2487 (1979).
9) K. I. Aspila, C. L. Chakrabarti, and V. S. Sastri, *Anal. Chem.*, **45**, 363 (1973).
10) H. Majima, *Sci. Rep. Res. Inst. Tohoku Univ., Ser. A*, **13**, 183 (1962).
11) The values for acetic acid were obtained by the analysis of the acid-base titration curve of acetic acid with sodium hydroxide solution in each medium by using the same pH meter.
12) R. H. Zucal, J. A. Dean, and T. H. Handley, *Anal. Chem.*, **35**, 988 (1963).
13) P. R. Wells, *Chem. Rev.*, **63**, 171 (1963).
14) R. Eisenberg, "Progress in Inorganic Chemistry," ed by S. J. Lippard, J. Wiley and Sons Inc., New York (1970), Vol. 12, p. 330.

The Differential Scanning Calorimetry of 1,3,5,7,2,4,6,8-Tetrathiatetrazocine

Yoshiyuki KUDO and Shuichi HAMADA*
Department of Applied Chemistry, Faculty of Science,
Science University of Tokyo, Kagurazaka, Shinjuku-ku, Tokyo 162
(Received November 18, 1985)

Synopsis. The molar heat of the decomposition of $S_4(NH)_4$ was obtained as 360±7 kJ mol^{-1} by means of differential scanning calorimetry. This value gave the standard enthalpy of the formation, $\Delta H_f(S_4(NH)_4, s, 298.15\,K)$, as 318±7 kJ mol^{-1}, which was comparable with that calculated (311 kJ mol^{-1}).

1,3,5,7,2,4,6,8-Tetrathiatetrazocine (tetrasulfur tetraimide, $S_4(NH)_4$) is finally pyrolyzed into sulfur, ammonia, and nitrogen in an argon atmosphere through step-by-step degradation.[1] However, little information on the thermodynamic properties is available, in contrast to those of tetrasulfur tetranitride (S_4N_4)[2,3] and tetrasulfur dinitride (S_4N_2).[2] In this work, the pyrolysis of this compound was studied by means of differential scanning calorimetry (DSC).

Experimental

The $S_4(NH)_4$ was prepared and purified by the method described in a previous paper.[1]

The heat of the decomposition of $S_4(NH)_4$ was measured at the heating rates of 16 and 32 K min^{-1} with a Perkin-Elmer, model DSC-1B, differential scanning calorimeter. The sample was carefully weighed with a microbalance and then tightly sealed in an aluminium container in an argon atmosphere. The DSC equipment was calibrated with an indium of 99.999% purity.

The molar heat capacity, C_p, of this compound was measured at the fixed heating rate of 8 K min^{-1} with the same equipment, using quartz as a reference. The sufficient reliability of this method was indicated by the agreement between the observed and the reported molar heat capacities of α-sulfur[4] (±1.4%) over the tempetarure range from 328 to 368 K.

Results and Discussion

Measurement of Heat of Decomposition of $S_4(NH)_4$. Figure 1 shows the DSC curve of $S_4(NH)_4$ taken at the heating rate of 16 K min^{-1} in the argon atmosphere. The DSC pattern consisted of sharp and broad exothermic peaks, in addition to an endothermic peak caused by its fusion. The former two peaks were attributable to the step-by-step degradation.[1] The dotted line in Fig. 1 was taken as the base line for estimating the heat of decomposition. The degradation immediately occurred after its fusion at the heating rates applied, though it took place even before fusion at such slow heating rates as 3 K min^{-1}.[1] Thus, the overall heat of decomposition was defined as the corresponding area by subtracting the endothermic peak area from the exothermic one in Fig. 1.

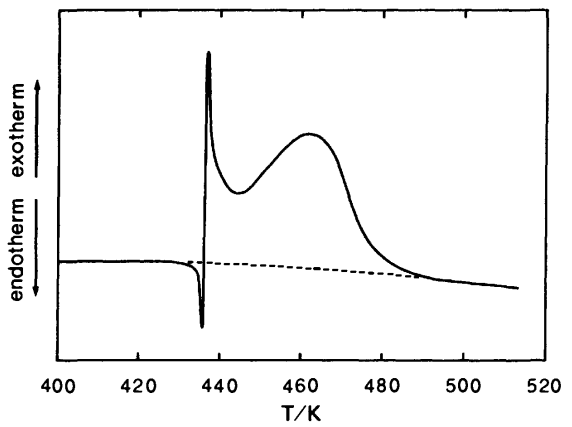

Fig. 1. DSC pattern of $S_4(NH)_4$ at heating rate of 16 K min^{-1}.

The molar heat of decomposition, Q, was obtained as 360±7 kJ mol^{-1} as the average for nine runs; the uncertainty value was defined as $\pm 3.0\sigma/\sqrt{n}$, where σ and n are the standard deviation and the number of data respectively. The value of Q was scarcely changed at either heating rate, i.e., 16 or 32 K min^{-1}, within the limits of experimental error shown above.

The molar heat capacity, C_p, of $S_4(NH)_4$ was measured over the temperatures from 328 to 363 K at the heating rate of 8 K min^{-1}. No chemical change in the sample was confirmed by thin-layer chromatography for 20 min after each run. Measurements below 323 K did not give reproducible results because of unstable base lines. The linear temperature dependence ($C_p = 0.153 + 1.26\times10^{-4}T$) gave the value of C_p as 0.191 kJ mol^{-1} K^{-1} at 298.15 K.

On the basis of stoichiometric correlation,[1] the overall pyrolytic reaction can be expressed as:[5]

$$S_4(NH)_4 = 1/2S_8 + 4/3N_2 + 4/3NH_3 \quad (1)$$

According to Eq. 1, the following equation yields the standard enthalpy of the formation of $S_4(NH)_4$:

$$\Delta H_f(S_4(NH)_4, s, 298.15\,K) = Q + 8/3RT + 1/2(\Delta H_t(\alpha,\beta) + \Delta H_m(\beta,\lambda) + X\Delta H_p) + 4/3\Delta H_f(NH_3, g, 298.15\,K) - \int_{298.15}^{T}\Delta C_p dT \quad (2)$$

where $\Delta H_t(\alpha,\beta)$ and $\Delta H_m(\beta,\lambda)$ are the enthalpy changes of transition from S_α to S_β (3.2 kJ mol^{-1})[6,7] and of the fusion of S_β (13.8 kJ mol^{-1});[6,7] ΔH_p, the enthalpy change of polymerization from S_λ to S_μ (13.3 kJ mol^{-1});[6,7] X, the fraction of S_μ (0.228 at 464 K);[8] $\Delta H_f(NH_3, g, 298.15\,K)$, the standard enthalpy of the formation of ammonia (−45.9 kJ mol^{-1}),[6] and ΔC_p, the difference in the molar heat capacities between the initial and final states.[6] The reaction temperature, T, was taken as 464 K at the maximum of the broad exothermic peak (Fig. 1), and the integral term was calculated as −1.5 kJ mol^{-1}.

According to Eq. 2, the standard enthalpy of the

formation of $S_4(NH)_4$, $\Delta H_f(S_4(NH)_4, s, 298.15\,K)$, was obtained as 318 ± 7 kJ mol^{-1}.

Calculation of Standard Enthalpy of the Formation of $S_4(NH)_4$. Sanderson's method[9] gave the S–N and N–H bond energies in $S_4(NH)_4$ as 247.7 and 363.8 kJ mol^{-1}, based on their respective bond lengths of 167.4[10] and 108 pm.[11] By combining these values with the standard enthalpies of the formation of atomic sulfur, nitrogen, and hydrogen,[12] the enthalpy of the formation of gaseous $S_4(NH)_4$, $\Delta H_f(S_4(NH)_4, g, 298.15\,K)$, was calculated as 426 kJ mol^{-1}.

The enthalpy of sublimation, ΔH_{sub}, is given as:[13]

$$\Delta H_{sub} = L^0 + RT \quad (3)$$

where L^0 is the lattice energy at 0 K. The lattice energy of the $S_4(NH)_4$ crystal was estimated by means of the Slater–Kirkwood equation,[14] assuming that the lattice energy is nearly equal to the London dispersion force, E, ($L^0=-E$),[13] and that the effect of hydrogen bonds in the crystal is negligible.[11] To calculate the value of E, the polarizabilities, α, of sulfur, nitrogen, and hydrogen atoms were taken as 2.836×10^{-24}, 9.437×10^{-25}, and 4.152×10^{-25} cm^3 respectively, which were deduced by the use of the Clausius-Mossotti relationship using corresponding atomic refractions.[15] Taking the 306 pairs of interatomic distances (less than 500 pm) which were given by the atomic coordinates,[10,11] the value of the ΔH_{sub} of $S_4(NH)_4$ was estimated as 115.0 kJ mol^{-1} ($E=-112.5$ kJ mol^{-1}).

For checking the reliability of this calculation, the enthalpies of the sublimation of tetrasulfur tetranitride and α-sulfur were also estimated in the same way.[16–18] The values thus calculated were 88.0 and 106.4 kJ mol^{-1} respectively; these values agreed closely with those observed (88.7[19] and 105.9 kJ mol^{-1} [12]).

The standard enthalpy of the formation, $\Delta H_f(S_4(NH)_4, s, 298.15\,K)$, was given as 311 kJ mol^{-1}, combined with the enthalpies of the formation at the gaseous state and of the sublimation. Consequently, the calculated value was in fair agreement with that obtained in this work (318 ± 7 kJ mol^{-1}).

References

1) S. Hamada and Y. Kudo, *Bull. Chem. Soc. Jpn.*, **52**, 1063 (1979).
2) Y. Kudo and S. Hamada, *Bull. Chem. Soc. Jpn.*, **56**, 2627 (1983).
3) C. K. Barker, A. W. Cordes, and J. L. Margrave, *J. Phys. Chem.*, **69**, 334 (1965).
4) J. Chao, *Hydrocarbon Process.*, **59**, 217 (1980).
5) It is assumed that the sulfur produced in this process exists as cyclooctasulfur, S_8.
6) "JANAF Thermochemical Tables," 2nd ed., Nat. Bur. Stand. (US), (1971).
7) The thermodynamic quantities of sulfur are expressed as S_8 units.
8) A. V. Tobolsky and A. Eisenberg, *J. Am. Chem. Soc.*, **81**, 780 (1959).
9) R. T. Sanderson, *J. Inorg. Nucl. Chem.*, **28**, 1553 (1966).
10) R. L. Sass and J. Donohue, *Acta Crystallogr.*, **11**, 497 (1958).
11) T. M. Sabine and G. W. Cox, *Acta Crystallogr.*, **23**, 574 (1967).
12) M. W. Chase, Jr., J. L. Curnutt, J. R. Downey, Jr., R. A. McDonald, A. N. Syverud, and E. A. Valenzuela, *J. Phys. Chem. Ref. Data*, **11**, 695 (1982).
13) K. Suzuki, S. Onishi, T. Koide, and S. Seki, *Bull. Chem. Soc. Jpn.*, **29**, 127 (1956).
14) J. C. Slater and J. G. Kirkwood, *Phys. Rev.*, **37**, 682 (1931).
15) The atomic refractions (7.153(S), 2.381(N), and 1.047 cm^3 (H)) were obtained as those at an infinitive wave length using the Cauchy equation.
16) B. D. Sharma and J. Donohue, *Acta Crystallogr.*, **16**, 891 (1963).
17) S. C. Abrahams, *Acta Crystallogr.*, **8**, 661 (1955).
18) A. S. Cooper, *Acta Crystallogr.*, **15**, 578 (1962).
19) S. Hamada, *Bull. Chem. Soc. Jpn.*, **46**, 3598 (1973).

Metal Complexes of Octabutyl- and Octaoctylporphyrins Preparation and Properties

Chang Quing YE,† Haruki TSURUTA,* and Sei OTSUKA††
Research Laboratory, Takasago Perfumery Co., Ltd. 5-36-31, Kamata, Ohta-ku, Tokyo 144
††Department of Chemistry, Faculty of Engineering Science, Osaka University, Toyonaka 560
(Received July 3, 1985)

Synopsis. Octabutyl- and octaoctylporphyrin complexes of Fe^{II}, Co^{II}, Ni^{II}, and Cu^{II} ions were prepared as a family of highly lipophilic metalloporphyrins.

In one phase of our investigations on metalloporphyrins, those which are highly soluble in non-polar organic solvents were required. Potential candidates were metal complexes of porphyrins having long alkyl chains.[1] Thus, 2,3,7,8,12,13,17,18-octabutyl- and octaoctylporphyrin complexes of several metal ions such as Fe^{II}, Co^{II}, Ni^{II}, and Cu^{II} were prepared. Since, no report, to our best knowledge, on these metal complexes has been made so far, we wish to report here briefly the preparation and some chemical properties of these complexes.

Results and Discussion

Preparations. The ligands, octabutyl- (H_2obp) and octaoctylporphyrin (H_2oop), were prepared by a slight modification of Callot's method[2,3] as shown in the Scheme.

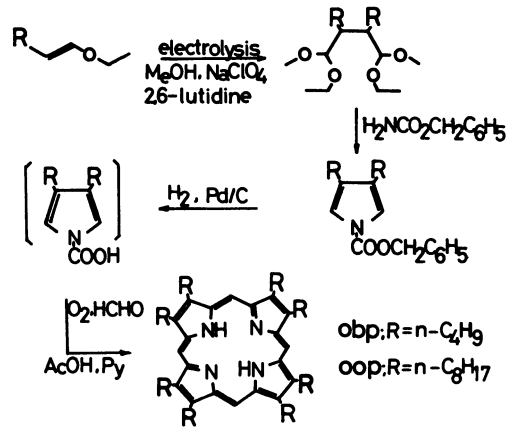

Scheme

Following essentially the literature methods[4—7] metal complexes of these porphyrins could be prepared. Thus, the reaction of acetates of Co(II), Ni(II), and Cu(II) with H_2obp or H_2oop gave the corresponding neutral metal complexes in a good to fair yield with a relative rate of formation, Co(II)<Ni(II)<Cu(II) complex. [FeCl(obp)] and [FeCl(oop)] were also prepared according to the literature procedures.[4]

As expected, they exhibited enhanced solubility in many organic solvents. Remarkably even hexane dissolves these complexes. On the other hand, they are practically insoluble in methanol, acetonitrile and dimethyl sulfoxide. The solubility trends are rather similar for the metal ions described above. The solubility differences between the two porphyrins obp and oop are also very small. However, their solubility in dioxane shows a salient feature. Namely, three neutral Co(II) complexes, [Co(oep)], [Co(obp)], and [Co(oop)] are moderately soluble in dioxane, whereas in the series of Cu(II) and Ni(II) porphyrins, only [Cu(oep)] and [Ni(oep)] are soluble in dioxane, all the other porphyrin complexes being sparingly soluble.

The UV-visible spectra of [M(oep)], [M(obp)], and [M(oop)] (M=Co, Ni, and Cu) were measured in $CHCl_3$ without adding axial ligands. As shown in Table 1 their α,β and Soret bands are very similar and in agreement with the spectra of oep complexes reported by Ogoshi.[8]

Table 1. UV-Visible Spectra of [M(obp)] and [M(oop)] (M=Co, Ni, and Cu) in $CHCl_3$

M(porp)		α		β		Soret	
		nm	log ε	nm	log ε	nm	log ε
oep[8]	Co	554	4.44	521	4.14	393	5.43
	Ni	554	4.52	519	4.07	394	5.32
	Cu	562	4.39	526	4.09	399	5.42
obp	Co	554	4.50	521	4.19	394	5.47
	Ni	554	4.53	519	4.08	395	5.30
	Cu	564	4.48	527	4.20	401	5.59
oop	Co	555	4.33	522	4.04	395	5.30
	Ni	555	4.51	519	4.11	396	5.32
	Cu	564	4.51	527	4.23	401	5.61

Experimental

Octaoctylporphyrin. A literature procedure[2] was employed with some modification. 1-Decenyl ethyl ether[9] (51.6 g) was electrolyzed in a cell with two 5 cm×15 cm graphite electrodes, to afford the acetal (15.1 g) (Scheme) in 25% yield. The acetal (14.4 g) was treated with benzyl carbamate (13.7 g) to give crude 1-benzyloxycarbonyl-3,4-dioctyl pyrrole, which was chromatographed on silica gel. A mixture of hexane and benzene (4:1) elution gave a yellow liquid (7.2 g) in 51% yield. ^{1}H NMR ($CDCl_3$) δ=0.89 [triplet, 6H, $-CH_2(CH_2)_6\underline{CH_3}$], 1.27 [singlet, 24H, $-CH_2(\underline{CH_2})_6CH_3$], 2.33 [triplet, 4H, $-\underline{CH_2}(CH_2)_6CH_3$], 5.33 [singlet, 2H, benzyl], 7.00 [singlet, 2H, pyrrole], 7.40 [singlet, 5H, benzyl]. MS $[M]^+$: 425. The *N*-benzyloxycarbonyl 3,4-dioctyl pyrrole (9.1 g) was submitted to hydrogenolysis at room temperature using Pd/C (5%, 700 mg) in a mixture of methanol and hexane (5:1) (100 ml). The resulting compounds were immediately treated with formaldehyde (35% aqueous solution, 2.2 ml), pyridine (76 ml), acetic acid (154 ml), and oxygen to afford octaoctylporphyrin (1.87 g) in 29% yield, mp 144—145 °C (lit, [10] 145.5 °C). The overall yield is 3.7% based on 1-decenyl ethyl ether. Octabutylporphyrin

†Study leave from Shanghai Institute of Organic Chemistry; A 1983 Takasago fellowship recipient.

mp 265—266 °C (lit, [10] 266—267 °C) was prepared in a similar manner in 6.8% from 1-hexenyl ethyl ether.

Chloro[octabutylporphyrianato(2)-]iron(III). Chloro[octabutylporphyrinato(2)-]iron(III) was prepared by the method described by Osa[5] in 89% yield, mp 202—203 °C. UV_{max} ($CHCl_3$): 382 (log ε, 5.01), 509 (3.98), 538 (3.99), 639 nm (3.68). MS $[M]^+$: 847 and 849 (Calcd, 846.9 and 848.9). Chloro-[octaoctylporphyrinato(2)-]iron(III) was prepared in the same way in 65%, mp 76—78 °C. UV_{max} ($CHCl_3$): 383 (log ε 5.02), 509 (3.99), 538 (4.00), 639 nm (3.68). MS $[M]^+$: 1295 and 1297 (Calcd, 1294.9 and 1296.9).

[Octaoctylporphyrinato(2)-]copper(II).[5-7] A mixture of octaoctylporphyrin (100 mg) dissolved in chloroform (50 ml) and a methanol solution (10 ml) saturated with copper acetate was reacted for 1 h at room temperature. Then methanol (100 ml) was added to precipitate a red solid, which was redissolved in chloroform. Methanol was added to give [octaoctylporphyrinato(2)-]copper(II) in 86% (90 mg) yield as red crystals, mp 185—187 °C. MS $[M]^+$: 1267 (Calcd, 1267.5). [Octabutylporphyrinato(2)-]copper(II) was prepared in a similar manner in 92% yield, mp>300 °C. MS $[M]^+$: 820 (Calcd, 819.5).

[Octabutylporphyrinato(2)-]cobalt(II). A methanol solution (10 ml) saturated with cobalt acetate was added to octabutylporphyrin (100 mg) disolved in chloroform (50 ml). The mixture was heated for 1 h. Methanol was added to the filtrate yielding a red solid. The solid was dissolved in dichloromethane and filtration was followed by concentration to a small volume. Methanol was then added to give [octabutylporphyrinato(2)-]cobalt(II) in 56% (60 mg) yield, mp>300 °C. MS $[M]^+$: 816 (Calcd, 815.9). [Octaoctylporphyrinato(2)-]cobalt(II) was obtained in the similar manner in 66% yield, mp 193—195 °C. MS $[M]^+$: 1263 (Calcd, 1262.9).

[Octabutylporphyrinato(2)-]nickel(II). A methanol solution (10 ml) saturated with nickel acetate was added to octabutylporphyrin (100 mg) dissolved in chloroform (50 ml) and heated under reflux for 5 h. Evaporation of chloroform and trituration with methanol afforded a crystalline product. [Octabutylporphyrinato(2)-]nickel(II) was obtained in 84% yield, mp 273—274 °C. ^1H NMR ($CDCl_3$) δ=1.14 (24H, $-CH_2CH_2CH_2C\underline{H}_3$), 1.77 (16H, $-CH_2CH_2C\underline{H}_2CH_3$), 2.21 (16H, $-CH_2C\underline{H}_2CH_2CH_3$), 3.87 (16H, $-C\underline{H}_2CH_2CH_2CH_3$), 9.75 (4H, $-C\underline{H}=$). MS $[M]^+$: 815 (Calcd, 814.7). [Octaoctylporphyrinato(2)-]nickel(II) was prepared in a similar manner in 58% yield, mp 150—151 °C. ^1H NMR ($CDCl_3$) δ=0.86 (24H, $-CH_2CH_2(CH_2)_5C\underline{H}_3$), 1.04—2.00 (80H, $-CH_2CH_2(C\underline{H}_2)_5CH_3$), 2.24 (16H, $-CH_2C\underline{H}_2(CH_2)_5CH_3$), 3.88 (16H, $-C\underline{H}_2CH_2(CH_2)_5CH_3$), 9.76 (4H, $-C\underline{H}=$). MS $[M]^+$: 1263 (Calcd, 1262.7).

One of the authors, Chang Qing Ye is grateful to Takasago Perfumery Co., Ltd. for the 1983 fellowship to carry out research work.

References

1) For reviews see: "Porphyrins and Metalloporphyrins," ed by K. M. Smith Elsevier Scientific Publishing Co., Amsterdam (1975); J. W. Buchler, "The Porphyrins" ed by D. Dolphin Academic Press, New York (1978), Vol. 1, pp. 390—483; P. D. Smith, B. R. James, and D. H. Dolphin, *Coord. Chem. Rev.*, **39**, 31 (1981).

2) H. J. Callot, A. Louati, and M. Gross, *Angew. Chem.*, **94**, 297 (1982).

3) H. J. Callot, A. Louati, and M. Gross, *Angew. Chem., Suppl.*, **1982**, 718.

4) H. Ogoshi, J. Setsune, T. Omura, and Z. Yoshida, *J. Am. Chem. Soc.*, **97**, 6461 (1975).

5) "Porphyrin Chemistry," ed by T. Osa, Kyoritsu Chemistry Library 20, Kyoritsu Publish Corp., Tokyo (1982).

6) H. H. Inhoffen, J. H. Fuhrhop, H. Voigt, and H. Brockmann Jr., *Ann. Chem.*, **695**, 133 (1966).

7) A. Shirazi and H. M. Goff, *Inorg. Chem.*, **21**, 3420 (1982).

8) H. Ogoshi, N, Masai, Z. Yoshida, J. Takemoto, and K. Nakamoto, *Bull. Chem. Soc. Jpn.*, **44**, 49 (1971).

9) J. L. E. Erickson and M. Z. Waskow, *J. Org. Chem.*, **23**, 670 (1958).

10) K. S. Chamberlin and E. LeGoff, *Heterocycles*, **12**, 1567 (1979).

Pseudo-Sugars. XV. A Facile Synthesis of Pseudo-β-DL-fructopyranose

Tetsuo SUAMI,* Seiichiro OGAWA, Yasushi UEMATSU, and Atsuo SUGA
Department of Applied Chemistry, Faculty of Science and Technology, Keio University, Hiyoshi, Yokohama 223
(Received November 8, 1985)

Synopsis. Pseudo-β-DL-fructopyranose, DL-(1,2/3,4)-1-*C*-hydroxymethyl-1,2,3,4-cyclohexanetetrol, has been synthesized from DL-1,2-di-*O*-acetyl-(1,3/2)-3-bromomethyl-5-cyclohexene-1,2-diol by the seven-steps sequence in 21% overall yield.

In recent years, biochemical properties of pseudo-sugars have stimulated considerable synthetic effort toward their stereoisomers. In continuation to the preceding paper,[1] since we required large quantities of pseudo-β-DL-fructopyranose (**1**) in order not only to carry out biological test in detail, but also to use as an intermediate for derivatization, the improved stereospecific route to **1** has been worked out. The present synthesis should be applied for preparation of an optically active **1**,[2] which would give an interesting knowledge on a sweet tasting property of sugars in terms of the molecular chirality.

O-Deacetylation of DL-1,2-di-*O*-acetyl-(1,3/2)-3-bromomethyl-5-cyclohexene-1,2-diol (**3**)[3] with hydrochloric acid in ethanol gave the dihydroxy compound (**4**) in 83% yield. Epoxidation of **4** with *m*-chloroperbenzoic acid (MCPBA) in dichloromethane, followed by acetylation, gave 80% yield of single epoxide (**5**) preferentially. The stereospecificity may be attributed to the *cis*-directing effect of the adjacent C-1 hydroxyl group.[4] Dehydrobromination of **5** with silver fluoride in pyridine at room temperature afforded the *exo*-methylene compound (**6**) in a quantitative yield. Reductive cleavage of the epoxide ring of **6** was carried out with lithium aluminum hydride (LAH) in tetrahydrofuran (THF), followed by acetylation with acetic anhydride in pyridine, gave the triacetate (**7**) in 52% yield. Epoxidation of the *exo*-methylene group of **7** with MCPBA gave 90% yield of a single spiro epoxide (**8**). Treatment of **8** with sodium acetate in refluxing aqueous 2-methoxyethanol, followed by acetylation in the presence of 4-dimethylaminopyridine, afforded the pentaacetyl derivative (**2**) of **1** in 66% yield.[5] This compound was identical with an authentic sample[1] in all respects. These results also supported the assigned structures of **5** and **8**. Compound **2** could readily be converted into the free pseudo-sugar **1** quantitatively.[1] Therefore, the overall yield of **1** from **3** was 21%.

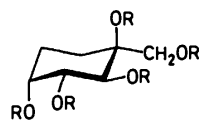

1 R = H
2 R = Ac

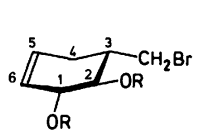

3 R = Ac
4 R = H

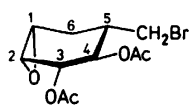

5

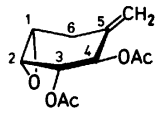

6

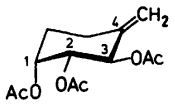

7

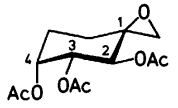

8

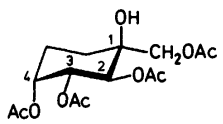

9

Experimental

General. The same method was used as described in the preceding paper.[1]

DL-(1,3/2)-3-Bromomethyl-5-cyclohexene-1,2-diol (4). A mixture of DL-1,2-di-*O*-acetyl-(1,3/2)-3-bromomethyl-5-cyclohexene-1,2-diol (**3**)[3] (10.0 g, 34 mmol) and ethanol (150 ml), and concd hydrochloric acid (50 ml) was stirred at room temperature for 13 h. The reaction mixture was treated with sodium hydrogencarbonate and then concentrated. The residue was extracted with ethanol several times and the extracts were concentrated to give a solid, which was purified by a silica-gel column (200 g) with ethyl acetate–hexane (1:3) as an eluant, giving 5.88 g (83%) of **4** as crystals: mp 80—80.5 °C; ^{1}H NMR ($CDCl_3$, 90 MHz) δ=1.74—2.35 (2H, m, H-3, 4), 3.36—3.85 (3H, m, H-2, 7, and 7′), 3.94—4.29 (1H, m, H-1), 5.37—5.87 (2H, m, H-5, 6).

Found: C, 40.43; H, 5.26; Br, 38.38%. Calcd for $C_7H_{11}BrO_2$: C, 40.60; H, 5.35; Br, 38.59%.

DL-3,4-Di-*O*-acetyl-1,2-anhydro-(1,2,3,5/4)-5-bromomethyl-1,2,3,4-cyclohexanetetrol (5). A mixture of **4** (0.10 g, 0.48 mmol) and MCPBA (0.16 g, 0.90 mmol) in dichloromethane (2 ml) was stirred at room temperature for 2 h. The reaction mixture was concentrated and the residue was treated with acetic anhydride (1 ml) and pyridine (2 ml) at room temperature overnight. The mixture was concentrated and the residue was taken up in ethyl acetate and the solution was washed with saturated sodium hydrogencarbonate and water thoroughly. Evaporation of the solvent gave a solid, which was purified by a silica-gel column to give 0.12 g (80%) of **5** as crystals: mp 110—110.5 °C. ^{1}H NMR ($CDCl_3$, 90 MHz) δ=2.05 (3H, s) and 2.10 (3H, s) (OAc), 1.58—2.54 (3H, m, H-5, 6, and 6′), 3.07—3.45 (4H, m, H-1, 2, 7, and 7′), 5.04 (1H, dd, *J*=8.1 and 9.2 Hz, H-4), 5.26 (1H, dd, *J*=8.1 and 2 Hz, H-3).

Found: C, 42.91; H, 4.92; Br, 25.76%. Calcd for $C_{11}H_{15}BrO_5$: C, 43.02; H, 4.92; Br, 26.02%.

DL-3,4-Di-*O*-acetyl-1,2-anhydro-(1,2,3/4)-5-methylene-1,2,3,4-cyclohexanetetrol (6). A suspension of **5** (0.20 g, 0.65 mmol), silver fluoride (0.20 g, 2 molar equiv), in pyridine (5 ml) was stirred at room temperature for 1 h. An insoluble material was removed by filtration and the filtrate was concentrated. The residue was purified by a silica-gel column (8 g) with ethyl acetate, giving 0.15 g (100%) of **6** as a syrup: ^{1}H NMR ($CDCl_3$, 90 MHz) δ=2.10 (3H, s) and 2.13 (3H, s) (OAc), 2.75—2.90 (2H, m, H-6 and 6′), 3.30—3.49 (2H, m, H-1 and 2), 4.87—5.03 (2H,

m, H-7 and 7'), 5.13 (1H, dd, J=8.3 and 2 Hz, H-3), 5.43 (1H, br d, J=8.3 Hz, H-4).

Found: C, 58.17; H, 6.36%. Calcd for $C_{11}H_{14}O_5$: C, 58.40; H, 6.24%.

DL-1,2,3-Tri-*O*-acetyl-(1,2/3)-4-methylene-1,2,3-cyclohexanetriol (7). To a solution of **6** (0.50 g, 2.2 mmol) in THF (24 ml) was added $LiAlH_4$ (0.42 g, 11 mmol) gradually, and the mixture was stirred at room temperature for 3 h. Then the mixture was filtered through a celite bed and the filtrate was concentrated and the residue was acetylated in the usual way. The product was purified by a silica-gel column (20 g) with ethyl acetate–hexane (1:5) as an eluant, giving 0.31 g (52%) of **7** as crystals: mp 60—61 °C; ^{1}H NMR ($CDCl_3$, 90 MHz) δ=2.01 (3H, s) and 2.13 (6H, s) (OAc), 1.45—2.56 (4H, m, H-5, 5', 6, and 6'), 4.85—5.08 (3H, m, H-1, 7, and 7'), 5.34—5.66 (2H, m, H-2 and 3).

Found: C, 57.60; H, 6.66%. Calcd for $C_{13}H_{18}O_6$: C, 57.77; H, 6.71%.

DL-2,3,4-Tri-*O*-acetyl-1,7-anhydro-(1,2/3,4)-1-*C*-hydroxymethyl-1,2,3,4-cyclohexanetetrol (8). A mixture of **7** (95 mg, 0.35 mmol), MCPBA (217 mg, 2.5 molar equiv), and dichloromethane (3 ml) was stirred at room temperature for 4 h. Excess peroxy acid was destroyed by sodium thiosulfate and the mixture was concentrated. The residue was processed as described in the preparation of **5** and the product was purified by a silica-gel column to give 90 mg (90%) of **8** as a syrup: ^{1}H NMR ($CDCl_3$, 90 MHz) δ=2.00 (3H, s), 2.06 (3H, s), and 2.10 (3H, s) (OAc), 2.68 (2H, s, H-7 and 7'), 1.35—2.93 (4H, m, H-5, 5', 6, and 6'), 4.89—5.53 (3H, m, H-2, 3, and 4).

Found: C, 54.51; H, 6.37%. Calcd for $C_{13}H_{18}O_7$: C, 54.54; H, 6.34%.

DL-2,3,4-Tri-*O*-acetyl-(1,2/3,4)-1-*C*-acetoxymethyl-1,2,3,4-cyclohexanetetrol (9). A mixture of **8** (0.47 g, 1.7 mmol), anhydrous sodium acetate (0.68 g, 8.3 mmol), and 90% aqueous 2-methoxyethanol (10 ml) was stirred at 80 °C for 6 h. The mixture was concentrated and the residue was acetylated in the usual way. The product was purified on a silica-gel column (40 g) with ethyl acetate–hexane (5:9) to give 0.45 g (78%) of **9** as crystals: mp 108—109 °C. ^{1}H NMR ($CDCl_3$, 90 MHz) δ=1.96 (3H, s), 2.08 (6H, s), and 2.10 (3H, s) (4 OAc), 3.90 and 4.00 (1H, d, J=11.4 Hz, $C\underline{H}_2OAc$), 5.25—5.50 (3H, m, H-2, 3, and 4).

Found: C, 52.17; H, 6.35%. Calcd for $C_{15}H_{22}O_9$: C, 52.02; H, 6.40%.

DL-1,2,3,4-Tetra-*O*-acetyl-(1,2/3,4)-1-*C*-acetoxymethyl-1,2,3,4-cyclohexanetetrol (2). A mixture of **8** (67 mg, 0.23 mmol), anhydrous sodium acetate (95 mg, 1.1 mmol), and 90% aqueous 2-methoxyethanol (2 ml) was heated at 80 °C for 6 h. The product was acetylated with acetic anhydride (1.5 ml) and pyridine (1.5 ml) in the presence of 4-dimethylaminopyridine (30 mg) at 60 °C for 14 h, and then at 90 °C for 4 h. The mixture was processed in the usual way and the product was purified by a silica-gel column with ethyl acetate–hexane (3:8) as an eluant, giving 60 mg (66%) of **2** as crystals: mp 147.5—148 °C. This compound was identical with an authentic sample[1] in all respects.

The authors express their sincere thanks to Mr. Saburo Nakada for the elementary analyses.

References

1) T. Suami, S. Ogawa, M. Takada, K. Yasuda, K. Takei, and A. Suga, *Bull. Chem. Soc. Jpn.*, **59**, 819 (1986).

2) The optically active **3** has been synthesized: S. Ogawa and T. Takagaki, *J. Org. Chem.*, **50**, 2356 (1985).

3) S. Ogawa, T. Toyokuni, T. Kondoh, Y. Hattori, S. Iwasaki, M. Suetsugu, and T. Suami, *Bull. Chem. Soc. Jpn.*, **54**, 2739 (1981).

4) H. B. Henbest and R. A. L. Wilson, *J. Chem. Soc.*, **1957**, 1958. H. O. House, "Modern Synthetic Reactions" 2nd ed., Benjamin, California (1972), p. 304.

5) When the product was treated with acetic anhydride and pyridine in the absence of 4-dimethylaminopyridine, the tetraacetate (**9**) was obtained mainly in 78% yield.

The Effect of Intermolecular Association on Kinetic Behavior. Rate Acceleration with Time in Oxidation of a Pair of Thiols

Masato M. Ito, Toshikazu Ogikubo, Hideki Ueda, Kazuomi Hagino, and Tadashi Endo*
College of Science and Engineering, Aoyama Gakuin University, Chitosedai, Setagaya-ku, Tokyo 157
(Received December 17, 1985)

Synopsis. In base-catalyzed oxidation of a pair of associating thiols [$HSCH_2$-CONHCONH-Ph and $HSCH_2CH_2$-NHCONHCO-C_6H_{13}], rate enhancement with time occurred in protic media, whereas the rate was reduced with time in aprotic solvents. For a pair of nonassociating thiols [$HSCH_2$-$CO_2C_2H_5$ and $HSCH_2CH_2OH$], the rate enhancement was neither observed in a protic solvent nor in an aprotic one.

Recently it has been shown that intermolecular association plays a significant role in chemical reactions.[1] In order to elucidate the effect of intermolecular association on kinetic behavior, we examined the rate of oxidation for pairs of associating (**1** and **2**, system A) and nonassociating thiols (**3** and **4**, system N) in various solvents, and report that the rate acceleration with time in the oxidation is only observed for the associating system.

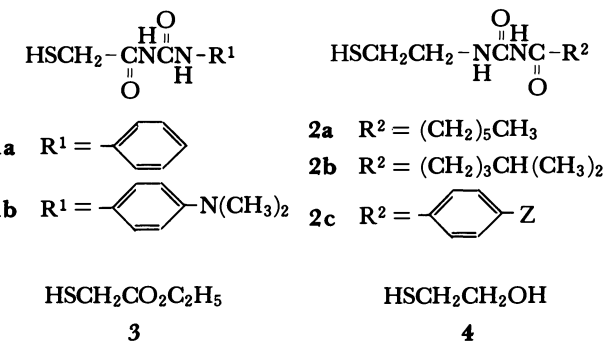

$HSCH_2CO_2C_2H_5$ **3**

$HSCH_2CH_2OH$ **4**

The ln([RSH]/[RSH]$_0$) was plotted against time for oxidation of a pair of associating thiols **1a** and **2a,b** (systems A_{aa} and A_{ab}) in oxygen-saturated acetonitrile (MeCN) and H_2O–MeCN [mole fraction of water (x_w)=0.42], at 35.0°C in the presence of triethylamine (Et_3N) as a catalyst (Fig. 1). In MeCN the oxidation follows pseudo first-order kinetics, as in the case of the oxidation in the presence of a large excess of a base.[2,3] On the other hand, sharp downward curvature is observed in aqueous MeCN,[4] suggesting that rate acceleration occurs with time. This has been confirmed by a plot of [RSH]/[RSH]$_0$ against time showing downward curvature (Fig. 2).

The [RSH]/[RSH]$_0$–time profiles were further investigated in various solvents for oxidation of system A_{aa} (Fig. 2). Also in H_2O–EtOH (x_w=0.20), the reaction has proved to be accelerated with time. This holds for the oxidation in nonaqueous protic solvents, EtOH and EtOH–MeCN (x_{EtOH}=0.42), but not in 1,4-dioxane even after 100 h. These observations suggest that rate acceleration with time in oxidation of system A occurs in protic media.[5]

Thiols **1** and **2** have been shown to associate strongly with each other in $CDCl_3$ via two NH···O intermolecular hydrogen bonds between the inner -NHCO-

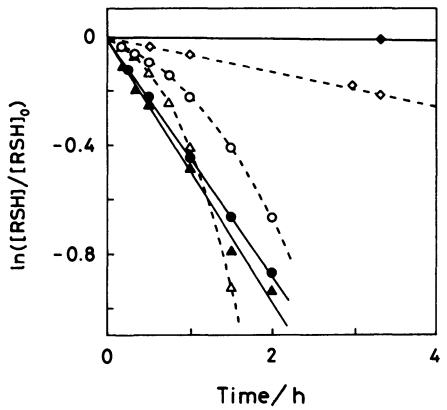

Fig. 1. First-order kinetic plots for oxidation of **1a** and **2a** (system A_{aa}), of **1a** and **2b** (system A_{ab}), and of **3** and **4** (system N) at 35.0°C. [RSH]$_0$=2.00×10^{-2} M, [Et_3N]=2.0×10^{-3} M. ●, System A_{aa} in MeCN; ○, system A_{aa} in H_2O–MeCN (x_w=0.42); ▲, system A_{ab} in MeCN; △, system A_{ab} in H_2O–MeCN (x_w=0.42); ◆, system N in MeCN; ◇, system N in H_2O–MeCN (x_w=0.42). Linear relationship for system N in aqueous MeCN is shown only until ca. 20% conversion in this figure.

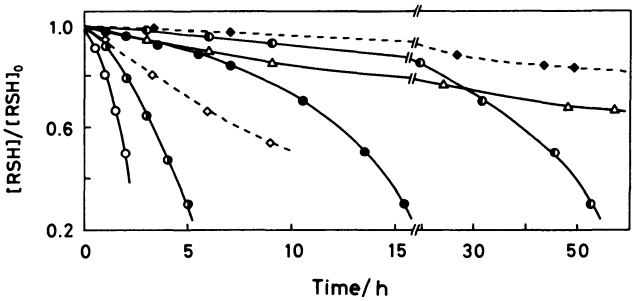

Fig. 2. Kinetic plots for oxidation of **1a** and **2a** (system A_{aa}) and **3** and **4** (system N) at 35.0°C. [RSH]$_0$=2.00×10^{-2} M, [Et_3N]=2.0×10^{-3} M. ○, System A_{aa} in H_2O–MeCN (x_w=0.42); ◑, system A_{aa} in MeCN–EtOH (x_{EtOH}=0.42); ●, system A_{aa} in H_2O–EtOH (x_{EtOH}=0.80); ◐, system A_{aa} in EtOH; △, system A_{aa} in 1,4-dioxane; ◇, system N in H_2O–MeCN (x_w=0.42); ◆, system N in MeCN.

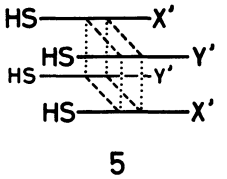

5

Fig. 3. Association scheme in a typical tetramer **5**. -----, Hydrogen bonds in dimers; ·····, noncovalent weak interactions responsible for stabilization of tetramers. The symbols X′ and Y′ represent R^1 and R^2, respectively.

units in the -CONHCONH- group to form tetramers (reaction intermediates) such as **5** (Fig. 3).[6]

Control experiments were performed using a pair of nonassociating thiols (**3** and **4**, system N) (Figs. 1 and 2). In H_2O–MeCN (x_w=0.42), the reaction follows pseudo first-order kinetics until at least 50% conversion (Fig. 1). In MeCN, the rate appears to follow second-order kinetics. These findings indicate that no rate enhancement occurs for system N regardless of the solvents employed.

From the results presented here, it seems reasonable to conclude that intermolecular association is responsible for the rate acceleration with time in the oxidation. Our work suggests the possibility that intermolecular association affects another aspect of kinetic behavior in chemical reactions.

Experimental

Materials. Thiols **1a** and **2a,b** were prepared as described previously.[3] Other thiols and Et_3N were purified by distillation through a fractionating column. Organic solvents were dried by proper procedures,[7] and purified by distillation. Water was purified through Millipore Milli-Q water purification system followed by distillation. The iodine solution (0.001 M (1 M=1 mol dm^{-3})) containing potassium iodide (0.005 M) was titrated with 1.00×10^{-3} M aqueous sodium arsenite standard solution before use.

Kinetics. The two thiols (**1** and **2** or **3** and **4**, 1.00×10^{-4} mol each) were weighed into a two-necked flask, and dissolved in 10.00 ml of the reaction solvent. The solution was stirred under an oxygen atmosphere for at least 4 h in a well-stirred water bath thermostated to ±0.1 °C. Oxidation of thiols was negligible in the absence of Et_3N. At time zero, 2.0×10^{-5} mol of Et_3N was added to the solution with a microsyringe, and time measurement was begun. At appropriate time intervals, a 0.50 ml portion of the reaction mixture was pipetted out, and quenched in 5 ml of a 1:9 mixture of 3 M hydrochloric acid with MeCN. The amount of remaining thiols in the quenched solution was then determined by titration with the 0.001 M iodine solution. Each plot in Figs. 1 and 2 represents the average of at least three, generally five, or more runs.

References

1) T. Endo, A. Kuwahara, H. Tasai, T. Murata, M. Hashimoto, and T. Ishigami, *Nature*, **268**, 74 (1977); T. Endo, Y. Takeda, H. Kamada, S. Kayama, and H. Tasai, *Chem. Lett.*, **1980**, 417; T. Endo, Y. Takeda, T. Orii, A. Kuwahara, M. Ohta, M. Sakai, R. Okada, and M. Hashimoto, *Bull. Chem. Soc. Jpn.*, **53**, 2687 (1980).

2) T. J. Wallace, A. Schriesheim, and W. Bartok, *J. Org. Chem.*, **26**, 1311 (1963).

3) T. Endo, M. Hashimoto, T. Orii, and M. M. Ito, *Bull. Chem. Soc. Jpn.*, **57**, 1562 (1984) and the references cited therein.

4) Similar rate profiles were observed for oxidation of **1b** and **2c** (Z=H, Me, and Et) in H_2O–MeCN (x_w=0.42) at 35.0 °C.[3]

5) The rate-determining step is generally regarded as that given by Eq. 1 or 2 [G. Capozzi and G. Modena, "Oxidation of Thiols," in "The Chemistry of the Thiol Group," ed by S. Patai, Wiley, London (1974), Part 2, Chap. 17]. One

$$RSH + Et_3N \overset{K}{\rightleftharpoons} RS^- + Et_3NH^+ \quad (1)$$

$$RS^- + O_2 \longrightarrow RS\cdot + O_2^{\cdot-} \qquad k_2 \quad (2)$$

possible explanation for the rate profiles in Figs. 1 and 2 is associated with the behavior of superoxide anion ($O_2^{\cdot-}$) in solvents.

First, in aprotic solvents such as MeCN, the steady state assumption can be applied to $O_2^{\cdot-}$, since the $O_2^{\cdot-}$ (the other oxidant) formed in situ is known to oxidize thiols readily

$$RSH + O_2^{\cdot-} \longrightarrow RS\cdot + O_2H^- \quad (3)$$

(Eq. 3) to disulfides [S. Oae, T. Takata, and Y. H. Kim, *Bull. Chem. Soc. Jpn.*, **54**, 2712 (1981)]. If the step shown by Eq. 2 is rate-determining, the rate for the oxidation may be expressed as

$$-d[RSH]/dt = 2k_2'[RSH] \quad (4)$$

where $k_2'=k_2[O_2]K[Et_3N]/[Et_3NH^+]$. Thus, the oxidation will follow pseudo first-order kinetics (Fig. 1).[2]

Second, in protic solvents, the $O_2^{\cdot-}$ reacts with solvent molecules to give the other oxidants (Ox·), such as $HO_2\cdot$ [J. Rabani and S. O. Nielsen, *J. Phys. Chem.*, **73**, 3736 (1969)], which may also oxidize thiols (Eq. 5) to disulfides. If the

$$RSH + Ox\cdot \longrightarrow RS\cdot + OxH \qquad k_5 \quad (5)$$

step shown by Eq. 2 is rate-determining, the rate for the oxidation may follow the expression

$$-d[RSH]/dt = k_2'[RSH] + k_5[RSH][Ox\cdot] \quad (6)$$

Rate acceleration will occur at least when $k_2'<k_5[RSH]_0$.

Similar results are obtained, even if the rate-determining step is given by Eq. 1.

6) T. Endo, Y. Takeda, T. Orii, Y. Kaneko, and M. Kondo, *Chem. Lett.*, **1979**, 1455.

7) J. A. Riddick and W. B. Bunger, "Organic Solvents," 3rd ed, Wiley, New York (1970).

Synthesis and Absolute Configuration of an Optically Active Bisnoradamantane Derivative, (−)-6-Oxotricyclo-[3.3.0.0^{3,7}]octane-2-carboxylic Acid

Koichiro NAEMURA,* Masanori KOMATSU, and Hiroaki CHIKAMATSU
Department of Chemistry, Faculty of Engineering Science, Osaka University, Toyonaka, Osaka 560
(Received November 12, 1985)

Synopsis. 6-Isopropylidenetricyclo[3.3.0.0^{3,7}]octane-2-carboxylic acid (**11**) was prepared from the dimethylfulvene–ethyl acrylate adduct **5**. Optical resolution of **11** was carried out via the (+)-1-(2-naphthyl)ethylamine salt, and (−)-**11** was transformed into (−)-6-oxotricyclo[3.3.0.0^{3,7}]octane-2-carboxylic acid (**14**) whose absolute configuration and absolute rotation were established.

The smallest rings in the tricyclo[3.3.0.0^{3,7}]octane (bisnoradamantane)[1] ring system are all five membered. Because of the highly symmetrical arrangement of the fused cyclopentane rings within this system, the hydrocarbon **1** is achiral ($3C_2$, $2\sigma_v$; D_{2d} symmetry) and four CH_2 groups in **1** are a pair of enantiotopic molecular subunits. Conversion of two of these CH_2 groups oriented coaxially along one of C_2 axes into π-systems desymmetrizes the D_{2d} symmetry inherent to **1**, leading to formation of chiral molecules, e.g. **2**, **3**, and **4**. Among these molecules, 6-methylenebisnoradamantan-2-one (**2**) (C_2 symmetry) and bisnoradamantane-2,6-dione (**3**) (D_2 symmetry) were prepared in racemic forms in our laboratory.[2] Gleiter and Kissler[3] reported the synthesis of (±)-2,6-dimethylenebisnoradamantane (**4**) (D_2 symmetry) and mentioned that this molecule is an interesting model for studying the intramolecular interaction of two π-fragments via a six membered ring. Our continuing interests in high-symmetry chiral cage-shaped molecules prompted us to prepare the bisnoradamantane derivative having two coaxially oriented unsaturated centers in an optically active modification.

In the preceding paper,[2] we reported that the eleven-step conversion of the maleic anhydride–cyclopentadiene adduct to 6-methylenebisnoradamantane-2-carboxylic acid (**17**) proceeded in 3% overall yield. The carboxylic acid **17** was the key intermediate for the preparation of **2**, **3**, and **4**.[2,3] We now chose 5-*endo*-ethoxycarbonyl-7-isopropylidenebicyclo[2.2.1]hept-2-ene (**5**) as the starting material for the preparation of bisnoradamantane derivative possessing two substituents. The Diels–Alder reaction of dimethylfulvene with ethyl acrylate yielded a 28% yield of **5**, which was transformed into **11** in 6% overall yield in seven steps.

The adduct **5**, without removing its *exo*-isomer, was reduced with $LiAlH_4$ to give **6** which was converted into **7** by tosylation followed by treatment with sodium cyanide. Alkaline hydrolysis of **7** yielded **8** in 42% overall yield from **5**. By use of Sauers' procedure,[4] **8** was converted into **10** via **9** in 27% overall yield. The cleavage reaction of **10** was accomplished with potassium *t*-butoxide and water. Contrary to our expectation that the ring opening of the cyclobutanone moiety in **10** should yield a mixture of two isomeric carboxylic acids depending upon the direction of bond cleavage, 6-isopropylidenebisnoradamantane-2-carboxylic acid (**11**) was the sole product isolated from the reaction mixture. Confirmation of structure **11** was obtained by its conversion into methyl 6-oxobisnoradamantane-2-carboxylate (**13**) which has been prepared in a racemic form.[2] Optical resolution of **11** was accomplished using (+)-1-(2-naphthyl)-ethylamine as the resolving agent. The resolved carboxylic acids, (−)-**11** ($[\alpha]_D$ −74.1°) and (+)-**11** ($[\alpha]_D$ +67.7°) were obtained respectively from the sparingly soluble and the soluble salts. Esterification of (+)-**11**, $[\alpha]_D$ +67.7°, with CH_2N_2 gave (+)-**12**, $[\alpha]_D$ +72.5°, which exhibited a singlet signal at δ 3.53 ppm due to CO_2CH_3 protons in its ^{1}H NMR spectrum. Addition of Eu(tfc)$_3$ [(+)-**12**/shift reagent=1.0/0.45 molar ratio] split the signal into two singlets at δ 5.90 and 5.98 ppm, and their integrated intensities indicated an enantiomer ratio of 90.5:9.5 corresponding to 81% optical purity.

Our next task is the determination of absolute configuration of these new compounds. Ozonization of (−)-**12**, $[\alpha]_D$ −77.5° (86.6% e.e.), followed by reductive work-up provided **13**. Its ^{1}H NMR spectrum and GLC behavior were identical with those of (±)-**13**.[2] Alkaline hydrolysis of **13** yielded (−)-**14**, $[\alpha]_D$ −60.8°. Calculation based on the optical purity of (−)-**12** assigns absolute rotation $[\alpha]_D$ −7.2° to (−)-**14**. The Wolff-Kishner reduction of (−)-**14** followed by esterification with CH_2N_2 furnished methyl (−)-(1*R*,3*R*,5*R*,7*R*)-bisnoradamantane-2-carboxylate (**16**) whose absolute configuration has been reported in our preceding paper.[5] The result eventually assigns the (1*R*,3*R*,5*R*,7*R*) configuration to (−)-**14**.

The optically active compounds **11** and **14** may serve as precursors for preparing bisnoradamantane derivatives having two coaxially oriented π-systems in an optically active form.

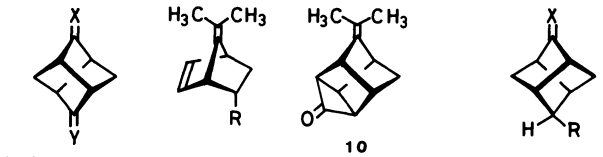

1 X= Y= H_2
2 X= O Y= CH_2
3 X= Y= O
4 X= Y= CH_2

5 R= $CO_2C_2H_5$
6 R= CH_2OH
7 R= CH_2CN
8 R= CH_2CO_2H
9 R= CH_2COCl

10

(−)-11 X= $C(CH_3)_2$ R= CO_2H
(−)-12 X= $C(CH_3)_2$ R= CO_2CH_3
13 X= O R= CO_2CH_3
(−)-14 X= O R= CO_2H
15 X= H_2 R= CO_2H
(−)-16 X= H_2 R= CO_2CH_3
17 X= CH_2 R= CO_2H

Experimental

Preparative GLC were done on a JGC-20K equipped with a TCD and using a 2 m×3 mm column of 10% PEG 20 M on

Chromosorb W.

5-Ethoxycarbonyl-7-isopropylidenebicyclo[2.2.1]hept-2-ene (5). A mixture of dimethylfulvene[6] (142 g, 1.34 mol) and ethyl acrylate (134 g, 1.34 mol) was heated at 100 °C for 44 h. Distillation of the product provided 78.5 g of **5** (28% yield); bp 78—82 °C (4 mmHg**). IR (neat film) 3060, 1735, 1180, 730 cm^{-1}.

Found: C, 75.72; H, 8.81%. Calcd for $C_{13}H_{18}O_2$: C, 75.69; H, 8.80%.

5-Hydroxymethyl-7-isopropylidenebicyclo[2.2.1]hept-2-ene (6). A solution of **5** (15.8 g, 0.0814 mol) in dry ether (200 mL) was added to a suspension of $LiAlH_4$ (2.50 g, 0.0658 mol) in dry ether (200 mL) and then the mixture was refluxed for 4.5 h. After a usual workup, the product was distilled to give 9.20 g of **6** (74% yield); bp 98—100 °C (4 mmHg). IR (neat film) 3450, 3060, 1030, 730, 710, 700 cm^{-1}.

Found: C, 80.31; H, 9.79%. Calcd for $C_{11}H_{16}O$: C, 80.44; H, 9.83%.

5-Cyanomethyl-7-isopropylidenebicyclo[2.2.1]hept-2-ene (7). Tosylation of **6** (9.20 g, 0.0605 mol) with tosyl chloride (13.9 g, 0.0728 mol) in pyridine (55 mL) gave 16.7 g of the tosylate as a viscous oil, which was mixed with NaCN (45.0 g, 0.918 mol) and *N,N*-dimethylformamide (520 mL). The mixture was heated at 110 °C for 20 h and a workup followed by distillation provided 7.22 g of **7** (80% yield); bp 114—118 °C (4 mmHg). IR (neat film) 3060, 2240, 730, 710, 700 cm^{-1}.

Found: C, 83.01; H, 8.70; N, 8.05%. Calcd for $C_{12}H_{15}N$: C, 83.19; H, 8.73; N, 8.09%.

5-Carboxymethyl-7-isopropylidenebicyclo[2.2.1]hept-2-ene (8). A mixture of **7** (36.7 g, 0.212 mol), KOH (35.7 g, 0.635 mol), and ethylene glycol (420 mL) was stirred at 140—150 °C for 8 h. A usual workup followed by distillation gave 31.2 g of **8** (77% yield); bp 142—146 °C (1 mmHg). IR (neat film) 1710, 720, 710 cm^{-1}.

Found: C, 74.88; H, 8.22%. Calcd for $C_{12}H_{16}O_2$: C, 74.97; H, 8.39%.

3-Isopropylidenetetracyclo[5.1.1.0^{2,6}.0^{4,8}]nonan-9-one (10). By use of a procedure similar to that reported by Sauers,[4] **8** (27.8 g, 0.145 mol) was converted into 6.80 g of **10** (32% yield) after alumina chromatography (pentane eluent) as a colorless oil; ^1H NMR (CCl_4) δ=1.60 (s, 3H), 1.63 (s, 3H), 1.4—1.6 (m, 2H), 2.2—3.0 (m, 6H). IR (neat film) 1780 cm^{-1}. The oily material was without further purification used in the next reaction.

6-Isopropylidenetricyclo[3.3.0.0^{3,7}]octane-2-carboxylic Acid (11). By use of a procedure similar to that reported by Sauers,[4] **10** (11.2 g, 0.0644 mol) was converted into **11** (3.84 g, 31% yield) after crystallization from pentane; mp 98—101 °C (in a sealed tube). IR (KBr) 1700 cm^{-1}.

Found: C, 75.13; H, 8.48%. Calcd for $C_{12}H_{16}O_2$: C, 74.97; H, 8.39%.

Optical Resolution of 11. To a solution of **11** (7.00 g, 0.0364 mol) in ethanol (70 mL) was added (+)-1-(2-naphthyl)ethylamine (6.23 g, 0.0364 mol). The deposited salt (6.26 g), $[\alpha]_D^{30}$ −8.71° (*c* 0.875, $CHCl_3$), was freed from the mother liquor which was reserved for isolation of the enantiomer (+)-**11**. Several times recrystallization of the salt from ethanol gave 3.49 g of the salt, $[\alpha]_D^{28}$ −32.6° (*c* 0.730, $CHCl_3$), which was stirred for 6 h with 10% HCl at room temperature. A usual workup provided 1.40 g of (−)-**11**, $[\alpha]_D^{28}$ −74.1° (*c* 0.805, $CHCl_3$). The carboxylic acid (−)-**11** (200 mg, 1.04 mmol) was treated with excess of a solution of diazomethane in ether with ice-cooling. A usual workup followed by prep. GLC separation (at 160 °C) gave 140 mg of (−)-**12** (65% yield); $[\alpha]_D^{27}$ −79.4° (*c* 0.903, $CHCl_3$). ^1H NMR (CCl_4) δ=1.7—1.9 (m, 4H), 1.51 (s, 6H), 2.4—2.8 (m, 5H), 3.53 (s, 3H). IR (neat film) 1730 cm^{-1}.

Found: C, 75.52; H, 8.75%. Calcd for $C_{13}H_{18}O_2$: C, 75.69; H, 8.80%.

From the dextrorotatory salt (1.44 g), $[\alpha]_D^{28}$ +53.3° (*c* 0.110, $CHCl_3$), isolated from the mother liquor, 550 mg of (−)-**11**, $[\alpha]_D^{28}$ +67.7° (*c* 0.950, $CHCl_3$), was obtained. Esterification of (+)-**11** (530 mg) gave 395 mg of (+)-**12**, $[\alpha]_D^{27}$ +72.5° (*c* 0.890, $CHCl_3$), after prep. GLC separation.

6-Oxotricyclo[3.3.0.0^{3,7}]octane-2-carboxylic Acid (14). Ozonization of (−)-**12**, $[\alpha]_D^{27}$ −77.5°, (900 mg, 4.37 mmol) followed by treatment with zinc powder and acetic acid was carried out by the similar procedure reported in our preceding paper[2] to give 235 mg of **13** (30% yield) after alumina chromatography (pentane–ether 1:1) followed by sublimation (75 °C at 30 mmHg); mp 63—65 °C (in a sealed tube) (lit,[2] (±)-**13**; mp 64—64.5 °C).

Found °C, 66.62; H, 6.78%. Calcd for $C_{10}H_{12}O_3$: C, 66.65; H, 6.71%.

The ester **13** (210 mg, 1.17 mmol) was stirred under reflux for 3 h in 4 mL of 50% aqueous methanol with KOH (205 mg) to give 158 mg of **14** (81% yield) after sublimation (110 °C at 10 mmHg); mp 120—121 °C (lit,[2] (±)-**14**; mp 125—126 °C). $[\alpha]_D^{25}$ −60.8° (*c* 0.875, MeOH). IR (KBr) 1760, 1710 cm^{-1}.

Found: C, 64.99; H, 6.09%. Calcd for $C_9H_{10}O_3$: C, 65.05; H, 6.07%.

Methyl (−)-Tricyclo[3.3.0.0^{3,7}]octane-2-carboxylate (16). By use of a procedure similar to that reported in our preceding paper,[2] the Wolff-Kishner reduction of (−)-**14** (130 mg, 0.783 mmol), $[\alpha]_D^{25}$ −60.8°, was carried out with KOH (282 mg) and hydrazine hydrate (310 mg, 6.20 mmol) in triethylene glycol (3 mL) to give 105 mg of **15**. Esterification of **15** with diazomethane yielded (−)-**16** (80 mg, 62% overall yield) after alumina chromatography followed by prep. GLC (at 120 °C); $[\alpha]_D^{26}$ −13.1° (*c* 0.655, $CHCl_3$) [lit,[5] bp 83—84 °C at 4 mmHg; $[\alpha]_D^{17}$ +14.5° ($CHCl_3$)].

Found: C, 72.34; H, 8.62%. Calcd for $C_{10}H_{14}O_2$: C, 72.26; H, 8.49%.

References

1) H. Park and L. A. Paquette, *J. Org. Chem.*, **45**, 5378 (1980) and references cited therein.

2) M. Nakazaki, K. Naemura, H. Harada, and H. Narutaki, *J. Org. Chem.*, **47**, 3470 (1982).

3) B. Kissler and R. Gleiter, *Tetrahedron Lett.*, **26**, 185 (1985).

4) R. R. Sauers and K. W. Kelly, *J. Org. Chem.*, **35**, 3286 (1970).

5) M. Nakazaki, K. Naemura, and N. Arashiba, *J. Org. Chem.*, **43**, 888 (1978).

6) C. Courtot, *Justus Liebigs Ann. Chem.*, **4**, 68 (1915).

**1 mmHg=133.322 Pa.

A New Synthesis of α-Phenylhomoallylnitriles from β-Nitrostyrene and Allylic Silanes

Hidemitsu UNO,* Satomi FUJIKI, and Hitomi SUZUKI*
Advanced Instrumentation Center for Chemical Analysis, Ehime University, Bunkyo-cho 2-5, Matsuyama 790
(Received October 18, 1985)

Synopsis. $TiCl_4$-catalyzed addition of allylic silanes to β-nitrostyrene affords γ,δ-unsaturated nitronates which, on treatment with low valent titanium in situ generated from Ti(IV) and zinc, are smoothly converted to γ,δ-unsaturated nitriles in moderate yields.

Michael-type additions of enol silyl ethers[1] and allylic silanes[2] to nitroalkenes have been used for the synthesis of 1,4-dicarbonyl compounds. In these reactions, an appropriate Lewis acid ($TiCl_4$, $SnCl_4$, or $AlCl_3$) is used as activator of nitroalkenes. Among the Lewis acids employed, $TiCl_4$ may be regarded as a potential reductant since, on treatment with zinc, it generates low valent titanium compound which can reduce carbonyl compounds to pinacols or olefins.[3] Based on this dual role of titanium compound, we have developed a new method of preparing α-phenylhomoallylnitriles **4**[4] from allylic silanes **1** and β-nitrostyrene (**2**).

In the presence of $TiCl_4$, allylic silanes **1** react smoothly with β-nitrostyrene (**2**) to give γ,δ-unsaturated silyl nitronates **3**. Subsequent addition of zinc dust to the reaction mixture produces low valent titanium from $TiCl_4$, which then converts nitronates **3** to γ,δ-unsaturated nitriles **4**.[5] Although the reaction is subject to extensive formation of phenylacetonitrile (**5**) as by-product, the yields of nitriles **4** are in most cases acceptable as shown in Table 1. In the absence of an allylic silane, β-nitrostyrene remained almost unaffected at low temperature, while by adding chlorodimethylphenylsilane or chlorotrimethylsilane instead of an allylic silane to the reaction system nitroolefin **2** was readily converted to nitrile **5** in good yield. Therefore, the formation of **5** as a common by-product would reasonably be attributed to the concurrent chlorinolysis of allylic silanes by $TiCl_4$.

Allylic groups usually entered into β-nitrostyrene (**2**) with allylic transposition (Entries 4—7).[6] However, buten-3-ylsilane **1h** afforded a mixture of two regioisomers (**4h**:**4d**=32:13) (Entry 8), while 2-methyl-2-propenylsilane **1i** suffered hydrochlorination of double bond of the final product (Entry 9).

The present reaction not only offers a new synthetic route to γ,δ-unsaturated nitriles, but also demonstrates a successful use of titanium compound as Lewis acid and reductant in a simple one-pot procedure.[7]

Experimental

Materials. Allylic silanes **1b** (bp 93 °C/2.27 kPa), **1h**[8] (bp 106 °C/2.67 kPa), and **1i** (110 °C/3.07 kPa) were prepared from chlorodimethylphenylsilane and the Grignard reagents. Crotylsilane **1d** (bp 106 °C/2.67 kPa) and prenylsilane **1e** (bp 115—118 °C/2.00 kPa) were prepared from silyllithium and allylic halides according to the literature.[9] Cinnamylsilane **1f** (bp 123 °C/27 Pa) was obtained by the reaction of a lithio derivative of allylbenzene with chlorodimethylphenylsilane. Allylic silane **1g** was prepared by our method.[10] Titanium tetrachloride was used after distillation. Products were identified by mass, IR, and ^1H NMR spectra as well as by direct comparison with authentic specimens. Purification of the products was performed by a silica-gel column chromatography (Wakogel C-200; hexane-CH_2Cl_2

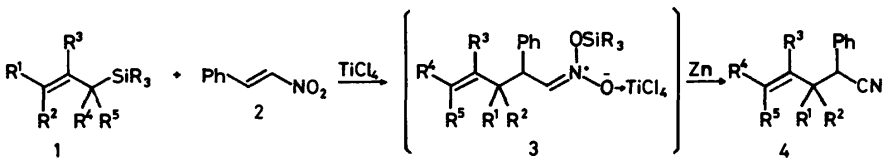

Scheme

Table 1. Homoallylnitriles Obtained from Allylic Silanes and β-Nitrostyrene

Entry		Allylic silane **1**						Homoallylnitrile **4**	Phenylacetonitrile **5**	Other product
		SiR_3	R^1	R^2	R^3	R^4	R^5	Yield/%[a]	Yield/%[a]	Yield/%[a]
1	a	$SiMe_3$	H	H	H	H	H	55	30	—
2	b	$SiMe_2Ph$	H	H	H	H	H	61	23	—
3	c	$SiPh_3$	H	H	H	H	H	69	15	—
4	d	$SiMe_2Ph$	Me	H	H	H	H	65[b]	21	—
5	e	$SiMe_2Ph$	Me	Me	H	H	H	33	21	—
6	f	$SiMe_2Ph$	Ph	H	H	H	H	41[c]	19	—
7	g	$SiMe_2Ph$	H	H	H	Me	CO_2Me	46	20	—
8	h	$SiMe_2Ph$	H	H	H	Me	H	32[d]	22	13[e]
9	i	$SiMe_2Ph$	H	H	Me	H	H	—	11	19[f]

a) Isolated yields. b) Diastereomeric mixture (75:25 estimated by 400 MHz ^1H NMR). c) Diastereomeric mixture (67:33 estimated by 400 MHz ^1H NMR). d) Stereoisomeric mixture (*E*-**4h**:*Z*-**4h**=ca. 1:1). e) 3-Methyl-2-phenyl-4-pentenenitrile **4d**. f) 4-Chloro-4-methyl-2-phenylpentanenitrile.

as eluent) and/or preparative GPC (Japan Analytical Industry, LC-08; JAI-1H (20 mmID×60 cm)+JAI-2H (20 mmID×60 cm)).

General Procedure. To a stirred solution of β-nitrostyrene (**2**, 164 mg, 1.1 mmol) and an allylic silane (**1**, 1 mmol) in CH_2Cl_2 (10 ml) was added $TiCl_4$ (1 M** CH_2Cl_2 solution, 1.5 ml) at −15 °C under argon. After disappearance of **2** (ca. 2 h), dry THF and zinc dust (200 mg, 3 mmol) were added successively and the resulting dark purple mixture was stirred for another hour. The reaction was quenched by adding aqueous $NaHCO_3$ and ether. The suspension was then filtered through a Celite pad. The filtrate was separated and the aqueous layer was extracted twice with ether. The combined extracts were washed with brine and dried over Na_2SO_4. Evaporation of the solvent gave an oily material which was chromatographed on silica gel.

2-Phenyl-4-pentenenitrile 4a. 60 MHz ^{1}H NMR (CCl_4) δ= 2.58 (2H, t, J=7 Hz), 3.78 (1H, t, J=7 Hz), 5.12 (2H, m), 5.68 (1H, ddt, J=16, 10, and 7 Hz), and 7.30 (5H,m); IR (NaCl) 3047 (m), 3010 (m), 2975 (m), 2960 (m), 2900 (m), 2225 (m), 1635 (s), 1450 (s), 990 (m), 920 (s), 750 (vs), and 690 cm^{-1} (vs); MS m/z (rel intensity) 157 (M^+, 63), 117 (37), 116 (100), and 90 (98).

3-Methyl-2-phenyl-4-pentenenitrile 4d. 400 MHz ^{1}H NMR ($CDCl_3$) (major isomer) δ=1.12 (3H, d, J=6.7 Hz), 2.66 (1H, m), 3.82 (1H, d, J=11.6 Hz), 5.15 (2H, m), 5.75 (1H, m), and 7.30 (5H, m); (minor isomer) δ=1.14 (3H, d, J=7.6 Hz), 2.66 (1H, m), 3.73 (1H, d, J=6.4 Hz), 5.05 (2H, m), 5.75 (1H, m), and 7.30 (5H, m); IR (NaCl) 3080 (m), 3055 (m), 2960 (vs), 2925 (m), 2230 (m), 1640 (m), 1490 (s), 1455 (vs), 995 (s), 925 (vs), 750 (s), and 700 cm^{-1} (vs); MS m/z (rel intensity) 171 (M^+, 24), 117 (59), 116 (100), 115 (100), and 90 (21).

3,3-Dimethyl-2-phenyl-4-pentenenitrile 4e. 60 MHz ^{1}H NMR (CCl_4) δ=1.16 (6H, s), 3.50 (1H, s), 5.02 (2H, m), 5.80 (1H, dd, J=16 and 10 Hz), and 7.20 (5H, m); IR (NaCl) 2955 (vs), 2920 (m), 2235 (w), 1490 (s), 1450 (s), 1000 (m), 730 (vs), and 700 cm^{-1} (vs); MS m/z (rel intensity) 185 (M^+, 15), 117 (100), 116 (80), 115 (22), and 90 (16).

2,3-Diphenyl-4-pentenenitrile 4f. Colorless solids; mp 116—117 °C; 400 MHz ^{1}H NMR ($CDCl_3$) (major isomer) δ=3.72 (1H, t, J=7 Hz), 4.07 (1H, d, J=7 Hz), 5.17 (2H, m), 6.05 (1H, ddd, J=16, 10, and 7 Hz), and 7.20 (10H, m); (minor isomer) δ=3.68 (1H, t, J=7 Hz), 4.15 (1H, d, J=7 Hz), 5.17 (2H, m), 6.23 (1H, ddd, J=16, 10, and 7 Hz), and 7.20 (10H, m); IR (NaCl) 3050 (m), 3000 (m), 2945 (s), 2910 (s), 2195 (vw), 1450 (m), 1110(vs), 790 (vs), 745 (m), and 695 cm^{-1} (vs); MS m/z (rel intensity) 234 (M^+, 4), 207 (3), 119 (84), 118 (100), and 117 (100); Anal. Found: C, 87.25; H, 6.53; N, 5.85%. Calcd for $C_{17}H_{15}N$: C, 87.51; H, 6.48; N, 6.00%.

Methyl 5-Cyano-2-methyl-5-phenyl-2-pentenoate 4g. 60 MHz ^{1}H NMR ($CDCl_3$) δ=1.76 (3H, broad s), 2.72 (2H, t, J=7 Hz), 3.70 (3H, s), 3.86 (1H, t, J=7 Hz), 6.64 (1H, m), and 7.29 (5H, m); IR (NaCl) 2930 (m), 2910 (m), 2225 (m), 1710 (vs), 1450 (s), 1120 (vs), 740 (s), and 690 cm^{-1} (vs); MS m/z (rel intensity) 229 (M^+, 26), 143 (14), 128 (15), and 117 (100).

2-Phenyl-4-hexenenitrile 4h. 400 MHz ^{1}H NMR ($CDCl_3$) (cis isomer) δ=1.55 (3H, d, J=7.0 Hz), 2.67 (2H, m), 3.80 (1H, m), 5.43 (1H, m), 5.65 (1H, dq, J=10.1 and 7.0 Hz), and 7.32 (5H, m); (trans isomer) δ=1.70 (3H, d, J=6.1 Hz), 2.56 (2H, m), 3.80 (1H, m), 5.43 (1H, m), 6.59 (1H, dq, J=15.6 and 6.1 Hz), and 7.32 (5H, m); IR (NaCl) 3020 (m), 2960 (m), 2910 (m), 2245 (m), 1600 (m), 1495 (s), 1455 (vs), 970 (s), 760 (s), and 700 cm^{-1} (vs); MS m/z (rel intensity) 171 (M^+, 39), 117 (100), 116 (96), and 90 (49).

4-Chloro-4-methyl-2-phenylpentanenitrile. 400 MHz ^{1}H NMR ($CDCl_3$) δ=1.63 (3H, s), 1.78 (3H, s), 2.22 (1H, dd, J=15.0 and 3.1 Hz), 2.47 (1H, dd, J=15.0 and 9.8 Hz), 4.18 (1H, dd, J=9.8 and 3.1 Hz), and 7.40 (5H, m); IR (NaCl) 3010 (m), 2230 (m), 1600 (m), 1490 (s), 1450 (s), 1115 (s), 750 (s), and 700 cm^{-1} (vs); MS m/z (rel intensity) 209 (M^++2, 4), 207 (M^+, 9), 172 (18), 157 (7), 131 (100), 130 (13), 129 (40), 128 (14), 117 (57), and 116 (81).

The authors express their appreciation for the measurement of 400 MHz ^{1}H NMR spectra to Mr. Hiroyuki Furuta (Kyoto Univ.) and also for gifts chlorosilanes from Shin-etsu Chem. Co. Ltd.

References

1) M. Miyashita, T. Yanami, and A. Yoshikoshi, *J. Am. Chem. Soc.*, **98**, 4679 (1976); M. Miyashita, T. Kumazawa, and A. Yoshikoshi, *Chem. Lett.*, **1980**, 1043.

2) M. Ochiai, M. Arimoto, and E. Fujita, *Tetrahedron Lett.*, **22**, 1115 (1981).

3) T. Mukaiyama, T. Sato, and J. Hanna, *Chem. Lett.*, **1973**, 1041.

4) D. S. Watt, *Tetrahedron Lett.*, **1974**, 707.

5) J. E. McMurry and J. Melton, *J. Org. Chem.*, **38**, 4367 (1973).

6) A. Hosomi, M. Saito, and H. Sakurai, *Tetrahedron Lett.*, **21**, 3783 (1980), and references cited therein.

7) Allylic stannanes are found to react similarly with 1-nitroalkenes, giving the corresponding homoallylnitriles in much better yields.

8) J. Slutsky and H. Kwart, *J. Am. Chem. Soc.*, **95**, 8678 (1973); I. Fleming and D. Waterson, *J. Chem. Soc., Perkin Trans. 1*, **1984**, 1809.

9) J. G. Smith, S. E. Drozda, S. P. Petraglia, N. R. Quinn, E. M. Rice, B. S. Taylor, and M. Viswanathan, *J. Org. Chem.*, **49**, 4112 (1984).

10) Y. Naruta, H. Uno, and K. Maruyama, *Chem. Lett.*, **1982**, 609.

**1M=1mol dm^{-3}.

Synthesis and Chiral Recognition of Optically Active Crown Ethers Incorporating a 9,9′-Biphenanthryl Moiety as the Chiral Center

Koji YAMAMOTO,* Tomohito KITSUKI, and Yoshio OKAMOTO
Department of Chemistry, Faculty of Engineering Science, Osaka University, Toyonaka, Osaka 560
(Received September 14, 1985)

Synopsis. Two chiral crown ethers incorporating a 9,9′-biphenanthryl moiety as the chiral center have been prepared, and their chiral recognition properties in transport of methyl (±)-phenylglycinate hydrochloride, (±)-1-phenylethylamine hydrochloride, and (±)-1,2-diphenylethylamine hydrochloride were examined.

As an extension of our recent synthetic studies on optically active crown ethers incorporating axially dissymmetric molecules,[1] we report here the preparation and chiral recognition properties of optically active crown ethers (**9**) having a 9,9′-biphenanthryl moiety as the chiral center.

Preparation of **9** was carried out according to the sequence of reactions illustrated in Scheme 1. In the

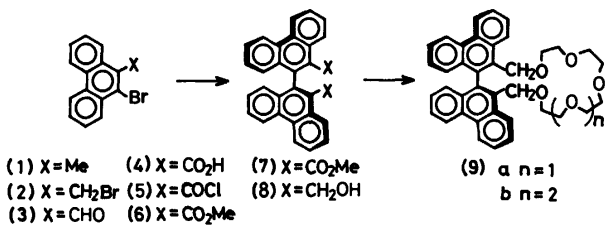

Scheme 1.

initial step 9-bromo-10-methylphenanthrene (**1**)[2] was converted into the corresponding bromomethyl derivative (**2**) by a side chain bromination, followed by a Sommelet reaction[3] and an oxidation to give the acid (**4**) (30% yield from 1). The latter was transformed into the corresponding acid chloride (**5**) and esterified to produce **6** (86.8% yield from **4**). The coupling of the bromo ester (**6**) to give the biphenanthryl diester (**7**) was effected under Ullmann conditions,[4] and the lithium aluminium hydride reduction of this ester gave the alcohol (**8**) (64.4% yield from **6**). Optical resolution of (±)-(**8**) was achived by HPLC with a column packed with (+)-poly(triphenylmethyl methacrylate);[5] elution with methanol gave optically pure (−)-(*S*)-(**8**)[6] and (+)- (*R*)-(**8**) with $[\alpha]_D$ (acetone) −70.0° and +69.7°, respectively. Condensation of (−)-(**8**) with tetraethylene glycol ditosylate (NaH–THF) afforded the (−)-(*S*)-9,9′-biphenanthryl-crown-5 (**9a**), mp 223—225 °C (55% yield). The (+)-(*R*)-biphenanthryl-crown-6 (**9b**) was prepared in the same way from (+)-(**8**). The (+)-alcohol (**8**) was condensed with pentaethylene glycol ditosylate to afford (+)-(*R*)-(**9b**), mp 201—203 °C (47% yield).

Table 1. Differential Transport of Enantiomeric Molecules

Host	Guest	Transport %	Configuration of dominant entiomer	Optical purity %
(−)-(*S*)-(**9a**)	a	1.4	*R*	21
	b	3.1	*S*	88
	c	3.5	*S*	49
(+)-(*R*)-(**9b**)	a	1.8	*S*	15
	b	4.1	*R*	20
	c	3.9	*R*	19

a) Methyl (±)-phenylglycinate hydrochloride. b) (±)-1,2-Diphenylethylamine hydrochloride. c) (±)-1-Phenylethylamine hydrochloride.

Table 1 gives the chiral recognition behavior of (−)-(*S*)-(**9a**) and (+)-(*R*)-(**9b**) with methyl (±)-phenylglycinate hydrochloride, (±)-1-phenylethylamine hydrochloride, and (±)-1,2-diphenylethylamine hydrochloride.

A few of the typical enantiomer selective crown ethers (**10**) prepared by Cram et al.[8] are shown in

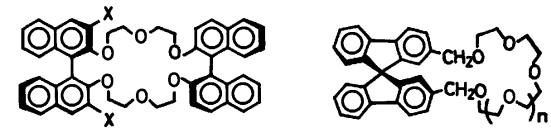

Figure. One of the most enantiomer selective of these compounds is the dimethyl derivative of the bis-(α,α′-binaphthyl)-22-crown-6 (**10**). With methyl (±)-phenylglycinate at 0 °C, a 90% optical purity was found for this crown by differential transport. Our results (Table 1) show that **9a** containing five oxygens has a higher enantiomer selectivity than **9b** containing six oxygens towards all substrates, and 1,2-diphenylethylamine of as high as 88% optical purity was 3.1% transported by (−)-(*S*)-(**9a**). These results are compatible with Prelog's experiment[9] which reveal that 9,9′-spiro-bifluorene-22-crown-5 (**11**) (n=1) possesses the highest enantiomer selectivity for several ammonium cations with a chiral substituent in a 9,9′-spiro-bifluorenocrown series (**11**).

Experimental

Melting points are uncorrected. IR and NMR spectra were recorded on a Hitachi 260-10 and a JNM-MH-100 spectrometer, respectively.

9-Bromo-10-(bromomethyl)phenanthrene (2). A stirred and refluxed solution of **1** (21.7 g, 80 mmol), *N*-bromosuccinimide (15.8 g, 80 mmol), and benzoyl peroxide (0.1 g) in CCl_4 (150 mL) was irradiated with a tungsten lamp (100 W) for 4 h. After a usual workup, the resulting solid was recrystallized from hexane to give **2** (19.6 g, 70% yield), mp 141—142 °C; ^{1}H-NMR (CCl_4) δ=5.13 (s, 2H), 7.48—8.60 (m, 8H) (Found: C, 51.42; H, 2.86%).

9-Bromo-10-formylphenanthrene (3). The aldehyde (**3**)

(4 g, 11.4 mmol) was synthesized from **2** under Sommelet conditions as described.[3] The crude product was recrystallized from benzene to yield **3** (2.4 g, 95%), mp 160—161 °C; IR (KBr) 1700 cm^{-1} (C=O); ^{1}H-NMR ($CDCl_3$) δ=7.54—9.05 (m, 8H), 10.92 (s, 1H) (Found: C, 63.26; H, 3.13; Br, 28.10%).

9-Bromo-10-phenanthrenecarboxylic Acid (4). The oxidation of **3** (8 g, 28 mmol) was carried out according to literature[10] using potassium permanganate (12 g). The resulting product was recrystallized from toluene to afford **4** (4.8 g, 56.8%), mp 221—223 °C; IR (KBr) 1710 cm^{-1} (C=O) (Found: C, 59.68; H, 2.96; Br, 26.66%).

Methyl 9-Bromophenanthrene-10-carboxylate (6). A mixture of **4** (5 g, 16.6 mmol), thionyl chloride (8.3 ml, 114 mmol), and toluene (20 ml) was gradually heated to boiling, whereupon the acid chloride dissolved. After refluxing for 3 h, the solvent was removed by vacuum distillation. The solid residue was recrystallized from benzene-hexane to give **5** (4.7 g, 88.6%), mp 73—74 °C; IR (KBr) 1780 cm^{-1} (C=O). A suspension of **5** (4.5 g, 14 mmol) in absolute methanol (20 ml) was stirred at room temperature untill dissolution had occured. The solution was then heated to reflux for 5 h, followed by evaporation under reduced pressure to give a crystalline solid. Recrystallization from benzene-hexane afforded **6** (4.2 g, 98%), mp 228—229 °C; IR (KBr) 1725 cm^{-1} (C=O); ^{1}H-NMR ($CDCl_3$) δ=4.07 (s, 3H), 7.54—8.68 (m, 8H) (Found: C, 60.95; H, 3.54; Br, 25.31%).

Dimethyl 9,9′-Biphenathryl-10,10′-dicarboxylate (7). The Ullmann coupling of **6** (1.0 g, 3.17 mmol) was carried out according to literature[11] using activated copper bronze (1.6 g), and dry DMF (15 ml). The resulting product was recrystallized from methanol to yield **7** (0.52 g, 69.7%), mp 226—227 °C; IR (KBr) 1725 cm^{-1} (C=O); ^{1}H-NMR ($CDCl_3$) δ=3.35 (s, 6H), 7.20—8.95 (m, 16H) (Found: C, 81.65; H, 4.71%).

10,10′-Bis(hydroxymethyl)-9,9′-biphenanthryl (8). A solution of **7** (3.3 g, 7 mmol) in dry THF (50 ml) was added to a suspension of $LiAlH_4$ (0.6 g, 15.8 mmol) in dry THF (90 ml). The mixture was refluxed for 0.5 h with stirring and cooled in an ice-bath. After a usual workup, the product was recrystallized from chloroform to give **8** (2.9 g, 92.4%), mp 292—294 °C; IR (KBr) 3450 cm^{-1} (OH); ^{1}H-NMR ($CDCl_3$) δ=1.57 (s, 2H), 4.72 (q, J=12 Hz, 4H), 7.16—8.90 (m, 16H) (Found: C, 81.75; H, 4.71%).

Optical Resolution of (±)-(8). Optical resolution of (±)-(**8**) was achieved by HPLC with a column packed with (+)-poly(triphenylmethyl methacrylate) as descrived.[12] A solution of (±)-(**8**) (15 mg) in methanol (15 ml) was injected on the column and eluted with methancl to give the first eluted (−)-isomer followed by (+)-isomer. The procedure was repeated to process a total of 1 g of **8**, and recrystallization of the resolved enantiomeric compounds from chloroform afforded optically pure (*S*)-(−)-(**8**) and (*R*)-(+)-(**8**) respectively. (*S*)-(−)-(**8**): 0.45 g (45%), mp 280—281 °C, $[\alpha]_D^{25}$ −70.0° (acetone); (*R*)-(+)-(**8**): 0.46 g (46%), mp 281—282 °C, $[\alpha]_D^{26}$ +69.7° (acetone).

(−)-(*S*)-Decahydrodiphenanthro[9,10-*o*:9′,10′-*q*][1,4,7,10,13]-pentaoxacyclononadecin (9a). To a boiling suspension of NaH (36 mg, 1.5 mmol) in dry THF (15 ml) was added a solution of (−)-(**8**) (170 mg, 0.41 mmol) and tetraethylene glycol ditosylate (180 mg, 0.41 mmol) in dry THF (30 ml) dropwise over 8 h period under N_2. The reaction mixture was refluxed for further 12 h, cooled in an ice-bath, and quenched with water (12 ml). After a usual workup, the crude product was chromatographed on alumina (benzene eluent) to give a solid which was recrystallized from benzene-hexane to furnish (−)-(**9a**) (130 mg, 55%), mp 223—225 °C, $[\alpha]_D^{23}$ −143.9° ($CHCl_3$); ^{1}H-NMR ($CDCl_3$) δ=3.05—3.78 (m, 16H), 4.70 (s, 4H), 7.15—9.10 (m, 16H); Found: C, 79.48; H, 6.35%. Calcd for $C_{38}H_{36}O_5$: C, 79.69; H, 6.34%.

(+)-(*R*)-Dodecahydrodiphenanthro[9,10-*r*:9′,10′-*t*][1,4,7,10,13,16]hexaoxacyclodocosin (9b). Condensation of (+)-(**8**) (400 mg, 0.965 mmol) with pentaethylene glycol ditosylate (480 mg, 0.965 mmol) was carried out by the same procedure as described for **9a**. The product was chromatographed on alumina (benzene eluent) followed by recrystallization from benzene-hexane to give (+)-(**9b**) (280 g, 47%), mp 201—203 °C, $[\alpha]_D^{25}$ +166° ($CHCl_3$); ^{1}H-NMR ($CDCl_3$) δ=3.10—3.75 (m, 20H), 4.69 (s, 4H), 7.20—8.97 (m, 16H); Found: C, 77.76; H, 6.48%. Calcd for $C_{40}H_{40}O_6$: C, 77.90; H, 6.54%.

Enantiomer Differential Transport. Differential transport was carried out in a conventional apparatus which consisted of an outer cylindrical gass vessel (24.5 mm inner diameter) and a central glass tube (15.5 mm inner diameter). The 0.01 M (1 M=1 mol dm^{-3}) $CHCl_3$ solution of the host separated the inner aqueous phase (0.1 M HCl) and the outer aqueous phase (0.08 M HCl) which contained $LiPF_6$ (0.4 M) and the racemic guest (0.08 M). The organic layer was stirred at 20 °C for 1 h, and transport was followed by monitoring the absorbance at 262 nm and $[\theta]_{262}$ of the inner aqueous phase.

References

1) M. Nakazaki, K. Yamamoto, T. Ikeda, T. Kitsuki, and Y. Okamoto, *J. Chem. Soc., Chem. Commun.*, **1983**, 787; K. Yamamoto, H. Fukushima, Y. Okamoto, K. Hatada, and M. Nakazaki, *ibid.*, **1984**, 1111; K. Yamamoto, K. Noda, and Y. Okamoto, *ibid.*, **1985**, 1065.

2) J. F. J. Gippy and V. Moss, *J. Chem. Soc.*, **1952**, 2205.

3) D. M. Hall and E. E. Turner, *J. Chem. Soc.*, **1955**, 1242.

4) P. E. Fanta, *Synthesis*, **1974**, 9.

5) Y. Okamoto, S. Honda, I. Okamoto, H. Yuki, S. Murata, R. Noyori, and H. Takaya, *J. Am. Chem. Soc.*, **103**, 6971 (1981).

6) Absolute configuration of (−)-(**8**) was determined by the chiral recognition method developed by Miyano and coworkers.[7] Intramolecular Ullmann reaction of (+)-2,2′-bis(10-bromo-9-phenanthrylcarbonyloxy)-1,1′-binaphthyl (prepared from **5** by reaction with optically pure (−)-(*S*)-1,1′-binaphthyl-2,2′-diol) followed by $LiAlH_4$ reduction gave recovered (−)-(*S*)-1,1′-binaphthyl-2,2′-diol and (−)-(**8**) ($[\alpha]_D^{25}$ −59.5° (acetone), 85% optical yield). This result unequvocally indicate that (−)-(**8**) has a same *S*-configuration.

7) S. Miyano, M. Tobita, and H. Hashimoto, *Bull. Chem. Soc. Jpn.*, **54**, 3522 (1981).

8) R. C. Helgeson and D. J. Cram, *J. Am. Chem. Soc.*, **96** 7367 (1974); M. Newcomb, J. L. Toner, R. C. Helgeson, and D. J. Cram, *ibid.*, **101**, 4941 (1979); D. J. Cram, R. C. Helgeson, S. C. Peacock, L. J. Kaplan, L. A. Domeir, P. Moreau, K. Koga, J. M. Mayer, Y. Chao, M. G. Siegel, D. H. Hoffman, and G. D. Y. Sogah, *J. Org. Chem.*, **43**, 1930 (1978).

9) V. Prelog, *Pure Appl. Chem.*, **50**, 893 (1978).

10) M. Nakazaki, K. Yamamoto, M. Ito, and S. Tanaka, *J. Org. Chem.*, **42**, 3468 (1977).

11) E. Weber, I. Csoregh, B. Stensland, and M. Czugler, *J. Am. Chem. Soc.*, **106**, 3297 (1984).

12) Y. Okamoto, E. Yashima, K. Hatada, and K. Mislow, *J. Org. Chem.*, **49**, 557 (1984).

Mössbauer Study of Tin in γ-AgI

Kazuhiro HIRAGA and Sumio ICHIBA*
Department of Chemistry, Faculty of Science, Hiroshima University,
Higashisenda-machi, Naka-ku, Hiroshima 730
(Received November 9, 1985)

Synopsis. Tin was deposited onto the surface of powdered γ-AgI and introduced into the matrix by solid-state diffusion at 300 °C. The ^{119}Sn Mössbauer spectra show that the deposit before heat treatment was epitaxially grown α-Sn and that the diffused tin was in the state of valency 4, occupying both the octahedral and tetrahedral interstices.

The state of tin in silver halides has been studied by means of Mössbauer spectroscopy. Meisel et al.[1] doped the AgCl polycrystals with 0.05 mol% ^{119}Sn and reported that tin atom existed as Sn^{4+}, occupying an interstice surrounded by four cation vacancies. Efimov et al.[2] also reported the presence of only Sn^{4+} in AgCl and AgI after study by means of emission Mössbauer spectroscopy. They introduced ^{119m}Sn into AgCl and AgI by fusing the corresponding salts with metallic ^{118}Sn and by then irradiating them with thermal neutrons. On the other hand, Lagunov and Polozenko[3] prepared alloys of AgCl and tin enriched with ^{119}Sn and reported that the spectrum of the state of Sn^{4+} in AgCl was due to SnO_2 particles in AgCl. As we have found a sophisticated method by which a small amount of tin can be introduced into the crystalline powder,[4] about 2.8 mol% of natural tin was introduced into the matrix of powdered AgI by the method; the Mössbauer spectra were then measured in order to elucidate the state of tin in AgI, which has not been clear hitherto.

Experimental

Freshly-prepared tin(II) chloride (8.4×10^{-5} mol) was dissolved in dry ethanol (20 cm^3), after which 3×10^{-3} mol of silver iodide (GR, Katayama Kagaku Kogyo Co., Ltd.), which has been sieved to 150—200 mesh, was added to the solution. The powder was suspended in the solution by means of supersonic waves and manual shaking. Sodium borohydride (5×10^{-4} mol) was then added to the solution at 3 °C. After the reduced tin has been deposited on the surface of the powder of AgI, the sediment was filtered out of the solution and washed thoroughly with oxygen-free water, dry ethanol, and finally dry ether under a nitrogen atmosphere in order to remove the reaction by-products. The sample powder was enveloped in an evacuated Pyrex glass ampoule, heated at 300 °C for 10 h, and then cooled to room temperature. The sample was identified as γ-AgI by the X-ray powder diffraction method before and after the heat treatment.

The Mössbauer spectra were recorded by the use of a constant-acceleration-type spectrometer with an accuracy of within 0.05 mm s^{-1}. The Mössbauer source of calcium stannate was used at room temperature, and the absorber was cooled at 93 K in a liquid nitrogen cryostat. The Mössbauer parameters were obtained from computer-fitted Lorentzian curves by the least-squares method.

Results and Discussion

The Mössbauer absorption spectra of the sample before and after heat treatment are shown in Fig. 1. The Mössbauer parameters obtained from the spectra are listed in Table 1. The isomer shift of tin deposited on the γ-AgI substrate was 2.12 mm s^{-1}, a value which agreed roughly with the value of α-Sn, 2.03 mm s^{-1}, but not with that of β-Sn, 2.56 mm s^{-1}. The α-form of tin was found for the first time, whereas the β-form of tin was found previously in our studies of colloidal tin suspension,[5] tin deposit on the surface of α-Fe_2O_3 particles,[4] and tin on NaCl and KCl particles.[6] The α-form of tin may be formed by epitaxial growth. The γ-AgI substrate has a cubic structure of the zincblende type, while the deposited α-Sn, in contrast to β-Sn, has its corresponding cubic structure of the diamond type. Their structures are similar not only topologically but also metrically, so that the lattice constants are 6.489 Å and 6.473 Å respectively. Thus, one element of group 4B, Sn, fits into the 1B–7B compound, γ-AgI, neatly. It should also be noted that the isomer shifts of tin deposited on the surface of the particles of AgBr and AgCl were 2.33 and 2.40 mm s^{-1} respectively.[7]

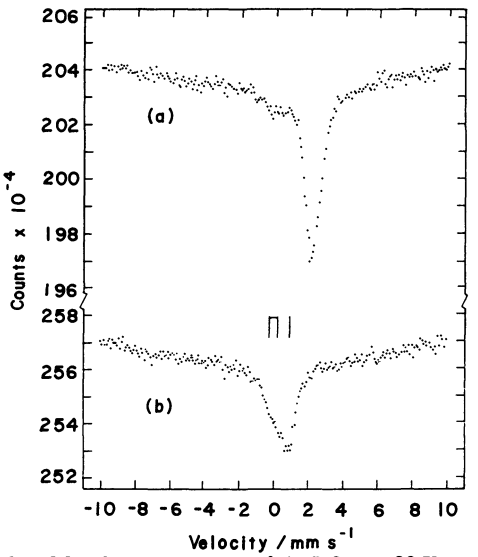

Fig. 1. Mössbauer spectra of AgI:Sn at 93 K.
(a) Before heating; (b) After heating at 300 °C for 10 h.

Table 1. ^{119}Sn Mössbauer Parameters for AgI : Sn at 93 K

	δ / mm s^{-1}	Δ / mm s^{-1}	Γ / mm s^{-1}	Relative area
(a)	2.12	—	1.05	1.00
(b)	0.86	—	0.91	0.47
	0.07	0.30	1.05	0.53

(a) Before heating. (b) After heating.

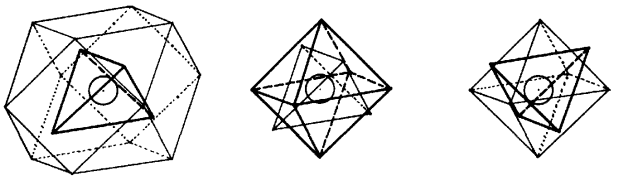

Fig. 2. Three models of the site for a tin atom in γ-AgI. (a) A site for the substitution; (b) and (c) Interstitial site. The circle shows the site for a tin atom. The polyhedra drawn in the thick line are the coordination polyhedra of iodine atoms and drawn in the thin line are the coordination polyhedra of silver atoms.

The absorption line of the tin in γ-AgI was near 0 mm s^{-1}, which corresponds to the Sn^{4+} oxidation state. The line shape was too complex to be attributed to a singlet peak, as in the results obtained by Efimov et al.[2] The parameters in Table 1(b) were derived on the assumption that the absorption line is a composite of a singlet component and a doublet component. The state of tin in γ-AgI will be inferred from the data thus obtained. Three models for the site of the foreign atom, Sn, are shown in Fig. 2. Figure 2(a) shows the silver atom site to be substituted, which is surrounded tetrahedrally by the first neighbors of four iodine atoms and cuboctahedrally by the second neighbors of twelve silver atoms. Two types of interstitial sites are examined; a wider one (Fig. 2(b)) and a narrower one which generates two subtypes in the vacancy distribution (Fig. 2(c)). The number of each site per unit cell is four. If it is assumed that the effective charge on a tin atom is four times as large as that on a silver atom, and that silver atoms nearest to the tin atom are removed to produce cation vacancies, only the tin atom at the interstitial site of Type b will give a singlet line due to the cubic symmetry, while any other sites, Type a or Type c, will give a doublet line. The data in Table 1(b) can be explained by the concurrent occupation of the sites of model b and c or a.

The plausibility of which models are occupied was examined by the use of the theories of the crystal potential and chemical bond.[8,9] Considering the electrostatic crystal potential of the doped crystal, the bond character of Ag–I, and the covalent or ionic radii of the three elements, we concluded that the occupation of the interstices is far more likely to occur than the substitution of a silver atom, and if the covalency (ca. 45%) acts predominantly, the Type c will be preferred to Type b.

References

1) W. Meisel, K. Hennig, and H. Schnorr, *Phys. Status Solidi*, **34**, 577 (1969).
2) A. A. Efimov, S. I. Bondarevskii, P. P. Seregin, and V. T. Shipatov, *Sov. Phys. Solid State*, **12**, 743 (1970).
3) V. A. Lagunov and V. I. Polozenko, *Sov. Phys. Solid State*, **15**, 1210 (1973).
4) S. Ichiba and T. Yamaguchi, *Chem. Lett.*, **1984**, 1681.
5) S. Ichiba, H. Ono, S. Kawasaki, S. Nakagawa, and M. Yamada, *Bull. Chem Soc. Jpn.*, **56**, 2837 (1983).
6) S. Ichiba et al., unpublished work, 1984.
7) S. Ichiba and K. Hiraga, unpublished work, 1984.
8) Y. Sakamoto, M. Miura, K. Hiraga, and H. Murata, *J. Sci. Hiroshima Univ., Ser. A*, **46**, 267 (1983).
9) L. Pauling, "The Nature of the Chemical Bond," 3rd ed, Cornell Univ. Press, Ithaca, New York (1960).

Synthesis and Characterization of Lanthanoid Complexes with 1,3-Bis(2-pyridylmethyleneamino)-2-propanol

Masatomi SAKAMOTO
Department of Industrial Chemistry, Faculty of Engineering, Ehime University, Bunkyo-cho, Matsuyama 790
(Received December 2, 1985)

Synopsis. Lanthanoid complexes of a general formula $[Ln(appy)(NO_3)_2]H_2O$ (Ln=La, Pr, Nd, Eu, or Gd) have been synthesized with 1,3-bis(2-pyridylmethyleneamino)-2-propanol (Happy). The complexes were characterized to be mononuclear and of nine-coordination in solid state with quinquedentate $appy^-$ and two bidentate NO_3^- ions. On dissolution in dimethyl sulfoxide, the complexes were shown to dissociate into $[Ln(appy)(dmso)_n]^{2+}$ based on ^{13}C-NMR spectra and molar conductance measurements.

Many mononuclear lanthanoid complexes have been obtained and structurally characterized.[1] On the other hand, less attention has been paid to binuclear lanthanoid complexes, in spite of much interest in physicochemical properties such as spin-exchange interaction and quantum efficiency of luminescence in condensed systems of f-block elements.[2]

Recently, Schiff base derived from 1,3-diamino-2-propanol and a carbonyl compound such as salicylaldehyde or 2,4-pentanedione was shown to form binuclear copper(II) complexes bridged by the deprotonated alcoholic oxygen of the Schiff base.[3] X-Ray crystallographic analyses for the complexes revealed the Cu-Cu distance to be considerably long (≈3.5 Å), suggesting that the Schiff bases can also function as binucleating ligands toward lanthanoid(III) ions of a large ionic radius.

In this study, lanthanoid complexes (Ln=La, Pr, Nd, Eu, or Gd) of 1,3-bis(2-pyridylmethyleneamino)-2-propanol (the 1:2 condensation product of 1,3-diamino-2-propanol and 2-pyridinecarbaldehyde, abbreviated as Happy hereafter) have been synthesized and characterized, to see the complexing behavior of Happy toward lanthanoid(III) ions.

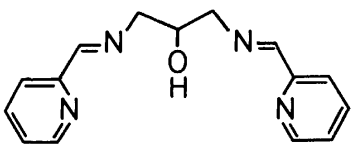

Fig. 1. Chemical structure of Happy.

Experimental

Preparation of Complexes. The metal nitrate (2 mmol) and 2-pyridinecarbaldehyde (2 mmol) were dissolved in methanol (20 cm^3). To this solution was added dropwise a methanolic solution (10 cm^3) of 1,3-diamino-2-propanol (1 mmol) under stirring at room temperature. The precipitate thus formed was filtered, washed with methanol and then with diethyl ether, and dried in vacuo. The yield based on the diamino alcohol was 30—50%.

Elemental analyses for the complexes are given in Table 1.

Measurements. Infrared spectra were measured with a JASCO IR-G spectrometer on KBr disks or nujol mulls. Electric conductivity measurements were carried out with a YOKOGAWA HEWLETT·PACKARD LCZ meter Model 4276A in dimethyl sulfoxide (DMSO) at 25 °C. Magnetic measurements were carried out by the Gouy method at room temperature. The apparatus was calibrated by the use of $Hg[Co(NCS)_4]$. ^{13}C-NMR spectra were recorded on a JEOL FX-100 spectrometer in DMSO-d_6 at 30 °C.

Results and Discussion

Analytical results demonstrated the stoichiometry of the complexes obtained to be $Ln(appy)(NO_3)_2H_2O$ (Table 1). It is presumed that the alcoholic group of the ligand is deprotonated and coordinated to the metal.

Infrared spectra of the complexes are essentially similar to each other. The coordination of the pyridine nitrogen to the metal is inferred from its in-plane deformation band located at 630 cm^{-1}.[4,5] The intense vibration at 1655 cm^{-1} is attributed to the C=N stretching mode. The azomethine nitrogen is probably coordinated to the metal, since Schiff bases are generally stabilized thermally when coordinated to a metal at the azomethine nitrogen.[6] In fact, it was impossible to isolate Happy in the metal-free state.

Table 1. Analytical, Magnetic, and Molar Conductance Data of Complexes

Complex	Found(%)(Calcd (%)[a])				μ_{eff} (B.M.)	Λ_M[b] (S cm^2mol^{-1})
	Ln	C	H	N		
La	24.67 (25.34)	32.64 (32.86)	2.85 (3.13)	15.71 (15.32)	dia.	78
Pr	25.93 (25.61)	32.06 (32.74)	2.79 (3.11)	15.22 (15.27)	3.34	77
Nd	26.29 (26.06)	32.32 (32.55)	2.95 (3.10)	15.06 (15.18)	3.31	77
Eu	27.92 (27.07)	31.73 (32.10)	2.79 (3.05)	14.99 (14.97)	3.31	77
Gd	28.43 (27.75)	31.82 (31.80)	2.76 (3.02)	14.86 (14.83)	7.95	76

a) Values for $Ln(appy)(NO_3)_2H_2O$. b) For 10^{-3} mol dm^{-3}.

The bands due to the nitrate ion appeared at 1450, 1300, 1035, and 815 cm^{-1}. This fact implies that the nitrate ion coordinates to the metal as a bidentate ligand.[7] The nitrate coordination is also supported by the splitting of the combination band in the 1700—1800 cm^{-1} region into two components;[8] the separation of the components for the La, Pr, Nd, Eu, and Gd complexes being 25, 27, 29, 32, and 34 cm^{-1}, respectively. The spectra on nujol mulls showed a broad band at 3500 cm^{-1}, suggesting that the H_2O molecule is not coordinated to the metal in each complex. Room-temperature magnetic moments for the complexes given in Table 1 are quite common for tervalent lanthanoid ions, respectively. Judging from these facts, the $[Ln(appy)(NO_3)_2]H_2O$ complexes are presumably mononuclear and of nine coordination with quinquedentate $appy^-$ and two bidentate NO_3^- ions, though the detailed structure for the complexes is unclear at present.

^{13}C-NMR spectrum of the La complex in DMSO-d_6 exhibited eight singlets at 163.62, 153.76, 149.71, 137.67, 125.76, 122.06, 70.04, and 64.41 ppm. The spectrum of 2-pyridinecarbaldehyde showed the carbonyl carbon signal at more lower field (193.33 ppm). Therefore, any indication of the cleavage of $appy^-$ into its components was not recognized from the spectrum of the La complex. It is likely that the coordination of $appy^-$ to the metal is maintained even in DMSO. The assignments of the signals for the La complex are as follows: 163.62 (azomethine carbon);[9] 153.76—122.06 (pyridine carbons);[9] 70.04 (methine carbon); 64.41 ppm (methylene carbon).

Electrical conductance measurements, on the other hand, revealed the complexes to become electrolytes in DMSO (Table 1). For 1:1 and 1:3 electrolytes, the molar conductances in DMSO are reported to be 37—43[10] and 110 Scm^2mol^{-1},[11] respectively. Molar conductances for $[Ln(appy)(NO_3)_2]H_2O$ (76—78 Scm^2mol^{-1}) clearly indicate that they behave as 1:2 electrolytes in DMSO. Evidently the nitrate ions are displaced with the solvent molecules to form $[Ln(appy)(dmso)_n]^{2+}$ species, though the number (n) of the coordinated solvent molecules is unknown.

From the above discussion, it is evident that Happy acts as a quinquedentate ligand toward lanthanoid ions to form 1:1 complexes with these ions. It should be mentioned that the complexing behavior of Happy differs from that of the macrocyclic Schiff base H_2apdapy (Fig. 2) bearing a structural relation to Happy. Recently, this macrocyclic Schiff base was shown to form 1:2 complexes with lanthanoid ions.[12]

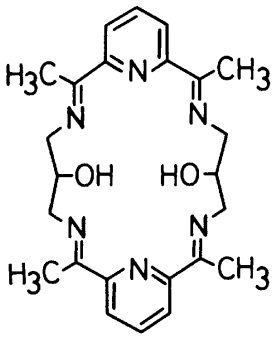

Fig. 2. Chemical structure of H_2apdapy.

The author is greatly thankful to Prof. Dr. Tomitaro Ishimori of Ehime University for his helpful discussion and encouragement throughout this work.

References

1) G. D. Smith, C. N. Caughlan, Mazhar-ul-Haque, and F. A. Hart, *Inorg. Chem.*, **12**, 2654 (1973); J. D. J. Backer-Dirks, C. J. Gray, F. A. Hart, M. B. Hursthouse, and B. C. Schoop, *J. Chem. Soc., Chem. Commun.*, **1979**, 774; K. K. Abid and D. E. Fenton, *J. Chem. Soc., Dalton Trans.*, **1984**, 351.

2) M. Nakamura, H. Ōkawa, S. Kida, and S. Misumi, *Bull. Chem. Soc. Jpn.*, **57**, 3147 (1984).

3) Y. Nishida, M. Takeuchi, K. Takahashi, and S. Kida, *Chem. Lett.*, **1983**, 1815; **1985**, 631.

4) W. Radecka-Paryzek, *Inorg. Chim. Acta*, **45**, L147 (1980); **52**, 261 (1981).

5) K. Nakamoto, "Infrared and Raman Spectra of Inorganic and Coordination Compounds," 3rd ed., Wiley-Interscience, New York (1978), pp. 211—213.

6) M. M. Jones, "Ligand Reactivity and Catalysis," Academic Press, New York (1968), Chap. 2.

7) R. B. King and P. R. Heckley, *J. Am. Chem. Soc.*, **96**, 3118 (1974).

8) A. B. P. Lever, E. Mantovani, and B. S. Ramaswany, *Can. J. Chem.*, **49**, 1957 (1971).

9) D. E. Fenton and M. Vidali, *Inorg. Chim. Acta*, **95**, 187 (1984).

10) P. G. Sears, G. R. Lester, and L. R. Dawson, *J. Phys. Chem.*, **60**, 1433 (1956).

11) S. K. Ramalingan and S. Soundararajan, *J. Inorg. Nucl. Chem.*, **29**, 1763 (1967).

12) M. Sakamoto, represented at the 35th Symposium of Coordination Chemistry in Japan, Hiroshima, October 12, 1985.

Asymmetric Oxidation of Sulfides with Optically Active Hydroperoxides Prepared by Singlet Oxygenation of Thiazolidine Derivatives

Toshikazu TAKATA and Wataru ANDO*
Department of Chemistry, The University of Tsukuba, Sakura, Ibaraki 305
(Received September 20, 1985)

Synopsis. Asymmetric oxidation of prochiral sulfides with optically active hydroperoxides prepared in situ by photo-sensitized oxygenation, gives chiral sulfoxides with moderate optical yields which are enhanced by addition of $Ti(OPr^i)_4$.

Asymmetric oxidation of sulfides is an essential and universal entry for synthesizing optically active sulfoxides with easy performance and less limitation, among several preparative methods with a variety of cptical yields.[1-7] However, the simplest oxidation with optically active peroxy acids resulted in low optical yields (0—5% e.e.),[1] in contrast to those with mixed oxidation systems, especially with modified Sharpless oxidation system (91% e.e.),[5,6] and electrochemical method (≈85% e.e.),[4] which were reported recently. The main reason is considered to be due not only to the distance between the chiral and reaction centers, but also to the lack of close interaction in the transition state. There has hitherto been no appropriate experimental verification for such a hypothesis, but the use of chiral hydroperoxide shortens the distance and therefore it would be expected to enhance the optical yield.

Although organic hydroperoxide is a relatively weak but useful oxidant for many organic substaces such as sulfides, to our knowledge it has not previously been used as a chiral oxidant for asymmentric oxidation of sulfides. In this paper, the optically active hydroperoxides that we have recently prepared by singlet oxygenation of thiazolidine derivatives,[8] are examined in the asymmetric oxidation of prochiral sulfides (Eq. 1).

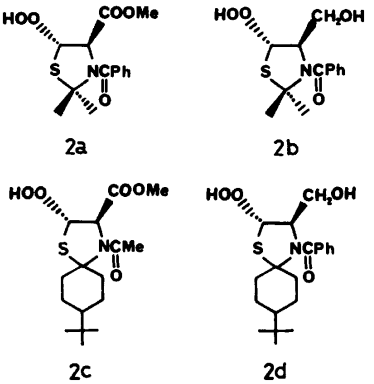

The asymmetric oxidation was carried out in a single reaction adding a prochiral sulfide to a solution of a hydroperoxide freshly prepared in situ by photosensitized oxidation of thiazolidine derivative **1**. The results obtained for a few sulfides with four hydroperoxdes, are summarized in Table 1.

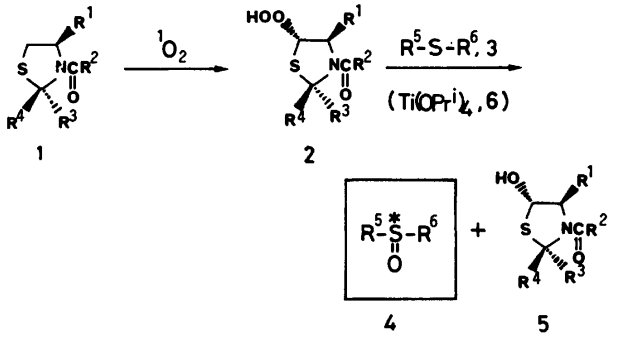

Fig. 1.

Table 1. Asymmetric Oxidation of Prochiral Sulfides with Optically Active Hydroperoxides

Run	Oxidant	Sulfide	Sulfoxide yield/%	Abs. confgn.	Optical purity/%[a]
1	**2a**	p-TolSMe(**4a**)	84	(+)-R	10.0(11)
2	**2b**	**4a**	95	(+)-R	3.6(7)
3	**2c**	**4a**	95	(−)-S	26.7(22)
4	**2a**	$PhSC_6H_4$-OMe-p(**4b**)	79	(+)-R	7.4
5	**2d**	$PhCH_2SBu^t$(**4c**)	93	(−)-S	9.2
6	**2c**	$PhCH_2STol$-p(**4d**)	80	(−)-S	17.2
7	**2a**+**6**	**4a**	59	(−)-S	10.3(12)
8	**2c**+**6**	**4a**	75	(−)-S	—[b](37)
9	**2c**+**6**	**4b**	41	(−)-S	5.3
10	**2c**+**6**	**4c**	80	(−)-S	25.8
11	**2c**+**6**	**4d**	81	(−)-S	21.3

a) Optical purity determined from specific optical rotation of purified sulfoxide (as for max. rotation, see Ref. 7. Parenthesis indicates enantiomer excess calculated from ^1H NMR integration using shift reagent Eu(hfc)3(tris[3-(heptafluoropropylhydroxymethylene)-*d*-camphorato], europium derivative) (error: ±ca. 5%). b) Not determined.

Table 1 indicates that some asymmetric induction on the sulfur atoms of the sulfides took place. The chemical yields of the sulfoxide product were satisfactory, while the optical purities were not high. However, these values are higher than those obtained in asymmetric oxidation with peroxy acids.[1] Direct comparison may be difficult because of the structural differences of the parent skeleton between these two oxidants. Among the hydroperoxieds used,[9] **2c** afforded good results with higher optical yields. As shown in Table 1 the absolute configuration of the excess enantiomer is variable depending on the structure not only of the hydroperoxides but also of the substrate sulfides. We believe that Mislow's suggestion is always operative where a small energy difference in the transition state would change the reaction course so as to give different results.[1]

The effect of the addition of $Ti(OPr^i)_4$ was examined, in expectation of a closer interaction in the transition state in the light of both the Sharpless[6,10] and the modified Sharpless[5] systems for asymmetric oxidations. In fact, enhancement of the optical purity was observed in the case of sulfides **4a** and **4b** (Runs 3 and 7, and 6 and 11). The absolute configuration, however, was changed by addition of **6** from *dextro* to *levo* rotatory for sulfide **4a** (Runs 1 and 7).

In this paper the first asymmetric oxidation of prochiral sulfides with optically active hydroperoxides is described. Since the increasing bulkiness of the oxidant peroxy acids does not always give rise to higher asymmetric induction,[1] the short distance between the reaction and chiral centers is important as well as the close interaction in the transition state during the oxidation. Therefore, the hypothesis that the low asymmetric induction in the peroxy acid oxidation is carried by two factors, is then justified by the results obtained here. Rough calculations[11] indicate the distances for peroxy acids are 361 pm and for hydroperoxide 225 pm. Such clear shortening of the distance in the hydroperoxide unambiguously causes the higher asymmetric induction. Addition of $Ti(OPr^i)_4$ (**6**) seems to affect the closeness in the transition state to some extent, although the exact structure of the transition state is still uncertain.[10]

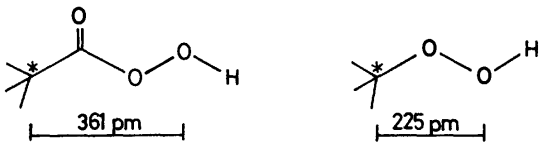

Fig. 2.

Experimental

Thiazolidines (1) were prepared from L-cysteine as described in the previous paper.[8] Sulfoxides (**4**) as products and alcohols (**5**)[12] as by-products were identified by reported physical and spectral data.

General Procedure. a) Without $Ti(OPr^i)_4$. A mixture of a thiazolidine derivative (1, 1—5 mmol) and TPP (5,10,15,20-tetraphenylporphyrin, 15 mg mmol^{-1} of 1) in dry THF ([C]=0.05—0.15 M (1 M=1 mol dm^{-3})) was photo-irradiated with a 500 W halogen lamp with bubbling dry oxygen at −30 °C. The reacton took 2 to 10 hs depending on the substrate (1) used.[8,12] To the resulting solution containing **2**, aprochiral sulfide (**3**, 2—10 mmol) was added and mixed well at −30 °C. The mixture was allowed to stand at −30 °C for 3 h and then at room temperature for a few hours in the dark to avoid further photo-oxidation of **3**. The resulting mixture was concentrated under reduced pressure and the residue was subjected to silica-gel chromatography (eluent: benzene-ethyl acetate-methanol=20:4:1). The products were eluted in the following order: TPP, sulfide **3**, sulfoxide **4**, and alcohol **5**. When further purification was necessary, the sulfoxide was purified by preparative high pressure liquid chromatography of sufficient sample for measurement of the optical rotation.

b) With $Ti(OPr^i)_4$. To the hydroperoxide (**2**) solution, $Ti(OPr^i)_4$ (1—5 mmol, equimolar of 1) and then sulfide **3** (2—10 mmol) were added subsequently at −30 °C. After the same treatment as above, to the reaction mixture concentrated, water (1—5 cm^3) and alumina (5—30 cm^3) were added. After allowing to stand for a few hours at room temperature and then drying with evaporator and vacuum pump, the resulting powder was poured onto the top of the column and chromatographed.

References

1) J. D. Morrison and H. S. Mosher, "Asymmetric Organic Reactions," Prentice-Hall Inc., New Jersey (1971), Chap. 1, p. 336.

2) E. Block, "Oxidation and Reduction of Sulfides," in "The Chemistry of Ether, Crown Ether, Hydroxy Groups, and Their Sulfur Analogues (Supplement E)," ed by S. Patai, John-Wiley, and Sons, New York (1980), Chap. 13, p. 570.

3) M. R. Barbachyn and C. R. Johnson, "Optical Activation and Utilization of Compounds Containing Chiral Sulfur Centers," in "Asymmentric Synthesis," ed by J. D. Morrison and J. W. Scott, Academic Press (1984), Vol. 4, Chap. 3, p. 230.

4) T. Komori and T. Nonaka, *J. Am. Chem. Soc.*, **106**, 265 (1984).

5) P. Pitched, E. Dunach, M. N. Deshmukh, and H. B. Kagan, *J. Am. Chem. Soc.*, **106**, 8188 (1984).

6) F. DiFuria, G. Modena, and R. Seaglia, *Synthesis*, **1984**, 325.

7) T. Takata, M. Yamazaki, K. Fujimori, Y. H. Kim, T. Iyanagi, and S. Oae, *Bull. Chem. Soc. Jpn.*, **56**, 2300 (1983).

8) T. Takata, K. Hoshino, E. Takeuchi, Y. Tamura, and W. Ando, *Tetrahedron Lett.*, **25**, 4767 (1984); T. Takata, Y. Tamura, and W. Ando, *Tetrahedron*, **41**, 2133 (1985); M. Iwakawa, B. M. Pinto, and W. A. Szarek, *Can. J. Chem.*, **56**, 326 (1978).

9) The structures of the thiazolidines 1c and 1d have not yet been determined although both are single stereoisomers.[12] The absolute configuration of the carbon atom bearing the tert-butyl group on the cyclohexane ring is not clear in each case.

10) K. B. Sharpless, S. S. Woodward, and M. G. Finn, *Pure Appl. Chem.*, **55**, 1823 (1984).

11) The distances were calculated from both reported bond lengths and angles: S. Oae and N. Furukawa, "Physical Organic Chemistry (Japanese)," Sankyo Shuppan (1980), Chap. 1.

12) T. Takata, L. Huang, and W. Ando, *Chem. Lett.*, **1985**, 1705.

Hydrogenation and Dimerization of Bicyclo[2.2.1]hepta-2,5-diene Catalyzed by Cobalt(I) Complexes

Hiroyoshi KANAI,* Yoshiyuki WATABE, and Taisei NAKAYAMA
Department of Hydrocarbon Chemistry and Division of Molecular Engineering, Faculty of Engineering, Kyoto University, Sakyo-ku, Kyoto 606
(Received October 9, 1985)

Synopsis. Bicyclo[2.2.1]hepta-2,5-diene **1** was hydrogenated to bicyclo[2.2.1]hept-2-ene **2** and tricyclo[2.2.1.$0^{2,6}$]heptane **3** in a 70:30 ratio and dimerized to Binor-S **4** by [CoX-(PPh_3)$_3$]-BF_3·Et_2O catalysts (X=halogen). **1** was dimerized to **4**—**7** having tricyclo[2.2.1.$0^{2,6}$]heptane skeletons by a [Co(SCN)(PPh_3)$_3$]-$ZnBr_2$-Zn system in THF.

Conjugated dienes were selectively hydrogenated to terminal olefins by [CoX(PPh_3)$_3$]-BF_3·Et_2O systems (X=halogen),[1] but to *cis*-olefins by [Co(SCN)(PPh_3)$_3$]-$ZnBr_2$-Zn systems.[2] Although bicyclo[2.2.1]hepta-2,5-diene **1** is a nonconjugated diene, π-electron systems are supposed to interact through the through-space overlap.[3] When **1** was treated with the [Co(SCN)-(PPh_3)$_3$]-$ZnBr_2$-Zn catalyst in the presence of hydrogen in 1,2-dimethoxyethane, bicyclo[2.2.1]hept-2-ene **2** (37%) and tricyclo[2.2.1.$0^{2,6}$]heptane **3** (31%) were formed with dimers (32%).[2]

The hydrogenation of **1** with a [CoBr(PPh_3)$_3$]-BF_3·Et_2O catalyst was attempted to give small amounts of **2** and **3** and large amounts of dimers (Table 1). The yield of hydrogenation increased slightly when **1** and BF_3·Et_2O were dropwise added to the cobalt complex solution. The ratio of **3**/**2** is lower than that (45/55) in the [Co(SCN)(PPh_3)$_3$]-$ZnBr_2$-Zn system.

Table 1. Hydrogenation and Dimerization of **1** with [CoX(PPh_3)$_3$]-BF_3·Et_2O Catalysts

X	Time min	Yield/%	
		Hydrogenated products (**2**:**3**)	Dimers (**4**)[a]
Cl	60	5.5 (72:28)	84 (94)
Br[b]	90	19 (68:32)	81 (99)

a) Selectivity of **4** in dimers. b) **1** (2.0 mmol) and BF_3 Et_2O (0.4 mmol) in C_6H_5Cl (5 ml) was added dropwise over 55 min.

Table 2. Dimerization of **1** with [CoX(PPh_3)$_3$]-Lewis Acid Systems

X	Lewis acid[a]	Solvent	Time	Conv.	Yield[b]/%	
			h	%	**4**	Other dimers
Br	BF_3Et_2O (0.14)	C_6H_5Br	2	100	98	0
	(4.1)			100	100	0
	(2.0)	C_6H_5Cl	0.17	—	75	0
		C_6H_5Br		—	85	0
		o-$CH_3C_6H_4Cl$		—	72	0
Cl	BF_3Et_2O (2.0)[c]	C_6H_5Br	10	99	95	0
	$ZnBr_2$ (1.0)		2	46	32	1.6
	(2.0)		14	50	35	1.4
	$AlCl_3$ (1.0)		2	18	2.2	0.5
	$AgClO_4$ (2.0)		14	55	53	0

a) The number in parentheses is the ratio of Lewis acid to the cobalt complex. b) Based on **1** added. c) **1** (21.8 mmol, **1**/Co=218) was reacted at 0 °C.

The dimers exclusively consist of endo-*cis*-endo-heptacyclo[5.3.1.$1^{2,6}$.$1^{4,12}$.$1^{9,11}$.$0^{3,5}$.$0^{8,10}$]tetradecane, **4**, usually designated as "Binor-S."[4] [CoX(PPh_3)$_3$] alone has no activity toward the reaction of **1**. When **1** was treated with [CoX(PPh_3)$_3$] and BF_3 in bromobenzene under a nitrogen atmosphere, **4** was selectively produced in a short time. BF_3·Et_2O is superior to $ZnBr_2$ and $AlCl_3$ as the cocatalyst (Table 2). Silver perchlorate reacted with [CoCl(PPh_3)$_3$] to give a cationic complex, [Co(PPh_3)$_3$]$^+$,[1] which was highly selective for the formation of **4** although the yield was low. Lewis acids serve as the production of cationic cobalt complexes. Only slight differences were observed on the reactivity and product composition between halogens in [CoX(PPh_3)$_3$].

Schrauzer et al. have stressed that the formation of **4** with [Zn[Co(CO)$_4$]$_2$] proceeds via a π-complex multicenter process which involves an intermediate containing one molecule of **1** coordinated to each of two cobalt atoms.[4] However, dimerization of **1** to **4** has occurred over mononuclear cationic complexes, binuclear catalysts not being uniquely active for its formation.[5] It is now recognized that monomeric cationic d^8 phosphine complexes including Co, Rh, and Ir are active for the selective formation of **4**.[6]

Haloarenes and arenes are suitable solvents for the reaction, but ethers (tetrahydrofuran and anisole) and dichloromethane are ineffective. Excess of **1** had no effect on the composition of dimers unlike the case with [Zn[Co(CO)$_4$]$_2$] that **4** was obtained exclusively using only a high catalyst to **1** ratio.[4a]

The dimerization of **1** with the [Co(SCN)(PPh_3)$_3$]-$ZnBr_2$-Zn system in THF gave dimers, **4**—**7** and an unidentified dimer(4%):

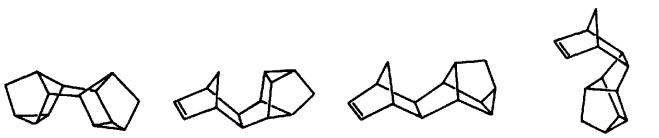

4 (36%) **5** (40%) **6** (9%) **7** (18%)

The dimers, **4**—**7**, consist at least of one tricyclo-[2.2.1.$0^{2,6}$]heptane skeleton. The catalytic activity and selectivity of the [Co(SCN)(PPh_3)$_3$]-$ZnBr_2$-Zn system are lower than those of [CoX(PPh_3)$_3$]-BF_3·Et_2O.

Deuteration of **1** by the [Co(SCN)(PPh_3)$_3$]-$ZnBr_2$-Zn system occurs specifically via the endo-addition of deuterium.[2] The tricyclo[2.2.1.$0^{2,6}$]heptane skeleton of dimers by both Co(I) complex systems suggests the following likely intermediates:

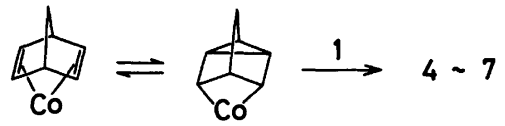

Tetracyclo[3.2.0.0^{2,7}.0^{4,6}]heptane (quadricyclane) **8** was treated with [CoBr(PPh$_3$)$_3$]–BF$_3$·Et$_2$O to give **4** exclusively. **1** was detected during the formation of **4**—**7** by the reaction of **8** with the [Co(SCN)(PPh$_3$)$_3$]–ZnBr$_2$–Zn system.

Experimental

Chlorobenzene, bromobenzene and *o*-chlorotoluene were commercially purified materials and used without further purification. Tetrahydrofuran was heated over lithium aluminium hydride and distilled just before use. Boron trifluoride–diethyl ether complex, zinc bromide, aluminium chloride and silver perchlorate were used without further purification. [CoX(PPh$_3$)$_3$] (X=Cl, Br) was prepared according to the method described earlier.[7] ^{1}H and ^{13}C NMR spectra were recorded on a Nicolet NT-300 and a JEOL FX-100 spectrometer, respectively.

Hydrogenation and Dimerization of 1 with [CoX(PPh$_3$)$_3$]–BF$_3$·Et$_2$O Catalysts. In a three-necked 100-ml flask [CoX(PPh$_3$)$_3$] (0.1 mmol) was placed. Chlorobenzene (10 ml) was added and the flask was dipped in an ice-water bath after several freeze-thaw operations. The flask was filled with atmospheric pressure of hydrogen and BF$_3$·Et$_2$O (0.2 mmol) and **1** (2.0 mmol) were added successively. After 60 min the products were analyzed by a Shimadzu 6A gas chromatograph (column for hydrogenated products: 30% Apiezon grease L 2 m, 80 °C; column for dimers: 20% SE-30, 2 m, 160 °C, and 20% PEG-20M 2 m, 175 °C). Hydrogenated products were identified as **2** and **3**.[8] **4** was identified by comparing its ^{1}H NMR spectrum with that of an authentic sample.[4]

Dimerization of 1 with [CoX(PPh$_3$)$_3$]–Lewis Acid. To a solution of [CoX(PPh$_3$)$_3$] (0.1 mmol) and Lewis acid in a solvent (10 ml) under nitrogen was added **1** (5.45 mmol) at r.t. and the mixture was stirred for an appropriate period. Dimers were analyzed by GLC.

Dimerization of 1 with [Co(SCN)(PPh$_3$)$_3$]–ZnBr$_2$–Zn System. The catalyst was prepared in situ from the reduction of [Co(SCN)$_2$(PPh$_3$)$_2$] (0.3 mmol) with Zn (3.0 mmol) and ZnBr$_2$ (1.0 mmol) in THF (10 ml) under nitrogen at 17 °C.[2] After the color of the solution changed from purple to brown (2—3 h), **1** (2.0 mmol) was added and the mixture was stirred at 17 °C for 20 h. Dimers were separated by a preparative gas chromatograph (20% SE-30, 2 m, 175 °C) and identified by comparing their ^{1}H and ^{13}C NMR spectra with those of authentic samples.[9]

References

1) K. Kawakami, T. Mizoroki, and A. Ozaki, *J. Mol. Catal.*, **5**, 175 (1979).

2) T. Nakayama and H. Kanai, *Bull. Chem. Soc. Jpn.*, **58**, 16 (1985).

3) R. Hoffmann, E. Heilbronner, and R. Gleiter, *J. Am. Chem. Soc.*, **92**, 706 (1970).

4) a) G. N. Schrauzer, B. N. Bastian, and G. A. Fosselius, *J. Am. Chem. Soc.*, **88** 4890 (1966); b) G. N. Schrauzer, R. K. Y. Ho, and G. Schlesinger, *Tetrahedron Lett.*, **1970**, 543.

5) a) R. R. Schrock and J. A. Osborn, *J. Am. Chem. Soc.*, **93**, 3089 (1971); b) M. Ennis, R. M. Foley, and A. R. Manning, *J. Organomet. Chem.*, **166**, C18 (1979).

6) Schrauzer et al.[4] assumed that **1** in conjuction with BF$_3$·Et$_2$O reduced [CoCl$_2$(PPh$_3$)$_2$], [RhCl(PPh$_3$)$_3$], and [IrCl(CO)(PPh$_3$)$_2$] to afford [(Lig)$_n$M-M(Lig)$_n$] (M=Co, Rh, Ir, Lig=PPh$_3$, CO). The assumption is less probable since the addition of AgClO$_4$ to a [CoCl(PPh$_3$)$_3$] solution or that of PPh$_3$ to [Rh(NBD)$_2$]$^+$ (NBD=1)[5a] results in the selective production of **4**.

7) a) H. Kanai and K. Ishii, *Bull. Chem. Soc. Jpn.*, **54**, 1015 (1981); b) M. Aresta, M. Rossi, and A. Sacco, *Inorg. Chim. Acta*, **3**, 227 (1969).

8) P. von R. Schleyer, *J. Am. Chem. Soc.*, **80**, 1700 (1958).

9) a) J. J. Mrowca and T. J. Katz, *J. Am. Chem. Soc.*, **88**, 4012 (1966); b) N. Acton, R. J. Roth, T. J. Katz, J. K. Frank, C. A. Maier, and I. C. Paul, *ibid.*, **94**, 5446 (1972); c) T. J. Katz, J. C. Carnahan, and R. Boecke, *J. Org. Chem.*, **32**, 1301 (1967).

2-Allylisourea as a Starting Material for Palladium-Catalyzed Wittig-Type Allylidenation of Aldehydes

Yoshio INOUE,* Masanori TOYOFUKU, and Harukichi HASHIMOTO
Department of Applied Chemistry, Faculty of Engineering, Tohoku University, Aoba, Aramaki, Sendai 980
(Received November 21, 1985)

Synopsis. 2-Allylic-substituted isoureas underwent Wittig-type allylidenation of aldehydes in the presence of triphenylphosphine and 2 mol% of [Pd(PPh$_3$)$_3$] to give the corresponding conjugated olefins in tolerable to good yields.

π-Allylpalladium chloride complex reacts with several nucleophiles such as stabilized carbanions (pK_a 10—20), enamines, and amines.[1a] The reaction is a well-established and useful synthetic method.[1b] Phosphines are also good nucleophiles, and an excess of triphenylphosphine has actually been shown to react with π-allylpalladium chloride in aqueous acetone to give [Pd(PPh$_3$)$_4$] and an allylic phosphonium salt.[2a] However this finding has not been fully utilized in organic syntheses.[2b,c] For example, the reaction of several aldehydes with allylic alcohols and triphenylphosphine under palladium catalysis has been reported.[2b]

Previously we reported that 2-allyl-1,3-dicyclohexylisourea (**1a**) was an efficient allylating agent for ketones,[3a] imides,[3b] and amides[3c] in the presence of a palladium (0) complex. The suggested reaction pathway involves the π-allyl intermediate **2** which is formed by the oxidative addition of **1a** to a palladium (0) complex. If triphenylphosphine reacts with **2** as a nucleophile, the phosphonium salt **3** may be formed. The isourea anion in **3** is a strong base and is expected to abstract an α-proton to afford allylidenetriphenylphosphorane (**4**). On this consideration we attempted Wittig-type allylidenation of aldehydes catalyzed by palladium (0) employing 2-allylisourea **1a** as the starting material.

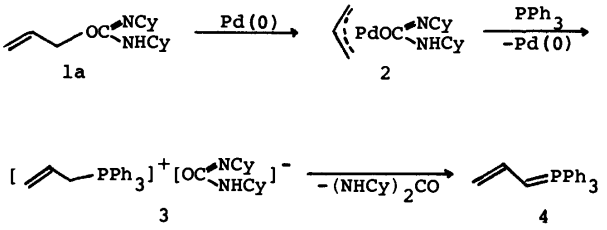

A DMF solution of **1a** (1.0 equiv), triphenylphosphine (1.0 equiv), and benzaldehyde (1.0 equiv) was stirred at 50 °C for 3 h in the presence of 2 mol% of [Pd(PPh$_3$)$_3$]. 1-Phenyl-1,3-butadiene (**5a**) was obtained in 86% yield (*E*:*Z*=33:67) after chromatographic work-up. Ketones such as acetone, acetophenone, and benzophenone did not participate in the reaction. Tributylphosphine gave significantly lower yields of the products. Benzene could be used as a solvent in place of DMF without altering appreciably the product composition. Various conjugated olefins could be prepared from aldehydes and allylic-substituted isoureas **1** in tolerable to good yields. The results are shown in Table 1. Employment of an excess **1** increased the yields of the products. Linear dienes were obtained predominantly even though starting from an α-branched isourea, i.e., 2-(1-methyl-2-propenyl)isourea **1b′**. The same mixture as above was also obtained starting from 2-(2-butenyl)isourea **1b** indicating that the intermediate for each should be

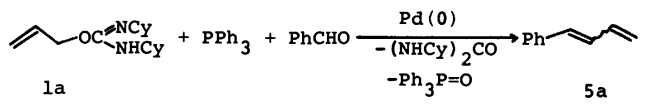

Table 1. Olefinization of Aldehydes with Allylic-Substituted Isoureas **1**[a]

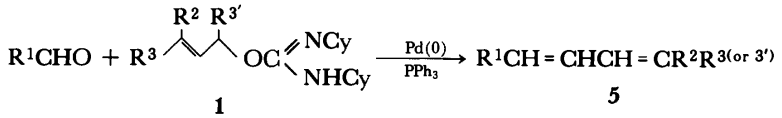

Aldehyde R^1		Isourea **1** R^2,	R^3,	R$^{3'}$	Reaction temp /time °C/h	Yield **5**[b] %	Composition[c] %
Ph	**1a**	H,	H,	H	50/3	**5a** 86 (98)[d]	*Z*:*E*=67:33
	1b	H,	CH_3,	H	80/3	**5b** 47 (68)[d]	1*Z*,3*E*:1*E*,3*E*=52:32[e]
	1b′	H,	H,	CH_3	80/3	**5b** (69)[d]	1*Z*,3*E*:1*E*,3*E*=54:30[e]
	1c	H,	C_3H_7,	H	80/3	**5c** 40 (94)[d]	1*Z*,3*E*:1*E*,3*E*=61:30[f]
	1d	H,	Ph,	H	80/3	**5d** 94	1*Z*,3*E*:1*E*,3*E*=64:36
	1e	CH_3,	CH_3,	H	80/3	**5e** 47	*Z*:*E*=69:31
	1f	CH_3,	C_6H_{11}, (geranyl)	H	80/3	**5f** 48	1*Z*,3*E*:1*E*,3*E*=75:25
C_3H_7	**1d**	H,	Ph,	H	68/3	**5c** 38	1*E*,3*Z*: 1*E*,3*E*=51:49

a) Reaction conditions; see experimental part. b) Isolated yield. c) Area ratio of the GLC peaks. d) Excess isourea **1** (2.0 equiv) was used. e) In addition, 1*Z*,3*Z*-isomer (12%) and 2-methyl-1-phenyl-1,3-butadiene (4%) were formed. f) 1*Z*,3*Z*- and 1*E*,3*Z*-isomers were also obtained in 6 and 3%, respectively.

same and that triphenylphosphine attacked preferencially the less hindered end of the π-allylic group. The initial *E*-geometry in the isoureas was almost preserved during the course of the reaction, but the stereoselectivity about a newly-formed double bond was not observed.[4]

The present reaction generally provides higher yields of dienes 5 under milder reaction conditions compared to the similar palladium-catalyzed Wittig-type olefinization involving allylic alcohols.[2b] It should be noted that this reaction proceeds under neutal conditions in contrast to the normal Wittig reaction in which basic conditions are adopted for the generation of phosphoranes from phosphonium salts.

Experimental

Materials. Allylic-substituted isoureas 1 were prepared from allylic alcohols and dicyclohexylcarbodiimide in the presence of a catalytic amount of copper(I) chloride according to the reported method.[5] [$Pd(PPh_3)_3$] was synthesized according to the known procedure.[6]

General Procedure for the Olefinization of Aldehydes with 1 (Table 1). A DMF solution (5 cm^3) of an allylic-substituted isourea **1** (2 mmol), triphenylphosphine (524 mg, 2 mmol), and an aldehyde (2 mmol) was stirred at 80 °C under nitrogen in the presence of [$Pd(PPh_3)_3$] (36 mg, 0.04 mmol). After 3 h, the reaction mixture was diluted with diethyl ether and the *N,N'*-dicyclohexylurea formed was filtered off. The filtrate was washed with saturated NaCl solution. The organic layer was dried over $MgSO_4$ and concentrated. The products were isolated by column chromatography on silica gel eluting with hexane. The isomer ratio was determined by GLC (Silicone GE SE-52, 20%, 2 m, for **5a—c**, **5e**, **5f**, or OV-1, 3%, 2 m, for **5d**). Individual isomer was separated by GLC (for **5a—c**, **5e**, **5f**) or TLC (for **5d**; silica gel, hexane/ethyl acetate=20/1).

1-Phenyl-1,3-butadiene (5a): *Z*-Isomer; ^1H NMR ($CDCl_3$) δ=5.05—5.49 (m, 2H), 6.00—7.02 (m, 3H), 7.28 (s, 5H). IR (neat) 1000, 900, 805, 770 cm^{-1}. *E*-isomer; ^1H NMR ($CDCl_3$) δ=4.98—5.54 (m, 2H), 6.15—7.18 (m, 3H), 7.18—7.46 (m, 5H). IR (neat) 1630, 1600, 1000, 950, 900 cm^{-1}.

1-Phenyl-1,3-pentadiene (5b): 1*Z*,3*E*-Isomer; ^1H NMR ($CDCl_3$) δ=1.80 (d, 3H), 5.96 (dq, 1H), 6.00—6.88 (m, 3H), 7.28 (s, 5H). IR (CCl_4) 1640, 1600, 985, 950, 930 cm^{-1}. 1*E*,3*E*-isomer; ^1H NMR δ=1.84 (d, 3H), 5.92 (dq, 1H), 6.00—6.86 (m, 3H), 7.04—7.58 (m, 5H). IR ($CDCl_3$) 1595, 1445, 980 cm^{-1}.

1-Phenyl-1,3-heptadiene (5c): 1*Z*,3*E*-Isomer; ^1H NMR ($CDCl_3$) δ=0.97 (t, 3H), 1.11—1.76 (m, 2H), 2.10 (q, 2H), 5.82 (dt, 1H), 5.88—6.10 (m, 3H), 7.08—7.54 (m, 5H). IR (neat) 1650, 1600, 1405, 980 cm^{-1}. 1*E*,3*E*-isomer; ^1H NMR ($CDCl_3$) δ=0.94 (t, 3H), 1.14—1.75 (m, 2H), 2.13 (q, 2H), 5.78 (dt, 1H), 6.02—6.99 (m, 3H), 7.06—7.52 (m, 5H). IR (neat) 1645, 1600, 990 cm^{-1}.

1,4-Diphenyl-1,3-butadiene (5d): The structures of the isomers (1*Z*,3*E*- and 1*E*,3*E*-) were determined by ^1H NMR and IR spectra comparing with the reported ones.[2c]

4-Methyl-1-phenyl-1,3-pentadiene (5e): *Z*-Isomer; ^1H NMR ($CDCl_3$) δ=1.82 (s, 6H), 6.36 (s, 3H), 7.03—7.41 (m, 5H). IR (neat) 1645, 1595, 790, 725 cm^{-1}. *E*-isomer; ^1H NMR ($CDCl_3$) δ=1.85 (s, 6H), 5.82—7.05 (m, 3H), 7.08—7.58 (m, 5H). IR (neat) 1645, 1595, 955 cm^{-1}.

4,8-Dimethyl-1-phenyl-1,3,7-nonatriene (5f): 1*Z*,3*E*-Isomer; ^1H NMR ($CDCl_3$) δ=1.60 (s, 3H), 1.69 (s, 3H), 1.82 (s, 3H), 2.12 (m, 4H), 5.09 (br, 1H), 6.35 (s, 3H), 7.08—7.50 (m, 5H). IR (neat) 1640, 1600, 795, 725 cm^{-1}. 1*E*,3*E*-isomer; ^1H NMR ($CDCl_3$) δ=1.62 (s, 3H), 1.69 (s, 3H), 1.89 (s, 3H), 2.15 (m, 4H), 5.13 (br, 1H), 5.95—7.07 (m, 3H), 7.10—7.59 (m, 5H). IR (neat) 1640, 1600, 965 cm^{-1}.

References

1) a) J. P. Collman and L. S. Hegedus, "Principles and Applications of Organotransition Metal Chemistry," University Science Books, Mill Valley, California (1980), p. 673; b) For reviews, see J. Tsuji, "Organic Synthesis with Palladium Compounds," Springer Verlag, Belrin (1980); B. M. Trost, *Tetrahedron*, **33**, 2615 (1977).

2) a) J. Powell and B. L. Shaw, *J. Chem. Soc., A*, **1968**, 774; b) M. M.-Manas and A. Trius, *Bull. Chem. Soc. Jpn.*, **56**, 2154 (1983); c) Y. Tsukahara, H. Kinoshita, K. Inomata, and H. Kotake, *Bull. Chem. Soc. Jpn.*, **57**, 3013 (1984).

3) a) Y. Inoue, M. Toyofuku, and H. Hashimoto, *Chem. Lett.*, **1984**, 1227; b) Y. Inoue, M. Taguchi, M. Toyofuku, and H. Hashimoto, *Bull. Chem. Soc. Jpn.*, **57**, 3021 (1984); c) Y. Inoue, M. Taguchi, and H. Hashimoto, *Bull. Chem. Soc. Jpn.*, **58**, 2721 (1985).

4) This non-stereoselectivity of allylic ylides is intrinsic; I. Gosney and A. G. Rowley, "Transformations via Phosphorus-stabilized Anions 1," in "Organophosphorus Reagents in Organic Synthesis," ed by J. I. G. Cadogan, Academic Press, London (1979), Chap. 2, p. 66.

5) E. Vowinkel and I. Büthe, *Chem. Ber.*, **107**, 1353 (1974).

6) P. Giannocca, A. Sacco, and G. Vasapollo, *Inorg. Chim. Acta*, **37**, 455 (1979).

On the Synthesis of Crystalline and Semicrystalline Tin(IV) Selenophosphate

Syed Ashfaq NABI and Zia Mahmood SIDDIQI*,†
Chemistry Department, Faculty of Education, University of Sebha, Sebha, Libya
†Department of Chemistry, Aligarh Muslim University, Aligarh, U.P., India
(Received October 24, 1984)

Synopsis. Samples of tin(IV) selenophosphate have been synthesized by mixing 0.05 M (1 M=1 mol dm^{-3}) aqueous solutions of tin(IV) chloride, sodium selenite, and sodium dihydrogenphoshate in different volume ratios and at different pH. A crystalline and a semicrystalline products are obtained when the precipitates are refluxed. Ion-exchange behavior of refluxed product is compared with the unrefluxed one.

Despite a large amount of work done on synthetic inorganic ion-exchangers only a little effort has been made to develop crystalline materials. In order to understand the mechanism of ion-exchange phenomenon in a systematic manner the crystallinity of the product is very important.[1] It is with this view in mind we have made an effort to synthesize tin(IV) selenophosphate in different sets of conditions. This report summarizes our findings in this direction.

Experimental

Reagents. Tin(IV) chloride (Baker Analyzed; U. S. A.), sodium selenite (BDH, England), and sodium dihydrogenphosphate (BDH, India) were used for the synthesis of tin(IV) selenophosphate. All other chemicals were of AnalarR grade.

Apparatus. The X-ray diffractometer PW 1140/90 was used for X-ray study.

Table 1. Synthesis and Properties of Tin(IV) Selenophosphate

Sample No.[a]	Conditions of synthesis					Appearance of bead after drying at 40 °C	Ion-exchange capacity for K^+ ions (meq/dry g)	X-Ray Results
	$SnCl_4 \cdot 5H_2O$ M	Na_2SeO_3 M	NaH_2PO_4 M	Mixing ratio (v/v/v)	pH			
P_1	0.05	0.05	0.05	1:1:2	−ve	White, shiny	1.55	Amorphous
R_1	0.05	0.05	0.05	1:1:2	−ve	White, shiny	1.60	Amorphous
P_2	0.05	0.05	0.05	1:1:2	0.0	Brownish, shiny	1.32	Amorphous
P_3	0.05	0.05	0.05	1:1:1	0.0	Light brown, shiny	1.35	Amorphous
P_4	0.05	0.05	0.05	3:1:2	0.0	White opaque	1.10	Amorphous
R_2	0.05	0.05	0.05	1:1:2	0.0	White, shiny	1.21	Amorphous
R_3	0.05	0.05	0.05	1:1:2	0.0	Brownish, shiny	1.60	Semicrystalline
R_4	0.05	0.05	0.05	1:1:2	0.0	White, fine powder	—	Crystalline
P_5	0.05	0.05	0.05	1:1:2	1.0	Brownish, shiny	1.21	Amorphous
P_6	0.05	0.05	0.05	1:1:2	2.0	Brownish, shiny	1.07	Amorphous
P_7	0.05	0.05	0.05	1:1:2	3.0	Brownish, shiny	0.72	Amorphous

a) R_1=Refluxed in concd HNO_3 for 6 h; R_2=Refluxed in 2M H_3PO_4 for 6 h; R_3=Refluxed in 2M H_3PO_4+2M selenious acid (1:1); R_4=Refluxed in 2M selenious acid.

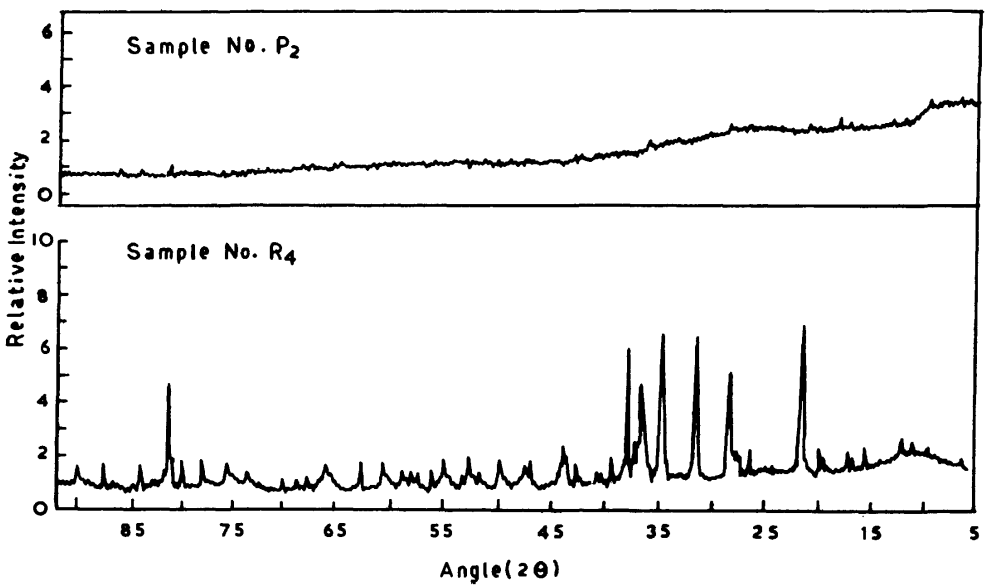

Fig. 1. X-Ray diffraction pattern of tin(IV) selenophosphate.

Table 2. Ion-Exchange Capacity (pH=6) of Tin(IV) Selenophosphates with Different Metal Ions at 25±1 °C

Ion	Salt used	Capacity (meq/g)	
		P_2 (Unrefluxed)	R_3 (Refluxed)
NH_4^+	NH_4Cl	0.87	1.1
Li^+	LiCl	0.83	0.84
Na^+	NaCl	0.91	0.65
K^+	KCl	1.32	1.60
Ca^{2+}	$Ca(NO_3)_2$	2.39	2.66
Sr^{2+}	$Sr(NO_3)_2$	0.97	1.36
Ba^{2+}	$Ba(NO_3)_2$	1.23	1.75

Table 3. X-Ray Data of Tin(IV) Selenophosphate (sample R_4)

θ/degree	d/Å	Intensity of the peak[a]
10.7	5.2136	S
13.1	4.2708	S
14.1	3.9734	S
15.7	3.5772	S
17.3	3.2551	S
18.3	3.0828	S
18.55	3.0427	M
19.0	2.9732	S
21.9	2.5952	M
23.75	2.4034	M
24.8	2.3077	M
26.25	2.1886	M
27.5	2.0963	M
30.3	1.9186	M
33.0	1.7773	M
37.6	1.5863	M
40.6	1.4874	M

a) S: sharp, M: medium.

Synthesis. Samples of tin(IV) selenophosphate were prepared by mixing 0.05M sodium dihydrogenphosphate and 0.05M sodium selenite solutions to 0.05M solution of tin(IV) chloride as described earlier.[2] The pH of mixture was adjusted by adding dilute sodium hydroxide or dilute hydrochloric acid solutions. The precipitate so formed was allowed to settle down for 24 h with mother liquor and then filtered, washed several times with distilled water, and then dried at 40 °C. The precipitate as obtained above was also refluxed for 6 h in various solutions. The refluxed precipitates (R_1, R_2, R_3, and R_4) were then filtered, washed with distilled water, dried at 40 °C, and converted into H^+ form by earlier method.[2] Conditions of synthesis, ion-exchange capacities and appearance of samples of tin(IV) selenophosphate are summarized in Table 1.

Ion-Exchange Capacity. The hydrogen-ion-liberation capacities of samples P_2 and R_3 with different metal ions were determined by column operations as reported earlier.[3] The results are given in Table 2.

X-Ray Diffraction Analysis. Manganese filtered Fe $K\alpha$ radiation was used for X-ray diffraction analyses of all samples. The results are reported in Table 3 and Fig. 1.

Discussion

It is clear from Table 1 that in general the ion-exchange capacity decreases by increasing the pH of solution at constant mixing ratio. It is also observed that there is no significant change in ion-exchange capacity of the material when the precipitate is refluxed for 6 h either in 2M nitric acid or in 2M phosphoric acid. The exchange capacity of tin(IV) selenophosphate (sample R_3) increases when the precipitate of sample P_2 is refluxed in a mixture of selenious acid and phosphoric acid. However, the product (sample R_4) becomes unstable when the precipitate is refluxed with selenious acid alone.

On comparing ion-exchange properties of refluxed product with unrefluxed material it is noted that the former has higher capacities with different metal ions (Table 2). The X-ray analysis of tin(IV) selenophosphate samples indicates that all samples are amorphous except samples R_4 and R_3 which appear to crystalline and semicrystalline. The diffraction pattern of R_4 is more pronounced and well defined (Fig. 1). It is interesting to note that amorphous tin(IV) selenophosphate (sample P_2) becomes crystalline when the precipitate is refluxed in 2M selenious acid for 6 h. The d-values of crystalline product of tin(IV) selenophosphate were calculated by Bragg's equation and are given in Table 3.

The authors are thankful to Professor M. S. Ahmad, Chairman, Department of Chemistry for research facilities and Council of Scientific and Industrial Research, New Delhi for financial assistance.

References

1) S. A. Nabi and Z. M. Siddiqi, *Bull. Chem. Soc. Jpn.*, in press.

2) S. A. Nabi, A. R. Siddiqi, and R. A. K. Rao, *J. Liq. Chromatogr.*, **7**, 1225 (1981).

3) S. A. Nabi, Z. M. Siddiqi, and W. U. Farooqi, *Bull. Chem. Soc. Jpn.*, **55**, 2642 (1982).

Hydrogen Bonding in Polyfluoride Ions

Tapas KAR and Abani Bhusan SANNIGRAHI*
Department of Chemistry, Indian Institute of Technology, Kharagpur 721302, India
(Received March 22, 1985)

Synopsis. Hydrogen bonding in the polyfluoride ions ($H_nF_{n+1}^-$, n=1 to 4) has been discussed in the light of atomic charges, bond ionicities, valencies and bond indices calculated from CNDO/2 wave functions. The hydrogen-bond energy in these ions is found to bear a qualitative relation with the bond index of the hydrogen bond.

The polyfluoride ions, in $H_nF_{n+1}^-$, wther n=1 to 4 have been experimentally characterized[1] as strong hydrogen-bonded systems. They are formed by the interaction of F^- with HF molecules. The experimentally determined structures of the polyfluorides show that the HF molecules are all hydrogen bonded to the central fluoride ion. Clark et al.[2] carried out ab initio SCF calculations and determined the electronic structure and hydrogen-bond energy of these systems. They found that HF_2^- possesses a symmetric linear structure, $H_2F_3^-$ a C_{2v} structure, $H_3F_4^-$ a D_{3h} structure and $H_4F_5^-$ a tetrahedral structure. All these ions contain adjacent strong hydrogen bonds and the average hydrogen-bond energy decreases with increasing n. We have in the present note discussed the hydrogen bonding in the polyfluoride ions in the light of atomic charges, bond ionicities, valencies and bond indices. All these quantities were obtained using CNDO/2 wave function.[3]

Method of Calculation. The experimental geometry being not available for all the species, calculations were performed at their ab initio SCF geometry.[2] Valencies (V_A) and bond indices (B_{AB}) where calculated using the following expressions: [4]

$$V_A = 2P_{AA} - \sum_{\lambda}^{A}\sum_{\sigma}^{A}(P_{\lambda\sigma})^2,$$

$$B_{AB} = \sum_{\lambda}^{A}\sum_{\sigma}^{B}(P_{\lambda\sigma})^2,$$

where, P_{AA} is the charge density on atom A and $P_{\lambda\sigma}$ is an element of the density matrix defined over the atomic orbitals. The percentage of ionic character or the ionicity of the bond A–B was calculated from the relation,

$$\%\ \text{Ionic character} = \frac{n_A - n_B}{n_A + n_B} \times 100,$$

where, n_A and n_B are the populations of atom A and B respectively. In order to calculate the atomic populations associated with a given bond, energy localized molecular orbitals (LMO) were obtained for each molecule using the criterion of Edmiston and Ruedenberg.[5]

Results and Discussion

All the LMO's were obtained with a high degree of localization. The nature of the LMO's indicates that the electronic structure of the polyfluoride ions can be described in a classical manner with an adequate numbers of HF bonds and lone pairs on the fluorine atoms. The hydrogen atom was found to be fractionally bonded in all the molecules.

Table 1. Bond Ionicities of the HF Bonds in Polyfluorides

Molecule	Bond	Population		% Ionic character
	X Y	X	Y	
HF	F-H	1.23	0.77	23.00
HF_2^-	F-H	1.63	0.35	63.78
$H_2F_3^-$	F-H	1.46	0.53	46.73
	F···H	1.82	0.14	85.71
$H_3F_4^-$	F-H	1.38	0.62	38.24
	F···H	1.90	0.08	91.92
$H_4F_5^-$	F-H	1.35	0.65	35.06
	F···H	1.93	0.06	93.46

Table 2. Atomic Charges, Valencies, and Bond Indices of Polyfluorides

Molecule	Atom	Atomic charge	Valency	Bond	Bond index
HF	F	−0.23	0.95	F-H	0.95
	H	+0.23	0.95		
HF_2^-	F	−0.65	0.58	F-H	0.46
	H	+0.30	0.92		
$H_2F_3^-$	F^t	−0.48	0.77	F^t-H	0.68
	H	+0.31	0.90	F^c···H	0.22
	F^c	−0.66	0.61		
$H_3F_4^-$	F^t	−0.40	0.84	F^t-H	0.78
	H	+0.30	0.91	F^c···H	0.13
	F^c	−0.70	0.56		
$H_4F_5^-$	F^t	−0.36	0.87	F^t-H	0.82
	H	0.29	0.91	F^c···H	0.09
	F^c	−0.72	0.55		

The percentage of ionic character of the HF bonds is given in Table 1. Of the four hydrogen-bonded species the HF_2^- ion is unique in the sense that it contains two equivalent bonds each of which can be described either by a normal H–F bond as in the HF molecule or by a dotted bond H···F as it is used to describe a hydrogen bond. The other species contain both types of bonds. The HF bond in HF_2^- is found to be more ionic compared to that in the isolated HF molecule, which indicates that the hydrogen-bond formation is accompanied by the weakening of the HF bond. In the other species the ionic character of the F–H bonds decreases and that of the F···H bonds increases as n increases. This implies that the strength of the hydrogen bond in polyfluorides should decrease with increasing n. Ab initio calculations of Clark et al.[2] support this prediction.

Atomic charges, valencies and bond indices of the

polyfluoride ions are given in Table 2. The atomic charge of the central fluorine increases as we go from HF_2^- to $H_4F_5^-$, which indicates that the magnitude of charge transferred from F^- (central fluorine) to HF molecules decreases with increasing n. Since charge transfer plays a very important role in the formation of the hydrogen bond, one may conclude that the strength of the hydrogen bond progressively decreases with the increasing number of HF molecules interacting with F^- ion to form polyfluorides.

Compared to that in the isolated HF molecule, the hydrogen valency decreases slightly upon hydrogen-bond formation. In HF_2^-, the status of the two H–F bonds and consequently that of the two fluorine atoms are identical. The valency of the terminal F atom increases and that of the central fluorine atom decreases with the increasing size of the polyfluoride ion.

The bond index of the F···H bonds gradually decreases and that of the F–H bond increases with increasing n. Since the bond index represents half the number of electrons engaged in covalent bonding, the above trend in bond index indicates that the strength of the hydrogen bond decreases gradually as we pass from HF_2^- to $H_4F_5^-$. Thus we find that the hydrogen-bond energy in the polyfluorides bears a qualitative relation with the bond index of the F···H bond. This can be understood from the fact that the diatomic contribution to the total CNDO/2 energy contains the term $-B_{AB}\gamma_{AB}/2$ which represents the exchange repulsion contribution to the binding energy. In order to verify whether the qualitative relation between bond index and hydrogen-bond energy holds good for other systems, we calculated the hydrogen-bond indices of the dimers and mixed dimers of NH_3, H_2O, and HF. The results are as follows: $(NH_3)_2$ (0.0026), $(H_2O)_2$ (0.0073), NH_3–H_2O (0.0106), $(HF)_2$ (0.0142), H_2O–HF (0.0199), and NH_3–HF (0.0302), where the figures in the parentheses indicate bond index. The experimental hydrogen-bond energy[6] in the above dimers follows the same order. It may be noted that the hydrogen-bond indices in these dimers are considerably less than those in the polyfluorides. It is consistent with the fact that the above dimers are weak hydrogen-bonded systems, while the polyfluorides are very strong hydrogen-bonded systems.

References

1) J. D. Forrester, M. E. Senko, A. Zalkin, and D. H. Templeton, *Acta Crystallogr.*, **16**, 15 (1963); B. A. Coyle, L. W. Schroeder, and J. A. Ibers, *J. Solid State Chem.*, **1**, 386 (1970); J. A. Ibers, *J. Chem. Phys.*, **40**, 402 (1964); I. Gennick, K. M. Harmon, and M. M. Potvin, *Inorg. Chem.*, **8**, 7033 (1977).

2) J. H. Clark, J. Emsley, D. J. Jones, and R. E. Overill, *J. Chem. Soc., Dalton Trans.*, **1981**, 1219.

3) J. A. Pople, and D. L. Beveridge, "Approximate molecular Orbital Theory," McGraw Hill Book Company, N. Y. (1970).

4) D. R. Armstrong, P. G. Perkins, and J. J. P. Stewart, *J. Chem. Soc., Dalton Trans.*, **1973**, 838.

5) C. Edmiston and K. Ruedenberg, *Rev. Mod. Phys.*, **35**, 457 (1963).

6) J. D. Dill, L. C. Allen, W. C. Topp, and J. A. Pople, *J. Am. Chem. Soc.*, **97**, 7220 (1975).

In Situ Trapping of NO. A Generalized Method for the Synthesis of Metal Nitrosyls

Mohammad Ishaque KHAN and Umesh Chandra AGARWALA*
Department of Chemistry, Indian Institute of Technology, Kanpur 208016, India
(Received February 4, 1985)

Synopsis. Several known nitrosyl complexes of Ru, Rh, Ir, Os, Co, and Mo have been synthesized using a more generalized method, using organic *N*-nitroso compounds. Physical methods such as IR, magnetic measurements, conductance measurements, melting points, and elemental analyses were used for the identification of the products of the reactions.

Although the coupling of gaseous NO with transition metal complexes to yield co-ordinated nitrosyls is a well documented process.[1] Its thermodynamic instability has surged interest in developing new synthetic routes for their synthesis. Our continuing interest in devising a new generalized procedure for introducing NO in metal complexes has suggested to us that the susceptibility of N-N bond cleavage in organic *N*-nitroso amino compounds resulting in the generation of NO in situ under mild experimental conditions could possibly provide a basis for such an attempt. This report suggests that such a goal is indeed realizable for incorporating NO in metal complexes.

Experimental

All the reagents used were of chemically pure grade. Carbon, hydrogen, and nitrogen analyses in the complexes were carried out by the microanalytical laboratory of Indian Institute of Technology.

Halide, cobalt, and rhodium in the complexes were analysed by standard methods. For the phosphorus estimation a weighed amount of the sample was decomposed by heating it for about 15 min with a mixture of sodium peroxide, sugar, and sodium nitrate in the ratio 20:1:3 in a Parr-Bomb crucible. The melt was extracted with water and filtered. After adding a few cm^3 of concentrated sulfuric acid to the filtrate it was evaporated to sulfur trioxide fumes. The resulting mixture was cooled, diluted with water, and filtered, if necessary. Phosphorus was estimated in the filtrate as ammonium molybdophosphate by standard procedure.

The IR spectra were recorded on Shimadzu IR-420 spectrophotometer in the region 4000—400 cm^{-1}. Conductivity measurements were carried out on an Elico Conductivity Bridge type-CM82T. Magnetic measurements were made with a Gouy balance at room temperature (25 °C).

In a typical run 10 cm^3 of a solution containing 0.5 mmol of the metal trihalide in methanol, ethanol, 2-methoxyethanol or benzene (as the ease may be, see Table 1) and 1 mmol of the desired *N*-nitroso amines were added successively to a well stirred, argon purged refluxing solution of about 2 mmol of coligand in the same solvent 15 cm^3. A slow stream of hydrogen chloride gas was also allowed to pass simultaneously through the reaction mixture while using *N*-nitroso alkyl amines, *N*-nitroso diethyl amine as nitrosylating agent (whereas dry chlorine gas was passed during the preparation of the dinitrosyl complex of molybdenum). The resulting reaction mixture was allowed to heat under reflux for about 15 to 20 min, where upon shining crystals of the corresponding nitrosyl in about 60% yield separated in most cases. In the case of molybdenum, a greenish yellow solution was obtained which on concentration to a small volume (5 cm^3), followed by addition of ethanol, gave greenish yellow crystals of the dinitrosyl. These crystals were collected by filtration, washed successively with ethanol, water, ethanol, and ether and dried in vacuo.

Results and Discussion

Table 1 illustrated the application of our procedure to the synthesis of various metal-nitrosyls. Since most of these nitrosyls are known, they have been identified by chemical analyses, and by comparing color, melting point, IR spectra, conductance, and magnetic susceptibility data with those reported.

The analytical data of the diamagnetic, non-conducting, greenish brown complex (mp 168 °C) obtained by the reaction of *N*-nitrosodiethylamine with $RuCl_3 \cdot xH_2O$ and PPh_3 in ethanol medium were in perfect agreement with empirical formula $[Ru\{(C_2H_5)_2N(NO)\}Cl_2(PPh_3)_2]$. Its IR spectrum exhibited bands at 1750(s) and 880(mw) cm^{-1}, assigned to ν(NO) and ν(C-N), respectively, in addition to all the characteristic bands of PPh_3 and the ligand.

In order to facilitate the release of NO by protonating the nitrogen atom N-NO, hydrogen chloride gas was passed through the reaction mixture while using *N*-nitrosodiethylamine as nitrosylating agent. The latter failed to nitrosylate without hydrogen chloride, probably because of its inability to acquire hydrogen ion from the reaction medium.

The purpose of passing dry chlorine gas in the reaction medium while preparing $[Mo(NO)_2Cl_2(PPh_3)_2]$, was two fold: (a) to oxidize molybdenum from zero to a higher oxidation state, and (b) to provide a source of chloride ions in the reaction after reduction.

Rapid perusal of Table 1 shows that the *N*-nitroso amino compounds having electron attracting substituents (R), ($\begin{matrix}R\\R\end{matrix}$>N-NO) effect the formation of nitrosyls with ease while the ones with electron-donating groups do not, but for the ruthenium case. The variations in the nitrosylating properties of *N*-nitroso amines may presumably be caused by the variation of electron density on nitrogen which will effect the N-N bond strength. The negative inductive effect (−I) resulting in the decrease of electron density at nitrogen might facilitate the scission of the N-N bond and vice versa. Thus, we expect that the presence of even one of the two substituents like C_6H_5, CN, CO, C_5H_5N, etc., on the nitrogen atom NO substituted will lead to nitrosylating reaction while the *N*-nitroso amines with both electron-donating groups like CH_3, C_2H_5,

Table 1. Preparation of Metal Nitrosyls

Reaction product	*N*-Nitroso derivative used	Metal used	Coligand	Reaction medium	Special conditions (if any)	ν(NO(cm^{-1}) for metal No synthesized
$[Ru(NO)Cl_3(PPh_3)_2]$[10]	Diphenyl *N*-Nitrosoamine	$MCl_3{\cdot}xH_2O$	$(C_6H_5)_3P$	Ethanol (for M=Ru)	—	1875(M=Ru)
$[Rh(NO)Cl_2(PPh_3)_2]$[11]	*N*-Nitroso-*N*-methylaniline[4]	(M=Ru, Rh, Ir)		or		1630(M=Rh)
$[Ir(NO)Cl_2(PPh^3)_2]$[11]	*N*-Nitrosodibenzylamine[5]			2-methoxyethanol		1560(M=Ir)
	N-Nitrosomethylurethane[6]			(for M=Rh, Ir)		
	N-Nitroso-*N*-phenylbenzylamine[4]					
	N-Nitroso ethylcynamide[7]					
	N-Nitroso-*N*-methylurea[8]					
	N-Nitrosomethylammiminopyridine[9]					
$[Ru(NO)_2(PPh_3)_2]$[12]	*N*-Nitrosodiphenylamine	$RuCl_3{\cdot}xH_2O$	$(C_6H_5)_3P$	Ethanol	In presence of $(C_2H_5)_3N$ in the reaction medium	1655, 1610
$[Ru(NO)Cl_3(PPh_3)_2]$[10]	*N*-Nitrosodiethylamine	$RuCl_3{\cdot}xH_2O$	$(C_6H_5)_3P$	Ethanol	In presence of HCl gas in the reaction medium	1875
$[Ru(C_2H_5)_2N(NO)Cl_2(PPh_3)_2]$[14]	*N*-Nitrosodiethylamine	$RuCl_3{\cdot}xH_2O$	$(C_6H_5)_3P$	Ethanol	—	1750
$[Os(NO)Cl_3(PPh_3)_2]$[12]	*N*-Nitrosodiphenylamine	$Na_2OsCl_6{\cdot}6H_2O$	$(C_6H_5)_3P$	2-Methoxyethanol	—	1850
$[Co(NO)(en)_2Cl]Cl$[15]	*N*-Nitrosodiphenylamine	$CoCl_2{\cdot}6H_2O$	Ethylenediamine (en)	Methanol	—	1630
$[Mo(NO)_2Cl_2(PPh_3)_2]$[13]		$Mo(CO)_6$	$(C_6H_5)_3P$	Benzene	In presence of Cl_2 gas in the reaction medium	1679, 1790

etc., on nitrogen atom, will not be effective nitrosylating agents but for ruthenium case. In the latter case the increased basicity of nitrogen (attached to NO group) because of the presence of alkyl groups, may cause *N*-nitroso amines preferentially coordinated to Ru through N atom attached to NO (i. e. $-Ru-N\langle^{R^1}_{R}$). Ruthenium being acid may withdraw electron density from nitrogen effecting the release of NO from the nitroso amines which subsequently attack on ruthenium with the formation of its nitrosyl. Thus, in case the metal ion is of low σ acidity (low oxidation states), the nitrosylation reaction may not take place.

Although the application of this new procedure has not yet been extensively extended, our present evidence indicates that the nitrosylation reactions will take place with *N*-nitroso amino compounds having at least one electron withdrawing group linked to NO substituted nitrogen atom. We believe that extension of the in situ, trapping of NO has an enormous potential for the effecient synthesis of metal nitrosyls which are rather difficult to synthesize under normal reaction conditions.

References

1) K. G. Caulton, *Coord. Chem. Rev.*, **14**, 317 (1975), and the references cited therein.

2) A. I. Vogel, "Text Book of Quantitative Inorganic Analysis," 3rd ed, Longmans Green and Co., London (1961).

3) F. E. Beamish, "A Textbook of Analytical Chemistry of Noble Metals," Pergamon, Oxford (1966).

4) A. I. Vogel, "A Textbook of Practical Organic Chemistry," 4th ed, English Language Book Society and Longman (1978).

5) C. G. Overberger, L. C. Palmer, B. S. Marks, and N. R. Byrd, *J. Am. Chem. Soc.*, **77**, 4100 (1955).

6) W. H. Hartman and R. Phillips, *Org. Synth.*, Coll. Vol. II, **1959**, 464.

7) S. S. Mirvish, L. D. Nagel, and J. Sams, *J. Org. Chem.*, **38**, 1325(1973).

8) F. Arndt, *Org. Synth.*, Coll., Vol. II, **1959**, 461.

9) A. E. Tschitschibakin and I. L. Khunjanz, *Ber.*, **61**, 2215 (1928).

10) K. R. Laing and W. R. Roper, *J. Chem. Soc., A*, **1970** 2149.

11) S. D. Robinson and M. F. Uttley, *J. Chem. Soc., A*, **1971** 1254.

12) N. Ahmad, J. T. Levison, S. D. Robinson, and M. F. Uttley, *Inorg. Synth.*, **15**, 45 (1974).

13) F. A. Cotton and B. F. G. Johnson, *Inorg. Chem.*, **3**, 1609 (1964).

14) M. I. Khan and U. C. Agarwala, unpublished results.

15) R. D. Feltham and R. S. Nyholm, *Inorg. Chem.*, **4**, 334 (1965).

A New Aspect of the Pressure Effect in Syngas Conversion to Ethylene Glycol

Takashi MASUDA, Kazuhisa MURATA, and Akio MATSUDA*
National Chemical Laboratory for Industry, Tsukuba Research Center, Yatabe, Tsukuba, Ibaraki 305
(Received October 18, 1985)

Synopsis. Pressure effect in syngas conversion to ethylene glycol (EG) is understood in terms of respective partial pressures of hydrogen (P_{H_2}) and carbon monoxide (P_{CO}). A new mechanism is proposed to explain an extraordinary effect of P_{H_2} on the selectivity to EG.

There has been observed a remarkable pressure effect on the rate and the selectivity of syngas conversion to ethylene glycol (EG) in the case of both cobalt,[1,2] and rhodium catalysis.[2,3] Although it has been presumed that both P_{H_2} and P_{CO} are responsible for this pressure effect, its dependency on each of them has never been fully established.[4] We have, therefore, undertaken to clarify the reason for this pressure effect by doing a series of experiments, varrying P_{H_2} at a fixed P_{CO}, and vice versa.

Results and Discussion

Cobalt-catalyzed reactions were performed in a mixed solvent consisting of phenol and *m*-cresol in a weight ratio of 5 to 1, since it is a good solvent for cobalt catalysis according to our previous exploration. While *N*-methyl-2-pyrrolidone (NMP) was used as a solvent for rhodium catalysis, since Rh–NMP is one of the well known system for the EG synthesis.[1] The results of experiments carried out with $Co_2(CO)_8$ 0.855 g (5 mg-atom as Co), phenol 25 g, *m*-cresol 5 g, under various P_{H_2} at 210 °C for 2 h, where P_{CO} was fixed at a constant, 150 kg cm^{-2}, are shown in Fig. 1. The dependency of the rate of EG formation on P_{H_2} is remarkable, the order of EG formation with respect to P_{H_2} being in the range of 2—3. On the other hand, almost linear relation is observed between the rate of methanol formation and P_{H_2}. As a result, the selectivity to EG increases and that to methanol decreases dramatically, as P_{H_2} is increased. The selectivity to methyl formate is almost independent of P_{H_2}.

The results of experiments carried out with Rh(acac)$_3$ 0.08 g (0.2 mg-atom as Rh), NMP 20 g, under various P_{H_2} at 260 °C for 2 h, where P_{CO} was fixed at a constant, 400 kg cm^{-2}, are shown in Fig. 2. As in the case of cobalt catalysis, the dependency of EG formation on P_{H_2} is fairly larger than that of methanol. The order of EG formation with respect to P_{H_2} is about 2, while the rate of methanol formation increases almost linearly with P_{H_2}. Consequently, the selectivity to EG increases and

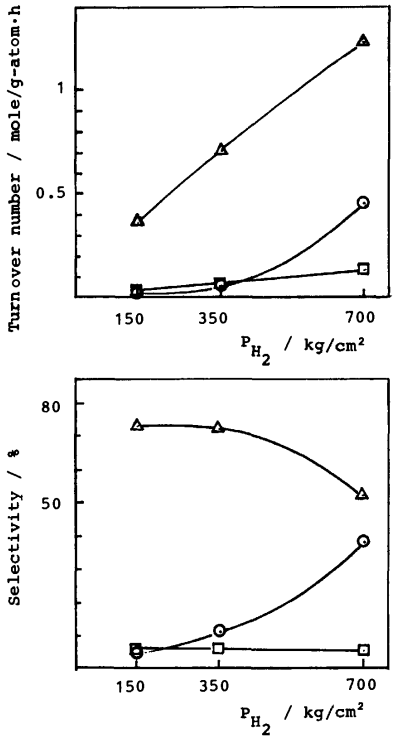

Fig. 1. Influence of H_2 partial pressure.
P_{CO}=150 kg cm^{-2}, 210 °C, Phenol 25 g+*m*-Cresol 5 g, Co 5 mg-atom, 2 h. Notations: O EG, Δ MeOH, □ HCOOMe, Selectivity to EG (Sel_{EG})=2EG/A, Sel_{MeOH}=MeOH/A, Sel_{HCOOMe}=HCOOMe/A, A=2(EG+EtOH)+MeOH+HCOOMe.

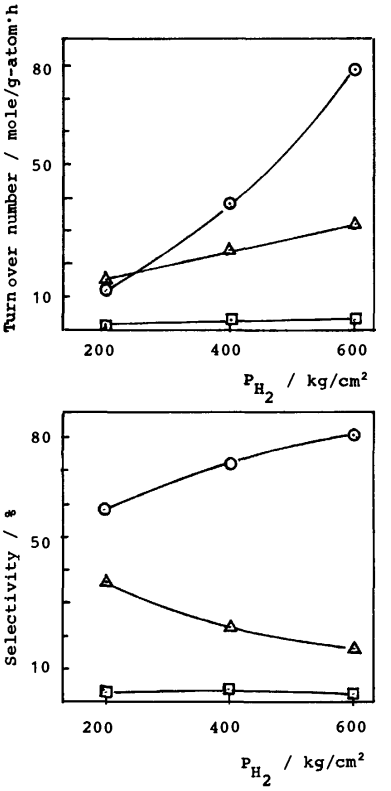

Fig. 2. Influence of H_2 partial pressure.
P_{CO}=400 kg cm^{-2}, 260 °C, NMP 20 g, Rh 0.2 mg-atom, 2 h. Notations: O EG, Δ MeOH, □ GL (Glycerol), Sel_{EG}=2EG/B, Sel_{MeOH}=MeOH/B, Sel_{GL}=3GL/B, B=3GL+2(EG+EtOH)+MeOH+HCOOMe.

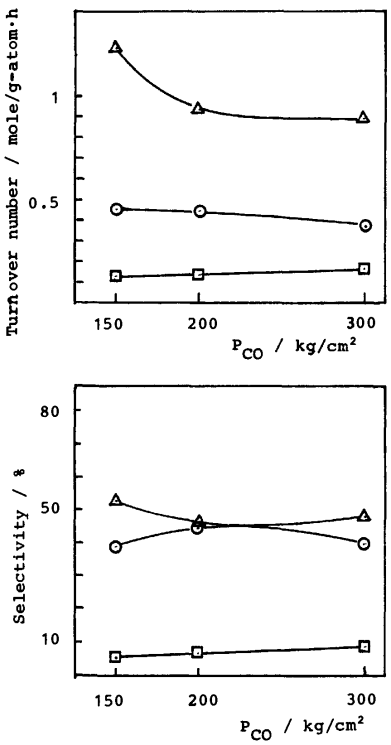

Fig. 3. Influence of CO partial pressure.
P_{H_2}=700 kg cm^{-2}, 210 °C, Phenol 25 g+*m*-Cresol 5 g, Co 5 mg-atom, 2 h. Notations: see Caption of Fig. 1.

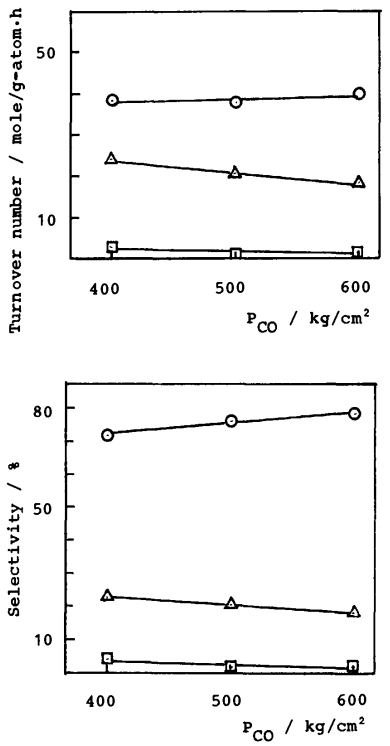

Fig. 4. Influence of CO partial pressure.
P_{H_2}=400 kg cm^{-2}, 260 °C, NMP 20 g, Rh 0.2 mg-atom, 2 h. Notations: see Caption of Fig. 2.

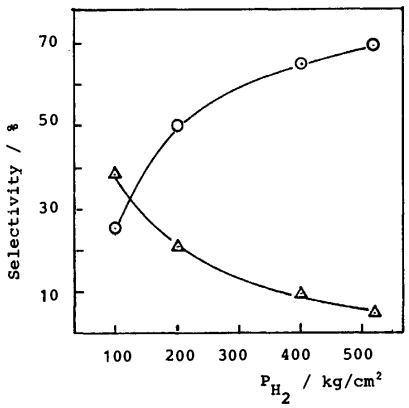

Fig. 5. Effect of H_2 partial pressure on the selectivity of the reaction of CH_2O with synthesis gas.
P_{CO}=100 kg cm^{-2}, 180 °C, CH_2O (37%aq) 40 mmol, Phenol 10 g+Toluene 10 g, Co 5 mg-atom, Ru 0.5 mg-atom, 2 h. Notations: O EG, Δ MEOH.

that to methanol decreases as P_{H_2} is increased. The selectivity to glycerol is almost independent of P_{H_2}.

The results of experiments carried out in the same manner as those shown in Fig. 1, except that P_{CO} was varied at a fixed P_{H_2}, 700 kg cm^{-2}, are shown in Fig. 3. The rate of EG formation is almost independent of P_{CO} in the range of 150—200 kg cm^{-2}, but it slightly declines as P_{CO} is increased above that range. On the other hand, the rate of methanol formation is independent of P_{CO} in the range of 200—300 kg cm^{-2}, whereas it sharply increases as P_{CO} is decreased below that range. As a result of these effects, the selectivity to EG showed a maximum and that to methanol a minimum, at the P_{CO} of about 200 kg cm^{-2}. The selectivity to methyl formate slightly increased with increasing P_{CO}. If value *A* (see caption of Fig. 1) is considered as representing the total CO hydrogenation activity, it is clear that the total rate of CO hydrogenation decreases as P_{CO} is increased.

The results of experiments carried out in the same manner as those shown in Fig. 2, except that P_{CO} was varied at a fixed P_{H_2}, 400 kg cm^{-2}, are shown in Fig. 4. Clearly, the rate of EG formation is almost independent of the P_{CO} in the range of 400—600 kg cm^{-2}, but the rate of methanol formation tends to decrease as P_{CO} is increased. As a consequence, the selectivity to EG slightly increases, and that to methanol declines as P_{CO} is increased. It is clear on calculating value *B* (see caption of Fig. 2), that the total rate of CO hydrogenation, in this case, is almost independent of P_{CO}.

In the course of our study of the cobalt catalyzed syngas reaction in the presence of formaldehyde, it was found that phenol-toluene mixture is a suitable solvent for EG formation,[5] and that the formation of unidentified products other than EG and methanol is dramatically suppressed by the presence of a small amount of ruthenium in addition to cobalt. Making use of these previous findings, the effect of P_{H_2} on the selectivity of syngas reaction with formaldehyde, where EG and methanol are the main products, was studied. The reactions were performed in an above mentioned solvent in the presence of $Co_2(CO)_8$ and $Ru_3(CO)_{12}$ in an atomic ratio of 10 to 1, where formaldehyde solution was fed, by means of a pump, to the reactor after the desired reaction temperature and pressure are reached in order to avoid the complexity arising from the reaction of formaldehyde occuring at a lower temper-

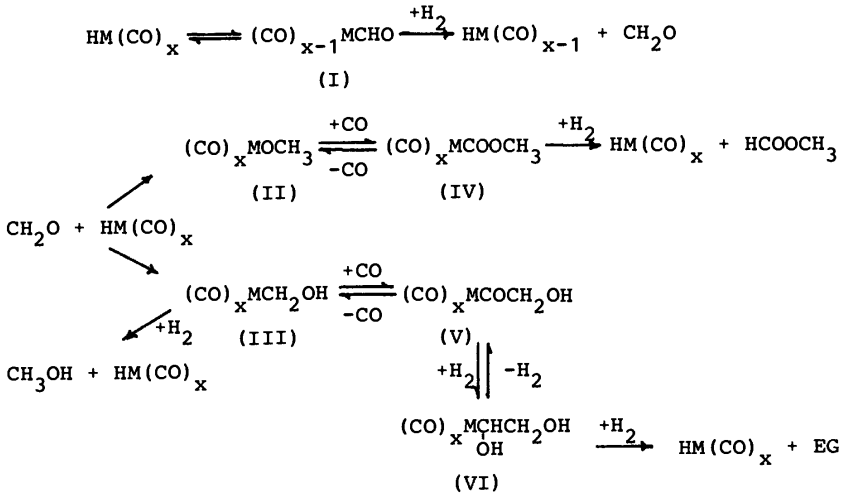

Scheme 1.

ature. The results are summarized in Fig. 5. A strikingly similar trend is observed as in the case of direct syngas conversion (cf. Figs. 1 and 2), i.e., the selectivity to EG increases and that to methanol decreases with increase in P_{H_2}.

Since a similar trend is observed in the P_{H_2} dependency of both cobalt- and rhodium-catalyzed reactions, the reactions in both cases are presumed to proceed by a generalized mechanism as shown in Scheme 1, where metal carbonyl hydride species is represented by $HM(CO)_x$ (M is Co or Rh). Formaldehyde intermediate, which is supposed to be produced by the hydrogenolysis of a formyl complex,[2] reacts with $HM(CO)_x$ to produce methoxy intermediate (II) and hydroxymethyl intermediate (III). EG and methanol is considered to be derived from a common intermediate (III), since there is always observed an opposite correlation between the selectivities of EG and methanol (cf. Figs. 1—4). On the other hand, methyl formate, the selectivity to which has any direct relation to neither EG nor methanol (cf. Figs. 1 and 3), is supposed to be derived from another intermediate (II). The hydroxyacetyl intermediate (V) is produced by the reversible addition of CO to intermediate (III), 1,2-dihydroxyethyl intermediate (VI) is produced by the reversible addition of H_2 to intermediate (V). Methanol is produced by the hydrogenolysis of intermediate (III), whereas EG is produced by the hydrogenolysis of intermediate (VI). Therefore, the order of EG formation with respect to P_{H_2} should be distinctively higher than that of methanol according to this scheme. Thus the reason for the effectiveness of hydrogen partial pressure on the EG selectivity is well understood by this mechanism.

Experimental

Apparatus. 100 ml Hastelloy C autoclave fitted with a stirrer; the autoclave is connected at the bottom through a valve to a gas-liquid separator, so that the reaction can be terminated at any desired time by opening the valve. The autoclave is brought to a desired temperature by heating under the pressure of CO or a mixed gas ($H_2/CO=1$), and pressure is readjusted to attain a desired P_{CO}. Then it is compressed with hydrogen to attain a desired P_{H_2}. Total pressure is kept constant (± 20 kg cm^{-2}) by supplying a mixed gas ($H_2/CO=2$) during the reaction.

This work is a part of "C_1-Chemistry Project," a National Research and Development Program of Agency of Industrial Science and Technologe, Ministry of International Trade and Industry (M.I.T.I.) Japan.

References

1) W. Keim, M. Berger, and J. Schlupp, *J. Catal.*, **61**, 359 (1980).
2) D. R. Fahey, *J. Am. Chem. Soc.*, **103**, 136 (1981).
3) A. Deluzarche, R. Fonesca, G. Jenner, and Kiennemann, *Erdoel. Kohle, Erdgas, Petrochem.*, **32**, 313 (1979).
4) L. C. Costa, *Catal. Rev. -Sci. Eng.*, **25** (3), **325** (1983).
5) Japan Kokai 58-90522 (1983).

A Reinterpretation for Ion Association at Micellar Surfaces Due to an Electrostatic Model

Tetsuo KANEKO*
Consulting Services Division, Electric Power Engineering Group, Japan NUS CO., Ltd.,
7-1 Nishi-Shinjuku 2 Chome, Shinjuku-ku, Tokyo 160
(Received September 26, 1985)

Synopsis. Ion association at the surface of a micelle is reinterpreted by considering that counter ions are bound by an electrostatic attraction with a spherical shell which is formed by the aggregation of the polar heads of amphiphilic molecules. It was found that the degree of ion association increased slightly with the increase in the aggregation number of amphiphilic molecules.

The association of counter ions with ionic micelles[1] has been suggested in experimental investigations, and an interpretation regarding it as an electrostatic interaction has been given to this association.[2,3] The investigations instigated by this interpretation have been performed on a basis of a micelle model with a uniform surface-charge density and the thermodynamics of micelle formation. Instead of the surface-charge density, the total charges, which are obtained by summing up the charges of the polar heads of the amphiphilic molecules and counter ions near a micellar surface, are introduced in this paper. As a result, the association of counter ions with an ionic micelle can be estimated according to electrostatics.

In this paper, the distribution of the counter ions which surround an ionic micelle is represented as forming a three-layered geometrical configuration as a result of electrostatic interaction. A reinterpretaton, for which the surface-charge density of a micelle is not introduced, is given to the characteristic of ion association on the basis of this distribution of the counter ions. The three-layered geometrical configuration is formed from a spherical shell composed of the polar head group of amphiphilic molecules, a layer composed of counter ions bound to the spherical shell, and an outermost layer where the movements of ions are not restricted strongly by the electrostatic field. In this investigation, it is assumed that the force which binds the counter ions within the spherical shell composed of the polar head group is electrostatic attraction. A micellar structure which includes counter ions within such a shell has been considered.[4] This micellar structure is taken into account when Gauss' law is applied to the first integration of the Poisson equation in order to obtain an approximate solution for the nonlinear Poisson-Boltzmann equation. An analytical approximate solution for the nonlinear Poisson-Boltzmann equation for a spherical micelle was given by Evans and Ninham.[3] In this paper, the surface potential for an ionized micelle is obtained on the basis of this analytical approximate solution and Gauss' law.

The association of counter ions with a micelle is estimated on the basis of this surface potential. This result gives an ion association independent of the counter-ion concentration if the aggregation number of amphiphilic molecules is constant with the change in the counter-ion concentration. It is interesting that the property independent of the counter-ion concentration is similar to that of a polyion solution. In addition, it was found that the degree of ion association increases slightly with the increase in the aggregation number of amphiphilic molecules. Thus, the dissociation of ionic micelle decreases slightly with an increase in the counter-ion concentration.

Model

In order to examine the association of counter ions with a micelle due to electrostatic attraction, the structure of the micellar surface should be taken into account.

It is assumed that the structure of the micellar surface is like that shown in Fig. 1. The polar heads of amphiphilic molecules in the assumed micellar model exist within a spherical surface ***D*** with a certain radius R, and the counter ions bound within ***D*** remain outside a spherical surface with the radius of $R-\delta R$, i.e., in a shell which has a thickness of δR. The surface potential on ***D*** is obtained by considering the micellar structure to be as is shown in Fig. 1.

The potential ψ around a spherical micelle is represented for a 1-1 electrolyte by this nonlinear Poisson-Boltzmann equation:

$$\frac{d^2\psi}{dr^2} + \frac{2}{r}\cdot\frac{d\psi}{dr} = \frac{8\pi n_0 e}{\varepsilon}\sinh\left(\frac{e\psi}{kT}\right), \tag{1}$$

where n_0 is the bulk electrolyte concentration, ε is the dielectric constant of the solvent, e is the unit charge, k is Boltzmann's constant, and T is the absolute temperature. The approximate solution[3] for the

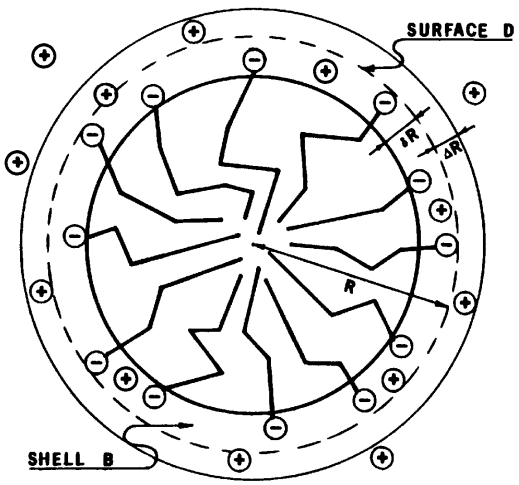

Fig. 1. Model of micelle. Polar head and counter ion are represented as (−) and (+) respectively.

surface potential ψ_0 on **D** which was obtained by Evans and Ninham from Eq. 1 is:

$$S^2 = 4\sinh^2\left(\frac{e\psi_0}{2kT}\right)\cdot\left\{1+\frac{4}{\kappa R}\cdot\frac{1}{\cosh(e\psi_0/2kT)+1}\right\}, \quad (2)$$

where $S \equiv -\frac{e}{\kappa kT}\cdot\left.\frac{d\psi}{dr}\right|_{r=R}$ and $\kappa^2 = 8\pi n_0 e^2/\varepsilon kT$.

In addition, the relation between the first and second terms on the left side of Eq. 1 for a larger r is:

$$\left|\frac{d^2\psi}{dr^2}\right| \gg \left|\frac{2}{r}\cdot\frac{d\psi}{dr}\right|,$$

as may be evaluated easily by the approximate solution of Debye-Hückel. Equation 2 is obtained by considering this relation and by integrating Eq. 1.

On the other hand, the first integration of Eq. 1 and Gauss' law lead to:

$$-\left.\frac{d\psi}{dr}\right|_{r=R} = \frac{Q}{\varepsilon R^2}, \quad (3)$$

where the charge Q has been in this investigation to consist of two terms. One term is caused by the charge of the polar head group; the other one is caused by the charge of the counter ions, which is bound by the potential within the spherical surface **D**. The charge Q which consists of these two terms is represented as:

$$Q = -eN + \int_{R-\delta R}^{R} en_0(\exp[-e\psi/kT] - \exp[e\psi/kT])\cdot 4\pi r^2 dr, \quad (4)$$

where N is the aggregation number of the amphiphilic molecules, assuming that the amphiphilic molecules are negatively ionized. Now, by substituting Eqs. 3 and 4 into Eq. 2, Eq. 2 is modified to the following equation:

$$\frac{e}{\varepsilon\kappa kT}\cdot\frac{1}{R^2}\cdot\{-eN + en_0\exp[-e\psi_0/kT]\cdot 4\pi R^2\cdot\delta R\}$$
$$\approx -\exp[-e\psi_0/2kT] - \frac{4}{\kappa R}, \quad (5)$$

where $e\psi_0/kT<0$ and $\exp[e\psi_0/kT] \ll 1 \ll \exp[-e\psi_0/kT]$ are taken into account, and where the integration in Eq. 4 is approximated by assuming that δR is small. Thus, from Eq. 5 we obtain for the surface potential ψ_0 the following equation:

$$\exp[-e\psi_0/kT] = \left(\frac{\varepsilon\kappa kT}{8\pi e^2 n_0\delta R}\right)^2\cdot$$
$$\left[-1+\sqrt{1+\frac{16\pi e^2 n_0\delta R}{\varepsilon\kappa kT}\left(\frac{e}{\varepsilon\kappa kT}\cdot\frac{eN}{R^2}-\frac{4}{\kappa R}\right)}\right]^2. \quad (6)$$

By using Eq. 6, the association of counter ions with an ionic micelle can be estimated and the behavior of ions known.

Results and Discussion

The number, N_c, of counter ions which are bound by electrostatic attraction within a spherical shell **B** is given by:

$$N_c = \int_{R-\delta R}^{R} n_0\exp[-e\psi/kT]\cdot 4\pi r^2 dr$$
$$\approx 4\pi R^2\delta R\cdot n_0\exp[-e\psi_0/kT].$$

Now, the degree of ion association β for counter ions bound in **B** is represented by the ratio of N_c to N, and, by using Eq. 6, β is represented as:

$$\beta = \frac{\chi_0 TR}{N}\cdot\frac{R}{2\delta R}\cdot\left[-1+\sqrt{1+2\cdot\frac{\delta R}{R}\left(\frac{N}{\chi_0 TR}-4\right)}\right]^2, \quad (7)$$

where $\chi_0=\varepsilon k/e^2$. It should be noted that n_0 does not appear in Eq. 7. This degree of ion association β, which does not include n_0, suggests that if an ionic micelle is associated with more counter ions, $|\psi_0|$ will decrease more and that, as a result, the thermal dissociation of counter ions will occur more easily. On the level of approximation used to obtain Eq. 7, the number of counter ions bound within the shell **B** is entirely independent of the counter-ion concentration if the change of N cannot be induced by the change in the counter-ion concentration. This result is similar to the result that Engström and Wennerström indicate for charged plates.[5] In addition, the characteristic of β shows that the degree of ion association decreases slightly with the increase in T and that it increases slightly with the increase in N.

Now, in order to estimate β, the radius R is determined from these relations:

$$R = (\text{hydrocarbon core radius } R') + (\text{thickness of shell } \delta R)$$

and:

$$(4\pi/3)R'^3 = Nv,$$

and thus:

$$R = (3Nv/4\pi)^{1/3} + \delta R. \quad (8)$$

For v, we use the volume of the hydrocarbon core given by:

$$v = 27.4 + 26.9\nu\ [\text{Å}^3],$$

where ν is close to the number of carbon atoms per chain.[6] In this paper, ν is regarded as the number of carbon atoms per chain. The values of β are shown in table 1, in which we use δR as 3 Å[2] and the R value given by Eq. 8 for lithium dodecyl sulfate (LDS) in order to calculate β.

Furthermore, another degree of ion association, β', for counter ions bond within the spherical surface with radius $R+\Delta R$ shown in Fig. 1 is defined as:

$$\beta' = \frac{1}{N}\cdot\int_{R-\delta R}^{R} n_0\exp[-e\psi/kT]\cdot 4\pi r^2 dr$$
$$+\frac{1}{N}\cdot\int_{R}^{R+\Delta R} n_0\exp[-e\psi/kT]\cdot 4\pi r^2 dr$$
$$\approx \beta + \frac{n_0}{N}\exp[-e\psi_1/kT]\cdot 4\pi(R+\Delta R)^2\Delta R, \quad (9)$$

where $\psi_1=\psi(R+\Delta R)$ and where it is assumed that ΔR is small. In order to estimate ψ_1, by using Gauss' law for the spherical surface with a radius of $R+\Delta R$ on the basis of the treatment introduced in the Model, we obtain:

$$-\left.\frac{d\psi}{dr}\right|_{r=R+\Delta R} = \frac{-eN}{\varepsilon(R+\Delta R)^2}$$
$$\cdot\left\{(1-\beta)-4\pi\Delta R(R+\Delta R)^2\frac{n_0}{N}\exp[-e\psi_1/kT]\right\},$$

Table 1. Values of β and β' Calculated for LDS

T	LDS	LiCl[a]	N[b]	β	β'
K	mol dm^{-3}	mol dm^{-3}			
308	0.074	0.0	57	0.32	0.43
308	0.074	0.2	81	0.37	0.50
308	0.074	0.4	92	0.39	0.52
308	0.074	1.0	103	0.40	0.53
308	0.325	0.0	79	0.37	0.49
308	0.598	0.0	86	0.38	0.51
308	0.845	0.0	93	0.39	0.52
308	0.985	0.0	94	0.39	0.52
308	1.107	0.0	96	0.40	0.53
295	0.294	0.0	75	0.37	0.50
310	0.294	0.0	71	0.36	0.47

a) Salt concentration in the solution of LDS. b) Data resulting from small-angle neutron-scattering data analysis for an LDS micellar system.[7]

and by substituting this equation into Eq. 2 for $r = R+\Delta R$, we obtain:

$$\exp[-e\phi_1/kT] = \frac{x_0 T}{8\pi n_0 \Delta R^2} \cdot \left[-1+\sqrt{1+\frac{2\Delta R}{R+\Delta R}\cdot\left\{\frac{N(1-\beta)}{x_0 T(R+\Delta R)}-4\right\}}\right]^2. \quad (10)$$

Therefore, by substituting Eq. 10 into Eq. 9, the following formula for β' is obtained:

$$\beta' = \beta + \frac{x_0 T(R+\Delta R)}{N}\cdot\frac{R+\Delta R}{2\Delta R}\cdot \left[-1+\sqrt{1+\frac{2\Delta R}{R+\Delta R}\left\{\frac{N(1-\beta)}{x_0 T(R+\Delta R)}-4\right\}}\right]^2. \quad (11)$$

The thickness of the shell ΔR included in Eq. 11 is:

$$\Delta R = 5.56 - \delta R\,[\text{Å}],$$

where 5.56Å is the mean diameter of a spherical polar head of dodecyl sulfate obtained by neutron scattering for an LDS solution.[7] It has been assumed here that the value of 5.56Å corresponds to $\delta R+\Delta R$ in the micellar model shown in Fig. 1. Thus, the values of β' obtained by Eq. 11 are shown in Table 1. These values of β' nearly all fall in the range of 0.5—0.8, indicating generally the degree of ion association. The change in β' with the change in the LDS concentration corresponds to the behavior of the degree of ion association obtained experimentally.[7] The values of β' in Table 1 indicate that the degree of ionic dissociation for an ionic micelle decreases slightly with the increase in the counter-ion concentration. Also, it is found that the micelles of smaller aggregation numbers have a higher degree of ionic dissociation; this is because of the characteristic of β' depending on the change in N.

If dissociation occurs in a micelle, the micelle becomes less stable due to an electrostatic repulsion between the polar heads of the amphiphilic molecules. The micelles of smaller aggregation numbers are less stable because of this electrostatic repulsion. On the contrary, instability due to the electrostatic repulsion decreases with the increase in N, because β values are larger for larger N values. As a result, we infer that the balance point between the hydrophobic effect for aiding micellar formation and an electrostatic repulsion disturbing micellar formation exists if N is larger than a certain value, although we can not discuss this balance point without the thermal influence factor.

We conclude that the characteristic of β' agrees well with the general property of ion association with an ionic micelle, although the value of δR has not yet been determined well enough.

Conclusions

Pictures of a micelle with wetted outer layers surrounded by spherical polar head groups with an average diameter equal to 5.56Å, pictures taken on the basis of neutron scattering, have been presented by Bendedouch, Chen, and Koehler.[7] We have divided such a wetted outer layer into two layers consisting of two spherical shells, as is shown in Fig. 1. The values of β' calculated by considering the two spherical shells nearly all fall in the range of 0.5—0.8, indicating generally the degree of ion association, although the value of δR used for calculating may have some uncertainty.

In addition, it has been found that the value of β' is independent of the counter-ion concentration, although the constancy of N is required as a condition. It is also noticed that this characteristic of β' may represent the property of a polyion solution.

The author wishes to express his thanks to Professor Tetsurou Ishiguro, Faculty of Science and Engineering, Chuo University, for valuable advice, and to Kazumi Kogure for reading and criticizing the manuscript.

References

1) D. Stigter and K. J. Mysels, *J. Phys. Chem.*, **59**, 45 (1955).
2) G. Gunnarsson, B. Jönsson, and H. Wennerström, *J. Phys. Chem.*, **84**, 3114 (1980).
3) D. F. Evans and B. W. Ninham, *J. Phys. Chem.*, **87**, 5025 (1983).
4) J. B. Hayler and J. Penfold, *J. Chem. Soc., Faraday Trans. 1*, **77**, 1851 (1981).
5) S. Engström and H. Wennerström, *J. Phys. Chem.*, **82**, 2711 (1978).
6) J. N. Israelachvili, D. J. Mithell, and B. W. Ninham, *J. Chem. Soc., Faraday Trans. 2*, **72**, 1529 (1976).
7) D. Bendedouch, S. H. Chen, and W. C. Koehler, *J. Phys. Chem.*, **87**, 2621 (1983).

Preparation and Stereochemistry of (Acetylacetonato)(2,2′-bipyridine)-chromium(III) Complexes with 2,2′-Bipyridine *N,N′*-Dioxide or Its 3,3′-Dimethyl Derivative

Hideaki KANNO,* Shunji UTSUNO, and Junnosuke FUJITA†
Department of Chemistry, Faculty of Science, Shizuoka University, Oya, Shizuoka 422
†Department of Chemistry, Faculty of Science, Nagoya University, Chikusa-ku, Nagoya 464
(Received December 3, 1985)

Synopsis. Four new mixed-ligand chromium(III) complexes, $[Cr(acac)(bpy)(L)]^{2+}$ and $[Cr(bpy)(phen)(L)]^{3+}$, where L denotes a seven-membered chelate ligand, 2,2′-bipyridine *N,N′*-dioxide (bpdo) or its 3,3′-dimethyl derivative (mbdo), were prepared and resolved. All of the complexes formed only one of two possible racemic pairs of diastereomers. The pair was assigned to have an *ob*($\Delta(\delta)$, $\Lambda(\lambda)$) structure on the basis of the circular dichroism spectra and the absolute configuration of optically active mbdo recovered from the resolved complex.

2,2′-Bipyridine *N,N′*-dioxide (bpdo)[1] and 3,3′-dimethyl-2,2′-bipyridine *N,N′*-dioxide (mbdo)[2] form a skew seven-membered chelate ring, δ and λ, upon coordination (Fig. 1). Recently, we found that the conformations of these dioxide ligands (L) in mixed-ligand chromium(III) complexes are greatly influenced by the other ligands in the complex. Thus, $[Cr(en)_2(bpdo)]^{3+}$ [3] and $[Cr(acac)_2(L)]^{+}$ [4] formed only a *lel*($\Delta(\lambda)$, $\Lambda(\delta)$) isomer, whereas $[Cr(bpy\text{ or }phen)_2(L)]^{3+}$ [5] formed an *ob*($\Delta(\delta)$, $\Lambda(\lambda)$) isomer of two possible ones, *lel* and *ob*. Here, en, acac, bpy, and phen denote ethylenediamine, acetylacetonate(−1), 2,2′-bipyridine, and 1,10-phenanthroline, respectively. An examination using molecular models indicated that such a difference in selectivity comes from steric interactions among the ligands in the complex.

In this paper, we report on the preparation and stereochemistry of chromium(III) complexes which consist of three different bidentate ligands, $[Cr(acac)(bpy)(L)]^{2+}$ and $[Cr(bpy)(phen)(L)]^{3+}$. Since acac, bpy, and phen form planar chelate rings in a complex, these complexes can have two racemic pairs of diastereomers, *lel* and *ob*.

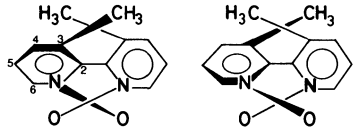

Fig. 1. A pair of enantiomers of mbdo.

Experimental

Since the new complexes are photosensitive causing hydrolysis, the following experiments were carried out in the dark.

Preparation of $[Cr(acac)_2(bpy)]Cl\cdot 2.5H_2O$. The complex was prepared according to a method similar to that for $[Cr(acac)_2(phen)]ClO_4$.[6] An aqueous ethanol solution (90%, 300 cm³) containing $[Cr(acac)_3]$ (3.0 g, 8.6 mmol), bpy (4.0 g, 25.6 mmol), and concd HCl (3 cm³) was kept at 80 °C for 2 d with stirring. The resulting solution was evaporated under reduced pressure to give pink crystals. They were collected by filtration, washed with 2 mol dm⁻³ HCl and acetone, and recrystallized from hot water. Yield: 1.9 g (45%). Found: C, 49.19; H, 5.30; N, 5.68%. Calcd for $C_{20}H_{22}N_2O_4ClCr\cdot 2.5H_2O$: C, 49.34; H, 5.59; N, 5.75%.

Preparation and Resolution of [Cr(acac)(bpy)(bpdo or mbdo)]$(ClO_4)_2$. An aqueous 0.2 mol dm⁻³ HCl solution (50 cm³) containing $[Cr(acac)_2(bpy)]Cl\cdot 2.5H_2O$ (2.0 g, 4.1 mmol) was kept at 60 °C for 2 d with stirring. To the resulting solution, $NaClO_4$ (2.5 g) and bpdo·H_2O[7] (1.2 g, 5.8 mmol) or racemic mbdo[2] (1.3 g, 6.0 mmol) were added. The solution was again kept at 60 °C for 8 h with stirring to give reddish-brown crystals. They were collected by filtration, washed with cold water, and recrystallized from hot water. Yield: the bpdo complex, 1.1 g (41%); the mbdo complex, 1.3 g (43%). Found for the bpdo complex: C, 42.99; H, 3.31; N, 7.99%. Calcd for $C_{25}H_{23}N_4O_{12}Cl_2Cr$: C, 43.24; H, 3.34; N, 8.07%. Found for the mbdo complex: C, 44.78; H, 3.76; N, 7.68%. Calcd for $C_{27}H_{27}N_4O_{12}Cl_2Cr$: C, 44.89; H, 3.77; N, 7.76%. Each complex gave only one racemic pair of diastereomers, no indication for the formation of another isomer being detected on column chromatograms.

The complexes were resolved by SP-Sephadex C-25 column chromatography. The perchlorate of each complex (0.08 g) was loaded on a column (ϕ2.2×130 cm) of SP-Sephadex and eluted with a 0.15 mol dm⁻³ Na_2SO_4 solution. Although only one band was observed on the column, the front and rear fractions of the band showed positive and negative rotations at 546 nm, respectively. The fractions which showed a constant specific rotation were combined, diluted with water, and poured again on a small column (ϕ2.2×3 cm) of SP-Sephadex. The adsorbed complex was eluted with a 2 mol dm⁻³ NaCl solution. The eluate was mixed with $NaClO_4$ to give reddish-brown crystals. They were collected by filtration, washed with a small amount of cold water, and recrystallized from hot water. Found for the $(+)_{546}$-isomer of the bpdo complex: C, 43.14; H, 3.33; N, 8.03%. Calcd for $C_{25}H_{23}N_4O_{12}Cl_2Cr$: C, 43.24; H, 3.34; N, 8.07%. Found for the $(+)_{546}$-isomer of the mbdo complex: C, 44.66; H, 3.73; N, 7.68%. Calcd for $C_{27}H_{27}N_4O_{12}Cl_2Cr$: C, 44.89; H, 3.77; N, 7.76%.

Preparation and Resolution of [Cr(bpy)(phen)(bpdo or mbdo)]$(ClO_4)_3\cdot H_2O$. The complexes were prepared by a method similar to that for $[Cr(phen)_2(bpdo)](ClO_4)_3$[5] using $[Cr_2(OH)_2(bpy)_2(phen)_2](NO_3)_4\cdot 6H_2O$[8] and the dioxide ligand. The complexes were obtained as orange crystals. Yield: the bpdo complex, 34%; the mbdo complex, 27%. Found for the bpdo complex: C, 42.98; H, 2.69; N, 9.48%. Calcd for $C_{32}H_{24}N_6O_{14}Cl_3Cr\cdot H_2O$: C, 43.04; H, 2.93; N, 9.41%. Found for the mbdo complex: C, 44.10; H, 2.98; N, 9.00%. Calcd for $C_{34}H_{28}N_6O_{14}Cl_3Cr\cdot H_2O$: C, 44.34; H, 3.28; N, 9.12%. Each complex gave only one racemic pair of diastereomers, no indication for the formation of another isomer being detected on column chromatograms.

The complexes were completely resolved by SP-Sephadex column chromatography using a 0.15 mol dm⁻³ $Na_2[Sb_2((+)_{589}\text{-tart})_2]$ solution as an eluent. The $(+)_{589}$-isomer was eluted faster from the column. The optically

active complex was isolated as the perchlorate by the same method as that for $(-)_{589}$-$[Cr(phen)_2(bpdo)]^{3+}$.[5] Found for the $(-)_{589}$-isomer of the bpdo complex: C, 43.15; H, 2.74; N, 9.41%. Calcd for $C_{32}H_{24}N_6O_{14}Cl_3Cr \cdot H_2O$: C, 43.04; H, 2.93; N, 9.41%. Found for the $(-)_{589}$-isomer of the mbdo complex: C, 44.13; H, 2.98; N, 9.10%. Calcd for $C_{34}H_{28}N_6O_{14}Cl_3Cr \cdot H_2O$: C, 44.34; H, 3.28; N, 9.12%.

Recovery of mbdo from the Complexes. The optically active mbdo was recovered from $(+)_{546}$-$[Cr(acac)(bpy)(mbdo)]^{2+}$ and $(-)_{589}$-$[Cr(bpy)(phen)(mbdo)]^{3+}$ by the same method as that for $[Cr(mbdo)_3]^{3+}$.[2] Both recovered mbdo showed positive rotations at 589 nm.

Measurements. Absorption and circular dichroism (CD) spectra were recorded on a Shimadzu MPS-50L spectrophotometer and a Jasco J-40 spectropolarimeter, respectively. Optical rotations were measured with a Union PM-101 polarimeter.

Results and Discussion

Each of the complexes, $[Cr(acac)(bpy)(L)]^{2+}$ and $[Cr(bpy)(phen)(L)]^{3+}$ (L=bpdo, mbdo), formed only one of two possible racemic pairs, *lel*($\Delta(\lambda)$, $\Lambda(\delta)$) and *ob*($\Delta(\delta)$, $\Lambda(\lambda)$). The bpy·phen complexes were completely resolved by SP-Sephadex column chromatography using $Na_2[Sb_2((+)_{589}\text{-tart})_2]$ as an eluent, but the acac·bpy complexes were not under the same chromatographic conditions. Their resolutions were achieved by SP-Sephadex column chromatography using an achiral eluting agent Na_2SO_4, although the columns showed only one band. All the active complexes in aqueous solutions were optically stable in the dark, but gradually hydrolyzed in the light.

The absorption and CD spectra of $(+)_{546}$-$[Cr(acac)(bpy)(L)]^{2+}$ and $(-)_{589}$-$[Cr(bpy)(phen)(L)]^{3+}$ are shown in Fig. 2. The spectral data in the region of the first absorption band are listed in the Table. The

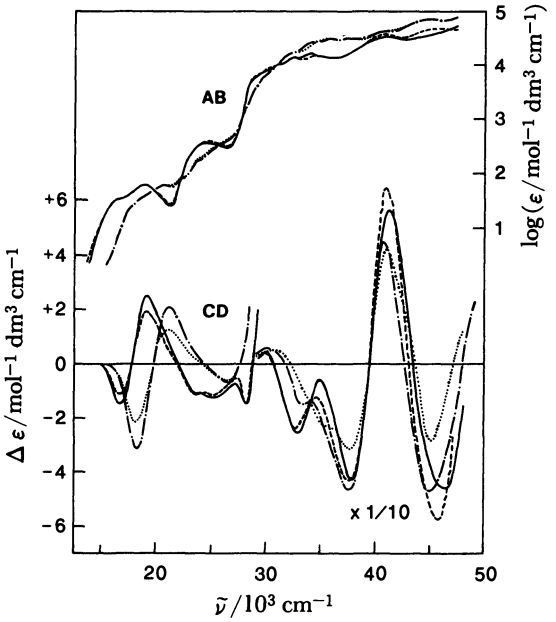

Fig. 2. Absorption (AB) and CD spectra of $(+)_{546}$-$[Cr(acac)(bpy)(mbdo)]^{2+}$ (——), $(+)_{546}$-$[Cr(acac)(bpy)(bpdo)]^{2+}$ (– – – –), $(-)_{589}$-$[Cr(bpy)(phen)(mbdo)]^{3+}$ (–·–·–), and $(-)_{589}$-$[Cr(bpy)(phen)(bpdo)]^{3+}$ (·····) in water.

Table Absoption and CD Spectral Data in the Region of the First Absorption Band

Complex	Absorption[a]	CD[a]
	$\tilde{\nu}/10^3\,cm^{-1}$ (log ε)	$\tilde{\nu}/10^3\,cm^{-1}$ (Δε)
$(+)_{546}$-[Cr(acac)-(bpy)(mbdo)]$^{2+}$	16.9 (1.5)[b]	17.06(−1.47)
	19.23(1.77)	19.53(+2.48)
$(+)_{546}$-[Cr(acac)-(bpy)(bpdo)]$^{2+}$	17.1 (1.5)[b]	17.06(−1.14)
	19.27(1.76)	19.53(+1.89)
$(-)_{589}$-[Cr(bpy)-(phen)(mbdo)]$^{3+}$	18.7 (1.6)[b]	18.35(−3.16)
	20.70(1.76)	21.32(+2.05)
$(-)_{589}$-[Cr(bpy)-(phen)(bpdo)]$^{3+}$	18.7 (1.5)[b]	18.25(−2.13)
	20.88(1.78)	21.28(+1.24)

a) Values of ε and Δε are given in $mol^{-1}\,dm^3\,cm^{-1}$. b) Shoulder.

absorption spectra of the bpdo and mbdo complexes are nearly the same over the whole region. The bands at ca. 19000 cm^{-1} with a shoulder (ca. 17000 cm^{-1}) for the acac·bpy complexes and at ca. 21000 cm^{-1} with a shoulder (18700 cm^{-1}) for the bpy·phen complexes can be assigned to the first absorption band ($^4T_{2g} \leftarrow {}^4A_{2g}$). In the higher energy region, the complexes show complicated spectra due to absorptions of the three kinds of ligands. In this region, however, the spectra of the bpy·phen and acac·bpy complexes are very similar to the average of those of the corresponding bis-bpy and bis-phen complexes,[5] and bis-acac,[4] and bis-bpy complexes, respectively.

The CD spectra of the complexes are similar in pattern over the whole region. This suggests that all the isomers have the same absolute configuration, including the chirality of the skew dioxide chelate ring. The spectra are very similar to those of $\Delta(\delta)$-$[Cr(bpy\text{ or }phen)_2(L)]^{3+}$,[5] but quite different from those of $\Delta(\lambda)$-$[Cr(acac)_2(L)]^+$.[4] Thus, all the isomers have the $\Delta(\delta)$ structure.

The free mbdo ligand is optically stable and can be recovered from the complex.[2] Both mbdo recovered from $(+)_{546}$-$[Cr(acac)(bpy)(mbdo)]^{2+}$ and $(-)_{589}$-$[Cr(bpy)(phen)(mbdo)]^{3+}$ showed positive rotations at 589 nm. The $(+)_{589}$-mbdo ligand was assigned to the *S* configuration and forms a δ skew chelate ring in a complex.[2] This is consistent with the structure ($\Delta(\delta)$) of the complexes assigned on the basis of the CD spectra. Since the bpdo complexes give CD spectra similar to those of the corresponding mbdo complexes over the whole region, it is concluded that the bpdo complexes also form an *ob*($\Delta(\delta)$, $\Lambda(\lambda)$) isomer stereoselectively. While it is expected that $[Cr(bpy)(phen)(L)]^{3+}$ forms the same *ob* isomer as $[Cr(bpy\text{ or }phen)_2(L)]^{3+}$, the selectivity of $[Cr(acac)(bpy)(L)]^{2+}$ differs from that of $[Cr(acac)_2(L)]^+$ which gives only a *lel* isomer.[4] Molecular models indicate that in *lel*-$[Cr(acac)(bpy)(L)]^{2+}$ the 6(6′)-hydrogen atom of bpy comes very close to the 6(6′)-carbon (and hydrogen) atom of the dioxide. There is no such extreme proximity between the acac and dioxide ligands in both *lel* and *ob* forms. In the *ob* form, one of the pyridine rings of the dioxide is nearly parallel to the diimine ligand to form a stable structure. The selective formation of *ob*-$[Cr(acac)(bpy)(L)]^{2+}$ is attributable to such steric conditions.

This work was partially supported by a Grant-in-Aid for Scientific Research No. 60740330 from the Ministry of Education, Science and Culture.

References

1) A. Vinciguerra, P. G. Simpson, Y. Kakiuti, and J. V. Quagliano, *Inorg. Chem.*, **2**, 286 (1963); A. R. Al-Karaghouli, R. O. Day, and J. S. Wood, *Inorg. Chem.*, **17**, 3702 (1978).
2) H. Kanno, K. Kashiwabara, and J. Fujita, *Bull. Chem. Soc. Jpn.*, **52**, 1408 (1979).
3) H. Kanno, K. Kashiwabara, and J. Fujita, *Bull. Chem. Soc. Jpn.*, **52**, 761 (1979).
4) H. Kanno, S. Utsuno, and J. Fujita, *Bull. Chem. Soc. Jpn.*, **57**, 3443 (1984).
5) H. Kanno, K. Kashiwabara, and J. Fujita, *Bull. Chem. Soc. Jpn.*, **53**, 2881 (1980).
6) D. Banerjea, J. Roy, and S. Sarkar, *Indian J. Chem.*, **8**, 372 (1970).
7) I. Murase, *Nippon Kagaku Zasshi*, **77**, 682 (1956).
8) S. Kaizaki, J. Hidaka, and Y. Shimura, *Bull. Chem. Soc. Jpn.*, **43**, 3024 (1970); *Inorg. Chem.*, **12**, 135 (1973).

4-Azidobutyryl Group for Temporary Protection of Hydroxyl Functions

Shoichi KUSUMOTO,* Keiichiro SAKAI, and Tetsuo SHIBA
Department of Chemistry, Faculty of Science, Osaka University, Toyonaka, Osaka 560
(Received September 24, 1985)

Synopsis. 4-Azidobutyryl esters formed from hydroxyl compounds and 4-azidobutyryl chloride were shown to be cleaved via reduction to 4-aminobutyrate followed by intramolecular O→N-acyl migrations to regenerate the free hydroxyl groups. High susceptibility of azide group to reduction enables the selective removal of this acyl group leaving many other functional groups unchanged.

In the synthetic studies on complex carbohydrates and other polyhydroxylated natural products, selective protection of particular hydroxyl groups is always required. For this purpose, various protecting groups have been proposed. However, during our recent synthetic studies on complex glycolipids, we realized that new types of protecting groups other than known ones are still required to facilitate the synthesis. We thus examined the use of 4-azidobutyryl group and found that this acyl group is versatile for temporary protection of hydroxyl functions.

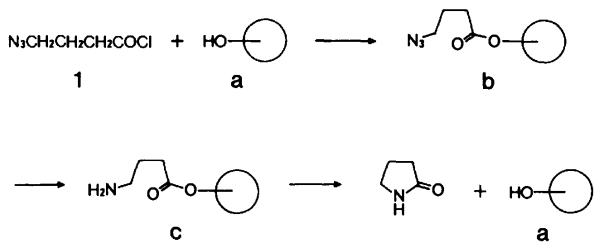

As the reagent for the introduction of 4-azidobutyryl group, the corresponding 4-azidobutyryl chloride (**1**) was prepared from γ-butyrolactone in four steps. Thus, opening of the γ-lactone[1] afforded ethyl 4-chlorobutyrate (**2**), which was then converted to ethyl 4-azidobutyrate (**3**).[2] Alkaline hydrolysis of **3** followed by reaction with thionyl chloride gave the desired chloride **1** as a colorless oil.[3]

Acylation of hydroxyl groups with this chloride (**1**) proceeded readily. The yields of the reaction with several substrates are summarized in Table 1.

We anticipated that the 4-aminobutyryl function which is formed on reduction of 4-azidobutyryl group would cause facile intramolecular O→N-acyl migration to regenerate the free hydroxyl group as shown in the scheme.[4] The only by-product formed thereby would be 2-pyrrolidinone which could be removed readily. Paulsen et al. described acylation of a trisaccharide with the chloride **1** and reduction of the resulting 4-azidobutyrate. However, they did not attempted the cleavage of the amino acyl group formed.[5]

One of the 4-azidobutyryl derivatives (**4b**) listed in Table 1 was then subjected to hydrogenolysis with palladium catalyst. TLC analysis revealed the presence of a small amount of the deacylated product (**4a**) in the reaction mixture together with the 4-aminobutyrate which gave a ninhydrin-positive spot. This indicated that the spontaneous deacylation certainly occurred even at room temperature, though the reaction rate was slow. The reaction was accelerated in boiling ethanol and completed within 1.5 h. The yield of deacylation step was 91% from **4b** as determined by HPLC analysis.

Owing to the high susceptibility of azide to catalytic hydrogenolysis, 4-azidobutyryl group can be selectively reduced and thus removed without affecting *O*-benzyl function in the same molecule as demonstrated in the deprotection of compound **5b**. Since benzyl ether is frequently employed as a persistent protecting group in many synthetic works, use of 4-azidobutyryl group would provide much flexibil-

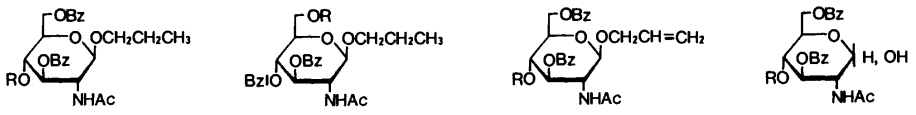

a R : H b R : $COCH_2CH_2CH_2N_3$ Bz : C_6H_5CO Bzl : $C_6H_5CH_2$

Table 1. Introduction and Removal of 4-Azidobutyryl Group

Compound	Introduction Yield/% (a→b)	Removal		
		Reduction (b→c)	Cleavage (c→a)	Yield/% (b→a)
4	96	H_2/Pd in EtOH[a]	Reflux in EtOH 1.5 h	91[b]
5	95	H_2/Pd in EtOH[a]	Reflux in EtOH 2.5 h	93
6	85	H_2S in Pyr-H_2O 2d[a]	Reflux in EtOH 2.0 h	95[b]
		PPh_3 in dioxane, reflux 2.5 h	then 80°C 1.5 h	78[b]

a) At room temperature. b) Determined by HPLC (see experimental section).

ity to the synthetic plan for complex target compounds.

Selective cleavage of 4-azidobutyryl group was next attempted in the presence of olefinic double bond. Though the hydrogenolysis of the azide group was faster than saturation of the allyl group in compound **6b**, fully selective reduction of the former was not possible with palladium-black.[6] Several other catalyst such as Raney nickel with absorbed hydrogen or palladium on calcium sulfate were examined but shown to give similar results. Selective reduction was effected chemically as follows. By use of triphenylphosphine, reduction to aminobutyryl group and its cleavage proceeded in boiling dioxane in rather short time in one step. In THF or ethanol, the reaction was slow even at reflux temperature and the yield of the deacylated product decreased due to the formation of an unidentified by-product. Use of hydrogen sulfide gave more satisfactory results. Thus, reduction of **6b** in a mixture of pyridine–water with hydrogen sulfide at room temperature[7] followed by cleavage by heating in ethanol as above gave **6a** in a high yield (Table 1). At higher temperature than 60 °C in the same solvent mixture,[7] reduction and cleavage took place successively but at such temperature the solution colored deeply and the yield of the product was very low.

In addition, the azidobutyryl group proved to survive under reaction conditions employed for cleavage of some other temporary protecting groups. For example, compound **6b** did not changed at all by heating in acetic acid–water (9:1) for 1 h. Thus, isopropylidene and benzylidene groups can be removed without affecting the azidobutyryl group. Furthermore, the allyl group in **6b** was removed through isomerization with an iridium complex,[8] followed by cleavage with iodine[9] to give **7b**, the azidobutyryl group being thereby unaffected.

In conclusion, 4-azidobutyryl group can be used as a new versatile acyl-type protecting group for hydroxyl functions. It can be easily introduced and has sufficient stability as well as a prominent feature to be cleaved preferentially to most of the other known protecting groups.

Experimental

All melting points and boiling points are not corrected. HPLC was performed with Shimadzu LC-5A liquid chromatograph apparatus equipped with a Cosmosil $5C_{18}$ column (4×125 mm); solvent: CH_3CN–H_2O (45:55); detection: absorbance at 254 nm. For quantitative determination of a deprotection product, a known amount of benzophenone was added to the reaction mixture as an internal standard, the peak area determined by use of an integrator (Shimadzu Chromatopac C-R1A) and amount of the product calculated.

Ethyl 4-Azidobutyrate (3). Sodium azide (34.4 g, 0.531 mol) and 15-crown-5 (5.8 g, 0.027 mol) were added to a solution of ethyl 4-chlorobutyrate (**2**)[1] (40 g, 0.266 mol) in CH_3CN (160 ml). The mixture was heated under reflux for 12 h. The completion of the reaction was confirmed with GLC (polyethylene glycol HT, 120 °C), After usual work-up, the product was distilled in vacuo; yield 39.6 g (95%), bp 96.5—98.5 °C/16 mmHg (1 mmHg=133.322 Pa). ^{1}H-NMR and IR spectra of this product were identical to the data given by Keschmann and Zbiral.[2]

4-Azidobutyryl Chloride (1). Azido ester **3** (13.0 g, 82.7 mmol) was heated in a solution of KOH (5.6 g, 100 mmol) in EtOH (270 ml) under reflux for 2 h. After evaporation of the solvent and acidification (HCl), the product was extracted with ether, and worked up as usual. Thionyl chloride (9.0 ml, 123 mmol) was added to a solution of the oily product in benzene. The mixture was stirred at room temperature for 30 min and then heated under reflux for 1.5 h. Evaporation in vacuo followed by vacuum distillation afforded the chloride 1; yield 9.66 g (79%), bp 90—91 °C/16 mmHg. EI-MS: *m/z* 147 (M^+). ^{1}H-NMR ($CDCl_3$) δ=1.94 (2H, quintet), 3.02 (2H, t, J=7.1 Hz), and 3.38 (2H, t, J=6.5 Hz).

Propyl 2-Acetamido-3,6-di-*O*-benzoyl-2-deoxy-β-D-glucopyranoside (4a). Allyl 2-acetamido-3,6-di-*O*-benzoyl-2-deoxy-β-D-glucopyranoside (**6a**)[10] (300 g, 6.39 mmol) was hydrogenated with Pd-black in EtOH (150 ml) at room temperature and recrystallized from EtOAc; yield 2.35 g (78%), mp 180—182 °C. Found: C, 63.42; H, 6.18; N, 2.95%. Calcd for $C_{25}H_{29}NO_8$: C, 63.88; H, 6.20; N, 2.95%.

Propyl 2-Acetamido-4-*O*-(4-azidobutyryl)-3,6-di-*O*-benzoyl-2-deoxy-β-D-glucopyranoside (4b). To an ice-cooled solution of **4a** (500 mg, 1.06 mmol) and pyridine (0.17 ml, 2.1 mmol) in CH_2Cl_2 (25 ml) was added the chloride **1** (235 mg, 1.59 mmol). The mixture was stirred at room temperature for 4.5 h. The mixture was worked up as usual and the product recrystallized from EtOAc–hexane; yield 590 mg (95%); mp 142—144 °C, IR (nujol) 2100 cm^{-1} (N_3); $[\alpha]_D^{15}$ +0.40° (*c* 1.00, $CHCl_3$). Found: C, 59.66; H, 5.83; N, 9.52%. Calcd for $C_{29}H_{34}N_4O_9$: C, 59.79; H, 5.88; N, 9.62%.

Propyl 2-Acetamido-3-*O*-benzoyl-4-*O*-benzyl-2-deoxy-β-D-glucopyranoside (5a). Allyl 2-acetamido-3-*O*-benzoyl-4-*O*-benzyl-2-deoxy-β-D-glucopyranoside[10] (494 mg, 1.08 mmol) was hydrogenated as described for **4a**. The completion of the reaction was checked by HPLC. After usual work-up the product was recrystallized from EtOAc; yield 437 mg (88%); mp 171—172 °C; $[\alpha]_D^{24}$ −46.9° (*c* 1.00, $CHCl_3$). Found: C, 65.53; H, 6.85; N, 3.08%. Calcd for $C_{25}H_{31}NO_7$: C, 65.63; H, 6.83; N, 3.06%.

Propyl 2-Acetamido-6-*O*-(4-azidobutyryl)-3-*O*-benzoyl-4-*O*-benzyl-2-deoxy-β-D-glucopyranoside (5b). Compound **5a** was acylated with 4-azidobutyryl chloride (1) and pyridine in CH_2Cl_2 as described above for the preparation of **4b**. The product was recrystallized from EtOAc–hexane; yield 1.19 g (96%); mp 110 °C; IR (nujol) 2100 cm^{-1} (N_3); $[\alpha]_D^{24}$ −15.3° (*c* 1.00, $CHCl_3$). Found: C, 61.26; H, 6.35; N, 9.80%. Calcd for $C_{29}H_{36}N_4O_8$: C, 61.26; H, 6.38; N, 9.85%.

Allyl 2-Acetamido-4-*O*-(4-azidobutyryl)-3,6-di-*O*-benzoyl-2-deoxy-β-D-glucopyranoside (6b). Compound **6a**[10] was acylated with the chloride **1** as described above. The product was recrystallized from EtOAc–hexane; yield 739 mg (85%); mp 127—128 °C; $[\alpha]_D^{24}$ −1.20° (*c* 1.00, $CHCl_3$). Found: C, 60.05; H, 5.52; N, 9.62%. Calcd for $C_{29}H_{39}N_4O_9$: C, 59.99; H, 5.56; N, 9.65%.

Removal of 4-Azidobutyryl Group of 4b and 5b via Catalytic Hydrogenolysis. a) Compound **4b** (290 mg, 0.500 mmol) was dissolved in EtOH (10 ml) and hydrogenolyzed in the presence of Pd-black (50 mg) at room temperature under atmospheric pressure of H_2. After 3 h disappearance of the starting material was confirmed by TLC. The catalyst was filtered off, and the filtrate was heated under reflux for 1.5 h. Yield of **4a** was 91% as determined by HPLC (see above). Isolation yield after recrystallization from EtOAc–hexane was 195 mg (83%); mp 178—180 °C. The product was identified with an authentic specimen of **4a** by means of TLC and ^{1}H-NMR.

b) Compound **5b** (569 mg, 1.00 mmol) was hydrogenolyzed and heated in ethanol as described above for **4b**.

Recrystallization from EtOAc gave a product which was identical with an authentic specimen of **5a**; yield 428 mg (93%); mp 169—171 °C.

Removal of 4-Azidobutyryl Group of 6b. a) With Triphenylphosphine: Triphenylphosphine (24.3 mg, 0.12 mmol) was added to a solution of **6b** (58.0 mg, 0.10 mmol) in dioxane (10 ml) heated under reflux. Heating was continued for 2.5 h.[11] The mixture was then kept at 80 °C for additional 1.5 h. The yield of **6a** was 78% (HPLC, see above). The product was isolated by silica-gel column chromatography (silica gel, 10 g; $CHCl_3$–MeOH 15:1) and recrystallized from EtOAc–hexane. It was identified with an authentic sample of **6a** by means of TLC, HPLC and ^{1}H-NMR.

b) With Hydrogen Sulfide: Hydrogen sulfide was bubbled through a solution of **6b** (21.0 mg, 36.2 mmol) in a mixture of pyridine–H_2O (2:1) (4 ml) at room temperature for 2 h. The mixture was then kept in a stoppered bottle at room temperature for 2 d. After the solvent had been removed in vacuo, EtOH was added to the residue and insoluble materials were filtered off. The filtrate was heated under reflux for 2 h. The yield of **6a** was 95% (HPLC, see above). The isolated product was identified with **6a** as above.

2-Acetamido-4-*O*-(4-azidobutyryl)-3,6-di-*O*-benzoyl-2-deoxy-D-glucose (7b). Compound **6b** (300 mg, 0.517 mmol) and $Ir(COD)[PCH_3(C_6H_5)_2]_2PF_6$[8] (15 mg) was dissolved in degassed THF (5 ml). The catalyst was activated as described in the literature.[8] The solution was then stirred at 50 °C for 1.5 h. After cooling, H_2O and I_2 (260 mg, 1.00 mmol) were added and the mixture was stirred at room temperature for 30 min. A 5% aqueous solution of $NaHSO_3$ was added to the mixture until the color of I_2 disappeared. The mixture was extracted with $CHCl_3$, the organic layer washed successively with aqueous $NaHSO_3$ solution and water. The product was purified with a silica-gel column (10 g, $CHCl_3$–acetone 5:1) and recrystallized from EtOAc–hexane; yield 230 mg (86%); mp 148—150 °C; IR (nujol) 2100 cm^{-1} (N_3); $[\alpha]_D^{24}$ +45.9° (*c* 1.00, $CHCl_3$). Found: C, 57.87; H, 5.27; N, 10.17%. Calcd for $C_{26}H_{28}N_4O_9$: C, 57.77; H, 5.22; N, 10.37%.

References

1) M. N. Galbraith, D. H. S. Horn, E. J. Middleton, and R. J. Hackney, *Aust. J. Chem.*, **22**, 1517 (1969).

2) E. Keschmann and E. Zbiral, *Justus Liebigs, Ann. Chem.*, **1973**, 1455. These authors described a preparation of ethyl 4-azidobutyrate (**3**) via different route.

3) This chloride could be kept in a refrigerator for several months without detectable decomposition.

4) Several protecting groups were proposed which can be removed by catalytic hydrogenation of aromatic nitro function followed by similar intramolecular cyclization reaction. For example; R. W. Holley and A. D. Holley, *J. Am. Chem. Soc.*, **74**, 3069 (1952); I. D. Entwistle, *Tetrahedron Lett.*, **1979**, 555.

5) H. Paulsen and H. Bottcher, *Chem. Ber.*, **112**, 3864 (1979).

6) Heating the reduction product in ethanol always gave a mixture of desired **6a** and the corresponding propyl glycoside.

7) H. Paulsen and H. Tietz, *Carbohydr. Res.*, **125**, 47 (1984).

8) J. J. Oltvoort, C. A. A. van Boeckel, J. H. de Koning, and J. H. van Boom, *Synthesis*, **1981**, 305.

9) M. A. Nashed and L. Anderson, *J. Chem. Soc., Chem. Commun.*, **1982**, 1274.

10) M. Imoto, H. Yoshimura, H. Yamamoto, T. Shimamoto, S. Kusumoto, and T. Shiba, *Tetrahedron Lett.*, **25**, 2667 (1984).

11) Though disappearance of the starting azidobutyrate was confirmed by TLC after this period, the mixture was further heated to assure the cleavage of the aminobutyrate.

Linear Furano Compounds: Synthesis of 7*H*-Furo[3,2-g][1]benzopyran-7-ones

Y. GEETANJALI, B. RAJITHA, and M. Kanakalingeswara RAO*
Department of Chemistry, Regional Engineering College, Warangal-506 004 A. P., India
(Received March 18, 1985)

Synopsis. A novel synthesis of 2-aroyl-7*H*-furo[3,2-*g*]-[1]benzopyran-7-ones, viz., **IIIa** and **b** was reported by condensing 2-benzoyl- and 2-(*p*-methoxybenzoyl)-3-methyl-5-acetyl-6-hydroxybenzofuran (**Ia** and **b**) with $C_6H_5CH_2$-COONa-Ac_2O. **VI** was synthesised by condensing 7-hydroxy-6-benzoyl-4,8-dimethylcoumarin (**IV**) with **V**. The basic ethers (**IIId—j**) were synthesised by demethylating **IIIb** with pyridinehydrochloride and resultant **IIIc** was condensed with *N,N*-dialkyl-2-haloalkanamine hydrochlorides. UV, IR, ^{1}H NMR, and Mass spectral data are also given.

2-(*p*-Hydroxybenzoyl)benzofuran,[1] 2-(*p*-hydroxybenzoyl)-3-ethylbenzofuran,[1] unsubstituted -7*H*-furo-[3,2-*g*][1]benzopyran-7-one, psoralene[2] and substituted -7*H*-furo[3,2-*g*][1]benzopyran-7-ones,[3] viz., 3-[*p*-(2-dimethylamino-1-methylethoxy)phenyl]-, 3-[*p*-[2-(diethylamino)ethoxy]phenyl]-, and 3-[*p*-(3-piperidinopropoxy)-phenyl]-substituted 2-phenyl-9-methyl-7*H*-furo-[3,2-*g*][1]benzopyran-7-ones have shown antifertility activity. The antifertility activity of these compounds is attributed to the presence of *p*-hydroxybenzoyl group and *p*-[2-(dialkylamino)alkoxy]-benzoyl and *p*-[2-(dialkylamino)alkoxy]phenyl groups.

Results and Discussion

Based on the above reports, 2-[*p*-[2-(dialkylamino)-alkoxy]-benzoyl]-7*H*-furo[3,2-*g*][1]benzopyran-7-ones-(**IIId—j**) were synthesised by developing the 2-pyrone ring on 2-benzoyl-and 2-(*p*-methoxybenzoyl)-3-methyl-5-acetyl-6-hydroxybenzofuran(**Ia** and **b**). 2-Benzoyl- and 2-(*p*-methoxybenzoyl)- 3,5-dimethyl-6-phenyl-7*H*-furo-[3,2-*g*][1]benzopyran-7-ones(**IIIa** and **b**) were synthesised to study structure and antifertility activity relationships.† **IIIa** and **b** were synthesised by refluxing a mixture of **Ia** and **b**, $C_6H_5CH_2COONa$ and Ac_2O at 180°C for 20—22 h in 70 and 80% yields. This method provides a convenient synthetic route for the synthesis of -7*H*-furo[3,2-*g*] [1]benzopyran-7-ones **IIIa** and **b** (Scheme 1). **IIIa** was also synthesised in 50% yield by refluxing a mixture of **Ia** with phenylacetyl chloride and freshly baked K_2CO_3 in dry acetone. **IIIb** was demethylated with pyridine hydrochloride to give 2-(*p*-hydroxybenzoyl)-3,5-dimethyl-6-phenyl-7*H*-furo[3,2-*g*][1]benzopyran-7-one(**IIIc**). **IIIc** was then, condensed with a number of *N,N*-dialkyl-2-haloalkanamine hydrochlorides in 1:1 mol ratio, and freshly baked K_2CO_3 in dry acetone for 20—22 h to give **IIId—j** (Scheme 1) in 60 to 70% yield.

2-Benzoyl-3-phenyl-5, 9-dimethyl-7*H*-furo[3, 2-*g*][1]-benzopyran-7-one(**VI**) (Scheme 2) was synthesised by condensing 7-hydroxy-6-benzoyl-4,8-dimethylcoumarin-(**IV**) with ω-bromoacetophenone (**V**) in 1:1 mol ratio freshly baked K_2CO_3 in dry acetone for 12 h (Scheme 2). The spectral data is summarized in Table 1. All the

†Antifertility activity is reported elsewhere.

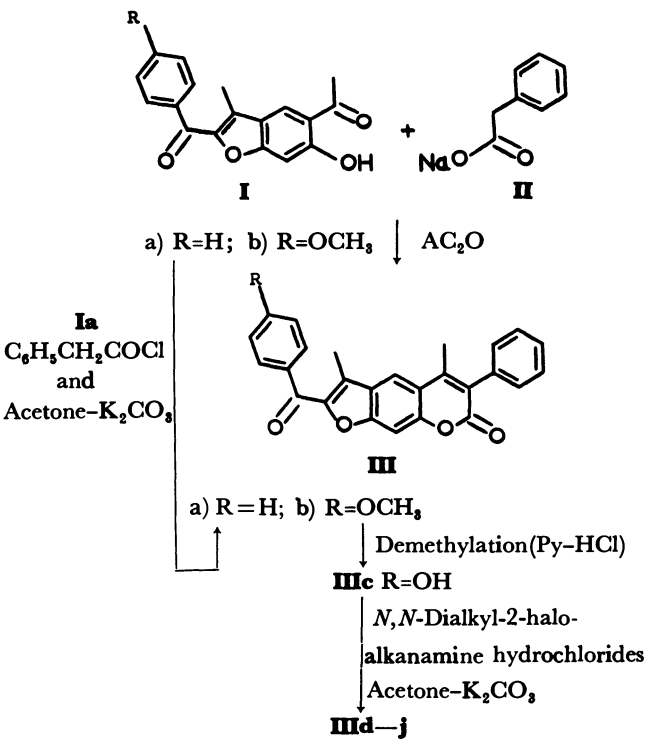

where R

d) $-O-CH_2-CH_2-N(CH_3)_2$
e) $-O-CH(CH_3)-CH_2-N(CH_3)_2$
f) $-O-CH_2-CH_2-N(Et)_2$
g) $-O-CH_2-CH_2-N$ (pyrrolidine)
h) $-O-CH_2-CH_2-N$ (piperidine)
i) $-O-CH_2-CH_2-CH_2-N$ (piperidine)
j) $-O-CH_2-CH_2-N$ (morpholine)

Scheme 1.

compounds exhibited two distinct UV absorption maxima in the region λ 288—292 nm and 355—358 nm. The IR spectra of these compounds have shown a lactone carbonyl group absorption at 1705—1720 cm^{-1} and an aroyl carbonyl group absorption at 1620—1630 cm^{-1}. The linear nature of the compounds **IIIa**, **b**, **d**, and **g** is confirmed by the observation of two singlets for the protons C_4 and C_9 in the ^{1}H NMR spectra of these compounds in the region δ 7.88—7.83 and δ 7.48—6.9 respectively. Further, the ^{1}H NMR spectrum, of compound **IIId** displayed two triplets at δ 4.1 and 2.8 respectively for

Table 1. Characterization Data of **IIIa—j** and **VI**

Compd[a-c]	Mp θ_m/°C	Formula	UV[d] λ_{max}/nm (log ε)	IR (KBr) -C=O/cm^{-1} Lactone	IR (KBr) -C=O/cm^{-1} Aroyl	^{1}H NMR ($CDCl_3$) δ (J in Hz)
IIIa	208	$C_{26}H_{18}O_4$,	290(4.23), 355(4.23)	1705	1625	7.98(m, 2H, 2′,6′-H), 7.83(s, 1H, 4-H), 7.35(m, 8H, 6-C_6H_5-H, 3′,4′,5′-H), 7.48(s, 1H, 9-H), 2.62(s, 3H, 5-CH_3), 2.38(s, 3H, 3-CH_3)
IIIb	270	$C_{27}H_{20}O_5$	290(4.48), 355(4.50)	1705	1625	8.25(d, 2H, J=9, 2′,6′-H), 7.88(s, 1H, 4-H), 7.32(m, 5H, 6-C_6H_5-H), 6.95(d, 2H, J=9, 3′,4′-H), 7.18(s, 1H, 9-H), 2.65(s, 3H, 5-CH_3), 2.38(s, 3H, 3-CH_3), 3.95(s, 3H, 4′-OCH_3-H)
IIIc	286	$C_{26}H_{18}O_5$	290(4.87), 358(4.92)	1680	1625	
IIId	110	$C_{30}H_{27}NO_5$	292(4.28), 358(4.36)	1715	1622	7.83(d, 2H, J=9, 2′,6′-H), 7.63(s, 1H, 4-H), 7.13(m, 5H, 6-C_6H_5-H), 6.75(d, 2H, J=9, 3′,5′-H), 7.0(s, 1H, 9-H), 4.1(t, 2H, J=6, -O-CH_2-), 2.8(t, 2H, J=6, -CH_2-N$\lesssim$), 2.61(s, 3H, 5-CH_3), 2.35(s, 6H, -N-$(CH_3)_2$), 2.30(s, 3H, 3-CH_3)
IIIe	103	$C_{31}H_{29}NO_5$	292(4.74), 355(4.77)	1710	1620	—
IIIf	95—97	$C_{32}H_{31}NO_5$	290(4.30), 355(4.36)	1710	1620	—
IIIg	101	$C_{32}H_{29}NO_5$	290(4.30), 358(4.36)	1715	1625	7.9(d, 2H, J=9, 2′,6′-H), 7.64(s, 1H, 4-H), 7.1(m, 5H, 6-C_6H_5-H), 6.71(d, 2H, J=9, 3′,5′-H), 6.9(s, 1H, 9-H), 4.1(t, 2H, J=6, -O-CH_2-), 2.8—2.74(m, 5H, -CH_2-N$\lesssim$, 5-CH_3), 2.7—2.2(m, 7H, -N-$(CH_2)_2$), 1.8(m, 4H,
IIIh	108	$C_{33}H_{31}NO_5$	290(4.42), 355(4.47)	1720	1625	—
IIIi	98	$C_{34}H_{33}NO_5$	292(4.44), 258(4.53)	1720	1625	—
IIIj	105	$C_{32}H_{29}NO_6$	288(4.33), 355(4.91)	1720	1625	—
VI	190—192	$C_{26}H_{18}O_4$	290(4.45), 358(4.50)	1715	1625	—

a) Satisfactory elemental analysis obtained for all the compounds. b) Compounds **IIIa—c** were obtained in 80, 70, and 90% yield, respectively. Compounds **IIId—j** and VI were obtained in 60—65 and 50% yield respectively. c) All the compounds were crystallized from dioxane. d) The UV spectra of compounds **IIIa—f, h, j,** and **IIIg, i** were recorded in chloroform and methanol respectively.

the protons of -O-CH_2- and -CH_2-N$\lesssim$ of (alkylamino)-alkoxyl group, whereas in the case of compound **IIIg**, the protons of -O-CH_2- have displayed a triplet and the protons of -CH_2-N$\lesssim$ and C_5-CH_3 groups have been observed as a multiplet in the region δ 2.80—2.74. The

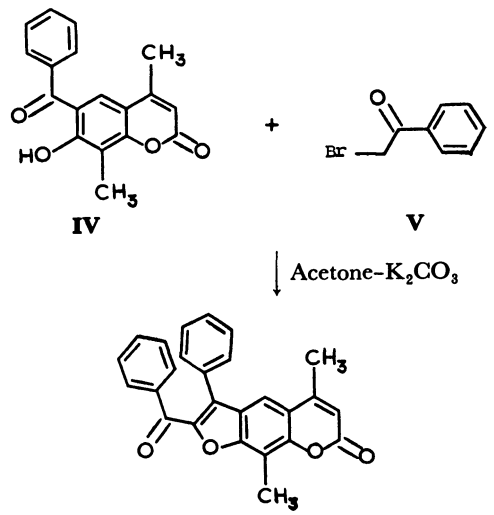

Scheme 2.

mass spectra of compounds **IIIa, b,** and **VI** showed molecular ions M$^+$394(8.1%), M$^+$424(100%), and M$^+$394(1.5%) respectively.

Experimental

Melting points of all the compounds **IIIa—j** and **VI** were taken in open capillaries and are uncorrected. UV absorption spectra were taken on Shimadzu UV 240 Ultraviolet Visible spectrophotometer, IR spectra were recorded on Perkin-Elemer spectrophotometer, and ^{1}H NMR spectra on a Varian EM 390-90 MHz NMR spectrophotometer with TMS as an internal standard.

The procedures given below are typical of the general procedure employed.

2-(*p*-Methoxybenzoyl)-3,5-dimethyl-6-phenyl-7*H*-furo[3,2-*g*]-[1]benzopyran-7-one (IIIb). Five ml of Ac_2O was added to an intimate mixture of **Ib** (16.20 g; 0.05 mol) and sodium phenylacetate (15.8 g; 0.1 mol), and the mixture was refluxed in an oil bath at 180° for 24 h. The reaction mixture was cooled and poured onto a crushed ice (5g). The solid obtained was recrystallized from dioxane. Yield: 14 g (70%), Found: C, 76.37; H, 4.65%. Calcd for $C_{27}H_{20}O_5$: C, 76.41; H, 4.71%

2-(*p*-Hydroxybenzoyl)-3,5-dimethyl-6-phenyl-7*H*-furo[3,2-*g*]-[1]benzopyran-7-one (IIIc). **IIIb** (12.72 g; 0.03 mol) was added to the freshly distilled pyridine hydrochloride (34.5 g;

0.3 mol), and the mixture was refluxed for 30 min. The cooled reaction mixture was poured into water, and the solid filtered off, washed with water, dried, and crystallized from dioxane. Yield: 10.8 g(90%). Found: C, 76.02; H, 4.31%. Calcd for $C_{26}H_{18}O_5$: C, 76.09; H, 4.39%.

2-[*p*-(2-Pyrrolidinylethoxy)benzoyl]-3,5-dimethyl-6-phenyl-7*H*-furo[3,2-*g*][1]benzopyran-7-one (IIIg). IIIc (1.23 g; 0.003 mol) was dissolved in acetone (400 ml) and to this 1-(2-chloroethyl)pyrrolidine hydrochloride (0.510 g; 0.003 mol) and freshly baked K_2CO_3 (3g) were added, and the mixture was refluxed for 22 h. The inorganic impurities were filtered off and the residue was poured into ice cold water, filtered, washed with water, and crystallized from aqueous dioxane as colorless flakes. Yield: 0.950 g(65%). Found: C, 75.69; H, 5.65; N, 2.69%. Calcd for $C_{32}H_{29}NO_5$: C, 75.73; H, 5.71; N, 2.76%

2-Benzoyl-3-phenyl-5,9-dimethyl-7*H*-furo[3,2-*g*][1]benzopyran-7-one(VI). A mixture of **IV** (0.294 g; 0.001 mol) and ω-bromoacetophenone (0.199 g; 0.001 mol) in acetone (300 ml) was refluxed for 12 h cooled, and the inorganic impurities were filtered off. Acetone was recovered by distillation and the residue was poured into ice cold water. The solid obtained was recrystallized from dioxane as shining needles. Yield: 0.908 g(50%). Found: C, 79.10, H, 4.49%. Calcd for $C_{26}H_{18}O_4$: C, 79.18; H, 4.56%.

We are grateful to Prof. K. Koteswara Rao, Principal, REC, Warangal for providing facilities and to the CSIR, New Delhi, for the award of a Senior research fellowship to YG.

References

1) M. Bisagni, NG. PH. Buu-Hoi, and R. Royer, *J. Chem. Soc.*, **1955**, 3693.
2) Pomashehenko, *Farmakol. Alkaloidov Glykozidov.*, **70**, 2231V(1967).
3) B. Rajitha, Y. Geetanjali, M. K. L. Rao, V. V. Somayajulu, and C. K. Atal, *Proc. Indian Acad. Sci.*, **90**, 291 (1981).

 © 1986 The Chemical Society of Japan Bull. Chem. Soc. Jpn., 59, 1303—1309 (1986)

Prediction of IR Intensities of Bending Fundamentals in 2,4-Pentadiynenitrile by the Combination of ab Initio Calculation and Experimental Parameters

Masakatsu UYEMURA
Department of Industrial Chemistry, Faculty of Engineering,
Tokyo Institute of Polytechnics, Atsugi, Kanagawa 243-02
(Received September 24, 1985)

2,4-Pentadiynenitrile is a H(C≡C)$_n$C≡N-type molecule. Molecules with n=0 to n=5 are known as interstellar molecules. Infrared spectra have not been observed yet, because the synthesis of a molecule of this type becomes more difficult as the molecular size increases. In the present study, the frequencies and infrared intensities of bending fundamentals in 2,4-pentadiynenitrile were predicted from an ab initio calculation coupled with empirical corrections. Calculation errors have been estimated by comparing calculated and experimental values in small reference molecules which have local structures similar to those of 2,4-pentadiynenitrile. The errors in 2,4-pentadiynenitrile have also been estimated.

Molecules designated as H(C≡C)$_n$C≡N are known as interstellar molecules and the microwave spectra for those with n=1 to 5 have been identified by radio-telescope observations.[1-5] The spectroscopic parameters of these molecules, especially those for the bending vibrations, are essential for an analysis of the radio-telescope data,[6] but laboratory infrared spectra are available only for hydrogen cyanide (n=0) and 2-propynenitrile (n=1). In the present work, the frequencies and the infrared intensities for the bending fundamentals of 2,4-pentadiynenitrile (n=2) were predicted based on an ab initio calculation. It is widely accepted that semiempirical MO theory, such as CNDO, is a powerful means for resolving sign ambiguities in dp/dQ. These are indeterminable from experiments alone.[7] However, the accuracy of semiempirical MO theory is still insufficient to predict infrared intensities with practical accuracy. Nowadays, ab initio MO theory has been applied to molecules of moderate size and it has become accepted that their accuracies are generally much superiror to those of semiempirical ones. In some cases, however, large discrepancies still remain between the calculated and experimental dipole-moment derivatives.[8] The major reason for these discrepancies is the fact that the electron repulsion is not properly taken into account in the Hartree–Fock MO theory. In fact, when elaborated CI calculations are performed, the above-mentioned discrepancies are significantly reduced.[9,10] Then, highly correlated wave functions are necessary for the accurate prediction of frequencies and infrared intensities. The ab initio calculation at this level, however, can be carried out at the present time only for small molecules (for example hydrogen cyanide) and can not be extended easily to larger molecules. Therefore, some alternate approaches must be explored. One of them may be an empirical correction of Hartree-Fock calculations, where the differences between calculated and experimental quantities are assessed. These are then used to obtain an empirical correction to the ab initio results. Essentially the same approaches have been employed in the determination of force fields, where the force constants from ab initio calculations were multiplied by empirical scale factors to obtain a more accurate prediction than the ab initio results themselves.[11,12] In the present study, the ab initio calculations were carried out to obtain the force fields and dipole-moment derivatives for bending vibrations of three H(C≡C)$_n$C≡N type molecules, i.e., HC≡N (n=0), HC≡CC≡N (n=1), and HC≡CC≡CC≡N (n=2), and two related molecules, i.e., HC≡CH and N≡CC≡N. First, the calculated values were compared with the experimental ones in cyanogen, acetylene, and hydrogen cyanide (hereafter, called reference molecules), in order to obtain the empirical correction parameters. Then, the frequencies and the infrared intensities in 2-propynenitrile were predicted and compared with the experimental values so as to estimate the error in the prediction employed here. Finally, the frequencies and the infrared intensities of the bending fundamentals in HC≡CC≡CC≡N and DC≡CC≡CC≡N were predicted in the same way by the use of empirical correction terms.

The same procedure can be applied, in principle, to other larger molecules. However, the CPU time available for each project is limited. Thus, the calculation of a large molecule can be performed at the sacrifice of the quality of the results. On the other hand, as described later, the error of an MO calculation is fairly large for the molecules treated in this work. Therefore, it is necessary to maintain a moderate calculation level for the purpose of this work. After all, the maximum-size molecule must be determined to take these conditions into account. Under the present computational condition, 2,4-pentadiynenitrile (n=2) is the largest member in this series of molecules that can be treated at the same calculation level as 2-propynenitrile (n=1) and other small reference molecules.

Calculation

The ab initio MO calculations were carried out after Hartree-Fock approximations using Pople's 4-31G** split valence plus polarization basis set. The alpha parameters for the polarization functions in H, C, and N were taken to be 1.0, 0.70, and 0.75 respectively.[13-15] The programs used are library programs IMSPAK and HONDOG at Computer Center of Institute for Molecular Science.

Force Fields. First, the theoretical equilibrium geometry was sought for each molecule; then, each atom was displaced 0.01 a.u. along a Cartesian coordinate perpendicular to the molecular axis. The energy gradients were calculated at every configuration; then these energy gradients were differentiated numerically with respect to atomic displacement to obtain $\boldsymbol{F}_x$ matrices. These calculations were performed using the program IMSPAK.

Internal coordinates $\boldsymbol{R}$ and laboratory fixed coordinates $\boldsymbol{X}$ are related by the following expression:[17]

$$\boldsymbol{X} = (\boldsymbol{A} \vdots \boldsymbol{a})\begin{pmatrix}\boldsymbol{R}\\ \boldsymbol{\rho}\end{pmatrix} \tag{1}$$

where $\boldsymbol{\rho}$ corresponds to the Eckart condition which must be fulfilled by molecular fixed coordinates $\boldsymbol{R}$. The inverse transformation of Eq. 1 is expressed as

$$\begin{pmatrix}\boldsymbol{R}\\ \boldsymbol{\rho}\end{pmatrix} = \begin{pmatrix}\boldsymbol{B}\\ \boldsymbol{\beta}\end{pmatrix}\boldsymbol{X}, \tag{2}$$

where $\boldsymbol{B}$ matrices are defined by Wilson[18] and an explicit expression of the $\boldsymbol{\beta}$ matrices is shown in Ref. 17. The $\boldsymbol{F}$ matrices for each molecule were obtained from $\boldsymbol{F}_x$ matrices by

$$\boldsymbol{F} = \tilde{\boldsymbol{A}}\,\boldsymbol{F}_x\,\boldsymbol{A}, \tag{3}$$

where $\tilde{A}$ stands for the transpose of $\boldsymbol{A}$.

Atomic Polar Tensors (APTs). Atomic coordinates were displaced 0.01 a.u. along the Cartesian coordinate around the equilibrium geometry and the dipole moments were calculated at these geometries; then the dipole moments were differentiated numerically to obtain $\boldsymbol{P}_x$ matrices (APTs).[16,17]

Fundamental Frequencies ν_i, and Infrared Intensities A_i. The $\boldsymbol{F}$ matrices obtained from Eq. 3 and the $\boldsymbol{G}$ matrices were used to determine the fundamental frequencies ν_i and $\boldsymbol{L}$ matrices. $\boldsymbol{P}_x$ matrices are related to the dipole-moment derivatives with respect to the internal coordinates $\boldsymbol{P}_R$ by the following Eq.,

$$\boldsymbol{P}_R = \boldsymbol{P}_x\,\boldsymbol{A}, \tag{4}$$

and $\boldsymbol{P}_R$ are related to $\boldsymbol{P}_Q$, i.e., the dipole-moment derivatives with respect to the normal coordiate, by

$$\boldsymbol{P}_Q = \boldsymbol{P}_R\,\boldsymbol{L}. \tag{5}$$

Then, the integrated molar absorption coefficients A_i are expressed as;[19]

$$A_i = \frac{N g_i P_{Q_i}^2}{3c^2(4\varepsilon_0)} \tag{6}$$

where N is Avogadro's constant and g_i is the degree of degeneracy.

Results and Discussion

Force Fields. Calculated and experimental force constants for N≡CC≡N, HC≡CH, and HC≡N are shown in Table 1. The force fields of these molecules have been thoroughly studied and the experimental values in Table 1 were obtained from harmonic frequencies.[20-22] The relative errors found in the calculated values in these molecules are generally larger than those obtained in other molecules at a similar calculation level (Hartree-Fock approximation using split valence basis set).[12] At the same time, it may be noted that the errors depend to some extent on the local structure of the molecules where the internal coordinate is defined; for example, the ratios of experimental diagonal force constants to calculated ones are 0.67—0.64 for H-C≡C and H-C≡N bending coordinates, and 0.58 for C-C≡N bending respectvely, which seems to reflect the extent of the electron correlation in a triple bond. As for the

Table 1. Experimental and Calculated (4-31G**) Force Constants (10^2 N m^{-1}) of the Reference Molecules[a,b]

	NCCN[c]		HCCH[d]		HCN[e]
	$r_0\Delta\phi_1$	$r_0\Delta\phi_2$	$r_0\Delta\phi_1$	$r_0\Delta\phi_2$	$r_0\Delta\phi_1$
Exp.					
$r_0\Delta\phi_1$	0.2918		0.2510		0.2596
$r_0\Delta\phi_2$	−0.0133	0.2918	0.0925	0.2510	
Calc.					
$r_0\Delta\phi_1$	0.4976		0.3729		0.4054
$r_0\Delta\phi_2$	−0.0408	0.4976	0.1081	0.3729	
Exp./Calc.					
$r_0\Delta\phi_1$	0.5864		0.6731		0.6404
$r_0\Delta\phi_2$	0.326	0.5864	0.8557	0.6731	

a) Bending coordinates ϕs are defined as follows;

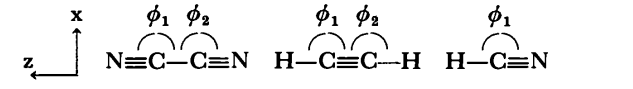

b) r_0 is a constant of 0.1 nm. c) Ref. 20. d) Ref. 21. e) Ref. 22.

off-diagonal force constants, the ratios of experimental to calculated values vary to a large extent. In one case, the ratio of experimental to calculated values is close to unity, and far from unity in the other case. However, it must be noted that the absolute values of the off-diagonal force constants are much smaller than the diagonal ones, so that in the off-diagonal force constants a small absolute error gives a large relative one.

The bending force constants for HC≡CC≡N and HC≡CC≡CC≡N were obtained at the same calculation level. Then, the correction factors were multiplied by the calculated force constants to give the most accurate prediction for the force fields. These correction factors were taken from the ratios of the experimental to the theoretical force constants obtained for similar or same bending coordinates in the reference molecules, i.e., the correction factor for H-C≡C was taken from the mean value (0.657) of ratios both in H-C≡N of HC≡N and in H-C≡C of HC≡CH. As for the C-C≡C bending force constant, there is no corresponding value among the reference molecules. Therefore, the correction factor for this constant was assumed to be equal to that for C-C≡N in N≡CC≡N (0.586). These two force constants are similar in that they are bending coordinates around a carbon atom which is involved in a conjugated triple bond. As for the off-diagonal force constants in 2,4-pentadiynenitrile, only those which are related to adjacent bending coordinates were considered here, since others are less important for the calculation of vibrational frequencies. These constants are further classified into two groups. The first group (group A) is composed of those between C-C≡C and C≡C-C bending coordinates; both of which have common C≡C bond. Group B is composed of those between C≡C-C and C-C≡C or C-C≡N bending coordinates; both of which have common C-C bond. Experimental values of the force constants in group A are positive, and fairly correctly predicted by the ab initio method in the reference molecules (for example, the ratio of the experimental value to the calculated one is 0.86 in HC≡CH), whereas those in group B are negative and the predicted magnitudes are too large (the above-mentioned ratio is 0.33 in N≡CC≡N). These ratios were used as correction factors for the force constants in the two groups. The force constants of HC≡CC≡N predicted in this way are compared with the experimental ones in Table 2(a) and the experimental and predicted frequencies of 2-propynenitrile are summarized in Table 2(b). The predicted freqencies are in the range of 0.95—1.04 of the experimental ones. Here, it may be noted that the predicted force constants in Table 2(a) are based on empirical correction factors and these were derived from harmonic frequencies of reference molecules, whereas the experimental force constants of 2-propynenitrile are based on the observed experimental frequencies. It is well known that the observed frequencies are generally lower than the harmonic ones because of the anharmonicities in potential functions. On account of the above effect, it might be reasonable that the predicted force constant of H-C≡C bending is 5% larger than the experimental one. On the contrary, the predicted values for the C≡C-C and C-C≡N bending force constants are about 2 to 6% less than the experimental ones. These discrepancies will be explained from the following two reasons. First, the frequencies of ν_6 and ν_7 are fairly near so that relatively large correlations exist between these force constants (diagonal constants for C≡C-C and C-C≡N bending coordinates) and the experimental uncertainties are relatively large in these force constants. Second, there is no C≡C-C bending force constant in the reference molecules, so that the correction factor for this bending force constant was assumed to be equal to that for C-C≡N. The force constants of 2,4-pentadiynenitrile which were pre-

Table 2(a). Experimental and Predicted Force Constants (10^2 N m^{-1}) of 2-Propynenitrile[a)]

Experimental[d)]	$r_0\Delta\phi_1$	$r_0\Delta\phi_2$	$r_0\Delta\phi_3$
$r_0\Delta\phi_1$	0.2397		
$r_0\Delta\phi_2$	0.0977	0.2732	
$r_0\Delta\phi_3$	0.0[b)]	0.0[b)]	0.3556
Predicted	$r_0\Delta\phi_1$	$r_0\Delta\phi_2$	$r_0\Delta\phi_3$
$r_0\Delta\phi_1$	0.2525		
$r_0\Delta\phi_2$	0.0836	0.2678	
$r_0\Delta\phi_3$	0.0[c)]	−0.0160	0.3361
Exp./Pred.	$r_0\Delta\phi_1$	$r_0\Delta\phi_2$	$r_0\Delta\phi_3$
$r_0\Delta\phi_1$	0.9493		
$r_0\Delta\phi_2$	1.169	1.0202	
$r_0\Delta\phi_3$	—	—	1.0580

a) Bending coordinates ϕs are defined as follows;

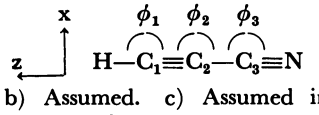

b) Assumed. c) Assumed in the present prediction. d) Ref. 23.

Table 2(b). Experimental and Predicted Bending Fundamental Frequencies (cm^{-1}) of 2-Propynenitrile

HCCCN	Exp.[a)]	Pred.	Exp. − Pred.
	663	690	−27
	499	504	−5
	223	215	8
DCCCN	**Exp.[a)]**	**Pred.**	**Exp. − Pred.**
	523	551	−28
	495	490	5
	213	205	8

a) Ref. 23.

Table 3. Rredicted Force Constants (10^2 N m^{-1}) of 2,4-Pentadiynenitrile[a]

	$r_0\Delta\phi_1$	$r_0\Delta\phi_2$	$r_0\Delta\phi_3$	$r_0\Delta\phi_4$	$r_0\Delta\phi_5$
$r_0\Delta\phi_1$	0.2476				
$r_0\Delta\phi_2$	0.0712	0.3087			
$r_0\Delta\phi_3$	0.0[b]	−0.0183	0.3275		
$r_0\Delta\phi_4$	0.0[b]	0.0[b]	0.0543	0.2678	
$r_0\Delta\phi_5$	0.0[b]	0.0[b]	0.0[b]	−0.0181	0.3554

a) Bending coordinates are defined as follows;

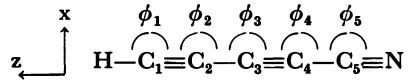

b) Assumed in the present prediction.

dicted in the same way are shown in Table 3.

Atomic Polar Tensors (APTs). Calculated and experimental atomic polar tensors (APTs) for N≡CC≡N, HC≡CH, and HC≡N are shown in Table 4.[24-26] In acetylene, good agreements were obtained between the calculated and the experimental APTs. On the other hand, fairly large errors were found in H and N of hydrogen cyanide. These errors are due to an overestimation of H–C and C≡N bond moments. This trend is also found in cyanogen in a more exaggerated way, where the calculated APT for N is 0.099*e* larger than the experimental one. This error is about 6-times larger than that in hydrogen cyanide. This error difference regarding the APTs for the N which participate in the C≡N bonds reflects a difference in the bonding characteristics in these C≡N bonds. This might be caused by a conjugation difference in these molecules. Therefore, when these APTs are used to predict those for 2-propynenitrile and 2,4-pentadiynenitrile, it becomes necessary to decide which of the reference molecules they are similar to. In the following calculation, the bonding characters of C≡N in 2-propynenitrile and 2,4-pentadiynenitrile were assumed to be the same as that in cyanogen. This is because these C≡N bonds participate in the conjugation. In this respect, hydrogen cyanide must be classified in a different category. The differences between the calculated and experimental APTs in the reference molecules are largest in C and N in cyanogen (0.099*e*) and the other differences are much smaller. Therefore, as a first approximation, it may be reasonable to correct errors only for C and N in a C≡N bond which participates in conjugation. In the following prediction of the APTs for C and N in a C≡N bond, 0.099*e* was subtracted from APTs for C and was added to those for N in 2-propynenitrile and 2,4-pentadiynenitrile to compensate the overestimation of the C≡N bond polarity. The other APTs were not subject to corrections and the ab initio results were used as the predicted values for the APTs. The predicted APTs of 2-propynenitrile and 2,4-pentadiynenitrile are shown in Table 5(a) and Table 6 respectively.

Table 4. Experimental and Calculated (4-31G**) APTs of the Reference Molecules[a),b)]

Cyanogen	N	C	
Exp.[c)]	−0.245	0.245	
Calc.	−0.344	0.344	
Exp. − Calc.	0.099	−0.099	
Acetylene	**H**	**C**	
Exp.[d)]	0.205	−0.205	
Calc.	0.206	−0.206	
Exp. − Calc.	−0.001	0.001	
Hydrogen cyanide	**H**	**C**	**N**
Exp.[e)]	0.237	0.084	−0.321
Calc.	0.254	0.081	−0.337
Exp. − Calc.	−0.017	0.003	0.016

a) Among nine elements of APTs for each atom, only those which are responsible for the bending intensities, $\partial P_x/\partial_x$, are listed. b) APTs are shown in *e*. c) Ref. 24. d) Ref. 25. e) Ref. 26.

Table 5(a). Calculated (4-31 G**), Predicted and Experimental APTs of 2-Propynenitrile[a)]

	H	C_1	C_2	C_3	N
Calc.	0.210	−0.137	0.024	0.267	−0.355
Corr.	—	—	—	−0.099	0.099
Pred.	0.210	−0.137	0.024	0.168	−0.256
Exp.[b)]	0.199	−0.117	0.034	0.149	−0.265
Exp. − Pred.	−0.011	0.020	0.010	−0.019	−0.009

a) See the footnote a) and b) in Table 4. b) Ref. 23.

Table 5(b). Experimental and Predicted Infrared Intensities (A/km mol^{-1}) of 2-Propynenitrile

	Exp.[a)]	Pred.(1)[b,c)]	Pred.(2)[b,d)]
HCCCN			
ν_5	68.4	80.3 (1.17)	84.6 (1.24)
ν_6	8.0	12.5 (1.56)	8.1 (1.01)
ν_7	0.18	0.087 (0.48)	0.16 (0.88)
DCCCN			
ν_5	21.0	20.5 (0.97)	21.0 (1.00)
ν_6	24.5	30.3 (1.24)	29.7 (1.21)
ν_7	0.22	0.079 (0.36)	0.12 (0.55)

a) Ref. 23. b) Values in the parentheses are the ratios of predicted to experimental intensities. c) Based on the predicted force constants and predicted APTs. d) Based on the force constants fitted to the observed frequencies and the predicted APTs.

The predicted infrared intensities in 2-propynenitrile are shown in Table 5(b). When the predicted values are used for both APTs and force fields (Pred. (1) in Table 5(b)) the ratios of the predicted to

Table 6. Predicted APTs of 2,4-Pentadiynenitrile[a)]

	H	C_1	C_2	C_3	C_4	C_5	N
Calc.	0.214	−0.149	−0.034	0.090	−0.026	0.248	−0.343
Corr.	—	—	—	—	—	−0.099	0.099
Pred.	0.214	−0.149	−0.034	0.090	−0.026	0.149	−0.244

a) See footnote a) and b) in Table 4.

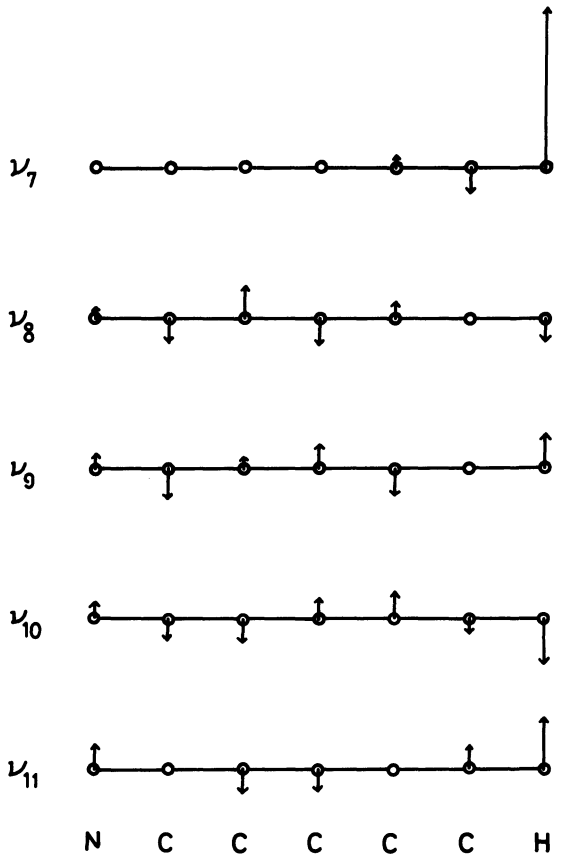

Fig. 1 (a). Normal modes of vibration in HCCCCCN.

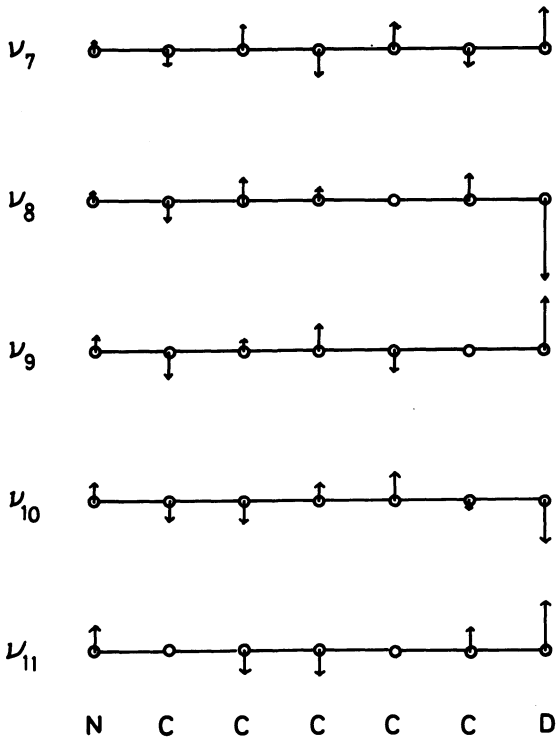

Fig. 1 (b). Normal modes of vibration in DCCCCCN.

experimental intensities lie between from 1.50 to 0.33. The value of this ratio for ν_5 in HCCCN is 1.17; this vibration results mainly from H–C≡C bending. The overestimated H–C polarity may be responsible for this overestimation. The errors in ν_7 intensities of HCCCN and DCCCN are much larger than those expected solely from the errors in APTs. In this mode, the molecules are bent mainly at the C–C≡N bending coordinate and the resultant changes of H–C and C≡N bond moments cancel each other. The net dipole-moment change becomes so small that a large relative error arises. Cancellations of this type occur more or less in ν_6 and ν_7 of HCCCN and DCCCN.

The sources of error in the predicted infrared intensities can be classified into two categories; one is the error in the APTs and the other is that in $\boldsymbol{L}$ matrices, which is mainly caused by the error in force fields. The $\boldsymbol{L}$ matrices determine the deformations of molecules, so that they determine the degree of cancellation or reinforcement of bond moments during the deformation. When this situation is taken into account, the general trend is well understood that the weak bands have large relative errors. To examine the influence of the error in the $\boldsymbol{L}$ matrix to the intensity A, another calculation was made for HCCCN and DCCCN, (Pred. (2) in Table 5(b)), where $\boldsymbol{L}$ matrices were determined from experimental force fields and the APTs were predicted as above. Here, it can be seen that the agreement between the experimental and predicted intensities of ν_6 and ν_7 in HCCCN and DCCCN have changed. This result seems to suggest that the errors in the predicted force fields are responsible to some extent for the errors in the predicted intensities, especially for low-intesity

bands.

Fundamental frequencies ν_i and infrared intensities A_i of bending vibrations in HCCCCCN and DCCCCCN were calculated using the predicted force fields (Table 3), and APTs (Table 6). Normal modes of vibrations for HCCCCCN and DCCCCCN are shown in Fig. 1. It can be seen that the ν_7 in the HCCCCCN is mainly localized at the H–C≡C bending coordinate. In the other vibrations, however, the vibrations delocalize more or less over the molecule. In the lowest vibrations (ν_{11} of HCCCCCN and DCCCCCN), the molecules are bent; thus the large bond moments of H–C (or D–C) and C≡N are inclined in the opposite direction and their moments cancel each other to give very low intensities. This situation is similar to that in ν_7 in 2-propynenitrile. As the vibrational frequency increases from ν_{11} to ν_8, the number of nodes in normal modes also increases, so that bond moments of H–C (or D–C) and C≡N cancel or reinforce each other, depending on the number of nodes. The resultant infrared intensities give rise to a intensity alternation.

As for the accuracy of the predicted force fields in 2-propynenitrile and 2,4-pentadiynenitrile, there may be no essential difference between them. Therefore, the predicted fundamental frequencies of 2,4-pentadiynenitrile are expected to have a comparable accuracy with that of 2-propynenitrile. The predicted frequency of ν_7 (mainly comprised from H–C≡C bending) in HCCCCCN may be about 4% too large as in HCCCN, since the correction factors for the H–C≡C diagonal force constants for these molecules were assumed to be equal. The other vibrations mainly consist of C≡C–C and C–C≡N bendings. Thus, their vibrational frequencies may be predicted too small, since the diagonal force constants for the C≡C–C and C–C≡N bendings have been predicted to be smaller than the experimental ones in 2-propynenitrile. These same correction factors were used for the prediction in 2,4-pentadiynenitrile.

It is more difficult to estimate the errors involved in the infrared intensities than those related to frequencies. This is because the former include errors from both the force fields and the APTs. However, it may be noted that the APTs for H, C, and N in H–C and C≡N bonds in these molecules are 2- to 7-times larger than those for other atoms. Thus, the $\boldsymbol{P}_R$ are dominated by APTs for these atoms and fairly good agreement were obtained between experimental and predicted APTs for H, C, and N in H–C and C≡N bonds in 2-propynenitrile. Therefore, the predicted APTs in 2,4-pentadiynenitrile are expected to have almost the same accuracy as those in 2-propynenitrile. The highest bending vibration (ν_7 in HCCCCCN) is mainly localized at H–C≡C bending. Thus, the infrared intensity is mainly donimated by the APTs of the H and C in H–C bond. At this point, it might be remembered that the APTs of H and C in the H–C bond in 2-propynenitrile were calculated to give an overestimated polarity with the direction (+)H–C(−), i.e, the magnitudes of APTs of H and C have been calculated too large by 6 to 17 percent. The calculated APT values for H and C in H–C≡C of 2,4-pentadiynenitrile are close to those in 2-propynenitrile. From this similarity in the APTs, it is inferred that the intensities of ν_7 in HCCCCCN and ν_5 in HCCCN may be predicted about 15 to 20% larger. In the other bending vibrations, it is difficult to estimate the errors in the predicted intensities since these vibrations delocalize over a molecule. Therefore, cancellations of bond moments occur to a larger extent. In such cases, some correlation may exist between the relative errors and the predicted intensities. In moderately strong bands (ν_7 and ν_{10} in HCCCCCN), their relative errors are expected to be 50% at most. In the weaker bands (ν_9 and ν_{11}), the predicted values may be regarded as order estimations.

Table 7. Predicted Frequencies (ν/cm^{-1}) and IR Intensities (A/km mol^{-1}) of Bending Fundamentals in HCCCCCN and DCCCCCN

HCCCCCN	ν_i	A_i	DCCCCCN	ν_i	A_i
ν_7	691	77.2	ν_7	580	2.33
ν_8	565	13.4	ν_8	537	41.1
ν_9	457	0.19	ν_9	444	2.9
ν_{10}	249	10.5	ν_{10}	242	11.1
ν_{11}	101	0.087	ν_{11}	98	0.098

The preliminary results of this work have been published previously,[27] and we should note that the intensity of the ν_8 fundamental in Table 1 in Ref. 27 was unfortunately misprinted and that the radiative transition rate through the ν_8 band was overestimated in the calculation. However, the total pump rate through the ν_8 and ν_7 bands decreases only by 15% due to this mistake and the main conclusion of the paper does not change.

The author wishes to express his thanks to Professor Keiji Morokuma and to Dr. Shigeki Kato of Institute for Molecular Science, for helpful discussions and kind advices. He also thanks to Professor Shuji Deguchi of the University of Illinois at Urbana-Champaign, for his encouragements throughout this work. The ab initio calculations were carried out at Computer Center, Institute for Molecular Science, using library programs IMSPAK and HONDOG. Normal coordinate calculations were carried out at Computer Center, The University of Tokyo.

References

1) L. E. Snyder and D. Buhl, *Astrophys. J.*, **163**, 147 (1971).

2) B. E. Turner, *Asptrophys. J.*, **163**, 138 (1971).

3) L. W. Avery, N. W. Broten, J. M. MacLeod, T. Oka, and H. W. Kroto., *Astrophys. J.*, **205**, L173 (1976).

4) N. W. Broten, T. Oka, L. W. Avery, J. M. MacLeod, and H. W. Kroto, *Astrophys. J.*, **223**, L105 (1978).

5) M. B. Bell, P. A. Feldman, S. Kwok, and H. E. Mattews, *Nature*, **295**, 389 (1982).

6) S. Deguchi, Y. Nakada, T. Onaka, and M. Uyemura, *Publ. Astron. Soc. Jpn.*, **31**, 105 (1979).

7) Roy E. Bruns, "Vibrational Intensities in Infrared and Raman Spectroscopy," ed by W. B. Person and B. Zerbi, Elsevier, Amsterdam (1982).

8) A. B. M. S. Bassi, *J. Chem. Phys.*, **68**, 5667 (1978).

9) B. Liu, K. M. Sando, C. S. North, H. B. Friedrich, and D. M. Chipman, *J. Chem. Phys.*, **69**, 1425 (1978).

10) J. E. Gready, G. B. Bacskay, and N. S. Hush, *J. Chem. Phys.*, **70**, 1071 (1979).

11) P. Pulay, G. Fogarasi, G. Pongor, J. E. Boggs, and A. Vargha, *J. Am. Chem. Soc.*, **105**, 7037 (1983).

12) G. Fogarasi and P. Pulay, *Ann. Rev. Phys. Chem.*, **35**, 191, (1984).

13) R. Ditchfield, W. J. Hehre, and J. A. Pople, *J. Chem. Phys.*, **54**, 724 (1971).

14) P. C. Hariharan and J. A. Pople, *Theor. Chim. Acta*, **28**, 213 (1973).

15) T. H. Dunning, Jr., and P. J. Hay "Modern Theoretical Chemistry," ed by H. F. Schaeffer III, Plenum, New York (1977), Vol. 3.

16) W. B. Person and J. H. Newton, *J. Chem. Phys.*, **61**, 1040 (1974).

17) W. B. Person, "Vibrational Intensities in Infrared and Raman Spectroscopy," ed by W. B. Person and B. Zerbi, Elsevier, Amsterdam (1982).

18) E. B. Wilson, J. C. Decius, and P. C. Cross, "Molecular Vibrations," McGraw-Hill, New York (1955).

19) D. Steele, *J. Mol. Struct.*, **117**, 163 (1984).

20) L. H. Jones, *J. Mol. Spectrosc.*, **49**, 82 (1974).

21) G. Strey and I. M. Mills, *J. Mol. Spectrosc.*, **59**, 103 (1976).

22) G. Strey and I. M. Mills, *Mol. Phys.*, **26**, 129 (1973).

23) M. Uyemura, S. Deguchi, Y. Nakada, and T. Onaka, *Bull. Chem. Soc, Jpn.*, **55**, 384 (1982).

24) K. Kim and W. T. King, *J. Chem. Phys.*, **80**, 974 (1983).

25) K. Kim and W. T. King, *J. Mol. Struct.*, **57**, 201 (1979).

26) K. Kim and W. T. King, *J. Chem. Phys.*, **71**, 1967 (1979).

27) S. Deguchi and M. Uyemura, *Astrophys. J.*, **285**, 153 (1984).

^{129}I Mössbauer Spectroscopic Studies on the Iodine Complexes of *N,N'*-Diphenyl-*p*-phenylenediamine and *N,N'*-Diphenylbenzidine

Hiroshi SAKAI* and Yutaka MAEDA
Research Reactor Institute, Kyoto University, Kumatori-cho, Sennan-gun, Osaka 590-04
(Received November 11, 1985)

^{129}I Mössbauer and resonance Raman spectroscopy have been applied to the iodine complexes of *N,N'*-diphenyl-*p*-phenylenediamine (DPPD-$I_{2.4}$) and *N,N'*-diphenylbenzidine (DPB-$I_{2.7}$), which exhibit relatively high electrical conductivities. The Mössbauer spectra of these complexes indicate the existence of two unequivalent iodine sites, corresponding to the central and terminal iodine atoms of a linear I_3^- unit. The resonance Raman spectra suggest that the I_3^- unit exists as a successive chain in these complexes. This is consistent with the crystallographic data of the DPPD-$I_{2.4}$ complex. The charge density of the I_3^- unit is slightly different from that of the isolated I_3^- ion because of a weak covalent bond between I_3^- units. It is confirmed that both complexes are partially oxidized mixed-valence compounds, formulated as $(DPPD)^{+0.8}(I_3^-)_{0.8}$ and $(DPB)^{+0.9}(I_3^-)_{0.9}$.

Some iodine complexes of oligoanilinic derivatives show interesting electrical and magnetic properties.[1] One of these complexes, *N,N'*-diphenyl-*p*-phenylenediamine-iodine (DPPD-I_x, x=1.8—2.4), exhibits relatively high electrical conductivity ($\approx$0.3 S cm^{-1}) at room temperature with a low activation energy (0.07 eV).[2,3] It is found from measurements of the thermoelectric power that in this complex (x=2.0—2.4) the electron conductivity is slightly more predominant than the hole conductivity near room temperature.[2,4] The complex is paramagnetic and shows a strong electron-spin resonance signal.[2] Crystallographic data of the complex (x=2.4) suggest that the iodine atoms are arranged in successive chains consisting of I_3^- units perpendicular to the layer of the planar DPPD molecule.[5] The iodine chain is coordinated to NH groups of the DPPD molecule. The interatomic distance in the I_3^- unit is approximately 2.99 Å, slightly longer than that of usual triiodide ions (2.92 Å).[6] The distance of 3.44 Å between I_3^- units along the chain is shorter than twice the van der Waals radius of iodine.

It is interesting to estimate the charge density of each iodine atom in order to understand the electrical and magnetic properties of the complex. The Mössbauer spectroscopy of ^{129}I is a powerful method for this purpose, since the electronic structure of iodine is directly derived from such Mössbauer parameters as the quadrupole coupling constant (e^2Qq) and its sign, the asymmetry parameter (η), and the isomer shift (δ). In this paper we report results of ^{129}I Mössbauer spectroscopy for the *N,N'*-diphenyl-*p*-phenylenediamine-$I_{2.4}$ (DPPD-$I_{2.4}$) and *N,N'*-diphenylbenzidine-$I_{2.7}$ (DPB-$I_{2.7}$) complexes. Furthermore, laser Raman spectra were measured for these complexes in order to clarify the configuration of iodine.

Experimental

Materials. The commercially available donor molecules, DPPD and DPB, were recrystallized from benzene. The ^{129}I labeled complexes used for measurements of the Mössbauer spectra were prepared from Na ^{129}I in an Na_2SO_3 solution. After oxidizing the iodide with 3 mol dm^{-3} H_2SO_4 and 10% H_2O_2, the resulting molecular iodine ($^{129}I_2$) was extracted with benzene. A dark-green DPPD-I_x complex with metallic luster was obtained upon adding a hot benzene solution of DPPD to the hot benzene solution of iodine. Lustrous, reddish-black crystals of DPB-I_x were obtained by mixing hot benzene solutions of DPB and excess iodine. The samples for measurements of resonance Raman spectra were prepared by using natural iodine in the same manner as the above procedures. The ratio of each component for these complexes was determined to be x=2.4 for DPPD-I_x and x=2.7 for DPB-I_x by iodometry.

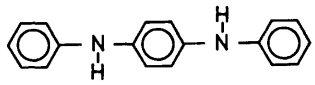

N,N'-diphenyl-p-phenylenediamine
(DPPD)

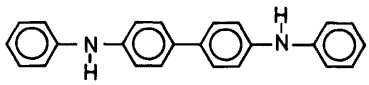

N,N'-diphenylbenzidine
(DPB)

Measuremens. A single-line $^{66}Zn^{129}Te$ Mössbauer source was prepared by irradiating 140 mg $^{66}Zn^{128}Te$ at a thermal neutron fluence rate of 2×10^{13} n cm$^{-2}\cdot$s^{-1} for 1 h in the Kyoto University Reactor (KUR). The source activity produced by the ^{128}Te (n,γ) ^{129}Te reaction was initially about 10 mCi, sufficient to obtain a reasonable spectrum in 3—4 h of data collection. The Mössbauer spectra were measured in a transmission geometry by cooling the source and the absorber to 16 K with a closed cycle helium refrigerator. The 27.8 keV Mössbauer γ-rays were detected with a 1 mm-thick NaI(Tl) scintillation counter. The Mössbauer spectrometer was calibrated with a six-line spectrum of an Fe foil.

Laser Raman spectra were recorded with Ar^+ (514.5 nm)

excitation usig a JEOL-JRS-400T triple monochromator and photon-counting detection. The data were obtained with compressed pellets of powdered samples by the front-surface reflection method using 60 mW laser power and a spinning cell. No decomposition was observed with this laser power.

Results and Discussion

Mössbauer Spectra. ^{129}I Mössbauer spectra of the DPPD-$I_{2.4}$ and DPB-$I_{2.7}$ complexes at 16 K are shown in Fig. 1(a) and (b). The spectra, consisting of two different quadrupole octets, were analyzed by the least-squares method using a double set of fitting parameters such as the quadrupole coupling constant (e^2Qq), the asymmetry parameter (η), the isomer shift (δ), the full-width at half-maximum (2Γ), and the intensity of each peak. The dashed curves in the figure represent the best fitted quadrupole-split octets, and the solid lines indicate the superimposed curves of the two octets. The obtained Mössbauer parameters are summarized in Table 1, together with results of the isolated I_3^- ions in the [Ru(η-C_5H_5)$_2$I]I_3[7] and β-carotene-I_3[8] complexes. The e^2Qq values are converted to that of the ^{127}I nucleus.

The existence of two unequivalent iodine atoms observed in the Mössbauer spectrum of the DPPD-$I_{2.4}$ complex is consistent with the results of the crystallographic analysis, in which the iodine atoms are arranged in chains of linear I_3^- units.[5] The similarity of the spectrum of the DPB-$I_{2.7}$ complex to that of DPPD-$I_{2.4}$ suggested that the iodine atoms build up an I_3^- unit. Later, this speculation was confirmed by the resonance Raman spectrum of the DPB-$I_{2.7}$ complex. It is now appropriate to assign the iodine with the larger quadrupole splitting to the central iodine atom (I_c) of the linear I_3^- unit, whereas the other to the two terminal iodine atoms (I_t). No broadening of the line width has been observed for I_t of the DPPD-$I_{2.4}$ complex, suggesting that the I_3^- unit is symmetric. On the other hand, the line width of I_t is broadened considerably in the DPB-$I_{2.7}$ complex compared with that of I_c and the broadening is enhanced in the region of higher velocity. This implies that the charge densities on the two I_t atoms are slightly different; i.e., the I_3^- unit is slightly asymmetric. Attempts to fit the spectrum with three unequivalent iodine sites were unsuccessful. Therefore, the values of e^2Qq, η, and δ given in Table 1 are

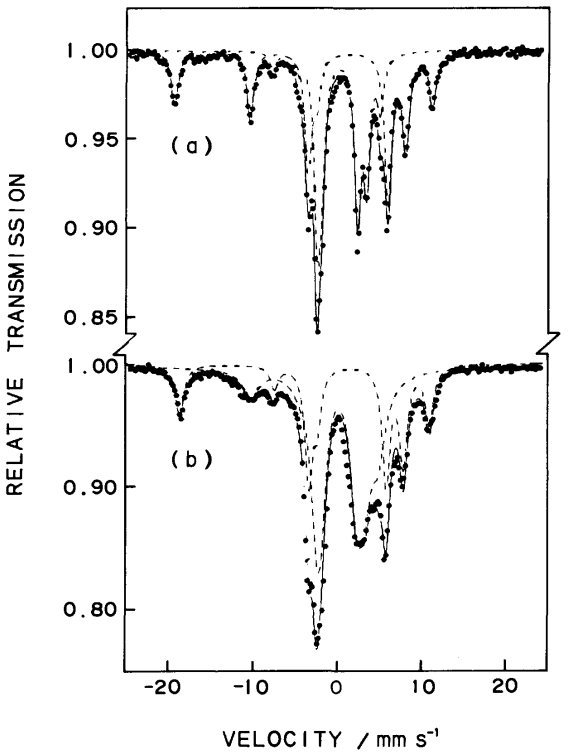

Fig. 1. ^{129}I Mössbauer spectra at 16 K of (a) *N,N'*-diphenyl-*p*-phenylenediamine-$I_{2.4}$ and (b) *N,N'*-diphenylbenzidine-$I_{2.7}$ complexes.

Table 1. ^{129}I Mössbauer Parameters for the Iodine Complexes of *N,N'*-Diphenyl-*p*-phenylenediamine and *N,N'*-Diphenylbenzidine, [Ru(η-C_5H_5)$_2$I]I_3, and β-Carotene-I_3

		e^2Qq[a] MHz	η	δ[b] mm s^{-1}	2Γ mm s^{-1}	Area Ratio	U_p	h_p	Ref.
DPPD-$I_{2.4}$	I_c	−2347±20	0.05±0.04	1.32±0.04	1.00±0.06	1.0	1.02	1.24	
	I_t	−1183±20	0.04±0.04	0.25±0.04	0.93±0.06	1.6	0.52	0.53	
DPB-$I_{2.7}$	I_c	−2282±20	0.10±0.04	1.35±0.04	1.09±0.06	1.0	1.00	1.26	
	I_t	−1166±20	0.06±0.04	0.22±0.04	1.60±0.06[c]	1.7	0.51	0.51	
[Ru(η-C_5H_5)$_2$I]I_3	I_c	−2460±35	0.06±0.04	1.48±0.05	0.83±0.08	1.0	1.07	1.35	(7)
	I_t	−1152±35	0.06±0.04	0.25±0.05	0.85±0.08	1.6	0.50	0.53	
β-Carotene-I_3	I_c	−2445±20	0.05±0.04	1.59±0.04	1.04±0.10	1.0	1.07	1.42	(8)
	I_t	−1152±20	0.06±0.04	0.23±0.04	1.20±0.10	1.4	0.50	0.51	

a) Quadrupole coupling constants (e^2Qq) are converted to the ^{127}I nucleus. b) Isomer shifts (δ) are relative to the ZnTe source. c) The value is of the line width at zero velocity.

the means of those for the two I_t atoms. The ratios of the absorption areas of I_t and I_c were found to be 1.6:1 and 1.7:1 for the DPPD–$I_{2.4}$ and DPB–$I_{2.7}$ complexes, respectively, as shown in Table 1. The same tendency is found in the I_3^- ions of [Ru(η-C_5H_5)$_2$I]I_3[7] and β-carotene–I_3[8] complexes. The deviation from the composition ratio of 2:1 in I_3^- is explained in terms of the recoilless fraction and the saturation effect. The I_t atom is bonded to one adjacent I_c atom, whereas the I_c atom is bonded to two I_t atoms with the same bond strength. Therefore, the I_t atom is expected to have a lower recoilless fraction than the I_c atom. Since the effective absorber thickness for the I_t atom is twice that for the I_c atom, the saturation for I_t is more dominant than for I_c. These effects result in the decrease in the absorption area of I_t.

The values of e^2Qq, η, and δ are closely related to the charge distribution and the charge density of 5p-electrons localized on the iodine atom as follows:[9,10]

$$U_p = -e^2Qq_{obsd}/e^2Qq_{atom} = -N_z + (N_x + N_y)/2, \quad (1)$$

$$\eta = 3(N_x - N_y)/2U_p, \quad (2)$$

$$\delta = 1.5\,h_p - 0.54 \text{ (mm s}^{-1}\text{, for ZnTe source)}, \quad (3)$$

$$h_p = 6 - (N_x + N_y + N_z), \quad (4)$$

where U_p is the number of unbalanced p-electrons, e^2Qq_{atom}, the atomic iodine quadrupole coupling constant, is equal to 2292.7 MHz for ^{127}I, and h_p is the number of 5p-electrons removed from the $5s^25p^6$ (I^-) configuration. N_x, N_y, and N_z are the populations of 5p-electrons in the x, y, and z directions, respectively. When the bonding of iodine is formed by only $5p_\sigma$-electrons, one expects the relationship $U_p=h_p=1\pm i$ to be valid; i is the ionic character. When 5s-electrons take part in bond formation (sp hybridization), the relationship $U_p>h_p$ is generally observed because of the decrease in the s-electron density at the nucleus. On the contrary, the participation of the $5p_\pi$-electrons (double bond character or intermolecular bonding in the x or y direction) leads to the relationship $U_p<h_p$. The values of U_p and h_p obtained for each iodine atom are given in Table 1, together with those for the isolated I_3^- ions in the [Ru(η-C_5H_5)$_2$I]I_3 and β-carotene-I_3 complexes.

DPPD-$I_{2.4}$ Complex: The U_p value is very close to the h_p value for the I_t atom in the DPPD–$I_{2.4}$ complex, suggesting that the bonding of I_t is mainly due to $5p_\sigma$-electrons. This result is consistent with the small η value of the atom, which implies that the bonding of the I_t atom is almost axially symmetric. Therefore, the I_t atom might not be interacting with the NH group of the DPPD molecule. Even if it should interact, the hydrogen bond with the NH group may be extremely weak. The I_t atom of the complex is found to be negatively charged by 0.48 e^- due to the values of U_p and h_p. It is generally observed that the terminal iodine is negatively charged by 0.50 e^- in the isolated I_3^- ion. The small deviation may be attributable to the weak covalent bond between I_3^- units. That is, the charge on the I_t atom is slightly delocalized along the chain of I_3^- units. This would lead to an increae in the charge density on the I_c atom. Actually, the values of U_p and h_p for I_c in this complex are smaller than those for I_c in the isolated I_3^- ions.

For the I_c atom in the DPPD–$I_{2.4}$ complex, the h_P value is larger than the U_P value. The same tendency is observed for the I_c atoms in the isolated I_3^- ions. This has been generally explained in terms of the presence of π-bonding in which the iodine donates $5p_\pi$-electrons to the neighbor atoms. However, it is quite difficult to consider the presence of a double bond or an intermolecular bond in the isolated I_3^- ion from the crystallographic data of [Ru(η-C_5H_5)$_2$I]I_3.[7] Furthermore, if the discrepancy is due to the π-bonding, the charge density on the I_c atom is estimated to be +0.24 e^- from the h_p value. This value is unreasonably high compared with the charge density calculated from the molecular orbital treatment of a delocalized three-center four-electron bonding. Lucken[11] has pointed out the contribution of $3d_\sigma$-electrons, on the central atom, to the linear Br_3^- bond formation. In his treatment the electronic structure of trihalide ions are descrided as a mixture of two extreme configurations, i.e., a delocalized three-center four-electron bond using only the valence p-electrons and covalent σ bonds between two $d_\sigma p_\sigma$ hybrid orbitals of the central atom and p_σ orbitals of two terminal atoms. This treatment is applicable to the interpretation of Mössbauer data for the triiodide ion. The contribution of the $4d_\sigma$ hybridization may lead to an increase in the effective s-electron density at the nucleus. This would markedly increase the δ value, but would hardly increase e^2Qq. In our previous paper[12] his treatment on the triiodide ion was concluded to be valid. It is interesting to apply $4d_\sigma$ hybridization to the central iodine atom of the bridging I_3^- unit in the complex, assuming no interaction with the NH group of the donor molecule. Using Eqs 4 and 5 in Ref. 12, the number of $4d_\sigma$ electrons promoted to the $5p_\sigma$-orbital can be easily estimated from the δ and e^2Qq. The h_p and h_d (the number of $4d_\sigma$-electron defect) obtained for the I_c atom are evaluated to be 0.84 and 0.17, respectively. That is, 0.17 e^- of the $4d_\sigma$-electron is promoted to the $5p_\sigma$-orbital. Consequently, the charge localized on the I_c atom is about +0.01 e^-. Thus, the I_c atom has a slight positive charge. If the hydrogen bond exists between the I_c atom and the NH group, the contribution of the $4d_\sigma$ hybridization

would decrease and, therefore, the charge density localized on the I_c atom would also decrease slightly. Judging from the small η value of the I_c atom, the hydrogen bond may be considerably weak. In the isolated I_3^- ion of $[Ru(\eta\text{-}C_5H_5)_2I]I_3$ the I_c atom is positively charged by $0.05\,e^-$ (evaluated in Ref. 12). This value is obviously larger than that of the bridging I_3^- unit.

It is concluded from the charge densities of the I_t and I_c atoms that in the bridging I_3^- unit a slight amount of charge is delocalized along the chain, ascribed to a weak covalent bond between the I_3^- units. It is likely that the delocalization of a small amount of charge is responsible for the electron conduction observed for the investigated complex. Furthermore, this complex is concluded to be a partially oxidized mixed-valence compound from the ratio of the iodine atom to the DPPD molecule, and the charge distribution of which is formulated as $(DPPD)^{+0.8}$ $(I_3^-)_{0.8}$. A stacking column consisting of the partially oxidized DPPD molecules may govern hole conductivity.

DPB-$I_{2.7}$ Complex: The agreement between the U_P and h_P values is good for the I_t atom of the DPB-$I_{2.7}$ complex, although these values represent the mean for the two I_t atoms. Furthermore, the η value is small. These results suggest that the bonding of the I_t atoms is mainly due to the valence $5p_\sigma$-electrons in a similar manner as the I_t atom of the DPPD-$I_{2.4}$ complex. The average charge density for the two I_t atoms was evaluated to be $-0.49\,e^-$. On the other hand, it has been found for the I_c atom of the complex that e^2Qq , i.e, U_p, is smaller and the η is larger than those for the I_c atom of DPPD-$I_{2.4}$. These facts anticipate that an intermolecular bond (a hydrogen bond) exists between the I_c atom and the NH group of DPB in the perpendicular to the linear I_3^- bond. However, since the δ value, i.e., h_p, for the I_c atom of the complex is nearly equal to that of DPPD-$I_{2.4}$ (within experimental error), the charge density localized on the I_c atom might be almost the same as that of the DPPD-$I_{2.4}$ complex. That is, the charge on the I_c atom of the I_3^- unit is slightly positive in the DPB-$I_{2.7}$ complex, but less than that for the isolated I_3^- ion. From the ratio of each composition the present complex is shown to also be a partially oxidized, mixed-valence compound, the charge distribution of which is formulated as $(DPB)^{+0.9}(I_3^-)_{0.9}$ (similar to the DPPD-$I_{2.4}$ complex). If the donor molecule is arranged in a stacking column, whose structure has not been revealed yet, a large electrical conductivity would be expected for the complex. It is not clear from only the Mössbauer data whether the I_3^- unit exists as a successive chain or as an isolated form, although the Mössbauer data of the complex are close to those for the bridging I_3^- unit of the DPPD-$I_{2.4}$ complex rather than the isolated I_3^- ion. This question may be solved by the resonance Raman spectrum of the complex.

Resonance Raman Spectra. In Fig. 2 (a) and (b) are presented resonance Raman spectra of the DPPD-$I_{2.4}$ and DPB-$I_{2.7}$ complexes excited by the Ar^+ 514.5 nm line. Both spectra are very similar to each other, suggesting that the iodine species of these complexes exist in a similar chemical form. This is consistent with the Mössbauer spectra. The Raman bands at 107 and 213 cm^{-1} can be assigned to the symmetric stretching vibration of a linear I_3^- unit and its first overtone, respectively. Teitelbaum et al.[13,14] have reported that the isolated I_3^- ion in $(C_6H_5)_4As^+I_3^-$ shows a Raman band of the symmetric stretching vibration at 113 cm^{-1}, whereas the corresponding band is observed at 108 cm^{-1} for the bridging I_3^- unit in $(benzamide)_2H^+I_3^-$. The spectral pattern of the latter compound is similar to those observed for the present complexes. It is, therefore, concluded that the iodine species in the DPPD-$I_{2.4}$ and DPB-$I_{2.7}$ complexes exist as a successive chain of I_3^- units. This is consistent with the crystallographic data of the former.

We would like to express our grateful acknowledgement to Prof. Takenobu Higashimura (Research Reactor Institute, Kyoto University) for his helpful discussions and encouragement. We wish to thank

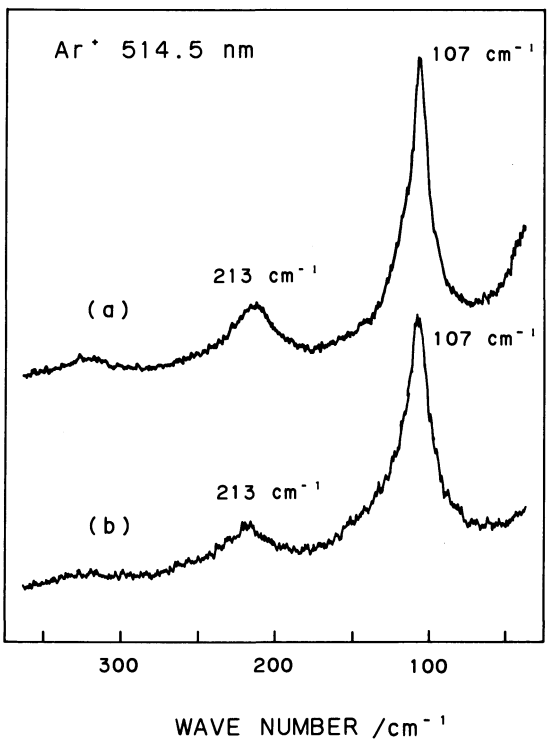

Fig. 2. Resonance Raman spectra excited by the Ar^+ 514.5 nm line of (a) *N,N'*-diphenyl-*p*-phenylenediamine-$I_{2.4}$ and (b) *N,N'*-diphenylbenzidine-$I_{2.7}$ complexes.

Mr. Shuichi Muraishi (JEOL Ltd.) for the measurements of the Raman spectra. This work was supported by the grant in aids of special research project on properties of molecular assemblies (No. 60104002) from the Ministy of Education, Science and Culture,.

References

1) J. Honzl, K. Ulbert, V. Hadek, and M. Tlustakova, *Chem. Commun.*, **1965**, 440.
2) V. Hadek, *J. Chem. Phys.*, **49**, 5202 (1968).
3) S. Doi, A. Fujita, S. Ikeura, T. Inabe, and Y. Matsunaga, *Bull. Chem. Soc. Jpn.*, **52**, 2494 (1979).
4) M. Sano, K. Ohno, and H. Akamatu, *Bull. Chem. Soc. Jpn.*, **44**, 3269 (1971).
5) K. Huml, *Acta Crystallogr.*, **22**, 29 (1967).
6) J. Runsink, S. S.-Walstra, and T. Migchelsen, *Acta Crystallogr., Sect. B* **28**, 1331 (1972).
7) M. J. Potasek, P. G. Debrunner, W. H. Morrison, Jr., and D. N. Hendrickson, *J. Chem. Phys.*, **60**, 2203 (1974).
8) T. Matsuyama, H. Sakai, H. Yamaoka, and Y. Maeda, *J. Chem. Soc. Dalton Trans.*, **1982**, 229.
9) N. N. Greenwood and T. C. Gibb, "Mössbauer Spectroscopy," Chapman and Hall, London (1971).
10) S. L. Ruby and G. K. Shenoy, "Mössbauer Isomer Shifts," ed by G. K. Shenoy and F. E. Wagner, North-Holland, Amsterdam (1978), Chap. 9b.
11) E. A. C. Lucken, "Nuclear Quadrupole Coupling Constants," Academic, London (1969), p. 290.
12) H. Sakai, Y. Maeda, S. Ichiba, and H. Negita, *J. Chem. Phys.*, **72**, 6192 (1980).
13) R. C. Teitelbaum, S. L. Ruby, and T. J. Marks, *J. Am. Chem. Soc.*, **101**, 7568 (1979).
14) R. C. Teitelbaum, S. L. Ruby, and T. J. Marks, *J. Am. Chem. Soc.*, **102**, 3322 (1980).

A Novel Development for the Simulater of Intermolecular Potentials

Tatsuya TAKAGI,* Akito TANAKA, Shigeo MAEDA, Sanshiro MATSUO, Hideaki FUJIWARA, and Yoshio SASAKI
Faculty of Pharmaceutical Sciences, Osaka University, 1-6 Yamada-Oka, Suita, Osaka 565
(Received December 17, 1985)

A novel treatment for the estimation of intermolecular interactions is proposed, incorporating intermolecular parameters into the semiempirical MNDO MO method. These parameters vary depending on the atomic species, but are constants to be reduced to the original MNDO formalism when the atomic pair belongs to a same molecule. The core–core repulsion and the two electron integral terms were modified using these parameters. The parameters introduced have been determined so as to reproduce well the interaction energies of the different model systems of molecular interaction. The resulting parameters permit calculations of large systems with sufficient accuracy within reasonably short CPU time.

Intermolecular interactions play an important role in various fields of chemistry such as solution chemistry,[1] quantum pharmacology,[2] and organic chemistry.[3] Although recently quantum-mechanical treatment has become accurate to be comparable to the experimental value in different systems, CPU time is still a limiting factor for the calculation of especially interaction energies in many-body systems. Semiempirical MO methods are expected to benefit short CPU time with reasonable accuracy of calculation. To this purpose, several investigators have made calculations.[4]

A total reparameterization of a semiempirical MO method would be necessary including the intermolecular potentials besides the molecular properties such as heat of formation which are reproduced in the MNDO[5] and MINDO/3[6] MO methods. But such reparameterization is likely to disturb the results hitherto attained satisfactorily. Quite recently, Dewar et al.[7] proposed a new semiempirical MO formula, AM1, which is the improved version of the MNDO MO method. This method is reported to have better reproducibilities in single molecular property as well as in energies of intermolecular interactions, whose results are compared with our calculations below.

Another method may be pointed out for the treatment of intermolecular potentials. That is, a partial reparameterization of a semiempirical MO formalism. Burstein and Isaev[8] proposed the MNDO/H method using a new function for the core–core repulsion term, while Mohammad and Hopfinger[9] proposed the CNDO/2H and the MINDO/3H methods using new treatments of the resonance integral and the core–core repulsion terms. These methods enabled us to calculate the hydrogen bonding systems of the intermolecular as well as intramolecular origin. However, there are some shortcomings of them. The user has to determine in advance which atoms are hydrogen-bonded or not, and the applications are limited to those systems where intermolecular forces other than the hydrogen bond of interest are exactly calculable by the semiempirical MO methods.

We propose here a new method of treating intermolecular potentials, i.e., introduction of new parameters, intermolecular parameters, which contribute only to the intermolecular potentials.

Calculation

We selected the MNDO MO formalism for the basis of new method which can be used to study with a number of properties of molecular systems large enough to be interesting to the organic chemists and biochemists. The CNDO/2 MO formalism[10] might also be useful for the basis. In fact, CNDO/2H method is reported to be more reliable than MINDO/3H method.[9] However, the CNDO/2 MO method sometimes fails to predict correctly the heat of formation, molecular geometries, etc., and hence it is not adopted in the present paper.

A *QCPE*[11] program was improved in great deal[12] and modified to include corrections stated below and the program NICER[13] was used as a diagonalization routine. The program SIMPLX[14] was used to optimize the intermolecular parameters. Ab initio MO calculations were carried out according to the IMSPAK program system[15] and its Osaka University version.[16] The 4-31G basis set[17] was adopted throughout. All molecular geometries were optimized using MNDO MO method. Numerical calculations were performed on an NEAC S1000 computer plus HFP system at the Computer Center, Osaka University and HITAC M-200H computer at the Computer Center, Institute for Molecular Science.

Formalism

There are some papers[18] which indicate that the MNDO MO method underestimates energies of intermolecular interactions, especially for hydrogen bonding systems. Energy decomposition analyses proposed by Kitaura and Morokuma[19] show that the unstabilization of the ES (electrostatic) term at longer distances is responsible for this underestimation (Fig. 1). Since the EX (exchange repulsion) term always

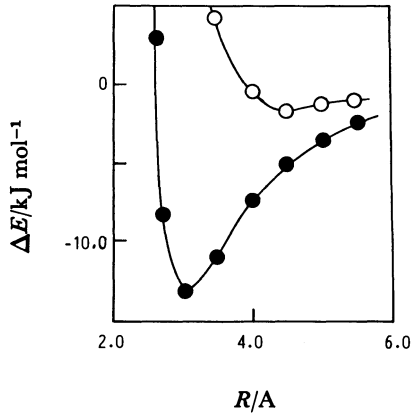

Fig. 1. Distance dependencies of the ES plus EX term for the $(H_2O)_2$ system. MNDO (●); ab initio (○).

vanishes in MNDO approximation, ES term in MNDO MO method is thought to correspond to the ES+EX term in ab initio MO method. The simplest way to correct for the ES term is to modify the core-core repulsion term. We tried to correct this as follows:

$$E_{ij}^{core}(SIMP) = E_{ij}^{core}(MNDO) - (A_i+A_j)[\exp\{-B_i(R_{ij}+\alpha)\} + \exp\{-B_j(R_{ij}+\alpha)\}]. \quad (1)$$

For atomic pairs of N-H and O-H a slightly different expression is used basing on the MNDO approximation:

$$E_{ij}^{core}(SIMP) = E_{ij}^{core}(MNDO) - (A_i+A_j)(R_{ij}+\alpha)[\exp\{-B_i(R_{ij}+\alpha)\} + \exp\{-B_i(R_{ij}+\alpha)\}], \quad (2)$$

where A_i, B_i, and α are intermolecular parameters. A's and B's vary depending on the atomic species, but A_i plus A_j is set to zero when i and j belong to a same molecule. A's and B's are determined empirically to fit to 110% of the most stable intermolecular distances and to 70% of the ES+EX calculated from 4-31G basis set. α is equal to 1.20 A in all cases. Although it would be better to fit to the experimental data, our attempt was interrupted by the insufficient data of intermolecular interactions in gas phase. The percentages, 110 and 70%, were taken by considering the characteristics of the relevant basis set, that is, the overestimation of electrostatic interaction energies and the underestimation of intermolecular distances.[20] The fifteen different systems which are illustrated in Fig. 2 were used for this parameterization. By these modifications, interaction energies from MNDO method were found to be improved in great deal except for the strongly hydrogen bonding systems. To take into account the latter systems, correction was made with the two

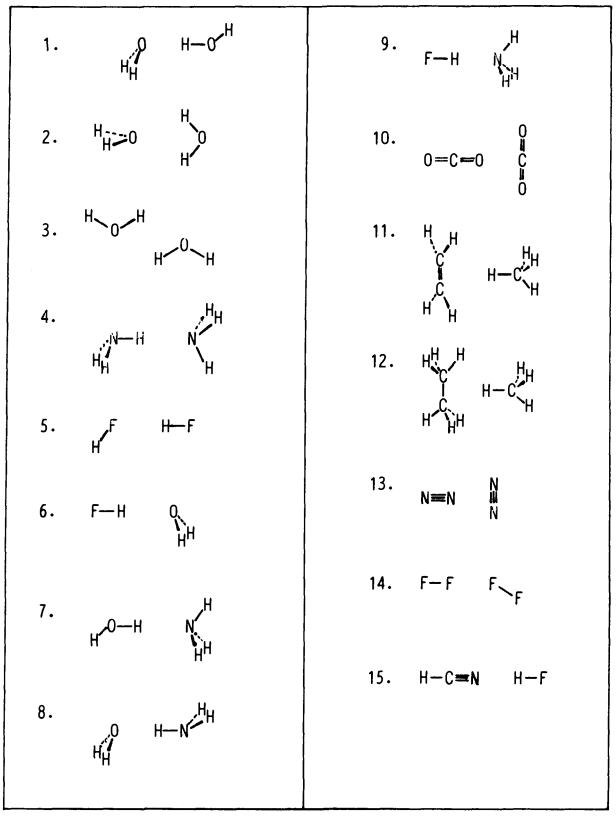

Fig. 2. Standard systems adopted for the SIMP parameterization.

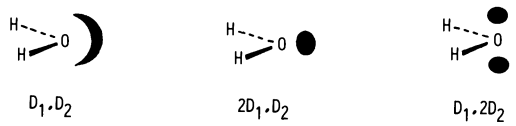

Fig. 3. Changes of the minimum point in molecular electrostatic potentials as a function of D_1 and D_2.

center repulsion integrals.

The two-center repulsion integrals are expanded in terms of multipole-multipole interactions [M^A_{lm}, M^B_{km}] in MNDO approximations. The formula for the integrals is expressed as follows:

$$\langle rs|tu\rangle = \sum_l \sum_k \sum_{m=-l\,\min}^{l\,\min} (e^2/2)^{l+k} \sum_{i=1}^{2^l} \sum_{j=1}^{2^k} [R_{ij}^2 + (\rho_i^A+\rho_k^B)^2]^{-1/2}, \quad (3)$$

where R_{ij} is the distance between the point charges i and j in the interacting configurations at atom A and B. For example, $\langle ss|sp_z\rangle$ is given by:

$$\langle ss|sp_z\rangle = [q^A, \mu_z^B] = -(e^2/2)[\{(R_{AB}-D_1^B)^2 + (\rho_0^A+\rho_1^B)^2\}^{-1/2}], \quad (4)$$

where D_1 and D_2 are the charge separations of the

multipole moments. Since D_1 and D_2 have been determined in MNDO approximation so as to reproduce well the molecular constants of each isolated molecule, it may be changed slightly in the interacting systems. In fact, the minimum point of molecular electrostatic potentials around H_2O molecule using MNDO formula[21] varies with the values of D_1 and D_2 (Fig. 3), and the molecular electrostatic potential map is different from the one using ab initio MO formula[22] when original values of D_1 and D_2 are used. This indicates that the changes in D_1 and D_2 may result in the correct map and the correct direction of the intermolecular interactions. Therefore, D_1 and D_2 are modified as follows:

$$D_l^{\mathrm{SIMP}} = f_l D_l \quad (l=1 \text{ or } 2). \tag{5}$$

f_l is the intermolecular parameters and set equal to 1.0 when atoms A and B belong to a same molecule but not when they belong to different molecules. Such definition of f_l, together with that of A_i in Eqs. 1 and 2, makes SIMP equivalent to MNDO for an isolated molecule. Equation 5 is applied only to the case of linear quadrupole, Q_{aa} and between hydrogen and heavy atoms when $l=2$. These parameters have been determined so as to reproduce well the interaction energies calculated from ab initio MO method for the different systems of molecular interaction illustrated in Fig. 2.

Results and Discussion

Table 1 lists the optimized values of the SIMP parameters for elements of H, C, N, O, and F. f_l values are approximately equal in the three atoms of N, O, and F, which indicates that the original MNDO MO method has made a similar error in the directions of the lone pairs of these atoms.

Tables 2 and 3 list the interaction energies and the most stable intermolecular distances calculated by SIMP, MNDO MO, AM1 MO, and ab initio (4-31G) MO method. It is clear that the results of SIMP reproduce well the one of ab initio MO method considering the aforementioned characteristics of 4-31G basis set. The regression analyses according to a relation $y=ax$ resulted in:

$$\Delta E(\mathrm{SIMP}) = 0.713\Delta E(4\text{—}31\ \mathrm{G}), \tag{6}$$
$$n = 15,\ R = 0.938,\ s = 4.85\ \mathrm{kJ\ mol^{-1}},$$

$$Re(\mathrm{SIMP}) = 1.033Re(4\text{—}31\ \mathrm{G}), \tag{7}$$
$$n = 15,\ R = 0.822,\ s = 0.37\ \mathrm{A}.$$

Table 1. Optimized SIMP Parameters

	A	B	f_1	f_2
H	4.281	1.7120	—	—
C	0.00211	2.8058	1.0	1.0
N	40.0	2.4059	1.402	2.658
O	54.0	2.8079	1.560	2.616
F	50.6	2.2920	1.497	2.147

Table 2. Comparison of Interaction Energies[a] Calculated by Various Procedures

No.[b]	SIMP	MNDO	AM1[c]	4-31G
1	−24.2	−2.5	−13.8	−32.6
2	−30.4	−4.1	—	−27.0
3	−21.6	−1.6	—	−25.5
4	−19.6	−1.3	—	−17.2
5	−22.2	−3.1	—	−31.8
6	−31.0	−5.8	—	−56.1
7	−27.9	−2.7	−11.3	−37.7
8	−17.2	−1.8	—	−17.2
9	−45.7	−6.4	—	−68.2
10	−1.8	−1.7	0.0	−7.8
11	−0.9	0.0	—	−2.7
12	−3.4	0.0	—	−0.2
13	−0.4	−0.4	—	−1.1
14	−0.3	0.0	—	−0.7
15	−28.4	−6.2	—	−36.2

a) Values in kJ mol^{-1}. b) See Fig. 2. c) Taken from Ref. 5.

Table 3. Comparison of Most Stable Intermolecular Distances[a] Calculated by Different Procedures

No[b]	SIMP	MNDO	4-31G
1	3.05	4.30	2.88
2	2.80	3.90	2.90
3	3.08	4.51	2.85
4	3.15	4.67	3.30
5	2.86	3.14	2.71
6	2.98	3.96	2.62
7	3.06	4.32	2.93
8	3.20	4.54	3.22
9	2.99	3.95	2.68
10	4.95	4.96	4.10
11	4.50	7.70	4.40
12	4.27	8.16	5.00
13	3.61	4.10	3.60
14	3.35	4.94	2.70
15	3.16	3.98	2.99

a) Values in A. b) See Fig. 2.

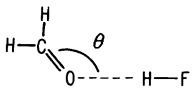

Fig. 4. Molecular configuration for the H_2CO plus HF system.

Table 4. Comparison of Interaction Energies and Optimized Intermolecular Distances Calculated from SIMP and ab initio (4-31G[a]) MO Methods[b]

H donor	H acceptor	*Re*/A	ΔE/kJ mol^{-1}
HCN	NH_3	3.18(3.15)	−32.4(−40.6[c])
CF_3H	$CHONH_2$	3.24(3.11)	−18.9(−32.0[d])
CH_4	NH_3	3.33(4.02)	−8.0(−4.6[c])
HF	H_2CO	3.10(2.73)	−24.8(−41.9[c])
H_2O	CO_2	3.34(3.10)	−10.6(−12.7[e])
NH_4^+	H_2O	2.56(2.68)	−91.7(−114.3[e])
H_2O	F^-	2.50(2.30)	−99.2(−101.6[f])

a) Except for H_2O plus F^- system. b) In parentheses listed are the results of ab initio MO method. c) Taken from Ref. 23. d) Taken from Ref. 24 e) Taken from Ref. 25. f) Near HF calculation. Taken from Ref. 26.

The regression coefficients are consistent with the initial purpose of fitting the results of the SIMP method to 110% of the *Re* values and to 70% of the ΔE values calculated from 4-31G basis set. The correlation coefficient is somewhat low in Eq. 7, but this is due to a small change in *Re* values.

We tested the SIMP method in the different 7 systems which were not used for the parametrization (Table 4). The reproducibility is satisfactory, considering the relations in Eqs. 6 and 7. SIMP also gives the correct molecular configurations in interacting systems. For example, although MNDO MO method gives 180 degree for the most stable values of θ in H_2CO plus HF system (Fig. 4), it gives 131 degree, which are approximately equal to that calculated from ab initio MO method.[22]

We expect that the SIMP method can be applied to various fields of chemistry–solvent effects on molecular structure, charge distribution, orbital energies, etc. These applications are currently under way in our laboratories.

The authours thank the Institute for Molecular Science for allotment of CPU time of the HITAC M-200H computer. Thanks are also due to Dr. Kizashi Yamaguchi for permitting us to use the IMSPAK program (Osaka University version) and to Dr. Yoshitaka Beppu for his advice in the development of SIMP program.

References

1) J. Detrich, G. Corongiu, and E. Clementi, *Chem. Phys. Lett.*, **112**, 426 (1984).
2) B. Pullman, H. Berthod, and Ph. Courriere, *Int. J. Quantum Chem.*, **1**, 93 (1974).
3) J. Jaume, L. L. Lluch, and J. Bertran, *Chem. Phys. Lett.*, **106**, 232 (1984).
4) P. Hobza and R. Zaharadnik, "Weak Intermolecular Interactions in Chemistry and Biology," Elsevier, Amsterdam (1980).
5) M. J. S. Dewer and W. Thiel, *J. Am. Chem. Soc.*, **99**, 4899, 4907 (1977).
6) R. C. Bingham, M. J. S. Dewar, and D. H. Lo, *J. Am. Chem. Soc.*, **97**, 1285, 1294, 1302, 1307 (1975).
7) M. J. S. Dewar, E. G. Zoebisch, E. F. Healy, and J. K. P. Stewart, *J. Am. Chem. Soc.*, **107**, 3902 (1985).
8) K. Ya. Burstein and A. N. Isaev, *Theor. Chim. Acta*, **64**, 397 (1984).
9) S. N. Mohammad and A. J. Hopfinger, *Int. J. Quantum Chem.*, **22**, 1189 (1982).
10) G. A. Segal and J. A. Pople, *J. Chem. Phys.*, **43**, S136 (1965); **44**, 3289 (1966).
11) W. Thiel, *QCPE*, **11**, 353 (1978).
12) T. Takagi, A. Tanaka, R. Tokura, and Y. Sasaki, MNDOA, The Library Program at the Computation Center Osaka University.
13) Y. Beppu and I. Ninomiya, *QCPE*, **14**, 409 (1981).
14) T. Kotani, SIMPLX, The Library Program at the Computation Center Osaka University.
15) K. Morokuma, S. Kato, K. Kitaura, I. Omine, S. Sakai, and S. Obara, IMS Computer Center Library Program, 1980, No. 0372.
16) K. Yamaguchi, private communication.
17) R. Ditchfield, W. Hehre, and J. A. Pople, *J. Chem. Phys.*, **54**, 724 (1971).
18) T. Takagi, H. Fujiwara, and Y. Sasaki, *Bull. Chem. Soc. Jpn.*, **57**, 1299 (1984); S. Scheiner, *Theor. Chim. Acta*, **57**, 71 (1980).
19) K. Kitaura and K. Morokuma, *Int. J. Quantum Chem.*, **10**, 325 (1976).
20) H. Umeyama and K. Morokuma, *J. Am. Chem. Soc.*, **99**, 1316 (1977).
21) A. Tanaka, T. Takagi, S. Maeda, S. Matsuo, H. Maezaki, and Y. Sasaki, to be published.
22) C. Giessner-Prettre and A. Pullman, *Theor. Chim. Acta*, **25**, 83 (1972).
23) P. Kollman, J. McKelvey, A. Johansson, and S. Rothenberg, *J. Am. Chem. Soc.*, **97**, 955 (1975).
24) P. Hobza, F. Mulder, and C. Sandorfy, *J. Am. Chem. Soc.*, **104**, 925 (1982).
25) P. Kollman, *J. Am. Chem. Soc.*, **99**, 4875 (1977).
26) H. Kistenmacher, H. Popkie, and E. Clementi, *J. Chem. Phys.*, **61**, 799 (1974).

Solvent Extraction of Palladium(II) from Aqueous Chloride Media with 1,2-Bis(*tert*-hexylthio)ethane

Yoshinari BABA,* Toshiya EGUCHI, and Katsutoshi INOUE
Department of Industrial Chemistry, Faculty of Science and Engineering, Saga University, Honjo-machi, Saga 840
(Received July 22, 1985)

The extraction equilibrium and kinetics of palladium(II) extraction from an aqueous chloride media with 1,2-bis(*tert*-hexylthio)ethane (mixture), abbreviated as *t*-BHTE and denoted by B, in toluene were studied at 303 K. Palladium(II) was extracted as a 1:1 Pd:extractant complex, $[PdCl_2B]$. The partition coefficient of this extractant was evaluated as $K_d=5.5\times10^4$ for hydrochloric acid and $K_d=2.5\times10^4$ for an aqueous ammonium chloride solution. The results of kinetic experiments were quantitatively explained in terms of a reaction scheme in which parallel reactions of *t*-BHTE with $[PdCl_3]^-$ and $[PdCl_4]^{2-}$ in an aqueous phase were the rate-determining steps:

$$[PdCl_3]^-_{aq.} + B_{aq.} \xrightarrow{k_1} [PdCl_2B]_{aq.} + Cl^-_{aq.}$$

$$[PdCl_4]^{2-}_{aq.} + B_{aq.} \xrightarrow{k_2} [PdCl_2B]_{aq.} + 2Cl^-_{aq.}$$

The reaction rate constants for the above were evaluated as $k_1=6.4\times10^4$ dm^3 mol^{-1} s^{-1} and $k_2=2.6\times10^2$ dm^3 mol^{-1} s^{-1} for extraction from an aqueous ammonium chloride solution, and $k_1=6.7\times10^4$ dm^3 mol^{-1} s^{-1} and $k_2=3.2\times10^2$ dm^3 mol^{-1} s^{-1} from a hydrochloric acid solution.

Precious metals such as gold, silver, and platinum group metals are the most important rare metals indispensable in the high-technology industries as raw materials of catalysts, electronic materials and so on. Therefore, it is very important to develop effective techniques to recover these metals from spent catalysts or various kinds of scrap. However, the current refining processes involving these metals are based on highly complicated selective-precipitation techniques which consume great amounts of energy and labour. Also, these are often insufficient in terms of the achieved separation efficiency.

A solvent-extraction process is a potential alternative refining technology as well as an ion-exchange process. The most important factor in the solvent extraction of metals is extractant selectivity to the specified metal ions to be recovered. Precious metals such as gold, silver, platinum, and palladium belong to the soft metals which possess a strong affinity to ligands containing donating-type sulfur atoms which act as soft bases.[1] Consequently, neutral organic compounds containing sulfur atoms are very selective and effective extractants for precious metals.[2-6]

In a previous paper,[7] the authors discussed the extraction equilibrium of mercury(II) from hydrochloric acids with 1,2-bis(hexylthio)ethane in 1,2-dichloroethane and found that it is extracted as a 1:1 metal:extractant complex. In the present study, the extraction of palladium(II) with 1,2-bis(*tert*-hexylthio)ethane† was investigated from a chloride media while stressing its kinetic aspect since the extraction rate of palladium(II) is very slow compared to that of mercury(II). Toluene was used instead of 1,2-dichloroethane as a diluent from the standpoint of practical application.

† It was impossible to carry out the experiment of the extraction of palladium(II) with 1,2-bis(hexylthio)ethane in toluene because of the formation of a precipitate at the interface during extraction.

Experimental

Reagents. 1,2-Bis(*tert*-hexylthio)ethane(mixture), abbreviated as *t*-BHTE and denoted by B hereafter, was synthesized by a method similar to that of 1,2-bis(hexylthio)ethane described in a previous paper.[7] The product was purified by vacuum distillation(156—159 °C/6 mmHg(1 mmHg=133.322 Pa)) and identified using IR and NMR spectra and element analysis. The results of element analyses are as follows. Found: C, 63.9; H, 11.3%. Calcd for $C_{14}H_{30}S_2$: C, 64.1; H, 11.5%. The product was a transparent liquid with a confirmed purity of about 97% by gas chromatography. Analytical-grade toluene was used without further purification. Organic solutions of *t*-BHTE were prepared on a gravimetric basis by diluting *t*-BHTE with toluene. Aqueous solutions of palladium(II) were prepared by dissolving palladium(II) chloride in hydrochloric acid or aqueous ammonium chloride solutions containing a small amount of hydrochloric acid(0.01 mol dm^{-3}).

Procedure for the Measurement of Extraction Equilibrium. Under an excess concentration of *t*-BHTE over the palladium(II) concentration in the aqueous phase, palladium(II) was almost completely extracted over the whole concentration region of hydrochloric acid. The remaining amount of palladium(II) was too small to make a precise quantitative analysis. Therefore, only a loading test was carried out to determine the molar ratio of palladium(II) extracted into the organic phase to *t*-BHTE by varying the concentration ratio of *t*-BHTE in the organic phase to that of palladium(II) in the aqueous phase under the conditions

of a large excess of the palladium(II) concentration.

Equal volumes (0.02 dm^3) of the organic and aqueous phases taken in a 0.1 dm^3 stoppered glass flask were shaken for 5 d in a water bath maintained at 303 K. The concentration of *t*-BHTE in the organic phase was varied from 1×10^{-3} to 1×10^{-2} mol dm^{-3} and that of palladium(II) was varied about from 1.5 to 10 times of the *t*-BHTE concentration. After separating the two phases, the palladium(II) concentration in the aqueous phase was determined using a Nippon Jarrell-Ash model AA-782 atomic absorption spectrophotometer and that in the organic phase was calculated from the mass balance of the palladium(II) concentration in the aqueous phase before and after equilibration.

Procedure for the Measurement of Aqueous Solubility of *t*-BHTE. The aqueous solubility of *t*-BHTE was measured spectrophotometrically at 303 K according to the following method. A toluene solution of *t*-BHTE and hydrochloric acid or an aqueous ammonium chloride solution of known concentrations was shaken vigorously for 24 h with a volume ratio of aqueous phase to organic phase 10:1 using Iwaki's mechanical shaker type V-VD. After phase separation, a sample of aqueous phase (0.19 dm^3) was transferred to a separatory funnel, to which 0.05 dm^3 of 2×10^{-3} mol dm^{-3} aqueous palladium(II) solution containing 0.01 mol dm^{-3} hydrochloric acid was added and shaken for 24 h by a mechanical shaker in order to completely convert any *t*-BHTE dissolved in the aqueous phase to its palladium(II) complex. A small amount of toluene (0.005 dm^3) was added and shaken vigorously for 24 h to transfer the palladium(II) complex into toluene. The absorbance of the palladium(II) complex was measured at 403 nm against a toluene blank using a Shimadzu UV 140 spectrophotometer. Then, the extractant concentration dissolved in the aqueous phase was calculated from the molar absorptivity and volume ratios.

Procedure for the Measurement of Extraction Rate. The experimental apparatus used was a batch-type stirred glass cell with a 10-cm inner diameter and a 15-cm depth as shown in Fig.1. The vessel was fitted with four baffles, each of which was 1-cm wide and 14-cm long. Stirring was carried out using a impeller with six flat blades connected to a speed controller. The baffles and impellers made of stainless steel or Teflon were used in the extraction from aqueous ammonium chloride solution and hydrochloric acid, respectively.

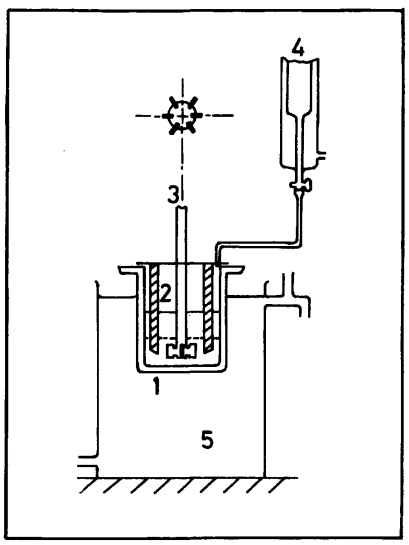

Fig. 1. Experimental apparatus.
1: Stirred glass cell, 2: baffle, 3: impeller, 4: reservoir with jacket, 5: thermostated bath.

Equal volumes (0.3 dm^3) of aqueous ammonium chloride solution or hydrochloric acid solution containing palladium(II) and *t*-BHTE solution of toluene were carefully introduced into the vessel. After that, stirring was initiated at a constant speed and samples were taken at definite time intervals. After phase separation, the palladium(II) concentration in the aqueous phase was determined using the atomic absorption spectrophotometer. The initial palladium(II) concentration was 5×10^{-4} mol dm^{-3} in all kinetic runs. The concentrations of the extractant and chloride ions were varied in the range of 5×10^{-3} to 0.1 mol dm^{-3} and of 0.1 to 6 mol dm^{-3}, respectively. Since the extraction rate was found to be independent of the stirring speed in a range greater than 1500 rpm, subsequent experiments were carried out at a constant stirring speed of 1500 rpm.

Results and Discussion

Equilibrium. The result of the loading test is shown in Fig.2. It indicates that the molar ratio of *t*-BHTE to palladium(II) in the organic phase asymptotically approaches unity. From this, the stoichiometric relation of this extraction reaction is considered to be generally expressed by

$$[PdCl_4]^{(i-2)-}_{aq.} + B_{org.} \rightleftharpoons [PdCl_2B]_{org.} + (i-2)Cl^-.$$

Aqueous Solubility of *t*-BHTE. The equilibrium distribution of *t*-BHTE between the aqueous phase and the organic phase is expressed by its physical partition to the aqueous phase as

$$B_{aq.} \rightleftharpoons B_{org.} \quad K_d' \qquad (1)$$

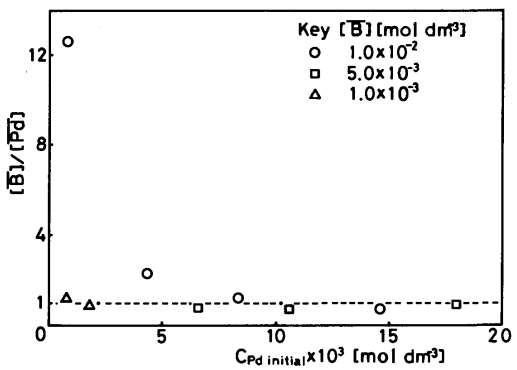

Fig. 2. Experimental results of the loading test at constant HCl concentration (1.0 mol dm^{-3}).

where K_d is the partition coefficient of *t*-BHTE and is expressed as

$$K_d = \frac{[\overline{B}]}{[B]}. \quad (2)$$

Here, the concentration of *t*-BHTE in the organic phase, $[\overline{B}]$, is nearly equal to its initial concentration since the partition coefficient is very large. The logarithm of Eq. 2 gives

$$\log [B] = \log [\overline{B}] - \log K_d. \quad (3)$$

Figure 3 shows the relation between the concentration of *t*-BHTE in the aqueous and organic phases based on Eq.3. The plotted points in this figure lie on a straight line with a slope of 1, regardless of the chloride ion concentration. There is, though, some scattering. From the intercept of the straight line with the ordinate, the partition coefficients, K_d, were evaluated as $K_d=5.5\times10^4$ and $K_d=2.5\times10^4$ for hydrochloric acid and aqueous ammonium chloride solution, respectively.

Kinetics. If it is assumed that the reaction rates in the forward and reverse directions are of pseudo-first-order with respect to the palladium(II) concentrations in the aqueous and organic phases, respectively. The relation between the palladium(II) concentration(a) in the aqueous phase and the contact time(t) is described as

$$\frac{a_i-a_e}{a_i}\ln\frac{a_i-a_e}{a_t-a_e} = k_f t, \quad (4)$$

where k_f denotes the observed reaction rate constant for the forward reaction and the subscripts i and e represent the initial and equilibrium states, respectively.

A typical experimental result is shown in Fig. 4. Here, the straight lines pass through the origin. The reaction-rate constants were obtained from the slopes of these straight lines.

Figure 5 shows the effect of the *t*-BHTE concentration on the observed extraction rate constant. In Fig. 5, the plots cluster along straight lines with slopes of 1; consequently, it can be concluded that the extraction rate is first order with respect to *t*-BHTE under these concentration regions.

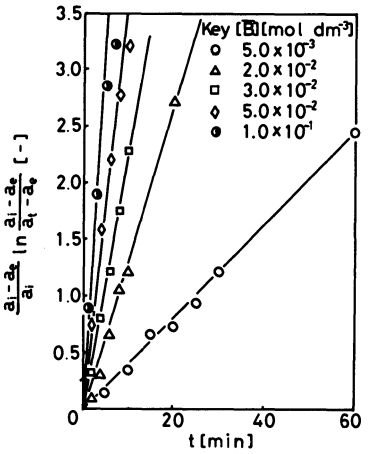

Fig. 4. Typical plot of the experimental results based on the pseudo-first-order rate expression at constant NH_4Cl concentration (0.5 mol dm^{-3}).

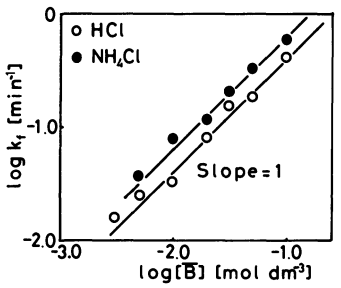

Fig. 5. Effect of *t*-BHTE concentration, at constant chloride ion concentration (0.5 mol dm^{-3}), on the observed extraction rate constant.

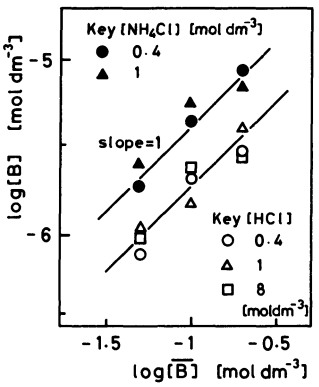

Fig. 3. Aqueous solubility of *t*-BHTE.

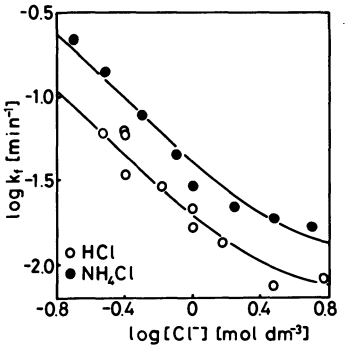

Fig. 6. Effect of chloride ion concentration, at constant *t*-BHTE concentration (1.0×10^{-2} mol dm^{-3}), on the observed extraction rate constant.

Similarly, the effect of chloride-ion concentration on the observed rate constants is shown in Fig. 6. For both aqueous media of hydrochloric acid and ammonium chloride, the plotted points lie on straight lines with slopes of −1 in the low-concentration range of chloride ions and approach constant values in the high-concentration range. Hence, it can be concluded that the extraction rate is inverse first order with respect to chloride ions in its low-concentration range and of zeroth order in its higher-concentration range.

In the concentration region of the chloride ions of the present study, the majority of palladium(II) exists as, tetrachloro complex, $[PdCl_4]^{2-}$, and a small amount of aquatrichloro complex, $[PdCl_3(H_2O)]^-$, coexists while the concentrations of the species, Pd^{2+}, $[PdCl(H_2O)_3]^+$, $[PdCl_2(H_2O)_2]$ can be negligible compared with those of the species, $[PdCl_3(H_2O)]^-$ or $[PdCl_4]^{2-}$. Among these, chloro complexes of palladium(II), the aquatrichloro complex, $[PdCl_3(H_2O)]^-$, is considered to be much more labile than other complexes as Rund[8] pointed out in their studies on the mechanism of substitution reactions of chloro complexes of palladium(II) with 1,10-phenanthroline and 2,2′-bipyridyl. Further, since *t*-BHTE has no interfacial activity, complexation with palladium(II) is not considered to take place at the interface between two phases but in the aqueous phase. Taking account of these facts, the following reaction scheme was put forward in order to explain the results of the extraction kinetics of palladium(II) mentioned above.

$$B_{org.} \rightleftharpoons B_{aq.} \qquad K_d^{-1} \tag{5}$$

$$[PdCl_3(H_2O)]^-_{aq.} + B_{aq.} \xrightarrow{k_1} [PdCl_2B]_{aq.} + Cl^-_{aq.} + H_2O \tag{6}$$

$$[PdCl_4]^{2-}_{aq.} + B_{aq.} \xrightarrow{k_2} [PdCl_2B]_{aq.} + 2Cl^-_{aq.} \tag{7}$$

$$[PdCl_2B]_{aq.} \rightleftharpoons [PdCl_2B]_{org.} \tag{8}$$

Assuming that the parallel reactions of $[PdCl_3(H_2O)]^-$ and $[PdCl_4]^{2-}$ with *t*-BHTE are the rate-determining steps, the rate expression can be described as follows:

$$-\frac{dC_{Pd}}{dt} = k_1[[PdCl_3(H_2O)]^-][B] + k_2[[PdCl_4]^{2-}][B] = (k_1\beta_3[Cl^-]^3/\alpha + k_2\beta_4[Cl^-]^4/\alpha)C_{Pd}[B]. \tag{9}$$

In the above equation, β_i is the stability constant of the *i*-th chloro complex of palladium(II) defined as follows.

$$Pd^{2+} + iCl^- \rightleftharpoons [PdCl_i]^{(i-2)-} \qquad \beta_i$$

$$\beta_i = [[PdCl_i]^{(i-2)-}]/[Pd^{2+}][Cl^-]^i. \tag{10}$$

In the present study, the following values[9] were used as the stability constants of the chloro complex of palladium(II): $\beta_1=10^{4.7}$, $\beta_2=10^{7.7}$, $\beta_3=10^{10.3}$, $\beta_4=10^{11.9}$. In Eq. 9, α is defined by

$$\alpha = 1 + \sum_{i=1}^{4} \beta_i[Cl^-]^i. \tag{11}$$

Under the present experimental conditions, Eq. 11 may be approximated by Eq. 12:

$$\alpha \simeq \beta_3[Cl^-]^3 + \beta_4[Cl^-]^4. \tag{12}$$

Eq. 9 is consequently approximated as

$$-\frac{dC_{Pd}}{dt} = \left\{\frac{k_1\beta_3[Cl^-]^3 + k_2\beta_4[Cl^-]^4}{\beta_3[Cl^-]^3 + \beta_4[Cl^-]^4}\right\} K_d^{-1}C_{Pd}[\overline{B}]. \tag{13}$$

In an even higher concentration range of chloride ions, it is further approximated by

$$-\frac{dC_{Pd}}{dt} = \{k_1(\beta_3/\beta_4)[Cl^-]^{-1} + k_2\}K_d^{-1}C_{Pd}[\overline{B}]. \tag{14}$$

C_{Pd} and $[\overline{B}]$ denote the total concentration of palladium(II) in the aqueous phase and that of *t*-BHTE in the organic phase, respectively.

Consequently, the proposed rate expression, Eq. 14, suggests that the extraction rate is first order with respect to *t*-BHTE in the organic phase and palladium(II) in the aqueous phase, respectively, and that it is of the inverse first order with respect to chloride ion in its low concentration region and of zeroth order in its high concentration region.

From the experimental results shown in Fig. 6, the reaction rate constants, k_1 and k_2, were evaluated by the least-square method according to Eq. 13 as $k_1=6.4\times10^4$ dm^3 mol^{-1}s^{-1} and $k_2=2.6\times10^2$ dm^3 mol^{-1}s^{-1} for the extraction from aqueous ammonium chloride solution, and as $k_1=6.7\times10^4$ dm^{3}mol^{-1}s^{-1} and $k_2=3.2\times10^2$ dm^3 mol^{-1} s^{-1} for that from hydrochloric acid using the distribution constants evaluated earlier. The values evaluated from two aqueous chloride media are in good agreement either for k_1 or for k_2. The large difference between k_1 and k_2 indicates that the aquatrichloro complex, $[PdCl_3(H_2O)]^-$, is much more labile than the tetrachloro complex, $[PdCl_4]^{2-}$, as mentioned earlier. However, these values are about two or three orders in magnitude greater than those obtained by Rund[8] in the complexation with 1,10-phenanthroline ($k_1=7.1\times10$ dm^3 mol^{-1}s^{-1} and $k_2=2.2$ dm^3 mol^{-1}s^{-1}). This might suggest the possibility of an interfacial reaction mechanism between two phases rather than the homogeneous reaction mechanism discussed above. More information regarding this system seems to be required.

The solid lines in Fig. 6 are the calculated results

from Eq. 13 using the evaluated values of k_1 and k_2, and the stability constants of the chloro complexes of palladium(II) and the partition coefficient of *t*-BHTE evaluated earlier. These lines are in fairly good agreement with the experimental results for both media. The difference between the rate of extraction from hydrochloric acid and that from aqueous ammonium chloride solution is attributable to that of the solubility of *t*-BHTE to both media.

The authors are indebted to Professor M. Takagi of Kyushu University for his instruction in the synthesis of 1,2-bis(*tert*-hexylthio)ethane.

References

1) R. G. Pearson, *J. Am. Chem. Soc.*, **85**, 3533 (1963); *J. Chem. Educ.*, **45**, 581, 643 (1968).

2) Yu. E. Nikitin, Yu. I. Murinov, and A. M. Rosen, *Russ. Chem. Rev.*, **45**, 1155 (1976).

3) V. A. Mikhailov, V. G. Torgov, E. M. Gil'bert, L. N. Mazolov, and A. V. Nikolaev, "Proceedings of International Solvent Extraction Conference 1971," Soc. Chem. Ind., London (1971), p. 1112.

4) V. A. Mikhailov, "Proceedings of International Solvent Extraction Conference 1977," Can. Inst. Min. Metall., Montreal (1979), p. 52.

5) V. A. Pronin, M. V. Usol'tseva, and S. M. Shostakovski, *Izv. Akad. Nauk SSSR, Ser Khim.*, **1971**, 2371.

6) V. A. Pronin, M. V. Usol'tseva, Z. N. Shastina, N. K. Gusarova, E. P. Vyalkh, S. V. Amosova, and B. A. Trofimov, *Russ. J. Inorg. Chem.*, **18**, 1016 (1973).

7) Y. Baba, Y. Ikeda, and K. Inoue, *Bull. Chem. Soc. Jpn.*, **58**, 881 (1985).

8) J. V. Rund, *Inorg. Chem.*, **13**, 738 (1974).

9) M. I. Gelfman and N. V. Kiseleva, *Zh. Neorg. Khim.*, **14**, 502 (1969).

Ylide-Metal Complexes. X.[1] An X-Ray Photoelectron Spectroscopic Study of Triphenylmethylenephosphorane and Gold- and Copper-Phosphorane Complexes

Yoshihisa YAMAMOTO* and Hidetaka KONNO†
Faculty of Pharmaceutical Sciences, Higashi Nippon Gakuen University, Ishikari-Tobetsu, Hokkaido 061-02
†Faculty of Engineering, Hokkaido University, Sapporo 060
(Received October 8, 1985)

Triphenylmethylenephosphorane, the bis(triphenylmethylenephosphorane)gold chloride and the corresponding copper chloride have been studied by X-ray photoelectron spectroscopy. For the phosphorane, the binding energies, E_B, for P 2s and P 2p peaks were observed at 190.1 and 132.6 eV, respectively. The E_B value for the P 2p peak agrees with that (132.6 eV) for the phosphonium ion in triphenylmethylphosphonium bromide. The C 1s spectrum was separated into two peaks at E_B=285.0 and 283.9 eV, assuming a ratio of 18:1. The peak at 285.0 eV corresponds to the phenyl carbons, and that at 283.9 eV can be assigned to the electron-rich methylene carbon. Thus, the structure of the phosphorane is considered to be an ylide formula, $(C_6H_5)_3\overset{+}{P}\text{-}\overset{-}{\ddot{C}}H_2$. In gold phosphorane complexes, E_B of the C 1s, P 2s, and P 2p peaks were close to those for the phosphorane. The E_B of the Cl $2p_{3/2}$, Au $4f_{7/2}$, and Au $4f_{5/2}$ peaks coincided with those for bis(triphenylphosphine)gold chloride. These results indicate the structure of the gold complex to be $(C_6H_5)_3\overset{+}{P}\text{-}\overset{-}{\ddot{C}}H_2$ / $(C_6H_5)_3\overset{+}{P}\text{-}\overset{-}{\ddot{C}}H_2$ $\diagdown\!\!\diagup\ \overset{+}{Au}$ ← Cl^-. The XPS results also indicate that the structure of the copper complex is similar to that of the gold complex.

Previously, we have been concerned with the preparation and properties of metal complexes with unstable triphenylmethylenephosphorane,[2] $(C_6H_5)_3P=CH_2$, and unstable triphenylmethylenearsorane[3] $(C_6H_5)_3As=CH_2$.

Many investigations regarding the XPS of metal complexes have been reported, especially, halogen complexes,[4] e.g., K_2MCl_6 (M: W, Re, Os, Ir, Pt); coordinated nitrogen-type complexes,[5] e.g., $[Co(NH_3)_5(NO_2)]Cl_2$; phosphine complexes,[6] e.g., $[(C_6H_5)_3P]_2CdCl_2$; olefine complexes,[7] e.g., $[(C_6H_5)_3P]_2Pt(CH_2=CH_2)$; metallocene,[8] e.g., $(\pi\text{-}C_5H_5)_2M$ (M: V, Cr, Mn, Fe, Co, Ni); carben complexes,[9] e.g., $(CO)_5CrC(OCH_3)CH_3$; and metal-carbonyl complexes,[10] e.g., $Fe(CO)_5$. However, the XPS study of ylide-metal complexes has not been reported so far, since preparation of complexes with unstable ylide was difficult.

The present paper deals with XPS measurements and the structure of triphenylmethylenephosphorane and its gold and copper complexes.

Experimental

XPS Measurements. Sample handling was always carried out in a 99.9995% pure nitrogen atmosphere to prevent possible decomposition. Samples were placed on a gold or nickel mesh holder and introduced into a spectrometer with a 99.9995% pure nitrogen atmosphere. After evacuating to better than 7×10^{-7} Pa (5×10^{-9}Torr†), the sample was cooled to 200 K, and irradiated with Mg $K\alpha$ X-ray (120 W). The instrument used was a VG ESCA 3 electron spectrometer. Analyzer energy was set to give a half width at half maximum [FWHM] of Au $4f_{7/2}$ peak of 1.18 eV. Peak separation of the spectra was made by the Gauss-Newton least-squares method, where a mixed Gaussian-Lorentzian curve shape having a fixed FWHM was utilized. The electron binding energies were calibrated by assigning 285.0 eV to the C 1s peak of the normal phenyl carbon.

Preparation of Phosphorane and Metal-Phosphorane Complexes. Triphenylmethylenephosphorane (**1**) was prepared from the triphenylmethylphosphonium bromide by the sodium amide method.[11] Bis(triphenylmethylenephosphorane)gold chloride (**6**), (triphenylmethylenephosphorane)(triphenylphosphine)gold chloride (**7**), and bis(triphenylmethylenephosphorane)copper chloride (**9**) were prepared by the method of the previous paper.[3b,11] Bis(triphenylphosphine)gold chloride (**8**) was prepared by the method of Baenziger.[12]

Results and Discussion

XPS of Triphenylmethylenephosphorane (1): The structure of phosphorane has been given in two formulae,[13] the ylide formula and the ylene formula as Scheme 1. The ylide formula shows a dipolar zwitterionic nature involving a carbanionic function and an onium center at the phosphorus element. In

$$\underset{\text{Ylide}}{R_3\overset{+}{P}-\overset{-}{\ddot{C}}H_2} \longleftrightarrow \underset{\text{Ylene}}{R_3P=CH_2}$$

Scheme 1.

† 1 Torr=133.322 Pa.

the ylene formula, a true double bond is postulated between the onium center and the phosphorane carbon. Although the P-C bond length of **1** was determined to be 1.66 Å by X-ray analysis[14](suggesting a double-bond character), the assignment of ylide or ylene formula for the phosphorane (**1**) remains unsolved so far.

The results by the XPS measurements of phosphorane (**1**) and the corresponding phosphonium salts are summarized in Table 1 with some reference values. The binding energy, E_B, value (132.6 eV) of the P 2p peak for triphenylmethylphosphonium bromide, $[(C_6H_5)_3\overset{+}{P}CH_3]Br^-$ (**2**), is in good agreement with that (132.5 eV) for phosphonium ion in benzyltriphenylphosphonium chloride,[15] $[(C_6H_5)_3\overset{+}{P}CH_2(C_6H_5)]Cl^-$ (**3**). In reference 16, the E_B of P 2p peak for **3** and methyltriphenylphosphonium chloride, $[(C_6H_5)_3\overset{+}{P}CH_3]Cl^-$ (**4**), are reported. However, those values are different from our results and also from those in reference 15. The E_B in reference 16, however, are somewhat ambiguous, because only E_B of the P 2p peak are given and there is no description of a calibration method. Therefore, the measured E_B for **2** is regarded as reasonable. Other reference values for **2** or **4** were not found by our literature survey. The E_B of the P 2p peak of **2** is different from that[6,15,17] for triphenylphosphine, $(C_6H_5)_3P$ (**5**), as is shown in Table 1. The E_B of **5** measured by different investigators show fairly large scattering, but the highest value is still lower than 132.6 eV of **2**.

In the XPS for phosphorane (**1**), the E_B of the P 2p peak was observed at 132.6 eV; i.e., phosphorus element in **1** can be assigned to the phosphonium ion. This suggests the ylide formula, $(C_6H_5)_3\overset{+}{P}-\overset{-}{C}H_2$. The C 1s spectrum for **1** showed a slightly distorted shape, a tailing at the lower binding-energy side and with a separate very weak satellite peak at the higher binding-energy side. The peak binding energy, E_B, was set at 285.0 eV as due to phenyl carbons. Assuming an 18:1 intensity ratio between phenyl carbons and a methylene carbon, the C 1s peak can be separated to two peaks at 285.0 eV and 283.9 eV. The E_B of the latter peak indicates an electron-rich carbon and is favorable to the ylide formula, but the results must be evaluated with caution since a few arbitrary factors are involved in the peak separation.

XPS of Bis(triphenylmethylenephosphorane)gold Chloride, $[(C_6H_5)_3PCH_2]_2AuCl$ (6), (Triphenylmethylenephosphorane)(triphenylphosphine)gold Chloride, $[(C_6H_5)_3PCH_2][(C_6H_5)_3P]AuCl$ (7), Bis(triphenylphosphine)gold Chloride (8) and Bis(triphenylmethylenephosphorane)copper Chloride, $[(C_6H_5)_3PCH_2]_2CuCl$ (9): The results of XPS for metal phosphorane and metal phosphine complexes are summarized in Table 2. The E_B of Au 4f and Cl $2p_{3/2}$ peaks for both gold complexes **6** and **7** are in good agreement with those for **8**. The E_B values for **8** coincide with those reported by others[18]: E_B[C 1s]=284.9 eV, E_B[P 2p]=131.8 eV, E_B[Cl $2p_{3/2}$]=197.5 eV, and E_B[Au $4f_{7/2}$]=85.2 eV, where oxidation number of gold has been assigned to +1. In addition, the structure of **8** has been found to be essentially trigonal planar by X-ray diffraction.[12] Therefore, the structure of **6** and **7** can be analogous to **8**, and the chloride in **6** and **7** can bond to Au(I). The E_B of C 1s, P 2s, and P 2p peaks for bonded phosphorane in **6** and **7** are very close to those for **1**, but are different from those for the coordinated phosphine. This suggests that the phosphorane in gold complexes can be the ylide formula; i.e., phosphorane-gold bonds are formed from the electron-pair in the carbanion and empty orbitals (sp^2) of gold. Then, the structure of **6** can be expressed as Scheme 2.

For copper complex **9**, the Cu 2p spectra showed no satellite peaks; thus the copper is monovalent

Table 1. Binding Energies Observed in the XPS of Phosphorane and Phosphonium Bromide, and Some Reference Values

No.	Compound	Binding energies of electrons, E_B/eV				Ref.
		C 1s		P		
				2s	2p	
1	$(C_6H_5)_3P=CH_2$	283.9	285.0	190.1	132.6	
2	$[(C_6H_5)_3PCH_3]Br$		285.0		132.6	
3	$[(C_6H_5)_3PCH_2(C_6H_5)]Cl$		285.0		132.5	15)
			(E_B[P 2p]=133.3 eV for $Na_4P_2O_7$)		130.5	16)
4	$[(C_6H_5)_3PCH_3]Cl$		(E_B[P 2p]=133.3 eV for $Na_4P_2O_7$)		130.2	16)
5	$(C_6H_5)_3P$		285.0		131.3	6a)
			285.0		131.9	6b)
			285.0		131.3	6c)
			285.0		130.6	15)
			285.0		130.9	17)

Table 2. Binding Energies Observed in the XPS of Metal Complexes with Phosphorane and Phosphine

No.	Complex	Binding energies of electrons, E_B/eV								
		C 1s		P		Cl	Au		Cu	
				2s	2p	$2p_{3/2}$	$4f_{7/2}$	$4f_{5/2}$	$2p_{3/2}$	$2p_{1/2}$
6	$[(C_6H_5)_3PCH_2]_2AuCl$	283.8	285.0	189.6	132.4	197.5	84.9	88.6		
7	$[(C_6H_5)_3PCH_2]$-$[(C_6H_5)_3P]AuCl$		285.0	189.8 189.3	132.9 131.6	197.7	85.0	88.7		
8	$[(C_6H_5)_3P]_2AuCl$		285.0	189.3	131.8	197.8	85.2	88.8		
9	$[(C_6H_5)_3PCH_2]_2CuCl$	283.6	285.0	189.5	132.4	197.8			933.5	953.3

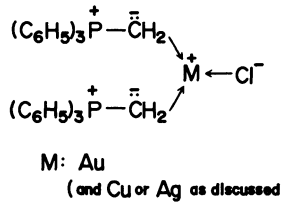

Scheme 2.

($3d^{10}$) or metallic.[19] The E_B of the Cu 2p peaks are much higher than those for commonly known complexes of Cu(I) or Cu(0),[19] but are in good agreement with those for triphenylphosphinecopper(I) chloride,[19a] $(C_6H_5)_3PCuCl$ (**10**), and tris(triphenylphosphine)copper(I) chloride, $[(C_6H_5)_3P]_3CuCl$ (**11**): E_B[Cu $2p_{3/2}$]=933.5 eV, and E_B[Cu $2p_{1/2}$]=953.2 eV assuming E_B[C 1s]=285.0 eV for phenyl carbons. The values for bis(triphenylphosphine)copper chloride, $[(C_6H_5)_3P]_2CuCl$ (**12**), were not found. Further, to distinguish the Cu(I) and Cu(0) Auger parameter, α, is known to be useful. It is defined as the kinetic energy of an intense Auger line minus that of an intense photoelectron line.[20] The measured $E_K[Cu_{LMM}] - E_K$[Cu $2p_{3/2}$] for copper in **9** was 361.3 eV. This value is very close to α=361.0 eV for CuCl and CuCN, but different from α=364.6 eV for metallic Cu.[20] Thus, the oxidation number of copper in **9** is one (or +1). Since other E_B values for **9** coincide with gold complex **6**, and the structure of **12**[21] is confirmed to be similar to that of **8**, the structure of **9** is as in Scheme 2. The XPS results strongly suggest that gold and copper complexes have the structure of Scheme 2. However, as a matter of course, X-ray diffraction may provide indisputable conclusions. So far, the diffraction is not conducted due to the difficulties of sample preparation, handling, and facilities.

The similarity of copper and gold complexes leads to a conclusion that the corresponding silver complex $[(C_6H_5)_3PCH_2]_2AgCl$ (**13**)[11] may have the same structure as is shown in Scheme 2.

Referenses

1) Part IX: Ref. 3a.

2) Y. Yamamoto, *Chem. Lett.*, **1980**, 311; Y. Yamamoto, *Bull. Chem. Soc. Jpn.*, **55**, 3025 (1982); **56**, 1772 (1983); **57**, 43 (1984).

3) a) Y. Yamamoto, *Bull. Chem. Soc. Jpn.*, **57**, 2835 (1984); b) Y. Yamamoto and Z. Kanda, *Bull. Chem. Soc. Jpn.*, **52**, 2560 (1979); c) W. Richter, Y. Yamamoto, and H. Schmidbaur, *Chem. Ber.*, **110**, 1312 (1977).

4) G. J. Leigh, and W. Bremser, *J. Chem. Soc., Dalton Trans.*, **1972**, 1216.

5) M. V. Zelber and R. G. Hayes, *J. Am. Chem. Soc.*, **95**, 3855 (1973); K. L. Cheng, J. C. Carver, and T. A. Carlson, *Inorg. Chem.*, **12**, 1702 (1973); P. Finn and W. L. Jolly, *Inorg. Chem.*, **11**, 893 (1972); G. J. Leigh, J. N. Murrell, W. Bremser, and W. G. Proctor, *J. Chem. Soc., Chem. Commun.*, **1970**, 1661; D. N. Hendrickson, J. M. Hollander, and W. L. Jolly, *Inorg. Chem.*, **8**, 2642 (1969).

6) a) P. A. Grutsh, M. V. Zeller, and T. P. Fehlner, *Inorg. Chem.* **12**, 1431 (1973); b) J. R. Blackburn, R. Nordberg, F. Stevie, R. G. Albridge, and M. M. Jones, *ibid.*, **9**, 2374 (1970); c) W. E. Morgan, W. J. Stec, R. G. Albridge, and J. R. Van Wazer, *ibid.*, **10**, 962 (1971).

7) R. Mason, D. M. P. Mingos, G. Russi, and J. A. Connor, *J. Chem. Soc., Dalton Trans.*, **1972**, 1729.

8) M. Barber, J. A. Connor, L. M. R. Derrick, M. B. Hall, and I. H. Hillier, *J. Chem. Soc., Faraday Trans. 2*, **1973**, 559.

9) W.B. Perry, T. F. Schaaf, W. L. Jolly, L. J. Todd, and D. L. Cronin, *Inorg. Chem.*, **13**, 2038 (1974).

10) M. Barber, J. A. Connor, M. F. Guest, M. B. Hall, I. H. Hillier, and W. N. E. Meredith, *Faraday Discuss. Chem. Soc.*, **54**, 219 (1972); M. Barber, J. A. Connor, I. H. Hillier, and V. R. Saunders, *J. Chem. Soc., Chem. Commun.*, **1971**, 682.

11) Y. Yamamoto and H. Schmidbaur, *J. Organomet. Chem.*, **96**, 133 (1975).

12) N. C. Baenziger, K. M. Dittemore, and J. R. Doyle, *Inorg. Chem.*, **13**, 805 (1974).

13) A. W. Johnson "Ylide Chemistry," Academic Press, New York, N. Y.(1966).

14) J. C. J. Bart, *J. Chem. Soc. (B).*, **1969**, 350.

15) M. Pelavin, D. N. Hendrickson, J. M. Hollander, and W. L. Jolly, *J. Phys. Chem.*, **74**, 1116 (1970).

16) W. E. Swartz, Jr., and D. M. Hercules, *Anal. Chem.*, **43**, 1066 (1971).

17) C. A. Tolman, W. M. Riggs, W. J. Linn, C. M. King, and R. C. Wendt, *Inorg. Chem.*, **12**, 2770 (1973).
18) A. McNeillie, D. H. Brown, W. E. Smith, M. Gibson, and L. Watson, *J. Chem. Soc., Dalton Trans.*, **1980**, 767.
19) a) D. C. Frost, A. Ishitani, and C. A. McDowell, *Mol. Phys.*, **24**, 861 (1972); b) P. E. Larson, *J. Electron Spectrosc.*, **1**, 251 (1972/73); c) B. Folkesson, P. Sundberg, L. Johansson, and R. Larson, *J. Electron Spectrosc. Relat. Phenom.*, **32**, 245 (1983).
20) C. D. Wagner, *Faraday Discuss. Chem. Soc.*, No. 60, 291 (1975).
21) P. H. Davis, R. L. Belford, and I. C. Paul, *Inorg. Chem.*, **12**, 213 (1973).

Proton-Catalyzed Formation of Methyl Carbamate in the Reaction of Isocyanic Acid in Methanol

Hitoshi YASHIRO,† Jun-ichi TAKESHITA,†† Akitsugu OKUWAKI,* and Taijiro OKABE
Department of Applied Chemistry, Faculty of Engineering, Tohoku University, Sendai 980
(Received August 14, 1985)

The rate of formation of methyl carbamate has been measured by a determination of the HNCO concentration. It can be expressed as follows: $r_c=k_c[HNCO][H^+]$. This rate equation was confirmed in the concentration range of HCl(0.76—1.53×10^{-3} mol dm^{-3}). Consequently, this reaction was subjected to a proton catalysis. However, at a H^+ concentration lower than 4×10^{-4} mol dm^{-3}, the observed rate was lower than that calculated by the rate equation, especially at a high HNCO concentration. This was explained by a reduction of the free HNCO concentration due to an association of HNCO with the formed carbamate.

Isocyanic acid reacts with alchohols to afford carbamates and allophanates.[1-2] The mechanism of the formation of carbamates via a rearrangement of the adduct without any consideration of catalysis was postulated by Blohm and Becker.[3] A detailed kinetic study of the HNCO-alcohol reaction, however, has been difficult since HNCO is produced in situ[4-6] because of its instability. Also a suitable method for determining HNCO or carbamates has not been developed.[7-8] The present authors have developed a method for a rapid determination of HNCO.[9] In this paper, the effects of HCl and triethylamine on the rate of formation of methyl carbamate are examined using the rapid method in a low-concentration range of HNCO(< 1.3 M) where the formation of methyl allophanate was negligible. Kinetic analyses show a proton-catalyzed mechanism for the reaction between MeOH and HNCO and a reduction mechanism regarding the rate by the formation of a complex.

Experimental

Reagents: Isocyanic acid was prepared and purified by Linhard's method.[10] The purity attained was 99.4% or greater. Methanol was purified by the usual method using magnesium activated by iodine. Methanolic hydrogen chloride solutions were prepared by bubbling HCl gas into MeOH. Sodium methoxide solution, 0.5 mol dm^{-3}, was prepared by addition of metallic Na pieces into MeOH.

Determination of HNCO: Excess MeONa was titrated with a standard HCl solution after adding a known amount of MeONa into a sample solution containing HNCO and filtering precipitated NaNCO.

Procedure: Methanol(20—30 cm^3) was placed in a 100-cm^3 round-bottomed flask with a ground-glass stopper and immersed in a thermostated bath. Isocyanic acid (0.7 g) was withdrawn with a pipet under a N_2 stream from a storage tube immersed in a Dry Ice-MeOH bath and added into the flask. After rapid agitation, a 2-cm^3 sample was quickly removed and the initial HNCO concentration was determined. Samples were then taken at certain intervals. The reaction mixture was not stirred during the reaction because no precipitate formed and the rate of formation of the carbamate was not altered by agitation.

Results

Effect of Isocyanic Acid, Triethylamine, and Hydrogen Chloride Concentrations. Isocyanic Acid Concentration: Figure 1 shows the effect of the initial HNCO concentration on the decrease in the HNCO concentration at 293 K. The rate of formation of methyl carbamate in MeOH, r_c, can be written as follows:

$$r_c = d[CH_3OCONH_2]_T/dt = -d[HNCO]_T/dt = k[HNCO]_T^{\alpha}, \quad (1)$$

where α is the order of the reaction, k the rate

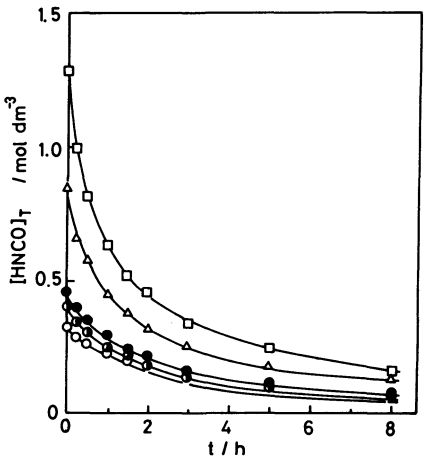

Fig. 1. Decreasing curves of concentration of HNCO at 293 K. $[HNCO]_0$(mol dm^{-3}): (□) 1.285, (△) 0.830, (●) 0.452, (◑) 0.406, (○) 0.319. Curves are calculated ones.

† Present address: Department of Applied Chemistry, Faculty of Engineering, Iwate University, Morioka 020.

†† Research Division, Japan Chemical Industrial Co. Ltd., Koto-ku, Tokyo 136.

constant for the formation of the carbamate, $[HNCO]_T$ the total HNCO concentration determined and $[CH_3OCONH_2]_T$ the total carbamate concentration. Then,

$$\log \tau_{1/m} = (1-\alpha)\log[HNCO]_0 + \log(m^{\alpha-1}-1)/k(\alpha-1), \quad (2)$$

where $\tau_{1/m}$ is the time required for decreasing the initial HNCO concentration to $1/m$ and $[HNCO]_0$ the initial HNCO concentration. Figure 2 shows plots of $\tau_{1/5}$ vs. $\log[HNCO]_0$. The order of the reaction, α, is 1.5 since the slope of the straight line is -0.5. From this data, we can write

$$2([HNCO]_T^{-1/2} - [HNCO]_0^{-1/2}) = kt. \quad (3)$$

This relationship is shown in Fig. 3. At an early stage, the relationship could be expressed by a dotted straight line. However the plots became lower than the straight line upon increasing the HNCO concentration and for a longer reaction time.

Triethylamine Concentration: In Fig. 4, 3/2 order rate plots are shown in the presence of triethylamine and methyl carbamate. The rate of formation was appreciably suppressed by triethylamine at about 10^{-4} mol dm^{-3}. The tendency is just reversed to the effect of bases on the reaction of phenyl isocyanate with MeOH in which the bases accelerated the formation of carbamates.[11] This discrepancy can be explained by the fact that triethylamine can not act as a base in the presence of a large excess of HNCO. Methyl carbamate also significantly reduced the rate.

Hydrogen Chloride Concentration: The rate of formation of methyl carbamate at 293 K was accelerated upon increasing the HCl concentration and became almost proportional to the first-order of the HNCO concentration at 4×10^{-3} mol dm^{-3}.

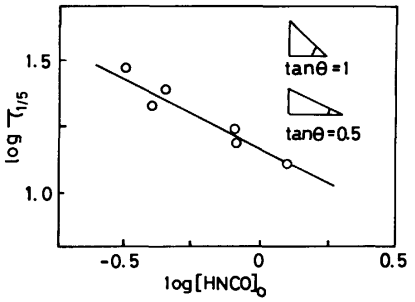

Fig. 2 Plot of log $\tau_{1/5}$ vs. log $[HNCO]_0$.

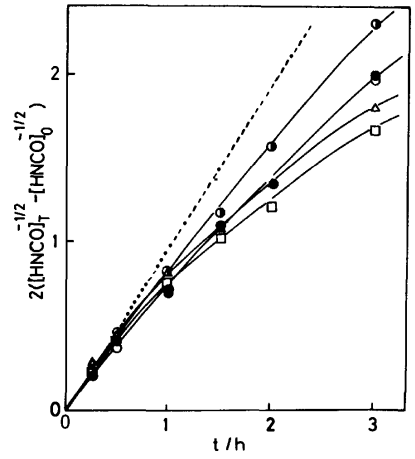

Fig. 3 Plot of $2([HNCO]_T^{-1/2}-[HNCO]_0^{-1/2})$ vs. t. $[HNCO]_0$(mol dm^{-3}): (□) 1.285, (△) 0.830, (●) 0.452, (◑) 0.406, (○) 0.319.

Discussion

Mechanism of the Formation of Methyl Carbamate. Rate Equation. The reactions ionvolved in the system can be considered as follows:

$$HNCO \overset{K_1}{\rightleftharpoons} H^+ + NCO^- \quad (4)$$

$$CH_3OH + HNCO \xrightarrow[k_c]{H^+} CH_3OCONH_2 \quad (5)$$

$$CH_3OCONH_2 + HNCO \overset{K_2}{\rightleftharpoons} CH_3CONH_2\cdot HNCO \quad (6)$$

$$HCl \longrightarrow H^+ + Cl^- \quad (7)$$

$$(C_2H_5)_3N + H^+ \longrightarrow (C_2H_5)_3NH^+, \quad (8)$$

where k_c is the rate constant. K_1 and K_2 are the equilibrium constants for Eqs.4 and 6, respectively.

Figure 5 shows the relationship between the HCl concentration and the slopes of the straight lines ($k_c[H^+]$) obtained from the first-order plots for the

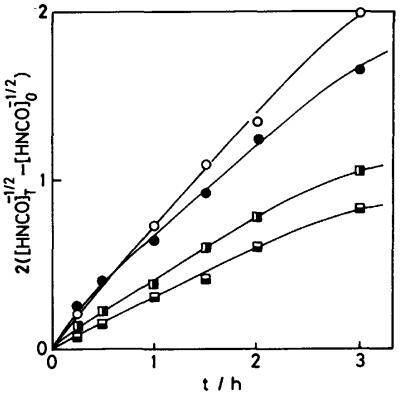

Fig. 4 Suppression of the rate of formation of methyl carbamate in the presence of triethylamine and methyl carbamate at 293 K.

	$[HNCO]_0$	$[(C_2H_5)_3N]$	$[CH_3OCONH_2]$ (mol dm^{-3})
(○)	0.406	—	—
(◨)	0.422	1.01×10^{-4}	—
(◧)	0.497	2.02×10^{-4}	—
(●)	0.468	—	0.480

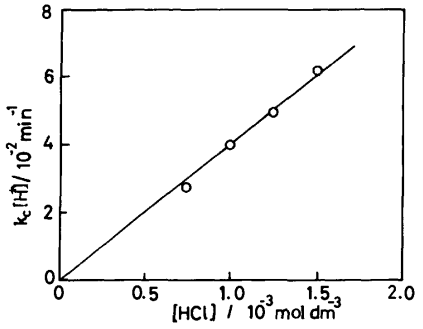

Fig. 5 Relationship between the apparent first-order rate constant($k_c[H^+]$) and concentration of HCl at 273 K.

HNCO concentration at 0.76—1.53×10^{-3} mol dm^{-3} of HCl and 273 K. This result supports the calculation that the rate of formation of the carbamate can be expressed by Eq. 9.

$$r_c = k_c[HNCO][H^+] \quad (9)$$

Rate-Determining Step. Blohm et al.[3] infered from an analogy to the mechanism of conversion of NH_4NCO to urea that carbamates are produced via a zwitterionic intermediate shown by Eq. 10(**a**). However, HNCO can hardly form such stable

$$CH_3OH + HNCO \overset{K_3}{\rightleftharpoons} CH_3\overset{+}{O}H\overset{-}{C}ONH \quad (10)$$

intermediate with MeOH since it is not a base such as NH_3. We considered simply that methyl carbamate was produced by a general acid-catalyzed reaction as shown by Eq. 9(**b**), since there were not enough data to discuss the proton-transfer process in the formation of methyl carbamate.

Mechanism of the Reduction of Rate by Methyl Carbamate. The plots in Fig. 3 became lower than the dotted line as the reaction proceeded. The tendency was enhanced at higher HNCO concentrations and for a longer reaction time. This may indicate that the formed methyl carbamate inhibited the reaction. This was confirmed by the result that the rate of formation decreased in the presence of 0.48 mol dm^{-3} methyl carbamate as shown in Fig. 4. From the rate Eq., there are the following three mechanisms by which the carbamate reduces its rate of formation: **A**) Reduction of the H$^+$ concentration, **B**) Reduction of the free HNCO concentration, **C**) Reduction of both concentrations. Each mechanism is discussed below.

In the case of **A**, the simplest mechanism is the formation of $CH_3OCO\overset{+}{H}NH_2$ as

$$CH_3OCONH_2 + H^+ \overset{K_4}{\rightleftharpoons} CH_3OCO\overset{+}{H}NH_2 \quad (11)$$

However, the decreasing curves of the HNCO concentration calculated by this mechanism could not be fitted with experimental data. The H$^+$ concentration was reduced remarkably by this mechanism; hence, the first-order linear relationship in Fig. 5 can not be obtained in such a low HCl concentration. Consequently, we did not consider any model composed of only case **A** as the mechanism of the reduction of rate. In the case of **B**, the simplest mechanism is the formation of a 1:1 complex as shown in Eq. 6. In this case, the H$^+$ concentration also slightly decreases through Eq. 4. In the case of **C**, the simplest mechanism is a combination of **A** and **B**.

Mechanism of the Formation of Methyl Carbamate. Four models can be made from the combination of the rate-determining step(**a** or **b**) and the mechanism of the reduction of rate(**B** or **C**) as follows: I **b-B**, II **b-C**, III **a-B**, IV **a-C**. In order to determine the optimum model, the decreasing curves of HNCO concentration as a function of time were simulated with these models.

In models III and IV, the decreasing curves could be fitted with the experimental ones only by model III. However, the formation constant (K_3) for the zwitterionic intermediate obtained was too great (1.0×10^{-2} mol^{-1} dm^3). Thus, model III is not reasonable since this value brings about a high concentration of the unstable intermediate.

In models I and II, the decreasing curves could be fitted with the experimental ones only by model I. The agreement could be obtained even in the presence of triethylamine, methyl carbamate, or HCl. In this model there is the problem that the formation of the 1:1 complex has not been confirmed by any other experiment. However, it is considered from the following facts that a weak interaction between an acid and base acts between methyl carbamate and HNCO to form the complex.

Isocyanic acid reacts quantitatively with strong bases such as MeONa or NaOH to precipitate the NaNCO[9] used in this study. An ion pair, $NH_4^+NCO^-$ is formed in DMSO between HNCO and NH_3 which is a weak base, and the formation constant is 79.6 at μ=0.0142.[12] It is known that carbamates promote the formation of those carbamates as base-catalyst.[11] In Fig. 4, it is shown that methyl carbamate is a very weak base.

Simulation. Theoretical Rate Equation. In order to calculate the rate of formation of methyl carbamate by Eq. 9, the concentrations of free HNCO and H$^+$ based on the model I shown by Eqs. 4—8 are derived as a function of initial and total concentrations of HNCO as follows. It will be shown that the first and 3/2 order rate equations can be derived by this model.

$$[HNCO] = [HNCO]_T - [NCO^-] - [CH_3OCONH_2 \cdot HNCO] \quad (12)$$

$$= [HNCO]_T/(1+K_2[CH_3OCONH_2]) \quad K_1/[H^+] \ll 1 \quad (13)$$

The concentration of free carbamate, $[CH_3OCONH_2]$, in Eq. 13 can be expressed as follows.

$$[CH_3OCONH_2] = [CH_3OCONH_2]_T - [CH_3OCONH_2 \cdot HNCO] \quad (14)$$

$[CH_3OCONH_2]_T$: total concentration; $[HNCO]_0 - [HNCO]_T$ (or $[CH_3OCONH_2]_0 + [HNCO]_0 - [HNCO]_T$)

$$[CH_3OCONH_2] = [CH_3OCONH_2]_T/(1+K_2[HNCO]) \quad (15)$$

This relationship is substituted in Eq. 13 and the expression is arranged.

$$K_2[HNCO]^2 + (1+K_2[HNCO]_0 - 2K_2[HNCO]_T)[HNCO] - [HNCO]_T = 0 \quad (16)$$

Thus, the HNCO concentration is expressed by Eq. 17 as the reasonable solution for Eq. 16.

$$[HNCO] = [-(1+K_2[HNCO]_0 - 2K_2[HNCO]_T) + \{(1+K_2[HNCO]_0 - 2K_2[HNCO]_T)^2 + 4K_2[HNCO]_T\}^{1/2}]/2K_2 \quad (17)$$

On the other hand, the concentration of H^+ can be expressed in the presence of HCl or triethylamine as follows.

In the Presence of HCl:

$$[H^+] = [HCl] + [NCO^-] \quad (18)$$

Consequently, the concentration of H^+ can be expressed by Eq. 19.

$$[H^+] = \{[HCl] + ([HCl]^2 + 4K_1[HNCO])^{1/2}\}/2 \quad (19)$$

In the Presence of Triethylamine:

$$[H^+] = [NCO^-] - [(C_2H_5)_3NH^+] \quad (20)$$

This can be solved similarly in the case of HCl, and the concentration of H^+ is expressed by Eq. 21.

$$[H^+] = \{-[(C_2H_5)_3N]_T + ([(C_2H_5)_3N]_T^2 + 4K_1[HNCO])^{1/2}\}/2 \quad (21)$$

Only HNCO: Hydrogen ion concentration can easily be derived from Eq. 19 or Eq. 21 as follows:

$$[H^+] = K_1^{1/2}[HNCO]^{1/2} \quad (22)$$

Thus, r_c can be expressed as Eq. 23.

$$r_c = k_c K_1^{1/2}[HNCO]^{3/2} \quad (23)$$

This Eq. is the differential form of Eq. 3 and k is equal to $k_c K_1^{1/2}$. Blohm and Becker[3] pointed out that if H^+ catalyzed the formation of carbamates, HNCO itself behaved as a catalyst. This was confirmed by the present work. In the presence of 10^{-3} mol dm^{-3} of HCl, the H^+ concentration is nearly equal to that of HCl since K_1 is very small and the free HNCO concentration can be replaced by that of the total HNCO at an early stage. Consequently, a first-order rate equation can be obtained. Thus, the two experimental rate equations could be derived from this mechanism.

Calculation of Rate and Equilibrium Constants. Generally, the rate equation is an ordinary differential equation

$$r_c = f([HNCO]_T, [HCl], [(C_2H_5)_3N], k_c, K_1, K_2). \quad (24)$$

These constants can be determined by solving Eq. 24 using the Runge-Kutta numerical-integration method to obtain the total concentration of HNCO at each reaction time by assuming these values.

The following values were obtained: k_c=131 mol^{-1} dm^3 min^{-1}, K_1=1.57×10^{-8} mol dm^{-3}, K_2=1.11 mol^{-1} dm^3 and σ=0.03622 mol^2 dm^{-6}. The value of $k_c K_1^{1/2}$ calculated from k_c and K_1 obtained is 1.01 h^{-1} and agreed with the observed value of 1.00+0.15 h^{-1} within experimental error. The solid lines in Fig. 1 are the decreasing curves of HNCO concentration calculated using these values. The calculated curves agreed well with the observed values.

Apparent Activation Energy and Dissociation Constant of HNCO. The relationships of Eq. 3 for 0.5 mol dm^{-3} HNCO solution at 273—303 K are shown in Fig. 6. In an early stage, linear relationships were observed. The apparent activation energy was 88 KJ mol^{-1} according to an Arrhenius plot of the slopes. The dissociation constant for HNCO at 273 K

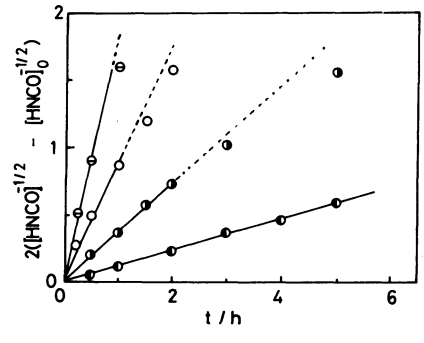

Fig. 6 Effect of temperature on the rate of formation. $[HNCO]_0$ (mol dm^{-3}): (⊖) 0.471, 303 K, (○) 0.406, 293 K (◑) 0.501, 283 K, (◐) 0.429, 273 K.

can be calculated from the values of $k_cK_1^{1/2}$ and k_c. These were 1.97×10^{-3} mol^{-1} dm$^{3/2}$min^{-1} and 40 mol^{-1} dm^3 min^{-1} from the slopes in Figs. 5 and 6, respectively. Thus, the dissociation constant of HNCO in MeOH is 2.40×10^{-9} mol dm^{-3} at 273 K and 1.57×10^{-8} mol dm^{-3} at 293 K.

Conclusion

In a kinetic study of the formation of methyl carbamate from HNCO in MeOH, we conclude that the rate-determining step is the reaction of MeOH and HNCO under the catalysis of proton and the product, methyl carbamate, reduces the apparent rate of its formation by association with HNCO to afford a complex.

References

1) "Gmelins Handbuch", **14**, C[D1], (1971), p 327.
2) D. J. Belson and A. N. Strachan, *Chem. Soc. Rev.*, **11**, 41 (1982).
3) H. W. Blohm and E. I. Becker, *Chem. Rev.*, **51**, 471 (1952).
4) R. A. Jacobson, *J. Am. Chem. Soc.*, **60**, 1742 (1938).
5) M. Amagasa, Y. Kasuga, Y. Saito, T. Yamaguchi, and H. Takekawa, *Kobunshi Kagaku*, **28**, 42 (1971).
6) E. S. Lane, *J. Chem. Soc.*, **1951**, 2764.
7) M. Spielman, J. D. Barnes, and W. J. Close, *J. Am. Chem. Soc.*, **72**, 2520 (1950).
8) W. J. Close, and M. A. Spielman, *J. Am. Chem. Soc.*, **75**, 4055 (1953).
9) H. Yashiro, J. Takeshita, A. Okuwaki, and T. Okabe, *Nippon Kagaku Kaishi*, **1984**, 1473.
10) M. Linhard, *Z. Anorg. Allg. Chem.*, **236**, 200 (1936).
11) J. W. Baker and J. B. Holdsworth, *J. Chem. Soc.*, **1947**, 713.
12) K. J. Hall and D. W. Watts, *Aust. J. Chem.*, **30**, 781 (1977).

 © 1986 The Chemical Society of Japan Bull. Chem. Soc. Jpn., 59, 1337—1340 (1986)

Liquid Crystal Materials with Sulfur Atoms Incorporated in the Principal Structure. V. New Liquid Crystal Compounds; 2,5-Diaryl-1,3-Oxathianes

Yuichiro HARAMOTO,* Makoto SANO, and Hiroyoshi KAMOGAWA
Department of Applied Chemistry, Yamanashi University, Takeda 4, Kofu 400
(Received October 1, 1985)

2,5-Bis(*p*-substituted phenyl)-1,3-oxathianes (**5**), new liquid crystal compounds, and some corresponding 1,3-dioxanes were synthesized by the acetal formation reaction. The mesomorphic behaviors of compounds **5** were compared with those of the corresponding 1,3-dioxanes and 1,3-dithianes. Compounds **5** exhibited the lowest transition temperatures between nematic and isotropic phases. This seems to originate in the bend at the 1,3-oxathiane ring containing two heteroatoms, oxygen and sulfur, different in size. Compounds **5** also tend to exhibit supercooling states in nematic phase.

In recent years, 2,5-disubstituted 1,3-dithianes and 2,5-disubstituted 1,3-oxathianes, new types of liquid crystal compounds, have been reported.[1-8] The present study relates to the synthesis and mesomorphic behavior of 2,5-bis(*p*-substituted phenyl)-1,3-oxathianes (**5**). The mesomorphic behavior of **5** were also compared with those of the corresponding 1,3-dioxanes and 1,3-dithianes.

Results and Discussion

2,5-Bis(*p*-substituted phenyl)-1,3-oxathianes (**5**) were synthesized via the route shown in Scheme 1. In step **1—2**, PBr_3 must be used for *p*-ethoxy and *p*-methoxy compounds to prevent the cleavage of the ether bond, but in the case of *p*-methyl compounds, $HBr-H_2SO_4$ condition could be used under conventional conditions. The amounts of PBr_3 were controlled so as to effect mainly the monobromination of the diols. Compounds **5** were purified by means of recrystallizations from hexane. Those compounds which could not be purified by recrystallizations were purified first by column chromatography, then by recrystallizations from hexane until only a single spot in TLC was obtained. Compounds **5** thus synthesized were

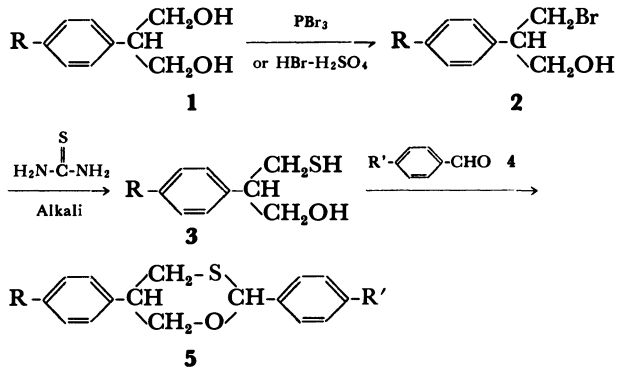

R: OCH_3, OC_2H_5, CH_3.
R′: OC_2H_5, $OC_3H_7{}^n$, $OC_4H_9{}^n$, $OC_5H_{11}{}^n$, CH_3, CN.

Scheme 1.

all colorless and odorless powders which were soluble in common organic solvents.

Absorption of C2, C4, and C6 carbons of the 1,3-oxathiane ring in ^{13}C-NMR, as determined by ^1H-complete decoupling (COM), ^1H-off resonance decoupling (OFR), and ^1H-selective decoupling (SEL) procedures, are located at δ=84.09, 35.16, and 75.58, respectively (R=CH_3O, R′=OC_4H_9). These values are almost equal to those of trans isomers of 2-(*p*-substituted phenyl)-5-alkyl-1,3-oxathianes.[6] Therefore, the obtained compounds must be trans isomers. The presence of 1,3-dithianes and 1,3-dioxanes can be detected by the examination of C2 proton signals at δ=5.25 and 5.50, respectively. Measurements of mesomorphic ranges and assignments of mesophases were carried out by means of a micro melting point apparatus equipped with polarizers.

Mesomorphic ranges of the synthesized 2,5-bis(*p*-substituted phenyl)-1,3-oxathianes and the corresponding 1,3-dioxanes and 1,3-dithianes are given in Table 1.

Transition temperatures of isotropic to nematic (Tn-i) for compounds **5** are lower than those for the corresponding 1,3-dioxanes and 1,3-dithianes. It is known generally that the larger the molecular width, the lower Tn-i is.[9] The molecular widths of the heterorings increase in the order: 1,3-dioxane,<1,3-oxathiane<1,3-dithiane. But compounds **5** bent at the 1,3-oxathiane ring due to the difference of atomic size between sulfur and oxygen. Therefore, the actual molecular widths of these three compounds must increase in the order: 1,3-dioxane<1,3-dithiane<1,3-oxathiane. This fact may explain lower values of Tn-i for compounds **5** as compared with those of the corresponding dioxanes and dithianes. However, Tn-i of the dithianes are higher than those of the corresponding dioxanes. This seems to originate from the dispersion force of 1,3-dithiane ring having two sulfur atoms. It is said generally that the main factor affecting Tn-i is molecular width.[10] Concerning the dithianes, however, this rule dose not appear to hold. Namely, the effect of the molecular width

Table 1. Transition Temperature of Compounds **5** and the Corresponding 1,3-Dioxanes and 1,3-Dithianes

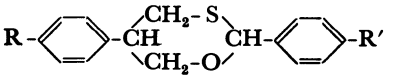

(**5**)

	R	R′	Transition temp/°C[a]
5-1	OC_2H_4	OC_2H_5	C $\underset{134}{\overset{144}{\rightleftharpoons}}$ N $\underset{171}{\overset{171}{\rightleftharpoons}}$ I
5-2	OC_2H_5	$OC_3H_7^n$	C $\underset{149}{\overset{149}{\rightleftharpoons}}$ N $\underset{159}{\overset{159}{\rightleftharpoons}}$ I
5-3	OC_2H_5	$OC_4H_9^n$	C $\underset{106}{\overset{106}{\rightleftharpoons}}$ N $\underset{160}{\overset{160}{\rightleftharpoons}}$ I
5-4	OC_2H_5	$OC_5H_{11}^n$	C $\underset{83}{\overset{93}{\rightleftharpoons}}$ N $\underset{152}{\overset{152}{\rightleftharpoons}}$ I
5-5	OC_2H_5	CH_3	C $\underset{109}{\overset{135}{\rightleftharpoons}}$ N $\underset{144}{\overset{144}{\rightleftharpoons}}$ I
5-6	CH_3	OC_2H_5	C $\underset{128}{\overset{139}{\rightleftharpoons}}$ N $\underset{147}{\overset{147}{\rightleftharpoons}}$ I
5-7	CH_3	$OC_3H_7^n$	C $\overset{135}{\rightleftharpoons}$ N $\underset{106}{\overset{113}{\rightleftharpoons}}$ I
5-8	CH_3	$OC_4H_9^n$	C $\overset{138}{\rightleftharpoons}$ N $\underset{109}{\overset{133}{\rightleftharpoons}}$ I
5-9	OCH_3	OC_2H_5	C $\underset{86}{\overset{115}{\rightleftharpoons}}$ N $\underset{163}{\overset{163}{\rightleftharpoons}}$ I
5-10	OCH_3	$OC_3H_7^n$	C $\underset{91}{\overset{132}{\rightleftharpoons}}$ N $\underset{139}{\overset{139}{\rightleftharpoons}}$ I
5-11	OCH_3	$OC_4H_9^n$	C $\underset{68}{\overset{105}{\rightleftharpoons}}$ N $\underset{144}{\overset{144}{\rightleftharpoons}}$ I
5-12	OCH_3	CN	C $\overset{141}{\rightleftharpoons}$ N $\underset{100}{\overset{106}{\rightleftharpoons}}$ I

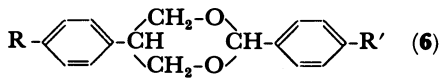

(**6**)

6-1	OC_2H_5	OC_2H_5	C $\underset{127}{\overset{127}{\rightleftharpoons}}$ N $\underset{174}{\overset{174}{\rightleftharpoons}}$ I
6-2	OC_2H_5	$OC_3H_7^n$	C $\overset{154}{\rightleftharpoons}$ S $\underset{135}{\overset{148}{\rightleftharpoons}}$ I
6-3	OC_2H_5	$OC_4H_9^n$	C $\underset{128}{\overset{148}{\rightleftharpoons}}$ S $\underset{149}{\overset{149}{\rightleftharpoons}}$ N $\underset{160}{\overset{160}{\rightleftharpoons}}$ I
6-4	OC_2H_5	CH_3	C $\underset{129}{\overset{136}{\rightleftharpoons}}$ N $\underset{147}{\overset{147}{\rightleftharpoons}}$ I

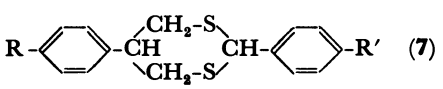

(**7**)

7-1	OC_2H_5	OC_2H_5	C $\underset{176}{\overset{176}{\rightleftharpoons}}$ N $\underset{195}{\overset{195}{\rightleftharpoons}}$ I
7-2	OC_2H_5	$OC_3H_7^n$	C $\overset{173}{\rightleftharpoons}$ N $\underset{167}{\overset{173}{\rightleftharpoons}}$ I
7-3	OC_2H_5	$OC_4H_9^n$	C $\underset{148}{\overset{148}{\rightleftharpoons}}$ N $\underset{182}{\overset{182}{\rightleftharpoons}}$ I
7-4	OC_2H_5	$OC_5H_{11}^n$	C $\underset{126}{\overset{126}{\rightleftharpoons}}$ N $\underset{175}{\overset{175}{\rightleftharpoons}}$ I
7-5	OC_2H_5	CH_3	C $\overset{165}{\rightleftharpoons}$ N $\underset{132}{\overset{165}{\rightleftharpoons}}$ I
7-6	CH_3	$OC_4H_9^n$	C $\overset{170}{\rightleftharpoons}$ N $\underset{110}{\overset{156}{\rightleftharpoons}}$ I
7-7	CH_3	$OC_5H_{11}^n$	C $\overset{146}{\rightleftharpoons}$ N $\underset{121}{\overset{142}{\rightleftharpoons}}$ I
7-8	CH_3	CN	C $\overset{180}{\rightleftharpoons}$ N $\underset{142}{\overset{160}{\rightleftharpoons}}$ I

b)

a) C=crystal; N=nematic; S=smectic; I=isotropic. b) Cited from Ref. 3.

may be smaller than that of the dispersion force of 1,3-dithiane ring having two sulfur atoms.

Compounds **5** having substituent R=CH_3 tend to become monotropic liquid crystal in contrast with those having substituent R=C_2H_5O or R=CH_3O. They also exhibited remarkable supercooling states in the nematic liquid crystal phase (R=CH_3C, R′=OC_4H_9:C–N 105 °C, N–C 68 °C).

Tn-i of a series of compounds **5** different only in substituent R decreased in the order: R=OC_2H_5>R=OCH_3>R=CH_3, and Tn-i of the compounds different only in substituent R′ exhibited somewhat higher values for those having alkoxyl groups of even carbon number (OC_2H_5, OC_4H_9).

Experimental

IR, ^{1}H-NMR, ^{13}C-NMR, and Mass spectra were obtained with a Hitachi 215 spectrophotometer, a JNM-PMX 60 spectrometer, a JNM-FX 90Q FT-NMR spectrometer, and a Hitachi RMU-6 MG spectrometer, respectively. Elemental analyses were carried out with a Perkin-Elmer 250 instrument. Transition temperatures and mesomorphic phases were determined by means of a Mitamura Riken micro melting point apparatus equipped with polarizers. The rates of heating and cooling were fixed to about 2 °C min^{-1}.

2-(*p*-Alkoxyphenyl)-3-bromo-1-propanols (2). To a solution of 2-(*p*-alkoxyphenyl)-1,3-propanediol (**1**; 0.08 mol),

anhyd benzene (150 ml), and pyridine (0.8 g) kept at 30 °C were added, dropwise, a solution of PBr_3 (0.027 mol), anhyd benzene (100 ml), and pyridine (0.3 g) (about 60 min). The solution was kept at 30 °C for 18 h. The reaction mixture was poured into ice water (400 ml) and extracted first with benzene (300 ml), then with ether (400 ml). The extract was washed with cold water (100 ml), dried over anhyd Na_2SO_4, and evaporated in vacuo at 30 °C.

3-Bromo-2-(*p*-methoxyphenyl)-1-propanol (2-1): Yield 50—60%. IR ($CHCl_3$) 3600 (OH), 2800—3000 (alkyl), 1600 (Ar), 1260 (ether) cm^{-1}. ^1H-NMR ($CDCl_3$) δ=2.5—4.2 (m, 9H, CH, CH_2Br, CH_3O, CH_2OH), 6.6—7.3 (q, 4H, ArH).

3-Bromo-2-(*p*-ethoxyphenyl)-1-propanol (2-2): Yield 45—50%. IR ($CHCl_3$) 3600 (OH), 2800—3000 (alkyl), 1600 (Ar), 1260 (ether) cm^{-1}. ^1H-NHR ($CDCl_3$) δ=1.4 (t, 3H, CH_3), 2.5—4.3 (m, 9H, CH, CH_2Br, CH_2OH, CH_3CH_2O), 6.7—7.4 (q, 4H, ArH).

3-Bromo-2-(*p*-methylphenyl)-1-propanol (2-3): To a solution of 48% HBr (33 g) and concd H_2SO_4 (10 g) cooled in an ice bath were added successively 2-(*p*-methylphenyl)-1,3-propanediol (**1**; 0.065 mol) and concd H_2SO_4 (17 g). The solution was kept at 70—75 °C for 15 h. The reaction mixture was then poured into ice water (200 g). The mixture was stirred and extracted twice with ether (each 300 ml). The extract was washed with cold 10% aq $NaHCO_3$ (100 ml), dried over anhyd Na_2SO_4, and evaporated in vacuo at 30 °C. Yield 50—60%. IR ($CHCl_3$) 3600 (OH), 2800—3000 (alkyl), 1600 (Ar) cm^{-1}. ^1H-NMR ($CDCl_3$) δ=2.3 (s, 3H, CH_3), 3.0—4.2 (m, 6H, CH, CH_2Br, CH_2OH), 7.2 (s, 4H, ArH).

2-(*p*-Substituted phenyl)-3-mercapto-1-propanols (3). To a solution of thiourea (0.064 mol) in triethylene glycol (10 ml) kept at 75 °C was added compound **2** (0.01 mol) in nitrogen atmosphere, followed by stirring at 75 °C for 18 h. Tetraethylenepentamine (0.01 mol) was then added, and the mixture was stirred at 75 °C for 2 h under a nitrogen atmosphere. The reaction mixture was poured into water (100 ml) and then extracted twice with ether (each 300 ml). The extract was washed with cold 5% aq HCl (100 ml), dried over anhyd Na_2SO_4, and evaporated in vacuo at 30 °C.

3-Mercapto-2-(*p*-methoxyphenyl)-1-propanol (3-1): Yield 60—65%. IR ($CHCl_3$) 3600 (OH), 2800—3000 (alkyl), 1600 (Ar), 1270 (ether) cm^{-1}. ^1H-NMR ($CDCl_3$) δ=0.9—1.5 (b, 1H, SH), 2.3—4.3 (m, 6H, CH_2OH, CH_3O), 6.5—7.4 (q, 4H, ArH).

2-(*p*-Ethoxyphenyl)-3-mercapto-1-propanol (3-2): Yield 65—70%. IR ($CHCl_3$) 3600 (OH), 2800—3000 (alkyl), 1600 (Ar), 1270 (ether) cm^{-1}. ^1H-NMR ($CDCl_3$) δ=0.9—1.5 (m, 4H, CH_3, SH), 2.4—3.0 (m, 3H, CH_2S, CH), 3.1—4.5 (m, 5H, CH_2O, CH_2OH), 6.5—7.4 (q, 4H, ArH).

3-Mercapto-2-(*p*-methylphenyl)-1-propanol (3-3): Yield 60—65%. IR ($CHCl_3$) 3600 (OH), 2800—3000 (alkyl), 1600 (Ar) cm^{-1}. ^1H-NMR ($CDCl_3$) δ=1.0—1.4 (m, 1H, SH), 2.3 (s, 3H, CH_3), 2.5—4.0 (m, 6H, CH_2S, CH, CH_2OH), 7.1 (s, 4H, ArH).

2,5-Bis(*p*-substituted phenyl)-1,3-oxathianes (5). To a solution of compound **3** (0.004 mol) and *p*-substituted benzaldehyde **4** (0.004 mol) in anhyd $CHCl_3$ (300 ml) cooled in an ice bath were added BE_3-$(C_2H_5)_2O$ (0.5 g) and Molecular Sieve (3A, 1/15; 3 g). The mixture was stirred at 0—5 °C for 8 h and then at 20—25 °C for 18 h. The solution was washed with 10% aq $NaHCO_3$ (400 ml), dried over anhyd Na_2SO_4, and evaporated in vacuo at 40 °C. The crude product was purified by recrystallizations from hexane, if necessary, by column chromatography and recrystallizations.

The spectral properties and analytical data of the synthesized compounds are given below.

2-(*p*-Substituted phenyl)-5-(*p*-ethoxyphenyl)-1,3-oxathianes: IR ($CHCl_3$) 2800—3000 (alkyl), 1600 (Ar), 1280 (ether) cm^{-1}. ^1H-NMR ($CDCl_3$) δ=0.8—2.3 (m, alkyl), 2.5—3.5 (m, 3H, CH, CH_2S), 3.7—4.5 (m, 6H, CH_2O), 5.8 (s, 1H, S-CH-O), 6.7—7.7 (m, 8H, ArH).

2-(*p*-Alkoxyphenyl)-5-(*p*-methylphenyl)-1,3-oxathianes: IR ($CHCl_3$) 2800—3000 (alkyl), 1600 (Ar), 1280 (ether) cm^{-1} ^1H-NMR ($CDCl_3$) δ=0.8—2.1 (m, alkyl), 2.3 (s, 3H, CH_3), 2.5—3.5 (m, 3H, CH, CH_3S), 3.7—4.5 (m, 4H, CH_2O), 5.8 (s, 1H, S-CH-O), 6.7—7.6 (m, 8H, ArH).

2-(*p*-Alkoxyphenyl)-5-(*p*-methoxyphenyl)-1,3-oxathianes: IR ($CHCl_3$) 2800—3000 (alkyl), 1600 (Ar), 1280 (ether) cm^{-1}. ^1H-NMR ($CDCl_3$) δ=0.9—2.1 (m, alkyl), 2.7—4.5 (m, 10H, CH_2S, CH, CH_2O, CH_3O), 5.8 (s, 1H, CH), 6.7—7.6 (m, 8H, ArH).

2,5-Bis(*p*-ethoxyphenyl)-1,3-oxathiane (5-1): Yield 43%. Found: C, 70.07; H, 6.99%. Calcd for $C_{20}H_{24}O_3S_1$: C, 69.73; H, 7.02%. MS (*m/z*) 344 (M^+).

5-(*p*-Ethoxyphenyl)-2-(*p*-propoxyphenyl)-1,3-oxathiane (5-2): Yield 35%. Found: C, 70.18; H, 7.17%. Calcd for $C_{21}H_{26}O_3S$: C, 70.36; H, 7.31%. MS (*m/z*) 358 (M^+).

2-(*p*-Butoxyphenyl)-5-(*p*-ethoxyphenyl)-1,3-oxathiane (5-3): Yield 47%. Found: C, 71.39; H, 7.54%. Calcd for $C_{22}H_{28}O_3S$: C, 71.02; H, 7.58%. MS (*m/z*) 372 (M^+).

5-(*p*-Ethoxyphenyl)-2-(*p*-pentyloxyphenyl)-1,3-oxathiane (5-4): Yield 39%. Found: C, 71.19; H, 7.68%. Calcd for $C_{23}H_{30}O_3S$: C, 71.46; H, 7.82%. MS (*m/z*) 386 (M^+).

5-(*p*-Ethoxyphenyl)-2-(*p*-methylphenyl)-1,3-oxathiane (5-5): Yield 32%. Found: C, 72.31; H, 6.93%. Calcd for $C_{19}H_{22}O_2S$: C, 72.57; H, 7.05%. MS (*m/z*) 314 (M^+).

2-(*p*-Ethoxyphenyl)-5-(*p*-methylphenyl)-1,3-oxathiane (5-6): Yield 40%. Found: C, 72.24; H, 7.08%. Calcd for $C_{19}H_{22}O_2S$: C, 72.57; H, 7.05%. MS (*m/z*) 314 (M^+).

5-(*p*-Methylphenyl)-2-(*p*-propoxyphenyl)-1,3-oxathiane (5-7): Yield 38%. Found: C, 73.46; H, 7.44%. Calcd for $C_{20}H_{24}O_2S$: C, 73.13; H, 7.37%. MS (*m/z*) 328 (M^+).

2-(*p*-Butoxyphenyl)-5-(*p*-methylphenyl)-1,3-oxathiane (5-8): Yield 44%. Found: C, 72.94; H, 7.72%. Calcd for $C_{21}H_{26}O_2S$: C, 73.64; H, 7.65%. MS (*m/z*) 342 (M^+).

2-(*p*-Ethoxyphenyl)-5-(*p*-methoxyphenyl)-1,3-oxathiane (5-9): Yield 23%. Found: C, 69.21; H, 6.83%. Calcd for $C_{19}H_{22}O_3S$: C, 69.06; H, 6.71%. MS (*m/z*) 330 (M^+).

5-(*p*-Methoxyphenyl)-2-(*p*-propoxyphenyl)-1,3-oxathiane (5-10): Yield 30%. Found: C, 69.65; H, 7.09%. Calcd for $C_{20}H_{24}O_3S$: C, 69.73; H, 7.02%. MS (*m/z*) 344 (M^+).

2-(*p*-Butoxyphenyl)-5-(*p*-methoxyphenyl)-1,3-oxathiane (5-11): Yield 35%. Found: C, 70.37; H, 7.31%. Calcd for $C_{21}H_{26}O_3S$: C, 70.36; H, 7.31%. MS (*m/z*) 358 (M^+).

2-(*p*-Cyanophenyl)-5-(*p*-methoxyphenyl)-1,3-oxathiane (5-12): Yield 24%. Found: C, 70.58; H, 5.98; N, 4.89%. Calcd for $C_{18}H_{17}NO_2S$: C, 69.43; H, 5.50; N, 4.50%. MS (*m/z*) 311 (M^+).

2-(*p*-Substituted phenyl)-5-(*p*-ethoxyphenyl)-1,3-dioxanes (6). Compounds **6** were synthesized by following the same procedure as for compounds **5** using **1** instead of **3**. IR

($CHCl_3$) 2800—3000 (alkyl), 1600 (Ar), 1300 (ether) cm^{-1}. ^1H-NMR ($CDCl_3$) δ=0.8—2.4 (m, alkyl), 3.7—4.5 (m, CH, CH_2O), 5.5 (s, 1H S-CH-O), 6.8—7.7 (m, 8H, ArH).

2,5-Bis(*p*-ethoxyphenyl)-1,3-dioxane (6-1): Yield 53%. Found: C, 72.81; H, 7.40%. Calcd for $C_{20}H_{24}O_4$: C, 73.14; H, 7.37%. MS (*m/z*) 328 (M^+).

5-(*p*-Ethoxyphenyl)-2-(*p*-propoxyphenyl)-1,3-dioxane (6-2): Yield 44%. Found: C, 73.63; H, 7.67%. Calcd for $C_{21}H_{26}O_4$: C, 73.66; H, 7.65%. MS (*m/z*) 342 (M^+).

2-(*p*-Butoxyphenyl)-5-(*p*-ethoxyphenyl)-1,3-dioxane (6-3): Yield 42%. Found: C, 74.03; H, 7.92%. Calcd for $C_{22}H_{28}O_4$: C, 74.13; H, 7.92%. MS (*m/z*) 356 (M^+).

5-(*p*-Ethoxyphenyl)-2-(*p*-methylphenyl)-1,3-dioxane (6-4): Yield 50%. Found: C, 76.39; H, 7.44%. Calcd for $C_{19}H_{22}O_3$: C, 76.48; H, 7.43%. MS (*m/z*) 298 (M^+).

References

1) Y. Haramoto and H. Kamogawa, *J. Chem. Soc., Chem. Commun.*, **1983**, 75.
2) Y. Haramoto, A. Nobe, and H. Kamogawa, *Bull. Chem. Soc. Jpn.*, **57**, 1966 (1984).
3) Y. Haramoto, K. Akazawa, and H. Kamogawa, *Bull. Chem. Soc. Jpn.*, **57**, 3173 (1984).
4) Y. Haramoto and H. Kamogawa, *Bull. Chem. Soc. Jpn.*, **58**, 477 (1985).
5) Y. Haramoto and H. Kamogawa, *Chem. Lett.*, **1985**, 79.
6) Y. Haramoto and H. Kamogawa, *Bull. Chem. Soc. Jpn.*, **58**, 1821 (1985).
7) Y. Haramoto and H. Kamogawa, *Mol. Cryst. Liq. Cryst.*, **131**, 101 (1985).
8) Y. Haramoto and H. Kamogawa, *Mol. Cryst. Liq. Cryst.*, **131**, 201 (1985).
9) G. W. Gray and B. W. Worrall, *J. Chem. Soc.*, **1959**, 1545 .
10) G. W. Gray, *Mol. Cryst.*, **1**, 333 (1966).

Versatile Synthesis of Cyclopropanecarboxylic Acid Derivatives by the $Ni(CO)_4$-Induced Reductive Carbonylation Reaction of *gem*-Dibromocyclopropanes

Toshikazu HIRAO,* Yoshiyuki HARANO, Yoshihiro YAMANA, Yuji HAMADA, Shinichiro NAGATA, and Toshio AGAWA
Department of Applied Chemistry, Faculty of Engineering, Osaka University, 2-1 Yamadaoka, Suita, Osaka 565
(Received October 22, 1985)

Reductive carbonylation of *gem*-dibromocyclopropanes was achieved by treatment with tetracarbonylnickel in the presence of alcohols, amines, thiols, or imidazole in DMF leading to the corresponding cyclopropanecarboxylic acid derivatives, respectively. Use of disulfides as an initial nucleophile resulted in carbonylation with sulfenylation at the geminal position. This method was applied to the intramolecular reductive carbonylation reaction of 2,2-dibromocyclopropanealkanols into bicyclic lactones. Nickel carbenoid and enolate complexes are assumed to be involved as key intermediates.

Cyclopropane derivatives are versatile synthetic intermediates since ring cleavage permits us to introduce three-carbon unit for selective carbon skeleton construction.[1] The methods for the cyclopropane ring formation have been advanced according to the development of carbene chemistry. On the other hand, the direct introduction of a functional group to a cyclopropane ring is fairly difficult although it diverses the utility of the cyclopropane ring transformation in organic syntheses. We already demonstrated[2] a versatile synthesis of cyclopropanecarboxylic acid derivatives by reductive carbonylation of *gem*-dibromocyclopropanes easily provided by the addition of dibromocarbene to olefinic compounds. The present paper describes a full account for this new method.

Results and Discussion

Treatment of the *gem*-dibromocyclopropane **1** with tetracarbonylnickel and amine in DMF gave a mixture of the *cis*- and *trans*-cyclopropanecarboxamides **2** (Eq. 1). This carbonylation reaction is

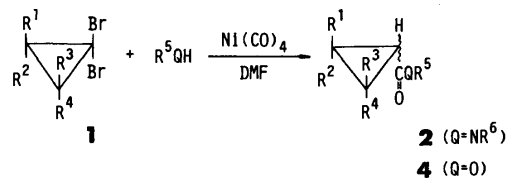

(1)

characterized by the simultaneous reduction of the geminal C–Br bond (reductive carbonylation). Our results are summarized in Table 1. A variety of *gem*-dibromocyclopropanes underwent reductive carbonylation with functional groups (e.g., methoxycarbonyl and cyano groups) inert under the conditions employed here. Aliphatic and aromatic amines reacted with almost equal ease. Use of excess tetracarbonylnickel increased the yields of **2**. The carbonylation reaction was suppressed substantially under CO flow and completely under 20 kg cm^{-2} of CO. This difference might be due to the occupation of coordination sites with CO.

1-Bromo-1-chloro-2-phenylcyclopropane (**3a**) was also converted to the amide **2a** via reductive carbonylation (Eq. 2), this being in sharp contrast to

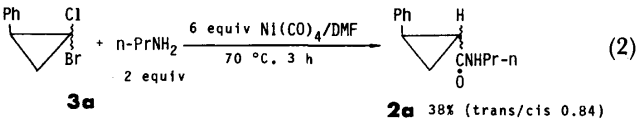

(2)

no reaction of 1,1-dichloro-2-phenylcyclopropane. The presence of one bromine atom is at least required for the success of the transformation.

Starting from 1-propanol or phenols, a stereoisomeric mixture of the cyclopropanecarboxylates **4** was produced. It is of interest that imidazole behaved as a nucleophile to give the 1-acylimidazoles **5** (Eq. 3). Since 1-acylimidazoles are known to be

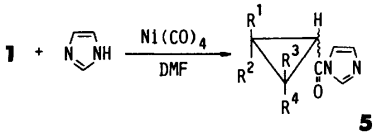

(3)

susceptible to nucleophilic attack,[3] this method will permit a facile synthesis of cyclopropyl ketones.

Thiols did not work as a selective nucleophile for reductive carbonylation (Eq. 4). A substantial

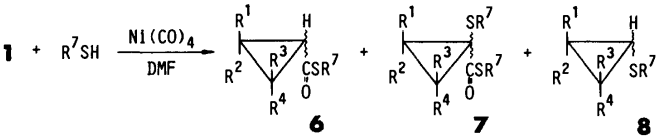

(4)

Table 1. Preparation of Cyclopropanecarboxylic Acid Derivatives

1					R^5QH	equiv	$Ni(CO)_4$ equiv	Time/h[a]	2—6 Yield/%		*trans/cis*
R^1	R^2	R^3	R^4								
Ph	H	H	H	**1a**	*n*-$PrNH_2$	2.5	6	3	**2a**	78	45 : 55
	1a				*n*-$PrNH_2$	2.5	2	3	**2a**	66	
	1a				*n*-$PrNH_2$	2.5	1	3	**2a**	52	
	1a				*n*-$PrNH_2$	1	1	3	**2a**	52	
	1a				*n*-$PrNH_2$	1	1[b]	3	**2a**	36	
	1a				*n*-$PrNH_2$	1	1[c]	3	**2a**	0	
	1a				$PhNH_2$	2.5	6	3	**2i**	63	
	1a				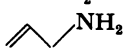	2.5	6	3	**2j**	56	
	1a				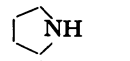	2.5	6	3	**2k**	66	50 : 50
CO_2Me	Me	H	H	**1b**	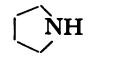	2.5	6	3	**2b**	44	
n-BuO	H	H	H	**1c**	*n*-$PrNH_2$	2.5	3	3	**2c**	16	
Me_3SiCH_2	H	H	H	**1d**	*n*-$PrNH_2$	2.5	6	6	**2d**	46	
	1a				*n*-PrOH	2.5	6	3	**4a**	62	34 : 66
	1a				PhOH	2.5	6	3	**4l**	57	
	1a				*m*-ClPhOH	2.5	6	3	**4m**	56	
	1b				*n*-PrOH	2.5	6	3	**4b**	75	
	1d				*n*-PrOH	2.5	6	13	**4d**	27	
CN	Me	H	H	**1e**	*n*-PrOH	2.5	6	3	**4e**	51	
Me_3Si	H	H	Ph	**1f**	*n*-PrOH	2.5	6	6	**4f**	43	
Me_3Si	H	*n*-Bu	H	**1g**	*n*-PrOH	2.5	6	6	**4g**	46	
	1a					2.5	6	6	**5a**	42	
	1d				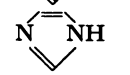	2.5	6	7	**5d**	73	
	1d				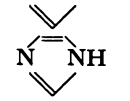	2.5	3	7	**5d**	69	
n-C_6H_{13}	H	H	H	**1h**	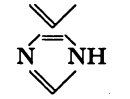	2.5	3	7	**5h**	58	
	1a				*t*-BuSH	2.5	6	8	**6a**	13[d]	
	1a				*n*-PrSH	2.5	6	8	**6n**	42[e]	
	1a				PhSH	2.5	6	8	**6o**	33[f]	

a) Reaction temperature, 70 °C. b) CO, flow. c) CO, 20 kg/cm². d) *S*-*t*-Butyl 1-*t*-butylthio-2-phenylcyclopropanecarbothioate (**7a**, 10%) and 1-bromo-2-phenylcyclopropane (33%) were obtained. e) 1-Phenyl-2-propylthiocyclopropane (**8n**, 5%) and 1-bromo-2-phenylcyclopropane (40%) were obtained. f) 1-Phenyl-2-phenylthiocyclopropane (**8o**, 32%) was obtained.

amount of *S*-*t*-butyl 1-*t*-butylthio-2-phenylcyclopropanecarbothioate (**7a**) or the cyclopropyl sulfide **8** was obtained as a by-product together with the desired cyclopropanecarbothioate **6** depending on thiols. For the selective preparation of **6**, the transformation from **5** was examined; 1-(2-phenylcyclopropylcarbonyl)imidazole (**5a**) was converted to **6a** in 65% yield on treatment with 2-methyl-2-propanethiol and a catalytic amount of $Mg(OEt)_2$.[3b] Furthermore, a one-pot transformation was performed only by the addition of 2-methyl-2-propanethiol to the crude resultant mixture of **5a** after removal of excess tetracarbonylnickel leading to **6a** selectively in 31% yield from 1,1-dibromo-2-phenylcyclopropane (**1a**) as shown in Scheme 1.

The formation of the 1-alkylthiocyclopropanecarbothioate **7a** is assumed to be explained by the

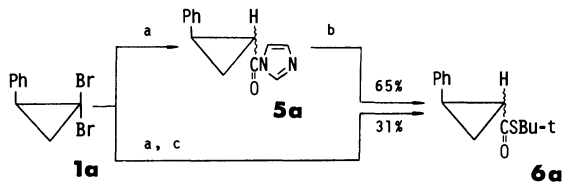

Reagents and conditions: (a) $Ni(CO)_4$ (6 equiv), Imidazole (2.5 equiv), DMF, 70 °C, 3 h; (b) *t*-BuSH (1.2 equiv), $Mg(OEt)_2$ (cat.), 25 °C, 14 h; (c) *t*-BuSH (1.2 equiv), 25 °C, 14 h.

Scheme 1.

intervention of the disulfide. Actually, the Ni(CO)$_4$-induced reaction of **1a** with dipropyl disulfide gave a mixture of *S*-propyl *cis*- and *trans*-2-phenyl-1-propylthiocyclopropanecarbothioates (**7n**) predominantly. Use of diphenyl or di-*t*-butyl disulfide resulted in the exclusive formation of **7** (Eq. 5, Table 2). This

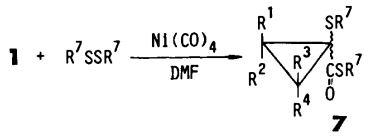

(5)

Table 2. Preparation of **7**[a]

1	$R^7_2S_2$	Product, Yield/%			
	R^7	**7**		**6**	
1a	*t*-Bu	**7a**	33	**6a**	2
1a	*n*-Pr	**7n**	34	**6n**	14
1a	Ph	**7o**	40	**6o**	0
1e	*n*-Pr	**7e**	40	**6e**	6

a) The reaction of **1** with Ni(CO)$_4$ (6 equiv) and $R^7_2S_2$ (2.5 equiv) was carried out at 70 °C for 20 h.

carbonylation accompanied by the simultaneous sulfenylation at the geminal position represents one of the scarcely investigated transition metal mediated reactions with disulfides.[4]

The *gem*-dibromocyclopropanes **9** bearing a hydroxyalkyl group (prepared by the addition of dibromocarbene to allylic or homoallylic alcohols[5]) were subjected to the intramolecular reductive carbonylation reaction giving the bicyclic *γ*- or *δ*-lactones **10**, respectively (Eq. 6, Table 3). It should be

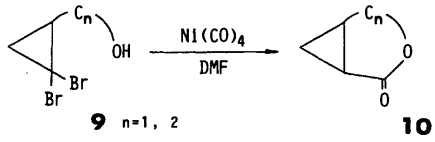

(6)

noted that the intramolecular reaction of **9a** provides a facile preparative method for *cis*-chrysanthemic acid from prenyl alcohol because the bicyclic lactone **10a** has been reported to be its key synthetic intermediate.[6] In the case of *trans*-2,2-dibromo-3-

Table 3. Preparation of **10**

9	Ni(CO)$_4$, equiv	Temp/°C	Time/h	**10**, Yield/%	
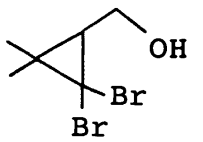 **9a**	2.2	80	11	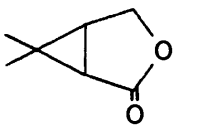 **10a**	37[a]
	7	75	3		73
	7	80	11[b]		27
	7	75	5[c]		60
	7	66	5[d]		3[e]
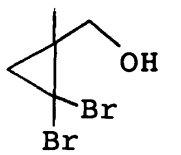 **9b**	7	75	3	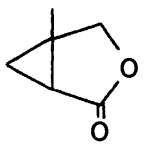 **10b**	82
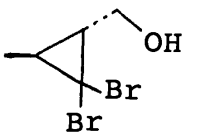 **9c**	1.2	80	11	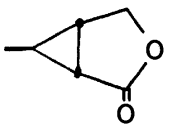 **10c**	43[f]
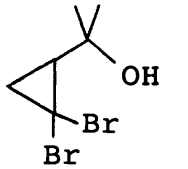 **9d**	7	75	3	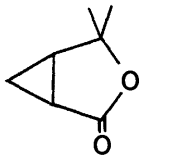 **10d**	70
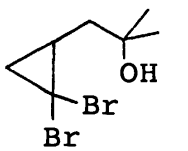 **9e**	7	75	3	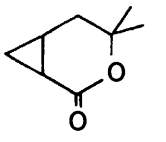 **10e**	51

a) *cis*-2-Bromo-3,3-dimethylcyclopropanemethanol (**11a**) was produced as a by-product (10%). b) CO, flow. c) 1-Methyl-2-piperidone was used as a solvent. d) THF was used as a solvent. e) A mixture of *cis*- and *trans*-2-bromo-3,3-dimethylcyclopropanemethanols (18%) was produced as by-products and 72% of **9a** was recovered. f) 6-*endo*-Methyl-3-oxabicyclo[3.1.0]hexan-2-one was not formed and *cis*-2-bromo-*trans*-3-methylcyclopropanemethanol (**11c**, 24%) was produced as a by-product.

methylcyclopropanemethanol (**9c**), 6-*exo*-methyl-3-oxabicyclo[3.1.0]hexan-2-one (**10c**) was produced selectively. Lactonization of tertiary-alcohols (**9d** and **9e**) proceeded well. Decrease in the amount of tetracarbonylnickel led to a small amount of by-product, the *cis*-2-bromocyclopropanemethanol **11**, derived by reduction of the bromine atom *trans* to the hydroxymethyl group of **9**. As observed in the intermolecular reactions, 2,2-dichloro-3,3-dimethylcyclopropanemethanol did not react even at the high reaction temperature (75 °C, 5 h or 120 °C, 7 h).

It is likely that tetracarbonylnickel serves an important role in the reduction step. The carbonylation reaction of **1a** with 1-propanol-*d* gave the corresponding α-deuteriocyclopropanecarboxylate, indicating that the α-proton is derived from the one of the hydroxyl group. No carbonylation of monobromocyclopropanes under the conditions employed above rules out their intervention. Moreover, oxidative addition of **1** to tetracarbonylnickel seems unlikely because the reaction of **1a** with tetracarbonylnickel in the absence of 1-propanol at 70 °C for 3 h resulted in its recovery (94%). Our first proposal refers to the intermediacy of the α-bromocyclopropanecarboxylate which is reduced to **4**.[2] This reaction path was supported by the reduction of α-bromo-β-methyl-γ-butyrolactone to β-methyl-γ-butyrolactone with tetracarbonylnickel and a small amount of water.[7] However, the independently prepared methyl 1-bromo-2-phenylcyclopropanecarboxylate (**12**) was recovered without carbonylation on treatment with tetracarbonylnickel and propylamine (Eq. 7). This finding suggests that an alternative

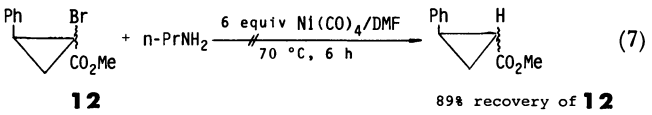

(7)

12 89% recovery of **12**

mechanism is operative.

A plausible reaction path is explained as depicted in Scheme 2. Tetracarbonylnickel is considered to contact with a nucleophile, e.g., alcohol to generate the complex **13**. A similar kind of intermediate has been reported to be present in carbonylation of vinyl halides.[8] This initial step is also ascertained by the following observations. Addition of **1a** to the DMF solution of tetracarbonylnickel pretreated with propylamine gave 50% yield of **2a**, but the reverse operation as shown in scheme 3 resulted in a poor yield of **2a** (16%). The interaction of amine with tetracarbonylnickel should be important to achieve the present transformation. The next step might be explained by invoking the attack of the complex **13** on **1** to form the nickel carbenoid complex **14**.[9] The migration of the alkoxycarbonyl group leads to the stable enolate complex **15**. Protonation with alcohol

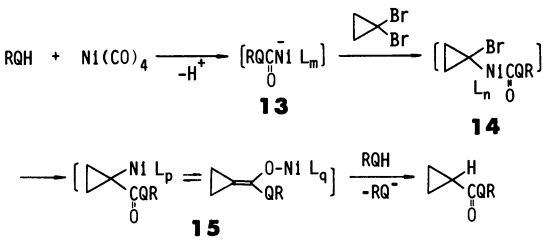

Scheme 2.

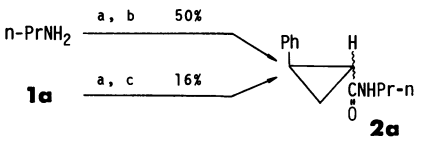

Reagents and conditions: (a) $Ni(CO)_4$ (1 equiv), DMF, 70 °C, 3 h; (b) **1a** (1 equiv), 70 °C, 3 h; (c) *n*-$PrNH_2$ (1 equiv), 70 °C, 3 h.

Scheme 3.

completes the debromination process giving the reductive carbonylation product together with the generation of **13** from tetracarbonylnickel. Checking a crude mixture of the intermolecular reaction, a small amount of the reduced monobromocyclopropane was detected. The formation of this monobromocyclopropane and **11** is assumed to be derived by the degradation of the carbenoid complexes **14**. The present scheme also accounts for the reaction with disulfides which play both roles of a nucleophile and an electrophile. Reductive carbonylation of *gem*-dibromocyclopropanes is considered to depend on the intermediacy of the novel nickel carbenoid and enolate complexes.

Experimental

IR spectra were taken on a JASCO IRA-1 spectrometer. NMR spectra were obtained on JEOL JNM PMX-60 and JEOL JNM FX-90Q spectrometers in $CDCl_3$ solutions with tetramethylsilane as an internal standard. Mass spectrometry was performed with Hitachi RMU-6E and JEOL JMS-DX 300 (high resolution) spectrometers. The *gem*-dibromocyclopropanes **1**[10] and **9**,[5] 1-bromo-1-chloro-2-phenylcyclopropane (**3a**),[10] and methyl 1-bromo-2-phenylcyclopropanecarboxylate (**12**)[11] were prepared according to the reported methods.

General Procedure for the Preparation of Cyclopropanecarboxylic Acid Derivatives. To a stirred solution of the *gem*-dibromocyclopropane **1** (5.0 mmol) and a nucleophile (11 mmol) in freshly distilled DMF (12 mL) was added dry tetracarbonylnickel (30 mmol) at room temperature. The mixture was stirred at 70 °C for 3 h unless otherwise stated in Table 1. Excess of tetracarbonylnickel was removed under the reduced pressure. Ether (15 mL) and 5% aq HCl (15 mL) were added to the resultant mixture, which was

stirred at room temperature for 1 h and extracted with ether (3×10 mL). The combined organic layers were washed with brine, dried over Na_2SO_4, and concentrated. The residue was flash chromatographed to give a mixture of *cis*- and *trans*-cyclopropanecarboxylic acid derivatives. To purify **5**, chromatography on normal silica-gel column was done eluting with 20% EtOAc-hexane.

2a (*cis*): Mp 71—72 °C (uncorrected); IR (neat) 1620 cm^{-1}; ^{1}H NMR (90 MHz) δ=0.67 (t, 3H, J=5.0 Hz), 1.0—1.5 (m, 2H), 1.22 (ddd, 1H, J=9.5, 8.6, 7.0 Hz), 1.67 (ddd, 1H, J=9.5, 8.5, 5.8 Hz), 1.89 (ddd, 1H, J=7.0, 5.8, 5.0 Hz), 2.40 (ddd, 1H, J=8.6, 8.5, 5.0 Hz), 2.99 (q, 2H, J=5.1 Hz), 5.5—5.9 (m, 1H), 7.22 (broad s, 5H); MS m/z 203 (M$^+$). (***trans***): Mp 107—112 °C (uncorrected); IR (neat) 1620 cm^{-1}; ^{1}H NMR (90 MHz) δ=0.90 (t, 3H, J=5.0 Hz), 1.0—1.7 (m, 5H), 2.3—2.6 (m, 1H), 3.0—3.4 (m, 2H), 5.0—6.2 (m, 1H), 6.9—7.4 (m, 5H); MS m/z 203 (M$^+$). Found (mixture): C, 76.90; H, 8.35; N, 7.01%. Calcd for $C_{13}H_{17}NO$: C, 76.81; H, 8.43; N, 6.89%.

2b: Oil; IR (neat) 1720, 1630 cm^{-1}; ^{1}H NMR (60 MHz) δ=1.27 (s, 3H), 1.43 (d, 2H, J=7.4 Hz), 1.7—2.1 (m, 4H), 2.32 (t, 1H, J=7.4 Hz), 3.3—3.6 (m, 4H), 3.70 (s, 3H). MS m/z 179 (M$^+$). Found: C, 62.10; H, 8.19; N, 6.49%. Calcd for $C_{11}H_{17}NO$: C, 62.54; H, 8.11; N, 6.63%. The other isomer was obtained in a small amount.

2c (*cis* and *trans*): Oil; IR (neat) 1620 cm^{-1}; ^{1}H NMR (60 MHz) δ=0.7—1.9 (m, 15H), 3.0—3.7 (m, 5H), 6.1—6.6 (broad, 1H); MS, Found 199.1572, Calcd for $C_{11}H_{21}NO_2$ 199.1571.

2d (*cis* and *trans*): Oil; IR (neat) 1640 cm^{-1}; ^{1}H NMR (60 MHz) δ=0.05 (s, 9H), 0.4—1.8 (m, 11H), 3.20 (dt, 2H, J=6.8, 6.0 Hz), 5.8—6.4 (broad, 1H); MS, Found 213.1547, Calcd for $C_{11}H_{23}NOSi$ 213.1547.

2i (*cis*): Mp 159—160 °C (uncorrected); IR (neat) 1640 cm^{-1}; ^{1}H NMR (90 MHz) δ=1.29 (ddd, 1H, J=8.6, 7.9, 5.0 Hz), 1.75 (ddd, 1H, J=7.1, 5.7, 5.0 Hz), 1.98 (ddd, 1H, J=8.9, 8.6, 7.1 Hz), 2.48 (ddd, 1H, J=8.9, 7.9, 5.7 Hz), 6.8—7.4 (m, 10H), 7.4—7.6 (broad, 1H); MS, Found 237.1154, Calcd for $C_{16}H_{15}NO$ 237.1153. (*trans*): Mp 162—163 °C (uncorrected); IR (neat) 1640 cm^{-1}; ^{1}H NMR (90 MHz) δ=1.1—1.4 (m, 1H), 1.5—1.9 (m, 2H), 1.4—2.7 (m, 1H), 6.8—7.6 (m, 10H), 7.6—8.0 (broad, 1H); MS, Found 237.1155, Calcd for $C_{16}H_{15}NO$ 237.1153.

2j: Oil; IR (neat) 1635 cm^{-1}; ^{1}H NMR (60 MHz) δ=1.0—2.7 (m, 4H), 3.5—3.9 (m, 2H), 4.6—5.1 (m, 2H), 5.3—5.9 (m, 2H), 7.30 (broad s, 5H); MS, Found 201.1153, Calcd for $C_{13}H_{15}NO$ 201.1153. **The Other Isomer**: Oil; IR (neat) 1635 cm^{-1}; ^{1}H NMR (60 MHz) δ=0.9—2.0 (m, 3H), 2.3—2.7 (m, 1H), 3.7—4.1 (m, 2H), 4.9—5.4 (m, 2H), 5.5—6.2 (m, 2H), 6.7—7.5 (m, 5H); MS, Found 201.1155, Calcd for $C_{13}H_{15}NO$ 201.1153.

2k (*cis* and *trans*): Oil; IR ($CHCl_3$) 1620 cm^{-1}; ^{1}H NMR (60 MHz) δ=1.1—3.7 (m, 12H), 7.14 (broad s, 5H); MS, Found 215.1309, Calcd for $C_{14}H_{17}NO$ 215.1309.

4a: IR (neat) 1735 cm^{-1}; ^{1}H NMR (90 MHz) δ=0.75 (t, 3H, J=6.6 Hz), 1.0—2.8 (m, 6H), 3.73 (t, 2H, J=6.6 Hz), 7.0—7.3 (m, 5H); MS, Found 204.1147, Calcd for $C_{13}H_{16}O_2$ 204.1149. **The Other Isomer:** IR (neat) 1735 cm^{-1}; ^{1}H NMR (90 MHz) δ=0.93 (t, 3H, J=6.4 Hz), 1.1—2.1 (m, 5H), 2.3—2.7 (m, 1H), 4.03 (t, 2H, J=6.4 Hz), 6.8—7.4 (m, 5H); MS, Found 204.1150, Calcd for $C_{13}H_{16}O_2$ 204.1149. Bp (mixture, Kugelrohr) 78—80 °C/0.25 mmHg (1 mmHg= 133.322 Pa).

4b: IR (neat) 1720 cm^{-1}; ^{1}H NMR (60 MHz) δ=0.97 (t, 3H, J=6.6 Hz), 1.2—1.9 (m, 7H), 2.40 (dd, 1H, J=6.6, 6.4 Hz), 3.70 (s, 3H), 4.10 (t, 2H, J=6.6 Hz); MS m/z 200 (M$^+$). **The Other Isomer:** IR (neat) 1720 cm^{-1}; ^{1}H NMR (60 MHz) δ=0.97 (t, 3H, J=6.6 Hz), 1.2—2.0 (m, 8H), 3.67 (s, 3H), 4.10 (t, 2H, J=6.6 Hz); MS m/z 200 (M$^+$). Bp (mixture, Kugelrohr) 78 °C/0.2 mmHg. Found (mixture): C, 59.91; H, 8.26%. Calcd for $C_{10}H_{16}O_4$: C, 59.98; H, 8.05%.

4d: IR (neat) 1720 cm^{-1}; ^{1}H NMR (60 MHz) δ=0.05 (s, 9H), 0.6—2.0 (m, 11H), 4.03 (t, 2H, J=6.4 Hz); MS m/z 214 (M$^+$). **The Other Isomer:** IR (neat) 1720 cm^{-1}; ^{1}H NMR (60 MHz) δ=0.10 (s, 9H), 0.5—2.0 (m, 11H), 4.07 (t, 2H, J=6.4 Hz); MS m/z 214 (M$^+$). Bp (mixture, Kugelrohr) 102 °C/0.2 mmHg. Found (mixture). C, 61.59; H, 10.49%. Calcd for $C_{11}H_{22}O_2Si$: C, 61.63; H, 10.34%.

4e (*cis* and *trans*): Bp (Kugelrohr) 85 °C/0.2 mmHg; IR (neat) 2220, 1720 cm^{-1}; ^{1}H NMR (60 MHz) δ=0.8—1.1 (m, 3H), 1.1—2.2 (m, 7H), 2.4—3.0 (m, 1H), 3.9—4.3 (m, 2H); MS m/z 167 (M$^+$). Found: C, 64.84; H, 8.10; N, 8.31%. Calcd for $C_9H_{13}NO_2$: C, 64.65; H, 7.84; N, 8.38%. One Isomer was Separated: IR (neat) 1720 cm^{-1}; ^{1}H NMR (60 MHz) δ=1.00 (t, 3H, J=6.6 Hz), 1.50 (s, 3H), 1.2—2.0 (m, 4H), 2.30 (dd, 1H, J=8.6, 6.8 Hz), 4.10 (t, 2H, J=6.6 Hz).

4f (R^1=Me_3Si, R^2=R^3=H, R^4=Ph, CO_2Pr-*n* *cis* to Ph): IR (neat) 1720 cm^{-1}; ^{1}H NMR (60 MHz) δ=0.07 (s, 9H), 0.70 (t, 3H, J=6.6 Hz), 1.07 (dd, 1H, J=8.8, 7.0 Hz), 1.1—1.5 (m, 2H), 1.90 (dd, 1H, J=8.4, 7.0 Hz), 2.37 (dd, 1H, J=8.8, 8.4 Hz), 3.72 (t, 2H, J=6.6 Hz), 6.9—7.4 (m, 5H); MS m/z 276 (M$^+$). (R^1=Me_3Si, R^2=R^3=H, R^4=Ph, CO_2Pr-*n* *trans* to Ph): IR (neat) 1720 cm^{-1}; ^{1}H NMR (60 MHz) δ=0.17 (s, 9H), 0.50 (dd, 1H, J=10.0, 8.6 Hz), 0.82 (t, 3H, J=6.8 Hz), 1.2—1.8 (m, 2H), 1.95 (dd, 1H, J=10.0, 4.4 Hz) 2.43 (dd, 1H, J=8.6, 4.4 Hz), 3.90 (t, 2H, J=6.8 Hz), 6.8—7.3 (m, 5H); MS m/z 276 (M$^+$). Bp (mixture, Kugelrohr) 117 °C/0.09 mmHg. Found (mixture): C, 69.71; H, 9.02%. Calcd for $C_{16}H_{24}O_2Si$: C, 69.52; H, 8.75%.

4g (*cis* and *trans*): IR (neat) 1720 cm^{-1}; ^{1}H NMR (60 MHz) δ=0.02 (s, 3.5 H), 0.07 (s, 5.5 H), 0.6—2.0 (m, 17H), 3.8—4.1 (m, 2H); MS, Found 256.1856, Calcd for $C_{14}H_{28}O_2Si$ 256.1857.

4m (*cis*): IR (neat) 1650 cm^{-1}; ^{1}H NMR (90 MHz) δ=1.39 (ddd, 1H, J=8.1, 7.8, 5.1 Hz), 1.84 (ddd, 1H, J=7.5, 5.6, 5.1 Hz), 2.24 (ddd, 1H, J=9.0, 7.8, 5.6 Hz), 2.71 (ddd, 1H, J=9.0, 8.1, 7.5 Hz), 6.3—7.4 (m, 9H). (***trans***): IR (neat) 1650 cm^{-1}; ^{1}H NMR (90 MHz) 1.45 (ddd, 1H, J=9.0, 7.0, 4.9 Hz), 1.73 (ddd, 1H, J=9.6, 5.0, 4.9 Hz), 2.08 (ddd, 1H, J=9.0, 5.0, 4.9 Hz), 2.65 (ddd, 1H, J=9.6, 7.0, 4.9 Hz), 6.8—7.4 (m, 9H); MS (mixture), Found 272.0603, Calcd for $C_{16}H_{13}O_2Cl$ 272.0604.

5a: Mp 85—87 °C (uncorrected); IR (neat) 1710 cm^{-1}; ^{1}H NMR (90 MHz) δ=1.59 (ddd, 1H, J=8.7, 8.5, 5.3 Hz), 2.10 (ddd, 1H, J=7.6, 5.6, 5.3 Hz), 2.64 (ddd, 1H, J=8.8, 8.7, 5.6 Hz), 2.91 (ddd, 1H, J=8.8, 8.5, 7.6 Hz), 7.04 (broad s, 1H), 7.20 (broad s, 5H), 7.42 (broad s, 1H), 8.17 (broad s, 1H); MS m/z 212 (M$^+$). Found: C, 73.47; H, 5.81; N, 13.32%. Calcd for $C_{13}H_{12}N_2O$: C, 73.56; H, 5.70; N, 13.20%. The other isomer was obtained in a small amount.

5d: Oil; IR (neat) 1720 cm^{-1}; ^{1}H NMR (90 MHz) δ=0.04 (s, 9H), 0.1—2.0 (m, 6H), 7.12 (broad s, 1H), 7.53 (broad s, 1H), 8.28 (broad s, 1H); MS m/z 222 (M$^+$). **The Other**

Isomer: Oil; IR (neat) 1720 cm^{-1}; ^1H NMR (90 MHz) δ=−0.07 (s, 9H), 0.7—0.8 (m, 2H), 1.2—2.0 (m, 3H), 2.2—2.5 (m, 1H), 7.11 (broad s, 1H), 7.56 (broad s, 1H), 8.23 (broad s, 1H); MS *m/z* 222 (M^+). Found (mixture): C, 59.31; H, 7.99; N, 12.91%. Calcd for $C_{11}H_{18}N_2OSi$: C, 59.42; H, 8.16; N, 12.60%.

5h (*cis* and *trans*): IR (neat) 1720 cm^{-1}; ^1H NMR (60 MHz) δ=0.5—2.4 (m, 17H), 7.12 (broad s, 1H), 7.42 (broad s, 1H), 8.15 (broad s, 1H); MS *m/z* 220 (M^+). Found: C, 71.02; H, 9.17; N, 12.65%. Calcd for $C_{13}H_{20}N_2O$: C, 70.87; H, 9.15; N, 12.72%.

6a: Bp (Kugelrohr) 162—163 °C/0.45 mmHg; IR (neat) 1680 cm^{-1}; ^1H NMR (90 MHz) δ=1.26 (s, 9H), 1.1—1.5 (m, 1H), 1.7—2.0 (m, 1H), 2.2—2.8 (m, 2H), 7.21 (broad s, 5H); MS, Found 234.1075, Calcd for $C_{14}H_{18}OS$ 234.1078. The other isomer was obtained in a small amount.

6n (*cis*): IR (neat) 1680 cm^{-1}; ^1H NMR (90 MHz) δ=0.81 (t, 3H, *J*=7.0 Hz), 1.2—1.6 (m, 4H), 1.90 (ddd, 1H, *J*=7.3, 5.6, 5.1 Hz), 2.3—2.8 (m, 1H), 2.69 (t, 2H, *J*=7.0 Hz), 7.25 (broad s, 5H); MS, Found 220.0921, Calcd for $C_{13}H_{16}OS$ 220.0921. **(*trans*):** IR (neat) 1680 cm^{-1}; ^1H NMR (90 MHz) δ=0.98 (t, 3H, *J*=7.1 Hz); 1.48 (ddd, 1H, *J*=8.2, 6.5, 4.4 Hz), 1.4—1.8 (m, 2H), 1.75 (ddd, 1H, *J*=8.6, 4.7, 4.4 Hz), 2.27 (ddd, 1H, *J*=8.2, 4.7, 3.8 Hz), 2.67 (ddd, 1H, *J*=8.6, 6.5, 3.8 Hz), 2.90 (t, 2H, *J*=7.1 Hz), 7.0—7.4 (m, 5H); MS, Found 220.0920, Calcd for $C_{13}H_{16}OS$ 220.0921. Bp (mixture, Kugelrohr) 114—118 °C/0.2 mmHg.

6o (*cis* and *trans*): White solid; IR (neat) 1680 cm^{-1}; ^1H NMR (60 MHz) δ=1.1—1.6 (m, 1H), 1.7—2.1 (m, 1H), 2.4—3.0 (m, 2H), 7.24 (broad s, 10H); MS, Found 254.0765, Calcd for $C_{16}H_{14}OS$ 254.0765.

Conversion of 5a to 6a. According to the reported method,[3b] treatment of **5a** with 1.2 equiv of 2-methyl-2-propanethiol and a catalytic amount of $Mg(OEt)_2$ at 25 °C for 14 h gave **6a** in 65% yield.

One-Pot Synthesis of 6a. After treatment of **1a** with tetracarbonylnickel and imidazole, excess tetracarbonylnickel was removed under the reduced pressure. Then, 1.2 equiv of 2-methyl-2-propanethiol was added to the resultant mixture, which was stirred at 25 °C for 14 h. Workup was done in the similar manner as mentioned above to give **6a** in 31% yield.

Preparation of 7. The reaction of **1** with disulfides was carried out in the similar manner as mentioned above. The conditions are shown in footnotes of Table 2.

7a: IR (neat) 1660 cm^{-1}; ^1H NMR (90 MHz) δ=1.06 (s, 9H), 1.2—1.6 (m, 1H), 1.40 (s, 9H), 1.68 (dd, 1H, *J*=5.2, 2.7 Hz), 2.71 (dd, 1H, *J*=13.0, 5.2 Hz), 7.18 (broad s, 5H); MS *m/z* 322 (M^+). **The Other Isomer:** IR (neat) 1660 cm^{-1}; ^1H NMR (90 MHz) δ=1.19 (s, 9H), 1.50 (s, 9H), 1.71 (dd, 1H, *J*=9.4, 5.6 Hz), 2.27 (dd, 1H, *J*=8.1, 5.6 Hz), 3.23 (dd, 1H, *J*=9.4, 8.1 Hz), 7.17 (broad s, 5H); MS *m/z* 322 (M^+). Found (mixture): C, 66.98; H, 8.20; S, 20.01%. Calcd for $C_{18}H_{26}OS_2$: C, 67.03; H, 8.13; S, 19.88%.

7e (*cis* and *trans*): Oil; IR (neat) 2250, 1665 cm^{-1}; ^1H NMR (90 MHz) δ=1.00 (broad t, 6H), 1.2—2.6 (m, 9H), 2.6—3.1 (m,4H); MS *m/z* 257 (M^+). Found: C, 56.08; H, 7.69; N, 5.51; S, 24.60%. Calcd for $C_{12}H_{19}NOS_2$: C, 55.99; H, 7.44; N, 5.44; S, 24.91%.

7n (*cis* and *trans*): Oil; IR (neat) 1680 cm^{-1}; ^1H NMR (90 MHz) δ=0.7—1.1 (m, 6H), 1.2—1.8 (m, 6H), 2.1—2.8 (m, 5H), 7.1—7.5 (m, 5H); MS *m/z* 294 (M^+). Found: C, 65.41; H, 7.47; S, 21.65%. Calcd for $C_{16}H_{22}NOS_2$: C, 65.26; H, 7.53; S, 21.78%.

7o: Oil; IR (neat) 1690 cm^{-1}; ^1H NMR (90 MHz) δ=1.71 (dd, 1H, *J*=9.1, 8.0 Hz), 2.71 (dd, 1H, *J*=8.0, 5.1 Hz), 3.21 (dd, 1H, *J*=9.1, 5.1 Hz), 7.1—7.6 (m, 15H); MS *m/z* 362 (M^+). Found: C, 72.76; H, 5.05; S, 17.80%. Calcd for $C_{22}H_{18}OS_2$: C, 72.89; H, 5.01; S, 17.69%. The other isomer was not isolated.

6e (*cis* and *trans*): Oil; IR (neat) 2250, 1670 cm^{-1}; ^1H NMR (90 MHz) δ=1.00 (broad t, 3H), 1.2—2.7 (m, 8H), 2.7—3.1 (m, 2H); MS, Found 183.0717, Calcd for $C_9H_{13}NOS$ 183.0717.

Preparation of 10. The reaction was carried out in the similar manner as mentioned above by mixing **9** and tetracarbonylnickel in DMF. The conditions are shown in Table 3.

10a: Bp (Kugelrohr) 90—94 °C/2.8 mmHg; IR (neat) 1760 cm^{-1}; ^1H NMR (60 MHz) δ=1.16 (s, 6H), 1.8—2.3 (m, 2H), 4.0—4.6 (m, 2H); ^{13}C NMR δ=14.4 (q), 23.0 (s), 25.2 (q), 30.1 (d), 30.6 (d), 66.5 (t), 174.8 (s); MS *m/z* 126 (M^+). Found: C, 66.68; H, 8.21%. Calcd for $C_7H_{10}O_2$: C, 66.65; H, 7.99%.

10b: Bp (Kugelrohr) 107—110 °C/4.0 mmHg; IR (neat) 1765 cm^{-1}; ^1H NMR (90 MHz) δ=1.01 (dd, 1H, *J*=4.6, 3.2 Hz), 1.20 (dd, 1H, *J*=8.8, 4.6 Hz), 1.40 (s, 3H), 1.84 (dd, 1H, *J*=8.8, 3.2 Hz), 4.06 (d, 1H, *J*=9.0 Hz), 4.14 (d, 1H, *J*=9.0 Hz); ^{13}C NMR δ=16.9 (q), 19.0 (t), 23.7 (d), 25.4 (s), 73.5 (t), 176.7 (s); MS *m/z* 112 (M^+). Found: C, 64.04; H, 7.32%. Calcd for $C_6H_8O_2$: C, 64.27; H, 7.19%.

10c: Bp (Kugelrohr) 80—82 °C/0.9 mmHg; IR (neat) 1765 cm^{-1}; ^1H NMR (90 MHz) δ=1.19 (s, 3H), 1.0—1.4 (m, 1H), 1.79 (dd, 1H, *J*=5.9, 2.8 Hz), 1.9—2.1 (m, 1H), 4.1—4.4 (m, 2H); ^{13}C NMR δ=16.0 (q), 21.0 (d), 25.1 (d), 25.2 (d), 69.5 (t), 175.9 (s); MS *m/z* 112 (M^+). Found: C, 64.33; H, 7.08%. Calcd for $C_6H_8O_2$: C, 64.27; H, 7.19%.

10d: Bp (Kugelrohr) 69—70 °C/0.4 mmHg; IR (neat) 1765 cm^{-1}; ^1H NMR (90 MHz) δ=0.8—1.4 (m, 3H), 1.36 (s, 3H), 1.48 (s, 3H), 2.0—2.2 (m, 1H); ^{13}C NMR δ=11.1 (t), 19.2 (d), 24.1 (q), 27.6 (d), 29.1 (q), 82.7 (s), 175.7 (s); MS *m/z* 126 (M^+). Found: 66.55; H, 7.63%. Calcd for $C_7H_{10}O_2$: C, 66.64; H, 7.99%.

10e: Bp (Kugelrohr) 85—87 °C/0.5 mmHg; IR (neat) 1725 cm^{-1}; ^1H NMR (90 MHz) δ=0.7—0.9 (m, 1H), 1.1—2.3 (m, 5H), 1.34 (s, 3H), 1.47 (s, 3H); ^{13}C NMR δ=11.9 (d), 12.5 (d), 18.8 (t), 27.5 (q), 29.1 (q), 35.8 (t), 83.1 (s), 172.4 (s); MS *m/z* 140 (M^+). Found: C, 68.32; H, 8.51%. Calcd for $C_8H_{12}O_2$: C, 68.54; H, 8.63%.

11a: Oil; IR (neat) 3300, 1250 cm^{-1}; ^1H NMR (60 MHz) δ=1.08 (dt, 1H, *J*=7.5, 7.4 Hz), 1.17 (s, 6H), 1.56 (broad s, 1H), 3.00 (d, 1H, *J*=7.4 Hz), 3.75 (d, 2H, *J*=7.5 Hz); MS, Found 160.9966, Calcd for $C_6H_{11}OBr$–OH 160.9965.

11c: Oil; IR (neat) 3480, 1250 cm^{-1}; ^1H NMR (90 MHz) δ=0.92 (ddt, 1H, *J*=7.7, 6.1, 4.0 Hz), 1.17 (ddq, 1H, *J*=5.7, 4.0, 3.6 Hz), 1.27 (d, 3H, *J*=5.7 Hz), 1.62 (broad s, 1H), 2.97 (dd, 1H, *J*=7.7, 3.6 Hz), 3.59 (d, 2H, *J*=6.1 Hz); MS, Found 163.9835, Calcd for C_5H_9OBr 163.9837.

This work was partially supported by a Grant-in-Aid for Scientific Research from the Ministry of Education, Science, and Culture.

References

1) D. Tunemoto and K. Kondo, *Yuki Gosei Kagaku Kyokai Shi*, **35** 1070 (1977); M. P. Doyle and D. V. Leusen, *J. Am. Chem. Soc.*, **103**, 5917 (1981); A. Tomazic and E. Ghera, *Tetrahedron Lett.*, **22**, 4349 (1981); S. P. Brown, B. S. Bal, and H. W. Dinnick, *ibid.*, **22**, 4891 (1981).

2) T. Hirao, Y. Harano, Y. Yamana, Y. Ohshiro, and T. Agawa, *Tetrahedron Lett.*, **24**, 1255 (1983).

3) a) H. A. Stabb, *Angew. Chem.*, **74**, 407 (1962). b) S. Ohta and M. Okamoto, *Tetrahedron Lett.*, **22**, 3245 (1981).

4) For example, S. Antebi and H. Alper, *Tetrahedron Lett.*, **26**, 2609 (1985).

5) K. Kleveland, L. Skattebøl, and L. K. Sydnes, *Acta Chem. Scad., Ser B*, **31**, 463 (1977).

6) M. Servin, L. Hevesi, and A. Krief, *Tetrahedron Lett.*, **1976**, 3915.

7) The related reduction reactions were reported: T. Kunieda, T. Tamura, and T. Takizawa, *Chem. Pharm. Bull.*, **25**, 1749 (1977); E. C. Chukovskaya, R. Kh. Freidlina, and N. A. Kuz'mina, *Synthesis*, **1983**, 773.

8) M. F. Semmelhack and S. J. Brickner, *J. Org. Chem.*, **46**, 1723 (1981), and references cited therein.

9) The corresponding lithium carbenoid complexes were reported: E. J. Corey and G. H. Posner, *J. Am. Chem. Soc.*, **90**, 5615 (1968); G. H. Posner, G. L. Loomis, and H. S. Sawaya, *Tetrahedron Lett.*, **1975**, 1373; T. Hiyama, S. Takehara, K. Kitatani, and H. Nozaki, *ibid.*, **1974**, 3295.

10) W. E. Keller, "Compendium of Phase-Transfer Reactions and Related Synthetic Methods," Fluka AG (1979).

11) U. Schöllkopf and M. Roetz, *Tetrahedron Lett.*, **1969**, 1541.

 © 1986 The Chemical Society of Japan Bull. Chem. Soc. Jpn., 59, 1349—1353 (1986)

Regioselectivity in the Catalytic Hydrogenolysis of 7-Fluoro-1-phenylbicyclo[4.1.0]heptanes

Koji Isogai,* Jun-ichi Sakai, and Katsuhiko Kosugi
Department of Applied Chemistry, Faculty of Engineering, Niigata University, Ikarashi, Niigata 950-21
(Received November 15, 1985)

The palladium-catalyzed hydrogenolysis of 7-chloro-7-fluoro-1-phenyl-, 7-fluoro-1-phenyl-, and 7,7-difluoro-1-phenylbicyclo[4.1.0]heptane was investigated. The hydrogenolysis of the cyclopropane ring occurs at the C_1–C_6 bond selectively, accompanied by the elimination of the *endo*-halogen. The hydrogenolysis of *endo*-7-fluoro-1-phenylbicyclo[4.1.0]heptane proceeded rapidly to give phenylcycloheptane as a sole product, whereas *exo*-7-fluoro-1-phenylbicyclo[4.1.0]heptane reacted slowly to give *trans*-1-fluoro-2-phenylcycloheptane, accompanied by a small amount of the C_1–C_7 bond-cleaved product. The different reactivity between the endo and exo derivatives became more considerably by the introduction of a methyl group at the 2-position. Thus, with the compounds having 2-methyl group the *endo*-fluoro derivative was cleaved at the C_1–C_6 bond accompanied by the C_1–C_7 bond cleavage, whereas the *exo*-fluoro derivative was cleaved at the C_1–C_7 bond exclusively.

Although many studies on the catalytic hydrogenolysis of vinyl, aryl, allyl, and benzyl fluorides have been reported,[1] little attention has been given to the catalytic hydrogenolysis of cyclopropyl fluorides. In the previous paper,[2] we reported the regioselective hydrogenolysis of 1,1-difluoro-3-methyl-2-phenylcyclopropane. The cyclopropane ring was cleaved at the C_2–C_3 bond exclusively using both palladium oxide (PdO) and Raney nickel (R-Ni), accompanied by a considerable extent of the carbon-fluorine bond hydrogenolysis. Mitsui et al.[3] reported that 1-phenylbicyclo[4.1.0]heptane and its 2-methyl derivative were hydrogenolyzed at the C_1–C_7 bond preferentially because of the difference of the catalyst hindrance between the C_1–C_6 bond and the C_1–C_7 bond on the catalyst surface. It seems to be interesting to investigate the behavior of the fluorine for the regioselectivity in the catalytic hydrogenolysis of the cyclopropane ring contained in such condensed ring systems. Here, we wish to report the palladium-catalzed hydrogenolysis of several 7-fluoro-substituted -phenylbicyclo[4.1.0]heptanes.

Results and Discussion

exo-7-Chloro-*endo*-7-fluoro-1-phenyl- (1-endo-F), *endo*-7-chloro-*exo*-7-fluoro-1-phenyl- (1-exo-F), *endo*-7-fluoro-1-phenyl- (2-endo-F), *exo*-7-fluoro-1-phenyl- (2-exo-F) and 7,7-difluoro-1-phenylbicyclo[4.1.0]heptane (**3**) were hydrogenated over PdO in ethanol solution at room temperature under atmospheric pressure. The results are shown in Table 1. The hydrogenolysis of the cyclopropane ring of these fluorocyclopropanes occurred at the C_1–C_6 bond selectively although only 2-exo-F was accompanied by a small amount of the C_1–C_7 bond cleaved product. Characteristic differences between the endo isomer and the exo isomer were observed in the reactivity and in the ratio of the products. The reaction of 1-endo-F proceeded very slowly and gave phenylcycloheptane (**5**) as a sole product, whereas the reaction of 1-exo-F proceeded rapidly than that of 1-endo-F to give **5** (37%) and *cis*-1-fluoro-2-phenylcycloheptane (**6**) (63%). On the other hand, 2-endo-F reacted very rapidly to give **5** as a sole product, whereas 2-exo-F reacted slowly to give mainly *trans*-1-

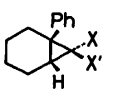

1-endo-F: X=F, X'=Cl
1-exo-F : X=Cl, X'=F
2-endo-F: X=F, X'=H
2-exo-F : X=H, X'=F
3 : X=F, X'=F

Fig. 1.

Table 1. Hydrogenolysis of 7-Fluoro-1-phenylbicyclo[4.1.0]heptanes

Substrate	Reaction time/h	Conversion %	Composition of products (%)				
			C_1–C_6 Fission				C_1–C_7 Fission
			5	**6**	**7**	**8**	**9**
1-endo-F	24	47	100	—	—	—	—
1-exo-F	4	95	37	63	—	—	—
2-endo-F	1	97	100	—	—	—	—
2-exo-F	24	96	10	—	78	—	12
3	0.5	100	20	27	—	53	—

Substrate: 20 mg, PdO: 20 mg.

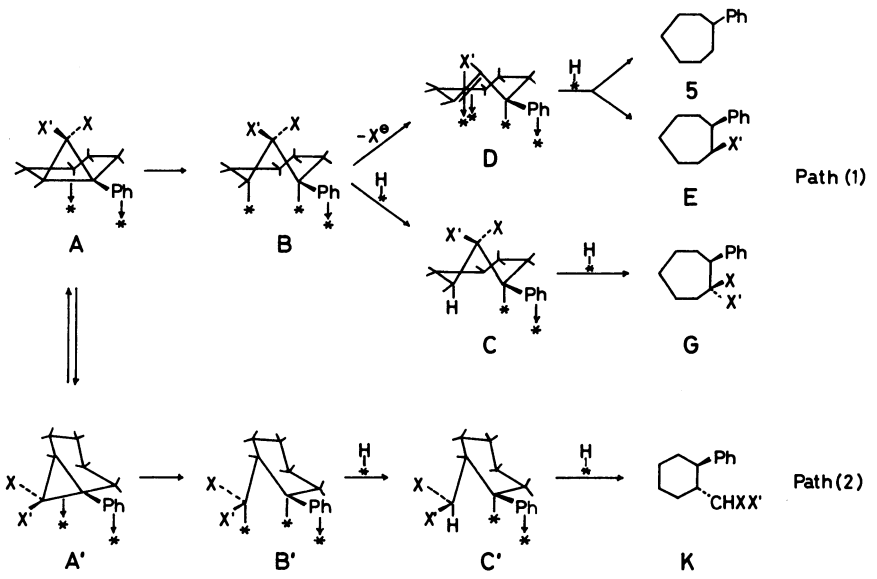

Scheme 1.

fluoro-2-phenylcycloheptane (**7**) (78%) with **5** (10%), accompanying a small amount of *trans*-1-fluoromethyl-2-phenylcyclohexane (**9**) formed by the C_1–C_7 bond cleavage. The hydrogenolysis of **3** proceeded more easily and gave **5**, **6**, and 1,1-difluoro-2-phenylcycloheptane (**8**) of the C_1–C_6 bond cleaved products.

It has been known that the bond lengths of cyclopropane are changed markedly by the fluorine substitution. The available data of ring bond length (Å) for C_1–C_2 and C_2–C_3 bonds in cyclopropane,[4] 1,1-dichloro-,[5] chloro,[6] fluoro,[7] and 1,1-difluorocyclopropane[8] are reported, respectively, as follows; 1.514, 1.514; 1.532, 1.534; 1.513, 1.515; 1.494, 1.527; 1.464, 1.552. In the case of 7-fluoro derivatives of 1-phenylbicyclo[4.1.0]heptane, analogous lengthening of the C_1–C_6 bond and shortening of the C_1–C_7 and C_6–C_7 bonds are expected which may cause an additional strain in the condensed ring system. In this hydrogenation, these effects may overcome the steric effect which is a dominant factor in the case of the parent compound and the C_1–C_6 bond hydrogenolysis occurs preferentially.

Additionally, the ease of hydrogenolysis of the cyclopropane ring and the carbon–fluorine bond seems to depend markedly upon whether the fluorine binds to endo- or exo-side. A similar stereochemical behavior was reported in the case of the ring-enlargement of 7-chlorobicyclo[4.1.0]heptanes by means of a thermal[9] and a solvolysis[10] reaction. The *endo*-chloro isomer reacts more easily than the *exo*-chloro isomer with the elimination of the chlorine as chloride ion. This stereospecific reaction is explained by a "concerted disrotatory process."[11] Similar fast progress of the ring-enlargement was observed in the hydrogenolysis of 1-exo-F, 2-endo-F, and **3**. Therefore, the elimination of the *endo*-halogen seems to contribute as one of fators to make easy the C_1–C_6 bond hydrogenolysis.

A probable pathway is shown in Scheme 1. The substrate adsorbs on the catalyst by the C_1–C_6 bond (adsorbed species A) or the C_1–C_7 bond (adsorbed species A′). In the case of the parent compound 1-phenylbicyclo[4.1.0]heptane (X=H, X′=H in A and A′), A has a larger catalyst hindrance than A′. Therefore, the C_1–C_7 bond cleaves preferentially.[3] In the hydrogenolysis of the fluorocyclopropanes, however, the weakening effect of the C_1–C_6 bond seems to overcome the catalyst hindrance and the hydrogenolysis proceeds easily through Path (1). Releasing the strain of the condensed ring by the ring-enlargement makes easy the formation of the C_1,C_6-diadsorbed species B from A. Additionally, in the case of 1-exo-F (X=Cl, X′=F) and 2-endo-F (X=F, X′=H), the elimination of the *endo*-halogen accelerates the C_1–C_6 bond cleavage to give cycloolefin intermediate D. Subsequent cis addition of hydrogen forms **5** and **6** (X′=F in E) competitively.

In this hydrogenation, 1-endo-F was ring-enlarged and gave **5**. The hydrogenolysis of 1-endo-F, therefore, seems to proceed via A, B, and D similarly to that of 1-exo-F and 2-endo-F. However, the reaction of 1-endo-F proceeded more slowly than that of 2-endo-F. Although the cause of the difference in the reactivity between 1-endo-F and 2-endo-F is not clear, it appears that the chlorine probably plays a role in the adsorption step. The role may be explained as one of examples of self-poisoning effects.[12] Because of the affinity of the chlorine to the catalyst is relatively stronger than that of the fluorine, the contribution of A′ in the adsorption state of 1-endo-F seems to be expected to some extent.

Table 2. Hydrogenolysis of 7-Fluoro-2-methyl-1-phenylbicyclo[4.1.0]heptanes

Substrate	Reaction time/h	Conversion %	Composition of products/%	
			C_1–C_6 Fission **10**	C_1–C_7 Fission **11**
4-endo-F	2	100	83	17
4-exo-F	8	86	—	100

Substrate: 20 mg, PdO: 100 mg.

The adsorption of the chlorine in A′ causes the lowering of the activity of catalyst. This effect makes difficult the hydrogenolysis of 1-endo-F from A′ which hinders the adsorption of 1-endo-F by the C_1–C_6 bond. By these factors, the lowering the activity of catalyst and the hindrance of adsorption by the C_1–C_6 bond, the hydrogenolysis of 1-endo-F seems to be retarded considerably. Although this self-poisoning effect affects in the case of 1-exo-F, the reaction seems to proceed smoothly by the assistance of the ready elimination of the *endo*-chlorine.

On the other hand, 2-exo-F reacted slowly than 2-endo-F and gave **7** (X=H, X′=F in G). The formation of **7** is explained by an alternative pathway in Path (1). Because the elimination of the *exo*-fluorine from B is disadvantageous stereoelectronically,[11] the cleavage of the C_1–C_6 bond of 2-exo-F proceeds more slowly than that of 2-endo-F and forms the half-hydrogenated state C (X=H, X′=F) without the elimination of the *exo*-fluorine. The half-hydrogenated state C receives hydrogen from the catalyst to give **7**. Furthermore, 2-exo-F gave a small amount of the C_1–C_7 bond cleaved product 9 (X=H, X′=F in K). The pathway of the C_1–C_7 bond cleavage may be explained by Path (2). Because the cleavage of the C_1–C_6 bond from A is relatively slow, the sterically less-hindered adsorption species A′ participated to some extent in this hydrogenation and causes the contamination of the C_1–C_7 bond cleaved product formed via B′ and C′.

In the case of the hydrogenolysis of **3** (X=F, X′=F), it was expected that **3** reacted in analogy with 1-exo-F to give **5** and **6**. However, **8** (X=F, X′=F in G) was obtained in an about 50% yield with **5** and **6**. It seems to be that the 7,7-difluoro-substitution weakens the C_1–C_6 bond more strongly and the C_1–C_6 bond cleaves easily without the assistance of the elimination of the *endo*-fluoine followed by the competitive formation of D (X′=F) and C (X=F, X′=F).

The difference observed in the hydrogenolysis of 2-endo-F and 2-exo-F appeared more strongly in the case of 2-methyl derivatives of 2-endo-F and 2-exo-F. The results of the hydrogenolysis of *t*-7-fluoro-*c*-2-methyl-*r*-1-phenylbicyclo[4.1.0]heptane (4-endo-F) and *c*-7-fluoro-c-2-methyl-*r*-1-phenylbicyclo[4.1.0]heptane (4-exo-F) are shown in Table 2. Since the rate of

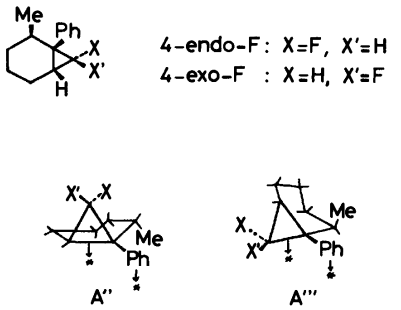

Fig. 2.

hydrogenolysis of 4-endo-F and 4-exo-F was considerably slower than that of 2-endo-F and 2-exo-F, PdO was used in the amount five times that for the other compounds. Although the hydrogenolysis of 4-endo-F proceeded more easily than 4-exo-F to give mainly *cis*-1-methyl-2-phenylcycloheptane (**10**), it was accompanied by *r*-1-fluoromethyl-*t*-3-methyl-*t*-2-phenylcyclohexane (**11**) which was arose by the C_1–C_7 bond cleavage. On the other hand, 4-exo-F was cleaved at the C_1–C_7 bond exclusively to give **11** as a sole product.

As can be seen from Fig. 2, the 2-methyl group increases the catalyst hindrance against the adsorption of the C_1–C_6 bond in the adsorbed species A.″ This steric effect seems to be large enough to retard the C_1–C_6 bond cleavage and 4-exo-F prefers the adsorbed species A‴ to give the C_1–C_7 bond cleaved product exclusively. This steric effect seems to affect even in the hydrogenolysis of 4-endo-F and causes the contamination of the C_1–C_7 bond cleaved product.

Experimental

^{1}H NMR spectra were recorded on a JNM-PMX 60 spectrometer with $Si(CH_3)_4$ as the internal standard. ^{19}F NMR spectra were recorded on a JNM-FX 90Q spectrometer with CF_3COOH as the external standard. Mass spectra were obtained with a HITACHI M-60 GC-MS spectrometer.

***exo*-7-Chloro-*endo*-7-fluoro-1-phenylbicyclo[4.1.0]heptane (1-endo-F) and *endo*-7-Chloro-*exo*-7-fluoro-1-phenylbicyclo-[4.1.0]heptane (1-exo-F).** According to the procedure of Ando et al.,[13] to a mixture of 1-phenylcyclohexene (20.5 g, 0.13 mol) and sodium hydride (3.1 g, 0.13 mol) was added

methyl dichlorofluoroacetate (30 g 0.13 mol) at 0—5 °C. After 2 h, methanol (4.2 ml) was added to the reaction mixture. A mixture of 1-endo-F and 1-exo-F (1:2) was obtained in a 24% yield; bp 110—113 °C/6 mmHg (1 mmHg=133.322 Pa). ^{19}F NMR ($CDCl_3$) δ=45.8 (d, J_{HFvic}= 19.5 Hz, cis), 68.8 (d, J_{HFvic}=3.0 Hz, trans). Found: C, 69.64; H, 6.33%. Calcd for $C_{13}H_{14}FCl$: C, 69.49; H,6.28%.

Isomers 1-endo-F and 1-exo-F were separated by preparative VPC. **1-endo-F:** MS *m/z* 224(M^+). ^{19}F NMR ($CDCl_3$): δ=68.8 (d, J_{HFvic}=3.0 Hz). **1-exo-F:** MS *m/z*: 224 (M^+). ^{19}F NMR ($CDCl_3$): δ=45.8 (d, J_{HFvic}=19.5 Hz). The value of ^{19}F NMR is comparable to that of each isomer of 7-chloro-7-fluorobicyclo[4.1.0]heptane.[9]

***endo*-7-Fluoro-1-phenylbicyclo[4.1.0]heptane (2-endo-F) and *exo*-7-Fluoro-1-phenylbicyclo[4.1.0]heptane (2-exo-F).** A mixture of 1-endo-F and 1-exo-F (0.5 g) was hydrogenated by use of Raney nickel (2 g) in ethanol in the presence of ethylenediamine (0.8 g) at room temperature under atmospheric pressure. The carbon-chlorine bond was hydrogenolyzed selectively with retention of configuration to give 2-endo-F and 2-exo-F, respectively, with a small amount of cyclopropane ring cleaved products. From the reaction mixture, the two isomers were separated by preparative VPC.

2-endo-F: MS *m/z* 190(M^+). ^{1}H NMR (CCl_4) δ=7.13 (5H, s, C_6H_5), 4.47 (1H, dd, J_{HFgem}=66.6 Hz, J_{HHvic}=7.0 Hz), 2.5—1.0 (9H, broad, ring). Found: C, 82.14; H, 8.09%. Calcd for $C_{13}H_{15}F$: C, 82.07; H, 7.95%.

2-exo-F: MS *m/z*: 190(M^+). ^{1}H NMR (CCl_4) δ=7.16 (5H, s, C_6H_5), 4.30 (1H, dd, J_{HFgem}=66.6 Hz, J_{HHvic}=2.5 Hz), 2.5—1.0 (9H, broad, ring). Found: C, 82.06; H, 8.16%. Calcd for $C_{13}H_{15}F$: C, 82.07; H, 7.95%. The values of ^{1}H NMR are comparable to those of each isomer of 7-fluoro-bicyclo[4.1.0]heptane.[9]

7,7-Difluoro-1-phenylbicyclo[4.1.0]heptane (3). A mixture of 1-phenylcyclohexene (9.0 g, 0.057 mol), chlorodifluoromethane (12 g, 0.4 mol), epichlorohydrin (28.3 g, 0.31 mol) and tetrabutylammonium chloride (1.1 g) was heated at 130 °C, 19 h, in an autoclave according to the procedure of Kamel.[14] The fraction, bp 93—96 °C/7 mmHg, 4.0 g, was purified by preparative VPC to give **3**. MS *m/z*: 208(M^+). ^{1}H NMR (CCl_4) δ=7.19 (5H, s, C_6H_5), 2.66—0.85 (9H, broad, ring). ^{19}F NMR ($CDCl_3$) δ=49.2 (dd, J_{FF}=148.4 Hz, J_{HFvic}=15.6 Hz), 64.6 (dd, J_{FF}=148.4 Hz, J_{HFvic}=3.0 Hz). Found: C, 74.78; H, 6.83%. Calcd for $C_{13}H_{14}F_2$: C, 74.97; H, 6.78%.

***t*-7-Fluoro-*c*-2-methyl-*r*-1-phenylbicyclo[4.1.0]heptane (4-endo-F) and *c*-7-Fluoro-*c*-2-methyl-*r*-1-phenylbicyclo[4.1.0]-heptane (4-exo-F).** To a mixture of 3-methyl-2-phenylcyclohexene (22.5 g, 0.13 mol) and sodium hydride (3.1 g, 0.13 mol) was added methyl dichlorofluoroacetate (30 g, 0.13 mol) at 0—5 °C followed by addition of methanol (4 ml) as described above. A mixture of endo and exo isomers of 7-chloro-7-fluoro-*c*-2-methyl-*r*-1-phenylbicyclo-[4.1.0]heptane (endo-F/exo-F=3/7) was obtained in a 20% yield, bp 115—120 °C/4 mmHg. MS *m/z*: 238(M^+). ^{19}F NMR ($CDCl_3$) δ=71.7 (d, J_{HFvic}=3.0 Hz) 48.0 (d, J_{HFvic}=22.4 Hz). Found: C, 70.24; H, 6.99%. Calcd for $C_{14}H_{16}FCl$: C, 70.43; H, 6.76%.

The chlorofluorocyclopropane was hydrogenated over Raney nickel according to the preceding procedure to give a mixture of 4-endo-F and 4-exo-F and the isomers were separated by preparative VPC, respectively.

4-endo-F: MS *m/z*: 204(M^+). ^{1}H NMR (CCl_4) δ=7.13 (5H, s, C_6H_5), 4.50 (1H, dd, J_{HFgem}=66.6 Hz, J_{HHvic}=6.6 Hz) 2.4—0.9 (8H, broad, ring), 0.67 (3H, d, J=7.0 Hz, CH_3). Found: C, 82.55; H, 8.55%. Calcd for $C_{14}H_{17}F$: C, 82.31; H, 8.39%.

4-exo-F: MS *m/z*: 204(M^+). ^{1}H NMR (CCl_4) δ=7.16 (5H, s, C_6H_5), 4.35 (1H, dd, J_{HFgem}=66.6 Hz, J_{HHvic}=2.4 Hz), 2.2—0.8 (8H, broad, ring), 0.67 (3H, d, J=6.4 Hz, CH_3). Found: C, 82.47; H, 8.43%. Calcd for $C_{14}H_{17}F$: C, 82.31; H, 8.39%.

General Procedure of Hydrogenation. Substrates (20 mg) were hydrogenated over PdO (20 mg, Kawaken Fine Chemical Co.) in ethanol (2 ml) at room temperature under atmospheric pressure. The composition of the products was determined by VPC at appropriate time intervals.

Identification of Products. After the hydrogenolysis proceeded appropriately, the reaction mixture was subjected to measurement of GC-MS. For measurement of NMR and elementary analysis, each component of products was separated by preparative VPC.

Phenylcycloheptane (5): Ms *m/z*: 174(M^+), which was identical with that of an authentic sample, bp 113—114 °C/10 mmHg, lit,[15] bp 114.5 °C/10 mmHg, prepared by the hydrogenation of 1-phenylcycloheptene over Pd-C.

***cis*-1-Fluoro-2-phenylcycloheptane (6):** MS *m/z*: 192(M^+). ^{1}H NMR (CCl_4) δ=7.14 (5H, s, C_6H_5), 4.88 (1H, mm, J_{HFgem}=48.0 Hz), 2.6—1.0 (12H, broad, ring). ^{19}F NMR ($CDCl_3$) δ=112.13 (m). Found: C, 81.37; H, 8.89%. Calcd for $C_{13}H_{17}F$: C, 81.21; H, 8.91%.

Compound **6** was identical with an authentic sample which was prepared as follows; hydrogenation of 1-phenyl-8-oxabicylo[5.1.0]octane (3.9 g) over Raney nickel (2 g) in hexane at room temperature under atmospheric pressure gave phenylcycloheptane (41%) and a mixture of *cis*- and *trans*-2-phenylcycloheptanol (51%, trans/cis=9/1). The fractional distillation of the reaction mixture gave *trans*-2-phenylcycloheptanol, 1.7 g, bp 130—137 °C/4 mmHg, lit,[16] bp 113—114 °C/0.5 mmHg, *p*-nitrobenzoate, mp 83—84 °C, lit,[16] mp 84—85 °C. To a methylene dichloride soluion (5 ml) of *trans*-2-phenylcycloheptanol (0.95 g, 5 mmol) was added a methylene chloride solution (5 ml) of hexafluoropropene-diethylamine (1.35 g, 6 mmol) at 0—5 °C and allowed to stand overnight. After removal of low boiling products, the residue was purified by a column chromatography to obtain **6** (70 mg). The values of NMR and elementary analysis were in agreement with those of **6** obtained by the hydrogenolysis of 1-exo-F and **3**. ^{1}H NMR (CCl_4) δ=7.14 (5H, s, C_6H_5), 4.85 (1H, mm, J_{HFgem}=48.0 Hz), 2.6—1.0 (12H, broad, ring). ^{19}F NMR ($CDCl_3$) δ=112.13 (m). Found: C, 80.86; H, 8.87%. Calcd for $C_{13}H_{17}F$: C, 81.21; H, 8.91%.

***trans*-1-Fluoro-2-phenylcycloheptane (7):** MS *m/z*: 192(M^+). ^{1}H NMR (CCl_4) δ=7.15 (5H, s, C_6H_5), 4.54 (1H, mm, J_{HFgem}=46.0 Hz), 2.4—1.2 (12H, broad, ring). ^{19}F NMR ($CDCl_3$) δ=86.38 (m). Found: C, 81.40; H, 9.05%. Calcd for $C_{13}H_{17}F$: C, 81.21; H, 8.91%.

Compound **7** was identical with an authentic sample which was prepared as follows; hydrogenation of 1-phenyl-8-oxabicyclo[5.1.0]octane (3.2 g) over Pd-C (0.36 g) in hexane solution in the presence of diethylamine (0.67 g) gave phenylcycloheptane (3%) and 2-phenylcycloheptanol (96%, cis/trans=95/5). The fractional distillation gave *cis*-2-phenylcycloheptanol, 2.5 g, bp 124—132 °C/3.5 mmHg,

lit,[16] bp 98.5—102.5 °C/0.25 mmHg, *p*-nitrobenzoate, mp 90—92 °C, lit,[16] mp 92—93 °C. Fluorination of the *cis*-alcohol (0.95 g) was carried out in a similar manner as described above to obtain **7** (0.45 g). The values of NMR and elementary analysis were in agreement with those of **7** obtained by the hydrogenolysis of 2-exo-F. ^{1}H NMR (CCl_4) δ=7.16 (5H, s, C_6H_5), 4.56 (1H, mm, J_{HFgem}=46.0 Hz), 2.4—1.2 (12H, broad, ring). ^{19}F NMR ($CDCl_3$) δ=86.38 (m). Found: C, 80.89; H, 8.91%. Calcd for $C_{13}H_{17}F$: C, 81.21; H, 8.91%.

1,1-Difluoro-2-phenylcycloheptane (8): MS *m/z*: 210(M^+). ^{1}H NMR (CCl_4) δ=7.17 (5H, s, C_6H_5), 2.7—0.8 (11H, broad, ring). ^{19}F NMR ($CDCl_3$) δ=4.80 (mm, J_{FFgem}=243.2 Hz), 23.27 (mm, J_{FFgem}=243.2 Hz). Found: C, 74.09; H, 7.80%. Calcd for $C_{13}H_{16}F_2$: C, 74.26; H, 7.67%.

***trans*-1-Fluoromethyl-2-phenylcyclohexane (9):** MS *m/z*: 192(M^+). ^{1}H NMR (CCl_4) δ=7.17 (5H, s, C_6H_5), 4.00 (2H, dd, J_{HFgem}=48.0 Hz, J_{HHvic}=3.0 Hz, CH_2F), 2.6—1.2 (10H, broad, ring). ^{19}F NMR ($CDCl_3$) δ=153.68 (m). Found: C, 80.92; H, 8.77%. Calcd for $C_{13}H_{17}F$: C, 81.21; H, 8.77%.

Compound **9** was identical with an authentic sample which was prepared as follows; to a methylene dichloride solution (5 ml) of *trans*-2-phenylhexahydrobenzyl alcohol (0.95g, 5 mmol), mp 46—48 °C, lit,[17] mp 46—48 °C, was added a methylene chloride solution (5 ml) of hexafluoropropene-diethylamine (1.35 g, 6 mmol) at 0—5 °C and the reaction mixture was allowed to stand overnight. The fraction, bp 107—110 °C/5 mmHg, 0.55 g, was purified by TLC and 0.17 g of **9** was obtained. The values of NMR and elementary analysis were in agreement with those of **9** obtained by the hydrogenolysis of 2-exo-F. ^{1}H NMR (CCl_4) δ=7.15 (5H, s, C_6H_5), 3.96 (2H, dd, J_{HFgem}=48.0 Hz, J_{HHvic}=2.8 Hz, CH_2F). ^{19}F NMR ($CDCl_3$) δ=153.68 (m). Found: C, 81.17; H, 8.97%. Calcd for $C_{13}H_{17}F$: C, 81.21; H, 8.91%.

***cis*-1-Methyl-2-phenylcycloheptane (10):** MS *m/z*: 188(M^+). ^{1}H NMR (CCl_4) δ=7.11 (5H, s, C_6H_5), 2.6—1.2 (12H, broad, ring), 0.73 (3H, d, *J*=6.0 Hz, CH_3). Found: C, 89.16; H, 10.73%. Calcd for $C_{14}H_{20}$: C, 89.29; H, 10.71%.

***r*-1-Fluoromethyl-*t*-3-methyl-*t*-2-phenylcyclohexane (11):** MS *m/z*: 206(M^+). ^{1}H NMR (CCl_4) δ=7.17 (5H, s, C_6H_5), 4.13 (2H, dd, J_{HFgem}=48.0 Hz, J_{HHvic}=3.0 Hz, CH_2F), 2.6—1.2 (9H, broad, ring), 0.78 (3H, d, *J*=7.0 Hz, CH_3). ^{19}F NMR ($CDCl_3$) δ=153.08 (m). Found: C, 81.74; H, 9.16%. Calcd for $C_{14}H_{19}F$: C, 81.51; H, 9.28%.

The authors are grateful to the Japan Association of Chemistry for financial support. We also thank Mr. Masakazu Okumiya, Osaka University, for elementary analysis and Mr. Takao Ohno, Analytical Instrument Laboratory of Niigata University, for ^{19}F NMR measurement.

References

1) A. R. Pinder, *Synthesis*, **6**, 425 (1980).
2) K. Isogai, N. Nishizawa, T. Saito, and J. Sakai, *Bull. Chem. Soc. Jpn.*, **56**, 1555 (1983).
3) S. Mitsui, Y. Sugi, M. Fujimoto, and K. Yokoo, *Tetrahedron*, **30**, 31 (1974).
4) W. J. Jones and B. P. Stoicheff, *Can. J. Phys.*, **42**, 2259 (1964).
5) W. H. Flygare, A. Narath, and W. G. Gwinn, *J. Chem. Phys.*, **36**, 200 (1962).
6) R. H. Schwendeman, G. D. Jacobs, and T. M. Krigas, *J. Chem. Phys.*, **40**, 1022 (1964).
7) S. Durmaz and H. Kollmar, *J. Am. Chem. Soc.*, **102**, 6942 (1975).
8) A. T. Perretta and V. W. Laurie, *J. Chem. Phys.*, **62**, 2469 (1975).
9) T. Ando, H. Hosaka, H. Yamanaka, and W. Funasaka, *Bull. Chem. Soc. Jpn.*, **42**, 2013 (1969).
10) S. J. Cristol, R. M. Sequeira, and C. H. DePuy, *J. Am. Chem. Soc.*, **87**, 4007 (1965).
11) C. H. DuPuy, L. G. Schnack, and J. W. Hausser, *J. Am. Chem. Soc.*, **88**, 3343 (1966).
12) E. B. Maxted, "Advances in Catalysis," ed by W. G. Frankenburg, V. I. Komarewsky, E. K. Rideal, P. H. Emmett, H. S. Taylor, Academic Press INC., Publishers, New York, N. Y. (1951), Vol. 3, p. 129.
13) T. Ando, H. Yamanaka, S. Terabe, A. Horike, and W. Funasaka, *Tetrahedron Lett.*, **1967**, 1123.
14) M. Kamel, W. Kimpenhaus, and J. Buddrus, *Chem. Ber.*, **109**, 2351 (1976).
15) S. I. Khromov and E. S. Balenkova, *Doklady Akad. Nauk SSSR.*, **89**, 1025 (1953).
16) J. Whuffman and J. E. Engle, *J. Org. Chem.*, **26**, 3116 (1961).
17) C. Buchanan and A. C. Ritchie, *J. Chem. Soc.*, **1954**, 4523.

Intramolecular "Diene-Regenerable" Diels-Alder Reaction of 2-Pyrone-6-carboxamides.[1] Preparation and Reaction of Fused 1,3-Cyclohexadiene Systems

Michihiko NOGUCHI,* Shinji KAKIMOTO, Hisao KAWAKAMI, and Shoji KAJIGAESHI
Department of Industrial Chemistry, Faculty of Engineering, Yamaguchi University, Tokiwadai, Ube 755
(Received November 25, 1985)

The 2-pyrone-6-carboxamides, prepared from 2-pyrone-6-carbonyl chloride and substituted allylamine, undergo an intramolecular Diels–Alder reaction spontaneously to give 3a,4,5,7a-tetrahydro-1-oxoisoindoline-5,7a-carbolactones, which regenerate the diene moieties by the decarboxylation to afford 3a,4-dihydro-1-oxoisoindolines. 3a,4,4a,5-Tetrahydro-1(2*H*)-isoquinolone and 2,3,4,5,5a,6-hexahydro-1*H*-2-benzazepin-1-one derivatives are obtained similarly from the corresponding amides. These fused 1,3-cyclohexadiene systems reveal to be versatile synthetic intermediates for polycyclic compounds by cycloaddition reaction and for benzo-fused heterocycles by dehydrogenation. The stereochemistries in the successive cycloaddition reactions are also discussed.

Previously, we reported that 2-pyrone-6-carboxylates bearing dienophiles at the ester moieties underwent "diene-regenerable" Diels–Alder reaction intramolecularly to give 3a,4-dihydrophthalide derivatives.[2] The 3a,4-dihydrophthalides behaved as novel functionalized 1,3-cyclohexadiene systems and provided a favorable method for the synthesis of 5,7a-ethanophthalides by the intermolecular Diels–Alder reaction with olefins[2] and of 4-substituted phthalides by oxidation.[3]

In this paper we wish to report that 2-pyrone-6-carboxamides, prepared from 2-pyrone-6-carbonyl chloride and substituted allylamines in situ, undergo an intramolecular Diels–Alder reaction to give tetracyclic adducts, which are smoothly converted to 3a,4-dihydro-1-oxoisoindolines by the extrusion of carbon dioxide. 1(2*H*)-Isoquinolone and 1*H*-2-benzazepin-1-one derivatives are obtained similarly by the intramolecular "diene-regenerable" Diels–Alder reaction of the corresponding 2-pyrone-6-carboxamides. The reaction of the fused 1,3-cyclohexadienes with *N*-phenylmaleimide and the oxidation of the 1,3-cyclohexadienes to benzo-fused heterocycles are also detailed.

Results and Discussion

Intramolecular Diels-Alder Reaction of 2-Pyrone-6-carboxamides. The reaction of 2-pyrone-6-carbonyl chloride (**1**) and *N*-allylaniline (**2a**) in the presence of triethylamine (Et_3N) at room temperature gave a crystalline product **4a** in 60% yield.

Unfortunately, **4a** did not provide satisfactory results on the elemental analysis, and the molecular ion peak on its mass spectrum was not observed because of its instability. Its IR spectrum, however, exhibited strong absorption bands at 1770 and 1700 cm^{-1} assignable to the lactone an lactam carbonyl streching vibrations, respectively. Also, its ^1H NMR spectrum (Table 2) showed two olefinic protons at δ=6.53 and 6.96 and the complicated signals over the region of δ=2 to 4 (total 6H) assigned to methylene and methine protons together with phenyl protons (5H). On the basis of these spectral data and the chemical conversions delineated later, **4a** was deduced to be not the expected *N*-allyl-2-pyrone-6-carboxanilide (**3a**) but 3a,4,5,7a-tetrahydro-1-oxo-2-phenylisoindoline-5,7a-carbolactone, an intramolecular Diels–Alder adduct of **3a**.

Similarly, the reaction of **1** with *N*-allylbenzylamine (**2b**), *N*-benzyl-*trans*-cinnamylamine (**2c**), *N*-(*trans*-2-butenyl)benzylamine (**2d**), and *N*-methyl-*trans*-cinnamylamine (**2e**) in the presence of Et_3N gave the corresponding Diels–Alder adducts **4b—e** in good yields. These results are summarized in Tables 1 and 2.

The stereochemistry at the 3-position of **4** could not be determined only on the basis of the coupling constants between 3-H and 3a-H or 3a-H and 4-H. However, its structure was deduced to be **4**-*endo* from the following inspections using the molecular models of **4**-*endo* and **4**-*exo* as well as the transition states. Firstly, the methylene protons at the 3-position of **4** were observed almost equivalently as shown in Table 2. The methylene protons at the 3-position of **4**-*endo* are possible to be equivalent and, on the other hand, those of **4**-*exo* are not so because of the anisotropic effect arising from the ether-

Table 1. Reactions of 2-Pyrone-6-carbonyl Chloride (**1**) with Alkenylamines (**2**)

Compd	R	R^1	Yield %	IR cm^{-1} ν_{CO}
4a[a]	Ph	H	60	1770, 1700
4b[b]	CH_2Ph	H	94	1765, 1700
4c[b]	CH_2Ph	Ph	88	1770, 1700
4d[b]	CH_2Ph	CH_3	83	1765, 1710
4e[a]	CH_3	Ph	68	1760, 1700

a) Colorless crystals. b) Colorless viscous oil.

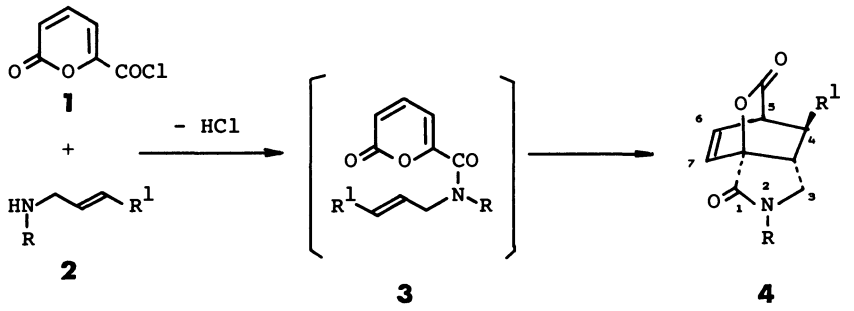

Scheme 1.

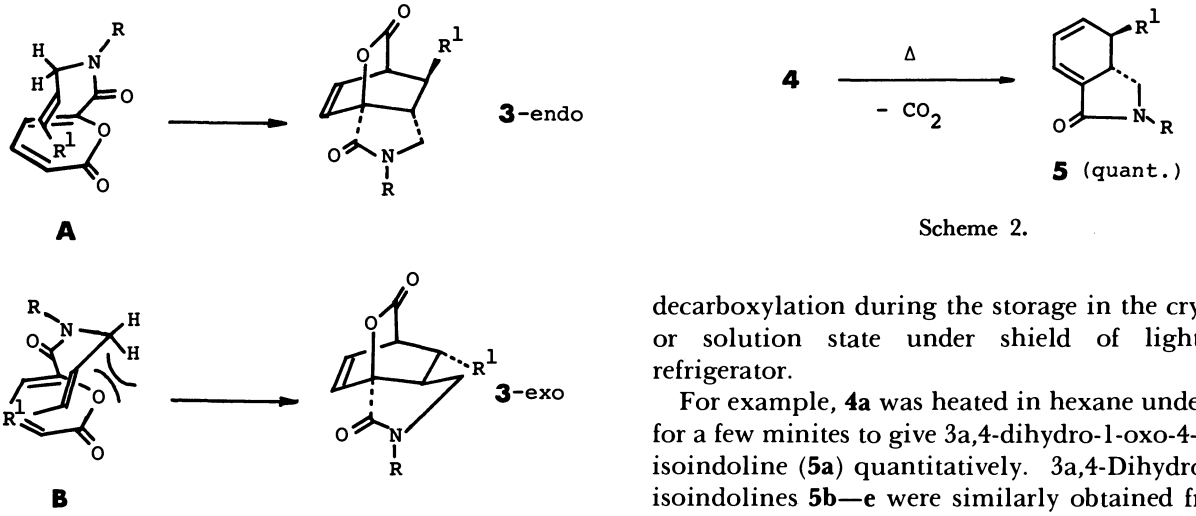

Scheme 2.

Fig. 1. Possible transition states for the intramolecular Diels–Alder reaction of **3**.

oxygen atom of the lactone moiety.

The configurations between 3a- and 4-positions of **4c**, **4d**, and **4e** were determined to be *trans* from those of the 3a,4-dihydro-1-oxoisoindoline derivatives, which were obtained by the decarboxylation of **4** as mentioned later.

The considerations using the molecular models of the possible transition states[4] in this reaction also indicate the predominant formation of **4**-*endo*, i.e., the orientation A leading to **4**-*endo* seems to be more favorable than B leading to **4**-*exo*, in which the sterical repulsion between one of the allylic methylene protons and the ether-oxygen atom of 2-pyrone part in **3** becomes serious along with the progress of the reaction (Fig. 1).

The Diels–Alder adducts from 2-pyrones and dienophiles are not so stable as well-known and only a few examples of the isolation have been reported.[5] To be emphasized is the isolation of the adducts **4**, because **4** possess further strained structures than the adducts reported previously.[5]

Predictively, the adducts **4** are thermodynamically and photochemically unstable and converted gradually to 3a,4-dihydro-1-oxoisoindoline derivatives by the decarboxylation during the storage in the crystalline or solution state under shield of light in a refrigerator.

For example, **4a** was heated in hexane under reflux for a few minites to give 3a,4-dihydro-1-oxo-4-phenylisoindoline (**5a**) quantitatively. 3a,4-Dihydro-1-oxoisoindolines **5b**—**e** were similarly obtained from the corresponding adducts **4b**—**e** in quantitative yields (Scheme 2).

The analytical and spectroscopic data of **5** were consistent with the proposed structures. Especially, their stereochemical confirmations at the 3a- and 4-positions were accomplished by the following ^{1}H NMR spectral data; for **5a** the vicinal coupling constants (5.9 and 2.2 Hz) between the olefin proton (5-H) and the methylene protons (4-H) were assigned to be $J_{5-4(a)}$ and $J_{5-4(b)}$, respectively. Nextly, the pronounced large coupling constants (17.2 and 9.7 Hz)[6] between 3a-H and 4-H were deduced to be *trans* and *cis*, respectively. These assignments were almost identical with those of 3a,4-dihydrophthalide.[2] Among **4c**, **4d**, and **4e**, the stereochemistry at the 3a- and 4-positions of **4c** was only determined to be *trans* on the basis of the vicinal coupling constants among the adjacent three protons at the 3a-, 4-, and 5-positions (J_{3a-4}=17.0 and J_{4-5}=0.8 Hz) (Table 3).

This means that the intramolecular Diels–Alder reaction of amide **3c** is carried out with the retention of the stereochemistry on the dienophile moiety. Taking the integrity of the stereocontrol in this reaction into consideration, the stereochemistries at the 3a- and 4-positions of **5d** and **5e** were suggested to be also *trans*.

The above findings revealed that the "diene-regenerable" Diels–Alder reaction of 2-pyrone-6-

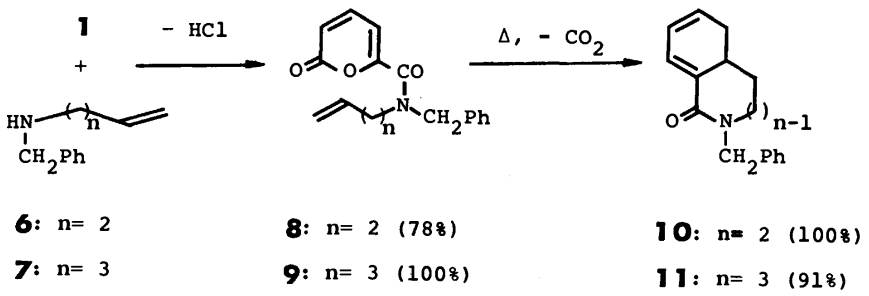

Scheme 3.

carboxamides **3** provided an attractive route to obtain 3a,4-dihydro-1-oxoisoindolines, so we attempted to apply this method to the preparation of the 1,3-cyclohexadiene systems fused by six- and seven-membered heterocycles containing nitrogen atom.

The reaction of **1** with *N*-(3-butenyl)benzylamine (**6**) and *N*-(4-pentenyl)benzylamine (**7**) in the presence of Et_3N at room temperature gave the 2-pyrone-6-carboxamides **8** and **9**. The successive intramolecular Diels–Alder reaction of **8** and **9** proceeded only under the severer conditions, i.e., under reflux in toluene for **8** and in *o*-dichlorobenzene for **9**, to give 2-benzyl-3,4,4a,5-tetrahydro-1(2*H*)-isoquinolone (**10**) and 2-benzyl-2,3,4,5,5a,6-hexahydro-1*H*-2-benzazepin-1-one (**11**), respectively (Scheme 3).

Cycloaddition Reaction of Fused 1,3-Cyclohexadienes 5a and 10 with *N*-Phenylmaleimide (NPMI). In order to obtain the stereochemical aspect on the Diels–Alder reaction of the fused 1,3-cyclohexadiene systems, the reaction of **5a** and **10** with NPMI was investigated.

The reaction of **5a** or **10** with an equimolar NPMI in xylene under reflux and the successive working-up gave the cycloadduct **12** or **13** as a sole product (Scheme 4).

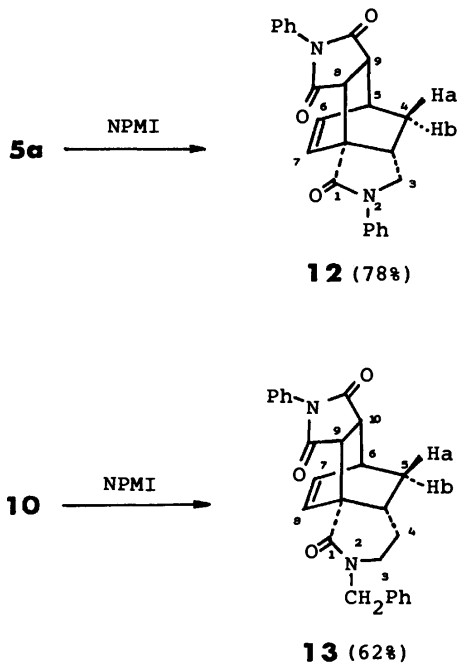

Scheme 4.

The structure of **12** was deduced to be a 3a,4,5,7a-tetrahydro-5,7a-ethano-1-oxoisoindoline derivative on the basis of its spectral data. It was confirmed that the stereochemistry at the 3a- and 7a-junctions was *cis* and the configurations of the protons at the 8- and 9-positions were both *exo* from the analysis of its ^1H NMR spectrum compared with that of cycloadduct[2] from 3a,4-dihydrophthalide and NPMI or of the related similar ring systems.[7]

The structure of **13** was deduced to be a 3,4,4a,5,6,8a-hexahydro-6,8a-ethano-1(2*H*)isoquinolone derivative also from its spectral data. The sufficient assignment of the signals in its ^1H NMR spectrum was not accomplished, because some of the methylene and methine protons were superimposed one another. However, the signal patterns[8] of the olefin protons of **13** were almost identical with those of **12**; δ=6.24 (dd, 1H, J=6.8 and 8.5 Hz) and 6.77 (d, 1H, J=8.5 Hz) for **12** and δ=6.26 (dd, 1H, J=5.7 and 9.0 Hz) and 6.86 (d, 1H, J=9.0 Hz) for **13**, so the stereochemistry at the 4a- and 8a- junctions of **13** was concluded to be also *cis*. Although the configurations of the protons at the 9- and 10-positions were obscure, they were tentitatively assigned to be both *exo* similarly to those of **12** according to the reaction pathway.

These findings indicate that the Diels–Alder reaction of **5a** and **10** with NPMI proceeds in a highly stereoselective manner. Therein, an only approarch of NPMI to 1,3-diene moiety of **5a** or **10** leading to *cis*-fused lactam ring seems to be possible owing to the less ring distorsion at the transition state in the reaction.

Dehydrogenation of Fused 1,3-Cyclohexadiene Systems 5, 10, and 11 to Benzo-Fused Heterocycles. As described above, 4-substituted phthalides were prepared by the facial oxidation of 3a,4-dihydrophthalides with palladium-charcoal (Pd/C), so we investigated the dehydrogenation of 3a,4-dihydro-1-oxoisoindolines **5** and their higher homologs, **10** and **11**, to the benzo-fused heterocycles.

The heating of **5** in refluxing xylene in the presence of Pd/C gave the expected 1-oxoisoindolines **14** almost quantitatively. While the similar treatment of **11** with Pd/C in refluxing *o*-dichlorobenzene yielded 2-benzyl-2,3,4,5-tetrahydro-1*H*-2-benzazepin-1-one (**16**)[9], **10** gave 2-benzyl-1(2*H*)-isoquinolone(**15**)[10] with the elimination of two equimolar hydrogen under similar dehydrogenating conditions (Scheme 5).

Finally, the possibility of the one-pot preparation of the benzlactams **15** and **16** from **8** and **9**, respectively, was surveyed. Heating of the amide **8** in refluxing toluene in the presence of Pd/C gave 2-benzyl-3,4-dihydro-1(2*H*)-isoquinolone (**17**;[9] 43%) and **14d** (47%). A similar reaction of **9** furnished 2-benzyl-3,4-dihydro-5-methyl-1(2*H*)-isoquinolone (**18**; 87%) as a sole product. In both cases, the terminal olefins of the dienophile moieties were isomerized by the Pd/C to the inner ones, which cycloadded to the 4π-components of 2-pyrones (Scheme 6). Interestingly, the dehydrogenation of the dihydro-1(2*H*)-isoquinolones **17** and **18** to 1(2*H*)-isoquinolone systems was suppressed under these reaction conditions.

In conclusion, the intramolecular "diene-regenerable" Diels–Alder reaction of 2-pyrone-6-carboxamides provided an attractive synthetic method for the 1,3-cyclohexadiene systems fused by pyrrole, pyridine, and azepine rings, which are versatile intermediates for polycyclic compounds and benzo-fused heterocycles. Among them, it should be emphasized that the stereochemistries of the final polycyclic compounds depend upon those of the successive intra- and intermolecular cycloaddition reactions.

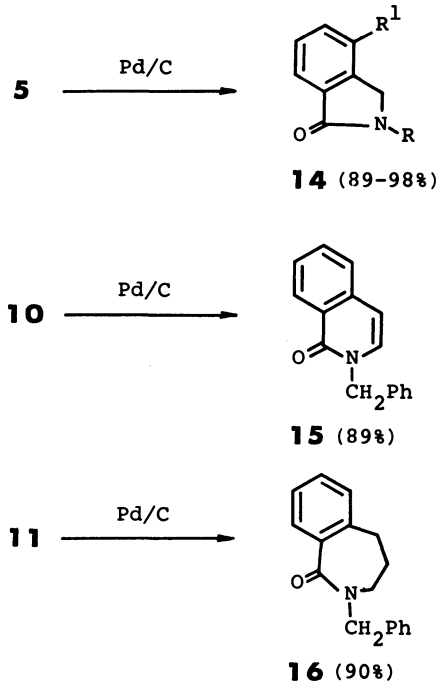

Scheme 5.

Experimental

General. All melting points are uncorrected. The IR spectra were measured on a JASCO IRA-1 spectrometer. The ^{1}H NMR spectra were obtained on JEOL FX-200 and JMN-MH-100 spectrometers with tetramethylsilane as an internal standard. The mass spectra were determined with JEOL JMS-012G-2 and JMS-D mass spectrometers equipped with direct inlets and at an ionization energy of 75 eV. The elemental analyses were performed on a Hitachi 026 CHN analyzer. The thin-layer chromatography was accomplished on 0.2 mm precoated plates of silica gel 60F-254 (Merck) or on 0.2 mm precoated plates of aluminium oxide 60F-254 Type E (Merck). The visualization was made with ultraviolet light (254 and 365 nm). For the preparative column chromatography, Wakogel C-300 was used.

Preparation of 3a,4,5,7a-Tetrahydro-1-oxoisoindoline-5,7a-carbolactones 4 from 2-Pyrone-6-carbonyl Chloride (1)

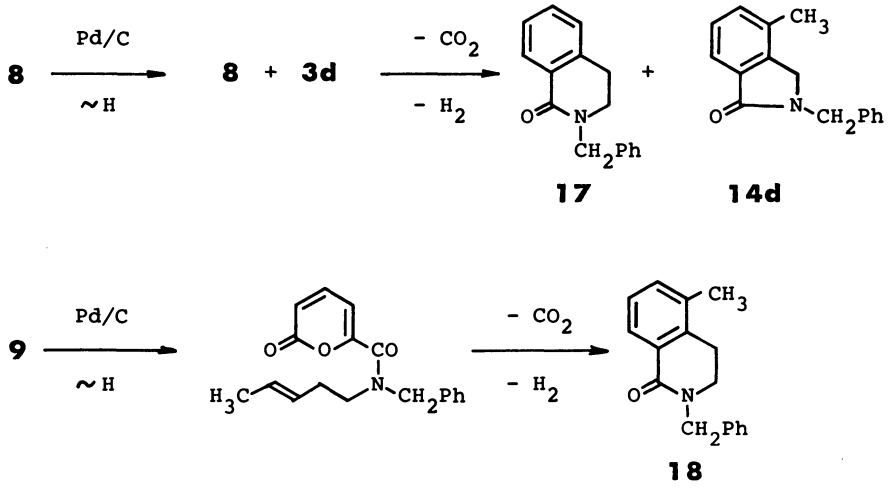

Scheme 6.

Table 2. ^{1}H NMR Spectral Data for 3a,4,5,7a-Tetrahydro-1-oxoisoindoline-5,7a-carbolactones **4** in $CDCl_3$: δ

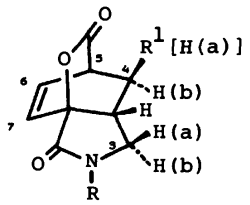

Compd	3-H(a)	3-H(b)	3a-H	4-H(a)	4-H(b)	5-H	6-H	7-H	Others
4a[a]	3.90	3.99	2.55	1.95	1.95	3.53	6.53	6.96	7.2—7.6 (phenyl)
	t	dd	dddd	ddd		ddd	dd	t	
	J (Hz) 3(a),3(b)=3(a),3a=9.0, 3(b),3a=9.2, 3a,4(a)=6.3, 3a,4(b)=6.0, 4(a),5=4(b),5=0.3, 5,6=7.2, 5,7=0.3, 6,7=8.0								
4b[b]	3.24	3.18	2.30	1.75	1.75	3.52	6.42	6.84	7.1—7.3 (phenyl)
	t	dd	m	m		m	t	d	4.5 (-CH_2-)
	J (Hz) 3(a),3(b)=3(a),3a=8.5, 3(b),3a=9.1, 5,6=6,7=7.0								
4c[a]	3.48	3.40	2.55	—	3.16	3.64	6.50	7.06	7.1—7.4 (phenyl)
	dd	t	ddd		dd	ddd	dd	dd	4.55 (-CH_2-)
	J (Hz) 3(a),3(b)=3(a),3a=6.2, 3(b),3a=5.4, 3a,4=6.0, 4,5=0.8, 5,6=5.9, 5,7=0.8, 6,7=6.4								
4d[b]	3.2 — 3.5		1.6——————2.0			2.94	6.34	6.80	7.2—7.3 (phenyl)
	m		m			m	dd	d	4.5 (-CH_2-)
	J (Hz) 5,6=5.5, 6,7=7.0								1.1 (Me)
4e[a]	3.58	3.58	2.62	—	3.20	3.69	6.50	7.02	7.2—7.4 (phenyl)
	d		dd		d	d	dd	d	2.98 (Me)
	J (Hz) 3(a),3a=3(b),3a=8.0, 3a,4=6.0, 4,5=0, 5,6=7.0, 6,7=7.5								

a) Measured at 200-MHz. b) Measured at 100-MHz.

and Allylamines 2. Typical Procedure: To a stirred and cooled at 0 °C solution of *N*-allylaniline (**2a**)(32 mmol) and Et_3N (35 mmol) in THF (40 mL), **1**[11] (32 mmol) in THF (10 mL) was added dropwise for 30 min and the reaction mixture was stirred for additional 12 h at room temperature. The resultant triethylamine hydrochloride was filtered off and the filtrate was evaporated in vacuo at room temperature. The crystallization and successive washing with ethanol gave 4.8 g (60%) of **4a**.

A similar reaction of **1** with **2e** gave **4e** also as a crystalline form. On the other hand, **4b**, **4c**, and **4d** were obtained as oily products, so their purification was accomplished with a column chromatography (silica gel-ether).

Some efforts to purify **4** enough to obtain the satisfactory elemental analyses, e.g., recrystalization or purification with a performance liquid chromatography, were made without success.

Heating of **4a** in a capillary at 45 °C showed some changes of its crystalline form and **4a** melted at 94—95 °C. The melting point was identical with that of the decarboxylated product **5a**. The mass spectrum of **4a** under the ordinarily-measured conditions was also identical with that of **5a**.

The results of these reactions and the spectral data of the products **5** are summarized in Tables 1 and 2, respectively.

Decarboxylation of 3a,4,5,7a-Tetrahydro-1-oxoisoindoline-5,7a-carbolactones 4. Typical Procedure: A solution of **4a** (500 mg, 1.96 mmol) in hexane (30 mL) was refluxed for a few minutes and cooled at −30 °C to give 410 mg (99%) of the crystalline **5a**.

5a: Colorless plates (hexane-ethanol); mp 94—95 °C; IR (KBr) 1675 cm^{-1} (CO); MS *m/z* (relative intensity) 211 (M^+, base peak), 107 (22), 106 (72), 105 (Ph-CH=NH$^+$, 92), 104 (27), 92 (M^+−PhNCO, 37), 91, 77.

Found: C, 79.75; H, 6.34; N, 6.68%. Calcd for $C_{14}H_{13}NO$: C, 79.59; H, 6.20; N, 6.63%; M, 211.

5b: Yield 100%; colorless plates (hexane-ethanol); mp 90—91.5 °C; IR (KBr): 1670 cm^{-1} (CO); MS *m/z* (relative intensity) 225 (M^+, base peak), 106 (42), 105 (Ph-CH=NH$^+$, 88), 91 (77), 77 (20).

Found: C, 80.13; H, 6.78; N, 6.19%. Calcd for $C_{15}H_{15}NO$: C, 79.97; H, 6.71; N, 6.22%; M, 225.

5c: Yield 100%; colorless needles (hexane-benzene); mp 139—141 °C; IR (KBr): 1680 cm^{-1} (CO); MS *m/z* (relative intensity) 301 (M^+, 11), 167 (Ph-$C_7H_6^+$, 44), 106 (13), 91 ($C_7H_7^+$, base peak).

Found: C, 83.65; H, 6.41; N, 4.74%. Calcd for $C_{21}H_{19}NO$: C, 83.69; H, 6.35; N, 4.65%; M, 301.

5d: Yield 97%; colorless plates (hexane-benzene); mp 136.5—138.5 °C; IR (KBr): 1680 cm^{-1} (CO); MS *m/z* (relative intensity) 239 (M^+, 13), 106 (33), 91($C_7H_7^+$, base peak), 77 (33).

Found: C, 80.31; H, 7.23; N, 5.81%. Calcd for $C_{16}H_{17}NO$: C, 80.30; H, 7.16; N, 5.85%; M, 239.

5e: Yield 99%; colorless prisms (hexane-benzene); mp 105.5—106.5 °C; IR (KBr): 1670 cm^{-1} (CO); MS *m/z* (relative intensity) 225 (M^+, base peak), 167 (Ph-$C_7H_6^+$, 40),

Table 3. ^{1}H NMR Spectral Data for 3a,4-Dihydro-1-oxoisoindolines **5** in $CDCl_3$: δ

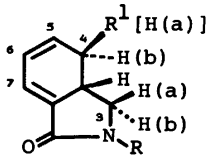

Compd	3-H(a)	3-H(b)	3a-H	4-H(a)	4-H(b)	5-H	6-H	7-H	Others
	4.13	3.51	2.90	2.62	2.09	6.15	6.29	6.86	7.1, 7.8 (phenyl)
	t	dd	m	ddd	dddd	dddd	ddd	t	
5a[a]	J (Hz) 3(a),3(b)=3(a),3a=9.0, 3(b),3a=9.6, 3a,4(a)=9.0, 3a,4(b)=17.2, 4(a),4(b)=17.0, 3a,5=1.2, 3a,7=3.2, 4(a),5=5.9, 4(b),5=4(b),6=2.2, 5,6=8.8, 6,7=3.2								
5b[b]	3.50	2.5——3.1		2.0——2.2		5.8——6.3		6.6	7.2 (phenyl)
	m	m		m		m		m	4.5 (-CH_2-)
	3.26	2.8——3.0			3.40	5.96	6.28	6.78	7.1—7.3 (phenyl)
5c[a]	m	m			ddd	dd	ddd	dd	3.95, 4.10 (-CH_2-)
	J (Hz) 3a,4=17.0, 3a,7=2.2, 4,5=0.8, 4,6=1.2, 5,6=8.8, 6,7=3.2								
	3.55	2.85	2.1——2.5			5.82	6.19	6.74	7.2—7.4 (phenyl)
5d[a]	t	dd	m			dd	ddd	dd	4.53, 4.60 (-CH_2-)
	J (Hz) 3(a),3(b)=3(a),3a=9.3, 3(b),3a=8.1, 3a,4=15.6, 3a,7=1.4, 4,5=0.7, 4,6=1.2, 5,6=9.0, 6,7=3.2								1.10 (Me)
	2.8——3.5					6.02	6.33	6.78	7.2—7.4 (phenyl)
5e[a]	m					dd	ddd	t	2.93 (Me)
	J (Hz) 3a,7=1.4, 4,5=0.8, 4,6=0.8, 5,6=9.0, 6,7=3.2								

a) Measured at 200-MHz. b) Measured at 100-MHz.

154 (70), 153 (47), 134 (M^+—C_7H_7, 92), 42 (60).

Found: C, 80.16; H, 6.79; N, 6.41%. Calcd for $C_{15}H_{15}NO$: C, 79.97; H, 6.71; N, 6.22%; M, 225.

The ^{1}H NMR spectral data of **5** are summarized in Table 3.

Preparation of 2-Pyrone-6-carboxamides 8 and 9 from 1 and Amines 6 and 7. Similarly to the preparation of **4**, the reaction of **1** (7.6 mmol) and **6** (7.6 mmol) in THF (40 mL) in the presence of a little excess of Et_3N at room temperature for 15 h gave an oily product, which was purified with a short column chromatography (aluminium oxide-ether) to afford 1.68 g (78%) of **8**.

8: Pale yellow viscous oil; IR (Neat) 1740 and 1635 cm^{-1} (CO); ^{1}H NMR ($CDCl_3$) δ=2.40 (m, 2H, >N-CH_2-), 3.40 (m, 2H, -CH_2-CH=), 4.50 (s, 2H, -CH_2-Ph), 5.15 (m, 2H, =CH_2), 5.7 (m, 1H, -CH=), 6.45 (m, 1H, 5-H), 6.65 (m, 1H, 4-H), and 7.3—7.4 (m, 6H, 3-H and phenyl protons); MS m/z (relative intensity) 283 (M^+, 17), 242 (M^+—C_3H_5, 85), 239 (M^+,—CO_2, 13), 95 (42), 91 ($C_7H_7^+$, base peak).

Found: C, 71.86; H, 6.09; N, 5.06%. Calcd for $C_{17}H_{17}NO_3$: C, 72.06; H, 6.05; N, 4.94%; M, 283.

9: Colorless viscous oil; IR (neat): 1740 and 1635 cm^{-1} (CO); ^{1}H NMR ($CDCl_3$) δ=1.6—2.2 (m, 4H, >N-CH_2-CH_2-), 3.4 (m, 2H, -CH_2-CH=), 4.65 (s, 2H, -CH_2-Ph), 4.90 (m, 2H, =CH_2), 5.68 (m, 1H, -CH=), 6.32 (m, 1H, 5-H), 6.60 (m, 1H, 4-H), and 7.2—7.3 (m, 6H, 3-H and phenyl protons); MS m/z (relative intensity) 297 (M^+, 4), 269 (M^+—CO, 5), 242 (M^+—C_4H_7, 5), 174 (30), 106, 104, 91 ($C_7H_7^+$, base peak).

Found: C, 72.92; H, 6.71; N, 4.99%. Calcd for $C_{18}H_{19}NO_3$: C, 72.70; H, 6.44; N, 4.71%; M, 297.

Diene-Regenerable Diels-Alder Reaction of 2-Pyrone-6-carboxamides 8 and 9. A solution of **8** (1.30 g, 4.6 mmol) in toluene (30 mL) was heated under reflux for one day and the toluene was evaporated to dryness, which was treated with a short column chromatography (silica gel-benzene) to give 1.10 g (100%) of **10**.

10: Colorless plates (hexane); mp 64—65 °C; IR (KBr): 1640 cm^{-1} (CO); ^{1}H NMR ($CDCl_3$) δ=1.68(m, 1H, 5-H), 1.96 (m, 2H, 4-H), 2.26 (m, 1H, 5-H), 2.72 (m, 1H, 4a-H), 3.3 (m, 2H, 3-H), 4.54, 4.83 (2d, 1H each, -CH_2-Ph, J=14 Hz), 6.12 (m, 2H, 6- and 7-H), and 7.16 (m, 1H, 8-H); MS m/z (relative intensity) 239 (M^+, base peak), 210 (17), 148 (M^+—C_7H_7, 17), 134 (23), 120 (23), 106 (27), 105 ($PhCO^+$, 70), 91 (45), 77 (41).

Found: C, 80.48; H, 7.21; N, 5.92%. Calcd for $C_{16}H_{17}NO$: C, 80.30; H, 7.16; N, 5.85%; M, 239.

Heating of **9** in *o*-dichlorobenzene under reflux for one day gave **11** in 91% yield.

11: Pale yellow viscous oil; IR(Neat): 1635—1610 cm^{-1} (CO); ^{1}H NMR ($CDCl_3$) δ=1.3—1.9 (m, 4H, 4- and 5-H), 1.9—2.3 (m, 2H, 6-H), 2.4 (m, 1H, 5a-H), 3.1—3.4 (m, 2H, 3-H), 4.62 (s, 2H, -CH_2-Ph), 6.0—6.1 (m, 2H, 7- and 8-H), 6.6 (m, 1H, 9-H), and 7.2—7.4 (m, 5H, phenyl protons); MS m/z (relative intensity) 253 (M^+, 11), 251 (M^+—H_2, 4), 106 (8), 105 (12), 104 (12), 91 ($C_7H_7^+$, base peak), 77 (26).

Found: m/z 253.1466. Calcd for $C_{17}H_{19}NO$: M, 253.1466.

Cycloaddition Reaction of 5a and 10 with *N*-Phenylmaleimide (NPMI). Typical Procedure: An equimolar (2.4 mmol) mixture of **5a** and NPMI in xylene (20 mL) was heated under reflux for 20 h and the xylene was evaporated in vacuo to give a residue. The residue was treated with a short column chromatography (silica gel-chloroform) to afford 0.71 g (78%) of **12**.

12: Colorless prisms (benzene-hexane); mp 280—281 °C;

IR (KBr): 1690 cm^{-1} (CO); ^1H NMR ($CDCl_3$) δ=1.45 (ddd, 1H, 4-H, J_{gem}=12.8, $J_{3a,4}$=8.6, and $J_{4,5}$=0.6 Hz), 1.91 (ddd, 1H, 4'-H, J_{gem}=12.8, $J_{3a,4'}$=10.2, and $J_{4',5}$=4.2 Hz), 2.25 (m, 1H, 3a-H), 3.16 (dd, 1H, 9-H, $J_{8,9}$=8.4 and $J_{5,9}$=3.8 Hz), 3.24 (d, 1H, 8-H, $J_{8,9}$=8.4 Hz), 3.49 (m, 1H, 5-H), 3.61 (t, 1H, 3-H, J_{gem}=$J_{3,3a}$=9.6 Hz), 4.00 (dd, 1H, 3'-H, J_{gem}=9.6 and $J_{3',3a}$=7.2 Hz), 6.24 (dd, 1H, 6-H, $J_{5,6}$=6.8 and $J_{6,7}$=8.5 Hz), 6.77 (d, 1H, 7-H, $J_{6,7}$=8.5 Hz), and 7.1—7.7 (m, 10H, phenyl protons); MS *m/z* (relative intensity) 384 (M^+, 63), 279, 265, 252, 236, 221 (M^+—NPMI, 36), 173 (NPMI$^+$, 18), 119 (PhNCO$^+$, 25), 105 (Ph-CH=NH$^+$, base peak), 77 (92).

Found: C, 75.14; H, 5.31; N, 7.39%. Calcd for $C_{24}H_{20}N_2O_3$: C, 74.98; H, 5.24; N, 7.29%; M, 384.

13: Yield 62%; colorless prisms (benzene-hexane); mp 229—230 °C; IR (KBr): 1700 and 1630 cm^{-1} (CO); ^1H NMR ($CDCl_3$) δ=1.16 (m, 1H, 5-H), 1.7—2.1 (m, 4H, 4-, 4'-, 4a-, and 5'-H), 3.08 (dd, 1H, 10-H, $J_{9,10}$=7.6 and $J_{6,10}$=3.4 Hz), 3.2—3.4 (m, 3H, 3-, 3'-, and 6-H), 4.07, 5.20 (2d, 1H each, $-CH_2-Ph$, J_{gem}=13.6 Hz), 6.26 (dd, 1H, 7-H, $J_{6,7}$=5.7 and $J_{7,8}$=9.0 Hz), 6.86 (d, 1H, 8-H, $J_{7,8}$=9.0 Hz), and 7.1—7.5 (m, 10H, phenyl protons); MS *m/z* (relative intensity) 412 (M^+, 18), 383, 357, 321, 252, 239 (M^+—NPMI, 16), 210 (23), 173 (NPMI$^+$, 16), 145 (6), 119 (PhNCO$^+$, 14), 105 (Ph-CH=NH$^+$, 51), 91 ($C_7H_7^+$, base peak), 77 (48).

Found: C, 75.70; H, 5.89; N, 6.89%. Calcd for $C_{25}H_{24}N_2O_3$: C, 75.70; H, 5.89; N, 6.79%; M, 412.

Dehydrogenation of Fused 1,3-Cyclohexadiene Systems 5, 10, and 11 to Benzo-Fused Heterocycles 14, 15, and 16. Typical Procedure: A solution of **4a** (300 mg, 1.4 mmol) in xylene (20 mL) in the presence of 10% Pd/C (150 mg) was heated under reflux for one day, the Pd/C was filtered off, and the filtrate was evaporated to dryness. The residue was chromatographed on silica gel (chloroform) to give 291 mg (98%) of 2-phenylphthalimidine (**14a**).

14a: Colorless plates (ethanol); mp 160—162 °C (lit,[12] mp 166—167 °C); IR (KBr): 1675 cm^{-1} (CO); ^1H NMR ($CDCl_3$) δ=4.65 (s, 2H, 3-H) and 7.0—7.9 (m, 9H, 4-, 5-, 6-, and 7-H and phenyl protons); MS *m/z* 209 (M^+).

14b: Yield 94%; colorless needles (hexane); mp 85—88 °C (lit,[12] mp 90 °C); ^1H NMR ($CDCl_3$) δ= 4.25 (s, 2H, 3-H), 4.82 (s, 2H, $-CH_2-Ph$), 7.30 (br s, 5H, phenyl protons), 7.3—7.5 (m, 3H, 4-, 5-, and 6-H), and 7.88 (m, 1H, 7-H); MS *m/z* 223 (M^+).

14c: Yield 89%; colorless plates (hexane); mp 135—136 °C; IR (KBr): 1680 cm^{-1} (CO); ^1H NMR ($CDCl_3$) δ=4.30 (s, 2H, $-CH_2-Ph$), 4.76 (s, 2H, 3-H), 7.2 (br s, 5H, phenyl protons), 7.3 (br s, 5H, phenyl protons), 7.4 (m, 2H, 5- and 6-H), and 7.9 (m, 1H, 7-H); MS *m/z* (relative intensity) 299 (M^+, base peak), 208 (M^+—C_7H_7, 43), 195 (29), 165 (52), 91 ($C_7H_7^+$, 71).

Found: C, 84.52; H, 5.88; N, 4.80%. Calcd for $C_{21}H_{17}NO$: C, 84.25; H, 5.72; N, 4.68%; M, 299.

14d: Yield 90%; colorless prisms (hexane); mp 116—117 °C; IR (KBr): 1680 cm^{-1} (CO); ^1H NMR ($CDCl_3$) δ=2.22 (s, 3H, $-CH_3$), 4.13 (s, 2H, $-CH_2-Ph$), 4.77 (s, 2H, 3-H), 7.1—7.4 (m, 2H, 5- and 6-H), 7.27 (br s, 5H, phenyl protons), and 7.67 (m, 1H, 7-H); MS *m/z* (relative intensity) 237 (M^+, base peak), 146 (M^+—C_7H_7, 41), 133 (34), 91 ($C_7H_7^+$, 94), 77 (32), 65 (38).

Found: C, 80.75; H, 6.47; N, 5.90%; Calcd for $C_{16}H_{15}NO$: C, 80.98; H, 6.37; N, 5.91%; M, 237.

14e: Yield 95%; colorless needles (hexane-benzene); mp 138.5—139.5 °C; IR (KBr): 1670 cm^{-1} (CO); ^1H NMR ($CDCl_3$) δ=3.44 (s, 3H, $-CH_3$), 4.50 (s, 2H, 3-H), 7.54 (br s, 5H, phenyl protons), 7.6 (m, 2H, 5- and 6-H), and 7.9 (m, 1H, 7-H); MS *m/z* (relative intensity) 223 (M^+, base peak), 194 (72), 165 (38), 91 ($C_7H_7^+$, 55).

Found: C, 80.96;·H, 5.90; N, 6.44%. Calcd for $C_{15}H_{13}NO$: C, 80.69; H, 5.87; N, 6.27%; M, 223.

Heating of **10** in xylene under reflux in the presence of Pd/C for 3 d gave similarly **15** in 90% yield.

15: Colorless needles (hexane); mp 67—69 °C (lit,[10] mp 69—71 °C); IR (KBr): 1640 cm^{-1} (CO); ^1H NMR ($CDCl_3$) δ=5.25 (s, 2H, $-CH_2-Ph$), 6.50 (d, 1H, 4-H, J=7 Hz), 7.13 (d, 1H, 3-H, J=7 Hz), 7.4 (br s, 5H, phenyl protons), 7.5—7.8 (m, 3H, 5-, 6-, and 7-H), and 8.5 (m, 1H, 8-H); MS *m/z* 235 (M^+).

16: Colorless prisms (hexane-benzene); mp 83—86 °C lit,[9] mp 82—85 °C); IR (KBr): 1635 cm^{-1} (CO); ^1H NMR ($CDCl_3$) δ=1.6—2.0 (m, 2H, 4-H), 2.75 (t, 2H, 3-H, J=7 Hz), 3.21 (t, 2H, 5-H, J=7 Hz), 4.90 (s, 2H, $-CH_2-Ph$), 7.1—7.6 (m, 8H, 6-, 7-, and 8-H and phenyl protons), and 7.95 (m, 1H, 9-H); MS *m/z* 251 (M^+).

One-Pot Preparation of Benzo-Fused Heterocycles from Amides 8 and 9. Typical Procedure: A solution of **8** (500 mg, 1.77 mmol) in toluene (20 mL) in the presence of 10% Pd/C (500 mg) was refluxed for one day and the solvent was evaporated to dryness. The residure was chromatographed on silica gel to give 190 mg (47%) of **14d** and 170 mg (43%) of **17** as benzene and benzene-chloroform (1:1) eluents, respectively.

17: Yellow oil; IR (Neat): 1640 cm^{-1} (CO); ^1H NMR ($CDCl_3$) δ=2.84 (t, 2H, 3-H, J=7 Hz), 3.44 (t, 2H, 4-H, J=7 Hz), 4.74 (s, 2H, $-CH_2-Ph$), 7.1—7.4 (m, 8H, 5-, 6-, and 7-H and phenyl protons), and 8.12 (m, 1H, 8-H); MS *m/z* 237 (M^+).

The above ^1H NMR spectral data were identical with the reported ones.[9]

18: Colorless plates (hexane); mp 79—80 °C; IR (KBr): 1640 cm^{-1} (CO); ^1H NMR ($CDCl_3$) δ=2.62 (s, 3H, $-CH_3$), 2.85 (t, 2H, 3-H, J=7 Hz), 3.44 (br t, 2H, 4-H, J=7 Hz), 4.76 (s, 2H, $-CH_2-Ph$), 7.2—7.4 (m, 7H, 6- and 7-H and phenyl protons), and 8.0 (m, 1H, 8-H); MS *m/z* (relative intensity) 251 (M^+, base peak), 174 (M^+—Ph, 18), 160 (M^+—C_7H_7, 31), 147 (26), 132 (30), 119 (PhCH$_2$CH=NH$^+$, 15), 104 (45), 91 (C_7H_7, 92), 77 (58).

Found: C, 81.52; H, 6.88; N, 5.69%. Calcd for $C_{17}H_{17}NO$: C, 81.24; H, 6.82; N, 5.57%; M, 251.

We wish to thank Professor Masashi Tashiro, Research Institute of Industrial Science, Kyushu University, for the measurement of high mass spectra and the elemental analyses. We are also grateful to Drs. Shigeki Nagai, Yoshiaki Ishida, and Keiji Saito, and Mr. Tsuyoshi Arai, Ube Research Laboratory, Ube Industries LTD, for the measurement of ^1H NMR spectra at 200-MHz.

References

1) Cycloaddition Reactions of 2-Pyrones and Related Compounds. Part IV. Part III of this series: M. Noguchi, S. Kakimoto, and S. Kajigaeshi, Heterocycles in press.

2) M. Noguchi, S. Kakimoto, and S. Kajigaeshi, *Chem. Lett.*, **1985**, 151.

3) M. Noguchi, S. Kakimoto, H. Kawakami, and S. Kajigaeshi, *Heterocyles*, **23**, 1085 (1985).

4) W. Oppolzer, *Angew. Chem. Int. Ed. Engl.*, **16**, 10 (1977).

5) H. Behringer and P. Heckmair, *Chem. Ber.*, **102**, 2835 (1969); T. Shimo, K. Somekawa, and S. Kumamoto, *Nippon Kagaku Kaishi*, **1982**, 1927 and references cited there.

6) After our report had appeared,[2] none of the comments for the assignments of the vicinal coupling constants between 3a- and 4-H of the 3a,4-dihydrophthalides have yet been obtained. We suggested, however, that the pronounced large coupling constants were owing to the ring distorsion of the 3a,4-dihydrophthalide and phthalimidine systems.

7) A. Krantz and C. Y. Linn, *J. Am. Chem. Soc.*, **95**, 5662 (1972).

8) It was reported that the signal patterns of olefin protons of *endo*- and *exo*-tricyclo[5.2.2.$0^{1,5}$]undec-8-en-2-ones were available for their structural determinations.[7]

9) Y. Ban, T. Wakamatsu, and M. Mori, *Heterocycles*, **6**, 1171 (1977); M. Mori, K. Chiba, and Y. Ban, *J. Org. Chem.*, **43**, 1684 (1978).

10) H. Iida, K. Kawano, T. Kikuchi, and F. Yoshimizu, *Yakugaku Zasshi*, **96**, 176 (1976).

11) R. H. Wiley and A. J. Hart, *J. Am. Chem. Soc.*, **76**, 1942 (1954).

12) C. J. M. Stirling, *J. Chem. Soc.*, **1960**, 255.

From Penicillin to Penem and Carbapenem. VIII.[1] Introduction of an Allyl Group at the C-4 Position of the Azetidinone Molecule, and the Synthesis of Dethiathienamycin

Katsumi FUJIMOTO, Yuji IWANO, and Koichi HIRAI*
Chemical Research Laboratories, Sankyo Co., Ltd. 1-2-58, Hiromachi, Shinagawa-ku, Tokyo 140
(Received November 29, 1985)

A new C_3-unit introduction reaction at the *C*-4 position of 4-acetoxy-2-azetidinone derivatives using tetraallyltin in the presence of 1/10 equiv of boron trifluoride etherate in dichloromethane is described. Dethiathienamycin was synthesized from (3*S*,4*R*)-4-allyl-3-[(*R*)-1-(*t*-butyldimethylsilyloxy)ethyl]-2-azetidinone via the ylide intermediate.

Thienamycin (**16**) and the majority of the carbapenems are extremely active antibiotics against a broad range of Gram-positive and Gram-negative bacteria and have natural stability against β-lactamases.

Naturally occurring carbapenems, however, are highly unstable compounds because of their ring strain and other factors.[2] They are sufficiently stable only in a limited pH range around neutrality. This and the fact that it has so far not been possible to increase fermentation yields by strain optimization have made their isolation in large quantities from culture filtrates difficult.

Therefore, considerable effort has been devoted to the synthesis of these compounds and the search for more stable derivatives.[2] In their syntheses a wide variety of compounds have been used as starting materials; in our case we used the azetidinone derivative **6**, which is easily obtainable from 6-APA (6-aminopenicillanic acid).

A fundamental problem for the synthesis of carbapenem derivatives from 2-azetidinone derivatives such as **6** is how to introduce a carbon substituent at the *C*-4 position of the 2-azetidinone molecule. As possible solutions several C–C bond formation methods at the *C*-4 position have been elaborated; they can be divided into the following five categories:

1. Utilization of active methylene compounds[3]
2. Utilization of organometallic reagents[4]
3. Utilization of silyl derivatives[5]
4. Utilization of carbene insertion to the C–S bond[6]
5. Utilization of potassium cyanide[7]

A common intermediate for the above reactions (excluding 4) is reasonably considered to be the azetinone (or 2-oxoazetidinium) one (**3** or its *N*-substituted one).

We took advantage of allyltin reagent for the introduction of the C_3-unit under the following working hypotheses. The properties of tin organyls are different from those of silicon and germanium in a greater tendency of Sn^{IV} to be able to coordinate in more than four centers and ionize more easily to give cationic species.[8] As shown in Chart 1 the coordination of Lewis acid would assist in the elimination of the acyloxy group to generate 2-oxoazetidinium intermediate **3**. Allyltin is apt to react with cationic derivative, and therefore under these conditions tetraallyltin should attack the acyliminium intermediate to give 4-allyl-2-azetidinone. The trialkyl(or triallyl)tin cation which is generated in this reaction process would react with the Lewis acid–acetoxy complex (e.g. $BF_3 \cdot OAc$) to generate the Lewis acid (e.g. BF_3). Under these hypotheses the reaction should proceed on inclusion of a catalytic amount of Lewis acid.

In this report we describe a mild and convenient method for the introduction of the allyl substituent at

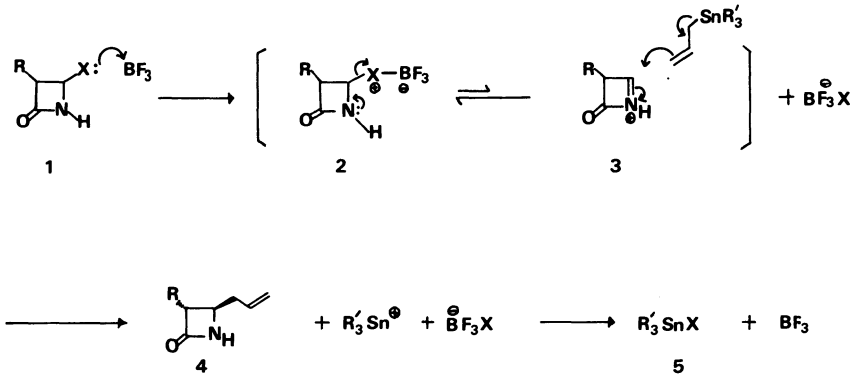

Chart 1.

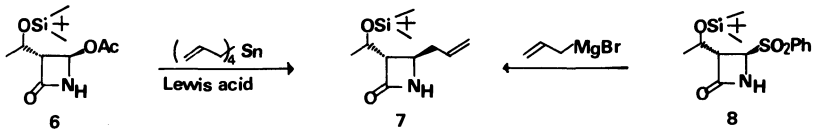

6 7 8

Chart 2.

Table 1. Effects of Lewis Acids

Lewis Acids	Yield/%
$SnCl_4$	30
$TiCl_4$	45
BF_3OEt_2	85
$ZnCl_2$	0
ZnI_2	0

the *C*-4 position of the azetidinone molecule, and application of this to the synthesis of dethiathienamycin (**17**).

First, we investigated the reaction between 4-acetoxy-3-[(*R*)-1-(*t*-butyldimethylsilyloxy)ethyl]-2-azetidinone (**6**) and tetraallyltin.

1) Effect of Lewis Acids. 4-Acetoxy-2-azetidinone derivative **6** was reacted with tetraallyltin in the presence of several kinds of Lewis acids. As shown in Table 1 zinc chloride and iodide failed to give the desired product. But tin tetrachloride and titanium tetrachloride gave **7** in moderate yields. Boron trifluoride etherate was the best of the five catalysts checked. 4-Acetoxy-2-azetidinone **6** was reacted with tetraallyltin in the presence of 0.1 equiv of boron trifluoride etherate in dichloromethane to give the 4-allyl-2-azetidinone (**7**) in 85% yield.

2) Effect of Amount of Tetraallyltin. Next we checked how many allyl groups in the tetraallyltin molecule could be used in this reaction. One, 0.5, and 0.25 mol of tetraallyltin was reacted with 1 mol of 4-acetoxy-2-azetidinone derivative **6** to give the desired product **7** in 85, 65, and 0% yield, respectively. These results suggest that two of the four allyl groups in the tetraallyltin molecule are effective enough in this allylation reaction. The same product **7** was also obtained using 1 equiv of allyltributyltin under the same conditions.

The 4-allyl-2-azetidinone produced was found to be identical with an authentic sample prepared from the corresponding 4-(phenylsulfonyl)-2-azetidinone derivative **8** and allylmagnesium bromide under the reported conditions.[9]

The simple 4-acetoxy-2-azetidinone (**9**) was also reacted with tetraallyltin in the presence of boron trifluoride etherate in dichloromethane to yield 4-allyl-2-azetidinone (**10**) in 74% yield.

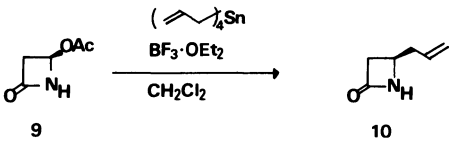

9 10

Chart 3.

In the case of tributylcrotyltin,[10] the 4-(1-methylallyl)-2-azetidinone **11** was obtained as a 1:1 mixture (^{1}H NMR, δ=1.17, 1/2 CH_3, d, J=6 Hz and 1.21, 1/2 CH_3, d, J=6 Hz) in 80% yield.

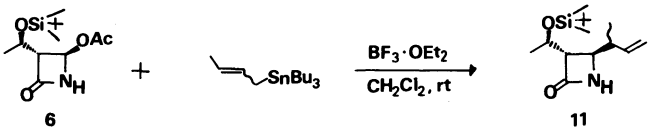

6 11

Chart 4.

It is well known that boron trifuoride etherate in chloroform is one set of conditions for the desilylation of the silyl ether.[11] Therefore the *p*-nitrobenzyloxycarbonyl (PNZ) protected azetidinone derivatives **12—14**, which are stable to the above conditions, were subjected to the above and the progress of the reaction was monitored on silica-gel TLC (UV detected). As shown in Table 2, regardless of the configurations of the *C*-4 acyloxy groups, the reaction completed in 6 h and the same 4-allyl substituted azetidinone product **15** was obtained in 93% isolated yield.

At this stage, out of interest in antibacterial activity, we turned our attention to the synthesis of dethiathienamycin (**17**) in which the sulfur atom is

Table 2. Reaction of 4-Acyloxy-2-azetidinone with Tetraallyltin

X	Isolated Yield/%
α-AcO	93
β-AcO	93
α-PhCOO	93

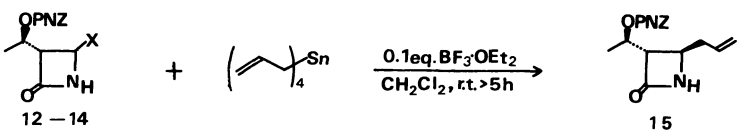

12—14 15

Chart 5.

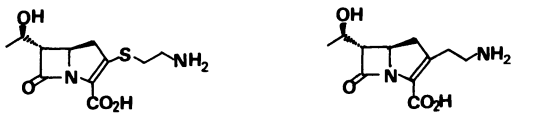

16 thienamycin 17 dethiathienamycin

Chart 6.

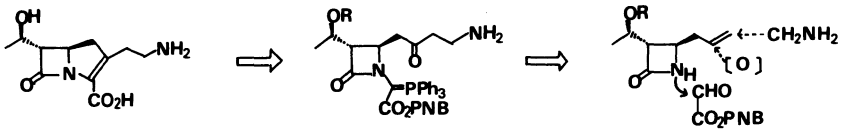

17 18

Chart 6′.

missing from the thienamycin molecule (**16**). Our strategy was as follows: i) The construction of the carbapenem skeleton was to be achieved by intramolecular Wittig reaction. ii) Compound **18** was to be synthesized from allylazetidinone **7** by the combination of 3 parts; *p*-nitrobenzyl glyoxylate, aminomethyl synthon, and the oxygen function at the 2-position of the allyl group.

We considered that the epoxidation of the double bond was useful for the introduction of the oxygen function, and the cyanide anion was taken advantage of for the aminomethyl synthon. Along these lines, the 4-allyl-2-azetidinone derivative **7** was oxidized with *m*-chloroperbenzoic acid in dichloromethane to the epoxide **19** as a mixture of two diastereomers, one of which crystallized: mp 83.5 °C $[\alpha]_D^{24}$ −18°(*c* 1, $CHCl_3$). The epoxide ring in **19** was opened regiospecifically to the cyano alcohol derivative **20**, one of the diastereomers of which also crystallized, mp 120—125 °C, on treatment with potassium cyanide in *N*,*N*-dimethylformamide–water (3:1) at room temperature for 15 h. The cyano group was then hydrogenated to the amino group using platinum oxide in acetic acid, and the succesive protection of the amino group by *p*-nitrobenzyloxycarbonyl chloride gave the compound **21** in 50% yield from **20**. The hydroxyl group in **21** was effectively oxidized to the ketone **22** with pyridinium chlorochromate in dichloromethane. Compound **22** was condensed with *p*-nitrobenzyl glyoxylate to afford the aminal derivative **23**, which was chlorinated by thionyl chloride and successively reacted with triphenylphosphine to give the ylide **24**. The intramolecular Wittig condensation reaction was easily performed by heating in benzene at 80 °C to afford the carbapenem **25**. The desilylation of this compound **25** could not be achieved under ordinary conditions (e.g. boron trifluoride etherate in acetonitrile, tetrabutylammonium fluoride and acetic acid, pyridine–acetic acid), presumably because of the instability of the carbapenem skeleton.

Therefore at the stage of **22** the silyl protective group was changed to the *p*-nitrobenzyloxycarbonyl group. The desilylation conditions, boron trifluoride

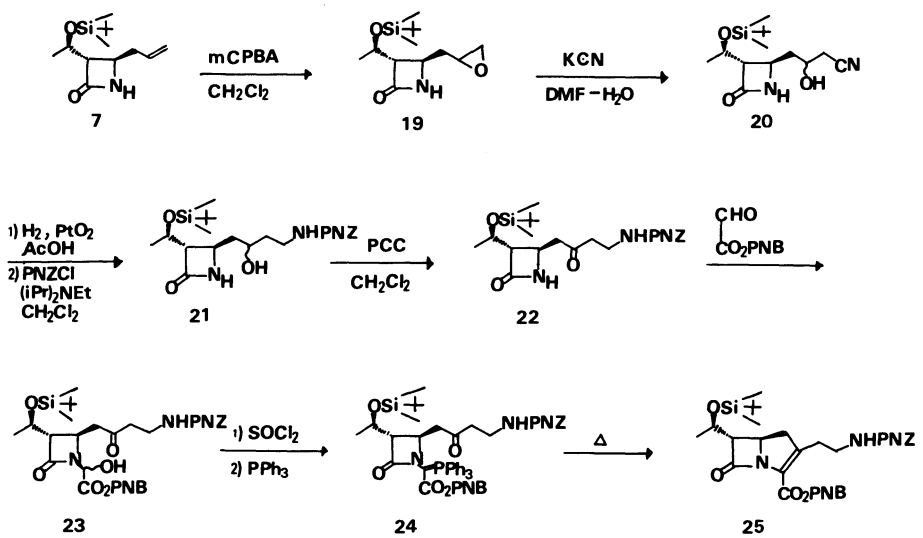

Chart 7.

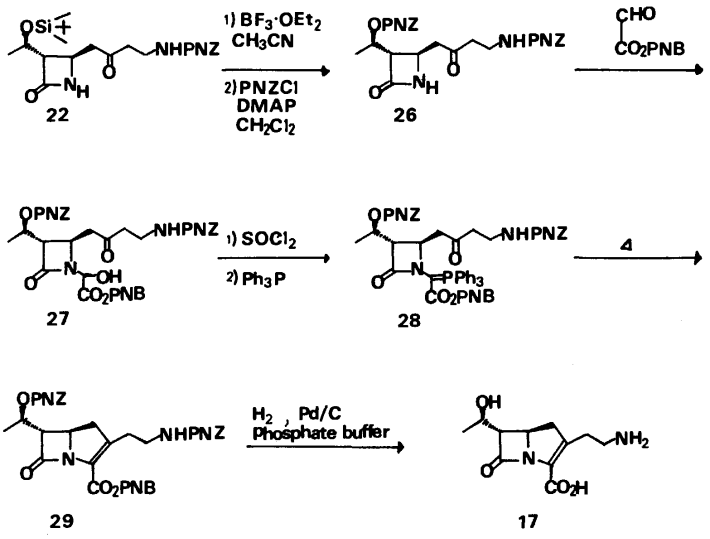

Chart 8.

etherate in acetonitrile were effectively applied to compound **22** to give the 1-hydroxyethyl compound, mp 115—116 °C. The hydroxyl group was reprotected with the *p*-nitrobenzyloxycarbonyl group using *p*-nitrobenzyloxycarbonyl chloride-4-(dimethylamino)-pyridine in dichloromethane to give the compound **26** in 50% isolated yield. The aminal formation reaction between **26** and *p*-nitrobenzyl glyoxylate (water was removed azeotropically before use) was smoothly performed in benzene in the presence of a catalytic amount of triethylamine at 40 °C for 5 min to afford the expected compound **27**. Chlorination and the ylide formation were performed under the standard conditions[12] to afford the ylide **28**. The intramolecular Wittig reaction was successfully applied to the ylide **28** by refluxing in benzene for 5 h to yield the desired carbapenem derivative **29**: IR(neat): 3400, 1775, 1745, 1720 cm^{-1}. The final stage of the synthesis; the deprotection of the *p*-nitrobenzyloxycarbonyl and *p*-nitrobenzyl group of the carbapenem derivative **29**, was achieved hydrogenetically by 10% palladium on carbon in phosphate buffer (pH 7.0), and the purification of the crude product was performed carefully on CHP 20P (75—150 μ) chromatography (water elution) to give the desired dethiathienamycin **17**. The antibacterial activity of dethiathienamycin (**17**) thus obtained is as follows: M.I.C. (μg/ml), Staphylococcus aureus FDA 209P JC 0.01, *Staphylococcus aureus* 56 (PCase+) 0.01, *Escherichia coli* NIHJ JC-2 0.2, *Escherichia coli* 609 (PCase+) 0.4, *Pseudmonas aeruginosa* 1001 12.5, *Klebsiela pneumoniae* 806 0.4. These activities are about one half of those of thienamycin (**16**).

Experimental

General. All melting points are uncorrected. Specific rotations were measured using a Perkin-Elmer 241 polarimater. IR spectra were recorded on JASCO A102 and A320 Infrared spectrometers. NMR spectra were taken using a Varian EM 360L spectrometer (60 MHz) and the chemical shifts are expressed in ppm units using TMS as internal standard: s, singlet; d, doublet; dd, doublet of doublet; ddd, doublet of doublet of doublet; t, triplet; q, quartet; dq, doublet of quartet; m, multiplet. Mass spectra (MS) were measured on JMS 01SG and JMS D300 mass spectrometers. (Preparative) TLC was carried out on Merck TLC-plates silica gel F_{254} Pre-coated, layer thickness: (2 mm) 0.25 mm and spots were made visible by ultraviolet irradiation.

(3*S*,4*R*)-4-Allyl-3-[(*R*)-1-(*t*-butyldimethylsilyloxy)ethyl]-2-azetidinone (7) Reaction of 6 with Tetraallyltin. General Procedure: To a stirred solution of 1 g (3.484 mmol) of (3*R*,4*R*)-4-acetoxy-3-[(*R*)-1-(*t*-butyldimethylsilyloxy)ethyl]-2-azetidinone (**6**) in 20 ml of anhydrous dichloromethane was added 1.46 g (5.166 mmol) of tetraallyltin and 49.5 mg (0.3484 mmol) of boron trifluoride etherate under a nitrogen atmosphere. The resulting yellow solution was stirred at room temperature (rt) for 15 h. Dichloromethane was added and the mixture was washed three times with water and dried over anhydrous magnesium sulfate. The solvent was removed under reduced pressure. Purification of the oil residue by flash column chromatography (cyclohexane-ethyl acetate, 2:1 v/v) afforded 800 mg (85%) of allylazetidinone (**7**):mp 70—77 °C; ^1H NMR ($CDCl_3$) δ=0.06 (6H, s), 0.87 (9H, s), 1.19 (3H, d, J=6 Hz), 2.2—2.5 (2H, m), 2.74 (1H, ddd, J=1.5, 3, and 5 Hz) 3.5—3.85 (1H, m), 3.95—4.35 (1H, m), 4.8—5.9 (3H, m).

Found: C, 62.47; H, 10.05; N, 5.20%. Calcd for $C_{14}H_{27}NO_2Si$: C, 62.40; H, 10.10; N, 5.20%.

Reaction of 6 with Allyltributyltin: To a solution of 60 mg (0.2091 mmol) of **6** in 6 ml of anhydrous dichloromethane was added 200 mg (0.6050 mmol) of allyltributyltin and 10 mg (0.0704 mmol) of boron trifluoride etherate under a nitrogen atmosphere. The resulting yellow solution was stirred at rt for 16 h. Dichloromethane was added and the mixture was washed three times with water and dried over anhydrous magnesium sulfate. The solvent was removed under reduced pressure. The residue was purified

by TLC (cyclohexane-ethyl acetate, 2:1 v/v) to give 40 mg (71%) of the desired product (**7**).

4-Allyl-2-azetidinone (9): To a solution of 550 mg (4.264 mmol) of 4-acetoxy-2-azetidinone in dichloromethane (10 ml) was added 1.4 g (4.95 mmol) of tetraallyltin and 60 mg (0.42 mmol) of boron trifluoride etherate under a nitrogen atmosphere. The resulting yellow solution was stirred at rt for 15 h. Dichloromethane was added and the mixture was washed with water and dried over anhydrous magnesium sulfate. The solvent was removed under reduced pressure. The residue was purified by TLC (cyclohexane-ethyl acetate, 2:1 v/v) to give 350 mg (74%) of the desired product **9**: mp 76—77 °C; ^{1}H NMR ($CDCl_3$) δ=2.2—2.5 (2H, t like), 2.4—2.75 (1H, m), 2.82—3.21 (1H, m), 3.45—3.8 (1H, m), 4.8—6.05 (3H, m), 6.9 (1H, br s).

(3*S*,4*R*)-3-[(*R*)-1-(*t*-Butyldimethylsilyloxy)ethyl]-4-(1-methyl-2-propenyl)-2-azetidinone (11): To a solution of 100 mg of **6** in 2 ml of dichloromethane was added 248 mg of 2-butenyltributyltin and 5 mg of boron trifluoride etherate. The mixture was stirred for 5 h and dichloromethane was added. The solution was washed with aqueous sodium hydrogencarbonate and water, dried over anhydrous magnesium sulfate, and evaporated. The residue was purified by flash column chromatography (cyclohexane-ethyl acetate, 2:1 v/v) to give 78.9 mg (80%) of the desired product **11**: ^{1}H NMR ($CDCl_3$) δ=0.08 (6H, s), 0.78 (9H, s), 1.05 (3H, d, J=6 Hz), 1.17 (3/2H, d, J=6 Hz), 1.21 (3/2H, d, J=6 Hz), 2.6—2.9 (1H, m), 3.2—3.6 (1H, m), 4.12 (1H, quintet, J=6 Hz), 4.8—5.3 (2H, m), 5.3—6.0 (1H, m), 6.0—6.7 (1H, m).

(3*S*,4*R*)-4-Allyl-3-[(*R*)-1-(*p*-nitrobenzyloxycarbonyloxy)ethyl]-2-azetidinone (15): To a solution of 115 mg (0.327 mmol) of (3*R*,4*S*)- or (3*R*,4*R*)-4-acetoxy-3-[(*R*)-1-(*p*-nitrobenzyloxycarbonyloxy)ethyl]-2-azetidinone (**12**, **13**) in 5 ml of anhydrous dichloromethane was added 115 mg (0.407 mmol) of tetraallyltin and 4.64 mg (0.0327 mmol) of boron trifluoride etherate under a nitrogen atmosphere. The resulting yellow solution was stirred at rt for 5 h. Dichloromethane was added and the mixture was washed 3 times with water, and dried over anhydrous magnesium sulfate. The solvent was removed under reduced pressure. The residue was purified by TLC (cyclohexane-ethyl acetate, 2:1 v/v) to give 101 mg (92.6%) of the desired product **15**: IR (neat): 3300 and 1740 cm^{-1} (lactam carbonyl); ^{1}H NMR ($CDCl_3$) δ=1.42 (3H, d, J=6.5 Hz), 2.36 (2H, t, J=6.5 Hz), 3.00 (1H, dd, J=2.5 and 7.5 Hz), 4.9—6.1 (4H, m), 5.20 (2H, s), 6.25 (1H, br s), 7.4—8.3 (4H, A_2B_2 type).

The same procedure with (3*R*,4*S*)-4-benzoyloxy-3-[(*R*)-(*p*-nitrobenzyloxycarbonyloxy)ethyl]-2-azetidinone (**14**) gave **15** in 93% yield.

(3*S*,4*R*)-4-(2,3-Epoxypropyl)-3-[(*R*)-1-(*t*-butyldimethylsilyloxy)ethyl]-2-azetidinone (19): To a solution of 800 mg (2.97 mmol) of 4-allylazetidinone **7** in 20 ml of anhydrous dichloromethane was added 780 mg (4.52 mmol) of *m*-chloroperbenzoic acid in an ice bath. The mixture was stirred at rt for 15 h. The reaction mixture was washed with 5% aqueous sodium hydrogenecarbonate and water successively, and dried over anhydrous magnesium sulfate. The solvent was removed under reduced pressure to give 650 mg of the desired product **19**. One of the diastereomers was recrystallized from petroleum ether: mp 83.5 °C;R_f= 0.45 (cyclohexane-ethyl acetate 1:2 v/v); IR (nujol) 3140, 3080, 1760, 1712 cm^{-1}; ^{1}H NMR ($CDCl_3$) δ=0.08 (6H, s), 0.89 (9H, s), 1.19 (3H, d, J=6 Hz), 1.5—2.1 (2H, m), 2.3—3.1 (5H, m), 3.6—4.4 (2H, m).

Found: C, 59.02; H, 9.45; N, 4.89%. Calcd for $C_{14}H_{27}NO_3Si$: C, 58.91; H, 9.53; N, 4.90%.

(3*S*,4*R*)-4-(3-Cyano-2-hydroxypropyl)-3-[(*R*)-1-(*t*-butyldimethylsilyloxy)ethyl]-2-azetidinone (20): To a solution of 500 mg (1.75 mmol) of **19** in 3 ml of DMF and 1 ml of water was added 250 mg (3.85 mmol) of potassium cyanide. The mixture was stirred at rt for 15 h. Ethyl acetate was added and the reaction mixture was washed with water and dried over anhydrous magnesium sulfate. The solvent was removed under reduced pressure. Purification of an oily residue by flash column chromatography (cyclohexane-ethyl acetate, 1:2 v/v) afforded 420 mg (77%) of the desired product **20**. One of the diastereomers crystallized from petroleum ether and ethyl acetate: mp 120—125 °C; IR (nujol) 3330, 2240(CN), 1700 cm^{-1} (lactam C=O); ^{1}H NMR ($CDCl_3$) δ=0.08 (6H, s), 0.89 (9H, s), 1.21 (3H, d, J=6 Hz), 1.7—2.1 (2H, m), 2.45—3.0 (3H, m), 3.5—4.4 (3H, m), 6.6 (1H, br s).

Found: C, 57.87; H, 9.05; N, 8.92%. Calcd for $C_{15}H_{28}N_2O_3Si$: C, 57.66; H, 9.03; N, 8.96%.

(3*S*,4*R*)-3-[(*R*)-1-(*t*-Butyldimethylsilyloxy)ethyl]-4-[(*p*-nitrobenzyloxycarbonylamino)-2-hydroxybutyl]-2-azetidinone (21): A mixture of 821 mg (2.63 mmol) of **20** and 42 mg of platinum oxide in 8 ml of glacial acetic acid was stirred under a hydrogen atmosphere at 1 atm for 5 h. The mixture was filtered through Celite and evaporated to give the desired amino derivative.

To a solution of the amino derivative thus obtained in 5 ml of dichloromethane was added 850.7 mg (3.95 mmol) of *p*-nitrobenzyl chloroformate and 1.02 g (7.91 mmol) of *N*,*N*-diisopropylethylamine. The mixture was stirred at rt overnight. Ethyl acetate (50 ml) was added and the mixture was washed with water two times and dried over anhydrous magnesium sulfate. The solvent was removed under reduced pressure. Purification of a residue by flash column chromatography (cyclohexane-ethyl acetate, 1:10 v/v) afforded 612.7 mg (47%) of the desired product **21** as a 3:5 mixture of diastereomers. Diastereomer I: R_f=0.55 (ethyl acetate); ^{1}H NMR ($CDCl_3$) δ=0.12 (6H,s), 0.89 (9H, s), 1.25 (3H, d, J=6 Hz), 1.4—2.0 (4H, m), 2.7—3.1 (1H, m), 2.0—4.4 (6H, m), 5.13 (2H, s), 5.63 (1H, t, J=6 Hz), 6.69 (1H, s), 7.3—8.3 (4H, m). Diastereomer II: R_f=0.50 (ethyl acetate); ^{1}H NMR ($CDCl_3$) δ=0.08 (6H, s), 0.88 (9H, s), 1.22 (3H, d, J=6 Hz), 1.4—2.1 (4H, m), 2.6—3.0 (1H, m), 3.0—4.1 (5H, m), 3.9—4.3 (1H, m), 5.16 (2H, s), 5.66 (1H, t, J=6 Hz), 6.65 (1H, s), 7.3—8.2 (4H, m).

(3*S*,4*R*)-3-[(*R*)-1-(*t*-Butyldimethylsilyloxy)ethyl]-4-[4-(*p*-nitrobenzyloxycarbonylamino)-2-oxobutyl]-2-azetidinone (22): To a solution of 368.6 mg (0.754 mmol) of **21** in 25 ml of dichloromethane was added 1.12 g (5.20 mmol) of pyridinium chlorochromate. The mixture was stirred at rt for 3 h and filtered through Celite. Dichloromethane was added to the filtrate and the solution was washed with water two times and dried over anhydrous magnesium sulfate. The solvent was removed under reduced pressure. The residue was purified by TLC (cyclohexane-ethyl acetate, 1:2 v/v) to give 242.9 mg (66%) of the desired product **22**: R_f=0.6

(cyclohexane-ethyl acetate, 1:2 v/v); ^{1}H NMR ($CDCl_3$) δ= 0.07 (6H, s), 0.86 (9H, s), 1.19 (3H, d, J=5.4 Hz), 2.4—3.0 (4H, m), 3.42 (2H, q like, J=6 Hz), 3.7—4.1 (1H, m), 3.9—4.4 (1H, m), 5.13 (2H, s), 5.70 (1H, br t, J=6 Hz), 6.52 (1H, br s), 7.3—8.2 (4H, m).

***p*-Nitrobenzyl 2-[(3*S*,4*R*)-3-[(*R*)-1-(*t*-Butyldimethylsilyloxy)-ethyl]-4-[4-(*p*-nitrobenzyloxycarbonylamino)-2-oxobutyl]-2-oxo-1-azetidinyl]-2-hydroxyacetate (23):** A mixture of 242.9 mg (0.4297 mmol) of **22** and 250 mg (1.10 mmol) of *p*-nitrobenzyl glyoxylate monohydrate in 100 ml of benzene was refluxed overnight. Triethylamine was added to this solution and the mixture was refluxed for 6 h. The solvent was removed under reduced pressure. A residue was purified by TLC (hexane-ethyl acetate-acetone, 8:6:3 v/v) to give 258.1 mg (86%) of the desired product **23** as a mixture of two diastereomers: R_f=0.55, 0.50 (hexane-ethyl acetate-acetone, 8:6:3 v/v); ^{1}H NMR ($CDCl_3$) δ=0.02 (3H, s), 0.05 (3H, s), 0.84 (9H, s), 1.22 (3H, d, J=6.4 Hz), 1.7—2.1 (1H, m), 2.4—3.2 (4H, m), 3.2—4.5 (5H, m), 5.0—6.0 (6H, m), 7.2—7.8 (4H, m), 7.9—8.5 (4H, m).

***p*-Nitrobenzyl 2-[(3*S*,4*R*)-3-[(*R*)-1-(*t*-Butyldimethylsilyloxy)-ethyl]-4-[4-(*p*-nitrobenzyloxycarbonylamino)-2-oxobutyl]-2-oxo-1-azetidinyl]-2-triphenylphosphoranylideneacetate (24):** To a solution of 258.1 mg (0.3677 mmol) of **23** in 22 ml of THF was added 0.064 ml of 2,6-lutidine. The mixture was cooled to −30 °C and 0.04 ml of thionyl chloride was added. The reaction mixture was stirred for 1 h and the precipitate formed was filtered through Celite. The solvent was removed under reduced pressure to give a crude chloro derivative.

The chloro derivative was dissolved in 14 ml of dioxane and 192 mg (0.733 mmol) of triphenylphosphine and 0.09 ml of 2,6-lutidine was added to this solution. The mixture was stirred at rt overnight. Ethyl acetate was added and the solution was washed with water two times and dried over anhydrous magnesium sulfate. The solvent was removed under reduced pressure. A residue was purified by TLC (hexane-ethyl acetate-acetone, 10:6:3 v/v) to give 93.5 mg (27%) of the desired product **24** and 24.7 mg (8%) of the desilylated phosphorane.

***p*-Nitrobenzyl (5*R*,6*S*)-6-[(*R*)-1-(*t*-Butyldimethylsilyloxy)-ethyl]-3-[2-(*p*-nitrobenzyloxycarbonylamino)ethyl]-7-oxo-aza-bicyclo[3.2.0]hept-2-ene-2-carboxylate (25):** To a solution of 165.8 mg (0.175 mmol) of **24** in 80 ml of dry benzene was added catalytic amount of hydroquinone. The mixture was refluxed for 5 h. The solvent was removed under reduced pressure and a residue was purified by medium pressure liquid chromatography on silica gel (cyclohexane-ethyl acetate, 2:3 v/v) to give 85 mg (73%) of the desired product **25**: R_f=0.4 (cyclohexane-ethyl acetate, 2:3 v/v); ^{1}H NMR ($CDCl_3$) δ=0.09 (6H, s), 0.86 (9H, s), 1.23 (3H, d, J=6.6 Hz), 2.4—3.7 (7H, m), 3.8—4.5 (2H, m), 4.8—5.4 (1H, m), 5.08 (2H, s), 5.1—5.4 (2H, m), 7.2—7.8 (4H, m), 7.8—8.4 (4H, m); IR(neat) 3380, 1765 (lactam C=O), 1715(NHC=O) cm^{-1}.

Found: C, 57.66; H, 6.15; N, 8.38%. Calcd for $C_{32}H_{40}N_4O_{10}Si$: C, 57.47; H, 6.03; N, 8.38%.

(3*S*,4*R*)-3-[(*R*)-1-Hydroxyethyl]-4-[4-(*p*-nitrobenzyloxycarbonylamino)-2-oxobutyl]-2-azetidinone: To a solution of 248.9 mg (0.5049 mmol) of **22** in 6 ml of acetonitrile was added 0.125 ml of boron trifluoride etherate under ice cooling. The mixture was stirred for 18 min in an ice bath and then cooled aqueous sodium hydrogencarbonate was added. The organic layer was extracted with ethyl acetate. The extracts were washed with water two times and dried over anhydrous magnesium sulfate. The solvent was removed under reduced pressure and a residue was purified by medium pressure liquid chromatography on silica gel (dichloromethane-ethanol, 10:1 v/v) to give 165.5 mg (90%) of the desired product as white crystals: mp 115—116 °C; R_f=0.1 (ethyl acetate); IR (KBr pellet) 3340, 1755 (lactam C=O), 1700, 1680 cm^{-1}; ^{1}H NMR (aceton-d_6) δ=1.18 (3H, d, J=6.2 Hz), 2.5—3.0 (4H, m), 2.89 (2H, d, J=6.2 Hz), 3.1—3.6 (2H, m), 3.6—4.2 (3H, m), 5.14 (2H, s), 7.3—7.8 (2H, m), 8.0—8.4 (2H, m).

Found: C, 53.69; H, 5.54; N, 11.07%. Calcd for $C_{17}H_{21}N_3O_7$: C, 53.75; H, 5.70; N, 11.06%.

(3*S*,4*R*)-4-[4-(*p*-Nitrobenzyloxycarbonylamino)-2-oxobutyl]-3-[(*R*)-1-(*p*-nitrobenzyloxycarbonyloxy)ethyl]-2-azetidinone (26): A solution of 471.5 mg (1.292 mmol) of the hydroxy derivative in 3 ml of dichloromethane was cooled in an ice bath and 315.9 mg (2.589 mmol) of 4-(dimethylamino)pyridine was added. A solution of 1.39 g (6.45 mmol) of *p*-nitrobenzyl chloroformate in 5 ml of dichloromethane was added slowly for 6.5 h and stirred for 30 min. The reaction mixture was washed with water, dil hydrochloric acid, and dil aqueous sodium hydrogencarbonate successively and dried over anhydrous magnesium sulfate. The solvent was removed under reduced pressure and the residue was purified by medium pressure liquid chromatography on silica gel (ethyl acetate) to give 465.2 mg (66%) of the desired product **26**: ^{1}H NMR ($CDCl_3$) δ=1.42 (3H, d, J=6 Hz), 2.3—4.1 (9H, m), 5.10 (2H, s), 4.2—4.7 (1H, m), 6.50 (1H, br s), 7.2—7.7 (4H, m), 7.9—8.4 (4H, m).

***p*-Nitrobenzyl 2-Hydroxy-2-[(3*S*,4*R*)-4-[4-(*p*-nitrobenzyloxycarbonylamino)-2-oxobutyl]-3-[(*R*)-1-(*p*-nitrobenzyloxycarbonyloxy)ethyl]-2-oxo-1-azetidinyl]acetate (27):** A mixture of 387.9 mg (1.709 mmol) of *p*-nitrobenzyl glyoxylate (water was removed azeotropically before use), 465 mg (0.855 mmol) of **26**, and 1 drop of triethylamine in 100 ml of benzene was stirred at 40 °C for 5 min. The solvent was removed under reduced pressure and a residue was purified by medium pressure liquid chromatography (dichloromethane-THF, 7:1 v/v) to give the desired products as a mixture of diastereomers. Diastereomer I: 208 mg (32%); R_f=0.4 (dichloromethane-THF, 7:1 v/v); ^{1}H NMR ($CDCl_3$) δ=1.39 (3H, d, J=6 Hz), 2.2—4.7 (11H, m), 5.10 (2H, s), 5.17 (2H, s), 5.21 (2H, s), 4.7—5.4 (1H, m), 7.2—7.6 (6H, m), 7.9—8.3 (6H, m). Diastereomer II: 322.1 mg (49%); R_f=0.3 (dichloromethane-THF, 1:1 v/v); ^{1}H NMR ($CDCl_3$) δ=1.39 (3H, d, J=6 Hz), 2.4—4.6 (11H, m), 5.10 (2H, s), 4.7—5.8 (3H, m), 5.17 (2H, s), 7.1—7.8 (6H, m), 7.8—8.4 (6H, m).

***p*-Nitrobenzyl 2-[(3*S*,4*R*)-4-[4-(*p*-Nitrobenzyloxycarbonylamino-2-oxobutyl]-3-[(*R*)-1-(*p*-nitrobenzyloxycarbonyloxy)-ethyl]-2-oxo-1-azetidinyl]-2-phosphoranylideneacetate (28):** To a solution of 530 mg (0.691 mmol) of **27** in 7 ml of THF was added 0.14 ml of 2,6-lutidine. The mixture was cooled to −20 °C and 0.07 ml of thionyl chloride was added. The reaction mixture was stirred for 30 min and the precipitate formed was filtered through Celite. The solvent was removed under reduced pressure to give a crude chloro derivative.

The crude chloro derivative was dissolved in 7 ml of dioxane, and 540.6 mg (2.063 mmol) of triphenylphosphine and 0.25 ml of 2.6-lutidine was added to this solution. The

mixture was stirred at rt for 3 h and at 40 °C for 13 h. After cooling, ethyl acetate was added and the solution was washed with water two times and dried over anhydrous magnesium sulfate. The solvent was removed under reduced pressure and the residue was purified by medium pressure liquid chromatography (cyclohexane–ethyl acetate, 1:10 v/v) to give 481 mg (69%) of the desired product **28**: R_f=0.3 (cyclohexane–ethyl acetate, 1:10 v/v); ^{1}H NMR ($CDCl_3$) δ=1.12 (3H, d, J=6.2 Hz), 2.3—3.0 (5H, m), 3.0—3.7 (4H, m), 4.5—4.9 (1H, m), 4.9—6.3 (6H, m), 7.1—8.0 (21H, m), 7.9—8.3 (6H, m).

***p*-Nitrobenzyl (5*R*,6*S*)-3-[2-(*p*-Nitrobenzyloxycarbonyl amino)ethyl]-6-[(*R*)-1-(*p*-nitrobenzyloxycarbonyloxy)ethyl]-7-oxo-1-azabicyclo[3.2.0]hept-2-ene-2-carboxylate (29):** To a solution of 503.3 mg (0.4973 mmol) of **28** in 100 ml of dry benzene was added catalytic amount of hydroquinone. The mixture was refluxed for 5 h and the solvent was removed under reduced pressure. A residue was purified by flash column chromatography (dichrolomethane–ether, 20:1 v/v) to give 194.5 mg (54%) of the desired product **29**: R_f=0.2 (dichrolomethane–ether, 20:1 v/v); IR(neat) 3400, 1775, 1745, 1720 cm^{-1}; ^{1}H NMR ($CDCl_3$) δ=1.46 (3H, d, J=6.2 Hz), 2.3—3.7 (7H, m), 3.7—4.5 (1H, m), 4.7—5.4 (8H, m), 7.1—7.8 (6H, m), 7.8—8.4 (6H, m).

(5*R*,6*S*)-3-(2-Aminoethyl)-6-[(*R*)-1-hydroxyethyl]-7-oxo-1-azabicyclo[3.2.0]hept-2-ene-2-carboxylic Acid (Dethiathienamycin) 17: A mixture of 194.5 mg (0.2705 mmol) of **29** and 58.3 mg of 10% palladium on carbon in 3.8 ml of THF and 3.8 ml of phosphate buffer (pH 7.0) was stirred under a hydrogen atmosphere (1 atm) for 2 h. The mixture was filtered through Celite and evaporated and the residue was chromatographed on CHP-20P (75—150 μ) (water elution) to give 14.9 mg (23%) of the desired product **17**: UV (water) 267 nm; ^{1}H NMR (D_2O, DSS) δ=1.22 (3H, d, J=6 Hz).

References

1) Part VII: K. Fujimoto Y. Iwano, S. Sugawara, and K. Hirai, *Chem. Pharm. Bull.*, in press; A part of this work was presented at the 51st National Meeting of the Chemical Society of Japan, Tokyo, April, 1985, Abstr., No. 4P17 Preliminary Communication: K. Fujimoto, Y. Iwano, and K. Hirai, *Tetrahedron Lett.*, **26**, 89 (1985).

2) W. J. Leanza, K. J. Wildonger, J. Hannah, D. H. Shih, R. W. Ratcliffe, L. Barash, E. Walton, R. A. Firestone, G. F. Patel, F. M. Kahan, J. S. Kahan, and B. G. Christensen, Recent Advances in the Chemistry of β-Lactam Antibiotics, second international symposium, Cambridge, England, ed. G. I. Gregory, The Royal Society of Chemistry p. 240 (1980).

3) A. Morimoto, T. Miyawaki, K. Yoshioka, the 101st Annual meeting of the Pharmaceutical Society of Japan, Kumamoto, April, 1981, Abstr., No. 3Na3-2.

4) T. Kametani, K. Fukumoto, and M. Ihara, *Heterocycles*, **17**, 463 (1982) and the references cited therein.

5) A. G. M. Barret and P. Quayle, *J. Chem. Soc., Chem. Commun.*, **1981**, 1076; A. Yosida, Y. Tajima, and S. Oida, *Tetrahedron Lett.*, **25**, 2793 (1984); S. Karady, J. S. Amato, R. A. Reamer, and L. M. Weinstock, *J. Am. Chem. Soc.*, **103**, 6765 (1981); P. J. Reider, R. Rayford, and E. J. J. Grabowski, *Tetrahedron Lett.*, **23**, 379 (1982).

6) I. Ernest, *Tetrahedron*, **33**, 547 (1977); K. Prasad, G. Schulz, C.-P. Mak, H. Hamberger, and P. Stütz, *Heterocycles*, **16**, 1305 (1981); K. Prasad, D. Kneussel, G. Schulz, and P. Stütz, *Tetrahedron Lett.*, **23**, 1247 (1982); T. Kametani, N. Kanaya, T. Mochizuki, and T. Honda, *Heterocycles*, **19**, 1023 (1982).

7) K. Hirai, Y. Iwano, and K. Fujimoto, *Tetrahedron Lett.*, **23**, 4025 (1982).

8) F. A. Cotton and G. Wilkinson, F. R. S., "Advanced Inorganic Chemistry," 3rd ed. John Wiley & Sons, Inc., New York, London, Sydney, Toronto (1972), pp. 309, 335.

9) T. Kobayashi, N. Ishida, and T. Hiraoka, *J. Chem. Soc., Chem. Commun.*, **1980**, 736.

10) Y. Yamamoto, H. Yatagai, Y. Naruta, and K. Maruyama, *J. Am, Chem. Soc.*, **102**, 7109 (1980); Y. Yamamoto, H. Yatagai, Y. Ishihara, N. Maeda, and K. Maruyama, *Tetrahedron*, **40**, 2239 (1984); Y. Yamamoto, T. Komatsu, and K. Maruyama, *J. Org, Chem.*, **50**, 3115 (1985); Y. Ueno, S. Aoki, and M. Okawara, *J. Am. Chem. Soc.*, **101**, 5414 (1979).

11) D. R. Kelly, S. M. Roberts, and R. F. Newton, *Synthetic Commun.*, **9**, 295 (1979).

12) R. Scartazzini, H. Peter, H. Bickel, K. Heusler, and R. B. Woodward, *Helv. Chim. Acta*, **15**, 408 (1972).

A Revised Primary Structure of Neocarzinostatin Using the Combination of Endopeptidase, Carboxypeptidase Y and Fast Atom Bombardment Mass Spectrometry

Kazuo HIRAYAMA,* Toshihiko ANDO, Rei TAKAHASHI, and Asao MURAI
Central Research Laboratories, Ajinomoto Co., Inc., Kawasaki, Kanagawa 210
(Received July 26, 1985)

The amino acid sequence of antitumor protein neocarzinostatin was revised and confirmed on the basis of mass spectrometric studies. Fast atom bombardment mass spectrometric experiments on neocarzinostatin and its tryptic, chymotryptic, staphylococcal protease, and carboxypeptidase Y digested peptides gave the molecular weights of various peptides and, in some cases, partial sequence information. These experiments gave a revised sequence, Glu(105)-Pro(106) to Pro(105)-Glu(106) and Asp(60) to Asn(60). The peptide fragments produced by these endopeptidase cleavage completely covered the full sequence of neocarzinostatin. Thirty-five of the 113 amino acids were determined by the carboxypeptidase Y digestion.

Mass spectrometric techniques have been used a number of times in the determination of the primary structure of peptides and proteins. Fragmentation of the electron impact method has been used for a long time in this area. Over the last year, new ionization techniques, field desorption (FD) mass spectrometry and fast atom bombardment (FAB) mass spectrometry, have been developed. These are paticularly suitable for underivatized peptides producing rather abundant molecular ions (M^+) or protonated molecular ions (MH^+). It is difficult to determine the primary structure of peptides by mass spectrometry alone. Shimonishi et al. established the combination of FD or FAB mass spectrometry with Edman degradation or exopeptidase digestion.[1-10] These techniques are suitable for peptide mixtures and may prove to be a valuable approach technique for the sequence determination of peptides and proteins.

Neocarzinostatin is an antitumor antibiotic protein[11-15] isolated from culture filtrates of *Streptomyces carzinostaticus*.[11] It is a single-chain polypeptide constituted of 113 amino acids and exists as an apoprotein and an associated nonprotein chromophore. The amino acid sequence of neocarzinostatin was first reported in 1972 by Maeda et al. using the Edman degradation method.[16,17] The structure of neocarzinostatin was corrected in 1982 by Biemann by a combination of tryptic and chymotryptic digestion, FABMS and GCMS (Fig. 1).[18] Recently, we found that there were a number of peptides from staphylococcal protease digests with m/z that conformed to the published sequence (Fig. 1), indicating the correctness of these regions, and two (m/z 706.9 and 2753.3) that did not. This clearly shows that the sequence is in error. Therefore, we reinvestigated the previously proposed primary structure of neocarzinostatin by a combination of endopeptidase, carboxypeptidase Y and FABMS without the Edman degradation method. Consequently, we found that Glu(105)-Pro(106) must be corrected to Pro(105)-Glu(106) and Asp(60) must be replaced with Asn(60) in Fig. 1. Recently, Biemann and coworkers published the revised primary structure of neocarzinostatin, in which Glu(105)-Pro(106) was corrected to Pro(105)-Glu(106) by our indication and by their GCMS data.[19] In addition, the structure of the chromophore was determined in 1985.[20]

We report in this paper the revised primary structure of neocarzinostatin and the reason for the exchange of Glu(105)-Pro(106) for Pro(105)-Glu(106)

```
                                        10                                  20
Ala-Ala-Pro-Thr-Ala-Thr-Val-Thr-Pro-Ser-Ser-Gly-Leu-Ser-Asp-Gly-Thr-Val-Val-Lys-

                                        30                                  40
Val-Ala-Gly-Ala-Gly-Leu-Gln-Ala-Gly-Thr-Ala-Tyr-Asp-Val-Gly-Gln-Cys-Ala-Trp-Val-

*                                       50                                  60
Asp-Thr-Gly-Val-Leu-Ala-Cys-Asp-Pro-Ala-Asn-Phe-Ser-Ser-Val-Thr-Ala-Asp-Ala-Asp-

                                        70                                  80
Gly-Ser-Ala-Ser-Thr-Ser-Leu-Thr-Val-Arg-Arg-Ser-Phe-Glu-Gly-Phe-Leu-Phe-Asp-Gly-

                                        90                                 100
Thr-Arg-Trp-Gly-Thr-Val-Asn-Cys-Thr-Thr-Ala-Ala-Cys-Gln-Val-Gly-Leu-Ser-Asp-Ala-

                                       110
Ala-Gly-Asp-Gly-Glu-Pro-Gly-Val-Ala-Ile-Ser-Phe-Asn
```

Fig. 1. The primary structure of neocarzinostatin.
* Asn of original report seems to be a misprint.

and the replacement Asp(60) with Asn(60) by the combination of the enzymatic cleavage (trypsin, chymotrypsin, staphylococcal protease), carboxypeptidase Y digestion and FABMS.

Experimental

Mass Spectrometry. Positive ion FAB mass spectra were recorded with a JMS HX-100 double focusing mass spectrometer fitted with a 23 kilogauss high field magnet, operating at accelerating voltages at 5 kV. The atom emission gun current of 20 mA was maintained at 6 kV for the generation of the xenon fast atom beam. Mass spectra were recorded with a JMA-3500 mass data system. A sample of the underivatized peptides was prepared by dissolving c. 5 μg samples in c. 1.5 μl of 1:1 glycerol–1 M† HCl. This solution was deposited on a stainless steel sample stage for introduction into the mass spectrometer ion source on the end of an axially mounted sample introduction probe.

Reagents and Enzymes. Dithiothreitol and iodoacetic acid were obtained from Wako Pure Chemical Industries Ltd., (Japan). Staphylococcal protease was purchased from Miles Laboratories Inc., (U.S.A.). Trypsin and chymotrypsin were from Sigma Chemical Co., (U.S.A.) and carboxypeptidase Y from Oriental Yeast Co., Ltd. (Japan).

Reduced and Carboxymethylated Neocarzinostatin. Commercially available neocarzinostatin (Yamanouchi Seiyaku Co., Inc.) was dialyzed against water and lyophilized. The crude neocarzinostatin was washed with methanol several times, dialyzed against water and lyophilized. Five μmol of neocarzinostatin was dissolved in 6 ml of Tris/HCl buffer (pH 8.0) containing 8 M urea and 0.2% EDTA. After addition of 300 μmol of dithiothreitol, the mixture was gassed with nitrogen for 10 min before heating for 3 h at 50 °C and was allowed to stand overnight in the dark at room temperature. To this mixture 100 mg of iodoacetic acid in 0.6 ml of 1 M NaOH were added. Alkylation was conducted at pH 8.0 or 8.5 by addition of 1 M NaOH. After 30 min the mixture was dialyzed against 0.2 M acetic acid and lyophilized.

Enzymatic Digestion (a) Trypsin: Under the standard conditions of 50:1 molar ratio of substrate to trypsin in 50 μl of 0.2 M ammonium acetate buffer (pH 8.0), 0.5 mg of the reduced and carboxymethylated neocarzinostatin was digested. The solution was incubated at 25 °C for 6 h. The hydrolysis was stopped by freezing and lyophilizing the solution.

(b) Chymotrypsin: The reduced and carboxymethylated neocarzinostatin (0.5 mg) or its endopeptidase digested peptides (0.5 mg) were treated under the conditions of 200:1 molar ratio of substrate to chymotrypsin in 50 μl of 0.2 M ammonium acetate buffer (pH 8.0). The solution was incubated at 25 °C for 30 min. The hydrolysis was stopped by freezing and lyophilising the solution.

(c) Staphylococcal Protease: The reduced and carboxymethylated neocarzinostatin (0.5 mg) was digested under the conditions of a 50:1 molar ratio of substrate to staphylococcal protease in 50 μl of 5 mM ammonium carbonate buffer (pH 8.8). The solution was incubated at 37 °C for 24 h. The hydrolysis was stopped by freezing and lyophilising the solution.

(d) Carboxypeptidase Y: After digestion by endopeptidase, the subpeptides were lyophilised and added to 100 μl of 0.05% pyridine–acetate buffer (pH 6.0) containing 20 μg of carboxypeptidase Y. The enzyme digestion was carried out at 37 °C, and aliquots were removed from the reaction mixture at different time intervals (1 min, 10 min, 1 h, 2 h) and isolated by freeze-drying.

Results and Discussion

(a) Chymotryptic Peptide: The positive ion FAB mass spectrum of the chymotryptic digest of the reduced and carboxymethylated neocarzinostatin indicated the presence of at least seven peptides shown in Fig. 2. Each peptide appears as the corresponding protonated molecular ions, MH^+. Five of the seven chymotryptic peptides (C1, C2, C5, C6, and C7) fit the published sequence on the basis of chymotrypsin specificity. The peptides C3 and C4 did not fit any fragment expected from the enzyme specificity (Table 1). If either Asp(57) or Asp(60) is replaced by Asn, C3 and C4 are matched to the position Ala(46)–Leu(67) and Ser(53)–Leu(67) in Fig. 1, respectively, on the basis of their m/z and chymotrypsin specificity.

(b) Tryptic Peptide: Only two of the four expected peptides could be found in the positive ion FAB mass spectrum of the tryptic peptides of the reduced and carboxymethylated neocarzinostatin; those with m/z=1859.0 (T1) and 1275.5 (T2) (data not shown). The other two peptides could not be found because they were too large to be observed by the spectrometer. The two tryptic peptides were matched with the sequence shown in Fig. 1 on the basis of

† 1 M=1 mol dm^{-3}.

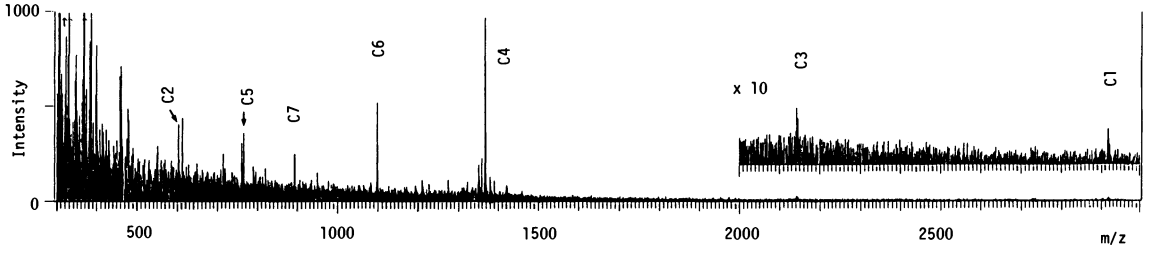

Fig. 2. The positive ion FAB mass spectrum of the chymotryptic digest of the reduced and carboxymethylated neocarzinostatin.

Table 1. Peptides Generated by Enzymatic Cleavage of the Reduced and Carboxymethylated Neocarzinostatin

Peptide	Observed mass value	Theoretical[a] mass value	Matching section (based on enzyme specificity) of:	
			Structure shown in Fig. 1.	Structure shown in Fig. 7.
C1	2918.8	2918.50	Ala (1)-Tyr (32)	Ala (1)-Tyr (32)
C2	603.3	603.33	Val (40)-Leu (45)	Val (40)-Leu (45)
C3	2144.0	2143.90	None	Ala (46)-Leu (67)
C4	1367.6	1367.62	None	Ser (53)-Leu (67)
C5	765.2	765.43	Thr (68)-Phe (73)	Thr (68)-Phe (73)
C6	1098.4	1098.56	Thr (68)-Phe (76)	Thr (68)-Phe (76)
C7	894.4	894.44	Leu (77)-Trp (83)	Leu (77)-Trp (83)
T1	1859.0	1858.97	Ala (1)-Lys (20)	Ala (1)-Lys (20)
T2	1275.5	1275.59	Ser (72)-Arg (82)	Ser (72)-Arg (82)
ST1	1374.5	1374.67	Ala (1)-Asp (15)	Ala (1)-Asp (15)
ST2	503.7	503.31	Gly (16)-Lys (20)	Gly (16)-Lys (20)
ST3	1193.2	1193.59	Val (21)-Asp (33)	Val (21)-Asp (33)
ST4	935.3	935.39	Val (34)-Asp (41)	Val (34)-Asp (41)
ST5	1725.8	1725.76	Thr (42)-Asp (58)	Thr (42)-Asp (58)
ST6	1163.3	1163.59	None	Ala (59)-Arg (70)
ST7	598.8	598.28	Gly (75)-Asp (79)	Gly (75)-Asp (79)
ST8	2439.5	2439.00	None	Trp (83)-Glu (106)
ST9	707.1	707.36	None	Gly (107)-Asn (113)
SC1	1374.6	1374.67	Ala (1)-Asp (15)	Ala (1)-Asp (15)
SC2	1677.7	1677.87	Gly (16)-Asp (33)	Gly (16)-Asp (33)
SC3	935.3	935.39	Val (34)-Asp (41)	Val (34)-Asp (41)
SC4	1165.3	1165.51	Thr (42)-Phe (52)	Thr (42)-Phe (52)
SC5	1367.4	1367.62	None	Ser (53)-Leu (67)
SC6	1007.5	1007.56	Leu (67)-Glu (74)	Leu (67)-Glu (74)
SC7	598.8	598.28	Gly (75)-Asp (79)	Gly (75)-Asp (79)
SC8	2753.1	2753.17	None	Gly (80)-Glu (106)
SC9	707.1	707.36	None	Gly (107)-Asn (113)

a) Calculated from the revised sequence.

their trypsin specificity (Table 1).

In order to determine the amino acid sequence of the tryptic peptides, they were subjected to chymotryptic cleavage and carboxypeptidase Y digestion. Figure 3 shows the positive ion FAB mass spectra of the chymotryptic peptides and of the digest with carboxypeptidase Y. The chymotryptic subpeptides TC1, TC2, TC3, TC5, TC6, and TC7 fit the sequence on the basis of their trypsin and chymotrypsin specificity. The peptide TC4 did not conform to enzyme specificity. After treatment with carboxypeptidase Y, subpeptide TC1(m/z 1858.6) gave mass peaks at m/z 1631.7, m/z 1532.8, and m/z 1431.5, on the FAB mass spectra. The results indicated that the C-terminal sequence of TC1 was -Thr-Val-[Val, Lys] (see Table 2). Similarly, the mass peaks at m/z 915.5, m/z 844.2, m/z 743.2, m/z 686.2, and m/z 615.0 from the subpeptide TC2 (m/z 1078.1) indicated that the C-terminal sequence of TC2 was -Ala-Gly-Thr-Ala-Tyr. In the same way, the mass peaks at m/z 490.2 from the subpeptide TC3 (m/z 603.7) showed that the C-terminus of TC3 was -Leu (or Ile). In the same manner, the mass peaks at m/z 1254.3, m/z 1167.5, m/z 1066.3, m/z 979.3, m/z 908.3, m/z 821.1, m/z 650.1, and m/z 579.6 from the subpeptide TC4 (m/z 1367.2) indicated that the C-terminal sequence of TC4 was -Ala-[Asn, Gly]-Ser-Ala-Ser-Thr-Ser-Leu(or Ile). If 60th amino acid residue is Asp, these mass peaks must be m/z 1255, m/z 1168, m/z 1067, m/z 980, m/z 909, m/z 822, m/z 650, and m/z 579. Accordingly it was necessary to replace Asp(60) with Asn in Fig. 1. Furthermore, the mass peaks at m/z 2666.9, m/z 2496.0, m/z 2439.1, and m/z 2309.8 from the subpeptide TC7(m/z 3126.9) indicated that the C-terminal sequence of TC7 was -Glu-Gly-[Val, Ala]-[Ile(or Leu), Ser, Phe, Asn]. These results show that the 106th amino acid residue of the sequence must be Glu.

(c) Staphylococcal Protease Digested Peptides: Two FABMS experiments were carried out on the staphylococcal protease digested peptides. First, the staphylococcal protease digested peptides were hydro-

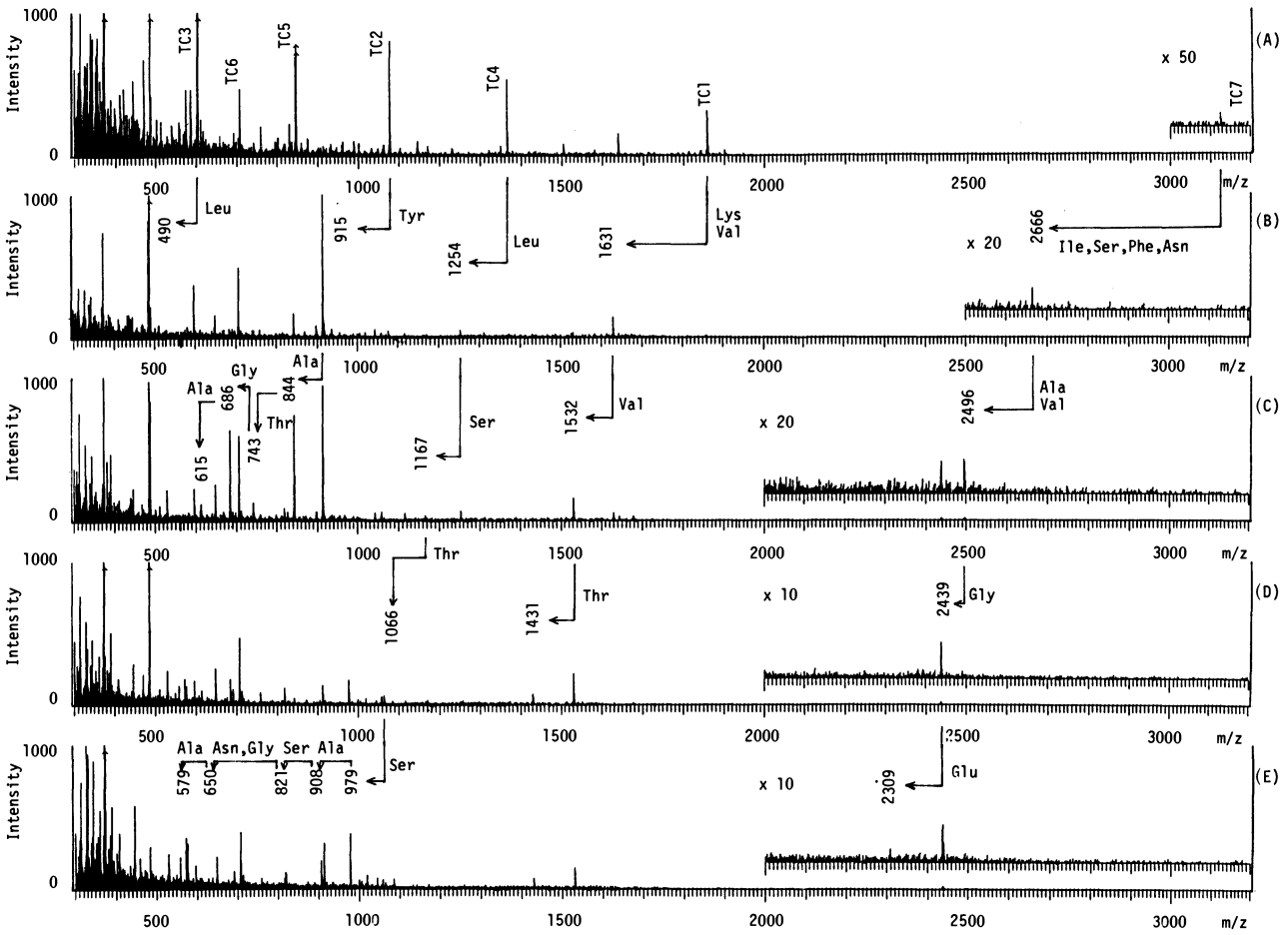

Fig. 3. The positive ion FAB mass spectra of the chymotryptic digest of the tryptic subpeptides (A) and of the digest with carboxypeptidase Y (B: 1 min, C: 10 min, D: 1 h, E: 2 h).

Table 2. Peptides Generated by Chymotryptic Cleavage of the Tryptic Peptides and of the Digest with Carboxypeptidase Y

Peptide	Observed mass value	Theoretical mass value	Matching section		C-terminal sequence
			Fig. 1.	Fig. 7.	
TC1	1858.6	1858.97	1—20	1—20	-Thr-Val-[Val, Lys]
TC2	1078.1	1078.55	21—32	21—32	-Ala-Gly-Thr-Ala-Tyr
TC3	603.7	603.33	40—45	40—45	-Leu(or Ile)
TC4	1367.2	1367.62	None	53—67	-Ala-[Asn,Gly]-Ser-Ala-Ser-Thr-Ser -Leu(or Ile)
TC5	846.9	846.40	72—78	72—78	
TC6	708.8	708.36	77—82	77—82	
TC7	3126.9	3127.35	None	83—113	-Glu-Gly-[Val, Ala]-[Ile(or Leu), Ser, Phe, Asn]

lyzed with trypsin or chymotrypsin, and the total hydrolysate was subjected to FABMS to give the molecular weights of the resulting peptides. Second, to determine the C-terminal sequence of staphylococcal protease digested peptides, they were subjected to carboxypeptidase Y digestion. The positive ion FAB mass spectrum of the tryptic peptides is shown in Fig. 4. Six tryptic peptides ST1, ST2, ST3, ST4, ST5, and ST7 fit the sequence shown in Fig. 1 on the basis of staphylococcal protease and trypsin specificity (Table 1). But the peptides ST6, ST8, and ST9 could not be matched with the published sequence on the basis of enzyme specificity.

If Asp(60) is replaced by Asn, ST6 fits the position Ala(59)-Arg(70) in Fig. 1 on the basis of its *m/z* and enzyme specificity. If Glu(105)-Pro(106) is Pro(105)-

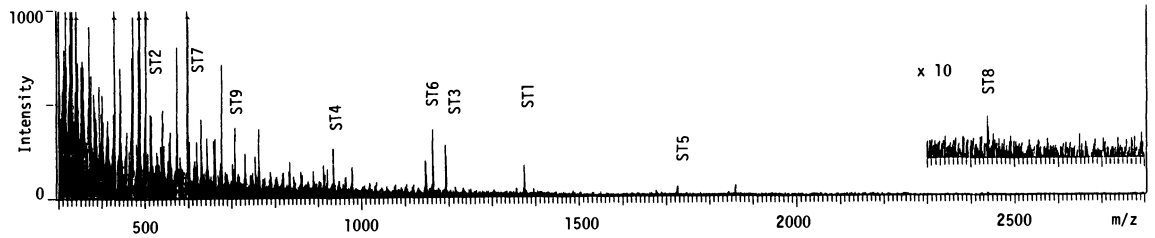

Fig. 4. The positive ion FAB mass spectrum of the tryptic digest of the staphyococcal protease digested subpeptides.

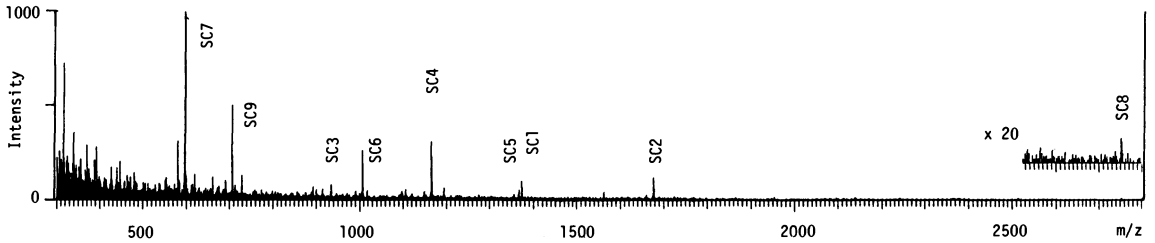

Fig. 5. The positive ion FAB mass spectrum of the chymotryptic digest of the staphylococcal protease digested subpeptides.

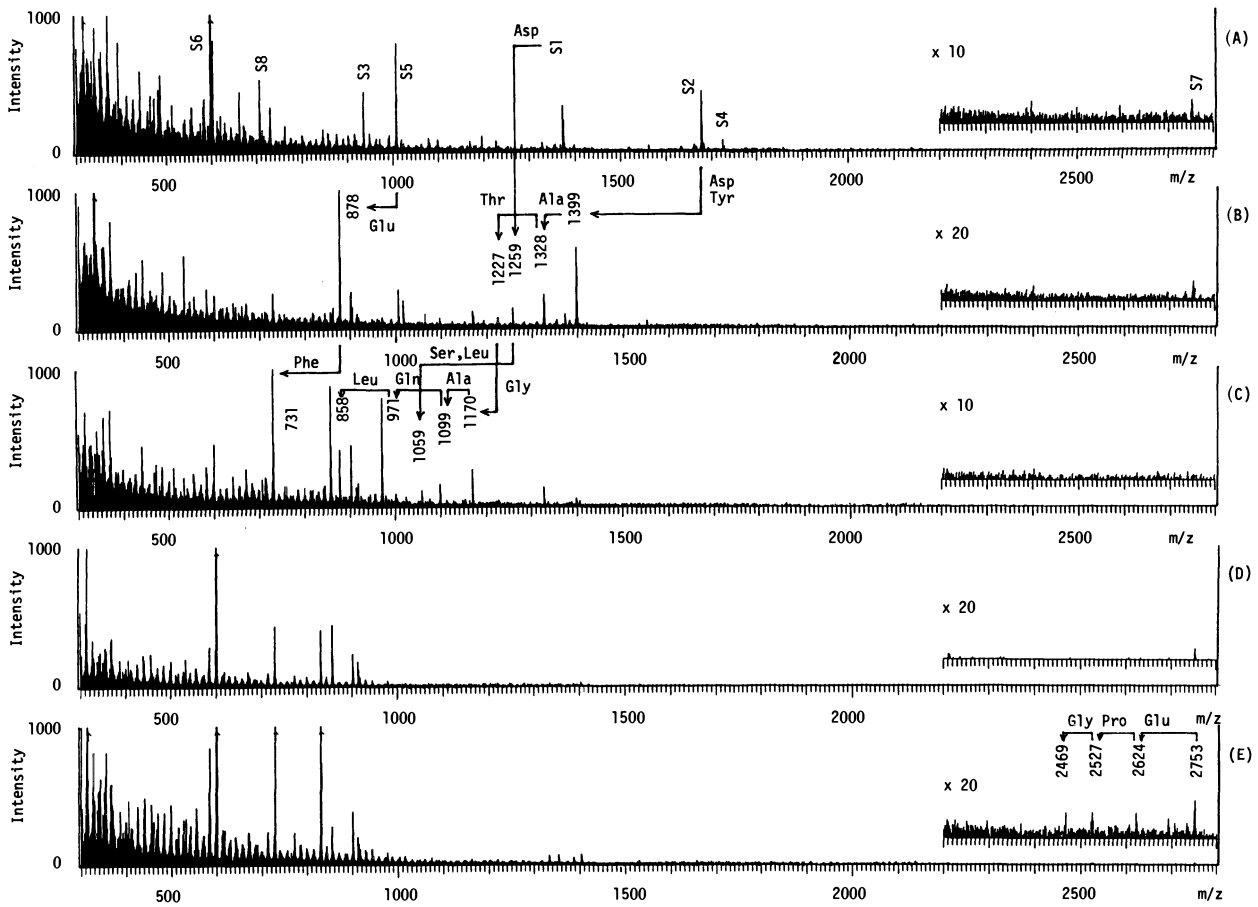

Fig. 6. The positive ion FAB mass spectra of the staphylococcal protease digested peptides of the reduced and carboxymethylated neocarzinostatin (A) and of the digest with carboxypeptidase Y (B: 1 min, C: 10 min, D: 1 h, E: 2 h).

Glu(106), ST8 and ST9 are matched to the position Trp(83)–Glu(106) and Gly(107)–Asn(113), respectively.

The positive ion FAB mass spectrum of the chymotryptic digest is shown in Fig. 5. Six chymotryptic peptides SC1, SC2, SC3, SC4, SC6, and SC7 fit the published sequence on the basis of staphylococcal protease and chymotrypsin specificity (see Table 1). The peptides SC5, SC8, and SC9 did not correspond to any fragment expected from the enzyme specificity.

If either Asp(57) or Asp(60) is replaced by Asn, SC5 corresponds to the position Ser(53)–Leu(67) in Fig. 1 on the basis of their *m/z* and enzyme specificity. If Glu(105)–Pro(106) is Pro(105)–Glu(106), SC8 and SC9 are matched to the position Gly(80)–Glu(106) and Gly(107)–Asn(113), respectively.

Figure 6 shows the positive ion FAB mass spectra of the staphylococcal protease digested peptides of the reduced and carboxymethylated neocarzinostatin and of their digest with carboxypeptidase Y. Six subpeptides S1, S2, S3, S4, S5, and S6 fit the published sequence on the basis of staphylococcal protease specificity. But the peptides S7 and S8 did not correspond to any fragment expected from the enzyme specificity (Table 3).

After treatment with carboxypeptidase Y, peptide S1 (*m/z* 1374.0) gave the mass peaks at *m/z* 1259.6

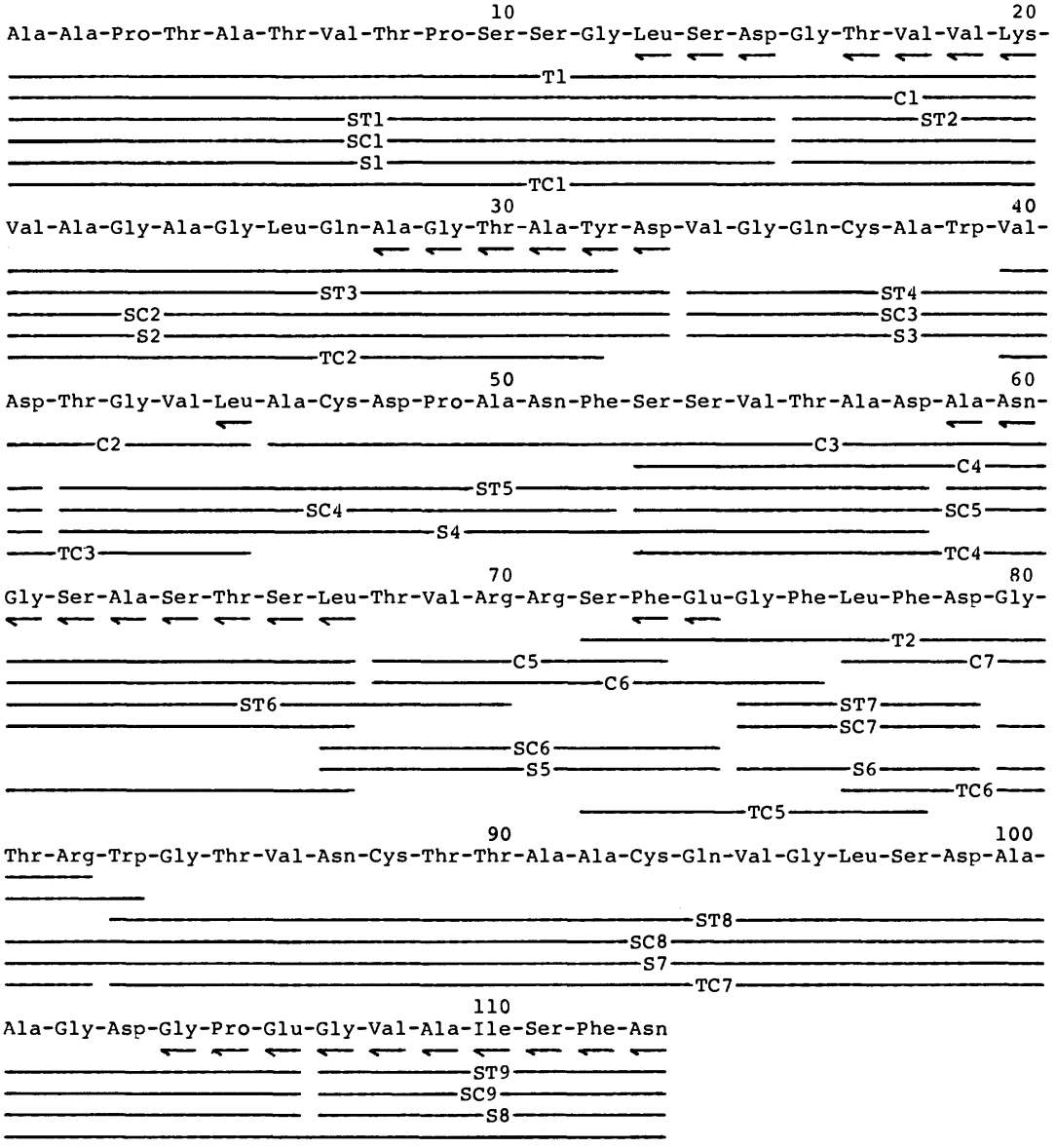

Fig. 7. The correct primary structure of neocarzinostatin and the sequence data with the results of endopeptidase and carboxypeptidase Y. ←—, Carboxypeptidase Y data; FABMS peptides produced by cleavage with trypsin (T), chymotrypsin (C), staphylococcal protease (S), staphylococcal protease and trypsin (ST), staphylococcal protease and chymotrypsin (SC), and trypsin and chymotrypsin (TC) are underlined.

Table 3. Peptides Generated by Staphylococcal Protease Cleavage of the Reduced and Carboxymethylated Neocarzinostatin and of the Digest with Carboxypeptidase Y

Peptide	Observed mass value	Theoretical mass value	Matching section		C-terminal sequence
			Fig. 1.	Fig. 7.	
S1	1374.0	1374.67	1—15	1—15	-[Leu(or Ile), Ser]-Asp
S2	1677.4	1677.87	16—33	16—33	-Leu-Gln(or Lys)-Ala-Gly-Thr-Ala-Tyr-Asp
S3	935.0	935.39	34—41	34—41	
S4	1725.3	1725.76	42—58	42—58	
S5	1007.1	1007.56	67—74	67—74	-Phe-Glu
S6	598.7	598.28	75—79	75—79	
S7	2753.3	2753.17	None	80—106	-Gly-Pro-Glu
S8	706.9	707.36	None	107—113	

and *m/z* 1059.5 on the FAB mass spectra. The results indicated that the C-terminal sequence of S1 was [Leu(or Ile), Ser] -Asp (see Table 3). Similarly, the mass peaks at *m/z* 1399.8, *m/z* 1328.8, *m/z* 1227.7, *m/z* 1170.6, *m/z* 1099.6, *m/z* 971.5 and *m/z* 858.3 from the peptide S2 (*m/z* 1677.4) indicated that the C-terminal sequence of S2 was -Leu-Gln(or Lys)-Ala-Gly-Thr-Ala-Tyr-Asp. In the same manner, the mass peaks at *m/z* 878.7 and *m/z* 731.2 from the peptide S5(*m/z* 1007.1) indicated that the C-terminal sequence of S5 was -Phe-Glu. Similarly, the mass peaks at *m/z* 2624.4, *m/z* 2527.1 and *m/z* 2469.8 from the peptide S7(*m/z* 2753.3) showed that the C-terminal sequence of S7 was -Gly-Pro-Glu. These results show that the position of Glu(105) and Pro(106) must be interchanged with each other.

The correct primary structure of neocarzinostatin and the sequence data are summarized in Fig. 7 with the results of carboxypeptidase Y digestion. This primary structure is the same as shown in Fig. 1 except Glu(105)-Pro(106) and Asp(60). Asp(60) would be caused by a variety of neocarzinostatin or by a mutation of *Streptomyces carzinostaticus* or by chemical change when it is isolated. Consequently, the subpeptides C3, C4, ST6, ST8, ST9, SC5, SC8, SC9, TC4, TC7, S7, and S8 correspond to the position 46—67, 53—67, 59—70, 83—106, 107—113, 53—67, 80—106, 107—113, 53—67, 83—113, 80—106, and 107—113 in Fig. 7. As shown in Fig. 7, the peptide fragments produced by the three kinds of enzymatic digestion completely covered the full sequence of neocarzinostatin. This implied the usefulness of the combination of enzymatic digestion and FAB mass spectrometry for the primary sequence studies of proteins.

We would like to thank Professors K. Biemann (Department of Chemistry, Massachusetts Institute of Technology), H. Matsuda and T. Matsuo (Institute of Physics, College of General Education, Osaka University) for much helpful discussion throughout this work and Mr. T. Higuchi of Jeol Ltd. for operating the FABMS system.

References

1) Y. Shimonishi, Y.-M. Hong, T. Matsuo, I. Katakuse, and H. Matsuda, *Chem. Lett.*, **1979**, 1369.

2) Y. Shimonishi, Y.-M. Hong, T. Kitagishi, T. Matsuo, H. Matsuda, and I. Katakuse, *Eur. J. Biochem.*, **112**, 251 (1980).

3) T. Matsuo, I. Katakuse, H. Matsuda, Y. Shimonishi, Y.-M. Hong, and Y. Izumi, *Mass Spectrosc. (Jpn.)*, **28**, 169 (1980).

4) Y. Shimonishi, Y.-M. Hong, I. Katakuse, and S. Hara, *Bull. Chem. Soc. Jpn.*, **54**, 3069 (1981).

5) Y. Shimonishi, Y.-M. Hong, T. Takao, S. Aimoto, H. Matsuda, and Y. Izumi, *Proc. Japan Acad.* **57B**, 304 (1981).

6) I. Katakuse, T. Matsuo, H. Matsuda, Y. Shimonishi, Y.-M. Hong, and Y. Izumi, *Biomed. Mass Spectrom.*, **9**, 64 (1982).

7) T. Takao, T. Hitouji, Y. Shimonishi, T. Tanabe, S. Inouye, and M. Inouye, *J. Biol. Chem.*, **259**, 6105 (1984).

8) Y.-M. Hong, T. Takao, S. Aimoto, Y. Shimonishi, H. Matsuda, and Y. Izumi, *Peptide Chemistry* **1981**: Proceedings of the 19th Symposium on Peptide Chemistry, ed. by T. Shioiri, p. 149. Protein Research Foundation, Minoh, Osaka (1982).

9) S. Aimoto, T. Takao, M. Hane, H. Ikemura, Y. Shimonishi, T. Takeda, Y. Takeda, and T. Miwatani, *Peptide Chemistry* **1982**: Proceedings of the 20th Symposium on Peptide Chemistry, edited by S. Sakakibara, p. 219. Protein Research Foundation, Minoh, Osaka (1983).

10) Y.-M. Hong, T. Takao, S. Aimoto, and Y. Shimonishi, *Biomed. Mass Spectrom.*, **10**, 450 (1983).

11) N. Ishida, K. Miyazaki, K. Kumagai, and M. Rikimara, *J. Antibiot.*, **18**, 68 (1965).

12) W. T. Bradner and D. J. Hutchison, *Cancer Chemother. Rep.*, **50**, 79 (1966).

13) K. Kumagai, H. Maeda, and N. Ishida, *Antimicrob. Agents Chemother.*, **1966**, 546 (1967).

14) M. Takahashi, K. Toriyama, H. Maeda, M. Kikuchi, K. Kumagai, and N. Ishida, *Tohoku J. Exp. Med.*, **98**, 273 (1969).

15) H. Maeda, K. Kumagai, and N. Ishida, *J. Antibiot. Ser.*

A. **19**, 253 (1966).
16) J. Meienhofer, H. Maeda, C. B. Glaser, J. Czomboz, and K. Kuromizu, *Science*, **178**, 875 (1972).
17) H. Maeda, C. B. Glaser, K. Kuromizu, and J. Meienhofer, *Arch. Biochem. Biophys.*, **164**, 379 (1974).
18) K. Biemann, *Int. J. Mass Spectrom. Ion Phys.*, **45**, 183 (1982).
19) B. W. Gibson, W. C. Herlihy, T. S. A. Samy, K.-S. Hahm, H. Maeda, J. Meienhofer, and K. Biemann, *J. Biol. Chem.* **259**, 10801 (1984).
20) K. Edo, M. Mizugaki, Y. Koido, H. Seto, K. Furihata, N. Otake, and N. Ishida, *Tetrahedron Lett.* **26**, 331 (1985).

Nature of Substituent Effect of Nitro and Methoxyl Group on Photocycloaddition of Polymethylene Dicinnamates

Masayuki KUZUYA,* Naohisa YOKOTA, Akihiro NOGUCHI, and Takachiyo OKUDA
Gifu Pharmaceutical University, 6-1, Mitahora-higashi 5-Chome, Gifu 502
(Received October 8, 1985)

The nature of the nitro substituent effect and topotactic assistance by the polymethylene chain of polymethylene dicinnamates upon the rate of photocyclization and the stereochemistry of photoproducts have been explored, in comparison with the similar effect of a methoxyl substituent; a striking rate enhancement and stereospecificity of the photoproduct were observed on a trimethylene dicinnamate derivative. However, the detailed study of the stereochemical course of the photoproduct has revealed that the dependence of the topotactic assistance of nitro derivatives on the polymethylene chain length largely differs from that of methoxy derivatives. Based on the results of the CNDO/S-CI excited state calculation of the model compounds, it is concluded that the acceleration character of the nitro substituent is mainly due to the odd electron density at the reaction site, i.e. the olefinic double bond; it is not due to the facile exciplex formation on the excited singlet state, unlike that of a methoxyl substituent.

In a previous paper of this series,[1] we have reported the excited state multiplicity responsible for an intramolecular photocycloaddition of polymethylene dicinnamates bearing methoxyl substituent at the benzene ring as studied by quenching experiments. We have shown a striking parallelism between the acceleration character of a 3-methoxyl substituent and the involvement of the excited singlet state in the reaction.

It is also known that a 4-nitro substituent in the benzene ring of cinnamate derivatives accelerates the photocycloaddition, and the participation of the excited singlet state is nearly the same as that of an unsubstituted cinnamate.[2] This indicates that the nature of the substituent effect on the rate of the photocycloaddition should differ from that of a methoxyl substituent.

Accordingly, it is of interest to study how a strong electron-withdrawing nitro substituent exerts an influence upon the photocycloaddition of polymethylene dicinnamates in comparison with that of a methoxyl derivatives.

In the present paper, we report an accelerating action of a nitro substituent and a polymethylene chain effect based upon the electronic structure and the stereochemistry of the photoproducts.

Experimental

Melting points were determined on a Shibata melting point apparatus and are uncorrected. IR spectra on KBr disks were recorded on a JASCO A-102 spectrometer, ^{1}H NMR spectra in $CDCl_3$ with TMS as internal standard on a Hitachi R-20 (60 MHz) spectrometer, UV spectra in acetonitrile on a Hitachi 323 spectrophotometer, and MS on a JEOL JMS-D300 spectrometer at 70 eV. Elemental analyses were carried out by the Microanalytical Laboratory, Gifu Parmaceutical University.

Materials. Polymethylene bis(nitrocinnamate)s **4b—j** and **5b—j** were prepared in 60—80% yields from α,ω-dibromoalkanes (n=2—6 and 10) and sodium nitrocinnamates according to the reported procedure.[3] The physical and spectral data are shown in Table 1.

UV-Irradiation. Each of the acetonitrile solutions of the di-trans-cinnamate derivatives (1.7×10^{-5} mol dm^{-3}) was irradiated with a grating monochromator (JASCO Model CRM-FM) with 2 kW Xenon lamp and 3 nm bandwidth. The resulting solution was subjected to UV spectral measurement at appropriate intervals.

The quantum efficiencies were determined in a similar manner to that previously reported[4] by the relative efficiencies approximated with the following formula on the basis of ethylene dicinnamates (**1b**).

$$\Phi_{rel} = (p\times\varepsilon)^{-1}$$

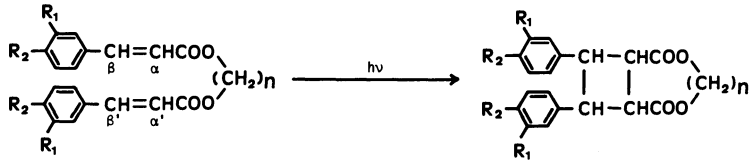

1—5 **11—15**

1, 11: $R_1=R_2=H$
2, 12: $R_1=OCH_3$, $R_2=H$
3, 13: $R_1=H$, $R_2=OCH_3$
4, 14: $R_1=NO_2$, $R_2=H$
5, 15: $R_1=H$, $R_2=NO_2$

b: $n=2$
c: $n=3$
d: $n=4$
e: $n=5$
j: $n=10$

Scheme 1.

Table 1. Physicochemical Properties of Polymethylene Dicinnamates

Compound	Mp θ_m/°C	$IR_{\nu_{c=0}}$	$UV_{\lambda_{max}(\varepsilon)}$	^1H NMR ($CDCl_3$) δ (ppm)					Anal		
				$-CH_2-CH_2-CH_2-$	$-O-CH_2-$	$C_\alpha-H$	$C_\beta-H$	Aromatic	Found (Calcd)		
4b	154.9—156.0	1715	261 (57000)	—	4.47 (s)	6.52 (d, J=16)	7.60 (d, J=16)	7.20—8.33 (m)	C, 58.10 (58.35)	H, 4.02 (3.92)	N, 6.79 (6.81)
4c	111.5—112.9	1710	261 (60000)	1.93—2.33 (quin)	4.23—4.43 (t)	6.45 (d, J=18)	7.59 (d, J=18)	7.26—8.33 (m)	C, 59.11 (59.16)	H, 4.23 (4.25)	N, 6.55 (6.57)
4d	139.8—141.2	1705	261 (64000)	1.66—2.00 (m)	4.10—4.40 (m)	6.45 (d, J=18)	7.59 (d, J=18)	7.20—8.30 (m)	C, 59.79 (60.00)	H, 4.54 (4.58)	N, 6.31 (6.36)
4f	156.1—157.0	1708	261 (60000)	1.41—2.00 (m)	4.00—4.30 (m)	6.46 (d, J=18)	7.60 (d, J=18)	7.18—8.23 (m)	C, 61.39 (61.54)	H, 5.11 (5.13)	N, 6.01 (5.98)
4j	94.5—96.0	1710	261 (55000)	1.21—5.50 (m)	4.07—4.27 (m)	6.46 (d, J=17)	7.63 (d, J=17)	7.17—8.23 (m)	C, 63.99 (64.11)	H, 6.17 (6.15)	N, 5.41 (5.34)
5b	186.0—187.3	1715	301 (42000)	—	4.43 (s)	6.47 (d, J=18)	7.59 (d, J=18)	7.62, 8.31 (d, J=9)	C, 58.05 (58.35)	H, 4.01 (3.92)	N, 6.71 (6.81)
5c	185.5—187.5	1712	301 (44000)	1.60—2.21 (quin)	4.10—4.30 (t)	6.45 (d, J=16)	7.59 (d, J=16)	7.65, 8.12 (d, J=9)	C, 59.08 (59.16)	H, 4.31 (4.25)	N, 6.53 (6.57)
5d[3]	175.1—176.0	1710	302 (43000)	1.60—2.10 (m)	4.12—4.30 (m)	6.45 (d, J=16)	7.59 (d, J=16)	7.65, 8.12 (d, J=9)	C, 59.97 (60.00)	H, 4.54 (4.58)	N, 6.45 (6.36)
5e	118.9—120.0	1709	301 (41000)	1.45—2.00 (m)	4.10—4.30 (m)	6.45 (d, J=16)	7.59 (d, J=16)	7.65, 8.12 (d, J=9)	C, 60.52 (60.79)	H, 4.97 (4.85)	N, 6.45 (6.17)
5f	122.0—123.5	1708	303 (38000)	1.30—1.90 (m)	4.10—4.30 (m)	6.45 (d, J=16)	7.59 (d, J=16)	7.65, 8.12 (d, J=9)	C, 61.31 (61.54)	H, 5.19 (5.13)	N, 6.07 (5.98)
5j	119.0—119.3	1709	302 (38000)	1.10—1.90 (m)	4.10—4.30 (m)	6.45 (d, J=16)	7.59 (d, J=16)	7.65, 8.12 (d, J=9)	C, 63.81 (64.11)	H, 6.13 (6.15)	N, 5.53 (5.34)

Here p is the irradiated photon number for the one-half decrease in concentration of total dicinnamate, which is calculated by an integrator of the grating monochromator used in the UV-irradiation and ε is the molar absorptivity at the irradiating wavelength.

Stereochemical Analysis of Photoproducts. A nitrogen saturated acetonitrile solution containing ca. 2×10^{-5} mol of each dicinnamate derivative was irradiated on a 400 W high pressure mercury lamp (RIKO Model RH 400-10 W) through a Pyrex filter for 10—100 h until the reaction proceeded to 90%. After the solvent was removed, the ^{1}H NMR spectrum of the residue was measured and the stereochemistry of the products was determined as follows: It is known that in the ^{1}H NMR spectrum the protons of *cis*-1,2-benzene rings on cyclobutane ring are shifted upfield owing to mutual shielding.[5] In fact, the aromatic proton signals of β-truxinate produced by the photolysis of **1c** appeared up field by ca. δ 0.36 above that of **1c**. The photolysate of **1d** showed two aromatic signals shifted upfield by δ 0.36 and 0.13 compared with that of **1d** so that the latter can be attributed to δ-truxinate. Based on these facts, the structures of the photoproducts were assigned; several selected ^{1}H NMR spectral features of the aromatic region of trimethylene series are listed in Table 2. Furthermore, in the MS no intermolecular photo-adduct was detected.

Table 2. Aromatic Proton Signals of Photoproduct

Photo-product No.	β-Truxinate		δ-Truxinate	
	Δδ	δ	Δδ	δ
11c	−0.36,	6.70—7.12 (m)	−0.11,	7.23 (s)
12c	−0.55,	6.30—6.60 (m)	−0.24,	6.61—6.90 (m)
13c	−0.02,	6.73 (d, J=8)	+0.35,	7.10 (d, J=8)
	−0.52,	6.83 (d, J=8)	−0.04,	7.27 (d, J=8)
15c	−0.65,	7.00 (d, J=8)	−0.39,	7.26 (d, J=8)
	−0.19,	7.93 (d, J=8)	−0.02,	8.10 (d, J=8)

Molecular Orbital Calculations. The electronic structures of substituted cinnamic acids as model compounds in excited states were calculated by the CNDO/S-CI method with standard parameters.[6] The planar structure (C_s symmetry) was assumed, and standard bond lengths and bond angles were employed for the geometric parameters.[7] Two-center two-electron repulsion integrals were evaluated according to the Mataga-Nishimoto formula.[8] In the CI procedure 20 singly excited configurations below 16 eV were used.

Results and Discussion

Nitro-Substituent Effect. The progressive spectral changes of trimethylene bis(3-nitrocinnamate)s (**4c**) and trimethylene bis(4-nitrocinnamate)s (**5c**) are

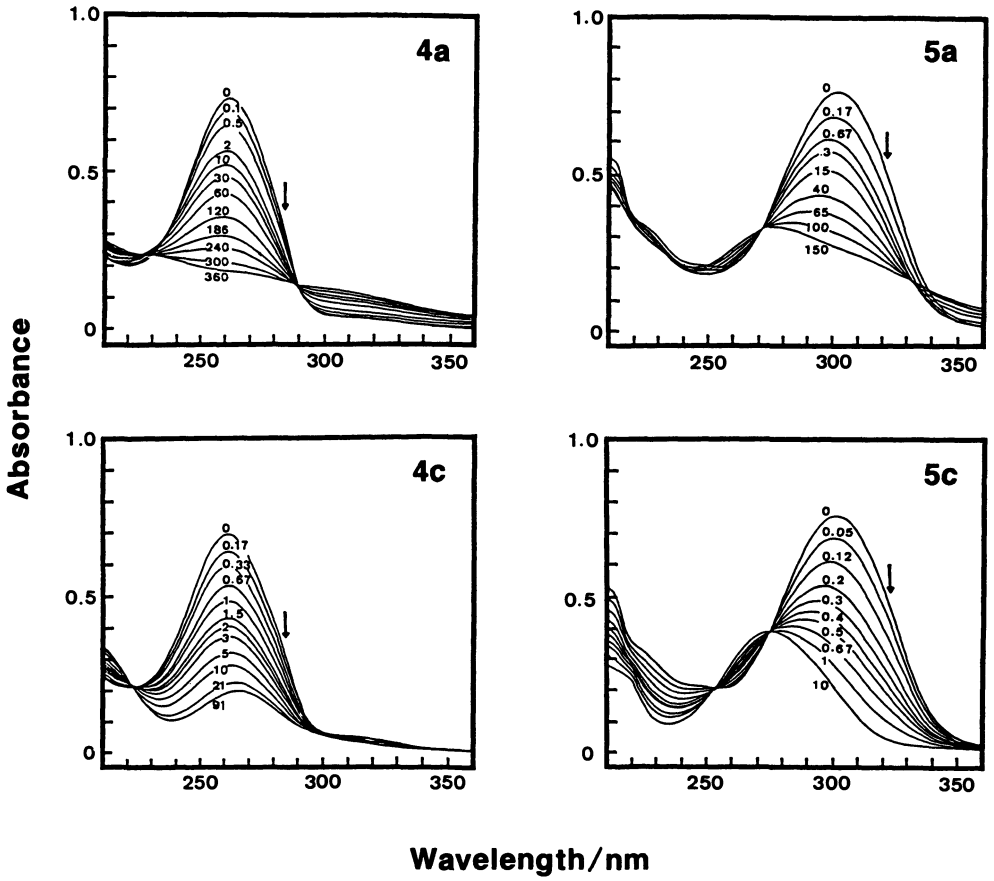

Fig. 1. Electronic spectral changes upon UV irradiation of methyl cinnamates and trimethylene dicinnamates. The arrows and numerical values in each spectrum indicate the irradiation wavelength and irradiation time (min), respectively.

shown in Fig. 1 together with those of methyl 3- and 4-nitrocinnamate (**4a** and **5a**) as unchained compound models for comparison.

It is seen from Fig. 1 that, on irradiation of methyl 3- and 4-nitrocinnamate (**4a** and **5a**), the absorption of the starting **4a** and **5a** decreased rapidly with isosbestic points at 235 and 272 nm, respectively. In the later stage of the reaction, such points disappeared or became faint. This result indicated that trans-cis photoisomerization proceeded until a photoequilibrium state was attained and then photocyclization occurred as an ensuing process in both cases. On the other hand, for trimethylene bis(3-nitrocinnamate)s (**4c**) and trimethylene bis(4-nitrocinnamate)s (**5c**), the decrease of the absorption of **4c** and **5c**, especially **5c**, was faster than that in the corresponding unchained compound **4a** and **5a**, and the isosbestic point was observed at 224 nm for **4c**, and 255 and 275 nm for **5c** throughout the reaction.

This result clearly indicated that the reaction of **4c** and **5c** involved a single photochemical process of photocyclization, and the rates of the photocyclization are far higher than those for the corresponding unchained cinnamates, due to the effect of the trimethylene chain.

The dependency of the relative quantum efficiencies for photocyclization on chain length were investigated and are shown in Fig. 2 together with those of the methoxy derivatives.

In fact, for the trimethylene compounds, the photocyclization of the 4-nitro derivative **5c** was three times as efficient as for 3-methoxy **2c** and 3-nitro **4c**. The quantum efficiencies diminished markedly with an increase or decrease in the number of methylene groups relative to those of the trimethylene compounds.

In order to compare the nature of the nitro substituent effect with that of methoxyl substituent on the photocylization, the electronic structure of the excited states of 3- and 4-nitrocinnamic acid (**4a'** and **5a'**) as model compounds were calculated by the

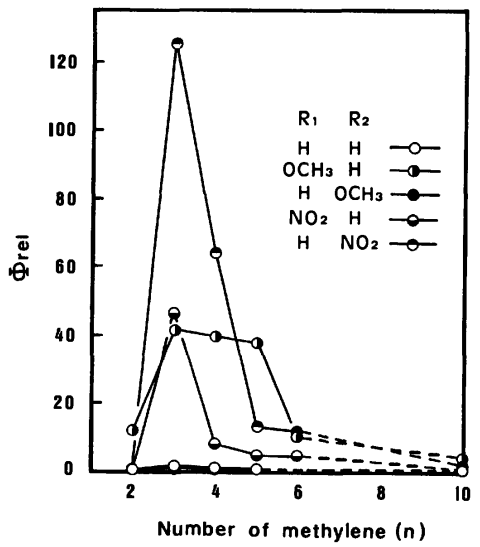

Fig. 2. Substituent effect on the photolability toward [2+2] cycloaddition on polymethylene dicinnamates.

CNDO/S-CI method. The reliability of this method for reproducing the experimental values of the lower transition energies of cinnamate derivatives has been proven in our previous paper.[4]

The calculated electronic structural features for **4a'** and **5a'** were summarized in Table 3.

The correlation between the experimental absorption wavelengths of **4a** and **5a** and the calculated transition energies of **4a'** and **5a'** was examined by a least square method. In fact, the lower transition energies of nitro derivatives were also found to be well reproduced and those thus corrected were shown in Fig. 3.

In general, the reactivity of a photochemical reaction can be discussed more reasonably on the basis of the partial atomic orbital population of the singly occupied orbital (SOMO) than of the total atomic orbital population. Thus the substituent effect on the reactivity for photocyclization can be estimated on the basis of the odd electron densities

Table 3. Computed Electronic Features for Excited States of Substituted Cinnamic Acids

Substituent		State	Transition energies	Oscillator strength	Odd electron density		π Charge density				π Bond order
R_1	R_2		eV/nm		C_α	C_β	C_α	C_β	Benzene ring	Nitro group	$C_\alpha=C_\beta$
NO_2	H	S_0	—	—	—	—	1.0825	0.8810	5.9115	4.0634	0.9039
		$S_1^{n\to\pi^*}$	3.9535 (314)	0.0001	0.0261	0.0522	1.0899	0.8860	6.2778	4.6814	0.8978
		$S_3^{\pi\to\pi^*}$	4.0562 (306)	0.0538	0.2406	0.1029	0.8686	0.8126	5.6971	4.6015	0.7390
		$S_5^{\pi\to\pi^*}$	4.8975 (253)	1.1413	—	—	1.0449	0.9197	5.5374	4.4091	0.7504
		$T_1^{\pi\to\pi^*}$	2.4793 (500)	—	0.0174	0.0160	1.0987	0.8954	6.2816	3.6530	0.8871
H	NO_2	S_0	—	—	—	—	1.0556	0.8931	5.9269	4.0666	0.9049
		$S_1^{n\to\pi^*}$	3.3795 (367)	0.0000	0.0966	0.0848	1.1470	0.9719	6.2573	4.5079	0.8229
		$S_3^{\pi\to\pi^*}$	4.2738 (290)	0.8008	0.3093	0.1355	0.8905	0.8320	5.7442	4.4980	0.6919
		$T_1^{\pi\to\pi^*}$	2.7228 (455)	—	0.2886	0.1446	0.9082	0.8577	5.7586	4.4264	0.6970

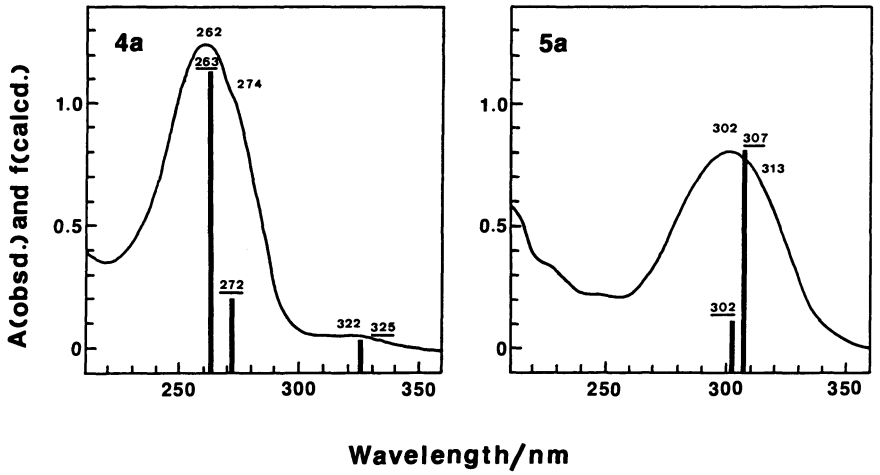

Fig. 3. Comparisons between the observed UV spectrum (solid curves) and the computed transition energy with correction (stick plot spectrum).
4a: Methyl 3-nitrocinnamate (ε=120000)
5a: Methyl 4-nitrocinnamate (ε=88000)

(Q_{odd}) of the lowest π-π^* excited state (S_3) calculated by the following formula, since S_3 state has a large value of Q_{odd} on C_α with the large oscillator strength.

$$Q_{odd} = \sum_i \alpha c_i^2, \quad \alpha = \sum_j C_i^2$$

c_i: The coefficient of i th MO (SOMO).
C_i: The CI coefficient of i th MO (SOMO) composed of each electronic configuration in S_3 state.
j: The number of electronic configuration involved i th MO (SOMO).

The correlation between the calculated Q_{odd} of the C_α at the lowest $S^{\pi-\pi^*}$ state (S_3) including those for methoxy derivatives of which detailed electronic structures were reported in a previous paper[4] and the relative quantum efficiencies (Φ_{rel}) for photocyclization of the trimethylene compounds was plotted, and is shown in Fig. 4.

It can be seen that the plots are linear demonstrating that the reactivity of the cinnamate derivatives was well correlated with the odd electron densities of the olefinic double bond at the lowest $S^{\pi-\pi^*}$ state. However, the plot of **5a** deviated considerably from the line. In the characteristics for the electronic structure of **4a'** and **5a'**, in the ground state the π-charge densities of the benzene ring are lower than that of cinnamic acid (=5.9664[4]) owing to a nitro group. In the S_3 state the further decrease in the π-charge density of the benzene ring was shown at the expense of the greater increase in that of the nitro group. These electronic features were considerably greater than those of the methoxy derivatives. This characteristic may cause electronic repulsion between the aromatic moiety in the excited state and that in the ground state. This repulsion would effect the transition state of the photocyclization reducing the exciplex formation. We believe this is one of the major reasons for the large deviation of 4-nitro derivatives shown in Fig. 4.

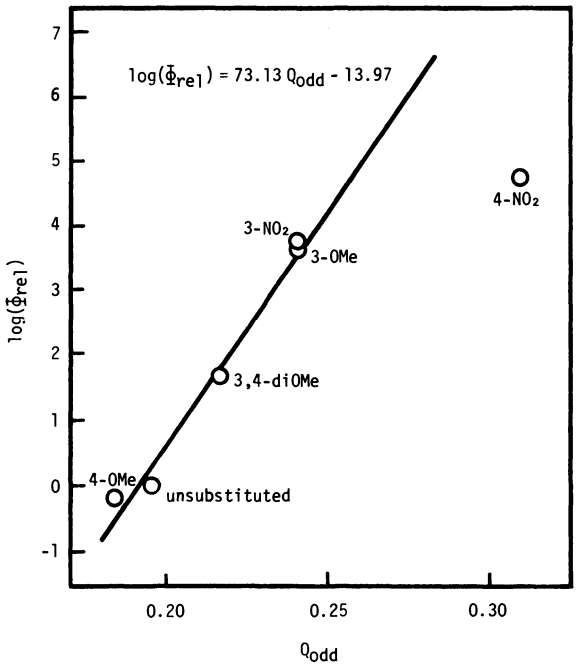

Fig. 4. Relationship between the calculated odd electron densities (Q_{odd}) of the C_α at the lowest $S^{\pi-\pi^*}$ state and the relative quantum efficiencies (Φ_{rel}) for photocyclization.

Stereochemistry of Photoproduct. The dependence of the stereochemistry of the photoproduct on the 4-nitro substituent and the number of methylene groups are shown in Fig. 5 together with those of other derivatives **1**—**3**.

As a general feature of Fig. 5, β-truxinate was exclusively formed for n=2, because of a difficulty in the production of δ-truxinate due to the geometrical

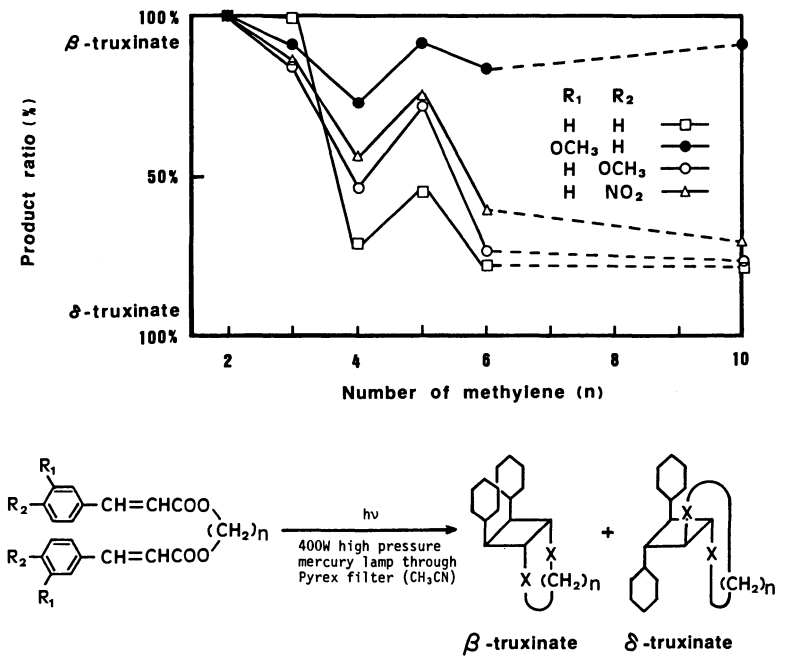

Fig. 5. Dependence of the stereochemistry of photoproduct upon alkane chain length and substituent.

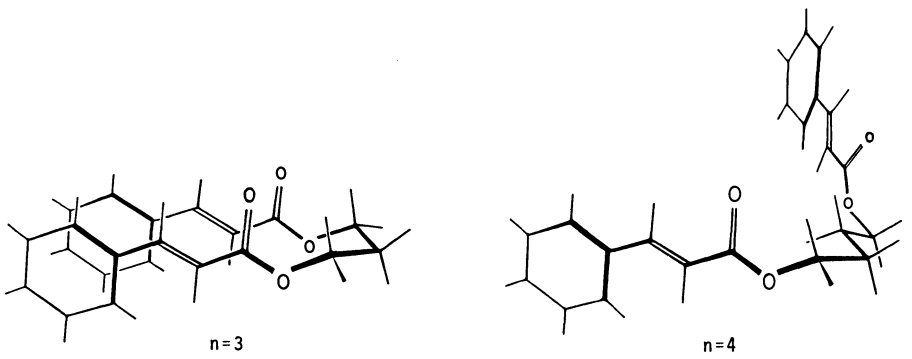

Fig. 6. The odd-even alternating effects of polymethylene chain on parallel arrangement of two cinnamoyl groups (Alkane chains are assumed to take an extended trans form).

restriction of ethylenic moiety. This tendency was shown also for n=3 and δ-truxinate was the main product. However, it was shown that the ratio of δ-truxinate in the total photoproduct markedly decreased for n=4 and that such a ratio increased again for n=5. These results indicated that the stereochemical course of the photoproduct are strongly depended on the odd or even number of the polymethylene chain. The most plausible geometrical situations of polymethylene dicinnamates are illustrated in Fig. 6 for n=3 and n=4 as representative examples.

Thus, an odd-even alternating effect of the methylene chain can be interpreted in terms of the vast difference in the geometric alignment between the two cinnamoyl moieties.[9,10] Another noteworthy feature in Fig. 5 is that only for 3-methoxy derivatives, was β-truxinate the main photoproduct irrespective of the number of methylene groups, unlike the case of the other derivatives.

From the above experimental results, it can be concluded that the high photocyclization efficiency of the trimethylene bis(4-nitrocinnamate)s (**5c**) is due to the high odd electron density in the olefinic moiety and the greater decrease of the efficiency and the less stereospecificity for the formation of β-truxinate product is due to the low efficiency for exciplex formation.

Conclusion

Pseudo-dimerization of the two cinnamoyl moie-

ties of polymethylene dicinnamates proceeds through both singlet and triplet pathways, but predominantly through the singlet pathway. The singlet pathway consists of two steps, i.e. the formation of an exciplex and its subsequent pseudo-dimerization. The topotactic assistance by the polymethylene chain mainly affects the formation of the exciplex and concomitantly the stereochemistry of the photocyclization; for n=3 the two cinnamoyl groups can assume the most preferable alignment for the formation of the exciplex resulting in the highest reactivity.[4,9] On the other hand, substituent perturbation could affect both steps. That is, the π-charge density of the benzene moiety and the odd electron density in the olefinic moiety affects the formation of the exciplex and the photodimerization, respectively. Thus, the observed rate enhancement of the pseudo-dimerization of 3-methoxy derivative can be concluded to be assisted by facile exciplex formation; accordingly the high stereoselectivity of the photoproducts was observed. That of the 4-nitro derivative can be ascribed to the high odd electron density of the olefinic double bond, not to the formation of the exciplex, demonstrated by the less stereoselectivity of the photoproduct of the derivatives linked with a longer polymethylene chain.

References

1) M. Kuzuya, N. Yokota, M. Tanaka, and T. Okuda, *Chem. Lett.*, **1985**, 1467.
2) T. Ishigami, T. Murata, and T. Endo, *Bull. Chem. Soc. Jpn.*, **49**, 3578 (1976).
3) J. L. Green and I. L. Honigberg, *J. Pharm. Sci.*, **61**, 802 (1972).
4) M. Kuzuya, M. Tanaka, M. Hosoda, A. Noguchi, and T. Okuda, *Nippon Kagaku Kaishi*, **1984**, 22.
5) B. S. Green and L. Heller, *J. Org. Chem.*, **39**, 196 (1974).
6) J. Del Bene and H. H. Jaffé, *J. Chem. Phys.*, **48**, 1807 (1968); **49**, 1221 (1968).
7) J. A. Pople and D. L. Beveridge, "Approximate Molecular Orbital Theory," McGrow-Hill, New York (1970), p. 111.
8) K. Nishimoto and N. Mataga, *Z. Phys. Chem. N. F.*, **12**, 335 (1957); N. Mataga and K. Nishimoto, *ibid.*, **13**, 140 (1957).
9) F. Hirayama, *J. Chem. Phys.*, **42**, 3163 (1965).
10) M. A. Winnik, *Chem. Rev.*, **81**, 491 (1981).

 © 1986 The Chemical Society of Japan Bull. Chem. Soc. Jpn., 59, 1387—1395 (1986)

Studies on Glycosylation of *erythro*-β-Hydroxy-L-histidine. A Key Step of Bleomycin Total Synthesis

Toshiaki MIYAKE, Tsutomu TSUCHIYA,* Sumio UMEZAWA,
Seiichi SAITO,† and Hamao UMEZAWA†
Institute of Bioorganic Chemistry, 1614 Ida, Nakahara-ku, Kawasaki 211
†Institute of Microbial Chemistry, 3-14-23 Kamiosaki, Shinagawa-ku, Tokyo 141
(Received November 16, 1985)

To improve the synthetic yield of bleomycin and its analogues, it is necessary to find the high yield procedure for condensation of sugar portion with the hydroxyl group of *erythro*-β-hydroxy-L-histidine moiety, preventing the *N*-glycosylation to imidazole. The present studies include the condensations of 4,6-di-*O*-acetyl-2,3-di-*O*-methyl-α-D-glucopyranosyl bromide (**10**) or 3,4,6-tri-*O*-acetyl-2-*O*-(2,4,6-tri-*O*-acetyl-3-*O*-carbamoyl-α-D-mannopyranosyl)-α-L-gulopyranosyl bromide (**3**) and 3,4,6-tri-*O*-acetyl-2-*O*-[2,4,6-tri-*O*-acetyl-3-*O*-(*N*-acetylcarbamoyl)-α-D-mannopyranosyl]-α-L-gulopyranosyl bromide (**28**) with a variety of protected derivatives of *erythro*-β-hydroxy-L-histidine. The results revealed that a) N^{im}-tosyl group is most effective to prevent the N^{im}-glycosylation, b) use of silver carbonate and silver perchlorate at low temperature (−55 °C) gave the desired α-glycosides in satisfactory yields, and c) among the esters (methyl and *p*-nitrobenzyl) and the *N*-protecting groups (Z, Boc, and pMZ) of *erythro*-β-hydroxy-L-histidine, methyl and Z were the best groups, respectively. Using the method thus improved, the desired *O*-α-L-guloside, that is, *erythro*-β-*O*-[3,4,6-tri-*O*-acetyl-2-*O*-(2,4,6-tri-*O*-acetyl-3-*O*-carbamoyl-α-D-mannopyranosyl)-α-L-gulopyranosyl]-N^{α}-benzyloxycarbonyl-$N^{im(\tau)}$-tosyl-L-histidine *p*-nitrobenzyl ester (**31**) was successfully prepared.

Bleomycin is an antitumor antibiotic clinically used in the treatment of squamous cell carcinoma, malignant lymphomas, and testis tumors.[1] The total synthesis of bleomycin A2 (**1**) had been accomplished by our group[2,3] and Hecht et al.[4] In our first total

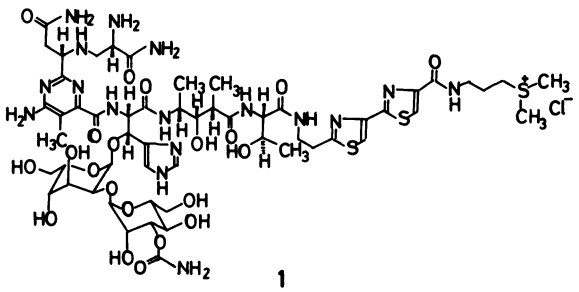

1

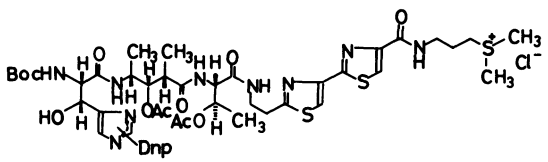

2

Boc: $COOC(CH_3)_3$
Dnp: $C_6H_3(NO_2)_2$(*o*, *p*)

Chart 1.

synthesis, the key step was the coupling of a protected suger, 3,4,6-tri-*O*-acetyl-2-*O*-(2,4,6-tri-*O*-acetyl-3-*O*-carbamoyl-α-D-mannopyranosyl)-α-L-gulopyranosyl bromide (**3**), with protected pentapeptide **2**[5] at the hydroxyl group of *erythro*-β-hydroxy-L-histidine. We therefore intended to improve the yield of the desired coupling product. In this paper we describe the basic experiments for this purpose, that is, coupling reactions of protected glucosyl and 2-*O*-mannopyranosyl-α-L-gulopyranosyl bromides with several protected *erythro*-β-hydroxy-L-histidine.

Glycosylation of a Derivative (14) of β-Hydroxy-L-histidine Protected with a Dnp Group at Imidazole Moiety. As a model glycosyl bromide for bleomycin synthesis, we prepared 4,6-di-*O*-acetyl-2,3-di-*O*-methyl-α-D-glucopyranosyl bromide (**10**). Methyl 4,6-*O*-cyclohexylidene-α-D-glucopyranoside (**4**)[6] was methylated with methyl iodide in *N*,*N*-dimethylformamide (DMF) to give the 2,3-di-*O*-methyl ether **5**.

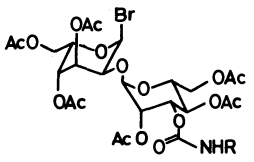

	R
3	H
28	Ac

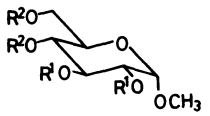

	R^1	R^2
4	H	$R^2R^2=C(CH_2)_5$
5	CH_3	$R^2R^2=C(CH_2)_5$
6	CH_3	H
7	CH_3	Ac

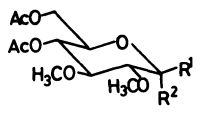

	R^1	R^2
8	H	OAc
9	OAc	H
10	H	Br

Chart 2.

Acidic hydrolysis of **5** followed by acetylation gave the 4,6-di-*O*-acetyl derivative **7**.[7] Acetolysis of **7** gave the corresponding 1-*O*-acetyl α- and β-D-glucoses **8** and **9** in 79 and 13% yield, respectively, with slightly accompanied methyl 2,3,4,6-tetra-*O*-acetyl-α-D-glucopyranoside (1.4%).[8] Treatment of the mixture of **8** and **9** with hydrogen bromide in acetic

acid gave the α-l-bromide **10**.

As a protected β-hydroxy-L-histidine for the condensation with **10**, we prepared a N^{im}-(2,4-dinitrophenyl) (=Dnp)-N^{α}-benzyloxycarbonyl(=Z) derivative[9] **14** of β-hydroxy-L-histidine. Since the low yield of our first condensation[2] was considered to be correlated to the presence of the bulky N^{α}-*t*-butoxycarbonyl (Boc) group near the hydroxyl group, the Boc group was replaced by a Z group. Treatment of **11** with *O*-benzyl *S*-(4,6-dimethyl-2-pyrimidinyl) thiocarbonate (Z–S reagent)[10] gave the N^{α}-Z-derivative **12** in high yield. Treatment of **12** with hydrogen chloride in methanol (to give **13**) followed by reaction with 2,4-dinitrofluorobenzene gave **14**.

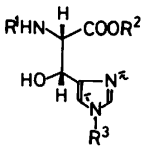

	R^1	R^2	R^3
11	H	H	H
12	Z	H	H
13	Z	CH_3	H
14	Z	CH_3	Dnp
21	Z	CH_3	Ts
22	Boc	CH_3	Ts
23	PMZ	CH_3	Ts
24	Z	H	Ts
25	Z	$CH_2C_6H_4NO_2(p)$	Ts

PMZ: $COOCH_2C_6H_4OCH_3(p)$
Z: $COOCH_2C_6H_5$

Chart 3.

The position of the Dnp group, which remained ambiguous in the previous papers,[2,5] was determined by the procedure of Bell and Jones.[11] Treatment of **14** with benzyl chloroformate and sodium hydrogen-

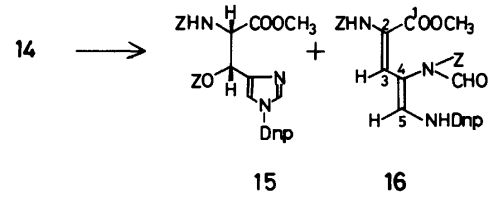

Chart 4.

carbonate in chloroform–water gave two main products. ^{1}H NMR spectroscopy provided evidences for their structural assignments: *O*-benzyloxycarbonyl derivative **15** of **14** and methyl 2,4-bis(benzyloxycarbonylamino)-4-*N*-formyl-5-(2,4-dinitroanilino)-2,4-pentadienoate (**16**). The ^{1}H NMR spectrum of **16** showed a doublet (J=12 Hz, NHDnp) at δ 10.64, which collapsed to a singlet on irradiation at δ 7.22 and disappeared on deuteration. The doublet at δ 7.22 (J=12 Hz, =C*H*–NHDnp) became a singlet on deuteration or irradiation at δ 10.64. Two singlets appeared at δ 7.49 (HC=) and 9.25 (*N*CHO), the latter being gradually disappeared on deuteration. These results indicate the hydrogen assignments to be described in the parentheses and, therefore, it was concluded that Dnp was attached to the nitrogen (*N*-5) bearing a hydrogen and a methine (C-5), not the nitrogen (*N*-4) bearing a formyl group. Thus, the structure of **16** was 2,4,5-tris(substituted amino)-2,4-diene, supporting the structure of **14**. The geometrical structure of **16** was not studied, however, from the expected reaction pathway and the NMR spectrum, a mixture of two isomers possibly composed of *E,Z* (major) and *Z,Z*-structures was presumed as follows. The compound **16** may be produced from **15** by a sequence of reactions including benzyloxycarbonylation of the $N^{im(\pi)}$ group, hydrolysis of the imidazole ring to give an *N*-formyl group,[12] and removal of a ZOH fragments (to give the 2,3-unsaturation).

According to the cross-ring coupling constant criterion suggested by Matthews and Rapoport,[13] the coupling constant between the two CH protons of imidazole ring is 0.9—1.0 Hz for the $N^{im(\pi)}$-substituted derivatives and 1.1—1.5 Hz for the $N^{im(\tau)}$-substituted derivatives. In the ^{1}H NMR spectrum of **14**, the broad singlet at δ 7.59 (H-2 of imidazole) measured at room temperature was resolved into a sharp doublet of 1.2 Hz at 55 °C, supporting the structure of **14** deduced from the structure of **16**.

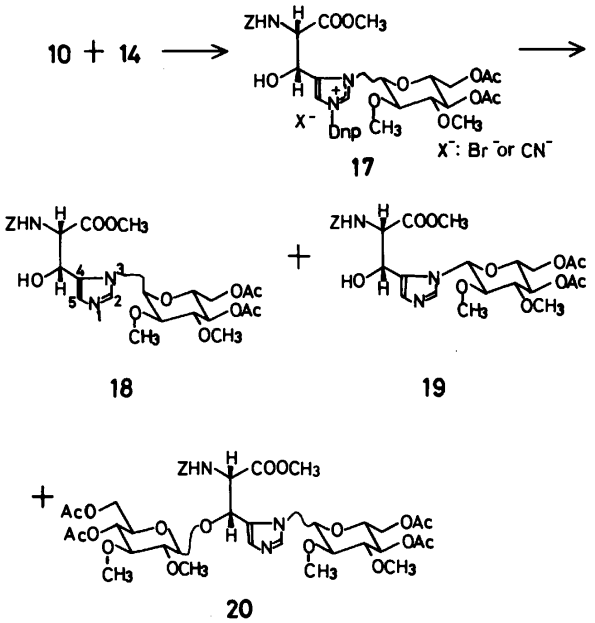

Chart 5.

Glycosylation of compound **14** with the bromide **10** according to the previous method[2] ($HgCN_2$ and molecular sieves in sulfolane, 40 °C, overnight) gave a complex mixture mainly comprised of two glucosides **17** having the Dnp groups. Since the mixture was unstable to light and cleavage of the Dnp group

occurred gradually during the purification, the Dnp group of **17** was removed beforehand by treatment with 2-mercaptoethanol to give the α- and β-$N^{im(3)}$-glucosides **18** and **19** in 34 and 26% yield (based on **14**) and a mixture of products (**20**, 6%) glucosylated both at $N^{im(3)}$ and OH-3. The positions of the glucosyl moieties in **18** and **19** were determined to be N^{im} from the low chemical shifts[14] of the anomeric protons (δ 6.30 and J=3.5 Hz, and δ 5.54 and J=9 Hz, respectively). The above results show that, glucosylation occurs at the $N^{im(3)}$ position in preference to the hydroxyl group in the presence of the $N^{im(1)}$-Dnp protecting group.

Preparation of the *O*-Glycosyl Derivatives of β-Hydroxy-L-histidine. As described previously in our communication,[3] N^{im}-tosyl group was revealed to be suitable for prevention of N^{im}-glycosylation. The *N*-tosyl compound **21** prepared from **13** showed a large

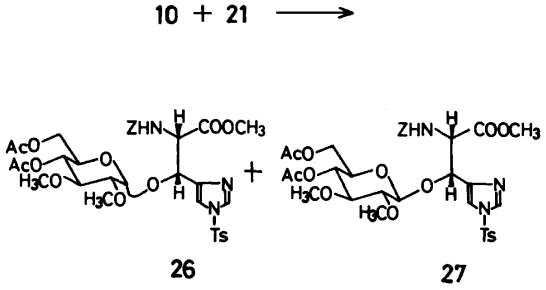

Chart 6.

cross-ring coupling constant ($J_{2,4}$=1.5 Hz) in its ^{1}H NMR spectrum, suggesting[13] the introduction of the tosyl group at $N^{im(\pi)}$. Condensation of **21** with the bromide **10** in the presence of mercury(II) cyanide and molecular sieves in dry dichloromethane at room temperature gave the desired α- and β-*O*-glucosides **26** and **27** in 21% yield in a ratio of 2:1, with the corresponding detosyl derivatives. Pure **26** and **27** were isolated by preparative high-performance liquid chromatography. The chemical shifts of the resonances of the anomeric protons of **26** and **27** in their ^{1}H NMR spectra (δ 4.89 and J=3.5 Hz for **26**, and δ 4.50 and J=7.5 Hz for **27**) supported the *O*-glucosides.

When the condensation was carried out in the presence of a mixture of silver carbonate and silver perchlorate as the catalysts at room temperature, the ratio of **26** and **27** was improved to 20:1 but without change of the yield (≈20%). Formation of the detosyl-di-N^{im},*O*-glucoside (≈25%) was also observed. However, the condensation yield was surprisingly improved to 67%, with the above ratio of **26** and **27** maintained, when the reaction was carried out at a low temperature (−55 °C). In this case, the yield of the detosyldiglucosyl derivative was lowered to 8%. It should be noted that sole lowering the reaction temperature remarkably suppressed the removal of the tosyl group and increased the yield of the desired *O*-α-glucoside. When mercury(II) cyanide was used as the catalyst, no reaction occurred at −55 °C, revealing the desirable effects of the silver catalysts.

The above reaction conditions were next applied to

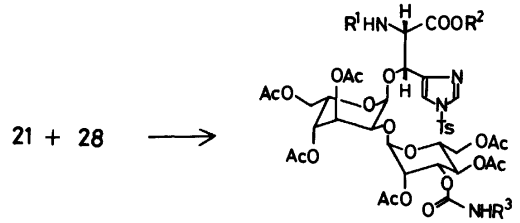

	R^1	R^3	R^3
29	Z	CH_3	Ac
30	Boc	CH_3	Ac
31	Z	$CH_2C_6H_4NO_2(p)$	H

Chart 7.

the condensation of **21** and a protected 2-*O*-[3-*O*-(*N*-acetylcarbamoyl)-α-D-mannopyranosyl]-α-L-gulopyranosyl bromide (**28**) prepared from 1,3,4,6-tetra-*O*-acetyl-2-*O*-(2,4,6-tri-*O*-acetyl-3-*O*-carbamoyl-α-D-mannopyranosyl)-β-L-gulopyranose[2] by bromination with hydrogen bromide–acetic acid–acetic anhydride. When **28** was used in 1.4 molar equivalents for **21**, the best yield (95%) of **29** was obtained. Incidentally, when 1.1, 1.2, 1.3 molar equivalents of **28** for **21** were used, 69, 77, and 89% of **29** were obtained. The structure of **29** was confirmed by the ^{1}H NMR spectrum (Fig. 1).

N^{α}-Protecting groups were further studied. When N^{α}-Boc- (**22**) and N^{α}-(*p*-methoxybenzyloxycarbonyl)(=PMZ) derivatives (**23**) of N^{im}-tosyl-β-hydroxy-L-histidine methyl ester were condensed with **28**, the yields of the desired *O*-α-L-gulosides were lower than the case when Z-group was used. The inspection of the ^{1}H NMR spectra of the mixtures of products obtained by the both reactions revealed that considerable part of these protecting groups were removed during the coupling reaction.

Finally, in view of easy removal of protecting group, methyl ester group of **21** was replaced by a *p*-nitrobenzyl, and the *N*-acetyl of the carbamoyl group was omitted. Compound **12** was treated with tosyl chloride as described for **21** to give the N^{im}-tosyl derivative **24**, which was led to the *p*-nitrobenzyl ester **25** by treatment with *p*-nitrobenzyl bromide. Condensation of **25** and 3,4,6-tri-*O*-acetyl-2-*O*-(2,4,6-tri-*O*-acetyl-3-*O*-carbamoyl-α-D-mannopyranosyl)-α-L-gulopyranosyl bromide (**3**) by the same procedure as above described for **29** gave the desired *O*-α-L-guloside **31** (43% from **25**) with recoverd **25** (25%). The product **31** is useful for the synthesis of bleomycin and its analogues.

In conclusion, the present studies revealed that (a) $N^{im(\pi)}$-tosyl group successfully prevented the glycosylation at $N^{im(\pi)}$, (b) use of a mixture of silver carbonate

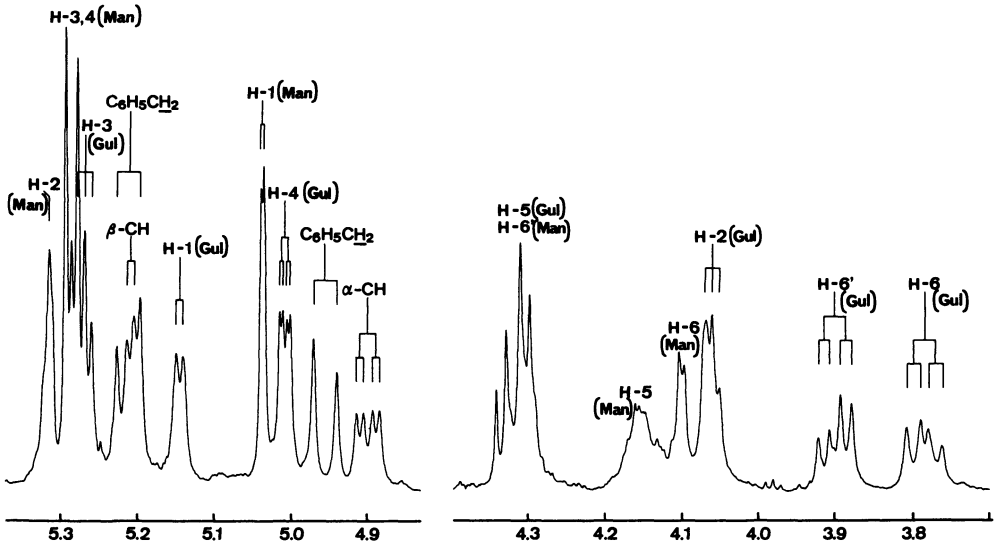

Fig. 1. Partial ^{1}H NMR spectrum of **29** (400 MHz, $CDCl_3$).

and silver perchlorate at low temperature (−55 °C) gave the desired *O*-α-glycosyl compounds almost selectively in satisfactory yields, and (c) among the protective groups of α-amino and carboxylic acid in the β-hydroxy-L-histidine portion, benzyloxycarbonyl and methyl groups, respectively, gave the best yield of the *O*-glycoside.

Experimental

IR spectra were determined in KBr disks on a Jasco A-202 infrared spectrophotometer. ^{1}H NMR spectra were recorded at 25 °C, unless otherwise stated, with Bruker WM-250 and WM-400 spectrometers (250 MHz and 400 MHz, respectively). Tetramethylsilane (δ=0.00) was used as an internal standard. Proton assignments of the products were confirmed by decoupling method if necessary. Secondary ion mass spectra (SIMS) and field desorption mass spectra (FDMS) were recorded on a Hitachi M-80 spectrometer. Optical rotations were measured in 0.1-dm cells of 0.5-ml capacity by using a Perkin-Elmer Model 241 polarimeter. Thin-layer chromatography (TLC) was carried out on E. Merck precoated TLC plates (silica gel 60 F-254). For column chromatography, silica gel (Wakogel C-200) was used, unless otherwise stated.

Methyl 4,6-*O*-Cyclohexylidene-2,3-di-*O*-methyl-α-D-glucopyranoside (5). To a solution of methyl 4,6-*O*-cyclohexylidene-α-D-glucopyranoside[6] (**4**, 505 mg) in dry *N*,*N*-dimethylformamide (DMF) (3 ml) were added silver oxide (2.15 g) and methyl iodide (0.6 ml), and the mixture was vigorously shaken at room temperature overnight. The resulting solution showed, on TLC with benzene–ethyl acetate (1:1), a single spot of **5** at R_f 0.64 (cf. **4**, R_f 0.16). The mixture was centrifuged and the residue was washed with DMF. The solutions combined were concentrated and the residue was extracted with chloroform. The organic solution was washed with water, dried ($MgSO_4$), and concentrated to give a pale yellow syrup (615 mg), that was purified by column chromatography with benzene–ethyl acetate (4:1) to give needles of **5**, 453 mg (81%), mp 82—83 °C; $[\alpha]_D^{23}$ +117° (*c* 1, $CHCl_3$); ^{1}H NMR (250 MHz, $CDCl_3$): δ=3.23 (1H, dd, H-2), 3.41, 3.53, 3.62 (each 3H, s, OCH_3), 4.80 (1H, d, H-1); $J_{1,2}$=3.5, $J_{2,3}$=8.5 Hz.

Found: C, 59.52; H, 8.49%. Calcd for $C_{15}H_{26}O_6$: C, 59.58; H, 8.67%.

Methyl 4,6-Di-*O*-acetyl-2,3-di-*O*-methyl-α-D-glucopyranoside (7). A solution of **5** (103 mg) in 80% aqueous acetic acid (1 ml) was heated at 50 °C for 1 h. The solution showed a single spot on TLC. Concentration gave a solid of **6** (83 mg) which partly crystallized on standing. A mixture of **6** and acetic anhydride (0.16 ml) in pyridine (1 ml) was kept at room temperature overnight. Addition of water (0.05 ml) followed by concentration gave a syrup, that was dissolved in chloroform. The solution was washed successively with 5% aqueous potassium hydrogensulfate, water, 5% aqueous sodium hydrogencarbonate, and water, dried ($MgSO_4$), and concentrated to give a syrup of **7**,[7] 104 mg (quantitative), $[\alpha]_D^{23}$ +109° (*c* 1, $CHCl_3$); IR (KBr): 1740 ($\nu_{C=O}$), 1240 cm^{-1} ($\nu_{C=O}$ of OAc); ^{1}H NMR (250 MHz, $CDCl_3$): δ=2.09, 2.10 (each 3H, s, OAc), 3.32 (1H, dd, H-2), 3.45, 3.53, 3.54 (each 3H, s, OCH_3), 3.59 (1H, t, H-3), 3.86 (1H, ddd, H-5), 4.05 (1H, dd, H-6), 4.24 (1H, dd, H-6′), 4.87 (1H, d, H-1), 4.95 (1H, dd, H-4); $J_{1,2}$=3.5, $J_{2,3}$=$J_{3,4}$=9.5, $J_{4,5}$=10.5, $J_{5,6}$=2.5, $J_{5,6'}$=5.0, $J_{6,6'}$=12.5 Hz.

Found: C, 50.93; H, 7.04%. Calcd for $C_{13}H_{22}O_8$: C, 50.97; H, 7.24%.

1,4,6-Tri-*O*-acetyl-2,3-di-*O*-methyl-α- and β-D-Glucopyranose (8 and 9). Compound **7** (3.89 g) was added to a mixture of acetic acid–acetic anhydride–sulfuric acid (10:10:1) (21 ml) under stirring at 0 °C, and the mixture was stirred at the temperature for 100 min. The resulting solution showed, on TLC with benzene–ethyl acetate (4:1), two spots at R_f 0.24 (**8**) and 0.30 (**9**). After dilution with chloroform (300 ml), the solution was successively washed with water, 5% aqueous sodium hydrogencarbonate, and water, dried ($MgSO_4$), and concentrated to give a pale yellow syrup, 4.13 g. Duplicate column chromatographies with benzene–ethyl acetate (4:1) and chloroform–2-butanone (15:1) gave syrups of **8**, 3.37 g (79%), **9**, 0.57 g (13%), and methyl 2,3,4,6-tetra-*O*-acetyl-α-D-glucopyranoside,[8] 57 mg (1.4%).

8: $[\alpha]_D^{23}$ +90° (*c* 1, $CHCl_3$); ^1H NMR (250 MHz, $CDCl_3$): δ=2.07, 2.10, 2.18 (each 3H, s, OAc), 3.42 (1H, dd, H-2), 3.48, 3.54 (each 3H, s, OCH_3), 3,55 (1H, t, H-3), 3.96 (1H, ddd, H-5), 4.03 (1H, dd, H-6), 4.24 (1H, dd, H-6′), 5.00 (1H, dd, H-4), 6.35 (1H, d, H-1); $J_{1,2}$=3.5, $J_{2,3}$=$J_{3,4}$=9.5, $J_{4,5}$=10, $J_{5,6}$=2.5, $J_{5,6'}$=4.5, $J_{6,6'}$=10 Hz.

Found: C, 50.53; H, 6.59%. Calcd for $C_{14}H_{22}O_9$: C, 50.29; H, 6.63%.

9: $[\alpha]_D^{23}$ −16° (*c* 1, $CHCl_3$) [lit,[15] $[\alpha]_D^{22}$ −18° (*c* 1.3, $CHCl_3$)]; ^1H NMR (250 MHz, $CDCl_3$): δ=2.07, 2.10, 2.17 (each 3H, s, OAc), 3.26 (1H, d, H-2), 3.34 (1H, t, H-3), 3.54, 3.56 (each 3H, s, OCH_3), 3.67 (1H, ddd, H-5), 4.05 (1H, dd, H-6), 4.24 (1H, dd, H-6′), 4.97 (1H, dd, H-4), 5.52 (1H, d, H-1); $J_{1,2}$=7.5, $J_{2,3}$=$J_{3,4}$=9, $J_{4,5}$=10, $J_{5,6}$=2.5, $J_{5,6'}$=5, $J_{6,6'}$= 12.5 Hz.

Found: C, 50.11; H, 6.39%. Calcd for $C_{14}H_{22}O_9$: C, 50.29; H, 6.63%.

4,6-Di-*O*-acetyl-2,3-di-*O*-methyl-α-D-glucopyranosyl Bromide (10). To a mixture of **8** and **9** (21.3 mg) was added a cold (0 °C) mixture of 30% hydrogen bromide in acetic acid–acetic acid-acetic anhydride (3:8:1, 0.4 ml) and the solution was kept at the temperature for 1 h, then at room temperature overnight in the dark. The resulting solution showed, on TLC with benzene–ethyl acetate (5:1), a spot at R_f 0.48. Concentration of the solution gave a syrup, that was dissolved in dichloromethane (1.5 ml) and the solution was washed successively with water, 5% aqueous sodium hydrogencarbonate, and water, dried ($MgSO_4$), and concentrated to give a syrup of **10**, 21.2 mg (94%), that was only slightly contaminated by the starting materials; ^1H NMR (250 MHz, $CDCl_3$): δ=2.08, 2.11 (each 3H, s, OAc), 3.30 (1H, dd, H-2), 3.52, 3.55 (each 3H, s, OCH_3), 3.63 (1H, dd, H-3), 4.07 (1H, dd, H-6), 4.17 (1H, ddd, H-5), 4.29 (1H, dd, H-6′), 5.03 (1H, dd, H-4), 6.55 (1H, d, H-1); $J_{1,2}$=4, $J_{2,3}$=9, $J_{3,4}$=9.5, $J_{4,5}$=10.5, $J_{5,6}$=2, $J_{5,6'}$=4.5, $J_{6,6'}$=12.5 Hz.

***erythro*-N^{α}-Benzyloxycarbonyl-β-hydroxy-L-histidine (12).** To an aqueous solution (2 ml) of *erythro*-β-hydroxy-L-histidine (**11**)[9] (305 mg, monohydrochloride) were added triethylamine (0.52 ml, 2.5 mol equiv for **11**) and a solution of *O*-benzyl *S*-(4,6-dimethyl-2-pyrimidinyl) thiocarbonate[10] (432 mg, 1.1 mol equiv for **11**) in 1,4-dioxane (2 ml) under stirring, and the solution was kept at room temperature for 2.5 h. The solution showed, on TLC with ethyl acetate–ethanol–water–formic acid (20:2:2:1), spots at R_f 0.12 (**12**) and 0 (trace, **11**). After addition of water (10 ml), the resulting solution was washed with ethyl acetate (10 ml×2) and the aqueous solution was concentrated to give a syrup, that was purified by column chromatography with the same solvent system described above to give a pale brown solid of **12**, 434 mg (97%), $[\alpha]_D^{17}$ +18° (*c* 1, CH_3OH); IR (KBr): 1705 (amide I), 1600 (aromatic), 1530 cm^{-1} (amide II); ^1H NMR (250 MHz, D_2O): δ=4.39 (1H, d, α-CH), 5.06 (2H, $C_6H_5CH_2$), 5.19 (1H, d, β-CH), 8.54 (1H, s, H-2 of Im); $J_{\alpha\text{-CH},\beta\text{-CH}}$=6.5 Hz.

Found: C, 54.11; H, 5.03; N, 13.21%. Calcd for $C_{14}H_{15}N_3O_5 \cdot 0.3\ H_2O$: C, 54.12; H, 5.06; N, 13.52%.

***erythro*-N^{α}-Benzyloxycarbonyl-β-hydroxy-L-histidine Methyl Ester (13).** Compound **12** was dissolved in 10% hydrogen chloride in methanol (6 ml) and the solution was kept at room temperature overnight, then at 40 °C for 7 h. The resulting solution showed, on TLC with chloroform–methanol (4:1), spots at R_f 0.45 (**13**) and 0.08 (trace, **12**). Concentration of the solution gave a yellow solid, that was purified by column chromatography with chloroform–methanol (5:1→5:2) to give a colorless, hygroscopic solid of **13**, 389 mg (78%, as the 0.8 hydrochloride), $[\alpha]_D^{20}$ −4° (*c* 1, CH_3OH); IR (KBr): 1720 ($\nu_{C=O}$ of ester, and amide I), 1615 (aromatic), 1525 cm^{-1} (amide II); ^1H NMR (250 MHz, CD_3OD): δ=3.74 (3H, s, $COOCH_3$), 4.60 (1H, d, α-CH), 5.05 (2H, $C_6H_5CH_2$), 5.12 (1H, d, β-CH), 7.32 (5H, $C_6H_5CH_2$), 7.35 [1H, s, H-5 of imidazole (=Im)], 8.65 (1H, s, H-2 of Im); $J_{\alpha\text{-CH},\beta\text{-CH}}$=7.5 Hz.

Found: C, 51.93; H, 5.33; N, 12.16; Cl, 8.21%. Calcd for $C_{15}H_{17}N_3O_5 \cdot 0.8$ HCl: C, 51.70; H, 5.15; N, 12.06; Cl, 8.14%.

***erythro*-N^{α}-Benzyloxycarbonyl-$N^{im(\tau)}$-(2,4-dinitrophenyl)-β-hydroxy-L-histidine Methyl Ester (14).** To a mixture of **13** (62.9 mg, 0.8 hydrochloride) and sodium hydrogencarbonate (40.0 mg, 2.6 mol equiv for **13**) in 50% aqueous 1,4-dioxane (1.2 ml) was added a solution of 2,4-dinitrofluorobenzene (49.1 mg, 1.5 mol equiv for **13**) in methanol (0.6 ml) and the solution was kept in the dark at room temperature for 3.5 h. Concentration of the solution gave a yellow solid, that was purified by column chromatography with benzene–ethyl acetate (1:2) to give a yellow solid of **14**, 74.1 mg (87%), $[\alpha]_D^{17}$ +8° (*c* 1, $CHCl_3$); IR (KBr): 1720 ($\nu_{C=O}$ of ester and amide I), 1610 (aromatic), 1540 (amide II and ν_{as} NO_2), 1500 (aromatic), 1350 cm^{-1} (ν_s NO_2); ^1H NMR (250 MHz, $CDCl_3$, at 55 °C): δ=3.75 (3H, s, $COOCH_3$), 4.86 (1H, dd, α-CH), 5.15 (2H, $C_6H_5CH_2$), 5.22 (1H, broad d, β-CH), 6.01 (1H, broad s, NH), 7.03 (1H, broad s, H-5 of Im), 7.3 (5H, $C_6H_5CH_2$), 7.56 (1H, broad d, H-2 of Im), 7.63 (1H, d, H-6 of Dnp), 8.53 (1H, dd, H-5 of Dnp), 8.81 (1H, d, H-3 of Dnp); $J_{NH,\alpha\text{-CH}}$=8.5, $J_{\alpha\text{-CH},\beta\text{-CH}}$=4, $J_{2,5(Im)}$=1.2, $J_{3,5(Dnp)}$=2.5, $J_{5,6(Dnp)}$=8.5 Hz.

Found: C, 50.18; H, 4.03; N, 13.69%. Calcd for $C_{21}H_{19}N_5O_9 \cdot H_2O$: C, 50.10; H, 4.21; N, 13.91%.

***erythro*-Bis-N^{α}:β-*O*-(benzyloxycarbonyl)-$N^{im(\tau)}$-dinitrophenyl-L-histidine Methyl Ester (15) and Methyl 2,4-Bis(benzyloxycarbonylamino)-4-*N*-formyl-5-(2,4-dinitrophenylamino)-2,4-pentadienoate (16).** A mixture of **14** (20.1 mg), sodium hydrogencarbonate (36.1 mg) and benzyl chloroformate (0.035 ml) in water–chloroform (0.6 ml each) was shaken at room temperature for 8 h. The chloroform layer showed, on TLC with benzene–ethyl acetate (3:1), two major spots at R_f 0.26 (**15**) and 0.46 (**16**). The organic layer separated was washed with water, dried ($MgSO_4$), and concentrated to give a dark-red syrup, that was column chromatographed with benzene–ethyl acetate (9:1) to give a yellow solid of **15**, 6.4 mg (26%), and a dark-red solid of **16**, 6.4 mg (26%).

15: $[\alpha]_D^{20}$ 0° (*c* 0.5, $CHCl_3$); ^1H NMR (250 MHz, $CDCl_3$): δ=3.73 (3H, s, $COOCH_3$), ≈5.15 (4H, $2C_6H_5CH_2$), 5.22 (1H, dd, α-CH), 6.19 (1H, d, β-CH), 6.47 (1H, d, NH), 7.13 [1H, broad s (d on irradiation at δ 6.19), H-5 of Im], ≈7.35 (10 H, $2C_6H_5CH_2$), 7.58 (1H, d, H-2 of Im), 7.66 (1H, d, H-6 of Dnp), 8.57 (1H, dd, H-5 of Dnp), 8.86 (1H, d, H-3 of Dnp); $J_{NH,\alpha\text{-CH}}$=9.5, $J_{\alpha\text{-CH},\beta\text{-CH}}$=4, $J_{2,5(Im)}$=1.3, $J_{3,5(Dnp)}$=2.5, $J_{5,6(Dnp)}$= 8.5 Hz.

16: ^1H NMR (250 MHz, $CDCl_3$): δ=3.66 (1H, s, $COOCH_3$), ≈5.2 (4H, $2C_6H_5CH_2$), 5.71 [1H, broad s (disappeared on deuteration), NHZ], 7.22 [1H, d, *J*=12 Hz (s on irradiation at δ=10.64 or on deuteration), H-5], 7.29 (1H, d, H-6 of Dnp), ≈7.35 (10 H, $2C_6H_5CH_2$), 7.49 (1H, s, H-3) 8.40 (1H, dd, H-5 of Dnp), 9.16 (1H, d, H-3 of Dnp), 9.25 (1H, s, CHO), 10.64 [1H, d, *J*=12 Hz (s on irradiation

at δ=7.22, or on deuteration), NHDnp]; $J_{3,5(Dnp)}$=2.5, $J_{5,6(Dnp)}$=9.5 Hz; FDMS: *m/z* 620 (MH^+), 619 (M^+), 591 ([M−CHO+H]$^+$).

***erythro*-$N^{im(3)}$-(4,6-Di-*O*-acetyl-2,3-di-*O*-methyl-α- and β-D-Glucopyranosyl)-N^{α}-benzyloxycarbonyl-β-hydroxyl-L-histidine Methyl Esters (18 and 19).** A mixture of 14 (41.0 mg), the bromide **10** (99 mg, ≈2.5 mol equiv for **14**) and powdered molecular sieves 4A (270 mg) in dry sulfolane (1 ml) was stirred in the dark at 40 °C for 3 h. Mercury(II) cyanide (170 mg) was added and stirring continued overnight. The mixture was charged on the top of a column with aid of benzene and chromatographed with benzene (120 ml)→benzene-ethyl acetate (1:2, 100 ml)→ethyl acetate-ethanol-water-formic acid (20:2:2:1, 120 ml) to give a mixture of products **17**, 56.4 mg, ^{1}H NMR (250 MHz, CD_3OD with slight CD_3COOD): δ=7.38 (H-5 of Im), 8.06 (H-6 of Dnp), 8.18 (H-2 of Im), 8.82 (H-5 of Dnp), 9.20 (H-3 of Dnp). To a solution of the solid in methanol (1 ml) was added 2-mercaptoethanol (10 mg) and the solution was kept at room temperature for 30 min. The resulting solution showed, on TLC with ethyl acetate-ethanol-water-formic acid (20:1:1:0.2), major three spots at R_f 0.20 (**18**), 0.30 (**19**), and 0.40 (**20**) (cf. **17**: R_f 0.05). The solution was concentrated and the syrup was chromatographed on a Sephadex LH-20 column with methanol and the products further purified by two silica-gel columns with chloroform-acetone (1:1) and ethyl acetate-ethanol-water-formic acid (20:1:1:0.2) to give solids of **18**, 16.8 mg (34% based on **14**), **19**, 12.8 mg (26% based on **14**), and **20**, 4.2 mg (6%).

18: Mp 69—71 °C, $[\alpha]_D^{21}$ +42° (*c* 0.5, $CHCl_3$); IR (KBr): 1740, 1530, 1235 cm^{-1}; ^{1}H NMR (250 MHz, $CDCl_3$): δ=2.00, 2.09 (each 3H, s, OAc), 3.40 (3H, s, OCH_3), 3.5 [1H, H-5 of glucoside portion (=G)], 3.59 (3H, s, OCH_3), 3.72 (3H, s, $COOCH_3$), 3.8 (2H, H-2,3 of G), 4.1 (2H, H-6,6′ of G), 4.71 (1H, dd, α-CH), 4.94 (1H, dd, H-4 of G), 5.1 (2H, $C_6H_5CH_2$), 5.34 (1H, d, β-CH), 5.79 (1H, d, NH), 6.30 (1H, d, H-1 of G), 7.08 (1H, s, H-5 of Im), 7.35 (5H, $C_6H_5CH_2$), 7.97 (1H, s, H-2 of Im); $J_{NH,\alpha\text{-}CH}$=8.5, $J_{\alpha\text{-}CH,\beta\text{-}CH}$=6, $J_{1,2(G)}$=3.5 Hz; SIMS: *m/z* 594 (MH^+), 320 ([**13**+H]$^+$), 302 ([**13**−OH]$^+$), 275 (G^+).

Found: C, 52.97; H, 5.73; N, 7.03%. Calcd for $C_{27}H_{35}N_3O_{12}\cdot H_2O$: C, 53.02; H, 6.10; N, 6.87%.

19: Mp 77—79 °C, $[\alpha]_D^{21}$ +20° (*c* 0.5, $CHCl_3$); IR (KBr): 1740, 1535, 1240 cm^{-1}; ^{1}H NMR (250 MHz, $CDCl_3$): δ=2.02, 2.12 (each 3H, s, OAc), 3.24 (3H, s, OCH_3), 3.34 (1H, t, H-3 of G), 3.39 (3H, s, OCH_3), 3.47 (1H, t, H-2 of G), 3.66 (1H, ddd, H-5 of G), 3.70 (1H, s, $COOCH_3$), 4.05 (1H, dd, H-6 of G), 4.16 (1H, dd, H-6′ of G), 4.95 (1H, dd, α-CH), 5.01 (1H, dd, H-4 of G), 5.07, 5.23 (each 1H, d, $C_6H_5CH_2$), 5.33 (1H, d, β-CH), 5.54 (1H, d, H-1 of G), 6.43 (1H, d, NH), 6.88 (1H, s, H-5 of Im), 7.38 (5H, $C_6H_5CH_2$), 7.70 (1H, s, H-2 of Im); $J_{NH,\alpha\text{-}CH}$=9, $J_{\alpha\text{-}CH,\beta\text{-}CH}$=5, $J_{1,2(G)}$=$J_{2,3(G)}$=$J_{3,4(G)}$=9, $J_{4,5(G)}$=10, $J_{5,6(G)}$=2, $J_{5,6'(G)}$=5, $J_{6,6'(G)}$=12.5, $J_{AB\ of\ C_6H_5CH_2}$=12 Hz; SIMS: *m/z* 594 (MH^+), 320 ([**13**+H]$^+$), 302 ([**13**−OH]$^+$), 275 (G^+).

Found: C, 52.73; H, 5.70; N, 6.83%. Calcd for $C_{27}H_{35}N_3O_{12}\cdot H_2O$: C, 53.02; H, 6.10; N, 6.87%.

20: ^{1}H NMR (250 MMz, $CDCl_3$): δ=4.52 and 4.58 [≈1H in total, each d, *J*=8 Hz, H-1 of *O*-G(β-anomer)], 4.82 and 4.92 [each d, *J*=4 Hz, H-1 of *O*-G (α-anomer)?], 5.50 and 5.59 [≈1H in total, each d, *J*=9 Hz, H-1 of *N*-G(β-anomer)], 6.31 and 6.41 [≈1H in total, each d, *J*=3.5 Hz, H-1 of *N*-G(β-anomer)].

***erythro*-N^{α}-Benzyloxycarbonyl-β-hydroxy-$N^{im(\tau)}$-tosyl-L-histidine Methyl Ester (21).** To a solution of **13** (317 mg, 0.8 hydrochloride) in 50% aqueous 1,4-dioxane (9 ml) were added sodium carbonate (116 mg) and then tosyl chloride (190 mg) in 1,4-dioxane (2 ml) and the mixture was stirred at 0 °C for 30 min, then at room temperature for 2 h. The solution showed, on TLC with chloroform-methanol (20:1), a major spot at R_f 0.44 (**21**). The solution was poured into a mixture of ether (5 ml) and water (3 ml) with stirring. The organic layer separated and the ether washings of the residual aqueous layer combined were dried ($MgSO_4$), and concentrated to give a solid of **21**, 415 mg (98%). Recrystallization from dichloromethane-ether gave needles, mp 112—114 °C, $[\alpha]_D^{24}$ +15° (*c* 1, $CHCl_3$); IR (KBr): 1755, 1720 ($\nu_{C=O}$ of ester, and amide I), 1600 (aromatic), 1530 (amide II), 1380 (ν_{as} SO_2), 1175 cm^{-1} (ν_s SO_2); ^{1}H NMR (250 MHz, $CDCl_3$): δ=2.42 (3H, s, CH_3 of Ts), 3.66 (3H, s, $COOCH_3$), 4.79 (1H, dd, α-CH), 5.10 (2H, s, $C_6H_5CH_2$), 5.15 [1H, broad s (d, after deuteration), β-CH], 5.85 (1H, d, NH), 7.24 (1H, broad s, H-5 of Im), 7.35 (7H, $C_6H_5CH_2$ and *m*-H of Ts), 7.79 (2H, *o*-H of Ts), 7.90 (1H, d, H-2 of Im); $J_{NH,\alpha\text{-}CH}$=8, $J_{\alpha\text{-}CH,\beta\text{-}CH}$=4, $J_{2,5(Im)}$=1.5 Hz; SIMS: *m/z* 474 (MH^+), 456 ([**21**−OH]$^+$), 320 ([**13**+H]$^+$), 302 ([**13**−OH]$^+$).

Found: C, 55.07; H, 4.96; N, 9.02; S, 6.58%. Calcd for $C_{22}H_{23}N_3O_7S\cdot 0.5\ H_2O$: C, 54.76; H, 5.01; N, 8.71; S, 6.64%.

***erythro*-β-Hydroxy-N^{α}-(*p*-methoxybenzyloxycarbonyl)-$N^{im(\tau)}$-tosyl-L-histidine Methyl Ester (23).** To an aqueous solution (0.5 ml) of **11**[9] (102 mg, monohydrochloride) were added triethylamine (0.2 ml) and a solution of *O*-(*p*-methoxybenzyl) *S*-(4,6-dimethyl-2-pyrimidinyl) thiocarbonate (PMZ-S reagent)[10] (184 mg) in 1,4-dioxane (0.5 ml), and the mixture was stirred for 3 h. Work-up as described for **12** gave a syrup, that was column-chromatographed with ethyl acetate-ethanol-water-formic acid (20:2:2:1) to give a solid of the corresponding N^{α}-PMZ derivative (185 mg). A mixture of the solid, sodium carbonate (72 mg), and tosyl chloride (116 mg) in H_2O-1,4-dioxane (3:4, 7 ml) was stirred at room temperature overnight. Concentration of the solution gave a residue, an aqueous solution of which was washed with ether and then ethyl acetate. The aqueous solution was concentrated to give a solid (263 mg), that was purified by column chromatography with chloroform-methanol (5:1) to give a solid of $N^{im(\tau)}$-tosyl derivative (163 mg). To a methanol solution (1.2 ml) of the solid was added a solution of ≈0.3 M† diazomethane in ether until the reaction mixture became yellow (≈0.5 ml). After concentration, the residue was column-chromatographed with chloroform-methanol (30:1) to give a solid of **23**, 35.9 mg (15% from **11**), ^{1}H NMR (250 MHz, $CDCl_3$): δ=2.45 (3H, s, CH_3 of Ts), 3.67 (3H, s, $COOCH_3$), 3.73 [1H, d (s on irradiation at δ 5.15; disappeared on deuteration), OH], 3.82 (3H, s, CH_3O of PMZ), 4.80 (1H, dd, α-CH), 5.04 (2H, s, CH_2 of PMZ), 5.15 (1H, dd, β-CH), 5.80 (1H, d, NH, disappeared on deuteration), 6.90 (2H, *m*-H of PMZ), 7.24 (1H, broad s, H-5 of Im), 7.30 (2H, *o*-H of PMZ), 7.35 (2H, *m*-H of Ts), 7.81 (2H, *o*-H of Ts), 7.90 (1H, d, H-2 of Im); $J_{NH,\alpha\text{-}CH}$=8, $J_{\alpha\text{-}CH,\beta\text{-}CH}$=3.5, $J_{\beta\text{-}CH,OH}$=7.5, $J_{2,5(Im)}$=1.5 Hz.

† 1 M=1 mol dm^{-3}.

***erythro*-N^{α}-Benzyloxycarbonyl-β-hydroxy-$N^{im(\tau)}$-tosyl-L-histidine *p*-Nitrobenzyl Ester (25).** To an aqueous solution (1 ml) of **12** (107 mg) and sodium carbonate (45 mg) was added tosyl chloride (80.6 mg) in 1,4-dioxane (1 ml) and the resulting clear solution was kept at room temperature for 5 h. The solution showed, on TLC with ethyl acetate-ethanol-water-formic acid (20:2:2:1), a spot at R_f 0.78 (**24**). Concentration gave a solid, that was column-chromatographed with chloroform-methanol (5:1) to give a solid of **24**, 164 mg, ^{1}H NMR (250 MHz, CD_3OD): δ=2.40 (3H, s, CH_3 of Ts), 4.53 (1H, d, *J*=5.5 Hz, α-CH), 7.30 (5H, $C_6H_5CH_2$), 7.42 (2H, *m*-H of Ts), 7.46 (1H, broad s, H-5 of Im), 7.90 (2H, *o*-H of Ts), 8.15 (1H, d, *J*=1.2 Hz, H-2 of Im). To a solution of **24** (88.6 mg) in dry DMF (1.7 ml) were added triethylamine (0.028 ml, dried over CaH_2, 1.1 mol equiv for **24**) and *p*-nitrobenzyl bromide (44.2 mg, 1.1 mol equiv for **24**) and the solution was kept at room temperature overnight. Concentration gave a residue, the solution of which was washed with water, dried ($MgSO_4$), and concentrated. The residue was column-chromatographed with chlorofom-methanol (30:1) to give needles of **25**, 53.6 mg (46% from **12**), mp 159—160 °C, $[\alpha]_D^{20}$ −6° (*c* 0.5, $CHCl_3$); IR (KBr): 1725, 1710, 1520 (amide II and $\nu_{as}NO_2$), 1380 ($\nu_{as}SO_2$), 1350 (ν_sNO_2), 1175 cm^{-1} (ν_sSO_2); ^{1}H NMR (250 MHz, $CDCl_3$): δ=2.42 (3H, s, CH_3 of Ts), 3.53 (1H, d, OH), 4.88 (1H, dd, α-CH), 5.89 (1H, d, NH), 7.18 (1H, broad s, H-5 of Im), 7.33 (2H, *m*-H of Ts), 7.34 (5H, s, $C_6H_5CH_2$), 7.41 (2H, broad d, *o*-H of $NO_2C_6H_4CH_2$), 7.78 (2H, dt, *o*-H of Ts), 7.84 (1H, d, H-2 of Im), 8.18 (2H, dt, *m*-H of $NO_2C_6H_4CH_2$); $J_{NH,\alpha\text{-}CH}$=8.5, $J_{\alpha\text{-}CH,\beta\text{-}CH}$=4, $J_{OH,\beta\text{-}CH}$=8, $J_{2,5(Im)}$=1.4 Hz.

Found: C, 56.31; H, 4.46; N, 9.22; S, 5.52%. Calcd for $C_{28}H_{26}N_4O_9S$: C, 56.56; H, 4.41; N, 9.42; S, 5.39%.

***erythro*-β-*O*-(4,6-Di-*O*-acetyl-2,3-di-*O*-methyl-α- and β-D-glucopyranosyl)-N^{α}-benzyloxycarbonyl-$N^{im(\tau)}$-tosyl-L-histidine Methyl Esters (26 and 27). A) Reaction Using Mercury(II) Cyanide as the Catalyst.** To a solution of **21** (20.8 mg) and the bromide **10** (26.0 mg, ≈1.5 mol equiv for **21**) in dry dichloromethane (0.5 ml) was added powdered molecular sieves 4A (50 mg) and the mixture was stirred in the dark at room temperature for 2 h. Mercury(II) cyanide (51 mg, 3 mol equiv for **10**) was added and the mixture was stirred at room temperature for 48 h (even after 24 h, **10** and **21** still remained). The resulting solution showed, on TLC with chloroform-methanol (20:1), several spots at R_f 0.48 (**26** and **27**), 0.30 (**21**), 0.22 (detosyldi-N^{im},*O*-glucosyl derivatives) and 0.12 (N^{im}-glucosyl derivatives) (cf. **10**: R_f 0.68). The mixture was centrifuged, and the supernatant solution and the dichloromethane washings of the residue combined were washed with water, dried ($MgSO_4$), and concentrated to give a pale yellow solid (42.6 mg), that was twice column-chromatographed with chloroform-methanol (50:1) to give a mixture of **26** and **27** (2:1, determined by the ^{1}H NMR spectrum), 5.8 mg (21% from **21**), a mixture of detosylglucosyl derivatives, 14.9 mg, and **21**, 3.2 mg (15%). Compounds **26** and **27** showed the same R_f value with several kinds of solvent systems tested but was separated by means of analytical high-pressure liquid chromatography (Waters Model 6000A, μ-porasil silica column) using chloroform as the developer. The physicochemical data of **26** and **27** described next were taken by the isolated products.

B) Reaction Using Silver Carbonate-Silver Perchlorate as the Catalyst. A mixture of **21** (43.6 mg), the bromide **10** (51 mg, ≈1.4 mol equiv for **21**) and powdered molecular sieves 4A (90 mg) in dry dichloromethane (1.8 ml) was stirred in the dark at room temperature for 2 h, then cooled to −55 °C. Silver carbonate (48.3 mg, 1.3 mol equiv for **10**) and silver perchlorate (43.1 mg, 1.4 mol equiv for **10**) were added and the mixture was stirred at −55 °C for 5.5 h. Work-up as described for A) gave a pale brown syrup (82 mg), that was thrice column-chromatographed with benzene-ethyl acetate (2:1), chloroform-methanol (50:1), and chloroform-acetone (10:1) to give a mixture of **26** and **27** (≈20:1, determined by the ^{1}H NMR spectrum), 45.9 mg (67% based on **21**), a mixture of detosyldiglucosyl derivatives, 6.0 mg (8%), and **21**, 3.0 mg (7%).

26: $[\alpha]_D^{19}$ +71° (*c* 0.5, $CHCl_3$), IR (KBr): 1745, 1600, 1520, 1380, 1240, 1175 cm^{-1}; ^{1}H NMR (250 MHz, $CDCl_3$): δ=2.07, 2.09 (each 3H, s, OAc), 2.43 (3H, s, CH_3 of Ts), 3.24 (1H, dd, H-2 of G), 3.31 and 3.50 (each 3H, s, OCH_3), 3.54 (1H, t, H-3 of G), 3.63 (3H, s, $COOCH_3$), ≈4.0 (2H, H-5,6 of G), 4.23 (1H, dd, H-6′ of G), 4.89 (1H, d, H-1 of G), 4.90 (1H, t, H-4 of G), ≈4.9 (1H, α-CH), ≈5.1 (3H, $C_6H_5CH_2$ and β-CH), 5.79 (1H, d, NH), 7.35 (7H, $C_6H_5CH_2$ and *m*-H of Ts), 7.45 (1H, apparent t, H-5 of Im), 7.80 (2H, *o*-H of Ts), 7.93 (1H, d, H-2 of Im); $J_{NH,\alpha\text{-}CH}$=9, $J_{1,2(G)}$=3.5, $J_{2,3(G)}$=$J_{3,4(G)}$=$J_{4,5(G)}$=9.5, $J_{5,6'(G)}$=5, $J_{6,6'(G)}$=13, $J_{2,5(Im)}$=1.5, $J_{\beta\text{-}CH,5(Im)}$=0.5 Hz; SIMS: *m/z* 748 (MH^+), 594 ([M−Ts+2H]$^+$), 4.74 ([**21**+H]$^+$), 456 ([**21**−OH]$^+$), 320 ([**13**+H]$^+$), 302 ([**13**−OH]$^+$), 275 (G^+).

Found: C, 53.32; H, 5.37; N, 5.14; S, 4.16%. Calcd for $C_{34}H_{41}N_3O_{14}S\cdot H_2O$: C, 53.33; H, 5.66; N, 5.49; S, 4.19%.

27: $[\alpha]_D^{22}$ +6° (*c* 0.2, $CHCl_3$); IR (KBr): 1740, 1510, 1375, 1230, 1175 cm^{-1}; ^{1}H NMR (250 MHz, $CDCl_3$): δ=2.05, 2.09 (each 3H, s, OAc), 2.43 (3H, s, CH_3 of Ts), 3.09 (1H, dd, H-2 of G), 3.26 (1H, t, H-3 of G), 3.48 and 3.51 (each 3H, s, OCH_3), 3.56 (3H, s, $COOCH_3$), 3.98 (1H, dd, H-6 of G), 4.07 (1H, dd, H-6′ of G), 4.50 (1H, d, H-1 of G), 4.87 (1H, apparent t, H-4 of G), 5.00 (1H, dd, α-CH), 5.11 (2H, $C_6H_5CH_2$), 5.17 (1H, broad d, β-CH), 6.18 (1H, d, NH), 7.33 (7H, $C_6H_5CH_2$ and *m*-H of Ts), 7.36 (1H, broad s, H-5 of Im), 7.81 (2H, *o*-H of Ts), 7.88 (1H, d, H-2 of Im); $J_{NH,\alpha\text{-}CH}$=9, $J_{\alpha\text{-}CH,\beta\text{-}CH}$=4, $J_{1,2(G)}$=7.5, $J_{2,3(G)}$=$J_{3,4(G)}$=9, $J_{4,5(G)}$=10, $J_{5,6(G)}$=2.5, $J_{5,6'(G)}$=5, $J_{6,6'(G)}$=12, $J_{2,5(Im)}$=1.5 Hz; SIMS: *m/z* 748 (MH^+), 594 ([M−Ts+2H]$^+$), 474 ([**21**+H]$^+$), 456 ([**21**−OH]$^+$), 320 ([**13**+H]$^+$), 302 ([**13**−OH]$^+$), 275 (G^+).

3,4,6-Tri-*O*-acetyl-2-*O*-[2,4,6-tri-*O*-acetyl-3-*O*-(*N*-acetylcarbamoyl)-α-D-mannopyranosyl]-α-L-gulopyranosyl Bromide (28). 1,3,4,6-Tetra-*O*-acetyl-2-*O*-(2,4,6-tri-*O*-acetyl-3-*O*-carbamoyl-α-D-mannopyranosyl)-β-L-gulopyranose[2] (31.3 mg) was dissolved in a cold (0 °C) mixture of 30% hydrogen bromide in acetic acid-acetic acid-acetic anhydride (3:8:1) (0.4 ml) and the solution was kept at the temperature for 1 h, then at room temperature in the dark overnight. The solution showed, on TLC with benzene-ethyl acetate (1:2), a single spot at R_f 0.44 (**28**; cf. the starting sugar: R_f 0.28). Work-up as described for **10** gave a pale brown solid of **28**, 32.3 mg (94%), ^{1}H NMR (250 MHz, $CDCl_3$): δ=2.09 (6H, s, 2OAc), 2.12, 2.14, 2.15, 2.23 (each 3H, s, OAc), 2.41 (3H, s, NAc), 4.05 [1H, dd, H-2 of gulose(=Gul)], 4.63 (1H, ddd, H-5 of Gul), 5.06 [1H, d, H-1 of mannose(=Man)], 5.11 (1H, dd, H-4 of Gul), 5.18 (1H, dd, H-3 of Man), 5.24 (1H, dd, H-2 of Man), 5.28 (1H, t, H-4 of Man), 5.36 (1H, dt, H-3 of Gul), 6.42 (1H, broad d, H-1 of Gul), 7.47 (1H, s, NH);

$J_{1,2(Gul)}$=4.5, $J_{1,3(Gul)}$=1, $J_{2,3(Gul)}$=$J_{3,4(Gul)}$=3.5, $J_{4,5(Gul)}$=1, $J_{5,6(Gul)}$≈5.5, $J_{5,6'(Gul)}$≈7, $J_{1,2(Man)}$=2, $J_{2,3(Man)}$=3, $J_{3,4(Man)}$=$J_{4,5(Man)}$=9.5 Hz.

***erythro*-β-*O*-[3,4,6-Tri-*O*-acetyl-2-*O*-[2,4,6-tri-*O*-acetyl-3-*O*-(*N*-acetylcarbamoyl)-α-D-mannopyranosyl]-α-L-gulopyranosyl]-N^{α}-benzyloxycarbonyl-$N^{im(\tau)}$-tosyl-L-histidine Methyl Ester (29).** A mixture of **21** (12.8 mg), the bromide **28**, (32.3 mg, ≈1.4 mol equiv for **21**) and powdered molecular sieves 4A (40 mg) in dry dichloromethane (0.6 ml) was stirred in the dark at room temperature for 2 h, then cooled to −55 °C. Silver carbonate (12.5 mg, 1.1 mol equiv for **21**) and silver perchlorate (10.5 mg, 1.1 mol equiv for **21**) were added and the mixture was stirred at −55 °C overnight. The solution showed, on TLC with benzene-ethyl acetate (1:2), a spot at R_f 0.30 (**29**; cf. **21**: R_f 0.55; **28**: R_f 0.42). Work-up as described for **26** gave a pale brown solid (40.4 mg), that was twice column-chromatographed with chloroform-methanol (30:1) and chloroform-acetone (3:1) to give a solid of **29**, 29.0 mg (95% based on **21**), mp 89—91 °C $[\alpha]_D^{27}$ −12° (*c* 0.5, $CHCl_3$); IR (KBr): 1740, 1600, 1510, 1375, 1220, 1175 cm^{-1}; ^1H NMR (400 MHz, $CDCl_3$): δ=1.97, 2.00, 2.08, 2.10, 2.11, 2.14 (each 3H, s, OAc), 2.35 (3H, s, NAc), 2.43 (3H, s, CH_3 of Ts), 3.55 (3H, s, $COOCH_3$), 3.79 (1H, dd, H-6 of Gul), 3.90 (1H, dd, H-6′ of Gul), 4.06 (1H, t, H-2 of Gul), 4.1 (1H, H-6 of Man), 4.15 (1H, H-5 of Man), 4.3 [2H, H-5(Gul) and H-6′(Man)], 4.90 (1H, dd, α-CH), 4.96 (1H, d, one of $C_6H_5CH_2$), 5.01 (1H, dd, H-4 of Gul), 5.01 (1H, d, H-1 of Man), 5.15 (1H, d, H-1 of Gul), 5.210 (1H, d, β-CH), 5.213 (1H, d, one of $C_6H_5CH_2$), 5.27 (1H, t, H-3 of Gul), 5.29 (2H, H-3,4 of Man), 5.31 (1H, H-2 of Man), 6.08 (1H, d, NH), 7.33 (5H, s, $C_6H_5CH_2$), 7.37 (2H, *m*-H of Ts), 7.47 (1H, broad s, H-5 of Im), 7.83 (2H, *o*-H of Ts), 7.97 (1H, d, H-2 of Im); $J_{NH,\alpha\text{-}CH}$=8.5, $J_{\alpha\text{-}CH,\beta\text{-}CH}$=3.5, $J_{1,2(Gul)}$=$J_{2,3(Gul)}$=$J_{3,4(Gul)}$=3.5, $J_{4,5(Gul)}$=1.5, $J_{5,6(Gul)}$=7, $J_{5,6'(Gul)}$=6, $J_{6,6'(Gul)}$=11.5, $J_{1,2(Man)}$=1, $J_{AB\ C_6H_5CH_2}$=12, $J_{2,5(Im)}$=1.5 Hz; SIMS: *m/z* 1135 (MH^+), 980 ([M−Ts+H]$^+$), 662 ([**28**−Br]$^+$), 474 ([**21**+H]$^+$), 456 ([**21**−OH]$^+$), 374 (mannose moiety$^+$), 320 ([**13**+H]$^+$), 302 ([**13**−OH]$^+$), 289 (gulose moiety$^+$).

Found: C, 51.73; H, 5.34; N, 4.69; S, 2.78%. Calcd for $C_{49}H_{58}N_4O_{25}S$: C, 51.85; H, 5.15; N, 4.94; S, 2.82%

***erythro*-β-*O*-[3,4,6-Tri-*O*-acetyl-2-*O*-[2,4,6-tri-*O*-acetyl-3-*O*-(*N*-acetylcarbamoyl)-α-D-mannopyranosyl]-α-L-gulopyranosyl]-N^{α}-*t*-butoxycarbonyl-$N^{im(\tau)}$-tosyl-L-histidine Methyl Ester (30).** Condensation of **22**[3] (6.8 mg) with **28** (15.7 mg) was carried out in the presence of powdered molecular sieves 4A (30 mg), silver carbonate (7.1 mg), and silver perchlorate (6.2 mg) in dry dichloromethane (0.5 ml) in a manner described for **29**. The solution showed, on TLC with benzene-ethyl acetate (1:2), a spot at R_f 0.20 (**30**). Usual work-up including column chromatography as described for **29** gave a solid of **30**, 3.2 mg (19% based on **22**), ^1H NMR (250 MHz, $CDCl_3$): δ=1.41 (9H, s, *t*-Butyl), 5.03 (1H, d, *J*=1 Hz, H-1 of Man), 5.13 (1H, d, *J*=3.5 Hz, H-1 of Gul).

***erythro*-β-*O*-[3,4,6-Tri-*O*-acetyl-2-*O*-(2,4,6-tri-*O*-acetyl-3-*O*-carbamoyl-α-D-mannopyranosyl)-α-L-gulopyranosyl]-N^{α}-benzyloxycarbonyl-$N^{im(\tau)}$-tosyl-L-histidine *p*-Nitrobenzyl Ester (31).** A mixture of **25** (27.2 mg), the bromide **3** (52 mg, ≈1.3 mol equiv for **25**), and powdered molecular sieves 4A (115 mg) in dry dichloromethane (1.6 ml) was stirred in the dark at room temperature for 2 h, then, after cooling to −55 °C, silver carbonate (18.6 mg) and silver perchlorate (14.8 mg) were added and the mixture was stirred at −55 °C overnight. The solution showed, on TLC with benzene-ethyl acetate (1:2), two spots at R_f 0.30 (**31**) and R_f 0.65 (**25**). Usual work-up as described for **26** gave a solid (66 mg), that was column-chromatographed with benzene-ethyl acetate (1:2) to give a solid of **31**, 24.4 mg (43% based on **25**) and **25**, 6.7 mg (25% recovered).

31: Mp 94—98 °C, $[\alpha]_D^{20}$ −12° (*c* 0.5, $CHCl_3$); IR (KBr): 1740, 1600, 1520, 1365, 1345, 1220, 1175 cm^{-1}; ^1H NMR (250 MHz, $CDCl_3$): δ=1.93, 1.99, 2.02, 2.06, 2.10, 2.14 (each 3H, s, OAc), 2.41 (3H, s, CH_3 of Ts), 3.75 (1H, dd, H-6 of Gul), 3.91 (1H, dd, H-6′ of Gul), 4.06 (1H, t, H-2 of Gul), ≈4.1 (2H, H-5, 6 of Man), ≈4.3 (2H, H-5 of Gul and H-6′ of Man), 4.61 (2H, broad s, $CONH_2$), 5.01 (1H, dd, H-4 of Gul), 5.03 (1H, d, H-1 of Man), 5.11 (1H, d, H-1 of Gul), ≈5.25 (H-3,4 of Man), 5.27 (1H, t, H-3 of Gul), 5.31 (1H, H-2 of Man), 6.10 (1H, d, NH), ≈7.3 (10H, $C_6H_5CH_2$, *o*-H of $NO_2C_6H_4CH_2$, H-5 of Im, and *m*-H of Ts), 7.79 (2H, dt, *o*-H of Ts), 7.90 (1H, d, H-2 of Im), 8.15 (2H, d, *m*-H of $NO_2C_6H_4CH_2$); $J_{NH,\alpha\text{-}CH}$=8, $J_{1,2(Gul)}$=$J_{2,3(Gul)}$=$J_{3,4(Gul)}$=3.5, $J_{4,5(Gul)}$=2, $J_{5,6(Gul)}$=7.5, $J_{5,6'(Gul)}$=6, $J_{6,6'(Gul)}$=11.5, $J_{1,2(Man)}$=1.5, $J_{2,5(Im)}$=1.3 Hz.

Found: C, 51.33; H, 4.94; N, 5.10; S, 2.27%. Calcd for $C_{55}H_{61}N_5O_{27}S\cdot 2H_2O$: C, 51.12; H, 5.07; N, 5.42; S, 2.48%.

We are grateful to Dr. Tomohisa Takita of Institute of Microbial Chemistry for kind discussions, to Dr. Hiroshi Naganawa for measurements of the SIMS and FDMS, and to Mr. Saburo Nakada of Keio University for elemental analyses. We are also grateful to Mrs. Yukiko Otsuka of Institute of Bioorganic Chemistry for measurements of the ^1H NMR spectra and Miss Sachiko Yanagida for preparation of the manuscript.

References

1) H. Umezawa, "Bleomycin: Chemical, Biochemical, and Biological Aspects," ed by S. M. Hecht, Springer-Verlag, New York, Heidelberg, and Berlin (1979), p. 24.

2) a) T. Takita, Y. Umezawa, S. Saito, H. Morishima, H. Umezawa, Y. Muraoka, M. Suzuki, M. Otsuka, S. Kobayashi, M. Ohno, T. Tsuchiya, T. Miyake, and S. Umezawa, "Peptides: Synthesis-Structure-Function," (Proceedings of the 7th American Peptide Symposium) (1981), p. 29; b) T. Takita, Y. Umezawa, S. Saito, H. Morishima, H. Naganawa, H. Umezawa, T. Tsuchiya, T. Miyake, S. Kageyama, S. Umezawa, Y. Muraoka, M. Suzuki, M. Otsuka, M. Narita, S. Kobayashi, and M. Ohno, *Tetrahedron Lett.*, **23**, 521 (1982).

3) S. Saito, Y. Umezawa, T. Yoshioka, T. Takita, H. Umezawa, and Y. Muraoka, *J. Antibiot.*, **36**, 92 (1983).

4) Y. Aoyagi, K. Katano, H. Suguna, J. Primeau, L.-H. Chang, and S. Hecht, *J. Am. Chem. Soc.*, **104**, 5537 (1982).

5) S. Saito, Y. Umezawa, H. Morishima, T. Takita, H. Umezawa, M. Narita, M. Otsuka, S. Kobayashi, and M. Ohno, *Tetrahedron Lett.*, **23**, 529 (1982).

6) F. H. Bissett, M. E. Evans, and F. W. Parrish, *Carbohydr. Res.*, **5**, 184 (1967).

7) a) H. G. Jones and J. K. N. Jones, *Can. J. Chem.*, **47**, 3269 (1969); b) Yu. N. Elkin, N. I. Shulga, T. I. Vakorina,

and A. K. Dzizenko, *Anal. Biochem.*, **68**, 9 (1975); c) Yu. N. Elkin, *J. Chromatogr.*, **180**, 163 (1979). Except for the retention time on gas-liquid chromatography, no physical data of **7** was reported in these references.

8) E. Pacsu, J. Janson, and B. Lindberg, "Methods in Carbohydrate Chemistry," ed by R. L. Whistler, M. L. Wolfrom, and J. N. BeMiller, Academic Press Inc., New York and London (1963), Vol. 2, p. 380.

9) Natural: T. Takita, T. Yoshioka, Y. Muraoka, K. Maeda, H. Umezawa, *J. Antibiot.*, **24**, 795 (1971). Synthetic: S. Saito, Y. Umezawa, T. Yoshioka, T. Takita, H. Umezawa, Y. Muraoka, *J. Antibiot.*, **36**, 92 (1983).

10) For the reagents of *t*-butyloxycarbonylation (Boc-S reagent) and *p*-methoxybenzyloxycarbonylation (PMZ-S reagent) see T. Nagasawa, K. Kuroiwa, K. Narita, and Y. Isowa, *Bull. Chem. Soc. Jpn.*, **46**, 1269 (1973).

11) J. R. Bell and J. H. Jones, *J. Chem. Soc., Perkin Trans. 1*, **1974**, 2336.

12) E. Babad and D. Ben-Ishai, *J. Heterocycl. Chem.*, **6**, 235 (1969).

13) H. R. Matthews and H. Rapoport, *J. Am. Chem. Soc.*, **95**, 2297 (1973).

14) "Nucleic Acid Chemistry, part one and two," ed by L. B. Townsend and R. S. Tipson, John Wiley & Sons, Inc., New York (1978).

15) F. Micheel and A. Klemer, *Chem. Ber.*, **91**, 194 (1958).

 © 1986 The Chemical Society of Japan Bull. Chem. Soc. Jpn., 59, 1397—1401 (1986)

Synthesis of 6-Amino-6-deoxy-L-idopyranosides

Keiji MATSUDA, Tsutomu TSUCHIYA,* Takahiro TORII, and Sumio UMEZAWA
Institute of Bioorganic Chemistry, 1614 Ida, Nakahara-ku, Kawasaki 211
(Received November 21, 1985)

Methyl 6-amino-6-deoxy-α- and -β-L-idopyranosides have been prepared from 3-*O*-acetyl-1,2-*O*-isopropylidene-D-glucofuranose via 5,6-anhydro-1,2-*O*-isopropylidene-L-idofuranose and the azide product derived from it. Isopropyl 6-amino-6-deoxy-α- and -β-L-idopyranosides were prepared from 6-azido-2,3,4-tri-*O*-benzyl-6-deoxy-α-L-idopyranosyl chloride and 2-propanol. Nonprotected α- and β-L-idopyranosides were distinguished by their $J_{1,2}$ proton couplings.

In the course of our synthetic studies on the analogs of aminoglycoside antibiotics containing 2,6-diamino-2,6-dideoxy-L-idopyranose, such as neomycin B, lividomycins, and paromomycin I, we needed to know the characteristics of the most basic 6-amino-6-deoxy-L-idopyranosides. In this paper we describe the syntheses of methyl and isopropyl 6-amino-6-deoxy-α-and-β-L-idopyranosides.

Sorkin and Reichstein[1] prepared methyl α-and β-D-idopyranosides from methyl 4,6-*O*-benzylidene-D-galactopyranosides by alkaline hydrolysis of the corresponding 2,3-anhydro-D-gulo- and -talo derivatives. In the synthesis of 3,6-diamino-3,6-dideoxy-D-idose, Hanessian and Haskell[2] used this kind of procedure. To prepare 6-deoxy-L-idosides, 5,6-unsaturated D-*xylo* compounds such as methyl 2,3,4-tri-*O*-acetyl-6-deoxy-α-D-*xylo*-hex-5-enopyranoside[3] were usually reduced catalytically. In the synthesis of 3-*O*-acetyl-2,6-diazido-4-*O*-benzyl-2,6-dideoxy-L-idopyranosyl chloride,[4] a precursor for the 2,6-diamino-2,6-dideoxy-L-idoside portion of neomycin B, we applied a head-to-tail inversion technique for a D-glucose derivative. Meyer and Reichstein[5] prepared L-idopyranose from 1,2-*O*-isopropylidene-5-*O*-tosyl-D-glucofuranose derivatives through hydrolysis of the 5,6-anhydro-L-idofuranoses derived from the D-glucofuranose. Since then most investigators used 5,6-anhydro compounds or similar methods using 5,6-epimine[6] or oxazoline[7,8] to prepare L-ido derivatives. In our present synthesis, the 6-amino-6-deoxy-L-idopyranosides (**13** and **14**) were also prepared by way of a 5,6-anhydro compound.

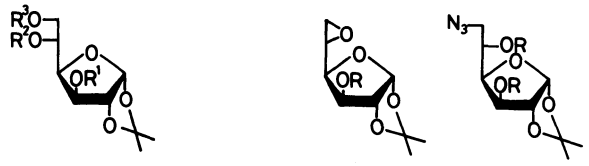

	R^1	R^2	R^3
1	Ac	H	H
2	Ac	H	$COC_6H_4NO_2(p)$
3	Ac	SO_2CH_3	$COC_6H_4NO_2(p)$
4	H	SO_2CH_3	H

	R
5	H
6	Ac

	R
7	H
8	Ac

Chart 1.

3-*O*-Acetyl-1,2-*O*-isopropylidene-D-glucofuranose[9] (**1**) was treated with *p*-nitrobenzoyl chloride in pyridine at −40 °C, when crystalline 6-*O*-(*p*-nitrobenzoyl) derivative **2** was obtained in high yield. No acetyl migration suggested[5] was observed. After mesylation of **2** (to give the 5-*O*-mesyl derivative,**3**) two acyl groups were removed by methanolic ammonia to give the diol **4**. Attempts to selectively remove the 6-*O*-(*p*-nitrobenzoyl) group by controlled reaction conditions were unsuccessful giving a mixture including a migration product, 6-*O*-acetyl derivative. Treatment of **4** with 1,8-diazabicyclo-[5.4.0]undec-7-ene (DBU) in oxolane gave the 5,6-anhydro derivative **5** of L-ido structure in a moderate yield. If methanolic ammonia or methanolic sodium methoxide was used instead of DBU, no pure **5** was obtained possibly by contamination of a 3,5-oxetane derivative as suggested by Buchanan and Oakes.[10] The structure of **5** was proved by the acetyl derivative **6** of **5**. From the ^1H NMR spectrum, it was clarified that the acetyl group was introduced at C-3, not at C-6, precluding the oxetane structure of **5**. Opening the 5,6-anhydro ring with a mixture[11] of sodium azide-ammonium chloride gave the 6-azido-L-idofuranose **7**. Reaction without the use of ammonium chloride gave **7** in only poor yield. Structure of **7** was proved by inspection of the ^1H NMR spectrum of the di-*O*-acetyl derivative **8**. Refluxing **7** with methanolic hydrochloric acid gave

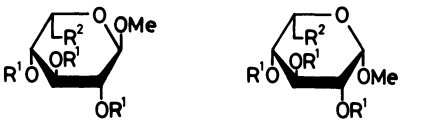

	R^1	R^2
9	Ac	N_3
11	H	N_3
13	H	NH_2

	R^1	R^2
10	Ac	N_3
12	H	N_3
14	H	NH_2

Chart 2.

a mixture of several products. Separation of them by usual silica-gel or resin column chromatography was found difficult; however, the portion of the anomeric mixture of 6-azidoglycopyranosides **11** and **12** was successfully isolated by a borate-form resin column chromatography using a borate buffer as the eluent.

The anomeric mixture was then acetylated and the tri-*O*-acetyl-6-azido-6-deoxy-α- (**9**) and -β-L-idopyranosides (**10**) were separated by silica-gel column chromatography. Removal of the acetyl groups from **9** and **10** gave pure methyl 6-azido-6-deoxy-α- (**11**) and -β-L-idopyranosides (**12**). Catalytic reduction of **11** and **12** gave the corresponding 6-amino-6-deoxy-α- (**13**) and -β-L-idopyranosides (**14**).

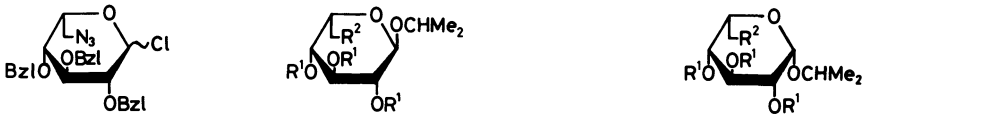

15

	R^1	R^2
16	$CH_2C_6H_5$	N_3
18	H	NH_2
20	H	$NHCO_2CH_2C_6H_5$

	R^1	R^2
17	$CH_2C_6H_5$	N_3
19	H	NH_2
21	H	$NHCO_2CH_2C_6H_5$

Chart 3.

Isopropyl 6-amino-6-deoxy-α-L-idopyranosides (**18** and **19**) were prepared from 6-azido-2,3,4-tri-*O*-benzyl-6-deoxy-L-idopyranosyl chloride[12] (**15**). Condensation of **15** with 2-propanol in the presence of mercury(II) cyanide in dichloromethane gave the isopropyl α- and -β-L-idopyranoside derivatives **16** and **17** in 1:4 ratio after chromatography. Reduction of the azido and removal of the benzyl groups of **16** and **17** with sodium in liquid ammonia gave the glycosides **18** and **19**. To confirm their structures, *N*-benzyloxycarbonyl derivatives **20** and **21** were prepared. Periodate oxidation of the both compounds gave one molar equivalent of formic acid, respectively, proving the presence of contiguous three hydroxyl groups.

One of the purposes of our syntheses was to examine the possibility to distinguish the anomers from their ^{1}H NMR spectra, especially from the $J_{1,2}$ values. Since hydrogens at C-1 and C-2 of both anomers (**9**, **10**, **11**, **12**, **13**, **14**, **18**, and **19**) are supposed to be situated in gauche relationship except for the $^4C_1$ conformation of the α-L-isomers, small $J_{1,2}$ proton coupling constants of all compounds are expected (see Fig. 1). Indeed, in the β-L-idosides **10**, **12**, **14**, and **19**, the $J_{1,2}$ proton coupling constants were all small (1—2 Hz) and, in **10**, **12**, and **19**, the $J_{2,3}$, $J_{3,4}$, and $J_{4,5}$ were so small (2—4 Hz) as those typical for the $^1C_4$(L) conformation of idopyranosides reported.[13,14] It should be stressed that both tri-*O*-acetyl-6-azido-6-deoxy-β-L-idoside (**10**) and the corresponding deacetylated idoside **12** had almost equal *J* values ($J_{1,2}$—$J_{4,5}$) suggesting that the presence of the *O*-acetyl groups of **10** did not necessarily contribute[15] the stability of the $^1C_4$(L) conformation. In the 6-amino-6-deoxy-β-L-idosides (**14** and **19**), although the *J* values of **14** except for $J_{1,2}$ could not be measured by overlapping with other signals, $^1C_4$ (L) conformations were presumed. Therefore it is concluded that all β-L-idosides described here take the $^1C_4$ (L) conformation exclusively. In the α-L-idosides **9**, **11**, **13**, and **18**, the $J_{1,2}$ values (3.5—6 Hz) of **11**, **13**, and **18** were larger than those (0.5—2 Hz) of the tri-*O*-acetyl-6-azido-6-deoxy-α-L-idoside (**9**), which, judging from the other *J* values (see Experimental), was suggested to take the ideal $^1C_4$ (L) conformation, stabilized[15] by the presence of the *O*-acetyl groups. Other nonprotected derivatives **11**, **18**, and possibly **13** will take a conformation equilibrated by two chair conformations ($^1C_4 \rightleftarrows {}^4C_1$), in NMR time-scale. It was further assumed that the isopropyl α-L-idopyranoside (**18**) took more $^4C_1$ (L) conformation than the methyl α-L-idosides **11**, **13**, the fact being ascribed to the tendency of the bulky isopropoxy group of **18** to take an equatrial position. Since $J_{2,3}$ and $J_{3,4}$ of **11** and **18** were almost equal,[16] respectively, contribution of a skew conformation will be negligible. In conclusion, α- and β-L-idopyranosides, so far described, can be distinguished by the $J_{1,2}$ values (α-L: 3.5—6 Hz, β-L: 1—2 Hz) if the protecting groups of the idopyranosides are absent. This affords a useful method for the discrimination of the anomers of nonprotected idopyranosides.

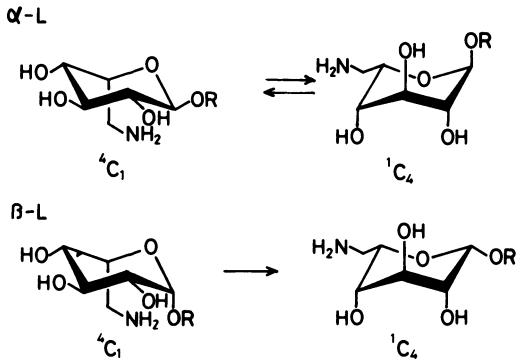

Fig. 1.

Experimental

General. ^{1}H NMR spectra were recorded at 90 MHz with a Varian EM-390 spectrometer unless otherwise stated.

The 250 MHz spectra were measured in the FT mode with a Bruker WM 250 spectrometer. IR spectra were recorded with a Hitachi 285 infrared spectrophotometer. Optical rotations were measured with a Perkin-Elmer 241 polarimeter. Thin-layer chromatography (TLC) was performed on precoated kieselgel 60, Merck. For column chromatography, silica gel (Wakogel C-200) was used.

3-*O*-Acetyl-1,2-*O*-isopropylidene-6-*O*-(*p*-nitrobenzoyl)-D-glucofuranose (2). A mixture of 3-*O*-acetyl-1,2-*O*-isopropylidene-D-glucofuranose[9] (**1**, 36.4 g) and *p*-nitrobenzoyl chloride (30.7 g) in pyridine (600 ml) was kept at −40 °C overnight. Addition of water (3 ml) followed by evaporation gave a residue, that was extracted with chloroform. The organic solution was washed with aqueous saturated potassium hydrogensulfate and aqueous saturated sodium hydrogencarbonate, dried (Na_2SO_4), and concentrated to give a solid. Recrystallization from chloroform–hexane gave pale-yellow crystals, 53.0 g (93%), mp 132—133 °C, $[\alpha]_D^{20}$ −14 ° (*c* 1, chloroform); IR (KBr): 1735 (ester); 1540 and 1350 cm^{-1}(nitro); ^1H NMR ($CDCl_3$): δ=1.37 and 1.54 (Me_2C), 2.20 (3H, s, Ac), 3.08 (1H, br m, OH), 3.98 (1H, dq, H-5), 4.32 (1H, dd, $J_{3,4}$=2.5, $J_{4,5}$=9 Hz, H-4), 4.48 (1H, dd, $J_{5,6}$=6, $J_{6,6'}$=12.5 Hz, H-6), 4.65 (1H, d, $J_{1,2}$=4, $J_{2,3}$=0 Hz, H-2), 4.80 [1H, dd, *J*=2.5 (=$J_{5,6'}$) and 12.5 Hz, H-6′], 5.33 (1H, d, *J*=2.5 Hz, H-3), 5.95 (1H, d, H-1), 8.32 (4H, s, phenyl).

Found: C, 52.43; H, 5.20; N, 3.36%. Calcd for $C_{18}H_{21}NO_{10}$: C, 52.56; H, 5.15; N, 3.40%.

3-*O*-Acetyl-1,2-*O*-isopropylidene-5-*O*-methylsulfonyl-6-*O*-(*p*-nitrobenzoyl)-D-glucofuranose (3). A solution of **2** (5.2 g) and methanesulfonyl chloride (2.94 ml) in pyridine (100 ml) was kept for 3 h at room temperature. Work-up as described above gave a solid of **3**, 5.8 g (94%), $[\alpha]_D^{20}$ −4 ° (*c* 1, chloroform); ^1H NMR ($CDCl_3$): δ=3.08 (3H, s, Ms), 5.32 (1H, dq, H-5), 5.42 (1H, d, H-3), 5.98 (1H, d, H-1).

Found: C, 46.35; H, 4.71; N, 2.63; S, 6.66%. Calcd for $C_{19}H_{23}NO_{12}S$: C, 46.63; H, 4.74; N, 2.86; S, 6.55%.

1,2-*O*-Isopropylidene-5-*O*-methylsulfonyl-D-glucofranose (4). A mixture of **3** (38 g) and 1 M† methanolic ammonia (680 ml) was stirred until the mixture became clear and the solution was kept at room temperature (totally 6 h). Neutralization with 1 M aqueous hydrochloric acid followed by evaporation gave a residue, that showed, on TLC with benzene–ethyl acetate (2:1), spots at R_f 0.38 (minor), 0.27 (**5**, minor) and 0.16 (**4**, major) (cf. **3**: R_f 0.63). The residue was extracted with chloroform and the soution washed with aqueous saturated sodium sulfate, dried (Na_2SO_4), and concentrated. Silica-gel (1 kg) column chromatography of the residue with benzene–ethyl acetate (1:2) gave an unknown product (R_f 0.38, 3.6 g), the 5,6-epoxy compound (**5**, 2.2 g) and a solid of **4**, 14.1 g (61%); **4**: $[\alpha]_D^{20}$ −3 ° (*c* 1, chloroform); ^1H NMR ($CDCl_3$; measured after shaking with slight D_2O): δ=1.34 and 1.55 (each s, Me_2C), 3.22 (3H, s, Ms), 3.85 (1H, dd, $J_{5,6}$=5.5, $J_{6,6'}$= 12.5 Hz, H-6), 4.10 (1H, dd, $J_{5,6'}$=3 Hz, H-6′), 4.15—4.4 (2H, H-3, 4), 4.58 (1H, d, $J_{1,2}$=4 Hz, H-2), 4.95 (1H, H-5), 5.96 (1H, d, H-1).

Found: C, 39.94; H, 6.35; S, 10.37%. Calcd for $C_{10}H_{18}O_8S$: C, 40.26; H, 6.08; S, 10.75.

5,6-Anhydro-1,2-*O*-isopropylidene-L-idofuranose (5). To a solution of **4** (14.0 g) in oxolane (300 ml) was added 1,8-diazabicyclo[5.4.0]undec-7-ene (DBU) (20 ml) and the solution was kept at room temperature overnight, then another DBU (8 ml) was added and kept likewise for further 24 h. TLC of the solution with benzene–ethyl acetate (1:2) showed spots at R_f 0.55 (**5**) and 0.45 (slight, **4**). After concentration to a small valume, chloroform was added and the organic solution was washed with 0.2 M phosphate buffer (pH 6) (a part of **5** was lost by dissolving in the solution), then aqueous saturated sodium sulfate, dried (Na_2SO_4), and concentrated. Silica-gel (250 g) column chromatography of the residue with benzene–ethyl acetate (1:2) gave **5** as crystals, 5.9 g (62%) and **4** recovered (0.9 g); mp 74—75 °C, $[\alpha]_D^{20}$ −26 ° (*c* 1, chloroform); ^1H NMR ($CDCl_3$): δ=1.35 and 1.52 (each s, Me_2C), 2.87 (2H, narrow m, H-6,6′), 3.02 (1H, d, *J*=5 Hz, OH-3; disappeared on deuteration), 3.35 (1H, q, $J_{5,6}$=$J_{5,6'}$=$J_{4,5}$=3.5 Hz, H-5), 4.22 [1H, dd, *J*=3 (=$J_{3,4}$) and 3.5 Hz, H-4], 4.38 (1H, dd, *J*= 3 and 5 Hz, H-3; on irradiation at δ 3.02 or on deuteration, the dd collapsed to a d), 4.56 (1H, d, $J_{1,2}$=3.5 Hz, H-2), 5.96 (1H, d, H-1).

Found: C, 53.18; H, 6.85%. Calcd for $C_9H_{14}O_5$: C, 53.46; H, 6.98%.

3-*O*-Acetyl-5,6-anhydro-1,2-*O*-isopropylidene-L-idofuranose (6). Compound **5** (490 mg) was treated with acetic anhydride (0.26 ml) in pyridine (15 ml) at 0 °C for 20 h. Usual work up gave amorphous powder of **6**, 496 mg (84%), $[\alpha]_D^{20}$ +15 ° (*c* 1, chloroform); ^1H NMR ($CDCl_3$): δ=1.36 and 1.55 (each s, Me_2C), 2.17 (3H, s, Ac), 5.38 (1H, d, *J*=3 Hz, H-3).

Found: C, 54.31; H, 6.58%. Calcd for $C_{11}H_{16}O_6$: C, 54.09; H, 6.60%.

6-Azido-6-deoxy-1,2-*O*-isopropylidene-L-idofuranose (7). A mixture of sodium azide (3.8 g) and ammonium chloride (3.6 g) in dry *N*, *N*-dimethylformamide (300 ml) was stirred at 100 °C for 1 h, then **5** (5.8 g) was added and further heated at the temperature for 1.2 h. TLC of the solution with chloroform–methanol (10:1) showed spots at R_f 0.5 (**5**, slight), 0.45 (**7**) and 0.4 (trace). After addition of chloroform (500 ml) the organic solution was washed with aqueous saturated sodium sulfate, dried (Na_2SO_4), and concentrated. Chromatography (silica gel, 260 g) of the residue with chloroform (300 ml), then chloroform–methanol (10:1) gave crystals of **7**, 4.7 g (68%) and **5** recovered (1.1 g, 19%); **7**: mp 97—99 °C, $[\alpha]_D^{20}$ −24 ° (*c* 1, chloroform); IR (KBr) 2100 cm^{-1} (N_3); ^1H NMR ($CDCl_3$; measured after shaking with slight D_2O): δ=1.36 and 1.50 (Me_2C), 3.53 (2H, double ABq, H-6,6′), 4.31 (1H, d, $J_{3,4}$=3 Hz; t before deuteration; H-3), 4.55 (1H, d, $J_{1,2}$=4 Hz, H-2), 6.01 (1H, d, H-1).

Found: C, 44.09; H, 5.99; N, 16.88%. Calcd for $C_9H_{15}N_3O_5$: C, 44.08; H, 6.16; N, 17.13%.

3,5-Di-*O*-acetyl-6-azido-6-deoxy-1,2-*O*-isopropylidene-L-idofuranose (8). Compound **7** (70 mg) was treated with acetic anhydride (0.08 ml) in pyridine (1.5 ml) in a usual manner to give a syrup, 80 mg (85%), $[\alpha]_D^{20}$ −26 ° (*c* 1, chloroform); *m/z* 330 $(M+1)^+$; ^1H NMR (benzene-d_6): δ=1.08 and 1.40 (Me_2C), 1.60 and 1.72 (each 3H, s, Ac), 5.28 (1H, d, H-3), 5.45 [1H, ddd, *J*=8 (=$J_{4,5}$), 4, and 5.5 Hz, H-5].

Methyl 6-Azido-6-deoxy-L-idopyranosides (11+12). A solution of **7** (100 mg) in 1.4 M methanolic hydrochloric acid (5 ml) was refluxed for 1.5 h. TLC of the solution

† 1M=1 mol dm^{-3}.

with chloroform–methanol (10:1) showed spots at R_f 0.38, 0.33, 0.27 (minor), and 0.15 (trace) (cf. **7**: R_f 0.52). The solution was neutralized with Dowex 1×2 resin (OH^- form), filtered, and concentrated. The residue was chromatographed on a column of Dowex 1×2 (borate form, 15 ml) with 0.0025 M aqueous $K_2B_4O_7$ solution (elution speed: 0.25 ml min^{-1}). The eluate (16—26 ml) containing the pyranosides (R_f 0.38 and 0.33) was passed through a column of Dowex 50W ×2 resin (H^+ form, 5ml) with water and concentrated. The residue was repeatedly concentrated with additions of methanol (until boric acid was undetected) to afford a syrup of a mixture of **11** and **12**, 55 mg (6%).

Methyl 2,3,4-Tri-*O*-acetyl-6-azido-6-deoxy-α- (9) and -β-L-idopyranosides (10). A solution of a mixture of **11** and **12** (54.8 mg) in pyridine (1.5 ml) was treated with acetic anhydride (0.2 ml) at room temperature overnight. TLC of the solution with benzene–ethyl acetate (3:1), showed spots of R_f 0.54 (**9**) and 0.48 (**10**). After addition of water (0.1 ml), the solution was concentrated. The chloroform solution of the residue was washed with water, dried (Na_2SO_4), and concentrated. The residue was chromatographed with benzene–ethyl acetate (5:1) to give a syrup (from the earlier fractions) of **9**, 43.4 mg (50%) and crystals of **10**, 30.8 mg (36%).

9: $[\alpha]_D^{20}$ −25° (*c* 1, chloroform); IR (KBr) 2100 cm^{-1} (N_3); *m/z* 346 $(M+1)^+$, 314 (M^+−MeO); ^1H NMR ($CDCl_3$): δ=2.15, 2.17 and 2.20 (each 3H, s, Ac), 3.25 (1H, dd, H-6), 3.50 (3H, s, OCH_3), 3.59 (1H, dd, H-6′), 4.37 (1H, ddd, H-5), 4.77 (1H, br s, half-height width was ≈3.5 Hz, H-1), 4.87 (2H, m, H-2,4), 5.02 (incomplete t with small splittings, H-3); $J_{1,2}$ ≈0.5, $J_{2,3}$ ≈3, $J_{3,4}$=3.5, $J_{4,5}$=2, $J_{5,6}$=4, $J_{5,6'}$=8.5 and $J_{6,6'}$=13 Hz.

In C_6D_6 at 250 MHz: δ=1.55, 1.60, and 1.65 (each s, Ac), 2.66 (1H, dd, H-6), 3.14 (3H, s, OCH_3), 3.20 (1H, dd, H-6′), 4.14 (1H, dt, H-5), 4.66 (1H, d, H-1), 4.85 (1H, t, H-4), 5.14 (1H, dd with small splittings, H-2), 5.26 (1H, t with small splittings, H-3); $J_{1,2}$=2, $J_{2,3}$=$J_{3,4}$=4, $J_{4,5}$ ≈3, $J_{5,6}$=8.5, $J_{5,6'}$= 3,5, $J_{1,3}$≈0.5, and $J_{2,4}$≈0.5 Hz.

10: Mp 107—108 °C, $[\alpha]_D^{20}$ +62° (*c* 1, chloroform); IR (KBr) 2100 cm^{-1} (N_3); ^1H NMR ($CDCl_3$) δ=2.18 (9H, s, Ac) (in pyridine-d_5: 2.08, 2.10 and 2.18, each 3H s), 3.30 (1H, dd, H-6), 3.62 (3H, s, OCH_3), 3.70 (1H, dd, H-6′), 4.16 (1H, ddd, H-5), 4.80 (1H, d, H-1), 4.88 [1H, dd with small splittings ($J_{2,4}$ ≈0.5 Hz), H-4], 4.98 [1H, dd with small splittings (≈0.5 Hz), H-2], 5.20 (1H, t, H-3); $J_{1,2}$=2, $J_{2,3}$= $J_{3,4}$=$J_{5,6}$=4, $J_{4,5}$=2.5, $J_{5,6'}$=8, and $J_{6,6'}$=13 Hz.

Found: C, 45.30; H, 5.59; N, 12.03%. Calcd for $C_{13}H_{19}N_3O_8$: C, 45.22; H, 5.55; N, 12.17%.

Methyl 6-Azido-6-deoxy-α- (11) and -β-L-Idopyranosides (12). To a solution of **9** (34.7 mg) in methanol (2 ml), barium hydroxide octahydrate (70 mg) was added and the mixture was stirred for 10 min at room temperature. After bubbling carbon dioxide, the mixture containing barium carbonate was concentrated and the residue was extracted with 1,4-dioxane. The extracted product was chromatographed on a short column of silica gel with chloroform–methanol (10:1) to give a syrup of **11**, 19.4 mg (88%), which crystallized on standing. In a similar manner a syrup of **12**, 15.1 mg (82%) was obtained from **10** (29.1 mg).

11: Mp 62—63 °C, $[\alpha]_D^{20}$ −74° (*c* 0.9, water); IR (KBr) 2100 cm^-; ^1H NMR (pyridine-d_5–D_2O=10:1): δ=3.58 (3H, s, OCH_3), 3.61 (1H, dd, H-6), 3.98 (1H, dd, H-6′), ≈4.13 (1H, H-4), 4.15 (1H, dd, H-2; on irradiation of H-1, the dd collapsed to a d), 4.46 [1H, dd with small splittings ($J_{1,3}$≦0.5 Hz), H-3], 4.62 (1H, ddd, H-5), 5.11 (1H, d with small splittings, H-1); $J_{1,2}$=3.5, $J_{2,3}$=5, $J_{3,4}$=$J_{5,6}$=4, $J_{4,5}$=2.5, $J_{5,6'}$=9, and $J_{6,6'}$=13 Hz.

Found: C, 38.53; H, 5.97; N, 18.85%. Calcd for $C_7H_{13}N_3O_5$: C, 38.36; H, 5.98; N, 19.17%.

12: $[\alpha]_D^{20}$ +54° (*c* 0.9, water): IR (KBr) 2100 cm^{-1}; ^1H NMR (pyridine-d_5–D_2O=10:1): δ=3.48 (1H, dd, H-6), 3.66 (3H, s, OCH_3), 4.00 (1H, narrow m, H-2), 4.01 (1H, dd, H-6′), 4.28 (1H, dd with small splittings, H-4), 4.53 (1H, ddd, H-5), 4.66 (1H, t, H-3), 5.14 (1H, d, H-1); $J_{1,2}$=1, $J_{2,3}$= $J_{3,4}$=$J_{5,6}$=4, $J_{4,5}$=2.5, $J_{5,6'}$=7.5, and $J_{6,6'}$=13 Hz.

Found: C, 38.27; H, 5.91; N, 18.88%. Calcd for $C_7H_{13}N_3O_5$: C, 38.36; H, 5.98; N, 19.17%.

Metyl 6-Amino-6-deoxy-α- (13) and -β-L-idopyranosides (14). An aqueous solution (1.5 ml) of **11** (16.5 mg) was hydrogenated (3 kg cm^{-2} of hydrogen) for 1 h in the presence of palladium black under shaking. Filtration followed by concentration gave a ninhydrin-positive solid of **13**, that was reprecipitated from methanol solution by addition of ethyl acetate, 13.0 mg (77% as hemicarbonate). In a similar manner **14** was obtained from **12** (12.9 mg) as a solid of hemicarbonate, 10.4 mg (79%).

13: $[\alpha]_D^{20}$ −88° (*c* 1, water): ^1H NMR (D_2O at 60 °C): δ=3.57 (3H, s, OCH_3), 4.75 (1H, d, $J_{1,2}$=4.5 Hz, H-1).

Found: C, 39.84; H, 7.02; N, 5.95%. Calcd for $C_7H_{15}NO_5 \cdot 1/2\ H_2CO_3$: C, 40.17; H, 7.19; N, 6.25%.

14: $[\alpha]_D^{20}$ +52° (*c* 0.9, water); ^1H NMR (D_2O at 60 °C): δ=3.65 (3H, s, OCH_3), 4.83 (1H, d, $J_{1,2}$=2 Hz, H-1).

Found: C, 40.32; H, 7.04; N, 6.08%. Calcd for $C_7H_{15}NO_5 \cdot 1/2H_2CO_3$: C, 40.17; H, 7.19; N, 6.25%.

Isopropyl 6-Azido-2,3,4-tri-*O*-benzyl-6-deoxy-α- (16) and -β-L-idopyranosides (17). A mixture of dry 2-propanol (0.8 ml), mercury(II) cyanide (680 mg) and Drierite ($CaSO_4$, 1.84 g activated at 235 °C for 3 h in vacuo) in dichloromethane (3 ml) was stirred for 1 h at room temperature. The 1-chloride[12] **15** (667 mg) dissolved in dichloromethane (3 ml) was added to the above suspension and the mixture was stirred overnight at room temperature. After addition of chloroform (50 ml), the mixture was filtered, and the solution was washed with aqueous sodium hydrogencarbonate, dried (Na_2SO_4), and concentrated. The residue was chromatographed on a silica-gel column with benzene–ethyl acetate (100:1) to give solids of **16**, 114 mg (16%), R_f 0.6 on TLC with benzene–ethyl acetate=30:1, and **17**, 425 mg (61%), R_f 0.48.

16: $[\alpha]_D^{26}$ −14.5° (*c* 1, chloroform). Found: C, 69.49; H, 6.77; N, 7.91%. Calcd for $C_{30}H_{35}N_3O_5$: C, 69.32; H, 6.77; N, 8.12%.

17: $[\alpha]_D^{26}$ +80° (*c* 1, chloroform). Found: C, 69.40; H, 6.79; N, 8.07%. Calcd for $C_{30}H_{35}N_3O_5$: C, 69.32; H, 6.77; N, 8.12%.

Isopropyl 6-Amino-6-deoxy-α-L-idopyranoside (18). A solution of **16** (76 mg) in oxolane (1.5 ml) was added to a solution of sodium metal (ca. 50 mg) in liquid ammonia (ca. 5 ml, −50 °C) and the deep-blue solution was kept at the temperature for 2 h. After addition of methanol to consume the residual sodium to give a colorless solution, ammonia was evaporated with gradual raise in temperature (finally under diminished pressure). The strongly alkaline

aqueous solution of the residue was passed through a column of Dowex 50 W×2 (NH_4^+ form) with water, and the ninhydrin-positive fractions combined were concentrated. The residue was chromatographed on a column of CM-Sephadex C-25 (10 ml) with water (30 ml), then 0.5 M aqueous ammonia to give a solid of **18**, 22 mg (65% as 1/6 carbonate), $[\alpha]_D^{24}$ −73° (*c* 1, water); ^{1}H NMR (in D_2O containing 20% ND_3 at 250 MHz): δ=1.19 and 1.24 (each 3H d, *J*=6 Hz, CH*Me*$_2$), ABq cendered at 2.85 (2H, H-6,6′), 3.35 (1H, dd, H-2), 3.72 (1H, dd, H-4), 3.96 (1H, m, H-5), 4.02 (1H, m, OC*H*Me$_2$), 4.72 (1H, d, H-1); $J_{1,2}$=6, $J_{2,3}$=8.5, $J_{3,4}$=7.5, $J_{4,5}$=4.5 Hz.

Found: C, 47.79; H, 8.22; N, 5.76%. Calcd for $C_9H_{19}NO_5 \cdot 1/6H_2CO_3$:C, 47.55; H, 8.36; N, 6.05%

Isopropyl 6-Amino-6-deoxy-β-L-idopyranoside (19). Compound **17** (160 mg) was treated smilarly as described for **18** to give a solid of **19**, 45 mg (63% as 1/6 carbonate), $[\alpha]_D^{24}$ +42° (*c* 1, water). ^{1}H NMR (in D_2O containing 20% ND_3 at 250 MHz): δ=1.19 and 1.24 (each 3H, d, *J*=6 Hz, CH*Me*$_2$), ABq centered at 2.86 (2H, H-6,6′), 3.58 (1H, dd, H-4), 3.62 (1H, ddd, H-2), 3.85 (1H, m, H-5), 3.99 (1H, t, H-3), 4.11 (1H, m, OC*H*Me$_2$), 4.91 (1H, d, H-1); $J_{1,2}$=1.5, $J_{2,3}$=$J_{3,4}$=4, $J_{4,5}$=2, $J_{2,4}$=1 Hz.

Found: C, 47.38; H, 8.23; N, 6.13%. Calcd for $C_9H_{19}NO_5 \cdot 1/6\ H_2CO_3$: C, 47.55; H, 8.36; N, 6.05%.

Isopropyl 6-Benzyloxycarbonylamino-6-deoxy-α-L-idopyranoside (20). To a solution of **18** (18 mg) in 50% aqueous methanol (2 ml) were added benzyl chloroformate (0.03 ml) and anhydrous sodium carbonate (50 mg), and the mixture was stirred for 2 h under ice-cooling. Concentration gave a residue, that was extracted with hot acetone. The isolated product was purified by silica-gel column chromatography with chloroform–methanol (20:1) to give a solid of **20**, 18 mg (65%). Recrystallization from chloroform–hexane gave needles, mp 157.5—159.5 °C, $[\alpha]_D^{25}$ −93° (*c* 1, chloroform). ^{1}H NMR ($CDCl_3$ containg slight D_2O): δ=1.20 and 1.25 (each 3H, d, CH*Me*$_2$), 5.02 (1H, d, *J*≈1 Hz, H-1), 5.19 (2H, s, PhC*H*$_2$CO$_2$).

Found: C, 57.20; H, 6.93; N, 3.82%. Calcd for $C_{17}H_{25}NO_7$: C, 57.46; H, 7.04; N, 3.94%.

Isopropyl 6-Benzyloxycarbonylamino-6-deoxy-β-L-idopyranoside (21). Compound **19** (55 mg) was treated similarly as described for **20** to give a solid of **21**, 67 mg (79%), $[\alpha]_D^{25}$ +10° (*c* 1, chloroform). ^{1}H NMR ($CDCl_3$ containing slight D_2O): δ=1.18 and 1.26 (each 3H, d, CH*Me*$_2$), 4.88 (1H, apparent s, H-1), 5.14 (2H, s, PhC*H*$_2$CO$_2$).

Found: C, 57.19; H, 7.06; N, 3.86%. Calcd for $C_{17}H_{25}NO_7$: C, 57.46; H, 7.04; N, 3.94%.

Periodate Oxidations of 20 and 21. A mixture of **20** or **21** (4.0 mg, each, 11.27 μM) and sodium periodate (12 mg, 56 μM) in water (1.2 ml) was stirred at 5 °C for 2 days. Analysis of the formic acid liberated by color detection method (at 450 mμ) by 5,5-diethyl-2-thiobarbituric acid[17] showed 14.20 and 14.75 μM (1.26 and 1.31 molar equiv for **20**), and 13.40 and 13.65 μM (1.19 and 1.21 molar equiv for **21**) formic acid.

References

1) E. Sorkin and T. Reichstein, *Helv. Chim. Acta*, **28**, 1 (1945).

2) S. Hanessian and T. H. Haskell, *J. Org. Chem.*, **30**, 1080 (1965).

3) B. Helferich and E. Himmen, *Chem. Ber.*, **61**, 1825 (1928).

4) T. Usui, Y. Takagi, T. Tsuchiya, and S. Umezawa, *Carbohydr. Res.*, **130**, 165 (1984).

5) A. S. Meyer and T. Reichstein, *Helv. Chim. Acta*, **29**, 152 (1946).

6) H. Saeki and E. Ohki, *Chem. Pharm. Bull.*, **16**, 2471 (1968).

7) W. M. zu Reckendorf, *Tetrahedron*, **1963**, 2033 (1963).

8) M. Miljković, T. Satoh, M. Konopka, E. A. Davidson, and D. Miljković, *J. Org. Chem.*, **38**, 716 (1973).

9) K. Josephson, *Ann. Chem.*, **472**, 217 (1929).

10) J. G. Buchanan and E. M. Oakes, *Carbohydr. Res.*, **1**, 242 (1965).

11) R. D. Guthrie and D. Murphy, *J. Chem. Soc.*, **1963**, 5288.

12) T. Torii, T. Tsuchiya, I. Watanabe, and S. Umezawa, *Bull. Chem. Soc. Jpn.*, **55**, 1178 (1982).

13) H. Paulsen and M. Friedmann, *Chem. Ber.*, **105**, 705 (1972).

14) A. S. Perlin, B. Casu, G. R. Sanderson, and J. Tse, *Carbohydr. Res.*, **21**, 123 (1972).

15) P. L. Durette and D. Horton, *Carbohydr. Res.*, **18**, 289, 389, and 403 (1971).

16) S. J. Angyal and Y. Kondo, *Carbohydr. Res.*, **81**, 35 (1980).

17) S. A. Barker and P. J. Somers, *Carbohydr. Res.*, **3**, 220 (1966).

 © 1986 The Chemical Society of Japan Bull. Chem. Soc. Jpn., 59, 1403—1410 (1986)

New Synthesis and Some Reactions of Vinyl Arenecarbodithioates. Wittig Reaction of (Triphenylphosphonio)methyl Arenecarbodithioate Iodides

Masaru ISHIDA, Koh-ichi KAGA, Hiroyuki SATO, Masato YOKOI, and Shinzi KATO*
Department of Chemistry, Faculty of Engineering, Gifu University, Yanagido, Gifu 501-11
(Received November 29, 1985)

Wittig reaction of new phosphonium salts, (triphenylphosphonio)methyl arenecarbodithioate iodides, with variety of aldehydes gave the corresponding vinyl arenecarbodithioates in moderate to good yields. Reaction of the vinyl dithiocarboxylate with nucleophiles such as potassium alkoxide or alkanethiolate was investigated and found to give the thioacylated products in high yields. Ab initio molecular orbital calculations of the model compound, vinyl dithioformate, are also discussed.

During the investigation on dithiocarboxylic acid derivatives,[1] the dithiocarboxylic ester containing a double bond α to the sulfide sulfur has attracted our attention, because of the interest in the spectral and physical properties and the potential usefulness as synthetic intermediates. Recently, the following three methods have been reported for the synthesis of vinyl alkanedithioates, 1) base-catalysed rearrangement of allyl dithiocarboxylate;[2] 2) base-induced ring opening of 2-ylidene-1,3-dithiolanes;[3] and 3) addition reaction of dithiocarboxylic acid to acetylene derivatives.[4] However, for the synthesis of vinyl arenecarbodithioates **6**, no general method has been developed.

In our preliminary report,[5] we have described a convenient and general synthesis of the esters **6** via Wittig reaction of (triphenylphosphonio)methyl arenecarbodithioate iodides **3**[6,7] with various aldehydes. In the present paper, we report full details of our study on the preparation of vinyl arenecarbodithioates and their synthetic applications together with results of molecular orbital calculation of vinyl dithioformate, which provide the estimation of the reactivity and structure of **6**.

Results and Discussion

Synthesis of the Phosphonium Salts. The phosphonium salts **3** are easily prepared by addition of piperidinium arenecarbodithioates **1**[8] to a chloroform suspension of (iodomethyl)triphenylphosphonium iodide (**2**)[9] at room temperature (Table 1). The crude salts **3** dried in vacuo were pure enough to be subjected to the following reactions. The structures of **3** were confirmed on the basis of spectral data and elemental analyses. For example, the ^{1}H NMR spectrum of the phosphonium salt **3c** showed a doublet peak at δ 6.08 with a coupling constant of 8 Hz (J_{H-P}). The IR spectrum of **3c** showed an absorption at 1240 cm^{-1} due to thiocarbonyl stretching frequency. The UV spectrum exhibited an absorption band at 360 nm (log ε=4.36) due to $\pi\rightarrow\pi^*$ transitions. At visible region, an absorption band was observed at 483 nm (log ε=2.53) due to $n\rightarrow\pi^*$ transitions of thiocarbonyl moiety with the hypsochromic shift from that of methyl 4-methoxybenzenecarbodithioate.[10]

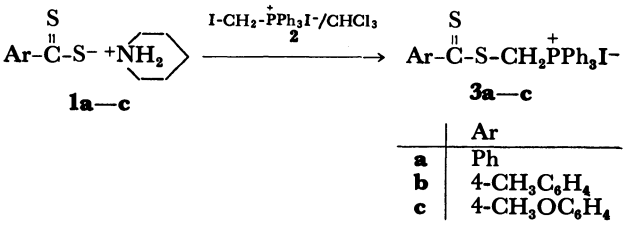

Scheme 1.

Table 1. Synthesis of (Triphenylphosphonio)methyl Arenecarbodithioate Iodide **3**

Product No.	Ar	Yield/%[a]
3a	Ph	53
3b	4-$CH_3C_6H_4$	77
3c	4-$CH_3OC_6H_4$	62

a) Isolated yield.

Synthesis of Vinyl Arenecarbodithioates. The Wittig reaction of the phosphonium salts **3** was carried out as follows. The salt **3** suspended in tetrahydrofuran (THF) was treated with an equimolar amount of potassium *t*-butoxide at −75 °C under argon atmosphere to give a deep purple solution of the ylide **4**.[11] Then, the aldehyde **5a, b, d,** or **e** was added to the solution and the mixture was gradually warmed to 0 °C (Method A). After workup, the corresponding vinyl arenecarbodithioates **6** were obtained in moderate to good yields. In the reaction with relatively inactive aldehydes **5c** and **f—i**, forcing conditions were required: The aldehyde **5** was added to the ylide solution at −30 °C and the reaction mixture was maintained at that temperature with stirring for 0.5—5 h (Method B). The cis/trans ratios of the products **6** seem to be dependent on the

Table 2. Synthesis of Vinyl Arenecarbodithioate **6**

Product No.	Ar	R	Yield/%[a]	Ratio[b] cis : trans
6a	Ph	4-$NO_2C_6H_4$	45 (A)	100 : 0
6b	4-$CH_3C_6H_4$	Ph	75 (A)	100 : 0
6c	4-$CH_3C_6H_4$	4-$NO_2C_6H_4$	89 (A)	100 : 0
6d	4-$CH_3OC_6H_4$	Ph	39 (A)	100 : 0
6e	4-$CH_3OC_6H_4$	4-$NO_2C_6H_4$	56[c] (A)	85 : 15
			69[c] (B)	50 : 50
6f	4-$CH_3OC_6H_4$	Ph-CH=CH	46[c] (B)	—
6g	4-$CH_3OC_6H_4$	4-$NO_2C_6H_4$-CH=CH	88[c] (A)	—
6h	4-$CH_3OC_6H_4$	2-$NO_2C_6H_4$-CH=CH	94[c] (A)	—
6i	4-$CH_3OC_6H_4$	Ph-C≡C	63[c] (B)	50 : 50
6j	4-$CH_3OC_6H_4$	Ph-$(CH=CH)_2$	55[c] (B)	—
6k	4-$CH_3OC_6H_4$	CH_3	65[c] (B)	40 : 60
6l	4-$CH_3OC_6H_4$	C_2H_5	28[c] (B)	50 : 50

a) Preparation methods are in parenceses; Method A; The reaction of the aldehyde and the ylide was carried out at −70°C, Method B; The reaction was carried out at −30 °C (See Experimental Section). b) Isomer ratios were determined on the basis of ^{1}H NMR. Those of the products **6f**, **g**, **h**, and **j** could not be determined, because of overlapping of olefin protons. c) Yield of a mixture of cis and trans isomers.

reaction conditions (Table 2). When the Wittig reaction of **3c** with 4-nitrobenzaldehyde was performed at −75 °C (Method A), **6e** was obtained as a 5:1 mixture of cis and trans isomers. While, under the conditions of method B, 1:1 mixture of *cis*-and *trans*-**6e** was obtained in 69% yield.

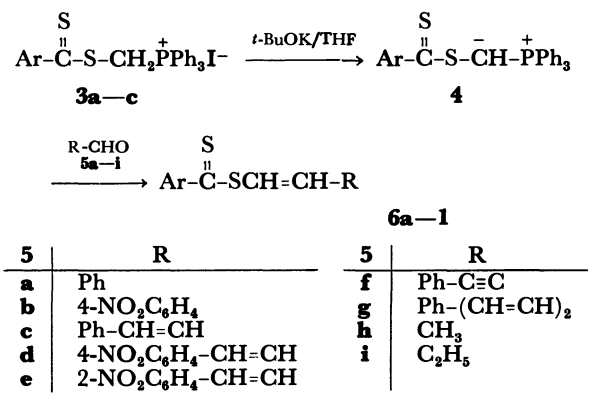

5	R	5	R
a	Ph	**f**	Ph-C≡C
b	4-$NO_2C_6H_4$	**g**	Ph-$(CH=CH)_2$
c	Ph-CH=CH	**h**	CH_3
d	4-$NO_2C_6H_4$-CH=CH	**i**	C_2H_5
e	2-$NO_2C_6H_4$-CH=CH		

Scheme 2.

Spectra of Vinyl Arenecarbodithioates. The typical spectra are exemplified by the vinyl dithiocarboxylate **6i**. The ^{1}H NMR spectrum of the crude **6i** showed two doublet peaks at δ 6.17 (J=10.0 Hz) and 6.29 (J=16.0 Hz) with an integration ratio of 1:1. The former resonance is due to the olefinic proton of *cis*-**6i** and the latter is due to that of *trans*-**6i**.[4] The geometrically pure samples were obtained from fractional recrystallization from methanol. The IR spectra of *cis*-and *trans*-**6i** showed C=S stretching absorptions at 1245 and 1240 cm^{-1}, respectively. The UV spectra of *cis*- and *trans*-**6i** showed absorption maxima due to $\pi\rightarrow\pi^*$ transitions of thiocarbonyl moieties at 362 (log ε=4.33) and 361 nm (log ε=4.41), respectively. In the visible spectra, the absorptions due to n→π^* transition were observed at 505 nm (*cis*-**6i**; log ε=2.41) and at 502 nm (*trans*-**6i**; log ε=2.51). It is noted that the wavelengths of the absorption maxima due to thiocarbonyl moieties of the vinyl dithiocarboxylates **6d**, **f**, and **j** (4-$CH_3OC_6H_4$-CS_2-$(CH=CH)_n$-Ph, n=1—3) are clearly dependent on the number of conjugated double bonds of enethiolate moieties (Table 3).

Table 3. The Absorption Bands of Electron Spectra with High Molar Absorptivities (log ε>4) of a Series of Vinyl Dithiocarboxylates **6d**, **f**, and **j**

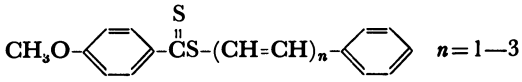

Compound No.	n	Absorption [nm] (log ε)[a]		
6d	1			356 (4.47)[b]
6f	2	296 (4.44)	350 (4.39)	400 (4.31)[c]
6j	3		334 (4.67)	418 (4.43)[c]

a) CH_2Cl_2 as a solvent. b) n→π^* transition band of thiocarbonyl moiety of **6d** was observed at 503 nm (log ε=2.53). c) Other absorption maxima were not observed at visible region.

Reaction of Vinyl Dithiocarboxylates with Nucleophiles. Since the enethiolate moiety of the ester **6** can be considered as a good leaving group, the reaction of **6** with some nucleophiles such as potassium alkoxides and alkanethiolates was investigated.

A solution of **6e** in THF was added to a solution of equimolar amount of potassium methoxide in

methanol at 0 °C under nitrogen atmosphere. The resulting deep purple solution[12] was stirred for 2 h at that temperature and then quenched with phenacyl bromide to give *O*-methyl 4-methoxybenzenecarbothioate (**7a**) in 80% yield.[13] The counter part, potassium ethenethiolate **8**, was isolated as a vinyl sulfide **10a** in 84% yield. High yield formation of **10a** may suggest that the vinyl dithiocarboxylate **6** can be considered as a useful precursor of enethiolate **8**. In a similar manner, potassium phenolate was converted into *O*-phenyl 4-methoxybenzenecarbothioate (**7d**) in 77% yield.

It is noteworthy that the reaction of **6e** with potassium 2-methyl-2-propanethiolate also gave *t*-butyl 4-methoxy-benzenecarbodithioate (**9c**) in 51% yield, which can not be prepared by esterification of piperidinium or alkali metal dithiocarboxylate with *t*-butyl bromide (Table 4).

The structural confirmation of the products **7**, **9**, and **10** were performed on the basis of the comparison of their spectra and physical properties with those of the authentic samples.[13–18]

Molecular Orbital Calculation. In order to estimate the reactivity and the structure of the vinyl dithiocarboxylates **6**, molecular orbital calculations were performed on the model compound, vinyl dithioformate (**11**). Two sets of the conformers, **11-I** and **11-II**, were optimized by the ab initio MO calculation with the minimal (STO-3G) basis set. The calculation of the total energy showed that the conformer **II** is more stable than the conformer **I** with the energy difference of 0.154 eV (14.9 kJ mol^{-1}) (Fig. 1).

The frontier orbitals of the conformers are illustrated in Fig. 2. The HOMO of the conformer I is a nonbonding orbital of thiocarbonyl sulfur. Whereas HOMO of the conformer **II** is a π-allyl type orbital at carbodithioate moiety. Thus, the [3+2] cycloaddition reactions[19] with dienophiles at dithiocarboxy moiety may be expected. The LUMO is π^* orbital of thiocarbonyl moiety and the coefficient is largest at thiocarbonyl carbons in both of the conformers. These calculation are well-compatible with experimental results.

In summary, the first general synthesis of vinyl arenecarbodithioate **6** via Wittig reaction of (triphenylphosphonio)methyl arenecarbodithioate iodide **3** have been developed. Some reactions of the vinyl

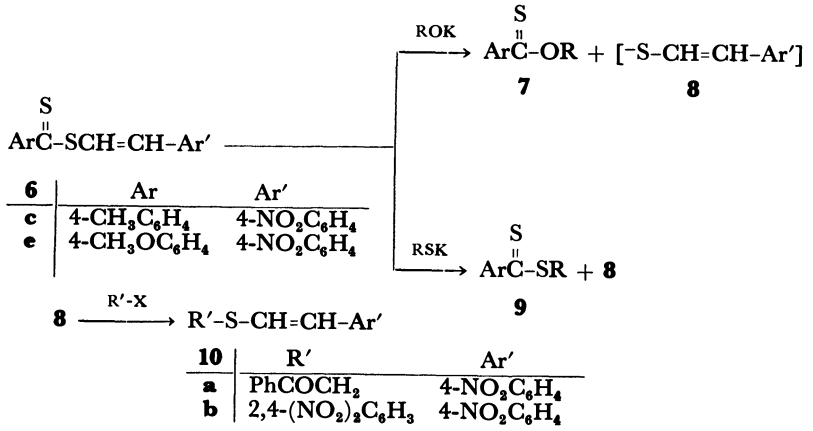

Scheme 3.

Table 4. Synthesis of *o*-Alkyl Thiobenzoates **7** and Dithiobenzoates **9** via the Reaction of Vinyl Arenecarbodithioate **6** with Alkoxides or Alkanethiolates

Product No.	Reagent No. Ar	Nucleophile	Yield[a] %	[Byproduct[b] (Yield/%)]
7a	**6e** 4-$CH_3OC_6H_4$	CH_3-O$^-$K$^+$	80	[**10a** (84)]
7b	**6c** 4-$CH_3C_6H_4$	CH_3-O$^-$K$^+$	82	[**10b** (43)]
7c	**6e** 4-$CH_3OC_6H_4$	C_2H_5-O$^-$K$^+$	57	[**10a** (15)]
7d	**6e** 4-$CH_3OC_6H_4$	Ph-O$^-$K$^+$	77	[**10b** (43)]
9a	**6e** 4-$CH_3OC_6H_4$	C_2H_5-S$^-$K$^+$	81	[**10a** (75)]
9b	**6c** 4-$CH_3C_6H_4$	C_2H_5-S$^-$K$^+$	67	[**10b** (56)]
9c	**6e** 4-$CH_3OC_6H_4$	*t*-C_4H_9-S$^-$K$^+$	51	[**10a** (70)]
9d	**6e** 4-$CH_3OC_6H_4$	Ph-S$^-$K$^+$	46	[**10a** (82)]

a) Yield of isolated product. b) **10a**: Phenacyl 2-(4-nitrophenyl)vinyl sulfide, **10b**: 2,4-Dinitrophenyl 2-(4-nitrophenyl)vinyl sulfide.

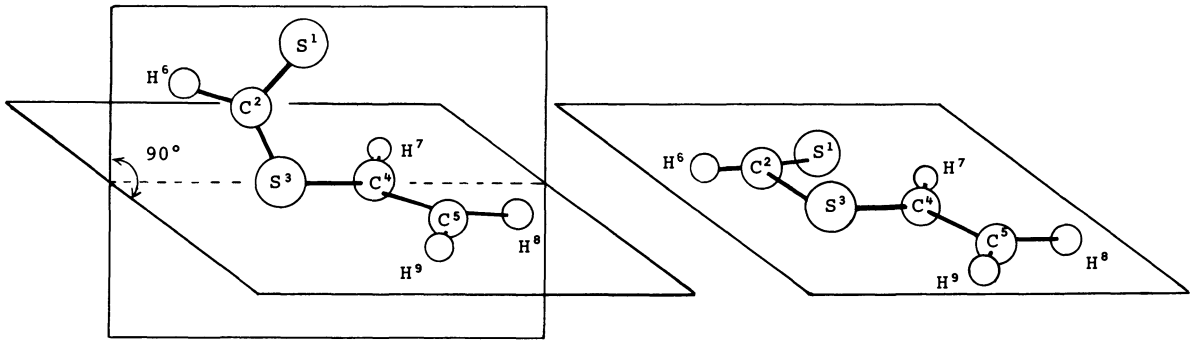

11-I

Total energy = −24492.86 eV

Bond length	[l/Å]	Bond angle	[ϕ/°]
S^1–C^2	1.582	S^1–C^2–S^3	130.0
C^2–S^3	1.760	S^1–C^2–H^6	122.2
C^2–H^6	1.102	S^3–C^2–H^6	107.7
S^3–C^4	1.779	C^2–S^3–C^4	101.6
C^4–C^5	1.309	S^3–C^4–C^5	123.1
C^4–H^7	1.086	S^3–C^4–H^7	116.6
C^5–H^8	1.083	C^5–C^4–H^7	120.4
C^5–H^9	1.083	C^4–C^5–H^8	122.2
		C^4–C^5–H^9	122.1
		H^8–C^5–H^9	115.7

11-II

Total energy = −24493.02 eV

Bond length	[l/Å]	Bond angle	[ϕ/°]
S^1–C^2	1.582	S^1–C^2–S^3	130.7
C^2–S^3	1.760	S^1–C^2–H^6	121.7
C^2–H^6	1.092	S^3–C^2–H^6	107.6
S^3–C^4	1.764	C^2–S^3–C^4	102.5
C^4–C^5	1.310	S^3–C^4–C^5	123.7
C^4–H^7	1.084	S^3–C^4–H^7	115.1
C^5–H^8	1.081	C^5–C^4–H^7	121.2
C^5–H^9	1.082	C^4–C^5–H^8	121.1
		C^4–C^5–H^9	123.0
		H^8–C^5–H^9	115.9

Fig. 1.

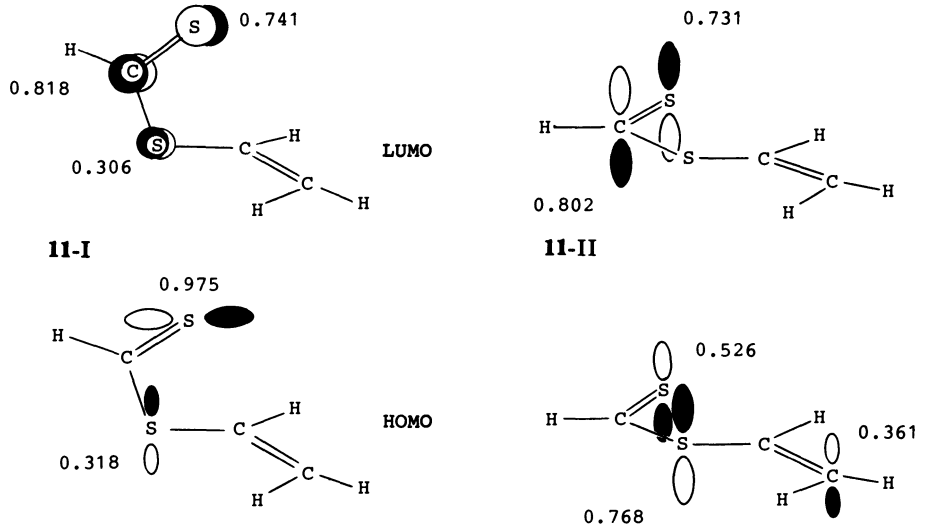

Frontier Orbitals and Frontier Orbital Coefficients[a] of Vinyl Dithioformate **11-I** and II
a) Coefficients of 3p-atomic orbitals of sulfurs and 2p-atomic orbitals of carbons.

Fig. 2.

dithiocarboxylate **6** proved to be useful as thioacylating reagent of alkoxides and alkanethiolate and as a precursor of ethenethiolate anion.

Experimental

Melting points were determined using a Yanagimoto melting point apparatus and are uncorrected. The IR spectra were measured on a JASCO grating IR spectrometer IR-G. The UV and Vis spectra were measured on a Hitachi 124 spectrophotometer. The ^{1}H NMR spectra were recorded on Hitachi R-24 (60 MHz), Hitachi R-22 (90 MHz), and JEOL-JNM-GX 270 (270 MHz) with tetramethylsilane as an internal standard. Mass spectra were recorded on Hitachi RMU-6M mass spectrometer at an ionizing voltage of 20 eV. Elemental analyses were performed by Elemental Analysis Center of Osaka Univer-

sity.

Preperation of [4-Methoxy(thiobenzoyl)thiomethyl]triphenylphosphonium Iodide (3c): Typical Procedure: To a solution of (iodomethyl)triphenylphosphonium iodide (**2**, 2.65 g, 5 mmol) in methanol/dichloromethane (1:3, 450 mL), piperidinium 4-methoxybenzenecarbodithioate (**1c** 1.34 g, 5 mmol) was added at room temperature. The mixture was stirred for an hour. After removal of the solvent in vacuo, the residue was poured into dichloromethane (100 mL), washed with water (3×50 mL), and dried over anhydrous sodium sulfate. Addition of ethyl acetate (50 mL) to the extracts followed by condensation in vacuo to ca. 50 mL gave the salt **3c** as orange precipitates (1.815 g, 62%). Recrystallization from dichloromethane/ethyl acetate (2:1) gave analytically pure **3c**: Mp 202—205 °C; IR (KBr) 1250 (C=S) cm^{-1}; UV and Vis (CH_2Cl_2) 360 nm (log ε=4.36), 483 nm (log ε=2.53); ^1H NMR ($CDCl_3$) δ=3.76 (3H, s, CH_3), 6.08 (2H, d, J=8 Hz, CH_2), 6.7 (2H, d, aromatic), 7.40—8.15 (17H, m, aromatic). Found: C, 55.43; H, 4.08%. Calcd for $C_{27}H_{24}OS_2PI$: C, 55.29; H, 4.12%.

[(Thiobenzoyl)thiomethyl]triphenylphosphonium Iodide (3a): Similarly to the synthesis of **3c**, from the salt **2** (2.65 g, 5.0 mmol) and piperidinium benzenecarbodithioate (**1a**, 1.19 g, 5.0 mmol) was obtained 1.46 g (53%) of the salt **3a**. Pure **3a** was recrystallized from dichloromethane/ethyl acetate (1:1): Mp 174—178 °C; IR (KBr) 1230 (C=S) cm^{-1}; UV and Vis (CH_2Cl_2) 308 nm (log ε=4.37), 483 nm (log ε=2.34); ^1H NMR ($CDCl_3$*) δ=5.90 (2H, d, J=9 Hz, CH_2), 7.20—8.20 (20H, m, aromatic). Found: C, 56.09; H, 4.03%. Calcd for $C_{26}H_{22}S_2PI$: C, 56.13; H, 3.99%. *Containing 5% of DMSO-d_6.

[4-Methyl(thiobenzoyl)thiomethyl]triphenylphosphonium Iodide (3b): Similarly to the synthesis of **3c** from the salt **2** (2.65 g, 5.0 mmol) and piperidinium 4-methylbenzenecarbodithioate (**1b**, 1.27 g, 5.0 mmol) was obtaind 2.20 g (77%) of the salt **3b**. Pure **3b** was recrystallized from dichloromethane/ethyl acetate (1:1): Mp 179—182 °C; IR (KBr) 1240 (C=S) cm^{-1}; UV and Vis (CH_2Cl_2) 321 nm (log ε=4.38), 487 nm (log ε=2.44); ^1H NMR ($CDCl_3$*) δ=2.42 (3H, s, CH_3), 5.85 (2H, d, J=9 Hz, CH_2); 7.20—8.15 (19H, m, aromatic). Found: C, 56.89; H, 4.19%. Calcd for $C_{27}H_{24}S_2PI$: C, 56.85; H, 4.24%. *Containing 5% of DMSO-d_6.

2-Phenylvinyl 4-Methoxybenzenecarbonditioate (6d): Typical Procedures (Method A): To the salt **3c** (0.587 g, 1.0 mmol) suspended in dry THF (30 mL) was added potassium t-butoxide (0.112 g, 1.0 mmol) under argon atmosphere at −75 °C. The mixture was stirred for 30 min. Then benzaldehyde (**5a**, 0.11 g, 1.0 mmol) was added and the mixture was gradually warmed to 0 °C within 3 h. The mixture was poured into water (50 mL), extracted with ether (3×50 mL), and the extract was dried over anhydrous sodium sulfate. After removal of the solvent, the residue was chromatographed on silica gel (benzene/hexane=1:10 as eluant) to give a red oil. After addition of ethanol, the oil was cooled at −20 °C to give 0.112 g (39%) of red crystalls of **6d**: Mp 49—50 °C; IR (KBr) 1245 (C=S) cm^{-1}; UV and Vis (CH_2Cl_2) 356 nm (log ε=4.47), 503 nm (log ε=2.53); ^1H NMR ($CDCl_3$) δ=3.85 (3H, s, CH_3), 6.90 (1H, d, J=11 Hz, vinyl), 6.75—8.20 (10H, m, aromatic and vinyl); MS m/z, 286 (M^+). Found: C, 66.98; H, 4.98; S, 22.41%. Calcd for $C_{16}H_{14}OS_2$: C, 67.00; H, 4.93; S, 22.36%.

2-(4-Nitrophenyl)vinyl Benzenecarbodithioate (6a): Similarly to the synthesis of **6d**, from the salt **3a** (0.556 g, 1.0 mmol) and 4-nitrobenzaldehyde (**5b**, 0.15 g, 1.0 mmol) was obtained 0.14 g (45%) of **6a** as red crystals. Recrystallization from ethanol gave pure **6a**: Mp 135—138 °C; IR (KBr) 1225 (C=S) cm^{-1}; UV and Vis (CH_2Cl_2) 328 nm (log ε=4.42), 512 nm (log ε=2.38); ^1H NMR ($CDCl_3$) δ=7.0 (1H, d, J=12 Hz, vinyl), 7.3—8.4 (10H, m, aromatic and vinyl); MS m/z, 301 (M^+). Found: C, 59.43; H, 3.75; N, 4.53%. Calcd for $C_{15}H_{11}NO_2S_2$: C, 59.78; H, 3.68; N, 4.65%.

2-Phenylvinyl 4-Methylbenzenecarbodithioate (6b): Similarly to the synthesis of **6d**, from the salt **3b** (0.571 g, 1.0 mmol) and benzaldehyde (**5a**, 0.11 g, 1.0 mmol) was obtained 0.20 g (75%) of **6b** as red crystals: Mp 50—51 °C; IR (KBr) 1245 (C=S) cm^{-1}; UV and Vis (CH_2Cl_2) 328 nm (log ε=4.32), 503 nm (log ε=2.40); ^1H NMR ($CDCl_3$) δ=2.35 (3H, s, CH_3), 6.95 (1H, d, J=11.3 Hz, vinyl), 7.10—8.20 (10H, m, aromatic and vinyl); MS m/z, 270 (M^+). Found: C, 70.82; H, 5.23; S, 23.51%. Calcd for $C_{16}H_{14}S_2$: C, 71.07; H, 5.22; S, 23.68%.

2-(4-Nitrophenyl)vinyl 4-Methylbenzenecarbodithioate (6c): Similarly to the synthesis of **6d**, from the salt **3b** (0.571 g, 1.0 mmol) and 4-nitrobenzaldehyde (**5b**, 0.15 g, 1.0 mmol) was obtained 0.28 g (89%) of **6c**. Recrystallization from ethanol gave pure **6c**: Mp 122—128 °C; IR (KBr) 1255 (C=S) cm^{-1}; UV and Vis (CH_2Cl_2) 332 nm (log ε=4.43), 507 nm (log ε=2.34); ^1H NMR ($CDCl_3$) δ=2.35 (3H, s, CH_3), 6.92 (1H, d, J=11.3 Hz, vinyl), 7.05—8.40 (9H, m, aromatic and vinyl); MS m/z, 315 (M^+). Found: C, 61.12; H, 4.15%. Calcd for $C_{16}H_{13}NO_3S_2$: C, 60.93; H, 4.15%.

2-(4-Nitrophenyl)vinyl 4-Methoxybenzenecarbodithioate (6e): Similarly to the synthesis of **6d**, from the salt **3c** (0.586 g, 1.0 mmol) and 4-nitrobenzaldehyde (**5b**, 0.151 g, 1.0 mmol) was obtained 0.186 g (56%) of **6e**. Recrystallization from methanol gave pure **6e** as orange needles (cis/trans=5:1): Mp 166—168 °C; IR (KBr) 1225 (C=S) cm^{-1}. UV and Vis (CH_2Cl_2) 367 nm (log ε=4.58), 504 nm (log ε=2.57); ^1H NMR ($CDCl_3$) δ=3.89 (3H, s, CH_3), 6.98 (0.8H, d, J=11.0 Hz, vinyl), 7.06 (0.2H, d, J=16.5 Hz, vinyl), 6.80—7.20 (2H, m, aromatic), 7.77 (0.8H, d, J=11.0 Hz, vinyl), 8.03 (0.2H, d, J=16.5 Hz, vinyl), 7.20—8.40 (6H, m, aromatic); MS m/z, 331 (M^+). Found: C, 57.95; H, 4.00; N, 4.21; S, 19.19%. Calcd for $C_{16}H_{13}NO_3S_2$: C, 57.99; H, 3.95; N, 4.23; S, 19.32%.

4-(4-Nitrophenyl)-1,3-butadienyl 4-Methoxybenzenecarbodithioate (6g): Similarly to the synthesis of **6d**, from the salt **3c** (0.586 g, 1.0 mmol) and 4-nitrocinnamaldehyde (**5d**, 0.177 g, 1.0 mmol) was obtained 0.32 g (88%) of the dithiocarboxylate **6g**. Recrystallization from dichloromethane/ethanol (2:1), gave pure **6g** as red crystals: Mp 192—194 °C; IR (KBr) 1245 (C=S) cm^{-1}; UV and Vis (CH_2Cl_2) 365 nm (log ε=4.55), 513 nm (log ε=2.96); ^1H NMR ($CDCl_3$) δ=3.90 (3H, s, CH_3), 6.65—8.20 (12H, m, aromatic and olefinic); MS m/z, 357 (M^+). Found: C, 60.24; H, 4.32; N, 3.67; S, 17.73%. Calcd for $C_{18}H_{15}NO_3S_2$: C, 60.48; H, 4.23; N, 3.92; S, 17.94%.

4-(2-Nitrophenyl)-1,3-butadienyl 4-Methoxybenzenecarbodithioate (6h): Similarly to the synthesis of **6d**, from the salt **3c** (0.586 g, 1.0 mmol) and 2-nitrocinnamaldehyde (**5e**, 0.177 g, 1.0 mmol) was obtained 0.33 g (94%) of the sulfide **6h** as red crystals. Recrystallization from dichoromethane/ethanol gave pure **6h**: Mp 96—100 °C; IR (KBr) 1250

(C=S) cm^{-1}; UV and Vis (CH_2Cl_2) 361 nm (log ε=4.52), 491 nm (log ε=2.72); ^1H NMR ($CDCl_3$) δ=3.85 (3H, s, CH_3), 6.5—8.3 (12H, m, aromatic and olefinic); MS *m/z*, 357 (M^+). Found: C, 60.35; H, 4.22; N, 3.98; S, 17.65%. Calcd for $C_{18}H_{15}NO_3S_2$: C, 60.48; H, 4.23; N, 3.92; S, 17.94%.

2-(4-Nitrophenyl)vinyl 4-Methoxybenzenecarbodithioate (6e): Typical Procedure (Method B): To the salt **3c** (0.587 mg, 1 mmol) suspended in 40 mL of dry THF was added potassium *t*-butoxide (0.112 g, 1 mmol) at −30 °C [Dry Ice/carbontetrachloride-chloroform (50:1)]. The solution was stirred for 30 min. Then, 4-nitrobenzaldehyde (**5b**, 0.151 g, 1 mmol) was added to the resulting deep purple solution of the ylide. The reaction mixture was gradually warmed to 0 °C with stirring within 3 h. After usual workup, was obtained 0.228 g (69%) of vinyl dithiocarboxylate **6e** as a mixture of cis and trans isomers (1:1). The ratio of the isomers was determined on the basis of ^1H NMR.

4-Phenyl-1,3-butadienyl 4-Methoxybenzenecarbodithioate (6f): Similarly to the synthesis of **6e** (Method B), from the salt **3c** (0.587 g, 1.0 mmol) and cinnamaldehyde (**5c**, 0.132 g, 1.0 mmol) was obtained 0.145 g (46%) of **6f** as red crystals. Recrystallization from methanol gave pure **6f**: Mp 95—97 °C; IR (KBr) 1250 (C=S) cm^{-1}; UV and Vis (CH_2Cl_2) 296 nm (log ε=4.44), 350 nm (log ε=4.39), 400 nm (log ε=4.31); ^1H NMR ($CDCl_3$) δ=3.90 (3H, s, CH_3), 6.70—8.20 (13H, m, aromatic and olefinic); MS *m/z*, 312 (M^+).

4-Phenyl-1-buten-3-ynyl 4-Methoxybenzenecarbodithioate (6i): Similarly to the synthesis of **6e** (Method B), from the salt **3c** (1.173 g, 2.0 mmol) and 3-phenyl-2-propynal (**5f**, 0.26 g 2.0 mmol) was obtained 0.39 g (63%) of red crystals of **6i** as a mixture of cis and trans isomers (1:1). Fractional recrystallization from dichloromethane/methanol gave geometrically pure samples: *cis*-**6i**: red crystals: Mp 69—73 °C; IR (KBr) 1240 (C=S) cm^{-1}; UV and Vis (CH_2Cl_2) 294 nm (log ε=4.19), 362 nm (log ε=4.33), 505 nm (log ε=2.41); ^1H NMR ($CDCl_3$) δ=3.87 (3H, s, CH_3), 6.17 (1H, d, *J*=10 Hz, vinyl), 7.70 (1H, d, *J*=8Hz, vinyl), 6.8—8.2 (9H, m, aromatic); MS *m/z*, 310 (M^+). Found: C, 69.56; H, 4.38%. Calcd for $C_{18}H_{14}OS_2$: C, 69.65; H, 4.55%. *trans*-**6i**: orange crystals: Mp 125—127 °C; IR (KBr) 1240 (C=S) cm^{-1}; UV and Vis (CH_2Cl_2) 293 nm (log ε=4.33), 361 nm (log ε=4.41), 502 nm (log ε=2.51); ^1H NMR ($CDCl_3$) δ=3.87 (3H, s, CH_3), 6.29 (1H, d, *J*=16 Hz, vinyl), 7.65 (1H, d, *J*=16 Hz, vinyl), 6.8—8.1 (9H, m, aromatic); MS *m/z*, 310 (M^+). Found: C, 69.68; H, 4.36%. Calcd for $C_{18}H_{14}OS_2$: C, 69.65; H, 4.55%.

6-Phenyl-1,3,5-hexatrienyl 4-Methoxybenzenecarbodithioate (6j): Similarly, from the salt **3c** (1.17 g, 2.0 mmol) and potassium *t*-butoxide (0.235 g, 2.0 mmol) was prepared 2.0 mmol of the ylide. Then, 5-phenyl-2,4-pentadienal (**5g**, 0.316 g, 2.0 mmol) was added at −30 °C and the reaction mixture was stirred at that temperature for 5 h. After usual workup, 0.369 g (55%) of **6j** was obtained as red crystals. Recrystallization from hot methanol gave pure **6j**: Mp 169—170 °C; IR (KBr) 1245 (C=S) cm^{-1}; UV and Vis (CH_2Cl_2) 334 nm (log ε=4.67), 418 nm (log ε=4.43); ^1H NMR ($CDCl_3$) δ=3.83 (3H, s, CH_3), 6.33—8.13 (15H, m, aromatic and olefinic); MS *m/z*, 338 (M^+). Found: C, 70.80; H, 5.38%. Calcd for $C_{20}H_{18}OS_2$: C, 70.97; H, 5.36%.

1-Propenyl 4-Methoxybenzenecarbodithioate (6k): Similarly to the synthesis of **6j**, from the salt **3c** (0.587 g, 1.0 mmol) and acetaldehyde (**5h**, 0.04 g, 0.9 mmol) was obtained 0.132 g (65%) of **6k** as a red oil (cis/trans=3:2). Analytically pure sample was obtained by preparative TLC (R_f=0.6, dichloromethane/hexane=2:3): IR (neat) 1235 (C=S) cm^{-1}; UV and Vis (CH_2Cl_2) 347 nm (log ε=3.72), 500 nm (log ε=1.71); ^1H NMR* ($CDCl_3$) δ=1.89 (1.8H, dd, *J*=1.5 and 7.0 Hz, CH_3), 1.97 (1.2H, dd, *J*=1.5 and 6.6 Hz, CH_3), 3.85 (3H, s, CH_3), 6.16 (0.4H, qd, *J*=6.6 and 15.6 Hz, vinyl), 6.16 (0.6H, qd, *J*=7.0 and 9.52 Hz, vinyl), 6.8—7.0 (2H, m, aromatic), 6.84 (0.4H, qd, *J*=1.2 and 15.6 Hz, vinyl), 7.02 (0.6H, qd, *J*=1.2 and 9.5 Hz, vinyl), 8.0—8.2 (2H, m, aromatic); MS *m/z*, 224 (M^+). Found: C, 58.68; H, 5.68%. Calcd for $C_{11}H_{12}OS_2$: C, 58.90; H, 5.39%. *270 MHz

1-Butenyl 4-Methoxybenzenecarbodithioate (6l): Similarly to the synthesis of **6j**, from the salt **3c** (0.587 g, 1.0 mmol) and propanal (**5i**, 0.06 g, 1.0 mmol) was obtained 0.066 g (28%) of **6l** as a red oil (cis/trans=1:1). Analytically pure sample was obtained by preparative TLC (R_f=0.8, dichloromethane/hexane=2:3): IR (neat) 1235 (C=S) cm^{-1}; UV and Vis (CH_2Cl_2) 345 nm (log ε=4.13), 498 nm (log ε=2.14); ^1H NMR* ($CDCl_3$) δ=1.07 (1.5H, t, *J*=7.7 Hz, CH_3), 1.13 (1.5H, t, *J*=7.3 Hz, CH_3), 2.2—2.4 (2H, m, CH_2), 3.85 (3H, s, CH_3), 6.07 (0.5H, td, *J*=7.3 and 9.5 Hz, vinyl), 6.20 (0.5H, td, *J*=6.6 and 15.8 Hz, vinyl), 6.86 (0.5H, td, *J*=1.5 and 15.8 Hz, vinyl), 6.8—6.9 (2H, m, aromatic), 7.00 (0.5H, td, *J*=1.5 and 9.5 Hz, vinyl), 8.0—8.2 (2H, m, aromatic); MS *m/z*, 238 (M^+). Found: C, 60.42; H, 6.18%. Calcd for $C_{12}H_{14}OS_2$: C, 60.47; H, 5.92%. *270 MHz-NMR

***O*-Methyl 4-Methoxybenzenecarbothioate (7a): Typical Procedures:** A solution of the dithiocarboxylate **6e** (0.083 g, 0.25 mmol) in 50 mL of dry THF was added dropwise at −70 °C to a solution of potassium methoxide (0.028 g, 0.24 mmol) in methanol (10 mL). The reaction mixture was warmed to 0 °C and the resulting deep purple solution (Vis; λ_{max}=493 nm) was stirred at 0 °C for 20 min. Then, to the enethiolate generated phenacyl bromide (0.05 g, 0.25 mmol) in 10 mL of methanol was added and stirred for 10 min. The mixture was quenched by addition of 5 drops of concentrated hydrochloric acid. The color of the solution turned to pale red then to yellow. After removal of the solvent, the residue was diluted with 50 mL of dichloromethane and washed with water (3×30 mL) and dried over anhydrous sodium sulfate. After concentration, the residue was purified by preparative TLC (hexane/dichloromethane=2:1 as eluant) gave 0.036 g (80%, R_f=0.63) of **7a** as yellow crystals together with 0.063 g (84%, R_f=0.11) of phenacyl 2-(4-nitrophenyl) vinyl sulfide (**10a**)[6] as pale yellow crystals. **7a**: Mp 43.5—45 °C [lit, mp 47 °C,[13a] 45 °C,[13a]]; IR (KBr) 1250 (C=S) cm^{-1}; ^1H NMR (CD_3COCD_3) δ=3.87 (3H, s, CH_3), 4.24 (3H, s, CH_3), 6.9—8.15 (4H, m, aromatic) [lit,[13a] ^1H NMR (CD_3COCD_3) δ=3.89 (3H, s, CH_3), 4.27 (3H, s, CH_3), 7.0—8.22 (4H, m, aromatic)]; MS *m/z*, 182 (M^+).

***O*-Methyl 4-Methylbenzenecarbothioate (7b):** Similarly to the synthesis of **7a**, a solution of the dithiocarboxylate **6c** (0.079 g, 0.25 mmol) in 40 mL of THF was treated with potassium *t*-butoxide (0.028 g, 0.25 mmol) in methanol (10 mL). In this case, the enethiolate generated was quenched by 2,4-dinitrochlorobenzene (0.051 g, 0.25 mmol). After usual workup, the residue was purified by preparative TLC (hexane/dichloromethane=1:1 as eluant) to give 0.034 g (82%, R_f=0.75) of **7b** as yellow oil together with

0.043 g (43%, R_f=0.05) of **10b**. **7b**: IR (neat) 1230 (C=S) cm^{-1}; ^1H NMR (CD_3COCD_3) δ=2.38 (3H, s, CH_3), 4.24 (3H, s, CH_3), 7.20—8.02 (4H, m, aromatic) [lit,[13a] ^1H NMR (CD_3COCD_3) δ=2.34 (3H, s, CH_3), 4.27 (3H, s, CH_3), 7.24—8.12 (4H, m, aromatic)]; MS *m/z*, 166 (M^+). The IR spectrum was well consistent with that of the authentic sample.[15] **10b**: Mp 153—158 °C; IR (KBr) 1330, 1510 (NO_2) cm^{-1}; ^1H NMR ($CDCl_3$) δ=6.73 (1H, d, *J*=10.5 Hz, vinyl), 7.20 (1H, d, *J*=10.5 Hz, vinyl), 7.6—7.9 (m, 3H, aromatic), 8.2—8.3 (m, 2H, aromatic), 8.43 (1H, dd, *J*=2.5 and 8.8 Hz, aromatic), 9.05 (1H, d, *J*=2.5 Hz, aromatic); MS *m/z*, 347 (M^+).

***O*-Ethyl 4-Methoxybenzenecarbothioate (7c):** Similarly to the synthesis of **7a**, the dithiocarboxylate **6e** (0.165 g, 0.5 mmol) was treated with potassium *t*-butoxide (0.056 g, 0.5 mmol) in ethanol (30 mL). After similar workup, the residue was purified by preparative TLC (ether/hexane=1:5 as eluant) to give 0.056 g (57%, R_f=0.45) of **7c** as yellow crystals together with 0.023 g (15%, R_f=0.1) of **10a**. **7c**: Mp 26—26.5 °C [lit,[16] mp 28—30 °C]; IR (KBr) 1220 (C=S) cm^{-1}; ^1H NMR ($CDCl_3$) δ=1.49 (3H, t, *J*=7.2 Hz, CH_3), 3.87 (3H, s, CH_3), 4.69 (2H, q, *J*=7.2 Hz, CH_2), 6.9—8.2 (4H, m, aromatic); MS *m/z*, 196 (M^+).

***O*-Phenyl 4-Methoxybenzenecarbothioate (7d):** Similarly to the synthesis of **7b**, a solution of the dithiocarboxylate **6e** (0.083 g, 0.25 mmol) in 40 mL of THF was added dropwise at 20 °C to a solution of potassium phenoxide prepared from potassium *t*-butoxide (0.028 g, 0.25 mmol) and phenol (0.024 g, 0.25 mmol) in 10 mL of THF. The enethiolate generated was quenched by 2,4-dinitrochlorobenzene (0.05 g, 0.25 mmol) in 10 mL of THF. After similar workup, the residue was purified by preparative TLC (hexane/dichloromethane=1:1) to give 0.047 g (77%, R_f=0.47) of **7d** as pale yellow crystals together with 0.035 g (43%, R_f=0.04) of 2,4-dinitrophenyl 2-(4-nitrophenyl)vinyl sulfide (**10b**). **7d**: Mp 111—112 °C (recrystallized from methanol); IR (KBr) 1260 (C=S) cm^{-1}; ^1H NMR ($CDCl_3$) δ=3.88 (3H, s, CH_3), 6.80—8.40 (9H, m, aromatic); MS *m/z*, 244 (M^+). Found: C, 68.35; H, 4.85%. Calcd for $C_{14}H_{12}O_2S$: C, 68.82; H, 4.95%.

Ethyl 4-Methoxybenzenecarbodithioate (9a): Typical Procedures: A solution of the dithiocarboxylate **6e** (0.083 g, 0.25 mmol) in THF (40 mL) was added dropwise to a solution of potassium ethanethiolate (0.25 mmol) prepared from potassium *t*-butoxide (0.028 g, 0.25 mmol) and ethanethiol (4 mL) in THF (10 mL) at −70 °C. The reaction mixture was stirred at that temperature for 1 h, then gradually warmed to −10 °C within 1 h. After standing for additional 1 h phenacyl bromide (0.05 g, 0.25 mmol) was added. After usual workup, the residue was purified by preparative TLC (hexane/dichloromethane=2:1 as eluant) to give 0.043 g (81%, R_f=0.48) of **9a** as reddish orange crystals, together with 0.056 g (75%, R_f=0.10) of **10a**. **9a**: Mp 20—21 °C [lit,[16] mp 22—25 °C]; IR (neat) 1235 (C=S) cm^{-1}; ^1H NMR ($CDCl_3$) δ=1.40 (3H, t, *J*=7.5 Hz, CH_3), 3.45 (2H, q, *J*=7.5 Hz, CH_3), 3.80 (3H, s, CH_3), 6.75—8.10 (4H, m, aromatic); MS *m/z*, 212 (M^+).

Ethyl 4-Methylbenzenecarbodithioate (9b): Similarly to the synthesis of **9a**, the dithiocarboxylate **6c** (0.079 g, 0.25 mmol) was treated with potassium ethanethiolate (0.025 g, 0.25 mmol) in ethanol (10 mL). The enethiolate generated was quenched by 2.4-dinitrochlorobenzene (0.05 g, 0.25 mmol). After usual workup, the residue was purified by preparative TLC (hexane/dichloromethane=1:1) to give 0.030 g (67%; R_f=0.80) of **9b** as a red oil, together with 0.044 g (56%; R_f=0.05) of **10b**. **9b**: IR (neat) 1230 (C=S) cm^{-1}; ^1H NMR ($CDCl_3$) δ=1.33 (3H, t, *J*=7.5 Hz, CH_3), 2.30 (3H, s, CH_3), 3.32 (2H, q, *J*=7.5 Hz, CH_2), 7.13 (2H, m, aromatic), 7.90 (m, 2H, aromatic) [lit,[17] ^1H NMR ($CDCl_3$) δ=1.3 (3H, t), 2.3 (3H, s), 3.3 (2H, q), 7.2 (2H, m), 7.9 (2H, m)]; MS *m/z*, 196 (M^+).

***t*-Butyl 4-Methoxybenzenecarbodithioate (9c):** Similarly to the synthesis of **9a**, a solution of the dithiocarboxylate **6e** (0.083 g, 0.25 mmol) in THF (40 mL) was treated with potassium 2-methyl-2-propanethiolate (0.032 g, 0.25 mmol) in THF (10 mL). After usual workup, the residue was purified by preparative TLC (hexane/dichloromethane=2:1 as eluant) to give 0.031 g (51%, R_f=0.55) of **9c** as reddish orange crystals, together with 0.052 g (70%, R_f=0.12) of **10a**. **9c**: Mp 37.5—39.5 °C; IR (KBr) 1240 (C=S) cm^{-1}; ^1H NMR ($CDCl_3$) δ=1.65 (9H, s, CH_3), 3.80 (3H, s, CH_3), 6.75—8.25 (4H, m, aromatic); MS *m/z*, 240 (M^+). All of the spectra were well consistent with those of authentic sample.[1c]

Phenyl 4-Methoxybenzenecarbodithioate (9d): Similarly to the synthesis of **9a**, the dithiocarboxylate **6e** (0.083 g, 0.25 mmol) was treated with potassium benzenethiolate (0.037 g, 0.25 mmol) in ethanol (10 mL). After usual workup, the residue was purified by preparative TLC (ether/hexane=2:1 as eluant) to give 0.03 g (46%; R_f=0.36) of **9d** as red crystals, together with 0.061 g (82%; R_f=0.07) of **10a**. **9d**: Mp 79.5—83.0 °C [lit,[18] mp 83 °C]; IR (KBr) 1240 (C=S) cm^{-1}; UV and Vis (CH_2Cl_2) 361 nm (log ε=4.23), 511 nm (log ε=2.27); ^1H NMR ($CDCl_3$) δ=3.80 (3H, s, CH_3), 6.75—8.25 (4H, m, aromatic), 7.4 (5H, s, aromatic); MS *m/z*, 260 (M^+).

We wish to acknowledge associate Prof. Dr. Satoshi Inagaki of Gifu University for his valuable advices on molecular orbital calculation. The calculation was carried out on a Hitachi computer of Institute for Molecular Science.

References

1) a) S. Kato, K. Sugino, Y. Matsuzawa, T. Katada, I. Noda, M. Mizuta, M. Goto, and M. Ishida, *Liebigs Ann. Chem.*, **1981**, 1798; b) S. Kato, S. Yamamoto, K. Ando, K. Itoh, M. Mizuta, and M. Ishida, *Z. Naturforsch.*, **37b**, 739 (1982); c) S. Kato, H. Shibahashi, T. Katada, T. Takagi, I. Noda, M. Mizuta, and M. Goto, *Liebigs Ann. Chem.*, **1982**, 1229; d) M. Ishida, H. Nakanishi, and S. Kato, *Chem. Lett.*, **1984**, 1961; e) M. Ishida, H. Nakanishi, and S. Kato, *Phosphorous and Sulfur*, **22**, 135 (1985); f) S. Kato, M. Goto, R. Hattori, K. Nishiwaki, M. Mizuta, and M. Ishida, *Chem. Ber.*, **118**, 1668 (1985).

2) M. Schoufs, J. Meijer, P. Vermeer, and L. Brandsma, *Synthesis*, **1978**, 439.

3) M. Saquet and T. Thuillier, *Tetrahedron Lett.*, **21**, 2165 (1980).

4) G. Levesque and A. Mahjour, *Tetrahedron Lett.*, **21**, 2247 (1980).

5) M. Ishida, H. Sato, and S. Kato, *Synthesis*, **1982**, 927.

6) S-(Triphenylphosphonio)methyl arenecarbothioate bromide was also prepared by us; M. Ishida, T. Iwata, M.

Yokoi, K. Kaga, and S. Kato, *Synthesis*, **1985**, 632.

7) The corresponding oxygen analogues, [1-(aryl- and alkylcarbonyl)oxyalkyl]phosphonium salts, were recently reported; E. Ander, T. Gassner, and A. Stankowiak, *Chem. Ber.*, **118**, 124 (1985).

8) S. Kato, T. Mitani, and M. Mizuta, *Int. J. Sulfur Chem.*, **8**, 359 (1973).

9) H. Hellmann and J. Bader, *Tetrahedron Lett.*, **1961**, 724.

10) a) J. Fabian, S. Scheithauer, and R. Mayer, *J. Prakt. Chem.*, **311**, 45 (1969); b) R. Mayer, E. Schinke, P. Rosmuss, and S. Sheithauer, *J. Prakt. Chem.*, **321**, 767 (1970).

11) We have previously reported the corresponding acylated salt; [$ArCS_2$–CH(CO–Ph)$\overset{+}{P}Ph_3$] $ArCS_2^-$; S. Kato, S. Imamura, and M. Mizuta, *Int. J. Sulfur Chem.* [A] **2**, 283 (1972).

12) The deep purple color (λ_{max}=493 nm) of the reaction mixture can be ascribed to the formation of potassium 2-(4-nitrophenyl)ethenethiolate (**8**), because the quite similar deep purple solution is formed from the reaction of *S*-[2-(4-nitrophenyl)vinyl] methoxybenzenecarbothioate (4-$CH_3OC_6H_4$-COS-CH=CH-$C_6H_4NO_2$(4-)) with potassium methoxide; See Ref. 6.

13) a) E. O. Fischer and S. Riedmüller, *Chem. Ber.*, **107**, 915 (1974); b) O. Exner, V. Jehlicka, and A. Ohno, *Collection Czechoslov. Chem. Commun.*, **36**, 2157 (1970).

14) a) W. Schroth, *Tetrahedron Lett.*, **1965**, 195; b) L. Brandsma, *Rec. Trav. Chim.*, **89**, 593 (1970); c) M. G. Missakian, R. Ketcham, and A. R. Martin, *J. Org. Chem.*, **39**, 2010 (1974).

15) T. Katada, S. Kato, and M. Mizuta, *Chem. Lett.*, **1975**, 1037.

16) H. Eilingsfeld, M. Seefelder, and H. Weidinger, *Chem. Ber.*, **96**, 2671 (1963).

17) J. Perregaard, I. Thomsen, and S.-O. Lawesson, *Bull. Chem. Soc. Belg.*, **86**, 321 (1977).

18) H. Viola, S. Scheithauer, and R. Mayer, *Chem. Ber.*, **101**, 3517, (1968).

19) V. N. Drozd and O. A. Popova, *Tetrahedron Lett.*, **1979**, 4491.

 © 1986 The Chemical Society of Japan Bull. Chem. Soc. Jpn., 59, 1411—1417 (1986)

Chemical Synthesis and Biological Activities of Two Disaccharide Dipeptides Corresponding to the Repeating Units of Bacterial Peptidoglycan

Shoichi KUSUMOTO, Koji YAMAMOTO, Masahiro IMOTO, Masaru INAGE, Masachika TSUJIMOTO,† Shozo KOTANI,† and Tetsuo SHIBA*

Department of Chemistry, Faculty of Science, Osaka University, Toyonaka, Osaka 560
†Department of Microbiology and Oral Microbiology, Osaka University Dental School, Suita, Osaka 565

(Received January 14, 1986)

Two disaccharide dipeptides, i.e., *O*-(*N*-acetyl-β-D-glucosaminyl)-(1→4)-*N*-acetylmuramyl-L-alanyl-D-isoglutamine (**2**) and *O*-(*N*-acetyl-β-muramyl-L-alanyl-D-isoglutamine)-(1→4)-*N*-acetyl-D-glucosamine (**3**), which correspond to partial structures of cell wall peptidoglycan were synthesized via the same glucosamine disaccharide as a common intermediate. Thus, selective introduction of lactic acid moiety on either one of the sugar moieties of the intermediate gave two disaccharides respectively which contain muramic acid on either reducing or nonreducing side. Coupling of the peptide moiety followed by deprotection afforded **2** and **3**. The results of biological tests showed that both **2** and **3** have the same magnitude of immunostimulating activities as those of *N*-acetylmuramyl-L-alanyl-D-isoglutamine which is the minimum structure required for expression of the activities.

Bacterial peptidoglycan is an integral part of the cell walls and known to exhibit a potent activity to modulate the defense mechanism of higher animals. Its structure is composed of glycan chains interlinked with peptide bridges. The former is β(1—4)glycan of alternating *N*-acetylglucosamine and *N*-acetylmuramic acid whose carboxyl group is the point of linkage to the peptide. It was independently demonstrated by us and a French group that the minimum structure required for the immunostimulation is *N*-acetylmuramyl-L-alanyl-D-isoglutamine (**1**), which is a common building block of the above architecture.[1,2] After this initial work, we prepared many derivatives and structural analogs of the muramyl peptide **1** and studied the relationship between their chemical structures and immunological activities.[3] In the meantime, comparison of immunopharmacological activities of various enzymatic digests of cell wall peptidoglycans has revealed that digests prepared with endopeptidases are generally more active than the muramyl dipeptide **1** as well as than digests obtained by use of glycosidases.[4] The endopeptidases are capable of hydrolyzing the cross linkages between the neighboring glycan chains, while the glycosidases split the glycan chain itself. These results seem to indicate that the presence of long glycan chain rather than the peptide network is required for efficient manifestation of these biological activities.

In view of the above findings, as the first step of a synthetic approach to a peptidoglycan polysaccharide peptides with stronger biological activities than the muramyl dipeptide **1**, we synthesized two disaccharide dipeptides, i.e., *O*-(*N*-acetyl-β-D-glucosaminyl)-(1→4)-*N*-acetylmuramyl-L-alanyl-D-isoglutamine (**2**) and *O*-(*N*-acetyl-β-muramyl-L-alanyl-D-isoglutamine)-(1→4)-*N*-acetyl-D-glucosamine (**3**), which correspond to structures having an *N*-acetylglucosamine unit β(1—4)-linked on either side of **1**. In other words, **2** and **3** are larger fragments of cell wall than **1** by one glucosamine residue.

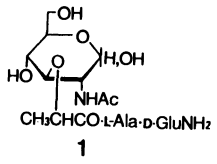

1

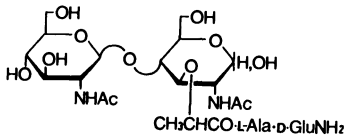

2

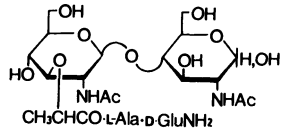

3

As reported in our preliminary communications,[5,6] the synthesis was performed via a common β(1—4)-linked disaccharide of glucosamine. One of its sugar residues was then selectively transformed into muramic acid to form the two alternative β(1—4)-linked disaccharides respectively. Coupling of the peptide moiety followed by deprotection afforded the desired products **2** and **3**. We describe in this paper the details of the synthesis. After our initial paper[5] on the synthesis of **2**, two other research groups also reported syntheses of both types of the disaccharide dipeptides via glucosamine disaccharides.[7,8] In the accompanying paper,[9] we also describe different approaches to form the corresponding disaccharide portions of **2** and **3** by means of a direct coupling of

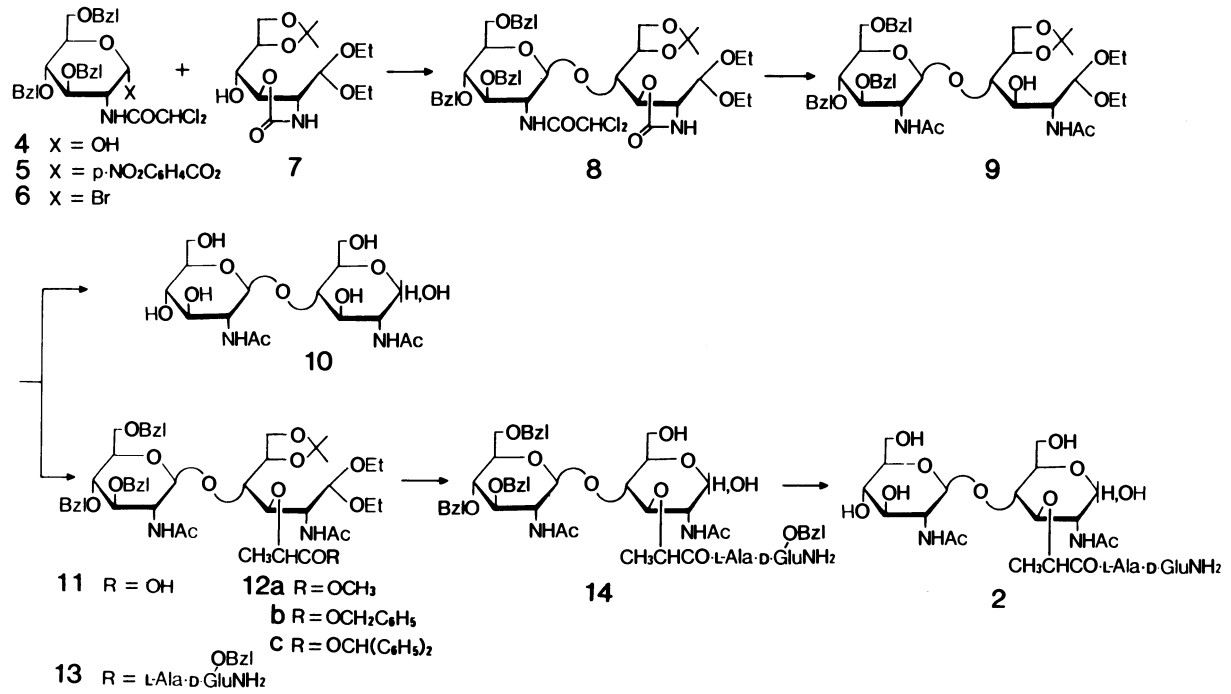

glucosamine and muramic acid residues.

In this investigation, an appropriate β(1—4)-linked glucosamine disaccharide which served as the common synthetic intermediate was prepared by coupling of the glycosyl bromide **6** with a known open-chain derivative of glucosamine, i.e., 2-amino-2-*N*: 3-*O*-carbonyl-2-deoxy-5,6-*O*-isopropylidene-D-glucose diethyl acetal (**7**).[10] The bromide **6** was prepared from 2-amino-3,4,6-tri-*O*-benzyl-2-deoxy-D-glucose.[11] After dichloroacetylation[12] of its amino group, the product **4** was converted into 1-*p*-nitrobenzoate **5** and then treated with dry hydrogen bromide in dichloromethane to give **6**.[13] The condensation of **6** with **7** in the presence of mercury(II) cyanide in benzene afforded the disaccharide **8** as the main product. The β-configuration of the newly formed glycosidic bond was ascertained chemically by converting **8** into *N,N'*-diacetylchitobiose. Thus, cleavage of the oxazolidone and dichloroacetyl protecting groups in **8** by alkaline hydrolysis gave **9**. *N*-Acetylation followed by further deprotection afforded the disaccharide **10** which was identified with an authentic sample of *N,N'*-diacetylchitobiose obtained from natural chitin.

For the preparation of the disaccharide which has the muramic acid residue on the reducing side, **9** obtained above was used as an intermediate. In this compound only one hydroxyl group remains free on C-3 where lactic acid moiety should be introduced to form muramic acid. The hydroxyl group of **9** was thus converted into the sodium alkoxide and treated with (*S*)-2-chloropropionic acid as described by Matsushima and Park.[14] However, when only dioxane was used as solvent as described,[14] the yield of the product **11** was quite variable. This seemed to be due to the difficulty in formation of alkoxide anion in that solvent in which **9** was only poorly soluble. Use of DMF as co-solvent improved the situation and the desired disaccharide derivative **11** could be obtained in a reproducible yield. The product was purified and isolated after esterification with diazomethane, phenyldiazomethane, or diphenyldiazomethane as methyl, benzyl, or diphenylmethyl ester (**12a**, **b**, **c**), respectively. Among these, only the diphenylmethyl derivative was crystalline. The structure of **12** was confirmed by converting **12a** into a known peracetylated derivative of *O*-β-D-glucosaminyl-(1→4)-muramic acid methyl ester.[15,16] The ester group of **12** was again hydrolyzed after purification and the resultant, free carboxyl group was coupled with L-alanyl-D-isoglutamine benzyl ester[1b] by means of the dicyclohexylcarbodiimide (DCC)–*N*-hydroxysuccinimide procedure to give the fully protected disaccharide dipeptide **13**. Deprotection of **13** was performed in two steps. Thus, the two acetal groups were first removed with hot aqueous acetic acid to give **14**, which in turn was subjected to hydrogenolysis. The final product **2** was isolated as a homogeneous hygroscopic powder.

Another disaccharide having the muramic acid residue on the nonreducing end was also synthesized from **9**. After the free hydroxyl group on position 3 had been protected with 2-methoxyethoxymethyl (MEM) group, the benzyl groups were hydrogenolyzed and the two hydroxyl groups on positions 4' and 6' again protected as benzylidene derivative to give a disaccharide **17** to be used for introduction of lactic acid moiety at position 3'. It was condensed with

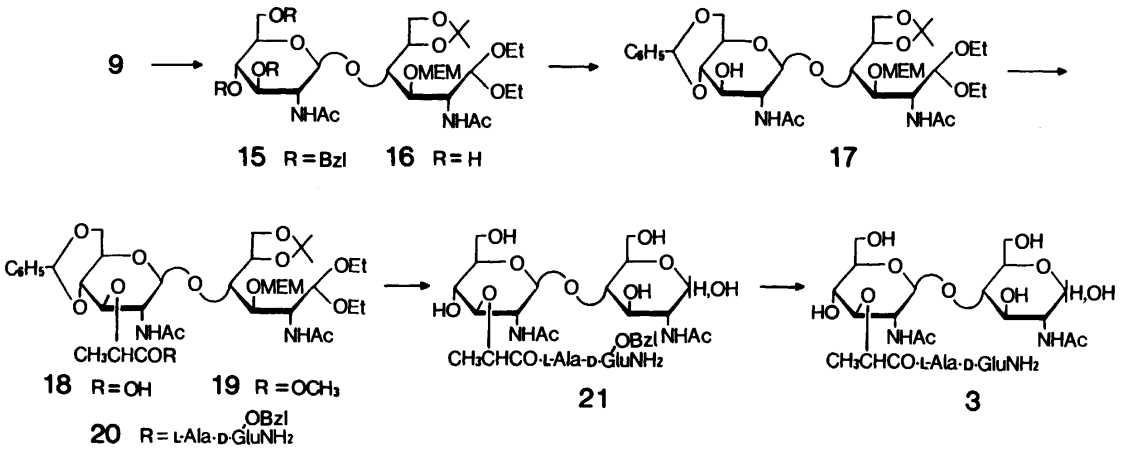

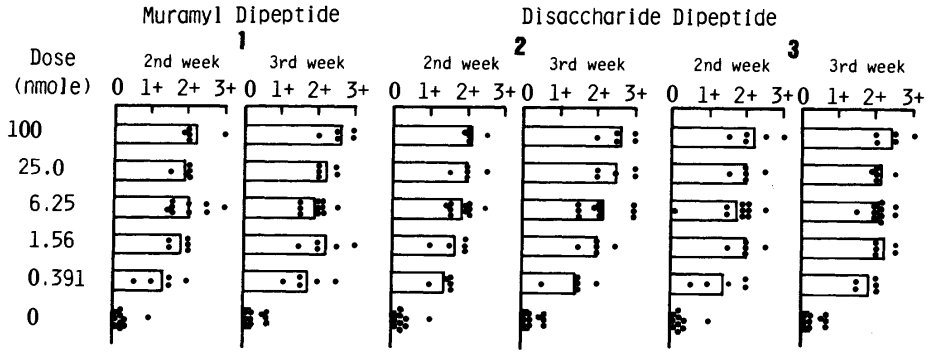

Fig. 1. Induction of delayed-type hypersensitivity against ovalbumin by **1**, **2**, and **3** in guinea pigs (corneal reaction). Each dot represents the score (arbitrarily graded with a maximum of 3+) for individual animal. Each column shows the mean score.

(*S*)-2-chloropropionic acid under similar conditions as above to afford the desired disaccharide **18** which was purified as the methyl ester **19** after esterification with diazomethane. Coupling of the dipeptide moiety as above gave a protected disaccharide dipeptide **20**, which was then subjected to deprotection reaction in two steps. In the first step when **20** was heated in aqueous acetic acid in order to remove all acetal-type protections, several by-products such as ethyl glycoside of the desired product were formed. However, by-products formation could be greatly suppressed by employing appropriate reaction conditions (see experimental section). The product **21** was isolated after purification with a column of porous polymer. It was then hydrogenolyzed to give the second disaccharide dipeptide **3**.

Immunoadjuvant activities of both disaccharide dipeptides prepared (**2** and **3**) were tested in guinea pigs by using ovalbumin as a test antigen. Their activities were compared with those of the muramyl dipeptide **1**. As shown in Figs. 1, 2, and 3, no significant differences were observed with the adjuvant activities among these compounds in terms of the induction of cellular immunity (as tested by corneal and tuberculin-type skin reactions) and the

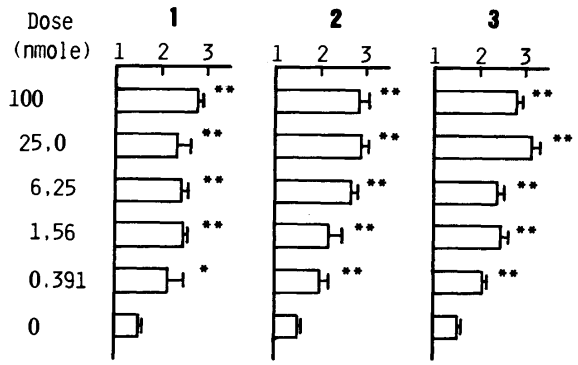

Fig. 2. Induction of delayed-type hypersensitivity against ovalbumin by **1**, **2**, and **3** in guinea pigs (tuberculin type of skin reaction). The extent of skin induration is expressed as ratios of the reading (48 h) at each test site to that at the control site. Significant difference from control group: $*P<0.05$, $**P<0.01$.

stimulation of humoral immunity (by determination of serum anti-ovalbumin level). We reported in a previous paper[17] that the glucosaminylmuramyl dipeptide **2** showed higher immunoadjuvant activities than **1**. Though discrepancy on this point might be due to the difference of antigen doses used for the

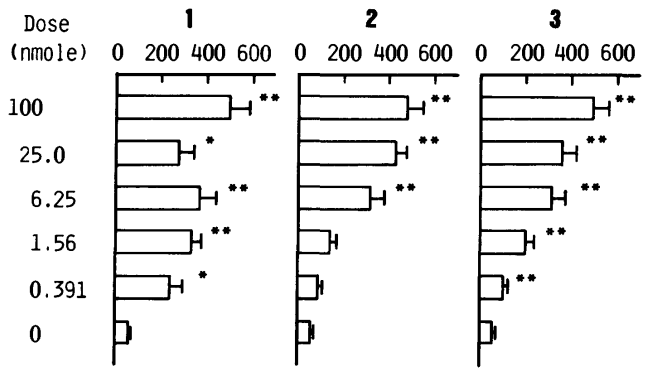

Fig. 3. Elevation of serum precipitating antibody levels against ovalbumin by **1**, **2**, and **3** in guinea pigs. Antibody level in serum is expressed as μg of antibody nitrogen per ml of serum. Significant difference from control group: $*P<0.05$, $**P<0.01$.

immunization (1 mg in the previous study and 0.1 mg in the present one), it should be concluded from the result obtained above that additional single glucosamine residue was not sufficient to induce a significant enhancement of the activities of **1**. Longer glycan chains might be required for effective potentiation. Synthesis of a peptidoglycan part structure with a longer saccharide is now being undertaken in our laboratory to confirm this assumption.

Experimental

All melting points are uncorrected. ^{1}H NMR spectra were measured for $CDCl_3$ solutions with tetramethylsilane as an internal standard (δ, ppm). FD-MS spectra were obtained with Si-emitter on JEOL OI-SG mass spectrometer. Optical rotations were measured with a Perkin-Elmer 141 polarimeter. Column chromatography and preparative thin-layer chromatography were carried out with Kieselgel 60 (0.063—0.2 mm) and with pre-coated Kieselgel F_{254} plates (0.5 mm thickness), E. Merck.

3,4,6-Tri-*O*-benzyl-2-deoxy-2-dichloroacetamido-D-glucopyranose (4). Pentachlorophenyl dichloroacetate (1.95 g, 5.16 mmol) and triethylamine (0.73 ml, 5.16 mmol) were added at room temperature to a stirred suspension of 2-amino-3,4,6-tri-*O*-benzyl-2-deoxy-D-glucose hydrochloride[11] (2.51 g, 5.16 mmol) in anhyd tetrahydrofuran (THF). After the mixture had been stirred at room temperature for 90 min, insoluble materials were filtered off, the filtrate evaporated in vacuo to give a gelatinous solid. It was purified by reprecipitation from dioxane–ether to give **4**; 2.38 g (82%); mp 217—219 °C(decomp). Found: C, 61.89; H, 5.56; N, 2.50; Cl, 12.50%. Calcd for $C_{29}H_{31}NO_6Cl_2$: C, 62.15; H, 5.58; N, 2.50; Cl, 12.56%.

3,4,6-Tri-*O*-benzyl-2-deoxy-2-dichloroacetamido-α-D-glucopyranosyl *p*-Nitrobenzoate (5). To an ice-cooled stirred solution of **4** (2.31 g, 4.12 mmol) in pyridine (50 ml) was added *p*-nitrobenzoyl chloride (2.30 g, 12.4 mmol) dissolved in a small amount of CH_2Cl_2. The mixture was stirred under ice-cooling for 2 h then at room temperature for 30 min. After usual work-up, the crude product was recrystallized from $CHCl_3$–ether; 2.50 g (86%); mp 173—174 °C; $[\alpha]_D^{20}$ +125° (*c* 1.00, $CHCl_3$). Found: C, 60.72; H, 4.82; N, 3.81; Cl, 9.89%. Calcd for $C_{36}H_{34}N_2O_9Cl_2$: C, 60.49; H, 4.83; N, 3.95; Cl, 9.99%.

3,4,6-Tri-*O*-benzyl-2-deoxy-2-dichloroacetamido-D-glucopyranosyl Bromide (6). A saturated solution of dry HBr in dry CH_2Cl_2 (5.5 ml) was added to a solution of **5** (2.00 g, 2.82 mmol) in dry CH_2Cl_2 (30 ml). The mixture was left stand at room temperature for 30 min. The precipitate of *p*-nitrobenzoic acid was removed by filtration. The residue obtained by evaporation of the solvent in vacuo at room temperature was dried over KOH and P_2O_5 in a desiccator overnight. It was used for the next coupling reaction without further purification.

2-Amino-4-*O*-(3,4,6-tri-*O*-benzyl-2-deoxy-2-dichloroacetamido-β-D-glucopyranosyl)-2-*N*: 3-*O*-carbonyl-2-deoxy-5,6-*O*-isopropylidene-D-glucose Diethyl Acetal (8). Dry benzene (30 ml) was added to 2-amino-2-*N*:3-*O*-carbonyl-2-deoxy-5,6-*O*-isopropylidene-D-glucose diethyl acetal (**7**) (0.90 g, 2.82 mmol) and powdered $Hg(CN)_2$ (2.14 g, 8.46 mmol). From this mixture, benzene (ca. 10 ml) was distilled off in order to remove the remaining trace of water. After cooling, a solution of the bromide **6** [obtained from **5** (2.00 g, 2.82 mmol)] in dry benzene (20 ml) was added and the mixture was stirred at room temperature for 24 h. The reaction mixture was diluted with $CHCl_3$, washed successively with 10% brine and H_2O, and dried ($MgSO_4$). The product was purified by chromatography on a silica-gel column ($CHCl_3$–acetone 6:1). Recrystallization from benzene–hexane gave **8**; 0.81 g (33%); mp 52—57 °C. $[\alpha]_D^{17}$ −11.0° (*c* 1.00, $CHCl_3$). Found: C, 59.74; H, 6.37; N, 3.23; Cl, 8.13%. Calcd for $C_{43}H_{54}N_2O_{11}Cl_2$: C, 59.92; H, 6.33; N, 3.25; Cl, 8.23%.

2-Acetamido-4-*O*-(2-acetamido-3,4,6-tri-*O*-benzyl-2-deoxy-β-D-glucopyranosyl)-2-deoxy-5,6-*O*-isopropylidene-D-glucose Diethyl Acetal (9). A mixture of **8** (4.25 g, 4.93 mmol) and $Ba(OH)_2 \cdot 8H_2O$ (18.6 g, 59.1 mmol) in dioxane (43 ml) and H_2O (43 ml) was heated at 100 °C with stirring for 16 h. The mixture was cooled, neutralized with CO_2 and filtered. The filtrate was concentrated in vacuo. The residue was dissolved in pyridine (50 ml), treated with acetic anhydride (13.9 ml), and worked up as usual. The crude acetylation product was dissolved in MeOH (80 ml), and 1M†† NaOMe in MeOH (8 ml) was added to it. The mixture was stirred at room temperature for 1 h and neutralized with Dowex 50 (H^+). Evaporation of the solvent in vacuo and purification with silica-gel column chromatography ($CHCl_3$–MeOH 15:1) afforded **9** as colorless syrup; 3.56 g (89%). ^{1}H NMR: 1.13 (6H, t, J=6.8 Hz $OCH_2C\underline{H}_3$), 1.28 and 1.40 (each 3H, s, isopropylidene CH_3), 1.90 (6H, s, $COCH_3$), 7.37 (15H, s, $OCH_2C_6\underline{H}_5$).

***N,N'*-Diacetylchitobiose (10).** Compound **9** (310 mg) was heated at 80 °C in 60% aq AcOH (10 ml) with stirring for 1 h. After evaporation of the solvent in vacuo, the residue was recrystallized from ethanol–hexane and then subjected to hydrogenolysis on Pd-black in 50% AcOH. The product was purified with preparative TLC (phenol–H_2O 3:1) to give a solid, 40 mg (27%), which was recrystallized from H_2O–acetone; mp 242—243 °C(decomp);

†† 1 M=1 mol dm^{-3}.

$[\alpha]_D^{22}$ +16.3° (*c* 0.40, H_2O; after equilibration). This product was identified with an authentic specimen of *N,N'*-diacetylchitobiose (mp 240—241 °C decomp, $[\alpha]_D^{22}$ +17.5°) by means of TLC and ^1H NMR.

2-Acetamido-4-*O*-(2-acetamido-3,4,6-tri-*O*-benzyl-2-deoxy-β-D-glucopyranosyl)-3-*O*-[(*R*)-1-(benzyloxycarbonyl)ethyl]-2-deoxy-5,6-*O*-isopropylidene-D-glucose Diethyl Acetal (12b). Sodium hydride (50% oil dispersion, 1.1 g, 23 mmol) was added to a solution of **9** (5.30 g, 6.56 mmol) in a mixture of dioxane (120 ml)–DMF(60 ml) at room temperature. After the mixture had been stirred at 60 °C for 20 min, (*S*)-2-chloropropionic acid (2.13 g, 20 mmol) and then NaH (1.3 g, 26 mmol) were added. The mixture was stirred at 60 °C for 8 h, cooled and the excess of NaH was decomposed by addition of ice. Acidification with 1 M HCl followed by extraction with $CHCl_3$ gave crude free acid **11**, which was treated with phenyldiazomethane in $CHCl_3$–hexane. The product was purified by silica-gel column chromatography (benzene–ethyl acetate 1:2) to give the benzyl ester **12b** as a pale yellow syrup; 3.0 g (47%); FD-MS: *m/z* 970 (M^+).

The corresponding methyl and diphenylmethyl esters **12a** and **c** were prepared in similar manners.

Compound 12a: Syrup; ^1H NMR: 1.12 (6H, t, *J*=7.0 Hz, $OCH_2C\underline{H}_3$), 1.25 and 1.38 (each 3H, s, isopropylidene CH_3), 1.25—1.38 (3H, $C\underline{H}_3CHCO_2$), 1.93 and 2.03 (each 3H, s, $COCH_3$), 3.73 (3H, s, CO_2CH_3), 7.33 (16H, C_6H_5 and $N\underline{H}COCH_3$).

Compound 12c: Mp 87—92 °C; $[\alpha]_D^{18}$ +21.0° (*c* 0.40, $CHCl_3$). Found: C, 68,99; H, 7.08; N, 2.56%. Calcd for $C_{60}H_{74}N_2O_{14}$: C, 69.05; H, 7.15; N, 2.68%.

2-Acetamido-4-*O*-(2-acetamido-3,4,6-tri-*O*-acetyl-2-deoxy-β-D-glucopyranosyl)-1,4,6-tri-*O*-acetyl-2-deoxy-3-*O*-[(*R*)-1-(methoxycarbonyl)ethyl]-α-D-glucopyranose. Methyl ester (**12a**) (50 mg) was heated in 60% AcOH (1 ml) at 60 °C for 1 h then at 80 °C for 1 h. The main product was isolated by means of preparative TLC on silica gel ($CHCl_3$–MeOH 9:1). Hydrogenolysis followed by acetylation with acetic anhydride and pyridine afforded peracetate of methyl ester as a mixture of the α- and β-anomers. It was again dissolved in acetic anhydride and treated with $ZnCl_2$ at 40 °C for 14 h to enrich the α-acetate, which was isolated as needles through recrystallization from acetone-ether; mp 231—233 °C; $[\alpha]_D^{18.5}$ +42.9° (*c* 0.07, $CHCl_3$).

Reported values for the natural specimen isolated from bacterial cells: Mp 235—236 °C; $[\alpha]_D^{22}$ +40° (*c* 0.20, $CHCl_3$).[14] Those for a synthetic specimen: Mp 237—238 °C; $[\alpha]_D$ +38° (*c* 0.23, $CHCl_3$).[15]

Benzyl L-Alanyl-D-isoglutaminate *N*-Acylated with 2-Acetamido-4-*O*-(2-acetamido-3,4,6-tri-*O*-benzyl-2-deoxy-β-D-glucopyranosyl)-2-deoxy-5,6-*O*-isopropylidene-3-*O*-[(*R*)-1-carboxyethyl]-D-glucose Diethyl Acetal (13). A solution of methyl ester **12a** (0.63 g, 0.70 mmol) in 0.5 M KOH in MeOH (14 ml) was stirred at room temperature for 24 h. The mixture was acidified with 3M citric acid, diluted with water and extracted with CH_2Cl_2. The organic layer was washed with H_2O, dried ($MgSO_4$) and evaporated in vacuo to give **11** as a syrup. It was dried by coevaporation with benzene in vacuo and then dissolved in dry THF. Benzyl L-alanyl-D-isoglutaminate hydrochloride (0.36 g, 1.1 mmol) and triethylamine (0.15 ml, 1.1 mmol) was added to the solution and the mixture was stirred in an ice bath for 30 min. *N*-Hydroxysuccinimide (0.12 g, 1.1 mmol) and DCC (0.14 g, 0.70 mmol) were added. Stirring was continued under cooling overnight. After addition of DCC (0.03 g, 0.14 mmol), the mixture was stirred at room temperature for further 3 h. Usual work-up and purification by column chromatography on silica gel ($CHCl_3$–MeOH 9:1) followed by reprecipitation form benzene-hexane afforded **13** as amorphous solid; 0.48 g (59%); mp 55—65 °C; $[\alpha]_D^{18}$ +9.5° (*c* 0.21, $CHCl_3$). Found: C, 63.11; H, 7.33; N, 5.90%. Calcd for $C_{62}H_{83}N_5O_{17}\cdot 1/2H_2O$: C, 63.14; H, 7.18; N, 5.94%.

Benzyl L-Alanyl-D-isoglutaminate *N*-Acylated with 2-Acetamido-4-*O*-(2-acetamido-3,4,6-tri-*O*-benzyl-2-deoxy-β-D-glucopyranosyl)-2-deoxy-3-*O*-[(*R*)-1-carboxyethyl]-D-glucose (14). Compound **13** (0.35 g, 0.30 mmol) was heated in 60% AcOH at 60 °C for 70 min. The product was purified by preparative TLC on silica gel ($CHCl_3$–MeOH 9:1). Precipitation by addition of ethyl acetate–hexane to a $CHCl_3$–MeOH (2:1) solution afforded colorless solid; 0.18 g (57%); mp 187—194 °C(decomp); $[\alpha]_D^{18}$ +8.5° (*c* 0.13, pyridine). Found: C, 61.25; H, 6.55; N, 6.42%. Calcd for $C_{55}H_{69}N_5O_{16}\cdot H_2O$: C, 61.49; H, 6.66; N, 6.51%.

L-Alanyl-D-isoglutamine *N*-Acylated with 2-Acetamido-4-*O*-(2-acetamido-2-deoxy-β-D-glucopyranosyl)-2-deoxy-3-*O*-[(*R*)-1-carboxyethyl]-D-glucose (2). Compound **14** (135 mg, 0.13 mmol) was suspended in MeOH and hydrogenolyzed in the presence of Pd-black catalyst at room temperature. The product was precipitated from MeOH–acetone to give hygroscopic powder, 90 mg (quantitative); mp 170—178 °C (decomp); $[\alpha]_D^{24}$ +0.6° $[\alpha]_{365}^{24}$ −21.7° (*c* 1.0, H_2O after equilibration). Found: C, 45.36; H, 6.40; N, 9.66%. Calcd for $C_{27}H_{45}N_5O_{16}\cdot H_2O$: C, 45.44; H, 6.44, N, 9.81%.

4-*O*-(2-Acetamido-3,4,6-tri-*O*-benzyl-2-deoxy-β-D-glucopyranosyl)-2-acetamido-2-deoxy-5,6-*O*-isopropylidene-3-*O*-(2-methoxyethoxymethyl)-D-glucose Diethyl Acetal (15). To a solution of **9** (1.60 g, 1.97 mmol) in a mixture of dioxane (32 ml)–DMF (16 ml) was added NaH (50% oil dispersion, 95 mg, 2.37 mmol). The mixture was stirred under Ar atmosphere at 60 °C for 30 min. The mixture was then cooled in an ice bath. 2-Methoxyethoxymethyl chloride (295 mg, 2.37 mmol) was added with stirring. After 70 min, a saturated aq solution of $NaHCO_3$ was added to the mixture. The solvent was removed in vacuo, the residue worked up as usual and subjected to silica-gel column chromatography ($CHCl_3$–acetone 2:1) to give **15** as colorless syrup; 1.00 g (57%); ^1H NMR: 4.75 (2H, s, OCH_2O) 3.80 (3H, s, OCH_3); FD-MS: *m/z* 919 $(M+Na)^+$. Further elution of the column afforded unchanged starting material (**9**); 0.65 g (41%).

4-*O*-(2-Acetamido-4,6-*O*-benzylidene-2-deoxy-β-D-glucopyranosyl)-2-acetamido-2-deoxy-5,6-*O*-isopropylidene-3-*O*-(2-methoxyethoxymethyl)-D-glucose Diethyl Acetal (17). Compound **15** (1.38 g, 1.54 mmol) was dissolved in EtOH (15 ml) and hydrogenolyzed at room temperature in the presence of Pd-black catalyst. The solid product **16** obtained by evaporation of the solvent in vacuo was used for the following reaction after drying by co-evaporation with benzene.

To a solution of **16** in DMF (20 ml) were added benzaldehyde dimethyl acetal (1.00 g, 6.61 mmol) and *p*-toluenesulfonic acid monohydrate (30 mg, 0.16 mmol). The mixture was kept at 40 °C and rotated on a rotary

evaporator in vacuo for 30 min. After usual work-up and purification with a silica-gel column ($CHCl_3$–acetone 1:2) afforded **17** as a pale yellow solid; 0.59 g (54% from **15**); FD-MS: *m/z* 737 $(M+Na)^+$.

4-*O*-[2-Acetamido-4,6-*O*-benzylidene-2-deoxy-3-*O*-[(*R*)-1-(methoxycarbonyl)ethyl]-β-D-glucopyranosyl]-2-acetamido-2-deoxy-5,6-*O*-isopropylidene-3-*O*-(2-methoxyethoxymethyl)-D-glucose Diethyl Acetal (19). To a solution of **17** (370 mg, 0.52 mmol) in a mixture of dioxane (8 ml)–DMF (4 ml) was added NaH (50% oil dispersion, 41 mg, 1.0 mmol). The mixture was stirred under Ar atmosphere at 60 °C for 30 min. Then (*S*)-2-chloropropionic acid (224 mg, 2.06 mmol) and NaH (103 mg, 2.6 mmol) were added. The mixture was treated and worked up as described for the preparation of **12b**. The crude product was treated with CH_2N_2 and purified by silica-gel column chromatography ($CHCl_3$-acetone 2:3). Lyophilization of a dioxane solution afforded a colorless solid; 274 mg (66%) $[\alpha]_D^{20}$ +0.4°, $[\alpha]_{365}^{20}$ −11.8° (*c* 1.00, MeOH), ^1H NMR: 3.90 (3H, s, CO_2CH_3), 1.20 (3H, d, *J*=7 Hz, CH_3 of lactyl residue); FD-MS: *m/z* 801 $(M+H)^+$, 823 $(M+Na)^+$. Found: C, 55.64; H, 7.33; N, 3.45%. Calcd for $C_{38}H_{60}N_2O_{16}\cdot H_2O$: C, 55.73; H, 7.63, N, 3.42%.

Benzyl L-Alanyl-D-isoglutaminate *N*-Acylated with 4-*O*-[2-Acetamido-4,6-*O*-benzylidene-2-deoxy-3-*O*-[(*R*)-1-carboxyethyl]-β-D-glucopyranosyl]-2-acetamido-2-deoxy-5,6-*O*-isopropylidene-3-*O*-(2-methoxyethoxymethyl)-D-glucose Diethyl Acetal (20). To a solution of **19** (264 mg, 0.33 mmol) in MeOH (3.3 ml) was added 1 M KOH in MeOH (3.3 ml). The mixture was stirred at room temperature for 2 h, acidified with aq citric acid solution. After evaporation of the solvent, the residue was extracted with $CHCl_3$ and worked up as usual. The free acid obtained was dissolved in dry THF and cooled in an ice-bath. To this solution were added benzyl L-alanyl-D-isoglutaminate trifluoroacetate (209 mg, 0.50 mmol), triethylamine (51 mg, 0.50 mmol), *N*-hydroxysuccinimide (58 mg, 0.50 mmol), and DCC (82 mg, 0.40 mmol). The mixture was stirred at 0 °C for 30 min and then at room temperature for 4 h. Usual work-up and purification with a silica-gel column (acetone) followed by lyophilization from dioxane afforded colorless powder; 313 mg (88%); mp 78—85 °C (with sintering at 65 °C); $[\alpha]_D^{17}$ −1.5°, $[\alpha]_{365}^{17}$ −9.3° (*c* 1.00, MeOH); FD-MS: *m/z* 1076 $(M+H)^+$. Found: C, 56.63; H, 7.03; N, 6.38%. Calcd for $C_{52}H_{77}N_5O_{19}\cdot 1.5H_2O$: C, 56.61; H, 7.31; N, 6.35%.

Benzyl L-Alanyl-D-isoglutaminate *N*-Acylated with 2-Acetamido-4-*O*-[2-acetamido-2-deoxy-3-*O*-[(*R*)-1-carboxyethyl]-β-D-glucopyranosyl]-2-deoxy-D-glucose (21). A solution of **20** (145 mg, 0.13 mmol) in 90% AcOH (5 ml) was heated at 100 °C for 30 min. After cooling and evaporation of the solvent, the residue was subjected to column chromatography on DIAION HP-20 (linear gradient from H_2O to MeOH) and lyophilized from water to give colorless powder; 42 mg (40%): $[\alpha]_D^{11}$ +18.6° (*c* 1.00, H_2O); FD-MS: *m/z* 786 $(M+H)^+$. Found: C, 50.80; H, 6.58; N, 8.47%. Calcd for $C_{34}H_{51}N_5O_{16}\cdot H_2O$: C, 50.80; H, 6.65; N, 8.71%.

L-Alanyl-D-isoglutamine *N*-Acylated with 2-Acetamido-4-*O*-[2-acetamido-2-deoxy-3-*O*-[(*R*)-1-carboxyethyl]-β-D-glucopyranosyl]-2-deoxy-D-glucose (3). Compound **21** (38 mg, 0.048 mmol) was dissolved in H_2O (4 ml) and hydrogenolyzed in the presence of Pd-black catalyst at room temperature. The product was lyophilized from water; 33 mg (quantitative); $[\alpha]_D^{11}$ +18.8° (*c* 1.00, H_2O); FD-MS: *m/z* 718 $(M+Na)^+$. Found: C, 46.50; H, 6.57; N, 9.67%. Calcd for $C_{27}H_{45}N_5O_{16}\cdot 1/4H_2O$: C, 46.32; H, 6.55; N, 10.00%.

Immunoadjuvant Activities. Immunoadjuvant activities of two disaccharide dipeptides, **2** and **3**, were tested in comparison with the muramyl dipeptide **1** by the methods previously described.[18,19] In brief, group of five guinea pigs [weight 300 to 400 g (strain Yodo, Nihon Rabbit Co., Osaka)] were immunized by intrafoot-pad injection of graded amount of test synthetic specimens or the muramyl dipeptide **1** and with 100 μg of ovalbumin (Sigma) incorporated into Freund incomplete adjuvant (Difco). Two and three weeks later, induction of delayed-type hypersensitivity was evaluated by corneal test, in which ovalbumin solution was injected intracorneally. The induction of delayed-type hypersensitivity was also determined by measuring the extent of induration of the skin site which received intracutaneous injection of 0.1 ml of ovalbumin solution (1 mg/ml) on day 26. Anti-ovalbumin precipitating antibody levels in serum were estimated with serum specimen drawn 4 weeks after the immunization by the quantitative precipitin reaction. The results are summarized in Figs. 1, 2, and 3.

References

1) a) S. Kotani, Y. Watanabe, F. Kinoshita, T. Shimono, I. Morisaki, T. Shiba, S. Kusumoto, Y. Tarumi, and K. Ikenaka, *Biken J.*, **18**, 105 (1975); b) S. Kusumoto, Y. Tarumi, K. Ikenaka, and T. Shiba, *Bull. Chem. Soc. Jpn.*, **49**, 533 (1976).

2) F. Ellouz, A. Adam, R. Ciorbaru, and E. Lederer, *Biochem. Biophys. Res. Commun.*, **59**, 1317 (1974).

3) For example: I. Azuma, K. Sugimura, M. Yamawaki, M. Uemiya, S. Kusumoto, S. Okada, T. Shiba, and Y. Yamamura, *Infect. Immun.*, **20**, 600 (1978).

4) The activities include arthritogenicity, activation of human complement, mitogenic activities, and so on. a) O. Kohashi, C. M. Pearson, Y. Watanabe, S. Kotani, and T. Koga, *J. Immunol.*, **116**, 1635 (1976); b) T. Koga, K. Maeda, K. Onoue, K. Kato, and S. Kotani, *Mol. Immunol.*, **16**, 153 (1979); c) A. Kawasaki, *J. Osaka Univ. Dent. Sch.*, **27**, 46 (1982); d) H. Takada, M. Tsujimoto, S. Kotani, S. Kusumoto, M. Inage, T. Shiba, S. Nagao, I. Yano, S. Kawata, and K. Yokogawa, *Infect. Immun.*, **25**, 645 (1979); e) K. Harada, S. Kotani, H. Takada, M. Tsujimoto, Y. Hirachi, S. Kusumoto, T. Shiba, S. Kawata, K. Yokogawa, H. Nishimura, T. Kitaura, and T. Nakajima, *Infect. Immun.*, **37**, 1181 (1982).

5) S. Kusumoto, K. Yamamoto, and T. Shiba, *Tetrahedron Lett.*, **1978**, 4407.

6) S. Kusumoto, M. Imoto, M. Inage, T. Ogiku, and T. Shiba, "Immunomodulation by Microbial Products and Related Synthetic Compounds-International Congress Series 563," ed by Y. Yamamura, S. Kotani, I. Azuma, A. Koda, and T. Shiba, Excerpta Medica, Amsterdam (1982) pp. 151—154.

7) a) P. L. Durette, E. P. Meitzner, and T. Y. Shen, *Tetrahedron Lett.*, **1979**, 4013; b) P. L. Durette, E. P. Meitzner, and T. Y. Shen, *Carbohydr. Res.*, **77**, C1 (1979).

8) a) M. Kiso, Y. Kaneda, R. Shimizu, and A. Hasegawa, *Carbohydr. Res.*, **83**, C8 (1980); b) M. Kiso, Y. Kaneda, R.

Shimizu, A. Hasegawa, and I. Azuma, *Carbohydr. Res.*, **104**, 253 (1982).

9) S. Kusumoto, M. Imoto, T. Ogiku, and T. Shiba, *Bull. Chem. Soc. Jpn.*, the accompanying paper.

10) Use of an open chain form of glucosamine was known to facilitate the condensation at the 4-hydroxyl group: K. Heins, K. Propp, R. Harrison, and H. Paulsen, *Chem. Ber.*, **100**, 2655 (1967).

11) T. D. Inch and H. G. Fletcher, Jr., *J. Org. Chem.*, **31**, 1810 (1967).

12) D. Shapiro, A. J. Acher, and E. S. Rachaman, *J. Org. Chem.*, **32**, 3767 (1967).

13) During this procedure no cleavage of the benzyl protecting groups was observed. Cf. M. Dejeter-Juszysky and H. M. Flowers, *Carbohydr. Res.*, **18**, 219 (1971).

14) Y. Matsushima and J. T. Park, *J. Org. Chem.*, **27**, 3581 (1962).

15) N. Sharon, T. Osawa, H. M. Flowers, and G. W. Jeanloz, *J. Biol. Chem.*, **241**, 223 (1966).

16) C. Merser and P. Sinaÿ, *Tetrahedron Lett.*, **1973**, 1029.

17) M. Tsujiomoto, F. Kinoshita, T. Okunaga, S. Kotani, S. Kusumoto, K. Yamamoto, and T. Shiba, *Microbiol., Immunol.*, **23**, 933 (1979).

18) S. Kotani, T. Narita, D. E. S. Stewart-Tull, T. Shimono, Y. Watanabe, K. Kato, and S. Iwata, *Biken J.*, **18**, 77 (1975).

19) S. Kotani, F. Kinoshita, I. Morisaki, T. Shimono, T. Okunaga, H. Takada, M. Tsujimoto, Y. Watanabe, K. Kato, T. Shiba, S. Kusumoto, and S. Okada, *Biken J.*, **20**, 95 (1977).

Synthesis of β(1—4)-Linked Disaccharides of *N*-Acetylglucosamine and *N*-Acetylmuramic Acid by Their Direct Condensation

Shoichi KUSUMOTO, Masahiro IMOTO, Tsuyoshi OGIKU, and Tetsuo SHIBA*
Department of Chemistry, Faculty of Science, Osaka University,
Toyonaka, Osaka 560
(Received January 14, 1986)

As a basic study in the synthetic approach to immunoactive cell wall peptidoglycan whose backbone is a β(1—4)-linked saccharide of alternating glucosamine and muramic acid, methods for the direct condensation of these sugar components were studied and *O*-(*N*-acetyl-β-muramyl)-(1→4)-*N*-acetyl-D-glucosamine and *O*-(*N*-acetyl-β-D-glucosaminyl)-(1→4)-*N*-acetylmuramic acid were synthesized. In the synthesis of the latter disaccharide, previous formation of an ester bond between the carboxyl group of muramic acid and the 6-hydroxyl group of glucosamine proved to facilitate the glycoside bond fromation between these sugar moieties.

In the preceding paper, we reported syntheses of two disaccharide-dipeptides which correspond to partial structures of cell wall peptidoglycan, i.e., *O*-(*N*-acetyl-β-D-glucosaminyl)-(1→4)-*N*-acetylmuramyl-L-alanyl-D-isoglutamine and *O*-(*N*-acetyl-β-muramyl-L-alanyl-D-isoglutamine)-(1→4)-*N*-acetyl-D-glucosamine.[1] Both of these structures contain additional one D-glucosamine unit linked to either position 1 or 4 of the muramic acid residue of *N*-acetylmuramyl-L-alanyl-D-isoglutamine which is the minimum structure responsible for the immunostimulating activity of cell wall peptidoglycan. Since cell wall fragments which retain long glycan chains generally show higher activity than the muramyl dipeptide, we expected similar enhancement of the activity for these disaccharide dipeptides as well. However, the result of biological tests revealed that only one additional glucosamine unit is not sufficient and a longer glycan structure would be required for significant enhancement of the activity.[1]

In this respect, we were interested in the synthesis of a larger cell wall structure whose backbone consists of an alternating glycan of glucosamine and muramic acid. For construction of such a glycan structure, direct coupling of the component sugar seemed to be necessary.[2] However, no direct synthesis of saccharides of muramic acid has been reported yet. We thus examined this approach and describe in this paper a preparation of both sequences of β(1—4) disaccharide consisting of glucosamine and muramic acid by their direct condensation.

The synthesis of the disaccharide in which muramic acid is located on the non-reducing side, i.e., O-(*N*-acetyl-β-muramyl)-(1→4)-*N*-acetyl-D-glucosamine, was performed as follows. At first, several glycosyl halogenides **1**—**4** were prepared[3] and subjected to reaction with glucosamine derivatives (**5** or **6**) in the presence of mercury(II) cyanide. However, no disaccharide was obtained in any combination of reaction partners, halogenides being transformed quantitatively to the corresponding oxazolines.[4] Therefore, glycosidation with oxazoline derivatives was next attempted. The oxazoline **7** derived from peracetylated methyl ester of muramic acid was subjected to acid-catalyzed reaction[5] with the glycosyl acceptor **5** or **6** as above. Again in these cases, no disaccharide was obtained. After prolonged reaction period, **7** was either hydrolyzed or changed to the corresponding glycal. Such low ability of the muramic acid derivative **7** to act as glycosyl donor seemed to be attributed to the steric hindrance caused by the lactic acid moiety, which might cover the upper face of the molecules, hindering the access of

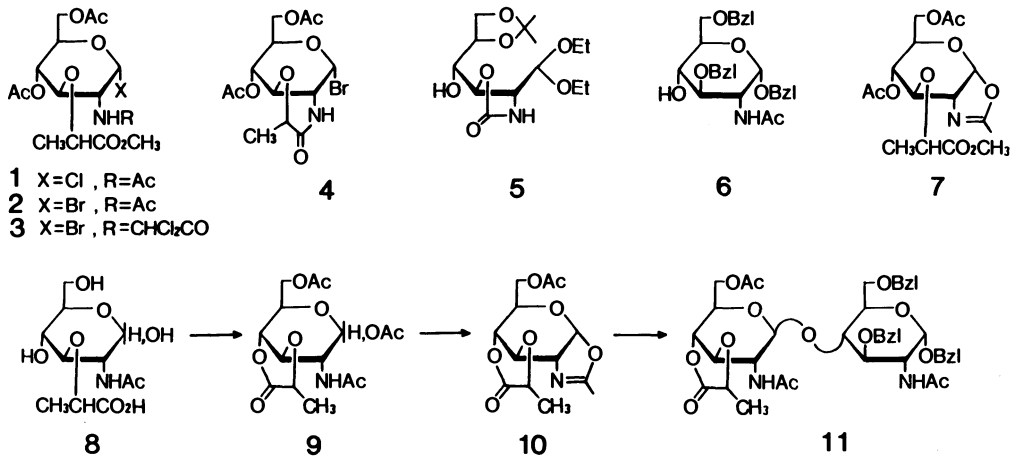

the glycosyl acceptor from the β-side.[6]

Relaxation of this steric hindrance could be expected in the oxazoline of an intramolecular ester form **10** where the lactic acid moiety is kept away from C-1. Formation of this ester also serves for the simultaneous protection of both carboxyl and 4-hydroxyl groups of the muramic acid moiety. In fact, by coupling of **10** with the glucosamine derivative **6** the desired β(1—4) disaccharide **11**[7] was obtained in 21% yield. The relatively low yield of **11** could be ascribed to the known very poor reactivity of the 4-hydroxyl group of glucosamine in the pyranoside form.

The next target of the synthesis was another disaccharide in which muramic acid is the reducing component. The first attempt to condense the simple peracetylated oxazoline **12** with the muramic acid derivative **13** failed to give a disaccharide. In addition to the known low reactivity of the 4-hydroxyl group described above, a steric hindrance due to the lactic acid moiety in **13** might be responsible in this case, too. Therefore, a novel device was required to facilitate the coupling. We thus tried to connect the two components prior to the glycosidation reaction with an ester linkage which can be formed more readily than a glycosidic bond. The muramic acid possesses a carboxyl function which can be used for this connection. The glycosidation reaction then becomes an intramolecular process and hence could be expected to proceed more easily. In the field of peptide chemistry, several examples of similar approaches had been described where two components to be coupled had been brought close together by auxiliary groups.[8,9]

Examination of molecular models indicated that an ester linkage between the carboxyl group of the muramic acid residue and the 6-hydroxyl groups of glucosamine is sterically most favorable for the formation of β(1—4) glycoside. According to this strategy, a synthetic precursor required for the glycosidation reaction, i.e., an oxazoline with an ester-linked muramic acid, was prepared as follows. The 6-hydroxyl group of the glucosamine derivative **14** was esterified with the protected muramic acid **17**.[10] Acetylation of the remaining free 4′-hydroxyl group in the product **18** followed by cleavage of the acetonide and 6-*O*-monoacetylation afforded **21**. All these transformations proceeded in satisfactory yields. When **21** was subjected to the standard conditions for allyl-propenyl isomerization described by Gent and Gigg[11] (in the presence of DABCO in ethanol-benzene-water), cleavage of the inter-sugar ester linkage occurred preferentially. This side reaction could be avoided by using dry benzene as solvent and eliminating DABCO. The propenyl glycoside **22** thus obtained was then treated with mercury (II) salt[12] to give the desired oxazoline **23** as syrup.

Glycosidation was effected in the presence of *p*-toluenesulfonic acid at 50 °C. The product was purified after cleavage of the ester linkage by methanolysis followed by re-*O*-acetylation.[13] The peracetylated methyl ester of *O*-(β-glucosaminyl)-(1→4)-muramic acid benzyl glycoside (**24**) was obtained in 20% yield from the oxazoline **23**. In contrast, no disaccharide was obtained at all under similar reaction conditions as described above in the reaction of the two corresponding monosaccharide units **12** and **13** which were not linked previously together with an ester bond. Consequently, the presence of the ester linkage which kept the two sugar moieties

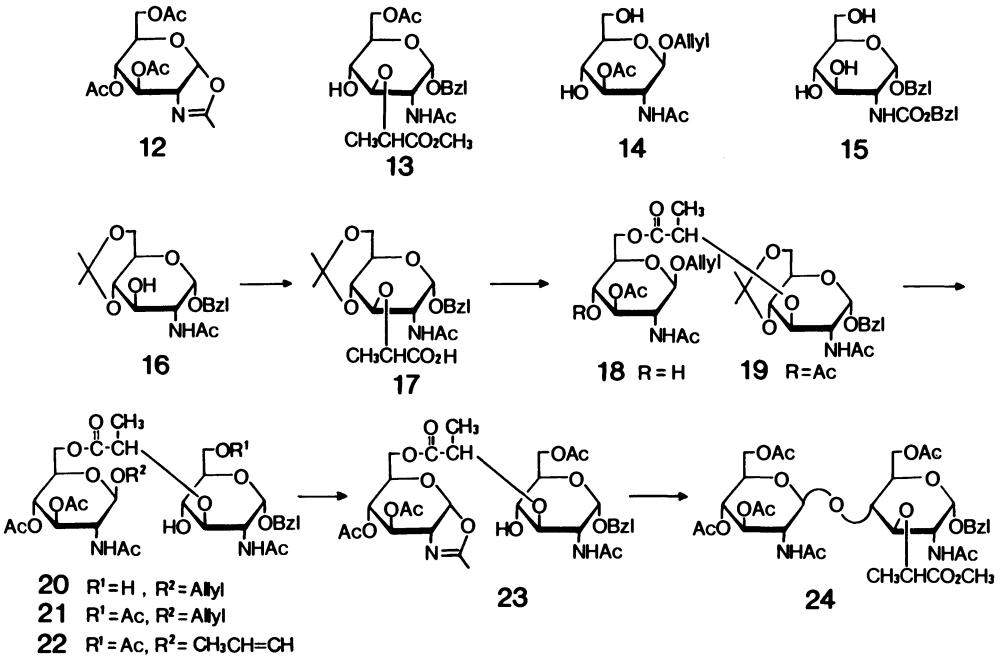

in close proximity to each other certainly favored the formation of the desired glycoside bond in the above experiment. Thus, this is the first example of the so-called "entropic activation"[9] in glycosidation reaction.

Since both sequences of β(1—4) disaccharide were prepared by direct condensation of glucosamine and muramic acid as described in this work, the basic problem was solved in the synthesis of cell wall glycan which consists of the alternating these two sugar moieties. Furthermore, the receipt of "entropic activation" demonstrated in this work seems to have wide applicability. Its some application even for glycosides without muramic acid were already attempted[14] by linking sugar moieties with dicarboxylic acids and the result will be reported in details elsewhere.

Experimental

All melting points are uncorrected. ^{1}H NMR spectra were measured for $CDCl_3$ solutions with tetramethylsilane as an internal standard (δ, ppm). Optical rotations were measured with a Perkin-Elmer 141 polarimeter. FD-MS spectra were obtained with Si-emitter on JEOL O1-SG mass spectrometer. Column chromatography and preparative thin-layer chromatography were carried out with Kieselgel 60 (0.063—0.2 mm) and with pre-coated Kieselgel F_{254} plates (0.5 mm thickness), E. Merck.

2-Acetamido-1,6-di-*O*-acetyl-3-*O*-[(*R*)-1-carboxyethyl]-2-deoxy-D-glucopyranose (Intramolecular Ester Form) (9). Acetic anhydride (10.0 ml, 106 mmol) was added to a suspension of *N*-acetylmuramic acid (**8**) (4.05 g, 15.3 mmol) in THF (130 ml). After the mixture had been stirred at 30 °C for 13 h and cooled to room temperature, pyridine (20 ml) was added to it. The mixture was stirred at room temperature for additional 8 h. The product isolated by usual work-up was recrystallized from $CHCl_3$–ether; 4.33 g (79%); mp 200—205 °C(decomp); $[\alpha]_D^{23}$ +151° (*c* 1.00, $CHCl_3$), ^{1}H NMR (100 MHz): 6.40 (1H, d, *J*=8 Hz, NH); 6.20 (1H, d, *J*=3 Hz, H-1), 2.15, 2.10, and 1.95 (each 3H, s, $COCH_3$), 1.50 (3H, d, *J*=7 Hz, lactyl CH_3). Found: C, 49.93; H, 5.87; N, 3.83%. Calcd for $C_{15}H_{21}NO_9$: C, 50.14; H, 5.89; N, 3.90%.

6-*O*-Acetyl-2-amino-3-*O*-[(*R*)-1-carboxyethyl]-2-deoxy-1-α-*O*:2-*N*,*N*-ethylidyne-D-glucopyranose (Intramolecular Ester Form) (10). Compound **9** (4.25 g, 11.8 mmol) was dissolved in a saturated solution of dry HBr in CH_2Cl_2 (80 ml), and the mixture was left stand at room temperature for 13 h. After the solvent had been evaporated in vacuo. The residue was dried in vacuo over KOH, overnight, and dissolved again in dry CH_2Cl_2 (80 ml). Pyridine (20 ml) was added to the solution. The mixture was stirred at room temperature for 1 h, washed with H_2O, dried ($MgSO_4$) and evaporated in vacuo to give syrup. It was used for the next reaction without further purification after co-evaporation in vacuo three times with toluene. ^{1}H NMR (60 MHz): 6.0 (1H, d, *J*=7 Hz, H-1), 2.10 and 2.15 (each 3H, s, oxazoline CH_3 and CH_3CO), 1.60 (3H, d, *J*=7 Hz, lactyl CH_3).

Benzyl 4-*O*-[2-Acetamido-6-*O*-acetyl-3-*O*-[(*R*)-1-carboxyethyl]-2-deoxy-β-D-glucopyranosyl]-2-acetamido-3,6-di-*O*-benzyl-α-D-glucopyranoside (Intramolecular Ester Form) (11). *p*-Toluenesulfonic acid monohydrate (80 mg, 0.42 mmol) was dehydrated by heating at 110 °C in vacuo. To this was added a solution of **10** (obtained from 4.25 g of **9** as described above) and benzyl 2-acetamido-3,6-di-*O*-benzyl-2-deoxy-α-D-glucopyranoside (**6**) (1.82 g, 3.70 mmol) in dry CH_2ClCH_2Cl (50 ml). The mixture was heated at 70 °C for 13 h. After evaporation of the solvent in vacuo, the product was purified by silica-gel column chromatography and recrystallized from $CHCl_3$–acetone; 604 mg (21% based on **6**); mp 262—265 °C (decomp); $[\alpha]_D^{20}$ +114° (*c* 1.01, $CHCl_3$). ^{1}H NMR (100 MHz): 7.40, 7.30, and 7.25 (each 5H, s, aromatic), 1.90, 1.85, and 1.70 (each 3H, s, CH_3CO), 1.45 (3H, d, *J*=7 Hz, lactyl CH_3). FD-MS: *m/z* 791 $(M+H)^+$, 813 $(M+Na)^+$. Found: C, 63.66; H, 6.34; N, 3.55%. Calcd for $C_{42}H_{50}N_2O_{13}$; C, 63.79; H, 6.37; N, 3.54%.

Benzyl 2-Benzyloxycarbonylamino-2-deoxy-α-D-glucopyranoside (15). To a suspension of 2-benzyloxycarbonylamino-2-deoxy-D-glucose[15] (120 g, 0.384 mol) in benzyl alcohol (900 ml) heated at 100 °C, a solution of dry HCl (29.9 g) in benzyl alcohol (180 ml) was added. The mixture was stirred at 100 °C till a homogeneous solution was obtained. After cooling, the mixture was poured into ether (1 l). The precipitate obtained on addition of hexane (2 l) was filtered and recrystallized form EtOH; 144 g (77%); mp 168—170 °C; $[\alpha]_D^{13}$ +123° (*c* 0.98, MeOH).[16]

Benzyl 2-Acetamido-2-deoxy-4,6-*O*-isopropylidene-α-D-glucopyranoside (16).[10] Compound **15** (20.0 g, 59.8 mmol) was hydrogenolyzed with Pd-black in a mixture of MeOH and THF (1:1, 400 ml). When the starting material disappeared as checked with TLC, the catalyst was filtered off, and acetic anhydride was (10.0 ml, 106 mmol) added to the filtrate. After 1 h at room temperature, the solvent was evaporated in vacuo. The residue was recrystallized from EtOH to give the acetamido derivative; 16.4 g (94%).

To a suspension of this product (10.0 g, 26.6 mmol) in dry acetone (150 ml), were added 2,2-dimethoxypropane (3.0 ml, 28 mmol) and *p*-toluenesulfonic acid monohydrate (0.25 g). The mixture was stirred at room temperature for 4 h and worked up as usual to give **16** as amorphous solid; 10.4 g (88% from **15**); $[\alpha]_D^{13}$ +98.3° (*c* 0.97, $CHCl_3$). ^{1}H NMR (60 MHz): 7.20 (5H, s, aromatic), 4.87 (1H, d, *J*=2.5 Hz, H-1), 1.67 and 1.47 (each 3H, s, isopropylidene CH_3).

Benzyl 2-Acetamido-3-*O*-[(*R*)-1-carboxyethyl]-2-deoxy-4,6-*O*-isopropylidene-α-D-glucopyranoside (17).[10] Sodium hydride (60% oil dispersion; 1.65 g, 68.4 mmol) was added to a solution of **16** (12.0 g, 34.2 mmol) in dry dioxane (700 ml). The mixture was heated to 60 °C and (*S*)-2-chloropropionic acid (8.00 g, 68.4 mmol) was added to it. Stirring was then continued at 60 °C for 1 h. After the excess NaH had been decomposed with ice, the solvent was evaporated in vacuo and the residue extracted with $CHCl_3$ after acidification. Usual work-up afforded a syrup which was dissolved in AcOEt and treated with an ethereal solution of CH_2N_2. Complete evaporation of the volatile materials (bath 50 °C at 5 mmHg) afforded a crystalline residue, which was once washed with a mixture of ether–hexane (5:1) and then hydrolyzed with KOH (2.0 g, 36 mmol) in MeOH (120 ml) at room temperature. Removal of the solvent after neutralization with Amberlite IRC-CG50 (H^+) afforded amorphous solid; 11.9 g (82%); $[\alpha]_D^{16}$ +127.3° (*c* 0.92, $CHCl_3$). ^{1}H NMR (90 MHz): 9.05 (1H, broad s, COOH),

7.95 (1H, d, J=2 Hz, NHAc), 7.28 (5H, s, aromatic), 5.35 (1H, d, J=2.5 Hz, H-1), 4.35 (1H, q, $CH_3\underline{C}H(O)$-COOH), 2.05 (3H, s, CH_3CO), 1.51 and 1.40 (each 3H, s, isopropylidene CH_3), 1.42 (3H, d, J=6.8 Hz, $\underline{C}H_3CH(O)$-COOH).

Allyl 2-Acetamido-3-*O*-acetyl-2-deoxy-β-D-glucopyranoside 6-*O*-Esterified with Benzyl 2-Acetamido-3-*O*-[(*R*)-1-carboxyethyl]-2-deoxy-4, 6-*O*-isopropylidene-α-D-glucopyranoside (18). Dicyclohexylcarbodiimide (3.80 g, 18.4 mmol) and 4-dimethylaminopyridine (0.02 g) were added to an ice-cooled solution of allyl 2-acetamido-3-*O*-acetyl-2-deoxy-β-D-glucopyranoside (**14**) (5.00 g 16.5 mmol) and **17** (7.70 g, 18.2 mmol) in a mixture of THF (20 ml) and dioxane (100 ml). After the mixture had been stirred at room temperature for 24 h, the product isolated by usual work-up and silica-gel column chromatography ($CHCl_3$–MeOH 30:1) was recrystallized from EtOAc–hexane; 10.0 g (86%); mp 107—111 °C; $[\alpha]_D^{16}$ +61.1° (c 1.11, $CHCl_3$). Found: C, 56.57; H, 6.99; N, 3.87%. Calcd for $C_{34}H_{48}N_2O_{14}\cdot 3/4H_2O$: C, 56.54; H, 6.91; N, 3.88%.

Allyl 2-Acetamido-3,4-di-*O*-acetyl-2-deoxy-β-D-glucopyranoside 6-*O*-Esterified with Benzyl 2-Acetamido-3-*O*-[(*R*)-1-carboxyethyl]-2-deoxy-4, 6-*O*-isopropylidene-α-D-glucopyranoside (19). Compound **18** (2.36 g, 3.33 mmol) was acetylated with acetic anhydride in pyridine. After usual work-up, the product was recrystallized from EtOAc–hexane; 1.89 g (76%); mp 168—170 °C; $[\alpha]_D^{16}$ +75.6° (c 0.93, $CHCl_3$). FD-MS: m/z 750 (M^+). Found: C, 57.55; H, 6.73; N, 3.70%. Calcd for $C_{36}H_{50}N_2O_{15}$: C, 57.59; H, 6.71 N, 3.73%.

Allyl 2-Acetamido-3,4-di-*O*-acetyl-2-deoxy-β-D-glucopyranoside 6-*O*-Esterified with Benzyl 2-Acetamido-6-*O*-acetyl-3-*O*-[(*R*)-1-carboxyethyl]-2-deoxy-α-D-glucopyranoside (21). Compound **19** (4.10 g, 5.47 mmol) was heated at 90 °C in 90% AcOH (100 ml) for 30 min. Evaporation of the solvent followed by co-evaporation with toluene in vacuo and trituration with ether afforded **20** as crystals, which were collected by filtration; 3.71 g (96%), mp 180—181 °C, $[\alpha]_D^{16}$ +58.4° (c 1.07, MeOH).

This compound (4.00 g, 5.6 mmol) was dissolved in pyridine (100 ml) and treated with acetic anhydride (2.3 ml, 23 mmol) under ice-cooling for 3 h. Usual work-up followed by purification with a silica-gel column ($CHCl_3$-MeOH, 30:1) gave an amorphous solid; 3.8 g (90%); $[\alpha]_D^{16}$ +98.4° (c 0.92, $CHCl_3$). Found: C, 55.52; H, 6.52; N, 3.67%. Calcd for $C_{35}H_{48}N_2O_{16}\cdot 1/4H_2O$: C, 55.51; H, 6.46; N, 3.70%.

1-Propenyl 2-Acetamido-3,4-di-*O*-acetyl-2-deoxy-β-D-glucopyranoside 6-*O*-Esterified with Benzyl 2-Acetamido-6-*O*-acetyl-3-*O*-[(*R*)-1-carboxyethyl]-2-deoxy-α-D-glucopyranoside (22). Compound **21** (2.00 g, 2.66 mmol) was heated under reflux with chlorotris(triphenylphosphine)rhodium(I) (200 mg) in anhyd benzene under Ar atmosphere for 16 h. After evaporation of the solvent in vacuo, the product was isolated by silica-gel column chromatography ($CHCl_3$–MeOH, 30:1) as pale yellow solid; 1.34 g (67%); $[\alpha]_D^{16}$ +9.06° (c 1.02, $CHCl_3$). ^{1}H NMR (90 MHz): 6.30—5.88 (1H, m, $OC\underline{H}$=$CHCH_3$), 1.53 (3H, dd, OCH=$CHC\underline{H}_3$).

3,4-Di-*O*-acetyl-2-amino-2-deoxy-1-α-*O*: 2-*N*,*N*-ethylidyne-D-glucopyranose 6-*O*-Esterified with Benzyl 2-Acetamido-6-*O*-acetyl-3-*O*-[(*R*)-1-carboxyethyl]-2-deoxy-α-D-glucopyranoside (23). After a solution of **22** (800 mg, 1.1 mmol) in anhyd CH_3CN (15 ml) had been stirred with powdered $CaSO_4$ (300 mg) at room temperature, $HgCl_2$ (450 mg, 1.7 mmol) and HgO (450 mg, 2.1 mmol) were added to it and the whole mixture was stirred at 60 °C under Ar atmosphere for 2 h. Usual work-up and column chromatographic purification on silica gel ($CHCl_3$–MeOH, 50:1) afforded colorless syrup; 313 mg (41%). ^{1}H NMR (100 MHz): 5.99 (1H, d, J=7.8 Hz, H-1 of oxazoline form). FD-MS: m/z 694 (M^+).

Benzyl 4-*O*-(2-Acetamido-3,4,6-tri-*O*-acetyl-β-D-glucopyranosyl)-2-acetamido-6-*O*-acetyl-2-deoxy-3-*O*-[(*R*)-1-(methoxycarbonyl)ethyl]-α-D-glucopyranoside (24). Compound **23** (225 mg, 0.32 mmol) was heated in dry CH_2ClCH_2Cl (4.5 ml) in the presence of p-toluenesulfonic acid (2 mg) at 50 °C for 16 h. The mixture was cooled and then treated with ethereal solution of CH_2N_2. The solvent was evaporated in vacuo and the residue was treated with 0.1 M† NaOMe (20 ml). After 3 h, the mixture was neutralized with Dowex 50×8 (H^+) and evaporated in vacuo. The residue was dried by co-evaporation with benzene and then acetylated with acetic anhydride (0.4 ml) and pyridine (5 ml). The product obtained by usual work-up followed by silica-gel column chromatography ($CHCl_3$–MeOH, 50:1) was recrystallized from EtOAc–ether; 47.9 mg (20%); mp 192—194 °C; $[\alpha]_D^{11}$ +102° (c 1.04, $CHCl_3$). FD-MS: m/z 768 (M^+). Found: C, 54.63; H, 6.32; N, 3.68%. Calcd for $C_{35}H_{48}N_2O_{17}$: C, 54.68; H, 6.29; N, 3.64%.

References

1) S. Kusumoto, K. Yamamoto, M. Imoto, M. Inage, M. Tsujimoto, S. Kotani, and T. Shiba, *Bull. Chem. Soc. Jpn.*, the preceding paper.

2) In our preceding synthesis,[1] the disaccharides of muramic acid and glucosamine were prepared via a glucosamine disaccharide by converting one of its sugar moieties into muramic acid. However, application of the same approach to a larger glycan seems to be not practical because complete and regio-controlled introduction of a desired number of 1-carboxyethyl ethers to a glucosamine oligosaccharide seems to be difficult.

3) The chloride (**1**) was prepared by treating *N*-acetylmuramic acid methyl ester with acetyl chloride, while the bromides were prepared by action of HBr in CH_2Cl_2 on the corresponding 1-*O*-acetates. Those of dichloroacetyl and intramolecular amide types were derived via removal of the *N*-acetyl group with $Et_3O\cdot BF_4$. *N*-Acetylmuramic acid itself was prepared according to Flowers and Jeanloz with slight modification as described for the preparation of **17**; *J. Org. Chem.*, **28**, 2983 (1963).

4) The glucosamine components were recovered unchanged. In case of **4**, the decomposition product could not be identified.

5) p-Toluenesulfonic acid, trifluoromethanesulfonic acid or $FeCl_3$ was used in CH_2ClCH_2Cl at 80 °C.

6) The same reason might also apply to the halogenides (**1**—**4**) described above.

7) For further confirmation of the structure, **11** was coupled with benzyl L-alanyl-D-isoglutaminate after alkaline hydrolysis. Hydrogenolytic deprotection of the coupling product afforded *O*-(*N*-acetyl-β-muramyl-L-alanyl-D-isoglutamine)-(1→4)-*N*-acetyl-D-glucosamine which was iden-

† 1M=1 mol dm^{-3}.

tical with the compound obtained in our previous work.[1)]

8) a) I. Ugi, *Angew. Chem.*, **74**, 9 (1962); b) H. v. Zychlinsky, I. Ugi, and D. Marquarding, *Angew. Chem.*, **86**, 517 (1974).

9) D. S Kemp, *Biopolymers*, **20**, 1793 (1981) and references cited in it.

10) A. Hasegawa, Y. Kaneda, M. Amano, M. Kiso, and I. Azuma, *Agric. Biol. Chem.*, **42**, 2187 (1978).

11) P. A. Gent and R. Gigg, *J. Chem. Soc., Perkin Trans. 1*, **1973**, 1858.

12) M . A. Nashed, C. W. Slife, M. Kiso, and L. Anderson, *Carbohydr. Res.*, **82**, 237 (1980).

13) When the condensation product was subjected directly to preparative silica gel TLC, a considerable cleavage of the inter-sugar ester linkage occurred to give a mixture.

14) A part of the preliminary result was already presented at the National Meeting of the Chemical Society of Japan, Kyoto 1983, Proceeding Vol. 2, p. 1151.

15) K. Heins, K. Propp, R. Harrison, and H. Paulsen, *Chem. Ber.*, **100**, 2655 (1967).

16) Though a small amount of the β-anomer was detected on TLC, this product was used for the following reaction.

Studies of Liquid Water by Computer Simulations. IV. Transport Properties of a 2-D Model

Yosuke KATAOKA
Department of Chemistry, Faculty of Science, Kyoto University, Kyoto 606
(Received September 5, 1985)

The constant-temperature constant-pressure molecular dynamics simulations of a water-like system are performed at many temperatures and pressures. A 2-dimensional model of water is used for the system with 576 molecules in a square cell. Thermodynamical quantities are anomalous as in liquid water. The temperature-dependences of the calculated self-diffusion coefficient and the shear viscosity are in agreement with the observed values at low pressures. The effects of compression on these transport coefficients are reproduced qualitatively. The bulk viscosity obtained is larger than the shear viscosity. The order of magnitude of the calculated thermal conductivity is in agreement with the experimental results. The contribution of the rotational motion to the thermal conductivity is calculated in order to discuss the anomalous temperature-dependence of this coefficient.

The behavior of the shear viscosity[1-6] and the self-diffusion coefficient[7-11] of liquid water at temperatures below about 300 K is unique. The initial application of pressure causes the viscosity to decrease, and the diffusion coefficient to increase. The Stokes-Einstein equation is valid even in supercooled water.[4-5] Although there are some molecular dynamics(MD) calculations of the self-diffusion coefficient,[12-14] it seems that a systematic study has not yet been performed on the viscosity nor on the thermal conductivity. The thermal conductivity of liquid water has a maximum as a function of temperature under constant pressure.[2,15,16] The thermal conductivity has considerable technical importance, but our understanding of the molecular behavior underlying the phenomenon is poorly developed.[2] Only a couple of phenomenological theories has been published concerning the anomaly of the thermal conductivity.[17,18] For this reason, we are planning to perform MD simulations at many temperatures and pressures to obtain the transport coefficients of liquid water.

Since the calculation of the transport coefficients is not easy,[19-22] we use the 2-D model of water,[23] as the first step. Despite theoretical predictions that transport coefficients in 2-D system diverge, a computer simulation of the small system can be used to study the transport properties.[24-27]

In the first paper of this series,[23] it was shown that a simple 2-D model of water can reproduce the main features of the thermodynamical behavior observed in real water. In the previous article,[28] dynamical properties of the 2-D water were studied by microcanonical MD simulation. The dipole direction relaxation time and the self-diffusion coefficient were calculated as functions of temperature and density. The effects of compression on these quantities are in good agreement with the experimental data.[28]

We use constant temperature and constant pressure MD(T-P-MD), because this method is more convenient to obtain the temperature dependence or pressure dependence of the system. Many methods are developed for the constant temperature MD.[29-34] Among them, Nosé's method[34] is used because this can conveniently be combined with Andersen's constant pressure MD.[31] By T-P-MD, the isothermal compressibility, the thermal expansion coefficient and the heat capacity at constant pressure are calculated from the fluctuations of the relevant quantities. Transport coefficients are calculated using the standard Kubo formula.[36]

As we have no experimental results on any 2-D water-like liquid, the absolute values obtained will be compared with those of the real water, where we shall use reduced units.[23] In the qualitative comparison of the temperature and pressure dependences, arbitrary scales will be used as follows.

The zero point of the thermal expansion coefficient and its maximum near the critical temperature are used to fix the temperature scale tentatively for the comparison of the calculated results with those of real water. By such a comparison, it is shown that the calculated transport coefficients are in agreement with those of real water. Although the maximum of the thermal conductivity as a function of temperature is not obtained, it is found that the contribution of the rotational motion to this coefficient has a maximum.

Molecular Dynamics Method

The 2-D model of water has been described in the first paper of this series.[23] The micro canonical molecular dynamics calculation was performed previously.[28] Therefore only the new aspects are described here.

The mass M of the molecule is 18 in units of atomic weight and the moment of inertia I is 3.34×10^{-44} gm^2. We use the following reduced units.[28] The energy E is measured in units of ε_0=24.68 kJ mol^{-1}($-\varepsilon_0$ is the absolute minimum of the

pair potential energy), the temperature in units of ε_0/k_B (k_B is the Boltzmann constant), the length in units of R_0=0.276 nm. The unit of time is

$$t_0 = (MR_0^2/\varepsilon_0)^{1/2} = 2.37\times 10^{-13}\ \text{s}. \quad (1)$$

The system consists of 576 molecules in a square unit cell with the periodic boundary condition. The dynamical equations are integrated with time increment

$$\Delta t = 0.435\times 10^{-15}\ \text{s} = 0.00184\, t_0 \quad (2)$$

by the predictor-corrector method.[37,38]

The constant temperature MD method of Nośe[34] is used in this paper. According to Nośe,[34] an additional degree of freedom s is introduced which acts as an external system on the system of N molecules. A constant Q appears in the kinetic energy part as $p_s^2/2Q$ in the total Hamiltonian, where p_s is the conjugate momentum of s. After some trial and error calculations, we have decided somewhat arbitrarily to choose 636 $\varepsilon_0 t_0^2$ for Q. The constant pressure MD method of Andersen is combined. In this method, the area A of the N molecular system is a variable. A constant W is introduced in the kinetic term as $p_A^2/2W$ where p_A is the conjugate momentum of A. We chose 1.92×10^{-3} $\varepsilon_0 t_0^2$ as the value of W after some preliminary simulations.

The total energy is conserved within 0.02% after 60000 steps, or 26 ps. In our standard run, 60000 steps are spent for the aging of the system. After this interval, the 60000-step run is performed at least twice, where the molecular dynamics statistical averages are obtained.

The shear viscosity, the bulk viscosity and the thermal conductivity are calculated by the standard Kubo type formula.[19,36] Averages of at least 6000 values are taken for the initial time in the standard 60000-step run. Some long runs are needed at low temperatures because of the long tail of the correlation function for the shear viscosity. In such cases, the MD run is as long as 120000 steps. The representative range of the time integration of the correlation function for the shear viscosity is $0\leq t\leq 3.6$ ps at T=0.194 ε_0/k_B, P=0.186 ε_0/R_0^2.

Thermodynamical Properties

The thermodynamic coefficients such as the thermal expansion coefficient, the isothermal compressibility and the heat capacity at constant pressure are easy to calculate because of the constant temperature and constant pressure MD method used in this paper. First the calculated thermodynamical quantities are compared with the experimental results. The temperature scale for the comparison is shown in this section. It will be used also in the comparison of the transport coefficients in the next section.

The thermal expansion coefficient at constant pressure, α, is calculated from the cross fluctuation of area A and enthapy H[35] (circle in Fig. 1)

$$\alpha = \frac{\langle AH\rangle - \langle A\rangle\langle H\rangle}{k_B T^2 \langle A\rangle}, \quad (3)$$

and also from the numerical differentiation of the area A of the N-molecule system (triangle in Fig. 1). The pressure P=0.186 ε_0/R_0^2 in Fig. 1 is the representative low pressure in 2-D water.[23] The results by these methods are in good agreement with the experimental values[1,2,39,40] if we use the temperature scale shown in Fig. 1. (The temperature scale for real water is shown in the upper part. The zero point and the scale of temperature for the real water are different from those for 2-D water. For this reason, the comparisons of the temperature dependences are only qualitative in the following figures.) In this figure, the experimental results are shown by the dotted line (normal pressure) and the dash-dotted line (P=100 MPa). As for the absolute value of the calculated expansion coefficient, the comparison is satisfactory at moderate temperatures. The coefficient obtained around the critical temperature T_c is small compared with the experimental results. This may result from the small number of molecules in the basic cell (N=576). The critical temperature of our 2-D water is about 0.263 ε_0/k_B and the critical pressure P_c is about 0.17 ε_0/R_0^2 which were estimated by the equation of state.[23]

The isothermal compressibility κ_T is calculated from the fluctuation[35] as shown below (triangle in

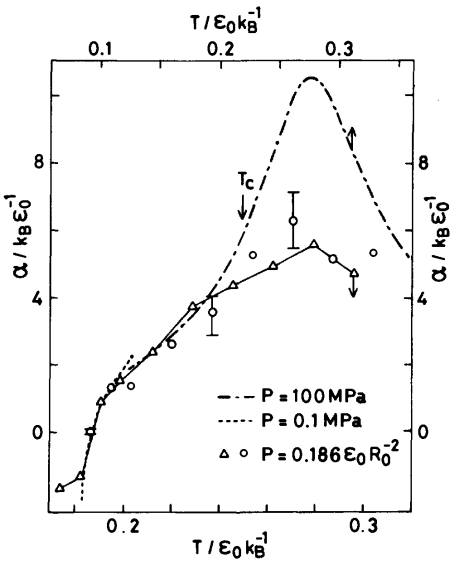

Fig. 1. Plot of the thermal expansion coefficient α vs. temperature T, at P=0.186 ε_0/R_0^2, ○ from the fluctuation, △ from the differentiation of the area. The dotted and the dash-dotted lines show the experimental results.[1,2,39,40]

Fig. 2):

$$\kappa_T = \frac{\langle A^2\rangle - \langle A\rangle^2}{k_B T \langle A\rangle}, \tag{4}$$

and by means of the radial distribution function $g(R)$[35] (circle in Fig. 2)

$$\kappa_T = \frac{\langle A\rangle}{k_B T N} + \frac{1}{k_B T}\int_0^\infty [g(R)-1]2\pi R dR. \tag{5}$$

The results are in agreement with the experimental ones.[1,2,40,41] We can see that the calculated compressibility has a reasonable value at moderate temperatures, and that the anomalies at low temperatures and at high temperatures are reproduced at least qualitatively.

The calculated heat capacity at constant pressure, C_p, is shown in Fig. 3, where the circles are the values

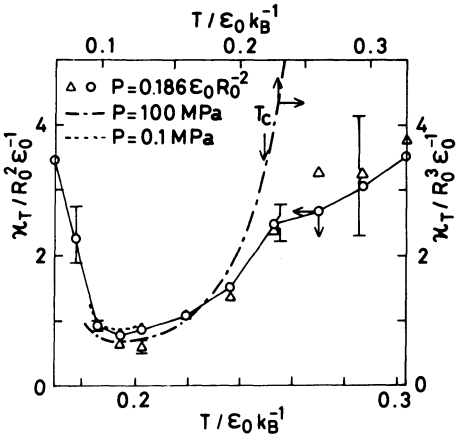

Fig. 2. Plot of the isothermal compressibility κ_T vs. temperature T, at $P=0.186\ \varepsilon_0/R_0^2$, △ from the fluctuation, ○ from the radial distribution function. The dotted and the dash-dotted lines show the experimental results.[1,2,40,41]

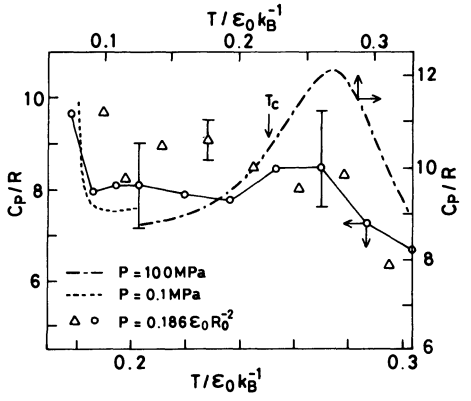

Fig. 3. Plot of the heat capacity at constant pressure C_p vs. temperature T, at $P=0.186\ \varepsilon_0/R_0^2$, ○ from the fluctuation, △ from the differentiation of H. The dotted and the dash-dotted lines show the experimental results.[1,2,40,42]

obtained from the fluctuation of the enthalpy H

$$C_p = \frac{\langle H^2\rangle - \langle H\rangle^2}{k_B T^2}, \tag{6}$$

and the triangles mean the result of the numerical differentiation of the enthalpy with respect to temperature. Unfortunately the calculated results scatter. We see however that the absolute values are in agreement with the experimental results. The temperature dependence is not inconsistent with that of the experimental values.[1,2,40,42]

Transport Coefficients

In this section, the calculated transport coefficients are compared with the experimental results and the time correlation functions are discussed.

The self-diffusion coefficient D is calculated from the mean square displacement $\langle \Delta r^2\rangle$ and from the velocity auto-correlation function.[38]

$$D = \lim_{t\to\infty} \frac{\langle \Delta r^2\rangle}{4t}, \tag{7}$$

$$D = \frac{1}{2}\int_0^\infty \langle v(t)\cdot v(0)\rangle dt. \tag{8}$$

The calculated coefficient D is plotted against pressure in Fig. 4 for several temperatures. The experimental results are shown by the dotted lines.[7-11] The anomaly of the self-diffusion coefficient is qualitatively reproduced as shown in Fig. 4 if we tentatively use the pressure scale for comparison with real water. The pressure scales and zero points are arbitrary for the purpose of qualitative comparison in Figs. 4 and 7.

The shear viscosity η and the bulk viscosity η_B are calculated from the relevant time correlation functions:[19,36]

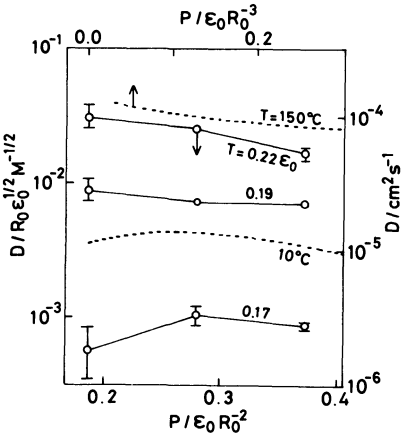

Fig. 4. Plot of the self-diffusion coefficient D vs. pressure P. Values of the temperature are indicated next to each curve.
The dotted lines are the experimental results.[7-11]

$$\eta = \frac{1}{k_B T\langle A\rangle}\int_0^\infty \langle J^{xy}(t)\cdot J^{xy}(0)\rangle \mathrm{d}t, \tag{9}$$

$$\eta_B = \frac{1}{4k_B T\langle A\rangle} \times \sum_{\alpha,\beta=x,y}\int_0^\infty \langle [J^{\alpha\alpha}(t)-\langle J^{\alpha\alpha}\rangle]\cdot[J^{\beta\beta}(0)-\langle J^{\beta\beta}\rangle]\mathrm{d}t, \tag{10}$$

$$J^{\alpha\beta} \equiv M\sum_i v_{i\alpha}v_{i\beta} + \sum_i r_{i\alpha}f_{i\beta}, \tag{11}$$

where M is the mass of the molecule and $v_{i\alpha}$ the α component of the velocity of i-th molecule. And r_i means the position of the i-th molecule and f_i is the force that the i-th molecule feels.

The viscosities obtained are shown in Fig. 5, where the results by several MD methods are compared. In this figure each circle (shear viscosity) and triangle (bulk vicosity) means the value obtained from each 60000-step run. The bar shows the average. Although the calculated values scatter, the shear viscosity can be obtained by the constant temperature and constant pressure MD (T-P-MD) as shown in this figure. Contrary to this, the orders of magnitude of the bulk viscosity by P-MD and T-P-MD were different from that of bulk viscosity by the micro canonical MD. This may arise from the fact that the bulk viscosity is related to the fluctuation of pressure P (see Eq. 10) and the area A is controlled in P-MD so the time dependence of P is artificial in this special MD.

Figure 5 shows that the bulk viscosity η_B is larger than the shear viscosity (at T=0.194 ε_0/k_B, P=0.186 ε_0/R_0^2):

$$\frac{\eta_B}{\eta} = 1.4 \tag{12}$$

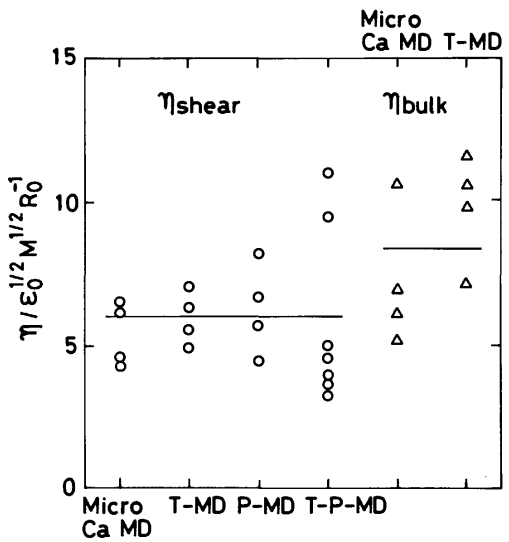

Fig. 5. Shear viscosity (○) and bulk viscosity (△) by several MD methods at T=0.194 ε_0/k_B, P=0.186 ε_0/R_0^2.

in accordance with the experimental results.[2,43] This feature is confirmed at another state (T=0.186 ε_0/k_B, P=0.216 ε_0/R_0^2), where the value of the ratio is also η_B/η=1.4.

The temperature dependence of the shear viscosity η at P=0.186 ε_0/R_0^2 is shown in Fig. 6, where the temperature scale is the same as that in Fig. 1. We see that the shear viscosity in the reduced units has a reasonable value as a function of temperature in Fig. 6. The calculated shear viscosity η is plotted against pressure P at several temperatures in Fig. 7. The experimental results are shown in the dotted lines.[1,6] The main anomalous feature in the shear viscosity of liquid water is seen in Fig. 7.

The shear viscosity η and the self-diffusion co-

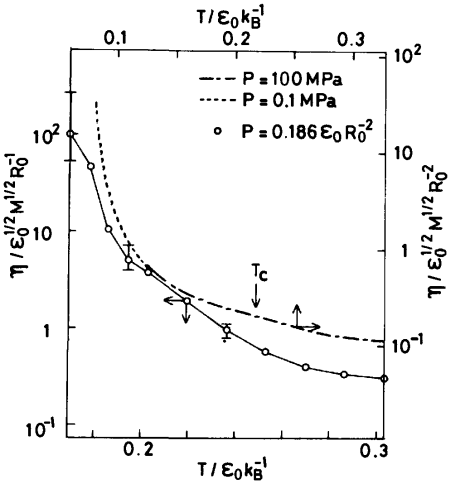

Fig. 6. Plot of the shear viscosity η vs. temperature T, at P=0.186 ε_0/R_0^2.
The dotted and the dash-dotted lines show the experimental results.[1-6]

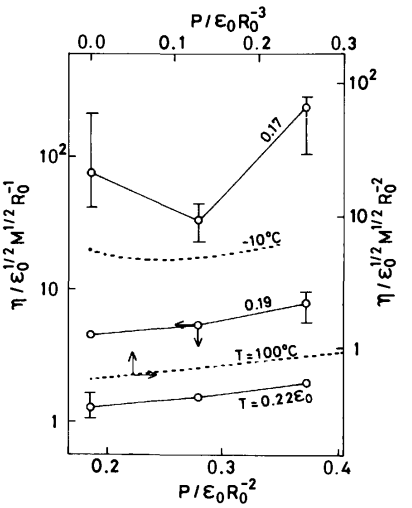

Fig. 7. Plot of the shear viscosity η vs. pressure P. Values of the temperature are indicated next to each curve.
The dotted lines are the experimental results.[1-6]

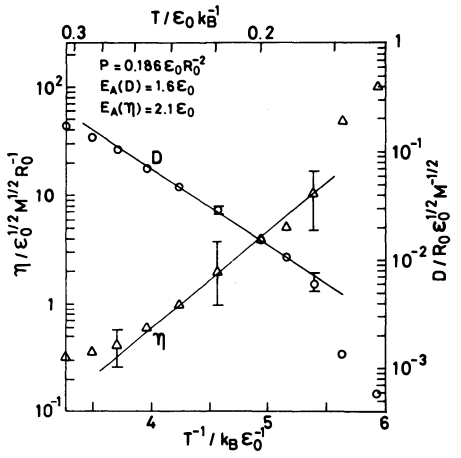

Fig. 8. Shear viscosity η and self-diffusion coefficient D vs. $1/T$ at $P=0.186\ \varepsilon_0/R_0^2$.

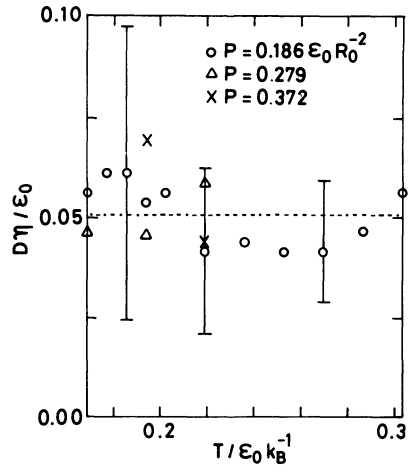

Fig. 9. Plot of the product ηD vs. T.

efficent D are plotted against $1/T$ in Fig. 8. As shown in this figture these quantities have about the same activation energy, so the product of these ηD is almost constant as a function of temperature as shown Fig. 9.

The thermal conductivity λ is calculated by the correlation function of the heat current $\boldsymbol{S}$(t):

$$\lambda = \frac{1}{2k_B T^2 \langle A \rangle} \int_0^\infty \langle \boldsymbol{S}(t) \cdot \boldsymbol{S}(0) \rangle \mathrm{d}t, \tag{13}$$

$$\boldsymbol{S}(t) \equiv \frac{\mathrm{d}}{\mathrm{d}t} \sum_i H_i \mathbf{r}_i, \tag{14}$$

were H_i is the contribution of the i-th molecule to the total Hamiltonian of the system $\mathscr{H}$:

$$\mathscr{H} = \sum_i H_i. \tag{15}$$

The calculated thermal conductivity λ is shown in Fig. 10 (open circle). The dotted line corresponds to the observed value at normal pressure.[2,15,16] The dash-dotted line means the experimental conductivity

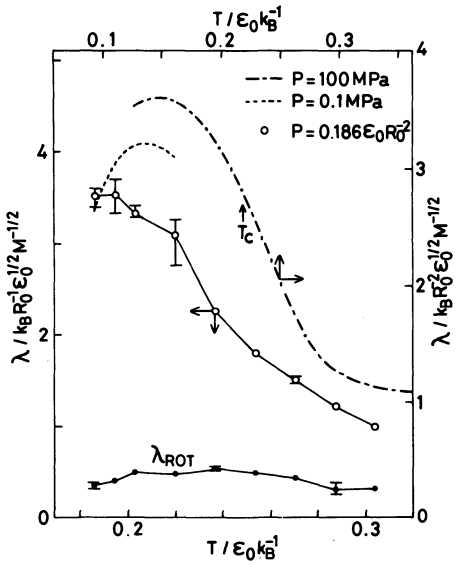

Fig. 10. Plot of the thermal conductivity λ vs. temperature T at $P=0.186\ \varepsilon_0/R_0^2$ (○).
The contribution from the rotational motion is also shown (●). The dotted and the dash-dotted lines show the experimental results.[2,15,16,44]

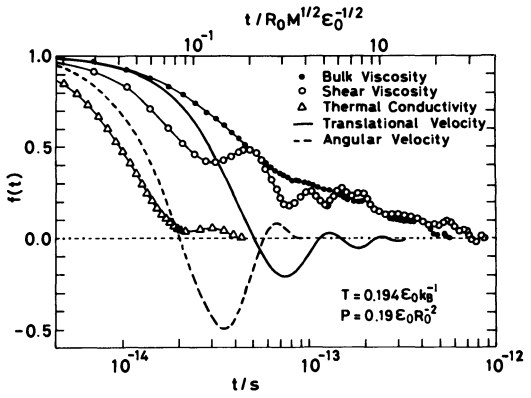

Fig. 11. The normalized correlation functions for the transport coefficients f(t) vs. time t, at $T=0.194\ \varepsilon_0/k_B$, $P=0.186\ \varepsilon_0/R_0^2$.

under pressure (P=100 MPa)[44] in this figure.

The order of magnitude of the calculated thermal conductivity is in agreement with those of the experimental results if we use the reduced quantities. The conductivity obtained has a tendency to saturate when the temperature is decreased. However, the maximum is not seen in the calculated temperature dependence of the conductivity. The contribution of the rotational motion is also shown in this figure (closed circle). This part has a maximum as a function of temperature. This contribution comes from the differentiation of the molecular Hamiltonian H_i with respect to the angle of the molecule φ:

$$\frac{\mathrm{d}H_i}{\mathrm{d}t} = \sum_j \left[\frac{\partial H_i}{\partial x_j}\dot{x}_j + \frac{\partial H_i}{\partial y_j}\dot{y}_j + \frac{\partial H_i}{\partial \varphi_j}\dot{\varphi}_j \right]. \tag{16}$$

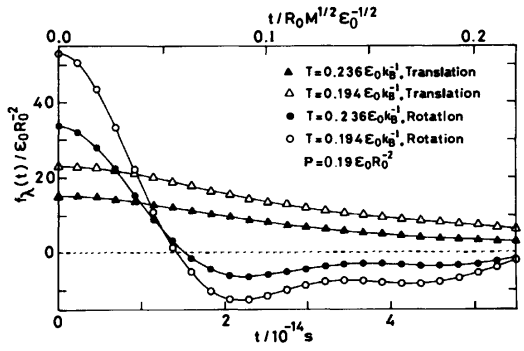

Fig. 12. The unnormalized correlation functions for the thermal conductivity $f_\lambda(t)$ vs. time t, at $P=0.186$ ε_0/R_0^2.

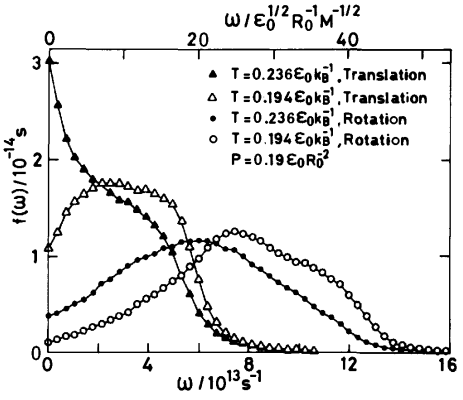

Fig. 13. The Fourier transforms of the correlation functions of velocity at $P=0.186$ ε_0/R_0^2.

We expect such a contribution is more important in real water than in 2-D water which has only one rotational degree of freedom.

The normalized correlation functions are shown in Fig. 11 in order to see the microscopic aspects of the transport coefficients (cf Ref. 19). The long tails are seen in the correlation functions for the shear viscosity (open circle) and bulk viscosity (closed circle). In contrast to these, the correlation function for the thermal conductivity has a short tail at this state ($T=0.194$ ε_0/k_B, $P=0.186$ ε_0/R_0^2). Its correlation time is about the same with as that of the correlation function of the rotational velocity.

The non-normalized correlation functions for the thermal conducvity $f_\lambda(t)$, defined as

$$\lambda = \int_0^\infty f_\lambda(t)\mathrm{d}t \tag{17}$$

are plotted in Fig. 12. In this figure, the contribution from the translational motion and that from the rotational one are compared and their temperature dependences are also compared. From this figure we can see the cancellation in the rotational part in the integration of the correlation function. This cancellation is more complete at $T=0.194$ ε_0/k_B than at $T=0.236$ ε_0/k_B. This is the reason for the increase of the rotational contribution when the temperature is increased from $T=0.194$ ε_0/k_B to $T=0.236$ ε_0/k_B. Such cancellation is due to the oscillatory feature of the rotational motion at these temperatures a shon in Fig. 13. In this figure, the auto-correlation functions of the velocity are compared. The oscillatory motion converts to diffusive motion in the translational motion when the temperature is raised from 0.194 ε_0/k_B to 0.236 ε_0/k_B. However, the oscillatory character persists in the rotational motion.

We summarize the above discussion as follows: The contribution from the rotational motion is important in order to understand the origin of the anomalous temperature dependence of the thermal conductivity of liquid water. This conclusion is different from the result of the previous theory,[18] where the anomaly is attributed to the translational motion of the cavity molecule. The estimated relaxation time of the cavity molecule[18] seems too long compared with the result of the MD calculation.[28] We plan to perform more MD calculations using a more realistic model for water.

Finally, we mention the effect of low dimensionality on the dynamical properties. It is difficult to see the long time tail in the velocity autocorrelation function in our system because of the oscillatoty behaviour (see Fig. 11). The values obtained for the transport coefficients are finite. This may come from the small number of molecules in the system and also from the short time range examined.

The author would like to thank Dr. Shuichi Nosé for letting us know his work on the constant temperature MD method prior to publication. The computation was done at the Computer Center of the Institute for Molecular Science and at the Kyoto University Data Procesing Center. The present work was partially supported by a Grand-in-Aid for Scientific Research No. 60129031 from the Ministry of Education, Science and Culture and by the Kyoto University Data Processing Center.

References

1) D. Eisenberg and W. Kauzmann, "The Structure and Properties of Water," Oxford U. P., New York (1969).

2) G. S. Kell, "Water, a Comprehensive Treatise," ed by F. Franks, Plenum, New York (1972), Vol. 1, p. 363.

3) K. E. Bett and J. B. Cappi, *Nature* **207**, 620 (1965).

4) E. M. Stanley and R. C. Batten, *J. Phys. Chem.*, **73**, 1187 (1969) and the references cited herein.

5) T. DeFries and J. Jonas, *J. Chem. Phys.*, **66**, 896 (1977); *ibid.* **66**, 5393 (1977).

6) J. Kestin, H. E. Khalifa, H. Sookiazian, and W. A. Wakeham, *Ber. Bunsenges. Phys. Chem.*, **82**, 180 (1978).

7) L. A. Woolf, *J Chem Soc., Faraday Trans., 1*, **71**, 784 (1975).
8) L. A. Woolf, *J. Chem Soc., Faraday Trans., 1*, **72**, 1267 (1976).
9) D. J. Wilbur, T. DeFries, and J. Jonas, *J. Chem. Phys.*, **65**, 1783 (1976).
10) K. Krynicki, C. D. Green, and D. W. Sawyer. *Faraday Discuss. Chem. Soc.*, **66**, 199 (1978).
11) K. R. Harris and L. A. Woolf, *J. Chem. Soc., Faraday Trans., 1*, **76**, 377 (1980).
12) F. H. Stillinger and A. Rahman, *J. Chem. Phys.*, **61** 4973 (1974).
13) R. W. Impey, M. L. Klein, and I. R. McDonald, *J. Chem. Phys.*, **74**, 647 (1981).
14) G. Jancsó, P. Bopp, and K. Heinzinger. *Chem. Phys.*, **85**, 377 (1984).
15) E. McLaughlin, *Chem. Eng.*, **64**, 389 (1964).
16) "Water and Steam, Their Properties and Current Industrial Applications," Proc. 9th Intern. Conf. on Prop. of Steam, held at München, 1979, ed by J. Straub and K. Scheffler, Pergamon, Oxford (1980).
17) M. Eigen, *Z. Elektrochemie*, **56**, 176 (1952).
18) I. S. Andrianova, O. Ya. Samoilov, and I. Z. Fisher, *J. Struct. Chem.*, **8**, 736 (1967).
19) D. Levesque, L. Verlet, and J. Kurkijarvi, *Phys. Rev.*, **A7**, 1690 (1973).
20) W. T. Ashurst and W. G. Hoover, *Phys Rev.*, **A11** 658 (1975); J. Vermesse and D. Levesque, *Phys. Rev.*, **A19**, 1801 (1979); W. G. Hoover, D. J. Evans, R. B. Hickman, A. J. C. Ladd, W. T. Ashurst, and B. Moran, *Phys. Rev.*, **A22**, 1690 (1980).
21) D. M. Heyes, *J. Chem. Soc., Faraday Trans., 2*, **79**, 1741 (1983).
22) G. Marechal and J.-P. Ryckaert, *Chem. Phys. Lett.*, **101**, 548 (1983).
23) K. Okazaki, S. Nosé, Y. Kataoka, and T. Yamamoto, *J. Chem. Phys.*, **75**, 5864 (1981).
24) W. G. Hoover, W. T. Ashurst, and R. J. Olness, *J. Chem. Phys.*, **60**, 4043 (1974).
25) D. J. Evans, *Phys. Rev.*, **A22**, 290 (1980).
26) T. E. Wainwright, B. J. Alder, and D. M. Gass, *Phys. Rev.*, **A4**, 233 (1971).
27) S. Toxvaerd, *Mol. Phys.*, **29**, 373 (1975).
28) Y. Kataoka, *Bull. Chem. Soc. Jpn.*, **57**, 1522 (1984).
29) L. V. Woodcock, *Chem. Phys. Lett.*, **10**, 257 (1971).
30) Y. Hiwatari, E. Stoll, and T. Schneider, *J. Chem. Phys.*, **68** 3401 (1978).
31) H. C. Andersen, *J. Chem. Phys.* **72**, 2384 (1980).
32) W. G. Hoover, A. J. C. Ladd, and B. Moran, *Phys. Rev. Lett.*, **48**, 1818 (1982); D. J. Evans, *J. Chem. Phys.*, **78**, 3297 (1983).
33) H. Tanaka, K. Nakanishi, and N. Watanabe, *J. Chem. Phys.*, **78**, 2626 (1983).
34) S. Nosé *Mol. Phys.*, **52**, 255 (1984); *J. Chem. Phys.*, **81**, 511 (1984).
35) See e.g. A. Ben-Naim, "Water and Aqueous Solutions," Plenum, New York (1974).
36) R. Zwanzig, *Ann. Rev. Phys. Chem.*, **16**, 67 (1965); R. Kubo, in Ref. 16, p. 303.
37) C. W. Gear, "Numerical Initial Value Problems in Ordinary Differential Equations," Prentice-Hall, Princeton (1971).
38) J. Kushick and B. J. Berne, "Statistical Mechanics, Part B: Time-Dependent Processes," ed by B. J. Berne, Plenum, New York (1967), p. 41.
39) H. Kanno and C. A. Angell, *J. Chem. Phys.*, **73**, 1940 (1980).
40) J. Kestin, J. V, Sengers. B. Kamgar-Parsi, and J. M. H. Levelt Sengers, *J. Phy. Chem. Ref. Data*, **13**, 175 (1984).
41) H. Kanno and C. A. Angell, *J. Chem. Phys.*, **70**, 4008 (1979).
42) C. A. Angell, M Oguni, and W. J. Sinchina, *J. Phys. Chem.*, **86**, 998 (1982); M. Oguni and C. A. Angell, *J. Chem. Phys.*, **73**, 1948 (1980); *ibid.*, **78**, 7334 (1983).
43) J. Rouch, C. C. Lai, and S.-H. Chen, *J. Chem. Phys.*, **65**, 4016, (1977); *ibid.*, **66**, 5031 (1977); J. Teixeira and J. Leblond, *J. de Phys.* **39**, L83 (1978).
44) J. Yata, T. Minamiyama, T. Kim, N. Yokogawa, and H. Murai, in Ref. 16, p. 431.

Formation of New Paramagnetic Complexes between Quinones and Their Semiquinone Anions in the Presence of a Cryptand or a Crown Ether

Kosaku SUGA,* Tsuyoshi TAKIGUCHI,† and Shigeru AOYAGUI
Department of Chemical Engineering, Tokyo Institute of Technology,
Ohokayama, Meguro-ku, Tokyo 152
(Received November 5, 1985)

The formation of new paramagnetic complexes is evidenced by the ESR spectra of anion radicals of duroquinone, *p*-benzoquinone, and 2,5-di-*t*-butyl-*p*-benzoquinone in tetrahydrofuran, which are recorded in the presence of their parent molecules and cryptand 222 or 18-crown-6. The numerical values for the equilibrium constant, standard enthalpy and standard entropy of the complex formation are also determined.

There are several reports about the formation of dimer cations between polyaromatic hydrocarbons and their cation radicals.[1,2] However, the formation of such dimer anions have scarcely been reported. In this paper, we report the formation of new paramagnetic complexes between several derivatives of *p*-benzoquinone and their semiquinone anions in the presence of a cryptand or a crown-ether in tetrahydrofuran at low temperature.

Experimental

p-Benzoquinone (BQ) was purified by sublimation. Other reagents; commercial duroquinone (DQ), 2,5-di-*t*-butyl-*p*-benzoquinone (DBQ), cryptand 222 (CRP) and 18-crown-6(CW) were used without further purification. The solvent, tetrahydrofuran (THF) was purified as described previously.[3] The method of deuteration followed the literature.[4] Semiquinone anion radicals (Q^-) were prepared in vacuo by reducing their parent molecules (Q) with anthracene anion radical, which was prepared by sodium or potassium reduction of anthracene. The respective test solutions used contained 0.5—1 mM (1 M=1 mol dm^{-3}) of Q^- ion-paired with an equivalent amount of Na^+ or K^+. When required, known amounts of Q, CRP, and CW were added. Simulated ESR spectra were calculated with a NEC PC-9801F2 personal computer.

Results and Discussion

The ESR spectra of Na^+DQ^- and K^+DQ^- recorded at −50 °C could be analyzed in terms of two sets of six equivalent hydrogens and one alkali metal atom, whose hyperfine splitting (hfs) constants (a) agree with the literature values.[5] An addition of DQ to these solutions caused electron-exchange broadening, but no new signals.

Figure 1 (a) shows an ESR spectrum of K^+DQ^- at −50 °C in the presence of CRP. Na^+DQ^- gave a similar spectrum under the same experimental conditions. These spectra, having no metal hfs, could be analyzed in terms of twelve equivalent hydrogens with a=1.9 G. This finding suggests that DQ^- should exist in the form of a free ion or an ion

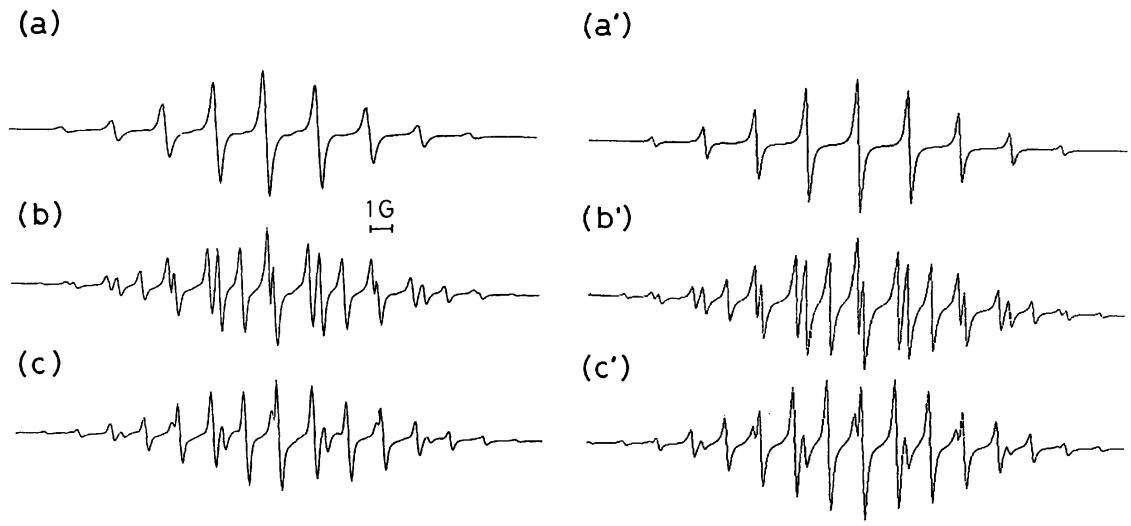

Fig. 1. ESR spectra of K^+DQ^- in THF containing 3.3 mM cryptand and (a) 0, (b) 6.4, (c) 12.8 mM DQ at −50 °C, and the corresponding computer simulated spectra; (a')—(c').

† Present address: Department of Electronic Chemistry, Graduate School at Nagatuta, Tokyo Institute of Technology, Nagatuta, Midori-ku, Yokohama 227.

pair whose cation is migrating rapidly between two oxygen sites.

Figure 1 (b) and (c) show that an increasing addition of DQ to the test solution gives rise to a new signal of increasing intensity, and the original signals of decreasing intensity. The new signal decreased in intensity with raising temperature, and became unobservable at 25 °C. This spectral change with temperature was reversible.

Figure 2 (a)—(c) show that a similar ESR pattern can be found for Na^+BQ^-, except that the hf structure is due to four equivalent hydrogens of a=2.38 G.

The ESR spectra of Na^+DBQ^- recorded at room temperature in the presence and absence of CRP exhibited hf structures due to two equivalent hydrogens and two nonequivalent hydrogens, respectively. The a value for the former hydrogens was 2.38 G, and the values for the latter agreed with the literature values.[6]

According to Fig. 3 (a)—(c), the effect of DBQ addition to the solution containing Na^+DBQ^- and CRP is the same as in Fig. 1 (a)—(c) and Fig. 2 (a)—

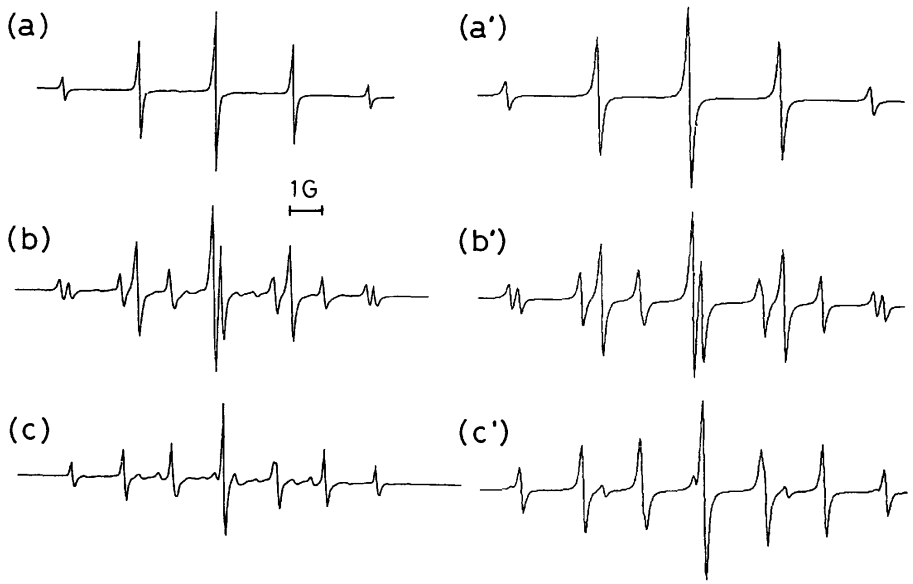

Fig. 2. ESR spectra of Na^+BQ^- in THF containing 3.1 mM cryptand and (a) 0, (b) 1.97 and (c) 4.12 mM BQ at −75 °C, and the corresponding computer simulated spectra; (a')—(c').

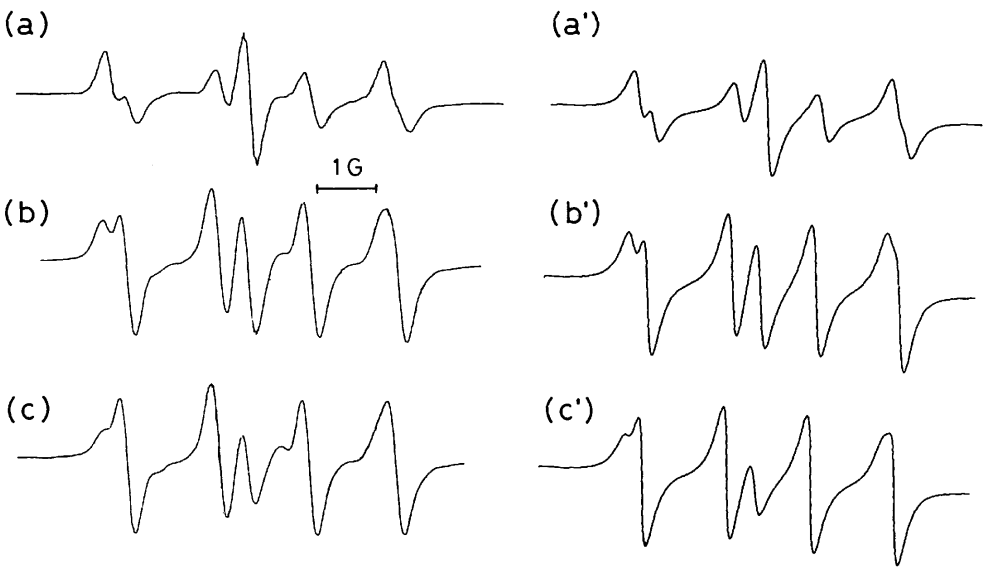

Fig. 3. ESR spectra of Na^+DBQ^- in THF containing 3.1 mM cryptand and (a) 0.3, (b) 17.1 and (c) 32.7 mM DBQ at −50 °C, and the corresponding computer simulated spectra; (a')—(c').

(c). Four new hf lines caused by DBQ addition, having equal intensities, can be attributed to two nonequivalent hydrogens of a=3.12 G and 1.56 G, respectively.

All features of the ESR spectra of Na^+DBQ^- with and without DBQ were not changed by substituting CW for CRP, except for the broadening of two inner peaks of the original four lines.

Figure 1 (a′)—(c′) show computer simulated ESR spectra assuming the following situations; (A) The new paramagnetic species have two nonequivalent groups of hydrogens including 6 members respectively. (B) The hf constants for these two hydrogen groups of the new species are 2.54 and 1.27 G, and the hf constant for the equivalent 12 hydrogens of the original species is 1.90 G. (C) The observed ESR spectrum is the superposition of the original spectrum and the new spectrum having intensities corresponding to their concentrations. (D) The difference of the center field of each spectrum due to the difference of g values is 0.25 G. These simulated spectra agreed well with the observed spectra.

Figure 2 (a′)—(c′) show the similarly simulated spectra assuming that the hf constants of the two groups of hydrogens (2 members) for the new species are 3.38 and 1.74 G respectively; the hf constant for the 4 hydrogens of the original species is 2.56 G; and the difference of the center field is 0.25 G. Figure 3 (a′)—(c′) show the simulated spectra assuming that the hf constants of the two nonequivalent hydrogens for the new species are 3.12 and 1.56 G; the hf constant for the 2 equivalent hydrogens of the original species is 2.38 G; and the differnce of the center field is 0.25 G. These simulated spectra also agreed well with the observed spectra.

The finding that these new signals can be found only in the presence of Q and increase in intensity with increasing Q concentration strongly suggests that they should be attributed to certain aggregates of Q and Q^-. Table 1 shows the equilibrium constants (K) for this association which were calculated from the relative intensities of the original and the new signals at different Q concentrations by assuming that the association occurred between one Q and one Q^-. The validity of this assumption may be supported by the K values which are nearly independent of the Q concentration.

Furthermore, the K values were little affected by the variations of the concentrations of CRP and CW, and of the kinds of alkali metal cations and crown compounds.

Figure 4 shows $\log K$ vs. T^{-1} plots for DBQ and BQ, and Table 2, the resultant values for the standard enthalpy ($\Delta H°$) and entropy ($\Delta S°$) of the association reaction. Both the $\Delta H°$ and $\Delta S°$ values are smaller for quinones of greater molecular size.

The results described above strongly suggests that

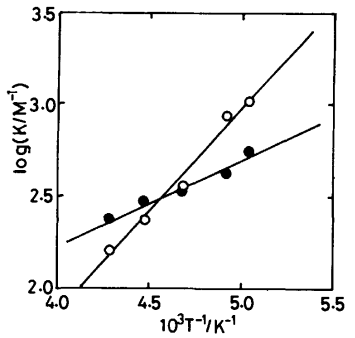

Fig. 4. Plots of $\log K$ vs. T^{-1} for the association reactions between (—●—) BQ and BQ^-, and (—○—) DBQ and DBQ^-, in the presence of Na^+ and cryptand.

Table 1. Equilibrium Constants, K, for Association Reactions between Q and Q^- in the Presence of CRP and Alkali Metal Cations

Q	[Q]/mM	$10^{-2}K/M^{-1}$ at T/K					
	T/K:	248	233	223	213	203	198
DBQ[a]	5.0		1.7	2.3	3.6	7.1	11.2
	14.3		1.5	2.4	3.8	10.4	9.4
BQ[b]	1.7		2.4	2.9	3.2	3.7	5.1
	6.2		2.5	3.2	3.7	5.1	6.3
DQ[c]	1.8	3.9		6.0			
	6.6	3.0		7.0			

a) The solution contains 3.1 mM CRP and equivalent concentration of Na^+ to DBQ^-. b) The solution contains 3.1 mM CRP and equivalent concentration of Na^+ to BQ^-. c) The solution contains 3.3 mM CRP and equivalent concentration of K^+ to DQ^-.

Table 2. Equilibrium Parameters at −50 °C for the Association Reactions between Q^- and Q in the Presence of CRP and Alkali Metal Cations

Q	$10^{-2}K/M^{-1}$	$\Delta H°$/kJ mol^{-1}	$\Delta S°$/J mol^{-1} K^{-1}
p-BQ[a]	3.0	−9	8
DQ[b]	7.0	−10	−4
DBQ[c]	2.4	−21	−50

a) The solution contains 3.1 mM CRP and equivalent concentration of Na^+ to DBQ^-. b) The solution contains 3.1 mM CRP and equivalent concentration of Na^+ to BQ^-. c) The solution contains 3.3 mM CRP and equivalent concentration of K^+ to DQ^-.

associations between quinones and their anion radicals occur in THF containing CRP and CW. If the associates are charge-transfer complexes like dimer cations,[1] the unpaired electron should be delocalized over two quinone molecules. Such a situation, however, is not in accord with the observed ESR pattern. On the contrary, if the unpaired electron is localized on one quinone molecule, the numbers of observed hf lines are reasonable. ESR

spectrum of the deuterated BQ (BQ-d_1) anion in THF containing CRP and BQ-d_1 supported this situation.

In this case, however, no simple structural model can explain the formation of such aggregates containing two Q molecules. A tentative model is given as follows: A quinone anion ion-paired with an alkali metal cation, which is captured by CRP and CW, can further associate with a quinone molecule, where an unpaired electron is localized on one quinone molecule and the migration of the cation is hindered. Then, the hf constants of the two sets of half number of equivalent hydrogens are not averaged, and the ratio of these happens to be about 2.0 as is seen in the case of the 2,5-DBQ anion ion pair: $a(H_3)$=1.50 G, $a(H_6)$=3.14 G at 0 °C.

We wish to thank Profs. Hiroshi Fukutomi and Hiroshi Tomiyasu for giving us facilities for the ESR measurements at The Research Laboratory for Nuclear Reactor in Tokyo Institute of Technology. We wish to thank Dr. Eiichi Ichikawa for his helpful suggestion to us about the method of deuteration of *p*-benzoquinone.

References

1) I. C. Lewis and L. S. Singer, *J. Chem. Phys.*, **43**, 2712 (1965).
2) O. W. Hawarth and G. K. Fraenkel, *J. Am. Chem. Soc.*, **88**, 4514 (1973).
3) K. Suga and S. Aoyagui, *Bull. Chem. Soc. Jpn.* **46**, 755 (1973).
4) H. Ziffer, E. Charney, and E. D. Becker, *J. Chem. Phys.*, **42**, 914 (1964).
5) M. P. Khakhar, B. S. Prabbananda, and M. R. Das, *J. Am. Chem. Soc.*, **89**, 3100 (1967).
6) A. W. Rutter and E. Warhust, *Trans. Faraday Soc.*, **64**, 2338 (1968).

 © 1986 The Chemical Society of Japan Bull. Chem. Soc. Jpn., 59, 1437—1441 (1986)

The Effect of the Substrate on the Epitaxial Growth of the Hexatriacontane Crystal

Michio ASHIDA, Yasukiyo UEDA, and Hisao YANAGI
Depertment of Industrial Chemistry, Faculty of Engineering, Kobe University, Rokko, Nada, Kobe 657
(Received November 5, 1985)

The epitaxial crystallization of hexatriacontane vacuum-evaporated onto a gold-covered KCl (001) surface was investigated as a function of the gold coverage. The hexatriacontane film on the KCl surface was composed of rod-like crystals taking the orientation of $(110)_H//(001)_{KCl}$ and $[001]_H//[110]_{KCl}$. The film on evaporated gold film was composed of lamellar crystals taking the orientation of $(001)_H$ parallel to the substrate and a random orientation in the azimuthal direction. The hexatriacontane film evaporated on the substrate which was partly covered with gold particles was composed of both rod-like and lamellar crystals. When the coverage ratio of the gold particles was low, the lamellar crystals in the hexatriacontane film took the orientation of $(001)_H//(001)_{KCl}$ and $[110]_H//[110]_{KCl}$. The numbers of lamellar crystals increased, and their orientation in the azimuth became more random, with and increase in the gold coverage.

In recent years thin films of organic compounds have attracted a good deal of attention because of their electronic and photoelectronic properties as semiconductors. The properties of ultrathin films are probably controlled by the molecular arrangement in the films. The main methods of preparing oriented thin films are the Langmuir-Blodgett (L-B) method and the vacuum-evaporation method. The former has been developed for preparing oriented organic thin films by mean of a wet process, and the properties of L-B films have been reported by many investigators.[1] In the case of vacuum-evaporation as a dry process, on the contrary, although there have been a number of reports on the structures of metals and inorganic compounds, there have been few reports on those of organic compounds.[2-5] We have investigated the orientation of vacuum-deposited films of organic compounds which consist of planar molecules, such as polycyclic aromatic compounds[6] and phthalocyanines.[7] The organic crystals composed of linear molecules, such as normal paraffins,[8] polyethylene[9] and polypropylene,[10] were also found to grow epitaxially in two modes on alkali halide, depending on the substrate temperature. When the substrate was preheated at 150 °C and kept at about 25 °C, the film was composed of rod-like crystals in which the linear molecules lay parallel to the substrate surface. On the substrate kept at temperatures in the vicinity of the respective melting points, the film was composed of disk-like crystals in which the molecules were oriented perpendicularly to the substrate. These two types of epitaxial crystallization have been reported for many polymers crystallizing on the surfaces of alkali halides and mica from organic solutions.[11-16] It has also been observed by X-ray diffraction that hexatriacontane film vacuum-evaporated on a copper block at room temperature is composed of crystals growing in such a way that the chain axes are oriented perpendicularly to the metal surface.[17] Those findings suggest that the orientation of vacuum-evaporated organic films depends on the substrate temperature and the substrate material. The interaction between the substrate surface and the linear molecules probably gives the nucleation of these two types of oriented crystals.

In the present work, in order to change the strength of the substrate-molecule interaction, a cleavage surface of a KCl single crystal was covered partly with either oriented gold particles or random ones and was then used as the substrate for vacuum-evaporated hexatriacontane film. The effect of the gold coverage and the substrate structure on the orientation of hexatriacontane crystal was investigated by using electron microscopy and electron diffraction.

Experimental

Gold was evaporated onto a cleavage surface of a KCl single crystal which had been maintained at room temperature (25 °C) or 400 °C in a vacuum of 10^{-5} Torr†. The amount of evaporated gold was controlled with a quartz-crystal microbalance. The coverage of gold particles on the KCl surface and the particle size were measured by means of electron micrographs by using a Laxer 450-particle analyzer. A clean KCl (001) surface and a gold-covered KCl surface were used as the substrates for preparing hexatriacontane films. The substrates were preheated at 150 °C for 1 h and were then kept at room temperature in a vacuum of 10^{-5} Torr, as has been described in a previous paper.[8] Hexatriacontane obtained from the Tokyo Chemical Industry Co., Ltd., was evaporated onto the substrate from a quartz crucible source heated with a tungsten coil. The deposition rate was about 2 nm min^{-1}. The thickness of the deposited films was controlled at about 100 nm by using a quartz-crystal microbalance. The specimens used for electron microscopy were prepared by dissolving the KCl crystal in water after the film had been backed with evaporated carbon film.

† 1 Torr=133.322 Pa.

The films were examined by means of a HU-11A Electron Microscope.

Results and Discussion

Figure 1 shows the stage of the growth of the gold evaporated onto a cleavage surface of KCl maintained at 400 °C. At the initial stage of deposition, fine particles were dispersed uniformly over the substrate surface, as is shown in Fig. 1(a), these gold particles grew larger (b, c), until they eventually joined to form isolated islands(d) and finally formed a continuous film, with an increase in the amount of the deposit. The electron-diffraction pattern from these films displayed the same single-crystal pattern as is shown in Fig. 2, indicating that the individual fine particles were single crystals with the same orientation of $(001)_{Au}//(001)_{KCl}$ and $[100]_{Au}//[100]_{KCl}$. The characteristics of the evaporated gold films shown in Fig. 1 are given in Table 1. In the case of gold evaporated on a cleavage surface of KCl at room temperature, gold particles were dispersed randomly over the surface in the initial stage and then accumulated to form a continuous film when the deposit increased. All films formed at room temperature gave a polycrystalline diffraction pattern, in contrast to the case at 400 °C.

As has been described in the previous paper,[8] hexatriacontane film on a cleavage surface of KCl without heat treatment was composed of small granules giving a ring-diffraction pattern. Epitaxial growth of hexatriacontane occurred on the cleavage surface of KCl which had been preheated at 150 °C for 1 h and then kept at about 25 °C. Therefore, the same heat treatment was carried out for all the substrates before the evaporation. The hexatriacontane film evaporated on a clean surface of KCl was composed of raft-like crystals crossing each other orthogonally, as is shown in Fig. 3(a). The electron-diffraction pattern from the film gave a superposition of two identical fiber diagrams rotated at 90° with respect to each other, as is shown in Fig. 3(b). The hexatriacontane crystal has an orthorhombic subcell with dimensions of a=7.42 Å, b=4.954 Å, and c=2.546 Å. It was found from the electron-diffraction pattern that the hexatriacontane crystal had its (110) plane parallel to the KCl (001) surface and its c-axis along the [110] direction of the KCl crystal; that is, the crystal took the parallel c-axis orientation.[8] When hexatriacontane was evaporated on the KCl surface 11% covered with gold particles, the film was composed of rod-rike crystals crossing each other

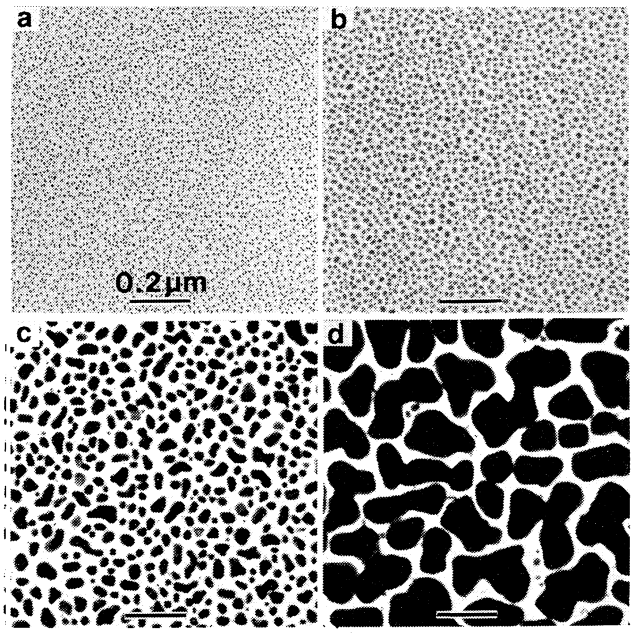

Fig. 1. A sequence of electron micrographs showing various stages of growth of gold films formed at 400 °C on KCl. The coverage of gold are (a) 11%, (b) 24%, (c) 54%, and (d) 74%.

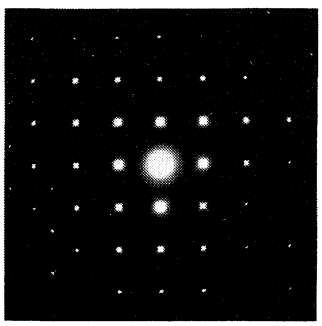

Fig. 2. Electron diffraction pattern of the gold films shown in Fig. 1.

Table 1. Character of Gold Deposits on (001) Surface of KCl

Substrate	Weight of Au mg/cm²	Particle number of Au μm⁻²	Mean diameter of Au Å	Coverage of KCl surface %
a	$1.0\times10^{-2}>$	1322	51.7	11.1
b	1.4×10^{-2}	1264	78.4	24.4
c	3.4×10^{-2}	563	218.1	54.3
d	5.2×10^{-2}	film	film	73.7

orthogonally and lamellar crystals filling in the space among the former, as is shown in Fig. 4(a). The electron-diffraction pattern in Fig. 4(b) shows the net pattern overlapping with arc spots, which indicates that the film contains two kinds of crystals with different orientations. The reflection spots are indexed as is shown in Fig. 5. The net-reflection spots with strong intensity coincide with the diffraction pattern observed from the film in Fig. 3(a). The arc-reflection spots on the ring pattern have the indices of $hk0$ and show a C_{4v} symmetry, whose mirror planes correspond to the (110) planes of KCl. These reflection spots suggest that the crystals take their c-axes perpendicularly to the substrate surface. Therefore, the arc pattern is composed of four sets of a net pattern, one of which is given by open circles, with C_{4v} symmetry. It is noted that the series of 110 and its higher-order reflection spots in the ring pattern coincide with the [110] direction of KCl and that this oriented direction agrees with that of the c-axes of the crystals illustrated in Fig. 3(b). On the basis of these diffraction patterns, the relative orientation between deposited gold particles and

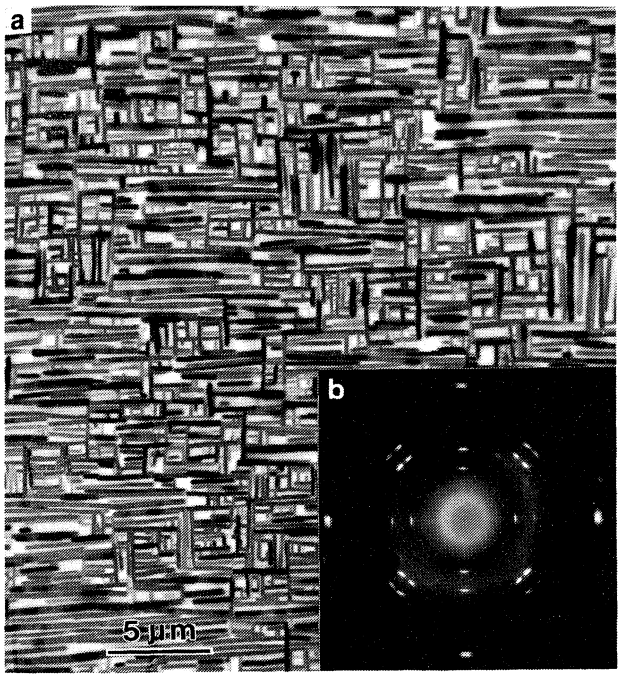

Fig. 3. Electron micrograph (a) and electron diffraction pattern (b) of hexatriacontane film evaporated on a clean cleavage surface of KCl.

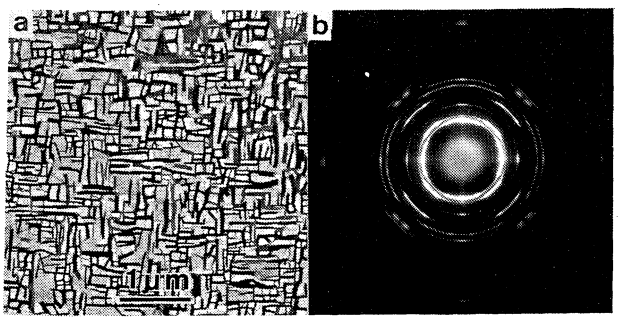

Fig. 4. Electron micrograph (a) and electron diffraction pattern (b) of hexatriacontane film evaporated on KCl surface covered with gold partices by 11%.

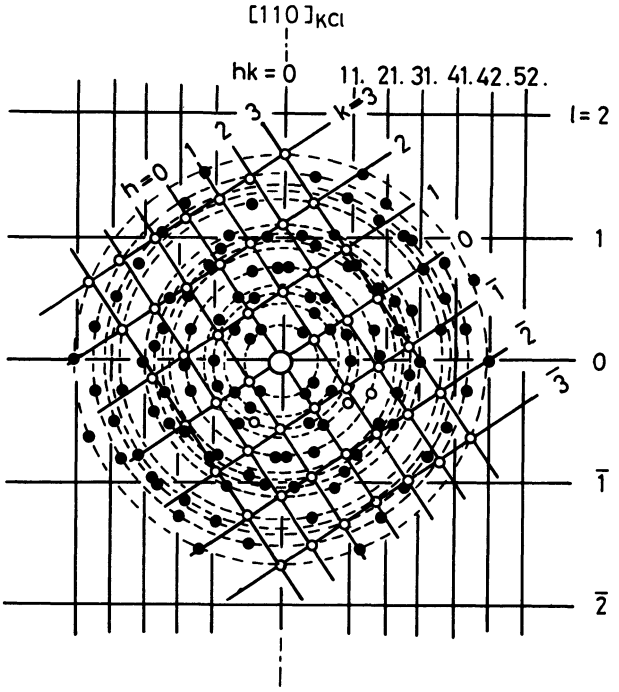

Fig. 5. The interpretation of the diffraction pattern shown in Fig. 4(b). Open circles are reperesentation of the basic single crystal pattern.

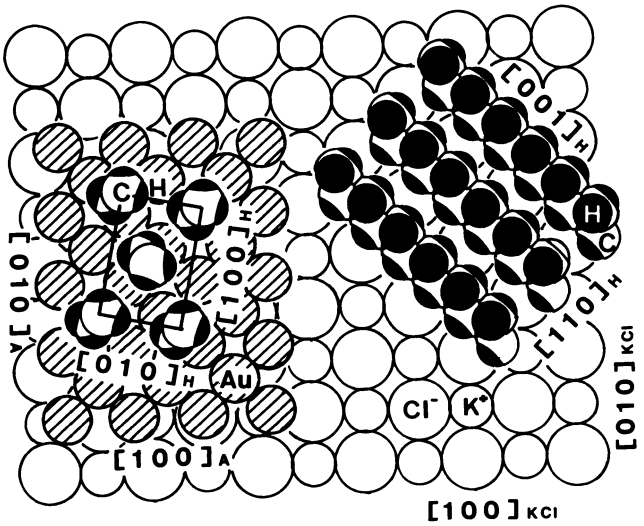

Fig. 6. Schematic diagram of the relative orientation of hexatriacontane crystals, gold and KCl (001) surface shown in Fig.4.

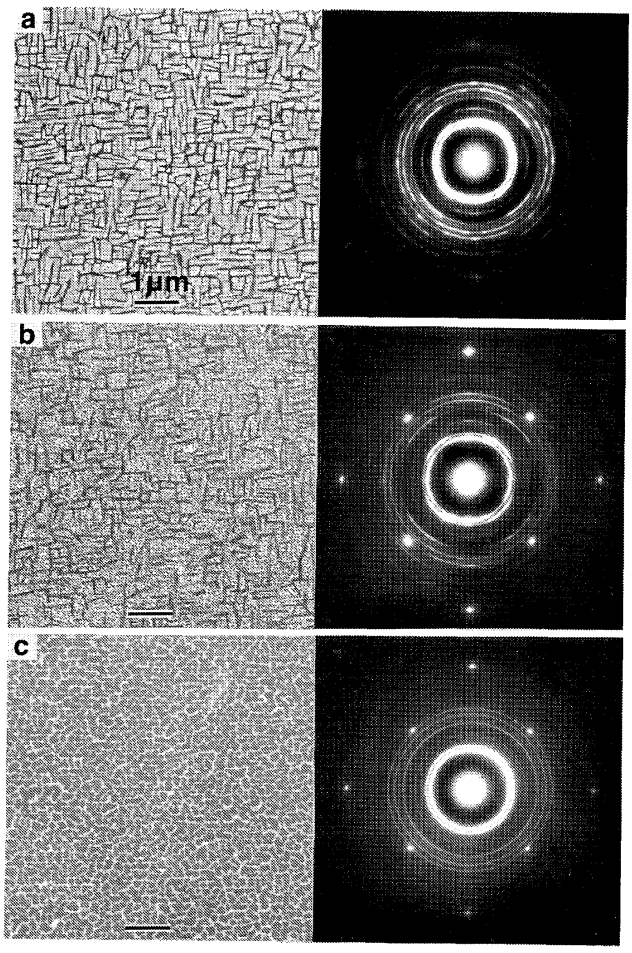

Fig. 7. Electron micrographs and electron diffraction patterns of hexatriacontane films evaporated on KCl surfaces covered with gold particles by(a) 24, (b) 54, and (c) 74%, respectively.

hexatriacontane crystals on the KCl surface can be explained in terms of a real lattice, as is shown schematically in Fig. 6. When the rod-like crystals take the orientation of $(110)_H//(001)_{KCl}$ and $[001]_H//[110]_{KCl}$, a closed-packing layer of the linear molecules lies adjacent to the KCl surface, with their long axes along the substrate [110] direction. On the other hand, it seems that the lamellar crystals nucleate on gold particles and grow over the surrounding KCl surface. The linear molecules in the lamellar crystal stand perpendicular to the substrate surface, and their closed-packing layers are arranged along the substrate [110] direction. Figures 7(a), (b), and (c) show electron micrographs and electron-diffraction patterns of the films deposited on the substrates covered about 24, 54, and 74% respectively with gold particles. The number of rod-like crystals decreased and the lamellar region increased with an increase in the coverage of the gold. Corresponding to these morphological variations, the more the substrate was covered with a gold deposit, the more predominancy

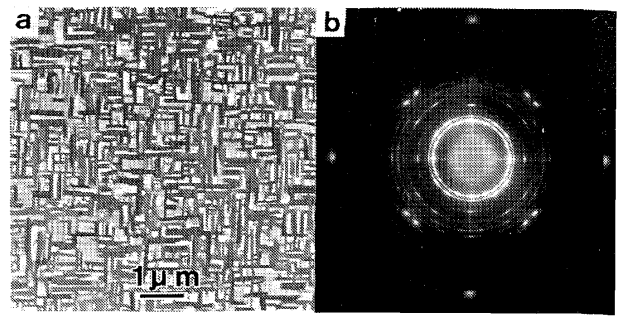

Fig. 8. Electron micrograph (a) and electron diffraction pattern (b) of hexatriacntane film evaporated on KCl surface covered by 12% with randomly-oriented gold particles.

of the ring pattern was observed in the electron-diffraction patterns. On the substrate with a gold coverage above 74%, the lamellar crystals covered the substrate uniformly, and the electron-diffraction pattern from the film showed a complete ring of ($hk0$) reflections of hexatriacontane crystals and net spots of gold crystals. These findings indicate that the film consists of polycrystals with their c-axes perpendicular to the substrate surface and with a random azimuthal orientation when the substrate surface is covered largely with a gold deposit. Figure 8 shows an electron micrograph and electron diffraction pattern of the hexatriacontane film evaporated on a substrate which is about 12% covered with gold particles taking a random orientation. The film was composed of rod-like and lamellar crystals as well as the film evaporated on the oriented gold. The ratio of the lamellar crystals to the rod-like crystals increased with an increase in the amount of gold deposited. This tendency was similar to the result for the films growing on the substrate surface covered with oriented gold. Consequently, it may be concluded that the orientation of hexatriacontane is dependent on the coverage of gold particles, but is independent of their orientation.

Alkali halide crystals have lines of unicharge ionic species which are aligned in the [110] direction of the (001) face, and the species exert a long-range dipole force which influences the orientation of long-chain molecules.[18] When hexatriacontane molecules are deposited on a clean surface of KCl, their long chains are arranged parallel to the [110] direction of KCl in the most closely packed way by means of an interaction between the KCl surface and the molecules, which causes the crystal to take the orientation of $(110)_H//(001)_{KCl}$ and $[001]_H//[110]_{KCl}$. On the other hand, the molecules deposited on gold particles yielded a nucleus of the oriented crystallite having $(001)_H//(001)_{Au}$. In the case of solution-grown polymers, two ways have been proposed for the nucleation of the crystals with their chain axes

perpendicular to the substrate surface; that is, nucleation in the solution[13] and nucleation at the side of the crystals already grown with their chain axes parallel to the substrate surface.[16] It has been concluded that a prerequisite condition for the formation of such oriented crystals is the presence of a weak interaction between the substrate surface and the polymer molecules.[15] It is well known that hexatriacontane crystals grow in lamellae, in which the long chains are arranged perpendicular to the flat face, from organic solutions.[19] This fact suggests that this crystal habit for hexatriacontane is the most stable form thermodynamically. Therefore, if there is little interaction between deposited molecules and a substrate, hexatriacontane molecules deposited on the substrate surface probably grow to a lamellar crystal on the surface. It seems that hexatriacontane molecules deposited on the gold surface form a nucleus of lamellar crystal, independently of the orientation of the deposited gold.

On the substrate surface covered partly with gold particles, some molecules deposited on the KCl surface grow to rod-like crystals, taking the parallel c-axis orientation, while the other molecules deposited on gold particles nucleate in lamellar crystals. Once nucleation and partial growth has occurred on fine gold particles, the reorientation of these "precrystals" to align with a preferential epitaxial growth direction on the KCl substrate would account for the regular crystalline orientation observed for epitaxy on KCl. Finally, the growth of these crystals directed by the epitaxial interaction with the KCl substrate may produce the unique azimuthal orientation of $[110]_H//[110]_{KCl}$. Alternatively, crystals growing on large gold particles and the gold substrate cannot experience these epitaxial interactions; thus, the hexatriacontane film may be composed of lamellar crystals with a random azimuthal orientation.

References

1) *Thin Solid Films*, **99**, Nos. 1—3 (1983).
2) N. Uyeda, M. Ashida, and E. Suito, *J. Appl. Phys.*, **36**, 1453 (1965).
3) Y. Murata, T. Kobayashi, N. Uyeda, and E. Suito, *J. Crystal Growth*, **26**, 187 (1974).
4) T. Kobayashi, Y. Fujiyoshi, and N. Uyeda, *Acta Crystallogr.*, **38**, 356 (1982).
5) M. Mitsuya, Y. Taniguchi, and M. Akagi, *J. Colloid Interface Scil*, **92**, 291 (1983).
6) M. Ashida and T. Watanabe, *Bull. Chem. Soc. Jpn.*, **45**, 2312 (1972).
7) M. Ashida, *Bull. Chem. Soc. Jpn.*, **39**, 2625 (1966); *ibid.*, **39**, 2632 (1966).
8) Y. Ueda and M. Ashida, *J. Electron Microscopy*, **29**, 38 (1980).
9) Y. Hattori, M. Ashida, and T. Watanabe, *Nippon Kagaku Kaishi*, **1975**, 496.
10) M. Ashida, Y. Ueda, and T. Watanabe, *J. Polym. Sci., Polym. Phys. Ed.*, **16**, 179 (1978).
11) J. A. Koutsky, A. G. Walton, and E. Baer, *J. Polym. Sci.*, **A-2**, 4, 611 (1966).
12) S. E. Rickert and E. Baer, *J. Appl. Phys.*, **47**, 304 (1976).
13) C. M. Balik and A. J. Hopfinger, *Macromolecules*, **13**, 999 (1980).
14) C. M. Balik, S. K. Tripathy, and A. J. Hopfinger, *J. Polym. Sci., Polym. Phys, Ed.*, **20**, 2003 (1982).
15) H. Ghavamikia and S. E. Rickert, *J. Mater. Sci. Lett.*, **2**, 103 (1983).
16) H. Ghavamikia and S. E. Rickert, *J. Mater. Sci.*, **18**, 2969 (1983).
17) K. Seki, S. Hashimoto, N. Sato, Y. Harada, K. Ishii, H. Inoguchi, and J. Kanbe, *J. Chem. Phys.*, **66**, 3644 (1977).
18) K. A. Mauritz, E. Baer, and A. J. Hopfinger, *J. Polym. Sci. Polym. Phys. Ed.*, **11**, 2185 (1973).
19) I. M. Dawson and V. Vand, *Proc. Roy. Soc.*, **A206**, 555 (1951).

 © 1986 The Chemical Society of Japan Bull. Chem. Soc. Jpn., 59, 1443—1448 (1986)

Phase Transition of Quaternary Alkyl Halide Salts of 1,4-Diazabicyclo[2.2.2]octane

Jun SHIMIZU, Kengo IMAMURA, Takashi NOGAMI,* and Hiroshi MIKAWA†
Department of Applied Chemistry, Faculty of Engineering, Osaka University, Yamada-oka, Suita, Osaka 565
(Received November 12, 1985)

A series of quaternary alkyl halide salts of 1,4-diazabicyclo[2.2.2]octane (DABCO) exhibited first-order phase transitions in the temperature range of 62—100 °C. Abrupt changes of halide anion conductivities were observed by two to three orders of magnitude at the transition temperatures. The transition temperature and the heat of transition tend to increase with the increase of the alkyl chain length. The temperature dependence of an IR spectrum showed that the band progressions due to long alkyl chain disappeared above the phase transition. This fact suggests that the *trans*-zigzag conformation of alkyl chains in the low temperature phase is destroyed by the internal rotation of the alkyl chain above the transition temperature.

Long-chain alkanes and their derivatives have attracted much attention for more than 50 years since the work by Müller.[1] He discovered a solid-state phase transition at a few degrees below the melting point. It has now been established that the phase transition is to be attributed to the hindered rotation of the alkyl chains.[2] The solid-state phase transition between an ordered phase (low temperature phase) and a rotator phase (high temperature phase) is interesting in relation to the melting process of polymer crystals as well as to the similar phase transition of some membranes (phospholipids).[3] The theoretical work on this problem before 1965 was surveyed by McClure.[4] Phase transitions involving conformational change were also observed for some *n*-alkanes.[5] Knowledge of the various types of polymethylene motions has accumulated substantially in the past few years, since the problems have been tackled both theoretically[6] and experimentally[7] with various independent techniques.

Independent of the above subjects, we have been studying halide anion conductivities by using several organic materials such as crown ether complexes,[8] cryptand complexes,[9] quaternary alkylammonium halides,[10] and quaternary alkylphosphonium halides.[11] As an extention of these studies, we have investigated the halide anion conductivities of a series of quaternary alkyl halide salts of 1,4-diazabicyclo[2.2.2]octane (DABCO), and found a first-order phase transition with concomitant and abrupt changes of the halide anion conductivities and crystal structures.[12] It has now been clarified that the phase transition in the present systems is to be attributed to the internal rotation of the C–C bonds of the alkyl chains in the solid state. Unlike alkanes and their derivatives, the phase transition temperature of the DABCO salts are more than one hundred degrees below their melting points (or decomposition points). This paper describes more details of the phase transition of the DABCO salts from the viewpoints of halide anion conductivities, thermal analyses, infrared absorption spectroscopy, and observations with a polarization microscope. The names of the quaternary alkyl halide salts of DABCO in the present study are abbreviated by the numbers of carbons of alkyl chains and the kinds of anions. For example, *N,N'*-didodecyl-1,4-diazoniabicyclo[2.2.2]octane dibromide is abbreviated as C_{12}-DABCO-Br. The materials studied are shown in Fig. 1.

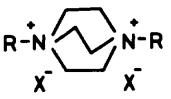

X^- = Cl^- : R = $C_{14}H_{29}$, $C_{16}H_{33}$, $C_{18}H_{37}$
X^- = Br^- : R = $C_{10}H_{21}$, $C_{11}H_{23}$, $C_{12}H_{25}$, $C_{13}H_{27}$, $C_{14}H_{29}$, $C_{15}H_{31}$, $C_{16}H_{33}$, $C_{17}H_{35}$, $C_{18}H_{37}$, $C_{22}H_{45}$
X^- = I^- : R = $C_{10}H_{21}$, $C_{12}H_{25}$, $C_{16}H_{33}$

Fig. 1. Quaternary alkyl halide salts of DABCO.

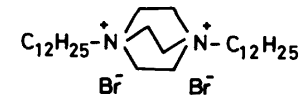

C_{12}-DABCO-Br

Experimental

Materials. Methyl alcohol was distilled without any drying procedures. Acetonitrile was passed through a column composed of several layers of basic, neutral, and acidic aluminas, refluxed over calcium hydride overnight, and then distilled. DABCO and all of alkyl halides were used without purifications.

Syntheses of Quaternary Alkyl Halide Salts of DABCO.

† Present address: Department of Environment and Safety Engineering, Faculty of Engineering, Fukui Institute of Technology, Gakuen-cho, Fukui 910.

Synthesis of quaternary alkyl halide salt of DABCO is described for C_{12}-DABCO-Br as a typical example. A methanol solution (30 ml) of DABCO (1.68 g, 15 mmol) and dodecyl bromide (7.48 g, 30 mmol) was refluxed for 36 h, and then allowed to cool to room temperature. It was then poured into benzene (500 ml) to obtain a white precipitate. It was filtered, dried, and then recrystallized three times from acetonitrile to obtain crystals of thin rectangular plates. For the chloride salts, acetonitrile was used as a reaction medium, and the reaction was conducted for 96 h. For the iodide salts, the same reaction conditions as described in the above example were adopted. In some cases, powders precipitate when the solution was cooled to room temperature after the reaction. In this case, a hot homogeneous solution was poured into benzene to obtain a precipitate. The solvents of recrystallization are as follows: acetonitrile for bromide salts possessing alkyl chains of C_{10}–C_{14}, and all of the chloride salts; ethyl alcohol for C_{14}-DABCO-I, C_{16}-DABCO-I, and bromide salts possessing longer alkyl chains than C_{14}

Measurements. Ionic conductivities were measured by a vector impedance meter 4800A (Hewlett Packard) in the frequency range of 25 Hz—500 kHz. Since all of the samples were hygroscopic, they were handled in a glove box until they were transferred to a glass vessel. The sample was compressed to a pellet (13 mm of diameter and ca. 0.5 mm of thickness) by applying a pressure of 300 kg cm^{-2} and sandwiched between platinum plates. After setting it was transferred to a sample holder made of Teflon, it was mounted in a glass vessel, dried under dynamic vacuum at 80 °C overnight, cooled to room temperature, and then subjected to measurement. After the drying procedure, the contribution of the proton conduction due to moisture seems to be negligible. Differential scanning calorimetry measurements of the samples were made on a SSC-560S (Daini Seikousha Co. Ltd) calorimeter with a scanning speed of 5 °C min^{-1}. The temperature dependence of the infrared spectra was measured by an A-102 (Japan Spectroscopic Co. Ltd.) for a KBr disk sample. The sample holder was surrounded by a ribbon heater.

Results and Discussion

Halide Anion Conductivities. All of the samples have already been confirmed as halide anion conductors.[12,13] Ionic conductivities were measured by an AC method. The impedance and a phase shift were measured, and the real and imaginary parts of the impedance were plotted for various frequencies (25 Hz—500 kHz). The impedance plot for C_{12}-DABCO-Br thus obtained at 78 °C is shown in Fig. 2 as a typical example. A semicircular arc was obtained in the high frequency range, which indicates that the equivalent circuit of the impedance is approximated by a parallel connection of a resistance and a capacitance. The linear relation with a 45° slope in the low frequency range might be due to a Warburg impedance. The resistance of the sample was estimated from the extrapolation of the semicircular arc to an abscissa. Temperature

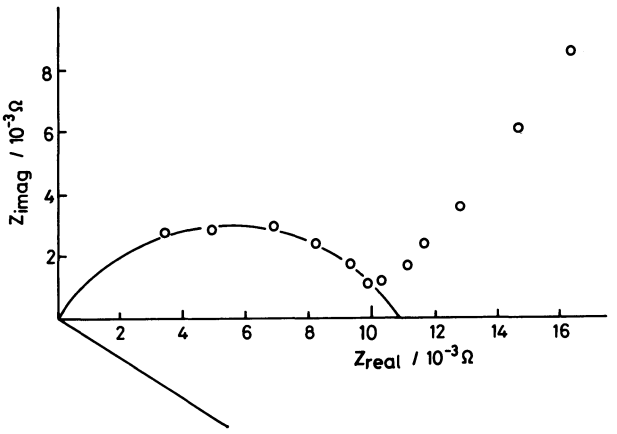

Fig. 2. The plots of the real and imaginary parts of impedance of C_{12}-DABCO-Br (a compressed pellet sample with an electrode area of 1.33 cm^2 and a thickness of 0.346 mm) at 78 °C in the frequency range of 25 Hz—500 kHz.

dependences of halide anion conductivities were measured with raising the temperature of the sample slowly from a room temperature; they are shown in Fig. 3 ((a) for chlorides, (b) for bromides, and (c) for iodides). Conductivities less than 10^{-9} S cm^{-1} are below the limit of our measurements. The following facts are noteworthy from this figure. (1) All of the samples show abrupt increases of the ionic conductivities by two to three orders of magnitude within narrow temperature ranges; this is attributed to a first-order phase transition as described later. (2) The order of the transition temperatures (T_c) of chlorides, bromides, and iodides is $Cl^- < Br^- < I^-$, when the carbon numbers of alkyl groups are fixed. (3) The longer the alkyl chains, the higher are the T_c, although a few exceptions are found.[14] (4) The order of the ionic conductivities of chlorides, bromides, and iodides is $Cl^- > Br^- > I^-$. (5) The longer the alkyl chain, the lower is the halide anion conductivity below T_c. However, the halide anion conductivities are close to each other above T_c; these points will be discussed later.

The close correspondence between T_c's and the lengths of the alkyl chains suggests that the phase transition is closely related to the structure of the alkyl group. The order of the ionic conductivities among three halides are due to the anionic size; the bigger the anionic size, the lower is its conductivity. Part of Table 1 shows materials, and the ratios of halide anion conductivities before (σ_l) and after (σ_h) the phase transition, i.e., σ_h/σ_l. The changes of the conductivities at T_c were found to be in the range of 150—180 for chloride salts, 630—3600 for bromide salts, and 140—350 for iodide salts. The abrupt change of the ionic conductivity showed hysteresis phenomena. Figure 4 shows the experimental results

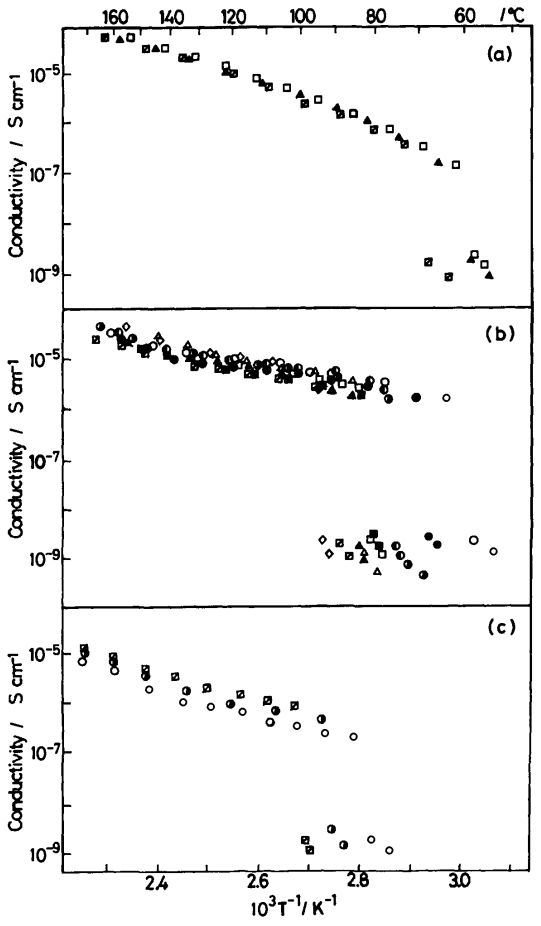

Fig. 3. Temperature dependences of halide anion conductivities.
(a) Chloride salts:
□: C_{14}-DABCO-Cl, ▨: C_{16}-DABCO-Cl, ▲: C_{18}-DABCO-Cl.
(b) Bromide Salts:
○: C_{10}-DABCO-Br, ●: C_{11}-DABCO-Br, ◑: C_{12}-DABCO-Br, ◐: C_{13}-DABCO-Br, □: C_{14}-DABCO-Br, ■: C_{15}-DABCO-Br, ▨: C_{16}-DABCO-Br, △: C_{17}-DABCO-Br, ▲: C_{18}-DABCO-Br, ◇: C_{22}-DABCO-Br.
(c) Iodide salts:
○: C_{10}-DABCO-I, ◑: C_{12}-DABCO-I, ▨: C_{16}-DABCO-I.

of C_{12}-DABCO-Br as an example, when the temperature was elevated above T_c and then cooled down again.

Differential Scanning Calorimetries. DSC measurements of the salts showed an endothermic transition at T_c when the temperature was elevated from room temperature across the T_c. An exothermic transition was observed at T_c when the temperature was lowered after it had been raised above T_c. Table 1 also shows T_c's and the endothermic (Q_{en}) and the exothermic (Q_{ex}) heats of transition. Owing to the hysteresis phenomenon, two T_c's are shown for each material. They were obtained by the onset of DSC peaks. The transition temperatures observed by heating the sample were, in general, higher than those observed by cooling the sample. The differences of the two T_c's were found to be in the range of 8—11 °C for chloride salts, 2—10 °C for bromide salts, and 2 °C for iodide salts. Figure 5 shows plots of the transition temperatures against the

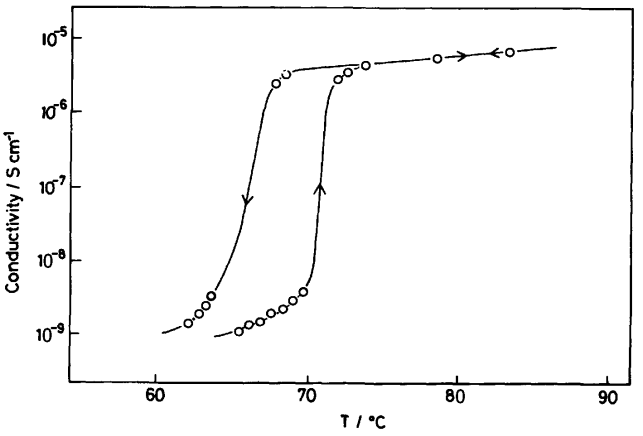

Fig. 4. Hysteresis of bromide anion conductivities of C_{12}-DABCO-Br.

Table 1. Quaternary Alkyl Halide Salts of DABCO, Phase-Transition Temperatures (T_c), Ratios of Halide Anion Conductivities Before (σ_l) and After (σ_h) Transition, and Endothermic (Q_{en}) and Exothermic (Q_{ex}) Heats of Transition

Materials	T_c[a] °C		σ_h/σ_l	Q_{en} kJmol^{-1}	Q_{ex} kJ mol^{-1}
(a) Chloride salts					
C_{14}-DABCO-Cl	61	51	150	41.4	38.5
C_{16}-DABCO-Cl	73	62	190	65.3	67.4
C_{18}-DABCO-Cl	61	53	180	68.7	71.2
(b) Bromide salts					
C_{10}-DABCO-Br	64	57	850	45.2	41.4
C_{11}-DABCO-Br	72	69	630	48.1	45.6
C_{12}-DABCO-Br	76	69	920	71.2	68.2
C_{13}-DABCO-Br	83	76	1500	67.4	62.8
C_{14}-DABCO-Br	88	78	1400	85.8	83.7
C_{15}-DABCO-Br	92	83	980	80.4	75.8
C_{16}-DABCO-Br	92	88	1200	96.3	101.7
C_{17}-DABCO-Br	96	86	3600	93.8	85.6
C_{18}-DABCO-Br	93	91	1400	105.5	105.9
C_{22}-DABCO-Br	99	96	2200	116.0	117.2
(c) Iodide salts					
C_{10}-DABCO-I	87	85	140	40.2	41.0
C_{12}-DABCO-I	93	91	190	54.8	53.2
C_{16}-DABCO-I	103	101	350	91.3	86.7

a) The temperatures in the left and right columns indicate the T_c's observed by heating and cooling the samples, respectively.

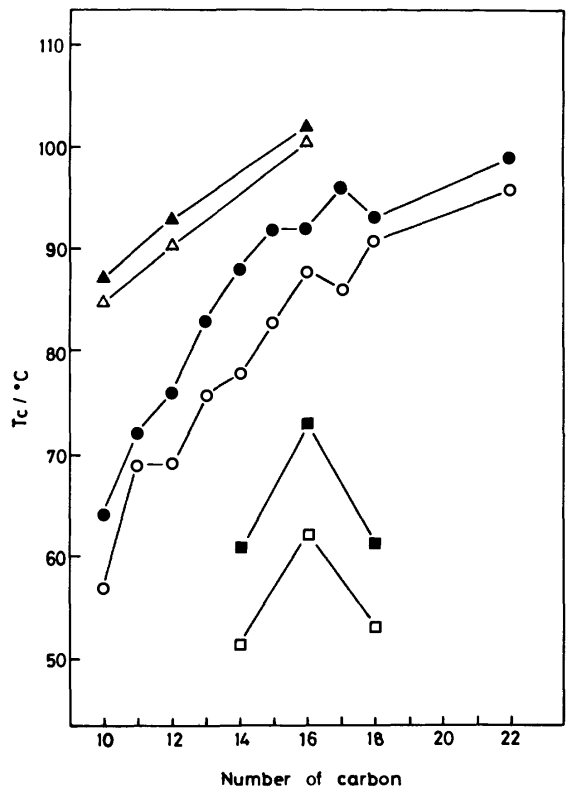

Fig. 5. Plots of phase transition temperatures against the number of carbons of alkyl group. The two transition temperatures of each material were obtained by the onset of the DSC peaks when the temperature was elevated or lowered across T_c's. The T_c's observed by heating the samples are higher than those observed by cooling the sample, and they are plotted independently. □, ■: chloride, ○, ●: bromide, △, ▲: iodide.

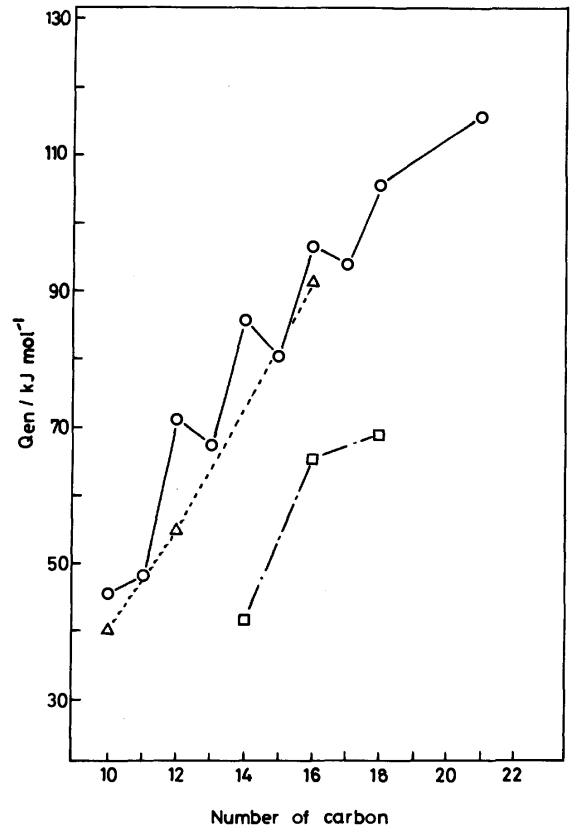

Fig. 6. Plots of endothermic heats of transition against the number of carbons of alkyl group. □: chloride, ○: bromide, △: iodide.

number of carbon atoms of the alkyl group attached to the DABCO nitrogen. This figure shows two T_c's for each material, corresponding to that observed by heating the sample and that observed by cooling. It is noteworthy that an even-odd number effect of carbons on the transition temperature was found for bromide salts in Fig. 5. The same type of effect on the phase transition temperature was also observed for a series of long chain alkanes and alcohols.[15] In most materials, the endothermic heats of transition were slightly larger than the exothermic heats of transition; this point will be discussed later. Figure 6 shows the plots of the endothermic heats of transition against the carbon numbers of the alkyl groups. This figure shows only the endothermic heats of transition, because they seem to represent the latent heats between the two phases more correctly than the exothermic heats of transition as described later. The heats of transition tend to increase as the alkyl group chains become longer. This suggests that the main factor controlling the transition is the change of the conformation of the alkyl chain. The order of the heats of transition of chlorides, bromides, and iodides is $Br^- > I^- > Cl^-$, if the number of carbon atoms in the alkyl group is fixed. It is noteworthy that an excellent even-odd number effect is observed for bromide salts as shown in Fig. 6.[15]

Infrared Absorption Spectroscopy. The temperature dependence of the infrared absorption spectra was measured to obtain more information on the phase transition. Figure 7 shows the temperature dependence of the IR spectra of C_{14}-DABCO-Br measured for a KBr disk sample at 30 and 100 °C as an example. The absorptions shown by the solid and dotted arrows at 30 °C are assumed to be due to band progressions,[16] which are well-known for long alkanes.[18] Many band progressions were smeared out at 100 °C. Detailed measurements revealed that this change of the absorption occurred exactly at the transition temperature. The disappearance of several band progressions in the high temperature range indicates that the *trans*-zigzag conformation of the alkyl chain in the low temperature phase is destroyed by the internal rotation of the C–C bonds of alkyl chain above the transition temperature.[19] Thus, the phase transition observed for DABCO salts is an order-disorder type.

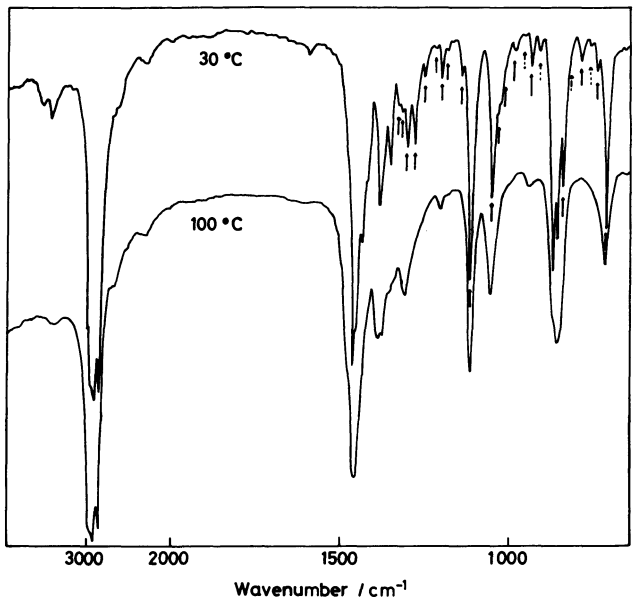

Fig. 7. Infrared absorption spectra of C_{14}-DABCO-Br for the KBr disk sample at 30 °C and 100 °C. The absorptions shown by the solid and dotted arrows at 30 °C are assigned to band progressions of the CH_2 vibrational mode.

Observation by Polarization Microscope. The above conclusion was also supported by observing the sample crystal in a polarization microscope under crossed Nicols condition. The bright transmitted light in the low temperature phase disappeared almost completely at the transition temperature, and the situation was unchanged even if the crystal were rotated above T_c. The abrupt decrease of the transmitted light above T_c reflects the lack of anisotropy of the crystal[20] due to the internal rotation of the C–C bonds of the alkyl chain.

Miscellaneous Discussions. The fact that the ionic conductivities become lower with the increase of the alkyl chain length below T_c is explained as follows. Judging from the crystal shapes of DABCO salts (very thin and rectangular) and from the crystal structures of related compounds,[21] the DABCO salts seem to possess layered structures, in which the long axes of the molecules are parallel with each other. The ion transport perpendicular to the long axis of a molecule seems not to be influenced so much by the length of the alkyl chain. On the other hand, the ion transport parallel to the long axis of the molecule will be retarded by the increase of the alkyl chain length, because the ion hopping length between anionic sites becomes longer. Thus, the latter effect accounts for the experimental observations. The reason why the ionic conductivities above T_c were similar to each other is as yet not clear. However, the following factors may be operative. The channel of the halide anion transport is greatly influenced by the packing of the individual molecule in the crystal. Since the material converts to the disordered phase above T_c, the peculiar pathway in the low temperature phase, which is closely related to the length of the molecule, and/or to the packing of molecules in the solid, would be destroyed or averaged by the movement of the alkyl group to give a structure-insensitive situation for anion transport.

The facts that the endothermic heats of transition are slightly larger than the exothermic heats of transition in most materials would be explained as follows. The former is caused by the transition from the ordered phase to the disordered phase. On the other hand, the latter is caused by the reverse transition. However, the disorder of the alkyl chain remains to some extent in the latter case, which gives rise to smaller exothermic heats of transition. This is consistent with the microscope observation that the surface of the crystal was wrinkled when the temperature was raised and lowered several times across T_c. Thus, the endothermic heat of transition seems to correspond to the latent heat between the ordered phase and the disordered phase more correctly than the exothermic heat of transition.

Summary. In conclusion, we have found that a series of quaternary alkyl halide salts of DABCO show first-order phase transitions, with concomitant and abrupt changes of halide anion conductivities, and infrared absorption spectra. The transition is caused by the change of the conformation of the alkyl group, possibly by the internal rotation of the C–C bonds of the alkyl chains. Therefore, the phase transition in the present study is closely related to the phase transitions of alkanes and their derivatives. The most distinct difference of the DABCO salts from others is that the transition temperatures are more than 100 degrees lower than the melting points (or decomposition points), because the latter are usually above 200 °C. The reason is that the present DABCO salts are ionic materials, and the lattice is more rigid than that of long alkanes and their derivatives which are covalent materials. The abrupt changes of the halide anion conductivities and the absence of birefringence above the transition temperature may be applicable to thermal switching devices. In this case, an output signal can be obtained both by electrical and optical techniques. The large differences between the transition temperatures and the melting points (or decomposition points) are favorable for such a device, because it ensures stability.

The authors are grateful to Professor Masamichi Kobayashi, Department of Macromolecular Science, Faculty of Science, Osaka University, for his discussions on the phase transitions of alkanes and on the assignment of the infrared absorption spectra of the present study. We are also grateful to Professor

Shigekazu Kusabayashi and Dr. Shunsuke Takenaka for the use of the DSC and the polarization microscope.

References

1) A. Müller, *Proc. Roy. Soc. (London)*, **A138**, 514 (1932).
2) J. D. Hoffmann, *J. Chem. Phys.*, **20**, 541 (1952).
3) D. A. Pink, T. J. Green, and D. Chapman, *Biochemistry*, **19**, 349 (1980).
4) D. W. McClure, *J. Chem. Phys.*, **49**, 1830 (1968).
5) R. G. Snyder, M. Maroncelli, H. L. Strauss, C. A. Ellinger, D. G. Cameron, H. L. Casal, and H. H. Mantsch, *J. Am. Chem. Soc.*, **105**, 133 (1983).
6) M. Kobayashi, *J. Chem. Phys.*, **68**, 145 (1978).
7) G. Zerbi, R. Magni, M. Gussoni, K. H. Horitz, A. Bigotto, and S. Dirlinkov, *J. Chem. Phys.*, **75**, 3175 (1981).
8) M. Fujimoto, T. Nogami, and H. Mikawa, *Chem. Lett.*, **1982**, 547.
9) M. Fujimoto, T. Nogami, and H. Mikawa, *Solid State Ionics*, **11**, 313 (1984).
10) J .Shimizu, T. Nogami, and H. Mikawa, *Solid State Ionics*, **14** 153 (1984).
11) K. Imamura, T. Nogami, and H. Mikawa, *Solid State Ionics*, **17**, 77 (1985).
12) J. Shimizu, T. Nogami, and H. Mikawa, *Solid State Commun.*, **54**, 1009 (1985).
13) A charge carrier was determined as a bromide or an iodide anion by a DC technique, using a graphite pellet electrode containing tetrabutylammonium tribromide or tetrabutylammonium triiodide (see Ref 12). In the case of the quaternary alkyl chloride salts of DABCO, we could not use the same technique, because of the instability of tetrabutylammonium trichloride. Judging from the similarity of the materials, however, the charge carrier of the chloride salts would be a chloride anion.
14) The exceptions were found for chloride salts and C_{17}-DABCO-Br.
15) A. A. Schaerer, C. J. Busso, A. E. Smith, and L. B. Skinner, *J. Am. Chem. Soc.*, **77**, 2017 (1955); A. Watanabe, *Bull. Chem. Soc. Jpn.*, **36**, 336 (1963).
16) The peak positions of the solid arrows are in fairly good accordance with the band progressions of n-$C_{15}H_{32}$, which have the same numbers of CH_2 units as the alkyl group of C_{14}-DABCO-Br. For the detailed assignments of the band progressions, see Ref. 17. The absorptions shown by the dotted arrows are due to the band progressions possessing the phase difference (ϕ_k) between adjacent CH_2 units given by $\phi_k=k\pi/14$, where k is an even number. These bands become IR-active because of the lower symmetry of the alkyl group of C_{14}-DABCO-Br than n-$C_{15}H_{32}$. The assignments of the band progressions in Fig. 7 have some ambiguities in the range of 1170—1310 cm^{-1}, because both the CH_2 wagging and CH_2 twisting-rocking modes have absorptions in this range. Since single absorption was observed at 720 cm^{-1} (CH_2-rocking mode) in Fig. 7, C_{14}-DABCO-Br seems to possess a parallel-packed molecular structure in the crystal. In this case, crystal field splitting does not appear. The separations of the absorptions shown by the arrows are too large to be the crystal field splittings, because these are usually less than 10 cm^{-1}.
17) R. G. Snyder and J. H. Schachtschneider, *Spectrochim. Acta*, **19**, 85 (1963).
18) H. Tadokoro, "Structure of Crystalline Polymers," Wiley Interscience, New York (1979), pp. 304—311.
19) J. R. Nielsen and C. E. Hathaway, *J. Mol. Spectroscopy*, **10**, 366 (1963). M. R. Barr, B. A. Dunell, and R. F. Grant, *Can. J. Chem.*, **41**, 1188 (1963).
20) Since the sample shows some powdered X-ray diffraction patterns above the transition temperature (see Ref. 12), the high temperature phase is not completely amorphous.
21) M. Kobayashi, T. Kobayashi, Y. Itoh, and K. Sato, *J. Chem. Phys.*, **80**, 2897 (1984).

 © 1986 The Chemical Society of Japan Bull. Chem. Soc. Jpn., 59, 1449—1454 (1986)

The Unreactive Nature of N(2^4S) to Unsaturated Hydrocarbons

Hironobu UMEMOTO,* Seiko NAKAGAWA, Shigeru TSUNASHIMA, and Shin SATO†
Department of Applied Physics, Tokyo Institute of Technology,
Ookayama, Meguro-ku, Tokyo 152
†Research Laboratory for Nuclear Reactors, Tokyo Institute of Technology,
Ookayama, Meguro-ku, Tokyo 152
(Received November 21, 1985)

The decay rates of ground-state atomic nitrogen in the presence of C_2H_4(ethene), $\Delta^{1,3}$-C_4H_6(1,3-butadiene), and C_2H_2(ethyne) were measured by using a pulse radiolysis-resonance absorption technique. It was found that the decay rates decrease drastically upon the addition of a small amount of I_2, an efficient radical scavenger. This suggests that the decay of N(^4S) in the absence of I_2 is due to the reactions between the N(^4S) and the free radicals. The rate constants for the reactions of N(^4S)+C_2H_4, $\Delta^{1,3}$-C_4H_6, and C_2H_2 were estimated to be much less than 10^3 m^3 mol^{-1} s^{-1}. The rate constant for the N+I_2→NI+I reaction was measured to be 2.4×10^4 m^3 mol^{-1} s^{-1}.

The reactions of active nitrogen with unsaturated hydrocarbons, especially with C_2H_4(ethene), have been studied very extensively. Two valuable reviews by Winkler and his co-workers appeared in 1968 and 1970 in which the studies on this subject prior to 1970 were summarized.[1,2] In 1949, Greenblatt and Winkler found that the major product of the reaction of active nitrogen with C_2H_4 is HCN; they proposed the following reaction mechanism:[3]

$$N(^4S) + C_2H_4 \longrightarrow C_2H_4N, \quad (1)$$
$$C_2H_4N \longrightarrow HCN + CH_3, \quad (2)$$
$$N(^4S) + CH_3 \longrightarrow HCN + 2H, \quad (3)$$

followed by the normal atom- and radical-recombination processes. This simple mechanism has been modified by many investigators, including Winkler and his co-workers.[4-6] In 1965, Herron proposed the following modified mechanism,[5] taking into account the observation that the concentration of N atoms determined by the NO titration technique, $[N]_{NO}$, is larger than that estimated from the amount of HCN produced in the presence of an excess amount of C_2H_4, $[N]_{HCN}$:[7]

$$N + C_2H_4 \longrightarrow HCN + CH_3, \quad (4)$$
$$N + CH_3 \longrightarrow HCN + 2H, \quad (3)$$
$$H + C_2H_4 \longrightarrow C_2H_5, \quad (5)$$
$$H + C_2H_5 \longrightarrow 2CH_3, \quad (6)$$
$$N + C_2H_5 \longrightarrow NH + C_2H_3, \quad (7)$$
$$N + NH \longrightarrow N_2 + H. \quad (8)$$

Here, Reactions 6—8 are important to explain the finding that the value of $[N]_{NO}$ approaches $[N]_{HCN}$ upon the addition of atomic hydrogen. Herron, in his later work, estimated the rate constant for Reaction 4 to be 8×10^3 m^3 mol^{-1} s^{-1} at 320 K.[8] Although the above mechanism could explain most features of the reaction of active nitrogen with C_2H_4, Safrany and Jaster questioned Reaction 4, the spin-forbidden internal rearrangement step.[9] They considered that the initial step must be the formation of free radicals. If active nitrogen contains atomic hydrogen as an impurity, even only a small amount, alkyl radicals can easily be produced by Reaction 5 and its succeeding chain processes. They also proposed the following reactions for the radical soures:

$$N + N + C_2H_4 \longrightarrow N_2 + C_2H_3 + H, \quad (9)$$

and:

$$N + N + M \longrightarrow N_2^* + M, \quad (10)$$
$$N_2^* + C_2H_4 \longrightarrow N_2 + C_2H_3 + H, \quad (11)$$

where N_2^* stands for electronically excited nitrogen molecules. Safrany's proposal was supported by Michael and his co-workers, who measured the reaction rates of N(^4S)+C_2H_4 at very low concentrations of N atoms ($\simeq10^{-6}$ mol m^{-3}) and found that the rate constant is less than 1×10^2 m^3 mol^{-1} s^{-1}.[10-12] In an earlier article from this laboratory, Sato et al. obtained the rate constant for the addition of N(^4S) to some unsaturated hydrocarbons by employing a pulse radiolysis-resonance absorption technique.[13] Their reported value for N+C_2H_4 was 4×10^4 m^3 mol^{-1} s^{-1}, the same order as that reported by Herron,[8] but more than two orders of magnitude larger than that reported by Michael.[12] Michael has insisted that, in the system of Sato et al., an intense electron beam must have produced a large amount of $N_2(A^3\Sigma_u^+)$, which must then have disturbed the measurement by producing free radicals.

There is no doubt that unsaturated hydrocarbons react with active nitrogen fairly rapidly, and that the reaction mechanisms are not simple. It is not certain, though, whether the initial step of the sequence is the addition of N atoms to the C=C double bonds or the formation of free radicals. Therefore, we re-measured the reaction rates for N+C_2H_4, $\Delta^{1,3}$-C_4H_6(1,3-butadiene), C_2H_2(ethyne), and C_2HCl_3(trichloroethene) in the presence of I_2, which scavenges free radicals as

well as quenches electronically excited molecular and atomic nitrogen.

Experimental

The experimental apparatus and the procedure were similar to those described elsewhere.[13,14] Briefly, a mixture of N_2 (typically 93±2 kPa), I_2 (0—4 Pa), and unsaturated hydrocarbons (0—7 Pa) was irradiated with a pulsed electron beam from a Febetron 706 apparatus (Hewlett Packard Co.). The change in the concentration of N(^{4}S) was measured by means of the absorption of the resonance lines ($3^4P_J \leftarrow 2^4S$) around 120 nm. The linear relationship between the optical density and the atomic concentration has been confirmed in a previous work.[13] The output of the photomultiplier tube (Hamamatsu R976) was amplified and processed with a wave memory (NF Circuit Design Block Co. WM-852) and a computer (NEC PC-9801F). All experiments were performed at 302±4 K.

Research-grade N_2 (Toyo Sanso) was used after having been passed through a furnace of copper chips at 590 K and a trap filled with a molecular sieve 4A at 77 K. Products of Takachiho Kako were used for $\Delta^{1,3}$-C_4H_6 and C_2H_2. The C_2H_4 was a product of Yokohama Chemical Co., while the C_2HCl_3 and I_2 were those of Koso Chemical Co.

Results

In the system of pure N_2, N(^{4}S) decayed very slowly; the decay rate was 3.2 s^{-1} (average of 13 runs). In the presence of a small amount of unsaturated hydrocarbons, however, N(^{4}S) decayed much more rapidly and the temporal profiles of the concentration were not single-exponential. These features were the same as those observed in a previous work.[13]

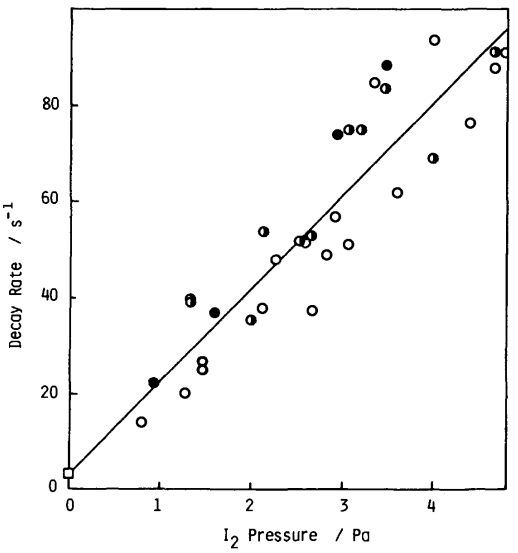

Fig. 1. The decay rate of N(^{4}S) as a function of the I_2 pressure. Total pressures are 53 kPa(◑), 93 kPa (○), and 133 kPa(●). The symbol □ stands for the average of 13 runs measured in the pure N_2 system.

In the system of N_2+I_2, the N(^{4}S) concentration decreased exponentially with the time, and the decay rate showed a linear dependence on the I_2 pressure, as is shown in Fig. 1. It was also found that the decay rate is independent of the total pressure between 53 kPa and 133 kPa.

In the system of the mixture of the three components, N_2, I_2, and unsaturated hydrocarbons, the decay of the N(^{4}S) concentration was again exponential, and the decay rates were much smaller than that observed in the system of the mixture of N_2 and the same amount of the hydrocarbon. Except in the case of C_2HCl_3, they were even smaller than that of the N_2+I_2 system. In other words, the decay rates of N(^{4}S) decreased in the following order, except for C_2HCl_3:

N_2 + unsaturated hydrocarbon $\gg$ N_2 + I_2

$>$ N_2 + I_2 + unsaturated hydrocarbon $>$ N_2 only.

Figures 2 and 3 illustrate the relationships between the decay rates of N(^{4}S) and the I_2 pressures in the presence of 3.3 and 6.7 Pa of C_2H_4 and $\Delta^{1,3}$-C_4H_6 respectively. The values in the absence of I_2 are rough and less reliable, since the decay was not single exponential. In the cases of $\Delta^{1,3}$-C_4H_6 and C_2H_2, the decay rates increased linearly with the I_2 pressure, and the apparent decay-rate constants were about half of that in the N_2+I_2 system, regardless of the hydrocarbon pressures. In the case of C_2H_4, a slight

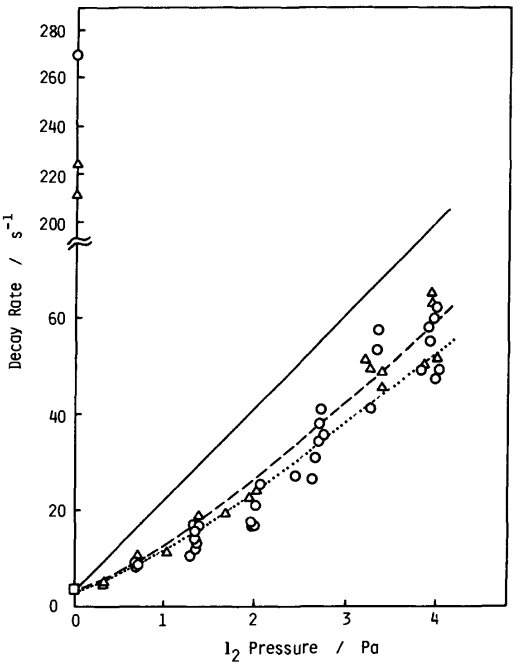

Fig. 2. The decay rate of N(^{4}S) as a function of the I_2 pressure in the presence of 3.3 Pa (△) and 6.7 Pa (○) of C_2H_4. The solid, broken, and dotted lines are results of the simulation in the absence and in the presence(3.3 Pa and 6.7 Pa) of C_2H_4, respectively.

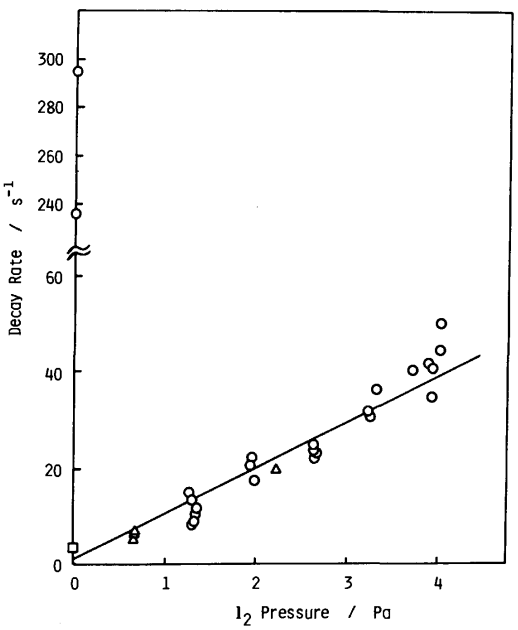

Fig. 3. The decay rate of N(⁴S) as a function of the I_2 pressure in the presence of 3.3 Pa (△) and 6.7 Pa (○) of $\Delta^{1,3}$-C_4H_6.

nonlinearity between the decay rate and the I_2 concentration could be observed, although the result was very similar to those for $\Delta^{1,3}$-C_4H_6 and C_2H_2 when the I_2 pressure was lower than 2.6 Pa. As for C_2HCl_3, the decay rate of N(⁴S) did not decrease so drastically as in the other cases upon the addition of I_2. In the absence of I_2, when the C_2HCl_3 pressure was around 7 Pa, the decay rate was in the order of 200 s^{-1}. In the presence of 1—4 Pa of I_2, the decay rate did not show any marked dependence on the I_2 pressure, and the average value was 58±11 s^{-1}.

Discussion

N_2+I_2 System. Phillips and his co-workers have studied this system by employing a discharge-flow technique. They proposed that the essential steps in this system are:[15-18]

$$N(^4S) + I_2 \longrightarrow NI(^3\Sigma^-) + I, \quad (12)$$
$$N(^4S) + NI(^3\Sigma^-) \longrightarrow N_2^* + I, \quad (13)$$
$$N_2^* + I_2 \longrightarrow N_2 + I_2^*, \quad (14)$$
$$N_2^* + I \longrightarrow N_2 + I^*, \quad (15)$$
$$NI + \text{wall} \longrightarrow (1/2)N_2 + (1/2)I_2, \quad (16)$$

where N_2^* is considered to be $N_2(W^3\Delta_u)$.[18] Since they have mentioned nothing about the quantum yield for the production of $N_2(W^3\Delta_u)$ in Reaction 13, some part of the product may be $N_2(A^3\Sigma_u^+)$ or vibrationally excited $N_2(X^1\Sigma_g^+)$. In the present system, since the total pressure was very high, it seems unlikely that Reaction 16 plays an important role. Termolecular processes, such as N+I+M→NI+M, may also be unimportant, because no total pressure dependence of the decay rate could be observed. If Reaction 13 is fast, and if it can be assumed that the concentration of NI is almost constant during the decay of N(⁴S), then the observed decay-rate constant must be twice the rate constant for Reaction 12, which has been calculated to be $(2.4\pm0.2)\times10^4$ m^3 mol^{-1} s^{-1}. This value is in fair agreement with that of Phillips, 1.4×10^4 m^3 mol^{-1} s^{-1}.[16] The assumption that the reaction rate for Reaction 13 is fast in this system is supported by the observation that the addition of unsaturated hydrocarbons decreases the apparent decay rates. This will be discussed in the next section.

N_2+I_2+C_2H_4 System. The addition of I_2 to the N_2+C_2H_4 system, even in only a tiny amount, drastically decreases the decay rate of N(⁴S). This strongly suggests that the rate for N+C_2H_4 is slow and that the apparent decay observed in the absence of I_2 is due to the reactions between the N(⁴S) and the free radicals. The finding that the decay rate in the three component system is even smaller than that in the N_2+I_2 system can be explained by assuming that NI is reactive to C_2H_4. However, it is impossible to account for the nonlinear relationship between the decay rate and the I_2 pressure shown in Fig. 2 by assuming the mechanism presented by Phillips. In order to explain this nonlinearity, we assumed the following reaction sequence:

$$N + I_2 \longrightarrow NI(^3\Sigma^-) + I, \quad (12)$$
$$N + NI \longrightarrow N_2(\text{or } N_2^*) + I, \quad (13)$$
$$NI + I_2 \longrightarrow NI_2 + I, \quad (17)$$
$$N + NI_2 \longrightarrow \text{Products}, \quad (18)$$
$$NI + C_2H_4 \longrightarrow \text{Products}. \quad (19)$$

In the absence of C_2H_4, this mechanism cannot, however, be distinguished from that proposed by Phillips if Reactions 13, 17, and 18 are much faster than Reaction 12. In the presence of C_2H_4, on the other hand, Reaction 19 competes with Reaction 17. When the I_2 pressure is high, Reaction 17 should be dominant and the result should agree with that in the absence of C_2H_4. When the I_2 pressure is low, however, Reaction 19 should be dominant and the apparent decay rate constant should be half of that in the absence of C_2H_4. Electronically excited molecular nitrogen is considered to be quenched by I_2 and C_2H_4 very rapidly. The alkyl and vinyl radicals produced from excited molecular nitrogen are considered to be scavenged by I_2 at an early stage. Atomic iodine may not disturb the system, either. The quenching of the first excited state of atomic iodine, $I(^2P_{1/2})$, by C_2H_4 is physical and slow. The rate constant has been measured as 4×10^4 m^3 mol^{-1} s^{-1}.[19] The reaction rate for $I(^2P_{3/2})$ should be even slower. If we assume that

the reaction rates for Reactions 13, 17—19 are much larger than that for Reaction 12, and that the rates for Reactions 17 and 19 are comparable, the nonlinear relationship can be deduced. The solid, broken, and dotted lines in Fig. 2 are the results of a simulation using the following rate constants (in units of $m^3\,mol^{-1}\,s^1$); $k_{12}=2.4\times10^4$, $k_{13}=6.0\times10^6$, $k_{17}=1.9\times10^6$, $k_{18}=6.0\times10^7$, $k_{19}=2.4\times10^6$. In the simulation, the inclusion of the NI+NI reaction had no effect on the results; the NI concentration must be very small compared with that of $N(^4S)$. It seems unlikely that $N(^4S)$ is reactive to C_2H_4, because the slope of the line in Fig. 2 at low pressures of I_2 (below 2.6 Pa), which is almost linear, is half of that in Fig. 1. By comparing these slopes, the rate constant for $N(^4S)+C_2H_4$ is calculated to be much less than $10^3\,m^3\,mol^{-1}\,s^{-1}$, which agrees with the result of Michael.[12]

In the absence of I_2, the reaction mechanism must be very complex. Safrany has presented the following mechanism, assuming that reactions which require drastic internal rearrangements, the rupture of double bonds, or a simultaneous rupture of more than one bond are unimportant:[20]

$$H + C_2H_4 \longrightarrow C_2H_5, \quad (5)$$
$$H + C_2H_5 \longrightarrow 2CH_3, \quad (6)$$
$$N + C_2H_5 \longrightarrow NH + C_2H_4, \quad (7)$$
$$N + C_2H_5 \longrightarrow CH_3 + H_2CN, \quad (20)$$
$$N + CH_3 \longrightarrow H + H_2CN, \quad (21)$$
$$N + C_2H_3 \longrightarrow NH + C_2H_2 \quad (22)$$
$$N + H_2CN \longrightarrow NH + HCN, \quad (23)$$
$$H + H_2CN \longrightarrow H_2 + HCN, \quad (24)$$
$$N + NH \longrightarrow N_2 + H, \quad (8)$$

and other atom- and radical-recombination reactions. Here, H atoms are considered to be formed by either Reaction 9 or Reactions 10 and 11. Although we do not think Safrany's assumptions are beyond question, the above mechanism is consistent with the present finding that $N(^4S)$ atoms do not react with C_2H_4 directly, and so this is probably the best starting point to an understanding of this complicated system. Safrany also considered that the H_2CN radical, which is isoelectronic to CHO and CH_3, must play an important role. The production of H_2CN in the active nitrogen/alkene system has also been confirmed by Takahashi and Miyazaki[6] and by Brooke and Mile.[21] Takahashi and Miyazaki detected D_2CN mass-spectrometrically in the system of active nitrogen and C_2D_4. They also detected CH_2 (CD_2) as an intermediate. As a source of CH_2 (CD_2), they proposed the following reactions:

$$N + C_2H_4 \longrightarrow CH_2 + H_2CN, \quad (25)$$
$$N + H_2CN \longrightarrow N_2 + CH_2. \quad (26)$$

As we have shown, however, the $N+C_2H_4$ reaction, including Reaction 25, is extremely slow. According to Safrany's suggestion, Reaction 26 can not occur, because it would require a rupture of the C=N double bond. Reactions such as:

$$N + C_2H_3 \longrightarrow HCN + CH_2, \quad (27)$$

can be excluded from the same reason. The abstraction of atomic hydrogen from CH_3 by H atoms or CH_3 radicals is 24 kJ mol^{-1} endothermic and must be very slow. On the other hand, abstraction by CN:

$$CH_3 + CN \longrightarrow CH_2 + HCN, \quad (28)$$

is exothermic. In spite of many efforts,[1,2,22,23] it is not yet clear how CN radicals are formed in active nitrogen/organic compound systems, but there is no doubt that CN is produced, since intense CN emission, in both red and violet systems, has been observed. Therefore, we would like to propose that CN is the precursor of CH_2. One possible source of CN is:[20]

$$N + N + HCN \longrightarrow N_2 + H + CN. \quad (29)$$

$N_2+I_2+\Delta^{1,3}$-C_4H_6 System. In this system, the decay rate of $N(^4S)$ showed a linear dependence on the I_2 pressure, and the slope of the linear plots was almost half of that of the N_2+I_2 system. These results can be explained by a reaction mechanism similar to that for C_2H_4 if the reaction rate for $NI+\Delta^{1,3}$-C_4H_6 is much faster than that for Reaction 17. The rate constant for $N+\Delta^{1,3}$-C_4H_6 is less than $10^3\,m^3\,mol^{-1}\,s^{-1}$.

$N_2+I_2+C_2H_2$ System. The situation in this system is analogous to that in the $N_2+I_2+\Delta^{1,3}$-C_4H_6 system. The rate constant for $N+C_2H_2$ is, again, less than $10^3\,m^3mol^{-1}s^{-1}$, which agrees with the result of Michael.[12] Safrany and Jaster have found that the reaction of C_2H_2 with active nitrogen is very different from those of alkenes or alkanes, and that it is rather similar to those of C_2N_2 and HCN.[20,24] One of the most characteristic features is that the fraction of N atoms initially present and converted to HCN is low, even in the presence of H atoms. It was also observed that the specific rate is strongly dependent on the C_2H_2 pressure. In order to explain these features, Safrany and Jaster considered that C_2N_2 is produced at the first stage of the sequence. They assumed the following replacement reaction:

$$N + C_2H_2 \longrightarrow CHCN + H, \quad (30)$$

follwed by:

$$N + CHCN \longrightarrow C_2N_2 + H. \quad (31)$$

From the length of the reaction flames, they estimaed the lower limit of the rate constant for Reaction 30 to be 4×10^3 m^3 mol^{-1} s^{-1}.[20,24] However, this value seems too large compared to the present upper limit, 10^3 m^3 mol^{-1} s^{-1}; we think Reaction 30 should be replaced by the following two reactions:

$$N_2^*(\text{or } N+N) + C_2H_2 \longrightarrow N_2 + C_2H + H, \quad (32)$$

$$N + C_2H \longrightarrow CHCN. \quad (33)$$

After the formation of CHCN and C_2N_2, the reaction sequence proposed by Safrany and Jaster seems to be enough to explain the experimental results.

N_2+I_2+C_2HCl_3 System. As has been mentioned, the decay rate of N(⁴S) showed no marked dependence on the I_2 pressure between 1—4 Pa. This suggests that 4 Pa of I_2 is not sufficient to scavenge free radicals completely in this system. Since I_2 is a very efficient scavenger for monoradicals, it may be supposed that biradicals, such as CCl_2, are produced and that they are less reactive to I_2. The C=C double bond is weakened by halogen substitution; this may be the cause for the production of biradicals. The upper limit of the rate constant for the N(⁴S)+C_2HCl_3 reaction is estimated to be 10^4 m^3 mol^{-1} s^{-1}.

Recently, Choo and Kim reported the bimolecular rate constant for N(⁴S)+C_2HCl_3 to be 1.6×10^4 m^3 mol^{-1} s^{-1}.[25] This value is a little larger than the present upper limit, and it is much larger than that for N(⁴S)+C_2H_4. The reaction path for N+C_2HCl_3 may be different from that for N+C_2H_4, but we are afraid they have not eliminated the contribution of the reactions of N(⁴S) with free radicals completely. In the systems of active nitrogen and fluoroethenes, Jones and Ahmed have shown that the hydrogen and fluorine atoms eventually formed play significant roles and that they must be the species initiating the reactions.[26]

Thermodynamical Considerations. Finally, it should be mentioned why N(⁴S) is so unreactive to hydrocarbons. Michael has discussed that intermediate quartet states are not crossed by potential surfaces which correlate with product states.[11,12] The following thermodynamical consideration suggests that the quartet states are physically unstable and that they decompose back into their initial components. The addition reaction of H(²S) to C_2H_4 to produce C_2H_5 is 160 kJ mol^{-1} exothermic. In the case of the O(³P)+C_2H_4 reaction to produce triplet biradicals, the exothermicity is much less. According to the ab initio Hartree-Fock calculation, it is 18 kJ mol^{-1}.[27] This small exothermicity may correspond to the weakness of the C-O single-bond strength compared to the C-H bond in most organic compounds.[28] Since the C-N single-bond strength is weaker still,[28] it is not surprising if the formation of quartet C_2H_4N triradicals is endothermic.

The next question is why NI($^3\Sigma^-$) is reactive. In order to explain the present experimental results, it is necessary to assume that the rate constant for Reaction 19, NI($^3\Sigma^-$)+C_2H_4, is larger than 10^5 m^3 mol^{-1} s^{-1}, while the order of the rate constant for NH($^3\Sigma^-$)+C_2H_4 has been estimated to be only 10^4 m^3 mol^{-1} s^{-1}.[29] The formation of triplet C_2H_4NI biradicals may not necessarily be endothermic, even if the formation of triplet C_2H_4NH biradicals is endothermic, but this seems less likely. One possibility is the production of stable ring compounds, such as cyclic C_2H_4NI. This process is spin-forbidden, but it may proceed fairly rapidly because of the heavy-atom effect of iodine atoms. For further discussion, accurate measurements of the rate constants for the NI reactions as well as those for NH are desired.

References

1) A. N. Wright and C. A. Winkler, "Active Nitrogen," Academic Press, New York (1968).
2) R. Brown and C. A. Winkler, *Angew. Chem. Internat. Edit.*, **9**, 181 (1970).
3) J. H. Greenblatt and C. A. Winkler, *Can. J. Res.*, **B27**, 721 (1949).
4) H. G. V. Evans, G. R. Freeman, and C. A. Winkler, *Can. J. Chem.*, **34**, 1271 (1956).
5) J. T. Herron, *J. Phys. Chem.*, **69**, 2736 (1965).
6) S. Takahashi and S. Miyazaki, *Bull. Chem. Soc. Jpn.*, **50**, 1627 (1977).
7) G. J. Verbeke and C. A. Winkler, *J. Phys. Chem.*, **64**, 319 (1960).
8) J. T. Herron, *J. Phys. Chem.*, **70**, 2803 (1966); J. T. Herron and R. E. Huie, *J. Phys. Chem.*, **72**, 2538 (1968).
9) D. R. Safrany and W. Jaster, *J. Phys. Chem.*, **72**, 518 (1968).
10) J. V. Michael and J. H. Lee, *Chem. Phys. Lett.*, **51**, 303 (1977).
11) J. V. Michael, *Chem. Phys. Lett.*, **68**, 561 (1979).
12) J. V. Michael, *Chem. Phys. Lett.*, **76**, 129 (1980).
13) S. Sato, K. Sugawara, and Y. Ishikawa, *Chem. Phys. Lett.*, **68**, 557 (1979).
14) H. Umemoto, K. Sugiyama, S. Tsunashima, and S. Sato, *Bull. Chem. Soc. Jpn.*, **58**, 3076 (1985).
15) C. G. Freeman and L. F. Phillips, *J. Phys. Chem.*, **68**, 362 (1964).
16) L. F. Phillips, *Can. J. Chem.*, **43**, 369 (1965).
17) D. I. Walton, M. J. McEwan, and L. F. Phillips, *Can. J. Chem.*, **43**, 3095 (1965).
18) L. F. Phillips, *Can. J. Chem.*, **46**, 1429 (1968).
19) R. J. Donovan, D. Husain, and C. D. Stevenson, *Trans. Faraday Soc.*, **65**, 2941 (1969); D. Husain and R. J. Donovan, *Adv. Photochem.*, **8**, 1 (1971).
20) D. R. Safrany, *Prog. React. Kinet.*, **6**, 1 (1971).
21) P. J. Brooke and B. Mile, *J. Chem. Soc., Chem. Commun.*, **1980**, 395.
22) D. Kley, N. Washida, K. H. Becker, and W. Groth, *Chem. Phys. Lett.*, **15**, 45 (1972); W. A. Rendall and J. M.

Roscoe, *J. Chem. Soc., Faraday Trans. 1*, **76**, 1757 (1980).
23) M. R. Gorbal and M. I. Savadatti, *Chem. Rev.*, **82**, 527 (1982).
24) D. R. Safrany and W. Jaster, *J. Phys. Chem.*, **72**, 3305 (1968).
25) K. Y. Choo and Y. K. Kim, *Chem. Phys. Lett.*, **102**, 281 (1983).
26) W. E. Jones and M. G. Ahmed, *Can. J. Chem.*, **60**, 2629 (1982).
27) M. Dupuis, J. J. Wendoloski, T. Takada, and W. A. Lester, Jr., *J. Chem. Phys.*, **76**, 481 (1982).
28) "CRC Handbook of Chemistry and Physics," ed by R. C. Weast, CRC Press, 61st ed., Florida (1980/81), p. F-243.
29) D. W. Cornell, R. S. Berry, and W. Lwowski, *J. Am. Chem. Soc.*, **88**, 544 (1966).

 © 1986 The Chemical Society of Japan Bull. Chem. Soc. Jpn., 59, 1455—1458 (1986)

Spectrophotometric and Analogue Derivative Spectrophotometric Determination of Chromium(III) with 2-(5-Bromo-2-pyridylazo)-5-(*N*-propyl-*N*-sulfopropylamino)phenol

Yoshio SHIJO* and Kaoru SAKAI
Department of Environmental Chemistry, Faculty of Engineering, Utsunomiya University, 2753, Ishii-cho, Utsunomiya 321
(Received August 26, 1985)

A sensitive method for the spectrophotometric determination of chromium(III) with 2-(5-bromo-2-pyridylazo)-5-(*N*-propyl-*N*-sulfopropylamino)phenol (5-Br-PAPS) is described. 5-Br-PAPS reacts with chromium(III) to form a 1:2 (metal:ligand) complex in weakly acidic media upon heating at 95 °C. The complex has an absorption maxima at 592 nm and gives a constant absorbance in the pH range of 3.4—6.2. The molar absorptivity and sensitivity for an absorbance of 0.001 are 8.94×10^4 dm^3 mol^{-1} cm^{-1} and 0.58 ng cm^{-2} respectively. The complex, once formed, is not decomposed by the addition of *trans*-1,2-cyclohexanediamine-*N*,*N*,*N*′*N*′-tetraacetic acid (CDTA). Thus, the selectivity of the method can be increased by the use of CDTA as a masking agent. The sensitivity of the method can be increased by employing analogue-derivative spectrophotometry, chromium(III) determination at parts-per-billion levels being feasible.

2-(5-Bromo-2-pyridylazo)-5-(*N*-propyl-*N*-sulfopropylamino)phenol (5-Br-PAPS) is a relatively new type of spectrophotometric reagent[1]. It is a water-soluble pyridylazo compound which has been developed by introducing a sulfoalkyl group into the amino group of the mother compound without sacrificing the oridinal spectrophotometric sensitivity. The reagent has the same chelating system as 4-(2-pyridylazo)-resorcinol (PAR), but is more sensitive than PAR for the determination of most metals, having molar absorptivities in the region of 1×10^5 dm^3 mol^{-1} cm^{-1} for several transition-metal complexes. 5-Br-PAPS has been reported to be a spectrophotometric reagent for the determination of zinc(II)[1] and vanadium(V).[2]

In the present work, a sensitive spectrophotometric method for the determination of chromium(III) with 5-Br-PAPS is descrived. The reagent reacts with chromium(III) to form a stable blue complex upon heating at 95 °C. The complex, once formed, is not decomposed by the addition of CDTA, whereas most other metal complexes are readily decomposed by CDTA. The conditions for the color development, the composition of the complex, and the influence of other metal ions are reported. The proposed method is very sensitive and selective for the determination of chromium(III). The sensitivity of the method is comparable to that of the 2-(5-bromo-2-pyridylazo)-5-diethylamino phenol (5-Br-PADAP) method (log ε=5.08)[3],but the former is better in selectivity than the latter because CDTA can be used as the masking agent. The method developed can be made even more sensitive by the use of an analogue derivative spectrophotometric technique.

Experimental

Reagents and Apparatus. The 5-Br-PAPS solution (5×10^{-3} M) was prepared by dissolving 0.120 g of 5-Br-PAPS (Dojindo Co., Ltd., Japan) in 50 cm^3 of water. The solution was stable for one week. The chromium(III) solution (1000 μg cm^{-3}) was prepared by dissolbing 0.500 g of metallic chromium (99.99% pure) in 45 cm^3 of hydrochloric acid by heating on a hotplate, and then by diluting the solution to 500 cm^3 with water. The solution was stable for at least six months. Working solutions were prepared by the dilution of this solution with 0.1 M† hydrochloric acid. All reagents were of an analytical-reagent grade, and all solutions were prepared with distilled, deionized water.

A Hitachi 100-10 spectrophotometer and a Hitachi 200-20 recording spectrophotometer were used. To obtain the derivative spectrum, a modified Hitachi 200-0576 derivative unit composed of two analogue-differentiation circuits (each having six different time-constants[4,5]) was connected in series between a Hitachi 200-20 recording spectrophotometer's output and a Hitachi 200 recorder's input. Cells with a 10-mm optical-path length were used throughout all the measurements unless stated otherwise.

Procedure. Ordinary spectrophotometry: To an aliquot containing less than 5 μg of chromium(III) in a 10-cm^3 test tube, 1 cm^3 of a 5×10^{-3} M 5-Br-PAPS solution and 1 cm^3 of a 2 M acetate buffer (pH 5) were added. The solution was diluted with water to 7 cm^3, and then heated 95 °C in a water bath for 20 min in order to complete the complexation. After cooling, the solution was transferred into a 10-cm^3 volumetric flask and diluted to the mark with water. The absorbance of the resultant solution was measured at 592 nm against a reagent blank prepared under the same conditions using 1-cm cells. Second-derivative spectrophotometry: When the chromium(III) content of the colored solution obtained by the procedure described above was too low to give a measurable absorbance, the procedure was carried out as follows. The second-derivative spectrum (from 700 to 500 nm) was recorded against a reagent blank by using a combination of both first-and second-order differentiation circuits of No. 6 and a scan speed of 120 nm min^{-1}, and the second-derivative value (the vertical

† 1 M=1 mol dm^{-3}.

distance from a peak to a trough) was measured.

Results and Discussion

Absorption Spectra. The absorption spectra of the chromium(III)-5-Br-PAPS complex at pH 5 is shown in Fig. 1, together with its second-derivative spectrum. The absorption spectra have an absorption peak at 592 nm and a shoulder on the shorter-wavelength side of the main absorption band. The absorption spectra of the complex was little affected by the addition of such cationic or anionic surfactants as tetradecyldimethylbenzylammonium chloride or dodecylbenzenesulfonic acid.

Effect of Experimental Variables. The pH dependence of the chromium(III) complex formation with 5-Br-PAPS by heating at 95 °C for 20 min is illustrated in Fig. 2. It was found that a constant absorbance at 592 nm was obtained in the pH range of 3.4—6.2. The absorbance of 5-Br-PAPS increases abruptly below pH 4 by increasing the protonated form of the amino group.

The reaction between chromium(III) with 5-Br-PAPS at room temperature is very slow. Therefore, the formation of the complex should be accelerated by heating. The effect of the heating time at 95 °C on the formation of the complex was examined. It was found that a constant absorbance was obtained by heating for more than 15 min at 95 °C. The complex, once formed at pH 5, was stable and gave a constant absorbance after 2 h.

The effect of the 5-Br-PAPS concentration on the absorbance of the complex was also examined. A concentration of more than 4×10^{-4} M was required to obtain a constant absorbance.

Composition of the Complex. The molar composition of the complex formed under the conditions described in the foregoing procedure was examined by Job's method of continuous variation. The results are shown in Fig. 3. The method indicated that the metal/ligand ratio of the complex was 1:2.

Calibration Graph. A straight-line calibration graph passing through the point of origin was obtained for chromium(III) concentrations of 0.04—0.6 $\mu g\,cm^{-3}$ using the foregoing procedure. The equation for the graph was Cr ($\mu g\,cm^{-3}$)=0.58 A (1), where A is the absorbance. The sensitivity for an absorbance of 0.001 and the molar absorptivity calculated from Equation (1) were 0.58 ng cm^{-2} and 8.94×10^4 $dm^3\,mol^{-1}\,cm^{-1}$ respectively.

Effect of Diverse Ions. The use of masking agents is required for the determination of chromium(III) with 5-Br-PAPS because many metal ions interfere with the formation of the colored complex. As masking agents, 0.2 cm^3 of 0.1 M tartaric acid was added before the addition of 5-Br-PAPS and 0.2 cm^3

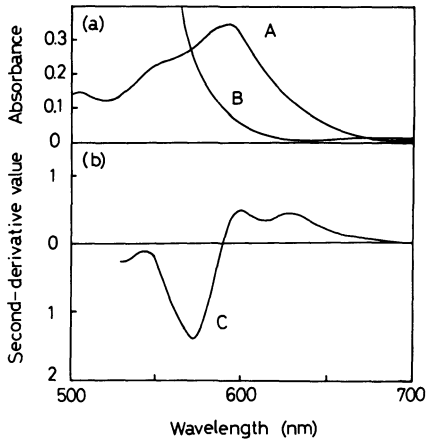

Fig. 1. (a) Absorption spectra of chromium (III)-5-Br-PAPS complex. (b) Second-derivative spectra of chromium-5-Br-PAPS complex. chromium (III), 0.2 $\mu g\,ml^{-1}$; 5-Br-PAPS, 5×10^{-4} M; pH, 5.
A: chrromium(III)-5-Br-PAPS complex, B: reagent blank, C: chromium(III)-5-Br-PAPS complex.

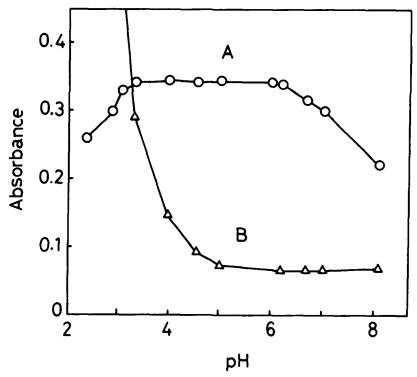

Fig. 2. Effect of pH.
chromium(III), 0.2 $\mu g\,ml^{-1}$; 5-Br-PAPS, 5×10^{-4} M; A: chromium(III)-5-Br-PAPS complex; B: reagent blank.

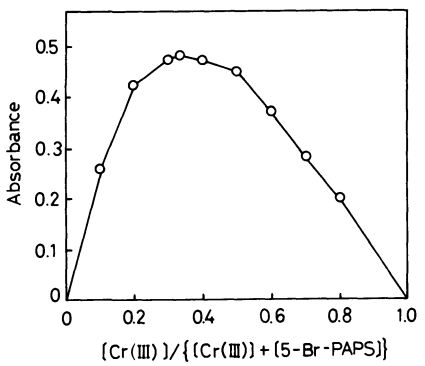

Fig. 3. Continuous variation plots of chromium(III)-5-Br-PAPS complex.
[chromium(III)] + [5-Br-PAPS] = 2×10^{-4} M; cell length, 2 mm; pH, 5.

Table 1. Tolerance Limits for Various Metal Ions in the Determination of 2 μg of Chromium(III). Tolerable Error: ±3%

Ions	Tolerance limit
Bi(III), La(III), Sc(III)	200 μg
Th(IV)	120 μg
Pb(II), Zr(IV)	40 μg
Fe(III), In(III), Mn(II), Mo(VI), Zn(II)	20 μg
V(V)[a]	4 μg
U(VI)[a]	2 μg
Ni(II)	400 ng
Co(II)	40 ng

a) Two hundred μl of 10% hydroxylamine hydrochloride was added after the formation of the chromium(III) complex.

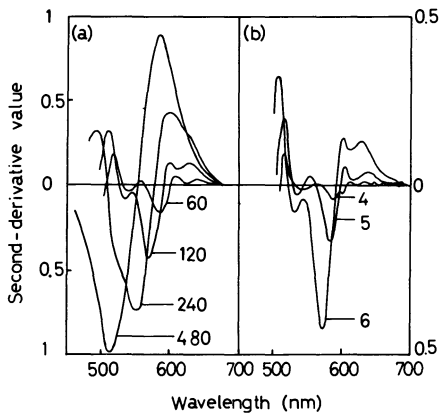

Fig. 4. Influence of (a) scan speed (with circuits all No.6) and (b) circuit number (with scan speed 120 nm min^{-1}) on second-derivative spectra of chromium–5-Br-PAPS complex. chromium(III), 60 ng ml^{-1}; 5-Br-PAPS, 5×10^{-4} M; pH, 5.

of 0.05 M CDTA after the formation of the chromium(III)–5-Br-PAPS complex in the foregoing procedure, then the mixture was heated at 95 °C for 5 min. Many metal complexes of 5-Br-PAPS decomposed upon the addition of CDTA. The absorbance of the chromium(III) complex, however, decreased only 5% compared with that in the absence of masking agents, because ligand exchange between CDTA with 5-Br-PAPS of the chromium(III) complex is very slow. The effects of foreign ions on the determination of chromium(III) when masking agents are used as has been described above are summarised in Table 1. The amounts of bismuth(III), lanthanum(III), scandium(III), thorium(IV), lead(II), zirconium(IV), iron(III), indium(III), manganese(II), molybdenum(VI), and zinc(II) tolerated are 200—20 μg. The masking of vanadium(V) and uranium(VI) with hydroxylamine hydrochloride are incomplete. Cobalt(II) and nickel(II) interfere seriously because these complexes with 5-Br-PAPS, once formed, are very stable and are little decomposed by the addition of CDTA.

Selection of Conditions for Measurement of the Second-Derivative Spectrum. Ishii and his coworkers have previously reported that derivative spectrophotometry using an analogue differentiation circuit is extremely effective in the sensitisation of ordinary spectrophotometry.[4,5] In this work, a derivative unit which is analogous to their apparatus was used. The second-derivative spectrum of the analyte is recorded, and the vertical distance from a peak to a trough, or from the base line to a trough of the spectrum, is measured. Since this distance(D) depends on both the time constant of the analogue differentiation circuits and the scanning speeds used, these need to be selected so as to give a large, well-resolved peak. The second-derivative spectra of the chromium(III)–5-Br-PAPS complex measured with varying circuit numbers and scan speeds are shown in Fig. 4. The largest peaks, but a poor linearity of the calibration graph, were obtained in the conditions of circuit No. 6 and a scan speed of 480 nm min^{-1}. The conditions of circuit No. 6 and a scan speed of 120 nm min^{-1} are found to be preferred for the determination of chromium(III) because reproducible data and a linear relationship for the chromium(III) concentration are obtained under these conditions.

Calibration Graph. The calibration graph, prepared by plotting the second-derivative value versus the chromium(III) concentration, was a straight line passing through the point of origin when either the peak-to-trough values or the base line-to-trough values were plotted. The equations for each graph, measured by employing a combination of circuit No.6 and a scan speed of 120 nm min^{-1}, are as follows; Cr(ng cm^{-3})=106 D (2) for the peak-to-trough measurements and Cr(ng cm^{-3})=134 D (3) for the base line-to-trough measurements, where D is the second-derivative value represented by the conversion of the value into the absorbance. From Eqs. 2 or 3, it can be seen that chromium(III) down to the 5 ng cm^{-3} level can be easily determined by the proposed method.

Comparison with Other Methods. Sensitive chromogenic reagents for the determination of chromium(III) include 5-Br-PADAP,[3] 2-(5-bromo-2-pyridylazo)-5-diethylaminophenol,[6] chromazurol S–hexadecyltrimethylammonium bromide,[7] phenylarsenazo,[8] PAR,[9] and diphenylcarbazide.[10] The first three are sensitive enough ($\log\varepsilon\fallingdotseq5$), but have a poor selectivity. The last three have a higher selectivity, but are they less sensitivity than the first two. In comparison with the methods using these reagents, the proposed method is sensitive ($\log\varepsilon=4.95$), selective, and stable. Further, the method can be applied

to more dilute samples by employing analogue-derivative spectrophotometry.

References

1) T. Makino, M. Saito, D. Horiguchi,and K. Kina, *Clin. Chim. Acta,* **120**, 127 (1982).
2) Y. Shijo and K. Sakai, *Bunseki Kagaku,* **33**, E 435 (1984).
3) Qiheng Xu and Rongshan Shi, *Huaxue Xuebao,* **42**, 151 (1984); *Chem. Abstr.,* **100**, 150302 x (1984).
4) H. Ishii and H. Koh, *Nippon Kagaku Kaishi,* **1980**, 203.
5) H. Ishii, T. Odashima,and T. Imamura, *Analyst,* **107**, 885 (1982).
6) F. Wei, Y. Zhu, P. Qu, F. Yin, and N. Shen, *Mikrochim. Acta,* **2**, 67 (1982).
7) W. Qi and B. Pu, *Huaxue Xuebao,* **42**, 27 (1984); *Chem. Abstr.,* **100**, 114193 d (1984).
8) S. Fu-sheng, *Talanta,* **30**, 446 (1983).
9) T. Yotsuyanagi, Y. Takeda, R. Yamashita, and K. Aomura, *Anal. Chim. Acta,* **67**, 297 (1973).
10) B. E. Saltman, *Anal. Chem.,* **24**, 1016 (1952).

 © 1986 The Chemical Society of Japan Bull. Chem. Soc. Jpn., 59, 1459—1465 (1986)

A New Method for Measuring 1:1 Association Constants Based on Releasing Rate of Free Ligand from Aqueous into Gaseous Phase, Applied to Determining Formation Constants of Metal Acetylacetonate Complexes

Isao SANEMASA,* Yuko NISHIMOTO, Akira TANAKA, and Toshio DEGUCHI
Department of Chemistry, Faculty of Science, Kumamoto University,
Kurokami 2-39-1, Kumamoto 860
(Received September 11, 1985)

A simple method is presented that allows estimation of 1:1 association constants between volatile and nonvolatile solutes in aqueous medium. On introducing an inert gas at a constant flow rate into the aqueous phase, the volatile solute is expelled from the solution, and the amount of the released solute is measured as a function of aeration time. Measurements are made in two separate runs at the same inert gas flow rate, one in the absence and the other in the presence of nonvolatile solutes. The releasing rate of the volatile solute is reduced with increasing association between both the solutes in the aqueous medium. The method was used to estimate formation constants of 1:1 acetylacetone complexes with metal ions, Cu(II), Ni(II), Co(II), Mg(II), Fe(II), Fe(III), and Al(III), at 25.0 °C and I=0.1 ($NaClO_4$), results being compared with literature values.

It has been shown that the disproportionation constant of mercury(I) in aqueous medium, i.e., the equilibrium constant for $Hg_2^{2+} \rightleftharpoons Hg^{2+}+Hg$, can be determined by combining two rate constants obtained from two independent experiments: one is concerned with measurement of the disproportionation rate while the equilibrium is caused to shift to the right by introducing nitrogen gas at a constant flow rate into the solution containing Hg(I) to expel Hg, and the other is concerned with measurement of the releasing rate of metallic mercury in the absence of Hg(II) at the same N_2 gas flow rate.[1] The present work was undertaken to demonstrate that the method might be applicable widely to systems where association occurs in aqueous medium between volatile and nonvolatile solutes.

In this work we are concerned with measurement of 1:1 formation constants of metal complexes. Acetylacetone was selected because this ligand is volatile[2] and because formation constants for a wide variety of metal ions are available from published compilations.[3] Various methods such as spectrophotometry, potentiometry, polarography, calorimetry, and solvent extraction have so far been used to determine formation constants for metal acetylacetonates.[3-8] Compared with these techniques, the present method is simple and not specific for the metal ions to be studied.

Experimental

Reagents and Materials. Distilled deionized water was used throuhout. Acetylacetone was of analytical reagent grade from Wako Pure Chemical. Stock solutions of 0.1 or 0.2 M (1 M=1 mol dm^{-3}) metal ions were prepared by dissolving their salts (ammonium iron(III) sulfate, aluminium potassium sulfate, sulfate and chloride for Cu(II), and chlorides for the other metals) in 0.01 M $HClO_4$, and standardizing gravimetrically (Fe: Fe_2O_3 converted to hydroxide; Al: 8-quinolinolate; Ni: dimethylglyoximate; Co: Co_3O_4 converted to α-nitroso-β-naphtholate) or titrimetrically (Mg: EDTA; Cu: iodometry). Amberlite XAD-2 resin, 20—50 mesh (Rohm and Hass), was ground in an agate mortar, a 50—80 mesh portion was collected and washed with ethanol by decantation until the supernatant became clear.

Preparation of Sample Solutions. A known amount of acetylacetone (5 to 50 μL) was added with a 25 or 100 μL micropipet to ca. 50 cm^3 of 0.1 M $NaClO_4$, a known volume of a metal ion stock solution was added, the pH was adjusted with a suitable buffer solution, and finally the solution was diluted to 100 cm^3 with 0.1 M $NaClO_4$ (the acetylacetone concentration was in the range of 4.87×10^{-4} to 4.87×10^{-3} M and the metal ion concentration was in the range indicated in Tables 1—3). The buffer solutions used are as follows: 0.2 M acetic acid-0.2 M sodium acetate (pH=3—6), 0.1 M sodium dihydrogenphosphate-0.1 M sodium hydroxide (pH=6—7.5), and 0.2 M boric acid-0.2 M potassium chloride-0.2 M sodium hydroxide (pH=7.5—10). For pHs lower than 3, perchloric acid (0.1 M) was used. The amount of the buffer or $HClO_4$ solution added to an aqueous solution containing both acetylacetone and metal ion was moderated so that the contribution of buffer salts to the increase in ionic strength was less than 0.01. The pH was measured with a Horiba Type F-7 pH meter to 0.01 pH unit.

Apparatus and Procedures. A 25 cm^3 portion of sample solution was transferred into a 100 cm^3 Erlenmeyer flask with a ground glass joint, the flask being immersed in a thermostated bath at 25.0±0.1 °C. A gas-inlet-type adaptor was mounted on the flask and nitrogen gas was dispersed through the solution via a sintered glass ball at a constant flow rate of 895 $cm^3\,min^{-1}$. The N_2 gas flow rate was adjusted by means of a needle valve and monitored during the aeration by a flow meter (Ueshima Brooks Rotameter); a deviation within 2% was observed around the adopted flow rate. The N_2 gas leaving the sample solution was

passed through a 5 mm×5 cm glass column which contained XAD-2 resin beads 3.5 cm in length and had its exit end plugged with glass wool. After a fixed time, the N_2 gas stream was interruted, the XAD column was replaced by another one, and the introduction of N_2 gas was resumed. This operation was repeated at regular time intervals. The acetylacetone adsorbed on the resin was completely eluted out with a 5 cm^3 ethanol, and the amount expelled from the solution during the fixed time was determined spectrophotometrically at 272 nm by reference to a calibration curve prepared in advance with acetylacetone-ethanol solutions of known concentrations. The XAD column, after subjected to elution with ethanol and air-dried, could be used repeatedly.

After completion of each aeration run, the pH of the sample solution was checked; no appreciable change in pH was found before and after aeration.

Results

Derivation of an Equation That Allows Estimation of 1:1 Metal Acetylacetonate Complex Formation Constants. The equilibria among the species that should be taken into account are

$$\text{acac}^- + \text{M}^{n+} \rightleftharpoons \text{M(acac)}^{n-1}, \ K_1, \quad (1)$$

$$\text{Hacac} \rightleftharpoons \text{H}^+ + \text{acac}^-, \ K_a, \quad (2)$$

$$\text{Hacac(aq)} \longrightarrow \text{Hacac(gas)}, \ k, \quad (3)$$

where K_1, is the formation constant of 1:1 metal acetylacetonate complex, K_a is the acid dissociation constant of acetylacetone (Hacac), and k is the rate constant for the expulsion of Hacac molecules from the aqueous into the gaseous phase. For convenience, symbol L^- will hereafter be used to denote species $acac^-$.

The solute HL expelled into the gaseous phase is to be trapped successively by XAD-2 columns, and the amount, Q_{HL}, trapped during a fixed time is measured as a function of aeration time, t. Here, we assume that the releasing rate of HL at a constant N_2 gas flow rate is of first-order dependence on the concentration of this species present in the solution, and thus

$$dQ_{HL}V^{-1}/dt = k[HL], \quad (4)$$

where V is the volume of the aqueous phase. We have mass-balance equations

$$C_M = [M^{n+}] + [ML^{n-1}], \quad (5)$$

$$\begin{aligned} C_{HL} &= [HL] + Q_{HL}V^{-1} + [ML^{n-1}] + [L^-] \\ &= [HL] + Q_{HL}V^{-1} + K_1[L^-][M^{n+}] + [L^-] \\ &= [HL] + Q_{HL}V^{-1} + (K_1[M^{n+}] + 1)K_a[HL][H^+]^{-1}, \end{aligned} \quad (6)$$

where C_M and C_{HL} indicate the total concentration of metal ions and that of acetylacetone, respectively. Substitution of Eq. 6 into Eq. 4 yields

$$dQ_{HL}V^{-1}/dt = k(C_{HL} - Q_{HL}V^{-1})/(1 + K_a[H^+]^{-1} + K_1K_a[M^{n+}][H^+]^{-1}), \quad (7)$$

which becomes, on integration and with $Q_{HL}=0$ at $t=0$,

$$\ln (C_{HL} - Q_{HL}V^{-1}) = -kt/(1 + K_a[H^+]^{-1} + K_1K_a[M^{n+}][H^+]^{-1}) + \ln C_{HL}. \quad (8)$$

Plots of $\ln(C_{HL}-Q_{HL}V^{-1})$ vs. t will give a straight line with a slope which corresponds to $-k/(1+K_a[H^+]^{-1}+K_1K_a[M^{n+}][H^+]^{-1})$ or to $-k/(1+K_a[H^+]^{-1})$ in the absence of metal ions. Under the condition that the total concentration of metal ions is sufficiently large compared to the concentration of the metal complex formed, that is, $C_M \gg [ML^{n-1}]$, we can set $[M^{n+}]$ in Eq. 8 equal to C_M.

Estimation of k and K_a. The constants k and K_a were determined from runs in the absence of metal ions. Figure 1 shows some plots constructed with the aid of Eq. 8. It is found that these plots give straight lines up to ca. 70% release of the acetylacetone initially present in the solution. This linearity verifies the validity of the assumption that the releasing rate of HL is first order in this species at a constant aeration rate. It can be seen from Fig. 1 that when the total concentration of HL is the same, the

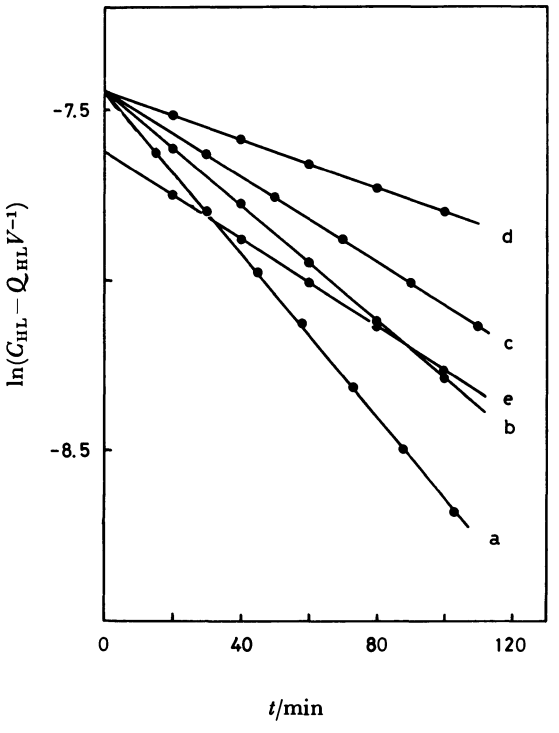

Fig. 1. The plots of $\ln (C_{HL}-Q_{HL}V^{-1})$ vs. t in the absence of metal ions. pH 2.30; N_2 gas flow rate: (a) 895, (b) 640, (c) 460, (d) 255, (e) 460 cm^3 min^{-1} ; C_{HL}: (a)—(d) 5.85×10^{-4}, (e) 4.87×10^{-4} mol dm^{-3}.

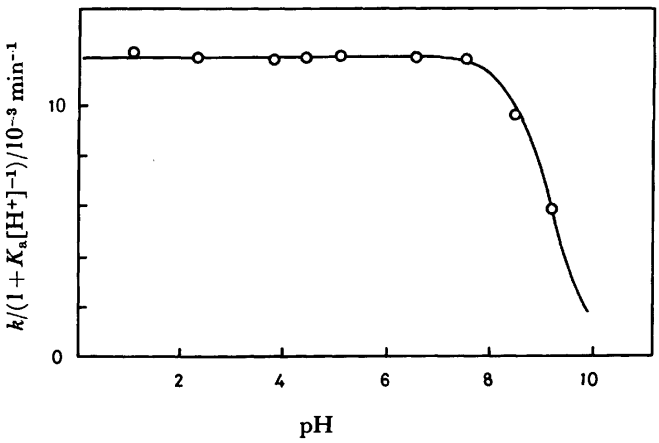

Fig. 2. The plots of $k/(1+K_a[H^+]^{-1})$ vs. pH in the absence of metal ions. N_2 gas flow rate 895 cm^3 min^{-1}; C_{HL} 5.85×10^{-4} mol dm^{-3}. The curve calculated using $k=1.20\times10^{-2}$ min^{-1} and $pK_a=9.17$ is depicted in a solid line.

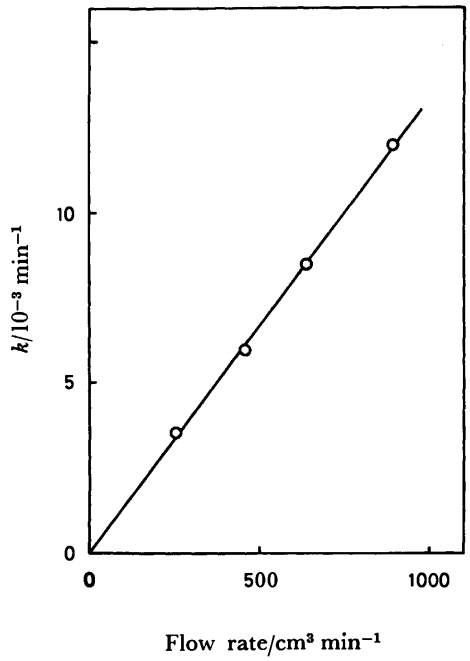

Fig. 3. k as a function of N_2 gas flow rate in the absence of metal ions. pH 2.30; C_{HL} 5.87×10^{-4} mol dm^{-3}.

slopes coincide with one another at the same aeration rate. This also supports the validity of Eq. 4.

At a constant N_2 gas flow rate, the slope of the straight line is almost constant in the acidic region, but steeply decreases in higher pH solutions, as seen from the plots of $k/(1+K_a[H^+]^{-1})$ vs. pH shown in Fig. 2. A least-squares calculation has revealed that k is 1.20×10^{-2} min^{-1} at an aeration rate of 895 cm^3 min^{-1} and that pK_a is 9.17. The K_a value thus determined is about half the reference one, 8.82 as pK_a,[9] reported at 25 °C and I=0.1(Na$^+$, H$^+$)ClO$_4$. The rate

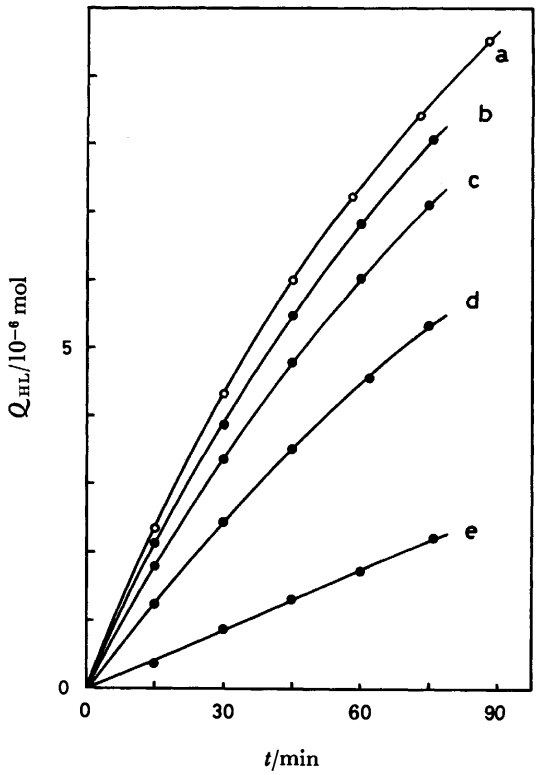

Fig. 4. The plots of Q_{HL} vs. t in the absence and presence of metal ions. N_2 gas flow rate 895 cm^3 min^{-1}; C_{HL} 5.85×10^{-4} mol dm^{-3}; (a): C_M=0, pH=2.30, (b): $C_{Mg}=2.05\times10^{-3}$ mol dm^{-3}, pH=7.37, (c): $C_{Ni}=9.85\times10^{-3}$ mol dm^{-3}, pH=4.76, (d): C_{Cu}(sulfate)$=1.98\times10^{-3}$ mol dm^{-3}, pH=3.68, (e): $C_{Fe(III)}=4.02\times10^{-3}$ mol dm^{-3}, pH=1.82.

constant, k is proportional directly to the N_2 gas flow rate in the range of 250 to 895 cm^3 min^{-1} studied, as shown in Fig. 3. In the subsequent runs, the flow rate was fixed at 895 cm^3 min^{-1} to reduce the time required for completing a single run.

Estimation of K_1. The amount of acetylacetone released into the gaseous phase was plotted against aeration time to give a parabolalike curve. Results for some metals are shown in Fig. 4, in which the result obtained in the absence of metal is included for comparison. Plots constructed with the aid of Eq. 8 gave straight lines for each run over the aeration time range investigated. Insofar as sample solutions are sufficiently acidic that the term $K_a[H^+]^{-1}$ can be neglected compared to unity, and provided also that the total concentration of metal ions is sufficiently large compared with the ligand concentration, the slope of the straight line can be taken as $-k/(1+K_1K_aC_M[H^+]^{-1})$. The effect of C_M and pH on the slope was examined for Cu and Ni. The results are shown in Fig. 5 ($C_{Ni}=1.97\times10^{-3}$—4.93×10^{-2} M, $C_{HL}=5.85\times10^{-4}$ M, and pH almost constant around 4.8) and in Fig. 6 ($C_{Cu}=1.98\times10^{-3}$ M, $C_{HL}=5.85\times10^{-4}$ M, and pH=1.02—4.89). As expected, the gradient of the straight line decreases as either C_M or pH increases.

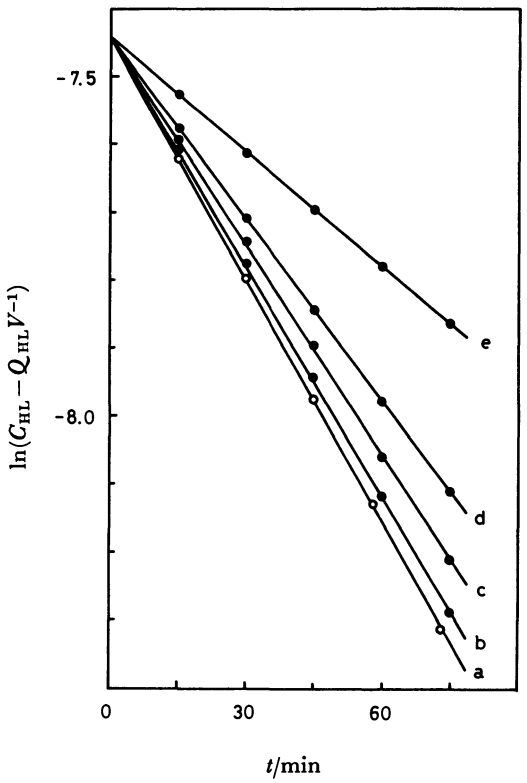

Fig. 5. The effect of C_M on the plots of $\ln(C_{HL}-Q_{HL}V^{-1})$ vs. t. N_2 gas flow rate 895 cm^3 min^{-1}; C_{HL} 5.85×10^{-4} mol dm^{-3}; (a): $C_M=0$, pH=2.30, (b): $C_{Ni}=1.97\times10^{-3}$ mol dm^{-3}, pH=4.80, (c): $C_{Ni}=4.93\times10^{-3}$ mol dm^{-3}, pH=4.80, (d): $C_{Ni}=9.85\times10^{-3}$ mol dm^{-3}, pH=4.76, (e): $C_{Ni}=4.93\times10^{-2}$ mol dm^{-3}, pH=4.63.

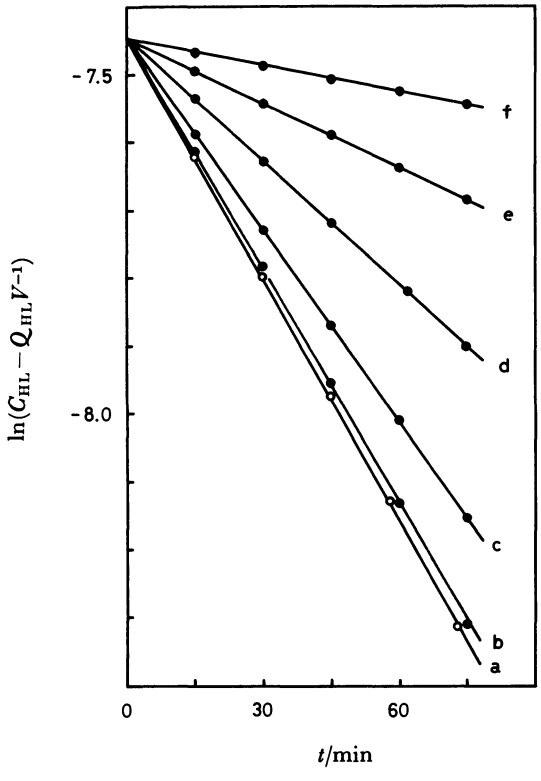

Fig. 6. The effect of pH on the plots of $\ln(C_{HL}-Q_{HL}V^{-1})$ vs. t. N_2 gas flow rate 895 cm^3 min^{-1}; C_{HL} 5.85×10^{-4} mol dm^{-3}; C_{Cu}(sulfate): (a) 0, (b)—(f) 1.98×10^{-3} mol dm^{-3}; pH: (a) 2.30, (b) 1.02, (c) 3.00, (d) 3.68, (e) 4.28, (f) 4.89.

The k and K_a values being known from the runs undertaken in the absence of metal, we can evaluate K_1 for each metal from the slope of the straight line. The K_1 values thus determined for Cu and Ni under various C_M and pH conditions are given in Table 1, and those for the other seven metals studied are summarized in Table 2, in which the K_1 values evaluated by using the reference pK_a(=8.82) are also listed together with those reported in the literature.[4-8] The K_1 values obtained by the present method are in reasonable agreement within 0.1 to 0.2 in the log unit with the literature values except for Al(III), which case differs by ca. 0.4 log unit.

Discussion

There are various factors which affect the precision and accuracy of the method proposed here for evaluating association constants between volatile and nonvolatile solutes. As was noted in a previous paper,[1] it is a requirement to carry out two separate runs, one in the absence and the other in the presence of nonvolatile solutes, under the same aeration conditions. To meet this requirement, the same sintered glass ball should be used in common, and the N_2 gas flow rate should be controlled to be as identical with each other as possible. Indeed, the rate constant, k, the absolute value of which is of no significance, is a function of the aeration rate (Fig. 3). In addition, the ionic strength and the kind of the electrolyte used to adjust it should be the same for the two runs, because the so-called salting-out effect may influence the volatility of the solute of interest, and hence the k value.

Particular attention should be paid to the presence of such electrolytes as may cause association with the nonvolatile solute to be studied, since this also affects the accuracy of the present method. For instance, the K_1 value for Cu decreases step by step as C_M increases, as can be seen from Table 1, when the sulfate salt is used; we first thought this arose from the salting-out of SO_4^{2-} ions, but it now seems more reasonable to consider ion-pair formation between Cu^{2+} and SO_4^{2-}.[10] The K_1 value of Cu(II) for the chloride salt is employed for this reason. Incidentally, the ion-pair formation constant has been reported to be ca. 200 at 25 °C and at ionic strengths corrected to zero.[3] The K_1 value of Cu(II) for the sulfate salt is to be underestimated unless the free metal ion concentration, $[M^{n+}]$, in the experimentally determined slope, $-k/(1+K_1K_a[M^{n+}][H^+]^{-1})$, is corrected for the

Table 1. Effects of the Total Concentration of Metal Ion and pH of Aqueous Solution on the Estimation of Formation Constants of Cu(II) and Ni(II) Acetylacetonate Complexes[a)]

Metal ion[b)]	$10^3 \times C_M$/mol dm^{-3}	pH	log K_1[c)]
Cu(II), SO_4^{2-}	1.98	3.00	8.3
	4.96	3.00	8.2
	9.92	3.00	8.2
	49.6	3.08	8.0
	1.98	1.02	9.4[d)]
	1.98	3.68	8.2
	1.98	4.28	8.0
	1.98	4.89	7.9
Cu(II), Cl^-	1.96	2.92	8.3
	4.90	2.88	8.3
	9.80	2.85	8.2
	49.0	2.79	8.2
Ni(II), Cl^-	1.97	4.80	5.9
	4.93	4.80	5.9
	9.85	4.76	6.0
	49.3	4.63	5.9
	1.97	3.80	6.5[d)]
	1.97	5.56	5.9
	1.97	6.36	5.7

a) The total concentration of acetylacetone is 5.85×10^{-4} mol dm^{-3}, temperature is 25.0±0.1 °C, and I=0.1 ($NaClO_4$). b) The counter anion is specified. c) Estimated with pK_a=9.17. d) See the text.

Table 2. Formation Constants, K_1, of Matal Acetylacetonates at 25.0±0.1 °C and I=0.1($NaClO_4$)

Metal ion[a)]	$10^3 \times C_M$ / mol dm^{-3}	pH	log K_1	
			This work[b)]	Literature
Cu(II)	1.96—49.0	2.79—2.92	8.3(7.9)[c)]	8.16[d)]
Ni(II)	1.97—49.3	4.63—6.36	5.9(5.5)[c)]	5.72[d)]
Co(II)	2.02	5.58	5.3(5.0)	5.10[e)]
Mg(II)	2.05	7.37	3.5(3.1)	3.34[e)]
Fe(II)	6.44	5.30	5.2(4.9)	5.07[f)]
Fe(III)	4.02	1.82	10.5(10.2)	9.27[g)], 10.5[h)]
Al(III)	4.98	2.00	8.7(8.3)	8.25[g)]

a) Chloride salt except for Fe(III) (ammonium iron(III) sulfate) and Al(III) (aluminium potassium sulfate). b) The total concentration of acetylacetone is 5.85×10^{-4} mol dm^{-3}, and the value are derived based on pK_a=9.17 estimated in this work, those on pK_a=8.82 (the literature value, Ref. 9) being given in the parentheses. c) The average of the chloride salts given in Table 1 (the value for Ni with the superscript d in Table 1 is excluded). d) Ref. 4, 25 °C, I=0.1($NaClO_4$). e) Recommended values cited in Ref. 5, 25 °C, I=0.1(Na^+, H^+)ClO_4^-. f) Ref. 6, 30 °C, I=0. g) Ref. 7, 25 °C, low ionic strength. h) Ref. 8, 25 °C, I=1.0.

ion-pair formation, that is, $[Cu^{2+}]=C_{Cu}-[Cu^{2+}SO_4^{2-}]$.

The choice of proper pK_a value is essential in estimating K_1. We have listed the two K_1 values in Table 2, one being evaluated based on pK_a=9.17 and the other on pK_a=8.82 reported in the literature. Although the K_a value determined in this work is appreciably lower, we are of the opinion that the use of this value leads to a better K_1 value since the same procedure employed to evaluate both pK_a and K_1 tends to compensate for systematic errors inherent in the present method.

An important point to keep in mind is the magnitude of the product, $K_1K_aC_M[H^+]^{-1}$. The value of K_1, cannot be evaluated accurately or at all when the term is too small compared with unity. This may be responsible for the unusual values observed for Cu at pH=1.02 and for Ni at pH=3.80 (Table 1). To get more reliable K_1, the solution pH and/or C_M should desirably be high for metals with relatively small stability constants. The choice of the solution pH, however, may be limited for metals subject to hydrolysis. For metals with large stability constants, on the other hand, these conditions are not necessarily desirable, because it takes a prolonged time to expel the free ligand from the aqueous phase.

When it is necessary to consider hydrolysis of metal ions, the concentration of M^{n+} should be modified by using $\alpha_{M(OH)}$, a side reaction coefficient, into $[M^{n+}]=C_M/\alpha_{M(OH)}$; with correction for the hydrolysis reaction, $M^{n+}+H_2O \rightleftarrows M(OH)^{n-1}+H^+$, the complex formation constant, $K_{1,correct}$, can be written as

$$\log K_{1,correct} = \log K_1 + \log \alpha_{M(OH)},$$

including the second term of the right hand side of the equation as a correction term. This correction term, however, is negligibly small at the solution pH adopted here except for Fe(III). The K_1 value of Fe(III) listed in Table 2 has been corrected by 0.1 in the logarithmic unit; for Fe(III) the literature value of −2.55 was used as $\log K_{hydrol}$, where K_{hydrol} is the hydrolysis constant and can be converted into the side reaction coefficient by the relationship, $\alpha_{M(OH)}=1+K_{hydrol}[H^+]^{-1}$.

An attempt was made to evaluate 1:2 formation constants for some metal acetylacetonato complexes on the basis of the equilibration

$$acac^- + M(acac)^{n-1} \rightleftharpoons M(acac)_2^{n-2},\ K_2 \qquad (9)$$

It is difficult in this case to derive a rate equation like Eq. 7 under the experimental condition $C_{HL}>C_M$ or $C_{HL}\approx C_M$. We therefore tried to estimate K_2 through the following three successive steps. The first step: $\log(Q_{HL}/V)$ is plotted vs. $\log t$ to give a straight line for each run, and the intercept, $\log a$, and the slope, b, are derived. The second step: on the assumption $Q_{HL}/V=a\ t^b$, $dQ_{HL}V^{-1}/dt$ is calculated at a selected aeration time, t, and then, the concentration of free

HL present in the solution at t is obtained based on the rate equation, Eq. 4. The third step: from the mass-balance equations

$$C_{HL} = [HL] + Q_{HL}/V + [L^-] + [ML^{n-1}] + 2[ML_2^{n-2}],$$
$$C_M = [M^{n+}] + [ML^{n-1}] + [ML_2^{n-2}],$$

Table 3. Change in Concentration of Free Ligand and Metal Complexes as a Function of Aeration Time and the Tentatively Estimated Formation Constants, K_2, of Metal Acetylacetonates at 25.0±0.1 °C, I=0.1(NaClO$_4$)

Aeration time/min	Concentration/10^{-4} mol dm^{-3}					log K_2
	Q_{HL}/V	HL	M^{n+}	ML^{n-1}	ML_2^{n-2}	
Cu(II)[a]						
15	1.71	8.26	0.83	6.51	2.46	6.9
30	3.23	7.45	0.98	6.92	1.90	6.9
45	4.53	7.01	1.13	7.49	1.19	6.6
60.5	5.73	6.71	1.27	8.10	0.43	6.2
76.5	6.77	6.49	1.41	8.65		
					Average	6.7
					Literature value[b]	6.84
Ni(II)[c]						
15	1.89	9.12	1.77	5.82	2.26	4.9
30	3.54	8.25	2.04	6.06	1.76	4.9
45	4.99	7.78	2.31	6.49	1.05	4.7
60	6.29	7.47	2.58	6.94	0.33	4.1
75	7.45	7.23	2.82	7.37		
					Average	4.8
					Literature value[d]	4.45
Fe(III)[e]						
15	2.25	11.08	6.43	20.08	11.31	9.7
30	4.28	10.01	6.96	19.63	11.03	9.7
45	6.09	9.43	7.40	19.66	10.40	9.7
60	7.83	9.03	7.80	10.85	9.67	9.7
75	9.43	8.74	8.15	20.07	8.96	9.7
90	10.93	8.51	8.49	20.36	8.21	9.7
					Average	9.7
					Literature value[b]	8.71
Al(III)[f]						
15	2.11	10.02	3.27	4.11	2.58	8.4
30	3.97	8.95	3.67	4.11	2.19	8.4
45	5.53	8.37	4.07	4.27	1.16	8.3
60	6.85	7.98	4.45	4.45	1.06	8.1
75	8.06	7.70	4.82	4.64	0.50	7.7
					Average	8.2
					Literature value[b]	7.35

a) As the chloride salt, $C_{Cu}=9.80\times10^{-4}$ mol dm^{-3}, $C_{HL}=2.14\times10^{-3}$ mol dm^{-3}, pH=4.89, and the data used are pK_a=9.17 and log K_1=8.3. b) Ref. 7. c) $C_{Ni}=9.85\times10^{-4}$ mol dm^{-3}, $C_{HL}=2.14\times10^{-3}$ mol dm^{-3}, pH=6.86, and the data used are pK_a=9.17 and log K_1=5.9. d) Ref. 5. e) $C_{Fe}=4.02\times10^{-3}$ mol dm^{-3}, $C_{HL}=4.87\times10^{-3}$ mol dm^{-3}, pH=2.12, and the data used are pK_a=9.17 and log K_1=10.5. f) $C_{Al}=9.96\times10^{-4}$ mol dm^{-3}, $C_{HL}=2.14\times10^{-3}$ mol dm^{-3}, pH=3.58, and the data used are pK_a=9.17 and log K_1=9.7.

we can derive

$$C_{HL} = [HL] + Q_{HL}/V + K_a[HL][H^+]^{-1} + 2C_M - [M^{n+}](2+K_1K_a[HL][H^+]^{-1}),$$

which allows us to estimate $[M^{n+}]$ by using the K_a and K_1 values evaluated by the present method, and in turn, $[ML^{n-1}]$ and $[ML_2^{n-2}]$ can be determined from the mass-balance relationships, from which K_2 is to be derived. The values thus determined are given in Table 3. Again, if it is necessary to make correction for the hydrolysis of metal ions, the product $[M^{n+}]\alpha_{M(OH)}$ must be employed instead of the simple $[M^{n+}]$; this correction was applied only to Fe(III).

It is informative to follow the change in concentration of such species as M^{n+}, ML^{n-1}, and ML_2^{n-2} as a function of aeration time. As aeration proceeds, $[ML_2^{n-2}]$ decreases with an accompanying increase in $[M^{n+}]$ (and also in $[ML^{n-1}]$ when C_{HL} is sufficiently large compared to C_M). In the case of Fe(III) given in Table 3, there was observed a steady state with respect to the ML^{n-1} species, which may result from C_{HL} being nearly equal to C_M. It appears that the K_2 value thus derived for each metal falls gradually as aeration proceeds. This is quite unreasonable and is probably caused by the assumption made in the second step, that is, the Q_{HL}/V vs. t plot follows a parabolic curve. In reality, the log(Q_{HL}/V) vs. log t plots show a slight deviation from the linearity and this trend is pronounced with prolonging aeration time. Therefore, the differential treatment of experimental results employed here to estimate K_2 led to erroneous evaluation of 1:2 association constants.

If it is convenient to follow the rate of decrease in the concentration of the associated species instead of measuring the releasing rate of the volatile solute expelled from the aqueous into the gaseous phase, the rate equation can be expressed as

$$-d[A\cdot B]/dt = kK^{-1}[A\cdot B][B]^{-1} = kK^{-1}[A\cdot B](C_M-[A\cdot B])^{-1},$$

which becomes, on integration and with $[A\cdot B]=[A\cdot B]_o$, the initial (t=0) concentration

$$C_B \ln [A\cdot B] - [A\cdot B] = -kK^{-1}t + C_B \ln [A\cdot B]_o - [A\cdot B]_o,$$

where A, B, and A·B denote the volatile, nonvolatile, and associated species, respectively, K is an association constant, and k is a rate constant of the expulsion of A from the aqueous phase in the absence of B. This is essentially the same form as that previously used to determine the disproportionation constant of mercury(I).[1] Implicit in this rate equation and also in Eq. 4 (and Eq. 7) is the assumption that the transfer of volatile solute from

the aqueous into the gaseous phase is the rate-determining step. If, on the other hand, an association equilibrium is the rate-determining step. the association constant cannot be estimated. This is a limitation on the applicability of the present method.

In general, it is somewhat difficult to measure association constants between nonvolatile and highly volatile solutes, because it is hard to maintain constant the concentration of the latter in the aqueous medium. The present method is applicable only to very volatile solutes, and in this respect seems complementary. The present technique need not maintain the volatile solute concentration constant, and its total concentration in the aqueous medium can easily be determined by aerating the medium with an inert gas for a prolonged period and by trapping the released solute during the aeration

An important application of the method proposed here will be encountered when hydrophobic interaction is to be studied in the aqueous environment between nonvolatile and volatile solutes.

The present work was partially supported by a Grant-in-Aid for Scientific Research (No. 6054037) from the Ministry of Education, Science and Culture.

References

1) I. Sanemasa and T. Hirata, *Bull. Chem. Soc. Jpn.*, **50**, 3255 (1977).

2) N. Nakashima and O. Tôyama, *Bull. Chem. Soc. Jpn.*, **45**, 3210 (1972).

3) L. D Sillén and A. E. Martell, "Stability Constants of Metal-Ion Complexes." The Chemical Society, Burlington House, London (1964), and its Suppliment No. 1 (Special Publication No. 25. 1971).

4) G. Gutnikov and H. Freiser, *Anal. Chem.*, **40**, 39 (1968).

5) J. Starý and J. O. Liljenzin, *Pure Appl. Chem.*, **54**, 2557 (1982).

6) R. M. Izatt, W. C. Fernelius, and B. P. Block, *J. Phys. Chem.*, **59**, 80 (1959).

7) A. Krishen and H. Freiser, *Anal. Chem.*, **31**, 923 (1959).

8) D. P. Fay, A. R. Nichols, and N. Sutin, *Inorg. Chem.*, **10**, 2096 (1971).

9) J. Rydberg, *Svensk. Kem. Tidskr.*, **67**, 499 (1955), cited in Ref. 3.

10) The authors are grateful to an Editor and to a reviewer who suggested the ion-pair formation for Cu(II) in the presence of sulfate ions.

 © 1986 The Chemical Society of Japan Bull. Chem. Soc. Jpn., 59, 1467—1470 (1986)

Nucleophilic Ring-Substitution Reactions of Unsymmetrical Quadridentate Schiff Base and Its Complex of Nickel(II) or Copper(II) with Ethyl Mercaptoacetate

Kuninobu KASUGA,* Hiroshi KURAMITSU, Mayumi KADOWAKI, Takeo NAGAHARA, and Yasuo YAMAMOTO

Department of Chemistry, Faculty of Science, Shimane University, Matsue 690

(Received September 24, 1985)

The nucleophilic replacement of halogen on the methine carbon of a Schiff base complex of nickel(II) or copper(II) by ethyl mercaptoacetate in dichloromethane proceeds via a four-centered intermediate, in which two polarizable atoms, such as bromine and sulfur, may stabilize strained bond angles. In the case of a free Schiff base ligand, a relatively stable adduct was spectrophotometrically confirmed. The adduct is thought to have a configuration analogous to that of a spiro compound containing a five-membered ring. Free ligands show no absorption bands in the wavelength region longer than 340 nm, while the adduct shows band at 375 nm assignable to a n-π* transition.

Many electrophilic substitutions of coordinated ligands have been reported; e.g. the methine protons of β-diketonato metal complexes have been replaced by such electrophiles as bromine, iodine, acyl derivatives, and sulfur.[1] The substitutions have also been reported on a quadridentate Schiff base complex of nickel(II) or copper(II), and those kinetics have been investigated.[2-4] On the other hand, only a few nucleophilic substitutions have been reported; the further conversion of the halogeno-substituted methine carbon of the β-diketone or a quadridentate Schiff base complex was been carried out with such nucleophiles as benzenethiol, its derivatives, and ethyl mercaptoacetate.[5-7] In this paper, we wish to report further studies of the nucleophilic substitution mechanism of the unsymmetrical quadridentate Schiff base and its complex of nickel(II) or copper(II) with ethyl mercaptoacetate, $HSCH_2CO_2C_2H_5$. The complexes used in this study are shown in Fig. 1.

Results and Discussion

The Substitution Reaction of the Nickel(II) or Copper(II) Complex. By the addition of ethyl mercaptoacetate, the spectrum of Ni(L-Br, CH_3) in dichloromethane changed to that of Ni(L-$SCH_2CO_2C_2H_5$, CH_3), with an isosbestic point at 288 nm (Fig. 2). The rate of reaction (1) was determined by means of the absorbance change at 385 nm by the use of a pseudo- first-order method:

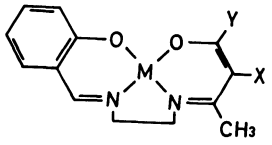

M(L-X,Y)

Fig. 1. Abbreviation of the Schiff base metal complexes.

$$Ni(L\text{-}Br,\ CH_3) + HSCH_2CO_2C_2H_5 \longrightarrow Ni(L\text{-}SCH_2CO_2C_2H_5,\ CH_3) + HBr \quad (1)$$

The plot of $-\ln(A_\infty - A_t)$ vs. the time was linear to at least 80% completion, where A_t and A_∞ represent the absorbances at time t and infinity respectively. The pseudo- first-order rate constant (k_{obsd}) was estimated from its slope. The rate was also measured at

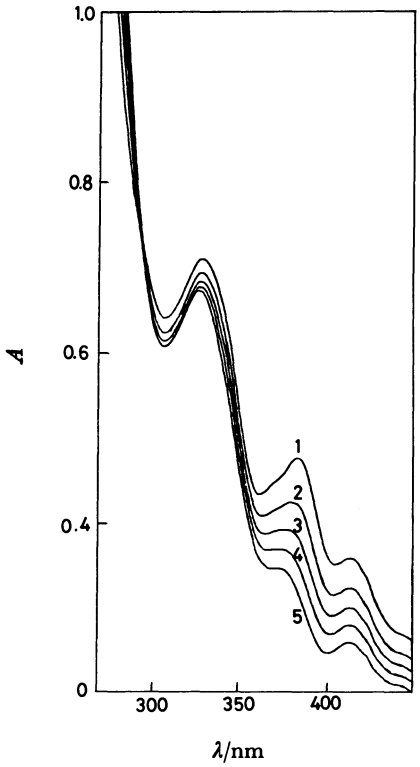

Fig. 2. Spectral change during the reaction of Ni(L-Br, CH_3) with ethyl mercaptoactate in dichloromethane at 20 °C: $[Ni(L\text{-}Br,CH_3)]_0 = 1.50 \times 10^{-4}$ mol dm^{-3}, $[HSCH_2CO_2C_2H_5]_0 = 3.00 \times 10^{-3}$ mol dm^{-3}. 1: 30 s, 2: 10 min, 3: 30 min, 4: 45 min, and 5: 80 min after the reaction.

Table 1. The Rate Constants for the Reactions of the Nickel(II) and Copper(II) Complexes with Ethyl Mercaptoacetate in Dichloromethane

Run	$k^{a)}_{obsd}/10^{-3}$ s^{-1}	Conditions
1	2.45±0.35	Ni(L-Br, CH_3) + $HSCH_2CO_2C_2H_5$ (2.25×10^{-3} mol dm^{-3})
2	2.71±0.55	(3.30×10^{-3} mol dm^{-3})
3	3.12±0.52	(3.75×10^{-3} mol dm^{-3})
4	4.44±0.63	(4.50×10^{-3} mol dm^{-3})
5	4.76±0.41	(5.25×10^{-3} mol dm^{-3})
	$k^{b)}$/mol^{-1} dm^3 s^{-1}	
6	$(9.20\pm0.98)\times10^{-1}$	Ni(L-Br, CH_3) + $HSCH_2CO_2C_2H_5$
7	$(1.12\pm0.15)\times10^{-3}$	Ni(L-Cl, CH_3) + $HSCH_2CO_2C_2H_5$
8	4.40±0.51	Ni(L-Br, C_6H_5) + $HSCH_2CO_2C_2H_5$
9	$(5.30\pm1.20)\times10$	Cu(L-Br, CH_3) + $HSCH_2CO_2C_2H_5$
	$k^{a,c)}_{obsd}/10^{-2}$ s^{-1}	Ni(L-Br, CH_3) + $HSCH_2CO_2C_2H_5$
10	0.53±0.11	$[EtOH]_0$ = 0.2%(v/v)
11	0.91±0.14	0.4%
12	1.25±0.18	0.6%
13	1.63±0.13	0.8%
14	1.94±0.21	1.0%
15	3.57±0.24	1.5%
16	4.33±0.28	2.0%

a) The first-order rate constants. b) The second-order rate constants. c) $[HSCH_2CO_2C_2H_5]_0 = 3.00\times10^{-3}$ mol dm^{-3}. $[complex]_0 = 1.50\times10^{-4}$ mol dm^{-3}.

327 nm. Both values were the same (within the limit of experimental error), showing no wavelength-dependence of the rate. The value of k_{obsd} was proportional to the concentration of ethyl mercaptoacetate, indicating that the reaction order is first in the concentration of the nucleophile (Runs 1—5 in Table 1).

Ni(L-Br, CH_3) did not react with ethyl hydroxyacetate under the same conditions as those used for ethyl mercaptoacetate. This corresponds to the finding that acetylacetone complexes of aluminum(III), chromium(III), iron(III), and cobalt(III) react with benzenethiols, but not with phenols.[5] The rate constant of the reaction for Ni(L-Cl, CH_3) was very small compared with that for Ni(L-Br, CH_3)(Runs 6 and 7). It has also been reported that the substitution for Ni(L-Br, C_6H_5) is performed with *N*-bromosuccinimide, but not with *N*-chlorosuccinimide.[8] That is, at least two polarizable atoms, such as sulfur and bromine, are required to promote the reaction facilely. The following four-centered intermediate might be proposed in view of the results concerning a solvent effect to be discussed later:

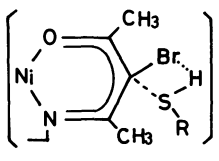

Scheme 1.

where R is $CH_2CO_2C_2H_5$.

A sulfur atom of the nucleophile is more polarizable than an oxygen atom; thus, the clouds of valence electrons about the sulfur atom are more easily distorted by methine carbon than those about the oxygen atom. A bromine atom might play the same role in the intermediate. Then, the polarizable sulfur and bromine atoms must stabilize the strained intermediate. By the addition of ethanol (>2% v/v) to the dichloromethane solution of Ni(L-Br, CH_3) and ethyl mercaptoacetate, the reaction was strongly depressed. Ethanol destabilizes the intermediate, with the formation of a hydrogen bond. However, the rate was increased up to 2% of ethanol (Runs 10—16). Probably, ethyl mercaptoacetate forms a dimer in a nonpolar solvent such as dichloromethane; thus, the concentrations of the monomer species which is active for the reaction might be increased by the addition of adequate amounts of ethanol.

A similar intermediate has been proposed for the nucleophilic substitution of the bromo-substituted methine carbon of the β-diketonato metal complexes for thiophenols; the reaction occurred in dichloromethane, but was depressed in a polar solvent, such as ethanol, acetone or ethyl ether. The reaction was also inhibited by the addition of small amounts of pyridine or piperidine.[5]

The rate constant for Ni(L-Br, C_6H_5) was about six times that for Ni(L-Br, CH_3) (Runs 6 and 8). A phenyl group attracts an electron from the chelate ring, promoting the nucleophilic substitution on the methine carbon. The rate constant for Cu(L-Br, CH_3)

is about fifty times that for Ni(L-Br, CH_3) (Runs 6 and 9). The electronegativities of the nickel(II) and copper(II) ions are almost the same,[9] which might exclude the inductive effect of the central metal ion on the reaction rate. The same tendency has been reported for the case of the electrophilic substitution reactions of M(L-H, CH_3), where M is H_2, Cu(II), or Ni(II), for *N*-chlorosuccinimide; e.g., the copper(II) complex shows an extremely large rate constant as compared with the nickel(II) complex and the free ligand.[4] As has been proposed for the electrophilic substitution, the copper(II) ion may catalyze the reaction via the formation of an ethyl mercaptoacetate adduct. However, the details are not known at present.

The Substitution Reaction of the Free Ligand. The spectral change of the free ligand, H_2(L-Br, CH_3) with ethyl mercaptoacetate is shown in Fig. 3. At first, the absorption band of H_2(L-Br, CH_3) at 328 nm was decreased, and then new peaks appeared at 284 and 375 nm; isosbestic points were found at 242, 263, 311, and 352 nm. Subsequently, both bands were gradually decreased, followed by the appearance of the band at 316 nm, where isosbestic points were not observed, probably because of the presence of side reactions. However, the final spectrum is consistent with that of hydrobromide of H_2(L-$SCH_2CO_2C_2H_5$, CH_3), the preparation of which will be discussed later. That is, a relatively stable adduct might be formed in the reaction of the free ligand and ethyl mercaptoacetate.

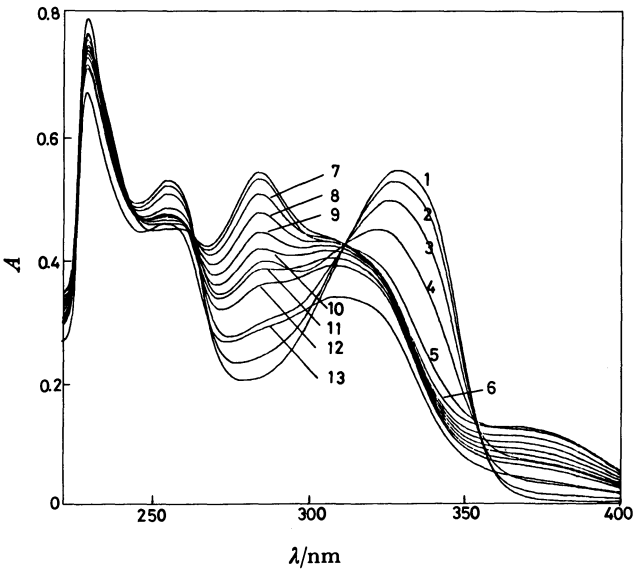

Fig. 3. Spectral change during the reaction of H_2(L-Br,CH_3) with ethyl mercaptoacetate in dichloromethane at 20 °C; $[H_2(L\text{-}Br,CH_3)]_0 = 1.00 \times 10^{-4}$ mol dm^{-3}, $[HSCH_2CO_2C_2H_5]_0 = 2.50 \times 10^{-4}$ mol dm^{-3}. 1: 1 min, 2: 30 min, 3: 1 h, 4: 1 h 30 min, 5: 2 h, 6: 2 h 30 min, 7: 3 h 30 min, 8: 4 h 30 min, 9: 5 h 50 min, 10: 7 h 10 min, 11: 10 h 20 min, 12: 11 h 20 min, and 13: 19 h 40 min after the reaction. The intensiry of absorption at 284 nm was increased in time courses from 1 to 6, whereas it was decreased from 7 to 13.

To elucidate the reaction mechanism, a few further experiments were carried out. The formation rate of the adduct in benzene was faster than that in dichloromethane, but the spectrum of H_2(L-Br, CH_3) did not change upon the addition of the nucleophile in ethanol. The spectrum of the free ligand also did not change with ethyl hydroxyacetate. In addition, the spectrum of H_2(L-H, CH_3) and H_2(L-Cl, CH_3) showed no change with ethyl mercaptoacetate. Thus, two polarizable atoms must be required to form the adduct. Attempts to isolate the adduct were unsuccessful because of decomposition during purification. As *p*-toluenethiol has been reported to act as a nucleophile toward a Schiff base nickel(II) complex,[7] it was added to the dichloromethane solution of the free ligand. The spectral change was similar to that of ethyl mercaptoacetate; e.g., at first, a band appeared around 375 nm, but subsequently its intensity was decreased. By the addition of 1-butanethiol, similar spectral change was also observed. That is, only the SH group of the nucleophile must play an important role in the formation of the adduct. The band at 375 nm disappeared in polar solvents, such as methanol, ethanol, and acetone. The free ligands, such as H_2(L-H, CH_3), H_2(L-Cl, CH_3), H_2(L-Br, CH_3), and H_2(L-$SCH_2CO_2C_2H_5$, CH_3), exhibit no band at wavelengths longer than 340 nm. Therefore, the new band may be ascribed to a n-π^* transition in the adduct.

It is known that the free Schiff base ligand has three tautomeric forms: The Schiff base, the keto enamine, and the imino enol.[10] Although the keto-enamine form exists predominantly in solution,[10] with the nucleophile, the Schiff base type might form an adduct with a five-membered ring system (see the following reaction Scheme). Because the strains of the bond angles must be less than those in the four-centered system, the free Schiff base ligand at first forms a relatively stable spiro-type adduct with the nucleophiles. On the other hand, the metal complex can not form the adduct because of the lack of the enol hydrogen atom.

The nucleophilic-substituted ligand was also prepared; pale yellow precipitates were immediately obtained by the reaction of H_2(L-Br, CH_3) and ethyl mercaptoacetate in a benzene solution, but could not be characterized because of their decomposition to a brownish, tarry material. A test of silver nitrate was positive for the precipitates, showing the presence of bromide. To characterize the precipitates, nickel(II) acetate was added to their methanol solution; the orange nickel(II) complex was thus obtained and identified as Ni(L-$SCH_2CO_2C_2H_5$, CH_3) by means of an elemental analysis and ^1H NMR measurements. Thus, the precipitates might be confirmed to be

hydrobromide of H_2(L-$SCH_2CO_2C_2H_5$, CH_3). In the ^1H NMR spectrum of the salt, an additional proton signal appeared in the low magnetic field (δ=11.02), probably arising from a -CH=N$\underline{H}^+$- proton. By the addition of an adequate amount of triethylamine to the salt, hydrogen bromide was liberated, resulting in an oily H_2(L-$SCH_2CO_2C_2H_5$, CH_3) compound which showed no band at 375 nm in dichloromethane. That is, the reaction might proceed as follows:

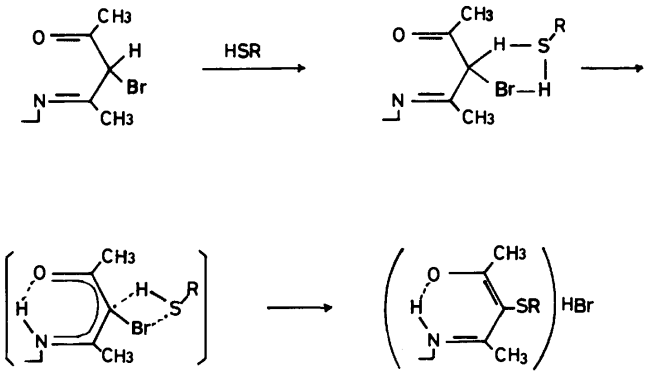

Scheme 2.

Consequently, the reaction of the Schiff base metal complex with ethyl mercaptoacetate proceeds via the four-centered intermediate, in which two polarizable atoms are required to stabilize the strained bond angles. On the other hand, the free Schiff base ligand at first forms the adduct with the five-membered ring system which shows the characteristic absorption band at 375 nm. Subsequently, the adduct slowly changes to the final product via the above intermediate.

Experimental

The Cu(L-Br, C_6H_5), Cu(L-Cl, C_6H_5), Ni(L-$SCH_2CO_2C_2H_5$, CH_3), and Ni(L-$SCH_2CO_2C_2H_5$, CH_3) complexes were prepared by the method described before.[4]

The Preparation of Cu(L-$SCH_2CO_2C_2H_5$, CH_3). A complex was prepared in a manner similar to those used for the nickel(II) complexes and was recrystallized with a mixture of methanol and water. Found: C, 50.37; H, 5.39; N, 6.61%. Calcd for $C_{18}H_{22}O_4SCu$: C, 50.75; H, 5.22; N, 6.57%. UV(CH_2Cl_2)λ_{max}(log ε) 268 (4.26), 328 (4.04), 384 (3.66), and 554 (2.65) nm. IR (ν CO) 1730 cm^{-1}.

The Preparation of Hydrobromide of H_2(L-$SCH_2CO_2C_2H_5$, CH_3). A benzene solution (20 cm^3) of 0.21 cm^3 (2.0 mmol) $HSCH_2CO_2C_2H_5$ was added to 50 cm^3 of a benzene solution containing 0.67 g (2.0 mmol) H_2(L-Br, CH_3); the mixture was then stirred at room temperature for 20 min. The pale yellow precipitates were filtered off and dried in a nitrogen atmosphere. The compound was sealed in a sample tube which had been purged with a nitrogen gas to prevent its decomposition into the brownish tarry material in air. ^1H NMR (DMSO-d_6) δ=1.39 (3H, t, CH_3), 2.67 (6H, s, CH_3), 3.43 (2H, s, SCH_2), 3.96—4.62 (6H, m, CH_2CH_2, $C\underline{H}_2CH_3$), 7.59—8.48 (4H, m, C_6H_4), 9.34 (H, s, -C$\underline{H}$=NH^+-), and 11.02 (H, s, -CH=N$\underline{H}^+$-) ppm.

The Preparation of H_2(L-$SCH_2CO_2C_2H_5$, CH_3). Adequate amounts of triethylamine were added to a dichloromethane suspension of the tarry hydrobromide salt, which then immediately dissolved. The hydrobromide of triethylamine was extracted with water for a few times, and the remaining dichloromethane solution was dehydrated on anhydrous sodium carbonate. When the solution was then concentrated under a reduced pressure, an oily material was obtained. ^1H NMR ($CDCl_3$) δ=1.25 (3H, t, CH_3), 2.34 (6H, d, CH_3), 3.33 (2H, s, SCH_2), 3.94 (4H, m, CH_2CH_2), 4.16—4.46 (2H, q, $C\underline{H}_2CH_3$), 7.44—8.09 (4H, m, C_6H_4), and 9.17 (H, s, CH=N) ppm. The orange nickel(II) complex was derived by adding an aqueous solution of nickel(II) acetate to the methanol solution of the oily material; it was then recrystallized with methanol. Found: C, 51.12; H, 4.95; N, 6.34%. Calcd for $C_{18}H_{22}N_2O_4SNi$: C, 51.33; H, 5.28; N, 6.65%. ^1H NMR ($CDCl_3$) δ=1.42 (3H, t, CH_3), 2.54 (3H, s, CH_3), 2.57 (3H, s, CH_3), 3.33—3.70 (6H, m, SCH_2, CH_2CH_2), 4.36—4.52 (2H, m, $C\underline{H}_2CH_3$), 7.16—7.99 (4H, m, C_6H_4), and 8.51 (H, s, CH=N) ppm. IR (ν CO) 1739 cm^{-1}.

Measurements. The ^1H NMR spectra were recorded with a JEOL-MH 100 spectrophotometer at a frequency of 100 MHz. The chemical shifts were determined in ppm, using TMS as the internal standard. The electronic spectra in solution and the infrared spectra using KBr pellets were measured on a Hitachi 124 spectrophotometer and a Hitachi 215 spectrophotometer respectively.

The authors wish to thank Mr. S. Kiyota for his preparation of some samples for kinetic measurements.

References

1) J. P. Collman, *Adv. Chem. Ser.* **37**, 78 (1963); J. P. Collman, *Angew. Chem.*, **77**, 154 (1965); K. C. Joshi and N. V. Patack, *Coord. Chem. Rev.*, **22**, 37 (1977).

2) T. Nagahara, K. Kasuga, and Y. Yamamoto, *Inorg. Nucl. Chem. Lett.*, **17**, 235 (1981).

3) Y. Fujii, M. Ito, and K. Akiyama, *Bull. Chem. Soc. Jpn.*, **54**, 2527 (1981).

4) K. Kasuga, T. Nagahara, T. Masuda, S. Kiyota, and Y. Yamamoto, *Bull. Chem. Soc. Jpn.*, **57**, 1631 (1984).

5) Z. Yoshida, H. Ogoshi, and Y. Shimizu, *Kogyo Kogaku Zosshi*, **72**, 1648 (1969).

6) Y. Yamamoto, K. Kasuga, and A. Sumita, *Bull. Chem. Soc. Jpn.*, **49**, 2021 (1976).

7) K. Kasuga, T. Nagahara, S. Kiyota, and Y. Yamamoto, *Inorg. Chim. Acta*, **87**, 165 (1984).

8) K. Kasuga, T. Nagahara, K. Kuramitsu, and Y. Yamamoto, *Inorg. Chim. Acta*, **113**, 13 (1986).

9) A. L. All-red, *J. Inorg. Nucl. Chem.*, **17**, 215 (1961).

10) G. O. Dudeck and R. H. Holm, *J. Am. Chem. Soc.*, **83**, 2099 (1961), **84**, 2691 (1962).

^{13}C NMR Study of the Cobalt(III) Complexes Containing Ethylenediamine-*N*-acetate (edma): $[Co(edma)_2]^+$ and [Co(ida)(edma)]

Tomoharu AMA,* Hiroshi KAWAGUCHI, and Takaji YASUI
Department of Chemistry, Faculty of Science, Kochi University,
Akebono-cho, Kochi 780
(Received November 13, 1985)

The ^{13}C NMR chemical shifts of the glycinate ring (G-ring) carbons of edma's in the six geometrical isomers of $[Co(edma)_2]^+$ were measured. It was shown that the trans ligands and chelation form (meridional or facial form) influence the ^{13}C NMR chemical shifts of the G-ring carbons in the same way as the magnetic anisotropy generated on the cobalt(III) center does. The chemical shifts of the ethylenediamine ring (E-ring) carbons of coordinating edma's were also influenced by the trans ligands and the chelation form, similarly to those of the G-ring carbons. Four geometrical isomers of [Co(ida)(edma)] were newly prepared and their structural assignments were made according to their ^{13}C NMR behavior.

It is known that the ^{13}C NMR chemical shifts of a ligand in the cobalt(III) complexes are influenced by the magnetic anisotropy of the cobalt center,[1] the chelation forms[2,3] (e. g. mer- and fac- forms), and the nature of the ligating atom in the trans position to the ligand. The latter influence has been studied for the glycinate ligand in the $[Co(ox)_x(gly)_y(en)_z]$ ($x+y+z=3$) series by Juranic et al.[4] However, their results have not yet been applied to the complexes of polydentate ligands having glycinate rings (G-ring).

In previous papers,[5,6] the structural assignments of the geometrical isomers of $[Co(edma)_2]^+$ (edma: $NH_2CH_2CH_2NHCH_2COO^-$) were reported. In this work we expand the results of Juranic et al. to the G-ring and to the ethylenediamine ring (E-ring) of edma in the six isomers of $[Co(edma)_2]^+$ and clarify which factor is the most important one to evaluate the ^{13}C chemical shifts of the coordinating edma's, comparing the three influences mentioned above. The result obtained for the $[Co(edma)_2]^+$ complex are applied to the newly prepared isomers of [Co(ida)(edma)] (ida: $NH(CH_2COO^-)_2$). The geometrical structures of the latter are discussed on the basis of absorption and ^{13}C NMR spectral data.

Experimental

Preparation of the Complexes. Four Isomers of the [Co(ida)(edma)] Complex: A solution containing 2.4 g of $CoCl_2 \cdot 6H_2O$, 1.3 g of iminodiacetic acid (H_2ida) and 2.3 g of ethylenediamine-*N*-acetic acid dihydrochloride dihydrate ($Hedma \cdot 2HCl \cdot 2H_2O$) in 100 cm^3 of water was adjusted to pH 5 with a 2 mol dm^{-3} NaOH solution. The pH being kept constant at 5, 24 g of PbO_2 was stirred into the solution in small portions at 30 °C. After 1 h, insoluble materials were removed by filtration. A solution containing neutral complexes was obtained by passing the filtrate through an SP-Sephadex (K^+ form) column and a QAE-Sephadex (SO_4^{2-} form) column (eluent: water). This solution was evaporated to about 10 cm^3 and poured onto a QAE-Sephadex (Cl^- form) column. A band adsorbed on the column was separated into three parts by recyclic developement with water: The first, a brown band; the second, two overlapped bands (violet and red-brown); and the third, a pink band. The second part was repeatedly developed on a QAE-Sephadex column (SO_4^{2-} form), by which means the violet (earlier eluate) and the red-brown (later eluate) bands were separated. Each solution eluted from the four bands was concentrated under reduced pressure, after which methanol was added to the concentrated solution to obtain crystals. Recrystallization was carried out from water by adding methanol except for the pink isomer which was recrystallized from warm water. Yields: The brown, 320 mg; the violet, 570 mg; the red-brown, 10 mg; and the pink isomer, 300 mg. Found for the brown isomer: C, 30.86; H, 4.76; N, 13.53%. Calcd for $[Co(ida)(edma)]=C_8H_{14}N_3O_6Co$: C, 31.28; H, 4.59; N, 13.68%. Found for the violet isomer: C, 29.24; H, 5.14; N, 12.74%. Found for the red-brown isomer: C, 29.54; H, 5.01; N, 12.96%. Found for the pink isomer: C, 29.51; H, 5.06; N, 12.90%. Calcd for $[Co(ida)(edma)] \cdot H_2O=C_8H_{16}N_3O_7Co$: C, 29.55; H, 4.96; N. 12.92%.

Six Isomers of the $[Co(edma)_2]X$ Complex: The preparation and separation were described in our previous paper.[5,6]

Spectral Measurements. The ^{13}C NMR spectra of the isomers were recorded on a JEOL FX-100 spectrometer, in the pulsed Fourier transform/proton noise decoupled mode. The field frequency ratio was stabilized by locking to internal D_2O. The peak positions were measured relative to internal dioxane (δ=67.40). No ^{13}C NMR spectra were obtained for the pink isomer of [Co(ida)(edma)] because of its low solubility in D_2O.

The two $-\underline{C}H_2-$ carbons neighboring to -NH- in coordinating edma ($-\underline{C}H_2NH\underline{C}H_2-$) were distinguished from one another by means of the ^1H selective decoupling method as the carbons were observed in the close magnetic fields in each isomer of $[Co(edma)_2]^+$; the methylene carbon of the G-ring appeared as a singlet peak when the glycinate $-CH_2-$ protons were decoupled. The signals which appeared near δ=180 and 40 were assigned to $-\underline{C}OO^-$ and $-\underline{C}H_2NH_2$ carbons, respectively.

The visible and UV absorption spectra were recorded on a HITACHI 557 spectrophotometer in aqueous solutions.

Results and Discussion

The numbering of the carbons in an edma ligand is as follows.

NH_2-CH_2-CH_2-NH-CH_2-COO^-
C-4 C-3 C-2 C-1

The $[Co(edma)_2]^+$ complex provides six geometrical isomers as shown in Fig. 1. The structural assignments of the geometrical isomers have been reported in the previous papers.[5,6] The ^{13}C NMR data of these isomers are listed in Table 1.

It is known that the chemical shifts of the ligands are influenced by the magnetic anisotropic effect of the cobalt(III) ion. The method of estimating this effect has been studied by Yoneda et al.[1] The anisotropy values (σ_{Co}) calculated for the coordinating edma's in $[Co(edma)_2]^+$ are presented in Table 1, together with the observed (δ^{obsd}) and corrected ($\delta^{cor}=\delta^{obsd}+\sigma_{Co}$) chemical shift values.

The ^{13}C NMR Chemical Shifts of the Complex Containing Facially Coordinating edma (*fac*-edma). The corrected chemical shift (δ^{cor}) of the C-1 carbons in coordinating edma's are classified into three types from the difference of two ligating atoms in the trans positions to two ligating atoms (N and O) of the G-ring of edma, as shown in Fig. 2(a); Types A, B, and C exhibit ^{13}C signals at lower, higher, and middle fields, respectively. Similarly to the C-1 carbons, the δ^{cor} values of the C-2 carbons can also be classified into three types as shown in Fig. 2(b). These results are in agreement with that obtained for the glycine ligand in the $[Co(ox)_x(gly)_y(en)_z]$ series by Juranic et al.[4] However, they do not describe the possibility of the classification for ethylenediamine (en) carbons. In the case of this series of the complex it is difficult to assign accurately each NMR signal to each carbon of

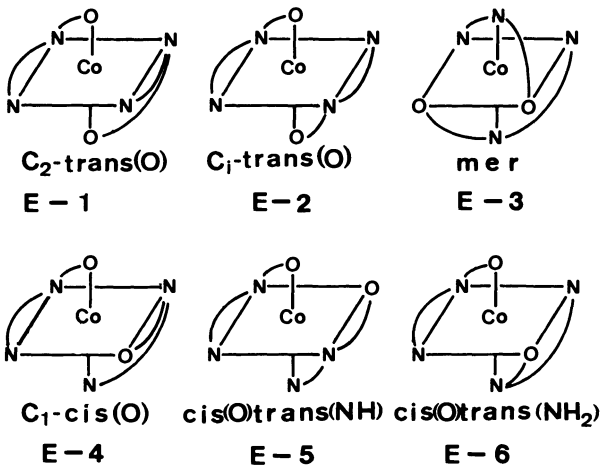

Fig. 1. The six geometrical isomers of the $[Co(edma)_2]^+$ ion.

Table 1. The Observed and Corrected ^{13}C Chemical Shifts and Magnetic Anisotropies from the Cobalt Center of the Isomers of $[Co(edma)_2]^+$ Ion

	C-1 Carbon				C-2 Carbon			
	δ^{obsd}	σ_{Co} c)	δ^{cor} d)	Type e)	δ^{obsd}	σ_{Co} c)	δ^{cor} d)	Type e)
C_2-*trans*(O)	185.61	+0.90	186.51	*fac* A	55.36	−0.06	55.30	*fac* B
C_1-*trans*(O)	185.41	+0.90	186.31	*fac* A	55.41	−0.06	55.35	*fac* B
C_1-*cis*(O)								
in-plane a)	184.30	+0.30	184.60	*fac* B	57.16	+0.27	57.43	*fac* A
out-of-plane b)	185.65	+0.13	185.78	*fac* C	57.16	−0.32	56.84	*fac* C
cis(O)*trans*(NH)	185.71	+0.13	185.84	*fac* C	57.16	−0.32	56.84	*fac* C
cis(O)*trans*(NH_2)	184.44	+0.30	184.74	*fac* B	56.53	+0.27	56.80	*fac* A
mer	184.74	+0.30	185.04	*mer* C	54.04	+0.27	54.31	*mer* C

	C-3 Carbon				C-4 Carbon			
	δ^{obsd}	σ_{Co} c)	δ^{cor} d)	Type e)	δ^{obsd}	σ_{Co} c)	δ^{cor} d)	Type e)
C_2-*trans*(O)	56.28	−0.53	55.75	*fac* C	41.76	−0.50	41.26	*fac* C
C_1-*trans*(O)	56.58	−0.53	56.05	*fac* C	42.25	−0.50	41.75	*fac* C
C_1-*cis*(O)								
in-plane a)	57.79	+0.06	57.85	*fac* A	40.59	−0.32	40.27	*fac* B
out-of-plane b)	55.99	−0.35	55.64	*fac* B	43.52	+0.02	43.54	*fac* A
cis(O)*trans*(NH)	55.36	−0.35	55.01	*fac* B	43.37	+0.02	43.39	*fac* A
cic(O)*trans*(NH_2)	58.53	+0.06	58.59	*fac* A	40.79	−0.32	40.47	*fac* B
mer	52.48	+0.06	52.54	*mer* B	47.51	−0.32	47.19	*mer* A

a) In-plane: in the plane of O-Co-O. b) Out-of-plane: out of the plane of O-Co-O. c) Anisotropies from cobalt(III), which were calculated according to Ref. 1. (+ value: to up-field). d) $\delta^{cor}=\delta^{obsd}+\sigma_{Co}$. e) See Fig. 2.

the en ligand because the chemical shifts of the en carbons are almost the same. On the contrary, as the chemical shift of C-3 is separated from that of C-4 in edma, it is to be easy to remove their erroneous signal assignments. In fact, our present data show that classifications similar to the C-1 and C-2 carbons are possible for the C-3 and C-4 carbons of the E-ring in edma (Table 1).

In both of the E- and G-rings, the difference in the chemical shifts between the Type A and Type B carbons (2—3 ppm) is larger than that caused by the magnetic anisotropy of a cobalt center (<1 ppm). However, the difference between the Types A and C or between the Types B and C is comparable to that caused by the anisotropy.

When a ligating N in the trans position to the ligating O of the G-ring is replaced by O, the C-1 carbon resonance is shifted to a lower field, while the C-2 carbon resonance is shifted to a higher field (alternation effect).[7] (On the contrary, when a ligating N in the trans position to -NH- nitrogen of the G-ring is replaced by O, the C-1 carbon resonance is shifted to a higher field and the C-2 carbon resonance to a lower field.) That is, an influence from the trans position works alternately on the chemical shifts of the C-1 and C-2 carbons in the G-ring. A similar alternation effect is also observed for two neighboring carbons in the E-ring. This effect has been observed for the substituted alkenes and for the protonation shifts of alkylamines.[8,9]

^{13}C NMR Chemical Shifts of the Complex Containing Meridionally Coordinating edma (*mer*-edma).

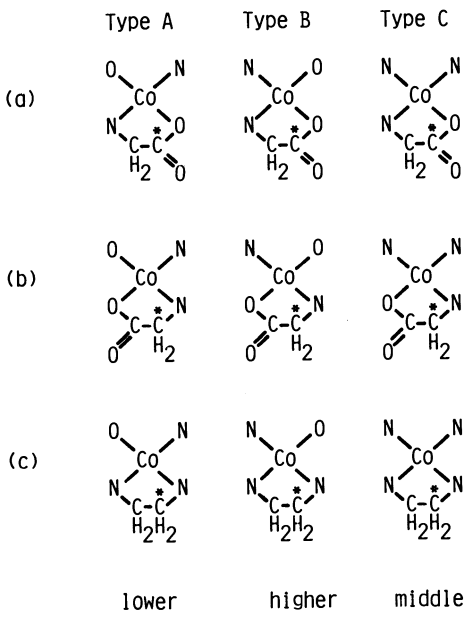

Fig. 2. Classification of the carbons in the coordinating edma: (a) for the C-1 carbon in the G-ring, (b) for the C-2 carbon in the G-ring, and (c) for the C-3 and C-4 carbons in the E-ring.

The chemical shifts of *mer*-edma are different from those of *fac*-edma, that is, the C-2 and C-3 carbons of *mer*-edma exhibit their chemical shifts in a higher field than those of *fac*-edma. This behavior is consistent with that of the $-CH_2NHCH_2-$ carbons of dien (dien: $NH(CH_2CH_2NH_2)_2$) and ida (The carbons in the mer-form resonate in a higher field than those in the fac-form.)[5,6] On the contrary, the C-4 carbon signal of *mer*-edma appears at a lower field than that of *fac*-edma.

The chemical shift difference of C-2 between *mer*- and *fac*-edma's is about 2.5 ppm, and those of C-3 and C-4 are about 3 and 3.5 ppm respectively. These values are much larger than the chemical shift difference caused by the magnetic anisotropy effect of the cobalt center.

Structural Assignments of the Isomers of [Co(ida)(edma)]. Figure 3 shows the geometrical structures of four possible isomers of [Co(ida)(edma)], and Fig. 4 shows their electronic absorption spectra. The pink isomer shows a sharp band in the first absorption band region, while the violet, brown and red-brown isomers show only a broad band or a shoulder band. This behavior makes it possible to assign the pink isomer to *fac*(O) and other three isomers to *mer*(O).[10] The red-brown isomer can be assigned to *mer*(O)*mer*(ch), because its first absorption band has the strongest intensity among the four geometrical isomers.[11] Although the geometrical structure (*mer*(O)*cis*(NH) or *mer*(O)*trans*(NH)) of the other two isomers (violet and brown) can not be assigned solely by the visible absorption spectra, it is possible to assign them from their ^{13}C NMR data.

The chemical shift of the C-4 carbon in *mer*(O)-*mer*(ch) [Co(ida)(edma)] (containing *mer* A Type C-4 carbon) can be calculated, assuming that its δ^{cor}(C-4) value is nearly equal to that of the mer isomer of $[Co(edma)_2]^+$ (which contains *mer* A Type C-4

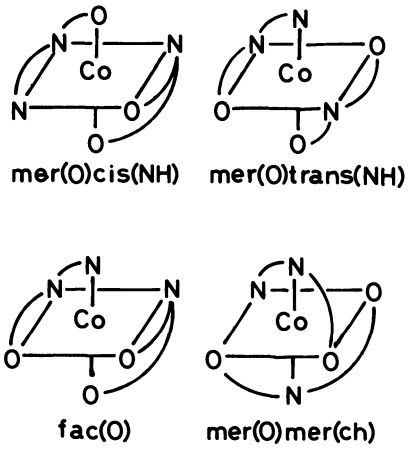

Fig. 3. The four geometrical isomers of [Co(ida)-(edma)].

Table 2. The Calculated and Observed Chemical Shifts of C-4 Carbons of edma in the Isomers of [Co(ida)(edma)]

	σ_{Co}	Type	Estimated δ^{cor} b)	δ^{cal} a)	Color of the isomer	δ^{obsd}
mer(O)*cis*(NH)	−0.5	*fac* B	40.4	40.9	Violet	41.08
mer(O)*trans*(NH)	−0.2	*fac* A	43.5	43.7	Brown	43.86
mer(O)*mer*(ch)	−0.2	*mer* A	47.2	47.4	Red-brown	47.22

a) $\delta^{cal}=\delta^{cor}-\sigma_{Co}$. b) The δ^{cor} values which appeared in Table 1 were averaged.

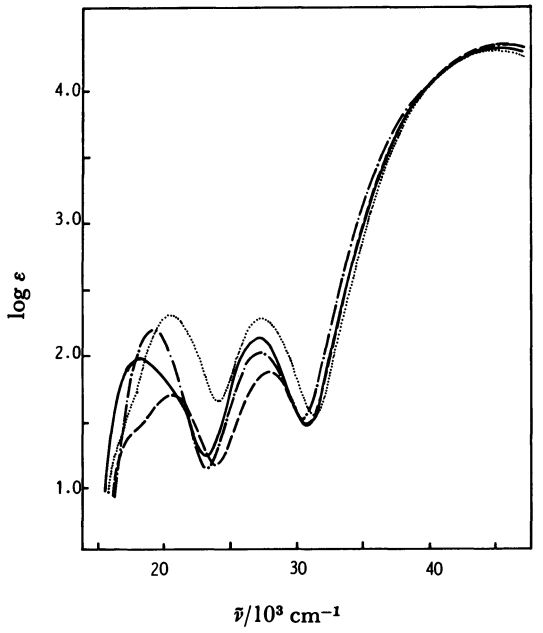

Fig. 4. Absorption spectra of the four isomers of [Co(ida)(edma)]; violet (——), brown (— —), red-brown (·····), and pink (—·—).

carbon, too; δ^{cor}(C-4)=47.2) and that the equation, $\delta^{cal}(=\delta^{obsd})=\delta^{cor}-\sigma_{Co}$, is applicable to the isomer of *mer*(O)*mer*(ch) [Co(ida)(edma)] (the σ_{Co} value (−0.2 ppm) of this isomer is calculated by the method described in Ref. 1.). The δ^{cal}(C-4) value (δ=47.4) of the *mer*(O)*mer*(ch) isomer is nealy equal to the δ^{obsd}(C-4) value of the red-brown isomer (δ=47.22), but not to that of either the violet (δ=41.08) or the brown (δ=43.86) isomer (Table 2). On the basis of these results, the red-brown isomer is assigned to the *mer*(O)*mer*(ch). In the similar manner, comparing the δ^{cal}(C-4) value of the *mer*(O)*cis*(NH) (δ=40.9) or *mer*(O)*trans*(NH) (δ=43.7) [Co(ida)(edma)] with the δ^{obsd}(C-4) values of the obtained *mer*(O)-form isomers of [Co(ida)(edma)], the violet isomer is assigned to *mer*(O)*cis*(NH) and the brown isomer to *mer*(O)-*trans*(NH).

References

1) H. Yoneda, U. Sakaguchi, and Y. Nakashima, *Bull. Chem. Soc. Jpn.*, **48**, 209 (1975).
2) T. Ama, H. Kawaguchi, and T. Yasui, *Bull. Chem. Soc. Jpn.*, **54**, 3597 (1981).
3) F. C. Ha, D. A. House, and J. W. Blunt, *Inorg. Chim. Acta*, **33**, 269 (1979).
4) N. Juranic, M. B. Celap, D. Vucelic, M. Malinar, and N. Radivojsa, *Inorg. Chem.*, **19**, 802 (1980).
5) T. Ama, H. Kawaguchi, and T. Yasui, *Bull. Chem. Soc. Jpn.*, **58**, 2561 (1985).
6) T. Yasui, H. Kawaguchi, and T. Ama, *Chem. Lett.*, **1983**, 1277.
7) J. A. Pople and M. S. Gordon, *J. Am. Chem. Soc.*, **89**, 4253 (1967).
8) J. B. Sothers, "Carbon-13 NMR Spectroscopy," Academic Press, New York (1972), p. 183.
9) I. Morishima, K. Yoshikawa, K. Okada, T. Yonezawa, and K. Goto, *J. Am. Chem. Soc.*, **95**, 165 (1973).
10) N. Matsuoka, J. Hidaka, and Y. Shimura, *Bull. Chem. Soc. Jpn*, **40**, 1868 (1967).
11) T. Yasui, H. Kawaguchi, N. Koine, and T. Ama, *Bull. Chem. Soc. Jpn*, **56**, 127 (1983).

 © 1986 The Chemical Society of Japan Bull. Chem. Soc. Jpn., 59, 1475—1480 (1986)

The Chromatographic Behavior of Alkali and Alkaline Earth Metal Cations on Crown Ether-Modified Silica Gels and Polymer Matrices

Tadashi IWACHIDO,* Hirohiko NAITO,† Fumihiko SAMUKAWA,† Kenji ISHIMARU,† and Kyoji TÔEI†

College of Liberal Arts, Okayama University, Tsushima-naka 2-1-1, Okayama 700
†Department of Chemistry, Faculty of Science, Okayama University, Tsushima-naka 3-1-1, Okayama 700

(Received December 9, 1985)

Alkali and alkaline earth metal cations were chromatographed over silica gels and polymer matrices which had been modified by the addition of benzo-15-crown-5, benzo-18-crown-6, and benzo-21-crown-7, using water as the mobile phase. The retention sequences of the cations agreed closely with the stability sequences of the corresponding crown-ether complexes. The best separation was attained on the silica gels modified by the use of benzo-18-crown-6. The retention times increased in this sequence: $Li^+ < Na^+ < Rb^+ < Cs^+ < K^+$; $Mg^{2+} < Ca^{2+} < Sr^{2+} < Ba^{2+}$. The retention sequences on the benzo-15-crown-5 and benzo-21-crown-7 columns were $Li^+ < Na^+ \approx Cs^+ < Rb^+ < K^+$ and $Li^+ \approx Na^+ < K^+ < Rb^+ \approx Cs^+$ respectively. The resin-based columns showed similar retention sequences, but were inferior in their separation ability to the silica-based ones. The retention times were affected by many factors, such as the cation concentration, the species of the counter anions, the kind and composition of the second solvents in the mixed mobile phase, and the column temperature.

Crown ethers are attractive to analytical chemists because of their selective cation-binding ability. In the field of chromatography, these substances have frequently been used as stationary phases. Four types of stationary phases have so far been developed depending on the method of crown-ether immobilization and on the kind of supporting material. Kimura et al.[1] chromatographed alkali metal cations over ODS-silica gels coated with dodecyl-18-crown-6 or decyl-cryptand 221. Igawa et al.[2-4] showed that silica gels coated with polyamide crown resins were useful for separating anions rather than cations. The stationary phases of this type are easy to prepare, but the loss of the crown ethers by elution is inevitable. The loss can be avoided by bonding them onto a certain supporting material. Blasius et al.[5,6] investigated extensively the chromatographic separation of many cations on crown ether- or cryptand-containing polymer matrices. Nakajima et al.[7-9] also studied the separation of alkali metal cations on crown-modified silica gels.

This paper will describe the immobilization of different crown ethers on silica gels and polymer matrices and the chromatographic separation behavior of the alkali and alkaline earth metal cations on these columns. Factors affecting the retention behavior were also investigated.

Experimental

Syntheses of Amino Crown Ethers. Benzo-15-crown-5 (B15C5), benzo-18-crown-6 (B18C6), and benzo-21-crown-7 (B21C7) were synthesized from catechol and 1,11-dichloro-3,6,9-trioxaundecane, 1,14-dichloro-3,6,9,12-tetraoxatetradecane, and 1,17-dichloro-3,6,9,12,15-pentaoxaheptadecane respectively by the method of Pedersen.[10] The dichloro compounds were prepared as follows: Polyethylene glycol (average mol. wt.=400) was treated with thionyl chloride in the presence of a small quantity of pyridine, and the product was fractionated by vacuum distillation. The crown ethers thus obtained were nitrated and then reduced to their respective amino compounds according to the method of Ungaro et al.[11]

Preparation of Crown-Modified Packings. Wakogel LC-5H (particle size: 5 μm, pore size: 60 nm) of an irregular type (Wako Chemical Industries, Ltd.) and LiChrosorb Si-100 (particle size: 5 μm, pore size: 100 nm) of a spherical type (Merck) were used as the supporting materials. The silica gels were activated by 6 M hydrochloric acid (1 M=1 mol dm^{-3}) under reflux with stirring for 8 h, washed thoroughly with water, and finally dried under a vacuum. A mixture of 5 g of the silica gels, 2 g of 6,7-epoxy-4-oxohexyltrimethoxysilane, and 100 cm^3 of dry toluene was heated under reflux with stirring for 10 h. After being separated from the mixture, the epoxy-modified silica gels were suspended in 100 cm^3 of dry toluene and then heated in the same manner in the presence of 3 g of the amino derivatives. The amount of crown ether moiety immobilized on the silica gels was determined to be 0.1—0.3 mmol per g of the dried crown-modified silica gels, judging from the weight loss on heating at 800 °C. Finally, the silica gels were treated with trimethylchlorosilane in order to endcap the residual silanol group. The estimated silica surface is shown in Fig. 1 (above).

Hitachi COOH type gels (No. 3011-C, 10—15 μm) were used as the polymer matrices. The crown ether moieties were introduced as follows: 2.6 g of the dry resins were dispersed in 40 cm^3 of toluene and treated with 4 cm^3 of thionyl chloride under reflux for 6 h. The resulting resins were washed well with dry toluene and then treated with 25 cm^3 of a pyridine solution containing 2.1 g of 4′-aminobenzo-18-crown-6 by occasional gentle swirling for two days at room temperature. The amount of the crown moiety immobilized was estimated to be 0.6 mmol per g of the crown-modified resin by measuring the amount of potassium picrate adsorbed on it. The estimated structure

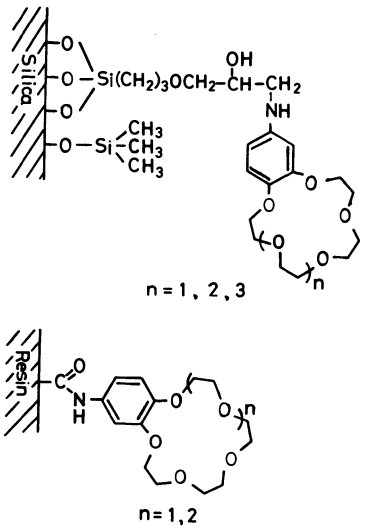

Fig. 1. Estimated structures of the crown-modified silica gel (above) and resin (below).

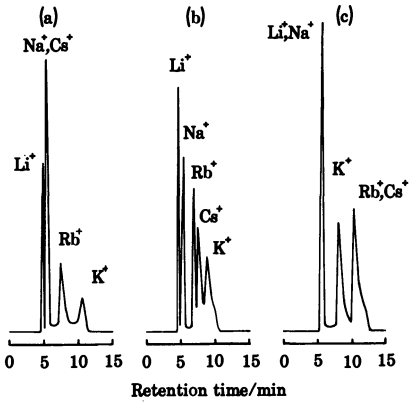

Fig. 2. Chromatograms of equimolar mixtures of alkali metal chlorides over the silica-based crown columns. (a): B15C5 ($n=1$), (b): B18C6 ($n=2$), (c): B21C7 ($n=3$).
Sample size: (a) 0.5 M, 3 μl (1l=1000 cm³); (b) 0.05 M, 5 μl; (c) 0.01 M, 5 μl.
Mobile phase: water, Flow rate: 0.5 ml min^{-1}.

is also shown in Fig. 1 (below).

Packing to Columns. The crown-modified silica-based packings were made balanced-density slurries by ultrasonic mixing with a Chemco C-type slurry solvent (Chemco Scientific Co., Ltd.) and pumped into stainless-steel columns (4 mm i.d., 250 mm length) with methanol according to a given pressure program by using a Model 124 Chemco Slurry-Packing Apparatus. The crown-modified resin-based packings were packed in a similar manner by using a methanol-chloroform mixture as the slurry solvent. The columns thus obtained were conditioned by elution with methanol and then a large quantity of water.

Materials. The alkali and alkaline earth metal salts were of an analytical grade. The water was purified by the use of an Auto Still (Model WAG-28, Yamato Scientific Co., Ltd.) equipped with ion-exchange resins and a glass-made distilling apparatus. The resulting water was distilled again with an all-quartz-made, non-boiling type distilling apparatus (HF-200, Fujiwara Seisakusho Co., Ltd.), preventing contamination of the water with CO_2 in the air.

Chromatographic Measurements. An assembly consisting of a pump (Shimadzu LC-5A), a sample injector (Rheodyne 7125), a conductometric detector (LDC conducto Monitor), and a recorder (YHP Reporting Integrator 3390A) was used for high-performance liquid chromatography. Freshly distilled water was used as the mobile phase. For the silica-based columns, the pressure drops were about 50 kg cm^{-2} at a flow rate of 0.5 cm^3 min^{-1} and for the resin-based ones, less than 20 kg cm^{-2} at a flow rate of 1.0 cm^3 min^{-1}. Chromatography was performed at 25 °C unless otherwise stated.

Results and Discussion

Separation of Alkali and Alkaline Earth Metal Cations. Typical chromatograms of the alkali metal cations on the crown-modified silica-gel columns are shown in Fig. 2. Li^+, Na^+, K^+, Rb^+, and Cs^+ were separated satisfactorily from each other on the B18C6-modified silica-gel (B18C6–Si) column. Na^+ was not separated from Cs^+ on the B15C5-Si column. Two pairs of ions, Li^+/Na^+ and Rb^+/Cs^+, were not separated on the B21C7–Si column. Figure 2 also shows that the retention sequences vary greatly according to the ring size of the crown ether moieties; the retention times on the B15C5–Si, B18C6–Si, and B21C7–Si columns increased in this sequence: $Li^+ < Na^+ \approx Cs^+ < Rb^+ < K^+$; $Li^+ < Na^+ < Rb^+ < Cs^+ < K^+$; and $Li^+ \approx Na^+ < K^+ < Rb^+ \approx Cs^+$ respectively.

Crown ethers are known to form 'metal-in-the-hole'-type complexes with many cations. Cations which fit into the hole of the crown ether form stable complexes of 1:1 stoichiometry. On the other hand, cations which are too large to fit into the molecular hole tend to form 1:2 (cation:crown) complexes, which are, in most cases, more stable than the 1:1 complexes. It is natural to consider that cations which can form more stable complexes are retained more strongly. The retention sequence on the B15C5-Si column can be elucidated on the basis of the stability sequence by assuming the 1:2 interactions for K^+ and Rb^+ (Table 1). The retention sequence on the B21C7–Si column was consistent with the stability sequence. For the B18C6–Si columns, both sequences agreed well; however, it was found that, in certain columns, Cs^+ appeared in the eluents before Rb^+, whereas, in other columns, it appeared as late as K^+. Nakajima et al.[8] indicated that poly(benzo-18-crown-6)- and bis(benzo-18-crown-6)-modified silica-gel columns possessing neighboring crown ether moieties were favorable for forming 1:2 complexes with Cs^+ and retained it most strongly among the alkali metal cations. Taking into account the fact that the densities of the crown ether moieties

Table 1. Stability Constants (logarithmic unit) of Crown Ether Complexes with Alkali and Alkaline Earth Metal Cations

Cation	r/nm[a]	B15C5[b] in 70% MeOH	18C6[c] in H_2O	21C7[d] in MeOH
Li^+	0.068			
Na^+	0.097	1.99	0.8	
K^+	0.133	1.5, 4.15[e]	2.03	4.41
Rb^+	0.147	1.8, 3.77[e]	1.56	
Cs^+	0.167	1.7	0.99	5.02
Ca^{2+}	0.099		<0.5[f]	
Sr^{2+}	0.112		2.72	
Ba^{2+}	0.134		3.87	

a) Ionic radii, Ref. 12. b) Benzo-15-crown-5, Ref. 13. c) 18-Crown-6, Ref. 14. d) 21-Crown-7, Ref. 15. e) 1:2 (Cation : crown) complex. f) Ref. 15.

of the present columns are as high as those of their columns (0.3 mm g^{-1}), it is probable that, even in the present columns, Cs^+ forms the 1:2 complexes to an appreciable extent, though the spatial arrangement of the crown ether moieties is less favorable than that of their columns. It seems, therefore, natural to consider that the columns with a high crown density retain Cs^+ longer.

The pore size of the silica gels showed no appreciable effect on the elution behavior of the cations.

Separation of Alkaline Earth Metal Cations. Chromatograms of the alkaline earth metal cations on the B15C5- and B18C6-Si columns are shown in Fig. 3((a) and (b)). The retention sequence on the former column was $Mg^{2+} \approx Ca^{2+} < Sr^{2+} < Ba^{2+}$; Mg^{2+} was not separated from Ca^{2+}. On the other hand, the retention sequence on the latter column was $Mg^{2+} < Ca^{2+} < Sr^{2+} < Ba^{2+}$; the separation of Mg^{2+} from Ca^{2+} was still unsatisfactory.

A mixture of the alkali and alkaline earth metal cations was chromatographed over the B18C6-Si column (Fig. 3(c)). Na^+, Sr^{2+}, and Rb^+ were separated from each other almost satisfactorily. The separation of Ca^{2+} from Li^+ was not achieved. The retention sequence agreed with the stability sequence. Sr^{2+}, however, was retained more weakly than had been expected from its stability constant.

A few univalent cations other than the alkali metal cations were chromatographed over the B18C6-Si column. Tl^+ was retained longer than K^+. Ag^+ was not detected as a peak. Quarternary ammonium salts were all eluted so rapidly that they were only poorly separated, the retention sequence being: benzyltrimethylammonium<trimethylammonium≈ammonium ions.

Counter Anions. Many investigators[3-8] have pointed out that the retention times of cations on crown-modified columns were affected markedly by

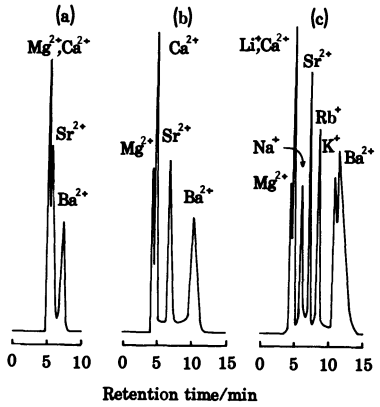

Fig. 3. Chromatograms of alkaline earth metal chlorides over the silica-based crown columns.
(a): B15C5, (b): B18C6, (c): B18C6.
Sample size: (a) 0.05 M (equimolar mixture), 3 μl; (b) 0.05 M (equimloar mixture), 5 μl; (c) 0.05 M (Li : Na : K : Rb=1 : 1 : 2 : 2 , Mg : Ca : Sr : Ba= 1 : 1 : 2 : 2), 5 μl.
Mobile phase: water, Flow rate: 0.5 ml min^{-1}.

Table 2. The Effect of Counter Anions on the Retention Time on the Silica-Based Columns[a]

Anion	B18C6		B21C7		r_{cryst}[b]
	Na^+	K^+	Na^+	K^+	
Cl^-	7.43	12.32	5.51	7.69	1.81
Br^-	7.55	12.50	5.69	8.13	1.96
I^-	8.17	14.97	6.34	9.71	2.20
NO_2^-	7.48		5.66		
NO_3^-	7.77	12.63	5.83	8.42	1.89[c]
$HCOO^-$	7.45		5.49		
CH_3COO^-	7.53		5.52		
ClO_2^-	7.48		5.52		
ClO_3^-	7.70	12.65	5.76	8.29	2.00[c]
ClO_4^-	8.85	15.93	7.22	11.88	2.36[c]
BrO_3^-		11.95		7.67	
IO_3^-		11.30		7.36	
SCN^-	9.97				
Pic^-[d]	21.83		18.71		
SO_4^{2-}	7.87	16.15	5.43	8.63	
$[Fe(CN)_6]^{3-}$		11.07		19.92	
$[Fe(CN)_6]^{4-}$		11.12		21.46	

a) Mobile phase: water, Flow rate: 0.4 cm^3 min^{-1}, Sample size: 0.1 mol dm^{-3}, 5 μl (1 l=1000 cm^3), Temp: 20 °C. b) Ref. 12. c) Ref. 16. d) 0.05 mol dm^{-3} picrate.

the anion species also present. In the present work, the effect of anions was investigated by using the B18C6- and B21C7-Si columns. The retention times obtained are summarized in Table 2, together with the anionic radii. From Table 2, it is clear that the retention times increase with an increase in the ionic size: $Cl^- < Br^- < NO_3^- < I^- < SCN^-$. This sequence

agreed with that reported by Igawa et al.[3] In the present experiment, however, SO_4^{2-} was not eluted so fast as they reported. The retention sequence for some oxyacid anions was $IO_3^-<BrO_3^-<ClO_3^-$, the sequence being difficult to explain from the size effect alone. In Fig. 4, the retention time is plotted against the lyotropic number,[17] which reflects the hydrophobic nature of anions. The higher the hydrophobicity, the longer the retention time becomes. It should be noted that ClO_4^- is retained much longer on the stationary phase. In Fig. 5, the retention time is plotted against the *A* value introduced by Motomizu.[18] He indicated that the extraction constants, K_{ex}, for the chloroform extraction of ion pairs could be divided into two terms: $\log K_{ex}=C+A$, where *C* and *A* represent the extractabilities of the cation and anion species respectively. The *A* value further reflects the hydrophobicity and the ion-pair formation ability of the anion. Figure 5 shows that, for many anions, the retention times are closely related to the *A* values. It is of interest to note that, in Fig. 5, the plot of ClO_4^- falls on a curve, unlike as in Fig. 4. It can be concluded that so-called soft anions are retained strongly on the crown-modified silica-gel columns. Table 2 shows that $[Fe(CN)_6]^{3-}$ and $[Fe(CN)_6]^{4-}$ are retained very weakly on the B18C6-Si column, whereas they are retained very strongly on the B21C7-Si column. The reason for this is not clear.

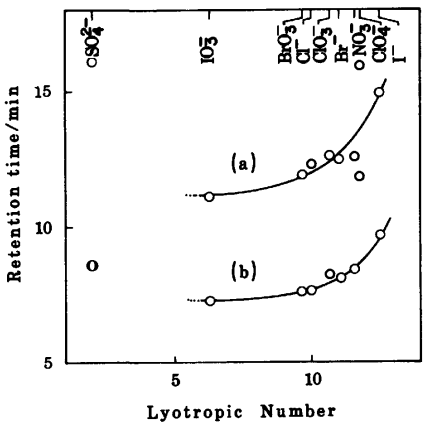

Fig. 4. Plots of retention time on the silica-based columns vs. the lyotropic number of anions.
(a): B18C6, (b): B21C7, Counter ion: K^+, Chromatographic conditions: see Table 2.

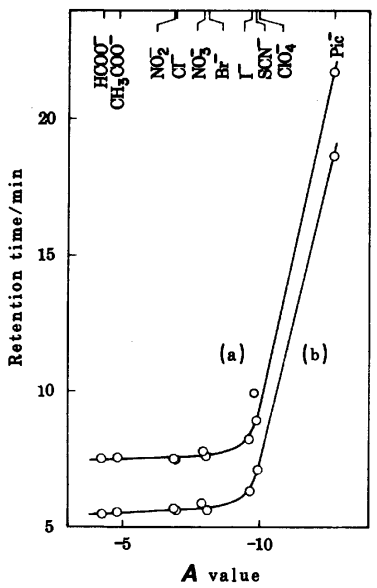

Fig. 5. Plots of retention time on the silica-based columns vs. the *A* value of anions.
(a): B18C6, (b): B21C7, Counter ion: Na^+, Chromatographic conditions: see Table 2.

Cation Concentration. The alkali metal cations were chromatographed separately over the B18C6-Si column by varying their concentrations (Fig. 6). The peak area yielded a straight line when plotted against the concentration, the linear range being from about 0.005 to 0.06 mol dm^{-3}. The lower concentration limit differed slightly with different cations; the limit appeared at somewhat higher concentrations for strongly retained cations (K^+, Cs^+, and Rb^+). Just outside the lower limit, the peak heights decreased rapidly with a decrease in the concentration, until finally the peak disappeared below the very broad, irregularly shaped background peak. The background peaks of this type were observed for all the cations tested, regardless of the species of the crown ether moieties. Therefore, the base-line separation among the strongly retained cations was not achieved (Figs. 2 and 3). Figure 7 shows that the retention time increases with a decrease in the cation concentration, the rate of increase being greater at lower concentrations. The peak assignment of the chromatograms must be made carefully because the

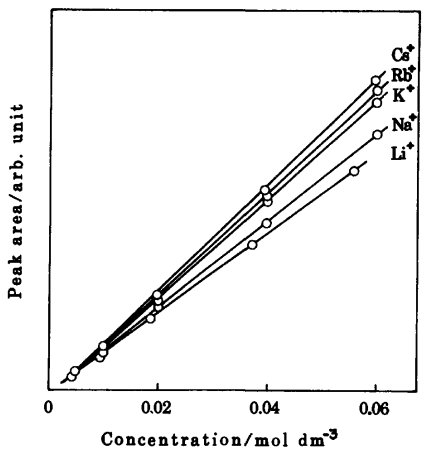

Fig. 6. Calibration curves of alkali metal chlorides on the silica-based B18C6 column.
Sample size: 5 μl, Flow rate: 0.2 ml min^{-1}.

retention time depends not only on the species of the counter anion, but also on the cation concentration.

Water-Methanol as the Mobile Phase. The stability constants of crown ether complexes are known to be three to four decades higher in methanol than in water.[19] Izatt et al.[13] showed clearly that the stability constants of benzo-15-crown-5 complexes increased regularly as the methanol portion of water–methanol mixtures was increased. Figure 8 shows that the retention times of the alkali metal cations increase with an increase in the methanol fraction, in accordance with the observation of Izatt et al. This figure also shows that the retention-time differences between any two cations become greater as the methanol portion increases; this finding implies that the addition of methanol improves the separation of the cations. With this in mind, the alkali metal cations were chromatographed over the B18C6–Si column by using a water–methanol (20% v/v) mixture as the mobile phase. However, little improvement was observed because of the broadening of the peaks. Pure water, therefore, is recommended as the mobile phase from the practical point of view.

Crown-Modified Resin Columns. The chromatographic behavior of the alkali metal cations was investigated on the resin-based B15C5 and B18C6 columns. Some typical chromatograms are shown in Fig. 9. The retention sequences of the cations on the B15C5- and B18C6–resin columns were $Li^+<Na^+\approx Cs^+<Rb^+<K^+$ and $Li^+<Na^+<Cs^+\approx Rb^+<K^+$ respectively. The retention behavior was very similar to that observed on the corresponding silica-based column (cf. Fig. 2 (a) and (b)). The separation patterns, however, were not so good as the silica-based columns. Na^+ was also not separated from Cs^+ on the B15C5–resin column. A linear relation between the peak area and the cation concentration was also observed with the resin-based columns in the range from about 0.01 to 0.1 M; the lower limit of the linear range was slightly higher than that of the silica-based column. It was noted that the retention time on the resin-based columns increased with an increase in the cation concentration, unlike the case with the silica-based columns.

Figure 10 shows that the retention time of the alkali metal cations depends to a considerable extent on the second solvent species. The addition of methanol increased the retention times, as has been mentioned above. On the other hand, the addition of

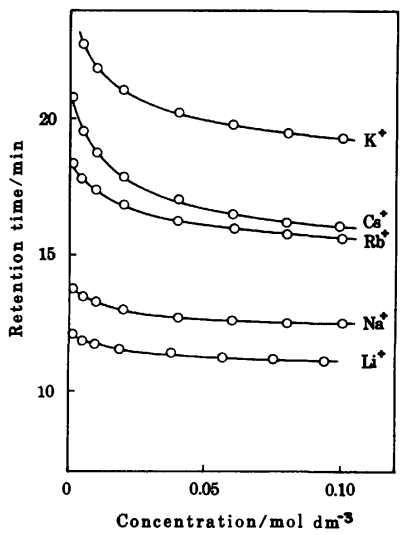

Fig. 7. Concentration dependence of the retention times of alkali metal cations on the silica-based B18C6 column.
Sample size: 5 μl, Flow rate: 0.2 ml min^{-1}.

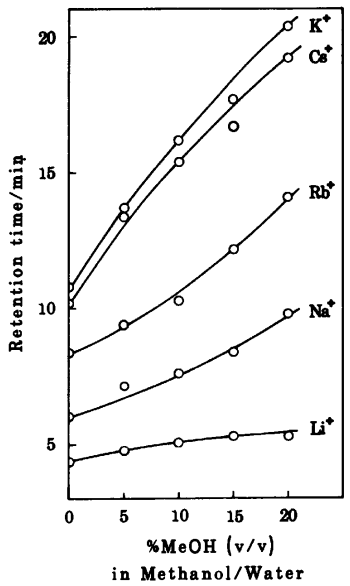

Fig. 8. Effect of methanol content on the retention times of alkali metal cations on the silica-based B18C6 column.
Sample size: 0.05 M, 1.5 μl, Flow rate: 0.5 ml min^{-1}.

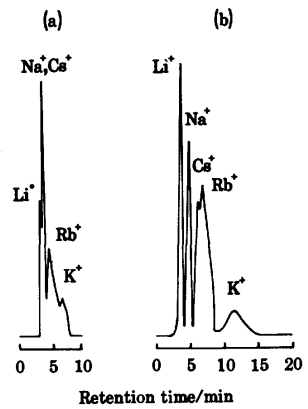

Fig. 9. Chromatograms of equimolar mixtures of alkali metal cations over the resin-based crown columns.
(a): B15C5, (b): B18C6.
Sample size: 0.1 M, 5 μl, Mobile phase: water, Flow rate: 1.2 ml min^{-1}.

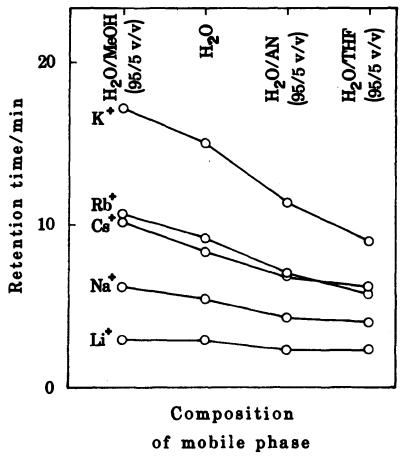

Fig. 10. Effect of the composition of mobile phase on the retention times of alkali metal cations.
AN: acetonitrile, THF: tetrahydrofuran.
Column: resin-based B18C6, Sample size: 0.1 M, 5 μl, Flow rate: 1 ml min^{-1}.

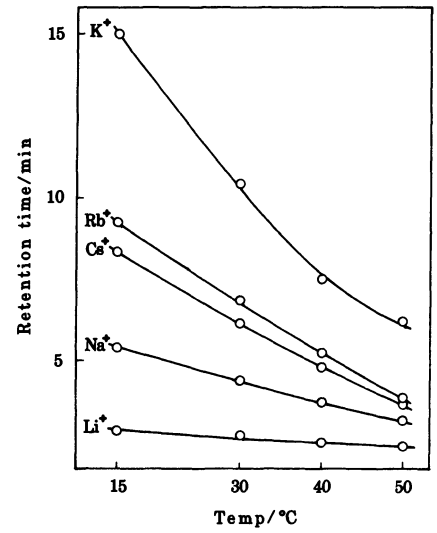

Fig. 11. Temperature dependence of the retention times of alkali metal cations.
Column: resin-based B18C6, Sample size: 0.1 M, 5 μl, Flow rate: 1 ml min^{-1}.

acetonitrile or tetrahydrofuran decreased the retention times. This phenomenon can not be elucidated in terms of the stability of the complexes, for the alkali metal–B18C6 complexes are more stable in these solvents than in water.[20,21]

The effect of the temperature on the retention times can be seen from Fig. 11. It was observed that, at lower temperatures, the separation was slightly improved. However, Cs^+ was not separated successfully from Rb^+, not even at 15 °C.

Silica- and Resin-Based Columns. The alkali and alkaline earth metal cations were most successfully separated on the B18C6-modified columns, without distinction of the matrices. However, a detailed comparison of the matrices of different types is difficult because conditions, such as the particle size, the pore size, and the density of the crown moiety, are not the same for both types of matrices. The separation ability of the resin-based columns seems to be inferior to that of the silica-based ones. However, further research on the resin-based columns is not hopeless if the fact that the chromatographic peaks on these columns show a better symmetry is taken into account.

References

1) K. Kimura, E. Hayata, and T. Shono, *J. Chem. Soc., Chem. Commun.*, **1984**, 271.

2) M. Igawa, I. Ito, and M. Tanaka, *Bunseki Kagaku*, **29**, 580 (1980).

3) M. Igawa, K. Saito, J. Tsukamoto, and M. Tanaka, *Anal. Chem.*, **53**, 1942 (1981).

4) M. Igawa, K. Saito, M. Tanaka, and T. Yamabe, *Bunseki Kagaku*, **32**, E137 (1983).

5) E. Blasius, K.-P. Janzen, W. Adrian, G. Klautke, R. Lorscheider, P.-G. Maurer, V. B. Nguyen, T. Nguyen-Tien, G. Scholten, and J. Stockemer, *Z. Anal. Chem.*, **284**, 337 (1977).

6) E. Blasius, K.-P. Janzen, W. Klein, H. Klotz, V. B. Nguyen, T. Nguyen-Tien, R. Pfeiffer, G. Scholten, H. Simon, H. Stockemer, and A. Toussaint, *J. Chromatogr.*, **201**, 147 (1980).

7) M. Nakajima, K. Kimura, and T. Shono, *Anal. Chem.*, **55**, 463 (1983).

8) M. Nakajima, K. Kimura, and T. Shono, *Bull. Chem. Soc. Jpn.*, **56**, 3052 (1983).

9) M. Nakajima, K. Kimura, E. Hayata, and T. Shono, *J. Liquid Chromatogr.*, **7**, 2115 (1984).

10) C. J. Pedersen, *J. Am. Chem. Soc.*, **89**, 7017 (1967).

11) R. Ungaro, B. El Haj, and J. Smid, *J. Am. Chem. Soc.*, **98**, 5198 (1976).

12) "Handbook of Chemistry and Physics," 53rd ed, ed by R. C. Weast, The Chemical Rubber Co., Cleveland (1972), p. F-177.

13) R. M. Izatt, R. E. Terry, D. P. Nelson, Y. Chan, D. J. Eatough, J. S. Bradshaw, L. D. Hansen, and J. J. Christensen, *J. Am. Chem. Soc.*, **98**, 7626 (1976).

14) R. M. Izatt, R. E. Terry, B. L. Haymore, L. D. Hansen, N. K. Dalley, A. G. Avondet, and J. J. Christensen, *J. Am. Chem. Soc.*, **98**, 7620 (1976).

15) J. J. Christensen, D. J. Eatough, and R. M. Izatt, *Chem. Rev.*, **74**, 351 (1974).

16) R. Kiriyama and H. Kiriyama, "Kozo Muki Kagaku, I," Kyoritsu, Tokyo (1965), p. 283.

17) K. Miyajima, "Kagaku no Ryoiki, Zokan No. 106," ed by M. Nakagaki, Nankodo, Tokyo (1974), p. 90.

18) S. Motomizu, *Bunseki Kagaku*, **33**, 31 (1984).

19) H. K. Frensdorff, *J. Am. Chem. Soc.*, **93**, 600 (1971).

20) A. Hofmanova, J. Koryta, M. Brezina, and M. L. Mittal, *Inorg. Chim, Acta*, **28**, 73 (1978).

21) K.-H. Wong, M. Bourgoin, and J. Smid, *J. Chem. Soc., Chem. Commun.*, **1974**, 715.

Acid-Dissociation Behavior of *para*-Hydroxyl Group in the *N,N,O*-Terdentate Ligand, 4-(4-Methyl-2-pyridylazo)resorcinol, Coordinated to a Transition Metal Ion

Yoshihiro KUDO, Noboru YOSHIDA, Masatoshi FUJIMOTO,* Katsumi TANAKA,† and Isamu TOYOSHIMA†

Department of Chemistry II, Faculty of Science, Hokkaido University, Sapporo 060

†Research Institute for Catalysis, Hokkaido University, Sapporo 060

(Received December 16, 1985)

The acid-dissociation behavior of 1:1 and 1:2 complexes of transition metals with an *N,N,O*-terdentate ligand, 4-(4-methyl-2-pyridylazo)resorcinol (4-MePAR), is spectrophotometrically studied in ethanol at 25 °C. The values of apparent pK_a of the *p*-hydroxyl group of the ligand in the metal complexes are found to be in the order, Pd(II)<Co(III)<Ni(II)<Mn(II). The electronic structures of the *p*-hydroxyl oxygen atoms in the solid complexes of Mn(II), Ni(II), Pd(II), and Co(III) are examined on the basis of the data of X-ray photoelectron spectroscopy (XPS). The decrease in the electron density on the *p*-hydroxyl oxygen atom caused by the inductive effect through the azo nitrogen and the benzene ring of the coordination of the ligand to the central metal atom is larger in the Pd(II) and Co(III) complexes compared with that in the Ni(II) and Mn(II) complexes.

It is well-known that the reactivity and the electronic structure of organic compounds are affected by the coordination to the metal atom.[1,2] Corsini et al. potentiometrically pointed out that in aqueous dioxane solution the acid dissociation of *p*-hydroxyl group in an *N,N,O*-terdentate ligand, 4-(2-pyridylazo)resorcinol (PAR), is accelerated by the coordination to the transition metal ions.[3] However, despite the importance of the ligand PAR in the field of analytical chemistry and of coordination chemistry, no work on the electronic structures of PAR and its metal chelates has been reported so far. Recently, we found out, by the application of X-ray photoelectron spectroscopy (XPS), the characteristics of the chemical bonding of bivalent metal ions with donor atoms in analogous complexes of an *N,N,O*-terdentate ligand.[4] It is of interest to obtain the detailed information on the electronic structures of multidentate complexes in order to understand the reaction behavior of the complexes in solutions.

In the present paper, we report the acid-dissociation behavior of the metal chelates of an *N,N,O*-terdentate ligand, 4-(4-methyl-2-pyridylazo)resorcinol (4-MePAR), in ethanol; the electronic structures of

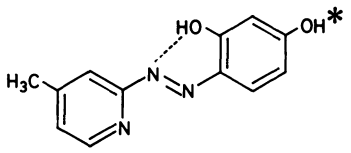

4-MePAR (LHH*)†

the isolated complexes are discussed on the basis of XPS measurements. The results of XPS measurements are correlated to the acid-dissociation behavior in ethanol of the *p*-hydroxyl groups in the metal–4-MePAR complexes.

† The ligand 4-MePAR is abbreviated to be LHH*, where H and H* denote the *ortho*- and the *para*-hydroxyl protons, respectively.

Experimental

Materials. Ethanol was dried with Molecular Sieves 3A or 4A for several days and distilled under argon atmosphere immediately before use. The ligand 4-MePAR (LHH*), its Ni(II) complex, $[Ni(LH^*)_2]^0$, and a terdentate Pd(II) complex of 5-dimethylamino-2-(2-pyridylazo)phenol (DAPAP) were prepared according to the literature.[4–6] The *N,N,O*-terdentate complexes of other bivalent or tervalent metal ions with 4-MePAR were prepared by the analogous method as described in the previous papers.[7,8] $[Pd(LH^*)Cl]^0$: Color: dark green. Found: C, 37.11; H, 3.05; N, 10.75; Cl, 8.97%. Calcd for $Pd(C_{12}H_{10}N_3O_2)Cl\cdot H_2O$: C, 37.14; H, 3.12; N, 10.83; Cl, 9.13%. The configuration around Pd(II) in the complex, $[Pd(LH^*)Cl]^0\cdot H_2O$, was identified to be essentially four-coordinated form by the XPS measurements: The $Pd(3d_{5/2})$ binding energy of the Pd(II)–4-MePAR complex, 338.6 eV, was almost equal to that of the corresponding four-coordinated complex of Pd(II) with DAPAP, $[Pd(dapapH_{-1})Cl]^0$, 338.0 eV.[9] $[Mn(LH^*)_2]^0$: Color: dark wine red. Found: C, 52.78; H, 3.87; N, 15.34%. Calcd for $Mn(C_{12}H_{10}N_3O_2)_2\cdot 0.6\,NaCl$: C, 52.75; H, 3.69; N, 15.38%. $[Co^{III}L(LH^*)]^0$: Color: dark wine red. Found: C, 53.13; H, 3.37; N, 15.97%. Calcd for $Co^{III}C_{24}H_{19}N_6O_4\cdot 0.5\,NaCl$: C, 53.03; H, 3.52; N, 15.46%. Bases employed here were of guaranteed reagent grade (Wako or Tokyo Kasei).

Measurements. Samples for XPS measurements were prepared in the form of a thin layer mounted on a nickel substrate covered with a fine gold mesh and dried overnight under 10^{-5}—10^{-7} Pa. XPS spectra of the samples were measured on a VG ESCA 3 spectrometer employing Mg $K\alpha$ (1253.6 eV) radiation under ca. 10^{-7} Pa at room temperature. In order to compensate for the charging of the insulating samples during the photoelectron ejection process, we referenced the spectra of all elements in each sample to the photoelectron line of C(1s). All raw binding energies were corrected to C(1s) value, 285.0 eV, of a

hydrocarbon.[6] The O(1s) peak in each complex was deconvoluted using two or three symmetric Gaussian curves.[4]

Visible absorption spectra of the samples in absolute ethanol were measured at 25.0±0.3 °C with a Hitachi EPS-3T spectrometer equipped with a 1 cm quartz cell. The preparations of the ethanol solutions for the measurements of visible spectra were carried out in a glove bag filled with argon. The concentrations of the solutions of the free ligand and the complexes were calculated from the weighed amount or the absorbance of the solution.

Results and Discussion

Reactions between Brønsted Bases and Metal-4-MePAR Complexes in Ethanol. Figure 1 shows the spectral change in the reaction of the *N,N,O*-terdentate chelate of Pd(II) with 4-MePAR with a Brønsted base, 2,6-lutidine, in ethanol. 2,6-Lutidine behaves exclusively as a Brønsted base; a very weak coordinating property of this base could be neglected. The spectrum of the Pd(II) complex has two absorption maxima in visible region at 442 ($\varepsilon_{max}=1.54\times10^4$) and around 590 nm ($\varepsilon_{max}=0.78\times10^4$ mol^{-1} dm^3 cm^{-1}) (Curve 1). Upon addition of a Brønsted base, 2,6-lutidine (pK_a in water (pK_a^W)=6.75), the absorbance around 440 nm decreased with the increase of that around 530 nm. The color of the solution changes from green to pink.[10] A set of isosbestic points for the spectral change was observed at 470 and 596 nm. This result shows the simple equilibrium for the reaction between the Pd(II)-4-MePAR complex and 2,6-lutidine. The final spectrum of the Pd(II) complex (Curve 4) possesses an absorption maximum at 535 nm ($\varepsilon_{max}=3.34\times10^4$ mol^{-1} dm^3 cm^{-1}). The reaction of [Pd(LH*)Cl]^0 is similar to the deprotonation in ethanol of the Mn(II)-4-MePAR complex or the Ni(II)-4-MePAR complex by triethylamine (pK_a^W=10.9), $[M(LH^*)_2]^0 \rightleftarrows [ML(LH^*)]^- + H^+ \rightleftarrows [ML_2]^{2-} + 2H^+$ (Fig. 2a).[11] The reaction of the Mn(II) and/or Ni(II) complexes with 2,6-lutidine showed no spectral change. On the other hand, a reaction of 2,6-lutidine with the Pd(II)-DAPAP complex, [Pd(dapapH$_{-1}$)Cl]^0, which has no dissociable hydroxyl group, did not indicate a large spectral change in the visible region. The above results exhibit that the large spectral change observed in the reaction of the Pd(II) complex, [Pd(LH*)Cl]^0, with 2,6-lutidine is attributed to the deprotonation of *p*-hydroxyl group, $[Pd(LH^*)Cl]^0 \rightleftarrows [PdLCl]^- + H^+$ (Fig. 1). The reaction of the Co(III) complex, [Co^{III}L(LH*)]^0, with 2,6-lutidine was interpreted in the same manner (Fig. 2b).[8]

The order of the values of the pK_a's of uni-positive conjugate acids does not show appreciable change with respect to the change in medium from water to ethanol.[12,13] Therefore, the values of acid-dissociation constants of the ligand 4-MePAR and its com-

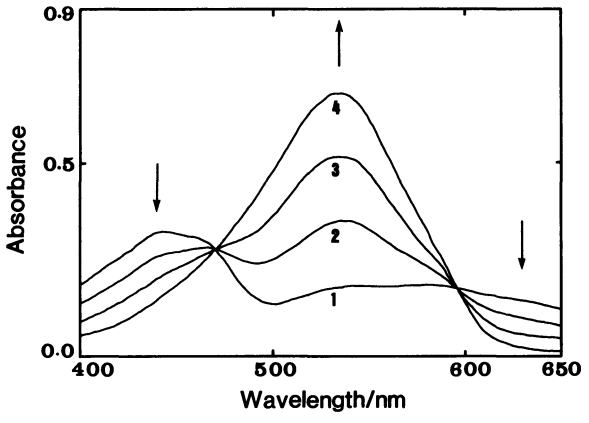

Fig. 1. Spectral change in the reaction between the Pd(II)-4-MePAR complex, [Pd(LH*)Cl]^0, and 2,6-lutidine in ethanol at 25 °C.
[Pd(LH*)Cl]$_t=2.04\times10^{-5}$ mol dm^{-3}. [2,6-lutidine]$_t$ =0.00 (1), 1.66×10^{-4} (2), 6.14×10^{-4} (3), 0.0858 mol dm^{-3} (4).

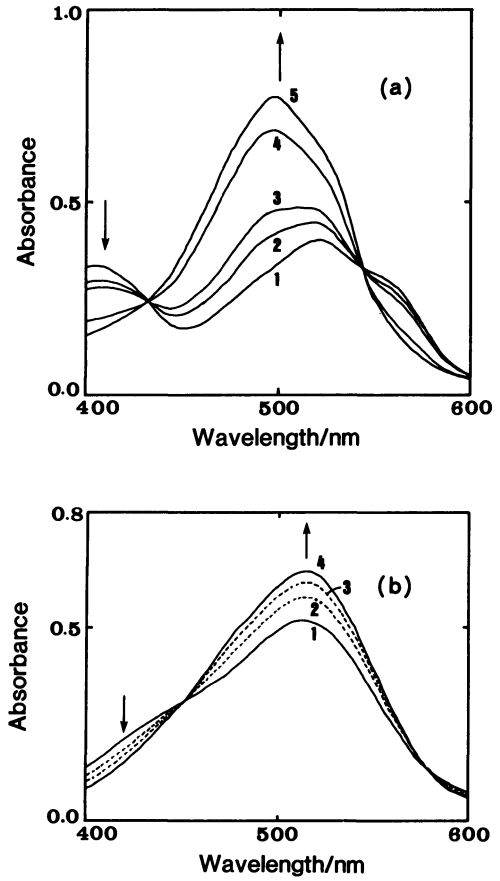

Fig. 2. Spectral changes upon additions of Brønsted bases to the ethanol solutions of the *N,N,O*-terdentate complexes of 4-MePAR at 25 °C.
(a) Ni(II)-4-MePAR complex-triethylamine. [Ni(LH*)$_2$]$_t=1.31\times10^{-5}$ mol dm^{-3}. [triethylamine]$_t$= 0.00 (1), 1.39×10^{-4} (2), 4.92×10^{-4} (3), 2.16×10^{-2} (4), 0.144 mol dm^{-3} (5).
(b) Co(III)-4-MePAR complex-2,6-lutidine. [Co^{III}L(LH*)]$_t=1.01\times10^{-5}$ mol dm^{-3}. [2,6-lutidine]$_t$=0.00 (1), 8.24×10^{-3} (2), 3.09×10^{-2} (3), 0.172 mol dm^{-3} (4).

plexes in water and in ethanol can be estimated by the spectral change in the reactions of these species with a Brønsted base of known pK_a value in two solvents. Figure 3 shows the plot of the absorbance of the Co(III) complex of 4-MePAR at 420 and 510 nm against the values of pK_a^{EtOH} of the added bases. From Fig. 3, the value of apparent pK_a of the Co(III) complex in ethanol was obtained; 6.4 for the reaction, $[Co^{III}L(LH^*)]^0 \rightleftarrows [Co^{III}L_2]^- + H^+$, 5.6 for $[Pd(LH^*)Cl]^0 \rightleftarrows [PdLCl]^- + H^+$, 7.3 for $LHH^* \rightleftarrows LH^- + H^+$.[14] The values of $(pK_{a1}^{EtOH} + pK_{a2}^{EtOH})/2$ for the reactions, $[M(LH^*)_2]^0 \rightleftarrows [ML(LH^*)]^- + H^+$, pK_{a1}^{EtOH}, and $[ML(LH^*)]^- \rightleftarrows [ML_2]^{2-} + H^+$, pK_{a2}^{EtOH}, were determined to be 9.3 and 10.1 for M=Ni(II) and Mn(II), respectively.[14] The order of the value of pK_a of the *p*-hydroxyl group of 4-MePAR and its complexes in ethanol was found to be Pd(II)<Co(III)<4-MePAR< Ni(II)<Mn(II). The order of acid-dissociation constants in the metal-4-MePAR system in ethanol was in good agreement with the corresponding order for the metal-PAR system in 50% aqueous dioxane solution, Pd(II) (5.38)<Cu(II) (5.5)<Co(III) (6.0)< PAR (7.0)<Ni(II) (pK_{a1}=7.7, pK_{a2}=9.2)≈Zn(II) (7.7, 9.3)<Mn(II) (8.8, 10.3).[3,15]

Possible Structures of the Species Formed in the Reactions of 4-MePAR or Its Complexes with Brønsted Bases in Ethanol. Ethanol is classified to a solvent of relatively low dielectric constant (24.3 at 25 °C).[16] The reaction equilibria, $AH + B \rightleftarrows A^- \cdot HB^+ \rightleftarrows A^- + HB^+$, would be present in ethanol, where AH and B denote a Brønsted acid and a Lewis base, respectively.[17] If an ion-pair species mainly formed under the experimental conditions,[18] then the association constant for the above reaction is approximately expressed by the equation, $K_A(B) = [A^- \cdot HB^+]/([AH][B])$. The absorbance A at wavelength λ (nm) of a mixed solution of the acid AH and the base B with initial concentrations $[AH]_0$ and $[B]_0$ (mol dm^{-3}) respectively is related to $K_A(B)$ as in the equation, $\log\{[B]_0 - (A-A_1)/\Delta\varepsilon\} = \log\{(A-A_1)/(A_2-A)\} - \log K_A(B)$, where $A_1 = \varepsilon_1[AH]_0$, $A_2 = \varepsilon_2[A^- \cdot HB^+] \simeq \varepsilon_2[AH]_0$, $\Delta\varepsilon = \varepsilon_2 - \varepsilon_1$, and ε_1 and ε_2 are the molar absorption coefficients (mol^{-1} dm^3 cm^{-1}) at λ of the acid, AH, and the ion pair, $A^- \cdot HB^+$, respectively.[18] If the above approximation is appropriate in ethanol, then the plot of $\log\{[B]_0 - (A-A_1)/\Delta\varepsilon\}$ (=log [B]) against $\log\{(A-A_1)/(A_2-A)\}$ (=$\log\{[A^- \cdot HB^+]/[AH]\}$) should give a straight line with a slope=1 and an intercept=$\log K_A(B)$. The plot of log [B] vs. $\log\{[A^- \cdot HB^+]/[AH]\}$ for the Co(III) complex in ethanol gave a straight line with a slope of 1.0. The similar results were obtained as for the plots for the Pd(II) complex (slope=0.9) and the free ligand 4-MePAR (1.3). The logarithms of the association constants, $\log K_A(B)$, are listed in Table 1 together with the spectral data. The order in $\log K_A(B)$ reflected the order of the acid-dissociation constants in ethanol of the *p*-hydroxyl group of the free ligand and its complexes. Further studies are necessary to clarify the structures of these ion-pair species in ethanol.

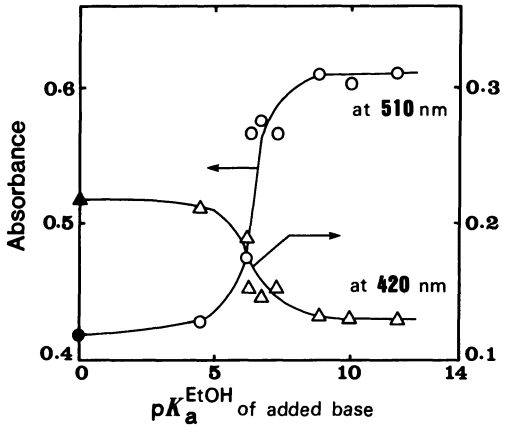

Fig. 3. Change of absorbance of the Co(III)–4-MePAR complex upon addition of a large excess of various Brønsted bases in ethanol at 25 °C.
$[Co^{III}L(LH^*)]_t = 9.30 \times 10^{-6}$ mol dm^{-3}. $[base]_t/[Co^{III}L(LH^*)]_t = 10^3$—$10^4$. Added base: *m*-chloroaniline (pK_a^{EtOH}=4.5), *p*-toluidine (6.24), 2,6-lutidine (≃6.8), imidazole (6.30, 7.3), triethanolamine (8.9), diethanolamine (10.0), triethylamine (11.9).[12,13] Full circle and triangle indicate the absorbance of the Co(III) complex in the absence of the Brønsted base.

XPS Evidence for the Increased Acid Dissociation of the *para*-Hydroxyl Group in Metal Complexes of 4-MePAR. Table 2 lists the XPS data for 4-MePAR and its metal complexes investigated here together with the electronegativities of the central metal atoms. The higher value of the core electron binding energy (BE) of the donor atom generally corresponds to the lower electron density on the donor atom.[4,19] Namely, the higher BE's of the N(1s) and the O(1s) in the *N,N,O*-terdentate complexes of 4-MePAR are attributed to the decrease in the electron densities on the donor atoms due to the formation of coordination bond. In general, the relative order of the O(1s) BE in a series of the same type of compounds is $O^{\delta-}$<M-O<M-OH.[20] From this fact, the highest peak of deconvoluted O(1s) BE was assigned to the peak of the *p*-hydroxyl oxygen in the *N,N,O*-terdentate complexes of 4-MePAR.[21] The ratio of the intensity of the deconvoluted O(1s) BE of the coordinated and the non-coordinated phenolic oxygen atoms was found to be almost 1:1 for the Ni(II) and the Mn(II) complexes. On the other hand, the ratio of the intensity in the deconvoluted O(1s) BE's for the Co(III) complex was found to be 1:2:1 from the lower BE to the higher BE, where the largest intensity ratio does indicate the presence of two atoms of the coordinated phenolic oxygen (see Table 2).

On the basis of the above assignments, the order of the values of BE of the *p*-hydroxyl oxygen atom in

the 4-MePAR complexes was obtained to be Pd(II)[22]≃Co(III)>Ni(II)≃Mn(II). The above order seems to reflect the acid-dissociation constants of the *p*-hydroxyl group in the complexes. The results of the O(1s) BE's deconvoluted show at least that the electron densities on the *p*-hydroxyl oxygen atoms in the Pd(II) and the Co(III) complexes are lower than those in the Ni(II) and the Mn(II) complexes.

The N(1s) BE's are directly affected by the electron-withdrawing effect of the central metal atom due to the formation of the M–N (azo and pyridyl) bonds, whereas the O(1s) BE's of the coordinated *o*-hydroxyl oxygen atoms in the resorcinol ring are not largely influenced by the coordination to the metal atom.[4] Therefore, the difference between the raw O(1s) and the raw N(1s) BE's, O(1s)−N(1s), in each complex appears to be the characteristic parameter for the extent of electron-withdrawing effect of the azo group on the *p*-hydroxyl group. The above discussion was supported by the linear correlation between the differences of BE's and the electronegativities of the central metal atoms: the lower value of O(1s)−N(1s) corresponds to the higher electron-withdrawing effect of the central metal atom. The plot of the difference of BE's, O(1s)−N(1s), against the apparent pK_a^{EtOH} of the *p*-hydroxyl group in the metal-4-MePAR com-

Table 1. Visible Absorption Spectral and Equilibrium Data for the Free Ligand 4-MePAR and Its Metal Complexes in Ethanol at 25 °C

Compounds	λ_{max}/nm(ε_{max})[a]		Added base[b]	log K_A(B)[c]
	AH	AH+B		
LHH*	388 (2.24)	406 (3.44)	NEt_3	4.02±0.18
		407 (3.52)	$HN(CH_2CH_2OH)_2$	3.88±0.16
		406 (3.44)	$N(CH_2CH_2OH)_3$	3.00±0.16
		—[d]	2,6-Lutidine	
$[Co^{III}L(LH^*)]^0$	514 (4.73)	514 (6.32)	NEt_3	≃6
		515 (6.52)	$HN(CH_2CH_2OH)_2$	5.74±0.13
		514 (6.58)	$N(CH_2CH_2OH)_3$	
		514 (6.12)	2,6-Lutidine	2.11±0.06
$[Pd(LH^*)Cl]^0$	442 (1.54)	535 (3.34)	2,6-Lutidine	3.48±0.14
	≃590 (0.78)			

a) $\varepsilon_{max}/10^4\,mol^{-1}\,dm^3\,cm^{-1}$. b) pK_a^w: NEt_3, 10.9; $HN(CH_2CH_2OH)_2$, 9.0; $N(CH_2CH_2OH)_3$, 7.9; 2.6-lutidine, 6.75. See Ref. 12. c) $K_A(B)/mol^{-1}\,dm^3$. d) No reaction was observed.

Table 2. Core Electron Binding Energies of O(1s) and N(1s) Levels[a] in the Ligand 4-MePAR and Its Metal Complexes

Compounds	Binding Energy/eV					χ_M[b]
	O(1s)			N(1s)	O(1s)−N(1s)	
	Raw	Deconvolution[c]	Assignment[d]			
LHH*[e]	528			395		
	531.3			398.3		
$[Mn(LH^*)_2]^0$	531.8	530.1 (0.42)	Mn–O	399.1	132.7	1.5
		532.6 (0.58)	H–O			
$[Ni(LH^*)_2]^0$	531.9	529.7 (0.44)	Ni–O	399.8	132.1[f]	1.8
		532.7(0.56)	H–O			
$[Co^{III}L(LH^*)]^0$	531.3	527.1 (0.34)	$O^{\delta-}$	399.8	131.5	>1.8
		531.1 (0.46)	Co–O			
		533.1 (0.20)	H–O			
$[Pd(LH^*)Cl]^0$	532.3	—[g]		401.3	131.0	2.2

a) All raw BE's were corrected to C(1s) value of the hydrocarbons, 285.0 eV.[6] b) Pauling's electronegativity value. c) Deconvoluted peaks with an error of ±0.5 eV and the value in parentheses shows the relative intensity of the peak. d) Assignments of the deconvoluted peaks. e) Ref. 6. f) The value was reported to be 131.8 eV in the previous work (see Ref. 6). g) Unable to deconvolute due to a very small O(1s) signal.

plexes is shown in Fig. 4. The acid dissociation of the *p*-hydroxyl group in the 4-MePAR complexes increased with the increase in the extent of the electron-withdrawing effect of the azo group coordinated to the central metal ions.

From XPS results, it is concluded that the coordination of the ligand 4-MePAR to the metal atom tends to decrease in the electron density on the *para*-hydroxyl oxygen atom in the ligand through inductive effect, thereby facilitating the acid dissociation of the *para*-hydroxyl group.

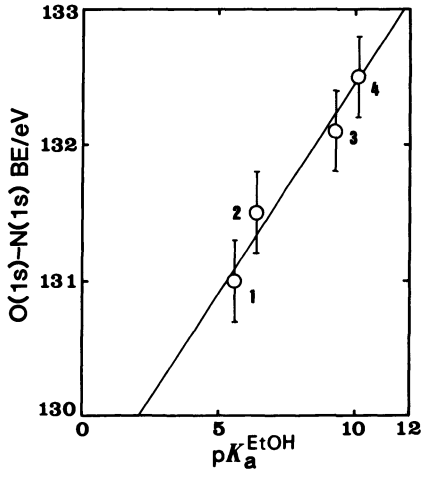

Fig. 4. Plot of the difference of BE's, O(ls)−N(1s), vs. the values of apparent pK_a in ethanol of the *N,N,O*-terdentate metal-4-MePAR complexes. Metal=Pd(II) (1), Co(III) (2), Ni(II) (3), and Mn(II) (4).

References

1) M. F. Hoq and R. E. Shepherd, *Inorg. Chem.*, **23**, 1851 (1984); H. Hoshino and T. Yotsuyanagi, *Talanta*, **31**, 525 (1984).

2) S. P. Bag, Q. Fernando, and H. Freiser, *Inorg. Chem.*, **1**, 887 (1962); C. Djordjević, J. Lewis, and R. S. Nyholm, *J. Chem. Soc.*, **1962**, 4778; T. R. Harkins and H. Freiser, *J. Am. Chem. Soc.*, **78**, 1143 (1956); D. S. Sigman, G. M. Wahl, and D. J. Creighton, *Biochemistry*, **11**, 2236 (1972).

3) A. Corsini, Q. Fernando, and H. Freiser, *Inorg. Chem.*, **2**, 224 (1963).

4) Y. Kudo, N. Yoshida, M. Fujimoto, K. Tanaka, and I. Toyoshima, *Chem. Lett.*, **1985**, 1573.

5) W. J. Geary and F. Bottomley, *Talanta*, **14**, 537 (1967).

6) Y. Kudo, N. Yoshida, T. Imamura, and M. Fujimoto, *Bull. Chem. Soc. Jpn.*, **57**, 3099 (1984).

7) K. Mochizuki, T. Ito, and M. Fujimoto, *Bull. Chem. Soc. Jpn.*, **52**, 441 (1979).

8) K. Mochizuki, T. Imamura, T. Ito, and M. Fujimoto, *Bull. Chem. Soc. Jpn.*, **51**, 1743 (1978).

9) The abbreviation dapapH$_{-1}$ denotes the monoanionic form of the free ligand, DAPAP, in the complex.

10) The color change of the Pd(II) complex, $[Pd(LH^*)Cl]^0$, from green at pH≃4 to pink at pH≃7 was observed in aqueous solution.

11) The spectral change in ethanol coincided with that observed in the pH titration of $[Ni(LH^*)_2]^0$ in 10%(v/v) dioxane-water. In the pH titration, the *N,N,O*-terdentate complex, $[Ni(LH^*)_2]^0$, was found to dissociate two *p*-hydroxyl protons in the ligand to form $[NiL_2]^{2-}$.[6] From these results, the change observed upon addition of triethylamine is attributed to a liberation of two protons of *p*-hydroxyl groups in the terdentate 1:2 complex. The spectrum of the final complex, $[NiL_2]^{2-}$, showed a single absorption maximum at 498 nm (ε_{max}=5.89×10^4 mol^{-1} dm^3 cm^{-1}) in absolute ethanol.

12) The correlation between the value of pK_a for the conjugate acid HB^+ ($\rightleftarrows H^+ + B$) in aqueous solution and that in absolute ethanol is generally expressed by the equation, pK_a in ethanol (pK_a^{EtOH})=pK_a^W +1.0. See, M. Tanaka, "San to Enki (Acids and Bases)," 4th ed, Syokabo, Tokyo (1977), p. 69.

13) B. Gutbezahl and E. Grunwald, *J. Am. Chem. Soc.*, **75**, 559 (1953); H. C. Brown and X. R. Mihm, *ibid.*, **77**, 1723 (1955); H. K. Hall, Jr., *ibid.*, **79**, 5441 (1957); C. H. Rochester, *J. Chem. Soc. (B)*, **1967**, 33; J. Oszczapowicz and M. Czurylowska, *Talanta*, **31**, 559 (1984).

14) Values of apparent pK_a were obtained from the data at the half-neutralization, where [acid] = [conjugate base] and therefore the pK_a^{EtOH} of the added Brønsted base is equal to the pK_a of the Brønsted acid titrated. The values of pK_a^{EtOH} of the Mn(II) and Ni(II) complexes were obtained with average values for the pK_a^{EtOH}'s of the two *p*-hydroxyl groups.

15) T. Yotsuyanagi, H. Hoshino, and K. Aomura, *Anal. Chim. Acta*, **71**, 349 (1974). In this paper, they pointed out that the green Pd(II)-PAR complex in 50% aqueous dioxane solution has an *N,N,O*-terdentate structure with undissociated *o*-hydroxyl group or an *N,N*-bidentate one. However, in the present work, on the basis of the spectral data (see text) and the elemental analysis of the isolated complex, $[Pd(LH^*)Cl]^0 \cdot H_2O$, it is reasonable to assign the green Pd(II)-4-MePAR complex to the *N,N,O*-terdentate structure with the coordinated *o*-hydroxyl group. Also, in aqueous solution, it is impossible to form the *N,N*-bidentate complex. See, Y. Kudo, N. Yoshida, and M. Fujimoto, *Bull. Chem. Soc. Jpn.*, **59**, 795 (1986); Ref. 6.

16) E. J. King, "Acid-base Behavior," in "Physical Chemistry of Organic Solvent Systems," ed by A. K. Covington and T. Dickinson, Plenum Press, London (1973), p. 375.

17) The species, $A^- \cdot HB^+$ and A^-, could not generally be distinguished by the spectroscopic measurements used in the present work, so one may write the apparent equilibrium constant as $K_A(B)=[A^- \cdot HB^+ + A^-]/([AH][B])$. See, N. Tokura, "Yōbaiwa (Solvation)," 1st ed, Kagaku Dōjin, Kyoto (1972), p. 23; O. D. Bonner and P. R. Prichard, *J. Solution Chem.*, **8**, 113 (1979).

18) It has been reported that, in nonaqueous solvents of relatively low dielectric constants (D<30), the salts of bulky ions predominantly form the ion-pairing species, i.e., *p*-nitrophenol-amine complexes or imidazolium picrate. See, R. Scott, D. De Palma, and S. Vinogradov, *J. Phys. Chem.*, **72**, 3192 (1968); H. Collaer, M. C. Haulait-Pirson, and P. Huyskens, *J. Solution Chem.*, **6**, 73 (1977); M. Nakahara and J. Osugi, *Kagaku (Chemistry)*, **25**, 1026 (1969).

19) D. N. Hendrickson, J. M. Hollander, and W. L. Jolly, *J. Chem. Phys.*, **49**, 3315 (1968); *Inorg. Chem.*, **8**, 2642 (1969); Y. Niwa, H. Kobayashi, and T. Tsuchiya, *ibid.*, **13**, 2891

(1974); S. O. Grim, L. J. Matienzo, and W. E. Swartz, Jr., *ibid.*, **13**, 447 (1974).

20) K. S. Kim, W. E. Baitinger, J. W. Amy, and N. Winograd, *J. Electron Spectrosc. Relat. Phenom.*, **5**, 351 (1974).

21) The intensity ratio of the peak of O(ls) BE's for *o*-hydroxypyridylazo compounds, represented by 4-MePAR, is complicated by the presence of keto-enol (hydrazone-azo) tautomers. See, T. Yoshida, *Bull. Chem. Soc. Jpn.*, **53**, 498 (1980). The fraction of keto tautomer of 4-MePAR was estimated to be 44% in solid state from the XPS measurements.

22) For the metal-4-MePAR and the M(II)-DAPAP systems, it was observed that the order of the deconvoluted N(ls) and O(ls) peaks with higher BE's between the complexes is nearly parallel to that of the raw N(ls) and O(ls) peaks. Y. Kudo, unpublished data. Therefore, it is suggested that the deconvoluted O(ls) BE of the *p*-hydroxyl group in the Pd(II) complex is higher than that in the Co(III) complex.

 © 1986 The Chemical Society of Japan Bull. Chem. Soc. Jpn., 59, 1487—1491 (1986)

Potentiometric and Calorimetric Studies on Formation of Glycinato Complexes of Nickel(II) in Water and in an Aqueous Dioxane Solution

Shin-ichi ISHIGURO, Taweesri PITHPRECHA,† and Hitoshi OHTAKI*
Department of Electronic Chemistry, Tokyo Institute of Technology at Nagatsuta,
4259, Nagatsuta-cho, Midori-ku, Yokohama 227
(Received December 26, 1985)

Protonation equilibria of glycinate (gly^-) ion and complex formation equilibria between nickel(II) and glycinate ions have been studied by potentiometry and calorimetry in water and in 0.2 mole fraction (55.0%w/w) dioxane-water mixture, each containing 3 mol dm^{-3} $LiClO_4$ as a constant ionic medium at 25 °C. A series of mononuclear complexes, $[NiL_n]^{(2-n)+}$ (L^-=gly^- and n=1—3) were found in both solutions and their formation constants, enthalpies and entropies were determined. It elucidated that the stepwise Gibbs energies of formation of the metal complexes varied in the sequence, $\Delta G_1^\circ < \Delta G_2^\circ < \Delta G_3^\circ$, and the stepwise enthalpies, $\Delta H_1^\circ > \Delta H_2^\circ > \Delta H_3^\circ$, and thus, the stepwise entropies markedly decreased in the order, $\Delta S_1^\circ > \Delta S_2^\circ > \Delta S_3^\circ$. The result was discussed in relation to changes in the metal-water and metal-ligand bond lengths within $[NiL_n(H_2O)_{6-2n}]^{(2-n)+}$ (n=1—3) with n. As to the solvent effects, the formation constants of each metal complex increased with the addition of dioxane to water, the increase was caused by both enthalpies and entropies of formation of the complexes, the former mainly contributing to the formation of $[NiL_2]$ and the latter to $[NiL]^+$ and $[NiL_3]^-$. The Gibbs energies of transfer of single species from water to the dioxane-water mixture were also evaluated. The enthalpy and entropy of transfer of any ionic species mostly compensated each other, so that the Gibbs energies of transfer of ions were rather small.

In previous papers,[1,2] we discussed about the complex formation equilibria between ethylenediamine and bivalent metal ions, Ni(II) and Cu(II), in water and in dioxane–water mixtures.

Since ethylenediamine is a neutral ligand, charges of the ethylenediamine complexes of Ni(II) and Cu(II) are kept +2 for all the complexes formed. The stepwise formation constants of each metal complex in dioxane–water mixtures examined were appreciably larger than those in water. The corresponding enthalpies of formation became less negative by the addition of dioxane to water. Consequently, the corresponding entropies of formation markedly increased to result in more favorable formation of the complexes in the mixtures than that in water.

In the nickel(II)–glycinate system in contrast to the metal–ethylenediamine system, charges of the complexes change with the bound ligand number and a different solvent effect on the complex formation equilibria is expected.

In this work, therefore, the complexation of nickel(II) with glycinate ions has been studied by potentiometry and calorimetry in water and in 0.2 mole fraction dioxane–water mixture. The protonation equilibria of the ligand ion were separately investigated in the same solutions. On the basis of these results, the Gibbs energies of transfer of related species from water to the dioxane–water mixture were then evaluated.

Experimental

Reagents. *Nickel(II) perchlorate* was prepared as described elsewhere.[1] Bis(glycinato)nickel(II) crystals were prepared by dissolving freshly precipitated nickel(II) carbonate to an aqueous glycine solution, and then recrystallized from water. *Glycine* was recrystallized three times from an aqueous ethanol and was dried at 80—100 °C in an electric oven.

Other chemicals used were prepared and purified as described previously.[1]

Measurement. All of potentiometric and calorimetric measurements were carried out in a room thermostated at (25.0±0.2) °C. All test solutions used involved 3 mol dm^{-3} $LiClO_4$ as a constant ionic medium throughout potentiometric and calorimetric titrations.

Potentiometric measurements were carried out in a liquid paraffin bath controlled at (25.00±0.02) °C. pH of a test solution was determined by using a glass electrode in combination with an Ag–AgCl reference electrode. The method of measurements was the same as that used in a previous work.[1]

Calorimetric measurements were carried out in a water bath thermostated at (25.000±0.007) °C. Details of measurements were described elsewhere.[1,3,4]

Solubilities of glycine and bis(glycinato)nickel(II) complex in water and in 0.2 mole fraction dioxane–water mixture were gravimetrically determined after the salts were equilibrated with the solvents without ionic medium for more than two weeks in a thermostated room at (25.0±0.2) °C.

Analysis of Potentiometric and Calorimetric Data. The protonation constants and enthalpies of protonation of glycinate ion, which had been determined in advance by separate experiments, were kept constant in the course of determining the formation constants and enthalpies of the metal–ligand complexation. Details of the analysis of potentiometric and calorimetric data were described previously.[1]

† Present address: Department of Chemistry, Faculty of Science, Prince of Songkla University, Songkla, Thailand.

Results and Discussion

The formation function $\bar{n}$ plotted against $-\log([L^-]/\text{mol dm}^{-3})$($L^-$=gly$^-$) for the nickel(II)-glycinate system in water and in the 0.2 mole fraction dioxane-water mixture are depicted in Fig. 1. In each solvent experimental points obtained at various metal concentrations fell on a single curve, indicating that the only mononuclear complexes were formed in the solutions. Since the $\bar{n}_{exp}$ values in each solution approached 3, the potentiometric data were analyzed by assuming the formation of the $[NiL_n]^{(2-n)+}$ (n=1—3) complexes in both solutions. As shown by the solid lines in Fig. 1, the theoretical formation functions well fitted the experimental ones over the whole range of $-\log([L^-]/\text{mol dm}^{-3})$ examined.

Calorimetric titration curves obtained for the nickel(II)-glycinate system in water and in the dioxane-water mixture are depicted in Figs. 2 and 3, respectively. Enthalpies $\Delta H°/\text{kJ mol}^{-1}$ calculated by $\Delta H° = -q/(\delta v C_{H,tit})$ were plotted against the degree of neutralization X of glycinate ion in a solution, where q and δv denote the heat evolved and the volume of the titrant added at each titration point, respectively, and $C_{H,tit}$ stands for the concentration of $HClO_4$ in the titrant solution. The solid lines in Figs. 2 and 3 show the curves calculated by using the formation constants and enthalpies of formation of the complexes finally obtained, which well reproduced the experimental points.

The overall formation constants β_n and overall enthalpies $\Delta H°_{\beta_n}$ of formation of $[H_nL]^{(n-1)+}$ (n=1 and 2) and $[NiL_n]^{(2-n)+}$ (n=1—3) in these solutions are summarized in Tables 1 and 2, respectively.

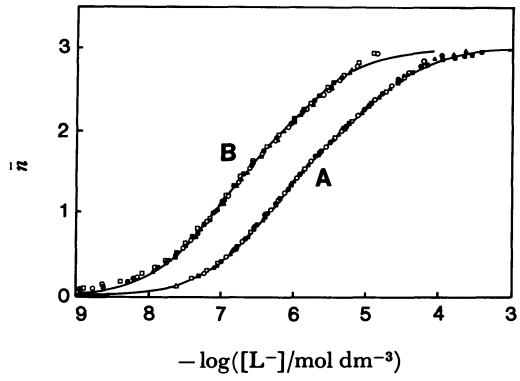

Fig. 1. Formation functions of the nickel(II) glycinate complexes in water (A) and in the 0.2 mole fraction dioxane-water mixture (B). Initial concentrations of metal and ligand ions, C_M and C_L/mol dm^{-3}: 0.00413, 0.02030(▲); 0.00609, 0.02014(○ and △); 0.00688, 0.03383(■); 0.01015, 0.03357 (□); 0.01522, 0.05035 (●) in water and 0.00201, 0.01108(□); 0.00335, 0.01847(○); 0.00405, 0.01405(■); 0.00503, 0.02270 (●); 0.00675, 0.02342(▲); 0.01012, 0.03512(△) in the mixture.

The solid lines show the curves calculated by using the formation constants in Tables 1 and 2.

Thermodynamic quantities, $\log(K_n/\text{mol}^{-1}\text{ dm}^3)$, $\Delta G°_n/\text{kJ mol}^{-1}$, $\Delta H°_n/\text{kJ mol}^{-1}$, and $\Delta S°_n/\text{J K}^{-1}\text{ mol}^{-1}$, for the stepwise formation of $[H_nL]^{(n-1)+}$ and $[NiL_n]^{(2-n)+}$ are listed in Table 3, together with the differences, $P_n(\text{mix})-P_n(\text{w})$ (P=log K, $\Delta G°$, $\Delta H°$, and $\Delta S°$), in water (w) and in the dioxane-water mixture (mix).

Formation of Glycinato Complexes of Ni(II). As seen in Table 3, the $\Delta G°_n$ values in any solution examined varied, as usual, in the sequence, $\Delta G°_1 < \Delta G°_2 < \Delta G°_3$, the $\Delta H°_n$ values in the sequence, $\Delta H°_1 > \Delta H°_2 > \Delta H°_3$ and the $\Delta S°_n$ values, $\Delta S°_1 > \Delta S°_2 > \Delta S°_3$. Therefore, the decrease in $\Delta S°_n$ with n is responsible to the increase in $\Delta G°_n$.

The decreased values of $\Delta H°_n$ and $\Delta S°_n$ with n might be expected if stronger metal-ligand bonds are

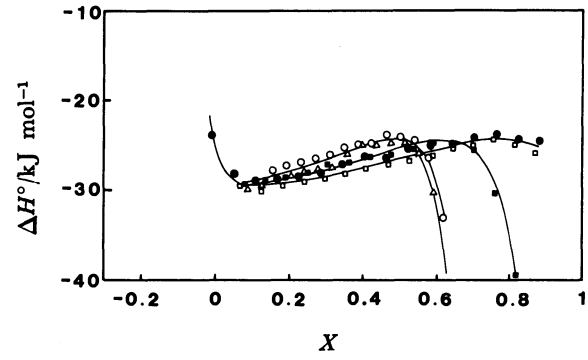

Fig. 2. Calorimetric titration curves of nickel(II) glycinate aqueous solution. Initial concentrations of metal and ligand ions, C_M and C_L/mol dm^{-3}: 0.01015, 0.0288(□); 0.01202, 0.0343(●); 0.01022, 0.0360 (■); 0.01085, 0.0499(△); 0.01159, 0.0520(○).

The solid lines show the curves calculated by using the formation constants in Tables 1 and 2.

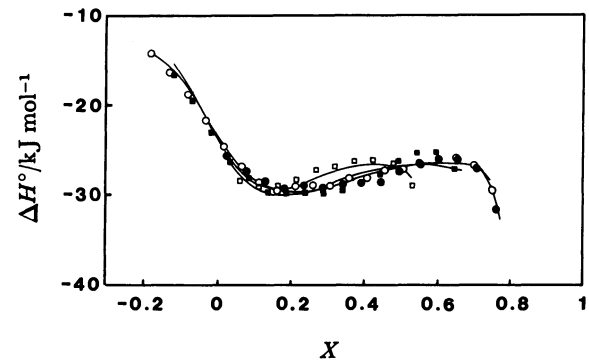

Fig. 3. Calorimetric titration curves of nickel(II) glycinate aqueous dioxane solution (0.2 mole fraction dioxane). Initial concentrations of metal and ligand ions, C_M and C_L/mol dm^{-3}: 0.00603, 0.02971(□); 0.00777, 0.03112(■); 0.01030, 0.03764 (○); 0.01191, 0.04405 (●).

The solid lines show the curves calculated by using the constants in Tables 1 and 2.

Table 1. The Overall Formation Constants β_n and Enthalpies, $\Delta H^\circ_{\beta n}$/kJ mol^{-1}, of Formation of $[H_nL]^{(n-1)+}$ ($L^- = gly^-$) in Solutions Containing 3 mol dm^{-3} $LiClO_4$ at 25 °C
$\beta_n = [H_nL^{(n-1)+}]/[H^+]^n[L^-]$

	Water	0.2 Mole Fraction Dioxane-Water Mixture
$\log \beta_1$	9.94 (0.01)	10.22 (0.01)
$\log \beta_2$	12.62 (0.01)	13.81 (0.01)
$\Delta H^\circ_{\beta 1}$	−57.9 (0.4)	−62.7 (0.5)
$\Delta H^\circ_{\beta 2}$	−63.4 (0.5)	−73.0 (0.5)

The values in parentheses refer to three standard deviations.

Table 2. The Overall Formation Constants β_n and Enthalpies, $\Delta H^\circ_{\beta n}$/kJ mol^{-1}, of Formation of $[NiL_n]^{(2-n)+}$ ($L^- = gly^-$) in Solutions Constaining 3 mol dm^{-3} $LiClO_4$ at 25 °C
$\beta_n = [NiL_n^{(2-n)+}]/[Ni^{2+}][L^-]^n$

	Water	0.2 Mole Fraction Dioxane-Water Mixture
$\log \beta_1$	5.74 (0.02)	6.47 (0.02)
$\log \beta_2$	10.70 (0.02)	12.20 (0.03)
$\log \beta_3$	14.44 (0.03)	16.85 (0.03)
$\Delta H^\circ_{\beta 1}$	−27.3 (0.6)	−27.6 (0.9)
$\Delta H^\circ_{\beta 2}$	−59.5 (0.5)	−63.5 (0.8)
$\Delta H^\circ_{\beta 3}$	−95.0 (0.6)	−100.2 (0.9)

The values in parentheses refer to three standard deviations.

formed within higher complexes. However, according to the results from the X-ray diffraction study of the structures of the complexes in water, the Ni–N bonds as well as the Ni–OH_2 bonds within $[NiL_n(H_2O)_{6-2n}]^{(2-n)+}$ elongate with n,[5-7] due, probably, to an electron donation from the ligands to the central metal ion, so that both metal-ligand and metal-water bonds are expected to be weaker within a higher complex. The enthalpy data obtained indicate that weakening of metal-ligand bonds may be more pronounced at the formation of a higher complex, and thus, the more negative values of ΔH°_n and ΔS°_n with n may result. The same conclusion was also obtained for the nickel(II)-ethylenediamine system.[1]

As to solvent effects, all the $\log K_n$ (n=1—3) values of the glycinatonickel(II) complexes, as well as the ethylenediamine ones,[1] increased by the addition of dioxane to water. In the nickel(II)-ethylenediamine system, the increase in the $\log K_n$ (the decrease in ΔG°_n) values was fully caused by the increase in the ΔS°_n (n=1—3) values, because the ΔH°_n (n=1—3) values also increased. On the other hand, in the nickel(II)-glycinate system as seen in Table 3, the ΔH°_n (n=1—3) values decreased and the ΔS°_n (n=1—3) values increased, and thus, both values were responsible to the increase in the $\log K_n$ (n=1—3) values. However, at the formation of $[NiL_2]$ the contribution of ΔH°_2 to the increased $\log K_2$ value in the mixture was more important than that of ΔS°_2 and the reverse was the case for the $[NiL]^+$ and $[NiL_3]^-$.

Table 3. Thermodynamic Quantities, $\log(K_n/\text{mol}^{-1}\,\text{dm}^3)$, ΔG°_n/kJ mol^{-1}, ΔH°_n/kJ mol^{-1} and ΔS°_n/J K^{-1} mol^{-1}, for the Stepwise Reactions, $H^+ + [H_{n-1}L]^{(n-2)+} = [H_nL]^{(n-1)+}$ ($L^- = gly^-$) and $[NiL_{n-1}]^{(3-n)+} + L^- = [NiL_n]^{(2-n)+}$, in Water and in Aqueous Dioxane of 0.2 Mole Fraction Dioxane Containing 3 mol dm^{-3} $LiClO_4$ at 25 °C, and their Differences in the Solvents

	Water	0.2 Mole Fraction Dioxane-Water Mixture	Difference
$[H_nL]^{(n-1)+}$ system			
$\log K_1$	9.94	10.22	0.28
$\log K_2$	2.68	3.59	0.91
ΔG°_1	−56.6	−58.3	−1.7
ΔG°_2	−15.3	−20.5	−5.2
ΔH°_1	−57.9	−62.7	−4.8
ΔH°_2	−5.5	−10.3	−4.8
ΔS°_1	−3	−15	−12
ΔS°_2	33	34	1
$[NiL_n]^{(2-n)+}$ system			
$\log K_1$	5.74	6.47	0.73
$\log K_2$	4.96	5.73	0.77
$\log K_3$	3.74	4.65	0.91
ΔG°_1	−32.8	−36.9	−4.1
ΔG°_2	−28.3	−32.7	−4.4
ΔG°_3	−21.3	−26.7	−5.4
ΔH°_1	−27.3	−27.6	−0.3
ΔH°_2	−32.2	−35.9	−3.7
ΔH°_3	−35.5	−36.7	−1.2
ΔS°_1	18	31	13
ΔS°_2	−13	−11	2
ΔS°_3	−48	−34	14

In a previous paper,[3] we reported the enthalpies of transfer ΔH°_t of the ethylenediamine and glycinato complexes of Ni(II) from water to the dioxane-water mixture. The ΔH°_t values of each species have significantly large absolute values. However, relatively small differences between the ΔH°_n values of the complexes in water and in the mixture was observed as seen in Table 3, because each difference involve the contributions of ΔH°_t of all species pertaining to the complex formation reaction which mostly compensate each other. The differences between the corresponding ΔG°_n values of the complexes in Table 3 were also small. The Gibbs energies of transfer of species involved in the complex formation reactions were then estimated as described in the following section.

Gibbs Energies of Transfer of Species from Water to the Dioxane-Water Mixture. The Gibbs energies of transfer of proton $\Delta G^\circ_t(H^+)$ from water to the

0.2 mole fraction dioxane-water mixture was 1.9 kJ mol^{-1} and the corresponding value of glycinate ion $\Delta G_t^\circ(L^-)$ was approximately estimated to be 6.0 kJ mol^{-1}.[8]

The Gibbs energies of transfer of $[H_nL]^{(n-1)+}$, $\Delta G_t^\circ(H_nL)$ (L^-=gly$^-$ and n=1 and 2), were then calculated by knowing the $\Delta G_t^\circ(H^+)$ and $\Delta G_t^\circ(L^-)$ values together with the overall Gibbs energies of formation of $[H_nL]^{(n-1)+}$, $\Delta G_{\beta n}^\circ$ (H_nL) ($=-RT\ln \beta_n$), in water and in the mixture given in Table 1:

$$\Delta G_t^\circ(H_nL) = \Delta G_{\beta n}^\circ(H_nL, \text{mix}) - \Delta G_{\beta n}^\circ(H_nL, \text{w}) + n\Delta H_t^\circ(H^+) + \Delta H_t^\circ(L^-). \quad (1)$$

Since the enthalpies of transfer ΔH_t° of the relevant species from water to the mixture have been reported,[3] the corresponding entropies of transfer ΔS_t° were calculated. The thermodynamic quantities of transfer of proton, glycinate ion and $[H_nL]^{(n-1)+}$ (n=1 and 2) thus obtained are summarized in Table 4.

The ΔG_t°(HL) value for glycine zwitterion thus obtained was 6.3 kJ mol^{-1}. The solubilities (α/mol dm^{-3}) of glycine zwitterion in water (α_w) and in the mixture (α_{mix}) were 3.23 and 0.154 mol dm^{-3}, respectively, which gave the $-RT\ln(\alpha_{mix}/\alpha_w)$ value to be 7.5 kJ mol^{-1}. The $-RT\ln(\alpha_{mix}/\alpha_w)$ value may be compared with the calculated ΔG_t°(HL) of glycine zwitterion as the first approximation.

The solubilities of the bis(glycinato)nickel(II) complex determined in water and in the dioxane-water mixture are given in Table 5. Since several glycinatonickel(II) complexes coexisted in the solutions, the distribution of species was calculated by using the formation constants of the complexes in each solution. The Gibbs energy of transfer of the neutral $[NiL_2]$ complex ΔG_t° (NiL_2) from water to the mixture was then calculated according to $\Delta G_t^\circ(NiL_2) = -RT\ln\{\alpha_{mix}(NiL_2)/\alpha_w(NiL_2)\}$, which, although being an approximate value, may be sufficient for the discussion given in a later section. By using the $\Delta G_t^\circ(NiL_2)$ and $\Delta G_t^\circ(L^-)$ values together with the Gibbs energies of formation $\Delta G_{\beta 2}^\circ$ of $[NiL_2]$ in water and in the mixture given in Table 2, the Gibbs energy of transfer of nickel(II) ion $\Delta G_t^\circ(Ni^{2+})$ from water to the mixture was calculated:

$$\Delta G_t^\circ(Ni^{2+}) = \Delta G_{\beta 2}^\circ(NiL_2, \text{w}) - \Delta G_{\beta 2}^\circ(NiL_2, \text{mix}) + \Delta G_t^\circ(NiL_2) - 2\Delta G_t^\circ(L^-). \quad (2)$$

The corresponding ΔG_t° values for $[NiL]^+$ and $[NiL_3]^-$ were then calculated by the similar procedure to that employed above. The ΔG_t° values of the glycinatonickel(II) complexes from water to the mixture thus obtained are summarized in Table 4, together with the corresponding enthalpies and entropies of transfer of the complexes.

As seen in Table 4, both enthalpy and entropy of transfer of proton from water to the mixture are significantly negative but compensate each other to result in a positive $\Delta G_t^\circ(H^+)$ value. The same trend is oserved for the corresponding ΔG_t°, ΔH_t°, and ΔS_t° values of $[H_2L]^+$. On the contary, both ΔH_t° and ΔS_t° values of glycinate ion are significantly positive but almost compensate each other to yield a relatively small positive $\Delta G_t^\circ(L^-)$ value. As to glycine zwitterion, the ΔH_t° value is positive and the ΔS_t° value negative, so that both values contribute to the positive ΔG_t°(HL) value.

Both ΔH_t° and ΔS_t° values for nickel(II) ion are especially largely negative, which also compensate each other to lead to a relatively small positive ΔG_t° value. Although the ΔH_t° values for $[NiL_n]^{(2-n)+}$ (n=1—3) vary from negative to positive with n, each ΔH_t° value is compensated with the corresponding ΔS_t° value and the resultant ΔG_t° values of the complexes are all positive.

As noted in a previous paper,[3] a negative or positive ΔH_t° value of an ion from water to the dioxane-water mixture may reflect the enhanced or weakened solvation structure around the ion in the secondary solvation shell in the mixture compared to that in water. It was then suggested that the solvation structures were enhanced around cations

Table 4. Thermodynamic Quantities of Transfer, ΔG_t°/kJ mol^{-1}, ΔH_t°/kJ mol^{-1}, and ΔS_t°/J K^{-1} mol^{-1}, of Single Species from Water to the 0.2 Mole Fraction Dioxane Mixture at 25 °C

Species	ΔG_t°	ΔH_t° [a]	ΔS_t°
H^+	1.9[b]	−22.7	−83
L^-	6.0[b]	28.7	76
[HL]	6.3	1.2	−17
$[H_2L]^+$	4.1	−26.3	−100
Ni^{2+}	2.7	−41.1	−147
$[NiL]^+$	4.6	−12.7	−58
$[NiL_2]$	6.2[c]	12.3	21
$[NiL_3]^-$	6.8	39.8	111

L^-: $NH_2CH_2COO^-$ (gly$^-$), [HL]: $NH_3^+CH_2COO^-$ (Hgly), $[H_2L]^+$: $NH_3^+CH_2COOH$ (H_2gly^+).
a) Ref. 4. b) Ref. 7. c) From solubility measurements.

Table 5. The Solubilities, α/mmol dm^{-3}, of the Bis(glycinato)nickel(II) Complex in Water and in an Aqueous Dioxane of 0.2 Mole Fraction Dioxane at 25 °C

Solvent	α_{tot}	$\alpha([NiL]^+)$	$\alpha([NiL_2])$	$\alpha([NiL_3]^-)$
Water	110.1	17.4	73.4	18.7
0.2 Mole Fraction Dioxane-Water Mixture	9.8	1.7	6.1	1.8

The distribution of species was calculated by using the formation constants in Tables 1 and 2.

but weakened around anions. If this consideration is applied to the entropies of transfer of ions, it is also indicated that the negative or positive values of ΔS_t° for cations or anions from water to the mixture should result. As seen in Table 4, the ΔS_t° values obtained were significantly negative for H^+, $[H_2L]^+$ and $[NiL]^+$ but positive for L^- and $[NiL_3]^-$, the result being consistent with those expected from the consideration above.

To conclude, it was also suggested by the entropies of transfer of ions from water to the dioxane–water mixture that the solvation structure around cations is enhanced but that around anions is weakened by the addition of dioxane to water. The change in the solvation structures around the ions with varying solvent compositions in dioxane–water mixtures may be related to the partially destroyed hydrogen-bonding structure of water in the bulk solvent mixtures. A dioxane molecule has oxygen atoms which can act as an electron donor and through which the hydrogen-bonds can be formed with water molecules, but it has a very poor electron acceptor ability. By forming the dioxane–water bonds, oxygen atoms of water which can not form sufficient hydrogen-bonds are generated in the mixture. The amount of the non-hydrogen-bonding oxygen atoms of water may increase with an increase in the dioxane content in the mixtures, so that the non-hydrogen-bonding oxygen atoms of water can favorably solvate to cations in the dioxane–water mixture, but solvation of anions may become less favorable due to the decreased acceptor ability of the solvent.

References

1) S. Ishiguro, Y. Oka, and H. Ohtaki, *Bull. Chem. Soc. Jpn.*, **56**, 2426 (1983).
2) S. Ishiguro, Y. Oka, and H. Ohtaki, *Bull. Chem. Soc. Jpn.*, **57**, 391 (1984).
3) S. Ishiguro and H. Ohtaki, *Bull. Chem. Soc. Jpn.*, **57**, 2622 (1984).
4) S. Ishiguro, K. Yamamoto, and H. Ohtaki, *Anal. Sci.*, **1**, 263 (1985).
5) H. Ohtaki, T. Yamaguchi, and M. Maeda, *Bull. Chem. Soc. Jpn.*, **49**, 701 (1976).
6) K. Ozutsumi and H. Ohtaki, *Bull. Chem. Soc. Jpn.*, **56**, 3635 (1983).
7) K. Ozutsumi, T. Yamaguchi, H. Ohtaki, K. Toji, and Y. Udagawa, *Bull. Chem. Soc. Jpn.*, **58**, 2786 (1985).
8) S. Ishiguro, H. Suzuki, and H. Ohtaki, to be published.

Synthesis and Properties of Oxo Complex of Ruthenium(IV), *trans*-[RuCl(O)(py)$_4$]$^+$, which is Formed by the Oxidation of Nitrosyl Complex of Ruthenium(II), *trans*-[RuCl(NO)(py)$_4$]$^{2+}$

Kimitake AOYAGI, Yasuhiko YUKAWA, Kunio SHIMIZU, Masao MUKAIDA*
Toshio TAKEUCHI, and Hidetake KAKIHANA
Department of Chemistry, Faculty of Science and Technology, Sophia University, Kioicho, Chiyoda-ku, Tokyo 102
(Received December 26, 1985)

Oxidation of *trans*-[RuCl(NO)(py)$_4$]$^{2+}$ with NaClO gives oxo complex of Ru^{IV}, *trans*-[RuCl(O)(py)$_4$]$^+$, with bond breaking of the metal-nitrosyl ligand. An X-ray structural study revealed that the complex has a much longer Ru–O bond distance (1.862(8) Å) than those of known mono-oxo complexes. A facile reactivity of the oxoruthenium(IV) complex was observed: with methanol methoxo complex, *trans*-[RuCl(OMe)(py)$_4$]$^+$, was formed. With PPh_3, a two-electron transfer process was indicated by the formation of Ph_3PO.

Considerable attention has been focused on the chemistry of high-valent ruthenium complexes with Ru^{IV}=O^{2-} unit, in connection with their usefulness as an oxygen-transfer agent in the selective oxidation of oganic substrates.[1] Although several other oxoruthenium(IV) complexes have recently been prepared,[2,3] there was no structural information concerning the Ru^{IV}=O^{2-} unit until a preliminary report of the present work and a work by Che et al. appeared.[4,5] Here we describe the syntheses, properties and structures of new mono-oxo complexes of ruthenium(IV), *trans*-[RuX(O)(py)$_4$]$^+$ (X=Cl, Br), which were prepared by the oxidation of the corresponding nitrosyl complex, *trans*-[RuX(NO)(py)$_4$]$^{2+}$, with sodium hypochlorite solution. The present work to afford the mono-oxo complex by the oxidation of the nitrosyl complex appears to be valuable as a synthetic route for the mono-oxo type of complexes.

The nitrosyl ligand coordinated to Ru^{II} atom is believed to be remarkably stable and to persist through a variety of substitution reactions. This is certainly true for most complexes with Ru^{II}NO$^+$ moiety studied so far. The nitrosyl ruthenium complex described above was nevertheless used as a starting material, in order to explore a possible oxidation reaction for the nitrosyl ligand. Recently, Meyer et al. have studied the oxidation of a nitrosyl complex of Ru^{II}, *cis*-[RuCl(NO)(bpy)$_2$]$^{2+}$ (bpy: 2,2′-bipyridine), which gives the corresponding nitrato complex via a reactive nitro complex of Ru^{III}.[6] Their work, however, was mainly a survey on the oxidation at acidic or neutral conditions. The oxidation reaction under a basic condition has not been reported.

Experimental

IR spectra were measured on a Hitachi EPI G2 spectrometer. UV-vis spectra were recorded on a Hitachi 200-20 spectrophotometer. Magnetic moments were measured by the Gouy method using mercury tetrakis(thiocyanato)cobaltate(II) as the calibrant. Elemental analyses were performed by both the Sophia University Analytical Facility and the Institute of Chemical and Physical Research, Wako, Saitama 351. The cyclic voltammetry and the normal pulse voltammetry were carried out by using a Fuso Polarograph Model 321 and a Fuso Potential Scanning unit Model 321 with a stationary platinum disk electrode(ϕ=1.99 mm). All the potentials were measured against a silver-silver ion electrode (Ag/0.1 mol dm^{-3} $AgClO_4$ in acetonitrile). The measurements were carried out at 25 °C. Deoxygenation of solution was carried out with argon gas, which had been passed through two wash bottles containing acetonitrile kept at 25 °C.[7]

Syntheses. Starting material in this work, *trans*-[RuX(NO)(py)$_4$]Y$_2$ (X=Cl, Br. Y=ClO_4, PF_6) were prepared according to the method reported previously.[8]

Chloro(oxo)tetrakis(pyridine)ruthenium(IV) Perchlorate, [RuCl(O)(py)$_4$]ClO_4 1A: To a solution of *trans*-[RuCl(NO)(py)$_4$](ClO_4)$_2$ (0.5 g) in H_2O (15 cm^3), aqueous solution of NaClO (2 cm^3) was added.[9] A yellow precipitate, which formed immediately, became light green with stirring for 4 h at 23—26 °C. The crystalline product obtained was kept for 3 more hours, without stirring, and then filtrated out, washed with cold water, and dried in vacuo. Yield 90—95%. It should be noted that effective stirring of the mixed solution and keeping it warm (at 23—26 °C) are necessary for the synthesis in order to avoid contamination by the unoxidized material of the yellow precipitate described above. The mono-oxo complex is stable as a solid and remained unchanged for several months when stored in a desiccator. Found: C, 42.2; H, 3.4; N, 9.9%. Calcd for $C_{20}H_{20}O_5N_4Cl_2Ru$: C, 42.2; H, 3.5; N, 9.9%.

Chloro(oxo)tetrakis(pyridine)ruthenium(IV) Hexafluorophosphate, [RuCl(O)(py)$_4$]PF_6 1B, and Bromo(oxo)tetrakis(pyridine)ruthenium(IV) Perchlorate, [RuBr(O)(py)$_4$]ClO_4 2, were prepared by the same procedure using the corresponding nitrosyl complexes. For **1B** yield 90%. Found: C, 39.0; H, 3.2; N, 9.2; PF_6, 23.5%. Calcd for $C_{20}H_{20}N_4OClPF_6Ru$: C, 39.1; H, 3.3; N, 9.1; PF_6, 23.6%. For **2** yield 90%. Found: C, 39.0; H, 3.2; N, 9.1%.

Calcd for $C_{20}H_{20}O_5N_4BrRu$: 39.2; H, 3.3; N, 9.1%.

Chloro(nitro)tetrakis(pyridine)ruthenium(II), [RuCl(NO_2)(py)$_4$] 3: As was described in the preparation of **1A**, addition of NaClO solution to aqueous solution of *trans*-[RuCl(NO)(py)$_4$](ClO_4)$_2$ gave immediately a yellow precipitate. The precipitate filtered out, washed with water and dried in vacuo. Found: C, 46.1; H, 4.0; N, 13.2%. Calcd for $C_{20}H_{22}N_5O_3ClRu$ (as monohydrate): C, 46.4; H, 4.3; N, 13.5%.

Chloro(methoxo)tetrakis(pyridine)ruthenium(III) Hexafluorophosphate, [RuCl(OMe)(py)$_4$]PF_6 4A: Complex **1B** (50 mg) was dissolved in methanol (25 cm^3), using a Erlenmeyer flask, and kept at room temperature for 2 d in dark, until the solution color changed to greenish yellow. The volume of the solution was reduced to 5 cm^3 using a rotary evaporator to produce a red crystalline material. The product was filtered out, washed with acetone and then ether, and dried in vacuo. Yield 70%. Found: C, 40.0; H, 3.6; N, 8.8%. Calcd for $C_{21}H_{23}N_4OClPF_6Ru$: C, 40.1; H, 3.7; N, 8.9%.

Chloro(methoxo)tetrakis(pyridine)ruthenium(III) Perchlorate, [RuCl(OMe)(py)$_4$]ClO_4 4B, was prepared by almost the same procedure using the corresponding mono-oxo complex **1A**. Found: C, 43.4; H, 4.0; N, 9.6%. Calcd for $C_{21}H_{23}N_4O_5ClPF_6Ru$: C, 43.2; H, 4.0; N, 9.6%.

Intensity Data Collection. A crystal with dimensions of 0.16×0.14×0.30 mm^3 was used for the measurement without shaping. The crystallographic data are: $RuC_{20}H_{20}N_4O_5Cl_2$, F. W. 568.4, tetragonal, space group *P4/ncc*, Z=16, a=25.781(5), c=14.130(4) Å, U=9391(4) Å^3, D_x=1.61, D_m=1.59 g cm^{-3}, μ(Mo $K\alpha$) 9.21 cm^{-1}. The reflections were collected by the ω scan technique ($2\theta<55°$) on a Rigaku AFC-6A automated four-circle diffractometer, with graphite monochromated Mo $K\alpha$ radiation (0.7107 Å). The 2122 independent reflections with $|F_o|>3\sigma(|F_o|)$ were used for the structure refinement. The intensities were corrected for Lorentz and polarization factors, but no correction was made for the absorption. All the calculations were carried out on a HITAC M-200H computer at the Computer Center of the University of Tokyo, using the local version of UNICS.[10] The atomic scattering factors were taken from the table.[11]

Structure Determination. The structure was solved by a heavy-atom method. The position of ruthenium and chlorine atoms were obtained from a three-dimensional Patterson function, while the positions of all the non-hydrogen atoms were succesively located by Fourier syntheses. Since the positions of only a few hydrogen atoms were obtained by a difference-Fourier syntheses, all of the positions were calculated and fixed. Their isotropic temperature factors were assumed to be 5.0 Å^2.

All other positions and thermal parameter were refined by a repeated block-diagonal least-squares method. The weighting scheme was $W=1/[\{\sigma(|F_o|)\}^2+(0.04\times|F_o|)^2]$. In the last cycle of the refinement with anisotropic temperature factors for all non-hydrogen atoms, all the parameter shifts were less than one-third of the corresponding standard deviations. The final R value ($R=\sum||F_o|-|F_c||/\sum|F_o|$) was 0.076. The F_o—F_c data and the anisotropic temperature parameter are deposited as Document No. 8627 at the Office of the Editor of the Bulletin of the Chemical Society of Japan.

Results and Discussion

Syntheses. The reaction of *trans*-[RuX(NO)(py)$_4$]$^{2+}$ (X=Cl, Br) in a basic aqueous solution containing NaClO as an oxidant gave the mono-oxo complex, *trans*-[RuX(O)(py)$_4$]Y (**1A**; for X=Cl, Y=ClO_4. **1B**; for X=Cl, Y=PF_6. **2**; for X=Br, Y=ClO_4), in high yield. In the initial step of the reaction, nitro complex, [RuCl(NO_2)(py)$_4$] **3**, was formed by the known nitrosyl-nitro conversion reaction (Eq. 1)[12]

$$[Ru^{II}Cl(NO)(py)_4]^{2+} \xrightarrow{OH^-} [Ru^{II}Cl(NO_2)(py)_4] \quad (1)$$

The nitro complex **3** was isolable and its identity was confirmed by a direct comparison with an authentic sample reported previously.[8] The next step of the reaction appears to be an oxidation of the nitro complex of Ru^{II} to Ru^{III} which is followed by a Ru^{III}–NO_2^- bonding rupture, resulting in the corresponding hydroxo complex (Eqs. 2 and 3):

$$[Ru^{II}Cl(NO_2)(py)_4] \xrightarrow{-e^-} [Ru^{III}Cl(NO_2)(py)_4]^+ \quad (2)$$

$$\xrightarrow{-NO_2^-} [Ru^{III}Cl(OH)(py)_4]^+ \quad (3)$$

The oxidation was also attempted for the corresponding hydroxo nitrosyl complex, *trans*-[Ru(OH)(NO)(py)$_4$]$^{2+}$, which has been known as a poor electrophile compared to *trans*-[RuCl(NO)(py)$_4$]$^{2+}$ used as the starting material of the present reaction.[8] In this case, however, the nitrosyl–nitro conversion reaction did not occur under the conditions, and the isolated product, by adding PF_6^-, was *trans*-[Ru(OH)(NO)(py)$_4$]$^{2+}$.[13]

Nitro complex of Ru^{III} has been found to be chemically unstable.[6] In the electrochemical experiment, in fact, a facile reaction due to a decomposition of the nitro complex of Ru^{III} was observed when **3** in CH_3CN undergoes a one-electron oxidation. As is shown in cyclic voltammogram (Fig. 1), **3** in CH_3CN displays a one-electron oxidation wave (E_{pa}=0.28 V vs. Ag/$AgClO_4$ (0.1 mol dm^{-3} in CH_3CN)) in the potential region expected for the Ru^{II}/Ru^{III} couple. On scan reversal, a small reduction wave appeared at −0.12 V with decreasing of a cathodic responce, corresponding to a pair of oxidation wave observed at 0.28 V.[14] The next cycle showed a new oxidation peak at −0.07 V, not present in the original anodic cyclic voltammogram, which is presumed to be the couple with the small reduction wave at −0.12 V. The lack of the cathodic responce and the appearance of the new couple are evidently due to a rapid decomposition of the oxidized species [Ru^{III}Cl(NO_2)(py)$_4$]$^+$, although more study with coulometric experiments is needed to clarify the electrochemical

behavior in the oxidation reaction of **3**. The cyclic voltammogram observed here is similar to that of *cis*-$[RuCl(NO_2)(bpy)_2]$, where nitro-nitrito isomerization has been known to occur by the oxidation of the Ru^{II}-NO_2^- moiety.[6] The fate of the NO_2^- ligand released (Eq. 3) could not be elucidated; it is probably changed into NO_3^-.

The final step to generate $Ru^{IV}=O^{2-}$ moiety from the hydroxo complex (Eq. 4) is the same reaction as found in *cis*-$[RuCl(O)(bpy)_2]^+$ [1b]:

$$[Ru^{III}Cl(OH)(py)_4]^+ \xrightarrow{-e^-} [Ru^{IV}Cl(O)(py)_4]^+ \quad (4)$$

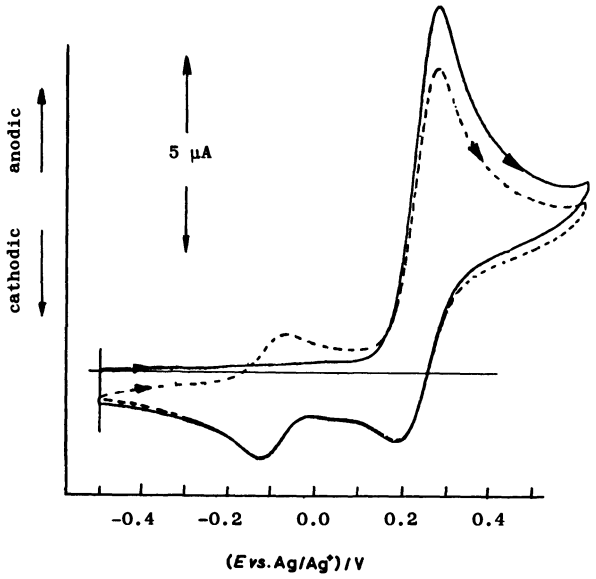

Fig. 1. The cyclic voltammogram of $[RuCl(NO_2)(py)_4]$ **3** (1.00 mol dm^{-3}) at a stationary platinum electrode (50 mV S^{-1}) in 0.1 mol dm^{-3} TEAP+AN at 25 °C. Initial potential: −0.5 V. The dashed curve shows the result of the second scan.

In the solid state, the complexes **1A**, **1B**, and **2** are stable indefinitely at room temperature. It was found, however, that the magnetic susceptibility of the complexes decreased markedly when the complexes were washed with organic solvents such as alcohols or acetone. Therefore, further purification by recrystallization was not attempted.

IR Spectra. The IR absorption band ascribed to Ru-O stretching vibration in **1A**, **1B**, and **2** was observed at the same frequency region, 800 cm^{-1} (Table 1). As reported previously, the absorption band due to the stretching vibration of the terminal oxo ligand occurs in 800—900 cm^{-1} for a variety of oxidation states of metal complexes.[15] This IR region, however, is almost the same as those for an antisymmetric stretching vibration (ν_3) of μ-oxo ruthenium complexes.[16] The absorption band due to ν_3 mode of a linear or quasi-linear M-O-M system has usually been regarded as a diagnostic for identifying the μ-oxo complexes.[16] Thus, the overlapping of these regions characteristic for both terminal- and bridging-oxo ruthenium complexes did not provide further information for identifying the present complex, and the choice in the correct formula between the mono-oxo complex, $[RuX(O)(py)_4]^+$, and the μ-oxo complex, $[Ru_2O(X)_2(py)_8]^{2+}$, could only be established by an X-ray structural determination.

Structure. The final atomic parameters are listed in Table 2, the interatomic distances in Table 3, and the bond angles in Table 4. The perspective drawing of the complex **1A** and the numbering scheme of the atoms are in Fig. 2. The cation is an oxo ruthenium(IV) complex ion, with trans octahedral geometry; it has four equatorial pyridine ligands, while the oxo and chloro ligands are coordinated in the axial direction. The oxo complex has a propeller-like

Table 1. Ru-O Distances and Stretching Frequencies in Selected Terminal- and Bridging-Oxo Ruthenium Complexes

Complex	Ru-O/Å	νRu-O/cm^{-1}	μ_{eff}/B.M.[c]	Refs.
Ru=O system				
$[RuCl(O)(py)_4]ClO_4$ **1A**	1.862(8)	805	2.94	this work
$[RuCl(O)(py)_4]PF_6$ **1B**		805	2.92	this work
$[RuBr(O)(py)_4]ClO_4$ **2**		805	2.93	this work
$[Ru(O)(tmc)(MeCN)](PF_6)_2$	1.765(5)		2.93	5
$[Ru(O)(bpy)(trpy)](ClO_4)_2$		792 (752)[a]	2.92	1
Ru-O-Ru system				
$[\{RuCl_5\}_2O]^{4-}$	1.801(2)	886[b]		18
$[\{Ru(NO_2)(bpy)_2\}_2O]^{2-}$	1.883(6)			19
$[\{Ru(TPP)(p\text{-}OC_6H_4CH_3)\}_2O]$	1.789(11)			20
$[\{Ru(OEP)(OH)\}_2O]$	1.847(13)			21
$[(NH_3)_5RuORu(en)_2ORu(NH_3)_5]^{6+}$	1.87			22

a) νRu-^{18}O. b) Raman spectra. c) 1 B.M. = 9.274078(36) 10^{-24} J T^{-1}. Abbreviations: tmc, 1,4,8,11-tetramethyl-1,4,8,11-tetraazacyclotetradecane; TPP, 5,10,15,20-tetraphenylporphine; OEP, 2,3,7,8,12,13,17,18-octaethylporphine; trpy, 2,2′ : 6′,2″-terpyridine.

Table 2. Positional Parameters ($\times 10^4$ for Non-Hydrogen Atoms Except to the Atoms of Perchlorate Anions; $\times 10^3$ for others) and Equivalent Isotropic Temperature Factors (B_{eq}/Å^2), with the Estimated Standard Deviations

Atom	x	y	z	B_{eq}/Å^2	Atom	x	y	z	B_{eq}/Å^2
Ru	41.5(4)	1836.8(4)	1462.2(8)	3.06	O(51)	−73(2)	445(2)	182(2)	15.77(13)
Cl	−22(2)	2446(1)	164(2)	4.17	O(52)	16	454	226	10.00
O(1)	102(3)	1385(3)	2488(6)	3.47	O(53)	−10	482(1)	337(2)	13.90(11)
N(1)	567(4)	1385(4)	673(8)	4.36	O(54)	−89(1)	483(1)	267(2)	12.58(10)
N(2)	649(4)	2278(4)	2033(7)	3.21	O(61)	250	250	370(2)	7.86(6)
N(3)	−580(4)	2267(4)	2206(7)	3.03	O(62)	213	210	494	9.20
N(4)	−544(4)	1374(4)	896(7)	3.75	O(63)	234	299	513	9.20
C(11)	954(6)	1138(6)	1126(12)	6.45	O(64)	300	237	513	9.20
C(12)	1297(6)	825(7)	598(16)	7.98	O(71)	−249(1)	205(1)	444(1)	11.07(4)
C(13)	1233(7)	753(7)	−342(17)	8.67					
C(14)	825(7)	996(6)	−773(12)	7.21	H(11)	100	118	192	7.14
C(15)	496(6)	1313(6)	−255(11)	5.20	H(12)	162	62	97	7.99
C(21)	654(5)	2397(5)	2969(9)	3.99	H(13)	150	51	−77	8.39
C(22)	1046(6)	2670(5)	3361(9)	4.54	H(14)	77	95	−153	7.21
C(23)	1446(5)	2843(5)	2820(11)	4.66	H(15)	17	151	−63	5.38
C(24)	1453(5)	2725(5)	1887(10)	4.33	H(21)	34	227	342	4.22
C(25)	1045(5)	2442(5)	1492(9)	3.81	H(22)	105	275	413	4.66
C(31)	−903(5)	2014(5)	2635(11)	4.44	H(23)	177	307	313	4.75
C(32)	−1288(6)	2268(6)	3094(11)	5.49	H(24)	177	285	144	4.34
C(33)	−1305(6)	2808(6)	3094(11)	5.69	H(25)	105	236	73	3.93
C(34)	−909(6)	3061(5)	2663(11)	5.31	H(31)	−91	159	263	4.10
C(35)	−522(6)	2794(5)	2205(10)	4.16	H(32)	−159	204	346	5.46
C(41)	−498(6)	857(5)	989(12)	5.29	H(33)	−163	302	345	5.67
C(42)	−873(6)	529(6)	612(14)	6.53	H(34)	−90	349	268	5.28
C(43)	−1278(7)	717(7)	131(13)	7.14	H(35)	−21	301	184	4.31
C(44)	−1329(6)	1270(7)	58(11)	5.48	H(41)	−16	70	139	5.55
C(45)	−954(6)	1568(6)	447(10)	4.65	H(42)	−85	11	70	6.20
					H(43)	−157	47	−23	6.48
Cl(5)	−38(1)	468	250	11.68(3)	H(44)	−167	141	−31	5.35
Cl(6)	250	250	471(1)	8.76(3)	H(45)	−100	200	39	4.59
Cl(7)	−250	250	500	6.02(2)					

Table 3. Selected Interatomic Distances with the Estimated Standard Deviations in Parentheses

	l/Å		l/Å
Ru-Cl	2.419(4)	N(1)-C(11)	1.38(2)
Ru-O	1.862(8)	C(11)-C(12)	1.46(2)
Ru-N(1)	2.107(11)	C(12)-C(13)	1.41(3)
Ru-N(2)	2.096(9)	C(13)-C(14)	1.38(2)
Ru-N(3)	2.089(9)	C(14)-C(15)	1.39(2)
Ru-N(4)	2.094(10)	C(15)-N(1)	1.38(2)
Cl-C(15)	3.25(2)	C(11)-C(25)	3.41(2)
Cl-C(25)	3.33(1)	C(21)-C(35)	3.36(2)
Cl-C(35)	3.27(2)	C(31)-C(45)	3.32(2)
Cl-C(45)	3.30(1)	C(41)-C(15)	3.33(2)
O-C(11)	2.95(2)	O-C(21)	3.04(2)
O-C(31)	3.06(2)	O-C(41)	2.91(2)

Table 4. Selected Bond Angles with the Estimated Standard Deviations in Parentheses

	ϕ/°
Cl -Ru-O	178.2(3)
Cl -Ru-N(1)	90.4(3)
Cl -Ru-N(2)	89.2(3)
Cl -Ru-N(3)	89.2(3)
Cl -Ru-N(4)	91.6(3)
N(1) -Ru-N(4)	176.6(4)
N(1) -C(11)-C(12)	116(2)
C(11)-C(12)-C(13)	120(2)
C(12)-C(13)-C(14)	118(2)
C(13)-C(14)-C(15)	122(2)
C(14)-C(15)-N(1)	119(1)

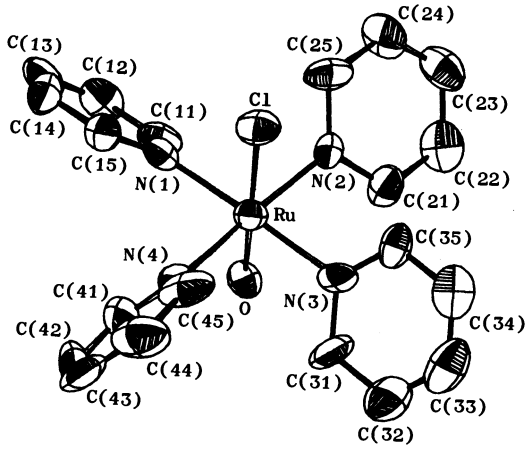

Fig. 2. The perspective drawing of $[RuCl(O)(py)_4]ClO_4$ **1A** and the numbering scheme of non-hydrogen atoms.

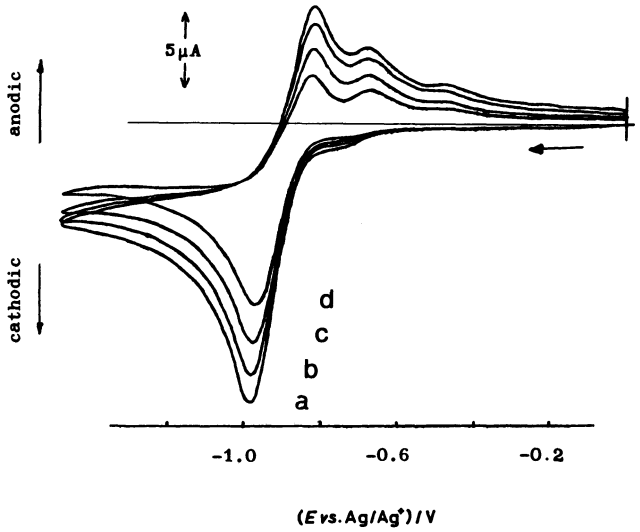

Fig. 3. The cyclic voltammograms of $[RuCl(O)(py)_4]ClO_4$ **1A** (1.07 mol dm^{-3}) at a stationary platinum disk electrode (scan rate/mV S^{-1}): (a) 100; (b) 80; (c) 60; (d) 40 in 0.1 mol dm^{-3} TEAP+AN at 25 °C.

structure similar to that of the nitrosyl complex, *trans*-$[RuCl(NO)(py)_4]^{2+}$, used as starting material for the present oxidation reaction.[17] The oxo and chloro ligands are almost on the line including the ruthenium: O-Ru-Cl, 178.2(3)°. The Ru-O bond distance, 1.862(8) Å, is considerably shorter than the sum of the single bond radii for Ru^{IV}-O^{2-} (1.97 Å) and it is significantly longer than the value 1.756 Å reported recently for similar mono-oxo complex, *trans*-$[Ru(O)(tmc)(MeCN)]^{2+}$, of which the bond length is consistent with the expected bond order of two.[5] The remarkably long bond distance of the Ru-O observed here may be important factor to the reactivity of the mono-oxo moiety in **1A**. It is worth noting that the observed Ru-O distance is comparable with values reported for both μ-oxo complexes of Ru^{III} and Ru^{IV}, as shown in Table 1.[18-22]

The Ru^{IV}-Cl distance, trans to the oxygen atom, is 2.419(4) Å. The distance is longer than Ru^{IV}-Cl distances, 2.317—2.364 Å reported in the complexes, $[Ru_2OCl_{10}]^{4-}$ and $[Ru_2NCl_8(H_2O)_2]^{3-}$.[23] An elongation of metal-Cl distance trans to nitrido ligand (N^{3-}), which has a multiple bonding order, has been reported in $[Os^{IV}NCl_5]^{2-}$;[24] the Os-Cl bond distance trans to the nitrido is 2.61 Å and that to cis is 2.36 Å, whereas such a lengthening has not been found for the Ru^{IV}-Cl distance, trans to bridging oxo ligand in $[Ru_2OCl_{10}]^{4-}$ (Ru-Cl(*trans*), 2.317(7) Å; Ru-Cl(*cis*), 2.362(2) Å.[18b] The Ru-N distance vary from 2.089(6) to 2.107(11) Å. These Ru-N distances are slightly shorter than those previously reported for *trans*-$[RuCl(NO)(py)_4]^{2+}$ (2.103—2.118 Å), $[Ru(py)_6]^{2+}$ (2.10—2.14 Å) and $[(py)_4Ru(ox)Ru(py)_4]^{2+}$ (2.096—2.113 Å).[17,25,26] The dihedral angles between the best plane of RuN_4 and those of the pyridine rings range from 44.1—54.1°. The angle between the two pyridine planes in trans position are 80.6—82.7°, which are little larger than those of *trans*-$[RuCl(NO)(py)_4]^{2+}$. The distances between adjacent pyridine carbons and those between pyridine carbon and axial chloro ligand are slightly longer than the corresponding distances in the nitrosyl complex. On the other hand, the distances between pyridine carbon and the chloro ligand are shorter.

One counter anion, ClO_4^-, is on the four-fold rotatory inversion axis, the second is on the four-fold rotation axis, and the third is on the two-fold rotation axis. A statistical distribution was observed at the oxygen of ClO_4^- on the four- and two-fold rotation axis, and their positions could not be determined.

The effective magnetic moments were found to be 2.92—2.94 B.M., as shown in Table 1. These are almost the same as those observed in the known oxoruthenium(IV) complexes and are close to spin-only value for two unpaired spins. The observation of two unpaired electrons is consistent with the orbital splitting scheme proposed by Meyer et al.,[1b] in which the existence of the half filled dπ* orbitals results in an extensive stabilization of the Ru-O bonding through a pπ(O^{2-})-dπ(Ru) interaction.

Electrochemical Behavior. A cyclic voltammogram of **1A** in acetonitrile is shown in Fig. 3.[27] The reductive sweep shows a single wave at a much more negative potential than those of the known Ru^{IV}/Ru^{III} couple (E_{pc}=−0.99 V vs. Ag/$AgClO_4$(0.1 mol

dm^{-3} in CH_3CN)). The cyclic voltammogram also shows an indistinct reduction wave observable near −0.85 V. The origin of the dim reduction wave is not clear, but it is thought to be caused by a partial decomposition of **1A** in the organic solvent. In the back sweeping, a small oxidation wave, which is the pair to the reduction wave at −0.99 V, appeared at −0.92 V with two additional oxidation waves. We compared the current heights, observed by the normal pulse voltammetry at the same experimental conditions, of the reduction wave at −0.99 V with those of other Ru^{IV}/Ru^{III};[28] the reduction wave appeared to be a metal-centered two-electron transfer comprising the Ru^{IV} and Ru^{II} oxidation states

$$[Ru^{IV}Cl(O)(py)_4]^+ + 2e^- \longrightarrow [Ru^{II}Cl(O)(py)_4]^- \quad (5)$$

Fig. 3 also illustrates that the electrochemically produced $[RuCl(O)(py)_4]^-$ is not stable and probably undergoes a facile solvolysis to give $[RuCl(CH_3CN)(py)_4]^+$, which is responsible for the appearance of the oxidation waves at −0.84 V. A one-electron reduced species involving $Ru^{III}-O^{2-}$ moiety was unobtainable by the electrochemical reduction in the aprotic solvent, while a succesive reduction of $Ru^{IV}=O^{2-}$ to give $Ru^{III}-OH^-$ and $Ru^{II}-OH_2$ moieties has been observed in aqueous solvent for certain oxoruthenium(IV) complexes.[1b] As was described above, **1A** exhibited the two-electron reduction wave at a surprisingly negative potential region, where the Ru^{III}/Ru^{II} redox potential is generally observed. The very negative potential in **1A**, compared to those of known Ru^{IV}/Ru^{III} couples, could be understood as showing that the presence of the oxo ligand leads to extensive stabilization of Ru^{IV} state.[1b]

Reactivity. The oxoruthenium(IV) complex in CH_3CN reacts easily with PPh_3. Such a reaction, which produces Ph_3PO with a reducing of the oxidation state of the metal atom, is characteristic for the complexes containing a reactive oxygen ligand. When **1A** in CH_3CN was mixed with PPh_3 (mole ratio 1:1.5) at room temperature, the mixed solution changed immediately from green to yellow. A brown material could be obtained by adding an excess amounts of ether to the yellow solution. The composition of the brown material agreed well with that of $[RuCl(CH_3CN)(py)_4]PF_6$. IR spectra of this material exhibited a sharp absorption band at 2245 cm^{-1}; this is assignable to ν(CN) of the coordinated CH_3CN. Another product, Ph_3PO, could also be obtained as a white precipitate from the filtrate of $[RuCl(CH_3CN)(py)_4]PF_6$ by adding ether (ν(P=O), 1182 cm^{-1}). While a stoichiometric study of the reaction could not be achieved, the above results giving both $[RuCl(CH_3CN)(py)_4]^+$ and Ph_3PO can be understood by the following equation:

$$[RuCl(O)(py)_4]^+ + PPh_3 \longrightarrow [RuCl(S)(py)_4]^+ + Ph_3PO \quad (6)$$
$$(S=CH_3CN)$$

The oxoruthenium(IV) complex **1A** is reactive even for organic solvents, such as alcohols and acetone. Upon recrystallization with methanol, the effective magnetic moment decreased from 2.94 to near 2.5 B.M. (calculated for the same formula as the mono-oxo complex), as was described above. Although the oxo ligand in $(Ru^{IV}=O^{2-})$ unit has been known to act as an oxygen-transfer agent toward organic substrates, there was no example where a product was isolated from these reactions, except for the case of the Ph_3PO. Attempt to isolate the solvolysis product from methanol, in the present case, yielded a red crystalline product. The experimental data obtained so far for the product as follows. Satisfactory elemental analyses were obtained, from which *trans*-$[RuCl(OMe)(py)_4]^+$ **4** could be confirmed.[29] The effective magnetic moment (2.32 B.M.), which was measured by the Gouy method, is in the range expected for Ru^{III} complexes. IR spectra show new bands at 2860, 2786, 1422, 1038, and 549 cm^{-1}, with disappearance of the ν(Ru=O) band characteristic of the oxo complexes. The assignment of the methoxo bands was verified by a comparison of those for the deuterated complex, $[RuCl(OCD_3)(py)_4]^+$, with the results reported by Hill et al.[30] Upon the deuteration, the methoxyl CH stretching vibration bands at 2860 and 2786 cm^{-1} shifted to 2172 and 2040 cm^{-1}, respectively. The methoxyl CH bending vibration band at 1422 cm^{-1} disappeared, and it is thought to shifted to near 1100 cm^{-1} region, where a strong absorption band due to ClO_4^- was observed. The band at 1038 cm^{-1}, which is believed to be methoxy CO stretching vibration, shifted to 1004 cm^{-1}. The Ru-O stretching vibration at 549 cm^{-1} is also shifted to 526 cm^{-1} in its deuterated complex. These shifts found in C-O and Ru-O stretching vibrations are regarded to be reasonable for the deuteration of a methoxo ligand coordinated to metal.[30]

Although further investigation is now in progress on the oxoruthenium(IV) complex, which acts as an oxidant toward organic substrates, we assume that the methoxo formation reaction involves a water condensation reaction between methanol and a hydroxo complex of Ru^{III}, $[RuCl(OH)(py)_4]^+$, which is formed by a one-electron reduction of **1A** (reverse of Eq. 4) with interaction of another methanol molecule

$$[RuCl(OH)(py)_4]^+ + MeOH \longrightarrow [RuCl(OMe)(py)_4]^+ + H_2O \quad (7)$$

The existence of the hydroxo complex could be presumed before the methoxo formation reaction occured.[31]

The authors wish to express their thanks to Professor Akira Ouchi and Dr. Mamoru Shimoi, the University of Tokyo, for the X-ray diffraction measurements and for their helpful discussions. They also would like to thank Dr. F. Scott Howell, Sophia University, for correcting the manuscript. Thanks are also due to Misses Mieko Kurihara and Kuniko Shirai for their technical assistance. The present work was partially supported by a Grant-in-Aid for Scientific Research No. 59540401 from the Ministry of Education, Science and Culture, and also by a grant from the Morimura Homei-kai (1983).

References

1) a) M. S. Thompson and T. J. Meyer, *J. Am. Chem. Soc.*, **104**, 4106, 5070 (1982); b) B. A. Moyer and T. J. Meyer, *Inorg. Chem.*, **20**, 436 (1981); c) M. S. Thompson, W. F. Giovani, B. A. Moyer, and T. J. Meyer, *J. Org. Chem.*, **49**, 4972 (1984); d) K. J. Takeuchi, M. S. Thompson, D. W. Pipes, and T. J. Meyer, *Inorg. Chem.*, **23**, 1845 (1984).

2) S. Goswami, A. R. Chakravarty, and A. Chakravorty, *J. Chem. Soc., Chem. Commun.*, **1982**, 1288.

3) Chi-Ming Che, Tin-Wu Tang, and Chung-Kwong Poon, *J. Chem. Soc., Chem. Commun.*, **1984**, 641.

4) Y. Yukawa, K. Aoyagi, M. Kurihara, K. Shirai, K. Shimizu, M. Mukaida, T. Takeuchi, and H. Kakihana, *Chem. Lett.*, **1985**, 283.

5) Chi-Ming Che, Kwork-Yin, and T. C. W. Mark, *J. Chem. Soc., Chem. Commun.*, **1985**, 546.

6) F. R. Keene, D. J. Salmon, J. L. Walsh, H. D. Abruna, and T. J. Meyer, *Inorg. Chem.*, **19**, 1896 (1980).

7) A. Endo, *Bull. Chem. Soc. Jpn.*, **56**, 2733 (1983).

8) F. Bottomley and M. Mukaida, *J. Chem. Soc., Dalton Trans.*, **1982**, 1933.

9) The use of fresh NaClO solution (Wako Co., available chlorine 10%) is necessary for the synthesis.

10) "The Universal Crystallographic Computation Program System (UNICS)," ed by Tosio Sakurai, Crystallographic Society of Japan, Tokyo (1967).

11) "International Tables for X-Ray Crystallography," Kynoch Press, Birmingham, U. K. (1974), Vol IV.

12) J. H. Swinehart, *Coord. Chem. Rev.*, **2**, 385 (1967).

13) It has been found that *trans*-$[Ru(OH)(NO)(py)_4]^{2+}$ reacts with OH^- at very high pH (approx. 13) to produce $[Ru(OH)(NO_2)(py)_4]$.[8] An unidentified material, which is believed to contain oxo ligand (ν(Ru=O), 795 cm^{-1}), could be obtained when an excess of NaClO was added to aqueous solution of *trans*-$[Ru(OH)(NO)(py)_4]^{2+}$.

14) In this potential region, the cyclic voltammogram of the corresponding dichloro complex, $[RuCl_2(py)_4]ClO_4$, exhibits only a redox wave at $E_{1/2}$=−0.14 V, which is ascribed to a reversible one-electron reduction of Ru^{III}/Ru^{II} couple.

15) F. A. Cotton and R. M. Wing, *Inorg. Chem.*, **4**, 867 (1965).

16) a) D. J. Howkin and W. P. Griffith, *J. Chem. Soc., A*, **1966**, 472; b) W. P. Griffith, *ibid.*, **1966**, 211.

17) T. Kimura, T. Sakurai, M. Shima, M. Mukaida, T. Togano, and T. Nomura, *Inorg. Chim. Acta*, **69**, 135 (1983).

18) A. M. Mathieson, D. P. Mellor, and N. C. Stephenson, *Acta Crystallogr.*, **5**, 185 (1952); b) J. P. Deloume, R. Faure, and G. T. David, *ibid., Sect. B*, **35**, 558 (1979).

19) D. W. Rhelps, E. M. Kahn, and D. J. Hodgeson, *Inorg. Chem.*, 14, 2486 (1975).

20) J. P. Collman, C. E. Barnes, P. J. Brothers, T. J. Collins, T. Ozawa, J. C. Gallucci, and J. A. Ibers, *J. Am. Chem. Soc.*, **106**, 5151 (1984).

21) H. Masuda, T. Taga, K. Osaka, H. Sugimoto, M. Mori, and H. Ogoshi, *J. Am. Chem. Soc.*, **103**, 2199 (1981).

22) P. M. Smith, T. Fealey, J. H. Farley, and J. V. Silverton, *Inorg. Chem.*, **10**, 1943 (1971).

23) a) M. Ciekanovicz and A. C. Skapski, *J. Chem. Soc.*, **1971**, 1972; b) R. J. D. Gee and H. M. Fowell, *ibid.*, **1971**, 1975.

24) D. Bright and J. A. Ibers, *Inorg. Chem.*, **8**, 709 (1969).

25) J. L. Templeton, *J. Am. Chem. Soc.*, **101**, 4906 (1979).

26) P. T. Cheng, B. R. Loescher, and S. C. Nyburg, *Inorg. Chem.*, **10**, 1275 (1971).

27) UV spectra of **1A** in CH_3CN (680—690 nm, ε=130 $mol^{-1}\,dm^3\,cm^{-1}$) did not change during the time for the measurement (30—45 min), though the complex is reactive toward organic solvents.

28) Y. Takeuchi, A. Endo, K. Shimizu, and G. P. Sato, *J. Electroanal. Chem.*, **185**, 185 (1985).

29) Trans geometry of the complex is indicated by its X-ray structure which is still being studied (R=8%). The result will be published separately.

30) M. J. Camenzind, F. J. Hollander, and C. L. Hill, *Inorg. Chem.*, **21**, 4301 (1982).

31) The chlorohydroxotetrakis(pyridine)ruthenium(III) complex has not been reported yet. The product obtained at this stage could reasonably be formulated as $[RuCl(OH)(py)_4]PF_6$ based on the following results. Anal. Found: C, 39.6; H, 3.6; N, 9.1%. Calcd for $C_{20}H_{21}N_4ClOPF_6Ru$: C, 39.1; H, 3.4; N, 9.1%. The IR spectra of the product (4000—750 cm^{-1}) are almost the same as to those of $[RuCl_2(py)_4]PF_6$, except that the product obtained exhibits a sharp absorption band which is assignable to ν(OH) at 3544 cm^{-1} (KBr). The cyclic voltammogram of the product in CH_3CN exhibits a reversible one-electron reduction wave at −0.68 V which is indicative the oxidation state of Ru^{III}.

 © 1986 The Chemical Society of Japan Bull. Chem. Soc. Jpn., 59, 1501—1504 (1986)

Synthesis of Photosensitive Poly(2,5-Norbornadien-7-yl Acrylate and Methacrylate)

Hiroyoshi KAMOGAWA* and Makoto YAMADA
Department of Applied Chemistry, Yamanashi University, Takeda 4, Kofu 400
(Received November 25, 1985)

2,5-Norbornadien-7-yl acrylate and methacrylate were synthesized by the esterification of 2,5-norbornadien-7-ol with acryloyl and methacryloyl chlorides, respectively. Polymerization of the monomers with AIBN provided vinyl polymers with pendant norbornadiene units, which could be made to clear films from CH_2Cl_2. UV-irradiations brought about remarkable changes in the 200 nm region of the absorption spectra of the films, indicating the formation of quadricyclane units. These could be partially converted back by immersion in a cobalt(II) 5,10,15,20-tetraphenylporphyrin solution.

It is well-known that norbornadiene (**1**) undergoes a reversible intramolecular [2+2] cycloaddition reaction on irradiation with ultraviolet light to afford the corresponding compound bearing a cyclobutane ring, quadricyclane (**1'**), as indicated in Eq. 1.[1-3]

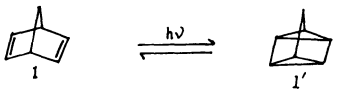

(1)

When the **1** unit is incorporated into the side chain of a vinyl polymer as pendant, a photosensitive polymer is obtained. This exhibits a reversible absorption spectrum change in response to UV irradiation in the solid state such as in a film.

The present study describes the first synthesis and polymerization of vinyl monomers bearing the **1** unit and the investigation of the photosensitivities of the films made of the resulting polymers from the standpoint of photomemory. The polymers made here may also be the first example of photosensitive polymers by the [2+2] cycloaddition mechanism.[4]

The polymers were synthesized via the following route (Eq. 2).

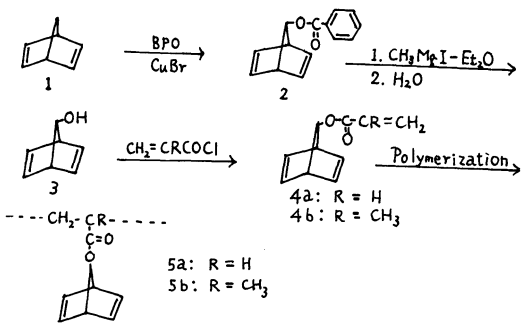

(2)

Absorption spectrum changes of **5a** and **5b** films in response with UV irradiations were also investigated.

Results and Discussion

The 2,5-norbonadien-7-yl group was chosen as the pendant in acrylic and methacrylic ester polymers because this pendant at the 7 position should exert the least steric hindrance to polymerization of the corresponding vinyl monomers as well as the subsequent photoreaction (Eq. 1).

2,5-Norbornadien-7-ol (**3**) was prepared starting with norbornadiene (**1**) via 2,5-norbornadien-7-yl benzoate (**2**).

Table 1. Polymerization Behavior of Norbornadiene Monomers

Monomer	Polymer						
	Conversion %	$[\eta]^{25}_{THF}$	IR(KBr) cm^{-1}	C[a] %	H[a] %	Iodine[a,b] Value	$\lambda^{CH_2Cl_2}_{max}$ nm
4a	27	0.45	3070, 2930, 2860, 1720, 1160	73.70 (74.06)	6.60 (6.22)	158 (157)	228 (ε 550)
4b	55	0.49	3070, 2980, 2930, 1720, 1150	74.68 (74.98)	7.07 (6.86)	149 (144)	228 (ε 400)

a) Figures in parentheses indicate calcd values. b) Wjis' method.

The 7h-reaction of **1** following the method of Tanida and Tsuji[5] provided **2** with satisfactory purity. Attempts to hydrolyze **2** under normal alkaline conditions using potassium hydroxide failed, so that the reaction of a Grignard reagent with the carbonyl group of **2** followed by hydrolysis as in the case of 2,5-norbornadien-7-yl acetate[6] was adopted to afford **3** in 61% yield. The latter was converted to acrylic and methacrylic esters (**4a** and **4b**) by conventional procedures. Thus, the reaction of **3** with acryloyl chloride in the presence of *N,N*-dimethylaniline as proton acceptor provided **4a** in 65% yield. With freshly distilled methacryloyl chloride, in the presence of pyridine, a 45% yield of **4b** was obtained. The purity of both products after column chromatography was satisfactory.

Free radical polymerizations of the monomers **4a** and **4b** with α,α'-azobisisobutyronitrile (AIBN) under mild conditions (50 °C, 72 h) provided soluble polymers as indicated in Table 1. Under more severe conditions (e.g., 10 fold monomer concentration) higher conversions were achieved accompanied by lower solubility, presumably due to the participation of the double bonds of the norbonadienyl moiety in polymerization. However, the polymers listed in Table 1 corresponded with **5a** and **5b** structures in all respects. The ultraviolet (UV) absorption spectra of polymer **5a** are indicated in Fig. 1.

The absorption maximum (228 nm) and shape of the curve in CH_2Cl_2 solution are almost identical with those of norbornadiene (**1**) as well as those (229 nm) of the corresponding monomer **4a** in the same solvent. For a film of **5a**, however, no peak is recognized above 200 nm and the absorbance continues to increase down to 189 nm with the decrease of the wavelength. Almost the same results were obtained for polymer **5b**. Both polymers **5a** and **5b** provided clear colorless films from CH_2Cl_2 solutions. This difference of absorption spectra between the film and solution states can be attributed to a solvent effect: Ethanol gives absorption peaks at 209, 212, and 208 nm for **4a**, **4b**, and **1**, respectively.

Films of **5a** and **5b** deposited on the inside walls of quartz cells were irradiated with UV light in a nitrogen atmosphere. Figure 2 and Table 2 indicate the results thus obtained.

The absorbance around 200 nm decreased with irradiation with simultaneous reductions in the iodine value and the 3070 cm^{-1} peak in the IR spectrum, indicating that the reaction given in Eq. 3 occurred.

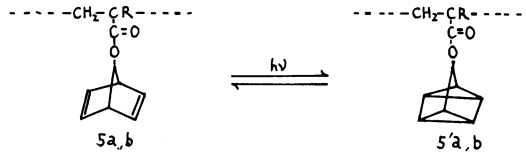

(3)

This reaction is intramolecular and appears to require little dimensional change, so that a smooth photoconversion of **5a,b** to **5'a,b** may take place even in the solid state. The use of a triplet photosensitizer was avoided to assure [2+2] cycloaddition by the pericyclic mechanism.

It is known that Co(II) porphyrins catalyze the back reaction in Eq. 1.[7] When the films subjected to 48 h irradiation were immersed in a solution of cobalt(II) 5,10,15,20-tetraphenylporphyrin for 24 h, the UV and IR spectra and the iodine values recovered to some extent, indicating that the back

Table 2. Photosensitivities of Norbornadiene Polymer Films

Polymer	Irradiation[a] time / h	Absorbance (200 nm)	Iodine Value	IR (3070 cm^{-1})
5a	0	0.540	158(100)[c]	Strong
	24	0.395	—	Weak
	48	0.303	73(46)[c]	Weak
	After immersion[b]	0.345	92(58)[c]	Weak
5b	0	0.510	149(100)[c]	Strong
	24	0.320	—	Weak
	48	0.215	20(13)[c]	Weak
	After immersion[b]	0.382	110(74)[c]	Medium

a) In a nitrogen atmosphere. b) With Cobalt(II) 5, 10,15,20-tetraphenylporphyrin. c) Residual **1** unit in %.

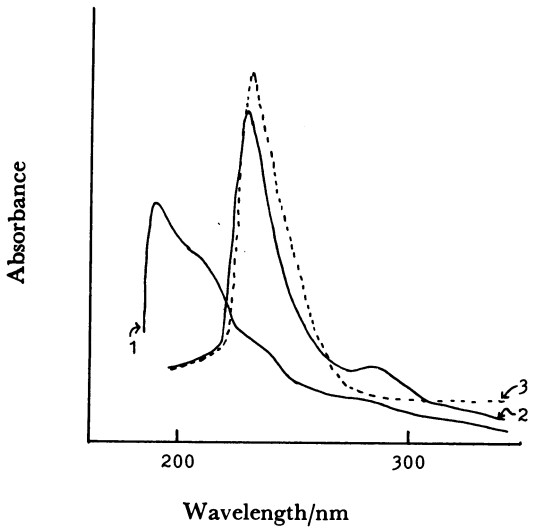

Fig. 1. Ultraviolet absorption spectra of norbornadiene polymer. 1: **5a**-Film; 2: **5a** in CH_2Cl_2; 3: Norbornadiene in CH_2Cl_2. The ordinate has no meaning other than to show the shapes of absorption curves.

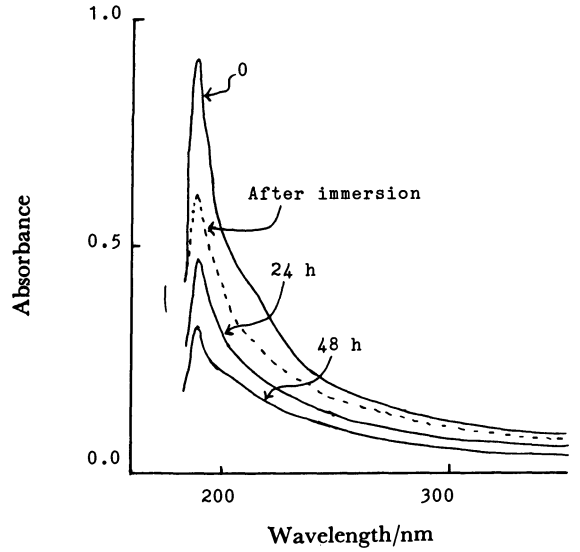

Fig. 2. Change of the absorption spectrum of a norbornadiene polymer (**5b**) film with UV irradiation. Figures in the diagram indicate the irradiation times in nitrogen atmosphere and the immersion was carried out after 48 h irradiation.

reaction shown in Eq. 3 occurred in the films. The rate and extent of the back reaction depend upon the diffusion of the catalyst into the films, so that a complete reversal would depend on the experimental conditions and the state of the films.

There was no indication of any degradation of the principal polymer chains or decomposition of the carboxyl portion judging from the values of intrinsic viscosity and IR spectra. In fact, the conversion as indicated in Eq. 3 could be repeated.

Experimental

Infrared, ^{1}H NMR, mass, and ultraviolet spectra were recorded on a Hitachi 215 spectrophotometer, a JNM-PMX 60 spectrometer, a Hitachi RMU-6 spectrometer, and a Hitachi 200-10 spectrophotometer, respectively, under standard conditions. Elemental analyses were carried out with a Perkin-Elmer 250 instrument.

2,5-Norbornadien-7-yl Benzoate (2). Refluxing for 7 h of a mixture of norbornadiene (9.2 g, 0.10 mol), copper(I) bromide (50 mg), and benzoyl peroxide (BPO; 6.0 g, 0.025 mol) in benzene (80 ml) and subsequent working up provided colorless needles (mp 54—56 °C, bp 109 °C/0.4 mm; lit,[5] mp 53—54 °C) in 34% yield. Found: C, 79.26; H, 5.66%. Calcd for $C_{14}H_{12}O_2$: C, 79.23; H, 5.70%. IR (KBr) 3070 (CH=CH); 1730, 1280 (ester) cm.$^{-1}$ ^{1}H NMR (CCl_4) δ=3.7 (m, 2H, 2CH), 4.8 (s, 1H, CHO), 6.7 (d, 4H, 2CH=CH), 7.5 (m, 3H, ArH), 8.1 (m, 2H, ArH). Ms (*m/z*) 212 (M^+).

2,5-Norbornadien-7-ol (3). To a Grignard reagent, prepared from magnesium (2.4 g, 0.10 mol) and methyl iodide (14.2 g, 0.10 mol) in anhydrous ether (100 ml), **2** (4.2 g, 0.020 mol) was added slowly under a nitrogen atmosphere. The reaction mixture was stirred at room temperature for 1 h. Saturated aqueous sodium sulfate was added. The ether solution was decanted, washed with water, and dried over anhydrous sodium sulfate. The ether was removed and the product distilled to yield a VPC-pure fluid (bp 81 °C/57 mm; lit,[6] 79 °C/57 mm) in 61% yield. Found: C, 77.75; H, 7.21%. Calcd for C_7H_8O: C, 77.75; H, 7.46%. IR (CCl_4) 3560 (OH), 3070 (CH=CH) cm.$^{-1}$ ^{1}H NMR (CCl_4) δ=2.9 (s, 1H, OH), 3.4 (m, 2H, 2CH), 3.8 (s, 1H, CHO), 6.6 (m, 4H, 2CH=CH). Ms (*m/z*) 108 (M^+).

2,5-Norbornadien-7-yl Acrylate (4a). To a stirred solution of **3** (2.2 g, 20 mmol), hydroquinone (0.1 g), *N,N*-dimethylaniline (4.2 ml, 33 mmol) in anhydrous acetonitrile (50 ml) cooled in an ice bath was added dropwise acryloyl chloride (2.5 ml, 30 mmol) with exclusion of moisture. The reaction mixture was stirred at room temperature for 15 h and poured into ice-water containing conc. hydrochloric acid (20 ml). Ether extraction followed by conventional working up provided a crude product, which was subjected to silica-gel column chromatography (Wakogel C-300) using hexane-benzene (1:1 v/v) as eluting solvent to afford a clear fluid in 65% yield. Found: C, 73.70; H, 6.60%. Calcd for $C_{10}H_{10}O_2$: C, 74.06; H, 6.22%. IR (CCl_4) 3070 (CH=CH); 1720 (ester); 980, 900 (vinyl) cm^{-1}. ^{1}H NMR (CCl_4) δ=3.7 (m, 2H, 2CH), 4.6 (s, 1H, CHO), 5.8—6.4 (m, 3H, CH_2=CH), 6.7 (m, 4H, 2CH=CH). λ_{max}^{EtOH} 209 nm (ε 3400), $\lambda_{max}^{CH_2Cl_2}$ 229 nm (ε 440). MS (*m/z*) 162 (M^+).

2,5-Norbornadien-7-yl Methacrylate (4b). The same procedure as that for **4a** was applied using methacryloyl chloride (3.9 ml, 40 mmol), freshly distilled, and pyridine (3.6 ml, 44 mmol) instead of acryloyl chloride and *N,N*-dimethylaniline, respectively. Column chromatographic purification using hexane-benzene (1:1 v/v) as eluting solvent provided a clear fluid in 45% yield. Found: C, 74.63; H, 6.95%. Calcd for $C_{11}H_{12}O_2$: C, 74.98; H, 6.86%. IR (CCl_4) 3070 (CH=CH), 1720 (ester), 930 (methacryloyl) cm.$^{-1}$ ^{1}H NMR (CCl_4) δ=1.8 (s, 3H, CH_3), 3.6 (m, 2H, 2CH), 4.6 (s, 1H, CHO), 5.5 (s, 1H, CH_2=), 6.0 (s, 1H, CH_2=), 6.7 (m, 4H, 2CH=CH). λ_{max}^{EtOH} 212 nm (ε 8100), $\lambda_{max}^{CH_2Cl_2}$ 229 nm (ε 1100). Ms (*m/z*) 176 (M^+).

Polymerization of the Monomers. A solution of monomer (0.4 g) and α,α'-azobisisobutyronitrile (AIBN; 0.02 g) in tetrahydrofuran (8 ml) was put into a glass ampule, which was evacuated and sealed in a conventional manner. Polymerization was carried out at 50 °C for 72 h and the resulting polymer was precipitated into hexane-benzene (1:1 v/v) to afford a white powder. The result thus obtained are given in Table 1.

The IR-spectra of the polymers showed absorption in the 2900 cm^{-1} region characteristic of the vinyl polymer backbone with disappearance of the monomeric vinyl absorptions.

Measurements of Ultraviolet (UV) Spectra. Film: A solution of the polymer in dichloromethane was spread over either a quartz plate or an inside wall of a quartz cell, which was air-dried at room temperature overnight and stored for at least a week before measurement. The average thickness of the films thus prepared was 0.01 mm.

Measurement: UV-absorption spectra of films were recorded on a spectrophotometer. The UV irradiation source was a 75W mercury lamp (Toshiba SHL-100UV-2) and irradiation was effected at a distance of 10 cm from the lamp.

Treatment of Irradiated Film for Spectrum Recovery: The films subjected to irradiation were immersed in a 1% solution of cobalt(II) 5,10,15,20-tetraphenylporphyrin in benzene–dichloromethane (4:1 v/v) for 24 h, washed thoroughly with the same solvent mixture, and dried.

References

1) W. G. Dauben and R. L. Cargill. *Tetrahedron*, **15**, 197 (1961).
2) G. S. Hammond, N. J. Turro, and A. Fisher, *J. Am. Chem. Soc.*, **83**, 4674 (1961).
3) N. J. Turro, "Modern Molecular Photochemistry," The Benjamin/Cummings Pub. Co. Inc. (1978), p. 427.
4) H. Kamogawa, *Kōbunshi Kakō*, **33**, 66 (1984).
5) H. Tanida and T. Tsuji, *Chem. Ind. (London)*, **1963**, 211.
6) P. R. Story, *J. Org. Chem.*, **26**, 287 (1961).
7) R. R. Hantala, R. B. King, and C. Kutal, "Solar Energy," The Humana Press (1979), p. 333.

Preparation of Alkyl Dihydrogenphosphates with Monomeric Metaphosphate Anion Generated by Photochemical C-P Bond Cleavage of *p*-Nitrobenzylphosphonic Acid

Narimasa IWAMOTO, Yoshiki OKAMOTO,* and Setsuo TAKAMUKU
The Institute of Scientific and Industrial Research, Osaka University, 8-1 Mihogaoka, Ibaraki, Osaka 567
(Received November 30, 1985)

Alkyl dihydrogenphosphates were prepared by a procedure that probably involves a monomeric metaphosphate anion as an intermediate. The monomeric metaphosphate anions used in this reaction were generated by a photochemical C-P bond cleavage of the *p*-nitrobenzylphosphonate dianion. The photolysis of a 1:2 molar mixture of *p*-nitrobenzylphosphonic acid and 1,8-diazabicyclo[5.4.0]undec-7-ene (or 2,2,6,6-tetramethylpiperidine) in excess alcohol gave alkyl dihydrogenphosphate in fairly good yield.

In our previous study of the photolysis of *p*-nitrobenzylphosphonic acid (**1**) in an alkaline 80% ethanol solution, we observed the heterolytic cleavage of the C-P bond and the generation of monomeric metaphosphate anions (**2**) with a high efficiency (Eq. 1—4).[1]

For almost 30 years, metaphosphate (**2**) has been postulated as an intermediate in the hydrolysis of phosphate esters and has been suggested as an essential phosphorylating agent in reactions involving intermediary metabolism.[2] Excellent evidence that **2** acts as a phosphorylating agent in solution has been accumulating.[3-9] Recently, Ramirez et al. reported that alkyl dihydrogenphosphates were conveniently prepared by a procedure involving **2** as an intermediate: An acetonitrile solution of 2,4-dinitrophenyl dihydrogenphosphate, or (*erythro*-1-phenyl-1,2-dibromopropyl)-phosphonic acid containing 2 molar equivalents of the hindered tertiary amine behaves thermally as a source of **2** at ambient temperature. By this method, sensitive and valuable alcohols can be converted into alkyl dihydrogenphosphates.[10]

Kirby reported the photochemical phosphorylation of methanol with 3,5-dinitrophenyl dihydrogenphosphate.[11] When a 70% methanol solution of cyclohexylammonium 3,5-dinitrophenyl hydrogenphosphate (2.8 mmol dm^{-3}) at pH 9 was irradiated at room temperature, methyl dihydrogenphosphate was obtained in 58—68% yield.

We have now established a novel procedure for the photochemical phosphorylation of alcohol using **2** generated by the photolysis of **1** in the presence of an organic base. The acid **1** was readily made available through the nitration of benzylphosphonic acid.

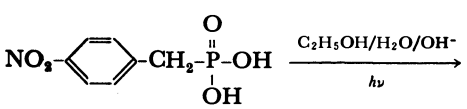

1

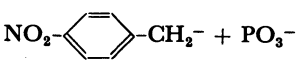

(1)

2

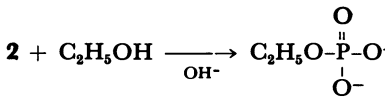

(2)

3b

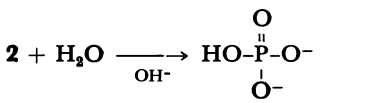

(3)

4

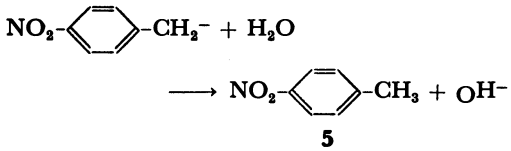

(4)

5

Results and Discussion

An 80% ethanol solution of **1** (50 mmol dm^{-3}) at pH 12, was adjusted with sodium hydroxide in a Pyrex tube. Upon irradiation by a high-pressure mercury lamp at ambient temperature, a highly efficient C—P bond cleavage of **1** occurred. The course of the reaction was followed by a GLC analysis of 4-nitrotoluene (**5**). The quantum yield was 0.86, which was larger than that of the photolysis of sodium 3-nitrophenyl hydrogenphosphate (ϕ= 0.05—0.24).[12] The phosphorus compounds were analyzed by ^{31}P NMR spectrometry. The photolysis was completed within about 30 min, and dianions of ethyl dihydrogenphosphate $C_2H_5OPO_3^{2-}$ (**3b**), ^{31}P NMR (80% C_2H_5OH, pH 12) δ=3.6 (t, J_{PH}=5.6 Hz), and orthophosphoric acid $HOPO_3^{2-}$ (**4**), δ=2.6 (s) were formed in 28 and 72% yields, respectively.

The disodium salt of **1** is only slightly soluble in anhydrous alcohol, but its amine salts are soluble. The anhydrous ethanol solutions of **1** (30 mmol dm^{-3}) containing 1,8-diazabicyclo[5.4.0]undec-7-ene (DBU, pK_a 11.5) were irradiated to give **3b**. The yield of **3b** reached a maximum upon the addition of 2 molar equivalents of DBU and decreased upon a further excess addition of the base (Fig. 1). This was explained by the inner filter effect of the DBU itself

and its photoproducts.[13] The quantum yield of the C–P bond cleavage of **1** under the best conditions was 0.57. The use of 2,2,6,6-tetramethylpiperidine (pK_a 11.1) also gave good results. However, the quantum yield of the C–P bond cleavage was low (ϕ=0.13). The yield of **3b** was not reduced even though an excess amount of the base was used. A large excess amount of triethylamine (pK_a 10.65) was required for obtaining **3b** in 50—60% yield, and the quantum yield of C–P bond cleavage was lower (ϕ=0.025). With pyridine (pK_a 5.17), the C–P bond cleavage did not occur. The photochemical C–P bond cleavage of **1** occurred only during its dianion.[1] The effect of the organic base can be explained by the degree of dissociation of **1**; with a weak base, triethylamine or pyridine, the acid **1** did not completely ionize into dianion. Thus, **2** was not generated.

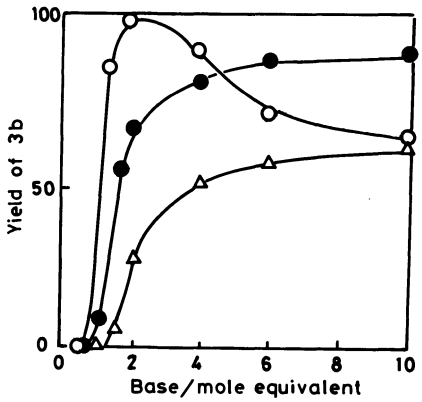

Fig. 1. Change of yields of **3b** by addition of organic bases.
○: DBU, ●: 2,2,6,6-tetramethylpiperidine, △: triethylamine.

Various alcohols were phosphorylated by a method in which a large excess amount of alcohol containing 2 molar equivalents of DBU were used. The phosphorylation proceeded without any detectable amount of a by-product. The yields and ^{31}P NMR chemical shifts of dianion of alkyl dihydrogenphosphates **3**, and the quantum yields of a C–P bond cleavage of **1** are summarized in Table 1. The quantum yields decreased in the order CH_3OH=C_2H_5OH>*i*-C_3H_7OH>*n*-C_4H_9OH>*n*-$C_5H_{11}OH$=*s*-C_4H_9OH>*t*-C_4H_9OH. This order is essentially the same as that for the polarity of alcohol used in these reactions. With increasing alcohol polarity, the acid **1** dissociated more completely and underwent highly efficient C–P bond cleavage.

Reactions using one molar equivalent of alcohol were performed in dichloromethane. The dichloromethane solutions of **1** (50 mmol dm^{-3}) containing a molar equivalent of alcohol and 2 molar equivalents of DBU were irradiated for 1 h. When cholesterol, borneol, and 1-dodecanol were used, the dianions of cholesteryl (**3j**), bornyl (**3k**), and dodecyl dihydrogenphosphate (**3l**) were obtained in 25, 35, and 27% yields, respectively. However, 72—78% of **1** were consumed during the irradiation. It was revealed by a ^{31}P NMR investigation that the greater part of **2** generated by irradiation was consumed during the formation of pyrophosphate ions (**8** or **9**) and a metastable intermediate (**10**) by a reaction with DBU.[4]

In the presence of a large excess of alcohol, metaphosphate (**2**) can react predominantly with the alcohol to give **3** in a quantitative yield (Eq. 2). When a comparable amount of alcohol was used, metaphosphate (**2**) reacted with alcohol (Eq. 2), its source (**1**) (Eq. 5), itself (**2**) (Eq. 6), **3** (Eq. 7), and

Table 1. The Yields of Alkyl Phosphates Ions (**3**) and Quantum Yields of C–P Bond Cleavage of **1**[a]

ROH	Product	Yield/%[b] of **3**	^{31}P NMR[c] δ ppm	Quantum yield[d] of C–P bond cleavage
CH_3OH	**3a**	94	4.4	0.72
C_2H_5OH	**3b**	97	2.6	0.72
i-C_3H_7OH	**3c**	77	0.5	0.49
n-C_4H_9OH	**3d**	80	3.0	0.40
s-C_4H_9OH	**3e**	55	0.2	0.30
t-C_4H_9OH	**3f**	32	−3.9	0.11
n-$C_5H_{11}OH$	**3g**	81	2.4	0.30
$HOCH_2CH_2OH$	**3h**	85	4.7	—
$C_6H_5CH_2OH$	**3i**	81	3.6	—

a) Five ml alcohol solutions of **1** (50 mmol dm^{-3}) containing 2 molar equivalent of DBU were irradiated by a high-pressure mercury lamp at ambient temperature for 1 h. b) Yields were determined by ^{31}P NMR spectrometry, based on **1** used. c) ^{31}P NMR chemical shifts of **3** were determined in the reaction mixtures (pH 12), which agreed with the values of authentic samples. d) These quantum yields were determined from the yield of **5**. The photolyses were carried out with no more than 20% decomposition. (see Experimental).

DBU (Eq. 8). When the amount of alcohol was reduced, the yield of **3** decreased remarkably, and other products were given through other reactions (Eqs. 5, 6, 7, and 8).

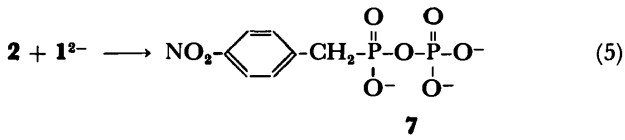

(5)

7

(6)

8

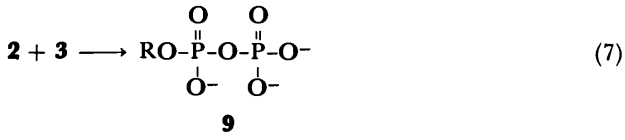

(7)

9

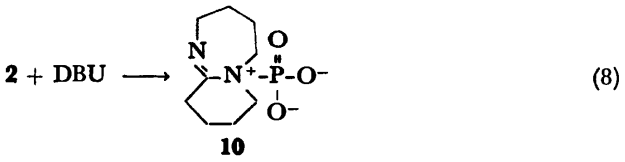

(8)

10

R=Alkyl-

The same experiment with 2,2,6,6-tetramethylpiperidine was unsuccessfully carried out since the piperidinium salt of **1** is only slightly soluble in dichloromethane or acetonitrile. In another preparative experiment, **3l** was isolated in 32% yield.

Experimental

All the melting points are uncorrected. ^{31}P NMR spectra were recorded at 40.25 MHz on a JNM FX 100 using triphenylphosphine as an external standard (δ=−5.6 ppm) for measurements of their chemical shifts, and diethyl methylphosphonate as an internal standard (δ=29.7 ppm) for quantitative analysis, respectively. Chemical shifts are expressed in ppm from 85% H_3PO_4, higher positive values indicated lower shieldings. Quantitative measurements were carried out under the conditions of proton decoupling while taking into account the differences in T_1 and nuclear Overhauser effects.[14] GLC analyses were performed on a Shimadzu GC-7A using a 1-m glass column packed with Silicone OV 17 (2%) on Chromosorb W AW DMCS.

Materials. Dichloromethane and other solvents were dried and distilled by the usual method. Cholesterol, borneol, and 1-dodecanol were of reagent grade and used without further purification. Other alcohols and amines were used after distillation. *p*-Nitrobenzylphosphonic acid (**1**) was prepared by the nitration of benzylphosphonic acid and recrystallized from 50% ethanol, mp 228—229 °C; ^1H NMR (D_2O, DSS, pH 12), δ=2.98 (2H d, J_{HH}=20 Hz, CH_2), 7.2—8.2 (5H, m, arom.); ^{31}P NMR (80% C_2H_5OH, pH 12) δ=15.2 (t, J_{HP}=20 Hz); Dissociation constant (80% C_2H_5OH) pK^1_a 3.9; pK^2_a 9.3; UV_{max} (80% C_2H_5OH, pH 12) 305 nm (ε 10,500).

Irradiation of 1 in 80% Ethanol Solution. Five ml of an ethanol solution of **1** (50 mmol dm^{-3}) was adjusted at pH 12 with a 10% aqueous solution of sodium hydroxide. Nitrogen was bubbled through the solution before irradiation. The solution was irradiated in a Pyrex tube (ϕ 10 mm) with a high-pressure mercury lamp (350 W) for 1 h under cooling with running water. The progress of the photolysis was monitored by a GLC analysis of **5**. After irradiation, a fixed amount of a chloroform-*d* solution of diethyl methylphosphonate was added to the mixture, which was submitted to a ^{31}P NMR analysis using triphenylphosphine as an external standard.

Preparation of 3. Irradiation of 1 in Excess Alcohol: A 5-ml alcohol solution of **1** (50 mmol dm^{-3}) containing DBU (100 mmol dm^{-3}) was irradiated in the same manner previously described. After the irradiation, the mixture was employed for a ^{31}P NMR analysis (Table 1).

Irradiation of 1 in Dichloromethane: A 5 ml dichloromethane solution of **1** (50 mmol dm^{-3}) containing alcohol (50 mmol dm^{-3}) and DBU (100 mmol dm^{-3}) was irradiated in the same manner previously described. After irradiation, the mixture was employed for a ^{31}P NMR analysis. In the case of 1-dodecanol, besides the signals of dianion of dodecyl dihydrogenphosphate (**3l**, δ=1.50 ppm, yield 19%) and **4** (δ=1.98 ppm, 9%), two peaks were observed at δ=−11.22 (t, J_{PH}=16 Hz, yield 5.6%) and −8.97 (s, 19%). The former was assumed to be a metastable reaction intermediate (**10**), formed by the reaction of **2** with DBU[4] and the latter was pyrophosphate ion (**8**).[15] Fifty-three percent of the unreacted dianion of **1** remained.

Isolation of 3l: The acid **1** (1.1 g, 5 mmol) was added to a 100 ml dichloromethane solution of 1-dodecanol (0.9 g, 0.5 mmol) and DBU (1.5 g, 10 mmol). The homogeneous solution was irradiated employing a Pyrex doughnut-type cell at 20 °C in a nitrogen atmosphere for 2 h. After the solvent was evaporated, the residue was triturated with ether to remove **5** and any unreacted alcohol. The residue was dried for a few minutes at 20 °C (0.1 mmHg).† The diammonium hydrogenphosphate was dissolved in a 2:1 V/V chloroform/ethanol mixture. The solution was treated with 3:48:47 V/V chloroform/methanol/1 mol dm^{-3} aqueous HCl reagent (15 ml) in order to liberate the free phosphoric acid under the mildest conditions. The two-phase system was stirred for a few minutes. The lower organic phase was separated and resubmitted to the same acidification procedure. Finally, this phase was washed with 3:48:47 V/V chloroform/methanol/water (10 ml). The organic phase was evaporated at 20 °C (0.1 mmHg), and the residue was triturated with ether (10 ml) to remove any unreacted 1-dodecanol that may have remained as a contaminant. The product **3l** was dried at 20 °C for 3 h (0.1 mmHg). Yield 0.46 g (35%), mp 55—56 °C.[16]

Measurement of the Quantum Yield. The quantum yields were determined on the basis of generated **5** and chemical actinometry using 2-hexanone. The quantum yield of acetone formation was taken as 0.25 in 2,2,4-trimethylpentane at room temperature;[17] A 2 ml 2,2,4-trimethylpentane solution of 2-hexanone with the absorbance identical with that of the solution of **1** was

† 1 mmHg=133.322 Pa.

irradiated for 1 h in a merry-go-round apparatus employing 313-nm monochromatic light using a filter solution of 0.1% K_2CrO_4–0.1% K_2CO_3. The yields of **5** and acetone were determined by a GLC analysis. The photolyses were carried out with no more than 20% decomposition.

The authors are grateful to Mr. Yoshio Takai of Material Analysis Center in the Institute of Scientific and Industrial Research, Osaka University, for the measurement of ^{31}P NMR spectra.

References

1) Y. Okamoto, N. Iwamoto, and S. Takamuku, *Chem. Lett.*, 1984, 2091.

2) F. H. Westheimer, *Chem. Rev.*, **81**, 313 (1981).

3) F. Ramirez and J. F. Marecek, *J. Am. Chem. Soc.*, **101**, 1460 (1979).

4) F. Ramirez and J. F. Marecek, *Tetrahedron*, **35**, 1581 (1979).

5) F. Ramirez and J. F. Marecek, *Tetrahedron*, **36**, 3515 (1980).

6) F. Ramirez, J. F. Marecek, and S. S. Yemul, *J. Am. Chem. Soc.*, **104**, 1345 (1982).

7) F. Ramirez and J. F. Marecek, *Pure Appl. Chem.*, **52**, 1021 (1980).

8) F. Ramirez, J. F. Marecek, and S. S. Yemul, *Tetrahedron Lett.*, **23**, 1515 (1982).

9) K. C. Calvo and F. H. Westheimer, *J. Am. Chem. Soc.*, **106**, 4205 (1984).

10) F. Ramirez, J. F. Marecek, and S. S. Yemul, *J. Org. Chem.*, **48**, 1417 (1983).

11) A. J. Kirby and A. G. Varvoglis, *J. Chem. Soc., Chem. Commun.*, **1967**, 405.

12) R. O. de Jongh and E. Havinga, *Recl. Trav. Chem. Pays-Bas*, **87**, 1327 (1968).

13) When the ethanol solution of DBU without **1** was irradiated, a broad absorption band (310—340 nm) also appeared. It is unkown what the absorption band resulted from.

14) Gated broadband decoupling and longer pulse intervals (50 s) were used. See, for example, A. D. Edward "Phosphorus-31 NMR of Phospholipids in Micelles" in "Phosphorus-31 NMR Principles and Applications," ed by D. G. Gorenstein, Academic Press, Inc. Orlando, Florida (1984), Chap. 14, p. 431.

15) J. R. Van Wazer, C. F. Callis, J. N. Shoolery, and R. C. Jones, *J. Am. Chem. Soc.*, **78**, 5715 (1956).

16) Y. Okamoto, *Bull. Chem. Soc. Jpn.*, **58**, 3393 (1985).

17) D. R. Coulson and N. C. Yang, *J. Am. Chem. Soc.*, **88**, 4511 (1963).

 © 1986 The Chemical Society of Japan Bull. Chem. Soc. Jpn., 59, 1509—1513 (1986)

Preparations and Thermal Isomerization of Some Tricarbonyl(1-silacyclohexadiene) Iron Complexes. Silyl and Hydrogen Migration in the Diene and the Diene Complex[1)]

Yasuhiro NAKADAIRA,* Toshiaki KOBAYASHI, and Hideki SAKURAI*
Department of Chemistry, Faculty of Science, Tohoku University, Sendai 980
(Received December 24, 1985)

The reaction of 1,1-dimethyl-2,5-diphenyl-1-silacyclohexa-2,4-diene with iron pentacarbonyl or diiron nonacarbonyl gave a mixture of tricarbonyl(1,1-dimethyl-2,5-diphenyl-1-silacyclohexa-2,4-diene)iron and tricarbonyl(1,1-dimethyl-3,6-diphenyl-1-silacyclohexa-2,4-diene)iron. Similarly, on treatment with iron pentacarbonyl 1,1-dimethyl-2,5-diphenyl-4-trimethylsilyl-1-silacyclohexa-2,5-diene yielded a mixture of tricarbonyl-(1,1-dimethyl-3,6-diphenyl-4-trimethylsilyl-1-silacyclohexa-2,4-diene)iron, tricarbonyl(1,1-dimethyl-2,5-diphenyl-4-trimethylsilyl-1-silacyclohexa-2,4-diene)iron, and tricarbonyl(1,1-dimethyl-2,5-diphenyl-6-trimethylsilyl-1-silacyclohexa-2,4-diene)iron as a result of migration of the hydrogen on the ligand competing with silyl migration. On thermolysis, 1,1-dimethyl-2,5-diphenyl-4-trimethylsilyl-1-silacyclohexa-2,5-diene underwent only 1,3-silyl-migration to yield 1,1-dimethyl-2,5-diphenyl-6-trimethylsilyl-1-silacyclohexa-2,4-diene. The mechanism of transition-metal assisted hydrogen-migration is discussed.

We have reported previously an interesting chemistry of the transition-metal complexes of silacyclopentadienes,[2)] which has been followed by several other workers.[3)] Our investigations of tricarbonyl-(silacyclopentadiene)iron complexes have shown that the exo-substituent on the silicon is highly activated toward electrophilic substitution; for example, tricarbonyl(1,1-dimethyl-2,5-diphenyl-1-silacyclopentadiene)iron (**1**) is readily converted stereospecifically into the silanol complex **2** by the treatment with mercury(II) acetate in the presence of perchloric acid.[2)] There are a few reports on the homologous complex, namely the transition-metal complexes of 1-silacyclohexadienes.[4,5)] We now describe our own result on the preparation and thermal isomerization of some tricarbonyl(1-silacyclohexadiene)iron complexes as well as of their ligands, 1-silacyclohexadienes.

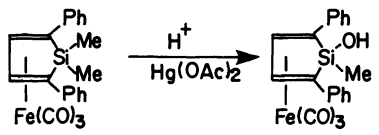

1 2

Results and Discussions

Treatment of 1,1-dimethyl-2,5-diphenyl-1-silacyclohexa-2,4-diene (**3**)[6)] with $Fe(CO)_5$ in xylene at 130 °C for 30 h afforded an isomeric mixture of tricarbonyl(1,1-dimethyl-3,6-diphenyl-1-silacyclohexa-2,4-diene)-iron (**5**) in 48.7% yield together with tricarbonyl(1,1-dimethyl-2,5-diphenyl-1-silacyclohexa-2,4-diene)iron (**4**) in 39.0% yield. **5** is a product of 1,5-H shift. These isomers could be separated each other by TLC on silica gel. Spectral properties, in particular NMR spectra served to distinguish between the two isomers, **4** and **5**. **4** shows two olefinic proton signals (H_3 and H_4) at 5.90 and 6.17 as doublet ($J_{3,4}$=5.4 Hz) together with AB type methylene proton signals (H_{6N} and H_{6X}, $J_{6N,6X}$=16.5 Hz) at 2.10 and 1.25, respectively. In contrast, with only one "internal" olefinic proton signal H_4 at 5.88, **5** has two "outside" complexed olefinic proton signals (H_2 and H_5) at 2.19 and 3.15, respectively. One proton signal due to H_6 is observed at 2.93. The configuration of H_6 is endo as described below. When **3** was allowed to react with diiron nonacarbonyl in benzene for 5 h at 90 °C, only **4** could be isolated in 78% yield together with the unreacted diene **3**. The equilibration between **4** and **5** was demonstrated as follows. When **4** was heated in a sealed tube at 130 °C for 48 h, it was converted into a 56:44 mixture of **4** and **5** without appreciable decomposition. Similarly, the thermolysis under similar conditions (140 °C, 22 h in a sealed tube), **5** gave a 48:52 mixture of **4** and **5**.[7)] These isomer ratios were determined after careful TLC separation of these thermolysates on silica gel. Inspection of these findings above indicates that treatment of the diene **3** with an iron carbonyl reagent gives **4** at first, which is then isomerized thermally to **5**, and the equilibrium constant between **4** and **5** is nearly unity.

1,1-Dimethyl-2,5-diphenyl-4-trimethylsilyl-1-silacyclohexa-2,5-diene (**6**) was obtained quantiatively by quenching the anion derived from **3** with trimethylchlorosilane. Thermolysis of **6** in a sealed tube at 170 °C for 38 h caused 1,3-sila-allyl rearrangement and gave 1,1-dimethyl-2,5-diphenyl-6-trimethylsilyl-1-silacyclohexa-2,4-diene (**7**) in high yield.[8,9)] The other possible isomers such as **8** and **9** were not detected in the reaction mixture and this shows that the trimethylsilyl group migrates to C_6 not to C_2 and 1,3- or 1,5-hydrogen migration does not compete with 1,3-silaallyl rearrangement effectively.[10)] 1,1-

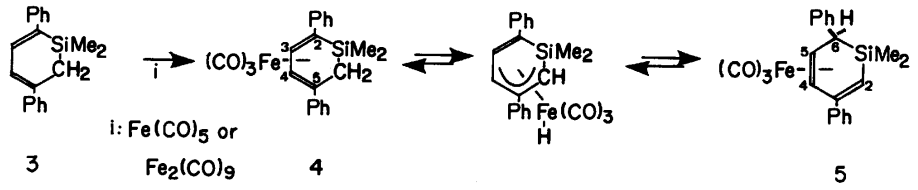

Scheme 1.

Table 1. Thermal Interconversion between 4 and 5

Complex	Temp	Time	Fe(CO)3(diene)		
	°C	h	% yield[a]		Relative yield
			4	5	4:5
4	130	48	52	42	56:44
5	140	22	41	43	48:52

a) Isolated Yields by TLC.

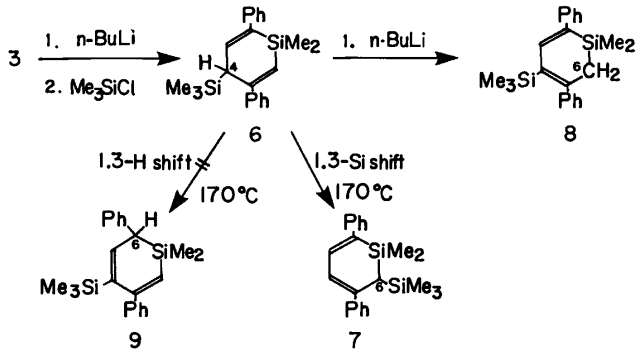

Scheme 2.

Dimethyl-2,5-diphenyl-4-trimethylsilyl-1-silacyclohexa-2,4-diene (**8**) was obtained by quenching the anion derived from **6** with water.

Treatment of dienes **6**, **7**, and **8** with $Fe(CO)_5$ led to the mixtures of complexes **10**, **11**, and **12** as shown in Table 2 and Scheme 3. These isomers could be separated by careful TLC on silica gel and their structures were readily characterized on the basis of NMR spectra. Thermolyses of **11** and **12** resulted in isomerization to give the equilibrium mixture as shown in Table 3. The results obtained here indicate that 1,3 and 1,5-hydrogen shift is considerably enhanced by the transition metal and can compete with the sila-allyl migration observed in thermolysis of **6**. This can be explained by assuming the intermediacy of a (π-allyl)metal hydrides such as **13**.[7,11] Coordination of the metal complex should occur from the less sterically hindered side of the diene and hence the trimethylsilyl group necessarily turns out to be exo in **10**.[15] This always allows to migrate the endo hydrogen to the metal center to form a π-allyl metal hydride such as **13**, which reverts to the diene complex, either **11** or **12**.

Table 2. Reactions of Dienes **6**, **7**, and **8** with $Fe(CO)_5$

Diene	Temp	Time	Fe(CO)3(diene)			
	°C	h	% yield[a]			
			10	**12**	**11**	**7**[b]
6	165	20	20.5	trace	26.4	42.0
7	170	37	44.0			34.3
8	160	22		23.4	37.5	

a) Isolated yields by TLC. b) A trace amount of **12** was detected on TLC.

Table 3. Thermal Interconversion of **11** and **12**

Complex	Temp	Time	Fe(CO)3(diene)		
	°C	h	% yield[a]		Relative yield
			11	**12**	**11**:**12**
11	170	7	71	27	72:28
12	155—180	123	50	24	68:32

a) Isolated yields by TLC.

On the other hand, **10** did not isomerize thermally, namely no metal-assisted hydrogen migration was observed. This may be ascribed to a large steric hindrance emerging in **15**. To examine the reactivity of the substituent on the silicon of the tricarbonyl(silacyclohexadiene)iron complex, **4** was allowed to react with $Hg(OAc)_2$ in presence of $HClO_4$,[2] and was found to remain unchanged under these conditions.[12]

It is noteworthy to add some comments on NMR signals, especially Si-Me signals of these carbonyl(silacyclohexadiene)iron complexes (Table 4). The assignment of these Si-Me signals is made by analogy to that made in tricarbonyl(silacyclopentadiene)iron complexes in which exo Si-Me resonance always occurs at higher field than the endo one.[13] The difference in chemical shift between endo- and exo-Me signals is similar in these two types of diene complexes. The similar trend is observed in the chemical shifts of C_6-methylene protons in **4**, and **12**.[14] The endo-proton signal always appears at lower field.[15]

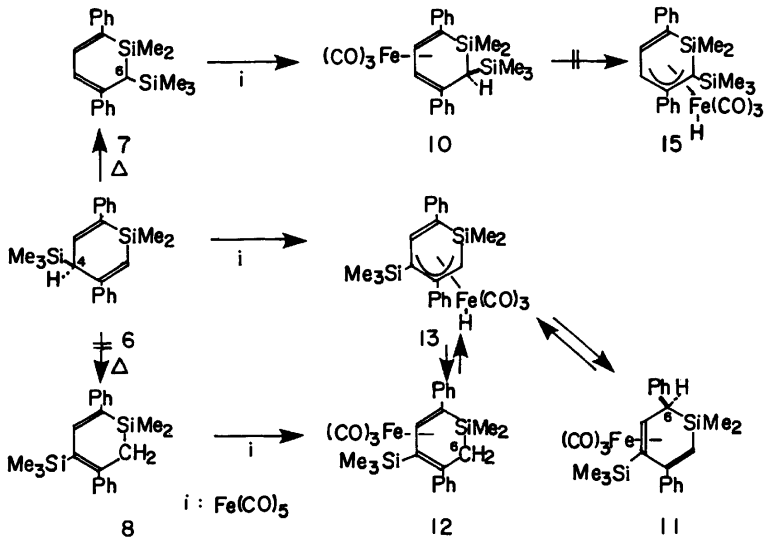

Scheme 3.

Table 4. NMR Spectra of Tricarbonyl(silacyclohexadiene)iron Complexes (δ in CCl_4)

Complex	Si-Me exo	Si-Me endo	H_{6X}[a]	H_{6N}[a]	H_2	H_3	H_4	H_5	$SiMe_3$
4	−0.02	0.44	1.25	2.10		6.17	5.90		
5	−0.42	0.35		2.93	2.19		5.88	3.14	
10	−0.05	0.38		1.71		6.03	5.91		−0.32
11	−0.22	0.47		3.00	1.91			3.25	0.05
12	0.06	0.42	1.37	1.73		5.91			0.20

a) H_{6X} and H_{6N} denote the exo- and endo-hydrogens at C_6, respectively.

Experimental

General Remarks. NMR spectra were obtained by using Varian A-60 and HA-100 instruments. Mass spectra were obtained by a Hitachi RMU-6 instrument. Infrared spectra were recorded on a Hitachi EPI-G2 grating spectrometer. NMR spectra were recorded in CCl_4 and chemical shift data are given in δ value. IR spectra were measured in a KBr disk and IR data are given in cm^{-1}.

Reaction of 1,1-Dimethyl-2,5-diphenyl-1-silacyclohexa-2,4-diene (3) with $Fe(CO)_5$. A mixture of **3** (478.5 mg, 1.73 mmol), $Fe(CO)_5$ (5 ml, ≈35 mmol) and dry xylene (5 ml) was heated in a small autoclave at 130 °C for 30 h. Solvent and excess $Fe(CO)_5$ were removed in vacuum and the residue was separated by TLC on silica gel. **4** (289.0 mg, 39.0%) and **5** (359.0 mg, 48.7%) were obtained. **4**: mp 80 °C; MS *m/z* M^+ 416; ^1H NMR −0.02 (3H, s, *exo*-SiMe), 0.44 (3H, s, *endo*-SiMe), 1.25 (1H, d, H_{6N}, $J_{6X,6N}$=16.5 Hz), 2.10 (1H, d, H_{6N}, $J_{6X,6N}$=16.5 Hz), 5.90 (1H, d, H_4, $J_{3,4}$=5.4 Hz), 6.17 (1H, d, H_3, $J_{3,4}$=5.4 Hz), 7.0—7.6 (10H, m, Ph); IR 2040, 1975, 1965 (CO), 1250 (SiMe); Anal. Calcd for $C_{22}H_{20}O_3SiFe$: C, 63.47; H, 4.84. Found: C, 63.49; H, 4.72, **5**: Mp 107 °C; MS *m/z* M^+ 416; ^1H NMR −0.42 (3H, s, *exo*-SiMe), 0.35 (3H, s, *endo*-SiMe), 2.19 (1H, d, H_2, $J_{2,4}$=1.8 Hz), 2.93 (1H, d, H_6, $J_{5,6}$=3.9 Hz), 3.14 (1H, dd, H_5, $J_{4,5}$=6.8 Hz, $J_{5,6}$=3.9 Hz), 5.88 (1H, dd, H_4, $J_{4,5}$=6.8 Hz, $J_{2,4}$=1.8 Hz), 6.8—7.6 (10H, m, Ph); IR 2050, 1990, 1970 (CO), 1250 (SiMe); Found: C, 63.39; H, 4.90%. Calcd for $C_{22}H_{20}O_3SiFe$: C, 63.47; H, 4.84%.

Reaction of 1,1-Dimethyl-2,5-diphenyl-1-silacyclohexa-2,4-diene (3) with $Fe_2(CO)_9$. A mixture of **3** (81.2 mg, 0.294 mmol), $Fe_2(CO)_9$ (148.2 mg, 0.407 mmol) and dry benzene (5 ml) was heated in an autoclave at 90 °C for 5 h. The solvent was removed under reduced pressure. The residual oil was separated by TLC on silica gel. Unchanged **3** (45.5 mg, 56.0%) was recovered and **4** (41.8 mg, 77.7%) was obtained.

Thermolysis of 4. **4** (54.0 mg, 0.130 mmol) was sealed under vacuum in a Pyrex tube and heated in an oil bath at 130 °C for 48 h. **4** (28.4 mg, 52.0%) were recovered and **5** (22.6 mg) were separated from the reaction mixture by TLC.

Thermolysis of 5. **5** (30.0 mg, 0.072 mmol) was sealed under vacuum in a Pyrex tube and heated in an oil bath at 140 °C for 22 h. The reaction mixture was separated by TLC. Starting material **5** (13.0 mg) was recovered and isomer **4** (12.2 mg) was obtained.

Preparation of 1,1-Dimethyl-2,5-diphenyl-4-trimethylsilyl-1-silacyclohexa-2,5-diene (6). In a 20 ml-flask was placed **3** (261.2 mg, 0.945 mmol) dissolved in dry ether (10 ml) containing *N,N,N',N'*-tetramethylethylenediamine (TMEDA) (0.5 g, ≈4 mmol). Then butyllithium in hexane

was added to the mixture and was stirred magnetically at room temperature for 10 min. Then excess amount of trimethylchlorosilane was added to the reaction mixture, and was hydrolyzed after 10 min and was extracted with ether. The ethereal solution was evaporated to dryness in vacuum. The residue was purified by TLC on silica gel to give **6** (301.0 mg, 91.4%). **6**: an oil; MS *m/z* M^+ 348; UV (hexane) $\lambda_{max}(\varepsilon)$ 245.5 nm (23900); ^{1}H NMR −0.08 (9H, s, $SiMe_3$), 0.27 (3H, s, SiMe), 0.41 (3H, s, SiMe), 3.70 (1H, d, H_4, $J_{3,4}$=5.4 Hz), 5.90 (1H, s, H_6), 6.83 (1H, d, H_3, $J_{3,4}$=5.3 Hz), 7.0—7.5 (10H, m, Ph); Found: C, 75.79; H, 8.29%. Calcd for $C_{22}H_{28}Si_2$: C, 75.59; H, 8.10%.

Preparation of 1,1-Dimethyl-2,5-diphenyl-6-trimethylsilyl-1-silacyclohexa-2,4-diene (7). **6** (121.2 mg, 0.248 mmol) was sealed under vacuum in a Pyrex tube and heated in an oil bath at 170 °C for 38 h. The reaction mixture was purified by TLC on silica gel. **7** (105.6 mg, 87.1%) was afforded as an oil. Other isomers such as **6** or **9** were not detected on TLC. **7**: an oil; MS *m/z* M^+ 348; UV (hexane) $\lambda_{max}(\varepsilon)$ 238 nm (14800), 350 nm (16800); ^{1}H NMR 0.02 (9H, s, $SiMe_3$), 0.43 (3H, s, SiMe), 0.45 (3H, s, SiMe), 1.89 (1H, s, H_6), 6.46 (1H, d, H_4, $J_{3,4}$=6.4 Hz), 6.83 (1H, d, H_3, $J_{3,4}$=6.4 Hz), 7.0—7.5 (10H, m, Ph); Found: C, 75.77; H, 8.10%. Calcd for $C_{22}H_{28}Si_2$: C, 75.79; H, 8.10%.

Preparation of 1,1-dimethyl-2,5-diphenyl-4-trimethylsilyl-1-silacyclohexa-2,4-diene (8). In a 30 ml-flask was placed 1,1-dimethyl-2,5-diphenyl-4-trimethylsilyl-1-silacyclohexa-2,4-diene (**6**) (166.5 mg, 0.478 mmol) dissolved in dry ether (10 ml) containing TMEDA (0.5 g, 4 mmol). Then butyllithium in hexane was added to the mixture and was stirred magnetically at room temperature for 10 min. The mixture was hydrolyzed and was extracted with ether. The ethereal solution was evaporated to dryness in vacuum. The residue was separated by TLC on silica gel to give unreacted **6** (61.0 mg, 36.6%) and **8** (55.5 mg, 52.6%). **8**: Mp 100 °C; MS *m/z* M^+ 348; UV (hexane) $\lambda_{max}(\varepsilon)$ 233 nm (11400), 322 nm (13200); ^{1}H NMR −0.16 (9H, s, $SiMe_3$), 0.25 (6H, s, $SiMe_2$), 1.96 (2H, s, H_6), 6.95 (1H, s, H_3), 7.0—7.4 (10H, m, Ph); Found: C, 75.89; H, 8.19%. Calcd for $C_{22}H_{28}Si_2$: C, 75.79; H, 8.10%.

Reaction of 4 with $Hg(OAc)_2$. In a 20 ml-flask equipped with a condenser and a nitrogen inlet tube, a mixture of **4** (38.0 mg, 0.0913 mmol), $Hg(OAc)_2$ (36.0 mg, 0.113 mmol), dioxane (10 ml) and one drop of 70% aq perchloric acid was placed and stirred magnetically at room temperature for 10 min. After addition of water, the reaction mixture was extracted with ether. The ethereal solution was evaporated to dryness to give an oil (37.0 mg). NMR spectrum of this oil indicated almost 100% recovery of **4**.

Reaction of 6 with $Fe(CO)_5$. In a small autoclave **6** (255.0 mg, 0.731 mmol), $Fe(CO)_5$ (5 ml, 35 mmol), dry toluene (10 ml) were heated at 165 °C for 20 h. The solvent and excess amount of $Fe(CO)_5$ are removed under vacuum and the residual oil was separated by TLC on silica gel. **10** (73.0 mg, 20.5%), **11** (94.0 mg, 26.4%) and **7** (107.4 mg, 42.0%) were afforded. Since **7** and **12** show same R_f value on TLC under various conditions, **7** thus obtained remained to be contaminated with a small amount of **12**. **10**: mp 140 °C; MS *m/z* M^+ 488; ^{1}H NMR −0.32 (9H, s, $SiMe_3$), −0.05 (3H, s, *exo*-SiMe), 0.38 (3H, s, *endo*-SiMe), 1.71 (1H, s, H_6), 5.91 (1H, d, H_4, $J_{3,4}$=5.1 Hz), 6.03 (1H, d, H_3, $J_{3,4}$=5.1 Hz), 6.9—7.4 (10H, m, Ph); IR 2040, 1975, 1950 (ν CO), 1250 (δ SiMe); Found: C, 61.64; H, 5.83%. Calcd for $C_{25}H_{28}O_3Si_2Fe$: C, 61.47; H, 5.78%. **11**: mp 95 °C; MS *m/z* M^+ 488; ^{1}H NMR −0.22 (3H, s, *exo*-SiMe), 0.05 (9H, s, $SiMe_3$), 0.47 (3H, s, *endo*-SiMe), 1.91 (1H, s, H_2), 3.00 (1H, d, H_6, $J_{5,6}$=4.2 Hz), 3.25 (1H, d, H_5, $J_{5,6}$=4.2 Hz), 6.8—7.6 (10H, m, Ph); IR 2050, 1980, 1970, 1960 (ν CO), 1260, 1250 (δ SiMe); Found: C, 61.73, H, 5.77%. Calcd for $C_{25}H_{28}O_3Si_2Fe$: C, 61.47; H, 5.78%. **12**: an oil; MS *m/z* M^+ 488; ^{1}H NMR 0.06 (3H, s, *exo*-SiMe), 0.20 (9H, s, $SiMe_3$), 0.42 (3H, s, *endo*-SiMe), 1.37 (1H, d, H_{6X}, $J_{6X,6N}$=16.5 Hz, 5.91 (1H, s, H_3), 7.0—7.6 (10H, m, Ph); IR (liquid film) 2050, 1975 (ν CO), 1250 (δ SiMe).

Reaction of 7 with $Fe(CO)_5$. A mixture of **7** (105.6 mg, 0.303 mmol), $Fe(CO)_5$ (2 ml, 14 mmol) and dry xylene (4 ml) was heated in an autoclave at 170 °C for 37 h. The solvent and excess $Fe(CO)_5$ were removed in vacuum. The residual oil was separated by TLC to give **7** (36.0 mg, 34.3%) and **10** (66.0 mg, 68.3%).

Reaction of 8 with $Fe(CO)_5$. A mixture of **8** (74.1 mg, 0.213 mmol), $Fe(CO)_5$ (2 ml, 14 mmol) and dry toluene (6 ml) was heated in an autoclave to 160 °C for 22 h. Solvent and unchanged $Fe(CO)_5$ were removed in vacuum. The residual oil was separated by TLC to afford **11** (39.1 mg, 37.5%) and **12** (24.3 mg, 23.4%). **12** was always contaminated with a trace of unidentified compound, which shows same R_f value as **12** on TLC under various conditions.

Thermolysis of 11. **11** (49.0 mg, 0.100 mmol) was sealed under vacuum in a Pyrex tube and was heated in an oil bath at 170 °C for 7 h. The reaction mixture was separated by TLC to give recovered **11** (34 mg) and isomer **12** (13.4 mg).

Thermolysis of 12. In an autoclave the mixture (87 mg) of **12** (0.0462 mmol) containing **7** (0.1848 mmol), $Fe(CO)_5$ (2 ml, 14 mmol) and dry toluene (5 ml) were placed, and heated in an oil bath at 155—180 °C for 123 h. The solvent and excess $Fe(CO)_5$ were removed in vacuum. The residual oil was separated by TLC to give **10** (43.2 mg, 0.0885 mmol), **11** (11.5 mg, 0.0236 mmol), and the mixture (21.0 mg) of **12** and **7**.

We thank Toshiba Silicone Co., Ltd. for a gift of chlorosilanes.

References

1) Chemistry of Organosilicon Compounds. 212.

2) a) H. Sakurai and J. Hayashi, *J. Organomet. Chem.*, **63**, C10 (1973); H. Sakurai, J. Hayashi, and T. Kobayashi, *J. Organomet. Chem.*, **110**, 303 (1976).

3) E. W. Able, T. Blackmore, and R. J. Whitley, *J. Chem. Soc., Dalton Trans.*, **1976**, 2484 and references cited therein; G. T. Burns, E. Colomer, and R. J. P. Corriu, *Organometallics*, **2**, 1901 (1983).

4) W. Fink, *Helv. Chim. Acta*, **58**, 1205 (1976); **59**, 276 (1976).

5) G. Märkl, C. Soper, P. Hofmeister, and H. Baier, *J. Organomet. Chem.*, **174**, 305 (1979); G. Märkl and O. Hofmeister, ibid., **187**, 31 (1980).

6) Y. Nakadaira, S. Kanouchi, and H. Sakurai, *J. Am. Chem. Soc.*, **96**, 5621 (1974).

7) T. H. Whitesides and J. P. Neilan, *J. Am. Chem. Soc.*,

98, 63 (1976); **95**, 5811 (1973).

8) J. Slutsky and H. Kwart, *J. Am. Chem. Soc.*, **95**, 8678 (1973).

9) Y. Nakadaira, S. Kanouchi, and H. Sakurai, *J. Am. Chem. Soc.*, **96**, 5623 (1974).

10) A. J. Ashe, III, *J. Am. Chem. Soc.*, **92**, 1233 (1970).

11) a) C. P. Casey and C. R. Cyr, *J. Am. Chem. Soc.*, **95**, 2248 (1973). b) J. U. Strauss and P. W. Ford, *Tetrahedron Lett.*, **1975**, 2917.

12) A tricarbonyl(1,2-disilacyclohexadiene)iron complex also is found to be inert under these conditions; Y. Nakadaira, T. Kobayashi, and H. Sakurai, *J. Organomet. Chem.*, **165**, 399 (1979).

13) H. Sakurai and J. Hayashi, *J. Organomet. Chem.*, **63**, C7 (1973).

14) T. H. Whitesides and K. W. Arhart, *J. Am. Chem. Soc.*, **93**, 5296 (1971).

15) This enables us to assign the H_6 methylene proton signals in NMR spectra of these complexes. Since H_{6N} signal of **10** is located at 1.71, the higher field signal (1.25 in **4** and 1.37 in **12**) and the lower field signal (2.10 in **4** and 1.73 in **12**) can be assigned to those of H_{6N} and H_{6N}, respectively, by considering the substituent effect of the trimethylsilyl group on the chemical shift of H_{6N}. The chemical shift of H_6 signal is almost the same in **5** and **11**, and this shows that the configuration of H_6 should be same in these two complexes. On considerations of the effect of the α-phenyl group on the chemical shift of the H_6 signal, H_6 is reasonably assigned to be endo in both **5** and **11**.

 © 1986 The Chemical Society of Japan Bull. Chem. Soc. Jpn., 59, 1515—1519 (1986)

Copper(I), Silver(I), Mercury(II), and Palladium(II) Complexes of Tetrathia[*n*]ferrocenophanes

Masaru SATO,* Shinsuke TANAKA, Sadatoshi AKABORI,† and Yoichi HABATA†
Chemical Analysis Center, Saitama University, Urawa, Saitama 338
†Department of Chemistry, Faculty of Science, Toho University, Funabashi, Chiba 274
(Received January 7, 1986)

The complexes of a series of macrocyclic tetrathioether ligands containing a ferrocene nucleus in the macrocycle, tetrathia[*n*]ferrocenophanes, with copper(I), silver(I), mercury(II), and palladium(II) salts were prepared and characterized. The stability of complexes seems to depend on the size of the macrocycles in tetrathia[*n*]ferrocenophanes. The interaction between the iron atom of a ferrocene nucleus and the metal ions incorporated in the macrocycles seems to be negligible in these complexes.

Much attention has recently been focused on organo heterobimetallic compounds from the catalytic and biochemical points of view.[1,2] An organometallic ligand can be an important starting material for preparing heterobimetallic complexes. It is well-known that sulfide ligands make stable complexes with soft metals,[3] and many complexes of the macrocyclic thioether with various metal salts were prepared and characterized.[4–9] The iron atom of ferrocene is a potential coordinate site and certain ferrocene derivatives can form complexes with metal salts.[10,11] We prepared a new type of macrocyclic thioether ligand containing a ferrocene nucleus; polythia[*n*]-[12] and oxathia[*n*]ferrocenophanes.[13] The complex of the latter with silver(I) nitrate was isolated and characterized.[13] We now report on the systematic preparation and some properties of the complex of tetrathia[*n*]ferrocenophanes (**1a—d**) with copper(I), silver(I), mercury(II), and palladium(II) salts.

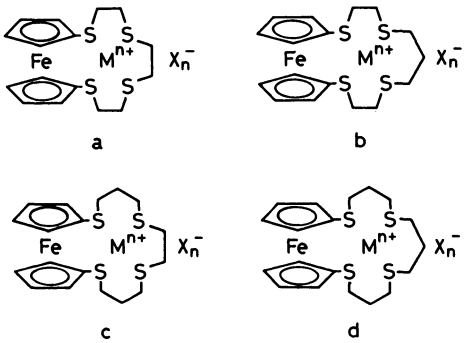

1. $M^{n+} = X_n^- =$ none
2. $M^{n+} = Cu^+$ $X_n^- = ClO_4^-$
3. $M^{n+} = Ag^+$ $X_n^- = ClO_4^-$
4. $M^{n+} = Hg^{2+}$ $X_n^- = Cl_2^-$
5. $M^{n+} = Pd^{2+}$ $X_n^- = Cl_2^-$

Results and Discussion

Copper(I) Perchlorate Complexes. The addition of anhydrous diethyl ether to a solution of tetrathia[*n*]ferrocenophanes (**1a—d**) and copper(I) perchlorate in acetonitrile afforded the 1:1 complexes (**2a—d**), respectively. The ^{1}H NMR spectra of these complexes (Table 1) shows the proton signals of the Cp-rings at δ ca. 4.4 as a broad singlet or a pair of triplets in acetonitrile-d_3. In the ^{13}C NMR spectra of **2a—d**, the α- and β-carbon signals appeared only as a pair of singlets (Table 2), indicating that complexes

Table 1. ^{1}H NMR Spectral Data of the Ligands **1** and the Complex **2—5** in Acetonitrile-d_3

Compd	Ring-H	SCH_2
1a	4.27(s, 8H)	2.85(m, 4H), 3.14(m, 4H), 3.06(s, 4H)
2a	4.42(m, 8H)	2.85—3.25(m, 8H), 3.08 (s, 4H)
3a	4.44(t, 4H), 4.36(t, 4H)	3.13(s, 8H), 3.07(s, 4H)
4a	4.47(s, 8H)	3.4—3.0(m, 8H), 3.20(s, 4H)
5a	4.45(m, 2H), 4.37(m, 6H)	3.8—3.0(m, 12H)[a]
1b	4.25(s, 8H)	3.14(m, 4H), 2.85(m, 4H), 2.81(t, 4H)
2b	4.45(m, 8H)	3.2—2.9(m, 8H), 2.84(t, 4H)
3b	4.42(m, 8H)	3.3—2.9(m, 12H)
4b	4.34(bs, 8H)	3.23(m, 4H), 2.88(m, 4H), 2.83(t, 4H)
1c	4.25(s, 8H)	2.92(t, 4H), 2.80(t, 4H), 2.82(s, 4H)
2c	4.59(t, 4H), 4.47(t, 4H)	2.90(t, 4H), 2.72(t, 4H), 3.04(s, 4H)
5c	4.71(m, 2H), 4.28(m, 6H)	3.8(m, 12H)[a]
1d	4.24(s, 4H)	2.89(t, 4H), 2.78(t, 4H), 2.62(t, 4H)
2d	4.51(m, 8H)	2.92(m, 12H)
4d	4.32(bs, 8H)	2.99(t, 8H), 2.74(t, 4H)

a) in DMSO-d_6.

2a—d have a symmetrical structure. However, it was confirmed by an X-ray analysis[14] that the Cu(I) atom had a tetrahedral coordination in the complex of 1,4,8,11-tetrathiacyclotetradecane with copper(I) perchlorate, although it was supposed[15] to be located in the central hole of a complex of 1,5,9,13-tetrathiacyclohexadecane with copper(I) tetrafluoroborate. Therefore, the appearance of symmetrical signals for the Cp-rings in the NMR spectra of **2a—d** seems to be due to a rapid dissociative equilibrium since in more coordinatable solvents (e.g. dimethyl-d_6 sulfoxide) complexes are completely dissociated to give NMR spectra of the corresponding free ligands. The IR spectra of **2a—d** (Table 3) showed a strong and broad band at 1140—1060 cm^{-1} and a sharp medium-strength band at about 620 cm^{-1}, indicating that there was only an uncoordinated perchlorate anion in the complexes.[16] A C–S–C medium-strength stretching vibration mode of the free ligand **1a—d** appeared near 680 cm^{-1}, but disappeared in **2b—d**. This suggests a considerably strong coordination of sulfur atoms to the copper(I) atom. In the ^{13}C NMR spectra (Table 2), complexes **2** showed a down-field shift of the α- and β-ring carbon signals, compared with the corresponding free ligands. The electronic spectra of **2** (Table 4) showed a hypsochromic shift and a decreased absorbance of the 440 nm band, assigned to the d–d transition.[17] These spectral data may suggest

Table 2. ^{13}C NMR Spectral Data of **1—4** in CD_3CN (22.5 MHz, ppm)

Compd	C_b[a]	C_α	C_β	Others
1a	87.3	73.0	70.2	39.2, 33.9, 32.5
2a	—	74.9	71.7	40.4, 36.2, 35.2
3a	82.9	73.5	71.8	36.2, 32.9, 32.5
1b	87.4	72.9	70.2	38.0, 33.2, 32.3, 31.0
2b	—	78.2	72.7	40.6, 35.4, 32.6, 24.6
3b	82.4	75.0	71.9	37.5, 35.1, 33.6
1c	86.6	73.7	70.2	35.9, 33.4, 31.3, 30.7
2c	—	77.6	73.0	41.2, 35.3, 32.1, 26.1
1d	86.4	73.7	70.2	36.0, 31.9, 31.8, 31.4, 30.7
2d	—	76.5	73.1	40.7, 35.4, 35.1, 25.9, 25.6

a) C_b means a bridge-head carbon.

Table 3. IR Spectral Data of **2—5** (KBr disk)

Compd	Frequency/cm^{-1}
2a[a]	3054m, 2860m, 1410s, 1384w, 1262s, 1140—1060vs, 1023s, 881m, 821s, 813s, 703w, 682w, 618s, 505s, 493s
2b	3050w, 2872w, 1412s, 1385w, 1256s, 1140—1065vs, 1027s, 885m, 817s, 621s, 502s, 484s
2c	3078m, 2906s, 1413s, 1385m, 1255m, 1140—1070vs, 1024s 888s, 813s, 623s, 503s, 480s
2d	3038m, 2866s, 1412s, 1384w, 1250s, 1150—1060vs, 1022s, 942m, 887m, 812s, 623s, 502s
3a	3046w, 2886m, 1412s, 1385m, 1257s, 1150—1065vs, 1024s, 882m, 810s, 684m, 623s, 512s, 493s, 480s
3b	3074w, 2902m, 1411s, 1383w, 1256s, 1145—1070vs, 1023s, 883m, 814s, 695w, 623s, 498s
4a[a]	3080w, 2920m, 1415s, 1385w, 1258m, 1195m, 1164m, 1130m, 1023s, 882m, 810s, 683, 516s, 492s, 480s
4b	3052w, 2880m, 1407s, 1380m, 1264m, 1256m, 1067m, 1062m, 1023s, 889m, 819s, 758m, 693w, 522s, 499s, 480s
4d[a]	3050w, 2870s, 1432s, 1427s, 1300m, 1254s, 1168m, 1162m, 1029s, 1024s, 892m, 885m, 817s, 812s, 519s, 503s, 484m
5a[a]	3076w, 2942m, 2886m, 1415s, 1403s, 1390m, 1280m, 1262m, 1218m, 1200m, 1165m, 1054m, 1031s, 1024s, 918s, 854s, 828s, 800s, 688w, 512s, 503s, 478s, 327m, 316m
5c[a]	3038w, 2866s, 1410s, 1332w, 1295m, 1253m, 1162m, 1024s, 925w, 890m, 882m, 815s, 512s, 493s, 470m, 340m, 320m

a) A CsI disk was used.

Table 4. Electronic Spectral Data of the Ligands 1 and the Complexes **2—4** in Acetonitrile

Ligands / Metal salts		**1a**	**1b**	**1c**	**1d**
None		442 nm (ε 223)	443 nm (ε 196)	443 nm (ε 191)	443 nm (ε 190)
$CuClO_4$	(2)	440 (ε 137)	434 (ε 129)	430 (ε 122)	434 (ε 139)
$AgClO_4$	(3)	438 (ε 195)	437 (ε 185)	—	—
$HgCl_2$	(4)	442 (ε 140)	447 (ε 140)	—	445 (ε 170)[a]

a) The 1:2 complex.

that for complex **2**, Cu(I) atoms coordinate to the sulfur atoms attached to ferrocene nuclei, although the definite structure is unknown at present. As a result, the electron density on a sulfur atom is decreased, resulting in a down-field shift of Cp-ring carbons and a change in the 440 nm band. In complex **2a**, the down-field shift of the Cp-ring carbons in the ^{13}C NMR spectrum and the hypsochromic shift of the 440 nm band in the electronic spectrum was rather small, compared with those of **2b—d**. This suggests that the coordination mode described above may be somewhat different in **2a**.

Silver(I) Perchlorate Complexes. When a solution of the ligand **1a** and silver(I) nitrate in acetonitrile was diluted with anhydrous diethyl ether, a 1:1 complex was precipitated. The 1:1 complexes (**3a** and **3b**) of the tetrathiaferrocenophanes **1a** and **1b** with silver(I) perchlorate were similarly isolated by the reaction of **1a** and **1b** with silver(I) perchlorate, respectively. However, the reaction of **1c** and **1d** with silver(I) salts gave no stable complex. Thus, the complex formation of tetrathia[n]ferrocenophanes with silver(I) salt depends on the size of the thiacrown ether rings. Although some complexes of oxathiacrown ethers with silver(I) nitrate were known,[13,18] the corresponding thiacrown ether complexes are rare. 1,4,8,11-Tetrathiacyclotetradecane has been shown to give the 1:1 and 1:2 complexes with silver(I) perchlorate, though their structures were not confirmed.[19] The absorption for the C–S–C stretching vibration of **3a** and **3b** appeared at about 690 cm^{-1} with decreased intensity compared with that of the corresponding free ligand, suggesting a weak coordination of the sulfur atom to the silver(I) atom in these complexes. In the electronic spectra of **3a** and **3b**, the absorption band near 440 nm, characteristic of a ferrocene nucleus, showed a hypsochromic shift and a decreased absorbance, the extent of which were rather small compared with those of the Cu(I) complexes (vide supra). A similar trend has been observed in the $AgNO_3$-added solution of oxathia[n]-[13] and polythia[n]ferrocenophanes in acetonitrile.[12] Thus, the complexation of silver(I) atoms in the complexes **3a** and **3b** appears to be loose. In the ^1H NMR spectrum of **3a**, the Cp-ring protons of the ferrocene nucleus appears as a pair of triplets at δ 4.44 and 4.36 (J=1.7 Hz) and the methylene protons resonates as two singlets at δ 3.13 and 3.07. The proton signals for the Cp-rings and the methylene groups in **3b** appears at δ 4.42 and 3.3—2.9 as multiplets, respectively. Similar spectra were also obtained upon the addition of silver(I) nitrate to a solution of **1a—d** in CD_3CN–CD_3NO_2 (1:4), suggesting that **1c** and **1d** also formed similarly 1:1 complexes **3c** and **3d** in the solution although they could not be isolated. The size of a silver(I) ion (1.26 Å) is too large to be incorporated into the central hole of the polythia-macrocycle in the ligands **1a** and **1b**. Thus, complexes **3a** and **3b** must have an unsymmetrical structure. Therefore, the symmetrical pattern of the ring proton signals observed in the ^1H NMR spectra, which suggests a symmetrical structure of complex **3**, seems due to a rapid dissociative equilibrium in the solution described in the copper(I) complexes. In the ^{13}C NMR spectra of **3a** and **3b** (Table 2), the bridge-head carbon signal is shifted up-field and the α- anf β-ring carbon signals down-field, compared with those in the corresponding ligands. This also seems to support a loose coordination of silver(I) atoms to the thiacrown moiety of ligands **1**.

Mercury(II) Chloride Complexes. It is well-known that a soft mercury(II) salt forms a wide range of complexes with thioethers,[3] particularly a stable complex with thiacrown ether.[20,21] When an ethereal solution of mercury(II) chloride was added to a solution of **1a** in diethyl ether, the stable 1:1 complex **4a** was isolated in good yield. Similarly, the 1:1 complex **4b** was prepared. However, in a similar manner, **1c** gave no stable complex and **1d** gave the stable 1:2 complex **4d** with mercury(II) chloride. Thus, the complex formation of tetrathia[n]ferrocenophanes with mercury(II) chloride depends on the size of the thiacrown ether ring. In complexes of the thioethers with mercury(II) chloride, of which the crystal structure were determined by X-ray analysis, the coordination about the mercury(II) atom was approximately tetrahedral in the most cases. For example, the coordination mode of a mercury(II) atom in the 1:2 complex of 1,4,8,11-tetrathiacyclotetradecane with mercury(II) chloride is a distorted tetrahedral,[22] while an octahedral coordination is suggested from its IR spectrum in the 1:1 complex of 1,4,8,11-tetrathiacyclotetradecane with mercury(II) chloride.[20] The 1:1 complexes **4a** and **4b** show no blue shifts in their electronic spectra, although their absorbances decrease to a considerable degree. Regarding their ^1H NMR spectra of **4a** and **4b**, a broading of the singlet as well as a small down-field shift (0.1—0.2 ppm) of the Cp-ring protons was observed; but non-symmetrization of the Cp-ring proton signals was not recognized. These spectral data suggests that in **4a** and **4b** the mercury(II) atoms coordinate only to sulfur atoms far away from the ferrocene nucleus of **1a** and **1b**. This may be due to a rather large ion radius (r_{ion}=1.10 Å)[23] that cannot be fitted to the central hole of the ligands **1a** and **1b**. The additional $HgCl_2$ in the 1:2 complex **4d** is probably bonded to the mercury(II) atom coordinated to the sulfur atoms of the macrocycle through the bridging chloro atoms, because the ^1H NMR spectrum of **4d** was very similar with those of **4a** and **4b**.

Palladium(II) Chloride Complexes. The addition of a solution of dichlorobis(acetonitrile)palladium(II)

in acetonitrile to a solution of **1a** and **1c** in acetonitrile gave the stable 1:1 complexes **5a** and **5c**, respectively. Unstable complexes were obtained from **1b** and **1d** by a similar procedure, but could not be characterized. The isolated complexes **5a** and **5c** were very insoluble in almost organic solvents. The ^{1}H NMR spectrum (dimethyl-d_6 sulfoxide) of **5a** showed broad signals at δ 4.45 and 4.37 (1:2), suggesting an unsymmetrical structure of complex **5a**. By contrast, the ring protons in dichloro[1,1′-(bis(isobutylthio)ferrocene)]palladium[24] appears as a symmetric pattern at δ 5.28 and 4.42. In the far-IR spectra of **5a**, the absorption at 327 and 316 cm^{-1} is in the range reported for *cis*-$PdCl_2$ moieties,[25] indicating a monomeric structure, where the Pd atom coordinated to the two sulfur atoms far from the ferrocene nucleus, because of the steric hindrance of large $PdCl_2$ moiety. However, the polymeric structure in which the Pd atom builds a bridge across two ferrocenophanes also cannot be ruled out. Recently, the X-ray analysis of the complex of 1,4,7,10-tetrathia[10]ruthenocenophane with palladium(II) chloride was reported and confirmed that the two sulfur atoms far from a ruthenocene nucleus coordinated to the palladium(II) atom.[26] Therefore, **5a** is suggested to have the same coordination mode with the above complex.

Mössbauer Spectra. The *IS* and *QS* values in ^{57}Fe Mössbauer spectra (300° K) of the free ligands **1** and the metal complexes **2**—**5** are summarized in Table 5. The Mössbauer parameters are little changed in going from the free ligands to the metal complexes. A similar small change was also observed in the complex of 1,1′-bis(diphenylphosphino)ferrocene with mercury(II) chloride.[27] A large change in the *QS* value observed in the complex of [2]ferrocenophanes with mercury(II) chloride[10] and tin(IV) chloride,[11] suggests the direct interaction between the iron atom of a ferrocene nucleus and the metal atoms. The relatively small change observed here seems to indicate that the metal atoms incorporated in the polythia-macrocycle has no strong interaction with the iron atom of a ferrocene nucleus.

Table 5. Mössbauer Parameters of **1**—**5**

Compd	*IS*	*QS*
1a	0.46	2.38
1c	0.42	2.39
2a	0.41	2.37
2b	0.41	2.37
3a	0.43	2.34
3b	0.42	2.36
4a	0.45	2.35
4b	0.45	2.32
4d	0.45	3.29
5a	0.42	2.33
5c	0.44	2.32

Experimental

Melting points are uncorrected. The electronic spectra were measured on a Hitachi 340 spectrometer. The IR spectra were measured on a JASCO IR-2 spectrometer. The ^{1}H and ^{13}C NMR spectra were obtained on a JEOL FX-90Q spectrometer, TMS being chosen as an internal standard.

Materials. Tetrathia[*n*]ferrocenophanes were prepared as described in a previous paper.[12] Mercury(II) chloride and silver(I) perchlorate were commercially available. Tetrakis(acetonitrile)copper(I) perchlorate[28] and dichlorobis(acetonitrile)palladium(II)[29] were prepared according to the literature.

(1,4,7,10-Tetrathia[10]ferrocenophane)copper(I) Perchlorate (2a). General Procedure. To a solution of 1,4,7,10-tetrathia[10]ferrocenophane (**1a**) (40 mg, 0.1 mmol) in hot acetonitrile (2.5 cm^3) was added a solution of tetrakis-(acetonitrile)copper(I) perchlorate (33 mg, 0.1 mmol) in acetonitrile (2.5 cm^3). The solution was refluxed for 15 min and then diluted with anhydrous diethyl ether (15 cm^3) to form yellow crystals. After the mixture was kept for 2 h in a refrigerator, the crystals were collected by filtration. Yellow leaflets (37 mg, 66%), mp 200 °C (decomp). Found: C, 34.63; H, 3.83%. Calcd for $C_{16}H_{20}ClO_4S_4FeCu$: C, 34.35; H, 3.61%.

(1,4,8,11-Tetrathia[11]ferrocenophane)copper(I) Perchlorate (2b). Yellow leaflets (68%), mp 208 °C (decomp). Found: C, 35.34; H, 3.92%. Calcd for $C_{17}H_{22}ClO_4S_4FeCu$: C, 35.61; H, 3.87%.

(1,5,8,12-Tetrathia[12]ferrocenophane)copper(I) Perchlorate (2c). Yellow crystals (75%), mp ≈214 °C (decomp). Found: C, 37.10; H, 4.16%. Calcd for $C_{18}H_{24}ClO_4S_4FeCu$: C, 36.80%; H, 4.16%.

(1,5,9,13-Tetrathia[13]ferrocenophane)copper(I) Perchlorate (2d). Yellow plates (55%), mp ≈204 °C (decomp). Found: C, 38.16; H, 4.45%. Calcd for $C_{19}H_{26}ClO_4S_4FeCu$: C, 37.93; H, 4.36%.

(1,4,7,10-Tetrathia[10]ferrocenophane)silver(I) Nitrate. To a solution of **1a** (400 mg, 1 mmol) in hot acetonitrile (20 cm^3) was added silver(I) nitrate (170 mg, 1 mmol). After heating for 15 min, the resulting crystals were filtered and washed with hot acetonitrile. Orange crystals (400 mg, 70%), mp ≈180 °C (decomp). ^{1}H NMR (CMSO-d_6) δ=4.46 (s, 8H), 3.18 (s, 8H) and 3.12 (s, 4H). IR (KBr): 2900, 1620, 1380, 1300, 1160, 1020, and 800 cm^{-1}. Found: C, 33.98%; H, 3.56; N, 2.74%. Calcd for $C_{16}H_{20}NO_2S_4FeAg$: C, 34.02; H, 3.56; N, 2.47%.

(1,4,7,10-Tetrathia[10]ferrocenophane)silver(I) Perchlorate (3a). General Procedure. To a solution of **1a** (40 mg, 0.1 mmol) in acetonitrile (10 cm^3) was added silver(I) perchlorate (21 mg, 0.1 mmol). The solution was evaporated up. The yellow oily residue was dissolved in acetonitrile (1 cm^3) and then diluted with anhydrous ether (ca. 2 cm^3). The solution was kept for overnight in a refrigerator. The crystals formed were filtered. Yellow rods (50 mg, 83%), mp ≈190 °C (decomp). Found: C, 32.08; H, 3.42%. Calcd for $C_{16}H_{20}ClO_4S_4FeAg$: C, 31.83; H, 3.34%.

(1,4,8,11-Tetrathia[11]ferrocenophane)silver(I) Perchlorate (3b). Yellow needles (88%), mp 185 °C (decomp). Found:

C, 33.05; H, 3.72%. Calcd for $C_{17}H_{22}ClO_4S_4FeAg$: C, 33.05; H, 3.56%.

Dichloro(1,4,7,10-tetrathia[10]ferrocenophane)mercury(II) (4a). General Procedure. To a solution of **1a** (50 mg, 0.13 mmol) in anhydrous ether (25 cm^3) was added a solution of mercury(II) chloride (35 mg, 0.13 mmol) in anhydrous ether (5 cm^3). The solution was refluxed for 15 min and then kept for overnight at room temperature. The resulting crystals were collected by filtration. Yellow leaflets (60 mg, 69%), mp ≈210 °C (decomp). Found: C, 28.77; H, 3.02%. Calcd for $C_{16}H_{20}Cl_2S_4FeHg$: C, 28.77; H, 3.02%.

Dichloro(1,4,8,11-tetrathia[11]ferrocenophane)mercury(II) (4b). Yellow fine needles (92%), mp 147 °C (decomp). Found: C, 30.11; H, 3.17%. Calcd for $C_{17}H_{22}Cl_2S_4FeHg$: C, 29.94; H, 3.25%.

Tetrachloro(1,5,9,13-tetrathia[13]ferrocenophane)dimercury(II) (4d). Yellow powdery crystals (46%), mp 151 °C (decomp). Found: C, 23.75; H, 2.97%. Calcd for $C_{19}H_{26}Cl_4S_4FeHg_2$: C, 23.25; H, 2.67%.

Dichloro(1,4,7,10-tetrathia[10]ferrocenophane)palladium (II) (5a). General Procedure. To a solution of **1a** (40 mg, 0.1 mmol) in acetonitrile (5 cm^3) was added a solution of dichlorobis(acetonitrile)palladium(II) (26 mg, 0.1 mmol). The solution was kept overnight at room temperature. The resulting crystals were collected by filtration. Brown needles (49 mg, 86%), mp ≈205 °C (decomp). Found: C, 33.80; H, 3.60%. Calcd for $C_{16}H_{20}Cl_2S_4FePd$: C, 33.50; H, 3.51%.

Dichloro(1,5,8,12-Tetrathia[12]ferrocenophane)palladium (II) (5c). Red brown fine crystals (87%), mp ≈185 °C (decomp). Found: C, 36.07; H, 3.91%. Calcd for $C_{18}H_{24}Cl_2S_4FePd$: C, 35.92; H, 4.02%.

^1H and ^{13}C NMR Spectra of the Complex of 1 with Silver(I) Nitrate. ^1H and ^{13}C NMR spectra were measured upon the addition of silver(I) nitrate (1.2 equiv) to a solution of **1a—d** in CD_3CN-CD_3NO_2 (1:4). The spectral data obtained were similar to those of **3a** and **3b** shown in Tables 1 and 2.

We thank Prof. I. Motoyama and Dr. M. Katada (Tokyo Metropolitan University, Department of Chemistry) for measurement of Mössbauer spectra. The present work was supported by a Grant-in-Aid for Science Research (No. 57540274) from the Ministry of Education, Science and Culture.

References

1) D. A. Roberts and G. L. Geoffroy, "Comprehensive Organometallic Chemistry," ed by G. Wilkinson, F. G. A. Stone, and E. Abel, Pergamon Press, Oxford, England (1982), Chap. 40.
2) D. Coucouvanis, *Acc. Chem. Res.*, **14**, 201 (1981).
3) S. G. Murray and F. R. Hartley, *Chem. Rev.*, **81**, 365 (1981).
4) W. Rosen and D. H. Bush, *J. Am. Chem. Soc.*, **91**, 4694 (1969); *Inorg. Chem.*, **9**, 262 (1970).
5) K. Travis and D. H. Bush, *Inorg. Chem.*, **13**, 2591 (1974).
6) T. E. Jones, D. B. Rorabacker, and L. A. Ochrymowycz, *J. Am. Chem. Soc.*, **97**, 7485 (1975).
7) T.-F. Lai and C.-K. Poon, *J. Chem. Soc., Dalton Trans.*, **1982**, 1465.
8) E. J. Hintsa, J. R. Hartman, and S. R. Cooper, *J. Am. Soc.*, **105**, 3738 (1983).
9) J. R. Hartman, E. J. Hinsta, and S. R. Cooper, *J. Chem. Soc., Chem. Commun.*, **1984**, 386.
10) M. Watanabe, H. Ichikawa, I. Motoyama, and H. Sano, *Bull. Chem. Soc. Jpn.*, **56**, 3291 (1983).
11) M. Watanabe, H. Ichikawa, I. Motoyama, and H. Sano, *Chem. Lett.*, **1983**, 1009.
12) M. Sato, H. Watanabe, S. Ebine, and S. Akabori, *Chem. Lett.*, **1982**, 1753; M. Sato, S. Tanaka, S. Ebine, and S. Akabori, *Bull. Chem. Soc. Jpn.*, **57**, 1929 (1984).
13) M. Sato, M. Kubo, S. Ebine, and S. Akabori, *Tetrahedron Lett.*, **1982**, 185; *Bull. Chem. Soc. Jpn.*, **57**, 421 (1984).
14) E. R. Dockal, L. L. Diaddario, M. D. Glick, and D. B. Rorabacker, *J. Am. Chem. Soc.*, **99**, 4530 (1977).
15) B. V. Gorewit and W. K. Musker, *J. Coord. Chem.*, **5**, 67 (1976).
16) B. J. Hathaway and A. E. Underhill, *J. Chem. Soc.*, **1961**, 3091.
17) M. Rosenblum, "Chemistry of the Iron Group Metallocenes," John Wiley Sons Inc., New York (1965), Chap. 3.
18) C. J. Pedersen, *J. Org. Chem.*, **36**, 254 (1971).
19) D. Sevdic and H. Meider, *J. Inorg. Nucl. Chem.*, **39**, 1403 (1977).
20) D. Sevdic and H. Meider, *J. Inorg. Nucl. Chem.*, **39**, 1409 (1977).
21) R. M. Izatt, R. E. Terry, L. D. Hansen, A. G. Avondet, J. S. Bradshaw, N. K. Dalley, T. E. Jensen, J. J. Christensen, and B. L. Haymore, *Inorg. Chim. Acta*, **30**, 1 (1978).
22) N. W. Alcock, N. Herron, and P. Moore, *J. Chem. Soc., Dalton Trans.*, **1978**, 394.
23) F. A. Cotton and G. Wilkinson, "Advanced Inorganic Chemistry," Interscience Publishers, New York (1966), p. 44.
24) B. McCulloch, D. L. Ward, J. D. Woolins, and C. H. Brubaker, Jr., *Organometallics*, **4**, 1425 (1985).
25) G. E. Coats and C. Parkin, *J. Chem. Soc.*, **1963**, 421.
26) S. Akabori, S. Sato, T. Tokuda, Y. Habata, K. Kawazoe, C. Tamura, and M. Sato, *Chem. Lett.*, **1986**, 121.
27) K. P. Mann, W. H. Morrison, and D. N. Hendrickson, *Inorg. Chem.*, **13**, 1180 (1974).
28) P. Hemmerich and C. Sigwart, *Experientia*, **19**, 488 (1963).
29) F. R. Hartley, S. G. Murray, and C. A. McAuliffe, *Inorg. Chem.*, **18**, 1394 (1979).

 © 1986 The Chemical Society of Japan Bull. Chem. Soc. Jpn., 59, 1521—1528 (1986)

Total Synthesis of Neomethynolide

Junji INANAGA,* Yasuhiro KAWANAMI, and Masaru YAMAGUCHI
Department of Chemistry, Faculty of Science, Kyushu University 33,
Hakozaki, Higashi-ku, Fukuoka 812
(Received January 16, 1986)

Neomethynolide (**1**), the aglycone of a twelve-membered ring macrolide, neomethymycin, was totally synthesized in its optically active form via 8,9-didehydro-**1**. The construction of the skeleton was carried out by condensing a stereoselectively synthesized fragment, 4-*t*-butyldimethylsiloxy-5-(2-methoxyethoxymethoxy)-3-methyl-1-hexyne, with Prelog-Djerassi lactonic ester, and mixed anhydride method was used for the lactonization of an intermediary hydroxy acid. The full stereochemistry of **1** was established by this synthesis.

A total synthesis and consequent establishment of whole stereochemistry of neomethynolide (**1**), the aglycone of a macrolide antibiotic, neomethymycin (**2**), have recently been communicated.[1] The full details of the work will be disclosed here.

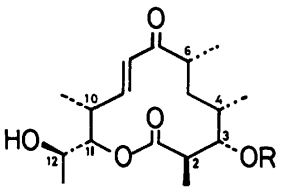

1 Neomethynolide (R=H)
2 Neomethymycin (R=Desosaminyl)

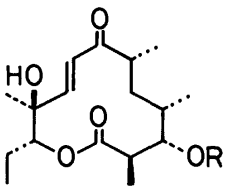

Methynolide (R=H)
Methymycin (R=Desosaminyl)

Neomethymycin belongs besides methymycin and YC-17,[2] to a twelve-membered ring family of typical macrolides and has been isolated from the culture filtrate of *Streptomyces* M-2140.[3a,c] Neomethynolide (**1**) was first obtained by the mild acid-hydrolysis of **2** as the authentic aglycone by Djerassi et al.,[3a,c] and Maezawa et al.[4] later reported that a mutant strain, *Streptomyces venezuelae* MCRL-0376 produced the aglcone **1** itself. Its chemical structure as 10-deoxy-12-hydroxymethynolide was given by Djerassi et al.[3b,c] and the partial stereochemistry, 2*R*, 3*S*, 4*S*, and 6*R*, was later established when Rickards et al.[5] carried out the precise ^{1}H NMR examination of a degradation product (Prelog–Djerassi lactonic acid) and its derivatives. From the analogy with methynolide[6] and on the basis of biogenetic consideration, **1** was also considered to have 10*R*, 11*S*, and 8,9-*trans* configuration though no experimental evidence was available. The present authors further postulated the 12*R* stereochemistry and carried out the synthesis of the compound having a structure represented by **1** in its optically active form.

The basic strategy in the present synthesis is similar in principle to that we previously adopted in the synthesis of methynolide.[7] The 8,9-double bond of the target molecule was introduced as triple bond and the latter was reserved until the later stage of the synthesis. This not only circumvented the instability of δ-hydroxy-α,β-enone structure in the molecule

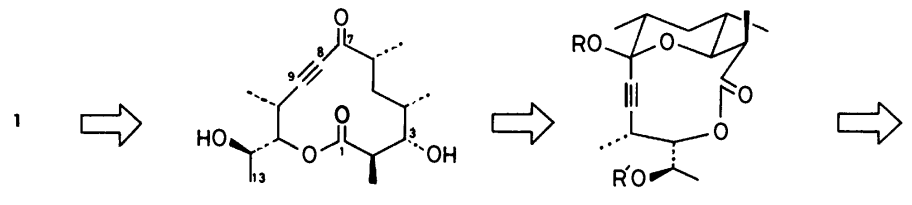

1 **20** **16 or 17**

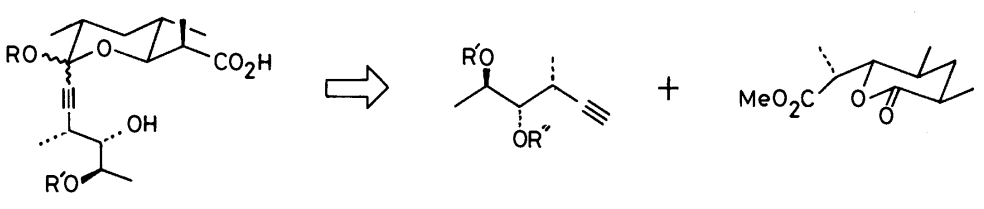

14 or 15 **7** **8**

which tended to undergo vinylogous retro-aldol type cleavage of 10,11-bond[8] but also enabled the choice of well-documented acetylenic ketone synthesis for the construction of basic skeleton by combining C(8)–C(13) (**7**) and C(1)–C(7) (**8**, Prelog–Djerassi lactonic ester) fragments. Instead of our previous procedure with silver acetylide and acid chloride,[7] the direct condensation[9] of lithiated **7** and **8** was adopted this time, which unnecessitated the tedious manipulation of **8** via several steps, and consequently much simplified the synthesis.

The next point is the use of hemi- or mixed acetal intermediates such as **9**—**17**. The 3-hydroxyl group and the conjugated 7-oxo group were thus intramolecularly protected at the same time minimizing protection-deprotection procedures and preventing the facile cleavage between triple bond and carbonyl group under alkaline hydrolytic conditions.

Lactonization to a highly strained bicyclic compound (**16** or **17**) by virtue of the very efficient mixed anhydride method[10] and the removal of 7-*O*-protection with the concomitant generation of 3-hydroxyl, 7-carbonyl, and monocyclic lactone structure should also be noted.

The stereoselective synthesis of the C(8)–C(13) fraction was started with 3,4-epoxy-2-pentanone (**3**).[11] We first examined the reduction of **3** to an *erythro*-epoxy alcohol (**4**) according to the method of Chautemps and Pierre[12] where the reduction with sodium borohydride in methanol at 0 °C was reported to give the *erythro*-isomer predominantly with over 95:5 ratio. However, we could not reproduce the result only obtaining a selectivity of about 72:28, and a number of other reducing agents were then examined under a variety of conditions to obtain higher selectivity. Some results are listed in the Table.

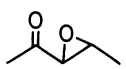

3

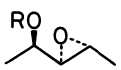

4 R=H
5 R=MEM

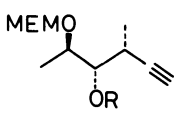

6 R=H
7 R=TBDMS

Although a sterically-crowded reagent prepared from sodium borohydride and 1-naphthol afforded fairly good *erythro*-selectivity (94:6), it was disadvantageous that excess reagent was required to complete the reaction and that the yield of the product was low (≈36%) mainly because of the difficulty of isolation from a large amount of naphthol which was liberated after aqueous workup (Entry 2). Reduction with sodium hydridobis(2-methoxyethoxy)aluminate (Red-Al), diisobutylaluminum hydride (DIBAL-H), or lithium tri-*t*-butoxyhydridoaluminate did not give satisfactory selectivity. Chelation controlled hydride reduction was then examined with a combination of sodium borohydride and appropriate metal salts. When zinc bromide or chloride was used, a highly stereoselective reduction took place accompanied with concomitant formation of 3-halo-1,2-diols as a result of nucleophilic attack of halogenide ions on epoxide ring (Entries 9 and 10). In order to prevent such ring openings, low nucleophilic counter anions such as fluoride or perchlorate were examined. Thus, by using a mixture of sodium borohydride and zinc perchlorate[13] in ether, the desired *erythro*-epoxy alcohol (**4**) was obtained exclusively in good yield (Entry 12).

Table 1. Reduction of Epoxy Ketone (**3**) with Various Reducing Agents[a]

Entry	Reducing agent	Solv.	Temp	Time	Ratio[b] (E:T)[c]
1	$NaBH_4$	MeOH	0 °C	30 min	72:28
2	$NaBH_4+3C_{10}H_7OH$[d]	THF	RT	13 h	94: 6
3	Red-Al	THF	−78~0 °C	6 h	81:19
4	DIBAL-H	Toluene	RT	10 min	58:42
5	$LiAlH(OBu^t)_3$	THF	0 °C	10 h	60:40
6	$Zn(BH_4)_2$	DME	0 °C	30 min	60:40
7	$NaBH_4+LiCl$	Et_2O	RT	12 h	76:24[e]
8	$NaBH_4+CaCl_2$	THF	−100 °C	20 min	87:13
9	$NaBH_4+ZnBr_2$	Et_2O	−78~−20 °C	3 h	>95: 5[f]
10	$NaBH_4+ZnCl_2$	THF	−78 °C	6 h	96: 4[g]
11	$NaBH_4+ZnF_2$	Et_2O	RT	10 min	83:17
12	$NaBH_4+Zn(ClO_4)_2$[h]	Et_2O	−78~0 °C	2 h	>95: 5

a) The reaction was carried out in 1 mmol scale with 1.0—1.1 equiv of reducing agent. b) Ratio was determined by ^{13}C NMR analysis of a mixture of epoxy alcohols and/or GLC analysis (Silicone GE, SE-30) of its acetates. c) E=% *erythro*; T=% *threo*. d) $NaBH_4$ (1 equiv) and 1-naphthol (3 equiv) was stirred in THF for several hours until no more hydrogen gas was evolved. e) 4-Chloro-2,3-pentanediol (ca. 20%) was produced as a by-product. f) 4-Bromo-2,3-pentanediol (ca. 8%) was also produced. g) 4-Chloro-2,3-pentanediol (ca. 10%) was also formed. h) Zinc perchlorate hexahydrate was used.

Hydroxyl group of **4** was protected with 2-methoxyethoxymethyl (MEM) chloride and *N,N*-diisopropylethylamine to afford the corresponding MEM ether (**5**) in 80% yield. Reaction of **5** with lithium acetylide-ethylenediamine complex was best performed in dimethyl sulfoxide (DMSO)–hexamethylphosphoric triamide (HMPA) at room temperature to give 65% yield of the desired acetylenic alcohol (**6**).

Resolution of **6** was carried out via its optically active *O*-methylmandelates. Treatment of **6** with (*S*)-(+)-*O*-methylmandelic acid chloride in the presence of 4-dimethylaminopyridine gave a mixture of diastereomeric esters which could be easily separated by column chromatography on silica gel. The early fraction gave, upon hydrolysis, the (−)-alcohol (**6**) in 95% yield. According to the following scheme (−)-**6** was degraded to 2-methylbutyric acid and, on correlation to (*R*)-(−)-*p*-phenylphenacyl 2-methylbutyrate (**iii**),[14] it proved to have a (2*R*,3*S*,4*R*)-configuration required for the synthesis of **1**.

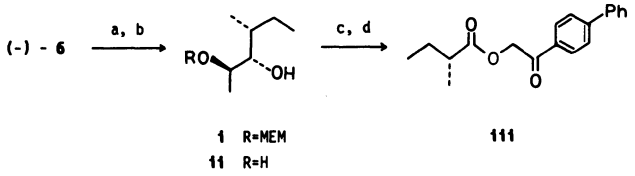

a: H_2/Pt, EtOH. b: HCl-MeOH. c: $NaIO_4$, $KMnO_4$, K_2CO_3, H_2O-Me_2CO. d: p-phenylphenacyl bromide, CsF.

The (−)-alcohol (**6**), thus obtained, was protected with *t*-butyldimethlysilyl (TBDMS) chloride and imidazole in *N,N*-dimethylformamide (DMF) to give the acetylenic silyl ether (**7**) in 98% yield as a key intermediate.

Another key intermediate, (+)-Prelog-Djerassi lactonic ester (**8**) was prepared in an non-stereoselective way according to the method used in the synthesis of methynolide.[15]

Condensation of the two fragments, lithium acetylide of (−)-**7** and (+)-**8**, was carried out in THF at −20 °C affording a mixture of hemiacetals (**9**, ca. 1:3.5 by ^{1}H NMR) in 90% yield. The major isomer was later found to have an equatorial hydroxyl group by converting the above mixture to the corresponding MEM ethers under nonequilibrium conditions followed by the examination of their ^{1}H NMR spectra as will be discussed later. The mixture **9** was treated with a catalytic amount of *p*-toluenesulfonic acid in methanol for 2 h to give an equilibrium mixture of the methyl acetals (**10**) which were difficult to separate. Since it is well-known that the anomeric methoxyl group of six-membered acetals preferentially occupies an axial position under equilibrium conditions,[16] the major isomer of the above methyl acetals (**10**) must have an axial methoxyl group. The relative intensity of the protons of anomeric methoxyl groups at C-7 in ^{1}H NMR spectrum was 3.5 (axial, δ=3.25):1 (equatorial, δ=3.35). On the other hand,

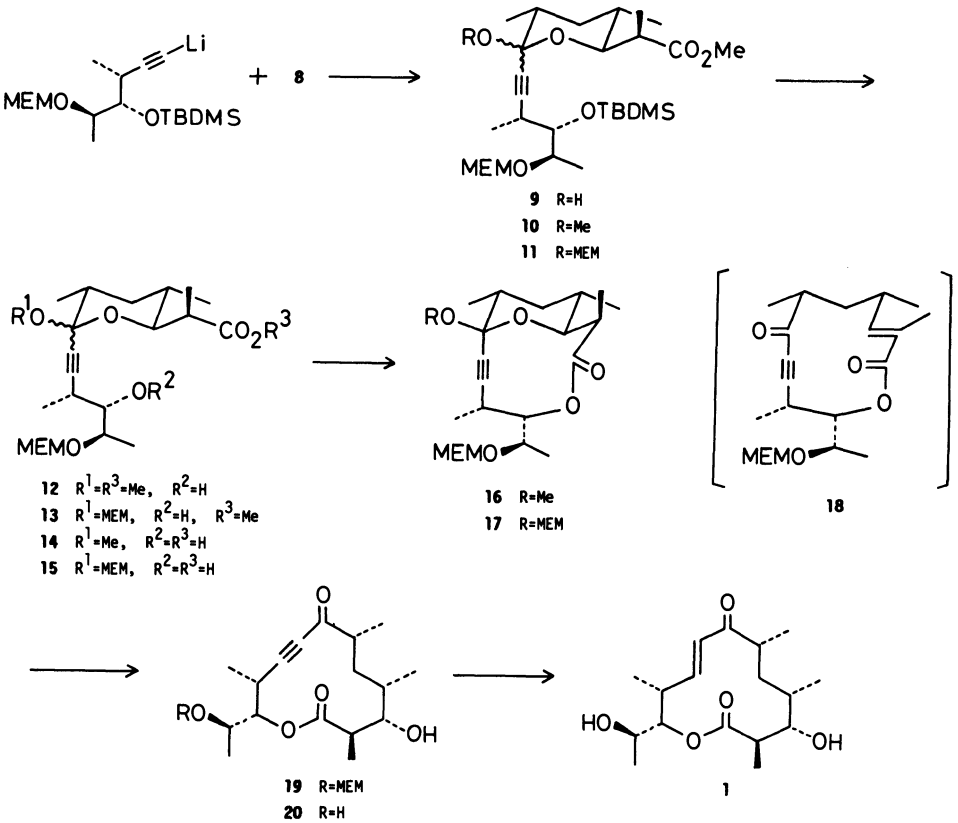

treatment of **9** with MEM chloride and *N,N*-diisopropylethylamine afforded a mixture of MEM ethers (**11**) in 90.4% yield which could be separated by preparative TLC on silica gel. Judging from ^{1}H NMR spectra of the above MEM ethers, the isomeric ratio of axial OMEM (δ=4.71 or 4.73)[17] to equatorial OMEM (δ=4.94)[17] was ca. 1:4, reflecting the original ratio of hemiacetals (**9**). The mixture of methyl acetals (**10**) was desilylated with tetrabutylammonium fluoride and the resulting alcohols (**12**) were hydrolyzed with aqueous methanolic sodium hydroxide to give a ca. 3 (axial OMe):1 (equatorial OMe) mixture of the hydroxy acids (**14**) in 83.3% overall yield. Alternatively, the major, less polar isomer with equatorial OMEM group **11** was converted into a single seco-acid (**15**) by the same procedures as above in 87.6% yield.

Lactonization of the seco-acid mixture **14** and that of **15** were carried out in refluxing benzene by mixed anhydride method using 2,4,6-trichlorobenzoyl chloride.[10] From the examination of molecular models it became apparent that the seco-acid having an axial methoxyl group (or OMEM group) has almost no chance of intramolecular cyclization, however it seems possible to lactonize the seco-acid having equatorial methoxyl group (or OMEM group) at C-7 position though they seem to still suffer from considerable strain in cyclization. In fact, the highly-strained bicyclic lactones (**16**) and (**17**) were obtained in 12.0% and 33.2% yield, respectively. The low yield of **16** compared with that of **17** seems to be due to the low content of the seco-acid with an equatorial methoxyl group in the mixture **14**. In both cases, the 2-unsaturated compound **18** was isolated as a by-product in 9—13% yield.

Deprotection of **16** with 1% trifluoroacetic acid (TFA) in dichloromethane for 14 h gave the mono-MEM ether (**19**) and the diol (**20**) in 61% and 16% yield, respectively. Prolonged reaction or high concentrations of TFA produced a complicated mixture. Pyridinium *p*-toluenesulfonate (PPTS) in refluxing ethanol did not give good result for the generation of the diol (**20**). Treatment of **17** with zinc bromide in dichloromethane also gave **19** and **20** in 38% and 44% yield, respectively. Since **19** could be further converted to **20** in 60% yield with zinc bromide, totally 67% yield of **20** was attained from **17**.

Reduction of 8,9-didehydroneomethynolide (**20**) by chromium(II) sulfate in aqueous DMF[18] at room temperature smoothly gave 65% yield of neomethynolide (**1**) as colorless needles. Melting point and combustion analysis of synthetic **1** revealed that it existed as monohydrate. All spectral data (NMR, IR, UV, Mass) of synthetic **1** as well as melting point of its diacetate were identical with those of the specimens of natural origin and hence the complete stereochemistry of neomethynolide (**1**) was established by the present total synthesis.

Experimental

Melting points and boiling points are uncorrected. IR spectra were determined on a Hitachi R-215, UV spectra on a Hitachi 200-10, and mass spectra on a Hitachi RML-6MG or JEOL JMS-OISG-2 spectrometer. ^{1}H NMR spectra were recorded at either 60 (Hitachi R-20B) or 90 MHz (JEOL JNM-FX90Q) as indicated and ^{13}C NMR spectra at 25 MHz (JEOL JNM-FX90Q) instrument. All NMR spectra were taken in deuteriochloroform solutions with tetramethylsilane as an internal standard. Optical rotations were determined on a Yanagimoto OR-50 Polarimeter.

Reactions were run under an atmosphere of nitrogen unless otherwise stated. Dry solvents were prepared according to the standard procedures. Anhydrous magnesium sulfate was used for drying solutions. Thin-layer chromatography (TLC) was carried out on Merck glass plates precoated with silica gel 60F-254 (0.25 mm).

3,4-Epoxy-2-pentanol (4). 3,4-Epoxy-2-pentanone[11] (**3**, 5.6 g, 56 mmol) was added to a cold (−78 °C) suspension of zinc perchlorate hexahydrate (23.5 g, 63 mmol) in dry ether (50 ml) and stirred for 10 min. Sodium borohydride (2.2 g, 58 mmol) was added all at once and the mixture was stirred vigorously at −78 °C for 1 h and at −78—0 °C for 1 h. The reaction was quenched carefully by the dropwise addition of saturated aqueous $NaHCO_3$ at 0 °C. The precipitate was filtered and washed well with ether. The combined ether solution was washed with saturated aqueous $NaHCO_3$, dried, and concentrated. The crude product was distilled to give **4** (4.4 g, 77%) as an oil: Bp 66—69 °C/2666 Pa; ^{1}H NMR (90 MHz) δ=1.25 (3H, d, J=6.4 Hz), 1.34 (3H, d, J=5.1 Hz), 2.73 (1H, dd, J=3.9 and 2.6 Hz), 3.07 (1H, dq, J=2.6 and 5.4 Hz), 3.18 (1H, broad s), and 3.86 (1H, dq, J=3.9 and 6.4 Hz); ^{13}C NMR δ=17.04, 18.69, 51.28, 62.55, and 65.07. This alcohol proved to be >95% pure *erythro*-**4** by the comparison of its ^{13}C NMR spectrum with that of an authentic mixture of the *erythro*- and the *threo*-epoxy alcohol which was obtained by sodium borohydride reduction of epoxy ketone (**3**) in methanol according to the literature.[12] *threo*-**4**: ^{13}C NMR δ=18.69, 19.42, 52.50, 63.50, and 67.36.

Gas chromatographic analysis (SE-30) of the acetate of **4** also showed the same purity of *erythro*-isomer. Retention time at 75 °C (column temp): *erythro*-**4**, 2.8 min; *threo*-**4**, 3.6 min.

2-(2-Methoxyethoxymethoxy)-3,4-epoxypentane (5). MEM chloride (2.22 ml, 19.4 mmol) was added dropwise to a cold (0 °C) solution of **4** (1.8 g, 17.6 mmol) and *N,N*-diisopropylethylamine (3.69 ml, 21.2 mmol) in methanol-free dichloromethane (18 ml) and the mixture was stirred at room temperature for 20 h. The solvent was evaporated in vacuo and the crude product was extracted with ether, washed successively with saturated aqueous NaCl, 3% aqueous phosphoric acid, and saturated aqueous $NaHCO_3$, dried, concentrated, and distilled to give **5** (2.69 g, 80%): A colorless oil; Bp 65 °C/400 Pa; ^{1}H NMR (60 MHz) δ=1.26 (3H, d, J=6.4 Hz), 1.33 (3H, d, J=5.2 Hz), 2.63 (1H, dd, J=4.8 and 2.4 Hz), 2.98 (1H, dq, J=2.4 and 5.4 Hz), 3.38 (3H, s) 3.3—3.9 (5H, m), and 4.73 (2H, s). Found: C, 56.62; H, 9.56%. Calcd for $C_9H_{18}O_4$: C, 56.82; H, 9.54%.

2-(2-Methoxyethoxymethoxy)-4-methyl-5-hexyn-3-ol (6). A mixture of **5** (190 mg, 1.0 mmol) and lithium acetylide-ethylenediamine complex (184 mg, 2.0 mmol) was stirred in a mixture of DMSO-HMPA (1:1, 2 ml) at room temperature for 60 h. After the addition of water (3 ml), the reaction mixture was saturated with NH_4Cl and extracted with diisopropyl ether. The extract was washed with aqueous NH_4Cl and brine, dried, and concentrated. The crude product was purified by preparative TLC (benzene-ethyl acetate, 8:2) to give the *dl*-acetylenic alcohol (**6**, 139 mg, 64%) as a colorless oil: R_f=0.4; ^{1}H NMR (60 MHz) δ=1.20 (3H, d, J=6.6 Hz), 1.32 (3H, d, J=6.6 Hz), 2.10 (1H, d, J=2.7 Hz), 3.40 (3H, s), 3.4—4.3 (6H, m), and 4.80 (2H, s). Found: C, 60.89; H, 9.42%. Calcd for $C_{11}H_{20}O_4$: C, 61.09; H, 9.32%.

Resolution of the *dl*-Alcohol (6). A mixture of the above *dl*-**6**, (2.40 g, 11.1 mmol), (*S*)-(+)-*O*-methylmandelic acid chloride[19] (2.46 g, 13.3 mmol), and 4-dimethylaminopyridine (1.76 g, 14.4 mmol) in dry dichloromethane was stirred at 40 °C for 65 h. The reaction mixture was diluted with ether and the resulting precipitate was filtered. The filtrate was washed successively with 2% aqueous phosphoric acid, saturated aqueous NaCl, and saturated aqueous $NaHCO_3$, dried, and concentrated. The crude mixture of diastereomeric esters was separated by column chromatography on silica gel (Merck) (petroleum ether-ethyl acetate, 9:1).

The less polar ester (1.83 g, 45.2%): A colorless oil; R_f=0.64 (benzene-ethyl acetate, 4:1); $[\alpha]_D^{23}$ +35.6° (*c* 1.41, $CHCl_3$); IR (neat) 3270 and 1750 cm^{-1}; ^{1}H NMR (90 MHz) δ=0.95 (3H, d, J=6.3 Hz), 1.11 (3H, d, J=6.8 Hz), 2.08 (1H, d, J=2.6 Hz), 2.67 (1H, m), 3.37 (3H, s), 3.44 (3H, s), 3.54 (4H, m), 4.02 (1H, m), 4.57 (2H, s), 4.80 (1H, s) 5.07 (1H, dd, J=8.1 and 4.2 Hz), and 7.2—7.6 (5H, m). Found: C, 65.57; H, 7.65%. Calcd for $C_{20}H_{28}O_6$: C, 65.91; H, 7.74%.

The more polar ester (1.69 g, 41.8%): A colorless oil; R_f=0.56 (benzene-ethyl acetate, 4:1); $[\alpha]_D^{23}$ +51.0° (*c* 1.35, $CHCl_3$); ^{1}H NMR (90 MHz) δ=0.79 (3H, d, J=6.0 Hz), 1.18 (3H, d, J=6.3 Hz), 2.00 (1H, d, J=2.6 Hz), 2.48 (1H, m), 3.39 (3H, s), 3.42 (3H, s), 3.63 (4H, m), 4.16 (1H, m), 4.67 (1H, d, J=7.2 Hz), 4.77 (1H, d, J=7.2 Hz), 4.79 (1H, s), 5.08 (1H, dd, J=8.8 and 3.7 Hz), and 7.2—7.6 (5H, m).

The less polar ester (1.839 g, 5.05 mmol) was stirred with NaOH (440 mg, 11 mmol) in methanol-water (1:1, 8.8 ml) at room temperature for 12 h. After the removal of methanol in vacuo and saturation of the solution with NaCl, the crude product was extracted with ethyl acetate, washed with saturated aqueous NaCl, dried, and concentrated to give (−)-**6** (1.036 g, 95%) as a colorless oil: $[\alpha]_D^{23}$ −24.4° (*c* 1.06, $CHCl_3$).

Similarly, the more polar ester was hydrolyzed to give (+)-**6**: $[\alpha]_D^{23}$ +23.1° (*c* 1.34, $CHCl_3$).

Determination of the Absolute Configuration of (+)-and (−)-Alcohol (6). A solution of (+)-**6** (197.4 mg, 0.913 mmol) in ethanol (2 ml) was shaken with platinum oxide (5 mg) at room temperature for 1 h under an atmosphere of hydrogen. After filtration of the catalyst, the filtrate was concentrated in vacuo to give a saturated alcohol (**i**, 191.6 mg, 95.3%) as a colorless oil: $[\alpha]_D^{23}$ +19.0° (*c* 1.16, $CHCl_3$); ^{1} NMR (60 MHz) δ=0.7—1.8 (12H, m), 2.3 (1H, broad s), 3.3—4.1 (6H, m) 3.40 (3H, s), and 4.77 (2H, s).

The alcohol (**i**, 218.1 mg, 0.99 mmol) was heated with 10% hydrochloric acid at 60 °C for 3 h. The reaction mixture was neutralized at 0 °C and then saturated at room temperature with anhydrous K_2CO_3. The crude product was extracted with ether, dried, concentrated, and subjected to preparative TLC (benzene-ethyl acetate, 1:1) to give the diol (**ii**, 75.3 mg, 58%) as a colorless oil: R_f=0.23; $[\alpha]_D^{23}$ −3.9° (*c* 1.28, $CHCl_3$); ^{1}H NMR (60 MHz) δ=0.7—2.0 (12H, m), 2.6 (2H, broad s), 3.40 (1H, dd, J=6.0 and 4.6 Hz), and 3.6—4.1 (1H, m).

A solution of the diol (**ii**, 25.5 mg, 0.19 mmol) in acetone (0.5 ml) was added to a stirred solution of $NaIO_4$ (123.8 mg, 0.58 mmol) in water (0.5 ml). To this mixture was added a solution of $KMnO_4$ (9.1 mg, 0.058 mmol) and K_2CO_3 (16.0 mg, 0.12 mmol) in acetone-water (1:1, 0.8 ml) and the whole mixture was stirred at 12 °C for 12 h. Insoluble material was filtered and washed with acetone. After evaporation of acetone, Na_2SO_3 (200 mg) was added and the mixture was acidified with 10% aqueous sulfuric acid to give a colorless solution, which was saturated with NaCl. The mixture was extracted with dichloromethane, dried, and concentrated to give crude 2-methylbutyric acid (13.8 mg) as a colorless oil. The acid thus obtained was mixed with CsF (44 mg) in acetonitrile (0.5 ml) and refluxed for 10 min. *p*-Phenylphenacyl bromide (58.4 mg) was added to this and the mixture was refluxed for 3 h. The precipitate was filtered and washed with acetone. After removal of solvents, the residue was subjected to preparative TLC (benzene) to give the pure ester (**iii**, 34.6 mg, 60% from the diol, **ii**) as a crystalline solid: R_f=0.30; $[\alpha]_D^{23}$ + 11.0° (*c* 1.73, C_6H_6); ^{1}H NMR (60 MHz) δ=1.01 (3H, t, J=6.9 Hz), 1.27 (3H, d, J=7.1 Hz), 1.4—2.0 (2H, m), 2.3—2.9 (1H, m), 5.37 (2H, s), and 7.3—8.2 (9H, m).

This ester (**iii**), upon hydrolysis, gave (*S*)-(+)-2-methylbutyric acid: $[\alpha]_D^{23}$ +25.2° (*c* 0.60, H_2O). Lit,[20] $[\alpha]_D^{21.2}$ +19.3° (neat).

(−)-**6** was also converted into the corresponding *p*-phenylphenacyl 2-methylbutyrate in the same manner: $[\alpha]_D^{23}$ −7.6° (*c* 1.06, C_6H_6). Lit,[14] $[\alpha]_D^{23}$ −4°.

4-*t*-Butyldimethylsiloxy-5-(2-methoxyethoxymethoxy)-3-methyl-1-hexyne (7). A mixture of (−)-**6** (1.03 g, 4.77 mmol), TBDMS chloride (1.44 g, 9.55 mmol), imidazole (1.30 g, 19.1 mmol), and dry DMF (5 ml) was stirred at room temperature for 65 h. After removal of solvent under reduced pressure the crude product was extracted with ethyl acetate, washed successively with 3% aqueous hydrochloric acid, saturated aqueous NaCl, and saturated aqueous $NaHCO_3$. Organic layer was dried and concentrated in vacuo to give the practically pure silyl ether (**7**, 1.55 g, 98.4%). Analytical sample was prepared by preparative TLC. A colorless oil; R_f=0.65 (benzene-ethyl acetate, 9:1); $[\alpha]_D^{23}$ −2.0° (*c* 1.01, $CHCl_3$); ^{1}H NMR (90 MHz) δ=0.09 (6H, s), 0.90 (9H, s), 1.14 (3H, d, J=6.3 Hz), 1.21 (3H, d, J=7.2 Hz), 2.07 (1H, d, J=2.6 Hz), 2.48 (1H, m), 3.39 (3H, s), 3.4—3.9 (5H, m), 4.06 (1H, dq, J=6.3 and 3.1 Hz), and 4.74 (2H, s). Found: C, 61.79; H, 10.34%. Calcd for $C_{17}H_{34}O_4Si$: 61.77; H, 10.37%.

Methyl (2*R*,3*S*,4*S*,6*R*,7*S*,10*R*,11*S*,12*R*)-11-*t*-Butyldimethylsiloxy-3,7-epoxy-7-hydroxy-12-(2-methoxyethoxymethoxy)-2,4,6,10-tetramethyl-8-tridecynoate and Its C-7 Epimer (9). A lithium acetylide solution was prepared from (−)-**7** (258 mg, 0.78 mmol) and butyllithium in hexane (1.6 mol

dm^{-3}, 819 μl) by stirring in dry THF (0.8 ml) at room temperature for 1 h. This solution was added dropwise to a cold (−20 °C) solution of (+)-Prelog-Djerassi lactonic acid methyl ester (**8**, 152 mg, 0.709 mmol) in THF (1.4 ml) and the reaction temperature was raised gradually to 0 °C over a period of 1 h. The reaction was quenched by the addition of saturated aqueous NH_4Cl. After evaporation of THF, the crude product was extracted with ethyl acetate, washed with saturated aqueous $NaHCO_3$, dried, and concentrated. The concentrate was subjected to preparative TLC (benzene–ethyl acetate, 3:1) to give a ca. 3.5:1 mixture of hemiacetals (**9**, 348 mg, 90%) as a colorless oil: IR (neat) 3350, 2200, and 1720 cm^{-1}; ^1H NMR[21] (90 MHz) δ=0.09 (3H, s), 0.10 (3H, s), 0.91 (9H, s), 3.38 (3H, s), 3.69 (3H, s), 4.68 (1H, d, J=7.2 Hz), and 4.78 (1H, d, J=7.2 Hz). Found: C, 61.68; H, 9.75%. Calcd for $C_{28}H_{52}O_8Si$: C, 61.73; H, 9.62%. The mixture was used for the next step without separation.

Methyl (2*R*,3*S*,4*S*,6*R*,7*R*,10*R*,11*S*,12*R*)-11-*t*-Butyldimethylsiloxy-3,7-epoxy-7-methoxy-12-(2-methoxyethoxymethoxy)-2,4,6,10-tetramethyl-8-tridecynoate and Its C-7 Epimer (10). A mixture of hemiacetals (**9**, 544 mg, 1.0 mmol) and *p*-toluenesulfonic acid monohydrate (9.7 mg, 0.05 mmol) in methanol (2.4 ml) was stirred at room temperature for 2 h. Saturated aqueous $NaHCO_3$ was added and methanol was removed in vacuo. The crude product was extracted with ethyl acetate, washed with saturated aqueous $NaHCO_3$, dried, and concentrated to give a practically pure mixture of C-7 epimeric methyl acetals (**10**, 550 mg, 98%), which were difficult to separate. The relative intensity of the protons of anomeric methoxyl groups at C-7 in NMR (90 MHz) spectrum was 3.5 (axial, δ=3.25):1 (equatorial, δ=3.35). Analytical sample was prepared by preparative TLC. A colorless oil: R_f=0.71 (benzene–ethyl acetate, 3:1). Found: C, 62.18; H, 9.67%. Calcd for $C_{29}H_{54}O_8Si$: C, 62.33; H, 9.74%.

Methyl (2*R*,3*S*,4*S*,6*R*,7*S*,10*R*,11*S*,12*R*)-11-*t*-Butyldimethylsiloxy-7,12-bis(2-methoxyethoxymethoxy)-3,7-epoxy-2,4,6,10-tetramethyl-8-tridecynoate and Its C-7 Epimer (11). A solution of **9** (458 mg, 0.84 mmol), MEM chloride (384 μl, 3.36 mmol), and *N*,*N*-diisopropylethylamine (644 μl, 3.70 mmol) in methanol-free dry dichloromethane (3.5 ml) was stirred at room temperature for 60 h. After removal of solvent, the crude product was extracted with ethyl acetate, washed with water, 3% aqueous phosphoric acid, brine, and saturated aqueous $NaHCO_3$. Organic layer was dried and concentrated to give a crude C-7 epimeric mixture of the MEM hemiacetals (**11**). The mixture was separated by preparative TLC (benzene–ethyl acetate, 3:1). The less polar zone gave the C-7 equatorial OMEM hemiacetal (384 mg, 72%) as a colorless oil: R_f=0.55; ^1H NMR (90 MHz) δ=0.08, 0.09, and 0.10 (6H, each s), 0.61 (3H, d, J=6.3 Hz), 0.91 (9H, s), 0.94 (3H, d, J=6.4 Hz), 1.11 (3H, d, J=6.1 Hz), 1.18 (3H, d, J=6.4 Hz), 1.26 (3H, d, J=7.0 Hz), 3.37 (3H, s), 3.38 (3H, s), 3.68 (3H, s), 4.73 (2H, s), and 4.94 (2H, s). Found: C, 60.97; H, 9.43%. Calcd for $C_{32}H_{60}O_{10}Si$: C, 60.73; H, 9.56%. The more polar zone gave C-7 axial OMEM hemiacetal (96 mg, 18%) as a colorless oil: R_f=0.41; ^1H NMR (90 MHz) δ=0.10 (6H, s), 0.90 (9H, s), 2.4—3.0 (2H, m), 3.3—4.1 (11H, m), 3.38 (6H, s), 3.68 (3H, s), 4.71 (2H, s), and 4.73 (2H, s).

Methyl (2*R*,3*S*,4*S*,6*R*,7*S*,10*R*,11*S*,12*R*)-3,7-Epoxy-11-hydroxy-7-methoxy-12-(2-methoxyethoxymethoxy)-2,4,6,10-tetramethyl-8-tridecynoate and Its C-7 Epimer (12). A solution of **10** (an epimeric mixture, 217 mg, 0.389 mmol) in dry THF (0.5 ml) was stirred with a THF solution of tetrabutylammonium fluoride (1 mol dm^{-3}, 1.93 ml, 0.82 mmol) at room temperature for 1.5 h. The reaction mixture was neutralized by the addition of saturated aqueous NH_4Cl. After removal of THF under reduced pressure, the crude product was extracted with ethyl acetate, washed with saturated aqueous $NaHCO_3$, dried, and concentrated. Purification by preparative TLC (benzene–ethyl acetate, 1:1) gave the alcohol (**12**, 147 mg, 85%, R_f=0.50) as a ca. 3.3 (axial OMe) : 1 (equatorial OMe) mixture of hemiacetals which were difficult to separate.

Methyl (2*R*,3*S*,4*S*,6*R*,7*S*,10*R*,11*S*,12*R*)-3,7-Epoxy-11-hydroxy-7,12-bis(2-methoxyethoxymethoxy)-2,4,6,10-tetramethyl-8-tridecynoate (13). To a stirred solution of **11** (the equatorial C-7 OMEM epimer, 344 mg, 0.544 mmol) in dry THF (1 ml) was added a tetrabutylammonium fluoride solution in THF (1 mol dm^{-3}, 2.14 ml) and the mixture was stirred at room temperature for 7 h. Similar workup as described above for desilylation of silyl ether (**10**) followed by preparative TLC (benzene–ethyl acetate, 1:1) of the crude product gave **13** (261 mg, 93%) as a colorless oil: R_f=0.43; ^1H NMR (90 MHz) δ=0.82 (3H, d, J=6.1 Hz), 0.94 (3H, d, J=6.6 Hz), 1.12 (3H, d, J=7.2 Hz), 1.26 (3H, d. J=6.1 Hz), 1.30 (3H, d, J=7.0 Hz), 2.46—2.94 (2H, m), 3.38 (3H, s), 3.40 (3H, s), 3.68 (3H, s), 4.78 (2H, m), 4.85 (1H, d, J=6.3 Hz), and 5.05 (1H, d, J=6.3 Hz). Found: C, 59.84; H, 8.85%. Calcd for $C_{26}H_{46}O_{10}$: C, 60.21, H, 8.94%.

(2*R*,3*S*,4*S*,6*R*,7*S*,10*R*,11*S*,12*R*)-3,7-Epoxy-11-hydroxy-7-methoxy-12-(2-methoxyethoxymethoxy)-2,4,6,10-tetramethyl-8-tridecynoic Acid and Its C-7 Epimer (14). An epimeric mixture of **12** (277 mg, 0.624 mmol), aqueous NaOH (1 mol dm^{-3}, 940 μl) and methanol (940 μl) was stirred at room temperature for 12 h. After removal of methanol under reduced pressure the crude product was diluted with a small amount of water and washed with ether. The aqueous alkaline layer was acidified (pH≈4) with 3% aqueous phosphoric acid. The organic acid was extracted with ethyl acetate, washed with saturated aqueous NaCl, dried, and concentrated to give **14** (263 mg, 98%) as a viscous oil. Anomeric isomers ratio was ca. 3 (axial OMe, δ=3.30) : 1 (equatorial OMe, δ=3.37).

(2*R*,3*S*,4*S*,6*R*,7*S*,10*R*,11*S*,12*R*)-3,7-Epoxy-11-hydroxy-7,12-bis(2-methoxyethoxymethoxy)-2,4,6,10-tetramethyl-8-tridecynoic Acid (15). A mixture of **13** (166.5 mg, 0.32 mmol), aqueous NaOH (1 mol dm^{-3}, 482 μl), and methanol (482 μl) was stirred at room temperature for 12 h. Usual workup as described above for saponification of **12** gave the hydroxy acid (**15**, 157 mg, 97%) as a viscous oil, which was dried over P_2O_5 under vacuum at 50 °C for 40 h. ^1H NMR (90 MHz) δ=0.84 (3H, d, J=6.1 Hz), 0.94 (3H, d, J=6.3 Hz), 1.12 (3H, d, J=6.8 Hz), 1.19 (3H, d, J=6.1 Hz), 1.35 (3H, d, J=6.8 Hz), 3.37 (3H, s), 3.40 (3H, s), 4.84 (2H, s), and 4.99 (2H, s).

(1*S*,2*R*,5*S*,6*R*,9*S*,10*R*,12*S*,1′*R*)-4,13-Dioxa-9-methoxy-5-[1-(2-methoxyethoxymethoxy)ethyl]-2,6,10,12-tetramethylbicyclo[7.3.1]tridec-7-yn-3-one (16). 2,4,6-Trichlorobenzoyl chloride[22] (90.9 μl, 0.566 mmol) was added to a solution of **14** (243.4 mg, 0.566 mmol) and triethylamine (85.8 μl, 0.679 mmol) in dry THF (1.5 ml). The mixture was stirred at room temperature for 4 h and then filtered through a Celite column. The filtrate was diluted with dry benzene (420 ml)

and added to a refluxing solution of 4-dimethylaminopyridine (414 mg, 340 mmol) in benzene (150 ml) over 24 h. After additional refluxing for 1 h the reaction mixture was washed successively with water, 3% aqueous phosphoric acid, saturated aqueous NaCl, and saturated aqueous $NaHCO_3$. Organic layer was dried and concentrated to give the crude product (219 mg), which was subjected to preparative TLC (benzene-ethyl acetate, 3:1). The bicyclic lactone (**16**, 28 mg, 12%): A coloress oil: R_f=0.60; $[\alpha]_D^{25}$ +5.64° (*c* 1.24, $CHCl_3$); ^1H NMR (90 MHz) δ=0.86 (3H, d, *J*=6.4 Hz), 0.89 (3H, d, *J*=6.3 Hz), 1.11 (3H, d, *J*=7.0 Hz), 1.24 (3H, d, *J*=5.1 Hz), 1.31 (3H, d, *J*=6.6 Hz), 2.6—3.2 (2H, m), 3.39 (6H, s), 3.4—4.0 (5H, m), 4.34 (1H, dd, *J*=10.3 and 2.2 Hz), 4.69 (1H, d, *J*=7.2 Hz), 4.83 (1H, dd, *J*=9.2 and 2.6 Hz), and 4.85 (1H, d, *J*=7.2 Hz). An elimination product (**18**, 26 mg, 12%): A colorless oil: R_f=0.53; $[\alpha]_D^{25}$ +97.3° (*c* 1.13, $CHCl_3$): IR ($CHCl_3$) 2200, 1700, and 1670 cm^{-1}; ^1H NMR (90 MHz) δ=1.07 (3H, d, *J*=6.8 Hz), 1.10 (3H, d, *J*=6.6 Hz), 1.33 (3H, d, *J*=6.1 Hz), 1.40 (3H, d, *J*=7.0 Hz), 1.87 (3H, d, *J*=1.3 Hz), 3.39 (3H, s), 4.72 (1H, d, *J*=7.2 Hz), 4.83 (1H, dd, *J*=3.5 and 7.4 Hz), 4.84 (1H, d, *J*=7.2 Hz), and 6.94 (1H, dq, *J*=10.9 and 1.3 Hz).

(1*S*,2*R*,5*S*,6*R*,9*S*,10*R*,12*S*,1′*R*)-4,13-Dioxa-9-(2-methoxyethoxymethoxy)-5-[1-(2-methoxyethoxymethoxy)ethyl]-2,6,10,12-tetramethylbicyclo[7.3.1]tridec-7-yn-3-one (17). 2,4,6-Trichlorobenzoyl chloride (50.0 µl, 0.311 mmol) was added to a solution of **15** (156.9 mg, 0.311 mmol) and triethylamine (47.1 µl, 0.342 mmol) in anhydrous THF (1 ml). After stirring at room temperature for 3 h, the resulting precipitate was filtered though a Celite column. The filtrate was diluted with dry benzene (150 ml) and added to a refluxing solution of 4-dimethylaminopyridine (227.6 mg, 1.87 mmol) in benzene (50 ml) over 20 h. Similar workup as described above for the lactonization of **14** gave the crude product (160.4 mg), which was subjected to preparative TLC (benzene-ethyl acetate, 3:1). The bicyclic lactone (**17**, 50.2 mg, 33.2%): A colorless oil: R_f=0.25; $[\alpha]_D^{25}$ +17.2° (*c* 0.29, $CHCl_3$): ^1H NMR (90 MHz) δ=0.85 (3H, d, *J*=5.6 Hz), 0.92 (3H, d, *J*=5.9 Hz), 1.08 (3H, d, *J*=7.0 Hz), 1.23 (3H, d, *J*=5.9 Hz), 1.30 (3H, d, *J*=6.3 Hz), 2.5—3.2 (2H, m), 3.39 (6H, s), 3.4—4.0 (8H, m), 4.36 (1H, dd, *J*=10.1 and 2.3 Hz), 4.68 (1H, d, *J*=7.2 Hz), 4.82 (1H, dd, *J*=9.0 and 2.6 Hz), 4.84 (1H, d, *J*=7.2 Hz), 4.93 (1H, d, *J*=5.9 Hz), and 5.06 (1H, d, *J*=5.9 Hz). Found: C, 61.65; H, 8.68%. Calcd for $C_{25}H_{42}O_9$: C, 61.70; H, 8.70%. The elimination product (**18**, 10.0 mg, 8.5%) was also isolated.

7,8-Didehydro-12-*O*-(2-methoxyethoxymethyl)neomethynolide (19) and 7,8-Didehydroneomethynolide (20). $ZnBr_2$ (42.8 mg, 0.19 mmol) was added to a solution of **17** (18.4 mg, 0.038 mmol) in dry dichloromethane (5 ml) and the mixture was subjected to ultrasonication at room temperature for 1 h. Another portion of $ZnBr_2$ (42.8 mg) was added and treated in a ultrasonic bath for 1 h. This procedure was repeated twice and then the mixture was further stirred at room temperature for 12 h. Saturated aqueous $NaHCO_3$ was added and the crude product was extracted with ethyl acetate, washed with saturated aqueous NaCl, dried, and concentrated. The concentrate was subjected to preparative TLC (benzene-ethyl acetate, 1:1) to give 8,9-didehydroneomethynolide (**20**) and its 12-*O*-MEM ether (**19**). **20**: colorless needles (5.5 mg, 44%): R_f=0.45; Mp 74—76 °C (monohydrate); $[\alpha]_D^{24}$ +27.0° (*c* 0.223, MeOH); IR ($CHCl_3$) 2200, 1725, 1660, and 1210 cm^{-1}; UV (EtOH) 220 nm (log ε=4.27); ^1H NMR (90 MHz) δ=0.97 (3H, d, *J*=6.3 Hz), 1.17 (3H, d, *J*=6.8 Hz), 1.22 (3H, d, *J*=6.1 Hz), 1.36 (6H, d, *J*=7.0 Hz), 3.24 (1H, m), 3.65 (1H, broad d, *J*=9.6 Hz), 3.86 (1H, m), and 5.03 (1H, dd, *J*=9.0 and 3.1 Hz); MS *m/z* 310 (M-18). Found: C, 62.21; H, 8.46%. Calcd for $C_{17}H_{26}O_5 \cdot H_2O$: C, 62.17; H, 8.59%.

19: A colorless oil (5.8 mg, 38%): R_f=0.59; $[\alpha]_D^{24}$ +15.5° (*c* 0.517, MeOH); ^1H NMR (90 MHz) δ=0.97 (3H, d, *J*=6.6 Hz), 1.16 (6H, d, *J*=6.3 Hz), 1.33 (3H, d, *J*=7.0 Hz), 1.35 (3H, d, *J*=6.6 Hz), 3.18 (1H, m), 3.39 (3H, s), 4.69 (1H, d, *J*=7.2 Hz), 4.83 (1H, d, *J*=7.2 Hz), and 5.11 (1H, dd, *J*=9.0 and 2.6 Hz).

19 (9 mg, 0.0226 mmol) and $ZnBr_2$ (127 mg, 0.564 mmol) were stirred in dichloromethane-nitromethane (10:1, 2.2 ml) at room temperature for 8 h. Similar workup as above followed by preparative TLC gave **20** (4.5 mg, 60%) and the starting **19** (1.5 mg, 17%).

8,9-Didehydroneomethynolide (20) from 16. A solution of **16** (8.8 mg, 0.0213 mmol) and trifluoroacetic acid (88 µl) in dry dichloromethane (8.8 ml) was stirred at room temperature for 14 h. Saturated aqueous $NaHCO_3$ was added and the crude product was extracted with ethyl acetate, washed with water, dried, and concentrated. The concentrate was subjected to preparative TLC (benzene-ethyl acetate, 1:1) to give **20** (1.1 mg, 16%) and **19** (5.2 mg, 61%).

Neomethynolide (1) Monohydrate. To a stirred solution of **20** (7.0 mg, 0.022 mmol) in absolute DMF (700 µl) was added an aqueous solution of chromium(II) sulfate[18] (1 mol dm^{-3}, 700 µl) and the mixture was stirred at room temperature for 10 h. The resulting deep green solution was saturated with ammonium sulfate, extracted with ethyl acetate, washed with saturated aqueous NaCl, dried, and concentrated in vacuo. The crude product was subjected to preparative TLC (benzene-ethyl acetate, 1:1) to give neomethynolide (**1**, 4.6 mg, 65%, R_f=0.28). Crystallization from acetone-hexane mixture gave colorless needles: Mp 92—93 °C (monohydrate) $[\alpha]_D^{24}$ +112.5° (*c* 0.160, MeOH); IR ($CHCl_3$) 1725, 1685, 1625, and 1215 cm^{-1}; UV (EtOH) 227 nm (log ε=4.08); ^1H NMR (90 MHz) δ=0.9—1.4 (15H, m), 3.57 (1H, broad d, *J*=10.7 Hz), 3.89 (1H, m), 4.83 (1H, dd, *J*=9.2 and 2.4 Hz), 6.42 (1H, dd, *J*=15.8 and 0.9 Hz), and 6.79 (1H, dd, *J*=15.8 and 5.0 Hz). Found: C, 61.54; H, 9.17%. Calcd for $C_{17}H_{28}O_5 \cdot H_2O$: C, 61.79; H, 9.15%. Found: *m/z* 312.1931. Calcd for $C_{17}H_{28}O_5$: M, 312.1935. Lit,[3c] Mp 90—120 °C (monohydrate); $[\alpha]_D$ +108° ($CHCl_3$); IR($CHCl_3$) 2.93, 5.75, 5.90, and 6.10 µ; UV (EtOH) 227.5 nm (log ε=4.10).

Neomethynolide Diacetate. This was prepared from **1** (monohydrate) and acetic anhydride in the presence of 4-dimethylaminopyridine. Colorless needles (acetone-hexane): Mp 198—199 °C; $[\alpha]_D^{25}$ +82° (*c* 0.123, MeOH); IR ($CHCl_3$) 1740, 1690, 1630, and 1240 cm^{-1}; ^1H NMR (90 MHz) δ=0.8—1.4 (15H, m), 2.08 (3H, s), 2.09 (3H, s), 4.9—5.3 (3H, m), 6.4 (1H, dd, *J*=5.5 and 0.9 Hz), and 6.76 (1H, dd, *J*=5.5 and 4.8 Hz); MS *m/z* 396 (M^+). Found: C, 63.53; H, 8.17%. Calcd for $C_{21}H_{32}O_7$: C, 63.61; H, 8.14%. Lit,[3c] Mp 199—201 °C; $[\alpha]_D$ +84° ($CHCl_3$); IR ($CHCl_3$) 5.71, 5.88, and 6.08 µ.

The authors are grateful to Dr. Akio Kinumaki of Microbiological Reseach Laboratory, Tanabe Seiyaku Company Ltd. for the generous supply of NMR data

of natural neomethynolide. This work was partially supported by a grant-in-Aid for Scientific Research No. 443008 from the Ministry of Education, Science and Culture.

References

1) J. Inanaga, Y. Kawanami, and M. Yamaguchi, *Chem. Lett.*, **1981**, 1415.

2) A. Kinumaki and M. Suzuki, *J. Chem. Soc., Chem. Commun.*, **1972**, 744.

3) a) C. Djerassi and O. Halpern, *J. Am. Chem. Soc.*, **79**, 2022 (1957); b) C. Djerassi and O. Halpern, *J. Am. Chem. Soc.*, **79**, 3926 (1957); c) C. Djerassi and O. Halpern, *Tetrahedron*, **3**, 255 (1958).

4) I. Maezawa, A. Kinumaki, and M. Suzuki, *J. Antibiot.*, **27**, 84 (1974).

5) R. W. Rickards and R. M. Smith, *Tetrahedron Lett.*, **1970**, 1025.

6) Total absolute configuration: Reference 3, 4, and D. G. Manwaring, R. W. Rickards, and R. M. Smith, *Tetrahedron Lett.*, **1970**, 1029.

7) J. Inanaga, T. Katsuki, S. Takimoto, S. Ouchida, K. Inoue, A. Nakano, N. Okukado, and M. Yamaguchi, *Chem. Lett.*, **1979**, 1021.

8) J. Inanaga, A. Takeda, N. Okukado, and M. Yamaguchi, *Mem. Fac. Sci., Kyushu Univ., Ser. C, Chem.*, **9**, 293 (1975).

9) For condensations of lithium acetylides and lactones: see J. C. Chabala and J. E. Vincent, *Tetrahedron Lett.*, **1978**, 937.

10) J. Inanaga, K. Hirata, H. Saeki, T. Katsuki, and M. Yamaguchi, *Bull. Chem. Soc. Jpn.*, **52**, 1989 (1979).

11) I. G. Tishchenco, A. A. Akhrem, and I. N. Nazarov, *Zh. Obschei Khim.*, **29**, 809 (1959).

12) J. L. Pierre and P. Chautemps, *Tetrahedron Lett.*, **1972**, 4371; P. Chautemps and J. L. Pierre, *Tetrahedron*, **32**, 549 (1976).

13) While the present study was in progress, a general, highly stereoselective reduction of α,β-epoxy ketones to *erythro*-epoxy alcohols by using $Zn(BH_4)_2$ in ether was reported: T. Nakata, T. Tanaka, and T. Oishi, *Tetrahedron Lett.*, **22**, 4723 (1981). We are gratefull to Dr. Oishi for his kind information on their results prior to publication.

14) D. H. Calam and D. A. H. Taylor, *J. Chem. Soc. (C)*, **1966**, 949.

15) A. Nakano, S. Takimoto, J. Inanaga, T. Katsuki, S. Ouchida, K. Inoue, M. Aiga, N. Okukado and M. Yamaguchi, *Chem. Lett.*, **1979**, 1019. See also Ref. 7.

16) For example: R. U. Lemieux, A. A. Pavia, J. C. Martin, and K. A. Watanabe, *Can. J. Chem.*, **47**, 4427 (1969).

17) Indicated chemical shifts were assigned to methylene protons between two oxygens of anomeric OMEM groups.

18) C. E. Castro, *J. Am. Chem. Soc.*, **83**, 3262 (1961); C. E. Castro and R. D. Stephens, *ibid.*, **86**, 4358 (1964).

19) E. J. Corey, P. B. Hopkins, S. Kim, S. Yoo, K. P. Nambiar, and J. R. Falck, *J. Am. Chem. Soc.*, **101**, 7131 (1979).

20) G. Odham, *Arkiv för Kemi*, **20**, 507 (1963).

21) Some characteristic peaks of major isomer were indicated.

22) R. C. Fuson, J. W. Bertetti, and Wm. E. Ross, *J. Am. Chem. Soc.*, **54**, 4380 (1932). Recently a very facile preparation of 2,4,6-trichlorobenzoic acid has been reported: M. A. Sutter and D. Seebach, *Liebigs Ann. Chem.*, **1983**, 939. We further modified the latter method as follows giving a higher yield: To a cold solution of 1,3,5-trichlorobenzene (290 mg, 1.6 mmol) in dry THF (10 ml) at −78 °C was added slowly a hexane solution of *n*-BuLi (1.63 mol dm^{-3}, 1.0 ml) and the mixture was stirred for 2 h at the same temperature. Dry carbon dioxide was bubbled in over 15 min at −78 °C and then the cooling bath was removed. Gas evolution started around 0 °C. After stirring for 30 min at room temperature, solvent was evaporated. The resulting solid was dissolved in water and washed with ether. The aqueous layer was saturated with NaCl and acidified by the addition of aqueous HCl (5 mol dm^{-3}). The product was extracted with ether, dried over anhydrous Na_2SO_4, and concentrated to give the acid as white crystalline solid (343 mg, 95%). The sample had an enough purity (^1H NMR) for the conversion to the corresponding acid chloride.

The Effect of Triple-Ion Formation on the Electron-Exchange Reaction Rate between Quinone and Semiquinone Anion Radical

Tsuyoshi TAKIGUCHI,† Kosaku SUGA,* and Shigeru AOYAGUI
Department of Chemical Engineering, Tokyo Institute of Technology,
Ohokayama, Meguro-ku, Tokyo 152
(Received October 23, 1985)

The rate constant and activation parameters of electron-exchange reactions between duroquinone, *p*-benzoquinone and 2,5-di-*t*-butyl-*p*-benzoquinone and their respective semiquinone anions which form ion-pairs or triple-ions with Na^+ and K^+ were determined. The rate constants of triple-ions were smaller than those of corresponding ion-pairs; the rate constants of potassium ion pairs and triple-ions were larger than those of the corresponding sodium aggregates; and the rate constants of triple-ions decreased upon increasing the size of the substituent for quinone. These results were explained on the basis of a mechanism which is generally accepted for electron-exchange reactions of ion pairs of anion radicals.

Although a considerable amount of work concerning the rates of electron-exchange reactions between aromatic compounds and their anion radicals, forming ion pairs, have been published, few results have been reported for anion radicals forming triple-ions.[1] Szwarc et al. compared the rate constant of the electron-exchange reaction for a duroquinone (DQ)/duroquinone anion (DQ^-) ion-pair system with that for a DQ/DQ^- triple-ion system.[1] Their results, unfortunately, only showed that the conversion of the ion-pair into the triple-ion influenced the rate of the electron-exchange reaction very little.

In the present work, we report on systematic measurements of the rate constants and activation parameters of electron-exchange reactions between DQ, *p*-benzoquinone (BQ), and 2,5-di-*t*-butyl-*p*-benzoquinone (2,5-DBBQ) and their respective semiquinone anions which form ion pairs or triple-ions with Na^+ and K^+ ions. We also examine whether the mechanism is applicable to the case of triple-ions which is generally accepted for the electron exchange of ion-pairs of anion radicals.[2,3]

Experimental

BQ was purified by sublimation. Commercial 2,5-DBBQ, 2,6-DBBQ, DQ, and sodium tetraphenylborate (NaTPhB) were used as obtained. Potassium tetraphenylborate (KTPhB) was prepared by a double decomposition of NaTPhB and potassium chloride. Tetrahydrofuran (THF) was purified in the same way as previously described.[4] Semiquinone anion radicals (Q^-) were prepared in vacuo by reducing their parent molecules (Q) with an anthracene anion radical. Solutions of triple ions were prepared by adding a weighed amount of dry alkali metal tetraphenylborate into the solutions of Q^- ion pairs. The rate constants of electron-exchange reactions were determined from the broadening of ESR spectra peaks which did not overlap each other. When direct measurements of line widths were difficult because of overlapping, rate constants were determined by computer simulation using a modified Bloch equation. X-band ESR spectra were recorded on a JEOL FE3X1 ESR spectrometer equipped with a variable-temperature adapter.

Results and Discussion

In Figs. 1 and 2, as tentative examples, we show the ESR Spectra for solutions of sodium ion-pair of DQ^- ($DQ^-\cdot Na^+$) and the sodium triple-ion of DQ^- ($DQ^-\cdot Na_2^{2+}$) containing different amounts of DQ at room temperature. The parameters for the ESR spectra of ion pairs and triple-ions measured in this

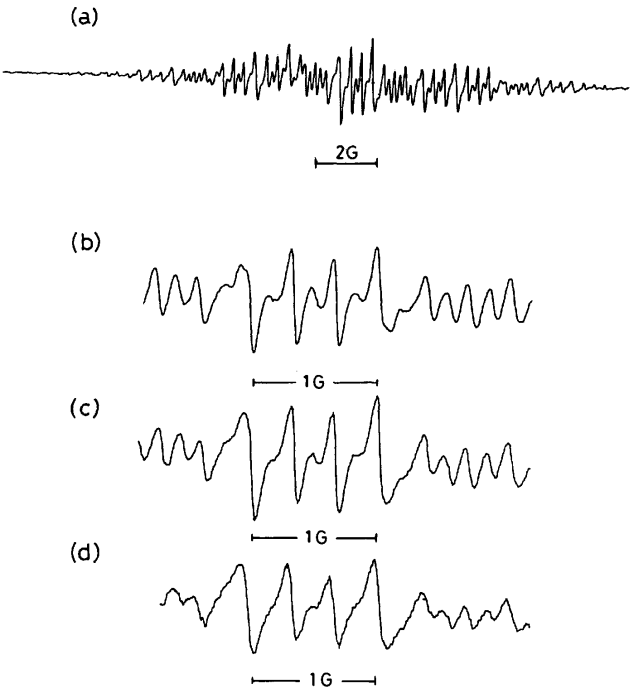

Fig. 1. ESR spectra for the ion-pair of DQ^- with sodium cation ($DQ^-\cdot Na^+$) in THF at 25 °C: (a) the whole spectrum; (b)—(d) central parts of the spectra in the presence of 0 mM, 0.67 mM, and 1.34 mM DQ respectively.

† Present address: Department of Electronic Chemistry, Graduate School of Nagatuta, Tokyo Institute of Technology, Nagatuta, Midori-ku, Yokohama 227.

experiment generally coincided with the values from the literatures.[5,6,7] In all cases, the line width of the ESR spectrum increased with the amounts of DQ as shown in Fig. 1 (b)—(d) and Fig. 2 (b)—(d). The rate constants and activation parameters obtained are shown in Table 1, where $Q^-\cdot M^+$ and $Q^-\cdot M_2^{2+}$ represent ion-pair and triple-ion, respectively. The free energy (ΔG^*), enthalpy (ΔH^*) and entropy (ΔS^*) of activation were determined by the use of Marcus' equation.

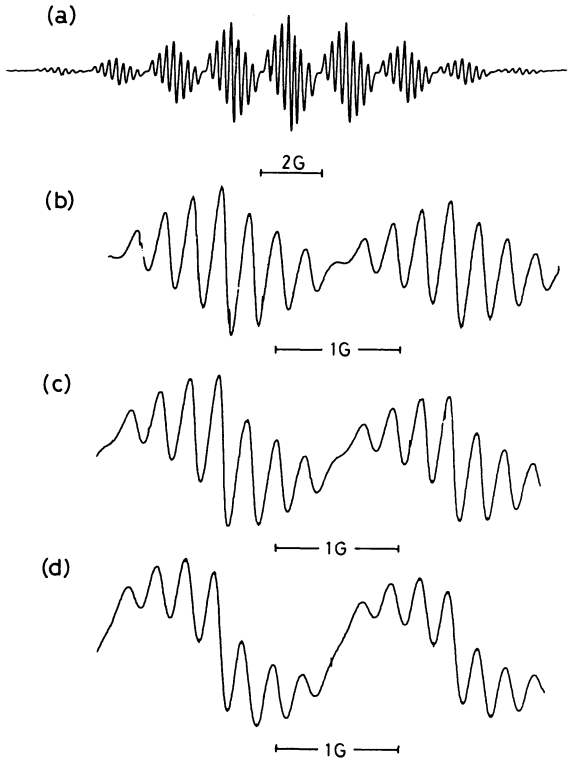

Fig. 2. ESR spectra for the triple-ion of DQ^- with sodium cations ($DQ^-\cdot Na_2^{2+}$) in THF containing 3.5 mM NaTPhB at 25 °C: (a) the whole spectrum; (b)—(d) the central parts of the spectra in the presence of 0 mM, 2.5 mM, and 5.0 mM DQ respectively.

The value of the rate constant for $DQ^-\cdot Na_2^{2+}/DQ$ listed in Table 1 agreed well with that reported by Szwarc et al.: $k=8.7\times10^7$ M^{-1} s^{-1}.[1] However, they have only showed that the rate constant for $DQ^-\cdot Na_2^{2+}/DQ$ was little different from k for $DQ^-\cdot Na^+$ in contrast to our results.

The results listed in Table 1 have the following marked trends without exceptions: (a) The rate constants for triple-ions are smaller than those for ion-pairs; (b) the rate constants for potassium ion-pairs and triple-ions are larger than those for the corresponding sodium aggregates respectively; (c) ΔG^* of $Q^-\cdot M_2^{2+}$ increases with the size of substituents of Q, and this tendency is more prominent in $Q^-\cdot Na_2^{2+}$ than in $Q^-\cdot K_2^{2+}$.

On the other hand, the activation parameters of these electron-transfer reactions, except ΔG^*, have no clear trends like the rate constants or ΔG^*. At present, it is difficult to discuss the contribution of ΔH^* and $-T\Delta S^*$ to ΔG^* in these electron-transfer reactions. Therefore, we will now discuss the trends of the rate constants or ΔG^* described above.

These trends can be explained as follows. According to studies on the electron exchange reactions of ion pairs and triple-ions of anion radicals, it has been concluded that counter cations should transfer simultaneously with electrons.[1,2] Cations which form ion-pairs and triple-ions with semiquinone anions are surrounded by solvation shells and, therefore, a substantial expenditure of energy is needed to reorganize them to make an activated complex with a symmetric configuration before and after an electron-exchange reaction. This energy may contribute to the activation free energy for the

Table 1. Rate Constants and Activation Parameters of Electron-Exchange Reactions between Quinones and Semiquinone Anions in the Form of Ion-Pairs or Triple-Ions

Ion aggregate	$k\times10^{-8}$ a)	ΔG^*	ΔH^*	ΔS^*
	dm^3 mol^{-1} s^{-1}	kJ mol^{-1}	kJ mol^{-1}	J mol^{-1} K^{-1}
$BQ^-\cdot Na_2^{2+}$	3.0	17	14	−10
$BQ^-\cdot K_2^{2+}$	5.3	15	6.2	−30
$DQ^-\cdot Na^+$	4.0	16	8.0	−26
$DQ^-\cdot Na_2^{2+}$	0.9	20	13	−23
$DQ^-\cdot K^+$	9.4	14	14	0
$DQ^-\cdot K_2^{+2}$	4.4	16	13	−11
2,5-DBBQ$^-\cdot Na^+$	0.62	21	16	−19
2,5-DBBQ$^-\cdot Na_2^{2+}$	0.01	30		
2,5-DBBQ$^-\cdot K^+$	1.3	19	13	−20
2,5-DBBQ$^-\cdot K_2^{2+}$	0.48	22	10	−30~−40
2,6-DBBQ$^-\cdot Na^+$	0.43 b)	21		
2,6-DBBQ$^-\cdot K^+$	2.4	18	14	−12

a) At 25 °C. b) At 0 °C.

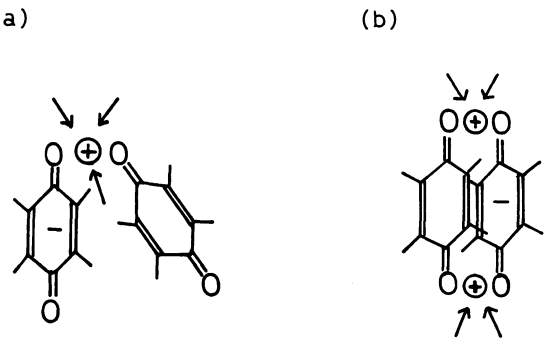

Fig. 3. Schematic illustration of activated complexes for the electron transfer reactions between quinone and its anion radical: (a) ion-pair; (b) triple-ion.

exchange reaction. When the cation is smaller, it is so much more strongly solvated that the energy barrier is higher and the rate of exchange reaction is smaller. Therefore, the rate constants of ion pairs or triple-ions with sodium ions are expected to be smaller than those for potassium aggregates. In the case of a triple-ion, where two counter ions interact with an anion, the reorganization energy of solvent molecules becomes larger than that in the case of an ion pair. Thus, trends (a) and (b) can be explained reasonably.

On the other hand, trend (c) can be interpreted as follows. The expected symmetric transition state involving semiquinone anion ion-pair might be schematically described as in Fig. 3(a). In this Figure, arrows indicate solvent orientations. It can be seen from this scheme that the relative angles between the both O–O axes and between the planes of two quinone molecules are variable. In contrast to the ion pair, in the case of triple-ion, the O–O axes of two quinone molecules must be parallel in symmetric transition state as illustrated schematically in Fig. 3(b). Therefore, as the size of substituents of Q become larger, the steric hindrance increases $\Delta G^{\ddagger}$ which is required to form the activated complex. This steric hindrance may be more prominent in $Q^{-}\cdot Na_2^{2+}/Q$ with smaller cation than in $Q^{-}\cdot K_2^{2+}/Q$. Thus, trend (c) also can be interpreted on the basis of the mechanism mentioned above, considering the steric hindrance in activation complexes.

These explanations indicate that the generally accepted mechanism of the electron-exchange reactions of ion-pairs of anion radicals can also be applied to the electron-exchange reactions of triple-ions.

We wish to thank Profs. Hiroshi Fukutomi and Hiroshi Tomiyasu for the use of facilities for the ESR measurement at The Research Laboratory for Nuclear Reactors in Tokyo Institute of Technology.

References

1) R. F. Adams, T. L. Staples, and M. Szwarc, *Chem. Phys. Lett.*, **5**, 474 (1970).

2) N. Hirota, "EPR Studies of Radical Anions in Solution," in "International Review of Science, Physical Chemistry Series II, Vol. 4, Magnetic Resonance," ed by C. A. McDowell, Butter-worth (1975), pp. 85—137.

3) M. Szwarc and J. Jagur-Grodzinski, "Ions and Ion Pairs in Electron Transfer Reactions of Radical Anions, Carbanions and Solvated Electrons," in "Ion and Ion Pairs in Organic Reactions," ed by M. Szwarc, John-Wiley Sons, (1974), Vol. 2, pp. 1—150.

4) K. Suga and S. Aoyagui, *Bull. Chem. Soc. Jpn.*, **46**, 755 (1973).

5) D. H. Chen, E. Warhurst, and A. Margaret Wilde, *Trans. Faraday Soc.*, **66**, 2561 (1967).

6) A. W. Rutter and E. Warhurst, *Trans. Faraday Soc.*, **64**, 2338 (1968).

7) M. P. Khakhar, B. S. Prabbananda, and M. R. Das, *J. Am. Chem. Soc.*, **89**, 3100 (1969).

Adsorption of Cationic Surfactants on Phospholipid Membranes and Its Contributions to Membrane-Surface Potential

Hideo MATSUMURA,* Miyako IWAMOTO,† and Kunio FURUSAWA†
Electrotechnical Laboratory, Sakura-Mura, Ibaraki 305
†Department of Chemistry, The University of Tsukuba, Sakura-Mura, Ibaraki 305
(Received October 31, 1985)

The adsorption behavior of cationic surfactants (alkyltrimethylammonium ions) on the phospholipid (phosphatidylethanolamine) membranes has been studied by means of interfacial electrostatic measurements, i.e., the surface potential of the monolayer and the zeta potential of the vesicles, in order to elucidate the balance between hydrophobic and electrostatic interactions. The data have been analyzed in terms of the interfacial electrochemical concept; these analyses have revealed that the hydrophobic interaction of a surfactant with the phospholipid membrane is the main motive force for adsorption and there is a critical alkyl-chain length to promote the surfactant adsorption. Furthermore, it was found that the electrostatic interactions between the surfactant and the phospholipid membrane, and among the surfactants themselves, also play a role in their adsorption.

The interaction of surfactants with the lipid membrane, especially with the lipid vesicles, has been studied extensively out of interest in the solubilization or fusion of biological membranes and their antibacterial action. The nonionic surfactant has been utilized as a solubilizer of the biological membrane because of its mild property of not destroying the biological function of the membrane components. On the other hand, studies of ionic surfactants have focused on their antibacterial properties. Quaternary ammonium compounds are typical cationic surfactants, and the antibacterial activity of a series of aliphatic quaternary ammonium salts have been studied.[1,2] The length of the hydrocarbon chain is one of the most significant factors controlling the antibacterial activity.[1] Shelton et al.[2] reported that an alkyltrimethylammonium bromide which contains less than eight carbon atoms in its alkyl group shows little antibacterial activity.

As well as the above practical interest, the adsorption of ionic surfactants on various interfaces has been studied out of interest in interfacial electrochemistry. For example, the effect of the surfactant adsorption on the zeta potential of a solid–water interface[3] and that on the electrocapillary curve at the oil–water interface[4] have been studied by many researchers.

In this work, the adsorption behavior of alkyltrimethylammonium bromides on the lipid membranes has been studied from the viewpoint of interfacial electrochemistry. As lipid membranes, phospholipid vesicles and monolayers spread on the aqueous solution were employed, and the change in the interfacial electrostatic potentials, i.e., the zeta potential of the vesicles and the surface potential of monolayers, caused by the adsorption of cationic surfactants, was studied. The main object in this work is to elucidate the contribution of electrostatic and hydrophobic interaction to the adsorption of cationic surfactants on phospholipid membranes.

Experimental

Materials. The monolayers and vesicles were prepared using L-α-dipalmitoylphosphatidylethanolamine (DPPE), which had been purchased from the Sigma Chemical Co., Ltd. (USA). As cationic surfactants, several alkyltrimethylammonium bromide (carbon numbers: 6,10,12,and 16) and tetrapentylammonium chloride, which had been purchased from the Tokyo Kasei Kogyo Co. Ltd., were used. These were used without any further purification. All the solutions of these compounds and the subphase solution in the monolayer experiment were prepared with deionized (Barnstead, NANO pure system) and doubly distilled water.

Zeta Potential. The DPPE vesicles were prepared by sonication without using any buffer to eliminate any unexpected effect of the included buffer ions. Vesicle suspensions were mixed with various concentrations of cationic surfactants; the final salt condition was 10^{-3} mol dm^{-3} NaCl. The electrophoretic mobilities of large-sized vesicles were measured with a Rank Brother microelectrophoretic apparatus (Model MK-2) using a rectangular glass cell at 20 °C. The zeta potentials were calculated from the mobility data according to the method of Wiersema.[5] In this calculation, the radius (a) of the vesicle was assumed to be 1000 Å.

Surface Potential of Monolayers. Phospholipid monolayers were prepared by spreading DPPE from a chloroform–ethanol (3:1) solution on the surface of a subphase solution containing 0.1 mol dm^{-3} NaCl in 80 ml a Teflon trough. The packing density of the monolayers prepared in these experiments was about 1/60 (molecule/Å^2). After the addition of a concentrated surfactant solution to the subphase solution, the solution was stirred for more than 30 min; then the surface potentials of the monolayers were measured by the vibrating-electrode method at 23 °C.

Results and Discussion

The electrostatic potential profile through the membrane-solution interface can be described ap-

proximately as a combination of an inside membrane potential which originates from dipoles of polar-head groups of phospholipid molecules and an ionic diffuse-double layer potential.[6] These potentials and their combination will change upon the adsorption of ionic compounds (a cationic surfactant in this case). Therefore, it is expected that their adsorption behavior can be analyzed by measuring both the surface potential of the monolayers and the zeta potential of the vesicles.[7]

Contribution of Alkyl-Chain Length. In Fig. 1, the change in the surface potential of the monolayer ($\Delta\Delta V$) is plotted against the concentrations of several kinds of alkyltrimethylammonium ions (abbreviated as alkyl-TMA) on a log scale. It is found that decyl-(C_{10}) and hexyl-(C_6) TMA have little effect on $\Delta\Delta V$, whereas dodecyl-(C_{12}) and hexadecyl-(C_{16}) TMA make a considerable contribution on $\Delta\Delta V$ in the present experimental concentrations. It is interesting to notice that there is a great difference in their contributions to $\Delta\Delta V$ between C_{10} and C_{12} TMA. This fact suggests that there is a critical hydrocarbon-chain length for the interaction between a surfactant and phopholipid membranes. A simillar tendency has been observed in the electrophoresis experiments. (Fig. 2). The electrophoretic mobility of DPPE vesicles changes the sign of its value with the concentration of C_{12} and C_{16} TMA, but not with that of C_{10} TMA. These data indicate that hydrocarbon numbers larger than ten are necessary for the alkyl chain of the surfactants to interact effectively with the DPPE membrane. Figure 3 shows the relationship between the $\Delta\Delta V$ of the DPPE monolayer membrane and the concentration of tetrapentylammonium bromide in the solution. As is shown in Fig. 3, this molecule has only a slight effect on the surface potential of the DPPE monolayer membrane. Those results suggest that these four alkyl chains are too short to enter the membrane interior of DPPE deep enough to interact with the hydrophobic part of the membrane and that a certain bulky effect of this molecule may play a role in this phenomenon.

Effect of Ionization State of DPPE. A DPPE molecule is an amphoteric molecule, and it has two dissociable groups, i.e., $-\overset{+}{N}H_3$ and $-PO_4H$. Depending on the pH in the bulk solution, these groups change their ionization state, as is shown in Fig. 4. (The ionization behavior of the PE membrane is

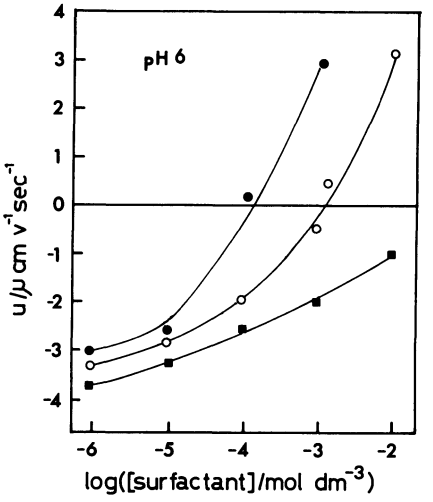

Fig. 2. Electrophoretic mobility of DPPE vesicles bathed in various concentration of several alkyltrimethylammonium bromide aqueous solution. (●): C_{16}, (○): C_{12}, (■): C_{10}.

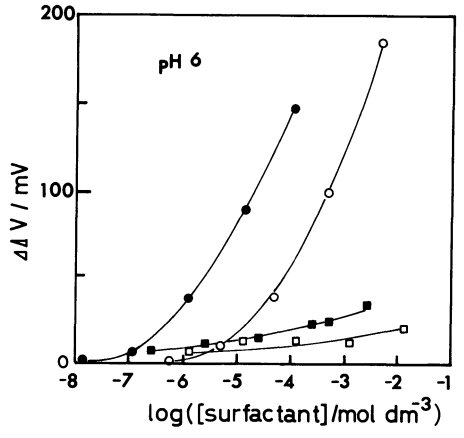

Fig. 1. Surface potential change of DPPE monolayer membrane vs. concentration of alkyltrimethyl ammonium bromide. (●): C_{16}, (○): C_{12}, (■): C_{10}, (□): C_6.

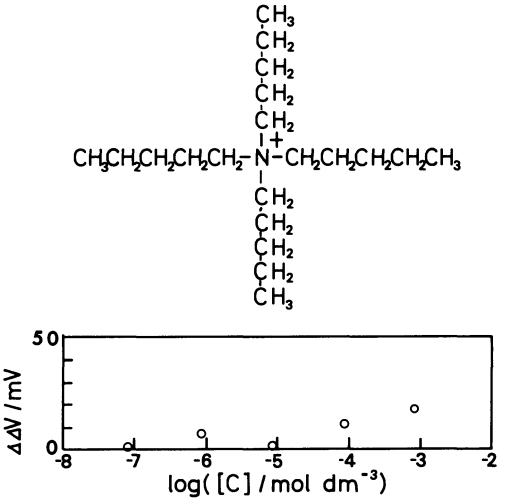

Fig. 3. Surface potential change of DPPE monolayer membrane vs. concentration of tetrapentylammonium bromide.

represented in Fig. 1 of Ref. 9.) Moreover, the ionization state of the phosphatidylethanolamine membrane has been reported by many researchers[8] to be different from that of the single molecule itself. In this work, three pH values, i.e., 3, 6, and 10, were selected in order to examine the effect of the ionization state on the adsorption of C_{12}-TMA onto the membrane. Figure 5 shows the change in the surface potential of the monolayer caused by the adsorption of C_{12}-TMA at the three pH values. $\Delta\Delta V$ begins to increase at a lower concentration of C_{12} TMA with an increase in the pH, i.e., in the order of: pH 10>pH 6>pH 3. This order is due to the change in the ionization state of the DPPE membrane; that is, at pH 10, the DPPE membrane has the most negative charges on the surface, whereas at pH 3, the DPPE membrane has the least negative charges or positive charges on it. As a result of the electrostatic interaction between C_{12} TMA and the DPPE membrane, the adsorption is promoted by the electrostatic attraction at pH 10, but is depressed by the repulsion at pH 3. Electrophoretic studies support this picture. Figure 6 shows the electrophoretic mobility of DPPE vesicles bathed in various concentrations of the C_{12} TMA solution at those three pH values. At pH 3, the DPPE vesicles have a positive value of mobility in the surfactant-free system. At pH 10, the electrophoretic mobility of the DPPE vesicles is comparable to that at pH 6. The adsorp-

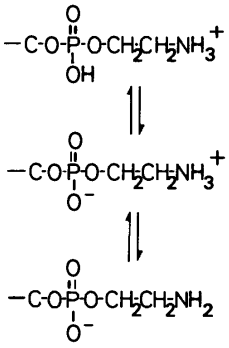

Fig. 4. Ionization state of PE.

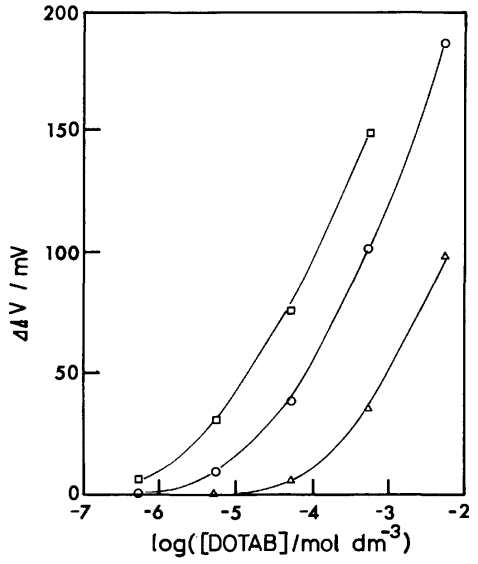

Fig. 5. Surface potential change of DPPE monolayer membrane vs. concentration of dodecyltrimethylammonium bromide at (△) pH 3, (○) pH 6, (□) pH 10.

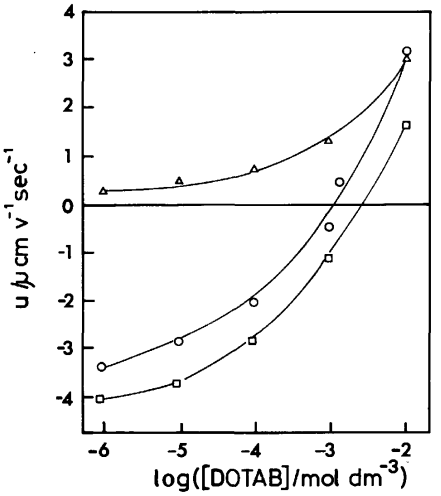

Fig. 6. Electrophoretic mobility of DPPE vesicles bathed in various concentration of dodecyltrimethylammonium bromide at (△) pH 3, (○) pH 6, (□) pH 10.

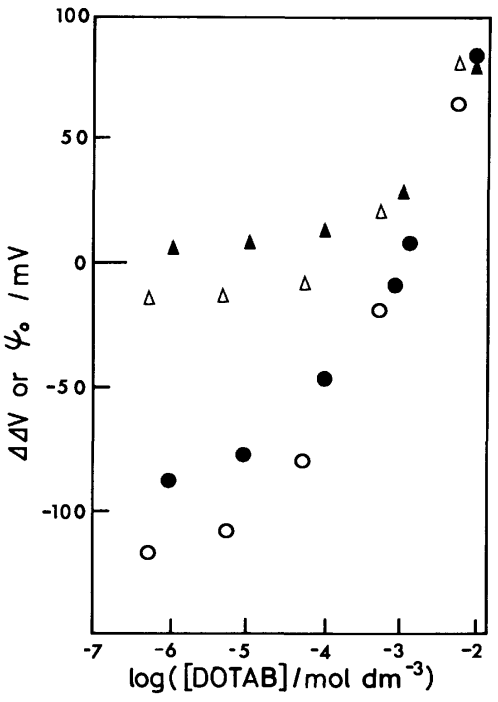

Fig. 7. Membrane surface potential (ψ_0; ▲,●) calculated from the data of electrophoretic mobility or surface potential change ($\Delta\Delta V$; △,○) of monolayer at pH 3 and pH 6, respectively.

tion of C_{12} TMA on the membrane causes a change in the zeta potential of the vesicles. The contribution of this surfactant to the mobility is greater at pH 6 and pH 10 than at pH 3. This behavior is almost the same as that shown in Fig. 5. In Fig. 7, the membrane surface potential (ψ_0), calculated from the data of electrophoretic mobilities by the method of Wiersema and the relation of $\psi_0=\zeta e^{\kappa d}$ (ζ: zeta potential, κ: Debye-Hückel parameter), is plotted together with the surface potential of the monolayer ($\Delta\Delta V$). In this calculation, the distance from the membrane surface to the slipping plane (d) is assumed to be 10 Å.[9] The two sets of data are compared with each other on the assumption that their values are equal at the surfactant concentration, 10^{-3} mol dm^{-3} (around this concentration the zeta potentials have a zero value at pH 6, and the surface potential can be taken to be zero.). This figure shows that $\Delta\Delta V$ resembles the change in the ψ_0 value of the vesicles (at pH 3 and pH 6). This means that the surfactants are adsorbed on the membrane surface in such a manner as their charges of the head group are located at the membrane-solution interface. The data of electrophoretic mobilities at pH 10 are not very different from those at pH 6. This may be due to the relaxation effect, because $\kappa a \simeq 5$ under these experimental condition; i.e., the electrophoretic mobility does not increase with the increase in the zeta potential above 100 mV.

Analytical Considerations

The adsorption behavior of charged molecules by the membrane can be described by the following simple relation:

$$[\text{surfactant}]_m = K_w K_e f [\text{surfactant}]_b, \quad (1)$$

where $[\text{surfactant}]_m$ is the concentration of C_{12} trimethylammonium ions adsorbed on the membrane; $[\text{surfactant}]_b$, its concentration in the bulk aqueous solution; K_w, the adsorption coefficient based on hydrophobic interaction, and f, the factor which originates from the mutual electrostatic repulsion of adsorbed ions and the next adsorbing ion and which determines the line shape of the adsorption curve. In other words, f denotes the discrete charge effects on the charged surface.[10] K_e is the constant of electrostatic interaction between the DPPE membrane and the surfactant molecules which arises from the ionization of DPPE molecules; it is denoted as follows:

$$K_e = e^{-\psi_0 e/kT}, \quad (2)$$

where ψ_0 is the membrane-surface potential.

The change in the surface potential of the monolayer ($\Delta\Delta V$) is approximated by the following equation:

$$\Delta\Delta V = \Delta q/C_c = e \cdot \Delta[\text{surfactant}]_m/C_c, \quad (3)$$

where Δq is the amount of charges adsorbed; e, the elementary electric charge, and C_c, the specific capacitance of the outer region of the monolayer.

The f factor, which determines the curvature of the figure, can be expressed as follows:

$$f = e^{-a \cdot \Delta\Delta V e/kT}, \quad (4)$$

where $0 \leqq a \leqq 1$. $a=0$ means that the mutual interaction of ions is absent, while $a=1$ means that the electrostatic potential produced by the adsorption of ions greatly influences the adsorption of the next adsorbing ion.

If one adopts here the diffuse double-layer theory instead of the simple capacitor model, Eq. 3 can be rewritten by the following equation:[11]

$$\sinh \frac{\Delta\Delta V}{51.4} = \frac{136.6 \cdot \Delta q}{\sqrt{C}}, \quad (5)$$

where C the concentration of indifferent ions.

These equations allow the analytical calculation of the a factor. The experimental data of $\Delta\Delta V$ for C_{12}-TMA are plotted, with their analytical curves, in Fig. 8. The solid lines are for Eq. 3, while the dashed ones are for Eq. 5. When we compare these data with the theoretical curves, $a=0.5$ is adequate. This means that these surfactant ions adsorb on the DPPE membrane partially hindered by electrostatic repulsion among the adsorbed ions themselves.

By comparing the data of $\Delta\Delta V$ and the electrophoretic mobility for C_{12}-TMA with those for C_{16}-TMA in Figs. 1 and 2, one can estimate the hydrophobic interaction per $-CH_2$ group. The adsorption coefficient of the hydrophobic part, K_w, is expressed as follows:

$$K_w = K \cdot e^{-(N-N_0)w/kT}, \quad (6)$$

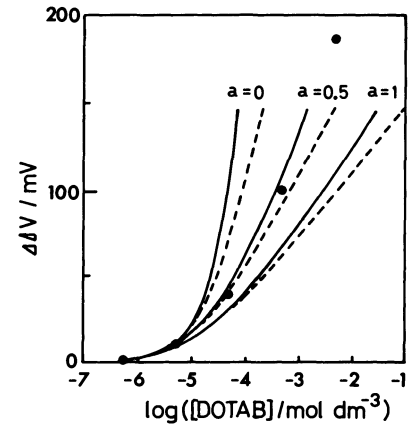

Fig. 8. Calculated curves from Eq. 3 —— and Eq. 5 ---- for surface potential change and experimental data of dodecyltrimethylammonium bromide.

where w is the hydrophobic interaction energy per CH_2 group; N, the number of CH_2 groups in the hydrocarbon chain; N_0, the critical number of CH_2 for hydrophobic interaction with the membrane, and K, the constant from other parts. The $\Delta\Delta V$ curves of C_{16}–TMA are shifted to the lower-concentration side by more than 1 order from that of C_{12}–TMA. Furthermore, the electrophoretic mobility curve of C_{16}–TMA is also shifted to a lower side by more than 1 order from that of C_{12}–TMA. These data make possible the calculation of the w-value through this relation: (shift value)$=e^{\Delta n \cdot w/kT}$; where $\Delta n=N(C_{16})-N(C_{12})=4$; i.e., Δn is the difference in CH_2 number. Then, w is obtained as $w=0.6—1.2\,kT$. By comparing this value with that of the hydrophobic interaction energy (1.1 kT) for the micelle formation of various surfactants, it can be said that the main motive force of adsorption is also hydrophobic interaction between the membrane and the ionic surfactants. In fact, Zaslavsky et al.[12] have studied the interaction between a series of N-acyl derivatives of amino acids and egg lecithin liposome and have reported that the binding free energy per CH_2 ranges from 0.24 Kcal mol^{-1}† (0.4 kT) to 1.05 Kcal mol^{-1} (1.8 kT).

† 1 cal=4.184 J.

References

1) J. A. Cella, D. N. Eggenberger, D. R. Noel, L. A. Harriman, and H. J. Harwood, *J. Am. Chem. Soc.*, **74**, 2061 (1952).

2) R. S. Shelton, M. G. Van Campen, C. H. Tilford, H. C. Lang, L. Nisomger, F. J. Bandelin, and H. L. Rubenkoenig, *J. Am. Chem. Soc.*, **68**, 753 (1946).

3) A. Watanabe, F. Tsuji, and S. Ueda, *Denki Kagaku*, **29**, 777 (1961).

4) A. Watanabe, M. Matsumoto, H. Tamai, and R. Gotoh, *Kolloid-Z*, **220**, 152 (1967).

5) P. H. Wiersema, A. L. Loeb, and J. TH. G. Overbeek, *J. Colloid Interface Sci.*, **22**, 78 (1966).

6) R. Aveyard and D. A. Haydon, "An Introduction to the Princples of Surface Chemistry," Cambridge Univ. Press, London/New York (1973), p. 34.

7) D. A. Haydon and V. B. Myers, *Biochim. Biophys. Acta*, **307**, 429 (1973).

8) H. Hauser and M. C. Phillips, "Progress in Surface and Membrane Science," 13, Academic Press, New York (1979), p. 297.

9) H. Matsumura, H. Kakoki, and K. Furusawa, *Bull. Chem. Soc. Jpn.*, **58**, 78 (1985).

10) O. S. Andersen, S. Feidberg, H. Nakadomari, S. Levy, and S. McLaughlin, *Biophys. J.*, **21**, 35 (1978).

11) A. G. Lee, *Biochim. Biophys. Acta*, **472**, 237 (1977).

12) B. Y. Zaslavsky, A. A. Borovskaya, A. K. Lavrinenko, A. Y. Lisichkin, Y. A. Davidovich, and S. V. Rogozhin, *Chem. Phys. Lipids*, **26**, 49 (1980).

 © 1986 The Chemical Society of Japan Bull. Chem. Soc. Jpn., 59, 1539—1543 (1986)

Kinetic Studies of Fast Equilibrium by Means of High-Performance Liquid Chromatography. XIV.[1] Separation of Rotamers of Phenyl Methylcarbamates and Their Rotational Energy Barriers

Masataka MORIYASU,* Chisako YAMAGAMI, Atsushi KATO, Yohei HASHIMOTO, and Narao TAKAO

Kobe Women's College of Pharmacy, Motoyamakita-machi, Higashinada-ku, Kobe 658

(Received December 9, 1985)

High-performance liquid chromatography(HPLC) of six phenyl methylcarbamates at low column temperatures on normal phase chromatography using hydroxyl-group chemically-bonded silica gel packing achieved the separation of rotamers. The population ratios of rotamers were determined for different conditions such as solvent composition and concentration. The rotational-energy barriers to intramolecular-bond rotation about the carbonyl-nitrogen bonds were determined for four *p*-substituted phenyl methylcarbamates, and it was found that the energy barriers were higher when electron-withdrawing groups were substituted.

In this research series, rotamers about the carbon–nitrogen bonds with partial double-bond characters, including metal dithiocarbamates,[2] anilides,[3–5] and *N*-alkylamides,[1] have been separated by means of HPLC at low column temperatures. The population ratios of rotamers in different conditions have been determined by this method, and the energy barriers to bond rotations have also been determined. This report deals with the separation of rotamers of *p*-substituted phenyl methylcarbamates and the determination of their rotational-energy barriers.[6]

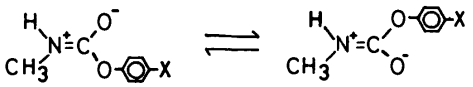

cis(Z) trans(E)

The restricted rotation about the carbonyl–nitrogen bonds of amides has been extensively investigated by many workers by means of NMR[7] with a special technique entitled the dynamic NMR method. Our previous reports[1,3–5] have demonstrated that HPLC has also been a powerful tool for examining the restricted bond rotation of amides and even better than NMR when the content of the minor rotamers is very low. Different from amides, the number of reports on dynamic NMR studies of carbamates is relatively few and they are restricted to symmetrical *N,N*-disubstituted carbamates. These are attributable to the following. (1) Different from amides, the differences in chemical shifts of two rotamers of carbamates are usually very small. This makes dynamic NMR studies of carbamates very difficult and once led to an erroneous conclusion that, different from amides, there were no large energy barriers to the carbonyl–nitrogen bond rotation of carbamates.[8] This difficulty was partially resolved by the use of a large amount of lanthanoid shift reagents; thus, the rotational-energy barriers were determined for dimethylcarbamates.[9] It is debatable, however, whether the rotational-energy barriers in the absence and presence of shift reagents are identical since it is probable that interactions between the shift reagents and carbamate molecules cause a variation in the energy barriers as well as the population ratios to a considerable extent. In addition, other difficulties exist for *N*-monosubstituted carbamates. (2) For symmetrically *N,N*-disubstituted carbamates, due to the equal population ratios of "two rotamers" simple T_c method[10] can be applied to determine the energy barriers. Contrary to this, complicated total line-shape analysis is inevitable for unsymmetrically *N*-substituted carbamates. The proximity of chemical shifts of two rotamers not only makes the total line-shape analysis impossible, but also prevents a determination of the population ratios of two rotamers. (3) Owing to a strong intermolecular association, such as the hydrogen bonding of *N*-monosubstituted carbamates, the overall process observed by means of NMR might involve the making and breaking of hydrogen bonds as well as bond rotation. Thus, it is not clear that the data obtained by means of dynamic NMR correctly indicate the rotational energy barriers, even though a total line-shape analysis is possible. For these reasons, a determination of the rotational-energy barriers has not hitherto been carried out for *N*-monosubstituted carbamates.

Experimental

The following six *p*-substituted phenyl methylcarbamates were prepared and purified as described elswhere;[11] phenyl methylcarbamate, *p*-methylphenyl methylcarbamate, *p*-fluorophenyl methylcarbamate, *p*-nitrophenyl methylcarbamate, *p*-hydroxyphenyl methylcarbamate, and *p*-cyanophenyl methylcarbamate.

The HPLC apparatus for use in low-temperature measurements was detailed elswhere.[3,12] Several column packings of two different types, i.e., silica-gel packings (LiChrosorb SI 60, LiChrosorb SI 100, and Polygosil 60-5)

and hydroxyl-group chemically-bonded packings (LiChrosorb DIOL and Nucleosil 7OH), were tested and it was found out that the latter gave better results. Complete base-line separation of rotamers by silica-gel packings was difficult because the retention times of rotamers were relatively close to each other. For the determination of the population ratios of rotamers, column effluent was passed through a narrow stainless-steel tube (0.5 mm in internal diameter and 10 m in length) which was thermostated at 80 °C in an air bath prior to detection by means of UV detector.[4] Thus, the equilibrium of rotamers in eluent was reequilibrated.

Results and Discussion

Separation of Rotamers. These six phenyl methylcarbamates were dissolved in chloroform or ethanol (0.01 mol dm^{-3}), and sample solutions were submitted to normal phase HPLC at different column temperatures. Figure 1 exemplifies the chromatograms of phenyl methylcarbamate in a chloroform solution on hydroxyl-group chemically-bonded packings. Two peaks corresponding to two rotamers appeared and were separated at low column temperatures. A complete base-line separation of rotamers was attained when the column temperature was below −55 °C, although the column efficiency gradually decreased with the falling temperature. With similar procedures, the separation of rotamers of other *p*-substituted phenyl methylcarbamates was possible below −55 °C.

The identification of each peak was not easy because different from anilides and amides hitherto NMR were not available. We consider, however, that the former small peak will be attributable to the cis-form (*Z*-form) for the following reason. Owing to the ability to form ring dimer,[13] the dielectric constants of cis-form (*Z*-form) rotamers of amides and carbamates are much smaller than those of trans-form (*E*-form) rotamers.[14] It is a well-known fact that in the adsorption or normal phase partition chromatography, nonpolar species are eluted faster than polar ones. This was actually observed for anilides and *N*-alkylamides as can be seen in our previous reports.[1,3,4] It is quite likely that a similar elution sequence can also be observed for carbamates. Hereafter, it is assumed that the former small peak can be assigned as cis-form (*Z*-form), although some ambiguity still remains on the peak identification.

Equilibrium Ratios of Rotamers. The ratios of two rotamers in chloroform and in ethanol were determined for these six carbamates (0.01 mol dm^{-3}, 25 °C), and the results are summarized in Table 1. For *p*-methylphenyl methylcarbamate, the ratios of two rotamers were determined in a variety of solvents (0.01 mol dm^{-3}, 25 °C), and the percentages of cis-form (*Z*-form) are determined which are as follows: 24% (in hexane), 22% (in benzene), 29% (in carbon tetrachloride), 14% (in diethyl ether), 14% (in ethyl acetate), 14% (in acetonitrile), 13% (in tetrahydrofuran), and 14% (in methanol). The effect of the concentration was also examined for *p*-methylphenyl methylcarbamates in chloroform. The percentages of cis-form (*Z*-form) were as follows; 17% (3.0 mol dm^{-3}), 22% (0.1 mol dm^{-3}), and 24% (0.01 mol dm^{-3}). By summarizing these results it can be concluded that the percentages of cis-form (*Z*-form) of these carbamates are higher in nonpolar solvents and in lower concentrations which is similar to the case for

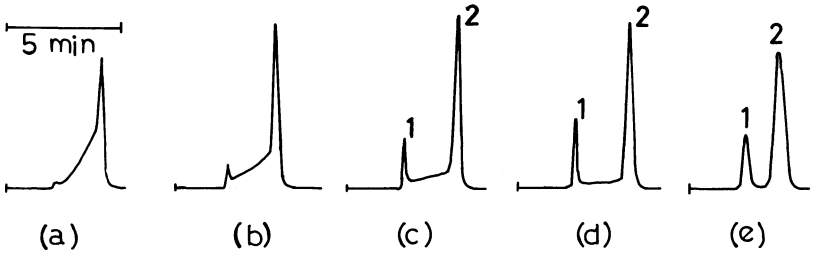

Fig. 1. HPLC chromatograms of phenyl methylcarbamate at various temperatures.
Column: Nucleosil 7OH (4.6 mm × 15 cm). Eluent: hexane: 1-propanol: acetic acid = 100 : 10 : 3, 2.5 cm^3 min. Detector: UV 254 nm. (a): −25 °C, (b): −30 °C, (c): −35 °C, (d): −40 °C, (e): −55 °C. 1 cis-form(*Z*-form), 2 trans-form(*E*-form).

Table 1. Percentage of Phenyl Methylcarbamates Existing as cis-Form (*Z*-Form) in Chloroform and Ethanol

	X					
	H	CH_3	OCH_3	NO_2	F	CN
In 0.01 mol dm^{-3} chloroform	23	24	26	13	21	15
In 0.01 mol dm^{-3} ethanol	19	17	17	8.8	16	7.4

25 °C.

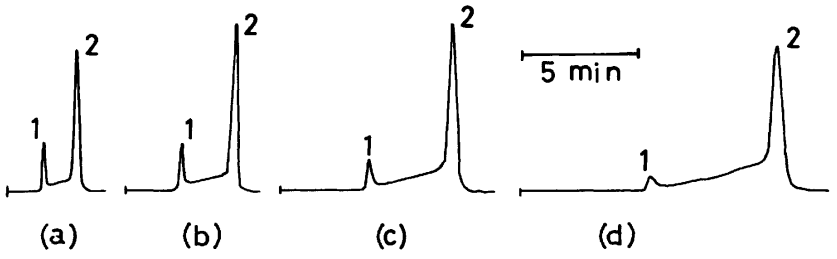

Fig. 2. HPLC chromatograms of phenyl methylcarbamate at −35 °C in different flow rate. Column: Nucleosil 7OH (4.6 mm × 15 cm). Eluent: hexane: 1-propanol: acetic acid = 100 : 10 : 3. Detector: UV 254 nm. Column temperature: −35 °C. Flow rate; (a): 4.3 cm^3 min^{-1}, (b): 2.5 cm^3 min^{-1}, (c): 1.4 cm^3 min^{-1}, (d): 0.8 cm^3 min^{-1}.

anilides and aliphatic amides.[1,4]

Determination of Rotational Energy Barriers. As described above, HPLC of phenyl methylcarbamates gave the separation of rotamers below −55 °C. Under the conditions of a baseline separation of rotamers, each peak was symmetrical and neither leading nor tailing was observed. With an increase in the column temperature, a partial transformation between two rotamers took place during the course of chromatography. In this case, complicated chromatograms were obtained. An approximate HPLC method for the determination of rotational-energy barriers[5] can be applied by observing the change in chromatographic patterns, provided that the rotational energy barriers are little affected by the adsorption or partition process of solute molecules on column packings. Figure 2 exemplifies the chromatograms of phenyl methylcarbamate at a column temperature of −35 °C for different flow rates. When the flow rate was low, a larger part of one rotamer transformed into other rotamer during the course of chromatography. The residual amount of cis-form (*Z*-form) was proportional to the product of the peak area of cis-form *S* and the flow rate *v* at a residence time *t* was plotted against *t*. Similar experiments were carried out at different column temperatures and the results are given in Fig. 3. From the slope of these linear curves, the rate constants to the bond rotation from cis-form (*Z*-form) to trans-form (*E*-form) k at different temperatures were calculated. The reverse rate constants k corresponding to the conversion from trans-form (*E*-form) to cis-form (*Z*-form) were also determined by the same way. The rate constants k and k_- for other carbamates including *p*-methylphenyl methylcarbamate, *p*-methoxyphenyl methylcarbamate, and *p*-nitrophenyl methylcarbamate were also determined with similar procedures. The activation energies of the forward E_a (from cis- to trans-form) and backward E_{-a} (from trans- to cis-form) reactions were calculated from the Arrhenius' plots as shown in Fig. 4. Thus, activation energies as well as rate constants can be determined. Table 2 summarizes the activation

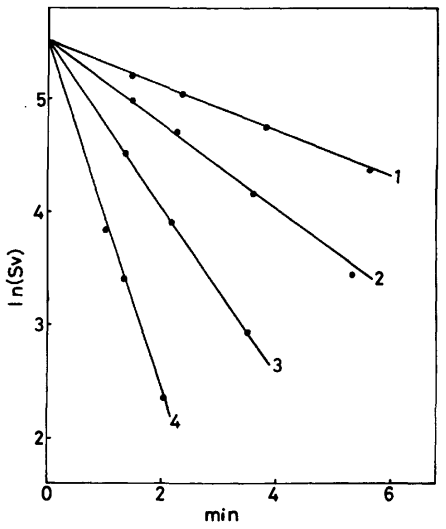

Fig. 3. Plots of residual amount of cis-form (*Z*-form) of phenyl methylcarbamate vs. residence time. 1: −40 °C, 2: −35 °C, 3: −30 °C, 4: −25 °C.

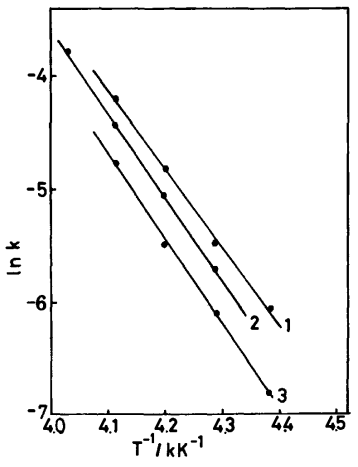

Fig. 4. Arrhenius' plot of intramolecular carbonyl-nitrogen bond rotation of phenyl methylcarbamates. 1: *p*-methoxyphenyl methylcarbamate, 2: phenyl methylcarbamate, 3: *p*-nitrophenyl methylcarbamate.

Table 2. Rate Constants and Energy Barriers of the Bond Rotation of Phenyl *N*-Methylcarbamates

	k(s^{-1}) at −30 °C trans→cis	k_{-}(s^{-1}) at −30 °C cis→trans	E_a(kJ mol^{-1}) cis→trans	E_{-a}(kJ mol^{-1}) trans→cis
p-Methoxyphenyl methylcarbamate	1.5×10^{-2}	1.2×10^{-3}	56.5	50.2
p-Methylphenyl methylcarbamate	1.3×10^{-2}	1.2×10^{-3}	59.0	53.2
Phenyl methylcarbamate	1.2×10^{-2}	1.0×10^{-3}	62.4	58.2
p-Nitrophenyl methylcarbamate	8.5×10^{-3}	*	64.4	*

* Due to the tailing of trans-form (*E*-form) rotamer, the rate constants and energy barriers of the reverse reaction were not calculated.

energies and rate constants at −30 °C for these four phenyl methylcarbamates. These energy barriers were found to be smaller than those of aliphatic amides[7] and close to those of anilides.[5,7] When a hydrogen in *p*-position in phenyl ring is replaced by an electron-withdrawing group, rotational energy barriers increase. On the other hand, the substitution by an electron-donating group decreases the energy barriers. These phenomena are explained by the following way. The contribution of the canonical form 2, which is responsible for the partial double

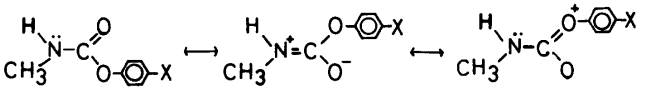

1 2 3

bond character of carbonyl-nitrogen bonds, is reduced by the contribution of another canonical form 3 for carbamates. Thus, the rotational energy barriers of carbamates are usually smaller than those of alkylamides. Similarly, the partial double bond character of carbonyl-nitrogen bonds of anilides is also reduced by dint of the contribution of the canonical forms 6 and 7. The substitution of a

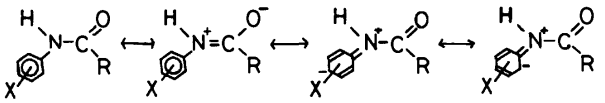

4 5 6 7

hydrogen atom in phenyl group by substituent X will bring about reverse effects on the rotatinal energy barriers for carbamates and anilides. In the case of anilides, the substitution of *o*- or *p*-hydrogen by an electron-donating group such as methoxy group will destabilize the canonical forms 6 and 7, and consequently the substitution will bring about an increase in the double-bond character and, thus, an increase in the energy barriers. Contrary to this, the substitution by an electron-withdrawing group such as nitro group will cause a decrease in the energy barriers. This phenomenon was actually observed by a dynamic NMR study for *p*-substituted *N*-methylformanilides.[15] The rotational energy barreirs of *p*-nitro-substituted *N*-methylformanilide and *p*-methoxy-substituted *N*-methylformanilide were 71.5 and 78.5 kJ mol^{-1}, respectively. The effects of substituents should differ for carbamates. The replacement of a hydrogen in the phenyl ring of phenyl methylcarbamates by an electron-donating group should stabilize the canonical form 3 and, thus, decreases the double-bond character of the carbonyl–nitrogen bonds. This is in agreement with the present experiments.

This work was partially supported by a Grant-in-Aid for Scientific Research from the Ministry of Education, Science, and Culture.

References

1) Part XIII. M. Moriyasu, A. Kato, and Y. Hashimoto, *Bull. Chem. Soc. Jpn.*, **59**, 939 (1986).

2) M. Moriyasu, Y. Hashimoto, and M. Endo, *Bull. Chem. Soc. Jpn.*, **56**, 1972 (1983).

3) M. Moriyasu, K. Kawanishi, A. Kato, and Y. Hashimoto, *Bull. Chem. Soc. Jpn.*, **57**, 1766 (1984).

4) M. Moriyasu, K. Kawanishi, A. Kato, Y. Hashimoto, and M. Sugiura, *Bull. Chem. Soc. Jpn.*, **58**, 2581 (1985).

5) M. Moriyasu, K. Kawanishi, A. Kato, Y. Hashimoto, M. Sugiura, and T. Sai, *Bull. Chem. Soc. Jpn.*, **58**, 3351 (1985).

6) Due to the strong double bond character of the carbonyl nitrogen bond, 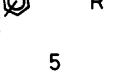 moiety is considered to lie on the same plane. In this report the prefixes cis- and trans- designate the configuration concerning C-O⁻ and N-H groups because the configuration seems to play an essential role. The alternative prefixes, *E*- and *Z*-, which were used for amides in our previous reports (Ref. 1,3,4, and 5), were shown in parentheses in this report because *Z*- and *E*-mean reverse configuration concerning C-O⁻ and N-H groups for amides and carbamates.

7) For the NMR study of the restricted bond rotation of amides, see the following review articles and the references cited therein: a) W. E. Stewart and T. H. Siddall, III, *Chem. Rev.*, **70**, 517 (1970); b) L. M. Jackman, "Dynamic Nuclear Magnetic Resonance Spectroscopy," Academic Press, New York (1975), p. 203.

8) Concerning the finding of the restricted bond rotation of carbamates, for example, see: a) T. M. Velga, *J. Org.*

Chem., **31**, 1150 (1966); b) M. T. Rogers and J. C. Woodbrey, *J. Phys. Chem.*, **66**, 540 (1962); c) E. Lustig, W. R. Benson, and N. Duy, *J. Org. Chem.*, **32**, 851 (1967).

9) S. R. Tanny, M. Pickering, and C. S. Springer, Jr., *J. Am. Chem. Soc.*, **95**, 6227 (1973).

10) For example, E. Breitmaier and W. Voelter, "^{13}C-NMR Spectroscopy," 2nd ed, Verlag Chemie, Weinheim (1978) p. 86.

11) C. Yamagami, N. Takao, T. Nishioka, T. Fujita, and Y. Takeuchi, *Org. Magn. Resn.*, **22**, 439 (1984).

12) M. Moriyasu, A. Kato, and Y. Hashimoto, *J. Chem. Soc., Perkin Trans. 2*, in press.

13) a) A. J. R. Bourn, D. G. Gilles, and E. W. Randall. *Tetrahedron*, **20**, 2811 (1964); b) L. G. Belinskaya, A. V. Lukashov, and E. S. Efremov, *Izv. Timiryazev. S-kh. Akad.*, **1974**, 162; *Chem. Abstr.*, **81**, 119752j (1974).

14) G. R. Leader and J. F. Gormley, *J. Am. Chem. Soc.*, **73**, 5731 (1951).

15) C. H. Yoder, J. A. Sandberg, and W. S. Moore, *J. Am. Chem. Soc.*, **96**, 2260 (1974).

Bulk Copolymerization of Acrylonitrile with Allyl Chloride and Thermal Analysis of the Products

Masao Okamoto,* Kiyoshi Suenaga, and Osamu Ishizuka
Department of Polymer Materials Engineering, Faculty of Engineering,
Yamagata University, Jonan, Yonezawa 992
(Received September 28, 1985)

The bulk copolymerization of acrylonitrile (M_1) with allyl chloride (M_2), carried out at 40 °C, was initiated by 0.05 mol% of α,α'-azobisisobutyronitrile under nitrogen. The compositions of six copolymers were in the range of allyl chloride units, 0.63—6.32 mol%. The monomer reactivity ratios r_1 and r_2 were calculated to be 6.04 and 0.035, respectively. Only three copolymers were soluble in *N,N*-dimethylformamide and their intrinsic viscosities were found to be greater than 4.5 dL g^{-1}. The chlorine contents, although 0.42, 0.87, and 1.03 wt%, were sufficiently effective to cause a change in the behavior of the thermal degradation of polyacrylonitrile (PAN). In DTA curves measured at a rate of 5 °C min^{-1} under nitrogen for copolymers containing ca. 1 wt% of chlorine, a sharp exotherm due to the polymerization of cyano groups shifted to the higher-temperature side (ca. 40 °C) and the differential temperature decreased to about 1/6. Moreover, the weight loss at 350 °C decreased from 19 wt% for PAN to 13 wt%. A similar thermal-degradation behavior was also observed for acrylonitrile-α-chloroacrylonitrile (CAN) copolymers. However, there was a great difference between allyl chloride and CAN units concerning the effect on the thermal degradation of PAN. Namely, only 1.5 mol% of allyl chloride units corresponded to 10 mol% of CAN units.

In a preceding study[1] hydrogen chloride (HCl) accelerated the rate of polymerization of cyano groups at 220 °C in an isothermal heat treatment of polyacrylonitrile (PAN). The acceleration was thought to be the result of the action of chlorine atoms which were formed by the reaction of thermally degraded polymer radicals with HCl. Moreover, it was demonstrated that in both DTA curves for the PAN samples heat-treated under an HCl atmosphere and for acrylonitrile-α-chloroacrylonitrile (CAN) copolymers, a sharper exotherm due to the polymerization of cyano groups appeared more at the higher-temperature side than that for pure PAN. The differential temperature ΔT decreased upon increasing the chlorine content. This type DTA behavior was also considered to be attributable to the action of chlorine atoms. Grassie and McGuchan[2] have already observed similar behavior for copolymers of acrylonitrile with vinyl chloride, vinylidene chloride, and CAN (comonomer units, more than 5 mol%). Acceleration effects on the polymerization rate of cyano groups are thought to appear even for a low content of comonomer units by changing its chemical component. In order to clarify the above-mentioned problem, we tried to prepare acrylonitrile (M_1)-allyl chloride (M_2) copolymers. So far, it has been reported that this system should be ideal and the relative reactivity of allyl chloride toward the acrylonitrile-type radical is 0.18 at 60 °C.[3] Since this indicates $r_1=1/0.18$ and $r_2=0.18$, it was expected that favorable copolymers will easily be obtained.

Experimental

Preparation of Copolymers. Commercial acrylonitrile and allyl chloride were distilled in a nitrogen atmosphere. Bulk copolymerization carried out at 40 °C was initiated by 0.05 mol% of AIBN under nitrogen. Polymerization conditions are listed in Table 1. The reaction vessel was sealed to prevent the loss of both monomers during copolymerization. After 1.25—36 h, the copolymerization was terminated by adding of a small amount of hydroquinone. The copolymer was filtered, washed thoroughly with methanol, and finally dried in a vaccum at 30 °C.

Chlorine Analysis. The method was reported in a previous paper.[4]

Determination of Intrinsic Viscosity. The intrinsic viscosity [η] was measured in *N,N*-dimethylformamide (DMF) at 35 °C.

Measurement of IR Absorption Spectra. IR spectra were measured by a Shimadzu IR-435 spectrophotometer using a pellet method.

Differential Thermal Analysis (DTA). The method was reported in a previous paper.[1] Samples were heated to 350 °C at 5 °C min^{-1} rate under nitrogen.

Results and Discussion

Composition of Copolymers. The chlorine content and [η] of copolymers are shown in Table 1. It was found from these results that the copolymers obtained in Expt Nos. 2, 3, and 4 contained little chlorine and that the molecular weights were sufficiently high. The content of allyl chloride units incorporated in each copolymer was calculated from the chlorine content (Table 1). Figure 1 shows the IR spectra of PAN and copolymers obtained in Expt Nos. 6 and 8. It was supposed from the spectra that a side reaction would proceed simultaneously with copolymerization in Expt Nos. 8 and 9, because a strong absorption appeared at 1738 cm^{-1}. Accordingly, these two copolymers were not analyzed in the present research. Although two new absorptions appeared at 685 and 725 cm^{-1} in all copolymers, they

Table 1. Copolymerization of Acrylonitrile (M_1) with Allyl Chloride (M_2) by AIBN at 40 °C

Expt No.	Reaction conditions			Analytical data of product			
	M_2	M_1+M_2	Time	Yield	Chlorine content	M_2 units	$[\eta]$
	mol%	g	h	wt%	wt%	mol%	dL/g
1	0	22.46	1.25	2.70	0	0	8.0
2	3.73	24.01	2.5	3.94	0.42	0.63	9.2
3	7.31	23.52	3	4.76	0.87	1.31	5.9
4	8.68	23.73	7	4.95	1.03	1.55	4.5
5	13.23	25.81	8	6.62	1.64	2.48	—[a]
6	20.28	25.64	8.75	—	2.31	3.51	—
7	29.57	23.68	11.25	4.32	4.11	6.32	—
8	35.04	25.19	16.2	1.12	5.45	—	—
9	41.49	27.65	36	0.07	7.19	—	—

a) The products in Expt Nos. 5—9 were insoluble in DMF.

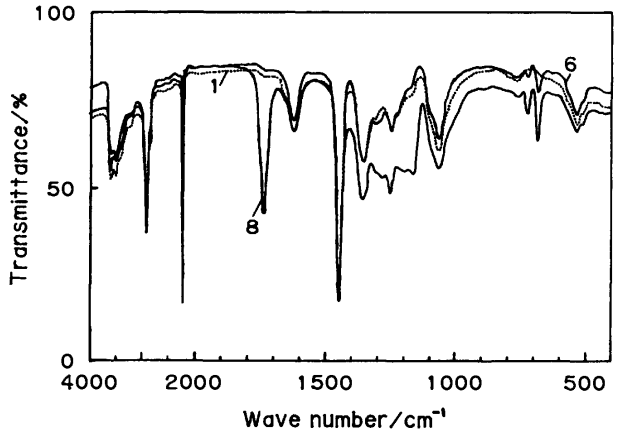

Fig. 1. IR absorption spectra of PAN and acrylonitrile-allyl chloride copolymers.
Arabic numerals used here are the same as Expt Nos. in Table 1. Concentration: Sample/KBr (mg/mg) = 1: 2.3/300, 6: 2.5/300, 8: 2.7/300.

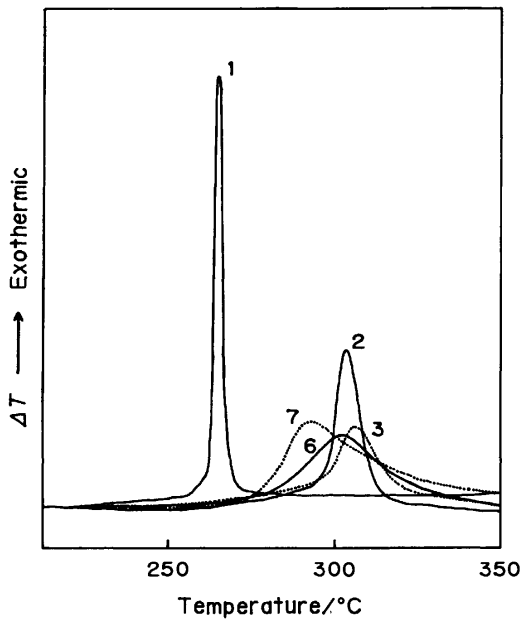

Fig. 2. DTA curves for PAN and acrylonitrile-allyl chloride copolymers.
Arabic numerals used here are the same as Expt Nos. in Table 1.

could be assigned to C–Cl stretching vibrations in allyl chloride units since their normalized absorbances[5] increased in proportion to the chlorine content.

During the present copolymerization the conversions were low as shown in Table 1. Therefore, the monomer reactivity ratios could be determined by the method of Fineman and Ross[6] using the composition of copolymers obtained in Expt Nos. 2—7. The values of r_1 and r_2 were calculated to be 6.04 and 0.035, respectively. Although the present copolymerization system was not ideal at 40 °C, it proved that favorable copolymers were obtained.

Thermal Analysis of Copolymers. Figure 2 shows the DTA curves for PAN and copolymers obtained in Expt Nos. 2, 3, 6, and 7. The weight losses at 350 °C are shown in Fig. 3. Even the DTA behavior of the copolymer which contained 0.42 wt% of chlorine (the content of allyl chloride units corresponding to 0.63 mol%) changed remarkably. Namely, the exotherm peak position due to the polymerization of cyano groups shifted more to the higher-temperature side (ca. 40 °C) than that for pure PAN. The value of ΔT became to about 1/3 in comparison with that for pure PAN. But the weight loss at 350 °C was not different from that for pure PAN (Fig. 3). When the chlorine content of the copolymer was 0.87, 1.03, or 1.64 wt% (the content of allyl chloride units corresponding to 1.31, 1.55, or 2.48 mol%), the exotherm peak position showed a somewhat greater shift to the higher-temperature side than that obtained for a

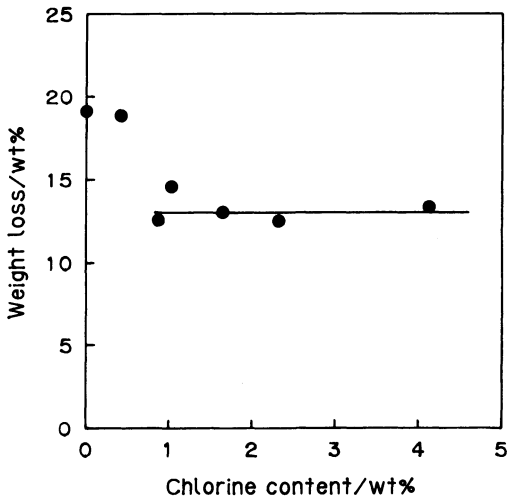

Fig. 3. Relationship between the chlorine content of copolymer and the weight loss at 350 °C.

copolymer containing 0.42 wt% of chlorine and ΔT decreased to about 1/6 in comparison with that for pure PAN. Moreover, the weight loss at 350 °C decreased from 19 wt% for PAN to 13 wt% for these copolymers (Fig. 3). Even if the chlorine content of copolymer was greater than 2 wt%, both ΔT and the weight loss didn't change again although the exotherm shifted to lower temperature side. Therefore, if allyl chloride is used as a comonomer, 1 wt% of chlorine is sufficient to change the behavior of the thermal degradation of PAN.

A similar behavior upon increasing the chlorine content has already been observed for acrylonitrile–CAN copolymers.[1,2] However, there was a great difference between allyl chloride and CAN units concerning the effect on the thermal degradation of PAN. When CAN was used as a comonomer, a sufficient chlorine content to change the behavior of thermal degradation of PAN was ca. 7 wt%. This indicates that regarding the effect of comonomer units, only 1.5 mol% of allyl chloride units corresponded to 10 mol% of CAN units. Consequently, HCl (and chlorine atoms) eliminated from the allyl chloride unit was more available than that eliminated from the CAN unit. This seems to have been caused by a difference in the temperature range in which each comonomer unit was dehydrochlorinated.

Finally, the chlorine and IR analyses of the copolymers which were heated to 350 °C at a rate of 5 °C min^{-1} were carried out. Since in every case both IR absorptions at 685 and 725 cm^{-1} disappeared after heating, it is clear that all allyl chloride units were dehydrochlorinated during heating. However, chlorine was detected in every case: after the heating of copolymers obtained in Expt Nos. 2—7, the chlorine contents were 0.11, 0.42, 0.44, 0.44, 1.06, and 1.35 wt%, respectively. The residual chlorine seems to have been combined as starting point of the polymerization of cyano groups.[1)]

References

1) M. Okamoto, T. Ogura, R. Ashikawa, and O. Ishizuka, *Nippon Kagaku Kaishi*, **1983**, 566.

2) N. Grassie and R. McGuchan, *Eur. Polym. J.*, **9**, 507 (1973).

3) F. R. Mayo, F. M. Lewis, and C. Walling, *J. Am. Chem. Soc.*, **70**, 1529 (1948).

4) M. Okamoto, C. Aoki, and O. Ishizuka, *Nippon Kagaku Kaishi*, **1977**, 103.

5) The absorbance a for w mg of copolymer was normalized by $A=a/w$, where A is the normalized absorbance.

6) M. Fineman and S. D. Ross, *J. Polym. Sci.*, **5**, 259 (1950).

Kinetics of Oxidation of Carbonyl Compounds by Peroxomonosulfate. Acetaldehyde, Propionaldehyde, and Butyraldehyde

M. S. RAMACHANDRAN,* T. S. VIVEKANANDAM, and V. ARUNACHALAM
School of Chemistry, Madurai Kamaraj University, Madurai-625 021, India
(Received April 25, 1985)

A kinetic study of oxidation of acetaldehyde, propionaldehyde, and butyraldehyde by peroxomonosulfate (PMS) in the presence of H^+ ion has been carried out. The reaction shows first order dependence each on [PMS] and [Aldehyde]. The reaction shows inverse first order over a particular concentration range of H^+ ion and beyond that first order dependence is observed with respect to [H^+]. The inverse hydrogen ion dependence on k_{obsd} may be due to the higher reactivity of SO_5^{2-} than HSO_5^- with aldehydes. The increase in k_{obsd} with increase in [H^+] beyond certain [H^+] can be explained by the formation of protonated carbonyl compounds. The Taft's plot gives ρ^* value of $\approx$5.0 indicating that the reaction is nucleophilic substitution at the carbonyl carbon which then rearranges to products.

In our previous paper[1] we have reported the results of kinetics of oxidations of formaldehyde, formic acid, and formate ion by peroxomonosulfate (PMS). We have observed, in the oxidation of formaldehyde by PMS, that SO_5^{2-} is more reactive than HSO_5^- and this is considered in favor of a nucleophilic substitution reaction of S_N2 type. Earlier workers[2] observed that the oxidation of aldehydes other than formaldehyde proceed through the enol form formed by the interaction between aldehydes and hydrogen ion. Since higher aldehydes, acetaldehyde, propionaldehyde, and butyraldehyde are enolizable, it would be interesting to study whether enol form of aldehydes will also involve in the kinetics. Aldehydes exist both in the hydrated form (*gem*-diol) as well as carbonyl form in aqueous solution.[3] Study of structure-reactivity relationship may throw some light on the nature of the aldehyde species involved in the oxidation reactions with PMS. With these views the kinetics of oxidations of the title aldehydes were undertaken and the results are discussed in this report.

Experimental

Acetaldehyde (SD's), propionaldehyde, butyraldehyde were purified by fractional distillation. Because of the high volatality of some of these aldehydes, the concentrations of the aqueous solutions were determined analytically; the Ponndorf's method[4] adopted by Seigel and Weiss[5] was used for all the aldehydes.

Potassium peroxomonosulfate (Du Pont) was used as such and all other chemicals were of analytical grade. The experimental details are discussed in Ref. 1.

Stoichiometry. The stoichiometry of the reactions were determined, at pH 4.0 and [H^+]=0.166 M (1 M=1 mol dm^{-3}), by taking a known excess of [PMS] over [Aldehydes]. The stoichiometry observed were identical at pH 4.0 and [H^+]=0.166 M and it could be represented as

$$RCHO + PMS \longrightarrow RCOOH \text{ (Product)}$$

Acetic acid was detected in the oxidation of acetaldehyde by spot tests.[6] Presence of carboxyl group in other two aldehydes were also confirmed.

Results and Discussion

Oxidations of the aldehydes were carried out under pseudo first-order conditions, with [Aldehydes] have been higher than, at least five times, that of [Peroxomonosulfate]. Analysis of the results indicates that the kinetics of oxidations of aldehydes by PMS are first order. Plots of log [PMS] versus time were linear even up to 70% conversion of [PMS]. The values of k_{obsd} were independent of [PMS]$_0$ and this shows that the order with respect to the [oxidant] is one.

An increase in the concentrations of the aldehydes causes a proportional increase in the rate constant at constant [H^+] and [PMS]. Plots of k_{obsd} versus [Aldehyde] are linear passing through origin (Fig. 1). This clearly proves the oxidations of aldehydes by PMS can be represented by the Eq. 1 as

$$\frac{-d[PMS]}{dt} = k'[\text{Aldehyde}][PMS], \quad (1)$$

where k' represents the rate constant at constant hydrogen ion concentration. The values of k' obtained are tabulated in Table 1.

The effect of hydrogen ion concentration on k_{obsd} was studied by varying the [H^+] from $\approx 10^{-4}$ to 0.166 M. In the high pH range, i.e. 4.4 to 3.6, the k_{obsd} decreases on decreasing the pH and the plots of k_{obsd} versus 1/[H^+] were linear with intercept (Fig. 2). The values of k_{obsd} are found to decrease with increase in [H^+] (3.5×10^{-3}—0.166 M) till a particular concentration of H^+ and then k_{obsd} increases with increase in [H^+] at constant [Aldehyde] (Table 2). The plots of k_{obsd} versus pH are found to be U-shaped curve (Fig. 3). This shows that different species are involved at different hydrogen ion concentration.

The change in ionic strength of the reaction medium shows a small increase in k_{obsd}. The kinetics

Table 1. Kinetic Parameters for the Oxidation of Aldehydes by PMS at 30 °C and μ=0.25

Substrate	k'[a]	k_1	k_2	$\Delta H^{\neq}$
	10^{-1} M^{-1} s^{-1}	10^{-2} M^{-1} s^{-1}	10^{4} M^{-1} s^{-1}	kcal mol^{-1}
Acetaldehyde	2.6	10.3	3.3	9.2
Propionaldehyde	2.0	5.1	3.3	10.1
Butyraldehyde	2.0	4.5	3.2	8.1

a) Values are at pH 4.0; 1 M=1 mol dm^{-3}. 1 cal=4.184 J.

Table 2. Dependence of k_{obsd} on [H$^+$] at 30 °C

[H$^+$]	$k_{obsd}/10^{-5}$ s^{-1}		
10^{-3} M	Acetaldehyde[a]	Propionaldehyde[b]	Butyraldehyde[c]
1.75	36.4	25.6	26.1
3.50	30.4	21.0	21.5
5.25	24.0	16.2	17.0
7.00	17.8	12.1	12.3
14.00	10.9	8.0	7.7
21.00	8.2	5.8	6.2
28.00	7.6	5.6	5.8
35.00	7.1	6.0	6.2
50.00	7.5	6.7	7.2
60.00	8.4	7.6	8.3
70.00	9.9	8.8	9.4
105.00	14.7	13.6	14.4
140.00	20.7	21.2	21.0
166.00	26.7	25.3	27.0

a) [Acetaldehyde]=5.6×10^{-3} M; [PMS]=10.5×10^{-4} M; μ=0.25. b) [Propionaldehyde]=7.05×10^{-3} M; [PMS]=10.5×10^{-4} M; μ=0.25. c) [Butyraldehyde]=6.65×10^{-3} M: μ=0.25.

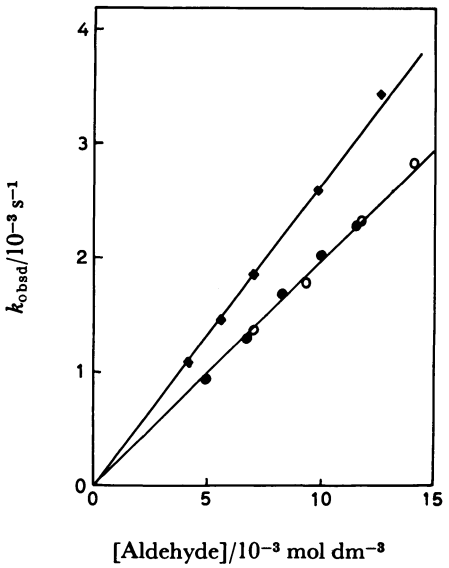

Fig. 1. Plot of k_{obsd} versus [Aldehyde]. [PMS]=10.5 × 10^{-4} mol dm^{-3}; pH=4.0; μ=0.25; t=30 °C. —■—: Acetaldehyde, —○—: Propionaldehyde, —●—: Butyraldehyde.

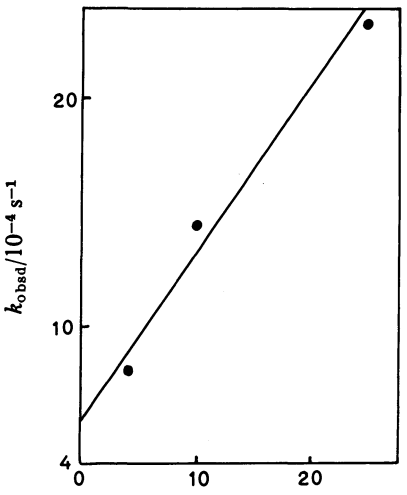

Fig. 2. Plot of k_{obsd} versus 1/[H$^+$] at 30 °C in the pH range 3.6—4.4. [Acetaldehyde]=5.6×10^{-3} mol dm^{-3}; [PMS]=10.5×10^{-4} mol dm^{-3}; μ=0.25.

of the reactions were studied at four different temperatures (30—45 °C) and from the temperature dependence of k_{obsd} the $\Delta H^{\neq}$ values are calculated and tabulated (Table 1).

In order that the proposed mechanism is realistic in accounting for many of the observed kinetic data, it is necessary to have a knowledge of the possible species of both the oxidant and the substrate and from this the choice of the correct or the most probable species responsible must be made under the existing conditions of the experiment. Peroxomonosulfate, in solution exists as HSO_5^- and SO_5^{2-} due to the equilibrium as in Eq. 2.

$$HSO_5^- \rightleftharpoons SO_5^{2-} + H^+ \quad (2)$$

The pK_a of the equilibrium[7] is 9.4 and therefore under the experimental conditions namely at pH 4.0 the oxidant exists predominantly as HSO_5^- and to a smaller extent as SO_5^{2-}.

It is well known that aliphatic aldehydes in aqueous solution are partially hydrated.[3] Aldehydes in acidic or neutral medium give various species due to different reactions such as keto-enol tautomerism, hydration, protonation or deprotonation of the *gem*-diol forms.

It was observed that in the oxidations of aliphatic aldehydes by some metal oxidants the rate determining reaction is the enolization of the aldehyde[2] and this enolization reaction is acid catalyzed as

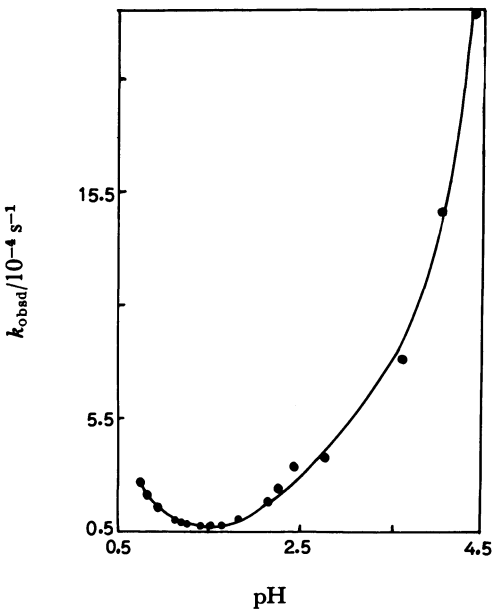

Fig. 3. Plot of k_{obsd} versus pH at 30 °C. [Acetaldehyde] $=5.6\times10^{-3}$ mol dm^{-3}; [PMS] $=10.5\times10^{-4}$ mol dm^{-3}; $\mu=0.25$.

$$RCH_2CHO + H^+ \overset{\text{fast}}{\rightleftharpoons} (RCH_2CHOH)^+, \quad (3)$$

$$(RCH_2CHOH)^+ \xrightarrow[\text{determining}]{\text{rate}} RCH{=}CHOH + H^+. \quad (4)$$

If this enolization were the rate determining reaction in the oxidation by PMS, then the rate of oxidations would be zero order with respect to PMS and the observed stoichiometry for the reaction should be greater than 1:1. The observed experimental facts namely the first order dependence of rate on [PMS] and 1:1 stoichiometry even at [H$^+$]=0.166 M clearly show that enolization reaction can be neglected and it would never be the rate determining reaction under the experimental conditions employed in the oxidations of aldehydes by PMS.

Carbonyl compounds are partially hydrated by water, the reaction being catalyzed by acids and bases.[3] The vast majority of the reactions with carbonyl compounds involve nucleophilic attack on the carbonyl carbon atom and the electrophilic attack, usually protonation, on the oxygen. The product formed between carbonyl compound and H$^+$ is responsible for acid catalysis.[8] Usually protonation of aliphatic carbonyl compounds are depicted as in Eq. 5.

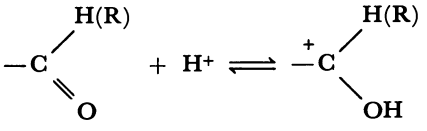

(5)

Extensive kinetic and spectral evidence indicates that protonated species is largely responsible for nucleophilic attack at the carbonyl carbon atom. Therefore we can safely assume that in aqueous solution and in the presence of hydrogen ion, aldehydes will exist as free aldehydic form, hydrated form (*gem*-diol) and protonated species.

Based on the experimental observation the most probable pathway will be

$$HSO_5^- \overset{K}{\rightleftharpoons} SO_5^{2-} + H^+, \quad (6)$$

$$\text{Aldehyde} + HSO_5^- \xrightarrow{k_1} \text{Products}, \quad (7)$$

$$\text{Aldehyde} + SO_5^{2-} \xrightarrow{k_2} \text{Products}. \quad (8)$$

As a first approximation, we can assume that at very low hydrogen ion concentration (pH 3.6 to 4.4) Eq. 5 can be neglected. Therefore at high pH the rate equation becomes

$$\frac{-d[PMS]}{dt} = k_1[\text{Aldehyde}][HSO_5^-] + k_2K\frac{[\text{Aldehyde}][HSO_5^-]}{[H^+]}$$

$$k_{obsd} = k_1[\text{Aldehyde}] + \frac{k_2K[\text{Aldehyde}]}{[H^+]}. \quad (9)$$

This equation explains the observed effect of [Aldehyde] and [H$^+$] (in the rage of pH 3.6 to 4.4) on k_{obsd}. At constant [H$^+$], the plots of k_{obsd} versus [Aldehyde] (Fig. 1) should give $(k_1+k_2K/[H^+])$ as slope which is equal to k' in Eq. 1. Similarly at constant [Aldehyde], plots of k_{obsd} versus $1/[H^+]$ should give k_2K[Aldehyde] as slope and k_1[Aldehyde] as intercept (Fig. 2). From the intercept and slope we can calculate the values of k_1 and k_2 knowing the literature value[7] of K as 3.98×10^{-10}. Perusal of the values in Table 1 shows that k_2 is approximately five order of magnitude greater than k_1. The higher reactivity of SO_5^{2-} than that of HSO_5^- may be considered to be in favor of nucleophilic attack by the peroxide.

Careful examination of the results in Table 2 shows that the protonation of the aldehydes (Eq. 5) is still less significant in the hydrogen ion concentration in the range of $1.75-21.0\times10^{-3}$ M (in the pH range of 1.68 to 2.76). In the k_{obsd} versus [H$^+$] curves, the effect of [H$^+$] in this range can also be explained by the Eq. 9. The values* for k_1' and k_2' are (at pH 1.68—2.76)

* For clarity the values of k_1 and k_2 obtained in the hydrogen ion concentrations ($1.75-21.0\times10^{-3}$ M) are denoted as k_1' and k_2'. In the plot of k_{obsd} versus $1/[H^+]$ the data point corresponding to [H$^+$] $=1.75\times10^{-3}$ M deviates from the straight line in all these three aldehydes. All other points fit well nicely in the plot and therefore the point corresponding to [H$^+$] $=1.75\times10^{-3}$ M was omitted in the plot to calculate k_1' and k_2'.

	k_1' $M^{-1}s^{-1}$	k_2' $M^{-1}s^{-1}$
Acetaldehyde	7.5×10^{-3}	4.5×10^{5},
Propionaldehyde	4.2×10^{-3}	3.4×10^{5},
Butyraldehyde	4.5×10^{-3}	2.6×10^{5}.

According to Eq. 9, the values of k_1 and k_2 should be independent of H^+ concentration range used. However, comparison of the values of k_1' and k_2' with those of k_1 and k_2 in Table 1 shows that k_1' is ten times smaller than k_1 and $k_2'\approx10k_2$. In this acid range (pH 1.68—2.76) the reactivity of SO_5^{2-} towards aldehyde is approximately eight order of magnitude greater than HSO_5^- which coincides with the results obtained in the oxidation of DMSO by PMS in acid media.[9] Similar discrepancy in the values of k_1 and k_2 with k_1' and k_2' was also observed in the oxidation of formaldehyde by PMS.[1] This discrepancy may probably be due to the fact that the equation used to calculate the concentrations of HSO_5^- and SO_5^{2-} may not be correct since the experimental pH was far away from the pK_a value of PMS (9.4).[7]

At very high hydrogen ion concentrations (35—166×10^{-3} M, pH 0.78 to 1.46), the observed effect of hydrogen ion on k_{obsd} can be explained by the catalytic effect of hydrogen ion due to the formation of protonated aldehydes as in Eq. 5. In this high hydrogen ion concentration range also the values of k_{obsd} were found to be independent of $[PMS]_0$ at constant $[H^+]$ and [Aldehyde]. This observation helps us to eliminate the possibility of the acid catalyzed hydrolysis of PMS similar to those observed in other peroxides. Further the plots k_{obsd} versus [Aldehyde] at constant $[H^+]$ were found to be linear passing through origin even at this high $[H^+]$. These observations clearly show that acid catalysis, the addition of H^+ on the RCHO to give $RCHOH^+$ which reacts with PMS to give product, is also occurring to a significant extent as

$$RCHO + H^+ \overset{K_1}{\rightleftharpoons} RCHOH, \quad (10)$$

$$RCHOH^+ + PMS \xrightarrow{k_3} \text{Products}, \quad (11)$$

$$RCHO + PMS \xrightarrow{k} \text{Products}. \quad (12)$$

Under these conditions, the rate law becomes

$$k_{obsd} = k_3K_1[RCHO][H^+] + k[RCHO] \quad (13)$$

and this equation explains the observed experimental facts at high $[H^+]$. The magnitude of K_1 may be small so that this catalytic effect have a pronounced effect on k_{obsd} only when $[H^+]>50\times10^{-3}$ M. No such catalytic effect was observed in the oxidation of formaldehyde by PMS even when $[H^+]>100\times10^{-3}$ M. The values of k_3K_1 obtained from the plot of k_{obsd} versus $[H^+]$ are grouped in Table 3.

So far the total analytical concentration of aldehyde is used to evaluate the kinetic parameters tabulated in Table 1. Turning now to the participation of the aldehydes in the keto or in the hydrated form, the relative rate constants can be computed by considering in turn one of the two forms as the only active species as

$$k^H = k_{total}(K_d+1)$$
$$k^{CO} = k_{total}(1+K_d^{-1})$$

where k^H, k^{CO}, and k_{total} represent the rate constants for the hydrated form, keto form, and observed rate constant for total analytical concentration of aldehydes, respectively. K_d represents the hydration equilibrium of aldehydes as

$$RCHO + H_2O \rightleftharpoons RCH(OH)_2$$
$$K_d=[RCHO]/[RCH(OH)_2]$$

In Table 4, the values of k_1, k_2, k_1^H, k_2^H, k_1^{CO}, and k_2^{CO} are given along with the values[10-13] of K_d and

Table 3.

Substrate	K_1k_3	$K_1k_3^{CO}$ a)
	10^{-2} $M^{-2}s^{-1}$	10^{-2} $M^{-2}s^{-1}$
Acetaldehyde	31.2	77.8
Propionaldehyde	24.8	42.4
Butyraldehyde	26.3	38.9

a) Values given in this heading correspond to the keto form values of [RCHO].

Table 4.

R in CHO	k_1 10^{-2} $M^{-1}s^{-1}$	k_2 10^{4} $M^{-1}s^{-1}$	k_1^H a) 10^{-2} $M^{-1}s^{-1}$	k_2^H a) 10^{4} $M^{-1}s^{-1}$	k_1^{CO} b) 10^{-2} $M^{-1}s^{-1}$	k_2^{CO} b) 10^{4} $M^{-1}s^{-1}$	K_d	σ^* c)
H	4.0	3.7	4.1	3.7	7204	6666	5.55×10^{-4} d)	0.490
CH_3	10.3	3.3	17.2	5.5	25.6	8.3	0.671e)	0.000
CH_3CH_2	5.1	3.3	12.2	7.9	8.7	5.7	1.408f)	−0.100
$CH_3CH_2CH_2$	4.5	3.2	13.9	9.9	6.7	4.8	2.083g)	−0.115

a) Rate corresponding to the hydrated form. b) Rate corresponding to the carbonyl form. c) Ref. 14. d) Ref. 10. e) Ref. 11. f) Ref. 12. g) Ref. 13.

Taft's polar substituent constants[14] σ^*.

If RCHO (keto form) is the active form, the reactivity would be depressed by a factor of ca. $\approx 10^3$ between the extremes in the order HCHO>BuCHO and the values in Table 4 bring out our expectation, whereas no regularity is observed for the hydrated form.

The rates of PMS oxidation of the aldehydes relative to that of acetaldehyde can be obtained by dividing k_1/k_2 of the aldehyde by that of acetaldehyde.** A plot of log $(k_1/k_{1\,\text{acetaldehyde}})^{H}$ or log $(k_2/k_{2\,\text{acetaldehyde}})^{H}$ versus σ^* was much less satisfactory whereas log $(k_1/k_{1\,\text{acetaldehyde}})^{CO}$ or log $(k_2/k_{2\,\text{acetaldehyde}})^{CO}$ versus σ^* is a good straight line (Fig. 4) with a slope (reaction susceptibility constant ρ^*) of +5.0 and +4.75, respectively.

According to reactivity-selectivity principle,[15-17] the more reactive substrate/oxidant should be less selective than the less reactive one. Since SO_5^{2-} is $\approx 10^6$ times more reactive than HSO_5^-, it should be less selective and hence the observed ρ^* should be less than that for the HSO_5^-. But it would be surprising to note that the reaction susceptibility constants (ρ^*) for the oxidations by HSO_5^- and SO_5^{2-} are almost same and it seems to be an apparent violation of reactivity-selectivity principle. This can be explained if the following reaction schemes are considered for the oxidations by SO_5^{2-} and HSO_5^-.

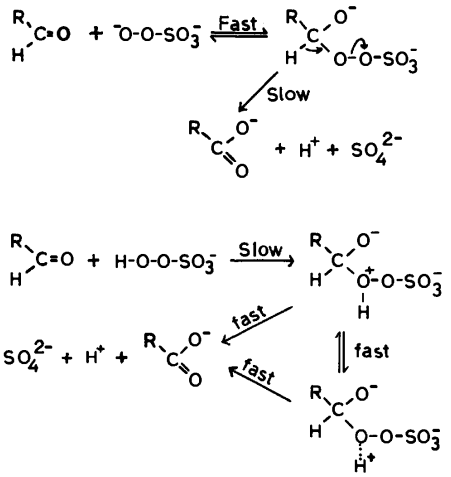

According to the tetrahedral mechanism of nucleophilic substitution at the carbonyl group,[18] the nucleophile adds on to the trigonal carbonyl carbon to give a tetrahedral intermediate which then decomposes in the rate determining step to give the product. The observed ρ^*_{obsd} for the oxidations of aldehyde by SO_5^{2-} is the combination of the ρ^*s for nucleophilic addition ρ^*_{NA} and the elimination ρ^*_{ES}, i.e. the decomposition into the product as

** Because the values of k_1 and k_2 obtained at high pH range are assumed to be free from other side reactions, these values are used in the correlation analysis.

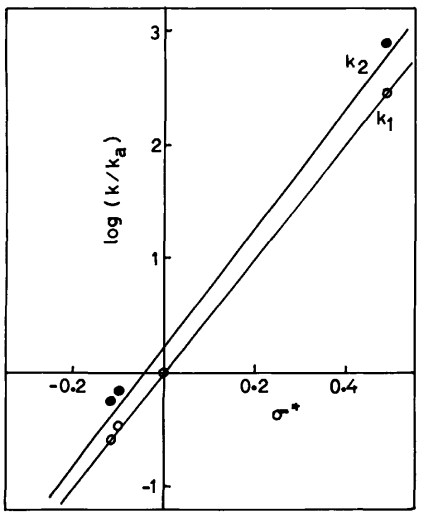

Fig. 4. Taft's plot. k_a represents the rate of acetaldehyde.

$$\rho^*_{obsd} = \rho^*_{NA} + \rho^*_{ES}$$

The value of ρ^*_{NA} should be positive and ρ^*_{ES} depends upon the combined opposing influence of the substituent on both the leaving groups/reactions; i.e. C–H which separates as H^+ and also C–O–O–SO_3^- group to give C=O and SO_4^{2-}. The large positive ρ^*_{obsd} shows that the ρ^*_{ES} may also be positive, otherwise ρ^*_{NA} would have a value greater than ρ^*_{obsd}. This means that the highly reactive nucleophile SO_5^{2-} is more selective and this is more unlikely. The observed ρ^*_{obsd} corresponding to k_1, i.e. oxidation by HSO_5^-, is only due to the nucleophilic substitution at the trigonal carbonyl carbon which may be a slow and rate determining step. This clearly explains that though it appears as a violation of reactivity-selectivity principle actually this is not the case since reactivity-selectivity principle can be applied only to the reactions involving same mechanistic pathways.[16,17] The same ρ^* values observed for k_1 and k_2 may be a fortuitous coincidence.

The structure-reactivity analysis can also be made for the acid catalyzed reaction also. The values of k_3K_1 corresponding to the keto form ($k_3K_1^{CO}$) are also given in Table 3. The electronic effect of the substituents would have opposing effects on K_1 and k_3; the electron-releasing substituents would increase the equilibrium constant K_1 whereas it would decreases the rate k_3. The Taft's plot for the hydrogen ion catalyzed reaction,

$$\log (k'/k'_{\text{acetaldehyde}}) = {}^{H^+}\rho^*_{obsd}\sigma^*,$$

where $k'=k_3K_1$, will give the susceptibility parameter (reaction constant) ${}^{H^+}\rho^*_{obsd}$ which is the combination of ${}^{H^+}\rho^*$ due to Eqs. 10 and 11 as

$${}^{H^+}\rho^*_{obsd} = {}^{H^+}\rho^*_{K_1} + {}^{H^+}\rho^*_{k_3}$$

The value of ${}^{H^+}\rho^*_{k_3}$ would be positive and greater than or at least equal to five since the ρ^* value for the aldehyde reactions with PMS is +5.0 (vide supra). Since the value of ${}^{H^+}\rho^*_{k_1}$ should be negative, the value of ${}^{H^+}\rho^*_{obsd}$ depends upon the magnitude of ${}^{H^+}\rho^*_{k_1}$. The value obtained for ${}^{H^+}\rho^*_{obsd}$ is +2.6 and this shows that the magnitude of ${}^{H^+}\rho^*_{k_1}$ is less than ${}^{H^+}\rho^*_{k_3}$. However it should be pointed out at this point that the above discussions are only qualitative since the Taft's plots are made only with the σ^* over a small and close range. The values of ρ^*s will not be accurate and we can not rely upon these numerical values. Therefore the above foregoing discussions should only be considered as an additional evidence which helps us in proposing the reaction scheme. However the value obtained in the analysis of acid catalyzed reaction helps us to explain why formaldehyde does not show the acid catalyzed reaction in our experimental conditions. According to the value of ${}^{H^+}\rho^*_{obsd}$, the value of k_3K_1 should be 8.3×10^{-3} which is hundred times lesser than the observed values of k_3K_1 for other aldehydes. Therefore we would have observed the acid catalyzed reaction of formaldehyde oxidation by PMS at very high hydrogen ion concentration. This shows although the results are qualitative in nature they are in the correct direction.

The authors acknowledge Prof. N. R. Subbaratnam for his constant encouragements and facilities. M. S. R. acknowledges the U. G. C., New Delhi for the financial assistance (Code No. 277). V. A. expresses his gratitude to the U. G. C. and the authorities of Thiruvalluvar College, Papanasam, for the grant of F. I. P. Fellowship. The authors also acknowledge the referees for their constructive criticisms and suggestions.

References

1) M. S. Ramachandran and T. S. Vivekanandam, communicated.
2) T. J. Kemp "Comprehensive Chemical Kinetics," ed by C. H. Bamford and C. F. H. Tipper, Elsevier, New York (1972), Vol. 7, p. 4.
3) R. P. Bell, *Adv. Phys. Org. Chem.*, **4**, 1 (1968).
4) W. Ponndorf, *Ber. Deutsch. Chem. Ges.*, **64**, 1913 (1931).
5) H. Seigel and E. T. Weiss, *Anal. Chem.*, **26**, 917 (1954).
6) F. Feigel, "Spot Tests in Organic Analysis," English edition, Elsevier, London (1956), p. 619.
7) D. O. Ball and J. O. Edwards, *J. Am. Chem. Soc.*, **78**, 1125 (1956).
8) W. P. Jencks, *Prog. Phys. Org. Chem.*, **2**, 63 (1964).
9) T. Pandurengan and P. Maruthamuthu, *Bull. Chem. Soc. Jpn.*, **54**, 3551 (1981).
10) P. Valenta, *Coll. Czech. Chem. Commun.*, **25**, 853 (1960).
11) R. P. Ball and J. C. Clunie, *Trans. Faraday Soc.*, **48**, 439 (1952).
12) E. Lombardi and P. B. Sogo, *J. Chem. Phys.*, **32**, 635 (1960).
13) L. C. Gruen and P. T. McTigue, *J. Chem. Soc.*, **1962**, 5217.
14) R. W. Taft "Steric Effect in Organic Chemistry," ed by N. S. Newman, Wiley, New York (1956), p. 619.
15) C. D. Johnson, *Chem. Rev.*, **75**, 755 (1975).
16) E. Buncell and C. Chuaqui, *J. Org. Chem.*, **45**, 2825 (1980).
17) E. Buncell, H. Wilson, and C. Chuaqui, *J. Am. Chem. Soc.*, **104**, 4896 (1982).
18) J. March, "Advanced Organic Chemistry: Reactions, Mechanisms and Structure," 2nd ed, McGraw-Hill International, Tokyo (1977), p. 307.

 © 1986 The Chemical Society of Japan Bull. Chem. Soc. Jpn., 59, 1555—1560 (1986)

Viscosity *B*-Coefficients of 1:1 Electrolytes in Acetonitrile-Water Mixtures at 25 and 35 °C

Gopu KUMAR,* Nibaran C. DEY, Birendra K. SAIKIA, and Inamul HAQUE†
Regional Research Laboratory, Jorhat, Assam, India
†Department of Chemistry, Dibrugarh University, Dibrugarh, Assam, India
(Received June 20, 1985)

Viscosity *B*-coefficients of the Jones-Dole equation were determined for KCl, KBr, KI, NaBr, CsI, Me_4NBr, Et_4NBr, n-Pr_4NI, n-Bu_4NBr, and $Na[BPh_4]$ at 25 and 35 °C in various acetonitrile–H_2O mixtures. The *B*-coefficients were split into the ionic components and a comparison was made among different methods available. The effective flow volume, V_e° obtained from $B=2.5\,V_e^\circ$ was compared with the crystal ionic volume, V_{cryst}° and the ionic partial molar volume, $\overline{V}_{ion}^\circ$ determined from the density experiments simultaneously carried out. Ion-solvent and solvent-solvent interactions were discussed in terms of the above parameters.

Microviscosity determination of electrolytes in aqueous solutions as well as in nonaqueous solutions have been carried out in order to throw light on the nature of ion-solvent interactions. Recently, such measurements have also been reported for water-organic binary solvent system. In a previous communication,[1] we have tried to evaluate the nature of ion-solvent interactions in DMF–H_2O binary solvent. We found that the use of a large number of electrolytes of known behavior provided useful information on the effects induced by the cosolvent on the 'water-structure'. Interesting results were obtained by previous workers on the viscosity and transport properties of electrolytes in pure acetonitrile.[2] Recently some works have been reported on the ultrasonic,[3] transport,[4] and thermodynamic[5] properties of the binary mixture of acetonitrile–H_2O system. However, no work has been reported on the viscosity of electrolytes in acetonitrile–H_2O solvent system. We therefore, thought it timely to extend our previous work[1] to this solvent system. In this paper we report the viscosity and density data of large number of uni-univalent electrolytes in various acetonitrile–H_2O mixtures at 25 and 35 °C. The primary objective of this study is to investigate the nature of ion-solvent interactions and hence throw light on the nature of effects induced by acetonitrile on the 'water-structure'.

Experimental

KCl, KBr (BDH, AR), KI, NaBr (E. Merck), CsI (Sisco, >99% pure), and $Na[BPh_4]$ (Sigma) were used without further purification. Laboratory grade Me_4NBr (Fluka, USA) and Et_4NBr (BDH) were purified as described elsewhere.[6] n-Pr_4NBr and n-Bu_4NBr (Fluka, puriss) were purified as described by Conway et al.[7] n-Pr_4NI (Fluka, puriss) was recrystallized from acetone (E. Merck) by adding ether. The salts were stored in vacuum desiccator and dried for 3 to 4 h at 100 °C prior to use. Acetonitrile was purified as described elsewhere.[8] Its density, viscosity, and refractive index at 25 °C compared well with the reported values.[9] Laboratory grade distilled water was redistilled over $KMnO_4$ in an all glass unit. Freshly distilled water was used to make all solutions.

Densities of the solutions were measured using a 45 ml single stem capillary pycnometer having a capillary diameter of 1.5 mm and were vacuum corrected. The values are precise to 5×10^{-5} g cm^{-3}. Viscosity of dilute solutions were measured using an Ubbelohde suspended level viscometer having a fall time of 1130.2 s for water at 25 °C. The kinetic energy correction term for the viscometer fell in the region of experimental error and, therefore, was neglected. All measurements were carried out in a thermostatic water bath with an accuracy of ±0.01 °C. The relative viscosities determined were precise to 0.05%.

Results and Discussion

The relative viscosity of KCl, KBr, KI, NaBr, CsI, Me_4NBr, Et_4NBr, n-Pr_4NI, and n-Bu_4NBr at 25 and 35 °C and for $Na[BPh_4]$ at 25 °C were determined in 20, 40, 60, and 80% weight percent acetonitrile–H_2O binary mixtures corresponding to 0.099, 0.226, 0.397, and 0.637 mol fraction of acetonitrile. Viscosity data were analyzed by the Jones-Dole equation:[10]

$$\eta_r = \eta/\eta_o = 1 + AC^{1/2} + BC. \quad (1)$$

Plots of $(\eta_r-1)/C^{1/2}$ vs. $C^{1/2}$ for observed viscosity data were found to be linear. The least square values of A, B, and δ, the RMS deviation of the experimental and calculated relative viscosity values are presented in Table 1. The *B*-coefficients of KCl, KBr, KI, NaBr, CsI, and Me_4NBr increase with increase in acetonitrile concentration of the binary solvent. Et_4NBr has a *B*-value fairly constant and increases only at higher acetonitrile concentration. However, for each composition of the solvent the *B*-value changes in the order KCl>KBr>KI>CsI and NaBr>KBr. The *B*-value of n-Pr_4NI and n-Bu_4NBr shows an initial decrease with increase in acetonitrile concentration, reaches a minimum between 40 and 60% acetonitrile concentration, and then increases with further increase in acetonitrile concentration. It has been observed[1] that n-Pr_4NBr behaved in a qualitatively similar fashion in DMF–H_2O mixtures. However, n-

Table 1. Least Square Values of Coefficients A($dm^{3/2}\,mol^{-1/2}$) and B($dm^3\,mol^{-1}$) of Eq. 1

% Acetonitrile[a]	Temp/°C		KCl	KBr	KI	CsI	NaBr	Me_4NBr	Et_4NBr	n-Pr_4NI	n-Bu_4NBr	$Na[BPh_4]$
0[b]	25	A	0.005	0.005	0.005	0.004	—	0.007	0.008	—	0.008	—
		B	−0.0140	−0.0490	−0.076	−0.118	0.053	0.101	0.343	0.82	1.148	—
	35	A	0.006	0.005	0.005	0.007	0.007	—	—	—	—	—
		B	0.0098	−0.026	−0.0485	−0.103	0.067	0.100	0.320	0.73	1.12	—
20	25	A	0.018	0.017	0.008	0.005	0.005	0.008	0.007	0.009	0.016	0.024
		B	0.015	−0.003	−0.031	−0.076	0.081	0.100	0.318	0.548	0.844	1.96
		$\delta\times10^4$	0.68	1.67	1.17	2.20	0.66	1.16	1.26	1.44	1.44	1.03
	35	A	0.020	0.014	0.016	0.015	0.008	0.009	0.006	0.013	0.012	—
		B	0.030	0.016	−0.012	−0.054	0.115	0.120	0.322	0.485	0.736	—
		$\delta\times10_4$	1.22	0.83	1.77	1.44	0.91	0.97	0.91	1.59	1.57	—
40	25	A	0.016	0.011	0.012	0.012	0.012	0.006	0.012	0.012	0.013	0.033
		B	0.181	0.143	0.071	0.052	0.193	0.219	0.322	0.474	0.750	1.77
		$\delta\times10^4$	1.05	2.48	2.09	0.49	2.72	1.61	0.76	0.58	2.76	0.89
	35	A	0.022	0.021	0.004	0.011	0.009	0.010	0.008	0.017	0.020	—
		B	0.196	0.163	0.106	0.081	0.234	0.247	0.320	0.393	0.626	—
		$\delta\times10^4$	1.52	3.97	2.26	1.55	2.61	3.73	2.75	2.38	0.00	—
60	25	A	0.020	0.016	0.015	0.021	0.031	0.010	0.019	0.005	0.009	0.017
		B	0.344	0.290	0.211	0.172	0.306	0.322	0.368	0.498	0.719	1.50
		$\delta\times10^4$	1.48	0.87	1.75	1.04	1.57	1.34	2.97	1.82	3.14	2.20
	35	A	0.020	0.013	0.013	0.016	0.017	0.008	0.027	0.018	0.021	—
		B	0.387	0.315	0.243	0.215	0.346	0.337	0.344	0.467	0.647	—
		$\delta\times10^4$	2.07	2.44	2.24	0.61	2.20	2.08	3.53	2.75	1.00	—
80	25	A	0.029	0.014	0.016	0.040	0.013	0.023	0.010	0.010	0.017	0.015
		B	0.508	0.417	0.372	0.300	0.490	0.403	0.530	0.602	0.748	1.12
		$\delta\times10^4$	0.73	1.00	2.48	0.73	1.55	1.59	2.42	1.90	1.75	1.57
	35	A	0.041	0.024	0.012	0.028	0.014	0.016	0.027	0.012	0.020	—
		B	0.552	0.468	0.413	0.338	0.540	0.434	0.473	0.587	0.719	—
		$\delta\times10^4$	0.76	1.31	2.28	2.05	2.14	2.51	1.31	2.11	1.99	—

a) Weight % AN. b) Values of A and B for pure water (except for data of CsI; $10^4\delta=2.00$ and NaBr; $10^4\delta=1.11$ at 35 °C) from Refs. 14, 19, and 20.

Bu_4NBr did not exhibit a minimum in DMF-H_2O solvent system.

In order to get an accurate information about the ion-solvent interactions, it is necessary to evaluate the contribution of the individual ionic species to the viscosity B-coefficients. However, no absolute method of such a computation is available even for pure water solvent. The most popular method of dividing the viscosity B-coefficients into ionic components arises from the observation that K^+ and Cl^- ions behave very similarly in ionic mobility and, therefore, it is likely that $B_{K^+}=B_{Cl^-}$. This method was used by Gurney[11] and subsequently by Kaminsky[12] and others. However, the method has never been free of criticism. Nightingale[13] considered that from mobility grounds RbCl or CsCl should have been more appropriate than KCl. Subsequently Desnoyers and Perron[14] proposed a splitting method in which they assumed that Et_4N^+ ion is neither a structure-breaker nor a structure-former. By assuming the hydrodynamic volume to be equal to the partial molar volume, they calculated the B_{ion} value for Et_4N^+ ion to be 0.3593 $dm^3\,mol^{-1}$. Using this value the B_{ion} values calculated for other ions in water showed comparable values to those obtained by the method of Kaminsky, i.e., $B_{K^+}=B_{Cl^-}$. Very recently Jenkins and Pritchett[15] made use of Krumgalz's suggestions alternative to Gurney's assumption and came to the conclusion that $B_{Cs^+}=B_{I^-}$ is a more reasonable approximation.

In the light of the above discussions it is imperative that any method of splitting B-coefficients into the ionic components for binary solvent system is not likely to be free of the criticisms which apply in pure water. We, therefore, decided to compare the B_{ion} values obtained by the various methods from the experimental B-values. Table 2 lists the B_{ion} values obtained by three different methods, i.e., (i) on the basis of $B_{K^+}=B_{Cl^-}$; (ii) assuming $B_{Et_4N^+}=0.3593$ $dm^3\,mol^{-1}$ and (iii) by using $B_{Cs^+}=B_{I^-}$.

From Table 2 we find that the B_{ion} values obtained by methods (i) and (iii) are comparable only in water

and low concentration of acetonitrile. However, with increasing acetonitrile concentration the values by the above two methods deviate beyond experimental error. Also, B_{ion} values obtained by method (ii) do not agree in any rate either with those obtained by method (i) or (iii). Interesting results are obtained in 80% acetonitrile concentration where all the three methods give close results for B_{ion} with a deviation of ± 0.032 dm^3 mol^{-1} between methods (i) and (iii) and the results by method (ii) falling in between. This close agreement is surprising considering the large magnitude of the B_{ion} values of alkali and halide ions and also the normally large values of tetraalkylammonium ions.

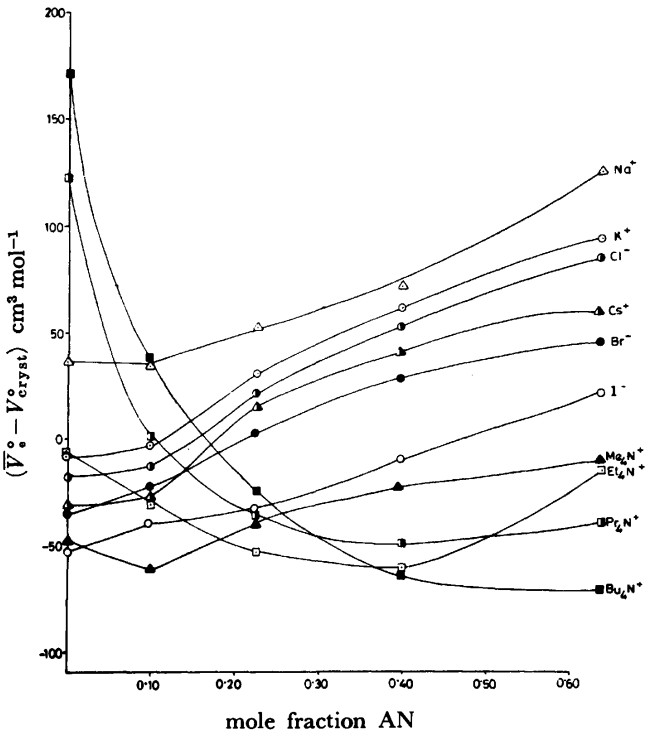

Fig. 1. Variation of $(\overline{V}^{\circ}_{e} - V^{\circ}_{cryst})$ with mole fraction of acetonitrile (AN) at 25 °C. B_{ion} on basis of $B_{K^+} = B_{Cl^-}$.

Eagland and Pilling[6] considered that $B = 2.5\, V^{\circ}_{e}$, where V°_{e} is the volume fraction of the solute molecules together with solvent molecules which are immobilized by the solute molecules because of the primary hydration. Like B_{ion}, $\overline{V}^{\circ}_{e}$ (for ion) would be sensitive to ion-dipole and structure-breaking effects. It would, therefore, be interesting to have a close look at the interaction effects by substracting V°_{cryst} from $\overline{V}^{\circ}_{e}$ values where V°_{cryst} is the crystal ionic volume derived from Pauling crystal radii. Figures 1—3 show the values of $(\overline{V}^{\circ}_{e} - V^{\circ}_{cryst})$ obtained by methods (i)—(iii), respectively. It is interesting to note that $(\overline{V}^{\circ}_{e} - V^{\circ}_{cryst})$ values for Na$^+$, K$^+$, Cs$^+$, Cl$^-$, Br$^-$, and I$^-$ in Fig. 1 increase slowly with increase in acetonitrile concentration of the binary solvent upto about 40% of acetonitrile followed by a steep increase with further increase of acetonitrile concentration. For n-Pr$_4$N$^+$ and n-Bu$_4$N$^+$, $(\overline{V}^{\circ}_{e} - V^{\circ}_{cryst})$ values steeply decrease initially with increase in acetonitrile concentration and finally show a slight increase for n-Pr$_4$N$^+$ only at 80% acetonitrile concentration. The behaviors of the above electrolytes are identical in Fig. 3. Me$_4$N$^+$ and Et$_4$N$^+$ show a more regular change in Fig. 3 compared to Fig. 1 (probably due to small experimental errors involved). However, a somewhat different trend is observed in Fig. 2; for K$^+$, Cs$^+$, and Me$_4$N$^+$ ions $(\overline{V}^{\circ}_{e} - V^{\circ}_{cryst})$ values first increase upto 60% acetonitrile concentration and then decrease at 80% acetonitrile concentration, and for Cl$^-$, Br$^-$, and I$^-$ ions the values first decrease and then increase. A

Table 2. Ionic B-coefficients at 25 °C

% Acetonitrile		Na$^+$	K$^+$	Cs$^+$	Cl$^-$	Br$^-$	I$^-$	Me$_4$N$^+$	Et$_4$N$^+$	n-Pr$_4$N$^+$	n-Bu$_4$N$^+$	[BPh$_4$]$^-$
0	i	0.095	−0.007	−0.049	−0.007	−0.042	−0.069	0.143	0.385	0.889	1.190	—
	ii	0.069	−0.033	−0.075	0.019	−0.016	−0.043	0.117	—	0.863	1.164	—
	iii	0.085	−0.017	−0.059	0.003	−0.032	−0.059	0.133	0.375	0.879	1.180	—
20	i	0.091	0.007	−0.038	0.007	−0.010	−0.038	0.110	0.328	0.586	0.854	1.87
	ii	0.123	0.039	−0.006	−0.025	−0.042	−0.070	0.142	—	0.618	0.886	1.84
	iii	0.091	0.007	−0.038	0.007	−0.010	−0.038	0.110	0.328	0.586	0.854	1.87
40	i	0.140	0.090	0.071	0.090	0.053	−0.019	0.166	0.269	0.493	0.697	1.63
	ii	0.231	0.181	0.162	0.000	−0.038	−0.110	0.257	—	0.584	0.788	1.54
	iii	0.095	0.045	0.026	0.136	0.098	0.026	0.121	0.224	0.448	0.652	1.68
60	i	0.188	0.172	0.133	0.172	0.118	0.039	0.204	0.250	0.459	0.601	1.31
	ii	0.298	0.282	0.243	0.062	0.008	−0.071	0.314	—	0.569	0.711	1.20
	iii	0.141	0.125	0.086	0.219	0.165	0.086	0.157	0.203	0.412	0.554	1.36
80	i	0.327	0.254	0.182	0.254	0.163	0.118	0.240	0.367	0.484	0.585	0.793
	ii	0.319	0.246	0.174	0.262	0.171	0.126	0.232	—	0.476	0.577	0.801
	iii	0.295	0.222	0.150	0.286	0.195	0.150	0.208	0.335	0.452	0.553	0.825

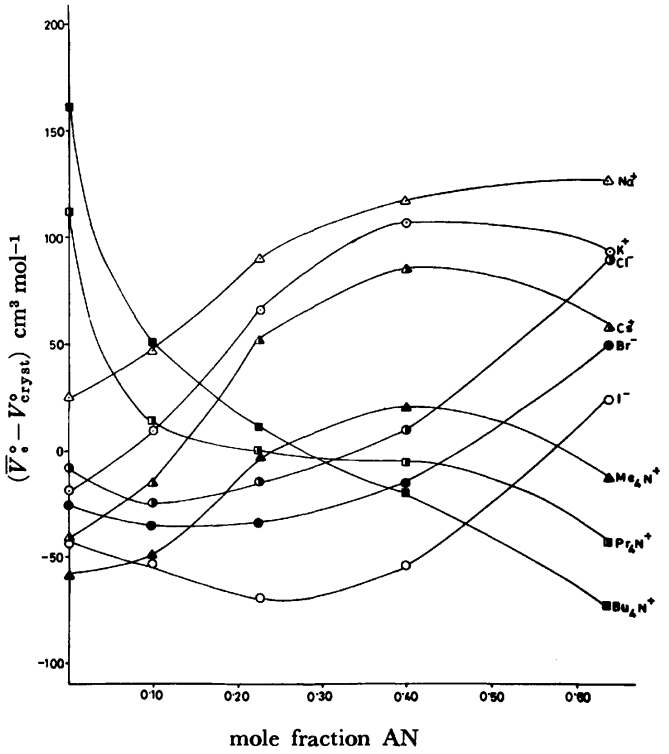

Fig. 2. Variation of $(\bar{V}_e^\circ - V_{cryst}^\circ)$ with mole fraction of acetonitrile (AN) at 25 °C. B_{ion} on the basis of $B_{Et_4N^+} = 0.3593$ mol^{-1} dm^3.

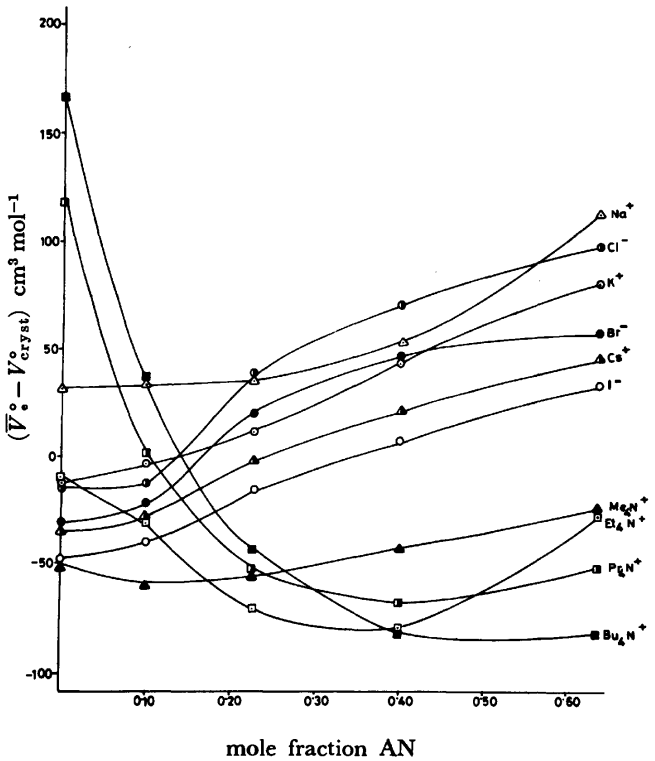

Fig. 3. Variation of $(\bar{V}_e^\circ - V_{cryst}^\circ)$ with mole fraction of acetonitrile (AN) at 25 °C. B_{ion} on basis of $B_{Cs^+} = B_{I^-}$.

Table 3. $\Delta B/\Delta T$ Coefficients in Acetonitrile-Water Mixtures in the Range 25—35 °C

$(\Delta B/\Delta T)$/dm³ mol⁻¹ K⁻¹	% Acetonitrile				
	0	20	40	60	80
KCl	0.0024	0.0016	0.0015	0.0043	0.0044
KBr	0.0023	0.0019	0.0020	0.0025	0.0051
KI	0.0027	0.0019	0.0035	0.0032	0.0041
CsI	0.0015	0.0022	0.0030	0.0043	0.0038
NaBr	0.0014	0.0034	0.0041	0.0040	0.0050
Me_4NBr	−0.0001	0.0020	0.0028	0.0015	0.0031
Et_4NBr	−0.0023	0.0004	−0.0002	−0.0024	−0.0057
n-Pr_4NI	−0.0090	−0.0063	−0.0081	−0.0031	−0.0015
n-Bu_4NBr	−0.0028	−0.0108	−0.0124	−0.0072	−0.0029

decrease of $(\bar{V}_e^\circ - V_{cryst}^\circ)$ for K^+, Cs^+, and Me_4N^+ ions with increase in acetonitrile concentration cannot be explained in view of the fact that all these ions have a stronger electrostriction in acetonitrile relative to water.[16] Therefore, $B_{Et_4N^+}$ probably cannot be taken as a constant for the splitting in this solvent. It is however, not possible to comment on the relative merit of methods (i) and (iii) without a detailed knowledge of the actual interactions taking place. But, for all practical purposes, both methods give B_{ion} values which are very close, particularly for mixtures of extreme composition (20 and 80% acetonitrile), so that a qualitative distinction is not possible.

It has been observed by earlier workers[17] that addition of acetonitrile to water breaks the ice-like structure of water liberating free water molecules thereby decreasing the structure. Therefore, *B*-values of the structure-breaking electrolytes should increase and that of the structure-forming electrolytes should decrease with the addition of acetonitrile as is observed in Table 1. However, in reality the picture does not seem to be so simple since $\Delta B/\Delta T$ for KCl, KBr, KI, and Et_4NBr first decreases and then increases with acetonitrile concentration (Table 3). In the case of NaBr, CsI, and Me_4NBr $\Delta B/\Delta T$ increases with acetonitrile concentration increasing. $\Delta B/\Delta T$ for *n*-

Table 4. Differences in B-Coefficients of Two Salts with a Common Ion

ΔB/dm^3 mol^{-1}	Temp/°C	% Acetonitrile				
		0	20	40	60	80
(KCl-KBr)	25	0.036	0.017	0.038	0.054	0.091
	35	0.036	0.014	0.033	0.072	0.084
(KCl-KI)	25	0.062	0.045	0.110	0.133	0.136
	35	0.058	0.042	0.090	0.144	0.139
(KI-CsI)	25	0.042	0.045	0.020	0.039	0.072
	35	0.054	0.042	0.025	0.028	0.075
(NaBr-KBr)	25	0.102	0.084	0.050	0.016	0.073
	35	0.093	0.099	0.071	0.031	0.072

Pr_4NI and n-Bu_4NBr which is negative for the entire composition of the solvent mixture studied, shows a maximum negative value between 20 and 40% acetonitrile concentration. Therefore, solute-solvent interactions sensitive to temperature change exist at all the studied concentrations. This suggests preferential solvation of the electrolytes by acetonitrile molecules.

Table 4 shows a similarly interesting trend in the data on the differences in B-coefficients of two alkali salts with either the cation or the anion as the common member. This observation is common to both the temperatures studied. In both cases the difference observed in pure water first decreases and then increases with the concentration of acetonitrile upto the highest concentration studied. The difference between the halide ions which are normally small in water are surprisingly high in 80% acetonitrile. However, the differences between the alkali cations which are significantly high in water relative to halides are not so prominent in 80% acetonitrile as in case of halides. A decrease in the intermediate region is probably due to a decrease in overall structure of the solvent. Increase on the other hand indicates increase in ion-dipole interactions, probably with free water molecules.

The apparent molar volumes (ϕ_v) of the electrolytes were calculated by using the density data. The limiting apparent molar volume, ϕ_v° ($=\overline{V}^\circ$) was then calculated by the least square method. In order to calculate the ionic partial molar volumes, the $\overline{V}^\circ$ values, for Me_4NBr, Et_4NBr, n-Pr_4NBr, and n-Bu_4NBr were plotted against respective r^3 [r=ionic radii of the ammonium ions[18]] and the intercept gave the values for Br^- ions. With increasing acetonitrile, the ionic partial molar volumes decrease and become negative for chloride and bromide ions but are positive for Na^+, K^+, Cs^+, and I^- ions. Not much change is observed in the case of tetraalkylammonium ions. Because of electrostriction it is not possible to make a comparison of the B-values with the $\overline{V}^\circ$ values of the alkali and halide ions with respect to acetonitrile concentration, though such a comparison is possible in the case of the tetraalkylammonium and tetraphenylborate ions. Table 5 shows the $\overline{V}^\circ_{ion}$ and the $(B/\overline{V}^\circ)_{ion}$ values of the electrolytes vs. acetonitrile concentration. The ratio increases for Me_4N^+ alone but decreases for Et_4N^+, n-Pr_4N^+, n-Bu_4N^+, and $[BPh_4]^-$ ions. Marginal increase is observed for Et_4N^+ and n-Pr_4N^+ ions in 80% acetonitrile concentration. It is interesting to note that for Me_4N^+ and Et_4N^+ ions, the ratio tends to the ideal value (2.5) at 80% acetonitrile concentration.

We may therefore, say that acetonitrile destroys the ice-like structure of water. Ionic B-coefficients of simple monovalent ions are large in acetonitrile-H_2O solvent mixture due to the participation of acetonitrile molecules in the solvation process and small for large tetraalkylammonium ions because of the disappearance of hydrophobic hydration.

Table 5. Ionic Partial Molar Volumes $\overline{V}^\circ_{ion}$ (dm^3 mol^{-1}) and $(B/\overline{V}^\circ)_{ion}$[a] Values of Different Ions in Acetonitrile-H_2O Mixtures at 25°C

Ion		% Acetonitrile				
		0	20	40	60	80
Cl^-	$\overline{V}^\circ_{ion}$	0.013	0.003	−0.001	−0.004	−0.009
Br^-	$\overline{V}^\circ_{ion}$	0.020	0.008	0.006	0.001	−0.003
I^-	$\overline{V}^\circ_{ion}$	0.031	0.022	0.018	0.014	0.007
Na^+	$\overline{V}^\circ_{ion}$	0.004	0.016	0.016	0.023	0.024
K^+	$\overline{V}^\circ_{ion}$	0.014	0.023	0.027	0.030	0.030
Cs^+	$\overline{V}^\circ_{ion}$	0.027	0.038	0.036	0.041	0.042
Me_4N^+	$\overline{V}^\circ_{ion}$	0.094	0.101	0.102	0.102	0.104
	$(B/\overline{V}^\circ)_{ion}$	1.521	1.089	1.628	2.000	2.308
Et_4N^+	$\overline{V}^\circ_{ion}$	0.154	0.161	0.162	0.163	0.162
	$(B/\overline{V}^\circ)_{ion}$	2.500	2.037	1.661	1.534	2.265
n-Pr_4N^+	$\overline{V}^\circ_{ion}$	0.220	0.232	0.229	0.233	0.230
	$(B/\overline{V}^\circ)_{ion}$	4.041	2.526	2.153	1.970	2.104
n-Bu_4N^+	$\overline{V}^\circ_{ion}$	0.280	0.297	0.300	0.300	0.303
	$(B/\overline{V}^\circ)_{ion}$	4.250	2.875	2.323	2.003	1.931
$[BPh_4]^-$	$\overline{V}^\circ_{ion}$	—	0.279	0.281	0.270	0.269
	$(B/\overline{V}^\circ)_{ion}$	—	6.703	5.801	4.852	2.948

a) Values of B_{ion} on the basis of $B_{K^+}=B_{Cl^-}$.

We thank Dr. J. N. Baruah, Director, Regional Research Laboratory, Jorhat, Assam for encouragement in carrying out the work.

References

1) N. C. Dey, G. Kumar, B. K. Saikia, and I. Haque, *J. Solution Chem.*, **14**, 49 (1985).
2) DF-T. Tuan and R. M. Fuoss, *J. Phys. Chem.*, **67**, 1343 (1963).
3) K. Subbarangaiah, N. M. Murthy, and S. V. Subrahmanyan, *J. Chem. Soc., Faraday Trans. 1*, **78**, 165 (1982).
4) M. I. Davis, *Thermochim. Acta*, **71**, 59 (1983).
5) M. I. Davis, *Thermochim. Acta*, **63**, 67 (1983).
6) D. Eagland and G. Pilling, *J. Phys. Chem.*, **76**, 1902 (1972).
7) B. E. Conway, R. E. Verrall, and J. E. Desnoyers, *Trans. Faraday Soc.*, **62**, 2738 (1966).
8) N. C. Dey, B. K. Saikia, and I. Haque, *Can. J. Chem.*, **58**, 1512 (1980).
9) C. Marsden and S. Mann, "Solvents Guide," 2nd ed, Interscience, New York (1963).
10) G. Jones and M. Dole, *J. Am. Chem. Soc.*, **51**, 2950 (1929).
11) R. W. Gurney, "Ionic Process in Solution," McGraw Hill, New York (1953).
12) M. Kaminsky, *Discuss. Faraday Soc.*, **24**, 171 (1957).
13) E. R. Nightingale Jr., *J. Phys. Chem.*, **66**, 894 (1962).
14) J. E. Desnoyers and G. Perron, *J. Solution Chem.*, **1**, 199 (1972).
15) H. D. B. Jenkins and M. S. F. Pritchett, *J. Chem. Soc., Faraday Trans. 1*, **80**, 721 (1984).
16) R. Zana, G. Perron, and J. E. Desnoyers, *J. Solution Chem.*, **8**, 10 (1979).
17) B. Z. Gorbunov and Yu. I. Naberukhin, *Zh. Strukt. Khim.*, **16**, 816 (1975).
18) E. R. Nightingale Jr., *J. Phys. Chem.*, **63**, 1381 (1959).
19) R. H. Stokes and R. Mills, "Viscosity of Electrolytes and Related Properties," Pergamon Press, New York (1965).
20) R. L. Kay, T. Vituccio, C. Zawayski, and D. F. Evans, *J. Phys. Chem.*, **70**, 2336 (1966).

Compensation Effect in the Electrical Conduction Process in Some Nucleic Acid Base Complexes with Acriflavine Dye

Deepali SARKAR, Kapur Mal JAIN,† and Tridibendra Narayan MISRA*
Optics Department, Indian Association for the Cultivation of Science,
Jadavpur, Calcutta-700 032, India
(Received July 11, 1985)

The validity of the compensation rule is studied for nucleic acid bases, adenine, cytosine, and uracil complexes with acriflavine dye. The value of the semiconduction activation energy of a complex varies with dye concentration. It is shown that at low dye concentration, these semiconducting complexes follow the three parameter equation $\sigma(T)=\sigma_0'\exp(E/2kT_0)\exp(-E/2kT)$, where σ_0' and T_0 are constant for a particular base, other notations have their usual meaning. Consistent values for σ_0' and T_0 have been obtained by using various methods of evaluation. These results suggest that compensation effect has a physical origin.

In some earlier communications we have demonstrated the validity of the compensation rule in the electrical conduction process in some polyene[1,2] and nitro aromatic[3] semiconductors. The variation in the semiconduction activation energy was obtained by adsorbing various chemical vapors on the crystallite surfaces in a polycrystalline sandwich cell configuration. It has been shown that these organic semiconductors follow the three constant equation

$$\sigma(T) = \sigma_0' \exp(E/2kT_0)\exp(-E/2kT), \quad (1)$$

where $\sigma(T)$ is the specific conductivity at TK, E is the semiconduction activation energy and k is the Boltzmann constant. The parameters σ_0' and T_0 are constants for a particular semiconductor.

The activation energy of a semiconductor may be varied by other methods also e.g. hydration, doping of impurity, complex formation, physical mixing etc. The interaction of acridine dyes with DNA and nucleic acid bases is of considerable biological significance. Such interaction is involved in frame shift mutation, antibacterial activities and photodynamic action. The spectroscopic studies confirm the complex formation between flavins and the purine and pyrimidine bases.[4] The binding of the dye molecules with the bases are believed to bring about the biological effects. For interaction with DNA two modes of interaction are suggested depending upon the DNA/Dye ratio.[4] For complex formation with nucleic acid base, the site of attack in a base depend on the electronic properties of the dye.[5] However, the modes of binding of nucleic acid bases with dyes also depend on dye concentration.[6] We have studied the semiconductive properties of the complexes of acriflavine dye with nucleic acid bases, adenine, cytosine, and uracil at various dye concentrations. In this paper we show that in the low dye concentration range ($\lesssim 10^{-1}$ mol mol^{-1}), these semiconducting complexes show compensation effect.

† Present address: Govt. Arts and Science College, Durg, M. P. 491002. (National Associate, University Grants Commission, India).

Experimental

The purine and pyrimidine bases used in the present study are adenine, cytosine, and uracil. These were obtained from Sigma Chemical Company, U. K., Acriflavine, a mixture of 2,8- and 3,6-diamino-10-methylacridinium chloride and 2,8- and 3,6-diaminoacridine was also obtained from the same commercial source. The bases and the dye were extensively purified by repeated crystallization from distilled water and methanol respectively and finally dried under vacuum before use. For preparing the complexes, acriflavine dye and the bases were taken in required proportions and dissolved in distilled water and then evaporated in vacuum. The finely powdered sample pressed in a sandwich cell between a conducting glass and a stainless steel electrode was maintained at moderate pressure by clips. The separation between the electrodes was maintained by a three mil thick teflon spacer. The cell was placed in a suitably designed conductivity chamber. A d.-c. voltage of 27 volts from a dry battery pack was applied across the cell. Dark conductivity was measured in both nitrogen atmosphere and vacuum using an Electrometer amplifier EA 815 of ECIL, India. The thermo emf was measured by a digital panel meter model HIL 2301, India. The experimental procedure for the measurement of activation energy was similar to that described earlier.[1]

Results and Discussion

The semiconduction activation energies of the crystalline powders of pure adenine, crytosine, uracil bases, and various base-dye complexes were measured several times in dry nitrogen atmosphere and also in vacuum (10^{-3} Torr (1 Torr=133.322 Pa)). All measurements gave consistent values. Almost the same values were obtained in dry nitrogen and in vacuum. The activation energies of pure adenine, cytosine, uracil, and acriflavine are 2.10, 2.12, 2.15, and 2.25 eV, respectively. The room temperature (30 °C) specific conductivities of the bases and also of the dye is typically of the order of 10^{-16}—10^{-18} Ω^{-1} cm^{-1}.

The current voltage characteristics of all the pure samples and the complexes are observed to be ohmic in the low voltage region (36 V) of our studies. In

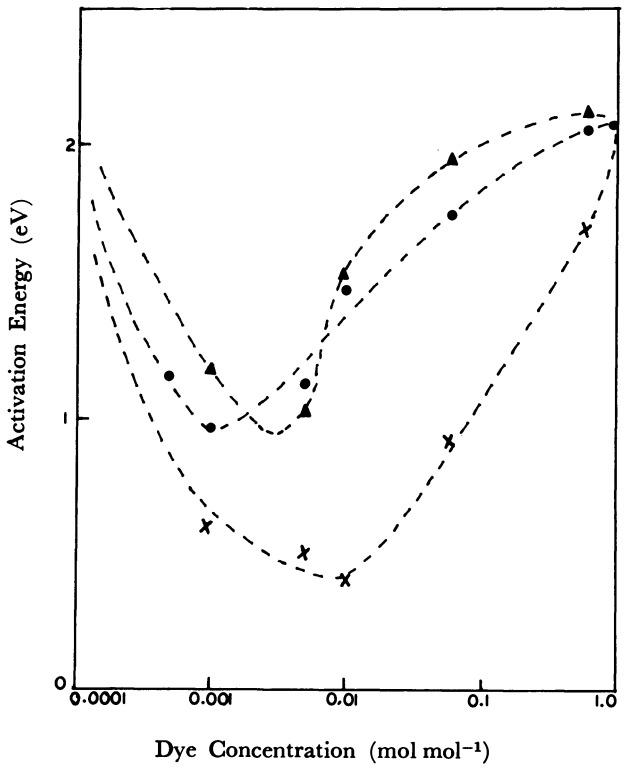

Fig. 1. Dye concentration dependence of semiconduction activation energy of various nucleic acid base-dye complexes. The lines are only for visual guide. Acriflavine complexes with i) Cytosine —×—. ii) Uracil —▲—. iii) Adenine —●—.

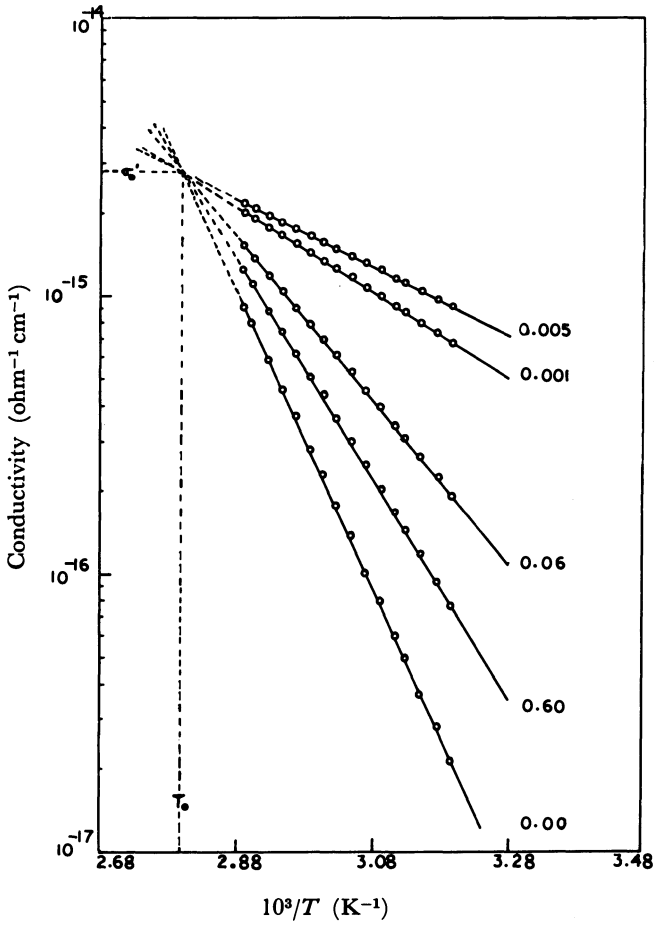

Fig. 2. $\log \sigma(T)$ vs. $1/T$ plot for cytosine-acriflavine dye complexes of different dye concentrations. The dye concentrations in mol mol^{-1} are shown in the diagram.

Fig. 1, we show the dye concentration dependence of activation energy for various complexes. As the dye concentration in a complex decreases from 1 mol mol^{-1} semiconduction activation energy decreases and reaches a minimum value at a certain dye concentration below which it starts increasing again and approaches the activation energy value of pure purine or pyrimidine base. For cytosine-acriflavine complex the minimum activation energy value obtained is 0.40 eV at 10^{-2} mol mol^{-1} dye concentration. For uracil-acriflavine and adenine-acriflavine complexes the minimum E value measured are 1.02 eV at 3×10^{-3} mol mol^{-1} dye concentration and 0.96 eV at 10^{-3} mol mol^{-1} dye concentration, respectively.

The binding of metal cations to nucleic acid bases and its relationship with electrostatic molecular potential of the bases have been discussed by Pullman and Pullman.[7] Their calculated electrostatic interaction energy is large for cytosine whereas it is small and is about the same magnitude for adenine and uracil. It is interesting to note that the change in semiconduction activation energy of our base-dye complexes also show a similar order.

In Fig. 2, we show the log σ (T) vs. $1/T$ plot for cytosine-acriflavine complexes of different dye concentration. It is seen that the extrapolated lines in these plots for complexes with different dye concentration intersect the ordinate at a wide variety of positions, but they all pass approximately through a single point at a temperature T_0. This result is in conformity with expression (1). At the characteristic temperature T_0, the value of $\sigma(T_0)$ gives the σ_0' value. For cytosine-acriflavine complexes, T_0=357 K and $\sigma_0'=2.8\times10^{-15}\ \Omega^{-1}\,\mathrm{cm}^{-1}$. In Figs. 3 and 4, we have shown similar log σ (T) vs. $1/T$ plot for uracil-acriflavine and adenine-acriflavine complexes. In these complexes, also the extrapolated lines pass through a single point. However in these complexes, the point of intersection is in the low temperature side of the working temperature region. From expression (1) we get that at any experimental temperature T_1K,

$$\sigma(T_1) = \sigma_0' \exp\left(\frac{1}{T_0} - \frac{1}{T_1}\right)\frac{E}{2k}.$$

The $\sigma(T_1)$ will show different behavior with variation of E depending on if $T_1>T_0$ or $T_1>T_0$. This is exactly what we see in the three complexes. In cytosine-acriflavine complex $\sigma(T_1)$ increases with

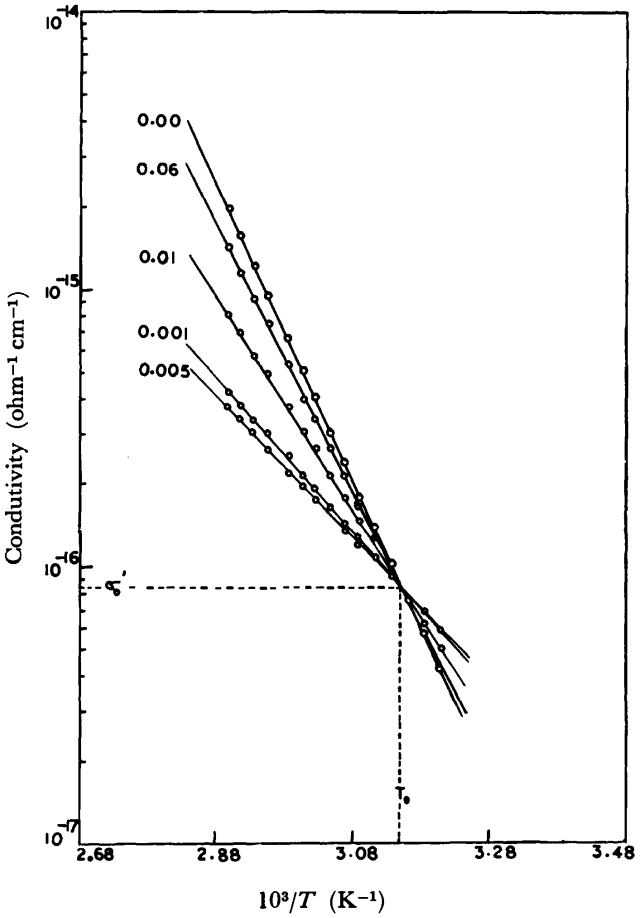

Fig. 3. $\log \sigma(T)$ vs. $1/T$ plot for uracil-acriflavine dye complexes of different dye concentrations. The dye concentrations in mol mol^{-1} are shown in the diagram.

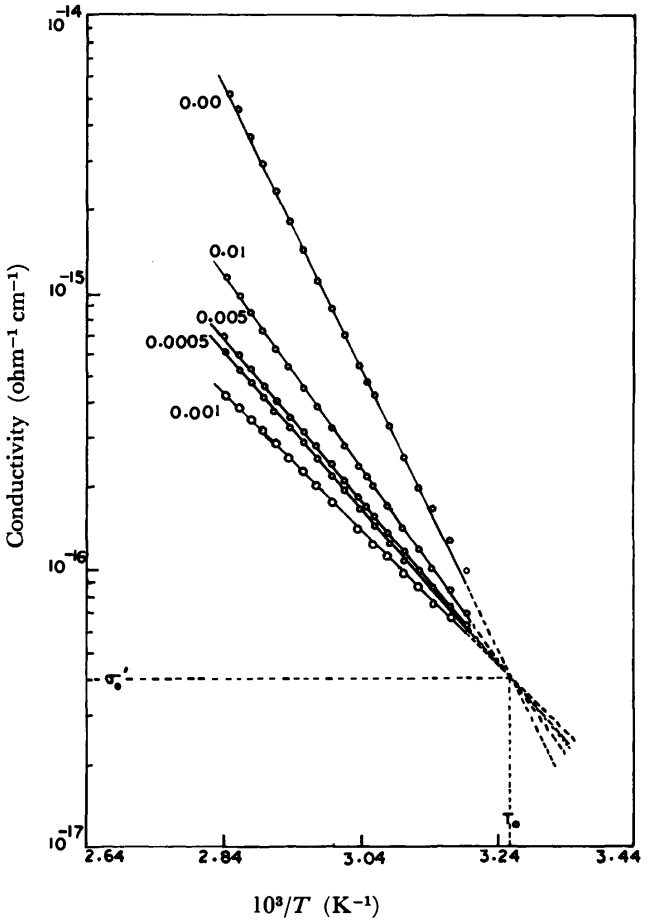

Fig. 4. $\log \sigma(T)$ vs. $1/T$ plot for adenine-acriflavine dye complexes of different dye concentrations. The dye concentrations in mol mol^{-1} are shown in the diagram.

decreasing E whereas in adenine-acriflavine and uracil-acriflavine complexes inverse behavior is observed. Inspite our measurement being limited by the electrometer sensitivity, we have been able to measure $\sigma(T)$ on both sides of T_0 in case of uracil-acriflavine complexes. To our knowledge, this is the first experimental demonstration of different behavior of change of $\sigma(T)$ with variation of E on two sides of a specific temperature in an organic semiconductor thus showing the physical significance of compensation temperature T_0.

It is now clear from experiments that the compensation temperature T_0 of a semiconductor plays an important role in dark conduction process. Acriflavine complexes with the three nucleic acid bases cytosine, adenine, and uracil have three distinct T_0 values. This result confirms our earlier observation with some polyenes[1,2] and some nitro aromatics[3] that T_0 is a molecular property.

"True" compensation effect is thought to arise from the existence of a linear relationship between the activation energy and the activation entropy of the system. It has been pointed out by Johnston and Lyons[6] that if a true linear free energy relation (LFER) does hold for dark conduction indicating a physical relationship between σ_0 and E, log (T_1) vs. E must also be linear where T_1 is a specific temperature. In Fig. 5, we show such plots for cytosine-acriflavine, adenine-acriflavine, and uracil-acriflavine complexes. T_0 and σ_0' are obtainable from the slopes and intercepts of these plots. These parameters can also be evaluated from plots made in alternate fashion as log σ_0 vs. E since log σ_0=log σ_0'+$E/2kT_0'$ σ_0 and E being experimentally measured. In Fig. 6, we show such plots for three different complexes. The plots are linear as expected from expression (1) and T_0 and σ_0' are obtained from the slopes and the intercepts respectively of these plots. In Table 1, we compare the values of T_0 and σ_0' for the complexes obtained by various methods of evaluation. The agreement is quite satisfactory. These results confirm that σ_0 and E are physically related and that T_0 has a physical origin. That we have observed compensation effect only in complexes of low dye concentra-

Table 1. Comparison of T_0 and σ_0' of Nucleic Acid-Base Acriflavine Dye Complexes Obtained by Various Methods of Calculation

Base	Different Parameter	Nucleic acid base/Dye ratio						
		1 : 0.00	1 : 0.0005	1 : 0.001	1 : 0.005	1 : 0.01	1 : 0.06	1 : 0.60
Cytosine	E / eV	2.12	—	0.60	0.50	—	0.92	1.70
	σ_T / ohm^{-1} cm^{-1}	8.70×10^{-18}	—	4.10×10^{-16}	6.10×10^{-16}	—	7.20×10^{-17}	2.00×10^{-17}
	σ_0 / ohm^{-1} cm^{-1}	3.87×10^{0}	—	5.40×10^{-11}	1.08×10^{-11}	—	7.50×10^{-9}	4.80×10^{-13}
	σ_0' / ohm^{-1} cm^{-1} from Fig. 2.	←			2.80×10^{-15}			→
	σ_0' / ohm^{-1} cm^{-1} from Fig. 6.	←			4.00×10^{-15}			→
	T_0/K from Fig. 2.	←			357.10			→
	T_0/K from Fig. 6.	←			344.00			→
Uracil	E / eV	2.15	—	1.25	1.02	1.53	1.90	—
	σ_T / ohm^{-1} cm^{-1}	2.50×10^{-18}	—	1.85×10^{-17}	2.15×10^{-17}	1.07×10^{-17}	3.30×10^{-18}	—
	σ_0 / ohm^{-1} cm^{-1}	1.58×10^{1}	—	8.50×10^{-7}	1.30×10^{-8}	1.70×10^{0}	1.57×10^{-1}	—
	σ_0' / ohm^{-1} cm^{-1} from Fig. 3.	←			8.40×10^{-17}			→
	σ_0' / ohm^{-1} cm^{-1} from Fig. 6.	←			6.80×10^{-17}			→
	T_0/K from Fig. 3.	←			317.50			→
	T_0/K from Fig. 6.	←			302.00			→
Adenine	E / eV	2.10	1.10	0.96	1.18	1.46	—	—
	σ_T / ohm^{-1} cm^{-1}	1.60×10^{-17}	2.30×10^{-17}	2.55×10^{-17}	2.40×10^{-17}	2.00×10^{-17}		
	σ_0 / ohm^{-1} cm^{-1}	1.12×10^{1}	1.4×10^{-7}	3.90×10^{-9}	1.56×10^{-6}	5.00×10^{-5}		
	σ_0' / ohm^{-1} cm^{-1} from Fig. 4.	←			4.00×10^{-17}			→
	σ_0' / ohm^{-1} cm^{-1} from Fig. 6.	←			2.20×10^{-17}			→
	T_0/K from Fig. 4.	←			306.40			→
	T_0/K from Fig. 6.	←			290.80			→

tion may imply that the nature of complex formation and hence the dye-base interaction at high and low dye concentrations is different.

We thank Prof. G. S. Kastha for his kind interest in the problem. One of us (KMJ) is thankful to the Secretary, Department of Higher Education, Govt. of M. P., India and to the Principal, Govt. Arts and Science College, Durg for the sanction of special leave.

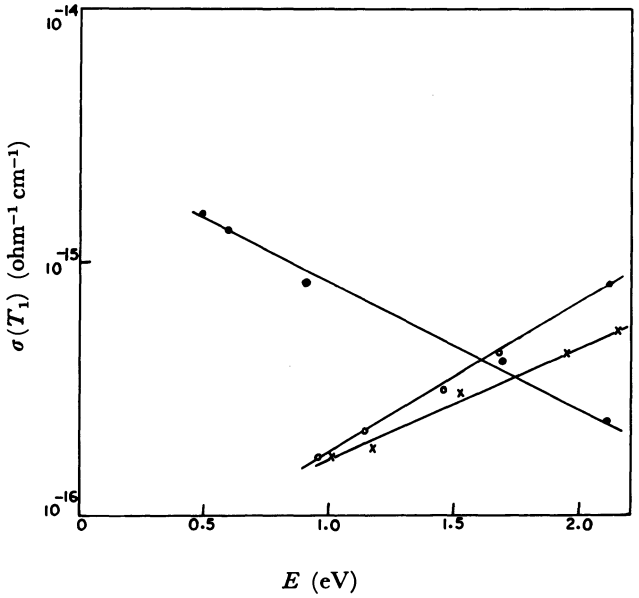

Fig. 5. Plot of log $\sigma(T_1)$ value at a constant temperture T_1(332.9 K) vs. E for a base-dye complexes, σ (T_1) and E change with dye concentration. (1) —●— for cytosine-acriflavine complex, (2) —×— for uracil-acriflavine complex, and (3) —○— for adenine-acriflavine complex.

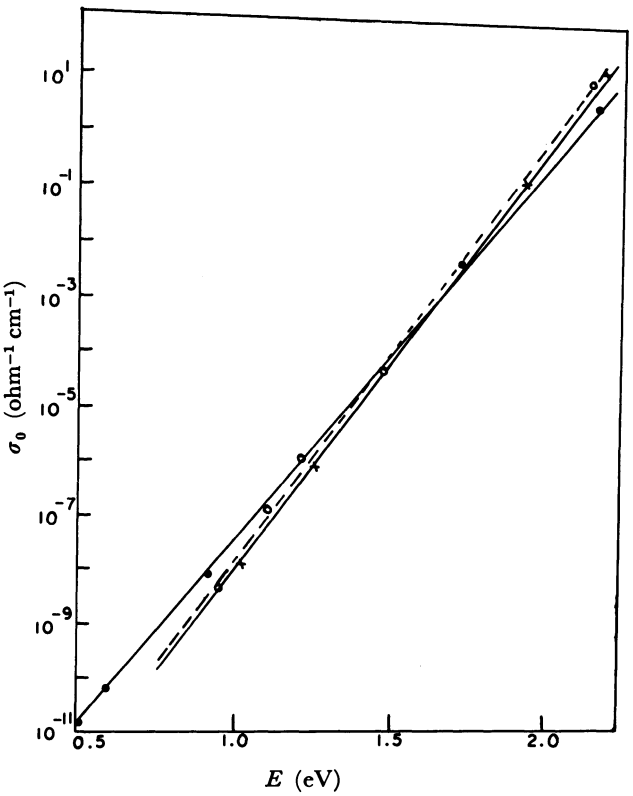

Fig. 6. Plot of log σ_0 value vs. E for base-dye complex as σ_0 and E change with dye concentration. (1) —●— for cytosine-acriflavine complex (2) —×— for uracil-acriflavine complex (3) —○— for adenine-acriflavine complex.

References

1) B. Mallik, A. Ghosh, and T. N. Misra, *Bull. Chem. Soc. Jpn.*, **52**, 2091 (1979).

2) B. Mallik, A. Ghosh, and T. N. Misra, *Phys. Status Solidi (a)*, **62**, 267 (1980).

3) A. Ghosh, K. M. Jain, B. Mallik, and T. N. Misra, *Jpn. J. Appl. Phys.*, **20**, 1059 (1981).

4) N. E. Geacintov, J. Waldmeyer, V. A. Kuzmin, and T. Kolubatev, *J. Phys. Chem.*, **85**, 3608 (1981).

5) A. Pullman and A. N. Armbruster, *Theor. Chim. Acta*, **45**, 249 (1977).

6) J. D. Buchanan, D. M. Power, G. O. Philips, and J. V. Davis, *Int. J. Radiat. Biol. (G. E.)*, **33**, 551 (1978).

7) A. Pullman, B. Pullman, "Biochem. Review, Golden Jubilee," Vol L1 (1980), p. 118.

8) G. R. Johnston and L. E. Lyons, *Aust. J. Chem.*, **23**, 2187 (1970).

 © 1986 The Chemical Society of Japan Bull. Chem. Soc. Jpn., 59, 1567—1569 (1986)

Studies in the Extraction of Cadmium with Some Sulfur Ligands

Roma LAHIRI and G. N. RAO*
Chemistry Department, Indian Institute of Technology, New Delhi-110016, India
(Received April 1, 1985)

Extraction of cadmium(II) with 2-(2-pyridyl)-2,3-dihydrobenzothiazole, *O,O'*-diethyl hydrogenphosphorodithioate, 1-phenyl-3-methyl-4-thiobenzoyl-5-pyrazolone, *N*-(2-naphthyl)mercaptoacetamide, and 2-(*o*-hydroxyphenyl)-2,3-dihydrobenzothiazole has been studied. Extraction constants (K_{ex}) have been calculated for these systems. These reagents have been compared with some common reagents used for the extraction of cadmium. Separation factors have been calculated for the separation of cadmium from zinc with some of these reagents.

Studies in the extraction of cadmium are somewhat limited. In spite of the fact that extraction of every metal has its own importance cadmium has a special significance owing to its toxicity and increasing concentration in the environment. In view of this a study has been undertaken to find effective reagents for cadmium extraction by investigating the extraction of cadmium with some sulfur ligands and by comparing the extraction data obtained with those for other reagents from the literature. Ligands containing donor sulfur atom have been chosen because cadmium which is a soft acid (in HSAB sense) is expected to form more stable complexes with soft bases.

The ligands chosen for the present study are 2-(2-pyridyl)-2,3-dihydrobenzothiazole(HPBT), *O,O'*-diethyl hydrogenphosphorodithioate(HDEDTP), 1-phenyl-3-methyl-4-thiobenzoyl-5-pyrazolone(HSBMPP), *N*-(2-naphthyl)mercaptoacetamide(HTN), and 2-(*o*-hydroxyphenyl)-2,3-dihydrobenzothiazole(H_2SATP).

Experimental

Apparatus and Reagents. A Pye Unicam SP 191 Atomic Absorption Spectrophotometer was used for measuring the metal concentrations. Measurements of pH was made using an expanded scale pH meter (Electronics Corporation of India Ltd.). A wrist action mechanical shaker was used for shaking.

Cadmium(II) solution was prepared by dissolving Analar grade cadmium acetate in distilled water, adding sufficient amount of acetic acid to prevent hydrolysis. The pH of the aqueous phase was maintained by using mixtures of potassium chloride and hydrochloric acid for pH 1—3, sodium acetate and acetic acid for pH 4—6, acetic acid and ammonia for pH 6—8 and ammonium chloride–ammonia for pH 8—10. A constant ionic strength (0.1) in the aqueous phase was maintained by using potassium nitrate solution. Where extraction was carried out from dilute hydrochloric acid solutions, potassium chloride was used to maintain the ionic strength.

The ligand HSBMPP was prepared by the method[1] reported by Chouhan and Rao. The compounds HPBT[2] and H_2SATP[3] were prepared by condensing 2-aminobenzenethiol (Kochlight) with 2-pyridinecarbaldehyde (Fluka), and salicylaldehyde(BDH), respectively. The other ligands used were HDEDTP (BDH) and HTN (E. Merck). Purity of the ligands was established on the basis of microanalysis and infrared spectra. Analar grade benzene, chloroform, carbon tetrachloride, and 1-butanol were used as solvents. Purification was done where necessary by standard methods.

Extraction Procedure. Ten ml of aqueous layer containing 2 ml of 100 ppm cadmium acetate solution, 5 ml of buffer solution and requisite volume of 1 M† potassium nitrate solution (to maintain the ionic strength at 0.1) was equilibrated with 10 ml of organic phase containing the required amount of the ligand in a stoppered bottle. The mixture was shaken in a mechanical shaker for a period sufficient for the attainment of equilibrium at 30±1 °C. The period of shaking was determined from preliminary experiments in all the systems studied. This was 60, 5, 120, 10, and 120 min with HPBT, HTN, HSBMPP, HDEDTP, and H_2SATP, respectively. Benzene was used as the solvent in the case of HSBMPP and H_2SATP while chloroform, carbon tetrachloride, and 1-butanol were used in the case of HTN, HDEDTP, and HPBT, respectively on the basis of preliminary solubility checks. After equilibration the aqueous layer was pipetted out. The concentration of the metal in the aqueous phase and the pH were then measured.

Results and Discussion

The extraction of a metal ion (M^{n+}) with a chelating ligand having a replaceable hydrogen atom (HA) may be represented as,

$$M^{n+}_{aq} + nHA_{org} \rightleftharpoons MA_{n\ org} + nH^{+}_{aq}. \quad (1)$$

The extraction constant (equilibrium constant) of this reaction is:

$$K_{ex} = \frac{[MA_n]_{org}[H^+]^n_{aq}}{[M^{n+}]_{aq}[HA]^n_{org}}. \quad (2)$$

Making the usual approximations[4] the ratio $[MA_n]_{org}/[M^{n+}]_{aq}$ in Eq. 2 may be considered equal to the distribution coefficient (D) and

$$K_{ex} = D\frac{[H^+]^n_{aq}}{[HA]^n_{org}} \quad (3)$$

or

$$\log K_{ex} = \log D - n\,pH - n \log [HA]_{org}. \quad (4)$$

Equation 4 implies that, (i) the slope of the plot

† 1 M=1 mol dm^{-3}.

of log D vs. pH at constant reagent concentration in the organic phase gives the number of protons released during complex formation and (ii) the slope of the plot of log D vs. log [HA] at constant pH gives the number of reagent molecules incorporated in the extracted complex.

Plots (Fig. 1) of log D vs. pH at constant ligand (HA) concentration and plots (Fig. 2) of log D vs. log [HA] at constant pH for HPBT, HTN, and HSBMPP gave slopes of ≈2. Thus the extraction of cadmium(II) with these ligands can be represented as occurring predominently according to the following equation:

$$Cd^{2+} + 2HA \rightleftharpoons CdA_2 + 2H^+$$

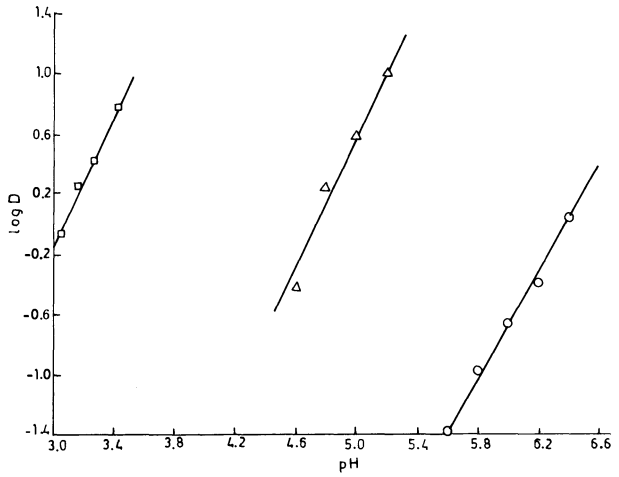

Fig. 1. Effect of pH on the extraction of Cd with HPBT, HTN, and HSBMPP.
○: HPBT (0.001 M), △: HTN (0.0025 M), □: HSBMPP (0.01 M).

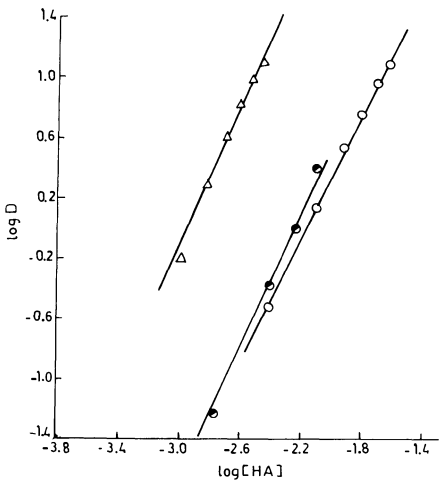

Fig. 2. Effect of ligand concentration on the extraction of Cd with HDEDTP, HSBMPP, and HTN.
○: HDEDTP ([HCl]=0.1 M, [KCl]=0.3 M), ◐: HSBMPP (pH=3.34), △: HTN (pH=5.1).

log K_{ex} values for these systems were calculated by using Eq. 4.

Since the extraction of cadmium(II) with HDEDTP took place from highly acidic solutions (quantitative extraction from 0.01—0.1 M HCl with 0.02 M reagent), a competing reaction in the aqueous phase would be the formation of the chloro complex of cadmium(II). A study of the effect of variation of chloride concentration showed that extraction fell with increase in chloride concentration. The plot (Fig. 2) of log D vs. log[HDEDTP] at constant hydrogen ion and chloride concentration gave a slope of ≈2 indicating the involvement of two moles of HDEDTP in the complex formation. The log K_{ex} value for this system was calculated from Eq. 5[5]

$$\log K_{ex} = \log D - n \log [HA]_{org} - n\,pH + \log \{1 + \beta_1[X^-] + \beta_2[X^-]^2 + \cdots\} \quad (5)$$

Here X^- is the complexing anion (Cl^-) and β_1 is the stability constant of the complex formation reaction.

The formula of the chelate species formed could not be determined in the case of Cd(II)-H_2SATP system as the log D vs. pH or log D vs. log [HA] plots were not regular. A $pH_{1/2}$ value (pH at 50% extraction) of 5.59 was obtained from the plot of percentage extration vs. pH with a 0.01 M solution of the ligand. An approximate K_{ex} value was calculated from this data assuming that the complex species formed here was similar to that in the other systems. Schweitzer et al. also observed irregularities in the extraction of cadmium(II) with salicylaldehyde oxime, acetylacetone, 2-methyl-8-quinolinol etc.[6]

The log K_{ex} values obtained in this study are listed in Table 1. The available K_{ex} values for the extraction of zinc(II) with these reagents are also included in this table.

From this data and other data available in literature[6,7,9,10] it may be concluded that ligands donating through sulfur would be more useful for the extraction of cadmium than their corresponding

Table 1. Extraction Constants for Cadmium(II) and Znic(II)

Reagent	log K_{ex} Cd(II)	Zn(II)	Solvent
2-(2-Pyridyl)-2,3-dihydrobenzothiazole	−6.8	−9.28[7]	1-Butanol
N-(2-Naphthyl)mercaptoacetamide	−4.27	−8.08[7]	Chloroform
3-Methyl-1-phenyl-4-thiobenzoyl-5-pyrazolone	−2.19	−2.68[8]	Benzene
O,O'-Diethyl hydrogenphosphorodithioate	3.67	—	Carbon tetrachloride
2-(*o*-Hydroxyphenyl)-2,3-dihydrobenzothiazole	−7.18	—	Benzene

Table 2. Separation Factors for Cadmium and Zinc

Reagent	Separation factor
2-(2-Pyridyl)-2,3-dihydrobenzothiazole	300
N-(2-Naphthyl)mercaptoacetamide	6500
3-Methyl-1-phenyl-4-thiobenzoyl-5-pyrazolone	3

oxygen analogues. The ligands HDEDTP, dithizone-(HDTZ),[11] sodium diethyldithiocarbamate (HDEDTC),[12] and HSBMPP appear to be most effective for the extraction of cadmium(II) if the K_{ex} values with these ligands are considered. The higher stability of HDEDTP in highly acidic solutions as compared to HDEDTC makes it a better reagent for analytical purposes.[13] Dithizone in spite of giving a high K_{ex} value is useful only at trace levels since the solubility of HDTZ itself and its chelates is very low in most of the organic solvents. On the other hand, both HDEDTP and its chelates are fairly soluble in organic solvents, and therefore can be useful at trace as well as macro levels. The ligands HPBT, HTN, 1,1,1-trifluoro-4-(2-thienyl)-4-mercaptobut-3-en-2-one,[10] 2-mercaptobenzothiazole,[6] 8-quinolinol,[14] and 5,7-dichloro-8-quinolinol,[6] by virtue of high K_{ex} values will also be useful for the extraction of cadmium. The oxygen donor ligands like β-diketones,[6,7,15] *N*-benzoyl-*N*-phenylhydroxylamine[15] etc. do not seem very attractive for the extraction of cadmium(II).

The possibility of utilizing these reagents for separating cadmium from zinc has been investigated by calculating the separation factor S which is the ratio of the distribution coefficients of the elements to be separated.[16] A separation in which not more than 1% of one element is coextracted will be obtained if $S \geq 10^4$ and the product of the distribution coefficients is close to unity. The separation factors for HPBT, HTN, and HSBMPP are given in Table 2.

Considering these separation factors and those for other reagents from literature[6-12,14,15,17] it can be concluded that benzoylacetone,[15] 1-phenyl-3-methyl-4-benzoyl-5-pyrazolone,[8,9] and HTN would be more useful for the separation of cadmium from zinc.

References

1) V. S. Chouhan and G. N. Rao, *Bull. Chem. Soc. Jpn.*, **55**, 301 (1982).
2) L. F. Lindoy, S. E. Livingstone, and T. N. Lockyer, *Aust. J. Chem.*, **18**, 1549 (1965).
3) A. Varadarajulu, Ph. D. Thesis, Indian Institute of Technology, Delhi (1977).
4) Yu. A. Zolotov, "Extraction of Chelate Compounds," Humphrey Science Publishers, INC., Ann Arbor, Michigan (1970), pp. 26—27.
5) E. B. Sandell and H. Onishi, "Photometric Determination of Traces of Metals," Wiley Interscience, New York (1978), p. 898.
6) A. K. Schweitzer and D. R. Randolph, *Anal. Chim. Acta*, **26**, 567 (1962).
7) R. Lahiri, Ph. D. Thesis, Indian Institute of Technology, Delhi (1984).
8) V. S. Chouhan, Ph. D. Thesis, Indian Institute of Technology, Delhi (1978).
9) H. C. Arora and G. N. Rao, *Indian. J. Chem.*, **11**, 488 (1973).
10) T. Honjo, S. Yashima, and T. Kiba, *Bull. Chem. Soc. Jpn.*, **46**, 3772 (1973).
11) Ref. 5, pp. 612—616.
12) Ref. 5, p. 519.
13) T. H. Handley, *Talanta*, **12**, 893 (1965).
14) Ref. 5, p. 428.
15) Ref. 5, Chap. 9B.
16) Ref. 4, pp. 152—154.
17) H. M. N. H. Irving and D. N. Edgington, *J. Inorg. Nucl. Chem.*, **27**, 1359 (1965).

 © 1986 The Chemical Society of Japan Bull. Chem. Soc. Jpn., 59, 1571—1573 (1986)

Determination of Iron in Drug Biochemical and Biological Samples as a Thiocyanato Mixed Ligand Complex with Hydroxyamidine

Raghunandan SINGH,* Lalta Prasad CHANDRAKAR, and Rajendra Kumar MISHRA†
Department of Chemistry, D. B. Science College, Gondia (M.S.), India
†Department of Chemistry, Ravishankar University, Raipur (M.P.), India
(Received April 25, 1985)

N-Hydroxy-*N*-*o*-tolyl-*N'*-phenylbenzamidine (HTPB) is presented as a new sensitive and highly selective reagent for determination of iron in drug, biochemical and biological samples in presence of thiocyanate. The red organge Fe(III)–HTPB–SCN mixed ligand complex is quantitatively extracted into benzene. The extraction of iron(III) as thiocyanato mixed ligand complex is quantitative in the acidity range between 0.2—0.7 M (1M=1 mol dm^{-3}) hydrochloric acid. The effective molar absorptivity of the complex is 12000 l mol^{-1} cm^{-1} with Sandell's sensitivity of 0.0046 μg of iron per cm^2. On the basis of this sensitive color reaction, a simple, rapid, selective, and highly reproducible method for the extractive spectrophotometric determination of microgram amounts of iron in various drug, biochemical and biological samples has been developed. The method is free from most of the common metal ions and commonly used sequestering agents.

Among the several methods reported for the spectrophotometric determination of iron in various complex materials,[1-13] the thiocyanate and 1,10-phenanthroline methods are used over a long period. The iron(III)–thiocyanate method is simple, rapid, and sensitive, but it suffers from interferences due to a large number of experimental factors. These include time of standing, thiocyanate concentration, deviation from Beer's law and reaction of the thiocyanate with other elements to give colored products. The iron(II)–1,10-phenanthroline method is widely applicable to routine determination of iron but it suffers from serious interference from common ions such as Ni(II), Cu(II), Bi(III), and Ag(I). Hence it is thought worthwhile to describe a better method for determination of iron in complex materials. In this communication, the reaction of *N*-hydroxy-*N*-*o*-tolyl-*N'*-phenylbenzamidine(HTPB) with iron(III) in

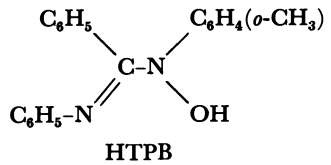

HTPB

presence of thiocyanate was investigated looking towards the possible use of this reagent for spectrophotometric determination of iron in biochemical and biological samples and separation from other metal ions associated in complex materials. The proposed method offers several advantages over other established methods.[1-13] It is sensitive and highly selective and can be used over wide acidity range. The reagent is easy to prepare and if kept in amber glass bottles, solution can be stored for at least a month without any deterioration. It is applicable for the determination of iron in all complex materials because most of the common ions do not interfere.

Experimental

Standard Iron(III) Solution. The standard solution of iron(III) was prepared by dissolving 1.0 g pure iron wire (E. Merck) in 50 ml of 1:3 nitric acid. The oxides of nitrogen were removed by boiling and diluted to one liter with distilled water. The metal content of the solution was evaluated gravimetrically with 8-quinolinol.[14]

Apparatus. A Carl-Zeiss specord recording ultraviolet spectrophotometer and an ECIL UV-VIS spectrophotometer model GS-865 equipped with 1-cm matched silica and quartz cells were employed for all photometric measurements.

Preparation of *N*-Hydroxy-*N*-*o*-tolyl-*N'*-phenylbenzamidine. *N*-*o*-Tolylhydroxylamine 3.2 g (0.027 mol) was taken in 50 ml absolute ether in a 500 ml conical flask. To this, 5.6 g (0.027 mol) of *N*-phenylbenzimidoyl chloride in 100 ml ether was added in small quantities during the course of 15 min with constant stirring. A light brown oil slowly separated out. Stirring and scratching were continued till the oil solidified and separated in the form of white crystals. This was filtered off and washed with 3×20 ml portions of ether and air dried. The resulting hydrochloride was treated with dilute aqueous ammonia to liberate the free base. This was recrystallized from petroleum ether–benzene (1:2) at 60—80°. Yield 45%, mp 131 °C. Analysis showed C, 79.08; H, 5.65; N, 8.98%. $C_{20}H_{18}N_2O$ requires: C, 79.47; H, 5.96; N, 9.27%.

Extraction Solution. A 0.1% W/v benzene solution of reagent was employed for the extraction work. 2% W/v aqueous solution of potassium thiocyanate was used throughout the experiment.

Recommended Procedure. Place and aliquot of iron(III) solution containing 40—80 μg of metal in a 100 ml separatory funnel. To this, add 5 ml of potassium thiocyanate solution. Adjust the volume of the solution to about 25 ml and the acidity to between 0.2 and 0.7 M with hydrochloric acid. Introduce 25 ml benzene solution of the reagent and equilibrate for 2 min. Allow the phases to separate. Dry the colored extract over anhydrous sodium sulfate 2 g in a 50 ml beaker. Measure the absorbance at wavelength of maximum absorption against reagent blank.

Results and Discussion

Absorption Spectra. The absorption spectra of the ternary iron(III) complex and the reagent in benzene are shown in Fig. 1. The Fe(III)-HTPB-SCN complex shows a sharp absorption maximum at 460 nm having the value for molar absorptivity to be 12000 l mol^{-1} cm^{-1}. As a reagent blank prepared under similar conditions does not absorb in the region 450—700 nm, it can be replaced by benzene.

Choice of Solvent. Various water immiscible organic solvents such as chloroform, benzene, carbon tetrachloride, toluene, xylene, etc. were found to extract the mixed ligand complex quantitatively. However, benzene was found to be the better extracting solvent as in this the sensitivity of the complex is enhanced and complete extraction is relatively rapidly accomplished.

Effect of Acidity. The acidity of the solutions was maintained with 2 M hydrochloric acid. If the hydrochloric acid concentration of aqueous phase lies in the range 0.01 to 1.0 M the position of the absorption band of the benzene extract remains intact. However, the optimum acidity range was found to be 0.2 to 0.7 M hydrochloric acid in which iron(III) was quantitatively extracted. The fatty acids and other inorganic acids were unsuitable for extraction work due to low absorbance of complex.

Effect of Reagents. A 30 and 120 fold molar excess of HTPB and thiocyanate respectively was found to be adequate for complete extraction of iron. A further excess of these (HTPB upto 100 fold and thiocyanate upto 5000 fold molar) did not interfere with the determination. The order of addition of reagents was not critical.

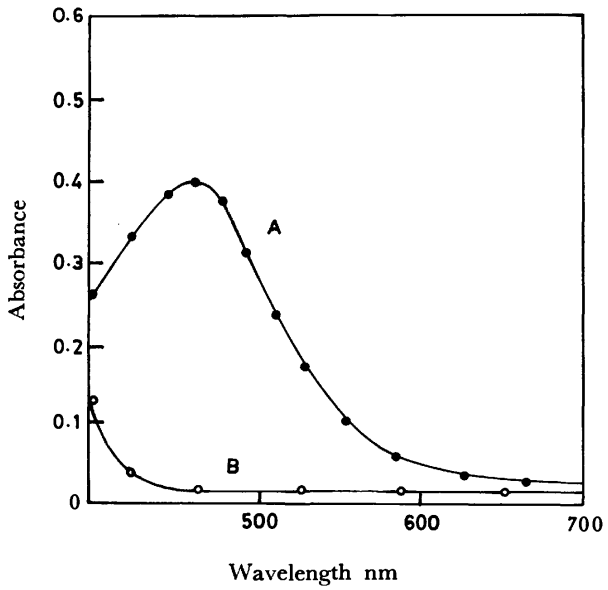

Fig. 1. Absorption spectra.
A: Fe(III)-HTPB-SCN complex (Fe=3.21×10^{-5}M),
B: *N*-Hydroxy-*N*-*o*-tolyl-*N'*-phenylbenzamidine 0.003 M in benzene.

Effect of Electrolytes, Volume of Aqueous Phase, Temperature, and Standing Time. The absorption of the colored system and the percentage extraction of iron(III) are not affected by electrolytes such as potassium chloride, ammonium chloride, and sodium chloride (2.0 M). The volume of the aqueous phase can vary between 10 to 60 ml without affecting the mixed complex formation and its subsequent extraction. Variation in temperature from 20 to 40 °C did not influence the absorbance value of the colored system. The extracts were stable for at least 40 h at 27±2 °C. A time of 1 min was sufficient for complete extraction of iron(III).

Beer's Law, Optimum Concentration, Sensitivity, and Precision. The orange-red iron(III) mixed complex adhered to Beer's law over the concentration range 0.2—4.5 ppm of the metal. The optimum concentration range on the basis of Ringbom plot[15] is 0.8 to 3.8 ppm of iron. The molar absorptivity and

Table 1. The Effect of Foreign Ions in the Determination of Iron(III) (45 μg/25 ml)

Ion	Added form	Tolerated amount[a]/ppm
Fe(II)	$FeSO_4(NH_4)_2SO_2 \cdot 6H_2O$	800
Cr(III)	$K_2SO_4Cr_2(SO_4)_3 \cdot 24H_2O$	1000
Al(III)	$Al(NO_3)_3$	1600
Bi(III)	$Bi(NO_3)_3$	1200
Cu(II)	$CuSO_4 \cdot 5H_2O$	300
Ni(II)	$Ni(NO_3)_2$	1400
Co(II)	$Co(NO_3)_2$	1400
Mn(II)	$MnCl_2 \cdot 4H_2O$	1000
Zn(II)	$ZnSO_4$	1600
Cd(II)	$CdSO_4$	2000
Pb(II)	$Pb(NO_3)_2$	1500
Ca(II)	$Ca(NO_3)_2$	3000
La(III)	$La(NO_3)_2$	2500
Th(IV)	$Th(NO_3)_4 \cdot H_2O$	1200
Zr(IV)	$Zr(SO_4)_2 \cdot 4H_2O$	80
Ti(IV)	$K_2TiO(C_2O_4) \cdot 2H_2O$	100
Nb(V)	Niobium Citrate	120
Ta(V)	Tantalum Citrate	120
Mo(VI)	$(NH_4)_6Mo_7O_{24} \cdot 4H_2O$	350
W(VI)	$Na_2WO_4 \cdot 2H_2O$	60
U(VI)	$UO_2(NO_3)_2 \cdot 6H_2O$	500
F^-	NaF	900
I	KI	900
$S_2O_3^{2-}$	$Na_2S_2O_3$	900
AsO_4^{3-}	Na_2HAsO_4	900
Phthalate	$KHC_8H_4O_4$	2500
Citrate	$Na_3C_6H_5O_7 \cdot 2H_2O$	800
Tartrate	$NaKC_4H_4O_6 \cdot 4H_2O$	800
Triethanolamine	$N(C_2H_4OH)_3$	2500
Urea	CH_4N_2O	2500
Thiourea	CH_4N_2S	2500

a) Causing an error of less than 2%.

Sandell's sensitivity of the color reaction are found to be 12000 l mol^{-1} cm^{-1} and 0.0046 μg of iron per cm^2 at 460 nm. The precision of the method was evaluated by measuring the absorbance value of 10 samples, each containing 45 μg iron per 25 ml. A mean absorbance value of 0.388 was observed with a standard deviation of ±0.0025 absorbance unit and relative standard deviation of ±0.69%.

Composition. In iron(III)-HTPB-SCN mixed ligand complex, the ratio of iron to reagent and thiocyanate was determined by curve fitting method[16] (by plotting log absorbance versus log concentration of reagents in terms of molarity). The results obtained indicate the formation of 1:1:2 (metal: HTPB:SCN) mixed ligand complex in benzene.

Influence of Diverse Ions. For studying the influence of diverse ions on the determination, an aliquot of iron(III) solution containing 45 μg of the metal was transferred to a separatory funnel and to this was added a solution containing a known weight of diverse ions. The acidity was adjusted to 0.5 M with hydrochloric acid and the total volume to about 25 ml and iron was extracted with the reagent as described earlier. The effect of various ions in the determination of iron(III) is summarized in Table 1.

Application of the Method. To test the validity of the method, various drugs, biochemicals and biological samples were selected. Iron presented in the form of iron(II) sulfate, iron(II) succinate, and fumarate can be conveniently determined by this method.

A weighed amount of the sample was transferred into a Kjeldahl flask and heated gently with a mixture of concentrated nitric and sulfuric acids (10:1 v/v) until charring commenced. Addition of concentrated nitric acid and boiling were continued until either a colorless or a pale yellow solution was obtained. This was then cooled, a few mililiters of water was added and then solution was evaporated until white fumes were evolved. The procedure was repeated two or three times. A few mililiters of dilute hydrochloric acid were added and heating was continued until fumes of nitric acid had been removed. The solution was then diluted to an appropriate volume. An aliquot of the solution was pipetted and iron was determined by the procedure recommended earlier. The results were compared with those obtained by 1,10-phenanthroline method (Table 2).

Table 2. Determination of Iron in Drug Biochemical and Biological Samples

No. Sample	Calculated iron content[a]/%	
	1,10-Phenanthroline method	Hydroxyamidine method
1 Iberol	0.105	0.103
2 Compoferon	0.110	0.109
3 Folitrin	0.350	0.347
4 Globintone	0.200	0.198
5 Ferronicum	0.325	0.324
6 Blood	0.057	0.057
7 Brassica Oleracia[b] varbotrytis (Leaves)	0.041	0.040

a) Average of six determinations. b) Value obtained from Ref. 17.

References

1) E. B. Sandell, "Colorimetric Determination of Traces of Metals," 3rd ed. Interscience, New York (1959), p. 97.
2) H. Nishida, *Bunseki Kagaku*, **19**, 221 (1970).
3) Y. Horiuchi and H. Nishida, *Bunseki Kagaku*, **19**, 930 (1970).
4) V. Panduranga Rao and P. V. R. B. Sarma, *Mikrochim. Acta*, **4**, 763 (1970).
5) H. Alexaki-Tzivanidou, *Anal. Chim. Acta*, **75**, 231 (1975).
6) M. Katyal, V. Kushwaha, and R. P. Singh, *Analyst*, **98**, 659 (1973).
7) K. Hayashi, Y. Sasaki, and K. Ito, *Bunseki Kagaku*, **21**, 1338 (1972).
8) H. L. Cluley and E. J. Newman, *Analyst*, **88**, 3, (1963).
9) J. M. Zehner and T. R. Sweet, *Anal. Chim. Acta*, **35**, 135 (1966).
10) B. M. Desai and J. V. Parghi, *J. Indian Chem. Soc.*, **54**, 1102 (1977).
11) B. J. Desai and V. M. Shinde, *Analyst*, **104**, 160 (1979).
12) A. J. Pandell, R. A. Montgomery, and R. A. Meissner, *Analyst*, **105**, 181 (1980).
13) D. T. Burns and M. E. M. Abdel Aziz, *Analyst*, **105**, 383 (1980).
14) A. I. Vogel, "A Text Book of Quantitative Inorganic Analysis," Longmans, Green London (1964), p. 524.
15) A. Ringbom, *Z. Anal. Chem.* **115**, 332 (1939).
16) L. G. Sillen, *Acta Chem. Scand*, **10**, 185 (1956).
17) C. Gopalan, B. V. Ramsastri, and S. C. Balasubramanian. "Nutritive Value of Indian Foods," National Institute of Nutrition, Indian Council of Medical Research, Hyderabad (1978), p. 65.

Reaction of 2-Aminobenzohydrazides with Schiff Bases. A New Route to 3-Benzylideneamino-4(3*H*)-quinazolinones and 2-[2-(Methylamino)-phenyl]-5-aryl-1,3,4-oxadiazoles

Padi PRATAP REDDY, Cheppala KISTA REDDY, and Padala SATYANARAYANA N. REDDY*
Department of Chemistry, Osmania University, Hyderabad-500 007, India
(Received November 19, 1984)

Reaction of 2-aminobenzohydrazides with Schiff bases in methanol followed by $KMnO_4$ oxidation has resulted in the respective formation of 3-benzylideneamino-4(3*H*)-quinazolinones and 2-[2-(methylamino)-phenyl]-5-aryl-1,3,4-oxadiazoles, characterized by spectral and analytical methods.

We have recently reported a facile one-step synthesis of 3,4-dihydro-5*H*-1,3,4-benzotriazepin-5-ones, the aza analogues of pharmacologically important 1,4-benzodiazepines, from isatoic anhydride and aroylhydrazines.[1] But the product yields in this reaction were moderate (30—50%) and the work-up involved extensive chromatography. We surmised that cyclization of 2-aminobenzohydrazide (**1**) by insertion of a carbon between the terminal nitrogens would provide a direct route to triazepin-5-ones. Schiff bases are known to participate in heterocyclization reactions acting as a source of carbon, sometimes more effectively than the corresponding carbonyl compounds.[2] Hence the reactions of 2-amino- and 2-(methylamino)benzohydrazides with *N*-benzylideneanilines were carried out and the results are discussed here.

Results and Discussion

2-Aminobenzohydrazide (**1**) reacts with *N*-(4-methoxybenzylidene)aniline (**2b**) in methanol at ambient temperature, to give a colorless crystalline product, mp 221 °C, whose elemental analysis and molecular weight (M^+ at *m/z* 387) tallies with the molecular formula $C_{23}H_{21}N_3O_3$, formally derived from one mole of **1** and two moles of the Schiff base. The same product was formed irrespective of the stoichiometry of reaction. The infrared (KBr, ν_{NH} 3280, $\nu_{C=O}$ 1660, $\nu_{C=N}$ 1610 cm^{-1}) and ^1H NMR (DMSO-d_6) spectra suggested *N*-[2-(4-methoxybenzylideneamino)benzoyl]-*N'*-(4-methoxybenzylidene)hydrazine (**3b**) structure for the product. The two azomethine protons could be discerned in ^1H NMR spectrum by the chemical shift values at δ 8.9 and 8.95. The hydrazone structure, **3b** was preferred also by its fragmentation behavior under electron impact which is characteristic of aroylhydrazones.[3] The mass spectrum of **3b** thus showed intense fragmentation peaks formed by N–N bond fission and α-cleavage reactions of the molecular ion.

Attempts to cyclize **3b** to the triazepinone by permanganate oxidation gave a product **4b**, mp 185 °C, whose molecular weight (M^+ at *m/z* 385). indicated loss of two hydrogens from **3b**. However, the spectral data is more in confirmity with 3-benzylideneamino-2-aryl-4-(3*H*)-quinazolinone structure. The IR spectrum is devoid of NH absorptions, and the carbonyl peak at 1680 cm^{-1} is similar to that of 3-substituted 4(3*H*)-quinazolinone.[4] The ^1H NMR showed the presence of only one azomethine proton (at δ 8.6) and successive loss of two 4-methoxybenzonitrile moieties from the molecular ion was indicated in the mass spectrum.

The reaction of **1** with Schiff bases has been extended to six other benzylideneanilines (**2a—g**) and good yields of the corresponding *N*-[2-(4-substituted benzylideneamino)benzoyl]-*N'*-(4-substituted benzylidene)hydrazines (**3**) were isolated except in the case of *N*-benzylideneaniline (**2a**). **3** was oxidized with permanganate to give quantitative yields of 3-benzylideneamino-4(3*H*)-quinazolinones, providing a

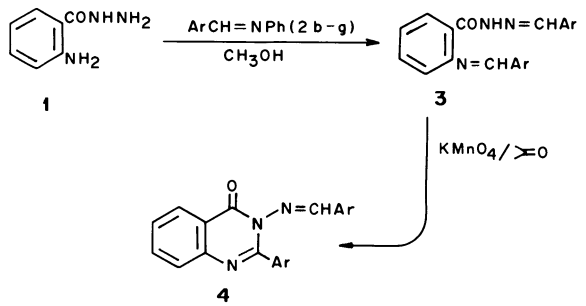

Scheme 1.

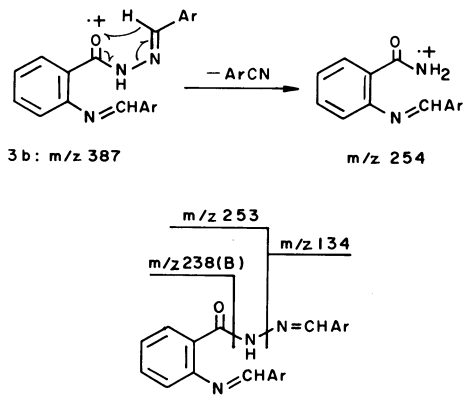

Scheme 2. Mass spectral fragmentation of product, **3b**.

new route for the synthesis of **4**.

The reaction of **1** with **2a** proceeded in a different way and gave a product, mp 190 °C whose M^+ (*m/z* 239) in the mass spectrum indicated it to be a 1:1 product. The electronic λ_{max} (log ε) [206 (3.63), 219 (3.90), 252 (3.70), 292 (4.05), 303 (2.97), 341 (3.10)] and IR spectra (ν_{NH} 3280, $\nu_{C=O}$ 1670 cm^{-1}) are consistent with 2-phenyl-1,2,3,4-tetrahydro-5*H*-1,3,4-benzotriazepin-5-one (**5**) structure. Compound **5** was found not soluble in benzene, chloroform, dimethyl sulfoxide, and acetone in such concentrations for obtaining a good continuous sweep ^1H NMR spectrum. **5** on permanganate oxidation, or on reaction with one mole of *N*-benzylideneaniline in methanol, gave a product **6**, mp 152 °C. The mass spectrum of **6** (M^+ at *m/z* 237) showed it to be a dehydrogenated product of **5** and the appearance of a peak at 1610 cm^{-1} (C=N) in addition to 1670 cm^{-1} (C=O) corroborates the assumption. Based on these data **6** was assigned 2-phenyl-1,4-dihydro-5*H*-1,3-4-benzotriazepin-5-one structure. **6** was also formed in the 1:2 molar reaction of **1** and **2a**.

The product **6** is an isomer of **6a** (mp 179 °C)[1] which may be formally derived from proton transfer. However, attempts to convert **6** to **6a** (or vice versa) by 4 M HCl (1 M=1 mol dm^{-3}) did not succeed. Hence, the structures of **5** and **6** were tentatively assigned on the basis of spectral data.

The reason why the reaction of **1** with **2a** gives **5** instead of **3a** is not clear.

To prevent the possibility of diarylidene compounds, 2-(methylamino)benzohydrazide (**7**) was reacted with *N*-benzylideneanilines. An equimolar mixture of **7** and **2b** in methanol gave a colorless crystalline product, mp 176 °C at room temperature, whose structure was confirmed as *N*-[2-(methylamino)benzoyl]-*N'*-(4-methoxybenzylidene)hydrazine (**8b**) from its mass (M^+ 283) and IR spectra (ν_{NH} 3240 $\nu_{C=O}$ 1670 cm^{-1}). The permanganate oxidation of **8b** gave a product which showed the molecular ion at *m/z* 281, two amu less than the starting **8b**. Surprisingly the IR (ν_{NH} 3190, $\nu_{C=N}$ 1600 cm^{-1}] was devoid of carbonyl absorption suggesting 2-[2-(methylamino)phenyl]-5-(4-methoxyphenyl)-1,3,4-oxadiazole (**9b**) structure. The carbonyl group absorbs around 1670 cm^{-1} in a triazepinone,[1] whose formation is possible in this oxidation reaction. **9b** was also obtained when the oxidation was carried out using lead tetraacetate (LTA). Synthesis of 1,3,4-oxadiazoles by oxidative cyclization of *N*-benzoylhydrazones or semicarbazones of aldehydes has been reported.[5] The reaction of **7** and five other *N*-benzylideneanilines afforded corresponding hydrazones, (**8a—f**). **8** Underwent both permanganate and LTA oxidation reactions to give good yields of **9**. Further evidence for the assigned structure of **9** was provided by comparison with authentic samples.[6] Formation of **9** from **8** is likely to proceed through the intermediacy of an enol form and the preference for oxadiazole ring is due to its thermodynamic stability and steric implications of methylamino group in the cyclization step.

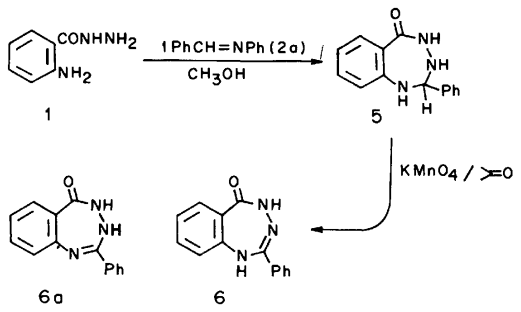

Scheme 3.

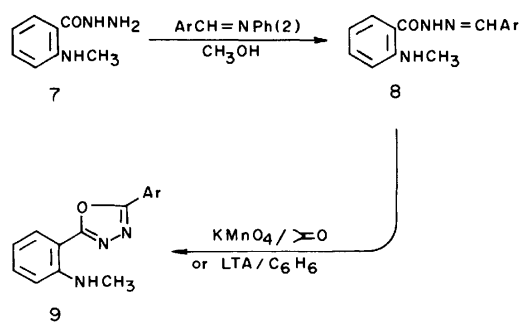

Scheme 4.

Experimental

Melting points are uncorrected. IR spectra were recorded on a Perkin-Elmer Infracord 337 spectrophotometer, ^1H NMR spectra on Varian A-60D instrument using TMS as internal standard and mass spectra on a Perkin-Elmer Hitachi RMU-6L instrument.

***N*-[2-(Benzylideneamino)benzoyl]-*N'*-benzylidene)hydrazines (3). General Procedure:** 2-Aminobenzohydrazide (**1**, 1 mmol) was dissolved in methanol (5 ml) and *N*-benzylideneaniline (**2**, 1 mmol) was added to it with thorough shaking and the mixture left aside for few minutes at room temperature. **3** Separated out from the clear solution, filtered and recrystallized from suitable solvent (Table 1).

3-Benzylideneamino-2-aryl-4-(3*H*)-quinazolinones (4). General Procedure: *N*-[2-(Benzylideneamino)benzoyl]-*N'*-benzylidenehydrazine (**3**, 10 mmol) was dissolved in dry acetone (100 ml) and $KMnO_4$ (1 gram) was added to it. The mixture was refluxed on water bath and further quantities of $KMnO_4$ were added to the boiling solution until pink color persisted. The solution was filtered and acetone was distilled off from the filtrate. The residue thus obtained was taken in water (25 ml) and excess $KMnO_4$ was destroyed with sodium sulfite solution (15 ml). The solution was extracted with chloroform (3×50 ml). The chloroform extract was dried over anhydrous sodium sulfate and the solvent was distilled off to yield crude product, **4**

Table 1. Characterisation Data of *N*-[2-(Benzylideneamino)benzoyl]-*N'*-benzylidenehydrazines (**3**), 3-Benzylideneamino-2-aryl-4(3*H*)-quinazolinones (**4**) and *N*-[2-(Methylamino)benzoyl]-*N'*-benzylidenehydrazines (**8**)

Compd	Ar	Mp (θ_m/°C)	Yield %	UV(MeOH) λ_{max}/nm (log ε)	IR(KBr) cm^{-1} NH	C=O	C=N	^{1}H NMR(δ)	Molecular formula		Calcd (%)	Found (%)
3b	4-$MeOC_6H_4$	221 (C_2H_5OH)	70	224 (3.17) 261 (3.26) 303 (3.33)	3280	1660	1610	3.9(s, 6H, $-2OCH_3$) 5.5(1H, NH) 7.9(m, 12H, aromatic) 8.9(s, 1H, azomethine) 8.95(s, 1H, azomethine)	$C_{23}H_{21}N_3O_3$	C H N	71.31 5.42 10.85	71.58 5.47 10.73
3c	4-MeC_6H_4	185 (C_6H_6)	68	226 (3.18) 257 (3.34) 305 (3.41)	3300	1660	1610	2.3(s, 6H, $-2CH_3$) 7.8(m, 12H, aromatic) 8.8(s, 1H) 8.85(s, 1H, azomethine)	$C_{23}H_{21}N_3O$	C H N	77.74 5.91 11.83	77.63 5.85 11.92
3d	4-$Me_2NC_6H_4$	238 (C_6H_6)	72	205 (3.14) 220 (3.16) 265 (3.42) 347 (3.28)	3250	1660	1610	3.3(m, 12H, $2NMe_2$) 8.0(m, 12H aromatic) 8.8(s, 1H) 8.84(s, 1H, azomethine)	$C_{25}H_{27}N_5O$	C H N	72.63 6.53 16.94	72.46 6.58 16.90
3e	4-ClC_6H_4	159 (C_6H_6/ C_2H_5OH)	73	224 (3.19) 253 (3.33) 295 (3.42) 308 (3.43) 340 (3.28)	3270	1660	1610	—	$C_{21}H_{15}N_3OCl_2$	C H N	63.63 3.78 10.60	63.42 3.83 10.49
3f	4-$NO_2C_6H_4$	234 (CH_3OH)	70	229 (3.20) 258 (3.27) 297 (3.34) 310 (3.41)	3280	1660	1610	7.9(m, 12H, aromatic) 5.1(s, 1H, NH) 8.9(s, 1H) 8.95(s, 1H)	$C_{21}H_{15}N_5O_5$	C H N	60.43 3.59 16.78	60.57 3.63 16.70
3g	2-ClC_6H_4	203 (pet. ether/ C_6H_6)	69	206 (3.18) 226 (3.32) 260 (3.41) 305 (3.41)	3250	1660	1610	—	$C_{21}H_{15}N_3OCl_2$	C H N	63.63 3.78 10.60	63.51 3.87 10.56
4b	4-$MeOC_6H_4$	185 (C_6H_6)	80	228 (3.54) 248 (3.59) 281 (3.62) 326 (3.74)	—	1680	1600	3.9(s, 6H, $-2OCH_3$) 7.9(m, 12H aromatic) 8.9(s, 1H)	$C_{23}H_{19}N_3O_3$	C H N	71.68 4.93 10.90	71.81 4.88 10.78
4c	4-MeC_6H_4	145 (C_2H_5OH)	82	225 (3.51) 253 (3.62) 284 (3.70) 324 (3.74)	—	1680	1600	2.3(s, 6H, $-2CH_3$) 7.8(m, 12H aromatic) 8.8(s, 1H)	$C_{23}H_{19}N_3O$	C H N	78.18 5.38 11.89	78.30 5.42 11.93

4d	4-$Me_2NC_6H_4$	204 (pet. ether/ C_6H_6)	78	222 (3.53) 261 (3.63) 277 (3.68) 352 (3.79)	—	1680	1600	3.3(m, 12H, $-2NMe_2$) 7.9(m, 12H, aromatic) 8.9(s, 1H)	$C_{25}H_{25}N_5O$	C H N	72.99 6.08 17.03	72.76 6.02 17.10
4e	4-ClC_6H_4	225 (C_6H_6)	82	228 (3.50) 255 (3.59) 280 (3.71) 342 (3.69)	—	1680	1600	—	$C_{21}H_{13}N_3OCl_2$	C H N	63.95 3.29 10.65	63.87 3.33 10.62
4f	4-$NO_2C_6H_4$	198 (C_2H_5OH)	78	235 (3.53) 250 (3.58) 273 (3.73) 317 (3.66)	—	1680	1600	—	$C_{21}H_{13}N_5O_5$	C H N	60.72 3.13 16.86	60.56 3.16 16.78
4g	2-ClC_6H_4	176 (C_6H_6)	80	212 (3.51) 258 (3.63) 282 (3.61) 313 (3.74)	—	1680	1600	7.8(m, 12H, aromatic) 8.8(s, 1H)	$C_{21}H_{13}N_3OCl_2$	C H N	63.95 3.29 10.65	64.07 3.22 10.60
8a	C_6H_5	192 (pet. ether/ C_6H_6)	82	220 (4.29) 257 (4.27) 362 (4.36)	3270	1670	1605	—	$C_{15}H_{15}N_3O$	C H N	71.14 5.92 16.60	70.96 5.86 16.63
8b	4-$MeOC_6H_4$	176 (C_6H_6)	82	212 (4.21) 224 (4.21) 263 (4.39) 358 (4.42)	3240	1670	1605	—	$C_{16}H_{17}N_3O_2$	C H N	67.84 6.00 14.84	67.78 5.95 14.88
8c	4-MeC_6H_4	212 (C_2H_5OH)	80	217 (4.25) 258 (4.31) 349 (4.19)	3280	1670	1605	—	$C_{16}H_{17}N_3O$	C H N	71.91 6.36 15.73	71.64 6.47 15.68
8d	4-$Me_2NC_6H_4$	171 (pet. ether)	83	215 (4.19) 226 (4.33) 264 (4.27) 368 (4.43)	3250	1670	1605	—	$C_{17}H_{20}N_4O$	C H N	68.91 6.75 18.91	69.06 6.79 18.86
8e	4-ClC_6H_4	231 (C_6H_6)	85	220 (4.22) 252 (4.36) 297 (4.38) 360 (4.43)	3300	1670	1605	—	$C_{15}H_{14}N_3OCl$	C H N	62.71 4.87 14.63	62.53 4.83 14.65
8f	4-$NO_2C_6H_4$	236 (C_2H_5OH)	83	224 (4.21) 253 (4.31) 310 (4.29) 372 (4.38)	3280	1670	1605	—	$C_{15}H_{14}N_4O_3$	C H N	60.40 4.69 18.79	60.53 4.66 18.69

Table 2. Characterization Data of 2-[2-(Methylamino)phenyl]-5-aryl-1,3,4-ozadiaxoles (**9**)

Compd	Ar	Mp θ_m/°C	Yield with $KMnO_4$ %	Yield with LTA %	UV(MeOH) λ_{max}/nm (log ε)	Molecular formula		Calcd (%)	Found (%)
9a	C_6H_5	142 (pet. ether)	85	66	253 (4.62) 272 (4.71) 280 (4.78) 293 (4.83) 375 (4.74)	$C_{15}H_{13}N_3O$	C H N	71.71 5.17 16.73	71.56 5.14 16.79
9b	4-$MeOC_6H_4$	143 (C_6H_6)	83	65	212 (4.56) 235 (4.67) 260 (4.89) 280 (4.68) 288 (4.77) 300 (4.76)	$C_{16}H_{15}N_3O_2$	C H N	68.32 5.33 14.94	68.51 5.35 14.88
9c	4-MeC_6H_4	125 (C_6H_6)	83	60	—	$C_{16}H_{17}N_3O$	C H N	71.91 6.36 15.73	71.79 6.39 15.71
9d	4-$Me_2NC_6H_4$	129 (C_2H_5OH)	82	61	—	$C_{17}H_{18}N_4O$	C H N	69.38 6.12 19.04	69.22 6.09 19.09
9e	4-ClC_6H_4	132 (pet. ether/ C_6H_6)	84	60	—	$C_{15}H_{12}N_3OCl$	C H N	63.04 4.20 14.71	62.89 4.23 14.69
9f	4-$NO_2C_6H_4$	210 (C_6H_6)	80	64	240 (4.65) 295 (4.82) 391 (4.76)	$C_{15}H_{12}N_4O_3$	C H N	60.81 4.05 18.91	61.06 4.07 18.84

IR (KBr) spectrum of all these compounds showed NH absorption around 3200 cm^{-1}; C=N absorption at 1600 cm^{-1}.

which was recrystallized from suitable solvent (Table 1).

2-Phenyl-1,2,3,4-tetrahydro-5*H*-1,3,4-benzotriazepin-5-one (5). 2-Aminobenzohydrazide (**1**, 0.15 g) was dissolved in methanol (6 ml) and *N*-benzylideneaniline (**2a**, 0.18 g) was added to it with thorough shaking and the mixture left aside for few minutes at room temperature. White-colored compound (**5**) that separated from the solution was filtered and recrystallized from benzene (mp 190 °C yield 76%).

Found: C, 70.44; H 5.41; N 17.45%. Calcd for: C, 70.30; H, 5.44; N, 17.57%.

2-Phenyl-1,4-dihydro-5*H*-1,3,4-benzotriazepin-5-one (6). Method 1. Oxidation of 5 Using $KMnO_4$. Tetrahydro compound **5** (0.24 g) was dissolved in acetone (50 ml) and $KMnO_4$ (1 g) was added to it. The mixture was refluxed on water bath for 8 h. The solution was filtered and acetone was distilled off from the filtrate. The residue thus obtained was taken in water (25 ml) and excess of $KMnO_4$ was destroyed with sodium sulfite solution (20 ml). The solution was extracted with chloroform (3×50 ml) and chloroform extract was dried over anhydrous sodium sulfate and the solvent was distilled off. The crude product thus obtained was recrystallized from pet. ether (60—80 °C)-benzene, mp 152 °C, yield 82%.

Found: C, 70.73; H, 4.60; N, 17.75%. Calcd for: C, 70.88; H, 4.64; N, 17.70%.

Method 2. Oxidation of 5 Using *N*-Benzylideneaniline (2a). Tetrahydro compound **5** (0.24 g) was dissolved in methanol (8 ml) and *N*-benzylideneaniline (**2a**, 0.18 g) was added to it. Reaction mixture was thoroughly shaken and left aside for few minutes. Separated light yellow-colored crystalline product (**6**) was filtered and recrystallized from pet. ether (60—80 °C)-benzene, mp 152 °C, yield 74%.

Method 3. From 2-Aminobenzohydrazide (1) and *N*-Benzylideneaniline (2a). 2-Aminobenzohydrazide (**1**, 0.15 g) was dissolved in minimum amount of methanol (6 ml) and *N*-benzylideneaniline (**2a**, 0.36 g) was added to it. Reaction mixture was thoroughly stirred and left aside for few minutes. Light yellow-colored crystalline compound separated out from the clear solution within few minutes. It was filtered and recrystallized from pet. ether (60—80 °C)-benzene, mp 152 °C, yield 72%.

***N*-(2-Methylaminobenzoyl)-*N'*-benzylidenehydrazines (8). General Procedure.** 2-(Methylamino)benzohydrazide (**7**, 1 mmol) was dissolved in methanol (7 ml) and an *N*-benzylideneaniline (**2**, 1 mmol) was added to it. The reaction mixture was stirred and left aside for few minutes. **8** separated immediately from the clear solution. It was filtered and recrystallized from suitable solvent (Table 1).

2-[2-(Methylamino)phenyl]-5-aryl-1,3,4-oxadiazoles (9). General Procedure. Method 1. Oxidation of Hydrazones 8 with $KMnO_4$. Hydrazone **8** (1 mmol) was dissolved in dry acetone (50 ml) and $KMnO_4$ (1 g) was added to it. The mixture was refluxed on water bath for 8 h. Further quantities of $KMnO_4$ were added to boiling solution until the pink color persisted. The solution was filtered and acetone was distilled off from the filtrate. The residue thus obtained was taken in water (20 ml) and excess of $KMnO_4$

was destroyed with sodium sulfite solution (20 ml). The solution was extracted with chloroform (3×50 ml) and chloroform extract was dried over anhydrous sodium sulfate and the solvent was distilled off. The crude product thus obtained was recrystallized from suitable solvent (Table 2).

Method 2. Oxidation of Hydrazones 8 with LTA. Hydrazone **8** (1 mmol) was dissolved in dry benzene (25 ml). Dry LTA (2 mmol, 0.886 mg) was added to it and the reaction mixture was refluxed on water bath for 15 min and then cooled. The mixture was extracted with 30% NaOH solution (3×50 ml). Benzene solution was dried over anhydrous sodium sulfate and the solvent removed under reduced pressure. The obtained brown residue was purified by recrystallization from suitable solvent (Table 2).

P. Pratap Reddy and Ch. K. Reddy are thankful to the CSIR, New Delhi, India, for the award of a JRF and SRF, respectively.

References

1) Ch. K. Reddy, P. S. N. Reddy, and C. V. Ratnam, *Synthesis*, **1983**, 842.

2) T. R. Govindachary, P. Chinnaswamy, S. Rajeswari, S. Chandrashekaran, M. S. Pramila, S. Natarajan, K. Nagarajan, and B. R. Pai, *Heterocycles*, **22**, 585 (1984).

3) W. D. Crow, J. L. Occolowitz, and R. K. Solly, *Aust. J. Chem.*, **21**, 761 (1968).

4) V. S. Misra, V. K. Saxena, and R. Srivastava, *J. Indian Chem. Soc.*, **60**, 610 (1983).

5) A. Hetzheim and K. Mockel, *Adv. Heterocycl. Chem.*, **7**, 190 (1966).

6) Ch. K. Reddy, P. S. N. Reddy, and C. V. Ratnam, *Indian J. Chem.*, in press.

Synthesis of Standardized Building Blocks as a β-D-Mannosyl Donors with a Temporary Protection to be 3,6-Di-*O*-glycosyl Acceptors, for Constructing the Inner Core of Glycoproteins and Artificial Antigens

El Sayed H. El Ashry*,† and Conrad Schuerch
Department of Chemistry, State University of New York,
College of Environmental Science and Forestry,
Syracuse, New York 13210, U.S.A.
(Received April 8, 1985)

A synthetic scheme has been achieved for the core block of glycoproteins having D-mannose configuration, which is standardized to be a 3,6-di-*O*-glycosyl acceptor and react stereoselectively as a β-D-mannosyl donor. The synthesis was started by methyl 2,3-*O*-isopropylidene-α-D-mannopyranoside, which upon benzylation, deisopropylidenation, and selective acetolysis of the 6-*O*-benzyl group afforded the corresponding tetraacetate, which could be converted to 3,6-di-*O*-allyl-4-*O*-benzyl-1,2-*O*-(1-methoxyethylidene)-β-D-mannopyranose. The orthoester could be separated into the *exo* and *endo* isomers. Hydrolysis of the orthoester ring followed by reaction with mesyl chloride gave 3,6-di-*O*-allyl-4-*O*-benzyl-2-*O*-mesytl-α-D-mannopyranosyl chloride, that upon reaction via its 1-*O*-trifluoroethanesulfonate with 2-[4-(*p*-toluenesulfonamido)phenyl]-ethanol gave the corresponding glycosides in β:α ratio of 3:1. Deallylation of the β-glycosides gave the diol which are suitable for branching and could react selectively at the 6-position allowing its potential for glycosylation by different glycosyl donors.

Many glycoproteins existing at cell surfaces and in inter-cellular systems have a common feature[1-4] in which a 3,6-di-*O*-(α-D-mannopyranosyl)-D-mannopyranosyl moiety is linked via a 1,4-β-linkage to a chitobiose residue which is linked in turn to asparagine. Glycan chains in these glycoproteins can be classified[4-12] into three types according to their origin as well as the kind of the monosaccharide existing in the branched units of the glycan chains. The first type (**1**) is oligosaccharides having high mannose content which was isolated from calf thyroglobule, the second type (**2**) which is considered as complex one and was isolated from immunoglobulin, and the third type (**3**) which is a hybrid and was isolated from ovalbumin. They have various biological functions such as the recognition signals at cell surfaces.

The artificial antigen, prepared by coupling a carbohydrate residue to a protein support, produces antibodies specific for the carbohydrate moiety, when immunized to animals. This led to great efforts towards the estimation of the immunological determinants of various antigens, via selecting artificial antigen containing particular oligosaccharide which may provide homogeneous antibody of predefined specificity.[13-16] The availability of homogeneous antibody specific for the synthetic hapten may provide an approach for studying the antigen-antibody interaction. The success in the synthesis of artificial antigen is largely due to the recent advances[17-22] in the stereoselective synthesis of the requisite oligosaccharides in high yield as well as their involvement of functional groups capable of coupling to proteins. α-D-Manp-(1→6)-α-D-manp, and α-D-manp-(1→2)-α-D-manp have been described[16] as the antigenic backbone and side chain of the yeast mannan. α-D-Manp-(1→3)-α-D-manp has been also described[23] as the antigenic branching point of the glycoproteins.

The object of this synthetic project aimed to provide an efficient synthetic approach for the synthesis of the protein conjugate of the trisaccharide 3,6-di-*O*-(α-D-mannopyranosyl)-D-mannose (**4**) as artificial antigen which represents the core structure in the glycoproteins.[1-3] The prerequisite for that is the synthesis of a core block of the mannose moiety, standardised (such as **4a**) to act as a glycosyl acceptor in the 3 and 6 positions, and meantime could act stereoselectively as a β-D-mannosyl donor toward a hydroxyl group, which is not yet reported elsewhere because it is de facto the most problematic part, and therefore its synthesis is described in the present work.

The available methods[24-27] for the stereoselective synthesis of 1,2-*cis* glycosides of gluco and galacto

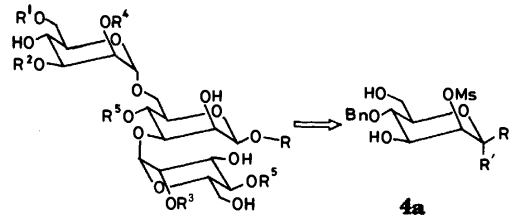

4a

R=4GlcNAcβ1→4GlcNaAcβ1→Asn

1 $R^4=R^5=H$, $R^1=R^2=R^3=$Man α1→2 Manα1-
2 $R^1=R^2=R^5=H$, $R^3=R^4=$SA α2→6 Gal β1→4 GlcNAcβ_1-
3 $R^3=R^4=H$, $R^1=R^2=$Man α1-, $R^5=$GlcNAcβ1-
4 $R=R^1=R^2=R^3=R^4=R^5=H$

Scheme 1.

† On leave of absence from Chemistry Department, Faculty of Science, Alexandria University, Alexandira, Egypt.

types are not of general utility for the synthesis of that of manno type. The use of glycosyl halides with *O*-2, *O*-3 bridging substituents that permit β-attack at *C*-1 has been reported.[28-31] This method does not allow the different temporary protection of *C*-2 and *C*-3 hydroxyl groups prior to the glycosidation of the mannosyl residue. The approach, which has found wide application in oligosaccharide synthesis,[32-35] utilises a suitably protected D-glucopyranosyl halide having a participating group at *C*-2 to favor β-linkage, followed by deacylation of *O*-2, oxidation and reduction of the resulting ketone to the manno epimer. A stereospecific synthesis of β-mannopyranosides with the use of insoluble silver catalysts has been also reported.[36] Enhancing the *C*-2-*O*-dipole by appropriate substitution has also been used to afford stereoselective synthesis[21,22] of β-D-mannosides. In a previous report,[22] a model study of the latter method with temporary blocking groups proved its successful application. Having this in mind, the design for the synthesis of 3,6-di-*O*-allyl-4-*O*-benzyl-2-*O*-mesyl-α-D-mannopyranosyl chloride (**17**) will provide a promising synthon to be used for synthesizing the target complex oligosaccharides by glycosidation to form the β-linkage followed by deallylation to generate hydroxyl groups at 3 and 6 positions, suitable for further construction.

Results and Discussion

Upon benzylation with benzyl chloride–powdered potassium hydroxide, methyl 2,3-*O*-isopropylidene-α-D-mannopyranoside (**5**)[37] gave the dibenzyl derivative (**6**) that upon deisopropylidenation afforded methyl 4,6-di-*O*-benzyl-α-D-mannopyranoside (**8**) in 82% yield. This dibenzyl derivative (**8**) is a potential starting material,* since it can be prepared on a large scale in crystalline form. The presence of two benzyl groups in **8** was confirmed form its ^{1}H and ^{13}C NMR spectra.

Moreover, the structure was also confirmed by its acetylation to give the diacetate (**9**) whose ^{1}H NMR spectrum showed the presence of two acetyl singlets at δ 2.15 and 1.93 and a downfield shift of H-2 and H-3 (δ 5.27 and 5.35, $J_{2,3}$ 4 Hz and $J_{3,4}$ 8 Hz). Acid hydrolysis of **8** by hydrochloric acid in aqueous dioxane afforded 89% yield of 4,6-di-*O*-benzyl-D-mannopyranose (**10**) based on the recovery of the starting material which could be recycled. The acetylation of **10** gave a mixture of the corresponding α- and β-tri-*O*-acetyl derivatives[23] in 55 and 30% yield, respectively. Acetolysis of **8** under controlled temperature and reaction time afforded 1,2,3,6-tetra-*O*-acetyl-4-*O*-benzyl-α-D-mannopyranose (**12**) in 73% yield. Compound **12** could also be obtained in 78 and 86% yield by acetolysis of **11**[38] and **10**, respectively. For convenience, direct conversion of **8** into **12** was found to be satisfactory. The structure of **12** was confirmed from ^{1}H NMR spectrum which showed the presence of four acetyl singlets in addition to the downfield shift of H-1, H-2, H-3, and H-6 signals, and from ^{13}C NMR spectrum which showed, in addition to the presence of one benzyl group, an upfield shift of the *C*-6. The acetate **12** was assigned the α-configuration based on its optical rotation. The reaction of **12** with hydrogen bromide afforded the bromide (**13**).

The orthoester **14** was prepared from **13** by reaction with methanol in the presence of 2,6-lutidine. It exists as a mixture of diastereoisomers in a ratio 1:12 as found from its ^{1}H NMR spectrum, and the major isomer could be crystallized in a pure form. Deacetylative allylation of the mixture of isomers of **14** gave the diallyl derivative (**15**), also as a mixture of isomers that could be separated by LC to give the major isomer **15a** as a crystalline derivative in 82% yield [singlets at δ 1.72 (CMe) and 3.30 (OMe)] and the minor isomer **15b** as a syrup in 6% yield [singlets at δ 1.53 (CMe) and 3.48 (OMe)]. For assignment of the diastereoisomeric orthoacetates, the chemical shifts for protons of the orthester ring could be used,[39] which fall into one of two patterns. From the fact that H-1, H-2, and CMe are less shielded and OMe more shielded in **15b**, than in **15a**, and the comparison of chemical shifts of OMe with that of

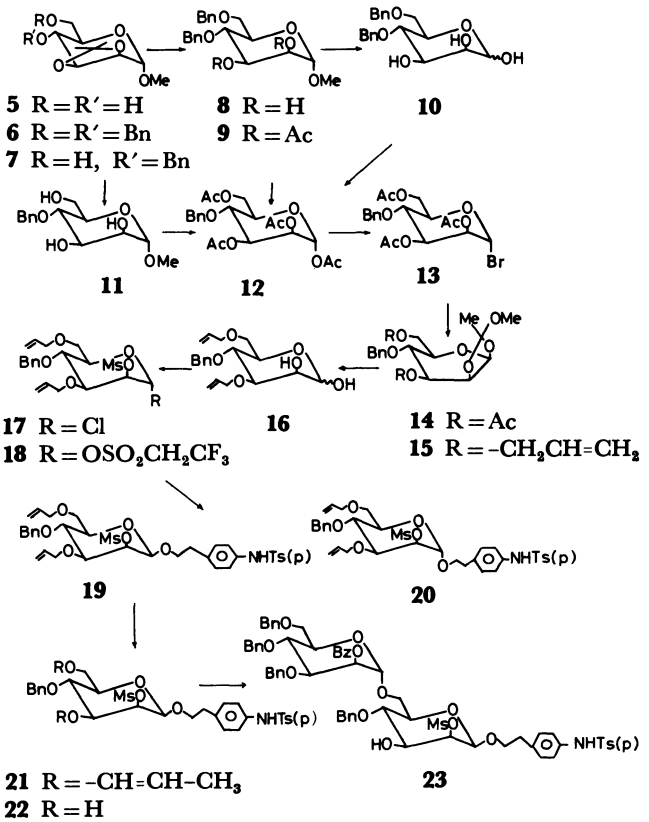

Scheme 2.

* This compound was used by V. K. Handa, V. V. Barlow, and K. L. Matta, *Carbohydr. Res.*, **76**, Cl (1979); but no data was given for it.

methanol, the isomer **15a** should tentataively have its OMe *exo*, and the other isomer *endo*. Opening of the orthoester ring of **15** with aqueous acetic acid afforded 85% yield of 3,6-di-*O*-allyl-4-*O*-benzyl-D-mannopyranose (**16**). Its ^{13}C NMR spectrum showed a ratio of ≈2.3:1.0 of α:β anomers, as indicated by the two signals of the anomeric carbon atoms at δ 94.17 and 94.63, respectively. The corresponding 3,4,6-tri-*O*-allyl analog[22] of **16** showed almost a similar ratio (≈2.5:1.0) for their anomeric carbon atoms. Reaction of **16** with mesyl chloride in 2,6-lutidine gave 68% yield of 3,6-di-*O*-allyl-4-*O*-benzyl-2-*O*-mesyl-α-D-mannopyranosyl chloride (**17**). Its ^{13}C NMR spectrum showed signals at δ 90.58 and 38.92 due to the anomeric carbon atom and the mesyl group, respectively.

The stereoselectivity and yield in glycosidation reactions can be optimized if the reactivity of *C*-1 is carefully balanced by an appropriate choice of *C*-1 leaving group. A wide spectrum of reactivities is now available by selecting the leaving group with the proper electronegativity, form the series of sulfonates (tosyl), 2,2,2-trifluoroethanesulfonyl (tresyl), or trifluromethanesulfonyl (triflyl). In the present work, the tresylate was selected as the leaving group, as it provides a moderate rate of glycosidation which may favor the β-glycosidation. Thus, reaction of **17** with silver tresylate followed by reaction with 2-[4-(*p*-toluenesulfonamido)phenyl]ethanol afforded 60% yield of the corresponding β-D-mannopyranoside (**19**) and 25% yield of α-anomer (**20**), after separation by LC. The assigned anomeric configurations was based on the comparison of the specific rotations of the two anomers, as well as their ^{1}H NMR spectral data. The β-anomeric proton appeared at δ 4.45 and that of α at δ 4.8, within the anticipated range[22,40] for β (δ 4.4—4.7) and α (δ 4.8—5.0), respectively. The ^{13}C NMR spectra showed *C*-1 at δ 98.03 and 98.64 for **20** and **19**, respectively. Rearrangement of the allyl groups in compound **19** into the 1-propenyl groups was achieved by action of tris(triphenylphosphine)rhodium chloride. Partial depropenylation of **21** was observed during the reaction and it was completed by the action with a mixture of mercury(II) oxide and mercury(II) chloride to give 77% yield of **22**. Although the 3- and 6-positions of **22** are available for glycosidation, but, the 6-position could be selectively glycosylated as shown by allowing its reaction with the tresylate derived from 2-*O*-benzoyl-3,4,6-tri-*O*-benzyl-α-D-mannopyranosyl chloride to give the disaccharide **23**.

In conclusion, the synthesis of the orthoesters **14** and **15** and the chloride **17** are of great value as precursors for complex oligosaccharides of biological significance, and actually the disaccharide **23** was successfully synthesized.

Experimental

Generals. ^{1}H NMR spectra were determined with a Varian A-60-A or XL-100-15 spectrometer for solutions in chloroform with tetramethylsilane as internal reference. ^{13}C NMR spectra were determined with Varian XL-100-15 or CFT-20 spectrometers in pulsed Fourier-transform proton-noise-decoupled mode on similar solutions. Optical rotations were determined with a Perkin-Elmer model 141 polarimeter in jacketed, 1-dm cells. Melting points were determined with a "Meltemp" apparatus with a 76-mm immersion thermometer. TLC was performed on "Baker flex" silica gel 1B-F (2.5×7.5 cm) plates; the solvents were ethyl acetate–hexane (1:1 solvent A; 2:1, solvent B; 1:3, solvent C). High pressure liquid chromatography (LC) was carried out using a Valvco septumless injector (1.0 ml), a Gleno pump, model HPLPS-1, and Waters differential refractometer R-401. A stainless-steel column (1×25 cm inside diameter) containing silica gel (Whatman, partisil M 9 10/25) was used. Preparative LC was performed on a Waters Prep-500 instrument, using a silica gel column.

Methyl 4,6-Di-*O*-benzyl-α-D-mannopyranoside (8). To a stirring mixture of methyl 2,3-*O*-isopropylidene-α-D-mannopyranoside[37] (46.8 g, 0.2 mol) and powdered potassium hydroxide (50 g) in toluene (200 ml) was added benzyl chloride (150 ml) gradually under heating. After 1 h, potassium hydroxide (50 g) was again added and the reaction was continued till TLC showed complete conversion into **6** (5 h). The mixture was cooled and filtered, and the filtrate wa washed with water, dried, and evaporated. The remaining oil was dissolved in methanol (200 ml) and 0.5 M hydrochloric acid (50 ml), and solution was heated under reflux until TLC showed complete hydrolysis (30 min), neutralized with excess of sodium hydrogencarbonate, and then filtered. The filtrate was evaported, and the residue was extracted with dichloromethane. The usual work-up of the extract gave the product which was crystallized from hexane (61.7 g, 82% yield); R_f=0.39 (solvent A); mp 101—103 °C; $[\alpha]_D^{29}$ +75.3° (c 2.0, chloroform); ^{1}H NMR δ=7.3 (m, 10 H, 2×Ph), 4.78, 4.64, 4.52, 4.50 (each d, 5 H, 2×CH_2Ph and hidden H-1), 3.7 (m, 6 H, H-2,3,4,5,6, and 6′), 3.32 (s, 3 H, OMe), 3.1 (bs, 2 H, 2×OH).

Found: C, 67.59; H, 6.95%. Calcd for $C_{21}H_{26}O_6$: C, 67.36; H, 7.00%.

1,2,3,6-Tetra-*O*-acetyl-4-*O*-benzyl-α-D-mannopyranose (12). a) A suspension of compound **8** (20.0 g, 0.05 mol) in acetic anhydride (80 ml) was cooled and treated with a cold solution on 1.0% sulfuric acid in acetic anhydride (160 ml). The mixture was stirred till complete dissolution and then kept at room temperature for 2 h. The resulting solution was poured onto crushed ice and the mixture was extracted with dichloromethane. The usual processing of the extract gave an oil that was purified by preparative LC with ethyl acetate–hexane (1:3) to give the pure product (17.0 g, 73% yield); R_f=0.59 (solvent B).

(b) A cooled solution of compound **8** (3.0 g, 8.0 mmol) in pyridine (10 ml) and acetic anhydride (6 ml) was left overnight in the ice box, poured onto crushed ice, and extracted with dichloromethane. The usual work-up of the

extract gave **9** that was purified by LC with ethyl acetate: hexane (1:3) as a solvent to give a pure product (3.1 g. 84% yield); $[\alpha]_D^{27}$+46.2° (c 1.0, chloroform); ^{1}H NMR δ=7.2 (m, 10 H, 2×Ph), 5.35 (dd, 1 H, $J_{2,3}$=4, $J_{3,4}$=8 Hz, H-3), 5.27 (dd, 1 H, H-2), 4.78—4.42 (m, 5 H, 2×CH_2Ph and H-1), 4.1—3.6 (m, 4 H, H-4,5,6, and 6′), 3.36 (s, 3 H, OMe), 2.15 and 1.93 (each s, 6 H, 2×Ac). Acetolysis of compound **9** showed similar results as in (a).

(c) Compound **7** was partially hydrolyzed with 0.5 M hydrochloric acid and the resulting compound **11** (0.2 g, 0.44 mmol) was treated with 0.67% sulfuric acid in acetic anhydride (2.5 ml) and the mixture was processed as before to give **12** (0.15 g, 78% yield).

(d) A solution of compound **8** (14.0 g, 0.04 mmol) in dioxane (150 ml) and 1 M hydrochloric acid (60 ml) was heated on a steam bath for 20 h. TLC indicated that further heating did not cause a complete transformation. The reaction mixture was cooled, neutralized with sodium hydrogencarbonate, concentrated under vacuum, and the remaining solid was extracted with ethyl acetate. The usual work-up of the extract gave a syrup that was crystallized from dichloromethane–hexane to give **10** (8.5 g); mp 110—112 °C. The mother liquor was evaporated and subjected to preparative LC with dichloromethane–ethyl acetate (1:1) to give a further crop (1.3 g) of **10**, in addition to the starting material (2.5 g) which could be recycled (the total yield based on recovery of the starting material was 89%); $[\alpha]_D^{27}$+29.8° (*c* 0.7, chloroform); ^{1}H NMR δ=7.2 (m, 10 H, 2×Ph), 5.22 (d, 1 H, $J_{1,2}\leq$1 Hz, H-1), 4.88—4.35 (m, 4H, 2×CH_2Ph, H-1), 4.1—3.3 (m, 6 H, H-2,3,4,5,6, and 6′), 3.08, 2.74, and 1.94 (each bs, 3 H, 3×OH).

A mixed cooled solution of **10** (1.8 g, 5.0 mmol) in acetic anhydride (7.0 ml) and 1.0% sulfuric acid in acetic anhydride (14.0 ml) was kept at room temperature for 1.5 h, poured onto crushed ice, and the mixture was processed as before to give, after separation by preparative LC the product (1.9 g, 86% yield); $[\alpha]_D^{27}$+60.2° (*c* 2.8 chloroform); ^{1}H NMR δ=7.3 (m, 5 H, Ph), 6.04 (d, 1 H, $J_{1,2}$=2 Hz, H-1), 5.37 (dd, 1 H, $J_{2,3}$=3.5, $J_{3,4}$=8.0 Hz, H-3), 5.26 (dd, 1 H, H-2), 4.7 and 4.6 (ABq, 2 H, *J*=12 Hz, CH_2Ph), 4.3 (m, 2 H, H-6 and 6′), 3.9 (m, 2 H, H-4 and 5), 2.12, 2.08, 2.04, and 1.99 (each s, 12 H, 4×Ac).

Found: C, 57.29; H, 5.84%. Calcd for $C_{21}H_{26}O_{10}$: C, 57.52; H, 5.98%.

2,3,6-Tri-*O*-acetyl-4-*O*-benzyl-α-D-mannopyranosyl Bromide (13). A cold solution of **12** (10.0 g, 22.8 mmol) in the least volume of dichloroemthane was added to a saturated solution of hydrogen bromide in dichloromethane (100 ml) at room temperature. The resulting solution was kept for 2 h, whereby TLC showed the disappearance of the starting material. Nitrogen was passed into the solution, then the usual processing gave a syrup that purified immediately by preparative LC with ethyl acetate–hexane (1:2) to give a pure product (7.1 g, 68% yield); R_f=0.63 (solvent B); ^{1}H NMR δ=7.3 (m, 5 H, Ph), 6.28 (d, 1 H, $J_{1,2}$=2 Hz, H-1), 5.71 (dd, 1 H, $J_{2,3}$=3.5, $J_{3,4}$=9 Hz, H-3), 5.45 (dd, 1 H, H-2), 4.70, and 4.64 (ABq, 2 H, *J*=12 Hz, CH_2Ph), 4.34 (m, 2 H, H-6 and 6′), 4.1 (m, 1 H, H-5), 3.95 (dd, $J_{4,5}$=9 Hz, H-4), 2.14, 2.07, and 1.99 (each s, 9 H, 3×Ac).

3,6-Di-*O*-acetyl-4-*O*-benzyl-1,2-*O*-(1-methoxyethylidene)-β-D-mannopyranose (14). A mixed solution of compound **13** (5.0 g, 10.9 mmol) in chloroform (15 ml), 2,6-lutidine (3 ml) and methanol (20 ml) was left at room temperature overnight, diluted with chloroform and water. The usual processing of the organic layer gave a crystallized product, that was recrystallized from dichloromethane–hexane to give colorless needles, (3.7 g, 83% yield); mp 150—151 °C; R_f=0.44 (solvent B); $[\alpha]_D^{23}$−4.3° (*c* 1.7, chloroform); ^{1}H NMR δ=7.3 (m, 5 H, Ph), 5.43 (d, 1 H, $J_{1,2}$=2.5 Hz, H-1), 5.14 (dd, 1 H, $J_{2,3}$=4, $J_{3,4}$=9 Hz, H-3), 4.7—4.6 (q, 2 H, CH_2Ph), 4.6 (m, 1 H, H-2), 4.36, and 4.21 (each q, $J_{5,6}$=3.0, $J_{5,6'}$=4.5, $J_{6,6'}$=12 Hz, H-6 and 6′), 3.89 (t, 1 H, H-4), 3.55 (m, 1 H, H-5), 3.27 (s, 3 H, OMe), 2.11, and 2.05 (each s, 6 H, 2×Ac), 1,72 (s, 3 H, CMe).

Found: C, 58.13; H, 6.29%. Calcd for $C_{20}H_{26}O_9$: C 58.53; H, 6.39%.

3,6-Di-*O*-allyl-4-*O*-benzyl-1,2-*O*-(1-methoxyethylidene)-β-D-mannopyranose (15). A hot solution of **14** (1.6 g, 2.4 mmol) and allyl bromide (6 ml) in benzene (30 ml) was treated with powdered potassium hydroxide (1.0 g), and the mixture was heated with stirring under reflux for 2 h, and then additional amount of powdered potassium hydroxide (1.0 g) was added and heating was continued for more 2 h. After cooling, the mixture was filtered. The usual processing of the filtrate gave a syrup composed from two diastereoisomers in a ratio 12:1, that separated on LC with 1:4 ethyl acetate–hexane as a solvent. The fast moving isomer was the minor product (0.1 g, 6% yield) R_f=0.55 (solvent B); $[\alpha]_D^{23}$ +13.1° (*c* 0.3, chloroform); ^{1}H NMR δ=7.3 (m, 5 H, Ph), 5.9 (m, 2 H, 2×CH in allyl), 5.2 (m, 4 H, 2×CH_2 in allyl), 5.16 (d, 1 H, $J_{1,2}$=3 Hz, H-1), 4.9, and 4.65 (ABq, 2 H, *J*=11 Hz, CH_2Ph), 4.3 (m, 2 H, H-2), 4.0 (m, 4 H, 2×OCH_2 in allyl), 3.7 and 3.5 (each m, 5 H, H-3,4,5,6, and 6′), 3.48 (s, 3 H, OMe), 1.53 (s, 3 H, CMe).

Found: C, 64.67; H, 7.58%. Calcd for $C_{22}H_{30}O_7$: C, 65.01; H, 7.44%.

The slow moving isomer was the major product that was crystallized from hexane (1.3 g, 82% yield); R_f=0.53 (solvent B); mp 43—44 °C; $[\alpha]_D^{23}$+25.8° (*c* 0.2, chloroform); ^{1}H NMR δ=7.3 (m, 5 H, Ph), 5.9 (m, 2 H, 2×CH of allyl), 5.34 (d, 1 H, $J_{1,2}$=3 Hz, H-1), 5.2 (m, 4 H, 2×CH_2 in allyl), 4.88, and 4.63 (ABq, 2 H, *J*=11 Hz, CH_2Ph), 4.48 (t, 1 H, H-2), 4.22 and 4.01 (each bd, 4 H, 2×OCH_2 in allyl), 3.65, and 3.45 (2m, 5 H, H-3,4,5,6, and 6′), 3.3 (s, 3 H, OMe), 1.72 (s, 3 H, CMe).

Found: C, 64.77; H, 7.88%. Calcd for $C_{22}H_{30}O_7$: C, 65.01: H, 7.44%.

3,6-Di-*O*-allyl-4-*O*-benzyl-D-mannopyranose (16). A solution of **15** (1.0 g, 2.46 mmol) in a mixture of glacial acetic acid (12 ml) and water (8 ml) was heated for 1 h on a steam bath and then concentrated in vacuo. The resulting syrup was dissolved in dichloromethane which was washed with aqueous sodium hydrogencarbonate, dried, and evaporated. The resulting syrup in a solution of methanol was deacetylated by catalytic amount of sodium methoxide for overnight at 5 °C, neutralized with acetic acid and evaporated. The residue was purified by LC with 1:1 ethyl acetate–hexane to give a pure syrup (0.74 g, 85%); $[\alpha]_D^{23}$+39.6° (*c* 1.3, chloroform); ^{1}H NMR δ=7.3 (m, 5 H, Ph), 5.9 (m, 2 H, 2×CH in allyl), 5.2 (m, 4 H, 2×CH_2 in allyl and H-1), 4.87 and 4.57 (ABq, 2 H, *J*=12 Hz, CH_2Ph), 4.68 (s, <1 H, H-1), 4.2—3.3 (m, 10 H, H-2,3,4,5,6,6′, and 2×OCH_2 in allyl).

Found: C, 64.51; H, 7.76%. Calcd for $C_{19}H_{26}O_6$: C, 65.12;

H, 7.48%.

3,6-Di-*O*-allyl-4-*O*-benzyl-2-*O*-mesyl-α-D-mannopyranosyl Chloride (17). To an ice-cooled solution of **16** (2.0 g, 5.7 mmol) in a mixture of dichloromethane (30 ml) and 2,6-lutidine (10 ml) was added dropwise with stirring mesyl chloride (2 ml), and the mixture was kept at 0 °C for 0.5 h and then at room temperature till TLC showed complete conversion (ca. 3 h). The usual processing of the reaction mixture gave a syrup which was purified by LC with 1:2 ethyl acetate-hexane (1.7 g, 68% yield); $[\alpha]_D^{27}$+75.3° (*c* 0.9, chloroform).

Found: Cl, 7.56%. Calcd for $C_{20}H_{20}ClO_7S$: Cl, 7.93%.

2-[4-(*p*-Toluenesulfonamide)phenyl]ethyl 3,6-Di-*O*-allyl-4-*O*-benzyl-2-*O*-mesyl-β- and α-D-Mannopyranoside (19 and 20). A solution of **17** (0.20 g, 0.45 mmol) in acetonitrile (2 ml) was treated with a solution of silver 2,2,2-trifluoroethanesulfonate in acetonitrile to form the corresponding 1-trifluoroethanesulfonate (**18**), whereby silver chloride precipitated out. After 1 h, the solution was filtered on 2-[4-(*p*-toluenesulfonamide)phenyl]ethanol (0.15 g, 0.51 mmol). All operations were performed on a high vacuum rack as described before. The reaction mixture was kept in the dark overnight, diluted with dichloromethane, washed with a solution of sodium hydrogencarbonate, sodium thiosulfate and water, and dried ($MgSO_4$). The usual processing of the extract and purification of the product with LC with 1:1 ethyl acetate-hexane as a solvent gave the major product **19** (0.19 g, 60% yield), in addition to a minor product 20 (0.08 g, 25% yield).

20: R_f=0.38 (solvent A); $[\alpha]_D^{23}$+22.1° (*c* 0.5, chloroform); ^{1}H NMR δ=7.65 (d, 2 H, *p*-substituted Ph), 7.2 (m, 12 H, aromatic and NH), 5.9 (m, 2 H, 2×CH in allyl), 5.2 (m, 4 H, 2×CH_2 in allyl), 4.8 (m, 2 H, H-1 and 2), 4.85 and 4.55 (ABq, 2 H, *J*=12 Hz, CH_2Ph), 4.1 (m, 5 H, H-3 and 2×OCH_2 in allyl), 3.6 (m, 6 H, H-4,5,6,6′ and OCH_2 in ethyl), 3.10 (s, 3 H, Ms), 2.8 (q, 2 H, CH_2 in ethyl), 2.36 (s, 3 H, Me).

Found: C, 57.94; H, 6.13%. Calcd for $C_{35}H_{43}NO_{10}S_2 \cdot H_2O$: C, 58.39; H, 6.02%.

19: R_f=0.33 (solvent A); $[\alpha]_D^{27}$−22.3° (*c* 0.3, chloroform); ^{1}H NMR δ=7.68 (d, 2 H, *p*-substituted Ph), 7.2 (m, 12 H, aromatic and NH), 5.9 (m, 2 H, 2×CH in allyl), 5.2 (m, 4 H, 2×CH_2 in allyl), 4.95 (m, 1 H, H-2), 4.9 and 4.55 (ABq, 2 H, *J*=11 Hz, CH_2Ph), 4.45 (s, 1 H, H-1), 4.1 (m, 5 H, H-3 and 2×OCH_2 in allyl), 3.6 (m, 6 H, H-4,5,6,6′ and OCH_2 in ethyl), 2.82 (bq, 2 H, CH_2 in ethyl), 2.80 (s, 3 H, Ms), 2.35 (s, 3 H, Me).

Found: C, 60.46; H, 6.00%. Calcd for $C_{35}H_{43}NO_{10}S_2$: C, 59.89; H, 6.18%.

2-[4-(*p*-Toluenesulfonamido)phenyl]ethyl 4-*O*-Benzyl-2-*O*-mesyl-β-D-mannopyranoside (22). The mixture of **19** (0.7 g, 1.0 mmol) and tris(triphenylphosphine)rhodium-(I) chloride (0.13 g) in 9:1 (v/v) ethanol-water (20 ml) was heated under reflux till TLC showed complete disappearance of **19** (2 h) and then evaporated to a syrup. The syrup was extracted with dichloromethane, and the usual processing of the extract gave a mixture of 1-propenyl and depropenylated derivatives which was heated with mercury(II) oxide (0.9 g) and mercury(II) chloride (0.9 g) in 9:1 (v/v) acetone-water under reflux for 15 min, filtered, and the filtrate was evaporated. The remaining residue was extracted with dichloromethane and the organic phase was washed with aqueous potassium iodide and water, dried ($MgSO_4$), and evaporated to a syrup, which was purified by using HPLC with ethyl acetate-hexane (0.48 g, 77% yield); $[\alpha]_D^{23}$ −20.0° (*c* 0.1, chloroform); ^{1}H NMR δ=7.66 (d, 2 H, *p*-substituted Ph), 7.3 (m, 12 H, aromatic and NH), 4.8 (d, 1 H, H-2), 4.83 and 4.63 (ABq, 2 H, *J*=11 Hz, CH_2Ph), 4.48 (s, 1 H, H-1), 4.01 (m, 1 H, H-3), 3.7—3.3 (m, 6 H, H-4,5,6,6′ and OCH_2 in ethyl), 2.81 (t, 2 H, CH_2 in ethyl), 2.8 (s, 3 H, Ms), 2.4 (bs, 2 H, 2×OH), 2.34 (s, 3 H, Me).

Found: C, 55.12; H, 5.75%. Calcd for $C_{29}H_{35}NO_{10}S_2 \cdot 0.5H_2O$: C, 55.22; H, 5.75%.

2-[4-(*p*-Toluenesulfonamide)phenyl]ethyl 6-*O*-(2-*O*-Benzoyl-3,4,6-tri-*O*-benzyl-α-D-mannopyranosyl)-4-*O*-benzyl-2-*O*-mesyl-β-D-mannopyranoside (23). Under high vacuum, **22** (0.1 g, 0.16 mmol), 2-*O*-benzoyl-3,4,6-tri-*O*-benzyl-α-D-mannopyranosyl chloride (1.5 equivalent) and silver tresylate were left in separate joined flask for 5 h at room temperature. Acetonitrile (2 ml) was distilled onto the chloride, and the resulting solution was mixed with silver tresylate. After 0.5 h, the solution of the tresylate was filtered over onto compound **22**. The resulting solution was kept for overnight at room temperature in the dark. The reaction mixture was diluted with dichloromethane, washed with saturated solution of sodium thiosulfate and sodium hydrogencarbonate, water and dried ($MgSO_4$). The resulting syrup after evaporation of the solvent, was separated on LC with ethyl acetate-hexane (2:3) to give the disaccharide as a syrup (0.12 g, 64% yield); $[\alpha]_D^{23}$ −4.3° (*c* 0.3, chloroform).

Found: C. 64.31; H, 5.75%. Calcd for $C_{63}H_{67}NO_{16}S_2 \cdot H_2O$: C, 64.32; H, 5.91%.

This work supported by Grant No. 5R01AI 12509 from the National Institute of Allergy and Infections Diseases, National of Health, U.S. Public Health Service. We thank Mr. R. Dushin for his skillfull techniques and efforts in preparing the starting material on large scale. We also thank Prof. J. Yoshimura and Dr. R. Eby for their helpfull discussions.

References

1) J. Montreuil, *Adv. Carbohydr. Chem. Biochem.*, **37**, 157 (1980).

2) R. Cornfeld and S. Kornfeld, *Annual Rev. Biochem.*, **45**, 217 (1976).

3) F. M. Winnik, J. P. Carver, and J. J. Krepinsky, Personnal communication.

4) T. Ogawa, K. Katano, K. Sasajima, and M. Matsui, *Tetrahedron*, **37**, 2779 (1981), and references cited in.

5) S. Ito, D. Yamashita, R. G. Spiro, and A. Kobata, *J. Biochem. (Tokyo)*, **81**, 1621 (1977).

6) J. Baenziger, S. Kornfeld, and S. Kochwa, *J. Biol. Chem.*, **249**, 1897 (1974).

7) J. Baenziger and S. Kornfeld, *J. Biol. Chem.*, **249**, 7260 (1974).

8) T. Tai, K. Yamashita, S. Ito, and A. Kobata, *J. Biol. Chem.*, **252**, 6687 (1977).

9) K. Yamashita, Y. Tachibana, and A. Kobata, *J. Biol. Chem.*, **253**, 3862 (1978).

10) J. Montreuil, *Pure Appl. Chem.*, **42**, 431 (1975).

11) D. Burke, L. Mendonca-previato, and C. E. Ballou,

Proc. Natl. Acad. Sci. U. S. A., **77**, 318 (1980).
12) R. C. Hughes and N. Sharon, *Nature*, **274**, 637 (1978).
13) W. F. Goebels and O. T. Avery, *J. Exp. Med.*, **50**, 521, 533 (1929).
14) W. F. Goebels, F. H. Babers, and O. T. Avery, *J. Exp. Med.*, **55**, 761 (1932).
15) W. F. Goebels, *J. Exp. Med.*, **64**, 29 (1936).
16) R. Eby and C. Schuerch, *Carbohydr. Res.*, **77**, 61 (1979).
17) R. U. Lemieux, K. B. Hendricks, R. V. Stock, and K. James, *J. Am. Chem. Soc.*, **97**, 4056 (1975).
18) S. Hannesian and J. Banoub, *Carbohydr. Res.*, **53**, c13 (1977).
19) R. Eby and C. Schuerch, *Carbohydr. Res.*, **34**, 79 (1974).
20) E. S. Rachaman, R. Eby, and C. Schuerch, *Carbohydr. Res.*, **67**, 147 (1978).
21) V. K. Srivastave and C. Schuerch, *J. Org. Chem.*, **46**, 1121 (1981).
22) E. S. H. El Ashry and C. Schuerch, *Carbohydr. Res.*, **105**, 33 (1982).
23) L. Awad, E. S. H. El Ashry, and C. Schuerch, *Carbohydr. Res.*, **122**, 69 (1983).
24) K. Igarashi, *Adv. Carbohydr. Chem. Biochem.*, **34**, 243 (1977).
25) G. Wulff and G. Röhle, *Angew. Chem., Int. Ed. Engl.*, **13**, 157 (1974).
26) C. Schuerch, "Anomeric Effect, Origin and Consequences," ed by W. A. Szarek and D. Horton, Am. Chem. Soc., Symp. Ser., **87**, 80 (1979).
27) J. R. Pougny and P. Sinay, *Tetrahedron Lett.*, **1976**, 4073.
28) S. Perlin, *Pure Appl. Chem.*, **50**, 1401 (1978).
29) R. J. Garegg and T. Iversen, *Carbohydr. Res.*, **70**, c13 (1979).
30) R. J. Garegg, T. Iversen, and R. Johansson, *Acta Chem. Scand., Ser. B.*, **34**, 505 (1980).
31) J. S. Brimacombe, *Specialist Periodical Repts. Chem. Soc. Carbohydrates*, **11**, 25 (1979).
32) O. Theander, *Acta Chem. Scand.*, **12**, 1883 (1958).
33) O. Theander, *Adv. Carbohydr. Chem.*, **17**, 223 (1962).
34) G. Ekborg, B. Lindberg, and J. Lönngren, *Acta Chem. Scand.*, **26**, 3287 (1972).
35) E. E. Lee, G. Keaveney, and P. S. O'Colla, *Carbohydr. Res.*, **59**, 268 (1977).
36) H. Paulsen and O. Lockhoff, *Chem. Ber.*, **114**, 3102 (1981).
37) M. E., Evans and F. W. Parrish, *Carbohydr. Res.*, **54**, 105 (1977).
38) R. Eby and C. Schuerch, *Carbohydr. Res.*, **100**, c41 (1982).
39) A. S. Perlin, *Can. J. Chem.*, **41**, 399 (1963).
40) R. Kasai, M. Okihara, J. Asakawa, K. Mizutani, and G. Tanaka, *Tetrahedron*, **35**, 1427 (1979).

 © 1986 The Chemical Society of Japan Bull. Chem. Soc. Jpn., 59, 1587—1592 (1986)

A Synthesis of Methyl 3-*O*-(β-D-Mannopyranosyl)-α-D-mannopyranoside from Sulfonate Intermediates

Laila Fathy AWAD, El Sayed H. EL ASHRY,†,* and Conrad SCHUERCH
Department of Chemistry, State University of New York,
College of Environmental Science and Forestry,
Syracuse, New York 13210, U.S.A.
(Received April 8, 1985)

Methyl 3-*O*-(β-D-mannopyranosyl)-α-D-mannopyranoside was synthesized by the reaction of 3,4,6-tri-*O*-benzyl-2-*O*-benzylsulfonyl-1-*O*-tresyl-D-mannopyranose with methyl 2,4,6-tri-*O*-benzyl- and 2,4,6-tri-*O*-(*p*-bromobenzyl)-α-D-mannopyranoside, followed by deprotection. The corresponding 1-*O*-(*p*-tolylsulfonyl) derivative gave better yield and stereoselectivity in the reaction with methanol, but was not sufficiently reactive to couple with a hindered secondary alcohol. The 2-*O*-benzylsulfonyl group is comparable in β-directing effect to 2-*O*-methylsulfonyl group, but its stereoselectivity is dependent on the structure of the reactant alcohol. It can be selectively removed by the reaction with sodium amide in *N*,*N*-dimethylformamide.

Stereoselectivity in syntheses of 1,2-*trans* and 1,2-*cis*-mannopyranosyl glycosides and oligosaccharides depends greatly on the protecting group at *O*-2 of the reactive mannosyl derivative and on its leaving group on *C*-1. In our previous paper[1] we investigated conditions for the formation of the 1,2-*trans* α-D-mannopyranosyl linkage using ester functions on *O*-2 and sulfonate leaving groups on *C*-1. β-D-Mannopyranosides are also of great interest because of their presence as structural elements in glycoproteins and the *O*-antigenic lipopolysaccharides,[2-8] and a number of methods have been proposed for their synthesis. Gorin and Perlin[9] first used 4,6-di-*O*-acetyl-2,3-*O*-carbonyl-α-D-mannopyranosyl bromide for the synthesis of β-D-mannopyranosides and it has since been used successfully for those of primary alcohols, while the stereoselectivity was uncertain[10-13] in cases of secondary alcohols. Garegg's method, using 2,3:4,6-di-*O*-cyclohexylidene-α-D-mannopyranosyl chloride and silver carbonate[14,15] or silver imidazole and mercury(II) chloride,[16] also gives better yields and stereoselectivity with primary alcohols. A widely used complex reaction sequence involves β-glucosidation, hydrolysis of a 2-*O*-acyl group, oxidation, and reduction.[17-21] 1,1-Dimannosides of various anomeric forms have been prepared with trifluoromethanesulfonyl (triflic) anhydride and 2,3,4,6-tetra-*O*-benzyl-D-mannose.[22] Silver silicate was successfully used by Paulsen and Lockhoff[23] as catalyst for the coupling of 6-*O*-acetyl-2,3,4-tri-*O*-benzyl-α-D-mannopyranosyl bromide to the equatorial 4-OH of a 1,6-anhydrogalactopyranose derivative to form the (1→4) β-linked disaccharide. β-D-Mannopyranosides have also been prepared by *O*-alkylation by Srivastava and Schuerch[24] and an interesting synthesis of β-D-mannopyranosides and -furanosides was recently reported by Schmidt, Reichrath and Morering,[25] in which 1-*O*-metallated derivatives are treated with alkyl triflates. The stereoselectivity is controlled by means of solvent and temperature. These methods are also presumably most useful for primary mannopyranosides. We have used a strongly electron-withdrawing, non-participating substituent on *O*-2 and a strongly electronegative leaving group at *C*-1 to control the stereoselectivity and yield of 1,2-*cis*-β-D-mannopyranosides and -β-L-rhamnopyranosides.[26-30] High β-selectivity has been observed in the formation of primary mannopyranosides, but results in the secondary positions of sugar derivatives were less satisfactory.[26,28,30]

The methylsulfonyl (mesyl) group has been used as a non-participating electron-withdrawing group on *O*-2, which can be removed selectively be reductive cleavage.[31] Herein we report the use of the benzylsulfonyl group as a substituent on *O*-2 and describe glycosidation results and the selective removal of the benzylsulfonyl group from the resultant glycosides and disaccharides.

Results and Discussion

3,4,6-Tri-*O*-benzyl-2-*O*-benzylsulfonyl-α-D-mannopyranosyl chloride (**2**) was prepared in 72% yield in one step by treating 3,4,6-tri-*O*-benzyl-D-mannose (**1**) in dichloromethane with excess benzylsulfonyl chloride in the presence of 2,6-lutidine. 3,4,6-Tri-*O*-benzyl-2-*O*-benzylsulfonyl-β-D-mannopyranose (**3**) was also separated as a by-product. The structure of both **2** and **3** was confirmed by ^{1}H and ^{13}C NMR spectroscopy. The methylene carbon of benzylsulfonyl group was found to have a characteristic signal in ^{13}C NMR, which resonate at δ 57.8 and 57.9 for **2** and **3**, respectively. The presence of the sulfonate function at *O*-2 caused a downfield shift of *H*-2 and it appeared as either a triplet in **2** or broad doublet in **3**. The β-configuration of **3** was confirmed by ^{13}C NMR and by its negative optical rotation. The chloride **2** was also obtained in 90% yield, when an ethereal solution of **3** was saturated with hydrogen chloride at 0 °C and worked up conventionally. The 1-*O*-(2,2,2-

† Present address: Chemistry Department, Faculty of Science, Alexandria University, Alexandria, Egypt.

trifluoroethylsulfonyl) (tresyl) derivative of **3** was prepared by the condensation of **2** and silver tresylate as described before[1] and was then coupled with absolute methanol to give methyl 3,4,6-tri-*O*-benzyl-2-*O*-benzylsulfonyl-α,β-D-mannopyranosides (**4**,**5**) in 57% yield with an α:β ratio of 2:3. When, instead of tresylate as leaving group, *p*-toluenesulfonate (tosylate) was used for the same coupling reaction, the stereoselectivity and the yield were improved with a 74% overall yield and α:β ratio of 18:82. Optical rotational values and ^1H and ^{13}C NMR spectra (see Experimental) confirmed the anomeric configuration of the anomers separated. When the 1-tosylate was prepared from **2** and treated with methyl 2,4,6-tri-*O*-(*p*-bromobenzyl)-α-D-mannopyranoside (**8**),[32] no reaction occurred and starting materials were recovered. However, the corresponding 1-tresytlate derived from **2** in the same reaction gave methyl 3-*O*-(3,4,6-tri-*O*-benzyl-2-*O*-benzylsulfonyl-α,β-D-mannopyranosyl)-2,4,6-tri-*O*-(*p*-bromobenzyl)-α-D-mannopyranosides (α:**10**, β:**14**) in 49% yield and in α:β ratio of 1:2. The structures of both **10** and **14** were confirmed by ^1H and ^{13}C NMR spectroscopy and optical rotation. The H-1′ proton of **10** and **14** appeared at δ 5.1—4.97 and 4.2—4.1, respectively. Anomeric carbons *C*-1′ in **10** and **14** resonated at δ 98.3 and 99.8, while the anomeric carbon *C*-1 of **14** resonated at δ 96.6. The *C*-5′ of β-isomer **14** was also observed in downfield as expected at δ 76.2.

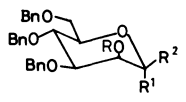

1 R=H, R^1, R_2=H, OH
2 R=O_2SBn, R^1=Cl, R^2=H
3 R=O_2SBn, R^1=H, R^2=OH
4 R=O_2SBn, R^1=OCH_3, R^2=H
5 R=O_2SBn, R^1=H, R^2=OCH_3
6 R=H, R^1=OCH_3, R^2=H
7 R=H, R^1=H, R^2=OCH_3

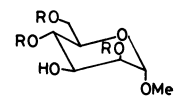

8 R=BnBr-*p*
9 R=Bn

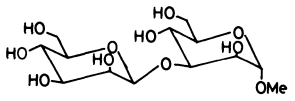

18

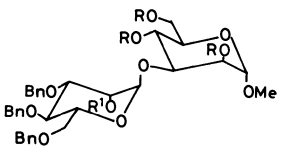

10 R=BnBr-*p*, R^1=O_2SBn
11 R=Bn, R^1=O_2SBn
12 R=BnBr-*p*, R^1=H
13 R=Bn, R^1=H

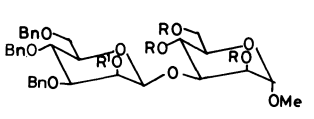

14 R=BnBr-*p*, R^1=O_2SBn
15 R=Bn, R^1=O_2SBn
16 R=BnBr-*p*, R^1=H
17 R=Bn, R^1=H

An analogous reaction was carried out on the 1-*O*-tresyl derivative from **2** with methyl 2,4,6-tri-*O*-benzyl-α-D-mannopyranoside (**9**).[33] The disaccharide methyl 2,4,6-tri-*O*-benzyl-3-*O*-(3,4,6-tri-*O*-benzyl-α,β-D-mannopyranosyl) α-D-mannopyranosides (α:**11**, β:**15**) were obtained in an improved yield (70%) but poorer β-selectivity (α:β of 61:39). As in the case of compounds **10** and **14**, the β-anomeric carbon resonates in upfield (δ=97.2) than α-anomeric carbon (δ=99.6), and C-5′ of **15** was found as expected at δ=76.2.

There is a surprising difference in stereoselectivity of the reactions of the 1-*O*-tresyl derivative from **2** with **8** and **9**. These results may reflect differences in reaction conditions rather than reactivity differences between **8** and **9**. In the reaction with **8**, the formation of tresylate was allowed to proceed for 6 h before the addition of **8**. In reaction with **9**, **2** and silver tresylate were allowed to react for only 1 h and silver halide precipitation was far from complete, when **9** was added. In the first case, therefore, there was a much better chance for an S_N2-like mechanism or shielded S_N1 mechanism to control stereoselectivity predominantly. In the second case, the cation generated directly by reaction of **2** with silver ion may be less shielded and steric control was less effective.

There is also an interesting difference between reaction of the tosylate and tresylate derived from **2** with alcohols. The tosylate gave better β-selectivity than the tresylate on reaction with methanol, but was insufficiently reactive to form product with relatively hindered secondary alcoholic functions, at least at ambient temperatures.

In summary, the benzylsulfonyl group is comparable to mesyl as a β-directing group in mannoside syntheses. In both cases stereoselectivity also depends on the nature of the alcoholic function reacting, and is usually better with primary alcohols. For separation of anomeric products, the benzylsulfonate group was preferable as the substituent.

A second objective of this research is to achieve a selective deblocking of the 2-*O*-benzylsulfonyl group. Sulfonate substituents have been removed in many cases by reductive cleavage[34-39] and this method has been applied to the cleavage of 2-*O*-mesyl groups.[37] Alternatively aryl *p*-toluenesulfonates have been hydrolyzed by bases.[40-42] The mechanism involves nucleophilic attack on sulfur by amine or hydroxide, causing sulfur–oxygen bond fission.[40,43,44] This mechanism apparently requires a good leaving group on sulfur. Mesyl chloride[45] and aryl benzylsulfonates are more readily hydrolyzed or aminolyzed, and these reactions proceed by a stepwise elimination-addition mechanism with the formation of a sulfene intermediate in the rate-determining step which is rapidly scavenged by amine or base.[46,47]

$$ArCH_2\text{-}SO_2\text{-}O\text{-}Ar' + Et_3N \rightleftharpoons Et_3\overset{+}{N}H + Ar\overset{-}{C}H\text{-}SO_2\text{-}O\text{-}Ar'$$

$$Ar'O^- + ArCH{=}SO_2 \xrightarrow{+OH} ArCH_2\text{-}SO_3^-$$

The latter approach was tried in the present instance.

Various amines under a variety of conditions failed to remove the benzylsulfonyl group, presumably because the sugar anion is a poor leaving group, and a stronger base is required to remove benzylic proton and to form the sulfene intermediate. However, the stronger base, sodium amide, in *N,N*-dimethylformamide at room temperature readily removed the substituent without the formation of by-product from **4**, **5**, **10**, **11**, **14**, and **15**. Yields of product ranged from 65 to 95% with the higher recoveries due to purer reagents and improved work-up procedures. ^{1}H and ^{13}C NMR and optical rotations of **6** and **7** agreed with those in the literature.[27,31,48,49] ^{13}C NMR of **12**, **13**, **16**, and **17** showed an upfield shift of *C*-2 and elimination of the benzylsulfonyl methylene carbons.

Methyl 3-*O*-(β-D-mannopyranosyl)-α-D-mannopyranoside (**18**) was obtained in quantitative yield by catalytic hydrogenation of **17**, while **16** gave **18** together with some decomposition products. A comparison of the ^{13}C NMR spectrum of **18** and **17** showed that the peak positions of *C*-2, *C*-3′, *C*-6, and *C*-6′ moved 6 to 7 ppm upfield on debenzylation as expected. The same was apparently true of *C*-4 and *C*-4′, although in **17** these positions could not be clearly distinguished from the six benzylic methylene carbons. Also as expected, *C*-1, *C*-1′, *C*-2′, and *C*-5′ moved downfield from δ 2.3 to 4.6, while the position of *C*-5 in **17** was also uncertain. A comparison of the ^{13}C NMR of **18** with those of methyl α- and β-D-mannopyranoside[50] confirmed these assignments and the specific rotation of **18**, $[\alpha]_D^{23}$+5.76°, was consistent with a β-linkage in comparison with the rotation of the corresponding α-linked disaccharide.[51]

Experimental

Generals. ^{1}H NMR spectra were determined with a Varian EM 360 MHz spectrometer for solution in chloroform-*d* with tetramethylsilane. ^{13}C NMR, optical rotations, melting point, TLC, high pressure liquid chromatography (LC) and coupling reactions were done as described previously.[1,29] *N,N*-Dimethylformamide (DMF) was distilled on the high vacuum rack and dried over Molecular Sieve. Silver 2,2,2-trifluroethanesulfonate was prepared as described.[1]

3,4,6-Tri-*O*-benzyl-2-*O*-benzylsulfonyl-α-D-mannopyranosyl Chloride (2). To a stirred solution of 3,4,6-tri-*O*-benzyl-D-mannopyranose (**1**) (1 g, 2.2 mmol) in dichloromethane (10 ml) and dry 2,6-lutidine (0.614 g, 5.7 mmol) was added benzylsulfonyl chloride (1.058 g, 5.5 mmol), and the reaction mixture was stirred overnight, and concentrated. The resulting residue was extracted with ether. The extract was washed with 1 M† hydrochloric acid, sodium hydrogencarbonate and water, dried, and concentrated. The resulting syrup was separated on LC using ethyl acetate-hexane (1:2) to give **2** (1 g) as syrup in 72.5% yield; $[\alpha]_D^{22}$ +31.3° (*c* 1.04, chloroform); ^{1}H NMR δ=7.1—7.35 (t, 20H, aromatic), 5.84—5.9 (d, 1H, H-1), 5.0—5.13 (t, 1H, H-2), 4.26—4.96 (m, 8H, 3×CH_2Ph and O_2SCH_2Ph), 3.53—4.2 (m, 5H, H-3,4,5,6, and 6′); ^{13}C NMR δ=90.2 (C-1), 77.9 (C-3), 76.4, 75.5, 74.8, 73.6, and 73.1 (C-2,4,5, and 3×CH_2Ph), 68.2 (C-6), 57.8 (O_2SCH_2Ph). 3,4,6-Tri-*O*-benzyl-2-*O*-benzylsulfonyl-β-D-mannopyranose (**3**) was also separated as syrup in 23% yield (0.3 g); $[\alpha]_D^{23}$−14.7° (*c* 1.06, chloroform), ^{1}H NMR δ=7.45 (20H, aromatic), 5.1—5.19 (d, 1H, H-2), 4.25—4.93 (m, 9H, H-1, 3×CH_2Ph and O_2SCH_2Ph), 4.1—3.4 (5H, H-3,4,5,6, and 6′), 2.59 (s, 1H, exchange with D_2O, OH); ^{13}C NMR δ=86.1 (C-1), 80.5 (C-3), 79.8 (C-5), 79.2 (C-4), 75.4, 73.7, 73.5, and 72.9 (C-2 and 3×CH_2Ph), 68.7 (C-6), 57.9 (O_2SCH_2Ph).

Compound **2** was also obtained from **3** in 90% yield. A solution of **3** (0.2 g, 0.33 mmol) in dry ether (10 ml) saturated with hydrogen chloride at 0 °C was left overnight with stirring at room temperature, swept by bubbling nitrogen to remove hydrogen chloride, washed with sodium hydrogencarbonate and water, dried, and concentrated. Separation of the product by LC using ethyl acetate-hexane (1:2) gave **2** (185 mg).

Found: C, 65.18; H, 5.80; Cl, 5.71; S, 5.09%. Calcd for $C_{34}H_{35}ClO_7S$: C, 65.52; H, 5.66; Cl, 5.68; S, 5.14%.

Methyl 3,4,6-Tri-*O*-benzyl-2-*O*-benzylsulfonyl-α,β-D-mannopyranosides (4,5). The chloride **2** (366 mg, 0.588 mmol), silver tresylate (159 mg, 0.588 mmol) and absolute methanol (25 mg, 0.78 mmol) were left separately under vacuum on a high vacuum rack for 3 h at room temperature. Acetonitrile (2 ml) was then distilled onto **2** and the resulting solution was left to react with silver tresylate for 1 h in the dark. The reaction mixture was then mixed with absolute methanol and kept for 70 h at room temperature in the dark. The reaction mixture was diluted with dichloromethane, filtered, washed with sodium thiosulfate, sodium hydrogencarbonate and water, dried, and concentrated. After separation of syrupy product by LC using ethyl acetate-hexane (1:3), compound **4** was obtained in 23% (64 mg) yield and **5** in 34% (94 mg) yield. The chloride **2** was recovered in 23% yield (85 mg).

Compounds **4** and **5** were also obtained in 14 and 61% yield, when **2** (468 mg, 751 mmol), silver *p*-toluenesulfonate (210 mg, 751 mmol), and absolute methanol (36 mg, 1.125 mmol) were treated as described above. Compound **4**: $[\alpha]_D^{23}$ +6.9° (*c* 1.1, chloroform); ^{1}H NMR δ=7.38—7.0 (d, 20 H, aromatic), 5.0—4.78 (t adjacent to d, 2H, H-2 and 1), 4.75—4.2 (m, 8H, 3×CH_2Ph, O_2SCH_2Ph) and 3.93—3.45 (5H, H-3,4,5,6, and 6′), 3.3 (s, 3H, OMe); ^{13}C NMR δ=99.0 (C-1), 78.1 (C-3), 76.3 (C-4), 75.3 (C-2), 71.98 (C-5), 69.1 (C-6), 57.7 (O_2SCH_2Ph), 55.2 (OMe). Compound **5**: $[\alpha]_D^{25}$−37.5° (*c* 0.98, chloroform); ^{1}H NMR δ=7.5—7.0 (d, 20H, aromatic), 5.2—5.06 (d, 1H, H-2), 4.95—4.25 (m, 9H, H-1, 3×CH_2Ph and O_2SCH_2Ph), 3.75—3.56 (m, 5H, H-3,4,5,6, and 6′), 3.5 (s, 3H, OMe); ^{13}C NMR δ=99.6 (C-1), 79.8 (C-3), 77.2 (C-5), 76.0 (C-4), 74.4 (C-2), 69.3 (C-6), 57.1 (O_2SCH_2Ph), 56.9 (OMe). The overall yield for this coupling was 74.6% (0.308 g) and the ratio of α:β was 18:82.

Found: C, 67.43; H, 6.02; S, 4.90%. Calcd for $C_{35}H_{38}SO_8$: C, 67.94; H, 6.12; S, 5.18%.

Methyl 3,4,6-Tri-*O*-benzyl-α-D-mannopyranoside (6). A solution of **4** (50 mg, 0.08 mmol) in DMF (5 ml) was treated with sodium amide (30 mg, 0.08 mmol) at room temperature overnight with stirring under anhydrous conditions. Methanol (2 ml) was then added and the

† 1 M=1 mol dm^{-3}.

reaction mixture was neutralized with acetic acid. The reaction mixture was evaportated on the high vacuum rack without heating. The resulting residue was extracted with ether, and the extract was washed with sodium hydrogencarbonate and water, dried, and concentrated. After separation of the residue on LC using ethyl acetate–hexane (2:3), **6** was obtained in 65% (24 mg) yield as a syrup; $[\alpha]_D^{23}$ +57.2° (*c* 0.5, chloroform), ^{1}H and ^{13}C NMR agree with those in the literature.[31,48,49]

Methyl 3,4,6-Tri-*O*-benzyl-β-D-mannopyranoside (7). A solution of **5** (0.1 g, 0.161 mmol) in DMF (5 ml) was treated with sodium amide (6.5 mg, 0.166 mmol) as described for **6**. Separation of the product by LC using ethyl acetate–hexane (1:1) gave **7** in 67% (50 mg) yield. $[\alpha]_D^{23}$ −13.1° (*c* 0.94, chloroform); lit,[27,31] $[\alpha]_D^{20}$ −10.2° (*c* 0.45, chloroform), $[\alpha]_D^{20}$ −8.77° (*c* 1.0, chloroform).

Methyl 3-*O*-(3,4,6-Tri-*O*-benzyl-2-*O*-benzylsulfonyl-α,β-D-mannopyranosyl)-2,4,6-tri-*O*-(*p*-bromobenzyl)-α-D-mannopyranoside (10,14). Compound **8**[32] (526 mg, 0.75 mmol), **2** (467 mg, 0.75 mmol), and silver tresylate (302 mg, 1.12 mmol) were left under vacuum for 5 h on the high vacuum rack. Acetonitrile was distilled onto **2**, and the resulting solution was left to react with silver tresylate for 6 h in the dark with stirring. The formed 1-*O*-tresyl derivative was then treated with **8** for 40 h in the dark. The reaction mixture was processed as described for **4** and **5** to give **10**, in 17% (160 mg) yield as a syrup. $[\alpha]_D^{23}$+6.9° (*c* 1, chloroform), ^{1}H NMR δ=7.4—6.8 (m, 32H, aromatic), 5.1—4.97 (d, 1H, H-1′), 4.95—4.8 (t, 1H, H-2′), 4.73—4.1 (m, 15H, H-1, 3×$CH_2C_6H_4Br$-*p*, 3×CH_2Ph, and O_2SCH_2Ph), 4.0—3.35 (m, 11H, H-2,3,3′,4,4′,5,5′,6, and 6′), 3.2 (s, 3H, OMe); ^{13}C NMR δ=99.8 (C-1′), 98.3 (C-1), 79.4 (C-3′), 77.7 (C-2 and 3), 76.4 (C-4), 69.2 and 69.5 (C-6 and 6′), 57.6 (O_2SCH_2Ph), 54.9 (OMe), 75.2, 74.8, 74.5, 74.2, 73.7, 72.7, and 71.9 (C-2′,4′,5,5′, 3×CH_2Ph, and 3×$CH_2C_6H_4Br$-*p*).

The β-disaccharide (**14**) was separated as a syrup in 32% (0.31 g) yield, which crystallized from ether; mp 113 °C; $[\alpha]_D^{22}$ −12.8° (*c* 0.86, chloroform); ^{1}H NMR δ =7.5—6.75 (m, 32H, aromatic), 5.13—5.03 (d, 1H, H-2′), 4.93 (s, 1H, H-1), 4.85—4.25 (m, 14H, 3×CH_2Ph, 3×$CH_2C_6H_4Br$-*p*, and O_2SCH_2Ph), 4.2—4.1 (bd, 1H, H-1′), 3.4—4.06 (m, 11H, H-2,3,3′,4,4′,5,5′,6, and 6′), 3.3 (s, 3H, OMe); ^{13}C NMR δ=99.1 (C-1), 96.6 (C-1′), 80.5 (C-3′), 78.1 and 77.6 (C-3 and 2), 76.2 (C-5′), 75.5 and 75.4 (C-4 and 4′), 74.3, 73.7, 73.2, 72.8, 72.7, 71.9, and 71.6 (C-2′,5, 3×CH_2Ph, and 3×$CH_2C_6H_4Br$-*p*), 69.5 and 69.2 (C-6 and 6′), 57.8 (O_2SCH_2Ph), 54.9 (OMe).

Found for **9**: C, 57.36; H, 5.02; S, 2.83; for **10**: C, 57.95; H, 4.79; S, 2.38%. Calcd for $C_{62}H_{63}O_{13}SBr_3$: C, 57.81; H, 4.93; S, 2.48%.

Methyl 3-*O*-(3,4,6-Tri-*O*-benzyl-α-D-mannopyranosyl)-2,4,6-tri-*O*-*p*-bromobenzyl-α-D-mannopyranoside (12). A well stirred solution of **10** (80 mg, 0.0621 mmol) and sodium amide (12 mg, 0.31 mmol) in DMF (5 ml) was processed as described for **6** to give **12** (50 mg) as a syrup in 70% yield. $[\alpha]_D^{24}$+19.5° (*c* 0.8, chloroform); ^{1}H NMR δ=7.45—6.85 (m, 27H, aromatic), 5.06 (s, 1H, H-1′), 4.86 (s, 1H, H-1), 4.75—4.21 (m, 12H, 3×CH_2Ph, and 3×$CH_2C_6H_4Br$-*p*), 4.1—3.5 (m, 12H, H-2,2′,3,3′,4,4′,5,5′,6 and 6′), 3.23 (s, 3H, OMe); ^{13}C NMR δ=101.6 (C-1′), 98.7 (C-1), 80.2 (C-3′), 78.9, and 77.9 (C-3 and 2), 75.3, 75.1, 74.7, 74.2, 73.7, 72.8, 72.2, 71.9, and 71.6 (C-5,5′,4,4′, 3×CH_2Ph, and 3×$CH_2C_6H_4Br$-*p*), 69.7 and 69.3 (C-6 and 6′), 68.8 (C-2′), 55.0 (OMe).

Found: C, 59.15; H, 4.56%. Calcd for $C_{55}H_{57}O_{11}Br_3$: C, 59.24; H, 5.06%.

Methyl 3-*O*-(3,4,6-Tri-*O*-benzyl-β-D-mannopyranosyl)-2,4,6-tri-*O*-(*p*-bromobenzyl)-α-D-mannopyranoside (16). A solution of **14** (0.1 g, 0.078 mmol) and sodium amide (15 mg, 0.387 mmol) in freshly distilled DMF (5 ml) was processed as described for **6** to give **16** (83 mg) in 95% yield as a syrup. $[\alpha]_D^{22}$+11.6° (*c* 1, chloroform); ^{1}H NMR δ=7.45—6.86 (m, 27H, aromatic), 4.93—4.8 (s, 1H, H-1), 4.76—4.2 (m, 14H, H-1′,5′, 3×CH_2Ph, and 3×$CH_2C_6H_4Br$-*p*), 4.0—3.4 (m, 11H, H-2,2′,3,3′,4,4′,5,6, and 6′), 3.23 (s, 3H, OMe), 2.5—2.26 (bs, 1H, OH); ^{13}C NMR δ=98.9 (C-1), 97.6 (C-1′), 81.8 (C-3′), 76.7, 75.9, 75.4, 75.2, 74.3, 73.7, 72.8, 71.9, and 71.7 (C-5,5′,4,4′,3,2, 3×CH_2Ph, and 3×$CH_2C_6H_4Br$-*p*), 69.5 (C-6 and 6′), 68.8 (C-2′), 54.9 (OMe).

Found: C, 57.78; H, 4.96%. Calcd for $C_{55}H_{57}O_{11}Br_3$: C, 58.24; H, 5.06%.

Methyl 2,4,6-Tri-*O*-benzyl-3-*O*-(3,4,6-tri-*O*-benzyl-2-*O*-benzylsulfonyl-α,β-D-mannopyranosyl)-α-D-mannopyranoside (11,15). Compound **9**[33] (405 mg, 0.874 mmol), silver tresylate (320 mg, 1.18 mmol), and **2** (0.7 g, 1.124 mmol) were left for 3 h on the high vacuum rack. Acetonitrile (3 ml) was distilled onto **2**, and the resulting solution was mixed with silver tresylate. The reaction mixture was left for 30—60 min with stirring in the dark, mixed with **9**, and then processed as described for **4** and **5** to give **11** (394 mg) in 43% yield as a syrup. $[\alpha]_D^{24}$ +9.8° (*c* 1.04, chloroform); ^{1}H NMR δ=7.36—7.37 (d, 35H, aromatic), 5.23—5.13 (d, 1H, H-1′), 5.13—5.15 (bs, 1H, H-2′), 4.92 (s, 1H, H-1), 4.8—4.17 (m, 14H, 6×CH_2Ph and O_2SCH_2Ph), 4.13—3.5 (m, 11H, H-2,3,3′,4,4′,5,5′,6, and 6′), 3.25 (s, 3H, OMe): ^{13}C NMR δ=99.6 (C-1′), 98.4 (C-1), 79.1 (C-3′), 77.8 and 77.6 (C-2 and 3), 76.7, 74.9, 74.4, 73.5, 72.8, 72.7, 72.3, 72.2, and 72.0 (C-5,5′,4,4′,2′, and 6×CH_2Ph), 69.3 and 68.9 (C-6 and 6′), 57.6 (O_2SCH_2Ph), 54.8 (OMe). The compound **15** was separated in 28% yield (252 mg) as a syrup. $[\alpha]_D^{24}$−17.2° (*c* 0.83, chloroform); ^{1}H NMR δ=7.5—7.7 (m, 35H, aromatic), 5.18—5.06 (d, 1H, H-2′), ca. 5.4 (bm, 18H, H-1,1′, 6×CH_2Ph, O_2SCH_2Ph and 2H of sugar protons), 4.0—3.46 (bm, 9H, rest of the sugar protons), 3.36 (s, 3H, OMe); ^{13}C NMR δ=99.3 (C-1), 97.2 (C-1′), 80.2 (C-3′), 77.8 (C-3), 77.4 (C-2), 76.2 (C-5′), 75.5, 75.3, 74.9, 74.3, 73.7, and 73.4 (C-5 and 6×CH_2Ph), 72.5 (C-4′), 72.2 (C-4), 71.5 (C-2′), 69.7, 69.3 (C-6 and 6′), 57.8 (O_2SCH_2Ph), 54.9 (OMe).

Found for **11**: C, 70.25; H, 6.25; S, 3.13, and for **15**: C, 70.00; H, 6.05; S, 2.86%. Calcd for $C_{62}H_{66}SO_{13}$: C, 70.83; H, 6.32; S, 3.05%.

Methyl 2,4,6-Tri-*O*-benzyl-3-*O*-(3,4,6-tri-*O*-benzyl-α-D-mannopyranosyl)-α-D-mannopyranoside (13). Compound **11** (129 mg, 0.127 mmol) in freshly distilled DMF (5 ml) was left to react with pure sodium amide (24 mg, 0.613 mmol) for 48 h as described for **6** to give **13** (90 mg) in 82% yield. $[\alpha]_D^{22}$+25.2° (*c* 0.85, chloroform,); ^{1}H NMR δ=7.4—7.05 (m, 30H, aromatic), 5.18 (s, 1H, H-1′), 4.9 (s, 1H, H-1), 4.83—4.43 (m, 12H, 6×CH_2Ph), 4.4—3.5 (bm, 12H, H-2,2′,3,3′,4,4′,5,5′,6, and 6′), 3.3 (s, 3H, OMe), 2.65—2.93 (bs, 1H, OH); ^{13}C NMR δ=101.5 (C-1′), 98.8 (C-1), 80.2 (C-3′), 78.7 (C-2), 77.8 (C-3), 75.5, 75.01, 74.7, 73.6, 72.4, 72.2, 72.1 (C-5,5′,4,4′ and 6×CH_2Ph), 69.6 and 69.4 (C-6 and 6′), 68.9 (C-2′), 54.9 (OMe).

Found: C, 73.05; H, 6.83%. Calcd for $C_{55}H_{60}O_{11}$: C, 73.63; H, 6,74%.

Methyl 2,4,6-Tri-*O*-benzyl-3-*O*-(3,4,6-tri-*O*-benzyl-β-D-mannopyranosyl)-α-D-mannopyranoside (17). Pure so-

dium amide (24 mg, 0.623 mmol) was left to react with compound **15** (132 mg, 0.125 mmol) in freshly distilled DMF (5 ml) for 48 h as described for **6** to give **17** (0.1 g) as a syrup in 90% yield. $[\alpha]_D^{22}$+16.6° (*c* 0.72, chloroform); ^{1}H NMR δ=7.37—7.17 (m, 30H, aromatic), 4.92—4.90 (d, 1H, H-1), 4.87—4.43 (m, 12H, 6×CH_2Ph), 4.35—4.21 (d, 1H, H-1′), 4.39 (s, 1H, one of sugar protons), 3.9—3.69 (m, 11H, rest of sugar protons), 3.31 (s, 3H, OMe), 2.65—2.50 (bs, 1H, OH). ^{13}C NMR δ=98.9 (C-1), 97.2 (C-1′), 81.6 (C-3′), 76.3 and 76.0 (C-2 and 3), 75.3 (C-5′), 74.6, 73.7, 73.5, 72.5, 71.9, 71.7, 71.4 (C-5,4,4′, and 6×CH_2Ph), 69.6, and 69.4 (C-6 and 6′), 68.6 (C-2′), 54.9 (OMe).

Found: C, 73.74; H, 7.14%. Calcd for $C_{55}H_{60}O_{11}$: C, 73.63; H, 6.74%.

Methyl 3-O-(β-D-Mannopyranosyl)-α-D-mannopyranoside (18). A suspension of **17** (84 mg) and palladium over carbon (0.04 g), in methanol (15 ml) and water (5 ml) was hydrogenated for 48 h at room temperature with stirring. After filtration and freeze drying, **18** was obtained in quantitative yield. $[\alpha]_D^{23}$+5.8° (*c* 0.59, water), ^{13}C NMR δ=103.03 (C-1), 99.5 (C-1′), 79.8 (C-3), 78.7 (C-5′), 75.2 (C-5); 74.7 (C-3′), 73.2 (C-2′), 69.4 (C-2), 69.1 (C-4′), 67.5 (C-4), 63.3 (C-6 and 6′), 57.1 (OMe). The same compound was obtained from **16** in 30% yield by the same procedure.

This work was supported by Grant No. AI-12509 from the National Institute of Allergy and Infections Diseases, National Institutes of Health, U.S. Public Health Service. We thank Dr. R. Eby for his helpful assistance and discussions, and Dr. L. Anderson who suggested the usage of the benzylsulfonyl protecting group. We also thank Prof. J. Yoshimura for his valuable discussions.

References

1) L. F. Awad, E. S. H. El Ashry, and C. Schuerch, *Carbohydr. Res.*, **122**, 69, (1983).
2) K. Jann and O. Westphal "The Antigens," ed by M. Sela, Academic Press, New York (1975), Vol. 3, p. 1.
3) J. Montreuil, *Adv. Carbohydr. Chem. Biochem.*, **37**, 157 (1980).
4) R. Kornfeld and S. Kornfeld, *Annual Rev. Biochem.*, **45**, 217 (1976).
5) J. Baenziger, S. Kornfeld, and S. Kochwa, *J. Biol. Chem.*, **249**, 1897 (1974).
6) J. Baenziger and S. Kornfeld, *J. Biol. Chem.*, **249**, 7260 (1974).
7) S. Ito, K. Yamashita, R. G. Spiro, and A. Kobata, *J. Biochem. (Tokyo)*, **81**, 1621 (1977).
8) J. Montreuil, *Pure Appl. Chem.*, **42**, 431 (1975).
9) P. A. J. Gorin and A. S. Perlin, *Can. J. Chem.*, **39**, 2474 (1961).
10) M. A. E. Shaban, I. E. Ray, D. A. Jeanolz, and R. W. Jeanolz, *Carbohydr. Res.*, **45**, 105 (1975).
11) N. K. Kochetkov, V. I. Torgov, N. N. Malysheva, and A. S. Shashkov, *Tetrahedron*, **39**, 1099 (1980).
12) V. I. Betaneli, M. V. Ovchinnikov, L. V. Backinowsky, and N. K. Kochetkov, *Carbohydr. Res.*, **84**, 211 (1980).
13) J. S. Brimacombe, *Special Periodical Repts. Chem. Soc. Carbohydr.*, **11**, 25 (1979).
14) P. J. Garegg and T. Iversen, *Carbohydr. Res.*, **70**, C13 (1979).
15) P. J. Garegg, T. Iversen, and R. Johansson, *Acta Chem. Scand., Ser. B*, **34**, 505 (1980).
16) P. J. Garegg, R. Johansson, and B. Samuelsson, *Acta Chem. Scand., Ser. B*, **35**, 635 (1981).
17) O. Theander, *Acta Chem. Scand.*, **12**, 1883 (1958).
18) O. Theander, *Adv. Carbohydr. Chem.*, **17**, 223 (1962).
19) E. E. Lee, G. Keaveney, and P. S. O'Colla, *Carbohydr. Res.*, **59**, 268 (1977).
20) H. B. Boren, G. Ekborg, K. Eklind, P. J. Garegg, A. Pilotti, and C. G. Swahn, *Acta Chem. Scand.*, **27**, 2639 (1973).
21) G. Ekborg, B. Lindberg, and J. Lonngren, *Acta Chem. Scand.*, **26**, 3287 (1972).
22) A. A. Pavia, J. M. Rocheville, and S. N. Ung, *Carbohydr. Res.*, **79**, 79 (1980).
23) H. Paulsen and O. Lockhoff, *Chem. Ber.*, **114**, 3102 (1981); *Tetrahedron Lett.*, **1978**, 4027.
24) V. K. Srivastava and C. Schuerch, *Tetrahedron Lett.*, **1979**, 3269.
25) R. R. Schmidt, M. Reichrath, and U. Morering, *Tetrahedron Lett.*, **21**, 3561 (1980); *Chem. Ber.*, **115**, 39 (1982).
26) V. K. Srivastava and C. Schuerch, *Carbohydr. Res.*, **79**, C13, (1980).
27) V. K. Srivastava and C. Schuerch, *J. Org. Chem.*, **46**, 1121 (1981).
28) V. K. Srivastava and C. Schuerch, *Carbohydr. Res.*, **100**, 411 (1982).
29) E. S. H. El Ashry and C. Schuerch, *Carbohydr. Res.*, **105**, 33 (1982).
30) E. S. H. El Ashry and C. Schuerch, unpublished results.
31) K. T. Webster, R. Eby, and C. Schuerch, *Carbohydr. Res.*, in press.
32) F. Kong and C. Schuerch, *Carbohydr. Res.*, **112**, 141 (1983).
33) V. K. Handa, J. Barlow, and K. L. Matta, *Carbohydr. Res.*, **76**, C1 (1979).
34) K. Freudenberg and R. Brauns, *Chem. Ber.*, **55**, 3233 (1922).
35) R. S. Tipson, *Method Carbohydr. Chem.*, **2**, 250 (1963).
36) H. Schmid and P. Kauer, *Helv. Chim. Acta*, **32**, 1371 (1949); H. R. Bolliger and P. Ulrich, ibid., **35**, 93 (1952).
37) M. A. Miljković, M. Pešić, A. Jokić, and E. A. Eavidson, *Carbohydr. Res.*, **15** 162 (1970); J. Kovar, *Can. J. Chem.*, **48**, 2383 (1970).
38) H. C. Jarrell, R. G. S. Ritchie, W. A. Szarek, and J. K. N. Jones, *Can. J. Chem.*, **51**, 1767 (1973).
39) Von F. Reber and T. Reichstein, *Helv. Chim. Acta*, **28**, 1164 (1945).
40) J. F. Bunnett and J. Y. Bassett, *J. Am. Chem. Soc.*, **81**, 2104 (1959).
41) J. L. Kice and G. J. Kasperek, *J. Am. Chem. Soc.*, **92**, 3393 (1970).
42) J. L. Kice, C. A. Walters, and S. B. Burton, *J. Org. Chem.*, **39**, 346 (1974).
43) E. T. Kaiser and O. R. Zaborsky, *J. Am. Chem. Soc.*, **90**, 4626 (1968).
44) T. Deacon, A. Steltiner, and A. Williams, *J. Chem. Soc., Perkin Trans. 2*, **1975**, 1778.
45) J. F. King and T. W. S. Lee, *J. Am. Chem. Soc.*, **91**, 6524 (1969).
46) A. Williams, K. T. Douglas, and J. S. Loran, *J. Chem. Soc., Chem. Commun.*, **1974**, 689.
47) J. F. King and R. P. Beatson, *Tetrahedron Lett.*, **1975**,

973.
48) E. S. Rechaman, R. Eby, and C. Schuerch, *Carbohydr. Res.*, **67**, 147 (1978).
49) N. E. Franks and R. Montgomery, *Carbohydr. Res.*, **6**, 286 (1968).
50) K. Bock and H. Thogersen, *Annual Reports on NMR Spectroscopy*, **13**, 1 (1982).
51) E. E. Lee and J. O. Wood, *Carbohydr. Res.*, **75**, 322 (1979).

Synthesis of New Arginine Derivatives as Substrates of Trypsin

Oyin SOMORIN* and Leo AMEGHASHITSI
Department of Chemistry, University of Lagos, Akoka, Yaba, Lagos, Nigeria
(Received July 10, 1985)

Eight new chromogenic arginine substrates: N^{α}-benzyloxy-carbonyl-L-arginine 3,5-dinitroanilide hydrochloride (L-ZADA·HCl), N^{α}-benzyloxycarbonyl-L-arginine 3-nitroanilide hydrochloride (L-ZANA·HCl), N^{α}-benzyloxycarbonyl-L-arginine 3-nitro-5-chloroanilide hydrochloride (L-ZANCA·HCl), N^{α}-benzyloxycarbonyl-L-arginine 3-nitro-5-bromoanilide hydrochloride (L-ZANBA·HCl), N^{α}-benzyloxycarbonyl-L-arginine 3-nitro-5-fluoroanilide hydrochloride (L-ZANFA·HCl), N^{α}-benzyloxycarbonyl-L-arginine 3-nitro-5-iodoanilide hydrochloride (L-ZANIA·HCl), N^{α}-benzyloxycarbonyl-L-arginine 3-nitro-5-(methylsulfonyl)anilide hydrochloride (L-ZANMA·HCl), and N^{α}-benzyloxycarbonyl-L-arginine 3-nitro-5-(trifluoromethyl)anilide hydrochloride (L-ZANTA·HCl) were synthesized by coupling 5-substituted 3-nitroanilines with N^{α}-benzyloxycarbonyl-L-arginine hydrochloride. These substrates were found to be susceptible to trypsin-catalyzed hydrolysis. These series of substrates are suitable for studying electronic effects on trypsin activity.

Several workers[1–12] have studied the dependence of the electronic effects of substituents in the substrate molecules on the reactivity of chymotrypsin, but there has been very few of such systematic studies on the activity of trypsin. Studies on the relationship of the electronic effects of substituents in the substrates and enzyme activity have been very useful in elucidating the mechanism of action of enzyme catalysis. Both chymotrypsin and trypsin exhibit some remarkable similarities. For example, trypsin and chymotrypsin are proteolytic enzymes which are protein in nature, containing no co-enzyme or prosthetic group and therefore the catalytic activity of these enzymes must be associated directly with the constituents of the protein.[13] Their precursors trypsinogen and chymotrypsinogen are both important constituents of pancreatic juice. These two strikingly similar enzymes are serine proteases with unique serine residue which reacts with organophosphorus compounds to yield inactive derivatives.[14] Besides possessing identical molecular weights both enzymes possess only one active site per molecule which is defined by the reactive serine residue and the common sequence Gly–Asp–Ser–Gly.[15,16] Chymotrypsin and trypsin have mechanistic similarities as evident from the various indications in the literature that trypsin-catalyzed hydrolyses, like those of chymotrypsin, proceed through an acyl-enzyme intermediate.[16] Hence it would be expected that the electronic factors which influence the reactivity of chymotrypsin could similarly influence the reactivity of trypsin.

In order to facilitate the study of these electronic effects, chromogenic substrates would be most desirable since such substrates offer the advantage of producing their own chromogen on enzymic hydrolysis which can easily be quantitatively estimated spectrophotometrically. Most of the substrates previously reported for the studies of the electronic effects on chymotrypsin activity are not chromogenic. In this paper, synthesis of new series of chromogenic substrates suitable for studying the electronic effects of substituents in the substrate molecules on the reactivity of trypsin is reported. The series include N^{α}-benzyloxycarbonyl-L-arginine 5-substituted 3-nitroanilide derivatives. The substrates are unique because of the presence of the nitro group at the 3-position (since the nitro group confers chromogenicity on the substrate) and the presence of various substituents at the 5-position which could be conveniently modified to yield a series of substrates that are suitable for studying the electronic effects on the trypsin activity. In this study the substituents at the 5-position include nitro, methylsulfonyl, trifluoromethyl, fluoro, chloro, bromo, and iodo groups.

Abbreviations: L-ZADA·HCl, N^{α}-benzyloxycarbonyl-L-arginine 3,5-dinitroanilide hydrochloride; L-ZANA·HCl, N^{α}-benzyloxycarbonyl-L-arginine 3-nitroanilide hydrochloride; L-ZANCA·HCl, N^{α}-benzyloxycarbonyl-L-arginine 3-nitro-5-chloroanilide hydrochloride; L-ZANBA·HCl, N^{α}-benzyloxycarbonyl-L-arginine 3-nitro-5-bromoanilide hydrochloride; L-ZANFA·HCl, N^{α}-benzyloxycarbonyl-L-arginine 3-nitro-5-fluoroanilide hydrochloride; L-ZANIA·HCl, N^{α}-benzyloxycarbonyl-L-arginine 3-nitro-5-iodoanilide hydrochloride; L-ZANMA·HCl, N^{α}-benzyloxycarbonyl-L-arginine 3-nitro-5-(methylsulfonyl)anilide hydrochloride; L-ZANTA·HCl, N^{α}-benzyloxycarbonyl-L-arginine 3-nitro-5-(trifluoromethyl)anilide hydrochloride, and DMF, *N,N*-dimethylformamide.

Experimental

All the reagents used throughout this investigation are of analytical grades. The ultraviolet and visible absorption spectra were measured with a Zeiss PMQ3 Spectrophotometer attached to Haake F3 thermostated water bath. The optical rotations were measured with a Perkin Elmer recording polarimeter, Model 241MC. Elemental analyses were carried out by Yanagimoto CHN Corder Model MT-2 at the Analytical Laboratory of Hokkaido University, Sapporo, Japan. Melting points were determined by Reichert melting point apparatus. The elemental analysis and melting points for all known compounds were found to agree with the theoretical and literature values.

Table 1. Elemental Analyses and Optical Rotations of New Chromogenic Arginine Substrates

Substrate	Mp θ_m/°C	$[\alpha]_D^{25}$	Fomula	Analyses					
				Calcd (%)			Found (%)		
				C	H	N	C	H	N
L-ZADA·HCl	222—224	−19.0°	$C_{20}H_{24}N_7O_7Cl$	47.09	4.75	19.23	47.10	4.77	19.04
L-ZANA·HCl	187—188	−19.3°	$C_{20}H_{25}N_6O_5Cl$	51.64	5.42	18.08	51.67	5.38	18.17
L-ZANCA·HCl	214—215	−15.8°	$C_{20}H_{24}N_6O_5Cl_2$	48.08	4.85	16.83	48.12	4.88	16.91
L-ZANBA·HCl	220—221	−14.6°	$C_{20}H_{24}N_6O_5ClBr$	44.15	4.45	15.45	44.09	4.38	15.35
L-ZANFA·HCl	215—216	−18.9°	$C_{20}H_{24}N_6O_5ClF$	49.72	5.01	17.40	49.88	5.09	17.66
L-ZANIA·HCl	203—204	− 9.6°	$C_{20}H_{24}N_6O_5ClI$	40.63	4.10	14.22	40.92	4.17	13.94
L-ZANMA·HCl	162—163	−20.3°	$C_{21}H_{27}N_6O_7ClS$	46.43	5.01	15.47	46.22	4.94	15.19
L-ZANTA·HCl	195—196	−14.7°	$C_{21}H_{24}N_6O_5ClF_3$	47.31	4.54	15.77	47.49	4.68	15.83

Buffer. 0.05 M(1 M=1 mol dm^{-3}) tris(hydroxymethyl)-aminomethane hydrochloride buffer solutions containing 0.04 M calcium chloride at pH values ranging from 6.5 to 9.5 were prepared.

Enzyme. Twice crystallized bovine pancreatic trypsin with a specific activity of 182 units mg^{-1} protein was purchased from Wako Pure Chemicals Industries, Japan. The trypsin activity was determined using L-TAME·HCl as a substrate according to the Worthington Procedure.[17]

Preparation of 5-Substituted 3-Nitroanilides. 3,5-Dinitroaniline, 3-nitro-5-chloroaniline 3-nitro-5-bromoaniline, 3-nitro-5-iodoaniline, 3-nitro-5-fluoroaniline, 3-nitro-5-(methylsulfonyl)aniline, and 3-nitro-5-(trifluoromethyl)-aniline were prepared according to the procedure reported by Dosumu.[18]

Synthesis of the Chromogenic Arginine Substrates, N^{α}-Benzyloxycarbonyl-L-arginine 5-Substituted 3-Nitroanilide Hydrochloride. The 3-nitro-5X-aniline (X=H, CF_3, NO_2, SO_2CH_3, F, Cl, Br, and I) was coupled to N^{α}-benzyloxycarbonyl-L-arginine hydrochloride by the method reported by Somorin et al.[19] Solution A containing the 3-nitro-5X-aniline (0.03 mol) and triethylamine (4.2 ml, 0.03 mol) in diethyl phosphonate (15 ml) was added to Solution B which contained phosphorus pentaoxide (8.55 g, 0.06 mol) in diethyl phosphonate (30 ml). Solution of N^{α}-benzyloxy-carbonyl-L-arginine (9.24 g, 0.03 mol) containing 85% phosphoric acid (2.1 ml, 0.03 mol) in diethyl phosphonate (30 ml) was added to the mixture of solutions A and B described above. The reaction mixture was heated on a water bath with stirring for 2 h in a well ventilated fume-cupboard. Diethyl phosphonate was removed in vacuo and the residual oil dissolved in 300 ml of 1M HCl after heating at 85 °C for about 5 minutes. On refrigerating, a semi-solid oil precipitated. The oil was separated by decanting off the acid solution, washed with cold water and dried. The oily product crystallized on triturating with ethyl acetate and was recrystallized from dilute hydrochloric acid. The mp, elemental analysis, and optical rotation of each chromogenic arginine substrate is recorded in Table 1.

Enzymatic Activity Determination. The initial rates of trypsin catalyzed hydrolyses of the anilide substrates were determined by continuous measurement of free 5-substituted 3-nitroaniline while the reaction proceeded in a themostated cuvette inserted in a Zeiss PMQ3 Model Spectrophotometer attached to a Haake F3 thermostated water bath. The concentration of the liberated substituted aniline was determined at 400 nm at which wavelength all the substrates have no contribution to the absorbance.

Results and Discussion

The synthesis of arginine substrates has always been a difficult task. The low basicity of the amino group in the 5-substituted 3-nitroaniline makes it difficult to couple with the carboxyl of arginine which has been activated by the azide, dicyclohexyl-carbodiimide or active ester method.[20] Therefore the activation of the amino group of the aniline derivatives seems to be essential for facilitating the coupling with the carboxyl group of arginine. The series of new arginine substrates reported in this paper were readily prepared without racemization through the condensation of 5-substituted 3-nitroanilines and N^{α}-benzyloxycarbonyl-L-arginine hydrochloride using the coupling procedure reported by Somorin et al.[19] The relative initial rates of trypsin catalyzed hydrolysis of the various substrates were determined and tabulated in Tables 2 and 3.

It has been reported that trypsin catalyses the hydrolysis of anilides via the acyl-enzyme intermediate.[16] The overall mechanism can be represented by the equation:

$$E + S \underset{k_{-1}}{\overset{k_1}{\rightleftharpoons}} ES \xrightarrow{k_2} ES^1 + P_1 \xrightarrow{k_3} E + P_2,$$

where k_2 and k_3 are the first-order rate constants for the acylation and deacylation steps respectively; P_1 and P_2 are products. It is known that the acylation step is the rate limiting step for amide and anilide substrates.[21,22] The same mechanism operates in the chymotrypsin-catalyzed hydrolysis of anilides and its acylation step has been studied in detail by varying the leaving group P_1. Through the determination of rate constant for the acylation step, k_2, several workers concluded that a proton transfer was involved in the acylation step.[5,6,8,11] Studies of

Table 2. Relative Rates of Trypsin Catalyzed Hydrolysis of Chromogenic Substrates

Substrate	Rate	Relative rates
	μmoles min^{-1}	ratio
L-ZANA·HCl	100	1.43
L-ZANTA·HCl	92	1.31
L-ZANMA·HCl	76	1.09
L-ZANFA·HCl	70	1.0

Table 3. Relative Rates of Trypsin Catalyzed Hydrolysis of the Halogen Derivatives of the New Arginine Chromogenic Substrates

Substrate	Rate	Relative rates
	μmoles min^{-1}	ratio
L-ZANFA·HCl	70	1.0
L-ZANCA·HCl	134	1.91
L-ZANBA·HCl	161	2.30
L-ZANIA·HCl	189	2.70

Parker and Wang[8] on the acylation step of α-chymotrypsin catalyzed hydrolysis of anilides suggest a pre-transition state protonation of the substrate followed by the usual nucleophilic attack of the protonated substrate by the serine residue.

The results in Table 1 suggest that the electron-withdrawing substituents (-F, $-CF_3$, and $-SO_2Me$) inhibit the rate of trypsin catalysed hydrolysis of the anilide substrates. It has been suggested that electron-withdrawing substituents hinder the rate of chymotrypsin catalyzed hydrolysis of anilides by inhibiting the proton transfer in the removal of the substituted aniline.[9] This is consistent with the mechanism proposed by Inward and Jencks[23] in which a conjugate acid of the catalyst (histidinium cation) donates a proton to the leaving group which is 5-substituted 3-nitroaniline.

The results in Table 2 show that the rates of enzyme-catalyzed hydrolysis of the halogen derivatives of the arginine substrates decrease in the order: iodo>bromo>chloro>fluoro. This unique sequence, which is characteristic of the halogen substituted chromogenic substrates, is the reverse of the order for the inductive effect which follows the order: fluoro>chloro>bromo>iodo. The details of the kinetics for the trypsin-catalyzed hydrolysis of these new arginine chromogenic substrates will be published elsewhere.

References

1) M. L. Bender and K. Nakamura, *J. Am. Chem. Soc.*, **84**, 2577 (1962).
2) M. Caplow and W. P. Jencks, *Biochemistry*, **1**, 883 (1962).
3) W. F. Sager and P. C. Parks, *J. Am. Chem. Soc.*, **85**, 2678 (1963).
4) W. F. Sager and P. C. Parks, *Proc. Nat. Acad. Sci. U.S.A.*, **52**, 408 (1964).
5) T. Inagami, S. S. York, and A. Patchornik, *J. Am. Chem. Soc.*, **87**, 126 (1965).
6) H. F. Bundy and C. L. Moore, *Biochemistry*, **5**, 808 (1966).
7) J. H. Wang and L. Parker, *Proc. Natl. Acad. Sci. U.S.A.*, **58**, 2451 (1967).
8) L. Parker and J. H. Wang, *J. Biol. Chem.*, **243**, 3729 (1968).
9) T. Inagami, A. Patchornik, and S. S. York, *J. Biochem.*, **65**, 809 (1969).
10) M. Caplow, *J. Am. Chem. Soc.*, **91**, 3639 (1969).
11) A. Williams, *Biochemistry*, **9**, 3383 (1970).
12) M. Philipp, R. M. Pollack, and M. L. Bender, *Proc. Nat. Acad. Sci., U.S.A.*, **70**, 517 (1973).
13) M. L. Bender, G. R. Schonbaum, and G. A. Hamilton, *J. Polymer Sci.*, **49**, 75 (1961).
14) B. S. Hartley, *Ann. Rev. Biochem.*, **29**, 45 (1960).
15) G. H. Dixon, D. L. Kauffman, and H. Neurath, *J. Am. Chem. Soc.*, **80**, 1260 (1958).
16) M. L. Bender, and F. J. Kezdy, *J. Am. Chem. Soc.*, **86**, 3704 (1964).
17) Worthington Descriptive Manual, (1972).
18) M. Dosumu, Ph. D. Thesis submitted to Chem. Dept. University of Lagos (1975).
19) O. Somorin, N. Nishi, and J. Noguchi, *Bull. Chem. Soc. Jpn.*, **51**, 1255 (1978).
20) J. P. Greenstein, and M. Winitz, "Chemical Procedures for Synthesis of Peptides" in "Chemistry of the Amino Acids," John Wiley and Sons, Inc. (1961) Vol. 2. p. 763.
21) B. Zerner and M. L. Bender, *J. Am. Chem. Soc.*, **85**, 356 (1963).
22) T. Inagami, and J. M. Sturtevant, *Biochem. Biophys. Res. Commun.*, **14**, 69 (1964).
23) P. W. Inward and W. P. Jencks, *J. Biol. Chem.* **240**, 1986 (1965).

Silver *cis*-Tetrachlorohydroxonitrosylruthenate (2–)

Yasuhiro KAMATA,† Eiichi MIKI, Kunihiko MIZUMACHI, and Tatsujiro ISHIMORI*
Department of Chemistry, College of Science, Rikkyo University,
3-Chome, Nishi-Ikebukuro, Toshima-ku, Tokyo 171
(Received January 13, 1986)

Synopsis. A new chloronitrosylruthenate ion was separated from the hydrolysis mixture of $[RuCl_5(NO)]^{2-}$ by the anion-exchange method, and it formed $Ag_2[RuCl_4(OH)(NO)]$ on the addition of silver nitrate. The anion of the silver salt was found to have the cis form on the basis of its IR spectrum.

Silver and ammonium salts of $[RuCl_4(OH)(NO)]^{2-}$ were prepared from the hydrolysis mixture of $[RuCl_5(NO)]^{2-}$ by Mercer et al.[1–3] The anion of these salts and its protonated aqua complex have been considered to have the trans form.[1–3] Separation of the possible isomers of $[RuCl_4(H_2O)(NO)]^-$ was reported without identification of the isomers.[4] The authors isolated *cis*-$Ag_2[RuCl_4(OH)(NO)]$ from a component of the hydrolysis mixture of $[RuCl_5(NO)]^{2-}$.

Experimental

$(NH_4)_2[RuCl_5(NO)]$ was prepared by Fletcher's method.[5] Electronic spectra of complexes in aqueous solutions were recorded on a Hitachi 340 spectrophotometer, and IR spectra of the isolated complexes on JASCO A-202 and IR-F spectrometers.

Preparation of *cis*-$Ag_2[RuCl_4(OH)(NO)]$. A solution of $(NH_4)_2[RuCl_5(NO)]$ (2.4 g) in 0.01 mol dm^{-3} $HClO_4$ (40 cm^3) was heated at 50 °C for 6 h, and stored at 5 °C overnight. The species in the solution were separated with a QAE Sephadex A-25 column (the nitrate form, ϕ 4 cm×40 cm) at below 10 °C. After $[RuCl_2(H_2O)_3(NO)]^+$ and $[RuCl_3(H_2O)_2(NO)]$ had been eluted out of the column with 0.05 mol dm^{-3} HNO_3, the elution was continued until three separate adsorption bands appeared. Since $[RuCl_5(NO)]^{2-}$ was strongly adsorbed on the uppermost part of the column, the uppermost part was taken out of the column by using a suction pump. *trans*-$[RuCl_4(H_2O)(NO)]^-$ in the lower adsorption band of the remaining bands was eluted out with 0.1 mol dm^{-3} HNO_3. The species in the final adsorption band was eluted with 1 mol dm^{-3} $HClO_4$. The effluent was collected under cooling with ice-water and it gave a silver salt on the addition of 5 wt% $AgNO_3$ solution. The silver salt was filtered off, washed with dilute HNO_3 containing a small amount of $AgNO_3$ and dilute HNO_3 successively, and then dried in a vacuum desiccator with $CaCl_2$ and NaOH. Yield, 80 mg. Found: Ru, 20.1; Cl, 28.35; N, 2.85%. Calcd for $Ag_2[RuCl_4(OH)(NO)]$: Ru, 19.99; Cl, 28.10; N, 2.77%.

Electronic spectra of $[RuCl_2(H_2O)_3(NO)]^+$, $[RuCl_3(H_2O)_2(NO)]$, and *trans*-$[RuCl_4(H_2O)(NO)]^-$ in the effluents were the same as those reported by Mercer et al.[1] *trans*-$Ag_2[RuCl_4(OH)(NO)]$ was prepared according to Ref. 1 by the addition of 5 wt% $AgNO_3$ solution to the *trans*-$[RuCl_4(H_2O)(NO)]^-$ solution separated.

Results and Discussion

The silver salt newly prepared had the formula, $Ag_2[RuCl_4(OH)(NO)]$, and was isomeric with *trans*-$Ag_2[RuCl_4(OH)(NO)]$ prepared by Mercer et al.[1]

The IR data of the new salt are shown in Table 1, together with those of *trans*-$Ag_2[RuCl_4(OH)(NO)]$ prepared. The IR bands were assigned by referring to Refs. 2, 6, and 7. The spectra of the trans salt were the same as those reported by Mercer et al.[2] The IR spectrum of the new salt in the Ru–Cl stretching region was clearly different from that of the trans salt. The trans salt gave two bands assigned to a doubly degenerate Ru–Cl stretching vibration and a totally symmetric Ru–Cl stretching vibration. The new salt gave three bands due to nondegenerate Ru–Cl stretching vibrations. *cis*-$[PtCl_4(NH_3)_2]$[8] and *cis*-$[SnCl_4(bpy)]$[9] gave typically four bands due to the metal–Cl stretching vibtations. However, it has been also observed that the number of the Sn–X stretching bands for *cis*-$[SnX_4(L\text{–}L)]$(X=Cl, Br, or I; L–L=phen, 1,2-bis(methylthio)ethane, or 1,2-bis(diphenylphosphino)ethane) ranges from two to four.[9] The three bands observed for the new salt strongly indicate that the new salt is the silver salt of *cis*-$[RuCl_4(OH)(NO)]^{2-}$.

The N–O stretching frequencies of the two salts show that the anions of both salts are of the linear

Table 1. Wavenumbers/cm^{-1} and Assignments of IR Bands for *trans*- and the New $Ag_2[RuCl_4(OH)(NO)]$

Assignment	O–H str	N–O str	O–H bend	a)	Ru–OH str	Ru–Cl str
Trans salt	3545 m	1888 vs	916 m, br	610 sh	519 s, br	327 vs
				597 m		297 vw
New salt	3500 m	1908 vs	810 m, br	585 sh	503 s, br	332 vs
				577 m		301 s
						275 m

a) Skeletal vibrations between Ru and NO. Abbreviations: str=stretching, bend=bending, vs=very strong, s=strong, m=medium, vw=very weak, sh=shoulder, br=broad.

† Present address: Nihon Tokushu Noyaku Seizo K. K., Toyota, Hino, Tokyo 191.

{RuNO}^{6} type.[10] Both OH^- and Cl^- are largely σ-bonding ligands, while π-donor ability of OH^- is greater than that of Cl^-. The NO in trans salt's anion is considered to withdraw more π electron density from the Ru than the NO in new salt's anion of the cis form. This can explain the results that the N–O stretching frequency of the trans salt was smaller than that of the new salt and the frequencies of the skeletal vibrations due to the RuNO group of the trans salt were greater than those of the new salt. The same results were observed for *trans*-$[RuL(NH_3)_4(NO)]^{2+}$(L=OH, or Cl)[11]; the N–O stretching frequency for the chloro complex (1880 cm^{-1}) was greater than that for the hydroxo complex (1841 cm^{-1}) and the frequencies of the skeletal vibrations due to the RuNO group for the chloro complex (562 and 603 cm^{-1}) were smaller than those for the hydroxo complex (589 and 630 cm^{-1}).

In complexes of the linear {RuNO}^{6} type, the NO is such a good π-acceptor and poor σ-donor that rather than a competition between the NO and the *trans*-L ligand for the same orbitals, there is mutual reinforcement in both Ru–NO and Ru–L bonds when L is a good σ-donor and poor π-acceptor, e.g. Cl^- or OH^-.[12] Therefore, the OH^- trans to the NO is considered to bind to the Ru more strongly than the OH^- cis to the NO. This can explain the results that each frequency of ν_{O-H}, δ_{O-H}, and ν_{Ru-OH} of the new salt was smaller than that of the trans salt.

On the basis of the IR data discussed above, the anion of the new salt can be assigned to the cis form.

In $[RuCl_5(NO)]^{2-}$, the Ru–Cl bonds cis to the NO were found to be longer than that trans to the NO[13] and were also indicated to be weaker than that trans to the NO.[14] Hydrolysis of the Cl ligand in *cis*-$[RuCl(NH_3)_4(NO)]^{2+}$ was found to be faster than the corresponding hydrolysis in *trans*-$[RuCl(NH_3)_4(NO)]^{2+}$.[15] Consequently, the formation of *cis*-$[RuCl_4(H_2O)(NO)]^-$ can be expected in the first step of the hydrolysis of $[RuCl_5(NO)]^{2-}$ in an acid solution. For the process of the preparation of the new salt, it can be also considered that the *cis*-$[RuCl_4(H_2O)(NO)]^-$ is separated from the hydrolysis mixture and it forms *cis*-$Ag_2[RuCl_4(OH)(NO)]$ on the addition of silver nitrate.

The present work was partially supported by a Grant-in-Aid for Scientific Research No. 58470038 from the Ministry of Education, Science and Culture.

References

1) E. E. Mercer, W. M. Campbell, Jr., and R. M. Wallace, *Inorg. Chem.*, **3**, 1018 (1964).
2) E. E. Mercer, W. A. McAllister, and J. R. Durig, *Inorg. Chem.*, **5**, 1881 (1966).
3) E. E. Mercer and A. B. Cox, *Inorg. Chim. Acta*, **6**, 577 (1972).
4) P. Polak, *Radiochim. Acta*, **24**, 193 (1977).
5) J. M. Fletcher, I. L. Jenkins, F. M. Lever, F. S. Martin, A. R. Powell, and R. Todd, *J. Inorg. Nucl. Chem.*, **1**, 378 (1955).
6) E. Miki, *Bull. Chem. Soc. Jpn.*, **41**, 1835 (1968).
7) M. J. Cleare, H. P. Fritz, and W. P. Griffith, *Spectrochim. Acta, Part A*, **28**, 2013 (1972).
8) D. M. Adams and P. J. Chandler, *J. Chem. Soc., A*, **1965**, 1009.
9) N. Ohkaku and K. Nakamoto, *Inorg. Chem.*, **12**, 2446 (1973).
10) J. H. Enemark and R. D. Feltham, *Coord. Chem. Rev.*, **13**, 339 (1974).
11) E. Miki, K. Mizumachi, T. Ishimori, and H. Okuno, *Bull. Chem. Soc. Jpn.*, **46**, 3779 (1973).
12) F. Bottomley, *Coord. Chem. Rev.*, **26**, 7 (1978).
13) J. T. Veal and D. J. Hodgson, *Inorg. Chem.*, **11**, 1420 (1972); *Acta Crystallogr., Sect. B*, **28**, 3525 (1972).
14) A. B. Nikol'skii, V. I. Baranovskii, N. V. Ivanova, and O. V. Sizova, *Russ. J. Inorg. Chem.*, **19**, 145 (1974).
15) F. Bottomley, E. M. R. Kiremire, and S. G. Clarkson, *J. Chem. Soc., Dalton Trans.*, **1975**, 1909.

The Positional Dependence of Anodic Peak Potentials in *N*-Substituted Adenines[1)]

Takeo SATO,* Kentaro FUKUZAKI, and Tozo FUJII†
Department of Chemistry, Tokyo Metropolitan University, Setagaya-ku, Tokyo 158
†Faculty of Pharmaceutical Sciences, Kanazawa University, Takara-machi, Kanazawa 920
(Received November 8, 1985)

Synopsis. In order to determine the structural dependence on the anodic potential, cyclic voltammetric measurements were carried out for 1-, 3-, 7-, 9-, and N^6-alkyladenines in *N*,*N*-dimethylformamide (DMF) or in acetonitrile (AN). The anodic peak potential, E_{pa}, in DMF was found to be sensitive to the substitution and shifted anodic in the order, 7-<1-<3-, N^6-<9-substituted derivatives. These data, with the aid of solvent effects, are useful for determining the substitution pattern in *N*-alkyladenines.

Only 9-substituted adenines were previously found in biologically important nucleosides and nucleotides,[2)] although five *N*-substituted derivatives are possible, namely, 1-, 3-, 7-, 9-, and N^6-substituted derivatives (**1**). Until now, however, all five de-

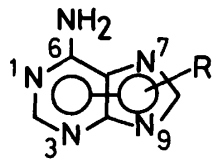

1

rivatives have been isolated from natural sources and have been synthesized.[2)] This has led to investigation of methods for the selective formation and structural determination of *N*-alkyladenines.[2,3)]

Besides chemical methods, three approaches have been reported[3)] to distinguish substitution in *N*-alkyladenines. UV spectral maxima in acidic or basic media were used to differentiate each of the 1-, 9-, and N^6-substitutions from a group of 3- and 7-substitutions. The pK_a' values were shown to differentiate 3- and 7- or 9-substitutions, and the value of λ_{min} (pH 1)$-\lambda_{min}$ (pH 7) was used to distinguish 3- from 7- or 9-substituted adenines. Sometimes, the first approach may not clearly differentiate substitution among imidazole rings, e.g. 7- from 9-substitution.[3)] In this note, we survey the anodic peak potentials of alkyladenines and related compounds in order to obtain a complementary method for structural determinations.

Dryhurst and Elving[4)] have carried out the anodic oxidation of adenine in aq acetic acid on a porous graphite electrode and observed an initial oxidation similar to an enzymatic type, followed by deep-seated fragmentation. We carried out cyclic voltammetric measurements for all the *N*-positional isomers of methyl-, ethyl-, and benzyladenines together with 9-phenethyladenine in acetonitrile (AN) or in *N*,*N*-dimethylformamide (DMF) using a platinum anode. All compounds except for 1-methyladenine showed an E_{pa} between +1.1 and +1.8 V vs. SCE at a scan rate of 50—500 mV s^{-1} but failed to show a reduction wave upon potential reversal. The data measured in DMF showed a significant positional dependence, the results determined at a scan rate of 250 mV s^{-1} are summarized in Table 1.

Adenine showed an E_{pa} at +1.75 V in DMF and +1.45 V in AN. In either solvent, the anodic peak potentials were found to depend on the substitution pattern and were essentially similar among the methyl, ethyl, and benzyl derivatives. In DMF, the 9-alkyl derivatives showed E_{pa}s at the highest anodic potential, observable only as a shoulder at ca. +1.7 V. Those having an N^6-substituent showed a slight cathodic shift with E_{pa}s at ca. +1.6 V. The 1- and 3-substituted adenines showed E_{pa}s at ca. +1.4 and 1.5 V, respectively. A significant cathodic shift was observed for the 7-alkyl derivatives which showed E_{pa}s at ca. +1.2 V. The E_{pa}s for alkyladenines in DMF increase in the order:

7-<1-<3-, N^6-<9-substituted derivatives

1-Methyladenine was practically insoluble in DMF and no voltammogram was recorded. Kinetin showed an E_{pa} at +1.63 V (+1.45 V in AN) as expected from N^6-substitution. Adenosine showed an E_{pa} at +1.23 V, a considerable cathodic potential. This was not expected from a 9-substituted derivative, and indicated that a one-electron transfer occurred on the sugar moiety. The above data showed that E_{pa} is sensitive to substitution and enables one to differentiate between 7- and 9-substitution quite easily.

The solvent effect on the CV measurements was then investigated. In *N*,*N*-dimethylacetamide, the 7-substituted derivatives showed E_{pa}s between +1.1 and 1.3 V, similar to those observed in DMF. In AN, however, a significant solvent-induced shift was noticed as compared with the amide solvents. Table 2 summarizes peak potentials for *N*-benzyladenines as well as the solvent shift in E_{pa}, ΔE_{pa} (AN-DMF).

Table 1. Anodic Peak Potential Data for *N*-Alkyladenines[a)]

Position of R	R			
	Me	Et	$PhCH_2$	$PhCH_2CH_2$
1	—[b)]	1.41	1.40	
3	1.54	1.54	1.52	
7	1.17	1.17[c)]	1.19	
9	1.68[c)]	1.68[c)]	1.70[c)]	1.76
N^6	1.58	1.54[c)]	1.56[c)]	

a) The cyclic voltammetry was carried out in DMF-TBAP (0.1 mol dm^{-3}) using a platinum inlay electrode as an anode and SCE as the reference at 250 mV s^{-1}. b) The compound is insoluble in DMF. c) Shoulder.

Table 2. The Anodic Peak Potential Data for *N*-Benzyladenines in Various Solvents[a)]

Position of R		E_{pa} DMF	E_{pa} DMAc[b)]	E_{pa} AN	ΔE_{pa} (AN-DMF)
Pyrimidine moiety	1	1.40		1.10	−0.30
	3	1.52		1.50	−0.02
	N^6	1.56[c)]		1.48	−0.08
Imidazole moiety	7	1.19	1.10[c)]	1.67	+0.48
	9	1.70[c)]		1.62	−0.08

a) The measurements were carried out in the same way as described in Table 1. b) *N*,*N*-dimethylacetamide. c) Shoulder.

In AN, the 1- and N^6-substituted derivatives having a substituent in the pyrimidine moiety showed cathodic shifts of 0.3 and 0.1 V, respectively, whereas the 7-substituted derivatives showed an anodic shift of 0.5 V. The anodic shift for both 7-methyl- and 7-ethyladenines in AN was 0.4 V. Those substituted at the 3- and 9-positions showed no solvent-induced shift. This phenomena might be ascribable to the selective association between the 1- and N^6-positions of adenine with the amide solvent as in the adenine–thymine pair.

Whereas the UV, pK_a', and λ_{min} methods have been used to differentiate substitution between pyrimidine and imidazole rings of alkyladenines, the present CV method independently could differentiate not only substitution between 7- and 9- positions but also among pyrimidine rings, namely, 1-, 3-, and N^6-substitution, with the aid of solvent effects.

Experimental

Materials. The substrates used for the CV measurements were obtained commercially or were taken from stocks which had been prepared according to published procedures: 1-,[5)] 3-,[6)] 7-,[7)] 9-,[8)] and N^6-methyladenines;[9)] 1-,[10)] 3-,[11)] 7-,[7)] 9-,[8)] and N^6-ethyladenines;[10)] 1-,[12)] 3-,[13)] 7-,[13)] 9-,[8)] and N^6-benzyladenines;[12)] 9-phenethyladenine.[8)]

Cyclic Voltammetry. The measurements were carried out using a generator, Hokuto HB-107A, and a potentiostat, Hokuto HA-101. As an anode, a platinum inlay electrode, Beckman No. 39273, was used. To avoid contamination from moisture, the reference SCE was connected to a modified H-cell through two junction bridges each filled with a sat KCl solution and DMF or AN–tetrabutylammonium perchlorate (TBAP). Molecular sieve 1A (Wako chemicals) was added to the bridge directly immersed in the cell.

Sample concentrations were between 10^{-4} and 10^{-5} mol dm^{-3}. 1-Methyladenine was insoluble in DMF and no voltammogram was recorded. As an anolyte, TBAP was added to the solution to make 0.1 mol dm^{-3} solutions. The results recorded at 250 mV s^{-1} are shown in Tables 1 and 2. The data are expressed in +V vs. SCE. Highly anodic peaks, especially determined in DMF, appeared as a shoulder.

References

1) Electron-organic Chemistry X. For Part IX; see T. Sato, T. Wada, Y. Komeichi, and M. Kainosho, *Bull. Chem. Soc. Jpn.*, **58**, 1452 (1985). T. S. and T. F. dedicate this short article to Professor N. J. Leonard on his 70th birthday.

2) J. H. Lister,"Fused Pyrimidines," ed by D. J. Brown, Wiley-Interscience, New York (1968); Part II; R. K. Robins, "Heterocyclic Compounds," ed by R. C. Elderfield, John Wiley and Sons, New York (1967), Vol. 8, Chap. 3; G. Shaw, "Comprehensive Heterocyclic Chemistry," ed by K. T. Potts, Pergamon Press, Oxford (1984), Vol. 5, Chap. 4.09.

3) N. J. Leonard and J. D. Deyrup, *J. Am. Chem. Soc.*, **84**, 2148 (1962)

4) G. Dryhurst and P. J. Elving, *J. Electrochem. Soc.*, **115** 1014 (1968).

5) J. W. Jones and R. K. Robins, *J. Am. Chem. Soc.*, **85**, 193 (1963).

6) J. W. Jones and R. K. Robins, *J. Am. Chem. Soc.*, **84**, 1914 (1962).

7) T. Fujii and T. Saito, *Heterocycles*, **17**, 117 (1982).

8) T. Fujii S. Sakurai, and T. Uematsu, *Chem. Pharm. Bull.*, **20**. 1334 (1972).

9) T. Fujii, T. Saito, and T. Muramoto, *Chem Pharm Bull.*, **31**, 4270 (1983).

10) Prepared from adenosine through a route similar to that used for the methyl homolog.[5,9)]

11) T. Fujii and T. Saito, *Chem. Pharm. Bull.*, **21**, 1954 (1973).

12) N. J. Leonard and T. Fujii, *Proc. Natl. Acad. Sci. U.S.A.*, **51**, 73 (1964).

13) T. Fujii, G. C. Walker, N. J. Leonard, D. C. DeLong, and K. Gerzon, *J. Med. Chem.*, **22**, 125 (1979).

Photochemical Isomerization of 2-Pyridyl- and 2-Pyrazinyl-1,2-benzisothiazol-3(2*H*)-ones

Nobumasa KAMIGATA,* Hirokazu IIZUKA, and Michio KOBAYASHI
Department of Chemistry, Faculty of Science, Tokyo Metropolitan University, Fukazawa, Setagaya-ku, Tokyo 158
(Received December 18, 1985)

Synopsis. The irradiation of 2-pyridyl- and 2-pyrazinyl-1,2-benzisothiazol-3(2*H*)-ones in benzene resulted in the formation of benzopyrido- and benzopyrazinothiazepinones, respectively. A mechanism involving a biradical species is proposed for this reaction.

Considerable attention has been focused in recent years on the photochemistry of five-membered heterocyclic ring systems. By far the greatest area of activity in this field has been a study of the photoisomerization that results in a change in the heterocyclic nucleus.[1] We have reported a novel photochemical ring-expansion reaction of such five-membered heterocyclic compound as 2-aryl-1,2-benzisothiazolinones to seven-membered heterocyclic compound, dibenzothiazepinones.[2] As we have continuous interest in this novel photoisomerization, the photochemical reaction of 2-pyridyl- and 2-pyrazinyl-1,2-benzisothiazol-3(2*H*)-ones has been studied and the results are described herein.

When a solution containing 2-(2-pyridyl)-1,2-benzisothiazol-3(2*H*)-one (**1**) in benzene was irradiated under argon with 300-nm light, a single photoproduct was obtained. This material was assigned as benzo[*f*]pyrido[3,2-*b*][1,4]thiazepin-10(11*H*)-one (**2**) on the basis of its spectral data.

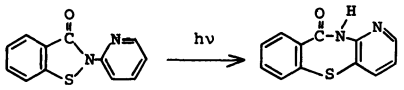

1 **2**

This reaction is of interest since it involves a medium-size seven-membered ring compound, is generally difficult to prepare and is obtained by photochemical isomerization from a five-membered compound involving a pyridine ring **1**. The photoreaction is presumed to proceeded via a homolytic cleavage of the S–N bond to generate a biradical **3**. The initially-formed thiyl radical of **3a** attacks the β-position of the *N*-(2-pyridyl) group to give a cyclized product **4**. A subsequent 1,7-hydrogen shift of the intermediate **4** leads to the final product **2** (Scheme 1).

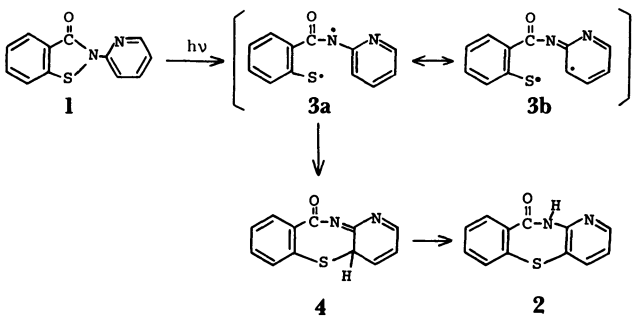

1 **3a** **3b** **4** **2**

Scheme 1.

For this proposed mechanism to be adequate, it was expected that a photochemical reaction of 2-(3-pyridyl)-1,2-benzisothiazol-3(2*H*)-one (**5**) would afford two photoisomerized products. As expected, the irradiation of **5** in benzene in a similar way afforded two isomeric photoreaction products. They were assigned as benzo[*f*]pyrido[2,3-*b*][1,4]thiazepin-6(5*H*)-one (**6**) and benzo[*f*]pyrido[4,3-*b*][1,4]thiazepin-10(11*H*)-one (**7**) on the basis of their spectral data.

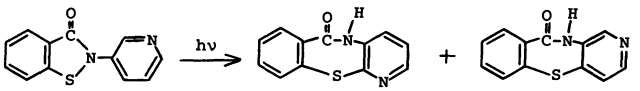

5 **6** **7**

The fact that almost equal amounts of photoisomeric products (**6** and **7**) were obtained in the photolysis of **5** suggests that the selectivity of the thiyl radical of the intermediate **8**, formed from **5** by the photochemical cleavage of the S–N bond, is extremely weak regarding on intramolecular attack on α- and γ-positions of the pyridine ring.

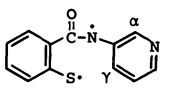

8

The photochemical reactions of 2-(4-pyridyl)-1,2-benzisothiazol-3(2*H*)-one (**9**) and 2-(2-pyrazinyl)-1,2-benzisothiazol-3(2*H*)-one (**10**) were also studied. In these cases, a single photoproduct, benzo[*f*]pyrido[3,4-*b*][1,4]thiazepin-6(5*H*)-one (**11**) and benzo[*f*]pyrazino[2,3-*b*][1,4]thiazepin-10(11*H*)-one (**12**) were isolated, respectively, for each reaction.

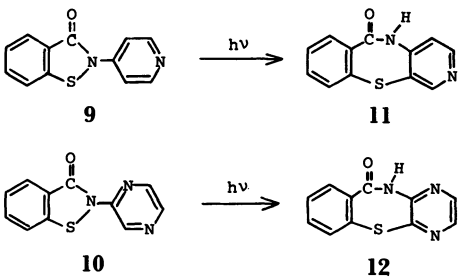

9 **11** **10** **12**

Experimental

All melting points were uncorrected. IR and UV spectra were recorded on a Hitachi EPI-G2 and a Hitachi 220A spectrometer. ^{1}H NMR spectra were measured with a

Hitachi R-90H (90 MHz) spectrometer using tetramethylsilane as an internal standard. Mass spectra were determined with a JEOL JMS-DX300 high-resolution mass spectrometer with a JEOL JMA5000 mass-data system at an ionization energy of 70 eV.

Materials. 2-Pyridyl- and 2-pyrazinyl-1,2-benzisothiazol-3(2*H*)-ones were prepared from 2,2'-dithiobis[benzoyl chloride] by treating with aminopyridine and aminopyrazine, respectively, according to a modified method of Reissert and Manns.[3] The yields, physical properties, and spectral data were as follows:

2-(2-Pyridyl)-1,2-benzisothiazol-3(2*H*)-one (1): Yield 84%; mp 194.5—195.5 °C (from $CHCl_3$); IR (KBr) 1675 cm^{-1}; ^1H NMR (DMSO-d_6) δ=7.07—7.90 (5H, m), 8.07 (1H, d, J=7.7 Hz), 8.41 (1H, d, J=5.1 Hz), and 8.75 (1H, d, J=8.4 Hz); ^{13}C NMR ($CDCl_3$) δ=114.39, 120.24, 120.61, 125.43, 126.57, 126.73, 132.74, 138.30, 140.98, 147.51, 150.36, and 163.95; MS, m/z 228 (M^+); HRMS, m/z 228.0419 ($C_{12}H_8N_2OS$ requires 228.0357); UV (methanol) 255 (log ε=3.98) and 335 nm (3.81).

2-(3-Pyridyl)-1,2-benzisothiazol-3(2*H*)-one (5): Yield 78%; mp 118.5—119.5 °C (from $CH_3CO_2C_2H_5$); IR (KBr) 1675 cm^{-1}; ^1H NMR (DMSO-d_6) δ=7.26—7.73 (4H, m), 8.11 (1H, dd, J=7.6 and 1.0 Hz), 8.15—8.27 (1H, m), 8.55 (1H, dd, J=4.7 and 1.3 Hz), and 8.95 (1H, d, J=2.4 Hz); ^{13}C NMR (DMSO-d_6) δ=120.18, 123.69, 124.01, 126.03, 127.13, 132.72, 134.41, 134.41, 139.60, 144.86, 147.46, and 164.27; MS, m/z 228 (M^+); HRMS, m/z 228.0339 ($C_{12}H_8N_2OS$ requires 228.0357); UV (methanol) 254 (log ε=4.11) and 330 nm (3.73).

2-(4-Pyridyl)-1,2-benzisothiazol-3(2*H*)-one (9): Yield 88%; mp 182.5—183.5 °C (from CH_3OH); IR (KBr) 1670 cm^{-1}; ^1H NMR ($CDCl_3$) δ=7.43—8.14 (6H, m), 8.66 (2H, dd, J=4.3 and 1.2 Hz); ^{13}C NMR ($CDCl_3$) δ=115.84, 122.20, 126.16, 126.16, 126.49, 133.63, 139.60, 144.21, 146.16, 149.08, and 164.21; MS, m/z 228 (M^+); HRMS, m/z 228.0339 ($C_{12}H_8N_2OS$ requires 228.0357).

2-(2-Pyrazinyl)-1,2-benzisothiazol-3(2*H*)-one (10): Yield 87%; mp 152—153 °C (from CH_3OH); IR (KBr) 1690 cm^{-1}; ^1H NMR ($CDCl_3$) δ=7.36—7.70 (3H, m), 8.08 (1H, d, J=7.9 Hz), 8.40 (1H, d, J=7.9 Hz), 8.42 (1H, s), and 10.03 (1H, s); MS, m/z 229 (M^+); HRMS, m/z 229.0294 ($C_{11}H_7N_3OS$ requires 229.0294); UV (methanol) 235 (log ε=3.60) and 345 nm (4.27).

Photolysis of 2-Pyridyl- or 2-Pyrazinyl-1,2-benzisothiazol-3(2*H*)-one. A solution containing 200 mg of **1**, **5**, **9**, or **10** in 230 cm^3 of benzene was irradiated using a 450-W Hanovia medium-pressure mercury lamp through a Pyrex filter sleeve for 40 h. The removal of the solvent under reduced pressure left a light-brown residue which was purified by silica-gel chromatography using dichloromethane–ethyl acetate 4:1 mixture as the eluent. The yield and physical and spectral data of these photoreaction products are as follows:

Benzo[*f*]pyrido[3,2-*b*][1,4]thiazepin-10(11*H*)-one (2): Yield 59%; mp 239—240 °C; IR (KBr) 2900—3200 (w, amide N-H) and 1650 cm^{-1} (s, amide C=O); ^1H NMR (DMSO-d_6) δ=7.20 (1H, dd, J=7.7 and 4.7 Hz), 7.46—7.75 (4H, m), 8.01 (1H, dd, J=7.7 and 1.8 Hz), 8.38 (1H, dd, J=4.7 and 1.8 Hz), and 10.98 (1H, s); MS, m/z 228 (M^+); HRMS, m/z 228.0465 ($C_{12}H_8N_2OS$ requires 228.0357).

Benzo[*f*]pyrido[2,3-*b*][1,4]thiazepin-6(5*H*)-one (6): Yield 23%; mp 300 °C; IR (KBr) 2900—3200 (w, amide N-H) and 1660 cm^{-1} (s, amide C=O); ^1H NMR (DMSO-d_6) δ=7.38—7.72 (6H, m), 8.28 (1H, dd, J=4.4 and 1.8 Hz), and 10.68 (1H, s); MS, m/z 228 (M^+); HRMS, m/z 228.0438 ($C_{12}H_8N_2OS$ requires 228.0357).

Benzo[*f*]pyrido[4,3-*b*][1,4]thiazepin-10(11*H*)-one (7): Yield 21%; mp 240—241 °C; IR (KBr) 2900—3200 (w, amide N-H) and 1660 cm^{-1} (s, amide C=O); ^1H NMR (DMSO-d_6) δ=7.40—7.77 (5H, m), 8.30 (1H, d, J=5.1 Hz), 8.43 (1H, s), and 10.82 (1H, s); MS, m/z 228 (M^+); HRMS, m/z 228.0384 ($C_{12}H_8N_2OS$ requires 228.0357).

Benzo[*f*]pyrido[3,4-*b*][1,4]thiazepin-6(5*H*)-one (11): Yield 40%; mp 244 °C; IR (KBr) 3170 (w, amide N-H) and 1660 cm^{-1} (s, amide C=O); ^1H NMR (DMSO-d_6) δ=7.20 (1H, d, J=5.3 Hz), 7.42—7.77 (4H, m), 8.42 (1H, d, J=5.3 Hz), 8.63 (1H, s), and 11.03 (1H, s); MS, m/z 228 (M^+); HRMS, m/z 228.0438 ($C_{12}H_8N_2OS$ requires 228.0357).

Benzo[*f*]pyrazino[2,3-*b*][1,4]thiazepin-10(11*H*)-one (12): Yield 45%; mp 232—233 °C; IR (KBr) 3100 (w, amide N-H) and 1650 cm^{-1} (s, amide C=O); ^1H NMR ($CDCl_3$) δ=7.40—7.47 (4H, m), 8.30 (2H, s), and 13.77 (1H, s); MS, m/z 229 (M^+); HRMS, m/z 229.0255 ($C_{11}H_7N_3OS$ requires 229.0305).

We are grateful to Dr. H. Matsumoto of Gunma University for recording the NMR spectra.

References

1) A. Padwa, "Rearrangements in Ground and Excited State," ed by P. de Mayo, Academic Press, New York (1980), Vol. 3, p. 501; A. Lablache-Combier, "Photochemistry of Heterocyclic Compounds," ed by O. Buchardt, Wiley, New York (1976), p. 123.

2) N. Kamigata, S. Hashimoto, S. Fujie, and M. Kobayashi, *J. Chem. Soc., Chem. Commun.*, **1983**, 765; N. Kamigata, S. Hashimoto, M. Kobayashi, and H. Nakanishi, *Bull. Chem. Soc. Jpn.*, **58**, 3131 (1985).

3) N. Kamigata, S. Hashimoto, and M. Kobayashi, *Org. Prep. Proc. Int.*, **15**, 315 (1983).

[Cr(acac)$_3$] as a New Calibrant for Magnetic Susceptibility Experiments

R. P. SHARMA* and K. K. BHASIN
Department of Chemistry, Panjab University, Chandigarh-160014, India
(Received August 12, 1985)

Synopsis. The merits of a common coordination compound, [Cr(acac)$_3$] obtained by a new and useful method, as a calibrant for magnetic susceptibility experiments are discussed.

Recently, we have described a new and useful method[1] for the preparation of a well documented coordination compound; tris(acetylacetonato)chromium(III), [Cr(acac)$_3$], in high yields by adding acetylacetone to a warm aqueous solution of $M_2Cr_2O_7$ ($M=NH_4^+$, Na^+, K^+) or M_2CrO_4 ($M=Na^+$, K^+). The purity of the sample has been checked by elemental analysis (C, H, Cr), melting point and infrared spectrum.

The advantages of our method over the already existing ones[2-4] are (i) the starting materials are readily available (ii) the method is quick (iii) the final product is purer and (iv) the yield of the product is not pH dependent.

One of the most important techniques used in coordination chemistry to find out the number of unpaired electrons in the transition metal ion so as to throw light on the environment around the central metal ion in a coordination compound is the magnetic susceptibility.[5] The first step to find out the magnetic susceptibility always involves the calibration of the Gouy's tube with a standard substance known as calibrant. A calibrant is selected so to fulfil the following requirements:

(i) The calibrant should be easy to prepare and the starting materials cheaply and readily available.
(ii) The method for its preparation should be simple and quick.
(iii) The calibrant should be of high purity and if need be, easy to purify.
(iv) The calibrant should be nonhygroscopic and fairly stable, i.e., it should possess good keeping properties.
(v) The magnetic moment value should be fairly large.

As it was relatively difficult earlier to prepare pure [Cr(acac)$_3$] (which may be usually contaminated with the buffer used) it was not thought as suitable for calibration purposes. The most commonly used calibrant[6-8] has always remained Hg[Co(SCN)$_4$] so far. In view of our convenient method for the preparation of [Cr(acac)$_3$] coupled with other advantages over Hg[Co(SCN)$_4$] (Table 1), the use of [Cr(acac)$_3$] as a calibrant is strongly recommended.

References

1) R. P. Sharma and K. K. Bhasin, *Polyhedron*, in Press (1985).
2) W. C. Fernelius and J. E. Blanch, *Inorg. Synth.*, **1957**, 130.
3) G. Brauer, "Handbook of Preparative Inorganic

Table 1. Comparison of the Physical Characteristics of Hg[Co(SCN)$_4$] and [Cr(acac)$_3$]

	Property	Hg[Co(SCN)$_4$]	[Cr(acac)$_3$]
1.	Color and physical state	Deep blue crystalline compound	Reddish violet crystalline compound
2.	Nature	Polymeric[a]	Monomeric[b]
3.	mp/bp (°C)	.....	216°/340°[c,d]
4.	Density(g/ml)	.....	1.37
5.	Solubility	Insoluble in conventional organic solvents	Soluble in conventional organic solvents
6.	Preparation and purity	Easy to prepare but difficult to purify	Easier to prepare as well as to purify
7.	Stability	Stable	Exceptionally stable
8.	Toxicity	Toxic	Nontoxic
9.	Number of unpaired electrons	3	3
10.	Magnetic moments(B. M.) (observed at 300 °K)	4.33[e]	3.86,[f] 3,88[g]
11.	Gram susceptibility	16.44×10^{-6}[c,h]	18.07×10^{-6}[f]
12.	Weiss constant	+2 °K[h]	+7 °K[f]

a) J. W. Jeffery, *Nature*, **159**, 610 (1947); J. W. Jeffery, *Acta Cryst. Supp.*, **6A**, 66 (1963). b) B. Morosin, *Acta Cryst.*, **19**, 131 (1965). c) G. Urbain and A. Debierne, *Compt. Rend.*, **129**, 302 (1899). d) J. Von. Hene, R. G. Charles, and W. M. Hickam., *J. Phys. Chem.*, **62**, 1098 (1958). e) B. N. Figgis., *Trans. Faraday Soc.*, **56**, 1553 (1960). f) B. N. Figgis., J. Lewis, and F. E. Mabbs, *J. Chem. Soc.*, **1961**, 3138. g) Present work. h) H.-St. Rade, *J. Phys. Chem.*, **77**, 424 (1973).

Chemistry," Academic Press, New York (1965) Vol. 2, p. 1384.
4) H. Ssekaalo and S. O. Wandiga, *J. Inorg. Nucl. Chem.*, **39**, 769 (1977).
5) B. N. Figgis and J. Lewis, *Progr. Inorg. Chem*, **6**, 37 (1964).
6) B. N. Figgis and R. S. Nyholm, *J. Chem. Soc.*, **1958**, 4190.
7) B. N. Figgis and R. S. Nyholm, *J. Chem. Soc*, **1959**, 338.
8) B. N. Figgis, *Trans. Faraday Soc*, **56**, 1553 (1960).

Molecular Rearrangements. XXIV. Thermolysis of Phenylhydrazones

Safaa Abd El-Salam MAHGOUB, Atiat Mohammed FAHMY, Morsy Mohammed ALY, and Mahmoud Zaif Amin BADR*
Department of Chemistry, Faculty of Science, Assiut University, Assiut, Egypt, A.R.E.
(Received April 10, 1984)

Synopsis. Thermolysis of acetophenone phenylhydrazone by reflux in air for 24 h gives ammonia, benzonitrile, acetophenone, biphenyl, aniline, *o*- and *p*-toluidines, together with 7-methyl-3-phenylindole, while that of benzophenone phenylhydrazone gives ammonia, benzophenone, *N*-benzhydrylideneaniline, biphenyl, aniline, benzonitrile, and 9-phenylacridine.

Thermolysis of phenylhydrazones of aldehydes and ketones was a matter of controversy, where Chattaway et al.[1] recorded the thermal breakdown of benzaldehyde phenylhydrazone into *N*-benzylideneaniline, stilbene, ammonia, benzene, and nitrogen.

Further extension of this reaction to other phenylhydrazones[2] leads to the conclusion that the reaction proceeds through a concerted fourcenter process rather than a free radical mechanism.

Repeating the above thermolysis reaction in one of our studies had resulted in different products than that recorded before. This prompted us to reinvestigate the reaction in an effort to gain further information about more generalized pyrolytic mechanism.

Thermolysis of benzophenone phenylhydrazone (**1**) by reflux in air for 24 h gives ammonia, benzophenone, biphenyl, aniline, benzonitrile, *N*-benzhydrylideneaniline (**2**), and 9-phenylacridine (**3**).

Formation of most of these products strongly points to a free radical mechanism starting by homolysis of N–N bond forming phenylaminyl and diphenylmethaniminyl radical pairs (Eq. 1) followed by H-abstraction to form aniline and diphenylmethanimine, respectively. The latter most probably on hydrolysis during working up procedure, gives rise to benzophenone and ammonia. Such a mechanism is to be expected on basis of bond energy values of the N–N and N–H bonds[3] being of the order 51 and 75 kcal mol^{-1}(1 cal=4.184 J), respectively.

However, such mechanism can not correlate for the formation of biphenyl, **2** and **3**. Consequently we have to take into consideration an alternative pathway involving isomerization of the phenylhydrazone **1** to the corresponding phenylazoalkane **4** as observed by other workers[4] through a free radical mechanism initiated by free radicals present in the reaction medium. The isomerized phenylazoalkane undergoes nitrogen extrusion forming phenyl and diphenylmethyl free radicals. Phenyl free radical substitution on the phenylazoalkane followed by its fragmentation gives biphenyl, whereas atmospheric oxidation of diphenylmethyl free radicals gives benzophenone as described by other workers[5] in the oxidation of benzyl radicals to benzaldehyde (Scheme 1). Furthermore, coupling of phenyl and dipenylmethaniminyl radicals leads to the formation of *N*-benzhydrylideneaniline.

The **3** (a pyrolysis product of **1**) is reasonably assumed to be formed via **5** which results from C–C coupling of diphenylmethyl and phenylaminyl radicals (Scheme 2).

Acetophenone phenylhydrazone (**6**) behaves similarly on thermolysis under the same conditions forming ammonia, acetophenone, biphenyl, aniline, benzonitrile, *o*- and *p*-toluidines, and 7-methyl-3-phenylindole. The formation of these products can be interpreted as in the case of **1**. Moreover, the formation of benzonitrile and *o*- and *p*-toluidines is in favor of the four-center mechanism proposed earlier by Crow and Solly[2] leading to the formation of *N*-methylaniline that ultimately rearranges to *o*- and *p*-toluidines as observed in a previous work.[6] On the other hand, fragmentation of diphenylmethaniminyl radicals leads to the formation of benzonitrile and phenyl radicals.[2]

However, the *o*-toluidine so formed have been consumed in the formation of 7-methyl-3-phenylindole (**7**) through condensation with styrene which is considered to be formed along with phenylethane as a disproportionation product of 1-phenylethyl radicals, as shown in Scheme 3. Such indole structure was further confirmed by its IR spectrum which shows ν NH at 3400 cm^{-1} and its electronic spectrum which shows absorption maxima at 272 nm (ε 2680) and 285 nm (ε 1920) characteristic for indole moiety.[7]

Repeating the pyrolysis of **6** in absence of air by heating in a sealed tube filled with nitrogen leads to a great decrease in the amount of acetophenone to about one third of that obtained in the case of reflux in air in addition to a corresponding increase in the yield of **7** as expected mechanistically.

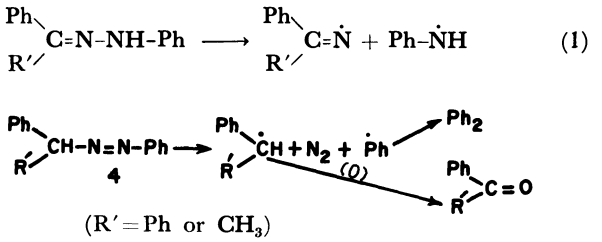

Scheme 1.

Dimerization of diphenylmethaniminyl radicals to form the corresponding azine was not observed due to the instability of the N–N bond.[8] Similarly, pyrolysis of **1** by heating in a sealed tube leads to an increase in the amount of **3** as compared with that obtained on reflux in air (cf. Table 1).

Table 1. Products of Thermolysis of Acetophenone Phenylhydrazone and Benzophenone Phenylhydrazone (20 g)

Products in g/%	Bp(θ_b/°C) 3 mm	Acetophenone phenylhydrazone		Benzophenone phenylhydrazone	
		Reflux	Seeled tube	Reflux	Seeled tube
Ammonia	—	Evolved	Evolved	Evolved	Evolved
Amine products:					
Aniline[a]	50—52	2.5(12.5)	2.3(11.5)	2.5(12.5)	1.5(7.5)
o-, *p*-Toluidine[b]	72—76	2.6(13)	1.8(9)	—	—
7-Methyl-3-phenylindole[c]	165—170	5.8(29)	7.5(37.5)	—	—
9-Phenylacridine[d]	215—220	—	—	5.6(28)	6.5(32.5)
Neutral products:					
Benzonitrile[e]	41—46	1.5(7.5)	1.3(6.5)	1.3(6.5)	1.0(5)
Acetophenone[f]	62—65	4.2(21)	1.5(7.5)	—	—
Biphenyl[g]	102—105	1.5(7.5)	1.2(6)	1.2(6)	1.0(5)
Benzophenone[h]	140—145	—	—	4.5(22.5)	4.2(21)
N-Benzhydrylideneaniline[i]	180—185	—	—	3.5(17.5)	3.0(15)
Residue	—	1.5(7.5)	3.6(16)	0.7(3.5)	2.2(11)

a) n_D^{20}: 1.5836; acetyl deriv. mp and mixed mp 113—114 °C. b) Found by GLC to consist mainly of *p*-toluidine together with traces (less than 1%) of *o*-toludine. c) MP and mixed mp 186—188 °C.[10] d) MP and mixed mp 182—183 °C, picrate mixed mp 185—186 °C.[12] e) Hydrolysis gives benzoic acid, mp and mixed mp 120—121 °C. f) D.N.P. deriv. mp and mixed mp 235—237 °C. g) MP and mixed mp 68—69 °C: 4,4′-dinitro deriv. mp and mixed mp 233 °C. h) MP and mixed mp 47—49 °C; D.N.P. deriv. mp and mixed mp 236—238 °C. i) MP and mixed mp 109—110 °C.[11]

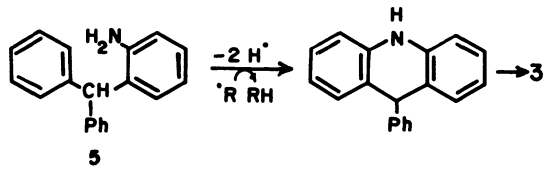

Scheme 2.

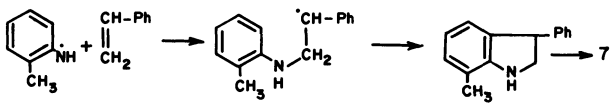

Scheme 3.

Experimental

All mp's are uncorrected. Thin-layer chromatography was carried out on glass plates covered with silica gel (25—40 mesh) and eluted with benzene/cyclohexane (2:1 v/v). The GLC analyses were carried out on a Pye-Unicam gas chromatograph, 'Series 104', equipped with a dual flame ionization detector, Model 24. The columns used were 4 ft(1 ft=0.3048 m)×5 mm packed with 20% SE 30 on Chromosorb W (35—80 mesh) or 10% SE 30 on Celite (60—80 mesh).

Thermolysis of Phenylhydrazones. **6** (mp 105—106 °C)[9] or **1** (mp 137 °C)[9] (20 g) was heated either under reflux in air or in a sealed tube under nitrogen atmosphere at 250 °C for 24 h. The ammonia evolved was detected by means of HCl and further absorbed in a trap containing sulfuric acid forming ammonium sulfate. The pyrolysate were treated similarly where in each case was dissolved in ether and shaken several times with dil HCl to extract the amine products. The ethereal layer containing either the neutral or the amine products was dried (Na_2SO_4) and evaporated to dryness leaving an oily material (15 g) which was separated by fractional distillation under reduced pressure into its constituents and identified by elemental analyses, TLC, GLC, UV, IR spectroscopy and/or mixed mp with authentic samples whenever possible. The results are shown in Table 1.

References

1) F. D. Chattaway, C. L. Cumming, and T. Wilsden, *J. Chem. Soc.*, **99**, 1950 (1911).
2) W. D. Crow and R. K. Solly, *Aust. J. Chem.*, **19**, 2119 (1966).
3) "CRC Handbook of Chemistry and Physics," 62nd ed. ed by R. C. Weast, CRC Press, Boca Raton. FL.FL 93 (1981—1982).
4) A. J. Bellamy and R. D. Guthrie, *J. Chem. Soc.*, **1965**, 3528.
5) A. E. Woodward and R. B. Mesrobian, *J. Am. Chem. Soc.*, **75**, 898 (1957).
6) M. Z. A. Badr and M. M. Aly, *Can. J. Chem.*, **52**, 293 (1974).
7) A. E. Gillam and E. S. Stern, "Electronic Absorption Spectroscopy," ed by E. Arnold, London (1960), pp. 151—152.
8) S. W. Benson, *J. Chem. Educ.*, **42**, 503 (1969).
9) R. Criegee and G. Lohaus, *Chem. Ber.*, **84**, 219 (1951).
10) M. Z. A. Badr, M. M. Aly, G. M. El-Naggar, and A. M. Fahmy, *Z. Naturforsch.*, **34b**, 1128 (1979).
11) D. Zoeppritz, *Ber.*, **35**, 991 (1902).
12) A. Bernthren, *Justus Liebigs Ann. Chem.*, **224**, 13 (1884).

Induced Cholesteric Mesophases as a Probe for the Stereochemistry of Chiral Biphenyls

Giovanni GOTTARELLI,* Gian Piero SPADA, Kaoru SENO,† Sanji HAGISHITA,† and Kaoru KURIYAMA†

Istituto di Scienze Chimiche, Universita' di Bologna, Via S. Donato 15, 40127 Bologna, Italy

†Shionogi Research Laboratories, Shionogi Co., Ltd., Fukushima-ku, Osaka 553

(Received July 6, 1985)

Synopsis. In the studies of the induced cholesteric mesophases, the twisting powers of cisoid- and transoid-bridged 2,2′-diaminobiphenyl derivatives having *R*-configuration were found to be negative and positive respectively. In the cases where CD spectroscopy is inadequate, the liquid crystal method is sensitive to the helicity of the biphenyl moiety. The conformation of 2,2′-diamino-6,6′-dimethylbiphenyl is discussed.

The stereochemistry of chiral biaryl derivatives is a subject of continuous interest.[1]

In particular, chiroptical techniques have been extensively employed for the configurational and conformational analysis of the system.[2,3]

In several cases the chiroptical techniques are unable to characterize the skew sense (i.e. the cisoid or transoid conformation) of the biaryl moiety. In the exciton approximation,[3,4] this indetermination is connected to the fact that the dipole–dipole interaction potential is not zero for a dihedral angle θ=90°; the value of θ at which the potential goes to zero depends in fact on the locations and directions of the electric dipole transition moments of the chromophores and therefore also on the substituents present. This point was emphasized in the recent work of Hagishita et al.[1] where cisoid- and transoid-bridged biphenyls having the same absolute configuration and therefore opposite helicity of the biphenyl skeleton, were shown to display very similar circular dichroism spectra in several cases.

In a recent work[5] we have shown that the configurations of a number of chiral cisoid-bridged biaryls, having various chemical structures, can be correlated by comparing the handedness of the cholesteric mesophases induced by traces of these derivatives dissolved in nematic liquid crystals of the biphenyl type.

Bridged biaryls having M-helicity induce M-cholesterics, while those of P-helicity induce P-cholesterics. The method, which allows the determination of configurations for cisoid-bridged systems, could be useful for the conformational analysis of non-bridged compounds of known absolute configuration; however, we needed experimental proof that rigid transoid derivatives also follow the helicity rule summarized above.

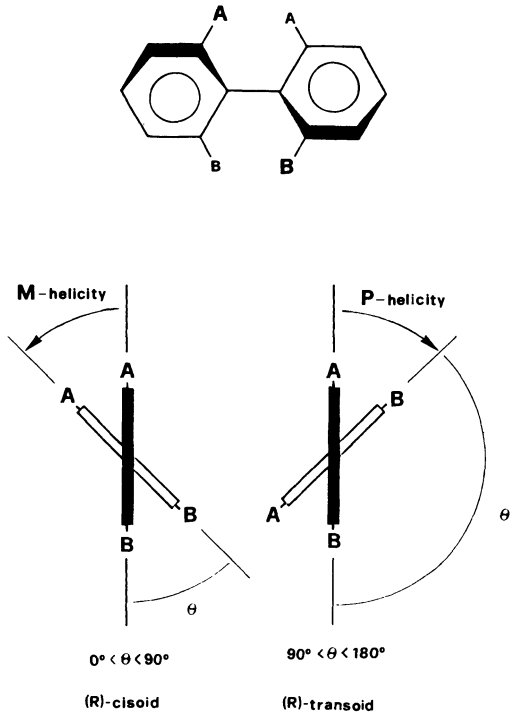

Fig. 1. Cisoid and transoid conformations of a chiral biphenyl derivative having *R*-configuration and the relative helicities of the biphenyl skeleton.

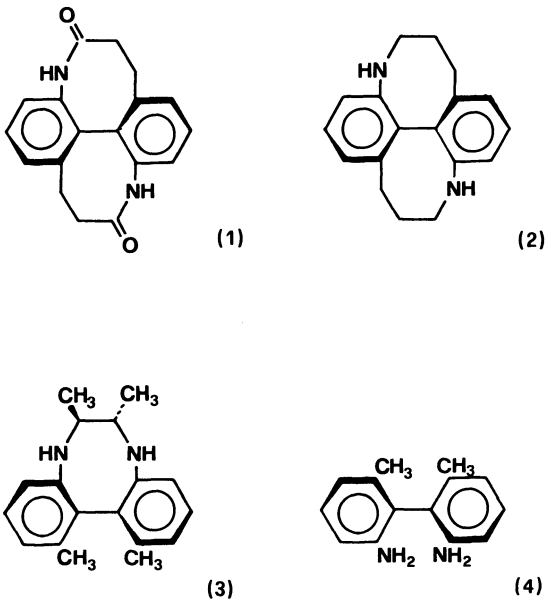

We report here the twisting powers β[6] of four diaminobiphenyls (Table 1), whose structure is known in detail from X-ray diffraction.[1] In particular, derivatives **1** and **2** constitute two examples of the rare trans-skew derivative (dihedral angle of 118° for **2**).[1]

Table 1. Characteristics of Derivatives **1**—**4** and Their Twisting Powers in a Biphenyl-Type Liquid Crystal

Compound	Absolute configur.	Dihedral angle[a]/°	Biphenyl helicity	$\beta/\mu m^{-1}$ in E7[b]	Cholesteric handedness
1	*R*		P	+58	P
2	*R*	118	P	+19.8	P
3	*R*	66	M	−21[c]	M
4	*R*	93	P	+2.0	P

a) From crystallographic data; Ref. 1. b) E7: A mixture of 4-cyano-4′-aryl and 4′-(normal alkyl)biphenyl from BDH Chemicals. c) The enantiomer was measured.

Indeed derivatives **1** and **2** also follow the rule proposed for cisoid compounds and show values of β of the order of magnitude expected:[7] their twisting powers have signs opposite to those of cisoid derivative **3** and other cisoid-bridged biaryls reported in Ref. 5. The liquid crystal method is therefore able to characterize the helicity of the biphenyl skeleton in the cases where CD spectroscopy fails.

Furthermore, derivatives **2** and **3**, which contain similar chemical groups, have quantitative values of β which are identical within the experimental error; this fact is a prerequisite for attempting the conformational analysis of non-bridged derivatives.

Derivative **4** has a small positive value of β indicating a P-helicity of the biphenyl system, which for the *R*-configuration is connected to a transoid conformation. The small value of β could be due either to the fact that the dihedral angle is very near to 90°,[7] or to the presence of cisoid and transoid conformers giving opposite contributions to the observed value with a slight prevalence of the transoid structure. X-Ray diffraction gives a dihedral angle of 93° (transoid), furthermore a comparison between the CD spectra measured in solution and in a KBr disc indicates a dihedral angle larger than 90°.[1]

The liquid crystal method therefore seems useful for the determination of the preferred conformation of chiral biphenyls in solution and could be a valid complement to circular dichroism studies. There are of course limitations due to the nature of substituents, which should not interfere with the alignment of the solute in the liquid crystal[7] or with the close contact between molecules of solvent and solute.[7]

Experimental

Measurements of the pitches were carried out with the "lens method"[8] with a standard Zeiss microscope.

The handedness of the cholesterics was deduced from the sign of the rotatory power[9] and cross-checked with the double spiral method.[10]

The synthesis and the characteristics of derivatives **1**—**4** are described in Ref. 1.

The liquid crystal mixture E7 is a commercial product from BDH Chemicals.

G. Gottarelli and G. P. Spada thank CNR and MPI (Rome) for financial support.

References

1) K. Seno, S. Hagishita, J. Sato, and K. Kuriyama *J. Chem. Soc., Perkin Trans. 1*, **1984**, 2013.

2) K. Mislow, M. A. W. Glass, H. B. Hopps, E. Simon, and G. H. Wahl Jr., *J. Am. Chem. Soc.*, **86**, 1710 (1964) and references therein.

3) S. F. Mason, "Molecular Optical Activity and the Chiral Discrimination," Cambridge University Press, Cambridge (1982), Chp. 6.

4) N. Harada and K. Nakanishi, "Circular Dichroic Spectroscopy-Exciton Coupling in Organic Stereochemistry," Oxford University Press, Oxford (1983).

5) G. Gottarelli, M. Hibert, B. Samori', G. Solladie', G. P. Spada, and R. Zimmermann, *J. Am. Chem. Soc.*, **105**, 7318 (1983).

6) The twisting power of a chiral solute in a nematic liquid crystal is defined as $\beta=(p.c.r)^{-1}$ where p the pitch (μm), c is the concentration (mol of solute/mol of solution) and r the enantiomeric excess of the dopant.

7) G. Gottarelli and G. P. Spada, *Mol. Cryst. Liq. Cryst.*, **123**, 377 (1985).

8) G. Heppke and F. Oestreicher, *Z. Naturforch.*, **A32**, 899 (1977).

9) J. P. Berthault, J. Billard, and J. Jacques, *C. R. Acad, Sci. Paris*, **C155**, 284 (1977).

10) G. Heppke and F. Oestreicher, *Mol. Cryst. Liq. Cryst.*, **41**, (letters), 245 (1978).

Synthesis and Characterization of Imidazolate-Bridged Binuclear Copper(II) Complexes

Naohide MATSUMOTO, Hiroyuki MURAKAMI, Toshifumi AKUI, Jukichi HONBO, Hisashi OKAWA,† and Akira OHYOSHI*
Department of Synthetic Chemistry, Faculty of Engineering, Kumamoto University, Kurokami 2-39-1, Kumamoto 860
†Department of Chemistry, Faculty of Science, Kyushu University, Hakozaki, Higashi-ku, Fukuoka 812
(Received October 4, 1985)

Synopsis. An unsymmetrical quadridentate copper(II) complex containing an imidazole moiety ([CuHL](ClO$_4$)) reacts with [1,4,7,10-tetraazacyclododecane]copper(II) perchlorate and [2-[2-(2-pyridyl)ethyliminomethyl]pyridine]-copper(II) perchlorate in the presence of one equivalent of triethylamine to give two discrete imidazolate-bridged binuclear copper(II) complexes, **1** and **2** respectively, where [H$_2$L] denotes the 1:1:1 condensation product of acetylacetone, ethylenediamine, and 4-formylimidazole. The analysis of the cryomagnetic data(ca. 80—300 K) on the basis of the Heisenberg model of a binuclear structure gave the antiferromagnetic interaction parameter($2J$) of -107.7 cm^{-1} for **2**.

Discrete imidazolate-bridged metal complexes are of current interest, since an imidazolate-bridged copper-(II)-zinc(II) center has been discovered in bovine erythrocyte superoxide dismutase (BESOD).[1] An X-ray crystallographic study of BESOD has indicated that the copper(II) and zinc(II) ions exist in distorted square planar and tetrahedral coordination environment respectively.[2] A number of imidazolate-bridged binuclear copper(II) complexes have been synthesized and characterized.[3] However, in most cases the two coordination spheres for the complexes are identical.

In this study, two imidazolate-bridged binuclear copper(II) complexes, **1** and **2**, in which the two coordination spheres of copper(II) ions are not identical, as is shown by the schemetic structures, have been prepared and characterized.

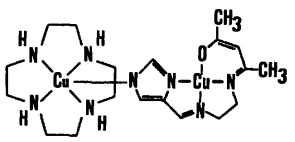

1

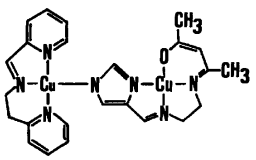

2

Experimental

Physical Measurements. The elemental analyses were performed by Mr. Shinichi Miyazaki at the Technical Service Center of Kumamoto University. The melting points were measured on a Yanagimoto micromelting points apparatus and were uncorrected. The electrical conductivity measurements were carried out on a Denki Kagaku AOC-10 conductometer on ca. 10^{-3} mol dm^{-3} solutions in methanol. The thermogravimetric analyses (TGA) were carried out on a Shimadzu TGC 20-type microthermobalance at the heating rate of 5 °C min^{-1}, using a ca. 10 mg sample for each run. The magnetic susceptibilities were obtained by the Faraday method from the temperature of liquid nitrogen to the ambient temperature, according to the procedure reported previously.[4] The susceptibilities were corrected for the diamagnetism of the component atoms by the use of Pascal's constants.

Syntheses. The copper(II) complex containing an imidazole moiety ([CuHL](ClO$_4$)) was prepared according to the method reported previously,[5] where [H$_2$L] denotes the unsymmetrical quadridentate Schiff-base ligand derived from acetylacetone, ethylenediamine, and 4-formylimidazole with a mole ratio of 1:1:1. [1,4,7,10-Tetraazacyclododecane]copper(II) perchlorate and [2-[2-(2-pyridyl)ethyliminomethyl]pyridine]copper(II) perchlorate hydrate were prepared by the method of the literature,[6,7] where the complexes are abbreviated as Cu[12]aneN$_4$(ClO$_4$)$_2$ and Cu(pip)(ClO$_4$)$_2$·H$_2$O respectively.

[CuLCu[12]aneN$_4$](ClO$_4$)$_2$·2.5H$_2$O 1. To a solution of [CuHL](ClO$_4$) (0.764 g, 2 mmol) in 30 cm^3 of 99% methanol was added a solution of triethylamine (0.202 g, 2 mmol) in 20 cm^3 of methanol. To the solution was added dropwise a solution of Cu[12]aneN$_4$(ClO$_4$)$_2$ (0.868 g, 2 mmol) in 20 cm^3 of methanol. The mixture was warmed at 50 °C for 30 min, after which the solution volume was reduced to one half. The solution was then kept for several days in a refrigerator. During that time, black prisms precipitated. They were collected by suction filtration, washed with methanol, and dried in vacuo. Attempts at recrystallization were unsuccessful. Found: C, 29.75; H, 5.24; N, 14.48%. Calcd for Cu$_2$Cl$_2$O$_9$N$_8$C$_{19}$H$_{34}$·2.5H$_2$O: C, 29.97; H, 5.16; N, 14.71%. Mp 225 °C(decomp), Λ_M 166.0 S mol^{-1} cm^2(MeOH), TGA, mass loss: 5.85 wt%; Calcd for 2.5H$_2$O: 5.91 wt%.

[CuLCu(pip)](ClO$_4$)$_2$·0.5H$_2$O 2. This complex was prepared by a similar method except that Cu(pip)(ClO$_4$)$_2$·H$_2$O instead of Cu[12]aneN$_4$(ClO$_4$)$_2$ was used. Blue-green microcrystalline material. Attempts at recrystallization were unsuccessful. Found: C, 37.60; H, 3.63; N, 12.78%. Calcd for Cu$_2$Cl$_2$O$_9$N$_7$C$_{24}$H$_{27}$·0.5H$_2$O: C, 37.71; H, 3.69; N, 12.84%. Mp 260 °C(decomp), Λ_M 174.1 S mol^{-1} cm^2(MeOH), TGA: mass loss, 1.15 wt%; Calcd for 0.5H$_2$O: 1.18 wt%.

Results and Discussion

The complex containing an imidazole moiety [CuHL]$^+$ reacts with [1,4,7,10-tetraazacyclododecane]-copper(II) and [2-[2-(2-pyridyl)ethyliminomethyl]pyridine]copper(II) in the presence of one equivalent of triethylamine to give the imidazolate-bridged binuclear copper(II) complexes, **1** and **2** respectively. The complexes crystallize as hydrates. The solvent molecules in the crystals were detected by TGA, where weight losses corresponding to those to be expected from the elemental analyses were observed. The molar electrical conductances of Complexes **1** and **2** are 166.0 and 174.1 S mol^{-1} cm^2 in methanol

respectively. These values are in the expected range of the 2:1 electrolyte in methanol (160—220 S mol^{-1} cm^2),[8] indicating that Complexes **1** and **2** have the formulas of [CuLCu[12]aneN$_4$]$^{2+}$(ClO$_4^-$)$_2$ and [CuLCu(pip)]$^{2+}$(ClO$_4^-$)$_2$ respectively.

The χ_A vs. T plots for Complexes **1** and **2** are shown in Fig. 1. The maximum in the χ_A vs. T plot of **1** is not observed in the temperature range studied(ca. 80—300 K), indicating that the magnetic interaction parameter ($|2J|$) is less than 89.5 cm^{-1} when obtained by means of the equation $|2J|=1.61\,kT_{max}$, where T_{max} is the temperature with the maximum magnetic susceptibility. The maximum at ca. 100 K in the plot of **2** is indicative of antiferromagnetic intramolecular exchange interaction. The magnetic susceptibility data of **2** were analyzed by means of a least-squares method using the SALS program,[9] in which the g and J values were refined as variable parameters on the basis of the Bleaney-Bowers Eq. 1 for isotropic exchange in a copper(II) dimer:

$$\chi_A = \frac{Ng^2\beta^2}{kT}\left[\frac{1}{3+\exp(-2J/kT)}\right] + N\alpha \qquad (1)$$

The temperature-independent paramagnetism($N\alpha$) was taken to be 60×10^{-6}, while the other symbols have their usual meanings. The best-fit values are $g=2.104$ and $2J=-107.7$ cm^{-1}, where the generalized R factor, $R=[\sum[\chi_A(\text{obsd})-\chi_A(\text{calcd})]^2/\sum\chi_A(\text{obsd})^2]^{1/2}$, using as a convenient statistical indicator of the quality of the least-squares fits, was calculated to be 0.005. In Fig. 1, theoretical curve with the parameters of g and J obtained is shown as a solid line.

Lippard and his co-workers pointed out that the magnitude of the exchange interaction parameter($2J$) for the imidazolate-bridged copper(II) complexes depends on the angles, ϕ and ϕ', defined in the drawing: i.e., increasing the ϕ and ϕ' angles leads to an increase in $|J|$.[3a] The X-ray analysis of

[CuHL](ClO$_4$) revealed the ϕ angle to be 143.1(1)°.[5] For the μ-Im[Cu(pip)]$_2$(NO$_3$)$_3$·2.5H$_2$O complex, it

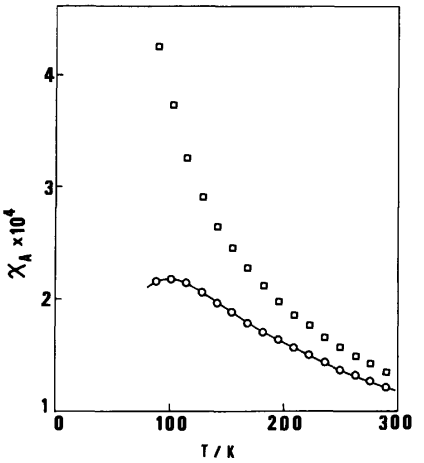

Fig. 1. Plots of χ_A vs. T for the binuclear copper(II) complexes **1** (□) and **2** (○), where the solid line represents the theoretical curve of Eq. 1 with the parameters of $g=2.104$, $2J=-107.7$ cm^{-1} for **2**.

was reported to have the ϕ angle of 120—128° and $2J=-53.8$ cm^{-1}.[3a] The larger $2J$ value of [CuLCu(pip)](ClO$_4$)$_2$·0.5H$_2$O **2** than that of μ-Im[Cu(pip)]$_2$(NO$_3$)$_3$·2.5H$_2$O is reasonable judging from the angles of ϕ and ϕ'.

References

1) J. A. Fee, *Biochim. Biophys. Acta*, **295**, 107 (1973).
2) J. S. Richardson, K. A. Thomas, B. H. Rubin, and D. C. Richardson, *Proc. Natl. Acad. Sci. U. S. A.*, **72**, 1349 (1975).
3) a) G. Kolks, S. J. Lippard, J. V. Waszczak, and H. R. Lilienthal, *J. Am. Chem. Soc.*, **104**, 717 (1982) and the references cited therein; b) M. Suzuki, I. Ueda, H. Kanatomi, and I. Murase, *Bull. Chem. Soc. Jpn.*, **56**, 3421 (1983) and the references cited therein.
4) M. Mikuriya, H. Okawa, and S. Kida, *Bull. Chem. Soc. Jpn.*, **54**, 2943 (1983).
5) N. Matsumoto, H. Murakami, T. Akui, J. Honbo, H. Okawa, and A. Ohyoshi, to be submitted for publication.
6) E. K. Barefield and F. Wagner, *Inorg. Chem.*, **12**, 2435 (1973).
7) G. Kolks, C. R. Frihart, P. K. Coughlin, and S. J. Lippard, *Inorg. Chem.*, **20**, 2933 (1981).
8) W. J. Geary, *Coord. Chem. Rev.*, **7**, 81 (1971).
9) T. Nakagawa and Y. Oyanagi, "Saishojijoho Niyoru Jikkendeta Kaiseki," The University of Tokyo Press (1982).

Spin-Equilibrium Behavior in Solution of an Iron(III) Complex [Bis-[3-(3-methoxysalicylideneamine)propyl]amino-*O,N,N',N'',O'*](pyridine)-iron(III) Tetraphenylborate

Akira Ohyoshi,* Jukichi Honbo, Naohide Matsumoto, Shoichi Ohta, and Shingo Sakamoto
Department of Synthetic Chemistry, Faculty of Engineering, Kumamoto University, Kurokami 2-39-1, Kumamoto 860
(Received November 28, 1985)

Synopsis. The title iron(III) complex with a spin equilibrium between high-spin(S=5/2) and low-spin(S=1/2) has been investigated by means of the temperature dependences of the magnetic susceptibilities (the Evans ^{1}H NMR technique), the electronic spectra, and the cyclic voltammetry. The pure electronic spectra for high-spin and low-spin species were evaluated from the observed electronic spectra and the equilibrium constants obtained from the magnetic data. The electron-transfer entropy for the $Fe^{3+}+e \rightarrow Fe^{2+}$ process(ΔS_{et}) was obtained as 205 $JK^{-1}mol^{-1}$ from the temperature dependence of the cyclic voltammogram.

We have previously reported the syntheses and characterizations of new families of spin-equilibrium mononuclear and binuclear iron(III) complexes, in which the spin-equilibrium behavior in the solid states has been investigated by the temperature dependences of the magnetic susceptibilities and the Mössbauer spectra.[1,2]

In this study, the spin-equilibrium behavior in the solution state of the title complex, whose schematic structure is shown in the drawing, has been investigated by means of the temperature dependences of the magnetic susceptibilities (the Evans ^{1}H NMR technique), the electronic spectra, and the cyclic voltammetry.

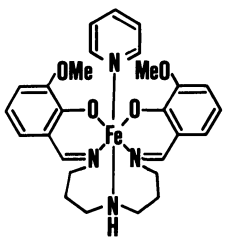

Experimental

Synthesis. The title complex [Fe(py)L][BPh_4] was prepared by the general method reported previously,[1] in which 3-methoxy-salicylaldehyde instead of salicylaldehyde was used for this complex. Found: C, 71.52; H, 6.13; N, 6.26%. Calcd for $FeC_{51}H_{52}N_4O_4B$: C, 71.93; H, 6.15; N, 6.58%. Mp 167—169 °C.

Physical Measurements. Magnetic susceptibility measurements in dichloromethane solution were performed by the Evans ^{1}H NMR method,[3] using a JEOL JNM-FX 100 spectrometer, where the Me_4Si was used as the reference compound. The magnetic susceptibility was corrected by the diamagnetism of the component atoms by the use of Pascal's constants. The effective magnetic moment was calculated by means of the equation; $\mu_{eff}=2.828\sqrt{\chi_A T}$. The temperature dependence of the electronic spectra in a dichloromethane solution was recorded with a Hitachi spectrophotometer model 340, according to the procedure of the literature.[4] Variable temperature cyclic voltammetric measurements were obtained with a three-electrode system using a Hokuto Denki HB-103 linear scanner and a HA-201 potentiostat with a Rika Denki model RW-11 XY-recorder. The working electrode was a platinum button, and a platinum wire served as the counter electrode. A commercial saturated calomel electrode(SCE) was used as the reference electrode and was separated from the bulk of the solution by a fritted glass bridge with the same solvent and supporting electrolyte (tetrabutylammonium perchlorate). The cell was cooled by circulating cold methanol. The temperature of the solution was monitored by means of a Yokogawa-Hokushin Denki digital multi-thermometer, type 2572, and was kept constant within ±0.2 °C during the measurement.

Results and Discussion

The [Fe(py)L][BPh_4] complex showed a striking thermochromism both in the solid and in the solution, changing its color from black in the solid and violet in the solution at the ambient temperature to green at the temperature of liquid nitrogen, which is characteristic of a spin equilibrium. The temperature dependence of the electronic spectra of the complex was measured in several organic solvents (dichloromethane, chloroform, acetonitrile, acetone, methanol, and ethanol) in order to examine the solvent effect on the spin-equilibrium behavior. Among the temperature dependences of the electronic spectra measured in various organic solvents, the spectrum measured in dichloromethane showed the most drastic thermochromic behavior with a set of isosbestic points, so that the spin-equilibrium behavior of the complex was thereafter studied in the dichloromethane solution by the use of variable-temperature techniques of magnetic susceptibility, electronic spectrum, and cyclic voltammetry.

The magnetic susceptibilities were measured in a dichloromethane solution by the Evans ^{1}H NMR method.[3] The effective magnetic moments at various temperatures are as follows (μ_B (K)): 5.55 (281), 5.50 (276), 5.45 (271), 5.33 (267), 5.24 (260), 5.07 (254), 4.98 (250), 4.85 (244), 4.60 (239), 4.44 (235). The μ_{eff} decreases from 5.55 μ_B at 281 K to 4.44 μ_B at 235 K, indicating a spin equilibrium between high-spin(S=

5/2) and low-spin(S=1/2). The equilibrium constant, defined as K=[high-spin]/[low-spin], was calculated from the expression: $K=(\mu_{eff}^2-\mu_{LS}^2)/(\mu_{HS}^2-\mu_{eff}^2)$, where μ_{HS} and μ_{LS} are the limitting high-spin and low-spin magnetic moments respectively. The value of μ_{HS} was fixed at 5.92, the spin-only value for the ^{6}A state. The value of μ_{LS} was taken as 2.0. The equilibrium constant, K, can be related to the entropy and enthalpy differences between high-spin and low-spin species by means of Eq. 1:

$$RT\ln K = \Delta H - T\Delta S \quad (1)$$

A plot of log K vs. T^{-1} is shown in Fig. 1. The data gives a straightline plot of log K vs. T^{-1}, with a ΔH value of 19.6 kJ mol^{-1} and ΔS value of 82.8 JK^{-1} mol^{-1}. The ΔH value is similar to the values reported for the spin-equilibrium iron(III) complexes [Fe(X-salmeen)$_2$]$^+$ and [Fe(X-sal)$_2$trien]$^+$,[5,6] where X-salmeen denotes the tridentate ligand derived from salicylaldehyde and *N*-methylethylenediamine and where (X-sal)$_2$trien denotes the hexadentate ligand derived from salicylaldehyde and bis(3-aminopropyl)amine. The ΔS value is somewhat larger than the values reported for the [Fe(X-salmeen)$_2$]$^+$ and [Fe(X-sal)$_2$trien]$^+$ complexes.

The temperature dependence of the electronic spectrum of the [Fe(py)L][BPh$_4$] complex in the dichloromethane solution is shown in Fig. 2. The spectrum changes with the set of isosbestic points at 420, 620, and 820 nm, suggesting a thermal equilibrium between two different electronic isomers, i.e., high-spin and low-spin species. At a single wavelength, the absorbance, A, is given by Eq. 2, where ε_{obsd} is the observed molar extinction coefficient, and where ε_{LS} and ε_{HS} are the molar extinction coefficients of the low-spin and high-spin species respectively:

$$\begin{aligned} A &= \varepsilon_{obsd}([LS]+[HS]) \\ &= \varepsilon_{LS}[LS]+\varepsilon_{HS}[HS] \end{aligned} \quad (2)$$

Equation 2 can be written as Eq. 3, using the equilibrium constant K=[HS]/[LS]:

$$(K+1)\varepsilon_{obsd} = \varepsilon_{LS} + K\varepsilon_{HS} \quad (3)$$

Therefore, a plot of $(K+1)\varepsilon_{obsd}$ vs. K gives the values of ε_{HS} from the slope and ε_{LS} from the intercept, where the values of K were estimated from the magnetic moments and where seven K values below 273 K were used. The electronic spectra of the pure high-spin and low-spin species were determined from this calculation; they are shown in Fig. 2 as dotted lines. The calculated electronic spectrum of the high-spin species exhibits two absorption maxima, at 450 and 560 nm, with the molar extinction coefficients of 3400 and 3400 mol^{-1} dm^3 cm^{-1}, while that of the low-spin species exhibits an absorption maximum at 670 nm, with the molar extinction coefficient of 3300 mol^{-1} dm^3 cm^{-1}.

The electrochemical reduction of the [Fe(py)L][BPh$_4$] complex involves a reversible one-electron transfer attributable to an Fe(III)/Fe(II) redox process. The half-wave potential for the reduction is observed at 0.018 V, and the peak separation, $E_{pa}-E_{pc}$, is 67 mV at 287 K. The electrochemical reduction was investigated in a dichloromethane solution as a function of the temperature between 287 and 257 K. A linear plot of $E_{1/2}$ vs. T was observed; it is shown in Fig. 3. The entropy change(ΔS_{et}) for the electrochemical reduction may be calculated from Eq. 4:[7]

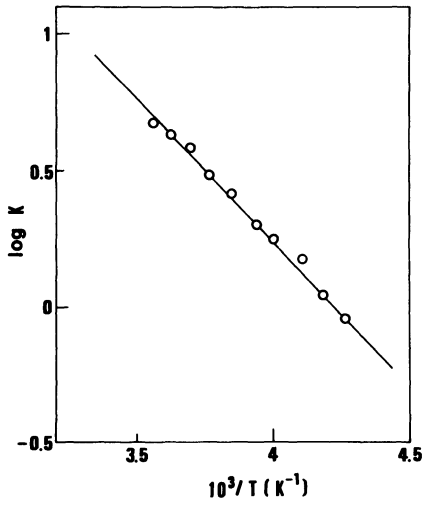

Fig. 1. A plot of log K vs. T^{-1} for [Fe(py)L][BPh$_4$], where K was calculated by the equation of $K=(\mu_{eff}^2-\mu_{LS}^2)/(\mu_{HS}^2-\mu_{eff}^2)$, and $\mu_{HS}=5.92$ and $\mu_{LS}=2.00$ were used.

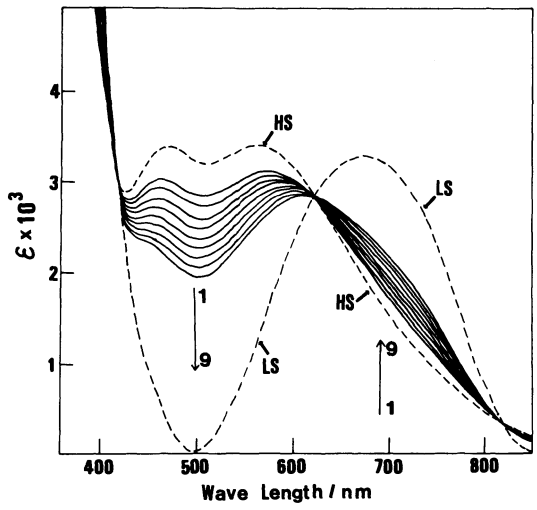

Fig. 2. Temperature dependence of the electronic spectrum for [Fe(py)L][BPh$_4$] in dichloromethane solution; 1(281.7 K), 2(277.7 K), 3(273.2 K), 4(268.2 K), 5(263.2 K), 6(258.2 K), 7(253.2 K), 8(248.2 K), 9 (243.2 K). The pure high-spin and low-spin spectra are shown as dotted lines.

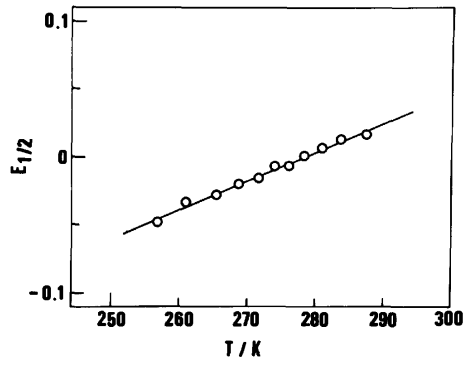

Fig. 3. A plot of $E_{1/2}$ vs. T for [Fe(py)L][BPh_4], where $E_{1/2}$ is relative to Saturated Calomel Electrode(SCE).

$$\Delta S_{et} = nF(\Delta E_{1/2}/\Delta T) \quad (4)$$

where n is the number of electrons transferred and where F is the Faraday constant. From Eq. 4, the value of ΔS_{et} was evaluated to be 205 $JK^{-1}mol^{-1}$. Kadish and his co-workers studied the electron-transfer properties of the spin-equilibrium iron(III) complexes and reported that the ΔS_{et} values varied from 88 to 146 $JK^{-1}mol^{-1}$ for [Fe(X-salmeen)$_2$]$^+$ and from 67 to 75 $JK^{-1}mol^{-1}$ for [Fe(X-sal)$_2$trien]$^+$.[8] Therefore, the ΔS_{et} value for the present complex is considerably larger than those for the [Fe(X-salmeen)$_2$]$^+$ and [Fe(X-sal)$_2$trien]$^+$.

We wish to thank the Institute for Molecular Science (Instrument Center) for use of the JEOL JNM-FX 100 NMR spectrometer and the Hitachi 340 spectrophotometer.

References

1) N. Matsumoto, S. Ohta, C. Yoshimura, A. Ohyoshi, S. Kohata, H. Okawa, and Y. Maeda, *J. Chem. Soc., Dalton Trans.*, **1985**, 2575.
2) S. Ohta, C. Yoshimura, N. Matsumoto, H. Okawa, and A. Ohyoshi, *Bull. Chem. Soc. Jpn.*, **59**, 155 (1986).
3) D. F. Evans, *J. Chem. Soc.*, **1959**, 2003.
4) M. Sugimoto, M. Nonoyama, T. Ito, and J. Fujita, *Inorg. Chem.*, **22**, 950 (1983).
5) R. H. Petty, E. V. Dose, M. F. Tweedle, and L. J. Wilson, *Inorg. Chem.*, **17**, 1064 (1978).
6) R. A. Binstead, J. K. Beattie, T. G. Deway, and D. H. Turner, *J. Am. Chem. Soc.*, **102**, 6442 (1980).
7) K. M. Kadish, *Phys. Bioinorg. Chem. Ser.*, **2**, 230 (1982).
8) T. Zhu, C. Su. Schaeper, B. K. Lemke, L. J. Wilson, and K. M. Kadish, *Inorg. Chem.*, **23**, 4345 (1984), and the references cited therein.

The Microwave Spectrum of Methyl Isoselenocyanate

Takeshi SAKAIZUMI,* Atsushi YASUKAWA, Hirobumi MIYAMOTO, Osamu OHASHI, and Ichiro YAMAGUCHI
Department of Chemistry, Faculty of Science and Technology, Sophia University, Kioi-cho, Chiyoda-ku, Tokyo 102
(Received December 9, 1985)

Synopsis. The microwave rotational spectra of two isotopic species of methyl isoselenocyanate(CH_3NCSe with ^{80}Se and ^{78}Se) in the ground vibrational state(A-species) have been assigned in the 9 to 40 GHz frequency range and the rotational and centrifugal distortion constants for the ground vibrational state have been determined. Three r_0 structural parameters have been determined from the observed rotational constants of the two species.

Molecules with an isoselenocyanato group form rather intriguring compounds since the isoselenocyanato(NCSe) group is ambidexterous: the isoselenocyanato group is able to bond at the site of either the N or the Se atom, forming either a R-NCSe or a R-SeCN molecule. The isoselenocyanic acid(H-NCSe)[1] exists only as R-NCSe type in the gas phase, while methyl derivatives have been identified as CH_3-SeCN[2] and CH_3-NCSe.[3] The presence of methyl isoselenocyanate(CH_3-NCSe) has been detected by infrared spectroscopy.[3]

In the CH_3-NCX(X=O and S) type, a barrier to the internal rotation of the methyl group in CH_3NCO[4] and CH_3NCS[4] has been found to be 83 and 304 cal mol^{-1} from the splitting of the $K_{-1}=0$, $m=\pm3$ lines. On the other hand, in the CH_3-XCN(X=S and Se) type, the barrier to internal rotation in CH_3SCN[5] and CH_3SeCN[2] has been found to be 1600 and 1240 cal mol^{-1}.

We are interested in the bond angle for R-NCX (R=H, CH_3, C_2H_5 and X=O, S, Se) molecules. The angle of H-N-C for H-NCO,[6] H-NCS,[7] and H-NCSe[1] has been determined to be 123.9°, 131.7°, and 143°. In methyl derivatives, the angle of C-N-C of CH_3-NCO[4] and CH_3-NCS[4] has been determined to be 139.98° and 147.5°. Recently, the C-N-C equilibrium angle for CH_3NCO[8] and CH_3NCS[9] has been found to be 140.2° and 152.5°, using a quasi-symmetric top molecule approach. These data show a large increase of 7 to 12° in the R-N-C angle for R-NCX molecules when the oxygen atoms of R-NCO molecules are replaced by sulfur atoms. A further increase in the C-N-C angle is anticipated upon the replacement of the sulfur atom in CH_3NCS by a selenium atom.

In this paper the microwave spectrum and three structural parameters of methyl isoselenocyanate in the ground vibrational state are reported.

Experimental

Methyl isoselenocyanate was prepared by heating in chloroform a mixture of methyl isocyanide, which was synthesized according to the method of Schuster,[10] and selenium powder for 96 hours.[3] The sample was purified by trap-to-trap vacuum distillation. The melting point and the IR spectrum agreed with the literature.[3]

The rotational spectrum was observed in the frequency region from 9 to 40 GHz with a conventional 100-kHz square-wave Stark modulation spectrometer. The microwave sources employed were a singnal generator(HP-8672A) in the frequency region of 9 to 23 GHz and a YIG-tuned GaAs oscillator(WJ-5610-302FD) in the frequency region of 26.5 to 40 GHz. The wave-guide cell was cooled with dry ice to about 0—10 °C.

Results and Discussion

The observed spectrum was quite dense, presumably due to the presence of several isotopic species (^{82}Se, ^{80}Se, ^{78}Se, and ^{76}Se), their vibrationally-excited states, and the A-E splitting due to the internal rotation of the methyl group.

A typical spectrum showed a-type R-branch transitions with the characteristic K-structure. The assignment of each line for the ^{80}Se species was made on the basis of the Stark effect, the relative population of the ^{80}Se species, and the fact that the line intensity for a ground state is the strongest. The assignment of the spectrum for the ^{78}Se species was made according to the estimated isotopic shifts of lines, keeping in mind that the spectrum lines have the same Stark effect as the corresponding lines of the ^{80}Se species. The observed and calculated line frequencies of ^{80}Se and ^{78}Se species are in good agreement, as shown in Tables 1 and 2. The rotational and centrifugal distortion constants were obtained by the least-squares method; they are listed in Table 3. The transitions listed in Tables 1 and 2 are ascribed to the A-species in the ground vibrational state for ^{80}Se and ^{78}Se species because of their Stark effects and line intensities. Since no Q-branch lines were observed because of their low intensity, the rotational constants A could not be determined accurately.

The observed spectra of CH_3NCO[4] and CH_3NCS[4] could not be fitted by the usual semirigid internal-rotation treatment. A reasonable fit of the $K_{-1}=0$ lines was obtained only if a semiempirical nonrigid correction factor[4] was used. The observed spectrum of CH_3NCSe could be fitted by the rigid-rotor approximation. This may mean that the barrier to internal rotation of the methyl group in CH_3NCSe may be higher than that in CH_3NCS(304 cal mol^{-1}). The E-species lines could not be assigned because the observed spectrum was quite dense.

Three structural parameters, r(C-N), r(N=C), and ∠C-N-C, have been adjusted to make the calculated values fit the four observed rotational constants of B and C. Some assumptions were made in this procedure: the methyl group has C_{3v} symmetry and

∠H-C-H=109.5°, r(C-H)=1.091 Å, and ∠N=C=Se=180°. Table 4 shows the assumed and derived structural parameters. If the estimation error of r(C=Se) from the similar molecules is ±0.010 Å, the errors of r(C-N), r(N=C), and ∠C-N-C are ±0.009 Å,

Table 1. Observed Rotational Transitions(MHz) of $CH_3NC^{80}Se$ in the Ground State

Transition	$CH_3NC^{80}Se$	
	ν_{obsd}	$\Delta\nu$[a]
$3_{22}-2_{21}$ } $3_{21}-2_{20}$ }	9858.74	−0.14
$3_{03}-2_{02}$	9860.80	0.14
$3_{12}-2_{11}$	9874.15	0.14
$4_{14}-3_{13}$	13128.61	0.07
$4_{13}-3_{12}$	13165.51	0.18
$5_{15}-4_{14}$	16410.79	0.15
$5_{14}-4_{13}$	16456.60	−0.02
$6_{16}-5_{15}$	19692.61	−0.11
$6_{06}-5_{05}$	19721.25	0.07
$6_{15}-5_{14}$	19747.69	−0.21
$7_{62}-6_{61}$ } $7_{61}-6_{60}$ }	22970.66	−0.03
$7_{17}-6_{16}$	22974.71	−0.06
$7_{53}-6_{52}$ } $7_{52}-6_{51}$ }	22982.09	0.01
$7_{44}-6_{43}$ } $7_{43}-6_{42}$ }	22991.43	−0.01
$7_{35}-6_{34}$ } $7_{34}-6_{33}$ }	22998.71	0.03
$7_{26}-6_{25}$ } $7_{25}-6_{24}$ }	23003.89	0.04
$9_{19}-8_{18}$	29538.58	−0.20
$9_{37}-8_{36}$ } $9_{36}-8_{35}$ }	29569.39	−0.14
$9_{28}-8_{27}$ } $9_{27}-8_{26}$ }	29576.16	−0.01
$9_{09}-8_{08}$	29581.52	0.08
$9_{18}-8_{17}$	29621.53	−0.02
$10_{1,10}-9_{1,9}$	32820.70	−0.02
$10_{3,8}-9_{3,7}$ } $10_{3,7}-9_{3,6}$ }	32854.71	−0.19
$10_{2,9}-9_{2,8}$ } $10_{2,8}-9_{2,7}$ }	32862.32	0.05
$10_{0,10}-9_{0,9}$	32868.21	0.10
$10_{1,9}-9_{1,8}$	32912.73	0.04
$11_{1,11}-10_{1,10}$	36102.70	0.08
$11_{3,9}-10_{3,8}$ } $11_{3,8}-10_{3,7}$ }	36140.40	0.18
$11_{2,10}-10_{2,9}$ } $11_{2,9}-10_{2,8}$ }	36148.50	0.17
$11_{0,11}-10_{0,10}$	36154.80	0.07
$11_{1,10}-10_{1,9}$	36203.62	−0.17
$12_{1,12}-11_{1,11}$	39384.37	−0.11
$12_{3,10}-11_{3,9}$ } $12_{3,9}-11_{3,8}$ }	39425.49	0.02
$12_{2,11}-11_{2,10}$ } $12_{2,10}-11_{2,9}$ }	39433.60	0.26
$12_{0,12}-11_{0,11}$	39441.11	−0.19
$12_{1,11}-11_{1,10}$	39494.78	−0.06

a) $\Delta\nu=\nu_{obsd}-\nu_{calcd}$

Table 2. Observed Rotational Transitions(MHz) of $CH_3NC^{78}Se$ in the Ground State

Transition	$CH_3NC^{78}Se$	
	ν_{obsd}	$\Delta\nu$[a]
$6_{16}-5_{15}$	19836.68	0.01
$6_{06}-5_{05}$	19865.33	−0.05
$7_{17}-6_{16}$	23142.76	0.06
$9_{19}-8_{18}$	29754.52	−0.14
$9_{37}-8_{36}$ } $9_{36}-8_{35}$ }	29785.60	−0.04
$9_{28}-8_{27}$ } $9_{27}-8_{26}$ }	29792.50	0.13
$9_{09}-8_{08}$	29797.70	0.01
$10_{1,10}-9_{1,9}$	33060.47	−0.10
$10_{3,8}-9_{3,7}$ } $10_{3,7}-9_{3,6}$ }	33095.00	−0.01
$10_{2,9}-9_{2,8}$ } $10_{2,8}-9_{2,7}$ }	33102.30	−0.17
$10_{0,10}-9_{0,9}$	33108.37	−0.01
$10_{1,9}-9_{1,8}$	33153.26	−0.09
$11_{1,11}-10_{1,10}$	36366.30	−0.13
$11_{3,9}-10_{3,8}$ } $11_{3,8}-10_{3,7}$ }	36404.30	−0.02
$11_{2,10}-10_{2,9}$ } $11_{2,9}-10_{2,8}$ }	36412.54	−0.02
$11_{0,11}-10_{0,10}$	36419.11	−0.10
$12_{1,12}-11_{1,11}$	39672.44	0.20

a) $\Delta\nu=\nu_{obsd}-\nu_{calcd}$

Table 3. The Observed and Calculated Rotational Constants for CH_3NCSe

	$CH_3NC^{80}Se$		$CH_3NC^{78}Se$	
	Obsd	Calcd[a]	Obsd	Calcd[a]
A/GHz	100 (50)		100[b]	
	102.700[c]		102.908[c]	
B/MHz	1648.045 (8)	1647.92	1660.104 (8)	1659.92
C/MHz	1638.848 (8)	1638.87	1650.826 (8)	1650.76
Δ_J/kHz	0.180 (23)		0.204 (28)	
Δ_{JK}/kHz	74.05 (28)		75.00 (48)	

Figures in parentheses indicate the uncertainty attached to the last figures, estimated from 2.5 times the standard deviations.

a) Calculated from the structural parameters in Table 4. b) Assumed. c) Calculated from assuming the inertia defect(−3.2 amuÅ²).

Table 4. Structural Parameters of CH_3NCSe

Assumed parameters	Derived parameters
r(C-H) : 1.091 Å	r(C-N) : 1.447±0.009 Å
r(C=Se) : 1.708 Å	r(N=C) : 1.205±0.010 Å
∠H-C-H : 109.5 Å	∠C-N-C : 157.0±4.0°
∠N=C=Se : 180°	

Table 5. Comparison of the Structural Parameters(Å) for Similar Molecules

	r(C-N)	r(N=C)	r(C=Se)	R-N-C(deg)
CH_3-NCSe[a]	1.447	1.205	(1.708)	157.0
CH_3-NCS	1.452[b]	1.216[b]		147.46[b]
	1.4123[c]	1.2068[c]		152.52[c]
CH_3-NCO	1.437[b]	1.207[b]		139.98[b]
	1.4342[d]	1.207[d]		140.18[d]
H-NCSe[e]		1.195	1.717	143.0
H-NCS[f]		1.207		131.7
H-NCO[g]		1.214		123.9
CH_2=C=Se[h]			1.706	
S=C=Se[i]			1.695	
O=C=Se[j]			1.7098	

a) This work, b) Ref. 4, c) Ref. 9, d) Ref. 8, e) Ref. 1, f) Ref. 7, g) Ref. 6, h) Ref. 11, i) Ref. 12, j) Ref. 13, ( ): assumed.

±0.010 Å, and ±4° respectively. The rotational constants calculated from the derived structural parameters are consistent with the observed ones, as shown in Table 3.

The derived values of the bond lengths, r(C-N) and r(N=C), are in agreement with those of similar molecules within less than 0.01 Å, as shown in Table 5. The angle of C-N-C of 157° is much larger than the ones of CH_3NCO and CH_3NCS. A similar trend is seen for the case of the H-N-C angle in HNCO (124°), HNCS(132°), and HNCSe(143°).

References

1) B. M. Landsberg, *Chem. Phys. Lett.*, **60**, 265 (1979).
2) T. Sakaizumi, Y. Kohri, O. Ohashi, and I. Yamaguchi, *Bull. Chem. Soc. Jpn.*, **51**, 3411 (1978); B. M. Landsberg, *Z. Naturforsh.*, **33a**, 1323 (1978); T. Sakaizumi, M. Obata, T. Takahashi, E. Sakaki, O. Ohashi, and I. Yamaguchi, *Bull. Chem. Soc. Jpn.*, to be published.
3) W. J. Franklin, R. L. Werner, and R. A. Ashby, *Spectrochimica Acta*, **30A**, 1293 (1974).
4) R. G. Lett and W. H. Flygare, *J. Chem. Phys.*, **47**, 4730 (1967).
5) S. Nakagawa, S. Takahashi, T. Kojima, and C. C. Lin, *J. Chem. Phys.*, **43**, 3583 (1965).
6) K. Yamada, *J. Mol. Spectrosc.*, **79**, 323 (1980).
7) K. Yamada, M. Winnewisser, G. Winnewisser, L. B. Szalanski, and M. C. L. Gerry, *J. Mol. Spectrosc.*, **79**, 295 (1980).
8) J. Koput, *J. Mol. Spectrosc.*, **106**, 12 (1984).
9) M. Kreglewski, *Chem. Phys. Lett.*, **112**, 275 (1984).
10) R. E. Schuster, J. E. Scott, and J. Casanova, Jr., *Org. Synth.*, **V**, 772 (1973).
11) B. Bak, O. J. Nielsen, H. Svanholt, and A. Holm, *Chem. Phys. Lett.*, **55**, 36 (1978).
12) C. Hirose and R. F. Curl, Jr., *J. Chem. Phys.*, **55**, 5120 (1971).
13) M. W. P. Strandberg, T. Wentink, and A. G. Hill, *Phys. Rev.*, **75**, 827 (1949).

Out-of-Plane Vibrations of [$^1H_5$]- and [$^2H_5$]Pyridines

Yoshimi Ozono, Masayoshi Maehara, Yoshinori Nibu,† Hiroko Shimada,* and Ryoichi Shimada†

Department of Chemistry, Faculty of Science, Fukuoka University, Jonan-ku, Fukuoka 814

†Department of Chemistry, Faculty of Science, Kyushu University 33, Hakozaki, Higashi-ku, Fukuoka 812

(Received December 10, 1985)

Synopsis. Assignments of the out-of-plane normal vibrations of [$^1H_5$]- and [$^2H_5$]pyridines were reexamined based on the polarization behavior of the Raman bands and also through the normal coordinate calculation.

The normal vibrations of [$^1H_5$]- and [$^2H_5$]pyridines have been studied by many workers. Very recently Wong and Colson reviewed the previous works and reexamined the assignments of the normal vibrations of [$^1H_5$]- and [$^2H_5$]pyridines through the analysis of the high resolution FT-IR spectra.[1] There are, however, some ambiguous arguments in the assignments for the out-of-plane vibrations. They assigned the a_2 vibrations empirically using weak Raman, infrared(combination) and fluorescence bands and their assignments for the b_1 vibrations are reliable only for the infrared bands showing clear rotational band contour in vapor. Therefore, definite experimental evidences are needed for the reasonable assignments for the a_2 and b_1 vibrations.

In this paper the authors intend to give the most reliable assignments for the out-of-plane vibrations of [$^1H_5$]- and [$^2H_5$]pyridines through the analysis of the polarized Raman spectra in single crystals and the normal coordinate calculations.

Experimental

Materials. [$^1H_5$]- and [$^2H_5$]pyridines, obtained from Nakarai Chemical Company and Commissariat a l'Energie Atomique, respectively, were purified by repeated distillation under reduced pressure.

Optical Measurement. The polarized Raman spectrum was observed in a single crystal with a JEOL 400 T Laser Raman Spectrophotometer at −45 °C. Although a block of single crystal of the sample could be obtained by the Bridgman method, a cubic crystal sample could not be cut off because the crystal is very hygroscopic and also melts by pressing with a razor blade even in a Dry Ice box. Thus a single crystal was grown in a capillary glass tube of about 3 mm in diameter and 70 mm in length having a sharp conical end by cooling gradually in a Mini Subzero Tabai MC-81 Refrigerator. The direction of the crystal growth was found to be one of the crystal axis and other two crystal axes were found by rotating the crystal specimen around the crystal growth direction under the polarized light. The crystal growth direction and other two crystal axes thus determined are referred to as u, v, and w axes, respectively. The polarized Raman spectrum was observed in the following two crystal orientations. The u axis was directed parallel to the polarization direction of the excitation laser beam. The v and w axes were directed parallel to the propagation direction of the laser beam in the first and second crystal orientations, respectively. The Raman scattering was observed at right angles with the excitation light beam. Thus the uu, uv, and uw polarized Raman spectra were obtained, where the first letter refers to the direction of the polarization of the excitation light and the latter to that of the scattering light. The sample was excited with the 514.5 nm line from an Ar^+ ion laser.

Results and Discussion

A normal coordinate calculation for pyridine was performed through the standard GF matrix methods with a FACOM M-200 computer at Computer Center of Fukuoka University. The geometric parameters of the molecule were taken from the data determined by Bak et al.[2] The force constants used for the calculation of the out-of-plane vibrations are listed in Table 1. The notation of Q, q, P, p, and t are the same as those used by Whiffen.[3] The calculated frequencies and modes are given in Table 2.

The crystal structure of pyridine was studied by Mootz and Wussow.[4] Pyridine crystalizes in the orthorhombic system of the space group C_{2v}^9 with sixteen molecules in the unit cell. No factor group splitting was observed in the Raman bands of the molecular vibrations and therefore the relationship between the Raman tensors for the free molecule and the crystal was derived based on the simplified oriented gas model. The Raman tensors were calculated in the same way as described previously[5,6] and the results are given in Table 3. This table suggests that (1) the a_2 vibrations can be observed strongly in the aa, bb, and cc spectra while the b_1 and b_2 vibrations strongly in the ab, ac, and bc spectra and (2) if the crystal growth direction is along the crystal a or b axis, the b_1 and b_2 vibrations show different polarization behavior in the uv and uw spectra while if the direction is along the c axis, these vibrations show the same polarization behavior. The polarized Raman spectra of [$^1H_5$]- and [$^2H_5$]pyridines are shown in Figs. 1 and 2, respectively. These figures show that the depolarized Raman bands in liquid show two different types of polarization behavior in single crystals, that is, the relative intensity of the bands belonging to the first type is strong in the uu spectrum and very weak in the uv and uw spectra and

Table 1. Force Constants for Out-of-Plane Vibrations

$Q_{C\text{-}N}$	0.22	q^o	−0.06	p^m	−0.03
$Q_{C\text{-}C}$	0.2	q^m	0.01	t^o	−0.02
P_H	0.30	P^o	0.03	t^m	−0.02

in aNmrad^{-2}(=mdyn Arad^{-2}) units.

Table 2. Out-of-Plane Vibrations of [$^1H_5$]- and [$^2H_5$]Pyridines

Sym. spec.	Mode	[$^1H_5$]pyridine				[$^2H_5$]pyridine			
		WC[a]	This work			WC[a]	This work		
		Infrared	Raman		Calcd	Infrared	Raman		Calcd
		$\tilde{\nu}$/cm^{-1} Pol	$\tilde{\nu}$/cm^{-1} Pol		$\tilde{\nu}$/cm^{-1}	$\tilde{\nu}$/cm^{-1} Pol	$\tilde{\nu}$/cm^{-1} Pol		$\tilde{\nu}$/cm^{-1}
		Vapor	Crystal			Vapor	Crystal		
	ν_{17a}	980[b]	975	uu	966	815[b]	813	uu	797
a_2	ν_{10a}	880[c]	882	uu	868	690[b]	688	uu	678
	ν_{16a}	373	377	uu	370	318.0	323	uu	319
	ν_{17b}	1007	952	uv uw	958	828.3	820	uv uw	814
	ν_5	936.6 C	878	uv uw	860	765.3 C	763	uv uw	746
b_1	ν_4	744.0 C	755	uv uw	754	630.8	627	uv uw	610
	ν_{11}	700.3 C	715	uv uw	728	525.8 C	528	uv uw	535
	ν_{16b}	403.3 C	408	uv uw	391	367.6	362	uv uw	349

a) Taken from Ref. 1. b) Taken from H. D. Stidham and D. P. DiLella, *J. Raman Spectrosc.*, **9**, 90 (1980), *ibid.*, **9**, 247 (1980). c) Taken from Y. Mochizuki, K. Kaya, and M. Ito, *J. Chem. Phys.*, **69**, 935 (1978).

Table 3 Squared Values of the Elements of the Derived Polarizability Tensors

	b_2	b_1	a_2
$(A_{aa})^2$	0.02	0.02	0.47
$(A_{bb})^2$	0.01	0.04	0.47
$(A_{cc})^2$	0.004	0.004	0.98
$(A_{ab})^2$	0.41	0.54	0.01
$(A_{ac})^2$	0.30	0.22	0.01
$(A_{bc})^2$	0.27	0.21	0.01

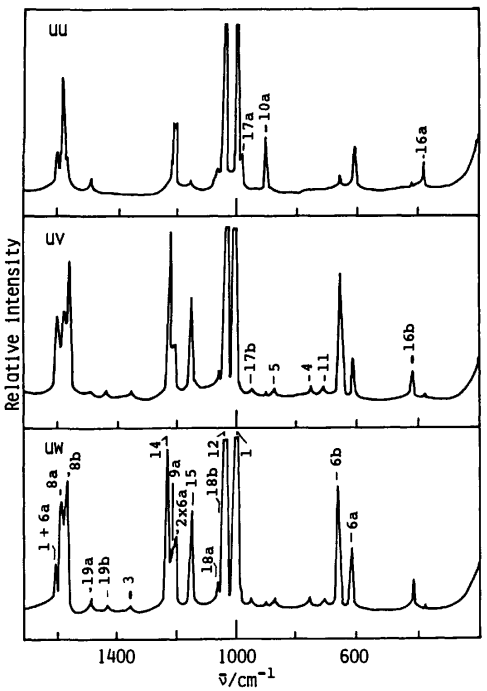

Fig. 1. Polarized Raman spectrum of [$^1H_5$]pyridine single crystal.

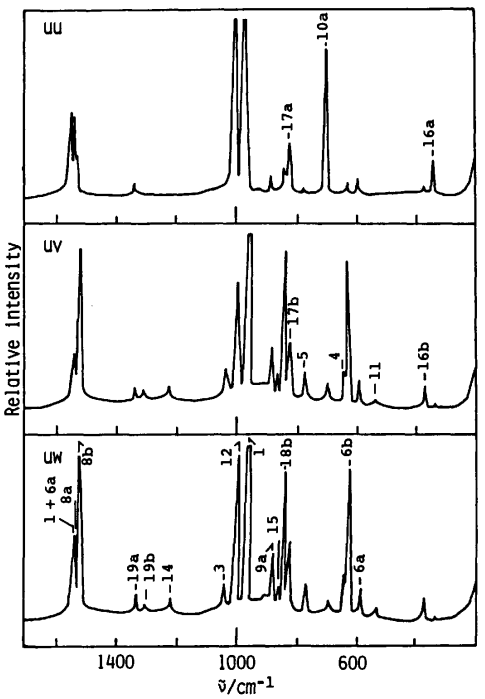

Fig. 2. Polarized Raman spectrum of [$^2H_5$]pyridine single crystal.

the relative intensity of the second type bands is strong in the uv and uw spectra and very weak in the uu spectrum. Comparing the observed relative intensity of the polarized Raman bands with the data given in Table 3, it can be concluded that the first type bands can be assigned to the a_2 vibrations and the second type bands to the b_1 or b_2 vibrations. These figures also show that the second type bands show almost equal polarization behavior in the uv and uw spectra. This observation indicates that the u axis should correspond to the crystal c axis. No infrared bands corresponding to the first type polarized Raman bands could be observed and this

fact supports the first type bands being to be assigned to the a_2 vibrations. The vibrational modes were determined based on the normal coordinate calculation.

[$^1H_5$]Pyridine. Depolarized Raman bands observed at 952, 878, 755, 715, and 408 cm^{-1} in liquid show the second type polarization in crystal. Thus these bands can safely be assigned to the ν_{17b}, ν_5, ν_4, ν_{11}, and ν_{16b} vibrations of b_1 species, respectively, because the non-totally symmetric in-plane vibrations except for the ν_{6b} vibration are expected to be observed in the region higher than 1000 cm^{-1} in this molecule. Although Wong and Colson[1] assigned the frequency of 1007 cm^{-1} to the b_1 vibration, this frequency could not be observed in the polarized Raman spectrum. Depolarized Raman bands at 975, 882, and 377 cm^{-1} in liquid show the first type polarization in crystal and thus these can definitely be assigned to the ν_{17a}, ν_{10a}, and ν_{16a} vibrations of a_2 species, respectively.

[$^2H_5$]Pyridine. Depolarized Raman bands at 763, 627, 528, and 362 cm^{-1} in liquid show the second type polarization in crystal. Thus these bands can be assigned to the ν_5, ν_4, ν_{11}, and ν_{16b} vibrations of b_1 species, respectively. A depolarized and broad Raman band around 820 cm^{-1} in liquid is clearly resolved into two bands at 820 and 813 cm^{-1} in crystal and show the second and first type polarization, respectively. Therefore, the former was assigned to the ν_{17b} vibration. Depolarized Raman bands at 813, 688, and 323 cm^{-1} in liquid show the first type polarization in crystal and thus these can be assigned to the ν_{17a}, ν_{10a}, and ν_{16a} vibrations of a_2 species, respectively. Wong and Colson presented the ν_5 and ν_{10b} modes for the hydrogen wagging vibrations of b_1 species in decreasing order of vibrational frequency, while the normal coordinate calculation used reasonably estimated force constants gives the ν_{17b} and ν_5 modes for these wagging vibrations, respectively.

The polarization behavior of the Raman bands gave clear and definite experimental justification for the assignments of the out-of-plane vibrations. The polarization behavior of the Raman bands also supports the assignments for the in-plane vibrations given by Wong and Colson except for the ν_{18b} vibration of [$^1H_5$]pyridine. Wong and Colson assigned weak infrared bands observed at 705.8 and 1690.9 cm^{-1} to the $\nu_{18b}-\nu_{16a}$ and $\nu_{18b}+\nu_{6a}$ vibrations, respectively, and gave the frequency of 1079 cm^{-1} for the ν_{18b} vibration. A Raman band observed at 1045 cm^{-1} as a shoulder of the strong ν_{12} band shows clearly the second type polarization in single crystal and the frequency is higher than 1000 cm^{-1}. Thus we assigned the frequency of 1045 cm^{-1} to the ν_{18b} vibration of [$^1H_5$]pyridine.

References

1) K. N. Wong and S. D. Colson, *J. Mol. Spectrosc.*, **104**, 129 (1984).
2) B. Bak, L. Hansen-Nygaard, and J. Rastrup-Andersen, *J. Mol. Spectrosc.*, **2**, 361 (1958).
3) D. H. Whiffen, *Philos. Trans. R. Soc. London, Ser. A*, **248**, 131 (1955).
4) D. Mootz and H. G. Wussow, *J. Chem. Phys.*, **75**, 1517 (1981).
5) Y. Ishibashi, R. Shimada, and H. Shimada, *Bull. Chem. Soc. Jpn.*, **55**, 2765 (1982).
6) Y. Ishibashi, F. Arakawa, H. Shimada, and R. Shimada, *Bull. Chem. Soc. Jpn.*, **56**, 1327 (1983).

The Microwave Spectrum of (*E*)-(Propinaldehyde Oxime)

Kazuhiko YOSHIDA, Takeshi SAKAIZUMI, Osamu OHASHI,* and Ichiro YAMAGUCHI
Department of Chemistry, Faculty of Science and Technology, Sophia University, Chiyoda-ku, Tokyo 102
(Received December 11, 1985)

Synopsis. Microwave spectra of propionaldehyde oxime and its deuterated derivatives ($CH_3CH_2CH{=}NOD$) were observed in the frequency region from 10 to 35 GHz. Several a-type R-branch transitions were identified and the following rotational constants(MHz) in the vibrationally ground state were determined to be: A=19400±400, B=2278.16±0.03, and C=2204.09±0.03 for the normal species, and A=19000±400, B=2194.31±0.02, and C=2128.40±0.02 for the deuterated species. The spectrum analyzed in this work has been concluded from the rotational constants to be due to a *ac*,*E*-conformer.

From its rotational spectrum propionic acid (CH_3CH_2COOH) has been shown to exist predominantly in a *sp*-conformation in which the methyl group eclipses the carbonyl bond and the hydroxyl hydrogen is located between the two oxygen atoms.[1] Acrylaldehyde oxime has been reported to exist predominantly in a *s-trans* form for both *E*- and *Z*-forms.[2,3]

Propionaldehyde oxime[4] has been reported by nuclear magnetic resonance spectroscopic study to exist in two stereoisomeric forms, termed *E*- and *Z*-forms with respect to the C=N bond, each form of which has four possible rotational conformations with respect to the C_2–C_3 bond if the OH bond is assumed to be at the trans position to the CN bond just as it has been found in such molecules as acrylaldehyde oxime[2,3] and acetaldehyde oxime,[6,7] as shown in Fig. 1.

Experimental

Propionaldehyde oxime was produced by reacting propionaldehyde with hydroxylamine hydrochloride according to Dunstan and Dymond's method.[5]

Deuterated species of propionaldehyde oxime ($CH_3CH_2CH{=}NOD$) was prepared in the absorption cell itself in the same way as that for acetylaldehyde oxime-d.[6,7]

The microwave spectrometer used was a conventional 100 KHz sinusoidal- and square-wave Stark modulation type with a phase sensitive detector. The spectra were observed at room temperature.

Results and Discussion

The rotational constants calculated from the assumed structural parameters as listed in Table 1 suggests that seven conformers of eight possible rotational conformers were near prolate symmetric top molecules in whose spectra bunches of the absorption lines are expected with the frequency interval of about (B+C).

A survey of the spectrum was made in frequency region of 8.5 to 32 GHz at the Stark fields between 200 and 300 V cm^{-1}. Groups of the absorption lines were found with the frequency interval of about 4500 MHz. The frequencies of the absorption lines which were assigned on the basis of their characteristic Stark effects are listed in Table 2 together with

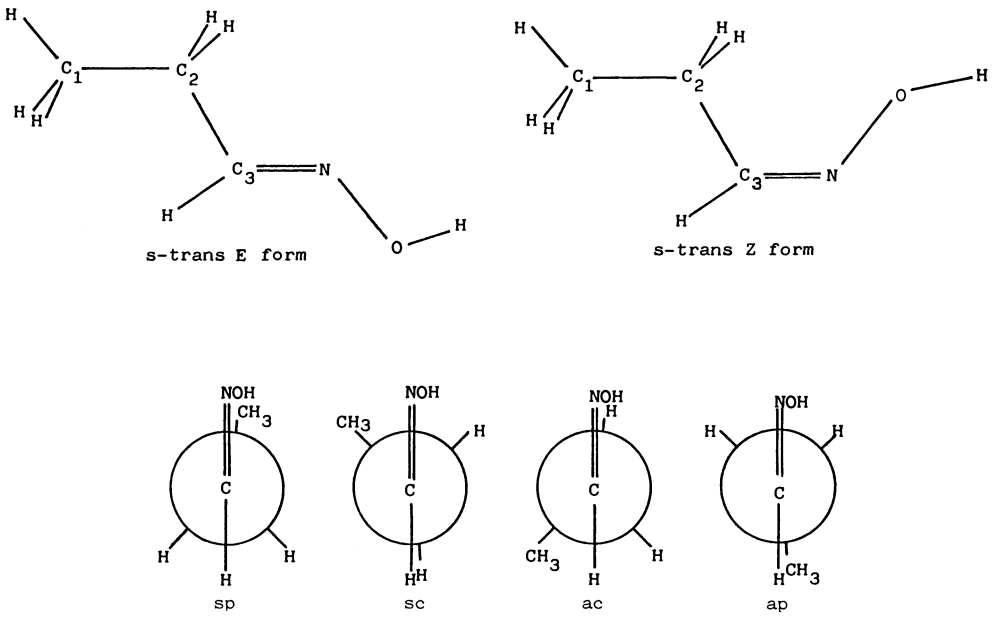

Fig. 1. Four possible rotational conformers and the numbering of carbon atoms of a *ap*-(*E*)-(propionaldehyde oxime) and a *ap*-(*Z*)-(propionaldehyde oxime).

Table 1. Structural Parameters Assumed for Propionaldehyde Oxime

Bond length	r/Å	Bond angle	θ/°
C_1-C_2	1.536	HC_1H	109.5
C_2-C_3	1.493	HC_2H	105.7
C_1-H	1.095	$C_1C_2C_3$	112.1
C_2-H	1.095	HC_1C_2	110.3
C_3-H	1.086	HC_2C_3	109.8
C_3=N	1.276	C_2C_3=N	125.4
N-O	1.408	HC_3=N	121.8
O-H	0.956	C_3=NO	110.2
		NOH	102.7

Table 2. Observed Transition Frequencies (MHz) of Propionaldehyde Oxime

Transition	Normal		Deuterated	
	Obsd	$\Delta\nu$[a]	Obsd	$\Delta\nu$[a]
3_{13}—2_{12}	13335.67	0.16	12869.42	0.24
3_{03}—2_{02}	13445.73	0.04	12967.33	0.04
3_{12}—2_{11}	13557.74	0.00	13066.77	−0.16
4_{14}—3_{13}	17780.43	0.11	17158.65	0.04
4_{04}—3_{03}	17926.33	−0.06	17288.71	0.04
4_{23}—3_{22}	17929.37	0.10		
4_{22}—3_{21}	17931.42	−0.24		
4_{13}—3_{12}	18076.51	−0.10	17422.30	0.03
5_{15}—4_{14}	22224.76	−0.04	21447.75	−0.04
5_{05}—4_{04}	22406.09	0.06	21609.26	−0.11
5_{24}—4_{23}	22411.36	0.22	21613.58	0.04
5_{23}—4_{22}	22415.78	−0.14	21617.44	0.04
5_{14}—4_{13}	22595.07	−0.09	21777.32	−0.04
6_{16}—5_{15}	26668.87	−0.03	25736.52	−0.13
6_{06}—5_{05}	26884.47	0.08	25928.99	0.04
6_{25}—5_{24}	26892.59	−0.12	25935.64	−0.09
6_{24}—5_{23}	26901.13	0.05	25942.45	−0.03
6_{15}—5_{14}	27113.30	−0.02	26132.25	0.12
7_{17}—6_{16}	31112.44	−0.09	30025.13	−0.01
7_{07}—6_{06}	31361.12	−0.09	30247.37	0.08
7_{26}—6_{25}	31373.97	0.04	30257.63	0.00
7_{25}—6_{24}	31387.36	0.04	30268.49	0.05
7_{16}—6_{15}	31631.11	0.13	30486.46	−0.05

a) $\Delta\nu=\nu_{obsd}-\nu_{calcd}$

the differences between the observed and calculated frequencies which were obtained by the least squares fitting. These lines should be attributable to a ground vibrational state because of their strong intensities, some of which were accompanied by relatively weak satellites in their vicinity and they might be ascribed to a vibrationally excited state.

The values of the rotational and centrifugal distortion constants were obtained from the least squares fit of all the assigned lines in which the Watson type Hamiltonian including the centrifugal distortion terms of Δ_J and Δ_{JK} was used and the results are listed in Table 3.

The spectrum of the deuterated species was analyzed with the same way as the normal species and its results are listed in Tables 2 and 3.

The derived values of the rotational constants and the values of $\Delta I=I_c-I_a-I_b$ have close correspondence with the values calculated for the *ac*,*E*-conformer as shown in Table 4.

The r_s coordinates of the hydroxyl hydrogen atom were calculated from the rotational constants of the normal and deuterated species, using the Kraitchman's equations,[8] as follows: $|a|=2.84\pm0.06$ Å, $|b|=0.3\pm0.5$ Å, and $|c|=0.7\pm0.3$ Å. These values are consistent with the values calculated for the *ac*,*E*-conformer which are $|a|=2.7$ Å, $|b|=0.06$ Å, and $|c|=0.53$ Å. Above discussion leads to the conclusion that the spectrum analyzed in this work is due to an *ac*,(*E*)-(propionaldehyde oxime).

Table 3. Observed Rotational Constants of Propionaldehyde Oxime

	Normal	Deuterated
A/MHz	194000 ±400	19000 ±400
B/MHz	2278.16± 0.03	2194.31± 0.02
C/MHz	2204.09± 0.03	2128.40± 0.02
Δ_J/kHz	0.8 ± 0.2	0.6± 0.2
Δ_{JK}/kHz	21 ± 5	18 ± 5
κ	−0.9914	−0.9922
ΔI/amu·Å^2	−18.5 ± 0.5	−19.4 ± 0.5

$\Delta I=I_c-I_a-I_b$, Conversion factor: 505376 MHz·amu·Å^2

Table 4. Observed and Calculated Rotational Constants of Propionaldehyde Oxime

	A/MHz	B/MHz	C/MHz	κ	ΔI/amu·Å^2
Obsd	19400	2278.16	2204.09	−0.9914	−18.5
E-form					
sp	15142	3076.49	2641.09	−0.9303	−6.3
sc	16458	2830.04	2582.00	−0.9642	−13.5
ac	21125	2487.06	2407.51	−0.9915	−17.2
ap	25342	2409.59	2262.37	−0.9872	−6.3
Z-form					
sp	9715	5519.52	3681.10	−0.3906	−6.3
sc	10493	4386.31	3506.58	−0.7482	−19.3
ac	14623	3215.38	2990.05	−0.9613	−22.7
ap	19361	2959.99	2652.29	−0.9632	−6.3

$\Delta I=I_c-I_a-I_b$

References

1) Otto L. Stiefvaster, *J. Chem. Phys.*, **62**, 233 (1975).
2) Manabu Niwase, Kyoko Kubota, Kazuhiko Yoshida, Takeshi Sakaizumi, Masao Onda, Osamu Ohashi, and Ichiro Yamaguchi, *Bull. Chem. Soc. Jpn.*, **57**, 2408 (1984).
3) Mariko Terashima and Osamu Ohashi, *Bull. Chem. Soc. Jpn.*, **58**, 3647 (1985).
4) W. D. Phillips, *Ann. N. Y. Acad. Sci.*, **70**, 817 (1958).
5) W. R. Dunstan and T. S. Dymond, *J. Chem. Soc.*, **65**, 206 (1894).
6) Osamu Ohashi, Ryoji Ishihara, Takeshi Sakaizumi, Masao Onda, and Ichiro Yamaguchi, *Bull. Chem. Soc. Jpn.*, **49**, 891 (1976).
7) Osamu Ohashi, Hisao Hara, Keiko Noji, Takeshi Sakaizumi, Masao Onda, and Ichiro Yamaguchi, *Bull. Chem. Soc. Jpn.*, **50**, 834 (1977).
8) J. Kraitchman, *Am. J. Phys.*, **21**, 17 (1953).

Spectrophotometric Determination of Scandium(III) with *o*-Hydroxyhydroquinonephthalein in Cationic Micellar Media

Itsuo Mori,* Yoshikazu Fujita, Kinuko Fujita, Atsuko Usami, Hiroshi Kawabe, Yozo Koshiyama, and Takeshi Tanaka
Osaka University of Pharmaceutical Sciences, 2-10-65, Kawai, Matsubara, Osaka 580
(Received October 21, 1985)

Synopsis. A spectrophotometric method for determining trace amounts of scandium(III) has been established which makes use of formation of its ternary complex with *o*-hydroxyhydroquinonephthalein (Qnph) and *N*-hexadecylpyridinium chloride (HPC) as a cationic surfactant at pH 5.4. The molar ratio of the ternary complex among Qnph, scandium(III), and HPC is 3:2:6 in a weakly acidic medium, and its maximum absorbance is at 555 nm against a reagent blank. Beer's law holds in the concentration range 0—4.5 μg of scandium(III) in a final volume of 10 cm^3 at 555 nm. The apparent molar absorptivity is 1.0×10^5 $dm^3\,mol^{-1}\,cm^{-1}$ with a Sandell sensitivity of 0.0005 μg cm^{-2}. The coefficient of variation was 0.6% (n=5) for 2.7 μg of scandium(III).

Ternary complex formation reactions among organic reagents, metal ions, and cationic surfactants have proved[1-4] to result in markedly improved spectrophotometric properties–high molar absorptivity, stability over a wide pH range, and large bathochromic shift–in comparison with binary complex formation reactions between organic reagents and metal ions.

For scandium(III), various spectrophotometric determinations using Xylenol Orange (XO),[5] Methylthymol Blue (MTB),[6] Arsenazo III,[7] or Bromopyrogallol Red (BPR)[8] have been reported. However, most of these methods have disadvantages such as lacks in reproducibility, selectivity, or simplicity.

We have already reported that *o*-hydroxyhydroquinonephthalein (Qnph) is a useful reagent for spectrophotometric determination of various metal ions.[9-13] We have also noticed that similar methods utilizing cationic surfactants such as *N*-hexadecylpyridinium chloride (HPC) and *N*-hexadecyltrimethylammonium chloride (HTAC) are in lower pH regions, very sensitive, sharp in selectivity, and excellent in repeatability, in comparison with methods utilizing binary complex formation reactions without cationic surfactants.

In the present research, color reactions between Qnph and scandium(III) in the presence of various surfactants were first studied, and then essential conditions for simple, rapid, and sensitive spectrophotometric determination of scandium(III) were established with Qnph in the presence of cationic surfactant.

Experimental

Absorption spectra and absorbances were measured with recording spectrophotometers, Shimadzu Model UV-200 and UV-240 and a Hitachi Model 150-20, with 1.0 cm silica cells. Hitachi-Horiba Model F-7AD and M-5 pH glass electrode meters were used for pH measurement.

A 1.0×10^{-3} mol dm^{-3} solution of Qnph was prepared according to Ref. 9 and stored in a brown bottle. A stock solution (1.0×10^{-2} mol dm^{-3}) of scandium(III) was prepared by dissolving scandium chloride with a small amount of hydrochloric acid and deionized water. The concentration of the stock solution was determined by chelatometric titration, and a working solution (5.0×10^{-4} mol dm^{-3}) was prepared by dilution of this stock solution. A 1.0×10^{-2} mol dm^{-3} HPC solution was prepared by dissolving HPC in 20% methanol or water. Sodium acetate–acetic acid buffer solution 2.0×10^{-1} mol dm^{-3}; pH 5.4 was used for pH adjustment.

All the other reagents and materials were of analytical grade and used without further purification. Deionized water was used.

To a series of solutions containing 0—4.5 μg of scandium(III) were added 2.0 cm^3 of 1.0×10^{-2} mol dm^{-3} HPC solution, 3.0 cm^3 of sodium acetate–acetic acid buffer solution (pH 5.4), and 1.5 cm^3 of 1.0×10^{-3} mol dm^{-3} Qnph solution, mixed and diluted in several 10 cm^3 calibrated flasks to obtain suitable working solutions. After 10 min, the absorbance of the Qnph–scandium(III) complex solution was measured at 555 nm against a reagent blank (Qnph solution). The concentration of scandium(III) was determined by using a calibration graph.

Results and Discussion

In Fig. 1, curves A, B, C, and D show absorption spectra of Qnph and Qnph–scandium(III) complex solutions in the presence or absence of HPC as a cationic surfactant at pH 5.4. The Qnph–scandium(III)–HPC mixed solution shows a considerable bathochromic shift, and the absorbance is greater and stabler than that in the presence of poly(oxyethylene)sorbitan monolaurate (LT-221) as a nonionic surfactant. A maximum difference in absorbance between Qnph–scandium(III) and Qnph solutions is distinctly observed at 555 nm in the presence of HPC.

The absorbance at 555 nm is maximal and practically independent of pH in the range 4.7—5.8. Subsequent measurements were carried out pH 5.4 for determination of scandium(III).

The absorbance at 555 nm was constant when the volume of 1.0×10^{-3} mol dm^{-3} Qnph solution was varied between 1.0—2.5 cm^3. Hence 1.5 cm^3 of 1.0×10^{-3} mol dm^{-3} Qnph solution was chosen for determination of scandium(III).

HPC, HTAC, and zephiramine (Zp) as cationic surfactants were tested, and HPC showed a remarkably increasing effect on the stabilization and sensitivity. The effect of changing the concentration of HPC was studied. A maximum and constant

Application of Xanthene Derivatives for Analytical Chemistry, Part LIV. Part LIII, I. Mori, Y. Fujita, K. Fujita, Y. Koshiyama, H. Kawabe, T. Tanaka, and R. Munakata, *Bull. Chem. Soc. Jpn.*, **59**, 958 (1986).

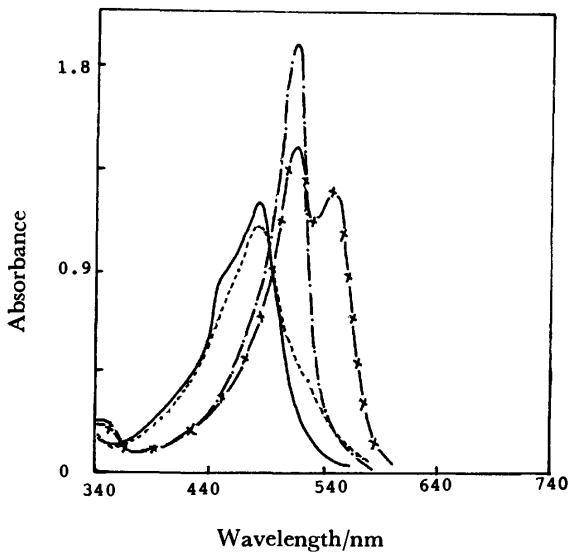

Fig. 1. Absorption spectra of scandium(III)-Qnph solution and Qnph solution in the presence and absence of HPC at pH 5.4.
Scandium(III): 1.0×10^{-5} mol dm^{-3}; Qnph: 4.0×10^{-5} mol dm^{-3}; HPC: 4.0×10^{-3} mol dm^{-3}; Reference: water; ——: Qnph solution in the presence of LT-221; ----: Qnph-scandium(III) solution in the presence of LT-221; —·—: Qnph solution in the presence of HPC; —×—: Qnph-scandium(III) solution in the presence of HPC.

absorbance of Qnph-scandium(III) solution against Qnph solution was observed upon addition of 1.0—4.0 cm^3 of 1.0×10^{-2} mol dm^{-3} HPC solution to the final volume of 10 cm^3. Thus, all further measurements were made with 2.0×10^{-3} mol dm^{-3} HPC as the final concentration.

A good linear relationship was observed over the range 0—4.5 μg of scandium(III) in the final volume of 10 cm^3 at 555 nm against a reagent blank. The apparent molar absorptivity is 1.0×10^5 dm^3 mol^{-1} cm^{-1}, and the Sandell sensitivity is 0.0005 μg cm^{-2}. The coefficient of variation (C.V.) for 5 replicate determinations is 0.6% for 2.7 μg of scandium(III), whereas C.V. in the presence of LT-221 is 4.5%.

The molar ratio of scandium(III) to Qnph was established by the molar-ratio and continuous-variation methods in the presence of high-concentration HPC. The results obtained indicate that the molar ratio of scandium(III) to Qnph is 2:3. On the other hand, the molar ratio of Qnph to scandium(III) in the coexistence of LT-221 is 3:2 as determined by both the molar-ratio and continuous-variation methods. Accordingly, the molar ratio of HPC to Qnph was subjected to determination by the molar-ratio method and found to be 2:1. Though further investigation is necessary, it is deduced from these results that the ternary complex formed in this reaction system may be expressed as $(Sc)_2(Qnph)_3(HPC)_6$.

Of the metal ions tested, iron(III), aluminium(III), thorium(IV), and copper(II), when each present in a small amount result in positive errors because of formation of colored complexes with Qnph in a weakly acidic medium. On the other hand, presence of iron(II), cobalt(II), or cadmium(II) causes no interference even when they are 2—50 times scandium(III) in amount, and large amounts of calcium(II) or magnesium(II) do not interfere. Though presence of citrate, oxalate, or phosphate ion results in negative errors, presence of tartrate or cyanide ion causes no interference when they are 5—20 times scandium(III). The results are summarized in Table 1.

Table 1. Effect of Foreign Ions

Foreign ions	Added as	Added		Absorbance at 555 nm	Found
		μg	molar ratio		μg
—	—	—	—	0.414	2.7
Th(IV)	Nitrate	5.8	1/2	0.511	3.4
Fe(III)	Sulfate	2.8	1	0.504	3.3
		0.6	1/2	0.420	2.7
Al(III)	Nitrate	0.7	1/2	0.477	3.1
Ce(III)	Nitrate	350.3	50	0.936	6.1
		7.0	1	0.435	2.8
Pb(II)	Nitrate	20.7	1	0.420	2.7
		103.6	10	0.445	2.9
Cu(II)	Nitrate	1.6	1/2	0.625	4.1
Co(II)	Nitrate	294.7	100	0.420	2.7
Zn(II)	Nitrate	326.9	100	0.564	3.7
Cd(II)	Nitrate	562.1	100	0.344	2.2
Mg(II)	Chloride	121.5	100	0.414	2.7
CN^-	Potassium	13.0	10	0.354	2.3
SO_4^{2-}	Sodium	480.3	100	0.414	2.7
NO_2^-	Sodium	115.0	50	0.375	2.5
F^-	Sodium	19.0	20	0.399	2.6
PO_4^{3-}	Potassium	0.5	1/10	0.365	2.4
Citrate	Sodium	7.8	1	0.285	1.9
Oxalate	Sodium	5.3	1	0.386	2.5
Tartrate	Sodium	147.1	20	0.418	2.7
		735.5	100	0.393	2.6

Scandium(III) taken: 2.7 μg/10 cm^3: Qnph: 1.5×10^{-4} mol dm^3; HPC: 2.0×10^{-3} mol dm^3; pH: 5.4; Reference: Reagent blank.

Scandium(III) is entirely masked by addition of large amounts of sodium fluoride solution as a masking agent. On the other hand, iron(III) or aluminium(III) is little affected by addition of small amounts (for example, 3.0×10^{-3} mol dm^{-3}) of sodium fluoride solution as a masking agent. Therefore, aluminium(III) or iron(III) can be determined by measuring at 555 nm absorbances, respectively, of Qnph-aluminium(III)-scandium(III)-sodium fluoride and Qnph-aluminium(III)-scandium(III) solutions, or Qnph-iron(III)-scandium(III)-sodium fluoride and Qnph-iron(III)-scandium(III) solutions, as shown in Fig. 2.

In conclusion, a simple, rapid, and sensitive spectrophotometric determination of scandium(III) by using Qnph-scandium(III)-HPC ternary complex has been established. The calibration curve is linear

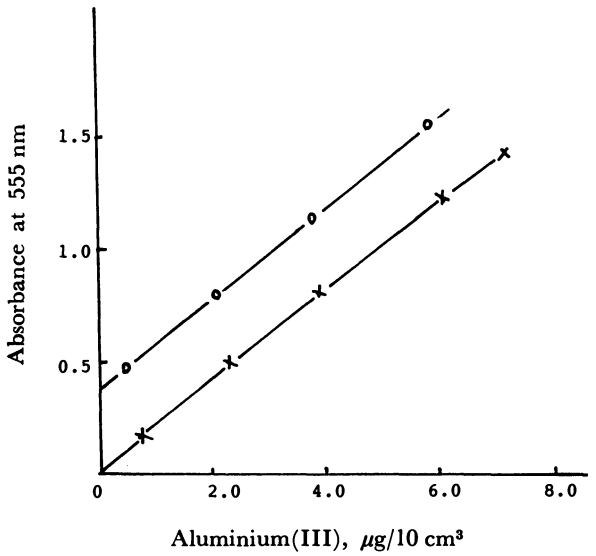

Fig. 2. Calibration curve for aluminium(III) in the presence of scandium(III) and fluoride ion.
Scandium(III): 5.0×10^{-6} mol dm^{-3}; HPC: 4.0×10^{-3} mol dm^{-3}; F^-: 3.0×10^{-3} mol dm^{-3}; Qnph: 1.5×10^{-3} mol dm^{-3}; pH: 5.4; Reference: Reagent blank; —×—: Aluminium(III)–F^-–scandium(III); —○—: Aluminium(III)-scandium(III).

in the concentration range 0—4.5 μg/10 cm³ for scandium(III). The apparent molar absorptivity is 1.0×10^5 dm³ mol^{-1} cm^{-1} for scandium(III) with a Sandell sensitivity of 0.0005 μg cm^{-2} at 555 nm. The sensitivity of the proposed method is about 4—5 times as high as those of the Arsenazo III, XO, MTB, and BPR methods.[5-8]

Moreover, the proposed method using the ternary complex may be used for separative assay of aluminium(III)-scandium(III) mixture or iron(III)-scandium(III) mixture solution by use of sodium fluoride as a masking agent.

References

1) V. N. Tikhonov, *Zh. Anal. Khim.*, **32**, 1435 (1977).
2) T. Yotsuyanagi, H. Hoshino, and S. Igarashi, *Bunseki*, **1985**, 496.
3) K. Ueno, *Bunseki Kagaku*, **20**, 736 (1971).
4) V. P. Antonich, M. M. Noveekeva, and V. A. Nazarenko, *Zh. Anal. Khim.*, **39**, 1971 (1984).
5) K. Tonosaki, and M. Otomo, *Bull. Chem. Soc. Jpn.*, **35**, 1863 (1962).
6) H. Okada, K. Kaneko, and S. Notizeki, *Bunseki Kagaku*, **12**, 822 (1963).
7) D. Kamimori, I. Taguchi, and K. Yoshikawa, *Bunseki Kagaku*, **15**, 458 (1966).
8) T. Shimizu, *Talanta*, **14**, 473 (1967).
9) I. Mori, Y. Fujita, and T. Enoki, *Bunseki Kagaku*, **25**, 388 (1976).
10) I. Mori, Y. Fujita, K. Sakaguchi, and S. Kitano, *Bunseki Kagaku*, **31**, E239 (1982).
11) S. Kitano, I. Mori, Y. Fujita, and Y. Kamada, *Bunseki Kagaku*, **33**, E163 (1984).
12) M. Yamazaki, I. Mori, Y. Fujita, S. Kitano, and Y. Kamada, *Bunseki Kagaku*, **33**, 170 (1984).
13) I. Mori, Y. Fujita, and K. Sakaguchi, *Bull. Chem. Soc. Jpn.*, **55**, 3649 (1982).

Site-Selective Photochemical Ene Reaction of 2-Methylene-1,2-dihydronaphthalene

Akira SUGIMOTO,* Satoshi SAKAMOTO, Kanji SUYAMA, and Shigeo YONEDA
Department of Applied Chemistry, College of Engineering, University of Osaka Prefecture, Mozu-Umemachi, Sakai, Osaka 591
(Received October 4, 1985)

Synopsis. The title compound, formed by the photolysis of 2-(2-anilinoethyl)naphthalene, reacted with olefins having a conjugated double bond to give an ene reaction product under irradiation conditions.

In the course of our studies on the intramolecular photochemical reactions of aromatic compounds with the anilino group, we came across the photolytical formation of *exo*-methylene compounds such as 9-methylene-9,10-dihydrophenanthrene (**1**).[1] A

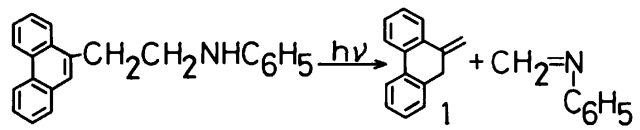

similar result was obserbed in the case of 1-(2-anilinoethyl)naphthalene.[2] Upon irradiation, 2-(2-anilinoethyl)naphthalene (**2**) afforded 2-[2-(2-naphthyl)ethyl]-1,2-dihydronaphthalene (**3**) seemed to be formed by the ene reaction of 2-methylene-1,2-dihydronaphthalene (**4**) (Scheme 1.).[2,3] We now give evidence for the transient existence of **4** and its ene reaction with various olefins.

Upon irradiation of a solution of **2** (1.6×10^{-2} mol dm^{-3}) in degassed benzene with a high-pressure mercury lamp, **3** was obtained as the main product.[4a] The identification of the structure of **3** was based on spectral data and the conversion of **3** to 1,2-di-2-naphthylethane.[5] The mass spectrum of **3**, isolated from the irradiated mixture in D_2O-saturated benzene, showed an M^+ ion peak at m/z=286.[4b] This indicated an incorporation of two deuterium atoms in **3** (vide infra).

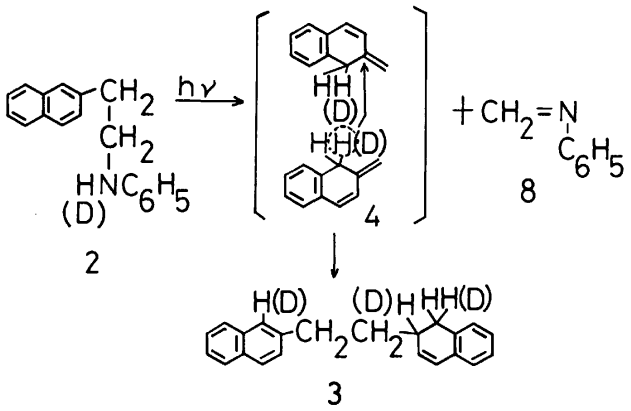

Scheme 1.

On the other hand, the irradiation of **2** in the presence of a large excess of styrene (30 times) gave 2-(3-phenylpropyl)naphthalene (**5**), but not **6** (Scheme 2, R=H). When the same irradiation was carried out in D_2O-saturated benzene, monodeuterated **5** (confirmed by mass spectrum) was obtained. The formations of **3** and **5** may be reasonably interpreted in terms of the ene reaction of **4**, as illustrated in Schemes 1 and 2. The deuteration examination demonstrated that an ene reaction occurred between **4** and an enophile molecule (**4** or styrene). In the formation of **3**, almost all of **4** formed was consumed and no other photoreactions occurred because the yield of **3** was comparable to that of imine (**8**).

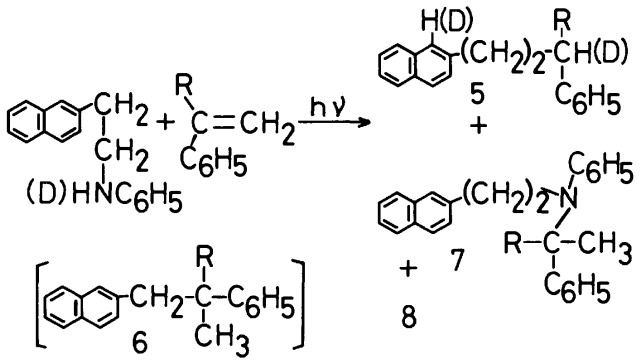

Scheme 2.

This ene reaction process was further confirmed by the irradiation of **2** in the presence of various olefins as an enophile. In these irradiations, the relative ratio of **2** and enophile had a great influence on the distribution of the photoproducts. For example, in the presence of equimolar of styrene, **2** exclusively afforded **3**, while in the presence of a large amount of styrene (10 times of **2** or more) it led to the formation of **5** together with **7**, the addition product of **2** to styrene (Scheme 2).[6] Similar results were observed in the presence of 2-phenylpropene. Therefore, irradiation of **2** was carried out in the presence of a large amount of olefins (30 times moles). The results are summarized in Table 1. Among the olefins shown, styrene, 2-phenylpropene, and 1,3-pentadiene afforded the ene reaction products together with **4**. Other olefins, however, gave no ene reaction product except for **3**. All isolated ene reaction products had such structures that a 2-naphthylmethyl group was site-selective bonded to the terminal carbon of the starting olefins. Namely, only terminal carbons were reactive. Terminal carbons of olefins such as 1,7-octadiene, hexene, and isobutyl vinyl ether, however, were not reactive. From these observations, it was deduced that the terminal carbon of a conjugated diene, including styrene and 2-phenylpropene, undergo an ene reaction with **4**. Upon irradiation without

Table 1. Isolated Yield of **3** and Those of the Other Ene Reaction Products[a)]

Enophile[b)]	Yield/%		Recovered **2**/%
	3	Other products	
None	37	—	37
C_6H_5-CH=CH_2	0	Compd **5**(R=H) 31	15
C_6H_5-C(CH_3)=CH_2	0	Compd **5**(R=CH_3) 21	30
C_6H_5-CH=CH-CH_3	26[c)]	0	54[c)]
CH_2=CH-$(CH_2)_3$-CH_3	35	0	46
CH_2=CH-$(CH_2)_4$-CH=CH_2	38	0	54
CH_2=CHCH=CH-CH_3	trace	20[c)]	41
CH=CH-$(CH_2)_4$	39	0	46
CH_2=CH-O-CH_2CH(CH_3)$_2$	22	0	51

a) Irrdiated for 7.5 h. b) 30 times of moles of **2** was used. c) Estimated values from the intensities of ^{1}H NMR signals because of the contamination with 1-phenylpropene. d) Yield of 2-hexylnaphthalene.

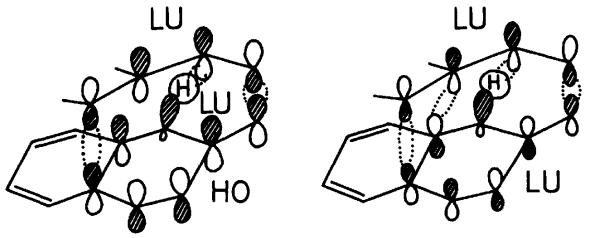

(a) (b)

Fig. 1.

such olefins, **4**, which has terminal conjugated double bonds, reacted as an enophile.

The interactions of the HOMO of π-bond of **4** with the LUMO of the C-H bond of the 1-position of **4**, and the LUMO of the π-bond of enophile led to the formation of ene reaction products[7] (Fig. 1a). As the carbon atoms having the largest coefficients of the LUMO or HOMO interact with each other, an enophile reacted with terminal methylene carbon of **4** at the terminal carbon.[8] On the other hand, the secondary orbital interaction between the LUMO of an enophile (Fig. 1b) may facilitate the reaction of **4** with olefins having a conjugated double bond.

According to Murata et al.,[9] **4** was reported to be isolated and gradually changed to 2-methylnaphthalene. In the present investigation, neither **4** nor 2-methylnaphthalene was detected in the irradiated mixture of **2**, even under high-diluted conditions (3×10^{-4} mol dm^{-3}). These results suggested that the dimerization reaction of **4** occurred photochemically and a significant contribution of the LUMO of **4** to the ene reaction.[10]

Experimental

All melting points were uncorrected. The mass spectra were obtained on a Shimadzu-LKB 9000 Gas chromatograph-Mass spectrometer. Other spectrometers used here were described previously.[11]

All preparative irradiation was performed in a way similar to that described previously.[11]

2-(2-Anilinoethyl)naphthalene (2). 2-Naphthaleneacetic acid was converted to the corresponding anilide by a standard method via acid chloride, yield 81%: mp 155—156 °C; IR (KBr) 3280 (NH), 1660 cm^{-1} (CO). Found: C, 83.00; H, 5.78; N, 5.30%. Calcd for $C_{18}H_{15}NO$: C, 82.73; H, 5.79; N, 5.36%. This anilide was treated with $LiAlH_4$ in THF-ether (1:1, v/v) in the usual manner to afford **2** (yield 60%): mp 54—56 °C; IR (KBr) 3380 cm^{-1} (NH); λ_{max}(hexane) 276 nm (log ε 3.83); ^{1}H NMR ($CDCl_3$) δ=2.7—3.8 (5H, CH_2CH_2NH) and 6.3—7.8 (12H, m, aromatic); m/z=247 (M^+). Found: C, 87.40; H, 6.68; N, 5.60%. Calcd for $C_{18}H_{17}N$: C, 87.41; H, 6.93; N, 5.66%.

Photolysis of 2. A solution of **2** (79 mg, 0.32 mmol) in benzene (20 cm^3) was irradiated. The residue after solvent evaporation was chromatographed (Silica gel with benzene) to yield **3** (17 mg, 37%) and was found to be contaminated by a trace of hydrocarbon which was isolated by repeated chromatography with benzene-hexane (1:3. v/v). A solvent evaporation of the second fraction of the latter chromatography gave pure **3** (13 mg): mp 81—85 °C; λ_{max}(hexane) 266 nm (log ε 4.14); ^{1}H NMR ($CDCl_3$) δ=1.6—2.1 (2H, m, CH_2), 2.3—3.0 (5H, m, CH and CH_2), 5.86 (1H, dd, J=10 and 3 Hz, CH=), 6.36 (1H, d, J=10 Hz, CH=), and 6.9—7.8 (11H, m, aromatic); m/z=284 (M^+). Found: C, 93.01; H, 7.26%. Calcd for $C_{22}H_{20}$: C, 92.91; H, 7.09%. This compound changed to an unidentified hydrocarbon upon irradiation of a solution for 7.5 h (25 mg from 64 mg of **3**, and 36 mg of **3** was recovered); mp 115—117 °C. Found: C, 92.63; H, 7.10%.

Photoreaction Products in the Presence of Additives (30 times mole to 2). Styrene: The first eluent of the chromatography on silica gel with benzene-hexane (1:3, v/v) yielded **5** (31%); viscous oil; ^{1}H NMR ($CDCl_3$) δ=1.8—3.0 (6H, m, $CH_2CH_2CH_2$) and 6.8—7.9 (12H, m, aromatic); m/z=246 (M^+). Found: C, 92.51; H, 7.45%. Calcd for $C_{19}H_{18}$: C, 92.64; H, 7.36%. The second eluent yielded *N*-[2-(2-naphthyl)ethyl]-*N*-(1-phenylethyl)aniline **7** (12%); viscous oil; ^{1}H NMR ($CDCl_3$) δ=1.4—1.8 (3H, m, CH_3), 2.7—4.0 (5H, m, CH and CH_2), and 6.5—7.9 (17H, m, aromatic); m/z=351 (M^+). Found: 88.63; H, 7.53; N, 3.89%. Calcd for $C_{26}H_{25}N$: C, 88.85; H, 7.17; N, 3.98%. The third eluent gave the starting amine **2** (15%).

2-Phenylpropene: The first eluent of the chromatography with benzene-hexane (1:3, v/v) yielded 2-(3-phenylbutyl)naphthalene (21%); viscous oil; ^{1}H NMR ($CDCl_3$) δ=1.28 (3H, d, CH_3), 1.8—2.9 (5H, m, CH_2CH_2CH), and 7.0—8.0 (12H, m, aromatic); m/z=260 (M^+). Found: C, 92.24; H, 7.90%. Calcd for $C_{22}H_{20}$: C, 92.26; H, 7.74%. The

second eluent yielded *N*-[2-(2-naphthyl)ethyl]-*N*-(1-methyl-1-phenylethyl)aniline (14%); viscous oil; ^{1}H NMR ($CDCl_3$) δ=1.30 (6H, s, CH_3), 2.4—3.4 (4H, m, CH_2), and 7.0—8.0 (17H, m, aromatic); *m/z*=365 (M^+). Found: C, 88.93, H, 7.58; N, 3.80%. Calcd for $C_{27}H_{27}N$: C, 88.72; H, 7.45; N, 3.83%. The third eluent gave **2** (30%).

1,3-Pentadiene: The first eluent of the chromatography with benzene–hexane (1:3, v/v) afforded a product mixture of *cis*-and *trans*-2-(4-hexenyl)naphthalene [suggested by ^{1}H NMR spectrum and GC–MS signals at *m/z*=210 (M^+)]. This mixture was hydrogenated over Pd/C (5%, 40 mg) in benzene (15 cm^3) to give 2-hexylnaphthalene (27 mg, 20% from **2**, 158 mg) which was purified by TLC; viscous oil; ^{1}H NMR ($CDCl_3$) δ=0.7—2.1 (11H, m, $CH_3(CH_2)_4$), 2.75 (2H, t, CH_2Ar), and 7.0—7.9 (7H, m, aromatic); *m/z*=212 (M^+). Found: C, 90.41; H, 9.78%. Calcd for $C_{16}H_{20}$: C, 90.51; H, 9.49%. The ^{1}H NMR spectral pattern of this compound at the region of δ=0.7—3.0 was almost identical to that of hexylbenzene.[12] The second eluent gave **2** (41%).

1,2-Di-2-naphthylethane: A solution of **3** (35 mg, 124 mmol) and DDQ (104 mg, 373 mmol) in benzene (100 cm^3) was refluxed for 6.5 h. After evaporating the solvent, the residue was chromatographed on alumina with benzene, and then purified by TLC to give 1,2-di-2-naphthylethane (79%); mp 183.5—185 °C (lit,[5] 185—186 °C).

The present work was partially supported by a Grant-in-Aid for Scientific Reserch No. 59550600 from the Ministry of Education, Science and Culture.

References

1) A. Sugimoto and S. Yoneda, *J. Chem. Soc., Chem. Commun.*, **1982**, 376.

2) A. Sugimoto, S. Sakamoto, K. Suyama, and S. Yoneda, Abstract of Symposium on Photochemistry 1983 (Tsukuba), p. 185.

3) Reviews on ene reaction: Hoffmann, H. M. R., *Angew. Chem. Int. Ed. Engl.*, **8**, 556 (1969); E. C. Keung and H. Alper, *J. Chem. Educ.*, **49**, 97 (1972); Y. Fujita, S. Suzuki, and K. Kanehira, *Yuki Gosei Kagaku Kyokai Shi*, **41**, 1152 (1983).

4) a) Small amounts of an unidentified hydrocarbon ($C_{22}H_{20}$) was isolated from the first elution of chromatography. This compound was formed from **3** on irradiation. Therefore, unless otherwise noted, the yield of this hydrocarbon was included in the yield of **3**. b) Calcd for $C_{22}H_{18}D_2$: M^+=286.

5) K. F. Lang and H. Buffleb, *Chem. Ber.*, **91**, 2866 (1958).

6) Addition of amine to olefin has been observed; e.g. R. C. Cookson, Miss S. M. de B. Costa, and J. Hudec, *Chem. Commun.*, **1969**, 753.

7) S. Inagaki, H. Fujimoto, and K. Fukui, *J. Am. Chem. Soc.*, **98**, 4693 (1976).

8) C. A. Coulson and A. Streitwiser Jr., "Dictionary of π-Electron Calculations," Pergamon Press (1965); I. Fleming, "Frontier Orbitals and Organic Chemical Reactions," John Wiley & Sons, Inc., (1976).

9) I. Murata, T. Nakazawa, M. Kato, T. Tatsuoka, and Y. Sugihara, *Tetrahedron Lett.*, **1975**, 1647.

10) Photo ene reactions and related reactions: N. D. Epiotis, "Theory of Organic Reactions," Springer-Verlag (1978), p. 150 and literatures were cited therein. R. N. Warrener, I. G. Pitt, and R. A. Russell, *J. Chem. Soc., Chem. Commun.*, **1982**, 1136.

11) A. Sugimoto, K. Sumi, K. Urakawa, M. Ikemura, S. Sakamoto, S. Yoneda, and Y. Otsuji, *Bull. Chem. Soc. Jpn.*, **56**, 3118 (1983).

12) The Aldrich Library of NMR Spectra, Aldrich Chem. Co. Inc., (1974), 4, p. 2-c.

Formation of Bis(2-oxazolidinone) Derivatives by Reactions of 2-Methoxy-3,3-dimethyl-2-phenyloxirane or α-Bromoisobutyrophenone with Carbon Dioxide and Aliphatic α,ω-Diamines

Norio SAITO,* Kiyotaka HATAKEDA, Shota ITO, Takashi ASANO, and Takashi TODA*,†

Government Industrial Research Institute, Tohoku, Nigatake, Sendai 983
†Department of Industrial Chemistry, Faculty of Engineering, Utsunomiya University, Ishii-cho, Utsunomiya 321

(Received December 4, 1985)

Synopsis. Reactions of 2-methoxy-3,3-dimethyl-2-phenyloxirane or α-bromoisobutyrophenone and carbon dioxide in the presence of aliphatic α,ω-diamines were investigated. 1,4-Butanediamine, 1,6-hexanediamine, 1,8-octanediamine, and 1,4-bis(aminomethyl)benzene afforded corresponding 3-(ω-aminoalkyl)-4-hydroxy-5,5-dimethyl-4-phenyl-2-oxazolidinones and 3,3′-polymethylenebis[4-hydroxy-5,5-dimethyl-4-phenyl-2-oxazolidinones] derivatives, while ethylenediamine gave only mono(2-oxazolidinone) derivative.

Since carbon dioxide is the most common, important and nontoxic C_1 resource, several attempts to utilize it have been reported.[1] In such attempts, reactions are carried out under high pressure, at high temperature, in the presence of metal catalysts or caustic alkali, and/or combinations of those methods and so far.[1] We noticed that carbon dioxide forms ammonium carbamates by the reactions with aliphatic amines, and some of the carbamate salts are fairly stable.[2,3] We, and Yoshida and Inoue, found that carbon dioxide reacts with oxiranes (or their synthons) in the presence of aliphatic amines to give 2-oxazolidinones,[2] carbamate derivatives,[4,5] and tetrahydro-2*H*-1,3-oxazin-2-ones.[5] Furthermore, we reported that thermolysis of the oxazolidone derivatives yielded isocyanate derivatives corresponding to the used amines.[6] These results prompted us to study further extention of reactions of carbon dioxide with oxiranes (or thier synthons) in the presence of α,ω-diamines such as ethylenediamine or 1,6-hexanediamine expecting to obtain bis(2-oxazolidinone) derivatives. Because thermolysis of this type of bis(2-oxazolidinone) would give bis(isocyanate)s of which importance is well recognized in polymer chemistry.

The reactions were carried out as follows. After carbon dioxide was saturated in a methanol solution of a diamine, 2-methoxy-3,3-dimethyl-2-phenyloxirane (**1**) (or α-bromoisobutyrophenone (**2**)) was added to this solution, and then the solution was heated. IR spectrum of the product (**3a**) derived from ethylenediamine showed free amino group's frequencies at 3390 and 3210 cm^{-1}, and a carbonyl absorption at 1750 cm^{-1} corresponding to that of 2-oxazolidinone.[2] The molecular formula and weight ($C_{13}H_{18}O_3N_2$, and *m/z*: M^+, 250) of **3a** indicate that only one amino group of ethylenediamine was incorporated into the 2-oxazolidinone skeleton. Thus, the structure of **3a** is presented as 3-(2-aminoethyl)-4-hydroxy-5,5-dimethyl-4-phenyl-2-oxazolidinone. On the other hand, 1,4-butanediamine, 1,6-hexanediamine, 1,8-octanediamine, and 1,4-bis(aminomethyl)-benzene gave two different kind of oxazolidone derivatives, respectivily. The first ones are mono(2-oxazolidinone) derivatives which possess a free amino group at the end of the methylene chain as shown in their IR spectra (see the Table). The second products did not show any free amino group frequencies, but showed very strong carbonyl absorption around 1750 cm^{-1}. Therefore, the latter products are bis(2-oxazolidinone) derivatives as shown in the Scheme such as **4**. The elemental analyses of them also support that those structures are correct. Fairly large amount (25—50%) of 1,1-dimethoxy-2-methyl-1-phenyl-2-propanol (**5**) was obtained together with **3** and **4**.

Table 1. Yields and IR Data of Reaction Products

R	product	Yield/%[a]		IR/cm^{-1}		
		1:1[b]	1:2[b]	C=O	NH	
$(CH_2)_2$	**3a**	37(Trace)	41(7)	1750	3320	3390
$(CH_2)_4$	**3b**	29(8)	25(20)	1750	3290	3365
	4b	1(1)	9(5)	1745		
$(CH_2)_6$	**3c**	35(21)	40(28)	1750	3310	3280
	4c	7(4)	5(3)	1750		
$(CH_2)_8$	**3d**	22(4)	21(19)	1745	3290	3360
	4d	7(8)	6(4)	1740		
$C_6H_4(CH_2)_2$(*p*-)	**3e**	13(Trace)	18(Trace)	1750	3300	3370
	4e	Trace(··)	Trace(-)	1750		

a) Yields are based on the oxirane (**1**), and yields in parenthesis are based on the bromo ketone (**2**). b) Mol ratio of **1** (or **2**): diamine.

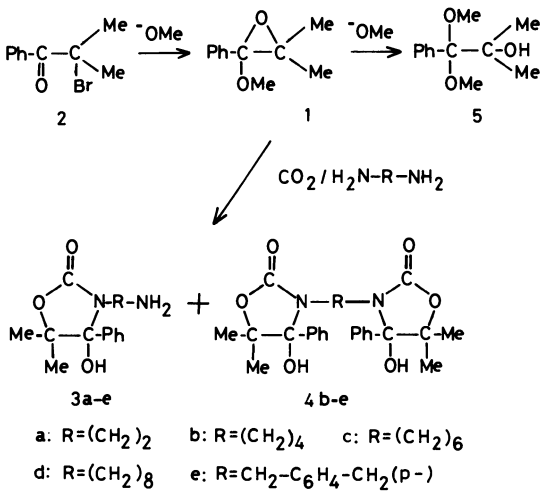

Scheme 1.

The results are listed in the Table. Further treatment of 3-(8-aminooctyl)-4-hydroxy-5,5-dimethyl-4-phenyl-2-oxazolidinone (**3d**) with the oxirane in the presence of carbon dioxide gave the corresponding bis(2-oxazolidinone) derivative (**4d**, 53%). However, **3a** did not give any bis(2-oxazolidinone) derivative under the same conditions. Although the reason was not clear, formation of oxazolidinones was not observed when 1,3-bis(aminomethyl)benzene was adopted as the diamine.

One of the reason for the low yield of the oxazolidinones formation is presumed to be steric hindrance of big carbamates derived from the diamines. Also, intra- or intermolecular hydrogen bond formation between the remained amino group and the formed carbamate carbonyl seems to make those group's reactivity toward the oxirane inactive. Formation of fairly large amount of **5** indicate that the attack of methoxide anion and carbamate anion take place in the same probability. Contrarily to this, carbamate anions smoothly react with the oxirane to give the oxazolidinones in good yields in the case of monoamines.[2] It seems likely that the reason why the second oxazolidinone ring does not form **3a** is as follows; the formed oxazolidinone ring near the remained amino group causes steric hindrance, and intramolecular hydrogen bond formation between the amino group and the carbonyl group in the oxazolidinone makes the amino groups inactive. The more data than we have now are needed in order to come the conclusion about the low yield of bis(2-oxazolidinone).

The yields are rather poor to fair, but the bis(2-oxazolidinone) formation suggests possibility of the bis(isocyanate)s formation from carbon dioxide and α,ω-diamines.

Experimental

All melting points were uncorrected. IR spectra were recorded on a Hitachi 285 spectrophotometer by KBr disk method. Mass spectra were measured on a JEOL JMS-300 mass spectrometer by EI, CI, and FD methods. The oxirane and the bromo ketone were prepared by the methods as reported previously.[2]

3-(2-Aminoethyl)-4-hydroxy-5,5-dimethyl-4-phenyl-2-oxazolidinone (3a): Carbon dioxide was bubbled through the solution of ethylenediamine (4.2 g, 0.07 mol) in methanol (100 cm^3) until the colorless precipitates produced in the solution, and then the oxirane (**1**, 6.3 g, 0.035 mol) (or bromo ketone (**2**)) was added dropwise to the solution. The mixture was gently refluxed for 18 h with bubbling of carbon dioxide. The methanol was removed in vacuo, and the residue was dissolved in chloroform, washed with water, and dried ($MgSO_4$). After removal of the chloroform, the residue was treated with petroleum ether to afford **3a** as a precipitate. **5** was obtained from the petrolem ether layer. **3a**: Yield, 3.6 g (41%); colorless prisms (ethanol), mp 191—192 °C. Found: C, 62.41; H, 7.33; N, 11.21%; MS (*m/z*) 250 (M^+). Calcd for $C_{13}H_{18}O_3N_2$: C, 62.38; H, 7.25; N, 11.19%.

3-(4-Aminobutyl)-4-hydroxy-5,5-dimethyl-4-phenyl-2-oxazolidinone (3b) and 3,3′-Tetramethylenebis[4-hydroxy-5,5-dimethyl-4-phenyl-2-oxazolidinone] (4b): Under the same conditions as described above, **1** (6.3 g, 0.035 mol) was allowed to react with carbon dioxide and 1,4-butanediamine (6.3 g, 0.07 mol). After removal of the solvent, the residue was dissolved in chloroform, and washed with water. When the choloform was removed in vacuo and the residue was treated with petroleum ether, a white precipitates was obtained. The precipitate was treated with benzene to give colorless solid of **4b** as an insoluble part. The benzene filtrate was evaporated, and then the residue was recrystallized to afford **3b**. **5** was obtained from the petroleum ether layer. **3b**: Yield, 2.4 g (25%); colorless powder (benzene-hexane), mp 106—107 °C. Found: C, 64.11; H, 7.98; N, 9.77%; MS (*m/z*) 278 (M^+). Calcd for $C_{15}H_{22}O_3N_2$: C, 64.72; H. 7.97; N, 10.07%. **4b**: Yield, 0.7 g (9%); colorless powder (acetone), mp 294—295 °C. Found: C, 66.90; H, 7.12; N, 5.82%; MS (*m/z*) 469 (M^++1). Calcd for $C_{26}H_{32}O_6N_2$: C, 66.65; H, 6.88; N, 5.98%.

3-(6-Aminohexyl)-4-hydroxy-5,5-dimethyl-4-phenyl-2-oxazolidinone (3c) and 3,3′-Hexamethylenebis[4-hydroxy-5,5-dimethyl-4-phenyl-2-oxazolidinone] (4c): These compounds were synthesized in the manner similar to that of **3b** and **4b**. **3c**: Yield, 4.3 g (40%); colorless powder (ethanol-water), mp 80—81 °C. Found: C, 66.85; H, 8.29; N, 8.85%; MS (*m/z*) 306 (M^+). Calcd for $C_{17}H_{26}O_3N_2$: C, 66.64; H, 8.55; N, 9.14%. **4c**: Yield, 0.5 g (5%); colorless powder (chloroform), mp 239—240 °C. Found: C, 67.10; H, 7.41; N, 5.59%; MS (FD, *m/z*) 496 (M^+), 519 (M^++23). Calcd for $C_{28}H_{36}O_6N_2$: C, 67.52; H, 7.31; N, 5.64%.

3-(8-Aminooctyl)-4-hydroxy-5,5-dimethyl-4-phenyl-2-oxazolidinone (3d) and 3,3′-Octamethylenebis[4-hydroxy-5,5-dimethyl-4-phenyl-2-oxazolidinone] (4d): Under the same conditions described above, **1** (6.3 g, 0.035 mol) was allowed to react with carbon dioxide and 1,8-octanediamine (10.1 g, 0.07 mol). The methanol was removed in vacuo and the residue was dissolved in chloroform, and then the chloroform layer was washed with hydrochloric acid. **3d** was obtained as a precipitate from the aqueuos layer by addition of aqueous sodium hydroxide. The chloroform layer was washed with water, and concentrated under reduced pressure. The residue was treated with ether to afford **4d** as a precipitate. **5** was obtained from the ether layer. **3d**: Yield, 2.5 g (21%); colorless needless (ethanol-water), mp 79—80 °C. Found: C, 67.66; H, 8.77; N, 8.13%; MS (*m/z*) 334 (M^+). Calcd for $C_{19}H_{30}O_3N_2$: C, 68.23; H, 9.04%; N, 8.38%. **4d**: Yield, 0.7 g (6%); colorless prisms (ethanol), mp 197—198 °C. Found: C, 68.45; H, 7.88; N, 5.19%; MS (*m/z*) 525 (M^++1). Calcd for $C_{30}H_{40}O_6N_2$: C,

68.68; H, 7.69; N, 5.34%.

3-[*p*-(Aminomethyl)benzyl]-4-hydroxy-5,5-dimethyl-4-phenyl-2-oxazolidinone (3e): This compound was obtained in the manner similiar to that of **3d**. **3e**: Yield, 2.3 g (18%); colorless powder (ethanol), mp 68—69 °C. Found: C, 69.58; H, 6.95; N, 8.52%; MS (*m/z*) 327 (M^++1). Calcd for $C_{19}H_{22}O_3N_2$; C, 69.92; H, 6.79; N, 8.58%.

1,1-Dimethoxy-2-methyl-1-phenyl-2-propanol (**5**, mp 54—55 °C, from hexane)[7] was obtained together with **3** and **4**; the yield of 5 varied (25—50%) for the each run of the reactions.

Preparation of 4d from 3d: After carbon dioxide was saturated in a methanol solution of **3d** (3.6 g, 0.02 mol), **1** (3.3 g, 0.01 mol) was added to the solution and then the mixture was gently refluxed for 24 h with bubbling of carbon dioxide. After the removal of the methanol in vacuo, the residue was dissolved in chloroform. The chloroform layer was washed with hydrochloric acid, water, and dried. The chloroform was evaporated in vacuo to afford a residue which was recrystallized from ethanol to give **4d** (2.8 g, 53%).

References

1) Y. Yoshida and S. Inoue, "Yuki Shigen no Kagaku," ed by S. Inoue, S. Sato, and H. Matsuda, Kagakudojin, Kyoto (1981), pp. 85—99; T. Osa, "Tansangasu no Kagaku," ed by Y. Kitani, M, Ichikawa, T. Osa, S. Inoue, and K. Asada, Kyoritu Shuppan, Tokyo (1976), Chap. 3.

2) T. Toda, *Chem. Lett.*, **1977**, 975; T. Toda, *Nippon Kagaku Kaishi*, **1982**, 282, and references therein.

3) T. Hayashi, *Riken Iho*, **11**, 1391 (1932); H. B. Wright and M. B. Moor, *J. Am. Chem. Soc.*, **70**, 3865 (1948).

4) Y. Yoshida and S. Inoue, *Chem. Lett.*, **1977**, 1375; Y. Yoshida and S. Inoue, *J. Chem. Soc., Perkin Trans. 1*, **1979**, 3146.

5) T. Asano, N. Saito, S. Ito, K. Hatakeda, and T. Toda, *Chem. Lett.*, **1978**, 311.

6) N. Saito, K. Hatakeda, S. Ito, T. Asano, and T. Toda, *Heterocycles*, **15**, 905 (1981).

7) T. I. Temnikova and N. I. Almashi, *Zh. Obshch Khim.*, **23**, 1338 (1953); *Chem. Abstr.*, **48**, 12025b (1954); C. L. Stevens and T. H. Coffield, *J. Am. Chem. Soc.*, **80**, 1919 (1958).

Selective Photooxidation of Alkali Mandelates by a Flavin Bearing a Crown Ring as a Metal Recognition Site[1)]

Seiji SHINKAI,* Hideki NAKAO, Kaori UEDA, Osamu MANABE, and Masayoshi OHNISHI

Department of Industrial Chemistry, Faculty of Engineering, Nagasaki University, Nagasaki 852

(Received November 4, 1985)

Synopsis. The quantum yields (Φ) for photooxidation of mandelate salts by a crown-containing flavin (CrFl) and 3-methyl-10-ethylisoalloxazine (MeEtIA) were determined in acetonitrile. MeEtIA photooxidized tetramethylammonium mandelate more selectively than potassium mandelate ($\Phi_{K^+}/\Phi_{Me_4N^+}$=0.42—0.64), while CrFl showed a high selectively for photooxidation of potassium mandelate ($\Phi_{K^+}/\Phi_{Me_4N^+}$=19—42).

The catalytic actions of coenzymes have attracted much attention of bioorganic chemists because they can catalyze the reactions to some extent even in the absence of apoenzymes. Thus, the model investigations on the coenzyme catalyses have provided many clues to elucidate the origin of the enzyme "activity" reasonably.[2,3)] In contrast, there are a few model investigations on the enzyme "selectivety" which is another important aspect of enzyme catalyses. In order to design such an enzyme model with a substrate selectivity one may add a recognition site (e.g., crown ether) to a coenzyme-based catalytic site.[4)] As an approach to model systems for flavoenzymes, we have synthesized a crown ether flavin mimic, 3,10-dimethyl-7,8-(1′,4′,7′,10′,13′,16′-hexaoxacyclooct-2′-eno)isoalloxazine (CrFl).[5)] Here we report that in photooxidation of mandelate salts CrFl not only acts as an excellent oxidizing agent but also shows a remarkable metal selectivity. In order to differentiate the contribution of the crown ring, we used 3-methyl-10-ethylisoalloxazine (MeEtIA) as a reference flavin.

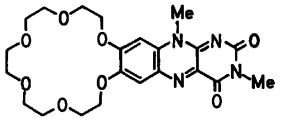

CrFl

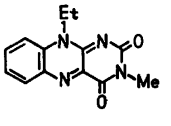

MeEtIA

Experimental

A standard actinometer (potassium trioxalatoferrate(III) was used for the quantum-yield determinations on the photochemical reaction of flavins and mandelate salts.[6)] Three-milliliter aliquots of the substrate solutions in a 1 cm quartz cell (10×10×45 mm) were deaerated and were irradiated under nitrogen with a 300 W high-pressure Hg lamp. The extraneous lines of the lamp other than 366 nm were filtered out using a combination of two solution filters ($CuSO_4$ and 5,7-dimethyl-1-azania-4-azacyclohepta-4,6-diene perchlorate) and of a glass filter (Corning 7-37). Light intensities at 366 nm were determined by trioxalatoferrate (III) actinometry.[6)] The quantum yields were determined by comparing the light intensities with the reduced flavins in the exactly same geometry.

Results and Discussion

The lowest singlet state (S1 band) of flavins corresponds to the polarization along the long axis of the molecule.[7)] The addition of $KClO_4$ (0.40 mM)* to CrFl (2.48×10^{-5} M) in acetonitrile (λ_{max} 459 nm, ε_{max} 19700) induced the blue shift of the absorption maximum (λ_{max} 455 nm, ε_{max} 18500). This indicates that the binding of K^+ to the crown ring suppresses the polarization from the benzene moiety to the uracil moiety along the long axis of CrFl. The addition of $NaClO_4$ and $CsClO_4$ also induced the blue shift although the magnitude was smaller than that in the presence of K^+. On the other hand, the absorption spectrum of MeEtIA was scarcely affected by these metal ions under the identical conditions. We estimated the association constants (K) for $MClO_4$+CrFl in acetonitrile at 30 °C from a decrease in the absorbance at 459 nm: $K=6.6\times10^3$ M^{-1} for Na^+, 2.5×10^4 M^{-1} for K^+, 4×10^3 M^{-1} for Cs^+, and less than 10^2 M^{-1} for Li^+.

Photoexcited flavins can oxidize mandelic acid to benzoic acid via dehydration followed by oxidative decarboxylation ($PhCH(OH)CO_2^- \rightarrow PhCOCO_2^- \rightarrow PhCO_2^- + CO_2$).[8)] We found that alkali and tetramethylammonium salts of mandelic acid are photooxidized by CrFl and MeEtIA in acetonitrile. The absorption bands of the oxidized flavins in the anaerobic solutions disappeared gradually with the photoirradiation time. Introduction of an O_2 stream

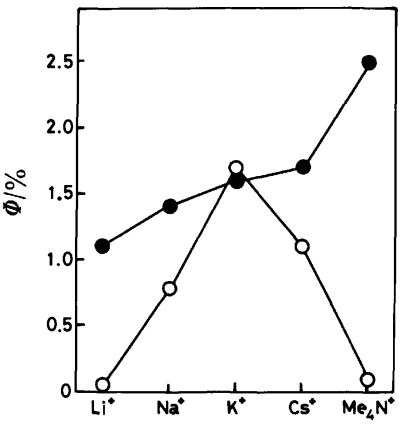

Fig. 1. Plots of Φ vs. alkali and tetramethylammonium cations in acetonitrile-methanol (70 : 30 v/v).
○: CrFl, ●: MeEtIA.

* 1 M=1 mol dm^{-3}.

Table 1. Photooxidation of Mandelate Salts ($PhCH(OH)CO_2^-M^+$) by Flavins[a)]

Flavin	M^+	B18C6	Φ/%			
		mM	MeOH(vol%)=0	10	20	30
CrFl	Li^+		*	*	*	0.05
CrFl	Na^+		*	1.7	0.87	0.77
CrFl	K^+		10.5	2.6	—	1.7
CrFl	K^+	0.21	9.4	—	—	—
CrFl	K^+	2.1	8.0	—	—	—
CrFl	Cs^+		4.7	1.6	—	1.1
CrFl	Me_4N^+		0.25	—	—	0.09
MeEtIA	Li^+		*	*	*	1.1
MeEtIA	Na^+		*	1.9	1.6	1.4
MeEtIA	K^+		3.4	2.3	—	1.6
MeEtIA	K^+	0.21	5.1	—	—	—
MeEtIA	K^+	2.1	7.0	—	—	—
MeEtIA	Cs^+		5.0	3.0	—	1.7
MeEtIA	Me_4N^+		8.1	—	—	2.5

a) Room temperature, $[PhCH(OH)CO_2^-M^+]=4.24\times10^{-3}$ M, $[flavin]=2.00\times10^{-4}$ M. * Denotes that the salt is not soluble sufficiently.

into the final solution regenerated the oxidized flavins quantitatively, indicating that the light-mediated oxidation of mandelate salts occurs without the intervention of side reactions. The results are summarized in Table 1.

The inherent reactivity of CrFl and MeEtIA may be compared by the quantum yields (Φ) for tetramethylammonium (Me_4N^+) mandelate, because Me_4N^+ ion does not interact with the crown ether ring. As shown in Table 1, the Φ values for MeEtIA are greater by 2.8—3.2 fold than those for CrFl. The difference is attributed to the electron-donating effect of the 7,8-polyether groups in CrFl. Examination of Table 1 reveals several interesting aspects characteristic of the crown-metal interaction: (i) The reactivity order for MeEtIA is $Me_4N^+>Cs^+>K^+>Na^+>Li^+$, whereas that for CrFl is $K^+>Na^+\approx Cs^+>Me_4N^+>Li^+$ (Fig. 1), (ii) the Φ for CrFl+potassium mandelate in acetonitrile is greater than MeEtIA+Me_4N^+ mandelate, (iii) the Φ values decrease with increasing methanol concentration and the decrease in CrFl occurs more sensitively than that in MeEtIA, and (iv) the addition of monobenzo-18-crown-6 (B18C6) enhances the Φ for MeEtIA (except that for Me_4N^+ mandelate), whereas it slightly decreases the Φ for CrFl.

It is well-known that decarboxylation is extensively affected by solvent effects[9-11]: The rates are enhanced in dipolar aprotic solvents because of desolvation of carboxylate anions. Hence, the decarboxylation rate ($PhCOCO_2^-\rightarrow PhCO_2^-+CO_2$) should be enhanced in dipolar aprotic solvents. Similarly, the dehydration process ($PhCH(OH)CO_2^-\rightarrow PhCOCO_2^-$) would be facilitated by desolvation of the carboxylate anion. The rate decrease caused by methanol addition is thus ascribed to specific solvation of the carboxylato group through hydrogen bonding. The Φ for MeEtIA+potassium mandelate increased on the addition of B18C6. At the high B18C6 concentration the Φ (7.0%) is comparable with that for Me_4N^+ mandelate (8.1%) which is believed to exist as a free ion pair.[11] The order of the reactivity for MeEtIA is parallel to the cation size and is rationalized in terms of the formation of loose (e.g., Cs^+) or tight (e.g., Li^+) ion pairs. These findings all support that photooxidation by MeEtIA is governed by solvation of mandelate salts.

Interestingly, the Φ for CrFl+potassium mandelate is unusually enhanced: The Φ augmentation relative to Me_4N^+ mandelate corresponds to 42-fold in acetonitrile and the Φ is even greater than that for MeEtIA+Me_4N^+ mandelate. It is reasonable to propose that the unusual reactivity stems from the crown-metal interaction, because the order of the reactivity is exactly in accord with the spherical recognition pattern for an 18-crown-6 analogue (Fig. 1). Therefore, one reason for the high Φ should be the desolvation of the carboxylato group by the crown-K^+ complexation. However, this effect cannot fully rationalize the fact that the Φ (10.5%) for potassium mandelate is much greater than that for free-ion-like Me_4N^+ counterpart (0.25%). Conceivably, one must take two more important effects into consideration. Firstly, CrFl should become electron-dificient through the binding of K^+ to the crown ether moiety. A similar trend has been observed for the thermal oxidation of 1-benzyl-1,4-dihydronicotinamide by CrFl.[5] Secondly, one may expect the contribution of the proximity effect between the anionic mandelate and the cationic CrFl·K^+ complex in acetonitrile. The contribution of these two effects is supported by the finding that the addition of B18C6 suppresses the photooxidation of potassium mandelate by CrFl (Table 1). It is likely that added B18C6 binds K^+ competitively and interferes with the "pseudo-intramolecular" reaction process via the CrFl·$K^+\cdots PhCH(OH)CO_2^-$ complex. It seems reasonable to conclude, therefore, that the specific Φ

increase for CrFl+potassium mandelate is achieved by several synergistic effects.

These results indicate that CrFl can imitate several biological concept important in enzyme chemistry. The crown ether moiety not only recognizes metal cations but also "activates" the flavin molecule through complexation with M^+. The close imitation is achieved because CrFl has within a molecule flavin as a catalytic site and crown ether as a recognition site, which are the minimum constituents for enzyme models.

References

1) Coenzyme Models. 44.
2) C. Walsh, "Enzymatic Reaction Mechanism," W. H. Freeman and Co., San Francisco (1979).
3) T. C. Bruice and S. J. Benkovic, "Bioorganic Mechanisms," Benjamin, New York (1966).
4) R. M. Kellog, *Top. Curr. Chem.*, **101**, 111 (1982).
5) S. Shinkai, Y. Ishikawa, H. Shinkai, T. Tsuno, H. Makishima, K. Ueda, and O. Manabe, *J. Am. Chem. Soc.*, **106**, 1801 (1984).
6) J. G. Galvert and J. N. Pitts, Jr., "Photochemistry," Wiley, New York (1966), pp. 734, 738.
7) P.-S. Song, "Flavins and Flavoproteins," ed by H. Kamin University Park Press, Baltimore (1981), p. 37.
8) W. H. Walker, P. Hemmerich, and V. Massey, *Eur. J. Biochem.*, **13**, 258 (1970).
9) D. S. Kemp and K. G. Paul, *J. Am. Chem. Soc.*, **92**, 2553 (1970).
10) D. H. Hunter, W. Lee, and S. K. Sim, *J. Chem. Soc., Chem. Commun.*, **1974**, 1018.
11) A. J. Parker, *Chem. Rev.*, **69**, 1 (1969).

Hydrolysis of *p*-Nitrophenyl Hexanoate in Hydrophobic Aggregate System

Masato KODAKA,* Toshio FUKAYA, and Masayoshi KIKKAWA
National Chemical Laboratory for Industry, Tsukuba 305
(Received December 5, 1985)

Synopsis. Hydrolysis of *p*-nitrophenyl hexanoate in the presence of azide ion (N_3^-) was accelerated by tetraheptylammonium bromide (**1**), which has four long alkyl chains. In contrast to **1**, the other tetraalkylammonium salts which have shorter alkyl chains, (**2**)—(**5**), did not elevate the reactivity. *p*-Nitrophenyl acetate, less hydrophobic substrate, was not hydrolyzed so efficiently even in the presence of **1**.

An enzyme holds a specific conformation in an aqueous solution, where hydrophilic groups are situated on the outer surface and hydrophobic groups are placed inside. As micelles resemble enzymes in this respect, lots of studies have been undertaken about micelle-system reactions from an enzyme-mimetic point of view.[1-6] In micelle systems substrates are incorporated into or adsorbed on micelles by electrostatic and/or hydrophobic interactions and activated in specific environments. Other enzyme-mimetic systems such as vesicles[7-9] and aggregate of methyltrioctylammonium chloride[10,11] are also studied intensively, where reactions are activated as compared with aggregate-free ones. In the present report, we describe the effect of a new type of hydrophobic aggregate made up of tetraheptylammonium bromide **1**, which possesses four long alkyl chains, upon the hydrolysis of an active ester (*p*-nitrophenyl hexanoate) in the presence of azide ion (N_3^-).

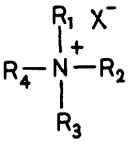

(1) $R_1=R_2=R_3=R_4=n\text{-}C_7H_{15}$, X=Br
(2) $R_1=R_2=R_3=R_4=n\text{-}C_6H_{13}$, X=I
(3) $R_1=R_2=R_3=R_4=n\text{-}C_5H_{11}$, X=Br
(4) $R_1=R_2=R_3=R_4=C_2H_5$, $X=ClO_4$
(5) $R_1=CH_2Ph$, $R_2=R_3=R_4=C_2H_5$, X=Br

Experimental

Tetraheptylammonium bromide (**1**) and tetrapentylammonium bromide (**3**) (Aldrich Chemical Co.), tetrahexylammonium iodide (**2**) (Tokyo Kasei Kogyo Co.), tetraethylammonium perchlorate (**4**) (Nakarai Chemicals), benzyltriethylammonium bromide (**5**) (Kanto Chemical Co.), sodium azide (Nakarai Chemicals), *p*-nitrophenyl hexanoate (*p*-NPH) (Tokyo Kasei Kogyo Co.), *p*-nitrophenyl acetate (*p*-NPA)(Aldrich Chemical Co.), and 8-anilino-1-naphthalenesulfonic acid magnesium salt (ANS) (Nakarai Chemicals) were used as supplied.

The reaction was carried out at pH 8.0, μ=0.5(KCl), buffered with 0.1 mol dm^{-3} KH_2PO_4–0.05 mol dm^{-3} $Na_2B_4O_7$. The reaction rate was determined by measuring the absorbance of liberated *p*-nitrophenol at 400 nm with a Beckman Model 34 spectrophotometer. Fluorescence intensity was measured under the same conditions as described above with a JASCO FP-4 fluorescence spectrophotometer.

Results

The reaction rate did not follow pseudo-first-order even when $[N_3^-] \gg [p\text{-NPH}]$, that is, $\ln\{c_0/(c_0-x)\}$ was not proportional to the reaction time (t) and the rate constant (the slope of the curve) decreased with time. Here, c_0 is the concentration of *p*-NPH at a time 0 and x is the concentration of *p*-nitrophenol at a time t. We have estimated the rate constant (k), therefore, from the slope of the curve at initial stage. On the other hand, the hydrolysis of *p*-NPH followed pseudo-first-order in the presence of N_3^- and hexadecyltrimethylammonium chloride (HTAC) micelle.

In Fig. 1 are shown the relations between k and the concentrations of the tetraalkylammonium salts (C), where k increased monotonously with increasing the concentration of **1** in the presence of N_3^- (5×10^{-4} mol dm^{-3}). In the absence of N_3^-, however, k remained fairly small in spite of the addition of **1** (5×10^{-5} mol dm^{-3}). The k value became more than 10 times larger upon addition of N_3^- (5×10^{-4} mol dm^{-3}), when the concentration of **1** was 5×10^{-5} mol dm^{-3}.

In the presence of **1** (5×10^{-5} mol dm^{-3}) k increased with increasing $[N_3^-]$, whereas the k value had a tendency to be saturated at higher $[N_3^-]$ (Fig. 2). When **1** was not present, k increased little even if N_3^- was added.

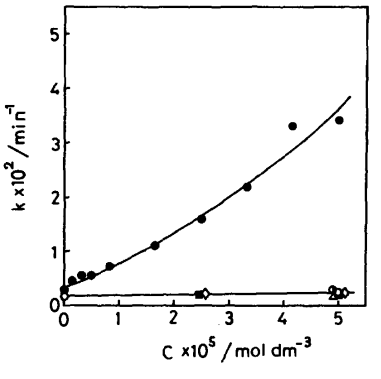

Fig. 1. Relationship between concentration of tetraalkylammonium (C) and rate constant (k) for hydrolysis of *p*-NPH in the presence of N_3^-; pH 8.0 (0.1 mol dm^{-3} KH_2PO_4–0.05 mol dm^{-3} $Na_2B_4O_7$ buffer solution), μ=0.5(KCl), 25 °C, [*p*-NPH]=5×10^{-5} mol dm^{-3}, [NaN_3]=5×10^{-4} mol dm^{-3}.
(—●—): **1**, (—○—): **1**, N_3^- free; (—■—): **2**, (—△—): **3**, (—◑—): **4**, (—◇—): **5**.

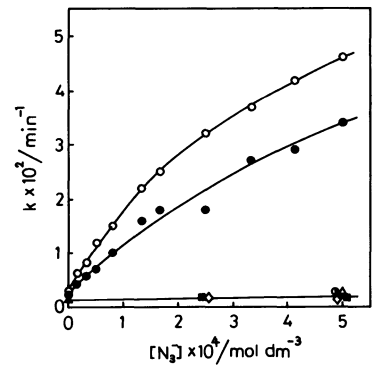

Fig. 2. Relationship between concentration of N_3^- ($[N_3^-]$) and rate constant (k) for hydrolysis of p-NPH in the presence of N_3^-; pH 8.0 (0.1 mol dm^{-3} KH_2PO_4 -0.05 mol dm^{-3} $Na_2B_4O_7$ buffer solution), μ=0.5 (KCl), 25 °C, [p-NPH]=5×10^{-5} mol dm^{-3}, [Tetraalkylammonium]=5×10^{-4} mol dm^{-3}. (—●—): **1**, (—○—): **1**, 29 °C, (—■—): **2**, (—▲—): **3**, (—◑—): **4**, (—◇—): **5**, (—△—): tetraalkylammonium free.

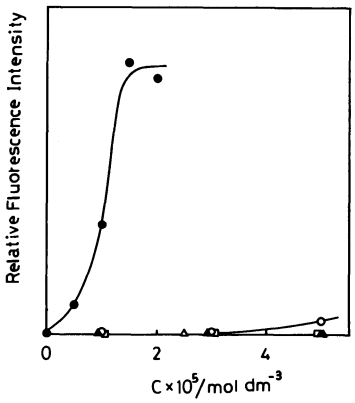

Fig. 3. Relationship between concentration of tetraalkylammonium (C) and relative fluorescence intensity of ANS; pH 8.0 (0.1 mol dm^{-3} KH_2PO_4-0.05 mol dm^{-3} $Na_2B_4O_7$ buffer solution), μ=0.5(KCl), 25 °C, [ANS]=1×10^{-4} mol dm^{-3}; excitation wavelength was 365 nm and emission wavelength was 490 nm. (—●—): **1**, (—○—): **2**, (—▲—): **3**, (—△—): **4**, (—□—) **5**.

Contrary to **1**, the other tetraalkylammonium salts, **2**—**5**, with less hydrophobic groups, did not accelerate the hydrolysis even in the presence of N_3^- (Figs. 1 and 2). Furthermore, the hydrolysis of p-NPA (less hydrophobic substrate than p-NPH) was not enhanced under the same conditions as those for p-NPH.

It is generally known that the fluorescence intensity of ANS is significantly increased when ANS is incorporated into hydrophobic environment.[12] Therefore we studied the effect of the tetraalkylammonium salts upon the fluorescence of ANS to see which ammonium salts form hydrophobic aggregates (Fig. 3). Relative fluorescence intensity was remarkably increased in the presence of **1** (≦2×10^{-5} mol dm^{-3}), while **2**—**5** scarcely increase the fluorescence.

Discussion

It seems very likely that the hydrolysis proceeds as follows.

$$CH_3(CH_2)_4COOC_6H_4NO_2 + N_3^- \longrightarrow CH_3(CH_2)_4CON_3 + {}^-OC_6H_4NO_2 \quad (1)$$

$$CH_3(CH_2)_4CON_3 + OH^- \longrightarrow CH_3(CH_2)_4COOH + N_3^- \quad (2)$$

Therefore in the present study we are discussing the first reaction (1) of the hydrolysis.

As described in the Results section, the hydrolysis of p-NPH in the presence of N_3^- and **1** did not follow pseudo-first-order plot. Taking into account the results that the hydrolysis was significantly accelerated upon addition of N_3^-, it seems very likely that N_3^- adsorbed on the aggregate should attack p-NPH very efficiently. As the concentration of **1** (≦5×10^{-5} mol dm^{-3}) is lower than that of N_3^- (≦5×10^{-4} mol dm^{-3}), the numer of N_3^- adsorbed on the aggregate is appreciably decreased as the reaction proceeds, for the liberated p-nitrophenol and/or hexanoic acid can be also adsorbed on the anion-binding site of the aggregate in competition with N_3^-. Therefore k will decrease as the hydrolysis proceeds. On the other hand, in the micelle system the concentration of HTAC (≧1×10^{-3} mol dm^{-3})was much higher than that of **1**, and so the number of N_3^- on the micelle may be virtually constant. The k value will be constant, therefore, during the reaction, as mentioned above.

In the presence of **1**, the k value increased but seemed to be saturated gradually as N_3^- was added (Fig. 2). This saturation may be attributed to the saturation of the amount of N_3^- on the **1**-aggregate. When **2**—**5** were added instead of **1**, the reaction was not accelerated even in the presence of N_3^- (Figs. 1 and 2). These results suggest that **2**—**5** cannot form aggregates in aqueous solution. This conclusion is also substantiated by the findings that the fluorescence intensity of ANS was remarkably increased by **1** but not by **2**—**5** (Fig. 3). An active ester, more hydrophilic than p-NPH, would not be included in **1**-aggregate. In fact, the hydrolysis of p-NPA was not activated in the presence of both **1** and N_3^-. Thus, it can be concluded that the rate enhancement of the hydrolysis of p-NPH in the presence of **1** and N_3^- is ascribed to the formation of the aggregate of **1** on which N_3^- and p-NPH are adsorbed and activated.

References

1) Y. Murakami, A. Nakano, A. Yoshimatsu, and K. Matsumoto, *J. Am. Chem. Soc.*, **103**, 2750 (1981).

2) K. Ogino, I. Tomita, K. Machiya, and W. Tagaki, *Chem. Lett.*, **1982**, 1875.

3) C. A. Bunton, S. E. Nelson, and C. Quan, *J. Org. Chem.*, **47**, 1157 (1982).

4) H. Al-Lohedan, C. A. Bunton, and M. M. Mhala, *J. Am. Chem. Soc.*, **104**, 6654 (1982).
5) H. Al-Lohedan and C. A. Bunton, *J. Org. Chem.*, **47**, 1160 (1982).
6) R. A. Moss, K. W. Alwis, and G. O. Bizzigotti, *J. Am. Chem. Soc.*, **105**, 681 (1983).
7) R. A. Moss and G. O. Bizzigotti, *J. Am. Chem. Soc.*, **103**, 6512 (1981).
8) Y. Murakami, A. Nakano, and K. Akiyoshi, *Bull. Chem. Soc. Jpn.*, **55**, 3004 (1982).
9) R. A. Moss and Y. Ihara, *J. Org. Chem.*, **48**, 588 (1983).
10) Y. Okahata, R. Ando, and T. Kunitake, *J. Am. Chem. Soc.*, **99**, 3067 (1977).
11) Y. Okahata, R. Ando, and T. Kunitake, *Bull. Chem. Soc. Jpn.*, **52**, 3647 (1979).
12) F. Cramer, W. Saenger, and H. Ch. Spatz, *J. Am. Chem. Soc.*, **89**, 14 (1967).

Structure Determination of Shinjulactones M and N, New Bitter Principles from *Ailanthus altissima* SWINGLE

Yoshio NIIMI, Takahiko TSUYUKI,* Takeyoshi TAKAHASHI,* and Kazuhiro MATSUSHITA†
Department of Chemistry, Faculty of Science, The University of Tokyo,
Hongo, Bunkyo-ku, Tokyo 113
†Application Center, Scientific Instrument Project, JEOL Co. Ltd.,
Nakagami, Akishima, Tokyo 196
(Received December 24, 1985)

Synopsis. Two new quassinoids, shinjulactones M and N were isolated from root bark of *Ailanthus altissima* SWINGLE. The structures of these compounds were determined to be 11β,20-epoxy-1β,11α,12α,13β,21-pentahydroxypicras-3-ene-2,16-dione and 11β,20-epoxy-1β,2α,11α,12α,15β-pentahydroxypicrasa-3,13(21)-dien-16-one, respectively, by spectral and chemical means.

As a continuation of studies on the bitter principles of Simaroubaceous plants, we have been investigating bitter principles of *Ailanthus altissima* SWINGLE (Japanese name: Shinju or Niwaurushi).[1] We further examined bitter principles in aqueous extracts of root bark of *A. altissima*, and obtained two new bitter principles, shinjulactone M (**1**; 0.0005%) and shinjulactone N (**2**; 0.0002%) together with known quassinoids, ailanthone (**3**),[2] $\Delta^{13(18)}$-dehydroglaucarubolone (**4**),[3] shinjulactone A (**5**)[2], shinjulactone D[4] and shinjuglycoside D.[5] This paper describes structure determination of shinjulactones M and N (**1** and **2**) and chemical derivation of **1** from ailanthone (**3**).

Shinjulactone M (**1**), mp 260—264 °C (decomp), showed the presence of hydroxyl, δ-lactone, and α,β-unsaturated ketone by IR and UV spectra and gave a molecular peak at *m/z* 410 in the EI-MS spectrum, suggesting the molecular formula, $C_{20}H_{26}O_9$. In the ^{13}C NMR of **1**, signals were observed at $\delta_{(C)}$ 66.5 and $\delta_{(C)}$ 75.8, which were assignable to a hydroxymethyl carbon atom and a carbon atom bearing a tertiary hydroxyl group, respectively. The ^1H NMR spectrum of **1** showed the presence of a tertiary methyl and a vinyl methyl groups and the spectral feature was similar to that of ailanthone (**3**)[2] except for the absence of an *exo*-methylene group. Since the molecular formula of **1** possesses extra two hydrogen and two oxygen atoms in comparison with that of ailanthone (**3**), the structure of **1** would be deduced to be a vicinal hydroxylation product of the *exo*-methylene in ailanthone (**3**) from the spectral evidence; the structure with the primary hydroxyl group at C-21 and the tertiary hydroxyl group at C-13 would be proposed for shinjulactone M (**1**). The COSY, NOESY spectra and ^{13}C-^1H J-correlated two-dimensional spectrum for **1** confirmed the location of the tertiary hydroxyl group. The configuration of the C-13 carbon atom was determined by difference NOE measurement. Irradiation of a signal due to one proton of C-21 methylene resonating at δ 4.42, resulted in increase in area of signals at δ 3.41 and 3.49 due to C-15 methylene and at δ 4.19 due to the other proton of C-21 methylene, respectively. This observation indicates that the hydroxymethyl group at C-13 locates in α-orientation and therefore the tertiary hydroxyl group at C-13 in β-orientation. Thus the structure of shinjulactone M was determined to be 11β,20-epoxy-1β,11α,12α,13β,21-pentahydroxypicras-3-ene-2,16-dione (**1**).

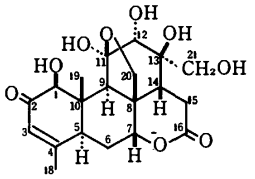

1

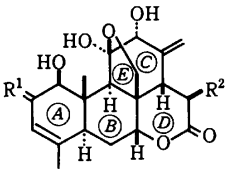

2 R¹=α-OH,β-H, R²=OH
3 R¹=O, R²=H
4 R¹=O, R²=OH
5 R¹=α-OH,β-H, R²=H

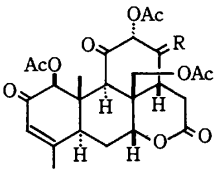

6 R=CH_2
7 R=α-CH_2OH,β-OH

Table 1. ^1H NMR Spectra of Shinjulactones M and N (**1** and **2**)[a] in C_5D_5N

	1[b]	2[c]
1-H	4.42 s	3.99 d (8.4)
2-H	—	4.62 m (overlapped with 7-H)
3-H	6.10 q (1.4)	5.79 br s
5-H	3.01 brd (12.6)	2.73 d (12.6)
6α-H	2.17 ddd (14.9, 2.9, 2.8)	2.08 d (14.3)
6β-H	2.07 ddd (14.9, 12.6, 2.7)	1.91 dd (14.3, 12.6)
7-H	4.61 dd (2.8, 2.7)	4.62 br s
9-H	3.39 s	3.41 s
12-H	4.32 d (1.5)	4.70 s
14-H	2.78 ddd (13.3, 6.0, 1.5)	3.01 d (11.9)
15α-H	3.41 dd (18.3, 13.3)	5.27 d (11.9)
15β-H	3.49 dd (18.3, 6.0)	—
4-Me	1.74 br s	1.61 s
10-Me	1.59 s	1.69 s
20-H	4.12 d (7.8)	3.77 d (8.4)
20-H′	4.83 d (7.8)	4.16 d (8.4)
21-H	4.19 d (11.2)	5.46 d (1.8)
21-H′	4.42 d (11.2)	5.52 d (1.8)

a) Coupling constants are expressed in Hz in parentheses. b) Measured at 400 MHz. c) Measured at 270 MHz.

Table 2. ^{13}C NMR Spectra of Shinjulactones M and N (1 and 2)[a] in C_5D_5N

No of carbon	1[b]	2[c]	No of carbon	1	2
1	84.6 d	83.1	11	110.5 s	110.2
2	197.5 s	72.3[d]	12	80.7 d	80.7
3	126.2 d	126.7	13	75.8 s	148.6
4	162.3 s	134.4	14	46.3 d	55.5
5	42.6 d	41.5[e]	15	31.0 t	67.8
6	26.1 t	25.5	16	170.1 s	173.0
7	78.3 d	78.6	18	22.4 q	20.9
8	46.3 s[f]	45.7	19	10.6 q	10.5
9	45.3 d	47.1	20	70.9 t	72.2[d]
10	45.3 s[f]	41.7[e]	21	66.5 t	120.2

a) Chemical shifts are expressed in δ downfield from TMS as an internal standard. b) Measured at 100 MHz. c) Measured at 67.5 MHz. d), e), and f) Signals may be reversed, respectively.

The structure (**1**) proposed for shinjulactone M was firmly confirmed by a chemical conversion of ailanthone (**3**) into shinjulactone M (**1**). Ailanthone (**3**), on treatment with osmium tetraoxide, afforded a product derived from an attack of the reagent on a conjugated olefin between C-3 and C-4, because the reagent could not be accessible to the *exo*-methylene due to a steric hindrance of E-ring. Ailanthone triacetate (**6**),[6,7] however, reacted with the reagent to afford a dihydroxy derivative (**7**), $C_{26}H_{32}O_{12}$. Treatment of **7** with potassium methoxide gave shinjulactone M, identical with a natural specimen including an optical property.

Shinjulactone N (**2**), mp 245—251 °C (decomp), gave a molecular formula, $C_{20}H_{26}O_8$ by high-resolution mass spectrum and showed the presence of hydroxyl and δ-lactone groupings. Comparison of the ^1H NMR spectrum of **2** with those of shinjulactone A (**5**)[2] and $\Delta^{13(18)}$-dehydroglaucarubolone (**4**)[3] led to the proposed structure with the same A, B, C, and E ring-structures as those of **5** and with the same β-equatorial hydroxyl group at C-15 as that in **4**, the coupling constant, $J_{14,15}$, being 11.9 Hz (see Table). Therefore, 11β,20-epoxy-1β,2α,11α,12α,15β-pentahydroxypicrasa-3,13(21)-dien-16-one (**2**) was proposed for shinjulactone N. The ^{13}C NMR spectrum of shinjulactone N was compatible with the proposed structure (**2**). Shinjulactone N (**2**) is corresponding to the hydrolyzate of 13,18-dehydroexcelsin obtained from *Ailanthus excelsa*.[8]

Although more than twenty quassinoids and four quassinoid glycosides have been isolated from *A. altissima* so far, shinjulactone M (**1**) is the first example of 11β,20-epoxypicrasane which possesses a hydroxyl group at $C_{(21)}$-atom, and the picrasane [B] bearing hydroxyl groups on $C_{(13)}$- and $C_{(21)}$-atoms may be one of biogenetical intermediates yielding methyl 13β,20-epoxypicrasan-21-oate [C], such as brusatol from ailanthone-type precursor [A] (Scheme 1).

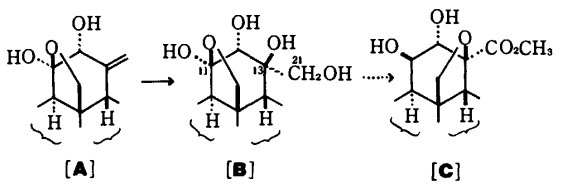

[A] [B] [C]

Scheme 1.

Experimental[9]

Extraction and Isolation of Shinjulactones M and N (1 and 2). The air-dried root bark (ca. 7 kg) was chipped and extracted with hot water twice (15 l and then 10 l). Evaporation in vacuo gave a concentrated extract (ca. 5 l), which was continuously extracted with dichloromethane (1 l×3) for 12 h. The aqueous layer was separated and concentrated to afford a solution (ca. 2 l), to which methanol (3 l) was added. After filtration, the filtrate was evaporated to give a residue (420 g), a part (317 g) of which was absorbed on silica gel (361 g) and placed on the top of silica-gel column (2 kg). Elution was performed with lower layer of chloroform–methanol–water in the following ratios successively; 50:12:3 (6.5 l), 65:35:10 (12 l), and 50:50:18 (5 l). Forty fractions (each 500 ml) were collected (column A).

Residues from fractions 19 and 20 of column A were combined (4 g) and separated by column chromatography on silica gel (80 g) eluted with 18% methanol in ethyl acetate (200 ml) and 20, 23, 26, 29, and 32% methanol in ethyl acetate (each 100 ml), and 8 fractions (each 100 ml) were collected (column B).

The residue from fraction 4 (581 mg) of column B was separated by partition chromatography on silicic acid (430 g) pretreated with water (287 g). Elution was performed with 0, 1, 3, 6, 9···24% ethanol in chloroform (each 1 l) and 33 fractions (each 250 ml) were collected (column C).

Residues from fractions 22—28 (117 mg) of column C were combined and separated by reversed phase chromatography using LiChroprep RP-8. Elution was performed with methanol-water (3:7) and 40 fractions (each 10 g) were collected. Fractions 13—17 afforded shinjulactone M (**1**; 32 mg). Combined residues (29 mg) of fractions 18—33 were further separated by gel column chromatography using Toyopearl HW-40S (2.4×100 cm) and methanol as an eluent. Seventy fractions (each 10 g) were collected. Fractions 50—52 gave shinjulactone N (**2**; 11 mg).

Shinjulactone M (1). Colorless prisms crystallized from methanol-ethyl acetate, mp 260—264 °C (decomp); $[\alpha]_D^{25}$ +37° (*c* 0.46, MeOH); IR (KBr) 3500, 2900, 1730, 1670, 1260, 1225, 1060, and 1030 cm^{-1}; UV (EtOH) 238 nm (ε 15600); ^1H and ^{13}C NMR (Tables 1 and 2); MS (EI) *m/z* (%) 410 (M^+; 2.2), 392 (3), 374 (13), and 107 (100); Found: *m/z* 410.1580. Calcd for $C_{20}H_{26}O_9$: M, 410.1577.

Shinjulactone N (2). Colorless amorphous solid from methanol-ethyl acetate, mp 245—251 °C; $[\alpha]_D^{25}$ +60.6° (*c* 0.32, MeOH), IR (KBr) 3420, 2870, 1720, 1625, 1610, and 1050 cm^{-1}; ^1H and ^{13}C NMR (Tables 1 and 2); MS (EI) *m/z* (%) 394 (M^+; 3.9), 376 (18), 361 (10), 332 (23), 105 (79), and 57 (100); Found: *m/z* 394.1616. Calcd for $C_{20}H_{26}O_8$: M, 394.1626.

Conversion of Ailanthone Triacetate (6) into Shinjulactone M (1). Ailanthone triacetate (**6**; 417.5 mg)[7] was treated with osmium tetraoxide (199 mg) in a mixture (8 ml) of pyridine-THF (1:1) at −72 °C for 9 h. After addition of sodium hydrogensulfite (0.36 g) in water (6 ml) and pyridine (3 ml), THF was removed by distillation in vacuo. The remaining solution was stirred at room temperature for 1 h. The usual work-up followed by separation by column chromatography on silica gel afforded shinjulactone M triacetate (**7**; 141 mg) together with the starting material (**6**; ca. 90 mg). **7**; colorless

needles from chloroform–ethyl acetate, mp 261—263 °C (decomp); $[\alpha]_D^{24}$ +10° (*c* 0.10, pyridine); IR (KBr) 3490, 3280, 1750, 1710, 1680, 1380, 1210, 1060, 1040, 900, and 600 cm^{-1}; UV (EtOH) 238 nm (ε 8800); ^1H NMR (C_5D_5N) δ 1.65 (3H, s; 10-Me), 1.79 (3H, s; 4-Me), 1.95, 2.10, and 2.15 (each 3H; OAc), 3.1—3.8 (3H, m; 14-H, 15-H, and 15-H′), 4.03 (2H, s; 21-H and 21-H′), 4.68 (1H, d, J=10.8 Hz; 20-H), 4.97 (1H, br s; 7-H), 5.31 (1H, d, J=10.8 Hz; 20-H′), 5.47 (1H, s; 1-H or 12-H), 5.66 (1H, s; 12-H or 1-H), and 6.03 (1H, br s; 3-H); ^{13}C NMR (C_5D_5N) δ 203.4, 191.6, 170.9, 170.3, 169.5, 169.2, 161.7, 126.5, 84.9, 81.0, 80.0, 78.0, 64.5, 64.1, 48.8, 44.7, 44.3, 42.1, 38.2, 28.4, 25.4, 21.9, 21.0, 20.7, 20.6, and 12.0; MS (EI) *m/z* (%) 536 (M^+; 6.2), 518 (2.4), 494 (5.6), 476 (13), 463 (4.3), 458 (5.4), 434 (9.6), 416 (11), 398 (20), 151 (19), 95 (32), and 60 (100); Found: *m/z* 536.1891. Calcd for $C_{26}H_{32}O_{12}$: M, 536.1892.

Shinjulactone M triacetate (**7**; 118 mg) was hydrolyzed with 0.3 M (1 M=1 mol dm^{-3}) potassium methoxide in methanol (10 ml) at room temperature for 1 h and, after the usual work-up, the hydrolyzate was purified by column chromatography on silica gel (5 g). Elution with 15% methanol in chloroform afforded shinjulactone M (**1**; 75.7 mg); mp 263—266 °C (decomp); $[\alpha]_D^{14}$ +20° (*c* 0.46, MeOH); the spectral data were completely identical with those of a natural specimen.

The authors wish to express their thanks to Associate Professor Hajime Nagano of Ochanomizu University for measurement of NMR, and Mr. Eiichi Ishii of the Botanical Gardens, the University of Tokyo, for collecting root of *A. altissima*.

References

1) M. Ishibashi, T. Tsuyuki, and T. Takahashi, *Bull. Chem. Soc. Jpn.*, **58**, 2723 (1985), and references cited therein.
2) H. Naora, M. Ishibashi, T. Furuno, T. Tsuyuki, T. Murae, H. Hirota, T. Takahashi, A. Itai, and Y. Iitaka, *Bull. Chem. Soc. Jpn.*, **56**, 3694 (1983).
3) J. Moron, J. Rondest, and J. Polonsky, *Experientia*, **22**, 511 (1966); S. M. Kupchan and J. A. Lacadie, *J. Org. Chem.*, **40**, 654 (1975).
4) T. Furuno, M. Ishibashi, H. Naora, T. Murae, H. Hirota, T. Tsuyuki, T. Takahashi, A. Itai, and Y. Iitaka, *Bull. Chem. Soc. Jpn.*, **57**, 2484 (1984).
5) S. Yoshimura, M. Ishibashi, T. Tsuyuki, T. Takahashi, and K. Matsushita, *Bull. Chem. Soc. Jpn.*, **57**, 2496 (1984).
6) J. Polonsky and J.-L. Fourrey, *Tetrahedron Lett.*, **1964**, 3983.
7) M. Ishibashi, T. Tsuyuki, and T. Takahashi, *Bull. Chem. Soc. Jpn.*, **58**, 2357 (1985).
8) S. A. Khan and K. M. Shamsuddin, *Phytochemistry*, **19**, 2484 (1980).
9) General procedures are the same as those described in lit. 5.

Induced Circular Dichroism in the Complexes of Sequential Lysine Polypeptides with Methyl Orange. On Intermolecular Aggregation of the Complexes and Distance between Lysine Residues

Hiroyuki YAMAMOTO,* Ayako NISHIDA, Tadao HAYAKAWA, Norio NISHI,† and Ryo YAMAMOTO†

Institute of High Polymer Research, Faculty of Textile Science and Technology, Shinshu University, Ueda 386

†Department of Polymer Science, Faculty of Science, Hokkaido University, Sapporo 060

(Received December 24, 1985)

Synopsis. Aggregation of the sequential poly(Lys HCl-X) (X: Gly, βAla, and εAhx)-Methyl Orange (MO) complexes was studied by means of a circular dichroism (CD) measurement. The intensity of the induced CD was affected by the concentration of the complexes and time after preparing the complex solutions. When MO molecules which are electrostatically bound to lysine residues are separated from each other, the aggregation of the complexes takes place to a lesser degree.

The origin of induced optical activities arises from dipole-dipole interactions between two transition dipoles of the chromophores under chiral environmental conditions.[1,2] Recently, several groups reported the results on an induced CD due to chiral interaction between cationic poly(Lys)[3] and anionic azo dyes.[4-8] The structural isomer εpoly(Lys) has also been examined from the standpoint of binding affinity to small molecules such as dyes and metals,[9] and of the induced CD properties on complexation with MO.[10] The εpoly(Lys)-MO complex caused an interchain aggregation. The differences in the results between poly(Lys) and εpoly(Lys) have mainly been attributed to the intramolecular distance between the ammonium groups, to which anionic azo dyes interacted electrostatically. To clarify the effect of distance between chromophores, sequential polypeptides containing functional groups may be one of the most suitable systems. In this Note a series of sequential lysine polypeptides are described in order to add some knowledge regarding the induced CD of cationic biopolymer-dye complexes.

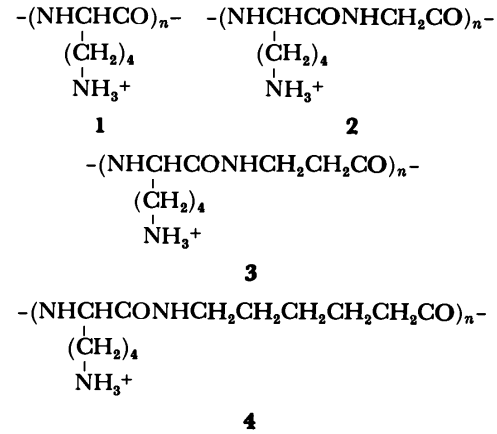

Scheme 1.

Experimental

Using lysyl-X dipeptides as precursors, three sequential lysine polypeptides, poly(Lys HCl-Gly) (2, degree of polymerization as total amino acid residues, DP,=40), poly(Lys HCl-βAla) (3, DP=60), and poly(Lys HCl-εAhx) (4, DP=90) were synthesized according to the racemization-free diphenyl phosphor azidate method.[11] Poly(Lys HBr) (1, DP=60) was purchased from Sigma and converted to poly(Lys HCl).[12] The chemical structures of the four polypeptides are shown in Scheme 1. Sodium 4-(4-dimethylaminophenylazo)benzenesulfonate (Methyl Orange, MO) was a guaranteed reagent from Wako. The mixtures were prepared by adding a dye solution to the polypeptide solutions. The final concentrations of lysine residues in polypeptides and MO were $1—7\times10^{-4}$ mol residue dm^{-3} and $2—14\times10^{-5}$ mol dm^{-3}, respectively, at residue/dye ratio (R/D)=5. The CD spectra were measured with a Jasco CD J-40A spectrometer. The molar ellipticity $[\theta]$ (degree $cm^2\,dmol^{-1}$) was expressed on the basis of the dye concentration.

Results and Discussion

The induced CD of the poly(Lys)-azo dye complexes has been studied[4-8] and the poly(Lys HCl)-MO complex used here (DP=60) exhibited intensities of $[\theta]_{371}=-25000$ and $[\theta]_{359}=25000$ at pH 6 and R/D=5. The induced CD spectra of the sequential lysine polypeptide-MO complexes were recorded by changing the concentration of the dye and keeping the R/D ratio constant at 5. Figure 1 shows the time dependence of the induced CD spectra of the poly(Lys HCl-Gly)-MO complex in water at pH 6 and dye concentration 10^{-4} mol dm^{-3}. Immediately after preparing the mixed solution, the complex exhibited no induced CD. After 1 h, a weak split-type induced CD spectrum with extrema at 371 nm (negative) and 359 nm (positive) was observed and their intensities at the extrema were found to increase on standing without stirring. After 23 h, the intensities were −16600 (371 nm) and 16100 (359 nm), and still increasing. Figure 2 shows the concentration and time dependence of the induced CD of the poly(Lys HCl-Gly)-MO complex in water at pH 6 (R/D=5). When the dye concentrations were less than 4×10^{-5} mol dm^{-3}, the system did not exhibit induced CD, even after 3 d. On the other hand, when the dye concentrations were greater than 6×10^{-5} mol

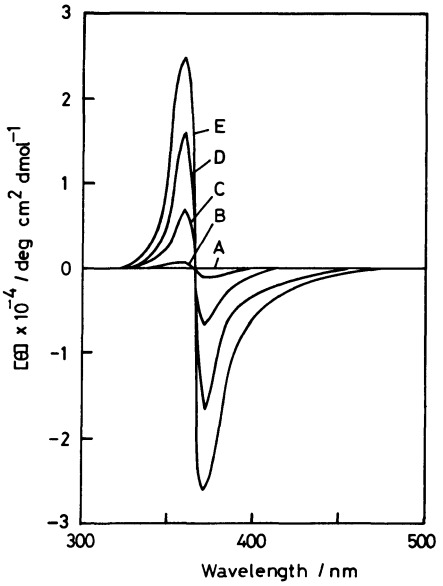

Fig. 1. Time dependence of the induced CD spectra of the poly(Lys HCl-Gly)-MO complex in water at pH 6 and R/D=5; MO, 10^{-4} mol dm^{-3}. A at 0 h, B after 1 h, C after 9 h, D after 23 h, and E after 47 h.

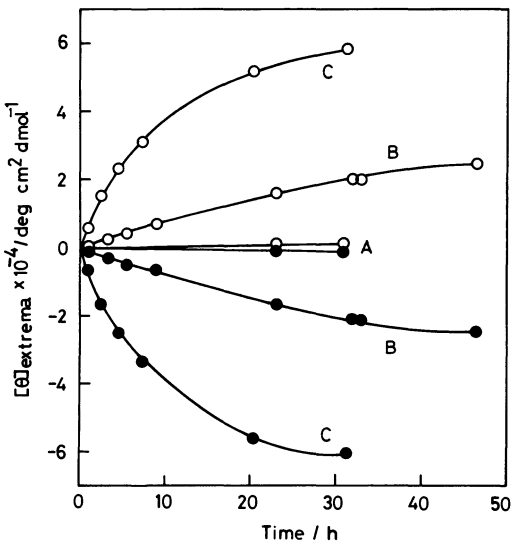

Fig. 2. Concentration and time dependences of the induced CD intensities of the poly(Lys HCl-Gly)-MO complex in water at pH 6 and R/D=5; ○ at 359 nm and ● at 371 nm.
Concentration of MO (mol dm^{-3}); A 6×10^{-5}, B 10^{-4}, and C 1.4×10^{-4}.

Table 1. Induced CD of MO Complexes with Sequential Lysine Polypeptides in Water at pH 6 and R/D=5

Polypeptide	Circular Dichroism[a]	
	Wavelength	[θ]
	nm	deg cm² dmol⁻¹
Poly(Lys HCl)	371	−25000
	364	0
	359	25000
Poly(Lys HCl-Gly)	371	−16600
	364	0
	359	16100
Poly(Lys HCl-βAla)	435	−8300
	412	0
	397	12100
Poly(Lys HCl-εAhx)	424	−7300
	405	0
	388	8200

a) MO 10^{-4} mol dm^{-3} and after 23 h.

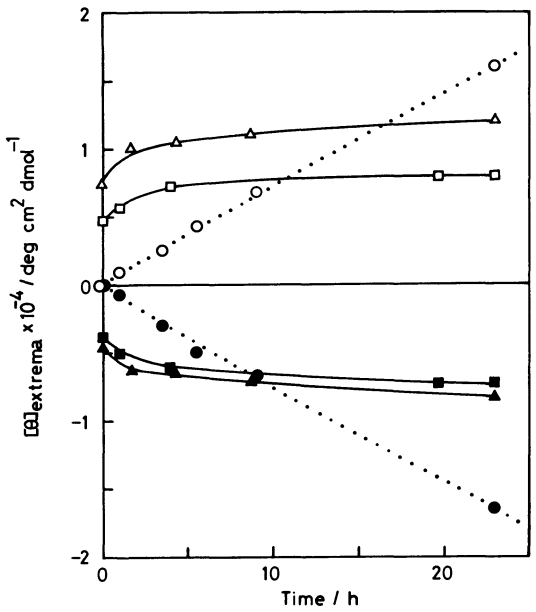

Fig. 3. Time dependence of the induced CD intensities of the poly(Lys HCl-X)-MO complexes in water at pH 6 and R/D=5; MO, 10^{-4} mol dm^{-3}. Poly(Lys HCl-βAla), △ at 397 nm and ▲ at 435 nm; poly(Lys HCl-εAhx), □ at 388 nm and ■ at 424 nm. Poly-(Lys HCl-Gly) (○ at 359 nm and ● at 371 nm) was partly reproduced from Fig. 2 (curve B).

dm^{-3}, the intensities of the induced CD were continued to increase after 2 d. This suggests that an intermolecular aggregation of the complex occurs. As listed in Table 1, the poly(Lys HCl-βAla)-MO complex exhibited the induced CD with the extrema at 435 nm (negative) and at 397 nm (positive), and poly(Lys HCl-εAhx)-MO complex at 424 nm (negative) and at 388 nm (positive). The induced CD spectra of the poly(Lys HCl-βAla)-MO and poly(Lys HCl-εAhx)-MO complexes, which have one and four more backbone atoms than poly(Lys HCl-Gly)-MO complex, exhibited smaller intensities and a little time dependence as depicted in Fig. 3. This suggests that, when MO molecules that are electrostatically bound to lysine residues are separated from each other, the intra- and intermolecular interactions are

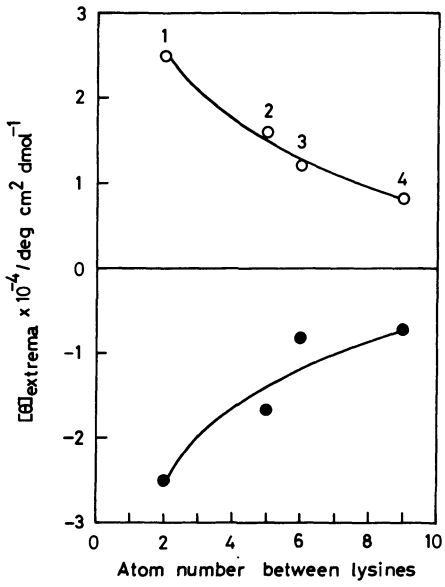

Fig. 4. Induced CD intensities at the extrema of the sequential polypeptide–MO complexes as a function of distance between lysine residues in water at pH 6 and R/D=5; MO, 10^{-4} mol dm^{-3}. After 23 h; samples 1—4, see text.

weaker.

At the beginning of the present study we expected to change the intramolecular interchromophoric distance using sequential polypeptides, although the problem was more complicated than anticipated. We tentatively plotted the induced CD intensities after 23 h at the extrema of four sequential polypeptide–MO complexes including poly(Lys HCl)–MO complex as a function of distance between C_α of the lysine residues in Fig. 4. Since the random coil conformations of the four sequential polypeptide–MO complexes did not allow an exact estimation of the distance between chromophores, the numbers of backbone atoms between lysine residues were plotted as abscissa. Boldly, it could be concluded that an increased distance between the N^ε-ammonium groups of lysine residues decreased the intensity of the induced CD (see also Fig. 3). The results in Fig. 4 are fundamentally similar to the results of the induced CD of the sequential poly(His)–MO complexes reported by us.[13] Since the DPs (40—90) of the sequential poly(Lys HCl–X) samples used here may be too low to investigate the intramolecular dye–dye interaction, very high DP samples with the same Lys HCl–X sequences might give additional information regarding the induced CD of the sequential lysine polypeptides.

References

1) R. E. Ballard, A. J. McCaffery, and S. F. Mason, *Biopolymers*, **4**, 97 (1966).
2) H. Yamamoto and A. Nakazawa, *Biopolymers*, **23**, 1367 (1984).
3) IUPAC-IUB nomenclature. *Biochem.*, **11**, 1726 (1972); *Biopolymers*, **11**, 321 (1972); εAhx, ε-aminohexanoic acid.
4) M. Hatano, M. Yoneyama, Y. Sato, and Y. Kawamura, *Biopolymers*, **12**, 2423 (1973).
5) Y. Ando, PhD Thesis, Tokyo Institute of Technology, 1981.
6) K. Murakami, T. Sano, N. Kure, K. Ishii, and T. Yasunaga, *Biopolymers*, **22**, 1935 (1983).
7) H. Yamamoto, A. Nakazawa, and T. Hayakawa, *J. Polym. Sci. Polym. Lett. Ed.*, **21**, 131 (1983).
8) H. Yamamoto, A. Nakazawa, T. Hayakawa, and M. Mitsuishi, *Polym. J.*, **16**, 791 (1984).
9) T. Takagishi, T. Ueno, N. Kuroki, S. Shima, and H. Sakai, *J. Polym. Sci. Polym. Chem. Ed.*, **22**, 1281 (1984).
10) T. Takagishi, N. Kuroki, S. Shima, H. Sakai, H. Yamamoto, and A. Nakazawa, *J. Polym. Sci. Polym. Lett. Ed.*, **23**, 329 (1985).
11) B. Nakajima and N. Nishi, *Polym. J.*, **13**, 183 (1981).
12) P. K. Sarker and P. Doty, *Proc. Natl. Acad. Sci. U. S. A.*, **55**, 981 (1966).
13) H. Yamamoto, A. Nakazawa, T. Hayakawa, and N. Nishi, *Int. J. Biol. Macromol.*, **7**, 167 (1985).

Aryliminodimagnesium Reagents. X. The Mild Reagent Derived from 2-Aminopyridine and Formation of Highly Reactive Azoxypyridines in the Reaction with Nitrobenzenes

Masao Ōkubo,* Chieko Sugimori, Mitsunao Tokisada, and Toshiki Tsutsumi
Department of Chemistry, Faculty of Science and Engineering, Saga University, Honjō-machi, Saga 840
(Received November 2, 1985)

Synopsis. The reaction of iminodimagnesium reagent derived from 2-amino-4-methylpyridine with nitrobenzenes was examined. The relative yields of the azoxypyridine formed via condensation and the azopyridines via deoxygenation and oxidative dimerization were explained in terms of weak electron-donating ability of the reagent and the strong electron-accepting ability of the azoxypyridine.

As an application of the procedure using aryliminodimagnesium reagents(ArN(MgBr)$_2$, aryl-IDMg), the reaction of reagent ***A*** derived from 1,2-benzenediamine with nitrobenzenes was reported.[1] The product distribution is governed by the sterically hindered but strongly electron-donating nature of ***A***. In the preliminary study on IDMg condensation with carbonyl compounds,[2] reagent $\boldsymbol{B}^{H}$ derived from 2-aminopyridine gave low yield of anil of fluorenone but no anil of benzophenone.

In order to study the reason for the low reactivity of the reagent derived from 2-aminopyridines for the purpose of developing the IDMg procedure, the reaction of nitrobenzenes with reagent $\boldsymbol{B}^{Me}$ derived from 2-amino-4-methylpyridine was examined. The product distribution was compared with that obtained in the reaction of reagent $\boldsymbol{C}^{MeO}$ derived from *p*-methoxyaniline.[3] The result will be explained by the quite weak electron-donating ability of $\boldsymbol{B}^{Me}$ and the very strong electron-accepting ability of azoxypyridine formed in the present reaction.

Results and Discussion

The reagents $\boldsymbol{B}^{H}$ and $\boldsymbol{B}^{Me}$ were prepared without difficulty from 2-aminopyridine and its 4-methyl derivative, respectively, by treating with EtMgBr in THF.[2] Attempts to convert 3- and 4-aminopyridines into IDMg failed; a voluminous white precipitate appeared and no evolution of ethane was observed. The results are quite similar to the successful preparation of IDMg (***A***) from 1,2-benzenediamine and the failure of preparation of IDMg from 1,3- and 1,4-isomers.[1] The reagent $\boldsymbol{B}^{Me}$ was allowed to react with *p*-(Me, Cl, MeO)-substituted nitrobenzenes. Four products identified are shown in Scheme 1: **1** is formed via condensation, **2** via deoxygenation of **1**, and **3** via oxidative dimerization of reagent molecules.[3] While the formation of **1**—**3** is expected from the previous study using the reagents derived from anilines,[3] the formation of the *ortho*-substitution product **4** is observed for the first time in IDMg reactions of nitrobenzenes. Reaction conditions and yields of **1**—**4** are summarized in Table 1 (Runs 1—9).

In Runs 2—4 using small excess of $\boldsymbol{B}^{Me}$, the yields of azopyridine **2** are higher than those of azoxypyridine **1**; the relative yield is distinct from the higher yields of symmetrical azoxybenzene than the those of azobenzene obtained by use of small excess of reagent derived from aniline.[3] For the complete consumption of the substrate, the large amount of $\boldsymbol{B}^{Me}$ and prolonged heating are needed (Runs 5—7). The azoxypyridine **1** is also consumed completely and

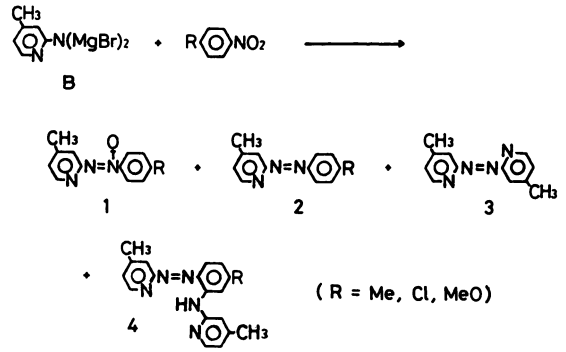

Scheme 1.

Table 1. Conditions and Yields of Products in the Reaction of Reagent $\boldsymbol{B}^{Me}$ with *p*-$RC_6H_4NO_2$

Run	R	[$\boldsymbol{B}^{Me}$]/Substr.	Reacn. time[a]/h	Yield[b]/% 1	2	3	4	Recovd.	Overall
1	Me	1.1	1.5	18	7	4	trace	71	100
2	Me	1.1	3.5	16	17	4	1	58	96
3	Me	2.5	1.5	16	31	7	2	39	95
4	Me	3.0	3.0	9	38	14	trace	30	91
5	Me	10.0	3.0	1	52	13	3	25	94
6	Me	10.0	5.0	0	74	13	5	0	92
7	Me	10.0	21.0[a]	10	20	5	1	63	99
8	Cl	2.5	1.5	24	29	12	3	30	98
9	MeO	2.5	1.5	22	26	5	3	37	93

a) Reaction mixtures were heated at 55 °C in Runs 1—6, 8, and 9, and at room temperature in Run 7.
b) Yields based on the amounts of substrates used.

Table 2. Correlation between EAA and Types of Products Formed in IDMg Reaction with Azoxyarenes
Ar^1-N=N(O)-Ar^2 + *p*-$MeOC_6H_4$-IDMg (at 55 °C for 3 h)

Azoxyarene				Products Formed *via*				
Ar^1	Ar^2	Redn. Pot./V	EAA	Deox. /%	Exchg. /%	Ox. Dim. /%	*ort.* Subs. /%	Decompn. /%
p-$MeOC_6H_4$	*p*-MeC_6H_4	−1.748	weak	O/16	—	—	—	—
C_6H_5	C_6H_5	−1.596		O/75	—	—	—	—
m-ClC_6H_4	C_6H_5	−1.423		O/75	O/21	—	—	—
2-4MPy[a]	*p*-ClC_6H_4	−1.312	strong	O/32	O/8	O/25	O/9	O/≥50

a) 2-(4-methyl)pyridyl.

good yield of **2** is obtained (Run 6).

It was postulated previously that the distribution of "normal and abnormal" products in the reactions of organomagnesium reagents depends principally on the combination of electron-donating and -accepting abilities (EDA and EAA) of reactants.[4,5] According to the EDA–EAA concept, the mechanism of reaction of benzophenones with ArMgBr was distinguished successfully from that with IDMg.[6] In order to apply the concept to the present result, the polarographic oxidation peak potential of $\boldsymbol{B}^{Me}$ (1.295 V) was measured in THF using ferrocene as internal standard.[5] The value higher than that of $\boldsymbol{C}^{MeO}$ (0.921 V)[5] indicates the weak EDA of $\boldsymbol{B}^{Me}$ which is responsible for the low reactivity shown by the large amount of recovery in Runs except 6. It is also responsible for the deoxygenation ability of $\boldsymbol{B}^{Me}$ in the reaction with azoxyarenes. By the treatment of azoxybenzene with five molar equivalents of $\boldsymbol{B}^{Me}$ and $\boldsymbol{C}^{MeO}$ at 55 °C for 3 h, deoxygenation proceeds to the extents of 0.5 and 75%,[5] respectively. Taking the previous results[1,5] into account, the order of EDA of IDMg's is shown as follows.

EDA: Electron-donating Ability

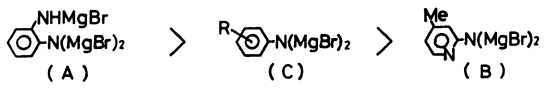

The reduction potentials of *p*-substituted nitrobenzenes (MeO: −1.508 V; Me: −1.418 V; Cl: −1.254 V) and those of azoxyarenes including $\mathbf{1}^{Cl}$ (See Experimental) were also measured in THF using bisbiphenylchromium(I)tetraphenylborate(BCTB) as internal standard,[7] the latters being listed in Table 2. The EDA of azoxyarene is affected greatly by the aryl group locating opposite to the positive nitrogen.[8] The products and yields obtained in the reaction of $\mathbf{1}^{Me}$ with reagent $\boldsymbol{C}^{MeO}$ are given in Scheme 2($\mathbf{2}^{Me}$ and **5**—**7**). The product $\mathbf{2}^{Me}$ is formed via "normal" deoxygenation,[8] **5** via exchange,[8] **6** via oxidative dimerization of IDMg molecules, and **7** via *ortho*-substitution. Table 2 includes also the types of products obtained under the same reaction conditions in the previous[8] and present studies.

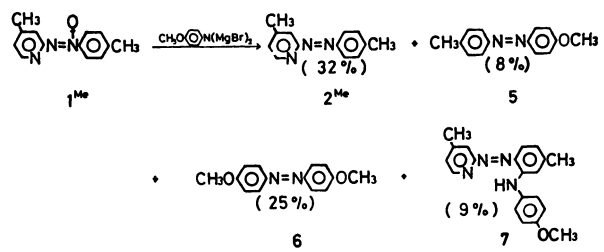

Scheme 2.

The results shown in Table 2 demonstrate that EAA of azoxyarenes are correlated to the distribution of types of products in IDMg reaction. In the reaction with $\boldsymbol{C}^{MeO}$ having strong EDA, azoxybenzenes having weak EAA undergo mild deoxygenation and those having strong EAA undergo rapid deoxygenation and exchange.[8] The azoxypyridine **1** having extremely strong EAA undergoes, additionally, oxidative dimerization of IDMg as well as *ortho*-substitution. The former process is indicative of involvement of electron transfer and is observed usually in the IDMg reaction with nitrobenzenes[3] having strong EAA. The latter process resembles the many examples of conjugate addition of Grignard reagents having strong EDA[5] with nitrobenzenes via electron transfer reported by Bartoli.[9] The strong EAA of $\mathbf{1}^{Me}$ and strong EDA of $\boldsymbol{C}^{MeO}$ are also responsible for the formation of an appreciable amount of unidentifiable black materials indicative of the decomposition via too much vigorous electron transfer.[4] Only a half amount of $\mathbf{1}^{Me}$ was converted into the identified products, $\mathbf{2}^{Me}$, **5**, and **7**.

In the reaction of Scheme 1, the large amounts of recovery in Runs except 6 are due to the weak EDA of $\boldsymbol{B}^{Me}$. In contrast to the reactions of nitrobenzenes with ordinary IDMg derived from anilines,[3] however, the azoxy compound formed first in the present reaction has EAA comparable to or stronger than that of substrate. Thus, the strong EAA of **1** not only gives rise to the higher yield of **2** than that of **1** (Runs 2—5 and 7—9) but also is responsible for the slight dependence of product distribution on the electronic effect of substituents of substrates (Runs 3, 8, and 9). The formation of **3** and **4** corresponding to **6** and **7**, respectively, is ascribed to the interaction of $\boldsymbol{B}^{Me}$ with **1**; the possibility of interaction with substrate is excluded from the large amount of recovery in Runs except 6.

The weak EDA of $\boldsymbol{B}^{H}$ and $\boldsymbol{B}^{Me}$ and also the strong EAA of **1** are ascribed to the electron-deficient pyridyl group shown by the lower reactivity of pyridines than that of benzenes toward electrophilic reagents.[10] The good yield of azopyridine (Run 6) suggests the further development of the present method.

Table 3. Melting Points, Elemental Analyses, and ^{1}H NMR Spectra of Products

No.	Mp θ_m/°C	Formula	C	H	N	^{1}H NMR/δ
			Found/(Calcd)			
$\mathbf{1}^{Me}$	110—110.5	$C_{12}H_{12}N_2O$	68.73 (68.71)	5.82 (5.77)	18.58 (18.49)	8.56 and 7.08(2H, ABq), 8.30 and 7.30(4H, ABq), 8.01(1H, s), 2.44(6H, s).
$\mathbf{1}^{Cl}$	121—122	$C_{12}H_{10}ClN_2O$	57.99 (58.19)	4.13 (4.07)	16.71 (16.97)	8.62 and 7.16(2H, ABq), 8.14 and 7.50(4H, ABq), 8.10(1H, s), 2.45(3H, s).
$\mathbf{1}^{MeO}$	79.8—80.2	$C_{12}H_{12}N_2O_2$	63.97 (64.19)	5.33 (5.39)	17.04 (17.27)	8.58 and 7.09(2H, ABq), 8.38 and 6.98(4H, ABq), 8.00(1H, s), 3.85(3H, s), 2.40(3H, s).
$\mathbf{2}^{Me}$	77—79	$C_{12}H_{12}N_2$	73.96 (73.91)	6.38 (6.20)	19.82 (19.82)	8.54 and 7.10(2H, ABq), 7.93 and 7.28(4H, ABq), 7.44(1H, s), 2.37(3H, s), 2.33(3H, s).
$\mathbf{2}^{Cl}$	92.5—93.0	$C_{12}H_{10}ClN_2$	62.03 (62.21)	4.36 (4.35)	18.01 (18.14)	8.62 and 7.19(2H, ABq), 7.02 and 7.50(4H, ABq), 7.59(1H, s), 2.39(3H, s).
$\mathbf{2}^{MeO}$	83.5—84.0	$C_{12}H_{12}N_2O$	68.70 (68.71)	5.87 (5.77)	18.48 (18.49)	8.59 and 7.14(2H, ABq), 8.10 and 7.04(4H, ABq), 7.60(1H, s), 3.82(3H, s), 2.36(3H, s).
3	143—146	$C_{12}H_{12}N_4$	68.01 (67.90)	5.92 (5.70)	26.43 (26.40)	8.60 and 7.30(4H, ABq), 7.84(2H, s), 2.48(6H, s).
$\mathbf{4}^{Me}$	62—64	$C_{11}H_{11}N_3$	71.63 (71.90)	6.19 (6.03)	21.94 (22.07)	12.65(1H, broad s), 8.83(1H, s), 8.50 and 7.06(2H, ABq), 8.17 and 6.78(2H, ABq), 7.82 and 6.86(2H, ABq), 7.55(1H, s), 6.78(1H, s), 2.45(3H, s), 2.40(3H, s), 2.29(3H, s).
$\mathbf{4}^{Cl}$	oil	$C_{10}H_8ClN_3$	— (64.00)	— (4.74)	— (20.74)	10.76(1H, broad s), 8.95(1H, d), 8.62 and 7.24(2H, ABq), 8.26(1H, d), 7.95(1H, d), 7.61(1H, s), 7.02 (1H, d), 6.80(1H, s), 2.51(3H, s), 2.35(3H, s).
$\mathbf{4}^{MeO}$	oil	$C_{11}H_{11}N_3O$	— (68.47)	— (4.80)	— (21.02)	12.60(1H, broad s), 8.90(1H, d), 8.56 and 7.10(2H, ABq), 8.22 and 6.67(2H, ABq), 7.87 and 6.60(2H, ABq), 7.63(1H, s), 6.87(1H, s), 3.97(3H, s), 2.43(3H, s), 2.34(3H, s).
7	96—100	$C_{20}H_{20}N_4O$	72.16 (72.27)	6.06 (6.06)	16.72 (16.86)	11.28(1H, broad s), 8.57 and 7.19(2H, ABq), 7.94 and 6.74(2H, ABq), 7.63(1H, s), 7.30 and 6.98(4H, ABq), 6.90(1H, s), 3.86(3H, s), 2.46(3H, s), 2.30 (3H, s).

Experimental

Melting points are uncorrected.

Materials, Reactions, and Products. 2-Amino-4-methylpyridine and nitrobenzenes were commercially available. The solution of $\boldsymbol{B}^{Me}$ in THF was prepared according to the reported procedure.[1,5] The reactions of Scheme 1 were carried out by adding the solution of nitrobenzenes (3.0 mmol) into the solution of given amount of $\boldsymbol{B}^{Me}$ at 0 °C. The reaction mixtures were stirred at 55 °C or at room temperature for the given period of time (See Table 1). Using the samples of $\mathbf{1}^{Me}$ formed in Runs 1—5 and 7, collected and purified, the reaction of Scheme 2 was carried out under the same conditions as those of the previous study.[8] The products formed in the reactions of Schemes 1 and 2 were separated by column and thin-layer chromatographies on silica gel.

The melting points, values of elemental analyses, and ^{1}H NMR spectra of products **1**—**4** and **7** are summarized in Table 3, those of the products **5** and **6** being reported previously.[3,8] The products $\mathbf{4}^{Cl}$ and $\mathbf{4}^{MeO}$ were not completely purified, and no elemental analysis was carried out.

Polarographic Measurements. The cyclic voltammetry was carried out by using a Yanaco P-1100 Model Voltammetric Analyzer. Using tetrabutylammonium perchlorate (0.2 M, 1 M=1 mol dm^{-3}) as supporting electrolyte, the oxidation peak potential of $\boldsymbol{B}^{Me}$ in THF was observed and normalized according to the reported procedure.[5] The reduction potentials of nitro- and azoxy-arenes given in the text are redox potentials observed and normalized similarly; no sample of $\mathbf{1}^{Me}$ was available because it had been used up for the reaction of Scheme 2. All the values of potentials are those vs. NHE. The two internal standard compounds used for the measurements of oxidation peak and reduction potentials, respectively, are given in the text.

The gift of samples of BCTB by Prof. G. Gritzner, University of Linz, and Prof. K. Izutsu, Shinshu University, is gratefully acknowledged. The authors thank Mr. Kōji Matsuo for the attempted preparation of IDMg from 3- and 4-aminopyridines. The authors are grateful to the Ministery of Education, Science, and Culture for a financial support by a Grant-in-Aid for Scientific Research (No. 60470026).

References

1) M. Ōkubo, M. Tokisada, and T. Gondo, *Nippon Kagaku Kaishi*, **1985**, 303.
2) M. Ōkubo, S. Hayashi, M. Matsunaga, and Y. Uematsu, *Bull. Chem. Soc. Jpn.*, **54**, 2337 (1981),
3) M. Ōkubo, T. Takahashi, and K. Koga, *Bull. Chem. Soc, Jpn.*, **56**, 199 (1983).
4) M. Ōkubo, M. Yoshida, K. Horinouchi, H. Nishida, and Y. Fukuyama, *Bull. Chem. Soc. Jpn.*, **56**, 1196 (1983).
5) M. Ōkubo, T. Tsutsumi, A. Ichimura, and T. Kitagawa, *Bull. Chem. Soc. Jpn.*, **57**, 2679 (1984).
6) M. Ōkubo, *Bull. Chem. Soc. Jpn.*, **58**, 3108 (1985).
7) G. Gritzner and J. Kuta, *Pure Appl. Chem.*, **56**, 461 (1984).
8) M. Ōkubo and K. Koga, *Bull. Chem. Soc. Jpn.*, **56**, 203 (1983).
9) G. Bartoli, M. Bosso, R. D. Pozzo, and F. Ciminale, *J. Org. Chem.*, **45**, 5227 (1982); G. Bartoli, *Acc. Chem. Res.*, **17**, 109 (1984).
10) R. M. Acheson, "An Introduction to the Chemistry of Heterocyclic Compounds," 3rd Ed., John Wiley & Sons Inc, New York (1976), Chap. 5.

Reductive and Regioselective Cleavage of Oxetanes Assisted by the Neighboring Hydroxyl

Michiharu KATO, Haruo KITAHARA, and Akira YOSHIKOSHI*
Chemical Research Institute of Non-Aqueous Solutions, Tohoku University, Sendai 980
(Received December 11, 1985)

Synopsis. On exposure to lithium aluminium hydride, 1,6-dioxadispiro[2.0.3.4]undecane and 5-methl-2-oxaspiro-[3.5]nonan-5-ol gave 1,2-dimethyl-*c*-2-(hydroxymethyl)-*r*-1-cyclohexanol (**5**) which was produced from regioselective C–O bond cleavage of oxetane rings by an intramolecular attack of hydride. The stereochemistry of **5** was confirmed by an unambiguous synthesis based on the Sharpless oxidation of 1-methyl-2-methylenecyclohexanemethanol.

On treatment with lithium aluminium hydride, oxetanes generally undergo reductive fission of their C–O bonds to produce alcohols.[1] On this reduction, it is known that boiling in tetrahydrofuran for several hours is an indispensable conditions for obtaining a reasonable reaction rate and yield.[2] While reduction of 2-oxaspiranes **1**(n=0—2) with this reductant led to the expected 1-methylcycloalkanemethanol **2**(n=0—2), 2-oxaspiro[3.5]nonane **1**(n=3) was reported to be exceptionally sluggish on the reduction.[3]

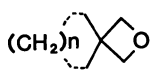

1

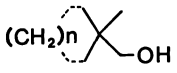

2

We wish to report here that treatment of 1,6-dioxadispiro[2.0.3.4]undecane (**3**) and 5-methyl-2-oxaspiro[3.5]nonan-5-ol (**4**),[4] derivatives of **1**(n=3) possessing additional oxygen functions, with lithium aluminium hydride resulted in unexpectedly facile and regioselective cleavage of their oxetane rings.

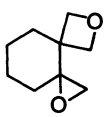

3

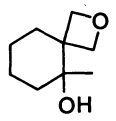

4

In the course of our synthetic study of a natural product, we have prepared hydroxy oxetane **4** in high yield by reduction of epoxy oxetane **3** with super hydride ($LiBHEt_3$).[4] When **3** was, on the other hand, treated with lithium aluminium hydride in place of the above reductant, the reduction proceeded smoothly even at room temperature, and the sole product obtained in 97% yield was not the hydroxy oxetane **4** but an unexpected diol, 1,2-dimethyl-*c*-2-(hydroxymethyl)-*r*-1-cyclohexanol (**5**). The diol **5** was also produced by treatment of **4** obtained above with lithium aluminium hydride under the same reaction conditions. Acetylation of the diol **5** with acetic anhydride in pyridine gave a crystalline acetoxy alcohol **6**, in which no evidence could be found for formation of its diastereomer.

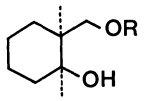

5 R=H
6 R=Ac

The stereochemistry of **5** was confirmed by an unambiguous synthesis starting with ethyl 1-methyl-2-oxo-cyclohexanecarboxylate.[5] Methylenation of the ester by the Wittig reaction with methylenetriphenylphosphorane provided unsaturated ester **7** in 60% yield, and the product was reduced with lithium aluminium hydride to the corresponding unsaturated alcohol **8** quantitatively. The alcohol **8** was then submitted to the Sharpless oxidation.[6] The reaction proceeded stereoselectively to provide hydroxy epoxide **9** in 73% isolated yield together with a small amount of its stereoisomer **10** (~1%).

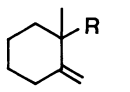

7 R=CO_2Et
8 R=CH_2OH

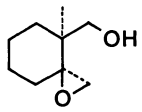

9

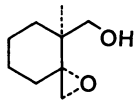

10

It is reasonable to surmise that the stereoselectivity of the above reaction would be controlled by the syn-directive effect of the homoallylic hydroxyl group in **8**. In other words, the epoxide oxygen of the major product **9** can be expected to have a syn configuration with respect to the hydroxymethyl group on the basis of the well-documented stereoselectivity.[6] Finally, reduction of **9** with lithium aluminium hydride afforded a single diol, whose physical properties (IR and ^1H NMR) were identical with those of the diol **5** prepared from **3** or **4**.

Mechanistic rationalization for the facile and regioselective cleavage of the oxetane ring would be given as follows. Since treatment of 5-methylene-2-oxaspiro[3.5]nonane (**11**)[4] with lithium aluminium hydride also resulted in recovery of **11** in the same way as the reduction of **1**(n=3), it is demonstrated that the presence of a hydroxyl group α to the oxetane ring plays an important role for the reductive cleavage with great facility. Apparently, the hydride reacts initially with the hydroxyl group in **4** to afford an alkoxy hydride **12**, which is also derived from preferential reduction of the epoxide ring in the

course of reduction of **3**. Thus the facile reductive cleavage of the oxetane ring would occur by internal hydride attack based on neighboring assistance. In the intermediate **12**, energetically favorable chelation between the aluminium and oxetane oxygen atoms would be attained with the equatorially oriented alkoxide group, and this conformational fixation would also be convenient for the intramolecular attack of hydride at the oxetane methylene carbon in the anti position regarding to the alkoxide group.

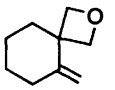

11

12

Experimental

Melting points are uncorrected. IR spectra were obtained with a JASCO A-3 infrared spectrometer. ^{1}H NMR spectra were recorded on a JEOL FX90Q spectrometer. Gas chromatography was carried out on a JEOL JGL-20K gas chromatograph. Dry tetrahydrofuran (THF) was obtained by distillation over sodium benzophenone ketyl. Column chromatography was performed by using silica gel (Merck, kieselgel 60, 70—230 mesh), and kieselgel GF_{254} was employed for preparative thin-layer chromatography as an absorbent.

Lithium Aluminium Hydride Reduction of Oxetane 3. A mixture of **3**[4] (80 mg, 0.52 mmol), lithium aluminium hydride (30 mg, 0.78 mmol), and THF (5 ml) was stirred at room temperature for 5 h under nitrogen and quenched with wet ether. A solid was filtered and washed with ether, and the combined ethereal solutions were dried ($MgSO_4$). Removal of the solvent left an oil, which was purified by preparative thin-layer chromatography (50% ether in hexane as an eluent) and subsequent solvent removal gave 79 mg (96%) of **5** as a viscous oil: IR (neat) 3300 cm^{-1}; ^{1}H NMR ($CDCl_3$) δ=0.82 (3H, s, C-CH_3), 1.21 (3H, s, O-C-CH_3), 1.0—2.2 (8H, m), 3.0—3.9 (3H, m, CH_2-OH). The oil was used in the next reaction.

Acetylation of Diol 5. A mixture of **5** (45 mg), acetic anhydride (0.8 ml), and pyridine (0.4 ml) was stirred at room temperature for 20 h under nitrogen, and poured into ice-water. The solution was extracted with ether and the combined extracts were washed successively with water and brine, and dried ($MgSO_4$). Evaporation of the solvent left 54 mg (95%) of **6** as crystals. Analysis by gas chromatography (10%-SE-30, 2 m×1 mm; vaporizer, 250 °C; column temperature, 170 °C; helium flow, 1 kg cm^{-2}) indicated a single peak with retention time 2.8 min. An analytically pure sample was obtained by recrystallization from ether–hexane (1:1): mp 88—89 °C; IR (KBr) 3480, 1720 cm^{-1}; ^{1}H NMR ($CDCl_3$) δ=0.99 (3H, s, C-CH_3), 1.21 (3H, s, O-C-CH_3), 1.2—1.8 (9H, m), 2.10 (3H, s, $COCH_3$), 4.13 and 4.23 (1H, d, J=11.1 Hz each, CH_2-O).

Found: C, 65.64; H, 10.02%. Calcd for $C_{11}H_{20}O_3$: C, 65.97; H, 10.07%.

Reduction of Hydroxy Oxetane 4 with Lithium Aluminium Hydride. A suspension of **4** (20 mg. 0.13 mmol) and lithium aluminium hydride (6 mg, 0.15 mmol) in THF (1 ml) was stirred at room temperature for 7 h under nitrogen and quenched with wet ether. A solid was filtered and washed with ether, and the combined extracts were dried ($MgSO_4$). Removal of the solvent left an oil, which was purified by filtration through a short silica gel column with 30% ether in hexane to give 18 mg (90%) of a viscous oil whose IR and ^{1}H NMR spectra were identical with those of diol **5** prepared above.

Ethyl 1-Methyl-2-methylenecyclohexanecarboxylate (7). To a stirred suspension of methyltriphenylphosphonium bromide (7.23 g, 20.2 mmol) in THF (40 ml) was added dropwise a solution of 1.5 M butyllithium in hexane (13.5 ml, 20.2 mmol) at 0 °C under nitrogen. The cooling bath was removed and the mixture was stirred at room temperature for 2 h. A solution of ethyl 2-methyl-2-oxo-1-cyclohexanecarboxylate (3.68 g, 20.2 mmol) in THF (5 ml) was added dropwise and stirring was continued for an additional hour at room temperature, and then at 60 °C for 10 h. After cooling to room temperature, water was added and the aqueous solution was extracted with ether. The combined extracts were washed successively with water and brine, and dried ($MgSO_4$). A residue obtained by concentration was chromatographed by eluting with 20% ether in hexane to give 2.04 g (60%) of **7** as a colorless oil: IR (neat) 3060, 1725, 1640, 890 cm^{-1}; ^{1}H NMR ($CDCl_3$) δ=1.23 (3H, t, J=7.2 Hz, $CO_2CH_2CH_3$), 1.30 (3H, s, C-CH_3), 1.1—1.8 (6H, m), 2.2 (2H, m, CH_2-C=), 4.18 (2H, q, J=7.2 Hz, $CO_2CH_2CH_3$), 4.78 and 4.87 (1H, br s each, C=CH_2).

Found: C, 72.15; H, 9.75%. Calcd for $C_{11}H_{18}O_2$: C, 72.49; H, 9.96%.

1-Methyl-2-methylenecyclohexanemethanol (8). To a stirred suspension of lithium aluminium hydride (237 mg, 6.25 mmol) in THF (10 ml) at 0 °C under nitrogen was added dropwise a solution of **7** (1.14 g, 6.25 mmol) in THF (2 ml). After removal of the cooling bath, stirring was continued for an additional 15 h at room temperature. The reaction was quenched by the addition of wet ether followed by a small amount of water. A solid was filtered and washed with ether, and the combined ethereal solutions were dried ($MgSO_4$). An oily residue obtained by evaporation was chromatographed by eluting with 50% ether in hexane to give 787 mg (90%) of **8** as a colorless oil: IR (neat) 3350, 3070, 1640, 900 cm^{-1}; ^{1}H NMR ($CDCl_3$) δ=1.08 (3H, s, CH_3), 1.1—1.8 (7H, m), 2.2 (2H, m, CH_2-C=), 3.38 (1H, d, d, J=10.4 and 7.2 Hz, C$H_a$$H_b$-O), 3.70 (1H, d, d, J=10.4 and 5.4 Hz, $CH_a$$H_b$-O), 4.75 and 4.87 (1H, s, with fine splittings each, =CH_2); ^{1}H NMR ($CDCl_3$-D_2O) δ=3.38 and 3.70 (1H, d, J=10.4 Hz each).

Found: C, 77.04; H, 11.80%. Calcd for $C_9H_{16}O$: C, 77.09; H, 11.50%.

Sharpless Oxidation of Homoallylic Alcohol 8. A solution of **6** (437 mg, 3.12 mmol) and vanadyl acetylacetonate (17 mg, 0.06 mmol) in dry benzene (8 ml) was warmed at 80 °C under nitrogen. A solution of 3M *t*-butyl hydroperoxide in toluene (1.2 ml, 3.43 mmol) was added dropwise to the above solution with stirring. Stirring was continued for an additional 2 h and, after cooling, the reaction was quenched by the addition of aqueous sodium hydrogensulfite solution followed by water. The benzene layer was separated and aqueous layer was extracted with benzene. The combined extracts were washed successively with water and brine, and dried ($MgSO_4$). An oily residue obtained by evaporation was chromatographed by eluting with 50% ether in hexane to give two products, **9** (355 mg, 73%) and **10** (4 mg, ~1%). **9**: IR (neat) 3400 cm^{-1}; ^{1}H NMR ($CDCl_3$) δ=0.98 (3H, s, CH_3), 1.1—2.2 (9H, m), 2.48 (1H, d, J=3.6 Hz, epoxide C$H_a$$H_b$), 2.9—3.58 (3H, m); ^{1}H NMR ($CDCl_3$-D_2O) δ=3.10 (1H, d, J=3.6 Hz, epoxide $CH_a$$H_b$), 3.15 and 3.44 (1H, d, J=11.2 Hz each, CH_2-O). Found: C, 69.20; H, 10.79%. Calcd for $C_9H_{16}O_2$: C, 69.19; H, 10.32%. **10**: IR (neat) 3400 cm^{-1}; ^{1}H NMR ($CDCl_3$) δ=1.13 (3H, s,

CH_3), 1.0—2.1 (9H, m), 2.55 (1H, d, J=3.6 Hz, epoxide CH_aH_b), 3.12 (1H, d, J=3.6 Hz with fine splittings, epoxide CH_aCH_b), 3.3—3.7 (2H, m); ^{1}H NMR ($CDCl_3$-D_2O) δ=3.25 and 3.55 (1H, d, J=11.2 Hz each, CH_2-O). Found: C, 68.90; H, 10.17%. Calcd for $C_9H_{16}O_2$: C, 69.12; H, 10.32%.

Reduction of Epoxy Alcohol 9 with Lithium Aluminium Hydride. A suspension of **9** (355 mg, 2.28 mmol) and lithium aluminium hydride (258 mg, 6.83 mmol) in THF (10 ml) was warmed with stirring at 50 °C for 15 h under nitrogen. After cooling to room temperature, the mixture was quenched with wet ether. A solid was filtered and the filtrate was dried ($MgSO_4$). Removal of the solvent left an oily residue which was purified by preparative thin-layer chromatography (70% ether in hexane as an eluent) to give 244 mg (93%) of a viscous oil, whose IR and ^{1}H NMR were identical with those of **5** prepared by reduction of **3**.

Treatment of Oxetane 11 with Lithium Aluminium Hydride. A suspension of **11** (25 mg, 0.18 mmol) and lithium aluminium hydride (14 mg, 0.36 mmol) in THF (2 ml) was stirred at room temperature for 20 h, and then at 60 °C for 5 h under nitrogen. After cooling to room temperature, the reaction was quenched with wet ether and a solid was filtered. The filtrate was dried ($MgSO_4$). An oily residue obtained by concentration was purified by passing through a short silica-gel column with 10% ether in hexane to give 21 mg of an oil whose ^{1}H NMR spectrum was identical with that of starting **11**.

References

1) S. Searles, Jr., K. A. Pollart, and E. F. Lutz, *J. Am. Chem. Soc.*, **79**, 948 (1957).

2) A. Rosowsky and D. S. Tarbell, *J. Org. Chem.*, **26**, 2255 (1961).

3) S. Searles, E. F. Lutz, and M. Tamres, *J. Am. Chem. Soc.*, **82**, 2939 (1960). The inertness has been accounted for the steric hindrance from axial hydrogens toward the bulky aluminium hydride ion.

4) M. Kato, H. Kitahara, and A. Yoshikoshi, *Chem. Lett.*, **1985**, 1785.

5) N. S. Vul'fson and V. I. Zaretskii, *Zh. Obschch. Khim.*, **28**, 369 (1953); *Chem. Abstr.*, **52**, 13658b (1958).

6) K. B. Sharpless and R. C. Michaelson, *J. Am. Chem. Soc.*, **95**, 6136 (1973); M. Kobayashi, S. Kurozumi, T. Toru, S. Ishimoto, *Chem. Lett.*, **1976**, 1341; K. Tsuzuki, Y. Nakajima, T. Watanabe, M. Yanagiya, and T. Matsumoto, *Tetrahedron Lett.*, **1978**, 989.

The H-1 NMR Solvent Shifts and Reactivity Parameters of Several Aromatic Compounds

Akihiro TAMAOKI and Kensuke TAKAHASHI*
Department of Industrial Chemistry, Nagoya Institute of Technology,
Gokiso-cho, Showa-ku, Nagoya 466
(Received September 25, 1985)

Synopsis. H-1 NMR solvent shifts were measured for 7 aromatic hydrocarbons and 13 heteroaromatic compounds. The chemical shifts can be correlated to the self-polarizabilities of the carbon atoms attached to the hydrogens in the aromatic hydrocarbons and will be of use in predicting the reactivities of the compounds. However, in the case of heteroaromatic compounds, no good correlation has been found between the reactivity parameters and the H-1 NMR solvent shifts.

The orientaion or, more quantitatively, the partial rate factor is an important problem in aromatic substitution reactions. The reactivities of the aromatic compounds can be expressed by various parameters. Several useful parameters are derived from the Hückel molecular orbital treatment.[1] Kuthan sought to present some correlation between the NMR chemical shifts and the reactivities.[2-6] However, Bartle and Jones[7,8] and Mallion[9] pointed out that the NMR shifts can be explained by the ring current and cannot be correlated with any reactivity parameters. We ourselves thought that the polarizability of the reaction center would be reflected in the solvent shifts of the relevant H-1 NMR and so have studied the correlation of the latter with various reactivity parameters.

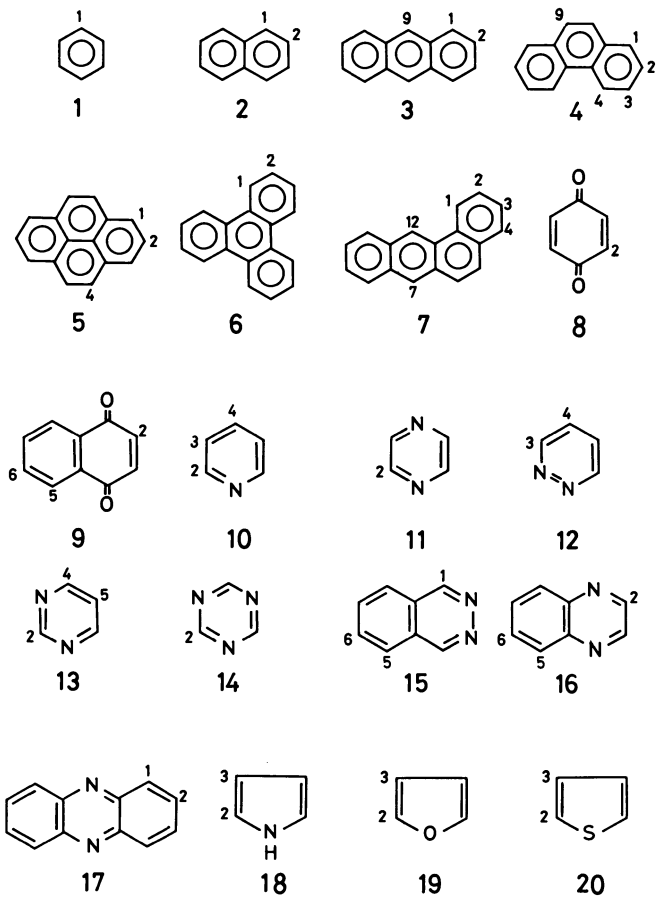

Scheme 1.

Experimental

The reagents and solvents are from commercial sources. The reagents used and their numberings are given in Scheme 1. Three solvents, acetone, carbon tetrachloride, and cyclohexane, were used (hereafter they will be abbreviated as **S1**, **S2**, and **S3**). The H-1 NMR chemical shifts were obtained by extrapolating to an infinitely diluted state in the solvents. The values were referred to an internal TMS, with errors of ±0.03 ppm. If the solution was measured at a concentration under 0.3 mol%, its singly measured value was taken as the infinitely diluted one. Here, D is defined as $D=\delta(\mathbf{S1})-\delta(\mathbf{S3})$. Therefore, D is the difference between two infinitely diluted shifts in acetone and cyclohexane. The H-1 NMR spectra were recorded on a Hitachi R-20B spectrometer at 60 MHz and 31.5 °C. The Hückel MO calculations were carried out by a HITAC-8400 computer system installed in this Institute. The parameters used in the calculation are mostly taken from Streitwieser's book.[1]

Results and Discussion

The chemical shifts and D's of 7 alternant aromatic hydrocarbons and 13 heteroaromatic compounds are tabulated in Tables 1 and 2, along with several calculated reactivity parameters. The chemical-shift data shown in the tables are almost entirely consistent with those previously reported.[10-19]

Alternant Hydrocarbons. The hydrogens in question will hereafter be divided into two groups. One is a sterically compressed hydrogen (i.e., "angular protons" in Kuthan's nomenclature[4]), while the other is an ordinary one. The former is hydrogen which has a mutual interaction, such as the H-4 and the H-5 of phenanthrene.[4] The D values can be correlated with the self-polarizability, (π_{rr}),[20,21] of the carbon atom carrying the hydrogen in question, as is shown in Fig. 1. The compressed hydrogens are situated under a correlation line in Fig. 1. This means that the compressed hydrogens have small π_{rr} values or large D's. A correlated equation is derived for π_{rr} and D as follows: $\pi_{rr}=0.85D+0.26$. The correlation coefficient is about 0.885 for 15 data points except for three compressed hydrogens. The data show that the relative reactivities of the positions in a molecule can be evaluated well from the D values, but that those between different molecules are difficult to evaluate. For example, the calculated order of the π_{rr} values of three similarly positioned carbons is **3**-1>**2**-1>**4**-1, but the experimentally

Table 1. H-1 Chemical Shifts of Several Alternant Aromatic Hydrocarbons in ppm[a] and Their Reactivity Parameters[b]

No.	δ(S1)	δ(S2)	δ(S3)	D	π_{rr}	L_r(E)	L_r^v(E)	S_r(E)
1	7.35	7.27	7.22	0.14	0.398	2.536	1.603	0.833
2-1	7.90	7.74	7.70	0.20	0.443	2.299	1.305	0.994
2-2	7.51	7.40	7.34	0.17	0.405	2.480	1.519	0.873
3-1	8.08	7.94	7.87	0.21	0.454	2.25	1.23	1.072
3-2	7.50	7.39	7.32	0.18	0.411	2.40	1.44	0.922
3-9	8.55	8.35	8.28	0.27	0.526	2.013	0.91	1.312
4-1	7.98	7.83	7.77	0.22	0.439	2.318	1.247	0.977
4-2	7.58	7.45	7.39	0.18	0.403	2.498	1.469	0.860
4-3	7.58	7.45	7.39	0.18	0.409	2.454	1.375	0.893
4-4	8.82	8.62	8.59	0.23	0.429	2.366	1.343	0.939
4-9	7.82	7.66	7.60	0.22	0.442	2.299	1.347	0.997
5-1	8.29	8.10	8.05	0.24	0.466	2.190	0.990	1.115
5-2	8.07	7.92	7.87	0.20	0.395	2.55	1.500	0.829
5-4	8.18	8.00	7.95	0.22	0.445	2.28	1.309	1.026
6-1	8.81	8.58	8.56	0.26	0.427	2.378	1.311	0.888
6-2	7.72	7.58	7.52	0.20	0.406	2.477	1.398	0.928
7-7	8.51	8.29	8.21	0.30	0.496	2.101	1.02	1.325
7-12	9.39	9.09	9.05	0.34	0.514	2.049	0.91	1.250

a) The chemical-shift values was obtained by extrapolation to the infinitely diluted state in each solvent, with an error of 0.03 ppm. b) The values and notations of the reaction parameters are mostly from Ref. 1, the others were calculated by the present authors.

Table 2. Infinitely Diluted H-1 Chemical Shifts of Heteroatom Compounds in ppm and Their Reactivity Parameters

No.	δ(S1)	δ(S2)	δ(S3)	D	π_{rr}	q_r
8	6.83	6.71	6.57	0.26	0.493	0.927
9-2	7.04	6.90	6.78	0.27	0.483	0.910
9-5	8.05	7.88	7.68	0.37	0.442	0.925
9-6	7.90	7.74	7.54	0.36	0.418	0.959
10-2	8.58	8.54	8.52	0.06	0.399	0.923
10-3	7.35	7.19	7.07	0.28	0.398	1.004
10-4	7.65	7.47	7.35	0.30	0.397	0.950
11	8.59	8.50	8.40	0.19	0.401	0.926
12-3	9.20	9.13	9.02	0.18	0.396	0.923
12-4	7.64	7.32	7.12	0.52	0.400	0.953
13-2	9.16	9.12	9.09	0.07	0.385	0.844
13-4	8.78	8.64	8.54	0.23	0.392	0.874
13-5	7.48	7.23	7.02	0.46	0.397	1.009
14	9.24	9.10	9.01	0.23	0.372	0.797
15-1	9.61	9.42	9.34	0.27	0.434	0.899
15-5	8.16	7.87	7.75	0.40	0.442	0.986
15-6	8.04	7.87	7.75	0.29	0.405	0.984
16-2	8.92	8.76	8.66	0.27	0.407	0.902
16-5	8.11	8.06	8.02	0.09	0.443	1.002
16-6	7.87	7.71	7.59	0.28	0.406	0.987
17-1	8.26	8.20	8.17	0.09	0.454	1.001
17-2	7.96	7.77	7.65	0.31	0.414	0.980
18-2	6.78	6.64	6.57	0.20	0.485	1.035
18-3	6.07	6.07	6.11	−0.04	0.380	1.106
19-2	7.54	7.36	7.28	0.26	0.504	1.015
19-3	6.42	6.29	6.24	0.18	0.382	1.090
20-2	7.48	7.26	7.18	0.29	0.451	1.000
20-3	7.15	7.05	6.99	0.16	0.400	1.000

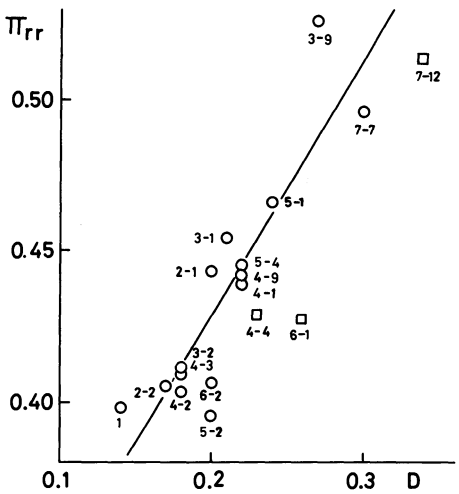

Fig. 1. Plot of self-polarizaility (π_{rr}, ordinate vs. solvent induced shift (D, abscissa). Rectangular show the values for the compressed hydrogens.

observed one of the D values is **4**-1>**3**-1>**2**-1. Here, **m**-n denotes the reference number of the compound (**m**) and the position (n) as given in Scheme 1. Large deviations of the self-polarizability from the correlation line in Fig. 1 were found for the hydrogens of **1**(0.019), **3**-9(0.037), **5**-2(−0.032), **6**-2(−0.024), and **7**-7(−0.019). It is strange that H(**3**-9) and H(**7**-7) show different signs for the deviation, although the hydrogens seem to be similar in their locations. The large deviation of **1** comes from its large π_{rr} value. Mallion stated that H(**5**-2) has a large deviation in the correlation between the chemical shifts and the free valences (F_r).[9] Bartle and Jones considered the

Table 3. Correlation between Solvent-Induced Shifts (D) and Reactivities (R) with 15 Data of 7 Alternant Hydrocarbons in the $R=aD+b$ Equation

R	a	b	r[a]	e[b]
π_{rr}	0.85	0.26	0.885	0.018
L_r(E)	−3.56	3.09	−0.877	0.081
L_r^{π}(E)	−4.56	2.26	−0.898	0.093
S_r(E)	3.59	0.25	0.924	0.062

a) Correlation coefficients. b) Standard deviations.

Table 4. Correlation between Solvent-Induced Shifts (D) and Reactivity Parameters (R) of 8 Nitrogen-containing Aromatic Compounds in the $R=aD+b$[a] Equation

R	a	b	r	e
L_r(E)	−2.03	2.72	−0.551	0.45
	(2.44)	(1.55)	(0.447)	(0.43)
L_r^{π}(E)	−1.66	0.98	−0.393	0.57
	(1.84)	(0.16)	(0.310)	(0.50)
S_r(E)	−0.41	0.97	−0.645	0.07
	(0.06)	(0.67)	(0.063)	(0.28)
q_r	−0.061	1.004	−0.412	0.020
	(−0.039)	(0.893)	(−0.071)	(0.049)
π_{rr}	−0.098	0.445	−0.616	0.018
	(0.080)	(0.383)	(0.364)	(0.018)

a) The values are given for 10 sites except for those adjacent to the hetero atom, whose values are given separately in parentheses.

cause of the deviation to be the ring-current effect in the case of **5**.[7] On the other hand, Haigh et al. stated that the deviation of H(**5**-2) is smaller than either H(**5**-1) or H(**5**-4) in the correlation of the chemical shifts and ring current.[22] Therefore, the abnormally large deviation of H(**5**-2)(−0.032 in π_{rr}) cannot be explained only by the ring-current effect, as has been stated by Bartle and Jones.[7]

There are many reactivity parameters in addition to π_{rr}; several of them are given in Table 1, the values of which are mostly cited from Streitwieser's book.[1] The correlations between such parameters and D can, then, be evaluated by the following linear equation: $R=aD+b$, where R is a reactivity parameter and where a and b are constant parameters. The results are shown in Table 3. Among the four parameters in the table, S_r(E) has the best correlation coefficient, while π_{rr} has the smallest standard deviation. The latter parameters can now be evaluated from the H-1 NMR chemical shifts in order to compare the local positions in a molecule or those of several related molecules.[23]

Hetroaromatic Compounds. The heteroaromatic compounds studied are divided into 3 types: (A) 2 quinones (**8** and **9**), (B) 8 nitrogen-containing compounds (**10**—**17**), and (C) 3 five-membered compounds (**18**—**20**). The hydrogens adjacent to heteroatoms sometimes give abnormal D values. The correlations between the reactivity parameters and D are given in Table 4. As the table shows, the correlations are poor. One of the reasons for this is that the reactivity parameters are derived by the Hückel MO method, the simplest MO method, which may not be suitable even for a qualitative discussion of the properties of heteroaromatic compounds. One of the other reasons is the heteroatom effect. The heteroatoms considered here have lone-pair electrons. These will significantly affect the D values in various complex manners.

References

1) A. Streitwieser, "Molecular Orbital Theory for Organic Chemists," John Wiley and Sons, Inc., New York (1961).
2) J. Kuthan, *Z. Chem.*, **6**, 150 (1966).
3) J. Kuthan and V. Skala, *Z. Chem.*, **6**, 422 (1966).
4) J. Kuthan, *Collection Czech. Chem. Commun.*, **33**, 1220 (1968).
5) J. Kuthan, Z. Donnerova, and V. Skala, *Collection Czech. Chem. Commun.*, **34**, 2398 (1969).
6) J. Kuthan, *Collection Czech. Chem. Commun.*, **35**, 714 (1970).
7) K. D. Bartle and W. W. Jones, *J. Phys. Chem.*, **73**, 293 (1969).
8) K. D. Bartle, *Org. Magn. Reson.*, **5**, 95 (1973).
9) R. B. Mallion, *Org. Magn. Reson.*, **5**, 91 (1973).
10) C. W. Haigh and R. B. Mallion, *Mol. Phys.*, **18**, 737 (1970).
11) N. Jonathan, S. Gordon, and B. P. Dailey, *J. Chem. Phys.*, **36**, 2443 (1962).
12) T. J. Batterham, L. Tsai, and H. Ziffer, *Aust. J. Chem.*, **17**, 163 (1964).
13) J. D. Memory and T. B. Cobb, *J. Chem. Phys.*, **38**, 1453 (1963).
14) J. A. Elvidge and P. D. Ralph, *J. Chem. Soc. B*, 249 (**1966**).
15) G. S. Reddy, R. T. Hobgood, Jr., and J. H. Goldstein, *J. Am. Chem. Soc.*, **84**, 336 (1962).
16) P. J. Black and M. L. Heffernan, *Aust. J. Chem.*, **18**, 707 (1965).
17) E. F. G. Herington and I. J. Lawrenson, *Spectrochim. Acta*, **21**, 1010 (1965).
18) T. Schaefer and W. G. Schneider, *J. Chem. Phys.*, **32**, 1224 (1960).
19) M. A. Cooper and S. L. Manatt, *J. Am. Chem. Soc.*, **92**, 1605 (1970).
20) C. A. Coulson and H. C. Longuet-Higgins, *Proc. Roy. Soc.*, **A191**, 39 (1947).
21) C. A. Coulson and H. C. Longuet-Higgins, *Proc. Roy. Soc.*, **A192**, 16 (1947).
22) C. W. Haigh, R. B. Mallion and E. A. G. Armour, *Mol. Phys.* **18**, 751 (1970).
23) A. Tamaoki and K. Takahashi, preliminary results presented at the 42nd National Meeting of the Chemical Society of Japan, Sendai, Sept. 1980, 4E09.

Dehydrogenation of Ethylbenzene on Potassium-Promoted Iron Oxide Catalysts Containing Various Transition Metal Oxides

Takenori HIRANO
Kasukabe Laboratory, Nissan Girdler Catalyst Co. Ltd.,
Ushijima 573, Kasukabe, Saitama 344
(Received November 12, 1985)

Synopsis. Various transition metal oxides, i.e., CeO_2, Cr_2O_3, ZrO_2, V_2O_5, WO_3, and MoO_3, were added to a potassium-promoted iron oxide catalyst to study their effects on the dehydrogenation activity of the catalyst. CeO_2 was found to promote styrene formation most strongly among the oxides examined, by lowering the activation energy.

The catalytic dehydrogenation of ethylbenzene is of importance in the manufacture of styrene, which is used for various processes such as the production of synthetic rubber and resins by polymerization. Potassium-promoted iron oxide with a minor amount of chromium oxide incorporated as a structural stabilizer, known as Shell 105, has widely been used in most dehydrogenation plants.[1] As the flow rate of ethylbenzene is high, even small improvements in the activity and selectivity of a catalyst bring about substantial advantages; it has recently been discovered that a potassium-promoted iron oxide catalyst containing minor but effective amounts of cerium oxide and molybdenum oxide but no chromium oxide exhibits a high selectivity at a high overall conversion level.[2] Dehydrogenation has extensively been studied on potassium-promoted iron oxide containing chromium oxide;[3] and reported in numerous patent papers, however, few basic studies on the catalysts containing other transition metal oxides, such as cerium oxide and molybdenum oxide, have been reported. In this work various transition metal oxides were added to the potassium-promoted iron oxide and the resulting effects upon the catalytic activity and selectivity were studied in the present work.

Experimental

All the catalysts examined were prepared by wet mixing of iron(III) oxide, potassium carbonate and a suitable amount of transition metal oxide; cerium(IV) oxide was initially added as carbonate, which decomposed to oxide in a calcination process. The resulting pastes were transformed into 3.2 mm dia. and 4—6 mm length extrudates; the extrudates were dried at 120 °C overnight and calcined at 600 °C for 4 h in the presence of air, then crushed into granules of 16/20 mesh before being used for the activity test. Each catalyst contained 28% potassium carbonate and 5 or 2.5% of a transition metal oxide, i.e., 5% of cerium(IV) oxide, chromium(III) oxide and zirconium(IV) oxide or 2.5% of vanadium(V) oxide, niobium(V) oxide, tungsten(VI) oxide, and molybdenum(VI) oxide, the rest was iron oxide. The activity test was carried out in a temperature range from 550 to 620 °C in the presence of steam; a steam to ethylbenzene molar ratio of 11.8 was maintained under atmospheric pressure. A differential-type reactor consisted of stainless steel (20 mm dia.) containing 3 g catalyst was used with a total SV of 39100 ml g^{-1} h^{-1}.** The products were condensed in an annular condenser; in addition to ethylbenzene (EB) and water, the condensate contained styrene (ST) and small amounts of benzene (Bz) and toluene (Tol). The surface area was measured by the BET method. The acidity and basicity of the catalysts were determined by the irreversibly adsorbed amounts of butylamine (nBA) at 80 °C and acetic acid (AA) at 130 °C, respectively, using the gas chromatographic pulse technique;[4] nBA pulses and AA pulses were fed into a U-tube containing 2 g of catalyst.

Results and Discussion

The activities measured for the various catalysts are given in Fig. 1: The natural logarithms of the rates of styrene, benzene and toluene formations at 580 °C are plotted against the electro-negativities (EN) of the transition metal oxides added; the EN values are the geometric means of Pauling's values[5] for the elements included in the oxides, calculated on the basis of the electronegativity equalization postulated by Sanderson.[6] It is found that all rates were

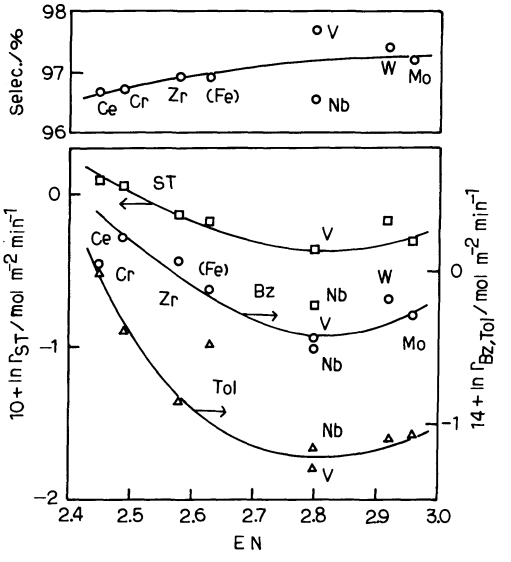

Fig. 1. Relations of the rates of ST, Bz, and Tol formation and the selectivity to ST with the EN of various transition metal oxides added to potassium-promoted iron oxide; 580 °C.

** The reaction rates were determined from the relation of $r=(F/S)\cdot X$, where F, S, and X represent the feed rate of ethylbenzene, the surface area of the catalyst, and the fraction of ethylbenzene converted into each product, respectively.

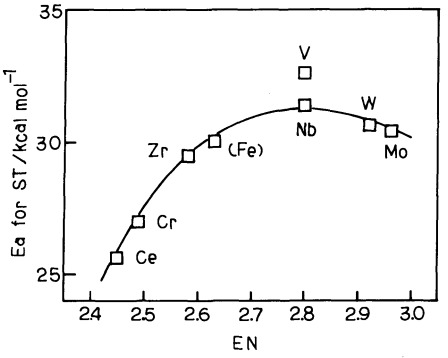

Fig. 2. Relation between the activation energies for ST formation and the *EN* of various transition metal oxides.

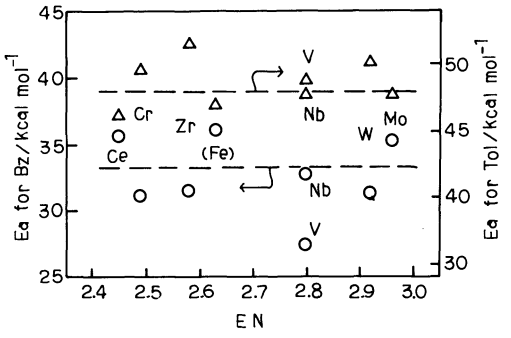

Fig. 3. Plots of the activation energies for Bz and Tol formations vs. *EN* of various transition metal oxides.

markedly influenced by the *EN* of the added oxides. All rates decreased with increasing the *EN*, then slightly increased after reaching the minimum at *EN* of 2.8, which corresponds to the promoters of vanadium oxide and niobium oxide. Since the extent of the initial reduction of the rate of toluene formation with the increase in *EN* was larger than those of styrene and benzene formations, the selectivity to styrene apparently increased with the increase in *EN*. Among the promoters examined, CeO_2 brought about the highest activity and V_2O_5 brought about the lowest activity, though the last promoter best improved the selectivity.

The activation energies (E_a) for the styrene, benzene and toluene formations over the various catalysts were obtained in a temperature range 550—620 °C, they are plotted in Figs. 2 and 3 against the *EN* values of the promoter oxides added. Indicated in Fig. 2 is a relation between the E_a for styrene formation and the *EN* of the promoters added. The change in E_a with *EN* seems to correspond to the behavior of the styrene formation rate with *EN*, given in Fig. 1: the E_a initially increased with the increase in *EN*, then slightly decreased after reaching a maximum. The CeO_2-containing catalyst had the lowest E_a of 25.6 kcal mol^{-1} (1 cal=4.184 J) and the highest rate of styrene formation. On the other hand,

Table 1. Surface Area (*SA*), Acidity and Basicity of Various Catalysts

Catalyst	*EN*[a]	*SA*	Acidity[b]	Basicity[c]
		$m^2 g^{-1}$	$\mu mol\ m^{-2}$	$\mu mol\ m^{-2}$
Fe-Ce-K	2.45	7.0	0.32	2.60
Fe-Cr-K	2.49	6.2	0.31	2.50
Fe-Zr-K	2.58	5.4	0.36	1.85
Fe-K	2.63	5.9	0.36	2.38
Fe-V-K	2.80	3.5	0.46	2.38
Fe-Nb-K	2.80	6.1	0.33	0.49
Fe-W-K	2.92	5.4	0.55	0.68
Fe-Mo-K	2.96	6.1	0.69	0.34
Fe	—	15.0	2.15	0.34

a) Electronegativity of the transition metal oxide (M_aO_b) added to the potassium-promoted iron oxide catalyst, determined from the relation of $EN=(X_M{}^a \cdot X_O{}^b)^{1/(a+b)}$, where X_M and X_O mean Pauling's electronegativity of each element.[5,6] b) Adsorbed amount of butylamine at 80 °C. c) Adsorbed amount of acetic acid at 130 °C.

there seems to be no relation between the E_a for benzene or toluene formation and the *EN* of various promoters, as shown in Fig. 3. It is therefore suspected that the changes in the benzene and toluene formation rates with *EN*, shown in Fig. 1, are caused by the changes in the numbers of active sites for these formations by the additions of various promoter oxides.

The acid-base properties of the catalysts containing various promoter oxides were determined by the adsorption of butylamine at 80 °C and acetic acid at 130 °C, and are given in Table 1. It can be seen from the table that the *EN* of the promoter oxides added apparently influenced the acid-base property of the potassium-promoted iron oxide, although the correlation between the *EN* of promoters and the measured acid-base properties of the catalysts was not complete however there is a tendency that a promoter oxide of lower *EN* would give higher adsorbed amount of acetic acid, basicity, and lower adsorbed amount of butylamine, acidity, on the catalyst.

Consequently, it was found that the styrene formation rate increased and its E_a decreased as the *EN* of the transition metal oxide added decreased. Decreasing the *EN*, i.e., increasing the basicity of the promoter may give rise to the dehydrogenation activity of the catalyst, because each basic site is considered to abstract hydrogen from hydrocarbons,[7] especially β-hydrogen from ethylbenzene.[8] Cerium oxide was found to be the best promoter for accelerating the styrene formation, and a hydrogen-transfer reaction on this oxide was reported,[9] though the dehydrogenation itself has never occurred on a pure cerium oxide. Interestingly, increasing the *EN*, i.e., acidity, decreased the formations of benzene and toluene; this result is opposite to what has been considered: the decomposition of ethylbenzene has been considered to take place on the acidic sites of the

potassium-promoted iron oxide catalyst.[10]

References

1) K. K. Kearby, *Catalysis,* **3**, 453 (1955).
2) F. J. O'Hara, U. S. Patent 3904552 (1975).
3) S. Carra and L. Forni, *Ind. Eng. Chem., Proc. Des. Dev.,* **4**, 281 (1965); B. D. Herzog and H. F. Rase, *Ind. Eng. Chem., Prod. Res. Dev.,* **23**, 187 (1984); T. Hattori, Y. Murakami, M. Ii, and H. Uchida, *Kogyo Kagaku Zasshi,* **72**, 2188 (1969).
4) M. Ai, *J. Catal.,* **52**, 16 (1978).
5) L. Pauling, *J. Am. Chem. Soc.,* **54**, 3570 (1932).
6) R. T. Sanderson, *Science,* **114**, 670 (1951); *J. Chem. Educ.,* **29**, 539 (1952).
7) T. Yamaguchi, N. Ikeda, H. Hattori, and K. Tanabe, *J. Catal.,* **67**, 324 (1981).
8) I. Wang, W. F. Chang, R. J. Shau, J. C. Wu, and C. S. Chung, *J. Catal.,* **83**, 428 (1983).
9) T. Yamaguchi and H. Shima, *Chem. Lett.,* **1979**, 899.
10) K. Shibata and T. Kiyoura, *Bull. Chem. Soc. Jpn.,* **42**, 871 (1969).

Effective Synthesis of 2-[4-(3-Methyl-2-butenyl)phenyl]propionic Acid via Hydromagnesation Reaction with Nickel or Titanium Catalysts

Takehiro AMANO,* Tomomi OTA, Kensei YOSHIKAWA, Tatsuhiko SANO, Yutaka OHUCHI, Fumie SATO,† Manzo SHIONO,†† and Yoshiji FUJITA††
Research Center, Taisho Pharmaceutical Co. Ltd., Yoshino-cho, Ohmiya, Saitama 330
†Department of Chemical Technology, Tokyo Institute of Technology, Meguro-ku, Tokyo 152
††Central Research Laboratories, Kuraray Co. Ltd., Sakazu, Kurashiki, Okayama 710
(Received December 12, 1985)

Synopsis. 2-[4-(3-Methyl-2-butenyl)phenyl]propionic acid was synthesized in 82% yield via nickel(II) chloride or dichlorobis[η^5-cyclopentadienyl]titanium-catalyzed hydromagnesation of 1-(3-methyl-2-butenyl)-4-vinylbenzene obtained in ca. 63—68% yield by the coupling reaction of 4-(3-methyl-2-butenyl)phenylmagnesium chloride with vinyl chloride.

In the course of our synthetic study of analgesic and antiinflammatory drugs, attention was focused on a convenient synthesis of 2-[4-(3-methyl-2-butenyl)-phenyl] propionic acid (**1**).[1] As the prenyl moiety of **1** was relatively unstable in acidic media or in the presence of oxygen, the method previously employed[1] required multi-step reactions with troublesome handlings to obtain **1** of a high purity. On the other hand, it has been well known that the hydromagnesation reaction of styrene with nickel[2] or titanium[3] catalysts afforded 1-phenylethylmagnesium halides in good yield, which prompted us to apply this reaction to 1-(3-methyl-2-butenyl)-4-vinylbenzene (**3**). Herein we wish to describe a practical three-step synthesis of **1** starting from 1,4-dichlorobenzene (Scheme).

The coupling reaction of the Grignard reagent of 1-chloro-4-(3-methyl-2-butenyl)benzene (**4**)[4] with vinyl chloride was carried out by using iron(III)[5] or nickel(II)[6] catalysts (0.4 mol% vs. **4**) such as iron(III) acetylacetonate, iron(III) chloride, or [1,3-bis(diphenylphosphino)propane]dichloronickel(II) to obtain **3** in 63, 64, and 68% yield, respectively. Rectification of **3** was carried out under reduced pressure to separate (3-

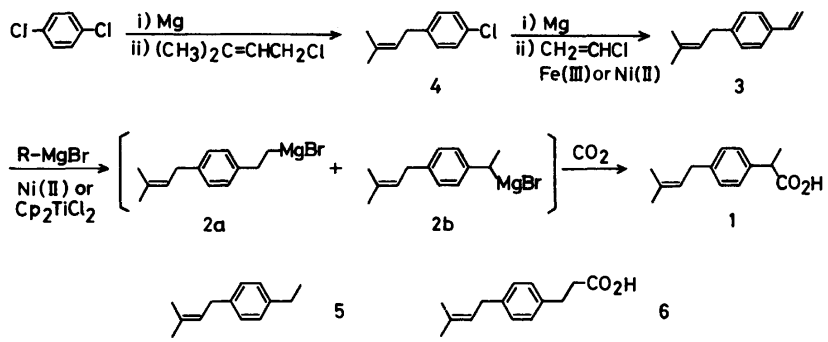

Table 1. Results of the Nickel-Catalyzed Hydromagnesation of **3**

Entry	R-MgBr[a]	Catalysts[b] (mol% vs. **3**)	Reaction Temperature/°C	Reaction Time/h	Yield of **5**/%[c]
1	*i*-C_4H_9	$NiCl_2$ (5)	17—20	4.25	57
2	C_2H_5	$NiCl_2$ (5)	0	5	51
3	C_2H_5	$NiCl_2$ (5)	15—20	1	52
				3	74
				5	79
4	C_2H_5	$NiCl_2$ (5)	30—40	1	36
5	C_2H_5	$NiCl_2$ (10)	15—20	1	55
6	C_2H_5	$NiCl_2$ (2.5)	15—20	2.5	64
7	*i*-C_4H_9	$NiBr_2$ (5)	15—20	4.5	34
8	*i*-C_4H_9	$Ni(acac)_2$ (5)	20	4.2	35
9	*i*-C_4H_9	$NiCl_2(PPh_3)_2$ (5)	20	5.2	6

a) 1.5 Equivalent (vs. **3**) of the Grignard reagent was used in THF. b) $Ni(acac)_2$: Nickel(II) acetylacetonate. c) Determined by GC (OV-1, 1m, 110 °C), using tridecane as the internal standard.

Table 2. Results of the Titanium-Catalyzed Hydromagnesation of **3**

Entry	R-MgBr[a]	Solvent	Catalyst[b] (mol% vs. **3**)	Reaction Temperature/°C	Reaction Time/h	Yield of **5**/%[c]
10	C_3H_7	Et_2O	5	30	5	64
11	*i*-C_3H_7	Et_2O	5	30	12	74
12	C_3H_7	THF	5	50	1	66
					5	90
13	C_3H_7	THF	2.5	50	5	70
14	C_3H_7	THF	10	50	5	58
15	C_3H_7	THF	5	reflux	5	65
16	*i*-C_3H_7	THF	5	50	5	87
17	*t*-C_4H_9	THF	5	50	5	40
18	*i*-C_4H_9	THF	5	50	5	—[d]

a) 1.22 Equivalent (vs. **3**) of the Grignard reagent was used. b) Catalyst: Dichlorobis[η^5-cyclopentadienyl]titanium. c) Determined by GC (OV-1, 1m, 110 °C), using tridecane as the internal standard. d) Only polymerization was observed.

methyl-2-butenyl)benzene (10%), unreacted **4** (ca. 2%), and a trace amount of 4-(3-methyl-2-butenyl)phenol (ca. 0.2%). Then, the optimum conditions of the hydromagnesation reaction of **3** with nickel(II) catalysts were investigated by measuring the yield of 1-ethyl-4-(3-methyl-2-butenyl)benzene (**5**) generated from the intermediary Grignard reagents (**2a,b**) by quenching with water (Table 1). The best yield of **5** was achieved by using ethylmagnesium bromide in the presence of nickel(II) chloride catalyst (5 mol% vs. **3**) at 15—20 °C in THF solvent (Entry 3). Variation of the reaction temperature or the amount of catalyst resulted in the decrease of the yield of **5**. The Grignard reagents (**2a,b**) prepared according to the procedure of Entry 3, in turn, was reacted with carbon dioxide at −10 °C to obtain **1** in 82% yield with a trace amount of 3-[4-(3-methyl-2-butenyl)-phenyl]propionic acid (**6**, 1.5%).

An alternative method for hydromagnesation of **3** was also studied by using dichlorobis[η^5-cyclopentadienyl]titanium catalyst (Table 2). The Grignard reagents (**2a,b**) prepared according to the best procedure of Entry 12 was reacted with carbon dioxide to obtain **1** in also 82% yield. In this case, however, the undesirable regio-isomer (**6**) was formed up to 8% yield, which made the purification process troublesome to some extent.

In conclusion, we employed nickel(II) chloride as the catalyst of the hydromagnesation reaction of **3** in large scale experiments and succeeded in developing a practical three-step method for **1** starting from 1,4-dichlorobenzene.

Experimental

The boiling and melting points were uncorrected. The IR spectra were recorded with a Digilab FTS-20 C/D spectrometer. The NMR spectra were taken with a Varian XL-200 (with hexamethyldisiloxane as an internal standard). GC analyses were made by Shimadzu GC-7AG gas chromatograph using a 3 mm×100 cm column of OV-1 on Celite 545 with He as the carrier gas. 1-Chloro-3-methyl-2-butene is commercially available from Kuraray Co. Ltd., NIC-division.

1-Chloro-4-(3-methyl-2-butenyl)benzene (4). The procedure previously reported was used.[4] Into a solution of 4-chlorophenylmagnesium chloride in THF (2500 ml), prepared from 1,4-dichlorobenzene (438 g; 3 mol) and magnesium (80 g; 3.3 atom) was added 1-chloro-3-methyl-2-butene (343 g 3.3 mol) at 10—15 °C during 2 h. After stirring for 3 h, the reaction mixture was poured into aqueous ammonium chloride and extracted with ether to obtain **4** (361 g; 1.95 mol) in 65% yield. Bp 64—65.5 °C/0.38 mmHg (1 mmHg=133.322 Pa) [lit,[4] bp 84—88 °C/1.5 mmHg].

1-(3-Methyl-2-butenyl)-4-vinylbenene (3). Into a mixture of magnesium (87.6 g; 3.6 atom) in THF (84 ml) was dropped a solution of **4** (542 g; 3 mol) in THF (300 ml) at 110—120 °C during 2 h under nitrogen atmosphere and the mixture was stirred further for 5 h. Thus obtained viscid Grignard reagent of **4** was immediately diluted to 1.5 M solution (1M=1 mol dm^{-3}) by addition of 1630 ml of THF. The Grignard solution was added slowly into a mixture of vinyl chloride (250 g; 4 mol) and iron(III) acetylacetonate (4.5 g; 0.12 mol) in THF (1500 ml) maintaining the reaction temperature at 25—32 °C. After stirring for 2 h, the resulting mixture was poured into aqueous ammonium chloride and extracted with ether. Rectification of the products with a Shibata Fractional Distillation Apparatus Model HPC-A-1500-B(packing column, 70 theoretical plates) gave **3** (325 g; 1.9 mol) in 63% yield with a small amount of lower boiling products [bp 35—58 °C/0.1 mmHg] consisted of (3-methyl-2-butenyl)benzene (41 g; 0.285 mol), unreacted **4** (11 g; 60 mmol), and 4-(3-methyl-2-butenyl)phenol (1 g; 6 mmol). Bp 68—70 °C/0.2 mmHg. IR(neat) 2960, 2900, 1625, 1505, 980, 900, 820 cm^{-1}. ^1H NMR(in $CDCl_3$) δ=1.57—1.73 (m, 6H, 2×CH_3); 3.25 (d, J=7 Hz, 2H, CH_2); 5.0—5.4 (m, 2H, 2×=CH); 5.6 (d, J=18 Hz, 1H, =CH), 6.62 (dd, J=11 and 18 Hz, 1H, =CH); 7.0—7.35 (m, 4H, arom.). Found: C, 90.51; H, 9.42. Calcd. for $C_{13}H_{16}$: C, 90.64; H, 9.36.

2-[4-(3-Methyl-2-butenyl)phenyl]propionic Acid (1). Nickel-Catalyzed Hydromagnesation: Into a mixture of **3** (258 g 1.5 mol) and nickel(II) chloride (9.8 g; 75 mmol) in THF was slowly added a 1 M solution of ethylmagnesium bromide in THF (2250 ml; 2.25 mol) at 15—20 °C to react for 5 h. The reaction mixture was cooled to ca. −20 °C, and dry gaseous carbon dioxide was passed through the bottom of the apparatus maintaining the temperature below −10 °C. After the exothermic reaction stopped, the reaction mixture was poured into aqueous ammonium

chloride and extracted with diisopropyl ether. The organic layer was extracted with 10% aqueous sodium hydroxide (1200 ml; 3 mol). Then, the aqueous layer was neutralized with 0.5 M sulfuric acid and extracted with hexane. The product was purified by distillation under reduced pressure to obtain **1** (268 g; 1.23 mol) in 82% yield. Bp 130—135 °C/0.1 mmHg. IR (neat) 3450—2500, 1700, 1225, 750 cm^{-1}. ^1H NMR (in CCl_4) δ=1.42 (d, J=7.2 Hz, 3H, CH_3), 1.68; 1.8 (s, 6H, 2×CH_3); 3.20 (d, J=7.2 Hz, 2H, CH_2); 3.54 (q, J=7.2 Hz, 1H, CH); 5.18 (t, J=7.2 Hz, 1H, =CH); 6.80—7.12 (m, 4H, arom.); 11.83 (s, 1H, OH). Found: C, 76.94; H, 8.39. Calcd. for $C_{14}H_{18}O_2$: C, 77.03; H, 8.31.

The distillation residue was purified by recrystallization from hexane to obtain 3-[4-(3-methyl-2-butenyl)phenyl]-propionic acid **6** (2.2 g; 10 mmol) in 0.7% yield. Mp 61—62 °C. IR (neat) 3300—2550, 1700, 1290, 940, 820 cm^{-1}. ^1H NMR (in $CDCl_3$) δ=1.72, 1.75 (s, 6H, 2×CH_3); 2.67 (t, J=8 Hz, 2H, CH_2) 2.92 (t, J=8 Hz, 2H, CH_2); 3.32 (d, J=7 Hz, 2H, CH_2); 5.33 (t, J=7 Hz, 1H, =CH); 7.13 (s, 4H, arom.); 10.88 (bs, 1H, OH). Found: C, 76.85; H, 8.35. Calcd. for $C_{14}H_{18}O_2$: C, 77.03; H, 8.31.

Titanium-Catalyzed Hydromagnesation: Dichlorobis[η^5-cyclopentadienyl]titanium (75 mg; 0.3 mmol) was added to a mixture of **3** (1 g; 6 mmol) and propylmagnesium bromide in THF (7.2 mmol in 6 ml) at room temperature under argon atmosphere and the mixture was stirred for 5 h successively. After addition of a small pieces of solid carbon dioxide (ca. 3 g), the resulting mixture was treated as the same manner described before. The products were esterified with diazomethane and analyzed by GC (OV-1, 1 m, 140 °C) using nonadecane as an internal standard. The result showed the formation of **1** in 82% yield and **6** in 8% yield.

References

1) T. Amano, J. Sawada, and M. Sasajima, Japan Kokai Patent, 1979-163545; *Chem. Abstr.*, **93**, 26117 (1980).

2) L. Farady and L. Marko, *J. Organomet. Chem.*, **28**, 159 (1971); T. A. Hilton, Japan Kokai Patent, 1981-97246.

3) H. L. Finkbeiner and G. D. Cooper, *J. Org. Chem.*, **27**, 3395 (1962); F. Sato, H. Ishikawa, and M. Sato, *Tetrahedron Lett.*, **21**, 365 (1980).

4) L. B. Jones and J. P. Foster, *J. Org. Chem.*, **35**, 1777 (1970).

5) M. Tamura and J. K. Kochi, *J. Am. Chem. Soc.*, **93**, 1487 (1971); S. M. Neumann and J. K. Kochi, *J. Org. Chem.*, **40**, 599 (1975).

6) R. J. P. Corriu and J. P. Masse, *J. Chem. Soc., Chem. Commum.*, **1972**, 144; K. Tamao, K. Sumitani, and M. Kumada, *J. Am. Chem. Soc.*, **94**, 4374 and 9268 (1972).

Thermically-Initiated Fluorinations at Saturated Carbon Atoms with Xenon Difluoride

Barbara ZAJC and Marko ZUPAN*
Institute "Jožef Stefan" and the Department of Chemistry, "E. Kardelj" University of Ljubljana, 61000 Ljubljana, Yugoslavia
(Received August 6, 1985)

Synopsis. The heating of several hydrocarbons with xenon difluoride at 95—120 °C in stainless steel reactors equipped with teflon jackets resulted in mono-, di-, and trisubstituted products.

It has been demonstrated that xenon difluoride reacts with several types of organic molecules but the main interest was directed towards the fluorination of alkenes, aromatic, and heteroaromatic molecules.[1-3] In most cases fluorinations have been carried out in a liquid phase and the presence of an appropriate catalyst has also been pointed out. On the other hand much less attention has been paid to reactions carried out at higher temperatures or in the vapor phase. Fourteen years ago Mackenzie and Fajer[4] reported that xenon difluoride also reacted with several aromatic molecules at temperatures between 100—200 °C but substitution reactions were also accompanied by the additional process, their extension depending on the structure of the substrate, molar ratio of xenon difluoride to the starting compound and temperature.

In our continuous interest in the fluorination of organic compounds with xenon difluoride we found it instructive to investigate reactions with several saturated hydrocarbons.

Results and Discussion

Direct substitution of hydrogen at a saturated carbon atom by fluorine represents a different problem from that of the introduction of chlorine or bromine[5] and several special techniques have been developed.[6] Adcock and coworkers[7] made an important contribution to direct fluorine introduction using a low temperature reaction of fluorine with an aerosol suspension of hydrocarbons. Barton and coworkers[8] recently found that functionalization of saturated carbon atoms is also possible with fluorine or CF_3OF but only one report on direct hydrogen atom substitution with xenon difluoride appeared and experimental details were so sparse that we were unable to repeat the direct fluorination of adamantane in CS_2 which should result in the formation of 1-fluoroadamantane.[9] Patrick and coworkers[10] have recently demonstrated that functionalization of a saturated carbon atom is also possible by xenon difluoride and they found that carboxylic acids are transformed to fluoro-substituted products by decarboxylation.

Mixtures of 2 mmols of several hydrocarbons, e.g. hexane or adamantane, with 2 mmols of xenon difluoride were heated in 20 ml sealed glass tubes up to 70 °C no reaction occurred. Further increases in temperature to 80—90 °C resulted in a violent reaction accompanied by flame and a complete decomposition of xenon difluoride, and the crude reaction mixture containing a small amount of unreacted substrate, hydrogen fluoride and tar was obtained. We then replaced the glass ampoules with 35 ml reflon jackets inserted in stainless steel containers and found that the heating of 2 mmols of cyclohexane and 2 mmols of xenon difluoride at 105 °C resulted in the complete decomposition of xenon difluoride. Again only tar was obtained. However, when the 35 ml teflon reactor was filled with 15 mmols of cyclohexane and 3 mmols of xenon difluoride and the mixture was heated for 2.5 h at 105 °C, the reaction mixture containing fluorocyclohexane with 18% yield (calculation based on xenon difluoride) was obtained. Reproducible fluorination of cyclohexane with xenon difluoride under the above-mentioned conditions could be observed only when the teflon jacket was thoroughly cleaned and dried.

The 2.5 h reaction of 15 mmols of hexane and 3 mmols of xenon difluoride at 105 °C resulted in the formation of three monofluoro-substituted products with a total yield of 15—20% (calculation based on xenon difluoride). Product distributions were determined by ^{19}F NMR and a good reproducibility of product distribution was observed (data stated in the Scheme are the average of three experiments and differ by only ±2%). It is evident from the product distribution that secondary carbon atoms are more reactive than primary to fluorine substitution by xenon difluoride.

Free radical reactions with adamantane have been studied in detail with the relative reactivity of C_1 and C_2 carbon strongly depending on the reagent, i.e. reaction with R_2N^+H proceeds 99% at C_1, reaction with $\cdot CCl_3$ proceeds 86% at C_1 while chlorination in CCl_4 yields nearly equivalent amounts of 1- and 2-chloroadamantane.[11] The 70 min reaction of 2 mmols of adamantane and 2 mmols of xenon difluoride in a teflon reactor at 105 °C gave a crude reaction mixture containing four fluoro-substituted products. Total yield of fluoro-substituted products, calculation based on xenon difluoride, was 18—20%. The yield of fluoro-substituted products was nearly doubled when instead of 2 mmols only 1 mmol of adamantane was used in the presence of 2 mmols of xenon difluoride while product distribution was only slightly influenced. Crude reaction mixtures were analyzed by ^{19}F NMR spectroscopy and product distribution resulting in the experiment using 2 mmols of adamantane is presented in the Scheme.

SCHEME

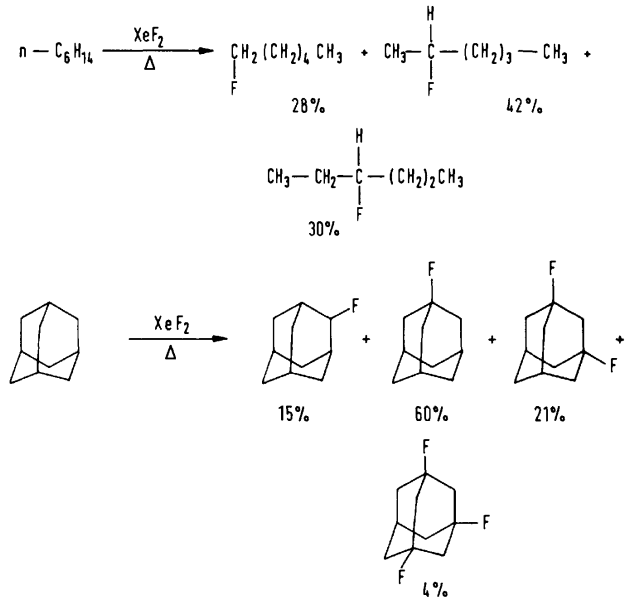

Pure samples of products were isolated by preparative GLC and structures were determined on the basis of spectroscopic data and their comparison with the literature. From the product distribution it is evident that the difference in reactivity between the secondary and tertiary carbon atoms in adamantane is much larger than that observed in hexane between the primary and secondary carbon atoms.

Experimental

IR spectra were recorded using a Perkin Elmer 727-B spectrometer and ^1H and ^{19}F NMR spectra by a Jeol JNM-PS-100 with Me_4Si or CCl_3F as the internal reference. Mass spectra and high resolution measurements were taken on a CEC-21-110 spectrometer. Gas liquid partition chromatography was carried out on a Varian 2700 Model.

Fluorination of Cyclohexane and Hexane. 15 mmols of hexane or cyclohexane and 3 mmols of xenon difluoride were placed in a teflon jacket (35 ml) which was inserted into a stainless steel container. The reaction mixture was heated for 150 min at 105±2 °C, cooled, after which 20 ml of ether was added to the reaction mixture, washed with aqueous $NaHCO_3$, water (twice), dried over Na_2SO_4, and the solvent partly evaporated under vacuum. Crude reaction mixtures were analyzed by ^{19}F NMR (octafluoronaphthalene was added as the internal standard). Fluorination of hexane resulted in the formation of three products with a total yield of 20% of fluoro-substituted products (calculation based on xenon difluoride). The crude reaction mixture contained the following three products: 1-Fluorohexane,[12] 2-fluorohexane,[13] and 3-fluorohexane[14] with relative yields of 28±2, 42±2, and 30±2%, respectively. The fluorination of cyclohexane gave only one product with a yield of 18% (calculation based on xenon difluoride) while pure fluorocyclohexane was isolated by preparative GLC (OV 17 10%, Chromosorb A 45/60, 60 °C), with 12% yield. Spectroscopic data are in agreement with those in the literature.[15]

Fluorination of Adamantane. 2 mmols of adamantane and 2 mmols of xenon difluoride were placed in a teflon jacket (35 ml) which was inserted into a stainless steel container. The reaction mixture was heated for 70 min at 105±2 °C, cooled and then 20 ml of ether were added to the reaction mixture, washed with aqueous $NaHCO_3$, water (twice), dried over Na_2SO_4, and the solvent evaporated under vacuum. The crude reaction mixture was analyzed by ^{19}F NMR, indicating the presence of four products: 1-fluoroadamantane, 2-fluoroadamantane, 1,3-difluoroadamantane, and 1,3,5-trifluoroadamantane with the following relative yields (determined by ^{19}F NMR): 60±2, 15±2, 21±3, and 4±0.5%, respectively. Separation of the combined crude reaction mixtures, obtained in three experiments, by GLC (OV-17 10%, Chromosorb A 45/60, 110 °C) gave pure 1-fluoroadamantane, 1,3-difluoroadamantane, and the mixture of 2-fluoroadamantane and 1,3,5-trifluoroadamantane, which were further separated by GLC (DNP 10% 3 m, Chromosorb W HP 80/100, 150 °C).

1-Fluoroadamantane: 35 mg (7.6%) of crystalline product, mp (sealed tube) 210—212° (mp_{lit} 210—212 °C),[16] NMR δF: −129.3 (broad s), δH: 1.6 (m, 6H), 1.9 (m, 6H), 2.2 (broad s, 3H). Mass spectrum: Calcd. for $C_{10}H_{15}F$ *m/z* 154.1158, found *m/z* 154.1155, *m/z* (rel intensity) 155 (M^++1, 11%), 154 (M^+, 87), 111 (20), 98 (39), 97 (100), 96 (34), 94 (21), 93 (31), 91 (10), 79 (19), 77 (14), 67 (12), 53 (10), 43 (26), 41 (24), 39 (27).

2-Fluoroadamantane: 8 mg (1.7%) of crystalline product, mp (sealed tube) 254—255 °C (mp_{lit} 254—255 °C),[17] NMR δF=−175 (dm, $^2J_{FH}$=51 Hz), δH=1.7 (m, 10H), 2.1 (m, 4H), 4.7 (dm, $^2J_{FH}$=51 Hz, 1H). Mass spectrum: Calcd for $C_{10}H_{15}F$ *m/z* 154.1158, found *m/z* 154.1160, *m/z* (rel intensity) 155 (M^++1, 12%), 154 (M^+, 100), 114 (41), 111 (12), 98 (14), 97 (27), 96 (13), 95 (15), 93 (34), 92 (26), 91 (19), 81 (13), 80 (21), 79 (51), 78 (15), 77 (17), 67 (17), 56 (12), 55 (10), 53 (12), 41 (25).

1,3-Difluoroadamantane: 13 mg (2.5%) of crystalline product, mp 239—240° (mp_{lit} 240—241 °C),[16] NMR δF=−137 (broad s), δH=1.5 (broad s, 2H), 1.8 (m, 8H), 2.1 (t, $^3J_{FH}$=5.5 Hz, 2H), 2.5 (broad s, 2H). Mass spectrum: Calcd for $C_{10}H_{14}F_2$ *m/z* 172.1063, found *m/z* 172.1065, *m/z* (rel intensity) 173 (M^++1, 8%), 172 (M^+, 66), 116 (25), 115 (89), 114 (31), 111 (32), 110 (10), 109 (10), 97 (52), 96 (17), 93 (15), 91 (10), 77 (13), 59 (14), 58 (44), 56 (19), 51 (10), 43 (100), 42 (13), 41 (22).

1,3,5-Trifluoroadamantane: 2.2 mg (0.5%) of crystalline product, mp (sealed tube) 243—245 °C (mp_{lit} 244—245 °C),[16] NMR δF=−142 (broad s), δH=1.8 (m, 6H), 2.1 (m, 6H), 2.5 (m, 1H). Mass spectrum: Calcd. for $C_{10}H_{13}F_3$ *m/z* 190.0969, found *m/z* 190.0966, *m/z* (rel intensity) 191 (M^++1, 10%), 190 (M^+, 91), 134 (22), 133 (81), 132 (28), 129 (28), 115 (100), 114 (14), 111 (26), 110 (10), 109 (16), 102 (10), 97 (18), 77 (13), 65 (10), 59 (26), 57 (14), 56 (67), 51 (17), 41 (18).

References

1) R. Filler, *Isr. J. Chem.*, **17**, 71 (1978).
2) M. Zupan, "Xenon Halide Halogenations" in "The Chemistry of Functional Groups, Supplement D," ed by S. Patai and Z. Rappoport, Wiley, New York (1983), p. 657.
3) M. Zupan, *Vestn. Slov. Kem. Druš.*, **31**, (Suppl.), 151 (1984).
4) D. R. MacKenzie, J. Fajer, *J. Am. Chem. Soc.*, **92**, 4994 (1970).
5) "The Chemistry of the Carbon-Halogen Bond," ed by S. Patai, Wiley, New York (1973), Vols. 1 and 2; de la Mare, P.B.D. "Electrophilic Halogenation," Cambridge University Press, Cambridge (1976).
6) W. A. Sheppard and C. M. Sharts, "Organic Fluorine Chemistry," W. A. Benjamin, New York (1969); R. D. Chambers, "Fluorine in Organic Chemistry," Wiley, New York (1973).

7) J. L. Adcock, K. Horita, and E. B. Renk, *J. Am. Chem. Soc.*, **103**, 6937 (1981).
8) D. H. R. Barton, R. H. Hesse, R. E. Markwell, and M. M. Pechet, *J. Am. Chem. Soc.*, **98**, 3034 (1976); D. Alker, D. H. R. Barton, R. H. Hesse, J. Lister-James, R. E. Markwell, M. M. Pechet, S. Rozen, T. Takeshita, and H. T. Toh, *Nouv. J. Chim.*, **4**, 239 (1980).
9) A. T. Podkhalyuzin and M. P. Nazarova, *Zh. Org. Khim.*, **11**, 1568 (1975).
10) T. B. Patrick, K. K. Johri, and D. H. White, *J. Org. Chem.*, **48**, 4158 (1983).
11) C. V. Smith and W. E. Billups, *J. Am. Chem. Soc.*, **96**, 4307 (1974).
12) G. Filipovich and G. V. D. Tiers, *J. Phys. Chem.*, **63**, 761 (1959).
13) R. A. Bartsch and J. F. Bunnett, *J. Am. Chem. Soc.*, **90**, 408 (1968).
14) J. K. Borchardt, J. C. Swanson, and W. H. Saunders Jr., *J. Am. Chem. Soc.*, **96**, 3918 (1974).
15) F. A. Bovey, W. W. Anderson, F. P. Hood, and R. L. Kornegay, *J. Chem. Phys.*, **40**, 3099 (1964).
16) K. S. Bhandari and R. E. Pincock, *Synthesis*, **9**, 655 (1974).
17) G. A. Olah, J. T. Welch, D. Y. Vankar, M. Nojima, I. Kerekes, and J. A. Olah, *J. Org. Chem.*, **44**, 3872 (1979).

Rapid Spectrophotometric Determination of Scandium(III) with (Pyridylazo)- and (Thiazolylazo)naphthols

Chander Dhar SHARMA, Sujansingh G. NAGARKAR, and Muppalla C. ESHWAR*
Department of Chemistry, Indian Institute of Technology, Bombay-400 076, India
(Received April 15, 1985)

Synopsis. Scandium(III) reacts with 1-(2-pyridylazo)-2-naphthol [PAN] and 1-(2-thiazolylazo)-2-naphthol [TAN] in weakly acidic media to yield red colored 1:1 and 1:2 chelates, respectively. These complexes are sparingly soluble in water but readily soluble in ≥24% (v/v) acetone and ≥32% (v/v) methanol, giving maximum absorbances at 545 and 570 nm for the PAN and TAN complexes, respectively. Beer's law is obeyed over the concentration ranges of 0.16 to 1.40 μg and 0.08 to 1.40 μg of Sc(III) per ml with PAN and TAN. The scandium(III) complexes formed with PAN and TAN have the molar absorptivities of 1.90×10^4 and 2.93×10^4 $dm^3\,mol^{-1}\,cm^{-1}$ at their absorption maxima, respectively. The effect of diverse ions on the determination of scandium with these reagents is also investigated.

Pyridylazo and thiazolylazo dyes are sensitive chromogenic reagents for metal ions and a wide range of applications in analytical chemistry have been reported with these dyes. 5-Ethylamino-2-(2-pyridylazo)-*p*-cresol and 5-ethylamino-2-(2-thiazolylazo)-*p*-cresol[1] yield intensely colored complexes with scandium, but these reagents are relatively less selective for scandium(III). The reaction of scandium with 4-(2-pyridylazo)resorcinol [PAR] requires 10 min for complete color development[2] at room temperature and a large number of ions have been reported[2,3] to interfere. The complex formation between scandium(III) and 4-(2-thiazolylazo)resorcinol [TAR] is quite sensitive but a preliminary separation of scandium(III) by ion-exchange chromatography[4] is needed to prevent metal interferences. Among various other types of dyes, chrome azurol S has been widely studied[5–8] for the spectrophotometric determination of scandium. It has been found that the addition of various surfactants is very effective for obtaining intensely colored complexes. In the absence of surfactants, the method requires 90 min for full color development at room temperature. Even in the presence of surfactants, the reaction is not always instantaneous.[7,8] Similarly, the color development for the complexes with xylenol orange,[9] arsenazo I[10] and chromotrope 2B[11] requires 10 to 30 min at room temperature. The present method involves the instantaneous reactions of scandium(III) with 1-(2-pyridylazo)-2-naphthol [PAN] and 1-(2-thiazolylazo)-2-naphthol [TAN] at room temperature in the absence of any surfactant.

Experimental

Apparatus and Reagents. All absorbance measurements were made on a EC Spectrophotometer GS 866C with 10-mm cells. The absorption spectra were recorded on a Varian Superscan 3 UV-Visible Spectrophotometer. An EC-pH meter (Model 822) was used for pH measurements.

A 0.768 g amount of scandium oxide (AnalaR) was heated with 30 ml of concentrated nitric acid. The clear solution obtained was diluted to 250 ml with doubly distilled water and the scandium content [2.227×10^{-2} M(1 M=1 mol dm^{-3})] was verified complexometrically. A 0.5 g amount of 1-(2-pyridylazo)-2-naphthol, PAN [Fluka A.G. purum] was dissolved in 250 ml of acetone to give a 0.2% solution. A 0.1% (w/v) methanolic solution of TAN was prepared from 1-(2-thiazolylazo)-2-naphthol [Fluka A.G. purum]. A buffer solution of pH 5.0 was prepared from 0.05 mol dm^{-3} hydrochloric acid and 0.05 mol dm^{-3} hexamine (AnalaR) solutions.

General Procedure. An aliquot of solution containing ≤35 μg of scandium was taken, for both systems, in a 25 ml volumetric flask containing 5 ml of hexamine buffer adjusted to pH 5.0. After the addition of 3.5 ml of 0.2% PAN, the scandium(III) complex formed was dissolved in 10 ml of acetone. On the other hand, the scandium(III)–TAN complex obtained with 3.0 ml of 0.1% TAN was dissolved in 10 ml of methanol. The content was made upto 25 ml with doubly distilled water and the absorbance of the complex was measured against a reagent blank at 545 nm for the PAN complex or 570 nm for the TAN complex.

Results and Discussion

Scandium(III) reacts instantaneously with PAN and TAN in weakly acidic media to form sparingly soluble red-colored chelates, which are soluble in acetone and methanol, respectively.

Effect of pH. The pH of the reaction mixture was varied in both the systems from 1.0 to 10.0. A constant maximum absorbance was observed in the pH range 4.5—5.5 and 4.2—5.6 for the scandium(III)–PAN and scandium(III)–TAN systems, respectively. Hence all the studies were carried out in a hexamine–hydrochloric acid buffer solution adjusted to pH 5.0.

Effect of Reagents Concentration. Volume of 0.2% PAN was varied from 0.2 to 5.0 ml for 25 μg of scandium(III), a constant maximum absorbance being obtained on addition of ≥3.0 ml reagent. Similarly for the same amount of scandium(III), a constant maximum absorbance was obtained on addition of ≥2.2 ml of 0.1% TAN. Thus, 3.5 ml of 0.2% PAN or 3.0 ml of 0.1% TAN was employed in further studies.

Choice of Solvent. It was found that, of the solvents examined, acetone and methanol were the best solvents for dissolving the PAN and TAN complexes, respectively. Since these complexes exhibited maximum absorbance in the solutions containing ≥24% (v/v) acetone and ≥32% (v/v) methanol, 10 ml each of acetone and methanol was employed to dissolve the complexes with PAN and TAN, respectively.

Table 1. Effect of Diverse Ions
(Amount of scandium(III) 25 μg/25 ml)

Sc(III)-PAN		Sc(III)-TAN	
Foreign ion added	Tolerance limit/μg	Foreign ion added	Tolerance limit/μg
Cl^-, Ca(II), Sr(II), Ba(II), As(III)	>25,000	Cl^-, Br^-, Mg(II), Ca(II), Sr(II), Ba(II)	>25,000
Br^-, urea, Mg(II)	20,000	Urea	20,000
$S_2O_3^{2-}$	8,000	I^-	15,000
NH_2OHHCl	7,000	Acetate	10,000
Thiourea	5,000	Thiourea	5,500
I^-	4,000	NH_2OHHCl, SCN^-	5,000
SCN^-, Ag(I)[a]	3,000	$S_2O_3^{2-}$, succinate	2,500
Pt(IV)[b]	1,400	Pt(IV)[d]	1,500
Acetate	1,000	CN^-, Al(III)	1,000
Au(III)	750	Rh(III)	750
Hg(II)	500	Au(III)	600
Sb(III)	400	Ag(I)[e]	450
Ce(III)	250	Citrate	400
Al(III), Rh(III), La(III)	200	Cr(III)	300
Cd(II), Cr(III), Ru(III), Th(IV)	150	Hg(II)[d]	200
Fe(III)	125	Cd(II)[d], La(III)	150
CN^-, citrate, succinate	100	Ascorbate, Ru(III)	100
$N_2H_4H_2SO_4$, phthalate, Sn(II), Mo(VI), U(VI)	50	Pb(II)[f], Sn(IV)	80
Ascorbate, Pb(II)[c], Zr(IV)	40	Ce(III)	60
In(III), Tl(III), Bi(III), Ti(IV), Hf(IV)	25	Fe(III)[g], Bi(III)[h]	40
$C_2O_4^{2-}$, Mn(II), Ga(III)	20	Mn(II)[g], Tl(III)[g], Th(IV)	30
F^-, $EDTA^{4-}$, Co(II), Ni(II), Cu(II), V(IV, V)	nil	Y(III), Se(IV), Zr(IV)[g], Hf(IV)[g], Mo(VI)	25
		Cu(II)[i], Sb(III)	20
		Fe(II)[g], Ni(II)[g]	10
		F^-, $C_2O_4^{2-}$, $EDTA^{4-}$, Co(II), Ti(IV), V(IV, V)	nil

Masked with a) $Na_2S_2O_3$ (2.02×10^{-3} M). b) NaSCN (1.48×10^{-3} M). c) $NaCH_3COO$ (4.87×10^{-4} M). d) NaSCN (2.47×10^{-3} M). e) $Na_2S_2O_3$ (6.32×10^{-4} M). f) $NaCH_3COO$ (4.87×10^{-3} M). g) KCN (6.14×10^{-4} M). h) KI (3.6×10^{-3} M). i) NH_2CSNH_2 (2.89×10^{-3} M).

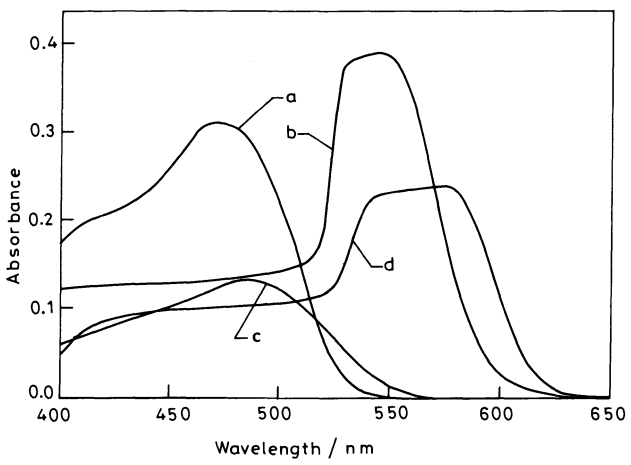

Fig. 1 Absorption Spectra.
Curves a): Reagent blank vs. solvent, [PAN] = 4.02×10^{-4} mol dm^{-3}. b): Sc(III)-[PAN] complex vs. reagent blank, [Sc(III)] = 1.78×10^{-5} mol dm^{-3}, [PAN] = 1.12×10^{-3} mol dm^{-3}. c): Reagent blank vs. solvent, [TAN] = 7.84×10^{-6} mol dm^{-3}. d) Sc(III)-TAN complex vs. reagent blank, [Sc(III)] = 7.77×10^{-6} mol dm^{-3}, [TAN] = 4.71×10^{-4} mol dm^{-3}.

Stability. The scandium(III) complexes thus formed are stable for 24 h (PAN complex) and 10 h (TAN complex).

Spectral Characteristics. The absorption spectra of the scandium(III) complexes with PAN and TAN and those of the respective reagent blanks are given in Fig. 1. The PAN and TAN complexes exhibited their absorption maxima at 545 and 570 nm, respectively.

Composition of Complex. The composition of the Sc(III)-PAN and Sc(III)-TAN complexes, established by the mole ratio method and the Job's method, was found to be 1:1 and 1:2, metal-to-ligand, ratios respectively.

Beer's Law and Sensitivity. The Sc(III)-PAN and Sc(III)-TAN complexes obeyed Beer's law over the concentration ranges 0.16 to 1.40 μg and 0.08 to 1.40 μg respectively of scandium(III) per ml, the molar absorptivities being 1.90×10^4 (at 545 nm) and 2.93×10^4 (at 570 nm) $dm^3\,mol^{-1}\,cm^{-1}$; the Sandell sensitivities, 2.30 and 1.50 ng cm^{-2}, respectively.

Effect of Diverse Ions. The effect of various anions and cations was studied in both the systems by setting the tolerance limit at an amount to cause an

error of ±2.0% in the determination of scandium. The effect of diverse ions is presented in Table 1.

Precision and Accuracy. The coefficient of variation and the relative mean error, calculated from ten replicate determinations with 25 μg of scandium(III), were found to be ±0.86 and ±0.98% for the scandium–PAN system and ±0.90 and ±1.41% for the scandium–TAN system.

References

1) S. I. Gusev and L. M. Shurova, *Uchen. Zap. Perm. Gos. Univ.*, **289**, 271 (1973), cf., *Anal. Abstr.*, **29**, 3B67 (1975).
2) L. Sommer and M. Hnilickova, *Anal. Chim. Acta*, **27**, 241 (1962).
3) A. I. Busev and C. Fan, *Talanta*, **9**, 101 (1962).
4) T. Shimizu and E. Momo, *Anal. Chim. Acta*, **52**, 146 (1970).
5) R. Ishida and N. Hasegawa, *Bull. Chem. Soc. Jpn.*, **40**, 1155 (1967).
6) V. N. Tikhonov and S. G. Danilova, *Zh. Anal. Khim.*, **35**, 1264 (1980).
7) Y. Zheng and S. Zhou, *Fenxi Huaxe*, **11**, 210 (1983), cf., *Anal. Abstr.*, **46**, 3B53 (1984).
8) Y. Ci, Y. Zhao, K. Hu, and L. Wen, *Fen Hsi Hua Hsueh*, **9**, 64 (1981), cf., *Anal. Abstr.*, **41**, 3B83 (1981).
9) O. V. Konkova, *Zh. Anal. Khim.*, **19**, 73 (1964).
10) V. A. Nazarenko and E. A. Biryuk, *Ukr. Khim. Zh.*, **29**, 198 (1963).
11) S. P. Sangal, *Microchem, J.*, **8**, 313 (1964).

 © 1986 The Chemical Society of Japan Bull. Chem. Soc. Jpn., 59, 1665—1669 (1986)

A Study of the Reactivity of Surface-Adsorbed Oxygen Species with C_2H_6 on V_2O_5/SiO_2

Eiji IWAMATSU, Ken-ichi AIKA,* and Takaharu ONISHI
Research Laboratory of Resources Utilization, Tokyo Institute of Technology, 4259 Nagatsuta, Midori-ku, Yokohama 227
(Received October 30, 1985)

The properties and reactivities of surface oxygen species including O^- on V_2O_5/SiO_2 were studied in connection with the oxidative dehydrogenation of C_2H_6 by N_2O. O^- was formed through N_2O on reduced V_2O_5 supported on SiO_2 which had been prepared from tetraethyl silicate, whereas it was not formed on V_2O_5 supported on SiO_2 obtained from other sources. One mole of O^- on V_2O_5/SiO_2 was found to react with one mole of C_2H_6 at 298K. No oxygen species other than O^- reacted with C_2H_6 at 298K. The surface reaction mechanism was discussed, and ethoxide was considered to be one of the surface intermediates. All the other surface oxygens but O^- reacted with C_2H_6 above 573K. Since a catalytic oxidative dehydrogenation reaction of C_2H_6 was active above 573K, the surface oxygens other than O^- were considered to be responsible for this reaction. The possibility of O^- as the reaction intermediate was also discussed.

Paramagnetic oxygen species, such as O^-, O_2^-, and O_3^- have been studied on oxide catalysts by means of EPR techniques.[1] O^- on the MgO surface has been found to react with alkanes under mild conditions, and the mechanism of the surface reaction has been studied.[2] On the other hand, as O^- is formed through N_2O, several attempts at getting useful products by means of the reaction of N_2O with alkane have been carried out. Methanol and formaldehyde have been obtained selectively over MoO_3/SiO_2 and other oxide systems by a reaction of CH_4 with N_2O in the presence of H_2O.[3,4] Phenol has also been obtained by a reaction of benzene with N_2O under similar conditions.[5] In these works, O^- is treated as an active intermediate.[3-5] However, since the conditions of O^- formation are very different from the conditions of the catalytic reactions, no relationship between the catalytic reactions and the surface reactions involving O^- have yet been studied well. The present authors intended to study both the catalytic reaction of C_2H_6 oxidation and the surface reaction of O^- with C_2H_6 on the same catalyst. C_2H_6 was used for the reactant because of the ease of handling and product analysis. V_2O_5/SiO_2 was chosen because it was an active catalyst of C_2H_6 oxidation and because it was a rare system in yielding O^- from O_2.[6] The reaction of O^- with hydrocarbons on this catalyst has not been studied extensively, although the reactivity of O_2^- has been studied well.[6] Thus, we will start by investigating the conditions of O^- formation and will thus study the surface reactivity of both O^- and other surface oxygen species on V_2O_5/SiO_2; finally, these results will be compared with the catalytic performance of the oxidative dehydrogenation reaction of C_2H_6 by the use of N_2O.

Experimental

Materials. Three kinds of SiO_2 were used as supports. SiO_2(A): A reference catalyst supplied by the Catalysis Society of Japan (JRC-SIO-1). SiO_2(B): Obtained by the hydration of tetraethyl silicate in a water–ethanol mixture at boiling point, followed by evaporation at 353K and calcination at 773 K for 5 h.[6] SiO_2(C): Commercial powdered silica (Cab-O-Sil). V_2O_5/SiO_2 was prepared by the impregnation of SiO_2 with 0.3 mol L^{-1} ammonia solution containing ammonium metavanadate (Wako Pure Chemical). The V_2O_5 content was 2.6% by weight. The supported catalysts were calcined at 773 K for 10 h. Unsupported V_2O_5 obtained from Wako Pure Chemical was also used.

Apparatus and Procedure. The surface reactions and catalytic reactions were carried out in a conventional closed-circulation system. Two g of the catalyst were used. The condensable gases are purified by vacuum distillation in the apparatus. The helium was purified through a copper-Kieselgur column. The reactants and products were analyzed by means of a gas chromatograph (FID, TCD) with Porapak Q and MS 5A columns. The EPR spectra were recorded with a JEOL JES-FE-1X spectrometer (X-band) at 77 K. The concentrations and g-factors of O^- were determined by a method similar to one described elsewhere.[2] The catalysts were evacuated at 773 K for 3 h and then oxidized with O_2 at the same temperature overnight before use (standard pretreatment). CO was used as a reduction agent, and the degree of reduction, as measured by CO_2 production, was represented by the percentage change of the V^{5+} ion to the V metal.

Results

Formations of Surface-Adsorbed Oxygen Species. N_2O decomposition took place at 298 K over V_2O_5/SiO_2(B), which had been reduced by CO at 693 K overnight. About 6×10^{-2} mmol of N_2 was produced in 15 min, but O_2 was not produced on this catalyst, unlike as in the Co-MgO system.[7] Following the N_2O decomposition, a concentration of the O^- thus produced was determined by the EPR measurement, while the amount of adsorbed oxygen was determined from the amount of N_2 produced. These values are plotted as a function of the reduction temperature in Fig. 1, where the degree of reduction is also shown. It may be seen that the amounts of O^- are much less than those of the total oxygen adsorbed. The material balance of N_2O suggested that a comparable number of N_2O atoms were also adsorbed as well as oxygen atoms. It

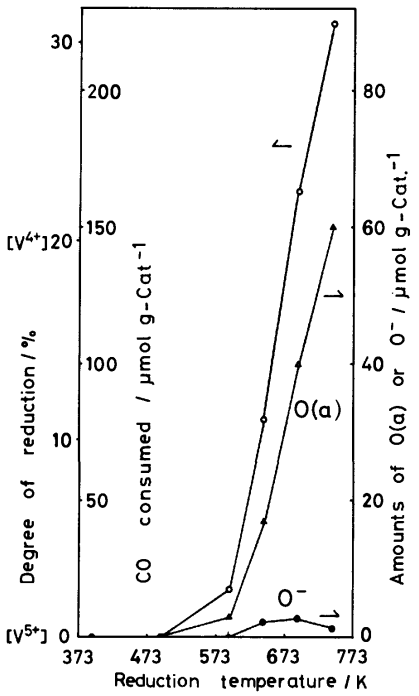

Fig. 1. Variation of the reduction degree of the catalyst and the amount of adsorbed oxygen and O^- after N_2O treatment as a function of the reduction temperature on 2.6wt%V_2O_5/SiO_2(B). 100% reduction corresponds to the whole reduction of V^{5+} ion to V metal.

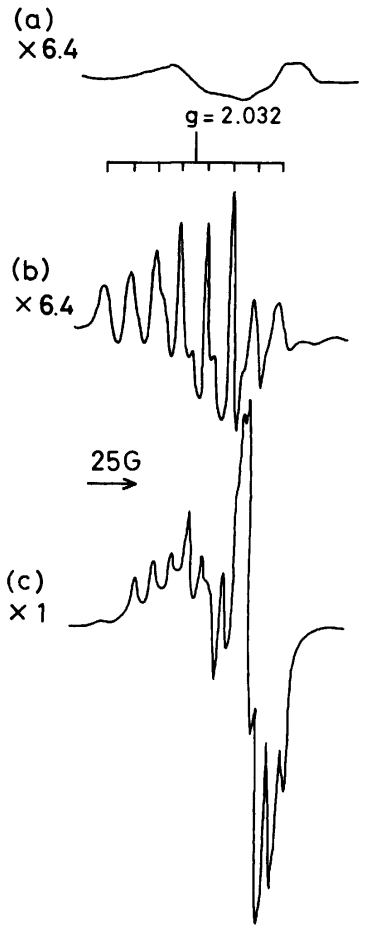

Fig. 2. EPR spectra of 2.6wt% V_2O_5/SiO(B); (a) sample reduced by CO at 693K for 15 h: (b) Sample contacted with N_2O at 298K after (a): (c) Sample contacted with O_2 at 298K after (b).

may also be seen that the concentration of O(a) is roughly proportional to the degree of reduction. It should be noted that O^- was not observed on other V_2O_5 systems, such as V_2O_5/SiO_2(A), V_2O_5/SiO_2(C), or unsupported V_2O_5, after the same pretreatment. O^- was not formed through O_2(1.5 Torr (1 Torr=133.3 Pa)), even on the well-reduced V_2O_5/SiO_2(B), where just O_2^- was produced. The amount of O_2^- produced from O_2 was about ten times more than that of the O^- produced from N_2O.

Stability of O^-. Figure 2 shows an EPR spectrum of V_2O_5/SiO_2(B) (a) after a standard pretreatment (reduction by CO at 693 K) and (b) after the introduction of N_2O at 298 K. The two peaks in Fig. 2(a) were assigned to parts of the octet spectra of the V^{4+} ions. The spectra in Fig. 2(b) was identified with O^- (g=2.032), for they show a hyperfine structure (A=13.2G) attributable to the V nucleus. After the gas phase had been evacuated, O_2 was introduced. The resultant EPR spectra are shown in Fig. 2(c); they should be identified with O_2^- ($g_{//}$=2.021, $A_{//}$=9.8G; $g_\perp$=2.003, $A_\perp$=6.0G).[6] Contrary to the cases of MgO[1] and Co-MgO,[7] where O^- reacted with O_2 giving O_3^-, no new signals showing O_3^- were observed. Instead, O_2^- was observed. The amount of O_2^- was about ten times that of O^-. As is observed at a low magnetic field in Fig. 2(c), a weak peak which is identified as a part of the O^- spectrum remains. This suggests that at least a part of the O^- does not react with O_2. Probably, O_2 is adsorbed on the other sites, independent of the sites for O^- formation.

The thermal stability of O^- was studied in an evacuated sample tube. The amounts of O^- were not changed, even after 260 h at 77 K. They decreased to two-thirds of the initial value after 100 h at 195 K. Finally, most of the O^- disappeared after 1 h at 373 K. The O^- on V_2O_5/SiO_2 was found to be thermally unstable above 373 K. Thus, it seems questionable that such O^- exists in a practical oxidation reaction at an elevated temperature.

A Surface Reaction between the O^- Anion Radical and C_2H_6. After the concentration of O^- had been determined, an excess amount of C_2H_6 was introduced to the catalyst at 298 K for 20 min. The O^- spectra (Fig. 2(b)) completely disappeared upon a reaction with C_2H_6 at 298 K. However, the V^{4+} signal (Fig. 2(a)) remained.

The reaction stoichiometry between O^- and C_2H_6 was also studied. The amount of O^- was controlled by changing the reduction conditions. The maximum concentration of O^- on V_2O_5/SiO_2(B) was several times larger than those on MgO[2] and Co-MgO.[9] As is shown

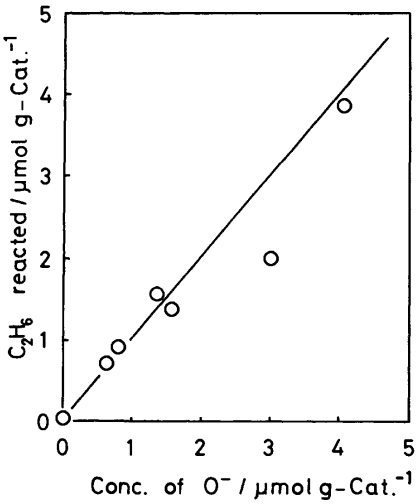

Fig. 3. Variation of the amount of C_2H_6 reacted with O^- at 298K as a function of the concentration of O^- evaluated from its EPR spectrum. 2g of 2.6wt% V_2O_5/SiO_2(B) was used as a sample.

in Fig. 3, one mole of O^- was proved to react with one mole of C_2H_6 as has been observed in the case of MgO.[2] It was also proved that C_2H_6 hardly reacted at all with other oxygen species on this catalyst at 298 K (see the zero point in Fig. 3). Contrary to this, it has been reported that adsorbed oxygen other than O^- also reacts with C_2H_6 at 298 K on Co-MgO.[9] No gas-phase products were observed by the surface reaction at 298 K.

TPD Behavior Following the Surface Reaction between O^- and C_2H_6 at 298 K. In order to assign the adsorbed species formed by the surface reaction between O^- and C_2H_6 on V_2O_5/SiO_2(B), temperature-programmed-desorption (TPD) experiments were carried out. After the gas phase had been evacuated, 100 Torr of He was introduced into the reactor. The temperature was then raised step-by-step while desorption products were trapped at 77 K in the closed circulation system. Figure 4 shows the accumulated amounts of desorption products as a function of the temperature. The main product, C_2H_4, desorbed above 473 K. The products recovered up to 773 K corresponded to 18% of the total carbon reacted. In order to discuss the adsorbed species, the TPD patterns of the model compounds were compared with the above results. The TPD pattern of adsorbed ethanol is shown in Fig. 5. However, the starting temperature of C_2H_4 desorption was higher in Fig. 5 that in Fig. 4. In this case, 94% of the adsorbed carbon source was recovered up to 773 K. On the other hand, the TPD products of adsorbed acetaldehyde, which were C_1 to C_4 alkanes and C_2H_4, were quite different from those in Fig. 4 and 5. In this instance, 41% of the adsorbed carbon source was recovered.

The Reaction between C_2H_6 and Adsorbed Oxygen Species other than O^- above 573 K. Following the N_2O decomposition on V_2O_5/SiO_2(B) at 298 K, the

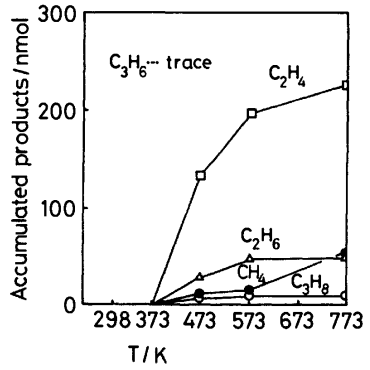

Fig. 4. TPD of surface species following the surface reaction of C_2H_6 and O^- at 298K on 2.6wt%V_2O_5/SiO_2(B) (2g).

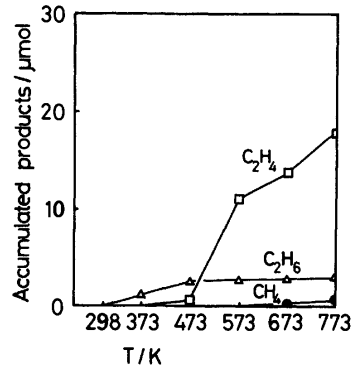

Fig. 5. TPD of C_2H_5OH adsorbed at 298K on 2.6wt%V_2O_5/SiO_2(B) (2g).

O^- produced was consumed by the reaction with C_2H_6 and the gas phase was evacuated. Then, C_2H_6-He gas was introduced again, and the temperature was raised. C_2H_6 reacted above 573 K yielding C_2H_4 as is shown in Fig. 6. The adsorbed oxygen was proved to be much less reactive than O^-.

Oxidative Dehydrogenation Reaction of C_2H_6 with N_2O above 573 K (Catalytic Reaction). In order to examine the role of O^- and the other oxygen species during the catalytic reaction over V_2O_5/SiO_2, a reaction between C_2H_6 and N_2O was carried out. Two kinds of catalysts, V_2O_5/SiO_2(A) and V_2O_5/SiO_2(B) (2 g each), were used. The catalysts were evacuated at 773 K for 3 h (Pretreatment a) or reduced by CO at 693 K overnight after the evacuation (Pretreatment b). Figure 7 shows a typical example of the time course of the reaction over V_2O_5/SiO_2(B) at 773 K after Pretreatment a. Both C_2H_4 and CO_2 were formed, while C_2H_4 was predominant in the early stage of the reaction. Figure 8 shows the conversions and the C_2H_4 selectivities of the reactions in 15 min over the two catalysts with the two kinds of pretreatments as a function of the reaction temperatures. When these figures are compared, the following facts are observed: 1) The reaction behavior over V_2O_5/SiO_2(B) (Fig. 8(c), (d)) and V_2O_5/SiO_2(A) (Fig. 8(a), (b)) resemble one another, although only the first sample can yield O^-. 2) The activity of N_2O

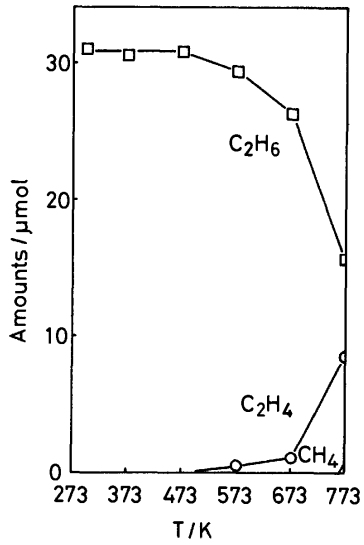

Fig. 6. Reaction of C_2H_6 with adsorbed oxygen other than O^- on 2.6wt%V_2O_5/SiO_2(B). Changes of the amount of the reactant and the products as a function of a reaction temperature.

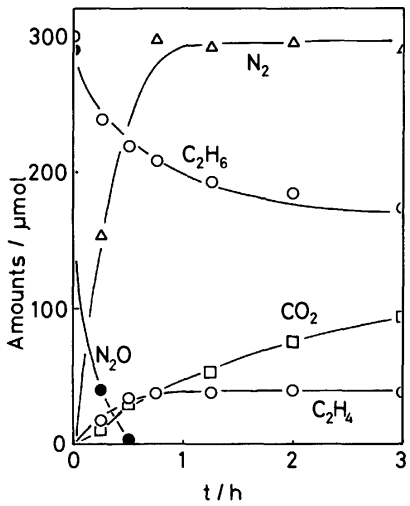

Fig. 7. Time course of the reaction between N_2O and C_2H_6 at 773K on V_2O_5/SiO_2(B) (2g) which is not reduced before the reaction.

decomposition at a lower reaction temperature was high over the samples treated with the Pretreatment b (Fig. 8(b), (d)), perhaps because N_2O was partly consumed to reoxidize the reduced V_2O_5. 3) On oxidized surfaces (Pretreatment a), the N_2O decomposition and the oxidation of C_2H_6 start at the same temperature (573 K in Fig. 8(a), (c)). This also roughly coincides with the temperature at which the adsorbed oxygen other than O^- reacts with C_2H_6 (Fig. 6). 4) The selectivity for C_2H_4 is rather high at higher temperatures (673 to 773 K).

Discussion

Conditions of O^- Formation. As is shown in Fig. 1, the O^- concentration is the highest under the reduc-

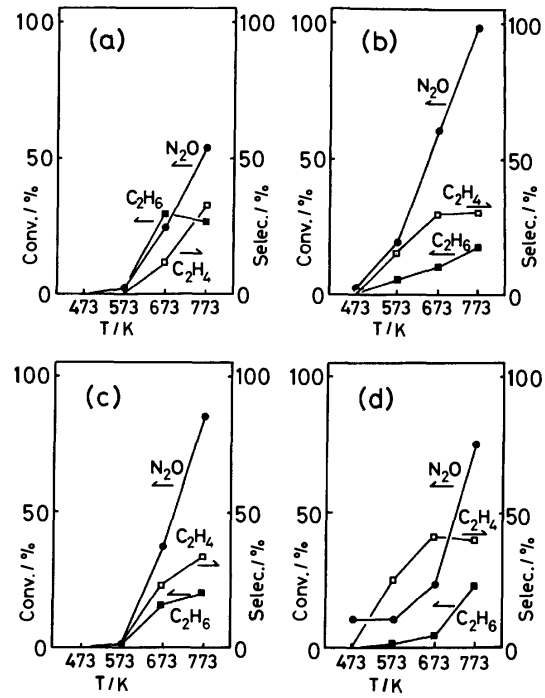

Fig. 8. Conversions and selectivities of the reaction between C_2H_6 and N_2O over 2g of various vanadium catalysts; (a) non reduced 2.6wt%V_2O_5/SiO_2(A): (b) reduced 2.6wt%V_2O_5/SiO_2(A): (c) non reduced 2.6wt%V_2O_5/SiO_2(B): (d) reduced 2.6wt%V_2O_5/SiO_2(B).

tion at 693 K, where the reduction of V^{5+} to V^{4+} is completed (22% of reduction). This suggests that V^{4+} ions are necessary for the formation of O^- ($V^{4+}+N_2O \rightarrow V^{5+}-O^-+N_2$). Furthermore, the formation conditions also depend upon the kind of support. Probably the circumstance of the vanadium ion, which might be controlled by the surface state of the SiO_2 support, is important. In order to investigate any differences among the vanadium ions of the samples, the EPR spectra of V^{4+} ions of the 4 samples used in this work were compared. The shapes of the EPR spectra of V^{4+} were classified into three kinds. However, the shapes of the spectra are not related to the conditions of O^- formation. V_2O_5/SiO_2(B) and V_2O_5/SiO_2(C) have spectra of the same shape, although only the former is active in O^- formation. The nature of the site for O^- formation could not be clarified in detail.

O^- could not be formed through O_2 under the same conditions as in the literature.[6] It has been reported that O^- is formed only when the pressure of O_2 is low (several Torr).[6] It seems that the conditions in our system are too restricted.

Surface Reactions of O^- and C_2H_6 at 298 K. One-to-one stoichiometry between O^- and C_2H_6 was found more clearly on V_2O_5/SiO_2 than on other systems. Thus, O^- is considered to abstract one hydrogen atom from C_2H_6, as has been suggested in the case of MgO.[2]

$$C_2H_6 + O^- \longrightarrow C_2H_5\cdot + OH^- \quad (1)$$

The subsequent reactions of the ethyl radical to form surface ethoxide and hydroxide are assumed to be as in Eqs. 2 and 3, because ethylene desorption still occurs at 573 K (Fig. 4), at which point ethoxide decomposition is observed (Fig. 5):

$$C_2H_5\cdot + O^{2-} + \square \longrightarrow C_2H_5O^- + \boxed{e^-} \quad (2)$$

$$C_2H_5O^- \longrightarrow C_2H_4 + OH^- \quad (3)$$

However, as is shown in Fig. 4, a majority of ethylene desorbs at lower temperature (473 K). This may suggest the existence of an other intermediate, for example, a carbonium ion, which releases ethylene at a lower temperature, as has been discussed in the case of MgO.[2]

$$C_2H_5\cdot + \square \longrightarrow C_2H_5^+ + \boxed{e^-} \quad (4)$$

$$C_2H_5^+ + O^{2-} \longrightarrow C_2H_4 + OH^- \quad (5)$$

Since the amount of recovered carbon atoms was low (18%), other processes, such as the polymerization of ethylene or further oxidation, might also occur.

Active Oxygen Species in the Oxidative Dehydrogenation of C_2H_6 by N_2O above 573 K. As has been described earlier, the adsorbed oxygen other than O^- is reactive above 573 K, where the catalytic reaction occurs. On the other hand, O^- reacts with C_2H_6 even at room temperature, and it is not thermally stable. After all, O^- is not considered to be present during the catalytic reaction conditions. The active species during the oxidative dehydrogenation above 573 K was considered to be the adsorbed oxygen other than O^-. This is also supported by the fact that the reactivity of V_2O_5/SiO_2 is not related to the ability to produce O^-.

If there are new circumstances under which only O^- is formed at a high temperature with a dynamic balance of O^- evolution and disappearance, the possibility that O^- is involved in the reaction should be discussed.[10] It should also be pointed out that an oxygen species which is not detected by EPR is also very active against C_2H_6, even at room temperature.[9] Regarding this system too, the authors suggest the importance of an adsorbed oxygen other than O^- as the active species of the reaction at the higher temperature.

Conclusions

The nature of O^- and the surface reaction mechanism between O^- and C_2H_6 were studied in order to elucidate the catalytic oxidative dehydrogenation of C_2H_6 with N_2O over V_2O_5/SiO_2. V_2O_5 must be supported on SiO_2 made from tetraethyl silicate in order to get O^-, and the amount of O^- formed is related to the concentration of V^{4+}. One mole of O^- is proved to react with one mole of C_2H_6 on V_2O_5/SiO_2 at 298 K. The adsorbed oxygen species other than O^- is less reactive than O^- toward C_2H_6. This species, EPR-undetectable oxygen, was found to be reactive with C_2H_6 above 573 K, and it is considered to be responsible for the catalytic reaction of C_2H_6 with N_2O above 573 K.

References

1) J. H. Lunsford, *Catal. Rev.*, **8**, 135 (1973).
2) K. Aika and J. H. Lunsford, *J. Phys. Chem.*, **81**, 1393 (1977).
3) R. Liu, M. Iwamoto, and J. H. Lunsford, *J. Chem. Soc., Chem. Commun.*, **1982**, 78.
4) H.-F. Liu, R.-S. Liu, K. Y. Liew, R. E. Johnson, and J. H. Lunsford, *J. Chem. Soc.*, **106**, 4117 (1984).
5) M. Iwamoto, J. Hirata, K. Matsukami, and S. Kagawa, *J. Phys. Chem.*, **87**, 903 (1983).
6) S. Yoshida, T. Matsuzaki, T. Kashiwazaki, K. Mori, and K. Tarama, *Bull. Chem. Soc. Jpn.*, **47**, 1564 (1974).
7) K. Aika, M. Isobe, M. Tajima, and T. Onishi, Proc. 8th. Intern. Congr. Catal., Dechema ed. Verlag Chemie., Wein heim (1984), p. III-335.
8) V. A. Shvets and V. B. Kazansky, *J. Catal.*, **25**, 123 (1972).
9) K. Aika, M. Tajima, and T. Onishi, *Chem. Lett.*, **1983**, 1783.
10) T. Ito and J. H. Lunsford, *Nature*, **314**, 721 (1985); T. Ito, J.-X. Wang, C.-H. Lin, and J. H. Lunsford, *J. Am. Chem. Soc.*, **107**, 5062 (1985).

Phase-Shift Studies of the Quenching of NH($c^1\Pi$) by HN_3, NO, CO, and CO_2

Shun-ichiro SASAKI, Shigeru TSUNASHIMA,* and Shin SATO†
Department of Applied Physics, Tokyo Institute of Technology, Ookayama, Meguro-ku, Tokyo 152
†Research Laboratory for Nuclear Reactors, Tokyo Institute of Technology, Ookayama, Meguro-ku, Tokyo 152
(Received December 26, 1985)

Absolute cross sections for quenching NH($c^1\Pi$) by the use of several inorganic molecules were determined at room temperature by using a phase-shift method. The NH($c^1\Pi$) radicals were produced by the photolysis of HN_3 using an amplitude-modulated Xe-resonance lamp. The results obtained were as follows: 0.01(He), 12(HN_3), 48(NO), 49(CO), and 30(CO_2) in units of 10^{-16} cm^2. In the case of NO, the 336 nm emission was enhanced, which suggests that NO quenches NH($c^1\Pi$) to NH($A^3\Pi$). From the phase difference between the 325 and 336 nm emissions, the quenching cross-section of NO for NH($A^3\Pi$) was estimated to be 60×10^{-16} cm^2.

A number of emission and absorption bands of NH radicals have been investigated by using the photolysis or electron impact of HN_3, NH_3, and HNCO.[1] The spectroscopic properties of NH radicals in the lower excited states are now well-known.[2] The energy-level diagram of the NH radical is shown in Fig. 1. The reactivities of these different states of NH radicals are, however, not well understood yet. Recently, we showed that the reactions of NH($a^1\Delta$) with hydrocarbons are very much similar to those of the isoelectronic species, O(^{1}D) and $CH_2(^1A_1)$: The NH($a^1\Delta$) radical inserts into the C–H bond and adds to the double bond of hydrocarbons.[3]

The quenching of the NH($b^1\Sigma^+$) state by various molecules was studied by Zetsch and Stuhl[4] and by Gelernt et al.[5] The rate constants of the quenching of NH($c^1\Pi$) and NH($A^3\Pi$) states by rare gases, H_2, and N_2 have been measured by Kawasaki et al., using the vuv photolysis of NH_3.[6] The quenching rates were estimated from the pressure dependence of the fluorescence intensities at 325 and 336 nm. On the other hand, the radiative lifetime of NH($c^1\Pi$) has been estimated to be 0.43[7] or 0.48[8] μs by the phase-shift method using a modulated electron beam. Since the bombardment of high-energy electrons produces not only NH($c^1\Pi$) but also the higher excited states of NH, the effect of the "cascading" from these excited states was taken into account.[7,8] Clerc et al. also estimated the lifetime of the NH($c^1\Pi$) state to be 0.50 μs from the decay rate of the fluorescence at 325 nm in the pulse radiolysis of NH_3.[9] Similar values were obtained in the studies of the pulse vuv photolysis of HNCO[10] and the 193-nm laser photolysis of HN_3.[11]

In the present study, a phase-shift method is used to determine the rate constants of the quenching of the NH($c^1\Pi$) state by several molecules, using an amplitude-modulated Xe resonance lamp. Here, the effect of the "cascading" may be ignored.

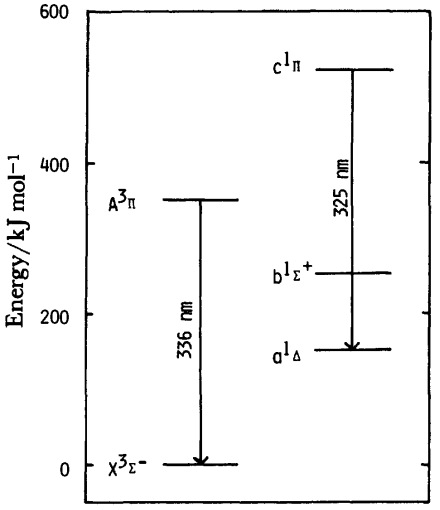

Fig. 1. An energy level diagram of NH radical.

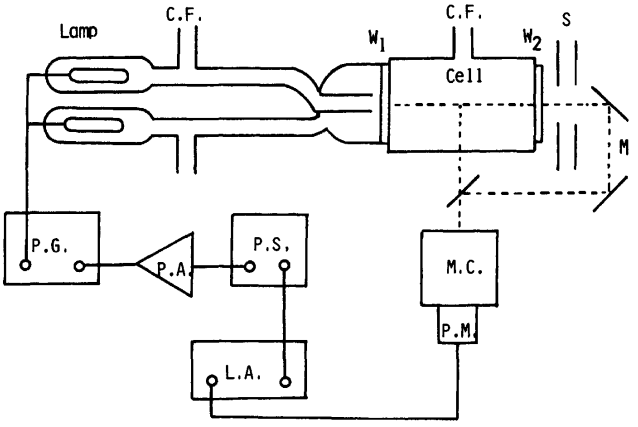

Fig. 2. A block diagram of the experimental apparatus: M; mirror, S; slit, W_1; LiF window, W_2; LiF window coated with sodium salicylate, C.F.; to circulating fan, M.C.; monochromator, P.M.; photomultiplier, L.A.; lock-in amplifier, P.S.; phase shifter, P.A.; pre-amplifier, P.G.; power generator.

Experimental

A block diagram of the experimental arrangement is shown in Fig. 2. The light source used was a home-made Xe-discharge lamp. The power of the lamp was supplied by a home-made power generator which had been used for previous studies of the mercury photosensitized luminescence.[12] The intensities were modulated at a frequency of 100 or 120 kHz, using the reference signal of a lock-in amplifier (NF Circuit Design Block Co., LI 573). A mixture of He (≈20 Torr; 1 Torr=133.3 Pa) and Xe

(≈0.06 Torr) was circulated in the lamp by means of an all-glass-made fan. This mixture was found to be suitable for effective modulation at high frequencies. The light from the lamp illuminated a Pyrex fluorescence cell, 50 mm in length and 30 mm o.d., through a LiF window. In order to detect the transmitted light, another LiF window coated with sodium salicylate was attached to the opposite side of the cell.[13] The emission from sodium salicylate was measured at 415.5 nm with a photomultiplier (Hamamatsu Photonics, 1P28) through a monochromator (Japan Spectroscopic Co., CT-25N). The signal from the photomultiplier was fed into the lock-in amplifier, and its phase angle was measured relative to the internal signal of the lock-in amplifier. Since the radiative lifetime of sodium salicylate is about 10 ns,[13] the phase angle thus measured can be considered to be equal to that of the excitation light from the lamp.

The fluorescence cell had two side arms for circulating the reaction mixture by means of an all-glass-made fan. The reaction mixture was diluted with He, typically 20 or 13 Torr. The fluorescence from the cell was measured at right angles to the excitation light using the same monochromator and photomultiplier as were used for the measurement of the emission from sodium salicylate. The phase angle of the fluorescence was also measured relative to that of the internal signal of the lock-in amplifier.

The phase-control dial of the lock-in amplifier was calibrated with a phase shifter (NF Circuit Design Block Co., UP 725), while the phase shifter was calibrated by drawing a Lissajous figure on an oscilloscope (Iwatsu Co., SS-5100). The phase shifter was also used to shift the phase angle of the reference signal so that the measured phase angle was kept in the linearly changing region of the phase-control dial.

The HN_3 was synthesized and purified by the method described in a previous paper.[3] The He (Suzuki Shokan Co.) was used after having been passed through a column packed with reduced copper at 300 °C and a trap packed with molecular sieve 4A at −196 °C. The NO, CO, CO_2, and Xe (Takachiho Shoji Co.) were used after having been distilled at low temperatures.

Results

When 0.1 Torr of HN_3 diluted with 20 Torr of He was irradiated with the Xe lamp, fluorescence was observed at about 325 nm. The spectrum was the same as that observed by Okabe,[14] and it was identified as the emission from $NH(c^1\Pi)$. The phase angle of the fluorescence was measured within the initial few minutes of irradiation, since a long irradiation caused a decrease in the emission intensity and its phase angle.

The difference in the phase angle between the 415.5 and 326 nm emissions, ϕ_1, was measured at the modulation frequencies of 100 and 120 kHz, and at various pressures of HN_3 and He. From the measurements of ϕ_1, the decay rate of $NH(c^1\Pi)$, R_1, was estimated by means of this relation: $R_1=2\pi f/\tan\phi_1$, where f denotes the frequency of the modulation (for details, see below). The decay rates thus determined are plotted in Figs. 3 and 4 as functions of the pressures of HN_3 and He respectively. The plots shown in Fig. 3 give a straight line with an intercept of $(2.2\pm0.1)\times10^6\,s^{-1}$ and a slope of $(5.2\pm0.7)\times10^{13}\,cm^3\,mol^{-1}\,s^{-1}$. The intercept and the slope of the straight line in Fig. 4 were $(2.8\pm0.1)\times10^6\,s^{-1}$ and $(1.1\pm0.1)\times10^{11}\,cm^3\,mol^{-1}\,s^{-1}$ respectively. All error limits quoted in this paper correspond to one standard deviation.

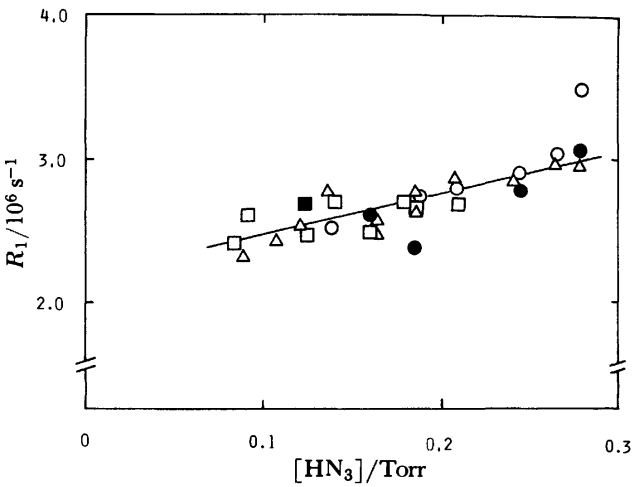

Fig. 3. Plots of R_1 against the pressure of HN_3: open symbols; f=100 kHz and closed symbols; f=120 kHz, [He]=20(○), 13.3(△), and 8.8(□) Torr.

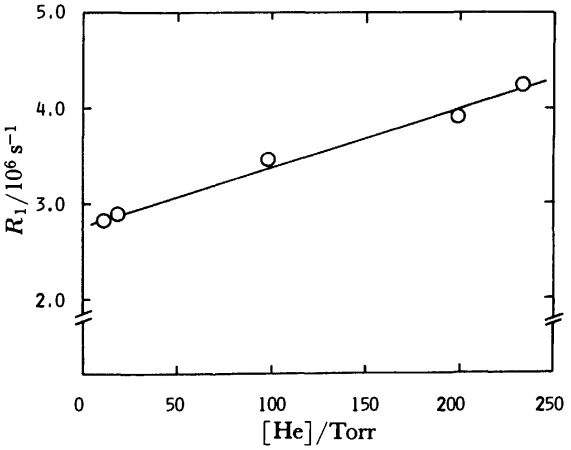

Fig. 4. Plots of R_1 against the pressure of He obtained at f=120 kHz and $[HN_3]$=0.244 Torr.

When a quencher, such as NO, CO, or CO_2, was added to a mixture of HN_3 (0.123 Torr) and He (20 Torr), the decay rate, R_1, increased. The decay rates are plotted as functions of the pressures of the quenchers in Fig. 5. The plots show straight lines for every quencher examined. The slopes and the intercepts of the straight lines are summarized in Table 1.

In the case of NO, a fluorescence at 336 nm was observed in addition to the 325-nm fluorescence. The spectrum was the same as that identified as the emission from $NH(A^3\Pi)$.[14] The phase difference between the 325 and 336-nm fluorescences, ϕ_3, was determined at various pressures of NO and HN_3. The $2\pi f/\tan\phi_3$

Table 1. The Intercepts and the Slopes of the Straight Lines Shown in Fig. 5 and the Quenching Cross-Sections

Quencher	Intercept	Slope	Cross-section[a]	
Q	$10^6\,s^{-1}$	$10^{14}\,cm^3\,mol^{-1}\,s^{-1}$	Obsd.	Ref.
CO_2	2.30±0.07	1.34±0.20	30	
CO	2.23±0.11	2.37±0.38	49	27,[b] 61[c]
NO	2.25±0.09	2.31±0.34	48	21[b]

a) In units of $10^{-16}\,cm^2$. b) Private communication from M. Kawasaki. c) Ref. 14.

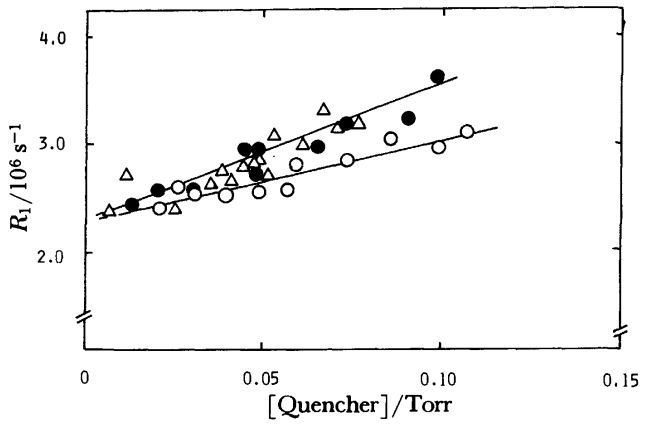

Fig. 5. Plots of R_1 against the pressure of CO(●), NO(△), and CO_2(○). For detail, see text.

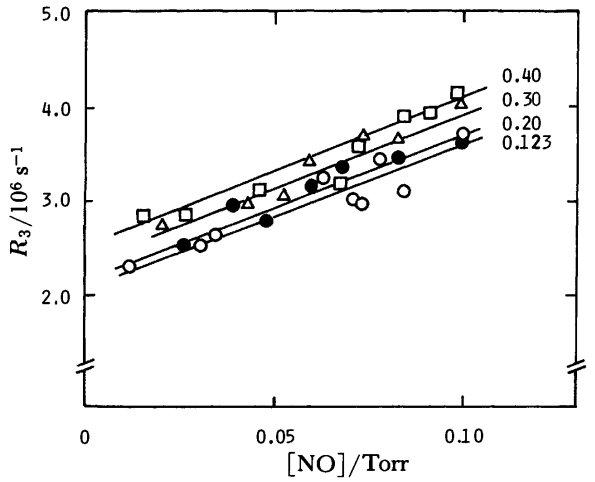

Fig. 6. Plots of R_3 against the pressure of NO. The values show the initial pressure of HN_3 in units of Torr.

(=R_3) values are plotted in Fig. 6 as a function of the pressure of NO. The plots showed straight lines for every pressure of HN_3 examined. The values of the intercepts, R_{30}, and the slopes are summarized in Table 2.

Table 2. The Intercepts and the Slopes of the Straight Lines in Fig. 6

[NH_3]	Intercept	Slope	Cross-section
Torr	$10^6\,s^{-1}$	$10^{14}\,cm^3\,mol^{-1}\,s^{-1}$	$10^{-16}\,cm^2$
0.123	2.16±0.21	2.59±0.58	54
0.20	2.20±0.13	2.70±0.38	57
0.30	2.27±0.13	3.24±0.37	68
0.40	2.43±0.15	2.97±0.42	62
	Average	2.88±0.53	60±11

Discussion

Photolysis of HN_3. The fluorescence of the NH ($c^1\Pi$) radicals appears at 325 nm. In order to explain the observed phase difference between the excitation light and the fluorescence at 325 nm, ϕ_1, the following reaction mechanism was considered:

$$HN_3 + h\nu \longrightarrow NH(c^1\Pi) + N_2 \quad (1)$$

$$NH(c^1\Pi) \longrightarrow NH(a^1\Delta) + h\nu(325) \quad k_{10} \quad (2)$$

$$NH(c^1\Pi) + HN_3 \longrightarrow \text{products} \quad k_{1a} \quad (3)$$

$$NH(c^1\Pi) + He \longrightarrow \text{products} \quad k_{1h} \quad (4)$$

Assuming the above mechanism, the decay rate, R_1, can be expressed as follows:

$$R_1 = 2\pi f/\tan\phi_1 = k_{10} + k_{1a}[HN_3] + k_{1h}[He] \quad (5)$$

Here, f denotes the frequency of the modulation. According to Eq. 5, the plots of the decay rates against the pressure of HN_3 will give a straight line with an intercept of $k_{10}+k_{1h}[He]$ and a slope of k_{1a}. Under a constant pressure of HN_3, the plots of the decay rates against the pressure of He will give a straight line with an intercept of $k_{10}+k_{1a}[HN_3]$ and a slope of k_{1h}. From the values of the intercepts and the slopes of the straight lines in Figs. 3 and 4, the values of k_{10}, k_{1a}, and k_{1h} are estimated to be $(2.2\pm0.2)\times10^6\,s^{-1}$, $(5.2\pm0.7)\times10^{13}$, and $(1.1\pm0.1)\times10^{11}\,cm^3\,mol^{-1}\,s^{-1}$ respectively. The radiative lifetime of NH($c^1\Pi$), the reciprocal of k_{10}, was estimated to be (0.48±0.03) μs. The value obtained here agreed well with those estimated by the various other methods.[7-11] The quenching by He was about two orders of magnitude smaller than that of HN_3 and agreed with that obtained by Kawasaki et al.[6] Recently, Haak and Stuhl estimated k_{1a} to be $4.4\times10^{14}\,cm^3\,mol^{-1}\,s^{-1}$ by using the ArF-laser photolysis of HN_3; this value is about one order of magnitude larger than the present value.[11] The reaction mechanism may not be simple in their laser-photolysis system, since they observed that (a) products were

formed in an appreciable concentration, (b) the intensities of the fluorescence of NH($A^3\Pi$) varied from 1.4 to 1.9 powers of the laser intensities, and (c) the decay rate of NH($A^3\Pi$) was not a single exponential. Thus, the quenching process can be considered to be disturbed by the side reactions.

If NH($c^1\Pi$) is formed via a long-lived intermediate, such as an excited HN_3 molecule, the observed decay rate should be dependent on the frequency of the modulation. This is, however, not the case, as is shown in Fig. 3.

Quenching of NH($c^1\Pi$). In the presence of a quencher, such as NO, CO, or CO_2, Eq. 5 should be changed:

$$R_1 = k_{10} + k_{1h}[He] + k_{1a}[HN_3] + k_{1q}[Q] \quad (6)$$

Here, k_{1q} represents the rate constant for the quenching of NH($c^1\Pi$) by a quencher, Q:

$$NH(c^1\Pi) + Q \longrightarrow \text{products} \quad k_{1q} \quad (7)$$

When the pressures of HN_3 and He are kept constant, the plots of R_1 against the pressure of a quencher will give a straight line with a slope of k_{1q} and an intercept of $k_{10}+k_{1h}[He]+k_{1a}[HN_3]$ (see Fig. 5). Using the values of k_{10}, k_{1a}, and k_{1h} estimated in this study, the intercept was calculated to be $2.5\times10^6\,s^{-1}$, a value which agreed well with the observed values of the intercepts shown in Table 1; i.e., the slopes shown in Table 1 can be considered to represent k_{1q}. The quenching cross-sections, σ_{1q}, were estimated by the use of Eq. 8 and are listed in the fourth column of Table 1:

$$\sigma_{1q} = k_{1q}(\pi\mu/8kT)^{1/2} \quad (8)$$

The symbols in Eq. 8 represent their usual meanings. In the fifth column of Table 1, the literature values are also listed. The NO, CO, and CO_2 efficiently quench the NH($c^1\Pi$) state.

Quenching by NO. In the case of NO, the formation of NH($A^3\Pi$) was detected by the fluorescence at 336 nm. The following reactions can be considered to explain the results:

$$NH(c^1\Pi) + NO \longrightarrow NH(A^3\Pi) + NO^* \quad \alpha \quad (9)$$

$$\longrightarrow \text{other reactions} \quad 1-\alpha \quad (10)$$

$$NH(A^3\Pi) \longrightarrow NH(X^3\Sigma^-) + h\nu(336) \quad k_{30} \quad (11)$$

$$NH(A^3\Pi) + NO \longrightarrow \text{products} \quad k_{3n} \quad (12)$$

$$NH(A^3\Pi) + HN_3 \longrightarrow \text{products} \quad k_{3a} \quad (13)$$

where α denotes the branching ratio for the formation of NH($A^3\Pi$). In the above reactions, the quenching by He is neglected. Assuming the above reactions, the decay rates of the NH($A^3\Pi$), R_3, can be expressed as follows:

$$R_3 = 2\pi f/\tan\phi_3 = k_{30} + k_{3a}[HN_3] + k_{3n}[NO] \quad (14)$$

The slopes of the straight lines in Fig. 6 correspond to k_{3n}. The values of the slopes shown in Table 2 are almost constant for every pressure of HN_3 examined. From the value of k_{3n}, the quenching cross-section of NO was calculated to be $60\times10^{-16}\,cm^2$. Recently, Hofzumahaus and Stuhl have estimated the cross section of NO for quenching rotationally hot NH($A^3\Pi$) to be $17\times10^{-16}\,cm^2$.[15] They pointed out that rotation of NH radicals reduces the effect of the quencher. The present result corresponds to the quenching rate for rotationally relaxed NH radicals.

The branching ratio, α, could not be determined from the phase-shift studies, because no formation rate of NH($A^3\Pi$), k_9, appeared in Eq. 14. Since the energy difference between NH($c^1\Pi$) and NH($A^3\Pi$) is 167 kJ mol^{-1}, the NO* formed by Reaction 9 is probably not an electronically excited one. Reaction 9, however, is a spin-allowed process for NO. For CO and CO_2, similar quenching reactions are spin-forbidden processes unless CO or CO_2 is excited to a triplet state. No triplet states of these molecules, however, are assigned in such a low energy region. This explains why only the NO molecule can quench NH($c^1\Pi$) to NH($A^3\Pi$).

References

1) H. Okabe, "Photochemistry of Small Molecules," John Wiley & Sons, New York (1978).
2) J. M. Lents, *J. Quant. Spectrosc. Radiat. Transfer*, **13**, 297 (1973); A. Gilles, J. Masanet, and C. Vermeil, *Chem. Phys. Lett.*, **25**, 346 (1974).
3) J. Hamada, S. Tsunashima, and S. Sato, *Bull. Chem. Soc. Jpn.*, **56**, 662 (1983) and the references cited therein.
4) C. Zetsch and F. Stuhl, *J. Chem. Phys.*, **66**, 3107 (1977).
5) B. Gelernt, S. V. Filseth, and T. Carrington, *J. Chem. Phys.*, **65**, 4940 (1976).
6) M. Kawasaki, Y. Hirata, and I. Tanaka, *J. Chem. Phys.*, **59**, 648 (1973).
7) E. Fink and K. H. Welge, *Z. Naturforsch.*, **A19**, 1193 (1964).
8) W. H. Smith, *J. Chem. Phys.*, **51**, 520 (1969).
9) M. Clerc, M. Schmidt, J. Hagge-Temman, and J. Belloni, *J. Phys. Chem.*, **75**, 2908 (1971).
10) Y. Mori, private communication.
11) H. K. Haak and F. Stuhl, *J. Phys. Chem.*, **88**, 3627 (1984).
12) H. Umemoto, S. Tsunashima, and S. Sato, *Chem. Phys. Lett.*, **53**, 521 (1978).
13) J. A. R. Samson, "Techniques of Vacuum Ultraviolet Spectroscopy," John Wiley & Sons, New York (1967), p. 212.
14) H. Okabe, *J. Chem. Phys.*, **49**, 2726 (1968).
15) A. Hofzumahaus and F. Stuhl, *J. Chem. Phys.*, **82**, 3152 (1985).

Phase-Shift Studies of the Quenching of NH($c^1\Pi$) and NH($A^3\Pi$) by Hydrocarbons

Shun-ichiro SASAKI, Akiko KANO, Shigeru TSUNASHIMA,* and Shin SATO†
Department of Applied Physics, Tokyo Institute of Technology, Ookayama, Meguro-ku, Tokyo 152
†Research Laboratory for Nuclear Reactors, Tokyo Institute of Technology, Ookayama, Meguro-ku, Tokyo 152
(Received December 26, 1985)

The cross-sections for quenching NH($c^1\Pi$) and NH($A^3\Pi$) by hydrocarbons were determined at room temperature by using a phase-shift method. The NH($c^1\Pi$) was produced by the photolysis of HN_3 using an amplitude-modulated Xe-resonance lamp. The apparent decay rate of the NH($c^1\Pi$) was estimated from the difference in phase angle between the excitation light and the fluorescence of NH($c^1\Pi$) at 325 nm. In the presence of Xe, the fluorescence of NH($A^3\Pi$) at 336 nm was enhanced. The difference in the phase angle between the fluorescences at 325 and 336 nm was found to correlate with the decay rate of NH($A^3\Pi$). From the decay rates obtained in the presence of hydrocarbons, the quenching cross-sections were determined.

The NH radical is known to be an important intermediate in astronomical emission sources. The electron configuration, $(2s\sigma)^2(2p\sigma)^2(2p\pi)^2$, of the NH radical gives rise to the $X^3\Sigma^-$, $a^1\Delta$, and $b^1\Sigma^+$ states, while the $(2s\sigma)^2(2p\sigma)(2p\pi)^3$ configuration gives rise to the $c^1\Pi$ and $A^3\Pi$ states. Figure 1 shows a correlation diagram of the NH radical and the O atom. Many similarities have been found in the reactions of NH radicals in the first excited state, NH($a^1\Delta$), with those of isoelectronic species, O(^{1}D) and $CH_2(^1A_1)$.[1-11] The measurements of the quenching processes of these excited states are important in elucidating the mechanism of the energy transfer. The rate constants of the reaction of the NH($a^1\Delta$) state with various molecules have been measured by McDonald et al.[10] and Piper et al.[11] Carrington and his co-workers[12] and Zetsch and Stuhl[13] have determined the rate constants of the quenching of the NH($b^1\Sigma^+$) state by several molecules and found that the NH($b^1\Sigma^+$) state is less reactive than NH($a^1\Delta$), although the former is energetically higher than the latter. This trend is similar to that observed in the case of O(^{1}D);[14] i.e., O(^{1}D) is more reactive than O(^{1}S), although the former is about 200 kJ mol^{-1} energetically lower than the latter. A limited number of quenching rates for the NH($c^1\Pi$) and NH($A^3\Pi$) states have been reported.[15-20] Recent studies of NH($A^3\Pi$) by Hofzumahaus and Stuhl have shown that the NH($A^3\Pi$) was quenched by every three collisions and that the quenching cross-sections of many inorganic molecules were correlated with the intermolecular well depth.[19] No systematic studies of the quenching of these highly excited states by hydrocarbons have been reported, probably because these quencher molecules absorb the vuv light and decompose. One our previous paper showed that the phase-shift method is a convenient and suitable method for the measurements of the quenching rate, especially for a quencher which absorbs the excitation light.[20] In this paper, the cross-sections for the quenching of NH($c^1\Pi$) and NH($A^3\Pi$) by hydrocarbons are reported and possible quenching mechanisms are discussed.

Experimental

The experimental method has been fully described in the previous paper,[20] and so only a brief outline will be given here.

The apparatus consists of an amplitude-modulated Xe-resonance lamp, an oxygen shutter, and a fluorescence cell. The oxygen shutter, which separates the lamp from the cell, was used to cut off the light of wavelengths shorter than 200 nm during the mixing of the reactants and the stabilizing of the lamp before irradiation. The transmitted vuv light was converted to longer wavelengths by using sodium salicylate and was measured at 415.5 nm. The phase angles of the

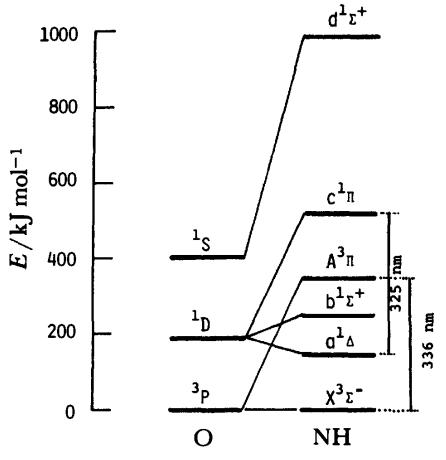

Fig. 1. Correlation diagram of NH and O.

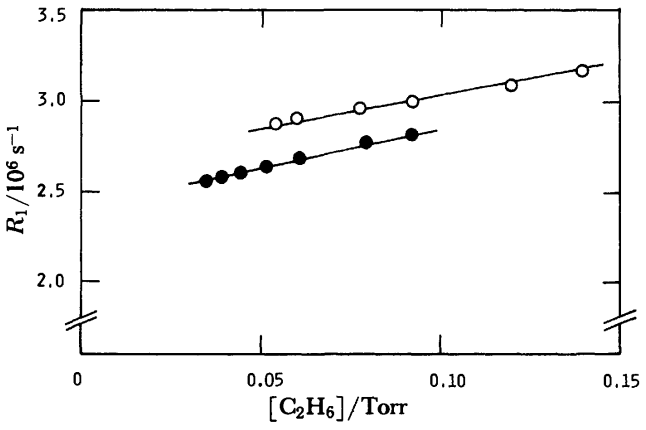

Fig. 2. Plots of R_1 against the pressure of C_2H_6 obtained at f=100 kHz and [He]=20 Torr. ○: [HN_3]= 0.123 Torr, ●: [HN_3]=0.081 Torr.

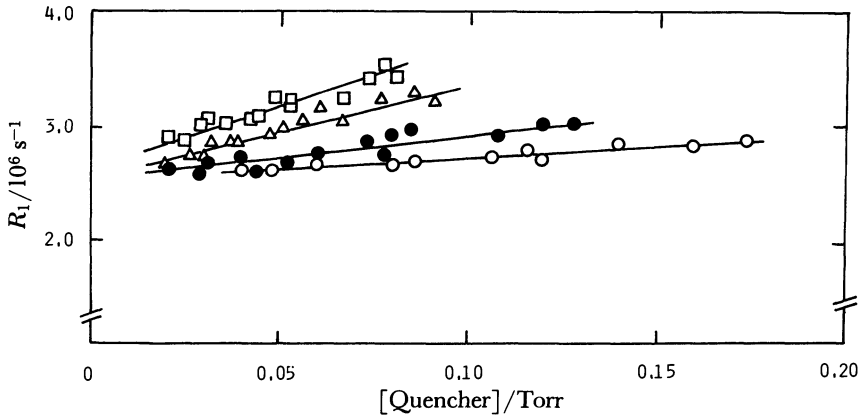

Fig. 3. Plots of R_1 against the pressure of a quencher obtained at f=100 kHz, [HN_3]=0.123 Torr, and [He]=20 Torr. ○: CH_4, ●: c-C_3H_6, △: C_3H_8, □: i-C_4H_{10}.

Table 1. Rate Constants and Cross-Sections for Quenching NH($c^1\Pi$) and NH($A^3\Pi$)[a]

	Quencher	k_{1q}[b]	σ_{1q}[c]	k_{3q}[b]	σ_{3q}[c]
1	CH_4	0.35±0.10	6.5	0.45±0.10	8.3
2	C_2H_6	0.86±0.11	18.1	1.13±0.12	23.9
3	C_3H_8	1.67±0.20	37.4	1.50±0.17	33.6
4	c-C_3H_6	0.75±0.10	16.7	0.88±0.09	19.5
5	n-C_4H_{10}	1.89±0.14	43.7	1.93±0.20	44.6
6	i-C_4H_{10}	1.94±0.29	44.8	1.83±0.15	42.3
7	C_2H_4	2.88±0.30	60.2	1.19±0.09	24.9
8	C_3H_6	2.65±0.20	58.9	1.84±0.11	40.9
9	1-C_4H_8	3.23±0.18	74.3	2.16±0.13	49.7
10	i-C_4H_8	3.19±0.11	73.4	3.50±0.22	80.5
11	t-Δ^2-C_4H_8	3.11±0.13	71.6	3.52±0.14	81.0
12	c-Δ^2-C_4H_8	3.24±0.18	74.6	3.59±0.18	82.6

a) The error limits are one standard deviation. b) In units of 10^{14} cm^3 mol^{-1} s^{-1}. c) $\sigma_q=k_q(\pi\mu/8kT)^{1/2}$, in units of 10^{-16} cm^2.

transmitted light and the fluorescence of the NH radicals were measured by using a lock-in amplifier relative to its reference signal.

Hydrogen azide was synthesized from sodium azide and stearic acid and purified by the method described in the previous paper.[20] Research-grade hydrocarbons were used after several distillations at low temperatures.

Results

Quenching of NH($c^1\Pi$). When a small amount of ethane was introduced into the reactant (0.1—0.3 Torr of HN_3 and 20 Torr of He: 1 Torr=133.3 Pa), the phase difference between the transmitted light and the fluorescence at 325 nm, ϕ_1, decreased. Figure 2 shows the plots of $R_1(=2\pi f/\tan\phi_1)$ as a function of the pressure of ethane. Here, f denotes the frequency of the modulation of the lamp. As is shown in Fig. 2, the plots give straight lines with the same slope for different initial pressures of HN_3. The intercepts increased with an increase in the pressure of HN_3. Similar plots were obtained with other quenchers, such as CH_4, C_3H_8, c-C_3H_6, n-C_4H_{10}, i-C_4H_{10}, C_2H_4, C_3H_6, 1-C_4H_8, i-C_4H_8, and *cis*- and *trans*-Δ^2-C_4H_8. All of the plots gave

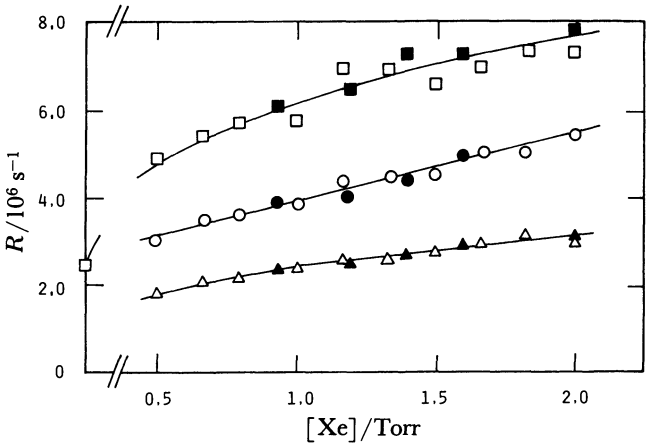

Fig. 4. Plots of R_1, R_3, and R_{13} against the pressure of Xe obtained at [HN_3]=0.07 Torr, and [He]=20 Torr. □: R_1, △: R_3, ○: R_{13}. Open symbols: f=100 kHz, closed symbols: f=120 kHz. The solid lines are calculated ones using Eqs. 18—20. For detail, see Text.

straight lines for every quencher examined. Some examples are shown in Fig. 3. The values of slope of each straight line are summarized in the third column of Table 1. The error limits show one standard deviation.

Effect of Xe on Fluorescence of NH. When Xe was added to a HN_3–He mixture, the intensity of the fluorescence of NH($c^1\Pi$) at 325 nm, decreased while that of NH($A^3\Pi$) at 336 nm increased. The phase-angle difference between the transmitted light and the emission at 336 nm, ϕ_3, was measured, like ϕ_1, at various pressures of HN_3 and Xe. The values of $R_1(=2\pi f/\tan\phi_1)$, $R_{13}(=2\pi f/\tan(\phi_1-\phi_3))$, and $R_3(=2\pi f/\tan\phi_3)$ are plotted as functions of the pressure of Xe in Fig. 4 and of that of HN_3 in Fig. 5.

Effect of Hydrocarbons on R_{13}. The phase-angle difference between the fluorescence of NH($c^1\Pi$) and that of NH($A^3\Pi$), $\phi_1-\phi_3$, was measured in the presence of hydrocarbon in a mixture of He(20 Torr)-HN_3(0.1 Torr)-Xe(0.7 Torr). The plots of R_{13} against the

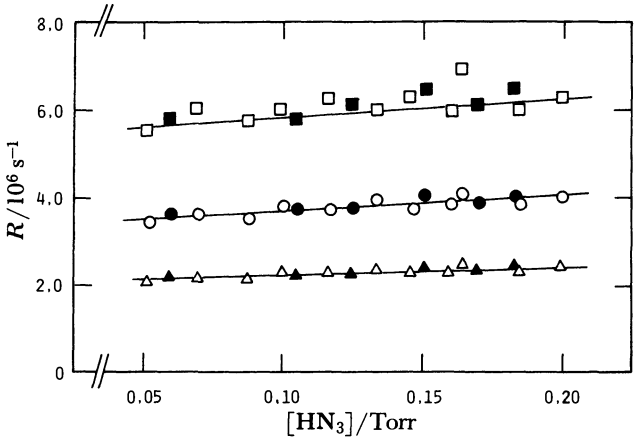

Fig. 5. Plots of R_1, R_3, and R_{13} against the pressure of HN_3 obtained at [Xe]=0.7 Torr, and [He]=20 Torr. For the other conditions, see footnote of Fig. 4.

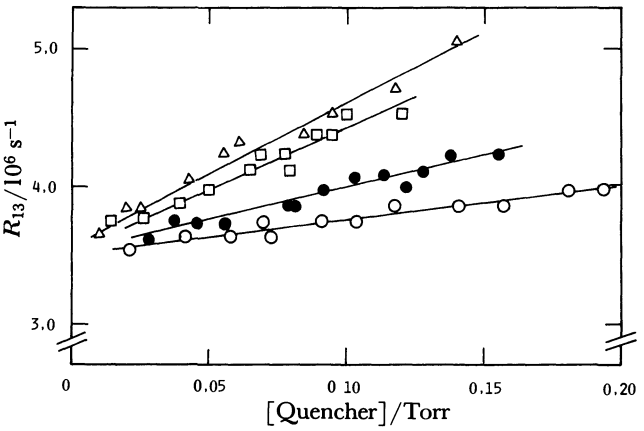

Fig. 6. Plots of R_{13} against the pressure of a quencher obtained at f=100 kHz, $[HN_3]$=0.1 Torr, [Xe]= 0.7 Torr and [He]=20 Torr. ○: CH_4, ●: c-C_3H_6, □: C_3H_8, △: i-C_4H_{10}.

pressure of hydrocarbon gave a straight line for every quencher examined. Some examples are shown in Fig. 6. The values of the slopes of the straight lines are summarized in the fifth column of Table 1.

Discussion

Quenching of NH(c¹Π) by Hydrocarbons. As was discussed in the previous paper,[20] the following reaction mechanism can be considered to explain the results shown in Figs. 2 and 3:

$$HN_3 + h\nu \longrightarrow NH(c^1\Pi) + N_2 \quad (1)$$

$$NH(c^1\Pi) \longrightarrow NH(a^1\Delta) + h\nu(325) \quad k_{10} \quad (2)$$

$$NH(c^1\Pi) + M \longrightarrow \text{products} \quad k_{1M} \quad (3)$$

where M denotes He, HN_3, or hydrocarbons.

Assuming the above reaction mechanism, the following relation can be derived for R_1:

$$R_1 = 2\pi f/\tan\phi_1 \quad (4)$$

$$= k_{10} + k_{1h}[He] + k_{1a}[HN_3] + k_{1q}[Q] \quad (5)$$

where k_{1h}, k_{1a}, and k_{1q} represent k_{1M} for He, HN_3, and the hydrocarbon used respectively. Under constant pressures of He and HN_3, the intercepts of the straight lines in Fig. 3 should be equal to $k_{10}+k_{1h}[He]+k_{1a}[HN_3]$. This R_1 value can be estimated to be $(2.3\pm0.4)\times10^6\ s^{-1}$ by using the previously obtained values of k_{10}, k_{1a}, and k_{1h} under the present experimental conditions; this value is in good agreement with the intercepts obtained in the present studies. Thus, the slope of the straight line shown in Table 1 corresponds to the value of k_{1q}. The quenching cross-sections were calculated from k_{1q} and are summarized in the fourth column of Table 1.

Effect of Xe. The results shown in Figs. 4 and 5 could not be explained by the addition of the following reactions to Reactions 1—3:

$$NH(c^1\Pi) + Xe \longrightarrow NH(A^3\Pi) + Xe \quad k_{1x} \quad (6)$$

followed by:

$$NH(A^3\Pi) \longrightarrow NH(X^3\Sigma^-) + h\nu(336) \quad k_{30} \quad (7)$$

$$NH(A^3\Pi) + M \longrightarrow \text{products} \quad k_{3M} \quad (8)$$

where M denotes a quencher such as He, HN_3, or Xe. If this mechanism is applicable, the following relation should hold for R_1:

$$R_1 = k_{10} + k_{1h}[He] + k_{1a}[HN_3] + k_{1x}[Xe] \quad (9)$$

That is, the plots of R_1 against the pressure of Xe should show a straight line with an intercept of $k_{10}+k_{1h}[He]+k_{1a}[HN_3]$, which is equal to $2.3\times10^6\ s^{-1}$ under the present experimental conditions. As is shown in Fig. 4, this is not the case. In order to explain the present results, then, the following reactions were considered in addition to Reactions 1—3 and 6—8:

$$Xe + h\nu(129.5) \longrightarrow Xe(^1P_1) \quad (10)$$

$$Xe + h\nu(147) \longrightarrow Xe(^3P_1) \quad (11)$$

$$Xe(^1P_1) \longrightarrow Xe + h\nu(129.5) \quad k_{20} \quad (12)$$

$$Xe(^1P_1) + HN_3 \longrightarrow Xe + NH(c^1\Pi) + N_2 \quad k_{2a} \quad (13)$$

$$Xe(^1P_1) + M \longrightarrow \text{products} \quad k_{2M} \quad (14)$$

$$Xe(^3P_1) \longrightarrow Xe + h\nu(147) \quad k'_{20} \quad (15)$$

$$Xe(^3P_1) + HN_3 \longrightarrow Xe + NH(A^3\Pi) + N_2 \quad k'_{2a} \quad (16)$$

$$Xe(^3P_1) + M \longrightarrow \text{products} \quad k'_{2M} \quad (17)$$

The spin-conservation rule was assumed to hold for Reactions 13 and 16.[21] Assuming the above reactions, the following relations were derived:

$$R_1 = AB/(A+B) \quad (18)$$

$$R_3 = (1/A+1/B+1/C)^{-1} \quad (19)$$

$$R_{13} = C \quad (20)$$

Here,

$$A = k_{10} + k_{1h}[He] + k_{1a}[HN_3] + k_{1x}[Xe] \quad (21)$$

$$B = k_{20} + k_{2a}[HN_3] \quad (22)$$

$$C = k_{30} + k_{3h}[He] + k_{3a}[HN_3] + k_{3x}[Xe] \quad (23)$$

where k_{3h}, k_{3a}, and k_{3x} represent k_{3M} for He, HN_3, and Xe respectively. To derive Eqs. 18—20, the following assumptions were made; (i) in the presence of Xe, the direct photolysis of HN_3 was negligible, (ii) the values of A, B, and C were larger than $2\pi f$, and (iii) $k'_{2a}[Xe(^3P_1)]$ was negligibly small compared with $k_{2a}[NH(c^1\Pi)]$ under the present experimental conditions.

From the slopes of the straight lines in the plots of R_{13} vs. [HN_3] and [Xe], the values of k_{3a} and k_{3x} were estimated to be $(6.0\pm1.1)\times10^{13}$ and $(2.8\pm0.1)\times10^{13}$ cm^3 mol^{-1} s^{-1} respectively. The latter value agreed well with that obtained by Hofzumahaus and Stuhl.[19] From the intercepts, the lifetime of NH($A^3\Pi$), $1/k_{30}$, was estimated to be 490 ± 40 ns using the value of $k_{3h}=4\times10^{10}$ cm^3 mol^{-1} s^{-1}.[19] The correction by the quenching of He at 20 Torr was less than 0.5%. The lifetime of NH($A^3\Pi$) estimated here agrees well with the literature value.[22] The solid lines in Figs. 4 and 5 are drawn by using Eqs. 18—20 with these values: $k_{10}+k_{1h}[He]=2.2\times10^6$ s^{-1}, $k_{1a}=5.2\times10^{13}$ cm^3 mol^{-1} s^{-1},[20] $k_{20}=2.1\times10^6$ s^{-1}, $k_{2a}=2.4\times10^{14}$ cm^3 mol^{-1} s^{-1}, and $k_{1x}=2.2\times10^{14}$ cm^3 mol^{-1} s^{-1}. Although the latter three values are not unique, the agreement is satisfactory, as Figs. 4 and 5 show.

Quenching of NH($A^3\Pi$) by Hydrocarbons. When a hydrocarbon is added to the He–HN_3–Xe mixture as a quencher, the following quenching reactions should be considered:

$$NH(c^1\Pi) + Q \longrightarrow \text{products} \qquad k_{1q} \quad (24)$$

$$NH(A^3\Pi) + Q \longrightarrow \text{products} \qquad k_{3q} \quad (25)$$

$$Xe(^1P_1) + Q \longrightarrow \text{products} \qquad k_{2q} \quad (26)$$

$$Xe(^3P_1) + Q \longrightarrow \text{products} \qquad k'_{2q} \quad (27)$$

By the addition of the above reactions, the terms of $k_{1q}[Q]$, $k_{2q}[Q]$, and $k_{3q}[Q]$ should be added to A, B, and C respectively. Under constant pressures of He, HN_3, and Xe, the following relation can be obtained:

$$R_{13} = 2\pi f/\tan(\phi_1-\phi_3) = C_0 + k_{3q}[Q] \quad (28)$$

where C_0 represents the R_{13} values in the absence of the quencher. That is, the slope of the straight line in Fig. 6 represents the k_{3q}. The cross-sections for quenching NH($A^3\Pi$), σ_{3q}, were calculated from the values of k_{3q}; they are listed in the sixth column of Table 1.

Comparison with Literature Values. No values have been reported for the cross-sections for quenching NH($c^1\Pi$) by hydrocarbons. For the quenching of NH($A^3\Pi$) by CH_4, the present results agree well with those obtained by Nishi et al.[17] and Hofzumahaus and Stuhl,[19] although the experimental methods are different.

Collision Complex Model. Recently, Hofzumahaus and Stuhl have measured the cross-sections for the quenching of NH($A^3\Pi$) by NH_3, NO, CH_4, H_2, CO, Xe, O_2, CO_2, Ar, N_2, and He, using the laser photolysis of NH_3. They found that the trend of the quenching cross-sections can be described by Parmenter's correlation, which suggests that the attractive force is effective for the quenching process.[19] In Parmenter's correlation, the quenching cross-sections, σ, are correlated with the intermolecular well depth, ε_{qq}:[23]

$$\ln\sigma = \ln C + \beta(\varepsilon_{qq}/k)^{1/2} \quad (28)$$

Here, $\beta=(\varepsilon_{A^*A^*}/kT^2)^{1/2}$, where $\varepsilon_{A^*A^*}$ is the well depth between the excited molecules, A*. Figures 7 and 8 show the plots for the quenching of NH($A^3\Pi$) and NH($c^1\Pi$) respectively by hydrocarbons. The numbers in Figs. 7 and 8 correspond to the compounds listed in Table 1. The well depth was approximated by $\varepsilon_{qq}/k=1.15\,T_b$, where T_b represents the boiling point.[24] The broken line in Fig. 7 shows the correlation obtained by Hofzumahaus and Stuhl. A good correlation is obtained for the quenching of NH($A^3\Pi$) by hydrocarbons:

$$\ln\sigma = (-1.2\pm0.8) + (0.30\pm0.05)(\varepsilon_{qq}/k)^{1/2} \quad (29)$$

The value of the slope is almost the same as that determined by Hofzumahaus and Stuhl.[19] The broken line in Fig. 8 is drawn by using Eq. 29. As is shown in Fig. 8, the trend of the cross-sections of paraffin for quenching NH($c^1\Pi$) is different from that of olefin, but it is similar to the case of the quenching of NH($A^3\Pi$). The quenching mechanism for olefin should be different from that of paraffin.

Following the method described by Hofzumahaus and Stuhl,[19] absolute cross sections were calculated. The method will be described here only briefly. The interaction potentilal, $V(r)$, is assumed to be in the form of Eq. 30:

$$V(r) = -C_3/r^3 - C_6/r^6 - C_6'/r^6, \quad (30)$$

where the C_3, C_6, and C_6' coefficients represent dipole–dipole ($C_3=2\mu_1\mu_2$), dipole-induced dipole ($C_6=2(\mu_1^2\alpha_2+\mu_2^2\alpha_1)$, and dispersion ($C_6'=1.5\,I_1I_2\alpha_1\alpha_2/(I_1+I_2)$) interactions respectively. The symbols μ, α, and I represent the dipole moment, the polarizability, and the ionization potential respectively. The effective potential, $V_{eff}(r)$, is given by Eq. 31 at the initial kinetic energy of E and the impact parameter of b:

$$V_{eff}(r) = V(r) + Eb^2/r^2 \quad (31)$$

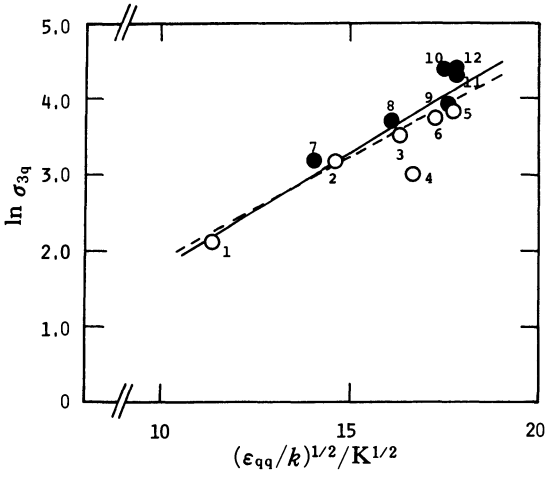

Fig. 7. Plots of $\ln\sigma_{3q}$ against $(\varepsilon_{qq}/k)^{1/2}$ for the quenching of NH($A^3\Pi$). The numbers correspond to the compound listed in Table 1. ○: paraffin, ●: olefin. The broken line shows the relation, $\ln\sigma=-0.82+0.275\,(\varepsilon_{qq}/k)^{1/2}$.[19]

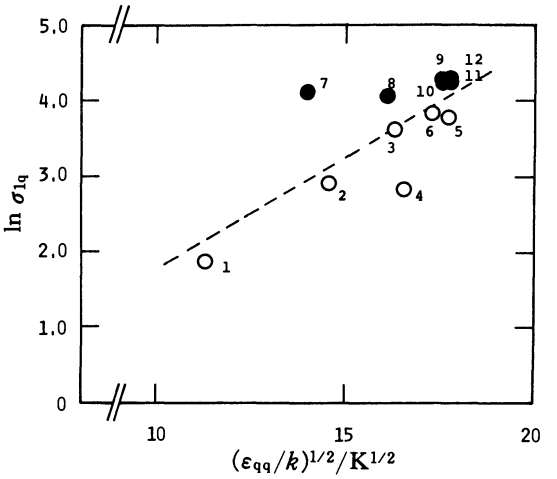

Fig. 8. Plots of $\ln\sigma_{1q}$ against $(\varepsilon_{qq}/k)^{1/2}$ for the quenching of NH($c^1\Pi$). The numbers correspond to the compound listed in Table 1. The broken line represents the best fit line obtained for the quenching of NH($A^3\Pi$).

The position of the centrifugal maximum, r_0, can be estimated, by the use of Eq. 32, as a function of E, where the orbiting condition, $E=V_{eff}(r_0)$, is satisfied:

$$\partial V_{eff}(r)/\partial r = 0 \quad \text{at } r = r_0 \tag{32}$$

Thus, the cross-section at the initial kinetic energy of E can be estimated by $\sigma(E)=\pi b^2=\pi r_0^2(1-V(r_0)/E)$. Thus, the thermally averaged cross-section, $\sigma(T)$, can be estimated by Eq. 33:

$$\sigma(T) = (1/kT)^2\int\sigma(E)\,E\exp(-E/kT)\mathrm{d}E \tag{33}$$

In Table 2, the calculated results are summarized, along with the parameters used in the calculation. Figures 9 and 10 show the plots of the cross-sections

Table 2. Quenching Cross-Sections Calculated by a Collision Complex Model and the Parameters Used for the Calculation

Compounds	μ[a]	α[b]	IP[c]	σ_{1q}[d]	σ_{3q}[d]
NH($c^1\Pi$)	1.70[e]	1.35[f]	7.48[g]		
NH($A^3\Pi$)	1.31[e]	1.35[f]	9.93[g]		
CH_4	0	2.60	12.6	55.8	56.2
C_2H_6	0	4.47	11.5	66.2	66.5
C_3H_8	0.084	6.29	11.10	78.3	77.5
c-C_3H_6	0	5.82	10.09	71.4	71.4
n-C_4H_{10}	0.050	8.42	10.63	83.7	83.2
i-C_4H_{10}	0.132	8.42	10.57	87.6	86.2
C_2H_4	0	4.26	10.50	64.6	64.7
C_3H_6	0.366	6.20	9.73	91.5	87.1
1-C_4H_8	0.34	8.14	9.63	96.2	92.3
i-C_4H_8	0.500	8.14	9.23	103.7	97.9
t-Δ^2-C_4H_8	0	8.14	9.13	79.1	78.7
c-Δ^2-C_4H_8	0.257[h]	8.14	9.13	91.8	88.6

a) Dipole moments in units of 3.3356×10^{-30} Cm; "CRC Handbook of Chemistry and Physics," 61st ed., CRC Press Inc., Boca Raton, (1980—1981), E-64, unless otherwise cited. b) Polarizabilities in units of $10^{-30}m^3$; estimated by the method described on p. 947 of Ref. 24, unless otherwise cited. c) Ionization potentials in units of 96.4846 kJ mol^{-1}; "CRC Handbook of Chemistry and Physics," 61st ed., CRC press Inc., Boca Raton, (1980—1981), E-69, unless otherwise cited. d) Calculated quenching cross sections in units of 10^{-16} cm^2. e) T. A. R. Irwin and F. W. Dalby, *Can. J. Phys.*, **43**, 1766 (1965). f) Assumed; see Ref. 19. g) Calculated from the ionization potential of NH($X^3\Sigma^-$) and the excitation energies of NH($c^1\Pi$) and NH($A^3\Pi$). h) Chemical Society of Japan, Ed., "Kagaku Binran Kisohen," 3rd ed., Maruzen Tokyo (1984), II-719.

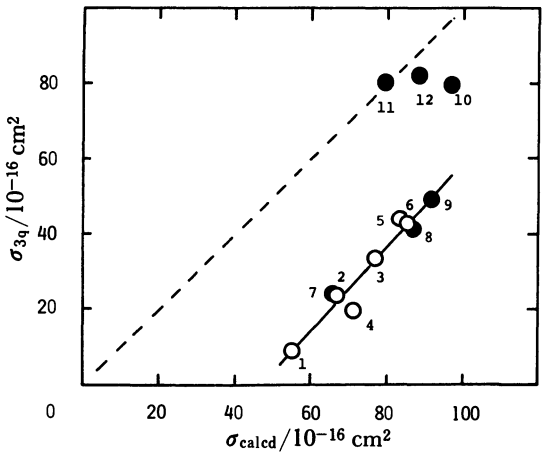

Fig. 9. Plots of the experimental cross sections, σ_{3q}, against those calculated by the collision complex model, σ_{calcd}, for quenching NH($A^3\Pi$). The numbers correspond to the compounds listed in Table 1.

observed against calculated ones. The observed cross-sections are smaller than the calculated ones except for higher olefins. Hofzumahaus and Stuhl evaluated the quenching probability $P=\sigma_{obsd}/\sigma_{calcd}$, to be about 0.3 by comparison with their results.[19] The results shown in Figs. 9 and 10, however, suggest that the probability depends on the molecular complexity.

Quenching Mechanism. In the case of O(^{1}D), the

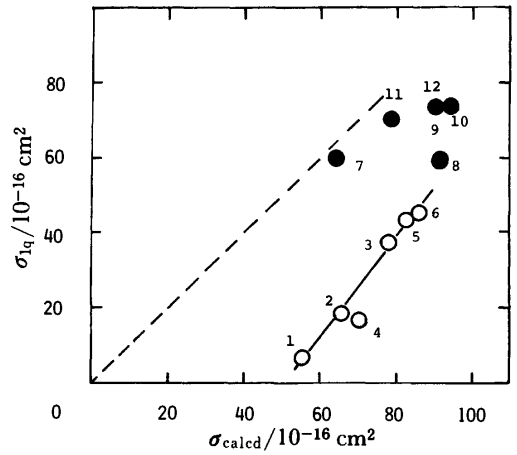

Fig. 10. Plots of the experimental cross sections, σ_{1q}, against those calculated by the collision complex model, σ_{calcd}, for quenching NH($c^1\Pi$). The numbers correspond to the compounds listed in Table 1.

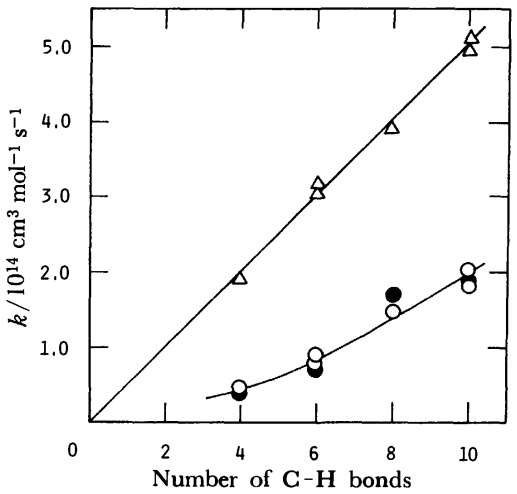

Fig. 11. Plots of reaction rates, k, against the number of C-H bonds included in paraffin. O: NH($A^3\Pi$), ●: NH($c^1\Pi$), and Δ: O(^{1}D).

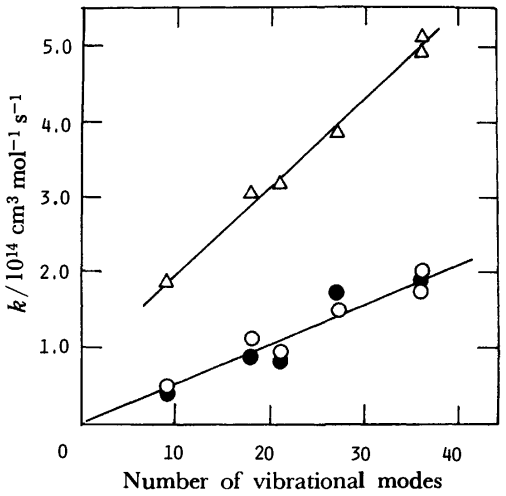

Fig. 12. Plots of reaction rates, k, against the number of vibrational modes of paraffin. O: NH($A^3\Pi$), ●: NH($c^1\Pi$), and Δ: O(^{1}D).

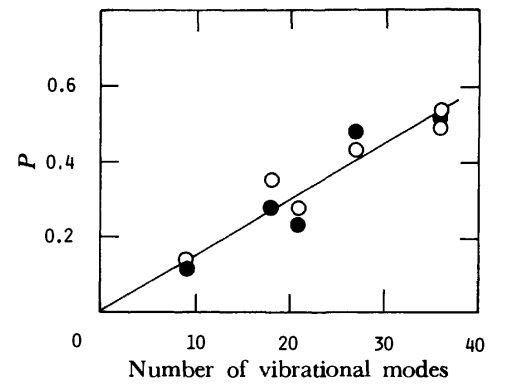

Fig. 13. Plots of quenching probabilities, P, against the number of vibrational modes of paraffin. O: NH($A^3\Pi$) and ●: NH($c^1\Pi$).

reaction rates of paraffin are known to be proportional to the number of C-H bonds included,[25] as is shown in Fig. 11. In the cases of the quenching of NH($A^3\Pi$) and NH($c^1\Pi$) by paraffin, the rate constants do not linearly increase with the number of C-H bonds included. This fact can not be explained by the term of the difference in the bond-dissociation energies, because n-C_4H_{10} quenches NH($A^3\Pi$) or NH($c^1\Pi$) as efficiently as i-C_4H_{10}, which has a weaker C-H bond than the former.

As is shown in Fig. 12, a good correlation was obtained between the quenching rates of paraffin and the number of the vibrational modes of quenchers in the cases of the quenching of NH($c^1\Pi$) and NH($A^3\Pi$). This fact may suggest that the intermolecular vibrational relaxation process in the collision complex is important. If the intermolecular vibrational relaxation is inefficient, the collision complex will decompose to the initial reactants; i.e., no quenching reactions will occur. That is, the quenching probability, P, becomes small for the molecules which have fewer vibrational modes. This trend is clearly shown in Fig. 13, where the quenching probabilities are plotted against the number of vibrational modes of the quenchers.

In the case of the quenching of NH($c^1\Pi$) by olefins, it is necessary to assign a large value of P, as may be seen from Fig. 10. A large value of P could not be explained by the term of the number of vibrational modes. In the above consideration, the rate of intermolecular vibrational relaxation is assumed to be an important factor in determining the probability. If the collision complex formed from olefin is considered to be tight enough for the efficient intermolecular vibrational relaxation, the collision probability will be high. Another possible explanation is that the rate of the decomposition to an exit channel is much faster than that of the returning to the initial reactants. At present, it is difficult to decide which mechanism is more important. The property of the collision complex is, in any event, an important factor in the quenching, although the validity of the assumption made for the

calculation of σ_{calcd} should be more carefully examined.

References

1) T. G. Slanger, "Reactions of Small Transient Molecules. Kinetics and Energetics," ed by A. Fontijin and M. A. A. Clyne, Academic Press, London (1983), p. 231.

2) S. Tsunashima, M. Hotta, and S. Sato, *Chem. Phys. Lett.*, **64**, 438 (1979); S. Tsunashima, J. Hamada, M. Hotta, and S. Sato, *Bull. Chem. Soc. Jpn.*, **53**, 2443 (1980); J. Hamada, S. Tsunashima, and S. Sato, *ibid.*, **55**, 1739 (1982); J. Kawai, S. Tsunashima, and S. Sato, *Nippon Kagaku Kaishi*, **1984**, 32.

3) S. Sato, T. Kitamura, and S. Tsunashima, *Chem. Lett.*, **1980**, 687; S. Tsunashima, T. Kitamura, and S. Sato, *Bull. Chem. Soc. Jpn.*, **54**, 2869 (1981).

4) T. Kitamura, S. Tsunashima, and S. Sato, *Bull. Chem. Soc. Jpn.*, **54**, 55 (1981); J. Hamada, S. Tsunashima, and S. Sato, *ibid.*, **56**, 662 (1983).

5) J. Kawai, S. Tsunashima, and S. Sato, *Chem. Phys. Lett.*, **110**, 655 (1984).

6) J. Kawai, S. Tsunashima, and S. Sato, *Bull. Chem. Soc. Jpn.*, **55**, 3312 (1983).

7) J. Kawai, S. Tsunashima, and S. Sato, *Chem. Lett.*, **1984**, 823.

8) O. Kajimoto and T. Fueno, *Chem. Phys. Lett.*, **80**, 484 (1981); O. Kondo, J. Miyata, O. Kajimoto, and T. Fueno, *Chem. Phys. Lett.*, **88**, 424 (1982).

9) S. Kodama, *Bull. Chem. Soc. Jpn.*, **56**, 2348 (1983); *ibid.*, **56**, 2355 (1983); *ibid.*, **56**, 2363 (1983); *ibid.*, **58**, 2891 (1985); *ibid.*, **58**, 2900 (1985).

10) A. P. Baronavski, R. G. Miller, and J. R. McDonald, *Chem. Phys.*, **30**, 119 (1978); J. R. McDonald, R. G. Miller, and A. P. Baronavski, *Chem. Phys.*, **30**, 133 (1978); W. S. Drozdoski, A. P. Baronavski, and J. R. McDonald, *Chem. Phys. Lett.*, **64**, 421 (1979); J. W. Cox, H. H. Nelson, and J. R. McDonald, *Chem. Phys.*, **96**, 175 (1985).

11) L. G. Piper, R. H. Krech, and R. L. Taylor, *J. Chem. Phys.*, **73**, 791 (1980).

12) B. Gelernt, S. V. Filseth, and T. Carrington, *J. Chem. Phys.*, **65**, 4940 (1976).

13) C. Zetsch and F. Stuhl, *J. Chem, Phys.*, **66**, 3107 (1977).

14) K. Schofield, *J. Photochem.*, **9**, 55 (1978).

15) H. Okabe, *J. Chem. Phys.*, **49**, 2726 (1968).

16) M. Kawasaki, Y. Hirata, and I. Tanaka, *J. Chem. Phys.*, **59**, 648 (1973).

17) N. Nishi, H. Shinohara, and J. Hanazaki, *Rev. Laser Eng.*, **10**, 394 (1982).

18) H. K. Haak and F. Stuhl, *J. Phys. Chem.*, **88**, 2201 (1984); *ibid.*, **88**, 3687 (1984).

19) A. Hofzumahaus and F. Stuhl, *J. Chem. Phys.*, **82**, 3152 (1985).

20) S. Sasaki, S. Tsunashima, and S. Sato, *Bull. Chem. Soc. Jpn.*, **59**, 1671 (1986).

21) D. H. Stedman, *J. Chem. Phys.*, **52**, 3966 (1970).

22) P. W. Fairchild, G. P. Smith, D. R. Crosley, and J. B. Jeffries, *Chem. Phys. Lett.*, **107**, 181 (1984).

23) H. M. Lin, M. Seaver, K. Y. Tang, A. E. W. Knight, and C. S. Parmenter, *J. Chem. Phys.*, **70**, 5442 (1979); C. S. Parmenter and M. Seaver, *ibid.*, **70**, 5458 (1979).

24) J. O. Hirschfelder, C. F. Curtiss, and R. B. Bird, "Molecular Theory of Gases and Liquids," 2nd ed., Wiley, London (1964).

25) P. Michaud, G. Paraskevopoulos, and R. J. Cvetanović, *J. Phys. Chem.*, **78**, 1457 (1974).

 © 1986 The Chemical Society of Japan Bull. Chem. Soc. Jpn., 59, 1683—1687 (1986)

Kinetic and Equilibrium Studies of Complex Formation of Nickel(II) with Carboxylate Ligands at High Pressure. IV. Nickel(II) Malate and Nickel(II) Tartrate

Tohru INOUE,* Kiyotaka KOJIMA, and Ryosuke SHIMOZAWA
Department of Chemistry, Faculty of Science, Fukuoka University, Nanakuma, Jonan-ku, Fukuoka 814-01
(Received January 21, 1986)

Kinetic and equilibrium measurements were carried out for the complexation reaction of nickel(II) malate and nickel(II) tartrate in an aqueous solution at 20 °C and at pressures up to 100 MPa. From the pressure dependence of the stability constant and the rate constant, the reaction volume, ΔV^0, and the activation volume, ΔV_f^*, for the complex formation were estimated as follows: $\Delta V^0=17.8\pm0.6\,cm^3\,mol^{-1}$ and $\Delta V_f^*=13.8\pm0.6\,cm^3\,mol^{-1}$ for nickel(II) malate, and $\Delta V^0=17.8\pm0.5\,cm^3\,mol^{-1}$ and $\Delta V_f^*=13.7\pm1.2\,cm^3\,mol^{-1}$ for nickel(II) tartrate. Comparing the ΔV^0 values with those obtained for other carboxylate ligands, it was inferred that both malate and tartrate ions form a six-membered chelate complex coordinated by carboxyl and hydroxyl oxygens. The rate-determining step of the overall complexation reaction was assigned to the first bond formation process based on the ΔV_f^* value with the correction for the volume change associated with the outer-sphere complex formation.

A pressure-variable study of a chemical reaction provides information about the volume change associated with the reaction.[1] The reaction volume and the activation volume are very useful parameters for understanding features of the reaction. We have been carrying out the kinetic and equilibrium measurements for the complexation reaction of nickel(II) with carboxylate ligands in an aqueous solution under pressure in order to interpret the course of the reaction through the volume profile.[2-4] Along the line of this series of studies, in the present study we investigated the complexation reactions of nickel(II) malate and nickel(II) tartrate under various pressures up to 100 MPa. From the pressure dependence of the stability constants and the rate constants of the complexation reactions, the values of reaction and activation volumes were estimated and compared with those previously obtained for other carboxylate ligand systems.

Experimental

Stock solutions of nickel(II) malate and nickel(II) tartrate were prepared from nickel sulfate and corresponding acids by the same procedure as described previously.[2] The concentration of the solution was determined by titrating with an EDTA solution standardized by a standard solution of zinc nitrate. Guaranteed grade reagents of nickel sulfate, L-malic acid, and DL-tartaric acid were obtained from Wako Pure Chemicals and used without further purification. Each sample solution was prepared by diluting the stock solution to the desired concentration. The pH's of the sample solutions were in the range of 6.1±0.2 for both nickel(II) malate and nickel(II) tartrate, where most of the ligands were considered to be in a fully dissociated form from the pK_a values of the acids; $pK_{a1}=3.28$ and $pK_{a2}=4.72$ for malic acid,[5] and $pK_{a1}=2.80$ and $pK_{a2}=3.96$ for tartaric acid.[5]

The stability constants of the complexes under various pressures were determined from conductivity measurements according to the Fuoss-Kraus method[6] as described previously.[2,4] The conductivity were measured for sample solutions of 20 different concentrations ranging from 2×10^{-4} to 1×10^{-3} mol dm^{-3} for nickel(II) malate and from 1×10^{-4} to 1.5×10^{-3} mol dm^{-3} for nickel(II) tartrate. A high-pressure pressure-jump apparatus[7] was used for kinetic measurements under pressure. The pressure-jump measurements were made for sample solutions of 11—13 different concentrations ranging from 8×10^{-4} to 1×10^{-2} mol dm^{-3} for nickel(II) malate and from 5×10^{-4} to 2×10^{-3} mol dm^{-3} for nickel(II) tartrate. The observed relaxation process was characterized by a single relaxation time. The temperature was kept at 20.0±0.1 °C and the pressure was maintained within ±0.5 MPa of the designated pressure for both equilibrium and kinetic measurements. The concentration in the molarity scale was corrected for compression under pressure using the density data of water.[8]

Results and Discussion

The complexation reaction under consideration is represented in Scheme 1.

$$Ni^{2+} + L^{2-} \overset{K}{\rightleftharpoons} NiL$$

L^{2-}: malate or tartrate

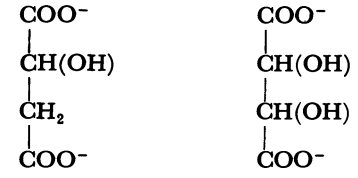

Scheme 1.

Stability constants of the complexes, K, determined from the conductivity data are listed in Table 1 (for details of the determination procedure, see Ref. 2). The reaction volume, ΔV^0, for the complexation reaction can be evaluated from the pressure dependence of the stability constant according to the relation[1]

$$RT\left(\frac{\partial \ln K}{\partial P}\right)_T = -\Delta V^0 - RT\kappa_0, \qquad (1)$$

where κ_0 represents the solution compressibility and other symbols have their usual meanings. In the above expression, $-RT\kappa_0$ is a correction term for the compression required when the concentration is expressed in terms of molarity and has a value of 1.1

Table 1. Stability Constants and Rate Constants for the Complexation Reaction of Nickel(II) Malate and Nickel(II) Tartrate as a Function of Pressure at 20°C and I→0[a)]

	Pressure/MPa					
	0.1	20	40	60	80	100
(a) Nickel(II) Malate						
$K/10^3\,mol^{-1}\,dm^3$	7.99(0.85)	7.15(0.67)	6.18(0.55)	5.14(0.44)	4.46(0.35)	3.80(0.29)
$k_f/10^5\,mol^{-1}\,dm^3\,s^{-1}$	2.00(0.07)	1.82(0.07)	1.61(0.06)	1.44(0.07)	1.28(0.06)	1.09(0.04)
$k_d/10\,s^{-1}$	2.50(0.28)	2.55(0.26)	2.60(0.25)	2.80(0.27)	2.86(0.26)	2.88(0.24)
(b) Nickel(II) Tartrate						
$K/10^3\,mol^{-1}\,dm^3$	2.80(0.08)	2.35(0.06)	2.01(0.06)	1.71(0.06)	1.51(0.06)	1.30(0.06)
$k_f/10^5\,mol^{-1}\,dm^3\,s^{-1}$	2.61(0.05)	2.20(0.07)	1.99(0.06)	1.73(0.06)	1.60(0.06)	—
$k_d/10\,s^{-1}$	9.33(0.32)	9.35(0.40)	9.90(0.43)	10.1(0.5)	10.7(0.6)	—

a) Standard deviations are shown in parentheses.

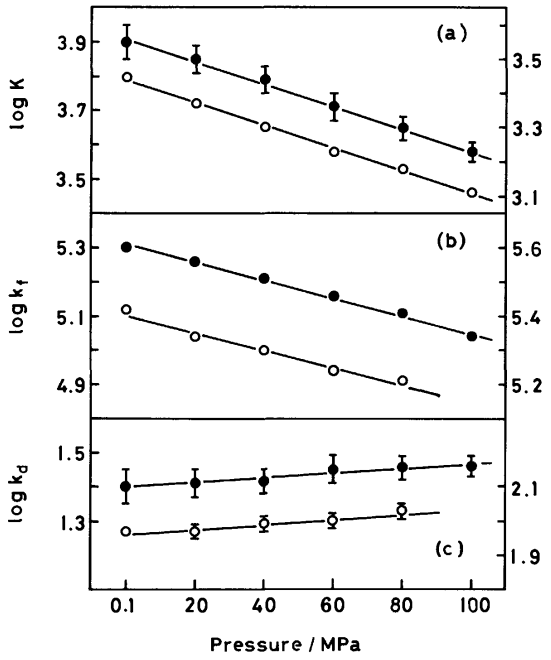

Fig. 1. Pressure dependence of (a) $\log K$, (b) $\log k_f$, and (c) $\log k_d$ at 20°C: ●, nickel(II) malate (left scale); ○, nickel(II) tartrate (right scale). Solid lines show the linear least-squares fits to the data points.

$cm^3\,mol^{-1}$ [1a)] for dilute aqueous solution as in the present case. Figure 1a shows plots of $\log K$ against pressure for nickel(II) malate and nickel(II) tartrate. In the measured pressure range, $\log K$ decreased linearly with increasing pressure. From the slope of the straight line fitted by a least-squares method, the values of reaction volume for the complexation reaction were estimated according to Eq. 1, and they are listed in Table 2 together with those obtained for other carboxylate ligands.

The rate constants for the complexation reaction were determined from the pressure-jump relaxation data according to the following relations; the details of the procedure were described elswhere.[2,4)]

$$1/\tau = k_f[\gamma_\pm^2(c_{Ni}+c_L) + 1/K]$$
$$k_d = k_f/K, \qquad (2)$$

where τ represents the relaxation time, k_f and k_d the rate constants for the complex formation and dissociation at zero ionic strength, c_{Ni} and c_L the equilibrium concentration of nickel(II) and ligand ions, and $\gamma_\pm$ the mean activity coefficient of the free ions at a given ionic strength. The values of the rate constants at various pressures are summarized in Table 1. The activation volume of the complexation reaction was estimated from the pressure dependence of the rate constants based on a relation analogous to Eq. 1.[1)] Plots of $\log k_f$ and $\log k_d$ against pressure are shown in Figs. 1b and 1c, respectively. In the measured pressure range, a linear relationship was obtained between the logarithm of the rate constant and the pressure. From the slope of the straight line, the values of the activation volume for the complex formation, ΔV_f^*, and dissociation, ΔV_d^*, were estimated. They are listed in Table 2 together with the activation volumes obtained for the complexation reaction with other carboxylate ligands.

It may be considered that the volume change associated with the complex formation in aqueous solution between metal ion and charged ligand consists of several contributions; i) the release of electrostriction due to the charge neutralization, ii) the elimination of solvated water around the coordinating group accompanied by the coordination bond formation, which produces free water, iii) the difference in coordination bond length between metal–water bond and metal-ligand bond, and iv) for chelating ligand, the increase of free volume, which is too small to be occupied by the solvent molecule, resulting from the formation of a ring structure. The contributions from i), ii), and iv) are positive for volume increase in the system, while the sign of the contribution from iii) may depend on the nature of the metal-ligand bond. According to the above consideration, it can be expected that the difference in the structure of the complex (e.g., monodentate or polydentate complex, or type of coordinating group(s) to metal ion) is reflected in the reaction volume.

The top five ligands in Table 2 have the same electrical charge(−2), and hence, the contribution i) is the same for these ligands. A succinate ion forms a

Table 2. Reaction Volumes, ΔV^0, and Activation Volumes, ΔV^*, for the Complex Formation of Nickel(II) with Carboxyl Ligands[a)]

Ligands	ΔV^0	ΔV_f^*	ΔV_d^*	$\Delta V_f^* - \Delta V_{os}^{0}$[b)]	Reference
Succinate	11.1±0.9	14.1±0.8	3.0±0.9	7.3	2
Malonate	13.5±1.0	14.7±0.5	1.2±1.2	7.5	4
Tartronate	13.3±0.7	15.2±0.5	1.9±0.8	8.0	4
Malate	17.8±0.6	13.8±0.6	−4.0±0.5	6.6	This work
Tartrate	17.8±0.5	13.7±1.2	−4.1±0.7	6.5	This work
Glycolate	17.3±1.0	14.7±0.5	−2.6±0.7	11.6	3
Lactate	17.6±0.9	13.5±0.4	−4.1±0.6	10.4	3

a) In $cm^3 mol^{-1}$; Errors are standard deviations estimated from the least-squares analysis. b) The values of ΔV_{os}^0 estimated from the Hemmes equation[14] are as follows; 6.8 $cm^3 mol^{-1}$ for succinate at 10°C, 7.2 $cm^3 mol^{-1}$ for malonate, tartronate, malate, and tartrate at 20°C, and 3.1 $cm^3 mol^{-1}$ for glycolate and lactate at 20°C.

monodentate complex rather than a seven-membered chelate complex,[9] while a malonate ion forms a six-membered chelate complex coordinated by two carboxyl oxygens.[10] This accords with a smaller ΔV^0 value for a succinate than for a malonate on considering the contributions ii) and iv). The similar ΔV^0 value for tartronate and malonate suggests that tartronate ion also forms a six-membered chelate complex by two carboxyl groups.[4]

Large ΔV^0 values for the complexation of nickel(II) malate and nickel(II) tartrate obtained in the present study indicate that malate and tartrate ions form a chelate complex with nickel(II). Some possible structures of the chelate complex are suggested from the molecular structure of malate and tartrate ions (shown in Scheme 1). Since a seven-membered chelate is unstable as seen in nickel(II) succinate, there remain two possibilities as a chelate structure; i.e., five-membered or six-membered ring coordinated by a carboxyl and a hydroxyl groups. The values of ΔV^0 for these two systems are quite similar, and they are also comparable to those for nickel(II) glycolate and nickel(II) lactate listed in Table 2. Glycolate and lactate ions form a five-membered chelate complex with nickel(II) by carboxyl and hydroxyl groups.[11,12] The similarity of ΔV^0 with glycolate and lactate systems might lead to the conclusion of a five-membered ring structure for nickel(II) malate and nickel(II) tartrate. However, the difference in the electrical charge between these two classes of ligands must be taken into account. Since glycolate and lactate ions have a charge of −1, the volume increase associated with charge neutralization (contribution i)) should be considerablly smaller than that for malate and tartrate ions. Thus, if nickel(II) malate and nickel(II) tartrate have a five-membered chelate ring, a somewhat larger ΔV^0 value should result rather than the observed value, because other contributions ii)—iv) may be regarded as to not differ significantly for these two classes of ligands. Hence, it may be considered that nickel(II) malate and nickel(II) tartrate form a six-membered chelate complex coordinated by carboxyl and hydroxyl groups.

The difference in ΔV^0 between malonate, tartronate systems and malate, tartrate systems, both of which form six-membered chelate complexes, may be attributed to the difference in coordinating groups. Since the interaction of a hydroxyl oxygen with a nickel(II) ion is weaker than that of a carboxyl oxygen, it may be expected that the bond length between a hydroxyl oxygen and a nickel(II) ion is longer than that between a carboxyl oxygen and a nickel(II) ion. Thus, larger ΔV^0 for malate and tartrate than malonate and tartronate can be partly explained in terms of contribution iii).

The metal complexation reaction has generally been interpreted in terms of a stepwise mechanism,[13] which can be represented by Scheme 2 for the bidentate chelate complex.

$$[Ni(H_2O)_6]^{2+} + L\text{-}L^{2-} \overset{K_{os}}{\rightleftharpoons} (H_2O)_5Ni(H_2O)L\text{-}L \qquad \begin{matrix} \text{I} \\ \\ \end{matrix} \qquad \begin{matrix} \text{II} \\ \\ \end{matrix}$$

$$\overset{k_1}{\underset{k_{-1}}{\rightleftharpoons}} (H_2O)_5Ni\text{-}L\text{-}L + H_2O \qquad \text{III}$$

$$\overset{k_2}{\underset{k_{-2}}{\rightleftharpoons}} (H_2O)_4Ni\begin{matrix}/L\\ \backslash L\end{matrix}\Big) + 2H_2O \qquad \text{IV}$$

Scheme 2.

In this scheme, I refers to the free ion, II the outer-sphere complex, III the monodentate complex, and IV the bidentate chelate complex, and K_{os} and k represent the outer-sphere complex formation constant and the rate constants of the respective steps.

It is reasonable to assume that the outer-sphere complex formation from the free ions is very rapid compared with the other steps because of its nature of an ion association process, and that the monodentate complex is in a steady state because an observed relaxation is characterized by a single relaxation time. Then, the observed rate constants for the complexation reaction are related to the outer-sphere complex formation constant and the rate constants of each step in Scheme 2 by

$$k_f = K_{os}k_1\left(\frac{k_2}{k_2+k_{-1}}\right) \qquad (3)$$

and

$$k_d = k_{-1}\left(\frac{k_{-2}}{k_2+k_{-1}}\right). \quad (4)$$

Two limiting cases can be distinguished, depending on the ratio of k_2/k_{-1}. If the first bond formation step (II⇄III) is rate-determining, i.e., $k_2 \gg k_{-1}$, Eq. 3 is reduced to

$$k_f \simeq K_{OS}k_1, \quad (5)$$

whereas, if the chelate-ring closure step (III⇄IV) is rate determining, i.e., $k_2 \ll k_{-1}$, Eq. 3 is reduced to

$$k_f \simeq K_{OS}K_1k_2, \quad (6)$$

where $K_1=k_1/k_{-1}$. The observed activation volume for these two limiting cases is approximately expressed by

$$\Delta V_f^* = \Delta V_{OS}^0 + \Delta V_1^* \text{ (for the former case)} \quad (7)$$

or

$$\Delta V_f^* = \Delta V_{OS}^0 + \Delta V_1^0 + \Delta V_2^* \text{ (for the latter case)}, \quad (8)$$

where ΔV_{OS}^0 is the reaction volume for the outer-sphere complex formation, ΔV_1^* and ΔV_1^0 are the activation volume and the reaction volume for the first bond formation after the outer-sphere complex formed, and ΔV_2^* is the activation volume for the ring-closure after the first bond formed. Thus, experimentally obtained ΔV_f^* is not a single but a composite term.

It is convenient to separate the outer-sphere complex formation process from the overall reaction. The value of ΔV_{OS}^0 can be estimated with considerable reliability according to Hemmes[14] as described in a previous paper.[2,3] The values of $\Delta V_f^*-\Delta V_{OS}^0$ for some carboxylate ligands are listed in Table 2. Those values for nickel(II) malate and nickel(II) tartrate obtained in the present study are regarded as essentially the same as that for nickel(II) succinate taking into account the error range. This leads to the conclusion that the rate-determining step for the complexation reaction of nickel(II) malate and nickel(II) tartrate is the first bond formation step, since the chelation step is lacking for nickel(II) succinate as mentioned before. The situation is also the same for nickel(II) malonate and nickel(II) tartronate. On the other hand, larger values of $\Delta V_f^*-\Delta V_{OS}^0$ for nickel(II) glycolate and nickel(II) lactate, for which the rate-determining step for the complexation reaction is the ring-closure step,[11,12] can be understood with the help of Eq. 8 as described in a previous paper.[3] Comparing the two classes of ligands, glycolate and lactate, and malate and tartrate, both of them form chelate complexes with nickel(II) coordinated by carboxyl and hydroxyl oxygens, but the size of chelate ring is different as mentioned before; the former class forms five-membered ring, whereas the latter forms six-membered ring. The difference in rate-determining step for these two classes of ligands may be attributed to

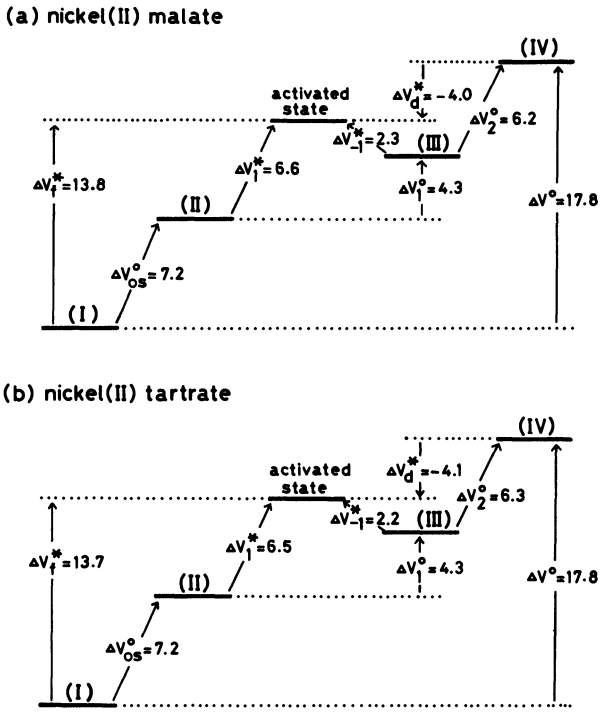

Fig. 2. Volume profile diagrams for the complexation reaction of nickel(II) malate (a) and nickel(II) tartrate (b). I, II, III, and IV in the figure correspond to the species in Scheme 2. The values of volume change in $cm^3\,mol^{-1}$ are shown in the figure.

the difference in the chelate-ring size. It is likely that a five-membered ring is imposed to take a sterically distorted structure, and hence, the ring closure becomes rate-determining for five-membered chelate formation.

It is worth noting that the values of $\Delta V_f^*-\Delta V_{OS}^0$ ($=\Delta V_1^*$) obtained for the complexation reaction for which the first bond formation is rate determining are very close to the activation volume of the water exchange of the aquanickel(II) ion, $\Delta V_{H_2O}^*=7.2\pm0.3$ $cm^3\,mol^{-1}$.[15] This suggests that the activated state for the first bond formation process is the same as that for the water exchange process, and is in accordance with the general picture drawn for the complexation reaction of labil metal ions.[13]

The volume profile diagrams obtained for the complexation reaction of nickel(II) malate and nickel(II) tartrate are shown in Fig. 2. The value of ΔV_1^0 representing the volume difference between II and III in Scheme 2 was estimated as $\Delta V^0-\Delta V_{OS}^0$ for nickel(II) succinate, based on the consideration that ΔV_1^0, the volume change associated with the first coordination-bond formation by a carboxyl group after the outer-sphere complex formed, is the same at different carboxylic acid. An initial volume increase occurs due to the release of electrostriction on forming the outer-sphere complex (II). It is followed by a volume increase due to the loosening of the water–nickel(II) bond to attain an activated state. Then, a volume decrease occurs on going from the activated state to the

monodentate complex (III) due to the completion of the first coordination-bond formation. It is again followed by a volume increase due to the second coordination-bond formation to lead a final chelate complex (IV). The remarkable feature of the volume profile for the complexation with malate and tartrate compared with those obtained previously with malonate and tartronate is that ΔV_d^* is negative for the former ligands, whereas ΔV_d^* for the latter ligands is positive. This difference can be partly attributed to the difference in the bond length of the second coordination bond; for nickel(II) malate and nickel(II) tartrate, the bond length between hydroxyl oxygen and metal ion may be longer and the final complex (IV) has a larger volume, which in turn results in the negative ΔV_d^*.

This work was supported financially in part by the Central Institute of Fukuoka University.

References

1) a) K. E. Weale, "Chemical Reactions at High Pressures," E. & F. N. Spon Ltd., London (1967); b) N. S. Isaacs, "Liquid Phase High Pressure Chemistry," John Wiley & Sons, New York (1981).

2) T. Inoue, K. Kojima, and R. Shimozawa, *Inorg. Chem.*, **22**, 3972 (1983).

3) T. Inoue, K. Sugahara, K. Kojima, and R. Shimozawa, *Inorg. Chem.*, **22**, 3977 (1983).

4) K. Kojima, T. Inoue, M. Izaki, and R. Shimozawa, *Bull. Chem. Soc. Jpn.*, **59**, 139 (1986).

5) C. F. Timberlake, *J. Chem. Soc.*, **1964**, 5078.

6) R. M. Fuoss and C. A. Kraus, *J. Am. Chem. Soc.*, **55**, 476 (1933); R. M. Fuoss, *ibid.*, **57**, 488 (1935).

7) T. Inoue, K. Kojima, and R. Shimozawa, *Chem. Lett.*, **1981**, 259.

8) P. W. Bridgman, "The Physics of High Pressure," G. Bell, London (1949).

9) S. Harada and T. Yasunaga, *Bull. Chem. Soc. Jpn.*, **46**, 502 (1973).

10) F. P. Cavasino, *J. Phys. Chem.*, **69**, 4380 (1965); J. L. Bear and C. T. Lin, *J. Phys. Chem.*, **72**, 2026 (1968).

11) S. Harada, Y. Okuue, and T. Yasunaga, *Bull. Chem. Soc. Jpn.*, **47**, 769 (1974).

12) S. Harada, H. Tanabe, and T. Yasunaga, *Bull. Chem. Soc. Jpn.*, **46**, 3125 (1973).

13) M. Eigen and R. G. Wilkins, "Mechanisms of Inorganic Reactions," Adv. Chem. Ser. No. 49, American Chemical Society, Washington, DC (1965); R. A. Wilkins, *Acc. Chem. Res.*, **3**, 408 (1974).

14) P. Hemmes, *J. Phys. Chem.*, **76**, 895 (1972).

15) Y. Ducommun, W. Earl, and A. E. Merbach, *Inorg. Chem.*, **18**, 2754 (1979); Y. Ducommun, K. E. Newman, and A. E. Merbach, *ibid.*, **19**, 3696 (1980).

 © 1986 The Chemical Society of Japan Bull. Chem. Soc. Jpn., 59, 1689—1694 (1986)

Studies of the Metal Complexes of Cyclohexane Derivatives. IX.[1] The Preparation and Properties of Platinum(II) Complexes Containing Methyl Derivatives of *cis*-1,2-Cyclohexanediamine

Reiko SAITO* and Yoshinori KIDANI†
Aichi Junior College of Nursing, Kamishidami, Moriyama-ku, Nagoya 463
†Faculty of Pharmaceutical Sciences, Nagoya City University, Tanabe-dori, Mizuho-ku, Nagoya 467
(Received November 2, 1985)

Four 1,2-diamine ligands, (1*RS*,2*SR*)-1-methyl-1,2-cyclohexanediamine(1m-chxn), (1*R*,2*S*,3*R*)-3-methyl-1,2-cyclohexanediamine(*R*,*S*,*R*-3m-chxn), (1*S*,2*R*,4*R*)-4-methyl-1,2-cyclohexanediamine(*S*,*R*,*R*-4m-chxn), and (1*R*,2*S*,4*R*)-4-methyl-1,2-cyclohexanediamine(*R*,*S*,*R*-4m-chxn), were prepared. The mixed-ligand complexes of the $[PtXL]^{2+}$ type (X=$(NH_3)_2$, 1,2-ethanediamine, *meso*-2,3-butanediamine, and 2,3-dimethyl-2,3-butanediamine, L=each m-chxn) were synthesized and characterized by means of their electronic, circular dichroism, and ^{13}C NMR spectra. The chelate ring formed by *S*,*R*,*R*-4m-chxn was almost conformationally fixed to take a δ conformation, while the chelate rings of 1m-chxn, *R*,*S*,*R*-3m-chxn, and *R*,*S*,*R*-4m-chxn easily interchange between δ and λ conformations. The stereochemistries of these three complexes are attributable to the conformational requirements for both the cyclohexane ring and the chelate ring, for which synchronous inversions are presumed.

The conformations of chelate rings of C-substituted 1,2-diamine complexes in solution have been extensively studied. Most of them may be classified into two types.

(1) In the complexes containing a chelate ligand with achiral carbon atoms or enantiotopic carbon atoms[2] in its chelate ring, such as 2,3-dimethyl-2,3-butanediamine(dmbn) and *meso*-2,3-butanediamine-(*m*-bn), the distributions of the two conformations in the $\delta \rightleftarrows \lambda$ equilibrium are equal as a result of the rapid interconversion.[3-5]

(2) In the complexes containing a chelate ligand with one chiral carbon atom or two diastereotopic carbon atoms,[2] such as (2*R* or 2*S*)-1,2-propanediamine and (2*R*,3*R* or 2*S*,3*S*)-2,3-butanediamine, the chelate rings take predominantly either a δ or a λ conformation.[3-5] However, the complexes formed by the other type of 1,2-diamine, which has an unsymmetrical structure due to constitutionally nonequivalent substituents attached to the chelate ring carbon atom(s), have not been so widely investigated.

Recently we have reported on the preparation and properties of the complexes containing the latter type of ligand, 1-aminomethyl-2-methylcyclohexylamine[6] or (1*R*,2*S*,3*S* or 1*S*, 2*R*,3*R*)-3-methyl-1,2-cyclohexanediamine (*R*,*S*,*S*- or *S*,*R*,*R*-3m-chxn).[1] In these complexs, the conformations of the chelate ring are almost fixed by means of the steric effect of the methyl group attached to the carbon atom outside the chelate ring. As an extention of these earlier studies, we have now synthesized some Pt^{II} complexes containing four new diamines (m-chxn), (1*RS*,2*SR*)-1-methyl-1,2-cyclohexanediamine-(1m-chxn), (1*R*,2*S*,3*R*)-3-methyl-1,2-cyclohexanediamine-(*R*,*S*,*R*-3m-chxn), (1*S*,2*R*,4*R*)-4-methyl-1,2-cyclohexanediamine(*S*,*R*,*R*-4m-chxn), and (1*R*,2*S*,4*R*)-4-methyl-1,2-cyclohexanediamine(*R*,*S*,*R*-4m-chxn). In this paper, the conformations of the m-chxn chelate rings will be discussed on the basis of the platinum-carbon coupling constants in the ^{13}C NMR spectra.

Experimental

Preparation of the Ligands. (1*RS*,2*SR*)-1-Methyl-1,2-cyclohexanediamine(1m-chxn): 1-Methyl-*r*-1,*c*-2-cyclohexanedicarboxylic acid was synthesized from butadiene and citraconic anhydride according to the literature.[7] From this acid, 1m-chxn was prepared by a method similar to that reported by Werner.[8] It was purified as the dihydrochloride. Found: C, 41.52; H, 8.99; N, 13.69%. Calcd for $C_7H_{16}N_2 \cdot 2HCl$: C, 41.80; H, 9.02; N, 13.93%.

(1*R*,2*S*,3*R*)-3-Methyl-1,2-cyclohexanediamine(*R*,*S*,*R*-3m-chxn): *t*-3-Methyl-*r*-1,*c*-2-cyclohexanedicarboxylic acid was obtained by a manner similar to that described in the literature.[9] (1*RS*,2*SR*,3*RS*)-3m-chxn was prepared by the same procedure as 1m-chxn. It was optically resolved using (2*R*,3*R*)-di-*O*-benzoyltartaric acid. The less soluble benzoyltartrate obtained, whose optical rotation could not be measured because of its low solubility, was recrystallized twice from EtOH–H_2O (1:2). Mp(decomp) 205—206°C. Anal. ($C_{25}H_{30}N_2O_8$) C, H, N. By treating this salt with a 3 mol dm^{-3} HCl solution, *R*,*S*,*R*-3m-chxn·2HCl was obtained. Found: C, 42.11; H, 9.18; N, 13.63%. Calcd for $C_7H_{16}N_2 \cdot 2HCl$: C, 41.80; H, 9.02; N, 13.93%. $[\alpha]_D = -33.8°$ (*c* 2.0, H_2O). The assignments of the absolute configurations of the three optically active diamines studied in this paper will be described in a later section.

(1*S*,2*R*,4*R*)- and (1*R*,2*S*,4*R*)-4-Methyl-1,2-cyclohexanediamine (*S*,*R*,*R*- and *R*,*S*,*R*-4m-chxn): Commercially available 4-methyl-1,2-cyclohexanedicarboxylic anhydride (Aldrich Co., Ltd.) was hydrolyzed. A white powder(**A**) was obtained nearly quantitatively; mp(decomp) 161—171°C. A suspension of 270 g of **A** in 480 cm^3 of 2-propanol was heated to bp and then cooled. A white powder (**B**, 150 g) was thus obtained; mp(decomp) 179—180°C. This was recrystallized twice from 2-propanol to give 48 g of acid **C**; mp(decomp) 185—186°C. This acid was *t*-4-methyl-*r*-1,*c*-2-cyclohexanedicarboxylic acid contaminated by a very small amount of the *c*,*c*-isomer. This contaminant could be removed during the course of optical resolution. To the

filtrate obtained after removing **B**, an excess amount of an aqueous ammonia solution was added. The resulting mixture was evaporated to dryness to yield 65 g of a crude mixture of monoammonium salt of *c,c*- and *t,c*-acid. This was recrystallized from EtOH–H_2O (1:2) to give 57 g of crystals. Treating this salt with a 3 mol dm^{-3} HCl solution gave 49 g of pure *c*-4-methyl-*r*-1,*c*-2-cyclohexanedicarboxylic acid(**D**; mp(decomp) 171—172°C).

From acid **D**, 1*SR*,2*RS*,4*RS*-4m-chxn was prepared by the same manner as was used for the synthesis of 1m-chxn and *R,S,R*-3m-chxn. This was optically resolved by the use of (2*R*,3*R*)-di-*O*-benzoyltartaric acid. The less soluble benzoyltartrate was recrystallized from EtOH–H_2O (1:2). Anal. ($C_{25}H_{30}N_2O_8 \cdot H_2O$) C, H, N. $[\alpha]_D = -68.6°$ (*c* 1.0, MeOH). Treating this salt with a 3 mol dm^{-3} HCl solution gave *S,R,R*-4m-chxn·2HCl. Found: C, 41.44; H, 9.04; N, 13.91%. Calcd for $C_7H_{16}N_2 \cdot 2HCl$: C, 41.80; H, 9.02; N, 13.93%. $[\alpha]_D = +23.0°$ (*c* 2.0, H_2O).

The *R,S,R*-4m-chxn compound was prepared from acid **C** by a similar Schmidt reaction.[8] It was optically resolved using the same resolving reagent as was used for *S,R,R*-4m-chxn. The less soluble diastereomeric salt obtained was recrystallized twice from H_2O–DMF (2:1); mp(decomp) 174—175°C. Anal. ($C_{25}H_{30}N_2O_8 \cdot 2H_2O$) C, H, N. $[\alpha]_D = -72°$ (*c* 0.5, MeOH). From this tartrate, *R,S,R*-4m-chxn·2HCl was obtained by a usual work up. Found: C, 42.05; H, 8.91; N, 13.87%. Calcd for $C_7H_{16}N_2 \cdot 2HCl$: C, 41.80; H, 9.02; N, 13.93%. $[\alpha]_D = +21.2°$ (*c* 2.1, H_2O).

Preparation of Complexes. $[Pt(NH_3)_2L]Cl_2$ (L= each m-chxn): These complexes were prepared by the reaction of $[PtCl_2L]$[10] with aqueous ammonia. Found: $[Pt(NH_3)_2$(1m-chxn)$]Cl_2 \cdot 0.5H_2O$, C, 19.00; H, 5.36; N, 12.74%. $[Pt(NH_3)_2$(*R,S,R*-3m-chxn)$]Cl_2 \cdot 0.5H_2O$, C, 19.11; H, 5.51; N, 12.98%. Calcd for $C_7H_{23}N_4O_{0.5}Cl_2Pt$: C, 19.23; H, 5.30; N, 12.81%. Found: $[Pt(NH_3)_2$(*S,R,R*-4m-chxn)$]Cl_2 \cdot H_2O$, C, 18.94; H, 5.35; N, 12.61%. Calcd for $C_7H_{24}N_4OCl_2Pt$: C, 18.84; H, 5.42; N, 12.55%. Found: $[Pt(NH_3)_2$(*R,S,R*-4m-chxn)$]Cl_2$, C, 19.61; H, 5.01; N, 12.92%. Calcd for $C_7H_{22}N_4Cl_2Pt$: C, 19.63; H, 5.18; N, 13.08%.

[Pt(en)L]Cl_2: These complexes were prepared by the reaction of $[PtCl_2(en)]$[11] with L in water. The aqueous solution of L was obtained from the m-chxn·2HCl solution by passing it through an anion-exchange resin column (Dowex, 1-X8, OH^- form). Found: [Pt(en)(1m-chxn)]-$Cl_2 \cdot 0.5H_2O$, C, 23.47; H, 5.28; N, 11.61%. [Pt(en)(*R,S,R*-3m-chxn)$]Cl_2 \cdot 0.5H_2O$, C, 23.00; H, 5.58; N, 12.15%. Calcd for $C_9H_{25}N_4O_{0.5}Cl_2Pt$: C, 23.33; H, 5.44; N, 12.09%. Found: [Pt(en)(*S,R,R*-4m-chxn)$]Cl_2$, C, 23.69; H, 5.22; N, 12.39%. [Pt(en)(*R,S,R*-4m-chxn)$]Cl_2$, C, 23.92; H, 5.26; N, 11.96%. Calcd for $C_9H_{24}N_4Cl_2Pt$: C, 23.79; H, 5.33; N, 12.33%.

[Pt(*m*-bn)L]Cl_2: The *m*-bn ligand was synthesized by a literature method.[12] The complexes were synthesized in a way similar to that used for the preparation of $[Pt(en)L]Cl_2$. Found: [Pt(*m*-bn)(1m-chxn)$]Cl_2$, C, 27.30; H, 5.79; N, 11.42%. [Pt(*m*-bn)(*S,R,R*-4m-chxn)$]Cl_2$, C, 27.39; H, 5.99; N, 11.93%. Calcd for $C_{11}H_{28}N_4Cl_2Pt$: C, 27.39; H, 5.85; N, 11.62%. [Pt(*m*-bn)(*R,S,R*-3m-chxn)$]Cl_2 \cdot 0.5H_2O$, C, 26.83; H, 5.93; N, 11.52%. [Pt(*m*-bn)(*R,S,R*-4m-chxn)$]Cl_2 \cdot 0.5H_2O$, C, 26.94; H, 5.89; N, 11.66%. Calcd for $C_{11}H_{29}N_4O_{0.5}Cl_2Pt$: C, 26.89; H, 5.95; N, 11.40%.

[Pt(dmbn)L]Cl_2: The dmbn ligand was prepared by the known procedure.[13] The complexes were obtained by the reaction of $[PtCl_2L]$ with an aqueous solution of dmbn. Found: [Pt(dmbn)(1m-chxn)$]Cl_2 \cdot 1.5H_2O$, C, 29.21; H, 6.34; N, 10.45%. [Pt(dmbn)(*R,S,R*-3m-chxn)$]Cl_2 \cdot 1.5H_2O$, C, 28.91; H, 6.47; N, 10.34%. [Pt(dmbn)(*S,R,R*-4m-chxn)$]Cl_2 \cdot 1.5H_2O$, C, 29.23; H, 6.47; N, 10.56%. Cacld for $C_{13}H_{35}N_4O_{1.5}Cl_2Pt$: C, 29.05; H, 6.56; N, 10.42%. Found: [Pt(dmbn)-(*R,S,R*-4m-chxn)$]Cl_2 \cdot H_2O$, C, 29.67; H, 6.55; N, 11.27%. Calcd for $C_{13}H_{34}N_4OCl_2Pt$: C, 29.55; H, 6.49; N, 10.60%.

Measurements. The CD and electronic spectra were measured using a JASCO J-40 spectropolarimeter and a Shimadzu UV-210-A spectrometer respectively. The optical rotations were measured with a JASCO DIP-4 polarimeter. The ^{13}C NMR spectra were recorded on a JEOL JNM-FX-100 spectrometer using D_2O as a solvent. The chemical shifts were reported relative to the dioxane (δ 67.70) added as an internal reference. The measurements of all the complexes except for the *R,S,R*-4m-chxn complexes were recorded with 8 K data points. For the *R,S,R*-4m-chxn complexes, the measurements were run with 16 K data words. The ^{13}C NMR spectra of some of the complexes, which were not sufficiently soluble in D_2O, were recorded after converting their counter anions to F^-.

Results and Discussion

Preparation of the Ligands. The diamines were

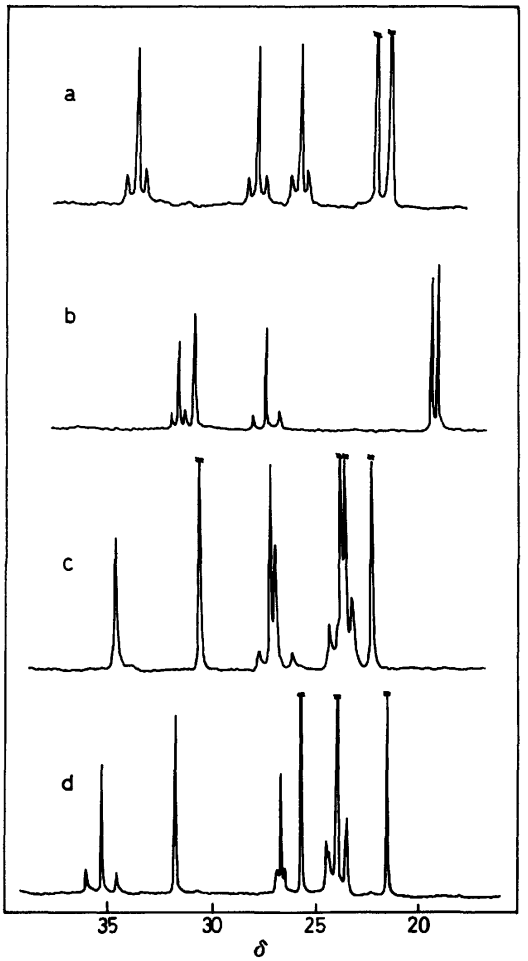

Fig. 1. ^{13}C NMR Spectra of $[Pt(NH_3)_2$(1m-chxn)$]$-Cl_2 (a), $[Pt(NH_3)_2$(*R,S,R*-3m-chxn)$]Cl_2$ (b), [Pt(dmbn)-(*S,R,R*-4m-chxn)$]Cl_2$ (c), and [Pt(dmbn)(*R,S,R*-4m-chxn)$]Cl_2$ (d).

Table 1. ^{13}C NMR Chemical Shifts[a] and Coupling Constants[b] for $[PtX(m\text{-chxn})]^{2+}$

Complex	m-chxn								X		
	α-Carbon		β-Carbon			Other carbon					
	(C_1, C_2)		C_3	C_6	CH_3	(C_4, C_5)		CH_3			
$[Pt(NH_3)_2(1m\text{-chxn})]^{2+}$	62.83	62.58	27.83 (22.0)	33.78 (23.2)	25.74 (20.8)	22.03	21.30	—			
$[Pt(en)(1m\text{-chxn})]^{2+}$	62.24	62.00	27.79 (20.8)	33.78 (23.2)	25.74 (20.8)	22.03	21.25	—	47.91		
$[Pt(m\text{-bn})(1m\text{-chxn})]^{2+}$	62.19	62.10	27.79 (19.5)	33.83 (23.2)	25.79 (20.8)	22.13	21.25	—	57.56	57.47	14.14 14.04 (25.6)
$[Pt(dmbn)(1m\text{-chxn})]^{2+}$	62.14	61.95	27.79 (19.5)	33.78 (23.2)	25.74 (20.8)	22.08	21.25	—	64.29		23.79 (23.2)
$[Pt(NH_3)_2(R,S,R\text{-3m-chxn})]^{2+}$	64.68 (7)	57.90	31.68 (18.3)	27.40 (33.0)	—	30.86	19.26	19.01			
$[Pt(en)(R,S,R\text{-3m-chxn})]^{2+}$	64.24 (9)	57.47	31.73 (18.3)	27.40 (33.0)	—	30.95	19.26	18.96	48.01	47.86	
$[Pt(m\text{-bn})(R,S,R\text{-3m-chxn})]^{2+}$	64.19	57.42[c]	31.68 (18.3)	27.35 (31.8)	—	30.81	19.21	18.91	57.51[c]		14.04 (26.9)
$[Pt(dmbn)(R,S,R\text{-3m-chxn})]^{2+}$	64.34[c]	57.37	31.68 (17.1)	27.40 (33.0)	—	30.91	19.21	18.91	64.19[c]		23.79 (23.2)
$[Pt(NH_3)_2(S,R,R\text{-4m-chxn})]^{2+}$	58.68	58.34	34.95	27.10 (44.0)	—	30.81	27.35	22.37			
$[Pt(en)(S,R,R\text{-4m-chxn})]^{2+}$	58.15	57.81	34.95	27.10 (42.8)	—	30.81	27.35	22.37	48.01	47.86	
$[Pt(m\text{-bn})(S,R,R\text{-4m-chxn})]^{2+}$	58.10	57.81	34.85	27.10 (42.8)	—	30.81	27.30	22.33	57.51	57.27	14.24 13.85 (28.1) (22.0)
$[Pt(dmbn)(S,R,R\text{-4m-chxn})]^{2+}$	58.10	57.76	34.90	27.10 (41.5)	—	30.81	27.30	22.33	64.39	64.19	23.89 23.69 (26.9)
$[Pt(NH_3)_2(R,S,R\text{-4m-chxn})]^{2+}$	59.05	58.59 (10)	35.44 (40.3)	26.54 (8.5)	—	31.98	25.59	21.62			
$[Pt(en)(R,S,R\text{-4m-chxn})]^{2+}$	58.44	58.17	35.39 (38.5)	26.59 (8.5)	—	31.78	25.62	21.40	47.96		
$[Pt(m\text{-bn})(R,S,R\text{-4m-chxn})]^{2+}$	58.54	58.03	35.46 (39.1)	26.54 (—)[d]	—	32.00	25.59	21.67	57.63	57.32	14.24 13.92 (27.5)
$[Pt(dmbn)(R,S,R\text{-4m-chxn})]^{2+}$	58.37	58.15	35.41 (37.9)	26.61 (9.8)	—	31.81	25.62	21.42	64.51	64.41	23.89 (25.0)

a) Carbon chemical shifts in ppm from external TMS measured vs. internal dioxane. b) Coupling constants (^{195}Pt-C) are found in parentheses in Hz. c) Two chemical shifts due to diamine-ring carbons of m-chxn and another diamine (X) appeared very close to one another. The signal with the stronger intensity was tentatively assigned to X. d) Platinum satellite peaks were observed as shoulders.

prepared from the corresponding methyl derivatives of *cis*-1,2-cyclohexanedicarboxylic acid. 1-Methyl-*r*-1,*c*-2-cyclohexanedicarboxylic acid was synthesized by the Diels-Alder reaction.[7] *t*-3-Methyl-*r*-1,*c*-2-cyclohexanedicarboxylic acid was prepared from the corresponding *c*,*c*-diastereomer by a literature method.[9] We found that the dicarboxylic aicd **A** obtained from commercially available 4-methyl-1,2-cyclohexanedicarboxylic anhydride was a mixture of *c*,*c*- and *t*,*c*-acid by comparing it with an authentic sample prepared according to the literature.[14] It could be separated into two isomers by the method presented in the Experimental section. The attempted optical resolution of 1m-chxn using (2*R*,3*R*)-di-*O*-benzoyltartaric acid was unsuccessful. For other diamines, each optically active enantiomer was prepared.

Conformations of the Chelate Rings. The possible conformations of the free m-chxn ligands and their chelate rings in each complex are shown in **1a—4d**. In the schematic structures of **c** and **d**, each ligand adopts a conformation illustrated in the corresponding structures, **a** and **b**. The symbols of (e) and (a) denote an equatorial and an axial methyl orientation respectively with respect to the cyclohexane ring. Some representative ^{13}C NMR spectra of the Pt^{II} complexes in the δ 10 to δ 40 region are shown in Fig. 1. The chemical shifts and platinum-carbon coupling constants are given in Table 1.

In the ^{13}C NMR spectra of 1m-chxn complexes, three platinum satellites were observed. Of the resonances with the satellite peak due to the skeletal carbons of the cyclohexane ring, one with $^3J_{Pt\text{-}C}$ of 23.2 Hz was assigned to C_6 carbon, applying the β-substituent parameter.[15] The methyl carbon and C_3 carbon, which occupy symmetrical positions about C_1–C_2 bond, showed a 20—22 Hz coupling. For $[Pt(NH_3)_2(m\text{-bn})]^{2+}$ and $[Pt(NH_3)_2(ibn)]^{2+}$ (ibn=2-methyl-1,2-propanediamine), both of which exist in equimolar conformations with a rapid ring inversion, the $^3J_{Pt\text{-}C}$ values have been reported to be 27.3 and 22.4 Hz respectively.[16] The small differences between $^3J_{Pt\text{-}C}$ values due to the three β carbons provide an indication of a roughly equal

probability of λ(**1c**) and δ(**1d**) conformations.

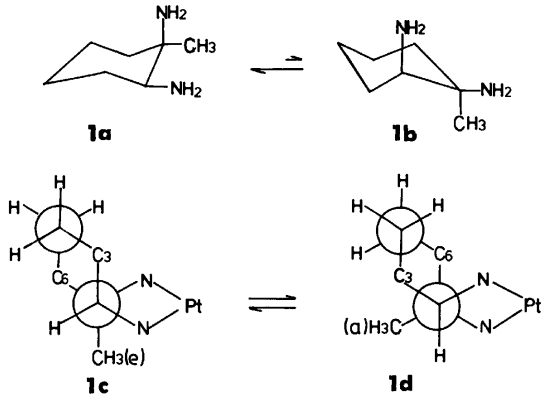

Based on the stereochemistry of the cyclohexane ring, the **1a** conformation, with the larger equatorial methyl and the smaller axial amino group, is more favorable than **1b**. Its conformational behavior prefers the **1c** conformation for the complex. On the other hand, concerning the effects of the substituents on the chelate ring, the **1c** conformation, having a chelate ring with C_3 carbon and the methyl group in axial orientations and C_6 carbon in an equatorial orientation, should be more unfavorable than the **1d** conformation. Because of these competitive steric effects, **1c** and **1d** conformations would seem to be almost equienergetic.

In the ^{13}CNMR spectra of the *R,S,R*-3m-chxn complexes, the signal around 32 ppm was assigned to the C_3 carbon by the aid of the off-resonance proton-decoupling technique. Two $^3J_{Pt-C}$ couplings, of about 18 and 32—33 Hz for C_3 and C_6 carbon respectively, were observed. The absense of additional peaks corresponding to each carbon indicated that the $\lambda \rightleftarrows \delta$ inversion was rapid on the NMR time scale. The

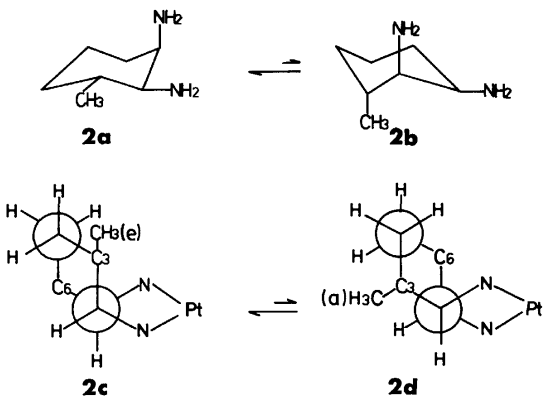

observed $^3J_{Pt-C_3}$ (and $^3J_{Pt-C_6}$) values must be the weighted averages of the **2c** and **2d** conformations, they can be expressed by the following equations:

$$^3J_{Pt-C_3}(\text{obsd}) = p\,{}^3J_{ax(2c)} + (1-p)\,{}^3J_{eq(2d)} \quad (1)$$

$$^3J_{Pt-C_6}(\text{obsd}) = p\,{}^3J_{eq(2c)} + (1-p)\,{}^3J_{ax(2d)} \quad (2)$$

where p denotes the population of the **2c** conformation and where $^3J_{eq(2c)}$ and $^3J_{ax(2c)}$ are, respectively, the values of $^3J_{Pt-C_6}$ and $^3J_{Pt-C_3}$ when the chelate ring is assumed to have exclusively a rigid conformation, **2c**. Similarly, $^3J_{eq(2d)}$ and $^3J_{ax(2d)}$ are, respectively, $^3J_{Pt-C_3}$ and $^3J_{Pt-C_6}$ when the **2d** conformation is assumed to be fixed. By refering to the literature,[17] $^3J_{eq(2c)}$ was assumed to be equal to $^3J_{eq(2d)}$, and $^3J_{ax(2c)}$ and $^3J_{ax(2d)}$ were assumed to be zero. Then, p is given by Eq. 3:

$$^3J_{Pt-C_6}(\text{obsd}) = p\{{}^3J_{Pt-C_3}(\text{obsd}) + {}^3J_{Pt-C_6}(\text{obsd})\} \quad (3)$$

A calculation from the data in Table 1 yielded p in the range of 0.64—0.67 for the *R,S,R*-3m-chxn complexes. Erickson et al.[17] have reported the p for [Pt(bpy)(pn)]$^{2+}$ (bpy=2,2′-bipyridine) to be 0.72. However, Yano et al.[18] have pointed out that a smaller $^3J_{Pt-C}$ value for an unsymmetrical complex such as a pn complex should be attributed to the puckering effect of the chelate ring rather than to the relative population. Our result showed one of a few cases in which the complex exhibited the intermediate relative population.

In both the **2c** and **2d** conformations of the *R,S,R*-3m-chxn complex, the two β carbons are located in an equatorial and an axial orientation respectively. The axial position in the **2d** conformation is less crowded than that in the **2c** conformation. Therefore the preference for the former conformation was expected. On the contrary, the **2d** conformer would not be preferable on the basis of the stereochemistry of the cyclohexane. The **2c**-conformation preference of about 65% obtained by the use of above NMR results indicated that this conformational equiribrium was influenced more pronouncedly by the stability of the cyclohexane ring than by the steric environment around the chelate ring.

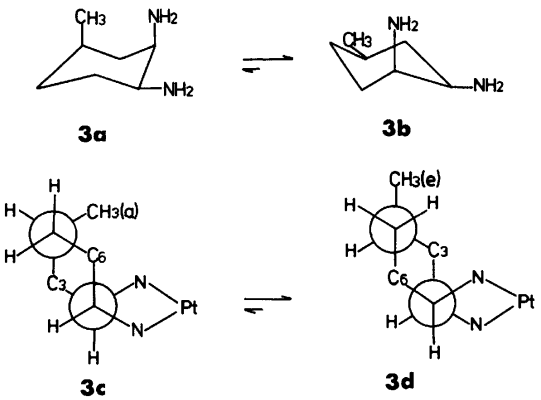

For the *S,R,R*-4m-chxn complexes, there is no large difference between the conformational situations with regard to the chelate rings of **3c** and **3d**, thus, the conformer distribution seems to be exclusively controlled by the stabilities of the cyclohexane ring. The ring inversion between **3a** and **3b** seems improbable because of the 1,3-diaxial interaction. This should lead to a strong preference of one extreme

Table 2. Electronic and CD Spectral Data of $[PtX(m\text{-}chxn)]^{2+}$

Complex	Electronic		CD	
	$\nu/10^3\,cm^{-1}$	(log ε)	$\nu/10^3\,cm^{-1}$	($\Delta\varepsilon$)
$[Pt(NH_3)_2(R,S,R\text{-}3m\text{-}chxn)]^{2+}$	36.0	(1.62)	34.8	(+0.11)
	42 sh	(2.1)	41.2	(−0.07)
	45.0	(2.70)	46 sh	(+0.1)
$[Pt(en)(R,S,R\text{-}3m\text{-}chxn)]^{2+}$	35.4	(1.63)	35.2	(+0.15)
	42 sh	(2.0)	41.5	(−0.07)
	44.6	(2.69)	46 sh	(+0.1)
$[Pt(m\text{-}bn)(R,S,R\text{-}3m\text{-}chxn)]^{2+}$	35.6	(1.60)	35.3	(+0.12)
	42 sh	(2.1)	41.7	(−0.06)
	44.6	(2.67)	46 sh	(+0.1)
$[Pt(dmbn)(R,S,R\text{-}3m\text{-}chxn)]^{2+}$	35.8	(1.66)	35.6	(+0.17)
	42 sh	(2.2)	41.8	(−0.08)
	44.7	(2.79)	46 sh	(+0.1)
$[Pt(NH_3)_2(S,R,R\text{-}4m\text{-}chxn)]^{2+}$	35.5	(1.61)	35.2	(−0.16)
	42 sh	(2.2)	41.2	(+0.13)
	45.5	(2.81)	45.0	(−0.26)
$[Pt(en)(S,R,R\text{-}4m\text{-}chxn)]^{2+}$	35.7	(1.63)	35.3	(−0.22)
	42 sh	(2.2)	41.3	(+0.13)
	44.6	(2.71)	46.5	(−0.32)
$[Pt(m\text{-}bn)(S,R,R\text{-}4m\text{-}chxn)]^{2+}$	35.7	(1.63)	35.6	(−0.26)
	42sh	(2.2)	41.3	(+0.18)
	44.6	(2.73)	46.5	(−0.37)
$[Pt(dmbn)(S,R,R\text{-}4m\text{-}chxn)]^{2+}$	35.8	(1.71)	35.7	(−0.25)
	42 sh	(2.3)	41.5	(+0.16)
	44.8	(2.80)	45.9	(−0.42)
$[Pt(NH_3)_2(R,S,R\text{-}4m\text{-}chxn)]^{2+}$	35.8	(1.63)	35.0	(−0.15)
	42 sh	(2.3)	41.0	(+0.11)
	45.0	(2.82)	44.8	(−0.27)
$[Pt(en)(R,S,R\text{-}4m\text{-}chxn)]^{2+}$	35.7	(1.63)	35.3	(−0.23)
	42 sh	(2.2)	41.2	(+0.09)
	44.6	(2.70)	45.5	(−0.32)
$[Pt(m\text{-}bn)(R,S,R\text{-}4m\text{-}chxn)]^{2+}$	35.7	(1.65)	35.3	(−0.25)
	42 sh	(2.3)	41.3	(+0.11)
	44.6	(2.74)	46.5	(−0.33)
$[Pt(dmbn)(R,S,R\text{-}4m\text{-}chxn)]^{2+}$	35.8	(1.65)	35.7	(−0.23)
	42 sh	(2.2)	41.3	(+0.10)
	44.8	(2.79)	46.5	(−0.37)

sh=shoulder.

conformation (**3d**) of the chelate ring. In the ^{13}C NMR spectra of these complexes, the $^3J_{Pt\text{-}C_6}$ coupling of 42—44 Hz and the $^3J_{Pt\text{-}C_3}$ coupling of ≈0 Hz were observed. These facts agree with the above prediction.

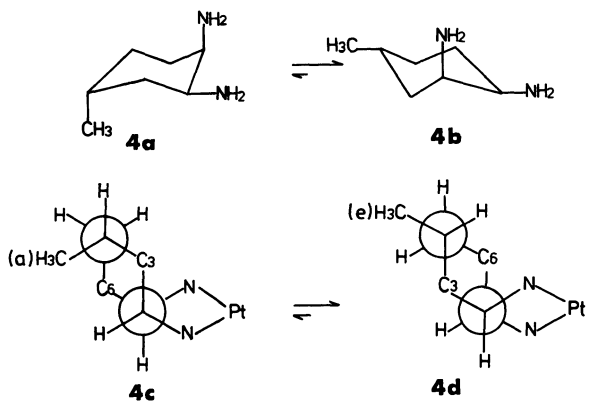

In the two conformations (**4c** and **4d**) of the *R,S,R*-4m-chxn complex, the steric effect of the methyl group attached to the γ carbon on the stability of the chelate ring seemed small, as in the *S,R,R*-4m-chxn complex.

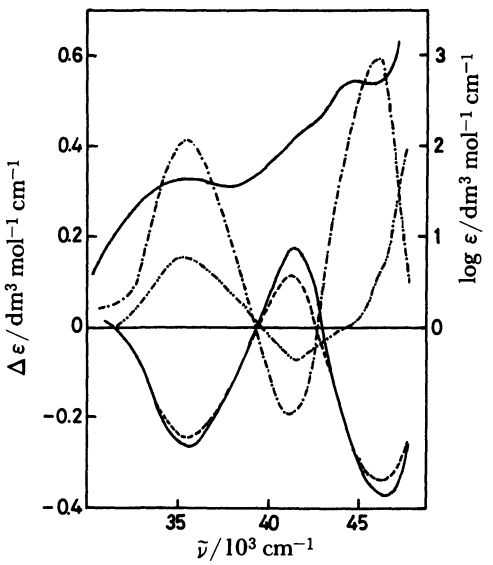

Fig. 2. Electronic and CD spectra of [Pt(en)(*R,S,R*-3m-chxn)]Cl_2 (—··—), [Pt(en)(*S,R,R*-3m-chxn)]Cl_2 (—·—),[1] [Pt(*m*-bn)(*S,R,R*-4m-chxn)]Cl_2 (——), and [Pt(*m*-bn)(*R,S,R*-4m-chxn)]Cl_2 (——).

Consequently, the conformer population of the chelate ring would seem to depend on the distribution of the two conformations of the free cyclohexane ring. The ^{13}C NMR spectra of the *R,S,R*-4m-chxn complexes indicated the existence of two conformers with a different molar ratio in the equilibrium, as in the case for the *R,S,R*-3m-chxn complexes. By a calculation similar to that used for the latter complexes, the population, *p*, of the **4d** conformation was found to be 0.80—0.83.

The conformational energy barriers for the complexes with a bulky counter ligand(X) might be expected to be higher than those with a smaller one. However, the spectral tendencies of the 1m-, *R,S,R*-3m, and *R,S,R*-4m-chxn complexes suggested that their conformational equilibrium was little affected by the mass of the X.

CD Spectra. The electronic and CD spectra of the complexes are shown in Fig. 2 and Table 2. The *R,S,R*-3m-chxn complexes showed a positive CD band(ca. 35000 cm^{-1}), a negative CD band(ca. 42000 cm^{-1}), and a positive CD band(shoulder ca. 46000 cm^{-1}). The signs and positions of the first two bands of these complexes were almost identical with those of the corresponding bands of the *S,R,R*-3m-chxn complexes[1] (Fig. 2), however, their CD strengths were weaker than those of the latter. Several reports[19-21] have shown that the chiral 1,2-diamine Pt^{II} complexes with a positive CD sign of the ^3E_g transition have a λ conformation. Thus, the λ conformation populated more largely was suggested for the *R,S,R*-3m-chxn complexes. Therefore, the absolute configuration of the present (−)-3m-chxn ligand can be identified as (1*R*,2*S*,3*R*). From the spectral results of both the 4m-chxn complexes, the δ conformations were reasonably deducible. It was concluded that the absolute configurations of the 4m-ligands, whose structures correspond to the *c,c*- and *t,c*-configurations, were (1*S*,2*R*,4*R*) and (1*R*,2*S*,4*R*) respectively.

Hawkins et al.[21] have reported the estimated value of the conformer population of $[Pt(NH_3)_2((S)$-3,3-dmbn$)]^{2+}$ (3,3-dmbn=3,3-dimethyl-1,2-butanediamine) from a comparison of the CD intensities of the ^1E_g band. Comparing the CD intensities of the present *R,S,R*-3m-chxn complexes with those of the *S,R,R*-3m-chxn complexes,[1] the intensity ratios were found to be 0.37 (the band around 35000 cm^{-1}) and 0.34 (the band around 41000 cm^{-1}) for $[Pt(NH_3)_2L]^{2+}$, and 0.37 (the band around 35000 cm^{-1}) and 0.35 (the band around 42000 cm^{-1}) for $[Pt(en)L]^{2+}$. If the contribution of the chiral atoms to the Cotton effect of the above bands is negligibly small, and if the $\Delta\varepsilon$ value of the *R,S,R*-3m-chxn complex, which presumably has an extremely fixed conformation, is nearly equal to that of the *S,R,R*-3m-chxn complex, the more favorable λ conformer populations of the *R,S,R*-3m-chxn complexes can be calculated to range from 0.65 to 0.68. These values were in excellent agreement with those estimated by means of NMR analyses. However, for the *R,S,R*-4m-chxn complexes the δ conformer population derived from a similar calculation did not agree with those obtained by NMR analyses. There remain some questions in these CD analyses, one of them being the lack of a common CD intensity value for the complexes with a fixed conformation.

We wish to thank the Instrument Center, Institute for Molecular Science, for the use of a NMR spectrometer (JEOL JNM-FX-100). We are also grateful to Miss Toshiko Naito of the Analytical Center of the Nagoya City University for her elemental analyses.

References

1) Part VIII of this series: R. Saito and Y. Kidani, *Bull. Chem. Soc. Jpn.*, **57**, 3430 (1984).
2) M. F. Gargallo, J. D. Mather, E. N. Duesler, and R. E. Tapscott, *Inorg. Chem.*, **22**, 2888 (1983).
3) E. J. Corey and J. C. Bailar, Jr., *J. Am. Chem. Soc.*, **81**, 2620 (1959).
4) A. J. MaCaffery, S. F. Mason, B. J. Norman, and A. M. Sargeson, *J. Chem. Soc. (A)*, **1968**, 1304.
5) C. J. Hilleary, T. F. Them, and R. E. Tapscott, *Inorg. Chem.*, **19**, 102 (1980).
6) R. Saito and Y. Kidani, *Bull. Chem. Soc. Jpn.*, **56**, 449 (1983).
7) J. J. Bloomfield and S. L. Lee, *J. Org. Chem.*, **32**, 3919 (1967).
8) N. W. Werner and J. Casanova, Jr., *Org. Synth.*, Coll. Vol V, 273 (1973).
9) J. F. Bussert, K. W. Greenlee, J. M. Derfer, and C. E. Boord, *J. Am. Chem. Soc.*, **78**, 6076 (1956).
10) T. G. Appleton and J. R. Hall, *Inorg. Chem.*, **9**, 1800 (1970).
11) F. Basolo, J. C. Bailar, Jr., and B. R. Tarr, *J. Am. Chem. Soc.*, **72**, 2433 (1950).
12) F. H. Dickey, W. Fickett, and H. J. Lucas, *J. Am. Chem. Soc.*, **74**, 94 (1952).
13) R. Sayer, *J. Am. Chem. Soc.*, **77**, 6686 (1955).
14) D. Craig, *J. Am. Chem. Soc.*, **72**, 1678 (1950).
15) D. K. Dalling and D. M. Grant, *J. Am. Chem. Soc.*, **94**, 5318 (1972).
16) S. Bagger, *Acta Chem. Scand., Ser. A*, **28**, 467 (1974).
17) L. E. Erickson, J. E. Sarneski, and C. N. Reilley, *Inorg. Chem.*, **14**, 3007 (1975).
18) S. Yano, T. Tukuda, M. Saburi, and S. Yoshikawa, *Inorg. Chem.*, **17**, 2520 (1978).
19) H. Ito, J. Fujita, and K. Saito, *Bull. Chem. Soc. Jpn.*, **40**, 2584 (1967).
20) B. Bosnich and E. A. Sullivan, *Inorg. Chem.*, 14, 2768 (1975).
21) C. J. Hawkins and J. Martin, *Inorg. Chem.*, **21**, 1074 (1982).

 © 1986 The Chemical Society of Japan Bull. Chem. Soc. Jpn., 59, 1695—1700 (1986)

Solvation of Anions in Water-Acetonitrile Mixtures

Kiyoshi MIYAJI* and Kenichi MORINAGA
Department of Chemistry, Faculty of Science, Saitama University, Urawa, Saitama 338
(Received December 26, 1985)

The enthalpies of transfer from water to mixtures with acetonitrile(ΔH_t°) for various anions reach maxima at a mole fraction of acetonitrile(x_{AN}) ca. 0.3, and decrease linearly and in parallel in the intermediate region. A linear relation is found between ΔH_t° at x_{AN} 0.3 and the hydration enthalpies for halide and symmetrical ions. This finding and the parallel x_{AN} dependence of ΔH_t° in the intermediate region are interpreted on the basis of the linear relation between the solvation enthalpies and the entropies for the halide ions. The reduction in the hydrogen-bonding interaction extending beyond the primary hydration sphere(ΔH_{INT}) for halide ions in the mixtures is estimated based on a modified Eley and Evans hydration model. At x_{AN} 0 to ca. 0.3, ΔH_{INT} compared with that in water agree well with the observed ΔH_t°, indicating that the increase in ΔH_t° is due to the reduction in the outer hydration sphere interaction. However, they split gradually at x_{AN} above 0.3. The adequacy of the modifications in the treatment of the solvation enthalpy cycle in the mixtures is re-evaluated from the structural viewpoint. The exothermic change in the intermediate region may be attributable to the reduction in the cavity formation energy.

Preferential solvation of ions has been studied in many kinds of mixed solvent systems by various methods.[1] Silver ion has been confirmed to be preferentially solvated by acetonitrile in water-acetonitrile mixtures by the measurements of the transference number,[2a] solubility,[2b] NMR,[2c] and the free energy of transfer.[2d] On the basis of this fact we have discussed the dependence of the ionic conductance[3] and ionic enthalpies of transfer (ΔH_t°)[4] on the solvent composition. Previously[4] the rapid changes of ΔH_t° for alkali and halide ions in the acetonitrile-rich region have been ascribed to the preferential hydration of smaller ions. The ΔH_t° maxima at a mole fraction of acetonitrile (x_{AN}) ca. 0.3 have been suggested to be due to the least favorable hydration for halide ions owing to the destruction of the water lattice caused by the addition of acetonitrile.

In this study we use a new approach to the discussion of the x_{AN} dependence of ΔH_t° for anions in the water-rich and in the intermediate regions from three viewpoints. The first viewpoint is ΔH_t° for anions in relation to the ionic enthalpy of hydration. Linear relations are found between ΔH_t° at x_{AN} 0.3 to 0.6 and the ionic hydration enthalpies, and the same relations are derived by using the entropies of transfer for halide ions. The second is an attempt to estimate the interaction in the outer hydration sphere for halide ions based on a modified Eley and Evans hydration model for the mixtures. It will be noted that the reduction in the interaction estimated from ionic solvation enthalpy cycle is found to be responsible for the endothermic process of ΔH_t° in the water-rich region. The third is ΔH_t° for anions in relation to the solvent structure of the mixtures. The adequacy of the correction for cavity formation energy in the mixtures arising from the change in the solvent structure is discussed. The change in ΔH_t° in the intermediate region is found to be due primarily to the reduction in the cavity formation energy.

Experimental

All chemicals used were of reagent grade. Sodium tetrafluoroborate was prepared from the acid and aqueous sodium carbonate solution, and recrystallized twice from water in a platinum dish. Other salts commercially available were once recrystallized from water. All salts were dried in vacuo, at 60 °C overnight and stored in a desiccator. Acetonitrile and water were distilled thrice and twice, respectively.[3] The enthalpy of solution was measured with a heat-exchange type calorimeter at 25±0.02 °C.[5] The reported standard enthalpy of solution (ΔH_s°) is the average of at least three determinations in a 10^{-3} to 10^{-2} mol dm^{-3} concentration range agreeing within ±0.4 kJ mol^{-1}.

Results and Discussion

The standard enthalpies of solution for electroly-

Table 1. The Enthalpies of Solution for Electrolytes in Water and Water-Acetonitrile Mixtures, ΔH_s°/kJ mol^{-1}

	x_{AN}							
	0	0.1	0.2	0.4	0.6	0.8	0.9	1.0
$NaNO_2$	+13.9	+9.8	+8.0	+3.3	−0.9			
$NaClO_3$	+21.5	+19.0	+15.7	+10.1	+7.1			
$NaBrO_3$	+26.8	+24.3	+21.7	+17.0				
NaN_3	+12.5	+6.7	+4.4	−0.7	−5.2			
$NaBF_4$	+27.4	+21.9	+14.4	+7.3	+2.4	−3.6		
$NaHCO_2$	+0.7	0	−1.7	−7.0	−11.4			
$NaCH_3CO_2$	−16.5	−14.4	−14.8	−18.9				
$NaCF_3CO_2$	−8.7	−6.4	−7.5	−10.9	−14.2	−16.5	−15.0	−6.3

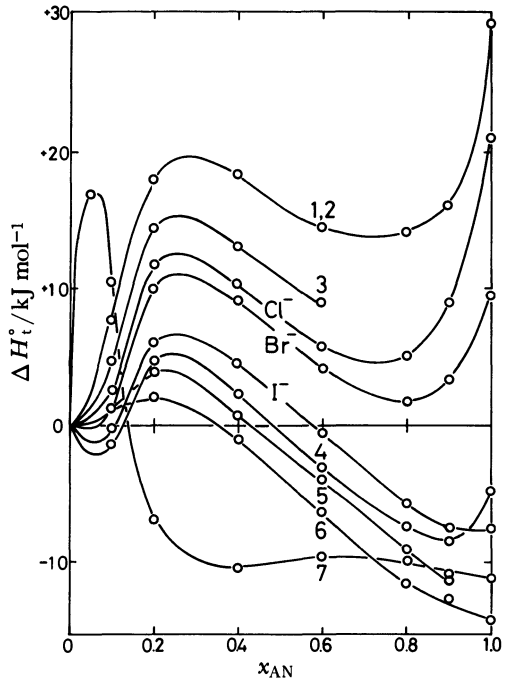

Fig. 1. The enthalpies of transfer from water to water-acetonitrile mixtures (ΔH_t°), for anions plotted against the mole fraction of acetonitrile, x_{AN}. 1,2: $CF_3CO_2^-$, $CH_3CO_2^-$, ($x_{AN} \leq 0.4$), 3: HCO_2^-, 4: NCS^-, 5: BF_4^-, 6: ClO_4^-, 7: Ph_4B^-.

tes are listed in Table 1. The ΔH_s° values for sodium bromate, chlorate and nitrite obtained in water agreed with the literature[6] values within ± 0.2 kJ mol^{-1} and ΔH_s° for sodium acetate within ± 0.8 kJ mol^{-1}.

The enthalpies of transfer from water to water-acetonitrile mixtures (ΔH_t°) for anions were calculated by using ΔH_t° value for Na^+ estimated previously[4] based on the TATB assumption ($\Delta H_t^\circ[Ph_4As^+] = \Delta H_t^\circ[Ph_4B^-]$).[7] Figure 1 shows the x_{AN} dependence of ΔH_t° for typical anions, although ΔH_t° for seventeen anions have been estimated in our laboratory.

The ΔH_t° values for anions reach maxima at x_{AN} ca. 0.3 except for some large anions containing phenyl groups. They decrease linearly and in parallel in the intermediate region, and reach minima at x_{AN} ca. 0.8. Those for small anions increase rapidly in the acetonitrile-rich region. From the extent of these rapid changes the order of the preference to water for anions has been determined.[4] The following order can be determined: $CF_3CO_2^- > Cl^- > Br^- > NCS^- > I^- > Pi^-$ (picrate) $> ClO_4^- \simeq BF_4^-$.

A Linear Relation between Enthalpies of Transfer at x_{AN} 0.3 and Enthalpies of Hydration for Anions. The enthalpies of transfer for anions from water to the mixtures at x_{AN} 0.3 ($\Delta H_t^\circ(x_{AN}=0 \rightarrow 0.3)$) are plotted against the ionic enthalpies of hydration (ΔH_W) in Fig. 2. The ΔH_W values for anions except BF_4^- were cited from the literature.[8] The ΔH_t° value for BF_4^- was estimated from a linear relation between ΔH_W and the reciprocal of the thermochemical radii of polyatomic anions.[9] Noticeably, the values for the halide and

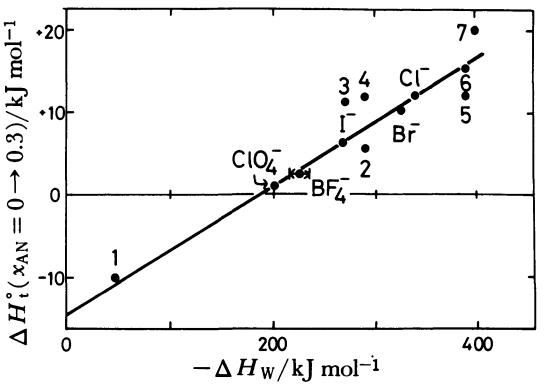

Fig. 2. The enthalpies of transfer from water to water-acetonitrile mixtures at the mole fraction of acetonitrile (x_{AN}) 0.3, ΔH_t° ($x_{AN}=0 \rightarrow 0.3$), plotted against the enthalpies of hydration, ΔH_W, for anions.

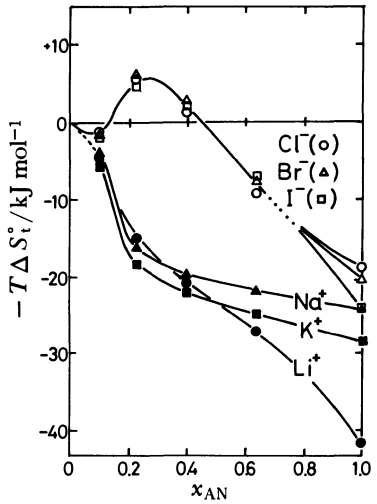

Fig. 3. The entropies of transfer from water to water-acetonitrile mixtures ($T\Delta S_t^\circ$) for alkali and halide ions plotted against the mole fraction of acetonitrile (x_{AN}).
○: Cl^-, △: Br^-, □: I^-, ●: Li^+, ▲: Na^+, ■: K^+.

symmetrical anions lie on a straight line. This finding means that the more strongly hydrated is an anion, the more unfavorable will be its solvation in the mixtures.

The same relation will be derived by using the ionic solvation entropy as follows. Fortunately, the free energies of transfer (ΔG_t°) for alkali metal and halide ions in these mixtures have been published on TATB assumption.[10] The entropies of transfer (ΔS_t°) for these ions can be estimated ($-T\Delta S_t^\circ = \Delta G_t^\circ - \Delta H_t^\circ$) and are plotted against x_{AN} in Fig. 3. The ΔS_t° values for anions are considered to be nearly equal to each other in the range of x_{AN} 0 to ca. 0.6, while those for cations are differentiated in this range.

As suggested by Eley and Evans,[11] the more negative the ionic hydration enthalpy, the more negative the corresponding entropy. The same relation would be expected to hold in the mixtures. Figure 4 shows the analysis of the thermodynamic functions in water and in the mixtures. The values of the thermodynamic

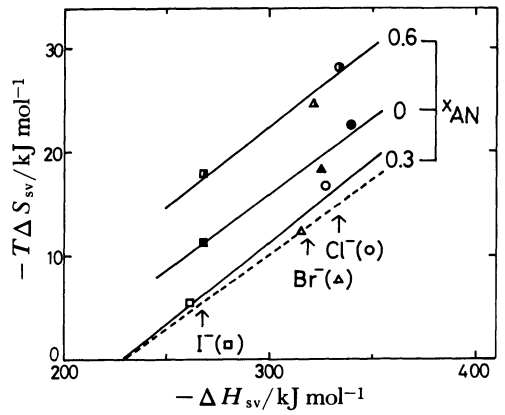

Fig. 4. The entropies of solvation, $-T\Delta S_{SV}$, plotted against the enthalpies of solvation, $-\Delta H_{SV}$, for halide ions in water and water-acetonitrile mixtures. Broken line indicates the plot of $-T\Delta S_{0.3}$ vs. $-\Delta H_W$.

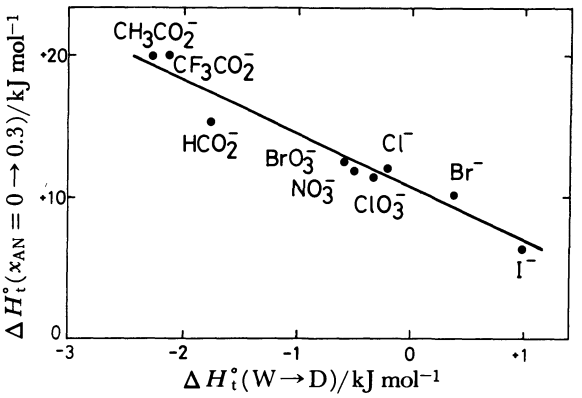

Fig. 5. The enthalpies of transfer from water to water-acetonitrile mixtures at the mole fraction of acetonitrile (x_{AN}) 0.3, $\Delta H_t^\circ(x_{AN}=0\rightarrow0.3)$, plotted against the enthalpies of transfer from normal water to heavy water, $\Delta H_t^\circ(W\rightarrow D)$ for anions.

functions in water (ΔS_W and ΔH_W) are cited from the literature,[8] and those in the mixtures are calculated from values of the transfer functions. The broken line represents $-T\Delta S_{0.3}$ plotted against $-\Delta H_W$ and intersects the line of $-T\Delta S_{0.3}$ plotted against $-\Delta H_{0.3}$ close to the same position on the abscissa.

Equations 1, 2, and 4 are derived from the plots of $-T\Delta S_{SV}$ vs. ΔH_{SV} in water and the mixtures of x_{AN} 0.3 and 0.5, respectively. Equation 3 is derived from the broken line. In those equations, the subscripts denote the solvent compositions.

$$-T\Delta S_w = -28.0 + 0.14_6(-\Delta H_w) \quad (1)$$

$$-T\Delta S_{0.3} = -36.3 + 0.15_8(-\Delta H_{0.3}) \quad (2)$$

$$-T\Delta S_{0.3} = -33.9 + 0.14_6(-\Delta H_w) \quad (3)$$

$$-T\Delta S_{0.5} = -29.0 + 0.15_9(-\Delta H_{0.5}) \quad (4)$$

$$\Delta H_t^\circ(x_{AN} = 0 \longrightarrow 0.3) = -15.2 + 0.076(-\Delta H_w) \quad (5)$$

By subtracting Eq. 1 from Eq. 2, the relation between ΔH_t° and ΔH_W is obtained. When the experimental value for $-T\Delta S_t^\circ$ (5.9 kJ mol^{-1}) is substituted in this relation, we obtain Eq. 5. The values of the slope and intercept of Eq. 5 are in good agreement with the experimental ones (slope 0.078, intercept 14.8).

In x_{AN} over the range 0.3 to 0.6, linear relations with the same slope as Eq. 5 can be derived in a similar manner as above, since the plots of $-T\Delta S_{SV}$ vs. $-\Delta H_{SV}$ have the same slope as that of Eq. 2. Therefore, the x_{AN} dependence of ΔH_t° is parallel in this range. Thus, we have been able to derive the linear relations between ΔH_t° at x_{AN} 0.3 to 0.6 and ΔH_W for halide ions by using ΔG_t° data.

Estimation of the Hydrogen-Bonding Interaction Extending beyond the Primary Hydration Sphere based on Modified Eley and Evans Hydration Model. The relation between $\Delta H_t^\circ(x_{AN}=0\rightarrow0.3)$ and the enthalpies of transfer from normal water to heavy water ($\Delta H_t^\circ(W\rightarrow D)$) is shown in Fig. 5. The $\Delta H_t^\circ(W\rightarrow D)$ values were cited from the literature.[12] Thus $\Delta H_t^\circ(x_{AN}=0\rightarrow0.3)$ was related closely to $\Delta H_t^\circ(W\rightarrow D)$. Anions which are more strongly hydrated by hydrogen-bonding interaction should have the more negative $\Delta H_t^\circ(W\rightarrow D)$ value, because heavy water has been shown to be more strongly hydrogen bonded than normal water.[12] Noticeably, those anions have the more positive $\Delta H_t^\circ(x_{AN}=0\rightarrow0.3)$ values. This finding suggests that the endothermicity in the mixtures results from an unfavorable interaction between the primary hydration sphere and the surroundings, since anions should be preferentially hydrated in the water-rich region. Accordingly we have developed the Eley and Evans treatment of the ionic hydration enthalpy cycle to estimate the outer sphere hydrogen-bonding interaction in the mixtures.

Several molecular models of the ionic hydration of the water structure, the orientation of the water dipole, various ion-water interactions and the water structure of the outer hydration sphere have been proposed,[13a-d] since Bernal and Fowler published their pioneer work in 1933. Eley and Evans have proposed a thought experiment involving the following steps to estimate theoretically the ionic hydration enthalpy for a tetrahydrated ion. (1) A cluster of five water molecules corresponding to the volume of the primary hydrated ion is removed from the liquid phase to the gas phase leaving a cavity in the liquid, $\Delta H_{CF}(>0)$. (2) The tetrahedral water cluster is dissociated into water monomers in the gas phase, $\Delta H_D(>0)$. (3) Four water molecules are coordinated to an ion in the gas phase, $\Delta H_{I\text{-}S(g)}(<0)$. (4) The hydrated ion is returned to the cavity, $\Delta H_{BC}(<0)$. (5) The water molecules of the returned hydrated ion interact with their neighbor, $\Delta H_{INT}(<0)$. In other words, ΔH_{INT} represents hydrogen-bonding interaction extending beyond the primary hydration sphere, namely the outer hydration sphere of anions. (6) Finally, one water molecule left in the gas phase is returned to the liquid phase, $\Delta H_C(<0)$.

Table 2. The Enthalpies of Solvation, ΔH_{SV}, the Enthalpies of Born Charging, ΔH_{BC}, the Enthalpies of Hydration in Gas Phase, $\Delta H_{1-S(g)}$, for Halide Ions and the Relative Partial Molar Enthalpies of Water in Water-Accetonitrile Mixtures, L_W/kJ mol^{-1}

		x_{AN}						
		0	0.1	0.2	0.3	0.4	0.5	0.6
Cl^-	$-\Delta H_{SV}$	340[a]	337.5	328.2	328.0	329.7	332.2	334.3
	$-\Delta H_{BC}$	153.2	153.0	153.5	153.6	152.9	152.9	152.4
	$-\Delta H_{1-S(g)}$[b]				203.3			
Br^-	$-\Delta H_{SV}$	320[a]	324.7	315.9	315.7	316.7	319.1	321.9
	$-\Delta H_{BC}$	148.3	148.0	148.3	148.3	147.8	147.7	147.2
	$-\Delta H_{1-S(g)}$[b]				197.9			
I^-	$-\Delta H_{SV}$	268[a]	268.3	262.0	261.7	263.5	266.0	268.6
	$-\Delta H_{BC}$	141.1	140.9	141.2	141.2	140.6	140.5	140.1
	$-\Delta H_{1-S(g)}$[b]				161.5			
	$-4L_W$[c]	0	+0.6	+0.2	−0.2	−1.2	−2.4	−3.6

a) From Ref. 8. b) From Ref. 4 (for tetrahedral hydration). c) From Ref. 24.

We propose a novel method to estimate the ΔH_{INT} term for the mixtures based on a modified hydration model.

Table 2 shows values of some terms used to estimate the sum of $\Delta H_{CF(W)}$ and ΔH_{INT} terms ($\Delta H_{CF(W)}+\Delta H_{INT}$) in aqueous solution according to the following equation:

$$\Delta H_{CF(W)} + \Delta H_{INT} = \Delta H_W - (\Delta H_{I-S(g)} + \Delta H_{BC} + \Delta H_D + \Delta H_C), \quad (6)$$

where $\Delta H_{1-S(g)}$ is the ionic hydration enthalpy in the gas phase measured with a mass spectrometer.[14] Stepwise enthalpies of hydration ($\Delta H_{3,4}$) for I^- are obtained by extrapolation of the $\Delta H_{n-1,n}$ vs. n plot. The ΔH_{BC} values are calculated by the Born equation in kJ mol^{-1}:

$$\Delta H_{BC} = 1398/2R_i \times (1 - 1/\varepsilon - 1/\varepsilon \times d\varepsilon/dT), \quad (7)$$

where $R_i(=r_c+2r_w)$ is the radius of the hydrated ion, r_c the crystal radius of the ion,[16] r_w the radius of the water molecule (1.38Å),[17] and $d\varepsilon/dT$ is the temperature coefficient of the dielectric constant of water (0.355/°C).[18] In this calculation the effect of dielectric saturation can reasonably be neglected, since the radius of the hydrated in is larger than 4Å in every case.[13b] The ΔH_D value is the enthalpy of breaking four hydrogen bonds in water (83.7 kJ mol^{-1})[15,17] and ΔH_C is the enthalpy of condensation of water (29.7 kJ mol^{-1}).[19]

Next we attempt to consider the solvation enthalpy cycle in the mixtures up to x_{AN} 0.6. We assume that an anion is preferentially hydrated in the primary hydration sphere in the mixtures. This assumption seems to be reasonable for the following reasons. An anion is more strongly solvated in water than in a dipolar aprotic solvent, since the positive charge end of the acetonitrile dipole is distributed over a large part of the molecule.[21] Furthermore, the activity of water in the intermediate region remains nearly constant as deduced from the marked positive deviation of the partial vapor pressure of water.[22] In fact, halide ions have been pointed out to be preferentially hydrated in those mixtures by the measurement of NMR on halide ion nucleus.[23]

Table 3. The Sum of the Enthalpies of Cavity Formation and Outer Hydration Sphere Interaction, $\Delta H_{CF(W)}+\Delta H_{INT}$, for Halide Ions in Water and Water-Acetonitrile Mixtures/kJ mol^{-1}

	x_{AN}						
	0	0.1	0.2	0.3	0.4	0.5	0.6
Cl^-	−37.5	−35.8	−25.6	−25.1	−26.3	−27.5	−29.0
Br^-	−34.5	−33.4	−23.9	−23.1	−23.8	−25.1	−27.2
I^-	−19.4	−20.5	−13.5	−12.6	−14.2	−15.6	−17.4

The ΔH_{CF} term in the mixtures is assumed to differ from that in water by $-5L_W$, the enthalpy of demixing five water molecules from the mixtures, and ΔH_C term by $+L_W$, the enthalpy of mixing one water molecule with the mixtures. Therefore, ($\Delta H_{CF}+\Delta H_C$) in the mixtures differ by $-4L_W$ from that in water, where L_W denotes the relative partial molar enthalpy for water in the mixtures and can be calculated from the excess enthalpy of mixing data[24,25] by an intercept method.[26] The ΔH_{BC} values in the mixtures are calculated in the same way as that in aqueous solution by using ε and $d\varepsilon/dT$ data.[18]

Values of ($\Delta H_{CF(W)}+\Delta H_{INT}$) estimated for the mixtures according to the following equation are shown in Tab. 3 together with those in water for comparison;

$$\Delta H_{CF(W)} + \Delta H_{INT(mix)} = -\Delta H_{SV(mix)} - (\Delta H_{I-S(g)} + \Delta H_{BC(mix)} + \Delta H_D + \Delta H_C) + 4L_W. \quad (8)$$

So, ΔH_t° is represented as follows:

$$\Delta H_t^\circ = -4L_W + \Delta\Delta H_{BC} + \Delta\Delta H_{INT}. \quad (9)$$

The smaller an anion, the more negative ($\Delta H_{CF(W)}+\Delta H_{INT}$) will be in water. If $\Delta H_{CF(W)}$ is assumed to be the latent heat of vaporization for water according to the suggestion of Buckingham,[13b] ΔH_{INT} for the chloride ion in water is approximately −60 kJ mol^{-1}.

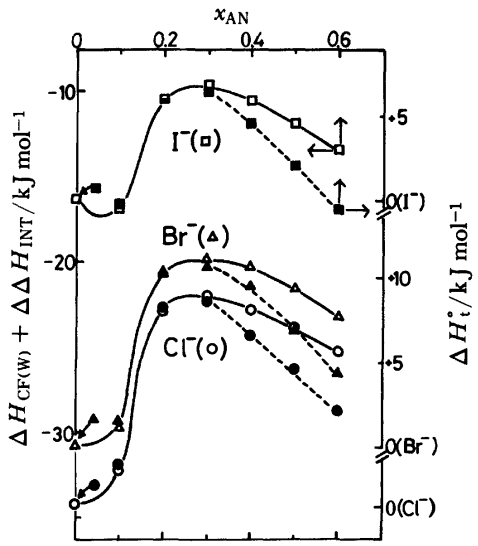

Fig. 6. The sum of the enthalpies of cavity formation and outer hydration sphere interaction, $\Delta H_{CF(W)}+\Delta H_{INT}$, and the enthalpies of transfer, ΔH_t°, for halide ions plotted against the mole fraction of acetonitrile (x_{AN}).

This means that several hydrogen bonds are formed in the outer hydration sphere for a halide ion through these cooperative effects.[20]

Figure 6 shows the comparison of $\Delta\Delta H_{INT}$ with ΔH_t° for halide ions. In this figure the broken curves represent the x_{AN} dependence of ΔH_t°, and the ordinate is adjusted so that the origin for each anion corresponds to $\Delta H_{CF(W)}+\Delta H_{INT}$ value in water. As shown in Tab. 2, the possibility of a ΔH_{BC} contribution to ΔH_t° is safely excluded, because the x_{AN} dependence of this term is negligible. If the ΔH_{CF} value in the mixtures can be correctly estimated by subtracting $5L_W$ from that in water, the left-hand ordinate will represent the $\Delta\Delta H_{INT}$. The two curves for each anion appear to show a similar trend in x_{AN} dependence. It can be said that the x_{AN} dependence of ΔH_t° at x_{AN} 0 to 0.6 may be explained semiquantitatively as the x_{AN} dependence of $\Delta\Delta H_{INT}$ based on the modified Eley and Evans hydration model. Noticeably, at x_{AN} 0 to ca. 0.3 the two curves agree well, while they split gradually with increasing x_{AN} beyond 0.3.

In the treatment of the solvation enthalpy cycle described above, hydration numbers for the halide ions were assumed to be four, although hydration numbers other than four have been reported.[27] The enthalpies of hydration in the gas phase have been reported up to the fourth water molecule for Cl^- and Br^-, and up to the third molecule for I^-, respectively.[14] It is possible to estimate approximately the hydration enthalpies in the gas phase up to the sixth water molecule by extrapolation. We have carried out a similar calculation to estimate ($\Delta H_{CF(W)}+\Delta\Delta H_{INT}$) for a hexahydrated ion by using such extrapolated values. The x_{AN} dependence of those values is very close to that for a tetrahydrated ion. So the same conclusion as before can be reached.

Solvation of Anions and Solvent Structure of Water–Acetonitrile Mixtures. In the previous section it has been clarified that the increase in ΔH_t° for halide ions in the range of x_{AN} 0 to ca. 0.3 was ascribed to the change in the ΔH_{INT} term. Accordingly the validity of the modified hydration model will now be discussed in relation to the solvent structure of the mixtures.

Three structurally different regions have been suggested to exist in those mixtures according to studies on the volumetric, viscosity and dielectric properties[18] and vapor pressure[22] measurements; (1) water-rich, (2) intermediate and (3) acetonitrile-rich regions. In the region (1) the voids inside the aqueous framework of the water lattice are considered to be progressively filled with acetonitrile. That is, no significant enhancement of the water lattice is caused by the addition of cosolvent in contrast to the other aqueous mixtures (water-*t*-butyl alcohol).[28a] This region, therefore, is stated as "essentially aqueous."[30] In the region (2), on the other hand, the large aggregates formed in the former region are considered to be progressively broken to smaller ones after the filling of the voids. The mixtures of x_{AN} ca. 0.3 seems to have the most compact solvent structure, since some physicochemical properties of the mixtures show extrema at this composition, such as excess volume[28a,b] and excess entropy[29] of mixing, energy-volume coefficient and isothermal compressibility.[30] Thus, this mixed solvent system can be classified as one of the simplest aqueous mixtures in which the added acetonitrile acts as a slightly weak structure maker of the water lattice in the water-rich region and a strong structure breaker in the intermediate region.

There is no doubt that the ΔH_t° maxima at x_{AN} ca. 0.3 may be closely associated with the most compact solvent structure at nearly the same solvent composition. As shown in Fig. 6, the estimated $\Delta\Delta H_{INT}(=\Delta H_t^\circ+4L_W-\Delta\Delta H_{BC})$ in x_{AN} range 0 to ca. 0.3 agree with the observed ΔH_t° better than expected. The proposed model may be applicable in this range, because the mixtures of x_{AN} 0 to ca. 0.3 can be regarded as the essentially aqueous solvent. Also from the above structural viewpoint, it is reasonable to interpret the increase in ΔH_t° with increasing x_{AN} in this region in terms of the reduction in the hydrogen-bonding interaction extending beyond the primary hydration sphere for smaller anions.

Since the observed ΔH_t° is clearly less than the estimated ΔH_{INT} in the intermediated region, the modified hydration model does not appear to work so well as in the water-rich region. As can be seen in Fig. 6, the x_{AN} dependence of $\Delta\Delta H_{INT}$ is reversed in going from the water-rich region to the intermediate region. If the correction for the ΔH_{CF} term has been made in the intermediate region as adequately as in the water-rich region, this reversal means the recovery of the outer hydration sphere disrupted somewhat in the water-rich

region. The possibility of this recovery, however, may be very low in consideration of the decrease in the water content. Reasonably, the outer hydration sphere which has been incompletely disrupted at x_{AN} ca. 0.3 is considered to reduce with increasing x_{AN} in this region though to a smaller extent. The interaction between the water cluster demixed from the mixtures and the surroundings was assumed to be equal to that in water in the above treatment of the solvation enthalpy cycle. This assumption, however, seems unreasonable in the intermediate region in which the water cluster has been broken to a certain extent. This interaction in the intermediate region should be weaker than that in water and should decrease with increasing x_{AN}. A consideration of this effect will lead to the reduction in the ΔH_{CF} value in this region. That is to say, the additional correction term besides $5L_W$ employed in this study seems to be needed for cavity formation in the intermediate region from the viewpoint of the solvent structure. Eventually, the exothermic change in ΔH_t° in the intermediate region may be considered to be due primarily to the decrease in ΔH_{CF} energy.

References

1) a) H. Schneider, "Solute-Solvent Interactions," ed by J. F. Coetzee and C. D. Richie, Marcel Dekker Inc., New York and Basel (1976), Vol. 2; b) A. K. Covington and Newman, *Adv. Chem. Ser.*, **155**, 153 (1976).

2) a) H. Strehlow and H.-M. Koepp, *Z. Electrochem.*, **62**, 373 (1958); b) H. Strehlow and H. Schneider, *J. Chim. Phys.*, **2392**, 118 (1969); c) H. Schneider and H. Strehlow, *Z. Phys. Chem. (Frankfurt)*, **49**, 44 (1968); d) B. G. Cox, R. Natarajan, and W. E. Waghorne, *J. Chem. Soc., Faraday Trans. 1*, **75**, 86 (1979).

3) K. Morinaga and K. Miyaji, *Denki Kagaku*, **50**, 736 (1982).

4) K. Miyaji and K. Morinaga, *Bull. Chem. Soc. Jpn.*, **56**, 1861 (1983).

5) M. Nakanishi and S. Fujieda, *Anal. Chem.*, **44**, 574 (1972).

6) "Kagaku Binran Kisohen," Maruzen, Tokyo (1975) Part 2, p. 910.

7) B. G. Cox, G. R. Hedwig, A. J. Parker, and D. W. Watts, *Aust. J. Chem.*, **27**, 477 (1974).

8) D. R. Rosseinsky, *Chem. Rev.*, **65**, 467 (1965).

9) T. C. Waddington, *Adv. Inorg. Chem. Radiochem.*, **1**, 157 (1959).

10) K. Das, A. K. Das, and K. K. Kundu, *Electrochim. Acta*, **26**, 471 (1981).

11) D. D. Eley and M. G. Evans, *Trans. Faraday Soc.*, **34**, 1093 (1938).

12) H. L. Friedman and C. V. Krishnan, "Water, A Comprehensive Treatise," ed by F. Franks, Plenum Publ., Co., New York (1973), Vol. 3, p. 1.

13) a) J. D. Bernal and R. H. Fowler, *J. Chem. Phys.*, **1**, 515 (1933); b) A. D. Buckingham, *Discuss. Faraday Soc.*, **24**, 151 (1957); c) S. Goldman and R. G. Bates, *J. Am. Chem. Soc.*, **94**, 1476 (1972); d) J. O'M. Bockris and P. P. S. Saluja, *J. Phys. Chem.*, **76**, 2298 (1972).

14) I. Dzidic and P. Kebarle, *J. Phys. Chem.*, **74**, 1466 (1970).

15) J. O'M. Bockris and A. K. N. Reddy, "Modern Electrochemistry," Plenum Pub. Co., New York (1976), Vol. 1.

16) "Landolt-Börnstein Zahlenwerte und Funktionen," 1 Band, Atom- und Molekular-physik, 4 Teil, Kristalle, Springer Verlag (1955), p. 522.

17) L. Pauling, "The Nature of the Chemical Bond," Cornell University Press, New York (1960).

18) C. Moreau and G. Dauhéret, *J. Chem. Thermodyn.*, **8**, 403 (1976).

19) J. F. Coetzee, "Recommended Methods for Purification of Solvents and Tests for Impurities," ed by J. F. Coetzee, Pergamon Press, Oxford (1982).

20) E. M. Arnett, B. Chawla, and N. J. Horrung, *J. Solution Chem.*, **6**, 781 (1977).

21) W. R. Davidson and P. Kebarle, *J. Am. Chem. Soc.*, **98**, 6125 (1976).

22) Von A-L. Vierk, *Z. Anorg. Chem.*, **261**, 283 (1950).

23) T. R. Stengle, Y-C. E. Pan, and C. H. Langford, *J. Am. Chem. Soc.*, **94**, 9037 (1972).

24) K. W. Marcom and R. W. Smith, *J. Chem. Thermodyn.*, **1**, 503 (1969).

25) The same values of L_W are obtained with the titration calorimetry method in our laboratory.

26) J. S. Rowlinson and F. L. Swinton, "Liquids and Liquid Mixtures," Butterworths, London (1982).

27) H. Ohtaki, M. Tanaka, and S. Funahashi, "Yooekihanno No Kagaku," Gakkai Shuppan Center, Tokyo (1977).

28) a) D. A. Armitage, M. J. Blandamer, M. J. Foster, N. J. Hidden, K. W. Marcom, M. C. R. Symons, and M. J. Wootten, *Trans. Faraday Soc.*, **64**, 1193 (1968); b) C. Moreau and G. Dauhéret, *Thermochim. Acta*, **13**, 358 (1975).

29) C. Treiner, P. Tzias, M. Chemla, and G. M. Poltoratskii, *J. Chem. Soc., Faraday Trans., 1*, **72**, 2007 (1976).

30) D. F. G-Taylor and D. D. Macdonald, *Can. J. Chem.*, **54**, 2813 (1976).

Preparation and Characterization of $[RhCl_2(edpp)_2]^+$ (edpp=(2-aminoethyl)-diphenylphosphine). Crystal Structures of *trans*(Cl,Cl), *cis*(P,P)-$[RhCl_2(edpp)_2]Cl \cdot 2C_2H_5OH$ and *cis*(Cl,Cl), *trans*(P,P)-$[RhCl_2(edpp)_2]Cl \cdot 4H_2O$

Frode GALSBØL,† Masaaki KOJIMA, Toshio ISHII,†† Shigeru OHBA,†††
Yoshihiko SAITO,††† and Junnosuke FUJITA*
Department of Chemistry, Faculty of Science, Nagoya University, Chikusa-ku, Nagoya 464
††Department of Chemistry, Chiba Institute of Technology, 2-17-1, Tsudanuma, Narashino 275
†††Department of Chemistry, Faculty of Science and Technology, Keio University, Hiyoshi 3, Kohoku-ku, Yokohama 223
(Received January 9, 1986)

Two of the five possible geometrical isomers of $[RhCl_2(edpp)_2]^+$ were formed by reaction of $RhCl_3 \cdot 2H_2O$ with edpp (edpp=(2-aminoethyl)diphenylphosphine) in 1:2 molar ratio in ethanol. The chlorides of the isomers were separated by fractional crystallization from ethanol. The structures of the more soluble (main product) and the less soluble (minor product) complexes were determined by X-ray analyses to have the trans(Cl,Cl), cis(P,P) and cis(Cl,Cl), trans(P,P) configurations, respectively. Crystal data are: for *trans*(Cl,Cl), *cis*(P,P)-$[RhCl_2(edpp)_2]Cl \cdot 2C_2H_5OH$, triclinic, space group $P\bar{1}$, with $a=10.024(3)$, $b=18.865(3)$, $c=9.833(2)$ Å, $\alpha=97.66(1)$, $\beta=103.92(2)$, $\gamma=82.30(2)°$, and $Z=2$, and for *cis*(Cl,Cl), *trans*(P,P)-$[RhCl_2(edpp)_2]Cl \cdot 4H_2O$, triclinic, space group $P\bar{1}$, with $a=11.341(4)$, $b=17.780(6)$, $c=8.712(3)$ Å, $\alpha=95.60(4)$, $\beta=112.31(3)$, $\gamma=82.56(4)°$, and $Z=2$. The trans influence of the P atom on the Rh-N and Rh-P bond lengths is observed. The mean Rh-N and Rh-P bond lengths (2.125(4) and 2.300(1)Å) in the trans(Cl,Cl), cis(P,P) isomer are respectively longer and shorter than those of the cis(Cl,Cl), trans(P,P) isomer (2.078(12) and 2.336(3)Å). ^{13}C NMR and absorption spectra of the isomers were recorded and are discussed.

In a previous paper,[1] we reported the preparation of $[CoCl_2(edpp)_2]^+$, where edpp denotes (2-aminoethyl)diphenylphosphine. Although five geometrical isomers are possible for the $[MCl_2(edpp)_2]$-type complex (Fig. 1), the cobalt(III) complex formed only one isomer and the structure was determined to have the trans(Cl,Cl),cis(P,P) configuration by X-ray analysis.[2] Of the two trans(Cl,Cl) isomers, the formation of the sterically less favorable trans(Cl,Cl),cis(P,P) isomer might be attributable to the strong trans effect of the phosphorus donor atoms.[2] For the rhodium(III) complex, $[RhCl_2(edpp)_2]^+$ the magnitudes of the steric and trans effects should be different from those of the cobalt(III) complex, and other isomers than trans-(Cl,Cl),cis(P,P) might be expected to be formed.

This paper describes the preparation and X-ray structure analyses of the trans(Cl,Cl),cis(P,P) and the cis(Cl,Cl),trans(P,P) isomers of $[RhCl_2(edpp)_2]^+$. Also, the absorption and ^{13}C NMR spectra of the isomers are compared with each other and with those of related complexes.

Experimental

The edpp ligand was prepared according to a literature method,[3] and handled under an atmosphere of nitrogen until it formed air-stable rhodium(III) complexes. Absorption and ^{13}C NMR spectra were recorded on a Hitachi 323 spectrophotometer and a JEOL JNM-GX 400 spectrometer, respectively.

Preparation of *trans*(Cl,Cl),*cis*(P,P)-$[RhCl_2(edpp)_2]Cl \cdot 2C_2H_5OH$ (isomer A) and *cis*(Cl,Cl),*trans*(P,P)-$[RhCl_2(edpp)_2]Cl \cdot H_2O$ (isomer B). A deaerated ethanol solution (8 cm³) of $RhCl_3 \cdot 2H_2O$ (0.587 g, 2.39 mmol) was added to a stirred solution of edpp (1.098 g, 4.79 mmol) in deaerated ethanol (3 cm³) over a period of 15 min. The mixture was heated at 70 °C for 7 h and gave a yellow solution together with a small amount of pale yellow precipitate. The mixture was evaporated to dryness in vacuo and the residue washed with diethyl ether to remove excess edpp before it was exposed to the air. The washed residue was shaken repeatedly with hot ethanol (ca. 175 cm³) to extract the products until the extracts were colorless. The combined extracts were heated (ca. 70 °C) and filtered while hot, and the filtrate on evaporation to a volume of ca. 75 cm³ gave a pale yellow precipitate. This was collected by filtration (The mother liquor was treated as described below.) and recrystallized from ethanol to yield a yellow powder of isomer B. Yield: 0.032 g. Found: C, 48.75; H, 5.22; N, 4.07%. Calcd for $C_{28}H_{34}N_2Cl_3OP_2Rh = [RhCl_2(edpp)_2]Cl \cdot H_2O$: C, 49.04; H, 5.00; N, 4.08%. UV-

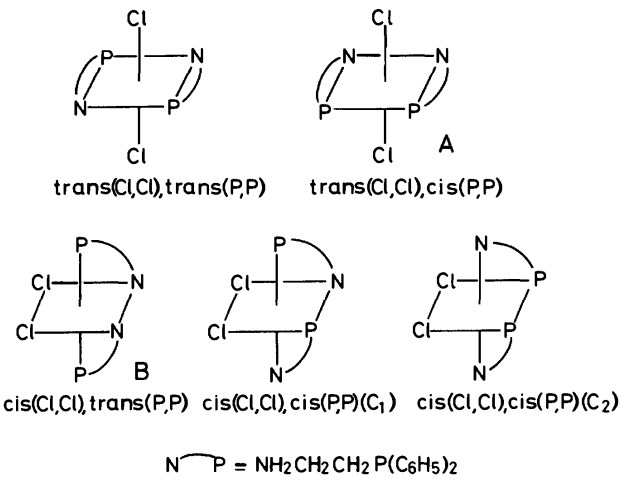

Fig. 1. The five possible geometrical isomers of $[M^{III}Cl_2(edpp)_2]^+$.

† On leave from Chemistry Department I, University of Copenhagen, Universitetsparken 5, DK-2100, Copenhagen φ, Denmark.

Table 1. Crystal Data and Experimental Details

	(A)	(B)
Chemical formula	$[RhCl_2(C_{14}H_{16}NP)_2]Cl\cdot 2C_2H_5OH$	$[RhCl_2(C_{14}H_{16}NP)_2]Cl\cdot 4H_2O$
Formula weight	759.9	739.8
Crystal system	Triclinic	Triclinic
Space group	$P\bar{1}$	$P\bar{1}$
a/Å	10.024(3)	11.341(4)
b/Å	18.865(3)	17.780(6)
c/Å	9.833(2)	8.712(3)
α/°	97.66(1)	95.0(4)
β/°	103.92(2)	112.31(3)
γ/°	82.30(2)	82.56(4)
V/Å^3	1778.6(6)	1591.2(10)
Z	2	2
D_x/g cm^{-3}	1.42	1.54
D_m/g cm^{-3}	1.41(1)	1.56(1)
μ(Mo $K\alpha$)/mm^{-1}	8.18	9.10
Color and Habit of crystals	Yellow prisms	Yellow prisms
Solvent used to recrystallize	Ethanol	Acetonitrile
Size of specimen/mm^3	0.27×0.55×0.55	0.5×0.2×0.15
Number of standard reflections, n and variation of their $\|F_o\|$ amplitudes, $(\|F_o\|/\|F_o\|_{initial})/n$	5 0.99—1.01	5 0.93—1.01
Number of reflections measured	8624	7771
Number of reflections observed with $\|F_o\|>3\sigma(\|F_o\|)$	7064	4575
Transmission factor	0.42—0.62	0.65—0.75
R	0.074	0.088
wR	0.089	0.116
Weight $w^{-1}=\sigma^2(\|F_o\|)+(c\|F_o\|)^2$	c=0.025	c=0.02
$S=[\sum w(\|F_o\|-\|F_c\|)^2/(m-n)]^{1/2}$	2.8	2.9
Number of observed unique reflections, m	6650	4353
Number of parameters, n	477	331
$(\Delta/\sigma)_{max}$ for non-hydrogen atoms	0.5	0.3
Peak height in the final difference synthesis/e Å^{-3}	−2.4—2.2	−1.6—2.8

(CH_3CN) 28000 (sh, log ε=3.41), 33000 (sh, 4.21), 35400 (4.28), 36100 (sh, 4.28), and 45000 cm^{-1} (sh, 4.51). Single crystals of isomer B, $[RhCl_2(edpp)_2]Cl\cdot 4H_2O$ suitable for X-ray crystallography were obtained by slow evaporation of an acetonitrile solution of the chloride at room temperature. The presence of four molecules of water of crystallization was suggested by the density and microanalytical data of the crystals. Found: C, 45.33; H, 4.72; N, 3.76%. Calcd for $C_{28}H_{40}N_2Cl_3O_4P_2Rh$: C, 45.41; H, 5.44; N, 3.79%.

By evaporating the mother liquor to a small volume isomer A was obtained as yellow-orange crystals. They were collected by filtration, washed with ethanol, and air dried. Yield: 0.25 g. Found: C, 50.88; H, 5.51; N, 3.84%. Calcd for $C_{32}H_{44}N_2Cl_3O_2P_2Rh=[RhCl_2(edpp)_2]Cl\cdot 2C_2H_5OH$: C, 50.58; H, 5.84; N, 3.69%. UV(C_2H_5OH) 24450 (log ε=2.24), 29000 (sh, 2.2), 34500 (sh, 3.97), 38900 (4.40), and 45700 cm^{-1} (sh, 4.67). The crystals effloresce in the air giving off the ethanol of crystallization.

Crystal Structure Determination. Crystal data and experimental details are given in Table 1. Crystals of both (A) and (B) were sealed into capillary tubes together with their mother liquors and mounted on an automated four-circle diffractometer, Rigaku AFC-5. Intensities were measured up to 2θ=55° by θ—2θ scan technique with scan speed 6° min^{-1} in θ, graphite monochromatized Mo $K\alpha$ radiation being used. Lattice constants were determined from 25 2θ values ($20°<2\theta<30°$) with (Mo $K\alpha$)=0.71073 Å. After absorption correction, the structures were solved by the Patterson-Fourier method. Two ethanol molecules in (A) could be found from Fourier synthesis. From the difference synthesis 30 of the 32 hydrogen atoms except those of the ethanol molecules were found and others were calculated. One of the phenyl groups bonded to the P(2) atom in (B) exhibited orientational disorder. The two sets of positions for the C(24)—C(28) atoms were included with 50% population. The dihedral angle between the least squares planes in two possible orientations for the disordered phenyl group is 77.8°. The water molecules as well as the Cl^- ion could not be found from Fourier synthesis. The difference synthesis gave five positions with peak heights 3.7—4.7 e Å^{-3}, the distances between them being longer than 2.65(2) Å. We were unable to distinguish the disordered water molecules from the disordered Cl^- ions on the basis of the difference synthesis. In the present study we have tentatively assumed that the five positions are all occupied by Cl^- ions and we have estimated their population parameters by the trial and error method with the restriction that the isotropic thermal parameters of the Cl^- ions remain almost equal. Positional parameters of all the hydrogen atoms in (B) were calculated and not refined, although eight hydrogen atoms were found from difference synthesis. By introducing these calculated hydrogen atoms, the R factor reduced from 0.092 to 0.088. Anisotropic thermal parameters

Table 2. Positional Parameters ($\times10^4$; for Rh$\times10^5$) and Equivalent Isotropic Temperature Factors

(A)	X	Y	Z	B_{eq}(Å^2)	(B)	X	Y	Z	B_{eq}(Å^2)
Rh	18897(4)	24027(2)	4348(3)	3.0	Rh	33210(8)	28037(5)	320(12)	2.8
Cl(1)	1923(1)	1153(1)	23(1)	4.1	Cl(1)	3463(3)	4103(2)	−130(4)	4.3
Cl(2)	2102(2)	3625(1)	1121(1)	4.8	Cl(2)	2160(3)	3003(2)	1810(4)	5.0
Cl(0)	6525(2)	2564(1)	−6344(2)	6.6	P(1)	5273(3)	2648(2)	2270(4)	3.3
P(1)	−429(1)	2475(1)	403(1)	3.2	P(2)	1477(3)	2900(2)	−2381(4)	3.7
P(2)	1987(1)	2556(1)	−1817(1)	3.1	N(1)	3295(10)	1654(5)	250(13)	4.4
N(1)	2153(4)	2302(2)	2619(4)	4.1	N(2)	4249(9)	2594(6)	−1639(12)	4.0
N(2)	4071(4)	2243(3)	768(5)	4.4	C(1)	5408(14)	1638(7)	2543(19)	5.8
C(1)	−292(6)	2185(3)	2148(6)	4.5	C(2)	4189(23)	1341(11)	1708(31)	13.7
C(2)	877(6)	2520(3)	3138(5)	4.9	C(3)	2227(13)	2930(8)	−3859(17)	5.6
C(3)	3797(5)	2728(3)	−1461(6)	4.1	C(4)	3426(13)	2434(8)	−3366(15)	5.1
C(4)	4618(5)	2165(4)	−511(6)	4.9	C(5)	5449(10)	3117(6)	4258(13)	3.3
C(5)	−1471(5)	3339(3)	379(5)	3.6	C(6)	6363(12)	2803(8)	5766(16)	5.0
C(6)	−1265(6)	3856(3)	−410(6)	4.5	C(7)	6478(15)	3194(9)	7238(15)	6.1
C(7)	−2140(7)	4495(3)	−513(7)	5.2	C(8)	5779(13)	3881(8)	7330(15)	4.9
C(8)	−3188(6)	4623(3)	155(8)	5.5	C(9)	4913(13)	4159(7)	5953(16)	4.7
C(9)	−3397(6)	4120(4)	952(8)	5.9	C(10)	4704(11)	3805(7)	4335(15)	4.1
C(10)	−2547(5)	3474(3)	1086(6)	4.5	C(11)	6684(10)	2853(7)	1962(14)	3.8
C(11)	−1544(5)	1885(3)	−870(5)	3.4	C(12)	6811(13)	3618(9)	1950(21)	6.4
C(12)	−2382(5)	2153(3)	−2084(5)	4.0	C(13)	7931(13)	3835(11)	1707(22)	7.7
C(13)	−3209(6)	1717(4)	−3078(6)	5.0	C(14)	8860(12)	3287(11)	1641(18)	6.8
C(14)	−3219(7)	1004(4)	−2872(7)	5.5	C(15)	8741(13)	2558(11)	1704(18)	7.0
C(15)	−2402(7)	739(3)	−1670(8)	5.4	C(16)	7645(13)	2313(9)	1846(17)	5.5
C(16)	−1569(6)	1178(3)	−677(6)	4.5	C(17)	520(10)	2096(6)	−2993(14)	3.3
C(17)	955(5)	3299(3)	−2716(5)	3.5	C(18)	389(16)	1671(7)	−4416(18)	5.8
C(18)	−252(5)	3208(3)	−3725(5)	3.9	C(19)	−413(21)	1090(10)	−4813(22)	9.0
C(19)	−1044(6)	3785(4)	−4322(6)	5.2	C(20)	−988(17)	934(9)	−3747(23)	8.0
C(20)	−670(7)	4462(4)	−3925(7)	5.7	C(21)	−795(15)	1361(8)	−2335(19)	6.0
C(21)	530(8)	4571(3)	−2927(7)	5.8	C(22)	−46(12)	1924(7)	−1925(17)	4.9
C(22)	1328(6)	3996(3)	−2318(6)	4.6	C(23)	296(11)	3722(7)	−2717(19)	5.8
C(23)	1794(5)	1793(3)	−3160(5)	3.4	C(24A)	−835(24)	3722(13)	−3943(30)	4.1
C(24)	2773(5)	1572(3)	−3983(6)	4.1	C(25A)	−1699(26)	4377(14)	−4098(33)	4.7
C(25)	2547(7)	1030(3)	−5070(6)	5.1	C(26A)	−1635(25)	4913(14)	−3036(31)	4.4
C(26)	1328(8)	705(3)	−5394(7)	5.6	C(27A)	−729(30)	4794(16)	−1450(38)	5.8
C(27)	339(7)	922(4)	−4585(8)	5.7	C(28A)	306(26)	4215(14)	−1173(33)	4.6
C(28)	614(6)	1445(3)	−3451(6)	4.4	C(24B)	−580(31)	3828(16)	−2411(38)	5.9
O(01)1	5029(5)	1215(3)	−6878(6)	6.7	C(25B)	−1544(28)	4557(15)	−2639(35)	5.3
C(01)1	5785(13)	532(7)	−7127(15)	11.3	C(26B)	−1240(28)	5042(15)	−3607(35)	5.1
C(01)2	6680(17)	514(10)	−8036(20)	15.0	C(27B)	−336(30)	4990(16)	−3951(38)	6.1
O(02)1	4078(5)	3084(3)	5023(6)	7.2	C(28B)	470(31)	4319(16)	−3814(38)	6.0
C(02)1	3760(10)	3863(6)	5125(12)	9.0	Cl(01)[a]	8254(15)	295(8)	584(19)	5.6
C(02)2	4792(13)	4191(7)	6251(15)	11.7	Cl(02)	1254(16)	841(9)	1837(20)	5.3
					Cl(03)	5915(16)	1060(9)	−1879(20)	5.2
					Cl(04)	3237(20)	331(11)	−2251(26)	5.1
					Cl(05)	3783(25)	287(13)	−4965(32)	4.6

a) Population parameters of disordered Cl^- ion: Cl(01), 0.25; Cl(02), 0.23; Cl(03), 0.22; Cl(04), 0.17; and Cl(05), 0.13.

were introduced for all the non-hydrogen atoms except for the ethanol molecules in (A) and for the disordered Cl^- ion and a phenyl group in (B). The function, $\sum w||F_o|-|F_c||^2$ was minimized by block-diagonal least squares. Complex neutral-atom scattering factors were used.[4] The calculations were carried out on a FACOM M380-R computer at Keio University with the UNICS III computation program system.[5] The final atomic parameters and bond lengths and bond angles are listed in Tables 2 and 3.[6]

Results and Discussion

Preparation, Absorption and ^{13}C NMR Spectra of the Two Isomers of $[RhCl_2(edpp)_2]^+$. Rhodium(III) chloride was reacted with edpp in a 1:2 molar ratio in ethanol to form a mixture of two isomers of $[RhCl_2(edpp)_2]Cl$. The mixture was separated into the isomers A and B by fractional crystallization from ethanol. Isomer B is much less soluble in ethanol than isomer A. The relative abundance of isomer B to isomer A was ca. 1:10. No isomerization of the isomers took place on refluxing in ethanol.

Figure 2 shows the absorption spectra of isomers A and B together with that of *trans*(Cl,Cl),*cis*(P,P)-$[CoCl_2(edpp)_2]^+$.[1,2] The spectral pattern of isomer A is quite similar to that of *trans*(Cl,Cl),*cis*(P,P)-$[CoCl_2(edpp)_2]^+$, although all the bands of isomer A are shifted by 7000—10000 cm^{-1} toward higher energy compared to the corresponding bands of the cobalt(III) complex. Thus isomer A is suggested to have the trans-(Cl,Cl),cis(P,P) configuration. The same structure was

Table 3. Bond Lengths (l/Å) and Bond Angles (ϕ/°)

		(A)	(B)			(A)	(B)
Rh - Cl(1)		2.335(2)	2.358(4)	P(2) - Rh - N(2)		83.7(1)	83.5(3)
Rh - Cl(2)		2.338(2)	2.362(4)	N(1) - Rh - N(2)		87.3(2)	92.6(4)
Rh - P(1)		2.303(1)	2.334(3)	Rh - P(1) - C(1)		98.9(2)	101.1(4)
Rh - P(2)		2.297(1)	2.337(3)	Rh - P(1) - C(5)		120.3(2)	120.1(4)
Rh - N(1)		2.131(4)	2.076(9)	Rh - P(1) - C(11)		120.2(2)	117.2(5)
Rh - N(2)		2.118(4)	2.079(12)	C(1) - P(1) - C(5)		105.9(3)	106.4(6)
P(1) - C(1)		1.838(6)	1.814(13)	C(1) - P(1) - C(11)		106.7(3)	108.2(6)
P(1) - C(5)		1.814(5)	1.798(12)	C(5) - P(1) - C(11)		103.2(2)	103.0(6)
P(1) - C(11)		1.829(5)	1.806(14)	Rh - P(2) - C(3)		98.4(2)	98.6(6)
P(2) - C(3)		1.828(5)	1.800(18)	Rh - P(2) - C(17)		121.0(2)	117.0(4)
P(2) - C(17)		1.822(5)	1.822(12)	Rh - P(2) - C(23)		118.9(2)	121.9(4)
P(2) - C(23)		1.816(5)	1.815(12)	C(3) - P(2) - C(17)		107.3(2)	108.0(7)
N(1) - C(2)		1.477(7)	1.402(23)	C(3) - P(2) - C(23)		106.1(2)	106.1(7)
N(2) - C(4)		1.471(8)	1.461(14)	C(17) - P(2) - C(23)		103.6(2)	103.9(5)
C(1) - C(2)		1.485(8)	1.439(27)	Rh - N(1) - C(2)		113.4(3)	116.3(10)
C(3) - C(4)		1.529(8)	1.460(19)	Rh - N(2) - C(4)		115.5(3)	115.6(8)
C(5) - C(6)		1.389(9)	1.439(15)	P(1) - C(1) - C(2)		107.5(4)	110.8(12)
C(5) - C(10)		1.397(8)	1.405(16)	N(1) - C(2) - C(1)		109.3(4)	120.7(19)
C(6) - C(7)		1.393(8)	1.367(19)	P(2) - C(3) - C)4)		106.3(4)	109.6(10)
C(7) - C(8)		1.347(11)	1.380(21)	N(2) - C(4) - C(3)		108.0(5)	111.9(11)
C(8) - C(9)		1.374(11)	1.320(16)	P(1) - C(5) - C(6)		120.5(4)	120.7(8)
C(9) - C(10)		1.392(8)	1.432(18)	P(1) - C(5) - C(10)		120.1(4)	119.6(8)
C(11) - C(12)		1.397(7)	1.388(21)	C(6) - C(5) - C(10)		119.2(5)	119.8(10)
C(11) - C(16)		1.376(8)	1.383(19)	C(5) - C(6) - C(7)		120.1(6)	118.1(12)
C(12) - C(13)		1.378(8)	1.468(26)	C(6) - C(7) - C(8)		120.7(6)	122.8(12)
C(13) - C(14)		1.388(11)	1.353(23)	C(7) - C(8) - C(9)		119.8(6)	119.2(12)
C(14) - C(15)		1.378(9)	1.329(28)	C(8) - C(9) - C(10)		121.4(6)	123.3(12)
C(15) - C(16)		1.383(8)	1.420(25)	C(5) - C(10) - C(9)		118.6(6)	116.8(10)
C(17) - C(18)		1.382(6)	1.355(18)	P(1) - C(11) - C(12)		119.4(4)	115.4(10)
C(17) - C(22)		1.395(8)	1.390(22)	P(1) - C(11) - C(16)		121.8(4)	124.8(11)
C(18) - C(19)		1.369(8)	1.396(26)	C(12) - C(11) - C(16)		118.8(5)	119.7(13)
C(19) - C(20)		1.360(11)	1.386(34)	C(11) - C(12) - C(13)		120.7(5)	119.0(14)
C(20) - C(21)		1.377(9)	1.339(24)	C(12) - C(13) - C(14)		119.9(6)	118.9(17)
C(21) - C(22)		1.373(8)	1.331(21)	C(13) - C(14) - C(15)		119.6(6)	121.2(17)
C(23) - C(24)		1.405(8)		C(14) - C(15) - C(16)		120.4(6)	122.2(16)
C(23) - C(28)		1.381(8)		C(11) - C(16) - C(15)		120.7(5)	118.8(14)
C(24) - C(25)		1.376(8)		P(2) - C(17) - C(18)		122.3(4)	121.3(11)
C(25) - C(26)		1.390(10)		P(2) - C(17) - C(22)		119.6(4)	117.4(10)
C(26) - C(27)		1.403(11)		C(18) - C(17) - C(22)		117.9(5)	121.2(12)
C(27) - C(28)		1.387(9)		C(17) - C(18) - C(19)		120.8(5)	116.9(17)
Cl(1) - Rh - Cl(2)		172.1(1)	95.2(1)	C(18) - C(19) - C(20)		120.8(5)	121.0(17)
Cl(1) - Rh - P(1)		88.7(1)	93.6(1)	C(19) - C(20) - C(21)		119.9(7)	119.3(18)
Cl(1) - Rh - P(2)		95.0(1)	87.6(1)	C(20) - C(21) - C(22)		119.7(6)	121.2(18)
Cl(1) - Rh - N(1)		88.0(1)	177.1(3)	C(17) - C(22) - C(21)		120.9(5)	120.2(13)
Cl(1) - Rh - N(2)		87.0(1)	86.6(3)	P(2) - C(23) - C(24)		121.8(4)	
Cl(2) - Rh - P(1)		95.7(1)	92.0(1)	P(2) - C(23) - C(28)		119.6(4)	
Cl(2) - Rh - P(2)		90.2(1)	93.5(1)	C(24) - C(23) - C(28)		118.5(5)	
Cl(2) - Rh - N(1)		86.0(1)	85.7(3)	C(23) - C(24) - C(25)		120.7(5)	
Cl(2) - Rh - N(2)		87.5(1)	176.4(3)	C(24) - C(25) - C(26)		120.4(6)	
P(1) - Rh - P(2)		105.4(1)	174.1(1)	C(25) - C(26) - C(27)		119.6(6)	
P(1) - Rh - N(1)		83.9(1)	83.6(3)	C(26) - C(27) - C(28)		119.2(7)	
P(1) - Rh - N(2)		170.3(1)	90.9(3)	C(23) - C(28) - C(27)		121.5(6)	
P(2) - Rh - N(1)		170.3(1)	95.1(3)				

suggested by the ^{13}C NMR spectrum, and the assignment was confirmed by the X-ray structure determination (vide infra). The lowest-energy absorption band at 24450 cm^{-1} of isomer A can be assigned to the split component (I_a) of the first absorption band, $^1A_{1g} \rightarrow {}^1T_{1g}$ (O_h). The band is at higher energy by 8550 cm^{-1} than the I_a band of the cobalt(III) complex. A similar energy difference (8550 cm^{-1}) is observed between the I_a bands of *trans*-$[RhCl_2(en)_2]^+$[7] and *trans*-$[CoCl_2(en)_2]^+$[8] (en=ethylenediamine). The *trans*-dichloro rhodium(III) complexes of dppe[9] (dppe=1,2-bis(diphenylphosphino)ethane) and en[7] show the I_a band at 23700 and 24600 cm^{-1}, respectively. Thus the spectrochemical series for the ligands can be determined as en≧edpp> dppe. The same order, en≧edpp has been reported for the *trans*-dichloro cobalt(III) complexes.[1,2] The spectral data of *trans*-$[CoCl_2(dppe)_2]^+$ is not available; the complex is reported to be extremely unstable.[10] However, dppe forms a stable cobalt(III) complex with two acac ligands (acac=2,4-pentanedionate ion). The

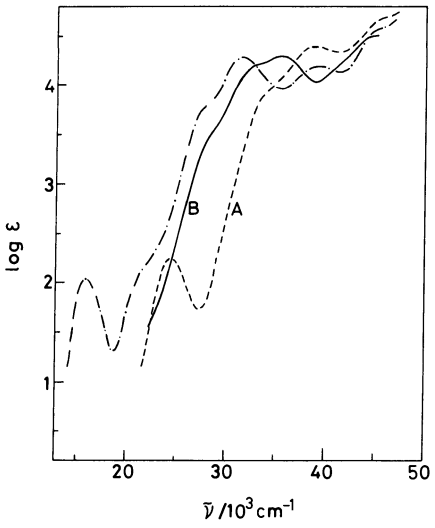

Fig. 2. Absorption spectra of *trans*(Cl,Cl), *cis*(P,P)-$[RhCl_2(edpp)_2]Cl \cdot 2C_2H_5OH$ (isomer A) in ethanol (---), *cis*(Cl,Cl), *trans*(P,P)-$[RhCl_2(edpp)_2]Cl \cdot H_2O$ (isomer B) in acetonitrile (——), and *trans*(Cl,Cl), *cis*(P,P)-$[CoCl_2(edpp)_2]Cl \cdot 2H_2O$ in methanol (—·—).

energy of the first absorption band of $[Co(acac)_2L]^+$ (L=dppe, edpp, en) decreases in the order dppe> edpp≧en.[11] This order is reversed to that for the *trans*-dichloro complexes. The apparent disagreement in the order may be ascribed to the difference in steric repulsion among the complexes. Examination of molecular models indicates that severe steric repulsions occur in *trans*-$[MCl_2(dppe)_2]^+$ (M=Co, Rh), whereas $[Co(acac)_2(dppe)]^+$ has no particular steric repulsions. In the absence of severe steric repulsions, therefore, it is apparent that the ranking of dppe in the spectrochemical series is higher than that of en. The I_b band of isomer A is observed as a shoulder (ca. 29000 cm^{-1}) and the second absorption band is hidden by the strong charge-transfer (CT) bands.

The first d-d absorption band of isomer B is almost hidden by strong bands in the higher energy region. However, the shoulder at ca. 28000 cm^{-1} can be assigned to a part of the first absorption band, since *cis*-$[RhCl_2(en)_2]^+$ shows the first d-d band maximum at nearly the same wavenumber (28400 cm^{-1}).[7] The shoulder of isomer B is at higher energy than that of the I_a band of isomer A. These positions correspond well to those of the lowest energy d-d transition bands of the cis (28800 cm^{-1}) and trans (24500 cm^{-1}) isomers of $[RhCl_2(dmpe)_2]^+$ [9] (dmpe=1,2-bis(dimethylphosphino)-ethane). From these results isomer B is suggested to have a cis(Cl,Cl) configuration. The first absorption band of isomer B is more intense than that of isomer A. Similar trends where cis-isomers exhibit more intense absorption bands than the corresponding trans-isomers were observed between the cis- and trans-isomers of $[RhX_2(en)_2]^+$ [7] (X=Cl, Br, I, etc.) and $[RhCl_2(dmpe)_2]^+$.[9] The bands around 33000 cm^{-1} in the absorption spectrum of isomer B may be assigned to a CT transition Rh^{III}–P.[10] Since the bands are at lower energy than the corresponding band of isomer A, isomer B would be assigned to have a trans(P,P) configuration. The trans(P,P) isomer of a bis(phosphine) cobalt(III) complex is reported to exhibit the Co^{III}–P CT band at lower energy than the corresponding cis(P,P) isomer.[12,13] Similar absorption spectral characteristics to those of isomers B and A have been observed for *cis*(NCS,NCS),*trans*(P,P)- and *trans*(NCS,NCS),*cis*(P,P)-$[Co(NCS)_2(edpp)_2]^+$.[14]

Figure 3 shows the ^{13}C NMR spectra of isomers A and B in dimethyl-d_6 sulfoxide. The spectral assignment was made according to previous work on bis(acac) cobalt(III) complexes of edpp and related ligands.[11] The mutual arrangement of the two chlorine donor atoms can be assigned on the basis of the number of the resonances. Isomer A exhibits six kinds of signals and can be assigned to either of the two trans(Cl,Cl) isomers (Figs. 1 and 3). This assignment is in accord with that given on the basis of the absorption spectrum. The spectrum of isomer B shows one kind of signal for each carbon of the two methylenes of the edpp ligands, while the two phenyl groups on each phosphorus atom are observed diastereotopically. Thus isomer B is suggested to have either cis(Cl,Cl),trans(P,P)(C_2) or cis(Cl,Cl),cis(P,P)(C_2) configuration from symmetry argument. One of the most noticeable aspects in the two spectra is the difference in line shape of the P–CH_2 and P–C_1 signals; the signals for isomer B appear as a 1:2:1 triplet, while those for isomer A as a five-line multiplet. Such differences can be explained on the basis of the difference in magnitude of the phosphorus–phosphorus coupling constant, $^2J_{PP}$ between the two isomers. The appearance of the phosphine α-carbon multiplet in the ^{13}C NMR spectrum of a bis(phosphine) complex has been shown to be a function of $^2J_{PP}$.[15,16] In a trans(P,P) complex $^2J_{PP}$ is usually large so that the signal appears as a 1:2:1 triplet (so-called virtually coupled triplet). On the other hand, a five-line multiplet is expected to appear only for a cis(P,P) complex. Hence isomers B and A can be assigned to cis(Cl,Cl),trans(P,P), and trans(Cl,Cl),cis-(P,P), respectively. These assignments are confirmed by the X-ray analyses.

Structures of (A) and (B). Figure 4 shows perspective drawings of the complex cations (A) and (B). The main product, (A) is the trans(Cl,Cl),cis(P,P) isomer. The lesser product, (B) is the cis(Cl,Cl),trans(P,P) isomer. The structures agree with the assignments based on the ^{13}C NMR and absorption spectra. Both complex cations have a pseudo twofold axis running through the Rh atom and the midpoint of the N(1) and N(2) atoms. The trans influence of the P atom on the Rh–N and Rh–P bond lengths is seen from Table 3. The mean Rh–N bond length, 2.125(4)Å, in (A) is longer than that in (B) by 0.047(12)Å. The mean Rh–P bond length, 2.336(3)Å, in (B) is longer than that in (A) by 0.036(3)Å. It is noted that the mean Co–P

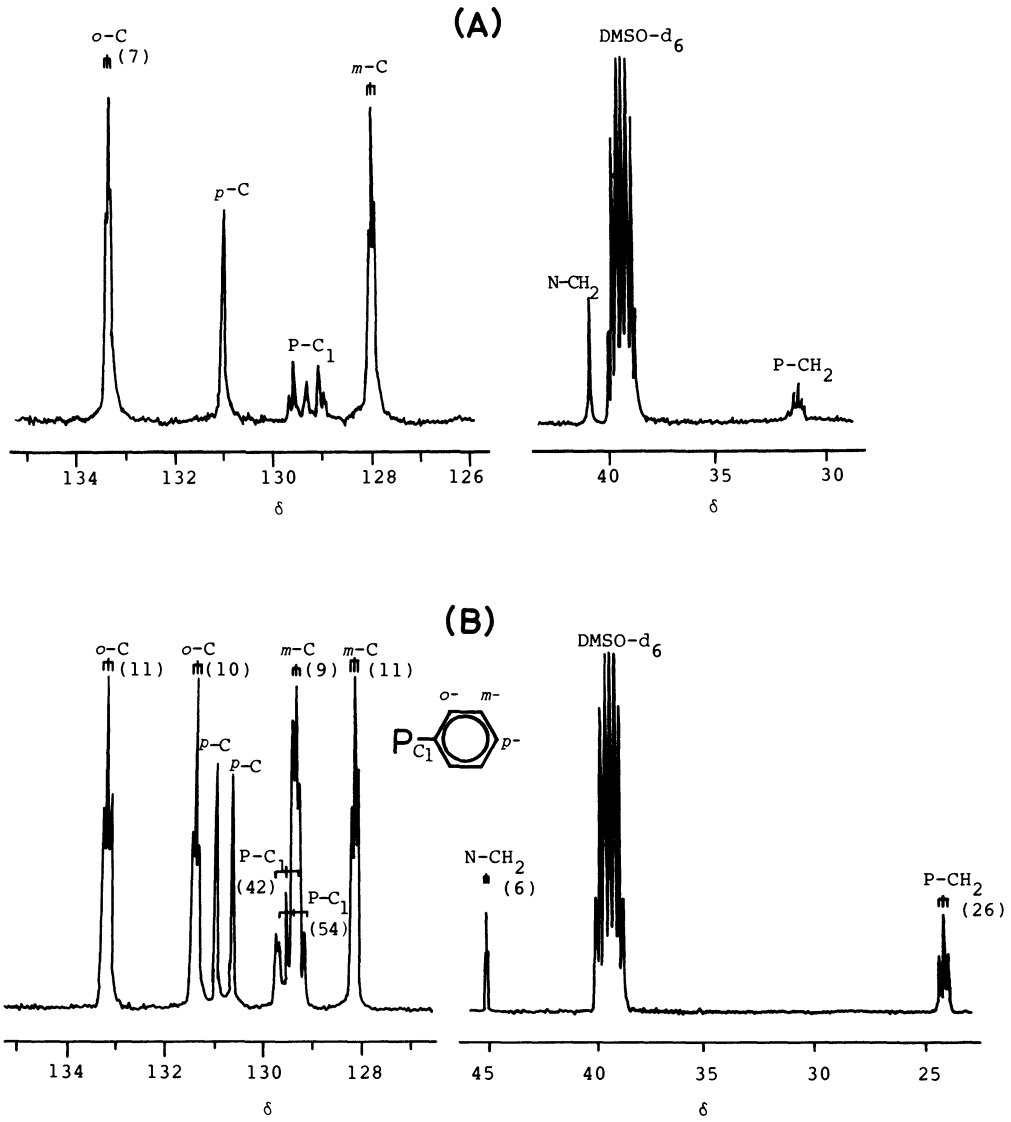

Fig. 3. ^{13}C NMR spectra of (A) *trans*(Cl,Cl), *cis*(P,P) (isomer A)- and (B) *cis*(Cl,Cl), *trans*(P,P) (isomer B)- $[RhCl_2(edpp)_2]^+$ in dimethyl-d_6 sulfoxide. The numbers in parentheses are the coupling constants in Hz of the triplet signals.

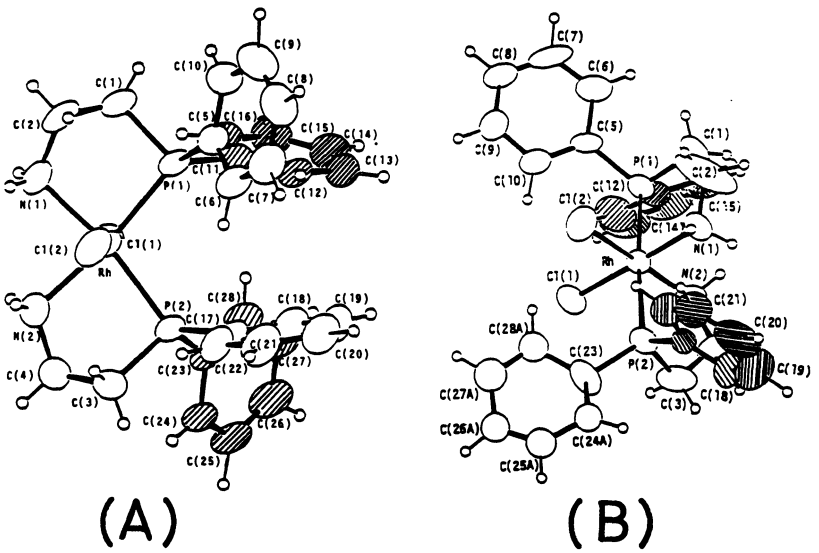

Fig. 4. Molecular structures of (A) and (B). Some of the phenyl rings are shaded for clarity.

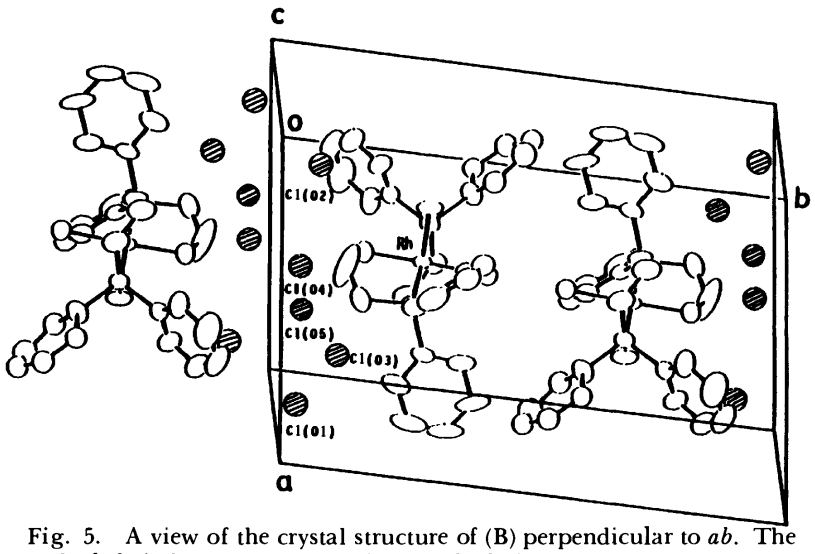

Fig. 5. A view of the crystal structure of (B) perpendicular to *ab*. The shaded circles represent the disordered Cl^- ion.

bond length in the trans(NCS,NCS),cis(P,P) isomer of $[Co(NCS)_2(edpp)_2]^+$ is almost the same as that in the cis(NCS,NCS),trans(P,P) isomer, although the mean Co–NH_2 bond length in the former is longer than that in the latter by 0.031(4) Å.[14] The molecular structure of (A) is essentially the same as that of the corresponding cobalt(III) complex.[2] The mean M–Cl and M–N bond lengths in (A) are longer than those in the cobalt(III) complex by ca. 0.10 Å.[2] On the other hand, the mean M–P bond length in (A) is longer than that in the cobalt(III) complex only by 0.045(3) Å. These results may indicate a stronger affinity of Rh^{3+} for P than Co^{3+} for P.

The close contact between the phenyl groups in (A) is avoided by the large P(1)–Rh–P(2) angle, 105.4(1)° and the appropriate orientations of the phenyl groups. The shortest non-bonded C···C distance is 3.516(8) Å for C(6)···C(17). The angle between the two coordination planes through Rh, N(1) and P(1), and through Rh, N(2) and P(2) atoms is 5.1°. The large thermal parameter of C(2) in (B) may be due to the puckering motion of the five-membered chelate ring. The crystal structure of (B) is shown in Fig. 5. The Cl^- ions are distributed over five sets of general positions with different population parameters and are between the layers of complex cations parallel to the *ac* plane; the shortest interatomic distance involving them is 3.04(2) Å for Cl(04)···N(1). Water molecules, which were not included in the structure refinement, might also be accommodated randomly in the hollow. The positional disorder of counter ions was also reported for $[Co\{(NH_2CH_2CH_2)_2NCH_2CH_2N(CH_2CH_2NH_2)_2\}]Br_3 \cdot H_2O$.[17]

Acknowledgement is made to Japan Society for the Promotion of Science for providing generous fellowship support for F. G. to work as a guest researcher at Nagoya University.

References

1) M. Atoh, I. Kinoshita, K. Kashiwabara, and J. Fujita, *Bull. Chem. Soc. Jpn.*, **55**, 3179 (1982).

2) I. Kinoshita, Y. Yokota, K. Matsumoto, S. Ooi, K. Kashiwabara, and J. Fujita, *Bull. Chem. Soc. Jpn.*, **56**, 1067 (1983).

3) K. Issleib and D. Haferburg, *Z. Naturforsch., B*, **20**, 916 (1965).

4) International Tables for X-ray Crystallography (1974). Vol. IV. Birmingham: Kynoch Press. (Present Distributor D. Reidel, Dordrecht.)

5) T. Sakurai and K. Kobayashi, *Rikagaku Kenkyusho Hokoku*, **55**, 69 (1979).

6) Tables of the coordinates of hydrogen atoms, the anisotropic thermal parameters of the non-hydrogen atoms, bond lengths and bond angles in the disordered phenyl group, and observed and calculated structure factors are kept as Document No. 8629 at the Chemical Society of Japan.

7) S. A. Johnson and F. Basolo, *Inorg. Chem.*, 1, 925 (1962).

8) M. Linhard and M. Weigel, *Z. Anorg. Chem.*, **271**, 101 (1952); Y. Shimura and R. Tsuchida, *Bull. Chem. Soc. Jpn.*, **28**, 572 (1955); M. Nakahara and M. Mitsuya, *ibid.*, **45**, 2209 (1972).

9) S. A. Butter and J. Chatt, *J. Chem. Soc. (A)*, **1970**, 1411.

10) V. M. Miskowski, J. L. Robbins, G. S. Hammond, and H. B. Gray, *J. Am. Chem. Soc.*, **98**, 2477 (1978).

11) K. Kashiwabara, I. Kinoshita, T. Ito, and J. Fujita, *Bull. Chem. Soc. Jpn.*, **54**, 725 (1981).

12) K. Kashiwabara, K. Katoh, T. Ohishi, J. Fujita, and M. Shibata, *Bull. Chem. Soc. Jpn.*, **55**, 149 (1982).

13) K. Katoh, H. Sugiura, K. Kashiwabara, and J. Fujita, *Bull. Chem. Soc. Jpn.*, **57**, 3580 (1984).

14) M. Atoh, K. Kashiwabara, H. Ito, T. Ito, and J. Fujita, *Bull. Chem. Soc. Jpn.*, **57**, 3139 (1984).

15) D. A. Redfield, L. W. Cary, and J. H. Nelson, *Inorg. Chem.*, **14**, 50 (1975).

16) P. S. Pregosin and R. W. Kunz," ^{31}P and ^{13}C NMR of Transition Metal Phosphine Complexes," Springer-Verlag, New York (1979), p. 65.

17) T. Ishii, S. Ohba, M. Ito, S. Fukushi, and Y. Saito, *Bull. Chem. Soc. Jpn.*, **58**, 826 (1985).

 © 1986 The Chemical Society of Japan Bull. Chem. Soc. Jpn., 59, 1709—1712 (1986)

Kinetic and Mechanistic Investigations of the Reduction by Radicals of Nitro to Hydroxyamino Groups in a Cobalt(III) Cage Compound

Keiichi TSUKAHARA
Department of Chemistry, Faculty of Science, Shimane University, 1060
Nishikawatsu-cho, Matsue, Shimane 690
(Received January 20, 1986)

A compound containing both a hydroxyamino and a nitro group in a cobalt(III) cage complex was detected and isolated in a $DQ^{\dagger}$ (1,1′-ethylene-2,2′-bipyridinium radical cation) reduction of the corresponding symmetric dinitro compound, $[Co(diNOsar)]^{3+}$ (diNOsar=1,8-dinitro-3,6,10,13,16,19-hexaazabicyclo[6.6.6]icosane). The nitro group of this compound was reduced to the hydroxyamino group by SO_2^-, $MDQ^{\dagger}$ (1,1′-ethylene-4,4′-dimethyl-2,2′-bipyridinium radical cation), and $PDQ^{\dagger}$ (1,1′-trimethylene-2,2′-bipyridinium radical cation). Rate constants for the various processes were obtained.

Sargeson et al.[1,2] have synthesized and developed the chemistry of a large number of macrocyclic metal cage compounds. The cobalt(III) cage complex containing two nitro groups $[Co(diNOsar)]^{3+}$ (**1**, X=Y=NO_2)[3] has interesting and unique redox properties. Compounds in various states of reduction between nitro and amino groups have been prepared by reductions with electrodes,[4] zinc dust,[1] and dithionite.[5] When the dithionite ion is used in excess, $[Co^{III}(diNOsar)]^{3+}$ is reduced to $[Co^{II}(diNOsar)]^{2+}$ and the latter is then followed by a reduction of the nitro to hydroxyamino groups with a concomitant oxidation of cobalt(II) to cobalt(III):[5]

$$[Co^{III}(diNOsar)]^{3+} \xrightarrow{e^-} [Co^{II}(diNOsar)]^{2+} \quad (1)$$

$$[Co^{II}(diNOsar)]^{2+} \xrightarrow{7e^-} [Co^{III}(diHAsar)]^{3+} \quad (2)$$

Dithionite ion is a very strong reductant of the formal redox potential −0.66 V at pH 7.[6] If we choose various reductants,[7] DQ^+ (**2a**, $E°=-0.35$ V), MDQ^+ (**2b**, −0.49 V), and PDQ^+ (**2c**, −0.55 V), it would be possible to obtain an intermediate compound in the formation process of $[Co^{III}(diHAsar)]^{3+}$ (**1**, X=Y=NHOH) from $[Co^{III}(diNOsar)]^{3+}$. Therefore, we decided to study the kinetics and to examine the products of this interesting reaction using the above radicals as well as SO_2^- ions which are effective reductants from dithionite ions. The kinetics of a one-electron reduction of $[Co(diNOsar)]^{3+}$ with viologen radicals as in Reaction 1 were reported previously.[8]

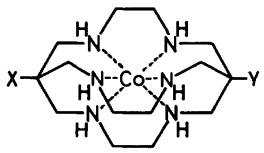

1

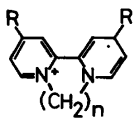

2a $DQ^{\dagger}$ (n=2, R=H)
2b $MDQ^{\dagger}$ (n=2, R=CH_3)
2c $PDQ^{\dagger}$ (n=3, R=H)

Fig. 1.

Experimental

Materials. $[Co(diNOsar)](ClO_4)_3 \cdot H_2O$ was prepared as described previously.[5,9] Its absorption spectrum in water (λ_{max}=474 nm (ε=159 $M^{-1}cm^{-1}$) and λ_{max}=345 nm (ε=128 $M^{-1}cm^{-1}$)) was in agreement with that described in the literature.[5] 1,1′-Ethylene-2,2′-bipyridinium dibromide, $(DQ)Br_2$, was obtained from Chemical Services. 1,1′-Ethylene-4,4′-dimethyl-2,2′-bipyridinium dibromide hydrate, $(MDQ)Br_2 \cdot H_2O$, and 1,1′-trimethylene-2,2′-bipyridinium dibromide hydrate, $(PDQ)Br_2 \cdot H_2O$, were prepared by the method of Homer and Tomlinson.[10] The other chemicals used were the purest commercial products. The viologen radicals (DQ^+, MDQ^+, and PDQ^+) were prepared by adding 0.95 equivalent of sodium dithionite to the oxidized viologens (DQ^{2+}, MDQ^{2+}, and PDQ^{2+}). $[Co(sep)]^{2+}$ was generated in situ by Zn/Hg reduction of $[Co(sep)]^{3+}$.[11] Aquapentacyanoferrate(II), $[Fe(CN)_5H_2O]^{3-}$, was prepared in situ by dissolving $Na_3[Fe(CN)_5NH_3]$ in water.

Kinetics. All kinetic measurements were carried out using a Gibson-Dionex stopped-flow spectrophotometer interfaced with an OLIS data-collecting system. The reactions with viologen radicals were followed by the loss of the radical at 760 nm, 25 °C, an ionic strength (I) of 0.50 M (1 M=1 mol dm^{-3}) with Na_2SO_4, and pH=7.8—8.2 (Tris-H_2SO_4 buffer, Tris=tris(hydroxymethyl)aminomethane) in an argon atmosphere. The molar absorption coefficients used were $\varepsilon_{760}=2.7\times10^3$ $M^{-1}cm^{-1}$ (DQ^+) and $\varepsilon_{760}=2.9\times10^3$ $M^{-1}cm^{-1}$ (MDQ^+).[7] The viologen radical (6.0×10^{-5}—2.9×10^{-4} M) was used in excess over the cobalt(III) complex (1.0×10^{-5}—5.0×10^{-5} M). Dithionite reductions were carried out at pH 6.3 (0.1 M MES buffer, MES=2-(*N*-morpholino)-ethane sulfonic acid) and pH 10.8 (0.02 M borate buffer), at 25 °C and I=0.50 M (Na_2SO_4). The cobalt(III) complex decomposed slowly at pH 10.8; therefore, neutral solutions of cobalt(III) complex in Na_2SO_4 were mixed with dithionite solutions at pH 11.1 (0.04 M borate buffer). The reactions were followed at the absorption maximum 505 nm of this complex at pH 10.8. Dithionite (5.0×10^{-3}—4.0×10^{-2} M) was used in excess over cobalt(III) complex (3.0×10^{-4}—5.0×10^{-4} M).

Product Analyses. Viologen radicals and dithionite ion

were used in five-to fifteen-fold excess over the cobalt(III) complex (1×10^{-4}—5×10^{-4} M). After the reactions were quenched by introducing air (reaction time was about half an hour at room temperature), the solutions were poured onto a CM-Sephadex C-25 (Na^+ form) column. The column was washed with water and the products were separated using different concentrations of NaCl solutions. Spectral measurements were carried out using a Cary 14 spectrophotometer and a Hitachi 260-50 IR spectrophotometer. Cyclic voltammetry was carried out in an argon atmosphere in an aqueous Tris-H_2SO_4 buffer (pH 7.8) with a BAS Model CV-1B Instrument. A three-electrode system was composed of a Pt auxiliary electrode and a Pt working electrode against a Ag/AgCl (3 M NaCl) reference electrode. Voltammograms were recorded on a Houston Instruments Omnigraphic 100 X-Y recorder at scan rate of 20—200 mV s^{-1}.

Results and Discussion

Product Analyses. When a viologen radical was mixed with $[Co(diNOsar)]^{3+}$, Reaction 1 was observed, being followed by a slow process. Stoichiometry determinations and kinetics were carried out on the MDQ^+ system where the slow process was sufficiently fast to be followed before an occurrence of a spontaneous decay of MDQ^+. Stoichiometric titrations monitored at an MDQ^+ radical peak showed $[MDQ^+]/[Co(III)]=8.0\pm0.1$ for the overall reaction; therefore a 7:1 stoichiometry was required for the second stage. The same result was obtained from the absorbance change in stopped-flow traces during the reaction; the ratio of the amplitude for the second stage and the first stage was 7.0±0.2 at 760 nm. The same stoichiometry was obtained in the PDQ^+ reduction.

When an excess of MDQ^+ was used over the cobalt(III) complex (at least 15 times), three products were separated on a Shephadex column. A pale-green species was eluted with a 0.1 M NaCl solution and was identified as MDQ^{2+}. A trace amount of a yellow species was eluted with a 0.4 M NaCl solution, but was not identified. A third orange species was eluted with a 0.5 M NaCl solution and was identified as $[Co(diHAsar)]^{3+}$ (>90%).

In the DQ^+ system the slow process could not be followed due to a spontanious decay of this radical. When an excess of DQ^+ was used over the cobalt(III) complex (ten times), four products were separated on the column. The first, a yellow species, was eluted with a 0.05 M NaCl solution and was found to be an air-oxidation product of DQ^+ (λ_{max}=419 nm), the yellow color being faded gradually. The same phenomenon has been reported in the O_2 oxidation of DQ^+ in methanol.[12] This is not the same species as that which arises from the oxidation of DQ^+ by hydrogen peroxide (λ_{max}=453 nm at pH 8). We have not identified these species. The second, a pale-brown species, was eluted with a 0.2 M NaCl solution and identified as DQ^{2+} which results from the oxidation of DQ^+ by cobalt(III). The third, an orange species,was eluted with a 0.4 M NaCl solution and identified as $[Co(diHAsar)]^{3+}$. It was isolated as a hydrogen chloride salt when it was eluted with 1 M HCl, evaporated to dryness, and washed with acetone. The IR spectrum showed the absence of an $-NO_2$ group. The fourth, an orange species, was eluted with a 0.5 M NaCl solution. The absorption spectrum in water has a λ_{max}=473 nm ($\varepsilon=150\pm20$ $M^{-1}cm^{-1}$) and there was no absorption maximum near 340 nm. It was isolated as a hydrogen chloride salt and its IR spectrum showed the presence of an $-NO_2$ group (1550 and 1350 cm^{-1}). From these results the fourth species was identified as $[Co(HANOsar)]^{3+}$ which contains a hydroxyamino and a nitro group (**1**, X=NHOH, Y=NO_2; analytical data for a hydrogen chloride salt, Found: C, 26.75; H, 6.10; N, 17.38%. Calcd for $[Co(C_{14}H_{33}O_3N_8)]Cl_4\cdot4H_2O$: C, 26.51; H, 6.53; N, 17.67%).

When a five-fold excess of DQ^+ was used over the cobalt(III) complex, an additional orange species was found on the top of the column. This was eluted with a 0.5 M NaCl solution and identified as the starting material, $[Co(diNOsar)]^{3+}$, by the IR and absorption spectra. This was easily recovered as a perchlorate salt.

These cobalt(III) complexes were also distinguished from each other using $[Fe(CN)_5H_2O]^{3-}$; with $[Co(diNOsar)]^{3+}$ a brown material, insoluble in water, is formed and with $[Co(diHAsar)]^{3+}$ a violet material is precipitated. Analytical data for the latter show the formula, $[Co(diHAsar)Fe(CN)_5]\cdot4H_2O$ (Found: C, 33.78; H, 5.62; N, 28.08%. Calcd: C, 34.39; H, 6.39; N, 27.45%). The IR spectrum shows the presence of -CN groups (2050 and 1620 cm^{-1}). $[Co(HANOsar)]^{3+}$ reacted with $[Fe(CN)_5H_2O]^{3-}$ to form a reddish violet species soluble in water (λ_{max}=490 nm). The absence of a nitroso group in $[Co(HANOsar)]^{3+}$ was confirmed by a Liebermann reaction[13] in which nitroso groups react with phenol to form deep-red species in sulfuric acid. These three complexes were also characterized by cyclic voltammetry. $[Co(diNOsar)]^{3+}$ and $[Co(diHAsar)]^{3+}$ showed quasi-reversible one-electron waves at +0.0 and −0.26 V vs. NHE, respectively. $[Co(HANOsar)]^{3+}$ showed a one-electron wave near −0.1 V, intermediate between those of $[Co(diNOsar)]^{3+}$ and $[Co(diHAsar)]^{3+}$. These values are in good agreement with those found in the literature.[4]

$[Co(sep)]^{2+}$ was also used as a reductant, its redox potential (−0.30 V) is slightly higher than that of DQ^+. When a five-fold excess of $[Co(sep)]^{2+}$ was used over $[Co(diNOsar)]^{3+}$, three orange species were separated on the column; these were identified as $[Co(sep)]^{3+}$, $[Co(HANOsar)]^{3+}$, and $[Co(diNOsar)]^{3+}$.

$[Co(HANOsar)]^{3+}$ was further reduced by MDQ^+ and dithionite. Two reactions were monitored in the dithionite reduction—a decrease in absorbance followed by an increase in absorbance at 480 nm. Stoichiometric titrations at 760 nm with MDQ^+ showed $[MDQ^+]/[Co(III)]=4.0\pm0.1$. This is in agreement with the $3e^-$ reduction for the second stage in which

Table 1. Rate Constants for Reduction of [Co(diNOsar)]$^{3+}$ by Dithionite at pH 10.8[a]

$[S_2O_4^{2-}]_0/10^{-3}$ M	First Stage[b] k_{obsd}/s^{-1}	Second Stage[c] k_{obsd}/s^{-1}	Third Stage $k_{obsd}/10^{-3}$ s^{-1}
7.0	0.91	0.042	1.3
14.3	1.30	0.073	1.9
20.0	1.61	0.083	2.2
30.0	1.90	0.108	2.1
40.0	1.89	0.129	2.1

a) 25 °C, I=0.50 M (Na_2SO_4), $[Co(III)]_0=5.0\times10^{-4}$ M, and λ=505 nm. b) Plots of k_{obsd} vs. $[S_2O_4^{2-}]_0^{1/2}$ were linear with zero intercept and k_1 was obtained as $(2.9\pm0.2)\times10^5$ M^{-1}s^{-1} using $K_d=1.4\times10^{-9}$ M^{-1} for the dissociation of $S_2O_4^{2-}$ to SO_2^-. D. O. Lambeth and G. Palmer, *J. Biol. Chem.*, **248**, 6095 (1973). c) Plots of k_{obsd} vs. $[S_2O_4^{2-}]_0^{1/2}$ were linear with zero intercept and k_2 was obtained as $(1.6\pm0.2)\times10^4$ M^{-1}s^{-1}.

[Co(diHAsar)]$^{3+}$ was produced.

When dithionite was used at pH 10.8 with [Co(diNOsar)]$^{3+}$, only [Co(diHAsar)]$^{3+}$ was produced. There was no evidence of further reductions of hydroxyamino to amino groups.

From the above observations it is considered that the following reactions occur successively after Reaction 1:

$$[Co^{II}(diNOsar)]^{2+} \xrightarrow{3e^-} [Co^{III}(HANOsar)]^{3+} \quad (3)$$

$$[Co^{III}(HANOsar)]^{3+} \xrightarrow{e^-} [Co^{II}(HANOsar)]^{2+} \quad (4)$$

$$[Co^{II}(HANOsar)]^{2+} \xrightarrow{3e^-} [Co^{III}(diHAsar)]^{3+} \quad (5)$$

Kinetics. Balahura et al.[5] have examined the dithionite reduction of [Co(diNOsar)]$^{3+}$ at pH 6.3. We have also measured this system at pH 10.8 and obtained similar results for the first and second stages (Table 1). A third very slow reaction, whose rate was independent of the concentrations of dithionite, may represent the decomposition of the cobalt(III) complex. The second-order rate constants are $(2.9\pm0.2)\times10^5$ M^{-1}s^{-1} (3.5×10^5 M^{-1}s^{-1} at pH 6.3[5]) for Reaction 1 and $(1.6\pm0.2)\times10^4$ M^{-1}s^{-1} (1.6×10^4 M^{-1}s^{-1} at pH 6.3[5]) for Reaction 2. This result is surprising because it is known that [Co(diNOsar)]$^{3+}$ is converted to a deprotonated species [Co(diNOsar-H)]$^{2+}$ (pK_a=8.85)[8] whose redox potential for the Co(III)/Co(II) couple shifts to a more negative value.[14] The rate-determining step of the reduction of the nitro to hydroxyamino groups in the cobalt(II) complex does not require hydrogen ions.

Dithionite reduction of [Co(HANOsar)]$^{3+}$ was carried out at pH 6.3 (0.1 M MES buffer), 25 °C and I=0.50 M (Na_2SO_4). The rate constants obtained are $k_4=(2.1\pm0.4)\times10^5$ M^{-1}s^{-1} for Reaction 4 and $k_5=(8.4\pm0.6)\times10^3$ M^{-1}s^{-1} for Reaction 5 (Table 2). Rates for Reactions 3 and 5 in the dithionite system are obviously comparable, suggesting that the attack of an electron on the $-NO_2$ group is rate determining and that the following intramolecular electron-transfer reactions and further reductions of nitroso groups are very fast ($\lessdot\gtrdot$ denotes sar),

Table 2. Rate Constants for Reduction of [Co(HANOsar)]$^{3+}$ by Dithionite[a]

$[S_2O_4^{2-}]_0/10^{-3}$ M	First Stage[b] k_{obsd}/s^{-1}	Second Stage[c] k_{obsd}/s^{-1}
5.0	0.68	0.022
10.0	0.72	0.030
20.0	1.4	0.046
30.0	1.6	0.053

a) 25 °C, I=0.50 M (Na_2SO_4), pH 6.3 (0.1 M MES buffer), $[Co(III)]_0=3.0\times10^{-4}$ M, and λ=480 nm. b) Plots of k_{obsd} vs. $[S_2O_4^{2-}]_0^{1/2}$ were linear with zero intercept and k_4 was obtained as $(2.1\pm0.4)\times10^5$ M^{-1}s^{-1} for the SO_2^- reduction. c) Plots of k_{obsd} vs. $[S_2O_4^{2-}]_0^{1/2}$ were linear with zero intercept and k_5 was obtained as $(8.4\pm0.6)\times10^3$ M^{-1}s^{-1} for the SO_2^- reducion.

Table 3. Rate Constants for Reduction of [Co(diNOsar)]$^{2+}$ and [Co(HANOsar)]$^{2+}$ by MDQ$^+$

$[Co(III)]_0$	$[MDQ^+]_0$	k_{obsd}	k_2 or k_5
10^{-6} M	10^{-4} M	s^{-1}	10^4 M^{-1}s^{-1}
[Co(diNOsar)]$^{2+}$			
10	1.03	—	1.36[b]
10	1.50	—	1.13[b]
[Co(HANOsar)]$^{2+}$			
2	0.90	1.28	1.4
2	1.30	3.05	2.3
2	1.50	3.96	2.6
17	1.43	—	1.7[c]

a) 25 °C, I=0.50 M (Na_2SO_4), pH 7.8 (0.1 M Tris-H_2SO_4 buffer) and λ=760 nm. b) Obtained from plots of $\ln[A_t/(A_t-A_\infty)]$ vs. t (Eq. 8). c) Obtained from plots of $\ln[A_t/(A_t-A_\infty)]$ vs. t (Eq. 9).

$$O_2N\lessdot Co^{II}\gtrdot NO_2^- \xrightarrow{fast} O_2N\lessdot Co^{III}\gtrdot NO \xrightarrow{fast} \quad (6)$$

$$HOHN\lessdot Co^{II}\gtrdot NO_2^- \xrightarrow{fast} HOHN\lessdot Co^{III}\gtrdot NO \xrightarrow{fast} \quad (7)$$

We also determined the rate constants for the MDQ$^+$ reductions of nitro to hydroxyamino groups in [Co(diNOsar)]$^{2+}$ and [Co(HANOsar)]$^{2+}$. Since the decay of MDQ$^+$ radical was monitored, the rate constants were obtained using the following equations, respectively:

$$\ln[A_t/(A_t-A_\infty)] = ([MDQ^+]_0-7[Co(II)]_0)k_2t + \ln[MDQ^+]_0/7[Co(II)]_0 \quad (8)$$

$$\ln[A_t/(A_t-A_\infty)] = ([MDQ^+]_0-3[Co(II)]_0)k_5t + \ln[MDQ^+]_0/3[Co(II)]_0 \quad (9)$$

where [ ]$_0$ represents the initial concentration of the given species and A_t and A_∞ denote the absorbances at time t and infinity, respectively. The plots of $\ln[A_t/(A_t-A_\infty)]$ vs. t for each system gave a linear relation for at least 3 half-lives. The second-order rate constant, k_2 or k_5, was calculated from the slope of this straight line. The results are shown in Table 3. Reaction-rate constants are similar to those for the dithionite system. Attempts to detect an intermediate

compound containing a nitroso group (-NO) were unsuccessful. However, we cannot completely rule out the possibility of the formation of a nitroso group since in these systems a small amount of cobalt(III) complex was separated which could not be identified.

The author would like to thank Professor Ralph G. Wilkins of New Mexico State University for support and encouragement. This work was supported by a grant from the National Science Foundation of U.S.A.

References

1) A. M. Sargeson, *Chem. Ber.*, **15**, 23 (1979).

2) I. I. Creaser, J. MacB. Harrowfield, A. J. Herlt, A. M. Sargeson, J. Springborg, R. J. Geue, and M. R. Snow, *J. Am. Chem. Soc.*, **99**, 3181 (1977).

3) diNOsar=1,8-dinitro-3,6,10,13,16,19-hexaazabicyclo-[6.6.6]icosane; HANOsar=1-hydroxyamino-8-nitro-3,6,10,13,-16,19-hexaazabicyclo[6.6.6]icosane; diHAsar=1,8-bis(hydroxyamino)-3,6,10,13,16,19-hexaazabicyclo[6.6.6]icosane; sar=3,6,-10,13,16,19-hexaazabicyclo[6.6.6]icosane; sep=1,3,6,8,10,13,16,-19-octaazabicyclo[6.6.6]icosane; DQ^+=1,1′-ethylene-2,2′-bipyridinium radical cation; MDQ^+=1,1′-ethylene-4,4′-dimethyl-2,2′-bipyridinium radical cation; PDQ^+=1,1′-trimethylene-2,2′-bipyridinium radical cation.

4) A. M. Bond, G. A. Lawrance, P. A. Lay, and A. M. Sargeson, *Inorg. Chem.*, **22**, 2010 (1983).

5) R. J. Balahura, G. Ferguson, B. L. Ruhl, and R. G. Wilkins, *Inorg. Chem.*, **22**, 3990 (1983).

6) S. G. Mayhew, *Eur. J. Biochem.*, **85**, 535 (1978).

7) K. Tsukahara and R. G. Wilkins, *J. Am. Chem. Soc.*, **107**, 2632 (1985) and references therein.

8) K. Tsukahara and R. G. Wilkins, *Inorg. Chem.*, **24**, 3399 (1985).

9) R. J. Geue, T. W. Hambley, J. MacB. Harrowfield, A. M. Sargeson, and M. R. Snow, *J. Am. Chem. Soc.*, **106**, 5478 (1984).

10) R. F. Homer and T. E. Tomlinson, *J. Chem. Soc.*, **1960**, 2498.

11) I. I. Creaser, R. J. Geue, J. MacB. Harrowfield, A. J. Herlt, A. M. Sargeson, M. R. Snow, and J. Springborg, *J. Am. Chem. Soc.*, **104**, 6016 (1982).

12) A. G. Evans, R. E. Alford, and N. H. Rees, *J. Chem. Soc., Perkin Trans. 2*, **1977**, 445.

13) F. Feigl, "Spot Tests in Organic Analysis," Elsevier, New York (1966), p. 164.

14) R. J. Geue, M. G. McCarthy, and A. M. Sargeson, *J. Am. Chem. Soc.*, **106**, 8282 (1984).

Syntheses and Properties of Hepta- and Dibenzopentafulvalene Derivatives Containing 13-, 15-, 17-, and 19-Membered Rings[1)]

Toyonobu Asao,* Noboru Morita, Jūro Ojima,†,* Masamitsu Fujiyoshi,†
Kazuyo Wada,† and Satoru Hamai†
Department of Chemistry, College of General Education, Tohoku University, Kawauchi, Sendai 980
†Department of Chemistry, Faculty of Science, Toyama University, Gofuku, Toyama 930
(Received, November 22, 1985)

5,10-Dimethyl-6,8-bisdehydroheptatridecafulvalene **10**, 10-methyl-6,8-bisdehydro-4,5-benzoheptatridecafulvalene **11**, 6,8-bisdehydro-4,5:10,11-dibenzoheptatridecafulvalene **12**, 5,10-dimethyl-6,8-bisdehydroheptapentadecafulvalene **13**, 5,10,15-trimethylheptapentadecafulvalene **14**, 7,12-dimethylheptaheptadecafulvalene **15**, and 7,12-dimethylheptanonadecafulvalene **16** were synthesized by a reaction of 8-oxoheptafulvene **8** with the corresponding bisdehydroannulenones **1**—**7**. Dibenzo derivatives of 5,10-dimethyl-6,8-bisdehydropentatridecafulvalene **23**, 10-methyl-6,8-bisdehydro-4,5-benzopentatridecafulvalene **24**, 6,8-bisdehydro-4,5:10,11-dibenzopentatridecafulvalene **25**, 5,10-dimethylpentapentadecafulvalene **26**, 5,10,15-trimethylpentapentadecafulvalene **27**, 7,12-dimethylpentaheptadecafulvalene **28**, and 7,12-dimethylpentanonadecafulvalene **29** were also synthesized by the reaction of 9-fluorenylidenemethanone **21** with the corresponding annulenones **1**—**7**. Furthermore, a benzo-annelated series of heptapentadecafulvalenes **30**—**35** was also synthesized. The ^{1}H NMR spectra of these hepta- and dibenzopentafulvalenes are discussed in connection with their tropicity. It can be concluded that a slight polarization of π-electrons through pinch bonds from the seven-membered rings to the many-membered rings in the heptafulvalene system and from the many-membered rings to the five-membered rings in the pentafulvalene system exist regardless of the size of the many-membered rings.

Recently, theoretical and experimental studies on the bicyclic polyene containing a cyclic cross conjugated π-electron system, fulvalene, have been extensively performed.[2)]

One group (A) of these compounds, in which one ring is $(4n+1)$-membered and the other is $(4n+3)$-membered, such as sesquifulvalene (pentaheptafulvalene) or triapentafulvalene (calicene), is potentially aromatic since the polarization of a π-electron through the central double bond (pinch bond) from $(4n+3)$ to $(4n+1)$-membered ring will make both rings a $(4n+2)$ π-electron system. The other group (B) in which both rings are $(4n+1)$- and/or $(4n+3)$-membered, such as pentafulvalene or heptafulvalene, is not potentially aromatic since the polarization of a π-electron through a pinch bond will make one ring a $(4n+2)$ system, and the other ring a $(4n)$ system.

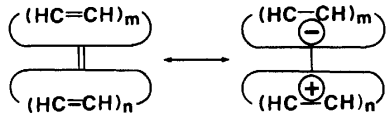

We have investigated the syntheses of fulvalene containing a cycloheptatrienylidene moiety by a reaction of 8-oxoheptafulvene with various annulenones.[3)]

The reaction of 8-oxoheptafulvene with various many-membered annulenones such as trideca-, pentadeca-, heptadeca-, and nonadeca-annulenones may give, by [2+2] cycloaddition followed by an extrusion of carbon dioxide, fulvalenes containing a seven-membered ring in one ring and a many-membered ring in the other ring belonging to the group (A) or (B), depending on the size of the many-membered rings. Furthermore, a similar reaction using 9-fluorenylidenemethanone instead of 8-oxoheptafulvene might give dibenzo derivatives of the pentafulvalenes containing many-membered ring belonging to either group (A) or (B).

Although derivatives of pentaundecafulvalene[4)] belonging to the group (A) and pentatridecafulvalene,[5)] pentaphenafulvalene,[6)] and undecafulvalene[7)] belonging to group (B) are known as macrocyclic compounds of these types, systematic investigations of the syntheses and properties of fulvalenes containing many-membered rings have not been undertaken. Recently, the syntheses of pentafulvalenes containing 13-, 15-, 17-, and 19-membered macrocyclic rings have been reported.[8)]

In this paper, two series of fulvalenes, heptafulvalenes containing 13-, 15-, 17-, and 19-membered macrocyclic rings and dibenzopentafulvalenes containing the similar macrocyclic rings have been synthesized, and their tropicities are discussed in terms of an inspection of their ^{1}H NMR spectra.

Results and Discussion

Syntheses. We have reported that a reaction of 8-oxoheptafulvene with tropone and its derivatives afforded heptafulvalenes and [2+8] cycloadducts in a variety of ratios depend on the substituents.[3)] We applied the reaction to derivatives of bisdehydro [13]-, [15]-, [17]-, and [19]annulenones and objective heptafulvalenes were synthesized. The reactions of 5,10-dimethyl-6,8-bisdehydro[13]annulenone **1**,[9)] 10-methyl-6,8-bisdehydro-4,5-benz[13]annulenone **2**,[10)] 6,8-bisdehydro-4,5:10,11-dibenz[13]annulenone **3**,[10)] 5,10-dimethyl-6,8-bisdehydro[15]annulenone **4**,[11)] 5,10,15-trimethyl-6,8-bisdehydro[15]annulenone **5**,[12)] 7,12-dimethyl-8,10-bisdehydro[17]annulenone **6**,[11)] and 7,12-dimethyl-8,10-bisdehydro[19]annulenone **7**[11)] with an excess of 8-oxoheptafulvene **8**[3,13)] formed in situ by a reaction of tropylcarbonyl chloride **9** and triethylamine

in dry benzene at refluxing or room temperature afforded 5,10-dimethyl-6,8-bisdehydroheptatridecafulvalene **10**, 10-methyl-6,8-bisdehydro-4,5-benzoheptatridecafulvalene **11**, 6,8-bisdehydro-4,5:10,11-dibenzoheptatridecafulvalene **12**, 5,10-dimethyl-6,8-bisdehydroheptapentadecafulvalene **13**, 5,10,15-trimethyl-6,8-bisdehydroheptapentadecafulvalene **14**, 7,12-dimethyl-8,10-bisdehydroheptaheptadecafulvalene **15**, and 7,12-dimethyl-8,10-bisdehydroheptanonadecafulvalene **16** in 3.9, 67.3, 23.8, 36, 86, 52, and 74% yields, respectively.

In the case of **1** and **3**, [2+8] cycloadducts **17** and **18** were obtained in yields of 41 and 14%, respectively, both as pale-yellow crystals. 2,13-Dideuterio derivative of **3**[14] afforded the corresponding fulvalene **19** and [2+8] adduct **20** which were very useful compounds for NMR assignment of compounds **12** and **18**,[15] respectively.

The fulvalenes **10**—**16** were recrystallized from benzene or hexane–benzene to give deep-colored (dark-reddish or dark-brownish) moderately stable crystals. These gradually decomposed upon standing at room temperature or upon exposure to air and diffused light.

On the other hand, reactions of the annulenones **1**—**7** with 9-fluorenylidenemethanone **21** formed in situ by a reaction of 9-chlorofluorene-9-carbonyl chloride

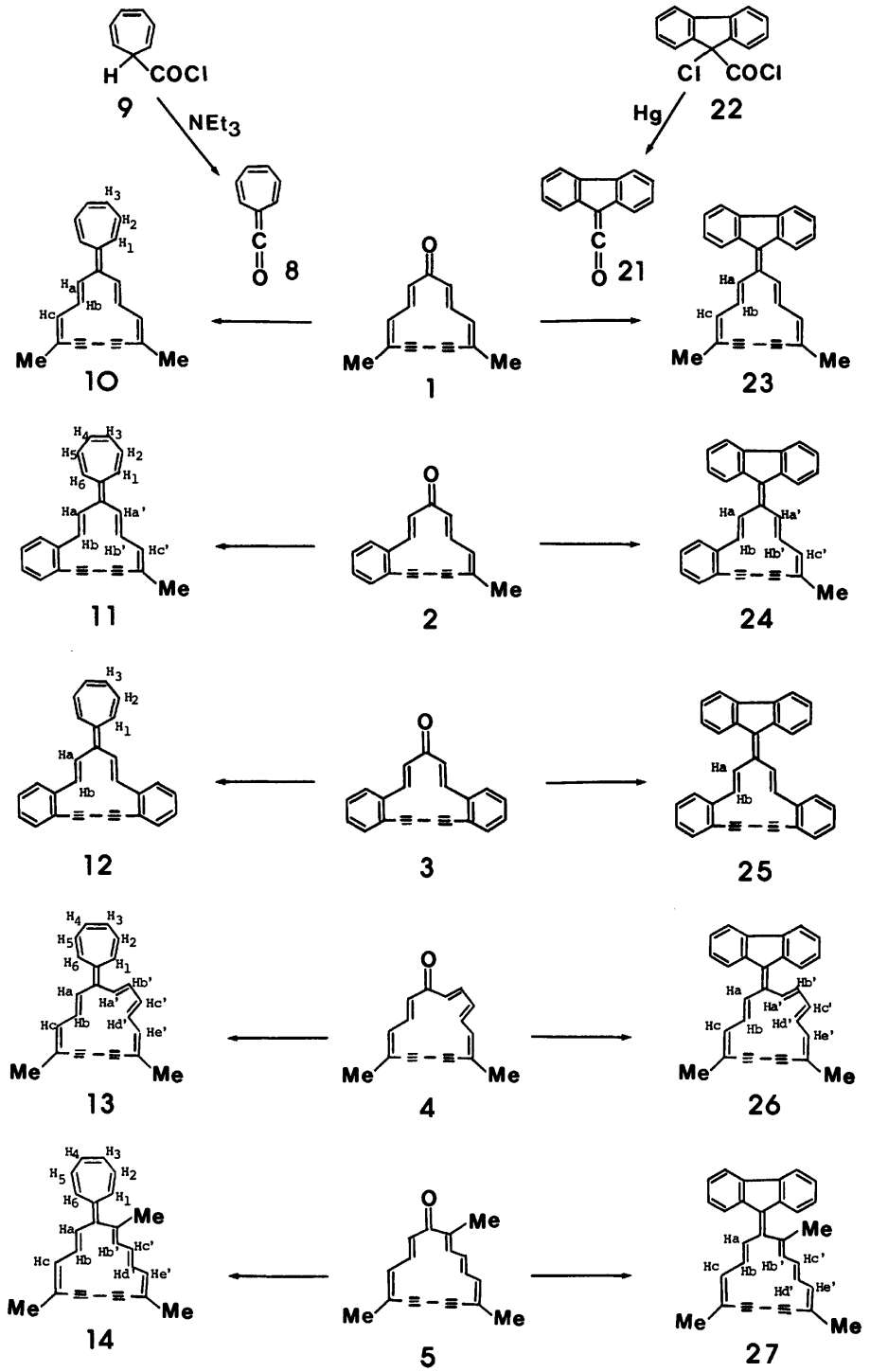

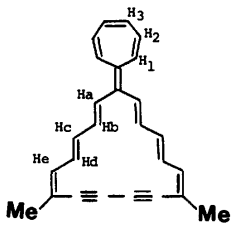

15

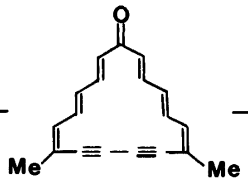

6

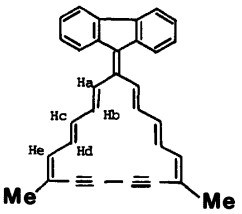

28

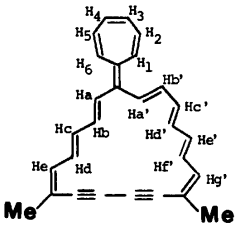

16

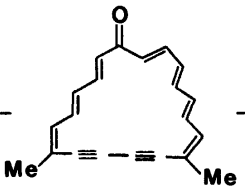

7

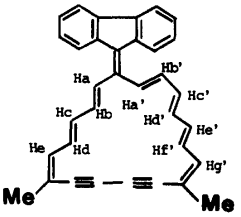

29

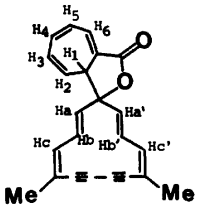

17

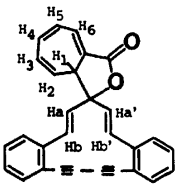

18

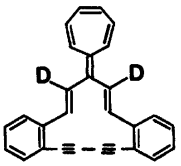

19

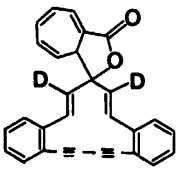

20

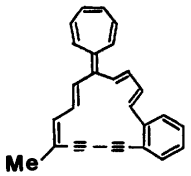

30

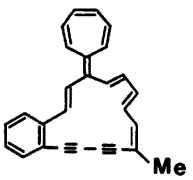

31

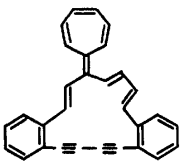

32

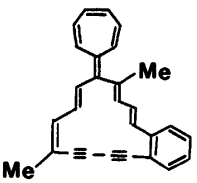

33

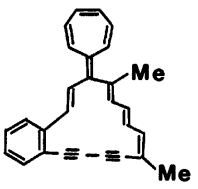

34

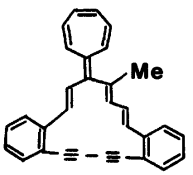

35

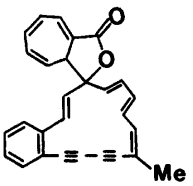

36

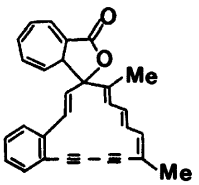

37

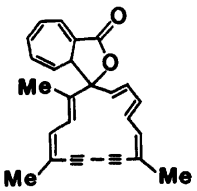

38

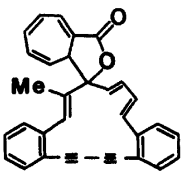

39

22 with mercury afforded the corresponding dibenzo derivatives of the pentafulvalenes **23—29** containing 13-, 15-, 17-, and 19-membered rings in 28, 27, 4.4, 47, 8.3, 38, and 36% yields, respectively. These fulvalenes were also deep-colored and moderately stable compounds at low temperature and under nitrogen atmosphere.

Furthermore, we studied the synthesis of the series of benzoannelated heptapentadecafulvalenes. The reactions of 10-methyl-4,5-benzo-,[16,17] 5-methyl-10,11-benzo-,[16,17] 4,5:10,11-dibenzo-,[18] 10,15-dimethyl-4,5-benzo-,[16] 5,15-dimethyl-10,11-benzo-,[16] and 15-methyl-4,5:10,11-dibenzo-6,8-bisdehydropentadecaannulenones[16] with 8-oxoheptafulvene **8** afforded the corresponding benzoannelated heptapentadecafulvalenes **30** [81%, mp 119—123 °C (decomp)], **31** [29.4%, mp 108—110 °C (decomp)], **32** [23.6%, mp 150 °C (decomp)], **33** [87%, mp 89 °C (decomp)], **34** (23%, mp not clear), and **35** (77%, mp not clear), and [2+8] cycloadducts **36** [mp 215—225 °C (decomp)] and **37** [mp 189—191 °C (decomp)] in some cases. However, the reactions of 2,5,10-trimethyl-6,8-bisdehydropentadecaannulenone[12] and 2-methyl-4,5:10,11-dibenzo-6,8-bisdehydropentadecaannulenone[12] with **8** were very slow and yielded only

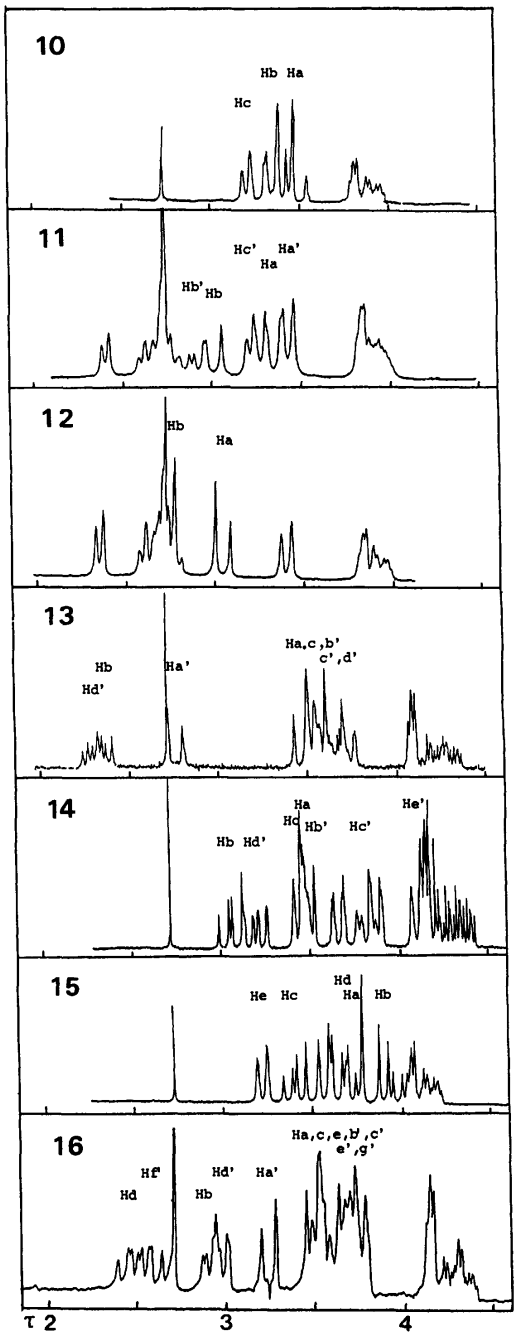

Fig. 1. ^{1}H NMR (200 MHz) Spectra (partial) of Heptafulvalenes **10—16** in $CDCl_3$ (τ values, internal standard, TMS).

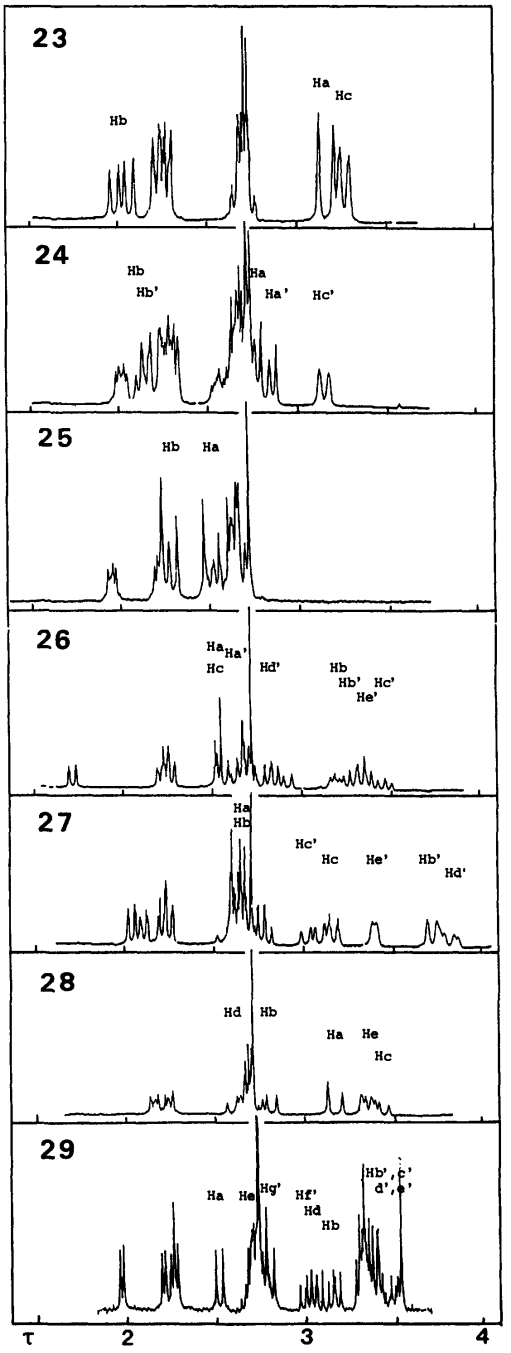

Fig. 2. ^{1}H NMR (200 MHz) Spectra (partial) of Pentafulvalenes **23—28** and ^{1}H NMR (400 MHz) Spectra of **29** in $CDCl_3$ (τ values, internal standard, TMS).

[2+8] cycloadducts **38** [mp 176°C (decomp)] and **39** [mp 193—194°C (decomp)], respectively.

^{1}H NMR. The ^{1}H NMR spectra at 200 MHz of the heptafulvalenes **10—16** and the pentafulvalenes **23—29** are illustrated in Figs. 1 and 2, respectively. The individual assignments were made on the basis of the multiplicities and coupling constants, which were determined by extensive decoupling experiments.

Differences of the outer and inner protons of the many-membered rings of all spectra were considerably smaller than those of starting annulenones; therefore, these fulvalenes have a more polyolefinic character than the starting annulenones.

Figure 1 shows that the seven-membered ring protons of **10**, **11**, **12**, and **15** resonate in a slightly higher magnetic field than those of **13**, **14**, and **16**; the former are almost the same as those of heptafulvalene itself[19] and the latter are almost the same as those of sesquifulvalene (pentaheptafulvalene).[20] On the other hand, the outer and inner protons of the many-membered rings of **10**, **11**, and **12** resonate with each other at lower and higher magnetic fields. The outer and inner protons of the many-membered rings of **13**, **14**, and **16** resonate with each other at higher and lower magnetic fields. These are in accord with that the compounds **10**, **11**, **12**, and **15**, belonging to the group (A), are potentially aromatic by polarization of the π-electrons which makes the seven-membered rings to 6π and the many-membered rings to 14π or 18π systems. Furthermore, it can be considered that the polarization of π-electrons from the seven-membered ring to the many-membered rings occurred even in compounds **13**, **14**, and **16**, belonging to the group (B). These make seven-membered rings to 6π and many-membered rings to paratropic having a 16π or a 20π system.

Figure 2 shows a reverse trend in the pentafulvalene compared to the heptafulvalene system. The outer and inner protons of the many-membered rings of **23**, **24**, **25**, and **28** resonate with each other at higher and lower fields. Those of **26**, **27**, and **29** resonate with each other at lower and higher fields. This shows that polarization of the π-electrons through a pinch bond from the many-membered rings to the five-membered rings occurred in all cases which make many-membered rings of **23**, **24**, **25**, and **28** to paratropic having 12π or 16π system and those of **26**, **27**, and **29** to diatropic having 14π or 18π system. In particular, relative chemical shifts of the corresponding inner protons of the many-membered rings of the hepta- and pentafulvalenes clearly show an inverse direction to each other. This indicates that the polarization of the π-electron from the seven-membered rings to the many-membered rings in the heptafulvalene series and from the many-membered rings to the five-membered rings in the pentafulvalene series occurred regardless of the size of the many-membered rings.

The ^{1}H NMR spectra of benzoannelated heptapentadecafulvalenes **30—35** were taken at 90 MHz, and the spectral patterns were similar to those of heptapentadecafulvalenes **11** and **12**; however, the signals were not separated. Therefore, we could not discuss the assignments and the tropicities.

Table 1. Chemical Shifts of Methyl Protons of Annulenones, and Hepta- and Pentafulvalenes

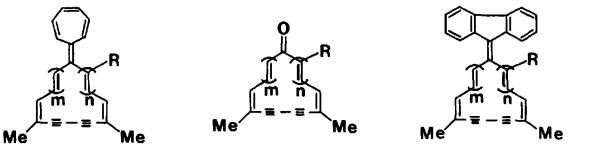

[13]-	R=H	**10** 8.08		**1** 8.26		**23** 8.12	
[15]-	R=H	**13** 8.18		**4** 7.82, 7.76		**26** 8.06, 8.02	
	R=Me	**14** 8.15, 8.06	8.13,	**5** 7.95, 7.79	7.90,	**27** 8.05, 7.77	8.04,
[17]-	R=H	**15** 8.00		**6** 8.23		**28** 8.06	
[19]-	R=H	**16** 8.14		**7** 7.87, 7.79		**29** 8.04, 8.00	

Furthermore, since the methyl groups of all fulvalenes were always outside of the rings and could be readily recognized in the NMR spectra, we inspected the methyl resonaces of these fulvalenes in the expectation of obtaining information concerning the tropicities.

The chemical shifts of the methyl resonances of the heptafulvalene **10**, **13**, **14**, **15**, and **16** and pentafulvalenes **23**, **26**, **27**, **28**, and **29** are listed in Table 1, together with those of the corresponding annulenones **1**, **4**, **5**, **6**, and **7**. We can see a remarkable alternation of the methyl resonace between $(4n+1)$ annulenones, [13]- and [17]annulenones which show a relatively high field, and $(4n+3)$ annulenones, [15]- and [19]annulenones which show relatively low field. These phenomena indicate paratropicity and diatropicity, respectively, owing to the polarization of the carbonyl group. The same alternation trend can be observed for the pentafulvalene series and a reverse alternation trend was observed for the heptafulvalene series, although the degree of the alternation for both series were much less than that for the annulenones.

Electronic Spectra. The electronic spectra of the heptafulvalenes **10**, **11**, and **12** and the pentafulvalenes **23**, **24**, and **25** are shown in Figs. 3 and 4, respectively. The electronic spectra of the heptafulvalenes **10**, **13**, **15**, and **16** and the pentafulvalenes **23**, **26**, **27**, **28**, and **29** are also shown in Figs. 5 and 6, respectively.

It can be seen from Figs. 3 and 4 that the longest wavelength bands exhibited absorption toward the longer wavelength in the order **10**>**11**>**12**, and **23**>**24**>**25**, respectively, as has been observed for the corresponding annulenones. This indicates that fused benzene rings inhibit the degree of conjugation of a π-electron systems in these fulvalene systems.

From Figs. 5 and 6, we can not see regularity depend on the ring size; the longest bands of nonadecafulvalenes **16** and **29** are shifted to shorter wavelength, which may due to the bending of the many-membered rings.

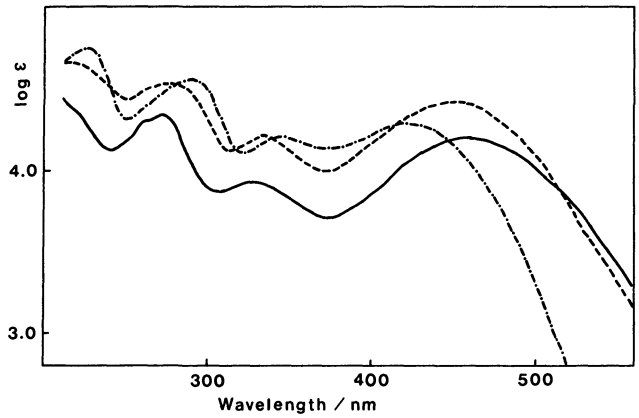

Fig. 3. Electronic Absorption Spectra of **10** (——), **11** (----), and **12** (-·-·-) in EtOH.

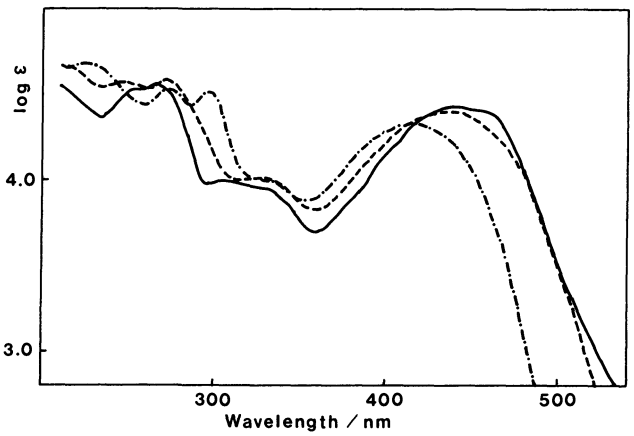

Fig. 4. Electronic Absorption Spectra of **23** (——), **24** (----), and **25** (-·-·-) in EtOH.

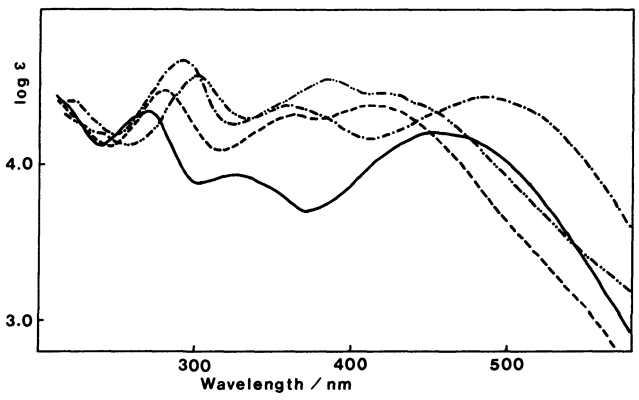

Fig. 5. Electronic Absorption Spectra of **10** (——), **13** (----), **15** (-·-·-), and **16** (-···-) in EtOH.

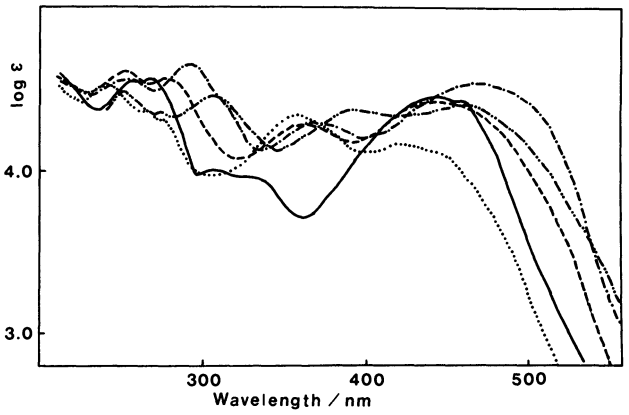

Fig. 6. Electronic Absorption Spectra of **23** (——), **26** (----), **27** (·····), **28** (-·-·-), and **29** (-···-), in EtOH.

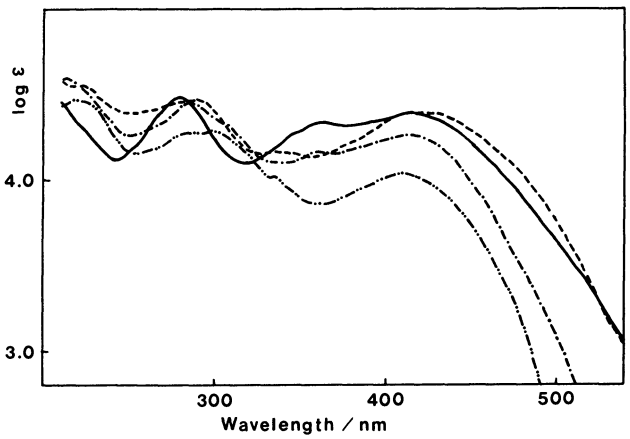

Fig. 7. Electronic Absorption Spectra of **13** (——), **30** (----), **31** (-·-·-), and **32** (-···-) in EtOH.

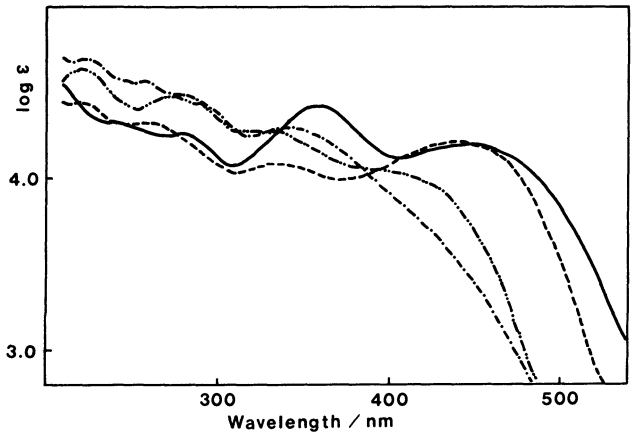

Fig. 8. Electronic Absorption Spectra of **14** (——), **33** (----), **34** (-·-·-), and **35** (-···-) in EtOH.

The spectral curves of the benzoannelated series of heptapentadecafulvelnes **30—32** and **33—35** are illustrated in Figs. 7 and 8 with those of **13** and **14**, respectively. The longest bands of the benzoannelated fulvalenes appeared at shorter wavelengths compared to those of **13** and **14**, as has been observed in Figs. 3 and 4.

Experimental

General. Melting points were determined on a hot-stage apparatus and were uncorrected. The IR spectra were obtained with a Hitachi 215 grating spectrophotometer. The electronic spectra were measured with a Hitachi 340

spectrophotometer. ^{1}H NMR spectra were recorded with a Varian XL-200 (200 MHz), JEOL JX-400 (400 MHz), or Hitachi R-22 (90 MHz) spectrometer in $CDCl_3$ solutions, tetramethylsilane being used as an internal standard; chemical shifts are reported in τ and coupling constants (J) show in Hz. Mass spectra were measured with a JMS D-200 spectrometer at 75 eV.

Reaction of [13]Annulenone 1 and 8-Oxoheptafulvene 8. A solution of tropylcarbonyl chloride **9** (154.6 mg, 1.0 mmol) in dry benzene (10 ml) was added dropwise to a solution of [13]annulenone **1** (104 mg, 0.5 mmol) and triethylamine (214 mg) in dry benzene (15 ml) during a period of 15 min at refluxing temperature under argon atmosphere, and the mixture was refluxed for further 15 min. The solution was submitted to column chromatography on silica gel, and eluted with a mixture of hexane and benzene. From reddish fraction heptatridecafulvalene **10** (5.5 mg, 3.9%) was obtained as dark reddish needles (from a mixture of hexane and benzene), color changed from around 110 °C and decomposed without melting.

From the yellow fraction, [2+8] cycloadduct **17** (67.0 mg, 41%) was obtained as pale-yellow prisms, mp 159—160 °C (decomp) (from benzene). **10**; IR (KBr) 2140 cm^{-1} (C≡C); ^{1}H NMR (200 MHz) τ=3.21 (d, J=9, Hc), 3.36 (d, J=12.5, H-1), 3.37 (d,d, J=15.5, 9, Hb), 3.51 (d, J=15.5, Ha), 3.79—3.98 (m, H-2,3), 8.08 (s, Me).

Found: C, 93.49; H, 6.16%. Calcd for $C_{22}H_{18}$: C, 93.57; H, 6.43%. **17**; IR (KBr) 2170 cm^{-1} (C≡C), 1745 (C=O); ES λ_{max} (EtOH) 258 nm (log ε 4.38), 316 (3.90); ^{1}H NMR (200 MHz) τ=2.86 (m, H-6), 3.25 (m, H-4, 5), 3.37 (d,d,q, J=5, 1, 1, Hc or Hc'), 3.49 (d,d,q, J=5, 1, 1, Hc' or Hc), 3.61 (d,d,q, J=15.5, 5, 1, Hb or Hb'), 3.75—3.95 (m, H-3), 3.95 (d,d,q, J=15.5, 5, 1, Hb' or Hb), 4.59 (d,d, J=9.6, 4, H-2), 4.79 (d,d, J=15.5, 1, Ha'), 4.83 (d,d, J=15.5, 1, Ha), 6.86 (m, H-1), 8.04 (d,d, J=1, 1, Me), 8.07 (d,d, J=1, 1, Me).

Found: C, 84.63; H, 5.53%. Calcd for $C_{23}H_{18}O_2$: C, 84.64; H, 5.56%.

Heptatridecafulvalene 11. A reaction of [13]annulenone **2** (34 mg, 0.14 mmol), chloride **9** (30 mg, 0.2 mmol), triethylamine (50 mg) in dry benzene (20 ml) was carried out in almost the same manner, conditions and purification procedure as in the case of 1. Heptatridecafulvalene **11** (29.8 mg, 67.3%) was obtained as dark-reddish crystals, mp 150 °C (decomp). IR (KBr) 2160 cm^{-1} (C≡C); ^{1}H NMR (200 MHz) τ=2.41 (d, J=7.5, 1H, Ar-H), 2.59—2.80 (m, 3H, Ar-H), 2.89 (d,d, J=16, 10.5, Hb'), 3.01 (d, J=16.5, Hb), 3.21 (d, J=10.5, Hc'), 3.26 (d, J=16.5, Ha), 3.43 (d, J=11.5, H-1,6), 3.45 (d, J=16, Ha'), 3.8—4.0 (m, H-2,3,4,5), 8.12(s, Me).

Found: C, 94.01; H, 5.61%. Calcd for $C_{25}H_{18}$: C, 94.30; H, 5.70%.

Heptatridecafulvalene 12. A solution of chloride **9** (154 mg, 1.0 mmol) in dry benzene (10 ml) was added dropwise to a solution of [13]annulenone **3** (140 mg, 0.5 mmol) and triethylamine (40 ml) at 80 °C under an argon atmosphere for 15 min. The reaction mixture was heated for an additional 30 min, submitted to column chromatography on alumina and eluted with benzene. From the reddish fraction heptatridecafulvalene **12** (42.2 mg, 23.8%) was obtained as dark-reddish crystals, mp decomposed from around 150 °C.

From pale yellow fraction, [2+8] cycloadduct **18** (29.1 mg, 14.5%) was obtained as pale-yellow crystals, mp 191—194 °C. **12**; IR (KBr) 2175 cm^{-1} (C≡C); ^{1}H NMR (200 MHz) τ=2.36 (d, J=8, 2H, Ar-H), 2.57—2.81 (m, 6H, Ar-H), 2.73 (d, J=16.5, Hb), 3.04 (d, J=16.5, Ha), 3.39 (d, J=11.5, H-1), 3.78—3.97 (m, H-2, 3).

Found: C, 94.62; H, 5.08%. Calcd for $C_{28}H_{18}$: C, 94.88; H, 5.12%. **18**; IR (KBr) 2190 cm^{-1} (C≡C), 1745 (C=O); ES λ_{max} (EtOH) 223 nm (log ε 4.81), 259 (4.52), 273 (4.50), 321 (4.18), 341 (4.16); ^{1}H NMR (200 MHz) τ=2.78 (m, 9H, H-6, Ar-H), 3.09 (d, J=16, Hb or Hb'), 3.22 (m, H-4, 5), 3.35 (d, J=16, Hb' or Hb), 3.54 (d, J=16, Ha'), 3.61 (d, J=16, Ha), 3.78 (d,m, J=10, H-3), 4.56 (d,d, J=10, 4, H-2), 6,99 (m, H-1).

Found: C, 87.37; H, 4.78%. Calcd for $C_{29}H_{18}O_2$: C, 87.41; H, 4.55%.

Heptapentadecafulvalene 13. A reaction of [15]annulenone **4** (78 mg, 0.33 mmol), chloride **9** (100 mg, 0.65 mmol), triethylamine (100 mg) in dry benzene (20 ml) was carried out in the almost same manner as in the case of 1. The usual work-up afforded the heptafulvalene **13** (36.9 mg, 36%) as dark-reddish crystals, mp 100—101.5 °C (decomp). IR (KBr) 2160 cm^{-1} (C≡C); ^{1}H NMR (200 MHz) τ=2.31 (d,d, J=14.5, 11, Hd'), 2.34 (d,d, J=15, 11.5, Hb), 2.76 (d, J=15.5, Ha'), 3.43—3.70 (m, Ha,c,b',c',e'), 3.56 (d, J=11.5, H-6), 3.73 (d, J=12, H-1), 4.08 (d,d, J=5, 3.5, H-3, 4), 4.25 (d,d,d, J=11.5, 5, 3.5, H-5), 4.27 (d,d,d, J=12, 5.5, 3.5, H-2), 8.18 (s, 2Me).

HRMS; Found: 308.1490. Calcd for $C_{24}H_{20}$: 308.1566.

Heptapentadecafulvalene 14. A reaction of a solution of [15]annulenone **5** (50 mg, 0.20 mmol) in dry benzene (10 ml) and a solution of chloride **9** (100 mg) in dry benzene (10 ml) was carried out in the similar manner in the case of **1**. The usual work-up afforded heptapentadecafulvalene **14** (45 mg, 86%) as dark-reddish crystals, mp 99—100 °C (decomp). IR (CCl_4) 2170 cm^{-1} (C≡C); ^{1}H NMR (200 MHz) τ=3.05 (d,d, J=15, 11.5, Hb), 3.19 (d,d,d, J=15.5, 10, 1, Hd'), 3.44 (d,d, J=11.5, 1.5, Hc), 3.49 (d, J=15, Ha), 3.51 (d, J=5, Hb'), 3.66 (d, J=11.5, H-6), 3.81 (d,d, J=15.5, 5, Hc'), 3.86 (d, J=12, H-1), 4.10 (d, J=10, He'), 4.15 (m, H-3, 4), 4.25 (d,d,d, J=11.7, 5.2, 3.7, H-5), 4.37 (d,d,d, J=12, 5, 4.5, H-2), 8.06 (d, J=1.5, Me), 8.13 (d,d, J=1.5, 1.5, Me), 8.15 (s, Me).

HRMS; Found: 322.1744. Calcd for $C_{25}C_{22}$: 322.1722.

Heptaheptadecafulvalene 15. A solution of [17]annulenone **6** (65 mg, 0.25 mmol), triethylamine (199 mg) in dry benzene (20 ml) and a solution of chloride **9** (100 mg, 0.6 mmol) in dry benzene (10 ml) was reacted, and the usual work-up afforded heptaheptadecafulvalene **15** (44.1 mg, 52%) as dark-brownish needles, mp 180—181 °C (decomp). IR (KBr) 2165 cm^{-1} (C≡C); ^{1}H NMR (200 MHz) τ=3.22 (br d, J=11, He), 3.39 (d,d, J=15, 10, Hc), 3.56 (d, J=11.5, H-1), 3.67 (d,d, J=15, 11, Hd), 3.73 (d, J=15.5, Ha), 3.93 (d,d, J=15.5, 10, Hb), 4.04 (d,d, J=4.5, 4, H-3), 4.15 (d,d,d, J=11.5, 4.5, 4, H-2), 8.00 (s, Me).

HRMS; Found: 334.1732. Calcd for $C_{26}H_{22}$: 334.1722.

Heptanonadecafulvalene 16. A solution of [19]annulenone **7** (50 mg, 0.17 mmol) and triethylamine (132 mg) in dry benzene (10 ml), and a solution of chloride **9** (100 mg) in dry benzene (10 ml) was reacted at room temperature for 20 min under argon atmosphere. The solution was passed through an alumina (deactivated by treating with ethyl acetate and water) column. The colored fraction was collected and purified by further column chromatography using the alumina to obtain heptafulvalene **16** (46.5 mg, 74%) as unstable dark-reddish crystals, mp 144—145 °C (decomp). IR (KBr) 2190 cm^{-1} (C≡C); ^{1}H NMR (200 MHz) τ=2.46 (d,d, J=15, 11, Hd), 2.57 (d,d, J=15, 11, Hf'), 2.93 (d,d, J=15, 11, Hb), 2.95 (d,d, J=15, 11, Hd'), 3.24 (d, J=16, Ha'), 3.45—4.00 (m, H-1, 6, a,c,e,b',c',e',g'), 4.14 (d,d, J=5, 3.5, H-3, 4), 4.19—4.39 (m, H-

2, 5), 8.14 (s, 2Me).

HRMS; Found: 360.1799. Calcd for $C_{28}H_{24}$: 360.1879.

Pentatridecafulvalene 23. A solution of [13]annulenone **1** (50 mg, 0.24 mmol), 9-chlorofluorene-9-carbonyl chloride **22** (150 mg, 0.57 mmol), in dry benzene (20 ml) in the presence of one drop of mercury was stirred at room temperature under an argon atmosphere for 3 d. The reaction mixture was directly submitted to column chromatography using silica gel, and the colored fraction was further purified by chromatography on silica gel. Pentatridecafulvalene **23** (24 mg, 28%) was obtained as dark-reddish crystals, mp 174—175 °C (decomp). IR (KBr) 2150 cm^{-1} (C≡C); ^1H NMR (200 MHz) τ=2.03 (d,d, J=16, 10, Hb), 2.20—2.30 (m, 4H, Ar-H), 2.64—2.77 (m, 4H, Ar-H), 3.07 (d, J=16, Ha), 3.27 (d, J=10, Hc), 8.12 (s, Me).

Found: C, 94.11; H, 5.44%. Calcd for $C_{28}H_{20}$: C, 94.34; H, 5.66%.

Pentatridecafulvalene 24. A solution of [13]annulenone **2** (50 mg, 0.2 mmol), chloride **22** (150 mg) in dry benzene (10 ml) in the presence of one drop of mercury was stirred at room temperature for 30 h under an argon atmosphere. The reaction mixture was submitted to column chromatography using alumina and eluted with benzene. The pentatridecafulvalene **24** (22 mg, 27%) was obtained as dark-reddish crystals, mp 190—192 °C (decomp). IR (KBr) 2165 cm^{-1} (C≡C); ^1H NMR (200 MHz) τ=1.97—2.31 (m, 5H, Hb, Ar-H), 2.10 (d,d, J=16.5, 10.5, Hb'), 2.49—2.72 (m, 8H, Ar-H), 2.78 (d, J=16.5, Ha), 2.82 (d, J=16.5, Ha'), 3.13 (d, J=10.5, Hc'), 8.00 (s, Me).

Found: C, 94.72; H, 4.84%. Calcd for $C_{31}H_{20}$: C, 94.86; H, 5.14%.

Pentatridecafulvalene 25. A solution of [13]annulenone **3** (50 mg, 0.18 mmol), chloride **22** (100 mg) and one drop of mercury in dry benzene (10 ml) was stirred at room temperature for 3 d. The usual work-up afforded pentatridecafulvalene **25** (3.4 mg, 4.4%) as dark-reddish crystals, mp 221—223 °C (decomp), and annulenone **3** (20 mg) was recovered. IR (KBr) 2190 cm^{-1} (C≡C); ^1H NMR (200 MHz) τ=1.97 (m, 2H, Ar-H), 2.20—2.32 (m, 2H, Ar-H), 2.26 (d, J=16.5, Hb), 2.46—2.71 (m, 12H, Ar-H), 2.49 (d, J=16.5, Ha).

HRMS; Found: 428.1488. Calcd for $C_{34}H_{20}$: 428.1566.

Pentapentadecafulvalene 26. A solution of [15]annulenone **4** (70 mg, 0.30 mmol), chloride **22** (150 mg) in dry benzene in the presence of one drop of mercury was stirred for 1 d at room temperature under an argon atmosphere. The usual work-up afforded pentapentadecafulvalene **26** (55 mg, 47%) as dark-reddish crystals, mp 153.5—155 °C (decomp). IR (KBr) 2160 cm^{-1} (C≡C); ^1H NMR (200 MHz) τ=1.70 (d, J=8, 1H, Ar-H), 2.30 (m, 3H, Ar-H), 2.58—2.86 (m, 4H, Ar-H), 2.52 (d, J=5, Ha), 2.53 (d, J=7, Hc), 2.60 (d, J=15.5, Ha'), 2.87 (d,d, J=15, 11, Hd'), 3.17 (d,d, J=7, 5, Hb), 3.28 (d,d, J=15.5, 7, Hb'), 3.32 (d, J=11, He'), 3.43 (d,d, J=15, 7, Hc'), 8.02 (s, Me), 8.06 (s, Me).

HRMS; Found: 382.1690. Calcd for $C_{30}H_{22}$: 382.1722.

Pentapentadecafulvalene 27. A solution of [15]annulenone **5** (50 mg, 0.20 mmol), chloride **22** (100 mg) and one drop of mercury in dry benzene (10 ml) was stirred at room temperature for 1 d under an argon atmosphere. The usual work-up afforded pentapentadecafulvalene **27** (6.6 mg, 8.3%) as dark-reddish crystals, mp 175—177 °C (decomp). IR (KBr) 2160 cm^{-1} (C≡C); ^1H NMR (200 MHz) τ=2.05 (d, J=7.5, 1H, Ar-H), 2.11 (br d, J=6.5, 1H, Ar-H), 2.21 (br d, J=6, 1H, Ar-H), 2.26 (br d, J=7.5, 1H, Ar-H), 2.52—2.82 (m, 6H, Ha,b, Ar-H), 3.05 (d,d,d, J=15, 11, 1.5, Hc'), 3.16 (d,m, J=9.5, Hc), 3.39 (br d, J=4.5, He'), 3.71 (d, J=11, Hb'), 3.81 (d,d, J=15, 4.5, Hd'), 7.77 (d, J=1.5, a'-Me), 8.04 (d, J=1.5, d-Me), 8.06 (d, J=1.5, f'-Me).

HRMS; Found: 396.1949. Calcd for $C_{31}H_{24}$: 396.1879.

Pentaheptadecafulvalene 28. A solution of [17]annulenone **6** (50 mg, 0.19 mmol), chloride **22** (150 mg, 0.57 mmol) and one drop of mercury in dry benzene (20 ml) was stirred at room temperature for 1 d under an argon atmosphere. The usual work-up afforded pentaheptadecafulvalene **28** (26.3 mg, 38%) as dark-reddish crystals, mp 273—274 °C (decomp). IR (KBr) 2155 cm^{-1} (C≡C); ^1H NMR (200 MHz) τ=2.15 (m, 2H, Ar-H), 2.24 (m, 2H, Ar-H), 2.65 (m, 4H, Ar-H), 2.63 (d,d, J=15.5, 11.5, Hd), 2.77 (d,d, J=15.5, 11, Hb), 3.17 (d, J=15.5, Ha), 3.34 (d, J=11.5, He), 3.40 (d,d, J=15.5, 11, Hc), 8.06 (s, Me).

HRMS; Found: 408.1868. Calcd for $C_{32}H_{24}$: 408.1879.

Pentanonadecafulvalene 29. A solution of [19]annulenone **7** (40 mg, 0.14 mmol), chloride **22** (150 mg) and one drop of mercury in dry benzene (10 ml) was stirred at room temperature for 1 d under an argon atmosphere. The usual work-up afforded pentanonadecafulvalene **29** (22 mg, 36%) as unstable dark-reddish-brown crystals, mp 123—124 °C (decomp). IR (KBr) 2160 cm^{-1} (C≡C); ^1H NMR (400 MHz) τ=1.97 (d, J=7, 1H, Ar-H), 2.21 (d, J=7, 1H, Ar-H), 2.26 (d, J=7, 1H, Ar-H), 2.28 (d, J=7, 1H, Ar-H), 2.56 (d, J=15, Ha), 2.65—2.8 (m, 4H, Ar-H), 2.7 (m, He), 2.7—2.8 (m, Ha'), 2.8 (m, Hg'), 3.0 (d,d, J=15, 11, Hf'), 3.06 (d,d, J=15, 11, Hd), 3.16 (d,d, J=15, 11, Hb), 3.3 (m, Hc), 3.35—3.65 (m, Hb',c',d',e'), 7.99 (s, Me), 8.04 (s, Me).

HRMS; Found: 434.2064. Calcd for $C_{34}H_{26}$: 434.2036.

References

1) Preliminary communications; T. Asao, N. Morita, J. Ojima, and M. Fujiyoshi, *Tetrahedron Lett.*, **1978**, 2795; N. Morita, T. Asao, J. Ojima, and K. Wada, *Chem. Lett.*, **1981**, 57; N. Morita, T. Asao, J. Ojima, and S. Hamai, *ibid.*, **1983**, 1887.

2) For reviews; E. D. Bergman, *Chem. Rev.*, **68**, 41 (1968); P. J. Garrat, "Aromaticity," McGraw Hill, London (1971); F. Pietra, *Chem. Rev.*, **73**, 293 (1973); D. Lloyd, "Non-Benzenoid Conjugated Carbocyclic Compounds," Elsevier, Amsterdam (1984).

3) Y. Kitahara, *Pure Appl. Chem.*, **44**, 833 (1975).

4) H. Prinzbach and L. Knothe, *Angew. Chem.*, **79**, 620 (1967); **80**, 698 (1968); H. Prinzbach, L. Knothe, and A. Dieffenbacher, *Tetrahedron Lett.*, **1969**, 2093.

5) G. M. Pilling and F. Sondheimer, *J. Am. Chem. Soc.*, **93**, 1977 (1971).

6) I. Murata, T. Nakazawa, and M. Okazaki, *Tetrahedron Lett.*, **1969**, 1921; H. Prinzbach and E. Woischnik, *Angew. Chem.*, **81**, 901 (1969); H. Prinzbach, *Pure Appl. Chem.*, **28**, 281 (1971); I. Murata "Topics in Nonbenzenoid Aromatic Chemistry," ed by T. Nozoe, R. Breslow, K. Hafner, S. Ito, and I. Murata, Hirokawa Publ., Tokyo (1973), Vol. 1, p. 159.

7) W. M. Jones, R. A. LaBar, U. H. Brinker, and P. Gebert, *J. Am. Chem. Soc.*, **99**, 6379 (1977).

8) J. Ojima, K. Itagawa, and T. Nakada, *Tetrahedron Lett.*, **24**, 5278 (1983), and the following paper.

9) T. M. Cresp, J. Ojima, and F. Sondheimer, *J. Org. Chem.*, **42**, 2130 (1977).

10) J. Ojima, Y. Yokoyama, and M. Enkaku, *Bull. Chem.*

Soc. Jpn., **50**, 1522 (1977); J. Ojima and M. Fujiyoshi, *J. Chem. Soc., Perkin Trans. 1*, **1980**, 466.

11) J. Ojima, Y. Shiroishi, K. Wada, and F. Sondheimer, *J. Org. Chem.*, **45**, 3564 (1980).

12) J. Ojima, K. Wada, K. Kanazawa, and Y. Nakazawa, *J. Chem. Soc., Perkin Trans. 1*, **1981**, 947.

13) T. Asao, N. Morita, and Y. Kitahara, *J. Am. Chem. Soc.*, **94**, 3655 (1972).

14) J. Ojima and M. Fujiyoshi, *Chem. Lett.*, **1978**, 569.

15) Inner protons of **19** resonate at τ 2.77 as singlet.

16) J. Ojima, K. Wada, and K. Kanazawa, *Chem. Lett.*, **1979**, 1035.

17) J. Ojima and Y. Shiroishi, *Bull. Chem. Soc. Jpn.*, **51**, 1204 (1978).

18) R. T. Weavers, R. R. Jones, and F. Sondheimer, *Tetrahedron Lett.*, **1975**, 104.

19) K. Kato, Y. Kitahara, N. Morita, and T. Asao, *Chem. Lett.*, **1977**, 873.

20) M. Neuenschwander and W. K. Schenk, *Chimia*, **26**, 194 (1972); R. Hollenstein, A. Mooser, M. Neuenschwander, and W. von Philipsborn, *Angew. Chem.*, **87**, 595 (1974); W. K. Schenk. R. Kybruz, and M.Neuenschwander, *Helv. Chim. Acta.*, **58**, 1099 (1975).

 © 1986 The Chemical Society of Japan Bull. Chem. Soc. Jpn., 59, 1723—1731 (1986)

Syntheses and Properties of Pentatrideca-, Pentapentadeca-, Pentaheptadeca-, and Pentanonadecafulvalene Derivatives

Jūro Ojima,* Kazunori Itagawa, and Tetsuya Nakada
Department of Chemistry, Faculty of Science, Toyama University, Gofuku, Toyama 930
(Received November 22, 1985)

5,10-Dimethyl-6,8-bisdehydropentatridecafulvalene **11**, 10-methyl-6,8-bisdehydro-4,5-benzopentatridecafulvalene **12**, 6,8-bisdehydro-4,5 : 10,11-dibenzopentatridecafulvalene **13**, 5,10-dimethyl-6,8-bisdehydropentapentadecafulvalene **14**, 7,12-dimethyl-8,10-bisdehydropentaheptadecafulvalene **15**, and 7,12-dimethyl-8,10-bisdehydropentanonadecafulvalene **16** were synthesized through the reaction of the corresponding bisdehydroannulenones **1**—**6** with cyclopentadienide. The tropic nature of these pentafulvalenes is discussed on the basis of ^{1}H NMR and electronic spectra as well as those of the corresponding heptafulvalene derivatives.

Syntheses of a series of paratropic dimethylbisdehydro[13]-**1**[1] and dimethylbisdehydro[17]annulenone **5**[2] and the diatropic dimethylbisdehydro[15]-**4**[2] and dimethylbisdehydro[19]annulenone **6**[2] as well as their α-methyl,[3] α-ethyl-substituted,[4] and benzo-annelated derivatives,[3] (e.g. **2** and **3**) have been described previously. Higher analogs of these annulenones, i.e., [21]-,[5] [23]-,[6] and [25]annulenone,[6] could also be synthesized, but only with difficulty. In view of the convenient and relatively easy preparation of compounds **1**—**6** they appeared to be the desirable starting materials for the synthesis of the cross-conjugated π-electron systems. In fact, the syntheses of the diphenylfulvene **7**[7] and the dichlorofulvene derivatives **8**[8] containing macrocyclic system by the reaction of these annulenones with diphenylketene and dichloroketene, respectively, have been achieved. Also, in the preceding paper,[9] of an another cross-conjugated system, fulvalene, which might be derived from the annulenones **1**—**6**, we reported the syntheses of heptafulvalenes **9** and dibenzo derivatives **10** of pentafulvalene using an addition reaction of ketene (8-oxoheptafulvene and 9-fluorenylidenemethanone) as similarly to preparation of **7** and **8**, and it was suggested that only a little π-electron polarization of the central double bond occurs in both the heptafulvalenes **9** and the dibenzopentafulvalenes **10** to form polar structures **9a** and **10a**. It can be seen from the polar structures that the heptafulvalene derivatives **9** polarize in such a way that the positive end of the dipole is localized in the 7-membered ring and the negative pole in the large ring, whereas the dibenzopentafulvalene derivatives **10** do in the reverse direction to **9**. Thus, the pentafulvalenes **10** are expected to exhibit the opposite polarization to those of the heptafulvalene derivatives **9**, but this potentiality would be diminished by benzo-annelation upon the 5-membered ring. Therefore, non-benzo-annelated pentafulvalene derivatives are more desirable to enhance the polarization of the central double bond and are expected to possess a greater extended π-electron system, compared with dibenzo-annelated fulvalenes **10**, and to show the reverse tropicity to the heptafulvalenes containing the same-membered large rings. Thus, starting from the annulenones, we were interested in syntheses of a series of the pentafulvalenes, in which the number of the double bond could be increased systematically and a study of their spectral properties and comparison with those of the heptafulvalene derivatives **9** appeared to be particularly informative.

This paper is concerned with the syntheses and

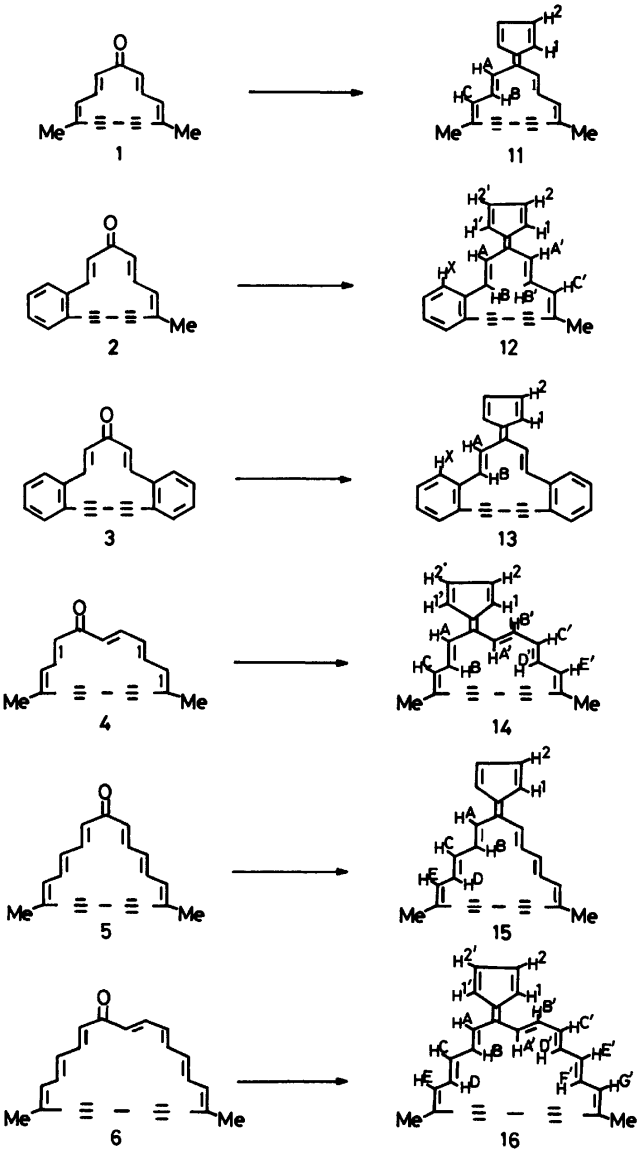

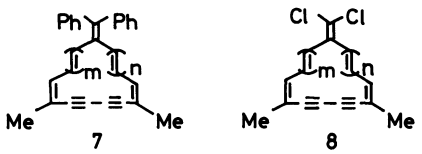

7

m : 1 ~ 2
n : 1 ~ 3

8

m : 1 ~ 2
n : 1 ~ 3

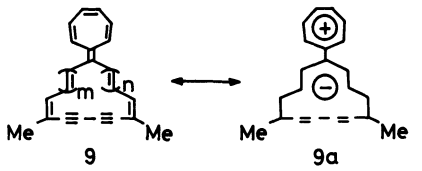

9 9a

m : 1 ~ 2
n : 1 ~ 3

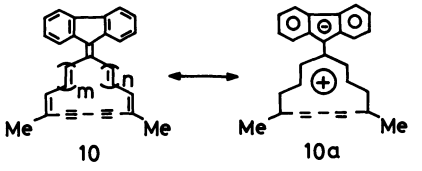

10 10a

m : 1 ~ 2
n : 1 ~ 3

properties of fulvalene derivatives containing cyclopentadienylidene moiety, **11**, **14**—**16**, and the benzoannelated derivatives **12**, **13** of the pentatridecafulvalene derivative **11**.[11] The ^{1}H NMR and electronic absorption spectra of these pentafulvalenes as well as comparison with those of the heptafulvalene derivatives are described in connection with tropicity.

Results and Discussion

Synthesis. In 1977, Howes and Sondheimer reported a synthesis of bis(cyclohexene)-annelated pentatridecafulvalene **17** through the reaction of the corresponding bisdehydroannulenone with a large excess of cyclopentadienide, but did a conjugative addition product when they used a little excess of cyclopentadienide. Thus, although only the pentatridecafulvalene **17** had been obtained, no systematic discussion of the tropicity has been done. We advantageously applied this procedure to the synthesis of pentafulvalenes derived from the annulenones **1**—**6**.

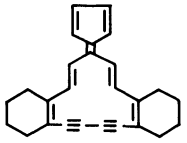

17

We first attempted the reaction of the acyclic ketones (precursors of annulenones), with a large excess of sodium cyclopentadienide, since the corresponding acyclic compounds for the desired fulvalenes would be the most appropriate compounds to examine the tropicity of fulvalenes, as has been made for the fulvene derivatives **7** and **8**.[7,8] However, all attempts to prepare the acyclic model compounds for the desired pentafulvalenes were unsuccessful. The objective pentafulvalene derivatives were synthesized by treatment of the annulenones **1**—**6** with cyclopentadienide according to the procedure of Howes and Sondheimer.[12] Reaction of 5,10-dimethyl-6,8-bisdehydro[13]annulenone **1**,[1] 10-methyl-6,8-bisdehydro-4,5-benz[13]annulenone **2**,[3a] 6,8-bisdehydro-4,5:10,11-dibenz[13]annulenone **3**,[3a] 5,10-dimethyl-6,8-bisdehydro[15]annulenone **4**,[2] 7,12-dimethyl-8,10-bisdehydro[17]annulenone **5**,[2] and 7,12-dimethyl-8,10-bisdehydro[19]-annulenone **6**,[2] with a large excess of sodium cyclopentadienide in tetrahydrofuran at −10—0°C gave 5,10-dimethyl-6,8-bisdehydropentatridecafulvalene **11** (11%), 10-methyl-6,8-bisdehydro-4,5-benzopentatridecafulvalene **12** (7.8%), 6,8-bisdehydro-4,5:10,11-dibenzopentatridecafulvalene **13** (3.9%), 5,10-dimethyl-6,8-bisdehydropentapentadecafulvalene **14** (4.9%), 7,12-dimethyl-8,10-bisdehydropentaheptadecafulvalene **15** (4.6%), and 7,12-dimethyl-8,10-bisdehydropentanonadecafulvalene **16** (6.8%), respectively. These fulvalene derivatives **11**—**16** thus obtained decomposed on attempted melting-point determination, and proved to be rather unstable. These substances decomposed gradually on exposure to diffused light and air.

^{1}H NMR Spectra. The ^{1}H NMR spectra of the fulvalenes **11**, **14**—**16** and the corresponding heptafulvalene derivatives **9** at 200 MHz are illustrated in Figs. 1 and 2, respectively. The individual assignments were made on the basis of the multiplicities and coupling constants, given in the Experimental section. In contrast to the cases of the heptafulvalenes **9** and in accord with the cases of the dibenzopentafulvalenes **10**, containing the same-membered ring, it is predicted that the compounds of **11** and **15** are not aromatic, since polarization of the central double bond would make one ring a $(4n+2)\pi$-system, but the other a $(4n)\pi$-system. On the other hand, the compounds **14** and **16** are aromatic since polarization of the central bond would make both rings $(4n+2)\pi$-systems.

From the Figs. 1 and 2, it is seen that the outer protons of the large rings of the pentatrideca- **11** and the pentaheptadecafulvalene **15** resonate in a higher field than the inner protons, while the reverse is seen in the spectra of the corresponding heptatridecafulvalene and heptaheptadecafulvalene. Thus, the large rings of **11** and **15** are suggested to be paratropic, as expected of 12π- and 16π-electron systems, respectively, owing to polarization of the central double bond. On the other hand, in the spectra of the pentapentadeca- **14** and the pentanonadecafulvalene **16**, the olefinic protons of the large rings resonate in a very narrow region, whereas the outer protons of the heptapentadecafulvalene and the heptanonadecafulvalene resonate in a higher field

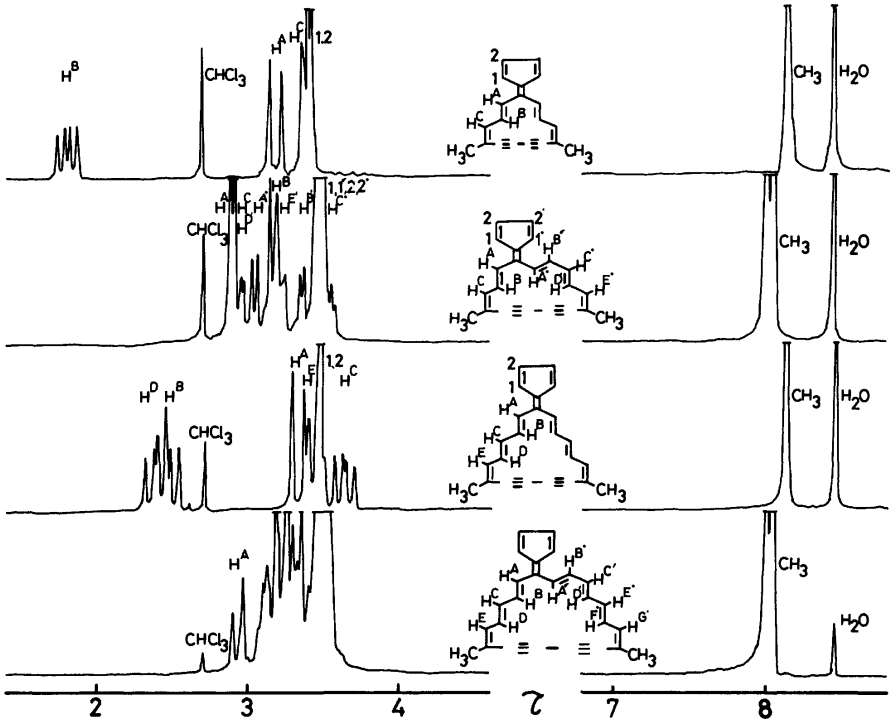

Fig. 1. ^{1}H NMR spectra of Pentatrideca- 11, Pentapentadeca- **14**, Pentaheptadeca- **15**, and Pentanonadecafulvalene **16** in $CDCl_3$ at 21 °C (200 MHz, τ values, internal standard, TMS).

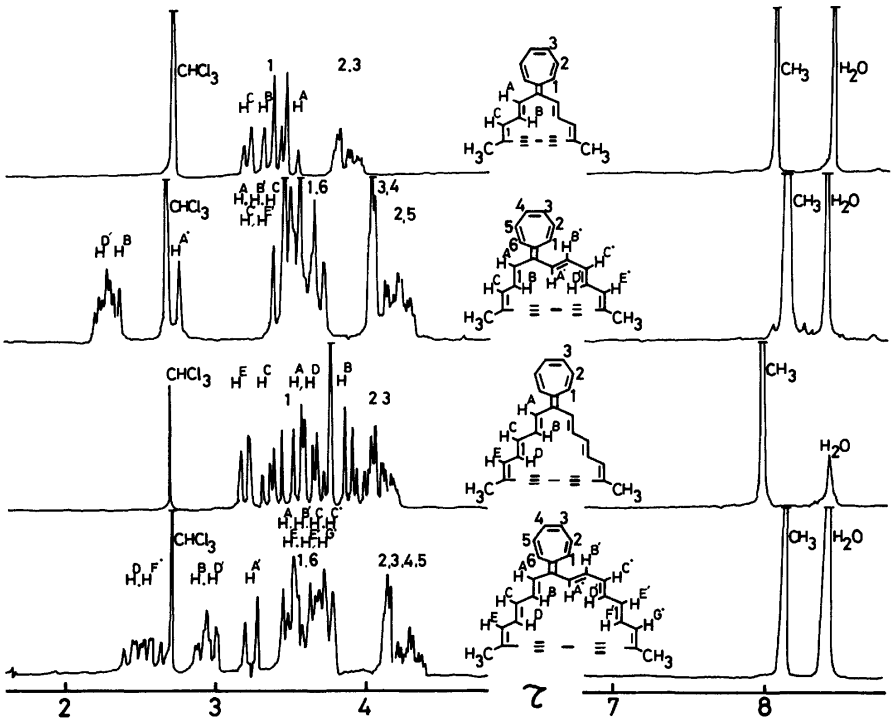

Fig. 2. ^{1}H NMR spectra of Heptatrideca-, Heptapentadeca-, Heptaheptadeca-, and Heptanonadecafulvalene in $CDCl_3$ at 21 °C (200 MHz, τ values, internal standard, TMS).

than the inner protons, as expected of 16π- and 20π-electron systems as before. Thus, although the large membered rings of **14** and **16** are suggested to be atropic, we considered that a systematic examination of the methyl resonances of these fulvalenes would provide a diagnostic tool to test the tropicity since the methyl groups must always be outside the ring and can readily be recognized.[2,6]

Table 1. The ^{1}H NMR Chemical Shifts of Methyl Protons of Compounds 1, **4—6** (90 MHz), **9** (200 MHz), and **11**, **14—16** (200 MHz) ($CDCl_3$, τ Value, at 21 °C

Large-membered ring	Annulenones **1**, **4—6**	Heptafulvalenes **9**	Pentafulvalenes **11**, **14—16**
[13]	8.26	8.08	8.13
[15]	7.76, 7.82	8.18	8.00, 8.05
[17]	8.23	8.00	8.12
[19]	7.79, 7.83	8.14	8.00, 8.04

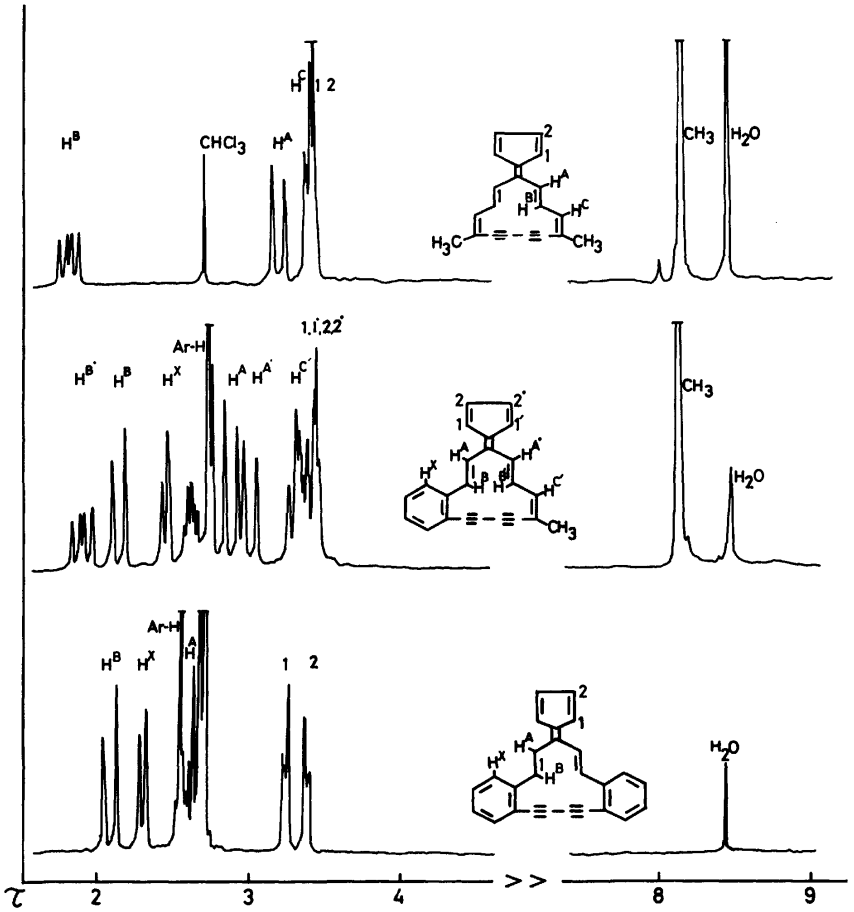

Fig. 3. ^{1}H NMR spectra of pentatrideca- 11, Benzpentatrideca- **12**, and Dibenzpentatridecafulvalene **13** in $CDCl_3$ at 21 °C (200 MHz, τ values, internal standard, TMS).

The chemical shifts of the methyl resonances of the pentafulvalenes **11**, **14—16** are listed in Table 1, altogether with those of the corresponding annulenones **1**, **4—6** and the heptafulvalenes **9**. As can be seen from the Table 1, the alternation of the methyl resonances between the [4*n*+1]annulenones ([13]- **1**, [17]annulenone **5**) (relatively high field) and [4*n*+3]annulenones ([15]- **4**, [19]annulenone **6**) (relatively low field) confirm the paratropicity of the former and the diatropicity of the latter,[2,6] owing to polarization of a carbonyl group. As expected from polarization of the central double bond of the pentafulvalenes, the alternation of the methyl resonances of the large-membered rings between the trideca- **11**, the heptadeca- **15** and pentadeca- **14**, the nonadecafulvalene **16** is seen in the same trend as that in the cases of annulenones **1**, **4—6**, albeit the degree of the alternation being much less than that of annulenones. On the other hand, the alternation of the methyl resonances between 13-, 17- and 15, 19-membered rings of the heptafulvalenes is seen in the reverse trend, as compared with that of annulenones and the pentafulvalenes, in agreement with that the heptafulvalenes **9** polarize from 7-membered ring to large ring. Thus, it can be suggested that a very little π-electron polarization from the large rings to 5-membered ring occurs in these pentafulvalenes **11**, **14—16**.

The ^{1}H NMR spectra of the pentatridecafulvalene **11** and its benzo-annelated derivatives **12**, **13** are shown in Fig. 3. As is seen from the Fig. 3, the differences of the chemical shifts between the inner

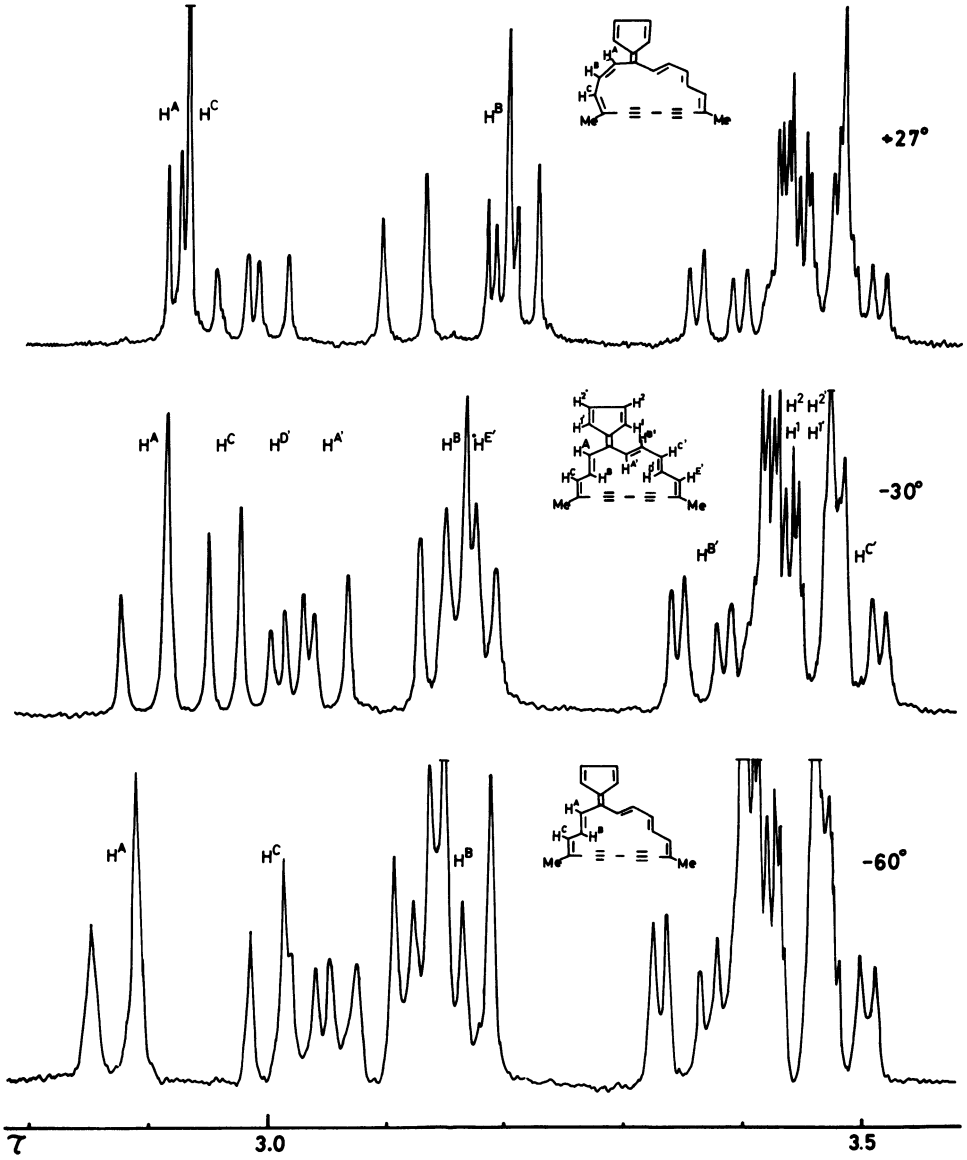

Fig. 4. ^{1}H NMR spectra of Pentapentadecafulvalene **14** at 27 °C, −30 °C, and −60 °C in $CDCl_3$ (400 MHz, τ values, internal standard, TMS).

protons and the outer protons of the large rings, which can be regarded as an approximate measure of the tropicity, become small in the sequence of **11**>**12**>**13**, with increasing number of fused benzene rings on the large rings. This fact suggests that the benzo-annelated fulvalenes **12**, **13** have less delocalized π-electron systems than that of non-benzo-annelated one **11**, as evidenced from the electronic absorption spectra of these compounds (vide infra) and has been demonstrated for the annulene,[10] dehydroannulene,[10] and dehydroannulenone[3] system.

Variable-temperature ^{1}H NMR spectra of these fulvalenes were run at 200 MHz over the range of −60 to 60 °C, and the results show the spectra of the fulvalenes **11**—**13**, **15**, **16** to be essentially temperature-independent, excluding any change of the indicated conformations between these temperatures. On the other hand, the spectra of the pentapentadecafulvalene **14** are temperature-dependent, as illustrated in Fig. 4 which shows the spectra taken at 400 MHz and the resonances of only the olefinic protons.

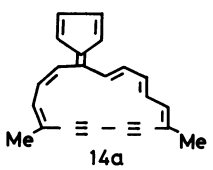

14a

In rather surprisingly contrast to the cases of **11**, **15**, and **16**, the pentadecafulvalene does not exist in the conformation **14**, but in the more unlike conformation **14a** at room temperature. This follows from the fact that the value of $J_{B,C}$ value is 4.5 Hz, indicating an s-cis relationship of the CH^B-CH^C bond, and both the H^A and H^C protons resonate in almost same field. On

Table 2. Electronic Absorption Spectra of the Fulvalenes **11**—**16** (a in THF, b in Acetonitrile); Maxima or Shoulders (sh) in nm (a, ε Values; b, Relative Extinction Coefficients, in Parentheses)

11	a	248 sh (15500),	261 (23200),	274 (21000),	310 (18900),	376 sh (25000),	397 (33600),	417 sh (28200)
	b	247 sh (0.58),	259 (0.79),	272 (0.69),	308 (0.60),	373 sh (0.76),	392 (1.00),	413 sh (0.84)
12	a		274 (25800),	285 (27000),	318 (19900),		392 (24300),	413 sh (19100)
	b		269 sh (0.98),	283 (1.00),	316 (0.73),		387 (0.75),	411 sh (0.59)
13	a		280 sh (32000),	294 (41800),	322 (28400),		379 (28900),	401 sh (20600)
	b		277 sh (0.75),	291 (1.00),	320 (0.71),		376 (0.70),	397 sh (0.51)
14	a	268 sh (19700),	279 (23700),		343 (29000),			432 (18200)
	b	260 sh (0.66),	277 (0.88),		338 (1.00),			427 (0.60)
15	a	276 sh (23000),	288 (34600),	304 (28800),	355 (25700),		428 (26500),	469 sh (15000)
	b	275 sh (0.74),	286 (1.00),	302 (0.82),	354 (0.74),		419 (0.75),	468 sh (0.51)
16	a		303 (35000),		371 (47900),		460 sh (20800)	
	b		302 (0.73),		369 (1.00),		458 sh (0.41)	

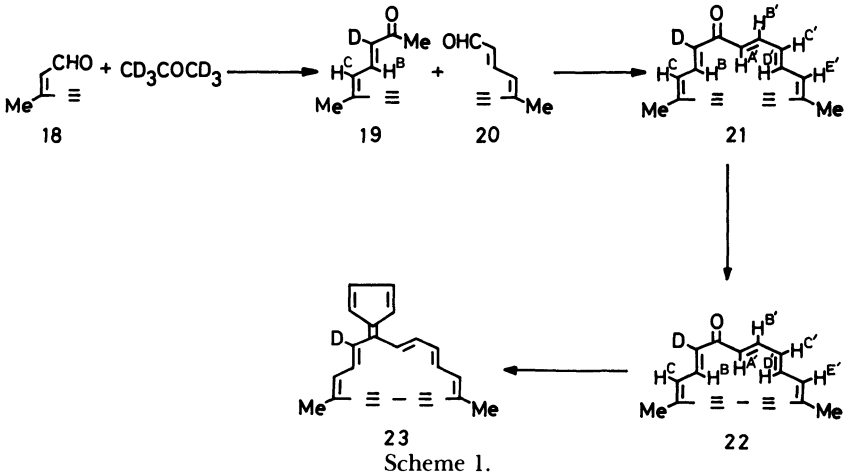

Scheme 1.

cooling, the H^A proton resonance moves to a slightly lower field and the H^C proton resonance to a slightly higher field, and the $J_{B,C}$ value varies to 10.5 Hz, indicating an s-trans relationship of the CH^B–CH^C bond at −30 °C. Further cooling results in an increasing separation of the H^A and H^C resonances. Thus, **14** exists in the similar conformation to those of **11**, **15**, and **16** at low temperature.

The observed temperature-dependency of the spectrum of **14** suggests that the molecular skeleton of **14** is mobile, particularly around CH^A–CH^B–CH^C moiety at room temperature, presumably due to a steric hindrance between H^1 and $H^{B'}$ protons. It is predicted that the pentanonadecafulvalene **16** would experience the similar hindrance, but the skeleton of **16** might presumably relieve the hindrance since a larger 19-membered ring would be more flexible than a 15-membered ring.[6]

We undertook a synthesis of 2-deuterio-labeled isomer **23** according to the reaction sequence in the Scheme 1 in order to understand the temperature-dependency of the ^1H NMR spectrum of **14** more exactly as well as to make the spectrum simple for assignment. However, the content of the deuterium of the isomer **23** obtained is quite small, and we could not get a significant result from comparison of the spectra between **14** and **23**.

We also attempted to obtain α-ethyl substituted pentafulvalenes as similarly as described for preparation of **11** and **14**, but we could not isolate any isomer from both 2-ethyl-5,10-dimethyl-6,8-bisdehydro-[13]annulenone (**24**)[4a] and 15-ethyl-5,10-dimethyl-6,8-bisdehydro[15]annulenone (**25**).[4b] From 2-ethyl-5,10-dimethyl-6,8-bisdehydro[15]annulenone (**26**),[4b] we isolated only the compound **27** which formed by conjugative addition between cyclopentadienide and **26**.

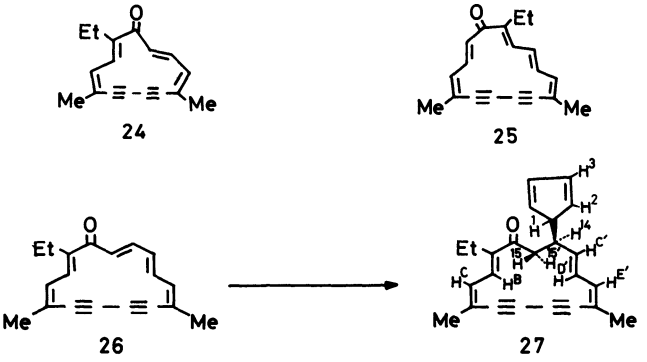

Electronic Spectra. The electronic absorption maxima of the pentafulvalenes **11—16**, determined in both tetrahydrofuran and acetonitrile, are listed in Table 2. As is seen from the Table 2, it is evident that all the bands of the fulvalenes **11—16** shows small bathochromic shift by changing the solvent from nonpolar (tetrahydrofuran) to polar solvent (acetonitrile). This solvent effect strongly supports the interpretation that a little π-electron polarization occurrs at the central double bond in the ground state of the pentafulvalene system, in agreement with the above-mentioned result from the examination of ^{1}H NMR spectra.

It is recognized that $(4n+2)\pi$-electron systems show the main maxima at higher wavelengths than $(4n)\pi$-systems in monocyclic annulenes,[13] dehydroannulenes,[13] dehydroannulenones,[2] and the fulvenes **7**, **8**.[7,8] Although the electronic spectra of these fulvalenes are not illustrated, the absorption curves are complex, but the spectra of the trideca- **11** and the pentadecafulvalene **14** are rather similar to those of the heptadeca- **15** and the nonadecafulvalene **16**, respectively. In the spectra of **11**, **14—16**, the main absorption bands exhibit a bathochromic shift as the ring size increases (Table 2), but it is not clear that the same sort of alternation of the main maxima occurrs between **11**, **15**, and **14**, **16**, as recognized in monocyclic $(4n+2)\pi$- and $(4n)\pi$-systems.[13]

The spectra of **11—13** are similar to one another as expected (Table 2),[11] and the medium bands shift to shorter wavelengths in the order of **13>12>11**, revealing that the fusion of benzene rings results in an appreciable bathochromic shift, as has been observed in benzo-annelated annulenes.[14] In contrast, the longest wavelength bands exhibit absorption toward longer wavelengths in the sequence of **11>12>13**, demonstrating that the fused benzene rings inhibit the degree of conjugation of π-electrons in these fulvalene system.[10]

Experimental

Melting points were determined on a hot-stage apparatus and are uncorrected. IR spectra were measured on Hitachi 260-50 spectrophotometer as KBr disk unless otherwise stated; only significant maxima are reported. Electronic spectra were determined on Hitachi 220A spectrophotometer (sh= shoulder). ^{1}H NMR spectra were measured on Varian XL-200 (200 MHz), JEOL FX-200 (200 MHz), or JEOL JX-400 (400 MHz) spectrometer and refer to solutions in $CDCl_3$, in τ-values with TMS as an internal standard. The coupling constants (J) are given in Hz. Assignments were assisted by decoupling experiments where necessary. Mass spectra were determined with JMS D-200 spectrometer at 75 eV using a direct inlet system. Alumina for column chromatography refers to Merck activity II-III. Reactions were followed by TLC aluminum sheets precoated with Merck Silica gel F_{254}. Freshly deoxygenated ether was used to minimize oxidation of the compounds employed for aldol condensation and was prepared by passing through a short column of Woelm basic alumina (activity I), followed by flushing with nitrogen, immediately before use. Organic extracts were dried over sodium sulfate prior to solvent removal.

5,10-Dimethyl-6,8-bisdehydropentatridecafulvalene (11). Freshly distilled cyclopentadiene (100 ml) was added to a stirred solution of sodium methoxide [from sodium (2.0 g) and dry methanol (350 ml)] during 15 min at −8 °C under nitrogen, and the solution was stirred for a further 10 min. A solution of [13]annulenone **1**[1] (453 mg, 2.17 mmol) in dry THF (100 ml) was then added at −8 °C during 25 min, and the solution was stirred for a further 1 h at the same temperature. After addition of ethyl acetate (50 ml), the mixture was poured into water. The separated aqueous layer was extracted with benzene and the combined organic extracts were washed with water. The residue after solvent removal was passed through a short column of alumina (3.7×3.0 cm) with 30% ether in hexane. The residual liquid obtained by concentrating the eluents was chromatographed on alumina (3.7×9.0 cm). The initial fractions, eluted with hexane, afforded fulvalene **11** (59.8 mg, 10.7%). It formed dark red needles, mp 103 °C, from hexane-benzene: MS m/z 256 (M^+, 39%) and 239 (100); mol wt 256.3; UV, see Table 2; IR 2150 (C≡C) and 970 cm^{-1} (*trans* HC=CH); ^{1}H NMR (200 MHz) τ=1.81 (dd, J=16, 10 Hz, 2H, H^B), 3.19 (d, J=16 Hz, 2H, H^A), 3.38 (d, J=10 Hz, 2H, H^C), 3.38—3.42 (m, 4H, H^1, H^2), 8.13 (s, 6H, Me), and see Fig. 1.

Found: C, 93.33; H, 6.43%. Calcd for $C_{20}H_{16}$: C, 93.71; H, 6.43%.

10-Methyl-6,8-bisdehydro-4,5-benzopentatridecafulvalene (12). To a cyclopentadienide solution, prepared from cyclopentadiene (100 ml), sodium (2.0 g), dry methanol (350 ml) as described for the preparation of **11**, was added dropwise a solution of benz[13]annulenone **2**[3a] (501 mg, 1.72 mmol) in dry THF (100 ml) during 25 min at −9 °C under nitrogen and the solution was stirred for a further 1 h at the same temperature. After work up as described for the isolation of **11**, the product was passed through a short column of alumina (3.0×4.0 cm) with hexane-ether (2:3). The residual red liquid after solvent removal was chromatographed on alumina (3.0×8.0 cm). The fractions eluted with 3% ether in hexane afforded fulvalene **12** (46.8 mg, 7.8%). It formed brown needles, mp 108 °C (decomp), from hexane-benzene: MS m/z 292 (M^+, 83%) and 276 (100); mol wt 292.3; UV, see Table 2; IR 2175 (C≡C) and 960 cm^{-1} (*trans* HC=CH); ^{1}H NMR (200 MHz) τ=1.91 (dd, J=16, 10.5 Hz, 1H, $H^{B'}$), 2.15 (d, J=16.5 Hz, 1H, H^B), 2.45 (d, J=7.5 Hz, 1H, H^X), 2.58—2.77 (m, 3H, Ar-H), 2.89 (d, J=16.5 Hz, 1H, H^A), 3.02 (d, J=16 Hz, 1H, $H^{A'}$), 3.29 (d, J=10.5 Hz, 1H, $H^{C'}$), 3.30—3.48 (m, 4H, H^1, $H^{1'}$, H^2, $H^{2'}$), 8.12 (s, 3H, Me), and see Fig. 3.

Found: C, 94.58; H, 5.32%. Calcd for $C_{23}H_{16}$: C, 94.48; H, 5.52%.

6,8-Bisdehydro-4,5:10,11-dibenzopentatridecafulvalene (13). To a cyclopentadienide solution, prepared from cyclopentadiene (100 ml), sodium (2.0 g), dry methanol (350 ml) as described above, was added dropwise a solution of dibenz[13]annulenone **3**[3a] (732 mg, 2.61 mmol) in dry THF (100 ml) during 30 min at −7 °C under nitrogen and the solution was stirred for a further 1.5 h at the same temperature. After work up as for the isolation of **11**, the product was passed through a short column of alumina (3.0×4.0 cm) with ether-hexane (1:1). The residue after solvent removal was chromatographed on alumina (3.7×7.5 cm). The fractions eluted with 3—5% ether in hexane afforded fulvalene **13** (33.0 mg, 3.85%). It formed brown needles, mp 173 °C (decomp), from hexane-benzene: MS m/z 328 (M^+, 96%)

and 326 (100); mol wt 328.3; UV, see Table 2; IR 2190 (C≡C) and 965 cm^{-1} (*trans* HC=CH); ^1H NMR (200 MHz) τ=2.09 (d, J=16.5 Hz, 2H, H^B), 2.30 (d, J=7.5 Hz, 2H, H^X), 2.59 (d, J=16.5 Hz, H^A), 2.52—2.74 (m, 6H, Ar-H), 3.22—3.26 (m, 2H, H^1), 3.36—3.40 (m, 2H, H^2), and see Fig. 3.

Found: C, 95.06; H, 4.75%. Calcd for $C_{26}H_{16}$: C, 95.05; H, 4.91%.

5,10-Dimethyl-6,8-bisdehydropentapentadecafulvalene (14). To a cyclopentadienide solution, prepared from cyclopentadiene (100 ml), sodium (2.0 g), dry methanol (300 ml) as described above, was added dropwise a solution of [15]annulenone **4**[2] (624 mg, 2.21 mmol) in dry THF (80 ml) during 20 min at −4 °C under nitrogen, and the solution was stirred for a further 40 min at the same temperature. After work up as for the isolation of **11**, the product was passed through a short column of alumina (3.7×3.5 cm) with ether. The residual red liquid after solvent removal was chromatographed on alumina (3.7×8.0 cm). The fractions eluted with 2% ether in hexane afforded fulvalene **14** (31.7 mg, 4.9%). It formed brown needles, mp 164 °C (decomp), from hexane-benzene: MS m/z 282 (M^+, 68%) and 265 (100); mol wt 282.3; UV, see Table 2; IR 2160 (C≡C), 980, and 960 cm^{-1} (*trans* HC=CH); ^1H NMR (400 MHz, 27 °C) τ=2.92 (d, J=7 Hz, 1H, H^A), 2.93 (d, J=4.5 Hz, 1H, H^C), 2.98 (dd, J=15, 11 Hz, 1H, $H^{D'}$), 3.13 (d, J=16 Hz, 1H, $H^{A'}$), 3.21 (dd, J=7, 4.5 Hz, 1H, H^B), 3.24 (d, J=11 Hz, 1H, $H^{E'}$), 3.41 (dd, J=16, 5 Hz, 1H, $H^{B'}$), 3.45—3.54 (m, 4H, H^1, $H^{1'}$, H^2, $H^{2'}$), 3.54 (dd, J=16, 5 Hz, 1H, $H^{C'}$), 8.00 (s, 3H, Me), 8.05 (s, 3H, Me), and see Figs. 1 and 4; (400 MHz, −60 °C) τ=2.87 (d, J=15 Hz, 1H, H^A), 3.00 (d, J=10.5 Hz, 1H, H^C), 3.04 (dd, J=15, 11 Hz, 1H, $H^{D'}$), 3.12 (dd, J=11 Hz, 1H, $H^{E'}$), 3.17 (d, J=15 Hz, 1H, $H^{A'}$), 3.18 (dd, J=15, 11 Hz, 1H, H^B), 3.35 (dd, J=16, 5 Hz, 1H, $H^{B'}$), 3.38—3.48 (m, 4H, H^1 and H^2), 3.49 (dd, J=16, 5 Hz, 1H, $H^{C'}$), 8.03 (s, 3H, Me), 8.07 (s, 3H, Me), and see Fig. 4.

Found: C, 93.52; H, 6.30%. Calcd for $C_{22}H_{18}$: C, 93.57; H, 6.43%.

7,12-Dimethyl-8,10-bisdehydropentaheptadecafulvalene (15). To a solution of cyclopentadienide, prepared from cyclopentadiene (100 ml), sodium (2.0 g), dry methanol (350 ml), was added dropwise a solution of [17]annulenone **5**[2] (808 mg, 3.10 mmol) in dry THF (100 ml) during 30 min at −5 °C under nitrogen, and the solution was stirred for a further 40 min at the same temperature. After work up as for the isolation of **11**, the product was passed through a short column of alumina (3.7×3.0 cm) with ether. The residual red liquid after solvent removal was chromatographed on alumina (3.7×8.0 cm). The fractions eluted with 2% ether in hexane afforded fulvalene **15** (44.1 mg, 4.61%). It formed dark brown needles, mp 177 °C (decomp), from hexane-benzene: MS m/z 308 (M^+, 53%) and 277 (100); mol wt 308.4; UV, see Table 2; IR 2170 (C≡C) and 985 cm^{-1} (*trans* HC=CH); ^1H NMR (200 MHz) τ=2.39 (dd, J=16, 11 Hz, 2H, H^D), 2.48 (dd, J=16, 11 Hz, 2H, H^B), 3.34 (d, J=16 Hz, 2H, H^A), 3.44 (d, J=11 Hz, 2H, H^E), 3.46—3.50 (m, 4H, H^1, H^2), 3.65 (dd, J=16, 11 Hz, 2H, H^C), 8.12 (s, 6H, Me), and see Fig. 1.

Found: C, 93.39; H, 6.53%. Calcd for $C_{24}H_{20}$: C, 93.46; H, 6.54%.

7,12-Dimethyl-8,10-bisdehydropentanonadecafulvalene (16). To a solution of cyclopentadienide, prepared from cyclopentadiene (100 ml), sodium (2.0 g), dry methanol (350 ml), was added dropwise a solution of [19]annulenone **6**[2] (704 mg, 2.46 mmol) in dry THF (100 ml) during 25 min at −6 °C under nitrogen and the solution was stirred for a further 50 min at the same temperature. After work up as for the isolation of **11**, the product was passed through a short column of alumina (3.7×3.5 cm) with hexane-ether (1:1). The residual red liquid after solvent removal was chromatographed on alumina (3.7×8.0 cm). The fractions eluted with 5% ether in hexane afforded fulvalene **16** (56.0 mg, 6.81%). It formed dark purple cubes, mp 158 °C (decomp), from hexane-benzene: MS m/z 334 (M^+, 78%) and 303 (100); mol wt 334.4; UV, see Table 2; IR 2170 (C≡C) and 985 cm^{-1} (*trans* HC=CH); ^1H NMR (400 MHz) τ=2.97 (d, J=15 Hz, 1H, H^A), 3.17 (dd, J=15, 11 Hz, 1H, H^D), 3.18 (dd, J=15, 11 Hz, 1H, $H^{F'}$), 3.18 (d, J=15 Hz, 1H, $H^{A'}$), 3.30 (d, J=11 Hz, 1H, $H^{G'}$), 3.32 (dd, J=15, 11 Hz, 1H, H^B), 3.32 (d, J=11 Hz, 1H, H^E), 3.41 (dd, J=15, 11 Hz, 1H, $H^{D'}$), 3.49—3.58 (m, 8H, $H^{B'}$, H^C, $H^{C'}$, $H^{E'}$, H^1, $H^{1'}$, H^2, $H^{2'}$), 8.00 (s, 3H, Me), 8.04 (s, 3H, Me), and see Fig. 1.

Found: C, 93.54; H, 6.70%. Calcd for $C_{26}H_{22}$: C, 93.37; H, 6.63%.

3-Deuterio-6-methyl-3,5-octadien-7-yn-2-one (19). An ice-cooled solution of sodium hydroxide (0.65 M (1 mol dm^{-3}), 5.0 ml) in heavy water (D_2O) and ethanol-d_4 (5.0 ml) was added in one portion to an ice-cooled solution of (*Z*)-3-methyl-2-penten-4-ynal **18**[15] (1.70 g, 18.1 mmol) in acetone-d_6 (10.0 ml). The solution was stirred for a further 1 h at 0 °C and dilute sulfuric acid (2 M, 10 ml) was then added. The solution was poured into water and extracted with benzene. The combined extracts were washed successively with aqueous sodium hydrogencarbonate and brine. The residue after solvent removal was chromatographed on alumina (3.7×10.0 cm). The fractions eluted with 5% ether in hexane afforded the ketone **19** (1.01 g, 40%) as a yellow liquid: MS m/z 135 (M^+, 41%) and 120 (100); mol wt 135.2; IR (neat) 3300, 3250 (C≡CH), 2100 (C≡C), 1660 (C=O), 1610 (C=C), and 990 cm^{-1} (*trans* HC=CH); UV (EtOH) λ_{max} 299 nm (ε 17800); ^1H NMR (90 MHz) τ=2.49 (d, J=11 Hz, 1H, H^B), 3.59 (d, J=11 Hz, 1H, H^C), 6.51 (s, 1H, C≡CH), 7.69 (s, 3H, Me), 7.96 (s, 3H, Me).

6-Deuterio-3,13-dimethyl-3,5,8,10,12-pentadecapentaene-1,14-diyn-7-one (21). An ethanolic sodium ethoxide (3.0 ml) from sodium (380 mg) and dry ethanol (50 ml) was added in one portion to a solution of ketone **19** (1.01 g, 7.29 mmol) and (2*E*,4*Z*)-5-methyl-2,4-heptadien-6-ynal **20**[16] (1.0 g, 8.3 mmol) in deoxygenated ether (50 ml). After being stirred for a further 6 h at 3—5 °C, the reaction was quenched by addition of 2 M sulfuric acid (10 ml). After work up as for the isolation of **19**, the residue after solvent removal was chromatographed on alumina (4.0×9.0 cm). The fractions eluted with 30% ether in hexane afforded ketone **21** (606 mg, 35%). It formed yellow needles, mp 105—106 °C, from hexane-benzene: MS m/z 237.1237, calcd for 237.1263; UV (Et_2O) λ_{max} 230 (sh, ε 8000), 246 (sh, 12100), and 360 nm (32300); IR 3280 (C≡CH), 2100 (C≡C), 1655 (C=O), 1605, 1595 (C=C), and 1005 cm^{-1} (*trans* HC=CH); ^1H NMR (90 MHz) τ=2.32 (d, J=11 Hz, 1H, H^B), 2.61 (dd, J=16, 11 Hz, 1H, $H^{B'}$), 2.92 (dd, J=16, 11 Hz, 1H, $H^{D'}$), 3.45—3.66 (m, 4H, $H^{A'}$, H^C, $H^{C'}$, $H^{E'}$), 6.51 (s, 1H, C≡CH), 6.57 (s, 1H, C≡CH), 7.96 (s, 3H, Me), 8.00 (s, 3H, Me).

2-Deuterio-5,10-dimethyl-6,8-bisdehydro[15]annulenone (22). A solution of ketone **21** (1.25 g, 5.26 mmol) in pyridine and dry ether (3:1, 120 ml) was added dropwise during 4 h to a stirred solution of anhydrous copper(II) acetate (6.8 g) in pyridine and dry ether (3:1, 400 ml) at 50—52 °C. The solution was stirred for a further 30 min at the same temperature and was then cooled. The reaction mixture was

poured into water and extracted with benzene. The combined extracts were washed with 5% hydrochloric acid until it turned acidic, then with aqueous sodium hydrogencarbonate solution, successively. The dark red liquid after solvent removal was chromatographed on alumina (3.7×8.0 cm). The fractions eluted with 30% ether in hexane afforded annulenone **22** (427 mg, 25%). It formed yellow needles, mp 159°C (decomp), from hexane-benzene: MS *m/z* 235.1107, Calcd for 235.1107; UV (Et_2O) λ_{max} 245 (ε 11600), 257 (13100), 302 (35800), and 382 nm (5900); IR 2180 (C≡C), 1635 (C=O), 1605 (C=C), and 980 cm^{-1} (*trans* HC=CH); ^1H NMR (90 MHz) τ=2.46 (dd, *J*=16, 5 Hz, 1H, $H^{B'}$), 2.80 (d, *J*=11 Hz, 2H, H^{C}, $H^{E'}$), 3.20 (dd, *J*=16, 5 Hz, 1H, $H^{C'}$), 4.22 (d, *J*=11 Hz, 1H, H^{B}), 4.39 (d, *J*=16 Hz, 1H, $H^{A'}$), 4.57 (dd, *J*=16, 11 Hz, 1H, $H^{D'}$), 7.76 (s, 3H, Me), and 7.82 (s, 3H, Me).

2-Deuterio-5,10-dimethyl-6,8-bisdehydropentapentadecafulvalene (23). To a solution of cyclopentadienide, prepared from cyclopentadiene (100 ml), sodium (2.0 g), dry methanol (300 ml), was added dropwise a solution of annulenone **22** (363 mg, 1.54 mmol) in dry THF (50 ml) during 20 min at −6°C and the solution was stirred for a further 1 h at the same temperature. After work up as for the isolation of **11**, the product was passed through a short column of alumina (3.7×4.0 cm) with hexane-ether (3:2). The residual red liquid after solvent removal was chromatographed on alumina (3.7×8.0 cm). The fractions eluted with hexane afforded fulvalene **23** (10.6 mg, 2.3%). It formed brown needles, mp 158°C (decomp), from hexane-benzene: MS *m/z* 283.1543, Calcd for 283.1472; The IR, UV, and ^1H NMR were almost the same as those of **14**.

Attempts to obtain α-ethyl-substituted fulvalenes from the α-ethyl-substituted [13]annulenone **24**[4a] and [15]annulenone **25**[4b] were carried out as the exactly same conditions as for the isolation of **11**. However, none of fulvalene was isolated.

14-(2,4-Cyclopentadienyl)-2-ethyl-5,10-dimethyl-2,4,10,12-cyclopentadecatetraene-6,8-diyn-1-one (27). Conjugative Adduct of Cyclopentadiene and 26. To a solution of cyclopentadienide, prepared from cyclopentadiene (100 ml), sodium (2.0 g), dry methanol (250 ml), was added dropwise a solution of [15]annulenone **26**[4b] (770 mg, 2.94 mmol) in dry THF (100 ml) during 30 min at −8°C under nitrogen and the solution was stirred for a further 1 h at the same temperature. After work up as for the isolation of **11**, the product was passed through a short column of alumina (4.0×3.0 cm) with 30% ether in hexane. The residual red liquid after solvent removal was chromatographed on alumina (3.7×7.5 cm). The fractions eluted with 10% ether in hexane afforded the adduct **27** (513 mg, 56.3%). It formed yellow needles, mp 139—140°C, from hexane-benzene: MS *m/z* 328 (M^+, 100%); mol wt 328.4; UV (THF) λ_{max} 239 (sh, ε 11700), 250 (sh, 14400), 276 (sh, 35500), 287 (43700), 381 (6350), and 423 nm (sh, 4260); IR 2170 (C≡C), 1665 (C=O), 1630, 1600 (C=C), and 970 cm^{-1} (*trans* HC=CH); ^1H NMR (90 MHz) τ=2.10 (d, *J*=11 Hz, 1H, H^{C}), 2.88—3.06 (m, 8H, H^{B}, $H^{C'}$, $H^{D'}$, $H^{E'}$, H^{2}, H^{2}, H^{3}, H^{3}), 5.96—6.22 (m, 1H, H^{14}), 6.39 (dd, *J*=16.5, 3 Hz, 1H, $H^{15'}$), 6.92 (dd, *J*=16.5, 11 Hz, 1H, H^{15}), 7.05 (s, 1H, H^{1}), 7.63 (q, *J*=7 Hz, 2H, $-C\underline{H}_2CH_3$), 7.99 (s, 3H, Me), 8.13 (s, 3H, Me), and 9.06 (t, *J*=7 Hz, 3H, $-CH_2C\underline{H}_3$).

Found: C, 87.46; H, 7.36%. Calcd for $C_{24}H_{24}O$: C, 87.76; H, 7.36%.

The present work was partially supported by a Grant-in-Aid for Scientific Research No. 58540306 from the Ministry of Education, Science and Culture.

References

1) T. M. Cresp, J. Ojima, and F. Sondheimer, *J. Org. Chem.*, **42**, 2130 (1977).

2) J. Ojima, Y. Shiroishi, K. Wada, and F. Sondheimer, *J. Org. Chem.*, **45**, 3564 (1980).

3) a) J. Ojima and M. Fujiyoshi, *Chem. Lett.*, **1978**, 569; *J. Chem. Soc., Perkin Trans. 1*, **1980**, 466; b) J. Ojima, K. Kanazawa, K. Kusaki, and K. Wada, *Chem. Lett.*, **1978**, 1009; *J. Chem. Soc., Perkin Trans. 1*, **1980**, 473; c) J. Ojima, K. Wada, and K. Kanazawa, *Chem. Lett.*, **1979**, 1035; J. Ojima, K. Wada, K. Kanazawa, and Y. Nakagawa, *J. Chem. Soc., Perkin Trans. 1*, **1981**, 947; d) J. Ojima, K. Wada, Y. Nakagawa, M. Terasaki, and Y. Juni, *Chem. Lett.*, **1980**, 225; *J. Chem. Soc., Perkin Trans. 1*, **1982**, 31.

4) a) J. Ojima, Y. Juni, Y. Yoneyama, K. Wada, and Y. Murosawa, *Bull. Chem. Soc. Jpn.*, **54**, 3466 (1981); b) J. Ojima and Y. Murosawa, *ibid.*, **54**, 3473 (1981).

5) J. Ojima, Y. Nakagawa, K. Wada, and M. Terasaki, *Chem. Lett.*, **1980**, 1209; *J. Chem. Soc., Perkin Trans. 1*, **1982**, 43.

6) J. Ojima, K. Wada, and M. Terasaki, *Tetrahedron Lett.*, **1981**, 457; *J. Chem. Soc., Perkin Trans. 1*, **1982**, 51.

7) S. Kuroda, K. Kitatani, and J. Ojima, *Tetrahedron Lett.*, **1982**, 2657; J. Ojima, S. Kuroda, and M. Kirita, *Chem. Lett.*, **1982**, 1371; S. Kuroda, J. Ojima, K. Kitatani, and M. Kirita, and T. Nakada, *J. Chem. Soc., Perkin Trans. 1*, **1983**, 2987.

8) J. Ojima, K. Itagawa, S. Hamai, T. Nakada, and S. Kuroda, *J. Chem. Soc., Perkin Trans. 1*, **1983**, 2997.

9) T. Asao, N. Morita, J. Ojima, and M. Fujiyoshi, *Tetrahedron Lett.*, **1978**, 2795; N. Morita, T. Asao, J. Ojima, and K. Wada, *Chem. Lett.*, **1981**, 57; N. Morita, T. Asao, J. Ojima, and S. Hamai, *Chem. Lett.*, **1983**, 1887; and see the preceding paper.

10) For reviews, see M. Nakagawa, *Pure Appl. Chem.*, **44**, 885 (1975); R. H. Mitchell, *Isr. J. Chem.*, **20**, 594 (1980).

11) Preliminary communication, see J. Ojima and K. Itagawa, and T. Nakada, *Tetrahedron Lett.*, **1983**, 5273.

12) P. D. Howes and F. Sondheimer, *J. Org. Chem.*, **43**, 2158 (1978).

13) P. J. Garratt and K. Grohmann, *Methoden Org. Chem. (Houben-Weyl)*, **5**, 533 (1972).

14) N. Darby, T. M. Cresp, and F. Sondheimer, *J. Org. Chem.*, **42**, 1960 (1977).

15) J. Ojima, T. Katakami, G. Nakaminami, and M. Nakagawa, *Bull. Chem. Soc. Jpn.*, **49**, 292 (1976).

16) J. Ojima, M. Kirita, Y. Murosawa, and T. Nakada, *Bull. Chem. Soc. Jpn.*, **56**, 1467 (1983).

Direct Diacetylmethylation of Aromatic Compounds with Tris-(2,4-pentanedionato)manganese(III)

Hiroshi NISHINO
Department of Chemistry, Faculty of Science, Kumamoto University, Kurokami 2-39-1, Kumamoto 860
(Received January 18, 1986)

The oxidation of naphthalenes with tris(2,4-pentanedionato)manganese(III) in acetic acid gave diacetylmethyl derivatives in good to moderate yields. Using excess amounts of the oxidant, the acetylmethyl-substituted naphthalenes were further oxidized and 3-acetoxy-3-naphthyl-2,4-pentanediones were obtained. The similar oxidation of anthracenes also produced (diacetylmethyl)anthracenes together with diacetylmethylene derivatives which were further oxidized. It was found that this direct diacetylmethylation was effective when the ionization potential of the aromatic compound was lower than 8.12 eV, and that the diacetylmethyl radical which was generated directly by the thermolysis of tris(2,4-pentanedionato)manganese(III) has an electrophilic nature based on the result of the oxidation of substituted naphthalenes. The reaction pathway for the oxidation of anthracene is also discussed.

Tris(2,4-pentanedionato)manganese(III), $Mn(acac)_3$, is a well-known catalyst in polymerization, autoxidation, and peroxide reactions.[1] However, the use as an oxidant itself is rare in the literature, although the oxidative coupling reaction of phenols[2] or thiols[3] and the oxidative intramolecular cyclization of phenolic oximes[4] have been reported. Recently, the present author has found that the oxidation of olefins with $Mn(acac)_3$ gave dihydrofurans in good yields.[5] This reaction has been explained as follows. Manganese(III) complexes generally tend to undergo a rapid exchange of ligands in a donor solvent such as acetic acid which can complex manganese(III) ions,[5] and therefore, $Mn(acac)_3$ will be easily decomposed in acetic acid to form diacetylmethyl radical, $\cdot CH(COCH_3)_2$. The attack of the $\cdot CH(COCH_3)_2$ radical on olefins and subsequent oxidative cyclization afforded dihydrofurans. In the case of 9-benzylidene-9,10-dihydroanthracene, the corresponding dihydrofuran was not obtained, but one of the methylenic hydrogens of the starting olefin was replaced by the $\cdot CH(COCH_3)_2$ radical (Scheme 1).[5] This led to the present investigation of

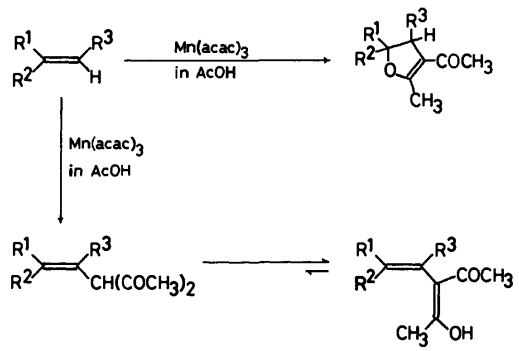

Scheme 1.

the reaction of aromatic compounds with $Mn(acac)_3$ in the hope that direct diacetylmethylation may take place. As for the similar reaction using manganese(III) complex, it is well-known that olefins are oxidized with manganese(III) acetate to give γ-lactones in good yields,[6] while the oxidation of aromatic compounds with manganese(III) acetate afforded carboxymethyl, acetoxymethyl,[7] diacetoxymethyl,[8] and carboxy derivatives.[9] These manganese(III) acetate oxidations involve the carboxymethyl radical, $\cdot CH_2CO_2H$.[7] In this paper, the author describes a new direct diacetylmethylation of aromatic compounds with $Mn(acac)_3$.

Results

When 2-methoxynaphthalene (**1a**) was oxidized with four molar equivalents of $Mn(acac)_3$ in acetic acid at 100 °C, the reaction was completed within 13 min to give **2a** (Table 1, Entry 1). The product **2a** showed a parent ion peak at m/z 256 in the mass spectrum and a broad absorption band in the IR spectrum which could be assigned to an enolized β-diketone. The ^1H NMR spectrum of **2a** indicated the presence of a 1-acetyl-2-hydroxy-1-propenyl group and an AB quartet (J=9.0 Hz) due to aromatic protons. Consequently, this spectroscopic evidence supported the structure of **2a** being 1-(1-acetyl-2-hydroxy-1-propenyl)-2-methoxynaphthalene. The reaction of **1a** with $Mn(acac)_3$ in another solvent, such as CH_3CN, did not occur.

Oxidation of 1-methoxynaphthalene (**1b**) under the same reaction conditions produced **3b** together with a diacetylmethyl derivative **2b** (Table 1, Entry 2). The structure of **3b** was determined to be 4-(1-acetoxy-1-acetyl-2-oxopropyl)-1-methoxynaphthalene on the basis of the spectral data. The ^{13}C-off-resonance decoupling of **3b** collapsed the peak at δ=102.613 (C-2) to a doublet, but the peak at δ=120.369 (C-4) did not collapse. This shows that the 1-acetoxy-1-acetyl-2-oxopropyl group was introduced at the C-4 position. Moreover, the position of the substituent group was also supported by comparing its ^1H NMR spectrum with that of **1b**. When this reaction was carried out at a molar ratio of 1:10 at reflux temperature, **3b** was obtained as the sole product (Table 1, Entry 3).

2,7-Dimethoxynaphthalene (**1c**) was oxidized with four molar equivalents of $Mn(acac)_3$ to give (acetylmethyl)naphthalene **2c**, while a nearly equimolar mixture of **2c** and **3c** was obtained in a 1:10 molar ratio reaction (Table 1, Entries 4 and 5). It was con-

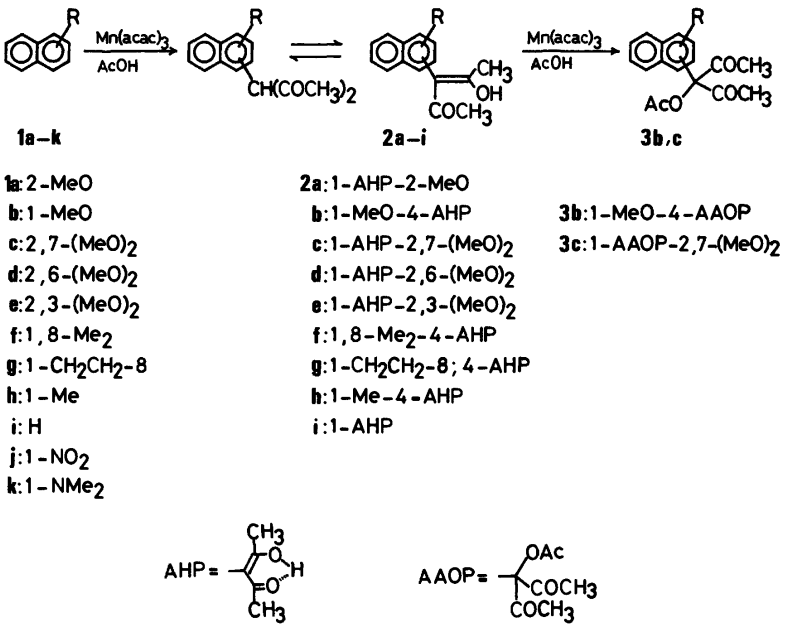

Fig. 1. Oxidation of naphthalenes (**1a—k**) with $Mn(acac)_3$ in AcOH at 100 °C.

Table 1. Oxidation of Naphthalenes with $Mn(acac)_3$ in Acetic Acid at 100 °C

Entry	Compound	Molar ratio of substrate : $Mn(acac)_3$	Time / min	Product (yield/%)[a]	
1	**1a**	1 : 4	13	**2a** (54)	
2	**1b**	1 : 2	10	**2b** (9)	**3b** (40)
3[b]	**1b**	1 : 10	2		**3b** (62)
4	**1c**	1 : 4	15	**2c** (52)	
5	**1c**	1 : 10	25	**2c** (36)	**3c** (31)
6	**1d**	1 : 4	14	**2d** (46)	
7	**1e**	1 : 4	10	**2e** (41)	
8	**1f**	1 : 4	14	**2f** (30)	
9	**1g**	1 : 4	13	**2g** (24)	
10	**1h**	1 : 4	15	**2h** (15)	
11	**1i**	1 : 4	15	**2i** (8)	
12	**2c**	1 : 2	3		**3c** (50)

a) The yields are based on the amount of the substrate consumed. b) The reaction was carried out at the reflux temperature.

firmed that the product **3c** was derived from the further oxidation of **2c** with $Mn(acac)_3$ since the diacetylmethyl derivative **2c** was oxidized under the same reaction conditions to give only the pentanedione **3c** (Table 1, Entry 12).

The oxidations of 2,6-dimethoxynaphthalene (**1d**), 2,3-dimethoxynaphthalene (**1e**), 1,8-dimethylnaphthalene (**1f**), acenaphthene (**1g**), 1-methylnaphthalene (**1h**), and naphthalene (**1i**) with $Mn(acac)_3$ were also carried out in acetic acid to yield the corresponding diacetylmethyl derivatives (**2d—i**) (Table 1, Entries 6—11). The reaction of 1-nitronaphthalene (**1j**) with $Mn(acac)_3$ did not occur under these conditions and **1j** was recovered. 1-Dimethylaminonaphthalene (**1k**) was oxidized with $Mn(acac)_3$ under the same reaction conditions to give intractable tarry materials and no diacetylmethylated products were detected.

Anthracene (**4**) gave four products (**5**, **6**, **7**, and **8**) (Table 2, Entries 1 and 2). The products **5** and **6** were determined to be anthracenes substituted by diacetylmethyl groups in their enol forms. The **7** showed characteristic carbonyl absorptions of diacetylmethyl group in the IR spectrum, and its ^1H NMR spectrum revealed an AB quartet (J=10.2 Hz) due to four protons which were assigned to methine protons of 9,10-dihydroanthracene and diacetylmethyl group. Therefore, the structure of **7** was considered to be 9,10-bis(diacetylmethyl)-9,10-dihydroanthracene. The spectroscopic data of **8** supported the symmetrical structure of 9,10-bis(diacetylmethylene)-9,10-dihydroanthracene which seemed to be formed by the further oxidation of **6** or **7**.

Acridine (**9**), xanthene (**11**), and pyrene (**17**) were oxidized with $Mn(acac)_3$ to give corresponding diacetylmethyl derivatives in good to moderate yields (Table 2, Entries 5, 6, 8, and 9). In the oxidation of

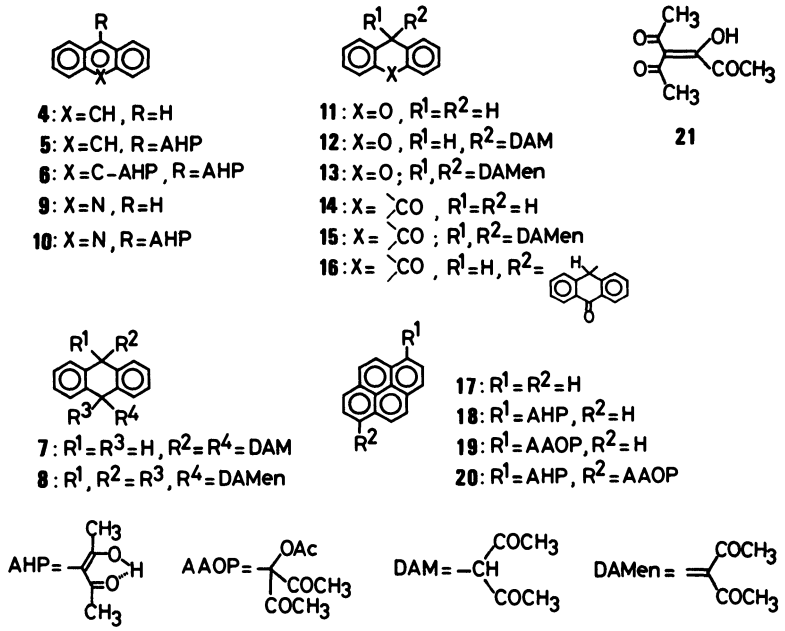

Fig. 2. Aromatic substrates and their oxidation products.

Table 2. Oxidation of Aromatic Compounds (**4**, **9**, **11**, **14**, and **17**) with $Mn(acac)_3$ in Acetic Acid at 100°C

Entry	Compound	Molar ratio of Substrate $Mn(acac)_3$	Time min	Product (yield/%)[a]
1	**4**	1:2	2	**5** (47) **6** (11) **7** (4) **8** (5)
2[b]	**4**	1:4	10	**5** (22) **6** (27) **7** (4) **8** (22)
3	**9**	1:4	14	**10** (49)
4	**11**	1:2	5	**12** (71) **13** (21)
5	**14**	1:4	19	**15** (7) **16** (78)
6	**17**	1:2	3	**18** (45) **19** (24) **20** (6)
7	**17**	1:4	8	**18** (35) **19** (23) **20** (24)

a) The yields are based on the amount of the substrate consumed. b) The reaction was carried out at the reflux temperature.

anthrone (**14**), however, a diacetylmethylene derivative **15** was obtained in poor yield, and a major product was a dimeric compound **16**. It has been reported that the product **16** was also obtained by the oxidation of **14** with manganese(III) acetate in acetic acid.[11b]

Discussion

The oxidation of aromatic compounds with manganese(III) acetate was studied in detail by Dewar et al.[10] and Heiba et al.[7] Methoxynaphthalenes (**1a** and **1b**) and anthracene (**4**) were oxidized with manganese(III) acetate in acetic acid to give naphthoquinones[10b,c] and anthraquinone,[11] respectively. These reactions were explained by the electron-transfer mechanism.[10] On the other hand, it is well-known that the free-radical mechanism involving the carboxymethyl radical, $\cdot CH_2CO_2H$, simultaneously competes with the electron-transfer process in the manganese(III) acetate-acetic acid system.[7] The attack of $\cdot CH_2CO_2H$ radicals on the aromatic ring and further oxidation mainly produces acetoxymethyl derivatives, $Ar\text{-}CH_2OAc$. Heiba and his co-workers proposed that the electron-transfer mechanism in the manganese(III) acetate-acetic acid system was observed only with aromatic compounds such as anthracene and 2-methylnaphthalene, having ionization potentials less than 8.0 eV.[7] It is also well-known that γ-lactones are obtained in good yields, when the $\cdot CH_2CO_2H$ radicals add to alkenes followed by oxidative cyclization. For this lactone annulation, it has been confirmed by subsequent experiments[12] that the lower ionization potential cutoff for useful alkenes was 8.2 eV; below this level the electron-transfer process occurred competitively. Accordingly, the free-radical mechanism in the manganese(III) acetate oxidation is characteristic for aromatic compounds and alkenes having ionization potential higher than about 8 eV.

The ionization potentials of the aromatic compounds used in this $Mn(acac)_3$ oxidation[13] and the total yields of their diacetylmethylated products are summerized in Table 3. As can be seen from this Table,

Table 3. Ionization Potentials of Aromatic Compounds and the Yields of Their Diacetylmethylated Products

Entry	Compound	Ionization potential / eV	Diacetylmethylated product yield/%[e]
1	Anthracene (**4**)	7.36[a]	75
2	Pyrene (**17**)	7.37[a]	82
3	2,6-Dimethoxynaphthalene (**1d**)	7.58[b]	46
4	1-Dimethylaminonaphthalene (**1k**)	7.59[c]	0[f]
5	1-Methoxynaphthalene (**1b**)	7.70[d]	62
6	2-Methoxynaphthalene (**1a**)	7.82[d]	54
7	1-Methylnaphthalene (**1h**)	7.96[b]	15
8	Naphthalene (**1i**)	8.12[a]	8
9	Anisole	8.39[d]	0[g]
10	1-Nitronaphthalene (**1j**)	8.59[d]	0[h]

a—d) Ref. 13. e) Total yields. f) An intractable mixture was obtained. g) No diacetylmethylated products were detected. h) This reaction did not occur and the starting material was recovered (see Experimental).

Table 4. Oxidation of Diacetylmethylated Products with $Mn(acac)_3$ in Acetic Acid at 100°C

Entry	Compound	Molar ratio of Subsrate:$Mn(acac)_3$	Time / min	Product (yield/%)[a]	Recovery / %
1	**5**	1:2	2	**6** (40) **8** (24)	29
2	**6**	1:2	2	**8** (66)	33
3	**7**	1:2	2		100
4	**7**	1:4	6	**8** (18)	77
5	**12**	1:2	2	**13** (29)	68

a) The yields are based on the amount of the substrated used.

it has been proved that the diacetylmethylation was effective when ionization potential of the aromatic compound was lower than 8.12 eV. This behavior as an oxidant is in contrast to that of manganese(III) acetate and it shows that $Mn(acac)_3$ is a weaker oxidant than manganese(III) acetate. The reason why the reaction of 1-dimethylaminonaphthalene (**1k**) with $Mn(acac)_3$ did not give any diacetylmethylated products in spite of the ionization potential was low is that a lone-pair electron on the nitrogen atom is more liable to be abstracted by $Mn(acac)_3$ than a π-electron of the aromatic ring, and then, another side-reaction such as polymerization might ensue.[15]

The existence of the $\cdot CH(COCH_3)_2$ radical in this reaction was proved indirectly by the isolation of 3-acetyl-4-hydroxy-3-hexene-2,5-dione (**21**), since **21** must be formed by a bimolecular coupling reaction of $\cdot CH(COCH_3)_2$ radicals. The **21** was produced regardless of the substrate used in the $Mn(acac)_3$-acetic acid system, and particularly, the formation of **21** was the best when the oxidation was carried out at room temperature (see Experimental and Reference).[14]

It has been suggested that the $\cdot CH(COCH_3)_2$ radical has an electrophilic nature like the $\cdot CH_2CO_2H$ radical generated in the manganese(III) acetate–acetic acid system,[7] since the diacetylmethyl group is situated at a position ortho or para to the electron-donating group in the oxidation of naphthalenes (Table 1 and Fig. 1).

When the enol **5** was oxidized with two molar equivalents of $Mn(acac)_3$, the bis(enol) **6** and the bis(diacetylmethylene)anthracene (**8**) were obtained (Table 4, Entry 1). The oxidation of **6** under the same reaction conditions gave only **8** (Table 4, Entry 2). Although 9,10-bis(diacetylmethyl)-9,10-dihydroanthracene (**7**), on the other hand, did not react with $Mn(acac)_3$ in a molar ratio of 1:2, a small amount of **8** was formed in a molar ratio of 1:4 (Table 4, Entries 3 and 4). Therefore, the route from **7** to **8** is not important. The reaction pathway for the oxidation of anthracene (**4**) with $Mn(acac)_3$ is illustrated in Scheme 2.

Thus, it is concluded that this new direct diacetylmethylation i) takes place in $Mn(acac)_3$-acetic acid system, ii) is characteristic for aromatic compounds having ionization potential lower than about 8 eV, and iii) the $\cdot CH(COCH_3)_2$ radical involved in this oxidation system is somewhat electrophilic.

Experimental

Measurements. Melting points were determined with an Electrothermal apparatus and are uncorrected. The IR spectra were taken on a JASCO A-102 infrared spectrophotometer, and the IR spectral data are expressed in cm^{-1}. The ^1H and ^{13}C NMR spectra were recorded on a Hitachi Perkin-Elmer R-24 (60 MHz) and a JEOL FX-100 instrument at room temperature. Chemical shifts are recorded in the δ scale, relative to TMS as an internal standard. The mass spectra were obtained with a JEOL JMS-DX-300 mass spectrometer using a direct-insertion probe at an ionizing voltage of 70 eV.

Materials. $Mn(acac)_3$ was prepared by the method de-

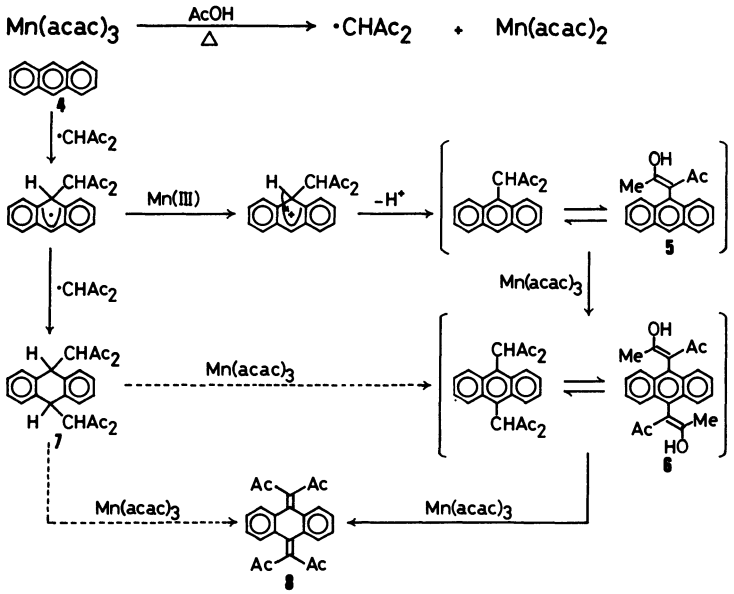

Scheme 2.

scribed in the literature.[16] Methoxynaphthalenes (**1a—e**) were synthesized by the methylation of the corresponding naphthols with dimethyl sulfate. Other starting materials (**1f—k**, **4**, **9**, **11**, **14**, and **17**) were obtained from commercial samples from the Wako Pure Chemical Industries, Ltd.

General Procedure for the Oxidation of Aromatic Compounds with $Mn(acac)_3$. The oxidation of aromatic compound (1 mmol) with a suitable amount of $Mn(acac)_3$ (indicated in the Tables) was carried out in acetic acid (25 cm^3) at 100°C until an opaque dark brown mixture changed to a clear brown solution. The solvent was removed in vacuo, and the residue was triturated with 2 M (1 M=1 mol dm^{-3}) HCl (25 cm^3) and then extracted with chloroform. The products were separated on TLC (Wako gel B-10), with chloroform as the developing solvent. The yields are summarized in Tables 1, 2, and 4.

Oxidation Products. 1-(1-Acetyl-2-hydroxy-1-propenyl)-2-methoxynaphthalene (2a): Colorless needles (from ethanol), mp 133.5—134.5°C; IR ($CHCl_3$) 1620 (COC=COH) and 3300—3600 (OH); ^1H NMR ($CDCl_3$) δ=1.71 (6H, s, 2×CH_3), 3.88 (3H, s, OCH_3), 7.29 (1H, d, J=9.0 Hz, H-3), 7.86 (1H, d, J=9.0 Hz, H-4), 7.2—7.9 (4H, m, ArH), and 16.90 (1H, s, OH); MS *m/z* (rel intensity), 256 (M^+, 100), 213 (40), 169 (30), 141 (20), and 43 (50). Found: C, 74.79; H, 6.18%. Calcd for $C_{16}H_{16}O_3$: C, 74.98; H, 6.29%.

4-(1-Acetyl-2-hydroxy-1-propenyl)-1-methoxynaphthalene (2b): Colorless needles (from methanol), mp 114.0—114.5 °C; IR ($CHCl_3$) 1610 (COC=COH) and 3300—3600 (OH); ^1H NMR ($CDCl_3$) δ=1.74 (6H, s, 2×CH_3), 3.96 (3H, s, OCH_3), 6.77 (1H, d, J=8.4 Hz, H-2), 7.17 (1H, d, J=8.4 Hz, H-3), 7.30—8.40 (4H, m, ArH), and 16.80 (1H, s, OH). Found: C, 74.67; H, 6.25%. Calcd for $C_{16}H_{16}O_3$: C, 74.98; H, 6.29%.

4-(1-Acetoxy-1-acetyl-2-oxopropyl)-1-methoxynaphthalene (3b): Colorless cubes (from ethanol), mp 179.5—180.0°C; IR ($CHCl_3$) 1722 and 1749 (C=O); ^1H-NMR ($CDCl_3$) δ=2.223 (6H, s, 2×CH_3), 2.336 (3H, s, OAc), 4.034 (3H, s, OCH_3), 6.795 (1H, d, J=8.3 Hz, H-2), 7.373 (1H, d, J=8.3 Hz, H-3), and 7.258—8.400 (4H, m, ArH); ^{13}C NMR ($CDCl_3$)[17] δ=20.827 (q, CH_3), 27.525 (q, 2×CH_3), 55.665 (q, OCH_3), 95.359 (s, >C<), 102.613 (d, C-2), 120.369 (s, C-4), 122.826 (d, C-8), 124.903 (d, C-7), 125.664 (d, C-6), 126.775 (s, C-8a), 126.980 (d, C-3), 127.536 (d, C-5), 132.128 (s, C-4a), 157.080 (s, C-1), 170.330 (s, C=O), and 200.810 (s, 2×C=O); MS *m/z* (rel intensity), 314 (M^+, 10), 272 (20), 230 (50), 158 (30), and 43 (100). Found: C, 68.83; H, 5.81%. Calcd for $C_{18}H_{18}O_5$: C, 68.78; H, 5.77%.

1-(1-Acetyl-2-hydroxy-1-propenyl)-2,7-dimethoxynaphthalene (2c): Colorless needles (from methanol), mp 120.0—120.5 °C; IR ($CHCl_3$) 1624 (COC=COH) and 3300—3600 (OH); ^1H NMR ($CDCl_3$) δ=1.77 (6H, s, 2×CH_3), 3.83 (3H, s, OCH_3), 3.88 (3H, s, OCH_3), 6.93—7.78 (3H, m, ArH), 7.15 (1H, d, J=9.6 Hz, H-3), 7.79 (1H, d, J=9.6 Hz, H-4), and 16.87 (1H, s, OH). Found: C, 71.16; H, 6.31%. Calcd for $C_{17}H_{18}O_4$: C, 71.31; H, 6.34%.

1-(1-Acetoxy-1-acetyl-2-oxopropyl)-2,7-dimethoxynaphthalene (3c): Colorless needles (from ethanol), mp 176—177°C; IR ($CHCl_3$) 1723 and 1760 (C=O); ^1H NMR ($CDCl_3$) δ=2.25 (9H, s, 2×CH_3 and OAc), 3.88 (3H, s, OCH_3), 3.92 (3H, s, OCH_3), 7.03 (1H, dd, J=9.0 and 2.4 Hz, H-6), 7.13 (1H, d, J=9.0 Hz, H-3), 7.39 (1H, d, J=2.4 Hz, H-8), 7.71 (1H, d, J=9.0 Hz, H-5), and 7.86 (1H, d, J=9.0 Hz, H-4). Found: C, 66.23; H, 5.96%. Calcd for $C_{19}H_{20}O_6$: C, 66.27; H, 5.85%.

1-(1-Acetyl-2-hydroxy-1-propenyl)-2,6-dimethoxynaphthalene (2d): Colorless prisms (from ethanol), mp 134—135°C; IR ($CHCl_3$) 1620 (COC=COH) and 3300—3600 (OH); ^1H NMR ($CDCl_3$) δ=1.75 (6H, s, 2×CH_3), 3.88 (6H, s, 2×OCH_3), 7.0—7.7 (3H, m, ArH), 7.25 (1H, d, J=9.6 Hz, H-4), 7.78 (1H, d, J=9.6 Hz, H-5), and 16.89 (1H, s, OH). Found: C, 71.07; H, 6.39%. Calcd for $C_{17}H_{18}O_4$: C, 71.31; H, 6.34%.

1-(1-Acetyl-2-hydroxy-1-propenyl)-2,3-dimethoxynaphthalene (2e): Colorless needles (from methanol), mp 117—118°C; IR ($CHCl_3$) 1600 (COC=COH) and 3300—3600 (OH); ^1H NMR ($CDCl_3$) δ=1.77 (6H, s, 2×CH_3), 3.89 (3H, s, OCH_3), 3.97 (3H, s, OCH_3), 6.91 (1H, s, H-4), 7.05—7.80 (4H, m, ArH), and 16.88 (1H, s, OH). Found: C, 71.10; H, 6.37%. Calcd for $C_{17}H_{18}O_4$: C, 71.31; H, 6.34%.

4-(1-Acetyl-2-hydroxy-1-propenyl)-1,8-dimethylnaphthalene (2f): Colorless needles (from methanol), mp 149—150°C; IR ($CHCl_3$) 1605 (COC=COH) and 3300—3600 (OH); ^1H NMR ($CDCl_3$) δ=1.750 (6H, s, 2×CH_3), 2.965 (6H, s, 2×CH_3), 7.151 (1H, d, J=7.1 Hz, H-2 or 3), 7.284 (1H, d, J=7.1 Hz, H-3 or 2), 7.275—7.734 (3H, m, ArH), and 16.70 (1H, s, OH); ^{13}C NMR ($CDCl_3$)[17] δ=23.762 (q, 2×CH_3), 26.161

(q, CH_3), 26.249 (q, CH_3), 113.125 (s, $\succeq C=$), 124.328 (d, C-3 or 6), 125.762 (d, C-6 or 3), 128.511 (d, C-5), 129.243 (d, C-2 or 7), 129.798 (d, C-7 or 2), 133.045 (s, C-8a), 133.689 (s, C-4), 134.830 (s, C-4a), 136.000 (s, C-1 or 8), 136.175 (s, =C-O and C-8 or 1), 191.519 (s, C=O). Found: C, 80.06; H, 7.13%. Calcd for $C_{17}H_{18}O_2$: C, 80.28; H, 7.13%.

5-(1-Acetyl-2-hydroxy-1-propenyl)acenaphthene (2g): Colorless needles (from methanol), mp 141.5—142.5 °C; IR ($CHCl_3$) 1603 (COC=COH) and 3100—3600 (OH); ^1H NMR ($CDCl_3$) δ=1.79 (6H, s, 2×CH_3), 3.40 (4H, s, 2×CH_2), 7.17—7.47 (5H, m, ArH), and 16.79 (1H, s, OH). Found: C, 80.77; H, 6.47%. Calcd for $C_{17}H_{16}O_2$: C, 80.92; H, 6.39%.

4-(1-Acetyl-2-hydroxy-1-propenyl)-1-methylnaphthalene (2h): Colorless plates (from methanol), mp 122 °C; IR ($CHCl_3$) 1600 (COC=COH) and 3200—3600 (OH): ^1H NMR ($CDCl_3$) δ=1.75 (6H, s, 2×CH_3), 2.74 (3H, s, CH_3), 7.21 (1H, d, J=7.2 Hz, H-2 or 3), 7.37 (1H, d, J=7.2 Hz, H-3 or 2), 7.20—8.11 (4H, m, ArH), and 16.80 (1H, s, OH). Found: C, 79.67; H, 6.73%. Calcd for $C_{16}H_{16}O_2$: C, 79.97; H, 6.71%.

1-(1-Acetyl-2-hydroxy-1-propenyl)naphthalene (2i): Pale orange needles (from methanol), mp 105—106 °C; IR ($CHCl_3$) 1600 (COC=COH) and 3200—3600 (OH); ^1H NMR ($CDCl_3$) δ=1.75 (6H, s, 2×CH_3), 7.2—8.0 (7H, m, ArH), and 16.80 (1H, s, OH). Found: C, 79.38; H, 6.25%. Calcd for $C_{15}H_{14}O_2$: C, 79.62; H, 6.24%.

9-(1-Acetyl-2-hydroxy-1-propenyl)anthracene (5): Colorless needles (from ethanol), mp 176—177 °C; IR ($CHCl_3$) 1597 (COC=COH) and 3200—3600 (OH); ^1H NMR ($CDCl_3$) δ=1.59 (6H, s, 2×CH_3), 7.32—8.17 (8H, m, ArH), 8.49 (1H, s, H-10), and 16.97 (1H, s, OH). Found: C, 82.43; H, 5.79%. Calcd for $C_{19}H_{16}O_2$: C, 82.58; H, 5.84%.

9,10-Bis(1-acetyl-2-hydroxy-1-propenyl)anthracene (6): Colorless needles (from ethyl acetate), mp over 300 °C; IR ($CHCl_3$) 1598 (COC=COH) and 3200—3600 (OH); ^1H NMR ($CDCl_3$) δ=1.65 (12H, s, 4×CH_3), 7.51—8.22 (8H, m, ArH), and 16.98 (2H, s, 2×OH). Found: C, 76.91; H, 6.05%. Calcd for $C_{24}H_{22}O_4$: C, 76.98; H, 5.92%.

9,10-Bis(diacetylmethyl)-9,10-dihydroanthracene (7): Colorless plates (from ethanol), mp 215—216 °C; IR ($CHCl_3$) 1695 and 1735 (C=O); ^1H NMR ($CDCl_3$) δ=2.10 (12H, s, 4×CH_3), 4.44 (2H, d, J=10.2 Hz, H-9 and H-10), 4.89 (2H, d, J=10.2 Hz, 2×$\succeq$CH-), and 7.12 (8H, s, ArH). Found: C, 76.69; H, 6.49%. Calcd for $C_{24}H_{24}O_4$: C, 76.57; H, 6.43%.

9,10-Bis(diacetylmethylene)-9,10-dihydroanthracene (8): Colorless needles (from ethanol), mp 219 °C; IR ($CHCl_3$) 1686 (C=O); ^1H NMR ($CDCl_3$) δ=2.27 (12H, s, 4×CH_3), and 7.24—7.56 (8H, m, ArH). Found: C, 77.34; H, 5.56%. Calcd for $C_{24}H_{20}O_4$: C, 77.40; H, 5.41%.

9-(1-Acetyl-2-hydroxy-1-propenyl)acridine (10): Pale yellow needles (from ethanol), mp 189—190 °C; IR ($CHCl_3$) 1610 (COC=COH) and 3100—3600 (OH); ^1H NMR ($CDCl_3$) δ=1.65 (6H, s, 2×CH_3), 7.35—8.44 (8H, m, ArH), and 17.05 (1H, s, OH). Found: C, 77.89; H, 5.60; N, 4.96%. Calcd for $C_{18}H_{15}O_2N$: C, 77.96; H, 5.45; N, 5.05%.

Oxidation of Xanthene (11). A mixture of xanthene (**11**) (364.4 mg; 2 mmol) and $Mn(acac)_3$ (1.4160 g; 4 mmol) was heated in acetic acid (25 cm^3) at 100 °C for 5 min, followed by treatment in a manner similar to that mentioned above, which gave a mixture of **12** and its enol form (263.3 mg), **13** (79.2 mg), and **11** (recovered 122.3 mg). The ratio of keto and enol was 2:1 based on the ^1H NMR spectrum. The mixture was recrystallized from ethanol and only the keto compound (**12**) was isolated.

9-(Diacetylmethyl)xanthene (12): Colorless needles (from ethanol), mp 142.5 °C; IR ($CHCl_3$) 1697 and 1731 (C=O); ^1H NMR ($CDCl_3$) keto form δ=1.84 (6H, s, 2×CH_3), 4.08 (1H, d, J=9.6 Hz, H-9), 4.84 (1H, d, J=9.6 Hz, $\succeq$CH-), and 6.95—7.30 (8H, m, ArH); enol form δ=1.84 (6H, s, 2×CH_3), 5.30 (1H, s, H-9), 6.8—7.4 (8H, m, ArH), and 17.16 (1H, s, OH). Found: C, 77.20; H, 5.90%. Calcd for $C_{18}H_{16}O_3$: C, 77.12; H, 5.75%.

9-(Diacetylmethylene)xanthene (13): Pale yellow needles (from ethanol), mp 144—145 °C; IR ($CHCl_3$) 1676 and 1706 (C=O); ^1H NMR ($CDCl_3$) δ=2.20 (6H, s, 2×CH_3) and 6.95—7.57 (8H, m, ArH). Found: C, 77.44; H, 5.06%. Calcd for $C_{18}H_{14}O_3$: C, 77.68; H, 5.07%.

Oxidation of Anthrone (14). 10-(Diacetylmethylene)anthrone (15): Colorless needles (from ethanol), mp 161 °C; IR ($CHCl_3$) 1669 and 1707 (C=O); ^1H NMR ($CDCl_3$) δ=2.22 (6H, s, 2×CH_3) and 7.5—8.4 (8H, m, ArH). Found: C, 78.59; H, 4.91%. Calcd for $C_{19}H_{14}O_3$: C, 78.60; H, 4.85%.

10,10′-Bianthrone (16): Pale yellow needles (from $CHCl_3$), mp 268—269 °C (lit, [11b] mp 230—250 °C); IR (KBr) 1657 (C=O); ^1H NMR ($CDCl_3$) δ=4.69 (2H, s, H-10 and 10′) and 6.70—7.98 (16H, m, ArH). Found: C, 86.91; H, 4.66%. Calcd for $C_{28}H_{18}O_2$: C, 87.02; H, 4.69%.

Oxidation of Pyrene (17). 1-(1-Acetyl-2-hydroxy-1-propenyl)pyrene (18): Pale orange needles (from ethanol), mp 158.0—158.5 °C; IR ($CHCl_3$) 1602 (COC=COH) and 3200—3600 (OH); ^1H NMR ($CDCl_3$) δ=1.76 (6H, s, 2×CH_3), 7.69—8.26 (9H, m, ArH), and 16.86 (1H, s, OH). Found: C, 83.87; H, 5.35%. Calcd for $C_{21}H_{16}O_2$: C, 83.98; H, 5.37%.

1-(1-Acetoxy-1-acetyl-2-oxopropyl)pyrene (19): Colorless needles (from ethanol), mp 178.0—178.5 °C; IR ($CHCl_3$) 1722 and 1749 (C=O); ^1H NMR ($CDCl_3$) δ=2.26 (6H, s, 2×CH_3), 2.39 (3H, s, OAc), and 7.82—8.43 (9H, m, ArH). Found: C, 76.79; H, 5.06%. Calcd for $C_{23}H_{18}O_4$: C, 77.08; H, 5.06%.

1-(1-Acetoxy-1-acetyl-2-oxopropyl)-6-(1-acetyl-2-hydroxy-1-propenyl)pyrene (20): Colorless needles (from methanol), mp 218—219 °C; IR ($CHCl_3$) 1603 (COC=COH), 1722 (C=O), 1749 (OAc), and 3300—3600 (OH); ^1H NMR ($CDCl_3$) δ=1.77 (6H, s, 2×CH_3), 2.26 (6H, s, 2×$COCH_3$), 2.39 (3H, s, OAc), 7.90 (1H, d, J=9.0 Hz, ArH), 7.99 (1H, d, J=9.0 Hz, ArH), 8.27 (1H, d, J=9.0 Hz, ArH), 8.47 (1H, d, J=9.0 Hz, ArH), 8.0—8.2 (4H, m, ArH), and 16.84 (1H, s, OH). Found: C, 73.46; H, 5.23%. Calcd for $C_{28}H_{24}O_6$: C, 73.67; H, 5.30%.

Oxidation of 1-Nitronaphthalene (1j). 1-Nitronaphthalene (**1j**) (198.7 mg; 1 mmol) was oxidized with $Mn(acac)_3$ (1.4298 g; 4 mmol) in acetic acid (25 cm^3) at 100 °C. The reaction was terminated after 15 min and **1j** (173.0 mg) was recovered.

Formation of 21 in the $Mn(acac)_3$ Oxidation. 1-Methoxynaphthalene (**1b**) (319.2 mg; 2 mmol) and $Mn(acac)_3$ (1.4240 g; 4 mmol) were heated at 100 °C in acetic acid (30 cm^3) for 10 min, affording **2b** (17.4 mg), **3b** (93.7 mg), and **21** (105.2 mg). The **21** was formed in all the $Mn(acac)_3$-acetic acid oxidation.

3-Acetyl-4-hydroxy-3-hexene-2,5-dione (21): Colorless prisms (from benzene), mp 115—116 °C; IR ($CHCl_3$) 1668, 1708 (C=O), and 3000—3600 (OH); ^1H NMR ($CDCl_3$) δ=1.607 (3H, s, CH_3), 2.389 (3H, s, CH_3), 2.605 (3H, s, CH_3), and 6.395 (1H, s, OH); ^{13}C NMR ($CDCl_3$) δ=197.558 (s, C=O), 196.910 (s, C=O), 194.919 (s, C=O), 112.959 (s, C=C), 106.294 (s, C=C), 29.648 (q, CH_3), 21.810 (q, CH_3), and 18.816 (q, CH_3); MS m/z (rel intensity), 170 (M^+, 6), 127 (80), 85 (50), 67 (100), and 43 (97). Found: C, 56.38; H, 5.95%. Calcd for $C_8H_{10}O_4$: C, 56.46; H, 5.92%.

Oxidation of 2c. The **2c** (102.2 mg; 0.36 mmol) and $Mn(acac)_3$ (258.5 mg; 0.72 mmol) were heated in acetic acid (15 cm^3) at 100 °C for 3 min. The reaction mixture was treated in a manner similar to that described above to give **3c** (29.0 mg) and **2c** (recovered 53.6 mg).

Oxidation of 5. The (diacetylmethyl)anthracene (**5**) (99.1 mg; 0.36 mmol) was oxidized with $Mn(acac)_3$ (266.4 mg; 0.72 mmol) in acetic acid (20 cm^3) at 100 °C for 2 min. After separation by TLC, **6** (53.9 mg; 40%), **8** (32.2 mg; 24%), and **5** (recovered 28.7 mg; 29%) were obtained.

Oxidation of 6. A mixture of bis(diacetylmethyl)anthracene (**6**) (103.5 mg; 0.28 mmol) and $Mn(acac)_3$ (198.2 mg; 0.56 mmol) was heated in acetic acid (20 cm^3) at 100 °C for 2 min, affording **8** (67.5 mg; 66%) and **6** (recovered 33.8 mg; 33%).

Oxidation of 7. The reaction of **7** (50.8 mg; 0.135 mmol) and $Mn(acac)_3$ (103.4 mg; 0.27 mmol) was carried out in acetic acid (10 cm^3) at 100 °C for 2 min. After work-up, however, only **7** was recovered. On the other hand, **7** (52.0 mg; 0.135 mmol) was oxidized with $Mn(acac)_3$ (199.5 mg; 0.54 mmol) in acetic acid (10 cm^3) at 100 °C for 6 min, giving **8** (9.2 mg; 18%) and **7** (recovered 40 mg; 77%).

Oxidation of 12. 9-(Diacetylmethyl)xanthene (**12**) (102.6 mg; 0.37 mmol) and $Mn(acac)_3$ (262.0 mg; 0.74 mmol) were heated on a water bath for 2 min. After the treatment described above, 9-(diacetylmethylene)xanthene **13** (29.9 mg; 29%) and **12** (recovered 69.3 mg; 68%) were obtained.

Oxidation of 1a with $Mn(acac)_3$ in CH_3CN. The reaction of **1a** (175.3 mg; 1 mmol) with $Mn(acac)_3$ (1.4146 g; 4 mmol) was carried out in CH_3CN (25 cm^3) at 100 °C for 3 h. The solvent was removed under diminished pressure and the residue was triturated with 2 M HCl (25 cm^3). The aqueous mixture was extracted with $CHCl_3$ and separated on TLC, which gave only **1a** (recovered 136.1 mg).

The author would like to express his grateful acknowledgment to Dr. Naoki Sato of the Department of Chemistry, Kumamoto University, for his helpful discussion and providing some data for ionization potentials of organic compounds. Thanks are also due to Mr. Teruyoshi Marunaka of the Taiho Pharmaceutical Co., Ltd., Tokushima, for his measurements of the mass and ^{13}C NMR spectra. The present work was partially supported by a Grant-in-Aid for Scientific Research No. 60740282 from the Ministry of Education, Science and Culture (1985).

References

1) D. Arndt, "Manganese Compounds as Oxidizing Agents in Organic Chemistry," Open Court Publishing Company, Illinois (1981), p. 3.

2) a) T. Shono, K. Yamanoi, T. Matsushita, and K. Shinra, *Kogyo Kagaku Zasshi*, **70**, 2062 (1967); b) M. J. S. Dewar and T. Nakaya, *J. Am. Chem. Soc.*, **90**, 7134 (1968); c) Y. Omote, Y. Takizawa, and N. Sugiyama, *Bull. Chem. Soc. Jpn.*, **45**, 2882 (1972); d) A. Ronlán and V. D. Parker, *J. Org. Chem.*, **39**, 1014 (1974); e) F. E. Ziegler and J. A. Schwartz, *J. Org. Chem.*, **43**, 985 (1978).

3) T. Nakaya, H. Arabori, and M. Imoto, *Bull. Chem. Soc. Jpn.*, **43**, 1888 (1970).

4) A. R. Forrester, R. H. Thomson, and Soo-On Woo, *J. Chem. Soc., Perkin Trans. 1*, **1975**, 2340.

5) H. Nishino, *Bull. Chem. Soc. Jpn.*, **58**, 1922 (1985).

6) J. B. Bush, Jr. and H. Finkbeiner, *J. Am. Chem. Soc.*, **90**, 5903 (1968); E. I. Heiba, R. M. Dessau, and W. J. Koehl, Jr., *ibid.*, **90**, 5905 (1968).

7) E. I. Heiba, R. M. Dessau, and W. J. Koehl, Jr., *J. Am. Chem. Soc.*, **91**, 138 (1969).

8) K. Kurosawa and H. Harada, *Bull. Chem. Soc. Jpn.*, **52**, 2386 (1979).

9) H. Nishino and K. Kurosawa, *Bull. Chem. Soc. Jpn.*, **56**, 474 (1983).

10) a) P. J. Andrulis, Jr., M. J. S. Dewar, R. Dietz, and R. L. Hunt, *J. Am. Chem. Soc.*, **88**, 5473 (1966); b) T. Aratani and M. J. S. Dewar, *ibid.*, **88**, 5479 (1966); c) P. J. Andrulis, Jr. and M. J. S. Dewar, *ibid.*, **88**, 5483 (1966).

11) S. A. Zonis, *Sbornik Statei Obshchei Khim.*, **2**, 1091 (1953); *Chem. Abstr.*, **49**, 5414 g (1955); b) R. Van Helden and E. C. Kooyman, *Recl. Trav. Chim. Pays-Bas*, **80**, 57 (1961).

12) W. E. Fristad and J. R. Peterson, *J. Org. Chem.*, **50**, 10 (1985); J. A. Norman, C. B. Thomas, and M. J. Burrow, *J. Chem. Soc., Perkin Trans. 1*, **1985**, 1087.

13) a) N. Sato, K. Seki, and H. Inokuchi, *J. Chem. Soc., Faraday Trans. 2*, **77**, 1621 (1981); b) O. B. Nagy, S. Dupire, J. B. Nagy, *Tetrahedron*, **31**, 2453 (1975); c) C. Utsunomiya, T. Kobayashi, and S. Nagakura, *Bull. Chem. Soc. Jpn.*, **48**, 1852 (1975); d) L. Klasinc, B. Kovač, and H. Güsten, *Pure Appl. Chem.*, **55**, 289 (1983).

14) The reaction of 1,1-diphenylethene (194.5 mg) with $Mn(acac)_3$ (707.7 mg) in acetic acid (25 cm^3) at room temperature for 12 h gave 3-acetyl-2-hydroperoxy-2-methyl-5,5-diphenyltetrahydrofuran (301.2 mg; 89%), 3-acetyl-2-methyl-5,5-diphenyl-4,5-dihydrofuran (17.1 mg; 6%),[5] and 3-acetyl-4-hydroxy-3-hexene-2,5-dione **21** (92.9 mg).

15) a) G. Galliani, B. Rindon, and C. Scolastico, *Tetrahedron Lett.*, **1975**, 1285; b) H. Nishino and K. Kurosawa, *Bull. Chem. Soc. Jpn.*, **56**, 1682 (1983).

16) M. N. Bhattacharjee, M. K. Chaudhuri, and D. T. Khathing, *J. Chem. Soc., Dalton Trans.*, **1982**, 669.

17) a) R. J. Highet and J. M. Edwards, *J. Magn. Reson.*, **17**, 336 (1975); b) D. H. Hunter and J. B. Stothers, *Can. J. Chem.*, **51**, 2884 (1973).

 © 1986 The Chemical Society of Japan Bull. Chem. Soc. Jpn., 59, 1741—1746 (1986)

NMR and XPS Studies of Some Diselenocarbamates. Bond Switch in Bis(dimethylselenocarbamoyl) Triselenide

Keiji KOBAYASHI,* Hideyuki TUKADA, Koichi KIKUCHI,† and Isao IKEMOTO†
Department of Chemistry, College of Arts and Sciences, The University of Tokyo, Komaba, Meguro-ku, Tokyo 153
†Department of Chemistry, Faculty of Science, Tokyo Metropolitan University, Fukazawa, Setagaya-ku, Tokyo 158
(Received January 23, 1986)

The hindered rotation about the C-N bond in dimethyldiselenocarbamates Me_2N-CSe-SeR has been investigated by variable temperature NMR spectroscopy. The barrier to the rotation was almost independent of the partial structure of R (R= -Me, -CSe-NMe_2), being 19 kcal mol^{-1}* at around 93 °C. However, for bis(dimethylselenocarbamoyl) triselenide (R= -Se-Se-CSe-NMe_2) (**1**), no splitting of *N*-methyl signals was observed in the ^1H and ^{13}C NMR spectra at subambient temperature. The equivalence of the methyl groups is discussed in terms of the bond switch between C=Se and C-Se moieties. The existence of the bond switch in **1** was also suggested by the XPS studies; the binding energy of the four selenium atoms was found to lie between those of C=Se and -Se- types of the selenium atoms, indicating that **1** takes an intramolecular coordination structure rather than a linear triselenide structure in the solid state, thereby facilitates the bond switch in solution.

There have been many examples of hindered internal rotation about the nitrogen-carbon bond in amide compounds since the classical studies of *N,N*-dimethylformamide.[1] Much of the subsequent work has been expanded to amide analogues involving sulfur in place of oxygen such as thioamide.[2] However, little attention has been given to the selenium analogues of amides.[3] Our present study began with the dynamic NMR of diselenocarbamates, as no data have been reported previously for the internal rotation of such selenium compounds. During the course of the study, we observed the magnetic equivalence of *N*-methyl protons in bis(dimethylselenocarbamoyl) triselenide (**1**) in sharp contrast to other selenocarbamates which exhibited nonequivalent *N*-methyl protons due to the restricted rotation about the C-N bond at room temperature. This unexpected behavior of **1** prompted us to suspect the triselenide structure of **1** represented as **A**. If **1** has the structure **B** composed of a positively charged central selenium atom and two negatively charged diselenocarbamato ligands, in analogy with bis(diselenocarbamato)metal (II) complexes, the NMR spectra of **1** should give the equivalent *N*-methyl protons, as was actually observed. The X-ray photoelectron spectra (XPS) might be helpful in distinguishing **A** from **B**, as these provide the ionic character of the selenium bond through inner-shell electron binding energies. Therefore, we have also made XPS studies. In this article we describe the results of the NMR and XPS studies of several diselenocarbamates, in particular, focussing on the characterization of the selenium bond in **1**. Based on these data we demonstrate the fast bond switch of carbamate **1** in solution and the intramolecular coordination structure in the solid state.

Results and Discussion

NMR Spectroscopy. The ^1H NMR spectra were measured for four diselenocarbamates, **1**, methyl dimethyldiselenocarbamate (**2**), bis(dimethylselenocarbamoyl) selenide (**3**), and bis(dimethyldiselenocar-

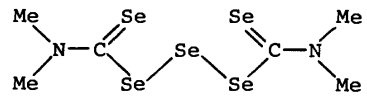

I -A

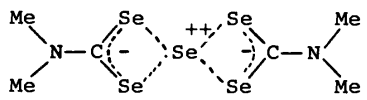

I -B

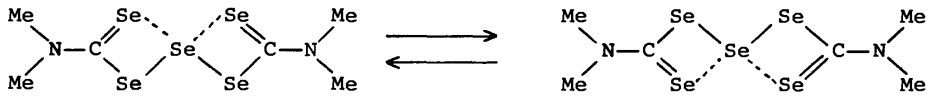

I -C (bond switch)

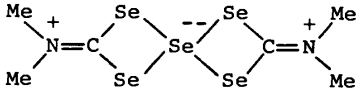

I -D

*1 cal=4.184 J.

Table 1. NMR Spectral Data

Compd	Solvent	^{1}H NMR[a]		^{13}C NMR[a]			^{77}Se NMR[b]	
		N-Me	Se-Me	N-Me	C=Se	Se-Me	-Se-	C=Se
1	DMSO-d_6	3.54		43.62	c)		c)	c)
2	$CDCl_3$	3.38	2.65				520.1	602.3
		3.67						
	C_6D_6	2.41	2.52					
		3.06						
	DMSO-d_6	3.36	2.55	44.16	194.76	18.55		
		3.58		49.02				
3	$CDCl_3$	3.39						
		3.57						
	DMSO-d_6	3.53		47.13	186.31			
		3.37		47.40			922.7	840.2
4	DMSO-d_6	3.30		c)	c)	c)	c)	c)

a) δ Values. b) Chemical shifts referred to MeSeMe in ppm. c) The NMR signals could not be recorded because of low solubility.

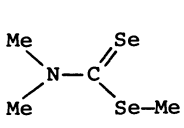

s-cis **2**

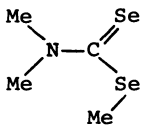

s-trans **2**

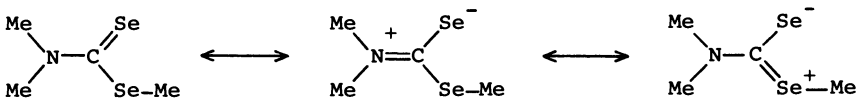

a b c

bamato)nickel (II) (**4**). The ^{1}H chemical shifts of these selenocarbamates are collected in Table 1. Also summarized in Table 1 are the ^{13}C and ^{77}Se NMR spectral data. Some of the ^{13}C and ^{77}Se chemical shifts could not be obtained because the solubility was extremely low for detecting the signals.

Carbamate **2** exhibited a singlet for the Se-Me protons and a doublet for the *N*-Me protons in the ^{1}H NMR spectra at room temperature. This was also the case in the ^{13}C NMR spectra. The nonequivalent methyl groups showed a large aromatic solvent-induced shift (ASIS) on the relative ^{1}H chemical shifts; the distance between the two peaks increased up to 0.65 ppm on replacement of $CDCl_3$ by benzene. The higher field peak was mainly responsible for this shift, being analogous to the ASIS behavior observed in *N,N*-dimethylacetamide.[4] Thus, the peak at δ 3.38 in $CDCl_3$ was assigned to the methyl protons *trans* to the selenocarbonyl group and the peak at δ 3.67 was to the *cis* protons.

For carbamate **2** two conformational isomers, *s-cis* and *s-trans* with respect to the CSe-Se single bond, may be considered. However, even on lowering the temperature down to −65 °C, no signals attributable to another conformer have been observed in the ^{1}H and ^{13}C NMR spectra. This indicates extremely high predominance of one isomer over another. The prefered isomer may be assigned to the *s-cis* conformer by analogy with the corresponding sulfur compound, methyl dimethyldithiocarbamate, for which the *s-cis* conformer has been reported to be more stable than the *s-trans* conformer on the basis of the NMR and MO studies.[5]

In compound **3** the nonequivalent *N*-Me protons were again observed, as shown in Table 1, indicating restricted rotation about the C-N bond. No additional peaks were observed in the ^{1}H NMR or in the ^{13}C NMR spectra at low temperature of −65 °C. Thus, solely one conformation of the possible three is permissible for **3**. Among the three conformers depicted below, the *s-cis*, *s-trans* conformer should exhibit four nonequivalent methyl signals. The *s-trans*, *s-trans* conformer is unlikely to exist because of the steric repulsion between the *N*-methyl groups. Therefore, the most stable isomer observed in the NMR spectra can be assigned to the *s-cis*, *s-cis* isomer.

On raising the temperature the *N*-Me doublet of **2** collapsed to a singlet, as shown in Fig. 1, due to rapid

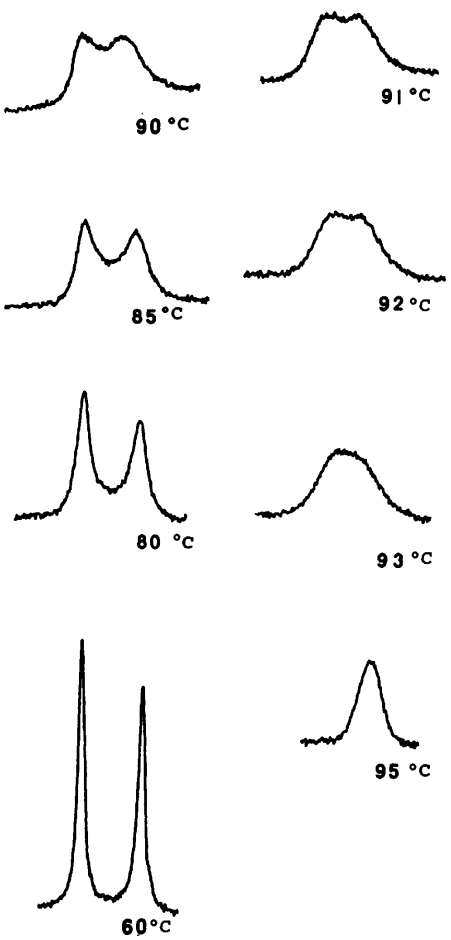

Fig. 1. Temperature dependent ^{1}H NMR of methyl dimethyldiselenocarbamate (**2**) in DMSO-d_6.

Table 2. Dynamic ^{1}H NMR Data

Compd	Solvent	T_c	$\Delta\nu_c$	$\Delta G^{\ddagger}$ [b]
		°C	Hz	kcal mol^{-1}
2	Tetrachloroethylene	59	27.2	16.8
	DMSO-d_6	93	19.3	18.8
3	DMSO-d_6	94	14.1	19.1
1 [a]	DMSO-d_6	(0>)	(15.0)	(14>)

a) Estimated value, see text. b) Values at T_c.

rotation about the C–N bond. The coalescence temperature of 93 °C and the chemical shift difference of 19.3 Hz allowed us to estimate the energy barrier to the rotation about the C–N bond in DMSO by means of the coalescence temperature method[6] and gave a value of 18.8 kcal mol^{-1} at 93 °C. In a nonpolar solvent such as tetrachloroethylene, the barrier was apparently lower than that obtained in DMSO, as shown in Table 2. It is reasonable to assume that the contribution of the polar resonance structure in the ground state is more enhanced in polar solvents than in nonpolar solvents, hence the double bond character of the CSe–N bond is increasing to raise the barrier to the rotation in DMSO.

Carbamate **3** showed a similar dynamic NMR behavior and led to the estimation of 19.1 kcal mol^{-1} for the barrier at the 94 °C of coalescence temperature. It is interesting to note that the barriers of **2** and **3** fall to almost the same value at the similar coalescence temperature. These observations suggest that the rotational barrier in dimethyldiselenocarbamates is almost independent of the residual structure other than the diselenocarbamate moieties. Close similarity of the rotational barrier has also been found among dithiocarbamates.[7]

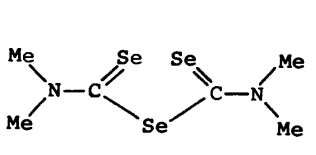

s-cis, s-cis **3**

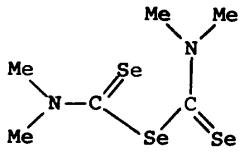

s-cis, s-trans **3**

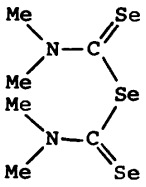

s-trans, s-trans **3**

The activation energies for the rotation in **2** and **3** seem to be slightly lower than those reported for *N*,*N*-dimethylselenoamide.[3] The resonance structure of the cross-conjugated species as represented in **c** probably contributes to the hybrid structure in diselenocarbamates, which should reduce the double bond character of the C–N bond and thus decrease the barrier to rotation.

Triselenide **1** exhibits the most unexpected part of this study; no splitting of *N*-methyl signals was observed in the ^{1}H NMR spectra at room temperature. Although the low temperature spectra could not be obtained below 5 °C in DMSO, down to this temperature the *N*-Me protons showed only a sharp singlet. Despite our anticipation that the ^{13}C chemical shift difference for the methyl signals might be relatively large, resulting in higher temperatures of decoalescence and permitting observations of the individual resonances at about 5 °C, the ^{13}C NMR spectra exhibited no splitting. By assuming 15.0 Hz for the chemical shift difference of the *N*-methyl protons, which corresponds to the value observed in **3**, and 0 °C for the coalescence temperature, the rotational barrier of **1** was estimated to be less than 14 kcal mol^{-1}. This energy value is apparently low as compared with those of **2** and **3** and unusual as well in view of the close similarity of the barrier in diselenocarbamates **2** and **3**.

It would be possible to interpret a single peak for the *N*-methyl protons of **1** by assuming the structure of a metal complex as represented in **B** rather than the triselenide structure **A**. The structure involving two diselenocarbamato ligands should show a singlet peak

Table 3. Binding Energies of the Se 3d Core Electron Peak/eV[a)]

1	3	4
54.5 (1 Se)	55.0 (2 C=Se)	55.0 (4 C⩵ Se⁻)
55.6 (4 Se)	56.5 (1 -Se-)	

a) Relative peak intensity and assignment are given in parentheses.

for the *N*-methyl signals, as was the case in the complex **4** which exhibited singlet signals at δ 3.30 in DMSO. An alternative explanation may be given by assuming the occurence of rapid interconversion of the *N*-methyl groups through a rate determining process other than bond rotation about the C–N bond. Thus, we can postulate the existence of the rapid bond switch as depicted in **c**, wherein the *N*-methyl protons should appear as a singlet even if the bond rotation is slow. To distinguish the structural possibilities **A**, **B**, and **C**, the ^{77}Se NMR spectrum and its low temperature variation should offer the most potentially useful means. However, the solubility of **1** was extremely low and we were unable to carry out dynamic NMR experiments by monitoring the ^{77}Se nuclei.

XPS Studies. We have also approached the problem on the binding character from the chemical shift differences in the XPS. The binding energies of Se 3d core levels obtained by the XPS measurements are listed in Table 3. All measurements were made on solid samples at room temperature. The data for compound **2** were not obtained, as the sample sublimed under the experimental conditions.

Among the three compounds, compound **4** exhibited the narrowest peak with a half width of 1.9 eV, since the four selenium atoms in **4** have all equivalent bonding properties. For the spectrum of **3** graphical separation of the overlapped peaks was accomplished on the bases of the peak profile of **4** and the normalization of the number of selenium atoms involved in the carbamates. Thus, the spectrum of **3** resulted in two peaks at 55.0 and 56.5 eV in an intensity ratio of 2:1 as shown in Fig. 2. The stronger peak with lower binding energy should be assigned to the C=Se selenium atoms and the weaker one with higher energy to the ether type of selenium atom. The energy value of the former peak is almost the same as that of **4**, indicating that negative charge is appreciably developed in the selenoketone type of selenium atom. On the other hand, the binding energy of the ether type of selenium atom is relatively high. The increase in binding energy corresponds to a more pronounced positive charge on the selenium atom and thus implies a great contribution of the dipolar structure due to cross-conjugation. This XPS result for the selenoether selenium atom in **3** is consistent with the ^{77}Se NMR chemical shift; the shift was significantly downfield as compared with that of **2**.

The peak profile of **1** was not broadened as much as for a triselenide structure with the three different types

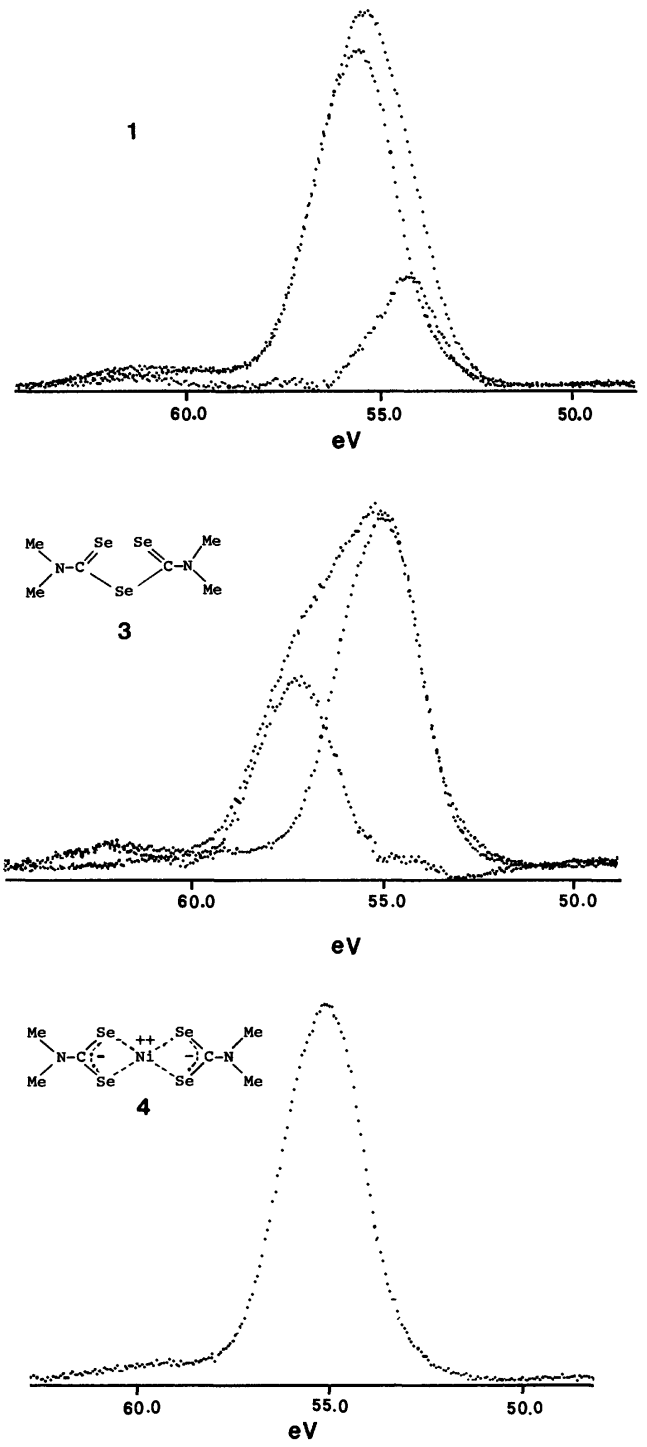

Fig. 2. The XPS peaks of Se 3d electrons in 1, 3, and 4.

of selenium atoms. The peak separation disclosed a small peak corresponding to one selenium atom at 54.5 eV besides a major peak at 55.6 eV due to four equivalent selenium atoms. Involvement of four equivalent selenium atoms in **1** rules out the linear triselenide structure **A** and is reminiscent of the metal complex structure **B**. The binding energy of these four selenium atoms, however, is larger than that observed in a typical bis(diselenocarbamato)metal (II) complex,

i. e. complex **4**. This may imply that four equivalent selenium atoms are not included as negatively charged diselenocarbamato ligands. Moreover, one selenium atom, which might correspond to the central one, has extremely low binding energy. On this selenium atom a negative charge must be developed rather than a positive charge. These observations clearly show that **1** is represented neither as the metal complex **B** nor the triselenide structure **A**; the XPS data suggest the contribution of the resonance form **D** to the overall structure of **1** even though it is less important than the others. This may be most reasonably explained by a structure in which the lone-pair electrons in the two selenocarbonyl groups are donated to the central selenium atom in the triselenide moiety. Thus, the bonding character of the selenium atoms in the selenocarbonyl functionality C=Se must be close to that of the selenium atoms of -Se-C- moiety and thereby exhibits approximately equal binding energies as was observed in the XPS.

Huesbye has reported the X-ray structure of the diselenocarbamate **5**, a compound of the same family of **1**.[8] This compound is a trapezoid planar four-coordinated complex, wherein two of the central atoms to the ligand bonds are intramolecular and the other two are weak intramolecular bonds. Binding energies of the selenium atoms involved in the former and the latter bonding probably could not be distinguished from the XPS spectra because the difference is small. Therefore, the present XPS data are consistent with the X-ray results.

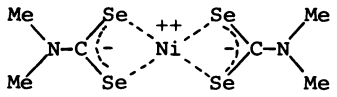

4

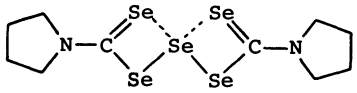

5

Concerning the structure of **1** in solution, the closer intramolecular approach of the two selenocarbonyl groups to the central selenium atom should facilitate the bond switch in the solution as illustrated in **C**. Thus both the bonding character revealed in the solid state and the equivalence of the *N*-methyl signals in the NMR spectra provide strong evidences for the occurence of the fast bond switch in bis(dimethylselenocarbamoyl) triselenide (**1**).

Experimental

The ^{1}H NMR spectra were measured on a Varian EM 390 spectrometer (90 MHz) with tetramethylsilane as the internal reference. The variable temperature ^{1}H NMR spectra were obtained on the EM 390 spectrometer equipped with a variable temperature probe and temperature controller, which was calibrated by the peak separations obtained with an ethylene glycol sample. The ^{13}C NMR spectra were obtained on a JEOL 400 GX spectrometer operating at 76.245 MHz equipped with a 10 mm probe. The spectra were recorded with proton noise decoupling for 5 kHz spectral width and with 45° pulse. Usually 100 scans were accumulated with a 3.5 s pulse interval after each pulse. The ^{77}Se NMR spectra were obtained on the JEOL 400GX spectrometer. About 2000—4000 average transients at a pulse repetition rate of 1 s with proton-noise decoupling were accumulated, employing 45° pulse. The chemical shifts were determined relative to external dimethyl selenide, which was observed to resonate at 76244285 Hz in $CDCl_3$.

The XPS data were obtained on a SHIMADZU ESCA 750 using Mg $K\alpha$ exciting radiation at room temperature, the source vacuum being ca. 10^{-7} mmHg**. Powdered samples were pressed onto an aluminum substrate. The binding energies of photoelectron peaks were calibrated by using the Au $4f_{7/2}$ peak (83.8 eV) of a thin gold film deposited on the sample surface. Peak positions and areas were obtained by graphical fitting of the peak profile of compound **4** to the experimental data.

Bis(dimethylselenocarbamoyl) triselenide (**1**) and bis(dimethylselenocarbamoyl) selenide (**3**) were prepared according to the procedures given in literature.[9] The melting points were in agreement with the literature values and the NMR spectra showed no trace of impurities.

Methyl Dimethyldiselenocarbamate (2). Hydrogen selenide, generated by the addition of water to 6.89 g (23.7 mmol) of aluminum selenide, was passed through a cooled solution (−10 °C) of 9.9 ml (71.0 mmol) of freshly distilled triethylamine in 250 ml of chloroform. The hydrogen selenide stream was then replaced by a stream of argon. To this solution 9.9 ml of triethylamine and 5.72 g (35.2 mmol) of *N,N*-dimethyldichloromethaniminium chloride were added at 0 °C in quick succession. The mixture was stirred at room temperature for 2 h and then treated with a solution of 4.50 g (31.9 mmol) of iodomethane in 10 ml of chloroform over 10 min. The resulting mixture was stirred at room temperature for 2 h, the solvent was removed under vacuum, and the residue was extracted with ether. The ether was evaporated to afford pale yellowish plates. Recrystallization from benzene-haxane gave 3.8 g (52%) of **2** as white plates, mp 85—86 °C. Found: C, 20.85; H, 4.22; N, 6.11%. Calcd for $C_4H_9NSe_2$: C, 20.96; H, 3.96; N, 6.12%.

Bis(dimethyldiselenocarbamato)nickel (II) (4). This complex was prepared by a modification of the method reported by Woodbridge,[10] using hydrogen selenide in place of carbon diselenide. A solution of 2.2 g (17.0 mmol) of unhydrous nickel chloride in a mixture of 150 ml of methanol and 20 ml of water was added to a solution of triethylammonium dimethyldiselenocarbamate in chloroform, which was prepared from 5.72 g of *N,N*-dimethyldichloromethaniminium chloride and hydrogen selenide as descrived above. The mixture was stirred for 2 h at room temperature and the resulting precipitate was filtered, washed with water, and dried to give 3.89 g (47%) of crude **4**. A portion of this solid was recrystallized from 1,1,2-trichloroethane to give pure **4** as dark greenish solids with

**1 mmHg=133.322 Pa.

high mp (>310°C). Found: C, 14.29; H, 2.59; N, 5.63%. Calcd for $C_6H_{12}N_2Se_4Ni$: C, 14.81; H, 2.49; N, 5.76%.

References

1) H. S. Gutowsky and C. H. Holm, *J. Chem. Phys.*, **25**, 1228 (1956).

2) M. Ōki, "Topics in Stereochemistry," ed by N. L. Allinger, E. L. Eliel, and S. H. Wilen, John Wiley and Sons, New York, N. Y. (1983), Vol. 14, p. 19.

3) G. Schwenker and H. Rosswag, *Tetrahedron Lett.*, **1967**, 4237; K. A. Jensen and J. Sandström, *Acta Chem. Scand.*, **23**, 1911 (1969).

4) J. B. Lambert, "Organic Structural Analysis," Macmillan, New York, N. Y. (1976), p. 31.

5) K. R. G. Devi, S. Manogaran, and D. N. Sathyanarayana, *Phosphorus Sulfur*, **11**, 47 (1981).

6) M. Ōki, H. Iwamura, and N. Hayakawa, *Bull. Chem. Soc. Jpn.*, **37**, 1865 (1964); R. J. Kurland, M. Rubin, and W. B. Wise, *J. Chem. Phys.*, **40**, 2426 (1964).

7) C. E. Holloway and M. H. Gitlitz, *Can. J. Chem.*, **45**, 2659 (1967); J. Sandström, *J. Phys. Chem.*, **71**, 2318 (1967).

8) S. Esperas, S. Husebye, and A. Rolandsen, *Acta Chem. Scand., Ser. A*, **29**, 608 (1975).

9) L. Henriksen, *Synthesis*, **1982**, 771.

10) D. Barnard and D. T. Woodbridge, *J. Chem. Soc.*, **1961**, 2922; K. A. Jensen and V. Krishnan, *Acta Chem. Scand.*, **21**, 2904 (1967).

 © 1986 The Chemical Society of Japan Bull. Chem. Soc. Jpn., 59, 1747—1752 (1986)

$AlCl_3$-Promoted Conjugate Reduction of α,β-Unsaturated Carbonyl Compounds with 1,3-Dimethyl-2-phenylbenzimidazoline

Hidenori CHIKASHITA* and Kazuyoshi ITOH
Department of Applied Chemistry, Faculty of Engineering, Kansai University, Suita, Osaka 564
(Received February 3, 1986)

The reduction of a variety of α,β-unsaturated carbonyl compounds, except for α,β-unsaturated aldehyde, to the corresponding saturated carbonyl compounds was effectively performed by using 1,3-dimethyl-2-phenylbenzimidazoline (DMBI) as a reducing agent with the aid of $AlCl_3$. The reduction is discussed on the basis of the hydride-donating ability of DMBI, together with the role of $AlCl_3$ as an electrophilic activator for the substrates. The catalytic efficiency of Lewis acids was found to be proportional to the efficiency to form a complex with a carbonyl group. The reduction of 2-cinnamoylpyridine with 2-deuterated DMBI revealed that in the reduction product, a deuterium atom was located at the β-position with respect to the carbonyl group. On the other hand, the reduction of the same substrate with DMBI followed by quenching with D_2O gave a reduced product which contained a deuterium label at the α-position. These results were interpreted in terms of a mechanism involving an enolate intermediate produced by either a one-step hydride transfer or a sequential transfer of an electron (e) and a hydrogen atom (H·) from the reducing agent to the substrate.

Many useful methods for obtaining functionalizing organic compounds have been developed in recent years by employing various types of heterocyclic compounds, either as mediate or immediate reagents.[1] On the other hand, the selective reduction of organic functional groups is one of the important and frequently encountered synthetic subjects in organic syntheses. However, despite much work in these fields, little attention has been given to the use of heterocycles having a hydrogen-donating ability as practical reducing agents for such selective reductions. Therefore, it could become one of the useful methods in this field if such heterocycles could be used as direct and selective reducing agents. Although more recently, several reports[2] have appeared concerning the use of 1,4-dihydropyridine derivatives (so-called NAD(P)H model compounds) such as 1,4-dihydronicotinamides or 3,5-bis(ethoxycarbonyl)-1,4-dihydro-2,6-dimethylpyridine as reducing agents from an above synthetic viewpoint, reductions with NAD(P)H-models have, so far, been mainly investigated with regard to biological, biomimetic, or mechanical interests. To the best of our knowledge, there has only been two sources[3] concerning the synthetic utility of other heterocycles as practical and selective reducing agents. In previous papers from our laboratory, it was revealed that dihydrobenzazoles such as 2-phenylbenzimidazoline or 2-phenylbenzothiazoline were useful reducing agents for the selective reduction of carbon–carbon double bonds of α,β-unsaturated dinitriles,[4] 2-aryl-1-nitroalkenes,[5] and α,β-unsaturated carbonyl compounds.[6] As a continuation of this work, we have investigated the potential reducing ability of *N*-methylated 2-phenylbenzazolines in a reduction of α,β-unsaturated carbonyl compounds in the presence of a Lewis acid. We found that 1,3-dimethyl-2-phenylbenzimidazoline (DMBI) is the most powerful component in this reaction relative to the other heterocycles. In this paper, we report on the details of an $AlCl_3$-promoted conjugate reduction of α,β-unsaturated carbonyl compounds with DMBI and show the mechanical features of these reactions.

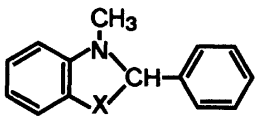

DMBI : X = N-CH_3
MBT : X = S
MBO : X = O

Scheme 1.

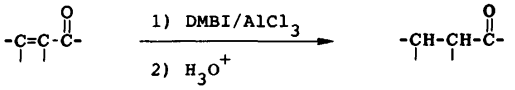

Scheme 2.

Results and Discussion

In contrast to 2-phenylbenzimidazoline, which should be prepared in situ from *o*-phenylenediamine and benzaldehyde in a solvent because it is an unstable intermediate and rapidly oxidized automatically to 2-phenylbenzimidazole in the absence of an appropriate hydrogen acceptor, DMBI can be prepared by a reaction of *N*,*N*′-dimethyl-*o*-phenylenediamine with benzaldehyde or the quaternization of 2-phenylbenzimidazole followed by a reduction with lithium aluminum hydride or sodium borohydride. It can be isolated as a handlable substance consisting of colorless needles.[7] DMBI is very stable in an atmospheric environment and can be stored in a sealed bottle for a long time.

For preliminary assays of the present study, we chose benzylideneacetone as a model compound and the reaction of the enone with DMBI in the presence or absence of a Lewis acid was carried out under the conditions shown in Table 1. Although the reduction of the enone with DMBI did not occur without a Lewis acid (Run 1), it was found that the reduction can proceed with 1 equivalent of DMBI in the presence of a slight excess of a Lewis acid in dry acetonitrile

Table 1. Reduction of Benzylideneacetone to Benzylacetone with DMBI in the Presence or Absence of Lewis Acid

Run	Lewis acid	Molar ratio[a] Enone:Lewis acid	Temp/°C	Time/h	Yield/%[b]
1	None	—	80	0.5	0
2	$ZnCl_2$	1:1.2	80	0.5	16
3	$SnCl_4$	1:1.2	80	0.5	36
4	$FeCl_3$	1:1.2	80	0.5	49
5	$AlCl_3$	1:1.2	80	0.5	100
6		1:1.2	r.t.	4	98
7		1:0.5	80	0.5	49
8		1:0.25	80	0.5	23

a) 1:1 Molar ratio of DMBI to the enone was used. b) Yield determined by GLC analysis.

Table 2. Reduction of Benzylideneacetone to Benzylacetone with MBT and MBO in the Presence or Absence of Lewis Acid[a]

Run	Reductant	Lewis acid	Molar ratio[b] Enone:Lewis acid	Time/h	Yield/%[c]
1	MBT	None	—	0.5	0
2		$ZnCl_2$	1:1.2	0.5	0
3		$FeCl_3$	1:1.2	0.5	34
4		$AlCl_3$	1:1.2	0.5	75
5		$AlCl_3$	1:1.2	48	100
6		$AlCl_3$	1:0.5	0.5	41
7		$AlCl_3$	1:0.25	0.5	20
8	MBO	$AlCl_3$	1:1.2	0.5	0

a) All the reactions were carried out in acetonitrile at 80°C. b) 1.2:1 Molar ratio of MBT and MBO to the enone was used. c) Yield determined by GLC analysis.

at 80°C. In all cases, the conjugate reduction product, 3-phenyl-2-butanone, was obtained in complete selectivity, and none of 4-phenyl-3-buten-2-ol, corresponding to the 1,2-reduction product, or 4-phenyl-2-butanol was detected. The change in the Lewis acid did not change the selectivity of the reduction, but the reaction employing $AlCl_3$ was very rapid and was completed within 30 min to give the product in quantitative yield (Run 5). In addition, this $AlCl_3$-promoted reduction proceeded well even at room temperature to give a nearly quantitative yield of the product (Run 6). As to the catalytic efficiency of the Lewis acid, Table 1 indicates that it is proportional to its efficiency to form a complex with a carbonyl group:[8] the latter efficiency increases in the order $ZnCl_2 < SnCl_4 < FeCl_3 < AlCl_3$. Thus, a Lewis acid can be regarded as an electrophilic activator to polarize a carbon–carbon double bond due to the formation of a complex with a carbonyl group of the enone. The use of a 1.2 equivalent of $AlCl_3$ to the enone is sufficient to promote the reaction, while the use of 0.5 or 0.25 equivalents of $AlCl_3$ to the enone gave the reduced product in 49 and 23% yields, respectively (Runs 7 and 8). This shows that the present conjugate reduction requires a stoichiometric amount of the Lewis acid.

A brief survey of the potential reducing ability of a series of *N*-methylated 2-phenylbenzazolines on the reduction of benzylideneacetone was conducted. As shown in Table 2, the reduction with 3-methyl-2-phenylbenzothiazoline (MBT) also proceeded in the presence of a Lewis acid with a similar trend shown on the DMBI-reduction (Runs 1—7) while the reduction with 3-methyl-2-phenylbenzoxazoline (MBO) did not occur at all (Run 8). Although the reaction with MBT proceeded well in the presence of $AlCl_3$ to give 3-phenyl-2-butanone in quantitative yield after a reaction time of 48 h (Run 5), it is apparent from Tables 1 and 2 that DMBI is superior to MBT in terms of its power.

We have demonstrated the general applicability of the present DMBI-reduction regarding a variety of α,β-unsaturated ketones. The results are summarized in Table 3. Generally, the reduction of linear enones by the present method can be performed easily to give nearly quantitative yields of the corresponding saturated ketones (Runs 1—7). β-Ionone, corresponding to an α,β:γ,δ-unsaturated carbonyl compound, was selectively reduced to dihydro-β-ionone in quantitative yield (Run 7). 1,2-Dibenzoylethylene, corresponding to an α,β-unsaturated diketone, was also reduced with no difficulty to 1,4-diphenyl-1,4-butanedione in quantitative yield (Run 3). In all cases, the conjugate reduction products were obtained in complete selectivity, and other by-products were not detected at all. Compared with a similar reduction with 2-phenylbenzothiazoline,[6] the present DMBI-reduction of linear enones is more rapid. In addition, 3-methyl-4-phenylbutenone could be effectively reduced with DMBI within 4 h, in contrast to the reduction by 2-phenylbenzothiazoline in which the butenone was

Table 3. Conjugate Reduction of α,β-Unsaturated Ketones with DMBI in the Presence of $AlCl_3$[a)]

Run	Enone	Product	Time/h	Yield/%[b)]	Bp or mp/°C/Torr[c)]
1	$C_6H_5CH{=}CHCOCH_3$	$C_6H_5CH_2CH_2COCH_3$	0.5	100	115—118/16[22)]
2	$C_6H_5CH{=}CHCOC_6H_5$	$C_6H_5CH_2CH_2COC_6H_5$	0.5	100	72.5—73.5[23)]
3	$C_6H_5COCH{=}CHCOC_6H_5$	$C_6H_5COCH_2CH_2COC_6H_5$	0.5	100	145—146[24)]
4	$(CH_3)_2C{=}CHCOCH_3$	$(CH_3)_2CHCH_2COCH_3$	1	96	45.5—46/80[25)]
5	$C_6H_5CH{=}C(CH_3)COCH_3$	$C_6H_5CH_2CH(CH_3)COCH_3$	4	94	104—105[22)]
6	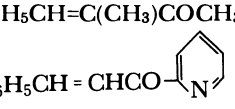	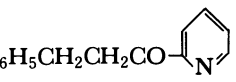	1[d)]	69[e)]	—
7	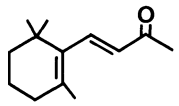	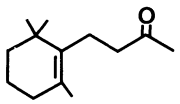	1	96	105—107/3[26)]
8	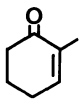	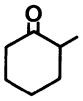	24	55	46.5—47/12[27)]
9	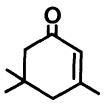	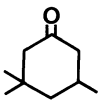	19	71	54—56/12[28)]
10	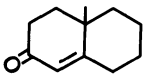	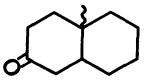	24	26[f)]	(*cis*)175—176.5[g),29)] (*trans*)178.5—180[g),29)]

a) 1.2:1 Molar ratio of DMBI and $AlCl_3$ to enone was used. b) Yield determined by GLC analysis. c) Spectral data of the reduced products were in satisfactory agreement with those of the corresponding authentic samples or expected values. d) Reaction at 60°C. e) Yield of isolated, pure product. f) Yield of isomeric mixture. g) Mp of 2,4-dinitrophenylhydrazone derivative.

sluggishly reduced to the same in 26% yield after a 24 h reaction. On the other hand, the reduction of cyclic enones was generally slower than that of linear enones but afforded moderate yields of saturated cyclic ketones (Runs 8—10). As pointed out regarding the reduction of linear enones, DMBI also seems to be more powerful in the reduction of cyclic enones than 2-phenylbenzothiazoline. In short, the $AlCl_3$-promoted conjugate reduction of a variety of α,β-unsaturated ketones can be practically performed in good yields with complete regiospecificity together with no side reactions. Thus, although there are several methods available to bring about such conversions, we consider the present method to be a useful addition. The relative reactivities of the enones were found to decrease in the order α,β-disubstituted linear enone>α,β,β-trisubstituted linear enone>α,α,β-trisubstituted linear enone>cyclic enone.

The conjugate reduction of an α,β-unsaturated ester and a similar aldehyde were also examined under similar conditions (Scheme 3). Methyl cinnamate

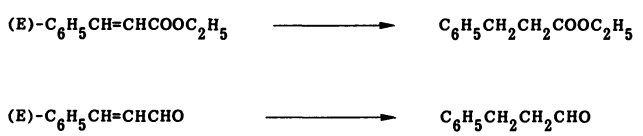

Scheme 3.

was less effectively reduced to the corresponding 3-phenylpropionate in 30% yield after a reaction time of 30 min. However, the reduction of cinnamaldehyde under the same conditions gave only a trace amount of the expected saturated aldehyde, 3-phenylpropanal. The latter result may show that the present method is, as yet, inapplicable to the conjugate reduction of α,β-unsaturated aldehydes.

The functional selectivity of the present DMBI-reduction should be noted since it is of importance in an organic synthesis and of interest to organic chemists. We have found that functional groups such as carbonyl, carboxylic ester, acid, nitro, isolated C=C, isolated C≡C, and the common carbon-halogen bond are inert to the present reducing system. These selective properties might enhance the utility of the present reducing method.

Mechanism. In an attempt to determine the destination of a hydrogen atom at the C-2 carbon of DMBI, we reduced 1-(2-pyridyl)-3-phenyl-2-propen-1-one (**1**) with 2-deuterated DMBI which can be easily prepared by the reduction of 2-phenylbenzimidazolium iodide with lithium aluminum deuteride (Scheme 4). The product of this reaction was found to be the saturated ketone (**2**) containing one deuterium atom at its β-carbon to the carbonyl group. This result shows that the hydrogen atom at C-2 carbon of DMBI surely transfers to the β-carbon of the substrate as a hydride, because the carbon at the β-position of the substrate is very nucleophilic due to the formation of a complex of $AlCl_3$ with the carbonyl group of the enone (**1**) and the pathway involving an isomerization of an allylic

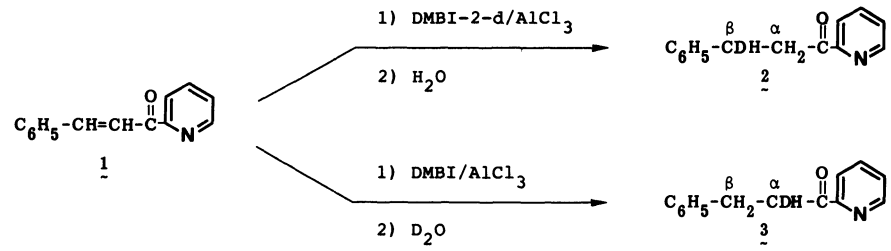

Scheme 4.

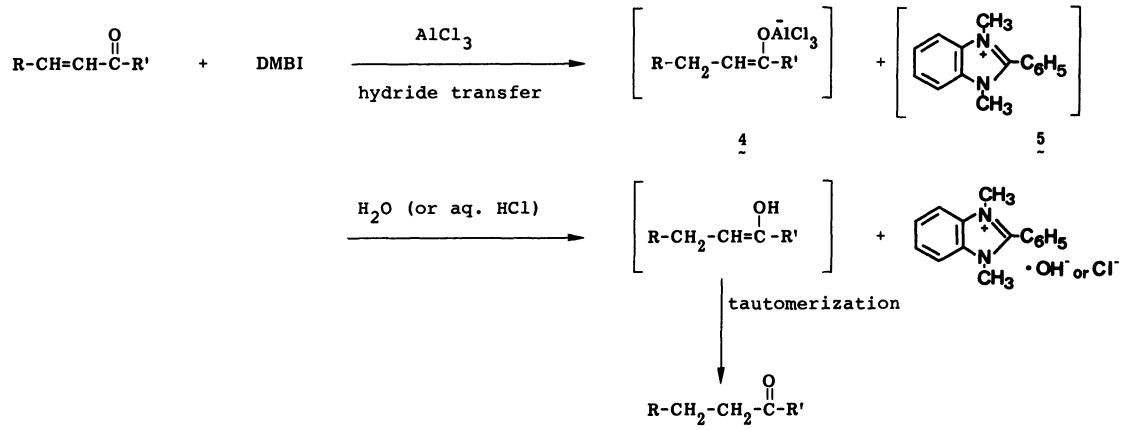

Scheme 5.

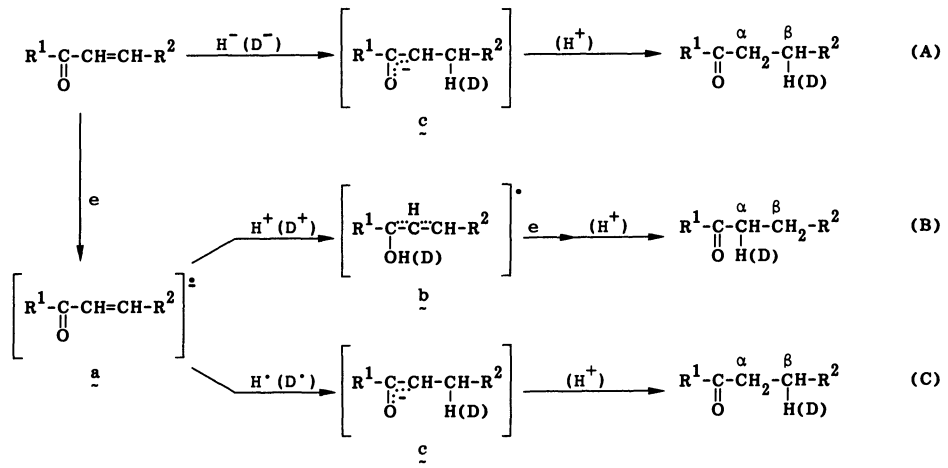

Scheme 6.

intermediate produced by the 1,2-reduction can be excluded according to the results reported by Gase et al.[9] When azachalcone (**1**) was reduced by DMBI, the α-deuterated ketone (**3**) was obtained in 65% yield after a workup with D_2O (Scheme 4). This indicates that the incorporation of a hydrogen atom from the water of the workup takes place and shows that the hydrogen atom at the α-position of the reduced product comes from the water for the workup after completion of the reaction. Considering these facts, a mechanism involving the hydride transfer followed by protonation of the aluminum enolate (**4**) by quenching water can be proposed for the present conjugate reduction as shown in Scheme 5. These processes fully conform to the driving force of the formation of stable benzimidazolium ion (**5**).

Recently, the mechanism of a hydride-equivalent transfer in a reduction with 1,4-dihydropyridine derivatives has been extensively discussed, and it has been proposed in some cases[10] that the reduction is most likely composed of an initial electron transfer followed by the transfer of a hydrogen nucleus or radical. Although the initial hydride transfer shown in Scheme 5 may be viewed as simply a one-step hydride transfer (mechanism A), schemes involving sequential transfers of e+H· (mechanism C) and e+H⁺+e (mechanism B) are also possible in theory (Scheme 6). The transfer of a hydride ion to the unsaturated ketone system (mechanism A) should give the saturated ketone in which the hydrogen atom of DMBI would be introduced at the β-carbon. In considering mechanisms B and C, it is expected that the radical

anion intermediate **a** formed by the addition of an electron to the substrate would undergo protonation (mechanism B) at the oxygen site to give the allylic intermediate **b**, while the addition of a hydrogen atom to the same (mechanism C) should result in anion **c**. As a consequence, upon completion of the reaction, the hydrogen atom of DMBI would be introduced at the α-carbon of the product obtained via mechanism B and that found via mechanism C would carry at the β-position. Thus, in light of the forementioned observation that the reduction of azachalcone (**1**) with 2-deuterated DMBI leads to the corresponding saturated ketone (**2**) which contains one deuterium atom at the β-carbon, mechanisms A and C are both candidates for the initial hydride transfer shown in Scheme 5. In addition, the role of the Lewis acid in the present reduction can be well understood according to these mechanisms as follows. First, a Lewis acid activates the substrate as an electrophilic activator. Second, a Lewis acid stabilizes the resulting enolate anion **c** by coordination.

Experimental

Melting points were recorded on a Yanagimoto micro melting-point apparatus and are uncorrected. ^{1}H NMR spectra were measured with a JEOL PMX-60 spectrometer at 60 MHz using tetramethylsilane as an internal reference. IR spectra were recorded on a JASCO A-202 spectrophotometer. Mass spectra were obtained on a JMS-QH100 GC-Mass spectrometer. GLC analyses were carried out on a Shimadzu Gas Chromatograph GC-6AM equipped with a hydrogen flame ionization detector using glass columns (1.5 m) packed with 2% Silicone OV-7 on Uniport HP (60—80 mesh). The yields by quantitative GLC were measured on the same columns by internal standard method, using pentylbenzene as an internal standard. Silica gel (Wakogel C-300) was used for short column chromatography.

Materials. DMBI, mp 97.5—98.5 °C (lit,[11] 96 °C) was prepared from 2-phenylbenzimidazole by the slight modification of the method of Craig et al.[12] DMBI-2-*d*, mp 97—98 °C was prepared by the reduction of 2-phenylbenzimidazolium iodide with $LiAlD_4$ according to the same procedure, that was fully deuterated material by ^{1}H NMR; no azomethine proton absorption was detected. MBT, mp 113—114.5 °C (lit,[13] 112—113 °C), and MBO, bp 151—152 °C/3 mmHg (lit,[14] 146—149 °C/2 mmHg (1 mmHg= 133.322 Pa)) were prepared according to the literature procedures.[13,14] Commercially available $AlCl_3$, $FeCl_3$, $SnCl_4$, and $ZnCl_2$ were used without purification. Acetonitrile was distilled three times on phosphorus pentaoxide before use. Mesityl oxide, β-ionone, isophorone, methyl cinnamate, and cinnamaldehyde were commercially supplied and purified by distillation. The following derivatives were prepared according to the literature and identified by spectroscopic (NMR and IR) methods: benzylideneacetone, bp, 110—112 °C/4.5 mmHg; mp 40—42 °C (lit,[15] bp 123—128 °C/8 mmHg; mp 40—42 °C); benzylideneacetophenone, mp 55—57 °C (lit,[16] 55—57 °C); (*E*)-1,2-dibenzoylethylene, mp 109—110 °C (lit,[17] 109—110 °C); (*E*)-3-methyl-4-phenyl-3-buten-2-one, bp 91 °C/2 mmHg (lit,[18] 80—93 °C/1 mmHg); 4a-methyl-4,4a,5,6,7,8-hexahydronaphthalen-2(3*H*)-one, bp 109—111 °C/1 mmHg (lit,[19] 112—115 °C/5 mmHg); 2-methyl-2-cyclohexen-1-one, bp 64.5—65.5 °C/16 mmHg (lit,[20] 83—85.5 °C/35 mmHg); 2-cinnamoylpyridine, mp 71—72 °C (lit,[21] 71—72 °C).

General Procedure for the Conjugate Reduction of α,β-Unsaturated Carbonyl Compounds with DMBI. A solution of an unsaturated carbonyl compound (1.0 mmol) in dry acetonitrile (2 ml) and $AlCl_3$ (0.16 g, 1.2 mmol) were mixed in a glass tube under ice-water cooling. After the $AlCl_3$ was completely dissolved, DMBI (0.27 g, 1.2 mmol) was added and the mixture was degassed several times in vacuo. The tube was sealed in vacuo and kept at 80 °C for the appropriate time (see Tables). After 0.1 M HCl (2 ml (1 M= 1 mol dm^{-3})) was added to the mixture in the tube under ice-water cooling, the aqueous mixture was extracted with chloroform. The chloroform extract was washed thoroughly with water and the organic layer was analyzed by quantitative GLC. The results are given in Tables. An identification of the products isolated by short-column chromatography on silica gel was performed by spectroscopic (NMR, IR, and MS) methods. These spectral data were in satisfactory agreement with those of the corresponding authentic samples or expected values.

In a large-scale synthesis, the reaction could be carried out in a three-necked flask under nitrogen and the same reaction conditions. After a workup, as previously described, the products could be isolated by distillation or short-column chromatography on silica gel.

Reduction of 2-Cinnamoylpyridine (1). A solution of azachalcone (1) (0.10 g, 0.5 mmol) in dry acetonitrile (1 ml) and $AlCl_3$ (0.08 g, 0.6 mmol) were mixed in a glass tube under ice-water cooling. After the $AlCl_3$ was completely dissolved, DMBI (0.13 g, 0.6 mmol) was added and the mixture was degassed several times in vacuo. The tube was sealed in vacuo and kept at 60 °C for 1 h. After water (1 ml) had been added to the mixture in the tube under ice-water cooling, the aqueous mixture was extracted with chloroform. The chloroform extract was thoroughly washed with water and dried with anhydrous Na_2SO_4. The oily residue obtained by evaporation of solvent was subjected to short column chromatography on silica gel to give 1-(2-pyridyl)-3-phenyl-1-propanone (73 mg, 69%), ^{1}H NMR ($CDCl_3$) δ=2.93 (t, 2H, β-CH_2), 3.43 (t, 2H, α-CH_2), 7.04 (s, 5H, Ph), and 7.17—8.42 (m, 4H, C_5H_4N); MS *m/z* 211 (M^+).

Azachalcone (1) (0.10 g, 0.5 mmol) was similarly reduced with DMBI-2-*d* (0.14 g, 0.6 mmol). The chromatographic purification of the crude product gave fully β-deuterated ketone (**2**) (81 mg, 76%), ^{1}H NMR ($CDCl_3$) δ=2.92 (t, 1H, β-CDH), 3.43 (d, 2H, α-CH_2), 7.04 (s, 5H, Ph), and 7.17—8.42 (m, 4H, C_5H_4N); MS *m/z* 212 (M^+).

Azachalcone (**1**) (0.10 g, 0.5 mmol) was similarly reduced with DMBI (0.13 g, 0.6 mmol). After quenching with D_2O (2 ml) under ice-water cooling, the aqueous mixture was extracted with chloroform and dried with anhydrous Na_2SO_4. Chromatographic purification of the crude product gave the fully α-deuterated ketone (**3**) (69 mg, 65%), ^{1}H NMR ($CDCl_3$) δ=2.92 (br, 2H, β-CH_2), 3.39 (t, 1H, α-CDH), 7.04 (s, 5H, Ph), and 7.17—8.42 (m, 4H, C_5H_4N); MS *m/z* 212 (M^+).

References

1) A. I. Meyers, "Heterocycles in Organic Synthesis,"

Wiley-Interscience, New York, N. Y. (1974); "Comprehensive Heterocyclic Chemistry," ed by A. R. Katritzky and C. W. Rees, Pergamon Press, New York (1984).

2) K. Nakamura, A. Ohno, and S. Oka, *Tetrahedron Lett.*, **24**, 3335 (1983); K. Nakamura, M. Fujii, A. Ohno, and S. Oka, *ibid.*, **25**, 3985 (1984); S. Yasui, K. Nakamura, and A. Ohno, *Chem. Lett.*, **1984**, 377; K. Nakamura, M. Fujii, S. Oka, and A. Ohno, *ibid.*, **1985**, 523; K. Nakamura, M. Fujii, H. Mekata, S. Oka, and A. Ohno, *ibid.*, **1986**, 87; S. Yasui, K. Nakamura, M. Fujii, and A. Ohno, *J. Org. Chem.*, **50**, 3283 (1985).

3) S. Tagani, C. Tabuchi, K. Morimoto, and D. Shiho, *Yakugaku Zasshi*, **94**, 929 (1974); S. H. Mashraqui and M. Kellogg, *Tetrahedron Lett.*, **26**, 1453 (1985).

4) H. Chikashita, S. Nishida, M. Miyazaki, and K. Itoh, *Synth. Commun.*, **13**, 1033 (1983).

5) H. Chikashita, Y. Morita, and K. Itoh, *Synth. Commun.*, **15**, 527 (1985).

6) H. Chikashita, M. Miyazaki, and K. Itoh, *Synthesis*, **1984**, 308.

7) D. M. Smith, "Dihydrobenzimidazoles, Benzimidazolones, Benzimidazolethiones, and Related Compounds," in "Chemistry of Heterocyclic Compounds," John Wiley & Sons, New York (1981), Vol. 3, Chap. 3, pp. 331—344; J. G. Smith and I. Ho, *Tetrahedron Lett.*, **1971**, 3541.

8) D. Cook, *Can. J. Chem.*, **41**, 522 (1963).

9) R. A. Gase and U. K. Pandit, *J. Am. Chem. Soc.*, **101**, 7059 (1979).

10) A. Ohno, T. Shio, H. Yamamoto, and S. Oka, *J. Am. Chem. Soc.*, **103**, 2045 (1981); and references cited therein.

11) A. V. El'tsov, *J. Org. Chem. USSR*, **3**, 191 (1967).

12) J. C. Craig, N. N. Ekwuribe, C. C. Fu, K. A. M. Walker, *Synthesis*, **1981**, 303.

13) K. Baker and H. E. Fierz-David, *Helv. Chim. Acta*, **33**, 2011 (1950).

14) A. V. El'tsov and M. Z. Girshovichi, *Zh. Org. Khim.*, **3**, 1332 (1967).

15) N. L. Drake and P. Allen, Jr., *Org. Synth.* Coll., Vol. I, 77 (1956).

16) E. P. Kohler and H. M. Chadwell, *Org. Synth.* Coll., Vol. I, 78 (1956).

17) R. E. Lutz, *Org. Synth.* Coll., Vol. III, 248 (1955).

18) C. E. Michael and N. H. Cromwell, *J. Org. Chem.*, **39**, 911 (1974).

19) C. H. Heathcock, J. E. Ellis, J. E. McMurry, and A. Coppolino, *Tetrahedron Lett.*, **1971**, 4995.

20) E. W. Warnhoff, D. G. Martin, and W. S. Johnson, *Org. Synth.* Coll., Vol. IV, 162 (1963).

21) C. S. Marvel, L. E. Coleman, Jr., and G. P. Scott, *J. Org. Chem.*, **20**, 1785 (1955).

22) A. Citterio and E. Vismara, *Synthesis*, **1980**, 291.

23) D. R. G. Brimage, R. S. Davidson, and P. F. Lambeth, *J. Chem. Soc., C*, **1971**, 1241.

24) J. P. Schaeter, *J. Org. Chem.*, **25**, 2027 (1960).

25) G. Dupont, *Bull. Soc. Chim. Fr.*, **3**, 1021 (1936).

26) A. Caliezi and H. Schinz, *Helv. Chim. Acta*, **33**, 1129 (1950).

27) P. D. Bartlett and R. H. Rosenwald, *J. Am. Chem. Soc.*, **56**, 1990 (1934).

28) A. Skita and W. A. Meyer, *Ber.*, **45**, 3589 (1921).

29) R. B. Woodward, F. Sondheimer, D. Taub, K. Heusler, and W. M. Mclamore, *J. Am. Chem. Soc.*, **74**, 4223 (1952).

Synthetic Approach toward Antibiotic Ezomycins. I. Synthesis of 5-Amino-5-deoxyoctofuranose-(1,4) Derivatives by Henry Reaction and Their Stereochemistry

Osamu SAKANAKA, Takashi OHMORI, Shuji KOZAKI, Tetsuo SUAMI,* Toshio ISHII,† Shigeru OHBA, and Yoshihiko SAITO*

Departments of Applied Chemistry and Chemistry, Faculty of Science and Technology, Keio University, Hiyoshi, Yokohama 223

†Department of Chemistry, Chiba Institute of Technology, Tsudanuma, Narashino 275

(Received January 7, 1986)

Ezomycins were discovered in a fermentation beer of Streptomyces species as antibiotics, which consisted of aminoocturonic acid, aminoglucuronic acid and base. As a part of a total synthesis of ezomycins, the title compounds have been synthesized. A KF-catalyzed Henry reaction between a nitropentose and a glyceraldehyde derivative gave a nitro alcohols mixture. Hydrogenation of the intact mixture, followed by *N*-acetylation afforded three diastereomers. The absolute configurations of the newly-introduced chiral centers were established by chemical methods and a X-ray crystal structure analysis.

Nucleoside antibiotic ezomycins were found in a fermentation broth of a strain which was very similar to Streptomyces Kitazawaensis.[1] The antibiotics exhibit antimicrobial activity against limited species of phytopathogenic fungi, such as Sclerotinia and Botritis. The molecular structures were established by a degradation study and a spectroscopic analysis.[2-4] A higher-carbon carbohydrate involved in ezomycins A_1, A_2, B_1, B_2, C_1, and C_2 is 5-amino-3,7-anhydro-5-deoxyocturonic acid, in which a furanoid ring is trans-

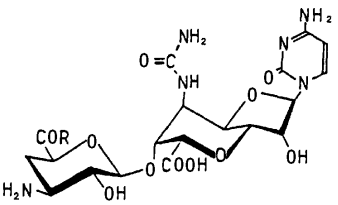

Ezomycin A_1 R = $NHCHCH_2CH_2SCH_2CHNH_2$ (COOH, COOH)

A_2 R = OH

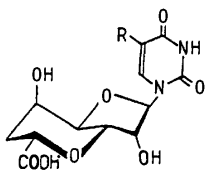

Octosyl acids A_1 R = COOH

A_2 R = CH_2OH

Scheme 1.

fused to a pyranoid ring. This particularly interesting structure was also found in antibiotic octosyl acids.[5] Several synthetic studies toward 3,7-anhydrooctose have been reported.[6-8] However, no derivatives with full function have been synthesized. Now, we have attempted to synthesize 5-amino-5-deoxyoctofuranose as a first step of the synthesis of ezomycins.

In a preceding paper,[9] a generally-applicable facile synthesis of higher-carbon carbohydrates has been developed by a KF-catalyzed Henry reaction between a nitro sugar and a sugar aldehyde, which is applied for the synthesis of 5-amino-5-deoxyoctofuranose-(1,4) derivatives in the present study.

Results and Discussion

In the KF-catalyzed Henry reaction, 5-deoxy-1,2-*O*-isopropylidene-3-*O*-methylthiomethyl-5-nitro-α-D-ribofuranose (**6**) was used as a nitro component and 2,3-*O*-isopropylidene-L-glyceraldehyde (**8**) was used as an aldehyde component. Compound **6** was prepared from known 1,2:5,6-di-*O*-isopropylidene-α-D-allofuranose[10] (**1**) by a **7** steps-reaction. Protection of 3-OH with chloromethyl methyl sulfide and sodium hydride in dioxane gave methylthiomethyl (MTM) ether (**2**) in 62%

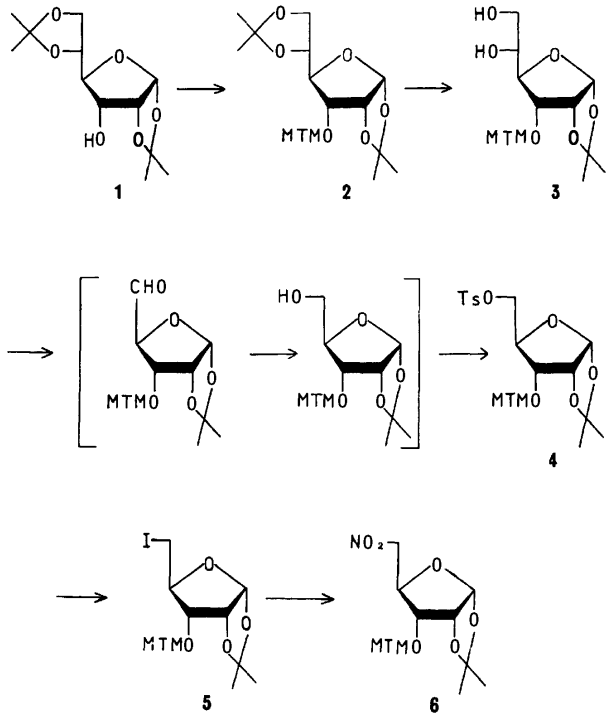

MTM: $-CH_2SCH_3$

Scheme 2.

yield. A selective removal of the 5,6-*O*-isopropylidene group by hydrolysis of **2** in aqueous acetic acid afforded the glycol (**3**) in 92% yield. Oxidative cleavage of the 5,6-diol with sodium periodate and successive reduction with sodium borohydride, followed by tosylation with *p*-toluenesulfonyl chloride in pyridine gave the tosylate (**4**) in 79% yield. Displacement of **4** with sodium iodide in 2-butanone afforded the iodide (**5**) in 94% yield. Replacement of **5** with sodium nitrite in dimethyl sulfoxide (DMSO) yielded the nitro compound (**6**) in 54% yield. On the other hand, the aldehyde **8** was prepared by a modified method of a known procedure.[11]

The Henry reaction of **6** and **8** was carried out in a toluene solution under the presence of KF and tetrabutylammonium iodide to give 5-deoxy-5-nitrooctose (**9**) as a mixture of diastereomers. Catalytic hydrogenation of the intact mixture **9** in the presence of Raney Ni, followed by *N*-acetylation afforded a mixture of three 5-acetamido-5-deoxyoctofuranoses (**11a**, **11b**, and **11c**). Compound **11c** was isolated in a homogeneous state by silica-gel chromatography in a poor yield of 5%. Compound **11b** was obtained by repeated fractional

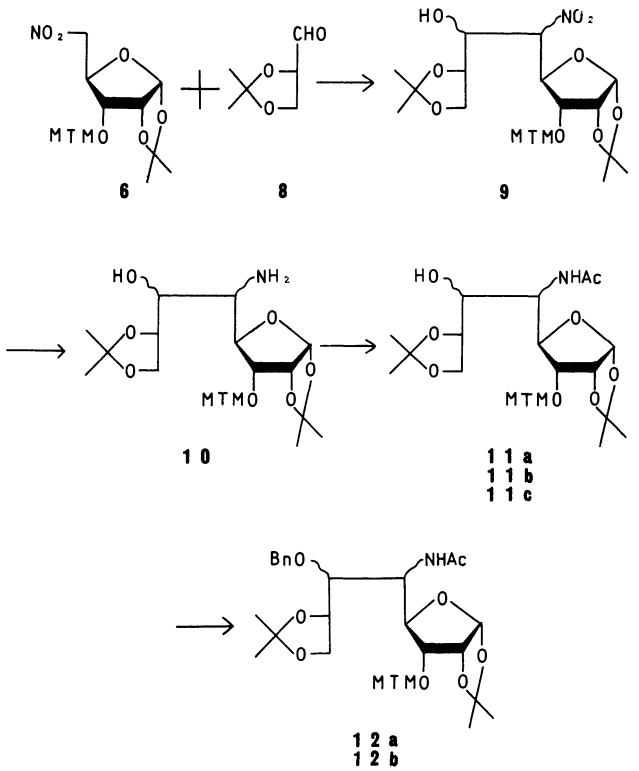

Scheme 3.

recrystallization. But the major product **11a** was contaminated with **11b** which showed the same chromatographic behavior in several solvent systems. *O*-Benzylation of a mixture (67% from **6**) of **11a** and **11b** with benzyl bromide and sodium hydride in *N*,*N*-dimethylformamide (DMF) gave the corresponding benzyl ethers (**12a** and **12b**), which were readily isolated in homogeneous states by silica-gel chromatography in 49 and 30% yield, respectively.

A stereochemistry of the newly-introduced chiral centers on C-5 and C-6 of the major product **12a** was established by converting **12a** to 2-acetamido-3-*O*-benzyl-2-deoxy-L-threitol (**18**) as follows. Hydrolysis of **12a** with aqueous acetic acid resulted in a preferential removal of the 7,8-*O*-isopropylidene group giving a diol (**13**). Oxidative cleavage of **13** with sodium

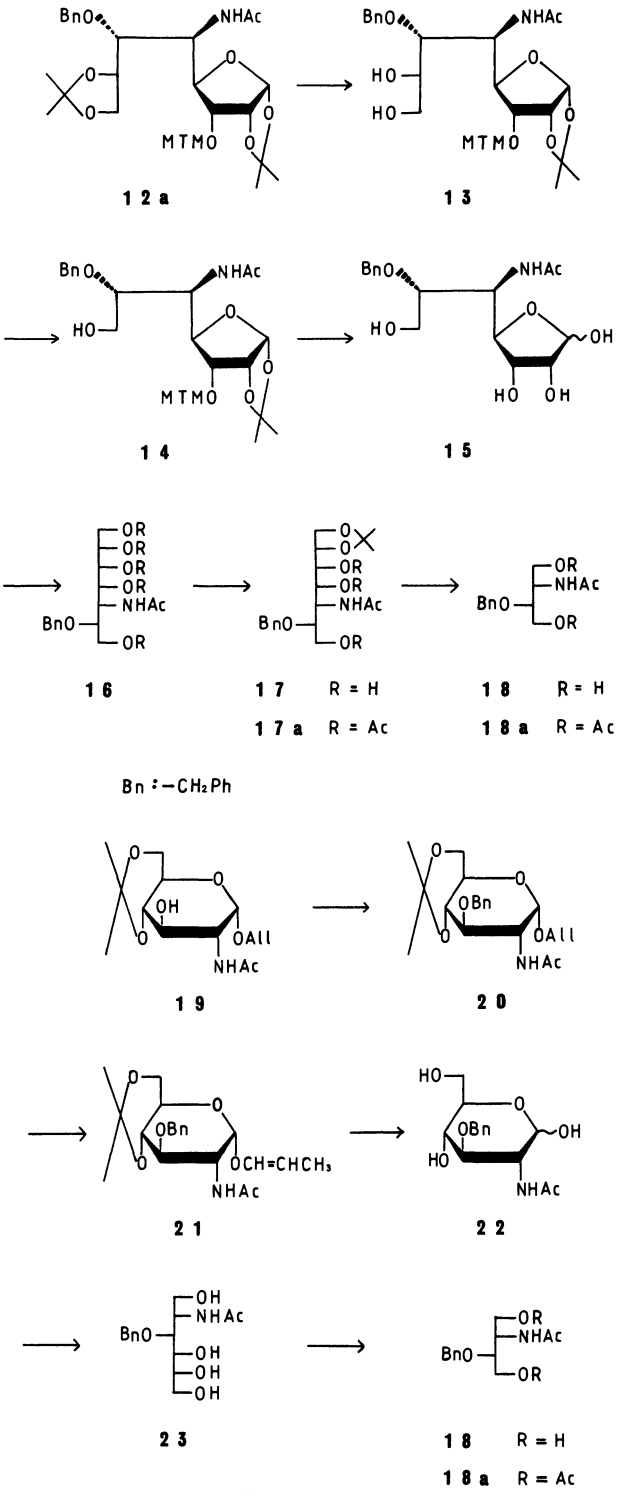

Scheme 4.

periodate and successive reduction with sodium borohydride afforded a heptose derivative (**14**). Removal of protective groups of **14** with aqueous trifluoroacetic acid gave a heptose derivative (**15**). Reduction of **15** with sodium borohydride afforded a heptitol derivative (**16**). Partial protection of **16** with 2-methoxypropene in the presence of *p*-toluenesulfonic acid yielded 1,2-*O*-isopropylidene derivative (**17**). Oxidative cleavage of **17** with sodium periodate and subsequent reduction with sodium borohydride afforded a C_4-alditol (**18**). Compound **18** was found to be identical with an authentic sample prepared as follows. *O*-Benzylation of allyl 2-acetamido-2-deoxy-4,6-*O*-isopropylidene-α-D-glucopyranoside[12] (**19**) with benzyl bromide and sodium hydride gave benzyl ether (**20**). Isomerization of the allyl group of **20** with Wilkinson's catalyst[13] afforded 1-propenyl ether (**21**). Hydrolysis of **21** with diluted hydrochloric acid resulted in a removal of the 1-propenyl and 4,6-*O*-isopropylidene groups giving **22**. Reduction of **22** with sodium borohydride yielded a hexitol (**23**). Oxidative cleavage of **23** with sodium periodate and successive reduction with sodium borohydride afforded the same C_4-alditol (**18**). Therefore, the absolute configurations on C-5 and C-6 were established as *R*-configurations. Consequently, **12a** has the same configurations on C-5 and C-6 as those of ezomycins.

A stereochemistry of **11b** was established by means of X-ray crystal structure analysis. Figure 1 shows a perspective drawing of **11b**. The absolute configurations on C-5 and C-6 are S and R, respectively. The torsion angle of both C(4)–C(5)–C(6)–C(7) and N–C(5)–C(6)–O(4) are almost 180°. Interatomic distance O(4)···O(5)($x-1/2$, $-y+3/2$, $-z+1$) is 2.722(7), suggesting an existence of an O(4)–H(04)···O(5) hydrogen bond.

The configurations of **11c** were determined by a fact that **11c** was derived from **11b** by oxidation with DMSO

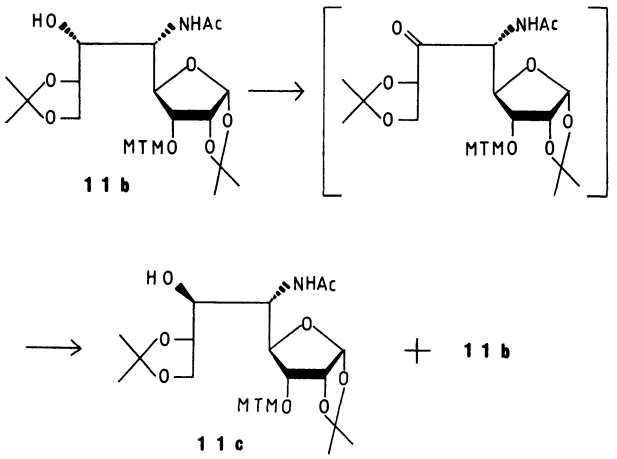

Scheme 5.

and dicyclohexylcarbodiimide (DCC) and successive reduction with sodium borohydride. That is, **11c** was an epimer of **11b** at C-6. Therefore, *S*-configurations were established on C-5 and C-6.

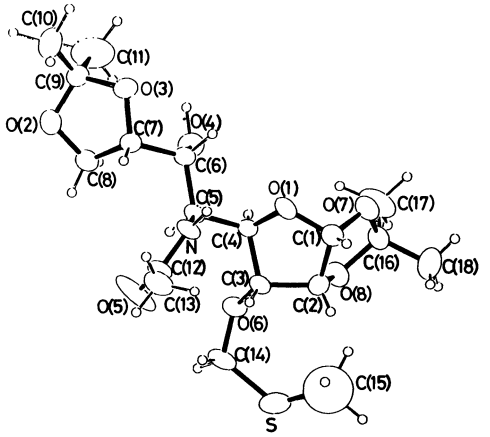

Fig. 1.

In the present case, the KF-catalyzed reaction between **6** and **8** seems to proceed without any predominant stereoselectivity.

Experimental

Melting points were determined on a Büchi 510 capillary melting point apparatus and are uncorrected. Optical rotations were measured with a Jasco DIP-4 polarimeter. IR spectra were recorded on a Hitachi 225 spectrometer. ^{1}H NMR spectra were recorded on a Varian EM-390 (90 MHz) spectrometer with a reference to tetramethylsilane as an internal standard. Mass spectra were recorded on a Hitachi M-80 or a Hitachi M-80A mass spectrometer. Solutions were dried over anhydrous sodium sulfate and concentrated below 45 °C. TLC was carried out on glass plates coated with Merck Kieselgel 60 F_{254}, and compounds were detected by spraying with a H_2SO_4 followed by heating. Chromatography was performed on a silica-gel (Merck Kieselgel 60 Art. 7734) column.

1,2:5,6-Di-*O*-isopropylidene-3-*O*-methylthiomethyl-α-D-allofuranose (2). To a stirred solution of **1** (20.0 g) in anhydrous dioxane (200 ml), sodium hydride (60% dispersion in mineral oil, 10.0 g) and chloromethyl methyl sulfide (10.0 ml) were added under ice cooling and the mixture was stirred overnight at room temperature. After addition of methanol, the reaction solution was concentrated and the residue was dissolved in ethyl acetate. The solution was washed with water repeatedly, dried and concentrated to dryness. The oily residue was chromatographed (5:1 (v/v) toluene–ethyl acetate) to give crystals. Recrystallization from hexane afforded 16.0 g (62%) of **2**: R_f=0.27 on TLC (5:1 (v/v) toluene–ethyl acetate); mp 58—60 °C; $[\alpha]_D^{23}$ +123° (*c* 0.8, $CHCl_3$); ^{1}H NMR ($CDCl_3$) δ=1.37, 1.43, 1.55 (total 12H, s×3, CMe_2×2), 2.17 (3H, s, SMe), 4.77 (2H, s, CH_2S), 5.75 (1H, d, *J*=4 Hz, H-1).

Found: C, 52.52; H, 7.45; S, 9.90%. Calcd for $C_{14}H_{24}O_6S$: C, 52.48; H, 7.55; S, 10.01%.

1,2-*O*-Isopropylidene-3-*O*-methylthiomethyl-α-D-allofuranose (3). Compound **2** (6.7 g) was dissolved in 80% aqueous acetic acid (100 ml) and the solution was allowed to stand overnight at room temperature. The solution was coevaporated with toluene and the residue was chromatographed (1:2 (v/v) toluene–ethyl acetate) to give 5.4 g (92%) of **3** as a colorless syrup: R_f=0.41 on TLC (ethyl acetate); $[\alpha]_D^{25}$ +198° (*c* 1.0, $CHCl_3$); IR ($CHCl_3$) 3550 cm^{-1} (OH); ^{1}H NMR ($CDCl_3$)

δ=1.33, 1.57 (total 6H, s×2, CMe_2), 2.20 (3H, s, SMe), 4.77 (2H, s, CH_2S), 5.78 (1H, d, J=4 Hz, H-1).

Found: C, 46.87; H, 6.97; S, 11.40%. Calcd for $C_{11}H_{20}O_6S$: C, 47.13; H, 7.19; S, 11.44%.

1,2-*O*-Isopropylidene-3-*O*-methylthiomethyl-5-*O*-*p*-tolylsulfonyl-α-D-ribofuranose (4). An aqueous solution (560 ml) of sodium periodate (44.9 g) was added dropwise to an aqueous solution (560 ml) of **3** (56.0 g) under ice cooling. After 20 min, sodium borohydride (10.6 g) was added to the solution and the mixture was stirred for 20 min under ice cooling. The mixture was extracted with chloroform and the organic layer was dried and concentrated to dryness. To a solution of the residue in dry pyridine (300 ml) was added *p*-toluenesulfonyl chloride (45.7 g). After 12 h at room temperature, the mixture was concentrated and the residue was partitioned between saturated aqueous sodium hydrogencarbonate and ethyl acetate. The organic layer was washed twice with water, dried and concentrated to dryness. The residue was recrystallized from cyclohexane to afford 63.6 g (79%) of **4**: R_f=0.32 on TLC (5:1 (v/v) toluene–ethyl acetate); mp 80—81 °C; $[\alpha]_D^{23}$ +99° (c 1.4, $CHCl_3$); IR (KBr) 1360 cm^{-1} (SO_2); ^1H NMR ($CDCl_3$) δ=1.33, 1.57 (total 6H, s×2, CMe_2), 2.13 (3H, s, SMe), 2.50 (3H, s, $SO_2C_6H_4Me$), 4.73 (2H, s, CH_2S), 5.67 (1H, d, J=4 Hz, H-1), 7.38 (2H, d, J=9 Hz, C_6H_4), 7.85 (2H, d, J=9 Hz, C_6H_4).

Found: C, 50.51; H, 5.95; S, 15.57%. Calcd for $C_{17}H_{24}O_7S_2$: C, 50.48; H, 5.95; S, 15.85%.

5-Deoxy-5-iodo-1,2-*O*-isopropylidene-3-*O*-methylthiomethyl-α-D-ribofuranose (5). To a solution of **4** (45.1 g) in 2-butanone (450 ml) was added sodium iodide (58.5 g) and the mixture was heated for 2 h under reflux. The solution was concentrated and the residue was partitioned between water and ethyl acetate. The organic layer was washed twice with water, dried and concentrated to dryness to give 37.7 g (93.9%) of **5** as an almost homogeneous syrup: R_f=0.55 on TLC (5:1 (v/v) toluene–ethyl acetate); ^1H NMR ($CDCl_3$) δ=1.37, 1.57 (total 6H, s×2, CMe_2), 2.20 (3H, s, SMe), 4.73 (2H, s, CH_2S), 5.80 (1H, d, J=4 Hz, H-1).

The product was used in the next step without any purification.

5-Deoxy-1,2-*O*-isopropylidene-3-*O*-methylthiomethyl-5-nitro-α-D-ribofuranose (6). To a solution of **5** (37.7 g) in DMSO (370 ml) were added phloroglucinol monohydrate (28.9 g) and sodium nitrite (14.5 g). After stirring for 4 d at ambient temperature, the mixture was poured into water and extracted with ethyl acetate. The organic layer was washed with water repeatedly, dried and concentrated to dryness. The residue was chromatographed (10:1 (v/v) toluene–ethyl acetate) to yield crystalline solids. Recrystallization from cyclohexane–toluene (2:1 v/v) afforded 15.8 g (54.2%) of **6**: R_f=0.36 on TLC (5:1 (v/v) toluene–ethyl acetate); mp 89—90 °C; $[\alpha]_D^{25}$ +167° (c 1.5, $CHCl_3$); IR (KBr) 1560, 1380 cm^{-1} (NO_2); ^1H NMR ($CDCl_3$) δ=1.37, 1.57 (total 6H, s×2, CMe_2), 2.17 (3H, s, SMe), 4.78 (2H, s, CH_2S), 5.80 (1H, d, J=4 Hz, H-1).

Found: C, 43.14; H, 6.09; N, 5.10; S, 11.61%. Calcd for $C_{10}H_{17}NO_6S$: C, 43.00; H, 6.13; N, 5.01; S, 11.48%.

2,3-*O*-Isopropylidene-L-glyceraldehyde (8). To an ice-cooled solution of 4,5-*O*-isopropylidene-L-arabinose diethyl thioacetal[14] (**7**, 10.0 g) in ethyl acetate (100 ml) was added lead tetraacetate (20.0 g) and the mixture was vigorously stirred for 5 min. To the mixture was added sodium carbonate (30 g) and the mixture was vigorously stirred for 2 h under ice cooling. After the salts were filtered off, the filtrate was concentrated to give a pale yellow syrup. It was rapidly chromatographed (3:2 (v/v) hexane–ethyl acetate) to afford 3.1 g (70%) of **8** as a colorless syrup: $[\alpha]_D^{29}$ −48.9° (c 1.02, C_6H_6) (lit,[15] $[\alpha]_D^{22}$ −67.9° (C_6H_6)). The IR and ^1H NMR spectra were superimposable on those of D-isomer, prepared by oxidative cleavage of 1,2:5,6-di-*O*-isopropylidene-D-mannitol.

The product was used in the successive reaction without further purification.

5-Acetamido-5-deoxy-1,2:7,8-di-*O*-isopropylidene-3-*O*-methylthiomethyl-β-L-erythro-L-talooctofuranose-(1,4) (11b) and 5-Acetamido-5-deoxy-1,2:7,8-di-*O*-isopropylidene-3-*O*-methylthiomethyl-β-L-threo-L-talooctofuranose-(1,4) (11c). To a solution of **6** (1.0 g) in toluene (3 ml) were added **8** (0.75 g), anhydrous potassium fluoride (0.25 g) and tetrabutylammonium iodide (0.75 g). The total mixture was stirred for 2 h 30 min at room temperature. The mixture was diluted with ethyl acetate, washed with water repeatedly, dried and concentrated to dryness. The residue was dissolved in a mixture of ethyl acetate (20 ml) and acetic acid (1 ml), and hydrogenated in the presence of Raney Nickel T-4[16] (ca. 2.5 g) under a pressure of 5.5 kg cm^{-2} for 20 h. After the catalyst was filtered off, the filtrate was added with sodium carbonate (5 g) and the mixture was stirred for 1 h at room temperature. The precipitates were filtered off, and the filtrate was concentrated to give a syrup. The residue was dissolved in a mixture of methanol (20 ml) and acetic anhydride (1 ml), and the mixture was allowed to stand for 10 min at room temperature. Coevaporation with toluene gave a syrup, which was chromatographed (ethyl acetate) to afford 1.01 g (67.0%) of a mixture of **11a** and **11b**, and 72 mg (4.7%) of **11c** as a colorless syrup. The mixture of **11a** and **11b** was dissolved in toluene (10 ml), and the solution was stored at −20 °C overnight. The crystals of **11b** were collected by filtration and washed with toluene. Recrystallization from toluene yielded an analytical sample. Furthermore, recrystallization from ethyl acetate–cyclohexane afforded nice single crystals for X-ray structure analysis.

11b: R_f=0.36 on TLC (ethyl acetate); mp 138—139 °C; $[\alpha]_D^{23}$ +25.9° (c 1.0, $CHCl_3$); IR (KBr) 1660 cm^{-1} (NHCO); ^1H NMR ($CDCl_3$) δ=1.33, 1.36, 1.42, 1.58 (total 12H, s×4, CMe_2×2), 2.04 (3H, s, NHAc), 2.18 (3H, s, SMe), 2.65 (1H, d, J=8 Hz, OH), 4.78 (2H, s, CH_2S), 5.72 (1H, d, J=4 Hz, H-1), 5.93 (1H, d, J=13 Hz, NH).

Found: C, 51.49; H, 7.29; N, 3.19%. Calcd for $C_{18}H_{31}NO_8S$: C, 51.29; H, 7.41; N, 3.32%.

11c: R_f=0.21 on TLC (ethyl acetate); $[\alpha]_D^{25}$+40.0° (c 1.08, $CHCl_3$); IR ($CHCl_3$) 1680 cm^{-1} (NHCO); ^1H NMR ($CDCl_3$) δ=1.36, 1.43, 1.56 (total 12H, s×3, CMe_2×2), 2.04 (3H, s, NHAc), 2.20 (3H, s, SMe), 2.92 (1H, d, J=4 Hz, OH), 4.70 (1H, dd, J=4, 4 Hz, H-2), 4.80 (2H, s, CH_2S), 5.79 (1H, d, J=4 Hz, H-1), 6.20 (1H, d, J=9 Hz, NH).

Found: C, 50.79; H, 7.23; N, 3.04%; M+H, 422.1823. Calcd for $C_{18}H_{31}NO_8S$: C, 51.29; H, 7.41; N, 3.32%. Calcd for $C_{18}H_{32}NO_8S$: m/z, 422.1846.

5-Acetamido-6-*O*-benzyl-5-deoxy-1,2:7,8-di-*O*-isopropylidene-3-*O*-methylthiomethyl-β-L-erythro-D-allooctofuranose-(1,4) (12a) and 5-Acetamido-6-*O*-benzyl-5-deoxy-1,2:7,8-di-*O*-isopropylidene-3-*O*-methylthiomethyl-β-L-erythro-L-talooctofuranose-(1,4) (12b). To a stirred solution of the intact mixture (6.19 g) of **11a** and **11b** in anhydrous DMF (60 ml) were added benzyl bromide (2.1 ml) and sodium hydride

(0.88 g) under ice cooling. After 95 min, the reaction mixture was partitioned between water and ethyl acetate. The organic layer was washed with water repeatedly, dried and concentrated to dryness. The residue was chromatographed (1:1 (v/v) toluene–ethyl acetate) to give 3.64 g (48.5%) of **12a** and 2.26 g (30.1%) of **12b**. Recrystallization from toluene–cyclohexane (1:2 v/v) and cyclohexane yielded analytical samples, respectively.

12a: R_f=0.58 on TLC (ethyl acetate); mp 144—145 °C; $[\alpha]_D^{22}$ +17.7° (*c*, 1.04, $CHCl_3$); IR (KBr) 3330 (NH), 1680 (NHCO) cm^{-1}; ^1H NMR ($CDCl_3$) δ=1.32, 1.36, 1.41, 1.54 (total 12H, s×4, CMe_2×2), 1.97 (3H, s, NHAc), 2.20 (3H, s, SMe), 5.66 (1H, d, *J*=10 Hz, NH), 5.79 (1H, d, *J*=4 Hz, H-1), 7.38 (5H, s, Ph).

Found: C, 58.75; H, 7.25; N, 2.47; S, 6.32%. Calcd for $C_{25}H_{37}NO_8S$: C, 58.69; H, 7.29; N, 2.74; S, 6.27%.

12b: R_f=0.53 on TLC (ethyl acetate); mp 108—109 °C; $[\alpha]_D^{20}$ +15.2° (*c* 1.57, $CHCl_3$); IR (KBr) 3310 (NH), 1680 (NHCO) cm^{-1}; ^1H NMR ($CDCl_3$) δ=1.32, 1.37, 1.41 (total 12H, s×3, CMe_2×2), 1.98 (3H, s, NHAc), 2.14 (3H, s, SMe), 5.57 (1H, d, *J*=4 Hz, H-1), 5.59 (1H, d, *J*=11 Hz, NH), 7.36 (5H, bs, Ph).

Found: C, 58.75; H, 7.17; N, 2.75; S, 6.24%. Calcd for $C_{25}H_{37}NO_8S$: C, 58.69; H, 7.29; N, 2.74; S, 6.27%.

5-Acetamido-6-*O*-benzyl-5-deoxy-1,2-*O*-isopropylidene-3-*O*-methylthiomethyl-β-L-erythro-D-allooctofuranose-(1,4) (13). Compound **12a** (2.0 g) was dissolved in 70% aqueous acetic acid (20 ml), and the solution was allowed to stand for 12 h at room temperature. The reaction solution was coevaporated with toluene to dryness, and the residue was chromatographed (ethyl acetate) to afford 1.68 g (90.7%) of **13** as crystals: R_f=0.42 on TLC (ethyl acetate); mp 147 °C; $[\alpha]_D^{22}$ +21.0° (*c* 1.03, $CHCl_3$); IR (KBr) 1650 cm^{-1} (NHCO); ^1H NMR ($CDCl_3$) δ=1.37, 1.55 (total 6H, s×2, CMe_2), 2.02 (3H, s, NHAc), 2.19 (3H, s, SMe), 5.84 (1H, d, *J*=4 Hz, H-1), 5.94 (1H, d, *J*=9 Hz, NH), 7.39 (5H, s, Ph).

Found: C, 56.07; H, 6.95; N, 3.04; S, 6.88%. Calcd for $C_{22}H_{33}NO_8S$: C, 56.03; H, 7.05; N, 2.97; S, 6.80%.

5-Acetamido-6-*O*-benzyl-5-deoxy-1,2-*O*-isopropylidene-3-*O*-methylthiomethyl-β-L-glycero-D-alloheptofuranose-(1,4) (14). To a stirred solution of **13** (103 mg) in 50% aqueous ethanol (2 ml) was added a solution of sodium periodate (49 mg) in 50% aqueous ethanol (2 ml) under ice cooling. After 60 min, the solution was diluted with water and extracted with dichloromethane repeatedly. The combined extract was dried and concentrated to dryness. The residue was dissolved in 50% aqueous ethanol (3 ml). To the stirred solution was added sodium borohydride (17 mg) under ice cooling. After 30 min, the reaction mixture was diluted with water and extracted with dichloromethane repeatedly. The extract was dried and concentrated to dryness. The residue was chromatographed (1:1 (v/v) toluene–ethyl acetate) to give 84 mg (87%) of **14** as crystals: R_f=0.44 on TLC (ethyl acetate); mp 148—150 °C; $[\alpha]_D^{26}$ +37.2° (*c* 1.02, $CHCl_3$); IR (KBr) 1665 cm^{-1} (NHCO); ^1H NMR ($CDCl_3$) δ=1.35, 1.55 (total 6H, s×2, CMe_2), 1.97 (3H, s, NHAc), 2.16 (3H, s, SMe), 5.77 (1H, d, *J*=4 Hz, H-1), 5.89 (1H, d, *J*=8 Hz, NH), 7.34 (5H, s, Ph).

Found: C, 57.21; H, 6.90; N, 2.92%. Calcd for $C_{21}H_{31}NO_7S$: C, 57.13; H, 7.08; N, 3.17%.

5-Acetamido-6-*O*-benzyl-5-deoxy-L-glycero-D-alloheptose (15). Compound **14** (83 mg) was dissolved in 90% aqueous trifluoroacetic acid (1.7 ml), and the solution was allowed to stand for 55 min under ice cooling. The reaction solution was concentrated to dryness, and the residue was chromatographed (10:1 (v/v) dichloromethane–methanol) rapidly to afford 58 mg (90%) of **15** as an amorphous solid. The compound was unstable and was not characterized.

3-Acetamido-2-*O*-benzyl-3-deoxy-L-glycero-L-altroheptitol (16). To an ice-cooled solution of **15** (70 mg) in 50% aqueous ethanol (4 ml) was added sodium borohydride (62 mg), and the solution was stirred for 2 h under ice cooling. After deionized with Amberlite IR-120 (H^+), the solution was concentrated to dryness. The residue was chromatographed (8:1 (v/v) dichloromethane–methanol) to yield 54 mg (78%) of **16** as a pale yellow syrup: R_f=0.44 on TLC (5:1 (v/v) dichloromethane–methanol); $[\alpha]_D^{30}$ −36.7° (*c* 1.25, MeOH); IR (neat) 1645 cm^{-1} (NHCO); ^1H NMR (CD_3OD) δ=1.99 (3H, s, NHAc), 7.32 (5H, bs, Ph).

Found: M+H, 344. Calcd for $C_{16}H_{26}NO_7$: *m/z*, 344.

3-Acetamido-1,4,5-tri-*O*-acetyl-2-*O*-benzyl-3-deoxy-6,7-*O*-isopropylidene-L-glycero-L-altroheptitol (17a). To a stirred solution of **16** (146 mg) in anhydrous DMF (2 ml) were added 2-methoxypropene (0.24 ml) and *p*-toluenesulfonic acid monohydrate (7 mg). After 5 h at room temperature, the solution was added with dry pyridine (6 ml) and acetic anhydride (6 ml) under ice cooling. After 1 h 45 min at room temperature, the solution was concentrated to dryness. The residue was dissolved in ethyl acetate, and the solution was washed three times with water. The organic layer was dried and concentrated to dryness. The residue was chromatographed (3:2 (v/v) toluene–ethyl acetate) to give 64 mg (30%) of **17a** as a colorless syrup: R_f=0.65 on TLC (ethyl acetate); $[\alpha]_D^{28}$ −27.6° (*c* 0.98, $CHCl_3$); IR ($CHCl_3$) 1735 (OAc), 1675 (NHCO) cm^{-1}; ^1H NMR ($CDCl_3$) δ=1.35 (6H, s, CMe_2), 2.00 (3H, s, NHAc), 2.04, 2.07 (total 9H, s×2, OAc×3), 6.36 (1H, d, *J*=10 Hz, NH), 7.33 (5H, s, Ph).

Found: M+H, 510. Calcd for $C_{25}H_{36}NO_{10}$: *m/z*, 510.

5-Acetamido-6-*O*-benzyl-5-deoxy-1,2-*O*-isopropylidene-L-glycero-D-alloheptitol (17). Compound **17a** (64 mg) was dissolved in ice-cooled 0.1 M methanolic sodium methoxide (2 ml (1 M=1 mol dm^{-3})). After 45 min under ice cooling, the solution was deionized with Amberlite IR-120 (H^+) and concentrated to dryness. The residue was chromatographed (1:8 (v/v) toluene–ethyl acetate) to afford 40 mg (83%) of **17** as a colorless syrup: R_f=0.16 on TLC (ethyl acetate); $[\alpha]_D^{29}$ −20.2° (*c* 1.98, $CHCl_3$); IR ($CHCl_3$) 1655 cm^{-1} (NHCO); ^1H NMR ($CDCl_3$) δ=1.34, 1.40 (total 6H, s×2, CMe_2), 2.00 (3H, s, NHAc), 6.41 (1H, d, *J*=9 Hz, NH), 7.34 (5H, s, Ph).

Found: M+H, 384. Calcd for $C_{19}H_{30}NO_7$: *m/z*, 384.

Allyl 2-Acetamido-3-*O*-benzyl-2-deoxy-4,6-*O*-isopropylidene-α-D-glucopyranoside (20). To a stirred solution of **19** (2.91 g) in anhydrous DMF (30 ml) were added benzyl bromide (1.35 ml) and sodium hydride (580 mg) under ice cooling. After 1 h under ice cooling, the solution was partitioned between water and ethyl acetate. The organic layer was washed twice with water, dried and concentrated to dryness. The residue was chromatographed (2:1 (v/v) toluene–ethyl acetate) to give 3.01 g (79.6%) of **20** as an amorphous solid: R_f=0.31 on TLC (1:1 (v/v) toluene–ethyl acetate); $[\alpha]_D^{20}$ +107° (*c* 0.62, $CHCl_3$); IR (KBr) 3290 (NH), 1640 (NHCO) cm^{-1}; ^1H NMR ($CDCl_3$) δ=1.42, 1.48 (total 6H, s×2, CMe_2), 1.89 (3H, s, NHAc), 5.47 (1H, d, *J*=8 Hz, NH), 5.72 (1H, m, $CH_2\underline{CH}{=}CH_2$), 7.32 (5H, m, Ph).

Found: M+H, 392. Calcd for $C_{21}H_{30}NO_6$: *m/z*, 392.

1-Propenyl 2-Acetamido-3-*O*-benzyl-2-deoxy-4,6-*O*-isopropylidene-α-D-glucopyranoside (21). To a solution of

20 (81 mg) in 75% aqueous ethanol (1.6 ml) were added 1,4-diazabicyclo[2.2.2]octane (12mg) and chlorotris(triphenylphosphine) rhodium(I) (38 mg). After refluxing for 20 min, the reaction mixture was filtered to remove the catalyst. The filtrate was concentrated and the residue was chromatographed (3:1 (v/v) toluene–ethyl acetate) to yield 70 mg (86%) of **21** as a colorless syrup: R_f=0.38 on TLC (1:1 (v/v) toluene–ethyl acetate); $[\alpha]_D^{29}$+134° (*c* 3.49, $CHCl_3$); IR ($CHCl_3$) 1670 cm^{-1} (NHCO); ^1H NMR ($CDCl_3$) δ=1.42—1.69 (total 9H, CMe_2, CH=CHC$\underline{H}_3$), 1.87 (3H, s, NHAc), 4.58 (1H, d, *J*= 12 Hz, CH_2Ph), 4.83 (1H, d, *J*=12 Hz, CH_2Ph), 4.99 (1H, d, *J*=3 Hz, H-1), 7.32 (5H, s, Ph).

Found: M+H, 392. Calcd for $C_{21}H_{30}NO_6$: *m/z*, 392.

2-Acetamido-3-*O*-benzyl-2-deoxy-D-glucose (22). A solution of **21** (40 mg) in 0.2 M HCl in 70% aqueous dioxane (4 ml) was allowed to stand for 20 h at room temperature. After neutralized with silver carbonate, the reaction mixture was filtered to remove the precipitates and the filtrate was concentrated to dryness. The residue was chromatographed (5:1 (v/v) dichloromethane–methanol) to give 29 mg (91%) of **22**: R_f=0.43—0.51 on TLC (5:1 (v/v) dichloromethane–methanol; $[\alpha]_D^{30}$ +2.7° (*c* 1.43, H_2O); IR (KBr) 1645 cm^{-1} (NHCO); ^1H NMR (CD_3OD) δ=1.93 (3H, s, NHAc), 5.08 (1H, d, *J*=3 Hz, H-1), 7.34 (5H, bs, Ph).

Found: M+Na, 334. Calcd for $C_{15}H_{21}NO_6Na$: *m/z*, 334.

2-Acetamido-3-*O*-benzyl-2-deoxy-D-sorbitol (23). To a stirred solution of **22** (37 mg) in water (2 ml) was added sodium borohydride (46 mg). After 12 h, the solution was deionized with Amberlite IR-120 (H^+) and concentrated to dryness. The residue was chromatographed (5:1 (v/v) dichloromethane–methanol) to give 28 mg (75%) of **23** as crystals. Recrystallization from 2-propanol yielded an analytical sample: R_f=0.38 on TLC (5:1 (v/v) dichloromethane–methanol); mp 125—127 °C; $[\alpha]_D^{30}$ −16.5° (*c* 1.19, MeOH); IR (KBr) 1635 cm^{-1} (NHCO); ^1H NMR (CD_3OD) δ=1.94 (3H, s, NHAc), 7.42 (5H, bs, Ph).

Found: C, 57.73; H, 7.32; N, 4.18%. Calcd for $C_{15}H_{23}NO_6$: C, 57.50; H, 7.40; N, 4.47%.

2-Acetamido-1,4-di-*O*-acetyl-3-*O*-benzyl-2-deoxy-L-threitol (18a) and 2-Acetamido-3-*O*-benzyl-2-deoxy-L-threitol (18). (A) from 17: To a stirred solution of **17** (21 mg) in methanol (0.5 ml) was added a solution of sodium periodate (47 mg) in water (1.0 ml) under ice cooling. After 1 h 35 min, sodium borohydride (21 mg) was added to the reaction solution under ice cooling. After 35 min, the reaction mixture was deionized with Amberlite IR-120 (H^+). The resin was filtered off, and the filtrate was concentrated to dryness. The residue was dissolved in a mixture of dry pyridine (1 ml) and acetic anhydride (0.5 ml) and the solution was allowed to stand for 1 h 10 min at room temperature. Coevaporation with toluene gave a syrupy residue, which was chromatographed (1:1 (v/v) toluene–ethyl acetate) to yield 12 mg (66%) of **18a** as a syrup: R_f=0.44 on TLC (ethyl acetate); $[\alpha]_D^{30}$ +14.7° (*c* 0.72, $CHCl_3$); IR ($CHCl_3$) 1735 (OAc), 1670 (NHCO) cm^{-1}; ^1H NMR ($CDCl_3$) δ=1.98, 2.06 (total 9H, s×2, NHAc, OAc×2), 4.52 (1H, d, *J*=12 Hz, CH_2Ph), 4.74 (1H, d, *J*=12 Hz, CH_2Ph), 5.79 (1H, d, *J*=9 Hz, NH), 7.36 (5H, s, Ph).

Found: M+H, 338. Calcd for $C_{17}H_{24}NO_6$: *m/z*, 338.

Compound **18a** (11.4 mg) was dissolved in ice-cooled 0.1 M methanolic sodium methoxide (1 ml), and the solution was stirred for 1 h under ice cooling. The reaction mixture was deionized with Amberlite IR-120 (H^+). The resin was filtered off, and the filtrate was concentrated to dryness. The residue was chromatographed (20:1 (v/v) dichloromethane–methanol) to give 8.5 mg (99%) of **18** as crystals: R_f=0.48 on TLC (5:1 (v/v) dichloromethane–methanol); mp 133—135 °C; $[\alpha]_D^{27}$ −46.5° (*c* 0.76, MeOH); IR (KBr) 1655 cm^{-1} (NHCO); ^1H NMR (CD_3OD) δ=1.96 (3H, s, NHAc), 7.37 (5H, bs, Ph).

Found: M+H, 254.1366. Calcd for $C_{13}H_{20}NO_4$: *m/z*, 254.1390.

(B) from 23: To a stirred solution of **23** (28 mg) in water (1.5 ml) was added a solution of sodium periodate (96 mg) in water (1.5 ml) dropwise under ice cooling. After 2 h, the reaction solution was added with sodium borohydride (17 mg) under ice cooling. After 40 min, the reaction solution was deionized with Amberlite IR-120 (H^+). The resin was filtered off, and the filtrate was concentrated to dryness. The residue was dissolved in a mixture of dry pyridine (4 ml) and acetic anhydride (3 ml), and the mixture was allowed to stand overnight at room temperature. The solution was coevaporated with toluene to dryness to give a pale brown syrup. The residue was chromatographed (1:1 (v/v) toluene–ethyl acetate) to afford 27 mg (89%) of **18a** as a colorless syrup: $[\alpha]_D^{30}$+14.7° (*c* 1.25, $CHCl_3$). IR, ^1H NMR and MS spectra were superimposable on those of the product derived from **17**.

The product was deacylated by the same procedure described in the preparation (A) to yield **18** (quantitative yield): mp 134—135 °C; $[\alpha]_D^{28}$ −46.3° (*c* 1.91, MeOH). IR, ^1H NMR and MS spectra were superimposable on those of the product derived from **17**.

Treatment of 11b with DMSO–DCC Followed by Sodium Borohydride. To a stirred solution of **11b** (300 mg), toluene (0.1 ml), phosphoric acid (0.02 ml) and pyridine (0.04 ml) in DMSO (1.5 ml) was added DCC (440 mg). After 3 h at room temperature, to the mixture was added a solution of oxalic acid (250 mg) in methanol (1 ml) under ice cooling. After 30 min under ice cooling, the mixture was diluted with ethyl acetate and the insoluble materials were filtered off. The filtrate was washed with aqueous sodium hydrogencarbonate and water, and concentrated to dryness. The residue was dissolved in 50% aqueous ethanol (6 ml), and to the solution was added sodium borohydride (40 mg). After 30 min at room temperature, the reaction mixture was deionized with Amberlite IR-120 (H^+). The resin was filtered off, and the filtrate was concentrated to dryness. The residue was chromatographed (ethyl acetate) to give 86 mg (29%) of **11c** and 126 mg (42%) of **11b**.

X-Ray Crystal Structure Analysis of 11b. A crystal of 0.4×0.4×0.6 mm^3 was mounted on an automated Rigaku AFC-5 four-circle diffractometer. The cell dimensions were refined from 25 2θ values (60°<2θ<70°) with λ(Cu $K\alpha_1$)= 1.54056 Å. The crystal data are: $C_{18}H_{31}NO_8S$, FW 421.5; orthorhombic, space group $P2_12_12_1$, a=13.938(1), b=27.866(2), c=5.5524(5) Å, V=2156.5(3) $Å^3$, Z=4, D_m(benzene/tetrachloromethane)=1.29(1), D_x=1.30 $Mg\,m^{-3}$, μ=1.66 mm^{-1}. Intensity measurement was performed to 2θ=120° by θ—2θ scan technique with scan speed 6° min^{-1} (θ). 2523 reflections were measured and 2322 reflections were observed [$|F_o|>3\sigma(|F_o|)$]. Absorption correction was neglected. The structure was solved by direct methods,[17] and refined by block-diagonal least square.[18] The minimized function is $\sum w||F_o|-|F_c||^2$, where $w=[\sigma^2(|F_o|)+0.025|F_o|^2]^{-1}$. The position of a methyl C(15) atom bonded to S was difficult to be found on Fourier synthesis, suggesting positional disorder. Only one possible position of C(15) was found on difference

Table 1. Positional Parameters ($\times 10^4$) and Equivalent Isotropic Thermal Parameters

Atom	x	y	z	B_{eq}/Å^2	Atom	x	y	z	B_{eq}/Å^2
S	8658(2)	9362(1)	−1241(5)	4.5	C(5)	7162(4)	7532(2)	571(12)	2.4
O(1)	6101(3)	8095(2)	2503(10)	3.2	C(6)	6435(4)	7119(2)	269(13)	2.5
O(2)	7442(4)	6022(2)	−2143(13)	4.1	C(7)	6936(4)	6639(2)	253(14)	2.6
O(3)	6227(4)	6265(2)	233(12)	3.7	C(8)	7527(5)	6515(2)	−2005(16)	3.4
O(4)	5972(3)	7188(2)	−1988(11)	3.5	C(9)	6496(6)	5900(3)	−1429(16)	3.6
O(5)	9114(4)	7567(4)	1117(12)	6.7	C(10)	6537(9)	5435(3)	165(34)	8.4
O(6)	7735(4)	8506(2)	−1944(10)	3.3	C(11)	5767(10)	5951(5)	−3480(23)	7.0
O(7)	5003(3)	8712(2)	1931(11)	3.6	C(12)	8645(4)	7525(2)	2946(13)	2.7
O(8)	6056(4)	9007(2)	−830(11)	3.5	C(13)	9092(5)	7503(3)	5379(15)	3.7
N	7685(3)	7498(2)	2819(10)	2.6	C(14)	8645(5)	8738(3)	−1950(22)	4.7
C(1)	5920(5)	8589(2)	2784(14)	3.0	C(15)	8009(20)	9578(7)	1034(48)	13.7
C(2)	6640(5)	8855(2)	1199(16)	3.1	C(16)	5094(5)	9053(2)	43(16)	3.2
C(3)	7315(4)	8457(2)	377(13)	2.7	C(17)	4411(7)	8914(4)	−1985(21)	5.6
C(4)	6664(4)	8026(2)	347(13)	2.5	C(18)	4896(8)	9545(3)	989(27)	6.2

synthesis. However, its thermal parameter became greater than 20Å^2 when anisotropic thermal parameters were introduced. In the last three cycles of least square calculation, the anisotropic thermal parameters of the C(15) atom were refined with damping factor 0.1. The positional parameters for all the hydrogen atoms were calculated and refined with damping factor 0.1 because only four hydrogen atoms among 31 hydrogen atoms could be found on difference synthesis. Final R=0.108, wR=0.169, and S=6.2.[19] Rather large R value may be attributed to the positional disorder of the MTM group. Any molecules of mother liquor, ethyl acetate and cyclohexane, will not exist judging from its density and the difference synthesis. Complex neutral-atom scattering factors were taken from International Tables for X-ray Crystallography.[20] The final atomic parameters are listed in Table 1. The absolute structure was determined with reference to the known absolute configuration of D-glucose.[21]

The authors express their sincere thanks to Mr. Masayuki Ito, Meiji Seika Kaisha, Ltd., and Dr. Kinichi Tadano for the mass spectra and Mr. Saburo Nakada and Mr. Akio Takahashi for their elemental analyses.

References

1) K. Takaoka, T. Kuwayama, and A. Aoki, Japanese Patent, 615332 (1971).

2) K. Sakata, A. Sakurai, and S. Tamura, *Agric. Biol. Chem.*, **37**, 697 (1973); **38**, 1883 (1974); **39**, 885 (1975); **40**, 1993 (1976); K. Sakata, A. Sakurai, and S. Tamura, *Tetrahedron Lett.*, **1974**, 1533; **1974**, 4327; **1975**, 3191.

3) K. Sakata and J. Uzawa, *Agric. Biol. Chem.*, **41**, 413 (1977).

4) K. Sakata, *Nippon Nogeikagaku Kaishi*, **49**, R51 (1975).

5) K. Isono, R. F. Crain, and J. A. McKloskey, *J. Am. Chem. Soc.*, **97**, 943 (1975).

6) K. Anzai and T. Saita, *Bull. Chem. Soc. Jpn.*, **50**, 169 (1977).

7) S. Hannesian, T. J. Liak, and D. M. Dixit, *Carbohyd. Res.*, **88**, C14 (1981); *Pure Appl. Chem.*, **53**, 129 (1981).

8) K. S. Kim and W. A. Szarek, *Can. J. Chem.*, **59**, 878 (1981); *Carbohydr. Res.*, **100**, 169 (1982).

9) Y. Fukuda, H. Sasai, and T. Suami, *Bull. Chem. Soc. Jpn.*, **55**, 1574 (1982).

10) R. Whistler and J. N. Beniller, "Methods in Carbohydrate Chemistry," **VI**, 123 (1972).

11) P. Kanda and M. A. Wells, *J. Lipid Res.*, **21**, 257 (1980).

12) T. Suami, H. Sasai, K. Matsuno, and N. Suzuki, *Carbohyd. Res.*, **143**, 85 (1985).

13) E. J. Corey and J. W. Suggs, *J. Org. Chem.*, **38**, 3224 (1973).

14) J. English and P. H. Griswold, *J. Am. Chem. Soc.*, **70**, 1390 (1948).

15) E. Baer and H. O. L. Fischer, *J. Am. Chem. Soc.*, **61**, 761 (1939).

16) S. Nishimura, *Bull. Chem. Soc. Jpn.*, **32**, 61 (1959).

17) P. Main, S. E. Hull, L. Lessinger, G. Germain, J. P. Declercq, and M. M. Woolfson, *MULTAN* **78**. A System of Computer Programs for the Automatic Solution of Crystal Structures from X-ray Diffraction Date. Univs. of York, England and Louvain, Belgium (1978).

18) T. Sakurai and K. Kobayashi, *Rikagaku Kenkyusho Hokoku*, **55**, 69 (1979).

19) Tables of bond lengths and bond angles, the coordinates of hydrogen atoms, the anisotropic thermal parameters of the non-hydrogen atoms and observed and calculated structure factors are deposited as Document No. 8631 at the Office of the Editor of *Bull. Chem. Soc. Jpn.*

20) "International Tables for X-ray Crystallography," Birmingham, Kynoch Press (1974), Vol. IV.

21) S. Neidle and D. Rogers, *Nature*, **225**, 376 (1970).

 © 1986 The Chemical Society of Japan Bull. Chem. Soc. Jpn., 59, 1761—1765 (1986)

Zeolite-Promoted Benzylation of Alcohols

Makoto ONAKA,* Motomitsu KAWAI, and Yusuke IZUMI
Department of Synthetic Chemistry, Faculty of Engineering, Nagoya University, Furo-cho, Chikusa-ku, Nagoya 464
(Received January 13, 1986)

Zeolite-promoted benzylation of alcohols with benzyl chloride has been investigated. By use of a series of cation-exchanged zeolites, which have the same crystalline structure but different acid and base properties, it is confirmed that the cooperative function of acid sites and base sites of zeolite is required for the effective benzylation of alcohols although both acid and base strengths are low. It is also found that alcohols show different reactivities in zeolite from those in solution depending on their molecular structures because the benzylation is promoted inside the narrow cavities of zeolite.

Recently heterogeneous organic reactions effected by inorganic porous solids or reagents adsorbed on those solids are attracting much attention to organic chemists because of attainment of high selectivity, mild reaction conditions, and simple operations.[1] However, what a role these porous solids play in promotion of organic reactions is still not completely elucidated.

Among inorganic porous solids we have been particularly concerned with zeolites and applied them to liquid-phase organic reactions.[2] The most remarkable feature of zeolites is that 1) zeolites have rigid and homogeneous crystalline structures (a definite pore size) and 2) acid-base properties of zeolites can be easily altered by exchange of cations in zeolite without any change of the crystalline structure.[3] We applied a series of cation-exchanged zeolites which have different acid and base properties with the same crystalline structure to benzylation of alcohols and investigated the influence of the zeolite properties on the benzylation. We have reported our preliminary results,[4] and this paper presents in detail our results of zeolite-promoted benzylation and a role of zeolite as an activator.

Results and Discussion

Benzylation of alcohols to benzyl ethers is one of familiar methods for protection of hydroxyl groups,[5] and is generally carried out by use of strong bases such as NaH[6] and KOH.[7] New benzylation methods under milder reaction conditions are required. Thus the application of inorganic porous solids to the benzylation of alcohols was examined.

$$ROH + PhCH_2Cl \longrightarrow ROCH_2Ph + HCl$$

The reaction of 1-decanol with an equimolar amount of benzyl chloride was chosen as a model reaction, and investigated in hexane in the presence of various types of inorganic solids such as alkali cation (M^+)-exchanged X and Y type zeolites (abbreviated as MX and MY, respectively) which have uniform cavities (about 13 Å in diameter),[3b] γ-alumina (neutral and basic) for column chromatography, and KF impregnated on γ-alumina (KF/Al_2O_3).[8] The results are summarized in Table 1.

Between the two types of zeolites, zeolite Y was more effective than zeolite X. Especially the use of potassium cation-exchanged Y type zeolite (KY) showed the highest yield (73%) and 23% of the starting alcohol was remained intact.

The zeolite acts not only as a promoter of the benzylation but also as a base which traps the hydrogen chloride evolved during the reaction.

Alumina (neutral and basic) and KF/Al_2O_3 also promoted the reaction. In these cases, however, dibenzyl ether was obtained as a by-product in 5—16% yields. Residual water on the alumina surface easily hydrolyzed benzyl chloride to benzyl alcohol which

Table 1. Benzylation of 1-Decanol with Benzyl Chloride[a]

Additive (Amount)	Yield/%[b]		Recovery/%[b]
	Benzyl decyl ether	Dibenzyl ether	1-Decanol
None	0	0	100
NaY (0.8 g)	15	0	47
KY (0.8 g)	73	0	23
CsY (0.8 g)	62	0	37
NaX (0.8 g)	4	0	86
KX (0.8 g)	8	0	92
Al_2O_3 (neutral, 1.2 g)	41	5	58
Al_2O_3 (basic, 1.2 g)	48	7	52
KF/Al_2O_3 (5.5 mmol)	62	16	20
K_2CO_3 (0.5 g)	0	0	100
Et_3N (1 mmol)	0	0	100

a) Reaction of 1-decanol (1 mmol) with benzyl chloride (1 mmol) and the additive in 5 ml of hexane was carried out under reflux for 5 h. b) Determined by GLC using diphenylmethane as an internal standard.

Table 2. Zeolite KY-Promoted Benzylation of 1-Decanol in Various Solvents

Solvent	Yield/%[b]	Recovery/%[b]
	Benzyl decyl ether	1-Decanol
Hexane	73	23
C_6H_6[c]	42	57
C_6H_5Cl[d]	77	21
CCl_4	77	23
$CHCl_3$	4	95
THF	0	100

a) Reaction of 1-decanol (1 mmol) with benzyl chloride (1 mmol) and KY (0.8 g) was carried out in a solvent under reflux for 5 h. b) Determined by GLC using diphenylmethane as an internal standard. c) Diphenylmethane was obtained in 28% yield as a by-product. d) Reaction was carried out at 80 °C for 5 h.

Table 3. Acid Strength Distribution of Zeolites and Alumina in Hexane (meq/g)

Porous solid	H_o				
	≦+1.5	≦+2.0	≦+3.3	≦+4.0	≦+6.8
NaY	0.006	0.008	0.012	0.028	0.25
KY	0	0	0.012	0.012	0.052
CsY	0	0	0	0	0.018
NaX	0	0	0	0.77	0.86
KX	0	0	0	0	0
Al_2O_3[a]	0	0	0.009	0.069	0.15

a) Neutral alumina.

Table 4. Base Strength Distribution of Zeolites and Alumina in Hexane (meq/g)

Porous solid	H_o				
	≧+1.5	≧+2.0	≧+3.3	≧+4.0	≧+6.8
NaY	0	0	0	0	0
KY	0.030	0.019	0	0	0
CsY	0.20	0.19	0.012	0.002	0
NaX	0.080	0.080	0.040	0	0
KX	0.93	0.42	0.014	0.003	0.002
Al_2O_3[a]	0.065	0.050	0	0	0

a) Neutral alumina.

Table 5. Zeolite KY-Promoted Benzylation of Various Alcohols[a]

Alcohol	Yield/%[b]	Recovery/%[b]
	Benzyl ether	Unreacted alcohol
Benzyl alcohol	57	33
1-Decanol	73 (84)[c]	23 (15)[c]
1-Octanol	69	24
2-Octanol	51 (61)[d]	25 (15)[d]
4-Octanol	40 (30)[e]	22 (64)[e]

a) Reaction of an alcohol (1 mmol) with benzyl chloride (1 mmol) and zeolite KY (0.8 g) was carried out in hexane under reflux for 5 h. b) Determined by GLC using diphenylmethane as an internal standard. c) Benzyl chloride (1.5 mmol) was used. d) Benzyl chloride (2 mmol) was used. e) Reaction was carried out at r.t. for 100 h.

was in turn benzylated to produce dibenzyl ether. In contrast with alumina, residual water in the zeolites did not cause the side reaction (Table 1).

Bases such as powdered potassium carbonate and triethylamine could not induce the benzylation of 1-decanol in hexane.

In various solvents was studied the benzylation of 1-decanol with zeolite KY as shown in Table 2. Nonpolar solvents such as hexane and carbon tetrachloride were most suitable for the reaction. In benzene was produced diphenylmethane in 28% yield based on benzyl chloride in addition to the benzyl ether. The acid sites of zeolite KY were considered to cause the Friedel-Crafts reaction of benzene with benzyl chloride. When chlorobenzene was employed as a solvent instead of benzene, the Friedel-Crafts reaction was suppressed and the yield of benzyl decyl ether improved.

The use of relatively polar solvents like chloroform and tetrahydrofuran (THF) drastically retarded the reaction. THF is relatively basic and hence acid sites of zeolite were neutralized by THF.

It is assumed that the difference of effectiveness in the benzylation between the zeolites was ascribed to those of intrinsic acid and base properties of zeolites. Thus we examined acid and base properties of the zeolites and alumina, and related them to the results of benzylation of 1-decanol.

According to the reported method[9] we measured distribution of acid-base strength of the zeolites and the alumina which were employed in the present study by use of Hammett indicators, butylamine, and trichloroacetic acid.

In the zeolite Y series, the maximum acid strength was in the order of NaY>KY>CsY (Table 3), whereas the maximum base strength was in the order of CsY>KY>NaY (Table 4).

When the effectiveness of the zeolites as a promoter was judged in terms of the yield of benzyl ether, the order was KY>CsY>NaY, which was not consistent with the order of the maximum base strength of the zeolites. This result indicates that the benzylation is not promoted only by a base site of the zeolite, but the cooperative function of an acid site and a base site of the zeolite is necessary for the effective benzylation of alcohols although both acid and base strengths are relatively low. We assume that, in the transition state of benzylation, within a cavity of the zeolite two molecules of an alcohol and benzyl chloride are oriented such a way that nucleophilicity of a hydroxyl group of the alcohol can be enhanced by a base site and benzyl chloride can be activated by an acid site concertedly depicted below.

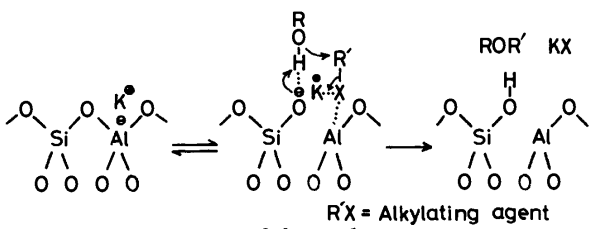

Scheme 1.

Table 6. Effects of Molecular Size of Alcohols on Benzylation

Alcohol	Method A[a]	Method B[b]
	Yield/%[c] (Relative yield)[e]	Yield/%[d] (Relative yield)[e]
1-Decanol	73 (1)	73 (1)
Benzyl alcohol	57 (0.78)	80 (1.10)
Cyclohexylmethanol	58 (0.79)	80 (1.10)
Neopentyl alcohol	53 (0.73)	77 (1.05)
1-Adamantylmethanol	15 (0.21)	80 (1.10)

a) Method A: Reaction of an alcohol (1 mmol) with benzyl chloride (1 mmol) and zeolite KY (0.8 g) was carried out in hexane under reflux for 5 h. b) Method B; Sodium alkoxide (20 mmol) which was prepared from an alcohol (20 mmol) and NaH (25 mmol) was treated with benzyl bromide (20 mmol) in THF under reflux for 5 h. c) Yield determined by GLC. d) Isolated yield. e) (Yield of corresponding benzyl ether of alcohol)/yield of benzyl decyl ether).

Neutral alumina was found to have analogous acid-base character to zeolite KY. The activity difference between the zeolite KY and the alumina may be attributed to the different mutual location of acid and base sites which is decisive to promote the reaction efficiently.

Table 5 shows the results of the benzylation of various alcohols. In comparison with primary alcohols, secondary alcohols were subject to dehydration and the yields of benzyl ethers decreased.

Zeolite Y consists of uniform cavities (13 Å in diameter) which incorporate various organic molecules and the external surface area of zeolite Y is only 0.5—1.3% of the total surface area.[3a] In Fig. 1 are shown adsorption isotherms for 1-decanol, cyclohexylmethanol, and 1-adamantylmethanol on zeolite KY in benzene at 30 °C. Bulky alcohols like 1-adamantylmethanol can be adsorbed in the zeolite. Hence in the present benzylation most of alcohols are considered to be adsorbed inside the cavities to undergo benzylation.

The molecular size of an alcohol and the steric bulkiness around a hydroxyl group of the alcohol are expected to influence the reaction rate of benzylation in zeolite. Thus the benzylation of five primary alcohols was studied by use of zeolite KY in comparison with the results obtained by a conventional method (the use of sodium hydride and benzyl bromide in THF) shown in Table 6. The steric hindrance around hydroxyl groups of the alcohols examined was estimated by use of the CPK molecular model in the following order: 1-decanol<benzyl alcohol<cyclohexylmethanol<neopentyl alcohol<1-adamantylmethanol. From the results of the conventional method it was confirmed that the five alcohols have almost the same reactivity in a solution. In the zeolite-promoted benzylation, however, it was observed that the reactivities of the alcohols decreased in the order of 1-decanol>benzyl alcohol≈cyclohexylmethanol≈neopentyl alcohol ≫1-adamantylmethanol. The adsorption isotherms for 1-decanol, cyclohexylmethanol, and 1-adamantylmethanol on zeolite KY in benzene in Fig. 1 show that the adsorption amount of cyclohexylmethanol is larger than those of 1-decanol and 1-adamantylmethanol. This fact means that the benzylation of alcohols inside the zeolite cavities is not governed by the ability of the alcohols to be adsorbed.

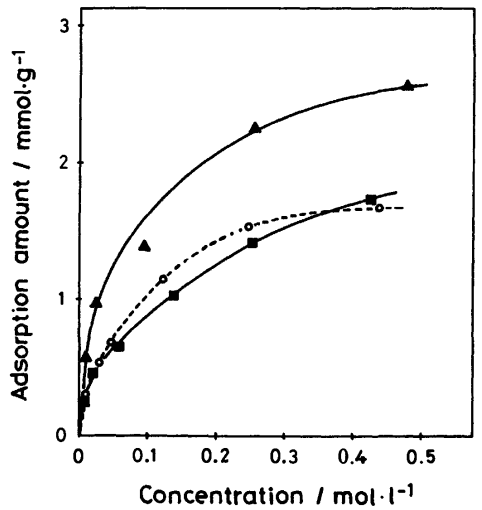

Fig. 1. Adsorption isotherms of alcohols on zeolite KY in benzene at 30 °C: 1-Decanol (○), Cyclohexylmethanol (▲), 1-Adamantylmethanol (■).

Table 7. Zeolite KY-Promoted Alkylation of 1-Octanol with Various Alkylating Agents[a]

R'X	Solvent	Yield of ether/%[b]
$PhCH_2Cl$	Hexane	69
$CH_2=CHCH_2Br$	CCl_4	58
n-$C_6H_{13}I$	Heptane	32
$CH_3OCH_2CH_2OCH_2Cl$	Hexane	0
CH_3SCH_2Cl	Hexane	0

a) Reaction of 1-octanol (1 mmol) with an alkylating agent (1 mmol) was carried out in solvent under reflux for 5 h. b) Isolated yield.

On the basis of the facts described above, we assume that the benzylation is greatly affected by whether the molecules of benzyl chloride and alcohol can be adequately arranged to the acid and base sites (Scheme 1) or not. Thus 1-adamantylmethanol may be too sterically hindered to be oriented in close proximity to a benzyl chloride molecule inside a cavity of zeolite.

In order to survey the limitations of reactions promoted by zeolite were investigated reactions of various

Table 8. Benzylation of Phenol[a)]

Additive	Yields/%[b)]			Recovery of PhOH/%[b)]
	1	2	3	
KY	12	20	12	43
CsY	24	4	5	66
KX	3	1	0	96
Al_2O_3[c)]	0	42	3	35

a) Reaction of Phenol (1 mmol) with benzyl chloride (1 mmol) and zeolite (0.8 g) or alumina (1.2 g) was carried out in CCl_4 under reflux for 5 h. b) Determined by GLC. c) Neutral alumina.

alkylating agents with alcohols and benzylations of phenolic hydroxyl groups and amino groups. In Table 7 are shown alkylations of alcohols by use of allyl bromide, hexyl iodide, 2-methoxyethoxymethyl chloride, and chloromethyl methyl sulfide.

Benzylation of phenol is expected to occur in two ways: *O*-benzylation and *C*-benzylation (Table 8).

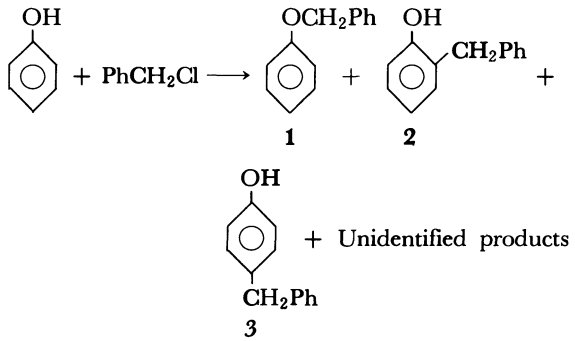

CsY, which is more basic than KY, induced *O*-benzylation more preferably than *C*-benzylation although the yield was low. Interestingly, by use of neutral alumina, *C*-benzylation products were mainly obtained and benzyl phenyl ether was not produced.

Besides alcohols, amines and amides were successfully benzylated to give the corresponding monobenzylation products selectively by use of zeolite KY.

$$PhNH_2 + PhCH_2Cl \xrightarrow[PhH,50^\circ C,5h]{KY} PhNHCH_2Ph + PhN(CH_2Ph)_2$$

84 % 6 %

$$CH_3CONH_2 + PhCH_2Cl \xrightarrow[PhCl,80^\circ C,5h]{KY} CH_3CONHCH_2Ph$$

80 %

Experimental

Materials. Unless otherwise noted, reagents were all commercial ones and used without further purification. THF was dried over sodium benzophenone ketyl. Chlorobenzene was distilled over calcium hydride. Chloroform was passed through a column of neutral alumina. Other solvents were dried over molecular sieve 3A. Zeolite NaX (Union Showa Co.), zeolite NaY (a reference catalyst from the Catalysis Society of Japan: JRC-Z-Y4.8, SiO_2/Al_2O_3=4.8), alumina (neutral)(Woelm 200 neutral, activity super I), and alumina (basic)(Woelm 200 basic, activity super I) were used. Potassium ion-exchanged X and Y type zolites were prepared from NaX and NaY according to the ion exchange technique. Preparation of KY from NaY shown as a typical example is as follows: Powdered zeolite NaY (100 g) was immersed in an aqueous 0.5 M (1 M=1 mol dm^{-3}) KCl solution (1000 ml) at 70 °C for 3 h with occasional stirring, and the zeolite was filtered on a Buchner funnel. This procedure was repeated 10 times. The ion-exchanged zeolite was washed with deionized water until no chloride ion could be detected in the washings by use of $AgNO_3$, dried at 110 °C for 12 h, and kept in a desiccator. Cesium ion-exchanged zeolite Y (CsY) was prepared by treatment of KY with an aqueous CsCl solution in the similar manner to that described above. The content of cations in zeolites was determined by atomic absorption analysis: NaX (Na^+ 100%), KX (K^+ 93%, Na^+ 7%), NaY (Na^+ 100%), KY (K^+ 99%, Na^+ 1%), and CsY (Cs^+ 68%, K^+ 32%). Zeolite and alumina were dried again at 500 °C for 5 h prior to the use. The activities of the zeolites and the aluminas remained unchanged after a few weeks' storage in a desiccator.

The KF impregnated on Al_2O_3 (Merck 90 neutral, Art. 1077) reagent was prepared according to the method reported by Ando et al.[8)]

All zeolites and aluminas were handled in the atmosphere as quickly as possible.

Analysis. GLC analyses were performed by a Shimadzu GC-8A gas chromatograph with columns (10% Silicone SE30 (Uniport B), 25% Silicone DC550 (Uniport B), and 10% PEG20M (Uniport B)), a flame ionization detector and a System Instruments 5000E integrator.

All the reaction products were identified as being identical with authentic samples. Yields of the products and recoveries of the starting materials were determined by GLC using internal standards unless otherwise mentioned.

Reaction Procedure. Use of Zeolite and Alumina: In a flask were placed zeolite (0.8 g)(or alumina (1.2 g)) and solvent (2 ml) under nitrogen. To the flask was added a solution of an alcohol (1 mmol) and an alkylating agent (1 mmol) in solvent (3 ml), and the suspended mixture was allowed to be stirred under the conditions shown in Tables. As work-up, water (3 ml) was added, and the resulting mixture was heated under reflux for 0.5 h. This work-up procedure is necessary in order to extract organic products in the zeolite completely. After the mixture was cooled, the zeolite was filtered off and organic products were extracted with ethyl acetate from the filtrate. The extract was dried over sodium sulfate, filtered and analyzed.

Use of NaH: To a suspension of sodium hydride (25 mmol) in 15 ml of THF under nitrogen at 0 °C was dropwise introduced a solution of an alcohol (20 mmol) in 15 ml of THF. The mixture was stirred at 50 °C for 1 h. To it was added a solution of benzyl bromide (20 mmol) in 15 ml of THF at 0 °C. The mixture was allowed to be stirred under reflux for 5 h. After the flask was cooled to 0 °C, excess 1 M HCl solution was added to quench the reaction. The organic layer was extracted with ethyl acetate, dried over sodium sulfate, filtered, and concentrated in vacuo. Distillation of the residue afforded benzyl ether.

Measurement of the Distribution of Acid and Base Strength. According to the literature,[9)] we measured acid-

base properties of zeolites and aluminas which were applied to the present study. The acid strengths and amounts of a solid were measured by titrating the solid suspended in hexane with a solution of butylamine in hexane using Hammett indicators (pK_a value): 4-phenylazo-*N*-phenylaniline (+1.5), 4′-amino-2,3′-dimethylazobenzene (+2.0), 4-dimethylaminoazobenzene (+3.3), 4-phenylazo-1-naphthylamine (+4.0), and Neutral Red (+6.8). The base strengths and amounts of a solid were measured by titrating the solid suspended in hexane with a solution of trichloroacetic acid in hexane using the same indicators as those listed above.

The authors thank Professors Yuichi Murakami and Tadashi Hattori and Drs. Miki Niwa and Hirofumi Itoh of Nagoya University for helpful advice concerning zeolites. They also thank Dr. Kuniyuki Kitagawa of Nagoya University for advising atomic absorption analyses.

References

1) a) G. H. Posner, *Angew. Chem., Int. Ed. Engl.*, **17**, 487 (1978); b) A. McKillop and D. W. Young, *Synthesis*, **1979**, 401, 481; c) M. Hojo and R. Masuda, *Yuki Gosei Kagaku Kyokai Shi*, **37**, 557, 689 (1979); M. Hojo, *ibid.*, **42**, 635 (1984).

2) M. Onaka, K. Ishikawa, and Y. Izumi, *Chem. Lett.*, **1982**, 1783; M. Onaka and Y. Izumi, *ibid.*, **1984**, 2007; M. Onaka, K. Ishikawa, and Y. Izumi, *J. Inclusion Phenomena*, **2**, 359 (1984); M. Onaka, M. Kawai, and Y. Izumi, *Chem. Lett.*, **1985**, 779; M. Onaka, A. Umezono, M. Kawai, and Y. Izumi, *J. Chem. Soc., Chem. Commun.*, **1985**, 1202; M. Onaka, H. Kita, and Y. Izumi, *Chem. Lett.*, **1985**, 1895.

3) a) P. B. Venuto and P. S. Landis, "Advances in Catalysis," ed by D. D. Eley, H. Pines, and P. B. Weisz, Academic Press, New York (1968), Vol. 18, p. 259; b) D. W. Breck, "Zeolite Molecular Sieves," John Wiley & Sons, New York (1974); c) "Zeolite Chemistry and Catalysis," ed by J. A. Rabo, American Chemical Society, Washigton, D. C. (1976).

4) M. Onaka, M. Kawai, and Y. Izumi, *Chem. Lett.*, **1983**, 1101.

5) J. F. W. McOmie, "Protective Groups in Organic Chemistry," Plenum Press, New York (1973), p. 95.

6) a) J. S. Brimacombe, D. Portsmouth, and M. Stacey, *J. Chem. Soc.*, **1964**, 5614; b) T. Iwashige and H. Saeki, *Chem. Pharm. Bull.*, **15**, 1803 (1967); c) S. Czernecki, C. Georgoulis, and C. Provelenghiou, *Tetrahedron Lett.*, **1976**, 3535.

7) H. G. Fletcher, *Methods Carbohydr. Chem.*, **2**, 166 (1963).

8) T. Ando, J. Yamawaki, T. Kawate, S. Sumi, and T. Hanafusa, *Bull. Chem. Soc., Jpn.*, **55**, 2504 (1982).

9) T. Yamanaka and K. Tanabe, *J. Phys. Chem.*, **79**, 2409 (1975).

Synthesis of 29-Norlanostane Derivatives[1)]

Misuzu NAORA (nee NAMIKAWA), Tatsushi MURAE, Takahiko TSUYUKI, and Takeyoshi TAKAHASHI*
Department of Chemistry, Faculty of Science, The University of Tokyo, Hongo, Bunkyo-ku, Tokyo 113
(Received January 16, 1986)

As authentic samples for identification of 29-norlanostane derivatives isolated from plant fossil, 29-norlanostan-24-one and -23-one, 29-norlanost-9(11)-en-24-one, -23-one, and -3-one, 29-norlanost-7-en-3-one, and 29-norlanostan-3-one were synthesized from a commercial lanosterol containing dihydrolanosterol.

The presence of 29-norlanostane derivatives in very minute quantities was demonstrated in a plant fossil collected at the south deposit, Ningyo-toge in Tottori Prefecture by gas chromatography-mass spectrometry, IR and ^{1}H NMR spectra. In order to identify these compounds, several 29-norlanostane derivatives were synthesized as authentic samples. This paper describes the synthesis of 29-norlanostan-24-one and -23-one (**1** and **2**), 29-norlanost-9(11)-en-24-one, -23-one, and -3-one (**3**, **4**, and **5**), 29-norlanost-7-en-3-one (**6**), and 29-norlanostan-3-one (**7**) from a commercial lanosterol (**8**) containing dihydrolanosterol (**9**).

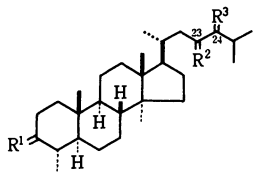

1 R^1=R^2=H_2, R^3=O
2 R^1=H_2, R^2=O, R^3=H_2
7 R^1=O, R^2=R^3=H_2

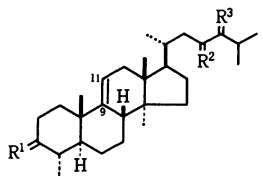

3 R^1=R^2=H_2, R^3=O
4 R^1=H_2, R^2=O, R^3=H_2
5 R^1=O, R^2=R^3=H_2

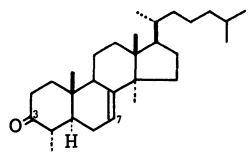

6

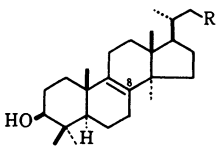

8 R= $-CH_2CH=C(CH_3)_2$
9 R= $-CH_2CH_2CH(CH_3)_2$

Demethylation of 4,4-dimethyl group of a commercial lanosterol (a mixture of lanosterol (**8**) and dihydrolanosterol (**9**)) was effected by the Pinhey's method.[2)] The mixture (**8** and **9**) was subjected to oxidation, oximation, and abnormal Beckmann rearrangement to afford a mixture of seconitrile (**10**) and dihydroseconitrile (**11**)[2)] in about 50% yield. On treatment with *m*-chloroperbenzoic acid (MCPBA) in dichloromethane at 0 °C, the seconitrile (**10**) afforded a seconitrile epoxide (**12**), which was easily separated from the dihydroseconitrile (**11**) remained intact by column chromatography. The epoxide (**12**) showed peaks at δ 1.28, 1.32, and 2.70 due to two methyl groups and a proton on the oxirane ring, respectively, and δ 1.77 (3H), 4.69 (1H), and 4.95 (1H) assignable to an isopropenyl group in the ^{1}H NMR spectrum. The epoxide (**12**) reacted with boron trifluoride etherate ($BF_3 \cdot OEt_2$)[3)] to give a mixture of a 24-keto derivative (**13**) and a rearranged aldehyde (**14**) in a ratio of 3:1. Optimization of the reaction conditions to improve the yield of the ketone (**13**) was attempted, but failed. Analytical samples of **13** and **14** were obtained by preparative thin-layer chromatography (TLC) and their structures were confirmed by ^{1}H NMR spectrum; the ketone (**13**) showed the signals at δ 1.10 (6H, d, J=7 Hz) and 2.50 (1H, septet, J=7 Hz), indicating the presence of an isobutyryl group, while the aldehyde (**14**) showed a singlet signal at δ 9.47 due to the aldehyde proton. Chromatographic behaviors of **13** and **14** being similar, the mixture of **13** and **14** in a large quantity was separated after reduction. Reduction with sodium borohydride followed by chromatographic separation afforded a secondary alcohol (**15**) and a primary one (**16**). In the ^{1}H NMR spectrum of 24-hydroxy seconitrile (**15**), a multiplet signal assignable to a methine proton of the secondary alcohol was observed at δ 3.30.

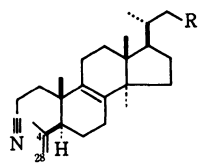

10 R= $-CH_2CH=C(CH_3)_2$
11 R= $-CH_2CH_2CH(CH_3)_2$

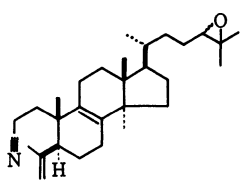

12

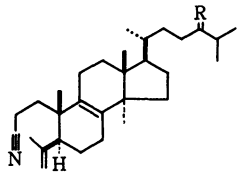

13 R=O
15 R=H,OH

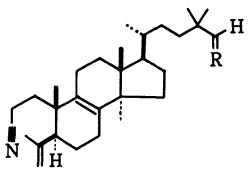

14 R=O
16 R=H,OH

The 24-hydroxy seconitrile (**15**) was epoxidized with MCPBA at 0 °C for 2 d to afford 4,28-epoxy-24-hydroxy seconitrile (**17**) in 86% yield together with its C-4 epimer in a small amount. The main hydroxy epoxide (**17**), after acetylation, was treated with $BF_3 \cdot OEt_2$ to yield 24-acetoxy-29-norlanost-8-en-3-one (**19**) in a good yield. The α-configuration of the methyl group at C-4 of **19** was demonstrated by the axial-axial coupling (J=11 Hz) observed between $C_{(4)}$–H and

$C_{(5\alpha)}$-H.

Oxidation of 24-acetoxy-29-norlanost-8-en-3-one (**19**) with chromium trioxide[4] afforded 24-acetoxy-29-norlanost-8-ene-3,7,11-trione (**20**), whose molecular formula, $C_{31}H_{46}O_5$, was determined by high-resolution mass spectrum (HR-MS). The Δ^8-triketo derivative (**20**) was then subjected to reduction with zinc in acetic acid[4] to yield a saturated triketone (**21**), to which the molecular formula, $C_{31}H_{48}O_5$, was assigned by HR-MS.

Wolff-Kishner reduction of the saturated triketone (**21**) under usual conditions[5] gave a mixture of 24-hydroxy-29-norlanostan-11-one (**22**) and 29-norlanostan-24-ol (**23**). Since an examination on the reaction conditions revealed that vigorous conditions enhanced the formation of **23**,[6] the following modification was made. The excess hydrazine hydrate was distilled off under reduced pressure before raising temperature. This additional process could suppress the formation of **23**. No occurrence of $C_{(4)}$-CH_3 epimerization in the Wolff-Kishner reduction was proved by the following observation. Reduction of 29-norlanost-8-en-3-one (**24**) (vide infra) under the same conditions as above gave a product (**25**), which was identical with that obtained by hydride reduction of 29-norlanost-8-en-3β-yl mesylate (**26**). 29-Norlanostan-24-ol (**23**) was oxidized to the corresponding 24-one (**1**).

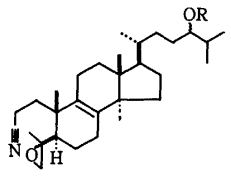

17 R=H
18 R=Ac

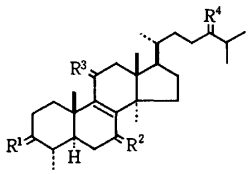

19 R^1=O, R^2=R^3=H_2, R^4=H,OAc
20 R^1=R^2=R^3=O, R^4=H,OAc
24 R^1=O, R^2=R^3=R^4=H_2
25 R^1=R^2=R^3=R^4=H_2
26 R^1=α-H,β-OMs, R^2=R^3=R^4=H_2

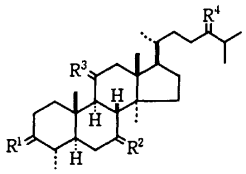

21 R^1=R^2=R^3=O, R^4=H,OAc
22 R^1=R^2=H_2, R^3=O, R^4=H,OH
23 R^1=R^2=R^3=H_2, R^4=H,OH
27a,b R^1=R^2=H_2, R^3=R^4=H,OH
28a,b R^1=R^2=H_2, R^3=H,OH, R^4=H,OAc

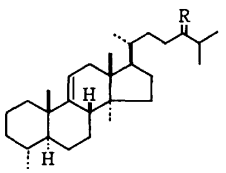

29a,b R=H,OAc
30a,b R=H,OH

Reduction of 24-hydroxy-29-norlanostan-11-one (**22**) with lithium aluminium hydride (LAH) afforded a pair of C-24 epimeric diols (**27a,b**)[5]. After selective acetylation of the hydroxyl group at C-24, dehydration of each acetoxy alcohol (**28a,b**) was effected by phosphoryl chloride in pyridine[5] to give 29-norlanost-9(11)-en-24-yl acetate (**29a,b**). On deprotection and oxidation, both **29a** and **29b** gave the same compound, 29-norlanost-9(11)-en-24-one (**3**), which showed a multiplet signal at δ 5.27 due to $C_{(11)}$-H and doublet signal at δ 1.09 (6H) due to geminal methyl groups on a carbon atom adjacent to the carbonyl group at C-24. Thus the synthesis of 29-norlanost-9(11)-en-24-one (**3**) was achieved from lanosterol (**8**) in ca. 2% total yield through 17 steps.

Next we investigated transposition of the carbonyl group at C-24 into C-23 without degradation of the side chain using lanost-8-en-24-one (**31**) as a model compound, which was prepared from lanosta-8,24-diene. Although several procedures for 1,2-carbonyl transposition have been reported,[7-10] most of them are limited to cyclic ketones. Application of these procedures to the conversion of 24-one into 23-one was unsuccessful due to unexpectedly large steric effect caused by the presence of bulky lanostane skeleton.

We developed a new synthetic route utilizing reduction of a masked α-diketone. Regioselective sulfenylation at C-23 of lanost-8-en-24-one (**31**) was accomplished by application of the inverse addition of the reagent.[9] The anion produced under kinetically controled conditions (see Experimental) was added a solution of diphenyl disulfide in tetrahydrofuran (THF) and hexamethylphosphoric triamide (HMPA) to give a mixture of 23-phenylthiolanost-8-en-24-ones (**32a,b**), which was shown to be C-23 epimers by characteristic septet of $C_{(25)}$-H at 2.92 and 2.97 and double doublet at δ 3.88 and 3.80 due to $C_{(23)}$-H in the ^{1}H NMR spectrum. The mixture was separated by TLC to afford **32a** and **32b**. According to the procedure reported by Trost et al.[9] the α-phenylthio ketones (**32a,b**) were treated with lead tetraacetate in benzene-acetic acid to yield a masked ketone (**33**), which was converted into a dimethyl acetal (**34**) by treatment with iodine in methanol. The carbonyl group in dimethyl acetal (**34**) was then reduced with LAH to give an α-ketol (**35**), the structure of which was supported by ^{1}H NMR spectrum; a double doublet signal at δ 4.66 (J=2.5 and 5 Hz) changed into a doublet signal on addition of D_2O. Acetylation of **35** gave an α-keto acetate (**36**), showing a characteristic signal at δ 4.87 (d, J=4 Hz) in the ^{1}H NMR spectrum. Finally the α-acetoxy ketone (**36**) was reduced with calcium in liquid ammonia to afford the expected product, lanost-8-en-23-one (**37**), total yield of which from the 24-one (**31**) was ca. 20% through 6 steps. Direct deoxygenation of **33**

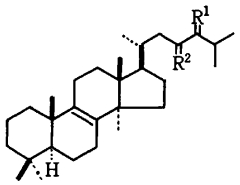

31 R^1=O, R^2=H_2
32a,b R^1=O, R^2=H,SPh
33 R^1=O, R^2=SPh,OAc
34 R^1=O, R^2=OCH_3,OCH_3
35 R^1=H,OH, R^2=O
36 R^1=H,OAc, R^2=O
37 R^1=H_2, R^2=O

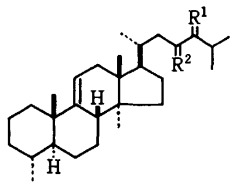

38a,b R^1=O, R^2=H,SPh
39 R^1=O, R^2=SPh,OAc
40 R^1=O, R^2=OCH_3,OCH_3
41 R^1=H,OH, R^2=O
42 R^1=H,OAc, R^2=O

and **34** by Wolff–Kishner reduction resulted in a formation of only a hydrocarbon mixture.

The method mentioned above was applied to the transposition of the carbonyl group of 29-norlanost-9(11)-en-24-one (**3**) into the corresponding 23-one (**4**). Sulfenylation of **3** afforded epimeric 23-phenylthio ketones (**38a,b**), which were subsequently converted into an α-acetoxy-α-phenylthio ketone (**39**), a dimethyl acetal (**40**), and an α-ketol (**41**). On acetylation followed by reduction with calcium in liquid ammonia, **41** gave 29-norlanost-9(11)-en-23-one (**4**) via **42**. The synthesis of a target molecule (**4**) from lanosterol (**8**) was successfully accomplished utilizing the newly developed reduction of a masked α-diketone in 0.4% total yield through 23 steps. 29-Norlanostan-23-one (**2**) was easily derived from **4** by hydrogenation and oxidation. The synthesis of 29-norlanost-9(11)-en-3-one and -7-en-3-one (**5** and **6**) and 29-norlanostan-3-one (**7**) was carried out through similar routes to the compounds **4** and **2**.

The dihydroseconitrile (**11**),[2] prepared from dihydrolanosterol (**9**) (vide supra), was converted into a demethyl derivative, 29-norlanost-8-en-3-one (**24**)[11] through a seconitrile epoxide (**43**). On reduction followed by acetylation, **24** gave an acetate (**45**), which was subjected to allylic oxidation, reduction with zinc, and Wolff–Kishner reduction in turn to afford 29-norlanostan-3β-ol (**48**) and 3β-hydroxy-29-norlanostan-11-one (**49**). The former (**48**), on Jones oxidation, afforded 29-norlanostan-3-one (**7**) and the latter (**49**) was converted into 29-norlanost-9(11)-en-3β-ol (**53**)[12] by reduction, partial acetylation, dehydration, and hydrolysis, which on oxidation gave 29-norlanost-9(11)-en-3-one (**5**).

On the other hand, oxidation of 29-norlanost-8-en-3β-yl acetate (**45**) with chromyl chloride afforded 3β-acetoxy-29-norlanost-9(11)-en-7-one (**54**), which was isomerized by treatment with $BF_3 \cdot OEt_2$ into a conjugate enone (**55**).[13] Wolff–Kishner reduction[14] of **55** following oxidation of the resultant alcohol afforded a mixture of 29-norlanost-7-en-3-one (**6**) and -8-en-3-one (**24**) in a ratio of ca. 2:1. The mixture showed a similar fragmentation to that of 9(11)-en-3-one (**5**) in the mass spectra. In the ^1H NMR spectrum of the mixture, three singlet signals at δ 0.69 (18-Me), 0.86 (30-Me), and 1.09 (19-Me) and a doublet signal at δ 1.00 (28-Me) are assignable to 7-ene (**6**) derivative. Separation of **6** from **24** could not be attained.

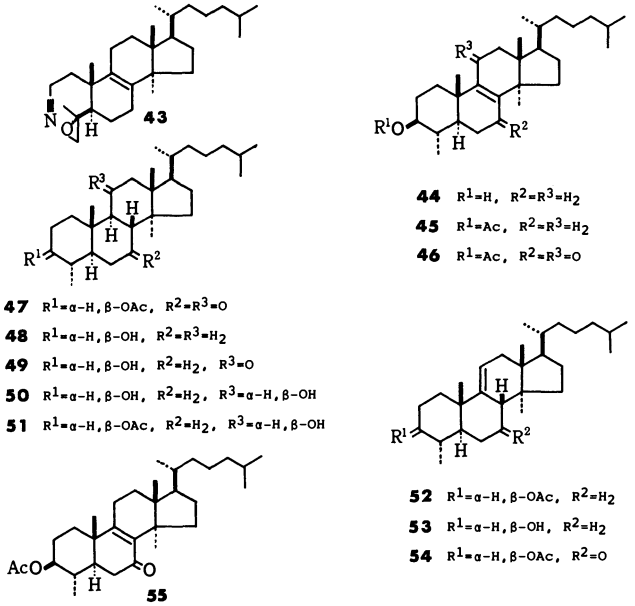

Experimental

General Procedures. Melting points were measured on a Mel-temp capillary melting point apparatus (Laboratory Devices) and uncorrected. IR spectra were obtained on a Hitachi 260-30 spectrometer in Nujol mull. ^1H NMR spectra were taken on a Hitachi R-20B (60 MHz) or a Varian EM-390 (90 MHz) or a Brucker WH-270 (270 MHz) spectrometer for solutions in $CDCl_3$ with tetramethylsilane as an internal standard. Mass spectra were run on a JEOL JMS-D300 mass spectrometer at 70 eV, and the relative intensities were indicated in the parentheses. Optical rotations were measured on a JASCO DIP-181 spectrometer in $CHCl_3$ (*c* 0.10) unless otherwise stated, and UV spectra on a Hitachi 340 spectrometer. TLC was carried out on Kieselgel 60 GF_{254} (E. Merck) coated in 0.25 mm thickness (for analytical) and in 0.5 mm thickness (for preparative). Wakogel C-200 (Wako) was used for column chromatography. Dry solvents were purified by distillation from desiccants as follows: ether/LAH; THF/Na-benzophenone; dichloromethane and carbon tetrachloride/P_2O_5; benzene/Na; toluene and HMPA/CaH_2; pyridine/BaO. Organic extracts were dried over anhydrous sodium sulfate.

Epoxidation of a Mixture of Seconitriles (10 and 11). The seconitrile mixture (**10** and **11**) was obtained by the method described by Pinhey et al.[2] in ca. 50% yield from a commercial lanosterol (**8**) (E. Merck, containing ca. 30% of dihydrolanosterol (**9**)).

The seconitrile mixture (43 g) in dichloromethane (3.4 l) was kept at 0 °C and reacted with MCPBA (16 g) in dichloromethane (0.4 l) in a refrigerator for 3 h. The reaction product was washed with successively cold 5% potassium iodide solution, water, and brine, and dried. Evaporation of the solvent and addition of hexane yielded crystals (6.67 g), which were identified as seconitrile epoxide (**12**), mp 119.5—121.5 °C (needles from hexane); IR 2240 and 1636 cm^{-1}; ^1H NMR (60 MHz) δ=0.75 (3H, s; 18-Me), 0.94 and 0.98 (each 3H, s; 19- and 30-Me), 1.28 and 1.32 (each 3H, s; $C\overset{O}{\diagup\!\diagdown}C(Me)_2$), 1.77 (3H, br s; C=C-Me), 2.70 (1H, t, *J*=6 Hz; $C\overset{O}{\diagup\!\diagdown}C$-H), 4.69 and 4.95 (each 1H, m; $C=CH_2$); Found *m/z* 437.3653. Calcd for $C_{30}H_{47}ON$: M, 437.3656.

The filtrate was separated by silica-gel chromatography (silica gel: 410 g). Elution (each fraction: 1/4 column volume) was performed with 10% ether–hexane (frs 1—10) and 20% ether–hexane (frs 11—25). Crystallization of frs 6—9 from methanol afforded dihydroseconitrile (**11**; 9.1 g).[2] Fractions 13—22 gave additional seconitrile epoxide (**12**; 14.5 g).

Treatment of Seconitrile Epoxide (12) with $BF_3 \cdot OEt_2$. $BF_3 \cdot OEt_2$ (1.5 ml) was added to a solution of the seconitrile epoxide (**12**; 1.2 g) in toluene (120 ml) and the reaction mixture was stirred at room temperature for 20 min.

Addition of water and extraction with ether furnished a mixture (1.18 g) of seconitrile ketone (**13**) and seconitrile aldehyde (**14**). A part of the mixture (145 mg) was separated by preparative TLC (developed three times with 20% ether–hexane) to afford seconitrile aldehyde (**14**; 21.7 mg) and seconitrile ketone (**13**; 67.9 mg). **13**: Mp 98—99 °C; IR 2240, 1705, 1635, and 894 cm^{-1}; ^1H NMR (60 MHz) δ= 0.74 (3H, s; 18-Me), 0.94 and 0.98 (each 3H, s; 19- and 30-Me), 1.10 (6H, d, J=7 Hz; O=C-CH<u>Me</u>$_2$), 1.78 (3H, br s; C=C-Me), 2.50 (1H, septet, J=7 Hz; O=C-C<u>H</u>Me$_2$), and 4.69 and 4.94 (each 1H, m; C=C<u>H</u>$_2$); MS m/z (%) 437 (M^+; 82), 422 (90), 394 (15), 383 (62), 254 (33), 242 (44), and 71 (100); Found: m/z 437.3663. Calcd for $C_{30}H_{47}ON$: M, 437.3656. **14**: An oil; ^1H NMR (60 MHz) δ=0.74 (3H, s; 18-Me), 0.94 and 0.98 (each 3H, s; 19- and 30-Me), 1.06 (6H, s; $C_{(24)}$-Me's), 1.78 (3H, br s; C=C-Me), 4.69 and 4.94 (each 1H, m; C=C<u>H</u>$_2$), and 9.47 (1H, s; H-C=O); MS m/z (%) 437 (M^+; 50), 422 (37), 409 (15), 383 (43), 254 (20), 242 (43), and 55 (100).

Reduction of the Mixture of Seconitrile Ketone (13) and Seconitrile Aldehyde (14). The mixture (6.8 g) of **13** and **14** was treated with sodium borohydride (0.6 g) in methanol (250 ml) at room temperature for 20 min. The usual work-up afforded a mixture (6.8 g) of alcohols, which was separated by silica-gel column chromatography (silica gel: 210 g) eluted with 30% ether–hexane (each fraction: 1/4 column volume). Fractions 7—10 gave a secondary alcohol (**15**; 3.9 g; 57% yield from **12**), and frs 12—14 a primary alcohol (**16**; 1.4 g; 20.5% yield from **12**). **15**: Mp 112.5—113 °C (needles from hexane); IR 3450, 2245, 1635, and 895 cm^{-1}; ^1H NMR (60 MHz) δ= 0.75 (3H, s; 18-Me), 0.83—1.04 (total Me×5), 1.77 (3H, br s; C=C-Me), 3.30 (1H, m; <u>H</u>-C-OH), and 4.68 and 4.93 (each, 1H, m; C=C<u>H</u>$_2$); MS m/z (%) 439 (M^+; 100), 424 (25), and 421 (2); Found: m/z 439.3787. Calcd for $C_{30}H_{49}NO$: M, 439.3812.

Epoxidation of 24-Hydroxy Seconitrile (15). To a solution of 24-hydroxy seconitrile (**15**; 610 mg) in dichloromethane (70 ml) was added MCPBA (453 mg) and the reaction mixture was stood for 2 d in a refrigerator. After the usual work-up, chromatographic separation (silica gel: 30 g, each fraction: 1/4 column volume) eluted with 30% ether–hexane afforded 4,28-epoxy-24-hydroxy seconitrile (**17**; 545.6 mg, 86.2% yield) from frs 25—34, and its epimer at C-4 from frs 21—23. **17**: Mp 112—113 °C; IR 3450 and 2245 cm^{-1}; ^1H NMR (60 MHz) δ=0.75 (3H, s; 18-Me), 0.91 (3H, s; Me), 0.80—1.03 (total Me×3), 1.08 (3H, s, 19-Me), 1.33 (3H, s; C<u>O</u>C-Me), 2.69 (2H, s; C<u>O</u>C<u>H</u>$_2$), and 3.30 (1H, m; <u>H</u>-C-OH); MS m/z (%) 455 (M^+; 45), 440 (18), 437 (15), 422 (72), 404 (28), 394 (12), 383 (42), and 354 (31); Found: m/z 455.3748. Calcd for $C_{30}H_{49}NO_2$: M, 455.3761.

Acetylation of 24-Hydroxy Seconitrile Epoxide (17). 24-Hydroxy seconitrile epoxide (**17**; 545 mg) was acetylated in the usual manner and the reaction product was purified by column chromatography (silica gel: 25 g). Elution with 40% ether–hexane afforded 24-acetoxy-4,28-epoxy-3,4-secolanost-8-ene-3-nitrile (**18**; 554 mg; 93% yield) as colorless oil, IR (liquid) 2250, 1740, and 1250 cm^{-1}; ^1H NMR (60 MHz) δ= 0.75 (3H, s; 18-Me), 0.80—1.0 (total Me×4), 1.09 (3H, s; 19-Me) 1.33 (3H, s; C<u>O</u>C-Me), 2.05 (3H, s; OAc), 2.69 (2H, s; C<u>O</u>C<u>H</u>$_2$), and 4.70 (1H, m; <u>H</u>-C-OAc); MS m/z (%) 497 (M^+; 12), 482 (10), 479 (3), 464 (3), 454 (4), 443 (12), 437 (10), 422 (100), 404 (28), 394 (20), and 383 (26).

Cyclization of 24-Acetoxy-4,28-epoxy-3,4-secolanost-8-ene-3-nitrile (18). $BF_3 \cdot OEt_2$ (1.5 ml) was added to a solution of the seconitrile epoxide (**18**; 553 mg) in toluene (200 ml) at room temperature under nitrogen and the reaction mixture was heated under reflux for 1.5 h. After addition of water, the reaction product was extracted with ether and the extract was washed with sodium hydrogencarbonate solution and brine, and dried. Evaporation and separation by chromatography on silica gel (25 g) eluted with 15% ether–hexane gave a mixture (58.5 mg) of olefinic compounds from frs 5 and 6 (each fraction: 1/4 column volume) followed by 24-acetoxy-29-norlanost-8-en-3-one (**19**; 229 mg, 44% yield) from frs 9—14. **19**: Mp 140—144 °C (needles from ether–hexane); IR (liquid) 1740, 1708, and 1240 cm^{-1}; $[\alpha]_D$ +35°; ^1H NMR (270 MHz) δ=0.73 (3H, s; 18-Me), 0.85—0.95 (total Me×4), 1.03 (3H, d, J=6 Hz; 28-Me), 1.21 (3H, s; 19-Me), 2.06 (3H, s; OAc), 2.32 (1H, dq, J=11 and 6 Hz; O=C-C<u>H</u>Me), and 4.73 (1H, m; <u>H</u>-C-OAc); MS m/z (%) 470 (M^+; 14), 455 (22), 410 (6), 395 (100), 311 (26), 283 (10), 257 (27), 243 (23), and 231 (25); Found: m/z 470.3757. Calcd for $C_{31}H_{50}O_3$: M, 470.3758.

Allylic Oxidation of 24-Acetoxy-29-norlanost-8-en-3-one (19). A solution of chromium trioxide (200 mg) in 90% acetic acid (2 ml) was added to a refluxing solution of 24-acetoxy-29-norlanost-8-en-3-one (**19**; 285 mg) in hexane–acetic acid (1:4, 10 ml). After reflux for 1.5 h, the reaction mixture was poured into a cold aqueous solution of sodium hydrogensulfite. The reaction product was extracted with ether and the extract was washed with 1 M (1 M=1 mol dm^{-3}) sodium hydroxide solution and then with brine. Evaporation gave a residue, which was chromatographed on silica gel (15 g) eluted with 35% ether–hexane (each fraction: 1/4 column volume) to give 24-acetoxy-29-norlanost-8-ene-3,7,11-trione (**20**; 115 mg from frs 16—24; 38% yield) as yellow needles or plates (from ether–hexane), mp 133.5—134.5 °C; IR 1735, 1715, 1690, 1670, and 1240 cm^{-1}; UV (EtOH) 269 nm (log ε 3.86); $[\alpha]_D^{26}$ +103.0°; ^1H NMR (90 MHz) δ=0.85 (3H, s; 18-Me), 0.91 (9H, d, J=7 Hz), 1.06 (3H, d, J=7 Hz; 28-Me), 1.20 (3H, s), 1.49 (3H, s), 2.05 (3H, s; OAc), 2.71 (1H, br s), 3.15 (1H, m), and 4.70 (1H, m; <u>H</u>-C-OAc), MS m/z (%) 498 (M^+; 20), 483 (3), 470 (3), 456 (6), 438 (45), 423 (15), 413 (10), 327 (15), 273 (20), 272 (25), 260 (27), 245 (30), 234 (15), and 55 (100); Found: m/z 498.3338. Calcd for $C_{31}H_{46}O_5$: M, 498.3343.

Reduction of 24-Acetoxy-29-norlanost-8-ene-3,7,11-trione (20). To a refluxing enone (**20**; 1.81 g) in acetic acid (100 ml), zinc dust (1.5 g) was added portionwise during 1.5 h and the heating was continued for 1 h. Zinc was filtered and washed with hot acetic acid. The filtrate and washings were combined and diluted with ether and the solution was washed with a saturated solution of sodium hydrogencarbonate and brine. The product was crystallized from methanol to give 24-acetoxy-29-norlanostane-3,7,11-trione (**21**; 1.28 g). The filtrate was subjected to silica-gel column chromatography to afford an additional **21** (240 mg). The total yield of **21** was 83.5%. **21**: Mp 182—185.5 °C (colorless stick); IR 1730, 1710, 1690, and 1240 cm^{-1}; $[\alpha]_D^{26}$ +47.5°; ^1H NMR (60 MHz) δ=0.76 (3H, s; 18-Me), 0.80—1.00 (total Me×3), 0.98 (3H, d, J=7 Hz; 28-Me), 1.23 (3H, s; 30-Me), 1.49 (3H, s; 19-Me), 2.05 (3H, s; OAc), and 4.70 (1H, m; <u>H</u>-C-OAc); MS m/z (%) 500 (M^+; 3), 485 (1), 456 (2), 440 (12), 425 (10), 370 (50), 328 (30), 302 (20), 260 (20), 220 (25), 193 (40), and 109 (100); Found: m/z 500.3492. Calcd for $C_{31}H_{48}O_5$: M, 500.3500

Wolff–Kishner Reduction of 24-Acetoxy-29-norlanostane-3,7,11-trione (21). A mixture of the trione (**21**; 200 mg), hydrazine hydrate (80%, 2 ml), and diethylene glycol (10 ml)

was refluxed at 130°C for 1.5 h, and the excess hydrazine hydrate was removed in vacuo. Potassium hydroxide (200 mg) was added to the mixture and nitrogen was bubbled for a while. After reflux for 3 h, the mixture was worked up as usual. Addition of methanol to the residue yielded crystals (58 mg), which were identified as 24-hydroxy-29-norlanostan-11-one (**22**). The filtrate was separated by column chromatography (silica gel: 10 g). Elution (each fraction: 1/4 column volume) with 20% ether–hexane (25 ml) and then with 30% ether–hexane (30 ml) gave 29-norlanostan-24-ol (**23**; 8.3 mg) from frs 6—8, and 24-hydroxy-29-norlanostan-11-one (**22**; 72 mg) from frs 13—17. **22**: Mp 156.5—157.5°C (needles from methanol); IR 3500 and 1695 cm^{-1}; $[\alpha]_D^{25}$ +63°; ^1H NMR (270 MHz) δ=0.72 (3H, s; 18-Me), 0.80 (3H, d, J=6 Hz), 0.90 (3H, d, J=7 Hz), 0.92 (6H, d, J=6 Hz), 1.02 (3H, s), 1.09 (3H, s), 2.01 (1H, d, J=13 Hz; $C_{(12)}$-H), 2.53 (1H, d, J=13 Hz; $C_{(12)}$-H'), 2.66 (1H, d, J=13 Hz; $C_{(9)}$-H), and 3.30 (1H, m; H-C-OH); MS m/z (%) 430 (M^+; 64), 415 (6), 412 (8), 397 (3), 387 (7), 319 (14), 311 (8), 273 (10), 260 (15), 233 (8), 223 (7), 191 (100), and 163 (16); Found: m/z 430.3768. Calcd for $C_{29}H_{50}O_2$: M, 430.3809. **23**: Mp 82.5—84.5°C (needles from methanol); IR 3400 cm^{-1}; $[\alpha]_D^{25}$ +35°; ^1H NMR (90 MHz) δ=0.78 (3H, s), 0.80 (3H, s), 0.84 (3H, s), 0.89 (3H, d), 0.93 (6H, d, J=6 Hz; 26- and 27-Me), and 3.31 (1H, m; H-C-OH); MS m/z (%) 416 (M^+; 12), 398 (13), 383 (10), 315 (12), 313 (9), 285 (82), 260 (15), 245 (100), 231 (10), 217 (32), 176 (70), 163 (38), and 109 (60); Found: m/z 416.4005. Calcd for $C_{29}H_{52}O$: M, 416.4016.

Retention of the Configuration at C-4 of 29-Norlanost-8-en-3-one (24) in the Wolff–Kishner Reduction. Wolff–Kishner reduction of 29-norlanost-8-en-3-one (**24**; 50 mg) under the same conditions as those used for 24-acetoxy-29-norlanostane-3,7,11-trione (**21**) afforded 29-norlanost-8-ene (**25**; 21.3 mg) after purification by silica-gel column chromatography, which was completely identical with that obtained by the following procedure.

To a solution of 29-norlanost-8-en-3β-ol (43 mg) in pyridine (5 ml), methanesulfonyl chloride (0.05 ml) was added and the mixture was allowed to stand overnight in a refrigerator. The usual work-up afforded 29-norlanost-8-en-3β-yl mesylate (**26**; 47 mg), a part (24 mg) of which was dissolved in THF (2 ml) and the solution was refluxed for 5 h with lithium triethylhydroborate (in excess) under nitrogen. The excess hydride was destroyed by addition of water and the mixture was extracted with ether. The crude mixture was separated by column chromatography on silica gel (3 g). Elution with hexane gave 29-norlanost-8-ene (**25**; 16.7 mg).

Oxidation of 29-Norlanostan-24-ol (23). A solution of the alcohol (**23**; 13 mg) in acetone (2 ml) was oxidized with Jones reagent at 0°C for 30 min. The usual work-up gave 29-norlanostan-24-one (1; 11 mg) as needles (from methanol), mp 92—93°C; IR 1705 cm^{-1}; $[\alpha]_D^{22}$ +22° (c 0.18, $CHCl_3$); ^1H NMR (90 MHz) δ=0.75—0.93 (total Me×5), 1.09 (6H, d, J=7 Hz; O=C-CH$\underline{Me}_2$), and 2.60 (1H, septet, J=7 Hz; O=C-C$\underline{H}$Me$_2$); MS m/z (%) 414 (M^+; 25), 399 (8), 328 (3), 313 (7), 287 (18), 260 (50), 245 (100), 231 (6), 217 (32), 204 (17), 190 (10), and 176 (38); Found: m/z 414.3843. Calcd for $C_{29}H_{50}O$: M, 414.3859.

Reduction of 24-Hydroxy-29-norlanostan-11-one (22). To a solution of 24-hydroxy-11-one (**22**; 300 mg) in ether (50 ml), LAH (50 mg) was added, and the reaction mixture was stirred for 2 h at room temperature. The usual work-up and chromatographic separation on silica gel (15 g) eluted with 20% ether–hexane (each fraction: 1/4 column volume) afforded 29-norlanostane-11,24-diol (**27a**; 83.5 mg) from frs 13—16 and its isomer (**27b**; 82.2 mg) from frs 19—24. Fractions 17 and 18 (100 mg) were further separated in the same manner to give **27a** (29.7 mg) and **27b** (46.0 mg). **27a**: Mp 140.5—141°C (fine needles from methanol); IR 3500 cm^{-1}; $[\alpha]_D^{25}$ +55°; ^1H NMR (90 MHz) δ=0.78 (3H, s), 0.80—1.10 (total Me×6), 3.30 (1H, m; H-$C_{(24)}$-OH), and 4.21 (1H, m; H-$C_{(11)}$-OH); MS m/z (%) 432 (M^+; 6), 414 (16), 399 (10), 396 (4), 381 (4), 285 (4), 276 (6), 258 (20), 245 (14), 243 (14), 240 (16), 229 (3), 217 (6), 193 (22), and 175 (12); Found: m/z 432.3935. Calcd for $C_{29}H_{52}O_2$: M, 432.3965. **27b**: Mp 160—163°C (needles from ether–methanol); IR 3300 cm^{-1}; $[\alpha]_D^{25}$ +39°; ^1H NMR (90 MHz) δ=0.78 (3H, s), 0.80—1.00 (total Me×6), 3.29 (1H, m; H-$C_{(24)}$-OH), and 4.22 (1H, m; H-$C_{(11)}$-OH); MS m/z (%) 432 (M^+; 4), 414 (18), 399 (14), 396 (3), 381 (10), 285 (4), 276 (4), 258 (17), 245 (10), 243 (14), 240 (10), 229 (6), 217 (6), 193 (17), and 175 (10); Found: m/z 432.3926. Calcd for $C_{29}H_{52}O_2$: M, 432.3965.

Acetylation of 29-Norlanostane-11,24-diols (27a and b). The diols (**27a**; 106.9 mg and **27b**; 114.9 mg) were dissolved in pyridine (3 ml) and acetic anhydride (1.5 ml) and stood for 5 h at room temperature, respectively. The usual work-up afforded 24-acetoxy-29-norlanostan-11-ols (**28a**; 123.8 mg and **28b**; 120.4 mg), respectively. **28a**: Mp 148.5—149.5°C (needles from methanol); IR 3540, 1715, and 1260 cm^{-1}; $[\alpha]_D^{26}$ +33°; ^1H NMR (90 MHz) δ=0.77 (3H, s; 30-Me), 0.88 (12H, d, J=7 Hz), 0.99 (3H, s), 1.07 (3H, s), 2.04 (3H, s; OAc), 4.20 (1H, m; H-C-OH), and 4.66 (1H, m; H-C-OAc); MS m/z (%) 474 (M^+; 5), 456 (38), 441 (38), 396 (24), 381 (78), 297 (14), 283 (100), 258 (22), 243 (30), 229 (26), 217 (26), 193 (28), and 109 (46); Found: m/z 474.4014. Calcd for $C_{31}H_{54}O_3$: M, 474.4071. **28b**: Mp 160.5—161°C (fine needles from methanol); IR 3545, 1712, and 1260 cm^{-1}; $[\alpha]_D^{26}$ +49°; ^1H NMR (90 MHz) δ=0.77 (3H, 30-Me), 0.89 (12H, d, J=7 Hz), 0.99 (3H, s), 1.07 (3H, s), 2.04 (3H, s; OAc), 4.22 (1H, m; H-C-OH), and 4.68 (1H, m; H-C-OAc); Found: m/z 474.4053. Calcd for $C_{31}H_{54}O_3$: M, 474.4071.

Dehydration of 24-Acetoxy-29-norlanostan-11-ols (28a and b). Phosphoryl chloride (0.2 ml) was added to a solution of the monoacetate (**28a**; 96.3 mg) in pyridine (5 ml), and the mixture was heated at 90—100°C for 3 h. The reaction mixture was poured into ice-water and extracted with ether. The usual work-up afforded 24-acetoxy-29-norlanost-9(11)-ene (**29a**) in a quantitative yield, mp 102—102.5°C (fine needles from methanol); IR 1730 and 1245 cm^{-1}; $[\alpha]_D^{23}$ +70°; ^1H NMR (90 MHz) δ=0.66 (3H, s; 18-Me), 0.75 (3H, s; 30-Me), 0.76—0.97 (total Me×5), 2.05 (3H, s; OAc), 4.68 (1H, m; H-C-OAc), and 5.28 (1H, m; C=C-H); MS m/z (%) 456 (M^+; 45), 441 (50), 396 (25), 381 (100), 297 (15), 283 (80), 257 (7), 243 (13), 229 (18), 217 (18), and 203 (9); Found: m/z 456.3983. Calcd for $C_{31}H_{52}O_2$: M, 456.3967.

The epimeric acetoxy alcohol (**28b**) was dehydrated in the same procedure to afford 24-acetoxy-29-norlanost-9(11)-ene (**29b**), mp 109.5—110.5°C (glistening plates from methanol); IR 1735 and 1240 cm^{-1}; $[\alpha]_D^{23}$ +81°; ^1H NMR (90 MHz) δ=0.65 (3H, s; 18-Me), 0.74 (3H, s; 30-Me), 0.76—0.97 (total Me×5), 2.04 (3H, s; OAc), 4.68 (1H, m; H-C-OAc), and 5.26 (1H, m; C=C-H); MS m/z (%) 456 (M^+; 27), 441 (40), 396 (26), 381 (100), 297 (14), 283 (75), 257 (6), 243 (14), 229 (18), 217 (16), and 203 (9); Found: m/z 456.3927. Calcd for $C_{31}H_{52}O_2$: M, 456.3967.

Deprotection of 24-Acetoxy-29-norlanost-9(11)-enes (29a and b). The acetate (**29a**; 58.9 mg) in ether was stirred with

LAH (ca. 20 mg) for 1 h at room temperature to afford 29-norlanost-9(11)-en-24-ol (**30a**; 54.9 mg), mp 91—92 °C (colorless plates from methanol); IR 3450 and 1630 cm^{-1}; $[\alpha]_D^{24}$ +76°; ^1H NMR (90 MHz) δ=0.67 (3H, s; 18-Me), 0.75 (3H, s; 30-Me), 0.75—0.97 (total Me×5), 3.30 (1H, m; H-C-OH), and 5.53 (1H, m; C=C-H); MS *m/z* (%) 414 (M^+; 52), 399 (86), 396 (14), 381 (58), 311 (4), 297 (14), 283 (20), 243 (15), 229 (20), 217 (20), and 203 (14); Found: *m/z* 414.3795. Calcd for $C_{29}H_{50}O$: M, 414.3860.

29-Norlanost-9(11)-en-24-ol (**30b**) was obtained from **29b** by the same method as above. **30b**: Mp 95—96 °C (fine needles from methanol); IR 3300 and 1635 cm^{-1}; $[\alpha]_D^{24}$ +54°; ^1H NMR (90 MHz) δ=0.66 (3H, s; 18-Me), 0.75 (3H, s; 30-Me), 0.82 (3H, d, *J*=7 Hz; 28-Me), 0.90 (6H, d, *J*=7 Hz), 0.92 (3H, d, *J*=6 Hz), 0.95 (3H, s; 19-Me), 3.32 (1H, m; H-C-OH), and 5.27 (1H, m; C=C-H); MS *m/z* (%) 414 (M^+; 50), 399 (100), 381 (64), 311 (4), 297 (15), 283 (22), 243 (20), 229 (24), 217 (25), 203 (15), and 119 (45); Found: *m/z* 414.3831. Calcd for $C_{29}H_{50}O$: M, 414.3860.

Oxidation of 29-Norlanost-9(11)-en-24-ols (30a and b). Jones reagent was added to a solution of 29-norlanost-9(11)-en-24-ol (**30a**; 42.6 mg) in acetone (5 ml) at 0 °C and the mixture was stirred for 20 min. The usual work-up afforded 29-norlanost-9(11)-en-24-one (**3**; 40.4 mg). The same ketone (**3**) was obtained from **30b** in the same manner. **3**: Mp 84—85 °C (colorless plates from methanol); IR 1712 and 1630 cm^{-1}; $[\alpha]_D^{24.5}$ +79°; ^1H NMR (90 MHz) δ=0.66 (3H, s; 18-Me), 0.76 (3H, s; 30-Me), 0.82 (3H, d, *J*=6 Hz; 28-Me), 0.87 (3H, d, *J*=5 Hz; 21-Me), 0.95 (3H, s; 19-Me), 1.09 (6H, d, *J*=7 Hz; O=C-CH$\underline{Me_2}$), 2.40 (2H, dd, *J*=6 and 7.5 Hz), 2.52 (1H, septet, *J*=7 Hz; O=C-C$\underline{H}$Me$_2$), and 5.27 (1H, m; C=C-H); MS *m/z* (%) 412 (M^+; 24), 397 (100), 379 (5), 311 (5), 273 (8), 243 (14), 229 (11), 217 (10), 203 (8), and 127 (30); Found: *m/z* 412.3798. Calcd for $C_{29}H_{48}O$: M, 412.3705.

Lanost-8-en-24-one (31). Lanosta-8,24-diene (540 mg) in THF (40 ml) was stirred with borane solution in THF (BH_3·THF, 1 M, 5 ml) for 1 h at 0 °C. Water (5 ml), 3 M sodium hydroxide (5 ml), and 30% hydrogen peroxide (7 ml) were added and the solution was warmed at ca. 40 °C for 2 h. After the usual work-up, the residue (585 mg) was crystallized from methanol to give lanost-8-en-24-ol (mp 85—89 °C, M^+ 428), which was oxidized with Jones reagent in acetone (20 ml) at 0 °C to afford lanost-8-en-24-one (**31**; 383 mg), mp 88—89 °C (colorless plates from methanol); IR 1715 cm^{-1}; ^1H NMR (270 MHz) δ=0.69 (3H, s; 18-Me), 0.84 (3H, s), 0.88 (6H, s), 0.89 (3H, d, *J*=7 Hz; 21-Me), 0.98 (3H, s; 19-Me), 1.09 (6H, d, *J*=7 Hz; O=C-CH$\underline{Me_2}$), 2.40 (1H, dd, *J*=6 and 8 Hz; O=C-C-H), and 2.53 (1H, septet, *J*=7 Hz; O=C-C$\underline{H}$Me$_2$); MS *m/z* (%) 426 (M^+; 34), 411 (100), 393 (4), 287 (6), 273 (8), 257 (5), 243 (6), 229 (9), and 127 (16); Found: *m/z* 426.3816. Calcd for $C_{30}H_{50}O$: M, 426.3859.

23-Phenylthiolanost-8-en-24-ones (32a and b). Diisopropylamine (0.3 ml; distilled from calcium hydride) was added to a solution of butyllithium (1.25 ml, 1.95 mmol) in THF (5 ml) containing 2,2′-bipyridyl as an indicator at −70 °C under argon atmosphere. After stirring for 40 min at room temperature, the solution was cooled to 0 °C and HMPA (1.5 ml) was added, and then the solution was cooled to −78 °C. A solution of the ketone (**31**; 393 mg, 0.92 mmol) in THF (5 ml) was added dropwise to the solution of lithium diisopropylamide (LDA) above obtained, and stirred for 30 min. Then the resulting anion was put into a solution of diphenyl disulfide (420 mg, 1.9 mmol) in a mixture of THF (2.5 ml) and HMPA (1.25 ml) at room temperature using a syringe. The mixture was stirred for 1.5 h and quenched with 10% ammonium chloride solution. The product was separated by column chromatography on silica gel (32 g). Elution (each fraction: 1/4 column volume) was performed with hexane (frs 1—12) and 2% ether-hexane (frs 13—30) to afford a mixture of α-phenylthio ketones (360 mg) from frs 25—27, which showed peaks at *m/z* 534 (M^+; 35), 519 (100), 463 (25), 411 (28), 409 (32), and 326 (33) in the mass spectrum. The mixture was further separated by preparative TLC (developed twice with 4% ether-hexane). The less polar isomer (**32a**; 153 mg) and the more polar one (**32b**; 180 mg) were obtained. **32a**: Mp 135—136 °C (colorless needles from methanol); $[\alpha]_D^{24}$ −61°; IR 1698, 1580, 1238, 1208, 1097, 900, 740, and 683 cm^{-1}; ^1H NMR (90 MHz) δ=0.62 (3H, s; 18-Me), 0.83 (3H, s; 30-Me), 0.87 (6H, s; 28- and 29-Me), 0.93 (3H, d, *J*=7 Hz), 0.96 (3H, s; 19-Me), 1.04 and 1.09 (each 3H, d, *J*=7 Hz; O=C-CH$\underline{Me_2}$), 2.92 (1H, septet, *J*=7 Hz; O=C-C$\underline{H}$-Me$_2$), 3.88 (1H, dd, *J*=3 and 12 Hz; O=C-C$\underline{H}$-SPh), and 7.3 (5H, m; SPh); Found: *m/z* 534.3878. Calcd for $C_{36}H_{54}OS$: M, 534.3893. **32b**: Mp 65—67 °C (amorphous powder from methanol); $[\alpha]_D^{24}$ +119°; IR (liquid) 1708, 1582, 1240, 908, 735, and 690 cm^{-1}; ^1H NMR (90 MHz) δ=0.72 (3H, s; 18-Me), 0.85 (3H, s; 30-Me), 0.89 (6H, s; 28- and 29-Me), 0.94 (3H, d, *J*=7 Hz; 21-Me), 0.99 (3H, s; 19-Me), 1.04 and 1.06 (each 3H, d, *J*=7 Hz; O=C-CH$\underline{Me_2}$), 2.97 (1H, septet, *J*=7 Hz, O=C-C$\underline{H}$-Me$_2$), 3.80 (1H, dd, *J*=3 and 11 Hz; O=C-C$\underline{H}$SPh), and 7.3 (5H, m; SPh); Found: *m/z* 534.3844. Calcd for $C_{36}H_{54}OS$: M, 534.3893.

Reaction of 23-Phenylthiolanost-8-en-24-ones (32a and b) with Lead Tetraacetate. To a solution of α-phenylthio ketone (**32a**; 45 mg) in a mixture of acetic acid (1 ml) and benzene (9 ml), lead tetraacetate (200 mg containing acetic acid) was added under nitrogen. The mixture was refluxed overnight and then ethylene glycol was added to destroy the excess lead tetraacetate. Brine was added and the mixture was extracted with toluene. After the usual work-up, a residue was purified by column chromatography on silica gel (5 g) eluted with 10% ether-hexane. The α-acetoxy-α-phenylthio ketone (**33**; 28.3 mg) was obtained. The isomeric α-phenylthio ketone (**32b**) afforded the same compound (**33**) on the same treatment. **33**: Mp 170—172 °C; IR 1750, 1720, 1240, 1230, 1210, 760, 750, 710, and 695 cm^{-1}; ^1H NMR (90 MHz) δ=2.08 (3H, s; OAc), 2.37 (1H, dd, *J*=2 and 14 Hz; $C_{(22)}$-H), 2.59 (1H, dd, *J*=2 and 14 Hz; $C_{(22)}$-H′), 3.03 (1H, septet, *J*=6 Hz; O=C-C$\underline{H}$Me$_2$), and 7.35 (5H, m; SPh); MS *m/z* (%) 592 (M^+; 2), 532 (100), 517 (48), 480 (27), 461 (27), 423 (37), 369 (20), 325 (24), 311 (42), 295 (31), 283 (24), and 233 (72); Found: *m/z* 532.3747. Calcd for $C_{36}H_{52}OS$ (M−AcOH): 532.3739.

23,23-Dimethoxylanost-8-en-24-one (34). The α-acetoxy-α-phenylthio ketone (**33**; 70 mg) and iodine (870 mg) were refluxed in methanol (70 ml) overnight. An aqueous solution of sodium thiosulfite was added to the mixture and the solvent was evaporated in vacuo. Extraction with ether and evaporation of the solvent afforded a solid, which was crystallized from methanol to afford 23,23-dimethoxylanost-8-en-24-one (**34**; 41.8 mg), mp 141—143 °C; $[\alpha]_D^{25}$ +46°; IR 1720, 1150, 1090, 1045, 975, and 951 cm^{-1}; ^1H NMR (90 MHz) δ=0.65 (3H, s; 18-Me), 0.77—1.0 (total Me×4), 1.08 (6H, d, *J*=7 Hz; O=C-CH$\underline{Me_2}$), 3.17 and 3.20 (each 3H, s; OMe); MS *m/z* (%) 454 (M^+−MeOH; 16), 439 (11), 415 (38), and 155 (100).

Reduction of Dimethyl Acetal (34). To a solution of the dimethyl acetal (**34**; 33 mg) in ether (6 ml), LAH (ca. 20 mg)

was added with stirring. After 20 min, aqueous ether was added to destroy the excess hydride, and then 0.2 M hydrochloric acid was added to acidify the mixture. The usual work-up gave 24-hydroxylanost-8-en-23-one (**35**; 23.9 mg), amorphous solid; ^{1}H NMR (90 MHz) δ=0.67—1.16 (total Me×8), 2.22 and 2.42 (each 1H, br d, J=9 Hz; $C_{(22)}$-H), 3.37 and 3.43 (total 1H, ca. 2:1, d, J=6 Hz; CH-OH, disappeared on addition of D_2O), 3.98 and 4.06 (total 1H, ca. 1:2, dd, J=3 and 6 Hz; O=C-CH-OH, changed to a doublet (J=3 Hz) on addition of D_2O); MS m/z (%) 442 (M^+; 38), 427 (100), 409 (10), 311 (50), 256 (18), and 230 (19); Found: m/z 442.3778. Calcd for $C_{30}H_{50}O_2$: M, 442.3808.

Acetylation of α-Ketol (35). The α-ketol (**35**; 23.9 mg) was acetylated to afford 24-acetoxylanost-8-en-23-one (**36**; 26.8 mg), an oil; ^{1}H NMR (90 MHz) δ=2.14 (3H, s; OAc), 4.84 and 4.87 (total 1H, ca. 1:2, d, J=4 Hz; O=C-CH-OAc); MS m/z (%) 484 (M^+; 23), 469 (97), 409 (20), 311 (100), 285 (17), and 255 (36); Found: m/z 484.3882. Calcd for $C_{32}H_{52}O_3$: M, 484.3915.

Lanost-8-en-23-one (37). A solution of the α-keto acetate (**36**; 29 mg) in ether (2 ml) was added dropwise to a solution of metalic calcium (20 mg) in liquid ammonia (10 ml, distilled from sodium) at −78 °C with stirring. After 1.5 h, ammonium chloride was added and then ammonia was evaporated. Brine was added and the mixture was extracted with ether. The ether extract was worked up and a residue crystallized from methanol to give lanost-8-en-23-one (**37**; 25.1 mg), mp 82—82.5 °C; $[\alpha]_D^{25}$ +54°; IR 1710 cm^{-1}; ^{1}H NMR (270 MHz) δ= 0.76 (3H, s; 18-Me), 0.87 (3H, s; 30-Me), 0.90 (3H, s), 0.91 (3H, s), 0.92 (3H, d, J=6 Hz), 0.93 (3H, d, J=6 Hz), 0.95 (3H, d, J=6 Hz), 1.00 (3H, s; 19-Me), 2.28 (2H, d, J=6 Hz; $C_{(24)}$-H), and 2.46 (1H, dd, J=2 and 15 Hz; $C_{(22)}$-H); MS m/z (%) 426 (M^+; 26), 411 (100), 393 (6), 369 (2), 326 (3), 311 (62), 273 (10), 257 (10), 229 (16), and 85 (52); Found: m/z 426.3883. Calcd for $C_{30}H_{50}O$: M, 426.3861.

Sulphenylation of 29-Norlanost-9(11)-en-24-one (3). The 9(11)-en-24-one (**3**; 124.8 mg) was treated in the same manner as **31** to yield epimers of 23-phenylthio-29-norlanost-9(11)-en-24-ones, **38a** (less polar; 61.0 mg) and **38b** (more polar; 60.5 mg). **38a**: Mp 131 °C (needles from methanol); IR 1710, 1700 (sh), 1630, 740, and 690 cm^{-1}; $[\alpha]_D^{24.5}$ −57°; ^{1}H NMR (90 MHz) δ=0.58 (3H, s; 18-Me), 0.73 (3H, s; 30-Me), 0.82 (3H, d, J=6 Hz; 28-Me), 0.90 (3H, d, J=6 Hz; 21-Me), 0.93 (3H, s; 19-Me), 1.05 and 1.10 (each 3H, d, J=7 Hz; O=C-CHMe$_2$), 2.93 (1H, septet, J=7 Hz; O=C-CHMe$_2$), 3.88 (1H, dd, J=4 and 12 Hz; H-C-SPh), 5.25 (1H, m; H-C=C), and 7.3 (5H, m; SPh); MS m/z (%) 520 (M^+; 7), 505 (4), 449 (100), 411 (6), 339 (14), 313 (10), 283 (7), 245 (8), 243 (8), 229 (16), 217 (20), 203 (21), and 109 (30); Found: m/z 520.3735. Calcd for $C_{35}H_{52}OS$: M, 520.3737. **38b**: An oil; IR (liquid) 1710, 1630, 745, 735, and 690 cm^{-1}; $[\alpha]_D^{24.5}$ +118°; ^{1}H NMR (90 MHz) δ=0.69 (3H, s; 18-Me), 0.73 (3H, s; 30-Me), 0.83 (3H, d, J=7 Hz; 28-Me), 0.93 (3H, d, J=7 Hz; 21-Me), 0.97 (3H, s; 19-Me), 1.04 and 1.07 (each 3H, d, J=7 Hz; O=C-CHMe$_2$), 2.97 (1H, septet, J=7 Hz; O=C-CHMe$_2$), 3.83 (1H, dd, J=4 and 10 Hz; H-C-SPh), 5.27 (1H, m; H-C=C), and 7.3 (5H, m; SPh); MS m/z (%) 520 (M^+; 8), 449 (100), 411 (8), 339 (14), 313 (10), 283 (6), 245 (12), 243 (12), 229 (16), 217 (20), 203 (24), 194 (30), and 109 (30); Found: m/z 520.3681. Calcd for $C_{35}H_{52}OS$: M, 520.3737.

Reaction of 23-Phenylthio-29-norlanost-9(11)-en-24-ones (38a and 38b) with Lead Tetraacetate. The α-phenylthio ketone (**38a**; 46.7 mg) reacted with lead tetraacetate in the same manner as **32a**, and the product was separated by column chromatography on silica gel (5 g). Elution with 10% ether-hexane gave the starting material (**38a**; 14.4 mg) and 23-acetoxy-23-phenylthio-29-norlanost-9(11)-en-24-one (**39**; 29 mg, 56% yield). The same compound (**39**) was obtained from the isomer (**38b**). **39**: Mp 137—138.5 °C (needles from methanol); IR 1750, 1720, 1630, 1215, 965, and 745 cm^{-1}; $[\alpha]_D^{25}$ +64°; ^{1}H NMR (90 MHz) δ=0.63 (3H, s; 18-Me), 0.72 (3H, s; 30-Me), 0.83 (3H, d, J=6 Hz; 28-Me), 0.94 (3H, s; 19-Me), 1.03 (3H, d, J=7 Hz; 21-Me), 1.08 and 1.14 (each 3H, d, J=7 Hz; O=C-CHMe$_2$), 2.08 (3H, s; OAc), 2.58 (1H, d, J=14 Hz; $C_{(22)}$-H), 3.03 (1H, septet, J=7 Hz, O=C-CHMe$_2$), 5.25 (1H, m; C=C-H), and 7.3 (5H, m; SPh); MS m/z (%) 518 (M^+−AcOH; 24), 503 (6), 447 (3), 409 (4), 297 (22), 283 (63), 243 (10), 234 (50), 217 (12), 206 (100), 191 (20), 163 (60), and 115 (70); Found: m/z 518.3571. Calcd for $C_{35}H_{50}OS$ (M−AcOH): 518.3581.

23,23-Dimethoxy-29-norlanost-9(11)-en-24-one (40). Treatment of **39** (81.8 mg) with iodine by the same method as **33** furnished a dimethyl acetal (**40**), which was purified by column chromatography on silica gel (5 g). Elution with 4% ether-hexane afforded 43.9 mg (66% yield) of **40** as needles (from methanol), mp 122.5—125 °C; IR 1720, 1630, 1270, 1150, 1090, 1065, 1040, 1020, 970, and 950 cm^{-1}; $[\alpha]_D^{26}$ +66°; ^{1}H NMR (90 MHz) δ=0.63 (3H, s; 18-Me), 0.74 (3H, s; 30-Me), 0.82 (3H, d, J=6 Hz; 28-Me), 0.94 (3H, s; 19-Me), 1.09 (6H, d, J=7 Hz; O=C-CHMe$_2$), 3.15 (1H, septet, J=7 Hz; O=C-CHMe$_2$), 3.19 and 3.22 (each 3H, s; OMe), and 5.27 (1H, m; C=C-H); MS m/z (%) 440 (M^+−MeOH; 2), 425 (0.2), 401 (100), 313 (2), 283 (2), 245 (2), 231 (1), 229 (1), 217 (2), and 203 (10); Found: m/z 440.3554. Calcd for $C_{30}H_{48}O_2$ (M−MeOH): 440.3652.

Reduction of 23,23-Dimethoxy-29-norlanost-9(11)-en-24-one (40). The dimethyl acetal (**40**; 43 mg) was reduced and hydrolyzed and the resulting product was purified by chromatography on silica gel (5 g) eluted with 10% ether-hexane to give 24-hydroxy-29-norlanost-9(11)-en-23-one (**41**; 31.6 mg, 81% yield) as white powder (from methanol), mp 112—115 °C; IR (liquid) 3500, 1710, 1635, 1280, 1260, 1180, 1130, 1020, and 760 cm^{-1}; $[\alpha]_D^{26}$ +53°; ^{1}H NMR (90 MHz) δ= 0.70 (3H, s; 18-Me), 0.76 (3H, s; 30-Me), 0.72 (3H, d, J=7 Hz; 21-Me), 0.84 (3H, d, J=6 Hz; 28-Me), 0.96 (3H, s; 19-Me), 0.91 and 1.09 (each 3H, d, J=7 Hz; CHMe$_2$), 2.55 (1H, br d, J= 13 Hz; $C_{(22)}$-H), 3.37 and 3.43 (total 1H, ca. 3:2, d, J=5 Hz; H-C-OH, disappeared on addition of D_2O), 3.97 and 4.06 (total 1H, ca. 2:3, dd, J=3 and 5 Hz; H-C-OH, changed into a doublet (J=3 Hz) on addition of D_2O), and 5.28 (1H, m; C=C-H); MS m/z (%) 428 (M^+; 22), 413 (100), 395 (8), 355 (15), 312 (15), 297 (60), 283 (13), 243 (18), 229 (13), 217 (17), 215 (20), 203 (20), and 189 (20); Found: m/z 428.3703. Calcd for $C_{29}H_{48}O_2$: M, 428.3653.

Acetylation of 24-Hydroxy-29-norlanost-9(11)-en-23-one (41). The α-ketol (**41**; 31 mg) was acetylated to give 24-acetoxy-29-norlanost-9(11)-en-23-one (**42**) quantitatively, mp 93.5—95 °C (needles from methanol); IR 1745, 1730, 1720, 1235, and 1025 cm^{-1}; $[\alpha]_D$ +71°; ^{1}H NMR (90 MHz) δ=0.70 (3H, s; 18-Me), 0.75 (3H, s; 30-Me), 0.81 (3H, d, J=8 Hz; 21-Me), 0.96 (3H, s; 19-Me), 0.91 and 0.99 (each 3H, d, J=7 Hz; CHMe$_2$), 2.15 (3H, s; OAc), 4.35 and 4.38 (total 1H, ca. 2:3, d, J=4 Hz; H-C-OAc), and 5.28 (1H, m; C=C-H); MS m/z (%) 470 (M^+; 12), 455 (80), 410 (3), 395 (12), 355 (12), 312 (26), 297 (100), 283 (15), 243 (18), 230 (11), 229 (10), 217 (13), 215 (17), 203 (14), 201 (14), and 189 (17); Found: m/z 470.3823. Calcd for $C_{31}H_{50}O_3$: M, 470.3760.

29-Norlanost-9(11)-en-23-one (4). The keto acetate (**42**;

26 mg) was treated in the same manner as **36**, and the product was separated by column chromatography on silica gel (5 g). Elution with 5% ether–hexane gave 29-norlanost-9(11)-en-23-one (**4**; 14.8 mg, 65% yield). Further elution with 10% ether–hexane afforded an epimeric mixture of 29-norlanost-9(11)-en-23-ols (4.3 mg). **4**: Mp 88—89 °C (needles from methanol); IR 1715 and 1630 cm^{-1}; $[\alpha]_D^{22}$ +89° (*c* 0.20, $CHCl_3$); ^1H NMR (270 MHz) δ=0.70 (3H, s; 18-Me), 0.75 (3H, s; 30-Me), 0.83 (3H, d, *J*=6 Hz; 28-Me), 0.88 (3H, d, *J*=7 Hz; 21-Me), 0.905 and 0.92 (each 3H, d, *J*=6 Hz; 26- and 27-Me), 0.95 (3H, s; 19-Me), 2.25 (2H, d, *J*=6 Hz; $C_{(24)}$-H_2), 2.43 (1H, dd, *J*=2 and 15 Hz; $C_{(22)}$-H), and 5.28 (1H, m; C=C-H); MS *m/z* (%) 412 (M^+; 21), 398 (20), 397 (100), 312 (45), 297 (67), 283 (8), 230 (20), 215 (16), and 119 (36); Found: *m/z* 412.3750. Calcd for $C_{29}H_{48}O$: M, 412.3705. HR-MS *m/z* 397.3490 ($C_{28}H_{45}O$), *m/z* 312.2837 ($C_{23}H_{36}$), *m/z* 297.2592 ($C_{22}H_{33}$), *m/z* 283.2430 ($C_{21}H_{31}$), *m/z* 230.2080 ($C_{17}H_{26}$), and *m/z* 215.1808 ($C_{16}H_{23}$).

29-Norlanostan-23-one (2). A solution of 29-norlanost-9(11)-en-23-one (**4**; 28 mg) in acetic acid (2 ml) was stirred with platinum oxide (25 mg) under hydrogen at 90 °C overnight. The catalyst was filtered off and washed with ether. The filtrate and washings were combined, evaporated, and chromatographed on silica gel (5 g). Elution (each fraction: 1/4 column volume) was performed with 5% ether–hexane (frs 1—8) and 20% ether–hexane (frs 9—22). An epimeric mixture of 29-norlanostan-23-ols was eluted in frs 12—21 (18 mg), and was treated with Jones reagent in acetone (5 ml) at 0 °C for 20 min. The usual work-up and crystallization from methanol afforded 29-norlanostan-23-one (**2**; 17.8 mg) as needles in 63.3% yield from **4**. **2**: Mp 103.5—105 °C; IR 1710 cm^{-1}; $[\alpha]_D^{22}$ +25° (*c* 0.39, $CHCl_3$); ^1H NMR (270 MHz) δ= 0.80 (3H, d, *J*=6 Hz), 0.80 (3H, s), 0.82 (3H, s), 0.83 (3H, s), 0.86 (3H, d, *J*=6 Hz), 0.90 (3H, d, *J*=7 Hz), 0.91 (3H, d, *J*= 6 Hz), 2.10 (1H, d, *J*=15 Hz; $C_{(22)}$-H), 2.24 (2H, d, *J*=6 Hz; $C_{(24)}$-H_2), and 2.42 (1H, br d, *J*=15 Hz; $C_{(22)}$-H′); MS *m/z* (%) 414 (M^+; 4), 399 (4), 314 (100), 299 (44), 245 (63), 217 (16), 203 (8), and 176 (46); Found: *m/z* 414.3810. Calcd for $C_{29}H_{50}O$: M, 414.3860. HR-MS *m/z* 399.3526 ($C_{28}H_{47}O$), *m/z* 314.3011 ($C_{23}H_{38}$), *m/z* 299.2772 ($C_{22}H_{35}$), *m/z* 245.2301 ($C_{18}H_{29}$), *m/z* 217.1930 ($C_{16}H_{25}$), *m/z* 203.1803 ($C_{15}H_{23}$), and *m/z* 176.1546 ($C_{13}H_{20}$).

29-Norlanost-8-en-3β-ol (44). 29-Norlanost-8-en-3-one (**24**, mp 105.5—107 °C; lit,[11] 109—111 °C), obtained from the dihydroseconitrile (**11**), was reduced with LAH to give 29-norlanost-8-en-3β-ol (**44**) in a quantitative yield, mp 140.5—142 °C (lit,[15] 135—137 °C); IR 3300 and 1020 cm^{-1}; ^1H NMR (90 MHz) δ=0.72 (3H, s; 18-Me), 0.84 (3H, s; 30-Me), 0.92 (Me×3), 0.99 (3H, s; 19-Me), and 3.11 (1H, m; H-C-OH); MS *m/z* (%) 414 (M^+; 20), 399 (100), 381 (20), 273 (10), 259 (12), and 245 (8).

Acetylation of 29-Norlanost-8-en-3β-ol (44). The alcohol (**44**; 100 mg) was acetylated to give 29-norlanost-8-en-3β-yl acetate (**45**; 80 mg) after crystallization from methanol, mp 98—98.5 °C (lit,[15] 89—90 °C); IR 1740 and 1245 cm^{-1}; ^1H NMR (90 MHz) δ=0.71 (3H, s; 18-Me), 0.84 (3H, s; 30-Me), 0.91 (Me×3), 0.99 (3H, s; 19-Me), 2.05 (3H, s; OAc), and 4.41 (1H, dt, *J*=5 and 10 Hz; H-C-OAc); MS *m/z* (%) 456 (M^+; 34), 441 (100), 396 (3), 381 (52), 287 (8), 273 (13), 259 (3), 241 (8), 229 (8), and 227 (10).

Allylic Oxidation of 29-Norlanost-8-en-3β-yl Acetate (45). The acetate (**45**; 417 mg) was oxidized with chromium trioxide in acetic acid, and the reaction product was separated by chromatography on silica gel (16 g). Elution (each fraction: 15 ml) was carried out successively with 5, 10, 15, 20, 25, and 30% ether–hexane (each 30 ml). Fractions 9—12 afforded 3β-acetoxy-29-norlanost-8-ene-7,11-dione (**46**; 327 mg), mp 154—155 °C (yellow needles from methanol); IR 1740, 1680, and 1245 cm^{-1}; ^1H NMR (90 MHz) δ=0.80—0.95 (total Me×3), 1.21 (3H, s), 1.33 (3H, s), 2.06 (3H, s; OAc), and 4.44 (1H, dt, *J*=5 and 10 Hz; H-C-OAc); MS *m/z* (%) 484 (M^+; 26), 424 (12), and 409 (4); Found: *m/z* 484.3512. Calcd for $C_{31}H_{48}O_4$: M, 484.3552.

3β-Acetoxy-29-norlanostane-7,11-dione (47). The dienone (**46**; 240 mg) was dissolved in acetic acid (10 ml) and treated with zinc dust (1.2 g). The resulting residue (240 mg) was crystallized from methanol to afford 3β-acetoxy-29-norlanostane-7,11-dione (**47**; 140 mg), mp 180.5—181 °C; IR 1730, 1710, and 1245 cm^{-1}; ^1H NMR (90 MHz) δ=0.72 (3H, s), 0.76—0.92 (total Me×4), 1.24 (3H, s), 1.27 (3H, s), 2.06 (3H, s; OAc), and 4.41 (1H, dt, *J*=5 and 10 Hz; H-C-OAc); MS *m/z* (%) 486 (M^+; 100), 471 (16), 426 (25), 373 (12), 318 (20), 287 (40), 250 (15), 237 (30), 220 (30), 207 (30), and 177 (52); Found: *m/z* 486.3683. Calcd for $C_{31}H_{50}O_4$: M, 486.3708.

Wolff–Kishner Reduction of 3β-Acetoxy-29-norlanostane-7,11-dione (47). A mixture of the dione (**47**; 230 mg), hydrazine hydrate (2 ml), and diethylene glycol (4 ml) was refluxed at 130 °C for 1.5 h, and then potassium hydroxide (0.8 g) was added after the reaction mixture was cooled to room temperature. The excess hydrazine hydrate was removed by distillation until the vapor temperature reached ca. 200 °C, and the solution was refluxed for 2 h. After the usual work-up, the reaction product was crystallized from methanol to give 29-norlanostan-3β-ol (**48**; 87 mg). The filtrate was chromatographed on silica gel (12 g) eluted with 10% ether–hexane (frs 1—2), 20% ether–hexane (frs 3—4), 30% ether–hexane (frs 5—6), 40% ether–hexane (frs 7—8), and 50% ether–hexane (frs 9—12). Fractions 9 and 10 afforded 29-norlanostan-3β-ol (**48**; 29 mg) and fractions 11 and 12 gave 3β-hydroxy-29-norlanostan-11-one (**49**; 60 mg). **48**: Mp 154.5—155 °C; IR 3300 cm^{-1}; ^1H NMR (90 MHz) δ=0.79—1.0 (Me× 7), and 3.09 (1H, dt, *J*=5 and 10 Hz; H-C-OH); MS *m/z* (%) 416 (M^+; 26), 411 (3), 276 (35), 261 (100), 232 (20), and 192 (66); Found: *m/z* 416.4022. Calcd for $C_{29}H_{52}O$: M, 416.4017. **49**: Mp 153 °C (needles from methanol); IR 3300, 1700, 1165, 1040, and 970 cm^{-1}; ^1H NMR (90 MHz) δ=0.72 (3H, s; 18-Me), 0.83—0.90, (Me×3), 0.95 (3H, d), 1.03 (3H, s), 1.09 (3H, s), 2.39 (1H, s), 2.48 (1H, br s), 2.76 (1H, dt, *J*=13.5 and 3 Hz), and 3.07 (1H, dt, *J*=5 and 10 Hz; H-C-OH); MS *m/z* (%) 430 (M^+; 26), 412 (5), 303 (26), 276 (8), and 207 (100); Found: *m/z* 430.3808. Calcd for $C_{29}H_{50}O_2$: M, 430.3809.

29-Norlanostan-3-one (7). Jones oxidation of **48** (29 mg) furnished 29-norlanostan-3-one (**7**; 27 mg), mp 118—119 °C (needles from methanol); IR 1710, 1180, 1140, and 980 cm^{-1}; $[\alpha]_D^{22}$ +42° (*c* 0.12, $CHCl_3$); ^1H NMR (270 MHz) δ=0.79 (3H, s), 0.81 (3H, s), 0.87 (9H, d, *J*=6 Hz), 0.97 (3H, d, *J*=6 Hz; 28-Me), and 1.11 (3H, s; 19-Me); MS *m/z* (%) 414 (M^+; 8), 399 (5), 274 (42), 259 (100), 245 (7), 231 (30), 218 (28), and 190 (48); Found: *m/z* 414.3857. Calcd for $C_{29}H_{50}O$: M, 414.3860.

29-Norlanostane-3β,11β-diol (50). A solution of the hydroxy ketone (**49**; 47 mg) in ether (5 ml) was refluxed with LAH (38 mg) for 2 h. The usual work-up gave a residue (52 mg), which crystallized from methanol to give 29-norlanostane-3β,11β-diol (**50**) as needles, mp 173.5 °C; IR 3400, 1040, 1030, and 975 cm^{-1}; ^1H NMR (90 MHz) δ=0.75—0.91 (Me×5), 1.01 (3H, s), 1.12 (3H, s), 3.09 (1H, dt, *J*=5 and

11 Hz; H-C(3)-OH), and 4.25 (1H, m; H-C(11)-OH); MS *m/z* (%) 432 (M^+; 3), 414 (13), 399 (15), 381 (15), 274 (44), 259 (26), 241 (16), 224 (66), 209 (40), and 208 (44); Found: *m/z* 432.3959. Calcd for $C_{29}H_{52}O_2$: M, 432.3965.

Acetylation of 29-Norlanostane-3β,11β-diol (50). The diol (**50**; 46 mg) was acetytlated to afford 3β-acetoxy-29-norlanostan-11β-ol (**51**; 51.3 mg), mp 167—168 °C (needles from methanol); IR 3480, 1710, 1280, 1035, and 980 cm^{-1}; ^1H NMR (90 MHz) δ=0.78 (3H, s; 30-Me), 0.87 (9H, d, *J*=6 Hz), 0.89 (3H, d, *J*=5 Hz), 1.00 (3H, s), 1.12 (3H, s), 2.05 (3H, s; OAc), 4.25 (1H, m; H-C-OH), and 4.40 (1H, dt, *J*=5 and 10 Hz; H-C-OAc); MS *m/z* (%) 474 (M^+; 2), 456 (6), 441 (6), 414 (1), 316 (28), 256 (15), 250 (38), 241 (24), and 224 (57); Found: *m/z* 474.4093. Calcd for $C_{31}H_{54}O_3$: M, 474.4073.

Dehydration of 3β-Acetoxy-29-norlanostan-11β-ol (51). Dehydration of the 11β-ol (**51**; 50 mg) was effected in the same way as that used for **28a** and **28b**. The product was purified by chromatography on silica gel (5 g) to afford 29-norlanost-9(11)-en-3β-yl acetate (**52**; 29 mg), mp 114 °C (needles from methanol) (lit,[12a] mp 113.5—115 °C); IR 1740, 1635, 1250, 1030, and 980 cm^{-1}; ^1H NMR (90 MHz) δ=0.66 (3H, s; 18-Me), 0.74—0.95 (total Me×5), 1.00 (3H, s; 19-Me), 2.05 (3H, s; OAc), 4.40 (1H, m; H-C-OAc), and 5.34 (1H, m; C=C-H); MS *m/z* (%) 456 (M^+; 68), 441 (100), 396 (7), and 381 (35); Found: *m/z* 456.3983. Calcd for $C_{31}H_{52}O_2$: M, 456.3967.

29-Norlanost-9(11)-en-3β-ol (53). The acetate (**52**; 27 mg) was hydrolyzed with potassium hydroxide in boiling methanol to give 29-norlanost-9(11)-en-3β-ol (**53**; 23 mg) after crystallization from methanol as needles. **53**: Mp 148—149 °C; IR 3300, 1635, 1040, 1020, and 975 cm^{-1}; ^1H NMR (90 MHz) δ=0.66 (3H, s; 18-Me), 0.75 (3H, s; 30-Me), 0.88 (9H, d, *J*=6 Hz), 0.97 (3H, d, *J*=6 Hz; 28-Me), 0.99 (3H, s; 19-Me), 3.10 (1H, dt, *J*=5 and 10 Hz; H-C-OH), and 5.35 (1H, m; C=C-H); MS *m/z* (%) 414 (M^+; 21), 399 (100), 381 (20), 311 (4), 273 (7), 259 (9), 245 (6), and 243 (8).

29-Norlanost-9(11)-en-3-one (5). The alcohol (**53**; 21 mg) was oxidized with Jones reagent to afford 29-norlanost-9(11)-en-3-one (**5**) quantitatively, mp 102—102.5 °C (needles from methanol); IR 1720, 1205, 1150, 1140, and 980 cm^{-1}; $[\alpha]_D^{22}$+71° (*c* 0.07, $CHCl_3$); ^1H NMR (270 MHz) δ=0.69 (3H, s; 18-Me), 0.74 (3H, s; 30-Me), 0.868 (3H, d, *J*=6.4 Hz), 0.872 (3H, d, *J*=6.6 Hz), 0.882 (3H, d, *J*=6.1 Hz), 1.01 (3H, d, *J*=6.4 Hz; 28-Me), 1.23 (3H, s; 19-Me), and 5.35 (1H, dd, *J*=5.5 and 4.5 Hz); MS *m/z* (%) 412 (M^+; 18), 397 (100), 299 (6), 285 (2), 257 (7), 243 (12), 231 (12), and 217 (4); Found: *m/z* 412.3726. Calcd for $C_{29}H_{48}O$: M, 412.3705.

Oxidation of 29-Norlanost-8-en-3β-yl Acetate (45) with Chromyl Chloride. Chromyl chloride (0.015 ml) in dichloromethane (0.8 ml) was added to a solution of 29-norlanost-8-en-3β-yl acetate (**45**; 50 mg) in dichloromethane (1 ml) at −60 °C, and the solution was stirred for 1 h at −30 °C. Sodium hydrogensulfite solution was added to the solution and the product was extracted with ether. The usual work-up afforded 9(11)-en-7-one (**54**), which was isomerized immediately by $BF_3 \cdot OEt_2$ in benzene (3 ml). After 2 d, the solution was diluted with ether and washed with sodium hydrogencarbonate solution and dried. On evaporation and crystallization from hexane, 3β-acetoxy-29-norlanost-8-en-7-one (**55**; 27.6 mg) was obtained. The filtrate was chromatographed on silica gel (5 g) eluted with 10% ether-hexane, 15% ether-hexane, and then 20% ether-hexane (each 20 ml) to afford additional crystals of **55** (8 mg) from frs 18—20 (each fraction: 1/4 column volume). **55**: Mp 143.5 °C (cubics from hexane); IR 1740, 1650, 1580, and 1245 cm^{-1}; UV (EtOH) 252 nm (log ε 4.0); ^1H NMR (90 MHz) δ=0.67 (3H, s), 0.87 (9H, d, *J*=7 Hz), 0.93 (3H, s), 1.19 (3H, s), 2.05 (3H, s; OAc), and 4.8 (1H, m; H-C-OAc); MS *m/z* (%) 470 (M^+; 50), 455 (100), 410 (3), 395 (4), 357 (10), 302 (11), 264 (6), 229 (12), and 215 (9); Found: *m/z* 470.3779. Calcd for $C_{31}H_{50}O_3$: M, 470.3759.

A Mixture of 29-Norlanost-7-en-3-one (6) and 29-Norlanost-8-en-3-one (24). A mixture of the enone (**55**; 25 mg), hydrazine hydrate (0.5 ml), and diethylene glycol (2 ml) was refluxed at 130 °C for 2 h. After cooling, potassium hydroxide (3 pellets) was added to the mixture and the temperature was raised at 220 °C. Reflux was continued for 2 h and the mixture was worked up as usual to afford a mixture of alcohols.

Without purification, the mixture of alcohols was oxidized with Jones reagent in acetone to afford a mixture of 29-norlanost-7-en-3-one (**6**) and 29-norlanost-8-en-3-one (**24**), which was purified by chromatography on silica gel (5 g). Elution (each fraction: 1/2 column volume) was performed with 10% ether-hexane. Fractions 4—6 gave crystals (13.6 mg), which were shown to be a 2:1 mixture of **6** and **24** by ^1H NMR measurement. The mixture of **6** and **24**: IR 1715, 1310, 1230, 1185, 1175, and 820 cm^{-1}; MS *m/z* (%) 412 (M^+; 36), 397 (100), 299 (6), 285 (4), 257 (16), 243 (13), and 231 (20). ^1H NMR (270 MHz) signals ascribable to **6** δ=0.69 (3H, s; 18-Me), 0.86 (3H, s; 30-Me), 1.00 (3H, d, *J*=7 Hz; 28-Me), 1.09 (3H, s; 19-Me), and 5.21 (1H, m; H-C=C≺).

The authors wish to express their thanks to Professor Tatsuo Miyazawa of The University of Tokyo for obtaining NMR spectra at 270 MHz.

References

1) A part of this work was reported in a preliminary form: M. Namikawa, T. Murae, and T. Takahashi, *Chem. Lett.*, **1981**, 733.

2) K. F. Cohen, R. Kazluskas, and J. T. Pinhey, *Chem. Commun.*, **1971**, 1419; *J. Chem. Soc., Perkin Trans., 1*, **1973**, 2076.

3) L. H. Briggs, J. P. Bartley, and P. S. Rutledge, *J. Chem. Soc., Perkin Trans., 1*, **1973**, 806.

4) C. Dorée, J. F. McGhie, and F. Kurzer, *J. Chem. Soc.*, **1948**, 988.

5) J. F. McGhie, M. K. Pardhan, and J. F. Cavalla, *J. Chem. Soc.*, **1952**, 3476.

6) D. H. R. Barton, D. A. J. Ives, and B. R. Thomas, *J. Chem. Soc.*, **1955**, 2056.

7) T. Nakai and T. Miura, *Yuki Gosei Kagaku Kyokai Shi*, **35**, 964 (1977).

8) T. Nakai and T. Miura, *Tetrahedron Lett.*, **1979**, 531.

9) B. M. Trost, K. Hiroi, and S. Koizumi, *J. Am. Chem. Soc.*, **97**, 438 (1975); B. M. Trost, T. N. Salzmann, and K. Hiroi, *ibid.*, **98**, 4887 (1976); B. M. Trost and G. S. Massiot, *ibid.*, **99**, 4405 (1977).

10) For review see V. V. Kane, V. Singh, A. Martin, and D. L. Doyle, *Tetrahedron*, **39**, 345 (1983).

11) R. Kazlayskas, J. T. Pinhey, J. J. H. Simes, and T. G. Watson, *Chem. Commun.*, **1969**, 945.

12) a) T. Itoh, T. Ishii, T. Tamura, and T. Matsumoto, *Phytochemistry*, **17**, 971 (1978); b) L. J. Goad, F. -X. Garneau, J. -L. Simard, J. W. ApSimon, and M. Girard, *Tetrahedron Lett.*, **26**, 3513 (1985).

13) E. V. Lassak, J. T. Pinhey, and J. J. H. Simes, *Aust. J. Chem.*, **26**, 1051 (1973); R. B. Boar, J. F. McGhie, and D. A. Lewis, *J. Chem. Soc., Perkin Trans., 1*, **1972**, 2590.
14) E. Ritshie, R. G. Senior, and W. C. Taylor, *Aust. J. Chem.*, **22**, 2371 (1969).
15) J. B. Barrera, J. L. Breton, J. D. Martin, and A. G. Gonzalez, *An Real. Soc. Espan. Fis. Quim. Ser B*, **63**, 191 (1967); *Chem. Abstr.*, **67**, 108792g (1967).

 © 1986 The Chemical Society of Japan Bull. Chem. Soc. Jpn., 59, 1777—1780 (1986)

Photochemical Reaction of 2,3-Dichloro-1,4-naphthoquinone with Enol Silyl Ethers

Kazuhiro MARUYAMA,* Seiji TAI, and Hiroshi IMAHORI
Department of Chemistry, Faculty of Science, Kyoto University, Kyoto 606
(Received January 17, 1986)

2-Oxoalkylated 1,4-naphthoquinones were obtained in the photochemical reactions of 2,3-dichloro-1,4-naphthoquinone with 2-trimethylsiloxy-1-alkenes. Application of this method afforded a wide variety of functionalized 2-oxoalkylated 1,4-naphthoquinones. The photochemical reactions of 2,3-dichloro-1,4-naphthoquinone with 1-alkyl-2-(trimethylsiloxy)ethylenes gave naphthol derivatives. However, 1,1-dialkyl-2-(trimethylsiloxy)ethylenes gave none of products.

The photochemistry of quinones with olefins is one of the most important fields of study because quinones exist widely in nature and play an important role. The photochemical reactions of 2,3-disubstituted 1,4-naphthoquinones with 2-methoxy-1-alkenes and subsequent hydrolysis were found to yield 2-oxoalkylated 1,4-naphthoquinones.[1,2] These quinones have possibilities to serve as precursors of naturally occurring and/or antitumor antibiotic quinonoid compounds. However, despite many studies on acylation[3-5] and allylation[3,4,6-10] of quinones, direct 2-oxoalkylation of quinones has never been reported.

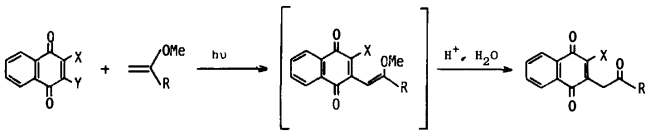

Fig. 1.

In this paper the photochemical reactions of 2,3-dichloro-1,4-naphthoquinone (**1**) with 2-trimethylsiloxy-1-alkenes **2** as well as other substituted enol silyl ethers **3** are discussed.

Results and Discussion

A benzene solution of quinone **1** and a mixture of 2-trimethylsiloxy-1-alkene **2** and its isomer **3** was irradiated with a high-pressure Hg arc lamp in the presence of pyridine at room temperature. Because **2** synthesized from 2-alkanone is contaminated with **3**, it is difficult to isolate **2** from the mixture of **2** and **3**. Then, the mixture of **2** and **3** was used for the reaction. Composite ratios of enol silyl ethers **2** and **3** in the mixture were summarized in Table 1. After hydrolysis of the reaction mixture, purification of products by column chromatography on silica gel gave two discrete classes of final products; 2-chloro-3-(2-oxoalkyl)-1,4-naphthoquinones **4** and 2,3-dichloro-4-(2-oxoalkoxy)-1-naphthols **5**. The results of the photochemical reactions of **1** with the mixture of **2** and **3** were summarized in Table 2. 2-Oxoalkylated 1,4-naphthoquinones **4** were obtained in good yields. In addition naphthol derivatives **5** were obtained. Products **5a—e** were obtained in yields of 10—30%, but **5f** was obtained only a little. On the other hand **4a—g** were obtained constantly as major products. From these results **5** were supposed to be derived from alkenes **3**, and **4** from **2**. To prove this pure enol silyl ethers **3** were synthesized from symmetrical ketones and an aldehyde, and were subjected to the photochemical reactions with quinone **1**. The results of the photochemical reactions of quinone **1** with substituted enol silyl ethers **3** were summarized in Table 2. Actually naphthol derivatives **5** were obtained from the photochemical reactions of quinone **1** with substituted enol silyl ethers **3m—n** and none of 2-oxoalkylated 1,4-naphthoquinones **4** were obtained at all.

These selectivities of products are attributed to the difference of steric effect between **2** and **3**. We have demonstrated that these reactions occur via photoinduced electron transfer and ion radical pair or exciplex exists as an intermediate.[2] In the reaction of **1** with **2**, radical cation $\mathbf{2}^{+}$ can easily attack the carbon atom at 2 or 3 site of radical anion $\mathbf{1}^{-}$ because of little steric effect and **4** is produced. But in the reaction of **1** with **3** (R_3=H, R_4=alkyl group), $\mathbf{3}^{+}$ is hard to approach to the carbon atom at 2 or 3 site of $\mathbf{1}^{-}$ owing to

Table 1. Isomer Ratio of Enol Silyl Ethers **2** and **3** (%)[a]

Enol silyl ether	**2**	**3**
2a : **3a**	80	20
2b : **3b**	94	6
2c : **3c**	90	10
2d : **3d**	91	9
2e : **3e**	79	21
2f : **3f**	99	1
2g : **3g**	99	1
2h : **3h**	100	0
2i : **3i**	100	0
2j : **3j**	100	0
2k : **3k**	73	27
2l : **3l**	94	6
2m : **3m**	—[b]	100
2n : **3n**	—[b]	100
2o : **3o**	—[b]	100
2p : **3p**	—[b]	100

a) The descriptions of **2a—p**, **3a—p** are listed in Table 2.
b) No **2** exist because enol silyl ethers are synthesized from symmetrical ketones and an aldehyde.

Table 2. Reaction of 2,3-Dichloro-1,4-naphthoquinone 1 with Enol Silyl Ether 2 and 3

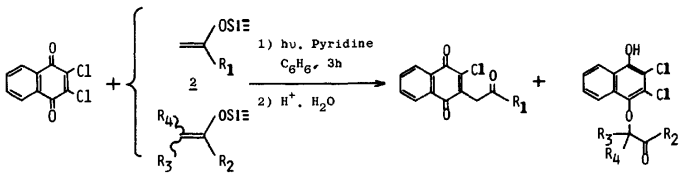

1 3 4 5

Alkene 2, 3				Quinone conversion/%	4 Yield/%[a]	5 Yield/%[a]
2a ;	$R_1=C_2H_5$	**3a** ;	$R_2=CH_3$, $R_3=H$, $R_4=CH_3$	43	**4a** ; 51	**5a** ; 19[b]
2b ;	$R_1=n$-C_3H_7	**3b** ;	$R_2=CH_3$, $R_3=H$, $R_4=C_2H_5$	33	**4b** ; 48	**5b** ; 18[b]
2c ;	$R_1=n$-C_4H_9	**3c** ;	$R_2=CH_3$, $R_3=H$, $R_4=n$-C_3H_7	34	**4c** ; 41	**5c** ; 18[b]
2d ;	$R_1=n$-C_5H_{11}	**3d** ;	$R_2=CH_3$, $R_3=H$, $R_4=n$-C_4H_9	26	**4d** ; 46	**5d** ; 19[b]
2e ;	$R_1=n$-C_6H_{13}	**3e** ;	$R_2=CH_3$, $R_3=H$, $R_4=n$-C_5H_{11}	26	**4e** ; 62	**5e** ; 31[b]
2f ;	$R_1=i$-C_4H_9	**3f** ;	$R_2=CH_3$, $R_3=H$, $R_4=i$-C_3H_7	37	**4f** ; 81	**5f** ; 5[b]
2g ;	$R_1=i$-C_3H_7	**3g** ;	$R_2=R_3=R_4=CH_3$	30	**4g** ; 63	**5g** ; 0[b]
2h ;	$R_1=$CHC_2H_5 CH$_2$OSi(CH$_3$)$_3$	**3h** ;	$R_2=CH_3$, $R_3=C_2H_5$, $R_4=CH_2OSi(CH_3)_3$	55	**4h** ; 68[c]	**5h** ; 0
2i ;	$R_1=$CH-n-C_3H_7 CH$_2$OSi(CH$_3$)$_3$	**3i** ;	$R_2=CH_3$, $R_3=n$-C_3H_7, $R_4=CH_2OSi(CH_3)_3$	64	**4i** ; 83[c]	**5i** ; 0
2j ;	$R_1=$CH-n-C_5H_{11} CH$_2$OSi(CH$_3$)$_3$	**3j** ;	$R_2=CH_3$, $R_3=n$-C_5H_{11}, $R_4=CH_2OSi(CH_3)_3$	32	**4j** ; 34[c]	**5j** ; 0
2k ;	$R_1=C_2H_4CH=CH_2$	**3k** ;	$R_2=CH_3$, $R_3=H$, $R_4=CH_2CH=CH_2$	52	**4k** ; 20	**5k** ; trace
2l ;	$R_1=C_2H_4CH=C(CH_3)_2$	**3l** ;	$R_2=CH_3$, $R_3=H$, $R_4=CH_2CH=C(CH_3)_2$	63	**4l** ; 24	**5l** ; 0
2m;	—	**3m**;	$R_2=C_2H_5$, $R_3=H$, $R_4=CH_3$	70(60)	**4m**; 0(0)	**5m**; 36(53)[d]
2n ;	—	**3n** ;	$R_2=n$-C_3H_7, $R_3=H$, $R_4=C_2H_5$	34	**4n** ; 0	**5n** ; 53
2o ;	—	**3o** ;	$R_2=H$, $R_3=R_4=CH_3$	19	**4o** ; 0	**5o** ; 0
2p ;	—	**3p** ;	$R_2=i$-C_3H_7, $R_3=R_4=CH_3$	59	**4p** ; 0	**5p** ; 0

a) Isolated yield based on starting quinone consumed. b) Irradiated for 2 h. c) R_1 contains a hydroxymethyl group. d) In the absence of pyridine.

the steric effect between chlorine atom and R_4. Thus, it is probable that 3^+ is trapped on the oxygen atom in 1^- and **5** is produced. In the reaction of **1** with **3** (R_3, R_4=alkyl group), 3^+ can approach to neither the carbon atom at 2 or 3 site of 1^- nor the oxygen atom in 1^- because of the large steric repulsion between the two reactive species. These are reflected in the fact that the chlorine atom is eliminated after coupling between radical cation and anion.

After all, the photochemical reactions of quinone **1** with enol silyl ethers **2** gave 2-oxoalkylated 1,4-naphthoquinones **4**. The reactions with enol silyl ethers **3a—f** and **3k—n** (R_3=H, R_4=alkyl group) gave naphthol derivatives **5a—f** and **5k—n**, respectively. However, the reactions with enol silyl ethers **3g,o,p** (R_3, R_4=alkyl group) gave no products.

Further, we introduced a hydroxyl group or a double bond into enol silyl ethers **2** as a functional group. The functionalized 2-trimethylsiloxy-1-alkenes **2** gave successfully the corresponding functionalized 2-oxoalkylated 1,4-naphthoquinones **3**. The results of the photochemical reactions of **1** with **2**, **3h—l** were summarized in Table 2.

In conclusion the photochemical reactions of quinone **1** with enol silyl ethers **2** and **3** afforded different products depending upon the substitution mode of enol silyl ethers.

Experimental

All melting points were determined with a Yanagimoto micro melting point apparatus and uncorrected. Mass spectra were taken on a JEOL JMS-DX300 mass spectrometer. ^{1}H NMR spectra were taken by using a JEOL PS-100 spectrometer and ^{13}C NMR were taken by using a JEOL FX-400 spectrometer. IR spectra were obtained by using a JASCO IRA-1 spectrometer on KBr pellets. Elemental analyses were performed at the Microanalysis Center of Kyoto University.

Material. Quinone **1** was used after recrystallization of commerical reagent. Enol silyl ethers **2** and **3** were synthesized according to the reported methods.[11-13]

General Procedures. Quinone **1** (1 mmol), enol silyl ether (2 mmol), and pyridine (2 mmol) were dissolved in benzene (25 ml) and irradiated in a Pyrex tube with a high-pressure Hg arc lamp for 2—3 h. After hydrolysis the reaction mixture was washed with brine, dried, concentrated, purified by chromatography on silica gel, and subjected to further examination for structure determination.

Identification of Products. 2-Chloro-3-(2-oxobutyl)-1,4-naphthoquinone (4a): Yellow needles from hexane-chloroform; mp 134—135 °C. MS; *m/z* 262 and 264 (M^+). Found: C, 63.74; H, 4.21; Cl, 13.58%. Calcd for $C_{14}H_{11}O_3Cl$: C, 64.01; H, 4.22; Cl, 13.50%. IR (KBr); 1705 and 1660 cm^{-1} (C=O). ^{1}H NMR ($CDCl_3$) δ=8.18 (2H, m), 7.82 (2H, m), 4.03 (2H, s), 2.70 (2H, q, J=7.0 Hz), and 1.15 (3H, t, J=7.0 Hz).

2-Chloro-3-(2-oxopentyl)-1,4-naphthoquinone (4b): Yellow plates from hexane-chloroform; mp 108—109.5 °C. MS;

m/z 276 and 278 (M^+). Found: C, 65.09; H, 4.61; Cl, 12.96%. Calcd for $C_{15}H_{13}O_3Cl$: C, 65.11; H, 4.74; Cl, 12.81%. IR (KBr); 1705 and 1670 cm^{-1} (C=O). ^1H NMR ($CDCl_3$) δ=8.11 (2H, m), 7.78 (2H, m), 3.98 (2H, s), 2.63 (2H, t, *J*=7.0 Hz), 1.69 (2H, sextet, *J*=7.0 Hz), and 0.98 (3H, t, *J*=7.0 Hz).

2-Chloro-3-(2-oxohexyl)-1,4-naphthoquinone (4c): Yellow plates from hexane–chloroform; mp 104—105.5 °C. MS; *m/z* 290 and 292 (M^+). Found: C, 66.04; H, 5.15; Cl, 12.23%. Calcd for $C_{16}H_{15}O_3Cl$: C, 66.10; H, 5.20; Cl, 12.19%. IR (KBr); 1705 and 1665 cm^{-1} (C=O). ^1H NMR ($CDCl_3$) δ=8.16 (2H, m), 7.80 (2H, m), 4.01 (2H, s), 2.66 (2H, t, *J*=7.0 Hz), 1.2—1.9 (4H, m), and 0.96 (3H, t, *J*=7.0 Hz).

2-Chloro-3-(2-oxoheptyl)-1,4-naphthoquinone (4d): Yellow needles from hexane–chloroform; mp 104—105 °C. MS; *m/z* 304 and 306 (M^+). Found: C, 66.77; H, 5.71; Cl, 11.70%. Calcd for $C_{17}H_{17}O_3Cl$: C, 67.00; H, 5.62; Cl, 11.63%. IR (KBr); 1710 and 1670 cm^{-1} (C=O). ^1H NMR ($CDCl_3$) δ=8.16 (2H, m), 7.77 (2H, m), 4.00 (2H, s), 2.66 (2H, t, *J*=7.0 Hz), 1.2—2.0 (6H, m), and 0.96 (3H, br-t, *J*=7.0 Hz).

2-Chloro-3-(2-oxooctyl)-1,4-naphthoquinone (4e): Yellow needles from hexane–chloroform; mp 107—108 °C. MS; *m/z* 318 and 320 (M^+). Found: C, 67.74; H, 6.04; Cl, 11.21%. Calcd for $C_{18}H_{19}O_3Cl$: C, 67.82; H, 6.01; Cl, 11.12%. IR (KBr); 1705 and 1670 cm^{-1} (C=O). ^1H NMR ($CDCl_3$) δ=8.18 (2H, m), 7.81 (2H, m), 4.01 (2H, s), 2.66 (2H, t, *J*=7.0 Hz), 1.1—1.9 (8H, m), and 0.92 (3H, br-t, *J*=7.0 Hz).

2-Chloro-3-(4-methyl-2-oxopentyl)-1,4-naphthoquinone (4f): Yellow needles from hexane–chloroform; mp 94—95.5 °C. MS; *m/z* 290 and 292 (M^+). Found: C, 65.86; H, 5.19; Cl, 12.17%. Calcd for $C_{16}H_{15}O_3Cl$: C, 66.10; H, 5.20; Cl, 12.19%. IR (KBr); 1705, 1675, and 1660 cm^{-1} (C=O). ^1H NMR ($CDCl_3$) δ=8.16 (2H, m), 7.18 (2H, m), 4.00 (2H, s), 2.53 (2H, d, *J*=7.0 Hz), 2.24 (1H, nonet, *J*=7.0 Hz), and 1.00 (6H, d, *J*=7.0 Hz).

2-Chloro-3-(3-methyl-2-oxobutyl)-1,4-naphthoquinone (4g): Yellow needles from hexane–chloroform; mp 112—113 °C. MS; *m/z* 276 and 278 (M^+). Found: C, 64.84; H, 4.67; Cl, 12.76%. Calcd for $C_{15}H_{13}O_3Cl$: C, 65.11; H, 4.74; Cl, 12.81%. IR (KBr); 1695, 1675, and 1655 cm^{-1} (C=O). ^1H NMR ($CDCl_3$) δ=8.14 (2H, m), 7.78 (2H, m), 4.06 (2H, s), 2.86 (1H, septet, *J*=7.0 Hz), and 1.24 (6H, d, *J*=7.0 Hz).

2-Chloro-3-(3-hydroxymethyl-2-oxopentyl)-1,4-naphthoquinone (4h): Yellow needles from hexane–chloroform; mp 116—118 °C. MS; *m/z* 307, 308, and 309 (M^+). Found: C, 62.73; H, 4.77; Cl, 11.55%. Calcd for $C_{16}H_{15}O_4Cl$: C, 62.65; H, 4.93; Cl, 11.56%. IR (KBr); 3360 (OH), 1700, and 1650 cm^{-1} (C=O). ^1H NMR ($CDCl_3$) δ=8.05 (2H, m), 7.69 (2H, m), 4.05 (2H, s), 3.74 (2H, m), 2.85 (1H, br-s), 2.63 (1H, tt), 1.57 (2H, m), and 0.91 (3H, t, *J*=8.4 Hz).

2-Chloro-3-(3-hydroxymethyl-2-oxohexyl)-1,4-naphthoquinone (4i): Yellow needles from hexane–chloroform; mp 118—120 °C. MS; *m/z* 321, 322, and 323 (M^+). Found: C, 63.42; H, 5.29; Cl, 11.28%. Calcd for $C_{17}H_{17}O_4Cl$: C, 63.66; H, 5.34; Cl, 11.05%. IR (KBr); 3380 (OH), 1720, 1680, and 1670 cm^{-1} (C=O). ^1H NMR ($CDCl_3$) δ=8.01 (2H, m), 7.68 (2H, m), 4.04 (2H, s), 3.74 (2H, m), 3.20 (1H, br-s), 2.71 (1H, tt), 1.39 (4H, m), and 0.90 (3H, t, *J*=6.0 Hz).

2-Chloro-3-(3-hydroxymethyl-2-oxooctyl)-1,4-naphthoquinone (4j): Yellow plates from hexane–chloroform; mp 87—88 °C. MS; *m/z* 349, 350, and 351 (M^+). Found: C, 65.70; H, 6.03; Cl, 10.29%. Calcd for $C_{19}H_{21}O_4Cl$: C, 65.42; H, 6.07; Cl, 10.16%. IR (KBr); 3360 (OH), 1700, 1670, and 1660 cm^{-1} (C=O). ^1H NMR ($CDCl_3$) δ=8.00 (2H, m), 7.66 (2H, m), 4.01 (2H, s), 3.79 (2H, d, *J*=6.0 Hz), 2.90 (1H, m), 2.38 (1H, br-s), 1.35 (8H, br-s), and 0.90 (3H, br-t).

2-Chloro-3-(2-oxo-5-hexenyl)-1,4-naphthoquinone (4k): Yellow needles from hexane–chloroform; mp 96—98 °C. MS; *m/z* 288 and 290 (M^+). Found: C, 66.82; H, 4.38; Cl, 12.56%. Calcd for $C_{16}H_{13}O_3Cl$: C, 66.56; H, 4.54; Cl, 12.28%. IR (KBr); 1700, 1670, and 1650 cm^{-1} (C=O). ^1H NMR ($CDCl_3$) δ=8.22 (2H, m), 7.86 (2H, m), 5.90 (1H, m), 5.15 (2H, dd, *J*=9.9 and 9.9 Hz), 4.04 (2H, s), 2.80 (2H, *J*=7.6 Hz), and 2.50 (2H, t, *J*=7.6 Hz).

2-Chloro-3-(6-methyl-2-oxo-5-heptenyl)-1,4-naphthoquinone (4l): Yellow needles from hexane–chloroform; mp 99—100.5 °C. MS; *m/z* 316 and 318 (M^+). Found: C, 67.97; H, 5.37; Cl, 11.29%. Calcd for $C_{18}H_{17}O_3Cl$: C, 68.25; H, 5.41; Cl, 11.19%. IR (KBr); 1700, 1660, and 1650 cm^{-1} (C=O). ^1H NMR ($CDCl_3$) δ=8.07 (2H, m), 7.72 (2H, m), 5.10 (1H, m), 3.94 (2H, s), 2.65 (2H, td, *J*=6.6 and 6.6 Hz), 2.38 (2H, t, *J*=6.6 Hz), 1.71 (3H, s), and 1.65 (3H, s).

2,3-Dichloro-4-(1-methyl-2-oxopropoxy)-1-naphthol (5a): Pink crystals from hexane–chloroform; mp 132.5—133.5 °C. MS; *m/z* 298, 300, and 302 (M^+). Found: C, 55.98; H, 3.77; Cl, 23.68%. Calcd for $C_{15}H_{14}O_3Cl_2$: C, 56.21; H, 4.04; Cl, 23.70%. IR (KBr); 3420 (OH) and 1730 cm^{-1} (C=O). ^1H NMR ($CDCl_3$) δ=8.11 (2H, m), 7.55 (2H, m), 6.30 (1H, br-s), 4.79 (1H, q, *J*=6.1 Hz), 2.53 (3H, s), and 1.39 (3H, d, *J*=7.0 Hz). ^{13}C NMR ($CDCl_3$) δ=208.3 (s), 145.1 (s), 143.5 (s), 128.3 (m), 127.4 (d), 126.6 (d), 122.8 (d), 122.2 (m), 122.1 (m), 121.2 (m), 112.4 (s), 84.2 (d), 26.0 (q), and 17.0 (q).

2,3-Dichloro-4-(1-ethyl-2-oxopropoxy)-1-naphthol (5b): Orange crystals from hexane–chloroform; mp 147—148 °C. MS; *m/z* 312, 314, and 316 (M^+). Found: C, 57.25; H, 4.43; Cl, 22.54%. Calcd for $C_{15}H_{14}O_3Cl_2$: C, 57.53; H, 4.51; Cl, 22.64%. IR (KBr); 3250 (OH) and 1690 cm^{-1} (C=O). ^1H NMR ($CDCl_3$) δ=8.17 (2H, m), 7.59 (2H, m), 6.14 (1H, br-s), 4.64 (1H, t, *J*=6.7 Hz), 2.48 (3H, s), 1.99 (2H, qd, *J*=6.7 and 7.0 Hz), and 0.99 (3H, t, *J*=7.0 Hz).

2,3-Dichloro-4-(1-propyl-2-oxopropoxy)-1-naphthol (5c): White needles from hexane–chloroform; mp 118—119 °C. MS; *m/z* 326, 328, and 330 (M^+). Found: C, 58.47; H, 4.92; Cl, 21.83%. Calcd for $C_{16}H_{16}O_3Cl_2$: C, 58.73; H, 4.93; Cl, 21.67%. IR (KBr); 3210 (OH) and 1700 cm^{-1} (C=O). ^1H NMR ($CDCl_3$) δ=8.12 (2H, m), 7.54 (2H, m), 6.11 (1H, br-s), 4.68 (1H, t, *J*=6.1 Hz), 2.44 (3H, s), 1.90 (2H, td), 1.48 (2H, qt), and 0.88 (3H, t, *J*=7.6 Hz).

4-(1-butyl-2-oxopropoxy)-2,3-dichloro-1-naphthol (5d): White crystals from hexane–chloroform; mp 103.5—104.5 °C. MS; *m/z* 340, 342, and 344 (M^+). Found: C, 59.99; H, 5.14; Cl, 20.85%. Calcd for $C_{17}H_{18}O_3Cl_2$: C, 59.84; H, 5.32; Cl, 20.78%. IR (KBr); 3200 (OH) and 1700 cm^{-1} (C=O). ^1H NMR ($CDCl_3$) δ=8.13 (2H, m), 7.55 (2H, m), 6.10 (1H, br-s), 4.67 (1H, t, *J*=5.8 Hz), 2.44 (3H, s), 1.91 (2H, td), 1.29 (4H, m), and 0.85 (3H, t, *J*=6.1 Hz).

2,3-Dichloro-4-(1-pentyl-2-oxopropoxy)-1-naphthol (5e): White crystals from hexane–chloroform; mp 52—54 °C. MS; *m/z* 354, 356, and 358 (M^+). Found: C, 60.68; H, 5.51; Cl, 19.75%. Calcd for $C_{18}H_{20}O_3Cl_2$: C, 60.86; H, 5.67; Cl, 19.96%. IR (KBr); 3520 (OH) and 1710 cm^{-1} (C=O). ^1H NMR ($CDCl_3$) δ=8.14 (2H, m), 7.55 (2H, m), 6.14 (1H, br-s), 4.68 (1H, t, *J*=6.1 Hz), 2.46 (3H, s), 1.88 (2H, td), 1.27 (6H, m), and 0.84 (3H, t, *J*=6.1 Hz).

2,3-Dichloro-4-(1-isopropyl-2-oxopropoxy)-1-naphthol (5f): White crystals from hexane–chloroform; mp 158—159 °C. MS; *m/z* 326, 328, and 330 (M^+). Found: C, 58.89; H, 4.82;

Cl, 21.92%. Calcd for $C_{16}H_{16}O_3Cl_2$: C, 58.73; H, 4.93; Cl, 21.67%. IR (KBr); 3290 (OH) and 1690 cm^{-1} (C=O). ^1H NMR ($CDCl_3$) δ=8.16 (2H, m), 7.55 (2H, m), 6.02 (1H, br-s), 4.65 (1H, d, J=4.2 Hz), 2.37 (3H, s), 1.68 (1H, m), and 1.08 (6H, d, J=6.7 Hz).

2,3-Dichloro-4-(1-methyl-2-oxobutoxy)-1-naphthol (5m): White needles from hexane–chloroform; mp 119—120 °C. MS; m/z 312, 314, and 316 (M^+). Found: C, 57.53; H, 4.51; Cl, 22.64%. Calcd for $C_{15}H_{14}O_3Cl_2$: C, 57.53; H, 4.51; Cl, 22.68%. IR (KBr); 3410 (OH) and 1690 cm^{-1} (C=O). ^1H NMR ($CDCl_3$) δ=8.05 (2H, m), 7.49 (2H, m), 6.24 (1H, br-s), 4.82 (1H, q, J=7.0 Hz), 2.93 (2H, q, J=7.3 Hz), 1.37 (3H, d, J=6.7 Hz), and 1.17 (3H, t, J=6.7 Hz).

2,3-Dichloro-4-(1-ethyl-2-oxopentyloxy)-1-naphthol (5n): White crystals from hexane–chloroform; mp 90.5—91.5 °C. MS; m/z 340, 342, and 344 (M^+). Found: C, 59.75; H, 5.32; Cl, 20.91%. Calcd for $C_{17}H_{18}O_3Cl_2$: C, 59.83; H, 5.32; Cl, 20.78%. IR (KBr); 3320 (OH) and 1690 cm^{-1} (C=O). ^1H NMR ($CDCl_3$) δ=8.12 (2H, m), 7.54 (2H, m), 6.07 (1H, br-s), 4.67 (1H, t, J=6.0 Hz), 2.78 (2H, qd), 1.93 (2H, t, J=7.2 Hz), 1.70 (2H, qd, J=7.2 and 7.2 Hz), and 0.95 (3H, t, J=4.8 Hz).

References

1) K. Maruyama, T. Otsuki, and S. Tai, *Chem. Lett.*, **1984**, 371.
2) K. Maruyama, T. Otsuki, and S. Tai, *J. Org. Chem.*, **50**, 52 (1985).
3) K. Maruyama, H. Uno, and Y. Naruta, *Chem. Lett.*, **1983**, 1767.
4) Y. Naruta, H. Uno, and K. Maruyama, *J. Chem. Soc., Chem. Commun.*, **1981**, 1277.
5) J. M. Bruce and E. Cutts, *J. Chem. Soc., C*, **1966**, 449.
6) Y. Naruta, H. Uno, and K. Maruyama, *Tetrahedron Lett.*, **22**, 5221 (1981).
7) T. Kometani, Y. Takeuchi, and E. Yoshii, *J. Org. Chem.*, **48**, 2311 (1983).
8) Y. Naruta, *J. Am. Chem. Soc.*, **102**, 3774 (1980).
9) Y. Naruta, *J. Org. Chem.*, **45**, 4097 (1980).
10) L. F. Fieser, *J. Am. Chem. Soc.*, **48**, 3201 (1926).
11) H. O. House, L. J. Czuba, M. Gall, and H. D. Olmstead, *J. Org. Chem.*, **34**, 2324 (1969).
12) P. Brownbridge, T. H. Chan, M. A. Brook, and G. J. Kang, *Can. J. Chem.*, **61**, 688 (1983).
13) P. J. Jerris and A. B. Smith, *J. Org. Chem.*, **46**, 577 (1981).

Synthesis of Oligodeoxyribonucleotides Involving a Rapid Procedure for Removal of Base-Protecting Groups by Use of the 4,4′,4″-Tris(benzoyloxy)trityl (TBTr) Group

Mitsuo SEKINE,* Narihiro MASUDA, and Tsujiaki HATA*
Department of Life Chemistry, Tokyo Institute of Technology, Nagatsuta, Midori-ku, Yokohama 227
(Received January 18, 1986)

Fully protected building units for oligodeoxyribonucleotide synthesis in the phosphoramidite approach were prepared in high yields by the 5′-dimethoxytritylation of *N*-[4,4′,4″-tris(benzoyloxy)trityl]deoxyribonucleosides followed by the 3′-phosphitylation with methoxymorpholinochlorophosphine. The solid phase synthesis of oligodeoxyribonucleotides on a controlled pore glass gel using the amidite units was examined. The efficiency of condensation was discussed in detail. The 4,4′,4″-tris(benzoyloxy)trityl (TBTr) group was removed rapidly from a protected tetramer synthesized on the controlled pore glass gel to give dGpCpApT.

Recent developments of oligodeoxyribonucleotide synthesis have enabled us to synthesize relatively long DNA fragments in short time.[1] Reaction velocity of condensation has been dramatically accelerated by introduction of new technologies such as the tetrazole-catalyzed phosphoramidite approach[2] and the *N*-methylimidazole[3] or 4-substituted pyridine-*N*-oxide-promoted phosphotriester approach.[4] The use of sterically hindered diaryl phosphorochloridates also improved markedly the condensation time.[5] However, only little attention has been paid to the deprotection procedure of fully protected DNA fragments.[6] Especially, removal of *N*-acyl protecting groups from oligomers was the most sluggish in the whole synthetic procedures. Some improvements have been reported in this direction but they required rather drastic conditions such as elevated temperatures.[7]

In this paper, we report basic studies on improvement of the deprotection procedure for *N*-protecting groups by the use of 4,4′,4″-tris(benzoyloxy)trityl (TBTr) as a universal base-protecting group.

Results and Discussion

In a previous paper,[8] we showed that the TBTr group could be introduced into the four common base moieties by using the transient protection strategy. The glycosyl bond of *N*-TBTr-deoxyadenosine (**2c**) was also found to be 4 times more stable to 2% dichloroacetic acid in dichloromethane (CH_2Cl_2) than that of N^6-benzoyldeoxyadenosine. Since the TBTr group was rather resistant to acids owing to its electronic effect derived from the three benzoyloxy substituents, the 4,4′-dimethoxytrityl (DMTr) group could be used as the 5′-hydroxy protecting group in combination with the TBTr group. Therefore, we chose the latter as the *N*-protecting group in the phosphoramidite approach using the morpholino group as an activatable phosphite protecting group.

Preparation of Fully-Protected Deoxyribonucleoside Amidite Units (3b—d). *N*-[4,4′,4″-Tris(benzoyloxy)-trityl]deoxyribonucleosides (**1b—d**) were allowed to

Table 1. Synthesis of *N*-TBTr-5′-*O*-DMTr-deoxyribonucleosides (**2b—f**)

Compd	Yield %	^{1}H NMR ($CDCl_3$) ppm	Formula	Elemental analysis Calcd (%) Found (%) C	H	N
2b	98	1.90—2.95 (2, m, 2′-H), 3.34 (2, m, 5′-H), 3.63 (6, s, OMe), 4.03 (1, m, 4-H′),4.43 (1, m, 3′-H), 4.84 (1, d, *J*=7Hz, 5-H), 6.33 (1, t, *J*=5Hz, 1′-H), 6.65 (4, d, *J*=8Hz, ArH), 6.91—7.76 (31, m, ArH), 8.10 (6, m, ArH)	$C_{70}H_{57}O_{12}N_3$	74.26 73.26	5.07 5.36	3.71 3.63
2c	92	2.08—3.16 (2, m, 2′-H), 3.40 (1, m, 5′-Ha), 3.74, 3.87 (6, s, OMe), 3.56—3.88 (1, m, 5′-Hb), 4.14 (1, m, 4′-H), 4.66 (1, m, 3′-H), 6.33 (1, m, 1′-H), 6.81 (4, m, ArH), 7.08—8.32 (32, m, ArH)	$C_{71}H_{57}O_{11}N_5$	73.75 73.13	4.97 4.83	6.06 5.90
2d	93	2.10 (2, m, 2′-H), 3.63 (3, m, 4′-H and OMe), 4.09 (2, m, 3′-H), 5.72 (1, m, 1′-H), 6.60—6.70 (4, m, ArH), 6.92—7.63 (32, m, ArH and 8-H), 8.02—8.10 (6, m, ArH)	$C_{71}H_{57}O_{12}N_5$	72.75 72.65	4.90 4.99	6.00 5.87
2f	93	2.06 (2, m, 2′-H), 3.32 (2, m, 5′-H), 3.68, 3.73 (6, s, OMe), 4.01—4.38 (2, m, 3′,4′-H), 5.74 (1, m, 2′-H), 6.39, 6.43 (2, s, N-CH-O), 6.74 (6, m, ArH), 7.00—7.77 (31, m, ArH), 7.99 (4, m, ArH), 8.17 (6, br d, *J*=8Hz, ArH)	$C_{87}H_{67}O_{12}N_5$	72.64 72.27	4.70 4.80	4.87 4.83

Table 2. Preparation of Phosphoramidite Units (**3b—f**)

Compd	Method for separation/ eluant	Isolated yield %	^{31}P NMR ($CDCl_3$) ppm	Elemental analysis: Formula	Calcd (%) / Found (%) C	H	N
3b	Basic alumina/0.5% Et_3N/ CH_2Cl_2–benzene	68	−144.5, −144.2	$C_{75}H_{67}O_{14}N_4P$	70.41 / 69.38	5.28 / 5.25	4.38 / 4.40
3c	Basic alumina/1% Me-N⟨ ⟩ / CH_2Cl_2–benzene	68	−144.3, −144.1	$C_{76}H_{67}O_{13}N_6P$	70.04 / 69.67	5.18 / 5.02	6.45 / 6.46
3d	Silica gel/1% Et_3N/ CH_2Cl_2–hexane	63	−144.4, −143.4	$C_{76}H_{67}O_{14}N_6P$	69.19 / 69.74	5.12 / 5.12	6.37 / 6.42
3e	Basic alumina/1% Me-N⟨ ⟩ CH_2Cl_2–benzene	68	−144.5	$C_{52}H_{54}N_7O_{10}P$	64.52 / 64.33	5.62 / 5.52	10.13 / 10.33
3f	Basic alumina/0.3% Et_3N/ CH_2Cl_2	95	−144.5, −143.7	$C_{92}H_{77}O_{18}N_6P$	69.69 / 69.98	4.90 / 4.77	5.30 / 5.49

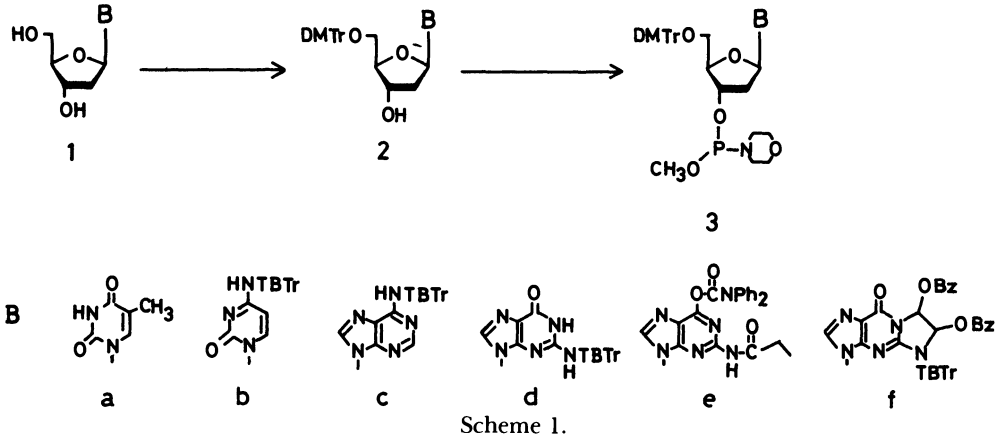

Scheme 1.

react with 4,4′-dimethoxytrityl chloride (DMTrCl) to give the corresponding 5′-tritylated products (**2b—d**) in 92—98% yields (Table 1). The amidite units (**3a—d**) were synthesized by a method similar to that described by Caruthers.[2b] Reaction of **2b—d** with methoxymorpholinochlorophosphine (MMCP) in the presence of *N,N*-diisopropylethylamine in CH_2Cl_2 gave the desired products (**3b—d**). The phosphoramidites **3b—d** were obtained in more than 90% yields by reprecipitation from CH_2Cl_2 into hexane. However, the purities of the precipitated materials were less than 70% from their NMR spectra. Several experiments were conducted to purify **3b—d** by using silica-gel or alumina column chromatography developed with various solvent systems. Because of the lability of the TBTr group to secondary amines such as morpholine the inert tertiary amines, triethylamine and *N*-methylpyrrolidine, were used with CH_2Cl_2–hexane or benzene. By the use of these solvent systems, **3b—d** were satisfactorily purified and their purities increased to more than 90% as shown in Chart 1. The impurities were found to be the hydrolyzed products (**4a—d**) of **3b—d** and the 3′–3′ linked dimer (**5b—d**). The former could be removed by chromatographic separation but the latter remained to a degree of 3—5% even after rechromatography. Nevertheless, the amidite units were used without further purification since the 3′–3′ by-products were inert during condensation and could be washed off from solid supports. The amidites appeared at −144 ppm in their ^{31}P NMR spectra as shown in Table 2.

Polymer Supported Synthesis of Oligodeoxyribonucleotides. Recent studies on the solid phase synthesis of oligodeoxyribonucleotides in the phosphoramidite approach pioneered by Caruthers[2] have shown that controlled pore glass (CPG)[9] was very effective as a nonswellable polymer support. Therefore, we employed two kinds of CPG gel supports, 3-aminopropyl CPG (P-CPG) and long-chain amino CPG (L-CPG) purchased from Funakoshi Co. Ltd. The latter has a hexamethylene chain in the spacer. Both the supports were bound to 4,4′-*O*-dimethoxytritylthymidine (DMTrT) via the succinate linker according to the well established procedure.[10] The loading amounts of DMTrT were 35.9 and 13.9 $\mu mol\,g^{-1}$ for P-CPG and L-CPG, respectively.

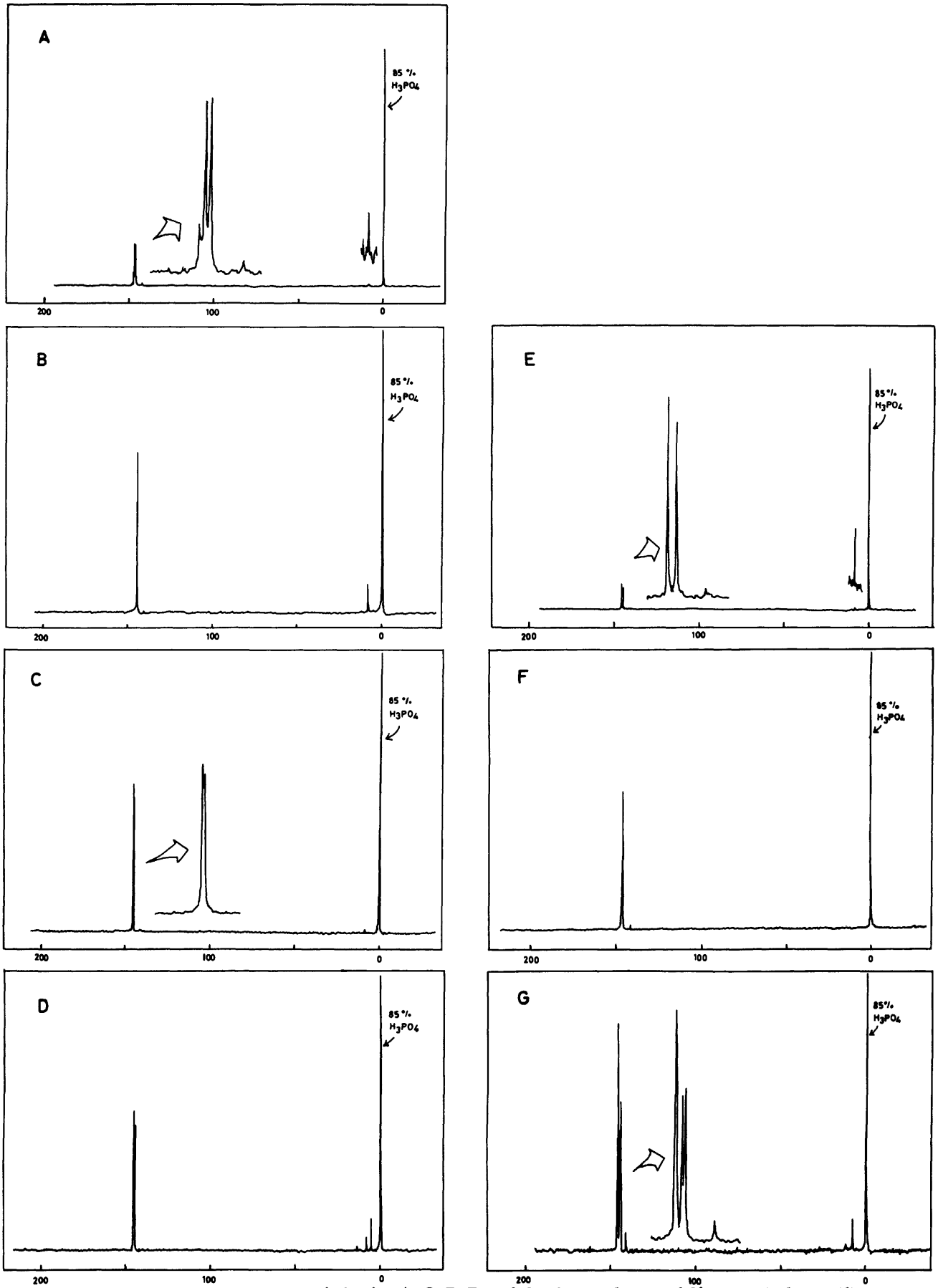

Chart 1. The ^{31}P NMR spectra of **3b**—f.· A, C, E, F, and G: **3b**, **3c**, **3d**, **3e**, and **3f**, respectively, purified by silica-gel or alumina column chromatography; B and D: **3c** and **3d**, respectively, obtained by reprecipitation from CH_2Cl_2 into hexane after the extractive workup.

Table 3. Elongation Cycle for Polymer Support Synthesis of Oligoribonucleotides

Step	Manipulation	Time/min	Volume/ml
1	1% TFA/CH_2Cl_2	2	3
2	Wash with CH_2Cl_2, MeCN	1	5
3	0.2M phosphoramidite (20 equiv)/MeCN (0.18 ml)+0.4M tetrazole (40 equiv)/MeCN (0.18 ml)	5 or 10	0.36
4	Wash with MeCN, THF		
5	0.1M I_2/2,6-lutidine-THF-H_2O (1:2:2, v/v/v)	1	1
6	Wash with MeCN, THF	1	5
7	0.07M DMAP/Ac_2O-THF-lutidine (2:6:1, v/v/v)	2	3
8	Wash with THF, CH_2Cl_2	1	5

DMTrT-CPG (35.9 μmol/g, 50 mg, 1.8 μmol) was used in each experiment.

Prior to condensation of **3b—d** on these supports, we reconfirmed suitable conditions of coupling cycle by using a modification of the procedure reported by Adams.[2c] The modified cycle for the polymer-supported synthesis is shown in Table 3.

Condensation of **3a** with T-L-CPG was repeated three times under the different conditions using 0.05 and 0.1 M† solutions of **3a**. However, the average coupling yields, which were estimated by the DMTr cation assay, were only 83 and 86% in the case of 0.05 and 0.1 M solutions of **3a**, respectively.

amidite(M)	time	solvent	T—T—T—T—— [L-CPG]
3a (0.05)	5 min	MeCN	87 87 74 (%) av. 83 %
3a (0.1)	5 min	MeCN	95 89 73 86

Although a relatively long spacer was involved in L-CPG like a long alkylated CPG (LA-CPG) used by Gilham,[9a] Adams,[2c] and Köster,[9d] the unexpected results were obtained. This is due probably to lack of affinity of the activated phosphorylated species of **3a** for the aliphatic hexamethylene chain. The presence of somewhat polar bonds like LA-CPG seems to be important for smooth coupling. However, the coupling of T-P-CPG with **3a** was found to proceed more effectively than that of T-L-CPG under the same conditions. Under the conditions of 10 min and 0.1 M solution of **3a**, the average coupling yield increased to 98% satisfactorily as reported in the original paper.[2b]

amidite(M)	time	solvent	
3a (0.1)	5 min	MeCN	
3a (0.1)	10 min	MeCN	
	T—T—T—T—T—T—T—— [P-CPG]		
	80 84 83 79 84 87 (%) av. 83 %		
	94 98 97 99 99 104 98		

We feel that the coupling time requires at least 10 min when the morpholino group is used. A relatively long reaction period has already been employed by Köster.[2d,8d]

However, the guanosine unit **3d** was found to form a gel in acetonitrile. The other new amidite units **3b,c** were soluble in this solvent. Therefore, a mixed solvent of 1,2-dichloroethane(DCE)-acetonitrile (1:1, v/v) was chosen during the condensation step to compare the reactivities of the three amidite units **3b—d** under the same conditions. In the case of the deoxycytidine unit **3b**, the coupling yields increased gradually with an increase in chain length and finally up to more than 95% after the five consecutive couplings. Compared with this result, the coupling yields in the case of **3c** were constant with an average yield of 79%. The average coupling yield was improved by the use of only acetonitrile to 89%.

amidite(M)	time	solvent	
3b (0.1)	10 min	DCE-MeCN	(1:1, v/v)
	C—C—C—C—C—C—T—— [P-CPG]		
	96 95 87 78 83 73 (%) av. 85 %		

amidite(M)	time	solvent	
3c (0.1)	10 min	DCE-MeCN	(1:1, v/v)
3c (0.1)	10 min	MeCN	
	A—A—A—A—A—A—T—— [P-CPG]		
	77 79 83 78 88 69 (%) 79 %		
	— 90 87 87 94 87 (%) 89 %		

A mixed solvent with 1,2-dichloroethane was somewhat inferior to acetonitrile in our coupling system. In an attempt to improve the coupling yield, a little more acidic catalyst, 5-(4-nitrophenyl)tetrazole (NPT), reported by Matteucci,[11] was employed. How-

† 1 M=1 mol dm^{-3}.

ever, this catalyst was ca. one-forth less soluble in acetonitrile than tetrazole so that a relatively dilute solution of NPT (0.1 M) had to be used. As a consequence, high yield couplings were attained at the second and third condensations although the first coupling was ineffective.

amidite(M)	NPT(M)	time	solvent
3c (0.1)	0.1	10 min	DCE–MeCN (1:1, v/v)

A—A—A—T—— [P-CPG]
97 89 35 (%) av. 74 %

However, a large amount of precipitate appeared 1 min after the tetrazole was added at every coupling stage. This precipitate, probably, morpholinium salt of NPT, caused difficult shaking during the reaction.

In the case of deoxyguanosine, the average coupling yield was very low in 1,2-dichloromethane–acetonitrile. It was observed that the coupling yields after the second condensation were considerably lower than that obtained in the first coupling. This low reactivity of **3d** led us to examine if the reagent was stable in 1,2-dichloroethane–acetonitrile. The same coupling cycle was repeated after **3d** was left in the mixed solvent in the presence of tetrazole for 5 h. However, a similar result was obtained.

amidite(M)	time	solvent
3d (0.1)	10 min	DCE–MeCN (1:1, v/v)
3d (0.1)*	10 min	DCE–MeCN (1:1, v/v)

G—G—G—T—— [P-CPG]
32 37 65 (%) av. 45 %
25 26 57 36

*In this case, **3d** was used 5h after tetrazole was added.

Next, in order to see if the low yield is due to side reactions at the guanine moiety, several experiments were conducted. First, the four consecutive couplings of T-P-CPG with a newly-synthesized amidite unit (**3e**) of deoxyguanosine were carried out. The compound **3e** was obtained in 67% yield from the deoxyguanosine derivative (**2e**) as the substrate which could eliminate any side reactions on the guanine moiety since the reactive amidite site was blocked completely with the diphenylcarbamoyl (DPC) group.[12]

amidite(M)	time	solvent
3c (0.1)	10 min	DCE–MeCN (1:1, v/v)

G*—G*—G*—G*—G*—G*—T—— [P-CPG]
83 85 83 79 81 89 (%) av. 83 %

G* refers to 2-*N*-propionyl-*O*^{6}-diphenylcarbamoyldeoxyguanosine.

Consequently, a nearly constant average yield of 83% was obtained. Since we aimed to develop rapid deprotection procedures through this study and removal of the DPC group required somewhat long periods of time, the double protection mode using glyoxal was employed. As expected from our previous paper, 1,2-bis(acyloxy)ethylene groups such as the 1,2-bis(isobutyryloxy)ethylene group[13] would be removed readily under mild basic conditions. The compound **1d** was treated with ethyl vinyl ether in the presence of trifluoroacetic acid in CH_2Cl_2 to give a bis(1-ethoxyethyl)ated derivative (**6**), which was in situ converted to a glyoxal adduct (**7**) by a method similar to that reported previously.[13] The two hydroxyl groups of **7** were further acylated with benzoic anhydride. The resulting product (**8**) was partially deblocked with 1 M zinc bromide in CH_2Cl_2–2-propanol[14] to give the key intermediate (**1f**) in an overall yield of 55% from **1d**.

It was found that the 1,2-bis(benzoyloxy)ethylene (BBE) group was rapidly eliminated from **1f** by treatment with 0.5 M NaOH–pyridine (1:1,v/v) at room temperature for 20 min. Under these conditions, the TBTr group was simultaneously removed to afford deoxyguanosine. It was also found that compound **1f** was stable to iodine in THF–lutidine–water like **1a**—

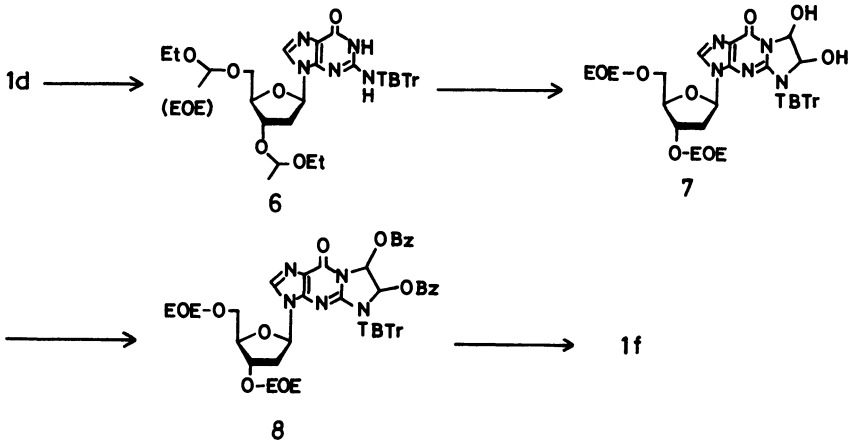

Scheme 2.

e. On the TFA treatment, **1f** has a relatively long half time of 24 h toward depurination. These results led us to synthesize a new deoxyguanosine amidite unit (**3f**). The compound **1f** was tritylated with DMTrCl to give **2f** in 93% yield. The subsequent phosphitylation of **2f** with MMCP gave **3f** in 95% yield. A high yield synthesis of **2f** was achieved with the aid of the highly lipophilic protecting groups contained in the molecule, which facilitated elution of the product from an alumina column.

The coupling reaction of the unit **3f** with T-P-CPG was tested under various conditions. However, unsatisfactory results were obtained. In 1,2-dichloroethane–acetonitrile, the coupling yields at the first and second condensations were 56 and 27% yields, respectively.

amidite(M)	time	solvent	
3f (0.1)	10 min	DCE–MeCN	(1:1, v/v)
3f (0.1)	60 min	DCE–MeCN	(1:1, v/v)
3f (0.1)	10 min	MeCN	

G′—G′—G′—G′—G′—T——	[P-CPG]
27 56 (%)	av. 47 %
23 32 66	40
60 62 47 49 74	58

G′ refers to 2-*N*-TBTr-N^1,N^2-bis(benzoyloxy)ethylene-deoxyguanosine.

When the time for the condensation was prolonged to 60 min, remarkable improvements were not made. When acetonitrile was used in place of the mixed solvent, somewhat better results were obtained. These results indicate that the low coupling yield in the case of **3d** may be due to the steric hindrance of the TBTr group attached to the exo amino group. In fact, the CPK model suggests that the TBTr residue can approach to the 3′-position. An alternative way to solve this problem should be studied.

In spite of the problem on the deoxyguanosine unit, we demonstrated rapid deprotection procedure after coupling using the four phosphoramidite units, **3a—c** and **3f**, on CPG gel. In order to see if the TBTr group can be smoothly removed from CPG gel, we synthesized a sequence of dGpCpApT on P-CPG. The results are shown below.

amidite(M)	time	solvent
3b, 3c, 3f (0.1 each)	10 min	MeCN

G′—C—A—T——	[P-CPG]
45 84 86 (%)	av. 72 %

The CPG gel loading this sequence was first treated with benzenethiol–Et_3N–dioxane (1:1:1, v/v)[2a] and then with 0.5 M NaOH–pyridine (1:1, v/v) at room temperature for 30 min. It was confirmed that under the latter conditions the succinate linker and the TBTr and BBE groups were rapidly removed as expected.[8,15] The reaction could be easily monitored by the strength of color of rosolic acid, which was generated as the deprotection proceeded. Since the sensitivity of this color test was as good as that of the DMTr cation assay under acidic conditions, the completion of deprotection can be confirmed directly by eyes.

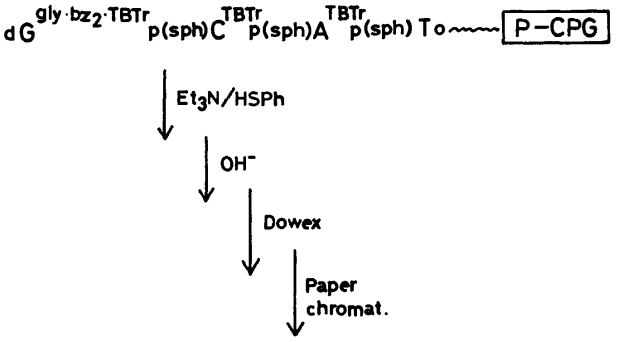

Scheme 3.

These properties will be advantageous when applied to automated synthesis of oligodeoxyribonucleotides. Rosolic acid and benzoic acid generated were easily removed by extraction with ether. The mixture obtained from the aqueous layer was chromatographed on Whatman 3 MM papers with 1-propanol–concentrated aqueous ammonia–H_2O (55:10:35, v/v/v) to afford dGpCpApT in 70% yield. The tetramer was characterized by enzymatic digestion with snake venom phosphodiesterase which gave G, pC, pA, and pT in the ratio of 1.08:0.85:1.00:0.88.

Conclusion

As shown in the present study, the TBTr and BBE groups could be removed promptly from the oligomer chain within 30 min. Since the phosphodiester linkage is rather stable under alkaline conditions[7] compared with phosphotriester linkage, relatively strong alkali like NaOH is available for removal of base protecting groups after elimination of the methyl group with benzenethiol. The conventional protecting groups of acyl-type were, however, resistant to alkali such as dilute NaOH except for labile acyl groups like the acetyl group on N^4-acetyldeoxycytidine[16] which can not be utilized in oligodeoxyribonucleotide synthesis. Therefore they have been removed mostly by treatment with concentrated aqueous ammonia. It is noteworthy that the TBTr and BBE groups are removed simply under mildly alkaline conditions that can be applied to the "full" automated-synthesis of DNA fragments which involves the deprotection procedure. The color

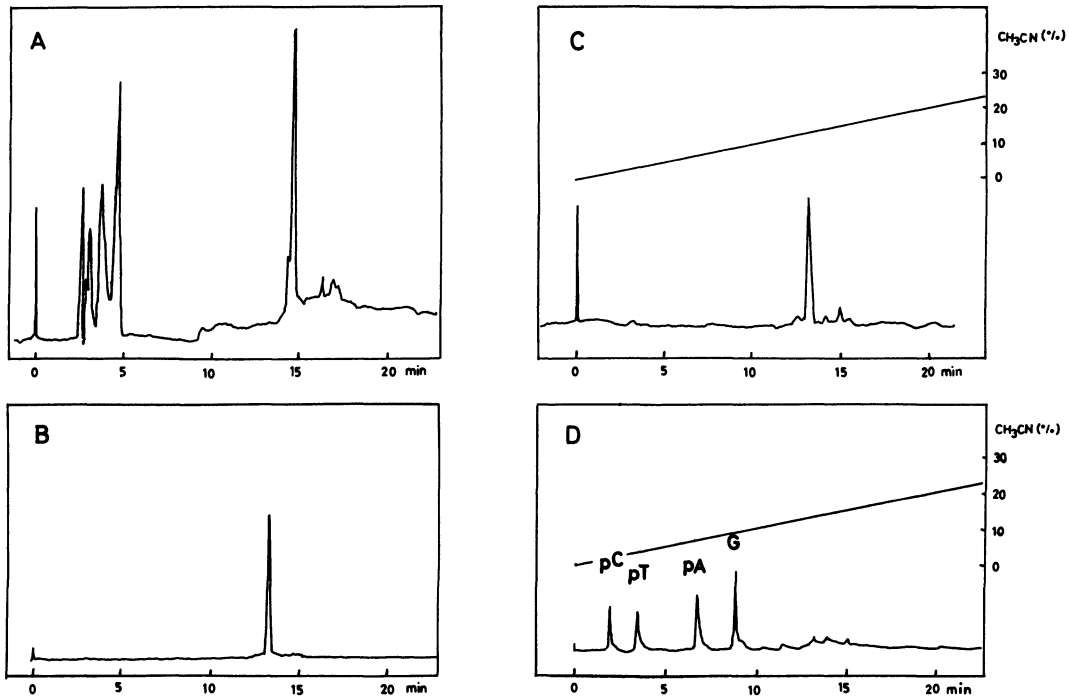

Chart 2. A: The ion-exchange HPLC profile of the mixture obtained after the protecting groups and linker were removed; B: The reverse-phase HPLC profile of dGpCpApT separated by paper chromatography; D: The reverse-phase HPLC profile of the mixture obtained by enzyme digestion of dGpCpApT with snake venom phosphodiesterase.

marker of rosolic acid enabled us to observe visibly the degree of the complete deprotection since the succinate linker and the BBE group were eliminated under the conditions where the TBTr group was removed. However, some improvements are needed for obtaining higher coupling yields. Especially, more suitable alkali-labile protecting groups should be explored for our purpose. We are now challenging to solve these problems in this derection.

Experimental

^{1}H NMR spectra were recorded at 100 MHz on a JEOL UNM PS-100 spectrometer using tetramethylsilane as an internal standard. UV spectra were obtained on a Hitachi 220A spectrophotometer. Paper chromatography was performed by use of a descending technique with Whatman 3 MM papers using the following solvent system: Solvent I (1-propanol–concentrated aqueous ammonia–water, 55:10:35, v/v/v). Column chromatography was performed with silica gel C-200 purchased from Wako Co. Ltd. or alumina Woelm B-Supper I from Kanto Co. Ltd., and a minipump for a goldfish bowl was conveniently used to attain sufficient pressure for rapid chromatographic separation. TLC was performed on precoated TLC plates of silica gel 60 F-254 (Merck) or aluminium oxide 60 F-254 (Merck).

Ion-exchange HPLC was performed on a JASCO TRI ROTAR type II apparatus equipped with a Whatman Partisil 10 SAX column (3.9×250 mm), a GP-A30 solvent programmer, a UVIDEC 100-II UV detecter and an RC-225 recorder. A linear gradient (0→99%) starting with buffer A (0.005 M KH_2PO_4, 20% CH_3CN, pH 6.54) and applying buffer B (0.5 M KH_2PO_4, 20% CH_3CN, pH 6.54) was used at a flow rate of 2 ml min^{-1} for 32 min for analysis and purification of dGpCpApT. Reverse phase HPLC was performed on a Waters Model A25 using a μ-Bondapack C-18 column using a linear gradient starting from buffer C (0.1 M NH_4OAc, pH 7.0) and applying CH_3CN at a flow rate of 2 ml min^{-1} for 30 min.

Deoxyribonucleosides were purchased from Yoshitomi Co. Ltd. Compounds **1b—d**,[8] **2a**,[17] and **2e**[12] were prepared to the published procedures. Pyridine was distilled two times from *p*-toluenesulfonyl chloride and from calcium hydride and then stored over molecular sieves 3A. Acetonitrile was distilled over calcium hydride and stored over molecular sieves 3A. 1,2-Dichloroethane was dried over P_4O_{10}, decanted, distilled over K_2CO_3, and stored over molecular sieves 3A.

Venom phosphodiesterase was purchased from Boehringer Co. Ltd. Elemental analyses were performed by the Microanalytical Laboratory, Tokyo Institute of Technology, at Nagatsuta.

General Procedure for Synthesis of 2b—f. An appropriate *N*-TBTr deoxyribonucleoside[7] (**1b—f**, 5 mmol) was rendered anhydrous by repeated coevaporation with dry pyridine and finally dissolved in dry pyridine (50 ml). To the solution was added DMTrCl (1.05—1.20 equiv), and the mixture was kept for 3—5 h. Then ice-water was added and the mixture was extracted with CH_2Cl_2. The organic layer was washed with satd $NaHCO_3$ solution, dried over Na_2SO_4, filtered, and evaporated to a gum. The residue was evaporated several times with toluene and chromatographed on silica gel (70 g) with CH_2Cl_2→CH_2Cl_2–MeOH in the presence of 0.3% pyridine to give **2b—f** as listed in Table 1.

General Procedure for Synthesis of 3b—f. An appropriate *N*-TBTr-5′-*O*-DMTr-deoxyribonucleoside (**2b—f**, 1 mmol) was

rendered anhydrous by coevaporation with dry pyridine and then with dry toluene two times each and finally dissolved in dry CH_2Cl_2 (10 ml). To the solution were added successively diisopropylethylamine (609 μl, 3.5 mmol) and MMCP (224 μl, 1.5 mmol). After being stirred at room temperature for 10 min, the mixture was dissolved with ethyl acetate (20 ml) which had been washed with satd $NaHCO_3$ solution. The organic phase was again washed with satd $NaHCO_3$ solution (20 ml). After drying over Na_2SO_4, the extract was filtered and evaporated to a foam. The foamy material was chromatographed on a silica-gel or alumina column as shown in Table 2. The elemental analyses and ^{31}P NMR spectra of **3b—f** are also given in Table 2.

Introduction of DMTrT to CPG. To a suspension of P-CPG (pore size 569 Å, NH_2 97 μmol g^{-1}) or L-CPG (pore size 569 Å, NH_2 123 μmol g^{-1}) were added triethylamine (3 equiv), 4-(dimethylamino)pyridine (0.75 equiv), and 5′-*O*-dimethoxytrityl-3′-*O*-[3-(pentachlorophenoxycarbonyl)propionyl]thymidine (1.5 equiv). After the mixture was rotated slowly in a sealed flask by using a rotary evaporator for 20 h, the gel was washed with CH_2Cl_2 and dried over P_4O_{10} and NaOH in vacuo. The resulting gel was used for condensation with **3**.

***N*²-[4,4′,4″-Tris(benzoyloxy)trityl]-*N*¹,*N*²-bis(benzoyloxy)-ethylenedeoxyguanosine (8).** To a mixture of **1d** (2.31 g, 2.61 mmol) and ethyl vinyl ether (5.07 ml, 53 mmol) was added trifluoroacetic acid (408 μl, 5.3 mmol). The solution was stirred at room temperature for 100 min and the solvent and the ether was removed under reduced pressure. The residue was coevaporated successively with toluene and dry pyridine two times each and then dissolved in 2.5 M solution of glyoxal in dry pyridine (10 ml). The mixture was evaporated ten times with dry pyridine (20 ml) and finally dissolved in CH_2Cl_2 (100 ml). The CH_2Cl_2 solution was washed five times with water (100 ml), dried over Na_2SO_4, filtered, and evaporated to a gum. The gum was rendered anhydrous by repeated coevaporation with dry pyridine and then evaporated several times with dry toluene to remove the last traces of pyridine. The residue was dissolved in dry CH_2Cl_2 (25 ml) and treated with benzoic anhydride (4.72 g, 20.9 mmol), triethylamine (2.9 ml, 20.9 mmol), 4-(dimethylamino)pyridine (32 mg, 0.26 mmol). After the resulting mixture was kept at room temperature for 17 h, water was added. The dibenzoate was extracted three times with CH_2Cl_2 and the extract was washed with satd $NaHCO_3$ solution. The extracts were combined and evaporated to dryness under reduced pressure. To the residue was added 1 M solution of zinc bromide in CH_2Cl_2–2-propanol (85:15, v/v, 26 ml), and the mixture was stirred for 1 h. Then pyridine was added and the resulting precipitate was removed by filtration. The filtrate was partitioned between CH_2Cl_2 and satd $NaHCO_3$ solution. The organic layer was collected, dried over Na_2SO_4, filtered, and evaporated to a foam under reduced pressure. The residue was chromatographed on silica gel with CH_2Cl_2–MeOH to give **8** (1.63 g, 55%); ^1H NMR ($CDCl_3$) δ=2.02 (2H, m, 2′-H), 3.52 (2H, m, 5′-H), 3.87 (1H, m, 4′-H), 4.29 (1H, m, 3′-H), 5.71 (1H, m, 1′-H), 6.24, 6.50 (2H, br s, N-CH-O), 7.04—7.80 (22H, m, ArH), 7.96 (4H, m, ArH), 8.17 (6H, br d, J=8 Hz, ArH). Calcd for $C_{66}H_{49}N_5O_{14}$: C, 69.77; H, 4.35; N, 6.16%. Found: C, 68.75; H, 4.10; N, 6.03%.

Solid Phase Synthesis of dGpCpApT on P-CPG. This synthesis was done by using DMTrT-P-CPG (50 mg, 1.8 μmol). The final DMTr cation assay showed that 0.575 μmol of the tetramer was formed.

Isolation of dGpCpApT. The P-CPG gel containing fully-protected tetramer was treated with benzenethiol–triethylamine–dioxane (1:1:2, v/v/v, 4 ml) at room temperature for 45 min with gentle rotation using a rotary evaporator. The gel was washed successively with MeOH and ether and then allowed to react with 0.5 M NaOH in pyridine–water (1:1, v/v, 1 ml) for 30 min using a rotary evaporator to keep constant rotation. The gel was removed by filtration and washed with pyridine–water (1:1, v/v, 5 ml). The eluant and washings were combined and passed through Dowex 50 W×2 (100—200 mesh, pyridinium form, 5 ml). The resin was washed with pyridine–water (1:1, v/v, 5 ml). The eluant and washing were combined and evaporated and then the residue was evaporated three times with a small amount of concentrated aqueous ammonia to remove the last traces of pyridine. Part (71%) of the residue was applied to Toyo Roshi No 51 Å papers. Chromatography developed with Solvent I afforded dGpCpApT (10.2 OD, 70% based on the assumption of 15% hypochromicity using ε 3.55×10⁴ at 258 nm).

Enzymic Assay of dGpCpApT. The tetramer (2.4 OD unit at 258 nm) was dissolved in Tris-HCl buffer (0.05 M, pH 8.0, 50 μl) and snake venom phosphodiesterase (10 μl) was added. The mixture was incubated at 37 °C for 1.5 h. After being heated at 100 °C for 3 min, the mixture was analyzed by reverse phase HPLC. The calculated ratio of dG, pC, pA, and pT was given in the text. The following ε values at 254 nm were used for calculation: 5630, 6080, 13400, and 14100 for pC, pT, pA, and dG, respectively.

References

1) a) V. Amarnath and A. D. Broom, *Chem. Rev.*, **77**, 183 (1977); b) C. B. Reese, *Tetrahedron*, **34**, 3143 (1978); c) M. Ikehara, E. Ohtsuka, and A. F. Markham, *Adv. Carbohy. Chem. Biochem.*, **36**, 135 (1978); d) G. A. Urbina, G. M. Sathe, W. C. Liu, M. F. Gillen, P. D. Duck, R. Bender, and K. K. Ogilvie, *Science*, **214**, 270 (1981); e) E. Ohtsuka, M. Ikehara, and D. Söll, *Nucleic Acids Res.*, **10**, 6553 (1982); f) K. Itakura, *Trends Biochem. Sci.*, **7**, 442 (1982); g) S. A. Narang, *Tetrahedron*, **39**, 3 (1983); h) W. Pfleiderer, *KONTAKTE* (Merck), 3 (1983); i) J. E. Davies and H. G. Gassen, *Angew. Chem. Int. Ed. Engl.*, **22**, 13 (1983); j) K. Itakura, J. J. Rossi, and R. B. Wallace, *Annu. Rev. Biochem.*, **53**, 323 (1984); k) "Oligonucleotide Synthesis, a Practical Approach," ed by M. J. Gait, IRL Press, Oxford (1984); l) M. H. Caruthers, *Science*, **230**, 281 (1985).

2) a) S. L. Beaucage and M. H. Caruthers, *Tetrahedron Lett.*, **23**, 1859 (1982); b) L. J. McBride and M. H. Caruthers, *ibid.*, **24**, 245 (1983); c) S. P. Adams, K. S. Kavka, E. J. Wykes, S. B. Holder, and G. R. Galluppi, *J. Am. Chem. Soc.*, **105**, 661 (1983); d) N. D. Sinha, J. Biernat, and H. Köster, *Tetrahedron Lett.*, **24**, 5843 (1983).

3) a) V. A. Efimov, S. V. Reverdatto, and O. G. Chakhmakhcheva, *Nucleic Acids Res.*, **10**, 6675 (1982); b) V. A. Efimov, S. V. Reverdatto, and O. G. Chakhmakhcheva, *Tetrahedron Lett.*, **23**, 961 (1982); c) V. A. Efimov, A. A. Buryakova, S. V. Reverdatto, O. G. Chakhmakhcheva, and Yu. A. Ovchinnikov, *Nucleic Acids Res.*, **11**, 8369 (1983).

4) V. A. Efimov, O. G. Chakhmakhcheva, and Yu. A. Ovchinnikov, *Nucleic Acids Res.*, **13**, 3651 (1985).

5) J. Matsuzaki, H. Hotoda, M. Sekine, and T. Hata,

Tetrahedron Lett., **25**, 4019 (1984).

6) K. K. Ogilvie, M. J. Nemer, G. H. Hakimelahi, Z. A. Proba, and M. Lucas, *Tetrahedron Lett.*, **23**, 2615 (1982).

7) T. P. Patel, M. A. Chauncey, T. A. Millican, C. C. Bose, and M. A. W. Eaton, *Nucleic Acids Res.*, **12**, 6853 (1984).

8) M. Sekine, N. Masuda, and T. Hata, *Tetrahedron*, **41**, 5445 (1985).

9) a) G. R. Gough, M. J. Brunden, and P. T. Gilham, *Tetrahedron Lett.*, **22**, 4177 (1981); b) H. Köster, A. Stumpe, and A. Wolter, *ibid.*, **24**, 747 (1983); c) B. S. Sproat and W. Bannwarth, *ibid.*, **24**, 5771 (1983); d) N. D. Sinha, J. Biernat, and H. Köster, *ibid.*, **24**, 5843 (1983); e) S. L. Beaucage, *ibid.*, **25**, 375 (1984); f) C. Claesen, G. I. Tesser, C. E. Dreef, J. E. Marugg, G. A. van der Marel, and J. H. van Boom, *ibid.*, **25**, 1307 (1984); g) W. J. Stec and G. Zon, *ibid.*, **25**, 5275 (1984); h) **25**, 5279 (1984); i) N. D. Sinha, J. Biernat, J. McManus, and H. Köster, *Nucleic Acids Res.*, **12**, 4539 (1984); j) R. T. Pon and K. K. Ogilvie, *Nucleosides & Nucleotides*, **3**, 485 (1984); k) C. Minganti, K. N. Ganesh, B. S. Sproat, M. J. Gait, *Anal. Biochem.*, **147**, 63 (1985); l) R. T. Pon, M. J. Damha, and K. K. Ogilvie, *Tetrahedron Lett.*, **26**, 2525 (1985); m) P. T. Pon, M. J. Damha, and K. K. Ogilvie, *Nucleic Acids Res.*, **13**, 6447 (1985).

10) K. Miyoshi, T. Miyake, T. Hozumi, and K. Itakura, *Nucleic Acids Res.*, **8**, 5473 (1980).

11) a) B. C. Froehler and M. D. Matteucci, *Tetrahedron Lett.*, **24**, 3171 (1984); b) W. G. Finnegan, R. A. Henry, and R. Lofguist, *J. Am. Chem. Soc.*, **80**, 3908 (1958).

12) a) T. Kamimura, M. Tsuchiya, K. Koura, M. Sekine, and T. Hata, *Tetrahedron Lett.*, **24**, 2775 (1983); b) T. Kamimura, K. Urakami, K. Koura, M. Sekine, K. Shinozaki, K. Miura, and T. Hata, *J. Am. Chem. Soc.*, **106**, 4552 (1984).

13) M. Sekine, J. Matsuzaki, and T. Hata, *Tetrahedron Lett.*, **23**, 5287 (1982).

14) R. Kierzek, H. Ito, R. Bhatt, and K. Itakura, *Tetrahedron Lett.*, **22**, 3761 (1981).

15) M. Sekine and T. Hata, *J. Org. Chem.*, **48**, 3011 (1983).

16) H. Köster, K. Kolikowski, T. Liese, W. Heikens, and V. Kohli, *Tetrahedron*, **37**, 363 (1981).

17) H. Schaller, G. Weimann, B. Lerch, and H. G. Khorana, *J. Am. Chem. Soc.*, **85**, 3821 (1965).

Syntheses and Properties of α-Alkyl-Substituted Bisdehydroaza[14]-annulenes and the Related Benzannelated Derivatives

Jūro Ojima,* Yasuhiro Yagi, Emiko Ejiri, Shuichi Ishizaka, and Tadahito Kato
Department of Chemistry, Faculty of Science, Toyama University, Gofuku, Toyama 930
(Received January 22, 1986)

14-Ethoxy-2,5,10-trimethyl-6,8-bisdehydroaza[14]annulene, 14-ethoxy-2-ethyl-5,10-dimethyl-6,8-bisdehydroaza-[14]annulene, 2-ethoxy-3,11-dimethyl-5,6-benzo-7,9-bisdehydroaza[14]annulene, and 2-ethoxy-11,14-dimethyl-5,6-benzo-7,9-bisdehydroaza[14]annulene were synthesized. Influence of α-alkyl substitution and benzannelation upon the skeleton of the bisdehydroaza[14]annulene ring system is discussed on the basis of ^{1}H NMR and UV spectra of these azaannulenes and their α-alkyl unsubstituted ones.

In a previous paper,[1] we reported the synthesis of the diatropic 14-ethoxy-5,10-dimethyl-6,8-bisdehydroaza-[14]annulene **1** and its benzannelated derivative **2** and showed that both the azaannulenes **1** and **2** proved to keep the conformations indicated between −60 to 60 °C, suggesting the rather high skeletal rigidity of **1** and **2**, in contrast to the cases of related 1,3-bisdehydro-[14]annulene series.[2]

This result as well as a prediction from molecular model led us to expect that the azaannulenes **1** and **2** might set α-alkyl substituent inside the ring properly. In order to investigate this possibility, it was decided to prepare α-alkyl derivatives of the compounds **1** and **2**. However, all the azaannulenes **3**—**6** obtained do not have α- or β-alkyl group inside the ring properly, by an analysis of their ^{1}H NMR spectra.[3]

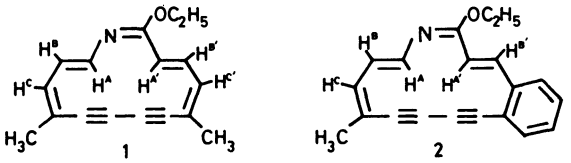

Results and Discussion

Synthesis. Aza[14]annulenes **3**—**6** were prepared by the same procedure to that for synthesis of compounds **1** and **2**.[1] Treatment of the trimethylbisdehydro[13]-annulenone (**7**)[4] with a large excess of hydroxyl-

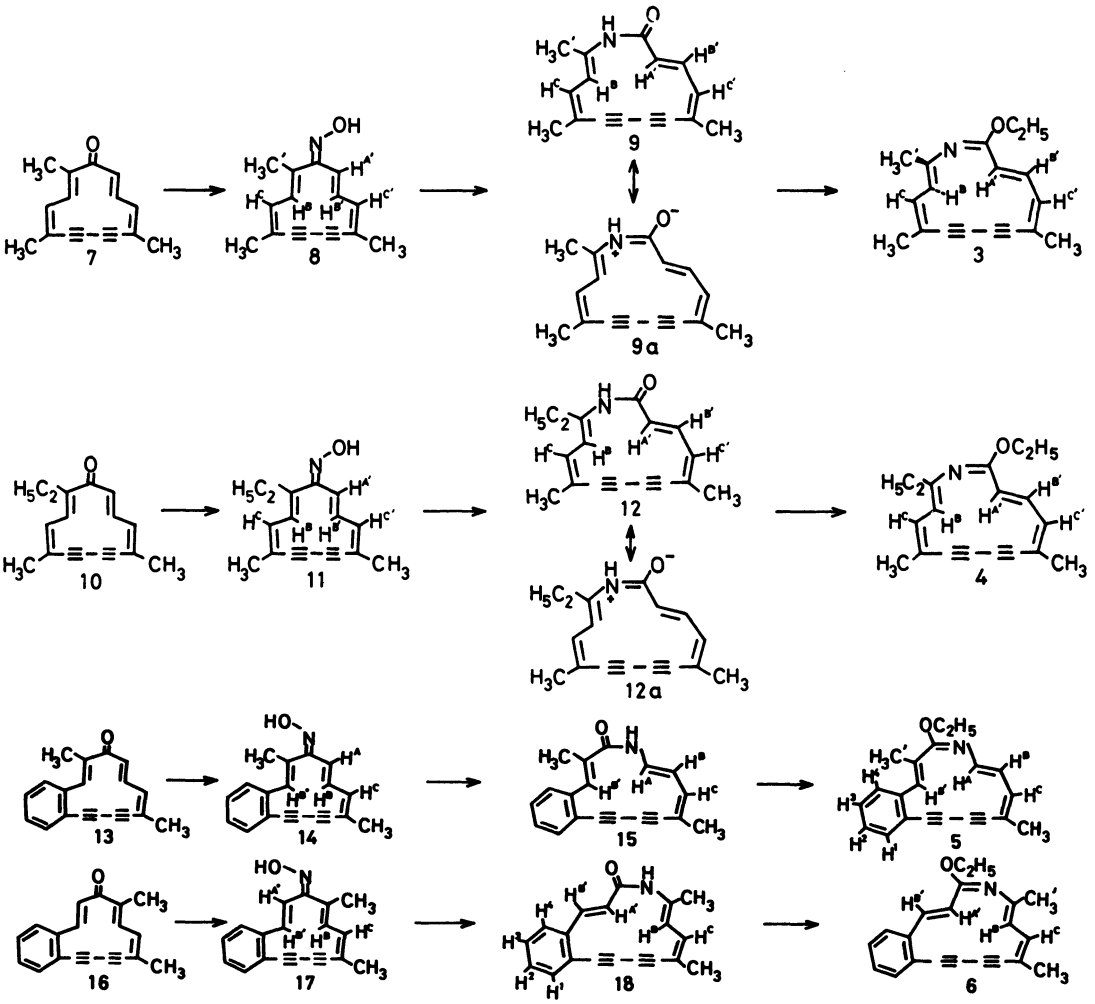

amine hydrochloride afforded only the isomer **8** of the two possible stereoisomeric oximes in 88% yield. The reaction of compound **8** with phosphorus pentachloride aroused Beckmann rearrangement to give the lactam **9** in 13% yield. The structure of compound **9** was determined by its ^{1}H NMR spectrum. Since Beckmann rearrangement is recognized to proceed usually in *anti*-migration with respect to hydroxyl group, the precursor of the lactam **9**, the oxime **8** should have the structure indicated.[5] The compound **9** reacted with a large excess of triethyloxonium tetrafluoroborate to yield the desired aza[14]annulene **3** in 38% yield. Similarly, the ethyldimethylbisdehydro[13]annulenone (**10**)[6] was led to the oxime **11** as a sole product in 52% yield, which was converted to the lactam **12** in 52% yield. Lactam **12** gave the azaannulene **4** in 14% yield. The dimethylbenzobisdehydro[13]annulenone (**13**)[4] was led to the oxime **14** (50%) as a sole product which was converted to the lactam **15** in 33% yield. The lactam **15** gave the benzazaannulene **5** in 10% yield. Thus, the formation of only the isomer **14** of the oxime from compound **13** prevented the possible preparation of an another α-methylated azaannulene, and instead led to the β-methylated one **5**. The oxime **17** (34%), obtained from the dimethylbenzobisdehydro[13]annulenone (**16**),[4] was led to the lactam **18** in 40% yield, which was

Table 1. ^{1}H NMR Chemical Shifts of **1**—**6** (in $CDCl_3$), and **1′**—**4′**, **6′** (CF_3COOD in $CDCl_3$) at 200 MHz, Determined at 21 °C (τ Value; internal standard, Me_4Si)

Compd	H^A	$H^{A'}$	H^B	$H^{B'}$	H^C	$H^{C'}$	$-OCH_2CH_3$	$-OCH_2CH_3$	CH_3	$CH_{3'}$	$-CH_2CH_3$	$-CH_2CH_3$	Benzenoid H
1[a]	6.25	7.06	2.99	2.19	2.62	2.70	5.40	8.51	7.49, 7.54				
1′[a]	(6.35)	(6.52)	(2.76)	(1.69)	(2.54)	(2.66)	(5.15)	(8.32)	(7.32), (7.52)				
3		4.99	6.04	2.55	2.93	3.22	5.74	8.63	7.79, 7.88	8.23			
3′		(4.29)	(4.18)	(2.36)	(3.19)	(3.19)	(5.29)	(8.45)	(7.76), (7.87)	(8.53)			
4		5.40	6.71	2.37	2.69	3.15	5.72	8.67	7.75, 7.85		7.65	9.01	
4′		(4.39)	(4.58)	(2.33)	(3.14)	(3.18)	(5.31)	(8.46)	(7.76), (7.87)		(8.07)	(9.16)	
2[a]	3.84	4.46	3.52	2.11	3.10		5.50	8.52	7.78				2.16—2.55
2′[a]	(3.12—3.20)	(4.14)	(3.12—3.20)	(1.53)	(4.16)		(5.17)	(8.30)	(7.73)				(1.98—2.24)
5[b]	2.09		3.85	3.38	3.58		5.67	8.62	8.04	8.21			2.48—2.74
6		3.24	4.80	2.43	3.36		5.74	8.60	8.02	8.24			2.51—2.74
6′		(2.95)	(3.74)	(1.95)	(3.48)		(5.26)	(8.35)	(7.94)	(8.23)			(2.33—2.45)

a) See Ref. 1. b) Addition of deuteriotrifluoroacetic acid to a solution of **5** in $CDCl_3$ resulted in decomposition of a sample.

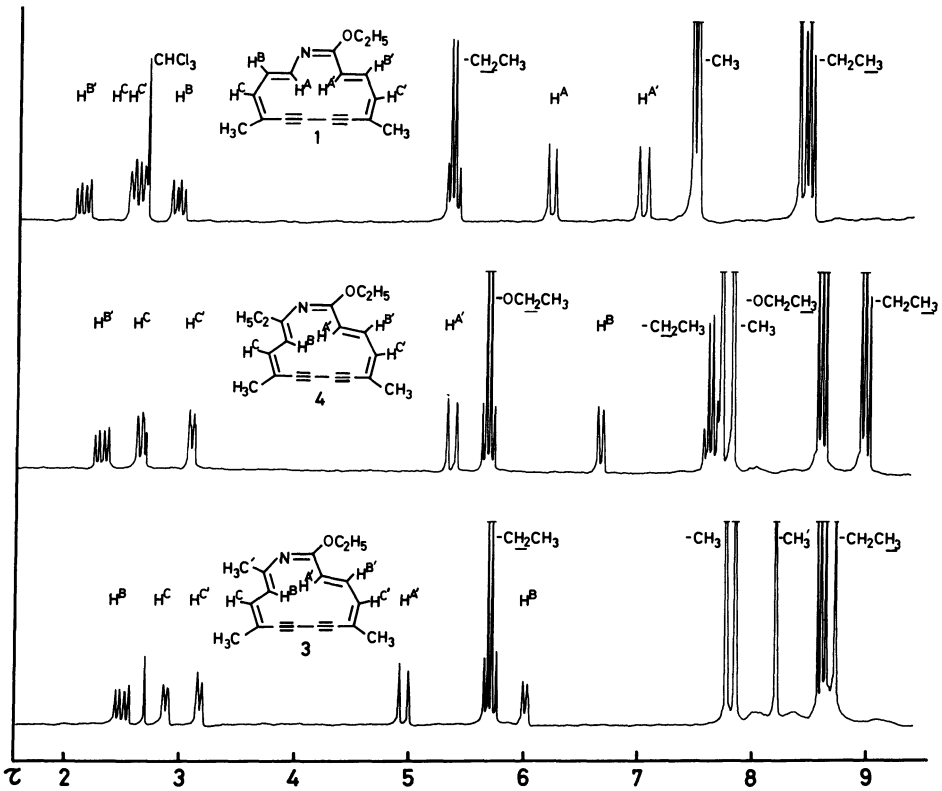

Fig. 1. The 200 MHz ^{1}H NMR spectra of **1**, **3**, and **4** in $CDCl_3$ (internal standard, TMS).

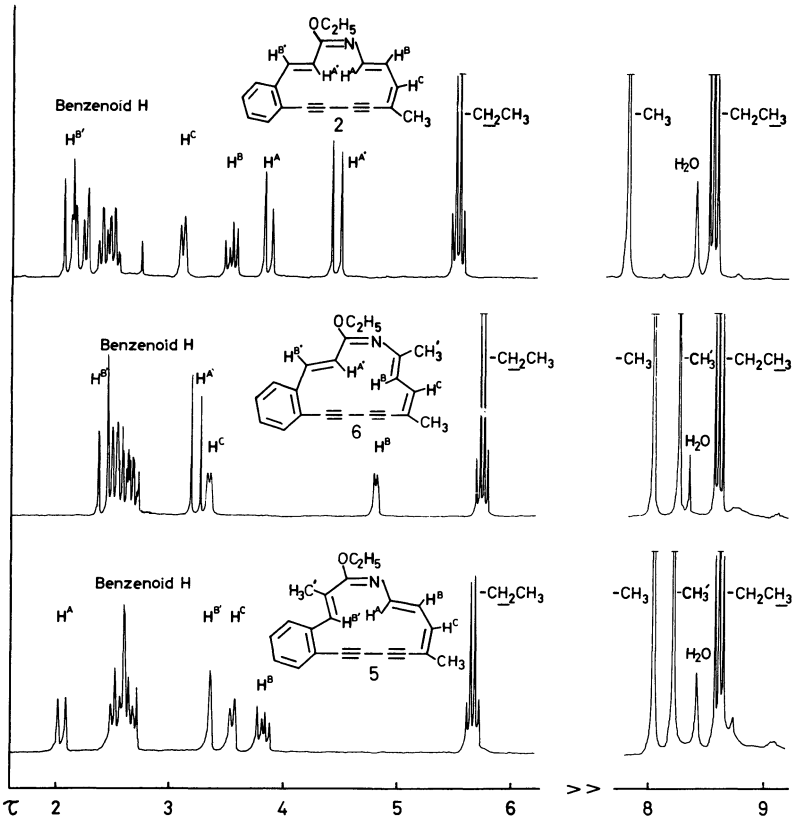

Fig. 2. The 200 MHz ^{1}H NMR spectra of **2**, **5**, and **6** in $CDCl_3$ (internal standard, TMS).

converted to the benzazaannulene **6** in 43% yield.

^{1}H NMR Spectra. The ^{1}H NMR chemical shifts of the azaannulenes **1**—**6** are listed in Table 1, and the spectra of the azaannulenes **1**, **3**, and **4** are shown in Fig. 1 and the spectra of the benzannelated azaannulenes **2**, **5**, and **6** are shown in Fig. 2. The assignments of the resonances in these azaannulenes are based on the multiplicities and coupling constants. As is seen from both the Table 1 and Fig. 1, it is noted that comparison of the chemical shift differences between the olefinic outer and inner protons which can be regarded as an approximate measure of tropicity, or of the chemical shifts of $-OC\underline{H}_2CH_3$ and CH_3 protons that the diatropicity of these azaannulenes decreases in the order of the dimethyl- **1**>the α-ethyl- **4**>the α-methyl-substituted azaannulene **3**, demonstrating that the perturbation caused by the α-alkyl substitution for the aza[14]annulene **1** greatly reduces the planarity of the molecular skeleton and it is larger in the α-methyl substitution than in the α-ethyl one. This also permits the safe conclusion that both **3** and **4** do not set their α-alkyl groups inside the ring properly.

The similar observation is made from comparison of the ^{1}H NMR chemical shifts (Table 1 and Fig. 2) of the benzannelated azaannulenes **2**, **5**, and **6**. Comparison of the chemical shifts of $-OC\underline{H}_2CH_3$ and CH_3 protons again indicates that the tropicity decreases in the order of benzaza- **2**>β-methylated benzaza- **6**>α-methylated benzazaannulene **5**, suggesting that the α- or β-methyl substitution in **2** reduces the planarity of the molecular skeleton. It eliminates the weak diatropicity of **2**,[1] rendering both **5** and **6** to be atropic.

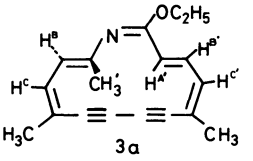

3a

Variable-temperature ^{1}H NMR spectra of these azaannulenes **1**—**6** were taken over the range of −60 to 60 °C and their chemical shifts are summarized in Table 2. As we see from Table 2, the spectra of **1** and **2** are essentially temperature-independent between these temperatures, although the resonances of the inner and outer protons of **1** and **2** move to a slightly higher and lower field, respectively, reflecting that the higher planarity of the azaannulene rings of **1** and **2** at lower temperature.[1] In contrast, the spectra of trimethylazaannulene **3** show temperature-dependency, as illustrated in Fig. 3. In particular, moving of the resonances of CH_3' and H^B proton toward higher and lower field, respectively, along with decreasing temperature, is notable. This fact as well as examination from molecular model leads us to believe the following. The molecule **3** exists in conformations such as **3** and **3a**, in which the vibrating CH_3'-C=CH^B

Table 2. ^{1}H NMR Chemical Shifts of Compounds **1—6** (In $CDCl_3$) at 90 MHz or 270 MHz (τ Value; internal standard, Me_4Si)

Compd	T/°C	H^A	$H^{A'}$	H^B	$H^{B'}$	H^C	$H^{C'}$	$-OCH_2CH_3$	$-OCH_2CH_3$	CH_3	CH_3'	$-CH_2CH_3$	$-CH_2CH_3$	H^4	H^1	H^2	H^3
1[a]	+60	6.18	6.97	3.03	2.24	2.64	2.72	5.38	8.52	7.50, 7.55							
	+23	6.25	7.06	3.02	2.20	2.63	2.71	5.41	8.52	7.50, 7.55							
	−30	6.35	7.16	3.01	2.16	2.62	2.69	5.45	8.51	7.50, 7.54							
	−60	6.40	7.21	3.02	2.15	2.61	2.68	5.48	8.51	7.48, 7.54							
2[a]	+60	3.78	4.37	3.53	2.12	3.11		5.48	8.53	7.79				2.16	2.27	2.39—2.55	
	+22	3.83	4.43	3.52	2.11	3.10		5.50	8.53	7.79				2.16	2.26	2.38—2.51	
	−30	3.91	4.50	3.52	2.09	3.09		5.54	8.52	7.79				2.14	2.24	2.36—2.51	
	−60	3.96	4.56	3.53	2.09	3.08		5.58	8.52	7.79				2.13	2.23	2.35—2.49	
3[b]	+60		5.01	6.11	2.55	2.93	3.24	5.73	8.64	7.81, 7.89	8.20						
	+22		5.00	6.06	2.55	2.94	3.23	5.74	8.63	7.80, 7.88	8.22						
	−30		4.86	5.77	2.58	2.98	3.22	5.77	8.60	7.79, 7.87	8.30						
	−60		4.73	5.52	2.63	3.12	3.24	5.78	8.58	7.79, 7.86	8.39						
4[b]	+60		5.38	6.71	2.38	2.71	3.16	5.71	8.64	7.77, 7.86		7.65	9.00				
	+23		5.41	6.71	2.37	2.71	3.15	5.72	8.63	7.75, 7.85		7.65	9.01				
	−30		5.37	6.62	2.39	2.69	3.13	5.74	8.61	7.74, 7.84		7.68	9.04				
	−60		5.28	6.50	2.39	2.75	3.13	5.76	8.59	7.74, 7.83		7.70	9.07				
5[b]	+60	2.07		3.87	3.43	3.59		5.67	8.64	8.06	8.22				2.51—2.87		
	+22	2.09		3.87	3.40	3.58		5.67	8.63	8.05	8.22				2.48—2.86		
	−30	2.13		3.85	3.28	3.54		5.68	8.59	8.02	8.23				2.45—2.82		
	−60	2.15		3.84	3.20	3.49		5.69	8.56	8.01	8.25				2.45—2.80		
6[b]	+60		3.25	4.84	2.40	3.35		5.72	8.60	8.02	8.22				2.44—2.80		
	+22		3.25	4.84	2.43	3.36		5.74	8.60	8.02	8.25				2.45—2.80		
	−30		3.24	4.72	2.50	3.42		5.78	8.60	8.03	8.31				2.45—2.80		
	−60		3.23	4.66	2.53	3.46		5.81	8.59	8.04	8.35				2.48—2.80		

a) At 270 MHz. b) At 90 MHz.

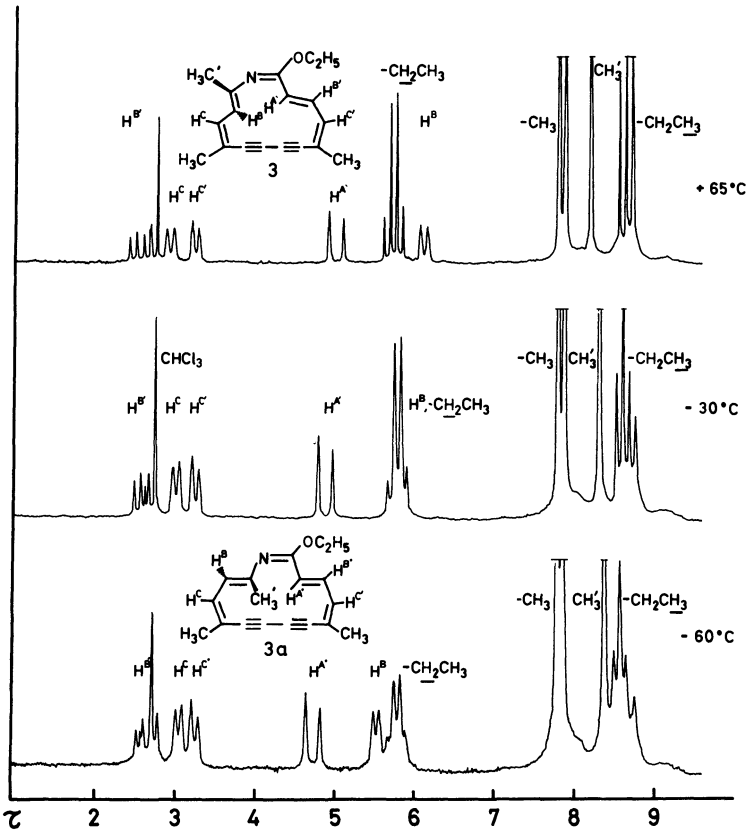

Fig. 3. The 90 MHz ^{1}H NMR spectra of **3** in $CDCl_3$ (internal standard, TMS).

Table 3. ^{1}H NMR Chemical Shifts of Lactams **9** and **12** at 200 MHz, Determined at 21 °C (τ Value; internal standard, Me_4Si)

Compd	$H^{A'}$	H^B	$H^{B'}$	H^C	$H^{C'}$	NH	CH_3	CH_3'	$-C\underline{H}_2CH_3$	$-CH_2C\underline{H}_3$
9	4.55	5.58	2.13	2.88	3.21	2.33	7.87, 7.91	7.79		
12	4.58	5.68	2.11	2.84	3.20	2.42	7.79, 7.91		5.01	8.85

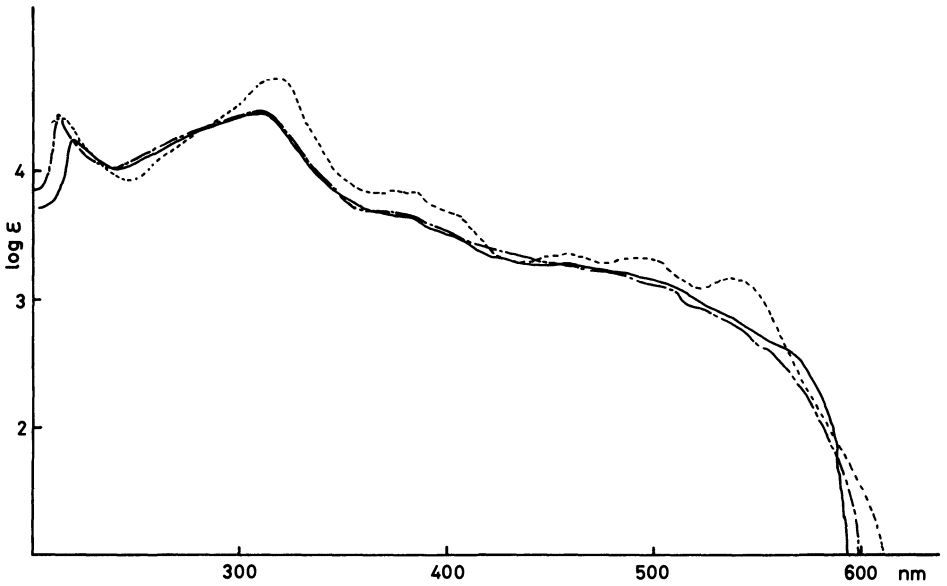

Fig. 4. Electronic spectra of **1** (------), **3** (—·—·—), and **4** (——) in THF.

moiety deviates from a molecular lane as depicted: The observed, relatively high-field, resonance of CH_3' protons and low-field resonance of H^B proton at −60 °C, suggests that the conformation **3a** is the preferred form at this temperature.

The similar behavior which is different from that for the cases of **1** and **2**, is observed in the variable-temperature spectra of **4**—**6** (Table 2), but the variation of their spectra is smaller than that of **3** between these temperatures. In the case of **4**, this might be attributable to the bulky α-ethyl group which hardly locates inside the ring, as compared with the case of **3**.

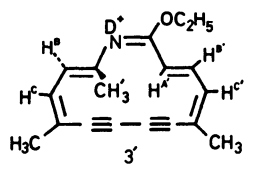

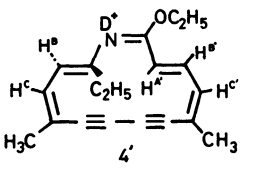

The ^{1}H NMR chemical shifts of the azaannulenes **1'**—**4'** and **6'**, taken in deuteriochloroform solution with a few drops of deuteriotrifluoroacetic acid, are also listed in Table 1. In these spectra, it is apparent that the resonances of almost all the protons including ethoxyl and methyl protons in these azaannulenes move to low field. This seems to be attributable to diminished π-electron perimeter, arising from withdrawal of electrons by deuteration. However, the movings of CH_3' and H^C protons in **3**, and of the CH_3, $-C\underline{H}_2CH_3$, and H^C protons in **4**, to high field, as compared with moving of the other protons in **3** and **4**, to low field, are rather large. This might also suggest that the CH_3'-C=CH^B-CH^C moiety in **3** and the C_2H_5-C=CH^B-CH^C one in **4** are mobile in their molecular perimeters. In particular, the high-field resonances of the CH_3' protons in the deuterated **3'** and the $-C\underline{H}_2CH_3$ and $-CH_2C\underline{H}_3$ protons in the deuterated **4'**, as compared with those of **3** and **4**, respectively, suggest that these deuterated species might exist in conformations indicated.

The ^{1}H NMR chemical shifts of the lactams **9** and **12**, which are the precursors of the azaannulenes **3** and **4**, respectively, are listed in Table 3. The fourteen-membered lactams **9** and **12** are also diatropic, since the inner $H^{A'}$ and H^B proton resonances appear at high field and the outer protons including CH_3, CH_3' protons in **9**, and $-C\underline{H}_2CH_3$, $-CH_2C\underline{H}_3$ protons in **12**, do at low field. Thus, the lactams **9** and **12** can be considered to exist in zwitter ionic forms **9a** and **12a**, as has been discussed previously.[1]

Electronic Spectra. The electronic absorption spectra, taken in tetrahydrofuran, of the bisdehydroaza-[14]annulenes **1**, **3**, and **4**, and of the benzannelated ones **2**, **5**, and **6** are illustrated in Figs. 4 and 5, respectively. As is seen from both Figs. 4 and 5, the longest wavelength band shift toward longer wavelength in the order of **1**>**4**>**3** (Fig. 4), **2**>**6**>**5** (Fig. 5), respectively, demonstrating the sequence for the degree of extended conjugation of π-electron system in these aza[14]annulene systems, conforming the results

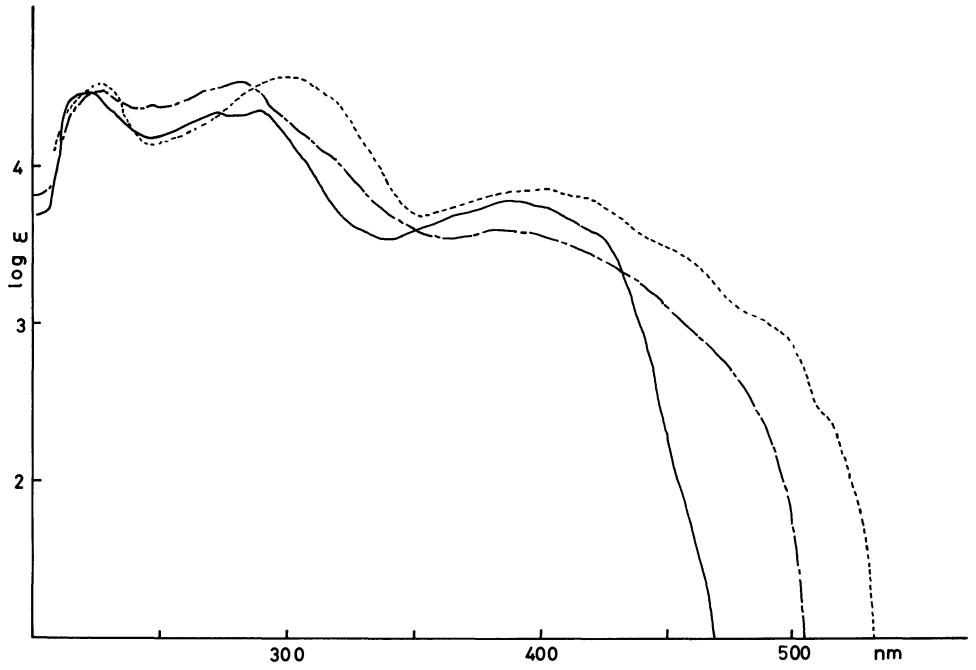

Fig. 5. Electronic spectra of **2** (------), **5** (——), and **6** (------) in THF.

from the ^{1}H NMR spectra.

All these results show that the conformation indicated for compound **1** is most appropriate for a conjugation of π-electrons in this bisdehydroaza[14]annulene system.

Experimental

All melting points are uncorrected. IR spectra were measured on Hitachi 260-50 spectrophotometer as KBr disk unless otherwise stated; only significant maxima are reported. Electronic spectra on Hitachi 220A spectrophotometer were measured in tetrahydrofuran solutions and recorded in nm. ε-Values are given in parentheses, shoulders being denoted by sh. Mass spectra were measured with JEOL JMS-200 spectrometer at 75 eV using a direct inlet system, ^{1}H NMR spectra were taken on JEOL FX-90Q (90 MHz) or Varian XL-200 spectrometer, and refer to solution in $CDCl_3$, unless otherwise specified, in τ-values with TMS as an internal standard. The coupling constants (J) are given in Hz. The individual assignments are made on the basis of multiplicities and coupling constants. Alumina (II–III) was used for column chromatography. Progress of most reactions was followed by TLC using Merck precoated alumina. Preparative TLC was carried out on 20×20 cm silica-gel plates (Merck, 0.5 or 2 mm thick). Dichloromethane was distilled over calcium hydride before use. Tetrahydrofuran (THF) was refluxed over potassium hydroxide pellets and distilled before use. Organic extracts with dichloromethane or chloroform were dried over anhyd calcium chloride prior to solvent removal.

1-Hydroxyimino-2,5,10-trimethylcyclotrideca-2,4,10,12-tetraene-6,8-diyne (8). To a stirred soln of the trimethylbisdehydro[13] annulenone (**7**)[4] (1.82 g, 8.20 mmol) in methanol (340 ml) and THF (85 ml) was added a soln of hydroxylamine hydrochloride (5.7 g, 82 mmol) in water (25 ml) at 38°C in one portion. After stirring for further 3 h at the same temp, further quantities of hydroxylamine hydrochloride (each 5.7 g in water (25 ml)) were added after every 10 h. After stirring for a total of 27 h, the soln was poured into an aq sodium hydrogencabonate soln. The mixture was extracted with chloroform. The combined extracts were washed with aq sodium chloride soln, dried, and evaporated. The residue after solvent removal was chromatographed on alumina (3.7×7 cm). The early fractions eluted with benzene gave the recovered annulenone **7** (64 mg). The following fractions eluted with 5% ethanol in chloroform gave the oxime **8** (1.71 g, 88%) as a solid. Recrystallization from hexane–chloroform afforded orange needles: Mp 164—165°C (decomp); MS m/z 237 (M^+, 89%) and 204 (100); mol wt 237.2; IR 3240 (-OH), 2170 (-C≡C-), and 980 cm^{-1} (trans C=C); UV_{max} 213 (29900), 275 (30900), and 350 nm sh (7740); ^{1}H NMR (90 MHz, DMSO-d_6) τ=−1.95 (s, 1H, OH, exchangeable with D_2O), 2.44 (d, 9, 1H, H^B), 2.45 (dd, 17, 9, 1H, $H^{B'}$), 2.99 (d, 10, 1H, $H^{C'}$), 3.23 (d, 10, 1H, H^C), 3.30 (d, 17, 1H, $H^{A'}$), 8.02 (s, 3H, CH_3'), and 8.18 (s, 6H, CH_3).

Found: C, 80.72; H, 6.22; N, 5.96%. Calcd for $C_{16}H_{15}NO$: C, 80.98; H, 6.37; N, 5.90%.

6,11,14-Trimethylazacyclotetradeca-3,5,11,13-tetraene-7,9-diyn-2-one (9). Phosphorus pentachloride (4.46 g, 21.4 mmol) was added in one portion to a stirred soln of the oxime **8** (1.01 g, 4.27 mmol) in THF (240 ml) at 1—3°C. After stirring for 4 h at the same temp, the soln was poured into water, and an aq sodium hydrogencarbonate soln was added (pH 8). The soln was warmed on a steam-bath, and then the mixture was extracted with chloroform. The combined extracts were washed with aq sodium hydrogencarbonate soln, and aq sodium chloride soln, and dried. The dark red semi-solid obtained after solvent removal was chromatographed on alumina (3.7×7.0 cm). The fractions eluted with 2% chloroform in benzene afforded the lactam **9** (129 mg, 13%) as a solid. Recrystallization from hexane–chloroform afforded dark red cubes: Mp 186—188°C (decomp); MS m/z 237 (M^+, 62%) and 194 (100); mol wt 237.2;

IR 3180, 3060 (NH), 2160 (-C≡C-), 1655 (C=O), 1605 and 1590 cm^{-1} (C=C); UV_{max} 298 sh (36700), 306 (38800), 365 sh (5330), and 436 nm (3280); ^1H NMR (200 MHz) τ=2.13 (dd, 15.5, 7.5, 1H, $H^{B'}$), 2.33 (br s, 1H, NH), 2.88 (d, 10, 1H, H^{C}), 3.21 (d, 7.5, 1H, $H^{C'}$), 4.55 (d, 15.5, 1H, $H^{A'}$), 5.58 (d, 10, 1H, H^{B}), 7.79 (s, 3H, CH_3'), 7.87 (s, 3H, CH_3), and 7.91 (s, 3H, CH_3).

Found: C, 81.09; H, 6.38; N, 5.93%. Calcd for $C_{16}H_{15}NO$: C, 80.98; H, 6.37; N, 5.90%.

14-Ethoxy-2,5,10-trimethyl-6,8-bisdehydroaza[14]annulene (3). To a stirred soln of the lactam **9** (93.4 mg, 0.394 mmol) in dichloromethane (50 ml) was added dropwise a soln of triethyloxonium tetrafluoroborate (2.2 g, 12 mmol) in dichloromethane (30 ml) during 30 min at room temp under argon. After stirring for 1 h, further quantities of the oxonium salt (each 1.5 g in dichloromethane (20 ml)) were added every day, and stirring was continued for 3 d. Then the soln was cooled in an ice-bath and aq 50% potassium carbonate soln (50 ml) was cautiously added. Then the mixture was poured into water and extracted with dichloromethane. The residue after solvent removal was chromatographed on alumina (3.7×6.0 cm). The initial fractions eluted with 5% ether in hexane gave the azaannulene **3** (39.2 mg, 37.5%) as a red liquid: MS *m/z* 265 (M^+, 54%) and 208 (100); mol wt 265.3; IR (neat) 2150 (-C≡C-), 1575 (C=C), 1290, 1255, and 1055 cm^{-1} (-O-); UV_{max} 277 sh (19200), 307 (26100), 386 sh (4030), 470 sh (1760), 511 sh (1160), and 553 nm sh (520), and see Fig. 4; ^1H NMR (200 MHz) τ=2.55 (dd, 16, 7, 1H, $H^{B'}$), 2.93 (d, 8, 1H, H^{C}), 3.22 (d, 7.5, 1H, $H^{C'}$), 4.99 (d, 16, 1H, $H^{A'}$), 5.74 (q, 7, 2H, $-OC\underline{H}_2CH_3$), 6.04 (d, 7.5, 1H, H^{B}), 7.79 (s, 3H, CH_3), 7.88 (s, 3H, CH_3), 8.23 (s, 3H, CH_3'), and 8.63 (t, 7, 3H, $-OCH_2C\underline{H}_3$), and see Figs. 1 and 3; **3'** (200 MHz, CF_3COOD in $CDCl_3$) τ=2.36 (dd, 16, 8, 1H, $H^{B'}$), 3.19 (d, 7.5, 2H, H^{C} and $H^{C'}$), 4.18 (s, 1H, H^{B}), 4.29 (d, 16, 1H, $H^{A'}$), 5.29 (q, 7, 2H, $-OC\underline{H}_2CH_3$), 7.76 (s, 3H, CH_3), 7.87 (s, 3H, CH_3), 8.45 (t, 7, 3H, $-OCH_2C\underline{H}_3$), and 8.53 (s, 3H, CH_3').

Found: C, 81.64; H, 7.50; N, 5.00%. Calcd for $C_{18}H_{19}NO$: C, 81.47; H, 7.22; N, 5.28%.

The later fractions eluted with chloroform gave the recovered lactam **9** (40 mg).

2-Ethyl-1-hydroxyimino-5,10-dimethylcyclotrideca-2,4,10,12-tetraene-6,8-diyne (11). To a stirred soln of the ethyldimethylbisdehydro[13]annulenone (**10**)[6] (1.24 g, 5.27 mmol) in methanol (150 ml) was added in one portion a soln of hydroxylamine hydrochloride (4.0 g, 5.8 mmol) in water (20 ml) was added. Then after stirring for 16 h, further quantities of hydroxylamine hydrochloride (each 4.0 g in water (20 ml)) were added after every 4 h. After stirring for a total of 34 h, the soln was worked up as in the preparation of **8**. The residue after solvent removal was chromatographed on alumina (4.0×7.5 cm). The early fractions eluted with benzene gave the recovered annulenone **10** (26 mg). The following fractions eluted with 2% ethanol in chloroform gave the oxime **11** (692 mg, 52%) as a solid. Recrystallization from hexane-chloroform afforded orange needles: Mp 155—156°C (decomp); MS *m/z* 251 (M^+, 84%) and 204 (100); mol wt 251.3; IR 3250 (-OH), 2170 (-C≡C-), 1000, and 990 cm^{-1} (trans C=C); UV_{max} 217 (20100), 274 (31000), and 351 nm sh (7200); ^1H NMR (90 MHz, DMSO-d_6) τ=−1.89 (s. 1H, OH, exchangeable with D_2O), 2.49 (dd, 17, 8.5, 1H, $H^{B'}$), 2.60 (d, 11, 1H, H^{B}), 3.03 (d, 10.3, 1H, H^{C}), 3.26 (d, 8.5, 1H, $H^{C'}$), 3.29 (d. 17, 1H, $H^{A'}$), 7.50 (q, 7.4, 2H, $-C\underline{H}_2CH_3$), 8.17 (s, 6H, CH_3), and 9.03 (t, 7.4, 3H, $-CH_2C\underline{H}_3$).

Found: C, 81.17; H, 6.92; N, 5.64%. Calcd for $C_{17}H_{17}NO$: C, 81.24; H, 6.82; N, 5.57%.

14-Ethyl-6,11-dimethylazacyclotetradeca-3,5,11,13-tetraene-7,9-diyn-2-one (12). A soln of phosphorus pentachloride (4.85 g, 23.3 mmol) in THF (330 ml) was added dropwise during 40 min to a stirred soln of the oxime **11** (1.17 g, 4.66 mmol) in THF (200 ml) under ice-bath. The soln was allowed to rise to room temp and stirring was continued for 3.5 h at same temp. Then the mixture was worked up as in the preparation of **9**. The residue after solvent removal was chromatographed on alumina (3.7×8.0 cm). The early fractions eluted with benzene-chloroform (2:3) gave the lactam **12** (610 mg, 52%) as a solid. Recrystallization from hexane-chloroform afforded red needles: Mp 189—191°C (decomp); MS *m/z* 251 (M^+, 75%) and 222 (100); mol wt 251.3; IR 3170, 3060 (NH), 2155 (-C≡C-), 1655 (C=O), 1600, and 1590 cm^{-1} (C=C); UV_{max} 218 (13800), 299 sh (28200), 307 (29900), and 441 nm sh (2500); ^1H NMR (200 MHz) τ=2.11 (dd, 15, 7, 1H, $H^{B'}$), 2.42 (br s, 1H, NH), 2.84 (d, 10, 1H, H^{C}), 3.20 (d, 6.4, 1H, $H^{C'}$), 4.58 (d, 15.7, 1H, $H^{A'}$), 5.68 (d, 10, 1H, H^{B}), 5.01 (q, 7.5, 2H, $-C\underline{H}_2CH_3$), 7.79 (s, 3H, CH_3), 7.91 (s, 3H, CH_3), and 8.85 (t, 7.5, 3H, $-CH_2C\underline{H}_3$).

Found: C, 81.31; H, 6.78; N, 5.33%. Calcd for $C_{17}H_{17}NO$: C, 81.24; H, 6.82; N, 5.57%.

The later fractions eluted with 5% ethanol in chloroform afforded the recovered oxime **11** (139 mg).

14-Ethoxy-2-ethyl-5,10-dimethyl-6,8-bisdehydroaza[14]annulene (4). To a stirred soln of the lactam **12** (703 mg, 2.80 mmol) in dichloromethane (250 ml) was added dropwise a soln of triethyloxonium tetrafluoroborate (7.97 g, 42 mmol) in dichloromethane (80 ml) during 1 h at room temp. After stirring for a further 2.5 h, further quantities of the oxonium salt (each 10 g in dichloromethane (50 ml)) was added every 15 h. After stirring for a total of 48 h, the mixture was worked up as in the preparation of **3**. The residue after solvent removal was chromatographed on alumina (3.7×8.0 cm). The early fractions eluted with 3% ether in hexane gave a red liquid, which was further purified by preparative TLC. The fast moving, red band on evaporation afforded the azaannulene **4** (111 mg, 14.2%) as a red liquid: MS *m/z* 279 (M^+, 51%) and 222 (100); mol wt 279.3; IR (neat) 2140 (-C≡C-), 1575 (C=C), 1290, 1250, and 1050 cm^{-1} (-O-); UV_{max} 219 (17100), 298 sh (27700), 308 (30900), 383 sh (4200), and 422 nm sh (1940), and see Fig. 4; ^1H NMR (200 MHz) τ=2.37 (dd, 15.5, 7.5, 1H, $H^{B'}$), 2.69 (d, 9, 1H, H^{C}), 3.15 (d, 7.5, 1H, $H^{C'}$), 5.40 (d, 15.5, 1H, $H^{A'}$), 5.72 (q, 7, 2H, $-OC\underline{H}_2CH_3$), 6.71 (d, 9, 1H, H^{B}), 7.65 (q, 7.5, 2H, $-C\underline{H}_2CH_3$), and 7.75 (s, 3H, CH_3), 7.85 (s, 3H, CH_3), 8.67 (t, 7, 3H, $-OCH_2C\underline{H}_3$), and 9.01 (t, 7.5, 3H, $-CH_2C\underline{H}_3$), and see Fig. 1; **4'** (200 MHz, CF_3COOD in $CDCl_3$) τ=2.33 (dd, 16, 8, 1H, $H^{B'}$), 3.14 (d, 5.5, 1H, H^{C}), 3.18 (d, 8, 1H, $H^{C'}$), 4.39 (d, 15.5, 1H, $H^{A'}$), 4.58 (d, 5.5, 1H, H^{B}), 5.31 (q, 7, 2H, $-OC\underline{H}_2CH_3$), 7.76 (s, 3H, CH_3), 7.87 (s, 3H, CH_3), 8.07 (q, 7.5, 2H, $-C\underline{H}_2CH_3$), 8.46 (t, 7, 3H, $-OCH_2C\underline{H}_3$), and 9.16 (t, 7.5, 3H, $-CH_2C\underline{H}_3$).

Found: C, 81.55; H, 7.88; N, 4.94%. Calcd for $C_{19}H_{21}NO$: C, 81.68; H, 7.58; N, 5.01%.

The later fractions eluted with chloroform gave the recovered lactam **12** (425 mg).

1-Hyroxyimino-2,10-dimethyl-4,5-benzocyclotrideca-2,10,12-triene-6,8-diyne (14). To a stirred soln of bisdehydrobenz-[13]annulenone (**13**)[4] (2.63 g, 10.2 mmol) in methanol (350 ml) and THF (200 ml) was added in one portion a soln of

hydroxylamine hydrochloride (14.2 g, 0.204 mmol) in water (30 ml) at room temp. After stirring for 13 h, further quantities of hydroxylamine hydrochloride (each 7.1 g in water (30 ml)) were added after every 5 h. After for a total of 27 h at 40 °C, the mixture was worked up as in the preparation of **8**. The residue after solvent removal was chromatographed on alumina (4.5×7.0 cm). The early fractions eluted with benzene gave the recovered annulenone **13** (26 mg). The following fractions eluted with benzene–chloroform (1:1) gave the oxime **14** (1.64 g, 59%) as a solid. Recrystallization from hexane–chloroform afforded yellow plates: Mp 160—162 °C (decomp); MS *m/z* 273 (M^+, 40%) and 258 (100); mol wt 273.2; IR 3250 (-OH), 2180 (-C≡C-), and 975 cm^{-1} (trans C=C); UV_{max} 225 (34100), 253 sh (25000), 266 (37800), 279 (47100), 328 sh (5820), 350 sh (7650), 371 (9460), and 392 nm sh (7520); ^1H NMR (90 MHz, DMSO-d_6) τ=−1.44 (s, 1H, OH, exchangeable with D_2O), 2.50 (dd, 16, 11, 1H, H^B), 2.42—2.80 (m, 4H, benzenoid H), 3.09 (d, 10, 1H, H^C), 3.49 (s, 1H, $H^{B'}$), 3.57 (d, 16, 1H, H^A), and 8.20 (s, 6H, CH_3).

Found: C, 83.47; H, 5.54; N, 5.41%. Calcd for $C_{19}H_{15}NO$: C, 83.49; H, 5.53; N, 5.13%.

3,11-Dimethyl-5,6-benzazacyclotetradeca-3,5,11,13-tetraene-7,9-diyn-2-one (15). A soln of phosphorus pentachloride (2.20 g, 10.6 mmol) in THF (120 ml) was added dropwise to a stirred soln of the oxime **14** (580 mg, 2.1 mmol) in THF (60 ml) during 40 min at 5 °C. After stirring for 3 h at room temp a soln of phosphorus pentachloride (0.35 g, 2.0 mmol) in THF (8 ml) was further added and the soln was stirred for a further 2 h. Then the soln was worked up as in the preparation of **9**. The residue after solvent removal was chromatographed on alumina (4.0×8.0 cm). The early fractions eluted with benzene–chloroform (1:1) gave the lactam **15** (195 mg, 33%) as a solid. Recrystallization from hexane–chloroform afforded yellow needles: Mp 220—222 °C (decomp); MS *m/z* 273 (M^+, 55%) and 230 (100); mol wt 273.3; IR 3180, 3070 (NH), 2220 (-C≡C-), 1650 (C=O), and 960 cm^{-1} (trans C=C); UV_{max} 257 sh (20900), 272 (28800), 286 (30700), 326 sh (4650), 388 (6980), and 422 nm sh (4650); ^1H NMR (200 MHz, DMSO-d_6) τ=−0.20 (d, 11, 1H, NH), 2.25 (dd, 14, 11, 1H, H^A), 2.37—2.61 (m, 4H, benzenoid H), 3.18 (s, 1H, $H^{B'}$), 3.58 (d, 8, 1H, H^C), 4.31 (dd, 14, 8, 1H, H^B), 8.13 (s, 3H, CH_3), and 8.24 (s, 3H, CH_3).

Found: C, 83.40; H, 5.44; N, 5.41%. Calcd for $C_{19}H_{15}NO$: C, 83.49; H, 5.53; N, 5.13%.

The later fractions eluted with chloroform gave the recovered oxime **14** (22 mg).

2-Ethoxy-3,11-dimethyl-5,6-benzo-7,9-bisdehydroaza[14]-annulene (5). A soln of triethyloxonium tetrafluoroborate (2.43 g, 12.8 mmol) in dichloromethane (30 ml) was added during 30 min dropwise to a soln of the lactam **15** (349 mg, 1.28 mmol) in dichloromethane (50 ml) at room temp under argon. After stirring for 15 h, the soln was worked up as in the preparation of **3**. The residue after solvent removal was chromatographed on alumina (3.7×7.0 cm). The fractions eluted with 10% ether in hexane gave the azaannulene **5** (39.8 mg, 10.3%) as a solid. Recrystallization from benzene afforded pale yellow needles: Mp 86.0—86.5 °C; MS *m/z* 301 (M^+, 64%) and 244 (100); mol wt 301.3; IR 2195 (-C≡C-), 1615, 1595 (C=C), 1295, 1270, and 1020 cm^{-1} (-O-); UV_{max} 260 sh (17700), 274 (21500), 288 (21800), 364 sh (4670), 387 (5420), and 418 nm sh (3940), and see Fig. 5; ^1H NMR (200 MHz) τ=2.09 (d, 13, 1H, H^A), 2.53 (d, 7.3, 1H, H^4), 2.59—2.74 (m, 3H, H^1, H^2, and H^3), 3.38 (s, 1H, $H^{B'}$), 3.58 (d, 8, 1H, H^C), 3.85 (dd, 13.5, 8, 1H, H^B), 5.67 (q, 7, 2H, $-OCH_2CH_3$), 8.04 (s, 3H, CH_3), 8.21 (s, 3H, CH_3'), and 8.62 (t, 7, 3H, $-OCH_2CH_3$).

Found: C, 83.73; H, 6.60; N, 4.72%. Calcd for $C_{21}H_{19}NO$: C, 83.69; H, 6.35; N, 4.65%.

1-Hydroxyimino-10,13-dimethyl-4,5-benzotrideca-2,10,12-triene-6,8-diyne (17). To a stirred soln of bisdehydrobenzo-[13]annulenone (**16**)[4] (1.62 g, 6.27 mmol) in methanol (180 ml) and THF (100 ml) was added in one portion a soln of hydroxylamine hydrochloride (4.50 g, 65 mmol) in water (10 ml) at room temp. After stirring for 13 h at the same temp, a further quantity of hydroxylamine hydrochloride (13.5 g) in water (30 ml) was added, and stirring was continued for further 15 h. The soln was then warmed to 38—39 °C and was stirred for further 7 h. Then the soln was worked up as in the preparation of **8**. After solvent removal, the residue was chromatographed on alumina (4.2×8.0 cm). The early fractions eluted with 3% ethanol in chloroform gave the oxime **17** (577 mg, 34%) as a solid. Recrystallization from hexane–chloroform afforded yellow needles: Mp 204—206 °C (decomp); MS *m/z* 273 (M^+, 88%) and 256 (100); mol wt 273.2; IR 3250 (-OH), 2180 (-C≡C-), and 980 cm^{-1} (trans C=C); UV_{max} 225 (30300), 272 (36300), 281 sh (35800), 380 (5460), and 412 nm sh (4140); ^1H NMR (90 MHz, DMSO-d_6) τ=−1.87 (s, 1H, OH, exchangeable with D_2O), 2.45 (d, 10.5, 1H, H^B), 2.61 (d, 17, 1H, $H^{B'}$), 2.52—2.75 (m, 4H, benzenoid H), 2.90 (d, 10.5, 1H, H^C), 3.15 (d, 17, 1H, $H^{A'}$), 7.98 (s, 3H, CH_3), and 8.16 (s, 3H, CH_3).

Found: C, 83.28; H, 5.42; N, 5.20%. Calcd for $C_{19}H_{15}NO$: C, 83.49; H, 5.53; N, 5.13%.

11,14-Dimethyl-5,6-benzazacyclotetradeca-3,5,11,13-tetraene-7,9-diyn-2-one (18). A soln of phosphorus pentachloride (2.63 g, 2.23 mmol) in THF (210 ml) was added to a stirred soln of the oxime **17** (869 mg, 3.18 mmol) in THF (150 ml) during 1 h under ice-bath. After stirring for 5 h at room temp the mixture was worked up as in the preparation of **9**. The residue after solvent removal was chromatographed on alumina (4.2×7.0 cm). The early fractions eluted with benzene–chloroform (1:1) gave the lactam **18** (346 mg, 39.8%) as a solid. Recrystallization from hexane–chloroform afforded orange needles: Mp 210—212 °C (decomp); MS *m/z* 273 (M^+, 84%) and 244 (100); mol wt 273.3; IR 3190, 3060 (NH), 2190 (-C≡C-), 1660 (C=O), and 980 cm^{-1} (trans C=C); UV_{max} 227 (28600), 268 sh (26200), 281 (32300), 295 sh (26300), 300 sh (23900), and 379 nm (7160); ^1H NMR (200 MHz, DMSO-d_6) τ=0.37 (s, 1H, NH), 1.90 (d, 16, 1H, $H^{B'}$), 2.21 (d, 7.7, 1H, H^4), 2.31 (d, 7.3, 1H, H^1), 2.30—2.48 (m, 2H, H^2 and H^3), 2.88 (d, 8.5, 1H, H^C), 3.53 (d, 16, 1H, $H^{A'}$), 4.77 (d, 8.5, 1H, H^B), 8.02 (s, 3H, CH_3), and 8.03 (s, 3H, CH_3).

Found: C, 83.19; H, 5.51; N, 5.25%. Calcd for $C_{19}H_{15}NO$: C, 83.49; H, 5.53; N, 5.13%.

The later fractions eluted with chloroform gave the recovered oxime **17** (166 mg).

2-Ethoxy-11,14-dimethyl-5,6-benzo-7,9-bisdehydroaza[14]-annulene (6). To a stirred soln of the lactam **18** (336 mg, 1.23 mmol) in dichloromethane (50 ml) was added dropwise a soln of triethyloxonium tetrafluoroborate (2.33 g, 12.3 mmol) in dichloromethane (30 ml) during 1 h at room temp under argon. After stirring for 2 h, a further quantity of the oxonium salt (1.2 g) in dichloromethane (20 ml) was added, and stirring was continued for further 8.5 h at room temp. Then the reaction mixture was worked up as in the preparation of **3**. The residue after removal of solvent was chromatographed on alumina (3.7×6.5 cm). The ini-

tial fractions eluted with 2% ether in hexane gave the azaannulene **6** (159 mg, 43%) as a solid. Recrystallization from hexane–benzene afforded orange plates: Mp 100—101 °C; MS *m/z* 301 (M^+, 75%) and 244 (100); mol wt 301.3; IR 2190, 2110 (-C≡C-), 1595 (C=C), 1250, 1050 (-O-), 975, and 960 cm^{-1} (trans C=C); UV_{max} 228 (29400), 245 sh (23800), 271 sh (30800), 281 (34200), 322 sh (9860), and 386 nm (3830), and see Fig. 5; ^1H NMR (200 MHz) τ=2.43 (d, 16, 1H, $H^{B'}$), 2.51—2.74 (m, 4H, benzenoid H), 3.24 (d, 16, 1H, $H^{A'}$), 3.36 (d, 5.5, 1H, H^{C}), 4.80 (d, 5.5, 1H, H^{B}), 5.74 (q, 7, 2H, $-OCH_2CH_3$), 8.02 (s, 3H, CH_3), 8.24 (s, 3H, CH_3'), and 8.60 (t, 7, 3H, $-OCH_2CH_3$), (200 MHz, CF_3COOD in $CDCl_3$) τ=1.95 (d, 16, 1H, $H^{B'}$), 2.33—2.45 (m, 4H, benzenoid H), 2.95 (d, 16, 1H, $H^{A'}$) 3.48 (s, 1H, H^{C}), 3.74 (s, 1H, H^{B}), 5.26 (q, 7, 2H, $-OCH_2CH_3$), 7.94 (s, 3H, CH_3), 8.23 (s, 3H, CH_3), and 8.35 (t, 7, 3H, $-OCH_2CH_3$).

Found: C, 83.91; H, 6.42; N, 4.76%. Calcd for $C_{21}H_{19}NO$: C, 83.69; H, 6.35; N, 4.65%.

The later fractions eluted with 5% ethanol in chloroform gave the recovered lactam **18** (192 mg).

This work was financially supported by a Grant-in-Aid No. 60540324 for Scientific Research from the Ministry of Education, Science and Culture.

References

1) a) J. Ojima, T. Nakada, M. Nakamura, and E. Ejiri, *Tetrahedron Lett.*, **26**, 635 (1985); b) J. Ojima, T. Nakada, E. Ejiri, and M. Nakamura, *J. Chem. Soc., Perkin Trans. 1*, in press.

2) R. T. Weavers and F. Sondheimer, *Angew. Chem.*, **86**, 167 (1974).

3) A part of this work has appeared as a preliminary form, J. Ojima, Y. Yagi, T. Nakada, S. Manaka, E. Ejiri, S. Ishizaka, and Y. Shiraiwa, *Chem. Lett.*, **1985**, 1767.

4) J. Ojima and M. Fujiyoshi, *J. Chem. Soc., Perkin Trans. 1*, **1980**, 466.

5) The structural determination of all the oximes described in this paper was made from examination of the structures of the subsequent lactams, on the basis of an assumption that all Beckmann rearrangements proceeded in *anti*-migration with respect to hydroxyl group; see L. G. Donaruna and W. L. Heldt, *Org. React.*, **11**, 1 (1960), and see also Ref. 1.

6) J. Ojima, Y. Juni, Y. Yoneyama, K. Wada, and Y. Murosawa, *Bull. Chem. Soc. Jpn.*, **54**, 3466 (1981).

 © 1986 The Chemical Society of Japan Bull. Chem. Soc. Jpn., 59, 1801—1807 (1986)

Syntheses and Properties of Two Ethoxytrimethylbisdehydroaza-[16]annulenes and Ethoxytrimethylbisdehydroaza[18]annulene

Jūro Ojima,* Yasuhiro Yagi, Sumio Manaka, Tetsuya Nakada, and Yasunao Shiraiwa
Department of Chemistry, Faculty of Science, Toyama University, Gofuku, Toyama 930
(Received January 22, 1986)

Syntheses of 2-ethoxy-3,6,11-trimethyl-7,9-bisdehydroaza[16]annulene, 2-ethoxy-6,11,16-trimethyl-7,9-bisdehydroaza[16]annulene, and 18-ethoxy-2,7,12-trimethyl-8,10-bisdehydroaza[18]annulene are described. It was found that the molecular skeletons of these α- or β-methylated aza[16]- and -[18]annulene are less planar than those of α- or β-methyl unsubstituted aza[16]- and aza[18]annulene, from examination of their ^{1}H NMR and electronic spectra.

In the previous paper, we have reported the synthesis of the paratropic dimethylbisdehydroaza[16]annulene (**1**) and the diatropic dimethylbisdehydroaza[18]-annulene (**2**).[1] In the preceding paper, we showed that the diatropicity, i.e., the planarity of the aza[14]annulene ring system decreases in the sequence of **3**> **5**>**4** on the basis of the chemical shifts of the olefinic protons. Also, the dimethylaza[14]annulene **3** can not set the α-alkyl group inside the ring and the trimethylaza[14]annulene **4** is a conformationally mobile molecule.[2]

Bearing these results in mind, we were interested in examining the properties of the higher analogs of the trimethylaza[14]annulene (**4**), and we expected that the aza[16]annulene **1** and the aza[18]annulene **2** with a larger π-electron cavity than the aza[14]annulene **3** might have the α-methyl group inside the ring. This paper is concerned with the syntheses and properties of the title compounds **6**—**8**, as well as comparison of the properties of **1** and **2**.[3]

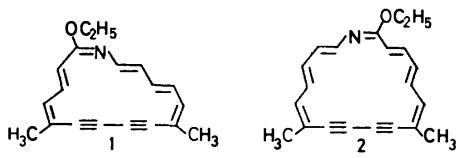

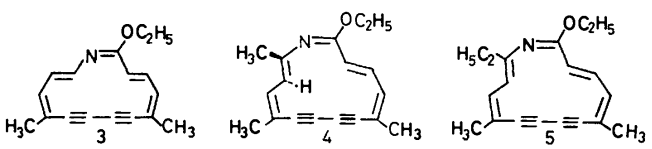

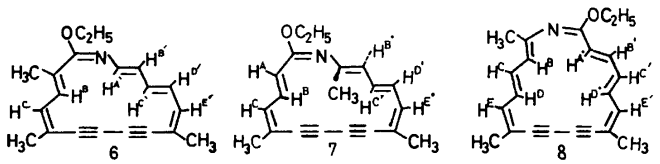

Results and Discussion

Synthesis. Synthesis of the azaannulenes **6**—**8** was carried out by the same procedure as that used for **1** and **2**. Treatment of the trimethylbisdehydro[15]annulenone (**9**)[4] with a large excess of hydroxylamine hydrochloride afforded only the isomer **10**[5] of the desired oxime in 58% yield. The reaction of **10** with phosphorus pentachloride led to the lactam **11** in 45% yield, which was converted to the unstable aza[16]annulene **6** in 0.4% yield by the reaction with triethyloxonium tetrafluoroborate. Similarly, the trimethylbisdehydro[15]annulenone (**12**)[4] was led to the

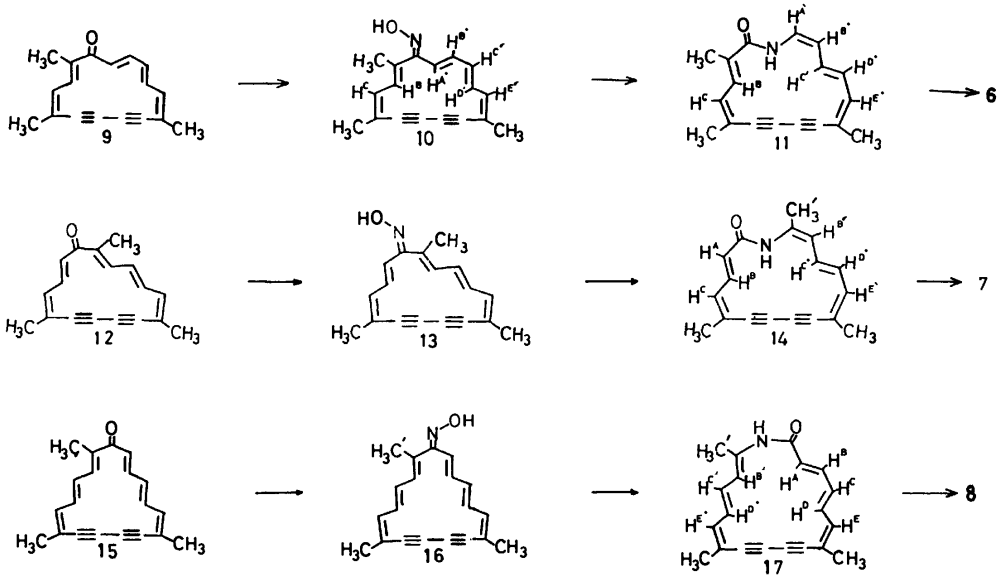

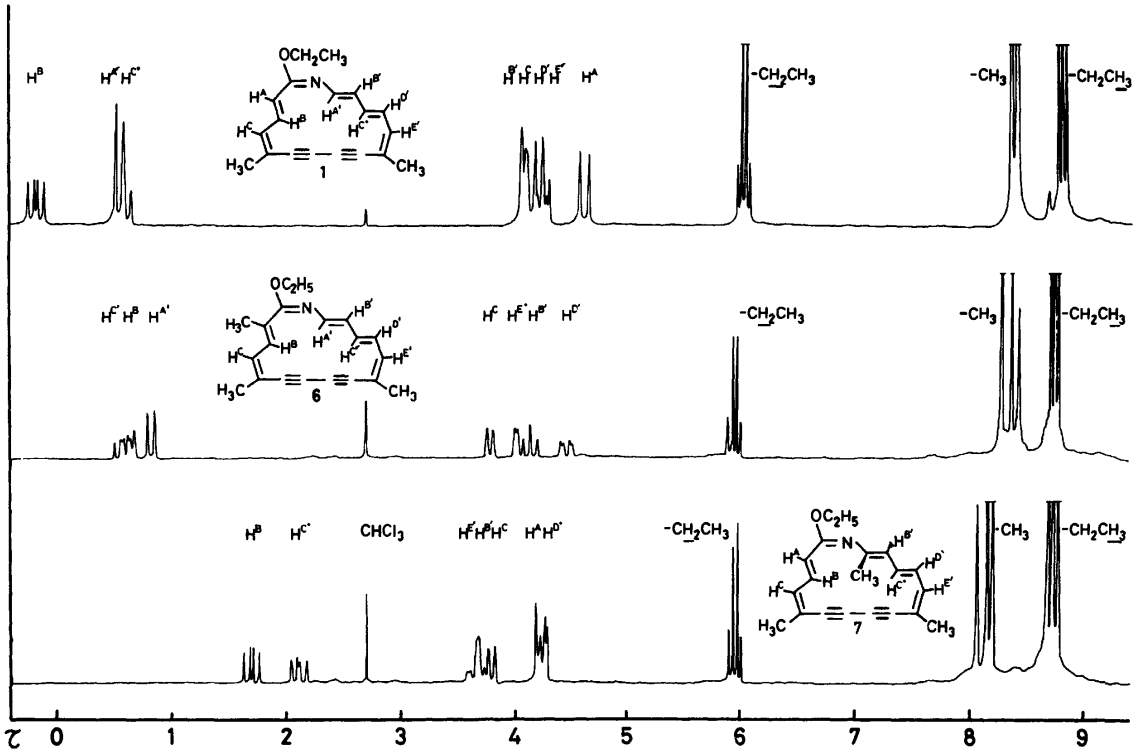

Fig. 1. The 200 MHz ^{1}H NMR spectra of the aza[16]annulenes **1**, **6**, and **7** in $CDCl_3$ (internal standard, TMS).

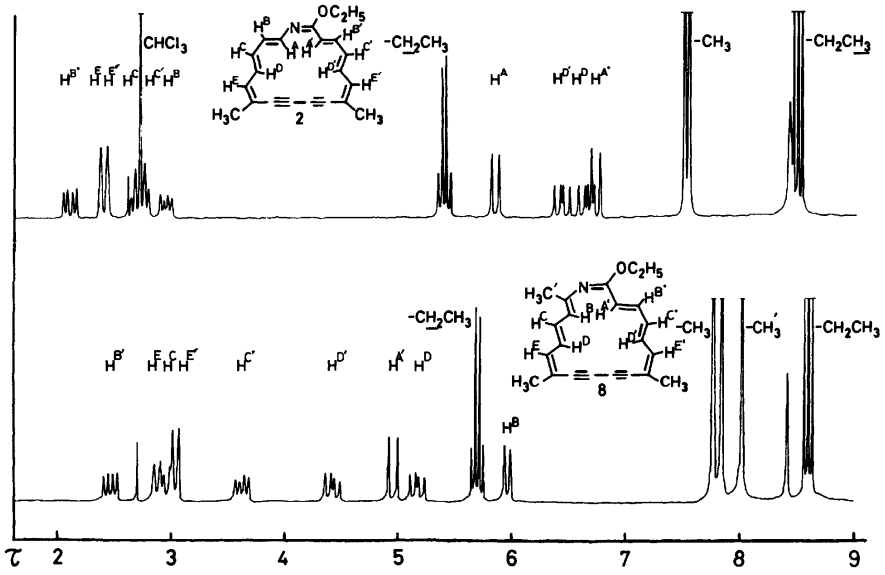

Fig. 2. The 200 MHz ^{1}H NMR spectra of the aza[18]annulenes **2** and **8** in $CDCl_3$ (internal standard, TMS).

oxime **13** (88%) as a sole product, which was converted to the lactam **14** in 47% yield. Lactam **14** gave the unstable aza[16]annulene **7** in 2.6% yield.

The oxime **16** (73%), obtained from the trimethylbisdehydro[17]annulenone (**15**)[6] was led to the lactam **17** in 46% yield, which was converted to the aza[18]annulene **8** as stable crystals in 11% yield.

^{1}H NMR Spectra. The ^{1}H NMR spectra of the trimethylaza[16]annulenes **6** and **7** are shown in Fig. 1, together with that of the dimethylaza[16]annulene **1**. The assignments of the resonances to the individual protons were made on the basis of multiplicities and coupling constants, and rigorously follow from decoupling experiments. Comparison of the chemical shift differences between the olefinic inner and outer protons indicate that the paratropicity of these azaannulenes decreases in the order of **1**>**6**>**7**, suggesting that the α-methyl substitution for the aza[16]annulene **1** greatly reduces the planarity of the molecular skeleton. This also indicates that the

Table 1. ^{1}H NMR Chemical Shifts of Aza[18]annulene **8** (In $CDCl_3$) at 90 MHz and **8′** (CF_3COOD in $CDCl_3$) at 200 MHz, Determined at 21 °C (τ Value: internal standard, Me_4Si)

T°/C	$H^{A'}$	H^{B}	$H^{B'}$	H^{C}	$H^{C'}$	H^{D}	$H^{D'}$	H^{E}	$H^{E'}$	$CH_{3'}$	CH_3	$-OCH_2CH_3$	$-OCH_2CH_3$
+60	4.96	5.95	2.54	3.05	3.67	5.16	4.43	2.95	3.10	8.05	7.81, 7.88	5.72	8.63
+25	4.99	5.99	2.51	3.04	3.66	5.20	4.47	2.91	3.08	8.04	7.79, 7.87	5.73	8.62
−30	5.06	6.08	2.44	2.95	3.65	5.29	4.55	2.86	3.02	8.01	7.79, 7.83	5.73	8.59
−60	5.13	6.15	2.44	2.92	3.63	5.35	4.58	2.86	3.02	8.01	7.77, 7.82	5.80	8.59
8′	5.46	5.74	1.84	3.05	3.91	5.25	3.78	2.75	2.92	7.87	7.64, 7.74	5.26	8.37

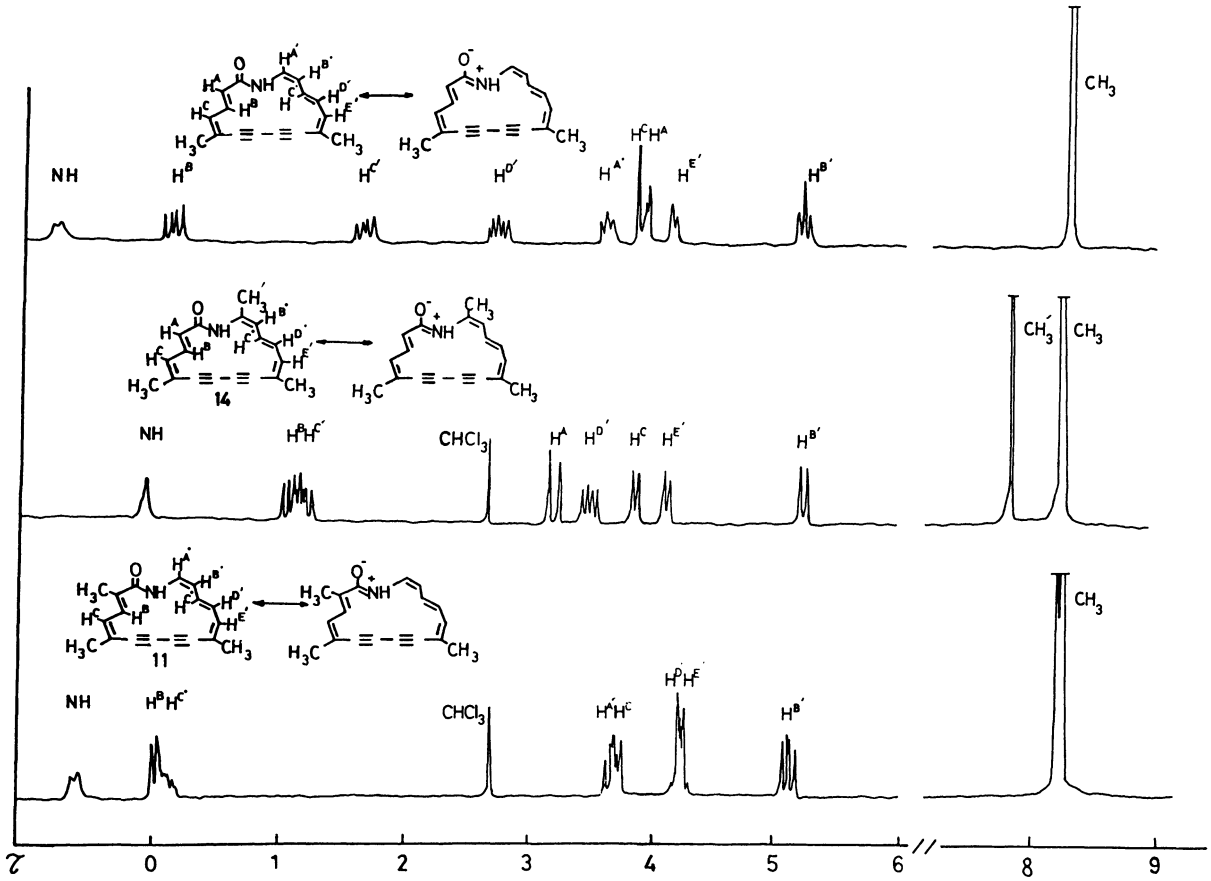

Fig. 3. The 200 MHz ^{1}H NMR spectra of the sixteen-membered lactams in $CDCl_3$ (internal standard, TMS).

trimethylaza[16]annulene **7** does not set the α-methyl group inside the ring properly. The extreme thermal unstability of **6** and **7**, as compared with **1**, might be due to low planarity of their molecular skeletons.

The ^{1}H NMR spectra of the dimethylaza[18]annulene **2** and the trimethylaza[18]annulene **8** are shown in Fig. 2. Comparison of the chemical shift differences of the olefinic inner and outer protons or of the chemical shifts of $-OCH_2CH_3$ and CH_3 protons between **8** and **2** indicates that the diatropicity of **8** is smaller than that of **2**. This again suggests that the perturbation caused by α-methyl substitution for the aza[18]annulene **2** changes the configuration and reduces the planarity of the molecular skeleton. It also indicates that the α-methyl group of **8** does not locate inside the ring.

Variable-temperature ^{1}H NMR spectra of the trimethylaza[18]annulene **8** were taken at 90 MHz over the range of −60 to 60 °C, and the chemical shifts of the protons are listed in Table 1. As we see from Table 1, the spectra of **8** which is the higher analog of the conformationally mobile trimethylaza[14]annulene **4**,[2] proved to be essentially temperature-independent between these temperatures. Thus, no notable change around the potentially mobile, CH_3-C=CH^B moiety occurred, in contrast to the case of the trimethylaza[14]annulene **4**, indicating that the molecular skeleton of **8** is more rigid and less strained than that of **4**. One possible explanation for this behavior is that in the case of aza[18]annulene **8**, the steric strain caused by α-methyl substitution can be relieved over the whole of a larger molecular skeleton of **8**, as compared with the case of **4**.

The ^{1}H NMR chemical shifts of the deuterated species **8′**, taken in deuteriochloroform solution admixed with a few drops of deuteriotrifluoroacetic acid are

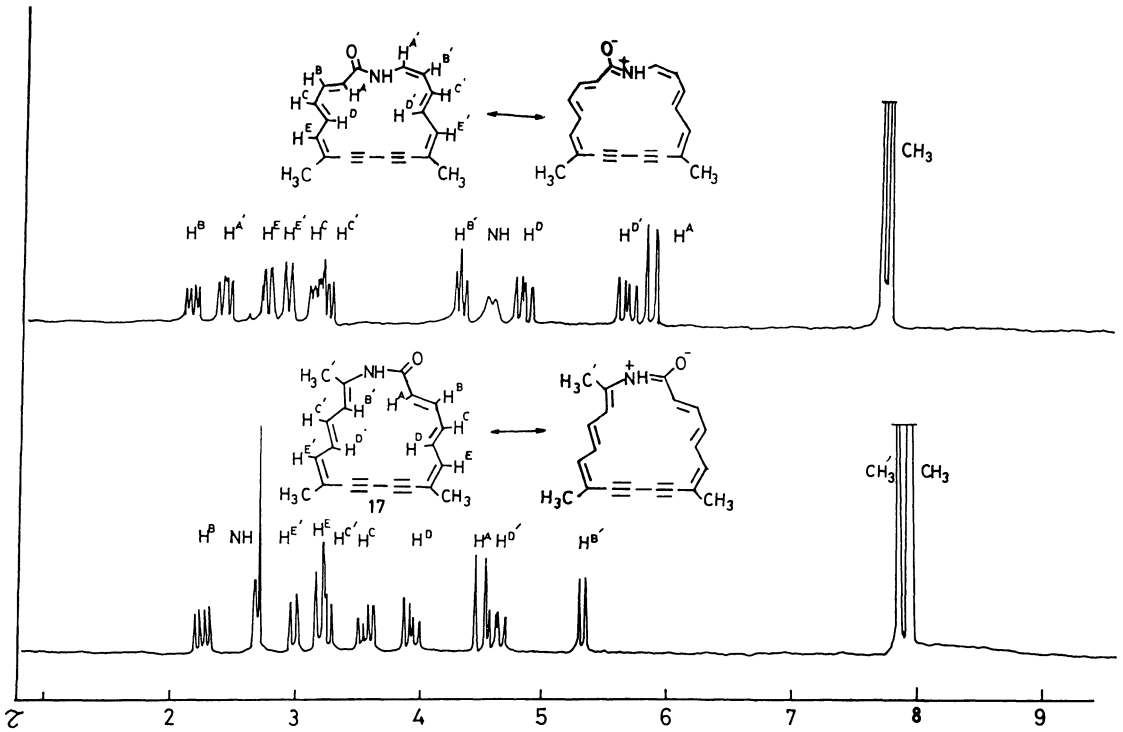

Fig. 4. The 200 MHz ^{1}H NMR spectra of the eighteen-membered lactams in $CDCl_3$ (internal standard, TMS).

also given in Table 1. It is apparent that the resonances of almost all the protons including ethoxyl and methyl protons in **8** shift toward lower field, except the protons nearby the nitrogen atom. This seems to be attributable to diminished π-electron perimeter in azaanulene **8**, arising from withdrawal of electrons by deuteration.

The ^{1}H NMR spectra of the lactams **11** and **14**, which are the precursors of the azaannulenes **6** and **7**, respectively, are shown in Fig. 3, together with that of the dimethylated lactam of the precursor of **1**, and the spectra of the lactam **17** and of the dimethylated lactam of the precursor of **2** are shown in Fig. 4. As can be seen from Fig. 3, the sixteen-membered lactams **11** and **14** as well as the dimethylated one show the inner proton resonances at low field and the outer proton (including methyl protons) resonances at high field. On the other hand, as we see from Fig. 4, the eighteen-membered lactam **17** as well as the dimethylated lactam shows the inner proton resonances at high field and the outer proton (including methyl protons) resonances at low field. Thus, it is noted that the spectra of these lactams are parallel to those of the corresponding azaanulenes with respect to the high-field and low-field shifts due to the olefinic and methyl protons. These results indicate that the sixteen-membered lactams **11** and **14** are paratropic, while the eighteen-membered lactam **17** is diatropic, and these lactams can be considered to exist in zwitter ionic forms, as indicated in Figs. 3 and 4, constructing fully conjugated macrocycles, as has been discussed previously.[1b] Furthermore, from Fig. 3, the chemical shift differences between the olefinic outer and inner protons as well as the chemical shifts of the methyl protons are almost the same in these lactams, indicating that the paratropicity, i.e., the planarity of the molecular skeletons of the sixteen-membered lactams are nearly the same. This fact is in contrast to the cases of the corresponding azaannulene series **1**, **6**, and **7** (Fig. 1), albeit both their lactams and the azaannulenes have the similar conformations each other. This suggests that the lactam ring have a more flexible perimeter for the steric strain, as compared with the azaannulene ring, presumably due to two single bonds on both sides of a nitrogen atom.

As we see from Fig. 4, the diatropicity decreases in the order of the dimethylated lactam>the trimethylated lactam **17** as similarly to the cases of the corresponding azaannulenes between **2** and **8**. This is reasonably attributed to the fact that the configurations both between the lactam **17** and the corresponding dimethylated lactam, and between the azaanulenes **2** and **8** are different.

Electronic Spectra. The electronic absorption spectra, taken in tetrahydrofuran, of the bisdehydroaza[16]annulenes **1**, **6**, and **7**, and of the bisdehydroaza[18]-annulenes **2** and **8** are illustrated in Fig. 5 and 6, respectively. As is seen from both Figs. 5 and 6, the longest wavelength bands shift toward longer wavelengths in the order of **1**>**6**>**7** (Fig. 5), **2**>**8** (Fig. 6), demonstrating the sequence for the degree of extended conjugation of π-electron system in these aza[16]- and

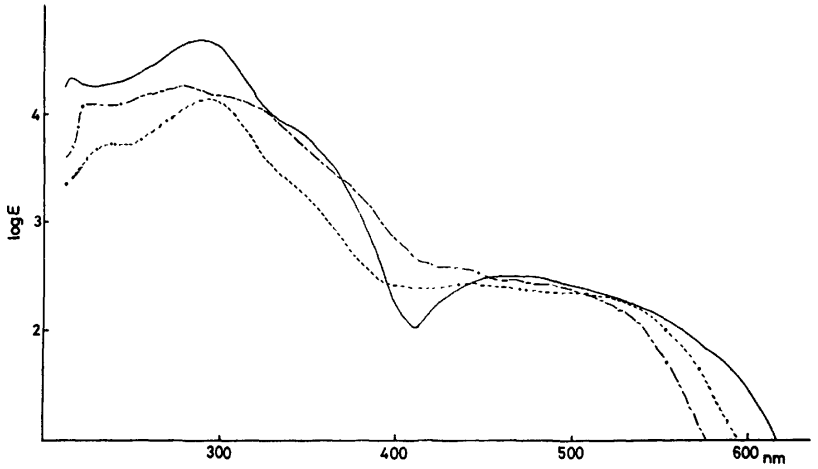

Fig. 5. Electronic spectra of the aza[16]annulenes **1** (——), **6** (------), and **7** (—·—·—) in THF.

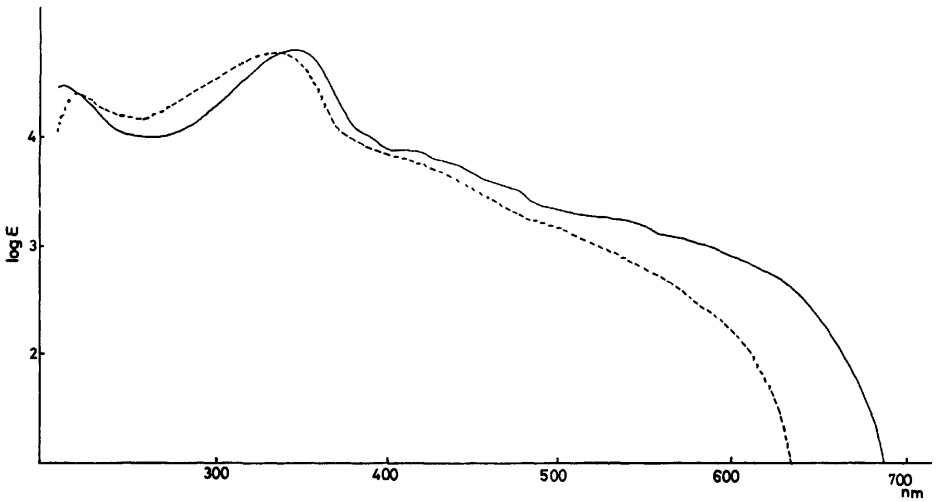

Fig. 6. Elelctronic spectra of the aza[18]annulenes **2** (——) and **8** (------) in THF.

-[18]annulene systems, respectively, as revealed above by examination from ^{1}H NMR spectra.

These results show that the conformations indicated for **1** and **2** are most appropriate for conjugation of π-electrons in these bisdehydroaza[16]- and -[18]annulene systems, respectively.

Experimental

All melting points are uncorrected. IR spectra were measured on Hitachi 260-50 spectrophotometer as KBr disk; only significant maxima are reported. UV spectra were taken on Hitachi 220A spectrophotometer and were recorded in nm, in tetrahydrofuran solution. ε-Values are given in parentheses, the shoulders being denoted by sh. Mass spectra were measured with JEOL JMS-200 spectrometer at 75 eV using a direct inlet system. ^{1}H NMR spectra were taken on JEOL FX-90Q (90 MHz) or Varian XL-200 (200 MHz) spectrometer, and refer to solutions in $CDCl_3$, unless othewise stated, in τ-values with TMS as an internal standard. The coupling constants (J) are given in Hz. Alumina (II-III) was used for column chromatography. Preparative TLC was carried out on 20×20 cm silica-gel plates (Merck, 0.5 or 2.0 mm thick). Dichloromethane was distilled over calcium hydride before use. Tetrahydrofuran (THF) was refluxed over potassium hydroxide pellets and distilled before use. Organic extracts with dichloromethane or chloroform were dried over anhyd calcium chloride prior to solvent removal.

1-Hydroxyimino-2,5,10-trimethylcyclopentadeca-2,4,10,12,14-pentaene-6,8-diyne (10). To a stirred soln of the trimethylbisdehydro[15]annulenone (**9**)[4] (1.70 g, 6.8 mmol) in methanol (250 ml) and THF (80 ml) was added a soln of hydroxylamine hydrochloride (19.0 g, 0.273 mol) in water (50 ml) at 38 °C in one portion. After stirring for further 24 h at 38—45 °C, further quantities of hydroxylamine hydrochloride (each 10 g in water (10 ml)) were added after every 24 h. After stirring for a total of 78 h, the soln was poured into aq sodium hydrogencarbonate soln and extracted with chloroform. The combined extracts were washed with aq sodium chloride soln, dried, and evaporated. The residue after solvent removal was chromatographed on alumina (3.7×7.5 cm). The early fractions eluted with hexane–chloroform (1:1) gave the recovered annulenone (**9**) (167 mg). The following fractions eluted with chloroform gave the oxime **10** (1.04 g, 58%) as a solid. Recrystallization from hexane–chloroform afforded orange needles: Mp 192 °C (decomp); MS m/z 263 (M^+, 37%)

230 (100); mol wt 263.3; IR 3230 (-OH), 2160 (-C≡C-), 990, and 970 cm^{-1} (trans C=C); UV_{max} 279 (27300), 309 (39200), and 395 nm sh (3400); ^1H NMR (90 MHz, DMSO-d_6) τ=−1.70 (s, 1H, OH, exchangeable with D_2O), 2.67 (dd, 16, 4, 1H, $H^{B'}$), 2.72—3.54 (m, 5H, H^B, H^C, $H^{C'}$, $H^{D'}$, and $H^{E'}$), 3.81 (d, 16.5, 1H, $H^{A'}$), 8.00 (s, 3H, CH_3), 8.02 (s, 3H, CH_3), and 8.08 (s, 3H, CH_3).

Found: C, 82.14; H, 6.45; N, 5.28%. Calcd for $C_{18}H_{17}NO$: C, 82.10; H, 6.51; N, 5.32%.

3,6,11-Trimethylazacyclohexadeca-3,5,11,13,15-pentaene-7,9-diyn-2-one (11). A soln of phosphorus pentachloride (5.0 g, 24 mmol) in THF (80 ml) was added to an ice-cooled, stirred soln of the oxime **10** (902 mg, 3.4 mmol) in THF (200 ml). The soln was stirred for a further 4 h at 25—28 °C, and then was poured into water. Then an aq sodium hydrogencarbonate soln was added (pH 8). The mixture was extracted with chloroform. The combined extracts were washed with aq sodium chloride soln, and dried. The residue after solvent removal was chromatographed on alumina (3.7×9.0 cm). The fractions eluted with hexane–benzene (3:2) gave the lactam **11** (405 mg, 45%) as a solid. Recrystallization from hexane–benzene afforded purple brown needles: Mp 187—189 °C; MS *m/z* 263 (M^+, 100%); mol wt 263.3; IR 3280 (NH), 2180 (-C≡C-), 1680 (C=O), 1620 (C=C), and 970 cm^{-1} (trans C=C); UV_{max} 265 sh (23500), 293 (38100), 310 sh (29200), 341 sh (9420), and 464 nm (1050); ^1H NMR (200 MHz) τ=−0.65 (d, 11, 1H, NH), −0.05 (d, 11, 1H, H^B), −0.04—0.12 (m, 1H, $H^{C'}$), 3.69 (dd, 11, 9.5, 1H, $H^{A'}$), 3.74 (d, 11.5, 1H, H^C), 4.24 (dd, 15, 11.5, 1H, $H^{D'}$), 4.28 (d, 11, 1H, $H^{E'}$), 5.16 (dd, 11, 9, 1H, $H^{B'}$), 8.25 (s, 3H, CH_3), 8.28 (s, 3H, CH_3), and 8.30 (s, 3H, CH_3), and see Fig. 3.

Found: C, 82.37; H, 6.46; N, 5.21%. Calcd for $C_{18}H_{17}NO$: C, 82.10; H, 6.51; N, 5.32%.

2-Ethoxy-3,6,11-trimethyl-7,9-bisdehydroaza[16]annulene (6). To a stirred soln of the lactam **11** (581 mg, 2.21 mmol) in dichloromethane (100 ml) was added dropwise a soln of triethyloxonium tetrafluoroborate (4.19 g, 22.1 mmol) in dichloromethane (30 ml) during 30 min at room temp under argon. After stirring for 1.5 h at the same temp, further quantities of the oxonium salt (each 4.19 g in dichloromethane (30 ml)) were added twice every 6 h. After stirring for a total 18 h, the soln was cooled in an ice-bath and an aq potassium carbonate soln was added dropwise (pH 8). The mixture was poured into water and extracted with dichloromethane. The combined extracts were washed with saturated aq sodium chloride soln, and dried. The residue after solvent removal was chromatographed on alumina (3.7×8.0 cm). The initial fractions eluted with 3% ether in hexane gave a dark red liquid, which was further purified by preparative TLC. The fast moving, red band on evaporation afforded the aza[16]annulene **6** (2.4 mg, 0.37%) as an unstable solid. Recrystallization from hexane–benzene afforded brown needles: Mp 114—115 °C; IR 2180 (-C≡C-), 1575 (C=C), and 1260 cm^{-1} (-O-); UV_{max} 237 (5270), 292 (13400), 340 sh (2210), and 455 nm (260), and see Fig. 5; ^1H NMR (200 MHz) τ=0.64 (dd, 16, 12, 1H, $H^{C'}$), 0.70 (d, 10, 1H, H^B), 0.88 (d, 13, 1H, $H^{A'}$), 3.83 (d, 11, 1H, H^C), 4.05 (d, 5.5, 1H, $H^{E'}$), 4.17 (t, 12, 1H, $H^{B'}$), 4.49 (dd, 16, 5, 1H, $H^{D'}$), 5.96 (q, 7, 2H, $-OC\underline{H}_2CH_3$), 8.28 (s, 3H, CH_3), 8.36 (s, 3H, CH_3), 8.43 (s, 3H, CH_3), and 8.74 (t, 7, 3H, $-OCH_2C\underline{H}_3$), and see Fig. 1.

HRMS: Found: 291.1607. Calcd for $C_{20}H_{21}NO$: 291.1620.

1-Hydroxyimino-5,10,15-trimethylcyclopentadeca-2,4,10,12,14-pentaene-6,8-diyne (13). To a stirred soln of the trimethylbisdehydro[15]annulenone (**12**)[4] (1.33 g, 5.34 mmol) in methanol (223 ml) and THF (65 ml) was added in one portion a soln of hydroxylamine hydrochloride (7.42 g, 0.107 mol) in water (8 ml) at room temp. After stirring for 17 h at room temp, a further quantity of hydroxylamine hydrochloride (14.8 g, 0.214 mmol) in water (15 ml) was added to the soln, and stirring was continued for a further 15 h. Then the soln was worked up as in the preparation of **10**. The residue after solvent removal was chromatographed on alumina (3.7×7.5 cm). The fractions eluted with 5% ethanol in chloroform gave the oxime **13** (1.24 g, 88%) as a solid. Recrystallization from hexane–chloroform afforded orange needles: Mp 198—200 °C (decomp); MS *m/z* 263 (M^+, 46%) and 231 (100); mol wt 263.3; IR 3250 (NH), 2150 (-C≡C-), 975, and 960 cm^{-1} (trans C=C); UV_{max} 278 sh (36100), 300 (50600), and 385 nm sh (20300); ^1H NMR (90 MHz, DMSO-d_6) τ=−1.37 (s, 1H, OH, exchangeable with D_2O), 2.79—3.94 (m, 7H, olefinic H), 8.02 (s, 3H, CH_3), 8.07 (s, 3H, CH_3), and 8.13 (s, 3H, CH_3).

Found: C, 82.19; H, 6.40; N, 5.46%. Calcd for $C_{18}H_{17}NO$: C, 82.10; H, 6.51; N, 5.32%.

6,11,16-Trimethylazacyclohexadeca-3,5,11,13,15-pentaene-7,9-diyn-2-one (14). A soln of phosphorus pentachloride (7.08 g, 34.0 mmol) in THF (210 ml) was added dropwise during 40 min to a soln of the oxime **13** (1.79 g, 6.80 mmol) in THF (210 ml) with stirring at 2—6 °C. After stirring for a further 2 h at the same temp, a further quantity of phosphorus pentachloride (1.42 g) in THF (22 ml) was added and stirring was continued for a further 1 h. Then the mixture was worked up as in the preparation of **11**. The residue after solvent removal was chromatographed on alumina (4.0×8.5 cm). The fractions eluted with 5% chloroform in benzene gave the lactam **14** (853 mg, 47%) as a solid. Recrystallization from hexane–chloroform afforded purple cubes: Mp 202—203 °C; MS *m/z* 263 (M^+, 100%); mol wt 263.3; IR 3300 (NH), 2180 (-C≡C-), 1650 (C=O), 1630, 1615 (C=C), and 970 cm^{-1} (trans C=C); UV_{max} 291 (26800), 342 sh (6380), and 459 nm (1110); ^1H NMR (200 MHz) τ=0.01 (s, 1H, NH), 1.17 (dd, 16.5, 9.0, 1H, H^B), 1.27 (dd, 15.8, 10.6, 1H, $H^{C'}$), 3.26 (d, 16.5, 1H, H^A), 3.56 (dd, 15.9, 8.6, 1H, $H^{D'}$), 3.93 (d, 9.2, 1H, H^C), 4.18 (d, 8.6, 1H, $H^{E'}$), 5.29 (d, 10.8, 1H, $H^{B'}$), 7.89 (s, 3H, CH_3'), 8.27 (s, 3H, CH_3), and 8.29 (s, 3H, CH_3), and see Fig. 3.

Found: C, 82.31; H, 6.51; N, 5.39%. Calcd for $C_{18}H_{17}NO$: C, 82.10; H, 6.51; N, 5.32%.

The later fractions eluted with 10% ethanol in chloroform gave the recovered oxime **13** (250 mg).

2-Ethoxy-6,11,16-trimethyl-7,9-bisdehydroaza[16]annulene (7). To a stirred soln of the lactam **14** (481 mg, 1.83 mmol) in dichloromethane (200 ml) was added a soln of triethyloxonium tetrafluoroborate (6.92 g, 36.5 mmol) in dichloromethane (60 ml) dropwise during 45 min with stirring at room temp under argon. After stirring for 3 h at the same temp, a further quantity of the oxonium salt (1.73 g) in dichloromethane (15 ml) was added, and stirring was continued for 21 h. Then the mixture was worked up as in the preparation of **6**. The dark red liquid after solvent removal was chromatographed on alumina (3.7×7.0 cm). The early fractions eluted with hexane gave an unstable red liquid, which was further purified by preparative TLC. The fast moving, red band on evaporation afforded the aza[16]-annulene **7** (13.6 mg, 2.6%) as a brown liquid: IR (neat) 2170 (-C≡C-), 1605 (C=C), and 1280 cm^{-1} (-O-); UV_{max} 266 sh (16700), 278 (18600), 304 (14800), 321 sh (11900), and 380

nm sh (1730), and see Fig. 5; ^{1}H NMR (200 MHz) τ=1.74 (dd, 16, 11, 1H, H^B), 2.16 (dd, 15.5, 11.5, 1H, $H^{C'}$), 3.71 (d, 4, 1H, $H^{E'}$), 3.73 (d, 11.5, 1H, $H^{B'}$), 3.82 (d, 11, 1H, H^C), 4.25 (d, 16, 1H, H^A), 4.27 (dd, 11.5, 4, 1H, $H^{D'}$), 5.91 (q, 7, 2H, $-OCH_2CH_3$), 8.07 (s, 3H, CH_3), 8.16 (s, 3H, CH_3), 8.20 (s, 3H, CH_3), and 8.73 (t, 7, 3H, $-OCH_2CH_3$), and see Fig. 1.

HRMS: Found: 291.1598. Calcd for $C_{20}H_{21}NO$: 291.1621.

The later fractions eluted with 5% ethanol in chloroform gave the recovered lactam **14** (76 mg).

1-Hydroxyimino-2,7,12-trimethylcycloheptadeca-2,4,6,12,14,16-hexaene-8,10-diyne (16). A soln of hydroxylamine hydrochloride (6.60 g, 95.0 mmol) in water (10 ml) was added in one portion to a stirred soln of trimethylbisdehydro[17]annulenone (**15**)[6] (657 mg, 2.40 mmol) in methanol (130 ml) and THF (40 ml) at room temp. After stirring for 19 h at 40 °C, a further quantity of hydroxylamine hydrochloride (6.6 g) in water (10 ml) was added and stirring was continued for a further 21 h at the same temp. Then the soln was worked up as in the preparation of **10**. The residue after solvent removal was chromatographed on alumina (4.2×7.5 cm). The fractions eluted with 5% ethanol in chloroform gave the oxime **16** (505 mg, 73%) as a solid. Recrystallization from hexane–chloroform afforded orange needles: Mp 218—220 °C (decomp): MS *m/z* 289 (M^+, 100%); mol wt 289.3; IR 3230, 3140 (-OH), 2170 (-C≡C-), 970, and 950 cm^{-1} (trans C=C); UV_{max} 300 (48800), 307 (48700), 370 sh (9490), and 398 nm sh (7180); ^{1}H NMR (90 MHz, DMSO-d_6) τ=−1.51 (s, 1H, OH, exchangeable with D_2O), 2.70—3.67 (m, 9H, olefinic H), 8.04 (s, 3H, CH_3'), and 8.15 (s, 6H, CH_3).

Found: C, 83.31; H, 6.63; N, 4.82%. Calcd for $C_{20}H_{19}NO$: C, 83.01; H, 6.62; N, 4.84%.

8,13,18-Trimethylazaoctadeca-3,5,7,13,15,17-hexaene-9,11-diyn-2-one (17). A soln of phosphorus pentachloride (2.44 g, 11.7 mmol) in THF (100 ml) was added dropwise during 30 min at −10 °C to a stirred soln of the oxime **16** (484 mg, 1.67 mmol) in THF (100 ml) and stirring was continued for a further 3.5 h at room temp. Then the soln was worked up as in the preparation of **11**. The residue after solvent removal was chromatographed on alumina (3.7× 9.0 cm). The fractions eluted with benzene–chloroform (1:1) gave the lactam **17** (221 mg, 46%) as a solid. Recrystallization from hexane–chloroform afforded dark brown cubes: Mp 202—204 °C (decomp); MS *m/z* 289 (M^+, 100%); mol wt 289.3; IR 3170, 3050 (NH), 2160 (-C≡C-), 1655 (C=O), 1605, 1585 (C=C), and 960 cm^{-1} (trans C=C); UV_{max} 327 (52100) and 403 nm sh (6250); ^{1}H NMR (200 MHz) τ=2.29 (dd, 15.5, 8.5, 1H, H^B), 2.70 (s, 1H, NH), 3.01 (d, 11, 1H, $H^{E'}$), 3.21 (d, 10.5, 1H, H^E), 3.25 (dd, 15, 11, 1H, $H^{C'}$), 3.58 (dd, 15.5, 8.5, 1H, H^C), 3.95 (dd, 15.5, 9.5, 1H, H^D), 4.50 (d, 15.5, 1H, H^A), 4.63 (dd, 15, 10.5, 1H, $H^{D'}$), 5.32 (d, 11, 1H, $H^{B'}$), 7.84 (s, 3H, CH_3'), 7.92 (s, 3H, CH_3), and 7.93 (s, 3H, CH_3), and see Fig. 4.

Found: C, 82.87; H, 6.80; N, 4.90%. Calcd for $C_{20}H_{19}NO$: C, 83.01; H, 6.62; N, 4.84%.

18-Ethoxy-2,7,12-trimethyl-8,10-bisdehydroaza[18]annulene (8). To a stirred soln of triethyloxonium tetrafluoroborate (4.05 g, 21.3 mmol) in dichloromethane (40 ml) was added a soln of the lactam **17** (206 mg, 0.712 mmol) in dichloromethane (35 ml) during 30 min at room temp under argon. After stirring for 17 h, a further quantity of the oxonium salt (2.5 g) in dichloromethane (20 ml) was added to the soln, and stirring was continued for a further 6 h. Then the soln was worked up as in the preparation of **6**. The residue after solvent removal was chromatographed on alumina (3.7×8.0 cm). The early fractions eluted with 2% ether in hexane gave the aza[18]annulene **8** (23.0 mg, 11.2%) as a solid. Recrystallization from hexane–benzene afforded dark brown needles: Mp 106—108 °C; MS *m/z* 317 (M^+, 88%) and 258 (100); mol wt 317.4; IR 2170 (-C≡C-), 1620, 1600, 1560 (C=N, C=C), 1280, 1265, 1055 (-O-), and 960 cm^{-1} (trans C=C); UV_{max} 291 sh (27000), 333 (55500), 412 sh (5660), and 510 nm sh (1270), and see Fig. 6; ^{1}H NMR (200 MHz) τ=2.51 (dd, 15.5, 8, 1H, $H^{B'}$), 2.92 (d, 10, 1H, H^E), 3.04 (dd, 15, 10.5, 1H, H^C), 3.08 (d, 10, 1H, $H^{E'}$), 3.66 (dd, 15, 8, 1H, $H^{C'}$), 4.46 (dd, 15, 10, 1H, $H^{D'}$), 4.99 (d, 15.5, 1H, $H^{A'}$), 5.20 (dd, 15, 10, 1H, H^D), 5.73 (q, 7, 2H, $-OCH_2CH_3$), 5.99 (d, 10.5, 1H, H^B), 7.79 (s, 3H, CH_3), 7.86 (s, 3H, CH_3), 8.04 (s, 3H, CH_3'), and 8.62 (t, 7, 3H, $-OCH_2CH_3$), and see Fig. 2, (200 MHz, CF_3COOD in $CDCl_3$) τ=1.84 (dd, 15.5, 8, 1H, $H^{B'}$), 2.75 (d, 10.5, 1H, H^E), 2.92 (d, 8, 1H, $H^{E'}$), 3.05 (dd, 15.5, 10.5, 1H, H^C), 3.78 (dd, 15.5, 8, 1H, $H^{D'}$), 3.91 (dd, 15.5, 8, 1H, $H^{C'}$), 5.25 (dd, 15.5, 10.5, 1H, H^D), 5.26 (q, 7, 2H, $-OCH_2CH_3$), 5.46 (d, 15.5, 1H, $H^{A'}$), 5.74 (d, 10.5, 1H, H^B), 7.64 (s, 3H, CH_3), 7.74 (s, 3H, CH_3), 7.87 (s, 3H, CH_3'), and 8.37 (t, 7, 3H, $-OCH_2CH_3$).

Found: C, 83.42; H, 7.24; N, 4.57%. Calcd for $C_{22}H_{23}NO$: C, 83.24; H, 7.30; N, 4.41%.

This work was financially supported by a Grant-in-Aid for Scientific Research No. 60540324 from the Ministry of Education, Science and Culture.

References

1) a) J. Ojima, T. Nakada, E. Ejiri, and M. Nakamura, *Tetrahedron Lett.*, **26**, 639 (1985); b) J. Ojima, T. Nakada, E. Ejiri, and M. Nakamura, *J. Chem. Soc., Perkin Trans. 1*, in press.

2) J. Ojima, Y. Yagi, E. Ejiri, S. Ishizaka, and T. Kato, the preceding paper.

3) A part of this work has appeared in a preliminary form, J. Ojima, Y. Yagi, T. Nakada, M. Manaka, E. Ejiri, S. Ishizaka, and Y. Shiraiwa, *Chem. Lett.*, **1985**, 1767.

4) J. Ojima, K. Wada, K. Kanazawa, and Y. Nakagawa, *J. Chem. Soc., Perkin Trans. 1*, **1981**, 947.

5) The structural determination of all the oximes described in this paper was made from examination of the structures of the subsequent lactams, and see Ref. 2.

6) J. Ojima, K. Kanazawa, K. Kusaki, and K. Wada, *J. Chem. Soc., Perkin Trans. 1*, **1980**, 473.

 © 1986 The Chemical Society of Japan Bull. Chem. Soc. Jpn., 59, 1809—1824 (1986)

Stereoselectivity of Cycloaddition of *N*-(Cyanomethyl)- and *N*-(α-Cyanobenzyl)imines with Olefinic Dipolarophiles. Synthetic Equivalents of Nitrile Ylide 1,3-Dipoles

Otohiko Tsuge,* Kazunori Ueno, Shuji Kanemasa, and Kiyotaka Yorozu
Research Institute of Industrial Science, and Department of Molecular Science and Technology, Interdisciplinary Graduate School of Engineering Sciences, Kyushu University, Kasugakoen, Kasuga 816
(Received January 27, 1986)

N-(Cyanomethyl)- and *N*-(α-cyanobenzyl)imines derived from a variety of aldehydes and ketones can tautomerize into *N*-protonated azomethine ylides which undergo cycloadditions with olefinic dipolarophiles. These cycloadditions are often accompanied by the elimination of HCN, mostly in a stereospecific manner, showing these imines to be synthetic equivalents of nonstabilized nitrile ylides. Stereoselectivity of the cycloadditions is discussed.

Since the discovery of imine–azomethine ylide tautomerism of the imines derived from α-amino esters,[1–3] a wide range of 1,3-dipolar cycloaddition reactions utilizing such imines have been applied to the synthesis of pyrrolidine- and pyrrole-2-carboxylates.[4,5] However, quite rare are cycloaddition examples leading to the formation of stereoselective cycloadducts.[1] Generally, a mixture of two or even more stereoisomers of cycloadducts is formed.[2,4,6]

It is only quite recent that stereochemical features of cycloaddition of heteroaromatic *N*-ylides as peripheral azomethine ylides with olefinic dipolarophiles have been unveiled.[7] Although a lot of examples for the cycloadditions of open-chained azomethine ylides have been reported,[8–15] it is so far very difficult to predict stereoselectivity of a given example of cycloaddition of an azomethine ylide with an olefin. This difficulty results partly from the lack of information on the structure of azomethine ylide which has participated in the cycloaddition.

An *N*-protonated azomethine ylide generated through tautomerism of imine lies in equilibrium with the starting imine under the conditions of cycloaddition. Therefore, the most stable isomer of all possible *N*-protonated azomethine ylides should participate in the cycloaddition. Geometry of the most stable ylide isomer may be readily predictable on the basis of structure of the starting imine.[16]

In the previous communications, we have found that *N*-benzylidene derivatives of cyanomethylamine[17] and α-cyanobenzylamine[18] undergo cycloadditions with olefins as *N*-protonated azomethine ylides of cyano-stabilized type. Elimination of HCN from the cycloadducts leads to pyrrolines which correspond to cycloadducts of nonstabilized nitrile ylides with olefins. It is important that these azomethine ylides directly afford cycloadducts one oxidation state higher than those expected from simple azomethine ylides, because there is no general route available for nonstabilized nitrile ylides.

The analysis of stereoselectivity in cycloadditions of *N*-protonated azomethine ylides of cyano-stabilized type is a major purpose of the present report. Structures incorrectly assigned for some cycloadducts described in the previous communication[18] are to be revised here.

Results and Discussion

A variety of *N*-(cyanomethyl)- **1a—d** and *N*-(α-cyanobenzyl)imines **1e—o** were examined as possible tautomeric precursors of *N*-protonated azomethine ylides of cyano-stabilized type (Scheme 1). The imines are readily accessible from reactions of aldehydes or ketones with cyanomethylamine or α-cyanobenzylamine. In some cases, imines were generated only in situ and used for the cycloadditions without isolation. Although the corresponding imines are similarly formed from cyanomethylamine and aliphatic aldehydes, they have a tendency to react further with the second molecule of the aldehyde as reactive enamines to give dienamines **A** even when no excess of the aldehyde is used.

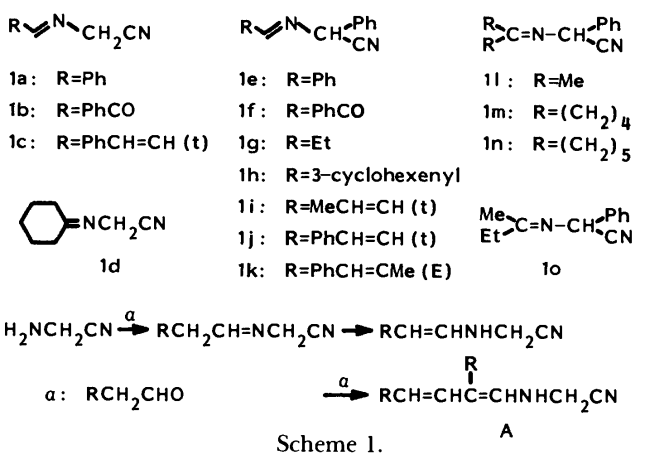

Scheme 1.

All the imines **1a—c** and **1e—k** derived from aldehydes are found to exist in single isomeric forms in solution (^{1}H NMR in $CDCl_3$), presumably in *E*-forms.[19]

In the present work, these imines **1** were subjected to react with olefinic dipolarophiles such as *N*-methyl- **2a**, *N*-(*p*-nitrophenyl)maleimide **2b**, dimethyl

Table 1. Cycloaddition of **1a** with **2** Under Various Conditions

Entry	Maleimide	Reaction conditions				Product	Yield/%[a]	Isomer ratio[b]
		Solvent	Catalyst/mol%	Temp	Time/h			
1	**2a**	Toluene	—	Reflux	6.5	**6**	100	
2		MeCN	—	Reflux	62	**6**+**10**	100	**6** : **10**=3:1
3		MeCN	AcOH (5)	rt	24	**6**+**10**	100	**6** : **10**=1:1
4		MeCN	$(COOH)_2$ (0.1)	Reflux	17	**6**+**10**	99	**6** : **10**=1:1
5		AcOH	—	rt	13	**6**+**10**	83	**6** : **10**=1.8:1
6	**2b**	Toluene	—	Reflux	16	**7**	100	
7		MeCN	AcOH (10)	rt	30	**7**	100	

a) Isolated yield. b) Determined by ^{1}H NMR.

fumarate **3**, dimethyl maleate **4**, and methyl acrylate **5**. On the basis of stereostructure of cycloadducts formed, geometry of *N*-protonated azomethine ylides involved in the cycloaddition as well as stereoselectivity

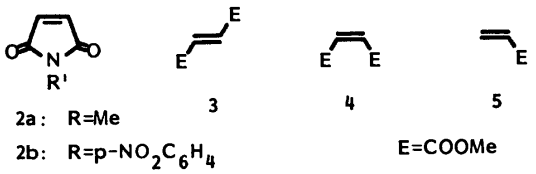

and stereospecificity of the cycloaddition is to be figured out. Synthetic versatility of these *N*-protonated azomethine ylides as synthons of nitrile ylides is next tested by elimination of HCN from the cycloadducts.

Reaction of *N*-(Cyanomethyl)imines with Maleimides. The reaction of *N*-(cyanomethyl)benzylideneamine **1a** with *N*-methylmaleimide **2a** took place cleanly, under reflux in toluene, to give a quantitative yield of cycloadduct **6** as a single stereoisomer (Scheme 2 and Table 1). However, under reflux in such a polar solvent as acetonitrile, the major product **6** was accompanied by its stereoisomer **10** in a 3:1 ratio (Entry 2 in Table 1). After investigation of the same reaction under a variety of conditions, it was found that this reaction was effectively catalyzed by weak acids such as acetic acid and oxalic acid (Entries 3 and 4).[20] Catalyzed cycloadditions occurred even at room temperature, a mixture of **6** and **10** being again obtained. Neither strong acids (CF_3COOH, *p*-TsOH) nor Lewis acids ($BF_3 \cdot Et_2O$, $Ti(OPr^i)_4$, $Al(OEt)_3$) were found to serve as effective catalysts, leading to recovery of the starting materials or complex mixture of many products.

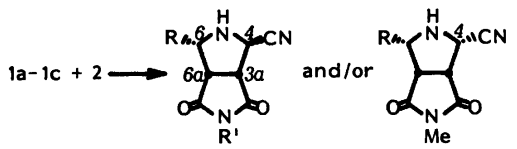

Scheme 2.

Similarly **1a** reacted with *N*-(*p*-nitrophenyl)maleimide **2b** to give single cycloadduct **7**, regardless of reaction conditions (Entries 6 and 7).

Stereostructures of **6** and **10** were assigned to be 3a,4-*trans*:6,6a-*cis* and 3a,4-*cis*:6,6a-*cis* cycloadducts, respectively, on the basis of spectral data, especially of the vicinal coupling constants (**6**: J_{3a-4}=0 and J_{6-6a}= 8.0 Hz; **10**: $J_{3a-4}=J_{6-6a}$=7.5 Hz). Signal assignment for the 6-H, a terminal of four consecutive methine hydrogens sitting on the newly formed five-membered ring, was accomplished by deuterium labeling. Monodeuterio derivatives **6**-d_1 and **10**-d_1 were prepared in the acid-catalyzed reaction of **1a**-d_1 with **2a** (Scheme 3).

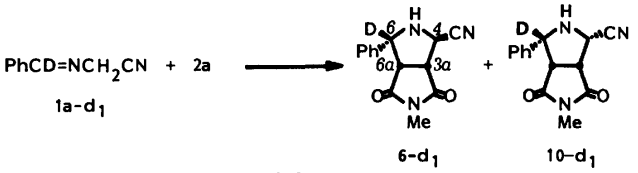

Scheme 3.

Under non-catalytic conditions, which have shown high stereoselectivity in the reaction of **1a**, *N*-(cyanomethyl)benzoylmethyleneamine **1b** and -cinnamylideneamine **1c** reacted with **2a** giving 3a,4-*trans*:6,6a-*cis* cycloadducts **8**, **9** and 3a,4-*cis*:6,6a-*cis* isomer **11** (Scheme 2 and Table 2).

Four geometrical isomers **B1**—**4** are possible for the *N*-protonated azomethine ylides formed through tautomerism of **1a**—**c**, and these ylides can be interconverted readily to each other via an imine form under the reaction conditions (Fig. 1). Relative stability

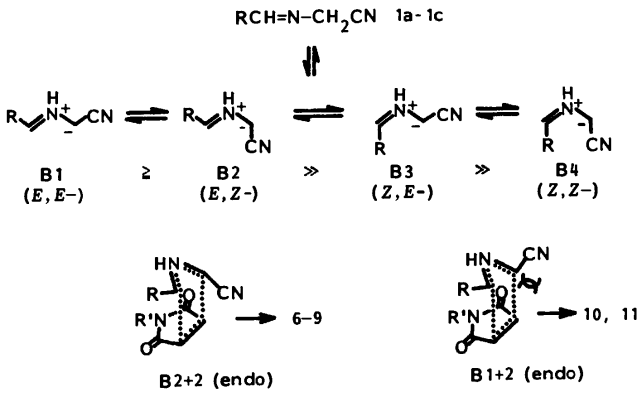

Fig. 1. Geometry of *N*-protonated azomethine ylides B generated from **1a**—**c** and stereochemistry of the cycloaddition with maleimides **2**.

Table 2. Cycloaddition of Imines **1** with Olefinic Dipolarophiles **2**—**5**

Imine	Olefin	Reaction conditions			Product	Yield/%[a]	Isomer ratio[b]	endo:exo[c]
		Solvent	Temp	Time/h				
1a	**2a**	Toluene	Reflux	6.5	**6**	100		100:0
	2b	Toluene	Reflux	16	**7**	100		100:0
1b	**2a**	$CHCl_3$	Reflux	4	**8**	100		100:0
1c	**2a**	Toluene	Reflux	14	**9**+**11**	100	**9** : **11**=2.3:1	100:0
1d	**2a**	Toluene	Reflux	15	**12**+**13**	15+50[d]		
1e	**2a**	Toluene	Reflux	6	**16**+**18**	92	**16** : **18**=2.3:1	70:30
		MeCN	Reflux	7	**16**+**18**	100	**16** : **18**=3.5:1	78:22
		MeCN[e]	Reflux	3	**16**+**18**+**20**+**22**	60+40[f]	**16** : **18**=6.7:1	87:13
	2b	Toluene	Reflux	6	**17**+**19**+**21**+**23**	92+8[g]	**17** : **19**=3.5:1	78:22
1f	**2a**	$CHCl_3$	Reflux	5 min	**14**	100		100:0
1g	**2a**	Toluene	Reflux	13	**24**	100		100:0
1h	**2a**	Toluene	Reflux	21	**25**	100		100:0
1i	**2a**	Toluene	Reflux	20	**26**+**29**	92	**26** : **29**=3.9:1	80:20
1j	**2a**	Toluene	Reflux	16	**27**+**30**	73	**27** : **30**=5:1	83:17
1k	**2a**	Toluene	Reflux	12	**28**	80		100:0
1l	**2a**	Toluene	Reflux	20	**31**	47		
1m	**2a**	Toluene	Reflux	36	**32**	83		
1n	**2a**	Toluene	Reflux	24	**33**	100		
1o	**2a**	Toluene	Reflux	19	**34**	30		
1a	**3**	Toluene	Reflux	24	**40**+**41**	86	**40** : **41**=1:1.9	100:0
		MeCN[h]	rt	38	**40**+**41**	72	**40** : **41**=2.2:1	100:0
1a	**4**	Toluene	Reflux	27	**42**	66		100:0
1e	**3**	Benzene	Reflux	8	**44**+**46**	100	**44** : **46**=3:1	75:25
		Toluene	Reflux	3	**44**+**47**+**46**	100	**44**+**47**:**46**=1.5+1.5:1	75:25
1e	**4**	Benzene	Reflux	15	**47**	100		100:0
1f	**3**	$CHCl_3$	Reflux	2	**45**	94		100:0
1j	**3**	Toluene	Reflux	20	**48**+**50**	76	**48** : **50**=2.5:1	71:29
	4	Toluene	Reflux	22	**48**+**52**	24+29[i]		100:0
1k	**3**	Toluene	Reflux	15	**49**+**51**	92	**49** : **51**=1.1:1	52:48
	4	Toluene	Reflux	23	**49**	76		100:0
1n	**3**	Toluene	Reflux	24	**53**	85		
	4	Toluene	Reflux	24	**53**	77		
1a	**5**	Neat	Reflux	12	**54**+**55**[j]	100	**54** : **55**=1.5:1	60:40
1e	**5**	Toluene	Reflux	6	**59**+**60**[k]	97	**59** : **60**=1.1:1	52:48[l]
1g	**5**	Neat	Reflux	22	**61**+**62**	93[m]		0:100[l]

a) All isolated yields as single isomer or as mixture of isomers. b) Determined on the basis of ^1H NMR spectrum of crude reaction mixture. c) The endo:exo ratio with respect to the imine carbon of **1**. d) The yields of **12** (15%) and **13** (50%). e) In the presence of AcOH (10 mol%). f) The yields of **16**+**18** (60%) and **20**+**22** (1:4, 40%). g) The yields of **17**+**19** (92%) and **21**+**23** (1:1, 8%). h) In the presence of AcOH (5 mol%). i) The yields of **48** (24%) and **52** (29%). j) Each two stereoisomers are included. k) **60** consists of two stereoisomers. l) The ratio of regioisomers (4-carboxylates: 3-carboxylates). m) The combined yield.

among them could be evaluated on the ground of steric repulsion.

Cyano moiety is only slightly bigger than hydrogen atom, while substituent R (Ph, PhCO, or PhCH=CH (t)) is much bulkier than any other substituents. Accordingly, the order of stability must be **B1**≧**B2**≫**B3**≫**B4**. The stereoselective cycloadducts **6**—**9** correspond to the ones formed through an endo approach of **2** to the second stable ylide **B2**, and the isomers **10** and **11** are endo cycloadducts of the most stable ylide **B1**. In the endo approach of **B1**, there exists some small steric repulsion between the cyano group and a carbonyl moiety of the maleimide **2**. So far we have no satisfactory explanation toward a question why acid catalysts have lowered stereoselectivity of the cycloaddition so much.

N-(Cyanomethyl)cyclohexylideneamine **1d**, generated in situ from cyclohexanone and cyanomethylamine under reflux in chloroform, reacted with **2a** under reflux in toluene to give only 15% of 3a,4-*cis* cycloadduct **12** (Scheme 4 and Table 2). Major product **13** was the Michael type adduct between cyclohexanone and **2a**. As described above (Scheme 1),

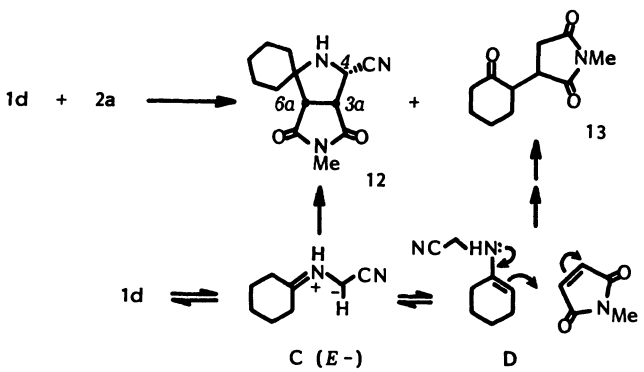

Scheme 4.

the imines derived from aliphatic aldehydes and cyanomethylamine readily tautomerize into enamines. In this case also, imine **1d** experienced competitive tautomerization, or the first formation of azomethine ylide and subsequent enamine formation, generating *N*-protonated azomethine ylide **C** and enamine **D**. The cycloaddition of **C**, that occupies sterically less hindered *E*-geometry, with **2a** produces **12** and the Michael addition of **D** forms a betaine intermediate which is then hydrolyzed into **13**.[21] Under acidic conditions (AcOH) both at room temperature and under reflux in acetonitrile, the Michael adduct **13** was the only product. This result looks reasonable since such polar conditions favor the Michael addition which is known to take place through a polar transition state.

Reaction of *N*-(α-Cyanobenzyl)imines with Maleimides. *N*-(α-Cyanomethyl)benzoylmethyleneamine **1f** is found reactive toward maleimides. Thus, the reaction of **1f** with **2a** was completed in 5 min under reflux in chloroform to give a stereoselective cycloadduct **14** in a quantitative yield, which was assigned as one of 6,6a-*cis* isomers as shown in Scheme 5. Stereochemistry at the 4-position was tentatively determined on the basis of the most stable geometry for the *N*-protonated azomethine ylide generated from **1f**. This point will be discussed later.

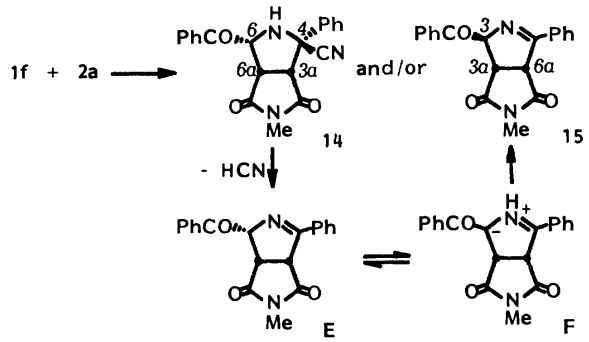

Scheme 5.

When chromatographed over silica gel,[22] **14** underwent quantitative elimination of HCN to give **15** as a single stereoisomer in which the configuration of the 3-position was inverted. The prolonged reaction of **1f** with **2a** also furnished **15** as a side product. Probably **14** was first transformed into cis isomer **E** which then isomerized into **15** as a thermodynamically more stable product via azomethine ylide tautomer **F** (Scheme 5). In this isomerization, such a strongly electron-withdrawing substituent as benzoyl moiety is essential since imine-azomethine ylide tautomerism takes place only if α-hydrogen of imine is highly acidic.

A mixture of cis **16** and trans isomer **18** of HCN-eliminated cycloadduct was obtained in the reaction of *N*-(α-cyanobenzyl)benzylideneamine **1e** with **2a** under reflux in acetonitrile or toluene (Scheme 6, **16**:**18**=3.5—2.3:1). Under catalytic conditions (AcOH),

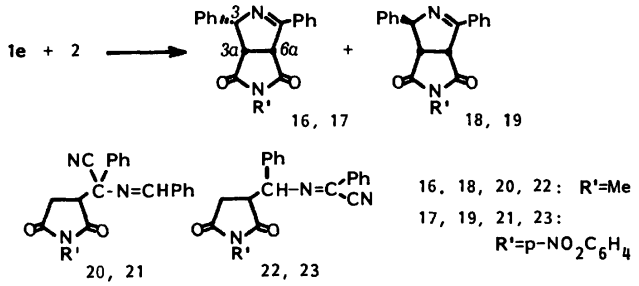

Scheme 6.

were formed two additional isomers **20** and **22** which were identified to be regioisomeric Michael adducts.

Similar reaction of **1e** with **2b** gave two HCN-eliminated cycloadducts **17**, **19** (3:1) and the Michael adducts **21**, **23** as minor products even under non-catalytic conditions (Table 2).[23]

This poor stereoselectivity between the 3- and 3a-positions of **16** and **18** (or **17** and **19**) is quite surprising. Four isomeric forms **G1—4** are again possible for the *N*-protonated azomethine ylide **G** formed by tautomerism of **1e** (Fig. 2). Unlike the preceding case (**B** in Fig. 1), **G1** must be by far the most stable since the additional phenyl moiety causes unfavorable steric repulsion in **G2**. Therefore, it is easily understood that only **G1** has participated in cycloaddition with **2**. Endo and exo approaches of **2a** to **G1** lead to the corresponding cycloadducts **H** and **I** whose stereospecific elimination of HCN produces cis **16** and trans isomer **18**. If this is the case, what is the reason for such poor stereoselectivity?

Before we try to explain this poor selectivity, we should rule out a possibility that **18** as a thermodynamically more stable isomer could have been secondarily derived from endo selective cycloadduct

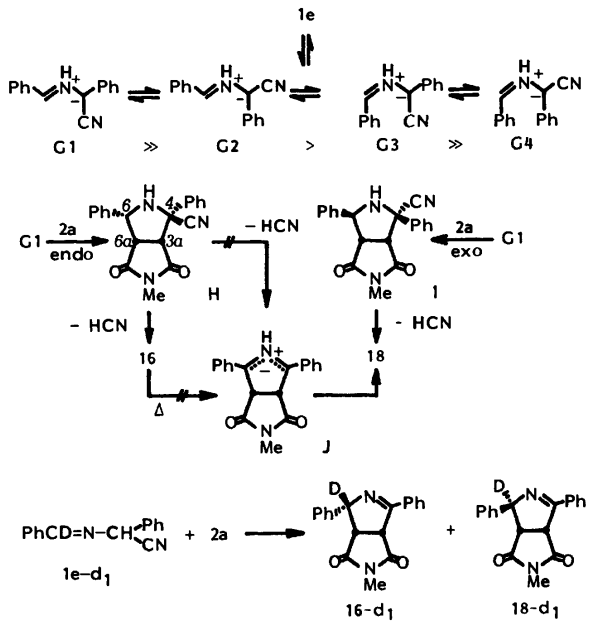

Fig. 2. Geometry of *N*-protonated azomethine ylide G generated from **1e** and stereochemistry of the cycloaddition with a maleimide **2a**.

H. Isomerization of **16** into **18** via azomethine ylide intermediate **J**, which resembles the inversion of **14** into **15** via **F** (Scheme 5), was first excluded by the fact that no trace of **18** was even detected on heating **16** under the reaction conditions of cycloaddition.[24] Direct formation of peripheral azomethine ylide intermediate **J** from **H** by 1,3-elimination of HCN was also excluded.[25] Cycloaddition of monodeuterio imine **1e**-d_1 with **2a** under the same conditions provided only a mixture of monodeuterio derivatives **16**-d_1 and **18**-d_1 of HCN-eliminated cycloadduct, indicating that stereochemistry at the 3-position of **16** and **18** has been already built up as it is now in the corresponding initial cycloadducts **H** and **I**. Thus, it is concluded that cycloaddition of **1e** with **2a** is nonstereoselective, forming two stereoisomeric cycloadducts **H** and **I**.

Both the phenyl substituents of **G1** can attractively interact with the carbonyl conjugation of **2a** allowing endo approach of both reagents.[26] However, this endo attractive interaction should be hindered by steric repulsion simultaneously growing among the same positions of these reacting molecules. As the phenyl groups are discouraged to share the same plane with the azomethine ylide triangle of **G1**,[27] steric repulsion on the endo approach becomes inevitable in this case. Accordingly the endo approach leading to **H** competes with the exo approach leading to **I**.

Similarly, *N*-(α-cyanobenzyl)alkylideneamines **1g—h** and -alkenylideneamines **1j—k** reacted with **2a** as *N*-protonated azomethine ylides to give 3,3a-*cis* **24—28** and/or 3,3a-*trans* isomers **29** and **30** of HCN-eliminated cycloadducts (Scheme 7 and Table 2). Stereoselectivity was found to depend upon substituents of imines **1**, and the cycloadditions of **1g—h** and **1k** were exclusively *endo*-selective.

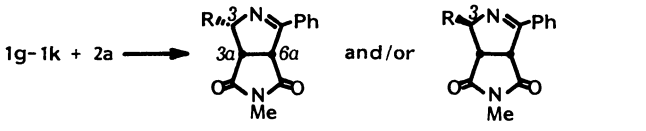

24: R=Et
25: R=3-cyclohexenyl
26: R=MeCH=CH (t)
27: R=PhCH=CH (t)
28: R=PhCH=CMe (E)
29: R=MeCH=CH (t)
30: R=PhCH=CH (t)

Scheme 7.

N-(α-Cyanobenzyl)imines **1l—o** derived from aliphatic ketones also reacted with **2a** giving HCN-eliminated cycloadducts **31—34** in good yields (Scheme 8 and Table 2).

Elimination of HCN from the Maleimide Cycloadducts. As mentioned above, most of the cycloadducts formed in the reactions of *N*-(α-cyanobenzyl)-imines **1e—o** with maleimides **2** undergo spontaneous elimination of HCN under the conditions of cycloaddition, indicating that these imines are useful

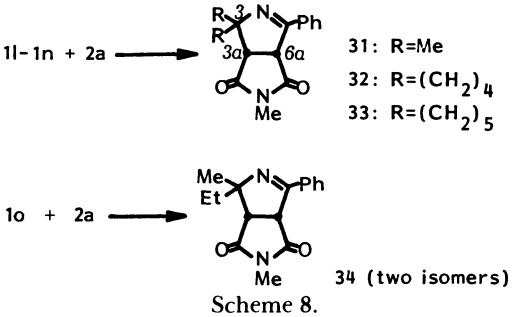

31: R=Me
32: R=$(CH_2)_4$
33: R=$(CH_2)_5$
34 (two isomers)

Scheme 8.

as synthetic equivalents of benzonitrile methylides. On the other hand, the cycloadducts from *N*-(cyanomethyl)imines **1a—d** are substituted with a cyano moiety. Therefore, some of these cycloadducts were subjected to thermal or base-catalyzed elimination of HCN.

On heating in xylene, the all-*cis* cycloadduct **10** underwent slow elimination of HCN to give **35** with retention of configuration (Scheme 9 and Table 3), while its isomer **6** was recovered unchanged under the same conditions. In the presence of a catalytic amount of DBU, elimination occurred to give a mixture of 3,3a-*trans* isomer **36** and double bond-migrated product **37** whose ratio was found to change depending upon reaction time. The thermodynamically most stable isomer **37** was quantitatively obtained when **36** was heated in xylene for a long time in the presence of DBU. It is understood that both inversion of stereochemistry at the 3-position and double bond migration have occurred via the common anionic intermediate **K**.

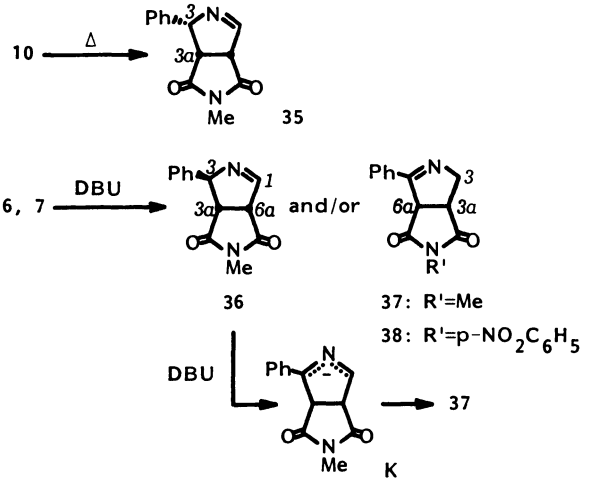

Scheme 9.

As spiro cycloadduct **12** has no possibility of secondary change after elimination of HCN, its elimination was carried out under reflux in xylene in the presence of a catalytic amount of DBU. A quantitative yield of **39** was obtained (Scheme 10 and Table 3).

Reaction with Fumarate, Maleate, and Acrylate. We further continued to study cycloaddition reactions of **1** with acyclic olefins such as dimethyl fumarate

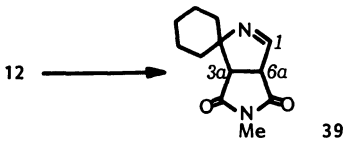

Scheme 10.

3 and maleate 4. Reaction of 1a with 3 gave two stereoisomeric cycloadducts 40 and 41 whose ratio was found to depend upon reaction conditions (Scheme 11 and Table 2). They were assigned as *r*-2, *c*-3, *t*-4, *t*-5 40 and *r*-2, *t*-3, *c*-4, *c*-5 isomer 41 on the basis of the corresponding coupling constants as well as the magnetic shielding by a phenyl group at the 5-position toward the adjacent ester moiety cis to the phenyl.

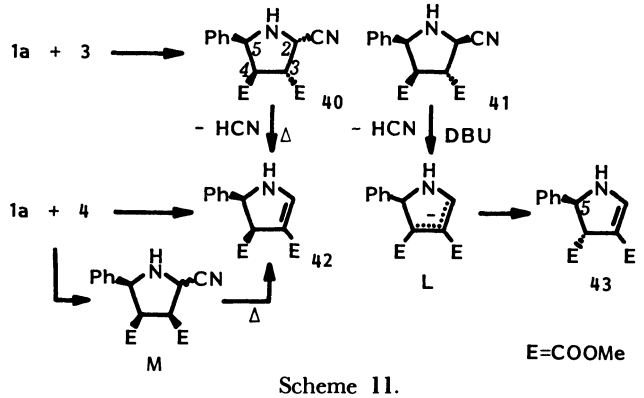

Scheme 11.

Cycloadduct 40 experienced slow elimination of HCN when heated in toluene to afford 4,5-*cis* 2-pyrroline 42 in which cis configuration at the 4- and 5-positions was retained. On the other hand, its isomer 41 suffered from no elimination until it was heated under reflux in toluene in the presence of a catalytic amount of DBU. The only product was 4,5-*trans* 2-pyrroline 43. This inversion leading to 43 as a thermodynamically more stable isomer was presumably caused via allyl anion intermediate L.

Reaction of 1a with the maleate 4 under reflux in toluene did not stop at a stage of cycloaddition but further reached to the complete elimination of HCN. The formation of 4,5-*cis* 2-pyrroline 42 as a single product indicates that cycloaddition between 1a and 4 was exclusively *endo*-selective to form cis cycloadduct M.

Thus, cycloadditions of 1a with both 3 and 4 are so highly stereoselective around one of the two newly formed C-C bonds that cycloadducts formed are exclusively 4,5-*cis* isomers. In contrast, reaction of 1e bearing an additional phenyl substituent with 3 showed poor stereoselectivity.

Reaction of 1e with 3 under reflux in benzene produced a mixture of 4,5-*cis* cycloadduct 44 and 4,5-*trans* isomer 46 of HCN-eliminated cycloadduct in a 3:1 ratio (Scheme 12 and Table 2). Under reflux in toluene, 4,5-*cis* isomer 47 of HCN-eliminated cycloadduct was newly formed (44:47:46=1.5:1.5:1), which was found to produce in a quantitative yield by thermal elimination of HCN of 44 with retention of stereochemistry. As 47 did not isomerize into 46 under the conditions of cycloaddition, 46 must be a product formed from 4,5-*trans* cycloadduct N through stereospecific HCN elimination reaction. After all, endoselectivity around the 4- and 5-positions was only 75% in this case.

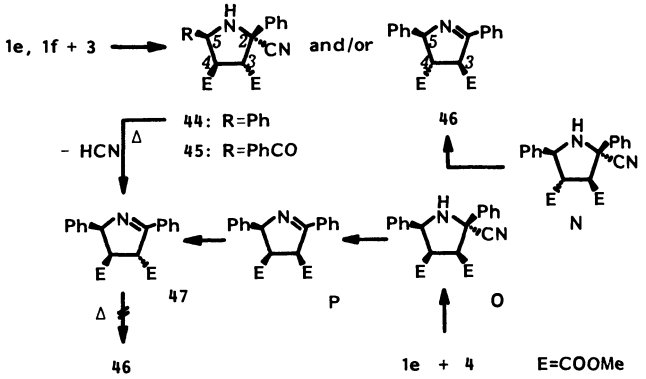

Scheme 12.

Similar cycloaddition of 1e with 4, however, occurred very cleanly to give a quantitative yield of 47 as a single isomer. As we now know that epimerization at the 5-position of 1-pyrroline hardly takes place under thermal conditions, formation of 47 is easily explained by the following mechanism: Cycloaddition between 1e and 4 first forms 4,5-*cis* cycloadduct O which then loses HCN under the conditions of cycloaddition. *r*-3, *c*-4, *c*-5 1-Pyrroline P undergoes epimerization at the 3-position through imine-enamine tautomerism.[28] Such tautomerization is frequently observed on pyrroline ring systems in which double bond is settled to the thermodynamically most stable location as seen in some examples 42, 43, 46, and 47.[29]

Not only to maleimides (Scheme 5) but also to 3, reactive imine 1f underwent stereoselective cycloaddition under mild reaction conditions to give 4,5-*cis* cycloadduct 45.

High stereoselectivity in cycloadditions of 1a with both 3 and 4 was predictable on the ground of attractive interaction working between the phenyl moiety of 1a and one of esters of 3 and 4. As shown in Fig. 3, this is the only possible attractive interaction and there exists no serious steric hindrance among substituents. As a result, stereochemistry of cycloaddition was controlled by this interaction providing 4,5-*cis* products 40—42 in all cases. On the other hand, there are two possible endo interactions in the reaction of 1e with 3 since 1e participates to cycloaddition in the most stable form G1. Accordingly, stereoselectivity between the 4- and 5-positions was poor and a mixture of 4,5-*cis* 44 and 4,5-*trans* cycloadduct N was formed. In the cycloaddition of 1e with 4, the both ester groups of 4 can possitively interact with the both phenyl groups of G1. Unlike the rigid

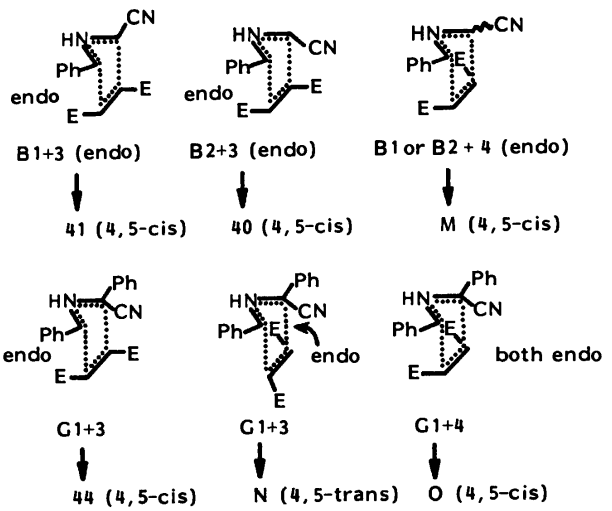

Fig. 3. Stereochemistry of cycloaddition of **1a** and **1e** with fumarate **3** and maleate **4**.

carbonyl conjugation of maleimides **2**, the ester groups of **4** can rotate around a C–C bond in such a direction as steric repulsion is minimized and also attractive interaction is maximized. Accordingly, the cycloaddition of **1e** with **4** was highly *endo*-selective forming cycloadduct **O**.

Similar reactions of **1j—k** with **3** furnished both mixtures of 4,5-*cis* **48**, **49** and 4,5-*trans* isomers **50**, **51** of HCN-eliminated cycloadducts (Scheme 13 and Table 2). However, the cycloadditions with **4** were exclusively *endo*-selective. 4,5-*cis* Isomers **48** and **49** were the only products in the reactions of **1j** and **1k**, respectively. Pyrrole **52** is the product formed by a 1,5-cyclization of imine **1j** followed by elimination of HCN. Spiro 1-pyrroline **53** carrying two ester groups trans to each other was obtained in either of reactions of **1n** with **3** and **4**.

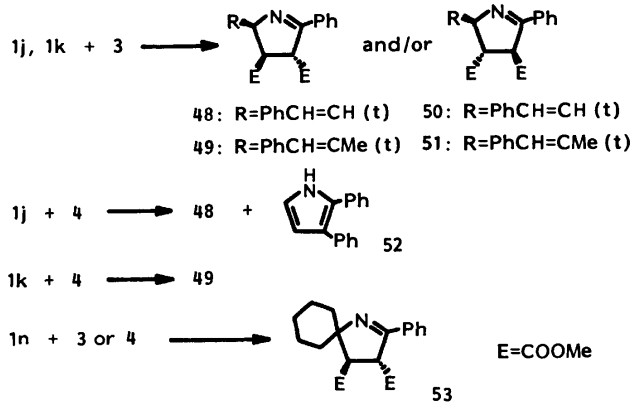

Scheme 13.

Although reaction of **1a** with methyl acrylate **5** gave only very poor yields of cycloadducts or HCN-eliminated cycloadducts under reflux in toluene or in acetonitrile in the absence or presence of AcOH, heating **1a** in **5** gave a quantitative yield of mixture of four cycloadducts. Two of the four were separated from the other two and they were assigned as mixtures of two isomers of 2,3-*cis* **54** and 2,3-*trans* cycloadduct **55** on the basis of the following conversion as well as spectral data (Scheme 14). The both mixtures **54** and **55** underwent smooth elimination of HCN affording 4,5-*cis* **56** and 4,5-*trans* 1-pyrroline **57** with retention of configuration, respectively. Both 1-pyrrolines **56** and **57** were further converted into the same pyrrole-3-carboxylate **58** by dehydrogenation with chloranil, indicating that the cycloaddition of **1a** with **5** was exclusively regioselective. As regioselectivity in this and related cycloadditions is most likely to result, at least in part, from endo attractive interaction among the substituents as shown later, comparable formation of *exo*-cycloadducts **55** in this case is

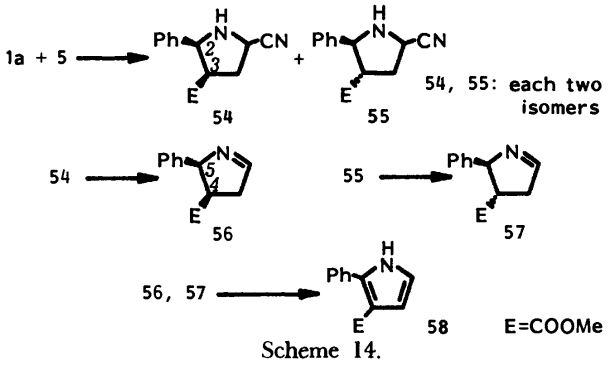

Scheme 14.

Table 3. Elimination of Hydrogen Cyanide from Cycloadducts

Cycloadduct	Reaction conditions				Product (yield/%)[a]			
	Solvent	Catalyst[b]	Temp	Time/h				
14	c)	silica gel	rt	—	**15** (100)			
10	Xylene	—	Reflux	19	**35** (60)			**10** (40)
6	Xylene	DBU	Reflux	7		**36** (19)	**37** (68)	
7	Xylene	DBU	Reflux	7			**38** (83)	
12	Xylene	DBU	Reflux	9	**39** (100)			
40	Xylene	—	Reflux	9	**42** (42)			**40** (58)
41	Toluene	DBU	Reflux	12.5		**43** (100)		
44	$CHCl_3$	silica gel	rt	—	**47** (100)			
	Toluene	—	Reflux	3	**47** (70)			
54	Toluene	DBU[d]	Reflux	17	**56** (82)			
55	Toluene	DBU	Reflux	18	**57** (81)			

a) All isolated yields. b) A catalytic amount of DBU was used. c) Chloroform–diethyl ether (3:1). d) Heating **54** under reflux in xylene in the absence of DBU gave a mixture of **56** and **54**.

quite surprising. We have so far no idea for the origin of exo cycloaddition.

Imine **1e** carrying two phenyl groups which can possitively interact with ester moiety reacted with **5** providing two regioisomeric HCN-eliminated cycloadducts **59** and **60** (Scheme 15 and Table 2). Stereochemistry at the 3-position of **60** is not important since easy epimerization is known to take place at this position.[29]

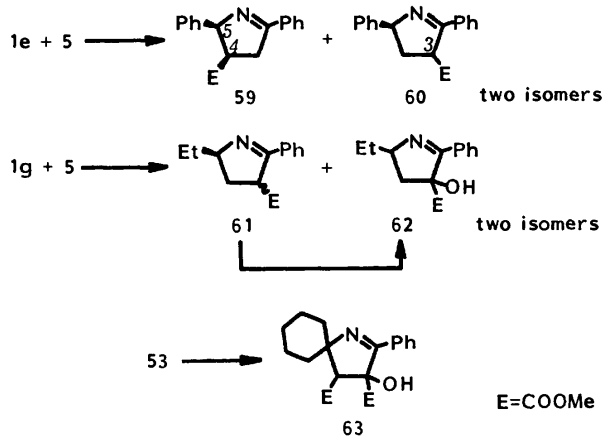

Scheme 15.

As anticipated, reaction of **1g** with **5** was regioselective giving single regioisomer **61** of HCN-eliminated cycloadduct. Probably endo interaction between the phenyl and ester groups resulted in such outstanding regioselectivity.

Surprisingly, **61** was easily air-oxidized at the 3-position forming mixture of two stereoisomeric 3-hydroxy-1-pyrrolines **62**. Similar air oxidation took place on **53** which was quantitatively oxidized into **63** under oxygen atmosphere.

Experimental

General. Melting points were determined on a Yanagimoto micro melting point apparatus and uncorrected. IR spectra were taken with a JASCO IRA-1 or a JASCO A-702 spectrometer. ^{1}H NMR spectra were recorded on a Hitachi R-40 (90 MHz) or a JEOL FX-100 instrument (100 MHz) and ^{13}C NMR spectra on a JEOL FX-100 spectrometer at 25.05 MHz. Chemical shifts are expressed in parts per million downfield from tetramethylsilane as internal standard. Mass spectra were measured with a JEOL JMS-01SG-2 spectrometer at 70 eV of ionization energy. Elementary analyses were performed on a Hitachi 026 CHN micro analyzer. Thin-layer chromatography (TLC) was accomplished on 0.2 mm precoated plates of silica gel 60 F-254 (Merck) or of aluminum oxide 60 F-254 type-E (Merck). Visualization was made with ultraviolet light (254 and 365 nm), iodine, molybdophosphoric acid (5% in ethanol), or *p*-anisaldehyde (5% in ethanol containing 5% of sulfuric acid). For preparative column chromatography, Wakogel C-200, C-300 (Wako) and Silicagel 60 (Merck) were employed. Flash chromatography was carried out on an EYELA EF-10 apparatus using a column (20×180 mm) packed with Silicagel 60 (Merck, size 0.04—0.063 mm). Preparative high performance liquid chromatography (HPLC) was performed on a Kusano KHLC-201 apparatus with a UV-detector Uvilog-III using a column (22×300 mm) packed with silica gel (Wakogel LC-50H). Solvents were evaporated with a Tokyo Rikakikai rotary evaporator type-V at about 50 °C unless otherwise cited.

Benzene, toluene, and xylene were distilled over sodium and stored on sodium wire.

General Procedure for the Preparation of 1. A mixture of each equimolar amounts of cyanomethylamine or α-cyanobenzylamine and carbonyl compounds was refluxed in an appropriate solvent under the elimination of water formed by means of a Dean-Stark trap. The solvents and reaction times are as follows: In chloroform: **1b** (10 min); **1c** (1.5 h); **1d** (5 h); **1e** (30 min); **1f** (5 min); **1g** (4 h); **1i** (30 min); **1k** (30 min); **1m** (4 h); **1n** (2.5 h); **1o** (2.5 h). In dichloromethane: **1a** (1 h). In toluene at 60 °C: **1j** (15 min). In acetone: **1l** (30 min). These imines are not highly stable and **1b**, **1f**, and **1j** are too unstable to be separated. Accordingly, the most imines **1** were prepared immediately prior to their use and they were used for the following cycloaddition reactions after the evaporation of solvent in vacuo. Some spectral and analytical data are given as follows: **1a**: IR (neat) 2240 and 1640 cm^{-1}; ^{1}H NMR ($CDCl_3$) δ=4.53 (2H, d, *J*=2.0 Hz, CH_2), 7.30—7.75 (5H, m, Ph), and 8.42 (1H, d, *J*=2.0 Hz, CH=N); ^{13}C NMR ($CDCl_3$) δ=45.73 (t, CH_2), 115.49 (s, CN), 128.06, 128.26, 131.23 (each d), 134.35 (s), and 164.27 (d, CH=N). **1c**: ^{1}H NMR ($CDCl_3$) δ=4.43 (2H, br, CH_2), 6.78—7.45 (7H, m, Ph and CH=CH), and 8.09 (1H, br d, *J*=7.5 Hz, CH=N). **1d**: ^{1}H NMR ($CDCl_3$) δ=1.55—1.90 (6H, m, CH_2), 2.15—2.40 (4H, m, CH_2), and 4.14 (2H, s, CH_2). **1e**: Colorless prisms (hexane); mp 51.5—52 °C; IR (KBr) 2210 and 1620 cm^{-1}; ^{1}H NMR ($CDCl_3$) δ=5.80 (1H, d, *J*=2.0 Hz, CH), 7.10—8.20 (10H, m. Ph), and 8.65 (1H, d, *J*=2.0 Hz, CH=N); MS *m/z* 220 (M^+). Found: C, 81.71; H, 5.46; N, 12.68%. Calcd for $C_{15}H_{12}N_2$: C, 81.79; H, 5.49; N, 12.72%. **1g**: ^{1}H NMR ($CDCl_3$) δ=1.10 (3H, t, Et), 2.36 (2H, m, Et), 5.41 (1H, br s, CH), 7.26 (5H, br s, Ph), and 7.95 (1H, br d, CH=N). **1h**: ^{1}H NMR ($CDCl_3$) δ=1.30—2.75 (7H, m, CH_2 and CH), 5.46 (1H, s, CH), 5.60 (2H, m, CH=CH), 7.26 (5H, br s, Ph), and 7.90 (1H, d, *J*=4.5 Hz, CH=N). **1i**: IR (neat) 2230 and 1620 cm^{-1}; ^{1}H NMR ($CDCl_3$) δ=1.84 (3H, d, *J*=5.0 Hz, Me), 5.45 (1H, s, CH), 6.20 (2H, m, CH=CH), 7.15—7.30 (5H, m, Ph), and 8.05 (1H, dd, *J*=7.0 and 1.5 Hz, CH=N); MS *m/z* 184 (M^+). HRMS Found: *m/z* 184.0970. Calcd for $C_{12}H_{12}N_2$: M, 184.0999. **1j**: ^{1}H NMR ($CDCl_3$) δ=5.55 (1H, d, *J*=1.5 Hz, CH), 6.80 (1H, dd, *J*=16.0 and 7.5 Hz, PhCH=CH), 7.05 (1H, d, *J*=16.0 Hz, PhCH=CH), 7.10—7.40 (10H, m, Ph), and 8.22 (1H, dd, *J*=7.5 and 1.5 Hz, CH=N). **1k**: Colorless prisms (hexane); mp 68—70 °C; IR (KBr) 2230 and 1615 cm^{-1}; ^{1}H NMR ($CDCl_3$) δ=2.07 (3H, s, Me), 5.55 (1H, s, CH), 6.80 (1H, br s, CH=), 7.10—7.40 (10H, m, Ph), and 8.14 (1H, s, CH=N); MS *m/z* 260 (M^+). Found: C, 82.85; H, 6.24; N, 10.78%. Calcd for $C_{18}H_{16}N_2$: C, 83.04; H, 6.20; N, 10.76%. **1l**: IR (neat) 2190 and 1640 cm^{-1}; ^{1}H NMR ($CDCl_3$) δ=1.95, 2.05 (each 3H, s, Me), 5.26 (1H, s, CH), and 7.10—7.50 (5H, m, Ph); ^{13}C NMR ($CDCl_3$) δ=19.65, 54.36, 119.19, 127.48, 129.24, 135.95, and 174.77. **1m**: ^{1}H NMR ($CDCl_3$) δ=1.70—2.30 (8H, m, CH_2), 4.89 (1H, s, CH), and 7.10—7.50 (5H, m, Ph). **1n**: ^{1}H NMR ($CDCl_3$) δ=1.50—2.50 (10H, m, CH_2), 5.43 (1H, s, CH), and 7.10—7.50 (5H, m, Ph). **1o**: ^{1}H NMR ($CDCl_3$) δ= 1.05 (3H, t, Et), 2.10 (3H, s, Me), 2.34 (2H, m, Et), 4.76 (1H, s, CH), and 7.10—7.50 (5H, m, Ph).

The deuterio derivatives **1a**-d_1 and **1e**-d_1 were similarly

prepared from the reactions with benzaldehyde-d_1 which was synthesized from phenylglyoxlic acid.[30]

General Procedure for the Cycloadditions of 1 with 2. The reactions of 1 with **2** were performed according to the following general procedure unless otherwise stated: A mixture of each equimolar amounts of 1 and **2** in a solvent (10—15 ml for 1 mmol of 1 or **2**) was allowed to react until either of the starting materials was all consumed (checked on TLC). The solvents and reaction conditions are listed in Tables 1 and 2. After the solvent was evaporated to dryness in vacuo, the residue was subjected to a ^{1}H NMR measurement to know the purity of products and then chromatographed over silica gel using chloroform, chloroform–diethyl ether, or chloroform–ethyl acetate (10—20:1 v/v). When a reaction was carried out in the presence of catalyst, the crude reaction mixture was first poured into water and extracted with chloroform or dichloromethane. The extract was washed with aqueous sodium hydrogencarbonate and water, dried over anhydrous magnesium sulfate, and evaporated in vacuo.

Reaction of 1a with 2a Leading to 6 and/or 10. The results are given in Table 1 (entries 1 to 5). **6**: Colorless prisms (benzene–hexane); mp 152—153 °C; IR (KBr) 3300, 2220, and 1690 cm^{-1}; ^{1}H NMR ($CDCl_3$) δ=2.40 (1H, br, NH), 2.85 (3H, s, NMe), 3.45 (1H, t, J_{6a-3a}=J_{6a-6}=8.0 Hz, 6a-H), 3.54 (1H, d, J_{3a-6a}=8.0 Hz, 3a-H), 4.66 (1H, s, 4-H), 4.78 (1H, d, J_{6-6a}=8.0 Hz, 6-H), and 7.18—7.38 (5H, m, Ph); ^{13}C NMR ($CDCl_3$) δ=25.14 (q, NMe), 47.66, 49.51, 49.85 (each d, 3a-, 4-, and 6a-C), 63.26 (d, 6-C), 118.66 (s, CN), 126.99, 128.45, 128.55, 136.00 (s), 174.01, and 175.24 (each s, CON); MS *m/z* (rel. intensity, %) 255 (M$^+$, 29), 144 (76), 143 (base peak), and 77 (49).

Found: C, 66.04; H, 5.13; N, 16.24%. Calcd for $C_{14}H_{13}N_3O_2$: C, 65.87; H, 5.13; N, 16.46%.

10: Colorless prisms (acetone–hexane); mp 199—200 °C; IR (KBr) 3300, 2250, and 1690 cm^{-1}: ^{1}H NMR (DMSO-d_6) δ=2.50 (1H, br, NH), 2.72 (3H, s, NMe), 3.42 (1H, t, J_{6a-3a}=J_{6a-6}=7.5 Hz, 6a-H), 3.56 (1H, t, J_{3a-4}=J_{3a-6a}=7.5 Hz, 3a-H), 4.22 (1H, d, J_{4-3a}=7.5 Hz, 4-H), 4.32 (1H, d, J_{6-6a}=7.5 Hz, 6-H), and 7.16—7.32 (5H, m, Ph); ^{13}C NMR (DMSO-d_6) δ=24.46 (q, NMe), 46.59, 47.85, 48.58 (each d, 3a-, 4-, and 6a-C), 62.91 (d, 6-C), 117.44 (s, CN), 127.09, 127.62, 137.62 (s), 174.40, and 174.99 (each s, CON); MS *m/z* (rel. intensity, %) 255 (M$^+$, 13), 228 (33), 144 (70), 143 (base peak), 117 (70), 115 (72), 90 (50), 89 (56), and 77 (39).

Found: C, 65.71; H, 5.09; N, 16.11%. Calcd for $C_{14}H_{13}N_3O_2$: C, 65.87; H, 5.13; N, 16.46%.

Reaction of 1a with 2b Leading to 7. The results are given in Table 1 (Entries 6 and 7): Colorless needles (benzene–hexane); mp 148—149 °C; IR (KBr) 3350, 2230, and 1720 cm^{-1}; ^{1}H NMR ($CDCl_3$) δ=2.53 (1H, br, NH), 3.64 (1H, t, J_{6a-3a}=J_{6a-6}=8.0 Hz, 6a-H), 3.76 (1H, d, J_{3a-6a}=8.0 Hz, 3a-H), 4.80 (1H, s, 4-H), 4.96 (1H, d, J_{6-6a}=8.0 Hz, 6-H), 7.22—7.40 (7H, m, Ar), and 8.10—8.30 (2H, m, Ar); ^{13}C NMR ($CDCl_3$) δ=47.56, 49.90, 50.20 (each d, 3a-, 4-, and 6a-C), 63.64 (d, 6-C), 118.13 (s, CN), 124.35, 126.28, 126.93, 128.75, 129.05, 135.39 (s), 136.62, 146.89 (each s), 172.20, and 173.43 (each s, CON); MS *m/z* (rel. intensity, %) 362 (M$^+$, 6), 143 (53), 117 (47), 115 (51), 90 (base peak), and 89 (53).

Found: C, 63.26; H, 3.91; N, 15.27%. Calcd for $C_{19}H_{14}N_4O_4$: C, 62.98; H, 3.89; N, 15.46%.

Reaction of 1b with 2a Leading to 8. A mixture of cyanomethylamine (162 mg, 2.89 mmol) and phenylglyoxal (440 mg, 2.89 mmol) in chloroform (30 ml) was heated under reflux for 10 min. After **2a** (321 mg, 2.89 mmol) was added, the mixture was allowed to react under the conditions shown in Table 2 to give **8**: Colorless prisms (benzene); mp 210—211 °C; IR (KBr) 3310, 2240, 1780, and 1700 cm^{-1}; ^{1}H NMR (CD_3CN) δ=2.71 (3H, s, NMe), 3.32 (1H, m, NH), 3.65 (1H, dd, J_{3a-4}=1.4 and J_{3a-6a}=7.7 Hz, 3a-H), 3.91 (1H, t, J_{6a-3a}=J_{6a-6}=7.7 Hz, 6a-H), 4.66 (1H, dd, J_{4-3a}=1.4 and J_{4-NH}=5.2 Hz, 4-H), 5.03 (1H, dd, J_{6-6a}=7.7 and J_{6-NH}=9.0 Hz, 6-H), 7.30—7.70 (3H, m, Ph), and 7.85—8.06 (2H, m, Ph); ^{13}C NMR (DMSO-d_6) δ=24.94 (q, NMe), 49.42, 50.18, 51.66 (each d, 3a-, 4-, and 6a-C), 64.59 (d, 6-C), 119.95 (s, CN), 128.42, 128.95, 133.77 (each d), 136.07 (s), 175.54 (2×C, s, CON), and 195.31 (s, PhCO); MS *m/z* (rel. intensity, %) 283 (M$^+$, 1), 178 (base peak), 106 (68), 93 (38), and 77 (25).

Found: C, 63.58; H, 4.67; N, 14.64%. Calcd for $C_{15}H_{13}N_3O_3$: C, 63.60; H, 4.63; N, 14.83%.

Reaction of 1c with 2a Leading to 9 and 11. A mixture of cyanomethylamine (112 mg, 2 mmol) and cinnamaldehyde (264 mg, 2 mmol) in chloroform (20 ml) was heated under reflux for 1.5 h on molecular sieves 4A. The molecular sieves was filtered off and the chloroform was evaporated in vacuo. To the residue were added dry toluene (20 ml) and **2a** (222 mg, 2 mmol). The mixture was allowed to react under the conditions shown in Table 2 to give a mixture of **9** and 11. **9**: Colorless needles (acetone–hexane); mp 175—176 °C; IR (KBr) 3450, 3320, 2220, 1765, and 1690 cm^{-1}; ^{1}H NMR (CD_3CN) δ=2.86 (3H, s, NMe), 3.44 (1H, t, J_{6a-3a}=J_{6a-6}=8.0 Hz, 6a-H), 3.60 (1H, d, J_{3a-6a}=8.0 Hz, 3a-H), 4.22 (1H, dd, J_{6-6a}=8.0 and $J_{6\text{-}CH=}$=7.2 Hz, 6-H), 4.51 (1H, s, 4-H), 6.10 (1H, dd, $J_{=CH\text{-}6}$=7.2 and J_{trans}=16.0 Hz, PhCH=C<u>H</u>), 6.66 (1H, d, J_{trans}=16.0 Hz, PhC<u>H</u>=CH), and 7.20—7.50 (5H, m, Ph); MS *m/z* (rel. intensity, %) 281 (M$^+$, 83), 170 (base peak), and 169 (74).

Found: C, 68.50; H, 5.44; N, 14.78%. Calcd for $C_{16}H_{15}N_3O_2$: C, 68.31; H, 5.37; N, 14.94%.

11: Colorless prisms (acetone–hexane); mp 209—210 °C; IR (KBr) 3450, 3310, 2230, 1765, and 1690 cm^{-1}; ^{1}H NMR (CD_3CN) δ=2.88 (3H, s, NMe), 3.30 (1H, t, J_{6a-3a}=J_{6a-6}=7.5 Hz, 6a-H), 3.49 (1H, t, J_{3a-4}=J_{3a-6a}=7.5 Hz, 3a-H), 3.89 (1H, dd, J_{6-6a}=7.5 and $J_{6\text{-}CH=}$=7.1 Hz, 6-H), 4.14 (1H, d, J_{4-3a}=7.5 Hz, 4-H), 6.14 (1H, dd, $J_{=CH\text{-}6}$=7.1 and J_{trans}=16.0 Hz, PhCH=C<u>H</u>), 6.60 (1H, d, J_{trans}=16.0 Hz, PhC<u>H</u>=CH), and 7.20—7.50 (5H, m, Ph); MS *m/z* (rel. intensity, %) 281 (M$^+$, 40), 254 (46), 170 (45), 169 (68), 168 (38), 143 (54), 115 (base peak), and 77 (35).

Found: C, 68.07; H, 5.31; N, 15.16%. Calcd for $C_{16}H_{15}N_3O_2$: C, 68.31; H, 5.37; N, 14.94%.

Reaction of 1d with 2a Leading to 12 and 13. A mixture of cyanomethylamine (153 mg, 2.73 mmol) and cyclohexanone (276 mg, 2.73 mmol) in dry chloroform (30 ml) was heated under reflux for 5 h. The solvent was removed by evaporation in vacuo. To the residue were added dry toluene (30 ml) and **2a** (303 mg, 2.73 mmol). The mixture was allowed to react under the conditions shown in Table 2 and chromatographed over silica gel. An elution with chloroform–diethyl ether (20:1) gave **13** (285 mg, 50%) and the followed fraction with chloroform–diethyl ether (10:1) afforded **12** (101 mg, 15%). The same reaction in the presence of acetic acid gave only **13** (70—72%).

12: Colorless prisms (benzene–hexane); mp 158—159 °C; IR (KBr) 3330, 2920, 2840, 2240, 1770, and 1695 cm^{-1}; ^{1}H NMR ($CDCl_3$) δ=1.20—2.20 (10H, m, CH_2), 2.50 (1H, br,

NH), 2.94 (1H, d, J_{6a-3a}=7.8 Hz, 6a-H), 3.00 (3H, s, NMe), 3.50 (1H, t, $J_{3a-4}=J_{3a-6a}$=7.8 Hz, 3a-H), and 4.28 (1H, d, J_{4-3a}=7.8 Hz, 4-H); ^{13}C NMR ($CDCl_3$) δ=22.59, 23.00 (each t, CH_2) 25.24 (2×C, t and q, CH_2 and NMe), 34.47, 36.00 (each t, CH_2), 47.06, 47.94, 53.59 (each d, 3a-, 4-, and 6a-C), 64.65 (s, 6-C), 117.59 (s, CN), 174.95, and 175.48 (each s, CON); MS *m/z* (rel. intensity, %) 247 (M^+, 20), 204 (base peak), 191 (28), and 119 (38).

Found: C, 62.99; H, 6.94; N, 16.92%. Calcd for $C_{13}H_{17}N_3O_2$: C, 63.14; H, 6.93; N, 16.99%.

13: Colorless needles (benzene-hexane); mp 122—123 °C; IR (KBr) 2900, 2830, and 1680 cm^{-1}; ^{1}H NMR ($CDCl_3$) δ=1.40—2.84 (12H, m, CH_2 and CH), and 3.00 (3H, s, NMe); ^{13}C NMR ($CDCl_3$) δ=24.94 (q, NMe), 24.77, 27.06, 31.83, 31.94 (each t, CH_2), 41.18 (d, CH), 41.77 (t, CH_2), 50.36 (d, CH), 177.01, 179.54 (each s, CON), and 210.54 (s, CO); MS *m/z* (rel. intensity, %) 209 (M^+, 35), 113 (base peak), and 97 (88).

Found: C, 63.27; H, 7.26; N, 6.82%. Calcd for $C_{11}H_{15}NO_3$: C, 63.14; H, 7.23; N, 6.69%.

Reaction of 1f with 2a Leading to 14 and/or 15. A mixture of α-cyanobenzylamine (563 mg, 3.7 mmol) and phenylglyoxal (489 mg, 3.7 mmol) in dry chloroform (30 ml) was heated under reflux for 5 min and **2a** (411 mg, 3.7 mmol) was added. The mixture was refluxed for 5 min and the solvent was evaporated in vacuo to give **14** (1.328 g, 100%). Continued heating for 1 h afforded a mixture of **14** and **15** (1:1). The latter **15** was obtained in a quantitative yield when **14** was chromatographed over silica gel with chloroform–diethyl ether (3:1).

14: Colorless prisms; mp 157—158 °C; IR (KBr) 3350, 1780, 1710, and 1685 cm^{-1}; ^{1}H NMR (DMSO-d_6) δ=2.70 (3H, s, NMe), 4.16 (1H, dd, J_{6a-3a}=9.0 and J_{6a-6}=10.0 Hz, 6a-H), 4.96 (1H, d, J_{3a-6a}=9.0 Hz, 3a-H), 6.20 (1H, br, NH), 6.36 (1H, d, J_{6-6a}=10.0 Hz, 6-H), and 7.20—8.10 (10H, m, Ph); MS *m/z* (rel. intensity, %) 332 (M^+—HCN, 10), 142 (22), 115 (65), and 105 (base peak).

Found: C, 70.14; H, 4.82; N, 11.58%. Calcd for $C_{21}H_{17}N_3O_3$: C, 70.18; H, 4.77; N, 11.69%.

15: Pale yellow prisms (acetone-hexane); mp 285—286 °C; IR (KBr) 1740 and 1690 cm^{-1}; ^{1}H NMR ($CDCl_3$) δ=2.88 (3H, s, NMe), 4.30 (1H, dd, J_{3a-3}=2.6 and J_{3a-6a}=8.5 Hz, 3a-H), 4.66 (1H, dd, J_{6a-3}=2.9 and J_{6a-3a}=8.5 Hz, 6a-H), 6.02 (1H, dd, J_{3-3a}=2.6 and J_{3-6a}=2.9 Hz, 3-H), and 7.20—8.30 (10H, m, Ph); ^{13}C NMR ($CDCl_3$) δ=25.25 (q, NMe), 45.79 (d, 3a-C), 56.60 (d, 6a-C), 79.55 (d, 3-C), 128.28, 128.63, 129.57, 131.45, 131.69, 133.86, 134.74, 167.44 (s, 1-C), 173.01, 177.54 (each s, CON), and 193.62 (s, PhCO); MS *m/z* (rel. intensity, %) 331 (M^+—H, 8), 330 (33), 140 (29), 113 (24), 105 (40), and 77 (base peak).

Found: C, 72.48; H, 4.30; N, 8.63%. Calcd for $C_{20}H_{16}N_2O_3$: C, 72.28; H, 4.85; N, 8.43%.

Reaction of 1e with 2a Leading to 16, 18 and/or 20, 22. Under the conditions shown in Table 2, a mixture of **16**, **18** and/or **20**, **22** was obtained. **16**: Colorless prisms (benzene); mp 178—179 °C; IR (KBr) 1780, 1700, and 1615 cm^{-1}; ^{1}H NMR ($CDCl_3$) δ=2.60 (3H, s, NMe), 3.94 (1H, dd, J_{3a-3}=10.0 and J_{3a-6a}=9.0 Hz, 3a-H), 4.60 (1H, dd, J_{6a-3a}=9.0 Hz, 6a-H), 5.85 (1H, d, J_{3-3a}=10.0 Hz, 3-H), 6.96—7.50 (8H, m, Ph), and 8.10 (2H, m, Ph); ^{13}C NMR ($CDCl_3$) δ=24.72 (q, NMe), 49.49 (d, 3a-C), 56.71 (d, 6a-C), 77.20 (d, 3-C), 127.11, 128.16, 128.34, 128.46, 129.57, 131.63, 131.86, 137.09, 144.59, 144.84, 167.26 (s, 1-C), 173.01, and 174.14 (each s, CON); MS *m/z* (rel. intensity, %) 306 (M^+, 5), 304 (base peak), 219 (23), and 115 (48).

Found: C, 74.10; H, 5.83; N, 9.27%. Calcd for $C_{19}H_{18}N_2O_2$: C, 74.49; H, 5.92; N, 9.15%.

18: Colorless prisms (benzene-hexane); mp 162—163 °C; IR (KBr) 1775, 1700, and 1610 cm^{-1}; ^{1}H NMR ($CDCl_3$) δ=2.95 (3H, s, NMe), 3.56 (1H, dd, J_{3a-3}=3.0 and J_{3a-6a}=8.5 Hz, 3a-H), 4.66 (1H, dd, J_{6a-3}=2.5 and J_{6a-3a}=8.5 Hz, 6a-H), 5.65 (1H, dd, J_{3-3a}=3.0 and J_{3-6a}=2.5 Hz, 3-H), 7.28—7.50 (8H, m, Ph), and 8.20 (2H, m, Ph); ^{13}C NMR ($CDCl_3$) δ=25.19 (q, NMe), 53.48 (d, 3a-C), 56.40 (d, 6a-C), 75.74 (d, 3-C), 126.17, 127.64, 128.40, 128.81, 129.57, 131.57, 131.75, 142.02, 166.32 (d, 1-C), 172.90, and 177.00 (each s, CON); MS *m/z* (rel. intensity, %) 306 (M^+, 4), 304 (base peak), 219 (15), and 115 (23).

Found: C, 74.66; H, 5.92; N, 9.22%. Calcd for $C_{19}H_{18}N_2O_2$: C, 74.49; H, 5.92; N, 9.15%.

20: Colorless prisms (benzene-hexane); mp 136—137 °C; IR (KBr) 2140, 1775, 1700, and 1610 cm^{-1}; ^{1}H NMR ($CDCl_3$) δ=2.68 (2H, d, J=7.0 Hz, CH_2), 2.82 (3H, s, NMe), 3.57 (1H, t, J=7.0 Hz, CH), 7.10—7.55 (8H, m, Ph), 7.80 (2H, m, Ph), and 8.53 (1H, s, CH=N); ^{13}C NMR ($CDCl_3$) δ=24.83 (q, NMe), 31.47 (t, CH_2), 50.24 (d, CH), 71.12 (s, q-C), 117.07 (s, CN), 126.18, 126.71, 129.13, 129.36, 129.66, 132.54, 134.60, 136.59, 163.13 (d, CH=N), 174.01, and 174.66 (each s, CON); MS *m/z* 333 (M^+, 15), 228 (base peak), and 115 (16).

Found: C, 72.03; H, 5.78; N, 12.68%. Calcd for $C_{20}H_{19}N_3O_2$: C, 72.05; H, 5.74; N, 12.61%.

22: Colorless viscous oil; IR (neat) 2210, 1775, 1700, and 1605 cm^{-1}; ^{1}H NMR ($CDCl_3$) δ=2.70 (2H, d, J=6.5 Hz, CH_2), 2.84 (3H, s, NMe), 3.46 (1H, q, J=6.5 Hz, CH), 5.43 (1H, d, J=6.5 Hz, CH), 7.20—7.55 (8H, m, Ph), and 8.00 (2H, m, Ph); ^{13}C NMR ($CDCl_3$) δ=24.71 (q, NMe), 31.24 (t, CH_2), 46.47 (d, CH), 71.65 (d, CH), 109.71 (s, CN), 126.72, 127.24, 127.83, 128.18, 128.95, 129.19, 133.01, 133.24, 137.83, 142.60 (s, C=N), 175.89, and 176.83 (each s, CON); MS *m/z* 333 (M^+, 10), 220 (18), 219 (base peak), 115 (27), and 105 (50).

Found: C, 71.84; H, 5.71; N, 12.64%. Calcd for $C_{20}H_{19}N_3O_2$: C, 72.05; H, 5.74; N, 12.61%.

Reaction of 1e with 2b Leading to 17, 19 and/or 21, 23. The result is given in Table 2. **17**: Colorless needles (benzene-hexane); mp 265—266 °C; IR (KBr) 1780, 1720, and 1610 cm^{-1}; ^{1}H NMR ($CDCl_3$) δ=4.20 (1H, t, $J_{3a-6a}=J_{3a-3}$=9.0 Hz, 3a-H), 4.90 (1H, d, J_{6a-3a}=9.0 Hz, 6a-H), 6.15 (1H, d, J_{3-3a}=9.0 Hz, 3a-H), and 6.90—8.40 (14H, m, Ar); MS *m/z* (rel. intensity, %) 411 (M^+, 77), 219 (31), 193 (base peak), and 115 (39).

Found: C, 70.16; H, 4.35; N, 10.15%. Calcd for $C_{24}H_{17}N_3O_4$: C, 70.06; H, 4.17; N, 10.21%.

19: Colorless prisms (benzene-hexane); mp 239—241 °C; IR (KBr) 1780, 1720, and 1610 cm^{-1}; ^{1}H NMR ($CDCl_3$) δ=3.85 (1H, dd, J_{3a-3}=3.0 and J_{3a-6a}=9.0 Hz, 3a-H), 4.95 (1H, dd, J_{6a-3}=3.0 and J_{6a-3a}=9.0 Hz, 6a-H), 5.90 (1H, t, $J_{3-3a}=J_{3-6a}$=3.0 Hz, 3-H), and 7.30—8.45 (14H, m, Ar); MS *m/z* (rel. intensity, %) 411 (M^+, 51), 219 (36), 193 (base peak), and 115 (46).

Found: C, 69.87; H, 4.03; N, 10.17%. Calcd for $C_{24}H_{17}N_3O_4$: C, 70.06; H, 4.17; N, 10.21%.

21: Colorless prisms (benzene-hexane); mp 250—252 °C; IR (KBr) 2250, 1780, 1720, and 1615 cm^{-1}; ^{1}H NMR ($CDCl_3$) δ=2.90 (2H, m, CH_2), 4.35 (1H, m, CH), 7.30—8.30 (14H, m, Ar), and 8.80 (1H, s, CH=N); MS *m/z* (rel. intensity, %) 438 (M^+, 14), 220 (18), 219 (base peak), and 115 (15).

Found: C, 68.27; H, 4.25; N, 12.50%. Calcd for $C_{25}H_{18}N_4O_4$:

C, 68.48; H, 4.14; N, 12.78%.

23: Colorless prisms (benzene-hexane); mp 195—196 °C; IR (KBr) 2240, 1775, 1710, and 1610 cm^{-1}; ^1H NMR ($CDCl_3$) δ=2.91 (1H, dd, J_{gem}=18.0 and J=9.0 Hz, one of CH_2), 3.10 (1H, dd, J_{gem}=18.0 and J=6.0 Hz, the other of CH_2), 3.63 (1H, ddd, J=9.0, 7.0, and 6.0 Hz, CH), 5.53 (1H, d, J=7.0 Hz, CH), and 7.22—8.32 (14H, m, Ar); MS *m/z* (rel. intensity, %) 438 (M^+, 13), 220 (21), 219 (base peak), and 115 (21).

Found: C, 68.12; H, 4.23; N, 12.49%. Calcd for $C_{25}H_{18}N_4O_4$: C, 68.48; H, 4.14; N, 12.78%.

Reaction of 1g with 2a Leading to 24. A mixture of propionaldehyde (300 mg, 5.17 mmol) and α-cyanobenzylamine (230 mg, 1.74 mmol) in dry chloroform was heated under reflux for 4 h. After the solvent and the excess aldehyde were removed by evaporation in vacuo, toluene (20 ml) and **2a** (215 mg, 1.94 mmol) were added to the residue. The mixture was allowed to react under the conditions given in Table 2 to give **24**: Colorless prisms (ethyl ether-hexane); mp 91—92 °C; IR (KBr) 2930, 1760, 1690, and 1610 cm^{-1}; ^1H NMR ($CDCl_3$) δ=1.16 (3H, t, Et), 1.20—1.32, 1.90—2.25 (each 1H, m, Et), 2.88 (3H, s, NMe), 3.66 (1H, t, J_{3a-3}=J_{3a-6a}=9.5 Hz, 3a-H), 4.32—4.64 (2H, m, 3- and 6a-H), 7.30—7.52 (3H, m, Ph), and 7.96—8.20 (2H, m, PH); ^{13}C NMR ($CDCl_3$) δ=12.12 (q, Et), 24.94 (q, NMe), 25.94 (t, Et), 47.18 (d, 3a-C), 56.89 (d, 6a-C), 75.18 (d, 3-C), 128.48, 129.48, 131.30, 132.48 (each d), 164.72 (s, 1-C), 173.54, and 175.95 (each s, CON); MS *m/z* 256 (M^+, 22), 228 (42), 170 (30), 145 (44), 144 (23), 143 (25), 142 (59), 130 (base peak), 115 (80), 104 (67), and 77 (30).

Found: C, 70.11; H, 6.27; N, 10.78%. Calcd for $C_{15}H_{16}N_2O_2$: C, 70.29; H, 6.29; N, 10.93%.

Reaction of 1h with 2a Leading to 25. A mixture of 3-cyclohexene-1-carbaldehyde (128 mg, 1.16 mmol) and α-cyanobenzylamine (119 mg, 0.902 mmol) was heated under reflux in dry chloroform (10 ml) for 2 h. The solvent was evaporated in vacuo. To the residue were added dry toluene (10 ml) and **2a** (111 mg, 1 mmol). The mixture was allowed to react under the conditions shown in Table 2 giving **25** as mixture of threo and erythro isomers (1:1): Colorless prisms (benzene-hexane); mp 167—168 °C; IR (KBr) 2980, 2860, 1750, 1670, and 1615 cm^{-1}; ^1H NMR ($CDCl_3$) δ=1.24—2.62 (7H, m, CH_2 and CH), 2.90 (3H, s, NMe), 3.68, 3.74 (each 0.5H, t, J_{3a-3}=J_{3a-6a}=9.0 Hz, 3a-H), 4.28—4.66 (2H, m, 3- and 6a-H), 5.70 (2H, m, CH=CH), 7.30—7.52 (3H, m, Ph), and 7.96—8.20 (2H, m, Ph); ^{13}C NMR ($CDCl_3$) δ=25.00 (q, NMe), 25.41, 25.41, 28.76, 31.18, 35.18, 36.18 (CH_2 and CH), 46.30, 46.53 (each d, 3a-C), 56.83 (d, 6a-C), 77.30, 78.59 (each d, 3-C), 126.30, 127.19, 128.42, 131.30 (each d), 132.42 (s), 165.07 (s, 1-C), 173.36, 175.89, and 176.18 (each s, CON); MS *m/z* (rel. intensity, %) 308 (M^+, 18), 228 (71), 200 (33), 170 (25), 143 (base peak), 142 (40), 116 (21), 115 (75), 104 (26), 91 (32), 80 (21), 79 (40), and 77 (51).

Found: C, 74.22; H, 6.52; N, 8.95%. Calcd for $C_{19}H_{20}N_2O_2$: C, 74.00; H, 6.54; N, 9.08%.

Reaction of 1i with 2a Leading to 26 and 29. The result is given in Table 2: **26**: Colorless prisms (benzene-hexane); mp 108—109 °C; IR (KBr) 1775, 1690, and 1615 cm^{-1}; ^1H NMR ($CDCl_3$) δ=1.68 (3H, d, J=7.0 Hz, Me), 2.85 (3H, s, NMe), 3.67 (1H, t, J_{3a-3}=J_{3a-6}=9.0 Hz, 3a-H), 4.46 (1H, d, J_{6a-3a}=9.0 Hz, 6a-H), 5.15 (1H, dd, J_{3-3a}=9.0 and $J_{3\text{-}CH=}$=6.0 Hz, 3-H), 5.40—5.85 (2H, m, MeC<u>H</u>=C<u>H</u>), 7.35 (3H, m, Ph), and 8.05 (2H, m, Ph); ^{13}C NMR ($CDCl_3$) δ=17.94 (q, Me), 25.00 (q, NMe), 48.47 (d, 3a-C), 56.71 (d, 6a-C), 74.48 (d, 3-C), 127.36, 128.65, 129.71, 129.89, 131.71, 132.18, 137.42, 166.30 (s, 1-C), 173.48, and 175.36 (each s, CON); MS *m/z* (rel. intensity, %) 268 (M^+, 20), 210 (11), 182 (22), and 115 (base peak).

Found: C, 71.39; H, 5.88; N, 10.22%. Calcd for $C_{16}H_{16}N_2O_2$: C, 71.62; H, 6.01; N, 10.44%.

29: Colorless prisms (hexane); mp 150—151 °C; IR (KBr) 1770, 1700, and 1605 cm^{-1}; ^1H NMR ($CDCl_3$) δ=1.70 (3H, d, Me), 2.90 (3H, s, NMe), 3.36 (1H, dd, J_{3a-3}=4.0 and J_{3a-6a}=8.0 Hz, 3a-H), 4.57 (1H, dd, J_{6a-3}=2.0 and J_{6a-3a}=8.0 Hz, 6a-H), 5.00 (1H, m, 3-H), 5.25—5.93 (2H, m, MeC<u>H</u>=C<u>H</u>), 7.35 (3H, m, Ph), and 8.05 (1H, m, Ph); ^{13}C NMR ($CDCl_3$) δ=17.77 (q, Me), 25.14 (q, NMe), 51.12 (d, 3a-C), 56.05 (d, 6a-C), 76.56 (d, 6-C), 114.55, 126.41, 128.56, 129.05, 129.59, 131.25, 131.64, 132.08, 165.87 (s, 1-C), 173.44, and 177.39 (each s, CON); MS *m/z* (rel. intensity, %) 268 (M^+, 21), 193 (base peak), 115 (30), and 105 (21).

Found: C, 71.54; H, 6.06; N, 10.27%. Calcd for $C_{16}H_{16}N_2O_2$: C, 71.62; H, 6.01; N, 10.44%.

Reaction of 1j with 2a Leading to 27 and 30. A mixture of cinnamaldehyde (264 mg, 2 mmol) and α-cyanobenzylamine (264 mg, 2 mmol) in toluene (10 ml) was heated at 60 °C for 5 min and then **2a** (222 mg, 2 mmol) was added. The mixture was allowed to react under the conditions given in Table 2.

27: Colorless needles (benzene-hexane); mp 153—154 °C; IR (KBr) 1780, 1700, and 1610 cm^{-1}; ^1H NMR ($CDCl_3$) δ=2.85 (3H, s, NMe), 3.88 (1H, dd, J_{3a-3}=9.0 and J_{3a-6a}=8.0 Hz, 3a-H), 4.64 (1H, d, J_{6a-3a}=8.0 Hz, 6a-H), 5.42 (1H, dd, J_{3-3a}=9.0 and $J_{3\text{-}CH=}$=6.0 Hz, 3-H), 6.30 (1H, dd, J=6.0 and J_{trans}=18.0 Hz, PhCH=C<u>H</u>), 6.60 (1H, d, J_{trans}=18.0 Hz, PhC<u>H</u>=CH), 7.20—7.54 (8H, m, Ph), and 8.20 (2H, m, Ph); MS *m/z* (rel. intensity, %) 330 (M^+, 53), 245 (23), 219 (23), and 115 (base peak).

Found: C, 76.36; H, 5.47; N, 8.41%. Calcd for $C_{21}H_{18}N_2O_2$: C, 76.34; H, 5.49; N, 8.48%.

30: Colorless prisms (benzene-hexane); mp 145—146 °C; IR (KBr) 1770 and 1700 cm^{-1}; ^1H NMR ($CDCl_3$) δ=2.95 (3H, s, NMe), 3.50 (1H, dd, J_{3a-3}=3.2 and J_{3a-6a}=8.3 Hz, 3a-H), 4.68 (1H, dd, J_{6a-3}=2.5 and J_{6a-3a}=8.3 Hz, 6a-H), 5.26 (1H, ddd, J_{3-3a}=3.2, J_{3-6a}=2.5, and $J_{3\text{-}CH=}$=6.0 Hz, 3-H), 6.26 (1H, dd, J=6.0 and J_{trans}=16.0 Hz, PhCH=C<u>H</u>), 6.68 (1H, d, J_{trans}=16.0 Hz, PhC<u>H</u>=CH), 7.20—7.50 (8H, m, Ph), and 8.18 (2H, m, Ph); MS *m/z* (rel. intensity, %) 330 (M^+, base peak), 245 (29), 219 (27), and 115 (96).

Found: C, 76.61; H, 5.58; N, 8.41%. Calcd for $C_{21}H_{18}N_2O_2$: C, 76.34; H, 5.49; N, 8.48%.

Reaction of 1k with 2a Leading to 28. The result is shown in Table 2: Colorless prisms (benzene-hexane); mp 149—150 °C; IR (KBr) 1770, 1690, and 1610 cm^{-1}; ^1H NMR ($CDCl_3$) δ=1.92 (3H, d, J=1.0 Hz, Me), 2.74 (3H, s, NMe), 3.72 (1H, t, J_{3a-3}=J_{3a-6a}=9.0 Hz, 3a-H), 4.42 (1H, d, J_{6a-3a}=9.0 Hz, 6a-H), 5.13 (1H, d, J_{3-3a}=9.0 Hz, 3-H), 6.13 (1H, br, PhC<u>H</u>=), 6.90—7.40 (8H, m, Ph), and 8.07 (2H, m, Ph); ^{13}C NMR ($CDCl_3$) δ=18.24 (q, Me), 25.00 (q, NMe), 48.18 (d, 3a-C), 56.77 (d, 6a-C), 79.47 (d, 3-C), 126.83, 127.71, 128.30, 128.65, 129.13, 129.77, 131.83, 132.12, 136.18, 136.48, 167.07 (s, 1-C), 173.30, and 175.07 (each s, CON); MS *m/z* (rel. intensity, %) 344 (M^+, 31), 233 (33), and 115 (base peak).

Found: C, 76.92; H, 5.92; N, 8.10%. Calcd for $C_{22}H_{20}N_2O_2$: C, 76.72; H, 5.85; N, 8.13%.

Reaction of 1l with 2a Leading to 31. A mixture of α-cyanobenzylamine (240 mg, 1.82 mmol) and acetone (20 ml) was heated under reflux for 30 min. The acetone was evaporated in vacuo and **2a** (222 mg, 2 mmol) was added to the residue. The mixture was allowed to react under the conditions shown in Table 2 to give **31**: Colorless prisms

(benzene-hexane); mp 176—177°C; IR (KBr) 2940, 1750, 1690, and 1610 cm^{-1}; ^1H NMR ($CDCl_3$) δ=1.33, 1.46 (each 3H, s, Me), 2.85 (3H, s, NMe), 3.25 (1H, d, J_{3a-6a}=8.5 Hz, 3a-H), 4.55 (1H, d, J_{6a-3a}=8.5 Hz, 6a-H), 7.20—7.50 (3H, m, Ph), and 7.90—8.20 (2H, m, Ph); ^{13}C NMR ($CDCl_3$) δ=24.94 (q, NMe), 25.47, 32.12 (each q, Me), 53.89 (d, 3a-C), 57.18 (d, 6a-C), 75.30 (s, 3-C), 128.48, 129.48, 131.30 (each d), 132.36 (s), 162.37 (s, 1-C), 173.43, and 176.01 (each s, CON); MS *m/z* (rel. intensity, %) 256 (M^+, 47), 255 (23), 170 (25), 156 (30), 145 (89), 115 (37), 104 (base peak), 103 (25), 96 (20), and 77 (30).

Found: C, 70.50; H, 6.35; N, 10.61%. Calcd for $C_{15}H_{16}N_2O_2$: C, 70.29; H, 6.29; N, 10.93%.

Reaction of 1m with 2a Leading to 32. A mixture of cyclopentanone (175 mg, 2.08 mmol) and α-cyanobenzylamine (238 mg, 1.80 mmol) in dry chloroform (20 ml) was heated under reflux for 4 h. The solvent was evaporated in vacuo and **2a** (222 mg, 2 mmol) in dry toluene (20 ml) was added to the residue. The mixture was allowed to react under the conditions shown in Table 2 giving **32**: Colorless prisms (benzene-hexane); mp 148—149°C; IR (KBr) 2930, 1750, 1680, and 1610 cm^{-1}; ^1H NMR ($CDCl_3$) δ=2.56—3.20 (8H, m, CH_2), 2.91 (3H, s, NMe), 3.38 (1H, d, J_{3a-6a}=8.7 Hz, 3a-H), 4.60 (1H, d, J_{6a-3a}=8.7 Hz, 6a-H), 7.24—7.50 (3H, m, Ph), and 7.92—8.16 (2H, m, Ph); ^{13}C NMR ($CDCl_3$) δ=23.65, 24.24 (each t, CH_2), 24.95 (q, NMe), 35.24, 43.24 (each t, CH_2), 52.65 (d, 3a-C), 56.89 (d, 6a-C), 85.42 (s, 3-C), 128.42, 129.42, 131.13 (each d), 132.60 (s), 162.01 (s, 1-C), 173.54, and 176.18 (each s, CON); MS *m/z* (rel. intensity, %) 282 (M^+, base peak) 281 (36), 241 (23), 171 (35), 170 (24), and 104 (22).

Found: C, 72.58; H, 6.51; N, 9.89%. Calcd for $C_{17}H_{18}N_2O_2$: C, 72.32; H, 6.43; N, 9.92%.

Reaction of 1n with 2a Leading to 33. A mixture of cyclohexanone (100 mg, 1.02 mmol) and α-cyanobenzylamine (119 mg, 0.902 mmol) in dry chloroform was heated under reflux for 2.5 h. The solvent was removed through evaporation in vacuo and **2a** (111 mg, 1 mmol) in dry toluene (10 ml) was added to the residue. The mixture was allowed to react under the conditions shown in Table 2 affording **33**: Colorless prisms (benzene-hexane); mp 200—201°C; IR (KBr) 2890, 1750, 1680, and 1640 cm^{-1}; ^1H NMR ($CDCl_3$) δ= 1.25—2.20 (10H, m, CH_2), 2.89 (3H, s, NMe), 3.24 (1H, d, J_{3a-6a}=8.5 Hz, 3a-H), 4.58 (1H, d, J_{6a-3a}=8.5 Hz, 6a-H), 7.25—7.50 (3H, m, Ph), and 8.00—8.20 (2H, m, Ph); ^{13}C NMR ($CDCl_3$) δ=23.18 (q, NMe), 22.88, 24.88, 25.77, 34.94, 41.83 (each t, CH_2), 54.47 (d, 3a-C), 56.30 (d, 6a-C), 78.24 (s, 3-C), 128.42, 129.54, 131.07 (each d), 132.83 (s), 161.77 (s, 1-C), 173.66, and 175.95 (each s, CON); MS *m/z* (rel. intensity, %) 296 (M^+, 40), 241 (20), 185 (36), 168 (24), 157 (20), 156 (82), 155 (240), 154 (23), 115 (base peak), and 104 (54).

Found: C, 73.13; H, 6.79; N, 9.36%. Calcd for $C_{18}H_{20}N_2O_2$: C, 72.95; H, 6.80; N, 9.45%.

Reaction of 1o with 2a Leading to 34. A mixture of 2-butanone (75 mg, 1.04 mmol) and α-cyanobenzylamine (119 mg, 0.902 mmol) in dry chloroform (10 ml) was heated under reflux for 2.5 h. The solvent was evaporated in vacuo and **2a** (111 mg, 1 mmol) in dry toluene (10 ml) was added to the residue. The mixture was allowed to react under the conditions shown in Table 2 giving **34** as mixture of two stereoisomers (1:1) whose separation through chromatography was unsuccessful: ^1H NMR ($CDCl_3$) δ=0.92 (2×3H, t, Et), 1.32, 1.44 (each 3H, s, Me), 1.55—2.10 (2×2H, m, Et), 2.86, 2.89 (each 3H, s, NMe), 3.26, 3.30 (each 1H, d, J_{3a-6a}= 9.0 Hz, 3a-H), 4.53, 4.61 (each 1H, d, J_{6a-3a}=9.0 Hz, 6a-H), 7.20—7.50 (2×3H, m, Ph), and 7.90—8.15 (2×2H, m, Ph).

General Procedure for the Elimination of HCN from the Maleimide Cycloadducts. The elimination reactions were performed under the conditions shown in Table 3. After the reactions were completed, the solvent was evaporated in vacuo and the residue was chromatographed over silica gel with hexane-ethyl acetate (9:1). The results are given in Table 3.

35: Obtained as mixture with the starting material **10** (**35**:**10**=6:4) which could not be removed through chromatography. ^1H NMR of **35** (in CD_3CN) δ=2.59 (3H, s, NMe), 3.69 (1H, dd, J_{3a-3}=10.0 and J_{3a-6a}=8.8 Hz, 3a-H), 4.19 (1H, dt, J_{6a-1}=J_{6a-3}=1.3 and J_{6a-3a}=8.8 Hz, 6a-H), 5.60 (1H, ddd, J_{3-1}=2.7, J_{3-3a}=10.0, and J_{3-6a}=1.3 Hz, 3-H), 6.85—7.10 (3H, m, Ph), 7.16—7.32 (2H, m, Ph), and 7.72 (1H, dd, J_{1-3}= 2.7 and J_{1-6a}=1.3 Hz, 1-H).

36: Colorless prisms (benzene-hexane); mp 153—154°C; IR (KBr) 1700 and 1620 cm^{-1}; ^1H NMR ($CDCl_3$) δ=2.99 (3H, s, NMe), 3.41 (1H, dd, J_{3a-3}=3.0 and J_{3a-6a}=8.5 Hz, 3a-H), 4.26 (1H, dd, J_{6a-3a}=8.5 and J_{6a-1}=2.0 Hz, 6a-H), 5.64 (1H, dd, J_{3-1}=5.5 and J_{3-3a}=3.0 Hz, 3-H), 7.16—7.50 (5H, m, Ph), and 7.78 (1H, br, 1-H); MS *m/z* (rel. intensity, %) 228 (M^+, 38), 143 (28), 117 (base peak), 115 (34), and 77 (17).

Found: C, 68.61; H, 5.40; N, 12.03%. Calcd for $C_{13}H_{12}N_2O_2$: C, 68.41; H, 5.30; N, 12.27%.

37: Colorless prisms (benzene-hexane); mp 125—126 °C; IR (KBr) 1765, 1700, 1690, and 1630 cm^{-1}; ^1H NMR ($CDCl_3$) δ=2.89 (3H, s, NMe), 3.64 (1H, dt, J_{3a-3}=6.0, 8.0 and J_{3a-6a}=8.0 Hz, 3a-H), 4.32—4.66 (3H, m, 1- and 6a-H), and 7.26—8.20 (5H, m, Ph); MS *m/z* (rel. intensity, %) 228 (M^+, 40), 117 (base peak), 115 (23), and 77 (13).

Found: C, 68.31; H, 5.38; N, 12.08%. Calcd for $C_{13}H_{12}N_2O_2$: C, 68.41; H, 5.30; N, 12.27%.

38: Yellow prisms (benzene-hexane); mp 133—134°C; IR (KBr) 1710 and 1610 cm^{-1}; ^1H NMR ($CDCl_3$) δ=3.90 (1H, ddd, J_{3a-3}=6.0, 7.5 and J_{3a-6a}=9.0 Hz, 3a-H), 4.57 (2H, m, 3-H), 4.79 (1H, dt, J_{6a-3}=2.0 and J_{6a-3a}=9.0 Hz, 6a-H), 7.20—7.60 (5H, m, Ar), and 8.00—8.32 (4H, m, Ar); MS *m/z* (rel. intensity, %) 335 (M^+, 21), 117 (base peak), and 77 (25).

Found: C, 64.80; H, 4.42; N, 12.00%. Calcd for $C_{18}H_{13}N_3O_4$: C, 64.48; H, 3.91; N, 12.53%.

39: Colorless needles (hexane); mp 92—93°C; IR (KBr) 2930, 2840, 1755, 1690, and 1620 cm^{-1}; ^1H NMR ($CDCl_3$) δ=1.20—2.20 (10H, m, CH_2), 2.90 (3H, s, NMe), 3.05 (1H, d, J_{3a-6a}=8.5 Hz, 3a-H), 4.14 (1H, dd, J_{6a-1}=1.0 and J_{6a-3a}=8.5 Hz, 6a-H), and 7.45 (1H, d, J_{1-6a}=1.0 Hz, 1-H); ^{13}C NMR ($CDCl_3$) δ=22.88, 23.00 (each t, CH_2), 24.94 (q, NMe), 25.47, 34.59, 41.24 (each t, CH_2), 51.77 (d, 3a-C), 58.71 (d), 90.36 (s, 3-C), 155.95 (d, 1-C), 173.54, and 175.83 (each s, CON); MS *m/z* (rel. intensity, %) 220 (M^+, 70), 113 (29), 109 (60), 108 (28), 81 (23), 66 (37), 58 (35), and 42 (base peak).

Found: C, 65.48; H, 7.35; N, 12.46%. Calcd for $C_{12}H_{16}N_2O_2$: C, 65.43; H, 7.32; N, 12.72%.

General Procedure for the Cycloadditions of 1 with 3 and 4. A mixture of each equimolar amounts of **1** and **3** (or **4**) in a solvent (10—15 ml for 1 mmol of **1**) was allowed to react until either of the starting materials was consumed (checked on TLC). After the solvent was evaporated in vacuo, the residue was subjected to a ^1H NMR measurement to know the purity of products and then chromatographed over silica gel using chloroform, chloroform-diethyl ether, or chloroform-ethyl acetate (10:1). The solvents, reaction conditions, and results are listed in Table 2.

Reaction of 1a with 3 Leading to 40 and 41. This reaction under reflux in toluene or at room temperature in acetonitrile in the presence of acetic acid gave **40** and **41** which were separated through column chromatography over silica gel with chloroform–diethyl ether (10:1). **40**: Colorless prisms (benzene–hexane); mp 123—124 °C; IR (KBr) 3320, 2980, and 1730 cm^{-1}; ^1H NMR ($CDCl_3$) δ=2.44 (1H, br, NH), 3.09 (3H, s, 4-COOMe), 3.77 (1H, dd, J_{4-3}=8.6 and J_{4-5}=9.6 Hz, 4-H), 3.78 (3H, s, 3-COOMe), 4.02 (1H, dd, J_{3-2}=7.2 and J_{3-4}=8.6 Hz, 3-H), 4.68 (1H, d, J_{2-3}=7.2 Hz, 2-H), 4.88 (1H, d, J_{5-4}=9.6 Hz, 5-H), and 7.16—7.40 (5H, m, Ph); ^{13}C NMR ($CDCl_3$) δ=49.47, 49.59 (each d, 3- and 4-C), 50.36, 51.83 (each q, COOMe), 52.89 (d, 2-C), 63.06 (d, 5-C), 118.65 (s, CN), 127.77, 128.36 (each d), 138.42 (s), 169.72, and 171.36 (each s, COOMe); MS *m/z* (rel. intensity, %) 288 (M^+, 5), 177 (82), 169 (39), 144 (56), 143 (base peak), 119 (26), 117 (31), 116 (44), 115 (67), 104 (34), and 77 (36).

Found: C, 62.60; H, 5.67; N, 9.78%. Calcd for $C_{15}H_{16}N_2O_4$: C, 62.49; H, 5.59; N, 9.72%.

41: Colorless prisms (benzene–hexane); mp 97—97.5 °C; IR (KBr) 3290, 2200, and 1720 cm^{-1}; ^1H NMR ($CDCl_3$) δ=2.50 (1H, br, NH), 3.18 (3H, s, 4-COOMe), 3.54 (1H, dd, J_{3-2}=8.4 and J_{3-4}=6.5 Hz, 3-H), 3.77 (3H, s, 3-COOMe), 3.90 (1H, dd, J_{4-3}=6.5 and J_{4-5}=9.6 Hz, 4-H), 4.30 (1H, d, J_{2-3}=8.4 Hz, 2-H), 4.60 (1H, d, J_{5-4}=9.6 Hz, 5-H), and 7.20—7.36 (5H, m, Ph); ^{13}C NMR ($CDCl_3$) δ=49.65, 50.53 (each d, 3- and 4-C), 51.95, 52.42 (each q, COOMe), 53.06 (d, 2-C), 64.48 (d, 5-C), 119.12 (s, CN), 127.24, 128.48 (each d), 137.95 (s), 170.89, and 171.18 (each s, COOMe); MS *m/z* (rel. intensity, %) 288 (M^+, 4), 177 (81), 169 (29), 162 (21), 144 (base peak), 143 (90), and 115 (29).

Found: C, 62.48; H, 5.54; N, 9.65%. Calcd for $C_{15}H_{16}N_2O_4$: C, 62.49; H, 5.59; N, 9.71%.

Reaction of 1a with 4 Leading to 42. The result is shown in Table 2: Colorless prisms (benzene–hexane); mp 120—122 °C; IR (KBr) 3300, 1720, and 1670 cm^{-1}; ^1H NMR ($CDCl_3$) δ=3.08 (3H, s, 4-COOMe), 3.61 (3H, s, 3-COOMe), 4.12 (1H, dd, J_{4-5}=12.3 and J_{4-2}=1.0 Hz, 4-H), 4.84 (1H, br, NH), 5.30 (1H, dd, J_{5-1}=1.6 and J_{5-4}=12.3 Hz, 5-H), 7.20—7.36 (5H, m, Ph), and 7.46 (1H, dd, J_{2-1}=3.0 and J_{2-4}=1.0 Hz, 2-H); ^{13}C NMR ($CDCl_3$) δ=50.48, 51.12 (each q, COOMe), 52.14 (d, 4-C), 66.08 (d, 5-C), 100.29 (s, 3-C), 127.14, 127.96 (each d), 137.66 (d), 150.62 (d, 2-C), 166.07, and 171.24 (each s, COOMe); MS *m/z* (rel. intensity, %) 261 (M^+, 35), 202 (base peak), 170 (45), 143 (50), 117 (21), and 115 (34).

Found: C, 64.38; H, 5.84; N, 5.57%. Calcd for $C_{14}H_{15}NO_4$: C, 64.36; H, 5.79; N, 5.36%.

Elimination of HCN from 40 and 41 Leading to 42 and 43. When **40** was heated under reflux in xylene, **42** was obtained. In the presence of a catalytic amount of DBU, **41** was converted into **43**. The reaction conditions and results are given in Table 3.

43: Colorless liquid; IR (neat) 3320, 1730, 1670, 1650, and 1585 cm^{-1}; ^1H NMR ($CDCl_3$) δ=3.64, 3.74 (each 3H, s, COOMe), 3.80 (1H, br, NH), 3.82 (1H, dd, J_{4-5}=7.0 and J_{4-2}=1.0 Hz, 4-H), 5.11 (1H, d, J_{5-4}=7.0 Hz, 5-H), 7.10—7.40 (5H, m, Ph), and 7.45 (1H, d, J_{2-4}=1.0 Hz, 2-H); ^{13}C NMR ($CDCl_3$) δ=50.77, 52.47 (each q, COOMe), 55.24 (d, 4-C), 67.65 (d, 5-C), 100.53 (s, 3-C), 126.07, 128.42, 129.13 (each d), 142.19 (s), 149.24 (d, 2-C), 166.19, and 174.60 (each s, COOMe); MS *m/z* (rel. intensity, %) 261 (M^+, 17), 202 (67), 201 (70), 170 (60), 158 (22), 143 (65), 142 (26), 131 (34), 117 (60), 116 (33), 115 (base peak), 104 (23), 103 (28), 90 (42), 89 (42), and 77 (39).

HRMS Found: *m/z* 261.0994. Calcd for $C_{14}H_{15}NO_4$: M, 261.1000.

Reaction of 1e with 3 Leading to 44, 46, and/or 47. The separation of these products was carried out as follows: Column chromatography of the mixture over silica gel with chloroform gave pure **44** and a mixture of **46** and **47**. This mixture was then subjected to HPLC (solvent: diethyl ether–hexane (7:3)), **46** and **47** being separated.

44: Colorless prisms (benzene–hexane); mp 131—133 °C; IR (KBr) 3350, 2230, and 1740 cm^{-1}; ^1H NMR (CD_3CN) δ=3.06 (3H, s, 4-COOMe), 3.56 (1H, br, NH), 3.62 (3H, s, 3-COOMe), 3.80—4.05 (2H, m, 3- and 4-H), 5.00 (1H, m, changed to dd (J=6.0 and 3.0 Hz) when treated with D_2O, 5-H), and 7.30—8.10 (10H, m, Ph); ^{13}C NMR ($CDCl_3$) δ=50.56 (d, 4-C), 51.72, 52.51 (each q, COOMe), 58.42 (d, 3-C), 62.13 (d, 5-C), 66.33 (s, 2-C), 119.20 (s, CN), 126.64, 127.80, 128.16, 128.34, 128.65, 129.38, 136.93 (s), 137.97 (s), 169.21, and 171.16 (each s, COOMe); MS *m/z* (rel. intensity, %) 337 (M^+—HCN, 43), 277 (base peak), and 115 (29).

Found: C, 69.21; H, 5.53; N, 7.69%. Calcd for $C_{21}H_{20}N_2O_4$: C, 69.09; H, 5.62; N, 7.61%.

46: Colorless prisms (benzene–hexane); mp 138—140 °C; IR (KBr) 1740 and 1620 cm^{-1}; ^1H NMR ($CDCl_3$) δ=3.50 (1H, t, J_{4-3}=J_{4-5}=8.0 Hz, 4-H), 3.60, 3.76 (each 3H, s, COOMe), 4.70 (1H, dd, J_{3-4}=8.0 and J_{3-5}=2.0 Hz, 3-H), 5.52 (1H, dd, J_{5-4}=8.0 and J_{5-3}=2.0 Hz, 5-H), 7.20—7.42 (8H, m, Ph), and 7.87 (2H, m, Ph); ^{13}C NMR ($CDCl_3$) δ=52.76 (2×C, q, COOMe), 56.30 (d, 4-C), 79.24 (d, 3-C), 127.13, 127.42, 127.90, 128.37, 128.83, 131.36, 133.01, 142.30, 168.54 (s, 2-C), 171.90, and 173.18 (each s, COOMe); MS *m/z* (rel. intensity, %) 337 (M^+, 19), 277 (base peak), and 115 (39).

Found: C, 71.12; H, 5.68; N, 4.21%. Calcd for $C_{20}H_{19}NO_4$: C, 71.20; H, 5.68; N, 4.15%.

47: Colorless prisms (benzene–hexane); mp 106—107 °C; IR (KBr) 1750 cm^{-1}; ^1H NMR ($CDCl_3$) δ=3.14, 3.70 (each 3H, s, COOMe), 4.00 (1H, dd, J_{4-3}=5.0 and J_{4-5}=9.0 Hz, 4-H), 4.92 (1H, dd, J_{3-4}=5.0 and J_{3-5}=2.0 Hz, 3-H), 5.95 (1H, dd, J_{5-3}=2.0 and J_{5-4}=9.0 Hz, 5-H), and 7.20—8.20 (10H, m, Ph); MS *m/z* (rel. intensity, %) 337 (M^+, 48), 277 (99), 193 (base peak), and 115 (36).

Found: C, 71.20; H, 5.83; N, 4.08%. Calcd for $C_{20}H_{19}NO_4$: C, 71.20; H, 5.68; N, 4.15%.

This compound **47** was also obtained from the reaction of **1e** with **4** (Table 2).

Reaction of 1f with 3 Leading to 45. The result is shown in Table 2: Colorless prisms (benzene–hexane); mp 96—97 °C; IR (KBr) 3300, 1730, and 1660 cm^{-1}; ^1H NMR ($CDCl_3$) δ=1.72 (1H, br, NH), 3.26, 3.66 (each 3H, s, COOMe), 3.86 (1H, d, J_{3-4}=9.0 Hz, 3-H), 4.22 (1H, t, J_{4-3}=J_{4-5}=9.0 Hz, 4-H), 5.30 (1H, d, J_{5-4}=9.0 Hz, 5-H), and 7.30—8.04 (10H, m, Ph); ^{13}C NMR ($CDCl_3$) δ=50.06, 52.18 (each q, COOMe), 52.83 (d, 3-C), 59.42 (d, 4-C), 62.00 (d, 5-C), 67.95 (s, 2-C), 119.30 (s, CN), 126.42, 128.77, 129.01, 129.19, 129.71, 134.18, 135.24, 136.42, 168.95 (s, COOMe), 170.77 (s, COOMe), and 196.25 (s, PhCO); MS *m/z* (rel. intensity, %) 365 (M^+—HCN, 9), 105 (base peak), and 77 (36).

Found: C, 67.47; H, 5.16; N, 7.10%. Calcd for $C_{22}H_{20}N_2O_5$: C, 67.34; H, 5.14; N, 7.14%.

Reaction of 1j with 3 Leading to 48 and 50. A mixture of cinnamaldehyde (132 mg, 1 mmol) and α-cyanobenzylamine (132 mg, 1 mmol) in toluene (10 ml) was heated under reflux for 15 min. After **3** (144 mg, 1 mmol) was added, the mixture was allowed to react under the conditions shown in Table 2. Although **48** and **50** could not be separated each other through

column chromatography, **48** was identical with one of two products (**48** and **52**) formed in the reaction of **1e** with **4** (Table 2).

48: Viscous liquid; IR (neat) 1700, 1680, and 1620 cm^{-1}; ^1H NMR ($CDCl_3$) δ=3.53, 3.60 (each 3H, s, COOMe), 3.75 (1H, dd, J_{4-3}=6.0 and J_{4-5}=9.0 Hz, 4-H), 4.72 (1H, dd, J_{3-4}=6.0 and J_{3-5}=2.0 Hz, 3-H), 5.30 (1H, ddd, J_{5-3}=2.0, J_{5-4}=9.0, and $J_{5\text{-}CH=}$=8.0 Hz, 5-H), 5.96 (1H, dd, J_{trans}=15.0 and J=8.0 Hz, PhCH=C<u>H</u>), 6.62 (1H, d, J_{trans}=15.0 Hz, PhC<u>H</u>=CH), 7.07—7.33 (8H, m, Ph), and 7.80 (2H, m, Ph); ^{13}C NMR ($CDCl_3$) δ=52.24 (2×C, q, COO<u>Me</u>), 52.89 (d, 4-C), 56.83 (d, 3-C), 75.89 (d, 5-C), 125.83, 126.78, 127.30, 128.01, 128.42, 128.77, 131.42, 132.96, 133.60, 136.83, 169.25 (s, <u>C</u>OOMe), and 171.42 (s, <u>C</u>OOMe); MS *m/z* (rel. intensity, %) 363 (M^+, 53), 304 (59), 272 (57), and 115 (base peak).

Found: C, 72.94; H, 5.64; N, 3.85%. Calcd for $C_{21}H_{21}NO_4$: C, 72.71; H, 5.82; N, 3.85%.

50: Contaminated with **48**; ^1H NMR ($CDCl_3$) δ=3.36 (1H, t, J_{4-3}=J_{4-5}=6.0 Hz, 4-H), 3.60, 3.70 (each 3H, s, COOMe), 4.60 (1H, dd, J_{3-4}=6.0 and J_{3-5}=2.0 Hz, 3-H), and 5.06 (1H, dt, J_{5-3}=2.0 and J_{5-4}=$J_{5\text{-}CH=}$=6.0 Hz, 5-H); MS *m/z* 363 (M^+).

Found: C, 72.58; H, 5.79; N, 4.02%. Calcd for $C_{21}H_{21}NO_4$: C, 72.71; H, 5.82; N, 3.85%.

52: Colorless prisms (hexane); mp 130—131 °C; IR (KBr) 3350 cm^{-1}; ^1H NMR ($CDCl_3$) δ=6.30 (1H, t, J_{4-5}=J_{4-NH}=2.0 Hz, 4-H), 6.72 (1H, t, J_{5-4}=J_{5-NH}=2.0 Hz, 5-H), 7.04—7.30 (10H, m, Ph), and 8.00 (1H, br, NH); MS *m/z* 219 (M^+).

Found: C, 87.70; H, 6.20; N, 6.38%. Calcd for $C_{16}H_{13}N$: C, 87.64; H, 5.98; N, 6.39%.

Reaction of 1k with 3 Leading to 49 and 51. This reaction under the conditions shown in Table 2 afforded a mixture of **49** and **51** which could not be separated each other through column chromatography. The isomer **49** was also obtained as a single product in the reaction of **1k** with **4** (Table 2).

49: Viscous liquid; IR (neat) 1730 and 1620 cm^{-1}; ^1H NMR ($CDCl_3$) δ=1.82 (3H, d, J=1.5 Hz, Me), 3.53, 3.62 (each 3H, s, COOMe), 3.85 (1H, dd, J_{4-3}=5.0 and J_{4-5}=9.0 Hz, 4-H), 4.75 (1H, dd, J_{3-4}=5.0 and J_{3-5}=1.5 Hz, 3-H), 5.26 (1H, dd, J_{5-3}=1.5 and J_{5-4}=9.0 Hz, 5-H), 6.47 (1H, br s, CH=), 7.10—7.40 (8H, m, Ph), and 7.85 (2H, m, Ph); MS *m/z* (rel. intensity, %) 377 (M^+, 42), 318 (35), and 115 (base peak).

Found: C, 72.84; H, 6.02; N, 3.58%. Calcd for $C_{23}H_{23}NO_4$: C, 73.19; H, 6.14; N, 3.71%.

51: Contaminated with **49**; ^1H NMR ($CDCl_3$) δ=1.90 (3H, d, J=1.5 Hz, Me), 3.50 (1H, dd, J_{4-3}=6.0 and J_{4-5}=5.0 Hz, 4-H), 3.57, 3.72 (each 3H, s, COOMe), 4.62 (1H, dd, J_{3-4}=6.0 and J_{3-5}=2.0 Hz, 3-H), 4.95 (1H, dd, J_{5-3}=2.0 and J_{5-4}=5.0 Hz, 5-H), and 6.40 (1H, br s, =CH); MS *m/z* 377 (M^+).

Found: C, 73.27; H, 6.18; N, 3.74%. Calcd for $C_{23}H_{23}NO_4$: C, 73.19; H, 6.14; N, 3.71%.

Reaction of 1n with 3 or 4 Leading to 53. The both reactions under the conditions shown in Table 2 gave the same product **53** as single isomer: Colorless viscous liquid; IR (neat) 1720 and 1610 cm^{-1}; ^1H NMR ($CDCl_3$) δ=1.16—2.20 (10H, m, CH_2), 3.20 (1H, d, J_{4-3}=7.5 Hz, 4-H), 3.60, 3.72 (each 3H, s, COOMe), 4.70 (1H, d, J_{3-4}=7.5 Hz, 3-H), 7.20—7.40 (3H, m, Ph), and 7.70—7.85 (2H, m, Ph); ^{13}C NMR ($CDCl_3$) δ=22.76, 23.41, 25.94, 34.47, 39.77 (each t, CH_2), 52.06, 52.53 (each q, COO<u>Me</u>), 56.77, 58.71 (each d, 3- and 4-C), 78.71 (s, 5-C), 128.02, 128.54, 130.60 (each d), 133.89 (s), 163.95 (s, 2-C), 172.25, and 172.30 (each s, <u>C</u>OOMe); MS *m/z* (rel. intensity, %) 329 (M^+, base peak), 270 (94), 242 (41), 210 (26), 185 (61), 182 (22), and 104 (35).

HRMS Found: *m/z* 329.1689. Calcd for $C_{19}H_{23}NO_5$: M, 329.1626.

General Procedure for the Cycloadditions of 1 with 5. These cycloadditions were carried out acoording to the general procedures mentioned above for the reactions with **2—4**, except that methyl acrylate **5** was used in large excess or as a reaction solvent. The reaction conditions and results are listed in Table 2.

Reaction of 1a with 5 Leading to 54 and 55. This reaction gave four stereoisomers of the corresponding cycloadduct. Mixture of two isomers **54** was separated from mixture of the other two **55** (**54**:**55**=1.5:1) through sequential procedures of column chromatography over silica gel (chloroform–diethyl ether (20:1)) and preparative thin layer chromatography on silica gel (the same eluent as above).

54: A 4:5 mixture of two stereoisomers; colorless liquid; IR (neat) 3330, 2230, 1730, and 1595 cm^{-1}; ^1H NMR ($CDCl_3$) δ=2.10—2.80 (3H, m, CH_2 and CH), 3.07, 3.15 (3H, each s, COOMe), 3.20—4.70 (3H, m, CH and NH), and 7.14 (5H, br s, Ph); ^{13}C NMR ($CDCl_3$) δ=32.41, 33.06 (each t, 4-C), 46.00, 47.12, 47.83, 48.77 (each d, 3- and 5-C), 63.65, 64.12 (each d, 2-C), 120.72, 121.30 (each s, CN), 126.89, 127.54, 127.71, 127.95 (each d), 138.48, 139.19 (each s), 171.66, and 172.31 (each s, <u>C</u>OOMe); MS *m/z* (rel. intensity, %) 230 (M^+, 13), 177 (19), 162 (19), 144 (base peak), 143 (79), 117 (25), and 104 (18).

HRMS Found: *m/z* 230.1050. Calcd for $C_{13}H_{14}N_2O_2$: M, 230.1054.

55: A 2:3 mixture of two stereoisomers; colorless liquid; IR (neat) 3320, 2205, 1725, and 1620 cm^{-1}; ^1H NMR ($CDCl_3$) δ=2.10—3.00 (3H, m, CH_2 and CH), 3.30—4.80 (3H, m, CH and NH), 3.57, 3.62 (3H, each s, COOMe), and 7.18 (5H, br s, Ph); MS *m/z* (rel. intensity, %) 230 (M^+, 30), 229 (42), 183 (22), 169 (22), 156 (55), 154 (69), 143 (47), 117 (57), 116 (61), 115 (base peak), and 91 (88).

HRMS Found: *m/z* 230.1048. Calcd for $C_{13}H_{14}N_2O_2$: M, 230.1054.

Elimination of HCN from 54 and 55 Leading to 56 and 57. The elimination was performed under the conditions listed in Table 3. The HCN-eliminated products **56** and **57** were purified through column chromatography over silica gel with chloroform–diethyl ether (5:1).

56: Pale yellow liquid; IR (neat) 1730 and 1625 cm^{-1}; ^1H NMR ($CDCl_3$) δ=2.80 (2H, m, 3-H), 3.08 (3H, s, COOMe), 3.50 (1H, ddd, J_{4-3}=9.6, 6.0 and J_{4-5}=9.2 Hz, 4-H), 5.52 (1H, ddd, J_{5-2}=2.0, J_{5-3}=4.0, and J_{5-4}=9.2 Hz, 5-H), 7.00—7.44 (5H, m, Ph), and 7.80 (1H, dt, J_{2-3}=1.0, 1.0 and J_{2-5}=2.0 Hz, 2-H); ^{13}C NMR ($CDCl_3$) δ=40.24 (t, 3-C), 46.30 (d, 4-C), 51.36 (q, COO<u>Me</u>), 78.83 (d, 5-C), 127.66, 128.13 (each d), 138.07 (s), 167.24 (d, 2-C), and 172.65 (s, <u>C</u>OOMe); MS *m/z* (rel. intensity, %) 203 (M^+, 15), 144 (34), 143 (20), 117 (42), 90 (23), and 43 (base peak).

HRMS Found: *m/z* 203.0932. Calcd for $C_{12}H_{13}NO_2$: M, 203.0945.

57: Pale yellow liquid; IR (neat) 1735, 1720, and 1620 cm^{-1}; ^1H NMR ($CDCl_3$) δ=2.90—3.04 (3H, m, CH_2 and CH), 3.70 (3H, s, COOMe), 5.36 (1H, m, 5-H), 7.00—7.44 (5H, m, Ph), and 7.66 (1H, br, 2-H); ^{13}C NMR ($CDCl_3$) δ=41.53 (t, 3-C), 49.18 (d, 4-C), 52.36 (q, COO<u>Me</u>), 79.89 (d, 5-C), 126.54, 127.60, 128.83 (each d), 142.54 (s), 165.59 (d, 2-C), and 174.77 (s, <u>C</u>OOMe); MS *m/z* (rel. intensity, %) 203 (M^+, 22), 144 (66), 143 (61), 117 (base peak), 116 (27), 115 (54), 104 (34), 91 (33), 90 (66), 89 (55), and 77 (28).

HRMS Found: *m/z* 203.0907. Calcd for $C_{12}H_{13}NO_2$: M,

203.0945.

Dehydrogenation of 56 and 57 Leading to 58. A mixture of equivalent amounts of **56** (or **57**) and DDQ in dry benzene was heated under reflux for 30 min. The residue was chromatographed over silica gel with chloroform–diethyl ether (10:1) to give pure **58** (41% from **56**: **42% from 57**): Beige liquid; IR (neat) 3310, 1700, 1685, and 1560 cm^{-1}; ^1H NMR ($CDCl_3$) δ=3.69 (3H, s, COOMe), 6.70, 6.74 (each 1H, d, J=1.0 Hz, 4- and 5-H), 7.20—7.60 (5H, m, Ph), and 8.50 (1H, br, NH); ^{13}C NMR ($CDCl_3$) δ=50.90 (q, COOMe), 111.68 (s, 3-C), 112.09 (d, 4-C), 117.88 (d, 5-C), 128.12, 128.88 (each d), 132.10 (s), 137.25 (s, 2-C), and 165.62 (s, COOMe); MS *m/z* (rel. intensity, %) 201 (M^+, 66), 170 (base peak), 115 (61), 114 (29), and 89 (17).

HRMS Found: *m/z* 201.0790. Calcd for $C_{12}H_{11}NO_2$: M, 201.0790.

Reaction of 1e with 5 Leading to 59 and 60. The crude reaction mixture was chromatographed over silica gel with chloroform to give pure **59** and mixture of stereoisomers **60** of HCN-eliminated cycloadduct. This mixture could not be separated by HPLC.

59: Colorless prisms (hexane); mp 104—105 °C; IR (KBr) 1730 and 1620 cm^{-1}; ^1H NMR ($CDCl_3$) δ=3.12 (3H, s, COOMe), 3.06—3.28 (1H, m, one of 3-H), 3.46—3.83 (2H, m, the other of 3-H and 4-H), 5.85 (1H, m, 5-H), 7.04—7.48 (8H, m, Ph), and 7.92 (2H, m, Ph); ^{13}C NMR ($CDCl_3$) δ=37.88 (t, 3-C), 47.89 (d, 4-C), 51.12 (q, COOMe), 78.39 (d, 5-C), 127.54, 127.95, 130.93, 133.66, 138.48, 172.41 (s, COOMe), and 173.18 (s, COOMe); MS *m/z* (rel. intensity, %) 279 (M^+, 35), 220 (72), 193 (base peak), and 115 (25).

Found: C, 77.48; H, 6.17; N, 5.10%. Calcd for $C_{18}H_{17}NO_2$: C, 77.39; H, 6.13; N, 5.01%.

60: A 2:1 mixture of two stereoisomers; colorless liquid; IR (neat) 1740 and 1620 cm^{-1}; ^1H NMR ($CDCl_3$) δ= 1.96—2.28 (1H, m, one of 4-H), 2.66—3.05 (1H, m, the other of 4-H), 3.54, 3.60 (3H, each s, COOMe), 4.16 (1/3H, dt, J=8.0, 2.0, and 2.0 Hz, 3-H), 4.34 (2/3H, dt, J=8.0, 2.0, and 2.0 Hz, 3-H), 5.26 (1/3H, dt, J=8.0, 8.0, and 2.0 Hz, 5-H), 5.47 (1H, dt, J=8.0, 8.0, 2.0 Hz, 5-H), 6.15—6.40 (8H, m, Ph), and 6.76—7.00 (2H, m, Ph); ^{13}C NMR ($CDCl_3$) δ=38.00, 38.88 (each t), 52.41 (q, 2×C), 54.29, 54.59 (each d), 75.55, 75.77 (each d), 124.36, 126.72, 127.00, 127.30, 128.01, 128.42, 128.71, 129.36, 130.89, 131.12, 133.36, 133.65, 143.12, 143.83, 169.40 (s), 169.77 (s), 172.42, and 173.12 (each s); MS *m/z* (rel. intensity, %) 279 (M^+, 40), 220 (65), 193 (93), 192 (base peak), and 115 (49).

Found: C, 77.14; H, 5.89; N, 4.94%. Calcd for $C_{18}H_{17}NO_2$: C, 77.39; H, 6.13; N, 5.01%.

Reaction of 1g with 5 Leading to 61 and 62. A mixture of propionaldehyde (530 mg, 9.14 mmol) and α-cyanobenzylamine (792 mg, 6 mmol) was heated under reflux in chloroform (60 ml) in the presence of molecular sieves 5A for 6 h. The molecular sieves was filtered off and the solvent was evaporated in vacuo. To the residue was added methyl acrylate **5** (3g, 30 mmol) and the mixture was refluxed for 22 h. The solvent was evaporated in vacuo and the residue was chromatographed over silica gel to give **61** (from chloroform–diethyl ether (20:1), 896 mg, 65%) and **62** (from chloroform–diethyl ether (10:1), 443 mg, 30%). Cycloadduct **61** gradually changes into **62** when its solution is allowed to stand on exposure to air. The other product **62** consists of two stereoisomers which can be separated by repeated column chromatography over silica gel.

61: Pale yellow liquid; IR (neat) 1730 and 1610 cm^{-1}; ^1H NMR ($CDCl_3$) δ=0.90—2.20 (7H, m, Et and CH_2), 3.56 (3H, s, COOMe), 3.60 (1H, m, 3-H), 4.20 (1H, m, 5-H), 7.10—7.40 (3H, m, Ph), and 7.60—7.90 (2H, m, Ph); MS *m/z* (rel. intensity, %) 231 (M^+, 19), 212 (55), 172 (19), 170 (36), 145 (29), 144 (base peak), 130 (40), 116 (42), 115 (27), and 104 (86).

HRMS Found: *m/z* 231.1256. Calcd for $C_{14}H_{17}NO_2$: M, 231.1258.

One isomer of **62**: Colorless needles (benzene–hexane); mp 129—130 °C; IR (KBr) 3100, 2960, 1755, and 1615 cm^{-1}; ^1H NMR ($CDCl_3$) δ=1.06 (3H, t, Et), 1.40—2.16 (2H, m, Et), 1.88 (1H, dd, J_{gem}=13.3 and J_{4-5}=7.0 Hz, one of 4-H), 2.66 (1H, dd, J_{gem}=13.3 and J_{4-5}=7.0 Hz, the other of 4-H), 3.74 (3H, s, COOMe), 3.86 (1H, s, OH), 4.12 (1H, m, 5-H), 7.20—7.48 (3H, m, Ph), and 7.70—7.90 (2H, m, Ph); ^{13}C NMR ($CDCl_3$) δ=10.82 (q, Et), 29.47 (t, Et), 44.83 (t, 4-C), 53.65 (q, COOMe), 71.24 (d, 5-C), 86.83 (s, 3-C), 128.01, 128.65, 130.65 (each d), 132.42 (s), 168.65 (s, 2-C), and 175.60 (s, COOMe); MS *m/z* (rel. intensity, %) 247 (M^+, 28), 144 (base peak), 130 (28), 104 (72), 102 (26), 85 (26), and 77 (24).

Found: C, 67.86; H, 6.93; N, 5.68%. Calcd for $C_{14}H_{17}NO_3$: C, 67.99; H, 6.93; N, 5.66%.

The other isomer of **62**: Colorless needles (benzene–hexane); mp 147—148.5 °C; IR (KBr) 3100, 1740, and 1620 cm^{-1}; ^1H NMR ($CDCl_3$) δ=1.04 (3H, t, Et), 1.40—2.45 (4H, m, Et and CH_2), 3.68 (3H, s, COOMe), 4.00 (1H, br s, OH), 4.30 (1H, m, 5-H), 7.20—7.44 (3H, m, Ph), and 7.64—7.84 (2H, m, Ph); ^{13}C NMR ($CDCl_3$) δ=11.13 (q, Et), 29.10 (t, Et), 45.21 (t, 4-C), 53.52 (q, COOMe), 72.27 (d, 5-C), 86.52 (s, 3-C), 127.83, 128.66, 130.61 (each d), 132.56 (s), 167.91 (s, 2-C), and 175.85 (s, COOMe); MS *m/z* (rel. intensity, %) 247 (M^+, 25), 144 (base peak), 130 (37), 104 (90), 103 (22), 102 (29), and 83 (29).

Found: C, 68.15; H, 6.96; N, 5.73%. Calcd for $C_{14}H_{17}NO_3$: C, 67.99; H, 6.93; N, 5.66%.

Air Oxidation of 53 Leading to 63. A solution of **53** in chloroform was stirred at room temperature under oxygen atmosphere for 2 d. The solvent was evaporated in vacuo to give a quantitative yield of **63**: Colorless prisms (hexane); mp 124—125 °C; IR (KBr) 3460, 1710, and 1605 cm^{-1}; ^1H NMR ($CDCl_3$) δ=1.01—2.20 (10H, m, CH_2), 3.24 (1H, s, 4-H), 3.71, 3.78 (each 3H, s, COOMe), 4.30 (1H, s, OH), 7.20—7.44 (3H, m, Ph), and 7.70—7.90 (2H, m, Ph); ^{13}C NMR ($CDCl_3$) δ=22.59, 23.48, 26.06, 33.77, 40.71 (each t), 52.18, 53.89 (each q, COOMe), 68.95 (d, 4-C), 78.53 (s, 5-C), 87.77 (s, 3-C), 128.25, 128.60, 130.72 (each d), 132.42 (s), 164.78 (s, 2-C), 170.77, and 173.99 (each s, COOMe); MS *m/z* (rel. intensity, %) 345 (M^+, 22), 242 (base peak), 210 (20), 185 (22), 183 (21), 182 (39), 155 (22), 129 (30), 123 (30), 122 (23), 104 (40), and 77 (22).

Found: C, 66.00; H, 6.69; N, 4.29%. Calcd for $C_{19}H_{23}NO_5$: C, 66.07; H, 6.71; N, 4.06%.

References

1) R. Grigg and J. Kemp, *Chem. Commun.*, **1978**, 109.
2) M. Joucla and J. Hamelin, *Tetrahedron Lett.*, **1978**, 2885.
3) O. Tsuge, K. Ueno, and K. Oe, *Chem. Lett.*, **1979**, 1407.
4) R. Grigg, *Bull. Soc. Chim. Belg.*, **93**, 593 (1984) as a review, and references cited therein.
5) B. Fouchet, M. Joucla, and J. Hamelin, *Tetrahedron Lett.*, **22**, 3397 (1981).
6) R. Grigg and J. Kemp, *Tetrahedron Lett.*, **21**, 2461

(1980); R. Grigg and S. Thianpatanagul, *J. Chem. Soc., Chem. Commun.*, **1984**, 180.

7) O. Tsuge, S. Kanemasa, and S. Takenaka, *Bull. Chem. Soc. Jpn.*, **58**, 3137 and 3320 (1985).

8) P. Gilgen, H. Heimgartner, H. Schimid, and H.-J. Hansen, *Heterocycles*, **6**, 143 (1977).

9) A. Padwa and L. Gehrlein, *J. Am. Chem. Soc.*, **94**, 4932 (1972).

10) J. W. Lown and B. E. Landberg, *Can. J. Chem.*, **52**, 798 (1974).

11) A. Padwa and H. Ku, *J. Org. Chem.*, **44**, 255 (1979).

12) R. Huisgen, K. Matsumoto, and C. H. Ross, *Heterocycles*, **15**, 1131 (1981).

13) J. W. Lown and K. Matsumoto, *Can. J. Chem.*, **48**, 2215 (1970).

14) J. W. Lown and M. H. Akhtar, *Can. J. Chem.*, **50**, 2236 (1972).

15) P. B. Woller and N. H. Cromwell, *J. Org. Chem.*, **35**, 888 (1970).

16) The imine consists of a sequence of sp^2-carbon-sp^2-nitrogen-sp^3-carbon, and *N*-protonated azomethine ylide sp^2-carbon-sp^2-nitrogen-sp^2-carbon. As the ylide bears a sterically insignificant hydrogen on the central nitrogen, the most stable geometry around the sp^2-carbon of ylide should be very close to that of the corresponding carbon of imine. Stable geometry at the both carbons of ylide can be estimated on the basis of stable configuration of imine.

17) O. Tsuge, S. Kanemasa, K. Yorozu, and K. Ueno, *Chem. Lett.*, **1985**, 1601.

18) O. Tsuge and K. Ueno, *Heterocycles*, **19**, 1411 (1982).

19) As a review on syn-anti isomerization of imine: S. Patai, "The Chemistry of Carbon-Nitrogen Double Bond," Interscience Publishers, London, New York, Sydney, Toronto (1970), Chap. 9, pp. 363—464.

20) Acid catalysis for cycloaddition of *N*-(α-methoxycarbonylbenzyl)imines is known: R. Grigg and H. Q. N. Gumaratne, *J. Chem. Soc., Chem. Commun.*, **1982**, 384.

21) Such competetive Michael addition is due to poor reactivity of azomethine ylide **C** in cycloaddition. Another azomethine ylide from **1n** was found much more reactive toward **2** and no Michael addition product was even detected (Scheme 8).

22) A mixture of chloroform–diethyl ether (3:1) was used as an eluent.

23) R. Grigg, H. Q. N. Gunaratne, and J. Kemp, *J. Chem. Soc., Perkin Trans. 1*, **1984**, 41.

24) An example of peripheral *N*-protonated azomethine ylide: R. Grigg, L. D. Basanagoudar, D. A. Kennedy, J. F. Malone, and S. Thianpatanagul, *Tetrahedron Lett.*, **23**, 2803 (1982).

25) 1,3-Elimination reactions leading to azomethine ylide: A. Padwa and Y.-Y. Chen, *Tetrahedron Lett.*, **24**, 3447 (1983); A. Hosomi, Y. Sakata, and H. Sakurai, *Chem. Lett.*, **1984**, 1117; N. Imai, Y. Terao, K. Achiwa, and M. Sekiya, *Tetrahedron Lett.*, **25**, 1579 (1984).

26) Such attractive interaction was recently reported (Z. Bende, L. Töke, L. Weber, G. Tóth, F. Janke, and G. Csonka, *Tetrahedron*, **40**, 369 (1984)).

27) Both phenyl groups can stabilize azomethine ylide **G** when they are in the same plane to the ylide triangle, but such coplanarity is sterically unfavored. Presumably the both phenyls are sitting at the position where stabilization of the ylide by conjugation through the phenyls is balancing with destabilization by steric repulsion.

28) P. W. Hickmott and B. Rae, *Tetrahedron Lett.*, **26**, 2577 (1985) and references cited therein.

29) O. Tsuge, S. Kanemasa, and K. Matsuda, *Chem. Lett.*, **1985**, 1411; O. Tsuge, S. Kanemasa, T. Yamada, and K. Matsuda, *Heterocycles*, **23**, 2489 (1985).

30) Phenylglyoxalic acid was first converted into an azine derivative. The azine was heated in D_2O to form *N*,*N*′-dibenzylidenehydrazine-d_2 which was then hydrolyzed with 10% hydrochloric acid. The yield of benzaldehyde-d_1 was 70—80% based on the acid (Our unpublished result).

 © 1986 The Chemical Society of Japan Bull. Chem. Soc. Jpn., 59, 1825—1827 (1986)

Cis-Trans Isomerism among the Octahedral Anionobis(*C*-substituted ethylenediamine)nickel(II) Complexes Obtained by Thermal Reactions

Yoshinori IHARA,* Yutaka FUKUDA,† and Kozo SONE†
Laboratory of Chemistry, Faculty of Education, Kanazawa University, Marunouchi, Kanazawa 920
†Department of Chemistry, Faculty of Science, Ochanomizu University, Otsuka, Bunkyo-ku, Tokyo 112
(Received December 24, 1985)

Ten octahedral anionobis(*C*-substituted ethylenediamine)nickel(II) complexes were obtained by thermal reactions of corresponding diaqua salts, and their electronic and IR spectra were examined to see whether they are cis or trans. Most of them were found to be trans, but $[Ni(NO_3)(m\text{-bn})_2](NO_3)$ and $[NiCl_2(i\text{-bn})_2]$ were cis.

We have previously reported on the thermal reactions of the nickel(II) complexes with *C*-substituted ethylenediamines in solid phase.[1] It was found that octahedral anionobis(diamine) complexes, $[NiX_2(NN)_2]$,[2] are obtained as the final products of the following thermal reactions:

a) $[Ni(H_2O)_2(NN)_2]X_2$ (Oh) $\xrightarrow[\Delta]{-2H_2O}$ $[NiX_2(NN)_2]$[2] (Oh′)

b) $[Ni(H_2O)_2(NN)_2]X_2$ (Oh) $\xrightarrow[\Delta]{-2H_2O}$ $[Ni(NN)_2]X_2$ (Sp) $\xrightarrow[\Delta]{}$ $[NiX_2(NN)_2]$[2] (Oh′)

c) $[Ni(NN)_2]X_2$ (Sp) $\xrightarrow[\Delta]{}$ $[NiX_2(NN)_2]$[2] (Oh′)

Here Oh (or Oh′) and Sp represent an octahedral species and square planar one, respectively.

Whether these aniono complexes are cis or trans is an interesting problem, which is also fundamental for understanding the nature of their formation reactions. Unfortunately, the literature on such geometrical isomers of octahedral Ni(II)-bis(diamine) complexes is scanty; the number of known examples of such isomers is not so many, and the methods of their identification by means of the visible and IR spectra are not so well-established as in the case of the Co(III) and Cr(III) complexes.

Recently, however, there appeared several experimental and theoretical works on the electronic spectra of tetragonal Ni(II) complexes.[3-7] In particular, Lever et al. studied the electronic states of the bis(*N*-substituted ethylenediamine)nickel(II) complexes by the normalized spherical harmonic Hamiltonian (NSH) method in detail,[8-13] showing that the feature of the electronic spectrum in near IR region is especially useful for the identification of a cis or a trans isomer of such a complex. In this study, we tried to apply their results to our nickel(II) complexes with *C*-substituted ethylenediamines to see whether each of them is cis or trans.

Experimental

Preparation of the ligands(1-phenyl-1,2-ethanediamine (phenen), 2-methyl-1,2-propanediamine(*i*-bn), *meso*- or *dl*-butanediamine(*m*-bn or *dl*-bn), and *dl*-1,2-diphenyl-1,2-ethanediamine(*dl*-stien)), and that of the anionobis(diamine)-nickel(II) complexes with them were described in the literature.[1,14,15] The electronic spectra in solid phase were measured by the diffuse reflectance method with a Hitachi 340 spectrophotometer equipped with reflection attachments for the visible (800—300 nm) and near IR (1400—800 nm) parts of the spectrum. The latter region was measured with special care for the discussion of the complex geometry. Common IR spectra were recorded with a JASCO IR-A3 spectrophotometer in Nujol mulls.

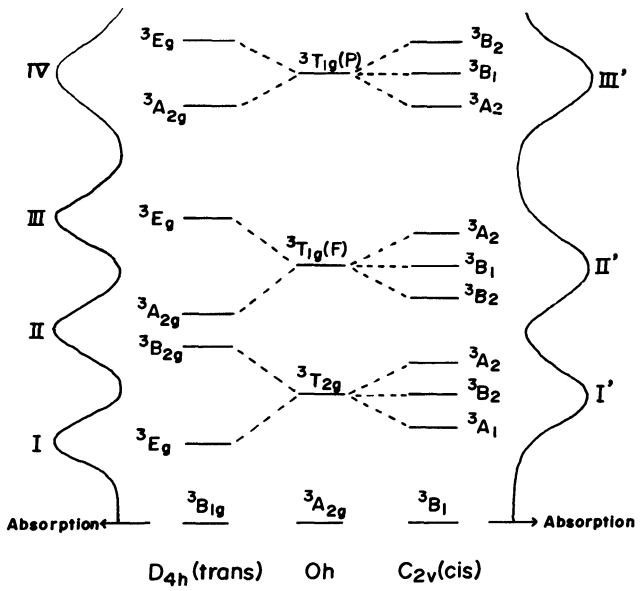

Fig. 1. Energy level diagrams of a d^8 system in ligand fields of different symmetries.[16] Sketches of the absorption spectra of the cis and trans isomers of NiX_2(diamine)$_2$ are also given. (After Lever[13]).

Results and Discussion

The energy levels derived from F and P terms of a d^8 system (Ni^{2+}) in ligand fields of different symmetries (Oh, D_{4h}(trans), and C_{2v}(cis)) are shown in Fig. 1. In a tetragonal system(D_{4h}), six spin-allowed transitions are anticipated, among which four or sometimes five bands are observed in practice.[7,8,13] The band due to the $^3B_{1g} \rightarrow {}^3A_{2g}$ (from $^3T_{1g}(P)$) transition is scarcely observable as a discrete band, but may appear as a

shoulder of the band of $^3B_{1g} \rightarrow {}^3E_g$ (from $^3T_{1g}(P)$) transition (Band IV shown in Fig. 1, which is sometimes obscured under the strong CT or ligand band in near UV region). The band due to $^3B_{1g} \rightarrow {}^3E_g$ (from $^3T_{1g}(F)$) transition, Band III, is normally observed at ca. 17—18×10³ cm⁻¹. The band of $^3B_{1g} \rightarrow {}^3A_{2g}$ (from $^3T_{1g}(F)$) transition seems to lie very close to that of $^3B_{1g} \rightarrow {}^3B_{2g}$ transition, giving only one peak, also around this region (Band II). The band at the lowest energy, Band I, is assigned to the $^3B_{1g} \rightarrow {}^3E_g$ transition.

On the other hand, in a C_{2v} system, the splittings of the respective terms are small; so, when the complex is cis, three rather broad bands (bands I′, II′, and III′ shown in Fig. 1) are observed as in the case of the regular Oh system.[7,12,13,18]

The electronic spectra of the three aniono complexes are now shown in Fig. 2, where the Roman numerals on the curves are the band assignments shown in Fig. 1. The spectra of [NiBr$_2$(*dl*-stien)$_2$] and [Ni(NO$_3$)$_2$(phenen)$_2$] have the same feature, differing from that of Ni(NO$_3$)$_2$(*m*-bn)$_2$ in the near IR region. The additional band observed at ca. 13×10³ cm⁻¹ in the *dl*-stien and phenen complexes can be attributed to Band II, i. e., the overlapping of the transition to $^3A_{2g}$ from $^3T_{1g}(F)$) and $^3B_{2g}$ (from $^3T_{2g}$) levels. The four bands observed are thus assigned to the transitions from $^3B_{1g}$ to the lowest ^3E_g (band I), $^3B_{2g}$ and $^3A_{2g}$ (band II), ^3E_g (band III), and $^3A_{2g}$ (from $^3T_{1g}(P)$) and ^3E_g (from $^3T_{1g}(P)$) (band IV), respectively, in the order of increasing energy. The shoulder at 12.5×10³ cm⁻¹ of the phenen complex is probably the transition to $^3B_{2g}$ state. Consequently, both of these complexes are clearly trans. On the other hand, the *m*-bn complex, whose spectrum scarcely show any splitting, is clearly cis.

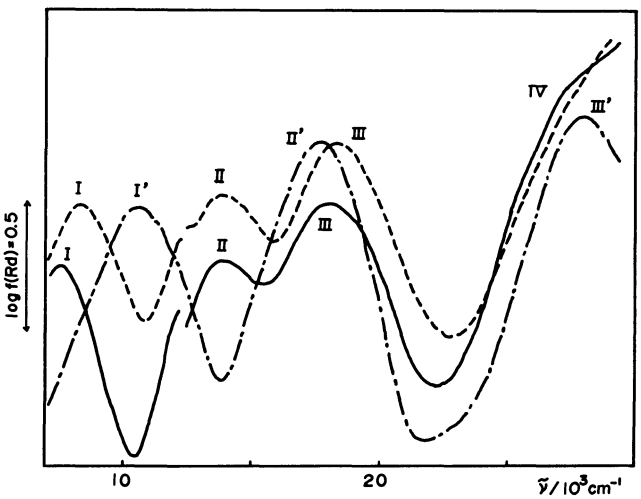

Fig. 2. Reflectance spectra of [NiBr$_2$(*dl*-stien)$_2$] (——), [Ni(NO$_3$)$_2$(phenen)$_2$ (----), and [Ni(NO$_3$)(*m*-bn)$_2$](NO$_3$) (—·—).

Table 1 summarizes the coordination structures of ten complexes deduced in the same way, their electronic spectral data and the thermochemical reactions used to prepare them. Most of these complexes are trans, and only two, i.e., Ni(NO$_3$)$_2$(*m*-bn)$_2$ and NiCl$_2$(*i*-bn),[19,20] are cis.

The mode of coordination in the three nitrato complexes in Table 1 was also studied by means of their IR spectra. In general, an NO_3^- ion in a metallic complex gives rise to a weak combination band in the range of 1700—1800 cm⁻¹. When it exists as an uncoordinated ion, this band is not split, but when it is coordinated as a monodentate ion, a small splitting into two components (less than 25 cm⁻¹) takes place. When it acts as a bidentate ligand, the splitting becomes much larger (20—50 cm⁻¹).[21,22]

Figure 3 indicates the IR spectra of the nitrate complexes of *dl*-stien and *m*-bn, together with those of their mother complexes having the free nitrate ions, [Ni(H$_2$O)$_2$(diamine)$_2$](NO$_3$)$_2$. A peak at 1746 cm⁻¹ assignable to the free NO_3^- ions in the spectrum of the mother complex with *dl*-stien is split into two peaks at 1749 and 1767 cm⁻¹ with a separation of 18 cm⁻¹ in that of the nitrato complex. This indicates that, in the latter, the two NO_3^- ions are coordinated at the axial positions as a unidentate ligands to form the *trans*-octahedral complex.[23] On the other hand, the nitrato

Table 1. Electronic Spectral Data of the Complexes

Complex	Absorption Bands $\tilde{\nu}/10^3\,cm^{-1}$				Preparation Method[a]
	I	II	III	IV	
trans-[NiCl$_2$(phenen)$_2$]	7.9	13.5	17.6	27.8 sh	(a)
trans-[NiBr$_2$(phenen)$_2$]	7.6	13.5	17.4	27.2	(a)
trans-[Ni(NO$_3$)$_2$(phenen)$_2$]	8.3	13.7	18.3	27.0<	(b)
trans-[NiCl$_2$(*dl*-bn)$_2$]	8.2	14.3	18.2	28.1	(b)
trans-[NiBr$_2$(*dl*-bn)$_2$]	7.6	14.3	17.9	29.4 sh	(b)
trans-[NiCl$_2$(*dl*-stien)$_2$]	8.1	14.3	17.9	26.5 sh	(b)
trans-[NiBr$_2$(*dl*-stien)$_2$]	7.6	13.9	18.1	26.1 sh	(b)
trans-[Ni(NO$_3$)$_2$(*dl*-stien)$_2$]	8.6	14.3	18.4	26.6 sh	(b)
	I′	II′	III′		
cis-[NiCl$_2$(*i*-bn)$_2$]	10.5	17.7	28.0		(c)
cis-[Ni(NO$_3$)(*m*-bn)$_2$](NO$_3$)	10.2	17.2	27.2		(c)

a) The symbols a, b, or c correspond to the thermal reactions used to obtain the complexes (see text).

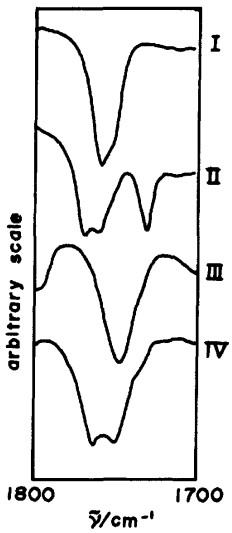

Fig. 3. IR spectra of $[Ni(m\text{-bn})_2](NO_3)_2$(I), $[Ni(NO_3)(m\text{-bn})_2](NO_3)$(II), $[Ni(H_2O)_2(dl\text{-stien})_2](NO_3)_2$(III), and $[Ni(NO_3)_2(dl\text{-stien})_2]$(IV).

complex with *m*-bn has the three peaks at 1732, 1758, and 1768 cm^{-1}. The peak at 1758 cm^{-1} appears at nearly the same position as that of the mother complex, showing that a part of the NO_3^- ions remains uncoordinated. The large separation (36 cm^{-1}) between the other two peaks indicates that the coordinated NO_3^- ions are acting as bidentate ligand. Therefore, the nitrato *m*-bn complex can be formulated as *cis*-$[Ni(NO_3)(m\text{-bn})_2](NO_3)$, having both free and bidentate nitrate ions.

The problem why only the nitrato complex of bis(*m*-bn) and the chloride complex of bis(*i*-bn) form the *cis*-octahedral structure is of interest. It is well known that the bis-type Ni(II) complexes with *m*-bn or *i*-bn strongly prefer a diamagnetic square planar structure,[1,24,25] so the generation of octahedral species with these diamines is quite unusual. In particular, the nitrato complex is the first example of an octahedral bis(*m*-bn) complex. Both of these novel complexes of *cis*-octahedral structure can be obtained only by the same type of thermal reaction (c), and they are converted into the original square planar complexes on cooling for some days, showing the reversibility of the structural changes.[26]

The work was partially supported by a Grant-in-Aid for Scientific Research No. 60303009 from the Ministry of Education, Science, and Culture.

References

1) Y. Ihara, T. Kamishima, and R. Tsuchiya, *Thermochim. Acta*, **67**, 28 (1983).

2) If X^- ion (e.g. NO_3^-) acts as a bidentate ligand, the formula is reperesented by $[NiX(NN)_2]X$ (see text).

3) I. Bertini, D. Gatleschi, and A. Scozzafava, *Inorg. Chem.*, **15**, 203 (1976).

4) D. A. Cruse and M. Gerboch, *J. Chem. Soc., Dalton Trans.*, **1977**, 152.

5) L. Y. Martin, C. R. Sperati, and D. H. Busch, *J. Am. Chem. Soc.*, **99**. 2968 (1977).

6) A. B. P. Lever, I. M. Walker, and P. J. McCarthy, *Spectrosc. Lett.*, **12**, 739 (1979).

7) A. B. P. Lever, *Coord. Chem. Rev.*, **43**, 63 (1982).

8) A. B. P. Lever, G. London, and P. J. McCarthy, *Can. J. Chem.*, **55**, 3172 (1977).

9) J. C. Donini, B. R. Hollebone, and A. B. P. Lever, *Prog. Inorg. Chem.*, **22**, 225 (1977).

10) A. B. P. Lever, I. M. Walker, and P. J. McCarthy, *Inorg. Chim. Acta*, **44**, L143 (1980).

11) I. M. Walker, A. B. P. Lever, and P. J. McCarthy, *Can. J. Chem.*, **58**, 823 (1980).

12) A. B. P. Lever, I. M. Walker, and P. J. McCarthy, *Can. J. Chem.*, **60**, 495 (1982).

13) A. B. P. Lever, "Inorganic Electronic Spectroscopy," 2nd ed., Elsevier, Amsterdam, 1985.

14) Y. Ihara and R. Tsuchiya, *Bull. Chem. Soc. Jpn.*, **57**, 2829 (1984).

15) Y. Ihara, *Bull. Chem. Soc. Jpn.*, **58**, 3248 (1985).

16) It is important to recognize that, depending upon the specific operators which survive from the cubic parent, there are three distinguishable C_{2v} systems, C_{2v}(I), C_{2v}(II), and C_{2v}(III), where the Roman numerals designate the surviving operators.[17] For example, *trans*(*X*,*Y*)-MX_2Y_2ZZ' is a C_{2v}(I) system, while *trans*-$M(X\text{-}X)_2ZZ'$ is a C_{2v}(II) one. The geometry of the cis complexes described in this study(*cis*-$M(X\text{-}X)_2Z_2$) just belongs to C_{2v}(III), and here the ground state($^3A_{2g}$) and $^3T_{2g}$ state of Oh system are transformed into $^3B_1$ and $^3A_1+^3A_2+^3B_2$, respectively,[9] as shown in Fig. 1.

17) J. C. Hempel, J. C. Donini, B. R. Hollebone, and A. B. P. Lever, *J. Am. Chem. Soc.*, **96**, 1693 (1974).

18) M. E. Farago, J. M. James, and V. C. G. Trew, *J. Chem. Soc., (A)*, **1967**, 820.

19) M. E. Farago, J. M. James, and V. C. G. Trew, *J. Chem. Soc., (A)*, **1968**, 48.

20) A. S. Antsyshkina and M. A. Porai-Koshits, *Dokl. Akad. Nauk. SSSR*, **143**, 105 (1962).

21) A. B. P. Lever, E. Mantovani, and B. S. Ramaswamy, *Can. J. Chem.* **49**, 1957 (1971).

22) Y. Fukuda, R. Morishita, and K. Sone, *Bull. Chem. Soc. Jpn.*, **49**, 1017 (1976).

23) The situation is quite similar in the case of *trans*-$[Ni(NO_3)_2(phenen)_2]$, the data of which are not shown in Fig. 3.

24) H. Nishimoto, T. Yoshikuni, A. Uehara, E. Kyuno, and R. Tsuchiya, *Bull. Chem. Soc. Jpn.*, **51**, 1068 (1978).

25) L. D. Pettit and J. L. M. Swash, *J. Chem. Soc., Dalton Trans.*, **1977**, 697.

26) The cis-trans isomerism among the diaqua complexes, which are the starting complexes of the thermal reactions, is also an interesting problem. Here, however, the situation is more complicated than in this study, and, in certain cases, mixtures of cis-trans isomers are obtained according to the preparative methods. Details on this topic will be reported elsewhere.

Ni(II)-Bearing Green Rust II and Its Spontaneous Transformation into Ni(II)-Bearing Ferrites

Yutaka TAMAURA
Department of Chemistry, Tokyo Institute of Technology, Ookayama, Meguro-ku, Tokyo 152
(Received January 25, 1986)

When solutions containing Fe(II), Ni(II), and SO_4^{2-} ions were oxidized by a mixed gas of air and nitrogen at pH 7.1 (25 °C), a Ni(II)-bearing green rust II (GR-II), which is a uniform crystalline precipitate with a definite chemical composition, was formed. The Ni(II) content in the Ni(II)-bearing GR-II increased with an increase in the Ni(II) concentration in the reaction solution. The Ni(II)-bearing GR-II was spontaneously transformed into Ni(II)-bearing ferrite under a nitrogen atmosphere without any oxidant. The metal mole ratio of $[Ni(II)/Fe(III)]_{fer}$ in the ferrite increased linearly with an increase in that of $[Ni(II)/Fe(III)]_{grn}$ in the Ni(II)-bearing GR-II (slope=0.193). From this relationship, the spontaneous transformation reaction was described as

$$2(Ni^{2+})_x(Fe^{2+})_{2-x}(Fe^{3+})(SO_4^{2-})(OH^-)_5 \longrightarrow Ni_{0.39x}Fe_{3-0.39x}O_4 + (2-1.61x)Fe^{2+} + 1.61xNi^{2+} + Fe(OH)_2 + 2SO_4^{2-} + 4H_2O.$$

This equation shows that Fe(II) ion in the GR-II is more readily incorporated into the ferrites than Ni(II) ion.

The formation and transformation of iron oxides, hydroxide oxides in aqueous systems have been studied by many workers.[1-15] The transformation reaction of γ-FeO(OH) to α-FeO(OH) was studied by Schwertmann and Taylor,[10] Oosterhout,[11] and Inoue et al.[15] Music et al.[1] reported the transformation reaction of β-FeO(OH) to α-FeO(OH). We reported that γ-FeO(OH) is transformed to Fe_3O_4 by the adsorption of Fe(II) ion.[12,13] Green rusts (hexagonal plates), which are composed of Fe(II), Fe(III), and sulfate or halogenide ions, are transformed to iron oxides or hydroxide oxides by oxidation of the Fe(II) ions. Recently,[14] we have found that the green rust II spontaneously transforms into Fe_3O_4 without any oxidation reaction (spontaneous transformation reaction). The term "spontaneous" will be used hereafter to distinguish from the oxidation reaction of the green rust II.

A green rust I is formed by the oxidation of Fe(II) ion in an aqueous solution containing Cl^-, Br^-, and F^- ions, and a green rust II, in that containing SO_4^{2-} ions. In the previous paper,[14] we presented a new method for the preparation of the green rust II having a definite chemical composition; The green rust II with the chemical composition of $(Fe^{3+})(Fe^{2+})_2(SO_4^{2-})(OH^-)_{5-2n}(O^{2-})_n$ was synthesized by air oxidation of Fe(II) ion in an aqueous solution containing a high concentration of SO_4^{2-} ion (the air oxidation method). For the reaction solutions containing Fe(II) and Zn(II) ions, Zn(II)-bearing green rust II's (GR-II) with definite chemical compositons were synthesized by the air oxidation method.[16] The present paper describes the synthesis of the Ni(II)-bearing GR-II's with definite chemical compositions by the air oxidation method, and the spontaneous transformation reaction of the Ni(II)-bearing GR-II's to Ni(II)-bearing ferrites.

Experimental

Chemicals. All the chemicals were of analytical grade, and distilled water was used for the preparation of solutions.

Apparatus. The reaction vessel (1 dm^3) of a separable type flask used in the previous paper was adopted.[14] The reaction solution was vigorously stirred with a magnetic stirring bar. An alkaline solution was added using a pH-stat instrument (TOA Electronics, Model HSM-10A). A teflon tube for the addition of the alkaline solution (φ 3 mm×40 cm) was connected to the pH-stat instrument, and the capillary tube (φ 0.2 mm×5 cm) was fitted to the end of the teflon tube. The tip of the capillary tube was fixed just above the stirring bar and near the glass electrode. A gas mixer with a gas flow controller was used to mix air and nitrogen.

Chemical Analysis. The Fe(II) and Fe_{total} contents were determined by means of the 2,2′-bipyridyl method[17] after dissolving the samples in an HCl solution (1:1). The Fe_{total} was determined after reducing Fe(III) to Fe(II) with hydroxylamine. The content of Ni(II) ions was determined using an atomic absorption spectrometer (Varian Model AA-875). The SO_4^{2-} content was determined by X-ray fluorescence (Toshiba X-ray spectrometer Model AFV 777) from the intensity of sulfur in a $BaSO_4$ precipitate collected on a glass fiber filter (Toyo Roshi GA 100 type). The OH^- content was estimated from the consumed amount of the alkaline solution during the reaction.

Synthesis of Ni(II)-Bearing GR-II. After passing nitrogen gas into a 0.7 dm^3 of the distilled water for 2 h to remove the dissolved oxygen, 25 g of Na_2SO_4, 10 g of $FeSO_4 \cdot 7H_2O$, and 0—2 g of $NiSO_4 \cdot 6H_2O$ were dissolved. The pH of the reaction solution was adjusted to 7.1 by adding a 2.0 mol dm^{-3} NaOH solution. The resultant reaction solution was almost transparent and slightly greenish. When the solution was turbid due to the formation of hydroxides, the solution was allowed to stand until the hydroxides dissolved completely. When the deaeration had not been enough to remove the dissolved oxygen, some Fe(III) hydroxide oxides were formed and we could not obtain the GR-II with definite chemical compositions.

The reaction was initiated by passing the mixed gas of air and nitrogen (air/N_2=1:1, flow rate; 3.0 dm^3 min^{-1}) at pH 7.1±0.1 and 25 °C. During the oxidation, an alkaline solution (2.0 mol dm^{-3}) was added to maintain a pH of 7.1. After 20 min, nitrogen gas was passed through in place of the mixed gas, and the reaction vessel was cooled in a water bath chilled

with ice. The greenish precipitates formed were collected by centrifugation in a nitrogen atmosphere, washed with distilled water freed from oxygen, and suspended in distilled water. The Ni(II)-bearing GR-II was stable in a nitrogen atmosphere at room temperature.

Electron Microscopy, IR Spectroscopy, and X-Ray Diffractometry for the Ni(II)-Bearing GR-II. A small portion of the Ni(II)-bearing GR-II suspension was taken into an evacuated glass capillary tube, and then sealed. The sample was mounted in a nitrogen atmosphere on a sample holder for electron microscopy. For the IR spectroscopy, the Ni(II)-bearing GR-II was washed with acetone freed from oxygen, dried in a nitrogen atmosphere, and suspended in Nujol. The IR spectrum was taken by a Shimazu IR spectrometer, Model IR 400, using a KBr cell in a nitrogen atmosphere.

Spontaneous Transformation Reaction of the Ni(II)-Bearing GR-II. The suspension of the Ni(II)-bearing GR-II (0.04 dm^3) was transferred in a nitrogen atmosphere to 0.3 dm^3 of a flask with a cap, sealed with Sealon Film (Fuji Co.), and wrapped with a nylon bag to prevent the oxidation. After keeping the flask in the water bath (60 °C) for 12 h, the product was isolated by transferring the reaction suspension to 0.6 dm^3 of a tartaric acid solution (10 w/v%, pH 5.5) and allowing to stand the suspension for 10 h. The product was collected by centrifugation in a nitrogen atmosphere, washed with oxygen-free water and acetone, successively, and dried in a nitrogen atmosphere. The dried product was examined by means of X-ray diffractometry and IR spectroscopy. The IR spectra were measured by the KBr-disc technique.

Results and Discussion

Synthesis of Ni(II)-Bearing GR-II. When the mixture of air and nitrogen gas was passed through the reaction solution, greenish precipitate was formed, and its amount increased with the oxidation time. The X-ray diffraction pattern of the precipitate obtained corresponded to that of the green rust II.[4] In the IR spectrum strong bands of SO_4^{2-} ion (1100 cm^{-1}) appeared. In the electron micrograph, hexagonal plate particles characteristic of the green rust II were observed. Chemical analysis showed that the greenish precipitate contained Fe(II), Fe(III), and Ni(II) metal ions. The metal mole fraction of Ni(II) in the greenish precipitate increased with an increase in the mole ratio of Ni(II)/Fe(II) in the initial reaction solution, as shown by Curve A in Fig. 1. Contrarily, the mole fraction of Fe(II) decreased (Curve C). However, the mole fraction of Fe(III) (Curve B) remained nearly constant. Table 1 shows the mole ratio of bivalent metal ions [Ni(II)+Fe(II)] to trivalent ions [Fe(III)] in the greenish precipitates. The mole ratios are nearly equal to 2:1, which corresponds to that of Fe(II) to Fe(III) ions in the green rust II having no other metal ions.[14] This suggests that the Fe(II) ions in the green rust II are preferentially replaced by the Ni(II) ions. As seen from Fig. 1, the Ni(II)-bearing GR-II having a Ni(II) mole ratio above 0.33 could not be obtained even from a solution of high Ni(II) concentrations. This

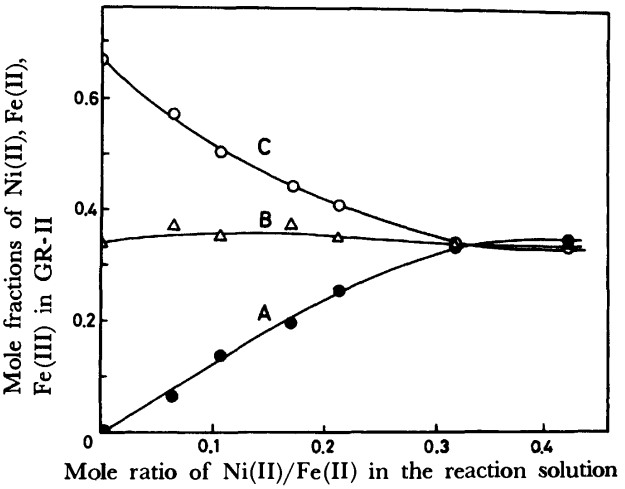

Fig. 1. The relationship between the mole fractions of metal ions [Ni(II); Curve A, Fe(III); B, and Fe(II); C] in the Ni(II)-bearing GR-II and the mole ratio of Ni(II)/Fe(II) in the initial reaction solution.

Table 1. Ratio of Bivalent Metal Ion [Fe(II)+Ni(II)] to Trivalent Metal Ion [Fe(III)] in the Ni(II)-Bearing GR-II

Mole ratio of Ni(II)/Fe(II) in the reaction solution	[Fe(II)+Ni(II)]/Fe(III) in the Ni(II)-bearing GR-II
0.0635	1.72
0.106	1.82
0.169	1.76
0.212	2.19
0.317	2.07
0.423	2.18

suggests that only one out of the two Fe(II) ions in the GR-II can be preferentially replaced by Ni(II) ion. The Chemical analysis showed that the chemical composition of the Ni(II)-bearing GR-II was given by $(Ni^{2+})_x(Fe^{2+})_{2-x}(Fe^{3+})(SO_4^{2-})(OH^-)_5$.

Formation of Ni(II)-Bearing Ferrites From the Ni(II)-Bearing GR-II. The X-Ray diffraction pattern of the black precipitate formed from the Ni(II)-bearing GR-II by the spontaneous transformation corresponded to that of a spinel type compound. Electron microscopic observation showed that the hexagonal particles characteristic of the GR-II changed to shperical or cubic particles characteristic of ferrites. In the IR spectrum, only bands corresponding to the ferrite appeared (strong band at 570 cm^{-1}). Thus, the Ni(II)-bearing GR-II spontaneously transformed into a Ni(II)-bearing ferrite in a nitrogen atmosphere without any oxidant (spontaneous transformation reaction).

When we used the Ni(II)-bearing GR-II's with various Ni(II) contents, the Ni(II)-bearing ferrites having various Ni(II) contents were formed by the spontaneous transformation reaction. Their chemical compositions are given by Fig. 2 [ternary diagram (FeO–Fe_2O_3–NiO)]. The broken line connecting Fe_3O_4 and $NiFe_2O_4$ shows the stoichiometric composition of

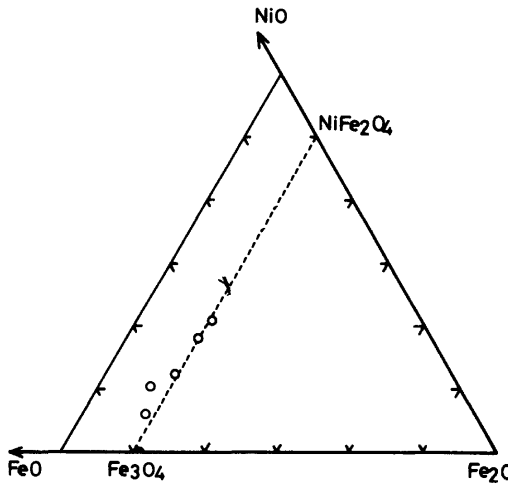

Fig. 2. Chemical compositions (FeO-Fe_2O_3-NiO system) of the Ni(II)-bearing ferrites formed from Ni(II)-bearing GR-II by the spontaneous transformation.

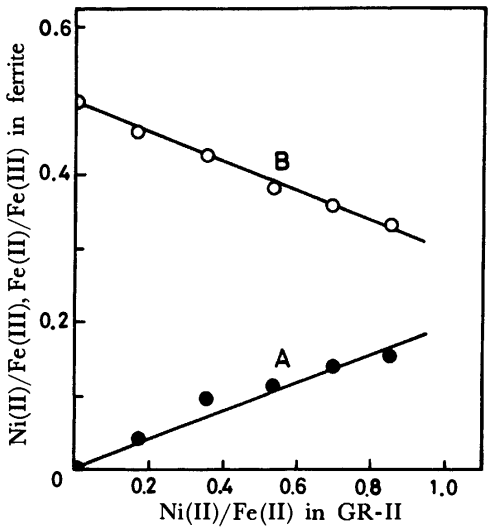

Fig. 3. The relationship between the mole ratios of $[Ni(II)/Fe(III)]_{fer}$ (Curve A) and $[Fe(II)/Fe(III)]_{fer}$ in the Ni(II)-bearing ferrites and the mole ratio of $[Ni(II)/Fe(III)]_{grn}$ in the Ni(II)-bearing GR-II.

the Ni(II)-bearing ferrites. As can be seen here, the chemical compositions of the Ni(II)-bearing ferrites formed by the spontaneous transformation are nearly stoichiometric with respect to oxygen. The limitation in the Ni(II) content in the ferrites is due to the fact that there is a limitation in the Ni(II) content in the Ni(II)-bearing GR-II as described above.

Incorporation of Ni(II) Ions into Ferrites in the Spontaneous Transformation Reaction. Figure 3 shows how the metal mole ratios of $[Ni(II)/Fe(III)]_{fer}$ (Curve A) and $[Fe(II)/Fe(III)]_{fer}$ (Curve B) in the ferrites change with the metal mole ratio of $[Ni(II)/Fe(III)]_{grn}$ in the Ni(II)-bearing GR-II. As can be seen here, the $[Ni(II)/Fe(III)]_{fer}$ increases linearly with an increase in the $[Ni(II)/Fe(III)]_{grn}$ (contrarily, the $[Fe(II)/Fe(III)]_{fer}$ decreases linearly). Since the spontaneous transformation reaction of M(II)-bearing GR-II is generally written by

$$2(M^{2+})_x(Fe^{2+})_{2-x}(Fe^{3+})(SO_4^{2-})(OH^-)_5 \longrightarrow M^{2+}{}_yFe^{2+}{}_{1-y}Fe^{3+}{}_2O_4 + (2x-y)M^{2+} + (3-2x+y)Fe^{2+} + 2SO_4^{2-} + 4H_2O + 2OH^-, \quad (1)$$

the linear relationship of Curve A in Fig. 3 is given by $y/2=0.193x$. With this, Eq. 1 is rewritten for the Ni(II)-bearing GR-II by

$$2(Ni^{2+})_x(Fe^{2+})_{2-x}(Fe^{3+})(SO_4^{2-})(OH^-)_5 \longrightarrow Ni_{0.39x}Fe_{3-0.39x}O_4 + (2-1.61x)Fe^{2+} + 1.61xNi^{2+} + Fe(OH)_2 + 2SO_4^{2-} + 4H_2O. \quad (2)$$

As reported previously[16] for the spontaneous transformation reaction of the Zn(II)-bearing GR-II, the linear relationship between $[Zn(II)/Fe(III)]_{fer}$ and $[Zn(II)/Fe(III)]_{grn}$ was obtained. Thus, in the spontaneous transformation reaction, there seems to exist a linear relationship betweeen $[M(II)/Fe(III)]_{fer}$ and the $[M(II)/Fe(III)]_{grn}$. When the slope of the line of the linear relationship is t, $y=2tx$. To evaluate what bivalent metal ions (M^{2+}) studied here are more readily incorporated into the ferrites in the spontaneous transformation reaction, we compared ratios of $[M(II)/Fe(III)]_{grn}$ with those of $[M(II)/Fe(III)]_{fer}$. These mole ratios are given by

$$[M(II)/Fe(III)]_{grn} = x, \quad (3)$$

and

$$[M(II)/Fe(III)]_{fer} = y/2 \quad (=tx). \quad (4)$$

For the ferrites, t and x should range from 0 to 1. The difference, D, bewteeen $[M(II)/Fe(III)]_{brn}$ and $[M(II)/Fe(III)]_{fer}$ is given by $(1-t)x$. Table 2 shows the relationship bewteen D and t in the spontaneous transformation reaction of the Zn(II)-, Fe(II)-, and Ni(II)-bearing GR-II's. The value of t for Zn(II)-bearing GR-II was evaluated from the data of the previous work ($t=0.48$).[16] For the Fe(II)-bearing GR-II, $t=0.25$, since $[Fe(II)/Fe(III)]_{grn}=2$, and $[Fe(II)/Fe(III)]_{fer}=1/2$. As can be seen from Table 2, Zn(II) ion is more readily incorporated into the ferrites in the spontane-

Table 2. Relationship between D ($[M(II)/Fe(III)]_{fer}$-$[M(II)/Fe(III)]_{grn}$) and t (Slope of the Linear Relationship between $M(II)/Fe(III)]_{fer}$ and $[M(II)/Fe(III)]_{grn}$ for the Transformation Reaction of the Zn(II)-, Fe(II)-, and Ni(II)-Bearing GR-II)

GR-II	t	D	$\log K_h$
Zn(II)-Bearing GR-II	0.460	0.540×	−8.96
Fe(II)-Bearing GR-II	0.250	0.750×	−9.5
Ni(II)-Bearing GR-II	0.193	0.807×	−9.86

$x=[M(II)/Fe(III)]_{grn}$, K_h; hydrolysis constant of MOH^+.

ous transformation reaction compared with Fe(II) and Ni(II) ions, and Ni(II) ion is the most difficult metal ion to be incorporated. This seems to come from the ease of the hydrolysis of those metal ions, considering the hydrolysis constants (log K_h) of −8.96, −9.5, and −9.86 for Zn^{2+}, Fe^{2+}, and Ni^{2+}, respectively.[18]

Since the particle shapes of the green rust II (hexagonal plate) and the ferrites (cubic) are different, it is assumed that the spontaneous transformation reaction proceeds via a dissolution-precipitation process. The mole ratio of the hydrolyzed species of the metal ions to the hydrolyzed Fe(II) ions is given by

$$\frac{[MOH^+]}{[FeOH^+]} = [M(II)/Fe(II)]_{grn} \frac{K_h^M}{K_h^{Fe}}, \quad (5)$$

where we assumed that the metal mole ratio of M(II)/Fe(II) near the surface of the GR-II, where the reaction takes place, is $[M(II)/Fe(II)]_{grn}$. K_h^M and K_h^{Fe} are the hydrolysis constants of M^{2+} and Fe^{2+} ions, respectively (in the pH range studied here, the main hydrolyzed species are $FeOH^+$ and MOH^+). On the other hand, from Eq. 1, the mole ratio of $[M(II)/Fe(II)]_{fer}$ in the ferrites is given by

$$[M(II)/Fe(II)]_{fer} = 2tx/(1-2tx). \quad (6)$$

The mole ratios of $MOH^+/FeOH^+$ evaluated from Eq. 5 for Zn(II) and Ni(II) with x in the range of 0—1, and those of $[M(II)/Fe(II)]_{fer}$ evaluated from Eq. 6 derived from the experimental results are given in Table 3. As can be seen here, the values evaluated from Eq. 5 are in fair agreement with those from Eq. 6. This suggests that the hydrolyzed species are preferentially incorporated into the ferrites, and that t can be related to the ease of the hydrolysis of the metal ions released from the green rust II.

The ligand field stabilizing energy (LFSE) would also affect the incorporation of metal ions into the spinel structure in the spontaneous transformation reaction. In theGR-II's, the metal ions occupy the octahedral sites. In the ferrites, Fe(II) and Ni(II) ions situate on the octahedral sites, but Zn(II) ion on the tetrahedral site. This means that differences in LFSE of these metal ions between GR-II's and ferrites are zero, indicating that the data (Table 2) can not be explained satisfactorily by LFSE.

Table 3. Comparison of the Values Evaluated from Eqs. 5 and 6 for Zn(II) and Ni(II) with x in the Range of 0—1

x	Ni(II)		Zn(II)	
	Eq. 5	Eq. 6	Eq. 5	Eq. 6
0.2	0.0484	0.0837	0.384	0.225
0.4	0.109	0.183	0.865	0.582
0.6	0.187	0.301	1.48	1.23
0.8	0.291	0.447	2.31	2.79

References

1) S. Music, A. Vertes, G. W. Simmons, I. Czado-Nagy, and H. Jr. Leidheiser, *J. Colloid Interface Sci.*, **85**, 256 (1982).
2) Z. A. Foroulis, *Corrosion*, **35**, 340 (1979).
3) R. J. Atkinson, A. M. Posner, and J. P. Qurik, *Clays Clay Miner.*, **25**, 49 (1977).
4) J. D. Bernal, D. R. Dasgupta, and A. L. Mackay, *Clay Miner. Bull.*, **4**, 15 (1959).
5) T. Misawa, T. Kyuno, W. Suetaka, and S. Shimodaira, *Corros. Sci.*, **11**, 35 (1971).
6) T. Misawa, K, Hashimoto, and S. Shimodaira, *Corros. Sci.*, **14**, 131 (1974).
7) M. Kiyama, *Bull. Chem. Soc. Jpn.*, **47**, 1646 (1974).
8) M. Kiyama and T. Takada, *Bull. Chem. Soc. Jpn.*, **45**, 1923 (1972).
9) J. Dousma, T. J. Van den Hoven, and P. L. de Bruyn, *J. Inorg. Nucl. Chem.*, **40**, 1089 (1978).
10) U. Schwertmann and R. M. Taylor, *Clays Clay Miner.*, **20**, 159 (1972).
11) G. W. V. Oosterhout, *J. Inorg. Nucl. Chem.*, **29**, 1235 (1967).
12) Y. Tamaura, P. V. Buduan, and T. Katsura, *J. Chem. Soc., Dalton Trans.*, **1981**, 1807.
13) Y. Tamaura, K. Ito, and T. Katsura, *J. Chem. Soc., Dalton Trans.*, **1983**, 189.
14) Y. Tamaura, T. Yoshida, and T. Katsura, *Bull. Chem. Soc. Jpn.*, **57**, 2411 (1984).
15) K. Inoue, K, Ichimura, K. Kaneko, and T. Ishikawa, *Corros. Sci.*, **16**, 507 (1976).
16) Y. Tamaura, *Bull. Chem. Soc. Jpn.*, **58**, 2951 (1985).
17) I. Iwasaki, T. Katsura, T. Ozawa, M. Mashima, H. Hamamura, and B. Iwasaki, *Bull. Volc. Soc. Jpn., Ser.*, **2**, 5, 75 (1960).
18) C. F. Baes, Jr., and R. Mesmer, "The Hydrolysis of Cations," Wiley-Interscience Publications, New York (1976).

 © 1986 The Chemical Society of Japan Bull. Chem. Soc. Jpn., 59, 1833—1838 (1986)

The Determination of a Small Amount of a Biological Constituent by the Use of Chemiluminescence. VI. The Flow-Injection Analysis of Protein Using a 1,10-Phenanthroline-Hydrogen Peroxide System

Tadashi HARA,* Takashi EBUCHI, Akihiro ARAI, and Masakatsu IMAKI†
Department of Chemical Engineering, Faculty of Engineering, Doshisha University, Karasuma Imadegawa, Kamigyo-ku, Kyoto 602
†Horiba Ltd., Kisshoin, Minami-ku, Kyoto 601
(Received November 13, 1985)

Since the catalytic activity of copper(II) for the chemiluminescent reaction between 1,10-phenanthroline and hydrogen peroxide decreased in the presence of protein, this phenomenon was applied to the determination of protein. The determination of protein was carried out by a flow-injection method, and the conditions for the determination of protein were established. The catalytic activity of copper(II) was enhanced by using an amino acid instead of the conventional biuret reagent. Similar calibration curves were obtained for human serum albumin, bovine serum albumin, human serum γ-globulin, bovine serum γ-globulin, and ovalbumin. According to the present flow-injection method using a chemiluminescent reaction, a small amount of protein could be conveniently and economically determined over a wide range of concentrations, 5.0×10^{-6} g dm^{-3}—1.0×10^{-1} g dm^{-3} at the rate of about 20 samples per hour, with the detection limit of 250 pg as the injected amount and the coefficient of variation of 5.9% (n=9). The sensitivity of the present method was about 40 times that of the previous luminol-hydrogen peroxide system.

In the previous paper,[1] several proteins in the concentration range of 2.0×10^{-4} g dm^{-3}—1.0×10^{-1} g dm^{-3} were determined by the use of the fact that the catalytic activity of copper(II) for the chemiluminescent (CL) reaction between 5-amino-2,3-dihydro-1,4-phthalazinedione(luminol) and hydrogen peroxide (H_2O_2) decreased in the presence of proteins. Though the method was sensitive, non-labeled, and applicable to the detection of an amino acid as well as protein,[2] its sensitivity was not yet satisfactory for the determination of a trace amount of a constituent in a human serum sample.

According to the authors' knowledge about the reaction between copper(II) and protein at high temperatures, a more sensitive method for the copper(II) determination was necessary for the determination of a smaller amount of protein than that in the previous paper. With this in mind, the CL reaction between 1,10-phenanthroline(phen) and H_2O_2, which had previously been used for the determination of ultratraces of copper(II),[3] was applied to the determination of a protein in the present paper. The present method showed a wider linear dynamic range and a smaller detection limit than those in the previous papers. The catalytic activity of copper(II) in a phen–H_2O_2 system was enhanced in the presence of an amino acid in opposition to that in a luminol–H_2O_2 system. On the basis of this phenomenon, bovine serum albumin (BSA) could be determined more sensitively in the presence of an amino acid.

Since the present method was expected to be useful for the development of a sensitive, rapid, and inexpensive detector by which a trace amount of protein could be determined without labeling it, the optimum conditions for the determination of protein, the improvement of the detection limit, and so on were examined.

Experimental

Reagents. All the reagents used were of a commercially available special grade. Ion exchange water was distilled for use. A 1.0×10^{-7} mol dm^{-3} copper(II) solution (biuret reagent) was prepared by diluting a 2.0×10^{-2} mol dm^{-3} copper(II) stock solution[4] with a buffer solution (pH 10.19) consisting of 0.1 mol dm^{-3} boric acid and 0.1 mol dm^{-3} potassium hydroxide. A phen solution containing ethylhexadecyldimethylammonium bromide (EHDAB), tetraethylenepentamine (TEPA), and sodium hydroxide (NaOH), and a H_2O_2 solution were prepared daily. The sample solution of BSA and bovine serum γ-globulin (BγG) from Sigma Chemical Co., and human serum albumin (HSA) and human serum γ-globulin (HγG) from ICN Pharmaceuticals, Inc., and control serum (Q-PAC-Chemistry Control Serum I) from HYLAND were prepared by diluting them in buffer solution. All α-amino acids were from Kyowa Hakko Co., Ltd.

Apparatus and Procedure. A schematic diagram of the apparatus used for the present flow-injection analysis is shown in Fig. 1. All the tubes and connectors used were made of Teflon except for the flow cell. Each solution of phen(a) and H_2O_2(b), held at 25°C by means of a thermostat(n) (Netsudenshi Kogyo Co., Ltd.), and copper(II) (c), held at room temperature, was fed by means of 5.0×10^5 Pa gauge pressure of nitrogen gas; the flow rates were all adjusted to 1.0 cm^3 min^{-1} by the use of a needle valve (h) (GILMONT). A buffer solution(d) was fed at the flow rate of 1.0 cm^3 min^{-1} by means of a pump(i) (Pharmacia High-precision Pump P-500).

A 50 mm^3 portion of a protein sample solution was injected into the buffer solution line through the sampling loop(k) and the six-way cock(j). The protein sample solution was first mixed with a copper(II) catalyst solution and then passed through a reaction tube(o) (0.40 m), held at 95°C, and a cooling tube(p) (0.64 m), held at 0°C, in that order. Then the reacting solution was further mixed with

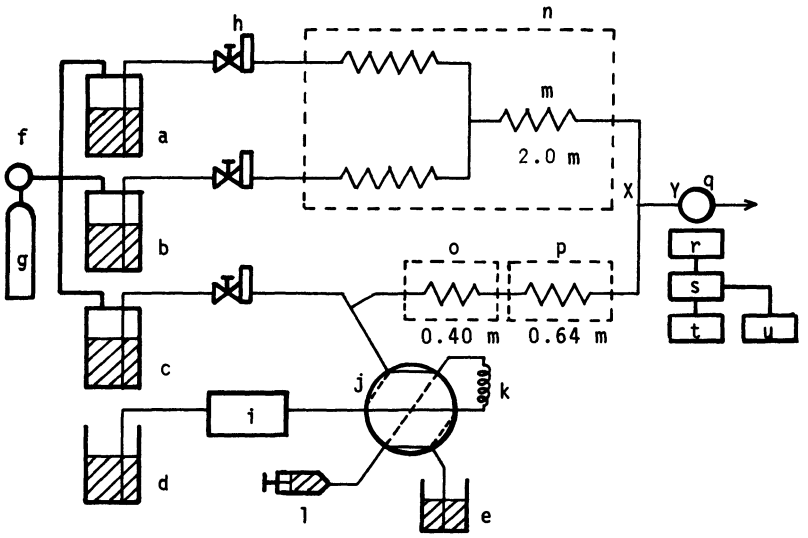

Fig. 1. Schematic diagram of the flow-injection system.
a: Phen solution, b: H_2O_2 solution, c: copper(II) catalyst solution, d: buffer solution, e: sample solution, f: regulator, g: N_2 cylinder, h: flowmeter equipped with a needle valve, i: pump, j: six-way cock, k: sampling loop, l: syringe, m: mixing coil, n: thermostat, o: reaction tube, p: cooling tube, q: flow cell, r: photomultiplier, s: amplifier, t: recorder, and u: integrator.

the phen-H_2O_2 solution, which had been thoroughly premixed by means of a 2.0 m mixing coil(m); the solution thus obtained was passed through a flow cell(q) (25 cm×0.8 mm i.d. poly(vinyl chloride) tube). The CL intensity of the solution passing through the cell was measured by means of a photomultiplier(r) (Hamamatsu TV Co., Ltd., R928), amplified with an amplifier(s) (Horiba Ltd., OPE-214), and recorded on a recorder(t) (Yokogawa Electric Works, Ltd., 3046), followed by the measurement of the peak area by the use of an integrator(u) (Shimadzu Chromatopac E1A or C-R2A). The distance between X and Y was 3 cm.

The CL intensity of a protein-free sample was recorded as a base line, while that of a protein-containing sample was recorded as a negative peak because the CL intensity was weakened due to the formation of a complex compound between copper(II) and protein.

Results and Discussion

Determination of Analysis Conditions. BSA was used as a model protein for the determination of the analysis conditions. The length of the reaction tube and the cooling tube and the reaction temperature were the same as in the previous paper. The flowing paths of both phen and H_2O_2 and the mixing coil were passed through a thermostat at 25 °C to keep them from the effect of the room temperature. A 2.0 m mixing coil was experimentally selected on the basis of its maximum CL intensity. The relationships between the peak area obtained by injecting a definite amount of BSA and phen, EHDAB, TEPA, NaOH, H_2O_2, and copper(II) solutions are shown in Figs. 2—7. From these results, the following optimum concentrations for the maximum peak area were chosen: 5.0×10^{-5} mol dm^{-3} phen; 4.0×10^{-5} mol dm^{-3} EHDAB; 2.0×10^{-7} mol dm^{-3} TEPA; 1.0×10^{-1} mol dm^{-3} NaOH; 5% H_2O_2; and 1.0×10^{-7} mol dm^{-3} copper(II).

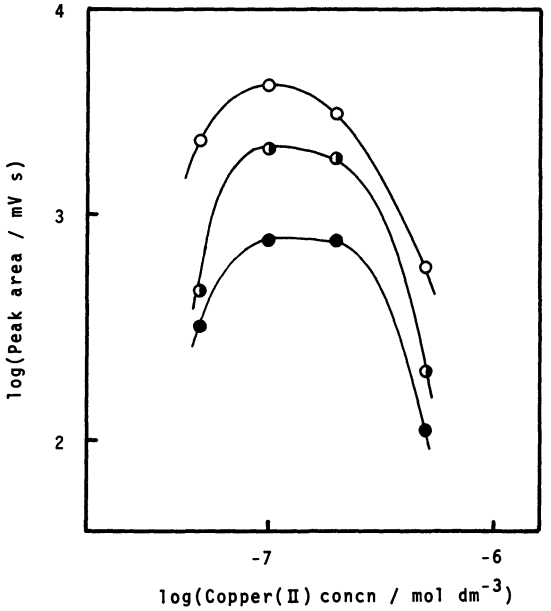

Fig. 2. Relationship between copper(II) concn and peak area.
○: 1.0×10^{-2} g dm^{-3}-, ◑: 5.0×10^{-3} g dm^{-3}-, and ●: 1.0×10^{-3} g dm^{-3}-BSA.
Conditions: 5.0×10^{-5} mol dm^{-3} phen, 4.0×10^{-3} mol dm^{-3} EHDAB, 2.0×10^{-7} mol dm^{-3} TEPA, 1.0×10^{-1} mol dm^{-3} NaOH, and 5% H_2O_2.

Determination of Various Proteins. The calibration curves of BSA and BγG were obtained under the above-mentioned conditions (Fig. 8). As can be seen from Fig. 8, each linear response was obtained over a wide range of concentrations, and 2×10^{-5}—1×10^{-1} g dm^{-3} BSA and 2×10^{-5}—5×10^{-2} g dm^{-3} BγG could

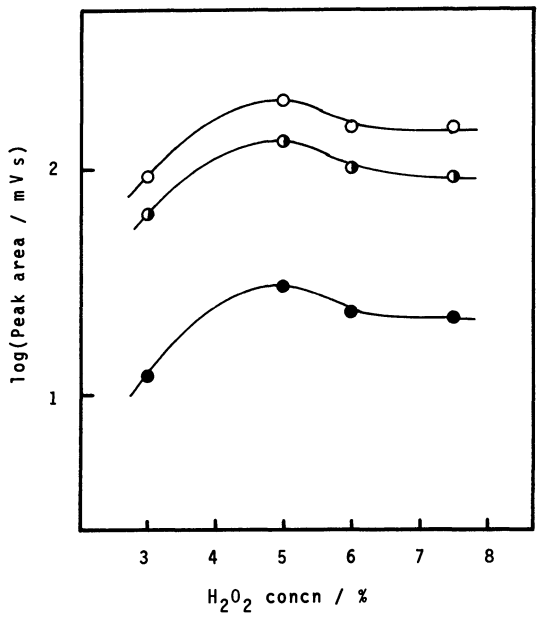

Fig. 3. Relationship between H_2O_2 concn and peak area.
○: 1.0×10^{-2} g dm^{-3}-, ◑: 5.0×10^{-3} g dm^{-3}-, and ●: 1.0×10^{-3} g dm^{-3}-BSA.
Conditions: 5.0×10^{-5} mol dm^{-3} phen, 4.0×10^{-3} mol dm^{-3} EHDAB, 2.0×10^{-7} mol dm^{-3} TEPA, 1.0×10^{-1} mol dm^{-3} NaOH, and 1.0×10^{-7} mol dm^{-3} copper(II).

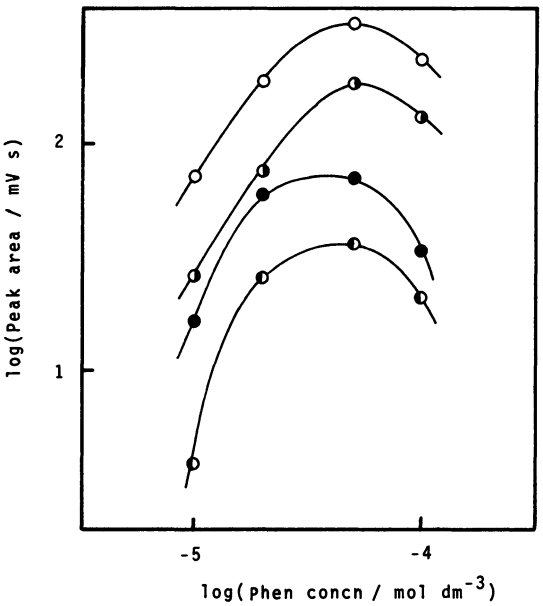

Fig. 4. Relationship between phen concn and peak area.
○: 1.0×10^{-2} g dm^{-3}-, ◑: 5.0×10^{-3} g dm^{-3}-, ●: 1.0×10^{-3} g dm^{-3}-, and ◐: 5.0×10^{-4} g dm^{-3}-BSA.
Conditions: 4.0×10^{-3} mol dm^{-3} EHDAB, 2.0×10^{-7} mol dm^{-3} TEPA, 1.0×10^{-1} mol dm^{-3} NaOH, 1.0×10^{-7} mol dm^{-3} copper(II), and 5% H_2O_2.

be determined. The detection limit (S/N=2) of the present method (a biuret reagent containing copper(II) and tartrate) was 1 ng BSA; this corresponded to one-tenth that in the previous paper. The coefficient of variation was 4.9% for ten measurements of 1×10^{-3} g dm^{-3} BSA.

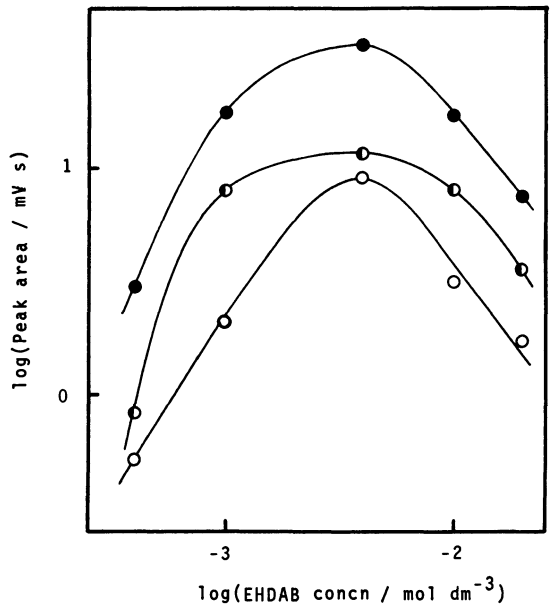

Fig. 5. Relationship between EHDAB concn and peak area.
●: 1.0×10^{-3} g dm^{-3}-, ◐: 5.0×10^{-4} g dm^{-3}-, and ○: 1.0×10^{-4} g dm^{-3}-BSA.
Conditions: 5.0×10^{-5} mol dm^{-3} phen, 2.0×10^{-7} mol dm^{-3} TEPA, 1.0×10^{-1} mol dm^{-3} NaOH, 1.0×10^{-7} mol dm^{-3} copper(II), and 5% H_2O_2.

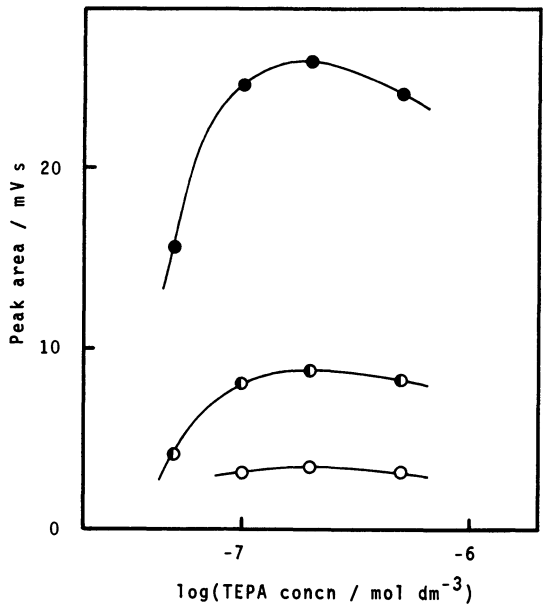

Fig. 6. Relationship between TEPA concn and peak area.
●: 1.0×10^{-3} g dm^{-3}-, ◐: 5.0×10^{-4} g dm^{-3}-, and ○: 1.0×10^{-4} g dm^{-3}-BSA.
Conditions: 5.0×10^{-5} mol dm^{-3} phen, 4.0×10^{-3} mol dm^{-3} EHDAB, 1.0×10^{-1} mol dm^{-3} NaOH, 1.0×10^{-7} mol dm^{-3} copper(II), and 5% H_2O_2.

A similar sensitivity was also obtained for HSA, HγG, and ovalbumin. Furthermore, the rapid formation of a very stable complex compound between copper(II) and protein by heating was suggested because the calibration curves were still linear, even at the limit of the detection of BSA and BγG. Therefore, the

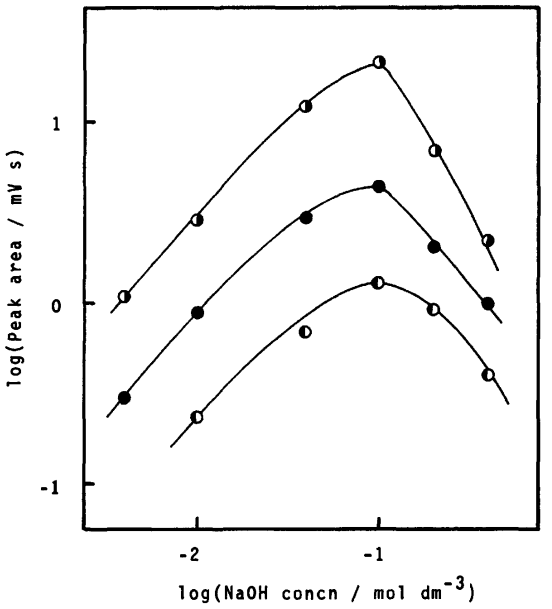

Fig. 7. Relationship between NaOH concn and peak area.
◑: 4.0×10^{-3} g dm^{-3}-, ●: 1.0×10^{-3} g dm^{-3}-, and ◐: 4.0×10^{-4} g dm^{-3}-BSA.
Conditions: 5.0×10^{-5} mol dm^{-3} phen, 4.0×10^{-3} mol dm^{-3} EHDAB, 2.0×10^{-7} mol dm^{-3} TEPA, 1.0×10^{-7} mol dm^{-3} copper(II), and 5% H_2O_2.

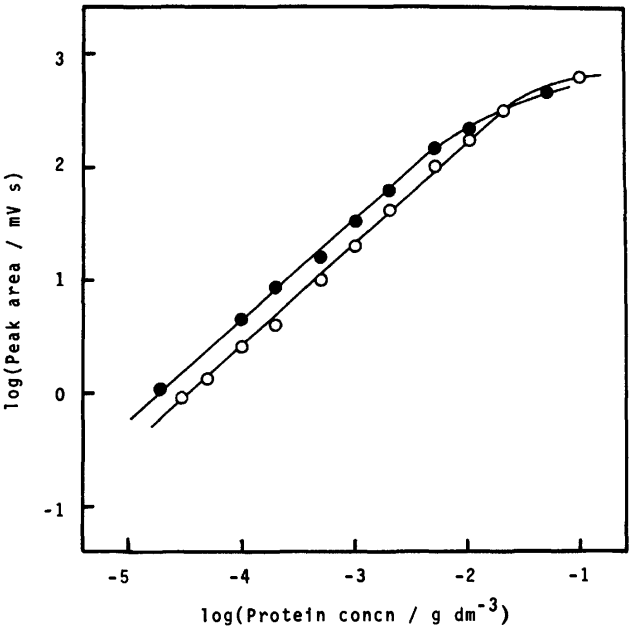

Fig. 8. Calibration curves of proteins.
○: BSA and ●: BγG.
Conditions: 5.0×10^{-5} mol dm^{-3} phen, 4.0×10^{-3} mol dm^{-3} EHDAB, 2.0×10^{-7} mol dm^{-3} TEPA, 1.0×10^{-1} mol dm^{-3} NaOH, 1.0×10^{-7} mol dm^{-3} copper(II), and 5% H_2O_2.

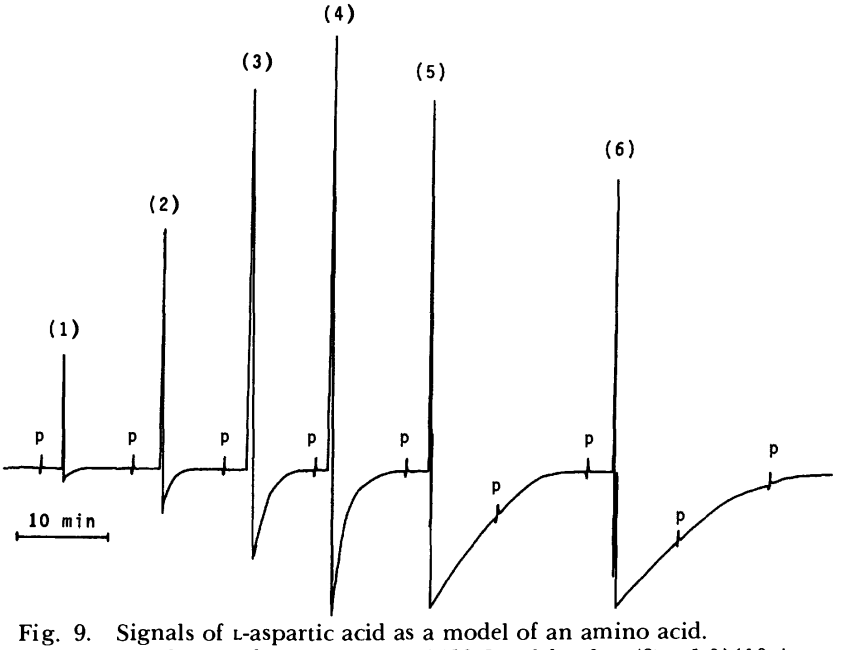

Fig. 9. Signals of L-aspartic acid as a model of an amino acid.
(1): 1.0×10^{-6} mol dm^{-3}-, (2): 1.0×10^{-5} mol dm^{-3}-, (3): 1.0×10^{-4} mol dm^{-3}-, (4): 1.0×10^{-3} mol dm^{-3}-, (5): 1.0×10^{-2} mol dm^{-3}-, (6): 2.0×10^{-2} mol dm^{-3}- Asp, and p: periodical shock peak accompanying with a reciprocation of the pump piston.
Conditions: 5.0×10^{-5} mol dm^{-3} phen, 4.0×10^{-3} mol dm^{-3} EHDAB, 2.0×10^{-7} mol dm^{-3} TEPA, 1.0×10^{-1} mol dm^{-3} NaOH, 1.0×10^{-7} mol dm^{-3} copper(II), and 5% H_2O_2.

feasibility for the determination of a much smaller amount of copper(II) was expected to improve the sensitivity of protein determination.

Copper(II) Catalyst Containing α-Amino Acid. The present method was applied to the determination of α-amino acid; the signals of L-aspartic acid (Asp) as a model are shown in Fig. 9. The shape of the signals was quite different from that in the luminol-H_2O_2 system; examination showed a first positive peak after the injection of an amino acid solution, followed by a second negative peak based on the formation of a copper(II)-Asp complex compound. The

Table 1. The Relative Responses of Various Amino Acids (5.0×10^{-5} mol dm^{-3}) Based on the Response of L-Aspartic Acid

α-Amino acid	Positive peak height	Positive peak area	Negative peak area	Formation constant*) $\log K_1K_2$
Asp	1.00	1.00	1.00	15.35[a)]
Gly	0.96	0.81	0.67	15.67
Pro	0.91	0.85	0.61	16.58[b)]
Ala	0.90	0.75	0.64	15.52
His	0.85	0.84	3.50	18.53
Glu	0.83	0.74	0.51	14.16
Lys	0.75	0.65	0.28	13.90
Arg	0.67	0.57	0.31	13.76

*) Temp: 25°C, Method: glass electrode, almost the same ionic strength. (The Chemical Society, "Stability Constant," Special Publication No. 17, London (1964)). a) 30°C. b) 20°C.

peak height corresponding to the positive catalytic activity increased with an increase in the Asp concentration and then decreased through the maximum value at 1×10^{-3} mol dm^{-3} Asp, while the peak area corresponding to the negative catalytic activity increased with an increase in the Asp concentration. These phenomena were also observed for such other amino acids as L-glutamic acid(Glu), L-glycine (Gly), L-alanine (Ala), L-proline (Pro), L-lysine hydrochloride (Lys), L-arginine hydrochloride (Arg), and L-histisine hydrochloride (His), and for ethylenediamine and 2,2′-bipyridine. However, a negative peak alone was obtained in the presence of such a ligand as triethylenetetramine, ethylenediaminetetraacetic acid, and diethylenetriaminepentaacetic acid, which contained more than four donor atoms and which formed a stable copper(II) complex compound. A negative peak alone was also obtained, even in the presence of ethylenediamine, when the mole ratio of ethylenediamine to copper(II) was very large ([ethylenediamine]/[copper(II)]=10^6). These results suggest that the final response rate has a close relation with the compositional structure of a copper(II) complex compound. A detailed investigation of the positive and negative peaks is now in progress. The response of each amino acid relative to that of Asp is shown in Table 1. Though the negative peak area of His was abnormally large, this seemed to be attributable to a larger formation constant of a copper(II)–His complex compound.

Since the positive cytalytic activity of copper(II) was much more enhanced in the presence of an amino acid than in that of a tartrate, while the negative catalytic activity alone of copper(II) was observed in the presence of protein, an attempt was made to determine microamounts of protein by using an amino acid instead of a tartrate contained in a biuret reagent. The relationship between the Arg concentration and the negative peak area was obtained by adding definite amounts of BSA to a solution containing a definite amount of copper(II) and various amounts of Arg as a coexisting amino acid (Fig. 10).

The calibration curves of BSA shown in Fig. 11 were obtained by adding various amounts of BSA to

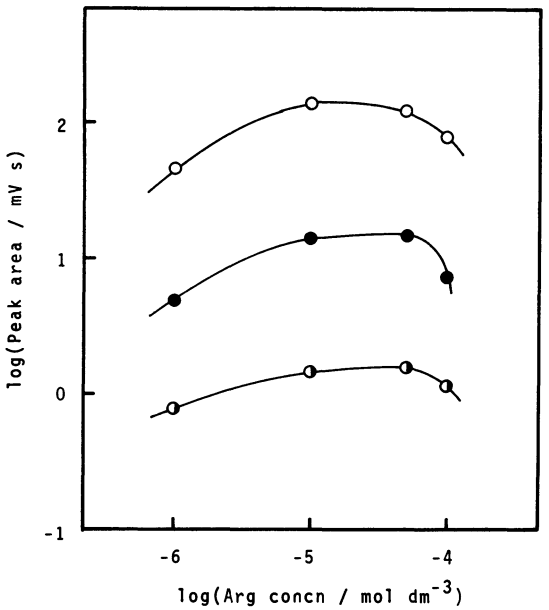

Fig. 10. Relationship between Arg concn and peak area.
○: 1.0×10^{-2} g dm^{-3}-, ●: 1.0×10^{-3} g dm^{-3}-, and ◑: 1.0×10^{-4} g dm^{-3}-BSA.
Conditions: 5.0×10^{-5} mol dm^{-3} phen, 4.0×10^{-3} mol dm^{-3} EHDAB, 2.0×10^{-7} mol dm^{-3} TEPA, 1.0×10^{-1} mol dm^{-3} NaOH, 1.0×10^{-7} mol dm^{-3} copper(II), and 5% H_2O_2.

a copper(II)–Arg solution, a copper(II)–biuret reagent solution, and a copper(II)–Asp solution, and by then measuring their peak areas. As can be seen from Fig. 11, the present modified method enabled us to determine 5.0×10^{-6}—1.0×10^{-1} g dm^{-3} BSA and showed the detection limit of 250 pg BSA. This value was one-fourth that in a biuret reagent and about one-fortieth that in the luminol–H_2O_2 CL system reported in the previous paper. The coefficient of variation obtained for nine measurements of 1×10^{-4} g dm^{-3} BSA was 5.9%. The other proteins, such as BγG, and HSA also showed a sensitivity similar to that in BSA (Fig. 12).

Though the present method was developed as a detector for high performance liquid chromatography, it was also applied to a human serum sample. First

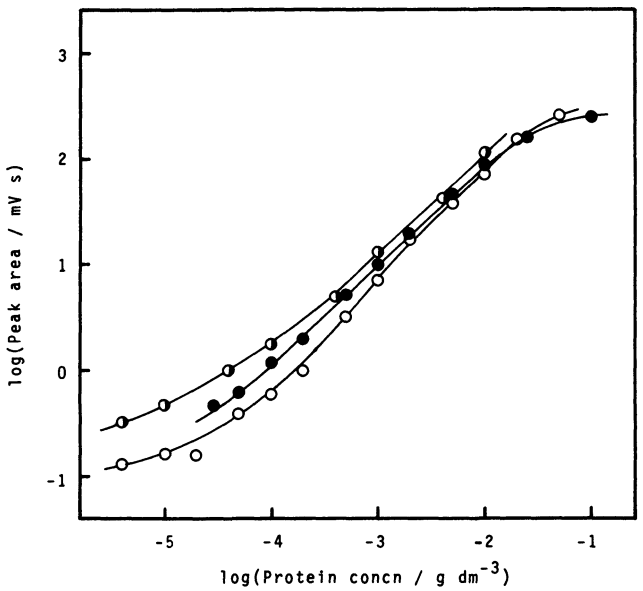

Fig. 11. Calibration curves of BSA in copper(II) catalyst solution.
◑: copper(II)-Arg soln, ●: copper(II)-biuret reagent soln, and ○: copper(II)-Arg soln.
Conditions: 5.0×10^{-5} mol dm^{-3} phen, 4.0×10^{-3} mol dm^{-3} EHDAB, 2.0×10^{-7} mol dm^{-3} TEPA, 1.0×10^{-1} mol dm^{-3} NaOH, 5% H_2O_2, 1.0×10^{-7} mol dm^{-3} copper(II), and 8.0×10^{-7} tartrate or 5.0×10^{-5} mol dm^{-3}-amino acids.

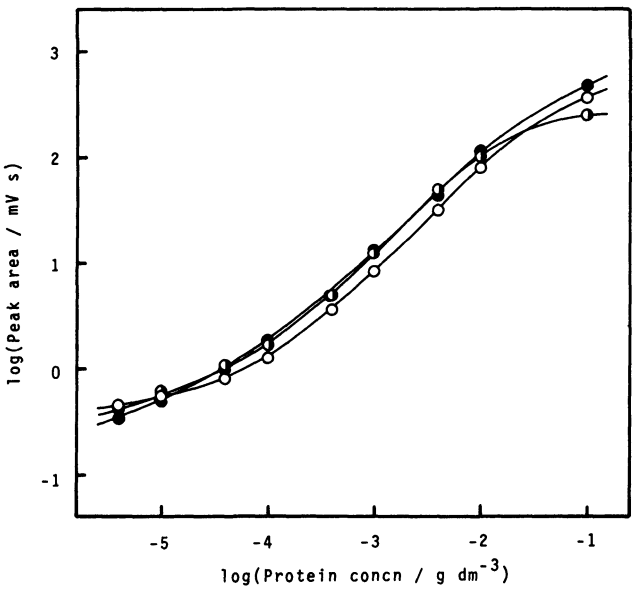

Fig. 12. Calibration curves of various proteins.
○: HSA, ●: BSA, and ◑: BγG.
Conditions: 5.0×10^{-5} mol dm^{-3} phen, 4.0×10^{-3} mol dm^{-3} EHDAB, 2.0×10^{-7} mol dm^{-3} TEPA, 1.0×10^{-1} mol dm^{-3} NaOH, 5% H_2O_2, 1.0×10^{-7} mol dm^{-3} copper(II), and 5.0×10^{-5} mol dm^{-3} Arg.

of all, the effect of the coexisting constituents in a human serum sample on the determination of HSA by the present modified method was examined. Various amounts of HSA were estimated in either the presence or absence of a definite amount of control serum (diluted to a volume of 10^5 times with a buffer solution), and the relationship between HSA concentration and

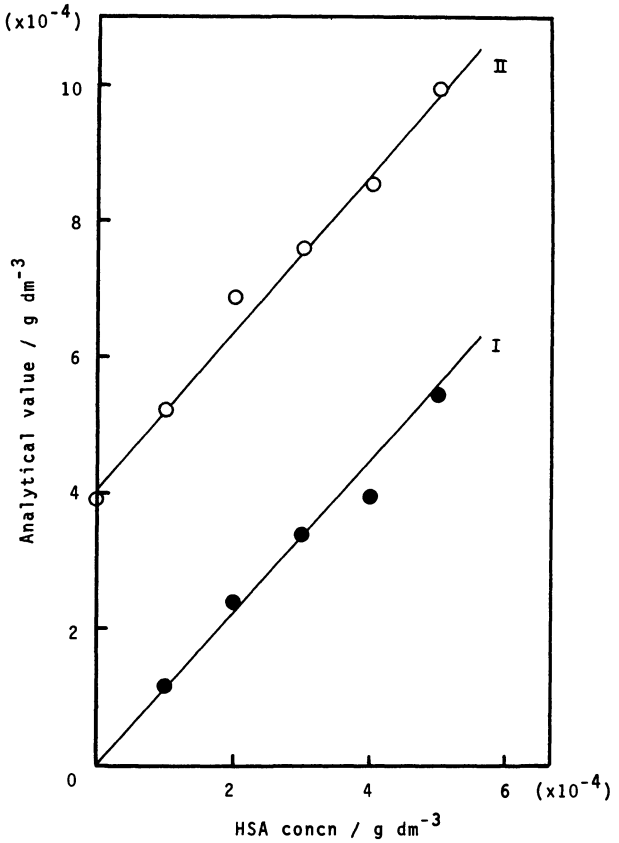

Fig. 13. Relationship between HSA concn and analytical value.
●: HSA and ○: HSA+control serum.
Conditions: 5.0×10^{-5} mol dm^{-3} phen, 4.0×10^{-3} mol dm^{-3} EHDAB, 2.0×10^{-7} mol dm^{-3} TEPA, 1.0×10^{-1} mol dm^{-3} NaOH, 5% H_2O_2, 1.0×10^{-7} mol dm^{-3} copper(II), and 5.0×10^{-5} mol dm^{-3} Arg.

the analytical value was obtained by the use of the calibration curve shown in Fig. 12. All the analytical values of the ordinate in Fig. 13 were represented as the amount of HSA. The difference between the two straight lines, I and II, in the analytical value was approximately equal to the amount of protein in the added control serum. This means that the present method was applicable to the sensitive determination of protein in a serum sample without being interfered with by coexisting constituents, when a sample solution is diluted to a volume of 10^5 times with a buffer solution and then measured.

The present method may be expected to be useful for the development of a sensitive, rapid, and inexpensive detector by which a trace amount of protein can be determined without labeling it.

References

1) T. Hara, M. Toriyama, and T. Ebuchi, *Bull. Chem. Soc. Jpn.*, **58**, 109 (1985).
2) T. Hara, M. Toriyama, T. Ebuchi, and M. Imaki, *Chem. Lett.*, **1985**, 341.
3) M. Yamada, S. Suzuki, *Anal. Lett.*, **17**, 251 (1984).
4) T. Hara, M. Toriyama, and K. Tsukagoshi, *Bull. Chem. Soc. Jpn.*, **56**, 1382 (1983).

Transition-Metal Complexes of Pyrrole Pigments. XXII. Photoredox Behavior of Oxo(tetra-*p*-tolylporphinato)-molybdenum(V) Complexes†

Yoshihisa MATSUDA, Toshihiko TAKAKI, and Yukito MURAKAMI*
Department of Organic Synthesis, Faculty of Engineering, Kyushu University, Hakozaki, Higashi-ku, Fukuoka 812
(Received November 16, 1985)

Photochemical reduction of oxomolybdenum(V) complexes of 5,10,15,20-tetra-*p*-tolylporphine, [$Mo^{V}O(X)$(ttp)], was investigated under irradiation with the visible light in benzene, where X stands for an axial ligand placed trans to the oxo group. Irradiation of [$Mo^{V}O(X)$(ttp)] resulted in a homolytic cleavage of the Mo-X bond to afford [$Mo^{IV}O$(ttp)] and a radical species generated from the axial ligand (X). The reduction rate was controlled by the nature of the Mo-X bond, and a complex with less ionic character of the axial bond was more reactive in the homolysis process. The bulkiness of the axial alkoxo ligands may provide two different effects which are opposite to each other on the reactivity: (i) The repulsive interaction between an axial ligand and the equatorial ttp accelerates the homolysis of the Mo-X bond; (ii) the diffusion rate of the radical species, generated by the photochemical cleavage of the axial coordinate bond, from the coordination sphere is progressively retarded as the bulkiness of the alkoxo ligand increases. The second effect seems to be more pronounced for the present photochemical reaction. The photochemical reduction of [$Mo^{V}O(X)$(ttp)] is essentially composed of two sequential steps, photochemical cleavage of the Mo-X bond and diffusion of the radical species from the coordination sphere. Reoxidation of [$Mo^{IV}O$(ttp)] under aerobic irradiation conditions afforded [$Mo^{V}O$-(OH)(ttp)] and [$(Mo^{V}O(ttp))_2O$] via the postulated intermediate formation of [$Mo^{V}(OO\cdot)$(ttp)].

The redox chemistry of metalloporphyrins and the reaction behavior of their various axial ligands have attracted much attention in connection with the development of oxygen carriers, oxygenation catalysts, and photochemical catalysts. We have investigated the redox behavior of some molybdenum[1] and niobium[2] complexes of 5,10,15,20-tetraphenylporphine by means of electrochemical methods. The redox potentials for couples of Mo^{V}/Mo^{IV} and Nb^{V}/Nb^{IV} as observed for these porphine complexes have been found to vary depending upon the nature of axial ligands, and fall in the region between 0 and −0.8 V vs. SCE. We have found recently that irradiation of tri-μ-oxo-bis(5,10,15,20-tetra-*p*-tolylporphinato)niobium(V) in benzene with the visible light under aerobic conditions afforded two paramagnetic species at room temperature.[3] One of the paramagnetic species, which is ESR silent, oxidized heterocyclic bases, while the other species, which is detectable by ESR, oxidized olefins catalytically to afford the corresponding epoxides selectively. On the other hand, Ledon and his associates have reported that the photo-assisted reduction of molecular oxygen to hydrogen peroxide took place in the presence of methoxooxo(5,10,15,20-tetraphenylporphinato)molybdenum(V).[4] In order to clarify axial ligand effects on the photoreduction process, oxo(tetra-*p*-tolylporphinato)molybdenum(V) complexes with various axial ligands, [$Mo^{V}O(X)$(ttp)] (X stands for an axial ligand placed trans to the oxo group), were employed and their photoreduction behavior was investigated from kinetic and structural viewpoints in this work. Reoxidation of the resulting oxomolybdenum(IV) species was also studied under aerobic conditions by spectroscopic means.

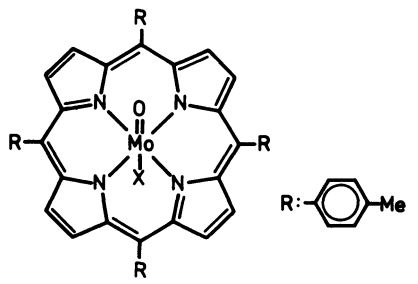

[$Mo^{V}O(X)$(ttp)] X: OCH_3, OC_2H_5, OC_4H_9, $OCH_2C_6H_5$, $OCOCH_3$, Cl

Experimental

ESR spectra were recorded on a JEOL JES-ME-3 X-band spectrometer equipped with a 100-kHz field modulation unit; a standard MgO/Mn^{II} sample calibrated with a NMR magnetometer was employed for calibration of the magnetic field. Electronic and IR absorption spectra were measured with a Hitachi 340 recording spectrophotometer and a JASCO DS-403G grating spectrophotometer, respectively.

Materials. Benzene was purified by the standard method and distilled under nitrogen just before use. Nitrosobenzene of Tokyo Kasei Kogyo Co. was purified by sublimation at 38 °C under reduced pressure (930 Pa). 5,10,15,20-Tetra-*p*-tolylporphine, H_2ttp, was prepared from pyrrole and *p*-tolualdehyde according to a procedure similar to that adopted for the synthesis of 5,10,15,20-tetraphenylporphine, H_2tpp.[5,6] Oxomolybdenum(V) complexes of the former equatorial ligand with methoxo, ethoxo, chloro, and acetato moieties as the axial ligands were prepared in the light of reported procedures for the preparation of the corresponding complexes of the latter equatorial ligand.[1,7]

Methoxooxo(5,10,15,20-tetra-*p*-tolylporphinato)molybdenum-

†Contribution No. 816 from this Department.

(V), [$Mo^{V}O(OCH_3)$(ttp)]: Yield 47%; Vis_{max} (benzene) 455, 583, and 623 nm; IR (KBr) 906 cm^{-1} (Mo=O). Found: C, 70.97; H, 4.42; N, 7.52%. Calcd for $C_{45}H_{31}N_4O_2Mo$: C, 71.52; H, 4.13; N, 7.42%.

Ethoxooxo(5,10,15,20-tetra-*p*-tolylporphinato)molybdenum-(V), [$Mo^{V}O(OC_2H_5)$(ttp)]: Yield 54%; Vis_{max} (benzene) 456, 580, and 620 nm; IR (KBr) 898 (Mo=O) and 519 cm^{-1} (Mo-O). Found: C, 72.70; H, 5.05; N, 6.78%. Calcd for $C_{50}H_{41}N_4O_2Mo$: C, 72.72; H, 5.00; N, 6.78%.

Chlorooxo(5,10,15,20-tetra-*p*-tolylporphinato)molybdenum-(V), [$Mo^{V}O(Cl)$(ttp)]: Yield 61%; Vis_{max} (benzene) 347, 422, 502, 630, and 677 nm; IR (KBr) 943 cm^{-1} (Mo=O). Found: C, 67.61; H, 4.37; N, 6.57%. Calcd for $C_{48}H_{36}ClN_4OMo \cdot HCl$: C, 68.00; H, 4.56; N, 6.43%.

Acetatooxo(5,10,15,20-tetra-*p*-tolylporphinato)molybdenum-(V), [$Mo^{V}O(OCOCH_3)$(ttp)]: Yield 51%; Vis_{max} (benzene) 409 sh, 482, 611, and 645 nm; IR (KBr) 914 and 947 cm^{-1} (Mo=O). Found: C, 69.48; H, 4.92; N, 6.33%. Calcd for $C_{50}H_{39}N_4O_3Mo \cdot CH_3CO_2H$: C, 69.41; H, 4.82; N, 6.23%.

Oxomolybdenum(V) complexes with butoxo and benzyloxo moieties as the axial ligands were prepared from [$Mo^{V}O(Cl)$(ttp)] according to the following procedure. An alcohol (1-butanol or benzyl alcohol; 20 mL) saturated with KOH was added to a dichloromethane solution (200 mL) containing [$Mo^{V}O(Cl)$(ttp)] (100 mg). After the mixture was evaporated to dryness in vacuo, the residue was extracted with dichloromethane. The extract was applied on a column of neutral aluminum oxide (Woelm, activity grade I) and eluted with dichloromethane containing the same alcohol species (1% v/v). The product fraction was evaporated to dryness in vacuo, and the residue was recrystallized from dichloromethane containing the same alcohol (ca. 1% v/v).

Butoxooxo(5,10,15,20-tetra-*p*-tolylporphinato)molybdenum-(V), [$Mo^{V}O(OC_4H_9)$(ttp)]: Yield 90%; Vis_{max} (benzene) 455, 582, and 622 nm; IR (KBr) 905 cm^{-1} (Mo=O). Found: C, 73.14; H, 5.31; N, 6.56%. Calcd for $C_{52}H_{45}N_4O_2Mo$: C, 72.54; H, 5.29; N, 6.38%.

(Benzyloxo)oxo(5,10,15,20-tetra-*p*-tolylporphinato)molybdenum (V), [$Mo^{V}O(OCH_2C_6H_5)$(ttp)]: Yield 70%; Vis_{max} (benzene) 458, 584, and 624 nm IR (KBr) 898 and 907 cm^{-1} (Mo=O). Found: C, 74.25; H, 5.20; N, 5.83%. Calcd for $C_{55}H_{43}N_4O_2Mo \cdot 1/4C_6H_5CH_2OH$: C, 74.50; H, 4.96; N, 6.12%.

Photoreduction Measurements. A benzene solution of [$Mo^{V}O(X)$(ttp)] (ca. 1×10^{-3} mol dm^{-3}) was sealed in a quartz tube (diameter, 5 mm) after evacuation of gas. The sample solution placed in an ESR cavity was irradiated with a 500-W tungsten lamp from a distance of 20 cm. ESR spectra were recorded under irradiation conditions. For detection of radical species, nitrosobenzene (ca. 5×10^{-2} mol dm^{-3}) was added to the sample solution to afford the corresponding spin adducts.

Benzene and [$Mo^{V}O(X)$(ttp)] were mixed in a spectrophotometric cell of 1-cm path length after both complex and solvent were degassed separately. The sample solution, containing ca. 4×10^{-6} mol dm^{-3} [$Mo^{V}O(X)$(ttp)], was irradiated with a 500-W tungsten lamp from a distance of 20 cm, and electronic absorption spectra were measured at appropriate time intervals.

Results and Discussion

Photoreduction of [$Mo^{V}O(X)$(ttp)]. The present oxomolybdenum(V) complexes, [$Mo^{V}O(X)$(ttp)], show characteristic ESR spectra in benzene, which consist of nine intense lines originated from the superhyperfine interaction of one d electron with four nitrogen nuclei of the equatorial ligand.[7] Although the ESR signals for the complexes with axial alkoxo ligands in benzene were subjected to change very slowly due to hydrolysis or dimerization of the complexes, the complexes dissolved in sufficiently dried and freshly distilled benzene remained stable without such decomposition for several hours in the dark at room temperature. The ESR signals for the present complexes except for [$Mo^{V}O(Cl)$(ttp)] underwent intensity decrease upon irradiation with the visible light under anaerobic conditions as shown in Fig. 1. The signals for the complexes with the alkoxo ligands disappeared in about 4 h and were recovered upon addition of alcohol species corresponding to the axial ligands under aerobic conditions, while the complexes remained ESR silent so long as anaerobic conditions were retained. These observations indicate that the irradiation results in reduction of the central metal atom along with elimination of the axial ligand as a radical species as shown by Eq. 1. The ESR signal for a benzene solution

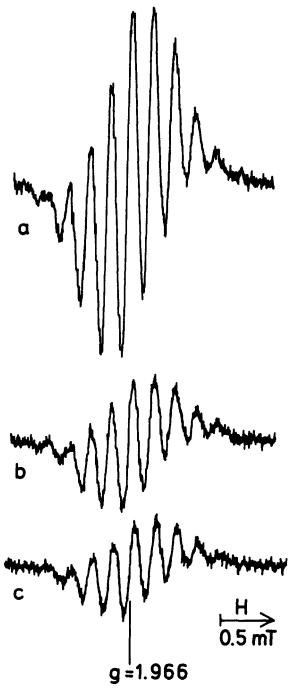

Fig. 1. ESR spectra for [$Mo^{V}O(OCH_3)$(ttp)] in benzene (ca. 1×10^{-3} mol dm^{-3}) under anaerobic conditions at room temperature: a, before irradiation; b, irradiated for 30 min; c, irradiated for 1 h.

$$\begin{array}{c} X \\ | \\ Mo^{V}(ttp) \\ \| \\ O \end{array} \xrightarrow{h\nu} \begin{array}{c} \\ \\ Mo^{IV}(ttp) \\ \| \\ O \end{array} + X\cdot \qquad (1)$$

of [$Mo^{V}O(X)$(ttp)] also underwent intensity decay in the presence of nitrosobenzene as a spin-trapping agent upon anaerobic irradiation, but a new signal, which is

Table 1. Spin Hamiltonian Parameters for Spin Adducts of Nitrosobenzene and Radical Species Generated from [$Mo^{V}O(X)(ttp)$] in Benzene under Aerobic Irradiation at Room Temperature

Mother complex	g-Value	(Hyperfine splitting constants)[a]$\times 10^4$/T			
		A_N	$A_{o,p}$	A_m	A_β
[$Mo^{V}O(OCH_3)(ttp)$]	2.01	14.85	2.98	0.92	0.92
[$Mo^{V}O(OC_2H_5)(ttp)$]	2.00	15.61	3.04	1.04	0.56
[$Mo^{V}O(OC_4H_9)(ttp)$]	2.00	15.54	3.07	1.06	0.68
[$Mo^{V}O(OCH_2C_6H_5)(ttp)$]	2.00	15.66	3.40	1.07	0.53

a) Hyperfine splitting constants are defined as follows: A_N, due to the nitrogen nucleus of nitrosobenzene; $A_{o,p}$, due to the proton nuclei placed at ortho and para positions of the benzene moiety; A_m, due to the proton nuclei placed at meta positions of the benzene moiety; A_β, due to the proton nuclei placed at β-position of the alkoxo moiety.

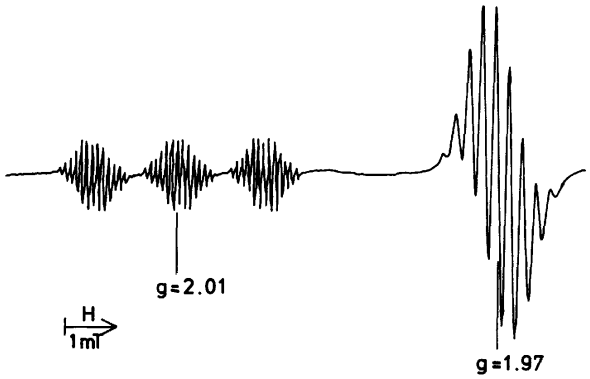

Fig. 2. ESR spectrum for [$Mo^{V}O(OCH_3)(ttp)$] in benzene (ca. 1×10^{-3} mol dm^{-3}) containing nitrosobenzene (ca. 5×10^{-2} mol dm^{-3}); irradiated for 30 min at room temperature.

attributed to the alkoxyl radical–nitrosobenzene adduct (**A**), appeared as shown in Fig. 2. Hyperfine splitting

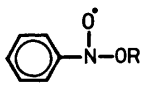

A

constants for several alkoxy adducts are listed in Table 1. The ESR behavior is in agreement with that observed during the photoreduction of methoxooxo(5,10,15,20-tetraphenylporphinato)molybdenum(V).[4]

The photoreduction of all the complexes other than [$Mo^{V}O(Cl)(ttp)$] was also examined by means of electronic spectroscopy as typically shown for [$Mo^{V}O(OC_2H_5)(ttp)$] in Fig. 3. The absorption bands at 456, 580, and 620 nm for the Mo^{V} species underwent intensity decay, and a new set of bands attributable to the Mo^{IV} species appeared at 434, 512(sh), 566, and 592 nm. The latter bands were further enhanced in their intensities along with the progress of photochemical reaction. Since isosbestic points were clearly observed at 396, 443, 535, 566, 598, and 648 nm, any additional reaction other than that given by Eq. 1 does not take place under the present conditions. Correlations between intensity of the Soret band and irradiation time are shown in Fig. 4. These correlations indicate that the photoreduction follows the first-order kinetics. Ledon et al. observed that the excitation of [$Mo^{V}O$-

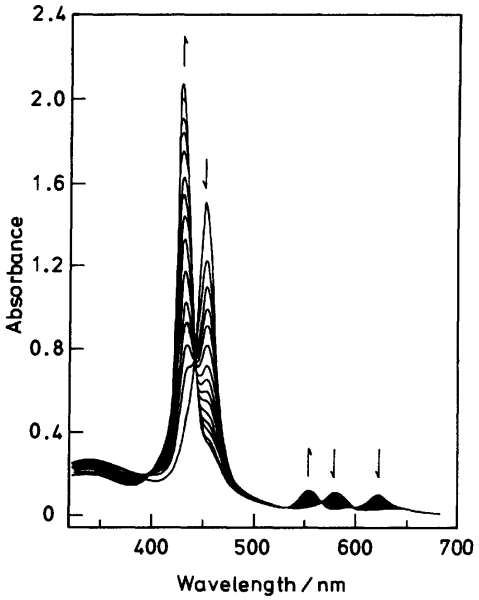

Fig. 3. Visible spectral change for [$Mo^{V}O(OC_2H_5)$-(ttp)] in benzene (ca. 4×10^{-6} mol dm^{-3}) under irradiation at room temperature. Trends of spectral change with time are shown by arrows; measurements were carried out at 20 s intervals.

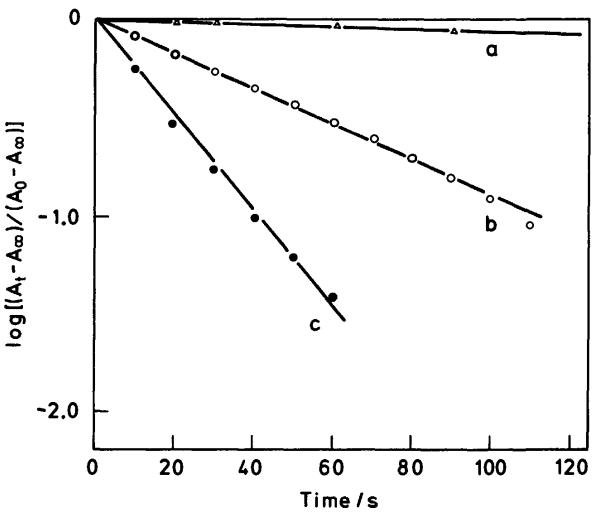

Fig. 4. First-order plots of Soret band intensity vs. irradiation time for [$Mo^{V}O(X)(ttp)$] in benzene at room temperature. Alkoxo moieties (X): a, $OCOCH_3$; b, $OCH_2C_6H_5$: c, OCH_3.

Table 2. Rate Constants of Photoreduction (k), Spectral Parameters, and Reduction Potentials for Molybdenum(V) Complexes

Complex	k[a]	Soret band[a]	IR (Mo=O)[b]	$E_{1/2}$(Mo)[c]
	s^{-1}	nm	cm^{-1}	V vs. SCE
$[Mo^{V}O(OCH_3)(ttp)]$	5.3×10^{-2}	455	906	−0.74
$[Mo^{V}O(OCOCH_3)(ttp)]$	4.1×10^{-4}	482	947, 914	−0.04
$[Mo^{V}O(Cl)(ttp)]$	No reaction	502	943	−0.06

a) Measured in benzene. b) KBr disc. c) Measured in dichloromethane for the corresponding tpp complexes, cited from Ref. 1.

Table 3. Rate Constants of Photoreduction (k) and Spectral Parameters for Molybdenum(V) Complexes with Various Axial Alkoxo Ligands

Complex	k[a]	Soret band[a]	IR (Mo=O)[b]
	s^{-1}	nm	cm^{-1}
$[Mo^{V}O(OCH_3)(ttp)]$	5.3×10^{-2}	455	906
$[Mo^{V}O(OC_2H_5)(ttp)]$	5.6×10^{-2}	456	898
$[Mo^{V}O(OC_4H_9)(ttp)]$	2.3×10^{-2}	455	905
$[Mo^{V}O(OCH_2C_6H_5)(ttp)]$	1.3×10^{-2}	458	907, 898

a) Measured in benzene. b) KBr disc.

$(OCH_3)(tpp)]$ was effective exclusively with the Soret band energy for the photoreduction.[4] Since the Soret bands of $[Mo^{V}O(X)(ttp)]$ and $[Mo^{IV}O(ttp)]$ do not show significant overlap between them (Fig. 3), light quanta absorbed by the former Mo^{V} species must be exclusively used for the photoreduction even after generation of the latter Mo^{IV} species. This may provide the reason why the clear first-order kinetics (Fig. 4) was observed for the present photochemical reaction.

Rate constants for the photoreduction are listed in Table 2 along with reduction potentials and Mo=O stretching frequencies for the oxomolybdenum(V) complexes having various axial ligands. The bonding mode of the axial coordinate bond, Mo–X, varies in a wide range as controlled by the electronegativity of axial ligand X. The covalent character decreases as goes downwards for the complexes listed in Table 2. The axial coordinate bond in $[Mo^{V}O(Cl)(ttp)]$ must be highly ionic in the light of structural determination of $[Mo^{V}O(Cl)(tpp)]$ by means of the single-crystal X-ray diffraction measurements.[8] The axial bonding character is reflected on the Soret band energy, the Mo=O stretching frequency, and the reduction potential for an electrochemical process given by Eq. 2.

$$\begin{array}{l} X \\ | \\ Mo^{V}(ttp) \\ \| \\ O \end{array} \xrightarrow{e^-} \begin{array}{l} \\ \\ Mo^{IV}(ttp) \\ \| \\ O \end{array} + X^- \qquad (2)$$

On the basis of the data listed in Table 2, a complex with less ionic character of the axial coordinate bond is more reactive in the photoreduction process. The Soret band is plausibly assigned to a charge-transfer transition from the porphine ligand to the metal.[9] Then, the excited electron seems to occupy ultimately an antibonding orbital localized in the Mo–X bond for complexes having a highly covalent axial bond, and consequently the axial coordinate bond is destabilized. The excited state is plausibly represented for the case of the axial coordination with large ionic character as $\{[Mo^{IV}O(ttp^+)]^+\cdots X^-\}$ which is regarded as a charge transfer complex, while the excited state for the covalent axial coordination may be given as $\{[Mo^{III}O(ttp^+)]\cdots X\cdot\}$. As a result, the electrostatic attraction between X^- and $[Mo^{IV}O(ttp^+)]^+$ is operative in the former case, while no such interaction would be expected in the latter. Therefore, a less electronegative axial ligand more readily undergoes the homolytic cleavage upon irradiation with the visible light.

Rate constants for the complexes with various axial alkoxo ligands are listed in Table 3 along with relevant spectral parameters. The rate of photoreduction decreases in the following order with respect to the alkoxo ligands: $OCH_3 \cong OC_2H_5 > OC_4H_9 > OCH_2C_6H_5$. In the light of the Soret band energies and the stretching frequencies of the Mo=O bond, there are no significant differences in the axial bonding character among these complexes. Therefore, differences in the reactivity must come from stereochemical origin. The bulkiness of the axial alkoxo ligand may provide two different effects which are opposite to each other on the reactivity. First, the repulsive interaction between an axial ligand, OR, and the equatorial one, ttp, accelerates the homolysis of the coordinate bond. Second, the diffusion rate of the radical species, generated by the photochemical cleavage of the axial coordinate bond, from the coordination sphere is progressively retarded as the bulkiness of the alkoxo ligand increases. The slow diffusion is in favor of recombination of the radical species and the reduced central metal. The second effect seems to be more pronounced for the present

photochemical reaction in the light of the kinetic data given in Table 3.

On the basis of the above discussion, the present photochemical reduction of [$Mo^{V}O(X)(ttp)$] is essentially composed of two sequential steps, photochemical cleavage of the axial coordinate bond and diffusion of the radical species from the coordination sphere as shown by Eq. 3. The overall reaction rate for the complexes with smaller axial ligands is primarily controlled by the first step which is enhanced as the axial coordinate bond becomes more covalent, while the second step becomes the rate-determining one for the reaction of the complexes with more bulky axial ligands.

$$X\text{-}Mo^{V}(ttp)(=O) \underset{\text{(step 1)}}{\overset{h\nu}{\rightleftharpoons}} \left[X\cdot \;\cdots\; Mo^{IV}(ttp)(=O) \right] \xrightarrow[\text{(step 2)}]{} Mo^{IV}(ttp)(=O) + X\cdot \qquad (3)$$

Reoxidation of [$Mo^{IV}O(ttp)$]. The photochemically reduced complex, [$Mo^{IV}O(ttp)$], was reoxidized under aerobic conditions in benzene to afford the starting complexes when the corresponding alcohols were added. The reoxidation process showed the second-order dependence on the molybdenum complex for all cases investigated here, and is in accord with the earlier work for [$Mo^{IV}O(tpp)$] in the presence of methanol.[4]

The fate of [$Mo^{V}O(X)(ttp)$] in benzene under aerobic irradiation conditions was monitored by electronic spectroscopy in the absence of an alcohol. The aerobic irradiation with the visible light resulted in appearance of absorption bands attributable to [$Mo^{IV}O(ttp)$]. The intensity increase of these bands, however, was found to level off within an hour at a lower level relative to that observed under anaerobic conditions; about 80% of the original complex was reduced. The observation indicates that the reoxidation of [$Mo^{IV}O(ttp)$] takes place by molecular oxygen under aerobic conditions. In a few hours under aerobic irradiation conditions, the absorption bands attributable to [$Mo^{IV}O(ttp)$] began to decrease in their intensities along with appearance of a new absorption band at 484 nm and precipitation of a dark crystalline material. The crystalline solid was slightly soluble in benzene and dichloromethane and exhibited electronic absorption spectra shown in Fig. 5. The absorption spectrum observed in benzene is identical with that for the μ-oxo dimer, [$\{Mo^{V}O(ttp)\}_2O$], while that in dichloromethane is identical with that for [$Mo^{V}O(OH)(ttp)$].[10] The ESR spectrum observed for the crystalline solid is shown in Fig. 6; $D=940\times10^{-4}\,cm^{-1}$, $E\cong0$. Consequently, this material is confirmed to be the μ-oxo dimer and hydrolyzed readily by a trace amount of water present in dichloromethane to afford [$Mo^{V}O(OH)(ttp)$]. Two fractions were recovered from the mother solution, obtained from the aerobic photochemical reaction of

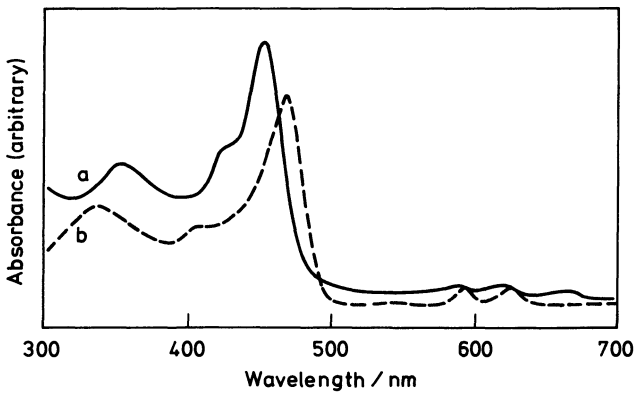

Fig. 5. Visible absorption spectra for the precipitated complex developed during reoxidation of [$Mo^{IV}O(ttp)$] in benzene without alcohols; measured in benzene (a) and dichloromethane (b).

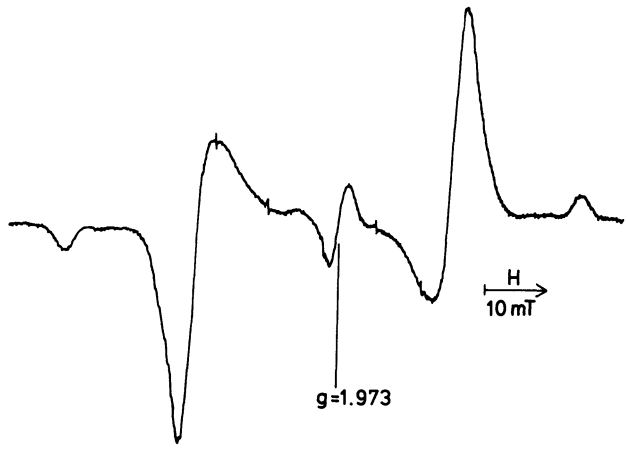

Fig. 6. ESR spectrum for the precipitated complex developed during reoxidation of [$Mo^{IV}O(ttp)$]; in solid state at room temperature.

[$Mo^{V}O(X)(ttp)$] in benzene, by column chromatography [aluminum oxide (Woelm), activity grade III; eluant, dichloromethane]. The first fraction was identified as [$Mo^{V}O(OH)(ttp)$], while the second fraction was not identified with known species; the latter showing a Soret band at 484 nm. However, we may plausibly assign the peroxo complex, [$Mo^{V}O(OO\cdot)(ttp)$], to this species on the following grounds. (i) The absorption due to [$Mo^{IV}O(ttp)$] decreased in its intensity along with appearance of the 484-nm band (vide supra). (ii) Imamura et al. reported that [$Mo^{V}O(X)(tpp)$] is reduced via its reaction with KO_2.[12] They assigned [$Mo^{V}O(OO\cdot)(tpp)$] to an intermediate showing a Soret band in the 480—490-nm range. (iii) Ledon et al. proposed that the reoxidation of [$Mo^{IV}O(tpp)$] takes place via intermediate formation of [$Mo(O_2)(OO\cdot)(tpp)$] in a benzene–methanol mixture.[4] However, they did not identify the intermediate. (iv) [$Nb^{IV}O(ttp)$], which was generated from [$\{Nb^{V}(ttp)\}_2O_3$] under photochemical conditions, was reoxidized by the atmospheric oxygen to afford [$Nb^{V}O(OO\cdot)(ttp)$].[3]

In addition to the above conclusion, [$Mo^{V}O(OH)$-

(tpp)] has been found to undergo dehydration to afford [{$Mo^{V}O(tpp)$}$_2O$] as precipitates in benzene.[11] Therefore, the reoxidation pathway for [$Mo^{IV}O(ttp)$] in benzene without an alcohol may be represented by Eq. 4 with participation of a trace amount of water from the open atmosphere.

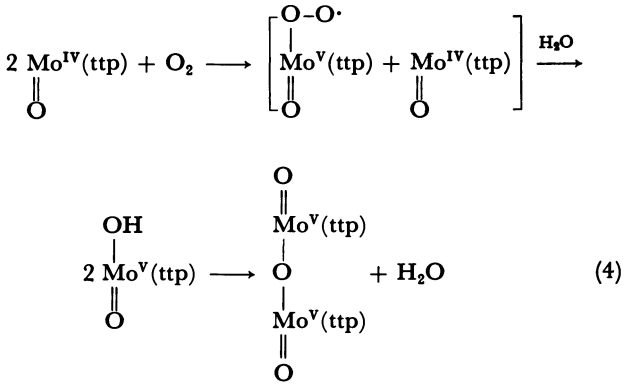

(4)

We have reported recently that tri-μ-oxo-bis(5,10,15,20-tetra-*p*-tolylporphinato)niobium(V) is capable of catalyzing the epoxidation of olefins by the atmospheric oxygen under irradiation with the visible light.[3] Since the catalytically active species in this reaction was confirmed to be [$Nb^{V}O(OO\cdot)(ttp)$], the peroxo molybdenum species, [$Mo^{V}O(OO\cdot)(ttp)$], which is likely formed under the present conditions, is also expected to act as an effective catalyst for the selective epoxidation of olefins in a similar manner.

References

1) Y. Matsuda, S. Yamada, and Y. Murakami, *Inorg. Chem.*, **20**, 2239 (1981).

2) Y. Matsuda, S. Yamada, T. Goto, and Y. Murakami, *Bull. Chem. Soc. Jpn.*, **54**, 452 (1981); Y. Matsuda, S. Sakamoto, T. Takaki, and Y. Murakami, *Chem. Lett.*, **1985**, 107.

3) Y. Matsuda, S. Sakamoto, H. Koshima, and Y. Murakami, *J. Am. Chem. Soc.*, **107**, 6415 (1985).

4) H. J. Ledon, M. Bonnet, and D. Galland, *J. Am. Chem. Soc.*, **103**, 6209 (1981).

5) A. D. Adler, F. R. Longo, J. D. Finarelli, J. Goldmacher, J. Assour, and L. Korsakoff, *J. Org. Chem.*, **32**, 476 (1967).

6) G. H. Barnett, M. F. Hudson, and K. M. Smith, *Tetrahedron Lett.*, **30**, 2887 (1973).

7) Y. Matsuda, F. Kubota, and Y. Murakami, *Chem. Lett.*, **1977**, 1281.

8) H. J. Ledon and B. Mantzen, *Inorg. Chim. Acta*, **31**, L393 (1978).

9) M. Gouterman, "The Porphyrins," ed by D. Dolphin, Academic Press, New York (1978), Vol. 3, Part A, Chap. 1.

10) [$Mo^{V}O(OH)(ttp)$] was prepared in a manner similar to that reported for the preparation of [$Mo^{V}O(OH)(tpp)$].[11] Electronic spectra of both complexes were found to be nearly identical. [$Mo^{V}O(OH)(ttp)$]: Soret band (dichloromethane), 460 nm; IR (KBr), 925 cm^{-1} (Mo=O).

11) H. J. Ledon, M. C. Bonnet, Y. Brigandat, and F. Varescon, *Inorg. Chem.*, **19**, 3488 (1980).

12) T. Imamura, K. Hasegawa, and M. Fujimoto, *Chem. Lett.*, **1983**, 705.

Flameless Atomic-Absorption Spectrometric and Differential-Pulse Polarographic Determination of Cadmium after Coprecipitation with Hafnium Hydroxide

Joichi UEDA* and Natsuko YAMAZAKI
Department of Chemistry, Faculty of Education, Kanazawa University, Marunouchi, Kanazawa 920
(Received December 11, 1985)

Using the coprecipitation method with hafnium hydroxide, the flameless atomic-absorption spectrometric and the differential-pulse polarographic determinations of cadmium have been studied. The collecting ability of hafnium hydroxide for cadmium is excellent; from 0.01 to at least 1000 μg of cadmium in 50—400 cm^3 of a sample solution is coprecipitated quantitatively. The presence of hafnium hydroxide does not interfere with either method of determining cadmium. Of the diverse ions examined, there are no ions which interfere with the flameless atomic-absorption spectrometric determination, even if they are present in a concentration of at least 5000 times that of cadmium; as for the differential-pulse polarographic determination, only indium interferes when present in small amounts. The linear calibration curves through the point of origin were obtained over the range of 0.4—4 ng cm^{-3} of cadmium for the former method and 0.04—40 μg cm^{-3} for the latter method. In the proposed methods, the flameless atomic-absorption spectrometric determination was successfully applied to the analysis for trace amounts of cadmium in river-water samples.

The coprecipitation method is one of the most useful methods for the concentration of cadmium, and various techniques for the determination of trace cadmium, coupled with a preconcentration procedure by means of coprecipitation, have been proposed; inductively coupled plasma-atomic emission spectrometry using hydroxide of indium[1] or lanthanum[2] as a coprecipitant; X-Ray fluorescence using 1,3:2,4-di-*O*-benzylidene-D-glucitol[3] and 1,10-phenanthroline-sodium tetraphenylborate;[4] flame atomic-absorption spectrometry using naphthalene,[5] soybean protein,[6] strontium carbonate,[7] aluminium hydroxide,[8] and tris(1-pyrrolidinecarbodithioato)cobalt(III),[9] and flameless atomic-absorption spectrometry using iron(III) hydroxide[10] and cobalt 1-pyrrolidinecarbodithioate(cobalt-APDC).[11] Moreover, tin(IV) hydroxide[12] has also been proposed as a useful collector of cadmium as a result of investigation using the radiotracer method.

In a previous paper,[13] the present authors suggested that hafnium hydroxide is effective as a collector of trace amounts of lead; it can be satisfactorily analyzed by means of differential-pulse polarography in the presence of large amounts of hafnium. This time, we have recognized that hafnium hydroxide also coprecipitates quantitatively over a wide concentration range of cadmium almost entirely without the coprecipitation of alkali and alkaline earth metals and that this concentration method can be successfully combined with the cadmium determination by means of flameless atomic-absorption spectrometry or differential-pulse polarography. Both methods proposed here are simple, fairly free from the effect of diverse ions, and give good reproducibilities. Cadmium determination by a combined coprecipitation-differential-pulse polarography has not yet been tried. Concerning combined coprecipitation-flameless atomic-absorption spectrometry, however, as has been mentioned above, several methods have been reported. Among those, though, the method using iron(III) hydroxide as a collector[11] can not avoid the coprecipitation of large amounts of alkaline earth elements which may interfere with cadmium determination, and in the case of cobalt-APDC,[12] it is troublesome to digest the precipitate in order to reduce the matrix effect because of the presence of cobalt-APDC itself. This paper will describe the fundamental conditions for the coprecipitation of cadmium with hafnium hydroxide and for the flameless atomic-absorption spectrometric and the differential-pulse polarographic determination of cadmium.

Experimental

Apparatus. All the atomic-absorption measurements were carried out with a Hitachi 170-70 Zeeman-effect atomic-absorption spectrometer with a hollow cadmium cathode lamp (Hitachi 2082008) and a cup-type graphite furnace (Hitachi 170-5104). A Yanagimoto voltammetric analyzer, model p-1000, was used for the differential-pulse polarographic measurements, operating in a three-electrode configuration with a dropping-mercury electrode, a saturated calomel reference electrode, and a platinum counter electrode. A Hitachi-Horiba model M-5 glass electrode pH meter was also used for the pH measurements.

Reagents. Standard Cadmium Solution: A solution containing about 1 mg cm^{-3} of cadmium was prepared by dissolving guaranteed reagent-grade cadmium nitrate in a small amount of nitric acid and by then diluting it with distilled water. The solution was subsequently standardized by complexometric titration.

Hafnium Solution: A solution containing about 5 mg cm^{-3} of hafnium was prepared by dissolving hafnium chloride (Nakarai Chemicals Co.) in 2 mol dm^{-3} of hydrochloric acid and standardized by complexometric back titration.

All the other reagents used were of a guaranteed reagent grade and were purified with a chelate resin when necessary.

Recommended Procedures. Flameless Atomic-Absorption Spectrometric Determination: To a sample solution (50—400 cm^3) containing 0.01—0.1 μg of cadmium, 10 mg of hafnium is added and the pH is adjusted to about 9.5

Table 1. Operating Conditions for Flameless Atomic-Absorption Spectrometry

Analytical wavelength	228.8 nm
Lamp current	8 mA
Slit width	No. 2 (1.1 nm)
Scale expantion	×2
Argon-gas flow rate	
Sheath gas	3 l min^{-1}
Carrier gas	0 l min^{-1}
Drying conditions	21A (ca. 100°C), 70s
Ashing conditions	80A (ca. 700°C), 30s
Atomizing conditions	250A (ca. 2250°C), 5s
Injection volume	20 μl

Table 2. Operating Conditions for Differential-Pulse Polarography

Scan range	−0.3 to −0.9 V
Scan rate	10 mV s^{-1}
Modulation amplitude	50 mV
Forced drop time	1s
Temp. of measurements	20±0.1°C

with 1:1 aqueous ammonia in order to precipitate hafnium hydroxide. After the solution has then been allowed to stand for more than 20 min, the precipitate is filtered by suction using a 3G4 sintered-glass filter, washed with aqueous ammonia of pH 9.5, and dissolved with 1 cm^3 of concd. nitric acid. After the solution is diluted to 25 cm^3 with distilled water, measurements of the atomic absorbance are carried out under the optimum operating conditions, which are shown in Table 1.

Differential-Pulse Polarographic Determination: To a sample solution (50—400 cm^3) containing 1—1000 μg of cadmium, 10 mg of hafnium is added and then precipitated as hafnium hydroxide at about pH 9.5 with 1:1 aqueous ammonia. After allowing the solution to stand for more than 20 min, the precipitate is filtered by suction using a 3G4 sintered-glass filter, washed with aqueous ammonia of pH 9.5, and dissolved with 2 cm^3 of concd hydrochloric acid (with two 1-cm^3 portions of concd hydrochloric acid at about a 5-min interval). The solution is then diluted to 25 cm^3 with distilled water and deaerated with pure nitrogen for 5 min. Then, the polarogram is recorded under the operating conditions shown in Table 2 and the cadmium is determined by the current peak height at −0.64 V.

Results and Discussion

Study of Optimum Conditions for Coprecipitation. The effect of the pH on the coprecipitation of cadmium with hafnium hydroxide was examined by coprecipitating 0.1 or 30 μg of cadmium from 100 cm^3 of the sample solution. As is shown in Fig. 1, almost 100% recoveries of cadmium were obtained over the pH range from 7.0 to 12.0 for 0.1 μg of cadmium and from 7.5 to 12.0 for 30 μg of cadmium. Hence, a pH of about 9.5 was used for the coprecipitation in the further experiments. The amount of hafnium which is required for the quantitative coprecipitation of cadmium increases gradually with an increase in

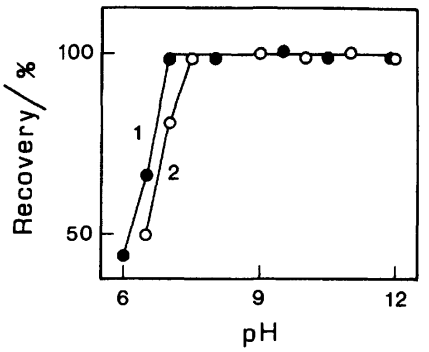

Fig. 1. Effect of pH on coprecipitation.
1: Measurements by flameless atomic absorption spectrometry, Cd 0.1 μg/25 cm^3, Hf 10 mg/25 cm^3, concd HNO_3 1 cm^3/25 cm^3.
2: Measurements by differential pulse polarography, Cd 30 μg/25 cm^3, Hf 10 mg/25 cm^3, concd HCl 2 cm^3/25 cm^3.

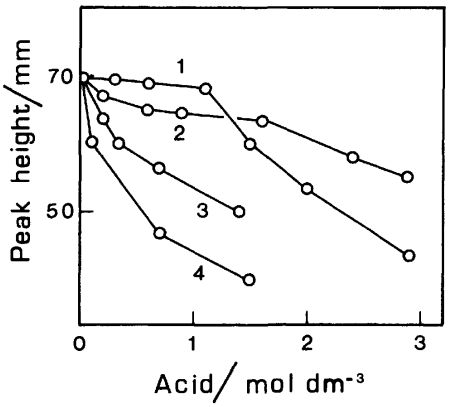

Fig. 2. Effect of acid concentration on peak height of cadmium.
Measurements by flameless atomic absorption spectrometry, Cd 0.1 μg/25 cm^3, Hf 10 mg/25 cm^3,
1: HNO_3, 2: HCl, 3: $HClO_4$, 4: H_2SO_4.

the volume of the sample solution. As a result of the examinations for portions of the sample solution from 50 to 400 cm^3, we found that more than 5 mg of hafnium was needed for 400 cm^3. In this study, 10 mg of hafnium was used. The coexistence of a large amount of hafnium does not interfere with the determinations; that is, the presence of 0.08 to at least 2 mg cm^{-3} of hafnium does not affect the flameless atomic-absorption spectrometric determination, nor does the presence of from 0.08 to at least 1 mg cm^{-3} interfere with the differential-pulse polarographic determination. The investigation of the aging time of the precipitate for the cadmium recovery led to the result that standing for more than 20 min at room temperature was suitable for the quantitative collection of cadmium, because almost a 100% recovery was attained about 15 min after the precipitation of hafnium hydroxide and this percentage remained almost constant for at least 10 h.

Choice of Acids for Dissolution of Precipitate. For the dissolution of hafnium hydroxide, several acids,

Table 3. Influence of Diverse Ions

Ion	A		B		Ion	A		B	
	Amount added	Cadmium found	Amount added	Cadmium found		Amount added	Cadmium found	Amount added	Cadmium found
	mg	ng	mg	μg		mg	ng	mg	μg
Li^+	1	100.0	5	30.3	Bi^{3+}	0.5	99.0	0.1	30.6
Na^+	10	99.5	—	—	Cu^{2+}	0.5	98.5	1	28.5
K^+	10	100.0	—	—	Zn^{2+}	0.5	104.8	5	30.3
Be^{2+}	0.5	105.0	5	29.6	La^{3+}	1	100.5	5	30.5
Mg^{2+}	10	102.0	5	30.0	Zr^{4+}	1	100.5	5	30.3
Ca^{2+}	10	102.5	5	30.8	Th^{4+}	1	98.9	5	30.0
Sr^{2+}	1	100.1	—	—	V(V)	—	—	0.1	29.1
Ba^{2+}	1	100.0	5	30.3	Cr^{3+}	0.5	104.5	0.1	29.1
Al^{3+}	1	101.7	5	28.5	Mo(VI)	1	97.3	5	30.0
Ga^{3+}	1	104.8	5	28.8	W(VI)	1	98.0	—	—
In^{3+}	0.5	105.0	0.05	62.2	Mn^{2+}	1	96.3[a)]	5	29.5
Sn^{4+}	1	95.5	0.05	29.2	Fe^{3+}	1	100.1	0.1	30.0
Pb^{2+}	1	100.0	0.1	29.5	Co^{2+}	1	99.0	1	30.1
Sb^{3+}	1	101.5	1	30.0	Ni^{2+}	1	99.5	1	29.7

A: The flameless atomic-absorption spectrometric determination (100 ng of cadmium was taken). B: The differential-pulse polarographic determination (30 μg of cadmium was taken). a) Hydrochloric acid was used to dissolve the precipitate.

such as nitric, hydrochloric, sulfuric, and perchloric acid, were examined. Hafnium hydroxide dissolves easily in nitric, hydrochloric, and perchloric acids, but not easily in sulfuric acid. The effects of these acids on the atomic absorbance or the polarogram of cadmium are diverse. In Fig. 2, the effects of the concentrations of these acids on the peak height on the flameless atomic-absorption spectrometric determination are shown. The addition of increasing amounts of these acids decreases the peak heights of cadmium. In the case of nitric acid, however, the magnitude of the decrease is small over the concentration range from about 0.3 to 1.1 mol dm^{-3}, and in this concentration range, the use of this acid gives the highest peak height. On the basis of these results, the nitric acid was used to dissolve the precipitate for the flameless atomic-absorption spectrometric determination. For the differential-pulse polarographic determination, it was found that the hydrochloric acid was adequate as a supporting electrolyte for the dissolution of hafnium hydroxide and for obtaining well-defined polarograms. Since the presence of this acid over the concentration range from 0.5 to at least 3 mol dm^{-3} did not affect the current peak height of cadmium, an acidity of about 1 mol dm^{-3} was adopted in this experiment.

Optimum Operating Conditions. According to the recommended procedure, the instrumental parameters, such as the drying, ashing, and atomizing conditions and the flow rate of argon gas, were examined using a solution which contained 0.1 μg/25 cm^3 of cadmium. An almost constant absorbance was obtained when the drying, ashing, and atomizing currents were within 19 to 22 A, 45 to 85 A, and 220 to 280 A respectively. The times of drying, ashing, and atomizing also did not affect the absorbance within the time ranges examined, that is, 50—90 s, 10—40 s, and 4—10 s respectively. The change in the flow rate of the sheath gas from 1 to 5 l min^{-1} had no effect on the cadmium absorbance, but the increase in the flow rate of the carrier gas made the absorbance decrease gradually. From these results and the results of the examinations of other instrumental conditions, such as the lamp current, the slit width, and the injection volume, the optimum conditions for the measurement of the cadmium absorbance were determined to be as shown in Table 1. For the differential-pulse polarography, the conditions which are summarized in Table 2 were adopted as the optimum operating conditions.

Calibration Curves. The straight lines through the point of origin were obtained over the concentration range from 0.4 to 4 ng cm^{-3} of cadmium for the flameless atomic-absorption spectrometry and from 0.04 to 40 μg cm^{-3} for the differential-pulse polarography. The reproducibility of the AAS method, expressed by the relative standard deviation obtained from five repeated determinations, was 2.8% for 4 ng cm^{-3} of cadmium, while that one of the polarographic method was 1.3% for 1.2 μg cm^{-3} of cadmium.

Influence of Diverse Ions. The results of the influence of the diverse ions examined by the recommended procedures are summarized in Table 3. For the flameless atomic-absorption spectrometry, large amounts of sodium, potassium, magnesium, and calcium were found not to interfere with the determination. Some ions, such as beryllium, indium, bismuth(III), copper(II), zinc, and chromium(III), can also coexist, at least up to 5000 times of the amount of cadmium, and there are no ions among the examined ones which have a serious influence on the determi-

Table 4. Amounts of Coprecipitation of Alkali and Alkaline Earth Metals

Ion*	Amount added	Recovery
	mg/100 cm³	%
Na^+	5	2.0
K^+	5	5.0
Mg^{2+}	5	5.1
Ca^{2+}	5	6.1
Sr^{2+}	5	5.0
Ba^{2+}	5	15.0

* Coprecipitated at about pH 9.5 using 10 mg of hafnium. The final volume of the solutions was made up to 25 cm³.

nation. For the differential-pulse polarographic determination, only indium interferes even present in only a small amount.

The Amounts of the Coprecipitation of Alkali and Alkaline Earth Metals. The amounts of the coprecipitation of alkali and alkaline earth metals were also studied. The amount of the coprecipitation of each ion was determined by measuring the amount of the ion remaining in the aqueous phase after the coprecipitation had been carried out and by subtracting this amount from the original amount of the ion. Flame photometry was used for the measurement of sodium, potassium, strontium, and barium, and the complexometric titration method, for magnesium and calcium. The results obtained are shown in Table 4. From this, it is obvious that alkali and alkaline earth metals hardly coprecipitate with hafnium hydroxide; this suggests that the use of hafnium hydroxide is effective for the separation of some kinds of elements from a sample solution containing large amounts of alkali and alkaline earth metals.

Application to River Water. Of the proposed methods, flameless atomic-absorption spectrometry was used for the determination of cadmium in the Kakehashi river system. The river-water samples were filtered through a membrane filter (Toyo Roshi TM-2p; pore size 0.45 μm) and acidified with hydrochloric acid to about pH 2 as soon as possible after sampling. Then cadmium was determined according to the recommended procedure. As is summarized in Table 5, the results which were obtained from the calibration and from the standard addition methods were in good agreement.

Table 5. Results for Cadmium in River Water

Kakehashi river system sampling point	Sample volume	A	B
		Cd found	Cd found
	cm³	ng cm⁻³	ng cm⁻³
Nunohashi	—[a]	0.79	0.82
Kanahira	—[a]	0.47	0.52
Shōrenji	100	0.22	0.20
Yūsenji	300	0.033	0.036
Kamonourahashi	300	0.035	0.034
Nomiōhashi	300	0.052	0.041
Kakehashiōhashi	300	0.043	0.039
Kakehashigawabashi	300	0.052	0.048

A: Determination by the calibration method. B: Determination by the standard addition method. a) Cadmium was determined without preconcentration.

References

1) M. Hiraide, T. Ito, M. Baba, H. Kawaguchi, and A. Mizuike, *Anal. Chem.*, **52**, 804 (1980).
2) K. Himeno, K. Yanagisawa, T. Yuki, and Y. Nakamura, *Bunseki Kagaku*, **33**, T43 (1984).
3) S. Takemoto, H. Kitamura, Y. Kuge, S. Nakagawa, K. Murata, and S. Ikeda, *Bunseki Kagaku*, **25**, 40 (1976).
4) C. Bergerioux and W. Haerdi, *Analusis*, **8**, 169 (1980); *Anal. Abstr.*, **40**, 1H26 (1981).
5) C. L. Sethi, B. K. Puri, and M. Satake, *Bunseki Kagaku*, **33**, E17 (1984).
6) S. Musha and Y. Takahashi, *Bunseki Kagaku*, **24**, 540 (1975).
7) T. Owa, K. Hiiro, and T. Tanaka, *Bunseki Kagaku*, **21**, 878 (1972).
8) M. Hiraide, Y. Yoshida, and A. Mizuike, *Anal. Chim. Acta*, **81**, 185 (1976).
9) K. V. Krishnamurty and M. M. Reddy, *Anal. Chem.*, **49**, 222 (1977).
10) V. Hudnik, S. Gomiscek, and B. Gorenc, *Anal. Chim. Acta*, **98**, 39 (1978).
11) E. A. Boyle and J. M. Edmond, *Anal. Chim. Acta*, **91**, 189 (1977).
12) A. Mizuike, H. Kawaguchi, K. Fukuda, Y. Ochiai, and Y. Nakayama, *Mikrochim. Acta*, **1974**, 915.
13) J. Ueda and C. Kita, *Bull. Chem. Soc. Jpn.*, **58**, 1899 (1985).

Analytical Use of Luminescence Induced Ultrasonically in Solution. I. Sonic Chemiluminescence of Luminol for Determination of Cobalt(II) at Sub-pg Levels by Flow Injection and Continuous Flow Methods

Takayuki KOMATSU, Minoru OHIRA, Masaaki YAMADA,* and Shigetaka SUZUKI
Department of Industrial Chemistry, Faculty of Technology, Tokyo Metropolitan University, Fukasawa, Setagaya-ku, Tokyo 158
(Received December 18, 1985)

Ultrasonic irradiation of alkaline luminol solution produces intense light emission (sonic chemiluminescence) as a result of the reaction of luminol with reactive species which are generated ultrasonically from water molecule. For the analytical application of ultrasound-induced luminescence, the sonic chemiluminescence of luminol is first utilized for the determination of ultratraces of cobalt(II) by flow injection and continuous flow methods. This novel method is based on the measurement of sonic chemiluminescence enhanced by the presence of cobalt(II); it provides analytical characteristics comparable to those for the conventional luminol chemiluminescence method using hydrogen peroxide as an oxidizing agent. The limit of detection is 0.06 pg(10-μl sample injection) or 0.06 pg ml^{-1} (continuous sample flow), the linear dynamic range is 3 orders of magnitude (10-μl sample injection), the sampling rate is 120 h^{-1}, and the relative standard deviation is 3.9% for 6 pg Co(II) ($n=10$). The method is successfully applied to real samples. Possible explanation of sonic chemiluminescence is also presented; the mechanism involving superoxide anion radical is proposed for the cobalt(II)-catalyzed sonic chemiluminescence.

Ultrasound is widely used in various fields, e.g., diagnosis and therapy, disintegration of biological materials, metal processing, cleaning, etc. Recently, the chemical uses of ultrasound have received considerable attention because of its chemical effects like redox-action and acceleration of chemical reaction.[1-7] Such chemical effects arise from acoustic cavitation which occurs when high intensity ultrasound (>3.5 kW m^{-2}) is propagated through a liquid medium. The acoustic cavitation is a three-stage process consisting of the formation, growth, and collapse of gas or vapor-filled bubbles suspended in the liquid phase; the presence of dissolved gas reduces the liquid strength and hence favors the initiation of cavity formation.[8] The most striking characteristics of the acoustic cavitation is the liberation of a high energy through the process; the collapse generates transient hot-spots with local temperatures and pressures of several thousand K and hundreds of atmospheres.[4] This leads to the thermal decomposition of the cavity contents and the formation of free radicals. For example, in aqueous solutions the primary reaction in the cavitation of water gives hydrogen atoms and hydroxyl radicals in the absence of any volatile solute.[1]

It is known that the cavitation is frequently accompanied by a faint light emission called sonoluminescence (SL).[9,10] The intensity and spectrum of SL depend on the nature of liquid, the nature of dissolved gas, the liquid temperature, the presence of solute, and the ultrasonic intensity.[11] In air-saturated water, the SL spectrum consists of characteristic bands based on OH*, H_2O^*, NO_2^*, and radiative recombination (HO_2+H) which are overlaying a broad continuum arising from the radiative recombination (H+OH).[10] The presence of inorganic species like metal ions sometimes provides their characteristic emissions.[12-14] On the other hand, in an alkaline aqueous solution of luminol (5-amino-2,3-dihydro-1,4-phthalazinedione) containing dissolved oxygen the cavitation causes an intense light emission (sonic chemiluminescence, SCL) which is essentially luminol chemiluminescence, in addition to the SL.[9,15,16] Our attention has been focused on the introduction of these luminescence phenomena into the field of analytical chemistry. We already made it clear in the preliminary works that the SL and SCL were likely to be usable as analytical tools. That is to say, the SL and SCL techniques permit the determinations of water in methanol with no use of reagents[17] and of traces of cobalt(II) by monitoring the cobalt(II)-catalyzed SCL of luminol,[18] respectively. Our ultimate goal is to evaluate the utility and limit in the analytical use of the ultrasonically induced luminescence. In this paper, we describes the details of the luminol SCL for the determination of cobalt(II) at sub-pg levels, namely, further exploration of the SCL technique, its analytical characteristics, the comparison with the conventional luminol chemiluminescence (CL), and the mechanistic study of the cobalt(II)-catalyzed SCL.

Experimental

Apparatus. A schematic diagram of the flow system is given in Fig. 1. It is basically as before,[18] except that a flow line R_2 is newly placed. An aqueous solution containing luminol and sodium hydroxide is supplied through a flow line R_1. R_2 represents a carrier stream for cobalt(II) and other species. This is an aqueous cobalt(II) solution for the continuous flow method, or pure water or surfactant solution when cobalt(II) and other species are injected by means of a 10-μl rotary valve injector S (injection method). The streams are delivered by peristaltic pumps P_1 and P_2. The alkaline luminol solution is sonicated in a glass sonication cell C

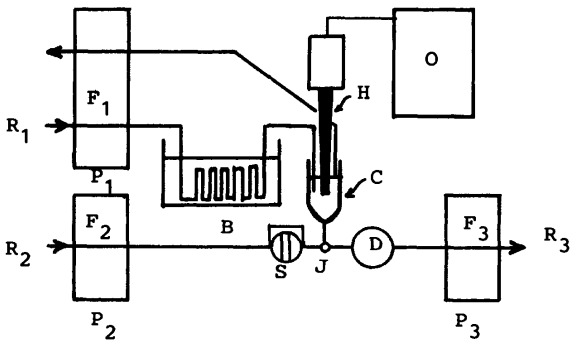

Fig. 1. Flow diagram for sonic chemiluminescence (SCL) method (for key, see text).
Recommended conditions: $R_1=5\times10^{-5}$ M luminol, 0.16 M NaOH, $R_2=0.03$ M SDS; Flow rates (ml min^{-1}) $F_1=1.3$, $F_2=1.6$, $F_3=2.8$.

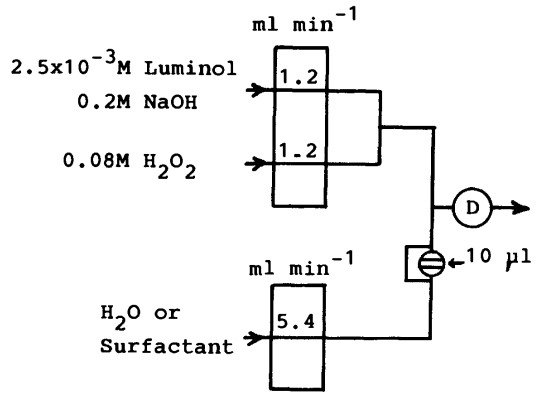

Fig. 2. Flow diagram for conventional chemiluminescence (CL) method.
Recommended conditions are specified in the figure.

by means of an exponential horn H (cross section: 0.05 cm^2) directly immersed in the solution, oscillated with an oscillator O (Tomy Seiko Co., Handy Sonic Model UR-20P; 28 kHz, max. 20 W). The luminol solution within the sonication cell is kept to be a constant volume (ca. 1.3 ml) during sonication by use of the pump tubes for the pump P_1 with different diameters. In order for adequate and stable cavitation to occur continuously, the luminol solution is cooled in an ice-water bath B before sonication. The luminol solution sonicated is drawn by a peristaltic pump P_3 and mixed with R_2 at a Y-joint J to be a flow line R_3. The cobalt(II)-catalyzed SCL is monitored at a spiral flow cell D ca. 15 cm apart from J, the minimum distance which can be achieved. Flow lines and a light-detecting device including the spiral flow cell have been described elsewhere.[19] In the system, there is no oxidizing agent intentionally added.

For the comparison of the present SCL method with an conventional CL method using hydrogen peroxide as an oxidizing agent, the flow system as shown in Fig. 2 was also assembled. Recommended conditions are given in the figure.

Absorption spectra of luminol were measured by a Shimadzu UV-240 spectrophotometer.

Reagents. Chemicals of analytical grade were used as received. The water used was prepared by distillation of Millipore (milli-R) water in an all-Pyrex glass apparatus, with a Teflon membrane inserted to block mist evolved. Stock solutions (10^{-2} M, 1 M=1 mol dm^{-3}) of various species were prepared by dissolving chlorides or nitrates, or sodium or potassium salts in water otherwise stated elsewhere. Luminol solution were prepared daily.

Analysis of Real Samples. Pepperbush or Pond Sediment (0.5 g) was boiled with 10—20 ml of concentrated nitric acid on a hot plate until the appearance of white fumes, and with concentrated sulfuric acid until the solution became colorless. After cooling, the solution was diluted to 100 ml. A 1 ml portion was added to each of several 100 ml volumetric flasks for standard addition of cobalt before dilution to volume, and cobalt was determined as described above.

Results and Discussion

Reagent Concentrations. The concentrations of luminol and sodium hydroxide were optimized at $F_1=1.8$, $F_2=2.7$, and $F_3=4.1$ ml min^{-1}, where F_1,F_2, and F_3 were the flow rates of R_1, R_2, and R_3, respectively. There is a reagent concentration giving the highest signal as shown in Figs. 3 and 4. The concentrations of 5×10^{-5} M for luminol and 0.16 M for sodium hydroxide were chosen for further experiments. These concentrations are several times higher than those in the previous system[18] because of the dilution of reagent solution with water of R_2, but the luminol concentration is one-fiftieth of that in the conventional CL system. From the absorption spectra, it was confirmed that there was no appreciable decrease in the luminol concentration due to the sonication.

Flow Rates of the Reagent Solutions. The effect of the flow rates F_1, F_2, and F_3 on the signal is represented in Fig. 5. In the experiment, F_1 is set at the lowest flow rate, 1.3 ml min^{-1} which can be achieved readily because the longer the resident time of luminol solution in the sonication cell, the higher the signal. As can be seen from the figure, the higher signal is obtained at each F_2 when F_3 is nearly equal to F_1+F_2, the highest signal being obtained at 1.6 for F_2 and 2.8 ml min^{-1} for F_3. With F_2 over 1.6 ml min^{-1}, further increased signal was not observed because of excess dilution of the sonicated luminol solution with water.

Effect of Surfactants. Surfactants (amphiphilic molecules) which have distinct hydrophobic and hydrophilic regions spontaneously form molecular aggregates in solution called micelles when they reach a certain concentration (critical micelle concentration, cmc). Organized molecular assemblies like micelles have currently been utilized in many types of analytical method,[20,21] because solutes accommodated in molecular assemblies often achieve a great degree of organization compared to homogeneous solution. In CL measurements, for instance, the use of micellar solution as reaction medium is very attractive because of the acceleration of CL reaction and the solubilization of CL reagents insoluble in water. So far there have been several reports on the analytical application of CL in micellar solution.[22-26]

In order to investigate whether micellar media func-

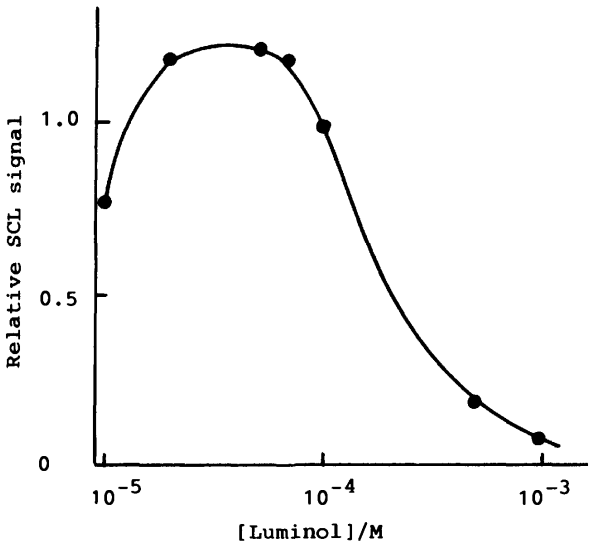

Fig. 3. Effect of luminol concentration on the SCL signal for Co(II).
0.16 M NaOH, 10^{-8} M Co(II), Flow rate (ml min^{-1}): F_1=1.3, F_2=2.7, F_3=4.1.

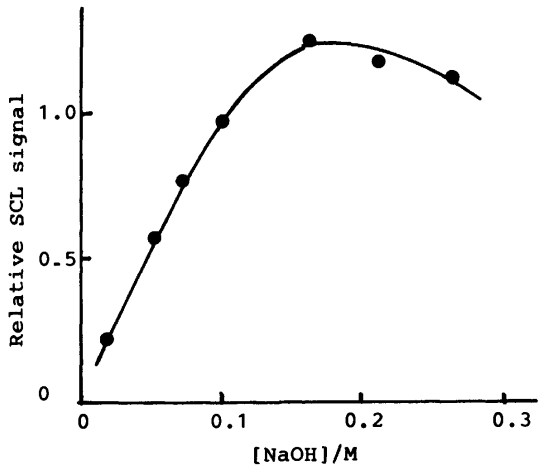

Fig. 4. Effect of sodium hydroxide concentration on the SCL signal for Co(II).
10^{-4} M luminol, 10^{-8} M Co(II), Flow rate (ml min^{-1}): F_1=1.3, F_2=2.7, F_3=4.1.

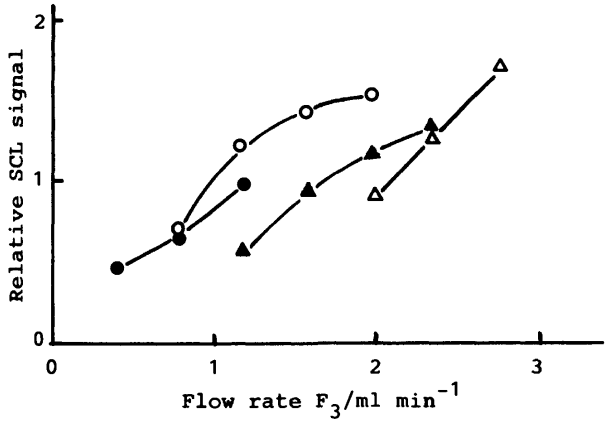

Fig. 5. Effect of flow rates on the SCL signal for Co(II).
0.16 M NaOH, 5×10^{-5} M luminol, 10^{-8} M Co(II), F_1=1.3 ml min^{-1}, F_2(ml min^{-1}): ●: 0, ○: 0.8, ▲: 1.2, △: 1.6.

Table 1. Effect of Surfactant Micelles on the Signal for Co(II)[a]

Surfactant[b]	Concentration[c] /10^{-3} M	Relative signal[d]	
		SCL method	CL method
CTAB	1.8	5	360
MDBAC	0.7	5	145
SDS	16	530	320
SDBS	16	120	250
Triton X-100	0.8	100	190
Brij 35	0.2	75	370

a) 10-μl injection of 10^{-8} M solution. b) CTAB: hexadecyltrimethylammonium bromide, MDBAC: tetradecylbenzylammonium chloride (zephiramine), SDS: sodium dodecyl sulfate, SDBS: sodium dodecylbenzenesulfonate. c) [CMC]×2. d) Normalized with respect to the value (=100) in the absence of surfactant.

tion effectively for the present SCL system, various surfactants were examined by adding to the carrier stream R_2. The results are shown in Table 1. Anionic surfactants increased the signal (max. 6 times increase for 0.03 M sodium dodecyl sulfate, SDS), whereas for cationic surfactants significant decreases in the signal were observed. This might be rationalized in terms of the following micellar effect. Owing to its charge, luminol monoanion (the most abundant species of luminol in the present alkaline solution) migrates easily on the cationic micellar surface. From the absorption spectra of luminol showing that λ_{max} at 300 and 349 nm in water are red-shifted by ca. 5 nm in the hexadecyltrimethylammonium bromide (CTAB) micellar solution, it is reasonable to consider that luminol monoanion is solubilized in the Stern layer where is less polar than in bulk water. This is supporte by the fact that the degree of the red shift is equivalent to that in 50% ethanol solution, namely, the hydrophobicity in the solubilization site is corresponding to that in 50% ethanol solution. For SDS, Triton X-100, and Brij 35 micellar solutions, no spectral changes were observed. This means that luminol monoanion is mainly solubilized in bulk water. Superoxide anion radical (a reactive species in the present SCL system) also migrates easily on the cationic micellar surface and hence reacts with luminol monoanion noncatalytically through a pathway in which cobalt(II) does not participate as stated later. On the other hand, cobalt ion is repelled electrostatically from the cationic micellar surface, but attracted to and concentrated on the anionic micellar surface. Consequently, the positively charged micellar surface causes the decrease in superoxide anion radical participating in Co(II)-catalyzed SCL reaction and/or the decreased cobalt ion-luminol monoanion interaction due to the charge separation, resulting in the suppression of Co(II)-catalyzed SCL reaction. In contrast, the concentration of cobalt ion on the negatively charged micellar surface favors the Co(II)-catalyzed

Table 2. Analytical Characteristics

Characteristic	SCL method[a]	CL method[b]
Background current, pA	48	250
Noise current, pA	1.2	5.0
Lower detection limit (S/N=3)		
10-μl injection, pg	0.06	0.04
continuous flow, pg ml^{-1}	0.06[b]	0.06
Linear dynamic range		
10-μl injection	1000	250
continuous flow	100	100
Sampling rate, h^{-1}	120	180
R.s.d. for 6 pg (n=10), %	3.9	5.7

a) With SDS. b) Without SDS.

SCL reaction.

The results for the conventional CL system are also shown in the table, indicating that any surfactants tested slightly increased the signal. This suggests that a cobalt(II)–hydrogen peroxide complex which is considered to work as a catalyst in the conventional CL system[27] may be noncharged species. And also this strongly suggests that the mechanism of SCL is different from that of the conventional CL.

Analytical Characteristics of the SCL System. Under the recommended conditions (as specified in Fig. 2), the analytical characteristics of the system were investigated. The results are summarized in Table 2. The SCL method has extremely high sensitivity and good reproducibility; the analytical characteristics are comparable to those for the conventional CL system. The detection limit is 10 times lower than that by the gallic acid CL method developed previously by the authors[28] which is more sensitive than any other method. For the measurement by continuous sample flow, the presence of SDS did not serve to improve sensitivity because it caused high background and severe noise; this was also the case for both types of the measurement in the conventional CL system. The logarithmic calibration graph for 10-μl sample injection exhibited a straight line with a slope of unity and linear dynamic range of 10^3. For continuous sample flow it gave a slightly larger slope and narrow linear dynamic range as well as in the conventional CL system.

Effect of Other Substances. Most of classical solution CL methods suffer from poor selectivity. Especially, the luminol CL method permits 30 species to enhance the luminescence reaction.[29] The present SCL system is very selective as shown in Table 3, despite of the use of luminol. Only strong oxidizing agents like hexacyanoferrate(III) and permanganate provided CL signals 0.1% of that for cobalt(II); other species enhanced the emission very weakly or gave rise to no emission. The selectivity for the conventional CL system is also represented in the table, the selectivity being equivalent to that for the SCL system. This means that the SCL technique itself does not yield such high selectivity. The high selectivity presumably derives from the measurement in flow. In general, a flow injection system often provides better selectivity than the corresponding batch system.

Table 3. Selectivity

Species[a]	Relative molar signal	
	SCL method	CL method
Co(II)	1000	1000
$[Fe(CN)_6]^{3-}$	2	0.2
MnO_4^-	1	0.02
Fe(II)	0.2	0.06
Ag(I)	0.04	
Fe(III)	0.03	0.03
Mo(VI)	0.02	
Cr(VI)	0.02	0.01
Mn(II)	0.007	0.02
Cr(III)	−0.04	0.3
Cu(II)	−0.08	0.1

a) 10-μl injection of 10^{-5} M solution of chloride or nitrate, or potassium salt except ammonium sulfate for Fe(II, III) and ammonium molybdate for Mo(VI), and of 10^{-8} M Co(II) solution.

Table 4. Effect of Other Substances on the CL Signal for Co(II)[a]

Species	SCL signal[b]		Species	SCL signal[b]	
	10^{-4} M	10^{-5} M		10^{-4} M	10^{-5} M
Fe(II)	130	120	MnO_4^-	7600	1700
Ag(I)	100		$[Fe(CN)_6]^{3-}$	1900	400
Cr(VI)	100		NH_4^+	90	100
Cd(II)	100		CO_3^{2-}	60	110
Zn(II)	90	100	S^{2-}	35	120
Al(III)	55	60	CN^-	−5	65
Pb(II)	50	70	EDTA	−20	−5
Mn(II)	35	90			
Cu(II)	25	20			
Mg(II)	25	40			
Fe(III)	15	50			
Cr(III)	15	45			
Ca(II)	10	25			
Ni(II)	−10	20			

a) 10-μl injection of 10^{-8} M solution. b) The value 100 means no interference.

To check the effect of concomitant species on the signal for cobalt(II), 10-μl of a 10^{-8} M Co(II) solution containing each common species(10^{-4} and 10^{-5} M) was injected. The results are shown in Table 4. Many

Table 5. Effect of the Addition of Trappers on the Signal for Co(II)[a)]

Reactive species	Trapper	Concentration/M	Relative signal[b)]	
			SCL method	CL method
·OH	HCOONa	10^{-5}	110	110
		10^{-4}	140	130
		10^{-3}	140	130
	2-C_3H_7OH	10^{-5}	120	95
		10^{-4}	130	95
		10^{-3}	130	90
$O_2^{\cdot-}$	NBT[c)]	10^{-5}	45	100
		10^{-4}	10	110
		10^{-3}	NS[e)]	110
$^1O_2$	NaN_3	10^{-5}	110	95
		10^{-4}	120	95
		10^{-3}	130	95
	DABCO[d)]	10^{-5}	110	100
		10^{-4}	140	100
		10^{-3}	130	90

a) 10-μl injection of 10^{-8} M solution. b) The value 100 means no effect. c) Nitro Blue Tetrazolium (Registry No. 38184-50-8). d) 1,4-Diazabicyclo[2.2.2]octane. e) No signal.

species eliciting no emission or very weak emission per se suppressed the Co(II)-catalyzed emission, except permanganate and hexacyanoferrate(III). The suppressions due to anionic species are based on the complexation or precipitation reaction with cobalt(II). Although the suppressions due to cationic species can not be fully explainable, such cationic species at high concentration levels may compete the site on the anionic micellar surface with cobalt, resulting in inhibition of the interaction between cobalt and luminol monoanion (and/or superoxide anion radical) and/or may catalyze effectively the disproportionation reaction of superoxide anion radical[30,31] on the anionic micellar surface, resulting in decrease in the superoxide anion radical concentration. Accordingly, the presence of SDS seems to cause or amplify the suppression . In fact, for instance, the suppressive interferences due to lead and calcium were no longer observable in the absence of SDS; these species at 10^{-4} M increased the Co(II)-catalyzed signals by 10 and 20%, respectively and 10^{-5} M they did not interfere. Therefore, no addition of SDS to the system may be recommended in order to reduce or eliminate interferences, although the sensitivity decreased slightly. Needless to say, the interferences can be reduced by dilution.

Mechanistic Study of the SCL. As stated above, the effect of surfactants on the Co(II)-catalyzed signal strongly suggests the difference in luminescent reaction mechanism between the SCL and the conventional CL. In order to confirm this suggestion, various trappers for reactive species which were considered to react luminously with luminol were added to the carrier stream R_3. The results are summarized in Table 5. Remarkable decrease in the Co(II)-catalyzed SCL signal was led to by the addition of Nitro Blue Tetrazolium (NBT), indicating that superoxide anion radical ($O_2^{\cdot-}$) contributed to the Co(II)-catalyzed SCL reaction. It is well known that luminol react with $O_2^{\cdot-}$ to emit light.[32] On the contrary, any trapper tested did not cause appreciable change in the Co(II)-catalyzed CL signal. Therefore, it can be said that these reactive species do not take part in the conventional CL reaction. This is consistent with the idea that a Co(II)–hydrogen peroxide complex plays an important role in the Co(II)-catalyzed CL reaction.[27]

Superoxide anion radical is generated ultrasonically in alkaline solution. The irradiation of strong ultrasound first leads to the dissociation of water molecule to hydrogen atom (·H) and hydroxyl radical (·OH). The ·H produced reacts with dissolved oxygen molecule to form hydroperoxide radical,[33,34] which immediately deprotonates to form $O_2^{\cdot-}$ in alkaline solution.

$$\cdot H + O_2 \longrightarrow HO_2^{\cdot}$$

$$HO_2^{\cdot} \rightleftharpoons O_2^{\cdot-} + H^+ \quad (pK_a = 4.8)$$

Superoxide anion radical is unstable in water, but its stability is greatly increased in alkaline solution;[35] the half-life of its decay is 10 s at pH 11.3.[32] In fact, the sonication of alkaline solution without luminol (in this case, luminol is added to the stream R_3) also provided Co(II)-catalyzed signal, about half the signal in the sonication of alkaline luminol solution. Although how much $O_2^{\cdot-}$ is produced by the sonication is unknown, its concentration will not exceed 10^{-5} M, the concentration produced upon electron irradiation of alkaline solution without luminol but with methanol or formate as a trapper for ·OH which consumes $O_2^{\cdot-}$.[32] In the present SCL system, the presence of luminol and furthermore the absence of such trapper will enable the $O_2^{\cdot-}$ concentration at the mixing joint J (see Fig. 1) to be far below 10^{-5} M. This low concentration of $O_2^{\cdot-}$ might cause in part

severe interferences due to other substances as stated above.

According to the pulse radiolysis experiments by Merényi et al.,[32] there are two routes where luminol (LH_2) may react with $O_2^{\cdot-}$ to chemiluminesce, that is,

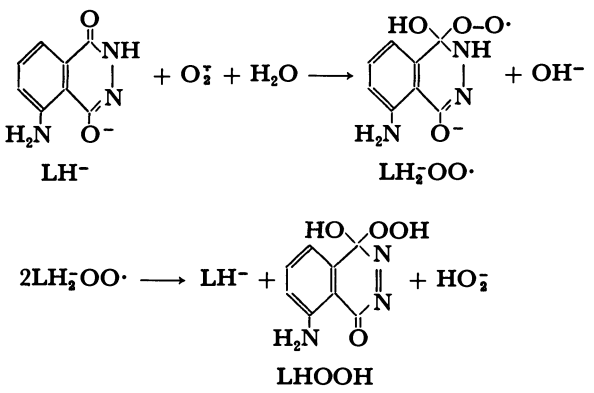

Scheme 1.

The hydroperoxide LHOOH formed, a short-lived CL intermediate, affords the excited aminophthalate through a rearrangement to the endoperoxide and a two-step decomposition.[36]

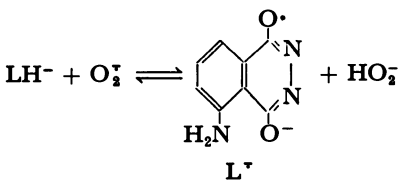

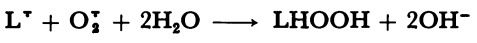

Scheme 2.

The SCL signal in the absence of Co(II), i.e., the background signal is conceivably based on reaction Scheme 1 with very small luminescence quantum efficiency (10^{-6}).[32] In contrast, the quantum efficiency for the luminescence arising from reaction Scheme 2 is 10^{-2}—10^{-3},[32] the same order of that for the conventional CL reaction whose reaction mechanism is proposed by Burdo and Seitz as shown in Scheme 3.[27]

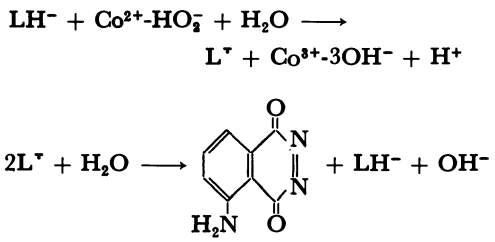

Scheme 3.

The diazaquinone L produced gives LHOOH through nucleophilic attack by hydroperoxide ion HO_2^-.[34,37] That the SCL method has the analytical sensitivity comparable to that for the conventional CL method, implies that both methods have the same order of luminescence quantum efficiency. Therefore, it is reasonable to consider that reaction Scheme 2 operates in the presence of cobalt(II). Furthermore, considering the similarity that the formation of luminol radical ($L^{\cdot-}$) appears in reaction Schemes 2 and 3, it seems likely that cobalt(II) works catalytically on the direct electron-transfer reaction to form $L^{\cdot-}$. At present stage, however, we can not say how cobalt(II) contributes to the electron transfer reaction.

Application to Real Samples. The applicability of the proposed method was evaluated by assaying NIES (National Institute for Environmental Studies) standard reference materials (Pepperbush[38] and Pond Sediment[39]). Standard additions of cobalt to acid-digested samples indicated that the results obtained for Pepperbush (23, 24 $\mu g\,g^{-1}$) by the 10-μl sample injection method with SDS and Pond Sediment (30, 29 $\mu g\,g^{-1}$) by the continuous sample flow method without SDS were within the certified values (23±3 and 27±3 $\mu g\,g^{-1}$, respectively).

Conclusion

In this paper, we have indicated the analytical utility of ultrasound-induced luminescence in solution through the determination of ultratraces of Co(II) using luminol SCL phenomenon. This novel SCL method is unique in being capable of detecting Co(II) selectively at sub-pg or sub-pg ml^{-1} levels with no use of oxidizing agents intentionally added, in contrast with the conventional luminol CL method. No other method can surpass the SCL method with regard to the sensitivity, the detection limit (0.00006 $ng\,ml^{-1}$) being much lower than those for flameless atomic absorption (0.2 $ng\,ml^{-1}$) and fluorescence methods (1 $ng\,ml^{-1}$), neutron activation analysis (0.5 $ng\,ml^{-1}$), and inductively coupled plasma emission method (0.1 $ng\,ml^{-1}$). We have also made it clear that the mechanism of SCL reaction is different from that of conventional CL reaction and ultrasonically generated $O_2^{\cdot-}$ plays a key role in the Co(II)-catalyzed SCL emission.

Although the SCL method could not be superior to the conventional CL method with respect to the analytical characteristics, the present work revealed that strong ultrasound was of great value as an energy source for eliciting luminescence. Accordingly, there is much possibility of finding out new luminescence systems usable in analysis because the reactive species ultrasonically generated react luminously with various organic compounds in solution and because the direct excitation of chemical species in solution by ultrasound leads to sonoluminescence (SL). These investigations are now in progress.

This work was supported by a Grant-in-Aid (Grant

No. 59550514) for Scientific Research from the Ministry of Education, Science and Culture.

References

1) K. Makino, M. M. Mossoba, and P. Riesz, *J. Phys. Chem.*, **87**, 1369 (1983).
2) K. S. Suslick, J. W. Goodale, P. F. Schubert, and H. H. Wang, *J. Am. Chem. Soc.*, **105**, 5781 (1983).
3) K. S. Suslick and P. F. Schubert, *J. Am. Chem. Soc.*, **105**, 6042 (1983).
4) K. S. Suslick, J. J. Gawlenowski, P. F. Schubert, and H. H. Wang., *J. Phys. Chem.*, **87**, 2299 (1983).
5) E. J. Hart and A. Henglein, *J. Phys. Chem.*, **89**, 4342 (1985).
6) C. Sehgal, R. G. Sutherland, and R. E. Verrall, *J. Phys. Chem.*, **84**, 2920 (1980).
7) C. Sehgal, T. J. Yu, R. G. Sutherland, and R. E. Verrall, *J. Phys. Chem.*, **86**, 2982 (1982).
8) C. Sehgal, R. P. Steer, R. G. Sutherland, and R. E. Verrall, *J. Phys. Chem.*, **81**, 2618 (1977).
9) E. N. Harvey, *J. Am. Chem. Soc.*, **61**, 2392 (1939).
10) C. Sehgal, R. G. Sutherland, and R. E. Verrall, *J. Phys. Chem.*, **84**, 388 (1980).
11) P. K. Chendke and H. S. Fogler, *J. Phys. Chem.*, **89**, 1673 (1985).
12) C. Sehgal, R. P. Steer, R. G. Sutherland, and R. E. Verrall, *J. Chem. Phys.*, **70**, 1 (1979).
13) C. Sehgal, R. G. Sutherland, and R. E. Verrall, *J. Phys. Chem.*, **85**, 315 (1981).
14) C. Sehgal, R. G. Sutherland, and R. E. Verrall, *J. Phys. Chem.*, **84**, 228 (1980).
15) E. W. Flosdorf, L. A. Chambers, and W. M. Malisoff, *J. Am. Chem. Soc.*, **58**, 1069 (1936).
16) H. Ojima, *Nippon Kagaku Zasshi*, **81**, 1785 (1960).
17) M. Yamada, T. Hobo, and S. Suzuki, *Chem. Lett.*, **1983**, 283.
18) M. Yamada and S. Suzuki, *Chem. Lett.*, **1983**, 783.
19) M. Yamada, H. Kanai, and S. Suzuki, *Bull. Chem. Soc. Jpn.*, **58**, 1137 (1985).
20) L. J. Cline Love, J. G. Habarta, and J. G. Dorsey, *Anal. Chem.*, **56**, 1133A (1984).
21) E. Pelizzetti and E. Pramauro, *Anal. Chim. Acta*, **169**, 1 (1985).
22) L. L. Klopf and T. A. Nieman, *Anal. Chem.*, **56**, 1539 (1984).
23) M. Yamada and S. Suzuki, *Anal. Lett.*, **17**, 251 (1984).
24) W. L. Hinze, T. E. Riehl, H. N. Singh, and Y. Baba, *Anal. Chem.*, **56**, 2180 (1984).
25) M. Kato, M. Yamada, and S. Suzuki, *Anal. Chem.*, **56**, 2529 (1984).
26) M. Yamada, S. Kamiyama, and S. Suzuki, *Chem. Lett.*, **1985**, 1597.
27) T. G. Burdo and W. R. Seitz, *Anal. Chem.*, **47**, 1639 (1975).
28) M. Yamada, T. Komatsu, S. Nakahara, and S. Suzuki, *Anal. Chim. Acta*, **155**, 259 (1983).
29) A. MacDonald, K. W. Chan, and T. A. Nieman, *Anal. Chem.*, **51**, 2077 (1979).
30) C. Bull, G. J. McClune, and J. A. Fee, *J. Am. Chem. Soc.*, **105**, 5290 (1983).
31) S. Goldstein and G. Czapski, *J. Am. Chem. Soc.*, **105**, 7276 (1983).
32) G. Merényi, J. Lind, and T. E. Eriksen, *Photochem. Photobiol.*, **41**, 203 (1985).
33) E. L. Mead, R. G. Sutherland, and R. E. Verrall, *Can. J. Chem.*, **54**, 1114 (1976).
34) G. Merényi, J. Lind, and T. E. Eriksen, *J. Phys. Chem.*, **88**, 2320 (1984).
35) P. F. Knowles, J. F. Gibson, F. M. Pick, and R. C. Bray, *Biochem. J.*, **111**, 53 (1969).
36) T. E. Eriksen, J. Lind, and G. Merényi, *J. Chem. Soc., Faraday Trans. 1*, **77**, 2137 (1981).
37) D. B. Paul, *Aust. J. Chem.*, **37**, 1001 (1984).
38) K. Okamoto, Y. Yamamoto, and K. Fuwa, *Anal. Chem.*, **50**, 1950 (1978).
39) Y. Iwata, K. Matsumoto, H. Haraguchi, K. Fuwa, and K. Okamoto, *Anal. Chem.*, **53**, 1136 (1981).

The Electrolyte Effect on the Chemical Equilibria of Bis(β-diketonato)-nickel(II) Complexes in Dimethyl Sulfoxide

Setsuko KUDO† and Akio IWASE*
Department of Chemistry, Faculty of Science, Yamagata University, Koshirakawa-machi, Yamagata 990
†Chemical Laboratory, Yamagata Building Service Co., Ltd., Iizuka-machi, Yamagata 990
(Received January 16, 1986)

The electrolyte effect on the homogeneous chemical equilibria of $Ni(bfac)_2$, $Ni(ftac)_2$, and $Ni(ttac)_2$ in dimethyl sulfoxide has been studied by means of polarographic and ultraviolet spectral measurements, where $bfac^-$, $ftac^-$, and $ttac^-$ represent the enolate anions of benzoyltrifluoroacetone, 2-furoyltrifluoroacetone, and 2-thenoyltrifluoroacetone respectively. The chemical equilibria of these complexes in 0.05 mol dm^{-3} TBAP solutions found previously:

$$Ni(bi\text{-}L)_2 \rightleftharpoons Ni(bi\text{-}L)(uni\text{-}L) \rightleftharpoons Ni(bi\text{-}L)^+ + L^- \rightleftharpoons Ni(uni\text{-}L)^+ + L^-$$

shifted more to the right in the presence of one of the electrolytes ($NaClO_4$, $KClO_4$, $RbClO_4$, $CsClO_4$, TMAP, or TEAP) at the same concentrations as TBAP; bi- and uni- mean that the ligands coordinate to the metal as bidentate and unidentate respectively. Under the conditions of $[NiL_2]=1$ mmol dm^{-3} and $[MClO_4]=0.05$ mol dm^{-3}, the molar fractions of the species of the $Ni(bi\text{-}L)_2$ type decreased with an increase in the inverse of the cationic radii. Such a tendency was explained mainly in terms of the interaction between the π-electron system of $Ni(bi\text{-}L)_2$ and those cations. For the same metal perchlorates, except $NaClO_4$, the stability of $Ni(bi\text{-}L)_2$ decreased in the order of: $bfac^- > ftac^- > ttac^-$.

The homogeneous chemical equilibria and the electrode reactions of ten bis(β-diketonato)nickel(II) complexes in dimethyl sulfoxide (DMSO) were investigated by means of conductivity and electronic spectral measurements, cryoscopy, polarography, and cyclic voltammetry.[1-5] It was found polarographically that five complexes, viz., $Ni(bzac)_2$,[1,6] $Ni(dbm)_2$,[2,6] $Ni(bfac)_2$,[2] $Ni(ftac)_2$,[2] and $Ni(ttac)_2$,[2] were involved in the following homogeneous chemical equilibria:

$$Ni(bi\text{-}L)_2 \rightleftharpoons Ni(bi\text{-}L)(uni\text{-}L) \rightleftharpoons Ni(bi\text{-}L)^+ + L^- \rightleftharpoons Ni(uni\text{-}L)^+ + L^- \quad (1)$$

where bi- and uni- mean that the ligands coordinate to the metal as bidentate and unidentate respectively.

The present paper deals with the electrolyte effect on the above chemical equilibria of $Ni(bfac)_2$, $Ni(ftac)_2$, and $Ni(ttac)_2$ in DMSO polarographically and spectrophotometrically, where $bfac^-$, $ftac^-$, and $ttac^-$ indicate the enolate anions of benzoyltrifluoroacetone, 2-furoyltrifluoroacetone, and 2-thenoyltrifluoroacetone respectively.

Experimental

Reagents. The alkali metal perchlorates,[1] tetrabutylammoium β-diketonates (n-Bu_4NL),[2] and DMSO[7] were the same as those described previously. Tetramethylammonium perchlorate (TMAP) and tetraethylammonium perchlorate (TEAP), purified for polarographic measurements, were obtained from Nakarai Chemicals, Ltd. These salts were recrystallized once from ethanol, followed by drying in vacuo at 60 to 70 °C for a minimum of 10 h. Tetrabutylammonium perchlorate (TBAP) was prepared in the usual way.[8]

Apparatus, etc. The apparatus was the same as that described in a previous paper.[7] The scan rate of polarographic measurements was 2 mV s^{-1}. Two dropping-mercury electrodes were used. The A electrode had an m value of 0.890 mg s^{-1} and a drop time, t_d, of 6.60 s at −1.0 V vs. SCE when measured in an air-free 0.05 mol dm^{-3} TBAP–DMSO solution at a height of 50 cm in the mercury reservoir. The B electrode had an m value of 1.055 mg s^{-1} and a t_d value of 5.48 s at −1.0 V when measured under the above conditions.

The current-potential curves and ultraviolet spectra were obtained at 25.0±0.2 and 25.0±0.5 °C respectively, except in the temperature-effect experiments.

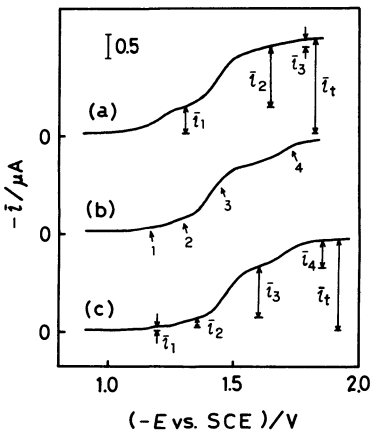

Fig. 1. d.c. Polarograms of 1 mmol dm^{-3} $Ni(bfac)_2$ in DMSO.
Supporting electrolyte; (a): $NaClO_4$, (b): $RbClO_4$, (c): TMAP. Each in 0.05 mol dm^{-3}. t_d=1.5 s. With the DME (A).

Results

Polarography. The polarographic behavior of $Ni(bfac)_2$, $Ni(ftac)_2$, and $Ni(ttac)_2$ was studied in DMSO containing 0.05 mol dm^{-3} TBAP as a supporting electrolyte.[2] In Fig. 1, three typical polarograms of $Ni(bfac)_2$ in other supporting-electrolyte solutions are shown in the potential range less negative than

Table 1. d.c. Polarographic Data of the Reduction of Ni(bfac)$_2$, Ni(ftac)$_2$, and Ni(ttac)$_2$ in DMSO

Complex	Supporting electrolyte[1]	($E_{1/2}$ vs. SCE)/V	Slope/mV	$\bar{i}_j/\bar{i}_t$[2]
Ni(bfac)$_2$	$NaClO_4$	−1.20[3]	39	0.26
		−1.40	70	0.68
		−1.66		0.06
	$KClO_4$	−1.08		0.03
		−1.20		0.11
		ca. −1.4 (Max.)		0.70
		ca. −1.6		0.16
Ni(ftac)$_2$	$NaClO_4$	−1.16[3]	45	0.32
		−1.36	75	0.63
		ca. −1.6		0.05
	$KClO_4$	ca. −1.1		0.86
		ca. −1.2		
		ca. −1.3 (Max.)		
		ca. −1.6		0.14
Ni(ttac)$_2$	$NaClO_4$	−1.12[3]		0.33
		−1.38	74	0.62
		−1.64		0.05
	$KClO_4$	ca. −1.1		0.15
		−1.19		
		ca. −1.35 (Max.)		0.74
		ca. −1.65		0.11

1) Each in 0.05 mol dm^{-3}. 2) The $\bar{i}_j/\bar{i}_t$ ratios were obtained at a concentration of 1 mmol dm^{-3} under a controlled drop time, where j=1—4. The meanings of $\bar{i}_j$ and $\bar{i}_t$ are shown in Fig. 1. 3) The first wave split into two peaks in differential-pulse polarography.

−2.0 V.[9] In this potential range, Ni(bfac)$_2$, Ni(ftac)$_2$, and Ni(ttac)$_2$ each gave four reduction waves in DMSO containing an electrolyte—$KClO_4$, $RbClO_4$, $CsClO_4$, TMAP, TEAP, or TBAP—at a concentration of 0.05—0.1 mol dm^{-3}. When $NaClO_4$ was used as the supporting electrolyte, these complexes each gave three d.c. polarographic waves, of which the first wave at less negative potential split into two peaks differential-pulse (DP) polarographically.[10] The d.c. polarographic data assembled in Table 1 are those for the complexes obtained in the presence of either $NaClO_4$ or $KClO_4$ at a concentration of 0.05 mol dm^{-3}.

Because of partial overlapping, the polarographic properties of the following waves could not be examined in detail: (a) the second and the third waves of Ni(bfac)$_2$ in a TEAP solution and of Ni(ftac)$_2$ in $KClO_4$, $RbClO_4$, $CsClO_4$, and TEAP solutions; (b) the first and the second waves of Ni(ttac)$_2$ in $KClO_4$, $RbClO_4$, and TEAP solutions. The temperature effect on these DP polarograms, however, was closely similar to that observed previously.[2]

In other cases except in $NaClO_4$ solutions, most of the polarographic and cyclic voltammetric properties were the same as those in 0.05 mol dm^{-3} TBAP solutions;[2] the $\bar{i}_j/\bar{i}_t$ values only were dependent on the cations of the supporting electrolytes used (the meanings of $\bar{i}_j$ and $\bar{i}_t$ are shown in Fig. 1). The half-wave potentials ($E_{1/2}$) of the four waves shifted to more negative potentials with a decrease in t_d. When either $KClO_4$, $RbClO_4$, $CsClO_4$, TMAP, or TEAP is chosen as the supporting electrolyte, therefore, it is reasonable to presume the same electrode reaction as that proposed previously.[2] That is to say, the four waves for the complexes are due to the irreversible two-electron reduction of different species with the Ni(II) involved in the homogeneous chemical equilibria (1) but for which the rate of the reestablishment of the equilibria is slow:[11,12] the first, the second, the third, and the fourth waves come from the reduction of Ni(uni-L)$^+$, Ni(bi-L)$^+$, Ni(bi-L)(uni-L), and Ni(bi-L)$_2$ respectively.

In $NaClO_4$ solutions, the first limiting currents ($\bar{i}_1$) were diffusion-controlled for all the complexes. The plots of $\bar{i}_1$ against the mole ratio (L/Ni) indicated that the respective first waves were due to the reduction of the corresponding mono-complexes. Furthermore, the polarographic properties of the second and the third waves in $NaClO_4$ solutions were similar to those of the third and the fourth waves respectively in the other supporting-electrolyte solutions. Thus, the polarographic behavior of the complexes in $NaClO_4$ solutions can be explained by the following electrode reaction:

$$\mathrm{NiL^+} \overset{\text{slow}}{\rightleftharpoons} \mathrm{Ni(bi\text{-}L)(uni\text{-}L)} \overset{\text{slow}}{\rightleftharpoons} \mathrm{Ni(bi\text{-}L)_2}$$

$$\downarrow 2e \qquad \downarrow 2e \qquad \downarrow 2e$$

1st wave 2nd wave 3rd wave

On the basis of the splitting of the d.c. polarographic first waves into DP polarographic peaks mentioned above, it seems likely that the respective first waves result from the reduction of the two mono-complexes.

Assuming that the diffusion coefficients for the different species in the solution are equal, the polarographic current ratios, the $\bar{i}_j/\bar{i}_t$ values, represent their molar fractions for the total complex concentration

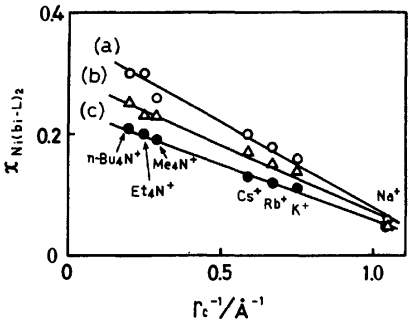

Fig. 2. Plots of the molar fraction of Ni(bi-L)$_2$ vs. the inverse of the cationic radii of supporting electrolytes.
Concn of supporting electrolyte: 0.05 mol dm^{-3}. Complex; (a): Ni(bfac)$_2$, (b): Ni(ftac)$_2$, and (c): Ni(ttac)$_2$ of 1 mmol dm^{-3}, respectively.

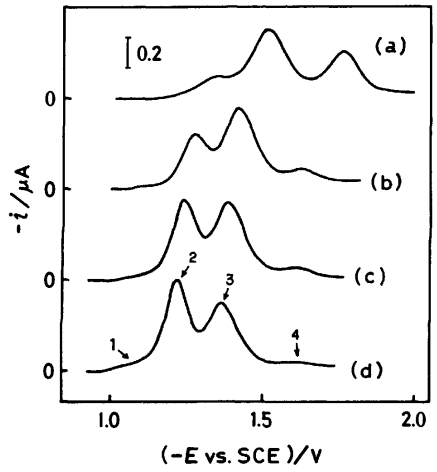

Fig. 3. Effect of sodium ion on DP polarogram of 0.5 mmol dm^{-3} Ni(ftac)$_2$ in DMSO.
Supporting electrolyte; (a): 0.1 mol dm^{-3} TBAP, (b): 0.02 mol dm^{-3} $NaClO_4$+0.08 mol dm^{-3} TBAP, (c): 0.05 mol dm^{-3} $NaClO_4$+0.05 mol dm^{-3} TBAP, (d): 0.1 mol dm^{-3} $NaClO_4$. Modulation amplitude: 50 mV, pulse interval: 1.0 s. With the DME (B).

(see Table 1). The degree of the dissociation of Ni(bi-L)$_2$ increased with a decrease in the crystallographic (unsolvated) radii of the cations of the supporting electrolytes; linear relationships were obtained between the molar fractions of species of the Ni(bi-L)$_2$ type, the $\bar{i}_4/\bar{i}_t$ values, and the inverse of the cationic radii ($1/r_c$), as is depicted in Fig. 2. For the same metal perchlorates, except $NaClO_4$, the stability of Ni(bi-L)$_2$ decreased in the order of: bfac$^-$>ftac$^-$>ttac$^-$. On the other hand, no difference in their stabilities could be detected in $NaClO_4$ solutions. As can be seen from the DP polarograms in Fig. 3, the sodium ion significantly influenced the chemical equilibria (1) (see also the $\bar{i}_j/\bar{i}_t$ values in Table 1). The first peak at the least negative potential in Curve (a) was detected only at a high sensitivity, because the complex concentration measured was low. It appears that the shift of the peak potentials (E_p) to less negative potentials with an

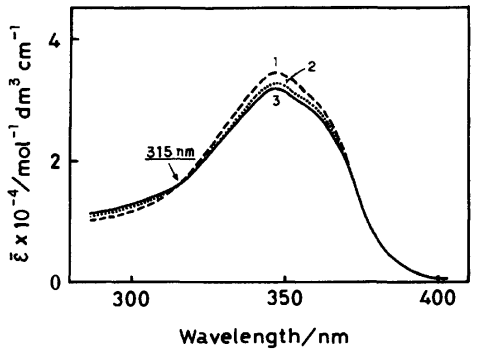

Fig. 4. UV spectra of Ni(ttac)$_2$ at different concentrations in DMSO.
Concn (mol dm^{-3}); (1): 4.0×10^{-6}—1.0×10^{-5}, (2): 1.0×10^{-4}, (3): 7.0×10^{-4}.

increase in the sodium-ion concentration is attributed to the interaction between the reduction products and the sodium ion, e.g., the formation of ion pairs.[13] In addition, the slope of the regression line is considered as the measure of the sensitivity of the stability of Ni(bi-L)$_2$ to the effect of electrolyte cations for a given complex. From this point of view, the stability of Ni(bi-L)$_2$ was subject to the cationic effect in the order of: bfac$^-$>ftac$^-$>ttac$^-$.

Ultraviolet Spectra. In Fig. 4, the electronic spectra of Ni(ttac)$_2$ in the near-ultraviolet region are shown at different concentrations. In this region, similar spectra were obtained for all the complexes. There were isosbestic points at 298, 308, and 315 nm respectively for Ni(bfac)$_2$, Ni(ftac)$_2$, and Ni(ttac)$_2$, though their spectra did not change with time. In the vicinity of the absorption maxima, the apparent molar absorption coefficients ($\bar{\varepsilon}$)[14] increased with a decrease in the concentration of the complexes. Such a tendency corresponds to the dissociation of the complexes, compared with that of some bis(β-diketonato)-nickel(II)[4] and -cobalt(II)[7,15] complexes in the same solvent.

The electronic spectra of the complexes varied slightly in the presence of any one of the electrolytes except $NaClO_4$, while they varied considerably upon the addition of $NaClO_4$. The effects of the sodium ion on the electronic spectra of Ni(bfac)$_2$ and Ni(ttac)$_2$ are illustrated in Figs. 5 and 6 respectively, where the total concentration of the electrolyte is adjusted to 0.1 mol dm^{-3} with TBAP. The addition of the sodium ion at different concentrations to a certain complex solution gave two isosbestic points, of which the one at the shorter wavelength was in agreement with that described above. The isosbestic points for Ni(bfac)$_2$, Ni(ftac)$_2$, and Ni(ttac)$_2$ at longer wavelengths were 347, 352, and 358 nm respectively. They were values near to the isosbestic points observed in the corresponding *n*-$Bu_4NL/NaClO_4$ media—that is, 342, 353, and 358 nm for L$^-$=bfac$^-$, ftac$^-$, and ttac$^-$ respectively.

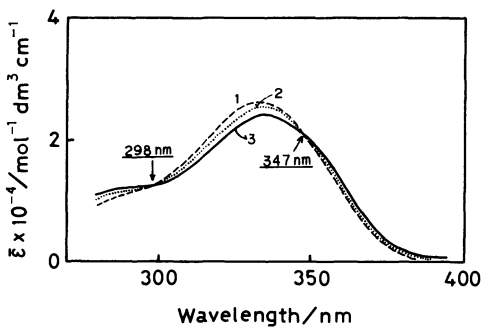

Fig. 5. Effect of sodium ion on the UV spectrum of 0.5 mmol dm^{-3} Ni(bfac)$_2$ in DMSO.
Coexisting electrolyte; (1): 0.1 mol dm^{-3} $NaClO_4$, (2): 0.02 mol dm^{-3} $NaClO_4$+0.08 mol dm^{-3} TBAP, (3): 0.1 mol dm^{-3} TBAP.

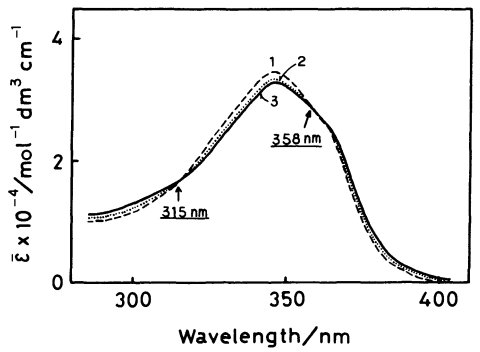

Fig. 6. Effect of sodium ion on the UV spectrum of 0.5 mmol dm^{-3} Ni(ttac)$_2$ in DMSO.
Coexisting electrolyte; (1): 0.1 mol dm^{-3} $NaClO_4$, (2): 0.02 mol dm^{-3} $NaClO_4$+0.08 mol dm^{-3} TBAP, (3): 0.1 mol dm^{-3} TBAP.

Discussion

It was described in a previous paper[2] that the dissociation of Ni(bfac)$_2$, Ni(ftac)$_2$, and Ni(ttac)$_2$ in DMSO was enhanced by the presence of TBAP as the supporting electrolyte for polarographic measurements. From the linear relationships given in Fig. 2, it may be concluded that the chemical equilibria (1) in 0.05 mol dm^{-3} TBAP solutions found previously[2] shift more to the right in the presence of one of the electrolytes ($NaClO_4$, $KClO_4$, $RbClO_4$, $CsClO_4$, TMAP, or TEAP) at the same concentrations as TBAP and that the sodium ion is the most effective among the cations used here.

The cationic effect on the chemical equilibria (1) is first considered from the standpoint of the lowering of the activity of the DMSO as a result of the solvation of the electrolyte cations. This effect can be estimated conveniently on the basis of the chemical equilibria (2):

$$\begin{aligned} &\text{Ni(bi-L)}_2\cdot(\text{DMSO})_m \\ &\rightleftharpoons \text{Ni(bi-L)(uni-L)}\cdot(\text{DMSO})_{m+1} \\ &\rightleftharpoons \text{Ni(bi-L)}^+\cdot(\text{DMSO})_{m+2} + \text{L}^-\cdot(\text{DMSO})_n \\ &\rightleftharpoons \text{Ni(uni-L)}^+\cdot(\text{DMSO})_{m+3} + \text{L}^-\cdot(\text{DMSO})_n \end{aligned} \quad (2)$$

Since the solvation of the Ni(II) species on the right hand requires more DMSO molecules, the above equilibria will shift to the left when the addition of a large amount of smaller cations lowers the activity of DMSO; this is contrary to the observed trend.

The isosbestic points at shorter wavelengths (shown in Figs. 4—6) are interpreted as being caused by one of the chemical equilibria (1), and those at longer wavelengths (shown in Figs. 5 and 6), by the interaction of the sodium ion with L^- or a free carbonyl oxygen of the unidentate ligand of Ni(bi-L)(uni-L). Such ion-pair or complex formation should shift the chemical equilibria (1) to the right; however, it seems unlikely to be responsible for the promotion of the dissociation of the Ni(II) complexes in the case of the other cations, especially tetraalkylammonium ions.

Kalinowski and Galazka[16] found that bis(acetylacetonato)copper(II) was involved in complicated equilibria in the presence of the lithium ion in various organic solvents. It was suggested spectrophotometrically that the lithium ion might interact in the unsolvated form. Furthermore, it was stated that the interaction of the lithium ion with the π-electron system of acetylacetonato groups in cyclic form was the more probable of the two possibilities. It is plausible that the linear relationships shown in Fig. 2 are also caused by such an interaction, that is, the interaction between the π-electron system of Ni(bi-L)$_2$ and the cations, though no definite statement can be made at the moment concerning the degree of solvation for the interacting cations. A smaller ion generates in its vicinity a more powerful electrostatic field than a large ion of the same charge. The above interaction seems to be the reason for the complication of the quantitative treatment of the chemical equilibria (1). The stability of Ni(bi-L)$_2$ observed, i.e., bfac$^-$> ftac$^-$>ttac$^-$, did not coincide in order with that to be expected from the aromaticity of the substituents,[17] the pK_a values of the ligands,[18] and the carbonyl ^{13}CNMR chemical shifts of the ligands in DMSO,[19] i.e., bfac$^-$>ttac$^-$>ftac$^-$. As has been suggested from the order of susceptibility of the stability of Ni(bi-L)$_2$ to the cationic effect, i.e., bfac$^-$>ftac$^-$>ttac$^-$, it is necessary to take into account the competitive interaction of the cations and the DMSO molecules with Ni(bi-L)$_2$.

The authors wish to acknowledge the useful suggestions of Professor Nobuo Suzuki, of Tohoku University, and Dr. Kazuko Tanaka, of the Institute of Physical and Chemical Research, in the field of solution chemistry.

References

1) S. Kudo, A. Iwase, and N. Tanaka, *Bull. Chem. Soc. Jpn.*, **55**, 1416 (1982).
2) S. Kudo, A. Iwase, and N. Tanaka, *Nippon Kagaku Kaishi*, **1983**, 1418.

3) S. Kudo, A. Iwase, and N. Tanaka, *Nippon Kagaku Kaishi*, **1983**, 1539.

4) S. Kudo and A. Iwase, *Nippon Kagaku Kaishi*, **1984**, 1341.

5) S. Kudo and A. Iwase, *Nippon Kagaku Kaishi*, **1985**, 263.

6) The abbreviations $bzac^-$ and dbm^- indicate the enolate anions of benzoylacetone and dibenzoylmethane respectively.

7) S. Kudo, A. Iwase, and N. Tanaka, *Inorg. Chem.*, **24**, 2388 (1985).

8) D. T. Sawyer and J. L Roberts, Jr., "Experimental Electrochemistry for Chemists," John Wiley & Sons, New York (1974), p. 212.

9) Sodium, potassium, rubidium, and caesium ions are reduced at ca. −2.0 V vs. SCE in 0.05 mol dm^{-3} TBAP-DMSO.

10) For the respective complexes, small DP polarographic peaks were observed in the potential range giving the foot of the first waves.

11) A. A. Vlček, *Prog. Inorg. Chem.*, **5**, 211 (1963).

12) The term "slow" means that the reaction proceeds so slowly that its occurrence can be neglected practically in the vicinity of the electrode surface during electrolysis.

13) G. Gritzner, H. Murauer, and V. Gutmann, *J. Electroanal. Chem.*, **101**, 185 (1979).

14) The $\bar{\varepsilon}$ value means the molar absorption coefficient obtained on the assumption that NiL_2 exists as the only species in the solution.

15) S. Kudo, *Nippon Kagaku Kaishi*, **1985**, 2099.

16) M. K. Kalinowski and A. Galazka, *Electrochim. Acta*, **25**, 1205 (1980).

17) J. B. Hendrickson, D. J. Cram, and G. S. Hammond, "Organic Chemistry," McGraw-Hill Book Company, New York (1970), p. 954.

18) L. G. Van Uitert, W. C. Fernelius, and B. E. Douglas, *J. Am. Chem. Soc.*, **75**, 457 (1953).

19) C. Shibata, T. Takeuchi, M. Yamazaki, and J. Niwa, *Nippon Kagaku Kaishi*, **1978**, 836.

The Distribution and Characterization of ^{137}Cs in Shallow Water Sediments

Kikuo TERADA,* Madoka HAMANO, Kazuhisa KOMURA,† and Ken MATSUMOTO
Department of Chemistry, Faculty of Science, Kanazawa University, Kanazawa, Ishikawa 920
†Low Level Radioactivity Laboratory, Faculty of Science, Kanazawa University, Wake, Tatsunokuchi, Ishikawa 923-12
(Received January 22, 1986)

The distribution and characterization of ^{137}Cs in shallow water sediments are investigated. The concentration of ^{137}Cs in surface sediments which have been collected from the 10—20 m depth of Tsukumo Bay, Noto Peninsula, tends to decrease with an increase in the distance from the inner part of the bay to the outer part. Vertically, ^{137}Cs contents gradually decrease to the 10 cm depth and then steeply decrease beyond this depth, until at the 15 cm depth no activity is observed. A sequential extraction technique with several kinds of extractants has been employed to survey the chemical form of the nuclide in the sediments. ^{137}Cs is completely extracted with an ammonium nitrate solution suggesting that the nuclide is strongly adsorbed in the crystal lattice of some clay minerals and is exchangedly desorbed from the sediment phase by ammonium ions in a high concentration. A core sample has been elutriated in five components of different grain sizes, and the contents of sodium, potassium, and ^{137}Cs have been determined. It has been revealed that a unit amount of the finest component contains about three times as much of the nuclide as that of the coarsest one. On the contrary, the potassium contents slightly decrease with the decrease in the particulate size.

The behavior of ^{137}Cs at the seawater/sediment interface, especially in esturine or shallow water, is of very interest because radionuclides of a moderately long half-life have been distributed a world-wide scale as a result of nuclear-weapons testing and reprocessing plants of nuclear power and have thus been introduced into the ecological system in these shallow water regions, closely correlated human activity.

Radiocesium is considered to be present in seawater, principally as a simple Cs^+ ion like ^{90}Sr, and to be scarcely captured at all by suspended substances such as marine planktons.[1,2] On the other hand, Nagaya et al.[3] have found that up to about 6% of ^{137}Cs exists in coastal seawater, bound to particulate materials. In addition, several investigations have been carried out studying the sorption behavior of the nuclide by means of some clay minerals, rocks, and soil components.[4-8] However, these studies have been concerned with purified soil components, a few synthetic mixtures of clay and soil, or laboratory experiments using natural sediment; little information has appeared in the literature on the distribution of ^{137}Cs in marine sediments. The present paper will describe the distribution and characterization of this nuclide, as correlated with other alkali metals in shallow water sediments which have been elutriated into five components of different grain sizes, the extraction property of ^{137}Cs with several kinds of extractants from the sediment, the sorption and desorption behavior of this nuclide on each elutriated component, and the determination of the sorption capacities of these components for ^{137}Cs.

Experimental

Apparatus and Reagents. An ORTEC 8501-1523S true coaxial Ge(Li) detector (80 cm^3; resolution of ^{60}Co at 1330 keV:1.9 keV; relative efficienty: 15.1%), coupled to an ORTEC Model-6200, 4000-channel pulse height analyzer, was used for the low-level background counting of ^{137}Cs at the Low Level Radioactivity Laboratory, Kanazawa University. A Shimadzu AA-646 atomic absorption/flame-emission spectrophotometer was used for the analyses of sodium and potassium. A Rigaku Denki X-ray powder diffractometer and a Hitachi 20PR refrigerated centrifuge and 500-cm^3 polyethylene centrifuge bottle were also used.

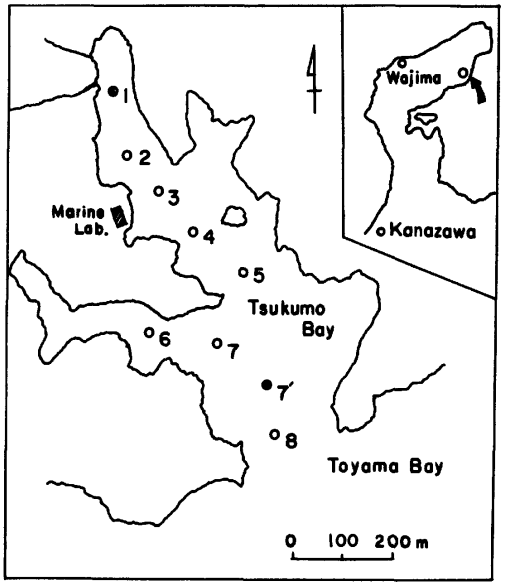

Fig. 1. Sampling Station in Tsukumo Bay.

All the reagents used were of a guaranteed reagent grade.

Materials. Sediment samples were collected from a depth of about 10—20 m in Tsukumo Bay, Noto Peninsula, with a Smith-Mackintire sampler and a Phleger gravity corer. The sampling sites are illustrated in Fig. 1. After sampling, core samples were immediately collected, by using a polyacrylic resin cylinder (i.d. 50 mm), from the sample collected by means of the Smith-Mackintire sampler. The core was cut into three layers, each 30 mm long. Each layer of the core was immediately centrifuged at 7000 G for 30 min at 5 °C to remove any interstitial water. The centrifuged samples were then submitted to elutriation as follows: About 30 g of the

sample was placed in a polycarbonate resin beaker, stirred with 800 cm^3 of distilled water, and then allowed to stand for 3 min. After thus standing, the suspension was transferred into another polycarbonate resin beaker. The residual sediment in the first beaker was treated as has been described above, using fresh distilled water, until the supernatant became almost clear. The suspensions were collected in the second beaker. The deposited fraction was named 3MP. The contents of the second beaker were stirred vigorously and then allowed to stand for 10 min. The suspensions obtained by the same procedure were collected in the third beaker. The deposited sediment fraction was named 10MP. Then, the suspension was sequentially elutriated into the fractions deposited after standing 1 h and 5 h and suspended after standing 5 h, these fractions being named 1HP, 5HP, and 5HS respectively. At the same time, in a small portion of the first suspension the chloride concentration was determined by Mohr's method in order to evaluate the contribution of seawater to the determination of sodium and potassium in the sediment.

Determination of ^{137}Cs. About 0.7—10 g of a dry sample was used for the γ-counting of ^{137}Cs. The samples available in amounts larger than 3 g were made into a disc 20 or 50 mm diameter by pressing, while the others were shielded in a small polyethylene pouch; then γ-counting was performed. In the sequential extraction procedure, about 30 g of the dry sample was used.

Determination of Sodium and Potassium. About 0.2 g of the sample was decomposed with an acid mixture (0.5 cm^3 of 60% perchloric acid+3 cm^3 of concd nitric acid+ 5 cm^3 of 47% hydrofluoric acid) in a PTFE beaker by heating on a hot plate at ca. 120 °C. This treatment was repeated 3—4 times. The residue was then dissolved in 5 cm^3 of 6 mol dm^{-3} hydrochloric acid and filtered through Toyo No. 5B filter paper. The filtrate was made up to 25 cm^3 with pure water. After appropriate dilution, sodium and potassium were analyzed by means of flame photometry at the wavelengths of 589.3 and 766.2 nm respectively.

Sequential Extraction of ^{137}Cs from the Sediment. About 30 g of a dry surface sediment sample containing 0.30± 0.014 pCi $^{137}Cs\,g^{-1}$ was put into a 100 cm^3 stoppered polyethylene centrifuge tube and shaken with 50 cm^3 of a methanol-acetone mixture (1:1 v/v) for 30 min. After centrifugation at 3000 rpm for 20 min, the supernatant was separated, evaporated to a small volume in a PTFE beaker, and then transferred into a shallow plastic dish 50 mm in diameter in order to dry it up. Finally, the contents of the dish were submitted to γ-counting. Next, to the sample remaining in the centrifuge tube 50 cm^3 of a 0.5 mol dm^{-3} magnesium chloride solution was added; the contents were then shaken and centrifuged as has been described above. The γ-counting of the magnesium chloride extract was also carried out. Then, the residual sediment was treated successively with a 0.5 mol dm^{-3} sodium hydroxide solution, 1 mol dm^{-3} hydrochloric acid, and a 50% ammonium nitrate solution. Finally, the residual sediment, which had been reduced to 23.6 g during the extraction procedure, was dried and pressed into a disc 50 mm in diameter for γ-counting.

Sorption Experiments of ^{137}Cs Using the Sediments. Filtered seawater which had been collected from the surface of Tsukumo Bay was spiked with ^{137}Cs (nitrate form) so as to make its concentration about 20000 cpm cm^{-3} and then allowed to stand for 1 d in order to attain equilibrium. An air-dried elutriated sample was pulverized to under 400 mesh with an agate mortar and placed (1.0 g) in a polycarbonate resin beaker. Then about 400 cm^3 of the ^{137}Cs-spiked sea water was added to it, after which the contents were vigorously stirred and allowed to stand with a loose cover. After one day, 3 cm^3 of supernatant was pipetted out and filtered through a small piece of dry filter paper. One cm^3 of the filtrate was pipetted out into a polyethylene test tube, and the radioactivity was measured by means of a NaI(Tl) scintillation counter. The contents of the beaker were then stirred and allowed to stand for one more day. The measurement of the radioactivity of the supernatant was carried out as has been described above until an equilibrium was attained.

Table 1. Contents of Potassium and ^{137}Cs in Surface Sediments (Tsukumo Bay, 1983-9-19)

Station	Depth	K	^{137}Cs	$^{137}Cs/K$
	m	%	pCi/g dry	pCi/meq
1	10	1.19	0.45±0.02	1.4_8
2	16	1.14	0.35±0.03	1.1_9
3	21	1.23	0.35±0.02	1.1_1
4	23	1.40	0.24±0.03	0.6_7
5	24	1.34	0.26±0.02	0.7_6
6	20	1.56	0.20±0.03	0.5_0
7	21	1.30	0.27±0.03	0.8_1
8	22	1.11	0.17±0.03	0.5_9

Measurement of Distribution Coefficient, K_d. Each sediment sample which adsorbed ^{137}Cs in the above experiment was separated from the supernatant by decantation, followed by centrifugation using a 50 cm^3 polyethylene bottle. The sediment in the bottle was washed with a small portion of seawater, and the washing was rejected by centrifugation. This procedure was repeated several times. Finally, 40 cm^3 of filtered seawater was put into the bottle, and the bottle was shaken for 24 h. After centrifugation, the radioactivity of the supernatant was measured as above.

Measurement of Sorption Capacity for ^{137}Cs. Cesium chloride (3.75 g) was dissolved in 200 cm^3 of the ^{137}Cs-spiked seawater. About 0.5 g of the powdered elutriated sample was then added to 25 cm^3 of the above seawater containing 1.39 meq of cesium (about three times the contents of sodium and potassium), and the contents were shaken for 20 h. After centrifugation, 1 cm^3 of the supernatant was submitted to γ-counting and the sorption capacity was calculated.

X-Ray Powder-Diffraction Measurement. In order to estimate the mineral composition of each elutriated sample, X-ray powder diffractometry was carried out. In particular, in order to distinguish the peaks of the clay minerals, measurements were performed after treating the sample with several kinds of reagents, e.g., ethylene glycol for montmorillonite and haloisite, ammonium nitrate for magnesium vermicurite, hydrochloric acid for kaolinite, vermicurite and chlorite, and potassium acetate for kaolinite minerals. The parameters used were Cu K_α (15 mA, 35 kV), a Ni filter, and a slit system (1°—0.3 mm—1°).

Results and Discussion

Distribution of ^{137}Cs in the Sediments. The ^{137}Cs contents of surface sediments of Tsukumo Bay are given in Table 1. The ^{137}Cs contents tend to decrease

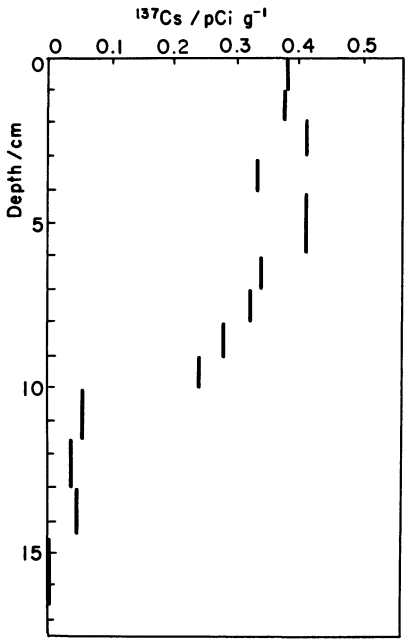

Fig. 2. Vertical distribution of ^{137}Cs in a sediment core.

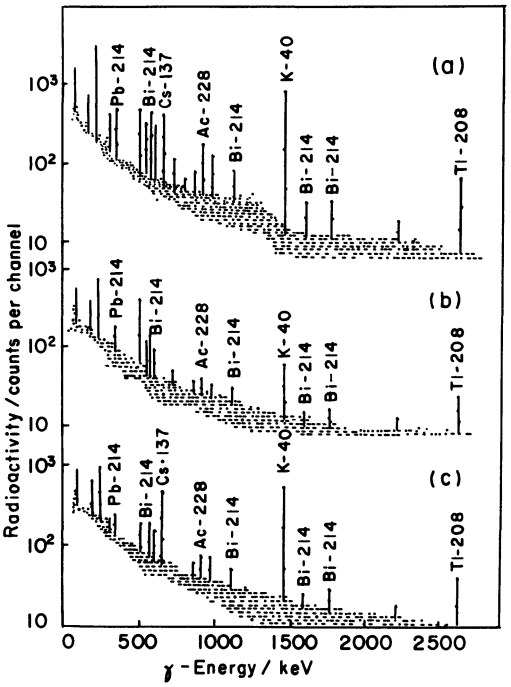

Fig. 3. Gamma-spectra of the raw sediment and extracts. (a) raw sediment, (b) extract with 1 mol dm^{-3} HCl, (c) extract with 50% NH_4NO_3.

with an increase in the distance from the inner part of the bay to the outer part. This fact suggests that, after ^{137}Cs has been transferred into the bay in several ways, e.g., through the river water and precipitation, and from the surroundings, this nuclide should sink down rather quickly and be captured by bottom sediments.

A core sample collected at St. 7' with the Phleger gravity corer was cut in 10 mm sections, and the γ-activity was measured. The vertical profile of the ^{137}Cs contents thus obtained is illustrated in Fig. 2. At 7—8 cm from the surface, the ^{137}Cs contents decrease to about one half-of that at the surface; beyond a depth of 10 cm the radioactivity of ^{137}Cs steeply decreases, until no activity is observed at the depth of 15 cm.

At the same time, the age of each section was determined by means of the ^{210}Pb method. The depth vs. time curve showed a straight line between depths of 30 mm and 110 mm, corresponding to about 44 years. As can be seen from Fig. 2 and the results of the age determination, ^{137}Cs can only slowly migrate downward through the sediment layers after deposition.

Extraction of ^{137}Cs from the Sediment Phase. Figure 3 (a)—(c) show the γ-spectra of the raw sediment, the extracts with 1 mol dm^{-3} hydrochloric acid, and 50% ammonium nitrate solutions. No measurable peak for ^{137}Cs is found in the spectra of the extracts with the methanol-acetone mixture, magnesium chloride, and sodium hydroxide solutions, as in the final residual sediment as hydrochloric acid extract (b). On the other hand, the extract with the ammonium nitrate solution gave a sharp peak of the nuclide, and the radioactivity of ^{137}Cs in the extract indicates that an almost complete extraction has been attained. Thus, scarcely ^{137}Cs seems to be present bound to any organic substances such as a humic substance, weakly or electostatically adsorbed on sediment surfaces, or in acid-soluble form. Miettinen et al.[9] have also reported that only 5% of the ^{134}Cs was eluted with 0.1 mol dm^{-3} hydrochloric acid from a ^{134}Cs-labelled sediment which had been collected from the Gulf of Finland. In the present experiments, however, about 15% of the initial amount of ^{137}Cs in the raw sediment was lost during the sequential extraction; this could not be measured in each extract. Therefore, an unmeasurable amount of the nuclide might be extracted in every extraction step according to the sorption-desorption equilibrium. On the other hand, the fact that almost all the ^{137}Cs was extracted in the 50% ammonium nitrate solution indicates that the nuclide in the sediments is contained in the phase of clay minerals and is exchangedly desorbed from the sediment by ammonium ions in a high concentration, because the effective ionic radii of ammonium ions and cesium ions resemble each other,[10] so the former ion can intrude into the crystal lattice of clay minerals and replace the latter ion.

Distribution of ^{137}Cs in the Components of Different Grain Sizes of the Sediments. Two samples collected from St. 1 and 7' were investigated for the distribution of ^{137}Cs, depending on the difference in the grain sizes of the components of the sediments.

The amount of each component obtained by elutriation, the contents of ^{137}Cs, sodium and potassium,

Table 2. Analytical Data of the Components Obtained by Elutriation of Sediment Core

Layer	Component[a)]	Weight %	Na %	K %	^{137}Cs pCi/g dry	^{137}Cs/K pCi/meq
Station 1						
Upper	3MP	62.6	1.10	1.28	0.26±0.03	0.7_8
	10MP	8.7	0.53	1.09	0.39±0.16	1.3_9
	1HP	9.2	0.41	1.09	0.43±0.14	1.5_9
	5HP	6.3	0.25	1.06	1.57±0.33	5.2_3
	5HS	13.0	0.11	0.31	0.76±0.16	4.4_7
Middle	3MP	63.6	1.17	1.23	0.31±0.04	1.0_0
	10MP	9.1	0.66	1.14	0.38±0.09	1.2_3
	1HP	8.9	0.43	1.13	0.59±0.14	2.0_3
	5HP	5.4	0.21	0.98	0.63±0.19	2.6_3
	5HS	12.9	0.09	0.48	1.01±0.13	6.7_3
Lower	3MP	66.6	1.24	1.33	0.31±0.03	0.9_7
	10MP	8.0	0.68	1.16	0.65±0.06	2.2_4
	1HP	8.9	0.62	1.17	0.62±0.08	2.2_1
	5HP	5.4	0.19	1.01	0.82±0.15	3.2_8
	5HS	11.7	0.11	0.51	1.05±0.04	6.1_8
Station 7′						
Upper	3MP	43.2	1.38	1.54	0.09±0.03	0.2_3
	10MP	12.1	1.06	1.31	0.19±0.08	0.5_7
	1HP	14.5	0.71	1.18	0.43±0.13	1.4_8
	5HP	13.6	0.32	0.89	0.57±0.08	2.4_8
	5HS	16.5	0.15	0.87	0.58±0.08	2.6_4
Middle	3MP	42.3	1.39	1.56	0.12±0.03	0.2_7
	10MP	10.0	1.05	1.31	0.46±0.09	1.3_9
	1HP	16.3	0.77	1.20	0.36±0.07	1.1_4
	5HP	13.5	0.30	0.89	0.51±0.09	2.1_7
	5HS	17.8	0.14	0.89	0.66±0.07	3.0_0
Lower	3MP	45.4	1.43	1.52	0.05±0.02	0.1_3
	10MP	12.1	1.05	1.39	0.32±0.15	0.8_9
	1HP	16.2	0.60	1.18	0.22±0.07	0.7_6
	5HP	12.4	0.32	0.95	0.67±0.07	2.7_9
	5HS	13.9	0.17	0.90	0.64±0.14	2.7_8

a) Grain sizes of the components are; 3MP: 31—16 μm, 10MP: 16—7.8 μm, 1HP: 7.8—3.9 μm, 5HP: 3.9—1.9 μm, 5HS: <1.9 μm.

and the ^{137}Cs/K ratios (pCi/meq) in these components are shown in Table 2. The weight percentages of the coarsest component most abundant in both sediments are above 62 and 42% respectively in St. 1 and 7′. The next most abundant component consists of the finest particulates in both sediments; their weight percentages are above 12 and 14% for St. 1 and 7′ respectively. This tendency is observed in every three layer of the sediment core. The concentration of ^{137}Cs in the unit amount of each component of the elutrilated sediment sample shows a more marked tendency, that is, the finer the grain size of the component, the higher the concentration of ^{137}Cs. The finest component contains about three times the quantity of the nuclide as the coarsest ones. On the contrary, the potassium contents slightly decrease with the decrease in grain size. Subsequently, the ^{137}Cs/K ratios show a remarkable increase with the decrease in the grain size of the components. In St. 1 and 7′, the ratios for the finest components amount to more than 6 and 10 times, respectively, those of the coarsest ones. These facts indicate that the nuclide tends to concentrate in the fine components of the sediment, in spite of its lower sodium and potassium contents. As a result of the X-ray powder diffraction measurements, it was observed that the peak height of potassium feldspar was highest for the coarsest component, while that of cristobalite was dominant in the finest component, except for calcite in St. 7′. However, because, unfortunately, no detailed information has been obtained on clay minerals in the present study, it is still obscure to what kinds of clay minerals the highest concentration of ^{137}Cs in the finest componet of the sediments should be attributed. In any event, it can be thought that the fine components contain a large number of exchangeable sites for cesium and that they probably exist in some clay minerals such as montmorillonite and kaolinite, as has been reported many authors.[4-8]

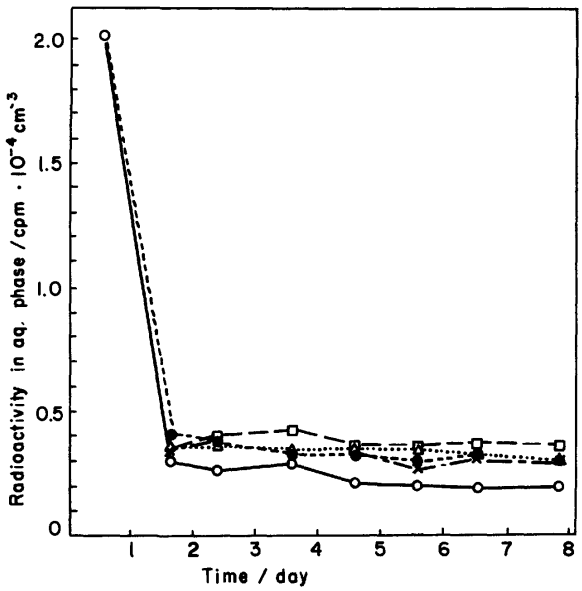

Fig. 4. Radioactivity change in aqueous phase according to sorption of ^{137}Cs on the elutriated components: 3MP —□—, 10MP —*—, 1HP, ····△····, 5HP ---●---, and 5HS —○—.

Table 3. Distribution Coefficients, K_d, for the Sorption of ^{137}Cs on the Components Obtained by Elutriation of Sediment Core (Upper Layer)

Component	amount used	K_d	K_d
	g dry	Sorption from 400 cm^3 of sea water	Desorption by 40 cm^3 of sea water
3MP	1.039	2050	2160
10MP	1.023	2630	—
1HP	1.029	2460	2610
5HP	1.030	2560	2990
5HS	1.105	3650	3850

Table 4. Sorption Capacity for Cesium and Exchange Balance between the Correlated Elements

Sample	Sorption capacity for Cs	Na contents	K contents	Cs sorbed/(Na+K) ratio
	meq g^{-1}	meq g^{-1}	meq g^{-1}	
3MP	0.32	0.61	0.39	0.32
10MP	0.15	0.46	0.34	0.19
1HP	0.20	0.30	0.31	0.33
5HP	0.23	0.13	0.23	0.64
5HS	0.29_7	0.06_5	0.23	1.01

In the present investigation, laboratory experiments using ^{137}Cs tracer have been performed to clarify the above postulation.

Sorption of ^{137}Cs on the Sediments. The results obtained by sorption experiments on the ^{137}Cs on the elutriated components of sediments are shown in Fig. 4. A blank experiment no sorption of the nuclide on the walls of the beakers used was observed. During 24 h standing, the sorption equilibrium seems almost to be attained, since the decrease in the radioactivity in the aqueous phase becomes significantly slow after one-day standing. After seven days, the sorption equilibrium is completely attained, when about 81.2% of ^{137}Cs has been adsorbed by the coarsest component, while by the finest component about 90% of the initial activity is captured from seawater in a volume 400 as much as the sediment phase. Furthermore, it was observed that the latter component adsorbed ^{137}Cs more quickly than the former one.

The distribution coefficients of ^{137}Cs between the sediments and seawater are shown in Table 3. (The 10MP sample was mistested because the sorption behavior very closely resembled the 5HP component.) The results show that the K_d values increase with the decrease in the grain size of the sediment components. In the present study, the components of different grain sizes were pulverized to under 400 mesh; therefore, the surface areas are thought to be not so very different and to have no effect on the K_d value or the sorption capacity. Thus, the K_d value for the finest component is about 1.8—1.9 times that for the coarsest ones. As can be seen from Table 3, a fairly good agreement is observed between the K_d values which were obtained by the two opposing experiments: the sorption of ^{137}Cs by the sediment component from 400 cm^3 of seawater and the desorption of nuclide adsorbed on the sample with 40 cm^3 of seawater.

In Table 4, the sorption capacities of the components for cesium are shown, together with the concentrations of sodium and potassium, and the ratio of cesium to sodium plus potassium. From the results given in the table, it can be seen that only 20—30% of the alkali metals are replaced by cesium for the coarsest components, while in the case of the finest component almost all the alkali metals are exhanged with cesium. Another experiment using seawater containing one half the amount of cesium and the tracer gave very similar capacity values. These results may indicate that the fine component of the elutriated sediments has a larger number of exchangeable sites for ^{137}Cs than the coarse ones; this is probably the reason for the higher ^{137}Cs contents in the finest component of the sediment in spite of the rather lower contents of sodium and potassium.

The present work was partially supported by a Grant-in-Aid for Scientific Research (No. 58380021) from the Ministry of Education, Science, and Culture.

References

1) F. Louman, "Disposal of Radioactive Wastes," IAEA, Vienna (1960), Vol. 2, p. 106.

2) S. A. Patin and N. I. Popov, "Disposal of Radioactive Wastes Into Seas, Oceans and Surface Waters," IAEA, Vienna (1966), Vol. 1, p. 443.

3) Y. Nagaya and K. Nakamura, *J. Oceanogr. Soc. Jpn*,

30, 179 (1974).

4) M. G. M. Bruggenwert and A. Kamphorst, "Soil Chemistry," ed. by G. H. Bolt, Elsevier, Amsterdam (1979), B., p. 141.

5) A. Maes and A. Cremers, "Soil Chemistry," ed by G. H. Bolt, Elsevier, Amsterdam (1979), B., p. 205.

6) A. Dloughy, "Disposal of Radioactive Wastes Into the Ground," IAEA-SM-93/18, Vienna (1967), p. 241.

7) H. Nishita, B. W. Kowalewsky, A. J. Steen, and K. H. Larson, *Soil Sci.*, **81**, 317 (1956).

8) K. Bunzl and W. Schultz, *J. Radioanal. Nucl. Chem.*, **90**, 23 (1985).

9) J. K. Miettinen and M. Lax, "Isotope Marine Chemistry," ed by E. D. Goldberg, Y. Horibe, and K. Saruhashi, Uchida Rokakuho, Tokyo (1980), p. 35.

10) "Lange's Handbook of Chemistry," 12-Ed., ed by J. A. Dean, McGraw-Hill, New York (1979), pp. 3—120.

 © 1986 The Chemical Society of Japan Bull. Chem. Soc. Jpn., 59, 1869—1876 (1986)

Double Diels-Alder Reaction of *trans*-3-Methylene-1,4-hexadiene and 1-Methyl-3-methylene-4-pentenyl Tosylate

Shuji KANEMASA, Hirohiko SAKOH, Eiji WADA, and Otohiko TSUGE*
Research Institute of Industrial Science, and Department of Molecular Science and Technology, Interdisciplinary Graduate School of Engineering Sciences, Kyushu University, Kasugakoen, Kasuga 816
(Received November 25, 1985)

A cross-conjugated triene, *trans*-3-methylene-1,4-hexadiene, is accessible from the Grignard reagent of chloroprene and methyloxirane via 1-methyl-3-methylene-4-pentenyl tosylate. The diene-transmissive Diels-Alder reaction of the triene and the stepwise sequence of double Diels-Alder reaction of the tosylate are investigated. Stereo- and regioselectivity of these reactions in the presence or absence of Lewis acid catalyst are discussed.

The diene-transmissive Diels–Alder reaction of cross-conjugated trienes such as 3-benzylidene- **A**,[1] 3-methoxymethylene-2,4-bis(trimethylsilyloxy)-1,4-pentadiene **B**,[2] and 2-ethoxy-3-methylene-1,4-pentadiene **C**[3] is useful for the synthesis of stereochemically defined and functionalized [6.6] bicyclic systems.[1–7] Stepwise sequence using synthetic equivalents of the cross-conjugated trienes offers a convenient route to cross bis-cycloadducts in which two different dienophiles are incorporated,[3,8,9]

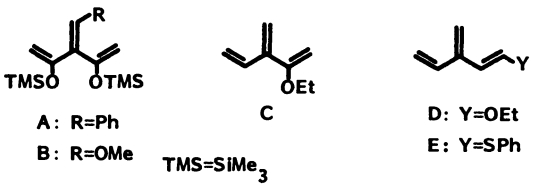

It has been found that triene **C** undergoes the first Diels–Alder reaction exclusively across the 2-monosubstituted diene moiety since the other 2,3-disubstituted diene moiety can hardly occupy an *s-cis* conformation which is essential in the transition state of Diels–Alder cycloaddition.[3] Although cross-conjugated trienes **D** and **E** carrying a diene-activating substituent at the 1-position selectively react with a dienophile across the 1,3-disubstituted triene, they are unfortunately too unstable to be employed as starting materials.[10]

The present article describes the diene-transmissive Diels–Alder reaction of *trans*-3-methylene-1,4-hexadiene (**1**) and the stepwise double cycloaddition of 1-methyl-3-methylene-4-pentenyl tosylate (**2**), a precursor of **1**.

Results and Discussion

In a study of organic synthesis utilizing cross-conjugated trienes, a general and simple preparative method of trienes starting from readily available materials is required. Our synthetic plan of **1** starts from an industrial material, chloroprene, and an epoxide as shown in Scheme 1. 4-Methylene-5-hexen-2-ol (**3**), which is readily accessible by the regioselective reaction of the Grignard reagent of chloroprene with

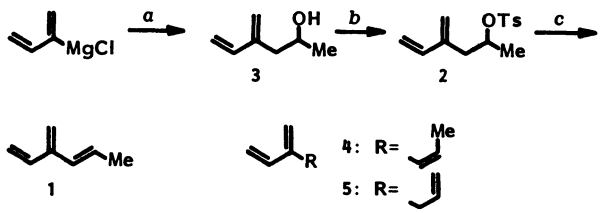

a: 2-methyloxirane, *b*: TsCl-pyridine, *c*: DBU

Scheme 1.

methyloxirane,[11] was tosylated in pyridine at 0 °C to give tosylate **2** in 80% yield. When **2** was heated at 100—110 °C with DBU under reduced pressure, the desired triene **1** was obtained in 64% yield as thermally labile liquid. Although the triene **1** thus obtained was only 90% pure (GLC), its separation from contaminants, the 2:1 mixture of **4** and **5**,[12] by vacuum distillation was unsuccessful. The contaminants could not be removed by distillation under higher vaccum, and under lower vacuum **1** underwent partial dimerization to give a mixture of **6** and **7** in the ratio 74:26 (GLC). Thus, the triene **1** of this purity was used for the following reactions.

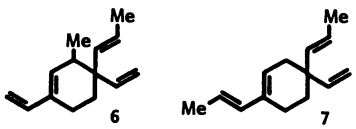

The reaction of **1** with an equivalent amount of *N*-phenylmaleimide (**8**) at room temperature gave a mixture of two isomeric bis-cycloadducts **11** and **12** in 92% yield in the ratio 5:1 (^{1}H NMR) as shown in Scheme 2. Even in a similar reaction below −50 °C, the bis-cycloadducts **11** and **12** (68%, **11**:**12**=4:1 by ^{1}H NMR) were formed together with two isomeric mono-cycloadducts **9** and **10** (24%, **9**:**10**=81:19 by GLC).

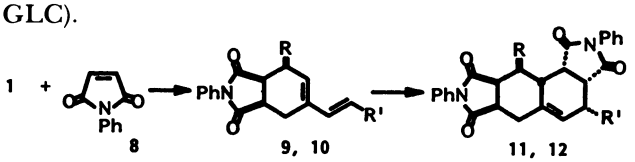

9, 11: R=Me, R'=H
10, 12: R=H, R'=Me

Scheme 2.

As it will be presented later, the minor bis-cycloadduct **12** can be obtained as a single stereoisomer in the reaction of **8** with **10** which is available from the cycloadduct derived from diene tosylate **2** and **8** (Schemes 4, 5, and 6). Accordingly, the major bis-cycloadduct **11** has to be the stereoselective cycloaddition product derived from the other mono-cycloadduct **9**. The structure of **11** was confirmed to be the endo cycloadduct of **8** across 1,3-disubstituted diene moiety of **1** on the basis of spectral data.[13] After all, the Diels-Alder reaction of **1** with **8** has occurred not only across the 1,3-disubstituted diene part but also across the 2-monosubstituted diene, and chemoselectivity between the both dienes does not depend upon the reaction conditions. The selectivity in favor of the methyl-substituted diene in the reaction with **8** was 81—83%.

On the other hand, the Diels-Alder reaction of **1** with an equimolar amount of dimethyl acetylenedicarboxylate (DMAD, **13**) at room temperature led to a mixture of two isomeric monocycloadducts **14** and **15** in 77% yield. The chemoselectivity between the 1,3-disubstituted and 2-monosubstituted dienes of **1** was 78:22 (GLC) (Scheme 3). When excess **13** was used and the reaction was carried out in refluxing benzene, a complex mixture containing two mono- and bis-cycloadducts along with their partly or fully aromatized derivatives.

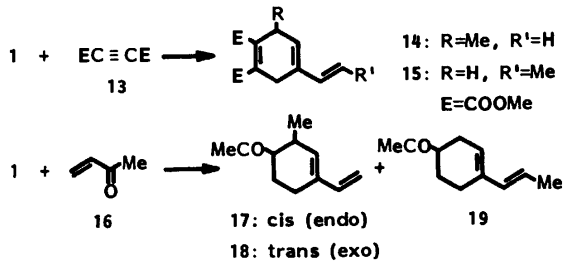

Scheme 3.

To our surprise, regioselectivity in the first Diels-Alder reaction of **1** was found unexpectedly high. For example, the reaction with methyl vinyl ketone (**16**) as an unsymmetrically substituted dienophile at room temperature gave three regioselective monocycloadducts in 76% yield, two of which are endo **17** and exo cycloadduct **18** across the methyl-substituted diene (**17**:**18**=70:30 by GLC) and the other **19** is the cycloadduct across the 2-monosubstituted diene (**17**+**18**:**19**=69:31 by GLC).[14] When this reaction was carried out in the presence of an equimolar amount of ethylaluminum dichloride as a Lewis acid in toluene at −78°C for 0.5 h, the *endo*-selectivity increased to 98% (**17**:**18**=98:2). However, the chemoselectivity could not be improved (**17**+**18**:**19**=71:29 by GLC).[15] Since the chemoselectivity between both diene moieties of **1** in the first Diels-Alder reaction was low, we had to give up the route involving diene-transmissive Diels-Alder cycloaddition of triene **1**. Therefore, stepwise sequence of double Diels-Alder reaction using diene tosylate **2** was instead investigated hereafter.

The Diels-Alder reactions of **2** with **8** or 1,4-naphthoquinone (**20**) gave cycloadduct **21** or **22** in 99 or 72% yield, respectively (Scheme 4). Although the regioselectivity found in the reaction of **2** with **16** in refluxing benzene was very low (74%, **23**:**24**=64:36 by GLC),[16,17] a similar reaction in the presence of ethylaluminum dichloride at −50 to −70°C was exclusively *para*-selective. 67% Yield of **23** was the only isolated product.

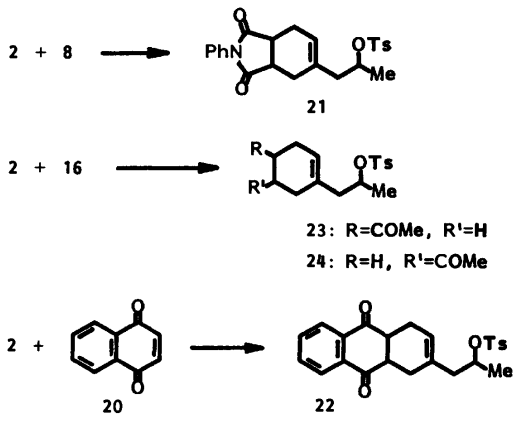

Scheme 4.

The elimination of *p*-toluenesulfonic acid from **21** was readily performed by heating with DBU under reflux in toluene to give a mixture of three elimination products in 73% yield (Scheme 5). It was found that purity of the expected trans diene **10** was 91%, and that the contaminants consisted of the corresponding cis isomer **25** and unconjugated diene **26** (9%, **25**:**26**=2:1 by ^{1}H NMR).[18] One-pot procedure for the Diels-Alder reaction of **2** with **8** and the diene formation into **10** was successful: **10** was obtained in 70% yield (**10**:**25**:**26**=91:6:3 by GLC).

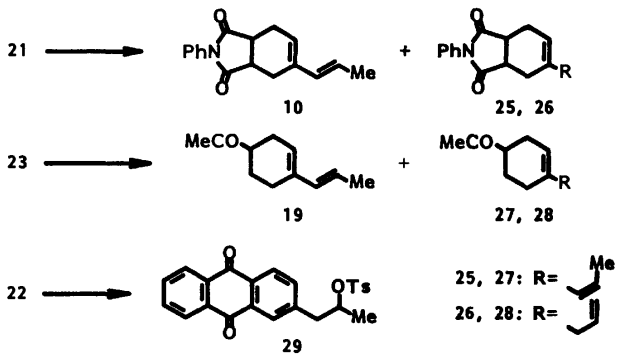

Scheme 5.

The elimination reaction of **23** under similar conditions afforded trans diene **19** as major product, which had been previously obtained as minor product in the reaction of **1** with **16**, together with two isomeric dienes **27** and **28** (76%, **19**:**26**:**27**=87:8:5 by GLC). However, naphthoquinone adduct **22** resulted in the dehydrogenation into **29** instead of the elimination of sulfonic acid.[19]

The second Diels–Alder reaction step of the stepwise sequence was investigated by utilizing diene **10**. Since it was unsuccessful to remove the contaminants **25** and **26**, the diene **10** of 91% purity was used for subsequent reactions. These isomeric dienes **25** and **26** did not affect the second Diels–Alder cycloaddition and were recovered unchanged.

The reaction of **10** with **8** readily took place at room temperature to give bis-cycloadduct **12** as a single stereoisomer in 78% yield, which is identical with the minor bis-cycloadduct formed in the reaction of **1** with **8** (Scheme 6). Therefore, both regioisomeric bis-cycloadducts **11** and **12** are now accessible from the triene **1** and the diene tosylate **2**, respectively, both as either major or single product. This facile and stereoselective cycloaddition may occur because the diene moiety of **10** is not sterically crowded at the side opposite to the fused five-membered ring to allow the endo approach **F** of **8** from this direction (Fig. 1).

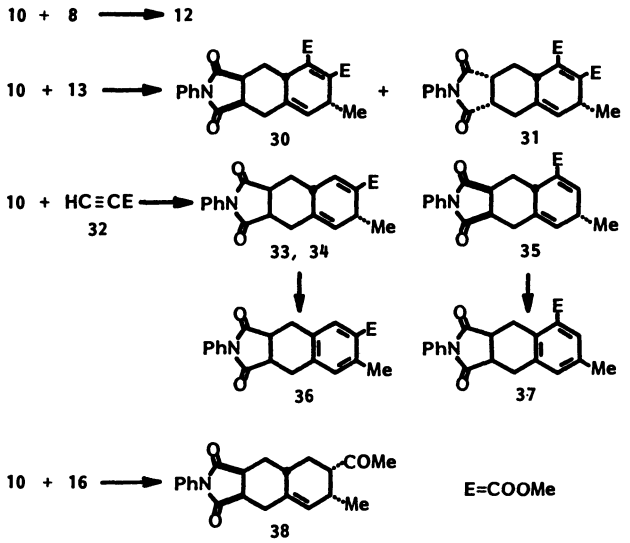

Scheme 6.

Compared to high stereoselectivity of the reaction with **8**, the reaction of **10** with DMAD **13** gave two stereoisomers **30** and **31** in 79 and 8% yields, respectively. The major product **30** corresponds to the cycloadduct formed by the attack of **13** from sterically less hindered side of diene **10**.

Regioselectivity of this type of reaction was found very low. For example, three isomers **33**—**35** were formed in 62% yield in the reaction with methyl propynoate (**32**) (**33**:**34**:**35**=2:1:1 by ^{1}H NMR, 25% of **10** was recovered). As **33** and **34** were converted into the same dehydrogenated derivative **36** and **35** was dehydrogenated into its isomer **37**, **33** and **34** are assigned as stereoisomers to each other and **35** is one of their regioisomers.

The stereochemistry of **30**, **31**, and **33**—**35** were determined on the basis of spectral data as well as the stereochemical mode of reactions which are illustrated in Fig. 1. Thus, the major cycloadduct **30** has

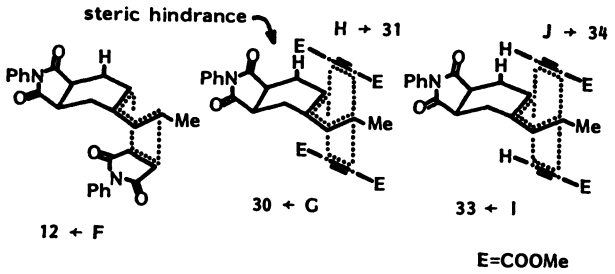

Fig. 1. Stereochemistry of the cycloaddition of **10**.

been formed through the approach **G** of **13** from the side opposite to the fused maleimide ring. The other approach **H** leading to **31** causes some steric repulsion between the ester moiety of **13** and a quasi-axial hydrogen adjacent to the diene moiety or the fused maleimide ring. On the other hand, in the approaches **I** and **J** giving **33** and **34**, one substituent on the dienophile **32** is hydrogen which brings about only negligible steric repulsion at both sides of the diene. Accordingly, the stereoselectivity on the formation of **33** and **34** may have been reduced. It is readily understood that **35** has been formed in a highly stereoselective manner.

The reaction of **10** with methyl vinyl ketone (**16**) as an unsymmetrically substituted dienophile was performed in the presence of ethylaluminum dichloride at −70 °C. The regioselective, *endo*-selective, and face-selective cycloadduct **38** was obtained in 78% yield (Scheme 6).

It is concluded that the stepwise sequence of double Diels–Alder reaction of **2** can be performed in a highly selective fashion for the combination of two different olefinic dienophiles, either in the presence or absence of Lewis acid.

Experimental

General. Melting points were determined on a Yanagimoto micro melting point apparatus and uncorrected. IR spectra were taken with a JASCO IRA-1 or a JASCO A-702 spectrometer. ^{1}H NMR spectra were recorded on a Hitachi R-40 (90 MHz) or a JEOL FX-100 instrument (100 MHz) and ^{13}C NMR spectra on a JEOL FX-100 spectrometer at 25.05 MHz. Chemical shifts are expressed in parts per million downfield from tetramethylsilane as internal standard. Mass spectra were measured with a JEOL JMS-OlSG-2 spectrometer at 70 eV of ionization energy. GC-Mass spectra as well as high resolution mass spectra were also obtained on the same instrument. Elementary analyses were performed on a Hitachi 026 CHN micro analyzer. Thin-layer chromatography (TLC) was accomplished on 0.2 mm precoated plates of silica gel 60 F-254 (Merck) or of aluminum oxide 60 F-254 type-E (Merck). Visualization was made with ultraviolet light (254 and 365 nm), iodine, molybdophosphoric acid (5% in ethanol), or *p*-anisaldehyde (5% in ethanol containing 5% of sulfuric acid). For preparative column chromatography, Wakogel C-200, C-300 (Wako) and Silicagel 60 (Merck) were employed. Flash chromatography was carried out on an EYELA EF-10 apparatus using a column (20×180 mm) packed with Silicagel 60 (Merck, size: 0.04—

0.063 mm). Preparative high-performance liquid chromatography (HPLC) was performed on a Kusano KHLC-201 apparatus with a UV-detector Uvilog-III using a column (22×300 mm) packed with silica gel (Wakogel LC-50H). Gas-liquid chromatography (GLC) was accomplished on a Yanaco G-2800 gas chromatograph (Yanagimoto) with an ionization detector using a glass column (SE-30, 3×2000 mm) or a glass capillary column (Sillicone GE, SE-30, 0.25×5000 mm). Micro vacuum distillation was carried out on a Sibata GTO-250R Kugelrohr distilling apparatus. Solvents were evaporated with a Tokyo Rikakikai rotary evaporator type-V at about 50 °C unless otherwise stated.

Tetrahydrofuran was distilled over sodium wire and then over lithium aluminum hydride prior to its use. Benzene and toluene were also distilled over sodium and stored on sodium wire. The solvents for column chromatography (hexane and ethyl acetate) were used without further purification.

4-Methylene-5-hexen-2-ol (3). Methyloxirane (7 ml, 0.1 mol) in dry THF (25 ml) was slowly added to the 0.1 M solution (1 M=1 mol dm^{-3}) of 1-methylenepropenylmagnesium chloride in THF (100 ml, 0.1 mol) and the mixture was heated at 50—60 °C for 2 h. After cooled to room temperature, the mixture was hydrolyzed with 3N-HCl. The organic layer was separated, and the aqueous layer was extracted with ether (100 ml). The combined organic layer was washed with 5% aqueous sodium hydrogen carbonate, then with brine, and dried over magnesium sulfate. After the solvent was removed by evaporation, the residue was distilled under vacuum (20 mmHg) to give **3** (purity 80% (GLC), 4.66 g, 42%). Repeated vaccum distillation gave pure **3**: Colorless liquid; bp 55—60 °C/2399 Pa (lit,[11] bp 56—60 °C/2660 Pa); ^{1}H NMR ($CDCl_3$) δ=1.20 (3H, d, J=6.5 Hz, Me), 2.29 (1H, ddd, J_{gem}=14.0, J_{2-1}=7.5, J_{long}=1.0 Hz, one of 2-H), 2.34 (1H, s, OH), 2.44 (1H, ddd, J_{gem}=14.0, J_{2-1}=5.0, J_{long}=1.0 Hz, the other of 2-H), 3.93 (1H, m, 1-H), 4.96—5.40 (4H, m, =CH_2), and 6.36 (1H, dd, J_{4-5}=11.0 and 17.5 Hz, 4-H).

1-Methyl-3-methylene-4-pentenyl Tosylate (2). A mixture of **3** (0.655 g, 5.84 mmol), *p*-toluenesulfonyl chloride (1.11 g, 5.84 mmol), and pyridine (2 ml) was allowed to stand in a freezer for 36 h. Pyridine hydrochloride precipitated was removed by filteration and the filtrate was chromatographed over silica gel with hexane-ethyl acetate (9:1) to give **2** (1.243 g, 80%): Colorless liquid; IR (neat) 1360, 1190, and 1175 cm^{-1}; ^{1}H NMR ($CDCl_3$) δ=1.25 (3H, d, J=6.0 Hz, Me), 2.34 (1H, dd, J_{gem}=14.0 and J_{2-1}=8.0 Hz, one of 2-H), 2.42 (3H, s, *p*-Me), 2.66 (1H, dd, J_{gem}=14.0 and J_{2-1}=6.0 Hz, the other of 2-H), 4.68 (1H, ddq, J_{1-2}=8.0, 6.0 and J_{1-Me}=6.0 Hz, 1-H), 4.84—5.16 (4H, m, =CH_2), 6.16 (1H, dd, J_{4-5}=11.0 and 17.5 Hz, 4-H), 7.28, and 7.74 (each 2H, d, J=8.0 Hz, ArH); ^{13}C NMR ($CDCl_3$) δ=20.47, 21.54 (each q, Me), 39.03 (t, 2-C), 78.36 (d, 1-C), 114.03, 119.53 (each t, 3-CH_2= and 5-C), 127.77, 129.62 (each d), 137.71 (d, 4-C), 140.93 (s, 3-C), 144.44 (s); MS m/z (rel. intensity, %) 266 (M^+, 4), 199 (9), 155 (96), 94 (53), 91 (base peak), and 79 (51).

Found: C, 63.06; H, 6.84%. Calcd for $C_{14}H_{18}O_3S$: C, 63.13; H, 6.81%.

***trans*-3-Methylene-1,4-hexadiene (1).** A mixture of **2** (0.62 g, 2.32 mmol) and DBU (0.709 g, 4.64 mmol) was heated in a micro distilling apparatus, at 110 °C at 2660 Pa for 30 min, to give **1** (0.141 g, 64%, purity 90% (GLC)) which was collected in a receiver cooled in a Dry Ice bath (−78 °C): Colorless liquid; ^{1}H NMR ($CDCl_3$) δ=1.78 (3H, d, J=5.0 Hz, Me), 5.00 (2H, s, 3-CH_2=), 5.04 (1H, dd, J_{gem}=1.5 and J_{1-2}=10.5 Hz, one of 1-H), 5.36 (1H, dd, J_{gem}=1.5 and J_{1-2}=17.5 Hz, the other of 1-H), 5.84 (1H, dq, J_{5-4}=16.0 and J_{5-6}=5.0 Hz, 5-H), 6.14 (1H, d, J_{4-5}=16.0 Hz, 4-H), and 6.40 (1H, dd, J_{2-1}=17.5 and 10.5 Hz, 2-H); ^{13}C NMR ($CDCl_3$) δ=18.32 (q, Me), 113.60, 115.13 (each t, 1-C and 3-CH_2=), 127.28 (d, 5-C), 129.75 (d, 4-C), 136.68 (d, 2-C), and 144.43 (s, 3-C); GC-MS m/z 94 (M^+).

Found: m/z 94.0769. Calcd for C_7H_{10}: M, 94.0782.

The residue which was left in a distilling flask after the vaccum distillation of **1** was chromatographed over silica gel using hexane-ethyl acetate (19:1) to afford a mixture of **6** and **7** (74:26 checked by GLC). **6**+**7**: Colorless liquid; ^{1}H NMR ($CDCl_3$) δ=0.92 (d, J=7.0 Hz, Me), 1.64, 1.68 (each d, J=5.0 Hz, Me), 1.40—2.40 (m, CH_2 and CH), 4.90—6.10 (m, CH_2= and CH=), and 6.31 (dd, J=17.5 and 11.0 Hz); ^{13}C NMR ($CDCl_3$) δ=16.66, 18.21, 18.31 (each q, Me), 21.53, 22.17, 30.08, 30.32, 32.08, 35.10 (each t, CH_2), 38.38, 38.62 (each d, CH), 41.11, 44.09 (each s), 110.55 (t), 111.96, 112.55, 113.72, 121.63, 122.95, 123.63, 124.61, 124.75, 134.47 (d), 134.71, 137.30, 137.55, 139.84 (each d), 142.67, and 145.26 (each s); GC-MS m/z (rel. intensity, %) **6**: 188 (M^+, 5), 95 (23), 94 (13), 79 (base peak), and 77 (12); **7**: 188 (M^+, 10), 95 (22), 94 (11), 79 (base peak), and 77 (11).

Reaction of 1 with 8 Leading to 11, 12 or 9—12. i) A mixture of **1** (purity 90%, 0.033 g, 0.32 mmol) and **8** (0.060 g, 0.35 mmol) in dry benzene (1 ml) was stirred at room temperature under nitrogen for 20 h. The solvent was evaporated in vacuo and the residue was chromatographed over silica gel with hexane-ethyl acetate (2:1) to provide the 5:1 mixture (^{1}H NMR) of **11** and **12** (0.071 g, 92%) which were separated from each other through HPLC using hexane-ethyl acetate (2:1). ii) To a solution of **1** (purity 90%, 0.104 g, 1 mmol) in dry toluene (2 ml) was added **8** (0.191 g, 1.1 mmol) at −70 °C. The mixture was stirred below −50 °C for 2 h. The solvent was removed by eveporation in vacuo and the residue was chromatographed over silica gel with hexane-ethyl acatate (4:1) to afford a mixture of **9** and **10** (0.7 g, 24%, 81:19 (GLC)) whose separation was unsuccessful. Further elution with hexane-ethyl acetate (2:1) gave the 4:1 mixture (^{1}H NMR) of **11** and **12** (0.163 g, 68% based on **8**). The data for **9**, **11**, and **12** are given below, and **10** was assigned by the comparison of its spectral data with those of the authentic sample prepared from the reaction of **21** with DBU.

9: ^{1}H NMR ($CDCl_3$) δ=1.39 (3H, d, J=7.0 Hz, Me), 2.00—3.40 (5H, m, CH_2 and CH), 5.02 (1H, d, J=11.0 Hz, one of =CH_2), 5.38 (1H, d, J=17.5 Hz, the other of =CH_2), 5.70 (1H, m, 5-H), 6.32 (1H, dd, J=11.0 and 17.5 Hz, 6-C<u>H</u>=CH_2), and 7.00—7.50 (5H, m, Ph); ^{13}C NMR ($CDCl_3$) δ=16.65 (q, Me), 22.88 (t, 7-C), 31.53 (d, 4-C), 40.30 (d, 7a-C), 44.42 (d, 3a-C), 113.12 (t, =CH_2), 126.60 (d, 2×C), 128.60 (d), 129.13 (d, 2×C), 132.13 (s, 6-C), 133.36, 136.72 (each d, 5-C and <u>C</u>H=CH_2), 137.36 (s), 177.07, and 178.66 (each s, CON); GC-MS m/z (rel. intensity, %) 267 (M^+, 42), 120 (base peak), and 105 (75).

11: Colorless prisms (ethanol); mp 242—243 °C; IR (KBr) 1765 and 1700 cm^{-1}; ^{1}H NMR ($CDCl_3$) δ=1.53 (3H, d, J=6.5 Hz, Me), 1.76—3.44 (10H, m, CH_2 and CH), 5.76 (1H, m, 5-H), and 7.00—7.52 (10H, m, Ph); MS m/z (rel. intensity, %) 440 (M^+, 73), 267 (base peak), and 174 (58).

Found: C, 73.51; H, 5.49; N, 6.45%. Calcd for $C_{27}H_{24}N_2O_4$: C, 73.62; H, 5.49; N, 6.36%.

12: Colorless needles (ethanol); mp 228—229 °C; IR (KBr) 1765 and 1700 cm^{-1}; ^{1}H NMR ($CDCl_3$) δ=1.44 (3H, d, J=7.0 Hz, Me), 2.00—3.48 (10H, m, CH_2 and CH), 5.60 (1H, br

s, 5-H), and 7.00—7.60 (10H, m, Ph); MS *m/z* (rel. intensity, %) 440 (M^+, base peak), 267 (21), and 174 (26).

Found: C, 73.88; H, 5.59; N, 6.33%. Calcd for $C_{27}H_{24}N_2O_4$: C, 73.62; H, 5.49; N, 6.36%.

Reaction of 1 with 13 Leading to 14 and 15. A mixture of **1** (purity 90%, 0.028 g, 0.27 mmol) and **13** (0.042 g, 0.3 mmol) in dry benzene (1 ml) was stirred at room temperature under nitrogen for 20 h. The solvent was evaporated in vacuo and the residue was chromatographed over silica gel using hexane-ethyl acetate (4:1) to afford a mixture of **14** and **15** (0.051 g, 77%, 78:22 (GLC)) as colorless liquid, which could not be separated from each other. Their spectral data are given below:

14: ^{1}H NMR ($CDCl_4$) δ=1.17 (3H, d, J=7.0 Hz, Me), 2.90—3.44 (3H, m, CH_2 and CH), 3.75, 3.76 (each 3H, s, COOMe), 5.04 (1H, d, J=11.0 Hz, one of $=CH_2$), 5.13 (1H, d, J=17.5 Hz, the other of $=CH_2$), 5.64 (1H, m, 4-H), and 6.36 (1H, dd, J=11.0 and 17.5 Hz, 5-C<u>H</u>=CH_2); GC-MS *m/z* (rel. intensity, %) 206 (M^+−30, 41), 205 (20), and 117 (base peak).

15: ^{1}H NMR ($CDCl_3$) δ=1.76 (dd, J=6.5 and 0.5 Hz, Me). Other signals are hidden in those of **14**; GC-MS *m/z* (rel. intensity, %) 235 (M^+−1), 234 (29), and 203 (base peak).

Reaction of 1 with 16 Leading to 17—19. i) A mixture of **1** (purity 90%, 0.065 g, 0.62 mmol) and **16** (0.097 g, 1.38 mmol) in dry benzene (1 ml) was stirred at room temperature under nitrogen for 20 h. The solvent was evaporated in vacuo and the residue was chromatographed over silica gel with hexane-ethyl acetate (19:1) to give a mixture of the dimers **6** and **7** (0.004 g, 7%, 79:21 (GLC)). Further elution with hexane-ethyl acetate (9:1) afforded a mixture of **17**, **18**, and **19** (0.084 g, purity 93% (GLC), 76%, **17**:**18**:**19**=48:21:31 (GLC)), none of which could be separated in pure form from the other two. ii) To a solution of **16** (0.078 g, 1.12 ml) in dry toluene (1 ml) was added the 1 M solution of ethylaluminum dichloride (in hexane, 1 ml) by use of a syringe at −78 °C. After 0.5 h, **1** (0.105 g, purity 90%, 1 mmol) in dry toluene (1 ml) was introduced and then the mixture was stirred for an additional 0.5 h at the same temperature. Usual hydrolytic work-up with aqueous sodium hydrogencarbonate was followed by the extraction with benzene (10 ml ×2). The benzene was dried over magnesium sulfate and evaporated in vacuo. The residue was chromatographed over silica gel using hexane-ethyl acetate (9:1) to provide a mixture of **17**, **18**, and **19** (0.077 g, 46%, **17**:**18**:**19**=71:2:26 (GLC)). Structural assignment of these products was carried out as follows: The isomer **19** was first identified by the comparison of its spectral data with those of the authentic sample prepared from the reaction of **23** with DBU. The signals of **19** were taken away from the spectrum of the mixture obtained in the Lewis acid-catalyzed reaction. The remaining signals are those of **17**, which make possible to assign the structure of **17**. Finally, the signals for **18** are available in the spectrum of the mixture obtained in the upper reaction. Their spectral data are given below:

17: ^{1}H NMR ($CDCl_3$) δ=0.86 (3H, d, J=7.0 Hz, Me), 1.50—2.92 (6H, m, CH_2 and CH), 2.14 (3H, s, COMe), 4.93 (1H, d, J=11.0 Hz, one of $=CH_2$), 5.08 (1H, d, J=18.0, the other of $=CH_2$), 5.56—5.76 (1H, m, 2-H), and 6.32 (1H, dd, J=11.0 and 18.0 Hz, 1-C<u>H</u>=CH_2); ^{13}C NMR ($CDCl_3$) δ=15.77 (q, Me), 23.59 (t, 2×C, 5- and 6-C), 28.59 (q, CO<u>Me</u>), 31.41 (d, 3-C), 51.47 (d, 4-C), 111.36 (t, $=CH_2$), 133.77 (d), 135.42 (s, 1-C), 139.54 (d), and 210.90 (s, <u>C</u>OMe); GC-MS *m/z* (rel. intensity, %) 164 (M^+, 73), 149 (45), 121 (92), 94 (98), 92 (48), and 79 (base peak).

18: ^{1}H NMR ($CDCl_3$) δ=0.96 (3H, d, J=7.0 Hz, Me), 2.15 (3H, s, COMe), 4.93 (1H, d, J=11.0 Hz, one of $=CH_2$), 5.06 (1H, d, J=18.0 Hz, the other of $=CH_2$), 5.56—5.76 (1H, m, 2-H), and 6.32 (1H, dd, J=11.0 and 18.0 Hz, 1-C<u>H</u>=CH_2); ^{13}C NMR ($CDCl_3$) δ=20.12 (q, Me), 25.53 (t, 2×C, 5- and 6-C), 32.24 (d, 3-C), 55.59 (d, 4-C), 111.07 (t, $=CH_2$), 134.54 (d), and 211.89 (s, <u>C</u>OMe). Other signals are overlapping with those of **17**; GC-MS *m/z* (rel. intensity, %) 164 (M^+, 71), 149 (54), 121 (base peak), 94 (91), 92 (52), and 79 (76).

Reaction of 2 with 8 Leading to 21. A mixture of **2** (0.346 g, 1.3 mmol) and **8** (0.225 g, 1.3 mmol) in dry benzene (5 ml) was heated under reflux under nitrogen for 15 h. The solvent was removed by evaporation in vacuo and the residue was chromatographed over silica gel with hexane-ethyl acetate (1:1) to afford the 1:1 mixture of two diastereomers of **21** (0.568 g, 99%): Colorless liquid; IR (neat) 1780, 1710, 1380, 1190, and 1175 cm^{-1}; ^{1}H NMR ($CDCl_3$) δ=1.12, 1.18 (each 3H, d, J=6.5 Hz, Me), 1.90—2.72 (6H, m), 2.36 (3H, s, *p*-Me), 2.92—3.10 (2H, m), 4.20—4.40 (1H, m, C<u>H</u>Me), 5.48—5.72 (1H, m, 6-H), 7.04—7.50 (5H, m, Ph), 7.24, and 7.72 (each 2H, d, J=8.0 Hz, ArH); ^{13}C NMR ($CDCl_3$) δ=20.22, 21.25 (each q, Me), 24.02, 24.12, 27.09, 27.83 (each t), 38.50, 38.59, 39.18 (each d), 44.10, 44.34 (each t), 77.09, 78.55 (each d, <u>C</u>HOTs), 123.97, 124.31 (each d, 6-C), 125.97, 127.23, 127.33, 128.06, 128.59, 129.48 (each d), 131.77, 133.81, 133.96, 134.83, 135.03, 144.24, 144.34 (each s), 178.30, and 178.55 (each s, CON); MS *m/z* (rel. intensity, %) 439 (M^+, 4), 267 (55), 120 (66), and 91 (base peak).

Found: C, 65.34; H, 5.82; N, 3.41%. Calcd for $C_{24}H_{26}NO_5S$: C, 65.59; H, 5.73; N, 3.19%.

Reaction of 2 with 20 Leading to 22. A mixture of **2** (0.141 g, 0.53 mmol) and **20** (0.084 g, 0.53 mmol) in dry benzene (2 ml) was refluxed under nitrogen for 36 h. The benzene was evaporated in vacuo and the residue was chromatographed over silica gel using hexane-ethyl acetate (3:1) to give the 1:1 mixture of two diastereomers of **22** (0.165 g, 72%): Colorless solid; IR (KBr) 1685, 1590, 1355, and 1170 cm^{-1}; ^{1}H NMR ($CDCl_3$) δ=1.04, 1.05 (each 3H, d, J=6.0 Hz, Me), 1.80—2.60 (8H, m), 2.39, 2.43 (each 3H, s, *p*-Me), 3.00—3.20 (2H, m), 4.68 (1H, m, C<u>H</u>OTs), 5.40 (1H, m, 3-H), 7.28, 7.30 (each 2H, d, J=8.0 Hz, ArH), and 7.60—8.10 (6H, m, ArH); MS *m/z* (rel. intensity, %) 424 (M^+, 5), 252 (51), and 91 (base peak).

Found: C, 68.08; H, 5.74%. Calcd for $C_{24}H_{24}O_5S$: C, 67.91; H, 5.70%.

Reaction of 2 with 16 Leading to 23 and/or 24. i) A mixture of **2** (0.246 g, 0.92 mmol) and **16** (0.3 ml, 3.7 mmol) in dry benzene (2 ml) was refluxed under nitrogen for 48 h. The solvent and excess **16** were evaporated in vacuo and the residue was chromatographed over silica gel with hexane-ethyl acetate (3:1) to give a mixture of **23** and **24** (0.222 g, 74%) whose separation failed. The isomer ratio was determined after their conversion into a mixture of **19** and its regioisomer by the reaction with DBU (**23**:**24** was calculated as 64:36). ii) To a solution of **16** (0.1 ml, 1.23 mmol) in dry toluene (1 ml) was added ethylaluminum dichloride (1 M solution in hexane, 0.6 ml, 0.6 mmol) at −70 °C. After 0.5 h at the same temperature, **2** (0.164 g, 0.62 mmol) in toluene (1 ml) was added and the mixture was allowed to react below −50 °C for 1 h. Usual hydrolytic work-up with aqueous sodium hydrogen carbonate was followed by the extraction with benzene (10 ml×2). The combined extracts were dried over magnesium sulfate and evaporated in vacuo. The re-

sidue was chromatographed over silica gel using hexane-ethyl acetate (3:1) to provide **23** (0.139 g, 67%).

23: Colorless liquid; IR (neat) 1710, 1355, 1190, and 1175 cm^{-1}; ^1H NMR ($CDCl_3$) δ=1.22, 1.24 (each 3H, d, J=6.2 Hz, Me), 1.30—2.50 (9H, m), 2.12 (3H, s, COMe), 2.42 (3H, s, *p*-Me), 4.64 (1H, m, CHOTs), 5.36 (1H, m, 2-H), 7.24, and 7.72 (each 2H, d, J=8.0 Hz, ArH); ^{13}C NMR ($CDCl_3$) δ=20.82, 21.59 (each q, Me), 24.65, 26.88, 27.94 (each t), 27.94 (q, Me), 44.59, 44.77 (each t), 46.65, 46.77 (each d, 4-C), 78.83 (d, CHOTs), 123.83 (d, 2-C), 127.83, 129.95 (each d), 132.54 (s, 1-C), 134.66, 144.77 (each s), and 211.48 (s, COMe); MS *m/z* (rel. intensity, %) 336 (M^+, 4), 164 (29), 121 (59), and 43 (base peak).

Found: C, 64.41; H, 7.23%. Calcd for $C_{18}H_{24}O_4S$: C, 64.26; H, 7.19%.

24: ^1H NMR ($CDCl_3$) δ=1.26 (3H, d, J=6.2 Hz, Me), 1.30—2.50 (9H, m), 2.12 (3H, s, COMe), 2.42 (3H, s, *p*-Me), 4.64 (1H, m, CHOTs), 5.36 (1H, m, 2-H), 7.24, and 7.72 (each 2H, d, J=8.0 Hz, ArH); ^{13}C NMR ($CDCl_3$) δ=44.89, 45.00 (each d, 5-C), 125.07 (d, 2-C), 131.30 (s, 1-C), and 211.19 (s, COMe). Other signals are overlapping with those of **23**.

Reaction of 21 with DBU Leading to 10. A mixtute of **21** (0.233 g, 0.53 mmol) and DBU (0.105 g, 0.69 mmol) in dry toluene (4 ml) was refluxed for 6 h. The toluene was evaporated in vacuo and the residue was subjected to a column chromatography over silica gel using hexane-ethyl acetate (2:1) to give a mixture of **10**, **25**, and **26** (0.104 g, 73%). The isomer ratio **10**+**25**:**26** was determined as 97:3 by GLC. Although **10** and **25** showed the same retention time in the GLC, the mixture of **25** and **26** was recovered unchanged in the reaction of the above mixture with **13** and their ratio was 2:1 (^1H NMR). After all, the ratio among them was calculated as **10**:**25**:**26**=91:6:3.

10 (purity 91% (GLC)): Colorless oil; IR (neat) 1780 and 1715 cm^{-1}; ^1H NMR ($CDCl_3$) δ=1.74 (3H, d, J=6.0 Hz, Me), 2.00—3.40 (6H, m, CH_2 and CH), 5.40—5.92 (2H, m, =CH), 6.04 (1H, d, J=16.0 Hz, 5-CH=CHMe), and 7.04—7.48 (5H, m, Ph); ^{13}C NMR ($CDCl_3$) δ=18.18 (q, Me), 23.41, 24.59 (each t, 4- and 7-C), 39.41 (d, 2×C, 3a- and 7a-C), 123.36, 124.42, 126.54, 128.54, 129.13 (each d), 131.89 (d), 132.25, 137.83 (each s), and 178.95 (s, 2×C, CON); MS *m/z* (rel. intensity, %) 267 (M^+, 20) and 91 (base peak).

Found: C, 76.38; H, 6.41; N, 5.24%. Calcd for $C_{17}H_{17}NO_2$: C, 76.45; H, 6.46; N, 5.34%.

25+**26**: ^1H NMR ($CDCl_3$) δ=1.74 (d, J=6.0 Hz, Me), 2.00—3.40 (m, CH_2 and CH), 5.00 (m, =CH_2), 5.32—5.90 (m, =CH), and 7.04—7.48 (m, Ph).

One-Pot Synthesis of 10. A mixture of **2** (0.39 g, 1.46 mmol) and **8** (0.254 g, 1.46 mmol) in dry toluene (6 ml) was heated at 80 °C under nitrogen for 15 h. After DBU (0.29 g, 1.9 mmol) was added, the mixture was refluxed for 6 h. The solvent was evaporated in vacuo and the residue was chromatographed over silica gel using hexane-ethyl acetate (2:1) to give **10** (0.272 g, 70%, purity 91% (GLC), the contaminants are **25** and **26** in the ratio 2:1 (GLC)).

Reaction of 23 with DBU Leading to 19. A mixture of **23** (0.119 g, 0.35 mmol) and DBU (0.07 g, 0.46 mmol) in dry toluene (3 ml) was refluxed under nitrogen for 12 h. The toluene was evaporated in vacuo and the residue was chromatographed over silica gel with hexane-ethyl acetate (9:1) to give a mixture of **19**, **27**, and **28** (0.044 g, 76%, **19**:**27**:**28**=87:8:5) whose separation failed.

19: ^1H NMR ($CDCl_3$) δ=1.73 (3H, d, J=6.5 Hz, Me), 1.40—2.70 (7H, m, CH_2 and CH), 2.16 (3H, s, COMe), 5.32—5.72 (2H, m, =CH), and 6.02 (1H, d, J=16.0 Hz, 1-CH=CHMe); ^{13}C NMR ($CDCl_3$) δ=18.18 (q, Me), 24.24, 24.71, 27.41 (each t, CH_2), 28.00 (q, COMe), 47.59 (d, 4-C), 122.36, 124.48, 134.01 (each d), 135.54 (s, 1-C), and 211.66 (s, COMe).

27+**28**: ^1H NMR ($CDCl_3$) δ=1.73 (d, J=6.5 Hz, Me), 1.40—2.70 (m, CH_2 and CH), 2.17 (s, COMe), 4.98 (m, =CH_2), and 5.32—5.72 (m, =CH).

Reaction of 22 with DBU Leading to 29. A mixture of **22** (0.092 g, 0.22 mmol) and DBU (0.043 g, 0.28 mmol) in dry toluene (2 ml) was stirred at room temperature under nitrogen for 2 h. The mixture was chromatographed over silica gel with hexane-ethyl acetate (3:1) to give **29** (0.051 g, 56%): Pale yellow needles (ethanol); mp 122—124 °C; IR (KBr) 1670, 1595, 1185, 1170, 885, 760, and 710 cm^{-1}; ^1H NMR ($CDCl_3$) δ=1.43 (3H, d, J=6.0 Hz, Me), 2.04 (3H, s, COMe), 2.96 (2H, d, J=6.5 Hz, CH_2), 4.78 (1H, tq, J=6.0 and 6.5 Hz, CHOTs), 6.96 (2H, d, J=8.0 Hz, ArH), 7.32—7.42, 7.68—7.86 (each 3H, m, ArH), 8.00 (1H, d, J=8.0 Hz, ArH), and 8.10—8.36 (2H, m, ArH); MS *m/z* (rel. intensity, %) 420 (M^+, 5), 248 (38), and 91 (base peak).

Found: C, 68.64; H, 4.91%. Calcd for $C_{24}H_{20}O_5S$: C, 68.56; H, 4.79%.

Reaction of 10 with 8 Leading to 12. A mixture of **10** (purity 91%, 0.042 g, 0.14 mmol) and **8** (0.027 g, 0.16 mmol) in dry benzene (1 ml) was stirred at room temperature for 20 h. The solvent was evaporated in vacuo and the residue was chromatographed over silica gel with hexane-ethyl acetate (1:1) to afford **12** (0.049 g, 78%) whose spectral data were shown above.

Reaction of 10 with 13 Leading to 30 and 31. A mixture of **10** (purity 91%, 0.102 g, 0.35 mmol) and **13** (0.108 g, 0.76 mmol) in dry benzene (3 ml) was refluxed under nitrogen for 60 h. The solvent was evaporated in vacuo and the residue was chromatographed over silica gel using hexane-ethyl acetate (2:1) to provide **30** (0.112 g, 79%) and then **31** (0.012 g, 8%).

30: Colorless needles (ethanol); mp 177—178 °C; IR (KBr) 1775, 1735, 1710, 1375, and 795 cm^{-1}; ^1H NMR ($CDCl_3$) δ=1.22 (3H, d, J=7.0 Hz, Me), 1.32—1.66, 1.92—2.26 (each 1H, m, CH_2), 2.64—3.32 (6H, m, CH_2 and CH), 3.76 (6H, s, COOMe×2), 5.55 (1H, dd, J_{5-6}=4.0 and J_{5-8a}=1.5 Hz, 5-H), and 7.10—7.56 (5H, m, Ph); ^{13}C NMR ($CDCl_3$) δ=21.83 (q, Me), 30.94 (t, 9-C), 33.41 (d, CH), 35.00 (t, 4-C), 36.53, 40.71, 42.00 (each d, CH), 52.30 (q, 2×C, COOMe), 124.06 (d), 126.36 (d, 2×C), 128.53 (d), 129.24 (d, 2×C), 131.66, 132.13, 133.42, 140.18 (each s), 167.31, 168.65 (each s, COOMe), 176.95, and 177.83 (each s, CON); MS *m/z* (rel. intensity, %) 409 (M^+, 2), 377 (22), and 362 (base peak).

Found: C, 67.29; H, 5.61; N, 3.58%. Calcd for $C_{23}H_{23}NO_6$: C, 67.47; H, 5.66; N, 3.42%.

31: Colorless solid; mp 63—65 °C; IR (KBr) 1775, 1735, and 1710 cm^{-1}; ^1H NMR ($CDCl_3$) δ=1.14 (3H, d, J=7.0 Hz, Me), 1.10—1.40, 2.26—2.56 (each 1H, m, CH_2), 2.68—3.40 (6H, m, CH_2 and CH), 3.76 (6H, s, COOMe×2), 5.56 (1H, dd, J_{5-6}=3.5 and J_{5-8a}=1.5 Hz, 5-H), and 7.10—7.56 (5H, m, Ph); MS *m/z* (rel. intensity, %) 409 (M^+, 3), 377 (49), and 362 (base peak).

Found: *m/z* 409.1517. Calcd for $C_{23}H_{23}NO_6$: M, 409.1524.

Reaction of 10 with 32 Leading to 33—35. A mixture of **10** (purity 91%, 0.152 g, 0.52 mmol) and **32** (0.24 g, 2.85 mmol) in dry benzene (3 ml) was refluxed under nitrogen for 40 h. The

solvent was evaporated in vacuo and the residue was chromatographed over silica gel using hexane-ethyl acetate (2:1) to give **33** (0.042 g, 23%), the mixture of **33**, **35**, **10**, **25**, and **26** (0.092 g, the isomer ratio was 26:16:40:7:3 (GLC)), and **34** (0.028 g, 15%). The isomer **35** was separated from the mixture through HPLC.

33: Colorless solid; mp 138—139 °C; IR (KBr) 1775, 1700, 1380, and 1250 cm^{-1}; ^1H NMR ($CDCl_3$) δ=1.16 (3H, d, J=7.0 Hz, Me), 1.45 (1H, dt, J_{gem}=14.5 and J_{9-8a}=J_{9-9a}=6.0 Hz, one of 9-H), 1.90—2.24 (1H, m, the other of 9-H), 2.52—3.32 (6H, m, CH_2 and CH), 3.72 (3H, s, COOMe), 5.57 (1H, m, 5-H), 6.77 (1H, d, J_{8-8a}=4.0 Hz, 8-H), and 7.16—7.56 (5H, m, Ph); MS m/z (rel. intensity, %) 351 (M^+, 3), 336 (27), 319 (35), and 304 (base peak).

Found: C, 71.95; H, 5.99; N, 4.28%. Calcd for $C_{21}H_{21}NO_4$: C, 71.78; H, 6.02; N, 3.99%.

34: Colorless solid; mp 149—151 °C; IR (KBr) 1775, 1705, 1375, and 1255 cm^{-1}; ^1H MMR ($CDCl_3$) δ=1.09 (3H, d, J=7.0 Hz, Me), 1.10—1.48 (1H, m, one of 9-H), 2.20—3.50 (7H, m, CH_2 and CH), 3.71 (3H, s, COOMe), 5.57 (1H, m, 5-H), 6.72 (1H, d, J_{8-8a}=4.0 Hz, 8-H), and 7.12—7.56 (5H, m, Ph); MS m/z (rel. intensity, %) 351 (M^+, 10), 336 (13), 319 (63), and 304 (base peak).

Found: C, 71.87; H, 6.14; N, 4.21%. Calcd for $C_{21}H_{21}NO_4$: C, 71.78; H, 6.02; N, 3.99%.

35: Colorless needles (ethyl acetate-hexane); mp 227—228 °C; IR (KBr) 1770, 1700, 1370, and 1255 cm^{-1}; ^1H NMR ($CDCl_3$) δ=1.16 (3H, d, J=7.0 Hz, Me), 1.10—1.54, 2.00—2.32 (each 1H, m, 9-H), 2.48—3.28 (6H, m, CH_2 and CH), 3.75 (3H, s, COOMe), 5.49 (1H, br s, 5-H), 6.89 (1H, dd, J_{7-6}=3.0 and J_{7-8a}=1.5 Hz, 7-H), and 7.10—7.56 (5H, m, Ph); MS m/z (rel. intensity, %) 351 (M^+, 6), 336 (38), 319 (40), and 304 (base peak).

Found: C, 71.77; H, 6.09; N, 4.16%. Calcd for $C_{21}H_{21}NO_4$: C, 71.78; H, 6.02; N, 3.99%.

Dehydrogenation of 33—35 Leading to 36 and 37. i) A mixture of **33** (0.026 g, 0.097 mmol) and chloranil (0.027 g, 0.11 mmol) in dry toluene (1 ml) was refluxed for 15 h. The toluene was evaporated in vacuo and the residue was chromatographed over silica gel with hexane-ethyl acetate (2:1) to afford **36** (0.025 g, 97%). ii) The isomer **34** was readily dehydrogenated giving **36** when exposed to the air. iii) A mixture of **35** (0.02 g, 0.057 mmol) and chloranil (0.021 g, 0.085 mmol) in dry toluene (1 ml) was refluxed for 15 h. The same procedure as mentioned above gave **37** (0.016 g, 80%).

36: Colorless prisms (ethanol); mp 170—171 °C; IR (KBr) 1770, 1700, 1390, and 1265 cm^{-1}; ^1H NMR ($CDCl_3$) δ=2.53 (3H, s, Me), 2.70—3.50 (6H, m, CH_2 and CH), 3.84 (3H, s, COOMe), 6.76—6.92 (2H, m, Ph), 7.04 (1H, s, 8-H), 7.20—7.40 (3H, m, Ph), and 7.72 (1H, s, 5-H); MS m/z (rel. intensity, %) 349 (M^+, 5), 318 (39), and 317 (base peak).

Found: C, 72.14; H, 5.47; N, 4.11%. Calcd for $C_{21}H_{19}NO_4$: C, 72.19; H, 5.48; N, 4.01%.

37: Colorless solid; mp 58—60 °C; IR (KBr) 1770 and 1700 cm^{-1}; ^1H NMR ($CDCl_3$) δ=2.30 (3H, s, Me), 2.80—3.48 (5H, m, CH_2 and CH), 3.86 (3H, s, COOMe), 4.06 (1H, dd, J_{gem}=15.0 and J_{4-3a}=3.0 Hz, one of 4-H), 6.70—6.96 (2H, m, Ph), 7.11 (1H, br s, 8-H), 7.20—7.40 (3H, m, Ph), and 7.56 (1H, br s, 6-H); MS m/z (rel. intensity, %) 349 (M^+, 18), 318 (31), and 317 (base peak).

Found: m/z 349.1306. Calcd for $C_{21}H_{19}NO_4$: M, 349.1313.

Reaction of 10 with 16 Leading to 38. To a solution of **16** (0.074 ml, 0.9 ml) in dry toluene (1 ml) was added ethylaluminum dichloride (1 M solution in hexane, 0.9 ml, 0.9 mmol) at −70 °C. After 0.5 h, **10** (purity 91 %, 0.237 g, 0.81 mmol) in toluene (1 ml) was added and the mixture was stirred at the same temperature for 2 h. Usual work-up with aqueous sodium hydrogen carbonate was followed by the extraction with benzene (10 ml×2). The benzene was dried over magnesium sulfate and evaporated in vacuo. The residue was chromatographed over silica gel with hexane-ethyl acetate (2:1) to give **38** (0.211 g, 78%): Colorless solid; mp 111—112 °C; IR (KBr) 1770 and 1700 cm^{-1}; ^1H NMR ($CDCl_3$) δ=0.78 (3H, d, J=7.0 Hz, Me), 1.10—3.28 (11H, m, CH_2 and CH), 2.10 (3H, s, COMe), 5.48 (1H, dd, J_{5-6}=4.0 and J_{5-8a}=2.0 Hz, 5-H), and 7.10—7.52 (5H, m, Ph); ^{13}C NMR ($CDCl_3$) δ=16.47 (q, Me), 25.65 (t), 28.35 (q, COMe), 29.01, 29.77 (each t), 31.00, 33.36, 39.41, 39.71 (each d), 51.36 (d, 7-C), 126.42 (d, 2×C), 127.95, 128.48 (each d), 129.13 (d, 2×C), 132.25, 134.18 (each s), 178.89 (s, 2×C, COOMe), and 210.31 (s, COMe); MS m/z (rel. intensity, %) 337 (M^+, base peak), 319 (42), 295 (65), 294 (99), 91 (54), and 77 (30).

Found: C, 74.88; H, 6.94; N, 4.40%. Calcd for $C_{21}H_{23}NO_3$: C, 74.75; H, 6.87; N, 4.15%.

We are grateful to Toyo Soda Manufactural Company for a generous sample of chloroprene.

References

1) O. Tsuge, E. Wada, and S. Kanemasa, *Chem. Lett.*, **1983**, 239.

2) O. Tsuge, S. Kanemasa, H. Sakoh, and E. Wada, *Chem. Lett.*, **1984**, 273.

3) S. Kanemasa, H. Sakoh, E. Wada, and O. Tsuge, *Bull. Chem. Soc. Jpn.*, **58**, 3312 (1985).

4) O. Tsuge, E. Wada, and S. Kanemasa, *Chem. Lett.*, **1983**, 1525.

5) O. Tsuge, S. Kanemasa, H. Sakoh, and E. Wada, *Chem. Lett.*, **1984**, 277.

6) O. Tsuge, E. Wada, S. Kanemasa, and H. Sakoh, *Bull. Chem. Soc. Jpn.*, **57**, 3221 (1984).

7) O. Tsuge, S. Kanemasa, H. Sakoh, and E. Wada, *Bull. Chem. Soc. Jpn.*, **57**, 3234 (1984).

8) O. Tsuge, E. Wada, S. Kanemasa, and H. Sakoh, *Chem. Lett.*, **1984**, 469.

9) O. Tsuge, E. Wada, S. Kanemasa, and H. Sakoh, *Chem. Lett.*, **1984**, 709.

10) The trienes **D** and **E** can be synthesized by the reaction of the Grignard reagent of chloroprene with 2-bromovinyl ethyl ether and 2-bromovinyl phenyl sulfide in the presence of Ni(dppp)Cl_2 at −78 °C to room temperature, respectively. They can be only isolated as solution in THF because of the ready polymerization. They react with *N*-methylmaleimide to give the corresponding bis-cycloadducts as single isomers (Our unpublished results).

11) S. Nunomoto and Y. Yamashita, *J. Org. Chem.*, **44**, 4788 (1979).

12) GLC analysis of this mixture showed only two peaks in the ratio 90:10. However, cycloaddition of this mixture with *N*-phenylmaleimide (**8**) produced bis-cycloadducts **11** and **12** as major products and two monocycloadducts of **4** and **5** (GLC and ^1H NMR).

13) Stereostructures of **9**, **11**, and **12** can not be determined only on the basis of the spectral data. Endo structure of **9** and that of the second six-membered ring of **12** are based on

a rule that cyclic dienophiles undergo highly *endo*-selective cycloaddition (J. Sauer, *Angew. Chem. internat. Edit.*, **6**, 16 (1967)). As **11** and **12** are the only stereoisomers formed, the second molecule of **8** is most likely to have attacked **9** and **10** from the less hindered side of diene, opposite to the preexistent fused maleimide ring. Similar stereoselectivity has been previously reported (Ref. 6).

14) Endo and exo structures of **17** and **18** were confirmed on the basis of chemical shifts of the ring methyl and also of the fact that **17** was mainly obtained in the Lewis acid-catalyzed cycloaddition (T. Inukai and T. Kojima, *J. Org. Chem.*, **31**, 2032 (1966)).

15) An example of Lewis acid-catalyzed Diels-Alder reaction: T. Inukai and T. Kojima, *J. Org. Chem.*, **32**, 869 (1967).

16) The ratio between **23** and **24** was determined by GLC analysis after their conversion into the corresponding dienes. The para:meta ration in the Diels-Alder reaction of 2-methyl-1,3-butadiene with **16** was reported as 71:29 (E. F. Lutz and G. M. Bailey, *J. Am. Chem. Soc.*, **86**, 3899 (1964)).

17) Regiochemistry of **23** and **24** was determined by the fact that **23** is the only regioisomer formed in the Lewis acid-catalyzed Diels-Alder reaction of **2** and **16**.

18) When **10** containing 9% of **25** and **26** is subjected to a Diels-Alder cycloaddition, **25** and **26** as contaminants can be recovered unchanged. It is known that cis 1-substituted 1,3-diene is much less reactive than the trans isomer (See the reference in Ref. 13).

19) Such dehydrogenation which presumably took place via an enol intermediate can be seen in a literature (K. Hayakawa, K. Ueyama, and K. Kanematsu, *J. Org. Chem.*, **50**, 1963 (1985)).

 © 1986 The Chemical Society of Japan Bull. Chem. Soc. Jpn., 59, 1877—1886 (1986)

Formation and Identification of Aryldiazenyl Radicals Using the ESR Technique[1)]

Tadashi SUEHIRO,* Seiichi MASUDA, Takaaki TASHIRO, Ryuichi NAKAUSA, Masamichi TAGUCHI, Akemi KOIKE, and Anton RIEKER†

Department of Chemistry, Faculty of Sciences, Gakushuin University, Mejiro, Toshima-ku, Tokyo 171
†Institut für Organische Chemie der Universität Tübingen, Auf der Morgenstelle 18, Tübingen D-7400, West Germany
(Received November 30, 1985)

Aryldiazenyl radicals were formed at −104 — −116 °C by photoirradiation of cyclopropane solutions of 1-aryl-2-(arylthio)diazenes and of 1-aryl-3,3-dimethyltriazenes in the presence or absence of olefins, and also by irradiation of cyclopropane solutions of substituted 1,2,3-benzothiadiazoles in the presence of di-*t*-butyl peroxide. The ESR spectra were analyzed and the hfs constants were assigned by reference to the spectra of methyl, ^{2}H, and ^{15}N-labelled aryldiazenyl radicals and to the results of CINDO calculations. Aryldiazenyl radicals are relatively persistent and the -N=N group rotates about the C-N^{2} bond axis. The preferred conformations of the radicals were considered.

Aryldiazenyl radicals have been the subject of much interest in organic chemistry during the last decades.[2)] The appearence of the radicals in transient states was suggested by chemical facts such as the formation of compounds derived from the aryldiazenyl radicals,[3,4)] and of isomeric azo compounds.[5)] The most conclusive evidence for the radicals was the isolation of phenylazotriphenylmethane in the thermolysis of α-(phenylazo)cumene in the presence of triphenylmethyl radicals.[6)] Aryldiazenyl radicals have, however, not yet been directly characterized by any spectroscopic method, and the physical and chemical properties of the radicals have remained unclear. We report here on the detection and identification of aryldiazenyl radicals by the ESR method and on their possible conformations by reference to theoretical calculation of the hfs constants.

Results and Discussion

(1) Formation and Detection of Aryldiazenyl Radicals. Cyclopropane solutions of ortho-, meta-, and para-substituted 1-phenyl-2-(arylthio)diazenes were irradiated in the ESR cavity using a Xe lamp (1 kW) through a filter of 420 nm at −104 — −116 °C to afford radicals which will be later identified as substituted phenyldiazenyl radicals (Reaction 1). From 1-(4-methylphenyl)- and 1-(4-methoxyphenyl)-3,3-dimethyltriazenes we obtained radicals with the same constitution as those from diazenes, more conveniently by using a N_2 Laser (Molectron UV-14) than by using a Xe lamp (Reaction 2). Starting with 1-(4-dimethylaminophenyl)-3,3-dimethyltriazene we could not observe the ESR spectrum of the corresponding radicals, because of its poor solubility in cyclopropane at low temperatures. From these two kinds of starting compounds we obtained the spectra of the same nitrogen-centered radicals. This confirmed that the radicals we observed were indeed the primary radicals formed by the photolysis of diazenes and triazenes, and not the radicals formed secondarily by any radical addition reaction to diazenes or triazenes. This conclusion was further supported by experiments using neat or mixed solvents of olefins and cyclopropane for 1-aryl-2-(arylthio)diazenes: Olefinic solvents such as 1-butene, *cis*-2-butene, and propene did not cause any change in the ESR spectra observed (Reaction 1). Olefinic solvents caused some acceleration in the decay rate of the aryldiazenyl radicals, on which we will reported in the next paper.

The third type of starting compounds for the nitrogen-centered radicals of the same sort were substituted 1,2,3-benzothiadiazoles, whose thiadiazole rings were opened photochemically by using di-*t*-butyl peroxide (Reaction 3).

$$\underset{(R=H,\ 4\text{-}Bu^t)}{Ar\text{–}N=N\text{–}S\text{–}C_6H_4\text{–}R} \xrightarrow[(CH_2)_3+R^1CH=CHR^2]{h\nu} Ar\text{–}N^2=N^1\cdot + \cdot S\text{–}C_6H_4\text{–}R \qquad (1)$$

$$Ar\text{–}N=N\text{–}N(CH_3)_2 \xrightarrow[(CH_2)_3]{h\nu} Ar\text{–}N=N\cdot + \cdot N(CH_3)_2 \qquad (2)$$

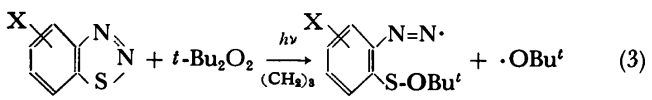

(3)

The hyperfine splitting constants of the radicals observed during these reactions together with *g*-values are listed in Table 1.

Photolysis of 1-(4-*t*-butylphenylthio)-2-phenyldiazene (No. 9) gave an ESR spectrum of nine 1:2:1 triplets (1.2 G†) in a pattern of 1:1:1 triplet (22.5 G) of 1:1:1 triplets (9.45 G). This pattern of triplet of triplets, together with the low *g*-value of 2.0002, is the characteristic feature of the spectra of all the radicals we observed in the reactions 1, 2, and 3. In the following, we are going to identify them as aryldiazenyl radicals by examining the reactions of their formation and by analyzing the ESR spectra.

(2) Identification of the Aryldiazenyl Radicals. The pattern of triplet (1:1:1) of triplets (1:1:1) characteristic of the ESR spectra obtained in this work, shows that the

†1 G=1×10^{-4} T.

Table 1. Hyperfine Splitting Constants of Aryldiazenyl Radicals[a)]
$Ar-N^2=N^1\cdot$

No.	Starting Compound of Ar-N=N·	g-Value (±0.0001)	Hfs. Const./G[b)]			(x-H)[c)]
			a_{N^1}	a_{N^2}	a_H	
1	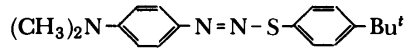	2.0005	9.4$_6$	22.0	1.0$_0$	(3,5-H)
2	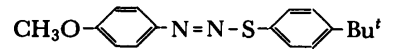	2.0004	9.6$_0$	22.4	1.0$_6$	(3,5-H)
3	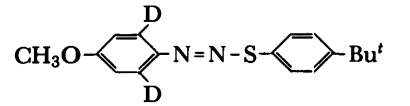	2.0004	9.4$_8$	22.5	1.1$_0$	(3,5-H)
4	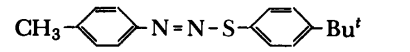	2.0004	9.3$_5$	22.7	1.1$_0$	(3,5-H)
5	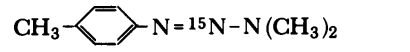	2.0004	13.4$_5$	23.0	1.1$_5$	(3,5-H)
6	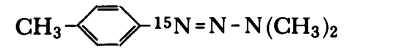	2.0003	9.6$_5$	31.6	1.1$_5$	(3,5-H)
7	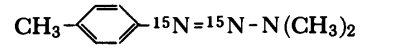	2.0002	13.3$_0$	31.4	1.2$_0$	(3,5-H)
8	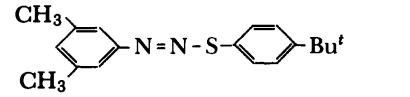	2.0003	9.4$_5$	22.7	None	
9	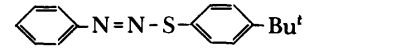	2.0002	9.4$_5$	22.5	1.2$_0$	(3,5-H)
10	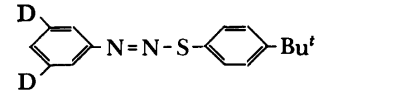	2.0003	9.4$_5$	22.9	None	
11	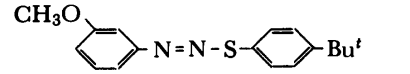	2.0004	9.5$_0$	22.8	1.1$_5$	(5-H)
12	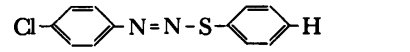	2.0003	9.1$_3$	22.8	1.2$_0$	(3,5-H)
13	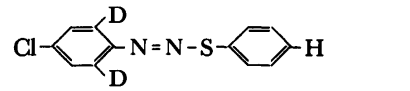	2.0004	9.3$_5$	23.1	1.0$_0$	(3,5-H)
14	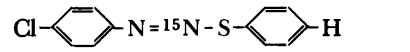	2.0002	13.3$_0$	23.0	1.1$_0$	(3,5-H)
15	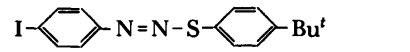	2.0006	9.4$_8$	23.0	1.0$_4$	(3,5-H)
16	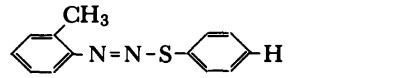	2.0002	9.5$_0$	23.0	1.8$_5$	(5-H)
17	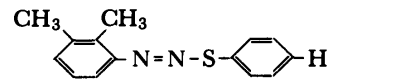	2.0003	9.2$_5$	23.1	2.0$_0$ 0.4$_7$	(5-H) (6-H)
18	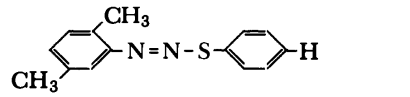	2.0003	9.3$_5$	22.8	None	
19	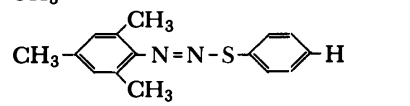	2.0001	9.7$_0$	22.0	0.7$_5$	(2,6-Me-H)
20	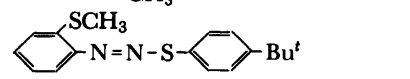	2.0004	9.4$_0$	22.8	1.2$_2$ 0.7$_0$	(5-H) (3-H)
21	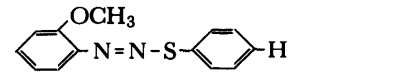	2.0005	9.7$_5$	24.5	1.3$_0$ 0.5$_0$	(5-H) (3-H)
22	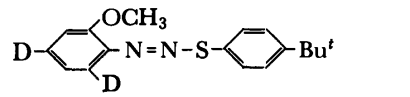	2.0003	9.6$_0$	24.3	1.3$_5$ 0.6$_0$	(5-H) (3-H)
23	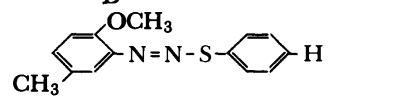	2.0002	9.7$_5$	24.5	0.5$_3$	(3-H)

Table 1. (Continued)

No.	Starting Compound of Ar-N=N·	g-Value (±0.0001)	Hfs. Const./G[b]			(x-H)[c]
			a_{N1}	a_{N2}	a_H	
24	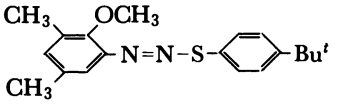	2.0004	9.5$_8$	22.8	None	
25	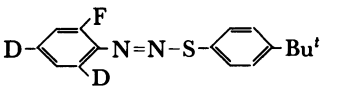	2.0003	9.6$_0$	25.7	0.9$_6$ 0.4$_8$	(5-H) (3-H) a_F:1.4$_4$
26	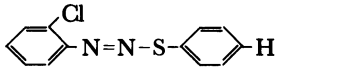	2.0006	9.3$_8$	25.3	1.6$_5$	(5-H)
27	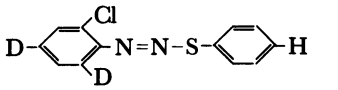	2.0008	9.3$_5$	25.4	1.7$_4$	(5-H)
28	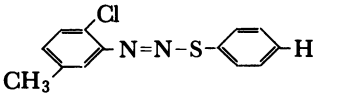	2.0007	9.6$_0$	25.5	None	
29	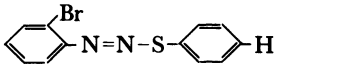	2.0024	9.4$_5$	25.6	1.9$_0$	(5-H)
30	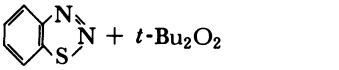	2.0002	9.3$_2$	20.9	1.3$_2$	(3-H)
31	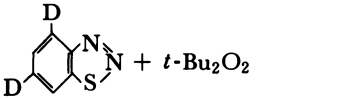	2.0002	9.3$_5$	20.8	1.3$_0$	(3-H)
32	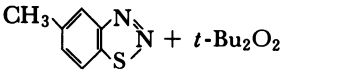	2.0002	9.2$_0$	21.0	1.3$_4$	(3-H)

a) The ESR spectra of (perdeuterio-, 2-F-, 4-Br-, 3- and 4-$CH_3C(O)$-, 3- and 4-NC-, 4-$CH_3OC(O)$-, and 5-CH_3-2-CH_3S-phenyl)diazenyl radicals showed the same pattern as those in Table 1 and the spectra were in accordance with the discussions in this report. b) 1 Gauss=1×10^{-4} T. c) x denotes the position of the hydrogen atom on the benzene ring which gives rise to the hfs constant a_H.

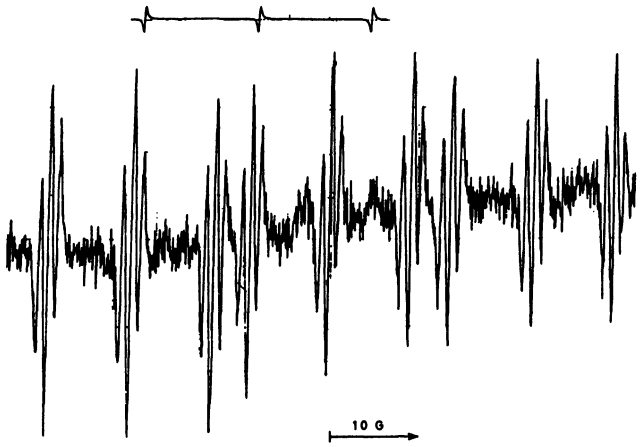

Fig. 1. ESR spectrum of (4-chloro-2,6-dideuteriophenyl)-diazenyl radical.

Fig. 2. ESR spectrum of (3-methoxyphenyl)diazenyl radical.

unpaired electron is coupled to two ^{14}N nuclei. This is further proved by the specific ^{15}N-labelling discussed below. The large splitting constants point to nitrogen centered radicals as expected for aryldiazenyls.

The additional small coupling of 0.5 to 2.0 G must then be ascribed to at least some of the aryl ring protons. In order to identify these protons, we compared the ESR spectra of specifically substituted or deuterated species.

Substitution of hydrogen-4 of the phenyl group by methoxyl (from No. 9 to No. 2) and by chlorine (No. 12), and further substitution of hydrogen-2 and -6 by deuterium (Nos. 3 and 13) did not cause any change of the 1:2:1 triplets, attributed to hydrogen hfs. (Fig. 1) In the case of 1-(4-*t*-butylphenylthio)-2-(3-methoxyphenyl)diazene (No. 11) the spectrum pattern was, however, converted into nine doublets (1.15 G). (Fig. 2)

1-(4-*t*-Butylphenylthio)-2-(3,5-dimethylphenyl)diazene (No. 8, Fig. 3) and 1-(4-*t*-butylphenylthio)-2-(3,5-dideuteriophenyl)diazene (No. 10) both gave nine singlets

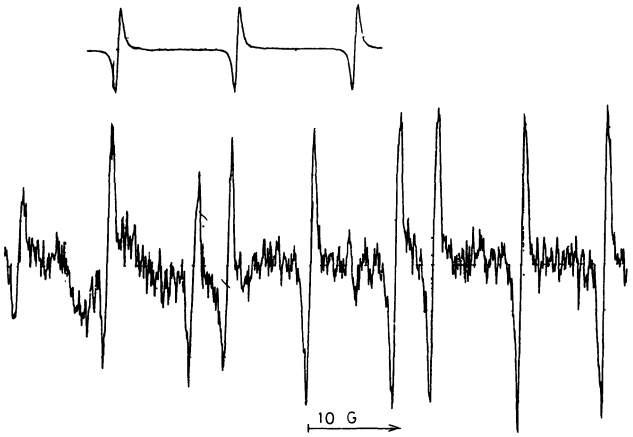

Fig. 3. ESR spectrum of (3,5-dimethylphenyl)diazenyl radical.

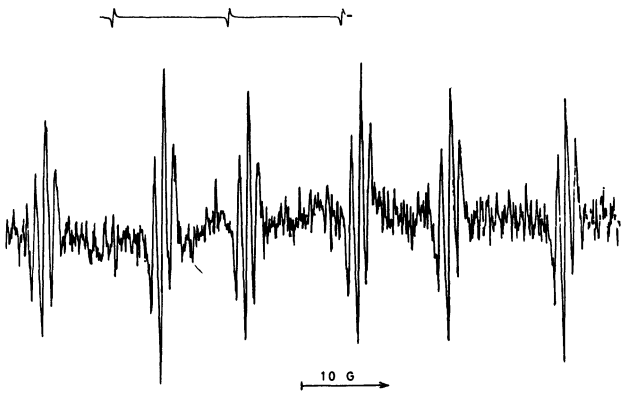

Fig. 4. ESR spectrum of (4-chlorophenyl)diazenyl-1-^{15}N radical.

in a pattern of 1:1:1 triplet (22.7 and 22.9 G, respectively) of 1:1:1 triplets (9.45 and 9.45 G, respectively). The successive disappearence of the hydrogen hfs from No. 9 to 11 to Nos. 8 and 10 proves that the hfs results from the meta hydrogens of the aryl group.

When 2-^{14}N of 1-(4-chlorophenyl)-2-(phenylthio)diazene was replaced by ^{15}N via diazotization of chloroaniline using sodium nitrite-^{15}N in the preparation of the diazene, the pattern of the ESR spectrum of the nitrogen nuclei changed from a triplet of triplets into a triplet of doublets: 1-(4-Chlorophenyl)-2-(phenylthio)diazene-2-^{15}N (No. 14) gave a spectrum composed of six 1:2:1 triplets (1.1 G) in an arrangement of 1:1:1 triplet (23.0 G) of doublets (13.3 G, Fig. 4).

A similar change in the spectrum pattern due to the nitrogen isotope was observed in the experiments using ^{15}N-triazenes. If 2-^{14}N of 1-(4-methylphenyl)-3,3-dimethyltriazene was replaced by ^{15}N (No. 5), then the spectrum pattern (triplet of triplets as in the case of No. 4) changed into a 1:1:1 triplet (23.0 G) of doublets (13.45 G, Fig. 5). If on the other hand the 1-^{14}N of the original triazene was replaced by ^{15}N (No. 6), then it gave a spectrum of a doublet (31.6 G) of 1:1:1 triplets (9.65 G, Fig. 6). Triazene-1,2-$^{15}N_2$ (No. 7) gave a spectrum of a doublet (31.4 G) of doublets (13.3 G, Fig. 7).

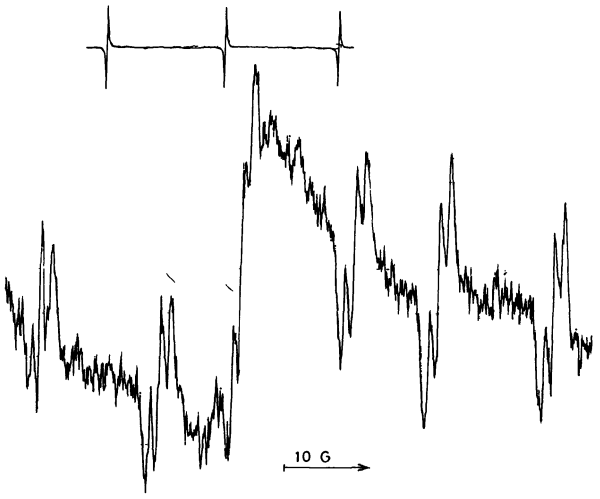

Fig. 5. ESR spectrum of (4-methylphenyl)diazenyl-1-^{15}N radical.

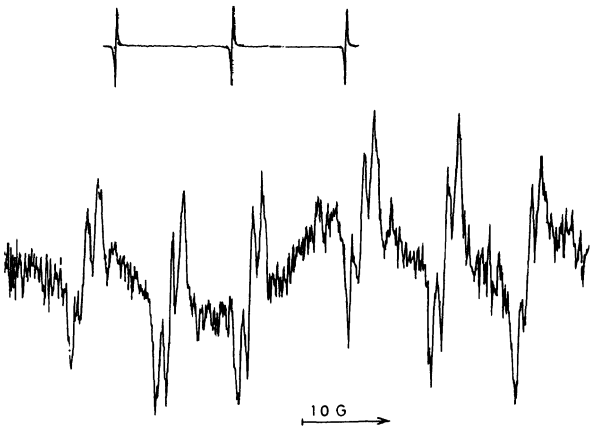

Fig. 6. ESR spectrum of (4-methylphenyl)diazenyl-2-^{15}N radical.

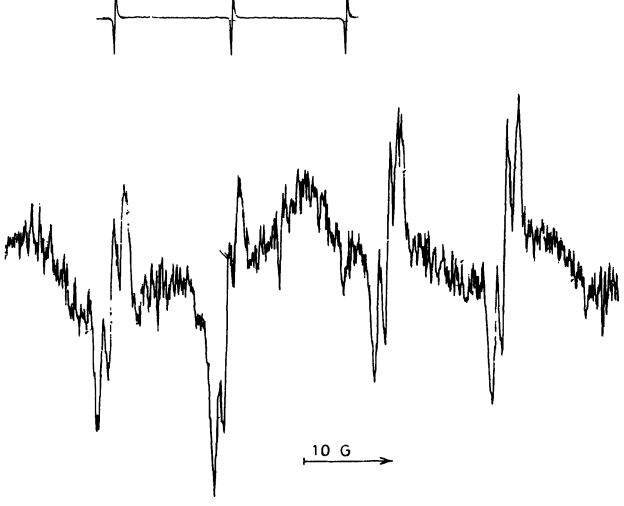

Fig. 7. ESR spectrum of (4-methylphenyl)diazenyl-1,2-$^{15}N_2$ radical.

In every case, the small triplet splitting (1.1—1.2 G), attributed to the meta ring protons, was also resolved. The ratios, 13.4 G/9.7 G and 31.5 G/23.0 G, are in

good accordance with the magnetogyric ratio of $|^{15}N/^{14}N|=1.40$. These results assigned the hfs constants of 23.0 G to 2-^{14}N and that of 9.7 G to 1-^{14}N of the aryldiazenyl radical structure.

The *g*-values of these nitrogen centered radicals were low, 2.0003 on the average, except for the *g*-value of (2-bromophenyl)diazenyl, 2.0024 (No. 29, see below). These values are lower than those of carbon radicals such as triphenylmethyl radical (2.00266[7]), aminyl radicals such as *N*-aryl-*t*-butylaminyls (2.0035[8]), and thiyl radicals derived from cysteine (2.025[9]). They are, however, very close to those of 2-butenoyl radicals, 2.0005,[10] to those of nitrosobenzene cation radicals, 2.0007,[11] and to those of benzoyl radicals, 2.0014.[12] The latter three radicals are reported to be σ-radicals.

From these remarkable ESR features (large nitrogen hfs, small *meta*-ring proton hfs, low *g*-values) we may draw two conclusions: (i) The data exclude the possibility of the radicals being some kind of *N*-centered radicals such as 2-substituted 2-(arylthio)-1-phenylhydrazyl, Ar-S-N(X)-$\dot{N}$-C_6H_5, because the hydrazyl radicals should have a *g*-value of about 2.0035, as high as that of phenylaminyl radicals.[8] Moreover, phenylaminyl radicals are π-radicals and afford measurable hfs constants of ortho and para hydrogens of the aryl ring, which is, however, not the case with the present radicals. The possibility that they are 2-substituted 1-(arylthio)-2-phenylhydrazyl radicals, C_6H_5-N(X)-$\dot{N}$-S-Ar, is also very small, because arylthioaminyl radicals should have a *g*-value of ca. 2.006,[13] a high value due to the conjugation of the nitrogen radical center with the arylthio group. Arylthioaminyl radicals should also give appreciable hfs constants of ortho and para hydrogens of the arylthio group, which in our case was not detected, on substitution of the 4-*t*-butyl group by hydrogen.

The assignment of the structure of hydrazyl radicals as those cited above to our nitrogen centered radicals can also be excluded if we consider the reaction conditions of radical formation in olefinic solvents, Reaction 1. Finally, such radicals should not be formed from triazenes, Reaction 2. (ii) The low *g*-values of the aryldiazenyl radicals can be explained by assuming a σ-radical structure.

The relatively high *g*-value of 2.0024 for the (2-bromophenyl)diazenyl (No. 29), contrary to the *g*-value of 2.0006 for the (4-iodophenyl)diazenyl radical (No. 15), is remarkable. The very small increase in the *g*-value for the (4-iodophenyl)diazenyl, (as compared to Nos. 9 and 12), thus gives evidence for a very small spin density at the 4-position of the phenyl group because of the σ-radical nature. The *g*-value of 2.0024 of (2-bromophenyl)diazenyl may also be an indication of a through-space interaction between bromine and the radical center. (2-Chlorophenyl)diazenyl radicals (Nos. 26—28) showed a much smaller increase in *g*-values, to ca. 2.0007. From 1-(4-*t*-butylphenylthio)-2-(2-iodophenyl)diazene we could not observe any definitely interpretable spectrum.

Phenyldiazenyl radical (No. 9), as already mentioned, revealed hfs due to the meta hydrogens, and not to the ortho and para hydrogens. Furthermore, methyl substitution for the meta hydrogens completely suppressed the original hydrogen hfs (No. 8). This fact is not generally true for π-radicals, and also gives support for the σ-radical nature of aryldiazenyl radicals.

(2,4,6-Trimethylphenyl)diazenyl radical (No. 19), on the other hand, revealed a hydrogen hfs which was ascribed to the protons of the ortho methyl groups. A similar methyl-hydrogen hfs was reported for 2,4,6-trimethylbenzenesulfonyl radicals.[14] (See discussion on page 1883.) Based on the chemical methods of formation, Reactions 1—3, and on the analysis of the ESR spectra observed, we concluded that the radicals obtained were aryldiazenyl σ-radicals.

Apparently, two groups of *ortho*-substituted phenyldiazenyl radicals exist, as based on the hydrogen hfs analysis: 1) (2-Substituted phenyl)diazenyl radicals showing two different hfs constants of the meta hydrogens, to which (2-fluoro-, 2-methoxy-, and 2-methylthiophenyl)diazenyl radicals belong, and 2) (2-substituted phenyl)diazenyl radicals revealing only one hydrogen hfs constant of hydrogen-5, to which (2-methyl-, 2-chloro-, and 2-bromophenyl)diazenyl radicals belong.

(2-Methoxyphenyl)diazenyl radical of group 1) showed hfs constants of 0.50 G for hydrogen-3 and of 1.30 G for hydrogen-5, and the assignment was confirmed by experiments Nos. 22—24. The hfs constants of (2-fluoro- and 2-methylthiophenyl)diazenyl radicals were assigned in analogy to (2-methoxyphenyl)diazenyl radical ($a_{H-5}>a_{H-3}$) and partly supported by experiments.*) In the case of (2-fluorophenyl)diazenyl, the highest non-nitrogen hfs constant observed was attributed to fluorine, based on the calculated values.

(2-Methyl- and 2-chlorophenyl)diazenyl radicals of group 2) revealed only one hydrogen hfs constant each, 1.85 and 1.65 G, respectively (Nos. 16 and 26), and the assignments were based on the experiments Nos. 18 and 28. The hydrogen hfs of (2-bromophenyl)diazenyl radical was assigned to hydrogen-5 in analogy to (2-chlorophenyl)diazenyl radical. Hydrogen hfs constants of some representative aryldiazenyl radicals are reproduced in Fig. 8.

(3) Possible Conformations of Aryldiazenyl Radicals. a) A Model of Rotation of the N=N Group about the C-N^2 Bond Axis, with a Preference of Staying in a Position out of the Plane of the Benzene Ring: Phenyldiazenyl radicals are very similar to benzoyl radicals, as regards σ-radical character and hydrogen hfs. In order to obtain a qualitative picture

*) (2-Fluorophenyl)diazenyl radical gave the same ESR spectrum as that of (2-fluoro-4,6-dideuteriophenyl)diazenyl (No. 25). The assignment of 1.22 G to hydrogen-5 for (2-methylthiophenyl)diazenyl was supported by comparison with (5-methyl-2-methylthiophenyl)diazenyl radical (g= 2.0002, a_{H-3}=0.50 G).

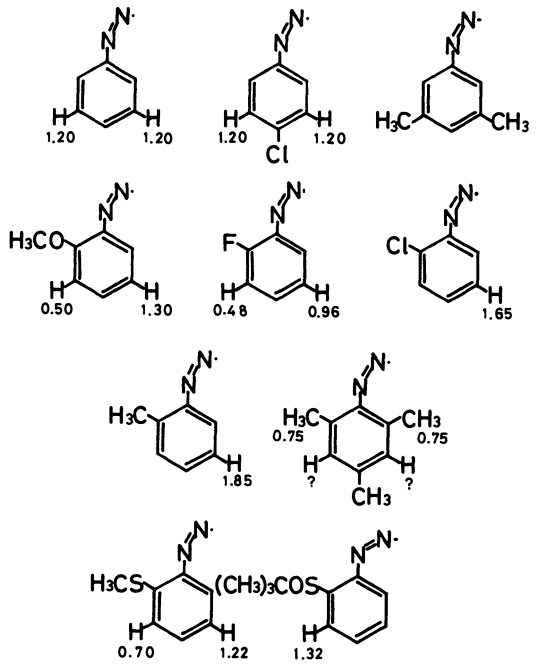

Fig. 8. Hyperfine splitting constants of aryldiazenyl radicals.

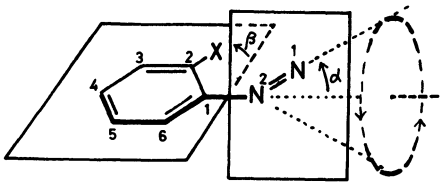

Fig. 9. Conformation of aryldiazenyl radicals with rotating N=N group about the C-N^2 bond axis. X stands for the substituent group.

of the conformation of aryldiazenyl radicals we performed INDO calculations[15] on phenyldiazenyl radical and on (2-fluoro-, 2-methyl-, 2-methoxy-, and 2,6-dimethylphenyl)diazenyl radicals. These calculations suggested that phenyldiazenyl radicals have conformations in which the azo group rotates about the C-N^2 bond axis with a preference in the "vertical" form: The N^1 atom of the radical is raised out of the plane of the benzene ring, forming an angle between the bonds C-N^2 and ^{1}N-N^2 (angle α, Fig. 9) of 40°, and an angle between the plane of the benzene ring and the plane C-N^2-N^1 (angle β) of 90°.

In the INDO calculations we have, first of all, searched for a conformation of the minimum total energy, and it was the vertical form for phenyldiazenyl radical with the total energy (T.E.)=−67.017750 a.u. The calculated highest hfs constants 0.80 G, of hydrogen-3 and -5 for this vertical conformation were in fairly good agreement with the symmetric spin distribution observed in the ESR experiments ($a_{H-3}=a_{H-5}=1.20$ G).

The molecular dimensions in the vertical form were as follows: Normal benzene ring; C-N^2=1.40 Å; N^1-N^2=1.20 Å; the angle α=40°, and the angle β=90°. The bond length C-N^2 used in the calculations was that of azobenzene,[16] but the length N^1-N^2 was shortened by 0.03 Å from that of azobenzene. The angle α was decreased from 60° of azobenzene to 40°.

Table 2. Hyperfine Splitting Constants of Phenyldiazenyl Radical, Calculated by INDO Method[a] (Gauss)[b]
Ph-N^2=N^1·

β=	a_{N^1}	a_{N^2}	$a_{2\text{-H}}$	$a_{3\text{-H}}$	$a_{4\text{-H}}$	$a_{5\text{-H}}$	$a_{6\text{-H}}$
0°	5.07	20.33	0.27	1.70	0.21	−0.33	1.76
10	5.10	20.04	0.24	1.66	0.15	−0.27	1.67
20	5.13	19.43	0.18	1.59	0.01	−0.13	1.45
30	5.18	18.78	0.15	1.48	−0.13	0.03	1.24
40	5.24	18.16	0.16	1.37	−0.25	0.17	1.06
50	5.30	17.61	0.20	1.24	−0.34	0.31	0.90
60	5.35	17.17	0.26	1.13	−0.41	0.44	0.78
70	5.39	16.85	0.33	1.01	−0.46	0.56	0.67
80	5.40	16.72	0.40	0.91	−0.49	0.69	0.56
90	5.41	16.64	0.48	0.80	−0.50	0.80	0.48
found	9.45	22.5	—	1.20	—	1.20	—

a) Calculation was performed using α=40°, C-N^2= 1.40 Å, and N^1-N^2=1.20 Å. b) 1 Gauss=1×10^{-4} T.

Similar calculations by this method were also reported by Kasukhin and others for phenyldiazenyl radicals with a planar conformation,[17a] and by Seifert and Gerhart on a vertical conformation.[17b] Our results of INDO calculations for the vertical form affording the highest hfs constant for the hydrogen-3 and -5 differed from those of Seifert and Gerhart[17b] which revealed the highest hfs constants for 2,6-hydrogens. This difference is probably due to the different molecular dimensions used by these authors.

The calculation on a planar form with the same molecular dimensions except for β=0°, yielded a total energy higher than that of the vertical form by 4.17 kcal/mol†, and an asymmetric spin distribution over the aromatic hydrogens, as was reported by Kasukhin and others[17a] (Table 2). Since the difference between the total energies of the vertical and planar conformations was rather low, it is plausible to assume that the azo group of the phenyldiazenyl radical rotates about the C-N^2 bond axis with a high probability that it stays in the vertical form.

By using the bond lengths of phenyldiazenyl radical, we also calculated the hfs constants for the planar conformations of (2-fluoro-, 2-methyl-, 2-methoxy-, and 2,6-dimethylphenyl)diazenyl radicals with a smaller extent of variation of α. It turned out that the angle α=40° characterized the most stable planar conformation for all aryldiazenyl radicals considered. The vertical form of these aryldiazenyl radicals were found to be more stable by 2 to 4 kcal/mol than the corresponding planar conformations.

To a first approximation, these minima in T. E. sug-

† 1 cal=4.184 J.

Table 3. Hyperfine Splitting Constants of 2-Substituted Phenyldiazenyl Radicals Found and Calculated by the INDO Method and the Difference in Total Energy between Conformations[a)]

2-Substituent in Ar-N=N·	found / calcd	β°	a_{N^1}	a_{N^2}	$a_{3\text{-H}}$	$a_{4\text{-H}}$	$a_{5\text{-H}}$	$a_{6\text{-H}}$	a_X	T.E.[c)]
			Gauss[b)]							kcal[d)]/mol
2-F	f.	—	9.60	25.7	0.48	—	0.96	—	a_F: 1.44	
	c.	90	5.25	18.02	1.00	−0.57	0.79	0.63	6.78	−3.61
	c.[e)]	110	5.32	18.27	0.73	−0.51	1.00	0.48	7.01	−3.29
2-CH_3O	f.	—	9.75	24.5	0.50	—	1.30	—	—	
	c.	90	5.31	17.84	1.02	−0.53	0.82	0.55	—	−2.82
	c.[e)]	120	5.25	18.38	0.58	−0.42	1.16	0.33	—	−2.19
2-CH_3	f.	—	9.50	23.2	—	—	1.85	—	—	
	c.	90	5.40	16.59	0.74	−0.48	0.84	0.37	$a_{Me\text{-H}}$: 0.67	−3.99
	c.[e)]	150	5.18	18.67	0.01	−0.21	1.54	0.09	0.14	−1.11
2,4,6-$(CH_3)_3$	f.	—	9.70	22.0	?	—	?	—	$a_{Me\text{-H}}$: 0.75	
2,6-$(CH_3)_2$	c.[e)]	90	5.39	16.57	0.78	−0.46	0.78	—	0.68	−2.51

a) The molecular dimensions for the calculations were α=40°, C-N^2=1.40 Å, and N^1-N^1=1.20 Å. b) 1 Gauss=1×10^{-4} T. c) The difference in total energies: T.E.$_\beta$−T.E.$_{\beta=0°}$. d) 1 cal=4.184 J. e) The angle β which gave the best fit of calculated hyperfine splitting constants to the experimental data.

gest that for aryldiazenyl radicals carrying 2-fluoro, 2-methyl, 2-methoxy-, and 2,6-dimethyl substituents, the N=N group rotates about the C-N^2 bond axis. A best fit of the calculated hydrogen hfs constants and the experimental data was, however, not found in the conformation with β=90° but in a certain nonplanar form except for (2,6-dimethylphenyl)diazenyl radical (Table 3). We are not going into further discussion on the conformations of the aryldiazenyl radicals, because of the limited accuracy of our calculations. In any case, it is plausible to assume a rotation of the N=N group with energy barriers of several kcal/mol, with a preference of a certain specified conformation.

In benzoyl radical[12] and in benzenesulfonyl radicals,[14] the groups C=O and SO_2 were reported to rotate about the bond connecting them to the benzene ring. Nitrosobenzene cation radical was presumed to be in a specified conformation, holding the oxygen atom above the plane of the benzene ring at an angle β of ca. 70°.[11]

The (2,4,6-trimethylphenyl)diazenyl radical revealed a hfs of nine septes (0.75 G). This suggested a symmetrical spin distribution on the six ortho methyl hydrogens. The INDO calculations for (2,6-dimethylphenyl)diazenyl in the vertical conformation gave hfs constants of 0.68 G for the ortho methyl hydrogens and 0.78 G for the 3,5-hydrogens. Thus, the observed proton hfs may also be of the nonet type, with two signals disappearing in the wings of the spectrum due to low intensity. At present, we cannot finally decide between a septet or a nonet structure.

We do not know why (2-methylphenyl)diazenyl radical (No. 16) gave a doublet and (2-methoxyphenyl)-diazenyl (No. 21) a double doublets structure of the proton hfs. Comparison of the calculated hydrogen-3 hfs constants of these radicals in the vertical form may give some indication. The constant of (2-methoxyphenyl)diazenyl, 1.02 G, was higher than that of (2-methylphenyl)diazenyl, 0.74 G, and this higher value might lead to the experimantally observed hfs of hydrogen-3 in the methoxy compound. We could not ascribe these differences simply to the electronegativity of the substituents.

b) A Model of Planar Conformation with N^1 in the Side Opposite to the 2-Substituent, Maintaining a High Angle α: The ESR experiments Nos. 30—32 suggested that the hfs constant of (2-*t*-butoxythiophenyl)diazenyl radical resulted from hydrogen-3. In order to gain insight into this exceptional hfs, we carried out CNDO calculations on (2-methylthiophenyl)diazenyl radical as a model by varying the angle α from +80° to −80° for the planar conformations (β=0°), and also by varying α for the vertical forms (β=90°). Although the agreement of the calculated hfs constants with the experimental ones was very poor, the best fit of the hydrogen hfs in the case of (2-*t*-butoxythiophenyl)diazenyl radical was found in the conformation with α=−80° in a planar form. The results of calculations for the vertical forms were completely unsatisfactory. It is of significance here to see that the INDO calculation for the planar conformation of (2-methylphenyl)diazenyl radical with α=−80° afforded the highest hydrogen hfs constant for hydrogen-3.*)

The angle of α=−80° may be understood, if one assumes that the ring opening of the thiadiazole by the attack of a *t*-butoxyl radical on the sulfur atom is followed by the rotation of the azo group about the C-N^2 bond axis by 180° to the opposite side of the 2-*t*-butoxythio substituent, and that the repulsion between the substituent and the lone pair electrons of N^2 is very high.

Experimental

(1) Syntheses of 1-Aryl-2-(arylthio)diazenes. 1-Aryl-2-

*) The calculation on (2-methylphenyl)diazenyl radical using α=−80°, β=0°, C-N^2=1.42 Å, and N^1-N^2=1.20 Å, gave $a_{N}1$=7.89 G, $a_{N}2$=8.30 G, $a_{3\text{-H}}$=0.99 G, $a_{4\text{-H}}$=0.49 G, $a_{5\text{-H}}$=−0.15 G, and $a_{6\text{-H}}$=−0.09 G.

(arylthio)diazenes were prepared according to the method of Zwet and Kooyman[18] by the reaction between arenediazonium chloride and sodium arenethiolate at ca. −5°C, and recrystallized from methanol or ether–methanol. The diazenes prepared are listed in Table 4.

(2) Syntheses of 1,2,3-Benzothiadiazoles. 1,2,3-Benzothiadiazoles were prepared by the method of Jacobson and Janssen[20] by diazotization of 2-mercaptoanilines and purified by distillation (Table 5).

(3) Syntheses of Triazenes. 1-Aryl-3,3-dimethyltriazenes (Ar=4-tolyl, 4-methoxyphenyl) were prepared by the reaction of arenediazonium salts with dimethylamine in aqueous alkaline solution,[21] and purified by sublimation.[22,23] 1-(4-Dimethylaminophenyl)-3,3-dimethyltriazene was obtained by a variant of this method, described by Rondestvedt and Davis.[24] However, the yield was only poor, and the compound decomposed slowly even at room temperature. The triazenes prepared are listed in Table 6.

(4) Isotope-Labelling Experiment. a) Deuterium-Labelling: The deuterium-labelled compounds were prepared by heating the parent anilines to 100°C in an excess of deuterium oxide (Merck UVASOL, *d*-99.75%)–deuterium chloride for 24 h whereupon the process was repeated 3 times each with a freshly prepared mixture of deuterium oxide–deuterium chloride.

The deuterium exchange was monitored and determined by ^{1}H NMR spectroscopy of aniline deuteriochloride in deuterium oxide.

Diazotization of the deuteriated aniline was also performed in deuterium oxide–deuterium chloride.

For the preparation of 1-(4-*t*-butylphenylthio)-2-(3,5-dideuteriophenyl)diazene, we used 3,5-dideuterioaniline (*d*-98%), obtained from perdeuterioaniline (Merck Co.) by ^{1}H-exchange reaction using H_2O–hydrogen chloride.

b) ^{15}N-Labelling: For the preparation of 1-(4-chlorophenyl)-2-(phenylthio)diazene-2-^{15}N, we diazotizated 4-chloroaniline using sodium nitrite-^{15}N (Prochem Co., ^{15}N-95%).

The ^{15}N-labelled triazenes (Nos. 5—7) were prepared according to the general procedure[21,22] using the respective ^{15}N-labelled starting materials (sodium nitrite-^{15}N, *p*-toluidine-^{15}N, ^{15}N-95%).

(5) ESR Experiment. ESR spectra were taken on a Varian E-109E spectrometer at −104 — −116°C. About 50 mg of azo sulfide and 2 ml of cyclopropane were sealed in vac. in a Pyrex tube (ϕ 10 mm), carrying a quartz side arm (ϕ 4 mm). The irradiation of the sample was carried out by using a Xe lamp (1 kW) of USHIO Electric Co. Type UXL-1000D-0, Pyrex cylinder lens, a filter glass (420 nm), and a 10 cm water cell filter. Triazenes were irradiated with a Molectron UV-14 and a quartz cylinder lens.

1,2,3-Benzothiadiazoles were illuminated using a Xe lamp and a quartz lens without 420 nm filter in the presence of di-*t*-butyl peroxide, ca. 200 mg.

The *g*-values were determined by reference to the *g*-value of 2.0054[25] of potassium nitrosodisulfonate in a slightly ammoniacal solution.

(6) CINDO Calculations. We employed the standard CNDO and INDO programs[15] on a MELCOM-COSMO 700

Table 4. 1-Aryl-2-(arylthio)diazenes, Ar–N=N–S–C_6H_4–R

No.	Substit. on Ar	R	Mp θ_m/°C	Remarks and Elemental Analysis (%)		
				C	H	N
1	4-$(CH_3)_2N$	4-*t*-C_4H_9	77—78°C, d	f. 69.23	7.57	13.32
				c. 68.97	7.40	13.41
				for $C_{18}H_{23}N_3S$		
2	4-CH_3O	4-*t*-C_4H_9	50—52°C, d	lit,[18] mp 50—51°C		
3	4-CH_3O-2,6-d_2	4-*t*-C_4H_9	48—50°C, d	*d*-atom% 92%		
4	4-CH_3	4-*t*-C_4H_9	58—61°C, d	lit,[18] mp 58.5—59.5°C		
8	3,5-$(CH_3)_2$	4-*t*-C_4H_9	37—38°C, d	f. 72.38	7.53	9.58
				c. 72.44	7.43	9.39
				for $C_{18}H_{22}N_2S$		
9	H	4-*t*-C_4H_9	34—35°C, d	lit,[18] mp 33.5—34.5°C		
10	3,5-d_2	4-*t*-C_4H_9	34—35°C, d	*d*-atom% 98%		
11	3-CH_3O	4-*t*-C_4H_9	33—34°C, d	f. 67.81	6.79	9.38
				c. 67.97	6.71	9.32
				for $C_{17}H_{20}N_2OS$		
12	4-Cl	4-H	59—60°C, d	lit,[18] mp 59.0—59.5°C		
13	4-Cl-2,6-d_2	4-H	59—60°C, d	*d*-atom% 94%		
14	4-Cl-2-^{15}N	4-H	59—60°C, d			
15	4-I	4-*t*-C_4H_9	57—58°C, d	f. 48.45	4.39	7.30
				c. 48.49	4.32	7.07
				for $C_{16}H_{17}IN_2S$		
16	2-CH_3	4-H	19—20°C, d	f. 68.27	5.25	12.13
				c. 68.39	5.30	12.27
				for $C_{13}H_{12}N_2S$		
17	2,3-$(CH_3)_2$	4-H	37—38°C	f. 69.36	5.92	11.58
				c. 69.39	5.82	11.56
				for $C_{14}H_{14}N_2S$		
18	2,5-$(CH_3)_2$	4-H	39—40°C, d	f. 69.49	5.82	11.57
				c. 69.39	5.82	11.56
				for $C_{14}H_{14}N_2S$		

Table 4. (Continued)

No.	Substit. on Ar	R	Mp θ_m/°C	Remarks and Elemental Analysis (%)		
				C	H	N
19	2,4,6-$(CH_3)_3$	4-H	28—29°C, d	f. 70.37	6.46	10.46
				c. 70.28	6.29	10.93
				for $C_{15}H_{16}N_2S$		
20	2-CH_3S	4-*t*-C_4H_9	61—62°C, d	f. 64.59	6.63	8.42
				c. 64.52	6.37	8.85
				for $C_{17}H_{20}N_2S_2$		
21	2-CH_3O	4-H	59—60°C, d	f. 64.19	4.90	11.41
				c. 63.91	4.95	11.47
				for $C_{13}H_{12}N_2OS$		
22	2-CH_3O-4,6-d_2	4-*t*-C_4H_6	78—80°C, d	f. 67.49		9.14
				c. 67.52		9.26
				for $C_{17}H_{18}D_2N_2OS$		
				NMR of $D_3N^+C_6H_2D_2OCH_3$ (D_2O) 7.03 (s, 1H), 6.91 (s, 1H)		
23	2-CH_3O-5-CH_3	4-H	23.5—24.5°C, d	f. 65.01	5.43	11.05
				c. 65.09	5.46	10.84
				for $C_{14}H_{14}N_2OS$		
24	2-CH_3O-3,5-$(CH_3)_2$	4-*t*-C_4H_9	28—29°C, d	f. 69.59	7.66	8.82
				c. 69.48	7.36	8.53
				for $C_{19}H_{24}N_2OS$		
25	2-F-4,6-d_2	4-*t*-C_4H_9	44—45°C, d	NMR of $D_2HC_6H_2D_2F$ (D_3Cl) 6.97 (d, $J_{H\text{-}F}$: 10 Hz, 1H), 6.91 (s, 1H)		
26	2-Cl	4-H	46—47°C, d	f. 57.78	3.56	11.41
				c. 57.95	3.65	11.26
				for $C_{12}H_9ClN_2S$		
27	2-Cl-4,6-d_2	4-H	45.5—47°C, d	f. 57.53		11.33
				c. 57.48		11.17
				for $C_{12}H_7ClD_2N_2S$		
				NMR of $D_3N^+C_6H_2D_2Cl$ two singlets of arom-H		
28	2-Cl-5-CH_3	4-H	30—32°C, d	f. 59.34	4.18	10.64
				c. 59.43	4.22	10.66
				for $C_{13}H_{11}ClN_2S$		
29	2-Br	4-H	44—45°C, d	f. 49.03	3.01	9.60
				c. 49.16	3.09	9.56
				for $C_{12}H_9BrN_2S$		

Table 5. Benzothiadiazoles

No.	Substit. on Benzene Ring	Mp θ_m/°C	Remarks			
30	(H)	34—36°C	lit,[20] mp 35.5—36°C			
31	4,6-d_2	34—35°C	*d*-atom%: 4-*d* 97%, 6-*d* 99%			
32	5-CH_3	29—30.5°C	C%	H%	N%	S%
			f. 56.30	3.93	18.84	20.96
			c. 55.98	4.03	18.65	21.35
			for $C_7H_6N_2S$			

Table 6. 1-Aryl-3,3-dimethyltriazenes
Ar-N^1=N^2-$N(CH_3)_2$

No.	Substit. on Ar	Mp θ_m/°C	Remarks
—	4-CH_3	49—50°C	lit,[21] mp 46.5—47.5°C
—	4-CH_3O	oil	lit,[21] bp 59°C/0.75 Torr[a]
—	4-$(CH_3)_2N$	89—91°C	lit,[24] mp 92—93.5°C
5	4-CH_3-2-^{15}N	49—50°C	—
6	4-CH_3-1-^{15}N	49—50°C	—
7	4-CH_3-1,2-$^{15}N_2$	49—50°C	—

a) 1 Torr=133.322 Pa.

computer (MITSUBISHI Electric Co.).

References

1) Preliminary results of this study were reported in *Chem. Lett.*, **1980**, 1339. The g-values were recalculated by reference to the standard value of nitrosodisulfonate (Ref. 24). The assignment of the hydrogen hfs of (2-*t*-butoxythiophenyl)diazenyl radical should be corrected as a_{3-H}=1.32 G instead of a_{5-H} (Ref. Nos. 30—32 of Table 1).

2) A. Tsolis, S. G. Mylonakis, M. T. Nieh, and S. Seltzer, *J. Am. Chem. Soc.*, **94**, 829 (1972); R. C. Neuman, Jr., G. D. Lockyer, Jr., and M. J. Amrich, *Tetrahedron Lett.*, **1972**, 1221; N. A. Porter, L. J. Marnett, C. H. Lochmüller, G. L. Closs, and M. Shobataki, *J. Am. Chem. Soc.*, **94**, 3664 (1972); E.-L. Dreher, P. Niederer, A. Rieker, W. Schwarz, and H. Zollinger, *Helv. Chim. Acta*, **64**, 488 (1981).

3) R. Kerber, O. Nuyken, and L. Weithmann, *Chem. Ber.*, **108**, 1533 (1975).

4) K. Chakravorty, J. M. Pearson, and M. Szwarc, *J. Phys. Chem.*, **73**, 746 (1969).

5) N. A. Porter and P. M. Iloff, Jr., *J. Chem. Soc., Chem. Commun.*, **1971**, 1575.

6) N. A. Porter, G. R. Dubay, and J. G. Green, *J. Am. Chem. Soc.*, **100**, 920 (1978).

7) J. Sinclair and D. Kivelson, *J. Am. Chem. Soc.*, **90**, 5074 (1968).

8) S. F. Nelsen, R. T. Landis, L. H. Kiehle, and T. H. Leung, *J. Am. Chem. Soc.*, **94**, 1610 (1972); W. C. Danen, C. T. West, and T. T. Kensler, *J. Am. Chem. Soc.*, **95**, 5716 (1973).

9) K. Akasaka, S. Ohnishi, T. Suita, and I. Nitta, *J. Chem. Phys.*, **40**, 3110 (1964).

10) A. G. Davies and R. Sutcliffe, *J. Chem. Soc., Chem. Commun.*, **1979**, 473.

11) G. Cauquis, M. Genies, H. Lemaire, A. Rassat, and J. P. Ravet, *J. Chem. Phys.*, **47**, 4642 (1967).

12) P. J. Krusic and T. A. Rettig, *J. Am. Chem. Soc.*, **92**, 722 (1970).

13) Y. Miura and M. Kinoshita, *Bull. Chem. Soc. Jpn.*, **50**, 1142 (1977).

14) C. Chatgilialoglu, B. C. Gilbert, and R. O. C. Norman, *J. Chem. Soc., Perkin Trans. 2*, **1979**, 770.

15) J. A. Pople, D. L. Beveridge, and P. A. Dobosh, *J. Chem. Phys.*, **47**, 2026 (1967); *J. Am. Chem. Soc.*, **90**, 4201 (1968); D. L. Beveridge and P. A. Dobosh, *J. Chem. Phys.*, **48**, 5532 (1968).

16) J. J. de Lange, J. M. Robertson, and I. Woodward, *Proc. Roy. Soc.*, **171**, 398 (1939).

17) a) L. F. Kasukhin, M. P. Ponomarchuk, and A. L. Buchachenko, *Chem. Phys.*, **3**, 136 (1974); b) K. G. Seifert and F. Gerhart, *Tetrahedron Lett.*, **1974**, 829.

18) H. van Zwet and E. Kooyman, *Rec. Trav. Chim.*, **86**, 993 (1967).

19) A. Hantzsch and H. Freese, *Ber.*, **28**, 3237 (1895); T. Yamada, N. Tanaka, T. Morisawa, M. Nishikuri, and A. Kaji, *Bull. Chem. Soc. Jpn.*, **43**, 908 (1970).

20) P. Jacobson and H. Janssen, *Ann.*, **277**, 218 (1893).

21) J. Elks and D. H. Hey, *J. Chem. Soc.*, **1943**, 441; see also M. H. Akhtar, R. S. McDaniel, M. Feser, and A. C. Oehlschlager, *Tetrahedron*, **24**, 3899 (1968).

22) K.-M. Dangel and A. Rieker, unpublished.

23) K.-M. Dangel, Thesis, University of Tübingen, 1979.

24) C. S. Rondestvedt, Jr., and S. F. Davis, *J. Org. Chem.*, **22**, 200 (1957).

25) G. E. Pake, J. Townsend, and S. I. Weissman, *Phys. Rev. Ser. 2*, **85**, 682 (1952).

From Penicillin to Penem and Carbapenem. IX. C_1-Unit Introduction and the Carbapenam Synthesis from the Penicillin Molecule[1)]

Katsumi FUJIMOTO, Yuji IWANO, and Koichi HIRAI*
Chemical Research Laboratories, Sankyo Co., Ltd., 1-2-58, Hiromachi, Shinagawa-ku, Tokyo 140
(Received December 18, 1985)

An effective method for (*R*)-1-hydroxyethylation of benzyl bis(phenylseleno)penicillanate is described. The hydroxyethylated product was transformed into the 4-methylsulfonyl- and 4-phenylsulfonyl-2-azetidinone derivatives. These monocyclic compounds were reacted with potassium cyanide under two-phase conditions to give the 4-cyano-2-azetidinone derivative (C_1-unit introduction) in high yield. The cyano group was then converted into the iodomethyl group. Using the 4-iodomethyl-2-azetidinone derivative an isopenam derivative was synthesized. Furthermore, carbapenam derivative were also constructed by a novel [3+2] cyclization reaction between 4-iodomethyl-2-azetidinone and dimethyl 2-methylthio- and 2-phenylthiofumarate.

Since the discovery of thienamycin (**1**),[2)] a potent new broad spectrum antibiotic from Streptomyces cattleya, intense studies on the synthesis and structure-activity relationship of this and related compounds have revealed that the high antibiotic activity and stability against β-lactamase are linked to the combination of the *R* configuration of the 1-hydroxyethyl substituent and the trans configuration on the β-lactam ring.[3)]

There have been several reported syntheses starting from various materials; for example, 3-oxopentadioate, acetoxybutadiene, 2,2-dimethoxypropiononitrile oxide, L-aspartic acid, D-glucose, 6-bromo-3-oxobicyclo[2.2.1]heptan-7-carboxylate etc.[4)] We planned to utilize the β-lactam ring in the penicillin molecule for the synthesis of the carbapenem derivatives; in this case, however, there seemed to be three problems to be solved. The first one is how to introduce the (*R*)-1-hydroxyethyl substituent at the 6-position in the penicillin molecule, the second is concerned with introduction of a carbon substituent at the C-4 position of the 2-azetidinone ring, and the last is associated with the construction of the carbapenem skeleton. In this report we describe our approach for solving these three problems.

Concerning the first problem, we have already reported a method using methyl dibromopenicillanate[5)] as a starting material. However, our continuing interest in developing new methods prompted us to develop another route for the introduction of the (*R*)-1-hydroxyethyl substituent utilizing benzyl 6,6-bis(phenylseleno)penicillanate **3a**.

The starting materials **3a**, **4a**, and **5a** were prepared from the known diazo compound **2**[6)] by the reported method as shown in Scheme 1.

The phenylthio analogues **3b** (mp 100—103 °C), and **5b** (mp 84—86 °C) were prepared analogously, but **4b** could not be obtained by tributylstannane reduction of **3b**.

The compounds **3**—**5** were treated with methylmagnesium bromide or butyllithium in tetrahydrofuran (THF) to generate the enolates, which were reacted with acetaldehyde to yield the desired 6-hydroxyethylated products (**6**, **7**, and **8**).

As shown in Table 1, the diphenylthio derivative **3b** (Entries 1 and 2) gave no hydroxyethylated products. This is due to the well-known phenomena that

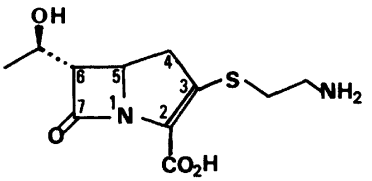

1

Fig. 1.

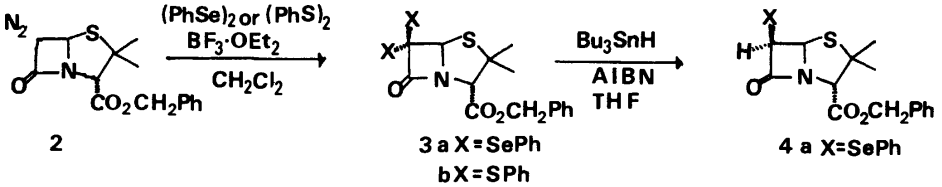

2 **3a** X=SePh, **b** X=SPh **4a** X=SePh

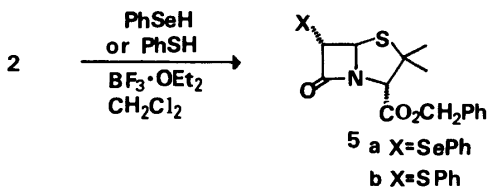

5 **a** X=SePh, **b** X=SPh

Scheme 1.

Table 1. The Results of the Introduction of the 1-Hydroxyethyl Group

Entry	X	Y	Z	Base	Yield/%	6:7:8	s.m./%
1	PhS	PhS	—	MeMgBr	—	—	100
2	PhS	PhS	—	BuLi	—	—	100
3	PhSe	H	—	MeMgBr	—	—	—
4	H	PhSe	PhSe	BuLi	48	1 : 2 : 1	—
5	H	PhSe	PhSe	MeMgBr	5	1 : 0 : 0	70
6	PhSe	PhSe	PhSe	BuLi	56	2 : 3 : 2	—
7	PhSe	PhSe	PhSe	MeMgBr	78	30 : 1 : 0	
8	H	PhS	PhS	BuLi	38	0 : 1 : 0	—

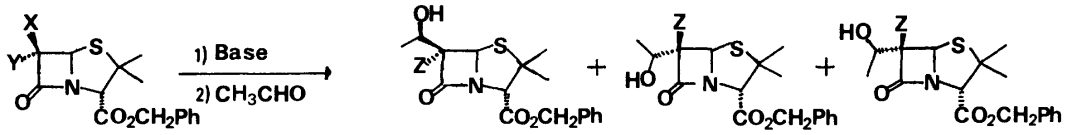

3 6 7 8

Scheme 2.

the selenoacetal generates a carbanion by releasing one of the seleno-parts on base treatment (i.e. pseudo halide), but this is not the case for the thioacetal. It is noteworthy that the α-phenylseleno (**5a**, Entries 4 and 5) and α-phenylthio (**5b**, Entry 8) derivatives gave the desired products, but the β-phenylseleno (**4a**, Entry 3) derivative gave only the diphenyldiselenide (about 50%). The diphenylseleno derivative (**3a**, Entries 6 and 7) gave **6**, **7**, and **8** in the ratio of 2:3:2 using butyllithium as base, and when methylmagnesium bromide was used as base **3a** gave **6** highly selectively in the ratio of **6**:**7**:**8**=30:1:0 in 78% isolated yield.

The structure of these products was determined by ^{1}H NMR and degradation study. As shown in Table 2, the two methyl groups of the compounds with β-phenylseleno group appeared at 1.70—1.78 and 1.31—1.45, and those of the compounds with an α-phenylseleno group appeared at 1.55—1.57 and 1.28—1.33. In the case of **6** and **7** these methyl group appeared at 1.55 and 1.28, and 1.78 and 1.45, respectively. These data strongly suggested that the product **6** has an α-phenylseleno group at C-6, and the product **7** has a β-phenylseleno group. Furthurmore the structures were confirmed by the chemical degradation study.

The high stereoselectivity observed in Entry 6 (Table 1) can be explained as follows: The magnesium enolate is less reactive than lithium enolate, therefore the transition state is rather product like and the bulkiness of the phenylseleno group affected the course of the approach of acetaldehyde to attack preferentially from the β-side of the molecule. In this approach the steric repulsion between the thiazolidine group and the methyl group in acetaldehyde forced the direction of aldehyde approach as shown in Fig. 2, therefore the β-(*R*)-1-hydroxyethylated product was obtained in a high selectivity.

Recently, Ishiguro and Nakatsuka calculated the energy of the enolate configuration by means of MNDO, and they announced that the most stable

Table 2. The Chemical Shifts of Methyl Groups

Compound	Me^1	Me^2
4a	1.40	1.70
5a	1.33	1.57
3a	1.31	1.70
6	1.28	1.55
7, **8**	1.45	1.78

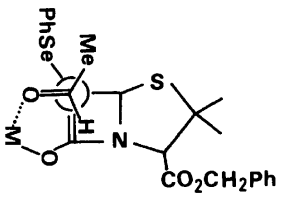

Fig. 2.

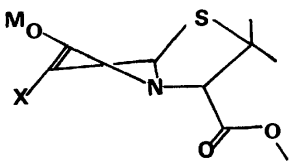

A

Fig. 3.

conformer is that as shown in Fig. 3.[7] In this conformer the upper face (β-face) is less sterically hindered than the α-face, so the metal coordination occurs on the β-face, and acetaldehyde has more chance to come from the β-face of the conformer.

With the desired product **6** in hand, we next turned our attention to conversion of **6** to 3,4-*trans*-disubstituted 2-azetidinone derivative. By tin hydride reduction, the phenylseleno group was removed to give 6β-(*R*)-1-hydroxyethylated product **9** in 95% isolated yield.[8] The coupling constant between the protons on the β-lactam ring is 4.4 Hz (cis) and the structure was confirmed as **11a** by comparison with an authentic

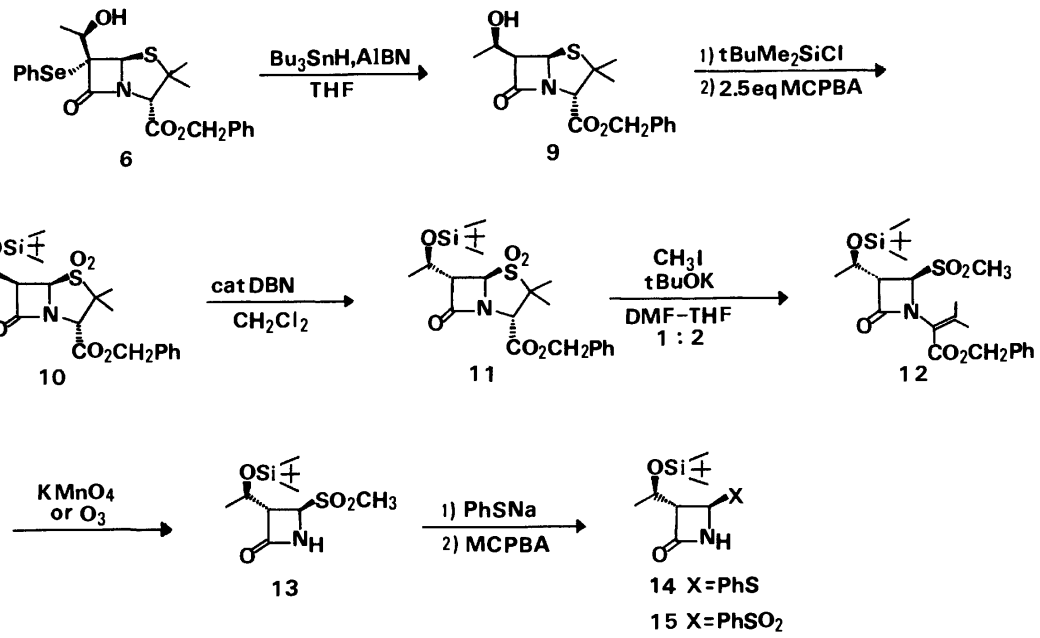

Scheme 3.

sample prepared from the known benzyl 6α-bromo-6β-(*R*)-1-hydroxyethylpenicillanate[9] by tin hydride reduction. After the protection of the hydroxyl group in 6, the product was oxidized with 2.5 equiv of *m*-chloroperbenzoic acid to afford the cis sulfone derivative **10** (mp 118 °C).

The crucial step for the isomerization of *cis*-**10** to *trans*-**11** was satisfactorily achieved by adding a catalytic amount of 1,5-diazabicyclo[4.3.0]non-5-ene (DBN) to a solution of **10** in dichloromethane at 20—25 °C. The isomerization occurred within 30 min to afford the trans product **11**.

The ring opening of the trans sulfone **11** was smoothly achieved by excess methyl iodide and potassium *t*-butoxide (2.5 equiv) in THF: DMF (1:2) to yield the monocyclic β-lactam **12**. In this ring opening reaction sodium hydride was not effective. The *N*-substituent in **12** was oxidatively removed by potassium permanganate or ozonolysis to give the desired monocyclic β-lactam **13**, mp 100 °C, $[\alpha]_D^{22}$ −12.8° (*c* 1, $CHCl_3$). The sequence of the reaction in Scheme 3 was successfully applicable to benzyl 6α-bromo-6β-(1-hydroxyethyl)penicillanate to afford the same monocyclic β-lactam **13**. The methylsulfonyl group in **13** was transformed into phenylthio group in **14**, which was oxidized to the phenyl sulfone derivative **15** by the reported procedure.[10]

The next step to be solved was the carbon unit introduction at the C-4 position of the 2-azetidinone ring. To the best of our knowledge no method has been reported for the cyano group substitution at the C-4 position of 4-acetoxy-2-azetidinone.[11] In the case of our β-lactams **13**, **15**, and **16** which have a 1-hydroxyethyl substituent at the C-3 position we found that the cyano group was introduced in high yield at the desired position. Thus, the 2-azetidinone **15** or **16** was treated with an excess of potassium cyanide in THF in the presence of 18-crown-6 (0.1 equiv) or more conveniently with potassium cyanide under two-phase conditions (benzene–water, catalytic amount of tetrabutylammonium bromide) for 18 h to give the crystalline cyano derivative **17** in 68% isolated yield.

The dimeric product **24** was obtained in 10% yield as a by-product, but when the methylsulfonyl derivative **13** was used instead of **15** or **16** the formation of the dimeric product **24** was supressed to less than 10% of the monomer **17**. Manipulation of the cyano group in **17** was carried out as follows. Alkaline hydrolysis of **17** in the presence of hydrogen peroxide gave the amide derivative **18** in 85% isolated yield, which was further hydrolyzed to the acid **19**. Esterification with diazomethane gave the ester derivative **20**; $[\alpha]_D^{20}$ −12.8 (*c* 1.01, $CHCl_3$), which was then converted to the alcohol **21**. This was tosylated to the tosyl derivative **22**. The Finkelstein substitution reaction (NaI in acetone) of **22** was successfully performed to afford the 4-(iodomethyl)-2-azetidinone derivative **23** in 95% yield.

Compound **23** has been previously converted to thienamycin (**1**),[12] and was thought to be a useful precursor for the synthesis of isopenam derivative **29**. The aminal **25**, prepared via reaction of **23** with *p*-nitrobenzyl glyoxylate refluxing benzene, was chlorinated (thionyl chloride, 2,6-lutidine/THF) to give **26**, which was then transformed into isopenam derivative **27a** and **27b** (5:3) with hydrogen sulfide and triethylamine in dichloromethane. These structures were deduced from ^1H NMR spectra. The NMR spectra of 4,5-fused β-lactam system (i.e. penicillin) normally show the C-2 proton in the "natural" series

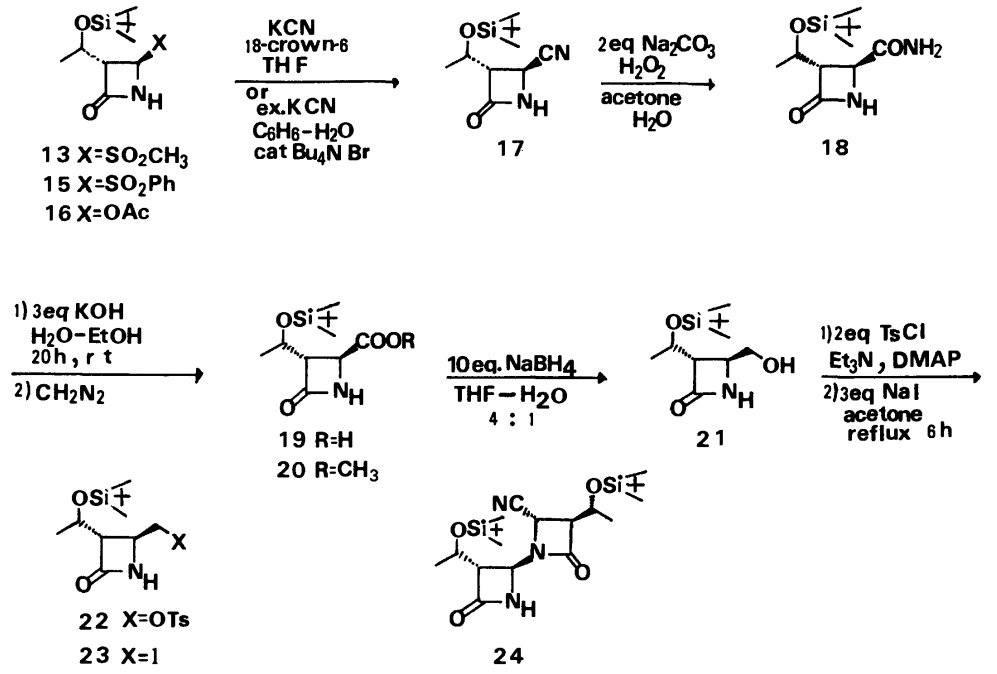

Scheme 4.

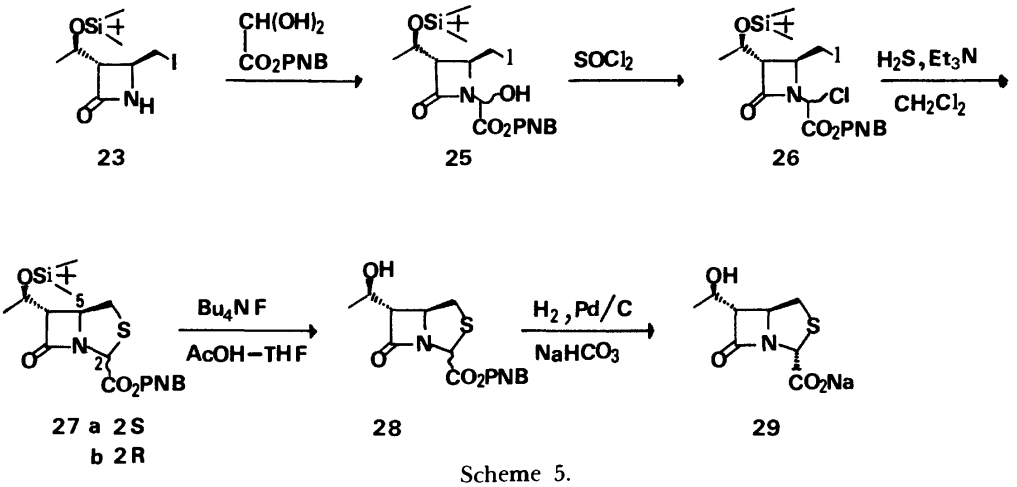

Scheme 5.

(2,5-trans) at a 0.5—1 ppm lower field than that of the corresponding "unnatural" series (2,5-cis).[13] In our case **27a** and **27b** showed the C-2 protons at δ 4.82 and 5.49 respectively. Therefore **27b** was the "natural" form (2,5-trans). Under the deprotection conditions (tetrabutylammonium fluoride, acetic acid–THF) both **27a** and **27b** gave the same alcoholic derivative **28**. In the presence of one equivalent of aqueous sodium hydrogencarbonate **28** was subjected to hydrogenolysis to give the sodium salt **29**, which has no remarkable antibacterial activity, MIC: Staphylococcus aureus 56, 200 $\mu g\,ml^{-1}$.

The following two methods are representative for constructing the carbapenem (or carbapenam): The first one is the internal Wittig type of reaction between C-2 and C-3 originally developed by Woodward in the field of penem synthesis, and the second one is the Merck method of the carbene insertion reaction between C-2 and N1-H to build up the 3-oxocarbapenam molecule. Beside these, several other methods have been reported, one of which is the aldol type reaction between C-2 and C-3, or C-3 and C-4 under basic conditions. We have already succeeded in the synthesis of Δ^3-carbapenem by aldol condensation between C-3 and C-4 using a dialdehyde intermediate.[14] Our continuing interest in constructing the carbapenam molecule by ring closure between C-3 and C-4 prompted us to develop another method for the synthesis of this unique carbapenam molecule.

Our 4-iodomethyl-2-azetidinone (**23**) has the nucleophilic center and at the same time the electrophilic center in itself. The nitrogen anion of **23** is sufficiently active to attack the α,β-unsaturated carbonyl compound (the Michael reaction) and the resulting

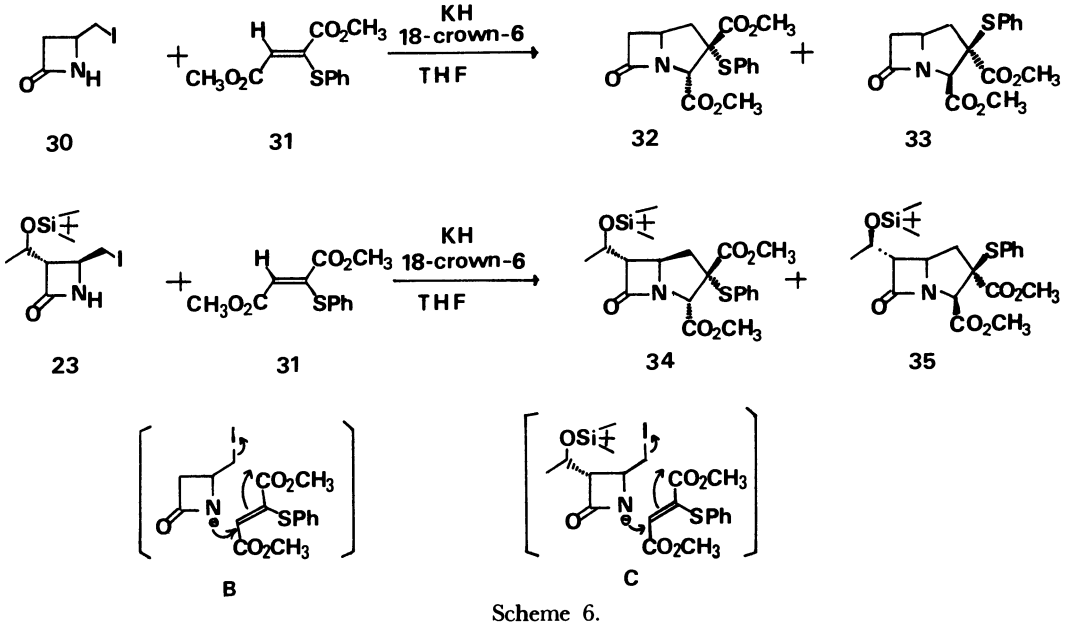

Scheme 6.

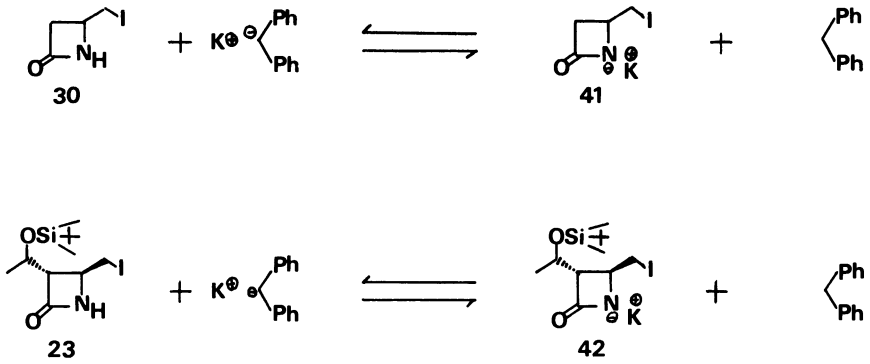

Scheme 7.

enolate has a chance to capture the electrophilic center (e.g. iodomethyl part) to give the cyclic compound.

On the basis of these hypotheses we investigated the reaction of 4-iodomethyl-2-azetidinone (**30**) with dimethyl 2-(phenylthio)fumarate (**31**) under basic conditions. The nitrogen anion **41** was generated by treatment of **30** with potassium hydride and 18-crown-6 in THF and reacted with **31** for 3 h at −78—0 °C. After the usual work-up the products were purified by careful TLC method to give **32** and **33** (1:1) in 27% isolated yield.

Likewise, the compound **23** gave the corresponding cyclized products (**34** and **35**) under the same conditions in 15% isolated yield.

As compounds **32**, **33**, **34**, and **35** have both phenylthio substituent and methoxycarbonyl group at C-3 position, we attempted an oxidative decarboxylation, but the desired 3-oxopenam derivative was not obtained on *N*-chlorosaccinimide (NCS) treatment of the corresponding sodium salt. Therefore we changed the phenylthio group to methylthio group.

The reaction of 2-(methylthio)fumarate (**36**) with **30** and **23** did not give the expected cyclized products. Therefore, we checked the base effect on our cyclization and found that 1,8-diazabicyclo[5.4.0]undec-7-ene (DBU), potassium fluoride, triphenylmethylpotassium, and lithium diisopropylamide faild to give the desired compound, but gave the polymeric or intractable products. We thought that these undesirable side reactions occured because of the high concentration of the nitrogen anions. In other to suppress these side reactions the nitrogen anion **41** and **42** should be kept in low concentration. Therefore we took advantage of the generation of these anions under the equilibrium conditions using diphenylmethanide (pK_a=33).

Diphenylmethylpotassium was prepared by the reaction of diphenylmethane with potassium hydride and 18-crown-6 in THF at room temperature. The 2-azetidinone **23** was added to the above solution and the mixture was stirred for 2 h at −40 °C to generate the nitrogen anion **42**. Dimethyl 2-(methylthio)fumarate was added to react with **42** for 2 h at −40—−20 °C to give **39** and **40** (2:1) in 18% yield.

Under the same conditions compound **30** gave the carbapenams **37** and **38** in 9% yield.

The purified compound **39** was carefully hydrolyzed

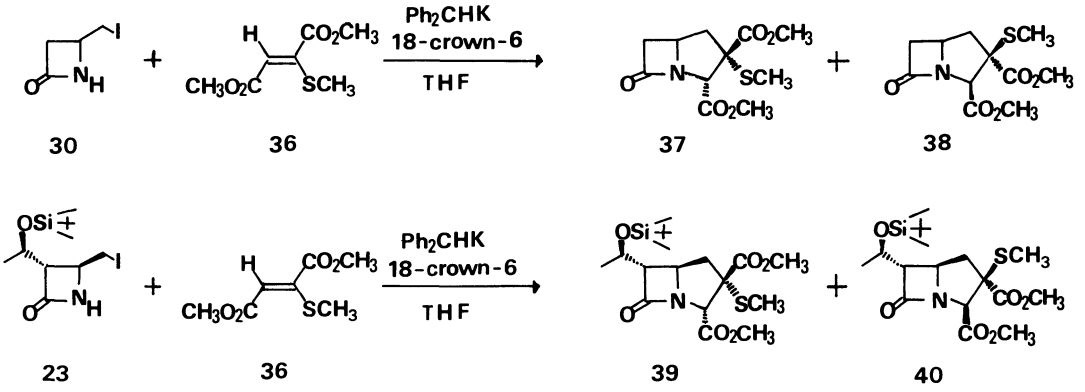

Scheme 8.

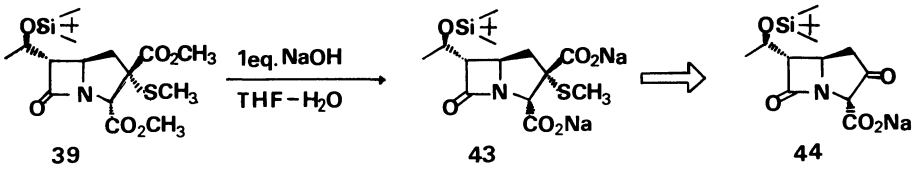

Scheme 9.

with aqueous sodium hydroxide to give the disodium salt **43**.

The structure of **32**, **33**, **34**, **35**, **37**, **38**, **39**, and **40** were determined by the same considerations as described for isopenam derivatives.

We are now investigating conversion of **43** to the 3-oxocarbapenam derivative (**44**) via Trost's oxidative decarboxylation method.[15] Compound **44** is an important intermediate for the synthesis of thienamycin and related carbapenem antibiotics.

Experimental

General. All melting points are uncorrected. Specific rotations were measured on a Perkin-Elmer 241 polarimeter. IR spectra were recorded on JASCO A102 and JEOL A320 Infrared spectrometers. NMR spectra were taken using a Varian EM 360L spectrometer (60 MHz) and the chemical shifts are expressed in ppm units using TMS as internal standard: s, singlet; d, doublet; dd, doublet of doublet; ddd, doublet of doublet of doublet; t, triplet; q, quartet; dq, doublet of quartet; m, multiplet; br, broad. Mass spectra (MS) were measured on JEOL JMS 01SG and JMS D300 mass spectrometers. (Preparative) TLC was carried out on Merck TLC-plates silica-gel F_{254} Pre-coated, layer thickness: (2 mm) 0.25 mm and spots were made visible by ultraviolet irradiation.

Benzyl (2*S*,5*R*,6*S*)-3,3-Dimethyl-7-oxo-6-phenylseleno-4-thia-1-azabicyclo[3.2.0]heptane-2-carboxylate [(2*S*,5*R*,6*S*)-6-(Phenylseleno)penicillanate] (5a), Benzyl (2*S*,5*R*,6*S*)-6-(Phenylthio)penicillanate (5b), and Benzyl (2*S*,5*R*)-6,6-Bis(phenylseleno)penicillanate (3a): These materials were synthesized according to the method of Giddrings et al.[16]

5a: ^{1}H NMR ($CDCl_3$) δ=1.32 (3H, s), 1.57 (3H, s), 4.45 (1H, s), 4.46 (1H, d, J=2 Hz), 5.08 (2H, s), 5.17 (1H, d, J=2 Hz), 7.0—7.8 (10H, m).

5b: ^{1}H NMR ($CDCl_3$) δ=1.36 (3H, s), 1.59 (3H, s), 4.43 (1H, d, J=2 Hz), 4.50 (1H, s), 5.10 (2H, s), 5.19 (1H, d, J=2 Hz), 7.0—8.2 (10H, m).

3a: Mp 104—105 °C (recrystallized from ethanol); ^{1}H NMR ($CDCl_3$) δ=1.30 (3H, s), 1.70 (3H, s), 4.36 (1H, s), 4.90 (1H, AB type, J=12.6 Hz), 5.00 (1H, AB type, J=12.6 Hz), 5.33 (1H, s), 7.0—8.1 (15H, m).

Benzyl (2*S*,5*R*)-6,6-Bis(phenylthio)penicillanate (3b): To a mixture of benzyl 6-diazopenicillanate and diphenyldiselenide in dichloromethane was added a catalytic amount of boron trifluoride etherate. The solvent was removed under reduced pressure to give **3b**: Mp 99—103 °C (recrystallized from acetone-hexane); ^{1}H NMR ($CDCl_3$) δ=1.35 (3H, s), 1.70 (3H, s), 4.41 (1H, s), 5.04 (2H, s), 5.46 (1H, s), 7.15—7.80 (15H, m).

Found: C, 63.97; H, 4.93; N, 2.55%. Calcd for $C_{27}H_{25}NO_3S_3$: C, 63.82; H, 4.96; N, 2.76%.

Benzyl (2*S*,5*R*,6*R*)-6-(Phenylseleno)penicillanate (4a): To a solution of 317 mg (0.527 mmol) of benzyl 6,6-bis(phenylseleno)penicillanate (**3a**) in 10 ml of THF was added 367 mg of tributylstannane and a catalytic amount of AIBN. The solution was refluxed for 2 h and the solvent was removed under reduced pressure. The residue was purified by flash column chromatography (benzene-ethyl acetate, 10:1 v/v) to give 153 mg (65%) of **4a**: ^{1}H NMR ($CDCl_3$) δ=1.40 (3H, s), 1.70 (3H, s), 4.52 (1H, s), 4.76 (1H, d, J=4 Hz), 5.15 (2H, s), 5.54 (1H, d, J=4 Hz), 6.9—7.9 (10H, m).

Benzyl (2*S* 5*R*,6*S*)-6-[(*R*)-1-Hydroxyethyl]-6-(phenylselenopenicillanate (6): To a solution of 6.0 g of methyl 6,6-bis(phenylseleno)penicillanate (**5a**) in 60 ml of THF was added 15 ml of methylmagnesium bromide in THF (1 mol dm^{-3}, Tokyo Kasei), keeping the reaction temperature below −50 °C. After stirring for 80 min at −78 °C, 4 ml of acetaldehyde was added and the whole mixture was stirred for 40 min. The reaction was quenched at −78 °C with 60 ml of a saturated aqueous ammonium chloride. The Dry-Ice acetone bath was removed, and the mixture was stirred to become two phase at ambient temperature. The organic phase was separated and the aqueous phase was extracted with ethyl acetate three times. The combined extracts were washed with saturated aqueous sodium chloride, and dried over anhydrous magnesium sulfate. After removal of the solvent

under reduced pressure the crude product was purified by dry column chromatography (benzene–ethyl acetate, 5:1 v/v) to give 3.68 g of **6** (74%): R:S=30:1.

Benzyl (2*S*,5*R*,6*R*)-6-[(*S*)-1-Hydroxyethyl]-6-(phenylseleno)-penicillanate (7): R_f=0.5 (benzene–ethyl acetate, 10:1 v/v); mp 195 °C; ^{1}H NMR ($CDCl_3$) δ=1.28 (3H, d, J=6.4 Hz), 1.45 (3H, s), 1.78 (3H, s), 1.8—2.5 (1H, m), 3.5—4.1 (1H, m), 4.53 (1H, s), 5.17 (2H, s), 5.47 (1H, s), 7.0—8.0 (10H, s).

Found: C, 56.25; H, 5.15; N, 2.77; S, 6.53%. Calcd for $C_{23}H_{25}NO_4SSe$: C, 56.32; H, 5.14; N, 2.86; S, 6.53%.

Benzyl (2*S*,5*R*,6*S*)-[(*R*)-1-Hydroxyethyl]-6-(phenylseleno)-penicillanate (6): R_f=0.41 (benzene–ethyl acetate, 10:1 v/v); ^{1}H NMR ($CDCl_3$) δ=1.28 (3H, s), 1.33 (3H, d, J=6.0 Hz), 1.55 (3H, s), 2.89 (1H, br s), 4.30 (1H, s), 4.46 (1H, q, J=6.0 Hz), 4.7—5.3 (2H, m), 5.12 (1H, s), 6.9—7.8 (10H, m).

All other aldol type reactions were performed by the same procedure.

Benzyl (2*S*,5*R*,6*R*)-6-[(*S*)-1-Hydroxyethyl]-6-(phenylthio)-penicillanate (7): Mp 179 °C; IR (nujol) 3475, 1780, 1750 cm^{-1}; ^{1}H NMR ($CDCl_3$) δ=1.23 (3H, d, J=6.5 Hz), 1.38 (3H, s), 1.70 (3H, s), 3.7—3.9 (1H, m), 4.49 (1H, s), 5.19 (2H, s), 5.58 (1H, s), 7.2—7.85 (10H, m).

Found: C, 62.14; H, 5.63; N, 3.16; S, 14.57%. Calcd for $C_{23}H_{25}NO_4S_2$: C, 62.28; H, 5.68; N, 3.16; S, 14.46%.

Benzyl (2*R*,5*R*,6*R*)-6-[(*R*)-1-Hydroxyethyl]penicillanate (9): A solution of 3.5 g of **6**, 4.0 g of tributylstannan, and catalytic amount of AIBN in 35 ml of THF was stirred for 2 h at 60 °C. The solvent was removed under reduced pressure and the residue was purified by TLC (benzene–ethyl acetate, 5:1 v/v) to give 2.65 g of **9** (quantitative): R_f=0.2 (benzene–ethyl acetate, 10:1 v/v); ^{1}H NMR ($CDCl_3$) δ=1.22 (3H, d, J=6 Hz), 1.41 (3H, s), 1.66 (3H, s), 2.88 (1H, OH), 3.49 (1H, dd, J=4.4 and 9 Hz), 3.8—4.5 (1H, m), 4.48 (1H, s), 5.20 (2H, s), 5.40 (1H, d, J=4.4 Hz), 7.43 (5H, m).

Benzyl (2*S*,5*R*,6*R*)-6-[(*R*)-1-(*t*-Butyldimethylsilyloxy)ethyl]-penicillanate 1,1-Dioxide (10): To a stirred solution of 2.65 g of **9** in 20 ml of DMF was added 680 mg of imidazole and 1.5 g of *t*-butylchlorodimethylsilane at room temperature. After 20 h ethyl acetate was added to the mixture, and the solution was washed with water and dried over anhydrous magnesium sulfate. The solvent was removed under reduced pressure and the residue was purified by column chromatography (benzene–ethyl acetate, 20:1 v/v) to give 1.9 g of the silyl ether.

To a stirred solution of 1.9 g of the silyl ether thus obtained in 25 ml of dichloromethane was added 2.2 g of *m*-chloroperbenzoic acid at room temperature. After 2 h the mixture was diluted with dichloromethane and washed with 5% aqueous potassium hydroxide. The solvent was removed under reduced pressure and the residue crystallized from ether to give **10**: Mp 118 °C (recrystallized from ether); R_f=0.36 (benzene–ethyl acetate, 20:1 v/v); IR (nujol) 1810, 1750 cm^{-1}; ^{1}H NMR ($CDCl_3$) δ=0.10 (3H, s), 0.15 (3H, s), 0.91 (9H, s), 1.26 (3H, s), 1.28 (3H, d, J=7 Hz), 1.52 (3H, s), 3.80 (1H, dd, J=5.5 and 10 Hz), 4.46 (1H, s), 4.59 (1H, d, J=5.5 Hz), 4.85 (1H, m), 5.20 (2H, br s), 7.40 (5H, s).

Found: C, 57.29; H, 7.31; N, 2.87; S, 6.60%. Calcd for $C_{23}H_{35}NO_5SSi$: C, 57.35; H, 7.32; N, 2.91; S, 6.60%.

Benzyl (2*S*,5*R*,6*R*)-[(*R*)-1-(*t*-Butyldimethylsilyloxy)ethyl]-penicillanate 1,1-Dioxide (11): To a stirred solution of 1 g of the cis sulfone derivative **10** in 5 ml of chloroform was added 0.05 ml of DBN. After 1 h the completion of the reaction was checked by ^{1}H NMR. The mixture was washed successively with 1% hydrochloric acid and water and dried over anhydrous magnesium sulfate. The solvent was removed under reduced pressure to give 980 mg of **11**: ^{1}H NMR ($CDCl_3$) δ=0.10 (6H, s), 0.91 (9H, s), 1.26 (3H, d, J=7 Hz), 1.31 (3H, s), 1.55 (3H, s), 3.66 (1H, dd, J=2.0 and 3.8 Hz), 4.2—4.55 (1H, m), 4.39 (1H, s), 4.61 (1H, d, J=2 Hz), 5.22 (2H, s), 7.42 (5H, s).

Benzyl 2-[(3*S*,4*R*)-3-[(*R*)-1-(*t*-Butyldimethylsilyloxy)ethyl]-4-methylsulfonyl-2-oxo-1-azetidinyl]-3-methyl-2-butenoate (12): To a stirred solution of 100 mg (0.208 mmol) of the trans sulfone **11** in 2 ml of THF–DMF (2:1) was added 0.5 ml of methyl iodide and 70 mg of potasium *t*-butoxide successively. After about 30 min the completion of the reaction was checked by TLC and ethyl acetate was added. The mixture was washed with water and dried over anhydrous magnesium sulfate. The solvent was removed under reduced pressure and the residue was purified by TLC (benzene–ethyl acetate, 10:1 v/v) to give 78 mg of **12**: IR (neat): 1780, 1722, 1630 cm^{-1}; ^{1}H NMR ($CDCl_3$) δ=0.07 (3H, s), 0.13 (3H, s), 0.92 (9H, s), 1.30 (3H, d, J=7 Hz), 2.06 (3H, s), 2.22 (3H, s), 2.56 (3H, s), 3.55 (1H, dd, J=2.5 and 4 Hz), 4.1—4.6 (1H, m), 5.17 (1H, d, J=2.5 Hz), 4.9—5.5 (2H, m), 7.35 (5H, s).

(3*S*,4*R*)-3-[(*R*)-1-(*t*-Butyldimethylsilyloxy)ethyl]-4-(methylsulfonyl)-2-azetidinone (13): To a stirred solution of 68 mg of the seco derivative **12** and 0.05 ml of acetic acid in 8 ml of acetone was added slowly a solution of 50 mg of potassium permanganate in 5 ml of water. After 16 h the reaction mixture was filtered through Celite, and the solvent was evaporated. The residual solution was extracted with ethyl acetate and the combined extracts were washed with water and dried over anhydrous magnesium sulfate. The solvent was removed under reduced pressure and the crude product was purified by TLC (benzene–ethyl acetate, 1:1 v/v) to give 40 mg (94%) of **13**: Mp 100 °C; $[\alpha]_D^{20}$ −12.8° (*c* 1 $CHCl_3$); IR (nujol): 3350, 1795, 1780, 1737 cm^{-1}; ^{1}H NMR ($CDCl_3$) δ=0.09 (6H, s), 0.88 (9H, s), 1.28 (3H, d, J=6 Hz), 2.94 (3H, s), 3.54 (1H, t, J=2 Hz), 4.1—4.5 (1H, m), 4.70 (1H, d, J=2 Hz), 6.95 (1H, br s).

Found: C, 46.66; H, 8.18; N, 4.33; S, 10.57%. Calcd for $C_{12}H_{25}NO_4SSi$: C, 46.87; H, 8.20; N, 4.56; S, 10.43%.

(3*S*,4*R*)-3-[(*R*)-1-(*t*-Butyldimethylsilyloxy)ethyl]-4-(phenylthio)-2-azetidinone (14): To a stirred solution of 3.38 g (10.99 mmol) of 4-(methylsulfonyl)-2-azetidinone **13** in 40 ml of absolute ethanole was added sodium phenyl sufide in absolute ethanol (prepared from 12.86 mmol of sodium ethoxide in ethanol and 12.05 mmol of thiophenol) at 5 °C. After 2 h, 600 ml of ethyl acetate was added, washed successively with neutral phosphate buffer (pH 6.86) three times and brine, and dried over anhydrous magnesium sulfate. The solvent was removed under reduced pressure and the residue was purified by flash chromatography (benzene–ethyl acetate, 95:5 v/v) to give 3.42 g (95%) of **14**: ^{1}H NMR ($CDCl_3$) δ=0.07 (6H, s), 0.83 (9H, s), 1.22 (3H, d, J=6.0 Hz), 3.08 (1H, dd, J=2.0 and 4.0 Hz), 3.90—4.5 (1H, m), 4.85 (1H, d, J=2.0 Hz), 6.70 (1H, br s), 7.20—7.60 (5H, m).

(3*S*,4*R*)-3-[(*R*)-1-(*t*-Butyldimethylsilyloxy)ethyl]-4-(phenylsulfonyl)-2-azetidinone (15): A solution of 4.12 g (12.2 mmol) of phenylthioazetidinone **14** in 150 ml of ethyl acetate was cooled in an ice bath. Sodium acetate (1.66 g, 12.2 mmol), 0.26 g of manganese(II) acetylacetonate, and 12.4 ml (73.2 mmol) of 40 % peracetic acid was added and the mixture was stirred for 2 h. Ethyl acetate was added and the reaction mixture was washed successively with aqueous sodium hydro-

gensulfite two times, saturated sodium hydrogencarbonate and brine two times and dried over anhydrous magnesium sulfate. The solvent was removed under reduced pressure, and the residue was purified by flash column chromatography (benzene–ethyl acetate,95:5 v/v) to give 3.3 g (73%) of **15**: ^{1}H NMR ($CDCl_3$) δ=0.05 (6H, s), 0.83 (9H, s), 1.25 (3H, d, J=6.0 Hz), 3.45 (1H, dd, J=2.0 and 3.5 Hz), 3.90—4.40 (1H, m), 4.56 (1H, d, J=2.0 Hz), 6.85 (1H, br s), 7.6—8.1 (5H, m).

(3*S*,4*S*)-3-[(*R*)-1-(*t*-Butyldimethylsilyloxy)ethyl]-4-cyano-2-azetidinone (17): i) To a solution of 57 mg of methyl sulfone **13** in 2 ml of benzene was added a solution of 57 mg of potassium cyanide in 2 ml of water and a catalytic amount of tetrabutylammonium bromide. The mixture was stirred for 24 h and the organic layer was separated. The aqueous layer was extracted with dichloromethane. The combined extracts were dried over anhydrous magnesium sulfate and evaporated. The residue was purified by TLC (benzene–ethyl acetate, 5:1 v/v) to give 42 mg (89%) of **17**.

ii) To a solution of 150 mg of **16** in 4 ml of anhydrous THF was added 100 mg of finely powdered potassium cyanide and 14 mg of 18-crown-6. The mixture was stirred vigorously for 2—8 h. The completion of the reaction was checked by TLC (benzene–ethyl acetate, 5:1 v/v). Ethyl acetate was added and the solution was washed with brine and dried over anhydrous magnesium sulfate. The solvent was removed under reduced pressure and the residue was purified by TLC (benzene–ethyl acetate, 5:1 v/v, R_f=0.38) to give 70 mg of **17**: Mp 136—138 °C (recrystallized from dichloromethane–hexane); IR (nujol): 3220, 2240, 1780, 1755 cm^{-1}; ^{1}H NMR ($CDCl_3$) δ=0.08 (6H, s), 0.88 (9H, s), 1.25 (3H, d, J=6 Hz), 3.65 (1H, t, J=2.5 Hz), 4.35 (1H, d, J=2.5 Hz), 4.30 (1H, dq, J=2.5 and 6 Hz), 6.65 (1H, br s).

Found: C, 56.57; H, 8.66; N, 11.00%. Calcd for $C_{12}H_{22}N_2O_2Si$: C, 56.65; H, 8.72; N, 11.01%.

(3*S*,4*R*)-[(*R*)-1-(*t*-Butyldimethylsilyloxy)ethyl]-4-[(3*S*,4*S*)-3-[(*R*)-1-(*t*-butyldimethylsilyloxy)ethyl]-4-cyano-2-oxo-1-azetidinyl]-2-azetidinone (24): Mp 158 °C (recrystallized from chloroform–hexane); IR (nujol): 3225, 1775 cm^{-1}; ^{1}H NMR ($CDCl_3$) δ=0.10 (12H, s), 0.90 (18H, s), 1.25 (6H, d, J=5.6 Hz), 3.5—3.9 (2H, m), 4.0—5.3 (2H, m), 4.48 (1H, d, J=2 Hz), 5.45 (1H, d, J=2 Hz), 6.23 (1H, br s).

(3*S*,4*S*)-3-[(*R*)-1-(*t*-Butyldimethylsilyloxy)ethyl]-4-carbamoyl-2-azetidinone (18): To a stirred solution of 163 mg of **17** in 3 ml of acetone was added 0.1 ml of 30% aqueous hydrogen peroxide and 1.4 ml of 0.5 mol dm^{-3} aqueous sodium carbonate at room temperature. After 30 min ethyl acetate was added and the organic layer was washed with water and dried over anhydrous magnesium sulfate. The solvent was removed under reduced pressure and the residue was purified by TLC (benzene–ethyl acetate, 1:2 v/v, R_f=0.2) to give 130 mg of **18** as crystals: Mp 87 °C (recrystallized from acetone–hexane); IR (nujol): 3100—3600, 1750, 1730, 1685, 1670 cm^{-1}; ^{1}H NMR ($CDCl_3$) δ=0.09 (6H, s), 0.90 (9H, s), 1.26 (3H, d, J=6.5 Hz), 3.21 (1H, dd, J=2.5 and 4.0 Hz), 4.15 (1H, d, J=6.5 Hz), 4.20 (1H, dq, J=4.0 and 6.5 Hz), 6.76 (2H), 7.36 (1H).

Found: C, 52.48; H, 8.98; N, 10.15%. Calcd for $C_{12}H_{24}N_2O_3Si$: C, 52.91; H, 8.88; N, 10.28%.

Methyl (3*S*,4*S*)-3-[(*R*)-1-(*t*-Butyldimethylsilyloxy)ethyl]-2-oxoazetidine-4-carboxylate (20): i) To a stirred solution of 210 mg of **17** in 6 ml of ethanol was added a solution of 100 mg of sodium hydroxide in 2.6 ml of water and 0.15 ml of 30% aqueous hydrogen peroxide. After 15 min the mixture was warmed up to 50 °C and stirred for 1.5 h at that temperature. After cooling, water and ethyl acetate was added and the organic layer was separated. From the organic layer 60 mg of **17** was obtained. The aqueous layer was acidified (about pH 2) with hydrochloric acid and the mixture was extracted with ethyl acetate. The combined extracts were washed with water and dried over anhydrous magnesium sulfate. After filtration, a solution of diazomethane in ether was added to the filtrate. The solvent was removed under reduced pressure to give 95 mg of **20** as crystals.

ii) To a solution of 180 mg of **18** in 4 ml of ethanol was added a solution of 40 mg of sodium hydroxide in 1 ml water. The reaction mixture was warmed up to 50 °C and stirred for 1 h at 50 °C. After cooling the solution was washed with ethyl acetate and acidified with hydrochloric acid. The organic layer was extracted with ethyl acetate and dried over anhydrous magnesium sulfate. After filtration a solution of diazomethane in ether was added and the solvent was removed under reduced pressure to give 90 mg of **20**: R_f= 0.4 (cyclohexane–ethyl acetate, 2:1 v/v); mp 78 °C; $[\alpha]_D^{25}$ −12.8° (c 1.01, $CHCl_3$); ^{1}H NMR ($CDCl_3$) δ=0.09 (6H, s), 0.89 (9H, s), 1.24 (3H, d, J=6 Hz), 3.25 (1H, m), 4.28 (1H, d, J=2.5 Hz), 4.2 (1H, m), 6.4 (1H, br s).

Found: C, 54.22; H, 8.86; N, 4.82%. Calcd for $C_{13}H_{25}NO_4Si$: C, 54.43; H, 8.77; N, 4.87%.

(3*S*,4*S*)-3-[(*R*)-1-(*t*-Butyldimethylsilyloxy)ethyl]-4-(hydroxymethyl)-2-azetidinone (21): A solution of 100 mg of **20** in 3 ml of water–THF (9:1) was cooled to 0 °C and 25 mg of sodium tetrahydroborate was added. The mixture was stirred for 15 min and ethyl acetate was added. The solution was washed with water and dried over anhydrous magnesium sulfate. The solvent was removed under reduced pressure to give 70 mg (78%) of **21**: Mp 90 °C (recrystallized from ether–hexane).

Found: C, 55.51; H, 9.84; N, 5.13%. Calcd for $C_{12}H_{25}NO_3Si$: C, 55.55; H, 9.71; N, 5.40%.

(3*S*,4*S*)-3-[(*R*)-1-(*t*-Butyldimethylsilyloxy)ethyl]-4-(*p*-tolylsulfonyloxymethyl)-2-azetidinone (22): To a solution of 100 mg of **21** in 2 ml of anhydrous THF–dichloromethane (1:1) was added 0.1 ml of pyridine and 100 mg of *p*-toluenesulfonyl chloride. The mixture was stirred overnight and dichloromethane was added. The solution was washed with water and dried over anhydrous magnesium sulfate. The solvent was removed under reduced pressure and the residue was purified by TLC (benzene–ethyl acetate, 5:1 v/v) to give 110 mg (68%) of **22**: Mp 89 °C (recrystallized from ether–hexane); IR (neat): 3300, 1778, 1375, 1170 cm^{-1}; ^{1}H NMR ($CDCl_3$) δ=0.08 (6H, s), 0.88 (9H, s), 1.18 (3H, d, J=6 Hz), 2.47 (3H, s), 2.7—3.0 (1H, m), 3.7—4.3 (4H, m), 6.00 (1H, br s), 7.2—7.85 (4H, m).

Found: C, 55.06; H, 7.47; N, 3.23; S, 7.75%. Calcd for $C_{19}H_{31}NO_5SSi$: C, 55.18; H, 7.55; N, 3.39; S, 7.75%.

(3*S*,4*S*)-3-[(*R*)-1-(*t*-Butyldimethylsilyloxy)ethyl]-4-iodomethyl-2-azetidinone (23): Sodium iodide (200 mg) was added to a solution of 100 mg of **22** in 3 ml of acetone. The mixture was warmed up to 60 °C and stirred for 7 h at the same temperature. After cooling the reaction mixture was filtered and the filtrate was evaporated. The residue was purified by TLC (benzene–ethyl acetate, 5:1 v/v) to give 85 mg of **23**: Mp 129 °C; IR (nujol): 3200, 1745 cm^{-1}; ^{1}H NMR ($CDCl_3$) δ=0.08 (6H, s), 0.88 (9H, s), 1.26 (3H, d, J=6 Hz), 2.85 (1H, dd, J=2 and 5 Hz), 3.2—3.5 (2H, m), 3.7—4.5 (2H, m), 6.24

(1H, br s).

Found: C, 38.94; H, 6.49; N, 3.60%. Calcd for $C_{12}H_{24}NO_2SiI$: C, 39.02; H, 6.50; N, 3.79%.

***p*-Nitrobenzyl 2-[(3*S*,4*S*)-3-[(*R*)-1-(*t*-Butyldimethylsilyloxy)-ethyl]-4-iodomethyl-2-oxo-1-azetidinyl]-2-hydroxyacetate (25):** A solution of 301.8 mg of **23** and 371.3 mg of *p*-nitrobenzyl glyoxylate hydrate in 100 ml of benzene was refluxed with stirring for 10 h. The solvent was removed under reduced pressure and the residue was purified by flash column chromatography (cyclohexane–ethyl acetate, 2:1 v/v) to give 318 mg (67%) of **25** as a mixture of the two diastereomers: R_f= 0.3 and 0.4 (cyclohexane–ethyl acetate, 2:1 v/v); ^{1}H NMR ($CDCl_3$) δ=0.07 (6H, s), 0.75 (9H, s), 1.28 (3H, d, J=6.4 Hz), 2.91 (1H, dd, J=2 and 4 Hz), 3.25—3.60 (2H, m), 3.75—4.45 (3H, m), 5.35 (2H, s), 5.25—5.65 (1H, m), 7.35—8.45 (4H, m).

***p*-Nitrobenzyl 2-[(3*S*,4*S*)-3-[(*R*)-1-(*t*-Butyldimethylsilyloxy)-ethyl]-4-iodomethyl-2-oxo-1-azetidinyl]-2-chloroacetate (26):** To a solution of 321 mg of **25** in 18 ml of THF was added 0.18 ml of 2,6-lutidine and 0.12 ml of thionyl chloride at −40 °C. After stirring for 20 min the reaction mixture was filtered through Celite and evaporated to give the crude chloro derivative **26**.

***p*-Nitrobenzyl (2*S*,5*S*,6*S*)-6-[(*R*)-1-(*t*-Butyldimethylsilyloxy)-ethyl]-7-oxo-3-thia-1-azabicyclo[3.2.0]heptane-2-carboxylate (27a) and *p*-Nitrobenzyl (2*R*,5*S*,6*S*)-6-[(*R*)-1-(*t*-Butyldimethylsilyloxy)ethyl]-7-oxo-3-thia-1-azabicyclo[3.2.0]-heptane-2-carboxylate (27b):** To a solution of **26** in 9 ml of dichloromethane was added 0.23 ml of triethylamine at 0 °C. Hydrogene sulfide was bubbled through this solution for 2 h at that temperature. The mixture was washed with water and dried over anhydrous magnesium sulfate. The solvent was removed under reduced pressure and the residue was purified by TLC (hexane–acetone–ethyl acetate, 25:3:6) to give 92.5 mg (36%) of **27b** and 157.5 mg (60%) of **27a**.

27a: R_f=0.8 (hexane–acetone–ethyl acetate, 25:3:6 v/v); mp 95 °C (recrystallized from hexane–ether); IR ($CHCl_3$): 1770, 1745 cm^{-1}; ^{1}H NMR ($CDCl_3$) δ=0.10 (6H, s), 0.90 (9H, s), 1.25 (3H, d, J=6 Hz), 2.7—3.3 (3H, m), 3.9—4.6 (2H, m), 4.82 (1H, s), 5.33 (2H, s), 7.4—8.5 (4H, m).

Found: C, 53.99; H, 6.41; N, 5.99; S, 6.83%. Calcd for $C_{21}H_{30}N_2O_6SSi$: C, 54.05; H, 6.48; N, 6.00; S, 6.87%.

27b: R_f=0.9 (hexane–acetone–ethyl acetate, 25:3:6 v/v); IR ($CHCl_3$): 1770, 1750 cm^{-1}; ^{1}H NMR ($CDCl_3$) δ=0.09 (6H, s), 0.88 (9H, s), 1.24 (3H, d, J=6 Hz), 2.7—3.7 (3H, m), 3.8—4.7 (2H, m), 5.26 (2H, s), 5.49 (1H, s), 7.3—8.4 (4H, m).

***p*-Nitrobenzyl (2*R*,5*S*,6*S*)-6-[(*R*)-1-Hydroxyethyl]-7-oxo-3-thia-1-azabicyclo[3.2.0]heptane-2-carboxylate (28):** To a solution of 180 mg of **27** in 4 ml of THF was added 0.21 ml of acetic acid and 0.552 mg of tetrabutylammonium fluoride trihydrate at 0 °C. After stirring overnight the reaction mixture was poured into a large quantity of ethyl acetate, washed with water, and dried over anhydrous magnesium sulfate. The solvent was removed under reduced pressure and the residue was purified by TLC (cyclohexane–ethyl acetate–acetone, 8:6:3 v/v) to give 37 mg (27%) of the diastereomer I and 35 mg (26%) of the diastereomer II. When the reaction time was overnight, diastereomer II changed to diastereomer I. Diastereomer I **28**: R_f=0.5 (cyclohexane–ethyl acetate–acetone, 8:6:3 v/v); ^{1}H NMR ($CDCl_3$) δ=1.37 (3H, d, J= 6 Hz), 2.0—2.5 (1H, br s), 2.8—3.8 (3H, m), 3.9—4.9 (2H, m), 5.28 (2H, s), 5.62 (1H, s), 7.3—8.5 (4H, m). Diastereomer II: R_f=0.4 (cyclohexane–ethyl acetate–acetone, 8:6:3 v/v); ^{1}H NMR ($CDCl_3$) δ=1.30 (3H, d, J=6 Hz), 1.7—2.5 (1H, br s), 2.7—3.6 (3H, m), 3.8—4.6 (2H, m), 4.76 (1H, s), 5.16 (2H, s), 7.3—8.5 (4H, m).

Sodium (2*R*,5*S*,6*S*)-6-[(*R*)-1-Hydroxyethyl]-7-oxo-3-thia-1-azabicyclo[3.2.0]heptane-2-carboxylate (29): To a solution of 46 mg of **28** in 5 ml of THF was added a solution of 11 mg of sodium hydrogencarbonate in 1.0 ml of water and 144.5 mg of 10% palladium on carbon. The mixture was shaken under a hydrogen atmosphere at 1 atm for 2 h, filtered through Celite, washed with ethyl acetate, and decolorized by activated carbon powder. The solution was lyophilized to give 11.4 mg (37%) of **29**: ^{1}H NMR (D_2O, DSS) δ=1.27 (3H, d, J=6 Hz), 2.7—3.4 (3H, m).

Methyl *dl*-[(2*R,3*S**,5*R**)-7-Oxo-3-phenylthio-1-azabicyclo[3.2.0]heptane]-2,3-dicarboxylate (32) and Methyl *dl*-[(2*R**,3*S**,5*S**)-7-Oxo-3-phenylthio-1-azabicyclo[3.2.0]heptane]-2,3-dicarboxylate (33):** Potassium hydride (35% in mineral oil, 8.015 mmol) was placed in the reaction flask and washed three times with dry hexane. The solid reagent was then slurried in 10 ml of dry THF and cooled to −40 °C. A solution of iodomethyl derivative **30** (1.127 g, 5.343 mmol) in 5 ml of THF and 2.12 g (8.015 mmol) of **31** in 5 ml of THF was added and the mixture was stirred at −25—−40 °C for 3 h. The reaction was quenched with sat. ammonium chloride and the organic layer was extracted with ethyl acetate. The combined extracts were dried over anhydrous magnesium sulfate. The solvent was removed under reduced pressure and the residue was purified by flash column chromatography (cyclohexane–ethyl acetate, 2:1 v/v) to give 478.9 mg (27%) of a mixture of **32** and **33**. These diastereomers were separated by TLC (cyclohexane–ether, 1:2 v/v).

32: R_f=0.35 (cyclohexane–ether, 1:2 v/v); ^{1}H NMR ($CDCl_3$) δ=2.2—3.3 (4H, m), 3.48 (3H, s), 3.86 (3H, s), 3.8—4.3 (1H, m), 5.28 (1H, s), 7.3—7.8 (5H, m).

33: R_f=0.30 (cyclohexane–ether, 1:2 v/v); mp 137—139 °C (recrystallized from hexane–ether); IR (KBr pellet): 1765, 1740 cm^{-1}; ^{1}H NMR ($CDCl_3$) δ=2.22 (1H, dd, J=10 and 14 Hz), 2.74 (1H, dd, J=5 and 14 Hz), 2.8—3.3 (2H, m), 3.46 (3H, s), 3.5—3.9 (1H, m), 3.88 (3H, s), 4.69 (1H, s), 7.0—7.7 (5H, m).

Found: C, 57.36; H, 4.93; N, 4.20; S, 9.63%. Calcd for $C_{16}H_{17}NO_5S$: C, 57.47; H, 4.82; N, 4.19; S, 9.59%.

Dimethyl (2*R*,3*S*,5*R*,6*S*)-6-[(*R*)-1-(*t*-Butyldimethylsilyloxy)-ethyl]-7-oxo-3-phenylthio-1-azabicyclo[3.2.0]heptane-2,3-dicarboxylate (34) and Dimethyl (2*S*,3*R*,5*R*,6*S*)-6-[(*R*)-1-(*t*-Butyldimethylsilyloxy)ethyl]-7-oxo-3-phenylthio-1-azabicyclo-[3.2.0]-heptane-2,3-dicarboxylate (35): Starting with **23** and **31**, the above procedure gave a mixture of **34** and **35**. Reaction time 2.5 h. Reaction temperature −70—−10 °C. Yield 15%. ^{1}H NMR ($CDCl_3$) δ=0.05 (6H, s), 0.81 (9H, s), 1.20 (3/2H, d, J=6 Hz), 1.23 (3/2H, d, J=6 Hz), 1.5—2.0 (1H, m), 2.7—3.6 (2H, m), 3.66 (3/2H, s), 3.69 (3/2H, s), 3.71 (3/2H, s), 3.84 (3/2H, s), 3.8—4.5 (1H, m), 5.48 (1/2H, s), 5.61 (1/2H, s), 6.9—7.7 (5H, m).

Dimethyl *dl*-(2*R,3*S**,5*S**)-3-Methylthio-7-oxo-1-azabicyclo[3.2.0]heptane-2,3-dicarboxylate (37) and Dimethyl *dl*-(2*R**,3*S**,5*R**)-3-methylthio-7-oxo-1-azabicyclo[3.2.0]heptane-2,3-dicarboxylate (38):** Potassium hydride (35% in mineral oil, 2.59 mmol) was placed in the reaction flask and washed twice with dry hexane. The solid reagent was then slurried in 5 ml of THF and cooled to −78 °C. Catalytic amount of 18-crown-6 and 435.1 mg (2.59 mmol) of diphenylmethane was added and stirred for 2 h at −78—20 °C.

The mixture was cooled to −40 °C and a solution of 273.2 mg (1.30 mmol) of **30** in 5 ml of THF and 509.4 mg (2.68 mmol) of **36**. The reaction mixture was stirred for 3 h at −40—−20 °C. The reaction was quenched with sat. ammonium chloride and the organic layer was extracted with ethyl acetate. The combined extracts was dried over anhydrous magnesium sulfate. The solvent was removed under reduced pressure and the residue was purified by flash column chromatography (cyclohexane–ethyl acetate, 2:1 v/v)to give 15 mg (4%) of a mixture of **37** and **38**.

The diastereomer **38**: ^{1}H NMR ($CDCl_3$) δ=2.14 (3H, s), 2.43 (1H, dd, J=6 and 15 Hz), 2.87 (1H, dd, J=1 and 6 Hz), 2.9—3.6 (2H, m), 3.76 (3H, s), 3.80 (3H, s), 3.8—4.4 (1H, m), 5.31 (1H, s).

Dimethyl (2*R*,3*S*,5*R*,6*S*)-6-[(*R*)-1-(*t*-Butyldimethylsilyloxy)-ethyl]-3-methylthio-7-oxo-1-azabicyclo[3.2.0]heptane-2,3-dicarboxylate (39) and Dimethyl (2*S*,3*R*,5*R*,6*S*)-[(*R*)-1-(*t*-Butyldimethylsilyloxy)ethyl]-3-methylthio-7-oxo-1-azabicyclo[3.2.0]heptane-2,3-dicarboxylate (40): Potassium hydride (35% in mineral oil, 2.26 mmol) was placed in the reaction flask and washed with dry hexane. The solid reagent was then slurried in 2 ml of THF and cooled to −78 °C. Diphenylmethane (384.6 mg, 2.289 mmol) and 18-crown-6 (599.9 mg, 2.272 mmol) was added and stirred for 2.5 h at −78—20 °C. The reaction mixture was cooled to −40 °C and a solution of 804 mg (2.179 mmol) of **23** in 6 ml of THF was added to the mixture. After stirringfor 5 min a solution of 858.8 mg (4.520 mmol) of **36** in 4 ml of THF was added slowly. The reaction mixture was stirred for 2.75 h at −40—−20 °C. The reaction was quenched with sat. aqueous ammonium chloride and the organic layer was extracted with ethyl acetate. The combined extracts were dried over anhydrous magnesium sulfate. The solvent was removed under reduced pressure and the residue was purified by flash column chromatography (cyclohexane–dichloromethane, 10:1 v/v) to give 165.9 mg (18%) of the products as a mixture of two diastereomers which were separated by TLC (cyclohexane–ethyl acetate, 1:1 v/v).

39: R_f=0.65 (cyclohexane–ether, 1:1 v/v); IR ($CHCl_3$): 1772, 1735 cm^{-1}; ^{1}H NMR ($CDCl_3$) δ=0.05 (6H, s), 0.88 (9H, s), 1.19, (3H, d, J=6.6 Hz), 2.16 (3H, s), 2.1—2.5 (1H, m), 2.7—3.2 (2H, m), 3.79 (3H, s), 3.80 (3H, s), 3.8—4.4 (2H, m), 5.34 (1H, s).

Found: C, 52.83; H, 7.89; N, 3.33%. Calcd for $C_{19}H_{33}NO_6SSi$: C, 52.88; H, 7.70; N, 3.25%.

40: R_f=0.60 (cyclohexane–ether, 1:1 v/v); IR (neat) 1770, 1735 cm^{-1}; ^{1}H NMR ($CDCl_3$) δ=0.04(6H, s), 0.84 (9H, s), 1.15 (3H, d, J=6 Hz), 2.10 (3H, s), 2.18 (1H, d, J=12.6 Hz), 2.71 (1H, dd, J=6 and 12.6 Hz), 3.08 (1H, dd, J=3 and 6 Hz), 3.3—3.8 (1H, m), 3.77 (3H, s), 3.87 (3H, s), 3.8—4.4 (1H, m), 4.69 (1H, s).

Disodium (2*R*,3*S*,5*R*,6*S*)-6-[(*R*)-1-(*t*-Butyldimethylsilyloxy)-ethyl]-3-methylthio-7-oxo-1-azabicyclo[3.2.0]heptane-2,3-dicarboxylate (43): To a solution of 92.4 mg (0.214 mmol) of **39** in 10 ml of THF–water (1:1) was added 1 equiv of 0.1 mol dm^{-3} aqueous sodium hydroxide for 8 h. The mixture was stirred for 3 d and evaporated. The solution was lyophilized to give 88.4 mg (92%) of **43**: ^{1}H NMR ($CDCl_3$) δ=0.17 (6H, s), 0.93 (9H, s), 1.28 (3H, d, J=5.4 Hz), 2.10 (3H, s), 2.0—2.5 (3H, m), 5.36 (1H, s).

References

1) Part VIII, K. Fujimoto, Y. Iwano, and K. Hirai, submitted for publication in this journal. Preliminary communications: a) K. Hirai, Y. Iwano, and K. Fujimoto, *Tetrahedron Lett.*, **23**, 4021 (1982); *ibid.*, **23**, 4025 (1982); K. Fujimoto, Y. Iwano, and K. Hirai, *ibid.*, **25**, 1151 (1984).

2) J. S. Kahan, F. M. Kahan, R. Goegelman, S. A. Currie, M. Jackson, E. O. Stapley, T. W. Miller, A. K. Miller, D. Hendlin, S. Mochales, S. Hernandez, H. B. Woodruff, and J. Birnbaum, *J. Antibiot.*, **32**, 1 (1979); G. Albers-Schönberg, B. H. Arison, O. D. Hensens, J. Hirshfield, K. Hoogsteen, E. A. Kaczka, R. E. Rhodes, J. S. Kahan, F. M. Kahan, R. W. Ratcliffe, E. Walton, L. J. Ruswinkle, R. B. Morin, and B. G. Christensen, *J. Am. Chem. Soc.*, **100**, 6491 (1978).

3) W. J. Leanza, K. J. Wildonger, J. Hannah, D. H. Shih, R. W. Ratcliffe, L. Barash, E. Walton, R. A. Firestone, G. F. Patel, F. M. Kahan, J. S. Kahan, and B. G. Christensen, "Recent Advances in the Chemistry of β-Lactam Antibiotics," ed by G. I. Gregory second international symposium, Cambridge, England, The Royal Society of Chemistry p. 240 (1980); W. Drückheimer, J. Blumbach, R. Lattrell, and K. H. Scheunemann, *Angew. Chem. Int. Ed. Eng.*, **24**, 189 (1985).

4) P. A. Grieco, D. L. Flynn, and R. E. Zelle, *J. Am. Chem. Soc.*, **106**, 6414 (1984) and the references cited therein.

5) K. Hirai, Y. Iwano, and K. Fujimoto, *Heterocycles*, **17**, 201 (1982).

6) J. C. Sheehan, Y. S. Lo, J. Loliger, and C. C. Podewell, *J. Org. Chem.*, **39**, 1444 (1974).

7) M. Ishiguro and T. Nakatsuka, the 105th Annual Meeting of the Pharmaceutical Society of Japan, Kanazawa, April. 1985, Abstr. No. 4P 9—3, p. 623.

8) J. A. Aimetti, E. S. Hamanaka, D. A. Johnson, and M. S. Kellog, *Tetrahedron Lett.*, **1979**, 4631.

9) F. A. Bouffard and B. G. Christensen, *J. Org. Chem.*, **46**, 2208 (1981).

10) K. Clauss, D. Grimm, and G. Prossel, *Liebig's Ann. Chem.*, **1974**, 539.

11) Recent Review: T. Kametani, K. Fukumoto, and M. Ihara, *Heterocycles*, **17**, 463 (1982).

12) K. Hirai, Y. Iwano, and K. Fujimoto, *Tetrahedron Lett.*, **24**, 3251 (1983).

13) T. C. Smale, *J. Chem. Soc., Perkin Trans. 1*, **1980**, 187; E. G. Brain, A. J. Eglington, J. H. C. Nayler, N. F. Osbone, R. Southgate, and P. Tolliday, *J. Chem. Soc., Perkin Trans. 1*, **1977**, 2479; A. G. Brown, D. F. Corbett, and T. T. Howarth, *J. Chem. Soc., Chem. Commun.*, **1977**, 359.

14) K. Hirai, K. Fujimoto, Y. Iwano, T. Hiraoka, T. Hata, and C. Tamura, *Tetrahedron Lett.*, **22**, 1021 (1981).

15) B. M. Trost and Y. Tamaru, *J. Am. Chem. Soc.*, **99**, 3101 (1977).

16) P. J. Giddings, D. I. John, and E. J. Thomas, *Tetrahedron Lett.*, **1978**, 995; *ibid.*, **21**, 399 (1980).

Total Synthesis of (−)-Vitrenal and Its Biological Activity

Mitsuaki KODAMA,** Usman S. F. TAMBUNAN, Tetsuto TSUNODA, and Shô ITÔ*
Department of Chemistry, Faculty of Science, Tohoku University, Aramaki-aza-Aoba, Sendai 980
(Received December 25, 1985)

(−)-Vitrenal, the enantiomer of the natural sesquiterpene aldehyde isolated from a liverwort, has been synthesized starting from (+)-3-carene, and its activity as a plant-growth regulator has been tested.

(+)-Vitrenal ((+)-**1**) is a tricyclic sesquiterpene aldehyde isolated by Matsuo et al. from a liverwort, *Lepidozia vitrea*, together with its possible biogenetic precursor, isobicyclogermacrenal (**2**), and lepidozenal (**3**).[1] All of these compounds have been shown to possess potent plant-growth inhibitory activity.[1] Because

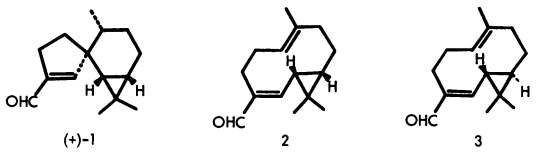

of its unique carbon skeleton as well as the biological activity, we have attempted a total synthesis of (−)-vitrenal ((−)-**1**), the enantiomer of the natural product, from easily accessible (+)-3-carene. Successful synthesis of (−)-**1** would provide us with a rare chance to test the growth-regulating activity of unnatural enantiomer. Although a synthesis of (±)-vitrenal has been reported by Magari et al.,[2] and our approach is somewhat similar to theirs, we describe our synthesis herein because we have successfully achieved stereocontroled C–C bond formation in two crucial steps by employing Claisen rearrangement. We also describe the result of our biological test.

Results and Discussion

Our synthetic strategy is shown in the form of retrosynthesis. The first Claisen rearrangement (A→B) would proceed in high stereoselectivity. The reduction of double bond in B would proceed from β-face due to the presence of a bulky dimethylcyclopropyl ring. Introduction of double bond, the formation of C, may not be selective, but both geometrical isomers would afford the same carboxylic ester E after the 2nd Claisen rearrangement, as long as the vinyl terminus approaches the allyl part from the less hindered and therefore favored β-face. Elongation of ester chain and cleavage of double bond in E to the dialdehyde F, and its aldol condensation should be unambiguous.

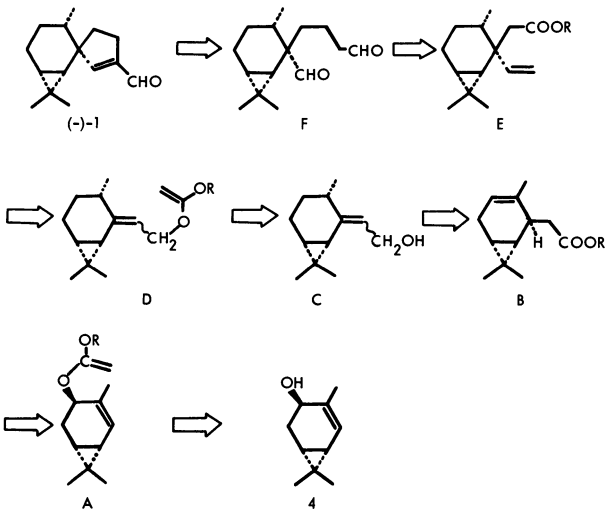

Starting with 2-caren-4β-ol (**4**), obtained by the known procedure,[3] the first Claisen rearrangement was performed: Heating **4** at 137° with excess triethyl orthoacetate in the presence of propionic acid induced vinyl ether formation and its Claisen rearrangement in one pot to afford, after hydrolysis and methylation, the methyl ester **5** in 65% yield. Catalytic hydrogenation (Pd–C) of **5** afforded the saturated ester **6** in quantitative yield. However, gas chromatographic analysis of **6** revealed the presence of stereoisomers in the ratio of 95:5. Assignment of the stereochemistry for the major isomer rests on the consideration of steric requirement in hydrogenation described above. Since the separation of the isomers was possible only by gas chromatography, the mixture was used in the following steps.

Phenylselenylation followed by oxydative deselenylation of **6** gave the unsaturated ester **7** in 75% yield. As was expected (vide supra), **7** was a 1:1 mixture of geometrical isomers. Although the isomers were separated by gas chromatography and properly characterized, the mixture was used without separation for further steps. The ester **7** was reduced with diisobutylaluminum hydride (DIBAL) to give the allylic alcohol **8** in 91% yield. The geometrical isomers were

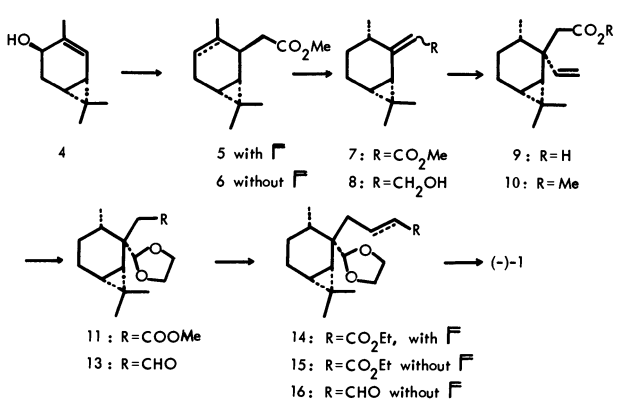

**Present address: Faculty of Pharmaceutical Sciences, Tokushima Bunri University, Tokushima 770.

possible to separate only by gas chromatography.

For the introduction of the second carbon chain, Claisen rearrangement was again applied on the mixture **8**. Heating **8** with excess triethyl orthoacetate under the conditions similar to the previous reaction, and the subsequent alkaline hydrolysis furnished a single crystalline acid **9** in 56% yield. Its methyl ester **10** gives a single peak on GLC, while the methyl ester of the acidic mother liquor exhibited the same major peak along with a minor peak. Thus both geometrical isomers must have yielded the same acid **9** as expected.[4] We have thus removed the undesired stereoisomer on the secondary methyl group simultaneously at this stage.

With chemically and optically pure acid **9** in hand, we have proceeded to the construction of the cyclopentene ring. The double bond in the ester **10** was ozonized and the formyl group formed was protected by ethylene glycol to give the acetal carboxylate **11** in 72% yield. When the protection was attempted with trimethyl orthoformate in the presence of *p*-toluenesulfonic acid, the product **12** obtained has the rearranged structure. It may be formed through the sequence shown.

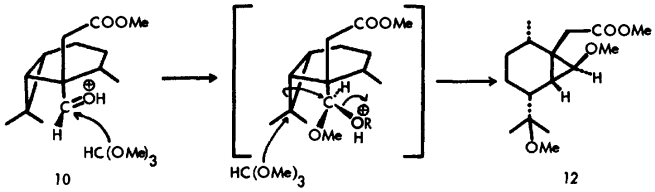

DIBAL reduction of **11** and pyridinium chlorochromate (PCC) oxidation of the resulted alcohol gave the acetal aldehyde **13** in 90% yield. Wittig reaction of **13** with (ethoxycarbonylmethylene)triphenylphosphorane went smoothly and the unsaturated ester **14** was obtained in 95% yeild. Catalytic reduction of **14** (to **15**) and subsequent DIBAL reduction followed by PCC oxidation afforded the acetal aldehyde **16**. Finally, treatment of **16** with hydrochloric acid accomplished deacetalization and aldol condensation in one pot to afford (−)-**1**. IR and NMR spectra of the product were identical and the specific rotation ($[\alpha]_D^{18}$ −113°) is completely opposite with those of natural vitrenal ($[\alpha]_D$ +107°).[1]

Although the biological activities of enantiomers have extensively been investigated in the field of insect pheromones,[5] the similar studies on growth regulators are rather scarce probably because natural regulators usually have rather complicated structures and synthesis of the unnatural enantiomer is not easy. The present synthesis of (−)-**1** gave us a good opportunity to compare the activity of the enantiomeric pair. Thus, we have carried out biological test using rice seedling and lettuce hypocotyl. While natural (+)-**1** shows a strong inhibition (I_{50}=18 ppm),[1] (−)-**1** exhibited a weak promotion (P_{50}=2.18×10³ ppm) in the former test and a weak inhibition (I_{50}=27.79×10³ ppm) for the latter. To the best of our knowledge, this is the first enantiomeric pair tested for the growth-regulating activity in higher plants.

Experimental

General. Melting points reported herein were taken with a YANACO melting point apparatus and are uncorrected. The ^{1}H NMR spectra were obtained on a Varian EM-390, a Varian XL-200 and/or a JEOL FX 90Q spectrometer. Chemical shifts are reported in ppm downfield from internal tetramethylsilane. Infrared spectra were recorded on a JASCO IR-2 diffraction grating infrared spectrometer. Mass spectra were measured on a HITACHI M-52 mass spectrometer and high resolution mass spectra on a JEOL JMS-01S02 mass spectrometer. Elemental analyses were performed on a YANAGIMOTO-CHN Coder. Gas chromatogram were recorded on a Shimadzu GC-6A. Optical rotation was measured on a UNION Automatic Digital Polarimeter, PM101.

(+)-Methyl 2β-(3-Caren-2-yl)acetate (5). A mixture of 2-caren-4-ol[3] (**4**, 10.6 g), propionic acid (0.6 ml) and triethyl orthoacetate (129 ml, 6.0 equiv) was heated at 136—137 °C for 20 h, and the reaction mixture was hydrolyzed with KOH (25.76 g) in 50% aq methanol (600 ml) under reflux for 4 h. After cooling, the reaction mixture was diluted with water and washed with ether. Separated aqueous layer was neutralized with 2 M HCl (1 M=1 mol dm^{-3}), and then extracted with ether. After washed with water and brine and dried over anhydrous $MgSO_4$, the ether extract was treated with diazomethane at room temperature for 30 min, and the solvent was distilled off. The residue was chromatographed on SiO_2 column (hexane:ether=10:1) to give 9.437 g (65% yeild) of **5**. Bulb-to-bulb distillation at 75 °C, 0.05 mmHg (1 mmHg=133.322 Pa), furnished the analytical sample as a colorless oil: IR (neat) 1734 cm^{-1}; ^{1}H NMR (CCl_4) δ=0.88, 1.03 (2s, 6H, $2CH_3$), 1.63 (s, 3H, CH_3), 3.63 (s, 3H, $COOCH_3$), 5.21 (s, b, 1H, C=CH); MS *m/z* 208 (M^+); $[\alpha]_D^{24}$ +6.5° (*c* 1.75, MeOH). Found: C, 75.25; H, 9.70. Calcd for $C_{13}H_{20}O_2$: C, 74.96; H, 9.68.

(−)-Methyl 2β-(2-Caranyl)acetate (6). **5** (3.00 g) was hydrogenated (3 Atm) in methanol (75 ml) at room temperature over palladium charcoal (600 mg) for 3 h. Filtration of the catalyst and evaporation of the solvent gave 3.027 g (100% yield) of **6**, colorless liquid. Gas chromatography of **6** disclosed the presence of two isomers in the ratio of 95:5 (DEG-S 15%, 130 °C). Preparative gas chromatography furnished the analytical sample of **6**, colorless oil: IR (neat) 1734 cm^{-1}; ^{1}H NMR ($CDCl_3$) δ=0.93 (d, 3H, *J*=10.5 Hz, CH_3), 0.96 (s, 6H, $2CH_3$), 3.66 (s, 3H, $COOCH_3$); MS *m/z* 210 (M^+); $[\alpha]_D^{24}$ −150° (*c* 1.28, MeOH). Found: C, 73.96; H, 10.56. Calcd for $C_{13}H_{22}O_2$: C, 74.24; H, 10.54.

Methyl 2-Caranylideneacetate (7). To a solution of lithium diisopropylamide (22.8 mmol) in dry tetrahydrofuran (50 ml) was added **6** (11.4 mmol) dropwise at −78 °C under argon atmosphere. After stirring for 30 min, benzeneselenenyl chloride (4.336 g) in dry tetrahydrofuran (5 ml) was added dropwise rapidly, and stirring was continued overnight at room temperature. Addition of water, extraction with ether, drying over anhydrous $MgSO_4$ and evaporation of the solvent gave, after short SiO_2 column chromatography (hexane:ether=10:1), 3.281 g (76% yield) of phenylseleno

compound.

To the phenylseleno compound in methanol (50 ml) was added $NaIO_4$ (4.438 g) in water (50 ml) with vigorous stirring. After 2 h, the product was extracted with ether. The extract was washed with water, saturated $NaHCO_3$ and brine, and dried over anhydrous Na_2SO_4. Evaporation of the solvent and SiO_2 chromatography of the residue (hexane:ether=50:1) gave 1.790 g (75%) of **7** as a colorless oil. Gas chromatographic analysis showed two peaks in the ratio of nearly 1:1 (DEG-S 15%, 160°C). Each peak was separated by preparative gas chromatography to give analytical specimens. **7a**: IR (neat) 1710, 1610 cm^{-1}; ^1H NMR ($CDCl_3$) δ=0.82, 1.04 (2s, 6H, $2CH_3$), 1.19 (d, 3H, J=7.2 Hz, CH_3), 3.71 (s, 3H, $COOCH_3$), 5.82 (t, 1H, J=1.8 Hz,C=CH); MS m/z 208 (M^+). **7b**: IR (neat) 1704, 1604 cm^{-1}; ^1H NMR ($CDCl_3$) δ=0.95 (s, 3H, CH_3), 1.09 (d, 3H, J=7.2 Hz, CH_3), 1.10 (s, 3H, CH_3), 3.67 (s, 3H, $COOCH_3$), 5.84 (s, 1H, C=CH); MS m/z 208 (M^+).

2-(2-Caranylidene)ethanol (8). A mixture of **7a** and **7b** (800 mg) in dry hexane (20 ml) was stirred at 0°C for 2 h with 1 M DIBAL solution (11 ml) under argon atmosphere. After saturated NH_4Cl (10 ml) was added, organic layer was separated and aqueous layer was extracted with ether. The organic layer was washed with water and brine, dried over anhydrous Na_2SO_4 and then solvent was evaporated. The residue was chromatographed on SiO_2 (hexane:ether=1:1) to give 700 mg (91%) of **8** with two components as a colorless oil. Preparative gas chromatography (DEG-S 15%, 160°C) separated each component **8a**: IR (neat) 3317, 1634 cm^{-1}; ^1H NMR ($CDCl_3$) δ=0.85 (s, 3H, CH_3), 1.02 (d, 3H, J=7.2 Hz, CH_3), 1.09 (s, 3H, CH_3), 4.24 (t, 2H, J=7.2 Hz, $=HCCH_2O$), 5.58 (t, 1H, J=7.2 Hz, C=CH); MS m/z 180 (M^+). **8b**: IR (neat) 3300, 1635 cm^{-1}; ^1H NMR ($CDCl_3$) δ=0.89 (s, 3H, CH_3), 0.95 (d, 3H, J=7.2 Hz, CH_3), 1.05 (s, 3H, CH_3), 4.23 (m, 2H, $=CH-CH_2O$), 5.58 (t, 1H, J=7.2 Hz, C=CH); MS m/z 180 (M^+).

(−)-(2-Vinyl-2-caranyl)acetic Acid (9). A mixture of **8** (500 mg) and triethyl orthoacetate (6.3 ml) was heated in benzene (30 ml) at 140°C for 10 h in the presence of a trace of propionic acid. After evaporation of the excess triethyl orthoacetate, the reaction mixture was heated under reflux overnight with KOH (454 mg) in 50% aq methanol (50 ml). The reaction mixture was diluted with water and washed throughly with ether to remove neutral materials. The aqueous solution was neutralized with 2 M HCl, and then extracted with ether. The $MgSO_4$-dried ether extract gave, after evaporation of the solvent, 350 mg (56% yield) of crystals. Recrystallization in 20% aq methanol gave 311 mg of **9**, colorless needles, mp 85—87°C: IR (KBr) 1693, 1634 cm^{-1}; ^1H NMR ($CDCl_3$) δ=0.83 (d, 3H, J=6.5 Hz, CH_3), 0.99, 1.08 (2s, 6H, $2CH_3$), 2.62 (s, 2H, CH_2CO_2), 4.9—5.1 (m, 2H, $C=CH_2$), 5.96 (dd, 1H, J=17.5, 10.5 Hz, C=CH); MS m/z 222 (M^+); $[\alpha]_D^{24}$ −145° (c 1.12, MeOH). Found: C, 75.62; H, 10.06. Calcd for $C_{14}H_{20}O_2$: C, 75.63; H, 9.97.

(−)-Methyl(2-vinyl-2-caranyl)acetate (10). Treatment of **9** (250 mg) with diazomethane furnished, after SiO_2 chromatography (hexane:ether=10:1), the methyl ester **10** (267 mg, 100%) as a colorless oil. IR (neat) 1736, 1676 cm^{-1}; ^1H NMR ($CDCl_3$) δ=0.82 (d, 3H, J=7.5 Hz, CH_3), 1.02, 1.10 (2s, 6H, $2CH_3$), 2.58 (s, 2H, CH_2CO_2), 3.63 (s, 3H, OCH_3), 4.9—5.1 (m, 2H, $C=CH_2$), 5.94 (dd, 1H, J=17.5, 10.5 Hz, CH=C); $[\alpha]_D^{24}$ −125° (c 1.12, MeOH). Found: m/z 236.1787. Calcd for $C_{15}H_{24}O_2$: M, 236.1775.

Acetal Carboxylate 11. Ozone was passed through a solution of **10** (200 mg) in methanol (10 ml) at −78°C for 1 h and reductive (Me_2S) work up of the reaction mixture gave an oily aldehyde (180 mg) which was converted without purification to **11** by heating it with ethylene glycol in dry benzene in the presence of catalytic amount of p-toluenesulfonic acid. Chromatographic separation on SiO_2 column (hexane:ether=10:1) afforded 173 mg (72% yield) of **11** as a colorless oil: IR (CCl_4) 1726 cm^{-1}; ^1H NMR ($CDCl_3$) δ=0.93 (d, 3H, J=7.5 Hz, CH_3), 1.00, 1.15 (2s, 6H, $2CH_3$), 2.49 (d, 1H, J=13.5 Hz, CH_2CO_2), 2.70 (d, 1H, J=13.5 Hz, CH_2CO_2), 3.63 (s, 3H, OCH_3), 3.6—4.0 (m, 4H, $O(CH_2)_2O$), 4.78 (s, 1H, $HC<^{O}_{O}$); $[\alpha]_D^{24}$ −135° (c 1.12, MeOH). Found: m/z 282.1847. Calcd for $C_{16}H_{26}O_4$: M, 282.1830.

Compound 12. Methyl ester **10** (40 mg), OsO_4 (2 mg), and $NaIO_4$ (90 mg) were stirred overnight in 50% aq tetrahydrofuran. After dilution, the reaction mixture was extracted with ether. Normal work-up and evaporation yielded an oily aldehyde (40 mg). Without purification, the aldehyde was stirred overnight with trimethyl orthoformate (291 mg), and p-toluenesulfonic acid (catalytic amount). Neutralization, extraction with ether, drying, evaporation and finally SiO_2 chromatography afforded 31 mg (68%) of **12**, a colorless liquid. IR (neat) 1726 cm^{-1}; ^1H NMR ($CDCl_3$) δ=0.91 (d, 3H, J=7.0 Hz, CH_3), 1.18, 1.22 (2s, 6H, $2CH_3$), 2.25 (d, 1H, J=16.3 Hz, CH_2CO_2), 2.62 (d, 1H, J=16.3 Hz, CH_2CO_2), 3.04 (d, 1H, J=3.2 Hz, CHO), 3.19, 3.31 (2s, 6H, $2OCH_3$), 3.68 (s, 3H, CO_2Me); MS m/z 284 (M^+).

Acetal Aldehyde 13. Compound **11** (130 mg) was reduced with DIBAL in hexane at −78°C for 30 min. The reaction was quenched with water (1 ml) and the product was extract with ether. Evaporation of the solvent gave 123 mg of the mixture of **13** and the corresponding alcohol.

Without purification, the mixture (123 mg) was oxidized with pyridinium chlorochromate (278 mg) in dichloromethane (10 ml). After stirring for 1 h, ether (10 ml) was added and stirred for 5 min and then filtrated. Evaporation of the solvent, and SiO_2 chromatography (hexane:ether=1:1) of the residue gave 102 mg (90%) of **13**, a colorless oil: IR (CCl_4) 1710 cm^{-1}; ^1H NMR ($CDCl_3$) δ=0.96 (d, 3H, J=7.5 Hz, CH_3), 1.02, 1.17 (2s, 6H, $2CH_3$), 2.34 (dd, 1H, J=15.0; 3.6 Hz, CH_2CO), 2.76 (dd, 1H, J=15.0; 3.6 Hz, CH_2CO), 3.7—3.9 (m, 4H, $O(CH_2)_2O$), 4.78 (s, 1H, $HC<^{O}_{O}$), 9.89 (t, 1H, J=3.6 Hz, CHO); $[\alpha]_D^{24}$ −122.5° (c 1.12, MeOH). Found: m/z 208.1456 ($-C_2H_4O$). Calcd for $C_{15}H_{24}O_3$: M, 252.1724.

Wittig Reaction of 13 (synthesis of 14). Benzene (10 ml) solution of **13** (100 mg) and (ethoxycarbonylmethylene)triphenylphosphorane (331 mg) was heated under reflux for 12 h. The solvent was removed in vacuo, and the residue was chromatographed on SiO_2 column (CH_2Cl_2) to give **14** (116 mg, 95%) as a colorless oil: IR (CCl_4) 1713, 1642 cm^{-1}; ^1H NMR (CCl_4) δ=0.88 (d, 3H, J=6.6 Hz, CH_3), 1.01, 1.14 (2s, 6H, $2CH_3$), 1.28 (t, 3H, J=6.6 Hz, OCH_2CH_3), 2.45 (d, 2H, J=9.0 Hz, CH_2), 3.8—4.0 (m, 4H, $O(CH_2)_2O$), 4.11 (q, 2H, J=6.6 Hz, OCH_2CH_3), 4.73 (s, 1H, $HC<^{O}_{O}$), 5.73 (d, 1H, J=15.6 Hz, $CH=CHCO_2Et$), 6.91 (dd, 1H, J=15.6; 6.6 Hz, $CH=CH-CO_2Et$); $[\alpha]_D^{24}$ −83° (c 1.12, MeOH). Found: m/z 322.2142. Calcd for $C_{19}H_{30}O_4$: M, 322.2142.

Acetal Butanoate 15. Catalytic reduction of **14** (50 mg) in methanol (3 ml) over palladium charcoal (5 mg) furnished, after filtration of the catalyst and evaporation of the solvent, **15**, a colorless oil, in quantitative yield. IR (CCl_4) 1712 cm^{-1}; ^1H NMR ($CDCl_3$) δ=0.89 (d, 3H, J=7.2 Hz, CH_3), 0.99, 1.15 (2s, 6H, $2CH_3$), 1.26 (t, 3H, J=7.2 Hz, OCH_2CH_3), 3.4—3.9 (m,

4H, $O(CH_2)_2O$), 4.13 (q, 2H, J=7.2 Hz, OCH_2CH_3) and 4.75 (s, 1H, $HC(O)$); $[\alpha]_D^{24}$ −75° (*c* 1.12, MeOH). Found: *m/z* 324.2257. Calcd for $C_{19}H_{32}O_4$: M, 324.2299.

Acetal Aldehyde 16. Compound **15** (36 mg) was reduced with 1.2 equivalent of DIBAL at −78 °C in dry hexane (2 ml) under argon atmosphere. After stirring for 30 min, the reaction was quenched with water. Extraction with ether furnished a mixture (30.2 mg) of **16** and the corresponding alcohol.

The mixture was oxidized in CH_2Cl_2 (1 ml) with pyridinium chlorochromate (78 mg). After stirring for 1 h, ether (5 ml) was added and the reaction mixture was filtrated. Evaporation of the solvent and SiO_2 chromatography (hexane: ether=1:1) gave 28.6 mg (85%) of **16** as a colorless oil. IR (CCl_4) 1716, 1453 cm^{-1}; ^1H NMR ($CDCl_3$) δ=0.89 (d, 3H, J=7.2 Hz, CH_3), 0.99, 1.15 (2s, 6H, $2CH_3$), 3.66—3.99 (m, 4H, $O(CH_2)_2O$), 4.74 (s, 1H, $HC(O)$), 9.77 (t, 1H, J=2.3 Hz, CHO); $[\alpha]_D^{20}$ −102.5° (*c* 0.5, MeOH). Found: *m/z* 280.2037. Calcd for $C_{17}H_{28}O_3$: M, 280.2037.

(−)-Vitrenal ((−)-1). Compound **16** (20 mg) in THF (2.4 ml) was heated for 6 h under reflux with 10% of aq HCl (0.6 ml). The reaction mixture was diluted with water, neutralized by saturated aq $NaHCO_3$, and extracted with ether. Evaporation of the solvent and short column SiO_2 chromatography afforded 14.7 mg (94%) of (−)-**1**. IR (CCl_4) 1680, 1614, 854 cm^{-1}; ^1H NMR ($CDCl_3$) δ=0.77 (d, 3H, J=5.5 Hz, CH_3), 0.94, 1.17 (2s, 6H, $2CH_3$), 6.86 (t, 1H, J=1.5 Hz, CH=C), 9.76 (s, 1H, CHO); $[\alpha]_D^{18}$ −113° (*c* 0.4, MeOH). Found: *m/z* 218.1673. Calcd for $C_{15}H_{22}O$: M, 218.1670.

The authors express their gratitude to Dr. N. Okagami, Tohoku University, for the tests of biological activity and to Dr. A. Matsuo, Hiroshima University, for the spectra of natural vitrenal.

References

1) A. Matsuo, S. Uto, H. Nozaki, M. Nakayama, and S. Hayashi, *J. Chem. Soc., Chem. Commun.*, **1980**, 1220; A. Matsuo, H. Nozaki, N. Kubora, S. Uto, and M. Nakayama, *J. Chem. Soc., Perkin Trans. 1*, **1984**, 203; A. Matsuo, S. Uto, H. Nozaki, and M. Nakayama, *ibid.*, **1984**, 215.

2) H. Magari, H. Hirota, T. Takahashi, A. Matsuo, S. Uto, H. Nozaki, M. Nakayama, and S. Hayashi, *Chem. Lett.*, **1982**, 1143.

3) Z. Rykowski and K. Burak, *Roczniki Chemii.*, **50**, 1709 (1976); K. Gollnick, S. Schroeter, G. Ohloff, G. Shade, and G. O. Schenck, *Liebigs Ann. Chem.*, **687**, 14 (1965).

4) The Cope rearrangement from α-side would suffer from severe steric hindrance between the ethoxy group and a methyl group situated on the same side of the molecule for both geometrical isomers, no matter chair or boat conformation is assumed in transition state.

5) Inter al., R. G. Riley, R. M. Silverstein, and J. C. Moser, *Science*, **183**, 760 (1974); D. L. Wood, L. E. Browne, B. Ewing, K. Lirdahl, W. D. Bedard, P. E. Tilden, K. Mori, G. B. Pitman, and P. R. Hughes, *ibid.*, **192**, 876 (1976); J. H. Tumlinson, M. G. Klein, R. E. Doolittle, T. L. Ladd, and A.T. Proveaux, *ibid.*, **197**, 789 (1977); K. Mori, S. Tamada, and P. A. Hedin, *Naturwissenschaften*, **65**, 653 (1978); J. P. Vité, G. Ohloff, and R. F. Billings, *Nature*, **272**, 817 (1978).

Cyclodextrin-Catalyzed Hydrolysis of Enantiomeric Esters Showing Stereoselectivity

Yasuji IHARA,* Eiji NAKANISHI, Mamoru NANGO,† and Joichi KOGA†
Yamaguchi Women's University, 3-2-1 Sakurabatake, Yamaguchi 753
†Department of Applied Chemistry, University of Osaka Prefecture, Sakai, Osaka 591
(Received January 6, 1986)

The rate constants for hydrolysis of the enantiomers of amino acid nitrophenyl esters have been determined at pH 9.00 and pH 10.0 in the presence of α- or β-cyclodextrin. α- and β-Cyclodextrins cause stereoselective acceleration in the hydrolysis of *m*-substituted enantiomers. On the other hand, less stereoselectivity is observed in the hydrolysis of *p*-substituted enantiomers. The stereoselective properties are discussed in the light of cyclodextrin-ester dissociation constants and thermodynamic parameters of the reaction.

Stereoselectivity and high catalytic reactivity are among the most interesting properties of enzyme action.[1] Several model studies on micellar,[2-9] polymer,[2,10-14] and macrocyclic[2,15-19] catalyzed reactions have been investigated in order to gain further insight into the stereoselective nature of enzyme reactions. In the course of our study on stereoselective micellar catalysis,[20,21] we found that comicelles of optically active *N*-acylhistidine or dipeptide derivatives containing histidyl residues and cationic surfactant are effective stereoselective catalysts for the hydrolysis of enantiomeric esters.

Cyclodextrin (CD) is often used as models of enzymatic reactions[22] since particular interest has attended the processes in which a substrate binds into a CD cavity and then undergoes reaction with one of CD's secondary hydroxyl groups. Stereoselectivities by CD have been reported for a number of reactions, particularly a very large selectivity was exhibited in the cleavage of chiral organophosphates such as isopropyl methylphosphonofluoridate,[16] or in the acylation of specific rigid substrates such as *p*-nitrophenyl *trans*-2-ferrocenylpropenoate.[18b] Recently, a remarkable stereoselectivity has also been reported in the hydrolysis of activated enantiomeric ester.[23]

In the present paper, the rate constants for hydrolysis of the enantiomers of amino acid *m*- and *p*-nitrophenyl esters (**1a** and **1b**) have been determined at pH 9.00 and pH 10.00 in the presence of α- or β-cyclodextrin. The substrate-binding properties, and the effect of temperature and of added surfactant on the rate constants were investigated to study the kinetic stereoselectivity.

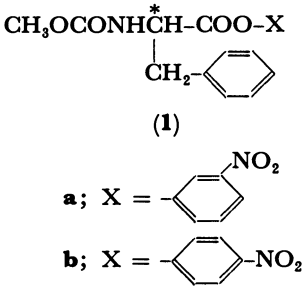

Experimental

Materials. α- and β-Cyclodextrins were commercially available highest grade reagents (Tokyo Kasei Co. and Nakarai Chemicals Co., Japan) and were used without further purification. *m*-Nitrophenyl esters of *N*-methoxycarbonyl-D- and L-phenylalanine were prepared by standard methods.[24] Other materials have been described elsewhere.[20,21]

Kinetic Measurements. Reactions were generally monitored on a Hitachi 200 spectrophotometer or a Shimadzu 140 spectrophotometer with a thermostated cell holder. In general procedure, a solution (25 μl) of substrate in aceto nitrile was added to a buffer solution (3.00 cm^3) containing the cyclodextrin or the catalyst and surfactant at desired concentrations. The formation of *m*- or *p*-nitrophenolate ion was followed spectrophotometrically at 390 or 400 nm, respectively. The pseudo-first-order rate constants were obtained from plots of log $(A_\infty - A_t)$ versus time (t) and calculated by the least-squares method. Correlation coefficients were >0.999.

Results and Discussion

Kinetics of Hydrolysis of 1 in the Presence of Cyclodextrin (CD). Kinetic studies were first examined at 25 °C using pH 9.00 sodium borate buf-

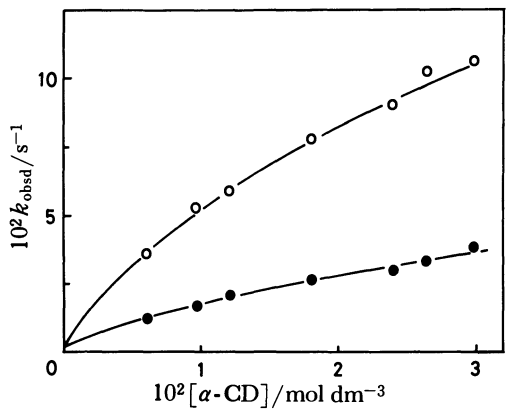

Fig. 1. Pseudo-first-order rate constants (k_{obsd}) for the hydrolysis of **1a** as a function of the concentration of α-CD at pH 9.00, 0.02 mol dm^{-3} borate buffer (I=0.2, KCl), and 25 °C; (●) D-**1a**, (○) L-**1a**, [**1a**]=1.00×10^{-4} mol dm^{-3}.

Table 1. Kinetic Parameters for Hydrolysis of **1a** and **1b** in the Presence of Cyclodextrin[a)]

Cyclodextrin	Ester	$10^3 k_{un}/s^{-1}$	$10^3 k_2/s^{-1}$	k_2/k_{un}	$10^2 K_{diss}$/mol dm^{-3}	k_2(L)/k_2(D)
α-CD	**1a** D	1.85	88.5	47.8	4.59	2.40
	L	1.93	212	110	3.12	
	1a D	(8.90)	(552)	(62.0)	(2.83)	(2.83)
	L	(8.96)	(1580)	(176)	(2.24)	
	1b D	2.92	24.6	8.45	12.0	1.16
	L	2.75	27.0	9.83	13.4	
β-CD	**1a** D	1.85	12.4	6.70	0.526	2.15
	L	1.93	26.6	13.8	0.574	
	1a D	(8.90)	(129)	(14.5)	(0.437)	(2.09)
	L	(8.96)	(269)	(30.0)	(0.486)	
	1b D	2.92	4.47	1.53	0.187	1.36
	L	2.75	6.08	2.21	0.379	
	1b D	(13.3)	(50.9)	(3.83)	(0.261)	(1.19)
	L	(13.0)	(60.5)	(4.65)	(0.428)	

a) At pH 9.00, 0.02 mol dm^{-3} borate buffer (I=0.2, KCl), and 25 °C, [**1a**]=1.0×10^{-4} mol dm^{-3}, [**1b**]=1.0×10^{-5} mol dm^{-3}. The values of parentheses are at pH 10.0, 0.02 mol dm^{-3} carbonate buffer (I=0.2, KCl).

fer or pH 10.00 sodium carbonate buffer, I=0.2 in 0.83% (v/v) acetonitrile-water. Under the conditions [CD]≫[substrate], pseudo-first-order rate constants (k_{obsd}) were evaluated by monitoring the release of *m*- or *p*-nitrophenoxide ion spectrophotometrically at 390 or 400 nm. Examples of the observed pseudo-first-order rate constants, k_{obsd}, against the varying cyclodextrin concentrations are shown in Fig. 1. The data were treated by the Michaelis-Menten pathway, applicable to much of enzyme kinetics described by Scheme 1, where CD is the cyclodextrin, S is the substrate, CD·S is the CD-substrate complex, K_{diss} is the dissociation constant, and k_{un} and k_2 are the rate constants for the alkaline hydrolysis and for the reaction of the complexed ester at infinite cyclodextrin concentration, respectively. The kinetic parameters are calculated by least squared method and given in Table 1.

$$\mathrm{CD} + \mathrm{S} \underset{}{\overset{K_{diss}}{\rightleftharpoons}} \mathrm{CD{\cdot}S} \xrightarrow{k_2} \mathrm{Products}$$
$$\mathrm{S} \xrightarrow{k_{un}} \mathrm{Products}$$

Scheme 1.

In the presence of CD, the rates of hydrolysis of **1a** are accelerated (6.7—180 fold) when compared (k_2/k_{un}) to alkaline hydrolysis under the same conditions. α-CD causes much greater rate accelerations than β-CD. Similarly, α-CD shows higher stereoselectivity, k_2(L)/k_2(D), than β -CD. The K_{diss} values are not very different for the enantiomeric D and L esters. Thus, the stereoselective rate accelerations are unrelated to the strength of binding. In this system, D and L esters may bind equally in the cavity of CD, but the binding of the D ester leads to the wrong orientation between the hydroxyl group of the CD and the carbonyl group of the esters.

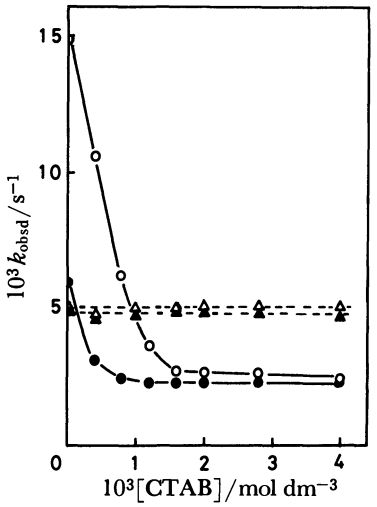

Fig. 2. Effect of CTAB on the hydrolysis of **1** catalyzed with α-CD at pH 9.00, 0.02 mol dm^{-3} borate buffer (I=0.2, KCl), and 25 °C; (——) **1a** (●) D-**1a**, (○) L-**1a**, (----) **1b**, (▲) D-**1b**, (△) L-**1b**; [**1a**]=1.00×10^{-4} mol dm^{-3}, [**1b**]=1.00×10^{-5} mol dm^{-3}, [α-CD]=2.0×10^{-3} mol dm^{-3}.

The rates of hydrolysis of **1b** are slightly accelerated (1.5—12 fold) at pH 9.00 and 10.0, and also a less stereoselectivity than **1a** is observed in the presence of α and β-CD. These results clearly indicate that the large stereoselective effect accords with the large rate enhancement of the reaction. Bender et al.[18a)] showed that β-CD hydrolyzed *N*-acetyl-L-phenylalanine *m*-nitrophenyl ester 2 times faster than the D-enantiomer, while β-CD inhibited the hydrolysis of both *N*-acetyl-L- and D-phenylalanine *p*-nitrophenyl esters. The data obtained by us are different from those of theirs in the case of *p*-substituted enantiomers. This may be mainly due to differences in experimental conditions such as the pH and the structure of substrates.

Effect of Surfactant on CD Catalyzed Hydrol-

ysis. The hydrolysis of **1** in the presence of CD and hexadecyltrimethylammonium bromide (CTAB) was carried out at pH 9.00 borate buffer and 25 °C. As shown in Fig. 2, reaction rates of **1a** are decreased upon addition of CTAB to the reaction mixture. This is attributed to the complex formation between the surfactant and CD. In contrast, hydrolysis of **1b** shows no significant effect on rates in the presence of CTAB. Thus, the hydrolysis of **1b** is not inhibited under the same conditions. It should be noted here that **1b** is more reactive than **1a** with increasing concentrations of CTAB. These results indicate that the inhibitive effect of CTAB on the reaction of **1a** is attributed to the strong interactions between CD and CTAB. On the other hand, no inhibitive effect on the reaction of **1b** indicates that there are no significant differences in reactivity between CD and CTAB. The strong binding of ionic surfactants with CD was widely discussed upon the basis of conductimetric measurements.[25a]

In the case of **1a**, the competitive inhibition constants, K_i, are determined by the method of Bender et. al,[26] Eq. 1. By plotting the inhibitor concentration, [I], against $(k_2-k_{obsd})/(k_{obsd}-k_{un})$ an approximately straight line is obtained with a y intercept of equal to $-K_i$ and a slope of $[CD]K_i/K_{diss}$, and the results are given in Table 2. The values of K_i obtained from both enantiomeric esters are very similar with those obtained from *m*-nitrophenyl acetate.[25b]

$$[I] = \left(\frac{k_2-k_{obsd}}{k_{obsd}-k_{un}}\right) \cdot \left(\frac{[CD]K_i}{K_{diss}}\right) - K_i \qquad (1)$$

Temperature Dependence of Reaction Rates. The effect of temperature change (5—35 °C) on the reaction rates for hydrolysis of **1a** in the presence of α- and β-cyclodextrin was examined at pH 9.00 in 0.02 mol dm^{-3} borate buffer (I=0.2 with KCl) and the kinetic parameters thus evaluated are listed in Tables 3 and 4. As discussed in previous section, stereoselective recognition is exercised in the reaction process rather than in the binding process over the whole temperature range. The stereoselectivity based on reaction rates slightly increases as the temperature is lowered. The highest stereoselectivity (2.71) is observed in the presence of α-CD at 5 °C.

In order to calculate the thermodynamic parameters accompanying the reaction process the least-squares slope was computed of the line formed by plotting $\ln(k_2/T)$ against $1/RT$. The calculated values are listed in Table 5. The $\Delta G^{\ddagger}$ values of α-CD are ca. 1.1—1.2 kcal mol^{-1} (1 cal=4.184 J) smaller than those of β-CD in both D and L esters. These results are compatible with those of Table 1. On the other hand, for both α- and β-CD, the $\Delta G^{\ddagger}$, $\Delta H^{\ddagger}$, and $\Delta S^{\ddagger}$ values of L substrate are ca. 0.4—0.5 kcal mol^{-1}, 1.0—1.1 kcal mol^{-1}, and 1.6—2.3 cal mol^{-1}K^{-1} smaller than those of D ester. The effect of enantiomeric selectivity is primarily to lower $\Delta H^{\ddagger}$ for activation. This is partly balanced by a small unfavorable change in the entropy of activation.

Stereoselective Nature of CD Catalysis. Although stereoselective effects in the present catalytic systems are relatively small, it is now clear that (1) α- and β-CD cause stereoselective acceleration in the hydrolysis of **1a**, while a less stereoselectivity is observed in the hydrolysis of **1b**. (2) The hydrolysis of **1a** with CD is inhibited by added CTAB, whereas there is no significant effect for **1b** hydrolysis in the presence of CTAB. For the reaction with CD, the esters are incorporated

Table 2. Inhibition by CTAB on the Hydrolysis of 1a Catalyzed with Cyclodextrin[a]

Ester	α-CD	β-CD
	10^4K_i/mol dm^{-3}	10^4K_i/mol dm^{-3}
D-1a	1.8±0.4	3.3±0.5
L-1a	1.3±0.3	3.6±0.7

a) At pH 9.00, 0.02 mol dm^{-3} borate buffer (I=0.2, KCl), and 25 °C, [α-CD]=2.00×10^{-3} mol dm^{-3}, [β-CD]=1.00×10^{-3} mol dm^{-3}, [1a]=1.0×10^{-4} mol dm^{-3}.

Table 3. Kinetic Parameters for the Hydrolysis of 1a in the Presence of α-CD[a]

	5 °C		15 °C		25 °C		35 °C	
	D	L	D	L	D	L	D	L
10^2k_2/s^{-1}	0.313	0.847	1.40	3.64	8.85	21.2	21.4	46.4
10^2K_{diss}/mol dm^{-3}	1.55	1.36	3.03	2.10	4.59	3.12	5.44	3.55
k_2(L)/k_2(D)	2.71		2.60		2.40		2.17	

a) At pH 9.00, 0.02 mol dm^{-3} borate buffer (I=0.2 with KCl), [1a]=1.00×10^{-4} mol dm^{-3}.

Table 4. Kinetic Parameters for the Hydrolysis of 1a in the Presence of β-CD[a]

	5 °C		15 °C		25 °C		35 °C	
	D	L	D	L	D	L	D	L
10^3k_2/s^{-1}	0.660	1.66	3.16	7.56	12.4	26.6	34.9	72.2
10^3K_{diss}/mol dm^{-3}	1.49	2.51	2.10	2.69	5.26	5.74	6.54	7.47
k_2(L)/k_2(D)	2.52		2.39		2.15		2.07	

a) At pH 9.00, 0.02 mol dm^{-3} borate buffer (I=0.2 with KCl), [1a]=1.00×10^{-4} mol dm^{-3}.

Table 5. Thermodynamic Parameters for Hydrolysis of **1a** in the Presence of Cyclodextrin[a]

	α-CD		β-CD	
	D	L	D	L
$\Delta G^{\ddagger}$[b]/kcal mol^{-1}	19.0	18.5	20.1	19.7
$\Delta H^{\ddagger}$/kcal mol^{-1}	24.9	23.9	22.0	20.9
$\Delta S^{\ddagger}$/cal mol^{-1} K^{-1}	19.8	18.2	6.45	4.14

a) At pH 9.00, 0.02 mol dm^{-3} borate buffer (I=0.2, KCl). The parameters were calculated by plotting the data of Tables 3 and 4 in the form of $\ln(k_2/T)$ versus $1/RT$. b) For the values at 298.2°K.

into the cavity of CD and react with a hydroxyl group. Thus, *meta* is better than *para* in stereoselectivity. This is attributable to the nature of the catalyst.

The differences in reactivity between D and L enantiomers in the hydrolysis of **1a** depend on the catalytic rate constants (k_2) rather than the dissociation constant of the complex formation (K_{diss}). In the cleavage of 2,2,5,5-tetramethyl-3-(*m*-nitrophenoxycarbonyl)-1-pyrrolidinyloxyl by α-CD,[17] k_2 for the (+) enantiomer is 6.9 times larger than that for the (−) enantiomer. However, the K_{diss} values are almost equal for the two enantiomers. On the other hand, in the cleavage of chiral organophosphates,[16] the reactivity depends on both k_2 and K_{diss}. Thus, the stereoselectivity is very large in this reaction. As described by Bender and Komiyama,[22] the larger enantiomeric specificity in the cleavage of organophosphates than in the cleavage of esters is attributable to the fact that the reaction takes place directly at the asymmetric center (phosphorus atom), whereas in the cleavage of esters it occurs at the carbonyl carbon atom, which is adjacent to the asymmetric center. However, a remarkable stereoselectivity has recently been reported in the hydrolysis of activated enantiomeric esters which contain relatively-long-chain alkyl groups.[23] These results suggest that more effective stereochemical features may be obtained by different combinations of substrates than those used in the present system. In connection with this work, we have also investigated in order to gain the stereoselective nature of micellar reaction.[20,21]

We thank Professor Myron L. Bender for helpful comments, Yoshimi Nakahara, Fumiko Nishimura, Satoe Furuya, Akemi Akiyama, and Hiroko Yamamoto for technical assistance.

References

1) M. L. Bender, "Mechanism of Homogeneous Catalysis from Protons to Proteins," Wiley, New York (1971).

2) a) J. H. Fendler and E. J. Fendler, "Catalysis in Micellar and Macromolecular Systems," Academic Press, New York (1975); b) C. A. Bunton, "Application of Biochemical Systems in Organic Chemistry," ed by J. B. Jones, C. J. Sih, and D. Perlman, Wiley, New York (1975), Part 2; c) U. Tonellato, "Solution Chemistry of Surfactant," ed by K. Mittal, Plenum, New York (1975).

3) a) C. A. Bunton, J. Robinson, and M. F. Stam, *Tetrahedron Lett.*, **1971**, 121; b) J. M. Brown and C. A. Bunton, *J. Chem. Soc., Chem. Commun.*, **1974**, 969; c) J. M. Brown, R. L. Elliott, C. G. Griggs, G. Helmchen, and G. Nill, *Angew. Chem. Int. Ed. Engl.*, **20**, 890 (1981).

4) a) R. A. Moss and W. L. Sunshine, *J. Org. Chem.*, **39**, 1083 (1974); b) R. A. Moss, T. J. Lukas, and R. C. Nahas, *Tetrahedron Lett.*, **1977**, 3851; c) R. A. Moss, R. C. Nahas, and T. J. Lukas, *Tetrahedron Lett.*, **1978**, 508.

5) J. Koga, M. Shoshi, and N. Kuroki, *Nippon Kagaku Kaishi*, **1978**, 1179.

6) a) K. Yamada, H. Shosenji, and H. Ihara, *Chem. Lett.*, **1979**, 491; b) K. Yamada, H. Shosenji, H. Ihara, and Y. Otubo, *Tetrahedron Lett.*, **1979**, 2529; c) H. Ihara, S. Ono, H. Shosenji, and K. Yamada, *J. Org. Chem.*, **45**, 1623 (1980); d) S. Ono, H. Shosenji, and K. Yamada, *Tetrahedron Lett.*, **1981**, 2391.

7) a) R. Ueoka, T. Terao, and K. Ohkubo, *Nippon Kagaku Kaishi*, **1980**, 462; b) K.Ohkubo, K. Sugahara, H. Ohta, K. Tokuda, and R. Ueoka, *Bull. Chem. Soc. Jpn.*, **54**, 576 (1981); c) R. Ueoka, Y. Matsumoto, Y. Ninomiya, Y. Nakagawa, K. Inoue, and K. Ohkubo, *Chem. Lett.*, **1981**, 785; d) K. Ohkubo, K. Sugahara, K. Yoshinaga, and R. Ueoka, *J. Chem. Soc., Chem. Commun.*, **1980**, 393; e) K. Ohkubo, N. Matsumoto, and H. Ohta, *J. Chem. Soc., Chem. Commun.*, **1982**, 738; f) R. Ueoka, Y. Matsumoto, and Y. Ihara, *Chem. Lett.*, **1984**, 1809.

8) a) K. Kon-no, M. Tosaka, and A. Kitahara, *J. Colloid Interface Sci.*, **79**, 581 (1981); b) K. Kon-no, M. Tosaka, and A. Kitahara, *ibid.*, **86**, 288 (1982).

9) a) Y. Murakami, A. Nakano, A. Yoshimatsu, and K. Fukuya, *J. Am. Chem. Soc.*, **103**, 728 (1981); b) Y. Murakami, A. Nakano, H. Ikeda, T. Imori, and K. Akiyoshi, *Bull. Chem. Soc. Jpn.*, **58**, 172 (1985).

10) a) C. G. Overberger and I. Cho, *J. Polym. Sci., A-1*, **6**, 2741 (1968); b) C. G. Overberger and K. W. Dixon, *J. Polym. Sci., Polym. Chem. Ed.*, **15**, 1863 (1977).

11) R. Fornasier and U. Tonellato, *J. Chem. Soc., Perkin Trans. 2*, **1984**, 1313.

12) Y. Okamoto, *Nippon Kagaku Kaishi*, **1978**, 870.

13) a) M. Nango, H. Kozuka, Y. Kimura, N. Kuroki, Y. Ihara, and I. M. Klotz, *J. Polym. Sci., Polym. Lett. Ed.*, **18**, 647 (1980); b) Y. Kimura, M. Nango, N. Kuroki, Y. Ihara, and I. M. Klotz, *J. Polym. Sci., Polym. Syn.*, **71**, 167 (1984); c) Y. Ihara, Y. Kimura, M. Nango, and N. Kuroki, *J. Polym. Sci., Polym. Chem. Ed.*, **21**, 1535 (1983); d) Y. Kimura, A. Tanaka, M. Nango, N. Kuroki, and Y. Ihara, *J. Polym. Sci., Polym. Chem. Ed.*, **22**, 407 (1984); e) Y. Kimura, M. Nango, Y. Ihara, and N. Kuroki, *Chem. Lett.*, **1984**, 429; f) Y. Kimura, S. Kanda, M. Nango, Y. Ihara, J. Koga, and N. Kuroki, *Chem. Lett.*, **1984**, 433.

14) a) M. Aglietto, G. Ruggeri, B. Tarquini, G. Ciardelli, and D. Gianni, *Polymer*, **21**, 541 (1980); b) M. G. Harun and A. Williams, *Polymer*, **22**, 946 (1981).

15) a) J. M. Von Ver Eijk, R. J. M. Nolte, V. E. M. Richters, and W. Drenth, *Recl. Trav. Chem. Pays-Bas*, **100**, 222 (1981); b) I. Cho and J-S. Shin, *Makromol. Chem.*, **183**, 2041 (1982); c) I. Cho and J-S. Shin, *Makromol. Chem.*, **184**, 147 (1983).

16) a) C. Von Hooidonk and J. C. A. E. Breebaart-Hansen, *Recl. Trav. Chim. Pays-Bas*, **89**, 289 (1970); b) C. Von Hooidonk and J. C. A. E. Breebaart-Hansen, *Recl. Trav. Chim. Pays-Bas*, **90**, 680 (1971); c) C. Von Hooidonk and J. C. A. E. Breebaart-Hansen, *Recl. Trav. Chim. Pays-Bas*, **91**, 1103 (1972).

17) a) K. Flohr, R. M. Paton, and E. T. Kaiser, *J. Chem. Soc., Chem. Commun.*, **1971**, 1621; b) K. Flohr, R. M. Paton, and E. T. Kaiser, *J. Am. Chem. Soc.*, **97**, 1209 (1975).

18) a) Y. Kitaura and M. L. Bender, *Bioorg. Chem.*, **4**, 237 (1975); b) G. L. Trainor and R. Breslow, *J. Am. Chem. Soc.*, **103**, 154 (1981).

19) a) Y. Chao and D. J. Cram, *J. Am. Chem. Soc.*, **98**, 1015 (1976); b) J. M. Lehn and C. Sirlin, *J. Chem. Soc., Chem. Commun.*, **1978**, 949.

20) a) Y. Ihara, *J. Chem. Soc., Chem. Commun.*, **1978**, 984; b) Y. Ihara, *J. Chem. Soc., Perkin Trans. 2*, **1980**, 1483; c) Y. Ihara, M. Nango, and N. Kuroki, *J. Org. Chem.*, **45**, 5009 (1980); d) Y. Ihara, R. Hosako, M. Nango, and N. Kuroki, *J. Chem. Soc., Chem. Commun.*, **1981**, 393.

21) a) Y. Ihara, N. Kunikiyo, T. Kunimasa, M. Nango, and N. Kuroki, *Chem. Lett.*, **1981**, 667; b) Y. Ihara, N. Kunikiyo, T. Kunimasa, Y. Kimura, M. Nango, and N. Kuroki, *J. Chem. Soc., Perkin Trans. 2*, **1983**, 1741.

22) M. L. Bender and M. Komiyama, "Cyclodextrin Chemistry," Springer-Verlag, New York (1977).

23) R. Fornaiser, P. Scrimin, and U. Tonellato, *Tetrahedron Lett.*, **1983**, 5541.

24) a) M. Bodanszky and V. Du. Vigneaud, *J. Am. Chem. Soc.*, **81**, 5688 (1959); b) D. T. Elmore and J. J. Smyth, *Biochem. J.*, **94**, 563 (1965).

25) a) T. Okubo, H. Kitano, and N. Ise, *J. Phys. Chem.*, **80**, 2661 (1976); b) H. Kitano and T. Okubo, *J. Chem. Soc., Perkin Trans. 2*, **1977**, 432.

26) R. L. Vanetten, J. F. Sebastian, G. A. Clowers, and M. L. Bender, *J. Am. Chem. Soc.*, **89**, 3242 (1967).

Kinetics and Mechanism of the Oxidative Deamination of Amines by Coenzyme PQQ

Shinobu ITOH, Yutaka KITAMURA, Yoshiki OHSHIRO,* and Toshio AGAWA
Department of Applied Chemistry, Faculty of Engineering, Osaka University, Yamadaoka 2-1, Suita, Osaka 565
(Received January 27, 1986)

Kinetic studies on the oxidative deamination of amines by coenzyme PQQ are carried out under anaerobic conditions. The reaction is first-order in the appearance of the reduced PQQ and in the total amine concentrations. A large kinetic isotope effect (k_H/k_D=7.24) in the oxidation of α,α-dideuteriobenzylamine indicates that the C-H bond cleavage is a rate-determining step. From the results of formation of two types of reduced PQQ (quinol and aminophenol) and low reactivities of secondary and tertiary amines, we propose the mechanism via covalent addition of the amine to the quinone followed by rate-limiting α-proton removal.

Amine oxidases are known to catalyze the oxidative deamination of amines in the presence of molecular oxygen as an electron acceptor to produce the corresponding carbonyl compounds, hydrogen peroxide, and ammonia (Eq. 1).[1]

$$RCH_2NH_2 + O_2 + H_2O \longrightarrow RCHO + H_2O_2 + NH_3 \quad (1)$$

They are divided into two classes: Copper-containing amine oxidases and FAD-containing ones. However, the chromophore of the former enzymes, which has a carbonyl function,[2] has not been identified despite of the presence of many investigations extended over a long period of time.[1-3] Recently, Ameyama and his coworkers demonstrated that 4,5-dihydro-4,5-dioxo-1*H*-pyrrolo[2,3-*f*]quinoline-2,7,9-tricarboxylic acid (PQQ, methoxatin) is the coenzyme of a methylamine dehydrogenase and copper-containing amine oxidases from beef plasma, pig kidney, and *Aspergillus niger*.[4] Duine and his co-workers simultaneously indicated the possible occurrence of PQQ in bovine serum amine oxidase, a mammalian copper-containing amine oxidase.[5]

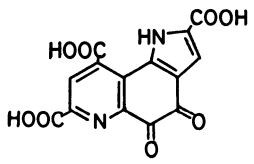

PQQ

PQQ is a novel coenzyme which was originally discovered and identified in methanol dehydrogenases of methylotropic bacteria.[6] In addition to methanol dehydrogenases from various methanol-grown microorganisms,[7] several types of alcohol, aldehyde, and glucose dehydrogenases have been revealed to be PQQ-containing enzymes (quinoproteins).[8] Methylamine dehydrogenase of *Pseudomonas* AM-1 has also been shown to be a quinoprotein in which PQQ is attached to the enzyme protein via a covalent bond.[9] Total syntheses[10] and some chemical properties[11] of PQQ have already been reported. A mechanism for alcohol and amine oxidation by quinoprotein, however, has not been clarified, though a few enzymological studies have been developed.[12,13]

As a model system of amine oxidases, we have already demonstrated the micellar enhanced oxidative deamination of amines catalyzed by coenzyme PQQ by two electron transferring from the amine to molecular oxygen.[14] We wish to demonstrate here the kinetics of the oxidative deamination of amines by PQQ and product analysis of the reduced PQQ to elucidate the mechanism of the reaction under anaerobic conditions.[15]

Experimental

PQQ was prepared according to the reported method.[10a] All amines investigated (except for α,α-dideuteriobenzylamine) and CTAB (hexadecyltrimethylammonium bromide) were obtained commercially and purified by the standard method.[16] α,α-Dideuteriobenzylamine was prepared according to the known method,[17] and the ^{1}H NMR indicated that the content of the deuterated compound was more than 99%.

Ultraviolet and visible absorption spectra were recorded on Shimadzu UV-240 spectrophotometer equipped with a temperature controlled cell holder, Shimadzu TCC-240. Measurements of pH were performed by using Horiba pH-meter F-8. HPLC analysis was performed by using Waters Model 510 (pump)-Lambda-Max Model 481 (UV-monitor)-Radial Compression Separation System (C_{18}).

Kinetics. The kinetic measurements of the oxidation of amines with PQQ were carried out in a carbonate buffer solution (0.05 M (1 M=1 mol dm^{-3}) pH 10.1, μ=0.2 with KCl) at 35 °C under anaerobic conditions. Typically, 1.5 ml of an aqueous bufffer solution containing CTAB (4.0×10^{-3} M) and an amine (8.0×10^{-3} M) was mixed with 1.5 ml of an aqueous buffer solution containing PQQ (8.0×10^{-5} M) in a Thunberg cuvette. Both solutions were degassed by bubbling N_2 through them before the reaction. The progress of the reaction was followed by monitoring the appearance of the reduced PQQ at 320 nm.

Product Analysis of Reduced PQQ. After the reaction of PQQ (20 mg, 5.7×10^{-2} mmol) and benzylamine (2.9×10^{-1} mmol) in a carbonate buffer solution (0.1 M, pH 10, 20 ml) under anaerobic conditions (N_2) for 24 h, the reduced product (19.2 mg) was precipitated by adding 2 M HCl (2 ml). HPLC analysis and UV spectrum revealed that there were at least two types of reduced compounds from PQQ;

HPLC, column: radial pack cartridge C_{18}(Waters), solvent: MeOH/H_2O/85% H_3PO_4, 45/54.5/0.5, v/v/v, flow rate: 2.0 ml min^{-1}, retention time: 4.9 min (for **1**) and 3.3 min (for **2**), (ratio of peak area, **1**:**2**=82:18), UV-spectrum (λ_{max}, CH_3CN), 320 nm (**1**) and 301 nm (**2**). Both products, **1** and **2**, were readily converted into PQQ by treating with an alkaline aqueous solution under aerobic conditions. The main product **1** was identical with $PQQH_2$ (quinol)[11b] in HPLC analysis, ^1H NMR spectrum, and UV spectrum in the mixture.

Results and Discussion

The reaction of benzylamine with PQQ was studied under pseudo-first-order conditions of total benzylamine concentration (4.0×10^{-3} M) greatly exceeding [PQQ]=4.0×10^{-5} M in the presence of CTAB (2.0×10^{-3} M) in a carbonate buffer solution (0.05 M, pH 10.1, μ=0.2 with KCl) at 35 °C. Monitoring of an appearance of the product from PQQ at 320 nm established a short lag phase followed by the first-order appearance of the product ($k_{obsd}=1.75\times10^{-3}$ s^{-1}, Fig. 1). Introduction of O_2 into the final reaction mixture led to quantitative regeneration of PQQ. The reaction was also first-order in total benzylamine concentrations (Fig. 2). In this oxidation reaction, the free amine is considered to be an active species.

$$k_{obsd} = k_2[\text{Amine}]_f = k_2\frac{K_a}{K_a+a_H}[\text{Amine}]_T \qquad (2)$$

$[\text{Amine}]_f$: free amine concentration

$[\text{Amine}]_T$: total amine concentration

Thus, the second-order rate constant k_2 is calculated to be 5.36×10^{-1} $M^{-1}s^{-1}$ (at pH 10.1) from Eq. 2 by using the pK_a value of 9.45 for benzylamine determined by volumetric titration under the kinetic conditions. The second-order rate constants at pH 10.1 for the other amines are listed in Table. Interestingly, β-phenethylamine and cyclohexylamine were oxidized faster than the benzylic amines. Incorporation of the substrates into the hydrophobic core of the micelle may be an important factor.[18]

It should be noted that *N*-methylbenzylamine was

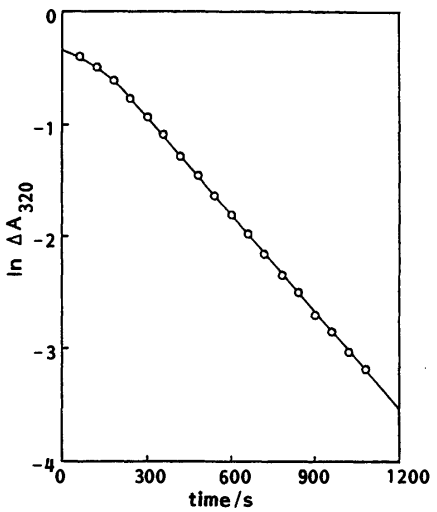

Fig. 1. Pseudo-first-order plot for the oxidation. PQQ (4.0×10^{-5} M), $PhCH_2NH_2$ (4.0×10^{-3} M), CTAB (2×10^{-3} M), pH 10.1 with 0.05 M carbonate buffer (μ=0.2 with KCl), 35 °C, anaerobic conditions (N_2).

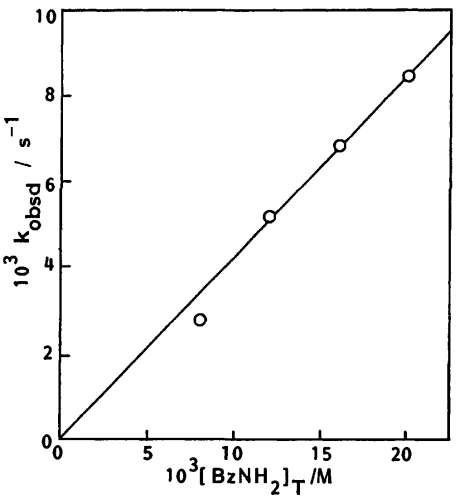

Fig. 2. Dependence on total benzylamine concentration of the pseudo-first-order rate constant (k_{obsd}). pH 10.1 with 0.05 M carbonate buffer (μ=0.2 with KCl), 35 °C.

Table. The Second-Order Rate Constant for the Oxidation of Amines by PQQ

Amine	$10^3 k_{obsd}$ / s^{-1}	pK_a	10^3[Amine]$_f$[a] / M	k_{obsd}/[Amine]$_f$ / $M^{-1}s^{-1}$
$PhCH_2NH_2$	17.5	9.45	3.26	0.536
$PhCH(CH_3)NH_2$	7.69	9.33	3.42	0.225
$Ph(CH_2)_2NH_2$	45.1	9.78	2.71	1.67
Cyclohexylamine	9.69	10.33	1.49	0.650
$PhCH_2NHCH_3$	0.81	9.57	3.10	0.026
$PhCH_2N(CH_3)_2$	0	9.02	3.70	0

a) Free amine concentrations at pH 10.1 calculated from the pK_a values determined by volumetric titration under the kinetic conditions. [PQQ]=4.0×10^{-5} M, [Amine]$_T$=4.0×10^{-3} M, 0.05 M carbonate buffer (μ=0.2 with KCl, pH 10.1) 35 °C, anaerobic conditions.

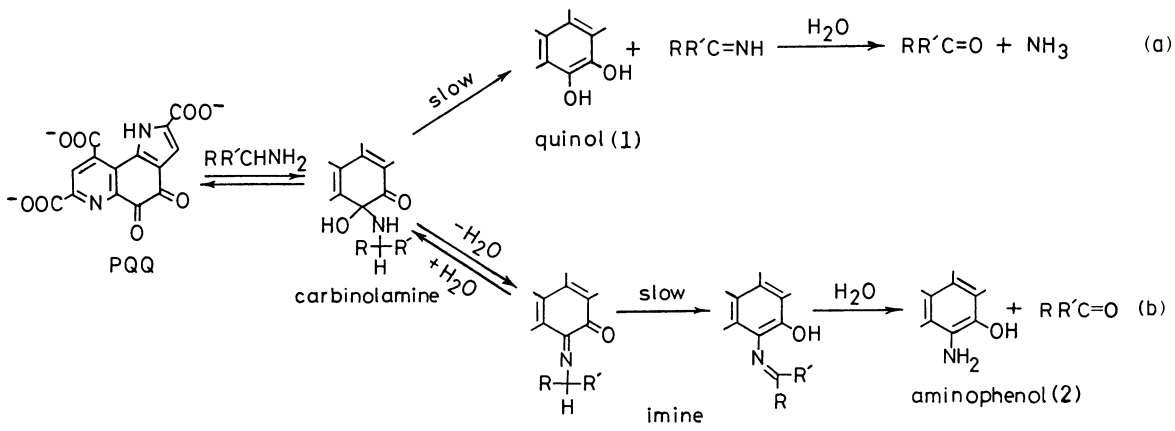

Scheme.

oxidized very slowly (k_2=2.6×10^{-2} $M^{-1}s^{-1}$) and *N,N*-dimethylbenzylamine was not oxidized under the same conditions. Thus, the order of the reactivities of the amines is primary>secondary≫tertiary. Furthermore, a large kinetic isotope effect (k_H/k_D=7.24) was observed for the reaction with benzylamine-d_2, indicating the C–H bond cleavage is a rate determining step.

Bruice and his co-workers recently investigated the chemical behavior of model compounds of PQQ and their reactions with various amines.[19,20] They suggested that the oxidation of primary amines by the model compounds proceeds via two competing covalent addition base-catalyzed elimination mechanisms through intermediate carbinolamine and imine, respectively, and they confirmed the formation of two types of reduced compounds (quinol and aminophenol).[20] Thus, we tried to isolate the reduced compound of PQQ in the reaction of PQQ with an amine, and found the formation of two types of reduced PQQ. Since the main product (**1**) was identical with $PQQH_2$ (quinol), the minor product (**2**) is assumed to be an aminophenol type one, though these two compounds could not be separated because of their instability in the mixture.

From these results, the mechanism of the reaction of the amines and PQQ is considered to be similar to that proposed by Bruice and his co-workers for the reaction of a PQQ-model, 7,9-didecarboxymethoxatin with amines (Scheme). That is to say, the oxidation of the amine by PQQ proceeds mainly via covalent addition of the amine to the quinone to form the carbinolamine intermediate followed by rate determining α-proton removal providing the quinol **1** (path a).[21] The reaction through the formation of the imine intermediate between PQQ and the amine followed by successive rearrangement and α-proton removal to provide the aminophenol **2** (path b) is considered to compete with the path a, but this may be the minor process. As in fact, appearance of absorptions at 385 and 403 nm which may be due to the imine intermediate were observed in the course of the reaction at pH 7 under anaerobic conditions. These absorptions are not for a semiquinone radical of PQQ because these absorptions do not disappear by aeration of the reaction mixture. On the other hand, the reaction was much decelarated above pH 12, which may be attributed mainly to hydration of the quinone group of PQQ.

At the present time, the mechanism via rate-determining one-electron transfer from the amine to PQQ may be dismissed because of lower reactivity of the secondary amine and of no reactivity of the tertiary amine. Considering the fact that the peak oxidation potentials of amines increase in general as in following order: primary>secondary>tertiary, the secondary and the tertiary amines should be oxidized more smoothly if the reaction should proceed via electron-transfer mechanism. It has been shown that the rate for chlorine dioxide oxidation of amines, which proceeds via electron transfer mechanism, increases with decrease of the peak oxidation potentials of amines.[22] A large kinetic isotope effect also contradicts the rate-limiting one-electron-transfer mechanism.

A possibility of the hydride-transfer mechanism from the α-position of the amine to the quinone is also considered to be discarded, since the oxidation potential of PQQ is relatively low ($E_{1/2}$=90 mV)[11b] compared with those of ordinary quinones in a neutral aqueous solution. As in fact, dehydrogenation of allylic and benzylic alcohols and carbonyl compounds such as succinate does not occur in the reaction with PQQ under suitable conditions. To obtain further insight into the mechanism of the oxidation, we are now synthesizing varieties of fused heteroaromatic *o*-quinones and examining their reactivities.

The present work was partially supported by a Grant-in-Aid for Special Project Research (No. 60104005) from the Ministry of Education, Science, and Culture to which our thanks are due.

References

1) a) H. Yamada and K. T. Yasunobu, *J. Biol. Chem.*, **237**,

1511, (1962); b) O. Oda, T. Manabe, and T. Okuyama, *J. Biochem.*, **89**, 1317 (1981).

2) a) A. Rinaldi, G. Floris, S. Sabatini, A. Finazzi-Agro, A. Giartosio, G. Rotilio, and B. Mondovi, *Biochem. Biophys. Res. Commun.*, **115**, 841 (1983); b) H. Ishizaki and K. T. Yasunobu, *Biochim. Biophys. Acta*, **611**, 27 (1980).

3) a) A. Finazzi-Agro, P. Guerrieri, M. T. Costa, and B. Mondovi, *Eur. J. Biochem.*, **74**, 435 (1977); b) R. Neumann, R. Hevey, and R. H. Abeles, *J. Biol. Chem.*, **250**, 6362 (1975); c) R. H. Suva and R. H. Abeles, *Biochemistry*, **17**, 3538 (1978); d) K. D. S. Yadav and P. F. Knowles, *Eur. J. Biochem.*, **114**, 139 (1981); e) S. Suzuki, T. Sakurai, A. Nakahara, T. Manabe, and T. Okuyama, *Biochemistry*, **22**, 1630 (1983); and references cited therein.

4) M. Ameyama, M. Hayashi, K. Matsushita, E. Shinagawa, and O. Adachi, *Agric. Biol. Chem.*, **48**, 561 (1984).

5) C. L. Lobenstein-Verbeek, J. A. Jongejan, J. Frank, and J. A. Duine, *FEBS Lett.*, **170**, 305 (1984).

6) S. A. Salisbury, H. S. Forrest, W. B. T. Cruse, and O. Kennard, *Nature (London)*, **280**, 843 (1979).

7) C. Anthony, "The Biochemistry of Methylotrophs," Academic Press Inc., New York (1982), pp. 152—194.

8) a) M. Ameyama, K. Matsushita, Y. Ohno, E. Shinagawa, and O. Adachi, *FEBS Lett.*, **130**, 179 (1981); b) M. Ameyama, E. Shinagawa, K. Matsushita, and O. Adachi, *Agric. Biol. Chem.*, **45**, 851 (1981); c) J. A. Duine, J. Frank, and J. K. Van Zeeland, *FEBS Lett.*, **108**, 443 (1979).

9) R. De Beer, J. A. Duine, J. Frank, and P. J. Large, *Biochim. Biophys. Acta*, **622**, 370 (1980).

10) a) E. J. Corey and A. Tramontano, *J. Am. Chem. Soc.*, **103**, 5599 (1981); b) J. A. Gainor and S. M. Weinreb, *J. Org. Chem.*, **46**, 4319 (1981); 47, 2833 (1982); c) J. Hendrickson and J. G. de Vries, *J. Org. Chem.*, **47**, 1150 (1982); 50, 1688 (1985); d) A. R. MacKenzie, C. J. Moody, and C. W. Rees, *J. Chem. Soc., Chem. Commun.*, **1983**, 1372; e) G. Büchi, J. H. Botkin, G. C. M. Lee, and K. Yakushijin, *J. Am. Chem. Soc.*, **107**, 5555 (1985).

11) a) J. A. Duine, J. Frank, and P. E. J. Verwiel, *Eur. J. Biochem.*, **108**, 187 (1980); b) J. A. Duine, J. Frank, and P. E. J. Verwiel, *Eur. J. Biochem.*, **118**, 395 (1981); c) R. H. Dekker, J. A. Duine, J. Frank, P. E. J. Verwiel, and J. Westerling, *Eur. J. Biochem.*, **125**, 69 (1982).

12) T. Mincey, J. A. Bell, A. S. Mildvan, and R. H. Abeles, *Biochemistry*, **20**, 7502 (1981).

13) R. De Beer, J. A. Duine, J. Frank, and J. Westerling, *Eur. J. Biochem.*, **130**, 105 (1983).

14) a) Y. Ohshiro, S. Itoh, K. Kurokawa, J. Kato, T. Hirao, and T. Agawa, *Tetrahedron Lett.*, **24**, 3465 (1983); b) S. Itoh, N. Kato, Y. Ohshiro, and T. Agawa, *Tetrahedron Lett.*, **25**, 4753 (1984).

15) Reoxidation of reduced PQQ by O_2 is investigated in the following paper.

16) D. D. Perrin, W. L. F. Armarego, and D. R. Perrin, "Purification of Laboratory Chemicals," Pergamon Press, Elmsford, New York (1966).

17) E. A. Halevi, M. Nussim, and A. Ron, *J. Chem. Soc.*, **1963**, 866.

18) S. Itoh, Y. Kitamura, and Y. Ohshiro, *YUKAGAKU*, **35**, 91 (1986).

19) a) T. S. Eckert, T. C. Bruice, J. A. Gainor, and S. M. Weinreb, *Proc. Natl. Acad. Sci. U.S.A.*, **79**, 2533 (1982); b) T. S. Eckert and T. C. Bruice, *J. Am. Chem. Soc.*, **105**, 4431 (1983).

20) P. R. Sleath, J. B. Noar, G. A. Eberlein, and T. C. Bruice, *J. Am. Chem. Soc.*, **107**, 3328 (1985).

21) A large difference of the kinetic isotope effect between PQQ (in our system) and model compounds[19,20] may be due to change of the rate-limiting step from the carbinolamine and imine formation to C–H bond cleavage by facilitation of the former step in the micellar system.

22) L. A. Hull, G. T. Davis, D. H. Rosenblatt, and C. K. Mann, *J. Phys. Chem.*, **73**, 2142 (1969).

Reaction of Reduced PQQ ($PQQH_2$) and Molecular Oxygen

Shinobu Itoh, Yoshiki Ohshiro,* and Toshio Agawa
Department of Applied Chemistry, Faculty of Engineering, Osaka University, Yamadaoka 2-1, Suita, Osaka 565
(Received January 27, 1986)

Reduced PQQ ($PQQH_2$) is prepared by the reaction of PQQ with thiophenol, 1-benzyl-1,4-dihydronicotinamide (BNAH), sodium dithionite, or sodium borohydride. Oxidation of $PQQH_2$ to PQQ by molecular oxygen in aqueous solutions is investigated kinetically. The oxidation is accelerated gradually with proceeding of the reaction, which may be attributed to the side reaction of $PQQH_2$ and H_2O_2 produced by the reaction of $PQQH_2$ and O_2. As in fact, the yield of H_2O_2 is found to be 50% based on $PQQH_2$. Initial rate is first-order in oxygen concentration. The pH-rate profile suggests that an active species in the reaction is $PQQH^-$. Autocatalysis of O_2^- and PQQ itself is scarcely detected in this reaction. The mechanism of the oxidation is also discussed.

It has been well-known that copper-containing amine oxidases constitute important sources of H_2O_2 in biological systems.[1] However, the reaction of this group of enzymes with O_2 has been less explored, because the true character of the second prosthetic group of the enzymes has not been clear. Meanwhile, Ameyama and Duine simultaneously indicated the possible occurrence of PQQ (4,5-dihydro-4,5-dioxo-1*H*-pyrrolo[2,3-*f*]quinoline-2,7,9-tricarboxylic acid, a newly discovered coenzyme) in copper-containing amine oxidases.[2,3]

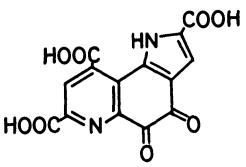

PQQ

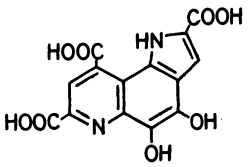

$PQQH_2$

We have already demonstrated the autorecycling PQQ-catalyzed oxidation of amines, which can be regarded as a model system of PQQ-containing amine oxidases.[4] And in the preceding paper, we investigated the mechanism of the reaction between PQQ and an amine under anaerobic conditions.[5] Moreover, existence of reduced PQQ (4,5-dihydroxy-1*H*-pyrrolo[2,3-*f*]-quinoline-2,7,9-tricarboxylic acid, $PQQH_2$) and its importance in a quinoprotein have also been reported by Duine and his co-workers.[6] Thus in this paper, we wish to investigate the reaction of $PQQH_2$ and O_2 in order to clarify the redox systems of PQQ in more detail. The reaction of hydroquinone and catechol derivatives with O_2 has not been studied so widely that the mechanism has not been clear.[7,8]

Experimental

Ultraviolet and visible absorption spectra were recorded on Shimadzu UV-240 spectrophotometer equipped with a temperature controlled cell holder, Shimadzu TCC-240. Measurements of pH were performed by using Horiba pH-meter F-8. Oxygen concentrations were determined by using Unicon oxygen meter. Superoxide dismutase (SOD) was obtained commercially, and catalase was supplied by Dr. K. Kobayashi (Osaka University). Other chemicals used were purchased at the highest purities available.

Preparation of $PQQH_2$ (quinol). Reduction of PQQ to $PQQH_2$ was performed with thiophenol, 1-benzyl-1,4-dihydronicotinamide (BNAH),[9] sodium dithionite, or sodium borohydride (Table). A typical procedure is as follows. After quantitative hydrolysis of PQQTME[10] (trimethyl ester of PQQ, 12.7 mg, 3.4×10^{-2} mmol) to PQQ in 0.05 M Na_2CO_3 (10 ml (1 M=1 mol dm^{-3})) at 30 °C for 24 h, the solution was neutralized (pH 6.8) with 2 M HCl. The solution was placed in the bottom of a Thunberg vessel (30 ml), and 10-fold excess of thiophenol (0.34 mmol) in acetonitrile (3 ml) was deposited in the side arm of the vessel. Both solutions were degassed for 30 min by bubbling N_2 through them, which were then mixed to start the reaction. After 2 h, the reaction mixture was acidified with 2 M HCl (1 ml), and was stood overnight. The precipitated product was collected by centrifugation and was washed with acetonitrile (5 ml). The product was dried in vacuo over P_2O_5, and recrystallized from dimethyl sulfoxide–acetonitrile (84% yield). The spectral data of the product were in good agreement with those reported by Duine and his co-workers.[6] BNAH, $Na_2S_2O_4$, $NaBH_4$ could also be reacted in the same way, and $PQQH_2$ was obtained in 77, 99, and 99% yield, respectively. Reduction of PQQ with phenylhydrazine (pH 3.1) and catalytic hydrogenation of PQQ (H_2 (1 atm)/PtO_2, pH 6.7) were carried out in the similar way reported elsewhere (82 and 65%, respectively).[6]

Oxidation of $PQQH_2$ by Molecular Oxygen. The reaction between $PQQH_2$ and O_2 was performed in 0.1 M acetate, phosphate, and carbonate buffer solutions (μ=0.3 with KCl, containing 5% dimethyl sulfoxide) at 30 °C under air atmosphere. An air saturated buffer solution (2.85 ml, $[O_2]=2.28\times10^{-4}$ M) was placed into a cuvette, and the reaction was started by adding 0.15 ml of an anaerobic DMSO solution of $PQQH_2$ (2.86×10^{-4} M). The reaction was followed by observing the disappearance of $PQQH_2$ at 320 nm. Hydrogen peroxide product was determined by adding 1 M NaI aqueous solution (0.5 ml) to the final reaction mixture, and monitoring the appearance of I_3^- at 353 nm (ε=25000 $M^{-1}cm^{-1}$). The rate constant was found to be identical with that for the reaction of I^- with authentic H_2O_2 at the pH employed. The yield of H_2O_2 was determined from the increase of A_{353} and was calculated to be about 50% based on $PQQH_2$. Oxygen concentration were controlled by mixing a O_2-saturated buffer solution and a N_2-saturated one.

Results and Discussion

Synthesis of $PQQH_2$. PQQ is reduced in the reac-

Table. Synthesis of $PQQH_2$[a]

Reductant[b] (Solvent, ml)	pH[c]	Time h	Isolated Yield[d] %
PhSH (CH_3CN, 3 ml)	6.8	2	84
BNAH (CH_3CN, 3 ml)[e]	6.8	3	77
$Na_2S_2O_4$ (H_2O, 1 ml)	11.4	5	99
$NaBH_4$ (H_2O, 1 ml)	7.2	4	99
$PhNHNH_2$ (CH_3CN, 3 ml)	3.1	3	82
H_2(1 atm)/PtO_2	7.0	5	65

a) PQQ was generated by hydrolysis of PQQTME (0.032—0.036 mmol) in 0.05 M Na_2CO_3 (10 ml). b) 10-fold excess over PQQ. c) The pH of a PQQ-aqueous solution was adjusted with 2 M HCl. d) Based on PQQ. e) In the dark.

tion with amines, but a mixture of the quinol and the aminophenol was obtained.[5] On the other hand, we found that only $PQQH_2$ (quinol) was produced in the reaction of PQQ with thiophenol,[11] BNAH, $Na_2S_2O_4$, and $NaBH_4$ (Table). Formation of PhSSPh and BNA^+ was detected in the reaction of PQQ with PhSH and BNAH by HPLC, respectively.

It should be noted that 99% of $PQQH_2$ was isolated in the reaction with $NaBH_4$, though Duine and his co-workers reported the formation of $PQQH_4$ in the reaction with $NaBH_4$.[12] Probably, they used so excess $NaBH_4$ over PQQ that further reduction might take place. The reaction with $PhNHNH_2$ (under acidic conditions) and catalytic hydrogenation (H_2/PtO_2, under neutral conditions) could be applied to the preparation of $PQQH_2$, but removal of the catalyst from the reaction mixture caused the autoxidation in the latter case.

The present methodology was applicable to the preparation of reduced PQQTME (trimethyl 4,5-dihydroxy-1*H*-pyrrolo[2,3-*f*]quinoline-2,7,9-tricarboxylate, $PQQTMEH_2$) which was obtained in 80% yield in the reaction of PQQTME and PhSH in acetonitrile under anaerobic conditions for 24 h.[13] BNAH, $NaBH_4$, and $PhNHNH_2$ were also applicable to the prepara-

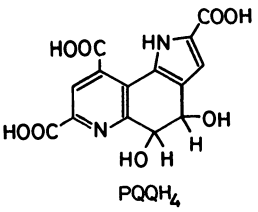

$PQQH_4$

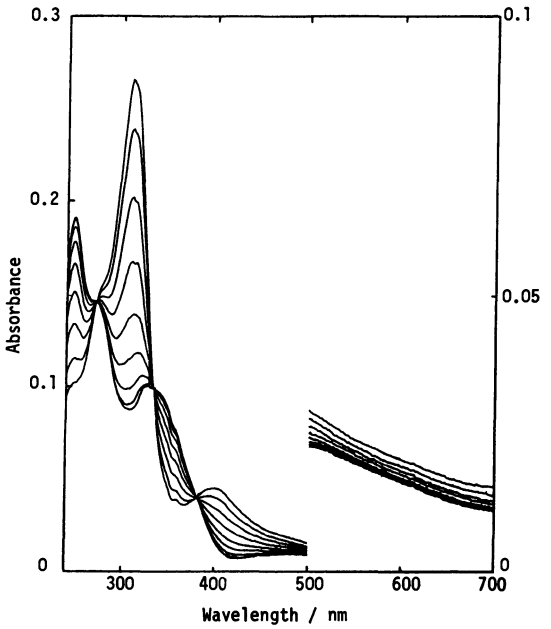

Fig. 1. Spectral change along the progress of the reaction of $PQQH_2$ (1.5×10^{-5} M), and O_2 (2.28×10^{-4} M), in 0.1 M acetate buffer (pH 3.81, μ=0.3 with KCl, containing 5% DMSO) at 30°C.

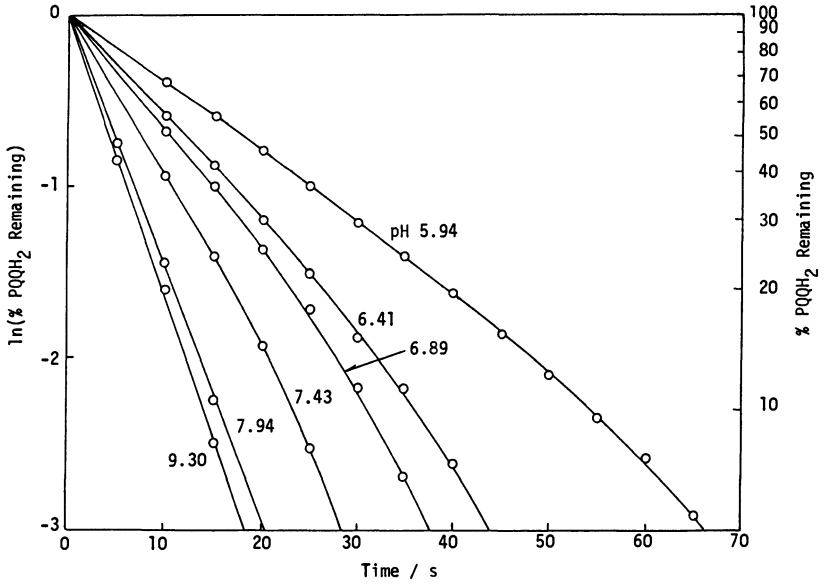

Fig. 2. Time course of the oxidation of $PQQH_2$ (1.5×10^{-5} M), by O_2 (2.28×10^{-4} M), in 0.1 M acetate (pH 5.94), phosphate (pH 6.41, 6.89, 7.43, 7.94), and carbonate (pH 9.30) buffer solutions (μ=0.3 with KCl, containing 5% DMSO) at 30°C.

tion of PQQTMEH$_2$ (70, 65, and 82% yield, respectively).

Oxidation of PQQH$_2$ by O$_2$ was studied under pseudo-first-order conditions of $[PQQH_2]_T=1.5\times10^{-5}$ M under air atmosphere ($[O_2]=2.28\times10^{-4}$ M at 30 °C) in 0.1 M buffer solutions (μ=0.3 with KCl, containing 5% DMSO). The progress of the reaction was followed by monitoring the disappearance of PQQH$_2$ at 320 nm (Fig. 1). PQQH$_2$ was oxidized rapidly to PQQ with isosbestic points at 272, 333, and 379 nm at pH 3.81 (0.1 M acetate buffer containing 5% DMSO) and the yield of H_2O_2 was determined to be about 50% based on PQQH$_2$ by iodometric titration. An intermediate such as a semiquinone or a covalent adduct of O$_2$ to PQQH$_2$ was not detected by UV-visible absorption spectroscopy in the course of the reaction.

The reaction did not follow the first-order kinetics, namely it is accelerated gradually with proceeding of the reaction (Fig. 2). Thus, the initial rate constant (k_i) was calculated from the initial slope of the pseudo-first-order plots. The initial rate (pH 6.90) was first-order in oxygen concentration (Fig. 3). As shown in Fig. 2, the rate increases as the pH is increased from 5.94 to 9, though the dependence of the initial rate on pH is somewhat complicated. The acid-base dissociation constant (K_a) for the quinol function of PQQH$_2$ was determined spectrophotometrically to be 7.08×10^{-10} M (pK_a=9.15) under the anaerobic kinetic conditions. Moreover, PQQH$_2$ was relatively stable in an organic solvent such as dimethyl sulfoxide even under aerobic conditions. These results indicate that PQQH$^-$ is considered to be an active species in the oxidation of PQQH$_2$ by O$_2$ as shown in Eq. 1.

$$PQQH_2 \underset{+H^+}{\overset{-H^+}{\rightleftharpoons}} PQQH^- \xrightarrow{k_2[O_2]} PQQ + H_2O_2 \qquad (1)$$

$$pK_a = 9.15$$

Why does the reaction deviate from the first-order rate law? To solve the problem, the reaction was carried out in the presence of catalase (10^{-7} M) under the same conditions (Fig. 4). In this case, the reaction followed the first-order rate law and such a deviation was not observed. On the other hand, the presence of SOD (superoxide dismutase, 10^{-7} M) in addition to catalase hardly affected the time course compared with the case of autoxidation of reduced flavins.[14] Furthermore, the presence of PQQ (1.5×10^{-5} M) in the reaction mixture also did not alter the time course of the reaction. From these results, we consider that the main cause for the deviation from the pseudo-first-order rate law is a side reaction of PQQH$_2$ with H_2O_2 (Eq. 4) formed by the reaction of PQQH$_2$ and O$_2$ (Eq. 3). As in fact, the yield of H_2O_2 was found to be about 50% based on PQQH$_2$, and PQQH$_2$ actually reacted with H_2O_2 comparably

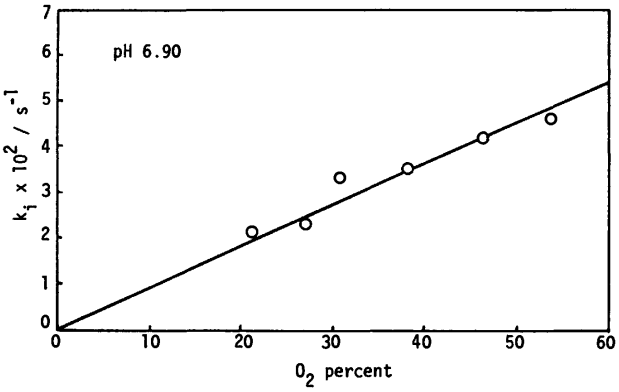

Fig. 3. Initial rate constant (k_i) for the O$_2$ oxidation of PQQH$_2$ (1.5×10^{-5} M) plotted as a function of O$_2$ percent (determined by oxygen meter based on O$_2$- saturated solution: 100%) in 0.1 M phosphate buffer (pH 6.90, μ=0.3 with KCl, containing 5% DMSO) at 30 °C.

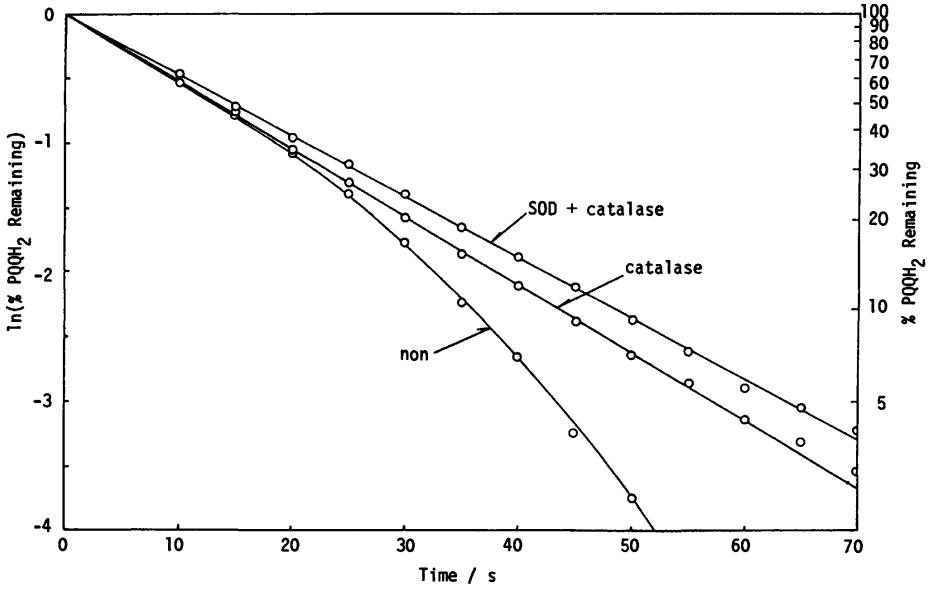

Fig. 4. Effect of catalase (10^{-7} M) and superoxide dismutase (SOD, 10^{-7} M) on the oxidation of PQQH$_2$ (1.5×10^{-5} M) by O$_2$ (2.28×10^{-4} M) in 0.1 M phosphate buffer (pH 6.90, μ=0.3 with KCl, containing 5% DMSO) at 30 °C.

fast in the absence of O_2. On the other hand, there may be little participation of autocatalysis by $O_2^{\cdot-}$ and PQQ itself (Eq. 5—7).

$$PQQH_2 + O_2 \longrightarrow PQQ + H_2O_2 \quad (3)$$

$$PQQH_2 + H_2O_2 \longrightarrow PQQ + 2H_2O \quad (4)$$

$$PQQH_2 + PQQ \rightleftharpoons 2PQQH^{\cdot} \quad (5)$$

$$PQQH^{\cdot} + O_2 \longrightarrow PQQ + O_2^{\cdot-} + H^+ \quad (6)$$

$$PQQH^{\cdot} + O_2^{\cdot-} \xrightarrow{H^+} PQQ + H_2O_2 \quad (7)$$

As molecular oxygen contains two unpaired electrons and is paramagnetic in the ground state, the concerted two electron reduction of O_2 to H_2O_2 is highly restricted by symmetry consideration.[15] Thus, the reduction of O_2 with $PQQH_2$ is assumed to occur in two ways: (a) By binding to the electron donor, $PQQH_2$, the molecular orbitals of O_2 are perturbed, or (b) the reduction of O_2 via two univalent electron transfer (stepwise). The standard redox potential (E_0') values (pH=7.0) of $O_2/HO_2^{\cdot}$ couple has been calculated to be −0.59 V (Eq. 8).[16] On the other hand, Duine and his co-workers determined the midpoint potentials (E_m) of the quinone/semiquinone and semiquinone/quinol couples for PQQ at pH 13.0 to be −0.218 and −0.242 V, respectively (Eqs. 10, 11).[6] Although the standard redox potentials (pH 7.0) for these couples of PQQ have not been defined, they are considered to be higher than those E_m (pH 13). Thus, one electron reduction of O_2 to $O_2^{\cdot-}$ by either $PQQH_2$ or the semiquinone appears thermodynamically unfavorable. Absence of autocatalysis by $O_2^{\cdot-}$ and the semiquinone may also discard the possibility of the reduction of O_2 via two univalent electron transfer (free radical mechanism, type b). Ultimately, it reminds us a mechanism via covalent addition of O_2 to quinol carbon of $PQQH^-$ followed by elimination of H_2O_2 (type a). The mechanistic details of the reaction is currently under investigation.

$$O_2 + H^+ + e^- \longrightarrow HO_2^{\cdot} \quad E_0' = -0.59\,V \quad (8)$$

$$HO_2^{\cdot} + H^+ + e^- \longrightarrow H_2O_2 \quad E_0' = 0.98\,V \quad (9)$$

$$\text{quinone/semiquinone} \quad E_m = -0.218\,V\ (pH=13) \quad (10)$$

$$\text{semiquinone/quinol} \quad E_m = -0.242\,V\ (pH=13) \quad (11)$$

The present work was partially supported by a Grant-in-Aid for Special Project Research from the Ministry of Education, Science, and Culture and by the Mishima-Kaiun Memorial Foundation to which our thanks are due. We also acknowledge Dr. Kazuo Kobayashi of Osaka University for his kind supply of catalase.

References

1) T. P. Singer and D. E. Edmondson, "Molecular Oxygen in Biology," ed by O. Hayashi, North-Holland Publish Campany (1974), p. 315.

2) M. Ameyama, M. Hayashi, K. Matsushita, E. Shinagawa, and O. Adachi, *Agric. Biol. Chem.*, **48**, 561 (1984).

3) C. L. Lobenstein-Verbeek, J. A. Jongejan, J. Frank, and J. A. Duine, *FEBS Lett.*, **170**, 305 (1984).

4) a)Y. Ohshiro, S. Itoh, K. Kurokawa, J. Kato, T. Hirao, and T. Agawa, *Tetrahedron Lett.*, **24**, 3465 (1983); b) S. Itoh, N. Kato, Y. Ohshiro, and T. Agawa, *ibid.*, **25**, 4753 (1984).

5) S. Itoh, Y. Kitamura, Y. Ohshiro, and T. Agawa, accompanying paper in this issue.

6) J. A. Duine, J. Frank, and P. E. J. Verwiel, *Eur. J. Biochem.*, **118**, 395 (1981).

7) T. H. James, J. M. Snell, and A. Weissberger, *J. Am. Chem. Soc.*, **60**, 2084 (1938).

8) H. Musso and H. Dopp, *Chem. Ber.*, **100**, 3627 (1967).

9) D. Mauzerall and F. H. Westheimer, *J. Am. Chem. Soc.*, **77**, 2261 (1955).

10) E. J. Corey and A. Tramontano, *J. Am. Chem. Soc.*, **103**, 5599 (1981).

11) S. Itoh, N. Kato, Y. Ohshiro, and T. Agawa, *Chem. Lett.*, **1985**, 135.

12) J. A. Duine, J. Frank, and P. E. J. Verwiel, *Eur. J. Biochem.*, **108**, 187 (1980).

13) Mp (decomp) 224—247 °C; ^{1}H NMR (DMSO-d_6, δ) 4.01, 4.09, 4.17 (each s, 3H, OCH_3), 6.1 (br s, quinol OH), 7.53 (d, J=2 Hz, 1H, aromatic 3-H), 8.79 (s, 1H, aromatic 8-H); IR (Nujol, cm^{-1}) 3200—3600 (quinol OH), 3480 (NH), 1725, 1735 (ester C=O); mass spectrum m/z 374 (M^+); Anal. Calcd for $C_{17}H_{14}N_2O_8$: C, 54.55; H, 3.77; N, 7.48%. Found: C, 54.03; H, 3.67; N, 7.50%; UV spectrum (CH_3CN) λ_{max}=325 nm (ε= 30400 $M^{-1}cm^{-1}$).

14) V. Massy, G. Palmer, and D. Ballon, "On the Reaction of Reduced Flavins and Flavoproteins with Molecular Oxygen" in "Flavins and Flavoproteins, Third International Symposium," ed by H. Kamin, University Park Press, Baltimore (1971), pp. 349—361.

15) H. Taube, *J. Gen. Physiol.*, **49**, 29 (1965).

16) N. Sutin, "Oxidase and Related Redox Systems," ed by E. T. King, H. S. Mason, and M. Morrison, Wiley, New York (1965), Vol 1, p. 34.

 © 1986 The Chemical Society of Japan Bull. Chem. Soc. Jpn., 59, 1915—1919 (1986)

Synthesis of ara-Cadeguomycin. 2-Amino-3,4-dihydro-4-oxo-7-(β-D-arabinofuranosyl)-7*H*-pyrrolo[2,3-*d*]pyrimidine-5-carboxylic Acid

Kaoru Okamoto, Tadao Kondo,†,* and Toshio Goto*
Laboratory of Organic Chemistry, Faculty of Agriculture, Nagoya University, Chikusa-ku, Nagoya 464
†Chemical Instrument Center, Nogoya University, Chikusa-ku, Nagoya 464
(Received January 31, 1986)

2-Amino-3,4-dihydro-4-oxo-7-(β-D-arabinofuranosyl)-7*H*-pyrrolo[2,3-*d*]pyrimidine-5-carboxylic acid, an analogue of cadeguomycin, has been synthesized via glycosylation of 3-methoxymethyl-5-methyl-2-methylthio-7*H*-pyrrolo[2,3-*d*]pyrimidin-4(3*H*)-one with 2,3,5-tri-*O*-benzyl-D-arabinofuranosyl chloride.

The arabinofuranosyl nucleosides such as ara-A[1] and ara-G[2] of naturally occurring purine and pyrimidine bases of nucleic acids have been synthesized to investigate their biological activities. It has been revealed that they act as inhibitors of ribonucleotide reductase or DNA polymerase.[3] 4-Amino-7-(β-D-arabinofuranosyl)pyrrolo[2,3-*d*]pyrimidine (ara-tubercidin),[4] resists to deactivation by deaminases and shows antiviral activity. Recently, 2-amino-7-(β-D-arabinofuranosyl)-pyrrolo[2,3-*d*]pyrimidin-4(3*H*)-one (7-deaza-ara-G) was also synthesized[5] to avoid deactivation by the above reason. These properties of arabinofuranosyl nucleosides prompted us to synthesize the ara-analogue (**2**) of cadeguomycin (**1**), which was isolated from the culture broth of *Streptomyces hygroscopicus* IM7912T as a minor component concomitant with tubercidin.[6] Cadeguomycin (**1**) inhibits growth of IMC carcinoma and metastasis of Lewis lung carcinoma, and enhances cell-mediated immunity and macrophage activity,[7] but shows no significant antimicrobial activity against bacteria and fungi in contrast to tubercidin.[6]

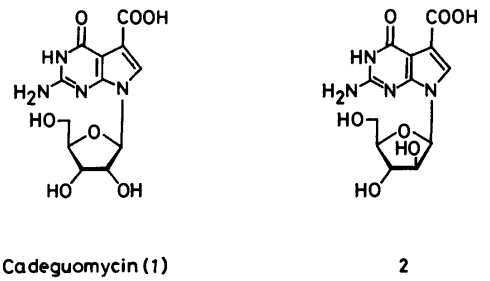

Fig. 1.

As a base moiety for the synthesis of ara-cadeguomycin (**2**) we have chosen 3-methoxymethyl-5-methyl-2-methylthio-7*H*-pyrrolo[2,3-*d*]pyrimidin-4(3*H*)-one (**3**) which has been applied to the syntheses of cadeguomycin (**1**),[8] nucleoside Q, preQ$_0$, and preQ$_1$.[9] The glycosylation reaction of the base **3** with 2,3,5-tri-*O*-benzyl-D-arabinofuranosyl chloride (**4**), which was prepared from 2,3,5-tri-*O*-benzyl-1-*O*-(*p*-nitrobenzoyl)-D-arabinofuranose according to the Fletcher's method,[10] was carried out in the same manner as the synthesis of cadeguomycin (**1**), etc.[8,9] Thus, treatment of **3** with **4** in the presence of sodium hydride in DMF gave **5αβ** as a 1:5 mixture of α and β isomer in 99% yield. The structural assignment of the anomers was achieved by comparison of chemical shifts of the anomeric protons in ^{1}H NMR spectra with those of known 7-(β-D-arabinofuranosyl)pyrrolo[2,3-*d*]pyrimidin-4(3*H*)-one analogues.[5,11] Generally the anomeric proton signal of the β isomer appears in a low field (≈6.53 ppm) compared with that of the α isomer (≈6.27 ppm) and has a larger vicinal coupling constant (5.4 Hz) in contrast to the α isomer (3.9 Hz) in ^{1}H NMR spectra. As this glycosylation products, **5αβ**, could not be separated by the usual silica-gel column chromatography, the mixture was subjected to the next acetylamination reaction. The conversion of the 2-methylthio group of **5αβ** into an acetylamino group was carried out by the method which has been used for the synthesis of nucleoside Q.[12] Thus, the mixture was treated at 100 °C with acetamide anion generated by fusion of sublimed acetamide and sodium hydride to give a mixture of **6α** and **6β** in 64% yield. In this stage, the anomeric mixture **6αβ** was easily separated into β (53% yield) and α isomer (11% yield) by use of a silica-gel column. The protecting benzyl groups on the sugar moiety were changed to acetyl groups since the benzyl groups are intolerable to the subsequent allylic bromination. Debenzylation of **6β** was accomplished with 10% Pd–C under hydrogen atmosphere to give the triol **7** in 67% yield. Treatment of **7** with acetic anhydride and anhydrous pyridine gave the acetylated compound **8** in 99% yield. The compound **8** was brominated with *N*-bromosuccinimide (NBS) in benzene at room temperature to afford the bromide **9** in 99% yield. The bromide **9** was further brominated with NBS in carbon tetrachloride to give a dibromide, which was converted into the bromo alcohol **10** by hydrolysis with silver carbonate in dioxane–water. The overall yield from **8** was 76%. Without isolation of the bromide **9** direct conversion of **8** with 2 equivalents of NBS into **10** resulted in a low yield (ca. 30%). Oxidation of the bromo alcohol **10** with active manganese (IV) dioxide in acetonitrile caused partial deacetylation and, therefore, the product was reacetylated with acetic anhydride and pyridine to give the aldehyde **11** in 67% yield. Further oxidation of **11** with NBS[13] in carbon tetrachloride under irradiation by a reflecting photolamp at room temperature gave the acid bromide, which was hydrolyzed by addition of water and then deacetylated with aqueous ammonia to afford the

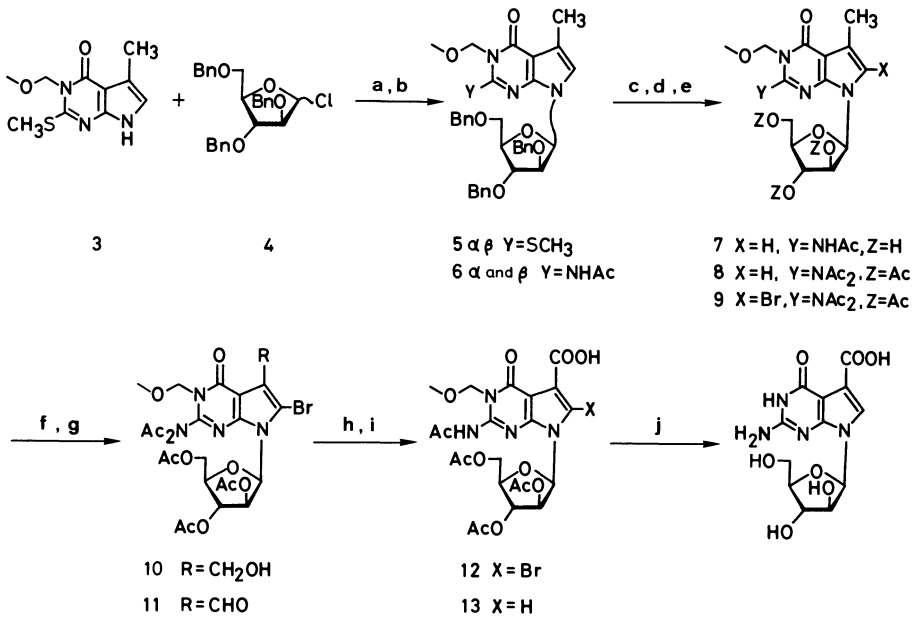

Scheme. 1. Reaction conditions: (a) NaH, DMF, 0°C, 2 h (97%); (b) NaH, CH_3CONH_2, 100°C, 40 min (64%); (c) 10% Pd-C/H_2, MeOH, rt, 7 h (67%); (d) Ac_2O, pyridine, rt, 1 h (99%); (e) NBS, benzene, rt, 30 min (99%); (f) NBS, benzoyl peroxide, K_2CO_3, CCl_4, reflux, 2 h; Ag_2CO_3, dioxane-water, rt, 1.5 h (76%); (g) MnO_2, CH_3CN, rt, 8 h (67%); (h) NBS, $h\nu$, K_2CO_3, CCl_4, rt, 45 min; 2M HCl (67%); (i) 10% Pd-C/H_2, MeOH-water, rt, 30 min (84%); (j) NH_4OH, MeOH, rt, 14 h; TFA-water (3/1), 70°C, 1 h (86%).

bromo carboxylic acid **12** in 64% yield. Finally, deprotection was accomplished stepwise. The compound **12** was debrominated with 10% Pd-C in the presence of potassium acetate giving the carboxylic acid **13** in 84% yield. Hydrolysis of **13** with aqueous ammonia in methanol followed by trifluoroacetic acid (TFA) afforded ara-cadeguomycin (**2**) in 86% yield, which was crystallized from ethanol-water to give pure ara-cadeguomycin (**2**).

Experimental

Melting points were determined on a Mitamura Riken flat-bulb thermometer with a heating metal block and uncorrected. Elemental analyses were performed on a Perkin-Elmer 240C elemental analyzer. Nuclear magnetic resonance spectra (NMR) were recorded with a JEOL FX-200 instrument in the FT mode. Chemical shifts were expressed in δ values relative to tetramethylsilane as an internal standard unless otherwise noted. Coupling constants (J) were given in hertz (Hz) and splitting pattern abbreviations are: s, singlet; d, doublet; t, triplet; q, quartet; dd, doublet of doublets; ddd, doublet of double doublets; br, broad; m, multiplet. Mass spectra (MS) were obtained on a JEOL DX-300 spectrometer. Infrared spectra (IR) were recorded on either a Shimadzu IR 435 or a JASCO A-3 spectrometer. Ultraviolet spectra (UV) were measured on a Hitachi 228 spectrometer. Optical rotations $[\alpha]_D$ were recorded on a JASCO DIP-181 digital polarimeter.

Analytical thin-layer chromatography (TLC) was done on precoated TLC glass sheets (silica gel 60F-254, layer thickness 0.25 mm) manufactured by E. Merck. Preparative silica-gel thick-layer chromatography was performed on 20×20 cm glass plates coated with silica gel PF-254 (E. Merck, Darmstadt). Column chromatography was performed with Merck silica gel 60 (70—230 mesh).

Glycosylation of the Base 3 with 4. Dry hydrogen chloride was bubbled into a solution of 2,3,5-tri-*O*-benzyl-1-*O*-(*p*-nitrobenzoyl)-D-arabinofuranose[7] (5.8 g, 10.2 mmol) in dichloromethane (36 ml) at 0°C until no further *p*-nitrobenzoic acid precipitated. After standing for 2 h, the precipitate was filtered and washed with dichloromethane. The combined filtrates were evaporated in vacuo to give the halogenose **4** as a viscous syrup, which was dissolved in anhydrous DMF (5.5 ml). A mixture of **3** (1.8 g, 7.5 mmol) and sodium hydride (50% oil suspension, 0.45 g, 9.4 mmol) in anhydrous DMF (7.0 ml) was stirred for 0.5 h and to this was added above DMF solution of **4** at 0°C under argon atmosphere. The reaction mixture was allowed to warm to room temperature, stirred for 6 h, poured into ice-water, and extracted with ethyl acetate. The extracts were washed with water and brine, dried over anhydrous Na_2SO_4, and evaporated in vacuo to give a viscous residue, which was applied to a silica-gel column and eluted with hexane-ethyl acetate (gradient elution from 3:1 to 2:1) to give 3-methoxymethyl-5-methyl-2-methylthio-7-(2,3,5-tri-*O*-benzyl-D-arabinofuranosyl)-7*H*-pyrrolo[2,3-*d*]pyrimidin-4(3*H*)-one (**5**$\alpha\beta$) (4.8 g, 99%) as a 1:5 mixture of α and β isomer (detected by ^{1}H NMR): UV (MeOH) 308 nm; ^{1}H NMR ($CDCl_3$)

δ=2.30 (d, J=1.0 Hz, β-CH_3-5), 2.36 (d, J=1.0 Hz, α-CH_3-5), 2.48 (s, α-CH_3S), 2.55 (s, β-CH_3S), 3.44 (s, β-CH_3O), 3.46 (s, α-CH_3O), 3.49—3.78 (m, α,β-H-5′), 4.0—4.7 (m, α,β-H-2′ and 3′, OCH_2Ph), 5.57 (br. s, OCH_2N), 6.27 (d, J=3.9 Hz, α-H-1′), 6.53 (d, J=5.4 Hz, β-H-1′), 6.70 (q, J=1.0 Hz, α-H-6), 6.82 (q, J=1.0 Hz, β-H-6), and 6.9—7.4 (m, ArH); IR (neat) 1685 (amide I), 1534 (amide II), and 1512 cm^{-1}; MS (EI) m/z 641 (M^+).

2-Acetylamino-3-methoxymethyl-5-methyl-7-(2,3,5-tri-*O*-benzyl-β-D-arabinofuranosyl)-7*H*-pyrrolo[2,3-*d*]pyrimidin-4(3*H*)-one (6β) and Its α Isomer (6α). To a mixture of sodium hydride (50% oil suspension, 1.3 g) and acetamide (13 g, sublimed just before use) was added **5αβ** (2.6 g, 4.1 mmol) and heated for 40 min at 100 °C under argon atmosphere. Excess acetamide was removed in vacuo and the residue was carefully acidified with acetic acid under ice-cooling and extracted with benzene. The extract was washed with water, saturated $NaHCO_3$, and brine, dried over anhydrous Na_2SO_4, and evaporated in vacuo to give a syrup, which was chromatographed on a silica-gel column (hexane–ethyl acetate, gradient elution from 2:1 to 1:1). The more rapidly migrating zone was the isomer **6α** (0.3 g, 11%) and the slower, the isomer **6β** (1.4 g, 53%) as a viscous syrup; **6α**: UV (MeCN) 306 nm (ε 9580); $[\alpha]_D^{21}$ +23.6° (c 0.1, $CHCl_3$); ^1H NMR ($CDCl_3$) δ=2.35 (3H, d, J=1.0 Hz, CH_3-5), 2.38 (3H, s, CH_3CON), 3.44 (3H, s, CH_3O), 3.60 (1H, dd, $J_{5',4'}$=5.1 Hz, $J_{5',5'}$=10.5 Hz, H-5′), 3.63 H, dd, $J_{5',4'}$=4.6 Hz, $J_{5',5'}$=10.5 Hz, H-5′), 4.15—4.28 (1H, m, H-4′), 4.35—4.66 (8H, m, H-2′ and 3′, 3×OCH_2Ph), 5.52 and 5.53 (2H, AB quartet, J=11.5 Hz, OCH_2N), 6.20 (1H, d, $J_{1',2'}$=3.9 Hz, H-1′), 6.77 (1H, q, J=1.0 Hz, H-6), 7.1—7.4 (15H, m, ArH), and 8.41 (1H, br. s, NH); IR (neat) 1685 (amide I) and 1570 (amide II) cm^{-1}; MS (EI) m/z 652 (M^+).

Found: C, 68.30; H, 6.15; N, 8.45%. Calcd for $C_{37}H_{40}N_4O_7$: C, 68.08; H, 6.18; N, 8.58%.

6β: UV (MeCN) 306 nm (ε 9660); $[\alpha]_D^{21}$ +45.8° (c 0.1, $CHCl_3$); ^1H NMR ($CDCl_3$) δ=2.29 (3H, d, J=1.2 Hz, CH_3-5), 2.40 (3H, s, CH_3CON), 3.43 (3H, s, CH_3O), 3.70 (1H, dd, $J_{5',4'}$=4.4 Hz, $J_{5',5'}$=10.5 Hz, H-5′), 3.73 (1H, dd, $J_{5',4'}$= 4.2 Hz, $J_{5',5'}$=10.5 Hz, H-5′), 4.09 (1H, ddd, $J_{4',3'}$=5.4 Hz, $J_{4',5'}$=4.2 and 4.4 Hz, H-4′), 4.21 and 4.27 (2H, AB quartet, J=11.5 Hz, OCH_2Ph), 4.22 (1H, t, $J_{2',1'}$=$J_{2',3'}$=5.4 Hz, H-2′), 4.31 (1H, t, $J_{3',2'}$=$J_{3',4'}$=5.4 Hz, H-3′), 4.52 and 4.56 (2H, AB quartet, J=12.0 Hz, OCH_2Ph), 4.60 and 4.64 (2H, AB quartet, J=12.0 Hz, OCH_2Ph), 5.50 and 5.51 (2H, AB quartet, J=11.5 Hz, OCH_2N), 6.41 (1H, d, $J_{1',2'}$=5.4 Hz, H-1′), 6.91 (1H, q, J=1.2 Hz, H-6), 6.9—7.4 (15H, m, ArH), and 8.38 (1H, br. s, NH); IR (neat) 1692 (amide I) and 1575 (amide II) cm^{-1}; MS (FAB) m/z 653 (M+H).

Found: C, 68.21; H, 6.05; N,8.63%. Calcd for $C_{37}H_{40}N_4O_7$: C, 68.08; H, 6.18; N, 8.58%.

2-Acetylamino-3-methoxymethyl-5-methyl-7-(β-D-arabinofuranosyl)-7*H*-pyrrolo[2,3-*d*]pyrimidin-4(3*H*)-one (7). A mixture of **6β** (1.2 g, 1.8 mmol) and 10% Pd-C (3.6 g) in methanol (50 ml) was stirred vigorously for 7 h at room temperature under hydrogen atmosphere. The catalyst was removed by filtration and washed well with methanol. The combined filtrates were evaporated in vacuo to give a syrup, which was chromatographed on a silica-gel column (chloroform–methanol, 5:1) to give a pale yellow syrup **7** (0.47 g, 67%): UV (MeCN) 305 nm (ε 7580); $[\alpha]_D^{21}$ +20.0° (c 0.1, MeOH); ^1H NMR (Acetone-d_6) δ=2.30 (3H, d, J=1.0 Hz, CH_3-5), 2.84 (3H, s, CH_3CON), 3.38 (3H, s, CH_3O), 3.83 (1H, ddd, $J_{5',4'}$=4.5 Hz, $J_{5',OH}$=5.1 Hz, $J_{5',5'}$=11.5 Hz, H-5′), 3.88 (1H, ddd, $J_{5',4'}$=4.5 Hz, $J_{5',OH}$=5.1 Hz, $J_{5',5'}$=11.5 Hz, H-5′), 3.95 (1H, q, $J_{4',3'}$=$J_{4',5'}$=4.5 Hz, H-4′), 4.16 (1H, ddd, $J_{2',1'}$=4.3 Hz, $J_{2',OH}$=7.5 Hz, $J_{2',3'}$=7.7 Hz, H-2′), 4.32 (1H, dd, $J_{3',2'}$=7.7 Hz, $J_{3',OH}$=$J_{3',4'}$=4.5 Hz, H-3′), 4.50 (1H, t, $J_{OH,5'}$=5.1 Hz, OH-5′), 4.70 (1H, d, $J_{OH,3'}$=4.5 Hz, OH-3′), 4.81 (1H, d, $J_{OH,2'}$=7.5 Hz, OH-2′), 5.52 and 5.55 (2H, AB quartet, J=10.8 Hz, OCH_2N), 6.34 (1H, d, $J_{1',2'}$=4.3 Hz, H-1′), 7.04 (1H, q, J=1.0 Hz, H-6), and 8.75 (1H, br. s, NH); IR (neat) 3370 (OH, NH) and 1675 (amide I) cm^{-1}; MS (FAB) m/z 383 (M+H).

Found: C, 50.03; H, 5.89; N, 14.91%. Calcd for $C_{16}H_{22}N_4O_7$: C, 50.26; H, 5.80; N, 14.65%.

2-Diacetylamino-3-methoxymethyl-5-methyl-7-(2,3,5-tri-*O*-acetyl-β-D-arabinofuranosyl)-7*H*-pyrrolo[2,3-*d*]pyrimidin-4(3*H*)-one (8). A solution of **7** (350 mg, 0.92 mmol) in acetic anhydride (1.7 ml) and anhydrous pyridine (3.5 ml) was stirred for 1 h at room temperature under argon atmosphere. The solution was evaporated to a syrup, which was chromatographed on a silica-gel column (ethyl acetate–hexane, 2:1) and crystallized from hexane–ethyl acetate to give **8** (500 mg, 99%) as white crystals: Mp 169—170 °C; UV (MeCN) 305 nm (ε 8640); $[\alpha]_D^{22}$ +15.8° (c 0.1, $CHCl_3$); ^1H NMR ($CDCl_3$) δ=1.85 (3H, s, CH_3COO), 2.14 (3H, s, CH_3COO), 2.17 (3H, s, CH_3COO), 2.31 (3H, s, CH_3CON), 2.41 (3H, d, J=1.0 Hz, CH_3-5), 2.45 (3H, s, CH_3CON), 3.42 (3H, s, CH_3O), 4.19 (1H, br. q, J=5.1 Hz, H-4′), 4.38 (1H, dd, $J_{5',4'}$=5.9 Hz, $J_{5',5'}$=11.7 Hz, H-5′), 4.44 (1H, dd, $J_{5',4'}$=4.6 Hz, $J_{5',5'}$=11.7 Hz, H-5′), 5.21 and 5.38 (2H, AB quartet, J=10.5 Hz, OCH_2N), 5.36—5.43 (2H, m, H-2′ and 3′), 6.48 (1H, d, $J_{1',2'}$=4.4 Hz, H-1′), and 6.85 (1H, q, J=1.0 Hz, H-6); IR (KBr) 1737 (COO), 1690 (amide I), and 1570 (amide II) cm^{-1}; MS (EI) m/z 550 (M^+).

Found: C, 52.33; H, 5.56; N, 10.14%. Calcd for $C_{24}H_{30}N_4O_{11}$: C, 52.36; H, 5.49; N, 10.18%.

6-Bromo-2-diacetylamino-3-methoxymethyl-5-methyl-7-(2,3,5-tri-*O*-acetyl-β-D-arabinofuranosyl)-7*H*-pyrrolo[2,3-*d*]pyrimidin-4(3*H*)-one (9). To a solution of **8** (575 mg, 1.0 mmol) in benzene (75 ml) was added NBS (210 mg, 1.2 mmol) at room temperature. After stirring for 30 min, the solvent was removed and the residue was chromatographed on a silica-gel column (ethyl acetate–hexane, 3:2) to give a pale yellow syrup **9** (650 mg, 99%): UV (MeCN) 310 (ε 8380) and 269 nm (5390); $[\alpha]_D^{22}$ −61.4° (c 0.1, $CHCl_3$); ^1H NMR ($CDCl_3$) δ=1.69 (3H, s, CH_3COO), 2.05 (3H, s, CH_3COO), 2.12 (3H, s, CH_3COO), 2.37 (3H, s, CH_3-5), 2.40 (3H, s, CH_3CON), 2.44 (3H, s, CH_3CON), 3.43 (3H, s, CH_3O), 4.14 (1H, ddd, $J_{4',3'}$=7.3 Hz, $J_{4',5'}$=3.4 and 7.6 Hz, H-4′), 4.25 (1H, dd, $J_{5',4'}$=7.6 Hz, $J_{5',5'}$=11.2 Hz, H-5′), 4.44 (1H, dd, $J_{5',4'}$=3.4 Hz, $J_{5',5'}$=11.2 Hz, H-5′), 5.28 and 5.34 (2H, AB quartet, J=10.5 Hz, OCH_2N), 5.50 (1H, t, $J_{2',1'}$=$J_{2',3'}$=7.3 Hz, H-2′), 6.26 (1H, t, $J_{3',2'}$= $J_{3',4'}$=7.3 Hz, H-3′), and 6.58 (1H, d, $J_{1',2'}$=7.3 Hz, H-1′); IR (neat) 1740 (COO), 1700, 1690 (amide I), and 1578 (amide II) cm^{-1}; MS (EI) m/z 628 and 630 (M^+).

Found: C, 45.71; H, 4.88; N, 9.12%. Calcd for $C_{24}H_{29}N_4O_{11}Br$: C, 45.80; H, 4.64; N, 8.90%.

6-Bromo-2-diacetylamino-5-hydroxymethyl-3-methoxymethyl-7-(2,3,5-tri-*O*-acetyl-β-D-arabinofuranosyl)-7*H*-pyrrolo[2,3-*d*]-pyrimidin-4(3*H*)-one (10). A mixture of **9** (650 mg, 1.0 mmol), NBS (210 mg, 1.2 mmol), anhydrous potassium carbonate (660 mg, 4.78 mmol), and benzoyl peroxide (20 mg) in carbon tetrachloride (60 ml) was refluxed with stirring for 2 h under argon atmosphere. The reaction mixture was cooled and the precipitate was removed through a glass filter and washed with carbon tetrachloride. The combined filtrates were

evaporated in vacuo to give a dibromide, which was dissolved in dioxane (40 ml) and water (14 ml). To this solution was added silver carbonate (800 mg, 2.9 mmol) and the mixture was stirred for 1.5 h at room temperature and filtered, and the filtrate was evaporated in vacuo to give a syrup, which was chromatographed on a silica-gel column (benzene–ethyl acetate, gradient elution from 1:1 to 2:3) to give **10** (507 mg, 76%) as a viscous syrup: UV (MeCN) 306 (ε 7290) and 269 nm (5830); $[\alpha]_D^{22}$ −44.7° (*c* 0.1, $CHCl_3$); ^1H NMR ($CDCl_3$) δ= 1.72 (3H, s, CH_3COO), 2.05 (3H, s, CH_3COO), 2.12 (3H, s, CH_3COO), 2.41 (3H, s, CH_3CON), 2.45 (3H, s, CH_3CON), 3.44 (3H, s, CH_3O), 4.16 (1H, ddd, $J_{4',3'}$=7.3 Hz, $J_{4',5'}$=3.7 and 7.6 Hz, H-4'), 4.24 (1H, dd, $J_{5',4'}$=7.6 Hz, $J_{5',5'}$=11.3 Hz, H-5'), 4.44 (1H, dd, $J_{5',4'}$=3.7 Hz, $J_{5',5'}$=11.3 Hz, H-5'), 4.73 (2H, s, OCH_2-5), 5.32 and 5.40 (2H, AB quartet, J=10.4 Hz, OCH_2N), 5.53 (1H, t, $J_{2',1'}=J_{2',3'}$=7.3 Hz, H-2'), 6.25 (1H, t, $J_{3',2'}=J_{3',4'}$= 7.3 Hz, H-3'), and 6.58 (1H, d, $J_{1',2'}$=7.3 Hz, H-1'); IR (neat) 3450 (OH), 1740 (COO), 1710, and 1690 (amide I); MS (EI) *m/z* 644 and 646 (M^+).

Found: C, 44.36; H, 4.37; N, 8.35%. Calcd for $C_{24}H_{29}N_4O_{12}Br$: C, 44.66; H, 4.53; N, 8.68%.

6-Bromo-2-diacetylamino-5-formyl-3-methoxymethyl-7-(2,3,5-tri-*O*-acetyl-β-D-arabinofuranosyl)-7*H*-pyrrolo[2,3-*d*]-pyrimidin-4(3*H*)-one (11). To a solution of **10** (480 mg, 0.74 mmol) in acetonitrile (25 ml) was added active MnO_2 (7.0 g) in seven portions every 30 min with stirring. After stirring for further 5 h, the mixture was filtered through a Celite 545 bed and the solid was washed well with acetone. The combined filtrates were evaporated in vacuo and the resultant syrup, which was deacetylated partially, was treated with acetic anhydride (1.5 ml) and anhydrous pyridine (3.0 ml) for 0.5 h at room temperature. The mixture was condensed to a syrup, which was purified by chromatography on a silica-gel column (benzene–ethyl acetate, 1:1) to give a colorless syrup 11 (319 mg, 67%): UV (MeCN) 296 (ε 12530) and 239 nm (14280); $[\alpha]_D^{22}$ −57.6° (*c* 0.2, $CHCl_3$); ^1H NMR ($CDCl_3$) δ=1.72 (3H, s, CH_3COO), 2.05 (3H, s, CH_3COO), 2.14 (3H, s, CH_3COO), 2.42 (3H, s, CH_3CON), 2.47 (3H, s, CH_3CON), 3.46 (3H, s, CH_3O), 4.15—4.32 (2H, m, H-5'), 4.35—4.50 (1H, m, H-4'), 5.34 and 5.42 (2H, AB quartet, J=10.7 Hz, OCH_2N), 5.59 (1H, t, $J_{2',1'}=J_{2',3'}$=7.3 Hz, H-2'), 6.27 (1H, $J_{3',2'}=J_{3',4'}$=7.3 Hz, H-3'), 6.74 (1H, d, $J_{1',2'}$=7.3 Hz, H-1'), and 10.47 (1H, s, CHO); MS(EI) *m/z* 642 and 644 (M^+).

Found: C, 44.47; H, 4.41; N, 8.93%. Calcd for $C_{24}H_{27}N_4O_{12}Br$: C, 44.80; H, 4.32; N, 8.71%.

2-Acetylamino-6-bromo-3,4-dihydro-3-methoxymethyl-4-oxo-7-(2,3,5-tri-*O*-acetyl-β-D-arabinofuranosyl)-7*H*-pyrrolo-[2,3-*d*]pyrimidine-5-carboxylic Acid (12). To a mixture of **11** 310 mg, 0.48 mmol) and anhydrous potassium carbonate (460 mg, 3.3 mmol) in carbon tetrachloride (70 ml) was added NBS (100 mg, 0.56 mmol). The mixture was irradiated by a 500 W reflecting photo-lamp with stirring for 45 min at room temperature. The mixture was cooled to 0°C and dioxane–water (3/1 v/v, 6 ml) was added to it. The reaction mixture was stirred for 30 min, acidified with 2 M HCl (1 M=1 mol dm^{-3}), and extracted with dichloromethane. The organic layer was washed with water and brine, dried over anhydrous Na_2SO_4, and evaporated in vacuo to give a syrup, which was treated with 28% aqueous ammonia (1 drop) in methanol (5 ml) for 5 min to hydrolyze the remaining *N,N*-diacetyl groups. After evaporation, the residual oil was purified by preparative silica-gel TLC (dichloromethane–methanol, 20:1) to give the bromo carboxylic acid **12** (190 mg, 64%) as a viscous syrup: UV (MeCN) 287 nm (ε 11650); $[\alpha]_D^{21}$ −71.4° (*c* 0.1, $CHCl_3$); ^1H NMR ($CDCl_3$) δ=1.78 (3H, s, CH_3COO), 2.07 (3H, s, CH_3COO), 2.14 (3H, s, CH_3COO), 2.38 (3H, s, CH_3CON), 3.51 (3H, s, CH_3O), 4.0—4.3 (2H, m, H-5'), 4.4—4.6 (1H, m, H-4'), 5.54 and 5.79 (2H, AB quartet, J=11.2 Hz, OCH_2N), 5.63 (1H, t, $J_{2',1'}=J_{2',3'}$=7.3 Hz, H-2'), 6.29 (1H, br. t, J=6.9 Hz, H-3'), 6.79 (1H, d, $J_{1',2'}$=7.3 Hz, H-1'), 8.40 (1H, br. s, NH), and 13.95 (1H, br, COOH); IR (neat) 1738 (COO), 1700 (sh, COOH), 1640 (amide I), and 1500 (amide II) cm^{-1}; MS (FAB) *m/z* 616 and 618 (M+H).

Found: C, 42.47; H, 4.13; N, 9.36%. Calcd for $C_{22}H_{25}N_4O_{12}Br$: C, 42.80; H, 4.08; N, 9.08%.

2-Acetylamino-3,4-dihydro-3-methoxymethyl-4-oxo-7-(2,3,5-tri-*O*-acetyl-β-D-arabinofuranosyl)-7*H*-pyrrolo[2,3-*d*]pyrimidine-5-carboxylic Acid (13). A mixture of **12** (150 mg, 0.24 mmol), 10% Pd-C (450 mg), and potassium acetate (1.2 g) in methanol (50 ml) was stirred vigorously for 30 min at room temperature under hydrogen atmosphere. The catalyst was filtered and washed with methanol. The combined filtrates were evaporated in vacuo and partitioned between chloroform and 1 M HCl. The organic layer was washed with water and brine, dried over anhydrous Na_2SO_4, and evaporated in vacuo to give a crude product, which was purified by preparative silica-gel TLC (dichloromethane–methanol, 20:1) to give a pale yellow viscous syrup **13** (110 mg, 84%): UV (MeCN) 297 (sh, ε 8990) and 281 nm (9180); $[\alpha]_D^{21}$ −10.5° (*c* 0.1, $CHCl_3$); ^1H NMR ($CDCl_3$) δ=1.90 (3H, s, CH_3COO), 2.17 (3H, s, CH_3COO), 2.20 (3H, s, CH_3COO), 2.51 (3H, s, CH_3CON), 3.51 (3H, s, CH_3O), 4.26 (1H, ddd, $J_{4',3'}$=4.4 Hz, $J_{4',5'}$=3.9 and 5.4 Hz, H-4'), 4.35 (1H, dd, $J_{5',4'}$=5.4 Hz, $J_{5',5'}$=11.7 Hz, H-5'), 4.46 (1H, dd, $J_{5',4'}$=3.9 Hz, $J_{5',5'}$=11.7 Hz, H-5'), 5.41 (1H, dd, $J_{3',2'}$=3.4 Hz, $J_{3',4'}$=4.4 Hz, H-3'), 5.47 (1H, dd, $J_{2',1'}$=4.9 Hz, $J_{2',3'}$=3.4 Hz, H-2'), 5.59 and 5.67 (2H, AB quartet, J=11.2 Hz, OCH_2N), 6.54 (1H, d, $J_{1',2'}$=4.9 Hz, H-1'), 7.89 (1H, s, H-6), 8.57 (1H, br. s, NH), and 13.17 (1H, br, COOH); IR (neat) 3310 (NH), 1750—1700 (COO), and 1654 (amide I) cm^{-1}; MS (FAB) *m/z* 539 (M+H).

Found: C, 49.28; H, 4.91; N, 10.26%. Calcd for $C_{22}H_{26}N_4O_{12}$: C, 49.07; H, 4.87; N, 10.40%.

2-Amino-3,4-dihydro-4-oxo-7-(β-D-arabinofuranosyl)-7*H*-pyrrolo[2,3-*d*]pyrimidine-5-carboxylic Acid (ara-cadeguomycin) (2). A solution of **13** (50 mg, 0.093 mmol) in 28% aqueous ammonia (2 ml) and methanol (2 ml) was stirred for 14 h at room temperature and evaporated in vacuo. The residue was heated for 1 h at 70°C in trifluoroacetic acid–water (3/1 v/v, 4 ml) and condensed to dryness, to which were added ethanol and water, and the precipitate was collected by filtration to give a crude material. Recrystallization from ethanol–water gave ara-cadeguomycin (**2**) (26 mg, 86%) as white crystals. A sample for analyses was obtained by purification with HPLC (Finepak SIL C_{18}; eluent: 30% methanol containing 1% acetic acid): Mp 240—255°C (decomp); UV (H_2O) 295 (ε 6890), 268 (7030), and 231 nm (16130); $[\alpha]_D^{26}$ +22.0° (*c* 0.1, DMSO); ^1H NMR (DMSO-d_6–D_2O, 2:1; internal standard: *t*-BuOH as 1.23 ppm) δ=3.78 (1H, dd, $J_{5',4'}$=5.4 Hz, $J_{5',5'}$=12.2 Hz, H-5'), 3.83 (1H, dd, $J_{5',4'}$=3.4 Hz, $J_{5',5'}$=12.2 Hz, H-5'), 3.93 (1H, ddd, $J_{4',3'}$=5.1 Hz, $J_{4',5'}$=3.4 and 5.4 Hz, H-4'), 4.20 (1H, t, $J_{3',2'}=J_{3',4'}$=5.1 Hz, H-3'), 4.30 (1H, t, $J_{2',1'}=J_{2',3'}$=5.1 Hz, H-2'), 6.32 (1H, d, $J_{1',2'}$=5.1 Hz, H-1'), and 7.84 (1H, s, H-6); IR (KBr) 3600—2200 (NH, OH, COOH), 1685 (COO, amide I), and 1654 (amide II) cm^{-1}; MS (FAB) *m/z* 327 (M+H).

Found: C, 44.15; H, 4.46; N, 17.02%. Calcd for $C_{12}H_{14}N_4O_7$:

C, 44.18; H, 4.32; N, 17.17%.

References

1) C. E. Cass, "Antibiotics," ed by F. E. Hahn, Springer-Verlag, West Berlin and Heidelberg (1979), Vol. 2.
2) E. J. Reist and L. Goodman, *Biochemistry*, **3**, 15 (1964).
3) R. T. Walker, E. De Clercq, and F. Eckstein, "Nucleoside Analogues," Plenum Press, New York (1979).
4) M. J. Robins, Y. Fouron, and W. H. Muhs, *Can. J. Chem.*, **55**, 1260 (1977); H.-D. Winkeler and F. Seela, *Chem. Ber.*, **113**, 2069 (1980).
5) F. Seela and H.-D. Winkeler, *J. Org. Chem.*, **47**, 226 (1982).
6) N. Tanaka, R.-T. Wu, T. Okabe, H. Yamashita, A. Shimazu, and T. Nishimura, *J. Antibiotics*, **35**, 272 (1982); R.-T. Wu, T. Okabe, M. Namikoshi, S. Okuda, T. Nishimura, and N. Tanaka, *ibid.*, **35**, 279 (1982).
7) B. D. Yuan, R.-T. Wu, I. Sato, T. Okabe, H. Suzuki, T. Nishimura, and N. Tanaka, *J. Antibiotics*, **38**, 642 (1985).
8) T. Kondo, K. Okamoto, M. Yamamoto, T. Goto, and N. Tanaka, *Tetrahedron*, **42**, 199 (1986).
9) T. Kondo, K. Okamoto, T. Ohgi, and T. Goto, *Tetrahedron*, **42**, 207 (1986).
10) R. Barker and H. G. Fletcher, Jr., *J. Org. Chem.*, **26**, 4605 (1961).
11) F. Harada and S. Nishimura, *Biochemistry*, **11**, 301 (1972); U. Lüpke and F. Seela, *Chem. Ber.*, **112**, 3432 (1979).
12) T. Ohgi, T. Kondo, and T. Goto, *J. Am. Chem. Soc.*, **101**, 3629 (1979).
13) Y.-F. Cheung, *Tetrahedron Lett.*, **1979**, 3809.

 © 1986 The Chemical Society of Japan Bull. Chem. Soc. Jpn., 59, 1921—1924 (1986)

Crystal Structue and Absolute Configuration of a New *cis*-Fused Caryophyllene Derivative. Naematlin 3-*p*-Bromobenzoate

Sei TSUBOYAMA,* Tosio SAKURAI, Kaoru TSUBOYAMA, and Kozo DOI†
Institute of Physical and Chemical Research (RIKEN), Wako, Saitama 351-01
†Department of Chemistry, Faculty of Science, Hirosaki University, Hirosaki 036
(Received January 31, 1986)

The molecular structure of naematolin 3-*p*-bromobenzoate has been determined by X-ray diffraction analysis. Unlike known caryophyllene derivatives isolated so far, the stereochemistry of the ring juncture is *cis* (1*S*,9*S*) form. The absolute configurations of five chiral centers of this compound are 1*S*,2*S*,3*R*,6*R*, and 9*S*, and the geometry of endocyclic double bond is *E* mode. This is the first example of a *cis*-fused 1*S*,9*S*-caryophyllane sesquiterpenoids confirmed by X-ray structure determination. Crystal data and the final *R* factor are: Mr=491.36, orthorhombic, space group $P2_12_12_1$, a=10.650(2), b=20.650(6), c=10.526(2) Å, U=2315(1) Å^3, Z=4, D_c=1.410 Mg m^{-3}, μ=1.791 mm^{-1}, R=0.084 for 1666 observed unique reflections.

Naturally occurring caryophyllane sesquiterpenoids either plant or animal origins consist generally of *trans*-bicyclo[7.2.0]undecane skeleton. Some of their structures were determined by X-ray analyses.[1-8] The structure of a sesquiterpenoid naematolin isolated from *Naematoloma sublateritium* by Backens et al. was also assigned to have *trans*-fused configuration on the basis of the spectral data.[9] With only exception, 9-*epi*-caryophyllene possessing *cis*-bicyclo[7.2.0]undecane skeleton, was described by Bohlmann et al.[10]

Very recently, the structure of naematolin (**1**) has been reported to be described as **1**, indicative of 1-e_imeric caryophyllene derivative.[11] This compound **1** was first isolated by Ito et al. in 1967 as one of metabolites of *Naematoloma fasciculare* (Basidiomycetes).[12]

In order to confirm the stereochemistry and to clarify the absolute configuration of naematolin, the structure determination of its 3-*p*-bromobenzoate (**2**) was carried out by X-ray analysis.

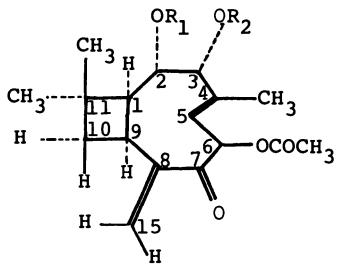

1 $R_1=R_2=H$
2 $R_1=H$, $R_2=p$-BrC_6H_4CO
3 $R_1=R_2=COCH_3$
4 $R_1=R_2=C_6H_5CO$

Experimental

Crystal Data. $C_{24}H_{27}O_6Br$, Mr=491.36, orthorhombic, space group $P2_12_12_1$, a=10.650(2), b=20.650(6), c=10.526(2) Å, U=2315(1) Å^3, Z=4, D_c=1.410 Mg m^{-3}, μ=1.791 mm^{-1}.

The sample for X-ray analysis was crystallized from ether-hexane. A 0.4×0.4×0.15 mm, colorless and plate crystal, was used for the measurement. The reflections within the range of $2\theta<55°$ were collected on a Rigaku AFC-5 four-circle automated X-ray diffractometer with graphite monochromatized Mo $K\alpha$ radiation (λ=0.7073 Å) by means of the ω scan ($2\theta<30°$) and ω—2θ scan ($2\theta>30°$) techniques. From the 2580 observed reflections, 1666 independent reflections with $|F_o|>3\sigma(F_o)$ were used for the structure analysis. The intensities were corrected for the Lorentz and polarization factors, and for the absorption. All the calculations were carried out on a FACOM M-380 computer at this Institute, using UNICS III program system.[13] The scattering factors and anomalous dispersion terms were taken from the International Tables.[14] The structure was solved by MULTAN,[15] and was refined by the block-diagonal least-squares method. The calculated hydrogen atom positions were included in the refinement with isotropic temperature factors. The final refinement was done through full-matrix least-squares method including extinction corrections with the weight $1/\sigma(F_o)^2$.[16] The final R was 0.084. Positional parameters for non-hydrogen atoms are given in Table 1.**

The Determination of the Absolute Configuration. The absolute configuration was determined with Mo $K\alpha$ data. The size of the crystal was 0.5×0.5×0.28 mm.

Eleven indices with $|\Delta F_c|/\sigma(F_o)>13$ were selected for the determination of the absolute configuration, where ΔF_c is the difference between the $|F_c|$ for the Bijvoet pairs. For each index, the diffraction intensities were measured for all eight combinations of plus and minus signs, and the mean values of equivalent indices were compared with the calculations. Signs of ΔF_o agree with those of ΔF_c without exception. Thus the parameters in Table 1 represent the correct absolute configuration without doubt.

Discussion of the Structure

A perspective drawing and the bond parameters are given in Figs. 1 and 2. The structure of **2** is best described as the conformation **5** (Fig. 3), where 4-membered ring having gem dimethyl groups is fused to 9-membered ring with *cis* fashion. The 9-membered ring moiety contains hydroxyl, *p*-bromobenzoyloxyl, allylic methyl, acetoxyl, carbonyl, and exocyclic methylene groups. The geometry of endocyclic double

** Tables of anisotropic temperature factors, atomic parameters of hydrogen atoms, and observed and calculated structure factors are kept at the Chemical Society of Japan, Document No. 8633.

Table 1. Atomic Parameters

Atom	X	Y	Z	B_{eq}/Å^2
BR	7020(2)	2241(1)	−1479(2)	5.7
O(2)	−253(13)	8(6)	−2564(10)	5.1
O(3)	1179(9)	927(5)	−1154(8)	3.0
O(6)	76(12)	1023(6)	3518(11)	4.6
O(7)	−1397(10)	−23(6)	3614(11)	4.6
O(16)	1071(15)	527(9)	5151(12)	6.6
O(18)	620(11)	1962(5)	−1422(14)	4.9
C(1)	529(12)	−442(6)	−614(12)	2.2
C(2)	−327(14)	66(8)	−1208(13)	3.2
C(3)	−94(15)	766(7)	−839(12)	3.0
C(4)	−364(14)	843(6)	575(15)	2.9
C(5)	608(15)	702(7)	1328(15)	3.6
C(6)	406(18)	463(8)	2709(12)	3.7
C(7)	−635(15)	−19(7)	2749(15)	3.1
C(8)	−760(14)	−500(7)	1644(16)	3.5
C(9)	378(14)	−677(6)	862(13)	2.6
C(10)	479(16)	−1375(8)	402(17)	4.2
C(11)	365(13)	−1144(8)	−1047(14)	3.2
C(12)	−893(16)	−1335(9)	−1627(19)	4.9
C(13)	1428(18)	−1413(10)	−1895(17)	5.5
C(14)	−1679(15)	955(8)	955(14)	3.9
C(15)	−1884(16)	−754(8)	1497(19)	5.2
C(16)	441(22)	977(12)	4786(19)	5.8
C(17)	−13(24)	1563(11)	5430(18)	6.9
C(18)	1430(15)	1561(7)	−1308(13)	3.2
C(19)	2793(14)	1700(6)	−1364(13)	2.8
C(20)	3171(15)	2286(8)	−1826(13)	3.5
C(21)	4418(17)	2470(7)	−1905(14)	3.9
C(22)	5294(13)	2043(7)	−1398(15)	3.4
C(23)	4945(16)	1450(8)	−860(15)	3.6
C(24)	3666(14)	1283(7)	−853(13)	2.8

Positional parameters are multiplied by 10^4. Thermal parameters are given by the equivalent temperature factors.

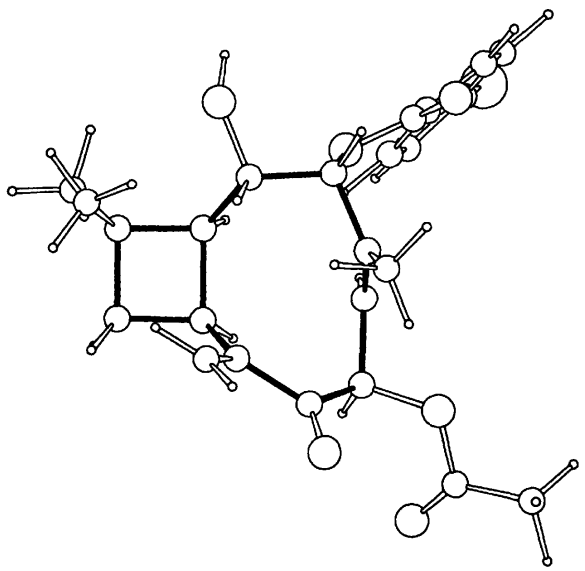

Fig. 1. Perspective drawing of the molecule.

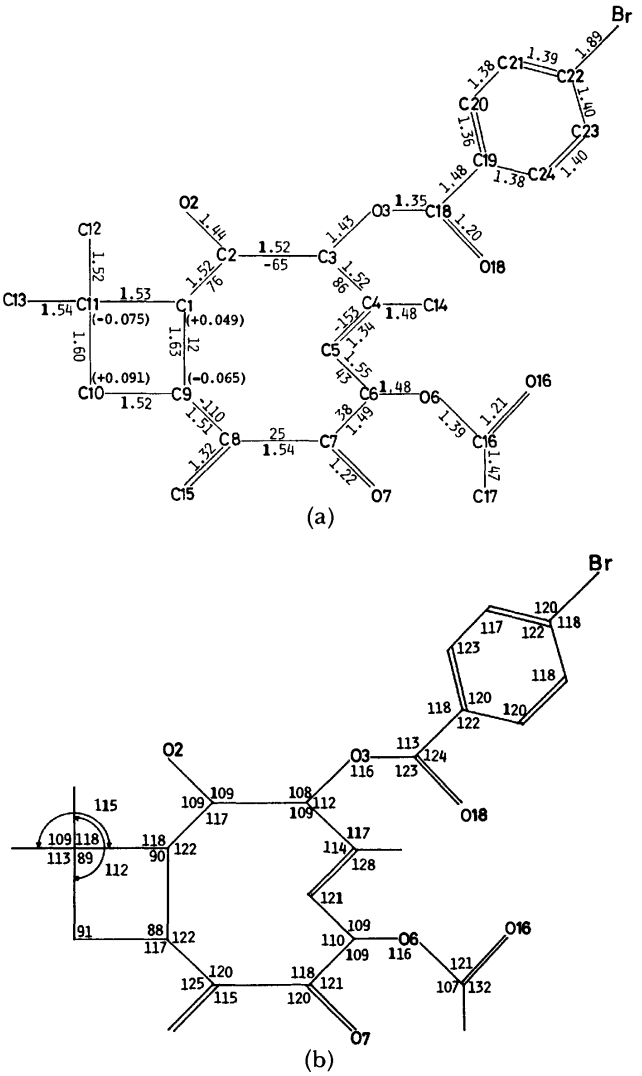

Fig. 2. Bond parameters.
(a) Bond lengths (l/Å) and torsion angles(ϕ/°). Torsion angles around the 9-membered ring are expressed by the figures inside the ring. The atomic displacements (Å) from the least-squares 4-membered plane are given in parentheses. (b) Bond angles (ϕ/°).
The standard deviations are: bond lengths: 0.03 Å; torsion angles: 2°; bond angles: 2°; atomic displacements: 0.008 Å.

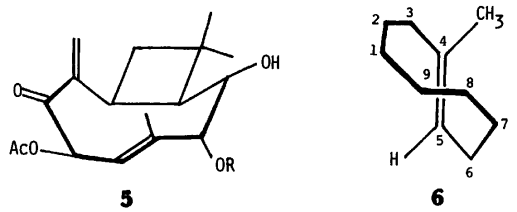

5 6

Fig. 3. Conformation of naematolin and chirality of 9-membered ring.

bond is E mode, and the configuration of the sp^2 plane chirality arising from the double bond is R as illustrated in **6**. (Fig. 3). Thus the configurations of the present compound are 1*S*, 2*S*, 3*R*, 4*E*, 6*R*, and 9*S*, respectively. Although *cis*-1*R*,9*R*-fused related compound has already been known as described above,[10] this is the first example of a *cis*-fused 1*S*,9*S*-caryophyllane sesquiterpenoid. The result agrees well with the

stereochemistry deduced from the spectral data, and the application of the dibenzoate chirality rule[17] to the dibenzoate **4** led also to the same conclusion.[11]

The markedly short nonbonded contacts are found between C(4) and C(8), and C(5) and C(8), 3.02(2), 2.90(2) Å, respectively. In fact, transannular cyclization in caryophyllene system occurs to give β-caryophyllene alcohol or the other tricyclic derivatives.[1,2,5]

Very large transannular H–H repulsions are supposed among hydrogen atoms H(C9), H(C5), and H(C6), and H(C2), H(C15-2) and H(C12-1) as observed by NOE experiments of ^{1}H NMR of the diacetate **3**.[11] The transannular hydrogen interactions may relieve even slightly by deviation of bond angle from the normal tetrahedral one and the carbonyl group occupies corner position. The conformation of fused 4-membered ring is essentially planar as given in Fig. 2(a), although that of *trans*-fused caryophyllene is usually nonplanar. The bond angles keep nearly 90°, and the fairly long bond lengths are observed between C(1) and C(9), and C(10) and C(11). This elongation of the bond lengths may release the repulsion between them.

The 9-membered ring takes [13113]*** and a boat-chair (BC) conformation as shown in Fig. 4. The lowest calculated conformation for flexible unsubstituted and saturated cyclononane is the triangular [333] and twist boat-chair (TBC) form of D_3 symmetry.[18] The corresponding cyclic ketone, cyclononanone, in a crystalline $HgCl_2$ complex has been shown to take an unsymmetric, quinquangular of type [12222], and a twist chair-boat (TCB) conformation of C_2 symmetry.[19,20] However, the ring in the present compound forces to take the BC conformation by the steric requirement.

β,γ-Unsaturated carbonyl compound can form inherently chiral chromophoric system.[21] In the circular dichroism spectrum of **1**, the negative relatively high rotational strength, $\Delta\varepsilon_{327}$ −3.16°, originates probably from this chirality. The sign of the n-π* Cotton effect agrees with the negative direction in the chirality rule as shown in Fig. 5. The dihedral angle of two planes in **2** is found to be 112°.

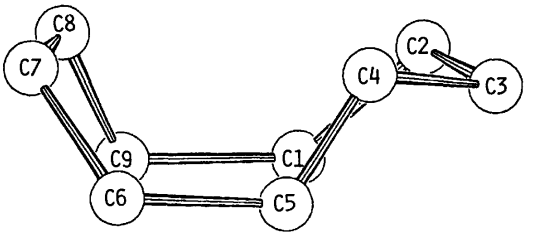

Fig. 4. Conformation of 9-membered ring.

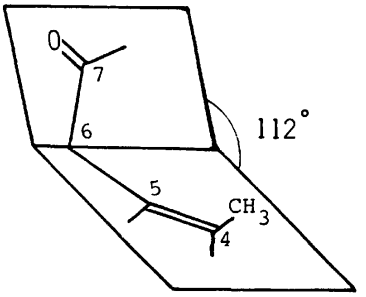

Fig. 5. Helicity with respect to β,γ-unsaturated ketone.

*** The conformation type is expressed by a series of numbers within brackets, each giving the number of bonds in one side. (Y. Dale, *Acta Chem. Scand.*, **27**, 115 (1973)).

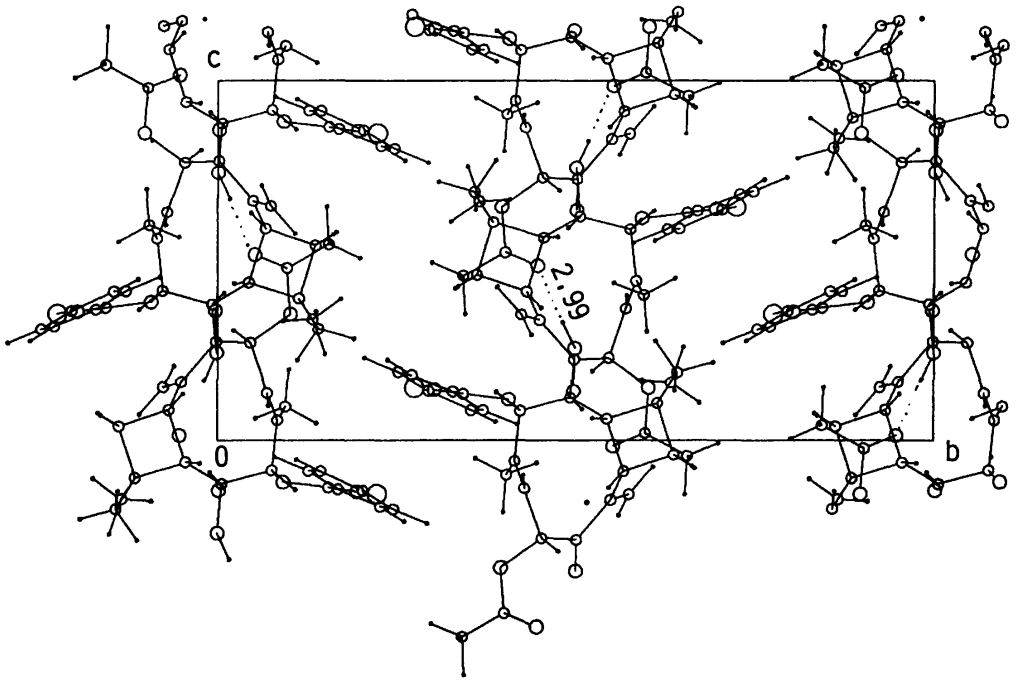

Fig. 6. Crystal structure, projection along **a**.

Conjugation of an α,β-unsaturated ketone tends to keep coplanarity unless a steric repulsion exists. In **2**, however, the terminal double bond and keto group are twisted to each other (23°). This means that a planar geometry is prevented by the unusual highly strained ring conformation. The deformation from coplanarity causes decrease in the optical density at the maximum in absorption spectrum of **1** compared with that of an isomer of naematolin, which was assgined to have trans juncture.[9]

Only one relatively weak intermolecular hydrogen bond is observed between O(2) and O(16), 2.99(2)Å, and there is no short (<3.3Å) intermolecular contacts as shown in Fig. 6. The relatively large R index may be due to the low-density packing.

Authors express their sincere thanks to Dr. Tetsuzo Ito of this Institute for his cooperation in extinction calculation. Helpful discussions with Dr. Yasuo Ohtsuka and the technical assistance of Mr. Tsuneharu Inoue are also gratefully acknowledged.

References

1) K. M. Robertson, and G. Todd, *J. Chem. Soc.*, **1955**, 1254.
2) D. M. Hawley, G. Ferguson, *J. Chem. Soc., (B)*, **1968**, 1255.
3) R. B. Bates, G. D. Rorsythe, G. A. Wolfe, G. Ohloff, and K.-H. Schulte-Eyte, *J. Org. Chem.*, **34**, 1059 (1969).
4) K. W. Gemmell, W. Parker, J. S. Roberts, and J. M. Robertson, *J. Chem. Soc., (B)*, **1970**, 947.
5) M-ul-Haque, D. Rogers, *J. Chem. Soc., Perkin Trans. 2*, **1974**, 228.
6) T. Yoshida, J. Nobuhara, M. Uchida, and T. Okuda, *Chem. Pharm. Bull.*, **26**, 2535 (1978).
7) Y. Asakawa, Z. Taira, T. Takemoto, T. Ishida, M. Kido, and Y. Ichikawa, *J. Pharm. Sci.*, **70**, 710 (1981).
8) W. M. Daniewski, P. A. Grieco, J. C. Huffman, A. Rymkiewcz, and A. Wawrzun, *Phytochem.*, **20**, 2733 (1981).
9) S. Backens, B. Steffan, W. Steglich, L. Zechlin, and T. Anke, *Liebigs Ann. Chem.*, **1984**, 1332.
10) F. Bohlmann, and C. Zdero, *Phytochem.*, **17**, 1135 (1978).
11) K. Doi, T. Shibata, M. Nara, S. Tsuboyama, T. Sakurai, and K. Tsuboyama, *Chem. Lett.*, **1986**, 653.
12) Y. Ito, H. Kurita, T. Yamaguchi, M, Sato, and T. Okuda, *Chem. Pharm. Bull.*, **15**, 2009 (1967).
13) T. Sakurai, and K. Kobayashi, *Rikagaku Kenkyusho Hokoku*, **55**, 69 (1979).
14) "International Tables for X-Ray Crystallography," Vol. IV. Birmingham (1974): Kynoch Press.
15) P. Main, S. E. Hull, L. Lessinger, G. Germain, J.-P. Declercq, and M. M. Woolfson (1978). *MULTAN* **78**. A "System of Computer Programs for the Automatic Solution of Crystal Structures from X-Ray Diffraction Data," Univs. of York, England, and Louvain, Belgium.
16) P. J. Backer, and P. Coppens, *Acta Crystallogr., Sect. A*, **31**, 417 (1975).
17) N. Harada, and K. Nakanishi, *Acc. Chem. Res.* **5**, 257 (1972).
18) F. A. L. Anet, and J. J. Wagner, *J. Am. Chem. Soc.*, **93**, 5266 (1971).
19) S. Dahl, and P. Groth, *Acta Chem. Scand.*, **25**, 1114 (1971).
20) Y. Dale, *Top. Stereochem.*, **9**, 199 (1976).
21) A. Moscowitz, K. Mislow, M. A. W. Glass, C. Djerassi, *J. Am. Chem. Soc.*, **84**, 1945 (1962).

Base-Catalyzed Hydrolysis of Acetylcholine Chloride in the Presence of Anionic and Nonionic Surfactants

Masayuki NAKAGAKI and Shoko YOKOYAMA*
Faculty of Pharmaceutical Sciences, Kyoto University, Yoshida-Shimoadachi-cho, Sakyo-ku, Kyoto 606
(Received July 1, 1985)

Base-catalyzed hydrolysis of acetylcholine chloride (Ach) in the presence of anionic and nonionic surfactants was investigated. The rate of hydrolysis was determined by measuring the rate of disappearance of Ach with a spectrophotometer. At a constant pH of 9.0, addition of heptaethylene glycol dodecyl ether (HED) at concentrations above the critical micelle concentration (cmc) results in a slight increase in the apparent rate, v, which is expressed by two reaction rates, v_f and v_m, in the aqueous and micellar phases, respectively. The increase in the apparent rate is due to increase in v_m. In the presence of sodium dodecyl sulfate (SDS), the apparent rate constant, k_{app}, is approximately constant at concentrations below the cmc, and k_{app} decreases above the cmc. In the presence of SDS-HED mixed micelles, k_{app} decreases with the mole fraction of SDS. In these cases, the decrease in the apparent rate is due to the decrease in both v_f and v_m. These two k_{app} decreases are due, respectively, to the decrease in Ach in the aqueous phase and the electrostatic repulsion between OH^- and DS^- at the micelle surface in conformity with the Gouy-Chapman theory.

Micellar catalysis has been a subject of interest in various fields: Hydrolysis of acetylcholine chloride (Ach) is widely studied in various kinetic model experiments for stability prediction,[1] and also studied in relation to its chemical and enzymatic stability. Studies carried out since 1930 have established the dependence on pH and temperature,[2-4,7] an salt effect,[5] and the enthalpy[6] of hydrolysis of Ach. Regarding the influence of surfactants on the hydrolysis of Ach, Nogami et al.[8] have revealed a retardation of base-catalyzed hydrolysis of Ach by sodium dodecyl sulfate (SDS) micelle by comparing half lives of Ach in the absence and presence of SDS. However, any kinetic analysis on the hydrolysis in the presence of surfactant has not yet been carried out.

In this investigation, a kinetic study on the base-catalyzed hydrolysis of Ach has been carried out in the presence of anionic surfactant, nonionic surfactant, or mixed micelles of anionic and nonionic surfactants. The relation between the rate of hydrolysis and the surface potential of micelle also has been made clear by taking into account the accurate critical micelle concentration (cmc) of surfactant in the presence of Ach[9] and the distribution of Ach between micellar and bulk phases.[10]

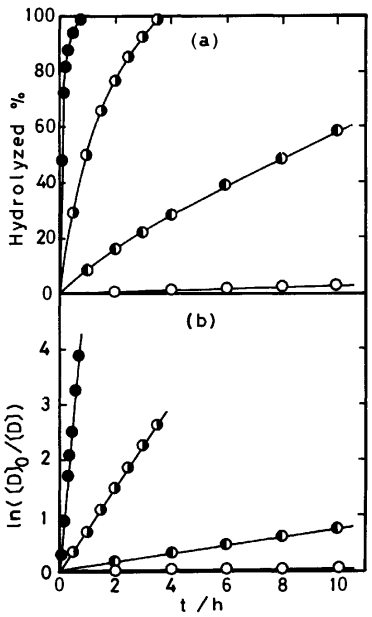

Fig. 1. Effect of pH on hydrolysis of Ach in the absence of surfactant.
(a) Hydrolyzed %, and (b) $\ln([D]_0/[D])$ vs. time.
pH: ○ 7.60, ◐ 9.00, ◑ 9.94, ● 11.00.
Concentration of Ach $[D]_0$: 5 mmol dm^{-3}.

Experimental

Materials. Acetylcholine chloride (Ach) from Nakarai Chemicals Co. was of guaranteed reagent grade and was used without further purification. Sodium dodecyl sulfate (SDS) supplied by Nihon Emulsion Co. was purified as described previously.[9-12] Heptaethylene glycol dodecyl ether (HED) from Nikkol Chemicals was of guaranteed reagent grade and was used without further purification. SDS-HED mixed micelles were prepared as described previously.[11]

Method of Measurement. The disappearance rate of Ach was followed at a constant pH and 25 °C by determining the concentration of Ach by the method described by Hestrin.[13] This method is the same as that employed in our previous study[10] and that used by Nogami et al.[8]

Procedures. Ach was dissolved in 100 ml of aqueous surfactant solution, and the pH was adjusted by adding aqueous sodium hydroxide solution. The test solution was connected with a pH-stat equipped with a 1 ml glass syringe as described previously[12] to keep the pH at a constant value during the reaction period, because acetic acid is produced by the hydrolysis of Ach.[14,15] The test solution was collected in 0.1 ml portions at suitable intervals, and the concentration of Ach was determined spectrophotometrically.

Results

Effect of pH on the Hydrolysis of Ach. The pH dependence of the hydrolysis of Ach in the absence of surfactant was examined. The percentage of Ach hydrolyzed is plotted against reaction time in Fig. 1(a).

The apparent rate constant for the hydrolysis, k_{app},

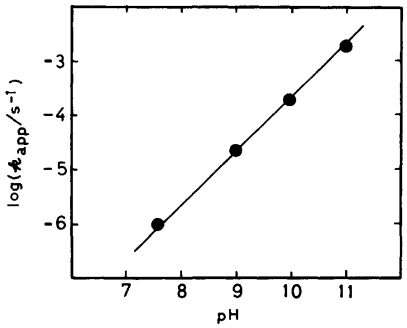

Fig. 2. Relation between pH and apparent rate constant for hydrolysis of Ach in the absence of surfactant.

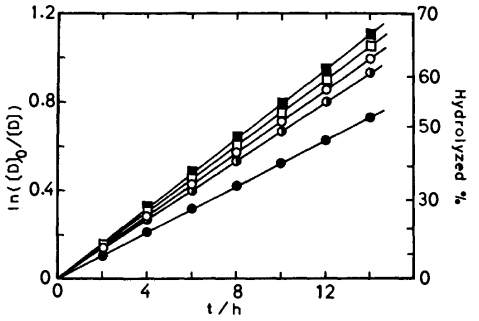

Fig. 3. Hydrolysis behavior of Ach in the presence of surfactants.
Hydrolyzed % vs. time, and ln([D]$_0$/[D]) vs. time.
Surfactants and concentrations: HED □: 2, ■: 20 mol dm^{-3} SDS ○: 2, ◑: 10, ●: 20 mmol dm^{-3}. pH: 9.0. [D]$_0$: 5 mmol dm^{-3}.

is defined by

$$\ln \frac{[D]_0}{[D]} = k_{app} \cdot t, \quad (1)$$

where [D]$_0$ is the initial concentration of Ach and [D] is the concentration of Ach at time t. Plots of ln([D]$_0$/[D]) vs. t are shown in Fig. 1(b), indicating a good proportionality. The relation between pH and the rate constant obtained from the slope of Fig. 1(b) is shown in Fig. 2.

As can be seen in Fig. 2, the plot of log k_{app} vs. pH is linear with a slope of +1, which indicates that the hydrolysis reaction is of apparent first order in hydroxide ion concentration and can be expressed by

$$k_{app} = k_{2,app}[OH^-], \quad (2)$$

where $k_{2,app}$ is the rate constant of second order reaction.

The value of k_{app} at pH 9 and 25 °C, 2×10^{-5} s^{-1}, is well consistent with the value, 1.9×10^{-5} s^{-1}, obtained by Showen et al.,[4] which is in support of the validity of the results obtained here.

Effect of Surfactant on the Hydrolysis of Ach. Effect of surfactants on the hydrolysis of Ach were examined at pH 9.0. It has been found that the surfactants used here are relatively stable at pH 9.0,[12,16-21] so that the decomposition of surfactants can be ignored.

In order to determine the value of k_{app}, values of ln([D]$_0$/[D]) are plotted against t according to Eq. 1 in Fig. 3 for several examples in the presence of surfactants. In Fig. 3, the percentage of Ach hydrolyzed also is given at the right-side ordinate. In all cases, good proportionality is observed. The hydrolysis of Ach in the presence of surfactants can, therefore, be expressed by the equation of apparent first order in hydroxide ion concentration.

Values of k_{app} obtained from Fig. 3 are shown in Fig. 4 against the total concentration of surfactants, C_t. In the presence of nonionic surfactants HED, k_{app} increases slightly above the cmc (0.066 mmol dm^{-3}).[11] In the presence of SDS, the dependence of k_{app} on surfactant concentration changes in three regions of

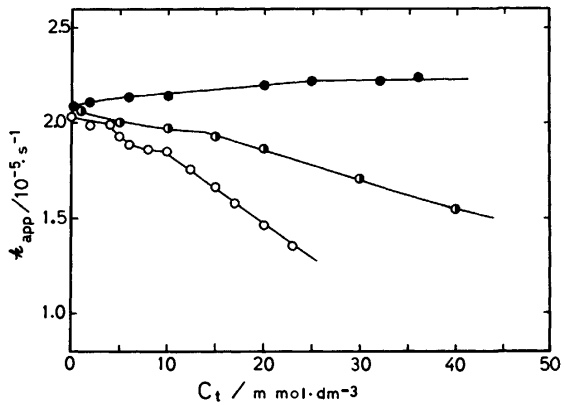

Fig. 4. Effect of surfactant on apparent rate constant for hydrolysis of Ach, k_{app}.
Surfactants: ●: HED alone, ○: SDS alone. ◑: HED-SDS mixed system (X_{SDS}=0.4). pH: 9.0. [D]$_0$: 5 mmol dm^{-3}.

surfactant concentration. In the presence of HED-SDS mixed micelle (X_{SDS}=0.4), the change in k_{app} is similar to that in the presence of SDS alone, but the first region cannot be found because the value of cmc is as low as 0.1 mmol dm^{-3} for the HED-SDS mixed system (X_{SDS}=0.4) in the presence of 5 mmol dm^{-3} Ach.

The effect on k_{app} of the composition of HED-SDS mixed system at the total concentration of 20 mmol dm^{-3} is shown by symbols ◑ in Fig. 5(a). The value of k_{app} decreases with the mole fraction of SDS, X_{SDS}.

Effect of Concentrations of Ach and SDS on the Hydrolysis of Ach. To investigate the effect of SDS on the hydrolysis of Ach in a little more detail, experiments were carried out with Ach solutions of 3 and 10 mmol dm^{-3} as well as 5 mmol dm^{-3}, plots of k_{app} against the concentration of SDS being shown in Fig. 6. The first break points correspond to the cmc of SDS in the presence of Ach of each concentration: 4.9, 4.0, and 2.5 mmol dm^{-3} for Ach of 3, 5, and 10 mmol dm^{-3}, respectively.[9] The k_{app} varies with the SDS concentration differently in three regions: k_{app} is approximately constant below the cmc (first region);

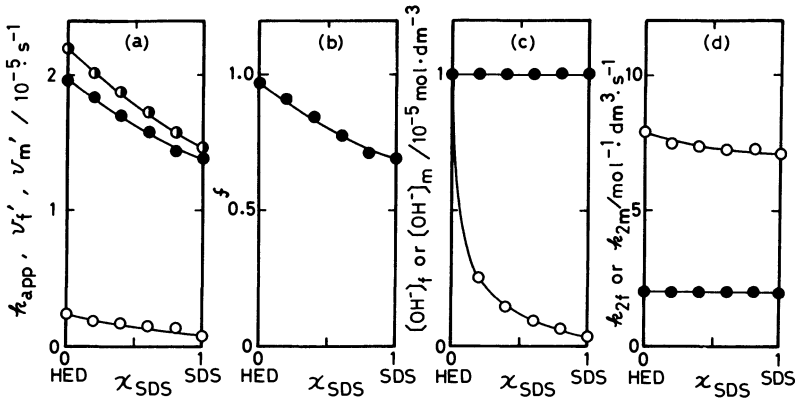

Fig. 5. Effect of HED-SDS mixed system on hydrolysis rate (a), Distribution ratio of Ach in the aqueous phase (b),[10] Concentration of OH^- (c) and Second order rate constant (d).
(a): ◑ k_{app}, ● v'_f, ○ v'_m. (b): $f=[D_f]/[D]$, $[D]=[D_f]+[D_m]$. (c): ● $[OH^-]_f$, ○ $[OH^-]_m$. (d): ● k_{2f}, ○ k_{2m}.
Total concentration of surfactants C_t: 20 mmol dm^{-3}. pH: 9.0. $[D]_0$: 5 mmol dm^{-3}.

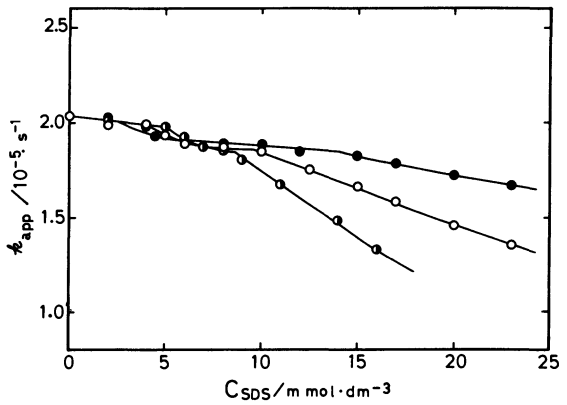

Fig. 6. Effect of SDS on k_{app} with varying concentration of Ach.
$[D]_0$: ◑ 3, ○ 5, ● 10 mmol dm^{-3}. pH: 9.0.

k_{app} decreases slowly above the cmc (second region); k_{app} decreases faster than in the second region (third region). The higher the concentration of Ach is, the longer the second region is and the slower the decrease in k_{app} in the third region is.

The decrease in k_{app} in the presence of SDS at concentrations above the cmc is considered to be due to the fact that the percentage of Ach included in the micellar phases increases with increasing concentration of the micelle[10] and that the approach of OH^- to Ach in the micellar phase is suppressed by the electrostatic repulsion of negatively charged micelle.

Discussion

Derivation of Rate Constants for the Hydrolysis of Ach in the Bulk and Micellar Phases. Ach is distributed between the micellar and bulk phases at surfactant concentrations above the cmc. The rate of the hydrolysis of Ach is, therefore, considered to be a sum of two terms:

$$-\frac{d[D]}{dt} = k_{app}[D] = v = v_f + v_m, \quad (3)$$

where v_f and v_m are the rates of hydrolysis in the aqueous and micellar phases, respectively.

Next, k_{app} can be represented as follows[22] by using the value of distribution ratio of Ach in the aqueous phase, f:[10]

$$k_{app} = k_f f + k_m(1-f), \quad (4)$$

where k_f and k_m are the first order rate constants of hydrolysis in the aqueous and micellar phases, respectively, and the value of $(1-f)$ means the distribution ratio of Ach in the micellar phase. Equation 4 is expressed from Eq. 2 as

$$k_{2,app}[OH^-] = k_{2,f} f[OH^-]_f + k_{2,m}(1-f)[OH^-]_m \quad (5)$$

where $k_{2,f}$ and $k_{2,m}$ are the second order rate constants of hydrolysis in the aqueous and micellar phases, respectively. When the total concentration of added surfactants, C_t, is lower than the cmc, namely C_t<cmc, Eq. 5 simply becomes

$$k_{2,app} = k_{2,f} \text{ (for } C_t < \text{cmc)}, \quad (6)$$

since f=1 and $[OH^-]_m$=0.

The rates of hydrolysis in the aqueous and micellar phases, v'_f and v'_m, are defined from Eq. 5 as

$$v'_f = k_{2,f} f[OH^-]_f, \quad (7)$$

$$v'_m = k_{2,m}(1-f)[OH^-]_m, \quad (8)$$

where v'_f and v'_m are related to v or k_{app} by

$$v'_f + v'_m = v' = \frac{v}{[D]} = k_{app}, \quad (9)$$

and $[OH^-]_m$ is expressed as

$$[OH^-]_m = [OH^-]_f \exp\left(-\frac{zF_A\psi}{RT}\right), \quad (10)$$

where z is the valency of OH^-, F_A is the Faraday constant, ψ is the surface potential at the micelle surface, T is the absolute temperature, and R is the gas constant. Therefore, $k_{2,m}$ is calculated from Eq. 11 as

$$k_{2,m} = \frac{(k_{2,app} - k_{2,f}f)}{(1-f)} \exp\left(\frac{zF_A\psi}{RT}\right). \quad (11)$$

With the values $z=-1$, $F_A=9.648\times10^4$ ($C\,mol^{-1}$), $R=8.314$ ($J\,mol^{-1}\,K^{-1}$), and $T=298.15$ K at 25 °C, Eq. 11 is rewritten into

$$k_{2,m} = \frac{(k_{2,app} - k_{2,f}f)}{(1-f)} \exp\left(0.03892\,\frac{\psi}{mV}\right). \quad (12)$$

Effect of HED–SDS Mixed Micelles on the Hydrolysis of Ach. The apparent rate of the hydrolysis of Ach in the presence of HED-SDS mixed micelles decreases with the mole fraction of SDS, as shown by symbols ◑ in Fig. 5(a). The values of $k_{2,f}$ are 2.02 $mol^{-1}\,dm^3\,s^{-1}$ for the HED-SDS mixed system (X_{SDS}= 0—0.8) and 1.99 $mol^{-1}\,dm^3\,s^{-1}$ for the single SDS system, as observed at the cmc (the first break point in Fig. 4) or estimated by Eqs. 2 and 6. Next, the values of $k_{2,m}$ in the presence of HED-SDS are calculated from Eq. 12 by using the values of f and ψ obtained in our previous study.[10] (Here, the values of $k_{2,m}$ and ψ are practically unknown quantities. In order to determine the value of $k_{2,m}$, we use the value of ψ[10] obtained for the HED-SDS mixed micelle system under conditions that C_t=20 mmol dm^{-3} and $[D]_0$=5 mmol dm^{-3}). The values of $k_{2,m}$ thus obtained are shown in Fig. 5(d), together with $k_{2,f}$, and the hydrolysis rates of Ach in the aqueous and micellar phases, v_f' and v_m' are calculated from Eqs. 7 and 8 and shown in Fig. 5(a), together with the data of k_{app}. In addition, the values of f[10] and $[OH^-]_m$ obtained from Eq. 10 are shown in Figs. 5(b) and (c), respectively.

The decrease in v_m' with the mole fraction of SDS (Fig. 5(a)) is due to the decrease in $[OH^-]_m$ as shown in Fig. 5(c). The electrostatic effect is well-known with micellar catalyses of various surfactants.[16,23-25]

Effect of Concentrations of Ach and SDS on the Hydrolysis of Ach. The second break point indicated in Fig. 6 may be considered to be the limit point where the number of negative charge supplied from SDS micelle is nearly equal to the number of positive charge supplied from Ach in the micelle (above the second break point, the number of negative charge> the number of positive charge). If the apparent distribution coefficient K' ($K'=([D_m]/[S])/([D_f])$[10]) of Ach between the micellar and aqueous phases is independent of the concentration of surfactant, the number of negative charge {(negative charge)−(positive charge)} increases with increasing concentration of SDS. Values of K' obtained for sufficient concentrations of micelle were found to be independent of the concentration of surfactant at a given concentration of Ach.[10] However, values of K' for insufficient concentrations of micelle were not exactly constant. This leads to the result that the number of negative charge is nearly equal to the number of positive charge below the second break point. The limit point was calculated on the basis of the result[10] on the distribution of Ach between the micellar and aqueous phases obtained by ultrafiltration. The dissociation degree, α, of micellar SDS was assumed to be 0.11 for the calculation. This value of α is in agreement with the previously obtained value of 0.102.[11] The limit points were found to be the points where C_{SDS} are 8.6, 9.6, and 14.0 mmol dm^{-3} in the presence of Ach of 3, 5, and 10 mmol dm^{-3}, respectively.

The third region is considered to be the region where the number of negative charge supplied by SDS micelle exceeds the number of positive charge supplied by Ach existing in the micelle. Therefore, the larger decrease in k_{app} in the third region is considered to be due to the larger decrease in v_m'. The decrease in v_m' in the third region can be explained in terms of the surface potential of the SDS micelle, ψ. For the hydrolysis rate of Ach in the third region shown in Fig. 6, the value of v_f' is calculated from Eq. 7 by using the values of f[10] and $k_{2,f}$ observed at the cmc of SDS in the presence of Ach of various concentrations shown in Fig. 6. The values of v_m' for the hydrolysis of Ach in the third region shown in Fig. 6 are calculated from Eq. 9 by subtracting the value of v_f' from the value of k_{app} ($=v_f'+v_m'$) which is obtained experimentally. The decrease in v_m' is considered to be due to the decrease in $[OH^-]_m$ which depends on the surface potential of the micelle, although $k_{2,m}$ of Eq. 8 is the same ($k_{2,m}$=7.023 $mol^{-1}\,dm^3\,s^{-1}$ for SDS micelle, which is shown in Fig. 5(d)). The value of $[OH^-]_m$ is, therefore, calculated from Eq. 8 by using the values of $k_{2,m}$ and f. The values of v_f', v_m', and $[OH^-]_m$ thus obtained are shown in Figs. 7(a) and (b). Furthermore, the values of surface potential of the SDS micelle, ψ, which have not been determined except the values of ψ[10] obtained for the HED-SDS mixed micelle system under conditions that C_t=20 mmol dm^{-3} and [D]=5 mmol dm^{-3}, are calculated by

$$\frac{\psi}{mV} = -59.16 \log\frac{[OH^-]_f}{[OH^-]_m}, \quad (13)$$

where the values of $[OH^-]_m$ can be calculated from Eq. 8 by using the values of v_m', $k_{2,m}$, and f which are obtained already. The values of ψ thus obtained are shown in Fig. 8.

The surface potential of the SDS micelle becomes more negative with increasing concentration of SDS.

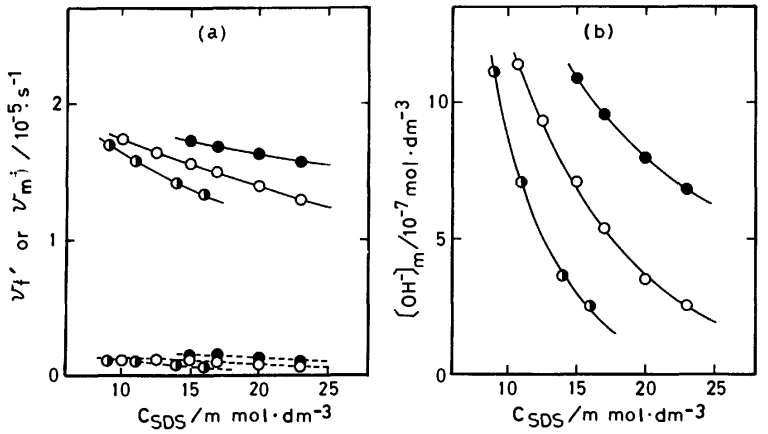

Fig. 7. Relation between (a) Hydrolysis rate and C_{SDS}, and (b) $[OH^-]_m$ and C_{SDS}.
(a) Solid line: $v't$, dotted line: v'_m. $[D]_0$: ◑ 3, ○ 5, ● 10 mmol dm^{-3}. These were calculated for the third region of relation between k_{app} and C_{SDS} shown in Fig. 6.

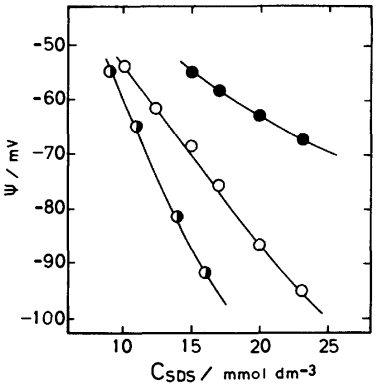

Fig. 8. Relation between surface potential of SDS micelle, ψ, and C_{SDS} in the presence of various concentrations of Ach $[D]_0$: ◑ 3, ○ 5, ● 10 mmol dm^{-3}. These were calculated for the third region in Fig. 6.

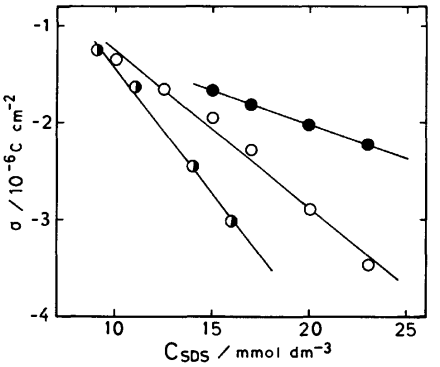

Fig. 9. Relation between surface charge of SDS micelle, σ, and C_{SDS} in the presence of various concentrations of Ach.
$[D]_0$: ◑ 3, ○ 5, ● 10 mmol dm^{-3}. These were calculated from the values of ψ shown in Fig. 8 by the Gouy-Chapman equation.

This is considered to be due to the decrease in the adsorbed amount of Ach per SDS micelle.

The change in the surface potential according to the increase in SDS concentration is largest when the concentration of Ach is as low as 3 mmol dm^{-3}.

According to the Gouy-Chapman theory, the relation between the surface potential, ψ, and the surface charge density, σ, is expressed as

$$\frac{\sigma}{C_{cm^{-2}}} = -5.8673 \times 10^{-6} \sqrt{\sum_i \left[\left(\frac{C_i}{\text{mol dm}^{-3}}\right)\left\{\exp\left(-\frac{z_i F_A \psi}{RT}\right)-1\right\}\right]}, \quad (14)$$

where 78.54[26] is used as the value of relative dielectric constant of water at 25 °C, C_i is the concentration of ion (Ach^+, Cl^-, Na^+, DS^-, OH^-, H^+), and z_i is the valency of ion. The value of σ obtained from ψ by using Eq. 14 is shown in Fig. 9. The value of σ becomes more negative with increasing concentration of SDS.

The relation between the surface charge density, $|\sigma|$, and the molar number of SDS per unit area, n, which contributes to the supply of the negative charge at the third region shown in Fig. 6, is expressed as

$$\frac{n}{\text{mol cm}^{-2}} = \frac{|\sigma|}{F_A}. \quad (15)$$

The relation between ($|\sigma|/F_A$) and (ΔC_{SDS}–[D_m]) is shown in Fig. 10, where ΔC_{SDS} is the concentration of micellar dissociated SDS (that is, $\Delta C_{SDS}=(C_{SDS}-\text{cmc})\times\alpha$). In Fig. 10, the zero value of (ΔC_{SDS}–[D_m]) corresponds to the second break point in Fig. 6 (the value of ψ is −52.5 mV). The relation between ($|\sigma|/F_A$) and (ΔC_{SDS}–[D_m]) is found to be embodied by a straight line independent of the concentration of Ach. Therefore, regarding the third region for the k_{app}–C_{SDS} profile shown in Fig. 6, it is evident that σ is determined by the subtraction of concentrations of micellar dissociated SDS and Ach existing in the micellar phase, which is caused by the increase in the molar

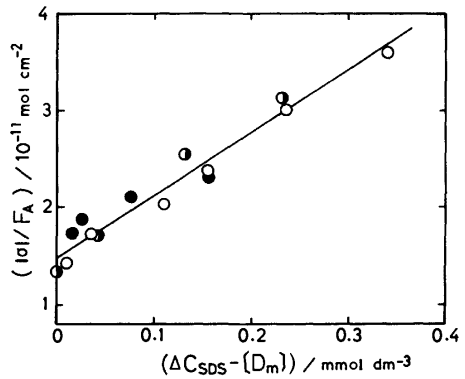

Fig. 10. Plot of ($|\sigma|/F_A$) vs. ($\Delta C_{SDS}-[D_m]$).
$[D]_0$: ◑ 3, ○ 5, ● 10 mmol dm^{-3}.
These were calculated from the values of σ shown in Fig. 9 and the results of distribution of Ach[10] for the third region in Fig. 6.

number of SDS per unit area.

Conclusion

The apparent rate of the base-catalyzed hydrolysis of Ach is decreased by the presence of SDS micelle or HED-SDS mixed micelles because of the decrease in both the rates in the aqueous and micellar phases. It has been concluded that this result can be explained in terms of two parameters, the distribution of Ach between the aqueous and micellar phases and the electrostatic effect at the micelle surface: (1) The decrease in the rate in the aqueous phase is due to the decrease in Ach in the aqueous phase, and (2) the decrease in the rate in the micellar phase is due to the approach of OH^- to Ach in the micellar phase being suppressed by the electrostatic repulsion of negatively charged micelle, which is in conformity with the Gouy-Chapman theory.

References

1) M. A. Zoglio, H. V. Maulding, W. H. Streng, and W. C. Vincek, *J. Pharm. Sci.*, **64**, 1381 (1975).
2) J. Butterworth, P. P. Eley, and G. S. Stone, *Biochem. J.*, **53**, 30 (1953).
3) L. Larsson, *Acta. Chem. Scand.*, **8**, 1017 (1954).
4) K. B. Schowen, E. E. Smissman, and W. F. Stephan, *J. Med. Chem.*, **18**, 292 (1975).
5) R. P. Bell and M. Robson, *Trans. Faraday Soc.*, **60**, 893 (1964).
6) G. S. Annis and D. D. Eley, *Biochem. J.*, **53**, 34 (1953).
7) H. Hofmann, *Helv. Chim. Acta.*, **13**, 138 (1930).
8) H. Nogami, S. Awazu, and M. Iwatsuru, *Chem. Pharm. Bull.*, 11, 1251 (1963).
9) M. Nakagaki and S. Yokoyama, *Bull. Chem. Soc. Jpn.*, **58**, 753 (1985).
10) M. Nakagaki and S. Yokoyama, *Chem. Pharm. Bull.*, **33**, 2654 (1985).
11) M. Nakagaki, S. Yokoyama, and I. Yamamoto, *Nippon Kagaku Kaishi*, **1982**, 1865.
12) M. Nakagaki and S. Yokoyama, *J. Pharm. Sci.*, **74**, 1047 (1985).
13) S. Hestrin, *J. Biol. Chem.*, **180**, 249 (1949).
14) Bender, Ginger, and Unik, *J. Am. Chem. Soc.*, **80**, 1044 (1958).
15) G. Aksnes and J. E. Prue, *J. Chem. Soc.*, 103 (1959).
16) J. H. Fendler and E. J. Fendler, "Catalysis in Micellar and Macromolecular Systems," Academic Press, New York (1975), p. 130.
17) S. J. Benkovic, *J. Am. Chem. Soc.*, **88**, 5511 (1966).
18) S. J. Benkovic and P. A. Benkovic, *J. Am. Chem. Soc.*, **88**, 5504 (1966).
19) J. L. Kice and J. M. Anderson, *J. Am. Chem. Soc.*, **88**, 5242 (1966).
20) E. J. Fendler and J. H. Fendler, *Chem. Commun.*, **1967**, p. 1261.
21) E. J. Fendler and J. H. Fendler, *J. Org. Chem.*, **33**, 3853 (1968).
22) "Physical Chemistry," ed by A. Ohtsuka and T. Kondo, Hirokawa, Tokyo (1973), p. 167.
23) E. F. J. Duynstee and E. Grunwald, *J. Am. Chem. Soc.*, **81**, 4540 (1959).
24) E. F. J. Duynstee and E. Grunwald, *J. Am. Chem. Soc.*, **81**, 4542 (1959).
25) K. G. Van Senden and C. Koningsberger, *Tetrahedron Lett.*, **1960**, 7.
26) "Kagaku Binran," ed by *Nippon Kagaku Kai*, Maruzen, Tokyo (1966), p. 1005.

Vapor-Phase Isomerization of *o*-Chlorotoluene over H-Mordenite Treated with CF_3Cl

Susumu OKAZAKI* and Hirofumi JOUHOUJI
Department of Industrial Chemistry, Faculty of Engineering, Ibaraki University, Nakanarusawa, Hitachi 316
(Received October 29, 1985)

Vapor phase-isomerization of *o*-chlorotoluene was somewhat promoted by H-mordenite (HM). The catalytic activity was appreciably enhanced by treatment with CF_3Cl and other chlorofluorocarbons such as CF_2ClCF_2Cl and CF_2ClCF_3. In particular, maintenance of the HM catalyst activity was remarkably improved by CF_3Cl treatment. The CF_3Cl-treated HM also promoted vapor phase isomerizations of *p*- and *m*-chlorotoluene. The catalytic activity was relatively long-lasting for the isomerization of *p*-chlorotoluene. Enlargement of the HM pore size on treatment with CF_3Cl and other chlorofluorocarbons may contribute to increasing the catalytic activity and then maintaing it.

Chlorotoluene is an important intermediate for syntheses of agricultural chemicals, dyes, and pharmaceuticals. It is prepared, in general, by chlorination of toluene, in which ortho isomer is preferably formed together with some para isomer owing to the directing effect of the methyl group. Accordingly, when *m*-chlorotoluene (MCT) is required in large amounts, it is desirable to isomerize the *o*-chlorotoluene (OCT) to MCT. In addition, the isomerization of OCT to *p*-chlorotoluene (PCT) is important because the para isomer is especially useful as a raw material for agricultural chemicals.

Hitherto isomerizations of halotoluenes have been known to occur only in the presence of a strong acid catalyst such as HF-BF_3[1] and $AlCl_3$.[2] However, these catalysts are unstable, and they are very difficult to recover. Furthermore, they are remarkably corrosive to reaction vessels.

Recently, acidic zeolites such as a proton-exchanged mordenite (HM) and H-ZSM-5 have been reported to be useful as a catalyst for the isomerization of chlorotoluene.[3] However, the isomerization, as catalyzed by the acidic zeolite, is carried out only in the liquid phase at a high temperature in a closed system.

From an industrial viewpoint, it is desirable for isomerization to proceed in the gas phase by using a continuous flow system under an atomospheric pressure. Hence, a search was carried out to seek a suitable catalyst for the gas phase isomerization of OCT. For comparison with the OCT isomerization, the vapor phase isomerizations of MCT and PCT were attempted in the presence of the treated HM. The results obtained for these isomerizations of chlorotoluenes are compared with those of the xylene isomerization, which is performed over the same catalyst, i.e., the CF_3Cl treated HM.[4]

Experimental

Materials. The HM used in this study was prepared by the heat-treatment of the NH_4 mordenite at 500 °C for 3 h. The NH_4 mordenite was prepared from a commercial Na mordenite (Toyo Soda Co., TSZ, SiO_2/Al_2O_3 mol ratio=9.75, 15.4, 19.0 or 22.7) by ion exchange with 1.0 M NH_4Cl (1 M=1 mol dm^{-3}) solution followed by the necessary washing. The proton-exchanged Y type zeolite (HY) was supplied by Toyo Soda Co. (TSZ 352). Before use as a catalyst or treatment with CF_3Cl, the HY was heat-treated in air at 500 °C for 3 h, similar to HM and other metal oxides. The treatments with CF_3Cl and other halocarbons were carried out by the previously reported methods.[4-6] Unless otherwise noted, the treatments were run at 450 °C for 15 min.

The Al_2O_3 catalyst was obtained by hydrolysis of aluminum isopropoxide (Wako Chemical Co.) followed by heat-treatment in air at 600 °C for 3h. The SiO_2–Al_2O_3 (Nikki Chemical Co., N-631L, Si/Al (atomic ratio)=85/15) was used to evaluate the catalytic activity of typical solid acid.

Reaction Procedure. The isomerization was carried out under ordinary pressure using a continuous flow reactor. The products were collected every 30 min and analyzed by gas chromatography using a column (3 mm×6.3 m) packed with 4,4′-azoxydianisole supported on Uniport HP (60—80 mesh) at 100 °C (oven temperature). Unless otherwise noted, the value representing the catalyic activity and activity maintenance was the one obtained for the first 30 min period.

Determination of Surface Properties. In order to know whether the Brönsted or the Lewis type acid site should promote the isomerization, the effect of 2,6-lutidine pretreatment[7] on the catalytic activity for the isomerization was examined together with that of pyridine pretreatment. In addition, CO_2 addition was examined for its effect on the basic sites of HM.

To evaluate the acid amount and acid strength, temperature-programmed desorption (TPD) of NH_3 (5 ml) was carried out on a sample (50 mg, 32—42 mesh) which was heat-treated in air at 500 °C for 3 h. Immediately before the TPD, the samples were heat-treated in the test apparatus at 500 °C for 1 h in an atmosphere of He. The temperature was raised to 500 °C at a rate of 40 °C min^{-1}.

Structure and Surface Composition. The structure of HM before and after treatment with CF_3Cl was determined from the powder-diffraction patterns obtained with a Rigaku Geigerflex X-ray diffractometer using filtered Cu $K\alpha$ radiation. The compositions in the surface layer were dertermined by XPS using a Shimadzu ESCA-750 apparatus. The spectra were measured with Mg $K\alpha$ radiation. The base pressure of the spectrometer was usually below 10^{-7} Torr (1 Torr=133,322 Pa) during the experiments. The compositions were calculated from the areas of the spectral peaks (i.e., the maximum in the counting rate) on the basis of the photoionization cross section at 1254 eV in units of the C ls cross section of

22200 barns.[8]

Results and Discussion

Comparison of Catalytic Activities of Various Solid Acids. Table 1 shows the results of the isomerization of OCT to other chlorotoluenes over various solid acids. Among these solid acids, HM exhibited the highest catalytic activity. HY also showed some catalytic activity, though the typical solid Lewis acid Al_2O_3 and the strong solid acid, $SiO_2 \cdot Al_2O_3$ were catalytically inactive. These facts are in contrast to observations that the isomerization of *o*- and *p*-xylenes are readily promoted by Al_2O_3–HX (X=halogen)[9] or SiO_2–Al_2O_3.[10]

After treatment with CF_3Cl at 450°C, HM became much more active, and SiO_2–Al_2O_3 became somewhat active. On the other hand, Al_2O_3 was still inactive as a catalyst, and HY completely lost its catalytic activity. It has been observed that Al_2O_3 becomes strongly acidic and catalytically active for paraffin isomerization[6] and CH_3OH conversion to olefins,[5] which are promoted by only extremely strong solid acids. So, the evidence that the CF_3Cl-treated Al_2O_3 was unable to promote the isomerization suggests that strong acidity is not the only essential factor for catalytic activity. Some other factors, for example the zeolytic structure, are needed for catalytic activity in the chlorotoluene isomerization. The loss of the catalytic activity of HY after the CF_3Cl-treatment is then explicible by the collapse of the zeolytic structure during the treatment with CF_3Cl, which was observed by XRD.

Table 1. Activities of Various Catalysts

	Conversion (mol%)	
	Before treatment	After treatment[a]
H-mordenite[b]	11.7	41.9
SiO_2–Al_2O_3	0	5.0
Al_2O_3	0	0
Y type zeolite	3.4	0

a) The treatment was carried out by using CF_3Cl at 450°C for 8 min. b) SiO_2/Al_2O_3 mol ratio=19.0.

Effects of Treatment with Various Fluorochlorocarbons or HF Acid. Table 2 summarizes the results relating to the effect of treatment using various simple fluoro- or fluorochlorocarbons, CCl_4 or HF acid.

As is shown in this table, CF_3Cl was the most effective treatment agent, while other chloropolyfluorocarbons such as CF_2ClCF_3, CF_2ClCF_2Cl, and CF_2Cl_2 also showed some effect. Abrupt increases in temperature were observed during the treatment of HM with these agents. Approximate values of the increase in temperature for the different agents were as follows: $CFCl_3$, 60°C; CF_2ClCF_2Cl, 50—60°C; CF_2Cl_2, 40°C; CF_3Cl, 30—40°C; CF_3CF_2Cl, 20°C; CF_4, CF_3CF_3, 0°C. For the CCl_4-treatment, the value could not be measured since the increase was too rapid and too sudden.

The increases in temperature are assignable to the surface reaction of HM with the treatment agent. Infact, the compositions were remarkably changed by the treatment. For example, as Table 3 shows, F and Cl components were incorporated in the surface layer by the treatment with CF_3Cl, and were retained after use as a catalyst. For the sample treated with fluoropolychlorocarbons or polychlorocarbon such as $CFCl_3$ and CCl_4, an extensive degradation of mordenite structure was confirmed by XRD determination. This probably resulted from the violent reaction between the HM surface and these polychlorocarbons which have a relatively weak C–Cl bond.[11] On the other hand, perfluorocarbons such as CF_4 and CF_3CF_3 were unable to react with the HM surface because of the very strong C–F bond in their molecules.[12] Thus the high bond strength in CF_4 and CF_3CF_3 may account for the inertness of the perfluorocarbons as a treatment agent for the HM surface.

Finally, chloropolyfluorocarbons such as CF_3Cl, CF_2ClCF_2Cl, and CF_2ClCF_3 may gently and moderate-

Table 2. Catalytic Activities of H-Mordenite Treated with Various Halocarbons or HF Acid

Treatment agent	Conversion mol%	Treatment agent	Conversion mol%
$CFCl_3$	9.5	CF_2ClCF_2Cl	28.4
CF_2Cl_2	19.1	CF_2ClCF_3	34.9
CF_3Cl	41.9	CF_3CF_3	7.8
CF_4	15.3	HF acid	7.4
CCl_4	tr.	no treatment	11.7

Table 3. Surface Composition of H-Mordenite[a]

Sample	Composition/atomic%					
	Si	Al	O	F	Cl	F/Al
Before treatment	28.7	3.7	67.6	0	0	—
After CF_3Cl treatment[b]	30.2	3.2	55.4	10.9	0.2	3.4
After use for 3 h	27.4	5.7	52.1	14.0	0.7	2.5

a) SiO_2/Al_2O_3 mol ratio=19.0. b) The treatment was carried out at 450°C for 8 min.

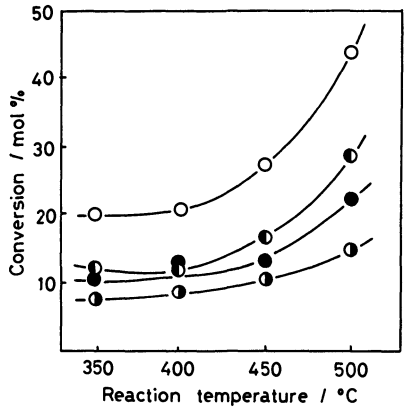

Fig. 1. Effect of reaction temperature on conversion of OCT. HM catalyst having SiO_2/Al_2O_3 mol ratio of 19.0 was used as a catalyst after treatment with CF_3Cl; the treatment was carried out at 450 °C for 8 min. W/F=64.9 gh/mol. Symbols used in this figure are as following.
○: Total conversion to MCT and PCT, ◐: conversion to MCT, ◑: conversion to PCT, ●: conversion to CB.

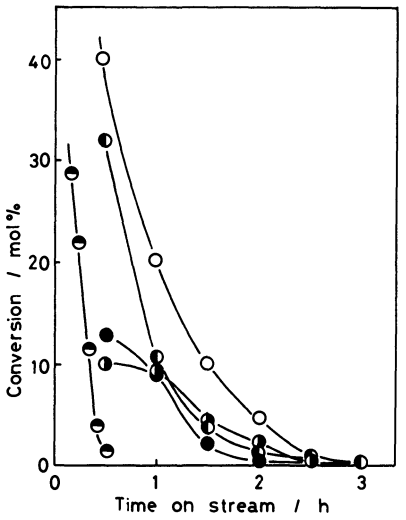

Fig. 2. Effect of process time on conversion of OCT. HM catalyst (SiO_2/Al_2O_3 mol ratio=19.0) was used after CF_3Cl-treatment. The CF_3Cl-treatment and the catalytic reactions were carried out under the same conditions as those described above (Fig. 1). Symbols are as following.
○: Total conversion to MCT and PCT, ◒: total conversion to MCT and PCT in the presence of untreated HM, ◐: conversion to MCT, ◑: conversion to PCT, ●: conversion to CB.

ly react with the HM surface through their C-Cl bonds of the right strength. That is, since these chloropolyfluorocarbons have a C-Cl bond which is fairly strong compared to those of chlorocarbons (such as CCl_4) and fluoropolychlorocarbons (such as $CFCl_3$), they are not so reactive as to destroy the mordenite structure. Similarly the C-F bond in the CF_2X group is fairly strong compared to that in the CFXY group (X and Y are atoms other than F),[12] although it is not as excessively strong as that in perfluorocarbon. Also this moderately high strength in the C-F bond should contribute to prevention of the violent reaction of the treatment agent with mordenite. Thus, CF_3Cl and chlofluoroethanes, containing not CFXY, but the CF_2X group may be the most suitable treatment agent for HM.

Although HF acid is widely used as the treatment agent for Al_2O_3, SiO_2-Al_2O_3 and various other metal oxides,[13] it was unsuitable for HM treatment. A significant formation of crystalline aluminum fluoride was observed by XRD measurement for the HF acid-treated HM, thus partial degradation of mordenite structure or deposition of the crystalline fluoride in the pores or channels of the mordenite may be the reason for the pronounced decrease in the catalytic activity.

Effect of Reaction Temperature. As Fig. 1 shows, the conversions of OCT to MCT and PCT considerably increased at temperatures higher than 400 °C. However, dechlorination or CB formation became important at high temperatures like 500 °C. So, the selectivity of the isomerization was maximal around 450 °C. Although the data are not shown here, other products such as benzene and polychloro aromatic compounds were formed in small amounts at temperature higher than 500 °C.

Changes of Catalytic Activity and Selectivity with Time on Stream. As is shown by the total conversion of OCT to other chlorotoluene in Fig. 2, the catalytic activity of HM abruptly decreased with reaction time. On treatment CF_3Cl at 450 °C, the catalytic activity was significantly enhanced, and a decrease in activity with process time became less prominent.

As Fig. 2 shows, at the beginning of OCT isomerization, MCT was preferentially formed. Then the amount of MCT product remarkably decreased with time, and finally became less than that of PCT.

It is probable that the pore size was decreased by the deposition of decomposed materials or carbonized products. So, transfer of the product from active sites by diffusion through the pore become more difficult for MCT than for PCT, because the former molecules have a larger cross-sectional area.

Isomerizations of MCT and PCT. As Figs. 3 and 4 show, the isomerizations of MCT and PCT were promoted by the CF_3Cl-treated HM as well as that of OCT. Furthermore, for these isomerizations of MCT and PCT, the activity maintenance of the treated HM catalyst was better than that for the OCT isomerization. Especially for the isomerization of MCT, the amount of PCT formation was still high even 3 h after the reaction was begun. This is explained as follows. Namely, the para isomer, which has the smallest cross-sectional area among the chlorotoluenes, should be most readily and easily transferred from the pores as soon as it is produced there. Thus, clogging of the pore is fairly slow in the isomerization of MCT when PCT is the main reaction product.

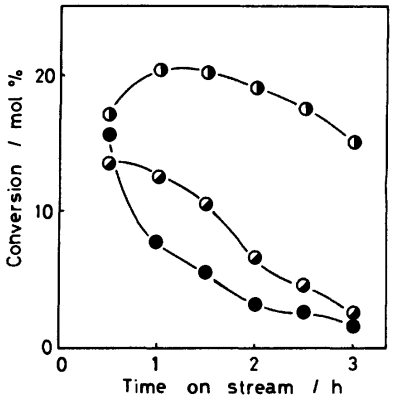

Fig. 3. Effect of process time on conversion of MCT. The HM catalyst (SiO_2/Al_2O_3=19.0) was used also in this reaction. The conditions employed in this reaction were the same as those employed in the OCT isomerization (shown in Figs, 1 and 2). The symbols used here were as following.
◑: Conversion to PCT, ◕: conversion to OCT, ●: conversion to CB.

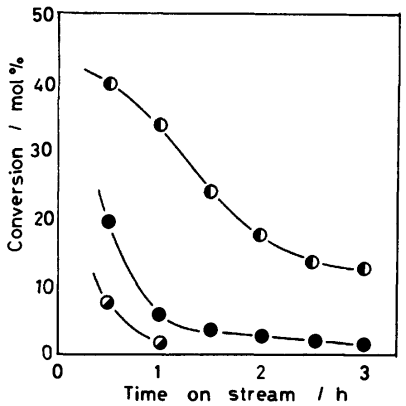

Fig. 4. Effect of process time on conversion of PCT. SiO_2/Al_2O_3 ratio of the HM catalyst=19.0. The conditions of the CF_3Cl treatment and the reaction were the same as those employed for the isomerization of OCT (Figs, 1 and 2) or MCT (Fig. 3). The symbols used in this figure are as following.
◐: Conversion to MCT, ◕: conversion to OCT, ●: conversion to CB.

Appreciably high conversion was obtained at the initial stage of the PCT isomerization process (Fig. 4). This result may be due to the ease with which the PCT molecule is able to reach the active sites in the mordenite pore as compared to other chlorotoluene molecules. However, the conversion decreased somewhat rapidly with reaction time, since the main product, MCT, was not readily removed from the active sites, in accordance with reduction of pore size which occurs with passing reaction time.

Poisoning of Active Sites. The results of poisoning with amines are shown in Table 4 together with those of CO_2 addition used as a reference. The active sites were poisoned with 2,6-lutidine as well as pyridine. It is already known that the 2,6-lutidine molecule is unable to react with Lewis acid sites because the electron-donating N atom in the molecule is sterically hindered by the two adjacent CH_3 groups.[7] Hence, the fact that the active sites were poisoned by the 2,6-lutidine suggests that the active sites on the treated HM are acid sites of not the Lewis, but the Brönsted type.

Table 4. Effect of Poisoning on Isomerization Activity of HM[a)]

	Product distribution/mol%		
	MCT	PCT	Chlorobenzene
Before treatment	31.6	10.8	13.0
Pyridine	4.4	6.0	2.4
2,6-Lutidine	8.1	6.0	9.1
Carbon dioxide	15.3	10.5	14.9
Ref.[b)]	16.6	12.9	13.6

a) SiO_2/Al_2O_3 mol ratio=19.0. b) The reference run was carried out by flowing 80 ml N_2, instead of CO_2, to examine the effect of CO_2 addition.

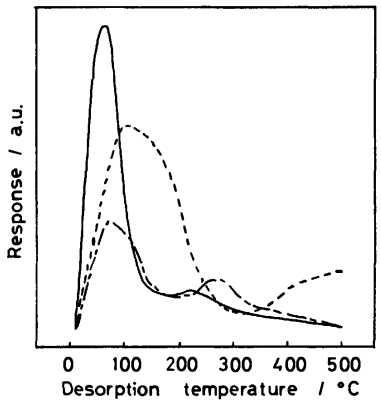

Fig. 5. TPD curves for H-mordenite.
---: Before treatment, ——: after treatment, ——: after use as a catalyst at 450°C for 3 h. The CF_3Cl treatment was carried out at 450°C for 8 min.

On the other hand, CO_2 addition gave almost the same results as that of the dilution with an inert gas, N_2. Thus, it is possible, that the basic sites, if they were present on the CF_3Cl-treated HM, had hardly any effect on the isomerization.

TPD Regarding Acid Strength Distribution. Figure 5 shows the TPD curves of HM before and after treatment with CF_3Cl. The TPD curve of the treated HM after use as a catalyst is also exhibited there.

As is represented by the dotted line, a fair amount of NH_3 was adsorbed by the untreated HM even at a temperature as high as 500°C. For HM treated with CF_3Cl, the adsorption of NH_3 at such a high temperature was no longer observed. Thus, two peaks around 80 and 280°C became observable in the TPD curve as is represented by the broken line. These facts suggested that excessibly strong acid sites on the untreated HM disappeared and moderately strong acid sites, relating to the peak around 280°C appeared during CF_3Cl treatment. For the treated HM which became catalytically less active after use as a catalyst for 3 h,

the peak at higher temperature almost completely disappeared, and a weak peak became observable around 220°C. Thus, the moderately strong acid sites represented by the peak around 280°C, may be most suitable for isomerization promotion.

Demethylation. As Figs. 1—4 show, demethylation also occurred in the early stages of the isomerization. The demethylation was especially pronounced at temperatures higher than 450°C as was exhibited in Fig. 1. On the other hand, hardly any dechlorination occurred under reaction conditions employed in this study, especially at temperatures lower than 500°C, although the bond strength of $Cl-C_6H_5$ (88 kcal mol^{-1} [14] (1 cal= 4.184 J)) is less than that of $H_3C-C_6H_5$ (91 kcal mol^{-1} [14]). So, demethylation is considered to be promoted by acid sites in a manner similar to the isomerization of chlorotoluene. In fact, the demethylation was subject to suppression by poisoning with amines as was already shown in Table 4. However, the acid strength essential to the promotion of demethylation must be fairly high, since demethylation was promoted only in beginning of a run, when appreciably strong acidity can be maintained without poisoning by product formation.

Reaction Pathway. In view of the evidence collected so far, the isomerization of chlorotoluene is expected to proceed similar to the isomerization of xylene.[15] However, the isomerization of chlorotoluene reached levels of 20—40% only with great difficulty at temperatures as high as 450°C in the presence of the CF_3Cl treated HM, while a conversion level of higher than 50% was obtained at the lower temperature of 300°C for xylene isomerization promoted by the same catalyst. Such a difference between the reactivities of chlorotoluene and xylene is ascribable to the difference in the activating effects of the substituent on the benzene ring. That is, when a carbon sp^3 orbital is attached to sp^2 orbital of carbon, there is an electron donation in the direction of sp^2 carbon, because the sp^2-hybridized carbon atom is somewhat more electronegative. Thus, a CH_3 group attached to the benzene ring activates it. In particular, the C atom directly bound to the CH_3 group is easily attacked by protons.

On the other hand, the chlorine atom should deactivate the benzene ring because the inductive effect of chlorine (−I) wins out over the resonance effect (+R). Thus, the activity of chlorotoluene is not as high as that of xylene.

Nevertheless chlorotoluene is less active than toluene as mentioned above, the electron-enriched C atom bound to the CH_3 group in chlorotoluene molecule should be first attacked by the Brönsted acid sites as in the case of the xylene isomerization.[4] Then, isomerization of the chlorotoluene can proceed according to the following reaction pathway.

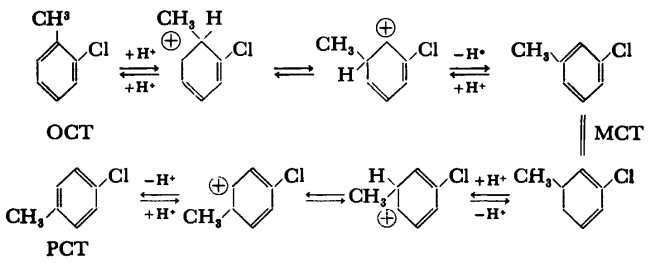

Since the C atom bound to Cl atom is expected to be positive in charge as described above, the C atom may not be attacked by the Brönsted acid on the HM catalyst. In fact, toluene which is produced by the dechlorination was not appreciably formed under the reaction conditions employed in this study.

Effect of CF_3Cl Treatment on Catalytic Activity of HM. In the isomerization of chlorotoluene, excessively strong acid sites are considered to be unsuitable because they do not readily release the product molecule, and thus they promote the decomposition or carbonization of the molecules in the mordenite pores. The treatment with CF_3Cl or some fluorochlorocarbons may be effective for modification of the too strong acidity of some active sites, possibly due to a slight change in the mordenite structure.

Besides the modification of the acid strength described above, the enlargement of the pore size of the HM seems to be another reason for enhancement of the catalytic activity and activity maintenance. It is well known that mordenite has only a one-dimentional channel.[16] Accordingly, resistance to molecular diffusion and clogging of the channel are serious problems in the reaction catalyzed by the mordenite. So, enlargement of the pores or channels through reaction of the CF_3Cl with the Si and Al components in the mordenite may contribute to the improvement of the catalytic activity and activity maintenance in this vapor phase isomerization of chlorotoluene. The enlargement of the pore by the treatment with CF_3Cl has already been seen in the increased amount of formation of the bulky molecule, 1,3,5-trimethylbenzene, in the isomerization and disproportionation of *m*-xylene.[4] Details of the pore enlargement are now being studied by adsorptions of gases of various cross-sectional areas.

The authors express their gratitude to K. I. Kasei Co., for their financial support to this study.

References

1) Gulf Research & Development Comp., Japan Patent 11809 (1971).
2) G. A. Olah, *J. Org. Chem.*, **27**, 3464 (1962).
3) Toray Comp., Japan Patent 40428 (1982), 85330 (1982).
4) S. Okazaki, T. Sudoh, R. Toba, and A. Kurosaki, *Shokubai*, **25**, 103 (1983).
5) A. Kurosaki, and S. Okazaki, *Bull. Chem. Soc. Jpn.*, **56**, 1279 (1983).
6) A. Kurosaki and S. Okazaki, *Chem. Lett.* **1983**, 1741.

7) P. A. Jacobs and C. F. Heylen, *J. Catal.*, **34**, 267 (1974).
8) J. H. Scofield, *J. Electron Spectros. Relat. Phenomena*, **8**, 129 (1976).
9) T. Shiba, T. Keii, and A. Ozaki, "Shokubai Kagaku Gailon, Kyoritsu Shuppan," Tokyo (1968), p. 134.
10) J. Ward and R. C. Hansford, *J. Catal*, **13**, 134 (1969).
11) N. N. Semenov, "Some Problems of Chemical Kinetics and Reactivities," Pergamon press, New York (1968), Vol. 1, p. 19.
12) G. Glocker, *J. Phys. Chem.*, **63**, 828 (1959).
13) A. N. Webb, *Ind. Eng. Chem.*, **49**, 261 (1957); S. Suzaki and S. Okazaki, *Nippon Kagaku Kaishi*, **1981**, 330; S. Okazaki, The Second Regular Meeting of Soviet-Japanese Fluorine Chemists, Moscow, June, **1981**, Abst. p. 109.
14) M. Szwarc, *Chem. Rev.*, **47**, 75 (1950).
15) H. W. Haynes, *Catal. Rev., Sci. Eng.*, **17**, 273 (1978).
16) T. Yashima, *Kagaku to Kogyo*, **34**, 897 (1981).

 © 1986 The Chemical Society of Japan Bull. Chem. Soc. Jpn., 59, 1937—1939 (1986)

The Formal Potentials of Quinones$^{0/-}$ and Quinones$^{-/2-}$ in an Aqueous Solution

Kosaku SUGA* and Shigeru AOYAGUI
Department of Chemical Engineering, Tokyo Institute of Technology, Ohokayama, Meguro-ku, Tokyo 152
(Received October 31, 1985)

Cyclic voltammograms of *p*-benzoquinone and its methyl derivatives are measured in a strongly alkaline aqueous solution. All of them have shown one reversible or quasi-reversible wave corresponding to the reduction of the quinones. Except for the 2,3,5,6-tetramethyl-*p*-benzoquinone (duroquinone), they have all also shown one or two additional small waves corresponding to the reduction of the OH^- adducts of the quinones. Their main waves can reasonably be explained by the calculated values of $E_1°$ and $E_2°$, which have been determined by the two-electron reduction potential and the several equilibrium constants of the quinones. The differences in the $E_1°$ and $E_2°$ values for these quiones are very small (0.007—0.046 V) in contrast to those in an aprotic solvent.

The quinone/hydroquinone (Q/QH_2) couple is known as a typical organic redox system in an aqueous solution.[1] In aprotic solvents, such as *N*,*N*-dimethylformamide (DMF) and acetonitrile (AN), the voltammograms for the reduction of *p*-benzoquinone and its methyl derivatives exhibit, respectively, two well-defined one-electron steps separated by ca. 0.6 V in the half-wave potential.[2] In an aqueous solution, however, they exhibit only one two-electron step each, the half-wave potential of which depends on the pH.[1] Such a situation as this is usually attributed to the fast protonation of the reduction products. If this is true, two one-electron waves should be observed in a highly alkaline solution, where protonation is negligible. However, this has never been realized, possibly because of the instability of these quinones in strong alkaline solutions.

This paper deals with the relation between the half-wave potentials of *p*-benzoquinone derivatives (Q) in a strongly alkaline aqueous solution and the formal potentials of $Q^{0/-}$ ($E_1°$) and $Q^{-/2-}$ ($E_2°$), which are calculated from the formal potential of Q/QH_2, the disproportionation constant of $2Q^- \rightleftarrows Q^{2-}+Q$, and the dissociation constants of QH_2 and QH^-. The $E_1°$ and $E_2°$ values may also easily be calculated from the corresponding formal potentials of protonated species, i.e., the formal potentials of Q/QH and QH/QH_2, which were calculated by Ilan et al.[3] However, their calculation makes use of the dissociation constant of QH, which is unnecessary for obtaining $E_1°$ or $E_2°$ values; this may introduce some additional errors into the resultant $E_1°$ and $E_2°$ values. Therefore, we have calculated the values of $E_1°$ and $E_2°$ directly from the original data.

Experimental

Commercial *p*-benzoquinone (BQ), 2-methyl-*p*-benzoquinone (MBQ), 2,5-dimethyl-*p*-benzoquinone (DMBQ), and 2,3,5,6-tetramethyl-*p*-benzoquinone (DQ) were purified by sublimation and recrystallization. The electrolysis cell used for cyclic voltammetry was of a three-electrode arrangement with a Mitsubishi Kasei Model 01 hanging-mercury-drop electrode (HMDE) as the working electrode and a saturated calomel electrode (SCE) as the reference electrode. Each test solution contained 0.5 mM (M=mol dm^{-3}) of a quinone, 0.1 M of Na_2SO_4, and 0.1 M of NaOH in water. Since the quinones used were unstable in a strongly alkaline solution, a 1 M NaOH solution was added to the test solution, which was deoxygenated by bubbling with nitrogen gas, immediately before measurement. Cyclic voltammetric experiments were carried out at (20±2)°C with a scan rate of 0.1 V s^{-1}.

Results and Discussion

Calculation of $E_1°$ and $E_2°$. The following equilibria in an aqueous solution and at an electrode have been established for a quinone and its reduced species in an aqueous solution:

$$Q + e^- \rightleftharpoons Q^-; E_1° \quad (1)$$

$$Q^- + e^- \rightleftharpoons Q^{2-}; E_2° \quad (2)$$

$$Q + 2H^+ + 2e^- \rightleftharpoons QH_2; E_m° \quad (3)$$

$$2Q^- \rightleftharpoons Q + Q^{2-}; K_d \quad (4)$$

$$Q^{2-} + H^+ \rightleftharpoons QH^-; K_1 \quad (5)$$

$$QH^- + H^+ \rightleftharpoons QH_2; K_2 \quad (6)$$

where $E_m°$ is the formal potential of Eq. 3 and where the K's are the conditional equilibrium constants defined as follows:

$$K_d = [Q][Q^{2-}]/[Q^-]^2 \quad (7)$$

$$K_1 = [QH^-]/[Q^{2-}][H^+] \quad (8)$$

$$K_2 = [QH_2]/[QH^-][H^+] \quad (9)$$

Among these quantities there exist the following relations (see Appendix):

$$(E_1° + E_2°)/2 = E_m° - (RT/2F)\ln[K_1K_2(C°)^2] \quad (10)$$

and:

$$E_1° - E_2° = (RT/F)\ln K_d \quad (11)$$

Table 1. Calculated One-Electron Reduction Potentials of Quinones in Aqueous Solutions and the Literature Values for E and K Used in the Calculation [a]

Quinone	$-E_1°$/V	$-E_2°$/V	$-E_m°$ [b]/V	$\log(K_1/M^{-1})$ [c]	$\log(K_2/M^{-1})$ [c]	$\log K_d$ [c]
BQ	0.150	0.187	0.458	11.4	9.85	4.2
MBQ	0.215	0.233	0.412	11.5	10.05	2
DMBQ	0.304	0.350	0.352	12.5	10.35	6
DQ	0.480	0.493	0.232	13.2	11.25	1.3

a) Oxidation-reduction potentials cited refer to SCE. b) Ref. 1. c) Ref. 3.

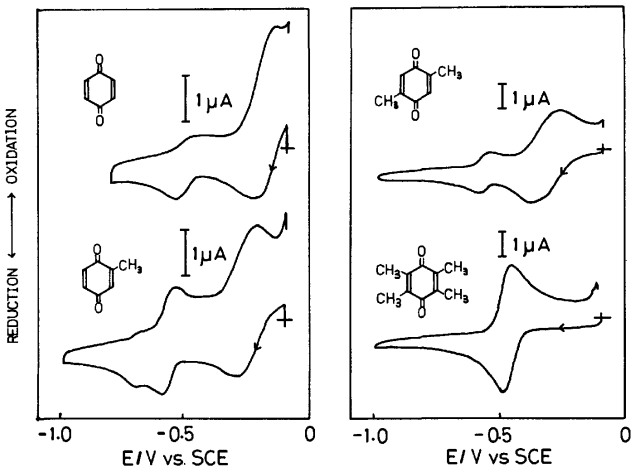

Fig. 1. Cyclic voltammograms for p-benzoquinone and its methyl derivatives in 0.1 M NaOH+0.1 M Li_2SO_4 aqueous solutions. Scan rate: 0.1 Vs^{-1}.

where C° is the standard molar concentration: C°=1 mol dm^{-3}. Table 1 lists the $E_1°$ and $E_2°$ values for BQ and related substitutes calculated from these equations and also the experimental values of $E_m°$, K_1, K_2, and K_d used in the calculation.

Cyclic Voltammetry of p-Benzoquinone and Its Methyl Derivatives in a Strongly Alkaline Aqueous Solution. Figure 1 shows cyclic voltammograms for the reduction of BQ, MBQ, DMBQ, and DQ in an aqueous 0.1 M NaOH solution. These quinones give one or more quasi-reversible steps: DQ gives one; MBQ, three; and the others, two. The most positive step of each cyclic voltammogram corresponds to the redox reactions of the quinones, and the others to the redox reactions of OH^- adducts which are in equilibrium with the parent quinones, as is shown by the following equation:[5]

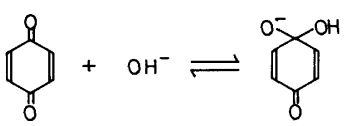

(12)

The finding that only the cyclic voltammogram of MBQ has three steps can be explained by the fact that only the OH^- adduct of MBQ has two isomers. The cyclic voltammogram of DQ, which has only one step suggests that this compound hardly forms the OH^- adduct at all, as has been pointed out by Bishop and Tong.[6]

The apparent half-wave potentials, $E_{1/2}$, determined from the midpoint of the cathodic and the anodic peak potentials of each first step are listed in Table 2, together with the peak separation, ΔE_p. The calculated values of $(E_1°+E_2°)/2$ and $E_1°-E_2°$ are also listed. Recently, Richardson and Taube[7] have calculated the simulation curve for a cyclic voltammogram which has two charge-transfer steps, with various half-wave potential differences. From their results, we can calculate the apparent peak separation, ΔE_p, of the cyclic voltammogram for two-step electron-transfer reactions with small half-wave potential differences. In Table 2, the $(\Delta E_p)_{th}$ values of the quinones thus calculated by using each value of $E_1°$ and $E_2°$ are shown together.

The agreement between the $E_{1/2}$ and $(E_1°+E_2°)/2$ values is excellent. The observed values of ΔE_p are generally somewhat larger than the calculated values, $(\Delta E_p)_{th}$, but the order of the magnitude of ΔE_p and $(\Delta E_p)_{th}$ are in fair agreement with each other. The small difference between the observed and calculated values of ΔE_p may be attributed to the difference between the standard electrode potential and the half-wave potential, or the difference in the compositions of the solution with which the half-wave potential and the other equilibrium constants have been measured.

The difference between the calculated values of $E_1°$ and $E_2°$ are very small in contrast to those in acetonitrile, as shown in Table 2. Peover[2] has measured the polarograms of several quinols in 75% ethanol containing 0.1 M NaOH as the supporting electrolyte; he has thus obtained a value of about 0.15 V as the difference between the first and second half-wave potentials. Hayano and Fujihira[4] have measured polarograms of p-benzoquinone in DMF–ethanol mixtures and have found that the difference between the two half-wave potentials decreased from about 0.8 V in DMF to 0.15 V in ethanol. These small differences between two half-wave potentials in a protic solvent such as ethanol have been explained by these authors as the effect of hydrogen bonding between the quinone and these protic solvents. The results obtained by us in water are, therefore, not unreasonable.

From the results presented above, we can conclude that the calculated one-electron reduction potentials shown in Table 1 are reasonable as the formal potentials for Q/Q^- and Q^-/Q^{2-} in an aqueous solution, and that the first and the second one-electron reduction potentials without protonation reactions for p-

Table 2. Half-Wave Potentials, $E_{1/2}$, and the Peak Separations, ΔE_p, of *p*-Benzoquinone Derivatives[a)]

Quinone	In water					In acetonitrile[b)]	
	Experimental		Calculated				
	$-E_{1/2}$/V	ΔE_p/V	$-(E_1°+E_2°)/2$	$(E_1°-E_2°)$	(ΔE_p)th/V	$-(E_{1/2})_1$/V	$-(E_{1/2})_2$/V
BQ	0.172	0.095	0.169	0.037	0.059	0.51	1.14
NBQ	0.231	0.075	0.224	0.018	0.048	0.58	1.10
DMBQ	0.331	0.090	0.327	0.046	0.070	0.67	1.27
DQ	0.490	0.048	0.487	0.007	0.045	0.84	1.45

a) The potentials cited refer to SCE. b) Ref. 2.

benzoquinone and its methyl derivatives in an aqueous solution have very close values in contrast to the values of the first and the second half wave potentials of these quinones in an aprotic solvent.

Appendix

Derivation of Equation 10. $E°^1$, $E°^2$, K_{2a1}, and K_{2a2} in Eqs. IIa and IIIa of Ref. 3 correspond to $E_1°$, $E_2°$, $1/K_2$, and $1/K_1$ respectively in this paper. Furthermore, E_o^1 and E_o^2 in these equations are the formal potentials of the following electrode reactions:

$$Q + H^+ + e^- \rightleftharpoons QH;\ E_o^1 \qquad (A1)$$

$$QH + H^+ + e^- \rightleftharpoons QH_2;\ E_o^2 \qquad (A2)$$

From Eqs. IIa and IIIa of Ref. 3, the following equation can be obtained:

$$(E_o^1 + E_o^2)/2 = (E°^1+E°^2)/2 - (RT/2F)\ln[K_{2a1}K_{2a2}(C°)^{-2}] \qquad (A3)$$

It is apparent from Eqs. A1 and A2 that $(E_o^1+E_o^2)/2$ is equal to $E_m°$ in this paper. Therefore, using the notation of this paper, Eq. 10 is obtained:

$$(E_1° + E_2°)/2 = E_m° + (RT/2F)\ln[K_1K_2(C°)^2] \qquad (10)$$

References

1) W. M. Clark, "Oxidation and Reduction Potentials of Organic Systems," The Williams and Wilkins Corp. (1960).
2) M. E. Peover, *J. Chem. Soc.*, **1960**, 4540.
3) Y. A. Ilan, G. Czapski, and D. Meisel, *Biochim. Biophys. Acta*, **430**, 209 (1976).
4) S. Hayano and M. Fujihira, *Bull. Chem. Soc. Jpn.*, **44**, 2051 (1971).
5) C. A. Bishop and L. K. J. Tong, *Tetrahedron Lett.*, **1964**, 41—42, 3043.
6) C. A. Bishop and L. K. J. Tong, *J. Am. Chem. Soc.*, **87**, 501 (1965).
7) D. E. Richardson and H. Taube, *Inorg. Chem.*, **20**, 1278 (1981).

Analysis of Proton-Transfer Reaction in Aqueous Solutions of Butylamines by Ultrasonic Methods

Yukio YOSHIDA and Sadakatsu NISHIKAWA*
Department of Chemistry, Faculty of Science and Engineering, Saga University, Saga 840
(Received November 2, 1985)

Ultrasonic absorption has been measured in an aqueous solution of *s*-butylamine over the frequency range 6.5—220 MHz and the concentration range 0.0115—3.18 mol dm^{-3} at 25 °C. The single relaxational phenomenon observed in a range less than 1 mol dm^{-3} was found to be associated with a perturbation of the equilibrium; R-NH_3^++OH^- ⇄ R-NH_3^+···OH^-. The rate constants of the forward and backward reactions, k_{12} and k_{21}, have been determined to be 2.1×10^{10} s^{-1} mol^{-1} dm^3 and 1.8×10^8 s^{-1}, respectively. It was also determined that the next step, R-NH_3^+···OH^- ⇄ R-NH_2+H_2O, which had been thought to have a considerable influence on the first step, was not very effective regarding the ultrasonic absorption observed in the MHz frequency range. The equilibrium constant in the second step, K_{32}, has been determined to be 3.5×10^{-2}. The standard volume change of the reaction has been calculated to be 26 cm^3 mol^{-1} from the concentration dependence of the maximum excess absorption per wavelength. The relaxation observed in a range greater that 1 mol dm^{-3} has been estimted to be associated with a molecular aggregation reaction. An ultrasonic study in an aqueous solution of butylamine has also been performed in order to determine the rate constants associated with a proton-transfer reaction at 25 °C.

The hydrogen atom has the simplest atomic structure and its properties have been experimentally and theoretically investigated.[1,2] Kinetic studies concerning proton-transfer reactions of amino acids, amines and carboxylic acids,[3-5] as well as the catalytic effect on the reaction[6-8] have been published using relaxation methods. Such information is very important in relation to biological reactions. It has been known that the proton-transfer process in aqueous amine solutions can be observed within the range of the ultrasonic pulse frequency 1—250 MHz. A theoretical approach which was originally proposed by Eigen,[9] seems to have become established. However, an analysis of the absorption associated with a proton-transfer may give us some unreasonable results, though the present authours[10,11] have also reported kinetic results regarding proton-transfer reaction in aqueous solutions of some amines according to his theory. In this situation, we consider that a reexamination of the analysis procedure should be undertaken. Another purpose of this report is to examine the isomeric effect of a proton-transfer reaction of butylamines. To this end, *s*-butylamine was chosen and the ultrasonic absorption and velocity results are given in this paper.

Experimental

s-Butylamine and butylamine were purchased from Tokyo Kasei Co. Ltd and Wako pure Chemicals, respectively, and distilled once. The desired concentrations of the aqueous solutions were prepared with doubly distilled water by weight. An improved ultrasonic pulse method was used for absorption measurements in the frequency range 6.5 to 220 MHz with 0.5, 5, and 20 MHz X-cut quartz transduceres. The procedure of the semiautomatic absorption measurement has been described elsewhere.[12] The sound velocity was measured by a sing around meter at 1.92 MHz and an interferometer at 2.5 MHz. The density of the solution was determined by a standard pyconometer of about 4 cm^3. The pH of the solution was measured by a HITACHI-HORIBA pH meter with a glass electrode. A saturated aqueous solution of $Ca(OH)_2$ was used as the standard reference of the electrode at pH=12.45 along with a standard buffer solution at 9.18 at 25 °C. All pH and ultrasonic measurements were carried out under a dry nitrogen gas because of the high basicity of the solution. They were all measured at 25 °C.

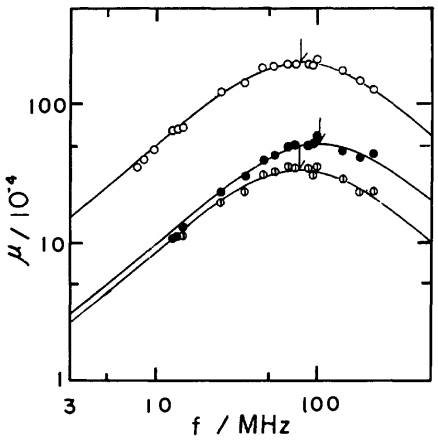

Fig. 1. The representative ultasonic absorption spectra in aqueous solution of *s*-butylamine at 25 °C. ○: 1.67 mol dm^{-3}, ●: 0.500 mol dm^{-3}, ⊕: 0.144 mol dm^{-3}.

Results and Discussion

Typical ultrasonic spectra for an aqueous solution of *s*-butylamine are shown in Fig. 1. In general, the frequency dependence of the absorption coefficient, α, due to a single process with a relaxation frequency, f_r, can be expressed as

$$\alpha/f^2 = A/\{1 + (f/f_r)^2\} + B \quad (1)$$

or

$$\mu = Afc/\{1+(f/f_r)^2\}, \quad (2)$$

were μ is the excess absorption per wave length, f the frequency, A the amplitude of the excess absorption,

Table 1. Thermodynamic and Ultrasonic Parameters in Aqueous Solution of *s*-Butylamine at 25°C

Concd	ρ	c	A	B	f_r	pH
mol dm^{-3}	g cm^{-3}	m s^{-1}	10^{-17} s^2 cm^{-1}		MHz	
0.0115	0.9970	1494.7	49	22	22	11.19
0.0225	0.9970	1497.9	48	20	39	11.28
0.0478	0.9967	1500.2	55	21	44	11.54
0.0510	0.9966	1499.2	55	21	46	11.40
0.0904	0.9965	1502.6	55	19	63	11.75
0.144	0.9956	1506.4	58	19	78	11.85
0.185	0.9949	1509.6	63	19	80	11.91
0.222	0.9946	1512.6	63	20	85	11.95
0.316	0.9940	1515.0	65	19	93	12.03
0.411	0.9923	1524.0	60	23	105	12.09
0.500	0.9910	1530.6	66	21	104	12.13
0.739	0.9875	1545.8	63	26	109	12.22
0.966	0.9844	1560.5	66	28	115	12.29

B the background absorption, and c the sound velocity. The solid curves in Fig. 1 were calculated using ultrasonic parameters determined by a nonlinear least-mean-square method. The agreement between experimental and calculated values was very good. The obtained ultrasonic parameters are listed in Table 1 along with the measured solution density, ρ. Figure 2 shows the dependence of the ultrasonic parameters on the concentration. In the concentration range less than 1 mol dm^{-3}, both A and B maintain a plateau. However, in a range greater than 1 mol dm^{-3}, A increases dramatically and shows a peak at about 2.4 mol dm^{-3} while B increases monotonously with the concentration. This indicates that the cause of the absorption in the high-concentration range is different from that observed in the low-concentration range.

In this paper, the relaxation phenomenon observed at less than 1 mol dm^{-3} is mainly considered. There have been many reports concerning ultrasonic absorption in aqueous solutions of various amines.[4,10,11,13–15] A process associated with an unimolecular reaction, such as rotational isomerization, might be ruled out since the relaxation frequency strongly depends on the concentration. In such a relatively dilute aqueous solution, the most feasible absorption mechanism is related to a hydrolysis of an amine. This can be expressed by

$$\text{R-NH}_3^+ + \text{OH}^- \underset{k_b}{\overset{k_f}{\rightleftharpoons}} \text{R-NH}_2 + \text{H}_2\text{O}, \qquad (3)$$

where k_f and k_b are the forward and backward rate constants, respectively. The relationship between the relaxation time, τ, and the reactant concentrations is given by

$$2\pi f_r = \tau^{-1} = \gamma^2 k_f\{[\text{R-NH}_3^+] + [\text{OH}^-]\} + k_b, \qquad (4)$$

where γ is an activity coefficient calculated using Davies equation,[16] $-\log\gamma = 0.5[I^{1/2}/(I^{1/2}+1) - 0.3I]$. I is the ionic strength. The ion concentrations were obtained from pH measurements in the solution. Plots of f_r vs. $\gamma^2[\text{OH}^-]$ which are shown in Fig. 3 provide us

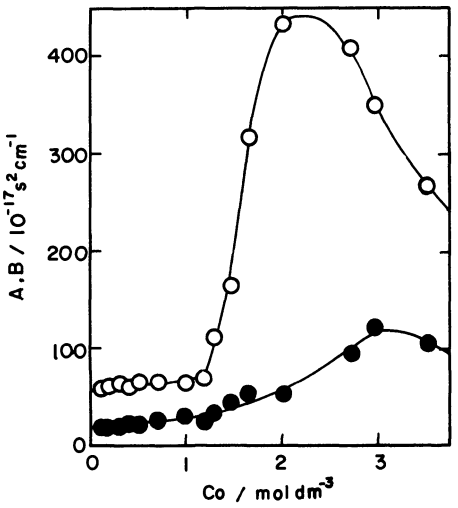

Fig. 2. Concentration dependences of the amplitude of the excess absorption (○), the background absorption (●) for aqueous solution of *s*-butylamine.

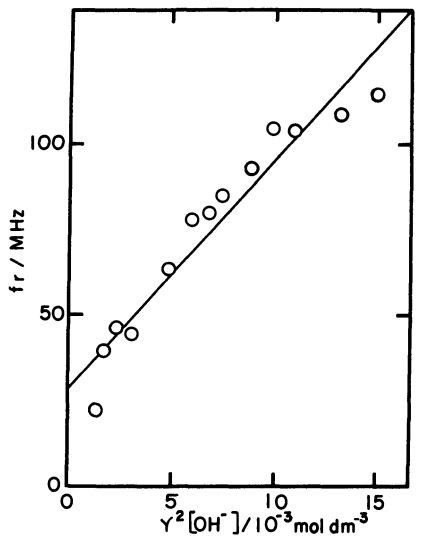

Fig. 3. The plots of f_r vs. $\gamma^2[\text{OH}^-]$ for aqueous solution of *s*-butylamine at 25°C.

Table 2. The Proton-Transfer Reaction Rate Constants for Four Butylamines

Solute	Temp	$k_{12}(k_f)$	k_{f0}	$k_{21}(k_b)$	k_{b0}	K_{32}	K_b[a)]	ΔV	Ref.
	°C	10^{10} mol^{-1} dm^3 s^{-1}		10^8 s^{-1}		10^{-2}	10^{-4} mol dm^{-3}	cm^3 mol^{-1}	
Normal	20	3.6±0.1	0.22±0.01	1.2±0.1	1.4±0.4	5.4±2.0	1.7±0.5	30	10)
	25	2.4±0.2	0.13±0.01	3.1±0.3	2.9±1.9	2.0±1.0	2.5±1.5	28	This work
Iso	20	1.3±0.1	0.052±0.002	3.1±0.2	2.9±0.3	0.93±0.5	2.2±1.2	31	20)
Tertiary	20	1.9±0.1	0.11±0.01	2.0±0.2	2.7±0.4	3.9±3.0	4.2±2.7	25	20)
Secondary	25	2.1±0.1	0.048±0.004	1.8±0.2	3.4±0.5	3.5±2.7	2.9±2.2	26	This work

a) The dissociation constants have been calculated by Eq. 12.

the rate constants from the slope and the intercept. The results are shown in Table 2. Though the equilibrium constant, which might be calculated from the ratio of the two rate constants, should be the same as that determined by a static methods,[17] they are different from each other by at least a factor of ten. Equation 4 can be expressed in terms of the analytical concentration, C_0, by

$$(2\pi f_r)^2 = \tau^{-2} = 4\gamma^2 k_f k_b C_0 + k_b^2. \quad (5)$$

Then, the forward and backward rate constants can also be obtained from the plots of f_r^2 vs. $\gamma^2 C_0$. They are also listed in Table 2 and are indicated as k_{f0} and k_{b0}. However, the rate constants, especially the forward rate constants, obtained by the above two procedures are very different as can be seen in Table 2. In order to test the accuracy of the ion concentrations in the solutions, we have estimated the dissociation constant using

$$K_b = \gamma^2[OH^-]^2/(C_0 - [OH^-]). \quad (6)$$

The calculated dissociation constant is $(2.8\pm1.6)\times10^{-4}$ mol. This is close to the literature value.[17] This means that the ion concentrations are not incorrect. These dynamic and static results indicate that the hydrolysis of amine proceeds through more complicate steps. The more detailed proton-transfer reaction mechanism has been originally proposed by Eigen,[9] which is expressed by Eq. 7 and it seems to have been successfully applied to the ultrasonic analysis for many aqueous solutions of amines and amino acids.[3,4]

$$R\text{-}NH_3^+ + OH^- \underset{k_{21}}{\overset{k_{12}}{\rightleftharpoons}} R\text{-}NH_3^+\cdots OH^- \underset{k_{32}}{\overset{k_{23}}{\rightleftharpoons}} R\text{-}NH_2 + H_2O \quad (7)$$

where k_{ij} represents the rate constant at each step. According to the procedure of the analysis used so far,[3,4,18] the rate constants of k_f and k_b in Eq. 3 are connected by the next equation on the assumption that the first step is much slower than the second.

$$k_f = k_{12} \text{ and } k_b = k_{21}k_{32}/k_{23} \quad (8)$$

If the above procedure is correct, the ratio k_b/k_f should be close to the dissociation constant, K_b, because $K_b \cong k_b/k_f = (k_{21}/k_{12})(k_{32}/k_{23})$. However, this did not hold since these values were calculated using the rate constants in Table 2. An agreement can not be produced, even if the error of the intercept is taken into account. In the analysis procedure previously used, the rate constant, k_f, was determined using Eq. 5 with the help of a dissociation constant in the literature. The backward rate constant was then calculated and the results appear to be consistent. However, the intercept of plots of the experimental relaxation frequency vs. the ion or analytical concentration seems to be an actual high value although it should have been very close to the origin of the coordinate axes. Also, there is no kinetic experimental evidence concerning the dissociation rate constant. Only an estimation using the theoretical equation proposed by Eigen has been performed. Dickson et al.[18] have analyzed the proton-transfer reaction for aqueous solutions of some diamines in terms of a strong coupling two-step reaction scheme. They seem to have considered the intermediate to consist of a hydrogen-bonded complex, although they have not touched upon the intermediate exactly. If the elementary step of the proton-transfer is taken into account, there should be an ion-pair formation process before the making of a hydrogen bond. Then, it should be necessary to assume another step between the reactants, $R\text{-}NH_3^+\cdots OH^-$ and $R\text{-}NH_2$, in Eq. 7. Such a step has been also proposed by Eigen.[1] Even if such a complicated reaction mechanismis considered, the reactants, $R\text{-}NH_3^+\cdots OH^-$ and $R\text{-}NH_2\cdots OH_2$, are not distinguishable because the intramolecular proton-transfer reaction is expected to be too fast to be detected. Then, the reaction scheme of Eq. 7 is the same as that being taken into account such another intermediate, $R\text{-}NH_2\cdots OH_2$. Under these circumstances, we have simply considered that the observed relaxation in the concentration range of 0.0115 to 1 mol dm^{-3} is assumed to be only due to the first step and the influence of the other steps is approximately negligible within the experimental error even if such process exists in a higher or lower frequency range. Then, the rate constants obtained from the plots of the relaxation frequency vs. $\gamma^2[OH^-]$ in Fig. 3 may be those of the first step, k_{12} and k_{21}. From this hypothesis, it is possible to estimate the equilibrium constants, K_{32} and K_b, as follows. The equilibrium constants of the first and second steps are expressed as

$$K_{21} = k_{21}/k_{12} = \gamma^2[\text{R-NH}_3^+][\text{OH}^-]/[\text{R-NH}_3^+\cdots\text{OH}^-] \quad (9)$$

and

$$K_{32} = k_{32}/k_{23} = [\text{R-NH}_3^+\cdots\text{OH}^-]/[\text{R-NH}_2],$$

respectively. The dissociation constant or the equilibrium constant, K_b, can be precisely expressed by the next equation when the intermediates are taken into account.

$$K_b = K_{21}/(1+K_{32}^{-1}) \quad (10)$$

When the concentration of the $\text{R-NH}_3^+\cdots\text{OH}^-$ is small, K_b is approximately equal to $(k_{21}/k_{12})(k_{32}/k_{23})$. It is possible to calculate the equilibrium constant, K_{32}, with the help of Eq. 10 since K_{21} is obtained from k_{12} and k_{21}. The result is shown in Table 2. The small value of K_{32} indicates that the intermediate of the amine hydrolysis does not exist to a great extent. Using Eqs. 9 and 10, and the analytical concentration, Eq. 4 is transformed to

$$2\pi f_r = \tau^{-1} = k_{12}\{-K_b+(K_b^2+4\gamma^2C_0K_b)^{1/2}\} + k_{21}. \quad (11)$$

Consequently, solving for K_b, we obtain

$$K_b = [(\tau^{-1})^2 + k_{21}^2 - 2\tau^{-1}k_{21}]/[k_{12}(4\gamma^2C_0k_{12} + 2k_{21} - 2\tau^{-1})] \quad (12)$$

Fig. 4 indicates the calculated K_b against C_0, where k_{12} and k_{21} obtained from the slope and the intercept in Fig. 3 are used. The obtained K_b listed in Table 2 is very close to that found in the literature.[17] The above analysis of the amine hydrolysis makes us believe that the observed relaxation is approximately due to a perturbation of the first step. In a determination of the rate constants, k_{12} and k_{21}, according to the analytical concentration, it is no wonder that the same rate constants, k_{12} and k_{21}, as those obtained by Eq. 4 are availabel if Eq. 11 is used in order to determine them. The rate constant, k_{12}, is consistent with the diffusion-controlled reaction predicted by Debye's equation.[9] However, the backward rate constant, k_{21} is small when compared to that predicted by the theoretical equation using the ordinary parameters such as the reaction radius, diffusion coefficient and dielectric constant. It should be of the order of $10^{10}\,s^{-1}$ according to the theory while the experimental value of k_{21} is of that of $10^8\,s^{-1}$. However, there is no direct observation that dissociation rate constant, k_{21}, is of the order predicted by theory. Applegate et al.[19] have also reported that in their proton-transfer reaction study, the decomposition of the reaction into two steps was arbitrary.

Another important parameter obtained by ultrasonic absorption and velocity measurements is the maximum absorption per wavelength, μ_{max}, expressed as

$$\mu_{max} = \pi\rho c^2\Gamma(\Delta V-\alpha_p\Delta H/\rho C_p)^2/2RT, \quad (13)$$

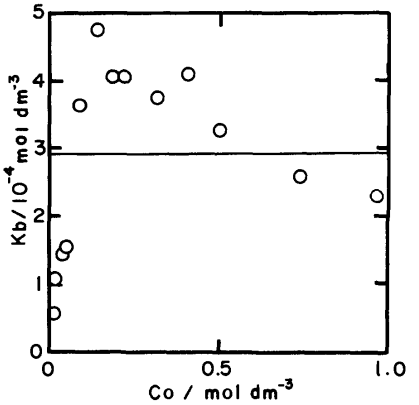

Fig. 4. The dissociation constants in aqueous solutions of *s*-butylamine calculated by Eq. 12 at 25 °C.

where ΔV is the standard volume change of the reaction, ΔH the standard enthalpy change of the reaction, α_p the thermal expansibility, C_p the specific heat, and Γ the concentration term which is expressed for the reaction under consideration as

$$\Gamma = \{1/[\text{R-NH}_3^+] + 1/[\text{OH}^-] + 1/[\text{R-NH}_3^+\cdots\text{OH}^-]\}^{-1}. \quad (14)$$

In the proton-transfer reaction, the enthalpy term can be quite small compared with the volume term in Eq. 13. Then, plots of μ_{max} vs. $\rho c^2\Gamma$ provide the standard volume change of the reaction. The result is given in Table 2.

A similar experiment and the analysis for an aqueous solution of butylamine have been performed at 25 °C. The kinetic results are also shown in Table 2. Also, the analyses of other butylamine solutions for which ultrasonic experimental results have been reported so far[10,21] have been performed. The calculated rate and thermodynamic constants are listed in Table 2. Inconsistent values are also obtained when it is assumed that the second step influences the first step. However, an analysis based on the assumption that the ultrasonic absorption is only due to the perturbation of the equilibrium associated with the first step has been shown to be reasonable.

In conclusion, the ultrasonic relaxation observed in the MHz frequency range in relatively dilute aqueous solutions of butylamines can be attributed to the hydrolysis which proceeds in an intermediate state. The first process of ion-pair formation is associated with the observed relaxation. However, it seems to be hard to distinguish the difference in the kinetic parameters of the four isomeric butylamines. This means that the association process is a diffusion-controlled reaction which depends mainly on the coefficients of the hydroxide ions in the solutions. However, it is hard to say whether the dissociation process is also the diffusion-controlled reaction as predicted by Eigen.

Next, we briefly discuss an excess absorption me-

chanism which was observed in a concentration range greater than 1 mol dm^{-3}. As can be seen in Fig. 2, the amplitude of the relaxational absorption has a maximum. The sound velocity also has a maximum. Such dependences on the concentration have been found in some aqueous solutions of amines with relatively large hydrophobic groups, such as in the solution of pentylamine.[20] On the other hand, such phenomena are not observed in solutions in which solutes consist of a small hydrophobic group.[11,20] From these experimental facts, we conclude that the aggregate associated with a hydrophobic interaction might be created in butylamine aqueous solutions. Unfortunately, it has not been possible to distinguish two relaxation processes at greater than 1 mol dm^{-3}. All measured spectra can be approximately expressed by a single relaxational equation, though the relaxation frequency shows a discontinuous dependence on the concentration at around 1 mol dm^{-3}. This means that the coupling between the hydrolysis and the aggregation reaction is quite strong in butylamine solutions. In the case of a pentylamine aqueous solution,[20] two such distinguishable relaxations have been clearly observed.

We are considering that the relaxation observed in the concentrated aqueous solutions of amines with relatively large hydrophobic groups might be closely related to those observed in aqueous solutions of some alcohols or ethers since both aqueous solutions may indicate quite similar ultrasonic characters. In order to determine the correlations between them, it is required to accumulate more ultrasonic data for aqueous solutions of various nonelectrolytes as functions of the concentration and frequency.

This work was partly supported by The Naito Foundation.

References

1) "Proton-Transfer Reactions," ed by E. Caldin and V. Gold, Chapman and Hall. London (1975).
2) S. Scheiner, *Acc. Chem. Rev.*, **18**, 174 (1985).
3) R. D. White, L. J. Slutsky, and S. Pattison, *J. Phys. Chem.*, **75**, 161 (1971).
4) M. Eigen, G. Maass, and G. Schwarz, *Z. Phys. Chem., (Frankfurt am Main)*, **74**, 319 (1971).
5) T. Sano, T. Miyazaki, N. Tatsumoto, and T. Yasunaga, *Bull. Chem. Soc. Jpn.*, **46**, 43 (1973).
6) T. Yamashita, H. Yano, S. Harada, and T. Yasunaga, *J. Phys. Chem.*, **87**, 5482 (1983).
7) T. Yamashita, H. Yano, S. Harada, and T. Yasunaga, *J. Phys. Chem.*, **88**, 2671 (1984).
8) T. Yamashita, H. Yano, S. Harada, and T. Yasunaga, *Bull. Chem. Soc. Jpn.*, **57**, 2352 (1984).
9) M. Eigen and L. DeMaeyer, "Technique of Organic Chemistry," ed by A. Weissberger, Jr., Wiley, New York N. Y. (1961), Vol. VIII, Part 2.
10) S. Nishikawa, T. Nakamoto, and T. Yasunaga, *Bull. Chem. Soc. Jpn.*, **46**, 324 (1973).
11) S. Nishikawa, U. Otani, and M. Mashima, *Bull. Chem. Soc. Jpn.*, **50**, 1716 (1977).
12) S. Nishikawa and K. Kotegawa, *J. Phys. Chem.*, **89**, 2896 (1985).
13) J. F. McKellar and J. H. Andrear, *Nature*, **195**, 778 (1962).
14) D. Grimshaw and E. Wyn-Jones, *J. Chem. Soc., Faraday Trans. II*, **69**, 168 (1973).
15) E. J. Williams, T. H. Thomas, E. Wyn-Jones, and W. J. Orville-Thoas, *J. Mol. Structure*, **2**, 307 (1968).
16) C. W. Davies, "Ion Association," Butterworths, London (1962).
17) J. J. Christensen, R. M. Igatt, D. P. Wrathall, and L. D. Hansen, *J. Chem. Soc. (A)*, 1212 (1969).
18) L. W. Dickson, H. Nomura, R. E. Verrall, T. Suzuki, and S. Kato, *J. Phys. Chem.*, **85**, 2273 (1981).
19) K. Applegate, L. J. Slutsky, and R. C. Parker, *J. Am. Chem. Soc.*, **90**, 6909 (1968).
20) S. Nishikawa, T. Yasunaga, and K. Takahashi, *Bull Chem. Soc. Jpn.*, **46**, 2992 (1977).
21) S. Nishikawa and M. Mashima, *Bull. Chem. Soc. Jpn.*, **52**, 655 (1979).

Chemical Effectiveness of Elastic and Inelastic Energy Loss of He^+, Ar^+, and Xe^+ Ions Bombarding Solid Potassium Nitrate†

Shin-ichi OHNO,* Katsutoshi FURUKAWA, and Takeshi SOGA
Department of Chemistry, Japan Atomic Energy Research Institute, Tokai-mura, Ibaraki 319-11
(Received December 5, 1985)

Decomposition of crystalline potassium nitrate due to He^+-, Ar^+-, and Xe^+-ion bombardment was studied in the energy range from 20 to 100 keV. The cross sections for producing nitrite ions were for the first time determined to be 5.7×10^{-20} m^2, 12.6×10^{-20} m^2, and 22.0×10^{-20} m^2 for 100 keV He^+, Ar^+, and Xe^+ ion, respectively. Comparing the values of these cross sections with the rate of an elastic and inelastic energy loss of these incident ions, which were calculated on the basis of the theory of Lindhard et al., it may be concluded that inelastic energy is about five times more efficient than elastic energy for the decomposition of the solid potassium nitrate.

Energetic particles lose energy in traversing matter because of two different processes:[2,3]

a) elastic collisions leading to atomic displacements, which are called "nuclear stopping" of the matter for the incident particle,

b) inelastic collisions leading to electronic excitations (ionizations and charge-exchange processes included), which are called "electronic stopping" of the matter. Both "nuclear" and "electronic" collisions may initiate chemical reactions in the material.[1,2,4]

Decomposition of potassium nitrate via electronic excitations has been studied in many works[1,5-12] using α-rays,[7] γ-rays,[5,8-10] or electron beams.[6,12] The only end-products reported are the nitrite ion and molecular oxygen, the initial process being the dissociation of an N-O bond:[7-9]

$$NO_3^- \longrightarrow NO_2^- + O. \quad (1)$$

On the other hand, elastic collisions are frequent phenomena at relatively low impact energies (≈keV region).[2,3] The energy transferred from incident ions to atomic constituents is so high compared to the binding energy for a molecular and crystalline structure that a chemical reaction may take place in the solid. Thus, Logan and Moore interpreted their results on the decomposition of potassium nitrate by incident 2 keV D^+ and He^+ as due to the atomic displacements.[11]

The present authors reported in a previous communication[1] that potassium nitrate decomposed during bombardment with 100 keV ions generated from discharge of deuterium, helium, nitrogen, and oxygen. The observed results suggested that the reaction proceeded mainly via electronic excitations.

The purpose of the present paper is to clarify the relative importance of electronic and atomic displacement excitations in chemical reactions in potassium nitrate. We aim at obtaining cross sections of the each ion decomposing potassium nitrate which should be determined from the yield-dose curve for He^+-, Ar^+-, and Xe^+-ion bombardment. These noble gas ions transfer their kinetic energy to KNO_3 without themselves taking part in chemical reaction. (cf. H_2^+ or O_2^+; see Ref. 1). The second step to our end is to know the relative amount of energy going into elastic and inelastic processes. We obtain this information from the calculation of stopping power according to the theory of Lindhard, Scharff and Schiøtt.[13,14]

By comparing the cross sections for the reaction with the electronic and nuclear stopping power thus obtained, one may determine the relative effectiveness of elastic and inelastic energy losses of the energetic particles bombarding solid potassium nitrate. Potassium nitrate was chosen because its radiolytic behavior toward ionizing radiations was well known; The only radiolytic products reported are nitrite ions and molecular oxygen.[10,11]

Experimental

Experimental method was the same as that reported previously.[1] Energetic ions were produced by discharge of He, Ar, and Xe in a radio-frequency source,[16] and accelerated at desired energies and were focussed through an aperture (8 mmφ) onto the sample.

The sample was a pressed disk of polycrystalline potassium nitrate. Irradiations were carried out at room temperature in vacuum (ca. 10^{-5} Pa). The current density was 10 μA cm^{-2}. After irradiations, the samples were dissolved in water and the concentration of nitrite ions produced was determined spectrophotometrically[17] by adding 1-naphthylamine and sulfanilic acid.

Results and Discussion

Yield-Dose Curve for the He^+-, Ar^+-, and Xe^+-Ion Bombardment. The amounts of nitrite ion as a function of the incident ion dose are shown in Figs. 1, 2, and 3 for the bombardment of He^+, Ar^+, and Xe^+ ion, respectively. As is seen from the figures, the yields depend on both the mass and energy of the bombarding ions. The rapid initial decomposition is followed by a decline in rate in all the cases examined.

We may assume here that each yield-dose curve includes of two regions: An initial decomposition the rate of which is linear with dose and a final plateau

†Chemical Reactions Induced by Energetic Particles. III.[1]

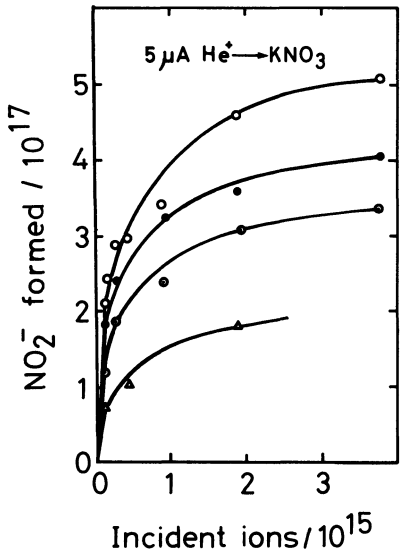

Fig. 1. Nitrite ion formation in potassium nitrate as a function of the energy of incident He^+ ions. Ion energy: (△) 20 keV, (⊙) 50 keV, (●) 80 keV, and (○) 100 keV; Ion beam intensity: 6.25×10^{13} ions $cm^{-2}s^{-1}$.

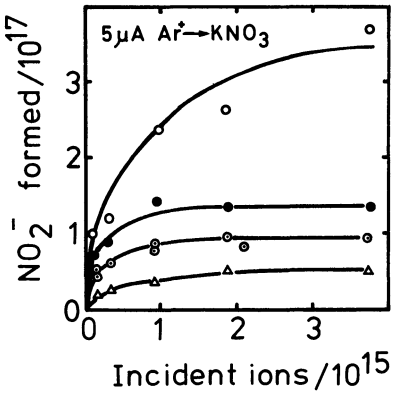

Fig. 2. Nitrite ion formation in potassium nitrate as a function of incident Ar^+ ion. Ion energy: (△) 20 keV, (⊙) 50 keV, (●) 80 keV, and (○) 100 keV; Ion beam intencity: 6.25×10^{13} ions $cm^{-2}s^{-1}$.

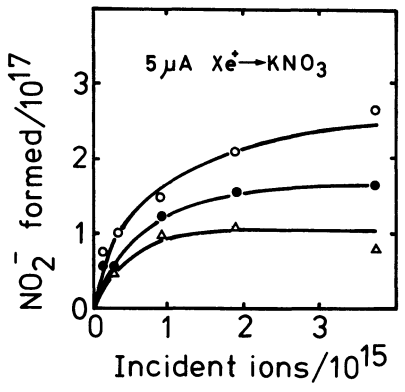

Fig. 3. Nitrite ion formation in potassium nitrate as a function of incident Xe^+ ions. Ion energy: (△) 50 keV, (●) 80 keV, and (○) 100 keV; Ion beam intensity: 6.25×10^{13} ions $cm^{-2}s^{-1}$.

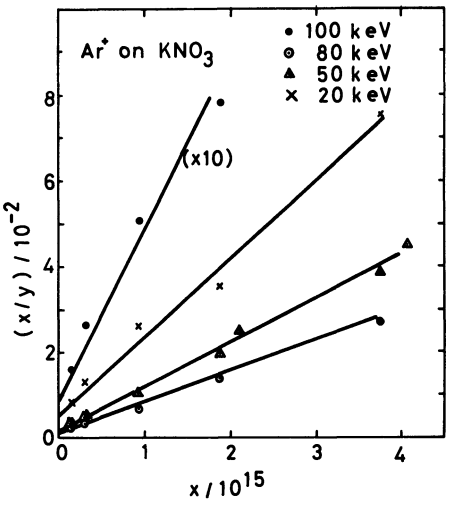

Fig. 4. Plots of x/y vs. x for 20 (×), 50 (△), 80 (⊙), and 100 (●) keV Ar^+ ions, where x and y are the number of incident ions and nitrite ions formed, respectively.

region which would be obtained at high doses. If we represent these relation as $y=ax$ and $y=b$, respectively, where y is the amount (=number) of nitrite ion and x is the dose (=number) with a and b being constants, we may obtain an expression:

$$\frac{x}{y}=\frac{1}{a}+\frac{1}{b}\cdot x. \tag{2}$$

The experimental points in Figs. 1—3 were replotted according to Eq. 2 (See Fig. 4, as an example) to obtain values of a and b for each yield-dose curve. Thus, an initial rate of NO_2^- formation, $Y=(dy/dx)_{x=0}$, and a "saturation yield," $(y)_{x=\infty}$, were calculated respectively from the values of a and b above obtained for incident He^+, Ar^+, and Xe^+ ions at an energy of T. The results are included in Fig. 5 and in Table 1, respectively.

The "saturation yields" shown in Table 1 probably represent a steady state between decomposition of NO_3^- to give NO_2^- (Reaction 1) and disappearence of NO_2^- either via a reverse reaction (Reaction 3) or via a further decomposition by incoming ions (Reaction 4):†

$$NO_2^- + 1/2O_2(O, O^+, O^-, O_2^-, \text{or } O_3) \longrightarrow NO_3^-, \tag{3}$$

$$NO_2^- \longrightarrow NO^- + O \text{ (or } NO+O^-). \tag{4}$$

Oxygen-containing species in Reaction 3 may diffuse away from the reaction zone; This prevents the reformation reaction of nitrate ion. Thus, analyses of the "saturation yield" seem very complex; we will hereafter strict our discussion on the initial rate of NO_2^- formation.

Calculation of the Stopping Power. The total stopping power, S_t, can be divided into two parts: $S_t=S_e+S_n$ where S_e and S_n are the electronic and nuclear

†In 1.4 keV electron-beam irradiation, there is no indication for futrher decomposition of the nitrite ion formed (Ref. 12).

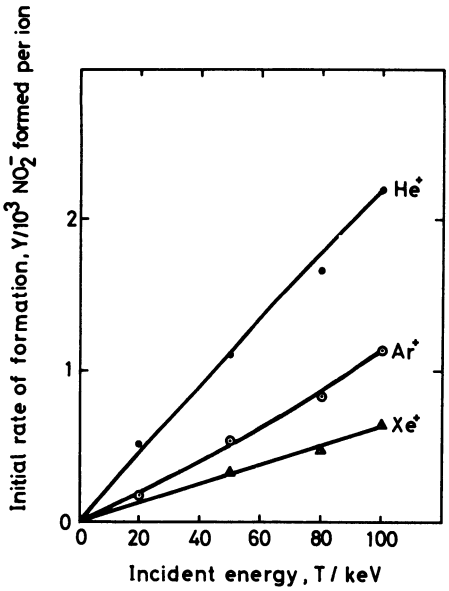

Fig. 5. The initial rate of formation of NO_2^-, $Y=(dy/dx)_{x=0}$, as a function of the incident ion energy, T, for He^+, Ar^+, and Xe^+ ions bombarding potassium nitrate.

Table 1. Saturation Yield (=b)/10^{17} NO_2^- for He^+, Ar^+, and Xe^+ Ions Incident on Potassium Nitrate at Various Energies

Ion energy/keV	20	50	80	100
He^+	2.1	3.7	4.3	5.5
Ar^+	0.56	0.96	1.45	4.0
Xe^+	—	1.46	1.9	3.0

stopping powers, respectively, as discussed in the introduction of this paper.

The electronic stopping power for a particle moving at the velocity v was calculated according to the theory of Lindhard, Scharff, and Schiøtt:[13,15]

$$S_e = 8\pi e^2 N a_0 Z_1^{7/6} Z_2 (Z_1^{2/3}+Z_2^{2/3})^{-3/2} v/v_0 \quad (5)$$

where a_0 is the Bohr radius of the hydrogen atom; v_0 is the Bohr velocity; Z_1 and Z_2 are the atomic number of the projectile and the target, respectively; N is the atom density of the target material.

The nuclear stopping power was calculated using[14,15]

$$S_n = s_n(8.462 Z_1 Z_2 M_1)/[(M_1+M_2)(Z_1^{2/3}+Z_2^{2/3})^{1/2}] \quad (6)$$

and

$$s_n = 0.5 \ln(1+\varepsilon)/(\varepsilon + 0.107^{0.375}) \quad (7)$$

Here, ε is the reduced energy of the ion and is defined as:

$$\varepsilon = 32.53 M_2 E/[Z_1 Z_2 (M_1+M_2)(Z_1^{2/3}+Z_2^{2/3})^{1/2}], \quad (8)$$

where the ion energy, E, is in keV; M_1 and M_2 are the ion and target masses in amu, respectively.

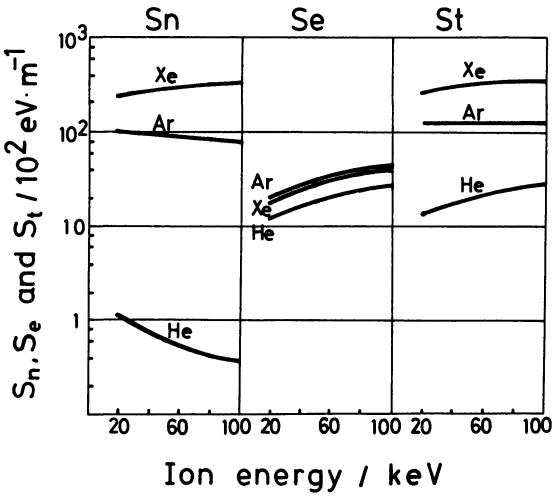

Fig. 6. The stopping powers of potassium nitrate (KNO_3: 10^{23} m^{-3}) for He^+, Ar^+, and Xe^+ ions in the energy range from 20 to 100 keV.
S_n: Nuclear stopping, S_e: Electronic stopping, S_t: Total stopping, $S_t=S_n+S_e$.

For the stopping power of compounds, e.g., KNO_3, the stopping powers of the constitutional element (i.e., K, N, and O) were weighted by their relative abundance; this is called Bragg's Rule. The results of the calculation are shown in Fig. 6, where the electronic, nuclear and total stopping powers in eV m^{-1} of potassium nitrate ($N=10^{23}$ m^{-3}) for He^+, Ar^+, and Xe^+ ions in the energy range 20—100 keV are plotted. We notice from Fig. 6 that He^+ ion in the energy range 20—100 keV dissipates most of their energy into electronic excitations, while Xe^+ ion in the same energy range into atomic displacement collisions.

Determining the Cross Sections for the Reaction Induced by Energetic Ions. The cross section for reaction of an energetic particle with a molecule in the solid is a function of the kinetic energy of the particle. The initial rate of NO_2^- formation, $Y=(dy/dx)_{x=0}$, for the incident energy at T_0, that is the number of the product formed per incident ion, is expressed as follows:

$$Y = N\int_0^{T_0} Q(T)\, ds \quad (9)$$

Here, N is the number density of KNO_3 in the medium, $Q(T)$ is the cross section that the product, NO_2^-, will be formed in a collision with the particle of the kinetic energy T, and ds is the distance traversed by the particle while in the energy range between $T+dT$ and T. In the continuous slowing-down approximation,[18] ds may be replaced by $dT/S(T)$, $S(T)$ being the total stopping power:

$$Y = N\int_0^{T_0} \frac{Q(T)}{S(T)}\, dT. \quad (10)$$

or

$$\frac{S(T)}{N}\frac{dY}{dT} = Q(T). \quad (11)$$

We assume here that the product yield from reaction of the recoil atoms or secondary electrons is negligibly small since their kinetic energy is no more sufficient in the majority of the case to initiate further chemical reactions. The cross sections, $Q(T)$, for producing NO_2^- from KNO_3 may be deduced from the slope of the Y-T curves of Fig. 5 and the total stopping-power values presented in Fig. 6 with the aid of Eq. 11. The results are included in Fig. 7; The cross sections for He^+, Ar^+, and Xe^+ ions at 100 keV are 5.7×10^{-20} m^2, 12.6×10^{-20} m^2, and 22.0×10^{-20} m^2, respectively, and they slightly depend on the ion energy T. These values are comparable to the cross sections estimated from the known atomic radius of He, Ar, and Xe, respectively.

Chemical Effectiveness of the Electronic and Nuclear Energy Losses in the Decomposition of Potassium Nitrate. Consider that an ion of the energy T travels a unit distance in the solid (KNO_3). From Eq. 2, the number of the product per unit path length of the ion of the energy at T is $N\,Q(T)$ where N is the number density of the target molecule. The energy expended in this reaction is provided from the energy deposited to this zone (=the unit path length) from the traversing ion, i.e., the total stopping power, $S_t=S_e+S_n$. If we designate the effectiveness of the energy contributed from S_e and S_n for the chemical reaction as f_e and f_n, respectively, the fraction of the deposited energy which is utilized to nitrite production, $N\,Q(T)$, is $f_eS_e+f_nS_n$. Thus, one may expect a linear relationship holds between $Q(T)$ and the value of $(f_eS_e+f_nS_n)/(f_e+f_n)$ or $(S_e+pS_n)/(1+p)$ where p represent f_n/f_f. In Fig. 8 are plotted the value of $Q(T)$ (shown in Fig. 7) as a function of $(S_e+pS_n)N^{-1}(1+p)^{-1}$ with p as a parameter. It is clearly demonstrated that an expected linear relationship holds when p is around 0.2. This suggests that, in the decomposition of KNO_3 due to the transmitted energy from the incident ion, an electronic energy is about five times more effective than a nuclear energy.

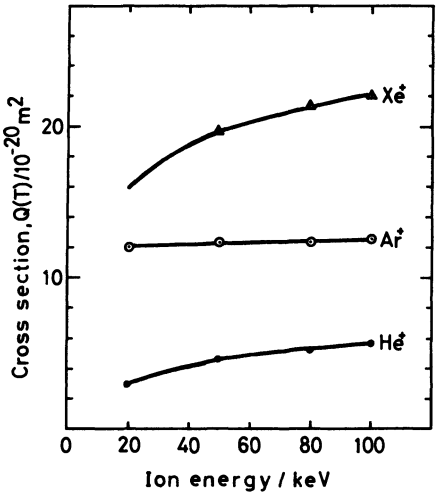

Fig. 7. Cross sections, $Q(T)$, for producing NO_2^- from KNO_3 for He^+, Ar^+, and Xe^+ ions in the energy range from 20 to 100 keV.

Mechanism of the Reaction. Mechanism of decomposition of the radiolyzed nitrates have been studied in many works.[5-11] An important role of atomic oxygen as an intermediate has repeatedly been emphasized (Reaction 1).[7-9]

Elastic "nuclear" collisions may lead to atomic displacements in potassium nitrate. However,the energy transmitted to potassium ions is most probably dissipated as heat; the collision with NO_3^- does not necessarily lead to breaking of the N-O bond. The momentum large enough to break the bond must be effectively trasferred to an O atom (the dissociation energy of the N-O bond is reported to be 3.9 eV[19]). Threshold energies for displacement of O-atoms from the oxide lattices, i.e. ZnO and MgO, are reported to be around 60 to 90 eV.[20] Though, a corresponding energy for KNO_3 has not yet been reported, it is very likely to exceed greatly the dissociation energy of the N-O bond. Thus, it is not surprising to notice that only a small portion of the deposited energy is converted to chemical energy and the remaining energy is degraded to thermal energy.

On the other hand, inelastic collisions may pro-

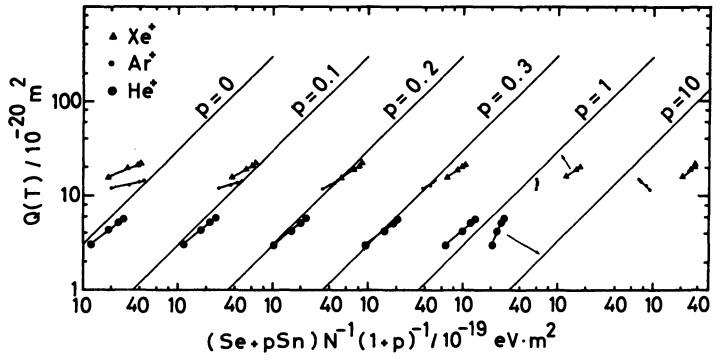

Fig. 8. Test of the linear relationship between $Q(T)$ and $(S_e+pS_n)N^{-1}(1+p)^{-1}$ with p as a parameter; Data taken from Figs. 6 and 7.

duce electronic excited states of the NO_3^- ion. A weak ($\pi^* \leftarrow n$) transition at about 4.1 eV and an allowed ($\pi^* \leftarrow \pi$) transition at about 6.2 eV are well-known.[21,22] These transitions may not lead to the N-O bond breaking, however, since in these transitions an electron is removed from an orbital which is not strongly bonding in nature. An oxygen atom, if it generates without sufficient kinetic energy, will not necessarily escape the parent NO_3^- group owing to some kind of a "cage effect."[10] Excitation of an electron from a bonding (=sp^2 hybrid) orbital is much more likely responsible for the bond dissociation. Excitations of an N- or O-core orbital followed by Auger processes[23] may be even more effective for the bond breaking. A dissociated O-atom may react with other NO_3^- ions,[7]

$$NO_3^- + O \longrightarrow NO_2^- + O_2 \quad (12)$$

or it may react with the NO_2^- ions produced (see Reaction 3):

$$NO_2^- + O \longrightarrow NO_3^-. \quad (13)$$

Reactions 12 and 13 have been studied in aqueous solutions and their rate constants relative to that for O_2 were reported to be 5.6 and 37, respectively.[24]

In both cases, i.e. elastic and inelastic collisions, an actual mechanism is probably more complex than above mentionned, possibly involving reactions of several ionic and free radical species. The cross sections which we have derived for the first time in this paper are for an overall reaction to give nitrite ions. Since the occurrence of the many thermal reactions are the same for the both cases, one may possibly state that an inelastic (=electronic) excitation is five times more efficient than an elastic (=atomic displacement) collision for the dissociation of the N-O bond in the solid potassium nitrate.

References

1) Part II: K. Furukawa and S. Ohno, *Bull. Chem. Soc. Jpn.*, **58**, 1831 (1985).

2) J. Kistemaker, F. J. De Heer, J. Sanders, and C. Snoek, "Radiation Research," ed by G. Silini, North-Holland, Amsterdam (1967), p. 68.

3) G. Dearnaley, J. H. Freeman, R. S. Nelson, and J. Stephen, "Ion Implantation," North-Holland, Amsterdam (1973).

4) O. Puglisi, G. Marletta, A. Torrisi, G. Foti, and L. Torrisi, *Radiat. Eff.*, **65**, 11 (1982).

5) J. Cunningham, *J. Phys. Chem.*, **65**, 628 (1961); *ibid.*, **70**, 30 (1966).

6) T. H. Chen and E. R. Johnson, *J. Phys. Chem.*, **66**, 755, 2249 (1962).

7) C. J. Hochanadel, *Radiat. Res.*, **16**, 286 (1962).

8) H. B. Pogge and F. T. Jones, *J. Phys. Chem.*, **74**, 1700 (1970).

9) J. Kalecinski, *Int. J. Radiat. Phys. Chem.*, **4**, 171, 181 (1972).

10) E. Chandunni and S. M. K. Nair, *Radiat. Eff. Lett.*, **58**, 5 (1981).

11) S. R. Logan and W. J. Moore, *J. Phys. Chem.*, **67**, 1042 (1963).

12) T. Sasaki, R. S. Williams, J. S. Wong, and D. A. Shirley, *J. Chem. Phys.*, **68**, 2718 (1978).

13) J. Lindhard and M. Scharff, *Phys. Rev.*, **124**, 128 (1961).

14) J. Lindhard, M. Scharff, and H, E. Schiøtt, *Mat. Fys. Medd. Dan. Vid. Selsk.*, **33**, No. 14 (1963).

15) J. F. Ziegler, "The Stopping and Ranges of Ions in Matter," Pergamon Press, New York (1980), Vol. 5.

16) K. Furukawa and S. Ohno, "100 kV-Ion Accelerator for Study of Chemical Reactions," JAERI-M 85-110 (1985).

17) F. D. Snell and C. T. Snell, "Colorimetric Methods of Analysis," Vol. 2, D. Van Nostrand, New York (1955), p. 802.

18) L. V. Spencer and U. Fano, *Phys. Rev.*, **93**, 1172 (1954).

19) Calculated using the constants of heat of formation: "CRC Handbook of Chemistry and Physics," ed by R. C. Weast, CRC Press, Florida (1985), p. D-50.

20) G. P. Pells, *Radiat. Eff.*, **64**, 71 (1982).

21) a) R. F. Barrow and A. J. Merer, Supplement to Mellor's Comprehensive Treatise on Inorganic and Theoretical Chemistry, ed by A. A. Eldridge et al., Longsmans (1967), Vol. VIII, Supplement II, p. 479; b) "Kagaku Benran," 3rd ed., ed by Chemical Society of Japan, II-595 (1985).

22) E. V. Sayre, *J. Chem. Phys.*, **31**, 73 (1959).

23) M. L. Knotek and P. J. Feibelman, *Surface Sci.*, **90**, 78 (1979); G. Stöcklin, "Radiation Research," ed by S. Okada et al., Jpn. Assoc. Radiat. Res, Tokyo (1979), p. 382.

24) O. Amichai and O. Tereinin, *Chem. Phys, Lett,*, **3**, 611 (1969).

Benzo-15-crown-5 Linked Spirobenzopyran. I. Photocontrol of Cation-Binding Ability and Photoinduced Membrane Potential Changes

Hiroshi SASAKI, Akihiko UENO, Jun-ichi ANZAI, and Tetsuo OSA*
Pharmaceutical Institute, Tohoku University, Aobayama, Sendai 980
(Received December 26, 1985)

Benzocrown ether-linked spirobenzopyran (**1**) and its analogue (**2**) which has no crown ring were synthesized. The binding abilities of **1** for alkali metal cations (Na^+, K^+, Rb^+, Cs^+) were found to change by UV light irradiation, while **2** did not bind these cations before and after UV light irradiation. The plasticized poly(vinyl chloride) (PVC) membrane entrapping **1** or **2** showed photoinduced potential changes reversibly by UV and visible light irradiation. In the membranes of both **1** and **2** showed normal photochromism of spirobenzopyran. In the case of **1**, the magnitude of the photoinduced potential change depended upon kind and concentration of alkali metal cations. However, the magnitude of photoinduced potential change of the membrane entrapping **2** was hardly affected by kind and concentration of alkali metal cations. The results are explained in terms of cooperative action of both crown ether and spiropyran.

Spirobenzopyran derivatives are well known photoresponsive organic compounds which can be reversibly isomerized by UV and visible light irradiation. This character was utilized to regulate polymer comformation,[1] viscosity of polymer solution,[2] enzyme activity,[3] membrane potential,[4-8] and ion permeation using liquid membrane,[9] etc. Crown ether derivatives have cation binding ability, and are widely studied not only in labolatory but also in industry. We have already reported the ion permeability[10,11] and the membrane potential change[12-17] which occurs reversibly upon photoirradiation across the poly(vinyl chloride) (PVC) membrane containing azobenzene-modified crown ethers.

In the present study, we synthesized spirobenzopyran derivatives bearing benzo-15-crown-5 and phenyl units (**1** and **2**, respectively), and examined photoresponsive cation binding ability of them by liquid–liquid extraction method, and by measuring membrane potentials across the PVC membranes entrapping **1** (PVC(**1**) membrane) and **2** (PVC(**2**) membrane).

From the different point of view, **1** is regarded as a photoresponsive crown ether. Photoisomerism of azobenzene has been used in many photoresponsive crown ethers.[10-22] The present system works based on the different isomerism performed by spiropyran, so **1** belongs to a new family of functional molecules showing photoresponsiveness.

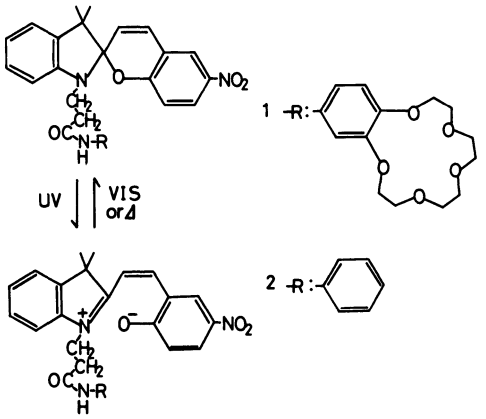

Experimental

Materials. Poly(vinyl chloride)(PVC) (polymerization degree of 1100) was purchased from Wako Pure Chemical Industry Ltd. and used without further purification. Dibutyl phthalate (DBP), tetrahydrofuran (THF), and alkali metal chlorides (NaCl, KCl, RbCl, and CsCl) were of extra pure reagent grade. Alkali metal picrates were prepared according to the Fuoss method.[23] Double-distilled water was used throughout.

3′,3′-Dimethyl-6-nitro-1′-[2-[3,4-(1,4,7,10,13-pentaoxatridecane-1,13-diyl)phenylcarbamoyl]ethyl]spiro[2*H*-1-benzopyran-2,2′-indoline] (1). 1′-(2-Carboxyethyl)-3′,3′-dimethyl-6-nitrospiro[2*H*-1-benzopyran-2,2′-indoline][24] (1 g, 2.62 mmol) and 4′-aminobenzo-15-crown-5[25] (0.75 g, 2.65 mmol) were dissoloved in 50 ml of the mixed solvent of chloroform and DMF (9:1 in volume). After dicyclohexylcarbodiimide (DCC) (0.54 g, 2.62 mmol) was added to the mixture at −5 °C, the mixture was stirred for 24 h, and then the formed *N,N′*-dicyclohexylurea was filtered off. The filtrate was subjected to silica-gel column chromatography (dichloromethane:EtOH=15:1 in volume). The obtained crude product was recrystallized from methanol to give 0.64 g (38%) of **1**. Mp 114 °C. Found: C, 64,49; H, 6.22; N, 6.47%. Calcd for $C_{35}H_{39}N_3O_9$: C, 65.10; H, 6.09; N, 6.51%. ^{1}H NMR ($CDCl_3$) δ=1.1, 1.25 (6H, s, CH_3 of pirrole ring), 1.5—1.9 (2H, broad, $-NCH_2-$), 2.4—2.8 (2H, m, $-CH_2-CO-$), 3.3—4.2 (16H, m, $-CH_2-$ crown ether), 5.75 (1H, d, J=16 Hz C<u>H</u>=CH-nitrobenzene), 6.3—7.2 (9H, m, aromatic H of 3*H*-indole and benzocrown, -NH-, and CH=C<u>H</u>-nitrobenzene), 7.7—8.1 (3H, m, aromatic of nitrobenzene). IR (KBr) $\delta_{C=O}$ 1655 cm^{-1} (amide I), ν_{N-H} 1610 cm^{-1} (amide II).

3′,3′-Dimethyl-6-nitro-1′-[2-(phenylcarbamoyl)ethyl]spiro[2*H*-1-benzopyran-2,2′-indoline] (2). Compound **2** was synthesized from 1′-(2-carboxyethyl)-3′,3′-dimethyl-6-nitrospiro[2*H*-1-benzopyran-2,2′-indoline] (0.5 g, 1.31 mmol) and aniline (0.12 g, 1.29 mmol) using a method analogous to that used for **1**. Purification of **2** was performed by recrystallization from isobutyl alcohol to give 0.40 g (68%) of **2**. Mp 120 °C. Found: C, 70.85; H, 5.93; N, 9.10%. Calcd for $C_{27}H_{25}N_3O_4$: C, 71.19; H, 5.53; N, 9.22%. ^{1}H NMR ($CDCl_3$) δ=1.1, 1.25 (6H, s, CH_3 of pirrole ring), 1.5—1.9 (2H, broad, NCH_2-), 2.4—2.9 (2H, m, $-CH_2-CO-$), 5.75 (1H, d, J=16 Hz -C<u>H</u>=CH-nitrobenzene), 6.5—7.3 (10H, m, aromatic H of 3*H*-indole and aniline, -NH-, and -CH=C<u>H</u>-nitrobenzene), 7.7—8.1

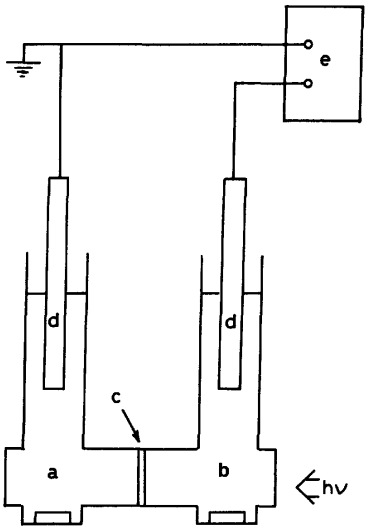

Fig. 1. Schematic sketch of the cell for membrane potential measurements.
a and b: Electrolyte solution, c: Membrane, d: Double junction type S.C.E.s, e: Potentiometer.

(3H, m, aromatic of nitrobenzene). IR (KBr) $\delta_{C=O}$ 1650 cm^{-1} (amide I), ν_{N-H} 1605 cm^{-1} (amide II).

Benzo-15-crown-5(**3**) was synthesised according to the Pedersen's method.[26]

Preparation of Membranes. (PVC(**1**)) or (PVC(**2**)) membrane was prepared by pouring the mixture of PVC (235 mg), DBP (0.54 ml), **1** (24.8 mg) or **2** (17.7 mg), and THF (20 ml) onto a flat Petri dish (9.2 cm diameter) and allowing the solvent to evaporate. The prepared membranes have a thickness of ca. 0.1 mm, and their mechanical strength was satisfactory for the spectroscopic and electrochemical measurements. The membrane entrapping both **2** and **3** was prepared in the same manner as that of PVC(**2**) membrane, except for addition of **3** (10.5 mg).

Absorption Spectra. Photoisomerization of **1** and **2**, which proceeds in solution or in the membranes, was monitored by measuring the absorption spectra.

Liquid–Liquid Extraction. At 25 °C, a 2 ml aqueous solution containing alkali metal picrate (1×10^{-5} mol dm^{-3}) and alkali metal chloride (1 mol dm^{-3}) was vigorously shaken in quartz UV cell with the equal volume of dichloromethane solution containing **1**, **2**, or **3**. After sufficient agitation, the picrate concentration in the aqueous layer was determined by the absorbance change at 354 nm. To obtain the data after UV irradiation, the liquid–liquid extraction was carried out under UV light.

Membrane Potential Measurements. All measurements were carried out at 25 °C with a U-shaped glass cell illustrated in Fig. 1. Double junction type of saturated calomel electrodes were employed. Both solutions were stirred vigorously. The effective membrane area of the cell was 2.54 cm^2. The composition of the electrochemical cell for the membrane potential measurements was as follows; Hg_2Cl_2 (s), Hg | KCl (sat.) | 0.1 mol dm^{-3} $(CH_3)_4NCl$ | electrolyte solution (c) | membrane | electrolyte solution (c) | 0.1 mol dm^{-3} $(CH_3)_4NCl$ | KCl (sat.) | Hg_2Cl_2 (s), Hg. The electrolyte solution of the left side was earthed. Photoirradiation was performed with 500 W xenon lamp (Ushio Electric Inc.) using cut off filters Toshiba UV D-35 and Y-45 for isolating UV ($320\,nm<\lambda<400\,nm$) and visible ($450\,nm<\lambda$) light, respectively. Photoirradiation was done from the right side.

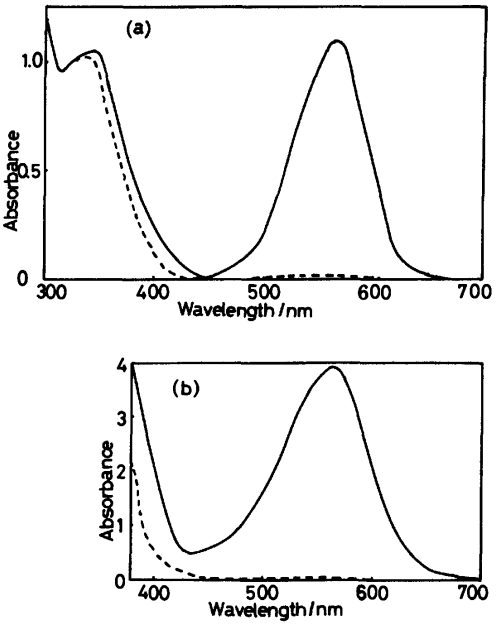

Fig. 2. (a) Absorption spectra of **1** in dichloromethane solution (1×10^{-4} mol dm^{-3}) before (---) and after (——) UV irradiation. (b) Absorption spectra of **1** in PVC membrane before (---) and after (——) UV irradiation.

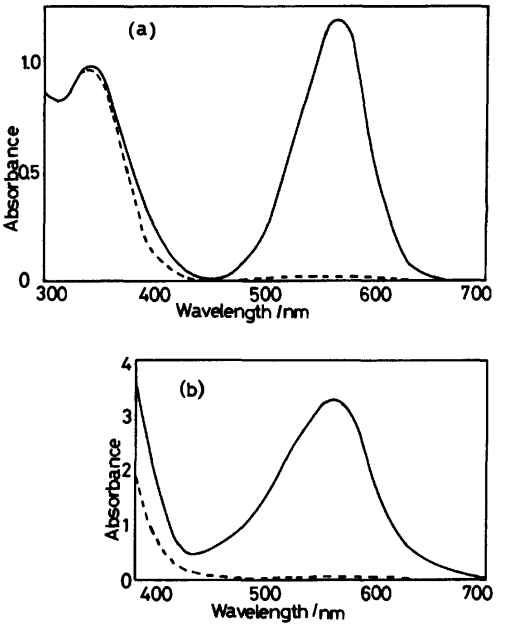

Fig. 3. (a) Absorption spectra of **2** in dichloromethane solution (1×10^{-4} mol dm^{-3}) before (---) and after (——) UV irradiation. (b) Absorption spectra of **2** in PVC membrane before (---) and after (——) UV irradiation.

Results and Discussion

Photochemical and Thermal Isomerization of 1 and

2. The absorption spectra of **1** and **2** in dichloromethane are shown in Fig. 2 (a) and Fig. 3 (a), respectively. In dichloromethane, the closed form of **1** showed an absorption band at 340 nm (ε=10200) and the solution was colorless. After UV irradiation (ca. 2 min), the absorption band at 340 nm was shifted to 345 nm (ε=10500) and a new absorption band was observed at 567 nm (ε=11000), the color of the solution being purple. This spectral change indicates that **1** was isomerized from closed form (closed-**1**) to opened form (opened-**1**).[4-7] By visible light irradiation of the solution of opened-**1**, the original spectral pattern of closed-**1** was recovered quickly (ca. 20 s). Opened-**1** was also isomerized thermally with the half life of ca. 80 s in the dark (at 25 °C). The compound **2** showed similar spectral changes to those of **1**. As shown by the absorption changes from 340 nm (ε=9700) of closed **1** to 345 nm (ε=10000) and 567 nm (ε=12000) of opened **2**. The photoinduced absorption changes of **2** in dichloromethane also occurred reversibly by alternate UV and visible light irradiation. The half life of opened **2** was ca. 80 s in the dark (at 25 °C).

The photoisomerization of **1** and **2** occurred also in PVC membranes. The absorption spectra of PVC(**1**) membrane and PVC(**2**) membrane were shown in Fig. 2 (b) and Fig. 3 (b), respectively. These membranes were soaked in 10 mmol dm^{-3} NaCl solutions. The closed forms of **1** and **2** showed no absorption in the wavelength region between 480 and 700 nm, so the membranes were colorless. After UV irradiation, the membranes turned purple, and a new absorption band appeared at 560 nm for PVC(**1**) and at 557 nm for PVC(**2**) membrane, respectively. These changes of the absorption spectra mean clearly that isomerization of **1** and **2** from closed form to opened one was achieved in the membranes. By visible light irradiation of the UV irradiated membranes, the colorless membranes were again obtained. The spectral changes completed within ca. 30 s. Opened **1** and **2** in PVC membranes were also isomerized thermally, with the half lives of ca. 4 and 3 min in the dark, respectively. The UV induced absorption changes of PVC(**2** and **3**) membrane were similar to those of PVC(**2**) membrane with a slightly different half life of ca. 6 min.

Liquid–Liquid Extraction. The results of liquid–liquid extraction with **1**, **2**, and **3** were shown in Table 1. In the dark, **1** showed different binding abilities for alkali metal ions, the magnitude of binding ability lying in the order of $K^+ > Na^+ > Rb^+ > Cs^+$. In contrast, **2** showed no cation-binding ability. The binding ability of the compound **3** was in the order of $K^+ > Na^+ > Rb^+ > Cs^+$, which was the same as that of **1**. The cation-binding ability of **1** slightly diminished for all alkali metal cations by UV irradiation. The depressed cation-binding ability of opened **1** might be explained in terms of the electrorepulsive interaction between a positive charge of the nitrogen atom of the spiropyran part and the alkali metal cation trapped by benzo-15-crown-5 moiety in **1**.

Table 1. Effect of UV Irradiation on Liquid–Liquid Extraction

	Condition	Picrate extracted/%			
		Na^+	K^+	Rb^+	Cs^+
1	Dark	38	58	31	24
1	UV irradiated	35	52	28	18
2	Dark	0	0	0	0
2	UV irradiated	0	0	0	0
3		23	36	17	13

a) Organic phase (2 ml of dichloromethane): [**1**], [**2**], or [**3**]=1×10^{-4} mol dm^{-3}. Aqueous phase (2 ml of water): [Alkali metal picrate]=1×10^{-5} mol dm^{-3}, [Alkali metal chloride]=1 mol dm^{-3}.

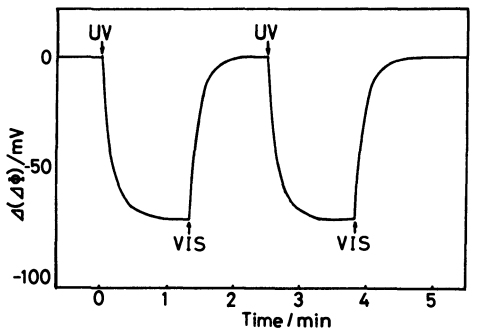

Fig. 4. Photoresponse of the membrane potential to alternate UV and VIS irradiation. PVC(**2**) membrane was used. Electrolyte was NaCl solution (1000 mmol dm^{-3}).

Photoinduced Potential Change. Figure 4 illustrates time response of the membrane potential change induced by alternate UV and visible light irradiation, which was obtained with the PVC(**2**) membrane. A negative shift of membrane potential was induced by UV irradiation. The membrane potential reached to a steady state under UV light within 30 s, and then returned to the initial potential by visible light irradiation within 30 s. It was reported in other membranes containing spirobenzopyran derivatives[4-8] that photoinduced potential changes occurred synchronously with photoisomerization between closed and opened forms. Since we also observed the purple-colorless change of the PVC(**2**) membrane associated with UV and visible light irradiation, the present photoinduced potential change should occur on the same basis. Table 2 shows the effects of the kind and concentration of alkali metal salts on the photoinduced potential change ($\Delta(\Delta\Phi)$) across the PVC(**2**) membrane. The $\Delta(\Delta\Phi)$ value was not dependent upon the kind of alkali metals except for Na^+, and was hardly affected by the alkali metal concentrations. Table 3 shows the photoinduced potential change $\Delta(\Delta\Phi)$ across the PVC(**1**) membrane. The $\Delta(\Delta\Phi)$ value remarkably depended upon both the kind and concentration of the alkali metals. With increasing concentration, the $\Delta(\Delta\Phi)$ value became less negative or more positive. The tendency for shifting toward more positive poten-

Table 2. Photoinduced Potential Changes, $\Delta(\Delta\Phi)$/mV, across PVC(2) Membrane

Electrolyte	Electrolyte concentration/mmol dm^{-3}		
	10	100	1000
NaCl	−78	−76	−71
KCl	−58	−59	−50
RbCl	−57	−59	−51
CsCl	−58	−56	−51

Photoirradiation was conducted from the compatment b side.

Table 3. Photoinduced Potential Changes, $\Delta(\Delta\Phi)$/mV, across PVC(1) Membrane

Electrolyte	Electrolyte concentration/mmol dm^{-3}		
	10	100	1000
NaCl	−33	−10	17
KCl	4	10	39
RbCl	2	3	19
CsCl	−21	−4	2

Photoirradiation was conducted from the compartment b side.

Table 4. Photoinduced Potential Changes, $\Delta(\Delta\Phi)$/mV, across PVC(2 and 3) Membrane

Electrolyte	Electrolyte concentration (mmol dm^{-3})		
	10	100	1000
NaCl	−74	−71	−61
KCl	−48	−44	−37
RbCl	−57	−53	−34
CsCl	−52	−39	−30

Photoirradiation was conducted from the compartment b side.

tial lay in the order of $K^+>Rb^+>Na^+>Cs^+$. In the case of PVC membrane entrapping azobenzene-linked (bis crown ethers),[3-8] which had stronger binding ability for alkali metal ions after UV irradiation, the $\Delta(\Delta\Phi)$ value was reported to be negatively shifted by photoinduced enhancement of cation-binding ability. The opposite shifts observed here therefore seem reasonable since cation-binding ability of **1** decreases by UV irradiation. Table 4 shows the photoinduced potential changes $\Delta(\Delta\Phi)$ across PVC(**2** and **3**) membrane. Although the extent was smaller than that for PVC(**1**) membrane, the $\Delta(\Delta\Phi)$ value was affected by both the kind and concentration of alkali metals, the absolute value of the negative potential change becoming smaller with increasing alkali metal concentration. This phenomenon may be due to the decreased contribution of the photoinduced charge density to total charge density on the membrane surfaces, which was caused by the amount of alkali metal cations trapped by crown ether **3**.

Conclusion

We have shown by liquid–liquid extraction that the cation selectivity of spirobenzopyran **1** changes by photoirradiation. When **1** was entrapped in PVC membrane, the membrane exhibited marked photoinduced membrane potential changes, which were dependent upon the alkali metal species. This kind of photoexcitable membranes will be useful for construction of new photosensors, with which alkali metal concentrations can be measured.

References

1) M. Irie, A. Menju, and K. Hayashi, *Macromolecules*, **12**, 1176 (1979).
2) A. Menju, K. Hayashi, and M. Irie, *Macromolecules*, **14**, 755 (1981).
3) I. Karube, Y. Nakamoto, and S. Suzuki, *Biochim. Biophys. Acta*, **445**, 774 (1976).
4) S. Kato, M. Aizawa, and S. Suzuki, *J. Membr. Sci.*, **1**, 289 (1976).
5) S. Kato, M. Aizawa, and S. Suzuki, *J. Membr. Sci.*, **2**, 39 (1977).
6) S. Kato, M. Aizawa, and S. Suzuki, *Kobunshi Ronbunshu*, **34**, 793 (1977).
7) M. Irie, A. Menju, and K. Hayashi, *Nippon Kagaku Kaishi*, **1984**, 227.
8) J. Anzai, A. Ueno, and T. Osa, *J. Chem. Soc., Chem. Commun.*, **1984**, 688.
9) T. Shimizu, and M. Yoshikawa, *J. Membr. Sci.*, **13**, 1 (1983).
10) J. Anzai, A. Ueno, H. Sasaki, K. Shimokawa, and T. Osa, *Makromol. Chem., Rapid Commun.*, **4**, 731 (1983).
11) J. Anzai, H. Sasaki, A. Ueno, K. Shimokawa, and T. Osa, *Nippon Kagaku Kaishi*, **1984**, 338.
12) J. Anzai, H. Sasaki, A. Ueno, and T. Osa, *J. Chem. Soc., Chem. Commun.*, **1983**, 1045.
13) J. Anzai, H. Sasaki, A. Ueno, and T. Osa, *Chem. Lett.*, **1984**, 1205.
14) J. Anzai, H. Sasaki, A. Ueno, and T. Osa, *MEMBRANE*, **9**, 277 (1984).
15) J. Anzai, H. Sasaki, A. Ueno, and T. Osa, *Bull. Chem. Soc. Jpn.*, **57**, 3331 (1984).
16) J. Anzai, H. Sasaki, A. Ueno, and T. Osa, *J. Chem. Soc., Perkin Trans. 2*, **1985**, 903.
17) H. Sasaki, J. Anzai, A. Ueno, and T. Osa, *Nippon Kagaku Kaishi*, **1985**, 1194.
18) S. Shinkai, T. Ogawa, T. Nakaji, Y. Kusano, and O. Manabe, *Tetrahedron Lett.*, **1979**, 4569.
19) S. Shinkai, T. Nakaji, T. Ogawa, K. Shigematsu, and O. Manabe, *J. Am. Chem. Soc.*, **103**, 111 (1981).
20) S. Shinkai, K. Shigematsu, Y. Kusano, and O. Manabe, *J. Chem. Soc., Perkin Trans. 1*, **1981**, 3279.
21) S. Shinkai, H. Kinda, and O. Manabe, *J. Am. Chem. Soc.*, **104**, 2933 (1982).
22) A. Kumano, O. Niwa, T. Kajiyama, M. Takayanagi, K. Kano, and S. Shinkai, *Chem. Lett.*, **1983**, 1327.
23) M. A. Coplan, and R. M. Fuoss, *J. Phys. Chem.*, **68**, 1177 (1964).
24) M. Aizawa, K. Namba, and S. Suzuki, *Arch. Biochem. Biophys.*, **180**, 41 (1977).
25) R. Ungaro, B. El Haj, and J. Smid, *J. Am. Chem. Soc.*, **98**, 5198 (1976).
26) C. J. Pedersen *J. Am. Chem. Soc.*, **89**, 7017 (1967).

 © 1986 The Chemical Society of Japan Bull. Chem. Soc. Jpn., 59, 1957—1966 (1986)

A High-Resolution Solid-State ^{23}Na NMR Study of Sodium Complexes with Solvents, Small Ligand Molecules, and Ionophores. ^{23}Na Chemical Shifts as Means for Identification and Characterization of Ion-Ion, Ion-Solvent, and Ion-Ligand Interactions

Ryoko TABETA, Misako AIDA, and Hazime SAITÔ*
Biophysics Division, National Cancer Center Research Institute, Tsukiji 5-Chome, Chuo-ku, Tokyo 104
(Received December 26, 1985)

We have recorded static and magic angle spinning (MAS) ^{23}Na NMR spectra of a variety of inorganic salts, solvent complexes, and complexes with small ligand molecules and ionophores in the solid state, in order to obtain the ^{23}Na chemical shifts of the ion-ion, ion-solvent, and ion-ligand interactions, respectively. In all cases, MAS resulted in considerable reduction of the linewidths. The observed ^{23}Na chemical shifts were corrected by subtracting the displacements by the quadrupole interaction when the quadrupole coupling constants cannot be ignored. We found that the range of the ^{23}Na chemical shifts found in the solid state is about 60 ppm and the ^{23}Na chemical shift of $NaBPh_4$ appears at the highermost region (−52 ppm). The ^{23}Na NMR chemical shifts of these complexes exhibited their characteristic peak positions, depending on variety of ligand molecules (H_2O, ether, or carbonyl) and Na-O interatomic distances but independent of the type of counterion. Finally, an attempt was made to relate the ^{23}Na chemical shifts to the magnitude of electron transfer from the ligand molecules to 3p orbital of Na^+ ion, by means of an ab initio molecular orbital method.

In recent years, coordination chemistry of alkali and alkaline earth metal ions has gained much interest in relation to understanding the vital role of these metal ions in biological systems and the manner of their specific interaction with naturally occurring ionophores or synthetic analogues such as crown ethers and cryptands.[1] As an excellent means of probing the behavior of the sodium ion in particular, high resolution ^{23}Na NMR spectroscopy has been extensively utilized to analyze the ion-ion, ion-solvent, and ion-ligand interactions in the solution state.[2-16] These ^{23}Na signals, however, cannot be observed separately but are seen as time-averaged single peaks due to rapid chemical exchange processes among several kinds of such short-lived species. Separate ^{23}Na NMR signals of free and complexed states were observed only when BPh_4 was used as a counterion stabilized as a solvent-separated ion pair[8] in solution or ligands of higher association constant such as cryptands were used.[10,12-16]

By contrast, it is expected that high-resolution ^{23}Na NMR studies in the solid state could provide unambiguous ^{23}Na chemical shifts of the individual species of the ion-ion, ion-solvent, and ion-ligand interactions, being free from interference due to chemical exchange processes as encountered in solution state. Undoubtedly, the collection of such data is invaluable because these parameters can be readily used as a diagnostic tool as well as reference data for the interpretation of solution ^{23}Na NMR studies. In addition, these data are very useful as viewed from the theoretical interpretation of the ^{23}Na chemical shifts in terms of electronic structures, because detailed molecular parameters are available from X ray diffraction studies. The displacement of the ^{23}Na chemical shifts was previously interpreted in terms of electron transfer from electron donors such as solvents to the 3p orbital of the Na^+ ion.[17] No detailed study, however, has been done as to the extent of such electron transfer to be compared with the experimental data.

For this purpose, it is known that magic angle spinning (MAS) can be effectively utilized for line-narrowing of the central $1/2 \leftrightarrow -1/2$ transition of quadrupolar nuclei with spin number of half-integer such as ^{23}Na in the solid state, if the line-splitting of the central line by the second-order quadrupole interaction can be neglected.[18] Otherwise, rapid sample spinning about an axis other than the magic angle is more favorable for line-narrowing.[19] In the present paper, we aimed to record ^{23}Na MAS NMR spectra of a number of inorganic salts,[20] solid solvent complexes, and complexes with small ligand molecules or ionophores, to obtain the ^{23}Na chemical shifts of the individual ion-ion, ion-solvent, and ion-ligand interactions, respectively. At the same time, static ^{23}Na NMR spectra were examined with the same samples to evaluate the quadrupole coupling constants, because the quadrupole interaction, if any, would cause the center of gravity in the ^{23}Na MAS NMR signals to shift upfield.[21]

Being consistent with our expectation, all samples studied here which possess octahedral or distorted octahedral arrangement of solvents or ligands gave single resonance lines because of negligible contribution of the quadrupole interaction, although correction of the ^{23}Na chemical shifts by the quadrupole interaction was necessary for crystals of inorganic salts such as rhombohedral, monoclinic and tetragonal structures. Interestingly, the range of the ^{23}Na chemical shifts in the solid state is about 60 ppm and the ^{23}Na NMR signal of $NaBPh_4$ is resonated at the highermost position (−52 ppm) which is very close to the data of the Na^- anion. In addition, the ^{23}Na chemical shifts of a variety of sodium complexes are varied significantly with type of ligand molecules (H_2O, ether or carbonyl group) and stereochemistry of these complexes including the Na-O distances as the most important parameter. Qualitatively, it appears

that the extent of electron transfer from the ligand molecules to Na^+ ion, as evaluated by an ab initio molecular orbital method with 6—31 G basis set, is in parallel with the displacement of ^{23}Na chemical shifts.

Experimental

Materials. Inorganic salts were of reagent grade and were used without further purification. The following sodium complexes were purchased from commercial sources: $Na_2SO_4 \cdot 10H_2O$ (Kanto Chemical Inc., Tokyo), sodium deoxyadenosine 5′-monophosphate hexahydrate (Na dAMP·$6H_2O$, Sigma Chemical Company, MI, USA), $Na_2HAsO_4 \cdot 7H_2O$, $Na(CH_3COO) \cdot 3H_2O$ (Wako Chemicals, Osaka), and trisodium nitrilotriacetate hydrate, sodium L-ascorbate and sodium D-isoascorbate hydrate (Tokyo Kasei Kogyo, Co. Ltd., Tokyo). These complexes were recrystallized from aqueous solution.

Solvent complexes of the Na ions with 1,4-dioxane,[22] methanol,[23] acetone,[24] and *N*,*N*-dimethylformamide[25] were prepared by the procedure described in the literatures. The sodium complexes with 1,4-dioxane are efflorescent and easily turn into anhydrous powder. By contrast, the complexes with methanol, acetone or *N*,*N*-dimethylformamide were decomposed very rapidly in air because of lower melting points (25—27°). Accordingly, several kinds of preparations were used to achieve unambiguous assignment of ^{23}Na signals whose relative peak-intensities were varied from sample to sample. For example, the following three kinds of samples were prepared for the complexes of $NaClO_4$ with 1,4-dioxane. $NaClO_4$ dissolved in small amount of water was mixed with 1,4-dioxane (mole ratio 1:3) and allowed to evaporate in air. After separation from solution, sample 3 was obtained by placing the colorless crystals thus obtained in vacuo for 3 h. Plate-shaped crystals were obtained by heating the above-mentioned crystals up to 60° and were allowed to evaporate in air. Sample 1 was obtained by blotting the crystals with a filter paper. Sample 2 was obtained by placing the sample in vacuo for 3 h.

(Ethylene glycol)(1-phenyl-1,3-butanedionato)sodium was obtained from ethanol solution containing sodium 1-phenyl-1,3-butanedionate and 4% ethylene glycol and was crystallized from toluene solution.[26] Glycine-sodium iodide-water (2/1/1) was obtained as crystal from aqueous solution containing glycine and NaI (mole ratio 2:1).[27] In a similar manner, triethanolamine-sodium iodide (1/1) was crystallized from methanol-1-butanol solution containing equimolecular amount of individual components.[28] A solution of acetic acid and half an equivalent of sodium hydroxide in water was allowed to evaporate to give crystals of $NaH(CH_3COO)_2$.[29]

Sodium complexes of valinomycin (Sigma Chemical Company, MI, U.S.A), nonactin (Boehringer-Manheim GmbH, Germany) and tetranactin (Chugai Pharmaceutical Co. Ltd., Tokyo) were obtained from ethyl acetate solution containing 10% excess NaSCN.[30] Complex formation was confirmed by the characteristic change of the ^{13}C chemical shifts in the solid state as determined by cross polarization-magic angle spinning (CP-MAS) NMR.[30,31] Monensin (Na salt) and lasalocid (Na salt) were purchased from Sigma Chemical Company, MI, U.S.A. These compounds were recrystallized from diethyl ether-petroleum ether (1:1) containing small amount of acetone or methanol.

Cryptands [2.2.2], [2.2.1], and [2.2] were purchased from Merck Chemical Company, Germany. 18-Crown-6 was purchased from Aldrich Chemical Company, WI, U.S.A. Sodium complexes with these ligands were prepared by dissolving in methanol, which was allowed to evaporate in air.[32] Complex formation was checked by examination of the ^{13}C CP-MAS NMR spectra.[32]

^{23}Na NMR Spectra. ^{23}Na MAS NMR spectra were recorded on a Bruker CXP-300 spectrometer operating at 79.35 MHz with a Z32DR MAS probe. Solid samples were contained in an Andrew-Beams type rotor machined from Delrin and spun as fast as 2—3 kHz by compressed air. Spectra were accumulated usually less than 200 times. Spectral width was 30 kHz and data points were 4 K. 90° pulse and repetition time were 6 μs and 2 s, respectively. ^{23}Na chemical shifts were referred to the signal of 1 M NaCl in aqueous solution (1 M=1 mol dm^{-3}).

Static ^{23}Na NMR spectra were recorded on the same spectrometer with a Z32vHP high power probe. The spectral width used was up to 500 kHz with 2 K data points. The quadrupole coupling constant was evaluated from the displacement of the satellite lines caused by the first-order (f.o.) quadrupole interaction or from the second-order (s.o.) splitting of the central line.[33]

Ab Initio Molecular Orbital Calculation. We calculated the electronic energies and electron densities of sodium complexes either with solvent molecules or ionophores as a function of the Na-O distance (R), by an ab initio molecular orbital method utilizing the IMSPACK program system[34] with a 6—31 G basis set.[35] As a geometry of complex,[36] we postulated an octahedral arrangment of six H_2O or six $H_2C{=}O$ molecules around the central Na^+ ion, representing also an ether (OH) or a carbonyl moiety of these ligand molecules, respectively. For comparison, we also calculated the electronic structure of some sodium complexes containing a single H_2O molecule having various orientations with respect to the sodium ion.

Results

Inorganic Salts. Figure 1 illustrates a typical example of the static ^{23}Na NMR spectrum of $NaClO_3$ in the solid state. The quadrupole coupling constant (e^2qQ/h) 785±2 kHz was readily evaluated either by the

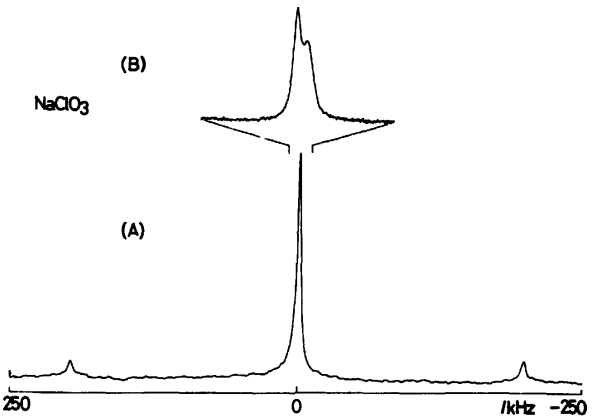

Fig. 1. 79.35 MHz static ^{23}Na NMR spectra of $NaClO_3$ in the solid state. (A) first-order split peaks (197 kHz from the central peak), spectral width 500 kHz. (B) second-order split central peaks (1.01 kHz), spectral width 20 kHz.

Table 1. ^{23}Na Chemical Shifts of Some Inorganic Salts in the Solid State (ppm from 1 M NaCl Soln)

	Static		MAS (ppm)			
	Type of spectrum[a]	$\frac{e^2qQ}{h}$ (kHz)	Obsd chemical shifts	Correction of chemical shifts by quadrupole interaction[b]	Corrected chemical shifts	Crystal structure
NaF	s	0	7.9±6	0	7.9±6	Cubic
NaCl	s	0	7.9±0.3	0	7.9±0.3	Cubic
NaBr	s	0	6.0±0.3	0	6.0±0.3	Cubic
NaHCOO	s	0	−0.2±0.7	0	−0.2±0.7	
NaB[C_6H_4F(p-)]	s	0	−0.5±0.3	0	−0.5±0.3	
$NaBiO_3$	s	0	−0.8±1.3	0	−0.8±1.3	
NaSCN	s	0	−2.1±0.6	0	−2.1±0.6	
NaI	s	0	−2.7±0.4	0	−2.7±0.4	Cubic
NaN_3	f.o.	286±2	−3.5±0.3	0.3	−3.2±0.3	Rhombohedral
$NaHCO_3$	s.o.	700±10	−5.4±0.6	1.9±0.1	−3.5±0.7	Monoclinic
$NaClO_3$	f.o./s.o.	785±2	−6.5±0.6	2.4	−4.1±0.6	
$NaNO_3$	f.o.	332±2	−7.3±0.2	0.4	−6.9±0.2	Rhombohedral
$NaBH_4$	s	0	−8.5±1.7	0	−8.5±1.7	Cubic
$NaIO_4$	f.o.	47±2	−12.5±0.4	0.02	−12.5±0.4	Tetragonal
$NaClO_4$	o	0	−20.0±0.5	0	−20.0±0.5	Tetragonal
$NaBF_4$	s.o.	1200±100	−24.8±1.2	5.7±1	−19.1±2.5	Tetragonal
$NaBPh_4$	s	0	−51.7±1.6	0	−51.7±1.6	

a) s stands for single line; f.o. stands for the first-order split signal; s.o. stands for the second-order split central peak.
b) Estimated errors smaller than 0.1 ppm are not shown.

first-order or second-order quadrupole-split peaks.[33] The quadrupole coupling constants thus obtained are summarized in Table 1, although type of spectrum designated by s gave single lines without quadrupole interaction. In all cases, it was found that these static ^{23}Na NMR spectra were analyzed as being due to a symmetrical field gradient (η=0). In fact, the asymmetry parameter of $NaNO_3$ was reported to be exactly zero[37] and that of $NaBF_4$ was assumed to be negligible.[38] High resolution ^{23}Na MAS NMR spectra were obtained by MAS experiments which resulted in a considerable reduction of the linewidths.[39] The ^{23}Na chemical shifts are summarized in Table 1. The upfield displacements of the ^{23}Na signals by the quadrupole interaction were corrected by the following formula given by Lippmaa and coworkers.[21]

$$\delta = \frac{1}{40}(e^2qQ/h)^2/\omega_L \qquad (1)$$

where ω_L stands for the Larmor frequency.

Solvent Complexes. Table 2 summarizes the ^{23}Na chemical shifts of a variety of solid solvent complexes, together with their bonding features as revealed by X-ray diffraction studies.[22–25,40–43] The static ^{23}Na NMR studies showed that all of these compounds gave single resonance lines, consistent with X-ray diffraction data in which solvent molecules such as H_2O, methanol, acetone, etc. are coordinated to the central sodium ions as an octahedral or a nearly octahedral arrangement.[22–25,40–43]

Figure 2 illustrates the ^{23}Na MAS NMR spectra of some sodium complexes with 1,4-dioxane. Many of

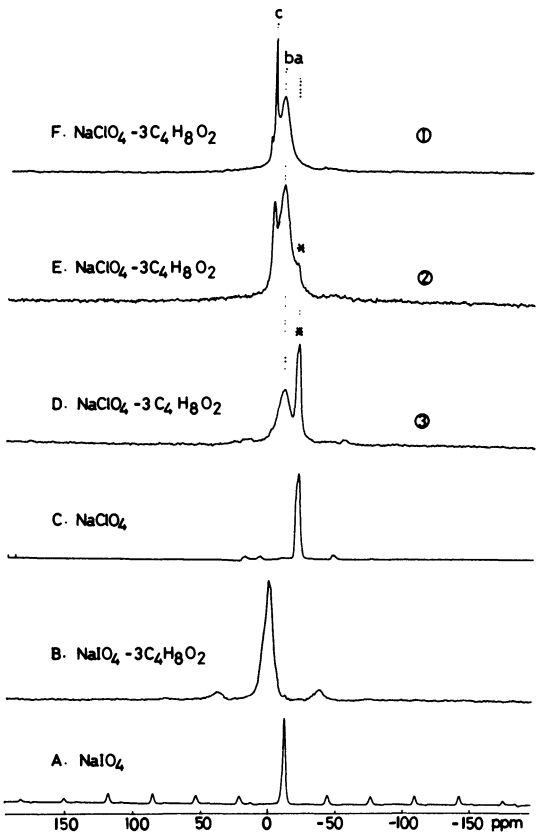

Fig. 2. 79.35 MHz MAS ^{23}Na NMR spectra of the sodium complexes ($NaClO_4$ and $NaIO_4$) with 1,4-dioxane. ①, ②, and ③ in Figure 2D-F stand for the sample number described in the text. The peaks asterisked arose from uncomplexed inorganic salts present in these complexes.

Table 2. ^{23}Na Chemical Shifts of Sodium Ions in Solvent Complexes, Complexes with Small Ligand Molecules and Complexes with Ionophores (ppm from 1 M NaCl Soln.)

	Static		MAS		Bonding features			
	Type of spectrum[a]	$\frac{e^2qQ}{h}$ (kHz)	Chemical shifts	Correction of chemical shifts by quadrupole interaction	Type of ligands[b]	Bond distance (Na-O, Å)	Coordination number	Ref
A. Solvent complexes								
$Na_2SO_4 \cdot 10H_2O$	s	0	2.3±1.5	0	H_2O	av. 2.43	6(Octahedral)	40
$Na_2HAsO_4 \cdot 7H_2O$	s	0	1.0±1.5	0	H_2O	2.35—2.48	6(Octahedral)	41
NadAMP·$6H_2O$	s	0	1.9±1.3	0	H_2O	2.37—2.45	6(Nearly octahedral)	42
$Na(CH_3COO) \cdot 3H_2O$	s	0	−0.2±1.7	0	$5H_2O$, COO	2.35—2.56	6(Distorted octahedral)	43
NaI·$3CH_3OH$	s	0	−2.9±0.4	0	CH_3OH	av. 2.47	6(Octahedral)	23
$NaClO_4 \cdot 3DX$	s	0	−11.3±1.5	0	DX	av. 2.43	6(Elongated octahedral)	22
$NaIO_4 \cdot 3DX$	s	0	−1.2±1.0	0	DX			
$NaBF_4 \cdot 3DX$	s	0	−11.6±1.6	0	DX	av. 2.43	6	22
NaI·3DX	s	0	−9.4±1.6	0	DX	av. 2.43	6	22
NaSCN·3DX	s	0	−10.0±1.0	0	DX			
NaI·3DMF	s	0	−11.7±1.0	0	DMF	av. 2.40	6(in between trigonal prism and octahedral)	25
NaI·$3(CH_3)_2C=O$	s	0	−6.2±0.9	0	$(CH_3)_2C=O$	av. 2.46	6(Octahedral)	24
B. Complexes with small ligands								
(Ethylene glycol)(1-phenyl-1,3-butanedionate)sodium	s	0	−8.7±2.8	0	3C=O, 2OH	2.29—2.36, 2.32—2.33	5(Tetragonal pyramid)	26
Trisodium nitrilotriacetate hydrate	s	0	−8.7±0.4	0	COO, H_2O	2.28—2.67	6(Distorted octahedron)	44
Sodium L-ascorbate	s	0	−9.6±1.9	0	4OH, C=O ether	2.42—2.72	6(Distorted octahedron)	45
Sodium D-isoascorbate hydrate	s	0	−0.6±1.5	0	3OH, 2 ether H_2O	2.30—2.39	6(Distorted octahedron)	46
NaI $2(NH_2CH_2COOH)H_2O$	s	0	0.4±0.2	0	COO, H_2O	2.32—2.64	6(Octahedral)	27
NaI $N(CH_2CH_2OH)_3$	f.o.	464	−3.8±1.9	0.9	OH	2.45—2.62	7(Irregular)	28
$NaH(CH_3COO)_2$	s	0	−0.6±0.9	0	COO	2.40—2.44	6(Trigonal prism)	29
C. Ionophores								
NaSCN-valinomycin	s	0	−23.3±4.7	0	C=O	2.69—2.83[c]	6(Octahedral)	47
NaSCN-nonactin	s	0	−18.2±1.0	0	C=O, ether	2.36—2.80	8(Distorted cubic)	48
NaSCN-tetranactin	s	0	−24.0±1.2	0	C=O, ether	2.43—2.95	8(Distorted cubic)	49
Lasalocid	s	0	−11.6±3.3	0	Ether	2.28—2.77	6(Monocapped pentagon)	50
Monensin	s	0	−14.2±3.4	0	Ether	2.35—2.52	6(Distorted octahedron)	51
NaSCN-[2.2.1]	s	0	−16.4±2.8	0	Ether	2.45—2.52	7	52
NaI-[2.2.2]	s	0	−16.2±1.7	0	Ether	2.57—2.58	8	53
NaSCN-[2.2]	s	0	−18.3±3.5	0	Ether		7	
NaSCN-18-crown-6	s	0	−16.0±0.9	0	Ether	2.45—2.62	7(Distorted pentagonal bipyramid)	54

a) s stands for single line; f.o. stands for the first-order split signal. b) DX and DMF stand for 1,4-dioxane and *N,N*-dimethylformamide, respectively. c) Data from potassium complex.

these complexes are efflorescent. In fact, the ^{23}Na MAS NMR spectra of $NaClO_4$–$3C_4H_8O_2$ complex gave three kinds of peaks whose relative peak intensities are significantly varied among three kinds of preparations (Figure 2D—F). The peak a is readily ascribed to the ^{23}Na NMR peak of uncomplexed $NaClO_4$, as compared with the peak position of $NaClO_4$ crystal (Fig. 2C). The peak c is assigned to the presence of Na^+ ion dissolved in a concentrated solution, because this peak is visible only for samples containing a wet fraction. In addition, it is emphasized that this sharp signal is still present in the static ^{23}Na NMR spectra. Accordingly, the peak b is unambiguously ascribed to the Na^+ ions complexed with 1,4-dioxane. By contrast, $NaIO_4$–$3C_4H_8O_2$ complex gave no residual peaks corresponding to the peaks a and c of $NaClO_4$–$3C_4H_8O_2$ complex (Fig. 2B). It is noteworthy that the ^{23}Na chemical shifts of these complexes are significantly displaced as compared with those of uncomplexed inorganic salts (Table 2).

Complexes with Small Ligand Molecules. In contrast to the cases of the solvent complexes described above, the sodium ions of the present complexes are coordinated to hydroxyl, carbonyl or ether moieties of small ligand molecules. The electric field gradient around the sodium ions is virtually zero as viewed from the appearance of single lines in the static ^{23}Na NMR, except for the case of 2-aminoethanol–sodium iodide(1/1) in spite of different type of oxygens around the sodium ions. For the latter, the bonding feature is that of an irregular geometry of 7 coordination which would cause non-zero quadrupole coupling constant (see Table 2).[28]

Complexes with Ionophores. Figure 3 illustrates the ^{23}Na MAS NMR spectra of crystalline sodium complexes with a variety of naturally occurring ionophores whose chemical structures differ substantially among them (see Fig. 4, for chemical structure[55]). Clearly, the ^{23}Na NMR signals of NaSCN complexes of nonactin, tetranactin, and valinomycin were displaced upfield by 16, 22, and 21 ppm, respectively, upon complex formation as compared with those of uncomplexed NaSCN, and the extent of the displacements

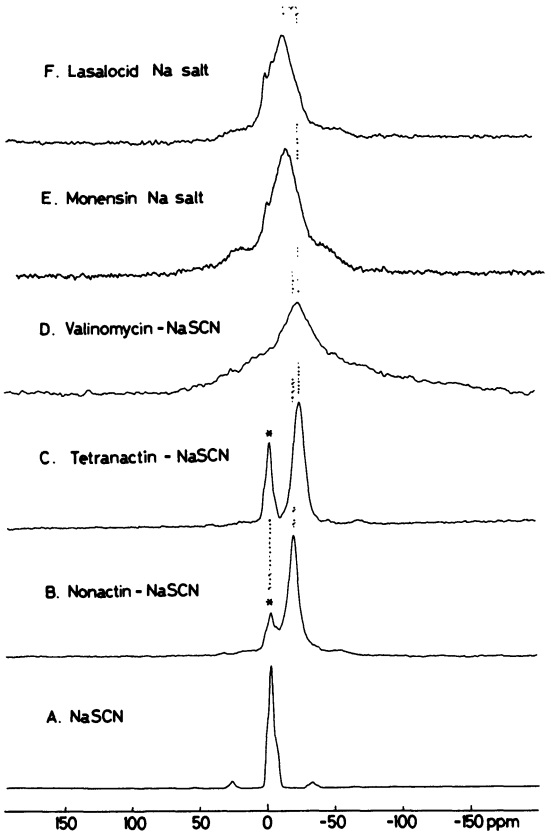

Fig. 3. 79.35 MHz MAS ^{23}Na NMR spectra of the sodium complexes with naturally occurring ionophores in the solid state. The peaks asterisked in Fig. 3B and C are from uncomplexed NaSCN.

of peaks in these cases is much larger than that of the solvent complexes described above (Table 2).

Figure 5 shows the ^{23}Na MAS NMR spectra of the sodium complexes with cryptands in the solid state (see Fig. 4). Again, it is clear that the ^{23}Na signals are displaced upfield by complexation with these cryptands and 18-crown-6 (spectrum not shown), consistent with the data of the naturally occurring ionophores (Table 2).

Ab Initio Calculation. Figure 6 summarizes the interaction energies and gross orbital charges of Na^+ ions complexed with H_2O or $H_2C{=}O$ molecules to form octahedra (a) and (b), respectively, or to form the plane (c). We consider the complexes (a) and (b) as models of the solvent complexes and complexes with ionophores, and the complex (c) as crown ethers. The total interaction energy (ΔE) was decomposed into the terms of polarization (PL), electrostatic (ES), charge transfer (CT), exchange (EX), and mixed term (mix) by the procedure of Morokuma et al.[56] Obviously, the interaction energy arises mainly from the electrostatic (ES) interaction and achieves the minimum value at about the Na–O distance of 2.4 Å, consistent with the experimental finding. The achieved stabilization energy increases in the following order: octahedral H_2CO<planar H_2O<octahedral H_2O. The largest amount of electron transfer from the ligand molecules to the 3p orbital of the Na^+ ion occurs at the bond length larger than 2.4 Å, and decreases with the following order: octahedral H_2O>octahedral $H_2C{=}O$>planar H_2O. Figure 7 summarizes the interaction energy and gross orbital charge of the Na^+ ion complexed with a H_2O molecule with various orientation. Similar results were obtained for the interaction with $H_2C{=}O$ molecule (data not shown).

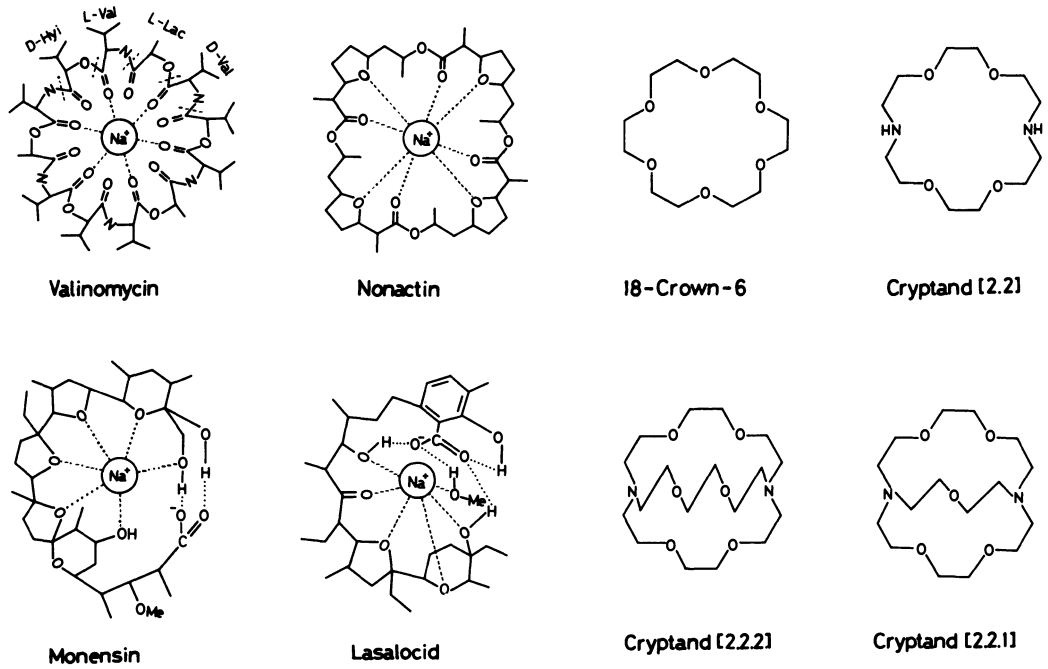

Fig. 4. Chemical structure of naturally occurring ionophores, 18-crown-6 and cryptands.

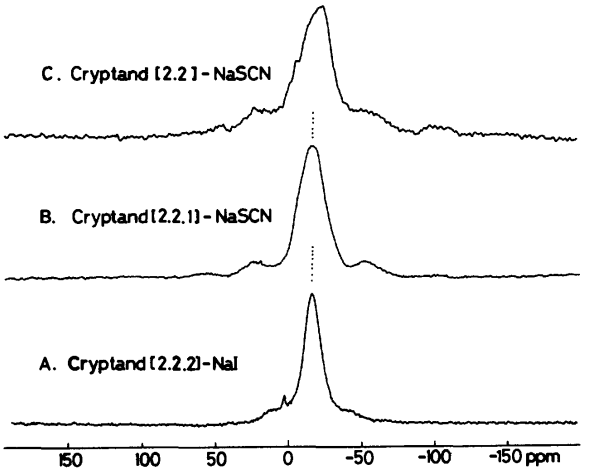

Fig. 5. 79.35 MHz ^{23}Na MAS NMR spectra of the sodium complexes with various types of cryptand molecules.

Discussion

Tables 1 and 2 show that the range of the ^{23}Na chemical shifts of inorganic salts and sodium complexes so far studied is about 60 ppm and these chemical shifts can be used as a diagnostic means of characterization of these compounds. These characteristic shifts, however, cannot be obtained by solution NMR spectra, because dissolution of these solid samples in solvents results in the disruption of the crystalline structure formed by ionic interactions.

It is noteworthy that the ^{23}Na NMR peak of $NaBPh_4$ resonates at −51.7 ppm (Table 1). This peak position is surprisingly high for a Na^+ ion. In contrast to Na^+ ions, the ^{23}Na chemical shift of Na^- ion is solvent-independent:[14-17] −61.9 ppm in $MeNH_2$, −61.8 ppm in 12-crown-4 and −63.1 ppm for the gas state. In

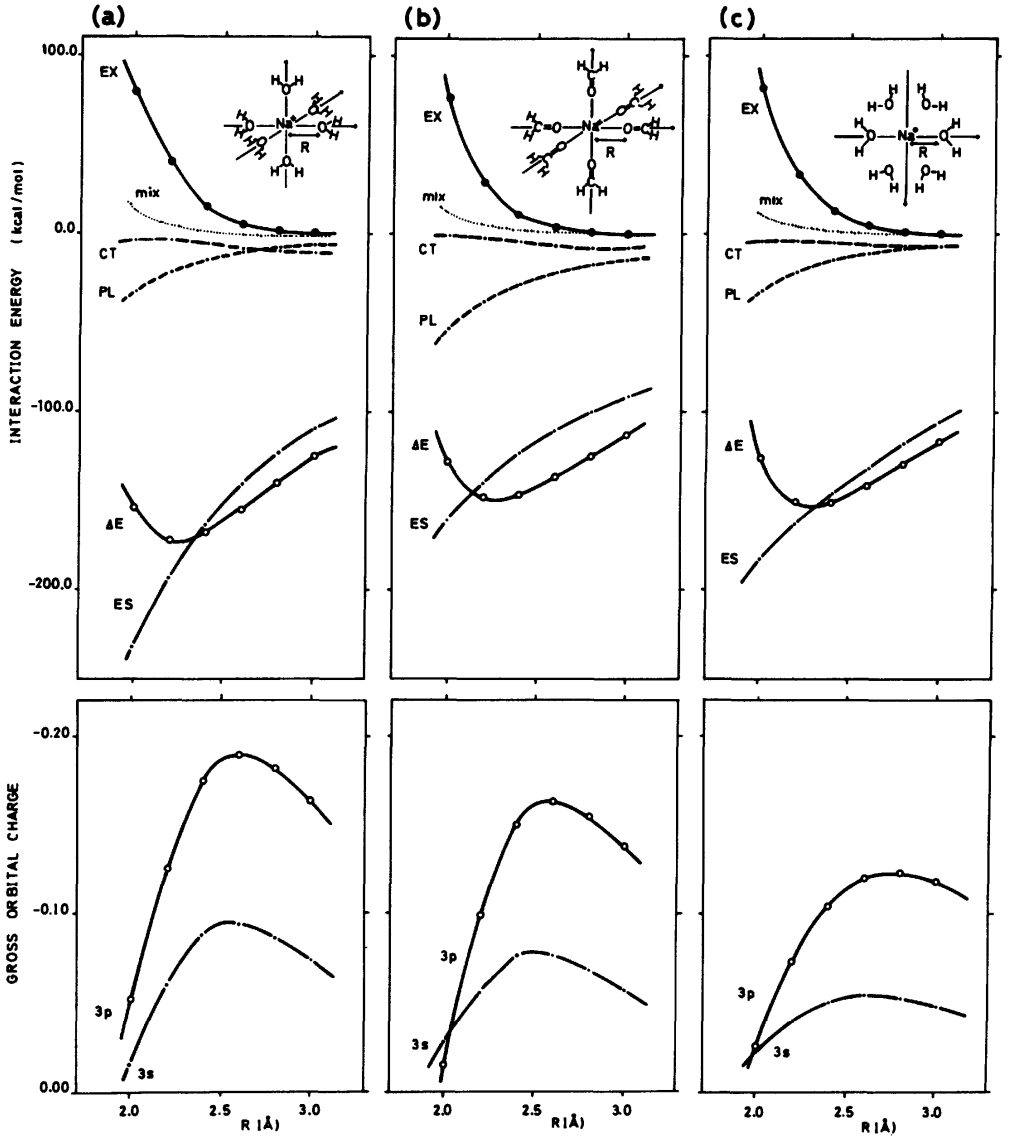

Fig. 6. The interaction energies and gross orbital charges of Na^+ ions complexed with H_2O and $H_2C{=}O$ molecules to form octahedron (a) and (b), respectively, or to form plane (c) as a function of the Na–O distance R (Å).

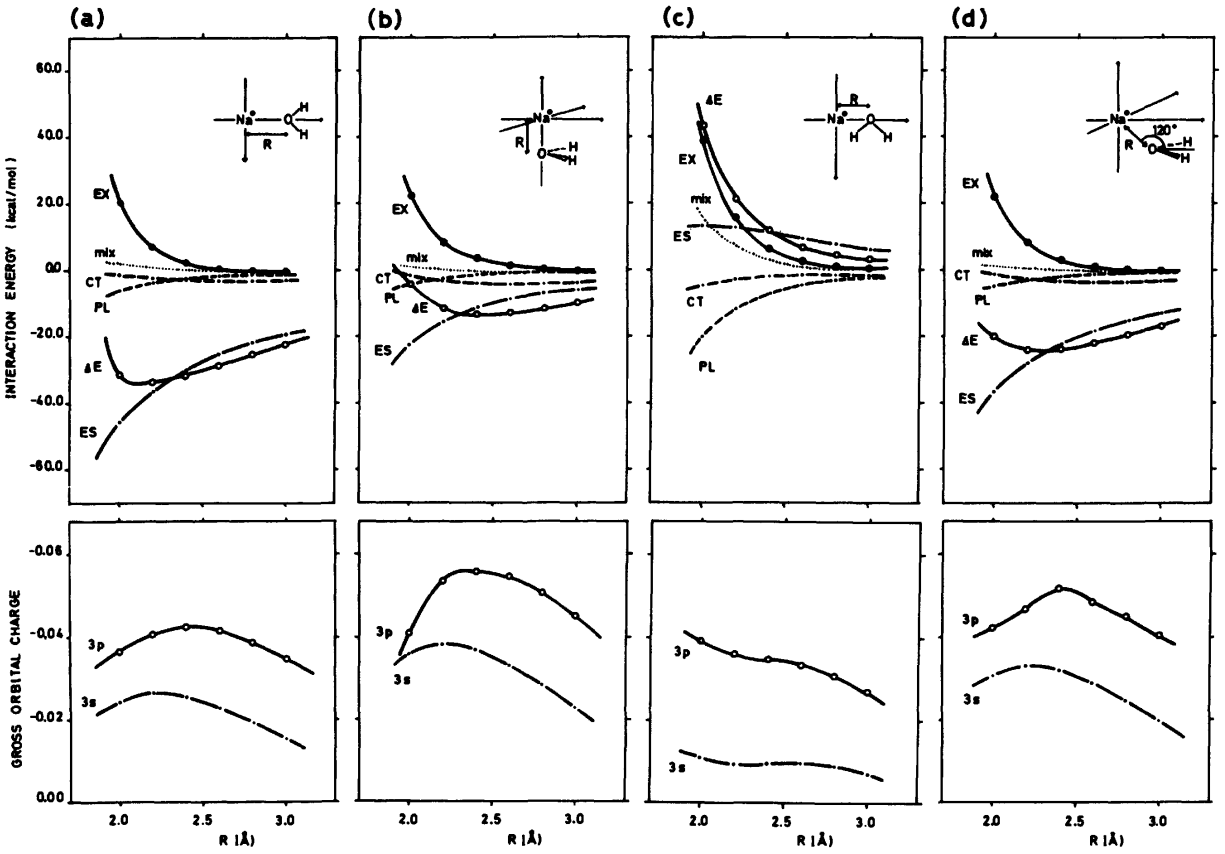

Fig. 7. The interaction energies and gross orbital charges of Na^+ ions complexed with a H_2O molecule with various orientation.

connection with this, Malli and Fraga[57] showed that the changes in nuclear shielding constants of Na^-(gas) with respect to Na^+(gas) are relatively small, amounting to a shielding of only 7.7 ppm for the addition of two 3s electrons to gaseous Na^+ to form Na^-(gas). Thus, it is possible to estimate the ^{23}Na chemical shift of Na^+(gas) as −55.4 ppm, on the basis of the data mentioned above. Accordingly, the electronic structure of the Na^+ cation in $NaBPh_4$ crystal seems to be very similar to that of the gaseous Na^+ ion, as manifested from a very small deshielding (+3 ppm). On the contrary, the large downfield shifts (≈+60 ppm) of a number of inorganic salts could be interpreted in terms of a large paramagnetic shielding contribution due to the presence of the 3p electron transferred from the counteranions, by analogy with the case of the ion-solvent interaction. As to the latter, the ^{23}Na chemical shifts can be correlated with the Gutmann donor strength of the solvents over a range of almost 20 ppm.[58]

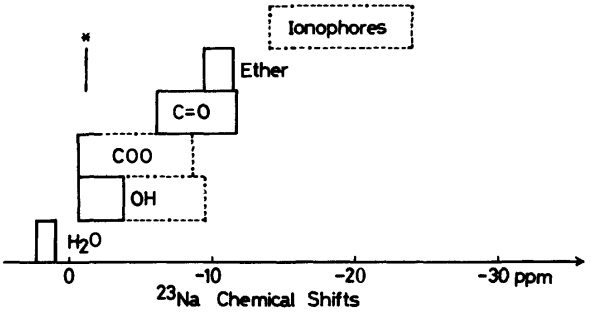

Fig. 8. Schematic representation of the displacements of the ^{23}Na chemical shifts as related to the type of ligand molecules. The data shown by the thick and dotted lines correspond with the complexes whose Na-O distance is in normal region (2.3—2.5 Å) and is larger than this range, respectively. The diagram asterisked arose from $NaIO_4$-$3C_4H_8O_2$ whose chemical shift is significantly lower than that of the other complexes indicated by the "ether".

In Figure 8, we summarized the range of the ^{23}Na chemical shifts of various sodium complexes as a function of the type of ligand molecule. For the complexes with mixed ligands, we plotted the range of the ^{23}Na chemical shifts by the type of ligands whose bonding numbers are larger than 3. In addition, we expressed the ^{23}Na chemical shifts of these complexes whose Na-O distances are in the normal range (2.3—2.5 Å) and are larger than this range by the thick and dotted lines, respectively. The following three features emerge from closer examination of Fig. 8 and Table 2.

First, the ^{23}Na chemical shifts of $Na_2SO_4 \cdot 10H_2O$, $Na_2HAsO_4 \cdot 7H_2O$, and NadAMP·$6H_2O$ are the same, 1.0—2.3 ppm, within the experimental error, regardless

of the variety of the counter-anions. Further, the ^{23}Na chemical shifts of four sodium complexes ($NaClO_4$, $NaBF_4$, NaI, and NaSCN) with 1,4-dioxane are the same, regardless of the different kinds of counteranions. These findings are rationalized by assuming that the Na^+ ions of these complexes are complexed with six (octahedral) H_2O molecules with Na–OH_2 distance 2.35—2.48 Å for the former,[40-42] and are complexed by six dioxane molecules with an average Na–O distance of 2.43 Å for the latter.[22] Accordingly, the counteranions have no direct effect upon the ^{23}Na chemical shifts because they are not directly coordinated to the sodium ions. It is not clear, however, why the ^{23}Na signal of the $NaIO_4$ complex appears at such a surprisingly lower field (−2.9 ppm). It is probable that the Na–O distance of this crystal might be different from the others, although no X-ray diffraction study is available. In a similar manner, the ^{23}Na chemical shift of $Na(CH_3COO)3H_2O$ is very close to the value of the sodium ions coordinated by six aqua ligands, because the Na ion in this case is coordinated by five H_2O molecules and one COO moiety.

Second, the ^{23}Na NMR signals of sodium complexes coordinated to COO or OH groups apprears at almost the same position (or slightly at higher field by 1—2 ppm) as those of the sodium complexes with H_2O (see Fig. 8). On the contrary, the ^{23}Na chemical shifts are displaced upfield by 5—10 ppm when the sodium ions are complexed with ether or the C=O moieties of ligands. Third, the ^{23}Na chemical shifts are significantly displaced upfield when the Na–O distances of the complexes are increased, as encountered for a variety of complexes with ionophores whose size of cavity is more preferrable to cations of larger ionic radii like potassium ions. In addition, the observation of the ^{23}Na chemical shift of trisodium nitrilotriacetate hydrate at rather higher field (−8.7 ppm) as H_2O and COO ligands could be interpreted in terms of the presence of a longer Na–O distance as compared with that of the other complexes.

A theoretical interpretation of the chemical shifts for alkali halide crystals was successfully performed by Kondo and Yamashita[59] and Ikenbery and Das[60] who took into account the overlap between the np-orbital of the metal and the outermost s- and p-orbitals of the halide ions. This approach, however, is not convenient for our purpose, because we are mainly concerned with a relation between the ^{23}Na chemical shifts and the magnitude of electron transfer from the ligand molecules. Alternatively, Bloor and Kidd showed that the paramagnetic term of the ^{23}Na chemical shifts amounts to ca. −270 ppm per electron donated to a 3p orbital of the sodium atoms,[17] using Schneider and Buckingham's "atom in a molecule" method.[61] The calculated electron density of 3p orbital at R=2.5 Å is 0.19, 0.16, and 0.11 for the coordinations of octahedral six H_2O (a), octahedral six H_2C=O (b) and planar six H_2O (c) molecules, respectively, as illustrated in Fig. 6. The resultant ^{23}Na chemical shifts for the models (a), (b), and (c) are −4, −12, and −25 ppm, respectively, by taking into account the fact that the paramagnetic shielding constant for the cases (a), (b), and (c) are −51, −43, and −30 ppm, respectively, following the formula of Bloor and Kidd[17] and the ^{23}Na chemical shift of the gaseous Na^+ ion is estimated as −54 ppm when referred to 1 M NaCl, as described already. The calculated ^{23}Na chemical shifts thus obtained are in good agreement with the experimental data, if the models (a), (b), and (c) are considered as representing the sodium complexes with ligands of H_2O, acetone or DMF, and 18-crown-6, respectively. Obviously from the data of Fig. 6, the electron density in the 3p orbital is decreased when the Na–O distance is increased further from 2.5 Å as in the cases of the complexes with ionophores, resulting in the upfield displacements of the ^{23}Na signals as a result of a reduction in the paramagnetic shielding contribution.

The extent of the electron transfer would be much influenced by the relative orientation of the lone-pair orbitals with respect to the direction of the Na–O vector, as shown in Fig. 7. Accordingly, the electron transfer is minimal for the arrangement of Na–H_2O as shown in Fig. 7(c), in which the lone-pair orbitals are perpendicular to the Na–O vector. On the contrary, the magnitude of the electron transfer is maximum for the arrangement of Fig. 7(b), although stabilization is not fully achieved. Similar results were obtained for the case of the Na–O=CH_2 system. For this reason, the relative orientation of the ligand molecule is a very important factor in the determination of the ^{23}Na chemical shifts in addition to the Na–O distance, because the magnitude of electron transfer is dependent on this separation. It is now obvious that the ^{23}Na chemical shifts of the sodium complexes can be well related to the extent of the electron transfer from the ligand molecules, although a more elaborate treatment is required to achieve a quantitative interpretation of the ^{23}Na chemical shifts in terms of electronic structure.[62]

Concluding Remarks

We have demonstrated that the ^{23}Na NMR signals of inorganic salts as well as a variety of sodium complexes in the solid state exhibit displacements of chemical shifts as large as 60 ppm and provide a convenient means of analyzing the following individual species, ion-ion, ion-solvent, and ion-ligand interactions which are present in the solution state. We found that these variations of the ^{23}Na chemical shifts are well related to the extent of electron transfer from the ligand molecules to the 3p orbital of the sodium ions which results in substantial deshielding due to a significant paramagnetic contribution. Accordingly, the ^{23}Na chemical shifts in the solid state are proven to be a very useful means for the characterization of these complexes as viewed from the type of ligand molecules, their relative

orientation, and the Na–O distances as well as reference data for solution NMR spectra.

The numerical calculations were carried out with a HITAC M-240H in the National Cancer Center and a HITAC M-200 H in the Institute for Molecular Sciences. This work was supported, in part, by a Grant-in-Aid for Scientific Research from the Ministry of Education, Science and Culture of Japan. Finally, we thank Dr. G. A. Webb, University of Surrey, England, for helpful discussion.

References

1) For review: a) B. C. Pressman, *Ann. Rev. Biochem.*, **45**, 501 (1976); b) C. J. Pedersen and H. K. Frensdorff, *Angew. Chem. Int. Ed. Engl.*, **11**, 16 (1972); c) N. S. Poonia and A. V. Bajaj, *Chem. Rev.*, **79**, 389 (1979); d) F. de Jong and D. N. Reinhoudt, *Adv. Phys. Org. Chem.*, **17**, 1 (1981); e) J. Lehn, *Struc. Bonding (Berlin)*, **16**, 1 (1973); f) B. Dietrich, in "Inclusion Compounds," ed by J. C. Atwood, J. E. D. Davies, and D. D. MacNicol, Academic Press, London (1984), Vol. 2, Chap. 10.

2) For review: a) P. Laszlo, *Angew. Chem. Int. Ed. Engl.*, **17**, 254 (1978); b) M. M. Civan and M. Shporer, "Biological Magnetic Resonance," ed by L. J. Berliner and J. Reuben, Plenum Press, New York and London (1978), Vol. 1, Chap. 1; c) B. Lindman and S. Forsen, "NMR and the Periodic Table," ed by R. K. Harris and B. E. Mann, Academic Press, London (1978), Chap. 6.

3) D. H. Haynes, B. C. Pressman, and A. Kowalsky, *Biochemistry*, **10**, 852 (1971).

4) M. Schporer, H. Zemel, and Z. Luz, *FEBS Lett.*, **40**, 357 (1974).

5) E. Shchori, J. Jagur-Grodzinski, Z. Luz, and M. Shporer, *J. Am. Chem. Soc.*, **93**, 7133 (1971).

6) E. Shchori, J. Jagur-Grodzinski, and M. Shporer, *J. Am. Chem. Soc.*, **95**, 3842 (1973).

7) M. Shamsipur and A. I. Popov, *J. Am. Chem. Soc.*, **101**, 4051 (1979).

8) B. O. Strasser, K. Hellenga, and A. I. Popov, *J. Am. Chem. Soc.*, **107**, 789 (1985).

9) B. Eliasson, K. M. Larson, and J. Kowalewski, *J. Phys. Chem.*, **89**, 258 (1985).

10) J. M. Ceraso and J. L. Dye, *J. Am. Chem. Soc.*, **95**, 4432 (1973).

11) J. P. Kintzinger and J. M. Lehn, *J. Am. Chem. Soc.*, **96**, 3313 (1974).

12) J. M. Ceraso, P. B. Smith, J. S. Landers, and J. L. Dye, *J. Phys. Chem.*, **81**, 760 (1977).

13) J. C. Lin and A. I. Popov, *J. Am. Chem. Soc.*, **103**, 3773 (1981).

14) R. C. Phillips, S. Khazaeli, and J. L. Dye, *J. Phys. Chem.*, **89**, 606 (1985).

15) J. M. Ceraso and J. L. Dye, *J. Chem. Phys.*, **61**, 1585 (1974).

16) J. L. Dye, C. W. Andrews, and J. M. Ceraso, *J. Phys. Chem.*, **79**, 3076 (1975).

17) E. G. Bloor and R. G. Kidd, *Can. J. Chem.*, **46**, 3425 (1968).

18) a) D. Muller and W. Gessner, *Chem. Phys. Lett.*, **79**, 59 (1981); b) E. Oldfield, R. A. Kinsey, B. Montez, T. Ray, and K. A. Smith, *J. Chem. Soc., Chem. Commun.*, **1982**, 254; c) D. J. Burton and R. K. Harris, *J. Chem. Soc., Chem. Commun.*, **1982**, 256; d) M. D. Meadows, K. A. Smith, R. A. Kinsey, T. M. Rothgeb, R. P. Skarjune, and E. Oldfield, *Proc. Natl. Acad. Sci. U.S.A*, **79**, 1351 (1982).

19) a) E. Oldfield, S. Schramm, M. D. Meadows, K. A. Smith, R. A. Kinsey, and J. Ackerman, *J. Am. Chem. Soc.*, **104**, 919 (1982); b) S. Ganapathy, S. Schramm, and E. Oldfield, *J. Chem. Phys.*, **77**, 4360 (1982).

20) R. Tabeta and H. Saitô, *Chem. Lett.*, **1984**, 293.

21) a) E. Kundla, A. Samoson, and E. Lippmaa, *Chem. Phys. Lett.*, **83**, 229 (1981); b) A. Samoson, E. Kundla, and E. Lippmaa, *J. Magn. Reson.*, **49**, 350 (1982).

22) a) J. C. Barnes and C. S. Duncan, *J. Chem. Soc., Dalton Trans.*, **1972**, 1732; b) J. C. Barnes and T. J. R. Weakely, *Acta Crystallogr., Sect. B*, **34**, 1984 (1978).

23) P. Piret and C. Mesureur, *J. Chim. Phys.*, **62**, 287 (1965).

24) P. Piret, Y. Gobillon, and M. van Meerssche, *Bull. Soc. Chim. Fr.*, **1963**, 205.

25) Y. Gobillon, P. Piret, and M. van Meerssche, *Bull. Soc. Chim. Fr.*, **1962**, 551.

26) D. Bright, G. H. W. Milburn, and M. R. Truter, *J. Chem. Soc. (A)*, **1971**, 1582.

27) J. Verbist, J.-P. Putzeys, P. Piret, and M. Meerssche, *Acta Crystallogr., Sect. B*, **27**, 1190 (1971).

28) J. C. Voegele, J. Fischer, and R. Weiss, *Acta Crystallogr., Sect. B*, **30**, 62 (1974).

29) J. C. Speakman and H. H. Mills, *J. Chem. Soc.*, **1961**, 1164.

30) R. Tabeta and H. Saitô, *Biochemistry*, **24**, 7696 (1985).

31) H. Saitô, R. Tabeta, A. Shoji, T. Ozaki, I. Ando, and T. Asakura, "Magnetic Resonance in Biology and Medicine," ed by G. Govil, C. L. Kheterapal, and A. Saran, Tata McGraw-Hill, New Delhi (1985), p. 195.

32) R. Tabeta and H. Saitô, *Bull. Chem. Soc. Jpn.*, **58**, 3215 (1985).

33) M. H. Cohen and F. Reif, "Solid State Physics," ed by F. Seitz and D. Turnbull, Academic Press, New York (1957) Vol. 5; A. Abragam, "The Principle of Nuclear Magnetism," Clarendon Press, Oxford (1961), Chap. VII; P. C. Taylor, J. F. Baucher, and H. M. Kriz, *Chem. Rev.*, **75**, 203 (1975).

34) K. Morokuma, S. Kato, K. Kitaura, I. Ohmine, S. Sakai, and S. Obara, Institute for Molecular Science Computer Center Library Program, 1980, No. 0372.

35) W. J. Hehre, R. Ditchfield, and J. A. Pople, *J. Chem. Phys.*, **56**, 2257 (1972).

36) For ligand molecules, the geometries were optimized with 6—31 G basis set by energy gradient techniques (P. Pulay, "Applications of Electronic Structure Theory," ed by H. F. Schaefer III, Plenum Press, New York (1977), pp. 153—185).

37) W. Gauss, S. Gunther, A. R. Haase, M. Kerber, J. Kronenbitter, H. Krüger, O. Lutz, A. Nolle, P. Schrade, M. Schule, and G. E. Siegloch, *Z. Naturforsch.*, **33a**, 934 (1978).

38) A. H. Silver and P. J. Bray, *J. Chem. Phys.*, **32**, 288 (1960).

39) The linewidths achieved by MAS experiments were less than 500 Hz for a number of inorganic salts, as reported previously (Ref. 20). Many of solvent complexes as well as complexes nonactin and tetranactin gave the linewidths of 500—1000 Hz. It appears, however, that the linewidths are increased to over 1000 Hz when the linebroadening by dipolar field from nearby proton(s) of counterions or ligands cannot

be completely removed by MAS experiments. In fact, the following complexes gave larger linewidths than 1500 Hz: Valinomycin (3000 Hz), monensin (2800 Hz), lasalocid (2100 Hz), [2.2.1] (1700 Hz) and [2.2] (2200 Hz). We found that the linewidths were in some instances significantly decreased by proton decoupling or removal of water molecules (Ref. 20). Further, the linewidths of $Na_2SO_4 \cdot 10H_2O$ and $Na_2HAsO_4 \cdot 7H_2O$ were decreased from 600 and 430 to 400 and 160 Hz, respectively, by recrystallization from D_2O solution. In this connection, it is mentioned that these linewidths studied herein were not affected by the second-order quadrupole interaction, because the quadrupole coupling constants from the static ^{23}Na NMR spectra were zero. Further, the linewidths of $NaBH_4$, $NaBPh_4$, and $NaBF_4$ are 1000, 1010, and 740 Hz, respectively, although the quadrupole coupling constants of the former two are zero and are 1.2 MHz for the latter.

40) H. A. Levy and G. C. Lisensky, *Acta Crystallogr., Sect. B*, **34**, 3502 (1978).

41) G. Ferraris and G. Chiari, *Acta Crystallogr.,Sect. B*, **26**, 1574 (1970).

42) B. S. Reddy and M. A. Viswamitra, *Acta Crystallogr., Sect. B*, **31**, 19 (1975).

43) K.-T. Wei and D. L. Ward, *Acta Crystallogr., Sect. B*, **33**, 522 (1977).

44) J. J. Daly, *J. Chem. Soc. (A)*, **1967**, 1708.

45) J. Hvoslef, *Acta Crystallogr., Sect. B*, **25**, 2214 (1969).

46) J. A. Kanters, G. Roelofsen, and B. P. Alblas, *Acta Crystallogr., Sect. B*, **33**, 1906 (1977).

47) K. Neupert-Laves, and M. Dobler, *Helv. Chim. Acta*, **58**, 432 (1975).

48) M. Dobler and R. P. Phizackerley, *Helv. Chim. Acta*, **57**, 664 (1974).

49) T. Sakamaki, Y. Iitaka, and Y. Nawata, *Acta Crystallogr., Sect. B*, **32**, 768 (1976).

50) C. C. Chang and I. C. Paul, *Science*, **196**, 1441 (1977).

51) M. Pinkerton and L. K. Steinrauf, *J. Mol. Biol.*, **49**, 533 (1970); W. K. Lutz, F. K. Winkler, and J. Dunitz, *Helv. Chim. Acta*, **54**, 4412 (1971).

52) F. Mathieu, B. Metz, D. Moras, and R. Weiss, *J. Am. Chem. Soc.*, **100**, 4412 (1978).

53) P. D. Moras and R. Weiss, *Acta Crystallogr., Sect. B*, **29**, 396 (1973).

54) M. Dobler, J. D. Dunitz, and A. P. Seiler, *Acta Crystallogr., Sect. B*, **30**, 2741 (1974).

55) Chemical structure of tetranactin is similar to that of nonactin, except for the presence of four ethyl groups in place of four methyl groups which are drawn inside the macrocyclic ring in Fig. 4 (see K, Ando, Y. Murakami, and Y. Nawata, *J. Antibiot.*, **24**, 418 (1971)).

56) K. Morokuma, *J. Chem. Phys.*, **55**, 1236 (1971); K. Kitaura and K. Morokuma, Int. *J. Quantum Chem.*, **10**, 325 (1976).

57) G. Malli and S. Fraga, Theoret. *Chim. Acta (Berl.)*, **5**, 275 (1966).

58) R. H. Erlich, E. Roach, and A. I. Popov, *J. Am. Chem. Soc.*, **92**, 4989 (1970).

59) J. Kondo and J. Yamashita, *J. Phys. Chem. Solid*, **10**, 245 (1959).

60) D. Ikenberry and T. P. Das, *J. Chem. Phys.*, **43**, 2199 (1965).

61) W. G. Schneider and A. D. Buckingham, *Discussions Faraday Soc.*, **34**, 147 (1962).

62) I. Ando and G. A. Webb, "Theory of NMR Parameters," Academic Press, London (1983); H. Nakatsuji, K. Kanda, K. Endo, and T. Yonezawa, *J. Am. Chem. Soc.*, **106**, 4653 (1984).

Conductivity of Lithium Salts in the Mixed Systems of High Permittivity Solvents and Low Viscosity Solvents

Yoshiharu MATSUDA, Masayuki MORITA,* and Fumitsugu TACHIHARA
Department of Industrial Chemistry, Faculty of Engineering, Yamaguchi University, Tokiwa-dai, Ube 755
(Received January 18, 1986)

Electrolytic conductivities of $LiClO_4$ and $LiPF_6$ have been investigated in the mixed systems of the high permittivity solvents and low viscosity solvents. Propylene carbonate (PC), sulfolane (S), and dimethyl sulfoxide (DMSO) were used as the high permittivity solvents, and 1,2-dimethoxyethane (DME) and tetrahydrofuran (THF) as the low viscosity solvents. The conductivity of 1 mol dm^{-3} $LiClO_4$ has a miximum in the mixed solvent with 40—80 m/o ether for every system. The conductance improvement by solvent-blending was qualitatively described in terms of a favorable combination of high permittivity and low viscosity of each component. The maximum conductivity of 1 mol dm^{-3} $LiClO_4$ increased in the order of S<PC<DMSO for the systems containing THF. The difference in the order of maximum conductivity between DME and THF was interpreted by ion-solvent interactions, whose measure is generally expressed by the donor and acceptor properties of the solvent. The $LiPF_6$ solutions had much higher conductance than those of $LiClO_4$, especially in high DME concentration regions.

A large number of aprotic organic solvent/lithium (Li) salt combinations have been examined as electrolyte solutions for Li batteries.[1] One of the basic requirements for battery electrolytes is high ionic coductivity. The conductivity of the electrolyte solution is much influenced by the permittivity and the viscosity of the solvent. The former relates to dissociation of the salt and the latter affects the motion of charged particles, or ions. With respect to these, a solvent with high permittivity and low viscosity should be suitable for the conductive electrolyte.[2] In general, however, few solvents satisfy these requirements concurrently. Hence, mixed systems consisting of two solvents, i.e., a high permittivity solvent and a low viscosity solvent, have sometimes been used for practical batteries.[3-5]

Previously, we have reported on the characteristics of some mixed electrolyte systems consisting of a high permittivity solvent and a low viscosity solvent for primary and secondary Li batteries.[6-11] As was expected, high conductivities were observed in the mixed solvent systems, and the electrode characteristics were also excellent in the mixed electrolyte systems.[8,10-13] However, both the conductance behavior and the electrode characteristics changed in response to the kinds of the solvent and the electrolyte salt.

In the present work, conductance behavior in some mixed solvent systems has been compared with one another. The high permittivity solvents used here were propylene carbonate (PC), sulfolane (S) and dimethyl sulfoxide (DMSO), and the low viscosity solvents were 1,2-dimethoxyethane (DME) and tetrahydrofuran (THF). The conductivities of $LiClO_4$ and $LiPF_6$ in the mixed systems are at first explained on the bases of the solvent permittivity and the solution viscosity. Differences in the conductance behavior among the systems are also discussed from the standpoint of the donor-acceptor properties of the solvents,[14,15] which concern the ion-solvent interactions to a great extent.

The structure of ionic solution with organic solvents has fairly been established by some workers,[16-18] but there have been few data on a comparison of the conductivities at moderate concentration of the salts.[19] This study concerns the conductivities at relatively high concentration (1 mol dm^{-3}). Thus the discussion will be rather qualitative, but be useful to develop the electrolyte of practical Li batteries.

Experimental

The purification of the solvents, PC, S, DME, and THF, was carried out as described previously.[9,11,19] DMSO was refluxed over CaH_2 and fractionally distilled.[20] The electrolytic salts were $LiClO_4$ (Ishizu Pharmaceutical) and $LiPF_6$ (Morita Chemical Industries). The solutions were prepared by dissolving the salts (normally 1 mol dm^{-3}) into the mixtures of the high permittivity solvents with the low viscosity solvents. These will be hereinafter represented by such formulas as "PC-DME/$LiClO_4$."

The conductivity of the electrolyte was measured with an AC impedance bridge (10 kHz). The relative permittivity (dielectric constant) of the solvent and the viscosity of the solution were determined by the same methods as described previously.[21] These measurements were carried out at 30 °C.

Results and Discussion

Table 1 shows the relative permittivity (ε_r), viscosity (η), donicity (DN) and acceptor number (AN) of the pure solvents. The values of DN and AN are those quoted from the literature.[1,14,15,24] PC, S, and DMSO have high permittivities as well as high viscosities. The ethers, DME and THF, are low viscosity-low permittivity solvents, whose η and ε_r are similar to each other.

Figure 1 shows the molar conductivity (Λ) of 1 mol dm^{-3} $LiClO_4$ in PC-DME, S-DME, and DMSO-DME as a function of the DME concentration (m/o) in the solvent. For every system, the conductivity in the mixed solvent was higher than that in the neat solvent. The molar conductivity became maximum at

Table 1. Selected Properties of the Solvents

Solvent	ε_r[a)]	η[a)]/10^{-3} Pa s	DN[b)]	AN[b)]
PC	66.8	2.25	15.1	18.3
S	42.5	9.87	14.8	19.0
DMSO	47.8	1.75	29.8	19.3
DME	6.92	0.40	24	(≃10)[c)]
THF	7.25	0.46	20.0	8.0

a) Measured at 30 °C. b) From references 1, 14, 15, and 24. c) 10.2 for diglyme (diethylene glycol dimethyl ether).

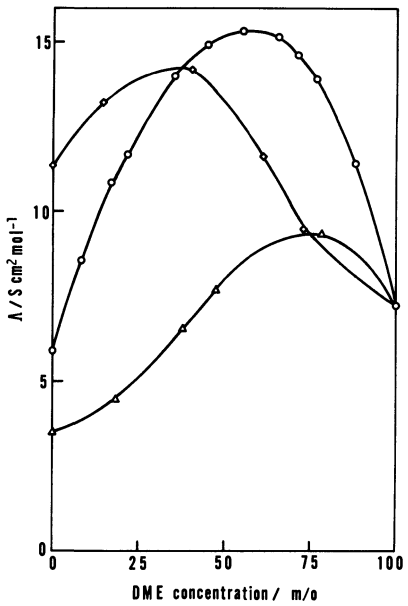

Fig. 1. Variation of the molar conductivity (Λ) of 1 mol dm^{-3} $LiClO_4$ with the solvent composition.
○: PC-DME, △: S-DME, ◇: DMSO-DME.

40—80 m/o DME. This conductivity enhancement is qualitatively explained by a favorable combination of high permittivity of PC, S, or DMSO with low viscosity of DME. The viscosity of the solution decreases with DME concentration. Thus, in the solution with relatively low DME content, the ionic mobility, or ionic conductance, increases with DME content in the solvents. On the other hand, the permittivity also decreases with DME content. This leads to an increase in the degree of ion association, which causes the conductivity to decrease, especially in the soltions with high DME content. Therefore, optimum solvent compositions are present for the conductance of these mixed electrolyte systems.

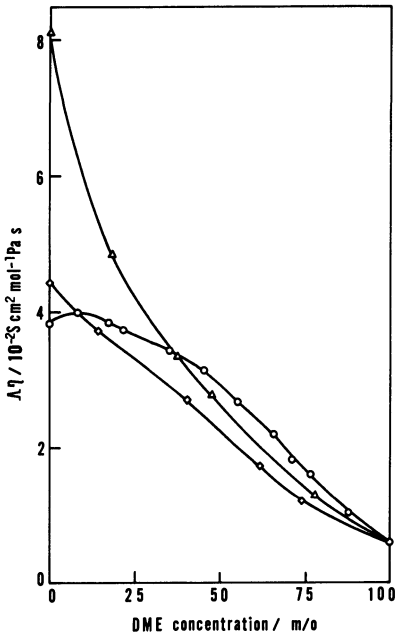

Fig. 2. Variation of the Walden product ($\Lambda\eta$) of 1 mol dm^{-3} $LiClO_4$ with the solvent composition.
○: PC-DME, △: S-DME, ◇: DMSO-DME.

Jansen and Yeager[25] have reported that the ion pair association constant K_a calculated by the Fuoss-Onsager theory was −1.0—−1.5 in PC(pure)/$LiClO_4$ at 25 °C. On the other hand, we have previously estimated the degree of association of $LiClO_4$ in the PC-DME and the PC-THF systems by using Bjerrum's equation.[9] The results showed that the degree of association would be very small (<0.1) in the solutions containing 0—40 v/o ethers, and that the ion association would significantly occur at the ether concentration range of 70 v/o or more. That is, it has been shown that the conductivity-solvent composition curves experimentally obtained in PC-DME/$LiClO_4$ and PC-THF/$LiClO_4$ were consistent with those calculated on the assumption that the conductivity is almost determined as the first approximation by the solution viscosity and the ion association.[9]

As shown in Fig. 1, there are some differences in the shape of the curve and in the DME concentration providing maximum conductivity among the three systems. This is first of all attributable to differences in the relative permittivity and the viscosity among PC, S, and DMSO. Figure 2 shows the Walden products ($\Lambda\eta$) of the 1 mol dm^{-3} $LiClO_4$ solutions as a function of DME concentration. The Walden products were approximately similar to one another in the solvents with DME concentration more than 40 m/o. The monotonous decrease of $\Lambda\eta$ with DME concentration in this region is related to the increase in ion association caused by increasing DME content in the solvents. If it is valid to assume that the conductivity is almost determined by the permittivity and the viscosity, differences in the Walden products among the solvent

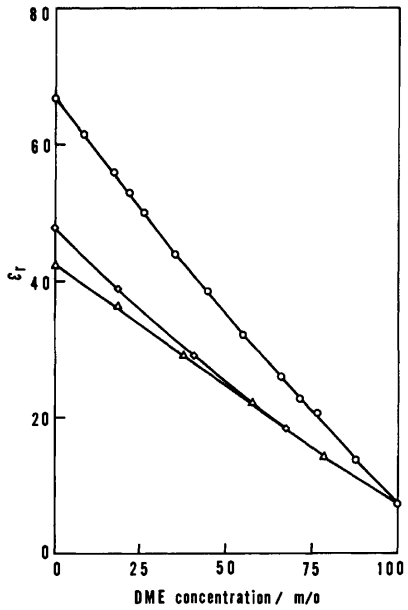

Fig. 3. Variation of the relative permittivity (ε_r) with the solvent composition.
O: PC-DME, △: S-DME, ◇: DMSO-DME.

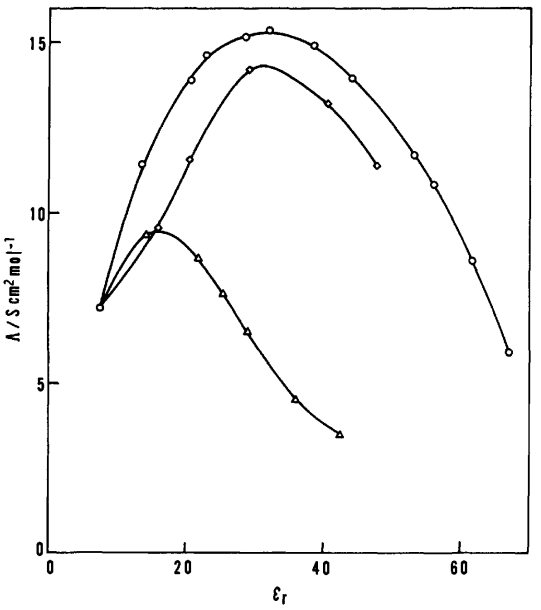

Fig. 4. Correlation between Λ of 1 mol dm^{-3} $LiClO_4$ and ε_r of the solvent.
O: PC-DME, △: S-DME, ◇: DMSO-DME.

systems would primarily originate in the permittivity of the solvent. The relative permittivities of the mixed solvents are shown in Fig. 3. In general, the permittivity of an binary system shows an additive property, i.e., a linear relationship between the permittivity and the composition. As shown in Fig. 3, the permittivity-composition curves for the present three systems bent downward. This is because the solvent compositions were represented by mole fractions. Relative permittivity can be assigned a significance in terms of the quantity per unit volume. In the present cases, the permittivities of the solvents varied almost linearly with the volume percent of the blended solvents.[9]

In Fig. 4, the molar conductivities of 1 mol dm^{-3} $LiClO_4$ solutions are plotted against the relative permittivities of the solvents. Since the permittivities had linear relationships to the solvent compositions, the Λ–ε_r relations also gave maximum values in the mixed systems. The ε_r providing the maximum Λ was about 30 in the systems of PC-DME and DMSO-DME, but it was 20 or less in S-DME. The relatively low Λ of 1 mol dm^{-3} $LiClO_4$ in S-DME might be attributable to the high viscosity of this system. Figure 5 shows the relation between the Walden products and the relative permittivities of the solvents. The differences in the $\Lambda\eta$–ε_r curves among the solvent systems originate probably in some characteristics of the systems, other than the permittivity and the viscosity, because the contributions of the latter parameters (ε_r and η) to the conductivity have already been reflected in the $\Lambda\eta$–ε_r relations. It must be taken into consideration that the dielectric saturation around ions[26] also affects the conductance behavior. However, this effect would be treated as a peculiar ion-solvent interaction. The ion-solvent interactions affecting the conductance behavior will be comprehensively discussed in the latter part of this section.

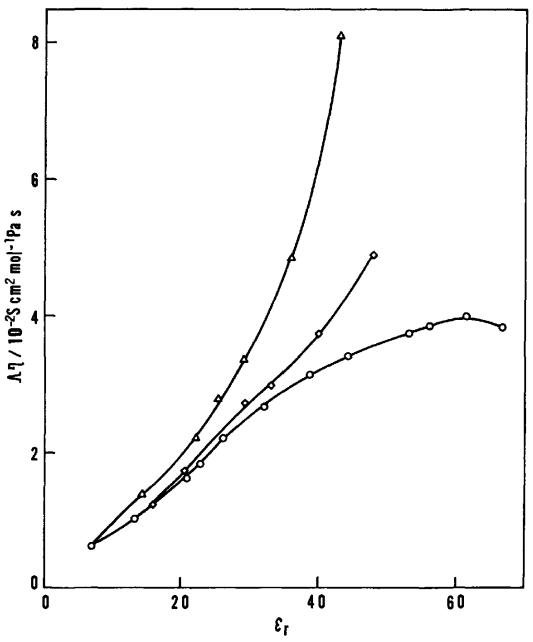

Fig. 5. Correlation between $\Lambda\eta$ of 1 mol dm^{-3} $LiClO_4$ and ε_r of the solvent.
O: PC-DME, △: S-DME, ◇: DMSO-DME.

In Fig. 5, the curve of DMSO-DME/$LiClO_4$ is almost consistent with that of PC-DME/$LiClO_4$ in the region of ε_r<40. The $\Lambda\eta$ in PC-DME tended to be unchangeable with increasing ε_r, especially in the high ε_r region. The $\Lambda\eta$ of DMSO-DME/$LiClO_4$ is higher than that of PC-DME/$LiClO_4$ in the DME

concentration region of 20 m/o or lower (ε_r>40). In S-DME, the $\Lambda\eta$ markedly increased with ε_r in the higher ε_r region (>30), compared with the PC- or DMSO-based system. This is mainly caused by high viscosity of S, since $\Lambda\eta$ in S-DME is rather lower than that in PC-DME or DMSO-DME. However, from the other point of view, it is considered that the S-DME/$LiClO_4$ system has relatively high conductance for its high viscosity.

The different $\Lambda\eta$–ε_r relations among the three systems in the low DME concentration (higher ε_r) region are explicable by the different donicities (*DN*) and acceptor numbers (*AN*) of PC, S, DMSO, and DME. According to Gutmann,[14,15] *DN* is defined as the negative ΔH-value in kcal mol^{-3} (1 cal=4.18 J) for the reaction (1) in 1,2-dichloroethane

$$D + SbCl_5 \longrightarrow D\cdot SbCl_5, \quad (1)$$

where D denotes the solvent in question. As $SbCl_5$ is a strong electron-acceptor, *DN* is a measure of the nucleophilic property of the solvent. On the other hand, *AN* is derived from the chemical shift of ^{31}P NMR of Et_3PO in the solvent under consideration. *AN* is expressed by a relative value when that of hexane is defined as 0 and the δ-value of the $Et_3PO\cdot SbCl_5$ adduct in 1,2-dichloroethane is arbitrarily normalized as 100. Thus *AN* is a measure of the electrophilic property of the solvent.

As DME has higher *DN* than PC, specific solvation (selective coordination) of DME to Li^+ comes out in the PC-DME system.[7,17] The *DN* of DMSO is higher than those of PC and DME. Thus the specific solvation of DME to Li^+ would not be expected in the DMSO-DME system. On the other hand, DME in the S-DME system would preferentially coordinate to Li^+ as in PC-DME because of the relatively low *DN* of S. Nevertheless, the Λ in S-DME was rather low compared with that in PC-DME. This result suggests that the other interactions, e.g., anion-solvent and ion-ion interactions, in the two systems differ from each other. These will be briefly discussed later again.

In Fig. 6, the molar conductivity of 1 mol dm^{-3} $LiClO_4$ in PC-THF is compared with that in PC-DME. As ε_r and η of pure THF are similar to those of DME, the variations of ε_r and η in PC-THF are also similar to those in PC-DME.[9] However, the molar conductivity in PC-THF was relatively low. In both systems Li^+ is probably coordinated by the ethers in preference to PC. It is considered that the primary solvation number of DME per Li^+ is two in PC-DME,[7] and the number of THF is four in PC-THF.[27] That is, the ionic radius of the solvated Li^+ would be larger in PC-THF than in PC-DME since there is no great difference in molecular volume between THF and DME. It is considered that there is little difference in the degree of association between the two systems containing the same concentrations of the ethers. Thus the relatively large size of

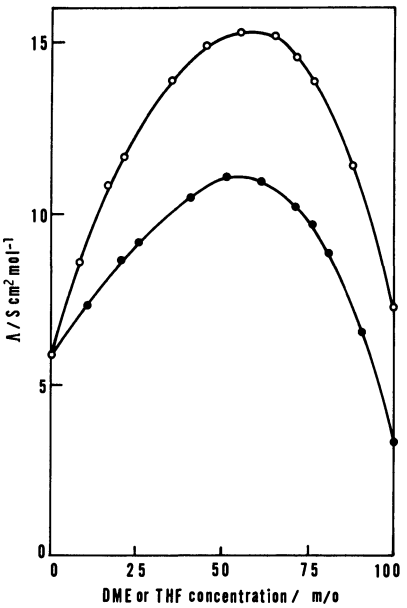

Fig. 6. Variation of Λ of 1 mol dm^{-3} $LiClO_4$ with the solvent composition.
○: PC-DME, ●: PC-THF.

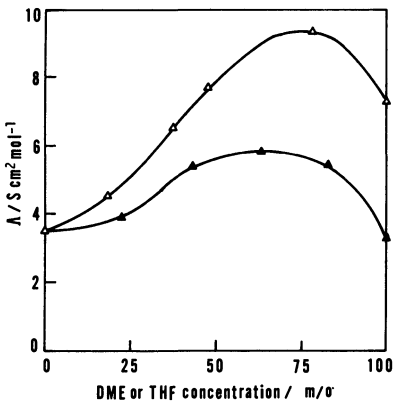

Fig. 7. Variation of Λ of 1 mol dm^{-3} $LiClO_4$ with the solvent composition.
△: S-DME, ▲: S-THF.

the Li^+–THF solvate would be responsible for the lower conductance in PC-THF than in PC-DME. An analogous explanation applies to the cases of S-DME and S-THF shown in Fig. 7. The S-THF/$LiClO_4$ (1 mol dm^{-3}) system shows a conductivity maximum at THF concentration of about 60 m/o. However, the maximum value of the conductivity in S-THF is only 70% of that in S-DME. On the other hand, the conductance in DMSO-THF was appreciably high unlike the cases of PC-THF and S-THF (Fig. 8). The conductivity of $LiClO_4$ in the DMSO-THF system varied in a similar manner and in the same magnitude as in the DMSO-DME system, except for the composition region of fairly high ether concentration. This means that the ion-solvent interaction, or the solvation, in the two systems is almost equivalent to each other. As DMSO has higher *DN* than DME

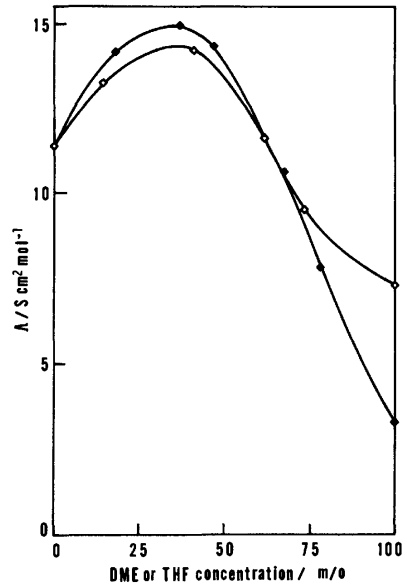

Fig. 8. Variation of Λ of 1 mol dm^{-3} $LiClO_4$ with the solvent composition.
◇: DMSO-DME, ◆: DMSO-THF.

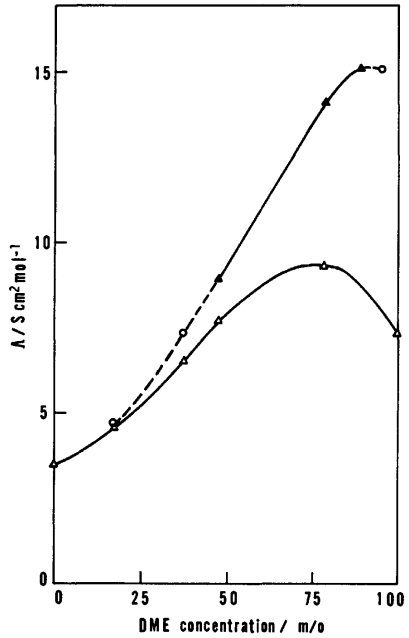

Fig. 10. Variation of Λ of 1 mol dm^{-3} $LiClO_4$ and $LiPF_6$ with the solvent composition.
△: S-DME/$LiClO_4$, ▲: S-DME/$LiPF_6$ (○: saturated $LiPF_6$).

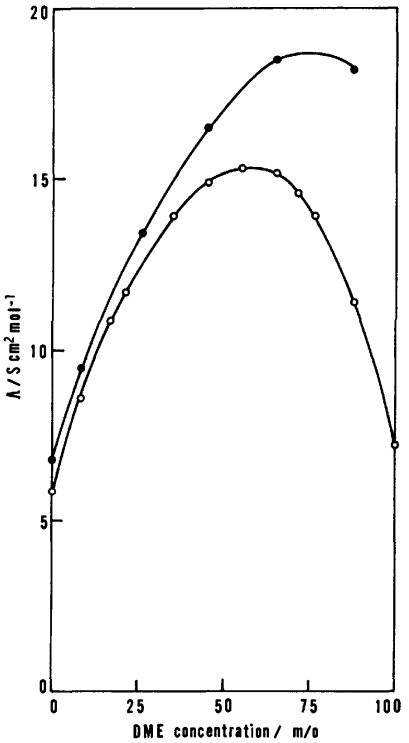

Fig. 9. Variation of Λ of 1 mol dm^{-3} $LiClO_4$ and $LiPF_6$ with the solvent composition.
○: PC-DME/$LiClO_4$, ●: PC-DME/$LiPF_6$.

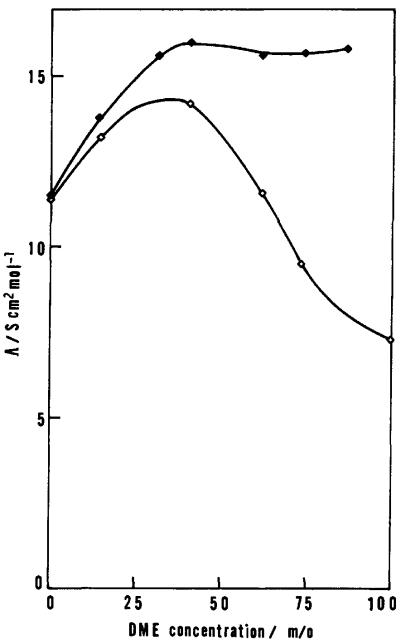

Fig. 11. Variation of Λ of 1 mol dm^{-3} $LiClO_4$ and $LiPF_6$ with the solvent composition.
◇: DMSO-DME/$LiClO_4$, ◆: DMSO-DME/$LiPF_6$.

or THF has, it is reasonable that DMSO coordinates preferentially to Li^+ in both systems. This description is consistent with the experimental results shown in Fig. 8. Besides the relatively low viscosity, the strong affinity of DMSO to Li^+, which leads to smaller size of solvated Li^+, might be related to the high conductance of $LiClO_4$ in neat DMSO compared with that in neat PC or S.

Influences of the anion on the conductance behavior of the Li salts were examined in PC-DME, S-DME, and DMSO-DME. Figures 9, 10, and 11 show the conductivity variations of 1 mol dm^{-3} $LiClO_4$ and $LiPF_6$. The solubility of $LiPF_6$ was rather low compared with that of $LiClO_4$. In S-DME, it was 1 mol

dm^{-3} or lower in the DME concentration range of < 40 or >95 m/o. The conductivity-solvent composition curves of $LiPF_6$ were almost identical to those of $LiClO_4$ in the DME concentration range up to about 40 m/o. The $LiPF_6$ solutions with high DME content showed relatively high conductance. A similar manner to this has been observed in the ether based electrolytes such as DME,[28] THF,[29,30] and 1,3-dixolane (DOL)[30] containing $LiAsF_6$ which is an analogous compound to $LiPF_6$. The reason why $LiAsF_6$ has higer conductance than $LiClO_4$ in these ether solvents has not sufficiently clarified yet.[30] The ion association will take place to a considerable extent in the ether-based electrolytes because of the low permittivity of the solvent and the relatively high concentration of the electrolyte. It is considered that the size of anion and hence the charge density at the spherical surface of anion would influence the ion-pair formation. It has been found that the two types of ion pairs may be present in solutions of high concentration or of low permittivity, i.e., solvent separated ion pairs and solvated contact ion pairs.[16,31] These are represented by the following chemical equilibria

$$(Li^+)S_n + A^- \rightleftharpoons (Li^+)S_nA^- \quad (2)$$

$$(Li^+)S_n + A^- \rightleftharpoons (Li^+A^-)S_{n-m} + mS, \quad (3)$$

where S represents a solvent molecule and A^- an anion.[1,31] It is possible that redissociation of solvent separated ion pairs occurs because of the long range nature of the coulomb force, and that the resulting free ions contribute to ionic conductance.[1] In other words, the difference in the types of ion pairs would appear in the difference of the ionic behavior, e.g., the association constants in the conventional treatment. The PF_6^- anion would be larger than ClO_4^- in its geometry[19] and hence the surface charge density of PF_6^- would be lower than that of ClO_4^-. Thus, in analogy with the $LiAsF_6$ solutions,[30] the solvent separated ion pairs would be liable to come out in the $LiPF_6$ solutions, while the contact ion pairs would be subject to form in the $LiClO_4$ solutions. These descriptions will interpret the result that the conductivities of the $LiPF_6$ solutions with high DME content were much higher than those of the $LiClO_4$ solutions.

The charge-discharge cycle characteristics of the Li electrode in S-DME/$LiPF_6$[11] and in DMSO-DME/$LiPF_6$[22] were much superior to those in the solutions containing $LiClO_4$. The $LiPF_6$ solutions consisting of the mixture of a high permittivity solvent and a low viscosity ether, which show high electrolytic conductivities, are very impressive for the practical use as the electrolytes of rechargeable Li batteries working at ambient temperatures.

The present work was partially supported by a Grant-in-Aid for Scientific Research No. 60490015 from the Ministry of Education, Science and Culture.

References

1) G. E. Blomgren, "Lithium Batteries," ed by J. P. Gabano, Academic Press, New York (1983), Chap. 2.
2) R. Jasinski, "Advances in Electrochemistry and Electrochemical Engineering," ed by P. Delahey and C. W. Tobias, Interscience, New York (1971), Vol. 8, p. 253.
3) H. Ikeda, T. Saito, and H. Tamura, *Denki Kagaku*, **45**, 314 (1977); H. Ikeda, S. Ueno, T. Saito, S. Nakaido, and H. Tamura, *ibid.*, **45**, 391 (1977).
4) M. Fukuda and T. Iijima, "Progress in Batteries and Solar Cells," ed by A. Kozawa et al., JEC Press, Cleveland (1978), Vol. 1, p. 26.
5) A. Morita, T. Iijima, T. Fujii, and H. Ogawa, *J. Power Sources*, **5**, 111 (1980).
6) Y. Matsuda and H. Satake, *Denki Kagaku*, **47**, 743 (1979); Y. Matsuda and H. Satake, *J. Electrochem. Soc.*, **127**, 877 (1980).
7) Y. Matsuda, H. Nakashima, M. Morita, and Y. Takasu, *J. Electrochem. Soc.*, **128**, 2552 (1981).
8) Y. Matsuda, Y. Yamamoto, and M. Morita, *Denki Kagaku*, **49**, 653 (1981).
9) Y. Matsuda, M. Morita, and K. Kosaka, *J. Electrochem. Soc.*, **130**, 101 (1983); Y. Matsuda, M. Morita, and K. Kosaka, *Denki Kagaku*, **51**, 119 (1983).
10) Y. Matsuda, M. Morita, and S. Kanameda, *Denki Kagaku*, **52**, 702 (1984).
11) Y. Matsuda, M. Morita, K. Yamada, and K. Hirai, *J. Electrochem. Soc.*, **132**, 2538 (1985).
12) S. Tobishima, J. Yamaki, and T. Okada, *Electrochim. Acta*, **29**, 1471 (1984).
13) S. Tobishima and T. Okada, *J. Appl. Electrochem.*, **15**, 317 (1985).
14) V. Gutmann, *Electrochim. Acta*, **21**, 661 (1976).
15) V. Gutmann, "The Donor-Acceptor Approach to Molecular Interactions," Plenum Press, New York (1978), Chap. 2.
16) R. Fernandez-Prini, "Physical Chemistry of Organic Solvent Systems," ed by A. K. Covington and T. Dickinson, Plenum Press, London (1973), Chap. 5.
17) J. Barthel, R. Watcher, and H.-J. Gores, "Modern Aspects of Electrochemistry," ed by B. E. Conway and J. O'M. Bockris, Plenum Press, New York (1979), Vol. 13, Chap. 1.
18) M. Salomon and E. Plichta, *Electrochim. Acta*, **28**, 1681 (1983).
19) S. Tobishima and T. Okada, *Electrochim. Acta*, **30**, 1715 (1985).
20) Y. Matsuda, Y. Ouchi, and H. Tamura, *J. Appl. Electrochem.*, **4**, 53 (1974).
21) C. K. Mann, "Electroanalytical Chemistry," ed by A. J. Bard, Marcel Dekker, New York (1969), Vol. 3, Chap. 2.
22) F. Tachihara, M. Morita, and Y. Matsuda, The 26th Battery Symposium in Japan, Kyoto, November 1985, Extended Abstr., No. 1A04.
23) Y. Matsuda, M. Morita, and T. Yamashita, *J. Electrochem. Soc.*, **131**, 2821 (1984).
24) Y. Marcus, "Introduction to Liquid State Chemistry," John Wiley and Sons, New York (1977), Chap. 3.
25) M. L. Jansen and H. L. Yeager, *J. Phys. Chem.*, **77**, 3089 (1973).
26) D. W. Watts, "Physical Chemistry of Organic Solvent

Systems," ed by A. K. Covington and T. Dickinson, Plenum Press, London (1973), Chap. 6.
27) S. Tobishima and A. Yamaji, *Electrochim. Acta*, **28**, 1067 (1983).
28) H. Farber, D. E. Irish, and S. Petrucci, *J. Phys. Chem.*, **87**, 3515 (1983).
29) J. Goldman, R. M. Mank, J. H. Young, and V. R. Koch, *J. Electrochem. Soc.*, **127**, 1461 (1980).
30) K. M. Abraham, *J. Power Sources*, **14**, 179 (1985).
31) I. R. Lantzke, "Physical Chemistry of Organic Solvent Systems," ed by A. K. Covington and T. Dickinson, Plenum Press, London (1973), Chap. 4.

Hydrogen Atom Transfer Reaction through Partial Charge-Transfer Triplet Complex. Chloranil and Mesitylene System

Harumichi KOBASHI,* Tadashi OKADA,† and Noboru MATAGA†
Department of Chemistry, Faculty of Engineering, Gunma University, Kiryu, Gunma 376
†Department of Chemistry, Faculty of Engineering Science, Osaka University, Toyonaka, Osaka 560
(Received January 20, 1986)

Mechanism and kinetics of hydrogen atom transfer reaction from mesitylene (M) to triplet chloranil (^{3}CA) in 1,2-dichloroethane (DCE) at room temperature have been studied by means of picosecond (ps) and nanosecond (ns) laser flash photolysis techniques. It was found that the hydrogen transfer resulting in the formation of chloranil semiquinone radical (CAH·) proceeded through a partial charge-transfer (CT) triplet complex between ^{3}CA and M as an intermediate. No ion-pair formation was observed. The triplet complex showed transient absorption bands in the visible and near infrared regions. The association constant (K_T=28 dm^3 mol^{-1}) and lifetime (τ_C=32 ns) of the complex were estimated from a kinetic analysis for ^{3}CA quenching. From these results, combined with those of the quantum yield of CAH· formation, the first order rate constants for the hydrogen transfer and intersystem crossing in the triplet complex were estimated to be (1.7 and 1.4)×10^7 s^{-1}, respectively.

Photoinduced H atom abstraction reactions of quinones exhibit very complicated features depending on properties of H donors and solvents. Although many investigations have suggested the participation of a triplet exciplex as an intermediate, detailed studies by direct observation of short lived triplet exciplexes are still rather scarce[1-4] and desirable to elucidate the reaction mechanisms.

In a previous paper we reported the intermediation of a triplet ion pair (or exciplex with complete CT) between chloranil radical anion (CA^-) and durene radical cation (DH^+) in the course of H atom transfer from durene (DH) to ^{3}CA in DCE; i.e., a two-step mechanism via the ion pair.[1] Simultaneously, we showed the existence of a fast H atom transfer competing with the ion-pair formation. The mechanism of the fast transfer was suggested to be, substantially, also a two-step mechanism via transitory electron transfer immediately followed by a proton transfer in a collision complex with a geometrical conformation favorable to cause the fast transfer. In relation to this, it is of interest whether such a fast H atom transfer can take place commonly for the case of CA (acceptor) and other methylated benzene (donor) systems where a complete electron transfer does not occur between the donor and acceptor. Since M has an ionization potential (I_P=8.4 eV)[5] higher than that of DH (I_P= 8.03 eV),[5] it is expected that such a complete electron transfer does not take place between ^{3}CA and M.

This paper describes a laser photolysis study of H abstraction for the system of CA and M in DCE. Results indicate that the production of CAH· proceeds through the partial CT triplet complex between ^{3}CA and M, $^3(CA^{\delta-}\cdots M^{\delta+})$, but not an ion pair, and that no fast H transfer competes with the complex formation. The first-order rate constants for the H transfer and intersystem crossing in the triplet complex have been estimated by kinetic analysis.

Experimental

Transient absorption spectra were measured by the same ps and ns ruby laser photolysis systems as used previously.[1] The R636 and R406 (Hamamatsu Photonics) photomultipliers were used for the ns photolysis in the 320—825 and 500—1000 nm regions, respectively. The ground state absorption spectra were measured with a Hitachi Model 200 spectrophotometer. Chloranil (CA: Tetrachloro-*p*-benzoquinone) was the same material as purified previously.[1] The GR grade mesitylene (M: 1,3,5-trimethylbenzene) was distilled under vacuum after dried with calcium hydride or Zeolite 4A. 1,2-Dichloroethane (DCE) as a solvent was purified by the usual method. Sample solutions for ns laser photolysis were degassed by freeze-pump-thaw cycles and those for ps laser photolysis were purged with dry nitrogen gas. Transient absorption measurements were carried out at 25 °C unless otherwise stated.

Results

Ground State Complex Formation. It is well-known that the present donor-acceptor pair forms an electron donor-acceptor (EDA) complex, CA···M, in the ground state.[6] We have confirmed this in DCE by means of the electronic absorption spectroscopy. Since a large part of the CT band of the complex overlapped the absorption band of free CA in the 350—450 nm range, we determined the values of the complex formation constant (K_G=0.31±0.08 dm^3 mol^{-1}) and the extinction coefficient of the CT band at 410 nm (ε_{410}= 3270±930 dm^3 mol^{-1} cm^{-1}) at 20 °C by the Rose-Drago's method.[7] This K_G value for the M donor is smaller than that for the DH donor (0.89 dm^3 mol^{-1})[1] as expected from the difference in their ionization potentials.

Quenching Curve of ^{3}CA. The T_n—T_1 absorption of ^{3}CA was quenched efficiently by added M. The decay kinetics monitored at 510 nm obeyed the first-order rate law throughout all concentrations (1.4×10^{-3}—0.32 mol dm^{-3}) of M examined. The plot of observed decay

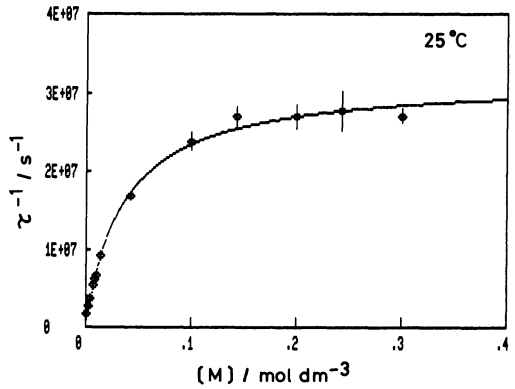

Fig. 1. A plot of the inverse lifetime τ^{-1} of ^{3}CA against the concentration of M at 25 °C. ○: The observed value with error bar, ——: the calculated curve with K_T=27.89 dm^3 mol^{-1}, τ_c=31.55 ns, and τ_0=4.325 μs obeying Eq. 5.

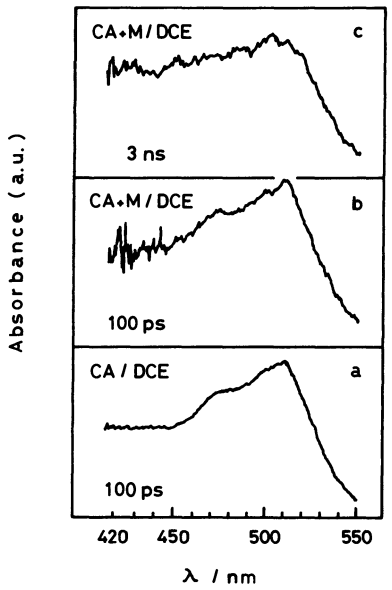

Fig. 2. Transient absorption spectra obtained by the ps laser photolysis for the solutions of CA (5.5×10^{-3} mol dm^{-3}) alone (a) and CA (5.5×10^{-3} mol dm^{-3}) plus M (0.32 mol dm^{-3}) (b and c) in DCE. Delay times: (a) 100 ps, (b) 100 ps, and (c) 3 ns. The absorbance is not corrected for the shot to shot variations of the excitation pulse intensity.

rate (τ^{-1}: the inverse of the lifetime) as a function of [M] is given in Fig. 1. The quenching curve tends to approach an asymptotic value on going to higher [M], which suggests the existence of a reverse process from a reaction intermediate such as exciplex.[8]

Picosecond Laser Photolysis. Figure 2 illustrates transient absorption spectra obtained by the ps laser photolysis. The spectrum observed for the solution of CA alone at 100 ps delay time (Fig. 2a) shows the band peaking at 510 nm, which is very similar to that of ^{3}CA obtained previously by the ns laser photolysis.[9] Since the intersystem crossing from the lowest excited singlet to the triplet state is very rapid,[1,10] the spectrum of Fig. 2a is assigned to the absorption band due to ^{3}CA. In the

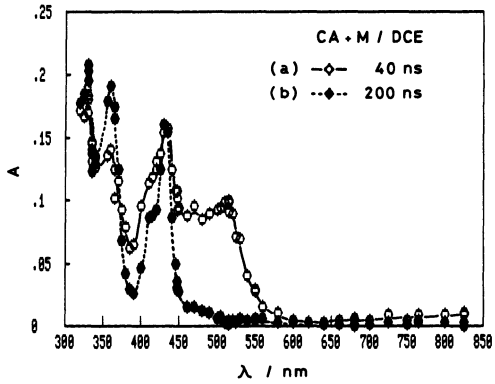

Fig. 3. Time-resolved absorption spectra obtained by the ns laser photolysis for the CA (3.0×10^{-3} mol dm^{-3}) and M (0.30 mol dm^{-3}) system in DCE. Delay times: (a) 40 ns and (b) 200 ns after the start of laser oscillation.

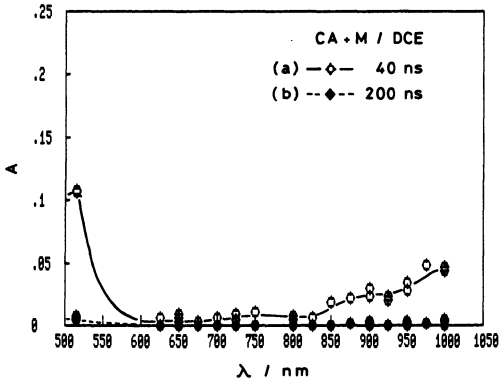

Fig. 4. Transient absorption spectra for the CA-M-DCE system in the long wavelength region. Delay times and concentrations of CA and M are the same as those in Fig. 3.

presence of M (0.32 mol dm^{-3}), the spectrum observed at 100 ps (Fig. 2b) resembles quite well with that of ^{3}CA (Fig. 2a). The spectrum at 3 ns (Fig. 2c) is also similar to that of Fig. 2a, although it shows slightly different features; the lack of vibrational structure and a slightly high absorbance in the 420—450 nm region relative to that at 510 nm. It should be noted that no absorption peaks were observed at 435 and 448 nm, which correspond to the characteristic bands of CAH· and CA^-, respectively.

Nanosecond Laser Photolysis. Time resolved absorption spectra obtained by the ns laser photolysis is given in Fig. 3. The spectrum immediately after excitation (Fig. 3a) shows an absorption band similar to that of Fig. 2c, in the 450—550 nm region. After the passage of time, this band around 510 nm disappears and strong absorption bands at 435, 360, and 325 nm, which are partly observed already in Fig. 3a, become remarkable (Fig. 3b). Among these bands, the 435 and 360 nm bands can be ascribed to CAH· produced by the H abstraction reaction by comparing them with those of CAH· observed previously in the CA and DH system[1] as well as in other related systems.[2,9] The

sharp band around 325 nm may be assigned to 3,5-dimethylbenzyl (M·) radical[11] produced by an H atom release from M, which is analogous to the formation of the benzyl-type 2,4,5-trimethylbenzyl (D·) radical observed in the CA–DH system.[1]

Figure 4 shows the transient spectra in the VIS and near IR region observed by using the R406 photomultiplier. The absorption from 800 to 1000 nm is clearly observed in the early stage after excitation, which was not detected in the absence of M. This long wavelength band disappears simultaneously with the band around 510 nm. The decay times observed at 975 as well as 1000 nm agree with that measured at 510 nm (τ=38±3 ns at 25 °C).

The decay kinetics of long lived CAH· was second-order; plot of the inverse of absorbance at 435 nm against time gave a straight line with the slope of 1.76×10^{6} s^{-1}. Using this value together with those of the molar extinction coefficient of CAH· at 435 nm ($\varepsilon_{CAH\cdot}(435)=1.0\times10^{4}$ dm^3 mol^{-1} cm^{-1})[1] and the effective length of optical path (l=0.90 cm), the second-order decay rate constant of CAH· is estimated to be 1.6×10^{9} dm^3 mol^{-1} s^{-1} at 25 °C. This value is approximately equal to that of CAH· (1.4×10^{9} dm^3 mol^{-1} s^{-1}) estimated previously in the CA–CAH_2 (tetrachlorohydroquinone)–DCE system.[9]

Determination of CAH· Yield. Under the condition of a constant laser intensity, the yield of CAH· (Φ_h) generated from ^{3}CA can be related to the following equation.

$$\Phi_h = \frac{A_{CAH\cdot}(435)/\varepsilon_{CAH\cdot}(435)}{A_{^3CA}(510)/\varepsilon_{^3CA}(510)} \quad (1)$$

where $A_{^3CA}(510)$ and $A_{CAH\cdot}(435)$ are the absorbance at 510 nm of ^{3}CA initially excited and that at 435 nm of produced CAH·, respectively, in a mixed solution of CA and M. $\varepsilon_{^3CA}(510)$ is the molar extinction coefficient of ^{3}CA at 510 nm; $\varepsilon_{^3CA}(510)=7.3\times10^{3}$ dm^3 mol^{-1} cm^{-1}.[1] On the addition of M of the concentration less than 2×10^{-2} mol dm^{-3}, the solution of CA (2.0×10^{-3} mol dm^{-3}) showed only little change (<3%) in the absorbance at 347 nm in the ground state, corresponding to little contribution of the ground state complex formation (<1%). Therefore, no correction for a small change in the concentration of the initially excited ^{3}CA was made in the photolysis at 347 nm for solutions involving a constant concentration of CA (2.0×10^{-3} mol dm^{-3}) regardless of the presence and absence of M when [M] was less than 2×10^{-2} mol dm^{-3}. At a relatively higher concentration of M in this concentration range, however, the quenching of ^{3}CA could not be neglected even at the time immediately after excitation by the laser pulse of ca. 25 ns fwhm. It was then necessary to estimate the true $A_{^3CA}(510)$ value using a separate solution as a reference. Since the absorbance change at 347 nm by the mixing of CA and M was negligible, a solution of CA alone containing the equal concentration to those of the mixed solutions could be used as a reference solution. Therefore, $A_{^3CA}(510)$ for the mixed solution can be replaced by the absorbance of ^{3}CA at 510 nm observed immediately after the excitation of the reference solution. $A_{CAH\cdot}(435)$ was obtained by observing the absorbance at 435 nm immediately after the decay of ^{3}CA in the mixed solution. CAH· did not show decay practically in the time range required for this estimation. Thus, Φ_h values were estimated to be 0.54 and 0.53 for the solutions of [CA]=2.0×10^{-3} mol dm^{-3} with [M]=4.0×10^{-3} and 1.6×10^{-2} mol dm^{-3}, respectively.

Discussion

Formation of a Partial CT Triplet Complex. As is shown in Figs. 2(b, c) and 3, no appreciable absorption band characteristic to CA^- was found around 450 nm both in ps and ns time regions. This result indicates clearly that an ion pair between CA^- and M^+ (mesitylene radical cation) is not formed in the present system,[12] contrary to the case of the CA–DH system[1] where dominant ion-pair formation takes place in the early stage after excitation. The reaction between ^{3}CA and M apparently leads to the formation of neutral radicals CAH· and M· as a result of H atom transfer from M to ^{3}CA (Fig. 3b).

The existence of intermediate complex which was suggested from the profile of quenching curve (Fig. 1) is supported also by the following results. It is expected that an EDA complex between CA and M is produced more efficiently in the triplet state than in the ground state, since ^{3}CA has a higher electron affinity than CA by the energy required for excitation from the ground to the triplet state; i.e., generally

$$E_A(^3A) = E_A(^1A) + E_T \quad (2)$$

where $E_A(^3A)$ is the electron affinity of the triplet state acceptor ^3A, $E_A(^1A)$ corresponds to that of the ground state acceptor ^1A, and E_T is the excitation energy to the triplet state. Combining Eq. 2 with the approximate relation,[13]

$$h\nu_{CT} = \text{const.} - E_A(^1A), \quad (3)$$

we can derive the following approximate equation,[2,14] assuming the same value for const.

$$h\nu_{^3CT} = h\nu_{CT} - E_T. \quad (4)$$

In Eqs. 3 and 4, $h\nu_{CT}$ and $h\nu_{^3CT}$ denote the transition energies of CT band of the ground and triplet state EDA complexes, respectively. When we use the values of E_T=2.13 eV for ^{3}CA[15] and $h\nu_{CT}$=3.02 eV (corresponding to the CT band of CA···M at 410 nm) in Eq. 4, the CT band of the triplet complex can be estimated to lie around ca. 1380 nm. The broad absorption band observed in the 800—1000 nm region (Fig. 4a),

which would have an absorption maximum beyond 1000 nm, may correspond to the CT band estimated above.

In view of the above results, we analyze the quenching data given in Fig. 1 on the basis of complex formation. Since the observed decay curves were exponential, the so called "dynamic equilibrium" would be established under the present experimental conditions.[16] In the equilibrium state, one can derive the following relation;[8,16]

$$\tau^{-1} = (\tau_0^{-1} + K_T[M]\tau_c^{-1})/(1 + K_T[M]) \quad (5)$$

where K_T is the formation constant of the triplet complex, τ and τ_0 are the decay times of ^{3}CA in the presence and absence of M, and τ_c is the lifetime of the complex. As is illustrated in Fig. 1, the experimental values of τ^{-1} are reproduced satisfactorily by the curve calculated with Eq. 5 employing the values, K_T=27.89 dm^3 mol^{-1}, τ_0=4.325 μs, and τ_c=31.55 ns which are determined by the least square method. The value of τ_0 (4.3 μs) is close to the observed one (5.6 μs) of pseudo first-order decay time of ^{3}CA in the absence of M.[9] The K_T value (28 dm^3 mol^{-1}) is significantly larger than the K_G value (0.31 dm^3 mol^{-1}), indicating that in the triplet state the complex formation is more favorable than in the ground state. This result agrees with the expectation from the larger electron affinity of ^{3}CA than CA mentioned above. Thus, the complex formation in the triplet state has been rationalized from the kinetic analysis as well as the detection of CT band.

We can estimate using the K_T value that in the equilibrium state 89% of ^{3}CA molecules are present as the triplet complex in the solution containing 0.30 mol dm^{-3} M. Hence, the intensity of absorption band around 510 nm in Fig. 3a (the spectrum at 40 ns) may be attributed mainly to the complex. That is, the triplet complex should have the absorption band around 510 nm as well as that in the near IR region. Since the absorption band around 510 nm is characteristic of ^{3}CA unit, the observed spectra in the presence of M may be assigned to the locally excited (LE) triplet state with a partial CT character; $^3(CA^{\delta-}\cdots M^{\delta+})$.

Reaction Mechanism of H Atom Transfer. In the solution of [CA]=5.5×10^{-3} and [M]=0.32 mol dm^{-3} submitted to the ps laser photolysis experiments, the absorbance due to the ground state complex reaches 38% of the total absorbance at 347 nm for the laser excitation, although CA is present by only 9% as the complex in the ground state. Under these conditions, therefore, the excellent similarity between Figs. 2a and 2b appears to indicate that a direct excitation of the ground state complex does not lead to the fast formation of CAH· as well as the ion pair.[17]

A rate constant for the formation of an outer complex can be usually approximated to be a diffusion controlled one (8.4×10^9 dm^3 mol^{-1} s^{-1} at 25 °C), so that ^{3}CA would collide with M of 0.32 mol dm^{-3} frequently enough to establish the equilibrium concerning the triplet complex formation during 3 ns delay time. Because the equilibrium in the triplet state shifts largely to the side of the complex formation (90% mole fraction), the spectrum at 3 ns (Fig. 2c) may be regarded mainly as that of the triplet complex. In addition, Fig. 2c can not be reproduced by the superposition of spectra of ^{3}CA (Fig. 2a) and CAH·. It is then implied that no CAH· is produced simultaneously with the triplet complex, if the spectrum of the triplet complex is almost the same as that of free ^{3}CA. Therefore, the fast H atom transfer competing with the formation of the triplet complex does not occur and CAH· is formed concomitantly with decrease of the triplet complex (Fig. 3).

Thus, a combination of ps and ns laser photolysis results allows us to conclude that the H atom transfer reaction proceeds via the triplet complex formation followed by H atom transfer from M to ^{3}CA in the complex. The reaction scheme may be written as follows.

$$\begin{array}{ccccc} {}^3CA + M & \overset{K_T}{\rightleftharpoons} & {}^3(CA^{\delta-}\cdots M^{\delta+}) & & \\ \tau_0^{-1}\downarrow & & k_d\downarrow & \searrow k_h & \\ CA + M & \overset{K_G}{\rightleftharpoons} & CA\cdots M & CAH\cdot + M\cdot & \end{array}$$

where τ_0 is the lifetime of ^{3}CA in the absence of M, k_d, and k_h are the rate constants for the intersystem crossing and H atom transfer processes in the triplet complex, respectively, and K_T and K_G are the equilibrium constants, respectively, as defined before.[18] The present mechanism of H abstraction is in a striking contrast with that for the case of CA and DH system where the H transfer proceeds mainly through the ion pair $CA^{\cdot-}\cdots DH^+$ formation followed by proton transfer and partly through the fast H transfer taking place competing with the ion-pair formation.[1] This difference in the mechanism seems to result from the level inversion between the zeroth order LE and CT states in the triplet complexes; i.e., the former state is lower than the latter one for the case of M donor and vice versa for the case of DH donor.

Estimation of k_h and k_d. Under the dynamic equilibrium condition between species A and B, in general, the mean rate parameter $\bar{k}$ for a certain process is given by the weighted mean of the corresponding rate parameters of A (k_A) and B (k_B) as follows:[16]

$$\bar{k} = k_A\chi_A + k_B\chi_B \quad (6)$$

where χ_A and χ_B are the mole fractions of A and B respectively. When A and B correspond respectively to ^{3}CA and $^3(CA^{\delta-}\cdots M^{\delta+})$, we can put $\bar{k}=\Phi_h/\tau$, $k_A=\phi_0/\tau_0$, $k_B=\phi_h/\tau_c$, $\chi_A=1/(1+K_T[M])$, and $\chi_B=K_T[M]/(1+K_T[M])$ for the H abstraction by ^{3}CA, so that Eq. 6 yields the following expression:

$$\Phi_h = \left(\frac{1}{1+K_T[M]}\cdot\frac{\phi_0}{\tau_0} + \frac{K_T[M]}{1+K_T[M]}\cdot\frac{\phi_h}{\tau_c}\right)\cdot\tau \quad (7)$$

Table 1. The Estimated Efficiencies (ϕ_h) of Hydrogen Transfer in the Triplet Complex along with the Observed Lifetimes (τ) of 510 nm Absorption and Yields (Φ_h) of CAH·

[CA]	[M]	τ	Φ_h	ϕ_h
10^{-3} mol dm^{-3}	10^{-3} mol dm^{-3}	ns		
2.0	4.0	297	0.54	0.56
2.0	16	103	0.53	0.54
				av. 0.55

where ϕ_0 is the efficiency of CAH· production by H abstraction of ^{3}CA from the solvent DCE, ϕ_h is the efficiency of CAH· formation from $^3(CA^{\delta-}\cdots M^{\delta+})$, and other parameters are the same as defined in Eqs. 1 and 5. According to Eq. 7, ϕ_h at each [M] can be estimated as far as Eq. 5 holds. Using the values of K_T=28 dm^3 mol^{-1}, τ_c=32 ns, τ_0=4.3 μs, and ϕ_0=0.19,[9] we obtained an average value ϕ_h=0.55 corresponding to the Φ_h values, 0.54 and 0.53, at [M]=4.0×10^{-3} and 1.6×10^{-2} mol dm^{-3}, respectively. Results are listed in Table 1. From these results, k_h=1.7×10^7 s^{-1} and k_d=1.4×10^7 s^{-1} are estimated. The k_h value is larger than the proton transfer rate constant k_p (2×10^6 s^{-1} at 20 °C) of the reaction $CA^{\cdot-}\cdots DH^+ \rightarrow CAH\cdot + D\cdot$, although the k_d value is the same order of magnitude as a corresponding rate constant k_d (1.3×10^7 s^{-1} at 20°C) of the ion pair.

Above results show clearly that the difference in nature of the intermediate complexes; i.e., the partial CT and the complete CT triplet complexes, is reflected in the rate constant of the hydrogen atom transfer between electron donor and acceptor pairs. It would be worthwhile to note that the difference by only one in the number of methyl group in the homologeous series of methylated benzene donors caused a drastic change in the mechanism of the quenching of ^{3}CA.

References

1) H. Kobashi, M. Funabashi, T. Kondo, T. Morita, T. Okada, and N. Mataga, *Bull. Chem. Soc. Jpn.*, **57**, 3557 (1984).

2) H. Kobashi, Y. Tomioka, and T. Morita, *Bull. Chem. Soc. Jpn.*, **52**, 1568 (1979).

3) H. Kobashi, E. Sunoh, and T. Morita, Symposium on Photochemistry, Tokyo December 1979, Abstr. No. BIII-210; *Chem. Abstr.*, **93**, 45538t (1980).

4) a) V. A. Kuzmin, A. P. Darmanyan, and P. P. Levin, *Chem. Phys. Lett.*, **63**, 509 (1979); b) P. P. Levin and T. A. Kokrashvili, *Bull. Akad. Sci. USSR, Div. Chem. Sci.*, **30**, 971 (1981); c) P. P. Levin, T. A. Kokrashvili, and V. A. Kuzmin, *Bull. Akad. Sci. USSR, Div. Chem. Sci.*, **32**, 251 (1983).

5) K. Watanabe, T. Nakayama, and J. Mottl, *J. Quant. Spectrosc. Radiat. Transfer*, **2**, 369 (1962).

6) a) G. Briegleb, "Elektron-Donor-Acceptor-Komplexe," Springer-Verlag, Berlin (1962); b) R. Foster, "Organic Charge-Transfer Complexes" Academic Press, London (1969).

7) N. J. Rose and R. S. Drago, *J. Am. Chem. Soc.*, **81**, 6138 (1959).

8) W. R. Ware, D. Watt, and J. D. Holmes, *J. Am. Chem. Soc.*, **96**, 7853 (1974).

9) H. Kobashi, H. Gyoda, and T. Morita, *Bull. Chem. Soc. Jpn.*, **50**, 1731 (1977).

10) a) E. F. Hilinski, S. V. Milton, and P. M. Rentzepis, *J. Am. Chem. Soc.*, **105**, 5193 (1983); b) P. M. Rentzepis, D. W. Steyert, H. D. Roth, and C. J. Abelt, *J. Phys. Chem.*, **89**, 3955 (1985).

11) K. Schested, H. Corfitzen, H. C. Christensen, and E. J. Hart, *J. Phys. Chem.*, **79**, 310 (1975).

12) In Fig. 3b, a weak absorption band in the 450—500 nm region remains as a tail of the strong absorption band of CAH· which has no absorption band in this wavelength region.[1] The time dependence of absorbance at 448 nm showed a small rise following a fast partial decay and then decayed slowly with nearly identical behavior to that of CAH·; i.e., the second-order decay. Since the spectral profile of this band is rather similar to that of $CA^{\cdot-}$, we attempted to measure a transient photocurrent by the same way as described previously.[1] The weak current was observed in the solution containing CA (3.0×10^{-3} mol dm^{-3}) and M (0.30 mol dm^{-3}). Its decay followed exactly the second-order kinetics but its rise time (ca. 49 ns) longer than the decay time of the triplet complex did not coincide with the rise time (ca. 0.9 μs) of the 448 nm absorption band. A similar absorption band was also observed with a long life in ethyl acetate as a solvent while the transient photocurrent did not flow at all. These results indicate that the absorption band decaying slowly with approximate second-order kinetics is not due to the ion pair $CA^{\cdot-}\cdots M^+$ produced from, or in the equilibrium with, the triplet complex. If $CA^{\cdot-}\cdots M^+$ was present, the decay time of $CA^{\cdot-}\cdots M^+$ would be short as supposed from similarity with the lifetime (49 ns) of the ion pair $CA^{\cdot-}\cdots D^+$.[1] Therefore, it may be plausible to consider that the weak band gives no evidence for the formation of $CA^{\cdot-}\cdots M^+$, although the origins of this band and the photocurrent in DCE are not clear at the present stage of investigation.

13) G. Briegleb, *Angew. Chem.*, **76**, 326 (1964).

14) K. Kawai, Y. Shirota, H. Tsubomura, and H. Mikawa, *Bull. Chem. Soc. Jpn.*, **45**, 77 (1972).

15) N. A. Shcheglova, D. N. Shigoline, G. G. Yakobson, and L. Sh. Tushishvili, *Zh. Fiz. Khim.*, **43**, 1984 (1969).

16) J. B. Birks, "Photophysics of Aromatic Molecules," Wiley-Interscience, London (1970), p. 309.

17) This result suggests that the excited singlet state of the complex which should be produced by the direct excitation undergoes an immediate relaxation to the $^3(CA^{\delta-}\cdots M^{\delta+})$ and/or $CA\cdots M$ state through ISC and/or IC. It is not clear whether the direct excitation of the EDA complex affords no triplet complex. At the present stage, however, it is sufficient to note that no CAH· forms immediately after the excitation of the EDA complex.

18) The process of a relatively slow H abstraction from the solvent DCE by ^{3}CA[9] is omitted in the scheme, but for a quantitative purpose one must take this process into consideration as being included in the relaxation process of ^{3}CA with the rate constant τ_0^{-1}.

Motions of Tetramethylammonium Cations and Phase Transitions in Solid $[(CH_3)_4N]_2CdX_4$ (X=Cl, Br, I) as Studied by ^1H NMR, Powder X-Ray Diffraction, and Differential Thermal Analysis Measurements

Setsuko SATO, Ryuichi IKEDA, and Daiyu NAKAMURA*
Department of Chemistry, Faculty of Science, Nagoya University, Chikusa-ku, Nagoya 464
(Received January 31, 1986)

The temperature dependences of ^1H spin-lattice relaxation times were determined at 20 MHz for $[(CH_3)_4N]_2CdCl_4$, $[(CH_3)_4N]_2CdBr_4$, and $[(CH_3)_4N]_2CdI_4$. For the last two complexes, the frequency dependence of the relaxation time was observed above room temperature. ^1H NMR second moments were observed for the bromide complex. At room temperature, the first two complexes were found to be isomorphous with the iodide complex which forms orthorhombic crystals. Differential thermal analysis experiments revealed that these complexes undergo four, one, and one solid-solid phase transitions in the above order between ca. 80 and 430 K. Two ^1H T_1 minima were clearly observed at lower temperatures for the chloride and bromide complexes, whereas at least three ^1H T_1 minima partly overlapped with each other were detected at lower temperatures for the iodide complex. For the former two complexes, the ^1H T_1 data were well analyzed by the general method already reported. For the bromide and iodide complexes, ^1H T_1 curves observed showed a maximum above room temperature. Motions of the cation activated in these complexes are discussed in relation to the crystal field experienced by the cation.

Dynamic behavior of tetramethylammonium $(tetMA)^+$ cations in various crystalline salts has been studied fairly in detail by means of ^1H NMR techniques.[1-11] The motions of the cation contributing to ^1H spin-lattice relaxation times (T_1) around room temperature have been shown to be random reorientations of CH_3 groups about each C–N bond axis by 120°, i.e., the C_3 reorientations, and overall reorientations of the cations about the center of gravity. It has been revealed through the temperature dependence measurements of ^1H T_1 that the activation energies (E_a) for the CH_3 C_3 reorientation of the above salts except $(tetMA)CdCl_3$[11] are in a range of 15—30 kJ mol^{-1}. The widely spread values of E_a observed indicate that the potential barriers to reorient arising from interionic as well as intraionic forces contribute to E_a for the CH_3 C_3 reorientation of the cation.

When the cations are located in a weak crystal field formed by surroundings such as those in $(tetMA)_2MBr_6$ (M=Sn, Te, Pt), E_a for the CH_3 C_3 reorientation is thought to be mostly determined by the intraionic potential barrier.[10] In these crystals, the four CH_3 groups in the cation are equivalent because of the position of the cation having a high site symmetry and the E_a values observed are ca. 17 kJ mol^{-1}. If the cation is placed at a low-symmetric lattice site, however, it is supposed that the cation is somewhat distorted owing to an asymmetric crystal field and the four CH_3 groups become nonequivalent. For the distorted cations, we can expect that they show ^1H T_1 through unique motional processes different from those found for the high symmetric cations. In the present investigation, we have selected $(tetMA)_2CdX_4$ (X=Cl, Br, I) as an example of the salts having the cations distorted and the measurements of the temperature dependences of ^1H NMR parameters, X-ray powder diffraction, and differential thermal analysis (DTA) have been undertaken to obtain detailed information about the motion of the slightly distorted cations.

Experimental

Wide-line ^1H NMR absorptions were recorded to evaluate ^1H NMR second moments (M_2) at several temperatures by use of a JEOL JNM-MW-40S spectrometer operated at 40 MHz. The temperature dependences of ^1H T_1 were measured at the Larmor frequencies of 9, 12, 20, and 45.7 MHz by means of pulsed spectrometers already reported.[9,12] The conventional inversion recovery method was employed to determine T_1 values. DTA experiments were performed using a homemade apparatus.[13] For the foregoing measurements, temperatures were determined by use of copper constantan thermocouples with the accuracy of ±3 K for the wide-line NMR and ±1 K for the other measurements. X-Ray powder patterns were recorded at room temperature using a Model D-3F diffractometer from Rigaku Denki Co. equipped with a copper anticathode.

$(tetMA)_2CdCl_4$ was synthesized by slowly evaporating the solvent after mixing two methanol solutions of $2CdCl_2 \cdot H_2O$ and (tetMA)Cl in a molar ratio of 1:8.[14] $(tetMA)_2CdBr_4$ was prepared in a similar manner from the corresponding bromides. Crystals of these salts obtained were purified by recrystallization from methanol by adding a small amount of the corresponding tetramethylammonium halides. $(tetMA)_2CdI_4$ was obtained by mixing the aqueous solutions of stoichiometric amounts of CdI_2 and (tetMA)I. The colorless crystals obtained were recrystallized from water. The above crystals prepared and purified were dried over phosphorus pentaoxide in a vacuum desiccator and were sealed in glass ampoules for the measurements of NMR and DTA after evacuating ambient air and then putting in a small amount of helium exchange gas. $(tetMA)_2CdCl_4$ and $(tetMA)_2CdBr_4$ were identified by chemical analysis. Anal. Calcd for $[(CH_3)_4N]_2CdCl_4$: Cl, 35.2; C, 23.9; H, 6.0%. Found: Cl, 35.1; C, 23.7; H, 6.1%. Calcd for $[(CH_3)_4N]_2CdBr_4$: Br, 55.1; C, 16.6; H, 4.2%. Found: Br, 55.0; C, 16.7; H, 4.2%. $(tetMA)_2CdI_4$ was identified by taking X-ray powder patterns. All diffrac-

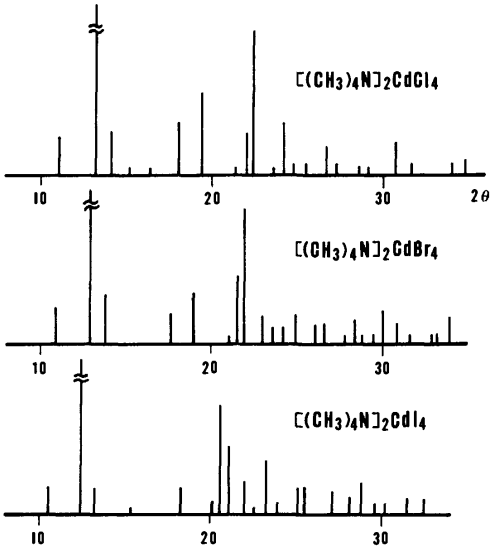

Fig. 1. X-Ray powder patterns taken at room temperature for tetramethylammonium tetrachloro- and tetrabromocadmate(II). Those of tetraiodocadmate-(II) are given for comparison.

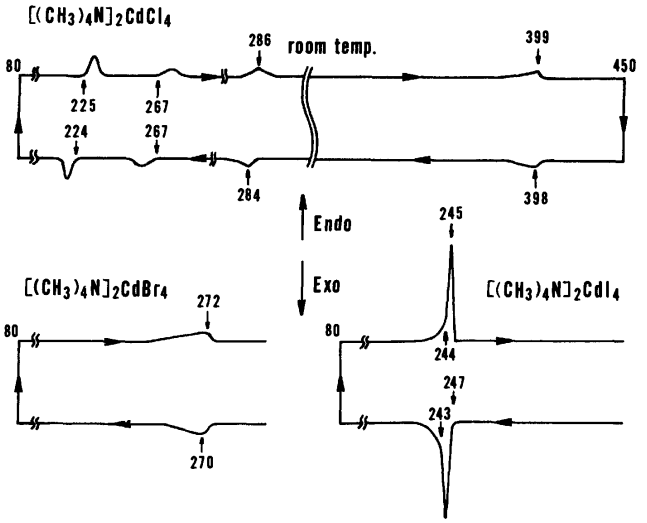

Fig. 2. DTA curves recorded for tetramethylammonium tetrachloro-, tetrabromo-, and tetraiodocadmate(II). Heat anomalies observed for tetrachlorocadmate(II) near 285 K are so small that they are enlarged about three times and shown in the figure. Temperatures measured in K are given only by figures.

tion lines detected were completely indexed in terms of an orthorhombic lattice having the lattice constants a=13.409, b=9.724, and c=16.894 Å already reported by Kallel et al.[15]

Results

From X-ray powder patterns taken at room temperature, the crystals of $(tetMA)_2CdCl_4$ and $(tetMA)_2CdBr_4$ were proved to be isomorphous with that of $(tetMA)_2CdI_4$. The powder patterns recorded for the three complexes are shown in Fig. 1. These patterns could be interpreted by the orthorhombic structure of many $(tetMA)_2MX_4$ type tetrahedral complexes[16–18] belonging to the space group *Pnma* with Z=4. The lattice constants determined were a=12.47, b=9.12, and c=15.81 Å for $(tetMA)_2CdCl_4$ and a=12.78, b=9.33, and c=16.19 Å for $(tetMA)_2CdBr_4$.

DTA curves recorded between ca. 80 and 450 K for the three complexes are shown in Fig. 2.

When $(tetMA)_2CdCl_4$ was heated from room temperature, a very small endothermic anomaly having a tail on the low temperature side appeared. The peak temperature of the anomaly was 399 K. An exothermic anomaly having a similar shape to the endothermic one and almost the same peak temperature appeared on cooling. Various methylammonium salts are known to show characteristic small heat anomalies showing no hysteresis phenomena about the peak temperature similar to the present one.[13,19–23] For these salts, we could unequivocally determine the phase transition temperature (T_{tr}) to be the peak temperature of DTA curves by comparing with the results of NQR studies which yield more accurate information about the alteration of crystal structure taking place especially in ionic crystals.[13,19–24] Accordingly, we can conclude that $(tetMA)_2CdCl_4$ undergoes a second order phase transition at 399 K.

When $(tetMA)_2CdCl_4$ was cooled from room temperature, three small exothermic anomalies appeared, the starting temperatures of which were 287, 267, and 224 K. Among these anomalies, the highest temperature one was very small. With increasing temperature, endothermic anomalies appeared at 225 and 267 K which were the initial temperatures and at 286 K determined as the peak temperature. Since the initiating temperature of the last one could hardly be determined because of its weakness and also broadness, we tentatively assigned T_{tr} of this phase transition as 286 K. Therefore, it is concluded that $(tetMA)_2CdCl_4$ undergoes three phase transitions at 286, 267, and 225 K below room temperature. Consequently, this complex experiences totally four phase transitions between ca. 80 and 450 K, yielding five structurally different solid phases.

Below room temperature, when $(tetMA)_2CdBr_4$ was cooled and warmed, an exothermic and an endothermic anomaly, respectively, appeared. Both anomalies are small and bear a strong resemblance to those observed at T_{tr} of 399 K for $(tetMA)_2CdCl_4$. They gave almost the same peak temperature. Except these, no heat anomaly could be recorded on both cooling and heating runs between ca. 80 and 430 K. Accordingly, one can conclude that $(tetMA)_2CdBr_4$ exhibits only one phase transition at 272 K, indicating the presence of two different crystalline phases.

With decreasing the temperature from room temperature, $(tetMA)_2CdI_4$ yielded a large exothermic peak which started very sharply at 247 K. From the peak

temperature, the curve returned back very sharply and almost symmetrically, but it became asymmetric from 243 K and gradually returned back to the base line with decreasing temperature. When the temperature was increased from 80 K, the base line was gradually deviated to the endothermic direction from ca. 235 K and a very sharp and large peak started from 244 K. The curve reached the maximum at 245 K, above which temperature the curve returned back to the base line very sharply. These experimental facts suggest that there exist two successive phase transitions around 245 K in the crystal of $(tetMA)_2CdI_4$. Since these phase transitions were not resolved, we could not determine T_{tr} exactly. Therefore, $(tetMA)_2CdI_4$ can be considered to undergo successive phase transitions having considerably different nature around 245 K. No heat anomaly except the above ones was recorded between ca. 80 and 450 K.

The temperature dependence of ^1H T_1 observed for $(tetMA)_2CdCl_4$ at the Larmor frequency of 20 MHz in a temperature range of 85—430 K is shown in Fig. 3. Two clearly separable T_1 minima with almost the same minimum value of 16 ms were observed. It is quite interesting that the observed T_1 curve is smooth and shows no marked anomaly at the phase transitions revealed by the DTA experiments although the gradient of the T_1 curve becomes milder just above T_{tr} of 286 K. This indicates that the phase transitions at 399, 267, and 225 K give negligible influence on the averaging of ^1H-^1H dipolar interactions in the cation.

The temperature dependences of ^1H T_1 observed for $(tetMA)_2CdBr_4$ at 12 and 20 MHz in the temperature ranges 300—465 K and 56—430 K, respectively, are

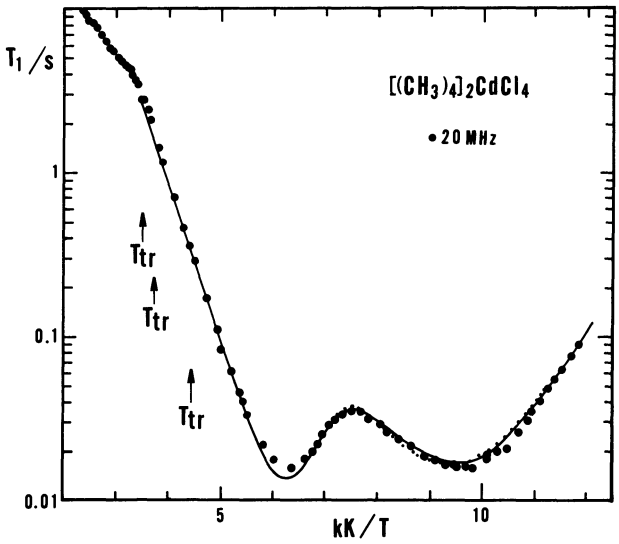

Fig. 3. Temperature dependence of ^1H T_1 observed for tetramethylammonium tetrachlorocadmate(II) at the Larmor frequency of 20 MHz (●). Solid line indicates the best fitted T_1 curve calculated based on the cationic model of C_{3v} while dotted line that based on the model of C_{2v}. Both curves agree very well with experimental values. The dotted line is written only in the temperature region where both calculated curves differ from one another. T_{tr} is the phase transition temperature determined by DTA.

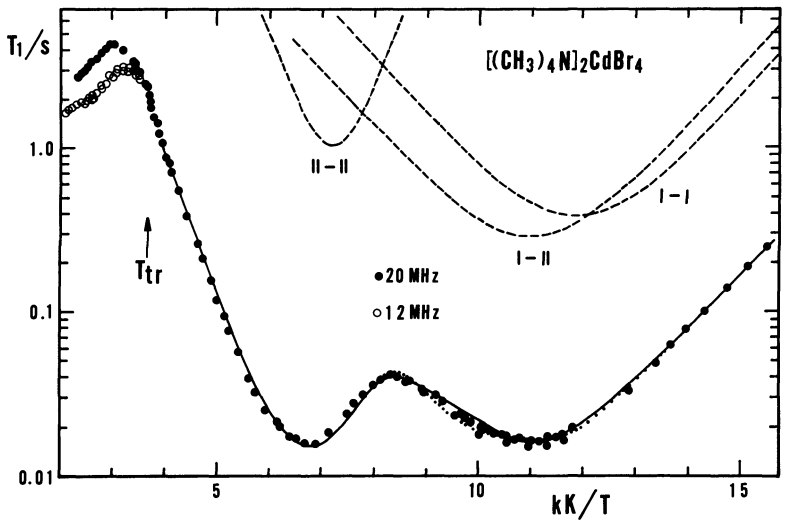

Fig. 4. Temperature dependence of ^1H T_1 observed for tetramethylammonium tetrabromocadmate(II) at the resonance frequencies of 20 (●) and 12 (○) MHz. Solid line shows the best fitted T_1 curve calculated using the cationic model of C_{3v} while dotted line that using the model of C_{2v}. The dotted curve is written only in the temperature region where both calculated curves differ from one another. Broken lines show calculated T_1 curves arising from inter-cationic dipolar interactions. Three curves were calculated for the cations between the same kind I(I-I), the different kinds I and II(I-II), and the same kind II(II-II). T_{tr} denotes the phase transition temperature determined from DTA.

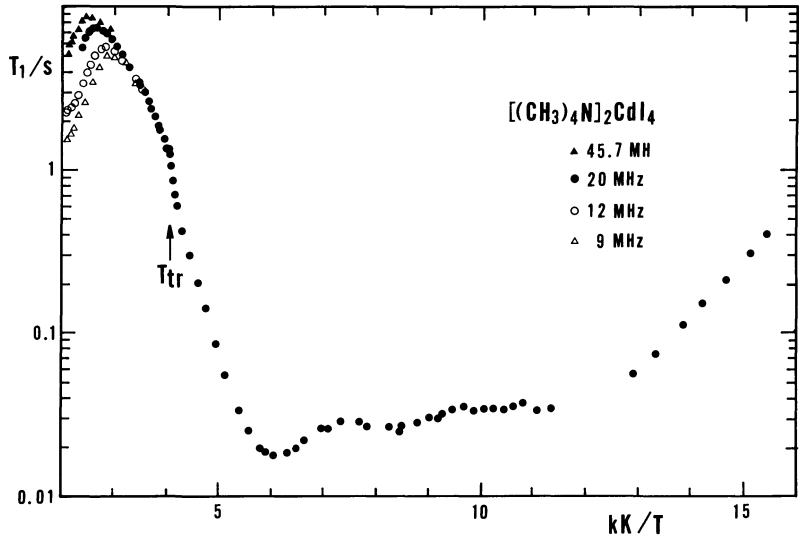

Fig. 5. Temperature dependence of ^1H T_1, observed for tetramethylammonium tetraiodocadmate(II) at 45.7 (▲), 20 (●), 12 (○), and 9 (△) MHz. T_{tr} indicates the phase transition temperature determined by DTA.

shown in Fig. 4. Two T_1 minima having almost the same minimum value of 16 ms were also obtained for this complex below T_{tr}. The T_1 curve yielding the low temperature minimum was very broad. The same is true for $(tetMA)_2CdCl_4$. Above T_{tr}, ^1H T_1 curves observed at both frequencies showed a maximum, above which temperature both T_1 values decreased almost linearly.

The temperature dependences of ^1H T_1 of $(tetMA)_2CdI_4$ measured at 9, 12, 20, and 45.7 MHz are shown in Fig. 5. T_1 observation was made in the temperature ranges of 65—430 K for 20 MHz and 300—465 K for the other three frequencies. Possibly, three or four T_1 minima partially overlapped to each other could be seen below T_{tr}. In a narrow temperature range below T_{tr} of ca. 245 K, ^1H T_1 observed at 20 MHz increased rapidly with increasing temperature and gave, above T_{tr}, a milder temperature gradient. With further increasing temperature, ^1H T_1 observed at the above Larmor frequencies yielded a maximum above which temperature each T_1 decreased almost linearly.

Discussion

It has been reported,[16-18] that half of the eight cations in a unit cell (Z=4) of the isomorphous $(tetMA)_2MX_4$ type complexes including $(tetMA)_2CdI_4$ occupies one of two kinds of nonequivalent lattice sites having low site symmetry. This means that the cation in these crystals may be distorted to some extent mainly through the electrostatic forces of the neighboring ions. In fact, the cations in the crystals of $(tetMA)_2CdI_4$ are known to be slightly distorted from T_d although the heavy atoms of the cation have very large thermal parameters.[15] In the following discussion, the same structures were roughly assumed for the cations also in $(tetMA)_2CdCl_4$ and $(tetMA)_2CdBr_4$ crystals because no atomic coordinates have been determined for these complexes as yet.

The present DTA experiments revealed the existence of phase transitions for both chloride and bromide complexes below room temperature. This means that the crystal structure of these complexes at lower temperatures is no more the same as that determined at room temperature. However, the heat anomalies recorded were so small that the structure was expected to be altered only slightly by the phase transitions. Furthermore, the ^1H T_1 data obtained show no marked anomaly at T_{tr} suggesting that the cations in these crystals keep almost the same structure from room temperature down to below 77 K.

According to the BPP theory, ^1H T_1 arising from the averaging of ^1H–^1H magnetic dipolar interactions due to molecular motions can be expressed as[25]

$$T_1^{-1} = Cg(\tau), \tag{1}$$

where

$$g(\tau) = \tau/(1+\omega^2\tau^2) + 4\tau/(1+4\omega^2\tau^2). \tag{2}$$

In these equations, C, τ, and ω denote the motional constant, the correlation time of the motion, and the angular Larmor frequency, respectively. By assuming the Arrhenius relationship for the motion, τ can be written using the activation energy E_a for the motion as

$$\tau = \tau_0 \exp(E_a/RT), \tag{3}$$

where τ_0 is the correlation time at the limit of infinite temperature.

The fact that the two T_1 minima with the same minimum value were observed for both chloride and

bromide complexes agrees very well with the crystal structure described above, showing the existence of two nonequivalent $(tetMA)^+$ cations in the crystal. Conceivable motional modes of the cation contributing to the T_1 minima are reorientations of the four CH_3 groups in the cation and also of the slightly distorted cation as a whole about its real and/or fictitious C_2 and C_3 symmetry axes. A possible explanation of the fairly deep T_1 minimum of 16 ms determined for each of the two nonequivalent cations is that all of these motional modes of each cation give a T_1 minimum at almost the same temperature and contribute as a whole to the T_1 minimum. This is because the ^1H T_1 minimum of the cation arising from these motional modes can be roughly estimated as 14 ms,[3] although this is obtained by assuming that all bond angles in the cation are tetrahedral and the bond lengths of C–H and C–N are 1.09 and 1.50 Å, respectively.[1]

$(tetMA)_2CdCl_4$ and $(tetMA)_2CdBr_4$ yielded very gentle gradients of $\log T_1$ vs. T^{-1} plots on the cold side of the lower temperature T_1 minimum. By using Eqs. 1—3, we roughly estimated E_a as 9 and 6.5 kJ mol^{-1} for the chloride and bromide complexes, respectively, from each slope. These values are too small to be considered mostly resulting from the CH_3 C_3 reorientation by the following reasons. The potential barriers for the internal CH_3 rotation in the cation have been estimated as 19.3 and 17.6 kJ mol^{-1} for $(tetMA)_2PtCl_6$ and $(tetMA)_2PtBr_6$, respectively, from the study of vibrational spectra.[26,27] For molecules having CH_3 groups in a similar situation to that of the cation, the torsional barriers of CH_3 groups in $(CH_3)_3N$ and $(CH_3)_4C$ molecules are reported to be 18.5 and 18.0 kJ mol^{-1}, respectively.[28,29] Moreover we also already obtained E_a for the CH_3 C_3 reorientation of the cation in $(tetMA)_2MBr_6$ (M=Sn, Te, Pt) crystals as 15.4, 17.8, and 18.4 kJ mol^{-1} respectively.[10]

In previous papers,[9,10] we explained shallow T_1 minima with extremely low E_a values ($\approx$8 kJ mol^{-1}) appearing at lower temperatures for $(tetMA)_2TeCl_6$, $(tetMA)_2PtCl_6$, and $(tetMA)_2MBr_6$ (M=Sn, Te, Pt) by the small-angle reorientation of the four CH_3 groups about their respective C_3 axis. However, this process can be permitted only for the cation placed in a highly symmetrical and weak crystal field such as that in the above complexes. This is because the correlated reorientation of the four CH_3 groups is an important condition for this motion. Since the cations in the present complexes are located at low symmetric lattice sites, their structure must be deformed from a tetrahedron. Therefore, the small-angle reorientation seems to be unsuitable for the explanation of the present T_1 minima with small E_a appearing at lower temperatures. For the cations deformed to some extent such as those in the present complexes, it can be expected that E_a for one or two CH_3 groups in the cation may be much lower than that for the others. This is because hindering barrier for the CH_3 C_3 reorientation is considered to be formed mainly by the intraionic forces.

For the present complexes, the CH_3 C_3 and overall reorientations give T_1 minima at almost the same temperature, where the condition necessary for the conventional treatment by Albert et al.[3] is not fulfilled. This indicates that this usual method cannot be used here. To interprete the present T_1 data, we employed the method of T_1 calculation reported by Takeda et al.,[30] which had been used for the interpretation of the data observed for neopentane. In this method, pairwise addition of intra- and inter-methyl ^1H magnetic dipolar interactions is taken for randomly jumping ^1H–^1H vectors through the respective CH_3 C_3 reorientations and also the reorientations of the whole cation about its C_2 and C_3 axes. Since jumping of each ^1H–^1H vector is regarded as representable by a Markov process, no correlation between these motions is considered as like in the case of the more convenient and widely used method developed by Albert et al.[3]

In the following analysis of T_1, the presence of two kinds of nonequivalent $(tetMA)^+$ cations is assumed in accordance with the crystal structure isomorphous with $(tetMA)_2CdI_4$ and the other $(tetMA)_2MX_4$ type complexes.[15–18] In the structure, each cation is placed on a mirror plane of the unit cell, indicating that there exist two equivalent carbon atoms in the cation. This means that each cation has two or three nonequivalent CH_3 groups. For favorable cases, the cations having C_{2v} or C_{3v} symmetry can be placed on the lattice sites. Therefore, the present T_1 calculation was performed for the two models of the cations having C_{2v} or C_{3v} symmetry so far as the motion of CH_3 groups is concerned. In other words, the geometry of the cation was roughly assumed to be T_d but the motional states of the four CH_3 groups to satisfy the above symmetry. The stable positions of hydrogen atoms were fixed at the all-staggered conformation,[27] and for C–H and C–N bond lengths the foregoing values were used.[3]

As the first model, we consider the cation having C_{2v} symmetry only in the motional states of the four CH_3 groups. Namely, two pairs, each of which consists of "equivalent" CH_3 groups, have different jumping rates and activation energies for the CH_3 C_3 reorientations from one another. For overall cationic reorientations, we assumed the presence of two kinds of nonequivalent C_2 reorientations about one genuine C_2 and two pseudo C_2 axes of the cation and, for simplicity, a single kind of C_3 reorientation about the four pseudo C_3 axes.

As the second model, we assumed the cation having C_{3v} symmetry in the same sense as above. In this model, we assumed that one CH_3 group of the cation has a more frequent jumping rate and a lower activation energy for the C_3 reorientation than the other three groups. The whole cationic motions are considered to consist of C_3 reorientations about the unique C_3 axis and the other three pseudo C_3 axes, and of C_2

reorientations about the three equivalent pseudo C_2 axes of the cation. In general, these reorientational modes should have different correlation times with the temperature dependence expressed by Eq. 3. However, the overall cationic C_3 and C_2 reorientations were reasonably assumed to have the same τ_0 and the same assumption could be made on the two kinds of CH_3 C_3 reorientations as well.

For the first C_{2v} model, the 12×12 transition matrix D[30] to calculate the intra CH_3 relaxation rate due to random jumpings of the ^1H–^1H vectors is given by

$$D = \begin{pmatrix} A & B & B' & B' \\ B & A & B' & B' \\ B' & B' & A' & B \\ B' & B' & B & A' \end{pmatrix}, \tag{4}$$

where

$$A = \begin{pmatrix} a_0 & a_1 & a_1 \\ a_1 & a_0 & a_1 \\ a_1 & a_1 & a_0 \end{pmatrix}, \qquad A' = \begin{pmatrix} a_0' & a_1' & a_1' \\ a_1' & a_0' & a_1' \\ a_1' & a_1' & a_0' \end{pmatrix}, \tag{5}$$

$$B = -\begin{pmatrix} \omega_2 & \omega_3' & \omega_3' \\ \omega_3' & \omega_2 & \omega_3' \\ \omega_3' & \omega_3' & \omega_2 \end{pmatrix}, \qquad B' = -\begin{pmatrix} \omega_2' & \omega_3' & \omega_3' \\ \omega_3' & \omega_2' & \omega_3' \\ \omega_3' & \omega_3' & \omega_2' \end{pmatrix}. \tag{5'}$$

In these equations,

$$a_0 = 2\omega_{CH_3} + 8\omega_3' + \omega_2 + 2\omega_2', \tag{6}$$

$$a_1 = -(\omega_{CH_3} + \omega_3'), \tag{7}$$

$$a_0' = 2\omega^*_{CH_3} + 8\omega_3' + \omega_2 + 2\omega_2', \tag{8}$$

$$a_1' = -(\omega^*_{CH_3} + \omega_3'). \tag{9}$$

Here, ω_{CH_3} and ω_{CH_3}* are the jumping rates of the C_3 reorientations of two nonequivalent CH_3 groups, and ω_2, ω_2', and ω_3' denote the jumping rates of the whole cationic reorientations about the C_2, pseudo C_2, and pseudo C_3 axes, respectively. These jumping rates were assumed to be the reciprocals of the correlation times of these motions.

The transition matrix due to jumping of the inter CH_3 ^1H–^1H vectors was calculated in a similar manner as used by Takeda et al.[30] Since diagonalization of these transition matrices which could be algebraically done for the T_d symmetric molecule was difficult for the present systems, it was carried out numerically using a FACOM-M382 computer in the Computation Center of Nagoya University.

Correlation times for the respective motional modes at a fixed temperature were calculated using Eq. 3 by substituting suitable trial values of E_a and τ_0. The numerical D matrix can be expressed in terms of these correlation times. By diagonalizing the D matrix thus constructed, we obtained a set of non-trivial eigenvalues which were reciprocals of the correlation times for the normal modes of reorientations for the intra CH_3 ^1H–^1H vectors at the temperature. The calculation for the D matrix of the jumping of the inter ^1H–^1H vectors was performed analogously. Finally, ^1H T_1 was obtained by the following equation,

$$T_1^{-1} = \sum_\ell K_\ell \left(\frac{\tau_\ell}{1+\omega^2\tau_\ell^2} + \frac{4\tau_\ell}{1+4\omega^2\tau_\ell^2} \right), \tag{10}$$

where τ_ℓ and K_ℓ indicate the correlation time of the ℓ-th normal mode associated with intra and inter ^1H–^1H vector jumpings and a constant depending on the mode and the structure as well, respectively. K_ℓ can be calculated numerically using the equations given by Takeda et al.[30]

T_1 values in a wide range of temperature were calculated as above by changing seven unknown parameters i.e., five E_a and two τ_0 values. From the T_1 curves calculated here, we selected several curves which agreed roughly with the observed values obtained from the cold side of the T_1 minimum, and derived approximate values of the unknown parameters.

For the other T_1 curve appearing at higher temperatures, the same method of calculation was applied. However, the T_1 curve having a rather steep slope may be interpreted by the usual "undistorted" cation. Therefore, the calculation was performed by simply assuming that all CH_3 groups in the cation are equivalent even in their motion. This results in the reduction of the number of unknown parameters.

The theoretical T_1 curve for the second model of the cation with C_{3v} symmetry for the motion of the CH_3 groups could be obtained similarly using the D matrix given by

$$D = \begin{pmatrix} A' & B_1 & B_2 & B \\ B_2 & A' & B_1 & B \\ B_1 & B_2 & A' & B \\ B & B & B & A \end{pmatrix}, \tag{11}$$

where

$$A = \begin{pmatrix} a_0 & a_1 & a_1 \\ a_1 & a_0 & a_1 \\ a_1 & a_1 & a_0 \end{pmatrix}, \qquad A' = \begin{pmatrix} a_0' & a_1' & a_1' \\ a_1' & a_0' & a_1' \\ a_1' & a_1' & a_0' \end{pmatrix}, \tag{12}$$

$$B_1 = -\begin{pmatrix} \omega_2' & \omega_3' & \omega_3 \\ \omega_3 & \omega_2' & \omega_3' \\ \omega_3' & \omega_3 & \omega_2' \end{pmatrix}, \qquad B_2 = -\begin{pmatrix} \omega_2' & \omega_3 & \omega_3' \\ \omega_3' & \omega_2' & \omega_3 \\ \omega_3 & \omega_3' & \omega_2' \end{pmatrix},$$

$$B = -\begin{pmatrix} \omega_2' & \omega_3' & \omega_3' \\ \omega_3' & \omega_2' & \omega_3' \\ \omega_3' & \omega_3 & \omega_2' \end{pmatrix}. \tag{13}$$

In these matrices,

$$a_0 = 2\omega_{CH_3} + 2\omega_3 + 6\omega_3' + 3\omega_2', \tag{14}$$

$$a_1 = -(\omega_{CH_3} + \omega_3), \quad (15)$$

$$a_0' = 2\omega_{CH_3}^* + 2\omega_3 + 6\omega_3' + 3\omega_2', \quad (16)$$

$$a_1' = -(\omega_{CH_3}^* + \omega_3'). \quad (17)$$

Here, ω_{CH_3} and ω_3 are the jumping rates of the ^1H–^1H vectors for the CH_3 C_3 and the whole cationic C_3 reorientations about the unique C_3 axis of the cation, respectively. $\omega_{CH_3}^*$ is the jumping rate of the other CH_3 C_3 reorientation while ω_3' and ω_2' denote those of the whole cationic reorientations about the other three pseudo C_3 and the three pseudo C_2 axes, respectively.

Since these ^1H–^1H vector reorientations in the cations should also average the interionic dipolar interactions which might be small, the interionic contribution to T_1 was roughly estimated by evaluating the difference of the inter-cationic second moment ΔM_2 between those in the rigid lattice and in the isotropically rotating state. The second moment M_2 in the rigid lattice could be roughly estimated for the present complexes by placing the T_d cations in the crystalline lattice isomorphous with $(tetMA)_2CdI_4$. From this model, we could calculate inter-protonic distances between protons belonging to the different cations. The interionic M_2 averaged by rapid ionic rotations was obtained by use of the method reported by Andrew and Eades.[31] In both crystals, there are two kinds of the cations I and II, which are considered to perform isotropic rotation with quite different correlation times from each other. Then, T_1 for the cation I giving rise to the low temperature minimum is expressed by[32,33]

$$T_1^{-1} = \frac{2}{3}\gamma^2\Delta M_2 g(\tau_{iso}) + \frac{2}{3}\gamma^2\Delta M_2' g(\tau_{iso}/2), \quad (18)$$

where γ and τ_{iso} indicate the gyromagnetic ratio of a proton and the correlation time of the isotropic rotation of the cation I, respectively.

The first term of Eq. 18 comes from the ^1H dipolar interactions between the cations I and II, while the second arises from those between protons belonging to the same kind of the cations I. The values of ΔM_2 and $\Delta M_2'$ calculated were 0.64 and 0.48 G^2, respectively. To evaluate τ_{iso} which is assumed to be expressed by Eq. 3, let the T_1 minimum temperature for the first term of Eq. 18 be equal to that of the observed low temperature one. Then, the temperature dependence of τ_{iso} was roughly estimated from the slope of the $\log T_1$ vs. T^{-1} curve. For the cation II yielding the high temperature T_1 minimum, the interionic T_1 can be given only by the second term of Eq. 18. $\Delta M_2'$ for this cation was calculated as 0.18 G^2 and τ_{iso} was obtained in the same way as for the cation I. The interionic contribution to the calculation of ^1H T_1 was taken into account only for $(tetMA)_2CdBr_4$ because it was turned out to be very small and the observed ^1H T_1 for $(tetMA)_2CdCl_4$ was assumed to be well explained only by intraionic contribution.

The refinement of the foregoing calculation was finally performed by changing the values of the adjustable parameters by stepwise finely to obtain the resultant best fitted T_1 curve which was the sum of the low and high temperature T_1 curves calculated separately as above. The evalution of the degree of fitting was determined by inspection.

The most appropriate T_1 curves calculated for the two kinds of the models of the cation are shown in Figs. 3 and 4 for the chloride and bromide complexes, respectively. The adjustable parameters giving rise to these T_1 curves are shown in Table 1. From these results, it is difficult to determine which model is more suitable for the present complexes. This is because both models provided the T_1 curves interpreting the observed T_1 data very well. However, it can be said that the observed T_1 curve having a normal minimum value but unusually small E_a can be explained by the motionally distorted T_d cation.

The values of E_a derived from the low temperature T_1 curve indicate that there is a distinct difference between the reorientations of the two kinds of CH_3 groups in the cation. It is noteworthy that E_a for the CH_3 reorientation whose rate is given by $\omega_{CH_3}^*$ is rather insensitive to the shape of the T_1 curve for both complexes and also for the choice of the model of the cation when E_a is larger than ca. 12 kJ mol^{-1}. On the other hand, the other E_a values listed in Table 1 gave an appreciable change on the shape of the curve when they were altered more than 0.5 kJ mol^{-1}. The larger E_a values of $(tetMA)_2CdCl_4$ than those of $(tetMA)_2CdBr_4$ obtained from both models are understandable by considering the size effect of the anion. Namely, the cations in the latter complex are thought to be more loosely packed in the crystal than those in the former crystal.

The T_1 curve observed for $(tetMA)_2CdI_4$ below room temperature is quite different from those of the foregoing two complexes, although the three complexes are isomorphous at room temperature. This difference may be due to the phase transition located at ca. 245 K, which exhibits a large heat anomaly suggesting a drastic change of the crystal structure. Therefore, the appearance of many T_1 minima successively in the low temperature phase is possibly attributed to the existence of more than two nonequivalent cations and/or CH_3 groups in the cation yielding their T_1 minima due to reorientations appearing in a fairly wide range of temperature. For this complex, E_a values were roughly estimated from the linear portions on the hot and cold sides of the T_1 curve below T_{tr} as 20.7 and 6.5 kJ mol^{-1}, respectively. Very small E_a of 6.5 kJ mol^{-1} was obtained also for this complex in the very low temperature region.

A T_1 decrease with increasing temperature was observed for both $(tetMA)_2CdBr_4$ and $(tetMA)_2CdI_4$ above room temperature, indicating the presence of at least one new relaxation process at higher temperatures.

Table 1. Best Fitted Activation Energies E_a and Correlation Times τ_0 for ^1H-^1H Vector Jumping Rates of the Cation in Tetramethylammonium (tetMA) Tetrachloro- and Tetrabromocadmate(II) Yielding High and Low Temperature T_1 Curves

Compound	High temp side			Low temp side		
[Motional model]	Jumping rate	E_a/kJ mol^{-1}	τ_0/s	Jumping rate	E_a/kJ mol^{-1}	τ_0/s
$(tetMA)_2CdCl_4$						
$[C_{3v}]$	ω_{CH_3}	17.5	3.3×10^{-12}	ω_{CH_3}	7.5	2.5×10^{-12}
				ω_{CH_3}*	>15.0	
	ω_3	19.7		ω_3	10.8	
		19.7	3.3×10^{-14}	ω_3'	18.0	6.3×10^{-14}
	ω_2	18.1		ω_2'	13.0	
$[C_{2v}]$	ω_{CH_3}	17.5	3.3×10^{-12}	ω_{CH_3}	8.1	1.7×10^{-12}
				ω_{CH_3}*	>12.0	
	ω_3	19.7		ω_2	11.0	
		19.7	3.2×10^{-14}	ω_2'	13.0	3.3×10^{-14}
	ω_2	18.0		ω_3'	14.5	
$(tetMA)_2CdBr_4$						
$[C_{3v}]$	ω_{CH_3}	14.0	1.3×10^{-11}	ω_{CH_3}	5.1	1.1×10^{-11}
				ω_{CH_3}*	>12.0	
	ω_3	17.5		ω_3	9.8	
		17.5	1.3×10^{-13}	ω_3'	12.7	3.3×10^{-14}
	ω_2	14.5		ω_2'	15.0	
$[C_{2v}]$	ω_{CH_3}	14.0	1.3×10^{-11}	ω_{CH_3}	5.7	8.3×10^{-12}
				ω_{CH_3}*	>12.0	
	ω_3	17.5		ω_2	9.5	
		17.5	1.3×10^{-11}	ω_2'	12.5	3.3×10^{-12}
	ω_2	14.5		ω_3'	12.5	

In these temperature regions, a clear frequency dependence of ^1H T_1 was observed for both complexes. However, the ratios of T_1 values determined at different frequencies and at the same temperature are much smaller than those of squared resonance frequencies. We determined M_2 for $(tetMA)_2CdBr_4$ at 450 K and yielded 0.5 G^2 which was almost the same as the value of 0.6 G^2 obtained at 302 K. This indicates that the T_1 decrease observed is difficult to explain through the magnetic dipolar relaxation mechanism.

It has been reported[34,35] that even bulky octahedral complex anions such as $[PtCl_6]^{2-}$ and $[PtBr_6]^{2-}$ reorient quite frequently at high temperatures and this motion appreciably shortens spin-lattice and also spin-spin relaxation times of the quadrupolar halogen nuclei. In the present complexes, rapid motions of the complex anions can be also expected to take place at high temperatures and the quadrupole resonance frequencies of iodine and bromine in both complexes are nearer to the NMR frequencies than that of chlorine in $(tetMA)_2CdCl_4$. Quadrupolar relaxation of iodine and bromine nuclei can provide an important relaxation process for ^1H in the cation through magnetic interactions between ^1H and halogen nuclei when the quadrupolar relaxation time becomes shorter than ^1H T_1 at high temperatures. This relaxation mechanism named dipolar relaxation of the second kind[36] seems to be the main origin of the frequency dependent T_1 decrease observed at higher temperatures.

This work was partially supported by a Grant-in-Aid for Scientific Research No. 59470009 from the Ministry of Education, Science and Culture.

References

1) E. R. Andrew and P. C. Canepa, *J. Magn. Reson.*, **7**, 429 (1972).
2) M. Mahajan and B. D. Nageswara Rao, *J. Phys. C*, **7**, 995 (1974).
3) S. Albert, H. S. Gutowsky, and J. A. Ripmeester, *J. Chem. Phys.*, **56**, 3672 (1972).
4) A. A. V. Gibson and R. E. Raab, *J. Chem. Phys.*, **57**, 4688 (1972).
5) H. Rager and A. Weiss, *Z. Phys. Chem.*, **NF93**, 299 (1974).
6) T. Tsuneyoshi, N. Nakamura, and H. Chihara, *J. Magn. Reson.*, **27**, 191 (1977).
7) H. Rager and A. Weiss, *Ber. Bunsenges. Phys. Chem.*, **80**, 138 (1976).
8) H. Rager and A. Weiss, *Ber. Bunsenges. Phys. Chem.*, **82**, 535 (1978).
9) L. S. Prabhumirashi, R. Ikeda, and D. Nakamura, *Ber. Bunsenges. Phys. Chem.*, **85**, 1142 (1981).
10) S. Sato, R. Ikeda, and D. Nakamura, *Ber. Bunsenges. Phys. Chem.*, **86**, 936 (1982).
11) T. Tsang and D. B. Utton, *J. Chem. Phys.*, **64**, 3780 (1976).
12) S. Gima, Y. Furukawa, R. Ikeda, and D. Nakamura, *J. Mol. Struct.*, **111**, 189 (1983).
13) Y. Kume, R. Ikeda, and D. Nakamura, *J. Magn. Reson.*, **33**, 331 (1979).
14) J. J. Foster and N. S. Gill, *J. Chem. Soc. (A)*, **1968**, 2625.
15) A. Kallel, J. W. Bats, and A. Daoud, *Acta Crystallogr., Sect. B*, **37**, 676 (1981).

16) B. Kamenar and A. Nagl, *Acta Crystallogr., Sect. B*, **32**, 1414 (1976).
17) J. R. Wiesner, R. C. Srivastava, C. H. L. Kennard, M. Divaiva, and E. C. Lingafelter, *Acta Crystallogr.*, **23**, 565 (1967).
18) P. Trouelan, J. Lefebvre, and P. Derollez, *Acta Crystallogr., Sect. C*, **40**, 386 (1984).
19) Y. Kume, R. Ikeda, and D. Nakamura, *J. Magn. Reson.*, **20**, 276 (1975).
20) Y. Kume, R. Ikeda, and D. Nakamura, *J. Phys. Chem.*, **82**, 1926 (1978).
21) H. Ishida, R. Ikeda, and D. Nakamura, *J. Phys. Chem.*, **86**, 1003 (1982).
22) H. Ishida, R. Ikeda, and D. Nakamura, *Phys. Stat. Sol. (a)*, **70**, K151 (1982).
23) H. Ishida, R. Ikeda, and D. Nakamura, *Bull. Chem. Soc. Jpn.*, **59**, 915 (1986).
24) G. Jugie and J. A. S. Smith, *J. Chem. Soc., Faraday Trans. 2*, **74**, 994 (1978).
25) N. Bloembergen, E. M. Purcell, and R. V. Pound, *Phys. Rev.*, **73**, 679 (1948).
26) R. W. Berg, *J. Chem. Phys.*, **69**, 1325 (1978).
27) R. W. Berg, *J. Chem. Phys.*, **71**, 2531 (1979).
28) W. G. Fateley and F. A. Miller, *Spectrochim. Acta*, **18** 977 (1962).
29) J. R. Durig, S. M. Craven, and J. Bragin, *J. Chem. Phys.*, **52**, 2046 (1969).
30) S. Takeda, G. Soda, and H. Chihara, *Mol. Phys.*, **47**, 501 (1982).
31) E. R. Andrew and R. G. Eades, *Proc. Roy. Soc. A*, **216**, 398 (1953).
32) G. Soda and H. Chihara, *J. Phys. Soc. Jpn.*, **36**, 954 (1974).
33) J. E. Anderson, *J. Chem. Phys.*, **43**, 3575 (1965).
34) K. R. Jeffrey and R. L. Armstrong, *Phys. Rev.*, **174**, 359 (1968).
35) M. Wiszniewska and R. L. Armstrong, *Can. J. Phys.*, **51**, 781 (1973).
36) M. O. Norris, J. H. Strange, J. G. Powles, M. Rhodes, K. Marsden, and K. Krynicki, *J. Phys. C*, 1, 422 (1968).

The Microwave Spectrum of Ethyl Isoselenocyanate

Takeshi SAKAIZUMI,* Kazuyuki IIDA, Osamu OHASHI, and Ichiro YAMAGUCHI
Department of Chemistry, Faculty of Science and Technology, Sophia University, Chiyoda-ku, Tokyo 102
(Received February 12, 1986)

The microwave spectra of two isotopic species (^{80}Se and ^{78}Se) of ethyl isoselenocyanate were measured in the frequency region of 10—28 GHz. Only a-type R-branch transitions in the ground vibrational state were identified. The rotational constants in MHz were obtained; $A=15140\pm23$, $B=1090.443\pm0.016$, and $C=1029.261\pm0.016$ for ^{80}Se species and $A=15112\pm28$, $B=1099.865\pm0.012$, and $C=1037.745\pm0.012$ for ^{78}Se species. The plausible structure of ethyl isoselenocyanate has deduced from the observed rotational constants to be the synperiplanar form with a plane of symmetry.

The microwave spectra of ethyl isocyanate[1] and ethyl isothiocyanate[2] have been reported and their structures have been determined to be planar synperiplanar conformers. A large increase in the C-N-C angle is seen when the oxygen atom of isocyanato group is replaced with a sulfur atom.[1,2] A similar trend is seen for the H-N-C angle of HNCO (124°),[3] HNCS (132°),[4] and HNCSe (143°)[5] and the C-N-C angle of CH_3NCO (140°)[6,7] and CH_3NCS (147.5°, 153°).[6,8] Recently, the C-N-C angle of methyl isoselenocyanate (CH_3NCSe)[9] has been found to be 157°. This angle is larger by about 10° than that of methyl isothiocyanate (CH_3NCS).

Franklin et al.[10] have reported the infrared spectrum of ethyl isoselenocyanate without inferring its geometrical conformation. It is very interesting to see what effect an atom heavier than oxygen or sulfur can produce on a molecular structure, particularly on the rotational conformation and the C-N-C angle.

The microwave spectra of two isotopic species (with ^{80}Se and ^{78}Se) of ethyl isoselenocyanate (CH_3CH_2NCSe) were measured in the frequency region between 10 and 28 GHz and assigned to a-type R-branch lines in the ground vibrational state. The rotational constants are reported and the molecular structure is discussed.

Experimental

Ethyl isoselenocyanate was prepared from ethyl isocyanide by refluxing in chloroform with finely divided black selenium for about 48 h.[11] Ethyl isocyanide was produced by adding silver cyanide to ethyl iodide and then adding potassium cyanide and water to the mixture.[12] Ethyl isoselenocyanate was purified by vacuum distillation and identified by comparing its infrared spectrum with the reported one.[10]

The spectrometer employed was a conventional 100 kHz square-wave Stark modulation type with a phase-sensitive detector. The microwave source was a HP8672A microwave synthesizer which was controlled by a HP9872A/S computer.

The temperature of the sample cell was kept between 0 and −10° to avoid any decomposition of the sample during the measurement of the spectrum. The absorption line widths could be kept at less than 1.5 MHz by cooling the sample cell, while the widths were about 2 to 3 MHz at room temperature.

Results and Discussion

There are four possible rotational conformers to be considered for ethyl isoselenocyanate as shown in Fig. 1. The calculation of the rotational constants for these four rotamers, using the assumed structural parameters, showed that all rotational conformers were nearly prolate symmetric top rotators, with Ray's

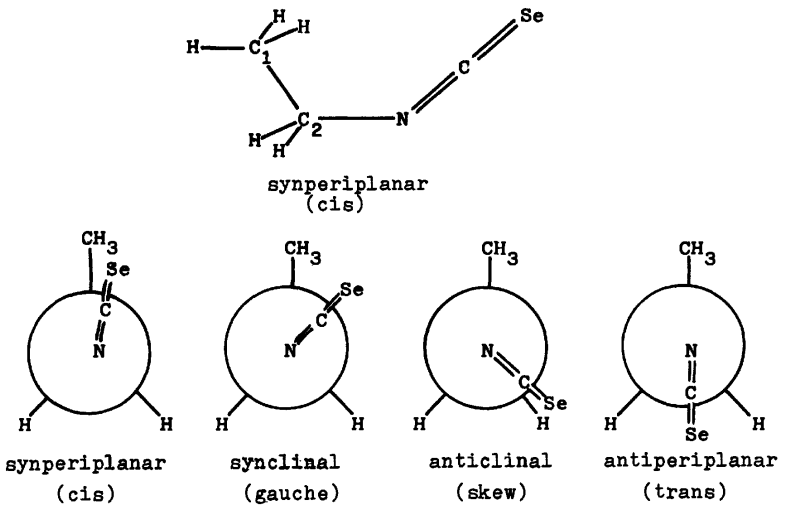

Fig. 1. Four possible rotational conformers and the numbering of carbon atoms on ethyl isoselenocyanate.

asymmetry parameter κ less than -0.99. Therefore, the rotational spectra for all four possible conformers were expected to have absorption lines with frequency intervals close to the quantity of (B+C), characteristic for a spectrum of near prolate symmetric top molecules. The ethyl isoselenocyanate has many isotopic species of selenium atom, among which ^{80}Se and ^{78}Se are dominant. The abundance ratio of ^{80}Se to ^{78}Se is about 2 and at higher frequency sides of each absorption line of ^{80}Se species, the absorption lines of ^{78}Se species were expected to appear with the intensities of about one half of the corresponding line intensities of ^{80}Se species.

The first survey of the spectrum in the frequency region of 18 to 24 GHz at the Stark field between 5 and 20 V cm^{-1} found groups of the strong lines with the frequency interval of about 2100 MHz; these were ascribed to ^{80}Se species. Groups of lines with the intensities of about one half of the corresponding line intensities of ^{80}Se species were found at frequencies higher by about 200 MHz than the absorption frequencies of ^{80}Se species. These weaker lines were assigned to ^{78}Se species.

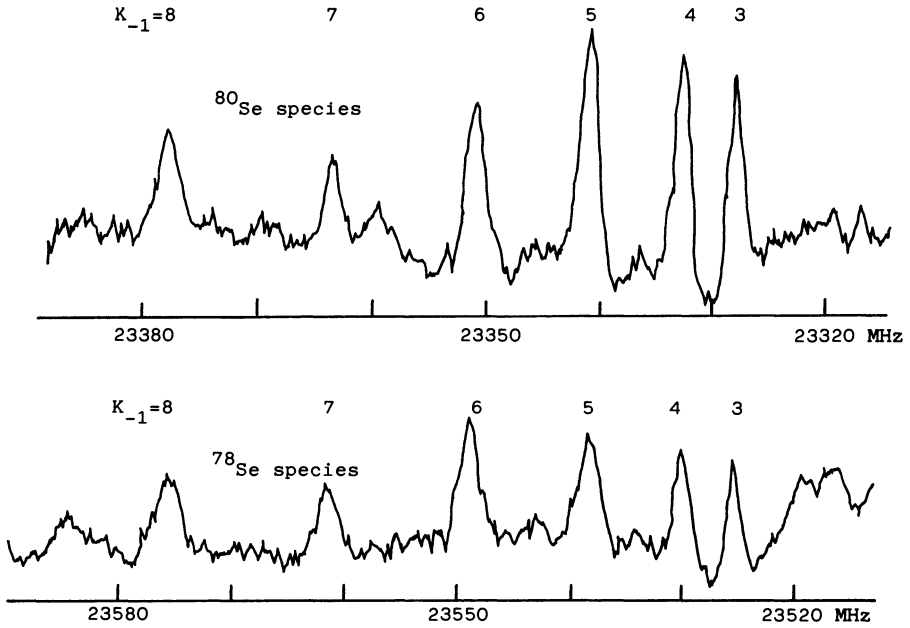

Fig. 2. The typical spectra of the J=11←10 transitions for $CH_3CH_2NC^{80}Se$ and $CH_3CH_2NC^{78}Se$, observed at the Stark field of 10 V cm^{-1}.

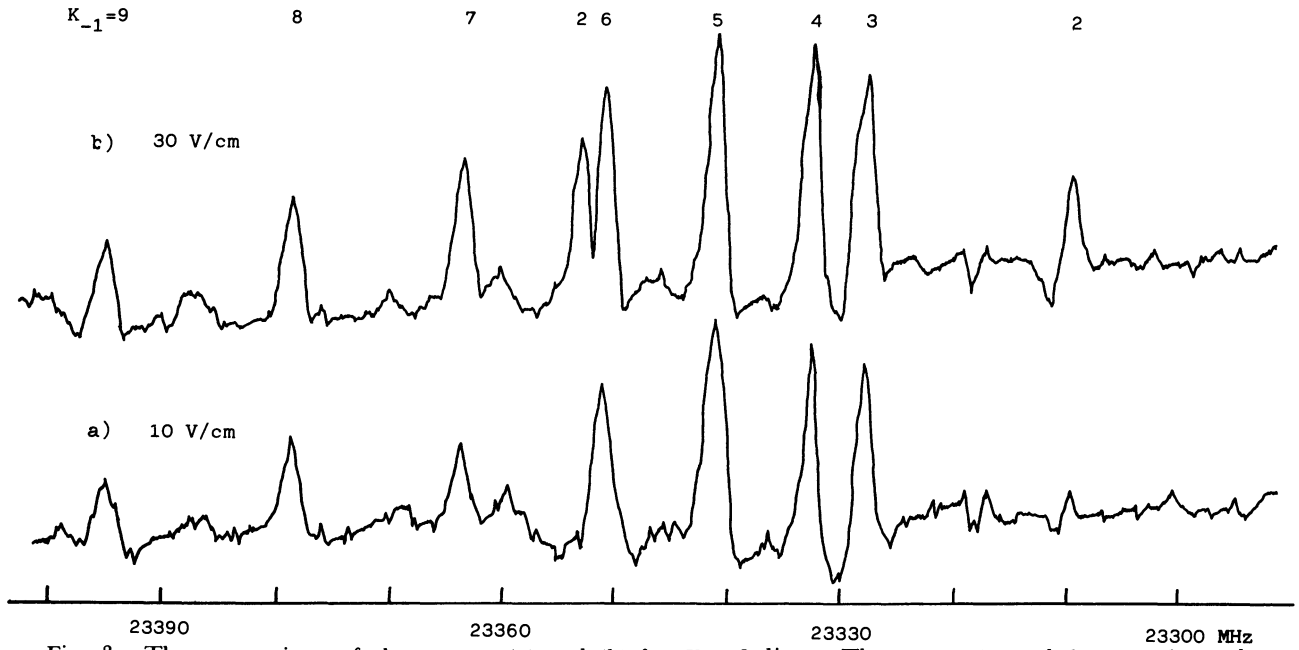

Fig. 3. The comparison of the spectra (a) and (b) for K_{-1}=2 lines. The spectra (a) and (b) were observed at the Stark fields of 10 and 30 V cm^{-1}, respectively.

Table 1. Observed Rotational Transitions(MHz) of $CH_3CH_2NC^{80}Se$

Transition	ν_{obsd}	$\Delta\nu$[a)]	Transition	ν_{obsd}	$\Delta\nu$[a)]
5_{15}–4_{14}	10444.92	0.08	10_6–9_6	21229.05	−0.17
5_{05}–4_{04}	10594.25	0.10	10_7–9_7	21240.62	−0.20
5_{14}–4_{13}	10750.45	−0.21	10_8–9_8	21254.21	0.14
6_{16}–5_{15}	12533.17	0.08	10_9–9_9	21268.94	0.16
6_{25}–5_{24}	12718.95	−0.03	10_{28}–9_{27}	21225.55	0.01
6_{15}–5_{14}	12900.24	0.23	10_{19}–9_{18}	21492.43	0.05
7_{17}–6_{16}	14621.05	0.11	11_{111}–10_{110}	22967.22	−0.04
7_{07}–6_{06}	14825.79	0.06	11_{011}–10_{010}	23269.09	0.03
7_{26}–6_{25}	14838.10	0.07	11_{210}–10_{29}	23310.05	−0.04
7_3–6_3	14844.72	0.13	11_4–10_4	23332.72	−0.08
7_5–6_5	14854.09	−0.14	11_5–10_5	23341.13	0.12
7_6–6_6	14861.06	−0.16	11_6–10_6	23351.71	0.06
7_{16}–6_{15}	15048.82	−0.11	11_7–10_7	23364.46	0.11
8_{18}–7_{17}	16708.23	−0.12	11_8–10_8	23378.86	−0.02
8_{08}–7_{07}	16939.46	0.11	11_9–10_9	23394.87	−0.18
8_{27}–7_{26}	16956.63	−0.08	11_{29}–10_{28}	23353.74	0.07
8_3–7_3	16965.47	0.10	11_{110}–10_{19}	23638.93	0.10
8_4–7_4	16969.76	0.05	12_{112}–11_{111}	25052.19	−0.08
8_5–7_5	16976.16	0.10	12_{012}–11_{011}	25374.50	−0.09
8_6–7_6	16984.03	0.04	12_{211}–11_{210}	25426.76	−0.06
8_7–7_7	16993.14	−0.21	12_4–11_4	25453.68	−0.04
8_{26}–7_{25}	16973.36	−0.06	12_5–11_5	25462.28	−0.17
8_{17}–7_{16}	17197.49	0.14	12_9–11_9	25521.09	−0.04
9_{19}–8_{18}	18795.25	0.01	12_{10}–11_{10}	25540.50	0.14
9_{09}–8_{08}	19051.16	−0.09	12_{210}–11_{29}	25483.45	0.09
9_{28}–8_{27}	19074.85	−0.13	12_{111}–11_{110}	25784.43	−0.04
9_3–8_3	19086.31	0.10	13_{113}–12_{112}	27136.61	−0.09
9_4–8_4	19090.83	0.05	13_{013}–12_{012}	27477.64	0.05
9_5–8_5	19097.82	0.02	13_{212}–12_{211}	27542.93	−0.22
9_6–8_6	19106.72	0.05	13_4–12_4	27574.57	−0.01
9_7–8_7	19117.10	−0.05	13_5–12_5	27583.83	0.07
9_{27}–8_{26}	19098.66	−0.17	13_6–12_6	27596.23	0.16
9_{18}–8_{17}	19345.20	0.01	13_7–12_7	27610.97	0.05
10_{110}–9_{19}	20881.63	0.07	13_8–12_8	27628.13	0.14
10_{010}–9_{09}	21161.20	−0.02	13_9–12_9	27647.02	−0.01
10_{29}–9_{28}	21192.78	−0.01	13_{10}–12_{10}	27667.81	−0.02
10_3–9_3	21207.13	0.16	13_{11}–12_{11}	27690.10	−0.06
10_4–9_4	21211.87	0.05			

a) $\Delta\nu=\nu_{obsd}-\nu_{calcd}$.

Table 2. Observed Rotational Transitions(MHz) of $CH_3CH_2NC^{78}Se$

Transition	ν_{obsd}	$\Delta\nu$[a)]	Transition	ν_{obsd}	$\Delta\nu$[a)]
8_{18}–7_{17}	16847.50	0.03	10_5–9_5	21390.88	0.15
8_{08}–7_{07}	17082.05	0.08	10_6–9_6	21408.45	−0.10
8_{27}–7_{26}	17099.88	0.09	10_7–9_7	21420.56	−0.11
8_3–7_3	17108.66	0.08	10_{28}–9_{27}	21405.34	−0.09
8_4–7_4	17112.94	0.04	10_{19}–9_{18}	21675.93	−0.14
8_{26}–7_{25}	17116.96	−0.11	11_{111}–10_{110}	23158.04	−0.07
8_{17}–7_{16}	17344.46	0.13	11_{011}–10_{010}	23464.28	−0.08
9_{19}–8_{18}	18951.66	0.01	11_{210}–10_{29}	23506.64	−0.01
9_{09}–8_{08}	19211.45	−0.05	11_4–10_4	23529.78	0.10
9_{28}–8_{27}	19236.05	0.15	11_5–10_5	23538.05	0.08
9_3–8_3	19247.37	0.10	11_6–10_6	23548.77	−0.13
9_4–8_4	19252.00	0.12	11_7–10_7	23562.05	−0.12
9_5–8_5	19258.86	−0.11	11_{29}–10_{28}	23551.62	−0.14
9_6–8_6	19268.07	0.01	12_{112}–11_{111}	25260.46	0.19
9_{27}–8_{26}	19260.46	−0.11	12_{012}–11_{011}	25587.16	−0.11
9_{18}–8_{17}	19510.99*	0.39	12_{211}–11_{210}	25641.10	−0.05
10_{110}–9_{19}	21055.00	−0.21	12_4–11_4	25668.60	0.10
10_{010}–9_{09}	21339.00	−0.03	12_5–11_5	25677.51	0.20
10_{29}–9_{28}	21371.55	0.02	12_6–11_6	25689.01	−0.10
10_3–9_3	21386.23	0.17	12_9–11_9	25739.68	0.07
10_4–9_4	21390.88	0.08	12_{210}–11_{29}	25699.70	−0.01

a) $\Delta\nu=\nu_{obsd}-\nu_{calcd}$. *) Not included in the least-squares fitting.

The typical spectra of ^{80}Se and ^{78}Se species observed with the Stark field of 10 $V cm^{-1}$ are shown in Fig. 2. The $K_{-1}=2$ doublet lines were observed at the Stark field of 30 $V cm^{-1}$ as shown in Fig. 3(b). The $K_{-1}=2$ lines show a first-order Stark effect because the value (−0.991) of Ray's asymmetry parameter in ethyl isoselenocyanate is very close to −1.00. The assignments of the $K_{-1}=0$ and 1 transition lines were based on the second-order Stark effect.

In the first place, the 27 absorption lines of $J=5\leftarrow4$ to $J=13\leftarrow12$ with $K_{-1}=0$ and 1 for ^{80}Se species in the ground vibrational state were fitted to obtain the preliminary rotational and centrifugal distortion constants. These were employed to predict and assign the other transition lines with K_{-1} values larger than 2. The 75 transition lines of ^{80}Se species in the ground vibrational state were used to determine the rotational parameters, including the centrifugal distortion terms up to sextic contributions. The results are given in Tables 1, 2, and 3, together with the results of ^{78}Se species, which were obtained by analyzing the spectrum in the same way as for ^{80}Se species.

The values of −5.83 and −5.94 u Å^2 of inertia defect (Δ) for ^{80}Se and ^{78}Se species in Table 4 suggest that there are a plane symmetry and four hydrogen and heavy atoms in the ethyl isoselenocyanate molecule locate out-of-plane and in-plane, respectively. This means that there are two possible rotamers, synperiplanar and antiperiplanar forms. The observed values of P_b and Ray's asymmetry parameters for ^{80}Se and ^{78}Se species are very close to the ones calculated for synperiplanar form, but very different from the ones for antiperiplanar form, as shown in Table 4. Furthermore, the observed rotational constants A, B, and C are comparable with the ones calculated for synperiplanar conformer.

The above discussion has led to the conclusion that the spectrum assigned in this work is due to a synperiplanar rotational conformer of ethyl isoselenocyanate. This rotational conformer has been formed in ethyl isocyanate[1] and ethyl isothiocyanate.[2]

Three structural parameters, ∠C-N-C, r(C-N), and r(N=C), have been fitted to all the observed rotational constants of B and C for ^{80}Se and ^{78}Se species. The results are listed in Table 5. Other structural parameters were transferred from ethyl isocyanate,[1] ethyl isothiocyanate,[2] and carbonyl selenide.[13] The observed and calculated rotational constants obtained from the structural parameters in Table 5 are given in Table 6.

The derived values of the bond lengths, r(C-N) and r(N-C), are in agreement with those of similar compounds within less than 0.01 Å, as shown in Table 7.

Table 3. Observed Rotational(MHz) and Centrifugal Distortion(kHz) Constants for $CH_3CH_2NC^{80}Se$ and $CH_3CH_2NC^{78}Se$

	$CH_3CH_2NC^{80}Se$	$CH_3CH_2NC^{78}Se$
A	15140(23)	15112(28)
B	1090.443(16)	1099.865(12)
C	1029.261(16)	1037.745(12)
Δ_J	0.770(16)	0.793(33)
Δ_{JK}	−48.37(12)	−47.64(98)
δ_J	0.085(33)	
H_{KJ}	−0.0327(12)	
Δ[a]	−5.83	−5.94

Values in parentheses denote 2.5 times standard deviation and apply to the last digits of the constants. Conversion factor: 505376 MHz μÅ^2. a) $\Delta=I_c-I_a-I_b$.

Table 5. Structural Parameters(Å and degree) of Synperiplanar Ethyl Isoselenocyanate

Assumed parameters		
C-H:	1.091	∠H-C-H: 108.8
C-C:	1.522	∠H_s-C-C: 109.6
C=Se:	1.709	∠C-C-H_a: 110.6
∠H=C=Se: 180		
Derived parameters		
C-N:	1.444±0.010	∠C-N-C: 158.0±3.0
N-C:	1.210±0.010	

H_s and H_a indicate the hydrogen atom located in symmetry plane and in out-of symmetry plane respectively.

Table 4. Observed and Calculated Rotational Constants(MHz), Δ (μÅ^2),[a] and P_b(μÅ^2)[b] of Ethyl Isoselenocyanate

	A	B	C	κ	Δ	P_b
			^{80}Se species			
Obsd	15140	1090.44	1029.26	−0.9913	−5.83	30.464
Synperiplanar	15553	1102.5	1042.9	−0.9918	−6.30	29.345
Synclinal	17491	1058.0	1013.7	−0.9946	−8.01	24.885
Anticlinal	24768	978.8	957.7	−0.9982	−9.00	15.890
Antiperiplanar	32338	945.4	929.4	−0.9990	−6.30	12.474
			^{78}Se species			
Obsd	15112	1099.87	1037.74	−0.9912	−5.94	30.476
Synperiplanar	15560	1112.1	1051.5	−0.9917	−6.30	29.335
Synclinal	17499	1067.1	1022.1	−0.9945	−8.01	24.865
Anticlinal	24775	987.2	965.7	−0.9982	−8.99	15.898
Antiperiplanar	32341	953.4	936.9	−0.9990	−6.30	12.481

a) $\Delta=I_c-I_a-I_b$. b) $P_b=(I_a+I_c-I_b)/2$.

Table 6. Observed and Calculated Rotational Constants(MHz) for $CH_3CH_2NC^{80}Se$ and $CH_3CH_2NC^{78}Se$

	$CH_3CH_2NC^{80}Se$		$CH_3CH_2NC^{78}Se$	
	Obsd	Calcd*)	Obsd	Calcd*)
A	15140	(14938)	15112	(14931)
B	1090.44	1090.31	1099.86	1099.73
C	1029.26	1029.24	1037.74	1037.66

*) Calculated using the structural parameters in Table 5.

Table 7. Comparison of Structural Parameters of R-NCX Molecules(R=H, CH_3, and C_2H_5; X=O, S, and Se)

	R-N-C/°	r(R-N)/Å	r(N=C)/Å	r(C=X)/Å
H-NCO[a]	123.9	0.995	1.214	1.1664
H-NCS[b]	131.7	0.993	1.207	1.5665
H-NCSe[c]	143.0	0.99	1.195	1.717
CH_3-NCO	139.98[d]	1.437[d]	1.207[d]	1.171[d]
	140.18[e]	1.4342[e]	1.207[e]	1.171[e]
CH_3-NCS	147.46[d]	1.452[d]	1.216[d]	1.561[d]
	152.52[f]	1.4123[f]	1.2068[f]	1.5665[f]
CH_3-NCSe[g]	157.0	1.447	1.205	1.708
C_2H_5-NCO[h]	142.11	1.461	1.207	1.171
C_2H_5-NCS[i]	151.0	1.454	1.210	1.550
C_2H_5-NCSe[j]	158.0	1.444	1.210	(1.709)

a) Ref. 3, b) Ref. 4, c) Ref. 5, d) Ref. 6, e) Ref. 7, f) Ref. 8, g) Ref. 9, h) Ref. 1, i) Ref. 2, j) Tis work, ( ): assumed.

The angle of C-N-C of 158° in ethyl isoselenocyanate is much larger than the ones of ethyl isocyanate and ethyl isothiocyanate. If the estimation error of r(C=Se) from OCSe is ±0.01 Å, the errors of r(C-N), r(N=C), and ∠C-N-C are ±0.010 Å, ±0.010 Å, and ±3°, respectively.

The R-N-C bond angle in R-NCX (R=H, CH_3, or C_2H_5 and X=O, S, or Se) molecules enlarges in order of oxygen, sulfur, and selenium atom as listed in Table 7.

References

1) T. Sakaizumi, O. Yamada, K. Ushida, O. Ohashi, and I. Yamaguchi, *Bull. Chem. Soc. Jpn.*, **49**, 2908 (1976).

2) T. Sakaizumi, O. Ohashi, and I. Yamaguchi, *Bull. Chem. Soc. Jpn.*, **49**, 948 (1976).

3) K. Yamada, *J. Mol. Spectrosc.*, **79**, 323 (1980).

4) K. Yamada, M. Winnewisser, G. Winnewisser, L. B. Szalanski, and M. C. L. Gerry, *J. Mol. Spectrosc.*, **79**, 295 (1980).

5) B. M. Landsberg, *Chem. Phys. Lett.*, **60**, 265 (1979).

6) R. G. Lett and W. H. Flygare, *J. Chem. Phys.*, **47**, 4730 (1967).

7) J. Koput, *J. Mol. Spectrosc.*, **106**, 12 (1984).

8) M. Kreglewski, *Chem. Phys. Lett.*, **112**, 275 (1984).

9) T. Sakaizumi, A. Yasukawa, H. Miyamoto, O. Ohashi, and I. Yamaguchi, *Bull. Chem. Soc. Jpn.*, **59**, 1614 (1986).

10) W. J. Franklin, R. L. Werner, and A. Ashby, *Spectrochim. Acta*, **30A**, 1283 (1974).

11) C. Collard-Charon and M. Renson, *Bull. Chem. Soc. Belg.*, **71**, 531 (1962).

12) H. L. Jackson and B. C. McKusick, Jr., *Org. Synth.* Coll. IV, 438 (1963).

13) Y. Morino and C. Matsumura, *Bull. Chem. Soc. Jpn.*, **40**, 1101 (1967).

Production of Carbon Monoxide by Direct Thermal Splitting of Carbon Dioxide at High Temperature

Yutaka NIGARA and Bernard CALES*,†
Research Institute for Scientific Measurements, Tohoku University, Sendai 980
†Centre de Recherches sur la Physique des Hautes Températures CNRS 45045 Orléans Cédex, France
(Received March 4, 1985)

The direct thermal decomposition of carbon dioxide CO_2 to produce carbon monoxide CO have been studied as a mean of conversion and storage of a thermal energy, such as the solar heat, into a gaseous fuel. The process under investigation consists to displace the dissociation equilibrium of carbon dioxide by a selective pumping of oxygen at high temperature through a semipermeable membrane. Large amounts of carbon monoxide have been produced after the extraction of the oxygen arising from the CO_2 dissociation with the aid of a membrane made of calcia-stabilized zirconia. The variations of the flow of CO evolved from the reactor vs. temperature and oxygen partial pressure are in good agreement with the theoretical variations that may be deduced from the general equations of electrochemical transport in stabilized zirconia. Thereby, the efficiency of this process appears to be directly limited by the low oxygen permeation rate through the material used as oxygen selective membrane.

In the last past years, many investigations have been devoted to the conversion and storage of primary energies, such as the solar heat.[1] Indeed, although inexhaustible, the solar energy is subject to considerable variations with the lattitude and also to diurnal or seasonal variations. Accordingly, the utilization of solar energy on a large scale needs its conversion into a convenient form for a subsequent use. Various ways have been investigated, in which the solar radiation could be used either through quantum effects, this is the case of the solar cells for a direct conversion to electricity[2] and the hydrogen production via a water photoelectrolysis process,[3] or as a source of thermal energy for a thermochemical conversion and storage.[4] Recently another approach has been considered, in which the solar heat could be used to perform a direct thermal splitting of water at high temperature and to produce hydrogen.[5,6] This process implies to separate the hydrogen and the oxygen arising from the steam dissociation, in order to avoid the recombination reactions at lower temperatures. This may be achieved at high temperature with the use of a membrane semipermeable to oxygen while impervious to other gaseous components.[7] Such a membrane must be characterized by a mixed, ionic and electronic, electrical conductivity and located in a gradient of oxygen chemical potential,[6] as shown in Fig. 1. The ionic component σ_i of the conductivity allows the oxygen to diffuse through the membrane as O^{2-} ions, while the electronic component σ_e ensures an internal partial short-circuit which is required for the reactions of oxygen exchange at the two electrolyte-gaseous phase interfaces (Fig. 1).

On using calcia-stabilized zirconia as oxygen semipermeable membrane, noticeable amounts of hydrogen have been produced by this technique.[6] However, the efficiency of such a process is unavoidably limited by the low dissociation rate of water vapor, which reaches only 4% about at 2300 K under normal pressure conditions. Thus, the use of a gaseous component characterized by a higher dissociation rate would be more convenient. Carbon dioxide CO_2 seems

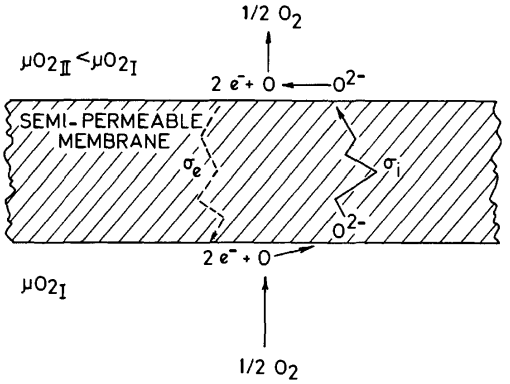

Fig. 1. Schematics of a membrane semipermeable to oxygen located between two different oxygen chemical potentials μO_2(I) and μO_2(II).

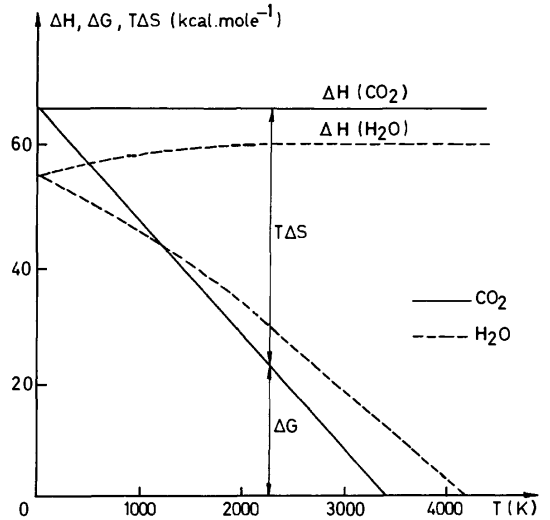

Fig. 2. Temperature dependences of the quantities of energy required for the dissociation of one mole of CO_2 or one mole of H_2O, after Ref. 8.

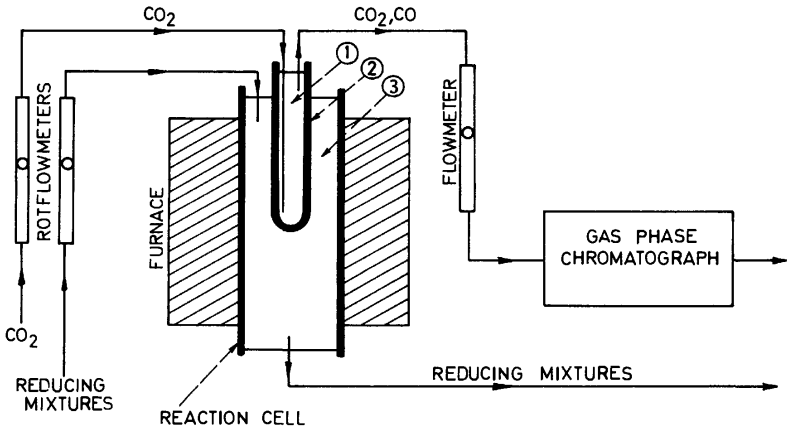

Fig. 3.Schematic illustration of the experimental set-up. ①: compartment I, ②: oxygen semipermeable membrane, ③: compartment II.

to be a good candidate owing to the potential applications of the gaseous fuel CO[2] which may be obtained by direct thermal splitting of CO_2. Moreover, the energy balance of the decomposition reaction is more propitious in the case of carbon dioxide than for water vapor.

The total quantity of energy ΔH required for the decomposition of one mole of CO_2 (or one mole of H_2O) may be supplied by means of a thermal energy $T\Delta S$ and/or an additional energy, such as a mechanical or an electrical energy, corresponding to the free enthalpy term ΔG[8] so that:

$$\Delta H = \Delta G + T\Delta S.$$

The temperature dependence of the various energies ΔH, ΔG, and $T\Delta S$ involved for the dissociation of one mole of CO_2 or one mole of H_2O may be deduced from the classical thermodynamic relationships and are depicted in Fig. 2. It clearly appears that, at high temperature, a major part of the total energy ΔH may be supplied by means of a thermal energy corresponding to $T\Delta S$. Furthermore, $T\Delta S$ is equal to 66% of the total energy required for the decomposition of one mole of CO_2 at 2250 K and only 50% in the case of one mole of H_2O at the same temperature.[8]

The purpose of the present work was to investigate the possibility of production of CO by direct thermal splitting of carbon dioxide on using a calcia-stabilized zirconia wall as oxygen semipermeable membrane.

Experimental

The experimental set-up mainly consists of a reaction cell, a laboratory built high temperature furnace working under oxidizing conditions,[9] a gas phase chromatograph and gas flowmeters (Fig. 3).[10]

The reaction cell is chiefly made up of a closed-end tube of calcia-stabilized zirconia, 2 mm thick and 10 mm in inner diameter, which acts as oxygen semipermeable membrane. Its chemical composition corresponds to 0.9 ZrO_2-0.1 CaO and the concentrations of the main impurities are ; 0.18 wt% Fe_2O_3, 0.81wt% SiO_2, 0.33wt% MgO, and 0.3 wt% Al_2O_3. The cell is located inside the high temperature furnace, the heating elements of wich are made of partially stabilized zirconia which allows the zirconia tube to be heated at temperatures up to 2500 K. However, owing to the difficulty of temperature measurements in the center of the reaction cell and to the thermomechanical characteristics of the cell itself, the usefull temperature range has been reduced to approximately 1700—2100 K.

The inner part of the zirconia tube, compartment I, is fed with pure carbon dioxide, with a flow-rate of 1000 $cm^3 h^{-1}$, under isobaric conditions (10^{-1} MPa). In the hot zone of the cell, carbon dioxide partially dissociates and the oxygen arising from the dissociation reaction diffuses through the zirconia wall into compartment II. The oxygen partial pressure in compartment II, pO_2(II), must be much lower than the oxygen partial pressure in compartment I, pO_2(I), that is fixed in dynamical conditions by the dissociation equilibrium of carbon dioxide. This has been conveniently achieved, in the present study, by the use of CO-CO_2 mixtures which allow to vary the oxygen partial pressure pO_2(II) in a large range, independently of the oxygen flux through the membrane. The flow-rate of CO-CO_2 mixtures in compartment II is equal to 18.5×10^3 $cm^3 h^{-1}$.

After migration of oxygen, the composition of the dissociated gas phase is checked out by chromatography at the gas outlet of compartment I.

Under stationary conditions, the mass flow balance implies that the flow of carbon monoxide D_{CO} evolved from the compartment I is twice the flow of oxygen D_{O_2}, through the effective permeation area S of the zirconia membrane, which is given by :

$$D_{co} = 2D_{O_2} = 2J_{O_2} \cdot S \qquad (1)$$

where J_{O_2} is the flow of oxygen per unit area of the semipermeable membrane.

From the measurement of temperature gradients along the zirconia tube,[10] the effective permeation area has been estimated to about 4 cm^2.

Theoretical Considerations

The partial current density $\vec{J_k}$ arising from the flow of charged species k in a solid electrolyte located in a chemical potential gradient is derived from the general equations of electrochemical transport and is given by:[11]

$$\vec{J_k} = -\frac{\sigma_k}{z_k q}\overrightarrow{\nabla \eta_k}, \tag{2}$$

where σ_k is the partial electrical conductivity of the electrolyte, z_k the valence of particles k and q the electronic charge. $\overrightarrow{\nabla \eta_k}$ denotes a gradient of electrochemical potential which results from gradients of chemical potential $\overrightarrow{\nabla \mu_k}$ and electrical potential $\overrightarrow{\nabla V}$:[12]

$$\overrightarrow{\nabla \eta_k} = \overrightarrow{\nabla \mu_k} + z_k q \overrightarrow{\nabla V}.$$

In the case of stabilized zirconia, the electrochemical transport at high temperature arises from the motion of both O^{2-} ions and electrons.[13] The total current density $\vec{J_t}$ is then the sum of the contributions due to ionic species $\vec{J}_{O^{2-}}$ and electrons $\vec{J_e}$. It is deduced from Eq. 2 and writes:

$$\vec{J_t} = \frac{\sigma_e}{q}\overrightarrow{\nabla \eta_e} + \frac{\sigma_i}{2q}\overrightarrow{\nabla \eta_{O^{2-}}}, \tag{3}$$

where σ_i and σ_e denote the partial ionic and electronic conductivities of stabilized zirconia.

Moreover, on assuming that the thermodynamic equilibrium between ionic and electronic species:

$$O^{2-} \rightleftharpoons 1/2\, O_2 + 2e^-$$

remains locally undisturbed by the partial current flows, it is possible to relate the total current density $\vec{J_t}$ to the chemical potential gradient of oxygen $\overrightarrow{\nabla \mu_{O_2}}$ by the following relationship:[11]

$$\vec{J_t} = \frac{\sigma_t}{q}\overrightarrow{\nabla \eta_e} + \frac{\sigma_i}{4q}\overrightarrow{\nabla \mu_{O_2}}, \tag{4}$$

where σ_t is the total conductivity of the material ($\sigma_t = \sigma_i + \sigma_e$).

Under stationary conditions, if no electrical current flows through an external circuit, the total current density in the material would be equal to zero and it follows from Eqs. 2 and 4:[11]

$$\vec{J}_{O^{2-}} = -\vec{J_e} = \frac{\sigma_e}{4q} t_i \overrightarrow{\nabla \mu_{O_2}}, \tag{5}$$

where t_i denotes the ionic transference number of stabilized zirconia ($t_i = \sigma_i/\sigma_t$).

Owing to the very wide electrolytic domain of stabilized zirconia,[14] the ionic transference number t_i is close to unity in large ranges of temperature and oxygen partial pressure. In the same domain, the electronic conductivity writes:[15]

$$\sigma_e = \sigma_e^\circ \exp(-\Delta E/k_B T)\, pO_2^{-1/4}, \tag{6}$$

where σ_e° is a constant, ΔE the activation energy, k_B the Boltzmann constant and pO_2 the oxygen partial pressure of the surrounding atmosphere. From the different values reported in the litterature, Heyne and Beekmans[15] have proposed a mean value of 3.7 eV for the activation energy of the n-type electronic conductivity of stabilized zirconia.

Combining Eqs. 5 and 6 with the condition $t_i \simeq 1$, the ionic current $J_{O^{2-}}$ through a stabilized zirconia membrane is obtained after integration over the thickness L of the membrane and is given by:

$$J_{O^{2-}} = \frac{k_B T}{qL}\sigma_e^\circ \exp(-\Delta E/k_B T)[pO_2(II)^{-1/4} - pO_2(I)^{-1/4}], \tag{7}$$

where $pO_2(I)$ and $pO_2(II)$ are the oxygen partial pressures at the two electrolyte-gaseous phase interfaces.

The oxygen flow J_{O_2} through the membrane is then derived from Eq. 7:

$$J_{O_2} = \frac{k_B T}{4qFL}\sigma_e^\circ \exp(-\Delta E/k_B T)[pO_2(II)^{-1/4} - pO_2(I)^{-1/4}], \tag{8}$$

where F is the Faraday constant.

The flow of carbon monoxide D_{CO} evolved from the reactor is directly related to J_{O_2} [Eq. 1] and would then obey the same dependences against temperature and oxygen partial pressures.

Results and Discussion

The composition of the gas phase evolved from compartment I is plotted in Fig. 4 vs. the cell temperature, for different values of the ratio CO_2/CO of the reducing mixtures flowing in compartment II. For CO_2/CO ratio lower than 10, the amount of produced carbon monoxide increases rapidly with the cell temperature. At 1954K, in the most reducing conditions ($CO_2/CO = 0.01$), which corresponds to an oxygen partial pressure $pO_2(II)$ of about 10^{-11} MPa, 21.5 mol% of carbon dioxide have been converted to CO.

Such a value is much higer than the dissociation rate of CO_2 which is expected to reach 1.2% at the same temperature without any transfer of oxygen through a semipermeable membrane. Thus, under the influence of the selective pumping of oxygen through the zirconia wall, the thermodynamical equilibrium

$$CO_2 \rightleftharpoons CO + 1/2\, O_2 \tag{9}$$

is strongly displaced to the right hand side.

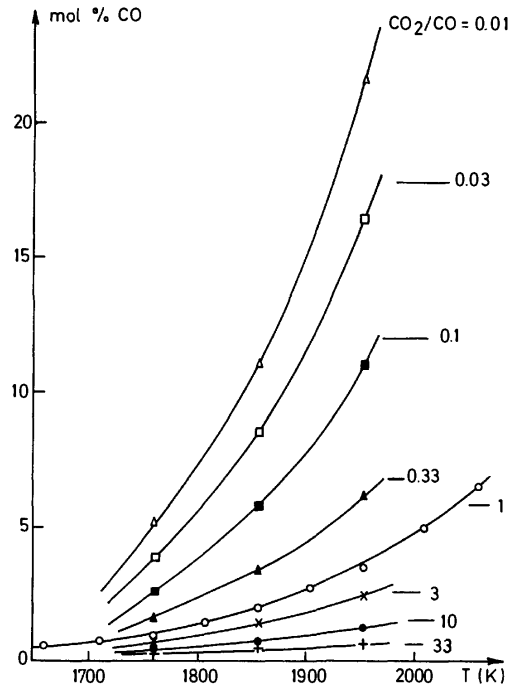

Fig. 4. Variations of the concentration of CO in the gas phase evolved from compartment I against temperature, for different composition of the $CO-CO_2$ mixtures flowing in compartment II.

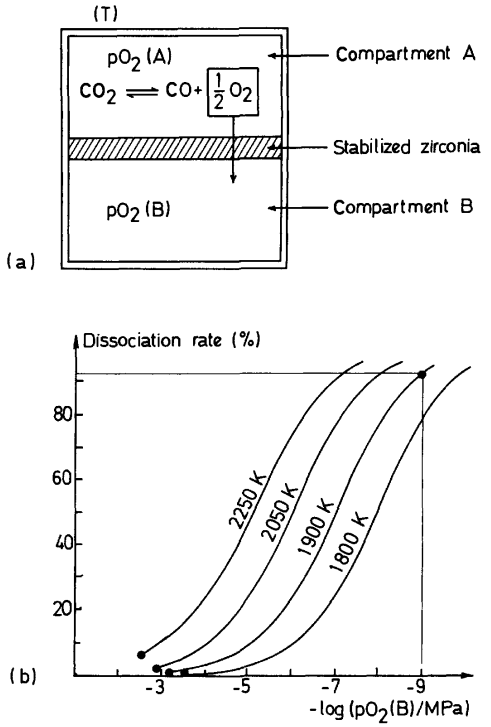

Fig. 5. Schematic of a reaction cell working under static conditions (a) and variations of the dissociation rate of CO_2 obtained with such a cell versus $pO_2(B)$ (b), after Ref. 8.

Nevertheless, due to the dynamical conditions used in the present technique, only a fraction of the introduced carbon dioxide is converted to CO. Indeed, let us consider a reaction cell working under static conditions and made up of a stabilized zirconia wall which separates two compartments A and B having the same volume (Fig. 5a). The calculated values of the dissociation rate of CO_2 that may be reached under these conditions are plotted in Fig. 5b as a function of the oxygen partial pressure $pO_2(B)$ fixed in compartment B before the experiment.[8] At a given temperature, the oxygen arising from the dissociation reaction would flow through the zirconia membrane until the oxygen partial pressures $pO_2(A)$ and $pO_2(B)$ are equal. Thus, at 1900 K, for an oxygen partial pressure $pO_2(B)$ initially fixed at 10^{-9} MPa, 93% about of the introduced carbon dioxide would be converted to CO before the system reaches the thermodynamical equilibrium.[8]

In the present case, the oxygen partial pressure $pO_2(I)$ in compartment I is smaller than the value predicted by the dissociation equilibrium of CO_2, owing to the oxygen transfer through the membrane. It has been however derived from the equilibrium constant K relative to equilibrium (9).

$$K = \frac{pCO\ pO_2(I)^{1/2}}{pCO_2} \qquad (10)$$

where the partial pressure of carbon monoxide, pCO, has been deduced from the CO content measured by chromatography in the gas phase evolved from compartment I.

The oxygen partial pressure $pO_2(II)$ is fixed by the $CO-CO_2$ mixtures. Due to the high buffer capacity of these mixtures, for CO_2/CO ratio higher than 0.03, the oxygen partial pressure $pO_2(II)$ is not affected by the oxygen transfer through the membrane. For CO_2/CO ratio smaller than 0.03, the quantity of oxygen flowing through the zirconia wall is high enough to slightly modify the composition of the $CO-CO_2$ mixtures and small corrections may be applied in the calculation of $pO_2(II)$.[10]

The flow of carbon monoxide D_{CO} evolved from compartment I has been plotted in Fig. 6 against the difference of oxygen partial pressures $\Delta pO_2^{-1/4} = [pO_2(II)^{-1/4} - pO_2(I)^{-1/4}]$, for three temperatures. The flow of CO appears to be directly proportional to $\Delta pO_2^{-1/4}$, since the log D_{CO} vs. log $\Delta pO_2^{-1/4}$ plots are characterized by straight lines, the slopes of which are not far from to unity. Owing to the proportionality relationship between D_{CO} and J_{O_2} [Eq. 1], this is in good agreement with the theoretical dependence of the oxygen flux J_{O_2} against $\Delta pO_2^{-1/4}$, predicted by Eq. 8.

Furthermore, according to Eq. 8, the semi-permeability coefficient, which is defined as the ratio of the oxygen flux to the difference $\Delta pO_2^{-1/4}$, varies with the temperature according to an Arrhenius law (Fig. 7), the activation energy of which amounts to about 3.55 eV. Such a value agrees with the mean activation energy for the n-type electronic conductivity of stabilized zirconia proposed by Heyne and Beekmans

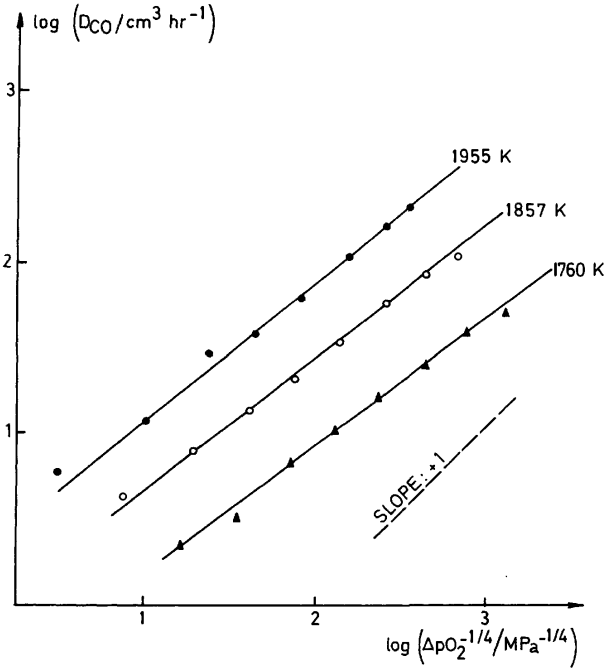

Fig. 6. Dependence of the flow of CO evolved from the reactor on the difference $\Delta pO_2^{-1/4}$.

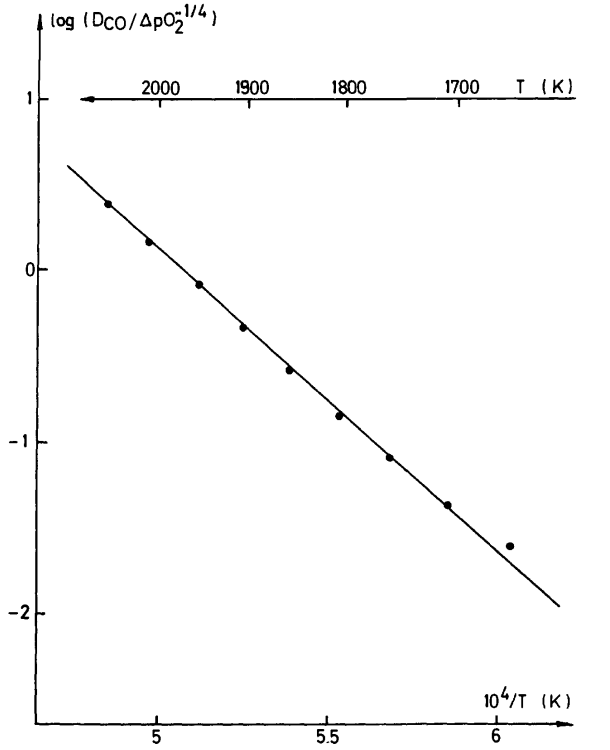

Fig. 7. Variation of the ratio $D_{CO}/\Delta pO_2^{-1/4}$ vs. temperature.

(3.7 eV).[15]

These two results clearly show that the oxygen flow J_{O_2} and the flow D_{CO} evolved from the compartment I correspond to the maximum flows that it is presently possible to obtain, since they directly depend on the specific characteristics of the oxygen semipermeable membrane. Thus, the efficiency of the process under investigation appears to be primarily limited by the low value of the electronic conductivity of the stabilized zirconia wall.

Indeed, the general expression of the current density $\vec{J}_{O^{2-}}$ due to the motion of O^{2-} ions in an oxide solid electrolyte [Eq. 5] may also be written:[16]

$$\vec{J}_{O^{2-}} = \frac{\sigma_t}{4q} t_i t_e \overrightarrow{\nabla \mu_{O_2}} \qquad (11)$$

where t_e is the electronic transference number of the material ($t_e=\sigma_e/\sigma_t=1-t_i$).

Thereby, the oxygen flux J_{O_2}, and consequently the amount of produced carbon monoxide, would be maximum for equal ionic and electronic transference numbers ($t_i=t_e=0.5$). The material used as oxygen semipermeable membrane would present equal ionic and electronic conductivities in the range of oxygen partial pressure [pO_2(I), pO_2(II)].

In the case of stabilized zirconia, such a behavior is observed for an oxygen partial pressure which is much smaller than pO_2(I) and pO_2(II) and rises from 10^{-21} MPa at 1673K to 10^{-13} MPa at 2073K.[17]

Conclusion

The present study has demonstrated the possibility of production of CO by direct thermal splitting of carbon dioxide at high temperature and extraction of oxygen by means of a semipermeable membrane.

On using calcia stabilized zirconia (10 mol% CaO) as oxygen semipermeable membrane, about 100 to 200 $cm^3 h^{-1}$ of CO have been produced at 1960 K for a CO_2 consumption of 1000 $cm^3 h^{-1}$. The variations of the flow of CO evolved from the reaction versus the cell temperature and the difference $\Delta pO_2^{-1/4}$ agreed with the theoretical variations deduced from the general equation of electrochemical transport in stabilized zirconia. Therefore, such a process appears to be very interesting with respect to energy conversion applications.

Various parameters could allow to appreciably increase the quantities of produced carbon monoxide. This would be the case on using a semipermeable membrane with a smaller thickness and/or a larger permeation area. Nevertheless, the efficiency of the process is primarily controlled by the electrical properties of the material used as oxygen selective membrane. Thus, in the present case, any improvement of this technique is submitted to an enhancement of the electronic conductivity of stabilized zirconia.

Fluorite type solid solutions may be observed between zirconia ZrO_2 and ceria CeO_2, which is known to exhibit an electronic conductivity, in large range of composition.[18] The addition of a third oxide, the cation of which has a lower valency than zirconium Zr(IV) or cerium Ce(IV) ions, such as yttria Y_2O_3, could enhance the ionic conductivity of these compounds. The study of the electrical properties of the solid

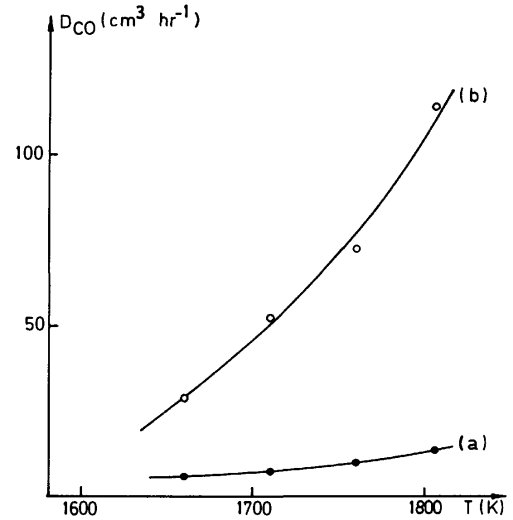

Fig. 8. Variations of the flow of CO evolved from the reactor against temperature in the case of a calcia stabilized zirconia membrane (a) or a ceria-doped stabilized zirconia memberane (b). The composition of the CO-CO_2 mixture in compartment II corresponds to $CO_2/CO=1$.

solutions of the ternary ZrO_2-CeO_2-Y_2O_3 system has shown that they would present, in the temperature and oxygen partial pressure ranges of interest for this process, a mixed electrical conductivity with equivalent ionic and electronic components.[19] Moreover, the solid solution containing about 20 mol% of cerium oxide CeO_2 appears to be the most suitable for this application.[16] This has been confirmed by preliminary results obtained on using such a solid solution as oxygen selective membrane. The flows of CO produced with the aid of either "pure" stabilized zirconia or ceria-doped stabilized zirconia as semipermeable membrane are compared in Fig. 8. They clearly indicate that the solid solution of the ZrO_2-CeO_2-Y_2O_3 system is characterized by a higher oxygen semipermeability. The use of this material in a process of thermal energy conversion and storage based on the direct thermal splitting of CO_2 is thus very promissing and presently under investigation.

References

1) J. O'M. Bockris, "Hydrogen Energy," ed by T. N. Veziroglu, Plenum Press, New York (1975), p. 9.
2) S. Wagner, "Solid State Chemistry of Energy Conversion and Storage," ed by J. B. Goodenough and M. S. Whittingham, American Chemical Society, Washington, (1977), p. 109.
3) J. R. Bolton, *Solar Energy*, **20**, 181 (1978).
4) M. Ducarroir, M. Tmar, and C. Bernard, *Rev. Phys. Appl.*, **15**, 513 (1980).
5) S. Ihara, "Solar-Hydrogen Energy Systems," ed by T. Ohta, Pergamon Press, New York (1979), p. 59.
6) B. Calès and J. F. Baumard, *High Temp. -High Pressures*, **14**, 681 (1982).
7) J. Lédé, F. Lapicque, J. Villermaux, B. Calès, A. Ounalli, J. F. Baumard, and A. M. Anthony, *Int. J. Hydrogen Energy*, **7**, 939 (1982).
8) J. Robieux, Internal Report, Academy of Sciences, France, 1981.
9) B. Calès and A. M. Anthony, "Progress in Solid Electrolytes," ed by T. R. Wheat, A. Ahmad, and A. K. Kuriakose, Energy Mines and Ressources, Ottawa (1983), p. 413.
10) A. Ounalli, Thesis, University of Orléans, France, 1981.
11) L. Heyne, "Mass Transport in Oxides," NBS Special Publication, Washington (1968), p. 149.
12) P. Kofstad, "Nonstoichiometry, Diffusion and Electrical Conductivity in Binary Metal Oxides," Wiley Interscience, New York (1972).
13) T. H. Etsell and S. M. Flengas, *Chem. Rev.*, **70**, 339 (1970).
14) J. W. Patterson, *J. Electrochem. Soc.*, **118**, 1033 (1971).
15) L. Heyne and N. M. Beekmans, *Proc. Brit. Ceram. Soc.*, **19**, 229 (1979).
16) B. Calès, Ph. D. Thesis, University of Orléans, France, 1983.
17) B. Calès and J. F. Baumard, *J. Mater. Science*, **17**, 3243 (1982).
18) E. Tani, M. Yoshimura, and S. Sōmiya, *J. Am. Ceram. Soc.*, **66**, 506 (1983).
19) B. Calès and J. F. Baumard, *J. Electrochem. Soc.*, **131**, 2407 (1984).

 © 1986 The Chemical Society of Japan Bull. Chem. Soc. Jpn., 59, 2003—2007 (1986)

Synthesis, Ion-Exchange Properties and Analytical Applications of Tin(IV) Tungstovanadophosphate

Syed Ashfaq NABI and Weqar Ahmad SIDDIQUI*,†
Chemistry Department, Faculty of Education, Post Box 18758, University of Sebha, Libya
†Department of Chemistry, Aligarh Muslim University, Aligarh-202001, India
(Received June 15, 1984)

Samples of tin(IV) tungstovanadophosphate have been synthesized under varying conditions and their ion-exchange properties are studied. Among the various samples of tin(IV) tungstovanadophosphate, sample $TTVP_7R$ is chosen for detailed study and its ion-exchange properties are compared with sample $TTVP_7$. Both the compounds are synthesized in excess of acid, i.e. at pH less than zero. Sample $TTVP_7$ is synthesized by adding 0.025 mol dm^{-3} sodium metavanadate, 0.025 mol dm^{-3} sodium tungstate and 1.0 mol dm^{-3} phosphoric acid to 0.1 mol dm^{-3} tin(IV) chloride in the volume ratio of 1:1:1:1 at pH=0. Sample $TTVP_7R$ was prepared by refluxing the precipitate of sample $TTVP_7$ in the reaction mixture. The chemical and thermal stabilities of this material have been determined. The reproducibility of the material is also checked. Distribution coefficients for numerous metal ions in formic acid-sodium formate buffer systems of different pH were determined. The utility of the material has been demonstrated by achieving a number of binary and ternary separations on its small columns.

Synthetic inorganic ion exchangers have attracted attention because of their versatility in separation science and in many other fields of diverse nature. The inorganic ion-exchange materials which have been synthesized and studied till now are mostly single and double salts of metals. In many instances it has been found that double salts exhibit ion-exchange properties and they are thermally and chemically more stable than single salts. For example tin(IV) vanadotungstate[1] has been found to behave entirely different from tin(IV) tungstate,[2] tin(IV) vanadate,[3] and tin(IV) phosphate.[4] It is our prediction that by incorporating three different types of anions in the matrix, the exchange properties of the material may be improved further. It is with this view in mind we have synthesized tin(IV) tungstovanadophosphate and studied its ion-exchange properties. The following pages summarize our findings in this direction.

Experimental

Reagents. Tin(IV) chloride pentahydrate (Reachim), sodium tungstate (BDH), sodium metavanadate (Riedel Germany), and phosphoric acid (BDH) were used for the synthesis of the material. All other chemicals were of analytical reagent grade.

Apparatus. Spectrophotometric studies were performed using spectrophotometer GS 866D (E. C.). ELICO Model LI-10 pH meter was used for pH measurements and Stanton thermobalance type H_4 for TGA. A temperature controlled shaker SICO was used for shaking.

Synthesis. Samples of tin(IV) tungstovanadophosphate were synthesized by mixing aqueous solutions of the appropriate reagents. The solutions used for the synthesis were 0.025 mol dm^{-3} in sodium tungstate, 0.025 mol dm^{-3} in sodium metavanadate, 0.5 mol dm^{-3} in phosphoric acid (1.0 mol dm^{-3} in phosphoric acid for the synthesis of samples $TTVP_7$ and $TTVP_7R$) and 0.1 mol dm^{-3} in tin(IV) chloride. Conditions of synthesis for different samples are indicated in Table 1. The pH for the sample solution in each case was adjusted by adding either concentrated hydrochloric acid or dilute sodium hydroxide solutions. The precipitate so formed was then allowed to settle down for 24 h at room temperature (25±2°C), washed several times with demineralized water (DMW) to remove excess reagent and finally

Table 1. Conditions of Synthesis and Few Properties of Different Samples of Tin(IV) Tungstovanadophosphate

Sample No.	Concentration/mol dm^{-3}				Mixing volume ratio v/v/v/v	pH	Appearance of precipitate	Appearance of beads after drying at 40°C	Ion-exchange capacity for K^+ /meq (dry g)$^{-1}$
	Tin(IV) chloride	Sodium tungstate	Sodium vanadate	Phosphoric acid					
$TTVP_1$	0.1	0.025	0.025	0.5	1:1:1:1	1	Yellow	Greenish yellow (shining)	1.50
$TTVP_2$	0.1	0.025	0.025	0.5	2:1:1:1	1	Yellow	Greenish yellow (shining)	1.35
$TTVP_3$	0.1	0.025	0.025	0.5	1:2:1:1	1	Yellow	Yellow (shining)	1.14
$TTVP_4$	0.1	0.025	0.025	0.5	1:1:2:1	1	Yellow	Yellow (shining)	1.21
$TTVP_5$	0.1	0.025	0.025	0.5	1:1:1:2	1	Yellow	Yellow (shining)	1.21
$TTVP_6$	0.1	0.025	0.025	P[a]	1:1:1:1	1	Yellow	Yellow (shining)	1.48
$TTVP_7$	0.1	0.025	0.025	1.0	1:1:1:1	<0	Yellow	Greenish yellow (shining)	2.06
$TTVP_7R$	0.1	0.025	0.025	1.0	1:1:1:1	<0	Yellow	Greenish yellow (shining)	2.15
$TTVP_8$	0.1	0.025	0.025	0.5	1:1:1:1	2.5—3	Yellow	Yellow (shining)	1.30

a) P=0.1 mol dm^{-3} Potassium dihydrogenorthophosphate.

Table 2. Data Showing the Reproducibility of Samples of Tin(IV) Tungstovanadophosphate

Sl. No.	Unrefluxed sample ($TTVP_7$)			Refluxed sample ($TTVP_7R$)		
	Appearance of the precipitate	Appearance of beads after drying at 40 °C	I.E.C. for K^+ meg (dry g)$^{-1}$	Appearance of the precipitate	Appearance of beads after drying at 40 °C	I.E.C. for K^+ meg (dry g)$^{-1}$
1	Yellow	Greenish yellow	2.00	Yellow	Greenish yellow	2.11
2	Yellow	Greenish yellow	1.98	Yellow	Greenish yellow	2.14
3	Yellow	Greenish yellow	2.04	Yellow	Greenish yellow	2.10
4	Yellow	Greenish yellow	1.96	Yellow	Greenish yellow	2.00
5	Yellow	Greenish yellow	2.01	Yellow	Greenish yellow	2.12
6	Yellow	Greenish yellow	1.98	Yellow	Greenish yellow	2.14

Table 3. Ion-Exchange Capacity [meq (dry g^{-1})] of Tin(IV) Tungstovanadophosphate for Various Cations

Cation	Salt used	pH	Hydrated radii[17]/nm	Sample $TTVP_7R$ meq (dry g)$^{-1}$	Sample $TTVP_7$ meq (dry g)$^{-1}$
Li^+	Lithium chloride	6.8	10.0	1.98	1.81
Na^+	Sodium chloride	6.8	7.9	1.72	1.83
K^+	Potassium chloride	6.8	5.3	2.15	2.06
Rb^+	Rubidium chloride	6.2	—	2.06	1.98
Mg^{2+}	Magnesium chloride	6.5	10.8	2.09	2.04
Ca^{2+}	Calcium chloride	6.5	9.6	2.13	2.08
Sr^{2+}	Strontium chloride	6.2	9.6	2.20	2.10
Ba^{2+}	Barium chloride	6.2	8.8	2.60	2.26

filtered under suction. It was then dried at 40 °C in an oven. The material was then immersed in DMW where it was broken into fine particles with slight evolution of heat. The material was then converted into hydrogen form by keeping it into 0.1 mol dm^{-3} nitric acid solution for 48 h. Excess of acid was removed by washing with DMW. Sample $TTVP_7R$ was prepared by refluxing the precipitate of sample $TTVP_7$ for 6 h in a mixture of 0.1 mol dm^{-3} sodium tungstate, 0.1 mol dm^{-3} sodium metavanadate and 1.0 mol dm^{-3} phosphoric acid in the volume ratio of 1:1:1. Concentrated hydrochloric acid was also added in sufficient quantity to adjust the pH of the mixture less than zero. The mixture was then allowed to cool. The supernatant liquid removed and the product was washed several times with water and finally filtered, dried, and converted into hydrogen form as described above. To check the reproducibility of the exchanger six sets of samples $TTVP_7$ and $TTVP_7R$ were prepared. Results are given in Table 2.

Ion-Exchange Capacity. The ion-exchange capacity of samples of tin(IV) tungstovanadophosphate was determined by column method.[3] The hydrogen ion liberation capacity with different mono and bivalent ions is reported in Table 3.

pH Titration. The titrations for samples $TTVP_7R$ and $TTVP_7$ were performed in NaOH-NaCl and KOH-KCl systems using the method.[5] The pH titration curves are shown in Figs. 1 and 2.

Thermal Treatment. The thermogravimetric analysis of tin(IV) tungstovanadophosphate in hydrogen form was performed at a heating rate of 10 °C min^{-1}. The resulting thermogram is shown in Fig. 3. To examine the effect of heating on the ion-exchange capacity, the material in the hydrogen form was heated at different temperatures (40, 100, 200, 400, 500, 600, and 800 °C) for 1 h in a muffle furnace.

Chemical Stability. The chemical stability of samples $TTVP_7R$ and $TTVP_7$ was studied in a number of solvents (0.1 to 4 mol dm^{-3} of HNO_3, HCl and H_2SO_4, 60% $HClO_4$, 1 mol dm^{-3} oxalic acid, 0.5 mol dm^{-3} aqueous NH_3, and 0.1 mol dm^{-3} NaOH) of analytical interest. One half gram of the ion-exchange material was equilibrated with 50 cm^3 of the solvent at room temperature (25±2 °C) and kept for 24 h with occasional shaking. Tin, tungsten, vanadium, and phosphorus in the solutions were determined spectrophotometrically using standard methods[6-9] respectively.

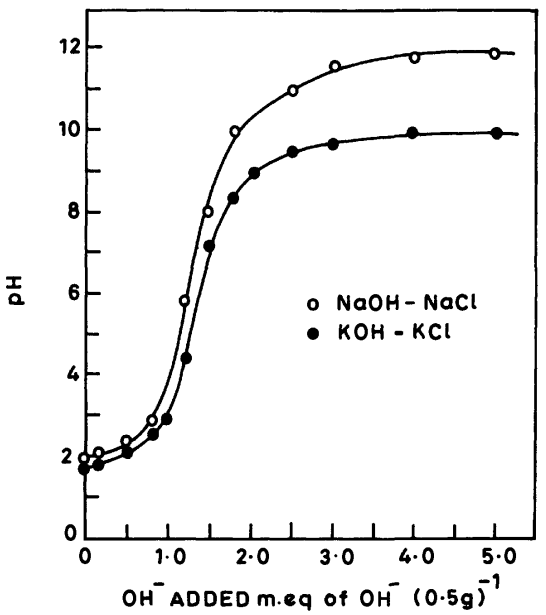

Fig. 1. pH Titration curves of tin(IV) tungstovanadophosphate (Sample $TTVP_7R$).

Chemical Composition. For the determination of chemical composition of various samples of tin(IV) tungstovanadophosphate, 0.2 g of the material was dissolved in hot concentrated hydrochloric acid. It was then diluted to

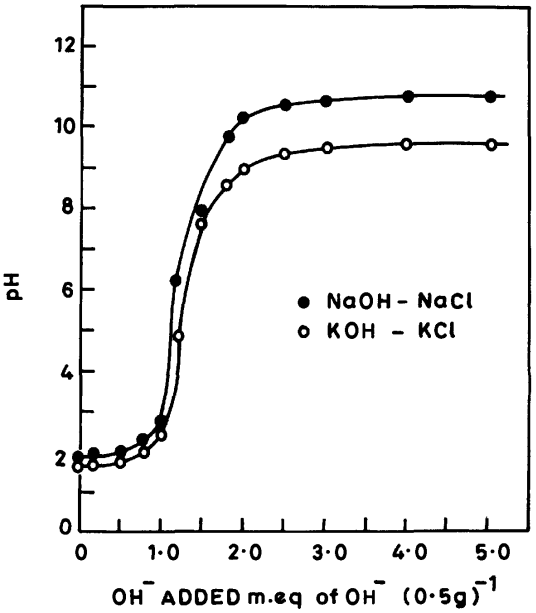

Fig. 2. pH Titration curves of tin(IV) tungstovanadophosphate (Sample $TTVP_7$).

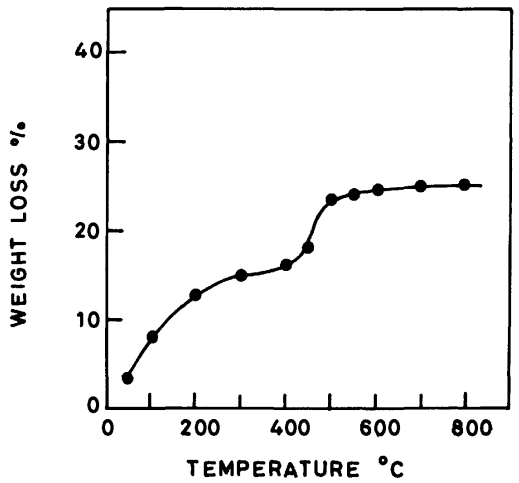

Fig. 3. Thermogram of tin(IV) tungstovanadophosphate($TTVP_7R$) in H^+ form.

100 cm^3 with DMW. Tin was determined spectrophotometrically[6] while tungsten and vanadium were determined by gravimetric[10] and titrimetric[11] methods respectively. Phosphate was determined titrimetrically using the standard method.[12]

Equilibrium Study. Equilibrium times for the adosorption of bivalent, tervalent, and quadrivalent metal ions (Mg^{2+}, Ba^{2+}, Cu^{2+}, Ni^{2+}, Al^{3+}, Fe^{3+}, Pr^{3+}, Zr^{4+}, and Th^{4+}) on tin(IV) tungstovanadophosphate ($TTVP_7R$, 50—100 mesh) in hydrogen form were determined by the earlier described method.[13]

Distribution Coefficient. Distribution coefficients of a number of metal ions in water and formic acid-sodium formate buffer systems of varying pH were determined. One half gram of the exchanger in hydrogen form (50—100 mesh) were added in 25 cm^3 cation solution in a 250 cm^3 Erlenmeyer flask. Concentration of metal ion in the solution was adjusted in such manner that it did not exceed 3% of the total ion-exchange capacity of the exchanger. The flask was then shaken in a shaker incubator at 25±2°C for 6 h. The amount of cation left in the solution after equilibrium was determined titrimetrically using 0.002 mol dm^{-3} EDTA as titrant. The K_d values were calculated according to the formula.[14] The results are given in Fig. 4.

Quantitative Separations of Metal Ions. Quantitative separations of some important metal ions of analytical utility were achieved on the columns of tin(IV) tungstovanadophosphate. Two grams of the exchanger in hydrogen form (50—100 mesh) was taken into a glass column of i. d. 0.6 cm. DMW was first run and then the mixture of metal ions was poured and allowed to be adsorbed. The metal ions were then eluted separately using suitable eluting reagents and determined by EDTA titrations. The flow rate of the effluent was maintained 1 $cm^3\,min^{-1}$ throughout the elution process. Results of separations achieved have been reported in Table 4.

Results and Discussion

Table 1 shows that the ion-exchange capacity of tin(IV) tungstovanadophosphate depends on the conditions of synthesis, that is on the mixing volume ratio of the reactants, the pH at which the precipitation is done and also on the refluxion. The maximum ion-exchange capacity [1.5 meq (dry g)$^{-1}$] is observed in the case of sample $TTVP_1$ prepared by mixing reagents in the volume ratio of 1:1:1:1 at pH 1. However, when the sample is prepared using the same ratio at pH less than zero, the capacity is found to increase significantly from 1.5 to 2.06 meq (dry g)$^{-1}$ (sample $TTVP_7$). It is interesting to observe that on refluxing the same product ($TTVP_7$) in a mixture of sodium metavanadate, sodium tungstate and phosphoric acid, the capacity of the final product ($TTVP_7R$) is further increased to some extent and it becomes chemically more stable. Both the refluxed product ($TTVP_7R$) and the unrefluxed product ($TTVP_7$) show reproducible properties as it is evident from the data given in Table 2.

It is clear from Table 3 that the hydrated radii of alkali metals and alkaline earths have no significant effect on the ion-exchange capacity of tin(IV) tungstovanadophosphate. The refluxed and the unrefluxed product both behave in a similar manner. The highest capacity is observed for Ba^{2+} ion [2.6 meq (dry g)$^{-1}$]. The order of exchange capacity for alkali metals, however, is as follows:

Sample $TTVP_7R$: $K^+ > Rb^+ > Li^+ > Na^+$

Sample $TTVP_7$: $K^+ > Rb^+ > Li^+ > Na^+$

In the case alkaline earths the same order is followed for both the ion-exchange materials

$$Ba^{2+} > Sr^{2+} > Ca^{2+} > Mg^{2+}$$

A comparison of the ion-exchange capacity of different tin(IV) based ion exchangers at 25±2°C shows

that tin(IV) tungstovanadophosphate ($TTVP_7R$) is much superior to other exchangers such as tin(IV) phosphate [(1.44 meq (dry g)$^{-1}$],[4] tin(IV) tungstate [0.58 meq (dry g)$^{-1}$][2] and tin(IV) vanadate [0.85 meq (dry g)$^{-1}$].[3] It is also interesting to note that stannic tungstovanadophosphate has higher ion-exchange capacity and chemical stability as compared to double salts such as tin(IV) vanadophosphate [1.98 meq (dry g)$^{-1}$].[1] The pH titration curves (Figs. 1 and 2) show that tin(IV) tungstovanadophosphate behaves as a monobasic acid. The uptake of ion depends on the pH of the solutions. The adsorption of K^+ is greater than

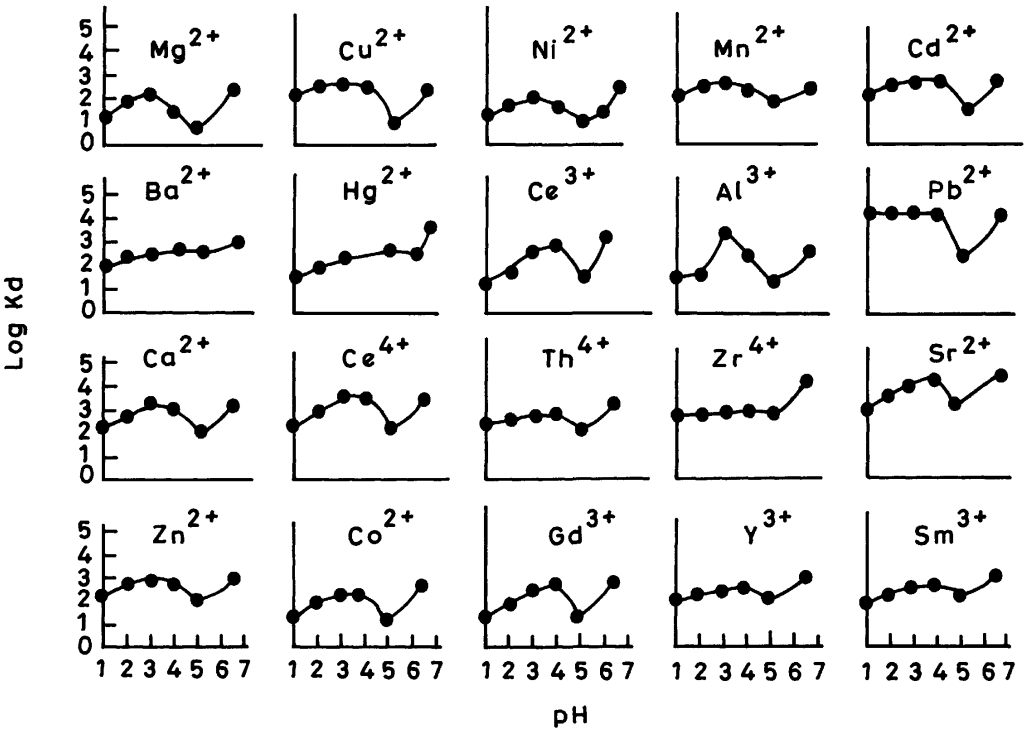

Fig. 4. Effect of pH of the solvent(formic acid–sodium formate system) on the adsorption of metal ion.

Table 4. Quantitative Separations of Metal Ions on Tin(IV) Tungstovanadophosphate (Sample $TTVP_7R$) Columns

Sl. No.	Separation	Amount fed to the column	Amount found after elution	Percent of metal ions eluted	Total elution volume	Eluent used
		μg	μg		cm^3	
1	Mg^{2+}	264	259.2	98.2	70	0.02 mol dm^{-3} HNO_3
	Ca^{2+}	272	256	94.1	40	0.05 mol dm^{-3} HNO_3
2	Cd^{2+}	1258.9	1213.9	96.4	70	0.02 mol dm^{-3} HNO_3
	Zn^{2+}	627.6	601.4	95.8	50	0.05 mol dm^{-3} HNO_3
3	Cd^{2+}	1258.9	1236.4	98	70	0.02 mol dm^{-3} HNO_3
	Pb^{2+}	2320.5	2237.7	96.4	40	0.05 mol dm^{-3} HNO_3
4	Mn^{2+}	582.4	560.4	96.2	60	Formic acid-sodium formate buffer (pH=5)
	Hg^{2+}	2046	1765.2	86.3	80	0.01 mol dm^{-3} HNO_3
5	Ba^{2+}	1428.3	1291	90.4	80	Formic acid-sodium formate buffer (pH=5)
	Ca^{2+}	272	264	97	40	0.05 mol dm^{-3} HNO_3
6	Hg^{2+}	2046	1805.3	88.2	80	0.01 mol dm^{-3} HNO_3
	Pb^{2+}	2320.5	2237.7	96.4	40	0.05 mol dm^{-3} HNO_3
7	Ce^{4+}	1652	1568	94.9	50	0.02 mol dm^{-3} HNO_3
	Th^{4+}	2505.6	2412.8	96.3	60	0.10 mol dm^{-3} HNO_3
8	Y^{3+}	1386.8	1315.7	94.9	70	0.05 mol dm^{-3} HNO_3
	Th^{4+}	2505.6	2366.4	94.4	60	0.10 mol dm^{-3} HNO_3
	Zr^{4+}	1237.6	1164.8	94.1	50	0.50 mol dm^{-3} HNO_3
9	Gd^{3+}	1130.4	1067.6	94.4	30	0.01 mol dm^{-3} HNO_3
	Y^{3+}	1386.8	1297.9	93.6	70	0.05 mol dm^{-3} HNO_3
	Zr^{4+}	1237.6	1183	95.6	60	0.50 mol dm^{-3} HNO_2

Na^+ in the pH region 2.5—10.

Tin(IV) tungstovanadophosphate has been found to be fairly stable in moderately concentrated nitric acid, hydrochloric acid, sulfuric acid, and perchloric acid. A comparison of the chemical stability data shows that the refluxed sample ($TTVP_7R$) is more stable than the unrefluxed one ($TTVP_7$). Equilibration study demonstrates the equilibrium is reached within 2 h of shaking for most of the metal ions studied except Cu^{2+} and Th^{4+} which take at least 4 h.

Thermogram of tin(IV) tungstovanadophosphate (Fig. 3) shows a continuous loss in weight upto 500 °C. A sharp weight loss upto a temperature of 250 °C may be due to removal of water molecules. It can also be inferred that the decomposition of tin(IV) tungstovanadophosphate starts after 250 °C and continues upto 500 °C. The gradual loss in weight in this temperature region is probably due to the loss of vanadium and phosphorus by volatilization. This conclusion is also supported from the ion-exchange capacity data [I. E. C. at 400 °C=0.2 meq (dry g)$^{-1}$ and at 500 °C=0.1 meq (dry g)$^{-1}$]. As vanadium and phosphorus contents of the material reduces the capacity becomes smaller and smaller. On increasing the temperature beyond 500 °C, the weight becomes constant due to the formation of stable tin oxide. The exchange capacity, therefore, reduces to a negligible value [0.4 meq (dry g)$^{-1}$].

Some interesting features are observed regarding the adsorption of metal ions on tin(IV) tungstovanadophosphate in sodium formate—formic acid buffer systems. It has been found that the pH of the buffer system affects the adsorption critically. It is apparant from Fig. 4 that the adsorption of metal ions on tin(IV) tungstovanadophosphate in sodium formate—formic acid buffer system vary with the pH. An increase in the pH of buffer system causes higher adsorption of almost all metal ions as expected. In the case of Zr^{4+}, the K_d value remains constant upto pH 5 and then increases sharply as the pH is increased. However, in other buffer systems studied, i. e. sodium citrate-citric acid and sodium acetate-acetic acid, distribution coefficients of metal ions do not vary with the pH of the buffer systems. This is also observed that the K_d values of metal ions are usually much more higher in demineralized water than in sodium formate-formic acid systems. The separation potentiality of tin(IV) tungstovanadophosphate has been demonstrated by achieving some important and difficult separations of metal ions quantitatively on its small columns.

Sphalerite and Calamine contain 0.1 to 0.5% of Cd^{2+}.[15] The binary separation of Cd^{2+}–Zn^{2+} may be utilized for the recovery of Cd^{2+} from these ores. Th^{4+}, Ce^{4+}, and Ca^{2+} may be eluted by different concentration of acid which can be applied for separation of these metal ions in cheralite[16] using tin(IV) tungstovanadophosphate columns.

Authors thank to Professor W. Rahman, Chairman, Department of Chemistry for research facilities and C. S. I. R. (New Delhi) for financial assistance.

References

1) M. Qureshi and R. C. Kaushik, *Sepn. Sci. Technol.*, **17**, 739 (1982).
2) M. Qureshi and K. G. Varshney, *J. Inorg. Nucl. Chem.*, **30**, 3081 (1968).
3) M. Qureshi and S. A. Nabi, *J. Inorg. Nucl. Chem.*, **32**, 2059 (1969).
4) Y. Inoue, *J. Inorg. Nucl. Chem.*, **26**, 2241 (1964).
5) N. E. Topp and K. W. Pepper, *J. Chem. Soc.*, **1949**, 323.
6) F. D. Snell and C. T. Snell, "Colorimetric Methods of Analysis," D. Van Nostrand Company Inc., Princeton, New Jersey (1959), Vol. IIA.
7) E. B. Sendell, "Colorimetric Determination of Traces of Metals," 3rd ed, Interscience, New York (1959), p. 886.
8) Ref. 6, p. 453.
9) Ref. 6, p. 560.
10) N. H. Furman, "Standard Methods of Chemical Analysis," 6th ed, D. Van Nostrand, Inc., princeton, New Jersey (1962), Vol. 1, p. 1161.
11) Ref. 10, p. 838.
12) Ref. 10, p. 814.
13) S. A. Nabi, R. A. K. Rao, and W. A. Siddiqui, *J. Liq. Chromatogr.*, **6**, 777 (1983).
14) S. A. Nabi, A. R. Siddiqui, and R. A. K. Rao, *J. Liq. Chromatogr.*, **4**, 1225 (1981).
15) I. M. Kolthoff, P. J. Elving, and E. B. Sandell, "Treatise on Analytical Chemistry," Interscience Publisher, New York, London (1961), Part 2. Vol. 3, p. 173
16) Ref. 15, Vol. 5, p. 142.
17) Wiklander, *Ann. Roy. Ag. Coll. Sweden*, **14**, 1 (1964).

Electrolytic Reduction of 1-Methylsulfinyl-1-methylthio-1-alkenes at Mercury Electrode in Nonaqueous Media

Akira KUNUGI,* Kyo ABE,† Toshio HAGI, and Taketsugu HIRAI
Department of Applied Chemistry, Faculty of Engineering, Osaka City University, Sugimoto, Sumiyoshi-ku, Osaka 558
†Department of Chemistry, Faculty of Science, Osaka City University, Sugimoto, Sumiyoshi-ku, Osaka 558
(Received December 18, 1985)

Synopsis. In the electrolytic reduction of organic sulfur compounds of general formular RCH=C$\begin{smallmatrix}\diagup\text{SMe}\\ \diagdown\text{S(O)Me}\end{smallmatrix}$, the substrates with R=aryl are much easier to reduce than those with R=alkyl, and the former substrates afford the desulfinylated compounds, E-isomers of RCH=CH(SMe), in good yields, but the later substrates do not give the corresponding desulfinylated compounds.

The title compounds, 1-methylsulfinyl-1-methylthio-1-alkenes (**1**), exhibit extremely interesting properties in their synthetic and mechanistic aspects.[1-5] Interestingly our preceding work[6] has shown that there is a sharp difference between the electrolytic and nonelectrolytic methods in the reduction of (*E*)-1-methylsulfinyl-1-methylthio-2-phenylethene (**1a**); the electrolytic reduction gives the desulfinylated compound, (*E*)-1-methylthio-2-phenylethene ((*E*)-**2a**), whereas the reduction with lithium aluminium hydride affords 2-phenyl-1,1-bis(methylthio)ethane.[1]

In the present work, the influence of a substituent group on the electrolytic reduction of **1** at a mercury electrode was examined in nonaqueous acetonitrile (MeCN) or *N*,*N*-dimethylformamide (DMF) containing excess phenol as a proton donor. The substrates investigated in this work are as follows.

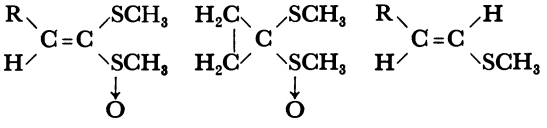

1a—h **1i** **2a—h**

a : R=C_6H_5,
b : R=*p*-$CH_3OC_6H_4$
c : R=*m*-$CH_3OC_6H_4$
d : R=*p*-FC_6H_4
e : R=1-naphthyl
f : R=2-naphthyl
g : R=$(CH_3)_3C$
h : R=$HOCH_2C(CH_3)_2$

Experimental

The substrates, **1a—h**, were prepared from methyl methylthiomethyl sulfoxide (FAMSO) and the corresponding aldehydes according to the publised method[1] and **1i** was synthesized from FAMSO and 1,2-bis(tosyloxy)ethane according to a method described in the literature.[4] Verification of the substrates was made by ^{1}H NMR spectroscopy and by comparision of the physical properties with published values.

Nonaqueous acetonitrile solutions were prepared from predeoxygenated MeCN and tetrabutylammonium tetrafluoroborate (TBAB) or tetrabutylammonium perchlorate (TBAP) which were purified and dried as described previously.[6] Nonaqueous *N*,*N*-dimethylformamide solutions were prepared from the predeoxygenated DMF and TBAB or tetrabutylammonium iodide (TBAI). DMF was purified in a manner similar to that described in the literature.[7] TBAI was recrystallized twice from acetone and dried in vacuo at 80°C for 3 d. The concentration of the supporting electrolyte was 0.1 mol dm^{-3}.

Controlled potential macroelectrolysis and polarography were carried out, using the same experimental set-up and procedure as reported in the previous paper.[6]

Indirect electrolysis of **1g** using phenanthrene as a mediator was carried out at the stirred mercury pool cathode of −2.8 V vs. Ag/Ag$^+$ in MeCN/TBAB without proton donor.

Results and Discussion

Polarography. d.c. Polarograms of **1a—f** in MeCN/TBAP or DMF/TBAI in the presence of excess phenol exhibited three waves. The third reduction wave is ascribed to the further reduction of the reduction products, **2a—f**, since controlled potential macroelectrolysis of **1a—f** at the plateau potential of the first wave afforded **2a—f** in high yields, respectively (vide infra). The half-wave potentials of the first reduction wave ($E_{1/2}$) of **1a—i** in MeCN/TBAP in the presence of excess phenol are summarized in Table 1, together with the results in DMF/TBAI. Among the substrates with R=substituted phenyl, **1a—d**, these $E_{1/2}$ seem to depend on the substituent constant sigma. The substrates with R=naphthyl, **1e** and **1f** were easy to reduce by 80—100 mV compared with **1a**. This can be interpreted in terms of stabilization of the le-reduction product due to the high delocalization of the charge of the radical anions of **1e** and **1f** through 1- and 2-naphthyl groups. On the other hand, the substrates with R=alkyl, **1g** and **1h**, were much more difficult to reduce than **1a**, but **1i** was not reducible in the accessible potential region.

Macroelectrolysis. Controlled potential macroelectrolyses of **1a—h** at the plateau potential of the first reduction wave at the stirred mercury pool electrode were conducted in MeCN/TBAB or DMF/TBAI in the presece of excess phenol. Table 2 summarizes the isolated yields of (*E*)-**2**, in which the coulometric *n*-values (electrons molecule^{-1}) also are included. The table shows that the substrates with R=aryl, **1a—f**, afford the desulfinylated compounds, (*E*)-**2a**–(*E*)-**2f**, in good yields, whereas the substrates with R=alkyl, **1g** and **1h**, do not give the corresponding desulfinylated compounds, **2g** and **2h**, but a complex mixture of products. The stereochemical structure of (*E*)-**2a**–(*E*)-**2f** was determined on the basis of the NMR spectra of their olefinic protons. The NMR spectra of the H exhibited

Table 1. Half-wave Potentials for the First Reduction Wave of **1a—i** in MeCN Containing 0.1 mol dm^{-3} TBAP and DMF Containing 0.1 mol dm^{-3} TBAI in the Presence of Excess Phenol at 27 °C[a)]

Substrate	$E_{1/2}$ in MeCN/V[b)]	$E_{1/2}$ in DMF/V[c)]
1a	−2.16	−1.41
1b	−2.27	−1.51
1c	−2.17	−1.40
1d	−2.16	−1.42
1e	−2.08	−1.31
1f	−2.08	−1.31
1g	−2.90	
1h	−2.90	
1i	no wave	

a) Concentrations of substrates and proton donor were 1.0—1.3×10^{-3} mol dm^{-3} and 4 times that of the substrate, respectively. b) Vs. Ag/0.1 mol dm^{-3} $AgNO_3$ in MeCN reference electrode. c) Vs. Ag/AgI 0.1 mol dm^{-3} TBAI in DMF reference electrode.

Table 2. Results of Controlled Potential Electrolysis of **1a—h** at the First Reduction Potential at an Hg Pool Cathode in Nonaqueous Media Containing Excess Phenol

Substrate	Electrolyte system	n-Value	Yield of (*E*)-**2**/%
1a	MeCN/0.1 mol dm^{-3} TBAB	3.6	85
	DMF/0.1 mol dm^{-3} TBAI	3.5	78
1b	MeCN/0.1 mol dm^{-3} TBAB	3.5	87
1c	MeCN/0.1 mol dm^{-3} TBAB	3.6	73
	DMF/0.1 mol dm^{-3} TBAI	3.4	78
1d	MeCN/0.1 mol dm^{-3} TBAF	3.5	79
1e	MeCN/0.1 mol dm^{-3} TBAB	4.2	80
	DMF/0.1 mol dm^{-3} TBAI	3.6	76
1f	MeCN/0.1 mol dm^{-3} TBAB	3.9	78
	DMF/0.1 mol dm^{-3} TBAI	3.4	78
1g	MeCN/0.1 mol dm^{-3} TBAB	2.1	0
1h	MeCN/0.1 mol dm^{-3} TBAB	2.1	0

the AB quartet splitting with J=15.3 Hz (cf. for (*Z*)-**2a**, AB_q J=10.6 Hz[8)]). Perusal of the NMR spectra of the reaction mixture indicated that no *Z*-isomers were produced in any experiment.

Table 2 also shows that there is no significant difference with regard to the product yield and the n-value between MeCN and DMF.

Indirect reduction of **1g** by means of the phenanthrene anion radical showed a catalytic current in the polarogram of phenanthrene in MeCN/TBAP. Nevertheless, the indirect macroelectrolysis of **1g** in MeCN/TBAB at −2.8 V vs. Ag/Ag$^+$ did not give **2g**. The indirect macroelectrolysis of **1i** was not undertaken because no catalytic current was observed.

The coulometric n-values for **1a—f** were 3.4—4.2, suggesting that the methylsulfinyl anion resulting from the cleavage of the carbon–sulfur bond will undergo further reduction to produce methanethiol. The production of methanethiol was confirmed experimentally: Benzyl methyl sulfide was isolated though low in yield (22% for **1a**) when the catholyte was allowed to react with benzyl bromide after the electrolysis.

In conclusion, polarography of organic compounds of general formular $\begin{matrix}R\\H\end{matrix}\!\!\searrow\!C{=}C\!\!\begin{matrix}\swarrow SMe\\\searrow S(O)Me\end{matrix}$ showed that $E_{1/2}$ for the first reduction wave in MeCN or DMF containing excess phenol as a proton donor is slightly dependent on the kind of R in **1** when R is an aryl group, whereas the substrates with R=alkyl are much more difficult to reduce than those with R=aryl. The electrolytic reduction of the substrates with R=aryl involves selective cleavage of one carbon-sulfur bond, resulting in formation of (*E*)-1-methylthio-2-arylethenes, (*E*)-**2a**–(*E*)-**2f**, in good yields with the consumption of about 4 electrons molecule^{-1}. On the other hand, the substrates with R=alkyl did not afford the corresponding desulfinylated compounds although about 2 electrons molecule^{-1} were consumed during the electrolyses. Neither could the corresponding desulfinylated compound be obtained by indirect electrolysis of **1g** by means of phenanthrene anion radical.

References

1) K. Ogura and G. Tsuchihashi, *Tetrahedron Lett.*, **1972**, 1383.
2) J. L. Herrmann, J. E. Richman, P. J. Wepplo, and R. H. Schlessinger, *Tetrahedron Lett.*, **1973**, 4707.
3) J. L. Herrmann, G. R. Kieczykowski, R. F. Romanet, P. J. Wepplo, and R. H. Schlessinger, *Tetrahedron Lett.*, **1973**, 4711, 4715.
4) K. Ogura, M. Yamashita, S. Furukawa, M. Suzuki, and G. Tsuchihashi, *Tetrahedron Lett.*, **1975**, 2767.
5) K. Ogura, *Yuki Gosei Kagaku Kyokai Shi*, **37**, 903 (1979).
6) A. Kunugi, T. Hagi, T. Hirai, and K. Abe, *Electrochim. Acta*, **30**, 1049 (1985).
7) J. P. A. Castrillon and H. H. Szmant, *J. Org. Chem.*, **30**, 1338 (1965).

Fluorescence Lifetimes of 9-Methylanthracene in Supersonic Free Jets. A Level Inversion between S_1 and T_2 States upon the Phase Change from Solution to Gas

Fujio TANAKA,* Satoshi HIRAYAMA,† Shigeru YAMASHITA, and Kosuke SHOBATAKE††
College of Integrated Arts and Sciences, University of Osaka Prefecture, Mozu-umemachi, Sakai 591
†Faculty of Textile Science, Kyoto Institute of Technology, Matsugasaki, Sakyo-ku, Kyoto 606
††Institute for Molecular Science, Myodaiji, Okazaki 444
(Received February 6, 1986)

Synopsis. Fluorescence lifetimes measured for 9-methylanthracene in supersonic free jets confirm the occurrence of nonradiative decay at the vibrationless level of S_1 that has been suggested from the measurement of the fluorescence yield. The nonradiative decay constants in the isolated and condensed phases have been compared from the viewpoints of relative positions of S_1 and T_2 levels and of the magnitude of the energy gap.

The fluorescence quantum yield (Φ_f) and lifetime (τ_f) for 9-substituted anthracenes strongly depend on temperature and medium.[1-8] In solution this behavior has been explained in terms of the intersystem crossing (ISC) from S_1 to T_2 lying above S_1. A recent measurement in supersonic free jets[9] showed that Φ_f of 9-methylanthracene(9MA) at the vibrationless level of S_1 is only 0.57 although the molecule is supercooled, making a sharp contrast to a Φ_f-value of unity at 77 K in the condensed phase.[1] On the basis of the solvent and pressure effects on the ISC rate, Tanaka et al. have suggested that S_1 should lie above T_2 in the isolated state as predicted from a large blue shift of the 0-0 band.[10] The fluorescence behavior of other 9-substituted anthracenes in solution and vapor phases has been interpreted similarly in terms of a S_1–T_2 level inversion model.[11] In the present work, in order to confirm these suggestions, the fluorescence lifetimes of 9MA in supersonic free jets have been measured and the heavy atom effect in the rare gas clusters has been investigated as well, along with the additional lifetime measurements in solutions. The radiative and nonradiative decay constants (k_r and k_{nr}) in the isolated and condensed phases were estimated, and the values of k_{nr} were compared from the viewpoints of relative positions of S_1 and T_2 levels and of the magnitude of the energy gap.

Experimental

9MA purchased from Tokyo Kasei was purified by column chromatography. The apparatus and the measurement system for laser induced fluorescence studies of jet-cooled molecules at the Institute for Molecular Scienece were described previously.[12] 9MA heated to ca. 80 °C in a furnace was expanded into vacuum with a carrier gas through a 150 μm nozzle.

The fluorescence lifetime in solution was measured by a time-correlated single photon counting system at Kyoto Institute of Technology.[13] Solvents of a spectroscopic grade were used. The composition of EPA was 5:5:2 in volume for diethyl ether, isopentane, and ethyl alcohol. Sample solutions of 2.5×10^{-5} mol dm^{-3} were deaerated by freeze-pump-thaw cycles.

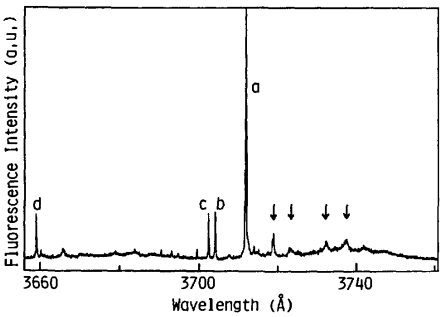

Fig. 1. The fluorescence excitation spectrum of 9MA expanded with 600 torr of Ar. The arrows indicate the Ar cluster bands of 9MA where the fluorescence lifetime was measured.

Table 1. Fluorescence Lifetimes for 9MA and Its Ar Clusters in Supersonic Free Jets

Bare 9MA		Ar Cluster	
Band position cm^{-1}	τ_f ns	Band position cm^{-1}	τ_f ns
26939 (a)	18.7	26891	11.6
26995 (b)	25.8	26859	13.2
27008 (c)	23.2	26797	13.3
27328 (b)	15.6	26758	14.3

Results and Discussion

The fluorescence excitation spectrum of 9MA expanded with 600 Torr (1 Torr=133.322 Pa) of Ar is shown in Fig. 1. The electronic origin band (a) of bare 9MA is located at 371.2 nm with a blue shift exceeding 1000 cm^{-1} from the corresponding transition in solution. The bare 9MA bands (a,b,c,d) are in good agreement with those reported by other investigators.[14,15] The Ar cluster bands on the longer-wavelength side of the origin band become prominent as the Ar pressure is increased.

Fluorescence lifetimes for the bare and cluster bands are listed in Table 1. τ_f for the 0-0 band is 18.7 ns while Zeweil et al. have obtained a value of 21 ns.[15] The vibronic bands b and c have longer lifetimes, and the vibronic band d has a shorter lifetime. Such an irregular change in the lifetime for 9MA, as well as for anthracene,[16] with an excess vibrational energy was observed in a wider range of excess energy.[15] The existence of longer lifetimes of 25.8 and 23.3 ns for b and c bands indicates that the lifetime of 18.7 ns for the 0-0 band contains the contribution from a nonradiative decay process besides radiative one. Sonnenschein et al.

Table 2. Radiative and Nonradiative Decay Constants for the S_1 Electronic Origin of Jet-Cooled 9MA and the Solution Values

Medium	temp °C	λ_{0-0}[a] nm	Φ_f	τ_f ns	k_r $\times10^7\,s^{-1}$	$k_r\cdot(1/n^2)$ $\times10^7\,s^{-1}$	k_{nr} $\times10^7\,s^{-1}$
Isolated		371.2	0.57[b]	18.7[c]	3.1		2.3
Pentane[d]	22	385.0	0.24	3.69	6.5	3.5	21
Hexane	R.T.[g]	385.6	0.29[e]	4.25[c]	6.8	3.6	17
Methylcyclohexane	R.T.	386.7	0.33[e]	5.20[c]	6.3	3.1	13
Toluene	R.T.	389.4	0.71[e]	9.20[c]	7.7	3.4	3.2
EPA	−196		1[f]	13.0[c]	7.7		≈0

a) Values from the absorption spectra. b) Ref. 9. c) Present work. d) Ref. 7. e) Ref. 5. f) Ref. 1. g) 20—25 °C.

obtained a value of Φ_f=0.57 for the 0–0 band of jet-cooled 9MA.[9] The present lifetime data are consistent with their result, concerning the occurrence of nonradiative decay from the vibrationless level of S_1. The radiative and nonradiative decay constants in solution and in free jet are compared in Table 2. Although the radiative decay constant for the jet-molecule is fairly smaller than that in solution, these values become comparable, after correcting for the refractive index, i.e. multiplying by $1/n^2$.[17]

The nonradiative decay route is the ISC from S_1 to T_2. In solution k_{nr} decreases as the S_1 energy is lowered from pentane to toluene since the S_1–T_2 energy gap increases when $S_1<T_2$.[5,10] The long lifetime in EPA at 77 K reflects only a radiative decay constant as indicated by the fluorescence quantum yield of unity at this temperature.[1]

Since an apparent activation energy of ca. 800 cm^{-1} has been obtained from the temperature dependence of k_{nr} in pentane and the S_1–T_2 gap has been estimated to be ca. 400 cm^{-1} by considering the shift of S_1 due to the temperature dependence of a dielectric constant,[7] the blue shift of ca. 1000 cm^{-1} in going from pentane solution to the isolated state probably results in the elevation of the S_1 energy above the T_2 level. This S_1–T_2 level inversion will enable energetically the ISC to occur in the isolated 9MA even though 9MA is supercooled.

Another evidence for the level inversion is provided by the fluorescence behavior of the rare gas clusters of 9MA. The fluorescence lifetimes at the Ar cluster bands are shorter compared with the value at the vibrationless bare band. If the vibrationless level of S_1 of bare 9MA lies below T_2, this result can not be understood since the lowering of the S_1 energy level by cluster formation will leave the ISC channel closed. Furthermore, when Kr or Xe was used as a carrier gas, no cluster bands were observed. This finding does not necessarily mean that no clusters are formed. On the contrary, it is reasonable to consider that Kr and Xe clusters are formed but their fluorescence intensities are very low since the ISC rates are extremely raised. In fact, as the pressure of Kr or Xe increases the 0–0 band intensity of the bare 9MA decreases significantly, indicating the formation of 9MA-Kr or Xe atom van der waals clusters which exhibit very short-lived excited states. These observations on the clusters of 9MA contrast with the case of 9-cyanoanthracene (9CNA).[12] For 9CNA its cluster bands with Ar, Kr, and Xe were detected and those lifetimes were almost identical with that (28 ns) of the vibrationless bare band, indicating the absence of the heavy-atom effect. In a supersonic free jet the fluorescence yield at the vibrationless level of bare 9CNA was found to be unity.[9] These results for 9CNA indicate that the ISC from S_1 to T_2 is energetically prohibited since $S_1<T_2$, and hence the heavy-atom effect was not observed. Conversely, for 9MA where the ISC route is open in the isolated state ($S_1>T_2$), the heavy-atom effect by Kr or Xe enhances the ISC rate remarkably. The shortened lifetime for the Ar clusters of 9MA may be ascribed to the change in the Franck-Condon factor between S_1 and T_2 caused by the decrease in the S_1–T_2 energy gap under the condition of $S_1>T_2$ because the heavy-atom effect by Ar, if any, seems to be insignificant.[18]

References

1) E. C. Lim, J. D. Laposa, and J. M. H. Yu, *J. Mol. Spectrosc.*, **19**, 412 (1966).
2) R. G. Bennett and P. J. McCartin, *J. Chem. Phys.*, **44**, 1969 (1966).
3) W. R. Ware and B. A. Baldwin, *J. Chem. Phys.*, **43**, 1194 (1965).
4) F. Tanaka and J. Osugi, *Chem. Lett.*, **1973**, 1279.
5) F. Tanaka, *Rev. Phys. Chem. Jpn*, **44**, 65 (1974).
6) B. Hammerich, R. Schmidt, and H.-D. Brauer, *Ber. Bunsenges. Phys. Chem.*, **83**, 198 (1979).
7) J. Rice, D. B. McDonald, L-K. Ng, and N. C. Yang, *J. Chem. Phys.*, **73**, 4144 (1980).
8) E. Blatt, F. E. Treloar, K. P. Ghiggino, and R. G. Gilbert, *J. Phys. Chem.*, **85**, 2810 (1981).
9) M. Sonnenschein, A. Amirav, and J. Jortner, *J. Phys. Chem.*, **88**, 4214 (1984).
10) F. Tanaka, M. Okamoto, S. Yamashita, and H. Teranishi, *Chem. Phys. Lett.*, **123**, 295 (1986).
11) S. Hirayama, R. A. Lampert, and D. Phillips, *J. Chem. Soc., Faraday Trans. 2*, **81**, 371 (1985).
12) S. Hirayama, K. Shobatake, and K. Tabayashi, *Chem. Phys. Lett.* **121**, 228 (1985).
13) S. Hirayama and Y. Shimono, *J. Chem. Soc., Faraday Trans. 2*, **80**, 941 (1984).
14) A. Amirav, U. Even, and J. Jortner, *Anal. Chem.*, **54**, 1666 (1982).
15) J. A. Syage, P. M. Felker, D. H. Semmes, F. Al Adel, and A. H. Zeweil, *J. Chem. Phys.*, **82**, 2896 (1985).
16) W. R. Lambert, P. M. Felker, and A. H. Zeweil, *J. Chem. Phys.*, **81**, 2209 (1984).
17) S. Hirayama and D. Phillips, *J. Photochemistry*, **12**, 139 (1980).
18) A. Amirav, U. Even, and J. Jortner, *J. Chem. Phys.*, **75**, 2489(1981).

The Crystal Structure of Bis(2,2′-bipyridyl)palladium(II) Picrate $[Pd(bpy)_2](pic)_2$. A Novel "Bow" Distortion

Shūichi MAEDA, Yuzo NISHIDA, Hisashi ŌKAWA,* and Sigeo KIDA
Department of Chemistry, Faculty of Science, Kyushu University 33, Hakozaki, Higashi-ku, Fukuoka 812
(Received December 10, 1985)

Synopsis. The title complex crystallized in the triclinic space group $P\bar{1}$ with a=8.228(2), b=13.493(2), c=7.753(1) Å; α=96.96(1), β=106.16(1), γ=99.99(1)°; Z=1. The structure was solved by the heavy-atom method and refined by the block-diagonal least-squares method to R=0.0366. It is found that picrate ions above and below the $[pd(bpy)_2]^{2+}$ cation stack with the bpy molecules and that this stacking leads to a novel bow distortion of the cation.

It is known that the bis(2,2′-bipyridyl)palladium(II) ion ($[Pd(bpy)_2]^{2+}$) is essentially planar, but is slightly distorted from a rigorous plane because of interligand steric repulsion.[1] Two types of distortions, i.e., bow and twist (Fig. 1), have been found for the cation. It seems that the type of distortion depends upon the counter ion, and bow distortion has been found for the salt with the tetracyano-*p*-quinonedimethane anion ($TCNQ^-$).[3,4] It is presumed that the stacking between bpy and $TCNQ^-$ is associated with the unique bow distortion. In this study, the crystal structure of $[Pd(bpy)_2](pic)_2$ with the 2,4,6-trinitrophenolate ion (picrate ion, pic^-) has been determined and discussed in terms of the noncovalent interaction between the bpy molecule of the $[Pd(bpy)_2]^{2+}$ cation and the pic anion.

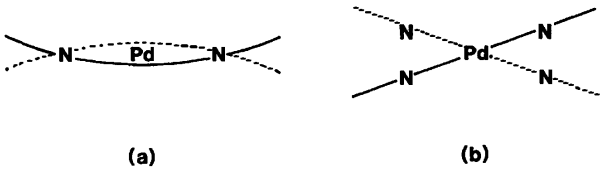

(a) (b)

Fig. 1. Schematical representation of (a) bow and (b) twist distortions.

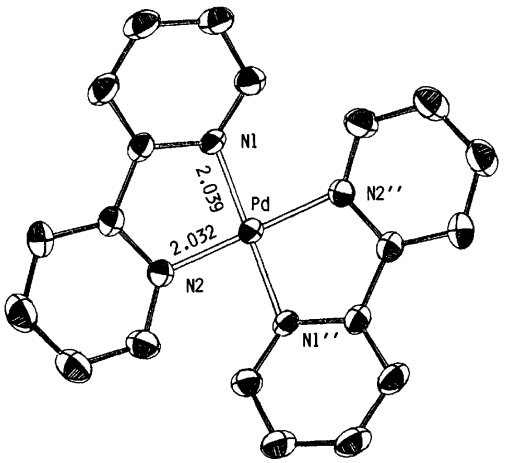

Fig. 2. Molecular structure of $[Pd(bpy)_2]^{2+}$ with bond distances.

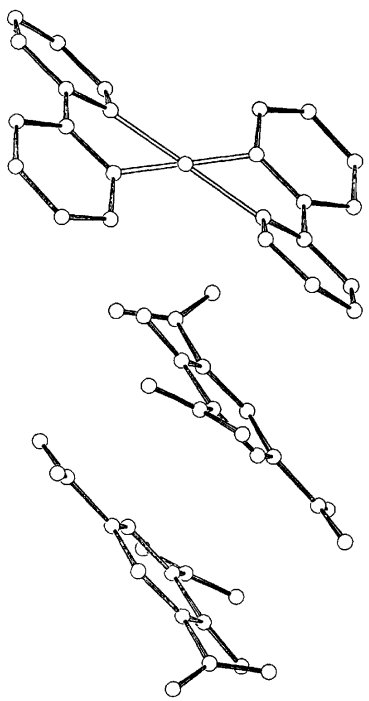

Fig. 3. Perspective view of the crystal packing.

Experimental

Preparation. $[Pd(bpy)_2](pic)_2$ was obtained as yellow crystals by the reaction of bis(2,2′-bipyridyl)palladium(II) perchlorate (1.25 g) and 2,4,6-trinitrophenol (1 g) in water. Anal. Found: C, 44.05; H, 2.39; N, 15.96%. Calcd for $C_{32}H_{20}N_{10}O_{14}Pd$: C, 43.83; H, 2.53; N, 15.97%. Single crystals were obtained by slow crystallization from a dilute methanolic solution.

X-Ray Analysis. A crystal with dimensions of 0.2×0.2×0.3 mm was used for the X-ray analysis. The unit-cell parameters and intensities were measured on a Rigaku AFC-5 Automated Four-circle Diffractometer with graphite monochromated Mo $K\alpha$ radiation (λ=0.71609 Å) at 291 K. The intensity data were collected by the 2θ—ω scan technique with a scan rate of 6° min^{-1}; they were corrected for the Lorentz and polarization effects, but not for absorption (μ=7.0 cm^{-1}). A total of 3821 reflections within the $2<\theta<55°$ range were collected, of which independent 3377 reflections ($|F_o| \geq 3\sigma(F_o)$) were employed in the solution and refinement.

Crystal Data: $[Pd(C_{10}H_8N_2)_2](C_6H_2N_3O_7)_2$, F.W.=874.99, triclinic $P\bar{1}$, a=8.227(2), b=13.493(2), c=7.753(1) Å; α=96.96(1), β=106.51(1), γ=99.99(1)°; D_m=1.81, D_c=1.81 g cm^{-3}, Z=1.

The structure was solved by the heavy-atom method, assuming the position of the palladium atom at (0,0,0), and was refined by the block-diagonal least-squares method to the final R value of 0.0366. The final atomic coordinates, the anisotopic temperature factors of the non-hydrogen atoms, a full list of bond distances (Å) and angles (°), and the complete F_o—F_c data are deposited as Document No. 8630 at the Office of the Editor of the Bulletin of the Chemical Society of Japan. All the calculations were carried out on a M-200 computer

at the Computer Center of Kyushu University using the local version[5] of the UNICS system.[6] The atomic-scattering factors were taken from the International Tables for X-Ray Crystallography.[7]

Results and Discussion

A perspective drawing of the $[Pd(bpy)_2]^{2+}$ cation is shown in Fig. 2, together with the bond lengths. The palladium atom lies at the center of the complex molecule; the mean Pd–N distance is 2.04 Å which is close to the previously reported Pd–N distances of the NO_3^-[8,9] and $TCNQ^-$[3,4] salts. The angles of N1–Pd–N2 and N1–Pd–N2″ are 78.9° and 101.1° respectively.

The $[Pd(bpy)_2]^{2+}$ cations are separated by pair of picrate ions, which are stacked with each other in a head-to-tail manner with an interplane distance of 3.41 Å, as is shown in Fig. 3. The picrate anions above and below the cation also stack with the bpy molecule with an interplane distance of ca. 3.57 Å. The picrate oxygens are located at the apical sites of the metal; however, the considerably long Pd–O distances (3.20 Å) suggest that there is no appreciable bonding.

In spite of the planar configuration of the PdN_4 part, the whole of the cation is not planar, and the two pyridine rings within one ligand are tilted by 21.3° to cause the bow distortion. Probably this distortion is attributable to the bpy/pic stacking interaction in the crystal. That is, when the pic stacks with the bpy, the nitro groups at the 2- and 6-positions exert a steric effect so as to bend the bpy molecule. So far as we know, this complex is only the second example of a bow distortion in the $[Pd(bpy)_2]^{2+}$ cation.

References

1) E. D. Mckenzie, *Coord. Chem. Rev.*, **6**, 187 (1971).
2) A. Hazell and A. Mukhopadhyay, *Acta Crystallogr., Sect. B.*, **36**, 1647 (1980).
3) V. Dung, H. Endres, H. J. Keller, W. Moroni, and D. Nothe, *Acta Crystallogr., Sect. B.*, **33**, 2428 (1977).
4) H. Endres, H. J. Keller, W. Moroni, D. Nothe, and V. Dung, *Acta Crystallogr., Sect. B.*, **34**, 1823 (1978).
5) S. Kawano, *Rep. Comp. Cent. Kyushu Univ.*, **13**, 39 (1980).
6) "Universal Crystallographic Computer Program System (UNICS)," ed by T. Sakurai, The Crystallographic Society of Japan, Tokyo (1964).
7) "International Tables for X-Ray Crystallography," Vol. III, Kynoch Press, Birmingham (1962).
8) P. C. Chieh, *J. Chem. Soc., Dalton Trans*, **1972**, 1643.
9) M. Hinamoto, S. Ooi,and H. Kuroya, *J. Chem. Soc., Chem. Commun.*, **1972**, 356.

Di-*n*-octyl Phenyl Phosphonate: A Plasticizer of Poly(vinyl chloride) Matrix Membrane Electrodes Behaving As a Li^+-selective Agent

Kazuhisa HIRATANI,* Tatsuhiro OKADA, and Hideki SUGIHARA
Industrial Products Research Institute, Higashi 1-chome, Yatabe-machi, Tsukuba-gun, Ibaraki 305
(Received November 7, 1985)

Synopsis. PVC matrix membrane electrodes, which are composed of dioctyl phenylphosphonate (DOPP) as a plasticizer and potassium tetrakis(4-chlorophenyl)borate (KTCPB) as a lipophilic anionic additive, without any other ionophore, exhibit appreciable Li^+-selectivity. The electrode has selectivity coefficients (log k^{Pot}_{LiM} for Li^+ over Na^+ up to -1.2, over K^+ up to -1.8, over Mg^{2+} up to -1.8, and over Ca^{2+} up to -1.2. The detection limit for Li^+ was about 5.0×10^{-5} mol dm^{-3}.

During the last decade much attention has been focused on the use of neutral carrier compounds as membrane components; they can be used together with different plasticizers in ion-selective membrane electrodes, especially for alkali and alkaline earth metal ions.[1] A number of neutral carriers for ion-selective electrodes have been reported thus far, such as noncyclic polyethers,[2,3] crown ethers,[4] and bis-crown ethers.[5] Moreover, the effects of the plasticizers on the behavior of the ion-selective electrodes have also been investigated, and the change in the selectivity coefficients brought about by plasticizers, together with neutral carriers, have been observed.[6] However, in order to discriminate among cations within a given group of the periodic system, the influence of the solvent/plasticizer with neutral carrier sensors has been considered of minor importance.[7] In this paper, we wish to report on the phenomenon that the selectivity for cations within a given group of the periodic system without any other neutral carrier changes completely depending on the kind of plasticizer.

Experimental

Materials. The plasticizers, dioctyl phenylphosphonate (DOPP) and *o*-nitrophenyl octyl ether (NPOE), and potassium tetrakis(4-chlorophenyl)borate (KTCPB), were commertially available (Dojin Lab.) and were used without further purification. Poly(vinyl chloride) (PVC) (degree of polymerization $n \fallingdotseq 1100$), which was also commertially available from Wako Pure Chemical Industries, Ltd., was used after the polymer had been dissolved in tetrahydrofuran (THF), followed by reprecipitation in methanol.

Preparation of Electrodes. A plasticizer (250 mg), PVC (100 mg), and KTCPB (3 mg) were dissolved in 4 ml of THF. The solution was then poured into a Petri dish (42 mm in diameter) which was held horizontally on a mercury pool, and the THF was evaporated slowly at room temperature. A transparent homogeneous membrane ca. 0.2 mm thick was thus obtained. A disk of the polymeric membrane 5 mm in diameter was cut out from the membrane obtained and was then mounted on an Orion model 92 electrode body for electromotive force (EMF) measurements. The cell assemblies of the ion-selective electrode were as follows: Ag/ AgCl/ 10^{-2}mol dm^{-3} LiCl//membrane// test solution/ 1 mol dm^{-3} $LiOCOCH_3$/ sat. KCl/AgCl/Ag, where a silver-silver chloride electrode in a double-junction configuration was used as the external reference electrode.

EMF-Response Measurements. Test solutions were prepared from analytical-grade chlorides of alkali and alkaline earth metals and deionized water (specific conductivity 5×10^{-7} $\Omega^{-1}cm^{-1}$). The EMF response of the testing solutions at 25 °C was measured with an Orion model 701A digital ionanalyzer (input impedance 10^{13} Ω) and was recorded by means of a strip-chart recorder and a printer. The time for the electrode to attain the stationary potential value within ±1 mV for the lapse of 30 sec. was referred to as the response time. The potentiometric selectivity coefficient $k^{Pot}_{i,j}$ of the i ion over the j ion was determined by the separate-solution method.[8] The concentrations of interference ions referred to by this calculation ranged from 10^{-1} to 1 mol dm^{-3}.

Results and Discussion

Figures 1 and 2 show the plots of the EMF response vs. the logarithm of ion activity (log *a*) when DOPP and NPOE respectively were used as plasticizers. In both cases, the PVC membrane electrodes show a near-Nernstian response for the ions examined except for those with a low EMF response. The electrode exhibits a marked Li^+-selectivity over Na^+, K^+, Mg^{2+}, and Ca^{2+} when DOPP is used, whereas the K^+-selectivity over Li^+, Na^+, Mg^{2+}, and Ca^{2+} is obtained when NPOE is used. When KTCPB was not included in the membranes, the near-Nernstian response for cations was not observed; rather, the response for anions was observed in the case of NPOE.[9] It has been reported

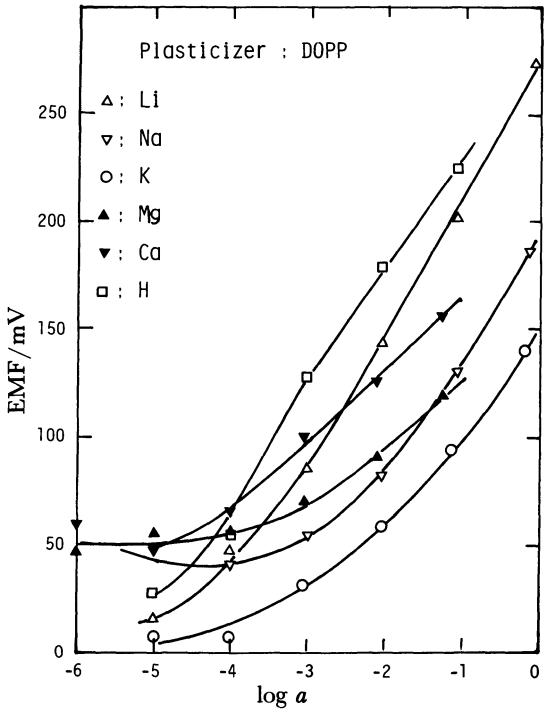

Fig. 1. EMF response of the PVC membrane containing DOPP (71 wt%) and KTCPB (3 wt%) (25 °C).

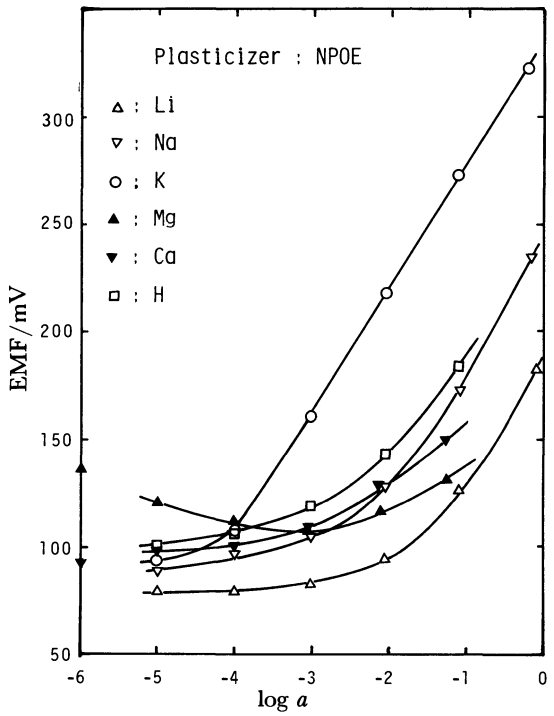

Fig. 2. EMF response of the PVC membrane containing NPOE (71 wt%) and KTCPB (3 wt%) (25 °C).

that DOPP is favorable for Ca^{2+}-selective electrodes containing an organophosphate salt-carrier.[10] It is also well known that a membrane based on tetraphenylborate in nitrobenzene or related solvents, e.g., NPOE, shows a monotonic preference for large over small cations, that is, for lipophilic over hydrophilic cations,[11] as is depicted in Fig. 2. However, when DOPP and KTCPB were used without any other ionophore, the electrode has appreciable selectivity coefficients for Li^+ over Na^+, K^+, Mg^{2+}, and Ca^{2+}. Apparently, DOPP can reverse its ion-selectivity from large to small alkali ions, that is, from lipophilic to hydrophilic cations.

Furthermore, the effect of the mixing of the plasticizers, DOPP and NPOE, on the selectivity coefficients for cations was investigated. The results are also summarized in Fig. 3. The mixing ratios apparently influence the selectivity for cations. The Li^+-selectivity is still retained even when the mixture composed of 3 wt% of DOPP and 68 wt% of NPOE is present in the membrane, as if DOPP hehaved as a Li^+-ionophore. This fact reminds us that certain organic phosphorous compounds and other compounds can improve ion-selectivity in the membrane electrodes.[13–15] It should be noted that the membrane electrode composed of a mixture of NPOE 57 wt% and DOPP 14 wt% as plasticizers has maximum selectivity coefficients for Li^+ over Na^+ of up to −1.3 compared with the other electrodes shown in Fig. 3. Thus, it is a new finding that appreciable Li^+-selectivity appears when a PVC membrane containing DOPP and KTCPB, without any other ionophore, is used.

We wish to thank Professor Toshiyuki Shono and Dr. Keiichi Kimura of Osaka University for their valuable discussions and suggestions.

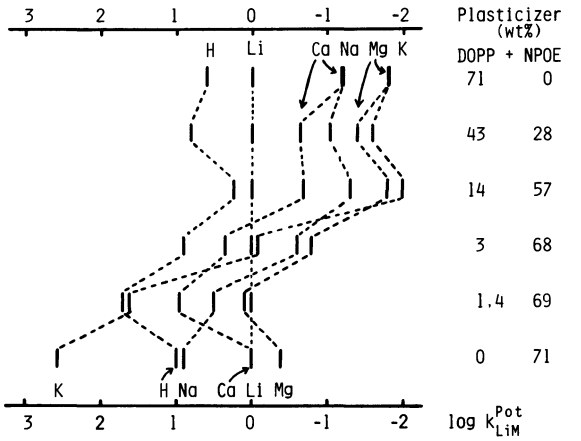

Fig. 3. Influence of the plasticizers on the potentiometric selectivity coefficients.[12]

References

1) "Ion-selective Electrodes in Analytical Chemistry," ed by H. Freiser, Plenum Press, New York and London (1978), Vol. 1.

2) D. Amman, W. E. Morf, P. Anker, P. C. Meier, E. Pretsch, and W. Simon, *Ion-selective Electrode Rev.*, **5**, 3 (1983).

3) H. Sugihara, T. Okada, and K. Hiratani, *J. Chem. Soc., Chem. Commun.*, **1985**, 957.

4) S. Kitagawa, K. Kimura, H. Yano, and T. Shono, *J. Am. Chem. Soc.*, **106**, 6978 (1984); J. Petránek and O. Ryba, *Anal. Chim. Acta*, **128**, 129 (1981).

5) H. Tamura, K. Kumai, K. Kimura, and T. Shono, *Mikrochim. Acta[Wien]*, **1983 II**, 287.

6) For example, H.-B. Jenny, C. Riess, D. Ammann, B. Magyar, R. Asper, and W. Simon, *Mikrochim. Acta[Wien]*, **1980 II**, 309; N. N. L. Kirsch, R. J. J. Funck, E. Pretsch, and W. Simon, *Helv. Chim. Acta*, **60**, 2326 (1977).

7) W. Simon, W. E. Morf, and P. C. Meier, "Structure and Bonding," ed by J. D. Dunitz, P. Hemmerich, J. A. Ibers, C. K. Jorgensen, J. B. Neilands, R. S. Nyholm, D. Reinen, and R. J. P. Williams, Vol. 16, Springer-Verlag, Berlin and New York (1973), p. 113.

8) K. Srinivasan and G. A. Rechnitz, *Anal. Chem.* **41**, 1203 (1969).

9) Unpublished result.

10) J. Růžička, E. H. Hansen, and J. Chr. Tjell, *Anal. Chim. Acta*, **67**, 155 (1973); A. Craggs, G. J. Moody, and J. D. R. Thomas, *Analyst*, **104**, 412 (1979).

11) R. Scholer and W. Simon, *Helv. Chim. Acta*, **55**, 1801 (1972).

12) This is defined by the weighting factor (k_{ij}^{Pot}) in the Nicolsky-Eisenman equation:

$$E = E_i^\circ + \frac{2.3RT}{Z_i F} \log[a_i + \sum_{j \neq i} k_{ij}^{Pot} (a_j)^{Z_i/Z_j}].$$

13) T. Imato, M. Katahira, and N. Ishibashi, *Anal. Chim. Acta*, **165**, 285 (1984).

14) G. H. Griffiths, G. J, Moody, and J. D. R. Thomas, *Analyst*, **97**, 420 (1972).

15) H. Hara, S. Okazaki, and T. Fujinaga, *Bull. Chem. Soc. Jpn.*, **53**, 3610 (1980).

The Synthesis of 3-Aryl-5-dialkylamino-1,4,2-dithiazol-1-ium Salts

Isao SHIBUYA* and Katsumi YONEMOTO
National Chemical Laboratory for Industry, Yatabe, Ibaraki 305
(Received December 24, 1985)

Synopsis. *N*-(Dialkylthiocarbamoylthio)arenecarboxamides, prepared by acylation of the corresponding *S*-dialkylthiocarbamoyl-substituted sulfenamides, cyclized with dehydration in a strong acidic media to form a number of 3-aryl-5-dialkylamino-1,4,2-dithiazol-1-ium salts in good yields.

The syntheses and reactions of 1,2- and 1,3-dithiolium cations have been investigated extensively, and their results have been summarized in some excellent reviews.[1-3] The synthesis of 3,5-diaryl-1,2,4-dithiazolium cations, the aza analogs of 1,2-dithiolium, were generalized by Liebscher and the author, and their reactivity has also been studied.[4-7] These five-membered heterocyclic cations are very reactive toward nucleophiles and produce many kinds of derivatives. Therefore, it can be anticipated that 1,4,2-dithiazolium cations, the aza analogs of 1,3-dithiolium, are also reactive and lead to many derivatives. It is interesting to investigate their syntheses and reactivies.

Recently, Paton et al prepared 3-aryl-5-methylthio derivatives by methylation of the corresponding 1,4,2-dithiazol-5-thiones;[8] however, by this method the dithiazol-5-thiones are given only in poor yields.

In addition, Sammes et al prepared 3-aryl-5-dialkylamino compounds quite recently by the reaction between sodium dithiocarbamate and α-chloro oxime *O*-sulfonate,[9] however the chloro oxime sulfonates are special reagents and not available easily.[10]

We now report that a number of 1,4,2-dithiazolium cations were obtained in high yields by another simple method. The approach to preparing 3-aryl-5-dialkylamino-1,4,2-dithiazol-1-ium salts, (**1**), was attained via the pathway shown as Scheme 1, which could be postulated based on the synthetic route of the corresponding 1,3-dithiolium salts.[11]

N-(Dialkylthiocarbamoylthio)arenecarboxamides, (**2**), the precursors for **1**, could not be obtained directly by a reaction of dithiocarbamic acids with *N*-bromoarenecarboxamides; however, the dithiocarbamic acids led to sulfenamides upon treating with hydroxylamine-*O*-sulfonic acid in aqueous sodium hydroxide. The sulfenamides were acylated smoothly with benzoic anhydride to give *N*-benzoyl sulfenamides, while other aroyl compounds were also accessible by treating with aroyl chlorides. Cyclization of **2** was carried out with dehydration in a strong acidic media to afford white crystalline compounds of **1a—g**. Their mps, yields, and analytical data are summarized in Table 1, and satisfactory analytical results were obtained for all products. The IR spectrum of **1a** was almost superimposable to that of 2-diethylamino-4-phenyl-1,3-dithiolium perchlorate. Two absorptions, at δ=166.79 and 192.47, are assignable to the C-3 and C-5 carbons of 1,4,2-dithiazolium ring, respectively. These were observed in the ^{13}C NMR spectrum of **1a**, and the spectral data agreed with the results of Sammes.[9] These facts showed that **1a** is identical with 3-phenyl-5-diethylamino-1,4,2-dithiazol-1-ium perchlorate, and it was found that a number of 3-aryl-5-dialkylamino compounds, **1a—g**, could be obtained in good yields using a simple method, Scheme 1. This process is more convenient and applicable than the two when 1,4,2-dithiazolium salts are supposed to be versatile intermediates to lead to various heterocycles. A study concerning the reaction of the 1,4,2-dithiazolium salts with nucleophiles is in progress.

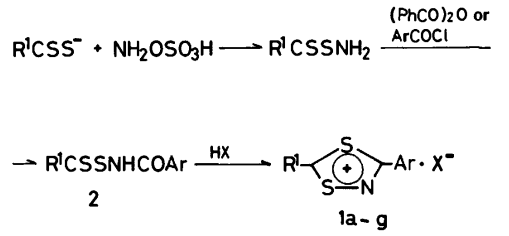

Scheme 1.

Experimental

***S*-Diethylthiocarbamoyl-Substituted Sulfenamide.** Into an aqueous solution (10 ml) of sodium diethyldithiocarbamate trihydrate (2.30 g, 0.01 mol) was added with stirring at a temperature below 10 °C an aqueous solution (10 ml) of hydroxylamine-*O*-sulfonic acid (1.70 g, 0.015 mol), neutralized with sodium hydroxide. The resulting precipitate was separated by filtration and air-dried. The crude product was dissolved in dichloromethane and filtered to remove any insoluble substance. The solvent was evaporated under a reduced pressure to give 1.56 g of the sulfenamide; yield 95%, mp 30—31 °C. ^1H NMR ($CDCl_3$) δ=1.26 (6H, t), 3.08 (2H, br s), 3.80 (4H, br q); IR (KBr): 3336, 3248, 2979, 2932, 1571, 1493, 1420, 1354, 1274, and 1205 cm^{-1}. Found: C, 36.77; H, 7.42; N, 16.80%. Calcd for $C_5H_{12}N_2S_2$: C, 36.59; H, 7.36; N, 17.05%.

Other *S*-dialkylthiocarbamoyl-substituted sulfenamides were also accessible in the same manner as described above almost quantitatively.

***N*-(Diethylthiocarbamoylthio)benzamide (2a). Reaction with Benzoic Anhydride:** Into a solution of *S*-diethylthiocarbamoyl-substituted sulfenamide (1.64 g, 0.01 mol) in chloroform (10 ml), benzoic anhydride (2.71 g, 0.012 mol) was added. The reaction mixture was then kept at 50 °C for 2 h. After removing the solvent under a reduced pressure, the resulting residue was washed with an excess of ether and recrystallized from ethanol to give 2.09 g of **2a**; yield 78%, mp 129 °C. ^1H NMR ($CDCl_3$) δ=1.34 (6H, br t), 3.87 (4H, br), 7.56 (3H, m), and 8.03 (2H, m). IR (KBr): 3315, 2980, 2935, 1672, 1503, 1455, 1423, 1278, and 710 cm^{-1}. Found: C, 53.85; H, 6.02; N, 10.40%. Calcd for $C_{12}H_{16}N_2S_2O$: C, 53.70; H, 6.01; N, 10.44%.

Reaction with Benzoyl Chloride: A solution of *S*-diethylcarbamoyl-substituted sulfenamide (0.82 g, 5 mmol) and

Table 1. 3-Aryl-5-dialkylamino-1,4,2-dithiazol-1-ium Salts, (**1a—g**)

Compd	R^1-	Ar-	X^-	Mp	Yield	Found (Calcd)/%		
				θ_m/°C	%	C	H	N
1a	Et_2N-	Ph-	ClO_4^-	141	80	41.08 (41.02)	4.31 (4.30)	7.98 (8.07)
1b	Et_2N-	*p*-$CH_3OC_6H_4$-	ClO_4^-	121	54	40.85 (41.00)	4.46 (4.50)	7.43 (7.27)
1c	Et_2N-	*p*-$CH_3C_6H_4$-	ClO_4^-	137	52	42.75 (42.79)	4.62 (4.70)	7.67 (7.68)
1d	Et_2N-	*p*-ClC_6H_4-	ClO_4^-	140	79	37.44 (37.41)	3.63 (3.66)	7.33 (7.68)
1e	Me_2N-	Ph-	ClO_4^-	175	63	37.18 (37.21)	3.39 (3.43)	8.70 (8.68)
1f	$(CH_2)_5N$-	Ph-	ClO_4^-	212	82	42.83 (43.03)	4.09 (4.17)	7.61 (7.72)
1g	Et_2N-	Ph-	BF_4^-	120	56	42.62 (42.58)	4.47 (4.43)	8.28 (8.29)

benzoyl chloride (1.05 g, 7.5 mmol) in ether (20 ml) was vigorously stirred with 2 mol dm^{-3} aqueous sodium hydroxide (20 ml) for 3 h at a temperature below 10 °C. The resulting precipitate was filtered, and recrystallized from ethanol to give 0.85 g of **2a**; yield 32%. Other *N*-benzoyl sulfenamide were given in 30—41% using the same procedure mentioned above.

Preparation of 3-Aryl-5-alkylamino-1,4,2-dithiazol-1-ium Salts (1a—g). To a solution of an *N*-benzoyl sulfenamide (0.01 mol) in acetic anhydride (20 ml), 70% perchloric acid (1 ml) or 40% tetrafluoroboric acid (2 ml) was added dropwise with stirring. The reaction mixture was kept at 60 °C for 2 h. After cooling to room temperature, the mixture was poured into an excess of ether to afford a white powder and recrystallized from acetonitrile to give **1a—g**. Their mps, yields, and analytical results are given in Table 1.

1a: ^{1}H NMR (DMSO-d_6) δ=1.38 (3H, t), 1.42 (3H, t), 3.87 (2H, q), 3.98 (2H, q), 7.02 (3H, m), and 7,99 (2H, m). ^{13}C NMR (DMSO-d_6, ppm from TMS) 10.36 (-CH_3), 54.47 (-CH_2-), 57.06 (-CH_2-), 128.82—133.44 (arom), 166,79 (C-3), 192.47 (C-5). IR (KBr): 1576, 1528, 1473, 1447, 1087, 769, 686, and 617 cm^{-1}.

References

1) N. Lozac'h and M. Stavaux, *Adv. Heterocyclic Chem.*, **27**, 151 (1980).
2) D. M. McKinnon, *Comp. Heterocyclic Chem.*, **6**, 783 (1984).
3) H. Gotthardt, *Comp. Heterocyclic Chem.*, **6**, 813 (1984).
4) J. Liebscher and H. Hartmann, *Liebigs Ann. Chem.*, **1977**, 1005.
5) J. Liebscher and H. Hartmann, *Heterocycles*, **23**, 997 (1985).
6) I. Shibuya, *Nippon Kagaku Kaishi*, **1979**, 389.
7) I. Shibuya, *Nippon Kagaku Kaishi*, **1982**, 1518.
8) D. J. Greig, M. McPherson, R. M. Paton, and J. Crosby, *J. Chem. Soc., Chem. Commun.*, **1985**, 696.
9) F. S. Y. Chan and M. P. Sammes, *J. Chem. Soc., Chem. Commun.*, **1985**, 1518.
10) W. E. Truce and A. R. Naik, *Can. J. Chem.*, **44**, 297 (1966).
11) E. Campaigne and N. W. Jacobsen, *J. Org. Chem.*, **29**, 1703 (1964).

Palladium(0)-Catalyzed Coupling Reaction of Isoprene Bromohydrin with Aromatic Organolithium Reagents

Shuki ARAKI, Masayuki OHMURA, and Yasuo BUTSUGAN*
Department of Applied Chemistry, Nagoya Institute of Technology, Gokiso-cho, Showa-ku, Nagoya 466
(Received January 28, 1986)

Synopsis. Palladium(0)-catalyzed reaction of isoprene bromohydrin with aromatic organolithium reagents selectively gave good yields of coupling products without rearrangement.

In our continuous study on the reaction of isoprene bromohydrin (1-bromo-2-methyl-3-buten-2-ol) (**1**) with organometallic reagents, we have recently reported the coupling reaction of **1** with Grignard reagents in the presence of a palladium(0) catalyst which gives exclusively vinyl-group-migrated products. With phenylmagnesium bromide, for example, **1** selectively gave 2-phenyl-4-penten-2-ol in 85% yield.[1] It is interesting to examine the palladium(0)-catalyzed coupling of **1** with organometallics other than Grignard reagent, because isoprene bromohydrin (**1**) shows diverse reaction behavior in the transition-metal-catalyzed coupling with various types of organometallic reagents.[2] We now report the palladium(0)-catalyzed reaction of **1** with aryllithium reagents which yields, in contrast with the reaction of Grignard reagents,[1] non-rearranged coupling products (**2**) with high selectivity (Eq. 1).

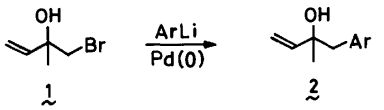

1 2 (1)

When the reaction of 1 with phenyllithium was conducted in the presence of a catalytic amount (0.1 mol%) of tetrakis(triphenylphosphine)palladium, 2-methyl-1-phenyl-3-buten-2-ol (**2a**) was obtained selectively in 53% isolated yield. No other coupling products could be found in the reaction mixture. In the absence of the catalyst, a mixture of **2a** and 2-methyl-4-phenyl-2-buten-1-ol (*E*/*Z* 52/48) was formed in the ratio 76:24 in 85% combined yield.

Results for other aryllithium reagents are summarized in Table 1, which shows that a variety of aryllithiums (phenyl, *p*-tolyl, 2-furyl, 2-thienyl, and 2-pyrrolyl) all give coupling products (**2a—f**) without rearrangement. However, the reactions of **1** with alkyl- and allyllithium reagents such as butyl- and prenyllithium in the presence of the Pd(0) catalyst gave complex product mixtures. For example, the coupling of **1** with prenyllithium under the similar reaction conditions described above gave complex mixture of products in which no trace of linalool could be found.

The present procedure provides a facile and synthetically useful method for introducing a 2-hydroxy-2-methyl-3-butenyl group, an isoprenoid C_5 synthon, to an aromatic nucleus.

Experimental

General. Infrared spectra were recorded on a JASCO IRA-1 spectrophotometer. ^{1}H NMR spectra were recorded on a Hitachi R-24A spectrometer (60 MHz) or on a Varian XL-200 spectrometer (200 MHz) with Me_4Si as internal standard. Mass spectra were determined using a Hitachi M-52 instrument at 20 eV. GLC analyses were performed on a Yanaco G1800 gas chromatograph equipped with a column packed with Apiezon grease L on Uniport B (15%). Elemental analyses were performed at the Elemental Analysis Center of Kyoto University. For Kugelrohr distillation, a Shibata GTO-250R glass tube oven was used.

Table 1. Pd(0)-Catalyzed Reaction of **1** with Aryllithiums

Aryllithium	Product	Yield/%
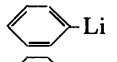	**2a**	53
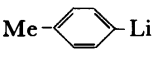	**2b**	86
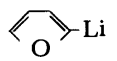	**2c**	60
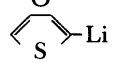	**2d**	78
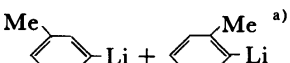 a)	**2e**[b]	92
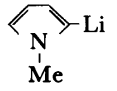	**2f**	70

a) Prepared by the lithiation of 3-methylthiophene.[4] b) Mixture of the products coupled at the 5- and 2-positions of 3-methylthiophene (7 : 3).

Palladium(0)-Catalyzed Coupling Reaction of Isoprene Bromohydrin (1) with Aryllithium Reagents. The following reaction with 2-furyllithium represents the general procedure. Tetrakis(triphenylphosphine)palladium (12 mg, 0.01 mmol) was added to a solution of 2-furyllithium, prepared from furan (680 mg, 10 mmol) and a hexane solution of butyllithium (1.6 M, 6.3 cm^3, 10 mmol (1 M=1 mol dm^{-3})) in ether (10 cm^3) according to the literature method,[3] and the mixture was stirred at 0 °C for 10 min. A solution of 1 (330 mg, 2 mmol) in ether (2 cm^3) was then added at 0 °C and the mixture was left overnight at room temperature. The reaction was quenched by the addition of saturated aqueous ammonium chloride and the product was extracted with ether. The extracts were dried (Na_2SO_4) and the solvent was evaporated. The residue was distilled (Kugelrohr) (bp 115 °C/ 18 Torr; 1 Torr≈133.322 Pa) to give a colorless oil (182 mg, 60%), which was found pure 2c by glc and ^{1}H NMR analyses.

The reactions with other aryllithium reagents were similarly carried out. Lithiation of thiophene,[4] 3-methylthiophene,[5] and 1-methylpyrrole[6] was performed according to literature. The structures of the coupling products (**2a—f**) were deduced by their spectral and analytical data, except for **2a** which was confirmed by the direct comparison with an authentic sample.[1]

2-Methyl-1-(*p*-tolyl)-3-buten-2-ol (2b): Bp 110 °C/3 Torr;

IR (neat) 3420, 2980, 1644, 1516, 1110, 920, and 812 cm^{-1}; ^1H NMR ($CDCl_3$) 1.29 (s, 3H, CH_3), 1.64 (bs, 1H, OH), 2.34 (s, 3H, CH_3), 2.80 (AB q, J=14 Hz, 2H, CH_2), 5.07 (dd, J=10, 2 Hz, 1H olefin), 5.14 (dd, J=17, 2 Hz, 1H, olefin), 6.00 (dd, J=17, 10 Hz, 1H, olefin), 7.13 (m, 5H, Ph); MS m/z 176 (M^+); Found: C, 81.47; H, 9.24%. Calcd for $C_{12}H_{16}O$: C, 81.77; H, 9.15%.

1-(2-Furyl)-2-methyl-3-buten-2-ol (2c): Bp 115 °C/18 Torr; IR (neat) 3430, 2980, 1642, 1594, 1504, 1146, 1010, 926, and 728 cm^{-1}; ^1H NMR (CCl_4) 1.22 (s, 3H, CH_3), 1.76 (bs, 1H, OH), 2.81 (s, 2H, CH_2), 5.00 (dd, J=10, 2 Hz, 1H, olefin), 5.21 (dd, J=17, 2 Hz, 1H, olefin), 5.92 (dd, J=17, 10 Hz, 1H, olefin), 6.08 (m, 1H, furan H-3), 6.27 (m, 1H, furan H-4), 7.32 (m, 1H, furan H-5); MS m/z 152 (M^+); Found: C, 70.96; H, 8.04%. Calcd for $C_9H_{12}O_2$: C, 71.02; H, 7.95%.

2-Methyl-1-(2-thienyl)-3-buten-2-ol (2d): Bp 120 °C/5 Torr; IR (neat) 3450, 2980, 1642, 1372, 1223, 1150, 994, 922, and 692 cm^{-1}; ^1H NMR ($CDCl_3$) 1.34 (s, 3H, CH_3), 1.73 (bs, 1H, OH), 3.06 (s, 2H, CH_2), 5.15 (dd, J=10, 2 Hz, 1H, olefin), 5.22 (dd, J=17, 2 Hz, 1H, olefin), 6.03 (dd, J=17, 10 Hz, 1H, olefin), 6.90 (m, 1H, thiophene H-3), 7.00 (m, 1H, thiophene H-4), 7.22 (m, 1H, thiophene H-5); MS m/z 168 (M^+); Found: C, 64.67; H, 7.37%. Calcd for $C_9H_{12}OS$: C, 64.25; H, 7.19%.

2-Methyl-1-(4-methyl-2-thienyl)-3-buten-2-ol and 2-Methyl-1-(3-methyl-2-thienyl)-3-buten-2-ol (2e) (7:3 Mixture): Bp 110 °C/ 3 Torr; IR (neat) 3450, 2980, 1642, 1370, 1120, 992, 920, 850, and 700 cm^{-1}; ^1H NMR ($CDCl_3$) 1.32 (s, 2.1H, CH_3), 1.33 (s, 0.9H, CH_3), 1.73 (bs, 1H, OH), 2.19 (s, 0.9H, CH_3), 2.22 (s, 2.1H, CH_3), 2.99 (s, 2H, CH_2), 5.12 (dd, J=10, 2 Hz, 1H, olefin), 5.21 (dd, J=17, 2 Hz, 1H, olefin), 6.01 (dd, J=17, 10 Hz, 1H, olefin), 6.69 (bs, 0.7H, thiophene H-3), 6.76 (bs, 0.7H, thiophene H-5), 6.85 (d, J=5 Hz, 0.3H, thiophene H-4), 7.12 (d, J=5 Hz, 0.3H, thiophene H-5); MS m/z 182 (M^+); Found: C, 65.78; H, 7.88%. Calcd for $C_{10}H_{14}OS$: C, 65.89; H, 7.74%.

2-Methyl-1-(1-methyl-2-pyrrolyl)-3-buten-2-ol (2f): Bp 130 °C/ 5 Torr; IR (neat) 3500, 2980, 1642, 1490, 1298, 1088, 1018, 920, and 704 cm^{-1}; ^1H NMR ($CDCl_3$) 1.32 (s, 3H, CH_3), 1.92 (bs, 1H, OH), 2.81 (AB q, J=15 Hz, 2H, CH_2), 3.57 (s, 3H, NCH_3), 5.11 (dd, J=10, 2 Hz, 1H, olefin), 5.18 (dd, J=17, 2 Hz, 1H, olefin), 5.99 (dd, J=17, 10 Hz, 1H, olefin), 6.04 (m, 1H, pyrrole H-3 or H-4), 6.11 (m, 1H, pyrrole H-4 or H-3), 6.60 (m, 1H, pyrrole H-5); MS m/z 165 (M^+); Found: C, 72.52; H, 9.21%. Calcd for $C_{10}H_{15}NO$: C, 72.69; H, 9.15%.

References

1) S. Araki, M. Ohmura, and Y. Butsugan, *Bull. Chem. Soc. Jpn.*, **58**, 1607 (1985).

2) Y. Butsugan, I. Kadosaka, and S. Araki, *Chem. Lett.*, **1979**, 527; S. Araki and Y. Butsugan, *ibid.*, **1980**, 185.

3) V. Ramanathan and R. Levine, *J. Org. Chem.*, **27**, 1216 (1962).

4) H. Gilman and D. A. Shirley, *J. Am. Chem. Soc.*, **71**, 1870 (1949).

5) V. Ramanathan and R. Levine, *J. Org. Chem.*, **27**, 1667 (1962).

6) N. Gjøs and S. Gronowitz, *Acta Chem. Scand.*, **25**, 2596 (1971).

Biomimetic Application of Natural Valinomycin and Nonactine Ionophores to Artificial Transport of Amino Acid Salts[1)]

Hiroshi TSUKUBE,* Kentaro TAKAGI, Tatsuo HIGASHIYAMA, Tadashi IWACHIDO, and Naomi HAYAMA
Department of Chemistry, College of Liberal Arts & Science, Okayama University, Okayama 700
(Received February 3, 1986)

Synopsis. Biological valinomycin and nonactine ionophores showed new and interesting transport abilities for important amino acid salts in the biomimetic membrane systems, which are of biological interest and of practical significance.

Valinomycin and nonactine are typical biological ionophores,[2)] which strongly bind K^+ ion in their macrocyclic cavities and effectively transport it across a biomembrane. A variety of investigations of molecular structures, biological activities, and other chemical properties of these ionophores have been investigated, but most of them have focussed only on K^+ cation transport phenomena.[3)]

Here we present a new biomimetic application of biological valinomycin and nonactine ionophores to the artificial membrane transport, in which amino acid derivatives are transported as anionic or cationic guest species. Although valinomycin and nonactine ionophores are believed to act as K^+ ionophores, we found that they showed excellent transport abilities for several amino acid guest salts. Their transport properties are compared with those of synthetic biscrown **3** and cryptand **4** (Fig. 2), because they are known to form three dimensional complexes with K^+ cation.[4)] Typical transport results, obtained by using a $CHCl_3$ liquid membrane, are summarized in Table 1.

Valinomycin **1** and nonactine **2** effectively transported several amino acid derivative anions together with alkali metal cations in the same direction, as observed in some biological amino acid symport systems.[5)] Table 1 demonstrates that valinomycin showed higher transport efficiencies than nonactine and other synthetic ionophores. Its transport properties were significantly controlled by combination of guest anion and cotransported cation. Optimal combination of Cs^+ and *N*-benzoylphenylalanine anion(Bz–Phe$^-$) provided suitably stable "valinomycin-guest anion-cotransported cation" type complex and allowed high transport efficiency.[6)] Since other employed ionophores had favourable combinations of guest salts, an effective transport of a given amino acid salt could be realized by appropriate choice of the employed ionophore and cotransported cation. These results clearly reveal new and potential transport functionalities of well-known bio-ionophores.

Table 1 also indicates that valinomycin **1** and nonactine **2** hardly mediated transport of amino acid ester salts, though the NH_3^+-moiety of amino acid ester has an ionsize similar to that of K^+ cation. Since synthetic ionophores **3** and **4** mediated transport of amino acid ester salts, the rigid backbones and bulky residues of biological valinomycin and nonactine ionophores would prevent stable complexations with guest ammonium cations of bulky amino acid esters.

The present results provide new and significant insights of biological and practical membrane transport systems. Other types of biological ionophores may offer further interesting transport functionalities for a new series of guest species, though several struc-

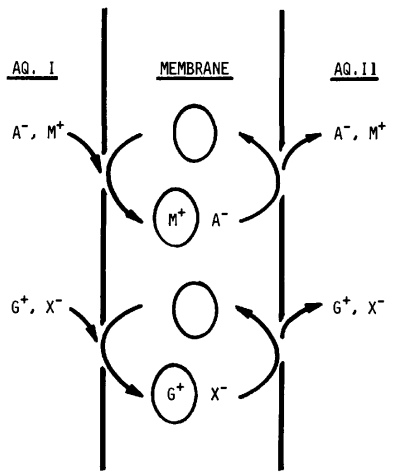

Fig. 1. Biomimetic membrane transport systems of amino acid salts.
O: Neutral ionophore; A^-M^+: *N*-Benzoylamino acid metal salt; G^+X^-: Amino acid ester salt.

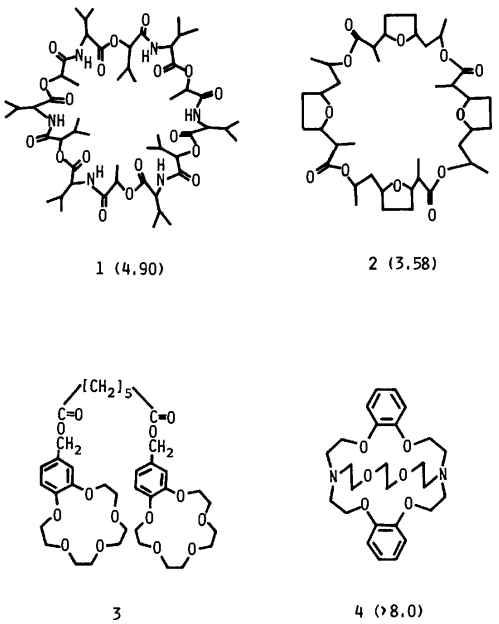

Fig. 2. Examined neutral ionophores.
The values indicated in parentheses were stability constants of the ionophores with K^+ ion in methanol as reported.

Table 1. Transport Properties of Amino Acid Salts by Neutral Ionophores

Guest Amino Acid Salt		Transport Rate $\times 10^6$ (mol/h)			
		1	2	3	4
A^-	M^+	"Condition A"			
Bz-Phe$^-$	Na^+	0.46	0.25	2.73	6.78
	K^+	8.80	4.88	2.68	1.57
	Cs^+	9.39	0.22	0.10	6.04
Bz-Leu$^-$	K^+	8.68	1.82	0.73	4.27
Bz-Val$^-$	K^+	7.56	0.72	0.24	4.29
Bz-Ala$^-$	K^+	4.57	0.16	0	2.11
G^+	X^-	"Condition B"			
H_3N^+-PheOEt	ClO_4^-	0	0.35	6.87	0.71
H_3N^+-TrpOMe	ClO_4^-	0	0	5.39	1.00

(Condition A) Aq. I: *N*-Benzoylamino acid, 0.5 mmol. MCl, 5.0 mmol. LiOH, 0.5 mmol/H_2O, 5 ml. Membrane: Ionophore, 0.0372 mmol/$CHCl_3$, 12 ml. Aq. II: H_2O, 5ml. (Condition B) Aq. I: Amino acid ester HCl, 0.5 mmol. $NaClO_4$, 1.0 mmol/H_2O, 5 ml. Membrane and Aq. II: same as Condition A.

tural modifications are required to suppress their high toxicities.

Experiments

1. Materials. Valinomycin, bis-crown, and cryptand ionophores were purchased from Aldrich, Dojindo, and Merck, respectively. Nonactine, obtained from Fluka, contained about 25% monactine. Special cares are required for usages of valinomycin and nonactine ionophores, because of their high toxicities. Other employed reagents were also commercially available and used without further purifications.

2. Transport Procedures. The transport experiments were carried out at room temperature in a U-tube glass cell (2.0 cm, i.d.) as reported before.[7] The ionophore in $CHCl_3$ (12 ml) was placed in the base of the U-tube, and two aqueous phases(5 ml, each) were placed in the arms of the U-tube, floating on the $CHCl_3$ membrane. The membrane phase was stirred with a magnetic stirrer. The amounts of amino acid derivative anions or cations transported into Aq. II phase were determined by spectroscopic method. Initial transport rates calculated are summarized in Table 1.

This research was supported in part by a Grant-in-Aid from the Ministry of Education, Science, and Culture.

References

1) Biomimetic application of biological monensin and lasalocid A to the cation transport have recently been developed: H. Tsukube, K. Takagi, T. Higashiyama, T. Iwachido, and N. Hayama, *J. Chem. Soc., Chem. Commun.*, **1986**, 448.

2) Recent review: G. R. Painter and B. C. Pressman, Topics in Current Chemistry, Springer-Verlag, Berlin (1982), Vol. 101, p. 83.

3) W. E. Morf, D. Ammann, E. Pretsch, and W. Simon, *Pure Appl. Chem.*, **36**, 421 (1973).

4) K. Kimura, T. Maeda, H. Tamura, and T. Shono, *J. Electroanal. Chem.*, **95**, 91 (1979); J. M. Lehn, *Structure and Bonding*, **16**, 1 (1973).

5) K. Ring, *Angew. Chem. Int. Ed. Engl.*, **9**, 345 (1970).

6) Valinomycin forms stable complexes with K^+ and Cs^+ ions, and their log *K* values have been determined in EtOH as 6.3(K^+) and 5.8(Cs^+): B. G. Cox, Ng van Truong, J. Rzeszotarsks, and H. Schneider, *J. Am. Chem. Soc.*, **106**, 5965 (1984).

7) H. Tsukube, *J. Chem. Soc., Perkin Trans. 1*, **1982**, 2359.

Titrations by Temperature Difference Electrode: Entropy Titrations

Tamio IKESHOJI
Government Industrial Research Institute, Tohoku; Nigatake 4-2-1, Sendai 983
(Received October 25, 1985)

Synopsis. A new type of potential-difference titration which has a relation with the entropy change of a reaction in a titrated solution was demonstrated using a Hg^{2+}–EDTA reaction on an Hg electrode. The potential difference between two identical electrodes, one kept at a different temperature from that of the solution, was monitored during titration. This difference changed from a minimum to a maximum at the equivalent point.

Many titrations concern Gibbs free-energy changes of reactions in titrated solutions. Some titration methods concern only enthalpy changes during reactions. A typical example of titrations concerning Gibbs free-energy changes is a potential-difference titration method in which the potential differences change due to Gibbs free-energy changes, i.e. the equilibrium constants of the reactions during titrations. Therefore, the equilibrium constants which this method concerns must be sufficiently large to determine the equivalent points and the equilibrium constants. In this note, the new type of titration method that is given mainly concerns entropy changes of reactions instead of the equilibrium constants. It is expected to be possible to precisely determine the equivalent points, even though the equilibrium constants are small, and to also calculate the entropy changes using only one titration curve. In ordinary potential-difference (OPD) titrations, entropy changes are calculated from at least two titration curves at different temperatures.

The new method presented here is one type of potential-difference titration in which the potential difference between two identical electrodes (one of which is kept at a different temperature from the titrated solution, called a "temperature difference electrode (TDE)") is monitored during titrations. The temperature of the other electrode is kept equal to that of the solution. In typical cases the potential difference during TDE titration is expected to change sharply from a minimum to a maximum at an equivalent point.[1] A sharp drop in potential was observed at this equivalent point in the case of OPD titration in which the electrode potential was monitored against a reference electrode in an iso-thermal condition. Since the configuration of these two identical electrodes was equal to that of a non-isothermal galvanic cell, their potential difference could be interpreted by the theory of non-isothermal galavanic cells containing a complexation reaction.

A demonstration of TDE titrations was performed using an Hg/Hg^{2+} electrode with disodium dihydrogen ethylenediaminetetraacetate ($EDTAH_2Na_2$) as a ligand for Hg^{2+}. This was done because the potential of Hg/Hg^{2+} is sufficiently stable to measure the small potential difference during TDE titration.

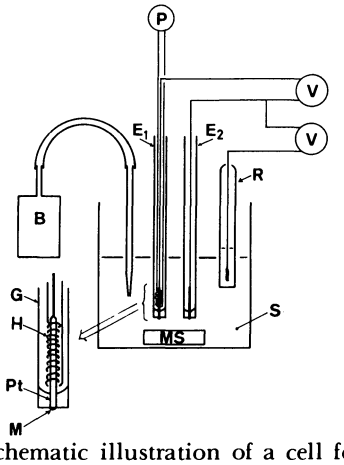

Fig. 1. Schematic illustration of a cell for temperature difference electrode titrations.
B: Motor driven syringe-burette, E_1: temperature difference electrode, E_2: the same type electrode as E_1 without a heater, H: small heater, G: glass tube, M: mercury hanging on Pt, P: power supply for small heater H, Pt: platinum rod, R: reference electrode, S: solution titrated, V: high impedance voltmeter.

Experimental

If a measurement cell for TDE titrations is built well, it will probably be complicated since it must have two compartments at different temperatures and a stirrer which can make all parts of the solution uniform. In this type measurement, the simple cell illustrated in Fig. 1 was used. Two electrodes, consisting of Pt rods (1 mmϕ) on which mercury was hanging, were placed in the cell. One of the electrodes was a TDE in which a small heater of chromel wire (13 Ω) insulated by Teflon was wrapped around the Pt rod in order to make the temperature of the TDE higher than the solution. Since the surface temperature of the TDE was a function of the current passing through this small heater and the speed of the magnetic stirrer, both were kept constant at 150 mA and ca. 150 rpm during titrations. A solution of 50 cm^3 containing $Hg(NO_3)_2$ (0.05 mmol) and sodium nitrate (1 mol dm^{-3}) at pH 1.3 or 2.2 adjusted by nitric acid were titrated by $EDTAH_2Na_2$ solution (0.01 mol dm^{-3}) with a motor-driven syringe-burette (ca. 0.2 $cm^3\,min^{-1}$) of TOA HSM-10A titrator. The cell was placed in a water bath kept at 29°C. The electrochemical system used here is, therefore, written as Hg (29°C)/Hg^{2+}, EDTA, $NaNO_3$/Hg(29°C+ΔT), where 29°C+ΔT is the surface temperature of the mercury of the TDE. The potential difference between two mercury electrodes hanging on the Pt rods and that between the mercury electrode at 29°C and an Ag/AgCl reference electrode which was used in the OPD titrations for comparison were monitored by a computer (HP-9845) with two high-impedance voltmeters (Hokuto HA-104 and ORION 811), a digital voltmeter (HP-3455A), and a scanner (Takeda TR-7216). All measurements were carried out at room temperature (29—30°C).

Results and Discussion

The potential difference measured during the TED

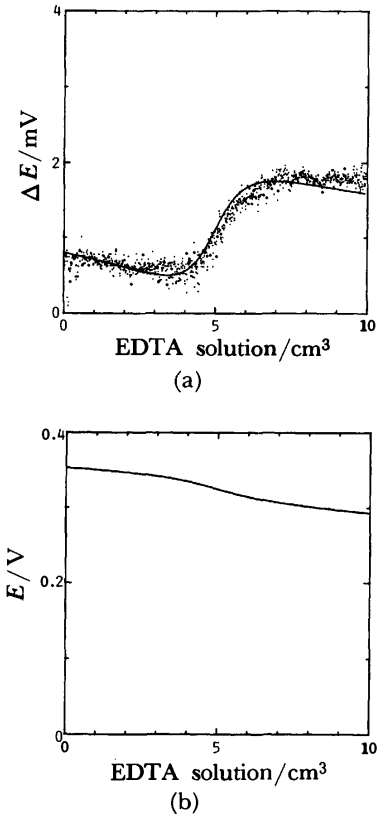

Fig. 2. Titration curves at pH 1.3. (a) by temperature difference electrode. (b) by ordinary potential difference titration.

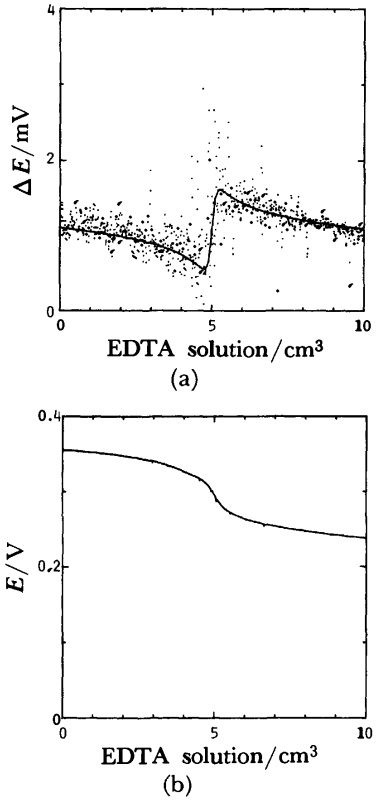

Fig. 3. Titration curves at pH 2.2. (a) by temperature difference electrode. (b) by ordinary potential difference titration.

titrations at pH 1.3 and 2.2 are plotted by dots in Figs. 2(a) and 3(a), and titration curves measured by the OPD ones in the same conditions are shown in Figs. 2(b) and 3(b).

An equivalent point for Hg^{2+} could be determined as the midpoint between the minimum and maximum peaks in the TDE titration curves. At pH 1.3, the equivalent point was determined to be 5.2 cm^3 in titrant volume from the TDE titration curve and 5.0 cm^3 from the OPD one. The difference was nearly within the experimental error. At pH 2.2 it was 5.0 cm^3 for both titration curves. The equivalent points can be seen more clearly in the TDE titration curves than in the OPD curves if measurements are performed under lower noise conditions. From the TDE and OPD titration curves at pH 1.3, regions where the apparent equilibrium constants of the complexation reaction were low, it was confirmed that a sharper change in the potential difference could be observed in case of TDE titration than in the case of OPD titration, even if the equilibrium constant was low. This is because the change in the potential difference during a TDE titration is not only due to the equilibrium constant, but also due to an entropy change of the complexation reaction.

The potential difference (ΔE) observed by the TDE titrations can be expressed by

$$\Delta E = \varepsilon \Delta T,$$

where ε is a thermoelectric power of this system, since two electrodes of the TDE titrations constitute a non-isothermal galvanic cell as described in Experimental. It is well known that the thermoelectric power of a non-isothermal galvanic cell is changed from the initial thermoelectric power (ε_i) at the uniform concentrations just after changing the temperature to the final value after a Soret equilibrium is attained.[2] For the experimental conditions mentioned in this note, the final thermoelectric power might be used for an interpretation of the observed thermoelectric power because of a thin thermal boundary layer on the mercury electrode of the TDE. In this layer, a Soret equilibrium could be attained within a short time. However, the final thermoelectric power in case of cells with a complexation reaction has not been theoretically derived yet. Therefore, in this note the initial thermoelectric power is used for a calculation of the TDE titration curves. This results in only a constant shift in the TDE titration curves since the difference between the initial and final thermoelectric power for general cases is due only to the constant terms of the transport numbers and Eastman entropies.[2] The initial thermoelectric power of the non-isothermal galvanic cells is expressed by the entropy change contributed from the electrode reaction and the transported entropies.[3] When an excess amount of indifferent salts is disolved in the solution, the transported entropies are constant. Therefore, the initial thermoelectric power of a cell $M(T)/M^{n+}$, Ligand/$M(T+\Delta T)$ with an excess amount of the indifferent salts is given as[1]

$$\varepsilon_i = \left(\frac{\partial E}{\partial T}\right)_{\text{iso}} + \text{const.}$$
$$= \frac{R}{nF} \ln C_{M^{n+}} + \frac{RT}{nF}\left(\frac{\partial \ln C_{M^{n+}}}{\partial T}\right) + \frac{\partial E^\circ}{\partial T} + \text{const.}, \quad (1)$$

where R and F are gas and Faraday constants, respectively. $(\partial E/\partial T)_{\text{iso}}$ is the temperature dependence of the isothermal electrode potential (E); i.e., it is determined from the electrode potentials measured against a reference electrode at various temperatures under the condition that the electrode and the reference electrode are kept at the same temperature. The term const. in Eq. 1 arises from transported entropies, activity coefficients, etc., and is constant for an excess of indifferent salts. $C_{M^{n+}}$ is the concentration of free M^{n+} which is not complexed with the ligand. $\partial E^\circ/\partial T$ is the temperature dependence of the standard electrode potential of M/M^{n+}. This term is also constant during titration. Details of the derivation of Eq. 1 is given elsewhere.[1] If the apparent complexation reaction with ligand L is simply written as

$$M^{n+} + L \rightleftarrows M^{n+}L \quad (2)$$

with equilibrium constant K

$$K = \frac{C_{M^{n+}L}}{C_{M^{n+}} C_L}, \quad (3)$$

where $C_{M^{n+}L}$ and C_L are the concentrations of complex $M^{n+}L$, and the free ligand, respectively, $C_{M^{n+}}$ can be calculated from Eq. 3 and the mass balances among them. The first term of Eq. 1 is dependent only on K but the second term of Eq. 1 is dependent on the standard entropy change (ΔS°) of the complexation reaction. Assuming K, ΔS°, and ΔT, it is possible to calculate the TDE and OPD titration curves. From the observed curves K, ΔS°, and ΔT can be determined as follows.

K: By a curve fitting of the OPD titration curve.

ΔT: From a slope of the TDE titration curve between 0 and a half of equivalent point in the titrant volume. In this region the slope of ε_i is not sensitive for K and ΔS° changes.

ΔS°: By a curve fitting of TDE titration curve. It is also possible to determine K from peak shapes in the TDE titration curve. The sharp peak means big K. The peak difference in height is corresponding to ΔS°.

In the above way, K, ΔS°, and ΔT under these experimental conditions were determined to be: log K= 4.9, $\Delta S^\circ = -18$ J K^{-1} mol^{-1}, and ΔT=10 K for pH 1.3 and log K=6.8, $\Delta S^\circ = -25$ J K^{-1} mol^{-1}, and ΔT=5 K for pH 2.2. The differences in ΔT are due to different electrode and stirrer configurations in the cells used. The calculated TDE titration curves are shown by solid lines in Fig. 2(a) and Fig. 3(a).

Since pK of the first proton release reaction of EDTA is 2.0,[4] EDTA forms mainly $EDTAH_4$ at pH 1.3. Therefore, the main complexation reaction at pH 1.3 can be expressed as

$$Hg^{2+} + EDTAH_4 \rightleftarrows HgEDTA^{2-} + 4H^+. \quad (4)$$

From data of stability constants of $EDTAH_4$ and $HgEDTA^{2-}$ found in the literature,[4] apparent $K(=C_{HgEDTA^{2-}}/C_{Hg^{2+}}C_{EDTAH_4})$ and ΔS° in a form of reaction scheme (2) at pH 1.3 are calculated as 6.8 in log K and -40 J K^{-1} mol^{-1}, respectively. The data used here were values at 25 °C and at an ionic strength 1.0 for K and 0.1 for ΔS°. Even though a simple complexation reaction (4) was assumed here, the difference in K and ΔS° between the calculations from values found in the literature and from observed curves was not large. Thus, since it is obvious that TDE titration is related to the entropy change, it might be called "Entropy titration."

The author wishes to thank Professor Signe Kjelstrup Ratkje of The Norwegian Institute of Technology for discussions about non iso-thermal galvanic cells by irreversible thermodydnamics and Mr. Ken Nozaki of Electrotechnical Laboratory for his suggestions to this work.

References

1) T. Ikeshoji and S. K. Ratkje *J. Electrochem. Soc.*, **133**, 1107 (1986).
2) J. Agar, "Advances in Electrochemistry and Electrochemical Engineering," ed by P. Delahay, Interscience, N.Y. (1961), Vol. 3.
3) Y. Ito, H. Kaiya, S Yoshizawa, S. K. Ratkje, and T. Førland, *J. Electrochem. Soc.*, **131**, 2504 (1984).
4) A. Martell and R. Smith, "Critical Stability Constants," Plenum Press, N.Y. (1982), Vol. 5.

Conformational Changes of 1,2,3-Triselena- and 1,2,3-Trithia-[3](1,1′)ruthenocenophane

Sadatoshi AKABORI,* Takeshi KUMAGAI, and Masaru SATO†
Department of Chemistry, Faculty of Science, Toho University, Funabashi, Chiba 274
†Chemical Analysis Center, Saitama University, Urawa, Saitama 338
(Received December 28, 1985)

Synopsis. 1,2,3-Triselena[3](1,1′)ruthenocenophane was obtained by the reaction of 1,1′-dilithioruthenocene with selenium powder in 22% yield. The energy barriers of the bridge reversal inversion of 1,2,3-triselena- and 1,2,3-trithia[3](1,1′)ruthenocenophane are 78.8 and 91.5 kJ mol^{-1}, respectively.

It is well-known that [3](1,1′)metallocenophanes are fluxional molecules and include bridge reversal processes. The high-temperature NMR spectra of 1,2,3-tricalcogena[3](1,1′)ferrocenophanes and their derivatives were recently interpreted as indicating the rigid nature of their medium-sized ring system.[1] For example, the activation energies required for the interconversion of 1,2,3-trithia[3](1,1′)ferrocenophane (**1**) and 1,2,3-triselena[3](1,1′)ferrocenophane (**2**) were estimated to be 80.3 and 68.4 kJ mol^{-1}, respectively. The difference in the activation energy between the two compounds is mainly attributable to the bond length of their bridge rings. In this connection, we have previously reported on the bridge reversal energy barriers of [3](1,1′)ruthenocenophane derivatives[2] containing calcogen atoms in the bridge. However, the bridge reversal energy barriers of 1,2,3-trithia[3]-(1,1′)ruthenocenophane (**3**) and 1,2,3-triselena[3](1,1′)-ruthenocenophane (**4**) have not previously been reported. It seemed interesting to compare the bridge reversal energy barriers of the metallocenophanes **1**, **2**, **3**, and **4**. Therefore, we prepared compound **3** and **4** and investigated the bridge reversal barriers in these ruthenocenophanes.

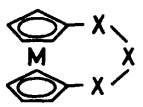

1: M=Fe, X=S
2: M=Fe, X=Se
3: M=Ru, X=S
4: M=Ru, X=Se

The reaction of 1,1′-dilithioruthenocene, which was prepared from ruthenocene and butyllithium in the presence of *N,N,N′,N′*-tetramethylethylenediamine (TMEDA), with selenium gave 1,2,3-triselena[3](1,1′)-ruthenocenophane (**4**) in 22% yield. The ^{1}H NMR spectrum of **4** in DMSO-d_6 showed the cyclopentadienyl (Cp) ring protons as an AMM′X pattern at δ 4.19, 4.79 and 5.00 as shown in Fig. 1, supporting the assigned structure. The multiplet at the highest field was assigned for H_X, due to the shielding effect of the lone pair electrons of the sulfur atoms located at the 1- and 3-positions in the bridge. Similarly, the lowest one was assigned for H_A. When the temperature was

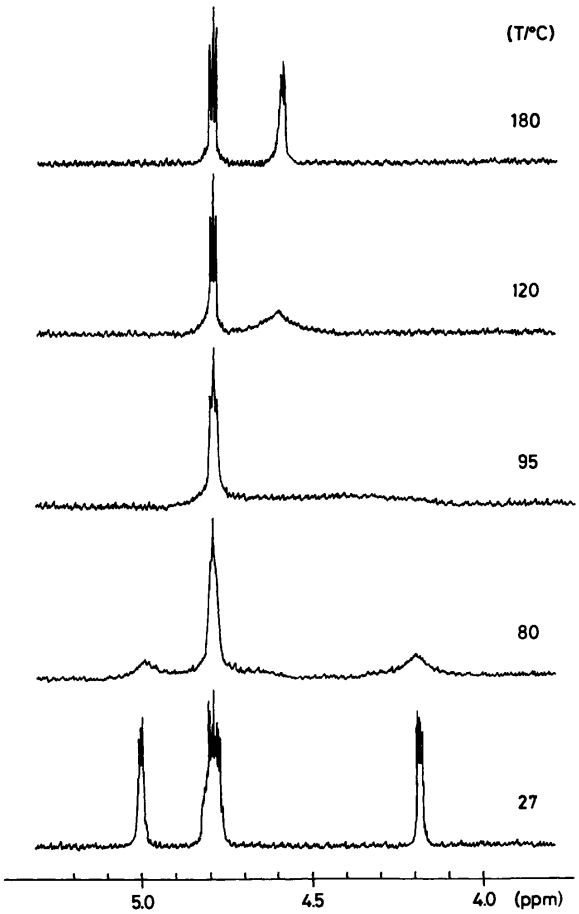

Fig. 1. Variable temperature 90 MHz ^{1}H NMR spectra of 1,2,3,-triselena[3](1,1′)ruthenocenophane in DMSO-d_6.

raised, these two multiplet peaks were broadened and coalesced at 95.2 °C. Above this temperature (180 °C) the broad peak due to H_α becomes sharp triplet. Also, the multiplet peak due to H_M at δ 4.79 was sharpened. The temperature dependence of the AMM′X pattern is in line with the exchange between the two α-ring protons, environments resulting from the bridge reversal inversion among conformer A and B (Fig 2). The rate of exchange k^1 at the temperature of coalescence T_c was calculated according to Gutowsky and Holm's method, from the Eq. 1,[3] where $\Delta\nu$ is the frequency separation of the resolved signals at room temperature.

$$k^1 = \pi\Delta\nu/\sqrt{2}, \quad (1)$$

$$k^1 = \kappa\frac{kT}{h}\exp\left(\frac{-\Delta G^{\ddagger}}{RT}\right). \quad (2)$$

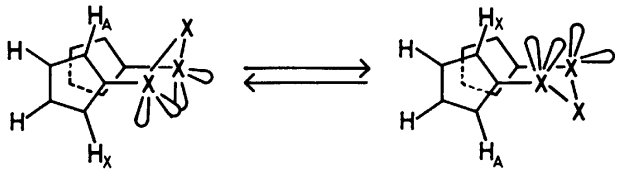

A B

Fig. 2. Bridge reversal mechanism of [3](1,1′)metallocenophane.

The values of $\Delta G^{\ddagger}$ were derived from the Eyring Eq. 2,[4] a unit transmission coefficient (k^1) being assumed. Equation 2 was transformed to Eq. 3 for the purpose of calculation.

$$\Delta G^{\ddagger} = 2.303RT_c(10.319 - \log_{10} k^1 + \log_{10} T_c) \quad (3)$$

When T_c=368 K, $k^1(s^{-1})$=161, and $\Delta\nu$(Hz)=72.6, the energy barrier for **4** was calculated to be about 75.2± 0.3 kJ mol^{-1}. This value is considerably greater than that of the bridge reversal barrier (67.2 kJ mol^{-1}) of corresponding ferrocenophane (**2**). This result is explainable by the fact that the distance between the two Cp rings of the ruthenocene nucleus was slightly longer than that of the ferrocene nucleus.[5,6] That is to say, the greater the angle of the bridge (X-X-X), the harder the bridge reversal. As shown in Fig. 3, the ^{1}H NMR spectra of 1,2,3-trithia[3](1,1′)ruthenocenophane (**3**) in DMSO-d_6 at room temperature also showed an AMM′X pattern at δ 4.28, 5.00, and 5.12. When the temperature was raised, the two multiplets of the H_A and H_X were broadened to ultimately coalesce at 170 °C. The bridge reversal barrier of **3** was calculated to be 91.5 kJ mol^{-1} ($\Delta\nu$=68.1 Hz, T_c=443 K, k^1=151 s^{-1}). The energy barrier was considerably greater than that of **4**. This result was in good agreement with the study previously reported by Abel et al. (1981).[1] They suggested that the bridge reversal barriers of [3](1,1′)-metallocenophane were correlated with the bridge length (Cp-X-X-X-Cp) determined from the covalent radii. That is, the longer the bridge length, the easier the inversion of the bridge. As the bridge length (8.56 Å) of **4** is longer than that (7.78 Å) of **3**, the value of the bridge reversal barrier of **4** is lower than that of **3**.

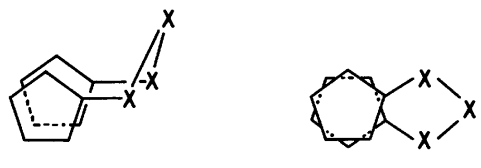

I II

Conformations I and II were possible as the low temperature limited conformation. For example, the structure of 1,2,3-trithia[3](1,1′)ferrocenophane took an eclipsed conformation I in a solid state and the energy of the staggered conformation II had to be higher than that of the eclipsed conformation I. Furthermore, in the [3](1,1′)ferrocenophanes, it has been proved and reported that the conformation I is the low temperature limiting conformation.[1] The conformation II is rather regarded as the transition state in the fluxional process. Accordingly, the 1,2,3-tricalcogena[3](1,1′)ruthenocenophanes (**3** and **4**) must take an eclipsed conformation as the low temperature limiting conformation.

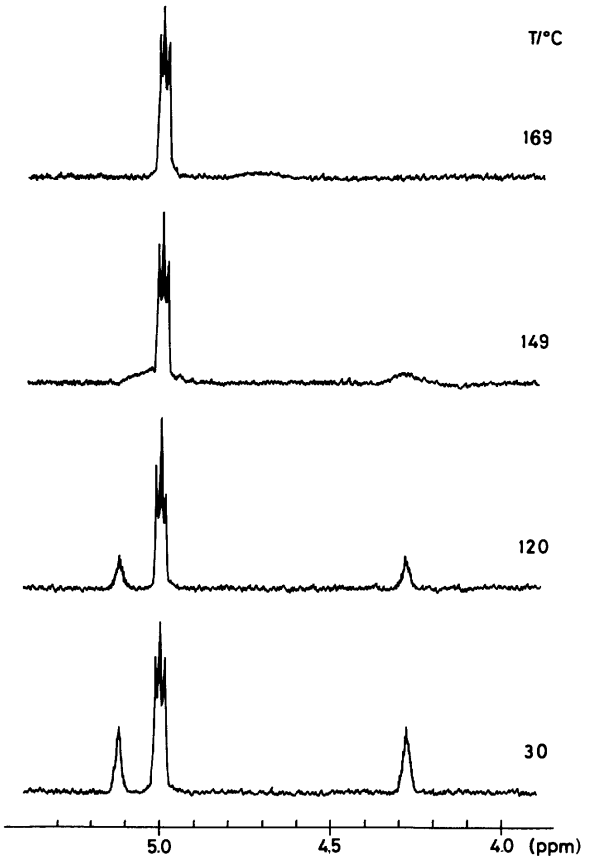

Fig. 3. Variable temperature 90 MHz ^{1}H NMR spectra of 1,2,3,-trithia[3](1,1′)ruthenocenophane in DMSO-d_6.

Experimental

1,2,3-Trithia[3](1,1′)ruthenocenophane (**3**) was prepared according to the previously reported method.[7] The variable temperature 90 MHz ^{1}H NMR of **3** and **4** were recorded in DMSO-d_6, on a JEOL FX-90 spectrometer, TMS being chosen as the internal standard. Mass spectra were taken on a Hitachi M-80 spectrometer. The melting point was not corrected.

1,2,3-Triselena[3](1,1′)ruthenocenophane (4). To a solution of ruthenocene (3.5 g, 15.2 mmol) in hexane (200 ml) was added a solution of TMEDA (5.6 ml, 37.7 mmol) and butyllithium (78.1 mmol) in hexane (50 ml) under nitrogen at a refluxing temperature. After the mixture was refluxed for 2 h, 1,2-dimethoxyethane (150 ml) and selenium powder (7.0 g, 88.6 mmol) were added to the mixture, and then refluxed for 16 h. After the mixture was cooled to room temperature, 10 ml of water was added. The supernatants were decanted and the residue was extracted with hot hexane until the extracts became colorless. The supernatants and the extracts were combined and concentrated in vacuo and the residue was chromatographed on activated alumina using a benzene : hexane (2:5) solution as the eluant. The yellow third fraction was collected and concentrated in vacuo. The residue

was recrystallized from hexane to give **4** as yellow plates in 22% yield, mp, 219.5—220.5 °C. Found: C, 25.96; H, 1.86%. Calcd for $C_{10}H_8RuSe_3$: C, 25.77; H, 1.73%. MS (70 eV), *m/z* 466 (M^+).

References

1) E. W. Abel, M. Booth, and K. G. Orrell, *J. Organomet. Chem.*, **208**, 213 (1981).

2) S. Akabori, T. Kumagai, and M. Sato, *J. Organomet. Chem.*, **286**, 69 (1985).

3) H. S. Gutowsky and C. H. Holm, *J. Chem. Phys.*, **25**, 1228 (1956).

4) S. Glastone, K. J. Laidler, and H. Eyring, "The Theory of Rate Process," McGraw-Hill Book Co., Inc., London (1941), Chap. 1.

5) G. L. Hardgrove and D. H. Templeton, *Acta Crystallogr.*, **12**, 28 (1959).

6) J. D. Dunitz, L. E. Orgel, and A. Rich, *Acta Crystallogr.*, **9**, 373 (1956).

7) S. Akabori, H. Munegumi, Y. Habata, S. Sato, K. Kawazoe, C. Tamura, and M. Sato, *Bull. Chem. Soc. Jpn.*, **58**, 2185, (1985).

Stereospecific Synthesis of the Fungal Prohormone (±)-Trisporol B via the Palladium-Catalyzed Cross-Coupling Reaction of 1-Alkenylborane with 1-Haloalkene

Norio MIYAURA, Yoshitaka SATOH, Shoji HARA, and Akira SUZUKI*
Department of Applied Chemistry, Faculty of Engineering, Hokkaido University, Sapporo 060
(Received January 20, 1986)

Synopsis. The synthesis of the titled C_{18} apocarotenoid prohormone by means of palladium-catalyzed cross-coupling reaction between (*E*)-1-alkenylbis(1,2-dimethylpropyl)-borane (**10**) and (*Z*)-6-iodo-5-hepten-2-one ethylene acetal (**9**) is described. The reaction is highly stereoselective and the demanded (7*E*) and (9*Z*) double bonds are readily introduced.

The development of a simple and convenient method for the preparation of functionalized conjugated alkadienes and trienes has long been attracting much attention, since they would be promising versatile intermediates for the synthesis of naturally occurring biologically active compounds. Recently, we have reported that 1-alkenylboranes react with 1-alkenyl halides in the presence of palladium catalyst and base to give stereodefined conjugated alkadienes while preserving their *E* and *Z*-configurations.[1]

In this paper, we describe a stereospecific synthesis of the benzyl ether of a fungal prohormone (±)-trisporol B[2] (**1**, R=CH_2Ph) which involves the cross-coupling reaction between (*E*)-1-alkadienylborane (**10**) and (*Z*)-1-alkenyl iodide (**9**).

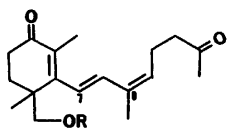

1 R = H, (±)-Trisporol B

The dienylborane derivative (**10**), required for the cross-coupling, was prepared via five steps from 2-methyl-3-ethoxy-2-cyclohexenone (**2**).[8] Thus, the methylation of **2** with lithium diisopropylamide (LDA) and methyl iodide in THF and HMPA, according to the method developed by Stork,[3] gave **3** in 91% yield as a white solid. Essentially the same procedure was applied for the benzyloxymethylation of **3** with LDA and benzyl chloromethyl ether to give **4** in 88% isolated yield. This enone **4** was then transformed into the enynone **5** by treatment with lithium trimethylsilylacetylide and the subsequent hydrolysis with aqueous hydrogen chloride. Desilylation[4] was performed with a saturated KF solution in 95% ethenol at room temperature in a quantitative yield. Subsequently, the carbonyl function of **5** was protected as its ethylene acetal. Thus, the overall yield from **2** to **6** was 56%, as shown in Eq. 1.

On the other hand, we have previously reported that the haloboration of terminal alkynes with 9-iodo-9-borabicyclo[3,3,1]nonane (B-I-9-BBN) proceeds highly regio- and stereoselectively to give the *syn*-adducts 9-[(*Z*)-2-iodo-1-alkenyl]-9-BBN's such as **7** in essentially quantitative yields, and the β-haloalkenyl-9-BBN (**7**) thus obtained reacts with α,β-unsaturated ketones via a Michael-type addition to yield haloalkenyl ketones like **8** in excellent yields.[5] This reaction sequence was applied to the synthesis of another necessary segment **9** for the cross-coupling (Eq. 2).

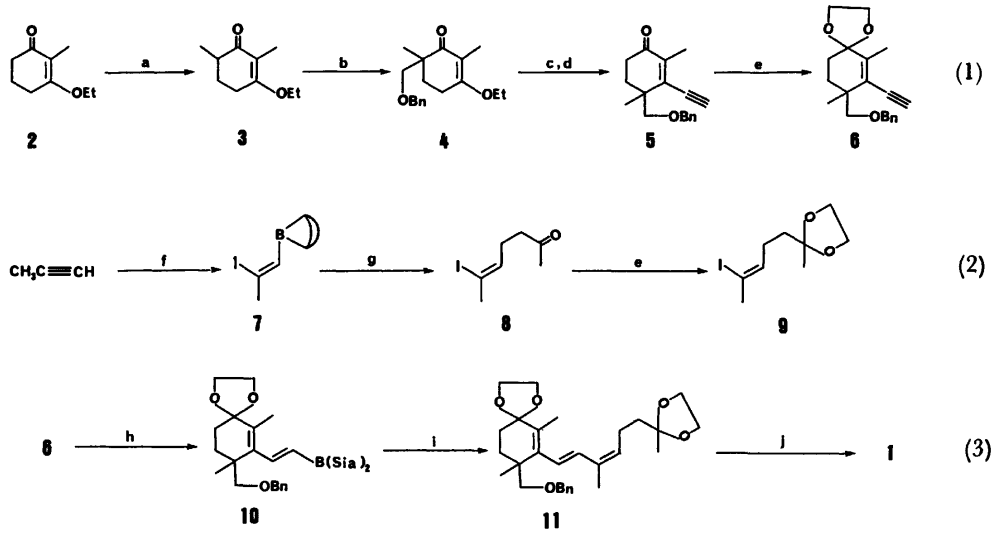

a) LDA, MeI b) LDA, $ClCH_2OCH_2Ph$ c) LiC≡CTMS d) KF e) EG, TsOH f) 9-iodo-9-BBN
g) MVK h) $HB(CHMe\text{-}CHMe_2)_2$ i) $Pd(PPh_3)_4$, NaOEt, **9** j) H^+

The coupling of these two fragments to **1** was carried out as outlined in Eq. 3. Namely, the enyne **6** in THF was subjected to hydroboration with bis(1,2-dimethylpropyl)borane[6] at room temperature by the usual procedure to give the dienylborane **10**. A mixture of **10** and the iodoalkene **9** in benzene containing $Pd(PPh_3)_4$[7] and sodium ethoxide was heated under reflux for 6 h in an atmosphere of nitrogen. The usual work-up and purification by TLC(silica gel-hexane) gave pure **11** in 52% yield, based on **6**. Finally, the deprotection of the ethylene acetal group with hydrogen chloride afforded the expected benzyl ether of trisporol B (**1**, R=CH_2Ph) as a pure form.

The present result clearly demonstrates that the novel two methodologies, the palladium-catalyzed cross-coupling reaction[1] and the haloboration-conjugate addition reaction,[5] both of which have been recently discovered by our group, provide a short step synthesis of trisporol B.

Experimental

The IR spectra were recorded on a Hitachi-Perkin Elmer Model 125 spectrometer. The ^1H NMR spectra of all compounds were measured with a Hitachi R-90H spectrometer (90 MHz) (solvent, $CDCl_3$; TMS as an internal reference). The measurement of mass spectra was carried out on a JEOL JMS-D 300 spectrometer (70 eV). Benzyl chloromethyl ether and trimethylsilylacetylene were commercial products and purified by distillation. THF was purified by distillation from benzophenone and sodium before use.

3-Ethoxy-2,6-dimethyl-2-cyclohexenone (3). To a solution of lithium diisopropylamide (LDA) (44 mmol) in THF (40 ml) was slowly added a solution of 3-ethoxy-2-methyl-2-cyclohexenone[8] (6.16 g, 40 mmol) in THF (20 ml) at −78 °C and the mixture was stirred for 1 h. To this solution was added HMPA (6 ml), and then methyl iodide (42 mmol) in THF (10 ml). The reaction mixture was stirred for 2 h at −78 °C, gradually warmed up to room temperature over 1 h, and then allowed to stand over night. The mixture was poured into ice water, extracted with ether, washed with brine, and dried over anhydrous $MgSO_4$. After evaporation of the solvent, the residue was chromatographed over silica gel with benzene/ethyl acetate (=10/1) to give **3** (6.1 g, 91%); Mp 49 °C; IR (nujol) 1630 cm^{-1}; ^1H NMR ($CDCl_3$) δ=1.14 (d, 3H, J=6.6 Hz), 1.34 (t, 3H, J=7.0 Hz), 1.70 (broad s, 3H), 1.8—2.4 (m, 3H), 2.4—2.7 (m, 2H), and 4.05 (q, 2H, J=7.0 Hz). Found: m/z 168.11495. Calcd for $C_{10}H_{16}O_2$: M, 168.11501.

6-Benzyloxymethyl-2,6-dimethyl-3-ethoxy-2-cyclohexenone (4). To a solution of LDA (36 mmol) in THF (30 ml) was slowly added a solution of the enone **3** (33 mmol) in THF (20 ml) at −78 °C and stirred for 1 h. Then, HMPA (5.5 ml) and benzyl chloromethyl ether (38 mmol) in THF (10 ml) were gradually added. The reaction mixture was stirred for 2 h at −78 °C, and then warmed up to room temperature. After the solution was allowed to stand overnight, a saturated brine solution was added. The mixture was extracted with benzene, washed with brine, and dried over $MgSO_4$. The chromatography over silica gel with benzene/ethyl acetate (=15/1) gave **4** (8.3 g, 88%); n_D^{20}=1.5410; IR (film), 1625, 1460, 1385, 1360, 1240, 1115, 740, and 700 cm^{-1}; ^1H NMR ($CDCl_3$) δ=1.08 (s, 3H), 1.33 (t, 3H, J=7.0 Hz), 1.69 (broad s, 3H), 1.7—2.2 (m, 2H), 2.4—2.6 (m, 2H), 3.32 (d, 1H, J=9.0 Hz), 3.66 (d, 1H, J=9.0 Hz), 4.03 (q, 2H, J=7.0 Hz), 4.49 (s, 2H), and 7.92 (s, 5H); Found: m/z 288.17359. Calcd for $C_{18}H_{24}O_3$: M, 288.17349.

4-Benzyloxymethyl-2,4-dimethyl-3-ethynyl-2-cyclohexenone (5) and Its Acetal (6). To a solution of trimethylsilylacetylene (20 mmol) in THF (20 ml) was added a solution of butyllithium in hexane (12.5 ml, 20 mmol) at −78 °C and the solution was stirred for 30 min. Anhydrous lithium bromide (6 mmol)[9] was added all at once, and then a solution of the enone **4** (14.3 mmol) in THF (10 ml). The reaction mixture was stirred for 1 h at −78 °C, and then warmed up to 0 °C over 1 h. After the solution was stirred for 1 h at 0 °C, aqueous 2 mol dm^{-3}-HCl (20 ml) was added slowly with vigorous stirring. After 20 min, the aqueous layer was separated and extracted with ether. The combined extracts were washed with a saturated brine solution, an aqueous 5% Na_2CO_3 solution and finally again with brine. After evaporation of the solvent, the residue was dissolved in 95% ethanol (100 ml) and treated with KF (9 g) for 3 h at room temperature. The removal of ethanol in vacuo (12 mmHg) gave a mixture of the product and an excess of KF. This mixture was extracted with benzene, washed with brine, dried over $MgSO_4$, and finally chromatographed over silica gel with benzene/ethyl acetate (=20/1) gave **5** (2.7 g, 70%), mp 57 °C; IR (nujol) 3260, 2150, 2090, 1670, 1590, 1100, 1025, 843, 730, and 695 cm^{-1}; ^1H NMR ($CDCl_3$) δ=1.22 (s, 3H), 1.99 (s, 3H), 1.6—2.6 (m, 4H) 3.36 (d, 1H, J=9.0 Hz), 3.64 (d, 1H, J=9.0 Hz), 4.53 (s, 2H), and 7.3 (s, 5H). Found: m/z 268.14526. Calcd for $C_{18}H_{20}O_2$: M, 268.14536.

A mixture of **5** (1.3 g, 4.8 mmol), ethylene glycol (6.3 mmol), trimethyl orthorformate (7 mmol), and a catalytic amount of p-toluenesulfonic acid in ether (20 ml) was stirred for 48 h at room temperature. After the usual work-up, the acetal was isolated by chromatography over silica gel with benzene/ethyl acetate (=20/1), 1.42 g (94%) of **6**; bp 160—165 °C/0.05 mmHg (the oven temperature of Kugelrohr) (1 mmHg=133.322 Pa); IR (neat) 3290, 2145, and 2095 cm^{-1}; ^1H NMR ($CDCl_3$) δ=1.14 (s, 3H), 1.9 (s, 3H), 1.5—2.1 (m, 4H), 3.13 (s, 1H), 3.34 (d, 1H, J=9.0 Hz), 3.48 (d, 1H, J=9.0 Hz), 3.99 (s, 4H), 4.52 (s, 2H), and 7.30 (s, 5H); Found: m/z 312.17185. Calcd for $C_{20}H_{24}O_3$: M, 312.17191.

(Z)-6-Iodo-5-hepten-2-one (8) and Its Acetal (9). The preparation of **8** from propyne was reported elsewhere,[5] which was protected as its ethylene acetal (**9**) by the usual procedure[10] by using ethylene glycol, methyl orthoformate, and p-TsOH in ether at room temperature. **9**: n_D^{18}=1.4980; IR (neat) 1670, 1150, 1055, 950, and 865 cm^{-1}; ^1H NMR ($CDCl_3$) δ=1.33 (s, 3H), 1.53—1.87 (m, 2H), 2.0—2.3 (m, 2H), 2.47 (s, 3H), 3.93 (s, 4H), and 5.43 (t, 1H, J=6.5 Hz).

The Benzyl Ether of (±)-Trisporol B (1, R=CH_2Ph). To a solution of **6** (1.8 mmol) in THF (2 ml) was added a solution of bis(1,2-dimethylpropyl)borane[6] in THF (4 ml of a 0.5 mol dm^{-3} solution, 2 mmol), and the mixture was stirred for 16 h at room temperature. After evaporation of the solvent in vacuo, the residue was dissolved in benzene (6 ml). To the solution of dienylborane **10** in benene thus obtained were added $Pd(PPh_3)_4$[7] (0.054 mmol), the alkenyl iodide acetal **9** (1.8 mmol) and a solution of sodium ethoxide in ethanol (1.8 ml of a 2 mol dm^{-3} solution), and then the mixture was refluxed for 6 h under N_2. After the flask was cooled to room temperature, NaOH (3 mol dm^{-3}, 2 ml) and 30%-H_2O_2 (0.5 ml) were added to decompose the unreacted borane. The product was then extracted with benzene, washed with a saturated brine solution, and dried ove $MgSO_4$. After evaporation of the solvent, the residue was chromatographed over silica gel with benzene/ethyl acetate (=10/1.5) to give **11** (0.435 g, 52%); n_D^{20}=1.4230; IR (film) 1663, 1075, 730, and 693 cm^{-1}; ^1H NMR ($CDCl_3$) δ=1.03 (s, 3H), 1.31 (s, 3H), 1.71 (s, 3H), 1.78 (broad s, 3H), 1.4—2.0 (m, 6H), 2.0—2.3 (m, 2H), 3.14 (d, 1H, J=9.0 Hz), 3.36 (d, 1H, J=9.0 Hz), 3.91 (s, 4H), 4.01 (s, 4H), 5.35 (t, 1H, J=7.0 Hz), 5.95 (d, 1H, J=16.3 Hz), 6.46 (d, 1H, J=16.3 Hz), and 7.29 (s, 5H); Found: m/z 468.28742.

Calcd for $C_{29}H_{40}O_5$: M, 468.28743.

A solution of **11** (0.101 g, 0.214 mmol) in THF (3 ml) was treated with aqueous 2 mol dm^{-3}-HCl (1 ml) for 6 h at room temperature. The product was extracted with ether, washed with brine, aqueous 5%-$NaHCO_3$, and finally with brine. TLC (silica gel) with benzene/ethyl acetate (=5/1) gave 75 mg (92%) of the benzyl ether of trisporol B (**1**, R=CH_2Ph): n_D^{20} =1.5650; λ_{max}^{EtOH}=301 nm; IR (neat) 1715, 1665, 1590, 1100, 965, 730, and 695 cm^{-1}; ^1H NMR ($CDCl_3$) δ=1.13 (s, 3H), 1.81 (broad s, 3H), 1.85 (s, 3H), 2.11 (s, 3H), 2.2—2.7 (m, 6H), 3.23 (d, 1H, J=9.0 Hz), 3.51 (d, 1H, J=9.0 Hz), 4.50 (s, 2H), 5.43 (broad t, 1H, J=7.2 Hz), 6.13 (d, 1H, J=16.0 Hz), and 6.60 (d, 1H, J=16.0 Hz); Found: m/z 380.23385. Calcd for $C_{25}H_{32}O_3$: M, 380.23397.

Although we could not compare the authentic sample of benzylether of trisporol B with the product 1 (R=CH_2Ph) obtained in this work, the spectral data of our benzyl ether are quite similar to those of trisporol B previously reported,[2b] except some points due to the benzyl ether group. For instance, the characteristic bands at 1715 and 1665 cm^{-1} in IR and λ_{max}^{EtOH}=301 nm in UV owing to the conjugated enone structure are almost super-imposable with those of trisporol B (1710 and 1665 cm^{-1}, and λ_{max}^{EtOH}=298 nm).[2b] The benzyl ether has the following ^1H NMR characteristics. The chemical shifts of vinylic protons in δ (7-H=6.60, 8-H=6.13, and 10-H=5.43) and the coupling constant (J_{7-8}=16 Hz) agree almost completely with those of trisporol B: Vinylic protons; 6.63, 6.20, and 5.40. J_{7-8}=16 Hz. Moreover, the chemical shifts of four methyl groups in the former compound, δ=1.13, 1.81, 1.85, and 2.11, are in fair agreement with those of trisporol B; 1.11, 1.81, 1.89, and 2.08.

From these spectral data, the structure of our product was concluded to be the benzyl ether of the expected compound.

References

1) N. Miyaura, K. Yamada, H. Suginome, and A. Suzuki, *J. Am. Chem. Soc.*, **107**, 972 (1985).

2) a) J. D. Bu'Lock, D. Drake, and D. J. Winstanley, *Phytochemistry*, **11**, 2011 (1972); b) M. P. Prisbylla, K. Takabe, and J. D. White, *J. Am. Chem. Soc.*, **101**, 762 (1979), and for the synthesis of related compounds, trisporic acid and its ester; c) B. M. Trost and P. L. Ornstein, *Tetrahedron Lett.*, **24**, 2833 (1983) and references cited therein.

3) G. Stork and R. L. Danheiser, *J. Org. Chem.*, **38**, 1775 (1973).

4) P. J. Stang and M. Ladika, *Synthesis*, **1981**, 29.

5) Y. Satoh, H. Serizawa, S. Hara, and A. Suzuki, *J. Am. Chem. Soc.*, **107**, 5225 (1985).

6) H. C. Brown, "Organic Synthesis via Boranes," John Wiley & Sons, New York (1975), p. 29.

7) D. R. Coulson, *Inorg. Synth.*, **13**, 121 (1972).

8) R. D. Clark, J. E. Ellis, and C. H. Heathcock, *Synth. Commun.*, **3**, 374 (1973); A. B. Mekler, S. Ramachandran, S. Swaminathan, and M. S. Newman, *Org. Synth.*, **41**, 56 (1961); W. F. Gannon and H. D. Houe, *ibid.*, **40**, 41 (1960).

9) In the absence of lithium bromide, the yield of **5** was considerably low: L. Brandsma and H. D. Verkruijsse, "Synthesis of Acetylenes, Allenes and Cumulenes," Elsevier Scientific Pub. Co., New York (1981).

10) T. W. Greene, "Protective Groups in Organic Synthesis," John Wiley & Sons, New York (1981).

Complex Formation between Heptylviologen and Cyclodextrin

Masato KODAKA* and Toshio FUKAYA
National Chemical Laboratory for Industry, Tsukuba 305
(Received January 24, 1986)

Synopsis. Complex formation between heptylviologen (**1**) and cyclodextrins (α and β) was confirmed indirectly. The absorption and circular dichroism (CD) spectra of *p*-nitrophenolate aqueous solution containing α- or β-cyclodextrin were changed, when **1** was added to the solution. Contrary to **1**, methylviologen (**3**) did not give the spectral changes.

Methylviologen (**3**) has been widely used as an electron mediator (a relay compound) for hydrogen formation[1-3] and fixation of carbon dioxide.[4,5] Recently attention has been directed to viologens possessing hydrophobic groups. For example, their inclusion complexes with cyclodextrin (CD_x) increase the stability of the pyridinium moiety of the viologens to hydrogenation,[6] and the viologens are promising for electrochromic display applications.[7] Okuno et al. have estimated the complex formation between hydrophobic viologen and CD_x by the measurement of fluorescence quenching of excited $[Ru(bpy)_3]^{2+}$ by hydrophobic viologens.[6] In the case of viologens with aromatic groups, inclusion compounds can be detected by NMR and Raman spectroscopy, too.[6,7] For heptylviologen (**1**), however, the complex formation can not be detected by these spectroscopic analyses.[7]

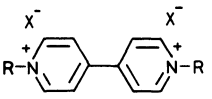

1 R = *n*-C_7H_{15}, X = Br
2 R = CH_2Ph, X = Cl
3 R = CH_3, X = Cl

As described above, the detection of the inclusion compounds for viologens having hydrophobic groups other than aromatic ones is not so easy. In the present study, we have indirectly confirmed the complex formation between **1** and CD_x and estimated the dissociation constant.

Experimental

Heptylviologen (**1**) (Aldrich Chemical Co.), benzylviologen (**2**) (Sigma Chemical Co.), methylviologen (**3**) (Nakarai Chemicals), α-CD_x and β-CD_x (Nakarai Chemicals), tri-*O*-methyl-β-CD_x(Funakoshi Chemicals), *p*-nitrophenol (p-NP) (Wako Pure Chemical Industries), and tris(2,2′-bipyridyl)-ruthenium(II) chloride (Strem Chemicals) were used as supplied.

Absorption, circular dichroism (CD) and fluorescence spectra were taken on a JASCO UVIDEC-1 spectrophotometer, a JASCO J-20 spectropolarimeter and a JASCO FP-4 fluorescence spectrophotometer, respectively, using 10 mm cells at room temperature. All measurements were carried out at pH 9.5 (0.1 mol dm^{-3} $KHCO_3$–0.1 mol dm^{-3} Na_2CO_3 buffer solution).

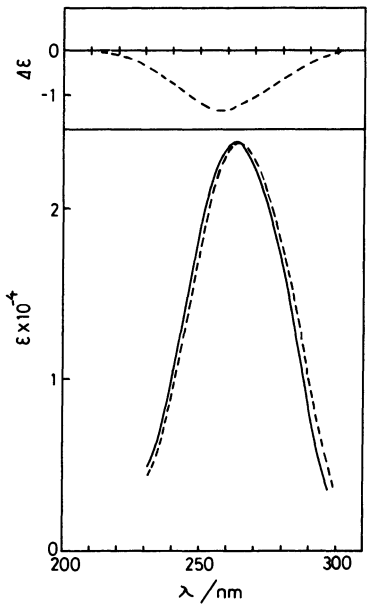

Fig. 1. Absorption and CD spectra of **1** (5×10^{-5} mol dm^{-3}) at pH 9.5.
Absorption: α-CD_x free (——); $[\alpha\text{-}CD_x]=4\times10^{-3}$ mol dm^{-3} (---).
CD: $[\alpha\text{-}CD_x]=4\times10^{-3}$ mol dm^{-3} (---).

Results and Discussion

As shown in Fig. 1, the absorption band of **1** was slightly red-shifted upon addition of α-CD_x. Corresponding to the change in the absorption spectrum, small negative Cotton effect was also observed in the CD spectrum, while **3** did not give any spectral changes. These results give the possibility that the hydrophobic chains of **1** should be included in the cavity of α-CD_x. Similar tendency was seen when β-CD_x was added into the solutions of **1** and **3** instead of α-CD_x. On the other hand, tri-*O*-methyl-β-CD_x caused little spectral change for **1**, suggesting that tri-*O*-methyl-β-CD_x has much smaller ability to form inclusion compounds.

To obtain more definitive evidence, we investigated the effect of **1** upon the absorption and CD spectra of p-NP in aqueous solution containing α-CD_x (Fig. 2). It should be noted that the addition of **1** caused appreciable changes in the spectra, which indicates that **1** undergoes complex formation with α-CD_x in competition with p-NP. On the other hand, **3** did not bring about the changes in the absorption and CD spectra. When β-CD_x was added instead of α-CD_x, similar spectral changes were observed upon addition of **1**. These findings suggest that the hydrophobic chains of **1** are included in α- or β-CD_x. The influence of tri-*O*-methyl-β-CD_x was not studied, for the spectral

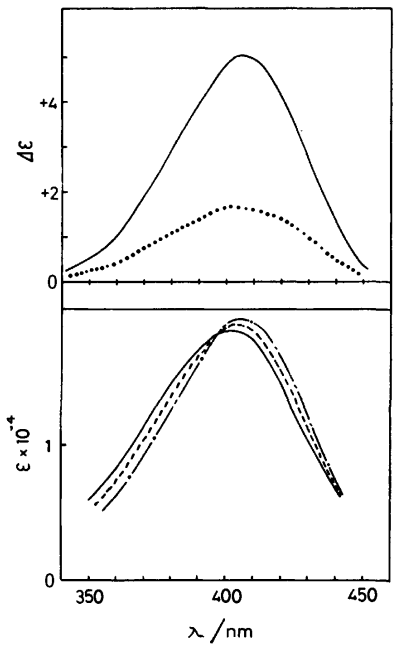

Fig. 2. Absorption and CD spectra of *p*-nitrophenol (5×10^{-5} mol dm^{-3}) at pH 9.5.
Absorption: α-CD$_x$ free, 1 free (——); [α-CD$_x$]= 5×10^{-4} mol dm^{-3}, 1 free (— — —); [α-CD$_x$]=5×10^{-4} mol dm^{-3}, [1]=1×10^{-3} mol dm^{-3} (---).
CD: [α-CD$_x$]=2.5×10^{-3} mol dm^{-3}, 1 free (——); [α-CD$_x$]=2.5×10^{-3} mol dm^{-3}, [1]=5×10^{-3} mol dm^{-3} (····).

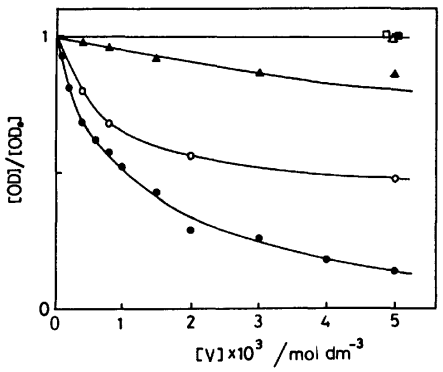

Fig. 3. Relation between relative absorbance ([OD]/[OD$_0$]) at 410 nm and concentration of various viologens ([V]) in *p*-nitrophenol/CD$_x$ solution (pH 9.5); [OD] and [OD$_0$] designate absorbance in the presence and absence of viologens, respectively.
[p-NP]=5×10^{-5} mol dm^{-3}, [CD$_x$]=5×10^{-4} mol dm^{-3}; 1/α-CD$_x$ (●), 1/β-CD$_x$ (○), 2/α-CD$_x$ (▲), 2/β-CD$_x$ (△), 3/α-CD$_x$ (■), 3/β-CD$_x$ (□).

changes of p-NP solution were small when it was added. Reasonable structure of 1/CD$_x$ (α and β) complex is shown below.

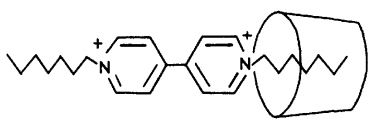

Figure 3 shows the changes in the relative absorbance of p-NP/CD$_x$ solution at 410 nm as a function of the concentration of the viologens. The results for benzylviologen (**2**) are also shown for comparison. It can be said from Fig. 3 that 1/CD$_x$ complex is more stable than 2/CD$_x$ one. From the relation in Fig. 3, we tried to estimate the dissociation constant of 1/α-CD$_x$ complex.

When the concentration of **1** is relatively higher than that of α-CD$_x$, the following two equilibriums can be expected to hold.

$$\text{p-NP} + \alpha\text{-CD}_x \rightleftarrows \text{p-NP}\cdot\alpha\text{-CD}_x \quad \text{[I]}$$

$$\mathbf{1} + \alpha\text{-CD}_x \rightleftarrows \mathbf{1}\cdot\alpha\text{-CD}_x \quad \text{[II]}$$

As the concentration of α-CD$_x$ (5×10^{-4} mol dm^{-3}) is much higher than that of p-NP (5×10^{-5} mol dm^{-3}), the dissociation constant of [I] (K_1) and that of [II] (K_2) are approximately described as follows.

$$K_1 = (p-x_1)(c-x_2)/x_1 \quad (1)$$

$$K_2 = (V-x_2)(c-x_2)/x_2 \quad (2)$$

p : total concentration of p-NP(5×10^{-5} mol dm^{-3}).
c : total concentration of α-CD$_x$(5×10^{-4} mol dm^{-3}).
V: total concentration of **1**.
x_1: concentration of p-NP·α-CD$_x$ complex.
x_2: concentration of **1**·α-CD$_x$ complex.

Eqs. 1 and 2 yield

$$K_2 = \frac{\{(p-x_1)(V-c) + K_1x_1\}x_1K_1}{\{c(p-x_1) - K_1x_1\}(p-x_1)}. \quad (3)$$

The x_1 value can be calculated from

$$x_1 = \Delta A/\Delta\varepsilon \quad (4)$$

where ΔA is the increase in the absorbance at 410 nm upon addition of CD$_x$ and **1** and $\Delta\varepsilon$ is the difference in the molar absorption coefficient between p-NP·α-CD$_x$ complex and p-NP. K_1 and $\Delta\varepsilon$ were obtained in a similar manner to that by Cramer et al.,[8] as to be 3.3×10^{-4} mol dm^{-3} and 3.4×10^{3} mol^{-1} dm^3 cm^{-1}, respectively. Therefore we could estimate K_2 from Eqs. 3 and 4 as a function of V (Fig. 4). K_2 was found to be approximately constant (ca. 2×10^{-4} mol dm^{-3}) under the conditions of $V>c$.

The complex formation between **1** and α- or β-CD$_x$ was also demonstrated by the measurement of fluorescence quenching of excited [Ru(bpy)$_3$]$^{2+}$ by **1** as reported by Okuno et al.[6] That is to say, Stern-Volmer constant ($k_q\tau$) in the presence of **1** (Fig. 5(a)) decreased much more than those in the presence of **2** or **3** (Fig. 5(b), (c)), when α- or β-CD$_x$ was added. However, tri-*O*-methyl-β-CD$_x$ did not essentially influence $k_q\tau$ values, probably due to the deficiency of ability to form inclusion complex.

As for the reduced form of **1** (cation radical), Yasuda et al. proposed an inclusion compound with β-CD$_x$, where it was more deeply situated in the cavity of β-CD$_x$.[7] Therefore we wish to mention some qualita-

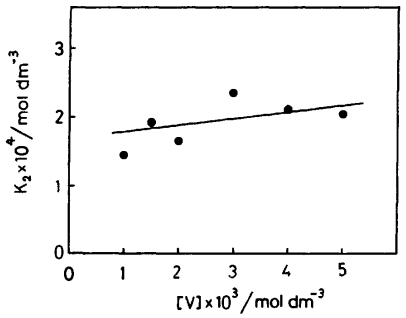

Fig. 4. Relation between dissociation constant (K_2) of 1/α-CD_x complex and concentration of 1 ([V]).

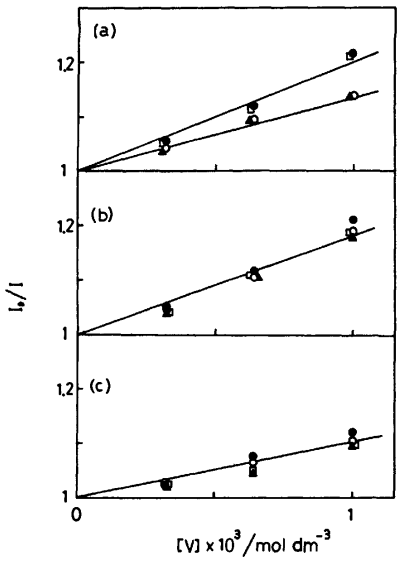

Fig. 5. Stern-Volmer plots for quenching of luminescence of $[Ru(bpy)_3]^{2+}$ (1×10^{-4} mol dm^{-3}) by viologen in the presence and absence of CD_x; (a) 1, (b) 2, (c) 3.
CD_x free (●), [α-CD_x]=2×10^{-3} mol dm^{-3} (○), [β-CD_x]=2×10^{-3} mol dm^{-3} (▲), [tri-*O*-methyl-β-CD_x]=2×10^{-3} mol dm^{-3} (□).

tive results about the reduced form of 1. When 1 was reduced with sodium dithionite ($Na_2S_2O_4$), the reduced form of 1 (purple) was precipitated in aqueous solution. In the presence of α- or β-CD_x, however, the aqueous solution of 1 turned blue by $Na_2S_2O_4$ without precipitation. Moreover, when p-NP was added to the above solution, the reduced form of 1 was again precipitated. On the other hand, when *o*-nitrophenol which is scarcely included in CD_x was added to the solution instead of p-NP, the precipitate was not formed. The findings mentioned above suggest that the reduced form of 1 is also included in α- or β-CD_x.

In the present study, the complex formation between 1 and α- or β-CD_x was definitely confirmed and the dissociation constant of the complex (1·α-CD_x) was estimated by making use of the competitive binding of 1 and p-NP with CD_x. The indirect method as shown in the present study will be useful, when the spectroscopic analyses such as absorption, NMR and Raman spectroscopy do not give fruitful information about the complex formation.

References

1) Y. Okuno, Y. Chiba, and O. Yonemitsu, *Chem. Lett.*, **1983**, 893.
2) K. Kalyanasundaram, J. Kiwi, and M. Grätzel, *Helv. Chim. Acta*, **61**, 2720 (1978).
3) M. Kirsch, J. M. Lehn, and J. P. Sauvage, *Helv. Chim. Acta*, **62**, 1345 (1979).
4) N. Kitamura and S. Tazuke, *Chem. Lett.*, **1983**, 1109.
5) B. A. Parkinson and P. F. Weaver, *Nature*, **309**, 148 (1984).
6) Y. Okuno, Y. Chiba, and O. Yonemitsu, *J. Chem. Soc., Chem. Commun.*, **1984**, 1638.
7) A. Yasuda, H. Mori, H. Kondo, and M. Itabashi, 51th National Meeting of the Chemical Society of Japan, Kanazawa, October 1985, Abstr., No.3A02.
8) F. Cramer, W. Saenger, and H. Ch. Spatz, *J. Am. Chem. Soc.*, **89**, 14 (1967).

Coupling Reaction of Grignard Reagents with α,ω-Dibromoalkanes in the Presence of Copper(I) Bromide-HMPA: Preparation of α,ω-Bis(vinylaryl)alkanes

Jun NISHIMURA,* Noriyuki YAMADA, Yuzuru HORIUCHI, Eiji UEDA, Akihiro OHBAYASHI, and Akira OKU

Department of Chemistry, Kyoto Institute of Technology, Matsugasaki, Sakyo-ku, Kyoto 606

(Received January 6, 1986)

Synopsis. The coupling reaction of Grignard reagents with α,ω-dibromoalkanes took place smoothly in THF/HMPA (12:1) in the presence of a catalytic amount of copper(I) bromide and gave the products in 60—100% yields. Several α,ω-bis(vinylaryl)alkanes were prepared in reasonable yields by the application of this reaction.

The coupling reaction of Grignard reagents with alkyl halides has been known to be induced by many transition metal halides[1-5] and sometimes to proceed without catalysts.[6] Recently we have found a facile coupling reaction of Grignard reagents with α,ω-dibromoalkanes in THF in the presence of a catalytic amount of copper(I) bromide and a small amount of HMPA. Our method gives comparable or even better yields in some cases than those using Tamura-Kochi's catalyst Li_2CuCl_4,[5,7] and we have successfully applied it to the preparation of several α,ω-bis(vinylaryl)alkanes of recent interest.[8,9]

$$ArMgBr \xrightarrow[CuBr/HMPA,\ THF]{Br(CH_2)_nBr} Ar(CH_2)_nBr + Ar(CH_2)_nAr \quad (1)$$

Results are summarized in Table 1. The reverse addition of the Grignard reagent and the use of copper(I)-HMPA as catalyst are essential for this coupling. Without the catalyst, the reaction gave products in much poorer yields. In the present method, only a small amount of HMPA is enough for dissolving copper(I) bromide and the recommended volume ratio of THF/HMPA is 12. Although the copper-catalyzed Grignard coupling is wellknown,[1,4,5,7] the present procedure seems to be more useful than the previous ones for the coupling of arylmagnesium halide because of its simplicity, comparatively high yields of products, and easy availability of necessary chemicals.

The reaction was successfully applied to the synthesis of several styrene derivatives which are less easily accessible by other methods based on Friedel-Crafts acylation of diarylalkanes.[8] The reaction sequence for the synthesis of α,ω-bis(*m*-vinylphenyl)alkanes **5** and **6** is shown in Eq. 2, and results of the preparations of diolefins **5** to **9** from the corresponding Grignard reagents **1** to **4** are summarized in Table 2.

Although compound **9** may be prepared through

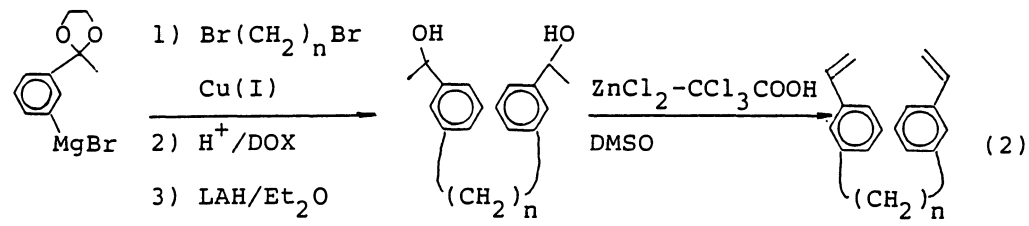

(2)

1

5 n=3

6 n=6

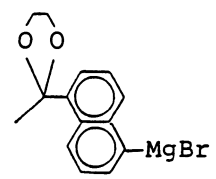

2

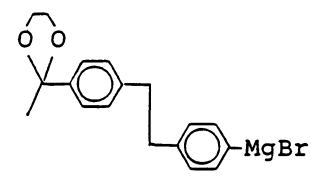

3

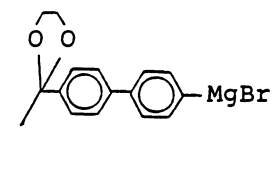

4

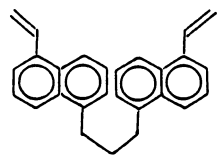

7

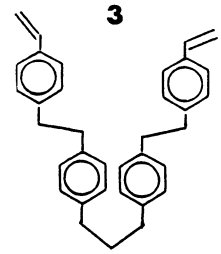

8

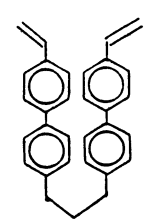

9

Table 1. Coupling Reaction of Grignard Reagents with α,ω-Dibromoalkanes[a]

RMgBr	$Br(CH_2)_nBr$ n	Yield/%			
		R-R[b]	$R(CH_2)_nBr$	$R(CH_2)_nR$	Total[c]
PhMgBr	3	3	81	16	100
1	3	tr (2)[d]	81 (43)[d]	11 (8)[d]	92 (53)[d]
1	4	tr	79	21	100
1	5	tr	76	18	94
1	6	tr	77	23	100
2-NaphMgBr	3	6	53	29	88
i-PrMgBr[e]	6	—[f]	44	16	60

a) Reaction conditions: RX, 10 mmol; dibromoalkane, 12 mmol; CuBr, 0.5 mmol; THF, 12 ml; HMPA, 1 ml; reflux for 4 h. b) Kharasch reaction products. c) Determined by GLC, using internal standards (based on RX). d) A solution of CuBr and 1,3-dibromopropane in HMPA was added to a THF solution of the Grignard reagent, free from any Mg turnings. e) At r.t. f) Not determined.

Table 2. Preparation of α,ω-Bis(vinylaryl)alkanes

RMgBr	$Br(CH_2)_n$-Br n	Mole ratio[a]	Yield/%		Product	Mp θ_m/°C	MS(M+·) Found (Calcd)	^{1}H NMR chem. shift δ (intensity, multiplicity, J in Hz)
			Glycol[b]	Diene[c]				
1	3	2:1	58	78	**5**	—[d]	248.1555 (248.1566 for $C_{19}H_{20}$)	1.91 (2H, m), 2.60 (4H, bt), 5.12 (2H, dd, 10.0 and 1.5), 5.62 (2H, dd, 18.1 and 1.5), 6.62 (2H, dd, 10.0 and 18.1), 7.10 (8H, m).
1	6	2:1	75	50	**6**	—[d]	290.2033 (290.2036 for $C_{22}H_{26}$)	1.50 (8H, m), 2.53 (4H, bt, 7.0), 5.10 (1H, dd, 10.8 and 2.0), 5.60 (1H, dd, 17.6 and 2.0), 6.62 (1H, dd, 10.8 and 17.6), 7.12 (8H, m).
2	3	2:0.7	73	79	**7**	79—80	348.1869 (348.1879 for $C_{27}H_{24}$)	2.22 (2H, quin, 7.1), 3.20 (4H, t, 7.1), 5.46 (2H, dd, 10.7 and 1.2), 5.76 (2H, dd, 17.9 and 1.2), 7.30—7.64 (10H, m), 7.91 (2H, d, 7.9), 7.99 (2H, d, 7.9).
3	3	2:0.7	81	81	**8**	152—154	456.2811 (456.2819 for $C_{35}H_{36}$)	1.94 (2H, m), 2.63 (4H, t, 7.1), 2.90 (8H, s), 5.20 (2H, dd, 11.2 and 1.2), 5.72 (2H, dd, 17.7 and 1.3), 6.72 (2H, dd, 17.7 and 11.2), 7.13 (8H, s), 7.25 (8H, A_2B_2).
4	3	2:0.7	63	75	**9**	162—164	400.2188 (400.2192 for $C_{31}H_{28}$)	2.02 (2H, quin, 7.1), 2.72 (4H, t, 7.1), 5.26 (2H, dd, 10.3 and 0.8), 5.78 (2H, dd, 17.1 and 0.8), 6.76 (2H, dd, 17.1 and 10.3), 7.22—7.64 (16H, m).

a) Grignard reagent vs. dibromide. b) Isolated yield of glycol (based on dibromoalkane). c) Isolated yield (based on glycol). d) Thick oil.

the Friedel–Crafts acetylation of 1,3-bis(4-biphenylyl)-propane derived from a poorly soluble aldol condensation product, 1,3-bis(4-biphenylyl)propenone, the present sequence allows its synthesis more conveniently, being carried out in a homogeneous system.

Experimental

^{1}H NMR spectra were recorded on Varian T-60A and XL-200 NMR spectrometers in $CDCl_3$ with tetramethylsilane as an internal standard. Mass spectra were recorded on a Hitachi M-80A mass spectrometer. GLC analyses were done by a Shimadzu GC-4CIT gas chromatograph (OV-17, 3%, 2 m, 250—300°C). Melting points were not corrected. Tetrahydrofuran was dried with benzophenone ketyl and distilled just before use. HMPA was heated over calcium hydride for prolonged time under a nitrogen atmosphere, then distilled in vacuo and stored over molecular sieves (3A) under the same atmosphere. Commercial copper(I) bromide of highest grade was used without purification.

Coupling Reaction of Arylmagnesium Bromide with α,ω-Dibromides (General Procedure). Grignard reagent **1** was prepared in dry THF (600 ml) from *m*-bromoacetophenone ethylene acetal (130 g, 0.552 mol) and Mg turnings (16.1 g, 0.662 mol) under a nitrogen atmosphere.[10] After the completion of reaction excess Mg turnings were removed[11] and the solution was added dropwise over 1 h to a vigorously stirred mixture of dry HMPA (50 ml), 1,3-dibromopropane (55.7 g, 0.552 mol),[12] and copper(I) bromide (1.98 g, 5 mol% to the Grignard reagent) under reflux. The dark green mixture was refluxed for further 4 h with stirring, then poured into ice–HCl mixture (500 ml) to decompose organometallic compounds. The aqueous phase was extracted with benzene three times. The combined extracts were washed successively with water three times, with aq NaOH, and again with water. The mixture was dried over Na_2SO_4 and then condensed by evaporation. The residue was distilled in vacuo; *m*-(3-bromopropyl)acetophenone ethylene acetal was obtained as a thick oil in a 33.8% yield (45.4 g, 103°C/0.05 mmHg) and 1,3-bis(*m*-acetylphenyl)propane bis(ethylene acetal) as a solid residue (mp, 95—96°C) in a 60.4% yield (59.0 g).

Preparation of 1,3-Bis(*m*-vinylphenyl)propane 5 (Typical Procedure). The above bis-adduct (59.0 g) was dissolved in dioxane (500 ml) without further purification. To this solution 10% aq HCl (500 ml) was added and the mixture was stirred overnight at room temperature. The reaction mixture was extracted with benzene three times, then the combined extracts were washed with aq $NaHCO_3$ followed by water three times, dried over Na_2SO_4, and condensed by evaporation to give 1,3-bis(*m*-acetylphenyl)propane. The diketone was reduced by $LiAlH_4$ in ether and the glycol obtained was purified by column chromatography (SiO_2, cyclohexane/AcOEt=4:1—1:1). The overall yield was 43.1 g (95.5%). The glycol (4.00 g) was dehydrated by the reported method[13] to afford 1,3-bis(*m*-vinylphenyl)propane **5**, which was purified by column chromatography (SiO_2, petroleum ether/cyclohexane).[14] Yield was 2.31 g (78.0%).

Support by a Grant-in-Aid for Special Project Research (No 60035037) from the Ministry of Education, Science and Culture is gratefully acknowledged.

References

1) For reviews, see a) H. Felkin and G. Swierczewski, *Tetrahedron*, **31**, 2735 (1975); b) E. Erdik, *ibid.*, **40**, 641 (1984); c) J. Lindley, *ibid.*, **40**, 1433 (1984).

2) K. Tamao, K. Sumitani, and M. Kumada, *J. Am. Chem. Soc.*, **94**, 4374 (1972).

3) R. J. P. Corris and M. J. P. Masse, *J. Chem. Soc., Chem. Commun.*, **1972**, 144.

4) K. Onuma and H. Hashimoto, *Bull. Chem. Soc. Jpn.*, **45**, 2582 (1972).

5) M. Tamura and J. K. Kochi, *Synthesis*, **1971** 303.

6) B. W. Palmer, *J. Label. Compds.*, **6**, 303 (1970).

7) L. Friedman and A. Shani, *J. Am. Chem. Soc.*, **96**, 7101 (1974).

8) R. H. Wiley and G. L. Maybery, *J. Polym. Sci., A.* **1**, 217 (1963).

9) J. Nishimura, Y. Yamada, T. Okuda, Y. Mukai, H. Hashiba, and A. Oku, *J. Org. Chem.*, **50**, 841 (1985).

10) Cl. Fengeas, *Bull. Soc. Chim. France*, **1963**, 1441.

11) Since the remaining Mg turnings readily react with 1,3-dibromopropane to afford cyclopropane, we used head-to-head connected hypodermic needles (ϕ 1.0 mm) to transfer the Grignard reagent by appling a nitrogen pressure.

12) Dibromomethane and 1,2-dibromoethane did not undergo the coupling reaction efficiently (see also Ref. 1a).

13) J. Nishimura, Y. Ishida, K. Hashimoto, Y. Shimizu, A. Oku, and S. Yamashita, *Polym J.*, **13**, 635 (1981).

14) For the purification of compounds **7**, **8**, and **9**, a cyclohexane–benzene mixture was used as an eluent.

Reaction of Nitromethane with Aryl Isocyanates in the Presence of Triethylamine. A Formation of 1,3-Diaryl-5-(hydroxyimino)-imidazolidine-2,4-diones

Tomio SHIMIZU,* Yoshiyuki HAYASHI, and Kazuhiro TERAMURA
Department of Color Chemistry and Technology, Faculty of Industrial Arts, Kyoto Institute of Technology, Matsugasaki, Sakyo-ku, Kyoto 606
(Received December 18, 1985)

Synopsis. 1,3-Diaryl-5-(hydroxyimino)imidazolidine-2,4-diones were obtained from the reactions of nitromethane with several aryl isocyanates in the presence of a trace amount of triethylamine and their structures were established from spectroscopic evidence and their chemical behavior.

Many preparative methods of nitrile oxides by dehydration of primary nitro compounds have been known.[1-5] One of the most useful methods consists of the use of phenyl isocyanate as the dehydrating agent in the presence of a catalytic amount of triethylamine.[2a] While the reaction has been applied successfully to various types of primary nitro compounds, the reaction takes a slightly different course with nitromethane since nitromethane reacts with phenyl isocyanate to give α-nitroacetanilide.[2c] In fact, 2-isoxazoline-3-carboxanilides are formed via a cyanoformanilide *N*-oxide from the reaction of nitromethane with phenyl isocyanate in the presence of olefins and trace of triethylamine.[2c] We investigated the reaction

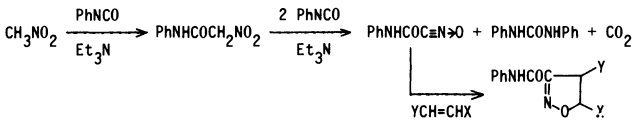

in expectation of obtaining a furazandicarboxanilide 2-oxide, a dimer of the cyanoformanilide *N*-oxide, in the absence of dipolarophiles. Though we could isolate none of the desired furazan oxides from the reaction mixture, we could isolate an unexpected and interesting compound. We report here the reaction in detail.

Results and Discussion

Treatment of an ethereal solution of nitromethane with two equivalents of phenyl isocyanate in the presence of a few drops of triethylamine gave colorless crystals (**1a**) in 27% yield besides a large amount of *N,N'*-diphenylurea and a small amount of phenyl isocyanate dimer. The structural assignment of **1a** as 5-(hydroxyimino)-1,3-diphenylimidazolidine-2,4-dione was based on the following results. The molecular ion

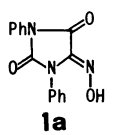

1a

peak (281.080) in the high resolution mass spectrum and the elemental analysis suggest its molecular formula as $C_{15}H_{11}N_3O_3$, formally a combination of 2 moles of phenyl isocyanate and one mole of formonitrile oxide (HCNO). Two singlets (δ 7.50 and 7.55) based on the protons of two phenyl groups and an acidic proton (δ 11.9) observed in the NMR spectrum and the formation of *N,N'*-diphenylurea by hydrolysis with ethanolic NaOH also suggested the structure of **1a**. 1,3-Diphenylimidazolidine-2,4-dione (**2**) and 1,3-diphenylimidazolidine-2,4,5-trione (**3**) were prepared by methods given in literatures for comparison. A sin-

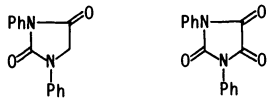

2 **3**

glet peak at δ 7.50 of phenyl protons of **3** in the NMR spectrum agreed well with that of **1a**. The product (**1a**) and the model compound (**3**) displayed carbonyl absorption peak in the IR spectra at a similar position (1730—1740 cm^{-1}). The structures of oxadiazole (**4** and **5**) are identical with those of the compounds expected from the 1,3-dipolar cycloaddition reaction of cyanoformanilide *N*-oxide with phenyl isocyanate.

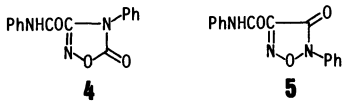

4 **5**

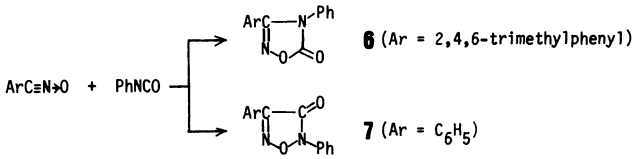

The formation of analogous oxadiazoles (**6** and **7**) has been known in the reaction of aromatic nitrile oxides with phenyl isocyanate.[6] The possibility of the structures (**4** and **5**) for the product could be ruled out by the evidence that **6** and **7** showed its carbonyl absorption at 1770[6a] and 1720 cm^{-1},[6b] respectively. The structure (**1a**) for the product was also supported by the formation of *O*-acyl oximes (**8**) by the acylation with several acyl halides. The compounds (**8**) showed an absorption of ester group at 1770 cm^{-1} in their IR spectra which agreed well with the *O*-acyl oxime structure and not with *N*-acylated compounds (ureas) of **4** and **5**. The chemical shifts of the alkyl protons in the acyl group of **8** appeared at a field higher than that of normal ones in the NMR spectra, and the effect may be ascribed to *Z*-configuration of *O*-acyl oximes.

Analogous oximes (**1b** and **1c**) and the O-acyl oxi-

Table Elemental Analyses of Compounds 1 and 8

Compd	Formula	Found (Calcd) (%)		
		H	C	N
1a	$C_{15}H_{11}N_3O_3$	4.18 (3.94)	64.32 (64.05)	14.72 (14.94)
1b	$C_{17}H_{15}N_3O_3$	4.97 (4.89)	66.30 (66.01)	13.42 (13.59)
1c	$C_{15}H_9N_3O_3Cl_2$	2.36 (2.59)	51.19 (51.45)	11.88 (12.00)
8a	$C_{17}H_{13}N_3O_4$	4.01 (4.05)	63.18 (63.15)	12.77 (13.00)
8b	$C_{18}H_{15}N_3O_4$	4.41 (4.48)	63.93 (64.09)	12.17 (12.46)
8c	$C_{19}H_{17}N_3O_4$	4.76 (4.88)	64.95 (64.95)	12.06 (11.96)
8d	$C_{21}H_{21}N_3O_4$	5.52 (5.58)	66.32 (66.48)	11.25 (11.08)
8e	$C_{22}H_{15}N_3O_4$	3.92 (3.92)	68.85 (68.56)	10.74 (10.91)
8f	$C_{19}H_{17}N_3O_4$	4.83 (4.88)	64.77 (64.95)	11.83 (11.96)
8g	$C_{17}H_{11}N_3O_4Cl_2$	2.70 (2.81)	52.11 (52.04)	10.69 (10.71)

Table 1. Yields[a] and Melting Points of 1 and 8

Compd	Ar	R	Yield %	Mp θ_m/°C
1a	C_6H_5	—	27	182—184
1b	$C_6H_4CH_3$-*m*	—	5	178—182
1c	C_6H_4Cl-*p*	—	32	215—219
8a	C_6H_5	CH_3	43	199—201
8b	C_6H_5	C_2H_5	25	218—221
8c	C_6H_5	C_3H_7-*n*	16	162—163
8d	C_6H_5	C_5H_{11}-*n*	20	154—155
8e	C_6H_5	C_6H_5	55	255—256
8f	$C_6H_4CH_3$-*p*	CH_3	4	208—209
8g	C_6H_4Cl-*p*	CH3	42	240—241

a) Yields of compounds (**1a**—**c**) were calculated on the basis of the aryl isocyanates. In the case of **8f**, the corresponding **1** (Ar=Tol-*p*) could not be isolated in crystalline state and the yield of **8f** is shown in over all yield from the isocyanate.

mes (**8f** and **8g**) were prepared by the reactions of nitromethane with some of aryl isocyanates and following acylation of the products. The results are shown in Table 1.

The mechanism of the formation of the oximes (**1**) is shown in Scheme 1; successive addition of aryl isocyanates to nitromethane gives *N*-(nitroacetyl)-*N,N'*-diarylureas (**9**), which undergo dehydration by the action of ArNCO/Et_3N to give nitrile oxides (**10**) and then, the nitrile oxides undergo intramolecular cyclization giving **1**. A similar addition of amines to nitrile oxides is well-known.[7]

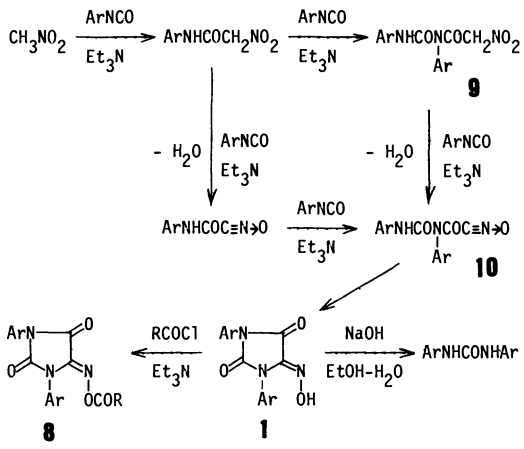

Scheme 1.

Experimental

Measurements. All melting points are uncorrected. The ^1H NMR spectra were measured on a Varian T-60A instrument with Me_4Si as an internal standard; chemical shifts are given in δ units and coupling constants (J) are in herz units: s=singlet; t=triplet; q=quartet; m=multiplet; br=broad singlet. The IR spectra were determined on a Hitachi 215 infrared spectrophotometer. The high-resolution mass spectra were measured on a Hitachi M-80 mass spectrometer. A part of these spectral data for all new compounds (**1** and **8**), 1,3-diphenylimidazolidine-2,4-dione (**2**), 1,3-diphenylimidazolidine-2,4,5-trione (**3**), 4-phenyl-3-(2,4,6-trimethylphenyl)-1,2,4-oxadiazol-5(4*H*)-one (**6**), and 2,4-diphenyl-1,2,5-oxadiazol-3(2*H*)-one (**7**) are shown in Table 2. All new products gave satisfactory elemental analyses (±0.3% for C, H, and N).

Materials. Nitromethane and isocyanates were commercially available and were without further purification. 1,3-Diphenylimidazolidine-2,4-dione (**2**)[8] and 1,3-diphenylimidazolidine-2,4,5-trione (**3**)[9] were prepared according to the methods described in the literatures.

Reactions of Nitromethane with Aryl Isocyanates. Typical Procedure. A few drops of triethylamine were added to a stirred dry ethereal solution (100 ml) of nitromethane (0.1 mol, 6.1 g) and phenyl isocyanate (0.2 mol, 24 g) at room temperature and the mixture was refluxed until an evolution of carbon dioxide ceased (ca. 6 h). Upon cooling to room temperature, a white solid crystallized out of the solution was filtered off. This colorless crystalline solid is a mixture of *N,N'*-diphenylurea, 5-(hydroxyimino)-1,3-diphenylimidazolidine-2,4-dione (**1a**), and phenyl isocyanate dimer. Upon exposing to atmosphere, the colorless products yellowed gradually at the surface owing to the presence of small amount of phenyl isocyanate dimer. The phenyl isocyanate dimer and a large part of **1a** could be extracted together with a small amount of *N,N'*-diphenylurea from the crystalline mixture by a Soxlet extractor using ethyl acetate. After evaporation of the solvent, the residual crystals were mixed with 100 ml of ethanol and the mixture was refluxed for 6 h for the purpose of conversion of phenyl isocyanate dimer into ethyl *N,N'*-diphenylallophanate[10] which shows better solubility in benzene than phenyl isocyanate dimer. Then, the solvent was evaporated and the crystalline residue was recrystallized from benzene to give analytically pure **1a**. The yields and melting points were shown in Table 1 along with those of analogous compounds prepared from similar reactions of nitromethane with other aryl isocyanates. Using a stoichiometric amount (0.4 mol) of phenyl isocyanate for the reaction, the yield of **1a** was not so varied.

Acylation of 1 with Acyl Chlorides. Typical Procedure. Seven mmol of acyl chloride was added to a stirred benzene solution (80 ml) of **1** (3.5 mmol) and triethylamine (7 mmol) at room termperature. The mixture was refluxed for 4 h and, then, washed with water several times. Evaporation of the solvent from the reaction mixture in a rotary evap-

Table 2. Spectral Data of **1**, **3**, **6**, **7**, and **8**

Compd	Ms; *m/z* Found (Calcd)	IR cm^{-1}	NMR[a] δ
1a	281.091 (281.091)	3270, 1740, 1670	7.50 (s, 5H), 7.55 (s, 5H), 11.9 (br, 1H, OH).
1b	309.126 (309.126)	3270, 1740, 1660	2.33 (s, 3H), 2.4 (s, 3H), 6.8—7.5 (m, 8H), 10.5 (s, 1H, OH).
1c	349.000 (349.000)	3250, 1725, 1660	7.45 (s, 4H), 7.55 (s, 4H), 11.9 (br, 1H, OH).
8a	323.103 (323.103)	1770, 1740, 1650	1.5 (s, 3H), 7.50 (s, 10H).
8b	337.121 (337.121)	1770, 1740, 1640	0.77 (t, 3H, J=7), 1.75 (q, 2H, J=7), 7.50 (s, 10H).
8c	351.138 (351.139)	1770, 1740, 1640	0.75 (t, 3H, J=7), 1.3 (sextet, 2H, J=7), 1.75 (t, 2H, J=7), 7.47 (s, 10H).
8d	379.174 (379.174)	1750, 1640	0.83 (t, 3H, J=7), 1.0—1.5 (m, 6H), 1.8 (t, 2H), 7.50 (s, 10H).
8e	385.121 (385.121)	1755, 1740, 1650	6.7—7.8 (m, 15H).
8f	351.138 (351.139)	1765, 1740, 1640	1.63 (s, 3H), 2.38 (s, 3H), 2.42 (s, 3H), 7.30 (s, 4H), 7.55 (s, 4H).
8g	391.012 (391.013)	1770, 1740, 1650	1.63 (s, 3H), 7.33 (s, 4H), 7.55 (s, 4H).
2	252.089 (252.090)	1700	4.3 (s, 2H), 7.47 (s, 5H), 7.1—7.8 (m, 5H).
3	226.069 (226.069)	1730	7.50 (s, 10H).
6[b]		1770	
7[b]		1720, 1650	about 7.25 (10H).

a) Compounds (**1b**, **8c**, **8d**, **8f**, and **2**) were dissolved in $CDCl_3$, the others were dissolved in DMSO-d_6. b) Spectral data of these compounds was cited from ref. 6.

orator gave crude crystalline product. The crude product was recrystallized from ethanol to give pure material of 5-(acyloxyimino)-1,3-diarylimidazolidine-2,4-dione (**8**) in the yields shown in Table 1.

Hydrolysis of 1a with Ethanolic NaOH. To a solution of sodium hydroxide (200 mg, 5 mmol) in 90% aqueous ethanol (50 ml) we added 280 mg (1 mmol) of **1a**, after which the mixture was stirred for 1 h at 50 °C. After evaporation of the solvent from the reaction mixture, the residue was treated with water and extracted with chloroform (100 ml). The organic layer was dried over anhydrous sodium sulfate. The evaporation of the solvent yielded *N,N'*-diphenylurea in 71% (150 mg) yield.

References

1) For review, see C. Grundmann and P. Grunanger, "The Nitrile Oxides," Springer-Verlag, New York (1971), pp. 51—53.

2) a) T. Mukaiyama and T. Hoshino, *J. Am. Chem. Soc.*, **82**, 5339 (1960); b) R. Paul and S. Tchelitcheff, *Bull. Soc. Chim. Fr.*, **1962**, 2215; c) *Idem, ibid.*, **1963**, 140; d) G. B. Bachmann and L. E. Strom, *J. Org. Chem.*, **28**, 1150 (1963); e) P. Vita-Finzi and P. Grunanger, *Chim. Ind. (Milan)*, **47**, 516 (1965).

3) a) A. Mckillop and R. J. Kobylecki, *Tetrahedron*, **30**, 1365 (1974); b) K. Harada, E. Kaji, and S. Zen, *Chem. Pharm. Bull.*, **28**, 3296 (1980); c) A. Rahman, N. Razzaq, and A. Jabbar, *Pak. J. Sci. Ind. Res.*, **30**, 91 (1978); d) A. Rahman, M. Younas, and N. A. Khan, *J. Chem. Soc. Pak.*, **5**, 243 (1983).

4) a) T. Shimizu, Y. Hayashi, and K. Teramura, *Bull. Chem. Soc. Jpn.*, **57**, 2531 (1984); b) R. G. Duranleau, J. M. Larkin, and S. R. Newman, U. S. Patent 4089867 (1978); *Chem. Abstr.*, **89**, 109515 (1978).

5) S. Tsushima, T. Tsujikawa, and O. Aki, Japan Patent 24902 (1968); *Chem. Abstr.*, **70**, 87344 (1969).

6) a) K. Bast, M. Christl, R. Huisgen, and W. Mack, *Chem. Ber.*, **105**, 2825 (1972); b) S. Hashimoto and K. Hiyama, *Nippon Kagaku Zasshi*, **89**, 412 (1968).

7) C. Grundmann and J. M. Dean, *J. Org. Chem.*, **30**, 2809 (1965).

8) H. Biltz and K. Slotta, *J. Prakt. Chem.*, **113**, 233 (1926).

9) H. Biltz and E. Topp, *Chem. Ber.*, **46**, 1399 (1913).

10) A. W. Hofmann, *Chem. Ber.*, **4**, 247 (1871).

Cyclic Peptides. XXII.[1] Synthesis of [2-Amino-2,3-dehydrobutanoic Acid[4]]AM-Toxin I

Hisakazu MIHARA,* Haruhiko AOYAGI, Tamio UENO,† Tetsuo KATO, and Nobuo IZUMIYA
Laboratory of Biochemistry, Faculty of Science, Kyushu University 33, Higashi-ku, Fukuoka 812
†Pesticide Research Institute, College of Agriculture, Kyoto University, Sakyo-ku, Kyoto 606
(Received February 21, 1986)

Synopsis. To investigate the role of the side chain of the 2,3-dehydroalanine (ΔAla) residue at position 4 in a cyclic tetradepsipeptide phytotoxin AM-toxin I on necrotic activity for apple leaf, [2-amino-2,3-dehydrobutanoic acid[4]] AM-toxin I was synthesized by two different routes. This analog showed no toxic activity, indicating that the side chain of the ΔAla residue can not be handled without loss of the activity.

AM-toxin I is a host-specific phytotoxic metabolite produced by *Alternaria mali*, which causes spot disease on apple leaf. The structure of AM-toxin I is a cyclic tetradepsipeptide containing a ΔAla[2] residue as shown in Fig. 1.[3] We have synthesized various analogs of AM-toxin I in order to study the relationship between structure and function (host-specific toxicity) of the toxin. According to our previous results,[4-8] for the induction of the full toxic activity, AM-toxin I requires factors such as specific ring conformation, the presence of the L-Hmb[2] and L-Amp[3] residues, and a double bond in the ΔAla[4] residue. However, significance of bulkiness of the side chain in the ΔAla[4] residue has not yet been explored. Thus, we synthesized an AM-toxin I analog (**1**) containing Δ^{Z}Abu which has a methyl group instead of a hydrogen atom in ΔAla (Fig. 1) and examined the activity of **1**.

Two synthetic routes for the cyclic peptide (**1**) are shown in Fig. 2. According to the successful synthesis of AM-toxin III and AM-toxin I analogs[6-9] using a D-amino acid residue as the precursor of ΔAla at the *N*-terminal of linear intermediates, a linear tetradepsipeptide, H-D-Thr-L-Ala-L-Hmb-L-Amp-ONSu (**6**), was selected as the precursor for the cyclization reaction. Lee et al.[10] reported that an L-Thr residue was converted to a Δ^{Z}Abu residue by the Photaki method[11] and Δ^{E}Abu was prepared similarly from an L-aThr residue, indicating that the D-Thr residue can be similarly converted to the Δ^{Z}Abu residue after cyclization. On the other hand, Ueda et al.[12] reported that cyclization of a linear tetradepsipeptide containing an L-Ser(Bzl) residue as the precursor of ΔAla residue at the *N*-terminal gave a desired cyclic tetradepsipeptide in high yield comparable to that of cyclization of a precursor containing a D-Ser residue.[13] Therefore, we also synthesized H-L-Thr(Bzl)-L-Ala-L-Hmb-L-Amp-ONSu (**7**) as a precursor of the cyclic peptide. Boc-D-Thr(or L-Thr(Bzl))-ONSu was coupled with H-L-Ala-L-Hmb-L-Amp-OH[6] to give Boc-D-Thr (or L-Thr(Bzl))-L-Ala-L-Hmb-L-Amp-OH (**2** or **3**).

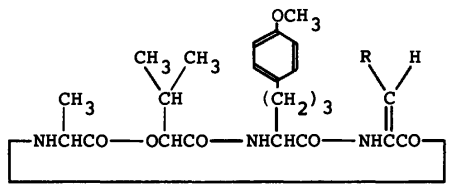

	R	X
AM-toxin I	H	ΔAla
[Δ^{Z}Abu[4]]AM-toxin I (**1**)	CH_3	Δ^{Z}Abu

Fig. 1. Structure of AM-toxin I and [Δ^{Z}Abu[4]]AM-toxin I.

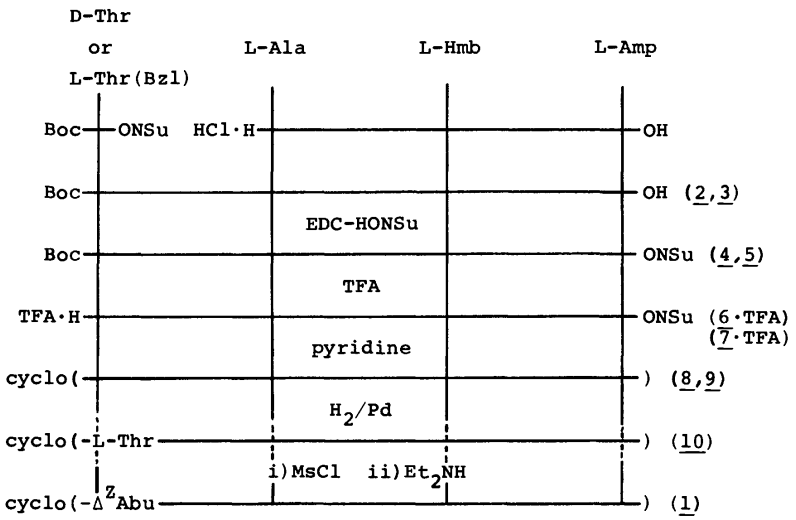

Fig. 2. Synthesis of [Δ^{Z}Abu[4]]AM-toxin I. H_2/Pd procedure was applied to L-Thr(Bzl) derivative (**9**).

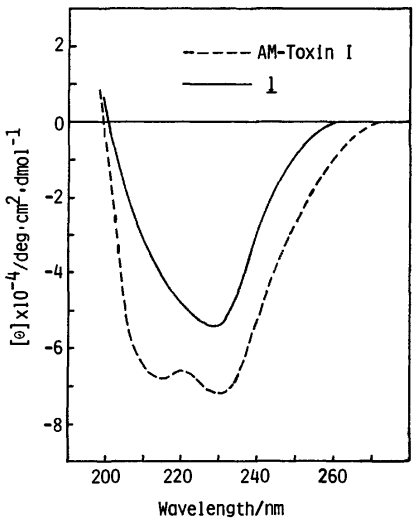

Fig. 3. CD spectra of AM-toxin I and [Δ^ZAbu^4]AM-toxin I in MeOH.

After the conversion of **2** and **3** to the corresponding active ester trifluoroacetates (**6**·TFA and **7**·TFA), their cyclizations at a concentration of 3 mM in pyridine gave cyclic peptides (**8** and **9**) in yields of 47 and 33%, respectively. The benzyl group of **9** was removed by catalytic hydrogenation. Both compounds **8** and **10** were treated with methanesulfonyl chloride and followed by diethylamine to give desired **1**. This was purified by silica-gel column chromatography followed by recrystallization. Although the yield in cyclization of **6** (D-Thr derivative) was higher than that of **7** (L-Thr(Bzl) derivative), compound **9** was converted to **1** in higher yield (16%) compared with **8** (7.2%). Noticeable difference was not observed between the total yields of **1** from **2** and **3**. Configuration of ΔAbu^4 in **1** was identified as Z form by means of ^{1}H NMR chemical shift of methyl proton in ΔAbu (1.7 ppm) compared with that reported by Lee et al.[10] (1.73 ppm for Z form and 2.05 ppm for E form).

CD spectra of **1** and AM-toxin I in methanol are shown in Fig. 3. Although AM-toxin I showed two negative ellipticity minima at 210 and 230 nm, **1** showed only a minimum at 230 nm. This result indicates that the conformation of **1** slightly differs from that of AM-toxin I.

Although minimum toxic activity of AM-toxin I for the induction of necrosis on an apple leaf (Indo) was 0.001 μg ml^{-1}, **1** did not show any toxicity at the concentration of 100 μg ml^{-1}. These results indicate that increasing the bulkiness of the side chain in the ΔAla^4 residue may result in alteration of the conformation of analog **1** and cause loss of the activity. This inactivity may also be due to the result that the unsaturated side chain of the ΔAbu residue in **1** can not react with a receptive substance in an apple leaf differing from the ΔAla residue in AM-toxin I. Combined with the results of no or very little activity of [L- or D-Ala^4]AM-toxin I,[4] the ΔAla residue in this toxin is certainly essential to induce the activity. Phytotoxic tentoxin is a cyclic tetrapeptide containing a *N*-Me-ΔPhe residue[14] and an antibacterial heptapeptide TL-119 contains a Δ^ZAbu residue in its cyclic tetrapeptide part.[15] Since the Δ^ZAbu residue in **1** can not be used as a substitute for the ΔAla residue in AM-toxin I, roles of the dehydroamino acid residues in these peptides on interactions with their receptive substances seem to be different from that of the ΔAla residue in AM-toxin I.

Experimental

Thin layer chromatography was carried out on Merck silica gel G with the following solvent systems: R_f^1,$CHCl_3$–MeOH (5:1); R_f^2, $CHCl_3$–MeOH (9:1); R_f^3, $CHCl_3$–MeOH–AcOH (95:5:1); R_f^4, $CHCl_3$–acetone (1:1). Optical rotation was measured with a Union high sensitivity polarimeter PM-71. Mass spectra were taken on a Nihondenshi mass spectrometer Model JMS-01SG-2 with a direct inlet system operating at 75 eV, CD on a JASCO J-40A spectropolarimeter, and ^{1}H NMR on a Jeol JNM-FX90Q.

Boc–D-Thr–L-Ala–L-Hmb–L-Amp–OH (2). To a solution of H–L-Ala–L-Hmb–L-Amp–OH·HCl[6] (410 mg, 0.95 mmol) and Et_3N (0.27 ml, 1.9 mmol) in a mixture (10 ml) of H_2O and dioxane (1:1) was added Boc–D-Thr–ONSu (250 mg, 0.8 mmol). The mixture was stirred at room temperature overnight. After evaporation, 10% citric acid was added to the residue. The separated oil was extracted with EtOAc, and the solution was washed with water and dried over Na_2SO_4. After evaporation, the product was obtained as an oil: Yield, 340 mg (72%); R_f^1=0.57.

Boc–L-Thr(Bzl)–L-Ala–L-Hmb–L-Amp–OH (3). Compound **3** was prepared from Boc–L-Thr(Bzl)–ONSu (610 mg, 1.5 mmol) and H–L-Ala–L-Hmb–L-Amp–OH·HCl[6] (780 mg, 1.8 mmol) as described for **2**. Compound **3** was crystallized from EtOAc–ether–petroleum ether: Yield, 800 mg (77%); mp 85—87 °C; $[\alpha]_D^{20}$ −7.2° (*c* 0.5, DMF); R_f^1=0.49. Found: C, 62.17; H, 7.50; N, 6.13%. Calcd for $C_{36}H_{51}N_3O_{10}\cdot 1/2H_2O$: C, 62.23; H, 7.54; N, 6.05%.

Boc–D-Thr–L-Ala–L-Hmb–L-Amp–ONSu (4). To a chilled solution of **2** (300 mg, 0.5 mmol) and HONSu (115 mg, 1.0 mmol) in DMF (3 ml) was added EDC·HCl (192 mg, 1.0 mmol). The mixture was stirred at 0 °C for 24 h. After evaporation, the residue was solidified by the addition of cold water and dried in vacuo: Yield, 320 mg (92%); R_f^1= 0.71. This was used to the next step without purification.

Boc–L-Thr(Bzl)–L-Ala–L-Hmb–L-Amp–ONSu (5). Compound **5** was prepared from **3** (690 mg, 1.0 mmol) as described for **4**: Yield, 770 mg (98%); R_f^2=0.70.

***cyclo*(–L-Ala–L-Hmb–L-Amp–D-Thr–) (8).** A solution of **4** (320 mg, 0.45 mmol) in TFA (2 ml) was allowed to stand at 0 °C for 30 min. After evaporation, the residual oil was solidified by the addition of ether. The powder was washed several times with ether by decantation to give H–D-Thr–L-Ala–L-Hmb–L-Amp–ONSu·TFA (**6**·TFA). This was dissolved in DMF (5 ml) and the solution was added dropwise into pyridine (130 ml) with stirring at room temperature. The stirring was continued for 3 d and the reaction mixture was evaporated. The residue was collected with the aid of water, and washed with 10% citric acid and water. This was recrystallized from DMF–EtOAc–ether; yield, 100 mg (47%); mp 242—244 °C (decomp); MS *m/z* 477 (M^+); R_f^1=0.76, R_f^2= 0.47. Found: C, 59.77; H, 7.38; N, 8.65%. Calcd for $C_{24}H_{35}N_3O_7\cdot 1/3H_2O$: C, 59.61; H, 7.36; N, 8.69%.

***cyclo*(–L-Ala–L-Hmb–L-Amp–L-Thr(Bzl)–) (9).** Compound **9** was prepared from **5** (780 mg, 1.0 mmol) as described for **8**. This was recrystallized from DMF–EtOAc: Yield, 190 mg (33%); mp 208—210 °C (decomp); MS *m/z* 567 (M^+); R_f^2=0.72, R_f^3=0.33. Found: C, 64.66; H, 7.14; N, 7.43%. Calcd for $C_{31}H_{41}N_3O_7\cdot 1/2H_2O$: C, 64.57; H, 7.34; N, 7.29%.

***cyclo*(-L-Ala-L-Hmb-L-Amp-Δ^ZAbu-) ([Δ^ZAbu^4]AM-toxin I, 1) from D-Thr Derivative (8).** To a chilled solution of **8** (67 mg, 0.14 mmol) in pyridine (3 ml) was added MsCl (0.055 ml, 0.7 mmol). After 24 h at 4°C, the solution was evaporated. The residue was solidified by the addition of cold water and washed with ether–petroleum ether (1:1) to give a powder of *cyclo*(-L-Ala-L-Hmb-L-Amp-D-Thr(Ms)-) (11): Yield, 69 mg (89%); R_f^2=0.82. This structure was confirmed by ^{1}H NMR spectrum. To a solution of 11 in DMF (1 ml) was added Et_2NH (0.026 ml, 0.26 mmol) at room temperature. The mixture was allowed to stand for 24 h at room temperature. After evaporation, the residue was solidified by the addition of cold water. This crude product (57 mg) was applied to a silica-gel column (1.1×27 cm) and eluted with $CHCl_3$–CH_3CN (1:1). The fraction was pooled and evaporated. The residue was recrystallized from EtOAc–petroleum ether: Yield, 4.6 mg (7.2%); mp 220—222°C (decomp); MS *m/z* 459 (M^+); R_f^2=0.38, R_f^4=0.34. Found: C, 62.50; H, 7.17; N, 9.21%. Calcd for $C_{24}H_{33}N_3O_6$: C, 62.72; H, 7.24; N, 9.14%.

[Δ^ZAbu^4]AM-toxin I (1) from L-Thr(Bzl) Derivative (9): Compound **9** (100 mg, 0.18 mmol) in DMF (25 ml) was hydrogenated for 4 h in the presence of Pd-black. After removal of the catalyst, the filtrate was evaporated and the residue was solidified by the addition of ether to give a powder of *cyclo*(-L-Ala-L-Hmb-L-Amp-L-Thr-) (**10**): Yield, 86 mg (100%); R_f^1=0.50. Compound **10** was treated with MsCl and Et_2NH, and then purified with a silica-gel column to give **1**; Yield, 13 mg (16%). This was identified to that obtained from **8** by mp, TLC and ^{1}H NMR spectrum.

We thank Dr. H. Nishikawa, Fukuoka University, for the measurement of CD spectra.

References

1) Part XXI of this series: H. Mihara, K. Ikesue, S. Lee, H. Aoyagi, T. Kato, T. Ueno, and N. Izumiya, *Int. J. Peptide Protein Res.*, in press.

2) Abbreviations: aThr, allothreonine; Abu, 2-aminobutanic acid; Amp, 2-amino-5-(*p*-methoxyphenyl)-pentanoic acid; Bzl, benzyl; Δ, 2, 3-dehydro; DMF, *N*,*N*-dimethylformamide; EDC·HCl, 1-ethyl-3-(3-dimethylaminopropyl)-carbodiimide; Hmb, 2-hydroxy-3-methylbutanoic acid; HONSu, *N*-hydroxysuccinimide; MsCl, methanesulfonyl chloride; TFA, trifluoroacetic acid.

3) T. Ueno, T. Nakashima, Y. Hayashi, and H. Fukami, *Agric. Biol. Chem.*, **39**, 1115 (1975).

4) Y. Shimohigashi, S. Lee, T. Kato, and N. Izumiya, *Bull. Chem. Soc. Jpn*, **51**, 584 (1978).

5) T. Higashijima, Y. Shimohigashi, T. Kato, N. Izumiya, T. Ueno, and T. Miyazawa, *Biopolymers*, **22**, 1167 (1983).

6) H. Mihara, H. Aoyagi, S. Lee, M. Waki, T. Kato, and N. Izumiya, *Int. J. Peptide Protein Res.*, **23**, 447 (1984).

7) H. Aoyagi, H. Mihara, S. Lee, T. Kato, T. Ueno, and N. Izumiya, *Int. J. Peptide Protein Res.*, **25**, 144 (1985).

8) H. Mihara, K. Ikesue, S. Lee, H. Aoyagi, T. Kato, T. Ueno, and N. Izumiya, *Int. J. Peptide Protein Res.*, in press.

9) T. Kanmera and N. Izumiya, *Int. J. Peptide Protein Res.*, **19**, 79 (1982).

10) S. Lee, T. Kanmera, H. Aoyagi, and N. Izumiya, *Int. J. Peptide Protein Res.*, **13**, 207 (1979).

11) I. Photaki, *J. Am. Chem. Soc.*, **85**, 1123 (1963).

12) K. Ueda, M. Kondo, M. Waki, and N. Izumiya, "Peptide Chemistry 1984," ed by N. Izumiya, Protein Research Foundation, Osaka (1985), pp. 157—160.

13) Y. Shimohigashi and N. Izumiya, *Int. J. Peptide Protein Res.*, **12**, 7 (1978).

14) G. E. Templeton, *Microb. Toxins*, **8**, 160 (1972).

15) J. Shoji, H. Hinoo, Y. Wakisaka, K. Koizumi, and M. Mayama, *J. Antibiot.*, **28**, 126 (1975).

Practical Synthesis of 1,1′-Binaphthyl-2-carboxylic Acids via Side Chain Oxidation of 2-Methyl-1,1′-binaphthyls

Sotaro MIYANO,* Shin-ichi OKADA, Toshiyuki SUZUKI,
Shigeru HANDA, and Harukichi HASHIMOTO
Department of Applied Chemistry, Faculty of Engineering, Tohoku University, Aramaki-Aoba, Sendai 980
(Received January 29, 1986)

Synopsis. Four 1,1′-binaphthyl-2-carboxylic acids were obtained in 38—53% isolated yield via three-stage oxidation of 2-methyl-1,1′-binaphthyls, that is, i) NBS-bromination to benzylic bromides, ii) treatment with sodium salt of 2-nitropropane to aldehydes, and iii) $KMnO_4$-oxidation to carboxylic acids.

In the past few years, there has been an intense interest in the asymmetric reactions by means of atropisomeric binaphthyls as the chirality recognizing units.[1] The main obstacle in carrying out these reactions, however, has been the difficulty to obtain the requisite axially chiral binaphthyl skeletons.[2] In this context, 1,1′-binaphthyl-2-carboxylic acids **1** are intriguing as the starting material for elaboration of such chiral auxiliaries, considering that the carboxyl substituent should be the most helpful resort for not only optical resolutions[3] but also transformations into various functionalities.[4] Actually, Goto et al. have shown that **1b** is useful for preparation of the derivatizing agents for liquid chromatographic resolution of enantiomeric hydroxy compounds.[5] Their preparation of **1b**, however, suffered from tedious manipulations which involved the synthesis of intermediate dimethyl 1,1′-binaphthyl-2,2′-dicarboxylate. On the other hand, Meyers and Lutomski,[6] and Wilson and Cram[7] reported nucleophilic substitution of 2-oxazoline-activated 1-alkoxynaphthalenes by a naphthyl Grignard or lithium reagent to give 2-(1,1′-binaphthyl-2-yl)oxazolines **2**, which are latent binaphthyl-2-carboxylic acids. Although the procedure can be applied for the construction of axially chiral binaphthyl linkage by the use of a substrate bearing chiral alkoxyl or oxazoline group, hydrolytic regeneration of the carboxyl function from the sterically crowded **2** is not so much easy, and it is still highly-desirable to provide an alternative, operationally more simple route to **1**.

Herein we wish to report our approach to **1** which is outlined in Scheme.[8,9] Ultrasonic irradiation remarkably facilitated the reaction of **3b** with magnesium turnings in ether to form the Grignard reagent **4**. The Kumada-Tamao method[10] was successfully utilized to promote cross-coupling of **4** with bromonaphthalenes **3** to give 2-methyl-1,1′-binaphthyls **5**. The use of 1.5—1.7 molar amounts of **4** appeared to be ample excess not to leave unchanged **3**. After usual workup of the reaction, recrystallization or distillation gave pure samples of **5** (55—82% yield). The significant upfield shift of ^1H NMR of the methyl groups for **5** is consistent with the binaphthyl structure where these protons are disposed over the shielding cone of the adjacent naphthalene rings (see Experimental).

The methyl substituents of **5** were readily brominated by treatment with 1.1 equiv of *N*-bromosuccinimide (NBS) in boiling CCl_4 in the presence of a catalytic amount of benzoyl peroxide. Filtration of the precipitated succinimide from the cool reaction mixture and evaporation of the solvent left crude

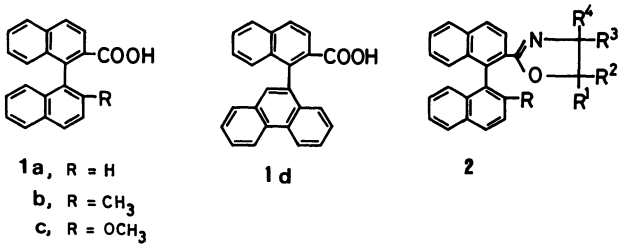

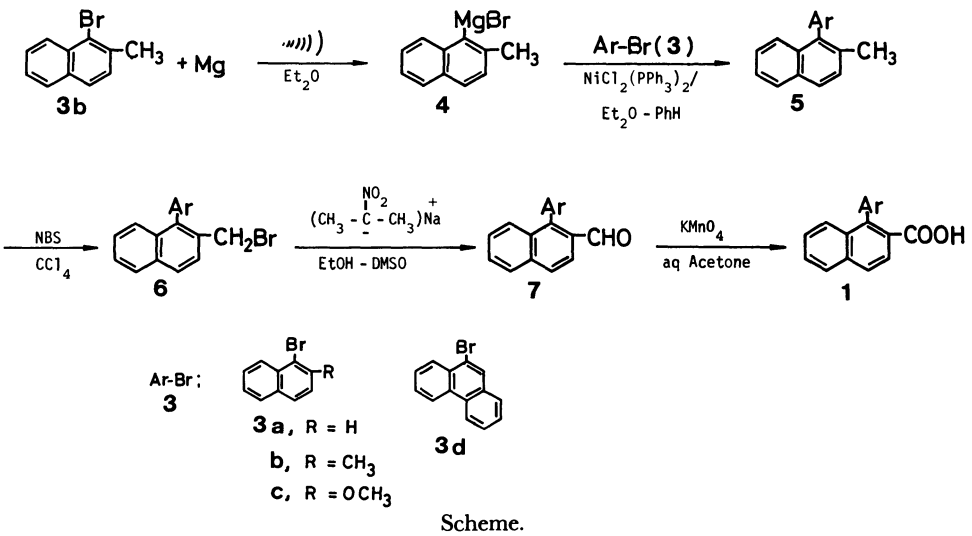

Scheme.

benzylic bromides **6**, which in turn were treated with sodium salt of 2-nitropropane in DMSO–EtOH to give aldehydes **7** according to the method of Klanderman;[11] the conventional Sommelet oxidation did not work well for these bulky benzylic bromides.[12] Conversion of **7** to carboxylic acids **1** was effected by $KMnO_4$–oxidation in boiling aqueous acetone applying the method of Hall and Turner with slight modifications.[13] Pure samples of **1** were readily obtainable by recrystallization, and were characterized by elemental analysis and spectral studies.

Although the yields of **1** were moderate (38—53% based on **5**), we believe that the procedure is synthetically useful; the starting bromonaphthalenes are readily available, and any stage of the procedure does not necessarily require chromatographic purification, rendering it suitable for preparative scale synthesis of **1**.

Experimental

Materials. **3c** was prepared by treating 1-bromo-2-naphthol with NaH in DMF, followed by addition of methyl iodide and stirring overnight at room temperature, mp 85—86°C (lit,[7] mp 83—84°C). Commercial **3d** (mp 63°C) was stored over silica gel in vacuo, and **3a** was distilled before use, bp 149—152°C/16 mmHg.* **3b**[13] (bp 115—118°C/1.5 mmHg) and $NiCl_2(PPh_3)_2$[14] were prepared as described in the literature.

2-Methyl-1,1′-binaphthyls (5). The synthesis of **5d** is representative. The Grignard reagent **4** was prepared under nitrogen in a flask immersed in the water bath of an ultrasonic laboratory cleaner (53 W, 41 kHz).

To an ultrasonically irradiated mixture of magnesium turnings (7.00 g, 0.288 g-atom) in 50 ml of ether was added a solution of **3b** (37.7 g, 0.171 mol) in ether (200 ml) over 1-h period; addition of a few drops of the bromide started the reaction quite readily, which was evidenced by clouding of the ether layer with a change of the magnesium surface from dull grey to metallic. During the addition, the temperature of the water bath was allowed to rise with sonication, which kept the reaction at rapid reflux. After the addition was complete, the sonication was continued for another 2 h. The Grignard reagent was obtained as a slightly yellow slurry, which was dissolved by adding 200 ml of benzene.

The Grignard solution was transferred to another dropping funnel by means of a cannula, and then added dropwise to a magnetically stirred solution of **3d** (26.0 g, 0.101 mol) and $NiCl_2(PPh_3)_2$ (0.655 g, 1 mol% of **3d**) in 150 ml of benzene at room temperature over 1-h period. After stirred overnight at room temperature, the mixture was heated at reflux for 3 h, and then bulk of the ether was distilled off through a short Vigreux column. The cooled reaction mixture was worked up as usual.[10] Solvents were removed in vacuo, and the residue was heated up to 150°C (bath temp) at 0.1 mmHg to remove volatiles comprised mainly of 2-methylnaphthalene. The crude product was dissolved in hexane, and passed through a silica-gel pad to remove colored materials. Evaporation of the solvent and crystallization from ethanol–acetone (9:5) gave pure **5d**, 26.5 g (82%); mp 145—148.5°C; IR (KBr) 3050, 1450, 1420, 810, 740, and 720 cm^{-1}; ^1H NMR ($CDCl_3$) δ=2.15 (3H, s, $-CH_3$),[15] 7.0—8.1 (13H, m, Ar-H), and 8.6—8.9 (2H, m, Ar-H). Found: C, 94.39; H, 5.93%. Calcd for $C_{25}H_{18}$: C, 94.30; H, 5.70%.

5a: **4** was prepared from 2.02 g (9.14 mmol) of **3b**, allowed to react with **3a** (1.09 g, 5.27 mmol), and worked up as above. Recrystallization from hexane gave 1.11 g (79%) of **5a** which melted at 86.0—88.0°C to an opaque liquid that cleared at ca. 103°C (lit,[16] mp 120—122°C)[17]; IR (KBr) 3050, 1500, 1360, 800, 780, and 740 cm^{-1}. ^1H NMR ($CDCl_3$) δ=2.10 (3H, s, $-CH_3$) and 7.0—8.1 (13H, m, Ar-H). Found: C, 94.21; H, 6.08%. Calcd for $C_{21}H_{16}$: C, 93.99; H, 6.01%.

5b: **4** was prepared from 4.55 g (20.6 mmol) of **3b**, and then allowed to react with another 2.78 g of **3b** (12.6 mmol). Trap-to-trap distillation gave 2.17 g (61%) of **5b** as a colorless glass; bp≈200°C (bath temp)/1 mmHg (lit,[2a] 190—210°C/0.2 mmHg); ^1H NMR ($CDCl_3$) δ=1.95 (6H, s, $-CH_3\times$ 2), 6.8—8.0 (12H, m, Ar-H). Found: C, 93.21; H, 6.11%. Calcd for $C_{22}H_{18}$: C, 93.58; H, 6.42%.

5c: **4** was prepared from 2.49 g (11.3 mmol) of **3b** and allowed to react with **3c** (1.45 g, 6.12 mmol). Crystallization from hexane gave 1.00 g (55%) of **5c**; mp 118—121°C; IR (KBr) 3050, 1620, 1570, 1240, 800, and 730 cm^{-1}. ^1H NMR ($CDCl_3$) δ=2.0 (3H, s, $-CH_3$), 3.64 (3H, s, $-OCH_3$), 6.7—8.0 (12H, m, Ar-H). Found: C, 89.01; H, 6.14%. Calcd for $C_{22}H_{18}O$: C, 88.56; H, 6.08%.

Oxidation of 5 to 1,1′-Binaphthyl-2-carboxylic Acids 1. The synthesis of **1d** is representative. A mixture of **5d** (3.18 g, 10.0 mmol), NBS (1.96 g, 11.0 mmol), and benzoyl peroxide (0.1 g) in CCl_4 (70 ml) was magnetically stirred and heated at reflux for 3 h, during which almost all of **5d** had disappeared as evidenced by ^1H NMR. Precipitated succinimide was filtered off from the cool mixture, and volatiles were removed in vacuo to give crude **6d**; δ ($-CH_2Br$)/(CCl_4-$CDCl_3$)=4.09 (1H, d, J=10.3 Hz) and 4.33 (1H, d).

The bromide was dissolved in 60 ml of DMSO under nitrogen. To the stirred solution was added slowly (0.5 h) a solution prepared by adding 3.25 g (36.5 mmol) of 2-nitropropane to a sodium ethoxide in ethanol, which had been obtained by dissolving 0.58 g of sodium (25.2 mg-atom) in 35 ml of ethanol. Stirring was continued for 3 h at room temperature, and then another 3 h at 60°C. The mixture was poured into ice-water (300 ml), extracted with dichloromethane, washed successively with 2 M† HCl, 1 M Na_2CO_3, and then water, and dried over Na_2SO_4. Evaporation of the solvent in vacuo left crude **7d**; ^1H NMR ($CDCl_3$) δ=9.72 (1H, -CHO); IR (KBr) 1680 cm^{-1}.

The aldehyde was dissolved in 60 ml of acetone and heated at reflux, to which was added dropwise (0.5 h) a solution of $KMnO_4$ (2.36 g, 15.0 mmol) in 60 ml of hot water, and heating was continued for an additional 1 h. To the dark brown mixture was bubbled sulfur dioxide till it became clear accompanying deposition of white precipitate. The solid was recovered by filtration, dissolved in hot toluene (200 ml), and then filtered hot after adding small amount of activated charcoal; concentration to about a third of the volume caused crystallization of **1d** on standing, 1.84 g (53%); mp 290—291.5°C; IR (KBr) 1680 cm^{-1}. ^1H NMR (DMSO-d_6) δ=6.8—8.4 (13H, m, Ar-H), 8.6—9.1 (2H, m, Ar-H), and 12.4 (1H, br, -COOH). Found: C, 86.24; H, 4.91%. Calcd for $C_{25}H_{16}O_2$: C, 86.19; H, 4.63%.

1c: The oxidation of **5c** (9.65 g, 32.4 mmol) was carried out as above and recrystallization from water–ethanol (2:1) gave 5.64 g (53%) of **1c**; mp 258.5—260°C; IR (KBr) 1680 cm^{-1}. ^1H NMR (DMSO-d_6) δ=3.69 (3H, s, $-OCH_3$), 6.5—8.3 (12H, m, Ar-H,), and 12.2 (1H, br, -COOH). Found: C, 80.28; H, 5.06%. Calcd for $C_{22}H_{16}O_3$: C, 80.47; H, 4.91%.

1a: The oxidation of **5a** (1.86 g, 6.94 mmol) was carried out as above except that, after treatment with SO_2, ca. 1 l of 28% aqueous ammonia was added to dissolve the acid which deposited as an oil and then passed through a silica-gel pad to remove colored precipitates. The aq layer was

*1 mmHg=133.322 Pa.

† 1 M=1 mol dm^{-3}.

made acidic by adding conc HCl, and the acid was taken into ether. Evaporation of the solvent and recrystallization from water–ethanol (1:1) gave 0.78 g (38%) of **1a**; mp 200—201.5 °C (lit,[7] mp 200—201 °C); IR (KBr) 1680 cm^{-1}; ^1H NMR (DMSO-d_6) δ=6.8—8.2 (13H, m, Ar-H) and 12.4 (1H, br, -COOH). Found: C, 84.46; H, 4.67%. Calcd for $C_{21}H_{14}O_2$: C, 84.54; H, 4.73%.

1b: The oxidation of **5b** (1.00 g, 3.55 mmol) was carried out according to the procedure used for **5a**, affording 0.451 g (41%) of **1b** after recrystallization from water–ethanol (1:1); mp 228—230 °C (lit,[5] 233 °C); IR (KBr) 1670 cm^{-1}; ^1H NMR (DMSO-d_6) δ=1.98 (3H, s, $-CH_3$), 6.6—8.3 (12H, m, Ar-H), and 12.4 (1H, br, -COOH). Found: C, 84.32; H, 5.33%. Calcd for $C_{22}H_{16}O_2$: C, 84.59; H, 5.16%.

We are grateful for support of this work by a Grant-in-Aid for Scientific Research No. 60119001 from the Ministry of Education, Science and Culture.

References

1) For example, a) R. Noyori, I. Tomino, Y. Tanimoto, and M. Nishizawa, *J. Am. Chem. Soc.*, **106**, 6709 (1984); b) K. Tani, T. Yamagata, S. Akutagawa, H. Kumobayashi, T. Taketomi, H. Takaya, A. Miyashita, R. Noyori, and S. Otsuka, *ibid.*, **106**, 5208 (1984).

2) a) N. Maigrot and J. P. Mazaleyrat, *Synthesis*, **1985**, 317; b) F. Cottineau, N. Maigrot, and J. P. Mazaleyrat, *Tetrahedron Lett.*, **26**, 421 (1985); c) N. Maigrot, J. P. Mazaleyrat, and Z. Welvart, *J. Org. Chem.*, **50**, 3916 (1985), and references cited therein.

3) P. Newman, "Optical Resolution Procedures for Chemical Compounds," Optical Resolution Information Center, Manhattan College, New York (1981).

4) For example, F. Bell and D. H. Waring, *J. Chem. Soc.*, **1949**, 1579.

5) J. Goto, N. Goto, and T. Nambara, *Chem. Pharm. Bull.*, **30**, 4597 (1982).

6) A. I. Meyers and K. A. Lutomski, *J. Am. Chem. Soc.*, **104**, 879 (1982); *Synthesis*, **1983**, 105.

7) J. M. Wilson and D. J. Cram, *J. Org. Chem.*, **49**, 4930 (1984).

8) Preparation of optically active **1a**,[7] **1b**,[5] **1c**,[7] have been reported.

9) Mazaleyrat et al. have reported modification of the methyl substituents of **5b** for the synthesis of various binaphthyl derivatives, which prompted us to disclose here our results; see Ref. 2).

10) M. Kumada, K. Tamao, and K. Sumitani, *Org. Synth.*, **58**, 127 (1978).

11) B. H. Klanderman, *J. Org. Chem.*, **31**, 2618 (1966).

12) S. J. Angyal, *Org. Reactions*, **8**, 197 (1954).

13) D. M. Hall and E. E. Turner, *J. Chem. Soc.*, **1955**, 1242.

14) L. M. Venanzi, *J. Chem. Soc.*, **1958**, 719.

15) 2-Methylnaphthalene: δ ($-CH_3$)=2.50.

16) A. D. Campbell, R. A. Elder, and G. W. Emerson, *J. Chem. Soc.*, **1959**, 3526.

17) We repeated the procedure twice, and got **5a** of similar thermal behavior.

Chemistry of 1,2-Thiaphosphole 2-Sulfides. III.[1] Cycloaddition Reactions with Some Acetylenic Dienophiles and Generation of Phosphorin 1-Sulfides

Hideyuki TANAKA and Shinichi MOTOKI*
Department of Chemistry, Faculty of Science, Science University of Tokyo, Kagurazaka, Shinjuku-ku, Tokyo 162
(Received December 20, 1985)

Synopsis. 1,2-Thiaphosphole 2-sulfides reacted with dimethyl acetylenedicarboxylate or phenylacetylene to afford 1-phosphabarrelene 1-sulfides (1-phosphabicyclo[2.2.2]octa-2,5,7-triene 1-sulfides) via phosphorin 1-sulfides.

Previously, we reported that 1,2-thiaphosphole 2-sulfides **2** generated by the thermolysis of 2,9-dithia-1-phosphabicyclo[4.3.0]nona-3,7-diene 1-sulfides **1** underwent cycloaddition reactions with various olefins to afford the stable 1:1 adducts **4**.[1]

Meanwhile, numerous studies have been devoted to the chemistry of phosphorin derivatives,[2] however, phosphorin 1-sulfides are little known because of their instability. Only one example was reported by Mathey et al. very recently. They treated 4,5-dimethyl-2-phenylphosphorin with an excess of sulfur in the presence of 2,3-dimethylbutadiene or dimethyl acetylenedicarboxylate (DMAD), and transiently formed phosphorin 1-sulfide was trapped as cycloadducts.[3,4]

In view of the recent investigation, we attempted the cycloaddition reactions of **1** (**2**) with acetylenic dienophiles and also expected the formation of the phosphorin 1-sulfides **6** from the adducts **5** by elimination of the bridged sulfur atom.

Results and Discussion

When the reaction of **1a—c** with DMAD was carried out in refluxing benzene, 1-phosphabarrelene 1-sulfides **7a—c** were obtained along with the other products **8a—c** (Table 1). This interesting results are explained as follows. Initially formed cycloadducts **5** are unstable under the reaction conditions and produce intermediary phosphorin 1-sulfides **6** by the elimination of the bridged sulfur atom. Subsequently, **6** react with DMAD to afford **7a—c** as reported by Mathey et al.[3] (Scheme 1).

The elementary analyses and the mass spectra indi-

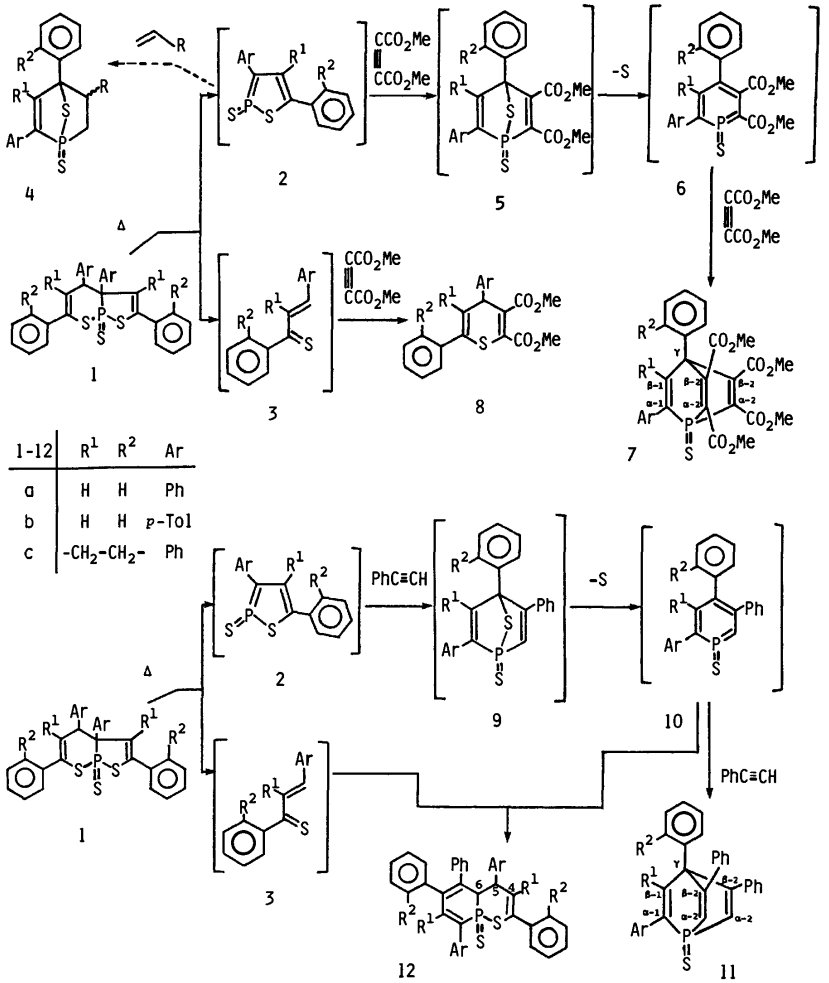

Scheme 1.

Table 1. Reactions of **1** with Acetylenic Dienophiles

Material	Dienophile	Reaction time/h	Product					
				Mp θ_m/°C[a]	Yield/%[b]		Mp θ_m/°C[a]	Yield/%[b]
1a	DMAD	1	**7a**	237—239	72	**8a**	c)	82
1b	DMAD	1	**7b**	202—204	59	**8b**	c)	70
1c	DMAD	1.5	**7c**	199—201	74	**8c**	103—105	61
1a	PhC≡CH	2	**11a**	218—220	38	**12a**	203—205	36
1b	PhC≡CH	2	**11b**	224—226	28	**12b**	180—182	54
1c	PhC≡CH	2	**11c**	228—230	86	**12c**	258—260	13

a) All the products decomposed at the melting points. b) The yield of products was based on **1**. c) Oil.

Table 2. ^{13}C NMR Spectral Data of **7** and **11** (δ(J_{CP}/Hz))

Compd	C(α-1)	C(α-2)	C(β-1)	C(β-2)	C(γ)	$J_{C(\alpha\text{-}1)P}$	$J_{C(\alpha\text{-}2)P}$	$J_{C(\beta\text{-}2)P}$	$J_{C(\gamma)P}$
7a	147.3	139.9	145.7	161.1	59.9	64.7	57.4	2.4	29.3
7b	147.1	139.9	144.8	161.0	59.5	64.7	57.4	2.4	29.3
7c	138.5	139.7	160.2	160.4	58.9	67.1	57.4	9.8	30.5
11a	148.9	134.1	145.0	170.9	66.3	61.0	67.1	3.7	30.5
11b	148.8	134.1	144.8	170.9	66.3	61.0	67.1	3.7	30.5
11c	140.7	134.4	157.9	170.5	65.6	63.5	65.9	3.7	31.7

a) **7** and **11**: $J_{C(\beta\text{-}1)P} \simeq 0$

Table 3. ^{1}H and ^{13}C NMR Spectral Data of **12** (δ(J/Hz))

Compd	H(4)	H(5)	H(6)	$J_{H(4)H(5)}$	$J_{H(5)H(6)}$	$J_{H(4)P}$	$J_{H(5)P}$	$J_{H(6)P}$	C(5)	C(6)	$J_{C(5)P}$	$J_{C(6)P}$
12a	6.41	4.28	3.75	4.5	10.0	2.5	14.5	14.0	50.7	53.6	2.5	48.8
12b	6.41	4.23	3.73	4.5	10.0	2.5	15.5	14.0	49.8	54.1	2.4	47.6
12c	—	4.16	3.78	—	8.0	—	22.0	14.5	47.0	52.0	4.9	48.8

cated that **7a—c** were 1:1 adducts of **6** with DMAD and the structures were confirmed by the ^{1}H and ^{13}C NMR spectral data. In the ^{1}H NMR spectrum of **7a**, the methoxycarbonyl groups resonated at δ=3.43 (s, 6H) and 3.89 (s, 6H). The doublet at δ=8.26 (1H, J_{HP}=30.0 Hz) was assigned to the olefinic H(β-1) proton. The ^{13}C NMR spectrum of **7a** showed signals of the C(α-1) and C(α-2) olefinic carbons at δ=147.3 (J_{CP}=64.7 Hz) and 139.9 (2×C, J_{CP}=57.4 Hz), respectively. The large C-P coupling constants suggest that these carbons are directly bonded to the phosphorus atom. The signals of the C(β-1) and C(β-2) carbons showed small C-P coupling constants ($J_{C(\beta\text{-}1)P} \simeq 0$ Hz, $J_{C(\beta\text{-}2)P}$=2.4 Hz). The signal of C(γ) carbon appeared at δ=59.9 and showed unusual large coupling constant (J_{CP}=29.3 Hz). These spectral data are closely similar to those of the 1-phosphabarrelene 1-sulfide reported previously.[3,5] The structures of **7b, c** were determined similarly (Table 2).

On the other hand, the mass spectra indicated that **8a—c** were 1:1 adducts of **3** with DMAD and their ^{1}H NMR spectral data suggested that they would be 4*H*-thiin derivatives. However, rearranged 2*H*-thiin structures can not be excluded strictly.[6]

The reaction of **1** with an excess of phenylacetylene gave the corresponding phosphabarrelene sulfides **11a—c** regioselectively. The orientation of phenyl group was determined by the ^{1}H NMR spectrum of **11b**. In this spectrum, signals of one proton (δ=8.45, J_{HP}=30.0 Hz), three protons (CH_3), two sets of two protons (*p*-Tol-H), and seventeen protons were observed. The first signal was assigned to the H(β-1) and the remaining two protons attached to the barrelene skeleton should be linked to the C(α-2) carbon atom. Signals of the H(α-2) couldn't be distinguished from those of other aromatic protons. Similarly, the structures of **11a** and **11c** were determined.

Cycloadducts of the thiones **3** with phenylacetylene were not obtained in this case, however, the analytical and the mass spectral data of the other products **12a—c** indicated that the compounds were 1:1 adducts of **10** and the thiones **3**. The ^{13}C NMR spectrum of **12a** showed a signal of the C(6) carbon at δ=53.6 with a large C-P coupling constant (J_{CP}=48.8 Hz), suggesting a direct bonding of the C(6)-P (Table 3).[1] In the ^{1}H NMR spectra, H(4), H(5), and H(6) protons resonated at δ=6.41 (dd, J_{HH}=4.5 Hz, J_{HP}=2.5 Hz), 4.28 (ddd, J_{HH}=4.5, 10.0 Hz, J_{HP}=14.5 Hz), and 3.75 (dd, J_{HH}=10.0 Hz, J_{HP}=14.0 Hz), respectively. These spectral data are in accord with the proposed structures. The structures of **12b, c** were determined similarly (Table 3). In these cycloaddition reactions, phosphorin sulfides **10** and α,β-unsaturated thiones **3** act as 2π- and 4π-electron components, respectively. Cycloadducts of this type did not form in the reaction of **1** and DMAD. From these results, it has been found that the sulfides **2** react with phenylacetylene more rapidly than the thiones **3**, and **3** are trapped by the generating **10** rather than phenylacetylene.

The mass spectra of **12** show fragments of thiones **3** and the phosphorin 1-sulfides **10**. So the preparation of the corresponding phosphorins[4] by the thermolysis of **12** in the presence of desulfurizing agent is now under investigation.

Experimental

All melting points are uncorrected. IR spectra were measured on a Hitachi Model 260-10 spectrometer. ^{1}H and

^{13}C NMR spectra were recorded on a JEOL JNM-FX 100 spectrometer in $CDCl_3$ solution using Me_4Si as an internal standard (^1H; at 100 MHz, ^{13}C; 25.05 MHz). ^{31}P NMR spectra were recorded at 36.21 MHz on a JEOL FX-90A spectrometer in $CDCl_3$ solution using 85% H_3PO_4 as an external standard. Mass spectra were recorded on a Hitachi double focusing mass spectrometer (RMU-7M), operating at an ionizing potential of 70 eV. Elemental analyses were performed using a Yanaco Model MT-3 CHN corder. 2,9-Dithia-1-phosphabicyclo-[4.3.0]nona-3,7-diene 1-sulfides **1** were prepared according to the previously described method.[1]

General Procedure for the Reaction of the Phosphabicyclo Compounds 1 with Acetylenic Dienophiles: A solution of **1** (2 mmol) and DMAD (7 mmol) or phenylacetylene (18 mmol) in 5 cm^3 of dry benzene was refluxed under a nitrogen atmosphere until **1** was consumed, as indicated by TLC. After evaporation of the solvent the residue was chromatographed on silica gel (Wakogel C-200) with benzene-ethyl acetate (10:1) or benzene-hexane (1:1) as an eluent to afford the products and were recrystallized from ethanol.

4,7-Diphenyl-2,3,5,6-tetrakis(methoxycarbonyl)-1-phosphabicyclo[2.2.2]octa-2,5,7-triene 1-Sulfide (7a): IR (KBr) 2970, 1740 (C=O), 1300, and 1260 cm^{-1}; ^1H NMR δ=3.43 (s, 6H, OCH_3), 3.89 (s, 6H, OCH_3), 7.22—7.62 (m, 8H, Ar-H), and 8.26 [d, 1H, J_{HP}=30.0 Hz, H(β-1)]; ^{31}P NMR δ=9.33 (d, J_{PH}=30.2 Hz); MS *m/z* 538 (M^+, 52), 506 (M^+—S, 35), 474 (15), 447 (506-$COOCH_3$, 14), 418 (11), 302 (M^+—4$COOCH_3$, 37), 271 (34), and 93 (100). Found: C,60.38; H, 4.27; S, 6.09%. Calcd for $C_{27}H_{23}O_8PS$: C, 60.22; H, 4.30; S, 5.95%.

4-Phenyl-2,3,5,6-tetrakis(methoxycarbonyl)-7-*p*-tolyl-1-phosphabicyclo[2.2.2]octa-2,5,7-triene 1-Sulfide (7b): IR (KBr) 2960, 1740 (C=O), 1280, and 1240 cm^{-1}; ^1H NMR δ=2.39 (s, 3H, CH_3), 3.42 (s, 6H, OCH_3), 3.88 (s, 6H, OCH_3), 7.08—7.56 (m, 9H, Ar-H), and 8.22 [d, 1H, J_{HP}=30.0 Hz, H(β-1)]; MS *m/z* 552 (M^+, 33), 520 (M^+—S, 21), 488 (7), 461 (520-$COOCH_3$, 9), 432 (10), 316 (M^+—4$COOCH_3$, 39), 285 (19), and 93 (100). Found: C, 60.80; H, 4.45%. Calcd for $C_{28}H_{25}O_8PS$: C, 60.87; H, 4.56%.

2,3-Benzo-7-phenyl-9,10,11,12-tetrakis(methoxycarbonyl)-8-phosphatricyclo[6.2.2.0^{1,6}]dodeca-6,10,11-triene 8-Sulfide (7c): IR (KBr) 2970, 1730 (C=O), 1285, and 1250 cm^{-1}; ^1H NMR δ=2.86 (s, 4H, $-CH_2CH_2-$), 3.44 (s, 6H, OCH_3), 3.88 (s, 6H, OCH_3), and 6.96—7.60 (m, 9H, Ar-H); MS *m/z* 564 (M^+, 70), 532 (M^+—S, 7), 500 (17), 473 (532-$COOCH_3$, 21), 444 (1), 328 (M^+—4$COOCH_3$, 48), 297 (21), 239 (54), and 93 (100). Found: C, 61.41; H, 4.56%. Calcd for $C_{29}H_{25}O_8PS$: C, 61.70; H, 4.46%.

2,3-Bis(methoxycarbonyl)-4,6-diphenyl-4*H*-thiin (8a): IR (neat) 2975, 1740 (C=O), 1260, and 1230 cm^{-1}; ^1H NMR δ= 3.58 (s, 3H, OCH_3), 3.77 (s, 3H, OCH_3), 4.87 (d, 1H, J_{HH}= 6.0 Hz), 6.08 (d, 1H, J_{HH}=6.0 Hz), and 7.00—7.60 (m, 10H, Ar-H); MS *m/z* 366 (M^+, 29), 334 (M^+—S, 13), 307 (M^+—$COOCH_3$, 100), and 289 (M^+—Ph, 53).

2,3-Bis(methoxycarbonyl)-6-phenyl-4-*p*-tolyl-4*H*-thiin (8b): IR (neat) 2950, 1720 (C=O), 1250, and 1220 cm^{-1}; ^1H NMR δ=2.26 (s, 3H, CH_3), 3.62 (s, 3H, OCH_3), 3.80 (s, 3H, OCH_3), 4.83 (d, 1H, J_{HH}=6.0 Hz), 6.08 (d, 1H, J_{HH}=6.0 Hz), and 6.83—7.60 (m, 9H, Ar-H); MS *m/z* 380 (M^+, 17), 348 (M^+—S, 19), 321 (M^+—$COOCH_3$, 100), and 289 (M^+-*p*-Tol, 35).

2,3-Bis(methoxycarbonyl)-1-phenyl-9,10-dihydro-1*H*-4-thiaphenanthrene (8c): IR (KBr) 2950, 1740 (C=O), 1260, and 1240 cm^{-1}; ^1H NMR δ=2.18—2.92 (m, 4H, $-CH_2CH_2-$), 3.68 (s, 3H, OCH_3), 3.84 (s, 3H, OCH_3), 4.77 (s, 1H), and 7.12—7.48 (m, 9H, Ar-H); MS *m/z* 392 (M^+, 30), 360 (M^+—S, 13), 333 (M^+—$COOCH_3$, 82), and 315 (M^+—Ph, 100).

3,4,5,7-Tetraphenyl-1-phosphabicyclo[2.2.2]octa-2,5,7-triene 1-Sulfide (11a): ^1H NMR δ=6.48—7.78 [m, 22H, H(α-2) and Ar-H] and 8.49 [d, 1H, J_{HP}=30.0 Hz, H(β-1)]; MS *m/z* 458 (M^+, 1), 395 (M^+—PS, 5), 356 (**10a**, 75), 324 (**10a**-S, 70), 254 (**10a**-PhC≡CH, 100), and 102 (PhC≡CH, 72). Found: C, 81.08; H, 5.08%. Calcd for $C_{31}H_{23}PS$: C, 81.20; H, 5.06%.

7-*p*-Tolyl-3,4,5-triphenyl-1-phosphabicyclo[2.2.2]octa-2,5,7-triene 1-Sulfide (11b): ^1H NMR δ=2.42 (s, 3H, CH_3), 6.56—7.40 [m, 17H, H(α-2) and Ar-H], 7.28 (d, 2H, J_{HH}=8.0 Hz, *p*-Tol-H), 7.62 (dd, 2H, J_{HH}=8.0 Hz, J_{HP}=1.5 Hz, *p*-Tol-H), and 8.45 [d, 1H, J_{HP}=30.0 Hz, H(β-1)]; MS *m/z* 472 (M^+, 10), 438 (M^+-H_2S, 4), 409 (M^+—PS, 12), 370 (**10b**, 100), 338 (**10b**-S, 98), 268 (**10b**-PhC≡CH, 83), and 102 (PhC≡CH, 98). Found: C, 81.20; H, 5.23%. Calcd for $C_{32}H_{25}PS$: C, 81.33; H, 5.33%.

2,3-Benzo-7,10,11-triphenyl-8-phosphatricyclo[6.2.2.0^{1,6}]-dodeca-6,10,11-triene 8-Sulfide (11c): ^1H NMR δ=2.98 (s, 4H, $-CH_2CH_2-$), 5.88—6.40 (m, 2H, Ar-H), and 6.60—7.60 [m, 19H, H(α-2) and Ar-H]; ^{31}P NMR δ=8.43 (t, J_{PH}= 20.3 Hz); MS *m/z* 484 (M^+, 11), 450 (M^+-H_2S, 9), 421 (M^+—PS, 21), 382 (**10c**, 25), 350 (**10c**-S, 27), 280 (**10c**-PhC≡CH, 50), and 102 (PhC≡CH, 100). Found: C, 81.83; H, 5.18; S, 6.26%. Calcd for $C_{33}H_{25}PS$: C, 81.79; H, 5.20; S, 6.62%.

3,5,7,8,10-Pentaphenyl-1-phospha-2-thiabicyclo[4.4.0]deca-3,7,9-triene 1-Sulfide (12a): ^1H NMR δ=3.75 [dd, 1H, J_{HH}= 10.0 Hz, J_{HP}=14.0 Hz, H(6)], 4.28 [ddd, 1H, J_{HH}=4.5, 10.0 Hz, J_{HP}=14.5 Hz, H(5)], 6.32—6.60 (m, 2H), 6.41 [dd, 1H, J_{HH}= 4.5 Hz, J_{HP}=2.5 Hz, H(4)], 6.72—7.52 (m, 22H), and 7.72—7.94 (m, 2H); ^{31}P NMR δ=49.39 (dddd, J_{PH}=2.5, 14.0, 14.5, 36.0 Hz); MS *m/z* 580 (M^+, 1), 356 (**10a**, 31), 324 (**10a**-S, 76), 254 (**10a**-PhC≡CH, 43), and 223 (**3a**-H, 100). Found: C, 78.52; H, 5.04; S, 11.03%. Calcd for $C_{38}H_{29}PS_2$: C, 78.59; H, 5.03; S, 11.04%.

5,10-Di-*p*-tolyl-3,7,8-triphenyl-1-phospha-2-thiabicyclo[4.4.0]-deca-3,7,9-triene 1-Sulfide (12b): ^1H NMR δ=2.26 (s, 3H, CH_3), 2.39 (s, 3H, CH_3), 3.73 [dd, 1H, J_{HH}=10.0 Hz, J_{HP}=14.0 Hz, H(6)], 4.23 [ddd, 1H, J_{HH}=4.5, 10.0 Hz, J_{HP}=15.5 Hz, H(5)], 6.32—7.44 [m, 22H, H(9) and Ar-H], 6.41 [dd, 1H, J_{HH}=4.5 Hz, J_{HP}=2.5 Hz, H(4)], and 7.75 (dd, 2H, J_{HH}= 8.0 Hz, J_{HP}=2.5 Hz, *p*-Tol-H); MS *m/z* 608 (M^+, 1), 370 (**10b**, 29), 338 (**10b**-S, 100), 268 (**10b**-PhC≡CH, 34), and 237 (**3b**-H, 56). Found: C, 78.84; H, 5.51%. Calcd for $C_{40}H_{33}PS_2$: C, 78.91; H, 5.46%.

7,15,16-Triphenyl-5,6,13,14,15,15a-hexahydro-7a-phospha-8-thiadibenzo[*a*,*j*]naphthacene 7a-Sulfide (12c): ^1H NMR δ=2.04—2.20 (m, 4H, $-CH_2-$), 2.48—2.92 (m, 4H, $-CH_2-$), 3.78 [dd, 1H, J_{HH}=8.0 Hz, J_{HP}=14.5 Hz, H(6)], 4.16 [dd, 1H, J_{HH}=8.0 Hz, J_{HP}=22.0 Hz, H(5)], and 6.50—7.70 (m, 23H, Ar-H); MS *m/z* 632 (M^+, 1), 382 (**10c**, 98), 350 (**10c**-S, 100), 280 (**10c**-PhC≡CH, 91), and 249 (**3c**-H, 51). Found: C, 79.68; H, 5.18%. Calcd for $C_{42}H_{33}PS_2$: C, 79.72; H, 5.26%.

The authors wish to thank JEOL LTD. for measuring the ^{31}P NMR spectra and also Mr. Yasuhiro Terauchi for technical assistance.

References

1) H. Yamaguchi, S. Kametani, T. Karakasa, T. Saito, and S. Motoki, *Tetrahedron Lett.*, **23**, 1263 (1982); T. Uchida, K. Kozawa, T. Saito, and S. Motoki, *Bull. Chem. Soc. Jpn.*, **57**, 1985; 1990 (1984); H. Tanaka, S. Kametani, T. Saito, and S. Motoki, *ibid.*, **58**, 667 (1985); H. Tanaka, T. Saito, and S. Motoki, *ibid.*, **59**, 59 (1986).

2) G. Märkl, *Angew. Chem., Int. Ed. Engl.*, **5**, 846 (1966) and later papers.

3) J.-M. Alcaraz and F. Mathey, *J. Chem. Soc., Chem. Commun.*, **1984**, 508.

4) J.-M. Alcaraz and F. Mathey, *Tetrahedron Lett.*, **25**, 4659 (1984).

5) G. Märkl and F. Lieb, *Angew. Chem., Int. Ed. Engl.*, **7**, 733 (1968).

6) E. T. Østensen, A. A.-A. Abdallah, S. H. Skaare, and M. M. Mishrikey, *Acta Chem. Scand., Ser. B*, **31**, 496 (1977).

A Convenient Synthesis of (±)-Dimorphecolic Acid and Its Analogs

Sadao TSUBOI, Seiji MAEDA, and Akira TAKEDA*
Department of Synthetic Chemistry, School of Engineering, Okayama University, Tsushima, Okayama 700
(Received January 22, 1986)

Synopsis. Dimorphecolic acid, self-defensive substances in rice plant against rice blast disease, and its analogs were prepared stereoselectively by the reaction of (2*E*,4*Z*)-2,4-decadienal with Grignard reagents.

Dimorphecolic acid (**1**) is one of self-defensive substances in rice plant against rice blast disease, which were isolated by Kato et al.[1] Compound **1** is also found in oil of vegetables and is shown to possess a unique ionophore activity.[2] Recently Morota et al. reported that dimorphecolic acid isolated from Lycium chinese Mill acts as an inhibitor against angiotensin I converting enzyme (ACE), namely as a hypotensive substance.[3] Rao et al. reported the first synthesis of **1** via several steps from epichlorohydrin.[4]

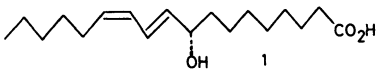

We present here a convenient synthesis of **1** via (2*E*,4*Z*)-2,4-decadienal. The synthetic sequence is shown in Scheme 1. The starting material, (2*E*,4*Z*)-2,4-decadienal (**2**) can be obtained by the reduction of ethyl (2*E*,4*Z*)-2,4-decadienoate, which was prepared by the stereoselective rearrangement of ethyl 3,4-decadienoate promoted with alumina, and the subsequent oxidation of the product.[5]

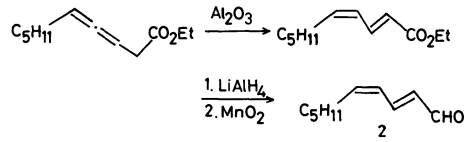

Reaction of **2** with Grignard reagent **3**[6] from 8-chloro-1-octanol gave the diol **4** in 59% yield. Oxidation of **4** with pyridinium dichromate in *N*,*N*-dimethylformamide (DMF) gave the keto acid **5**.[7] Reduction of **5** with $NaBH_4$–$CeCl_3$ in methanol afforded dimorphecolic acid (25% yield from **4**). On the other hand, one-pot synthesis of **1** was established by the reaction of **2** with 1,7-heptanediyldimagnesium dibromide (**6**)[8] followed by carboxylation and esterification (37% total yield as the methyl ester **7**). The ester **7** was converted to the benzoate, of which ^{13}C NMR data were identical with those of the literature.[1a] This carboxylation was accompanied by the formation of (2*E*,4*Z*)-2,4-decadien-1-ol (**8**) (15%) and tetraenediol **9** (42%), the reaction product of **6** with two equivalents of **2**. These compounds could be separated by HPLC or medium pressure chromatography. The present synthesis is one of rare examples[8d] of the application of di-Grignard reagents for the synthesis of natural products.

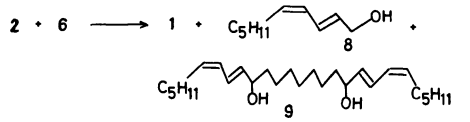

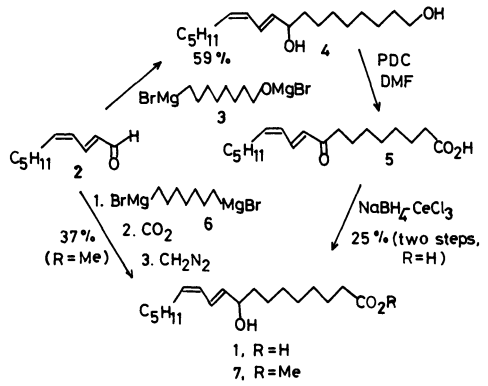

Scheme 1.

Furthermore, analogs of **1** were prepared in good yields by the reaction of **2** with Grignard reagents such as butylmagnesium bromide and octylmagnesium bromide as shown below. The biological activity of dienols **10** and **11** was examined against rice plant diseases. Neither **10** nor **11** showed any control activities against diseases such as rice blast, rice sheath blight, and rice brown spot. This fact shows clearly that a carboxyl group of **1** plays an important role for biological activity.

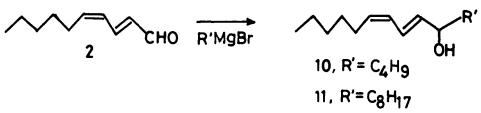

Although the present synthesis does not afford a high yield of **1**, the simplicity makes it more attractive than the previously reported ones.[4]

Experimental

The melting points and boiling points are uncorrected. Elemental analyses were carried out by Eiichiro Amano in our laboratory. Infrared (IR) spectra were obtained with a JASCO Model A-102 infrared spectrophotometer. High-performance liquid chromatography (HPLC) was performed with Hitachi Model 655 liquid chromatograph and Shodex Model SE-31 differential refractometer. ^1H NMR spectra (60 MHz) were recorded with a JEOL JNM-PMX60SI apparatus. ^{13}C NMR spectra were obtained with a JEOL JNM-FX100 apparatus, in $CDCl_3$ solvent. All chemical shifts are reported in δ units downfield from internal Me_4Si, and J values are given in herz. Column chromatography was accomplished with 100—200 mesh Wakogel C-200. Aldehyde **2** was prepared by the procedures described in the previous paper[5] and purified by column chromatography [silica gel, hexane–ethyl acetate (20:1—10:1)]. The purity (>95%) was checked by ^1H NMR spectrum.

(10*E*,12*Z*)-10,12-Octadecadiene-1,9-diol (4). To a mix-

ture of 73.6 mg (3.03 mg-atom) of magnesium and 0.5 ml of THF was added dropwise 0.115 ml (168 mg, 1.54 mmol) of ethyl bromide and the mixture was stirred for 1.5 h. After the dropwise addition of a solution of 8-bromo-1-octanol (316 mg, 1.51 mmol) in THF (1 ml) at 0 °C, the mixture was stirred for 30 min at 0 °C and then for 2.5 h at room temperature. At this interval 2—3 ml of THF was added. To the stirred mixture was added dropwise a solution of 152 mg (1 mmol) of **2** in 1 ml of THF at 0 °C. After the addition, the ice bath was removed and the mixture was stirred for 1.5 h. The reaction mixture was poured into aqueous NH_4Cl and extracted with ether. The organic layer was washed with water, dried over $MgSO_4$, and concentrated, and the resulting residue (410 mg) was chromatographed on 17 g of silica gel eluting with hexane–ethyl acetate–methanol (45:3:1) to give 149 mg (59%) of **4**: IR (neat) 3320 (OH), 2930, 1460, 1120, and 1060 cm^{-1}; ^1H NMR ($CDCl_3$) δ=0.90 (3H, t, J=6 Hz, CH_3), 1.33 (20H, br. S, $CH_3(CH_2)_3$, $(CH_2)_7CH_2OH$), 1.88 (2H, S, 2OH), 2.11 (2H, t, J=7 Hz, CH_2CH=CH), 3.58 (2H, t, J=6 Hz, CH_2OH), 4.15 (1H, m, $\succ$CHOH), 5.2—6.2 (3H, m, CH=CHCH=CHCHOH-), and 6.50 (1H, dd, J=10 and 15 Hz, CH=CHCHOH-). Found: C, 76.37; H, 12.27%. Calcd for $C_{18}H_{34}O_2$: C, 76.54; H, 12.13%.

Oxidation of 4 with Pyridinium Dichromate. To a solution of 1.28 g (3.40 mmol) of pyridinium dichromate[9] in 1 ml of DMF was added a solution of 160 mg (0.566 mmol) of **4** in 1.5 ml of DMF at 0 °C under an atmosphere of nitrogen. The mixture was stirred for 14 h at room temperature and then poured into water. The organic layer was extracted with ether, washed with water, dried over $MgSO_4$, and concentrated to give 124 mg of crude **5**: IR (neat) 3600—2500 (CO_2H), 1710 (C=O), 1590, 1460, and 1410 cm^{-1}; ^1H NMR ($CDCl_3$) δ=0.89 (3H, t, J=7 Hz, CH_3), 1.25 (16H, br. S, $CH_3(CH_2)_3$, $(CH_2)_5CH_2CO_2H$), 2.33 (4H, m, CH_2CH=CH, CH_2CO_2H), 3.38 (2H, t, J=5.5 Hz, CH_2COCH=), 5.5—6.4 (3H, m, CH=CHCH=CHCO), and 7.50 (1H, dd, J=10.5 and 16 Hz, CH=CHCO). The crude **5** was used for next step without purifucation.

Dimorphecolic Acid (1). To a solution of 313 mg (0.84 mmol) of cerium(III) chloride in 10 ml of methanol was added a solution of 124 mg (0.421 mmol) of **5** in 5 ml of methanol. Sodium borohydride (31.9 mg, 0.843 mmol) was added in several portions at 0 °C and the mixture was stirred for 4 h at 30—35 °C, and then poured into ice water, acidified with dilute HCl, and extracted with ether. The ethereal solution was washed with water, dried over $MgSO_4$, concentrated, and chromatographed on 7 g of silica gel eluting with hexane–ethyl acetate–methanol (45:4:1) to give 40.6 mg (25% yield estimated from **4**) of **1**:[1a] IR (neat) 3300—2500 (CO_2H), 1710 (C=O), 1460, 1410, and 980 cm^{-1}; ^1H NMR ($CDCl_3$) δ=0.90 (3H, t, J=6 Hz, CH_3), 1.28 (18H, m, $CH_3(CH_2)_3$, $(CH_2)_6CH_2CO_2H$), 2.0—2.5 (4H, m, CH_2CH=CH, CH_2CO_2H), 4.1 (1H, m, $\succ$CHOH), and 5.2—7.2 (5H, m, $\{CH=CH\}_2$, CO_2H).

Methyl Dimorphecolate (7) and (6*Z*,8*E*,19*E*,21*Z*)-6,8,19,21-Heptacosatetraene-10,18-diol (9). To a mixture of 53.7 mg (2.21 mmol) of magnesium and 1 ml of THF was added dropwise a solution of 0.17 ml (257 mg, 0.996 mmol) of 1,7-dibromoheptane in 1 ml of THF at 30—35 °C over 3 h. The mixture was stirred for 1 h and then 0.18 ml (175 mg, 0.98 mmol) of hexamethylphosphoric triamide (HMPA) was added at 15—18 °C. After 30 min, a solution of 120 mg (0.788 mmol) of **2** in 1.5 ml of THF was added dropwise, and the mixture was stirred for 1.5 h and then cooled at 0 °C. Carbon dioxide dried over anhydrous magnesium perchlorate was introduced and the mixture was stirred for 3 h under an atmosphere of carbon dioxide, and then poured into aqueous NH_4Cl cooled with ice. The mixture was acidified with dilute HCl and extracted three times with ether. The ethereal solution was washed with brine, dried ($MgSO_4$), and concentrated to give 286 mg of an oil, which was treated with diazomethane in ether. After concentration, the residual oil (288 mg) was analyzed by HPLC [column, SA-I (7.5 mmϕ×25 cm); elution, hexane–ethyl acetate–acetonitrile (10:3:1), 1 ml min^{-1}]. Peaks, retention times (min), integrated percentages are as follows: 1, 6.29, 9.9%; 2, 7.78, 45.5%; 3, 8.97, 31.7%; 4, 11.4, 12.9%. Each component was separated by preparative HPLC and assigned by spectral data.

Peak 1: 1,7-dibromoheptane.

Peak 2: **9**; 41% yield; IR (neat) 3350 (OH), 2950, 1462, and 980 cm^{-1}; ^1H NMR ($CDCl_3$) δ=0.89 (6H, t, J=6 Hz, $2CH_3$), 1.35 (26H, br. s, $2CH_3(CH_2)_3$, $(CH_2)_7CHOH$), 1.78 (2H, s, 2OH), 1.9—2.4 (4H, m, $2CH_2CH$=CH), 4.02 (2H, m, 2 $\succ$CHOH), 5.00—6.09 (6H, m, 2CH=CHCH=CHCHOH-), 6.32 (2H, dd, J=10 and 15 Hz, 2CH=CHCHOH-). Found: C, 80.37; H, 11.74%. Calcd for $C_{27}H_{48}O_2$: C, 80.14; H, 11.96%.

Peak 3: **7**;[1a] 37% yield; IR (neat) 3450 (OH), 2940, 1745 (CO_2CH_3), 1460, 1435, 1195, 1170, and 981 cm^{-1}; ^1H NMR (CCl_4) δ=0.90 (3H, t, J=5 Hz, CH_3), 1.35 (18H, br s, $CH_3(CH_2)_3$, $(CH_2)_6CH_2CO_2CH_3$), 1.9—2.4 (4H, m, CH_2-CH=CH, $CH_2CO_2CH_3$), 3.57 (3H, s, CO_2CH_3), 4.02 (1H, m, $\succ$CHOH), 5.03—6.06 (3H, m, CH=CHCH=CHCHOH-), and 6.35 (1H, dd, J=10 and 15 Hz, CH=CHCHOH). ^{13}C NMR data ($CDCl_3$, δ) were tentatively assigned.[10]

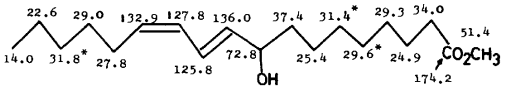

Found: C, 73.31; H, 10.80%. Calcd for $C_{19}H_{34}O_3$: C, 73.50; H, 11.04%.

Peak 4: **8**; IR and ^1H NMR spectra were identical with those of the literature.[5]

Methyl (10*E*,12*Z*)-9-benzoyloxy-10,12-octadecadienoate was prepared in 69% yield by the treatment of **7** (23 mg, 0.0744 mmol) with benzoyl chloride (13.2 mg, 0.0941 mmol) in pyridine (0.1 ml) at 20—25 °C for 5 h. Its ^{13}C NMR data was identical with those of the literature.[1a]

(6*E*,8*Z*)-6,8-Tetradecadien-5-ol (10). To a mixture of 162 mg (6.67 mmol) of magnesium in 0.5 ml of THF was added dropwise a solution of 0.59 ml (750 mg, 5.47 mmol) of butyl bromide in 1 ml of THF, occasionally cooling with water. After 2 h, a solution of 854 mg (5.47 mmol) of **2** in 1.5 ml of THF was added dropwise at 0 °C, and then the mixture was stirred for 30 min at 0 °C. After an additional stirring for 1 h at room temperature, the mixture was poured into aqueous NH_4Cl and extracted with ether. The organic layer was washed with brine, dried over $MgSO_4$, and concentrated to give 1.21 g of crude **10**. Preparative TLC gave 0.988 g (86%) of pure **10**: IR (neat) 3370 (OH), 2950, 1460, 1375, 980, and 950 cm^{-1}; ^1H NMR (CCl_4) δ=0.90 (6H, t, J=5 Hz, $2CH_3$), 1.36 (12H, br. s, $2CH_3(CH_2)_3$), 1.8—2.5 (3H, m, CH_2CH=, OH), 4.05 (1H, m, $\succ$CHOH), 5.28 (1H, m, CH=CHCH=CHCHOH-), 5.58 (1H, m, CH=CHCHOH-), 5.86 (1H, t, J=10 Hz, CH=CHCH=CHCHOH-), and 6.39 (1H, dd, J=10 and 15 Hz, CH=CHCHOH-). Found: C, 79.74; H, 12.62%. Calcd for $C_{14}H_{26}O$: C, 79.94; H, 12.46%.

(10*E*,12*Z*)-10,12-Octadecadien-9-ol (11). A solution of 850 mg (5.58 mmol) of **2** in 1.5 ml of THF was treated with a THF solution of octylmagnesium bromide prepared from magnesium (162 mg, 6.67 mmol), 1-bromooctane (1.33 g, 6.99 mmol) and THF (1 ml), as shown in the preparation of **10**. The reaction mixture was worked up as usual to give 1.63 g of crude **11**, which was purified by preparative TLC (silica gel, hexane–ethyl acetate (2:1)) to give 1.29 g (87%) of pure **11**: IR (neat) 3370 (OH), 2950, 1460, 1380, and 980 cm^{-1}; ^1H NMR (CCl_4) δ=0.89 (6H, t, J=5.5 Hz, $2CH_3$), 1.28 (2OH, br. s, $CH_3(CH_2)_3$, $CH_3(CH_2)_7$), 1.95—2.41 (2H, m, CH_2CH=CH),

4.01 (1H, m, >CHOH), 5.26 (1H, m, CH=CHCH=CHCHOH), 5.53 (1H, m, CH=CHCHOH), 5.82 (1H, t, J=10 Hz, CH=CH CH=CHCHOH), and 6.35 (1H, dd, J=10 and 15 Hz, CH= CHCHOH-). ^{13}C NMR data ($CDCl_3$, δ).[10] Assignments of

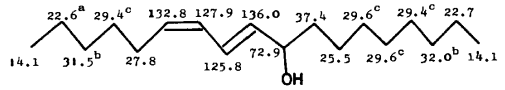

a, b, c may be interchangeable. Found: C, 81.38; H, 12.72%. Calcd for $C_{18}H_{34}O$: C, 81.13; H, 12.86%.

This work was supported in part by a Grant-in-Aid for Developmental Scientific Research (No. 59850144) from the Ministry of Education, Science and Culture in Japan. We thank Hokko Chemical Industry Co., LTD for the test of control activity against plant diseases. We also thank Professors J. F. Normant and A. Alexakis of the University of Pierre and Marie Curie for their suggestions concerning di-Grignard reagents.

References

1) a) T. Kato, Y. Yamaguchi, T. Hirano, T. Yokoyama, T. Uyehara, T. Namai, S. Yamanaka, and N. Harada, *Chem. Lett.*, **1984**, 409; b) T. Kato, Y. Yamaguchi, T. Uyehara, T. Yokoyama, T. Namai, and S. Yamanaka, *Tetrahedron Lett.*, **24**, 4715 (1983).

2) G. A. Blondin, Ann. N. Y. *Acad. Sci.*, **264**, 98 (1975).

3) a) T. Morota, H. Sasaki, M. Chin, T. Sato, N. Katayama, K. Fukuyama, and H. Mitsuhashi, the 32nd Annual Meeting of Pharmacognosical Society of Japan (October 12, 1985, Okayama), **2A**, 9-5; b) K. Niitsu, S. Iketani, T. Sato, N. Katayama, K. Fukuyama, M. Chin, H. Taguchi, and H. Mitsuhashi, *ibid.*, **2A**, 10-1.

4) A. V. Rama Rao, E. Rajarathnam Reddy, G. V. M. Sharma, P. Yadagiri, and J. S. Yadav, *Tetrahedron Lett.*, **26**, 465 (1985).

5) S. Tsuboi, T. Masuda, and A. Takeda, *J. Org. Chem.*, **47**, 4478 (1982).

6) G. Calriez, A. Alexakis, and J. F. Normant, *Tetrahedron Lett.*, **1978**, 3013.

7) L. Crombie and S. J. Holloway, *J. Chem. Soc., Chem. Commun.*, **1984**, 953.

8) Syntheses of similar di-Grignard reagents have been reported: a) L. H. Sommer and G. R. Ansul, *J. Am. Chem. Soc.*, **77**, 2482 (1955); b) M. Kumada, *J. Inst. Polytech. Osaka City Univ.*, **1**, 11 (1958); c) K. Diemert, P. Haas, and W. Kuchen, *Chem. Ber.*, 111, 629 (1978); d) T. Fujisawa, T. Sato, T. Kawara, and H. Tago, *Bull. Chem. Soc. Jpn.*, **56**, 345 (1983).

9) E. J. Corey and G. Schmidt, *Tetrahedron Lett.*, **1979**, 399.

10) Chemical shifts of olefinic carbons were estimated by proton selective decoupling experiments.

*Assignments may be interchangeable.

Oxidation Reactions of a System Composed of Chloro(5,10,15,20-tetraphenylporphyrinato)cobalt(III) and Its π Cation Radical with Phenols

Masahiro KOHNO
JEOL Ltd., Akishima, Tokyo 196
(Received May 31, 1985)

The reactions of a system composed of chloro(5,10,15,20-tetraphenylporphyrinato)cobalt(III), [Co^{III}Cl(tpp)], and its π cation radical coordinating axially two chloride anions, [Co^{III}(tpp)$^{+\cdot}$]Cl_2, with several phenols were investigated by using ESR and optical absorption spectroscopy. The phenols were oxidized to phenoxyl radicals. The phenols investigated were classified into two groups after taking into account the differences in the reaction activities and their redox potentials, the phenols mainly reacting with [Co^{III}(tpp)$^{+\cdot}$]Cl_2 and those reacting with both [Co^{III}Cl(tpp)] and [Co^{III}(tpp)$^{+\cdot}$]Cl_2. The oxidation reactions of phenols with [Co^{III}(tpp)$^{+\cdot}$]Cl_2 were the second-order. A linear relationship between the rate constants of oxidation and the redox potentials of phenols was recognized. Active species in the reactions were determined to be composed of a chlorine radical which originates from axial ligands of [Co^{III}Cl(tpp)] and [Co^{III}(tpp)$^{+\cdot}$]Cl_2, and the porphyrin ligand of [Co^{III}(tpp)$^{+\cdot}$]Cl_2 itself. A possible mechanism for the oxidation reactions is proposed. Finally, the reaction scheme of cobalt porphyrin, ([Co^{II}(tpp)], [Co^{III}Cl(tpp)], and [Co^{III}(tpp)$^{+\cdot}$]Cl_2) with phenols is compared with oxidation reactions of phenols with horseradish peroxidase.

Peroxidase enzymes catalyze oxidation reactions of various kinds of substrates in the presence of hydrogen peroxide or substituted peroxides in biological systems. Because of the biologically important function of peroxidases, their structures, physicochemical properties, and reactivities have been extensively studied by many workers.[1] It has been known that horseradish peroxidase (HRP) takes on five different oxidation states: iron(II), iron(III), Compound II, Compound I, and Compound III, as characterized in the order of increasing oxidation states, and that Compound I is a π cation radical of iron(IV) porphyrin.[2] The π cation radicals of synthetic metalloporphyrins were prepared by chemical, electrochemical, or photochemical oxidation and their chemical natures have also been investigated.[3]

Previously, the electronic and molecular structures of chloro(5,10,15,20-tetraphenylporphyrinato)cobalt(III), [Co^{III}Cl(tpp)], were investigated by X-ray analyses, optical absorption, ^{1}H NMR, and ESR.[4-11] We have determined by ESR that [Co^{III}Cl(tpp)] is converted partially and reversibly into a paramagnetic species in chlorinated hydrocarbons by thermal and light activations.[4] This species was identified to be a π cation radical of chloro(5,10,15,20-tetraphenylporphyrinato)cobalt(III) with two axially coordinating chloride anions, [Co^{III}(tpp)$^{+\cdot}$]Cl_2.[5,6] The formation of this species in a [Co^{III}Cl(tpp)] solution was inevitable, even if a careful purification process of [Co^{III}Cl(tpp)] by column chromatography was carried out. It was recently clarified that [Co^{III}Cl(tpp)] in an aerated dichloromethane solution undergoes photooxidation to produce [Co^{III}(tpp)$^{+\cdot}$]Cl_2.[12] Hereafter, we treated the [Co^{III}Cl(tpp)] solution with a small amount of [Co^{III}(tpp)$^{+\cdot}$]Cl_2, denoted as [Co^{III}Cl(tpp)]-[Co^{III}(tpp)$^{+\cdot}$]Cl_2.

In the present study, we characterized the function of [Co^{III}Cl(tpp)]-[Co^{III}(tpp)$^{+\cdot}$]Cl_2. through an investigation of the reaction between these complexes and phenol derivatives by means of ESR and optical absorption spectroscopy and cyclic voltammetry. A possible reaction mechanism of these complexes with the phenols is proposed. Finally, the redox reaction scheme of the cobalt porphyrins with phenols is compared with that of horseradish peroxidase with phenols that is already known.

Experimental

Materials. Chloro(5,10,15,20-tetraphenylporphyrinato)-cobalt(III), [Co^{III}Cl(tpp)], was provided by Dr. K. Yamamoto of The Institute of Physical and Chemical Research.

2,6-Di-*t*-butyl-4-(3,5-di-*t*-butyl-4-oxocyclohexadienylidene)-methylphenol(PG), 2,4,6-tri-*t*-butylphenol(TBP), and 2,6-di-*t*-butyl-4-(3,5-di-*t*-butyl-4-oxo-2,5-cyclohexadienylideneamine)phenol(BIP) were prepared according to the literature.[13] 2,6-Di-*t*-butyl-4-methylphenol(BHT), 2,3-di-*t*-butyl-4-methoxyphenol(BHA), and α-tocopherol (vitamin E; VE), supplied from Wako Junyaku Co., were used without further purification.

A spin trapping reagent, nitrosodurene was supplied by Mr. N. Takahashi of Sumitomo Chemical Co. Ltd.

Preparation of Sample Solutions. Benzene was used as a solvent. [Co^{III}Cl(tpp)] was dissolved in 2×10^{-3} mol dm^{-3}. The solution of [Co^{III}Cl(tpp)] contained a small amount of the π cation radical, [Co^{III}(tpp)$^{+\cdot}$]Cl_2.[4,6] The concentration of [Co^{III}(tpp)$^{+\cdot}$]Cl_2 (2.7×10^{-5} mol dm^{-3}) was determined by comparing its ESR intensity with that of 2,2,6,6-tetramethyl-4-hydroxy-1-piperidyloxyl (98% radical) dissolved in benzene as a standard.

Concentrations of phenols (PG, BHT, TBP, BIP, and BHA) were adjusted to be 1.0×10^{-2} mol dm^{-3} and a 1% solution was employed for the VE system. All solutions were prepared just before use.

Measurements. The ESR and optical absorption spectra of the reaction mixtures were measured under deaerated

conditions in order to avoid any oxidation of the phenols. The ESR measurements were carried out with a JEOL FE-2XG spectrometer equipped with a Takeda Riken TR-5211 microwave frequency counter. The *g*-value and hyperfine coupling constant(hfcc) were calculated from the resonance frequency and the magnetic field. The optical absorption spectra were measured by a Hitachi 330 spectrophotometer using quartz cells with optical path lengths of 1 and 0.1 cm. Cyclic voltammograms were measured for the phenols (1.0×10^{-3} mol dm^{-3}) dissolved in dichloromethane with 0.1 mol dm^{-3} of tetrabutylammonium-tetrafluoroborate ($TBAF_4$). The cyclic voltammograms were recorded by a Yanagimoto P-1000H instrument at 25 °C at a scan rate of 100 mV s^{-1}. The redox potentials($E_{1/2}$) obtained from the cyclic voltammograms were checked by simultaneous polarographic measurement.

Time-dependent ESR spectra were measured using a rapid-detection system. To 0.2 cm^3 of the [Co^{III}Cl(tpp)]-[Co^{III}(tpp)$^{+\cdot}$]Cl_2 solution, which was bubbled by dry nitrogen gas, was added 0.2 cm^3 of the phenol solution (1×10^{-2} mol dm^{-3}).

Results

Reactions of [Co^{III}Cl(tpp)]-[Co^{III}(tpp)$^{+\cdot}$]Cl_2 with Phenols (PG, BHT, TBP, BIP, BHA, and VE). The ESR spectra measured before and after the addition of PG to the [Co^{III}Cl(tpp)]-[Co^{III}(tpp)$^{+\cdot}$]Cl_2 solution are shown in Fig. 1. The solid line represents the signal of [Co^{III}(tpp)$^{+\cdot}$]Cl_2.[5,6] Upon an addition of PG, the intensity of the signal decreased and a new ESR signal with doublet-triplet splittings appeared. The new signal(dotted line) was identified as a phenoxyl radical of PG (PG·) on the basis of ESR parameters; g=2.0043, a_{H1}=0.85 mT, a_{H2}=0.17 mT, which coincide with the literature values within the experimental errors.[14] Both the concentrations of the reduced [Co^{III}(tpp)$^{+\cdot}$]Cl_2 and oxidized PG were estimated to be 1.2×10^{-5} mol dm^{-3} under equilibrium states. The corresponding optical absorption spectra are shown in Fig. 2. An intense band at 406 nm (Soret band) and a moderate one at 540 nm (Q band) were determined to represent the characteristic absorption of [Co^{III}Cl(tpp)].[8] The spectrum obtained after an addition of PG showed no appreciable change in the region of the Soret and Q bands, except for a slight decrease in the absorption intensity in the region of 640—740 nm; this was interpreted to be due to a decrease in [Co^{III}(tpp)$^{+\cdot}$]Cl_2.[12] These spectral changes suggest that PG was oxidized to PG· and

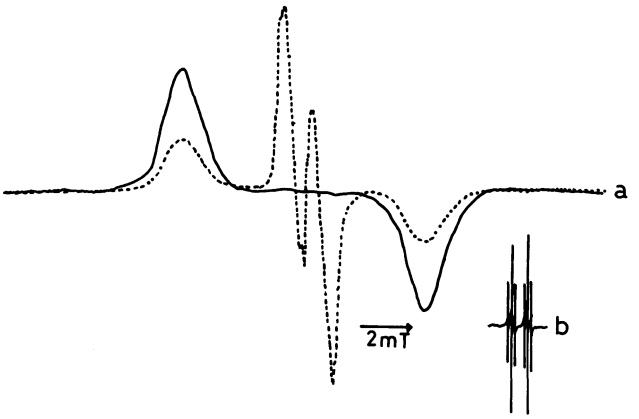

Fig. 1. a: ESR spectra measured before (——) and after (·····) addition of PG to [Co^{III}Cl(tpp)]-[Co^{III}(tpp)$^{+\cdot}$]Cl_2 in benzene at room temperature under degassed condition. b: The high resolution spectrum of center PG-phenoxyl radical.

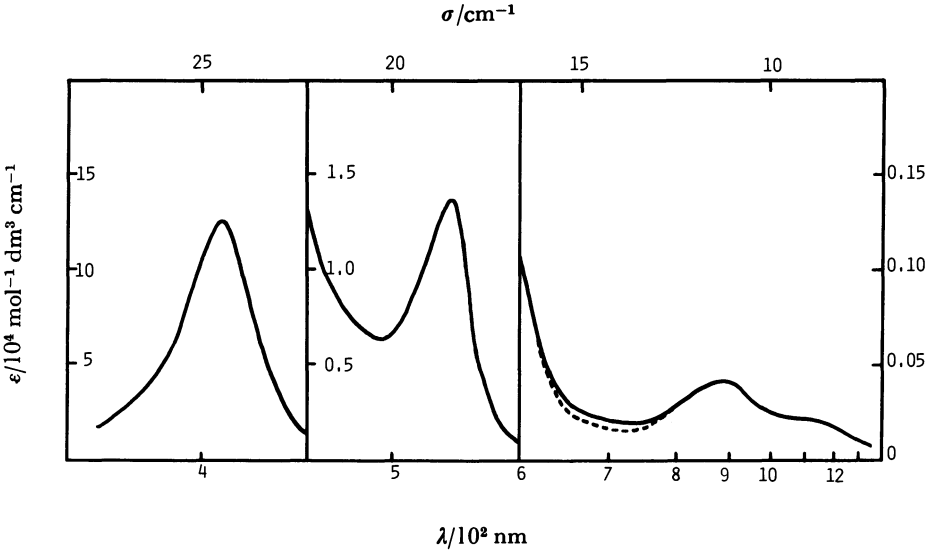

Fig. 2. Optical absorption spectra measured before (——) and after (·····) addition of PG to [Co^{III}Cl(tpp)]-[Co^{III}(tpp)$^{+\cdot}$]Cl_2 in benzene at room temperature under degassed condition.

$[Co^{III}(tpp)^{+\cdot}]Cl_2$ was reduced to $[Co^{III}Cl(tpp)]$, while the component $[Co^{III}Cl(tpp)]$ was unchanged.

In a reaction of $[Co^{III}Cl(tpp)]$-$[Co^{III}(tpp)^{+\cdot}]Cl_2$ with BHT or TBP, the phenol was oxidized to the corresponding phenoxyl radical (BHT· or TBP·),[15] and $[Co^{III}(tpp)^{+\cdot}]Cl_2$ was reduced to $[Co^{III}Cl(tpp)]$, as in the case of the PG system.

A reaction of $[Co^{III}Cl(tpp)]$-$[Co^{III}(tpp)^{+\cdot}]Cl_2$ with BIP also gave rise the formation of a phenoxyl radical (BIP·) (Fig. 3). The ESR parameters obtained from the spectrum are g=2.0036, a_N=0.21 mT, and a_H=0.104 mT. These values coincide with the reported values.[13] The concentrations of formed BIP· and the reduced $[Co^{III}(tpp)^{+\cdot}]Cl_2$ were 5.3×10^{-5} and 1.5×10^{-5} mol dm^{-3}, respectively. The concentration of formed BIP· was greater than that of reduced $[Co^{III}(tpp)^{+\cdot}]Cl_2$. This is different from the cases of the reaction with PG, BHT, or TBP. The optical spectrum of the reaction of $[Co^{III}Cl(tpp)]$-$[Co^{III}(tpp)^{+\cdot}]$-Cl_2 with BIP showed that the Soret band of $[Co^{III}Cl(tpp)]$ shifts from 406 to 410 nm with an increase in the absorption intensity. The red shift of the Soret band can be attributed to a further reduction of $[Co^{III}Cl(tpp)]$ to $[Co^{II}(tpp)]$[16] in the BIP system.

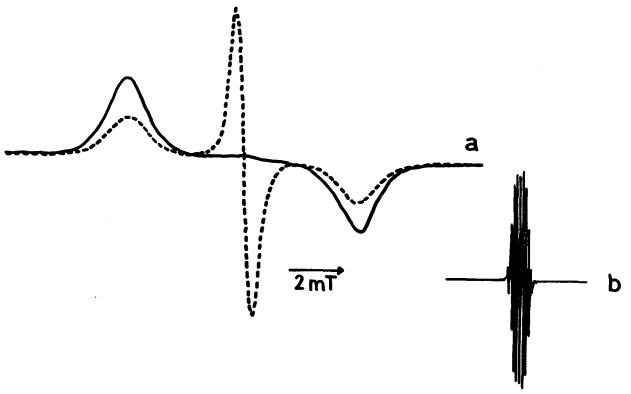

Fig. 3. a: ESR spectra measured before (——) and after (·····) addition of BIP to $[Co^{III}Cl(tpp)]$-$[Co^{III}(tpp)^{+\cdot}]Cl_2$ in benzene at room temperature under degassed condition. b: The high resolution spectrum of center BIP–phenoxyl radical.

When BHA and VE reacted with $[Co^{III}Cl(tpp)]$-$[Co^{III}(tpp)^{+\cdot}]Cl_2$, the ESR spectra of the reaction mixtures gave rise to new signals with a disappearance of the $[Co^{III}(tpp)^{+\cdot}]Cl_2$ signal. The new signals were assigned as BHA· and VE·, respectively.[17] The change in the optical absorption spectra of BHA is shown in Fig. 4. The absorption bands at 540 and 406 nm shifted to 530 and 410 nm, respectively, with an increase in absorption intensity. Furthermore, a weak band and a shoulder appeared at 1020 and 900 nm, respectively. The spectral change in the region of Q and the Soret bands indicates that a conversion of $[Co^{III}Cl(tpp)]$ to $[Co^{II}(tpp)]$ takes place in this system. The features of the ESR and optical absorption spectra show that BHA and VE react with both $[Co^{III}(tpp)^{+\cdot}]Cl_2$ and $[Co^{III}Cl(tpp)]$, as in the case of the BIP system. The appearance of new bands at the near-infrared region implies that isoporphyrin was formed. The absorption band is indeed complied with those of zinc- and iron-isoporphyrin.[18,19] For a comparison of such activities of phenols with their redox potentials, the oxidation potentials of the phenols under consideration were measured using cyclic voltammetry. The obtained potentials are listed in Table 1 with the ESR

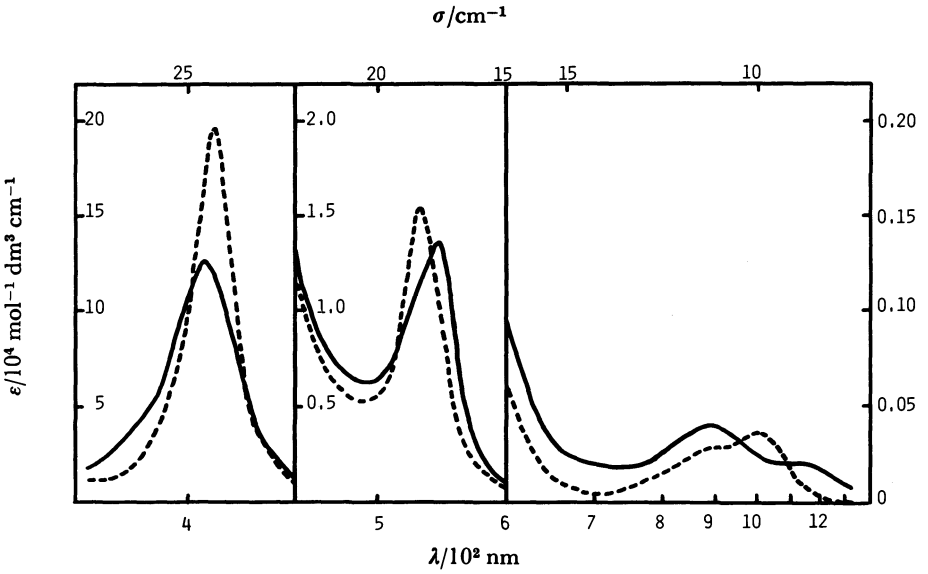

Fig. 4. Optical absorption spectra measured before (——) and after (·····) addition of BHA to $[Co^{III}Cl(tpp)]$-$[Co^{III}(tpp)^{+\cdot}]Cl_2$ in benzene at room teperature under degassed condition.

Table 1. ESR Parameters of Phenoxyl Radicals and Redox Potentials of Phenols[1] and Rate Constants(k_f) of the Reactions between [$Co^{III}(tpp)^{+\cdot}$]Cl_2 and the Phenols

Phenoxyl radical	ESR parameter		$E_{1/2}$ CV_1(eV) vs. SCE	k_f
	g-value	hfcc(mT)		$mol^{-1}\,s^{-1}$
PG·	2.0043	a_{H1}: 0.85	1.66	4.5×10^2
		a_{H2}: 0.17		
TBP·	2.0043	unresoluble	1.16	3.6×10^3
BHT·	2.0045	a_H: 1.12	1.10	
BHA·	2.0045	a_H: 0.48	0.97	7.2×10^3
BIP·	2.0036	a_N: 0.21	0.89	
		a_H: 0.104		
VE·	2.0047	a_{H1}: 0.58	0.75	
		a_{H2}: 0.44		

1) PG: 2,6-di-*t*-butyl-4-(3,5-di-*t*-butyl-4-oxocyclohexadienylidene)methylphenol. TBP: 2,4,6-tri-*t*-butylphenol. BHT: 2,6-di-*t*-butyl-4-methylphenol. BHA: 2,3-di-*t*-butyl-4-methoxyphenol. BIP: 2,6-di-*t*-butyl-4-(3,5-di-*t*-butyl-4-oxo-2,5-cyclohexadienylideneamine)phenol. VE: α-tocopherol (vitamin E).

parameters of all the obtained phenoxyl radicals.

Kinetics of the Reaction between [$Co^{III}(tpp)^{+\cdot}$]Cl_2 and BHA, TBP, or PG. The time-dependent ESR spectra of mixed solutions of [$Co^{III}(tpp)^{+\cdot}$]Cl_2 (2.7×10^{-5} mol dm^{-3}) with BHA in a range from 1×10^{-2} to 6.25×10^{-4} mol dm^{-3} were measured at 30 °C by using the rapid detection system combined with the method described in the Experimental section. In Fig. 5, the concentration of [$Co^{III}(tpp)^{+\cdot}$]Cl_2 estimated from the ESR signal intensities is plotted against the reaction time (in second). It is seen that the decay rates of [$Co^{III}(tpp)^{+\cdot}$]Cl_2 depend on the concentration of BHA, even in its excess range, as will be discussed later. The rate constants (k_f) for TBP and PG were determined in a similar manner as that of BHA (1×10^{-2} mol dm^{-3}) at 30 °C as is also listed in Table. 1.

The temperature dependence of a reaction between [$Co^{III}(tpp)^{+\cdot}$]Cl_2 and PG (1×10^{-2} mol dm^{-3}) was examined in order to obtain information regarding their activities. Upon increasing the temperature from 30 to 80 °C, the concentration of [$Co^{III}(tpp)^{+\cdot}$]Cl_2 decreased rapidly along with a concomitant increase in that of PG·. The enthalpy changes for [$Co^{III}(tpp)^{+\cdot}$]Cl_2 and PG· were estimated to be −1.7 and 7.1 kJ mol^{-1}, respectively, from the exponential portion.

Detection of Active Species Derived from [$Co^{III}Cl$(tpp)]-[$Co^{III}(tpp)^{+\cdot}$]Cl_2. The active species was detected using a spin-trapping method.[20] Among the various spin-trapping reagents tested for the detection, only nitrosodurene was effective to trap the

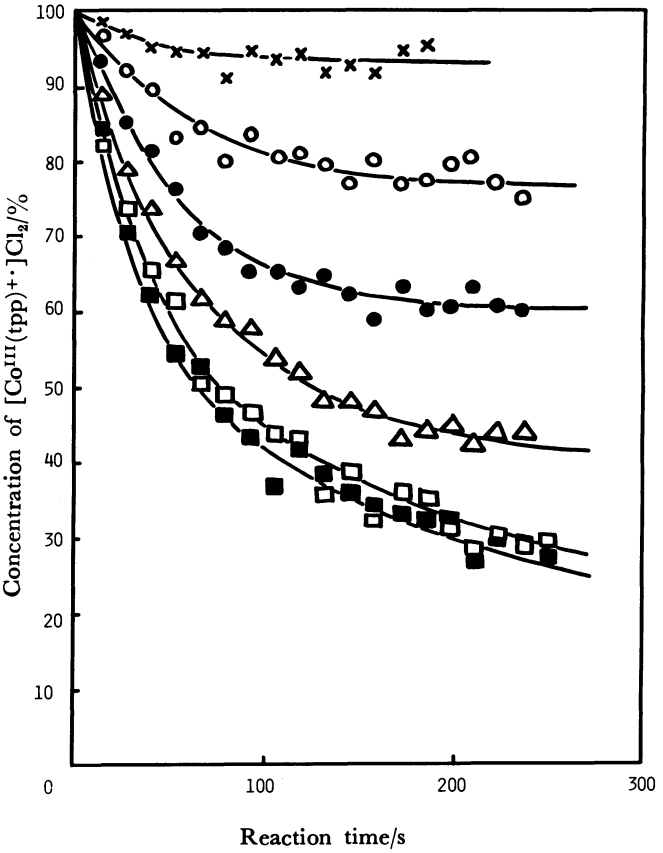

Fig. 5. Concentration decay of [$Co^{III}(tpp)^{+\cdot}$]Cl_2 in the reaction with BHA plotted against reaction time in second. Initial concentration of [$Co^{III}(tpp)^{+\cdot}$]Cl_2, 2.7×10^{-5} mol dm^{-3} and that of BHA, ■: 1.0×10^{-2}, □: 5.0×10^{-3}, △: 2.5×10^{-3}, ●: 1.25×10^{-3}, ○: 6.25×10^{-4} mol dm^{-3}, ×: blank.

species. To 1 cm^3 of the benzene solution of [$Co^{III}Cl$(tpp)]-[$Co^{III}(tpp)^{+\cdot}$]Cl_2, 3 mg of nitrosodurene was added under a degassed condition and the ESR spectrum was measured at room temperature.

The spin-trapping reaction is expressed as follows:

$$\text{R-N=O} + \text{X}\cdot \longrightarrow \text{R-N(X)-O}\cdot,$$

Scheme 1.

where X· is active species to be trapped. Figure 6 shows the ESR spectra of the spin adducts obtained by a reaction of [$Co^{III}Cl$(tpp)]-[$Co^{III}(tpp)^{+\cdot}$]Cl_2 with nitrosodurene. The spectra indicate the presence of two spin adducts (A and B). The following ESR parameters were obtained for A: one nitrogen (a_N=1.47 mT), one chlorine (a_{Cl}=0.284 mT), seven hydrogen (a_H=0.007 mT) nuclei, and for B; one nitrogen (a_N=1.47 mT) and seven hydrogen (a_H=0.007 mT) nuclei. From the ESR parameters, A was identified as a spin adduct of the nitrosodurene with a chlorine atom. The optical absorption spectrum which was measured after a reaction of [$Co^{III}Cl$(tpp)]-[$Co^{III}(tpp)^{+\cdot}$]Cl_2 with nitrosodurene in ben-

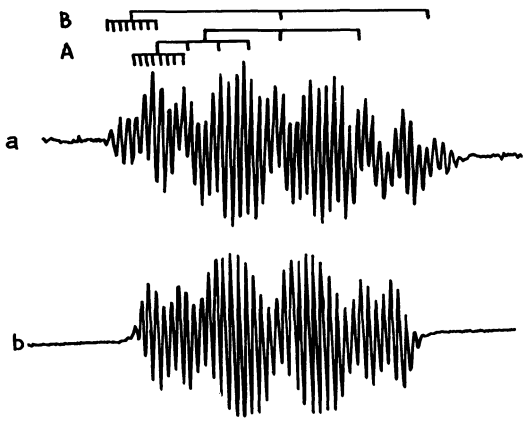

Fig. 6. ESR spectra of spin adducts (A and B) obtained from the reaction of nitrosodurene with [$Co^{III}Cl(tpp)$]–[$Co^{III}(tpp)^{+\cdot}$]Cl_2 in benzene at room temperature under degassed condition. Observed (a) and simulated for A (b) spectra.

zene at room temperature under a degassed condition showed the red shift of the Soret band, the blue shift of the Q band, and a decrease in the absorption intensity at around 600—700 nm. This spectral change was interpreted in terms of the formation of [$Co^{II}(tpp)$] from [$Co^{III}Cl(tpp)$] and [$Co^{III}(tpp)^{+\cdot}$]Cl_2. It is, thus, clear that the chlorine comes from axially coordinated chloride ligands in [$Co^{III}(tpp)^{+\cdot}$]Cl_2 and [$Co^{III}Cl(tpp)$]. This is the first case, to the auther's knowledge, that the active species in a reaction where metalloporphyrins participate has been directly detected. The second adduct B is probably a radical formed from nitrosodurene and a porphyrin ligand of [$Co^{III}(tpp)^{+\cdot}$]Cl_2.

Discussion

Based on the experiments described in the preceding section, phenols can be classified into two groups: group I (PG, TBP, and BHT) and group II (BHA, BIP, and VE). Phenols which belong to group II are more active than those of group I and are converted to phenoxyl radicals by both [$Co^{III}(tpp)^{+\cdot}$]Cl_2 and [$Co^{III}Cl(tpp)$], while phenols belonging to group I are oxidized only by [$Co^{III}(tpp)^{+\cdot}$]Cl_2. This difference in their activities can be explained in terms of the relative positions of the redox potentials of [$Co^{II}(tpp)$], [$Co^{III}Cl(tpp)$], [$Co^{III}(tpp)^{+\cdot}$]Cl_2, and phenols, as will be discussed in the following.

Regarding the oxidation process of the phenols, two oxidation mechanisms (1 and 2) have been proposed:[21]

$$POH \xrightarrow[CV_1]{-e} [POH]^{+\cdot} \xrightarrow{-H^+} PO\cdot \quad (1)$$

$$POH \xrightarrow{-H^+} PO^- \xrightarrow[CV_2]{-e} PO\cdot, \quad (2)$$

Scheme 2.

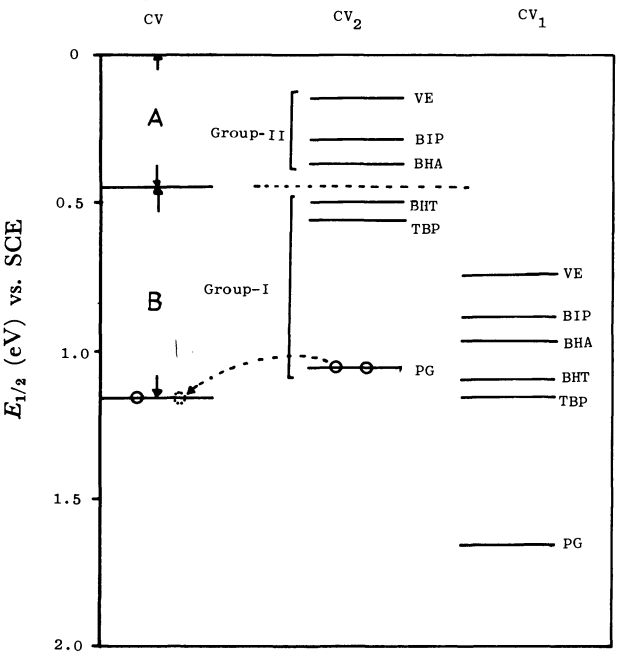

Fig. 7. Relative energy-level diagram of cobalt porphyrins and phenols. A and B represent half wave potential(CV) of [$Co^{II}(tpp)$]/[$Co^{III}Cl(tpp)$] and [$Co^{III}Cl(tpp)$]/[$Co^{III}(tpp)^{+\cdot}$]Cl_2, respectively. CV_1 represents half wave potential of phenols (POH)/phenol cation radicals ([POH]$^{+\cdot}$) and CV_2 phenolate anions (PO^-)/phenoxyl radicals ($PO\cdot$).

where phenols are abbreviated as POH. Process 1 means that first an electron is removed from phenol and then a proton is subtracted from the hydroxy group of the phenol to produce a phenoxyl radical.[22] In this process, the redox potential(CV_1) of POH/[POH]$^{+\cdot}$ obtained from a cyclic voltammogram should be the rate-determining factor. In process 2, first a proton is subtrated from the phenol, then, an electron transfer from phenolate anion follows. It has been reported[21] that the oxidation of 2,6-dimethylphenol(DMP) to diphenoquinone proceeds according to process 2 in the presence of a base(2,6-lutidine). A DMP–phenolate anion is formed through competition with the base. Such an ionic structure causes a decrease in the oxidation potential of the phenols. The redox potential (CV_2) of $PO^-/PO\cdot$ was estimated to be 0.6 eV lower than that of POH/[POH]$^{+\cdot}$(CV_1).[21]

In the present case, it is expected that the chloride anion of [$Co^{III}Cl(tpp)$] and/or [$Co^{III}(tpp)^{+\cdot}$]Cl_2 first forms an ion pair with the hydroxy proton of phenol and then process 2 proceeds predominantly. Here, we assume that in our case the oxidation potentials of phenolate anions formed are 0.6 eV lower than CV_1 of the precursor phenols. The energy-level scheme of phenols, [$Co^{III}(tpp)^{+\cdot}$]Cl_2, [$Co^{III}Cl(tpp)$], and [$Co^{II}(tpp)$] is given in Fig. 7 based on the cyclic voltammetries of these compounds. The CV_2 values of group I

phenols are lower than that of [Co^{III}Cl(tpp)]/[Co^{III}(tpp)$^{+\cdot}$]Cl$_2$[5] but higher than that of [Co^{II}(tpp)]/[Co^{III}Cl(tpp)], whereas the CV_2 values of group II phenols are higher than those of [Co^{III}Cl(tpp)]/[Co^{III}(tpp)$^{+\cdot}$]Cl$_2$ and [Co^{II}(tpp)]/[Co^{III}Cl(tpp)]. Consequently, the phenols of group I reduce only [Co^{III}(tpp)$^{+\cdot}$]Cl$_2$ but those of group II both [Co^{III}(tpp)$^{+\cdot}$]Cl$_2$ and [Co^{III}Cl(tpp)].

Possible Reaction Mechanism of [Co^{III}Cl(tpp)]-[Co^{III}(tpp)$^{+\cdot}$]Cl$_2$ with Phenols. When the concentrations of the phenols were of the same order as that of [Co^{III}(tpp)$^{+\cdot}$]Cl$_2$, the redox reaction did not proceeded. At concentrations 10^2 times higher than that of [Co^{III}(tpp)$^{+\cdot}$]Cl$_2$, however, the reaction process became spectroscopically detectable. A reaction of [Co^{III}Cl(tpp)]-[Co^{III}(tpp)$^{+\cdot}$]Cl$_2$ and PG showed that the amount of reduced [Co^{III}(tpp)$^{+\cdot}$]Cl$_2$ was equal to that of the generated PG phenoxyl radical. Furthermore, the redox reaction of [Co^{III}Cl(tpp)]-[Co^{III}(tpp)$^{+\cdot}$]Cl$_2$ by BHA proceeded depending on the concentration of BHA (Fig. 5). These facts give an indication that the reaction might be second order, as described by Eq. 1:

$$[Co^{III}(tpp)^{+\cdot}]Cl_2 + POH \rightarrow [Co^{III}Cl(tpp)] + PO\cdot + HCl \quad (1)$$

In our reaction condition, however, Eq. 1 should be reduced by the pseudo-first-order. We have tried to plot $\ln a/(a-x)$ as a function of time for the reaction with BHA (shown in Fig. 5), where a and x are initial and reduced concentration of [Co^{III}(tpp)$^{+\cdot}$]Cl$_2$, respectively. As shown in Fig. 8, before 50 s reaction time, the functions show linear relationships, but after 50 s they deviate downward from the linear relationships, which means that the reaction does not follow the pseudo-first-order reaction rate. Next, we assumed that the phenolate anion activated in part from BHA reacts with the cation radical, as discussed in process 2. This means that in Eq. 1, PO^- instead of POH takes part in the reaction. Thus, we have tried to simulate the second-order decay rates k_f of [Co^{III}(tpp)$^{+\cdot}$]Cl$_2$;

$$k_f t = \frac{1}{(a-b)} \ln \frac{b(a-x)}{a(b-x')}, \quad (2)$$

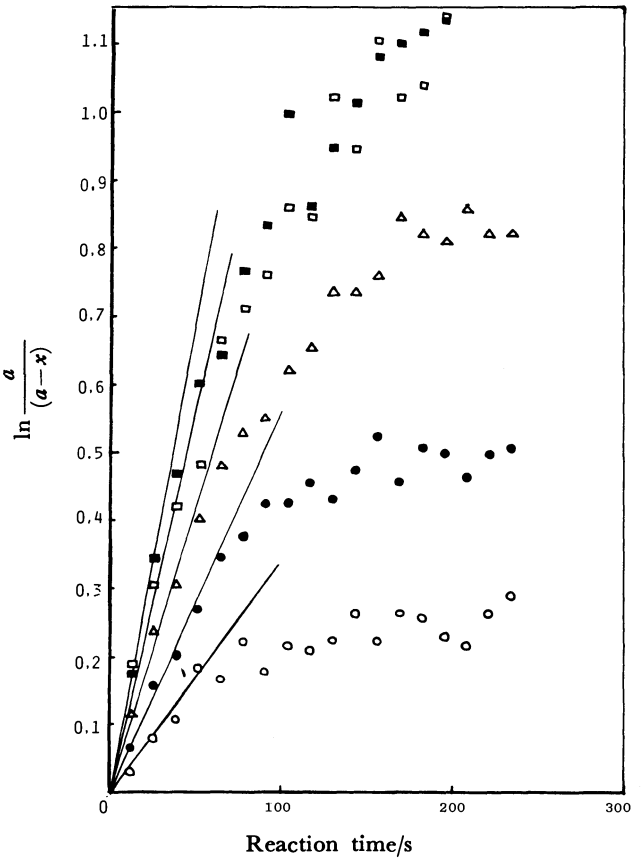

Fig. 8. In $a/(a-x)$ vs. time plot of the reaction between [Co^{III}(tpp)$^{+\cdot}$]Cl$_2$ and BHA, ■: 1.0×10^{-2}, □: 5.0×10^{-3}, △: 2.5×10^{-3}, ●: 1.25×10^{-3}, ○: 6.25×10^{-4} mol dm^{-3}.

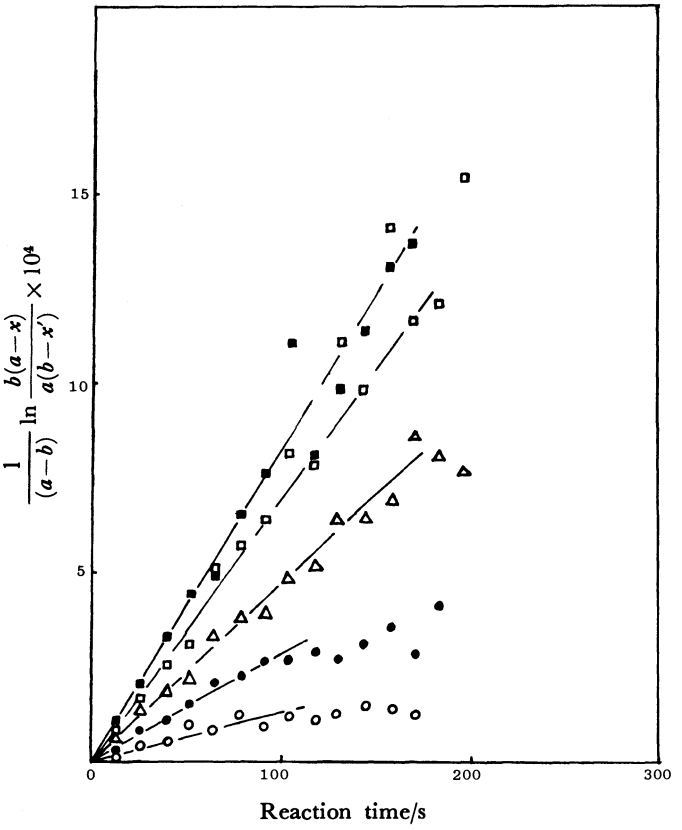

Fig. 9. $1/(a-b)\ln\{b(a-x)/a(a-x')\}$ vs. time plot of the reaction between [Co^{III}(tpp)$^{+\cdot}$]Cl$_2$ and BHA, ■: 1.0×10^{-2}, □: 5.0×10^{-3}, △: 2.5×10^{-3}, ●: 1.25×10^{-3}, ○: 6.25×10^{-4} mol dm^{-3}.

where a and x are the initial and reduced concentrations of $[Co^{III}(tpp)^{+\cdot}]Cl_2$ and b and x' are the initial and oxidized concentrations of the phenolate anion, respectively. Since b and x' are unknown, b has been substituted by trial values of 1.8 to 2.2×10^{-5} and x' is assumed to be equal to x. When the concentration of BHA anion is 2.1×10^{-5} mol dm^{-3}, the simulation accorded satisfactorily with the experimental data in whole concentration range of BHA (1.0×10^{-2}—6.25×10^{-4} mol dm^{-3}) as shown in Fig. 9. This means that the concentration of the phenolate anion is constant irrespective of the concentration change of phenol.

From these results, the reaction mechanism of $[Co^{III}(tpp)^{+\cdot}]Cl_2$ with the phenols may be written as follows:

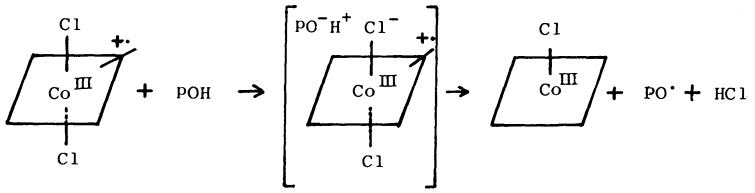

Scheme 3.

The chloride ligand of $[Co^{III}(tpp)^{+\cdot}]Cl_2$ attracts the hydroxy proton of phenol and a complex is formed, then, an electron transfer occurs from the phenolate anion to $[Co^{III}(tpp)^{+\cdot}]Cl_2$ in the complex to give a phenoxyl radical and $[Co^{III}Cl(tpp)]$. The fact that the reaction rates depend on the concentration of the phenols is related to the formation of the complex. In cases of reactions with group-II phenols, the chloride ligand of $[Co^{III}Cl(tpp)]$ also attracts its hydroxy protons. Thus, $[Co^{II}(tpp)]$ is formed through the formation of a similar complex:

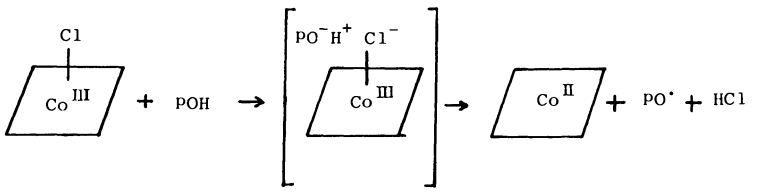

Scheme 4.

$[Co^{III}Cl(tpp)]$ and Horseradish Peroxidase(HRP). In the following we compare our results with the reaction of a typical enzyme HRP.[23] The function of $[Co^{III}Cl(tpp)]$–$[Co^{III}(tpp)^{+\cdot}]Cl_2$ and the enzymatic reaction of HRP are written in Schemes 5 and 6, respectively. The numbers in parentheses in these schemes represent the apparent oxidation states estimated on the basis of data from earlier work. $[Co^{III}(tpp)^{+\cdot}]Cl_2$ (+4) and Compound I (+5) of HRP are both π cation radicals and they perform two electron oxidation reactions. Here, we assume a correspondence of $[Co^{III}(tpp)^{+\cdot}]Cl_2$ with Compound I. Then, each of the other species in Scheme 5 can find a nice counterpart in Scheme 6. The change from $[Co^{III}(tpp)^{+\cdot}]Cl_2$ to $[Co^{III}Cl(tpp)]$ by a one-electron reduction corresponds to a reaction from Compound I to Compound II, and a change from $[Co^{III}Cl(tpp)]$ to $[Co^{II}(tpp)]$ to a reaction from Compound II to the native HRP–Fe(+3). This procedure enables us to write another correspondence: $[Co^{I}(tpp)]$ to HRP–Fe(+2), and $[Co^{III}(tpp)\text{-}O_2^{-\cdot}]$ to Compound III.[24] In our reaction system, the stable species is $[Co^{III}Cl(tpp)]$, corresponding to Compound II. The activity of $[Co^{III}Cl(tpp)]$ is considered to be due to its five-coordinate molecular structure[9] and the unique properties depending on the nature of the solvents[8] and the temperature.[10]

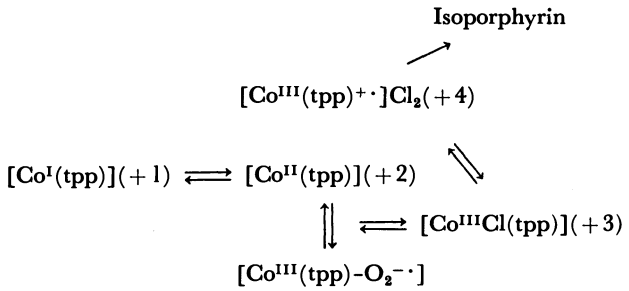

Scheme 5. Redox system of our case.

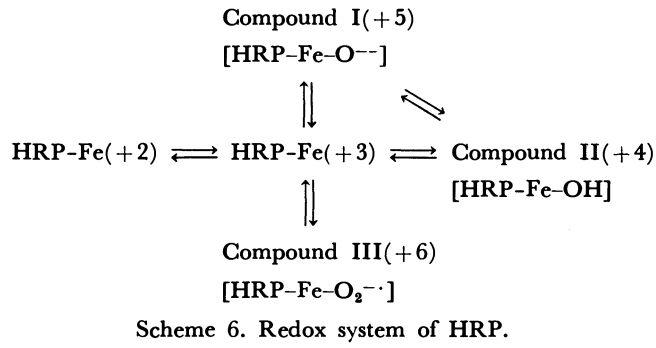

Scheme 6. Redox system of HRP.

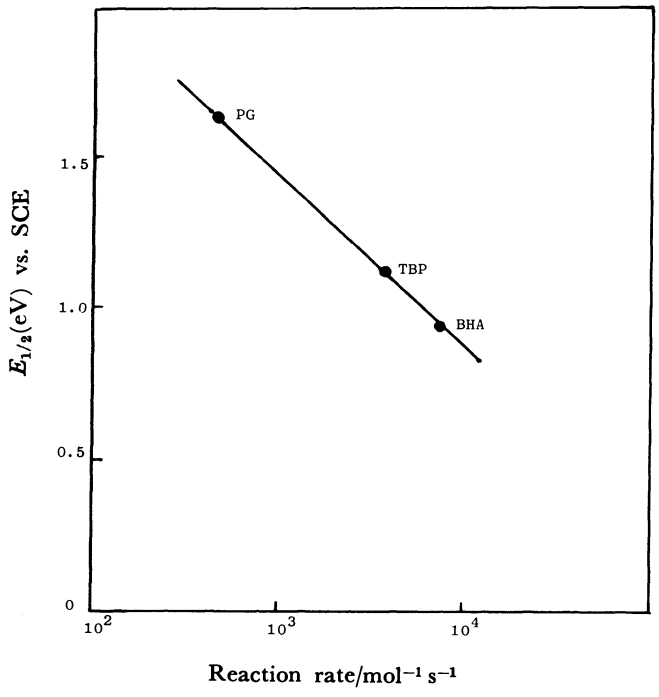

Fig. 10. Relation of reaction rates to redox potentials of phenols (PG, TBP, and BHA).

It should be noted that the active species conducting in our reactions was the chlorine radical, while the active species in the HRP system is considered to be an intermediate derived from H_2O_2.

Siga and Imaizumi[25] have reported that in the reactions of HRP-H_2O_2 and methemoglobin-H_2O_2, a phenoxyl radical formation from the phenols depends on their redox potentials. It has been found that the observed rate constants have a linear relationship with the redox potentials of the phenols. Therefore, the linear relationships shown in Fig. 10 indicate that the enzymatic reactions are correlated with the redox potentiels of the substrates. Furthermore, the concentration dependence of the rate constants shown in Fig. 9 has a similarity with that of the enzymatic reactions in which the concentration of the free radical formed depends upon that of the enzyme:[26] An excess amount of the substrates (more than 10^2 times that of the enzyme) is needed, and some activation mechanisms of the substrate are involved. Consequently, the good correspondence with [$Co^{III}Cl(tpp)$]-[$Co^{III}(tpp)^{+\cdot}$]Cl_2 and HRP suggests that knowledge of the molecular, electronic structure, and properties of [$Co^{III}Cl(tpp)$]-[$Co^{III}(tpp)^{+\cdot}$]-Cl_2 will give useful information for those of HRP.

The author wishes to express his deep gratitude to Prof. Hiroaki Ohya-Nishiguchi of Kyoto University and Dr. Kiyoko Yamamoto of The Institute of Physical and Chemical Research for their helpful discussions during the course of this study. The author is indebted to Mr. Akihiko Tajima of Ehime University for the measurements of cyclic voltammograms and useful discussions.

References

1) W. D. Hewson and L. P. Hager, "Peroxidases, Catalases, and Chloroperoxidase," in "The Porphyrins," ed by D. Dolphin, Academic Press. Inc., New York (1979), Vol. 7, p. 295 and other references cited therein.

2) a) D. Dolphin and R. H. Felton, *Acc. Chem. Res.*, **7**, 26 (1974); b) D. Dolphin, A. W. Addison, M. Cairns, R. K. Dinello, N. P. Farrell, B. R. James, D. R. Paulson, and C. Welborn, *Int. Quant. Chem.*, **16**, 311 (1979); c) J. E. Roberts, M. Hoffman, R. Rutter, and L. P. Hager, *J. Biol. Chem.*, **256**, 2118 (1981).

3) a) J. Fajer and M. S. Davis, "Electron Spin Resonance of Porphyrin π Cations and Anions," in "The Porphyrins," ed by D. Dolphin, Academic Press. Inc., New York (1979), Vol. 4, p. 197; b) M. A. Phillippi and H. M. Goff, *J. Am. Chem. Soc.*, **104**, 6062 (1982).

4) K. Yamamoto, M. Kohno, and H. Ohya-Nishiguchi, *Chem. Lett.*, **1981**, 255.

5) H. Ohya-Nishiguchi, M. Kohno, and K. Yamamoto, *Bull. Chem. Soc. Jpn.*, **54**, 1923 (1981).

6) M. Kohno, H. Ohya-Nishiguchi, K. Yamamoto, and T. Sakurai, *Bull. Chem. Soc. Jpn.*, **56**, 822 (1983).

7) M. Kohno, H. Ohya-Nishiguchi, K. Yamamoto, and T. Sakurai, *Bull. Chem. Soc. Jpn.*, **57**, 932 (1984).

8) K. Yamamoto, *Sci. Papers Inst. Phys. Chem. Res.*, **71**, 111 (1977).

9) T. Sakurai, K. Yamamoto, N. Naito, and N. Nakamoto, *Bull. Chem. Soc. Jpn.*, **49**, 3042 (1976).

10) K. Yamamoto, J. Uzawa, and T. Chijimatsu, *Chem. Lett.*, **1979**, 89.

11) K. Ichimori, H. Ohya-Nishiguchi, N. Hirota, and K. Yamamoto, *Bull. Chem. Soc. Jpn.*, **58**, 623 (1985).

12) K. Yamamoto, M. Hoshino, M. Kohno, and H. Ohya-Nishiguchi, *Bull. Chem. Soc. Jpn.*, **59**, 351 (1986).

13) G. M. Coppinger, *Tetrahedron*, **18**, 61 (1962).

14) a) K. Mukai, T. Mishina, K. Ishizu, and Y. Deguchi, *Bull. Chem. Soc. Jpn.*, **50**, 641 (1977); b) T. Yamamoto, M. Kohno, T. Miyamae, K. Mukai, and K. Ishizu, *Chem. Lett.*, **1972**, 681.

15) E. Mueller, K. Ley, K. Scheffer, and R. Mayer, *Chem. Ber.*, **91**, 2682 (1958).

16) G. D. Dorough, J. R. Miller, and F. M. Fuennekens, *J. Am. Chem. Soc.*, **73**, 4315 (1951).
17) a) K. Mukai, N. Tsuzuki, K. Ishizu, S. Ouchi, and K. Fukuzawa, *Chem. Phys. Lipids*, **29**, 129 (1981); b) K. Mukai, N. Tsuzuki, S. Ouchi, and K. Fukuzawa, *Chem. Phys. Lipids*, **30**, 337 (1982).
18) D. Dolphin, R. H. Felton, D. C. Borg, and J. Fajer, *J. Am. Chem. Soc.*, **92**, 743 (1970).
19) J. A. Guzinski and R. H. Felton, *J. Chem. Soc., Chem. Commun.*, **1973**, 715.
20) E. G. Janzen, *Acc. Chem. Res.*, **4**, 31 (1971).
21) K. Sasaki and A. Kunai, "Denkyoku-hanno Nyumon," Kagakudojin, Kyoto (1980), Chap. 5.
22) U. Svanholm, K. Bechgaard, and V. D. Parker, *J. Am. Chem. Soc.*, **96**, 2409 (1974).
23) I. Yamazaki and Y. Yokota, *Mol. Cell. Biochem.*, **2**, 39 (1973).
24) F. A. Walker, *J. Am. Chem. Soc.*, **92**, 4235 (1970).
25) T. Shiga and K. Imaizumi, *Arch. Biochem. Biophys.*, **167**, 469 (1975).
26) I. Yamazaki, H. S. Mason, and L. Piette, *J. Bio. Chem.*, **235**, 2444 (1959).

The Formation Process of Hydrous Gallium(III) Oxide Particles Obtained by Hydrolysis at Elevated Temperatures

Shuichi HAMADA,* Koji BANDO, and Yoshiyuki KUDO
Department of Applied Chemistry, Faculty of Science, and Institute of Colloid and Interface Science, Science University of Tokyo, Kagurazaka, Shinjuku-ku, Tokyo 162
(Received December 24, 1985)

Hydrous gallium(III) oxide was produced as monodispersed spherical particles by forced hydrolysis in the presence of sulfate ions, though they partially dissolved and recrystallized. The rate of the reaction degree was empirically expressed under the given conditions as $d\alpha/dt=1.60\alpha^{2/3}(1-\alpha)^{0.874}$, where α is the reaction degree. Polymeric hydroxo complexes were confirmed to act as precursors of the monodispersed spherical particles, judging from the fractional changes of the monomeric and polymeric species during the hydrolysis. The role of sulfate ions in the formation of hydrous gallium(III) oxide particles was discussed.

Recently, the preparation of monodispersed (hydrous) metal oxide particles has been extensively studied.[1-7] One method, the hydrolysis of metal ions at elevated temperatures, gives excellent monodispersed particles under suitable conditions. The morphology, composition, and size-distribution of the particles depend strongly, however, on several parameters, such as the concentration of metal ions, the pH, the temperature, and the kind of anion present, in the method of forced hydrolysis. Especially, a great influence of anions has usually been shown on the morphology and the composition of the particles. It has also been reported that the presence of sulfate ions in a solution is essential to produce monodispersed spherical particles of hydrous aluminium(III)[8] and chromium(III)[9] oxides. In a previous paper,[7] a remarkable effect of sulfate ions was also shown in making monodispersed spherical hydrous gallium(III) oxide particles by forced hydrolysis.

In this work, the role of sulfate ions in the formation of monodispersed hydrous gallium(III) oxide particles was studied, as was their formation process.

Experimental

Materials. All of the reagents used in this work were of a guaranteed grade and were employed without further purification. Stock solutions of gallium(III) sulfate and nitrate were prepared by dissolving the salts in doubly distilled water at room temperature, together with a known amount of the corresponding acid. These stock solutions, when kept in a cold place, did not show any visual change over three months.

Procedures. The sulfate and the nitrate solutions were prepared as the initial gallium(III) ion and acid concentrations of $[Ga^{3+}]_i=9.8\times10^{-4}$ and $[H^+]_{add}=1.0\times10^{-3}$ mol dm^{-3} respectively. The initial concentration ratio of sulfate to gallium(III) ions, $[SO_4^{2-}]_i/[Ga^{3+}]_i$, was specified as 1.9 by the use of potassium sulfate for the gallium(III) sulfate system. This composition has been confirmed as one of the optimum conditions for making monodispersed spherical particles.[7] The solutions were filtered through a membrane filter, 0.2 μm in pore size, before aging.

An aliquot of the solution was placed in a screw-capped Pyrex glass tube or a flask equipped with a condenser, and heated initially at the heating rate of 0.4 °C min^{-1},[7] followed by aging at a specified temperature (70—98 °C) in an oil bath. After the solution had been heated, particles were separated by centrifugation at 1700 g and then washed repeatedly with doubly distilled water. The morphology and size of the particles were observed with a transmission electron microscope.

The concentrations of gallium(III) and sulfate ions remaining in a supernatant solution were followed at regular time intervals after the solids had been completely separated by centrifugation at 45000 g. The supernatant solution thus obtained did not show any Tyndall cone. The total amount of gallium(III) species in the solution was determined spectrophotometrically as follows: A small portion of sulfuric acid was first added to the solution ($[H^+]\approx2.4\times10^{-2}$ mol dm^{-3}) to convert the polymeric gallium(III) species into monomeric ones, since the polymeric species did not complete the reaction with 8-quinolinol, not even within 60 min. Then all of the gallium(III) species were extracted by shaking the solution for 10 s at pH 5.1 with 10 cm^3 of chloroform, just after adding a buffer solution and a 8-quinolinol solution.

The concentration of the monomeric species was determined in the same way as above, but without the conversion process. Consequently, the concentration of polymeric gallium(III) species was estimated from the difference between the two values.

The concentration of sulfate ions in the supernatant solution was also determined colorimetrically with barium molybdate.[10]

Results

Morphology of Monodispersed Hydrous Gallium(III) Oxide Particles. Figure 1 shows the monodispersed spherical particles obtained by hydrolysis at 98 °C for 18 h. These particles were identified as amorphous-like hydrous gallium(III) oxide by means of X-ray powder diffractometry.[11]

Figures 2a—c show the change in the morphology of the particles during the reaction under the conditions shown in Fig. 1. The hydrous gallium(III) oxide was precipitated as monodispersed

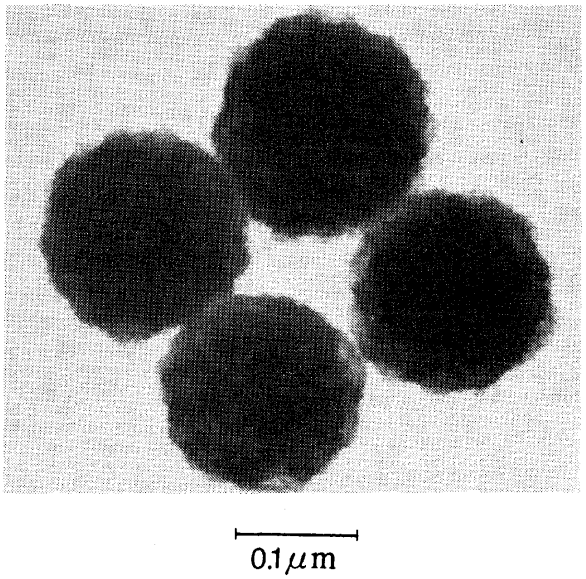

Fig. 1. Electron micrograph of monodispersed spherical hydrous gallium(III) oxide particles obtained at 98 °C. Aging conditions: $[Ga^{3+}]_I = 9.8 \times 10^{-4}$ mol dm^{-3}, $2[H_2SO_4] + [HNO_3] = 1.0 \times 10^{-3}$ mol dm^{-3}, and $[SO_4^{2-}]_I/[Ga^{3+}]_I = 1.9$ respectively.

spherical particles during a reaction for 3.5 h (Fig. 2a). The particles, however, dissolved in part after 4.5 h (Fig. 2b). Figure 2c indicates a mixture of spherical and rod-like particles which has been aged for 18 h. Such a mixture gave weak X-ray powder diffraction peaks attributable to gallium(III) hydroxide oxide. Accordingly, it is obvious that the monodispersed spherical particles became unstable as the reaction proceeded and that they were then transformed partially into crystalline particles through recrystallization.

Variations in the Fraction of Gallium(III) Species in the Supernatant Solution and in the Content Ratio of Sulfate to Gallium(III) in Particles during Reaction. Figure 3 shows the fractional change of soluble gallium(III) species during hydrolysis at 98 °C under the same conditions as are shown in Fig. 1. The fraction of gallium(III) species in the supernatant solution decreased quickly up to around 4 h, but it abnormally reached a maximum at around 4.5 h. This time corresponded to that when the particles partially dissolved (Fig. 2b).

The molar ratio of the sulfate to the gallium(III) contents, $n(SO_4^{2-})/n(Ga^{3+})$, in the particles was estimated by subtracting the concentrations of both gallium(III) and sulfate ions in the solution from their initial values, so that the value involved the amount of sulfate ions adsorbed on the surfaces. The sulfate ions incorporated in the particles were quickly excluded as hydrolysis was enhanced, as is shown in Fig. 4. A similar phenomenon has been observed in the case of hydrous chromium(III) oxide,

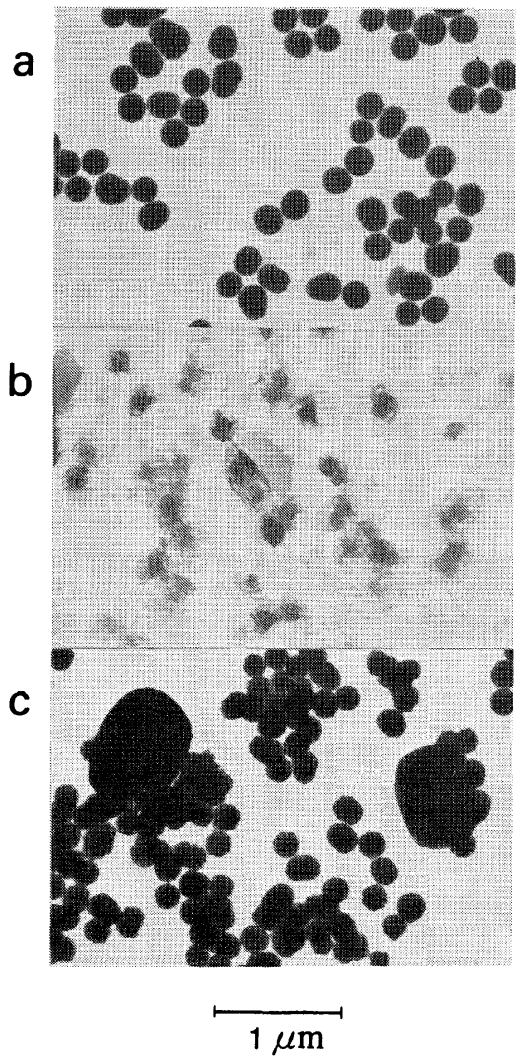

Fig. 2. Dissolution and recrystallization of hydrous gallium(III) oxide particles. Aging time: a; 3.5 h, b; 4.5 h, and c; 18 h.

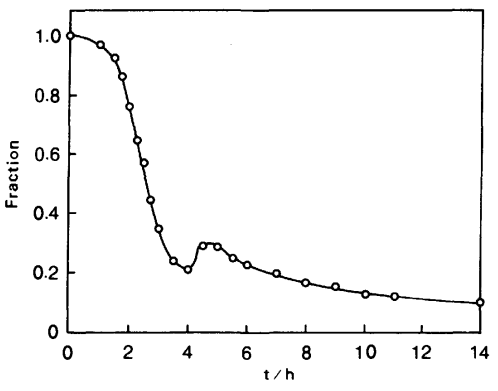

Fig. 3. Fractional change of gallium(III) species remained in supernatant solution during hydrolysis at 98 °C.

even though particular hydroxosulfato complexes acted as precursors of amorphous spherical particles.[9]

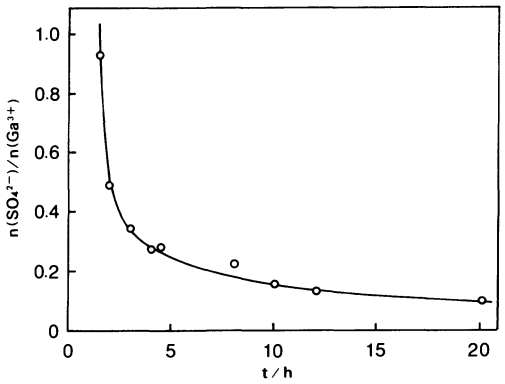

Fig. 4. Variation in composition of hydrous gallium (III) oxide particles during hydrolysis at 98 °C.

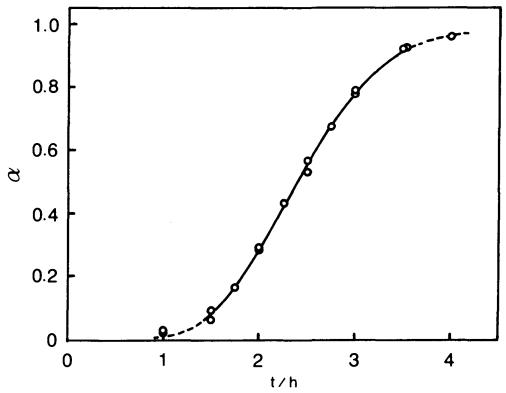

Fig. 5. Plots of reaction degree as a function of aging time at 98° C. O; Observed, —; Calculated.

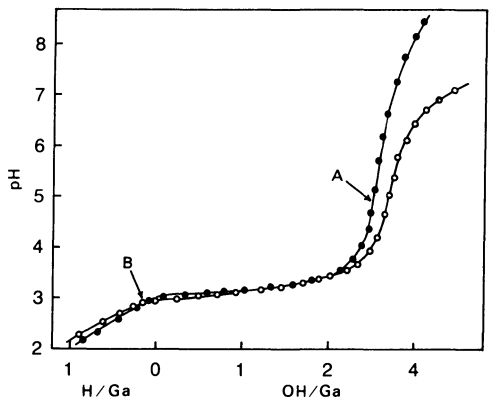

Fig. 6. Titration curves of gallium(III) nitrate (●) and sulfate (○) solutions. H/Ga and OH/Ga stand for $[H^+]_{add}/[Ga^{3+}]_t$ and $[OH^-]_{add}/[Ga^{3+}]_t$ respectively. Arrows A and B indicate points at which precipitates become visible for respective solution.

Change in Reaction Degree during Forced Hydrolysis. The rate of deposition of the solid phase during the growth of particles is approximately shown as:[12]

$$dP/dt = kS(C-C_s)^p \quad (1)$$

where P is the amount of solid formed; k, the apparent rate constant; S, the surface area of the particles; C, the concentration at the reaction time t; C_s, the final concentration, and p, the parameter of the concentration dependence. The P term can be expressed as mV, where m is the number of moles of gallium(III) species per unit volume and V, the volume of the particles. Thus,

$$dP/dt = mSdr/dt \quad (2)$$

where dr/dt is the radial growth rate. From Eqs. 1 and 2, the following equation can be obtained:

$$dr/dt = k'(C-C_s)^p \quad (3)$$

where k' is k/m.

On the other hand, the reaction degree, α, is defined as:

$$\alpha = (C_0-C)/(C_0-C_s) \quad (4)$$

where C_0 is the initial concentration. Accordingly, the modal diameter, r, of the monodispersed particles at t can be expressed as:

$$r = r_f\alpha^{1/3} \quad (5)$$

where r_f is the final modal diameter. Consequently, the following equation is obtained:

$$d\alpha/dt = K\alpha^{2/3}(1-\alpha)^p \quad (6)$$

where

$$K = 3k'(C_0-C_s)^p/r_f \quad (7)$$

Equation 6 was numerically integrated using the results obtained in Fig. 3. First, the parameters, p and K, were estimated as 0.874 and 1.60[13] respectively by a least-squares method using the logarithmic values of $d\alpha/dt$, α, and $1-\alpha$. Taking these values of the parameters, Eq. 6 was then integrated by the Runge-Kutta method. The solid curve in Fig. 5 displays the reaction degree thus calculated, which agreed very well with the experimental values over the wide range of reaction degrees from around 0.1 to 0.9. The rate of deposition, dP/dt or dV/dt, usually depends on the kinetic order between 1 and 2 with respect to the concentration during the growth process.[14,15] The value of the parameter p (0.874) obtained in this work was close to those presented above. Therefore, the hydrous gallium(III) oxide particles were confirmed to grow according to Eq. 1.

Fractional Changes of Monomeric and Polymeric Species in Partially Neutralized Gallium(III) Salt Solutions. The gallium(III) nitrate and sulfate solutions of 9.2×10^{-3} mol dm^{-3} containing a known amount of the corresponding acid were titrated very slowly with a potassium hydroxide solution of the

same concentration at room temperature. The arrows in Fig. 6 display points at which visual precipitation occurred. The two titration curves were almost identical, except at the later stages. Such a discrepancy in pH values at the later stages can be considered to arise from the replacement of sulfate ions incorporated in the precipitates by hydroxyl ions as neutralization proceeds. In the gallium(III) sulfate solution, however, precipitates appeared at an earlier stage (pH 2.9) ($[H^+]_{add}/[Ga^{3+}]_i=0.13$), while precipitation was retarded up to pH 4.8 ($[OH^-]_{add}/[Ga^{3+}]_i=2.5$) in the nitrate solution.

Such a clear difference in the precipitation process indicated that sulfate ions exerted a remarkable effect on the formation of hydrous gallium(III) oxide. Hek et al.[13] observed similar facts in aluminium(III) salt solutions.

The amounts of monomeric and polymeric aluminium(III) species have also been determined.[14-17] Turner[14] defined the respective amount on the basis of reactivity to 8-quinolinol. The definition for the monomeric and polymeric gallium(III) species was taken to be the same as that for aluminium(III). Furthermore, Iwase et al.[21] confirmed that a dimer, $[M_2(OH)_2]^{4+}$, was also easily extractable with 8-quinolinol, so that the term "monomer" will include this dimer hereafter.

The gallium(III) nitrate and sulfate solutions (9.2×10^{-3} mol dm^{-3}) were carefully neutralized with vigorous stirring to minimize the heterogeneity of the pH in the solutions; then, both the species were estimated in order to reveal their behavior, depending on neutralization. Figure 7 displays the fractions of the monomeric and polymeric species in the gallium(III) nitrate solution as a function of the degree of neutralization. The monomeric species was gradually polymerized as neutralization proceeded, while a solid phase did not appear in this $[OH^-]_{add}/[Ga^{3+}]_i$ range, even when a great amount of polymeric species existed.

On the contrary, the gallium(III) sulfate solution showed different features in the fractional change of the species, as is shown in Fig. 8. Precipitates appeared at a fraction of about 0.4 of the polymeric species. These results indicated that the precipitation of the polymeric gallium(III) species was enhanced in the presence of sulfate ions, combined with those produced on titration. This effect also takes place at forced hydrolysis, not only in the partially neutralized solutions.

Fractions of Monomeric and Polymeric Gallium(III) Species in Solutions during Forced Hydrolysis. Figures 9 and 10 show the changes in the fractions of the soluble gallium(III) species and the precipitates during the forced hydrolysis of the nitrate and the sulfate solutions at 98 °C. Though nearly identical fractions of the polymeric species were initially indicated in both salt solutions, the fraction of the monomeric species gradually decreased as it was converted into the polymeric species at an earlier stage of hydrolysis in the nitrate solution. The concentration ratio of the monomeric to the polymeric species, [monomer]/[polymer], decreased continuously as the hydrolysis was enhanced.

On the other hand, in the sulfate solution the precipitates appeared at an earlier stage of hydrolysis, even at a low fraction of the polymeric species. The [monomer]/[polymer] ratio gradually increased except around 4.5 h, while the fraction of the monomeric species changed similarly to that in the nitrate solution. These results clearly indicate that sulfate ions promote the deposition of hydrous gallium(III) oxide as spherical particles.

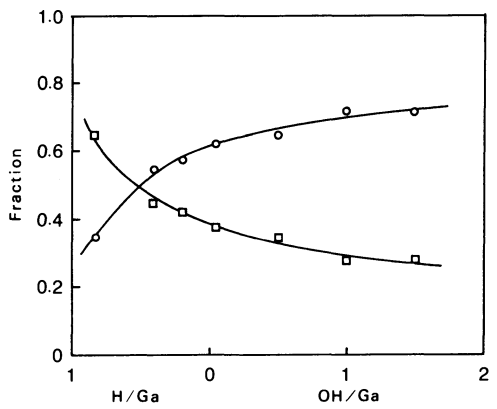

Fig. 7. Fractional changes of mono- and polynuclear hydroxo complexes in gallium(III) nitrate system at 25 °C. Symbols: □; Monomer, ○; polymer.

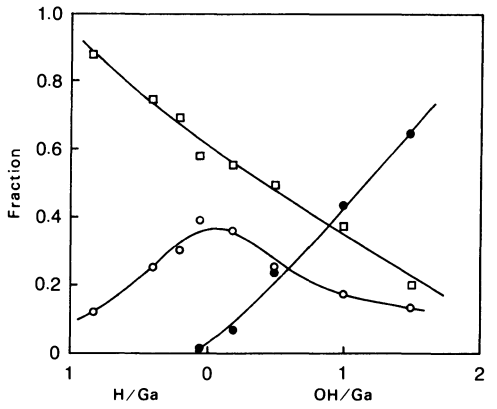

Fig. 8. Fractional changes of mono- and polynuclear hydroxo complexes in gallium(III) sulfate system at 25 °C. Symbols: □; Monomer, ○; polymer, ●; precipitate.

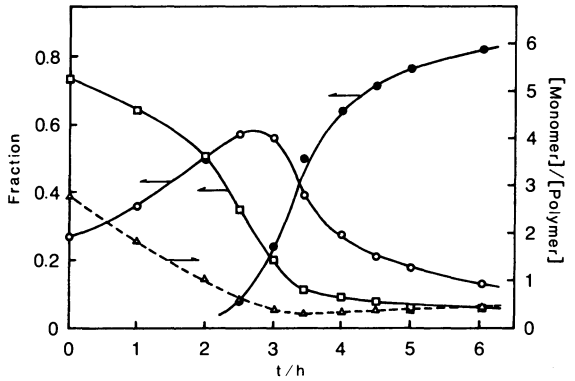

Fig. 9. Fractions of mono- and polynuclear hydroxogallium(III) complexes and precipitate during hydrolysis of nitrate solution at 98 °C. Symbols: □; Monomer, ○; polymer, ●; precipitate, △; [monomer]/[polymer] ratio. Aging conditions: $[Ga^{3+}]_i = 9.8 \times 10^{-4}$ mol dm^{-3}, $[HNO_3] = 1.0 \times 10^{-3}$ mol dm^{-3}.

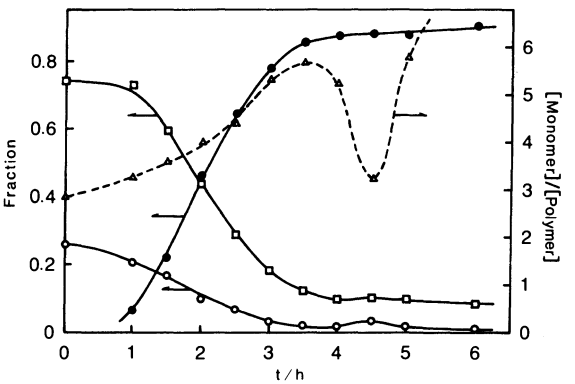

Fig. 10. Fractions of mono- and polynuclear hydroxogallium(III) complexes and precipitate during hydrolysis of sulfate solution at 98 °C. Symbols: □; Monomer, ○; polymer, ●; precipitate, △; [monomer]/[polymer] ratio. Aging conditions: $[Ga^{3+}]_i = 9.8 \times 10^{-4}$ mol dm^{-3}, $2[H_2SO_4] + [HNO_3] = 1.0 \times 10^{-3}$mol dm^{-3}, and $[SO^{2-}]_i/[Ga^{3+}]_i = 1.9$ respectively.

Discussion

On the formation of monodispersed spherical particles of amorphous hydrous aluminium(III) and chromium(III) oxides, it has been confirmed that polynuclear hydroxo and/or hydroxosulfato complexes act as precursors of such particles in the presence of limited amounts of sulfate ions.[8,9,22,23] The monodispersed spheres of hydrous gallium(III) oxide have also been clearly indicated to consist of polymeric species of hydroxo complexes.

According to the mass balance during the deposition of the solid phase, the following equation can be obtained:

$$df_{ppt}/dt = -df_{mono}/dt - df_{poly}/dt \quad (8)$$

Table 1. Rates of Change in Precipitate, Monomer, and Polymer Fractions in a Sulfate System

Reaction time / h	df_{ppt}/dt / h^{-1}	$-df_{mono}/dt$ / h^{-1}	$-df_{poly}/dt$ / h^{-1}
1.0	0.263	0.166	0.082
1.5	0.402	0.298	0.107
2.0	0.415	0.316	0.104
2.5	0.342	0.259	0.082
3.0	0.222	0.166	0.050
3.5	0.092	0.077	0.014

where f_{ppt}, f_{mono}, and f_{poly} are the fractions of the precipitate, the monomer, and the polymer respectively. Table 1 shows the values of the above three terms at different times in the sulfate system; these values were obtained from the respective fraction curves calculated by the least-squares method (Fig. 10). The results in Table 1 indicate that the values of $-df_{mono}/dt$ are 2.0—5.4 times those of $-df_{poly}/dt$. This fact implies that the reaction change in the monomer rather controlled the overall growth rate of the particles. However, a direct deposition of the monomer is unlikely, for the [monomer]/[polymer] ratio should decrease if the particles grow through this process. The [monomer]/[polymer] ratio may increase through a rapid degradation of the polymer, followed by a slow deposition of the monomer. This process is also unlikely, however, because the rate of the degradation of the polymer is usually not so fast.

Thus, the following reaction path, through slow polymerization and fast deposition steps, seems reasonable in the sulfate system:

$$\text{Monomer} \xrightarrow{\text{slow}} \text{Polymer} \xrightarrow{\text{fast}} \text{Amorphous particles.} \quad (9)$$

The first step can be accompanied by a build-up of the polymer as:

$$\text{Polymer}_{(a-b)} + b\,\text{Monomer} \longrightarrow \text{Polymer}_{(a)} \quad (10)$$

where $\text{Polymer}_{(a-b)}$ and $\text{Polymer}_{(a)}$ refer to species of a lower and higher degree of polymerization respectively.

On the other hand, a direct deposition of the polymer is hardly acceptable in the nitrate system, because the solid phase does not appear, even in the cases of large fractions of the polymer-for instance, around 0.5 at 2 h, as is indicated in Fig. 9. Additionally, the [monomer]/[polymer] ratio may decrease if the monomer species are polymerized faster than the deposition of the polymer, but this process is also improbable judging from the difference in df_{poly}/dt and df_{ppt}/dt at the early stages of the polymerization (up to 2 h) and of the deposition.

As is shown in Fig. 9, the rates of deposition

(df_{ppt}/dt) are comparable to those of the decrease in the polymer fraction ($-df_{poly}/dt$) after around 3 h. It has been reported in a previous paper[7] that only rod-like crystalline particles of gallium(III) hydroxide oxide were produced through the forced hydrolysis of the nitrate solution under the same conditions except for the kind of anion. Taking these facts into account, the rate of the particle growth would seem to be governed by that of the degradation of the polymer, and the monomer and/or low molecular-weight hydroxo complexes would seem to act as actual precursors of the crystalline particles. This process is supported by the fact that the [monomer]/[polymer] ratio increased again after 3.5 h and then returned to 2.8 at the final stage of forced hydrolysis (24 h).

Ruff and Tyree[24] expressed the cationic polymers of hydroxogallium(III) complexes as having a linear structure of $[Ga_{n+1}(OH)_{2n}]^{(n+3)+}$. They estimated, on the basis of pH measurements of a perchlorate solution, that the degree of polymerization, n, varied up to around 21 at the $[OH^-]_{add}/[Ga^{3+}]_i$ ratio of 1.75. Contrary to this, however, a much higher degree of polymerization (64) was observed by the light-scattering technique under the same conditions.[24] Patterson and Tyree,[25] by an isopiestic method, also estimated the degree of polymerization as 84 at the $[OH^-]_{add}/[Ga^{3+}]_i$ ratio of 2.0. It can be expected to have a feature similar to the hydrolysis of gallium(III) ions at elevated temperatures, though specified degrees of polymerization could not be obtained in this work.

Highly-polymerized hydroxogallium(III) complexes tend to reduce their large positive charges by converting the OH^--bridges in the polymers into O^{2-}-bridges. Cyclic structures composed of a hexamer unit are also possible, as are those of polymeric hydroxo complexes,[26] which have less positive charges than those of the linear structure for the same degree of polymerization. These highly-charged cationic polymers can more easily associate with sulfate ions compared with univalent anions, such as nitrate and perchlorate, while gallium(III) ions form sulfato complexes[27] in part. Hester and Plane,[28] by means of a Raman spectroscopic techique, have suggested that the sulfatogallium(III) complexes exist as outer-sphere complexes rather than as inner-sphere complexes. The sulfate ions thus paired with the polymers would effectively reduce the positive charge of the polynuclear hydroxo complexes and promote further polymerization.

After the nuclei were generated, their positively-charged surfaces would strongly adsorb sulfate ions in an acidic solution.[8] Then fine colloidal particles of hydrous gallium(III) oxide would easily associate according to the Schulze-Hardy rule, in addition to the surface nucleation of the polymeric species. Hek et al.[16] have confirmed, on the basis of the replacement behavior of labeled sulfate ions, that sulfate ions were incorporated in amorphous precipitates of hydrous aluminium(III) oxide as an adsorbed, but tightly-bound, state. The rapid exclusion of sulfate ions, as is shown in Fig. 4, would support this consideration. Such a spontaneous exclusion of sulfate ions may originate from the substitution by hydroxyl groups as the hydrolysis is enhanced. Hydrous aluminium(III) oxide particles also easily excluded the incorporated sulfate ions upon dialysis or repeated washings, and were transformed into crystalline α-AlOOH at elevated temperatures.[8,29]

In addition, there should be important conditions to obtain the monodispersed particles of hydrous gallium(III) oxide. As one of them, an appropriate formation rate of polynuclear hydroxo complexes is essential to gain a suitable supersaturation, leading to proper nucleation rates, whereas in general hydrolysis reactions take place faster than condensation.[30] These conditions have been shown in connection with the heating rate and the starting composition of the solutions.[7] The interfacial energy of embryos would be reduced according to the amount of sulfate ions adsorbed on the surfaces and would control the nucleation rate, in addition to the secondary surface-nucleation rate, though the detailed mechanisms are still not clear. This effect was distinctly reflected in the morphology of the particles during the forced hydrolysis of gallium(III) ions.[7] If many sulfate ions existed in the solutions ($[SO_4^{2-}]_i/[Ga^{3+}]_i > 2.0$), only polydispersed particles were produced because of the fast deposition rates.

References

1) J. H. L. Watson, R. R. Cardell, Jr., and W. Heller, *J. Phys. Chem.*, **66**, 1757 (1962).
2) E. Matijević, *Acc. Chem. Res.*, **14**, 22 (1981).
3) K. Miyata and K. Nakahara, *Shikizai Kyoukai Shi*, **49**, 349 (1976).
4) S. Hamada and E. Matijević, *J. Colloid Interface Sci.*, **84**, 274 (1981).
5) S. Hamada and E. Matijević, *J. Chem. Soc., Faraday Trans. 1*, **78**, 2147 (1982).
6) S. Hamada, T. Hanami, and Y. Kudo, *Nippon Kagaku Kaishi*, **1984**, 1065.
7) S. Hamada, K. Bando, and Y. Kudo, *Nippon Kagaku Kaishi*, **1984**, 1068.
8) R. Brace and E. Matijević, *J. Inorg. Nucl. Chem.*, **35**, 3691 (1973).
9) E. Matijević, A. D. Lindsay, S. Kratohvil, M. E. Jones, R. I. Larson, and N. W. Cayey, *J. Colloid Interface Sci.*, **36**, 273 (1971).
10) S. Sugano, *Bunseki Kagaku*, **8**, 180 (1959).
11) R. Roy, V. G. Hill, and E. F. Osborn, *J. Am. Chem. Soc.*, **74**, 719 (1952).
12) F. R. Duke and L. M. Brown, *J. Am. Chem. Soc.*, **76**, 1443 (1954).

13) The dimension of K is h^{-1} assuming that p equals unity.
14) J. W. Mullin, "Crystallisation," 2nd ed, Butterworths, London (1972).
15) A. G. Walton, "The Formation and Properties of Precipitates," Interscience Publishers, New York (1967).
16) H. de Hek, R. J. Stol, and P. L. de Bruyn, *J. Colloid Interface Sci.*, **64**, 72 (1978).
17) R. C. Turner, *Can. J. Chem.*, **47**, 2521 (1969).
18) R. C. Turner and G. J. Ross, *Can. J. Chem.*, **48**, 723 (1970).
19) T. Okura, K. Goto, and T. Yotsuyanagi, *Anal. Chem.*, **34**, 581 (1962).
20) K. Goto and T. Yotsuyanagi, *Nippon Kagaku Zasshi*, **89**, 49 (1968).
21) M. Iwase, T. Yotsuyanagi, and M. Nagayama, *Nippon Kagaku Kaishi*, **1985**, 2271.
22) E. Matijević and L. J. Stryker, *J. Colloid Interface Sci.*, **22**, 68 (1966).
23) A. Bell and E. Matijević, *J. Inorg. Nucl. Chem.*, **37**, 907 (1975).
24) J. K. Ruff and S. Y. Tyree, *J. Am. Chem. Soc.*, **80**, 5654 (1958).
25) C. S. Patterson and S. Y. Tyree, Jr., *J. Am. Chem. Soc.*, **79**, 1821 (1957).
26) R. J. Stol, A. K. van Helden, and P. L. de Bruyn, *J. Colloid Interface Sci.*, **57**, 115 (1976).
27) R. K. Nanda and S. Aditya, *Z. Phys. Chem. (Frankfurt am Main)*, **35**, 139 (1962).
28) R. E. Hester and R. A. Plane, *Inorg. Chem.*, **3**, 769 (1964).
29) E. Matijević, *Ann. Rev. Mater. Sci.*, **15**, 483 (1985).
30) K. H. Lieser, *Angew. Chem., Int. Ed. Engl.*, **8**, 188 (1969).

Electrochemical Properties of Electropolymerized Poly(1-pyrenamine) Films

Noboru Oyama,* Kazuhiko Hirabayashi, and Takeo Ohsaka
Department of Applied Chemistry for Resources, Tokyo University of Agriculture and Technology, Koganei, Tokyo 184
(Received December 25, 1985)

The electropolymerization of 1-pyrenamine (PA) in an acetonitrile solution led to the polymeric film formation on electrode surfaces. The chemical, spectroscopic, electrical and electrochemical characterization of the resulting poly(1-pyrenamine) (PPA) films was carried out. The number-average molecular weight of the PPA film, measured by gel permeation chromatography, was 1.8×10^3, corresponding to the degree of the polymerization of ca. 8. The PPA films were polymer-anion composites which contained ca. 0.3 anions (e.g., BF_4^-) per repeating aromatic unit, which is considered to be composed of three PA molecules. The oxidized form of the PPA film displayed the ESR response. The g factor was 2.0082 and the concentration of radical in the PPA film was determined to be 4.8×10^{19} e^-g^{-1}. The conductivities of the PPA films in the dry state at 300 K were in the range 10^{-11}—10^{-10} S cm^{-1}. The PPA film was electroactive in an aqueous solution as well as in a non-aqueous solution. The cyclic voltammetric responses depended on pH of aqueous solutions and supporting electrolyte in non-aqueous solutions. The thickness(ϕ) of the PPA film and the surface concentration(Γ) of the electroactive site in the PPA film were proportional to the amount (Q) of the charge passed during the electrolysis (when $Q<$ ca. 120 mC cm^{-2}). The volume concentrations of the electroactive site were 9.7×10^{-4} and 1.7×10^{-3} mol cm^{-3} for the PPA films prepared in the $NaClO_4$ and $TBABF_4$ (tetrabutylammonium tetrafluoroborate) electrolytes, respectively. From the normal pulse voltammetric, potential-step chronoamperometric and potential-step chronocoulometric experiments of the PPA films in a 0.2 M $NaClO_4$ aqueous solution (pH 1.0), the effective apparent diffusion coefficient (D_{app}) for the diffusion-like charge transport within the PPA films, and the standard rate constant (k°) and anodic transfer coefficient (α_a) of the heterogeneous electron-transfer reaction between the In_2O_3 electrode and the electroactive site in the PPA film were estimated to be $(1.5\pm0.5)\times10^{-10}$ cm^2 s^{-1}, $(1.9\pm0.4)\times10^{-5}$ cm s^{-1} and 0.67 ± 0.03, respectively.

In a series of recent papers,[1-9] we have reported (i) the preparation of polymeric films by electropolymerization of aniline, phenol and their derivatives, (ii) the electrochemical, spectroscopic, electrical and physicochemical characterization of the prepared polymeric films, and (iii) the applications of the polymer film-coated electrodes as "hybrid electrode materials." It has been demonstrated therein that whether or not the polymer film formation occurs and the structures and properties of the prepared films depend on the kind of the monomer used for polymerization as well as the experimental conditions used in their preparations (e.g., solvent, electrode material, supporting electrolyte, pH of electrolytic solution, current density, temperature, and electrolysis mode (potential sweep electrolysis, potentiostatic electrolysis, galvanostatic electrolysis, etc.)). Also, it has become apparent that one could prepare the polymeric films, chemical preparations of which are not always easy or in some cases very difficult, relatively easily by electropolymerization of commercially available reagents.

Along this line of investigation, the studies on the electropolymerization of polynuclear aromatic hydrocarbons containing hydroxyl or amino groups (e.g., 1-pyrenamine, 1-naphthylamine, and 1-naphtol) have been also started. The film formation during the electro-oxidation of a variety of polynuclear aromatic hydrocarbons has been previously observed by Peover and White,[10,11] and more recently the comprehensive study concerning their electropolymerization has been done by the IBM research group.[12-16] For polynuclear aromatic hydrocarbons containing hydroxyl or amino groups, only a few papers[17,18] concerning the electropolymerization of these compounds have appeared recently. The electrochemical oxidation of polynuclear aromatic amines (e.g., 1-naphthylamine,[19-21] 2-fluorenamine,[22] 10-phenyl-9-anthracenamine[23] and 9-(arylamino)anthracene[24]) has been recently studied by several investigators whose attention has been mainly directed to the mechanism of the formation of the dimeric products soluble in the electrolytic solutions used. Little attention has been paid to the formation of the polymeric films on the electrode surface, although the film formation has been obviously observed in some cases.[19,20] It would be worthwhile to examine the effect of a nucleus other than benzene in the electropolymerization of the aromatic amines and phenols.

In the present paper, we will report the preparation of the polymeric films by electropolymerization of 1-pyrenamine in an acetonitrile solution and the electrochemical, electrical, physicochemical and spectroscopic characterization of the resulting polymer films. It is demonstrated that the prepared polymeric films possess some interesting properties which differ from those obtained for the polymeric films[1-9,25-38] (e.g., polyaniline and polyphenol) prepared from mononuclear aromatic monomers with hydroxyl and/or amino groups.

Experimental

Materials. 1-Pyrenamine (PA)(Aldrich) was purified by

the following way: The commercially available PA reagent was dissolved in acetonitrile and then insoluble materials were filtered out, then the solvent was evaporated off and the resultant PA solids were purified by ordinary recrystallization techniques from hexane. Pyrene of reagent grade (Wako Chemical Co.) was purified by recrystallization from benzene. Acetonitrile (Wako) was distilled by ordinary technique after dehydration on molecular sieves (3A 1/16, Wako). Sodium perchlorate ($NaClO_4$) (Kanto Chemical Co.), tetrabutylammonium tetrafluoroborate ($TBABF_4$), tetrabutylammonium perchlorate(TBAP) (Tokyo Kasei Co.), tetraethylammonium chloride (TEACl) (Wako) which were used as supporting electrolytes were reagent grade. Tetrabutylammonium hexafluorophosphate($TBAPF_6$) (used as supporting electrolyte) was prepared from tetrabutylammonium bromide and potassium hexafluorophosphate and purified by recrystallization from H_2O/C_2H_5OH mixture. The basal-plane pyrolytic graphite(BPG) (Union Carbide Co.) and In_2O_3 were used as working electrodes. All other chemicals were reagent grade and were used without further purification.

Apparatus and Procedures. The electropolymerization and electrochemical measurements were conducted by using a standard three-electrode, two-compartment electrochemical cell. The electrode assembly consists of a BPG (or an In_2O_3) electrode as working electrode, a sodium chloride saturated calomel electrode(SSCE) as reference electrode and a spiral platinum wire as counter electrode. For cyclic voltammetry, potential-step chronoamperometry, potential-step chronocoulometry and normal pulse voltammetry, a home-made instrument was employed along with an X-Y recorder(Watanabe Co.).[39,40] The amounts (Γ) of the electroactive site in the electropolymerized poly(1-pyrenamine) (PPA) films were estimated in units of mol cm^{-2} by measuring the area of cyclic voltammograms(for the redox reaction of PPA film) obtained at slow potential scan rates(1—5 mV s^{-1}) in a 0.2 M (1 M=mol dm^{-3}) $NaClO_4$ aqueous solution (pH 1.0).[39-41] The molar concentration (in units of mol cm^{-3})of the electroactive site was calculated from the Γ thus obtained using the measured thicknesses of the PPA films. The electropolymerization of PA was carried out by a potential-sweep electrolysis and/or a constant potential electrolysis in an acetonitrile solution containing 5 or 10 mM PA+0.2 M supporting electrolyte (mainly $NaClO_4$ or $TBABF_4$). The film thicknesses of the resulting PPA films were measured with a Surfcom 550A (Surface Texture Measuring Instrument, Tokyo Seimitsu). An IR absorption spectroscopy (A-302 Infrared Spectrophotometer, Japan Spectroscopic Co., LTD.) was used to identify the PPA films formed on electrodes. ESR spectra were taken on JES-FEIX ESR Spectrometer for the oxidized forms of the PPA films. The conductivities (σ) of the PPA films in dry state were measured by using two-point probe technique at ambient temperature (300K) by means of d.c. power supply (Metronix Corp., Model 5126) and d.c. microvolt ammeter (Toa Electronic LTD., Model PM-18R). The weight- and number-average molecular weights of the PPA films were estimated by means of gel permeation chromatography by using narrow molecular weight polystyrene standards (Waters Assoc., Inc., Milford, Mass) as probe for measuring resolution and calibration.

Results and Discussion

Cyclic Voltammetric Behavior of PA Monomer. Typical cyclic voltammograms of PA at BPG electrode in an acetonitrile solution containing 0.2 M $TBABF_4$, and 10 mM PA are shown in Fig. 1 where the cyclic voltammograms of pyrene in the same supporting electrolytic solution are given for comparison. PA electro-oxidizes irreversibly and produces complicated cyclic voltammograms. The voltammograms contain multiple peaks which are broad and overlapping. In the first forward scan of the potential, the several anodic peaks were obtained at ca. 0.6, 0.95, 1.2, and 1.4 V vs. SSCE (at 50 mV s^{-1}). During the first reverse scan, the ill-defined cathodic peaks corresponding to the anodic peaks observed during the forward scan and the well-defined one at ca. 0.3 V were observed. In the second forward scan, the anodic peak corresponding to the cathodic one at 0.3 V was obtained at ca. 0.4 V. This paired anodic and cathodic peaks correspond to the redox reaction of the polymeric products being formed on the electrode surface. The oxidation potential (ca. 0.4 V) of the polymeric products is lower than that (ca. 0.6 V) of parent PA. Such a behavior seems to be a general feature of a number of families of homologous oligomers of aromatic compounds.[13,42] According to the fact,[13,42] the dimer or any higher oligomer is more easily oxidized than parent monomer. The

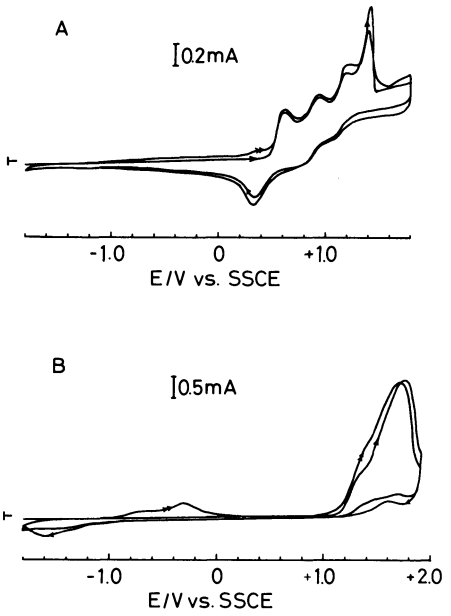

Fig. 1. Typical cyclic voltammograms of (A) PA and (B) pyrene at BPG electrodes in acetonitrile solutions under an atmosphere of nitrogen. Solution composition: (A) 10 mM PA+0.2 M $TBABF_4$, (B) 10 mM pyrene+0.2 M $TBABF_4$. Scan rate: 50 mV s^{-1}. Electrode area: 0.17 cm^2. The arrow indicates the direction of potential scan.

increase in the peak currents with successive potential scans indicates the build-up of the electroactive polymeric products on the electrode.

The cyclic voltammetric response of PA is considerably different from that for pyrene in that (i) the voltammetric responses are more complicated than those for pyrene, (ii) the first oxidation peak (ca. 0.6 V vs. SSCE) is much less positive than that (ca. 1.3 V) for pyrene, and (iii) the redox response of the polymeric product is observed at ca. 0.35 V, which is considerably negative compared with that (ca. 0.9 V) for the polymeric product from pyrene. Of course, PA as well as pyrene electro-oxidize and produce the respective polymeric films on electrode surfaces. The cyclic voltammetric data for pyrene shown in Fig. 1 are in good agreement with those reported previously by Diaz et al.[15]

By holding the electrode potential at the potential which is slightly over the first oxidation peak potential(typically this is 0.75 V vs. SSCE), the formation of the polymeric film on the electrode surface was observed. The electrolyses at more positive potentials (e.g., 1.0 V vs. SSCE) did not give the substantially different results: The cyclic voltammetric responses and IR spectra of the PPA films prepared by the electrolyses at 0.75 and 1.0 V vs. SSCE were the same. However, the electrolyses at much more positive potentials (e.g., 1.8 V vs. SSCE) did not lead a significant film formation on electrode surfaces. Thus, in the experiments mentioned below, the electrolysis was carried out at the potential which is slightly over the first oxidation peak potential. The typical cyclic voltammograms of this case are shown in Fig. 2. As the potential scan was cycled, the anodic peak current at 0.65 V decreased, while the new peaks at 0.35 and 0.45 V increased slowly. As a result, the formation of a purplish black thin film was observed on the electrode surface. The oxidized form of the film was purplish black and the reduced form was yellow. The redox response corresponding to the polymer film produced on the electrode surface was observed at ca. 0.3 V, when after the electrolysis the electrode was washed with benzene and then transferred into the supporting electrolytic solution containing no PA (0.2 M $NaClO_4$ aqueous solution, pH 1.0). The voltammetric response remained substantially unchanged even after the potential scan cycling of several hours.

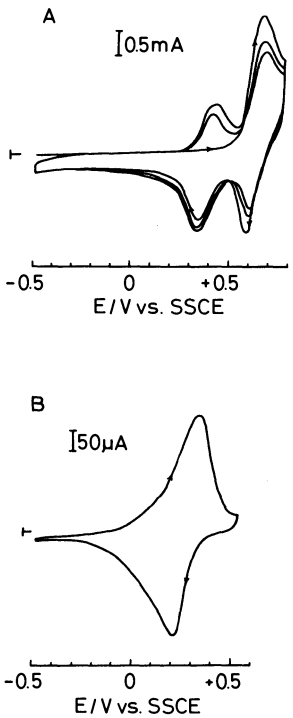

Fig. 2. (A) Typical cyclic voltammograms of PA at a BPG electrode in an acetonitrile solution containing 5 mM PA+0.2 M $TBABF_4$. Scan rate: 5 Vs^{-1}. Electrode area: 0.17 cm^2. (B) Cyclic voltammogram representing the electroactivity of the PPA film deposited on a BPG electrode in a 0.2 M $NaClO_4$ aqueous solution (pH=1.0). Scan rate: 50 mVs^{-1}.

Spectroscopic, Electrical and Chemical Characterization of PPA Film. The IR spectra of the PPA films formed on the In_2O_3 electrodes during the anodic oxidation of PA are shown in Fig. 3 in which the IR spectrum of PA monomer is also shown for comparison. These IR spectral data are summarized in Table 1. In the case of the oxidized form of the PPA film, the observation of the peak at 1660 cm^{-1}

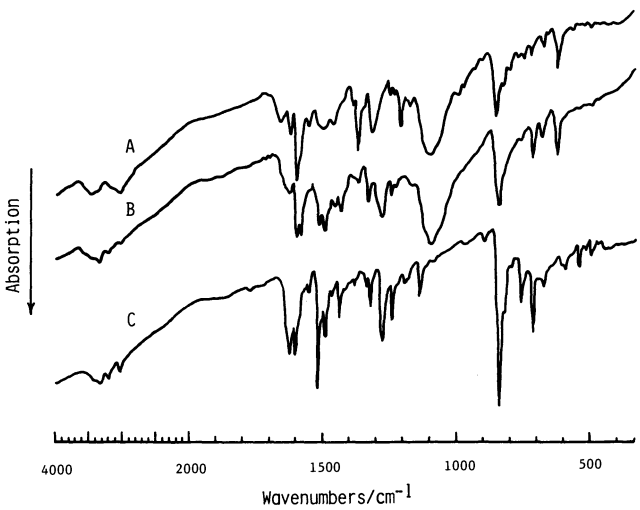

Fig. 3. IR spectra of (A) the oxidized form and (B) the reduced form of the PPA film and (C) PA monomer. The oxidized form of the PPA film was prepared on an In_2O_3 electrode by a constant-potential electrolysis (at 0.75 V vs. SSCE) in a 0.2 M $NaClO_4$ acetonitrile solution containing 10 mM PA and 10 mM pyridine. The reduced form was prepared by reducing electrochemically the oxidized form deposited on electrodes at −0.5 V vs. SSCE in a 0.2 M $NaClO_4$ aqueous solution (pH=1.0).

Table 1. IR Spectra of PPA Films and PA Monomer
(Fundamental Vibrations, Frequencies in cm^{-1})

Compound	Vibration mode[c,d,e]						
	ν(C=C)	ν(C-H)	γ(C-H)	ν(C=N)	ν(C-N)	ν(N-H)	ClO_4^-
PA	1600 s	3030 w	840 s	f	1280 s	3330 w	f
	1510 s		820 m				
	1490 m		760 m				
	1440 m		720 s				
			680 m				
Oxidized[a] form of PPA	1600 s	3030 w	850 s	1660 w	g	3350 w	1100 s
	1550 w		820 m				
	1490 w		760 w				
	1450 w		740 w				
			720 w				
			670 w				
Reduced[b] form of PPA	1600 s	3030 w	840 s	f	1280 s	3350 w	1100 s
	1580 s		820 m				
	1510 m		710 m				
	1430 m		680 w				

a) The oxidized form of the PPA film was prepared on an In_2O_3 electrode by a constant-potential electrolysis at 0.75 V vs. SSCE in an acetonitrile solution containing 10 mM PA+10 mM pyridine+0.2 M $NaClO_4$. b) The reduced form of the PPA film was prepared by reducing electrochemically the oxidized form deposited on electrodes at −0.5 V vs. SSCE in a 0.2 M $NaClO_4$ aqueous solution(pH 1.0). c) ν=Stretching vibration. d) γ= Out-of-plane bending vibration. e) Absorption intensity (not quantitative); s(strong), m(medium) and w(weak). f) No absorption. g) Absorption was observed as "shoulder".

corresponding to the stretching of the C=N bonds seems to point to polymers based on imine links of the type C-N=C.[43,44] This absorption peak was not observed with the reduced form of PPA as well as PA monomen The relatively strong absorption peaks at 1280 cm^{-1} which are ascribable to the stretching of C-N bonds[43,44] were observed with PA monomer and the reduced form of PPA, while in the case of the oxidized form the corresponding absorption peak was observed slightly as a "shoulder". The strong absorption peaks at 1100 cm^{-1} observed in the spectra of the oxidized and reduced forms of the PPA film are assigned to the presence of ClO_4^- ions,[43,44] which were used as an electrolytic anion during the film formation. The absorption peaks due to the N-H stretching at 3330—3350 cm^{-1} were observed for the oxidized and reduced forms of the PPA film and PA monomer. The other absorption peaks shown in Table 1 (i. e., ν(C=C), ν(C-H), and γ(C-H)), which are common to the PPA films and PA monomer, are characteristic of the various vibration modes of the C-H and C-C bonds of the aromatic nuclei.[43,44] From these results, the electropolymerization of PA seems to proceed via the formation of the C-N=C bonds and the C-NH-C bonds. In this point, the electropolymerization reaction of PA may be similar to that proposed recently for aniline and its derivatives.[2-4,6,7,27,30,46]

For the electropolymerized films of aniline and its derivatives,[2-4,6,7,46] an analysis of the absorption peak pattern between ca. 900 and 700 cm^{-1} which arises from the C-H out-of-plane bending modes[43,45] enabled us to assign correctively the substitution pattern of the aromatic ring and to elucidate the structures of the films. A fairly good correlation between the positions of the absorption bands and the substitution pattern in terms of numbers of adjacent hydrogen atoms was found for the condensed aromatic ring series (i.e., benzene, acene and phen series).[43,45,47,48] However, no conclusive results on the basis of the same idea were obtained for pyrene, which is a peri-condensed hydrocarbon. Recently, the empirical rules connecting substitution pattern and bond positions in a broad variety of substituted pyrenes (137 pyrene derivatives) has been suggested by Hansen and Berg.[49] According to their empirical rules, along with the above-mentioned discussions about the linkage between PA units in the PPA film, it can be concluded that the electropolymerization of PA proceeds via the coupling of the aromatic rings at the 1- and 6-positions and/or the 1- and 8-positions as follows:

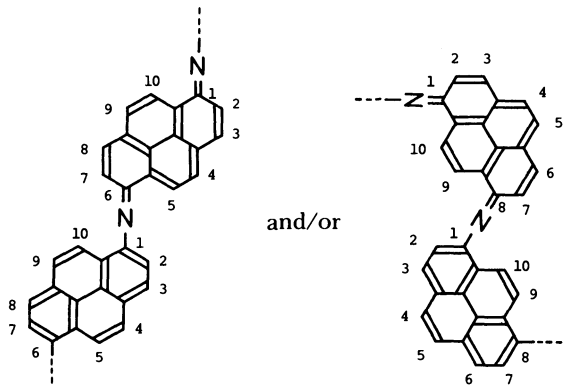

and/or

On the basis of the concept of radical cation dimerization, Bargon et al.[13] have recently suggested that the polypyrene, the polymeric product resulting from the electropolymerization of pyrene, is made up of 1,6-pyrenediyl and/or 1,8-pyrenediyl units. The PPA films were soluble in dimethyl sulfoxide and *N*,*N*-dimethylformamide(DMF). The weight- and number-average molecular weight ($\bar{M}_w$ and $\bar{M}_n$) of the PPA films were estimated by means of gel permeation chromatography (solvent: DMF). The values of $\bar{M}_n$ and $\bar{M}_w$ were 1.8×10^3 and 3.0×10^3, respectively which correspond to the degree of polymerization of 8 and 14, respectively. Note that the true molecular weight of the PPA film may be smaller than that estimated on the basis of polystyrene standards (as mentioned above), because PA is more rigid than styrene.

The elemental analysis of the PPA film (oxidized form) prepared in the $TBABF_4$ acetonitrile solution indicated that the weight percents of C, H, N, and BF_4^- in the PPA film are 78.07, 3.76, 5.72, and 12.45%, respectively which correspond to the molar ratios of 15.9(C), 9.1(H), 1.0(N) and 0.35(BF_4^-) (relative to the molar numer of N). This fact indicates that the PPA films are polymer-anion composites which contain ca. 12% BF_4^- by weight. From these molar ratios of C, H, N, and BF_4^- a possible structure of the repeating aromatic unit of the PPA film may be predicted as follows:

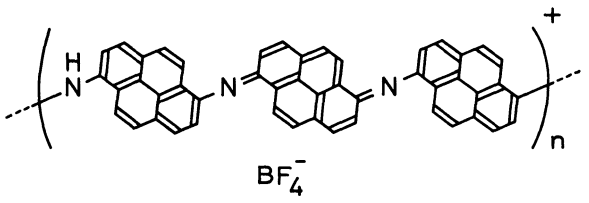

The molar ratios of C, H, N, and BF_4^- for the repeating unit structure predicted above are 16.0, 8.3, 1.0, and 0.33, respectively, which are in fair agreement with the experimental elemental analysis. Thus, the PPA film contains ca. 0.3 BF_4^- anions per repeating aromatic unit which is thought to be composed of three PA molecules. Further, it is worth noting that the elemental composition is somewhat hydrogen-rich. This may suggest that the double bonds of the pyrene rings of the PPA are partially hydrogenated, as previously proposed for the hydrogen-rich elemental compositions of the polymers prepared by the electropolymerization of polycyclic aromatic hydrocarbons such as pyrene and fluorene.[15]

In Fig. 4 is shown the ESR spectrum of the oxidized form of the PPA film. The ESR spectrum consists of a simple, symmetrical, narrow line with Lorentzian shape. The peak-to-peak line width was 0.90 mT at room temperature. The *g* factor measured against a 2,2-diphenyl-1-picrylhydrazyl radical standard was 2.0082. The concentration of radical in the PPA film was determined to be 4.8×10^{19} $e^- g^{-1}$, which is compared to the value ($(1-7)\times10^{19}$ $e^- g^{-1}$) for polyaniline[50,53] (oxidized form) and that (1.4×10^{19} $e^- g^{-1}$) for polyacetylene.[51] Assuming that the elemental composition of the PPA is $C_{48}H_{25}N_3(BF_4)_1$, it is thought that there is one unpaired electron per ca. 17 repeating units. Even after the reduction of the oxidized form of the PPA film by the chemical procedure (using the reductants such as $Na_2S_2O_4$ and C_2H_5SH) or by the electrochemical one (by holding the PPA-coated electrode at the potetial at which the PPA film could be reduced), no NMR spectra of the reduced form (as well as the oxidized form) of the PPA film were obtained.

The conductivities (σ) of the PPA films in the dry state, measured at 300 K by using the two-point probe technique, were in the range 10^{-11}—10^{-10} S cm^{-1} for both oxidized and reduced forms irrespective of the supporting electrolytes used (i.e., $NaClO_4$ and $TBABF_4$). Also, the σ values were nearly independent of the presence or absence of pyridine in the electrolytic solution. Note that the σ values for the PPA films are about 6 to 10 orders of magnitude smaller than those obtained for the other electropolymerized films, for example, the σ values (10^{-4}—10^{-1} S cm^{-1}) for polyaniline, poly(*o*-phenylenediamine) and poly(*N*-methylaniline).[3,5,53] Further, the

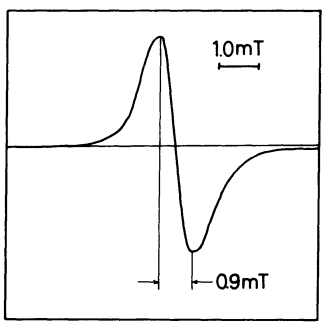

Fig. 4. ESR spectrum of the oxidized form of the PPA film at 298 K. The oxidized form of the PPA film was prepared by the same procedure as shown in Fig. 3.

following fact should be noted: In the case of the polyaniline films which were equilibrated with aqueous solutions of different pH's, washed in acetonitrile, and then dried under vaccum, changing pH from 0 to 6 has been reported to decrease σ by 6 orders of magnitude,[53] whereas in the case of the PPA film the slight dependence of σ on pH was observed, i.e., the σ values of the PPA films treated at pH 1.0 and 12.0 were ca. 10^{-10} and 10^{-12} S cm^{-1}, respectively. Such significant differences in the σ values and their pH dependences are considered to originate from the difference in the basic structures of the PPA and polyaniline, that is, the former contains polynuclear aromatic rings, while the latter contains mononuclear aromatic rings.

Electrochemical Response of PPA Film. Figure 5 shows the correlation between the thickness (ϕ) of the PPA film and the amount (Q) of the charge passed during the anodic oxidation of PA. In this case, the films were prepared by the anodic oxidation of PA at 0.75 V vs. SSCE in an acetonitrile solution containing 0.2 M $NaClO_4$ (or $TBABF_4$), 10 mM PA and 10 mM pyridine. The ϕ's are proportional to Q when $Q<$ca. 120 mC cm^{-2}. The proportionality constant of ϕ to Q is 4.2×10^{-3} cm^3 C^{-1} for the PPA film prepared in the $NaClO_4$ electrolyte and 1.9×10^{-3} cm^3 C^{-1} for that prepared in the $TBABF_4$ electrolyte. Thus, under the conditions of the same amount of the charge passed, the PPA film prepared in the $NaClO_4$ electrolyte is over twice thicker than that in the $TBABF_4$ solution. Such an observed proportionality is surprising in view of the fact that the film-forming reaction was accompanied by the formation of soluble, purplish products as can readily be seen from the colored (purplish) electrolytic solution. The similar proportionality of ϕ to Q has been also obtained in the electropolymerization of the other aromatic monomers (e.g., aniline,[1] N-methylaniline,[5] o-phenylenediamine[5] and N,N-dialkylanilines[6,7]), irrespective of the apparent observation of the production of the soluble products. The proportionality constants obtained for the PPA films are 5—10 times larger than that obtained for the electropolymerization of aniline. At any rate, the data shown in Fig. 5 indicate that the PPA film thickness can be arbitrarily controlled by the charge passed during the electrolysis.

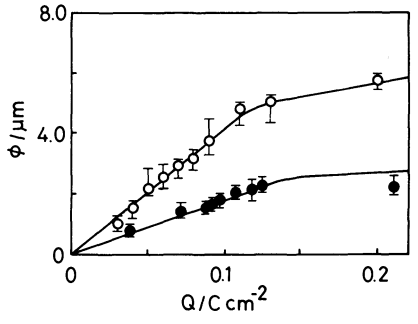

Fig. 5. Correlation between the PPA film thickness (ϕ) and the amount (Q) of the charge passed during the anodic oxidation of PA. The PPA films were prepared on BPG electrodes by a constant-potential electrolysis at 0.75 V vs. SSCE in acetonitrile solutions. Solution composition: (○) 10 mM PA+10 mM pyridine+0.2 M $NaClO_4$; (●) 10 mM PA+10 mM pyridine+0.2 M $TBABF_4$. Widths of error bars indicate uncertainties in thickness measurements.

Figure 6 shows the correlation between the Γ value and Q, where the Γ indicates the surface concentration of electroactive site in PPA films, measured by cyclic voltammetry in an aqueous $NaClO_4$ solution (pH 1.0). The Γ's are proportional to Q when $Q<$ca. 120 mC cm^{-2}. Thus, from the results shown in Figs. 5 and 6, the volume concentrations of electroactive site in the PPA films were estimated to be 9.7×10^{-4} and 1.7×10^{-3} mol cm^{-3} for the PPA films prepared in the $NaClO_4$ and $TBABF_4$ solutions, respectively. In this case, the current efficiency for the preparation of the PPA films was 30—40 per cent. This value is considerably high compared with those (several per cent) for polyaniline,[1] poly(N-methylaniline),[5] and poly(o-phenylenediamine)[5] films. It is interesting that the correlations between ϕ and Q, and Γ and Q depend on the supporting electrolyte used in the PPA film formation and as a result the volume concentrations of the electroactive site in the PPA films are different. This may probably be due to the different

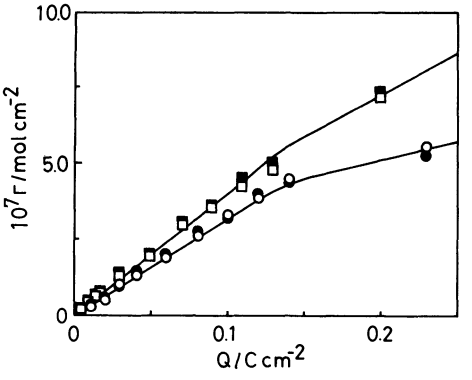

Fig. 6. Correlation between the surface concentration (Γ) of electroactive site in the PPA films and the amount (Q) of the charge passed during the anodic oxidation of PA. The PPA films were prepared by the same procedure as shown in Fig. 5. (□, ■): the PPA films prepared in the $NaClO_4$ electrolyte, (○, ●): the PPA films prepared in the $TBABF_4$ electrolyte. The estimation of the Γ values was conducted by measuring the area of cyclic voltammograms (for the redox reaction of the PPA film) obtained at the potential scan rate of 2 mVs^{-1} in a 0.2 M $NaClO_4$ aqueous solution (pH=1.0). The open and solid symbols indicate the Γ values estimated from the integration of the anodic and cathodic currents, respectively, of the cyclic voltammograms of the PPA films.

morphology of the PPA films formed in the different supporting electrolytes. The PPA films prepared from the $NaClO_4$ electrolyte appeared rough to the naked eye, while those from the $TBABF_4$ electrolyte appeared more lustrous. The latter PPA films were more adhesive to the electrode surface. Thus it may be thought that the PPA film prepared from the $NaClO_4$ electrolyte is more porous than that from the $TBABF_4$ electrolyte, so that the PA monomers can more easily penetrate the PPA film prepared from the $NaClO_4$ electrolyte to reach the electrode surface than that prepared from the $TBABF_4$ electrolyte. This is apparent from the Q vs. t curves obtained during the electrolysis at a constant potential (see Fig. 7).

The PPA films are electroactive in an aqueous solution. The pH-dependences of the cyclic voltammograms of the PPA films are shown in Fig. 8. For the PPA of Γ=2.2×10^{-9} mol cm^{-2}, corresponding to ca. 20 monolayers based on a monolayer coverage of ~10^{-10} mol cm^{-2}, the cyclic voltammetric response is similar to that obtained for the solution-phase redox species the electrode reaction of which is reversible, that is, the voltammograms are diffusion-like with broad peaks and diffusional tails and the cathodic and anodic peak currents are almost the same (Fig. 8A). The anodic and cathodic peak potentials (E_p^a and E_p^c) shifted to the negative potential with increasing pH (Fig. 9). The dependences of E_p^a and E_p^c on pH are complicated, indicating that proton (H^+) and electron (e^-) take part in the electrode reaction of the PPA film and in this case the numbers of H^+ and e^- involed in the electrode reaction vary with pH of the solution. However, in an acidic solution (pH<4.0) the slopes of E_p^a (and E_p^c) vs. pH plots are about −60 mV/pH. This suggests that the overall electrode reaction of the PPA film is the H^+/e^- reaction in an acidic

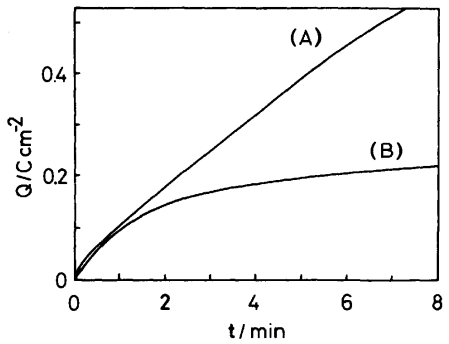

Fig. 7. Potential-step chronocoulometric responses for the anodic oxidation of PA at a BPG electrode in acetonitrile solutions. Solution composition: (A) 10 mM PA+10 mM pyridine+0.2 M $NaClO_4$; (B) 10 mM PA+10 mM pyridine+0.2 M $TBABF_4$. Electrode area: 0.17 cm^2. The electrode potential was stepped from 0.0 to 0.75 V vs. SSCE.

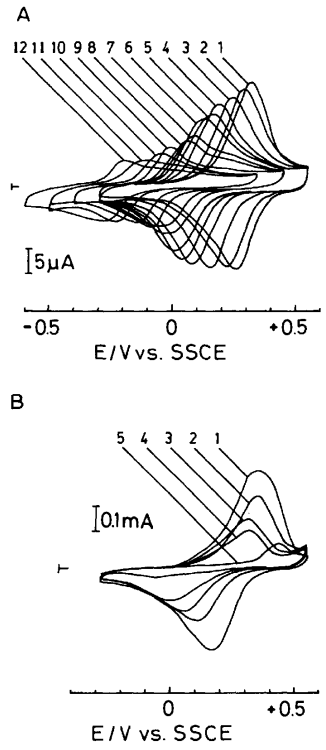

Fig. 8. Cyclic voltammetric responses of the PPA films on BPG electrodes in 0.2 M $NaClO_4$ aqueous solutions of various pH's. The Γ values of the PPA films: (A) 2.2×10^{-9} mol cm^{-2}; (B) 9.7×10^{-8} mol cm^{-2}. Scan rate: 100 mV s^{-1}. Electrode area: 0.19 cm^2. The PPA films were prepared by the same procedure as shown in Fig. 5. The numbers on respective cyclic voltammograms indicate pH values.

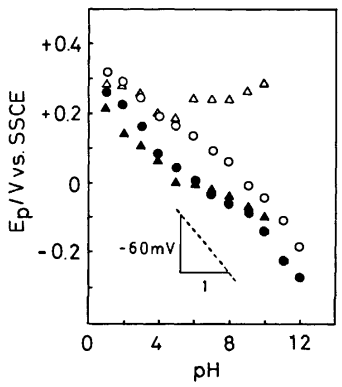

Fig. 9. Typical pH-dependences of the anodic and cathodic peak potentials of the cyclic voltammograms of the PPA films. The Γ values of the PPA films: (○, ●) 2.2×10^{-9} mol cm^{-2}, (△, ▲) 9.7×10^{-8} mol cm^{-2}. The open and solid symbols indicate the anodic and cathodic peak potentials (E_p^a and E_p^c), respectively. Other experimental conditions are the same as in Fig. 8.

aqueous solution. For the thicker film of $\Gamma = 9.7\times10^{-8}$ mol cm^{-2} corresponding to ca. 1000 monolayers, the cyclic voltammetric response is considerably complicated, compared with that for the thin film (Fig. 8B). In this case, the cyclic voltammetric response depended on the scan rate of the potential. The similar behavior has been also observed for the other electroactive electropolymerized films (e.g., polyaniline film[1,25,28]). It seems to be the reason for such a behavior that the PPA film contains the redox sites with slightly different redox potentials and/or its electrode reaction involves any chemical process which actually determines the rate of the overall electrode reaction at the time scale of the measurements. The decreases in the peak currents with increasing pH, shown in Fig. 8, are associated with the fact that a proton addition-elimination reaction is involved in the overall electrode reaction of the PPA film itself, as mentioned above. The magnitude of the peak currents reflects the apparent rate of the overall electrode reactions which decreases with a decrease in the concentration of proton. In this case, these decreases were found to be due to neither the dissolution of the PPA film on electrodes nor its chemical change to any electroinactive compounds (when soaked in alkaline solutions) from the following facts: The Γ values for a given PPA film-coated BPG electrode, measured in the solutions of different pH's, were the same within experimental errors. The coloration of the solution due to the dissolution was not observed. The IR spectra of the PPA films, which were equilibrated with the aqueous solutions of pH1.0 and 12.0 and then dried under vacuum, were essentially the same.

Figure 10 shows the typical normal pulse voltammograms for the oxidation of the PPA film on an In_2O_3 electrode in a 0.2 M $NaClO_4$ solution (pH 1.0). The PPA film was the electropolymerized one in the $NaClO_4$ acetonitrile solution. The plots of the anodic limiting current (i_{lim}) of these normal pulse voltammograms against the inverse square root of the sampling time (τ) were found to be linear (Fig. 11), indicating that the limiting currents were diffusion-controlled.[39,40] Thus the values of the apparent diffusion coefficients, D_{app}, for the charge-transport process within the PPA films were obtained from the slope of the i_{lim} vs. $\tau^{-1/2}$ plot by using the Cottrell equation, as has been done for other surface-confined polymers[39,40]: $D_{app}=1.3\times10^{-10}$ cm^2 s^{-1} (for anodic process). The potential-step chronoamperometric and chronocoulometric experiments (PSCA and PSCC) gave also the D_{app} values: from PSCA, the D_{app} values were determined to be 2.0×10^{-10} and 1.2×10^{-10} cm^2 s^{-1} for anodic and cathodic processes, respectively and from PSCC, the D_{app} values were determined to be 1.9×10^{-10} and 1.0×10^{-10} cm^2 s^{-1} for anodic and cathodic processes, respectively. The D_{app} values estimated by these different procedures are almost the same within experimental errors. These values of D_{app} are about 1—2 orders of magnitude smaller than those previously reported for other electroactive electropolymerized films.[1,8,52] Furthermore, from the analysis[39,40] of the rising part of the normal pulse voltammograms shown in Fig. 10, the standard rate constant (k°) and the anodic transfer coefficient (α) of the heterogeneous electron-transfer reaction were estimated to be $(1.9\pm0.4)\times10^{-5}$ cm s^{-1} and 0.67 ± 0.03, respectively.

The PPA films are also electroactive in a non-

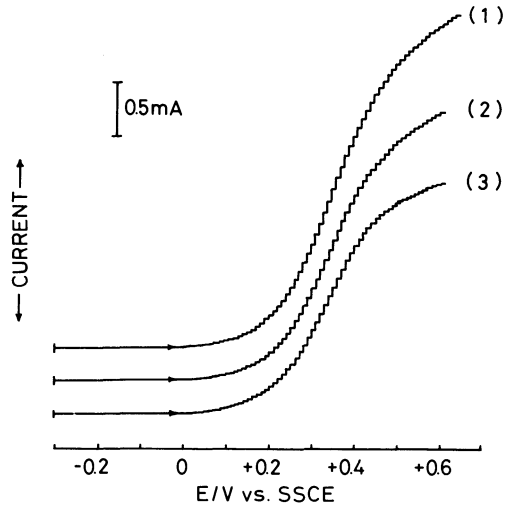

Fig. 10. Typical normal pulse voltammograms for the oxidation of the PPA film on an In_2O_3 electrode in a 0.2 M $NaClO_4$ aqueous solution (pH 1.0). The PPA film was prepared by the same procedure as in Fig. 5. Concentration of the electroactive site in the PPA film: 1.75×10^{-3} mol cm^{-3}. Thickness of the PPA film: 1.1×10^{-4} cm. Sampling time (τ): (1) 5, (2) 8 and (3) 10 ms. Electrode area: 0.16 cm^2.

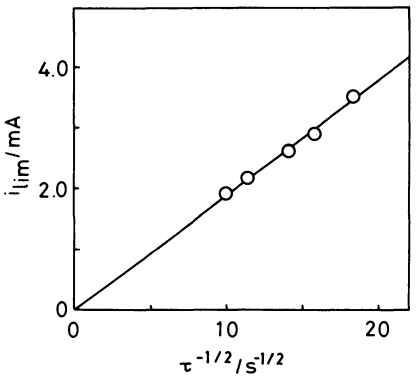

Fig. 11. Normal pulse voltammetric Cottrell plots of limiting current (i_{lim}) vs. (sampling time)$^{-1/2}$ for the oxidation of the PPA film on an In_2O_3 electrode in a 0.2 M $NaClO_4$ aqueous solution (pH 1.0). Other experimental conditions are the same as in Fig. 10.

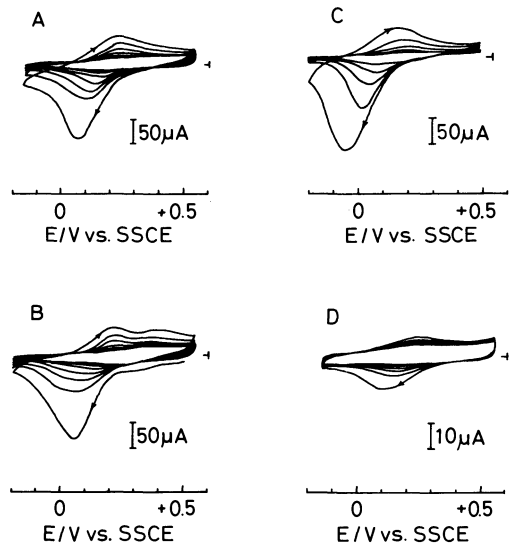

Fig. 12. Cyclic voltammetric responses of the PPA films on BPG electrodes in acetonitrile solutions containing different supporting electrolytes. Supporting electrolyte (0.2 M): (A) $TBABF_4$, (B) TBAP, (C) TEACl, and (D) $TBAPF_6$. Scan rate: 50 mVs^{-1}. Electrode area: 0.17 cm^2. The arrow indicates the direction of potential scan. The PPA films in (A)—(D) were prepared on BPG electrodes by a constant-potential electrolysis at 0.75 V vs. SSCE in acetonitrile solutions containing 10 mM PA+10 mM pyridine+0.2 M supporting electrolyte ((A) $TBABF_4$, (B) TBAP, (C) TEACl, and (D) $TBAPF_6$). In respective electrolysis, the amount of the charge passed was 30 mC cm^{-2}.

aqueous solution. For example, the cyclic voltammetric responses of the PPA film in acetonitrile solutions containing different supporting electrolytes are shown in Fig. 12. The peak current decreased with the cycling of potential scan, probably because of the relatively large solubility of the reduced form of the PPA film in an acetonitrile. The cathodic and anodic peak potentials seem to vary with the supporting electrolyte. The redox response of the PPA film in the acetonitrile solutions may be regarded as the so-called electrochemical doping-undoping process,[54,55] that is, the uptake/exclusion of the supporting electrolytic ions into/out of the film which is coupled to the electrode reaction proper of the PPA film. As mentioned above, the protons take part in the electrode reaction of the PPA in an aqueous solution and the bond formation (during the cathodic process) and cleavage (during the anodic process) of the N-H bonds occurs. Thus, the electrode reactions of the PPA film in aqueous and non-aqueous solutions are considered to be different from each other.

This work was partially supported by Grant-in-Aid for Scientific Research No. 59550510, for Noboru Oyama, from the Ministry of Education, Science, and Culture, Japan and the Nissan Science Foundation.

References

1) N. Oyama, Y. Ohnuki, K. Chiba, and T. Ohsaka, *Chem. Lett.*, **1983**, 1759.
2) Y. Ohnuki, T. Ohsaka, H. Matsuda, and N. Oyama, *J. Electroanal. Chem.*, **158**, 55 (1983).
3) T. Ohsaka, Y. Ohnuki, N. Oyama, G. Katagiri, and K. Kamisako, *J. Electroanal. Chem.*, **161**, 399 (1984).
4) Y. Ohnuki, H. Matsuda, and N. Oyama, *Nippon Kagaku Kaishi*, **1984**, 1801.
5) N. Oyama, K. Chiba, Y. Ohnuki, and T. Ohsaka, *Nippon Kagaku Kaishi*, **1985**, 1172.
6) N. Oyama, T. Ohsaka, and T. Shimizu, *Anal. Chem.*, **57**, 1526 (1985).
7) T. Ohsaka, T. Okajima, and N. Oyama, *J. Electroanal. Chem.*, **200**, 159 (1986).
8) T. Ohsaka, K. Chiba, and N. Oyama, *Nippon Kagaku Kaishi*, **1986**, 457.
9) N. Oyama, T. Ohsaka, and M. Nakanishi, *J. Macromol. Sci.-Chem.*, in press.
10) M. E. Peover and B. S. White, *J. Electroanal. Chem.*, **13**, 93 (1967).
11) M. E. Peover, "Electrochemistry of Aromatic Hydrocarbons and Related Substances," Electroanalytical Chemistry, Vol. 2, A. J. Bard, Ed., Marcel Dekker, Inc., New York (1967), pp. 1—51.
12) J. Bargon, S. Mohmand, and R. J. Waltman, *Mol. Cryst. Liq. Cryst.*, **93**, 279 (1983).
13) J. Bargon, S. Mohmand, and R. J. Waltman, *IBM, J. Res. Dev.*, **27**, 300 (1983).
14) R. J. Waltman, A. F. Diaz, and J. Bargon, *J. Electrochem. Soc.*, **131**, 1452 (1984).
15) R. J. Waltman, A. F. Diaz, and J. Bargon, *J. Electrochem. Soc.*, **132**, 631 (1985).
16) R. J. Waltman, A. F. Diaz, and J. Bargon, *J. Electrochem. Soc.*, **131**, 740 (1984).
17) M. C. Pham, A. Hachemi, and M. Delamar, *J. Electroanal. Chem.*, **184**, 197 (1985).
18) R. J. Waltman and J. Bargon, *J. Electroanal. Chem.*, **194**, 49 (1985).
19) N. Vettorazzi, J. J. Silber, and L. Sereno, *J. Electroanal. Chem.*, **125**, 459 (1981).
20) N. Vettorazzi, J. J. Silber, and L. Sereno, *J. Electroanal. Chem.*, **158**, 89 (1983).
21) M. Breitenbach and K. H. Heckner, *J. Electroanal. Chem.*, **33**, 45 (1971).
22) K. Yasukouchi, I. Taniguchi, H. Yamaguchi, K. Miyaguchi, and K. Horie, *Bull. Chem. Soc. Jpn.*, **52**, 3208 (1979).
23) G. Cauquis, J. Badoz-Lambling, and J. P. Billon, *Bull. Soc, Chim. Fr.*, **1965**, 1433.
24) J. P. Billon, G. Cauquis, J. Raison, and Y. Thiband, *Bull. Soc. Chim. Fr.*, **1967**, 199.
25) R. Noufi, A. J. Nozik, J. White, and L. F. Warren, *J. Electrochem. Soc.*, **129**, 2261 (1982).
26) F. Bruno, M. C. Pham, and J. E. Dubois, *Electrochim. Acta*, **22**, 451 (1977)
27) A. Volkov, G. Tourillon, P. C. Lacaze, and J. E. Dubois, *J. Electroanal. Chem.*, **115**, 279 (1980).

28) A. F. Diaz and J. A. Logan, *J. Electroanal. Chem.*, **111**, 111 (1980).
29) M. C. Pham, J. E. Dubois, and P. C. Lacaze, *J. Electroanal. Chem.*, **130**, 346 (1983).
30) D. M. Mohilner, R. N. Adams, and W. J. Argersinger, Jr., *J. Am. Chem. Soc.*, **84**, 3618 (1962).
31) T. Kobayashi, H. Yoneyama, and H. Tamura, *J. Electroanal. Chem.*, **161**, 419 (1984).
32) T. Kobayashi, H. Yoneyama, and H. Tamura, *J. Electroanal. Chem.*, **177**, 293 (1984).
33) A. Kitani, J. Izumi, J. Yano, Y. Hiromoto, and K. Sasaki, *Bull. Chem. Soc. Jpn.*, **57**, 2254 (1984).
34) J. Yano, A. Kitani, R. E. Vasquez, and K. Sasaki, *Nippon Kagaku Kaishi*, **1985**, 1124.
35) E. Tsuchida, H. Nishida, and T. Maekawa, *J. Macromol. Sci-Chem.*, **A21**, 1081 (1984).
36) G. Mengoli, S. Daolio, and M. M. Musiani, *J. Appl. Electrochem.*, **10**, 459 (1980).
37) M. C. Pham, J. E. Dubois, and P. C. Lacaze, *J. Electroanal. Chem.*, **99**, 331 (1979).
38) M. C. Pham, G. Tourillon, P. C. Lacaze, and J. E. Dubois, *J. Electroanal. Chem.*, **111**, 385 (1980).
39) N. Oyama, T. Ohsaka, M. Kaneko, K. Sato, and H. Matsuda, *J. Am. Chem. Soc.*, **105**, 6003 (1983).
40) N. Oyama, T. Ohsaka, and T. Ushirogouchi, *J. Phys. Chem.*, **88**, 5274 (1984).
41) N. Oyama and F. C. Anson, *J. Electrochem. Soc.*, **127** 640 (1980).
42) M. Genies and A. F. Diaz, *J. Electroanal. Chem.*, **98**, 305 (1979).
43) D. Dolphin and A. Wick, "Tabulation of Infrared Spectral Data," Wiley, New York, London, Sydney, Toronto (1977).
44) C. J. Pouchert, "The Aldrich Library of Infrared Spectra," 2nd. ed., Aldrich Chemical Company, Milwaukee, WI (1975).
45) A. D. Cross and R. A. Jones, "An Introduction to Practical Infrared Spectroscopy," 3rd. ed., Butterworth, London, (1969).
46) Y. Matsuda, A. Shono, C. Iwakura, Y. Ohshiro, T. Agawa, and H. Tamura, *Bull. Chem. Soc. Jpn.*, **44**, 2960 (1971).
47) S. E. Wiberley and R. D. Gonzales, *Appl. Spectrosc.*, **15**, 174 (1961).
48) N. B. Colthup, L. H. Daly, and S. E. Wiberley, "Introduction to Infrared and Raman Spectroscopy," Academic, New York, (1964).
49) P. E. Nansen and A. Berg, *Acta Chem. Scand., Ser. B*, **35**, 131 (1981).
50) S. C. Yang, S. Brahma, and D. Migneault, private communication.
51) I. B. Goldberg, H. R. Crowe, P. R. Newman, A. J. Heeger, and A. G. McDiarmid, *J. Chem. Phys.*, **70**, 1132 (1979).
52) T. Ohsaka, K. Chiba, and N. Oyama, manuscript in preparation.
53) J. P. Travers, J. Chroboczek, F. Devreux, F. Denoud, M. Nechtschein, A. Syed, E. M. Genies, and C. Tsintavis, *Mol. Cryst. Liq. Cryst.*, **121**, 195 (1985).
54) G. Tourillon and F. Garnier, *J. Phys. Chem.*, **87**, 2289 (1983).
55) A. G. McDiarmid and A. J. Heeger, "Molecular Metals," ed by W. E. Hatfield, Plenum Press, New York (1979), p. 161.

 © 1986 The Chemical Society of Japan Bull. Chem. Soc. Jpn., 59, 2081—2084 (1986)

The Crystal Structure of a Conformational Isomer of Teucrin P_1 from *Teucrium Gnaphalodes*

Zeyong ZHENG, Takashi YAMANE,* Tamaichi ASHIDA, Masaya MORITA,†
Natsuki KATO,† Takashi IWASHITA,†† and Koji NAKANISHI††
Department of Applied Chemistry, Nagoya University, Chikusa-ku, Nagoya 464
†Department of Agricultural Chemistry, Nagoya University, Chikusa-ku, Nagoya 464
††Suntory Institute for Bioorganic Research, Mishima, Osaka 618
(Received January 17, 1986)

The crystal structure of an isomer of Teucrin P_1 isolated from *Teucrium gnaphalodes* has been determined by the X-ray method. Crystal data: orthorhombic, $P2_12_12_1$, a=13.849(4), b=15.545(3), c=7.896(2) Å, Z=4. The final R value is 0.048 for 1247 observed reflections with $F_o>2\sigma(F_o)$. The structure is disordered, and two kinds of components (molecules) with different conformations coexist in the crystal. The major component exists with a probability of 0.74, while the minor one with 0.26. A tetrahydropyran ring in the former takes a boat form, while the latter a chair form, indicating that in this complex fused-ring system a boat form of the tetrahydropyran ring is more stable than a chair one. The conformation of the major component is the same as that of naturally occurring Teucrin P_1, apart from the orientation of a furan ring.

Teucrin P_1 with the trans-clerodane skeleton shows significant antifeeding activity against insects. It has been isolated from two different species, *T. gnaphalodes*[1] and *T. polium*,[2,3] in the family of Labiatae. The absolute structure of Teucrin P_1 isolated from *T. gnaphalodes* (abbreviated as TPG below) has been obtained by X-ray analysis and spectroscopic methods.[1] The X-ray analysis confirmed that ring **A** has a chair conformation and ring **B** and ring **E** take boat conformations.[1]

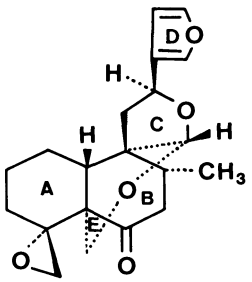

Scheme

It is interesting that $[\alpha]_D$ of TPG, −13.0°, is different from that of Teucrin P_1 from *T. polium* (abbreviated as TPP), +6.6°. The difference may reflect the boat/chair conformational difference of such **A**, **B**, and **E** rings in the skeleton of Teucrin P_1.

An isomer of TPG (abbreviated as TPG isomer) has been obtained by a chemical treatment which is expected for generating the conformational changes on ring **B** and/or **E**.[4] The $[\alpha]_D$ of TPG isomer is +2.9° and is rather close to that of TPP.

Therefore the X-ray structure analysis of TPG isomer is undertaken to make clear what kind of conformational change induces the shift of $[\alpha]_D$ as well as to obtain a clue to elucidate the conformation of TPP.

Experimental

TPG isomer was prepared by treating TPG in solution of hexamethylphosphoric triamide and tetrahydrofuran under the catalysis of lithium diisopropylamide at 253 K for 55 min., and crystallized from ethyl acetate solution.[4] Colorless rod crystals were obtained, in which a crystal with approximate dimensions of 0.5×0.4×0.8 mm was selected for the X-ray measurement.

Crystal Data: $C_{20}H_{24}O_5$, M=344.39, orthorhombic, $P2_12_12_1$, T=297 K, a=13.849(4), b=15.545(3), c=7.896(2) Å, V=1699.9(8) Å^3, Z=4, D_c=1.34 g·cm^{-3}, μ(Cu $K\alpha$)=7.41 cm^{-1}, F(000)=736.

A Rigaku four-circle diffractometer with graphite-monochromated Cu $K\alpha_1$ radiation (1.5405 Å) was used. The unit cell parameters were determined from 10 reflections with $13°\leqq 2\theta \leqq 21°$. Intensity data with $2\theta \leqq 115°$ were collected with the θ—2θ scan technique. The θ scan rates and background counting time at both ends of a scan were: 6.0° min^{-1} and 6.7 s for $0°\leqq 2\theta \leqq 60°$; 3.0° min^{-1} and 13.4 s for $60°\leqq 2\theta \leqq 85°$; 1.5° min^{-1} and 26.8 s for $85°\leqq 2\theta \leqq 100°$; 1.0° min^{-1} and 40.2 s for $100°\leqq 2\theta \leqq 115°$. The scan width was $\Delta\theta=(1.5+0.15\times\tan\theta)°$. 1367 reflections were collected, among which 120 reflections less than $2\sigma(F_o)$ were considered as unobserved. No intensity decreases of 3 standard reflections (002, 400, and 120) were observed during the experiment. Lorentz and polarization effects were corrected but no absorption correction was made.

The structure was determined by the direct method (*MULTAN* 78).[5] The absolute configuration of TPG isomer was conformed with that of TPG. The refinement was carried out by the block-diagonal least-squares method (*HBLS* VII).[6] The function minimized was $\sum w(|F_o|-|F_c|)^2$, and the weighting scheme was $w=[\sigma^2(F_o)+0.0042|F_o|^2]^{-1}$ at the final stage. In the course of the refinement, disorders were found at O(3) and O(4) atoms on ring **E** and **C** respectively. There are a major site (with higher probability of occurring, O(3A) and O(4A)) and a minor site (with lower one, O(3B) and O(4B)) for each of the two disordered O atoms. Their occupancies were estimated from the ratio of the integrated electron densities around each site, and the occupation ratio of O(3) is found to be

Table 1. The Final Fractional Coordinates($\times 10^4$) and Equivalent Isotropic Temperature Factors, with Their Estimated Standard Deviations in Parentheses

Atom	x	y	z	B_{eq}/Å^2
C (1)	−151 (3)	2373 (3)	9872 (6)	5.4 (2)
C (2)	102 (4)	2864 (3)	8239 (8)	6.7 (2)
C (3)	1179 (4)	2923 (3)	7983 (7)	7.0 (3)
C (4)	1657 (3)	2057 (2)	8051 (4)	4.5 (2)
C (5)	1401 (2)	1510 (2)	9596 (4)	3.8 (1)
C (6)	1797 (3)	607 (3)	9454 (6)	5.1 (2)
C (7)	1071 (4)	−99 (3)	9132 (7)	6.2 (2)
C (8)	228 (3)	−77 (2)	10440 (6)	5.1 (2)
C (9)	96 (3)	830 (2)	11222 (5)	4.4 (1)
C (10)	296 (2)	1481 (2)	9783 (4)	4.0 (1)
C (11)	−898 (3)	908 (3)	12069 (5)	4.9 (2)
C (12)	−713 (3)	1366 (2)	13738 (6)	5.4 (2)
C (13)	−1305 (3)	1073 (2)	15226 (5)	4.7 (2)
C (14)	−1267 (3)	263 (3)	16038 (6)	5.9 (2)
C (15)	−1887 (3)	277 (3)	17317 (6)	5.9 (2)
C (16)	−1942 (3)	1517 (3)	16085 (6)	6.5 (2)
C (17)	1968 (4)	1641 (3)	6468 (6)	6.4 (2)
C (18)	1839 (3)	1923 (3)	11197 (5)	5.5 (2)
C (19)	319 (4)	−806 (3)	11745 (9)	7.6 (3)
C (20)	794 (3)	1005 (3)	12745 (5)	4.7 (2)
O (1)	2657 (2)	2065 (2)	7542 (4)	5.7 (1)
O (2)	2646 (2)	454 (2)	9638 (5)	7.2 (2)
O (3A)	1223 (3)	1890 (2)	12588 (4)	4.6 (1)
O (3B)	1641 (6)	1122 (7)	12570 (12)	4.4 (4)
O (4A)	290 (2)	1046 (2)	14221 (4)	4.5 (1)
O (4B)	179 (6)	1530 (6)	13675 (12)	4.5 (4)
O (5)	−2328 (3)	1050 (2)	17387 (4)	7.3 (2)

identical with that of O(4). The occupancies of the major sites and the minor sites, 0.74 and 0.26 respectively, were fixed throughout the course of the refinement.

All the hydrogen atoms except for those attached to the carbon atoms directly bonded to the disordered O atoms with smaller occupancies are found in the difference Fourier map, and included in the refinements. The isotropic temperature factors of the H atoms are fixed to the equivalent temperature factors[7] of the corresponding carbon atoms to which they are bound. The final R and R_w are 0.048 and 0.064 respectively for 1247 reflections with $|F_o|>2\sigma(F_o)$. Atomic scattering factors were taken from International Tables for X-Ray Crystallography, VOL. IV.[8] The final atomic parameters with B_{eq}'s are given in Table 1.* All the computations were carried out on a FACOM M200 at Nagoya University Computation Center.

* The anisotropic thermal parameters of non-hydrogen atoms, the parameters of hydrogen atoms and the observed and calculated structure factors are preserved at the Chemical Society of Japan (Document No. 8634).

Discussion

The bond distances and angles are shown in Fig. 1, together with the numbering of atoms.

Extraordinariness occurs in the bond distances and angles concerning the disordered atoms O(3) and O(4). The bond distance of O(3B)–C(18) 1.674(12) Å is longer by about 0.20 Å than that of the normal O–C bond; while O(3B)–C(20) and O(4B)–C(12) distances, 1.195(11) Å and 1.263(11) Å respectively, come to short by about 0.20 Å as compared with the normal value. The large deviations from the tetrahedral angle are found in the bond angles of O(4B)–C(12)–C(13), 128.7(6)° and O(3B)–C(20)–O(4B), 125.1(7)°. Such extraordinariness will partly be due to the errors brought about by the small occupancies for O(3B) and O(4B). On the contrary, there is not a significant anomaly for the distances and angles concerning O(3A) and O(4A).

The disorder occurring at O(3) generates two different conformations on ring **E**, a boat conformation when O(3) is at the major site (O(3A)), and a chair conformation when at the minor site (O(3B)). The disorder of O(4) also affects the conformation of the five-membered ring **C**, although it always keeps an envelope shape. In the case of the major shape corresponding to O(4A), C(12) is out of the O(4A)–C(20)–C(9)–C(11) plane by 0.55(2) Å, whereas in the minor shape containing O(4B), C(20) is displaced by 0.47(3) Å from the plane defined by O(4B)–C(12)–C(11)–C(9).

On the molecular structure, four combinations are possible if the disorders are taken into account. However, the molecules in the crystal will take either the structure with ring **E** in a boat conformation (major) and ring **C** in the major shape or that with ring **E** in a chair conformation (minor) and ring **C** in the minor shape, if the two unreasonable combinations, O(3A)–O(4B) and O(3B)–O(4A), are excluded for the reasons described below. First, the combination of O(3A) and O(4B) may readily be rejected because of the too small angle of O(3A)–C(20)–O(4B), 75.5°. Then, as for the combination of O(3B) and O(4A), it is difficult to judge which combination, O(3B)–O(4B) or O(3B)–O(4A), is more rational only from the information of the corresponding bond angles, O(3B)–C(20)–O(4B) 125.1(7)° and O(3B)–C(20)–O(4A) 126.6(6)° respectively. However, it can also be reasonably excluded taking account of the equality between the occupation ratios of O(3) and O(4), because the existence of this combination in the crystal will make the ratios unequal in the absence of the conformer with O(3A) and O(4B).

Therefore, the conformations of the rings of the major component are ring **A**, chair; ring **B**, boat; ring **E**, boat; and ring **C**, envelope with C(12) at the flap. Those of the minor one are ring **A**, chair; ring **B**,

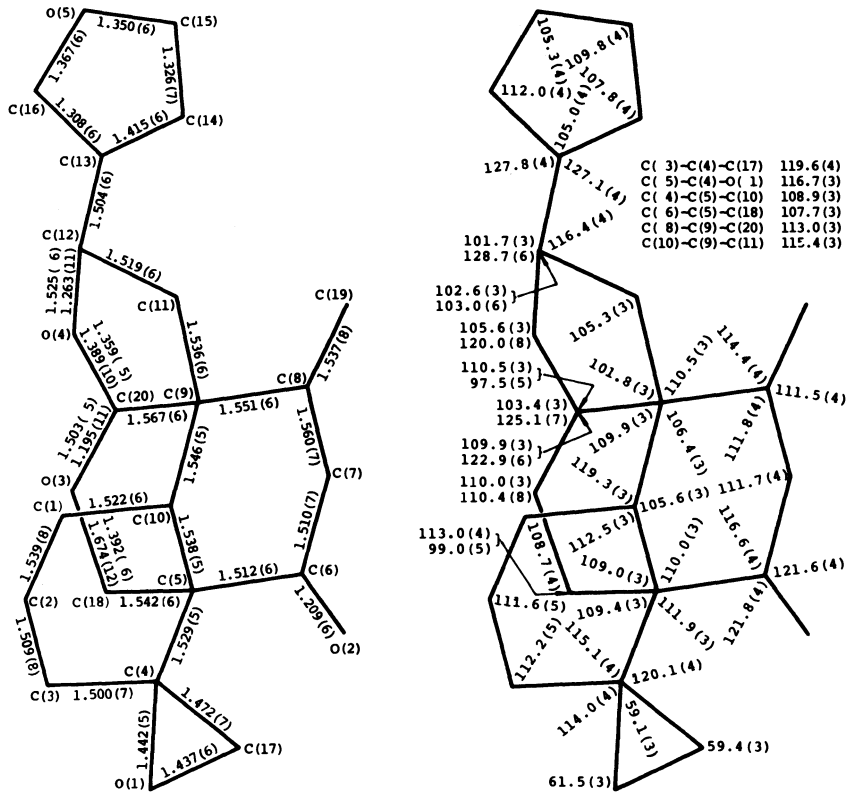

(a) (b)

Fig. 1. (a) Bond distances (l/Å) and (b) bond angles (ϕ/°) for the major component (upper) and the minor component (lower). The estimated standard deviations are in parentheses.

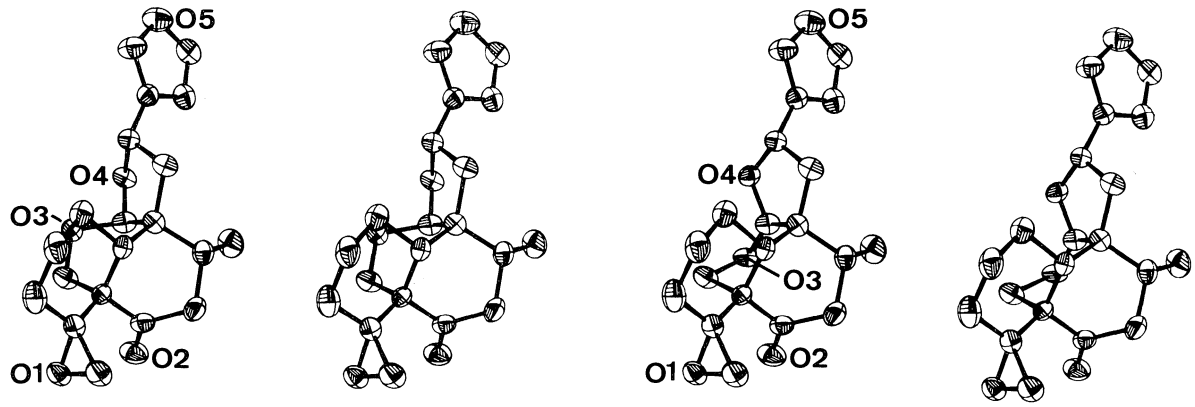

(a) (b)

Fig. 2. Stereoscopic drawing: (a) the major component and (b) the minor component. Atoms are drawn with 50% probability thermal ellipsoids.

boat; ring **E**, chair; and ring **C**, envelope with C(20) at the flap. The *ORTEP* II[10] drawing of the major and minor components are shown in Fig. 2.

The gross structure of the major component is the same as that of TPG, so far as the conformation of each ring is concerned. They differ only in the orientation of ring **D** with respect to ring **C**, but they can be related by a rotation of about 180° around the bond of C(12)–C(13).

The conformational change of ring **E**, from boat to chair, is induced in the naturally occurring molecule by the chemical reaction described above, and the consequent change of the puckering of ring **C** occurs to generate TPG isomer (here referring to minor

component) that has $[\alpha]_D$ of +2.9°. During the crystallization, however, the conformation of TPG isomer transforms to that of TPG. This shows that the molecule with ring **E** in a boat conformation (major) is more stable than that with ring **E** in a chair one (minor), though the opposite result has been expected by the conformational analysis (*MM2*).[4,9] The most stable structure anticipated by the conformational analysis possesses chair conformations for both ring **E** and ring **B**.

As for TPP, its structure may be different from those of TPG and TPG isomer, because its $[\alpha]_D$ (+6.6°) is remarkably different from that of TPG (−13.0°) and also shows a significant difference from that of TPG isomer (+2.9°). Therefore we expect that TPP might possess a chair conformation for ring **B**.

References

1) M. Martinez-Ripoll, J. Fayos, B. Rodrigues, M. C. Garcia-Alvarez, G. Savona, F. Pioozi, M. Paternostro, and J. R. Hanson, *J. Chem. Soc., Perkin Trans. I*, **1981**, 1186.

2) P. Y. Malakov, G. Y. Papanov, and N, M. Mollov, *Z. Naturforsch., Teil B.*, **34**, 1570 (1979).

3) D. P. Popa, Fan Tkhuk An', and L. A. Salei, *Khim. Prir. Soedin*, **13**, 49 (1977).

4) M. Morita, N. Kato, T. Iwashita, K. Nakanishi, Z. Y. Zheng, T. Yamane, and T. Ashida, *J. Chem. Soc., Chem. Commun.*, in press.

5) P. Main, S. E. Hull, L. Lessinger, G. Germain, J.-P. Declercq, and M. M. Woolfson, "*MULTAN* 78. A System of Computer Programs for the Automatic Solution of Crystal Structures from X-ray Diffraction Data," Univs. of York, England and Louvain, Belgium (1978).

6) T. Ashida, "UNICS-NAGOYA," Nagoya University, Nagoya, Japan (1981), p. 65.

7) W. C. Hamilton, *Acta Crystallogr.*, **12**, 609 (1959).

8) International Tables for X-Ray Crystallography, Vol. IV, Kynoch Press, Birmingham (1974), pp. 72—73.

9) N. L. Allinger, "Programme *MM2*: 77-Force field 1980," QCPE NO. 318.

10) C. K. Johnson, "ORTEP II," Report ORNL-5138, Oak Ridge National Laboratory, Tennessee, USA (1976).

Crystal Structures of 8-Oxa-6-azabicyclo[3.2.1]octan-7-one and the 4(*e*)-Bromo-substituted Derivative

Yuanxin Gu,†† Takashi Yamane,* Tamaichi Ashida, Kazuhiko Hashimoto,† and Hiroshi Sumitomo†

Department of Applied Chemistry, Faculty of Engineering, Nagoya University, Chikusa-ku, Nagoya 464

†Faculty of Agriculture, Nagoya University, Chikusa-ku, Nagoya 464

(Received February 13, 1986)

The crystal structures of the bicyclic oxalactam, 8-oxa-6-azabicyclo[3.2.1]octan-7-one(BOL) and the 4(*e*)-bromo-substituted derivative(Br-BOL) were determined by the X-ray diffraction method. Crystal data: (BOL) $P2_12_12_1$, a=10.926(3), b=9.115(2), c=6.280(2) Å, Z=4; (Br-BOL) $P2_12_12_1$, a=10.708(3), b=11.053(3), c=6.208(2) Å, Z=4. Refinements were carried out by the full-matrix least-squares method. R values are; (BOL) 0.050 for 601 reflections, (Br-BOL) 0.028 for 866 reflections. Both structures are quite similar to each other. The packing scheme of BOL is essentially the same as that of Br-BOL. Molecules are linked by N-H···O hydrogen bonds around a two-fold screw axis, giving rise to infinite chains extended along the c axis.

A bicyclic oxalactam, 8-oxa-6-azabicyclo[3.2.1]octan-7-one(abbreviated as BOL), is an interesting starting material for new functional polymers with permselectivity. The anionic solution polymerization of BOL leads to a high molecular weight polyamide (poly(BOL)) and the resulting poly(BOL) is easily cast to a hygroscopic membrane which has an excellent permeability for water and permselectivity for solutes of different sizes in an aqueous solution.[1-3] It may also be used as a component for graft and block copolymers.[4-6]

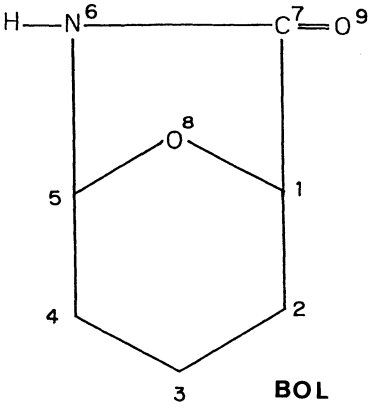

BOL

Anionic polymerization of BOL is known to proceed through the N^6–C^7 scission of the amide group.[1,2] The mechanism is the same as that in common lactams. On the other hand the cationic oligomerization of BOL was recently confirmed by the X-ray and NMR analyses of the resulting dimer [abbreviated as $(BOL)_2$],[7,8] to proceed through the C^5–N^6 scission of the amide group in the monomer unit.

The reactivity of such a novel bicyclic oxalactam should be closely related to the molecular structure. Therefore the 4-bromo-substituted derivative, 4(*e*)-bromo-8-oxa-6-azabicyclo[3.2.1]octan-7-one(abbreviated as Br-BOL), was synthesized in order to obtain an information on the structural and electronic effects upon their reactivity.[9] In this paper the structures of BOL and Br-BOL determined by the X-ray diffraction method were described.

Experimental

The BOL crystals obtained from a hexane solution were colorless plates and Br-BOL crystals grown from an ethyl acetate solution were colorless needles. The X-ray intensity data were collected on a Rigaku four-circle diffractometer, using graphite monochromated radiation; Cu $K\alpha$(λ=1.5405 Å) for BOL and Mo $K\alpha$(λ=0.70926 Å) for Br-BOL. Unit cell dimensions were obtained by the least-squares fit using 11 reflections with $40°<2\theta<56°$ for BOL and 14 reflections with $27°<2\theta<38°$ for Br-BOL. Crystal data and experimental conditions are shown in Table 1.

Both structures were solved by the direct method (*MULTAN* 80).[10] The refinement was carried out by the full-matrix least-squares method(*FMLS*).[11] The function minimized was $\sum w(|F_o|-|F_c|)^2$. After the anisotropic refinements of non-hydrogen atoms, all the hydrogen atoms were picked up on the difference-Fourier maps, and were included in the refinement with the isotropic temperature factors. The final R values were 0.050(R_w= 0.069) for BOL, and 0.028(R_w=0.035) for Br-BOL, respectively. The weighting scheme adapted was $w=(\sigma^2(F_o)+a|F_o|^2)^{-1}$ for the observed reflections with a=0.0 for BOL and 0.002 for Br-BOL. All the scattering factors were taken from the International Tables for X-Ray Crystallography, Vol. IV.[12] The atomic parameters of the non-hydrogen atoms with equivalent temperature factors(B_{eq})[13] are given in Table 2.* All the calculations were carried out on a

†† On leave from Institute of Physics, Chinese Academy of Science, Beijing, China.

* The anisotropic thermal parameters of non-hydrogen atoms, the parameters of hydrogen atoms, the equations of best-planes, and the tables of the observed and the calculated structure factors were kept at the Chemical Society of Japan(as Doc. No. 8637).

Table 1. Crystal Data and Experimental Conditions

	BOL	Br-BOL
Chemical formula	$C_6H_9NO_2$	$C_6H_8NO_2Br$
Mr	127.14	206.04
Space group	$P2_12_12_1$	$P2_12_12_1$
a/Å	10.926(3)	10.708(3)
b/Å	9.115(2)	11.053(3)
c/Å	6.280(2)	6.208(2)
V/Å^3	625.5(3)	734.7(4)
Z	4	4
d_{calcd}/(g cm^{-3})	1.350	1.862
μ/cm^{-1}	8.59(Cu $K\alpha$)	58.55(Mo $K\alpha$)
Crystal size/mm	0.2×0.2×0.5	0.2×0.2×0.4
Scan method	ω—2θ	ω—2θ
$\Delta\omega$/°	2.0+0.15 tan θ	1.0+0.35 tan θ
ω scan rate/(°min^{-1})	6—1*1	3—1*1
Background counting time/s	5—30*2	5—15*2
$2\theta_{max}$/°	125	55
No. of reflections measured	613	1004
No. of reflections observed($\|F_o\| \geq 3\sigma(F_o)$)	601	866

*1 The scan rate was varied as a function of 2θ angle.
*2 The background counting time is changed correlated with the scan rate.

Table 2. Final Fractional Coordinates(×10^4) and Equivalent Isotropic Temperature Factors, with Their Estimated Standard Deviations in Parentheses

(a) 8-Oxa-6-azabicyclo[3.2.1]octan-7-one

Atom	x	y	z	B_{eq}/Å^2
C (1)	6462(2)	3455(2)	45(4)	3.3(1)
C (2)	5100(2)	3619(4)	409(5)	3.8(1)
C (3)	4725(2)	2920(4)	2510(5)	4.4(2)
C (4)	5666(3)	3205(3)	4291(4)	4.4(1)
C (5)	6953(2)	3090(3)	3445(4)	3.9(1)
N (6)	7158(2)	1711(2)	2304(4)	3.9(1)
C (7)	6830(2)	1853(3)	277(4)	3.3(1)
O (8)	7100(2)	4135(2)	1771(3)	4.2(1)
O (9)	6783(2)	914(2)	−1118(3)	4.6(1)

b) 4-Bromo-8-oxa-6-azabicyclo[3.2.1]octan-7-one

Atom	x	y	z	B_{eq}/Å^2
Br	4295(1)	207(1)	2202(1)	4.31(2)
C (1)	6165(4)	2804(3)	−2550(7)	2.9(2)
C (2)	4776(4)	2625(4)	−3068(8)	3.5(2)
C (3)	4251(4)	1582(4)	−1750(7)	3.5(2)
C (4)	4685(4)	1671(4)	564(7)	2.9(2)
C (5)	6086(4)	1913(3)	676(7)	2.9(2)
N (6)	6797(3)	1125(3)	−718(6)	3.0(2)
C (7)	6843(3)	1591(3)	−2712(7)	2.6(2)
O (8)	6263(3)	3069(2)	−272(5)	3.3(1)
O (9)	7288(3)	1158(2)	−4351(5)	3.6(1)

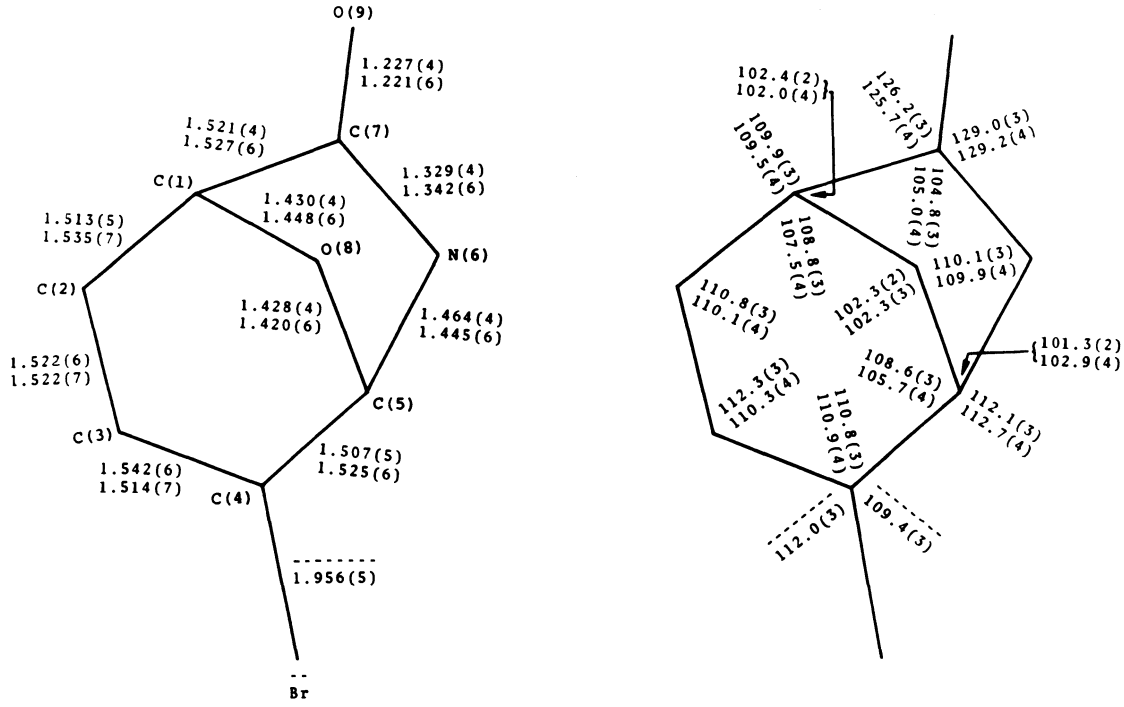

Fig. 1. (a) Bond distances (l/Å) and (b) bond angles (ϕ/°) for BOL (upper) and Br–BOL (lower). Estimated standard deviations are in parentheses.

FACOM M382 at Nagoya University Computation Center.

Results and Discussion

The bond distances and angles of BOL and Br–BOL are given in Fig. 1, with the numbering of atoms. The corresponding bond distances and angles between BOL and Br–BOL are in good agreements with each other, except for the C(3)–C(4) distance and the C(4)–C(5)–O(8) angle. The C(3)–C(4) distance of BOL seems slightly longer than that of Br–BOL. The C(4)–C(5)–O(8) angle, 108.6(3)°, of BOL is larger than that of Br–BOL, 105.7(4)°. The C(4)–C(5)–O(8) angle of BOL is similar to the corresponding ones in $(BOL)_2$,[7] 108.7(3) and 107.8(4)°, in which two molecules are included in the asymmetric unit, and the BOL skeleton is conserved at a terminus. The C(1)–C(7)–O(9) angle is smaller than the N(6)–C(7)–O(9) angle in both BOL and Br–BOL. These angles are, however, almost equal in the BOL moieties of $(BOL)_2$; that is, 127.3(4) and 127.1(4)° for ∠C(1)–C(7)–O(9), and 127.9(4) and 126.9(4)° for ∠N(6)–C(7)–O(9).

Stereoscopic views of BOL and Br–BOL drawn by *ORTEP* II[14] are shown in Fig. 2. The overall structures of both molecules are quite similar with each other, and they are also almost the same as the structures of the BOL moieties in $(BOL)_2$. The six-membered ring including C(1), C(2), C(3), C(4), C(5), and O(8) takes a chair conformation in each

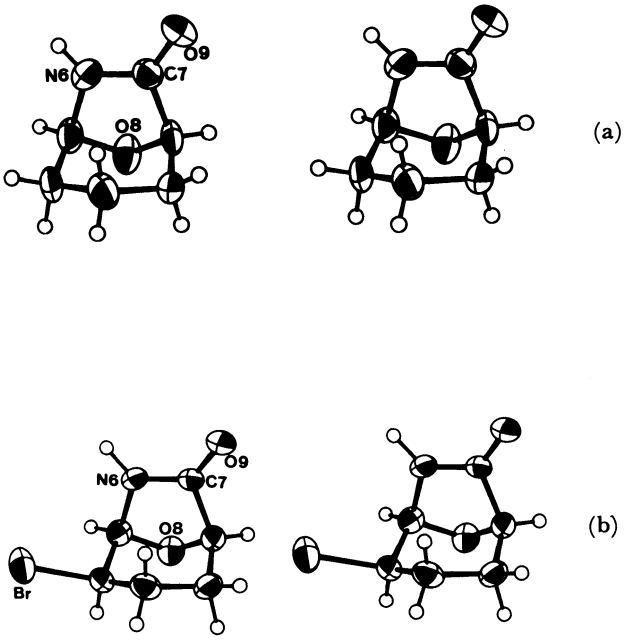

Fig. 2. Stereodrawings of (a) BOL and (b) Br–BOL. Atoms are drawn with 50% probability thermal ellipsoids.

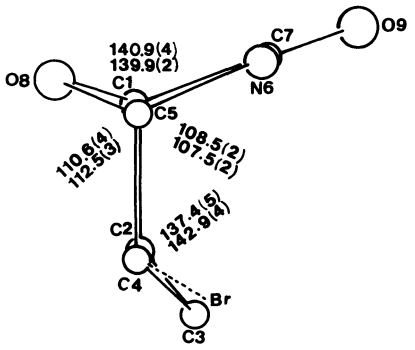

Fig. 3. Selected dihedral angles among the best-planes. Definitions are: plane I C(1), C(7), N(6), C(5), and O(9); plane II C(1), O(8) and C(5); plane III C(1), C(2), C(4) and C(5); plane IV C(2), C(3) and C(4). BOL upper, and Br–BOL lower.

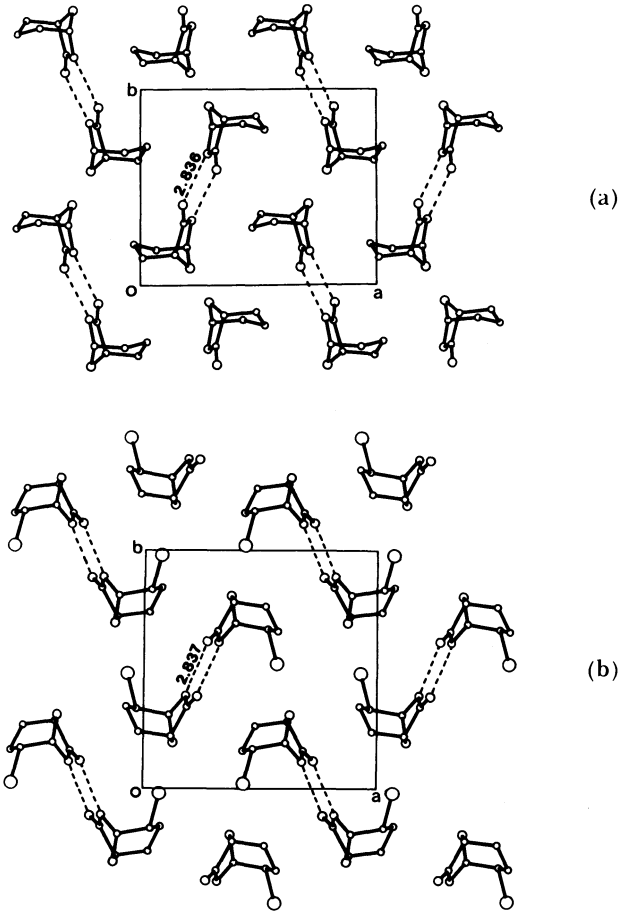

Fig. 4. Crystal structures of (a) BOL and (b) Br–BOL, projected along the c axis. Broken lines show the hydrogen bonds.

molecule. The C(1), C(7), N(6), C(5), O(8) five-membered ring shows an envelope conformation, with the O(8) out of plane[deviation: −0.604(5) Å for BOL and −0.59(1) Å for Br-BOL]. The Br atom is in equatorial with respect to the six-membered ring in Br-BOL. The molecule consists of four planes: plane I defined with C(1), C(7), N(6), C(5), and O(9); plane II C(1), O(8), and C(5); plane III C(1), C(2), C(4), and C(5); plane IV C(2), C(3), and C(4). The selected dihedral angles among the planes in the present two compounds are given in Fig. 3. A significant difference is found in the dihedral angles between the plane III and IV. The corresponding ones in $(BOL)_2$ are 139.7(5) and 140.6(5)°, which are intermediate between the present two compounds. Therefore marked changes on the molecular geometry of BOL skeleton are not observed by the substitution of Br at C(4), though the substitution may have significant effects on the intermolecular interactions due to the bulkiness and the strong electronegativity of the Br atom.

The packing of molecules in BOL and Br-BOL are drawn in Figs. 4(a) and (b), respectively. The packing schemes of both crystals are essentially the same, thus the present two compounds are isostructural. The elongation of the period of the b axis of Br-BOL, as compared with that of BOL, appears to be occured by the substitution of the bulky Br atoms, with the direction of C(4)-Br roughly parallel to the b axis. The hydrogen bonds occur between N(6)···O(9^{i}) 2.836(4) Å in BOL and N(6)···O(9^{ii}) 2.837(5) Å in Br-BOL. [Symmetry code: (i) $1.5-x$, $1-y$, $0.5+z$; (ii) $1.5-x$, $-y$, $0.5+z$] The H···O and ∠N-H···O are 1.99(5) Å and 167(5)° for BOL and 1.84(6) Å and 143(4)° for Br-BOL. Molecules are linked by hydrogen bonds around a two-fold screw axis, giving rise to infinite helical chains extended along the c axis.

One of the authors(Gu) thanks the Japan Society for the Promotion of Science for this research at Nagoya University.

References

1) H. Sumitomo and K. Hashimoto, *Macromolecules*, **10**, 1327 (1977).
2) K. Hashimoto and H. Sumitomo, *Macromolecules*, **13**, 786 (1980).
3) H. Sumitomo, K. Hahimoto, and T. Ohyama, *Polym. Bull.*, **1**, 133 (1978).
4) K. Hashimoto, H. Sumitomo, and M. Kawasumi, *Polym. Bull.*, **11**, 121 (1984).
5) K. Hashimoto, H. Sumitomo, and H. Yamamori, *Polym. J.*, **17**, 679 (1985).
6) K. Hashimoto, H. Sumitomo, and M. Kawasumi, *Polym. J.*, **17**, 1045 (1985).
7) T. Yamane, H. Nanayama, T. Ashida, K. Hashimoto, and H. Sumitomo, *Bull. Chem. Soc. Jpn.*, **58**, 2304 (1985).
8) K. Hashimoto and H. Sumitomo, *J. Polym. Sci., Polym. Chem. Ed.*, **22**, 1733 (1984).
9) K. Hashimoto, H. Sumitomo, and M. Suzuki, *Chem. Lett.*, **1986**, 767.
10) P. Main, S. J. Fiske, S. E. Hull, L. Lessinger, G. Germain, J.-P. Deqlercq, and M. M. Woolfson, "*MULTAN* 80. A System of Computer Programs for the Automatic Solution of Crystal Structures from X-ray Diffraction Data," Univs. of York, England, and Louvain, Belgium (1980).
11) T. Ashida, "*UNICS-NAGOYA*," Nagoya University, Nagoya, Japan p. 73 (1981).
12) "International Tables for X-Ray Crystallography," Kynoch Press, Birmingham (1974), Vol. IV, p. 71.
13) W. C. Hamilton, *Acta Crystallogr.*, **12**, 609 (1959).
14) C. K. Johnson, "*ORTEP* II," *Report ORNL*-5138, Oak Ridge National Laboratory, Tennessee, USA (1976).

Critical Behavior of the Correlation Function of Fluids Composed of Polar Diatomic Molecules

Masaharu OHBA and Kiyoshi ARAKAWA*
Research Institute of Applied Electricity, Hokkaido University, Sapporo 060
(Received February 17, 1986)

A critical behavior of fluids composed of polar diatomic molecules is studied by the use of the Ornstein-Zernike (OZ) theory of critical phenomena extended to the interaction site model. Firstly, the asymptotic forms of the atom-atom direct correlation functions $c_{\alpha\gamma}(r)$ for the polar fluids at large separation are obtained, which are valid off the critical point. Then, the OZ hypothesis that the asymptotic forms of $c_{\alpha\gamma}(r)$ do not change near and at the critical point is examined, and the critical behavior of the total correlation function is investigated. It is found to be completely analogous to the case of simple fluids. The relation between the OZ hypothesis and some integral equation theories is also discussed.

Properties of polar fluids are extensively explored on the basis of the interaction site model.[1-6] Recently, a phase diagram of the polar hard dumbbell fluid was obtained by the use of the interaction site approximation (ISA) of RISM-1, and the existence of the critical point was shown in the phase diagram.[7] It is interesting to investigate the behavior of the atom-atom pair correlation function near and at the critical point. In the case of simple fluids, it has been found that the Ornstein-Zernike (OZ) theory of critical scattering gives qualitatively correct results. An extension of the OZ theory to the primitive model of ionic fluids was performed, and the theory showed that the critical behavior of the pair correlation function of the ionic solutions is similar to that of simple fluids.[8]

In this paper, we attempt to extend the OZ theory to the interaction site model and to analyze the critical behavior of the atom-atom pair correlation function of polar fluids by using the OZ theory. In the next section, the asymptotic forms of the atom-atom direct correlation function at large separation are obtained, which is valid off the critical point. In the last section, the critical behavior of the atom-atom pair correlation function is investigated under the assumption that the atom-atom direct correlation function near and at the critical point is similar in its form to the obtained asymptotic formula.

The Asymptotic Forms of the Atom-Atom Direct Correlation Functions.

The system considered is a fluid composed of polar diatomic molecules whose bond length is l. The charges $+q$ and $-q$ are sited on the centers of atoms of the molecule. The total potential energy of the fluid is assumed to be the sum of all intermolecular interactions. The intermolecular interaction between the i-th and j-th molecules is given by

$$U(i,j) = \sum_{\alpha}\sum_{\gamma} u_{\alpha\gamma}(|\boldsymbol{r}_i^{\alpha} - \boldsymbol{r}_j^{\gamma}|), \tag{1}$$

where $u_{\alpha\gamma}(|\boldsymbol{r}_i^{\alpha} - \boldsymbol{r}_j^{\gamma}|)$ is the interaction potential between the α-th atom of the i-th molecule and the γ-th atom of the j-th molecule. $\boldsymbol{r}_i^{\alpha}$ denotes the position of the α-th atom of the i-th molecule. The atom-atom interactions are given as

$$u_{\alpha\gamma}(r) = u^{\mathrm{sr}}(r) + \frac{q_{\alpha}q_{\gamma}}{4\pi\varepsilon_0 r}, \tag{2}$$

where ε_0 is the dielectric constant of the vacuum. $u^{\mathrm{sr}}(r)$ is the short-range part of the potential including the repulsive and the dispersion forces. For simplicity, we assume that the short-range part of the potential is independent of α and γ.

The site-site Ornstein-Zernike (SSOZ) equation in Fourier transform space is given as

$$\tilde{\boldsymbol{h}} = \tilde{\boldsymbol{\omega}}\tilde{\boldsymbol{c}}\tilde{\boldsymbol{\omega}} + \rho\tilde{\boldsymbol{\omega}}\tilde{\boldsymbol{c}}\tilde{\boldsymbol{h}}, \tag{3}$$

where ρ is the number density of molecules and $\tilde{\boldsymbol{h}}$, $\tilde{\boldsymbol{c}}$, and $\tilde{\boldsymbol{\omega}}$ are matrices of Fourier transforms of the atom-atom total correlation function $h_{\alpha\gamma}(r)$, the atom-atom direct correlation function $c_{\alpha\gamma}(r)$, and the intramolecular pair correlation function $w_{\alpha\gamma}(r)$, respectively. The Fourier transform of $w_{\alpha\gamma}(r)$ is

$$\tilde{\omega}_{\alpha\gamma}(k) = \delta_{\alpha\gamma} + (1-\delta_{\alpha\gamma})\frac{\sin kl}{kl}, \tag{4}$$

where $\delta_{\alpha\gamma}$ is the Kronecker delta. Here, we introduce the total correlation function of the center of atoms $h_{\mathrm{s}}(r)$ and the total correlation function of charges $h_{\mathrm{d}}(r)$, which are defined as

$$h_{\mathrm{s}}(r) = \{h_{++}(r) + h_{+-}(r)\}/2, \tag{5}$$

and

$$h_{\mathrm{d}}(r) = \{h_{++}(r) - h_{+-}(r)\}/2. \tag{6}$$

$c_{\mathrm{s}}(r)$ and $c_{\mathrm{d}}(r)$ are also defined in a similar manner. Then, the matrix equation Eq. 3 separates into two scaler equations as follows,

$$\tilde{h}_{\mathrm{s}}(k) = (1+\tilde{w})^2\tilde{c}_{\mathrm{s}}(k) + 2\rho(1+\tilde{\omega})\tilde{c}_{\mathrm{s}}(k)\tilde{h}_{\mathrm{s}}(k), \tag{7}$$

and

$$\tilde{h}_{\mathrm{d}}(k) = (1-\tilde{\omega})^2\tilde{c}_{\mathrm{d}}(k) + 2\rho(1-\tilde{\omega})\tilde{c}_{\mathrm{d}}(k)\tilde{h}_{\mathrm{d}}(k), \tag{8}$$

where $\tilde{\omega}=\sin kl/kl$. From Eqs. 7 and 8, we have

$$\tilde{c}_{\mathrm{s}}(k) = \frac{\tilde{h}_{\mathrm{s}}(k)}{(1+\tilde{\omega})^2+2\rho(1+\tilde{\omega})\tilde{h}_{\mathrm{s}}(k)}, \tag{9}$$

and

$$\tilde{c}_{\mathrm{d}}(k) = \frac{\tilde{h}_{\mathrm{d}}(k)}{(1-\tilde{\omega})^2+2\rho(1-\tilde{w})\tilde{h}_{\mathrm{d}}(k)}. \tag{10}$$

For polar fluids, an asymptotic form of $h_{\alpha\gamma}(r)$ at large r off the critical point is[4,5]

$$h_{\alpha\gamma}(r) \simeq \frac{E}{r^6} + \frac{F}{r^7} + O(r^{-8}), \tag{11}$$

where E and F are constants independent of the indices α and γ. From Eq. 11, the small k expansion of the Fourier transform of $h_{\alpha\gamma}(r)$ is expressed as

$$\tilde{h}_{\alpha\gamma}(k) = \tilde{h}^{\mathrm{reg}}_{\alpha\gamma} + \tilde{h}^{\mathrm{sing}}_{\alpha\gamma}. \tag{12}$$

The regular term $\tilde{h}^{\mathrm{reg}}_{\alpha\gamma}$ and the singular term $\tilde{h}^{\mathrm{sing}}_{\alpha\gamma}$ are given by

$$\tilde{h}^{\mathrm{reg}}_{\alpha\gamma} = \tilde{h}(0) + k^2h^{(2)}_{\alpha\gamma} + k^4h^{(4)}_{\alpha\gamma} + O(k^6), \tag{13}$$

and

$$\tilde{h}^{\mathrm{sing}}_{\alpha\gamma} = E'k^3 + F'k^4\ln k + O(k^5), \tag{14}$$

where E', and F' are constants independent of indices α and γ. In Eq. 13, we use the fact that $\tilde{h}_{\alpha\gamma}(0)$ is independent of indices α and γ. By inserting Eqs. 12—14 into Eqs. 5 and 6, we have

$$\tilde{h}_{\mathrm{s}}(k) = \tilde{h}^{\mathrm{reg}}_{\mathrm{s}} + \tilde{h}^{\mathrm{sing}}_{\mathrm{s}}, \tag{15a}$$

$$\tilde{h}^{\mathrm{reg}}_{\mathrm{s}} = \tilde{h}(0) + k^2h^{(2)}_{\mathrm{s}} + k^4h^{(4)}_{\mathrm{s}} + O(k^6), \tag{15b}$$

$$\tilde{h}^{\mathrm{sing}}_{\mathrm{s}} = E'k^3 + F'k^4\ln k + O(k^5), \tag{15c}$$

and

$$\tilde{h}_{\mathrm{d}}(k) = \tilde{h}^{\mathrm{reg}}_{\mathrm{d}} + \tilde{h}^{\mathrm{sing}}_{\mathrm{d}}, \tag{16a}$$

$$\tilde{h}^{\mathrm{reg}}_{\mathrm{d}} = k^2h^{(2)}_{\mathrm{d}} + k^4h^{(4)}_{\mathrm{d}} + O(k^6), \tag{16b}$$

$$\tilde{h}^{\mathrm{sing}}_{\mathrm{d}} = O(k^5). \tag{16c}$$

By inserting Eqs. 15 and 16 into Eqs. 9 and 10, and by expanding the right hand side of Eqs. 9 and 10, we can obtain a small k expansion of $\tilde{c}_{\mathrm{s}}(k)$ and $\tilde{c}_{\mathrm{d}}(k)$. The results are as follows,

$$\tilde{c}_{\mathrm{s}}(k) = \tilde{c}^{\mathrm{reg}}_{\mathrm{s}} + \tilde{c}^{\mathrm{sing}}_{\mathrm{s}}, \tag{17a}$$

$$\tilde{c}^{\mathrm{reg}}_{\mathrm{s}} = c^{(0)}_{\mathrm{s}} + k^2c^{(2)}_{\mathrm{s}} + k^4c^{(4)}_{\mathrm{s}} + O(k^6), \tag{17b}$$

$$\tilde{c}^{\mathrm{sing}}_{\mathrm{s}} = C'k^3 + D'k^4\ln k + O(k^5), \tag{17c}$$

and

$$\tilde{c}_{\mathrm{d}}(k) = \frac{A}{k^2} + c^{(0)}_{\mathrm{d}} + O(k), \tag{18}$$

where $c_{\mathrm{s}}^{(0)}=\tilde{h}(0)/4(1+\rho\tilde{h}(0))$, $C'=E'/4(1+\rho\tilde{h}(0))$, $D'=F'/4(1+\rho\tilde{h}(0))$ and

$$A = \frac{36h^{(2)}_{\mathrm{d}}}{l^2(l^2+12\rho h^{(2)}_{\mathrm{d}})}. \tag{19}$$

Thus, the asymptotic forms of $c_{\mathrm{s}}(r)$ and $c_{\mathrm{d}}(r)$ off the critical point are given as

$$c_{\mathrm{s}}(r) \simeq \frac{C}{r^6} + \frac{D}{r^7} + O(r^{-8}), \tag{20}$$

and

$$c_{\mathrm{d}}(r) \simeq \frac{A}{4\pi r} + O(r^{-4}). \tag{21}$$

$h_{\mathrm{d}}^{(2)}$ is expressed in terms of the dielectric constant ε as[4-6]

$$4q^2h^{(2)}_{\mathrm{d}} = \frac{\mu^2}{9\rho}\left(\frac{\varepsilon-\varepsilon_0}{y\varepsilon}-3\right), \tag{22}$$

where $\mu=ql$ is the magnitude of the dipole moment of molecules, $y=\rho\mu^2/9\varepsilon_{\mathrm{O}}k_{\mathrm{B}}T$, k_{B} the Boltzmann constant and T the absolute temperature. Thus, we have

$$A = -\frac{3y\varepsilon-\varepsilon+\varepsilon_0}{3y(\varepsilon-\varepsilon_0)}\cdot\frac{q^2}{\varepsilon_0k_{\mathrm{B}}T}. \tag{23}$$

Equations 20 and 21 are the result of this section. The first term of Eq. 21 with Eq. 23 was already given in a different way.[9] Equation 20 and the second term of the right hand side of Eq. 21 are new results.

The Critical Behavior of Correlation Functions.

Here, we set up the hypothesis of the OZ theory for the system considered in this paper by assuming that the asymptotic forms of the atom-atom direct correlation function does not change near and at the critical point. Thus, the asymptotic forms near and at the critical point are given as

$$c_{\mathrm{s}}(r) \simeq O(r^{-6}), \tag{24a}$$

and

$$c_{\mathrm{d}}(r) \simeq \frac{A}{4\pi r} + O(r^{-4}). \tag{24b}$$

We define a new function $c_{\mathrm{e}}(r)$ by

$$c_{\mathrm{e}}(r) \equiv c_{\mathrm{d}}(r) - \frac{A}{4\pi r}. \tag{25}$$

From Eq. 24b, $c_e(r) \simeq O(r^{-4})$ as $r \to \infty$. Then, the Fourier transforms of $c_s(r)$ and $c_e(r)$ can be expressed as

$$\tilde{c}_s(k) = c_s^{(0)} + k^2 c_s^{(2)} + O(k^3), \tag{26}$$

and

$$\tilde{c}_e(k) = c_e^{(0)} + O(k), \tag{27}$$

where $c_s^{(0)}$, $c_s^{(2)}$ and $c_e^{(0)}$ are expressed as follows:

$$c_s^{(0)} = \int c_s(r) d\boldsymbol{r},$$

$$c_s^{(2)} = -\frac{1}{6}\int r^2 c_s(r) d\boldsymbol{r},$$

and

$$c_e^{(0)} = \int c_e(r) d\boldsymbol{r}.$$

The compressibility equation is

$$\rho k_B T \kappa_T = 1 + \rho \tilde{h}(0), \tag{28}$$

where κ_T is the isothermal compressibility of the fluid. This equation shows that in the approach to the critical point $\tilde{h}(0)$ tends to infinity. Thus, from Eq. 9, we have

$$c_s^{(0)} = \tilde{c}_s(0) \to 1/(4\rho_c), \tag{29}$$

where ρ_c is the number density at the critical point. This result confirms that $c_s^{(0)}$ is analytic at the critical point. However, the analyticity of $c_s^{(2)}$ and $c_e^{(0)}$ is not verified in general. Thus, the present OZ hypothesis for this system is expressed mathematically as follows: $c_s^{(2)}$ and $c_e^{(0)}$ are analytic near and at the critical point.

From Eqs. 7 and 8, we have

$$\tilde{h}_s(k) = \frac{(1+\tilde{\omega})^2 \tilde{c}_s(k)}{1-2\rho(1+\tilde{\omega})\tilde{c}_s(k)}, \tag{30}$$

and

$$\tilde{h}_d(k) = \frac{(1-\tilde{\omega})^2 \tilde{c}_d(k)}{1-2\rho(1-\tilde{\omega})\tilde{c}_d(k)}. \tag{31}$$

By inserting Eqs. 26 and 27 together with Eq. 23 into Eqs. 30 and 31, we have

$$\tilde{h}_s(k) = \frac{4c_s^{(0)} + (4c_s^{(2)} - 2l^2 c_s^{(0)}/3)k^2 + \cdots}{(1-4\rho c_s^{(0)}) + (\rho l^2 c_s^{(0)}/3 - 4\rho c_s^{(2)})k^2 + \cdots}, \tag{32}$$

and

$$\tilde{h}_d(k) = \frac{(Al^4/36)k^2 + \cdots}{3y\varepsilon/(\varepsilon-\varepsilon_0) - (\rho l^2/3)(c_e^{(0)} - l^2 A/20)k^2 \cdots}. \tag{33}$$

By taking Eq. 30 into consideration, the compressibility equation Eq. 28 can be expressed as

$$1 - 4\rho c_s^{(0)} = (\rho k_B T \kappa_T)^{-1} = \kappa_T^0/\kappa_T, \tag{34}$$

where $\kappa_T^0 = (\rho k_B T)^{-1}$ is the isothermal compressibility of the ideal gas. Equation 34 shows that $(1-4\rho c_s^{(0)}) \neq 0$ off the critical point. Thus, the asymptotic forms of $h_s(r)$ and $h_d(r)$ off the critical point obtained from the Eqs. 32 and 33 return to Eq. 11. However, since $(1-4\rho c_s^{(0)}) \to 0$ with the approach to the critical point, we obtain from Eq. 32.

$$h_s(r) \simeq \frac{c_s^{(0)}}{\pi(\rho l^2 c_s^{(0)}/3 - 4\rho c_s^{(2)})} \cdot \frac{1}{r} \cdot \exp(-\alpha r), \tag{35}$$

and

$$\alpha = \sqrt{\frac{1-4\rho c_s^{(0)}}{\rho l^2 c_s^{(0)}/3 - 4\rho c_s^{(2)}}} \to 0. \tag{36}$$

Thus, we find that $h_s(r)$ becomes a long-range function, that is, $h_s(r) \sim O(r^{-1})$ in the vicinity of the critical point. On the other hand, it is found from Eq. 33 that the asymptotic form of $h_d(r)$ at large r does not change at the critical point. This shows that near and at the critical point the density fluctuation diverges but the charge fluctuation remains finite. Identifing the correlation length ξ with α^{-1}, we obtain the critical exponent relation $2\nu = \gamma$. ν and γ are defined as

$$\kappa_T^0/\kappa_T \propto \varepsilon^{-\gamma}(1+\cdots),$$

and

$$\xi \propto \varepsilon^{-\nu},$$

where $\varepsilon = |(T-T_c)/T_c|$ and T_c is the critical temperature. These results are quite analogous with the case of simple fluids, which is in accordance with the prediction of Stell.[10]

Let us consider the relation of the OZ theory with integral equation theories. The ISA consists of the SSOZ equation Eq. 3 and the ISA closure given by

$$h_{\alpha\gamma}(r) = -1, \quad r < \sigma_{\alpha\gamma} \tag{37a}$$

and

$$c_{\alpha\gamma}(r) = -u_{\alpha\gamma}(r)/k_B T, \quad r > \sigma_{\alpha\gamma} \tag{37b}$$

where $\sigma_{\alpha\gamma}$ is the hard-sphere diameter of atoms. For the fluid composed of polar hard dumb-bells with the same diameter σ, Eqs. 37a and 37b can be expressed as

$$\begin{cases} h_s(r) = -1, & r < \sigma \\ c_s(r) = 0, & r > \sigma \end{cases} \tag{38}$$

and

$$\begin{cases} h_d(r) = 0, & r < \sigma \\ c_d(r) = -q^2/4\pi\varepsilon_0 k_B T r. & r > \sigma \end{cases} \tag{39}$$

Thus, the ISA satisfies the OZ hypothesis introduced in this section. Equations 7 and 38 becomes the PY-like integral equation of RISM-1[11,12] for neutral hard dumb-bell fluids (HDF), and so the quantity $(1-4\rho c_s^{(0)})$ is the same as that of the solution of the PY-like integral equation for HDF. Since the critical point does not exist for HDF, no critical point can be observed in the correlation function of the polar hard dumb-bell fluids in the ISA. However, if the phase behavior is investigated through the energy equation instead of the compressibility equation, it is possible to detect the critical point. In fact, Morriss and Isbister showed the existence of the critical point through the energy equation. The circumstances are quite similar to the case of the restricted primitive model of ionic solutions.[8] Since $h_s(r) \neq h(r)^{HDF}$ in the other approximations (for example, PY-like and HNC-like approximations), the critical point will be observed in the correlation function by using these approximations. The critical behavior obtained through these approximations will be different from the result in this work, because these approximations do not satisfy the OZ hypothesis presented here.

Appendix
The Critical Behavior of Nonpolar Fluids Composed of Homonuclear Diatomic Molecules.

The critical point of nonpolar fluids composed of homonuclear diatomic molecules was recently detected through the compressibility equation by using the PY-like integral equation of RISM-1.[13]

The asymptotic form of the atom-atom direct correlation function for this system off the critical point is expressed as[9]

$$c(r) \simeq -u(r)/k_B T \sim O(r^{-6}). \quad \text{as } r \to \infty \tag{A1}$$

Hereafter, the indices α and γ are omitted, because the atom-atom functions for this system are independent of the indices. For this system, the OZ hypothesis is expressed as follows: the first two coefficients of the small k expansion of the Fourier transform of $c(r)$ are analytic near and at the critical point. Thus, we have

$$\tilde{c}(k) = c^{(0)} + k^2 c^{(2)} + \cdots, \tag{A2}$$

where

$$c^{(0)} = \int c(r) d\boldsymbol{r},$$

and

$$c^{(2)} = -\frac{1}{6}\int r^2 c(r) d\boldsymbol{r}.$$

Then, from the similar discussion described in the last section, we have the same equations as Eqs. 35 and 36 in the approach to the critical point.

PY-like approximation for fluids interacting through the short-range interaction satisfies the OZ hypothesis presented in this appendix, and so it is found that the asymptotic form of $h(r)$ given by the PY-like approximation is $h(r) \sim O(r^{-1})$ at the critical point. On the other hand, HNC-like approximation does not satisfy the OZ hypothesis, and thus the critical behavior is different from that given by the PY-like approximation. In fact, we have found that $h(r)$ decays as r^{-2} in the HNC-like approximation, which is the same as that for simple fluids interacting through the short-range interactions.[14]

References

1) M. Ohba and K. Arakawa, *Bull. Chem. Soc. Jpn.*, **55**, 1387 (1982); **58**, 9 (1985); **58**, 3068 (1985).
2) G. P. Morriss and J. W. Perram, *Mol. Phys.*, **43**, 669 (1981).
3) F. Hirata and P. J. Rossky, *Chem. Phys. Lett.*, **83**, 329 (1981).
4) D. Chandler, *J. Chem. Phys.*, **67**, 1113 (1977).
5) J. S. Høye and G. Stell, *J. Chem. Phys.*, **65**, 18 (1976).
6) M. Ohba and K. Arakawa, *J. Phys. Soc. Jpn.*, **50**, 743 (1981).
7) G. P. Morriss and D. J. Isbister, *Mol. Phys.*, **52**, 57 (1984).
8) M. M. Noyola and D. A. McQuarrie, *J. Stat. Phys.*, **18**, 445 (1978).
9) P. T. Cummings and G. Stell, *Mol. Phys.*, **44**, 529 (1981); **46**, 383 (1982).
10) G. Stell, *Phys. Rev. Lett.*, **32**, 286 (1974).
11) D. Chandler and H. C. Andersen, *J. Chem. Phys.*, **57**, 1930 (1972).
12) K. Kojima and K. Arakawa, *Bull. Chem. Soc. Jpn.*, **51**, 1977 (1978); **53**, 1795 (1980).
13) P. A. Monson, *Mol. Phys.*, **53**, 1209 (1984).
14) M. E. Fisher, *J. Math. Phys.*, **5**, 66 (1964).

A High-Resolution Solid-State ^{13}C NMR Study of (1→3)-β-D-Glucans from Various Sources. Conformational Characterization as Viewed from the Conformation-Dependent ^{13}C Chemical Shifts and Its Consequence to Gelation Property

Hazime SAITÔ,* Ryoko TABETA, Takuma SASAKI,† and Yûko YOSHIOKA†
Biophysics Divison, National Cancer Center Research Institute, Tsukiji 5-Chome, Chuo-ku, Tokyo 104
†Chemotherapy Divison, National Cancer Center Research Institute, Tsukiji 5-Chome, Chuo-ku, Tokyo 104
(Received February 27, 1986)

High-resolution solid-state ^{13}C NMR spectra of a variety of (1→3)-β-D-glucans in the solid state were recorded by means of cross polarization-magic angle spinning (CP-MAS) NMR spectroscopy. We found that the C-1 and C-3 peak-positions of these glucans are significantly displaced (up to 8 ppm) depending upon variety of samples used. Interestingly, these glucans obtained by lyophilization or spray-drying possess regular secondary structures as detected by displacements of the conformation-dependent ^{13}C chemical shifts. In fact, at least four kinds of molecular conformations were distinguishable by ^{13}C NMR spectroscopy. Gel-forming ability of linear (1→3)-β-D-glucans, however, was related to the presence of a single particular conformation without involving any other form. By contrast, gel-formation was noted for a branched glucan whose conformation is similar to that of a linear glucan without gel-forming ability. Further, conformation of all these linear and branched (1→3)-β-D-glucans turned out to be the same when solid samples were prepared by lyophilization from DMSO solution.

It is well known that linear and branched (1→3)-β-D-glucans (Fig. 1) function as structural components in the cell walls of many plants and microorganism and also act as reserve polysaccharides.[1] Physical properties of (1→3)-β-D-glucans isolated from various sources are thus widely different: low molecular weight laminaran is water-soluble glucan, while pachyman (from *Poria cocos*) is not; curdlan (from *Alcaligenes faecalis*) is known to form elastic gel when aqueous suspension is heated at a temperature above 54 °C.[2,3] On the contrary, some fungal branched (1→3)-β-D-glucans such as lentinan (from *Lentinus edodes*) and schizophyllan (from *Schizophyllum commune*) form nonelastic gel without heating.[4] Our previous high-resolution ^{13}C NMR studies showed that these gel-structures are composed of rather flexible single-helical chains, a part of which being associated to give physical cross links such as multiple-helical junction-zones or these aggregates.[5–9] On the contrary, acid-degraded lower molecular weight fractions of these glucans ($\overline{DP}_n$<20 for linear glucans) are freely soluble in water.[6–8] In this connection, it is interesting to note that anti-tumor activity of these glucans is related to their solution properties:[10,11] higher molecular weight fractions with gel-forming ability are biologically active but water-soluble fraction is not.

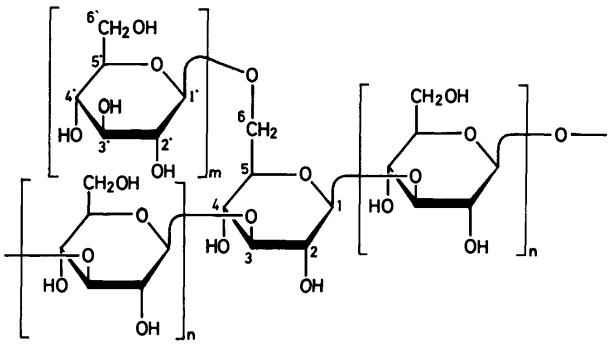

Fig. 1. Primary structures of linear and branched (1→3)-β-D-glucans: $m=0$, $\overline{DP}_n=540$, curdran; $m=0$, $\overline{DP}_n=38$, laminaran; $m=1$, $n=50$, pachyman; $m=1$, $n=2.5$, lentinan; $m=1$, $n=3$, HA β-glucan.

Accordingly, it appears that such a physical property might be also related to a secondary or tertiary structure of these glucans in addition to the degree of branching. As to the former, however, no detailed analysis for this purpose has been made, because these glucans obtained as spray-dried powder or lyophilized solid are naturally not at crystalline state and no X-ray diffraction study can be applied without extensive annealing of samples.[13,14] In addition, it is not yet clear whether or not glucans thus obtained do take any regular secondary structure. In order to reveal conformational features of noncrystalline as well as crystalline samples, high-resolution solid-state ^{13}C NMR spectroscopy has recently proven to be very useful for a various types of molecular systems.[15,16] The displacements of ^{13}C chemical shifts of backbone carbons (up to 8 ppm) are thus well related to variation of nearby torsion angles of respective carbons under consideration. In particular, the ^{13}C chemical shifts of the C-1 and C-X carbons of various types of glucans at the glycosidic linkages are well related to the torsion angles of the C-1–O_{gly} (ϕ) and C-X–O_{gly} (ψ), respectively.[17,18] Thus, conformational features of cellulose,[19–26] chitin,[27,28] (1→3)-β-D-,[29,30] and (1→4)-α-D-glucans[31] have been analyzed by the data of high-resolution

^{13}C NMR spectroscopy.

In this paper, we aimed to examine secondary structures of a variety of (1→3)-β-D-glucans from various sources by means of cross polarization-magic angle spinning (CP-MAS) ^{13}C NMR spectroscopy. First of all, we found that these glucans take various kinds of regular secondary structures, as viewed from the linewidths and displacements of ^{13}C NMR peaks, depending upon molecular weights and a manner of sample preparation. In fact, at least four kinds of different conformations can be distinguished by displacements of the C-1 and C-3 ^{13}C chemical shifts: form I (curdlan-type), form II (laminaran-type), form III (laminaripentaose-type), and form IV (DMSO-adduct). Then, it is found that paramylon granules which is over 90% crystalline is not consisting of molecular chains with a single conformation but a composite of several conformers. Further, conformational features of these glucans in the gel state were examined by observation of high resolution ^{13}C NMR spectra.

Experimental

Materials. Table 1 summarizes trivial names, degree of polymerization, physical properties, and sources of isolation for a variety of (1→3)-β-D-glucans studied in this paper. Lower-molecular-weight (1→3)-β-D-glucans were prepared from curdlan ($\overline{DP}_n$=540) by hydrolysis with formic acid or sulfuric acid by the method previously described.[10] Gel-filtration patterns of these preparations ($\overline{DP}_n$=14, 20, 82, and 131) on a Sephadex G-150 or Sepharose CL-4B column each gave a symmetrical peak. Curdlan with $\overline{DP}_n$=380 was obtained from the culture filtrate of *Alcaligenes faecalis* under different fermentation time. Numerically averaged degree of polymerization ($\overline{DP}_n$) was determined by the method of Manners et al.[32] The above-mentioned glucans were supplied by Takeda Chemical Industries, Osaka, Japan. Pachyman[33] was obtained from Sclerotium of *Poria cocos wolf* (Bukuryu) purchased from Shihira Shoten Ltd., Tokyo (by courtesy of Dr. G. Chihara of this Institute). Paramylon[34] (from *Euglena gracilis*) was a generous gift from Professor B. A. Stone of La Trobe University, Australia. Lentinan[35] was a generous gift from Dr. G. Chihara. Laminaran with $\overline{DP}_n$=38 (as determined by gel-filtration chromatography) was purchased from Nutritional Biochemical Corporation, Ohio, USA. Fractionated lower oligomers of (1→3)-β-D-glucans, laminaritriose, laminaripentaose, and laminariheptaose (Lot No. 407191), were purchased from Seikagaku Kogyo, Ltd., Tokyo, Japan. Isolation of fungal (1→3)-β-D-glucan, HA β-glucan (from *P. ostreatus (Fr.)* Quél.),[36] was reported previously. Some of these glucans were once dissolved in DMSO solution and lyophilized to obtain samples of DMSO-adduct. Curdlan gel was obtained by heating aqueous suspension (20 mg) at a temperature at 60 °C and cooling at an ambient temperature. Gels of fungal (1→3)-β-D-glucans were obtained by hydration of samples (20 mg) with excess water. To prepare gel samples for high resolution ^{13}C NMR spectroscopy, a few drops of concd NaOH solution were added stepwise to achieve 0.05 M.

^{13}C CP-MAS NMR Spectroscopy. Single contact 75.46 MHz ^{13}C CP-MAS NMR spectra were recorded on a Bruker CXP-300 spectrometer equipped with a CP-MAS accessory. Solid samples were contained in an Andrew-Beams type rotor machined from perdeuterated poly (methyl methacrylate), and spun as fast as 3—4 kHz. 90° pulse width was 5 μs and repetition time was 4 s. Spectra were usually accumulated 1000—2000 times. Chemical shifts were calibrated indirectly from the signal of liquid benzene (128.5 ppm) and converted to the value from tetramethylsilane.

Table 1. Characteristics of (1→3)-β-D-Glucan Samples Used

Sample No.	Trivial Name	Appearance	Linear or branched	$\overline{DP}_n$[a]	Solution properties in aqueous medium	Sources
1	Curdlan	Powder	Linear	540	Elastic gel	*Alcaligenes faecalis*
2	Curdlan	Powder	Linear	380	Elastic gel	*Alcaligenes faecalis*
3	Pachyman	Powder	Linear	250	Nonelastic gel	*Poria cocos*
4	Laminaran	Powder	Linear	38[b]	Not soluble	*Laminaria species*
5	Paramylon	Granule	Linear	—	Not soluble	*Euglena gracilis*
6	Lower-molecular-weight curdlans					
6a		Powder	Linear	14	Soluble	
6b		Powder	Linear	20	Soluble	
6c		Powder	Linear	82	Not soluble	
6d		Powder	Linear	131	Not soluble	
7	Laminaritriose	Lyophilized	Linear	3[c]	Soluble	
8	Laminaripentaose	Lyophilized	Linear	5[c]	Soluble	
9	Laminariheptaose	Lyophilized	Linear	7[c]	Soluble	
10	Lentinan	Powder	Branched	—	Nonelastic gel	*Lentinus edodes*
11	HA β-glucan	Lyophilized	Branched	—	Nonelastic gel	*Pleurotus ostreatus*(Fr.) Quél.

a) Determined by the method of Manners et al. b) By gel filtration chromatography. c) Single species.

Results

Figure 2 shows the ^{13}C CP–MAS NMR spectra of four representative linear (1→3)-β-D-glucans in the solid state. These glucans are classified into three groups as viewed from peak-positions of the C-3 (and C-2,5) carbons (Table 2): (1) pachyman and curdlan giving the C-3a peak at 89.6±0.3 ppm, (2) laminaran showing the C-3b peak (at 85.5 ppm) (in addition to a minor peak of the C-3a (89.6 ppm)), and (3) paramylon exhibiting the three peaks, the aforementioned C-3a, and C-3b, and an additional C-3c (82.4 ppm). The spread of the C-3 NMR signals in paramylon (C-3a -C-3c) turned out to be about 8 ppm, as shown in Table 2. The C-1 peak, on the other hand, appears as a singlet in most cases, but as a doublet peak in paramylon. Next, we illustrate the ^{13}C CP–MAS NMR spectra of branched (1→3)-β-D-glucans isolated from various fungi in the solid state (Fig. 3). Here, the presence of two distinct peaks is evident in the C-3 region: the C-3a peak position of lentinan is exactly the same as that of curdlan or pachyman within the experimental error (±0.3 ppm), whereas the C-3b peak position of HA β-glucan is identical to that of laminaran (Table 2). Again, the spectral profile of the C-2 and C-5 region of HA β-glucan resembles that of laminaran (Fig. 2). In Fig. 4, we demonstrate how the ^{13}C NMR peak profiles are varied with their numerically averaged degree of polymerization ($\overline{DP}_n$) of acid-degraded curdlan. Apparently, the glucans with $\overline{DP}_n$ 380 exhibit

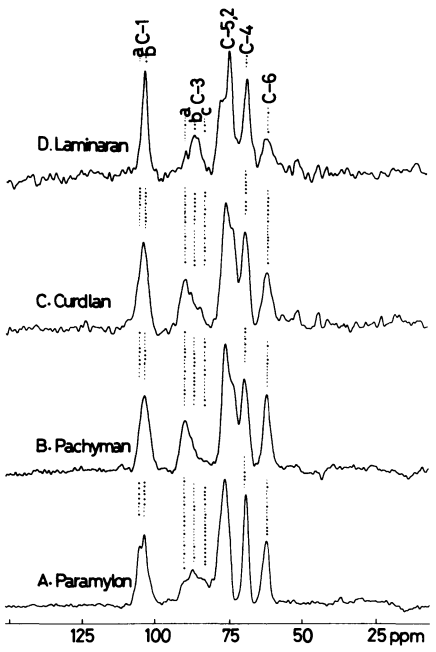

Fig. 2. 75.46 MHz ^{13}C CP–MAS NMR spectra of linear (1→3)-β-D-glucans in the solid state. A. paramylon, B. pachyman, C. curdlan, D. laminaran.

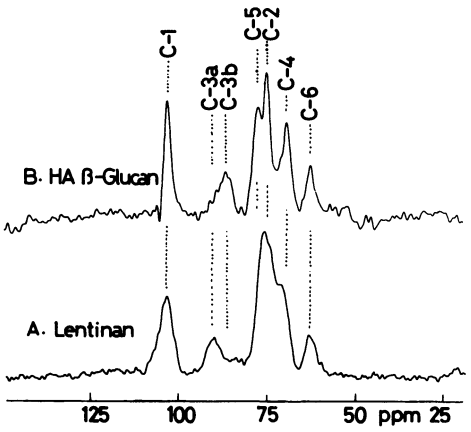

Fig. 3. 75.46 MHz ^{13}C CP–MAS NMR spectra of branched (1→3)-β-D-glucans in the solid state. A. lentinan, B. HA β-glucan. Number of transients is about 1000.

Table 2. ^{13}C Chemical Shifts of (1→3)-β-D-Glucans in the Solid State[a)]

	Form I		Form II			Form III		
	Laminari-heptaose	Laminari-pentaose	Curdlan	Pachyman	Lentinan	Laminaran	HA β-glucan	Paramylon
C-1	104.5	104.3	104.5	103.6	103.2	102.9	102.9	104.9
								103.3
C-2	72.9	73.0	73.5	73.0	73.3	73.9	73.6	75.6
C-3	91.3	91.1						90.2
			89.8	89.3	89.3			
						85.5	85.7	86.4
								82.4
C-4	69.8	69.4	68.8	69.6	69.1	67.8	67.9	68.6
C-5	76.1	75.8	75.5	75.5	75.0	76.6	76.0	75.6
C-6	61.5	61.6	61.8	61.6	61.8	61.7	61.5	61.7

a) ppm from TMS. experimental error ±0.3 ppm.

significant amount of the C-3b signals, although the peak height of the C-3a peak is higher than that of the C-3b peak.

In Figure 5, we summarized the ^{13}C CP-MAS NMR spectra of lower-molecular-weight oligomers, laminaritriose, laminaripentaose and laminariheptaose. Interestingly, all the ^{13}C NMR signals of these oligomers are identical within the experimental error (±0.3 ppm) by going from trimer to heptamer, except for the ^{13}C NMR signals arising from anomeric carbons of the terminal residues (peaks C-1a, and C-3a). The C-3 ^{13}C NMR peak positions of these oligomers (91 ppm) are significantly displaced downfield by about 1—2 ppm as compared with the corresponding peaks of curdlan, pachyman and lentinan, although the other carbon signals are identical to those of curdlan.

Further, Figure 6 summarizes the ^{13}C CP-MAS NMR spectra of a variety of (1→3)-β-D-glucans lyophilized from DMSO solution. The most notable feature is that DMSO molecule is incorporated into these polysaccharides as a quantitative manner (1/2 DMSO molecule per single residue), as manifested from the observed peak intensities. The linewidth of the C-3 peak as well as others is rather small for the samples prepared from DMSO solution as compared with that of samples lyophilized from aqueous medium. In addition, the peak positions of the C-3 signals were distinct from those of other preparations (Table 3) as shown in Figs. 1—3. On the contrary,

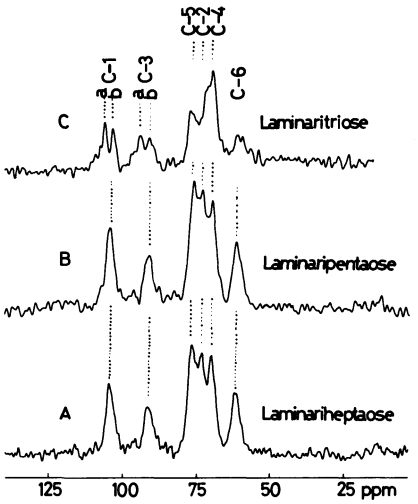

Fig. 5. 75.46 MHz ^{13}C CP-MAS NMR spectra of fractionated oligomers in the solid state. A. laminariheptaose, B. laminaripentaose, and C. laminaritriose.

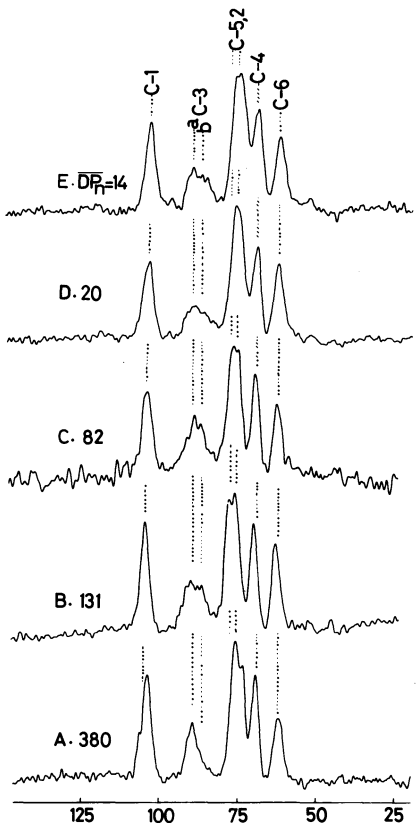

Fig. 4. 75.46 MHz ^{13}C CP-MAS NMR spectra of acid-degraded (1→3)-β-D-glucans and curdlan. $\overline{DP}_n$: A, 380; B, 131; C, 82; D, 20; and E, 14.

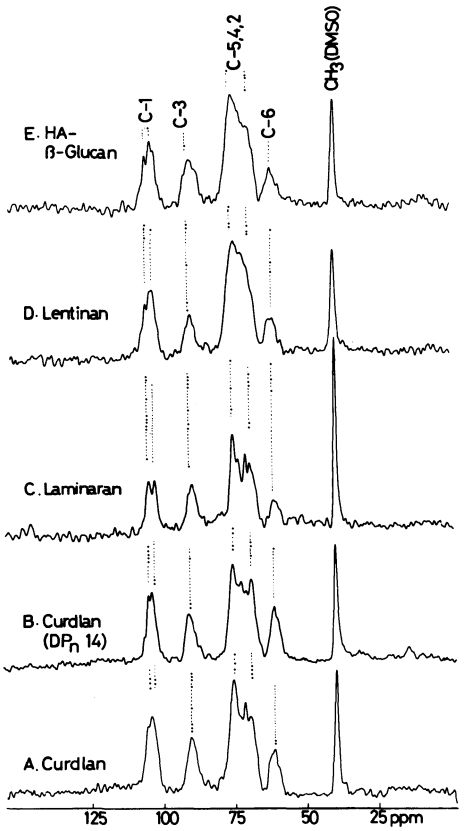

Fig. 6. 75.46 MHz ^{13}C CP-MAS NMR spectra of a variety of (1→3)-β-D-glucans lyophilized from DMSO solution in the solid state. A. curdlan, B. curdlan ($\overline{DP}_n$ = 14), C. laminaran, D. lentinan, and E. HA β-glucan.

Table 3. ^{13}C Chemical Shifts of (1→3)-β-D-Glucans Lyophilized from DMSO Solution[a)]

	Curdlan ($\overline{DP}_n=540$)	Curdlan ($\overline{DP}_n=14$)	Laminaran	Lentinan	HA β-glucan
C-1	106.3	105.5	105.5	105.7	105.9
	104.5	103.9	103.4	104.2	104.1
					102.7
C-2	71.5	73.5	71.1	—	72.6
C-3	90.3	91.2	90.2	89.7	90.1
C-4	68.8	69.0	69.1	—	69.0
C-5	75.5	75.7	75.6	74.4	75.2
C-6	61.0	61.4	61.0	61.4	61.7
CH_3 (DMSO)	39.5	39.4	39.6	39.5	39.5

a) ppm from TMS.

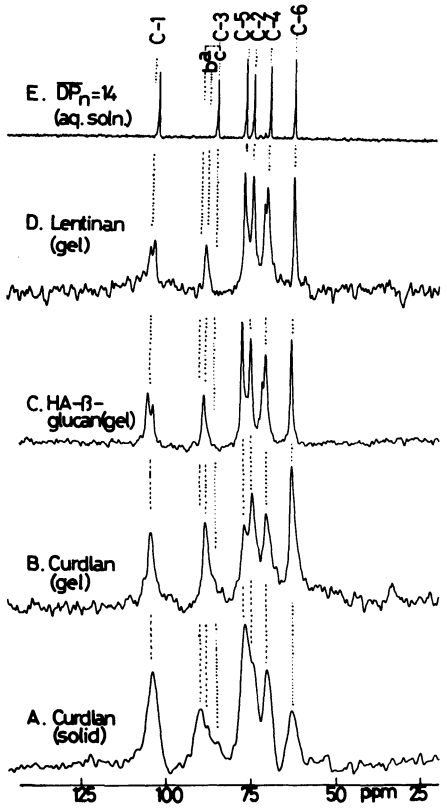

Fig. 7. Comparison of the ^{13}C NMR spectra of (1→3)-β-D-glucans among solid, gel and solution.

the C-1 signals are in many instances split into two separate peaks.

Finally, we recorded the ^{13}C NMR spectra of these (1→3)-β-D-glucans in the presence of excess water, as shown in Fig. 7. Interestingly, the ^{13}C NMR peaks of elastic gel of curdlan were well resolved at this higher frequency (75 MHz), in contrast to our previous observation at lower frequency (25 MHz).[6,7] Nevertheless, no ^{13}C NMR signals could be seen at neutral pH, in the case of nonelastic gels consisting of branched (1→3)-β-D-glucans. Consistent with our previous observation, ^{13}C NMR signals from these gel samples became visible when small amount of NaOH

Table 4. ^{13}C Chemical shifts of (1→3)-β-D-Glucans in the Gel and Solution State (ppm from TMS)

	Gel			soln
	Curdlan	HA β-glucan	Lentinan	
C-1	104.0	104.5, 102.9	104.3, 102.9	102.7
C-2	73.5	73.4	73.5	73.5
C-3	87.5	87.5	87.5	84.5
C-4	69.1	68.9	69.1, 70.0	68.4
C-5	75.9	76.0	76.1	75.8
C-6	61.4	61.1	61.2	61.0

(less than 0.2 M) was added. Again, the ^{13}C NMR chemical shifts of these samples were found to be identical among various types of (1→3)-β-D-glucans such as curdlan, lentinan and HA β-glucan, in the gel state (Table 4), although conformations of these glucans in the solid state are quite different. It appears that the peak position of the C-3 carbon in the gel state is slightly displaced upfield (2 ppm) as compared with that of the solid state. On the contrary, these peaks are more distinct from those of the homogeneous aqueous solution ($\overline{DP}_n$=14).

Discussion

Conformational Features in the Solid State. As previously demonstrated, ^{13}C chemical shifts of backbone carbons for a various types of molecular systems such as polysaccharides, polypeptides, and ionophores are significantly displaced (up to 8 ppm) together with their local conformations as described by a set of nearby torsion angles.[15,16,37-41] The advantage of ^{13}C NMR spectroscopy over other method is that conformational analysis can be done equally for noncrystalline as well as crystalline molecules. For polysaccharides, it is useful to examine displacements of ^{13}C NMR signals of carbons at the glycosidic linkages (C-1 and C-X carbons), because these ^{13}C signals are sensitively varied with any conformational change.[17,18,25] In fact, the maximal splitting of the C-3 chemical shifts

of (1→3)-β-D-glucans is found to be as large as 8 ppm for paramylon (Table 2).

Interestingly, curdlan, pachyman, and lentinan gave rise to almost identical spectral features (Fig. 2) and these ^{13}C chemical shifts are identical within the experimental error (±0.3 ppm) (Table 2) in spite of differences in the primary structure. In particular, curdlan is completely a linear glucan containing no other linkage than β-(1→3)-linkages with $\overline{DP}_n$=540, while pachyman ($\overline{DP}_n$=250) contains a branch for every 50 β-(1→3)-linked glucose residues and one or two internal β-(1→6)-linkages. Lentinan, on the other hand, is a branched (1→3)-β-D-glucan with two branches for every five residues. In a similar manner, two different kinds of glucans, laminaran (linear) and HA β-glucan (branched), gave identical spectral patterns whose peak positions of these two glucans are the same within the experimental error but distinct from those of the glucans as mentioned above (see Figs. 2 and 3, and also Table 2). These data indicate that the presence (or the degree of) of branching at the C-6 position does not affect secondary structures of these branched glucans in the solid state as compared with that of the linear glucans, although this factor plays dominant role in gelation conditions of the former.[5,8] In addition, the ^{13}C NMR peak positions are the same among lower molecular oligomers, laminaritriose, laminaripentaose and laminariheptaose (Fig. 5 and Table 2). Further, the ^{13}C chemical shifts are identical among lyophilized samples from DMSO solution (Table 3). These findings strongly indicate that (1→3)-β-D-glucans so far studied take regular ordered conformations in spite of lacking in any treatment to improve the degree of crystallinity. Otherwise, it is expected that very broad envelope of ^{13}C NMR signals whose linewidths are as large as 8 ppm should be observed, because random coil form in the solid state is considered to be superposition of any conceivable several kinds of conformations.[42]

It is now possible to claim that at least four types of conformations for these (1→3)-β-D-glucans can be distinguished by the aforementioned characteristic displacements of the C-1 and C-3 peaks due to the conformation-dependent ^{13}C chemical shifts. For the sake of convenience, we tentatively classified conformations of these polysaccharides into the following four forms, I—IV, as viewed from the C-1 and C-3 peak-positions (Tables 2 and 3). Naturally, spectral patterns of the C-2 and C-5 peaks also could be varied to some extent by going from one form to another. On the basis of the aforementioned discussion, it is now clear that paramylon is not consisting of a single conformation but is a composite of at least three kinds of different conformations, as judged from the C-1 and C-3 ^{13}C chemical shifts (Table 2): form I (laminaripentaose-type), form III (laminaran-type) and an additional conformation giving rise to the peak at 82.4 ppm for the C-3 carbon. In fact, Marchessault et al. found that these split signals were converted to a single peak as a result of conformational change due to hydration.[30] Obviously, this kind of conformational heterogeneity seems to be essential to achieve better crystalline packing of paramylon granules, by analogy with the cases of higher crystalline samples as in cellulose[19-26] and polyethylene.[43,44] In this connection, crystallinity of paramylon granules is highest (≈90%) among a series of (1→3)-β-D-glucans.[45] By contrast, crystallinity of curdlan powder is only 30%[45] which does not require the presence of conformations more than the single species, as judged from the ^{13}C NMR signals.

In this connection, it is worthwhile to point out that conformation of native curdlan obtained as surface matter stripped from the colonies grown on solid culture of *Alcaligenes faecalis* is essentially the same as that of alkaline regenerated curdlan reported herein, as judged from the similarity of the ^{13}C NMR spectra,[29] in contrast to the similar pair of native and regenerated celluloses.[19-26]

The C-3 ^{13}C NMR signals of laminariheptaose and laminaripentaose (form I) are resonated at the lowermost region (91.2±0.2 ppm) and are clearly distinguishable from those of other three forms as shown in Tables 2 and 3. In fact, this peak is displaced downfield by 1.6 ppm with respect to that of curdlan and pachyman (form II)(89.6±0.3 ppm). For this reason, conformation of higher-molecular-weight (1→3)-β-D-glucan ($\overline{DP}_n$=250), curdlan and pachyman, is not always identical to that of lower-molecular-weight glucans (DP_n=3, 5, and 7). Instead, the torsion angles ψ might be different to some extent as viewed from the difference in the C-3 signals, although the ϕ angle might be the same as indicated in the similarity of the C-1 signals among these glucans.

On the other hand, the C-1 and C-3 ^{13}C chemical shifts of laminaran and HA β-glucan are resonated at 103.2 and 85.7 ppm (C-3b of Figure 3), respectively, and these peak positions are resonated significantly at higher field, as compared with those of the forms I and II (Table 2). The presence of this form is ascribed to its lower molecular weight in the case of linear (1→3)-β-D-glucans as in laminaran ($\overline{DP}_n$=38). This view was further confirmed by the fact that lower-molecular-weight acid-degraded curdlans, whose $\overline{DP}_n$'s are between 14 and 131, contain significant amount of this form (40—10%), as seen from Fig. 8 where relative proportion of the form II (C-3a) is plotted against $\overline{DP}_n$'s (thus, contribution of the form III (C-3b) is 100-contribution of the form II %). In a similar manner, paramylon does not form a gel. Accordingly, lower-molecular-weight (1→3)-β-D-glucans

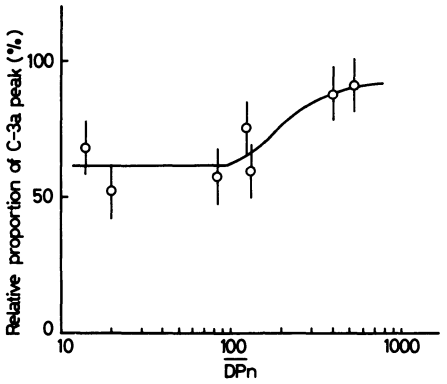

Fig. 8. A plot of the relative proportion of the C-3a peak (form II) against $\overline{DP}_n$.

taking either the forms I or III do not have gel-forming ability. In this connection, it is probable that molecular weight of HA β-glucan is rather low as in laminaran on the basis of the C-3 ^{13}C peak position (Fig. 3). Nevertheless, molecular weight of this sample estimated from a study of gel permeation chromatography is an order of 10^6 (unpublished finding). As to molecular weights of branched glucans, however, caution must be exercised about reliability of data, because aggregation phenomenon leading to infinite gel network at neutral pH or lower alkaline (<0.2 M NaOH) state would make apparent molecular weight significantly overestimated (infinite for gel!). To make situation more complicated, gelation condition as a function of molecular weight is strongly modified for branched glucans as compared with that of linear glucans. In particular, a lower-molecular-weight fraction of lentinan (fraction IV, M.W. 16200) was found to be gel-forming in spite of its lower molecular weight.[8] An explanation for this is that number of physical cross links is effectively increased for branched glucans.[8]

Alternatively, Marchessault et al.[30] suggested that the differences in the degree of hydration might strongly modify the spectral patterns of (1→3)-β-D-glucans as described above. This view, however, is not necessary true for an interpretation of the conformational heterogeneity as encountered for a variety of samples listed in Table 1, because there appears no distinct change about the degree of hydration among the samples of lyophilization or spray-drying, which were kept long time at an ambient temperature. It is also worthwhile to consider the difference in the degree of branching between lentinan and HA β-glucan. Lentinan has two branches for every five D-glucose residues,[11] while HA β-glucan has one branch for every four D-glucose residues[36] (see Fig. 1). Accordingly, there appears no direct relation between the degree of branching and molecular conformations so far elucidated.

As described already, lyophilized samples from DMSO solution take a regular conformation as manifested from observation of relatively narrow ^{13}C NMR signals. In particular, the C-1 ^{13}C signals of these samples are split into doublet signal at 105.8 and 104.0 ppm (Fig. 6). As an interpretation of this splitting, it is natural to postulate that there exist two kinds of different conformers in this form (form IV), although peak splitting of the C-3 ^{13}C signal is not pronounced. Alternatively, conformation of two chains is identical but splitting of peak is distinguishable by the effect of hydrogen bonding to one of chains with DMSO molecule.

Conformations in the Gel State. It appears that the ^{13}C NMR linewidths of the gel samples recorded at 75 MHz are much narrowed and excellent spectral separation is achieved in this study of higher frequency (especially at the region of C-2, 4, and 5) (Fig. 7). The observed linewidths in this case, however, are about 100 Hz and the extent of line narrowing as compared with the data of 25 MHz is about 30% for the C-1 and C-3 signals. This observation might be mainly ascribed to a plausible reduction in the number of effective cross links formed by multiple helical junction zones or aggregate of these regions, because the present spectra were recorded at a lower concentration (20 mg ml^{-1}) (one fifth of those of low frequency measurements). Naturally, the ^{13}C chemical shifts of gel samples in this study are in good agreement with our previous data.[4-9] However, more accurate data about the ^{13}C chemical shifts were obtained in this study because of much improved separation of peaks. Thus, it is now clear that the ^{13}C NMR peaks of curdlan gel are displaced downfield by 1.3 and 3.0 ppm for the C-1 and C-3 carbons, respectively, from those of water-soluble low-molecular-weight glucan taking random coil conformation, but the rest of peaks is unchanged by going from the gel to random-coil form (Table 4).

In spite of obvious differences in the conformations between curdlan (and lentinan) and HA β-glucan in the solid state, we found that exactly the same spectral features were observed between the two samples in the gel state (Fig. 7). In our previous papers,[5,29] we concluded that conformation of flexible molecular chains in curdlan, which is visible by high resolution ^{13}C NMR spectroscopy, is identical to that of the solid state. However, closer examination of the ^{13}C chemical shifts of these gel samples (Tables 2 and 4) shows that the C-3 ^{13}C chemical shifts of the gel samples appear at the midpoint of those of forms II and III, although no appreciable change was noted for the rest of peaks. The displacements of peaks in each case are 2—3 ppm and can be regarded as significant change, even if contribution of a plausible experimental error

(<1 ppm) is taken into account.[46] This finding implies that a sort of conformational rearrangement in association with hydration is required to form gel when solid samples of linear glucans with form II or of branched glucans with form II or III were used. It is conceivable that conformational change would be induced when these samples are hydrated to some extent. Consistent with this view, existence of polymorphic structures depending on humidity or hydration was demonstrated for curdlan by means of X-ray diffraction study.[12,30]

Concluding Remarks.

We found that (1→3)-β-D-glucans obtained either from lyophilization or spray-drying take regular secondary conformations as viewed from high-resolution solid-state ^{13}C NMR spectroscopy, in spite of inherent poor crystallinity. Obviously, this is the major advantage of the ^{13}C NMR spectroscopy as a new means of conformational elucidation complementary to X-ray diffraction. It is demonstrated that these secondary forms can be classified into at least four forms, on the basis of the conformation-dependent displacements of peaks at the C-1 and C-3 carbons. As a result, we concluded that paramylon with crystallinity of over 90% is not consisting of molecular chains of single conformation but a composite of at least three different conformers. In addition, we found that gelation property of linear glucans is related to the presence of particular conformation in the solid state. This view, however, must be modified to some extent in branched glucans, because gelation condition is not simple as in linear glucans.

We are grateful to Takeda Chemical Industries for providing us with curdlan and its acid-degraded samples, Dr. Goro Chihara for gift of lentinan and pachyman, and Professor B. A. Stone for gift of paramylon.

References

1) J. J. Marshall, *Adv. Carbohydr. Chem. Biochem.* **30**, 257 (1974).
2) T. Harada, A. Misaki, and H. Saito, *Arch. Biochem. Biophys.*, **124**, 292 (1968).
3) T. Harada, ACS Symp. Ser. No. 45, 265 (1977).
4) H. Saitô, T. Ohki, and T. Sasaki, *Carbohydr. Res.*, **74**, 227 (1979).
5) H. Saitô, ACS Symp. Ser., No. 150, 125 (1981).
6) H. Saitô, T. Ohki, and T. Sasaki, *Biochemistry*, **16**, 908 (1977).
7) H. Saitô, E. Miyata, and T. Sasaki, *Macromolecules*, **11**, 1244 (1978).
8) H. Saitô, T. Ohki, N. Takasuka, and T. Sasaki, *Carbohydr. Res.*, **58**, 293 (1977).
9) H. Saitô, T. Ohki, Y. Yoshioka, and F. Fukuoka, *FEBS. Lett.*, **68**, 15 (1976).
10) T. Sasaki, N. Abiko, Y. Sugino, and K. Nitta, *Cancer Res.*, **38**, 379 (1978).
11) T. Sasaki, and N. Takasuka, *Carbohydr. Res.*, **47**, 99 (1976).
12) R. H. Marchessault, Y. Deslandes, K. Ogawa, and P. R. Sundararajan, *Can. J. Chem.*, **55**, 300 (1977).
13) Y. Deslandes, R. H. Marchessault, and A. Sarko, *Macromolecules*, **13**, 1466 (1980).
14) H. Takeda, N. Yasuoka, N. Kasai, and T. Harada, *Polymer J.* **10**, 365 (1978).
15) H. Saitô, R. Tabeta, A. Shoji, T. Ozaki, I. Ando, and T. Asakura, "Magnetic Resonance in Biology and Medicine," ed by G. Govil, C. L. Kheterapal, and A. Saran, Tata McGraw-Hill, New Delhi, pp. 195, 1985.
16) H. Saitô, *Magn. Reson. Chem.*, in press.
17) H. Saitô, G. Izumi, T. Mamizuka, S. Suzuki, and R. Tabeta, *J. Chem. Soc., Chem. Commun.*, **1982**, 1386.
18) H. Saitô, G. Izumi, and R. Tabeta, Proc. 21th NMR Symp. 1982, pp. 37—44.
19) R. H. Atalla, J. C. Gast, D. W. Sindorf, V. J. Bartuska, and G. E. Maciel, *J. Am. Chem. Soc.*, **102**, 3249 (1980).
20) W. L. Earl and D. L. VanderHart, *J. Am. Chem. Soc.*, **102**, 2351 (1980).
21) R. L. Dudley, C. A. Fyfe, P. J. Stephenson, Y. Deslandes, G. K. Hammer, and R. H. Marchessault, *J. Am. Chem. Soc.*, **105**, 2469 (1983).
22) W. L. Earl and D. L. VanderHart, *Macromolecules*, **14**, 570 (1981).
23) G. E. Maciel, W. L. Kolodziejski, M. S. Bertran, and B. E. Dale, *Macromolecules*, **15**, 686 (1982).
24) F. Horii, A. Hirai and R. Kitamaru, *Polym. Bull.*, **8**, 163 (1982).
25) F. Horii, A. Hirai, and R. Kitamaru, ACS Symp. Ser., No. 260, 27 (1982).
26) F. Horii, A. Hirai, and R. Kitamaru, *J. Carbohydr. Chem.*, **3**, 641 (1984).
27) H. Saitô, R. Tabeta, and S. Hirano, *Chem. Lett.*, **1981**, 1479.
28) H. Saitô, R. Tabeta, and S. Hirano, "Chitin and Chitosan. Proceedings of the Second International Conference on Chitin and Chitosan," ed by S. Hirano and S. Tokura, Japanese Society of Chitin and Chitosan (1982), pp. 71—76.
29) H. Saitô, R. Tabeta and T. Harada, *Chem. Lett.*, **1981**, 571.
30) C. A. Fyfe, P. J. Stephenson, M. G. Taylor, T. L. Bluhm, Y. Deslandes, and R. H. Marchessault, *Macromolecules*, **17**, 501 (1984).
31) H. Saitô and R. Tabeta, *Chem. Lett.*, **1981**, 713.
32) D. J. Manners, A. J. Masson, and R. I. Sturgeon, *Carbohydr. Res.*, **17**, 109 (1971).
33) H. Saito, A. Misaki, and T. Harada, *Agr. Biol. Chem. (Tokyo)*, **32**, 1261 (1968).
34) A. E. Clarke and B. A. Stone, *Biochim. Biophys. Acta*, **44**, 161 (1960).
35) G. Chihara, Y. Y. Maeda, J. Hamuro, T. Sasaki, and F. Fukuoka, *Nature*, **222**, 687 (1969).
36) Y. Yoshioka, R. Tabeta, H. Saitô, N. Uehara, and F. Fukuoka, *Carbohydr. Res.*, **140**, 93 (1985).
37) H. Saitô, R. Tabeta, A. Shoji, T. Ozaki, and I. Ando, *Macromolecules*, **16**, 1050 (1983).
38) H. Saitô, R. Tabeta, A. Shoji, T. Ozaki, I. Ando, and T. Miyata, *Biopolymes*, **23**, 2279 (1984).

39) H. Saitô, R. Tabeta, T. Asakura, Y. Iwanaga, A. Shoji, T. Ozaki, and I. Ando, *Macromolecules,* **17**, 1405 (1984).
40) R. Tabeta and H. Saitô, *Biochemistry,* **24**, 7696 (1985).
41) R. Tabeta and H. Saitô, *Bull. Chem. Soc. Jpn.,* **58**, 3215 (1985).
42) T. Asakura, A. Kuzuhara, R. Tabeta, and H. Saitô, *Macromolecules,* **19**, 1841 (1985).
43) W. L. Earl and D. L. VanderHart, *Macromolecules,* **12**, 762 (1979).
44) I. Ando, T. Sorita, T. Yamanobe, T. Komoto, H. Sato, K. Deguchi, and M. Imanari, *Polymer,* **26**, 1864 (1985).
45) R. H. Marchessault and Y. Deslandes, *Carbohydr. Res.,* **75**, 231 (1979).
46) In this connection, it is important to consider a plausible contribution from the difference in molecular packing, by going from the solid to gel state, to the displacements of the ^{13}C chemical shifts (2—3 ppm for the C-3 carbon). As a means to estimate the extent of molecular packing, VanderHart compared the ^{13}C chemical shifts of *n*-alkane of different crystalline structure but the same molecular conformation and showed a separation of peaks 1.3 ppm in the resonance position of the internal methylene resonance.[47] In a same manner, Sorita et al. noticed the difference of the ^{13}C chemical shift due to molecular packing as large as 0.9 ppm for the system of *cyclo*- and *n*-alkanes.[48] Accordingly, it is obvious that such a contribution by molecular packing, if any, cannot well explain the observed displacements of peaks. Moreover, it is pointed out that significant displacements of peaks by going from the solid to gel state is limited to the C-3 peak alone, and the rest of peaks is unchanged within the experimental error. Therefore, it is reasonable to ascribe the significant displacements of peaks to a plausible conformational change, as treated in the present article.
47) D. L. VanderHart, *J. Magn. Reson.* **44**, 117 (1981).
48) T. Sorita, T. Yamanobe, T. Komoto, I. Ando, H. Sato, K. Deguchi, and M. Imanari, *Makromol. Chem. Rapid Commun.,* **5**, 657 (1984).

Mössbauer Spectroscopic Studies of Mercury(II) Chloride Adducts with Binuclear Metallocenes

Masanobu WATANABE, Izumi MOTOYAMA, and Hirotoshi SANO*
Department of Chemistry, Faculty of Science, Tokyo Metropolitan University, Fukasawa, Setagaya-ku, Tokyo 158
(Received December 25, 1985)

Biferrocene and ferrocenylruthenocene react with $HgCl_2$ to give very stable adducts. Large quadrupole splitting values (2.93 mm s^{-1} for biferrocene–$2HgCl_2$ and 2.99 mm s^{-1} for ferrocenylruthenocene–$5HgCl_2$, both at 78 K) indicate the presence of a direct interaction between the Fe and Hg atoms. The stabilities of their adducts suggest a chelating effect between the Fe and Fe or Fe and Ru atoms in biferrocene or ferrocenylruthenocene, respectively.

All attempts in preparing a stable adduct of mononuclear ferrocene with a Lewis acid such as Hg^{2+}, Sn^{4+}, and I^+ have been unsuccessful, whereas a number of the corresponding ruthenocene adducts were reported to be very stable.[1–4]

It was recently shown in our previous reports that [2]ferrocenophane derivatives react with various Lewis acids such as Sn^{4+}, Hg^{2+}, and I^+ to give stable adducts containing a chemical bond between the Fe and Lewis acid atoms.[5–7] The stabilities of [2]ferrocenophane adducts were ascribed to the distorted structure of [2]ferrocenophane which makes the nonbonding e_{2g} electrons of the iron atom in ferrocene easier to be ligated to a Lewis acid atom.

The other category of ferrocene derivatives which can provide a stable adduct with a Lewis acid, may be expected in binuclear metallocene derivatives, because their adducts with a Lewis acid are stabilized by a chelating effect of the binuclear ferrocene derivatives if they have a suitable molecular structure.[8] Fortunately, a number of binuclear ferrocene derivatives have been synthesized and reported in connection with studies of the mixed-valence state of iron atoms in their monocation salts. For instance, biferrocenium triiodide shows a so-called trapped valence state, while biferrocenylenium pentaiodide shows an averaged valence state.[9–11] It is also expected that ferrocenylruthenocene derivatives can provide much more stable adducts with a Lewis acid than the binuclear ferrocenes and that the electronic state of iron atoms in the adducts may provide information about the chelating effect.

Experimental

Materials. Biferrocene,[12] biferrocenylene,[13] diferrocenylmethane and diferrocenylethane,[14] 1,12-dimethyl[1.1]ferrocenophane,[15] [2.2]ferrocenophane,[16] ferrocenylruthenocene,[17] and ferrocenylruthenocenylmethane[18] were prepared by the methods reported previously.

Adducts of diferrocenylmethane, 1,2-diferrocenylethane, ferrocenylruthenocene and ferrocenylruthenocenylmethane with $HgCl_2$ were prepared in diethyl ether by a similar method to that used in the case of biferrocene–$2HgCl_2$ adduct.[8] Found: C, 25.71; H, 2.71%. Calcd for biferrocene–$2HgCl_2$, $C_{20}H_{18}Fe_2Hg_2Cl_4$: C, 26.29; H, 1.97%. Found: C, 12.52, H, 0.99; Fe, 5.54%. Calcd for diferrocenylmethane–$6HgCl_2$, $C_{21}H_{20}Fe_2Hg_6Cl_{12}$: C, 12.99; H, 1.10; Fe, 4.78%. Found: C, 13.02; H, 1.09; Fe, 5.51%. Calcd for 1,2-diferrocenylethane–$6HgCl_2$, $C_{22}H_{22}Fe_2Hg_6Cl_{12}$: C, 13.05; H, 1.10; Fe, 5.08%. Found: C, 14.17; H, 1.27%. Calcd for ferrocenylruthenocene–$5HgCl_2$, $C_{20}H_{18}FeRuHg_5Cl_{10}$: C, 13.55; H, 1.03%. Found: C, 22.96; H, 2.02%. Calcd for ferrocenylruthenocenylmethane–$2.5HgCl_2$, $C_{21}H_{20}FeRuHg_{2.5}Cl_5$: C, 22.75; H, 1.82%.

Reaction products of biferrocenylene, 1,12-dimethyl[1.1]ferrocenophane and [2.2]ferrocenophane were prepared in ethanol instead of diethyl ether because of better solubility, by following a method similar to that used for the biferrocene–$2HgCl_2$ adduct. The dark green precipitates that formed were filtered, washed with ethanol or diethyl ether and dried in a vacuum. Found: C, 16.86; H, 1.13; Hg, 54.00%. Calcd for biferrocenylenium$(HgCl_3^-)(HgCl_2)_3$, $C_{20}H_{16}Fe_2Hg_4Cl_9$; C, 16.11; H, 1.07; Hg, 53.86%. Found: C, 20.51; H, 1.71%. Calcd for 1,12-dimethyl[1.1]ferrocenophanium$(HgCl_3^-)(HgCl_2)_{2.5}$, $C_{24}H_{24}Fe_2Hg_{3.5}Cl_8$: C, 20.65; H, 1.70%. Found: C, 27.74; H, 2.31%. Calcd for [2.2]-ferrocenophanium$^{2+}(HgCl_3^-)_2$, $C_{24}H_{24}Fe_2Hg_2Cl_6$: C, 27.26; H, 2.37%.

Measurements. ^{57}Fe-Mössbauer measurements were carried out using a ^{57}Co(Pt) source moving in a constant acceleraion mode. The values of the isomer shifts were described with respect to metallic iron foil. The experimental error of the isomer shifts (I.S.) and quadrupole splittings (Q.S.) was ± 0.02 mm s^{-1}. Cyclic voltammograms were obtained by using a Hokuto Denko HB-107A function generator and a Hokuto Denko HA-201 potentiostat combined with a standard three-electrode configuration. A working electrode of platinum button-(Beckman) and an Ag/AgCl reference electrode were connected via a salt bridge containing (0.1 mol dm^{-3}) $[(C_4H_9)_4N]ClO_4$ in CH_3CN.

Results and Discussion

Biferrocene reacts with a large excess of $HgCl_2$ in diethyl ether, giving deep-red precipitates thought to be biferrocene–$2HgCl_2$, based on an elemental analysis. The adduct is stable in air for a long time (more than 200 d) at room temperature, while ferrocene–$7HgCl_2$ changes immediately into a ferricinium salt.[19] Other biferrocene derivatives, such as

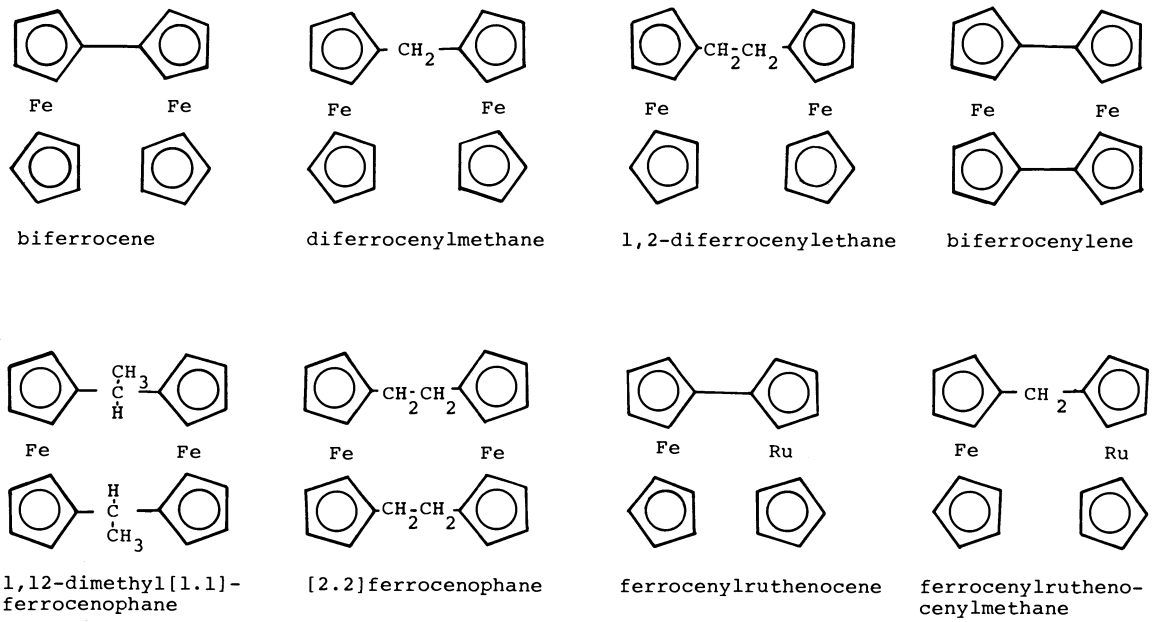

1′,1‴-dihalobiferrocene 1′,1‴-dialkylbiferrocene, react with $HgCl_2$ to give paramagnetic green precipitates. The results of Mössbauer spectroscopic studies of these precipitates show that these biferrocene are oxidized by $HgCl_2$, probably because of a steric hindrance of the substituents and that they give a trapped-valence state for each monocationic ferricinium salt.

Typical Mössbauer spectra of a biferrocene–$2HgCl_2$ adduct and the biferrocene itself, are shown in Fig. 1 and Mössbaur parameters are listed in Table 1. The Q.S. value (2.93 mm s^{-1} at 78 K) found in the biferrocene–$2HgCl_2$ adduct is a little smaller than that of [2]ferrocenophane–$3HgCl_2$ adduct (3.29 mm s^{-1} at 78 K)[6] but still larger than that of the original biferrocene. The results indicate that the biferrocene–$2HgCl_2$ adduct should have Fe–Hg bonds, as already verified in the $HgCl_2$ or $SnCl_4$ adducts of [2]ferrocenophane.[5,6]

A little lower Q.S. value and large stability of the

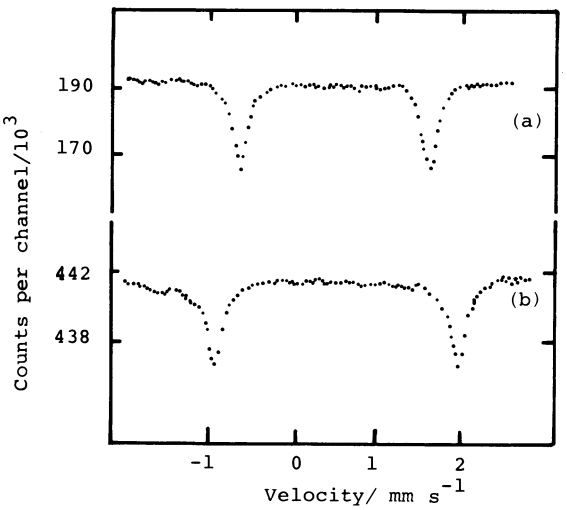

Fig. 1. Mössbauer spectra of (a) biferrocene and (b) biferrocene–$2HgCl_2$ adduct, both at 78 K.

Table 1. Mössbauer Parameters of Binuclear Ferrocene Derivatives and Their $HgCl_2$ Adducts and Salts

Compound	Temperature / K	Q.S. / mm s^{-1}	I.S. / mm s^{-1}
Biferrocene	78	2.33	0.53
Diferrocenylmethane	78	2.38	0.52
Diferrocenylethane	78	2.40	0.50
Biferrocenylene	78	2.44	0.53
1,12-Dimethyl[1.1]-ferrocenophane	78	2.45	0.54
[2.2]Ferrocenophane	78	2.43	0.52
Ferrocenylruthenocene	78	2.36	0.53
	300	2.29	0.46
Biferrocene–$2HgCl_2$	78	2.93	0.55
Diferrocenylmethane–$6HgCl_2$	78	3.02	0.53
Diferrocenylethane–$6HgCl_2$	78	3.00	0.50
Biferrocenylenium$^+$ $HgCl_3^-(HgCl_2)_3$	78	1.87	0.53
	200	1.83	0.47
	300	1.76	0.43
1,12-Dimethyl[1.1]ferrocenophanium$^+$ $HgCl_3^-(HgCl_2)_{2.5}$	78	1.93	0.52
		0.0	0.53
[2.2]ferrocenophanium^{2+}-$(HgCl_3^-)_2$	78	0.0	0.53
Ferrocenylruthenocene–$5HgCl_2$	78	2.99	0.57
Ferrocenylruthenocenylmethane–$2.5HgCl_2$	78	2.84	0.55
Biferrocenylenium$^+$ I_5^- [a]	4.2	1.756	0.542
	300	1.719	0.441
Ferrocene–$7HgCl_2$ [b]	275	2.94	0.45

a) Data were taken from Ref. 10. b) Data were taken for the fresh sample reported in Ref. 19.

biferrocene-$2HgCl_2$ adduct compared with ferrocene-$7HgCl_2$[19] suggest that biferrocene reacts with $HgCl_2$ as a chelating agent.

It is found that biferrocene reacts with $SnCl_4$ to give only green-colored precipitates in which iron atoms are not ligated to Sn^{4+} ions but partially oxidized to a mixed-valence state (Q.S. values, 2.26 and 0.29 mm s^{-1} at 78 K).[20] Also, biferrocene is oxidized to a dicationic biferricinium salt in the reaction with $SbCl_5$ (Q.S., 0.25 mm s^{-1} and I.S., 0.55 mm s^{-1} at 78 K, which are characteristic of ferricinium-like iron(III)). Although [2]ferrocenophane reacts with other Lewis acid species, such as $CdCl_2$, $ZnCl_2$, $CoCl_2$, to give corresponding adducts with them,[21] biferrocene does not react with these Lewis acids. The results may be interpreted by assuming that Hg^{2+} ions are a softer acid than Sn^{4+} and Sb^{5+} atoms, and that the e_{2g} electrons in biferrocene cannot be ligated to Lewis acids harder than Hg^{2+}.

Diferrocenylmethane and 1,2-diferrocenylethane also react with $HgCl_2$ as in the case of biferrocene, giving orange-yellow precipitates with a color that is very similar to that of ferrocene-$7HgCl_2$. The products are less stable than the biferrocene-$2HgCl_2$ adduct; i.e., they change color to blue-green after being allowed to stand at room temperature for several days after preparation. However, they are much more stable than the ferrocene-$7HgCl_2$ adduct which completely changes from orange-yellow to blue-green within a day.

The results indicate that the diferrocenylmethane- and 1,2-diferrocenylethane-$6HgCl_2$ adducts have Fe-Hg bonds, although the bonds seem to be a little weaker than the Fe-Hg bond in the biferrocene-$2HgCl_2$ adduct. Actually, the doublet component with a large Q.S. value decreases and a broad-line component with a small Q.S. value increases in their Mössbauer spectra (Fig. 2), if the compounds are placed in air for several days.

Biferrocene, 1,12-dimethyl[1.1]ferrocenophane and [2.2]-ferrocenophane react with $HgCl_2$ in ethanol giving dark-green paramagnetic precipitates. The ^{57}Fe-Mössbauer spectra of these reaction products are shown in Fig. 3, and the Mössbauer parameters are also listed in Table 1. A smaller Q.S. value (1.87 mm s^{-1} at 78 K) compared with that of biferrocenylene (2.44 mm s^{-1} at 78 K) was found and assigned to an averaged valence state of Fe(II) and Fe(III) as expected from the dark color of the adduct. The Q.S. value is close to that of biferrocenylenium

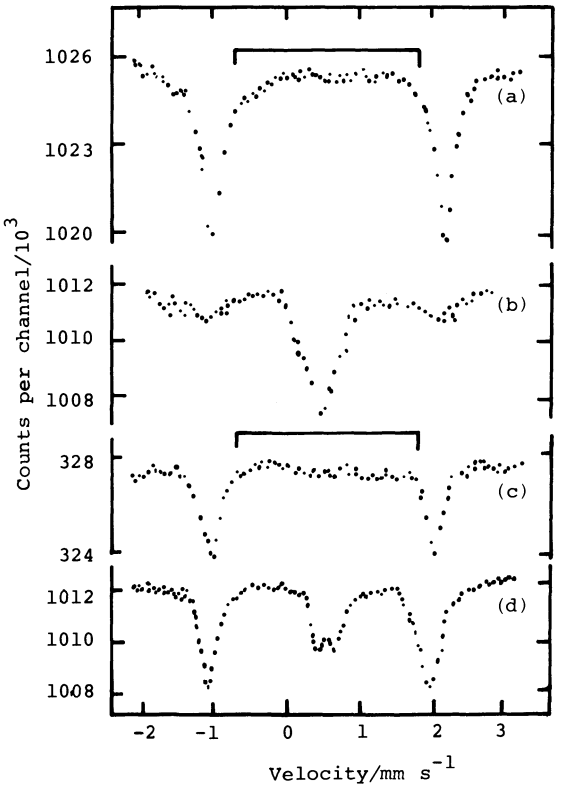

Fig. 2. Mössbauer spectra at 78 K of (a) diferrocenylmethane-$6HgCl_2$ adduct immediately, (b) 7 d after preparation, (c) 1,2-diferrocenylethane-$6HgCl_2$ adduct immediately, (d) 7 d after preparation. Peak position of diferrocenylmethane and 1,2-diferrocenylethane is shown.

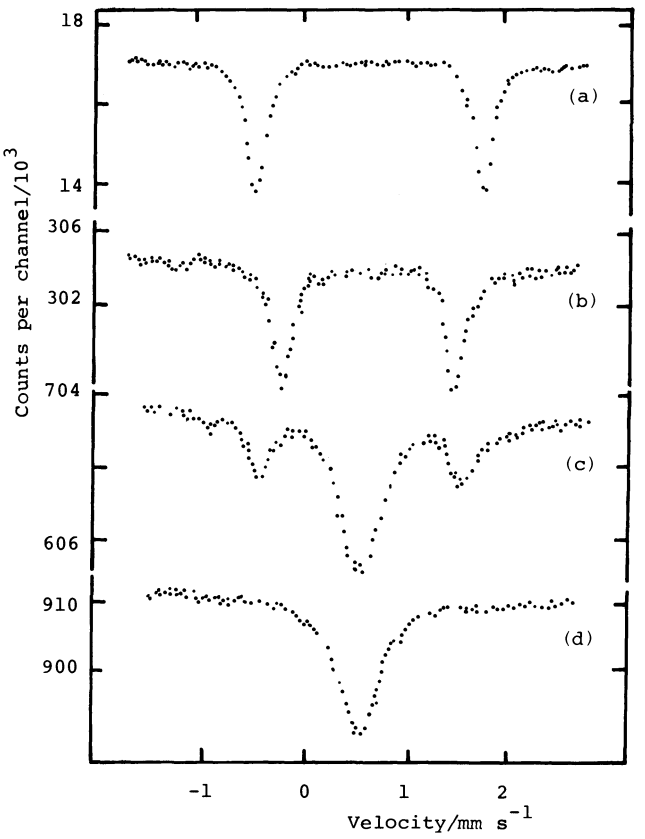

Fig. 3. Mössbauer spectra at 78 K of (a) biferrocenylene, and reaction products of (b) biferrocenylene, (c) 1,12-dimethyl[1.1]ferrocenophane, (d) [2.2]ferrocenophane with $HgCl_2$.

pentaiodide (1.756 mm s^{-1} at 4.2 K), which is known to show a typical averaged valence state.[10]

Magnetic susceptibility measurements showed that the monocationic biferrocenylenium salt is paramagnetic. The effective magnetic moment in a temperature range from 78 K to 120 K was found to be 2.02 BM, also close to the value characteristic of binuclear ferrocene derivatives in an averaged valence state (e.g., 1.90 BM for biferrocenylenium pentaiodide).[10] The results indicate that biferrocenylene is partially oxidized by $HgCl_2$ to form an averaged valence state of a monocationic biferrocenylenium salt.

The 1,12-dimethyl[1.1]ferrocenophane–$HgCl_2$ product showed two quadrupole splitting doublets (Q.S.; 1.93 mm s^{-1}. I.S.; 0.52 mm s^{-1} and Q.S.; 0.0 mm s^{-1}, I.S.; 0.53 mm s^{-1} at 78 K). These values are almost the same as those for the monocationic 1,12-dimethyl[1.1]ferrocenophanium triiodide salt.[10] This fact suggests that an interaction takes place between the iron atom, however, the interaction is not as strong as that of biferrocenylenium.

[2.2]Ferrocenophane reacts with $HgCl_2$ in ethanol giving dark green precipitates which are expressed as [2.2]ferrocenophanium^{2+}($HgCl_3^-$)$_2$. In the Mössbauer spectra of this compound, only a broad singlet peak is observed, suggesting that [2.2]ferrocenophane is oxidized by $HgCl_2$ completely to a dicationic [2.2]ferrocenophanium species.

In the cyclic voltammograms of biferrocenylene and 1,12-dimethyl[1.1]ferrocenophane, two kinds of one-electron oxidation peaks (0.26_5 and 0.85_5 V for biferrocenylene,[22] 0.38 and 0.61 V for 1,12-dimethyl-[1.1]ferrocenophane) were observed, while only one two-electron oxidation peak (0.42 V) was found in that of [2.2]ferrocenophane. The difference between the first and second half-wave potentials, $\Delta E_{1/2}$, has often been used as a parameter of the interaction between the Fe–Fe atoms in binuclear ferrocene derivatives. The fact that a larger value of $\Delta E_{1/2}$ (0.59 V) is observed in the biferrocenylene than the value (0.23 V) found in 1,12-dimethyl[1.1]ferrocenophane, is in accordance with the results of Mössbauer spectroscopic studies on binuclear ferrocenophanes' monocationic salts.

It can be concluded that doubly-bridged ferrocenophanes react with $HgCl_2$ gving only a ferricinium salt and not an adduct containing an Fe–Hg chemical bond. The reason that biferrocene, diferrocenylmethane, and 1,2-diferrocenylethane form adducts with $HgCl_2$ can be explained by assuming a more flexible molecular structure compared with the rigid structure of biferrocenylene, 1,12-dimethyl[1.1]ferrocenophane and [2.2]ferrocenophane. A large conformational change in such a way that the two Fe atoms are ligated to the $HgCl_2$ may occur, for instance, in biferrocene–2$HgCl_2$ but such a change can not be allowed in a rigid structure of binuclear ferrocenophanes.

Based on this speculation, more stable $HgCl_2$ adducts were prepared using ferrocenylruthenocene derivatives. The results of the cyclic voltammography of ferrocenylruthenocene show two one-electron oxidation peaks (E_{ox}; 0.45 and 0.92 V), one is ascribed to an oxidation of ferrocene-type iron atoms (0.45 V) and the other is to that of a ruthenocene-type ruthenium atoms (0.92 V); i.e., Ru atoms are oxidized less easily than Fe atoms by $HgCl_2$ in this compound. It is known that ruthenocene itself reacts with various kinds of Lewis acids such as I_2, $SnCl_4$, $SbCl_5$, and $HgCl_2$, to give relatively stable products containing a chemical bond between Ru and the Lewis acids.[1-4]

Ferrocenylruthenocene reacts with a large excess of $HgCl_2$ in diethyl ether giving diamagnetic orange-yellow precipitates. The product, expressed ferrocenylruthenocene–5$HgCl_2$, is more stable in air than biferrocene–2$HgCl_2$. The biferrocene–2$HgCl_2$ adduct changes color to green-blue upon standing at 80 °C for 2hr, while the color of ferrocenylruthenocene–5$HgCl_2$ remains upon standing under the same conditions.

Typical Mössbauer spectra of ferrocenylruthenocene and its $HgCl_2$ adduct are shown in Fig. 4. The Q.S. value of ferrocenylruthenocene is 2.36 mm s^{-1} at 78 K as shown in Table 1, which is nearly the same as that of biferrocene (2.33 mm s^{-1} at 78 K), suggesting there is no direct effect of ruthenocenyl group on Fe atoms in ferrocenylruthenocene.

A larger Q.S. value is observed in ferrocenylruthenocene–5$HgCl_2$ adduct (2.99 mm s^{-1} at 78 K) compared with the value of the original ferrocenylruthenocene.

Ferrocenylruthenocenylmethane reacts with $HgCl_2$

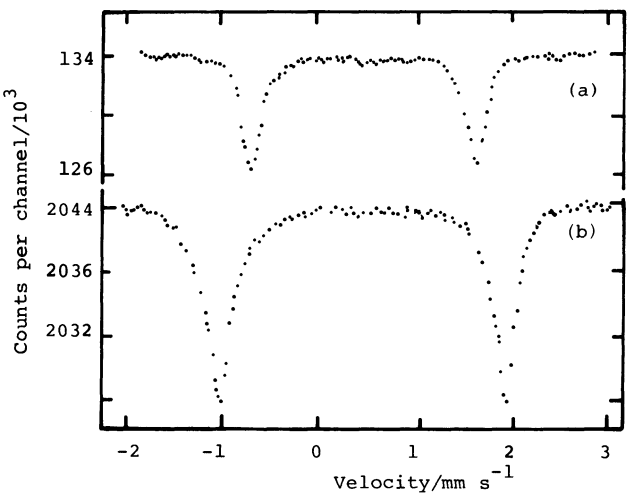

Fig. 4. Mössbauer spectra of (a) ferrocenylruthenocene and (b) its $HgCl_2$ adduct, both at 78 K.

in diethyl ether, giving a diamagnetic orange-yellow product. The Q.S. value found in this adduct (2.84 mm s^{-1} at 78 K) is a little smaller than those of binuclear ferrocene derivatives-$HgCl_2$ adducts or ferrocenylruthenocene-5$HgCl_2$ adduct, but still larger than that of the original ferrocenylruthenocenylmethane (2.44 mm s^{-1} at 78 K). The results indicate that the ferrocenylruthenocenylmethane adduct has an Fe-Hg bonding, although the bond should be a little weaker than the Fe-Hg bond in the $HgCl_2$ adduct of ferrocenylruthenocene.

Actually, the $HgCl_2$ adduct of ferrocenylruthenocenylmethane is not as stable as the $HgCl_2$ adduct of ferrocenylruthenocene. After being allowed to stand in air for several days after preparation, the color of the adduct gradually changed into blue-green, as in the case of diferrocenylmethane-6$HgCl_2$ and 1,2-diferrocenylethane-6$HgCl_2$ adducts. The reason that ferrocenylruthenocenylmethane forms a less stable adduct can be explained by the larger distance between the Ru and Fe atoms in the molecule compared in the ferrocenylruthenocene molecule; i.e., the distance of Fe-Ru atoms may be too large to make a stable chelation like ferrocenylruthenocene-5$HgCl_2$ adduct.

The facts that ferrocenylruthenocene can provide a more stable adduct than biferrocene and ferrocenylruthenocenylmethane with $HgCl_2$ and that the Q.S. value is similar to that of biferrocene-2$HgCl_2$ adduct, also suggest a possibility of chelation,

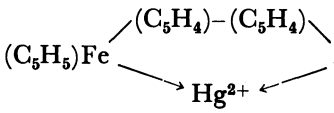

rather than a monodentated donation such as $-(C_5H_5)Ru\rightarrow Hg^{2+}\leftarrow Fe(C_5H_5)(C_{10}H_8)(C_5H_5)Ru\rightarrow Hg^{2+}\leftarrow Fe(C_5H_5)-$. It is tentatively concluded in this study that ferrocenylruthenocene and biferrocene form very stable adducts with $HgCl_2$ because of an appropriate distance between the Fe-Ru or Fe-Fe atoms for chelation to take place in these adducts. However, further studies must be conducted to provide direct evidece to prove the chelating bond in the adducts.

References

1) D. N. Hendrickson, Y. S. Sohn, W. H. Morrison, Jr, and H. B. Gray. *Inorg. Chem.*, **11**, 808 (1972).
2) W. H. Morrison, Jr. and D. N. Hendrickson, *Inorg. Chem.*, **11** 2912 (1972).
3) K. R. Mann, W. H. Morrison, Jr. and D. N. Hendrickson, *Inorg. Chem.*, **13**, 1180 (1974).
4) Y. S. Sohn, A. W. Schueter , D. N. Hendrickson, and H. B. Gray, *Inorg. Chem.*, **13**, 301 (1974).
5) M. Watanabe, H. Ichikawa, I. Motoyama, and H. Sano, *Chem. Lett.*, **1983**, 1009.
6) M. Watanabe, H. Ichikawa, I. Motoyama, and H. Sano, *Bull. Chem. Jpn.*, **56**, 3291 (1983).
7) M. Watanabe, K. Sato, I. Motoyama, and H. Sano, *Chem. Lett.*, **1983**, 1775.
8) M. Watanabe, K. Suto, I. Motoyama, and H. Sano, *Chem. Lett.*, **1984**, 1317.
9) W. H. Morrison, Jr. and D. N. Hendrickson, *J. Chem. Phys.*, **59**, 380 (1973).
10) M. H. Morrison, Jr. and D. N. Hendrickson, *Inorg. Chem.*, **14**, 2331 (1975).
11) D. O. Cowan, R: L. Collins, and F. Kaufman, *J. Phys. Chem.*, **75**, 2025 (1971).
12) M. D. Raush, *J. Org. Chem.*, **26**, 1802 (1961).
13) M. D. Raush, *J. Org. Chem.*, **28**, 3337 (1963).
14) P. L. Pauson and W. E. Watts, *J. Chem. Soc.*, **1962**, 3880.
15) T. H. Barr, H. L. Lentzner, and W. E. Watts, *Tetrahedron*, **25**, 6001 (1969).
16) K. Kasahara and T. Izumi, *Chem. Lett.*, **1978**, 21.
17) E. W. Neuse and M. S. Loonat, *Transition Met. Chem.*, **6**, 260 (1981).
18) S. P. Gubin and A. A. Lubovich, *J. Organomet. Chem.*, **22**, 183 (1970).
19) R. M. G. Roberts, J. Silver, and I. G. Harrison, *J. Organomet. Chem.*, **209**, 385 (1981).
20) M. Watanabe, I. Motoyma, and H. Sano, submitted to *Bull. Chem. Soc. Jpn.*
21)H. Sano, M. Watanabe, and I. Motoyama, *Hyperfine Interactions*, **28**, 833 (1986).
22) C. LeVanda, K. Bechgaard, and D. O. Cowan, *J. Org. Chem.*, **41**, 2700 (1976).

Mössbauer Spectroscopic Studies of Tin(IV) Halide Adducts with Ruthenocene and with [2]Ferrocenophanes

Masanobu WATANABE, Izumi MOTOYAMA, and Hirotoshi SANO*
Department of Chemistry, Faculty of Science, Tokyo Metropolitan University, Fukasawa, Setagaya-ku, Tokyo 158
(Received Junuary 13, 1986)

Adducts of tin(IV) halide with [2]ferrocenophane were prepared by treating SnX_4 (X=Cl or Br) with [2]ferrocenophane in hexane. The adducts were studied by means of ^{57}Fe- and ^{119}Sn-Mössbauer spectroscopy and other physicochemical measurements. Anomalously large quadrupole splittings (3.49 mm s^{-1} for [2]ferrocenophane-1.5$SnCl_4$ adduct and 3.47 mm s^{-1} for [2]ferrocenophane-1.5$SnBr_4$ adduct, both at 78 K) found in the ^{57}Fe-Mössbauer spectroscopy and organotin(IV) species (e.g., isomer shift value, 2.14 mm s^{-1} for the [2]-ferrocenophane-1.5$SnCl_4$ adduct and 2.10 mm s^{-1} for the [2]ferrocenophane-1.5$SnBr_4$ adduct, both at 78 K) found from the ^{119}Sn-Mössbauer spectroscopy suggest that a direct chemical bonding between Fe and Sn atoms is formed in the [2]ferrocenophane adducts, as the Ru-Sn bonding in the ruthenocene-1.5$SnCl_4$ adduct (isomer shift value, 2.08 mm s^{-1} at 78 K).

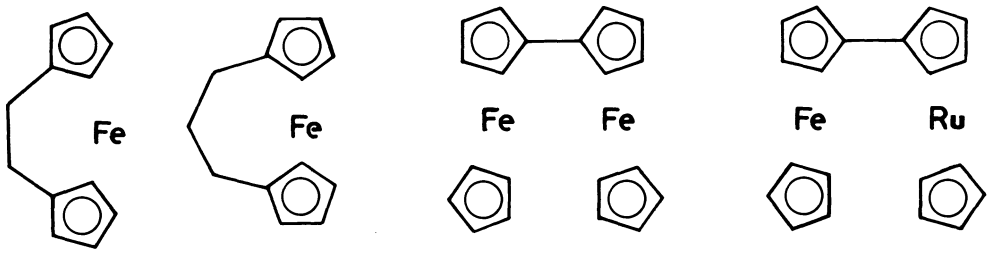

[2]Ferrocenophane [3]Ferrocenophane Biferrocene Ferrocenylruthenocene

Mann et al. reported that yellow-colored ruthenocene-tin(IV) halide adducts are prepared by the reaction of ruthenocene with $SnCl_4$ or $SnBr_4$ in a CCl_4 solution under nitrogen.[1] Based on the results of the IR spectra of these adducts, they proposed that the probable formula for the yellow products is $[(Cp)_2Ru\text{-}SnX_2\text{-}Ru(Cp)_2]^{2+}(SnX_5^-)_2$, where X=Cl or Br and Cp=C_5H_5, although no information was given about the ^{119}Sn-Mössbauer spectroscopy. The yellow SnX_4 adducts of ruthenocene are not as stable as the HgX_2 adducts of ruthenocene, in which Hg-Ru bonding is observed in X-ray analytical measurements.[2]

All attempts to prepare stable adducts of ferrocene with tin(IV) halide have been unsuccessful; e.g., ferrocene reacts with $SnCl_4$ giving not an adduct but only a paramagnetic ferricinium salt.

It has been shown in our recent reports that [2]ferrocenophanes react with various Lewis-acid species such as Hg^{2+}, Cd^{2+}, H^+, I^+, and Cl^+, giving their adducts by ligating electrons of iron atoms to the Lewis acids.[3-6] For instance, ^{57}Fe-Mössbauer spectroscopic studies of the [2]ferrocenophane-3$HgCl_2$ adduct show an anomalously large quadrupole splitting (Q.S.) value (3.29 mm s^{-1} at 78 K), suggesting a direct chemical bond between Fe^{2+} and Hg^{2+} atoms. The stability of [2]ferrocenophane-3$HgCl_2$ is ascribed to "naked" electrons around the iron atoms because the cyclopentadienyl rings are inclined by a bridged structure. In the case of the [2]ferrocenophane-$I^+I_3^-$ adduct, a direct interaction was verified by a single-crystal X-ray structural analysis; a similarly large Q.S. value is found in this adduct.[6]

From the similarity to ruthenocene-1.5SnX_4 adducts, it is expected that [2]ferrocenophane derivatives can provide a stable adduct of $SnCl_4$. The present study was planned to clarify the structure of the stable adducts of [2]ferrocenophane with SnX_4 (X=Cl or Br) and to provide further information about the chemical state of iron and tin by means of ^{57}Fe- and ^{119}Sn-Mössbauer spectroscopy.

Experimental

Materials. Biferrocene,[7] [2]ferrocenophane,[8] and [3]ferrocenophane[9] were prepared by the methods previously reported. The adduct of tin chloride with [2]ferrocenophane was prepared by the following method. To a solution of [2]ferrocenophane dissolved in dry hexane, a hexane solution of $SnCl_4$ was added in a nitrogen-filled dry box equilibrated with P_4O_{10}, and the produced red-orange precipitates were filtered, washed with a large excess of hexane, and dried under vacuum. The purity of the adduct was confirmed by elemental analysis: Found; C, 23.41; H, 2.77; Sn, 29.07%. Calcd for [2]ferrocenophane$(SnCl_4)_{1.5}$-(H_2O), $C_{12}H_{14}FeSn_{1.5}Cl_6O$: C, 23.19; H, 2.25; Sn, 28.67%. The red-orange product of [2]ferrocenophane with $SnBr_4$

was obtained by the same conditions as in the case of $SnCl_4$ adduct. The $SnBr_4$ adduct is very hygroscopic. Found: C, 16.21; H, 1.92%. Calcd for [2]ferrocenophane-$(SnBr_4)_{1.5}$-$(H_2O)_3$, $C_{12}H_{18}FeSn_{1.5}Br_6O_3$: C, 15.59; H, 1.95%. Reaction products of [3]ferrocenophane, biferrocene and ferrocene were obtained by the same procedure as described in the case of [2]ferrocenophane-1.5$SnCl_4$ adduct, but the color of the precipitates was dark-green characteristic of ferricinium salts. All the products prepared in the reactions of [2]-, [3]ferrocenophane and ferrocene with tin halides are so hygroscopic that the elemental analysis and IR spectroscopic data show an appreciable amount of water in each final product (as described in each empirical formula), even after keeping the samples in a desiccator. Found: C, 27.43; H, 2.93; Sn, 26.13%. Calcd for [3]ferrocenophanium-$(SnCl_4)_{1.25}(H_2O)_{1.5}$, $C_{13}H_{17}FeSn_{1.25}Cl_5O_{1.5}$: C, 26.96; H, 2.94; Sn, 25.64%. Found: C, 30.67; H, 2.44%. Calcd for biferrocenium$(SnCl_4)_{1.75}$, $C_{20}H_{18}Fe_2Sn_{1.75}Cl_7$: C, 29.07: H, 2.20%. Found: C, 20.10; H, 2.05; Sn, 28.85%. Calcd for ferricinium$(SnCl_4)_{1.5}(H_2O)_2$, $C_{10}H_{14}FeSn_{1.5}Cl_6O_2$: C, 19.58; H, 2.28; Sn, 29.05%. The adducts of [2]ferrocenophane-1.5$SnCl_4$ are hardly soluble in most organic solvents but are soluble in *N,N*-dimethylformamide. The solution shows only an absorption spectrum of [2]ferrocenophane, while the other precipitates such as [3]ferrocenophane-1.25$SnCl_4$ are soluble in *N,N*-dimethylformamide. The resulting green-colored solution gives an absorption spectra similar to that of the ferricinium salts.

Ruthenocene reacts with a large excess of $SnCl_4$ in dry hexane under nitrogen giving a yellow adduct. Found: C, 20.28; H, 1.78%. Calcd for ruthenocene$(SnCl_4)_{1.5}$, $C_{10}H_{10}RuSn_{1.5}Cl_6$: C, 19.29; H, 1.61%.

Measurements. ^{57}Fe-Mössbauer measurements were carried out by using a ^{57}Co(Pt) source moving in a constant acceleration mode, while ^{119m}Sn-Mössbauer spectra were measured against a $Ca^{119m}SnO_3$ source. The velocity calibration was made by the resonance lines of an ^{57}Fe-enriched metallic-iron absorber against the ^{57}Co(Pt) source. The isomer shift (I.S.) for ^{57}Fe was taken with respect to metallic iron and that for ^{119}Sn was descrided with respect to a $BaSnO_3$ absorber. The experimental error of the I.S. and Q.S. values were estimated to be within ± 0.02 mm s^{-1}.

Results and Discussion

The ruthenocene-1.5$SnCl_4$ adduct is not very stable and the yellow color gradually changes into green-yellow upon standing at room temperature for several days in air after preparation. The adduct is soluble in CH_3CN and gives a yellow solution. An absorption band at 360 nm in its fresh solution rapidly decreases in intensity while standing in air, and an absorption band characteristic of ruthenocene appears at 310 nm within a few minutes after preparing the solution. This is ascribed to a dissociation of the adduct into ruthenocene and $SnCl_4$.

The ^{119}Sn-Mössbauer parameters of the adducts and related compounds are listed in Table 1 and typical ^{119}Sn-Mössbauer spectra of $Ru(Cp)_2$-1.5$SnCl_4$ and related compounds are shown in Fig. 1. Measure-

Table 1. ^{119}Sn-Mössbauer Parameter for [2]Ferrocenophane-Tin Halide Adduct and Related Compounds

Compound	Temperature / K	I.S. / mm s^{-1}
[2]Ferrocenophane$(SnCl_4)_{1.5}(H_2O)$	4.2	0.54
		2.11
	40	0.53
		2.10
	78	0.54
		2.14
	97	0.53
		2.14
	138	0.51
		2.11
[3]Ferrocenophane$(SnCl_4)_{1.25}(H_2O)_{1.5}$	78	0.25
		0.77
		3.99
Ferrocene$(SnCl_4)_{1.5}(H_2O)_2$	78	0.18
		0.80
		4.07
Biferrocene$(SnCl_4)_{1.75}$	78	0.22
		0.86
		4.01
Ruthenocene$(SnCl_4)_{1.5}$	78	0.56
		2.08

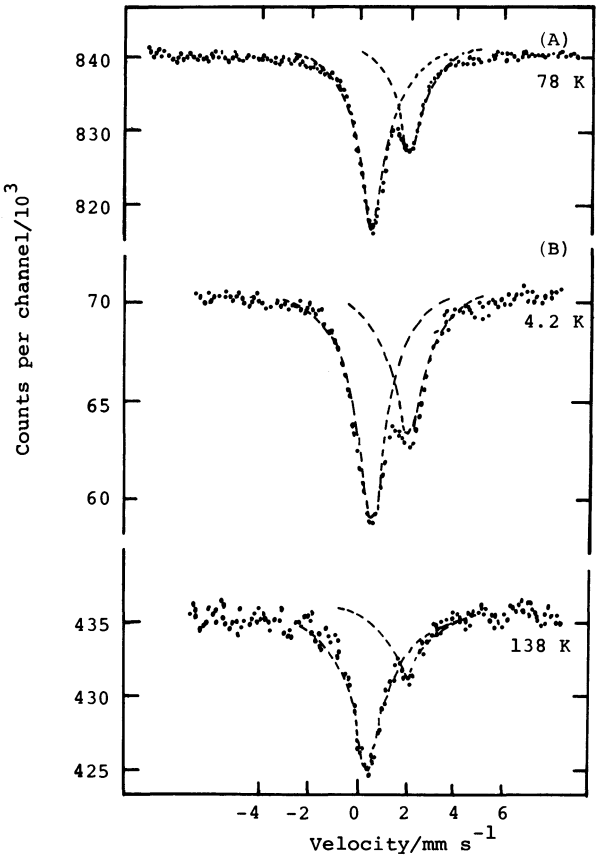

Fig. 1. ^{119}Sn-Mössbauer spectra of (A) ruthenocene-$SnCl_4$ adduct and (B) [2]ferrocenophane-$SnCl_4$ adduct, at indicated temperatures.

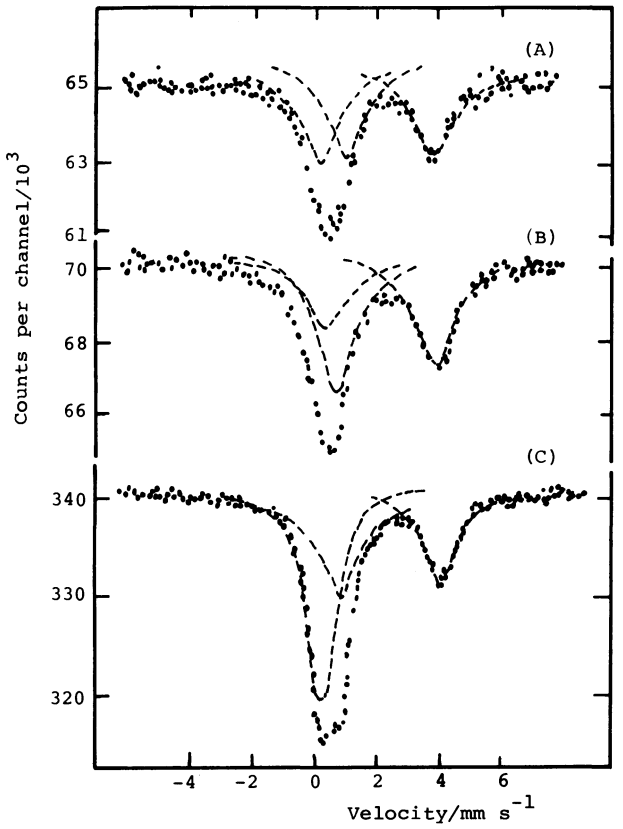

Fig. 2. ^{119}Sn-Mössbauer spectra of (A) reaction products with $SnCl_4$ and ferrocene, (B) [3]ferrocenophane, and (C) biferrocene, all at 78 K.

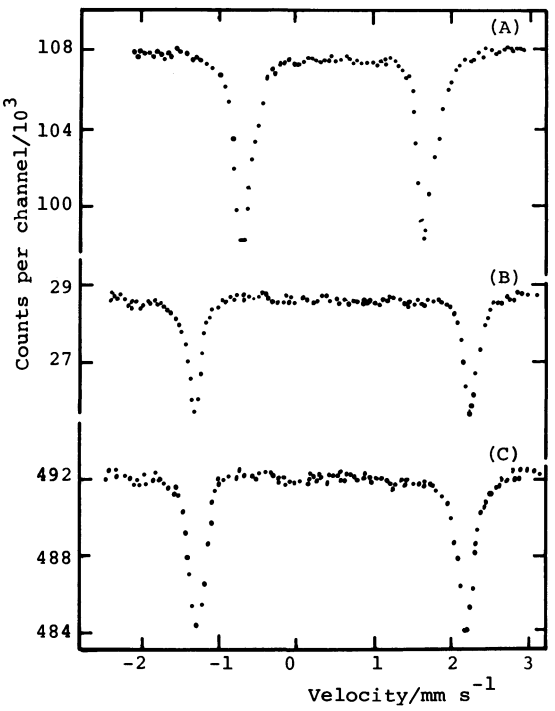

Fig. 3. ^{57}Fe-Mössbauer spectra of (A) [2]ferrocenophane, (B) [2]ferrocenophane-$SnCl_4$ adduct, and (C) [2]ferrocenophane-$SnBr_4$ adduct, all at 78 K.

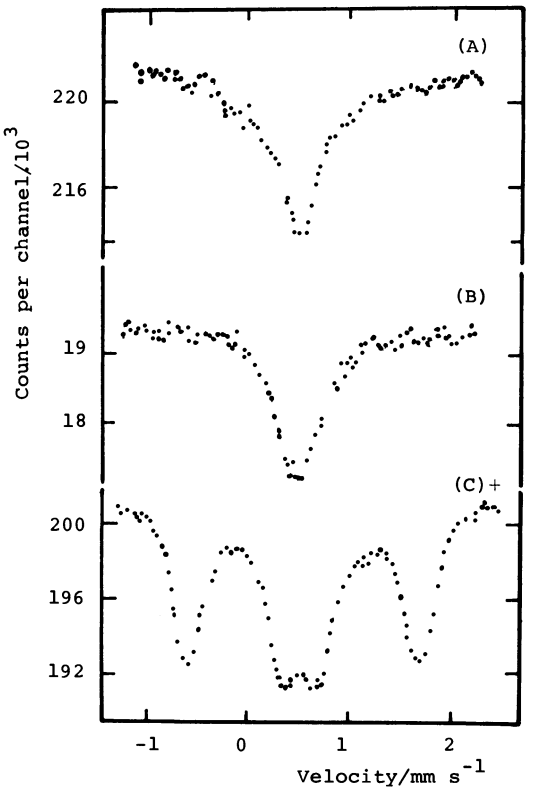

Fig. 4. ^{57}Fe-Mössbauer spectra of (A) reaction products with $SnCl_4$ and ferrocene, (B) [3]ferrocenophane, and (C) biferrocene, all at 78 K.

ments of the ^{119}Sn-Mössbauer spectra for the $SnCl_4$ adducts were limited to within a temperature range below 150 K because of their small recoil-free fraction. In the spectrum measured at 78 K of $Ru(CP)_2$-1.5$SnCl_4$, two kinds of chemical states of the tin(IV) species (I.S., 0.56 and 2.08 mm s^{-1}) were observed. The component with a higher I.S. value (2.08 mm s^{-1}) was ascribed to an organotin(IV) species and the other broad component with a lower I.S. value (0.56 mm s^{-1}) to a rather ionic $SnCl_5^-$ species, respectively. This was based on the systematics of the ^{119}Sn-Mössbauer spectroscopic parameters found in tetravalent organotin or organometallic tin chlorides and hexachlorotin(IV) species.

Mann et al. has already proposed $[(Cp)_2Ru\text{-}SnCl_2\text{-}Ru(Cp)_2]^{2+}(SnCl_5^-)_2$ as one of the probable structures for the yellow adduct on the basis of the IR spectroscopic studies.[1] In an analogy to the conclusion, it was also confirmed from the results of a ^{119}Sn-Mössbauer spectroscopic study that the component having a higher I.S. value is ascribable to a tin(IV) species of $(Cp)_2Ru\text{-}SnCl_2\text{-}Ru(Cp)_2$ and the lower one to $SnCl_5^-$.

Ferrocene reacts with $SnCl_4$ giving paramagnetic green precipitates. The ^{119}Sn- and ^{57}Fe-Mössbauer spectra of the product are shown in Figs. 2 and 4, respectively. In the ^{57}Fe-Mössbauer spectrum of this product, a broad singlet peak observed indicates the

Table 2. ^{57}Fe-Mössbauer Parameters for the [2]Ferrocenophane-Tin Halides Adducts and Related Compounds

Compound	Temperature K	Q.S. mm s^{-1}	I.S. mm s^{-1}
[2]Ferrocenophane	78	2.41	0.49
[2]Ferrocenophane-$(SnCl_4)_{1.5}(H_2O)$	4.2	3.53	0.52
	78	3.49	0.50
	300	3.40	0.41
[2]Ferrocenophane-$(SnBr_4)_{1.5}(H_2O)_3$	78	3.47	0.51
1,1,2,2-Tetramethyl[2]ferrocenophane$(SnCl_4)_{1.5}(H_2O)$	78	3.43	0.50
	200	3.37	0.46
Ferrocene$(SnCl_4)_{1.5}(H_2O)_2$	78	0.0	0.54
[3]Ferrocenophane-$(SnCl_4)_{1.25}(H_2O)_{1.5}$	78	0.0	0.52
Biferrocene$(SnCl_4)_{1.75}$	78	0.29	0.54
		2.26	0.50

presence of the ferricinium-like iron atoms as expected from the dark-green color of the product. The ^{119}Sn-Mössbauer spectrum shows that there are three components ascribed to two kinds of Sn(IV) species (I.S., 0.18 and 0.80 mm s^{-1}) and to a kind of Sn(II) species (I.S., 4.07 mm s^{-1}) at 78 K. The presence of Sn(II) peak suggests that ferrocene may be oxidized by $SnCl_4$ giving ferricinium salt, expressed as $[(Cp)_2Fe^+]_2(SnCl_3^-)(SnCl_5^-)(SnCl_4)(H_2O)_4$ in accord with the elemental analysis data.

Biferrocene, one of the typical binuclear ferrocene derivatives, is also known to react with $HgCl_2$ giving a more stable adduct than that of ferrocene. Biferrocene reacts with $SnCl_4$ in a hexane solution giving green-black paramagnetic precipitates. ^{57}Fe-Mössbauer spectroscopic measurements indicate that there are two kinds of iron atoms, one of which is ferrocene-like (Q.S., 2.26, I.S., 0.50 mm s^{-1}) and the other is ferricinium-like (Q.S., 0.29, I.S., 0.54 mm s^{-1}, at 78 K), showing a trapped-valence state. ^{119}Sn-Mössbauer spectroscopic measurements show that there are three components ascribed to two kinds of Sn(IV) species, ($SnCl_5^-$ and $SnCl_4 \cdot nH_2O$: I.S., 0.86 and 0.22 mm s^{-1} at 78 K, respectively) and to a kind of Sn(II) species ($SnCl_3^-$: I.S., 4.01 mm s^{-1} at 78 K). The spectral shape is similar to that of ferrocene-1.5$SnCl_4(H_2O)_2$. The product is expressed by a formula, (biferrocenium$^+$)$_2(SnCl_3^-)(SnCl_5^-)(SnCl_4)_{1.5}$, based on an elemental analysis.

It is reported that cyclopentadienyl rings are separated by 3.32 Å from each other in ferrocene molecules, and by 3.68 Å in ruthenocene molecules.[10,11] The larger separation of the Cp rings in ruthenocene provides a good explanation for the fact that ruthenocene can easily donate the e_{2g} electrons of the ruthenium atom to a Lewis acid, such as $SnCl_4$, $HgCl_2$, giving a stable coordination compound.[1,2,12]

Recently, the structure of the [2]ferrocenophane was investigated by an X-ray analysis and it was found that the crystals of [2]ferrocenophane are orthorhombic with a=12.444(2), b=19.969(4), c=7.467(1), space group, P_{bca}. The two five-membered rings are tilted 22.2° with respect to one another. The cyclopentadienyl rings are largely separated by 3.60 Å (in maximum) from each other,[13] and this value corresponds to that of ruthenocene (3.68 Å).[11]

[2]Ferrocenophane reacts with a large excess of $SnCl_4$ in dry hexane under the same condition as in the case of ruthenocene-1.5$SnCl_4$, giving an orange-yellow adduct with a formula of [2]ferrocenophane-1.5$SnCl_4(H_2O)$. This adduct is not as stable as the ruthenocene-1.5$SnCl_4$ adduct and its color gradually changes into dark-blue (ferricinium salt) upon standing in air at room temperature for a few hours, while the ruthenocene-1.5$SnCl_4$ adduct keeps its color for several days. The adduct of [2]ferrocenophane with $SnCl_4$ is soluble in *N*,*N*-dimethylformamide giving a solution exhibiting the original absorption spectrum of [2]ferrocenophane. This suggests a dissociation of the adduct into [2]ferrocenophane and $SnCl_4$.

The ^{119}Sn- and ^{57}Fe-Mössbauer spectra of this adduct are illustrated in Figs. 1, and 3, respectively. Anomalously large Q.S. values (3.49 mm s^{-1} at 78 K, 3.40 mm s^{-1} 300 K) are observed for the [2]ferrocenophane-1.5$SnCl_4$ adduct compared with that of [2]ferrrocenophane itself (2.41 mm s^{-1} at 78 K). The anamalously large Q.S. values are good evidence for a direct interaction between Fe and Sn atoms in this adduct, as already verified in the $HgCl_2$, I_2, $CdCl_2$ adducts with [2]ferrocenophane.[3-6]

The ^{119}Sn-Mössbauer spectra of [2]ferrocenophane-1.5$SnCl_4$ (Fig. 1) exhibit two peaks corresponding to two kinds of chemical states of the tin(IV) species (I.S., 0.54 mm s^{-1} and 2.14 at 78 K). Based on the assumption that the recoil-free fraction of both the tin atoms should become approximately equal at lower temperatures, the value of the areal intensity of the lower I.S. component is about two times larger than that of the higher I.S. component at 40 K to 4.2 K. Therefore, it seems reasonable to ascribe the component with higher I.S. (2.14 mm s^{-1}) to (Cp′)$_2$Fe-$SnCl_2$-Fe(Cp′)$_2$-type tin(IV) species and the other broad component with a lower one (I.S., 0.54 mm s^{-1} at 78 K) to a rather ionic $SnCl_5^-$-type tin(IV) species, in the ^{119}Sn-Mössbauer spectroscopic study of ruthenocene-1.5$SnCl_4$ adduct. A similar conclusion is obtained for [2]ferrocenophane-1.5$SnBr_4$ adduct. [2]Ferrocenophane reacts with directly $SnBr_4$ in hexane solution to give orange-yellow precipitates, with a formula of [2]ferrocenophane$(SnBr_4)_{1.5}(H_2O)_3$. Both the [2]ferrocenophane-tin(IV) halide adducts are hygroscopic. The $SnBr_4$ adduct is more hygroscopic than the $SnCl_4$ adduct and its orange-yellow color changes into black in an hour on standing in air at room temperature.

^{57}Fe- and ^{119}Sn-Mössbauer spectroscopic studies on the $SnBr_4$ adduct show an anomalously large quadrupole splitting (3.47 mm s^{-1} at 78 K, see in Fig. 3) for the iron atom and the presence of two kinds of chemical states of tin(IV) atoms (I.S., 0.92 mm s^{-1} for $SnBr_5^-$-type and 2.10 mm s^{-1} for $[(Cp')_2Fe-SnBr_2-Fe(Cp')_2]^{2+}$-type, at 78 K), respectively.

1,1,2,2-Tetramethyl[2]ferrocenophane also reacts with $SnCl_4$, giving an orange-yellow adduct. An anomalously large Q.S. value (3.43 mm s^{-1} at 78 K) is also observed by means of ^{57}Fe-Mössbauer spectroscopy, and two kinds of chemical state of tin(IV) species are found by means of ^{119}Sn-Mössbauer spectroscopy for this adduct.

These ^{119}Sn-Mössbauer results of [2]ferrocenophane–1.5$SnCl_4$ or –1.5$SnBr_4$ adducts are very similar to that of the $SnCl_4$ adduct of ruthenocene. Therefore, these adducts may be expressed as $[(Cp')_2Fe-SnX_2-Fe(Cp')_2]^{2+}(SnX_5^-)_2$, where X=Cl or Br. Similar direct chemical bonds between Fe and Sn atoms (Fe–Sn–Fe) were previously reported in $[Fe(Cp)(CO)_2]_2^{2+}(SnCl_2^{2-})$ by O'Connor and Corey.[14]

The magnetic susceptibility measurement shows that the adducts of [2]ferrocenophane–1.5$SnCl_4$ and –1.5$SnBr_4$ are diamagnetic at temperatures from 78 to 300 K, indicating no possibility of an oxidation of [2]ferrocenophane to a [2]ferrocenophanium cation. However, the color of these adducts gradually changes from orange-yellow to black upon standing at room temperature. These black substances are paramagnetic, probably because [2]ferrocenophane is oxidized by SnX_4 forming [2]ferrocenophanium cations.

On the other hand, [3]ferrocenophane, in which the two Cp rings are slightly inclined to each other (ca., 9°), reacts with $SnCl_4$ giving green-black precipitates. The effective magnetic moment (μ_{eff}) for these precipitates was found to be 2.60 BM; this is a characteristic value for normal ferricinium salts. The ^{57}Fe-Mössbauer spectrum of this salt is shown in Fig. 4-B, where a broad singlet peak is observed (I.S., 0.52 mm s^{-1} at 78 K), and the ^{119}Sn-Mössbauer spectrum (see in Fig. 2-B) also suggests the presence of three types of tin species, ascribed to two kinds of Sn(IV) components (I.S., 0.25 and 0.77 mm s^{-1}, assigned to $SnCl_4 \cdot nH_2O$ and $SnCl_5^-$, respectively) and to a kind of Sn(II) component (I.S., 3.99 mm s^{-1}, assigned to $SnCl_3^-$). The results indicate that the reaction product with [3]ferrocenophane with $SnCl_4$ is expressed as $[(C_5H_4)_2C_3H_6Fe^+]_4(SnCl_3^-)_2(SnCl_5^-)_2(SnCl_4)(H_2O)_6$, in accord with elemental analysis data.

All the results obtained in the present study lead to the conclusion that ruthenocene and [2]ferrocenophanes give adducts with SnX_4, containing coordination bonds between the ruthenium or iron atoms in metallocene and tin atoms. The coordination bonds may be stabilized by a decreased steric hindrance of Cp-rings both in ruthenocene and [2]ferrocenophanes; that is, the longer separation between the Cp-rings both in ruthenocene and [2]ferrocenophane than in ferrocene will make the e_{2g}-electrons of the metallocene easier to be ligated to SnX_4.

Lauher and Hoffmann suggested that the energy levels of frontier orbitals such as e_{2g}, a_{1g}, and e_{1g} in ferrocene depend on the bending angle of the molecule around iron atoms, ∠Cp–Fe–Cp.[15] For instance, one of the split e_{1g} levels goes down while the a_{1g} level and one of the split e_{2g} levels go up, as the angle decreases from 180°. It is not unreasonable to assume that the energy levels cross each other more dramatically if the iron atoms are involved in the ligation to a Lewis acid, giving an increased Q.S. value compared with that of the original [2]ferrocenophane.

References

1) K. R. Mann, W. H. Morrison, Jr., and D. N. Hendrickson, *Inorg. Chem.*, **13**, 1180 (1974).

2) W. H. Morrison, Jr. and D. N. Hendrickson, *Inorg. Chem.*, **11**, 2912 (1972).

3) M. Watanabe, H. Ichikawa, I. Motoyama, and H. Sano, *Bull. Chem. Soc. Jpn.*, **56**, 3291 (1983).

4) M. Watanabe, I. Motoyama, and H. Sano, *J. Radioanal. Nucl Chem. Lett.*, **96**, 585 (1985).

5) H. Sano, M. Watanabe, and I. Motoyama, *Hyperfine Interactions*, **28**, 833 (1986).

6) M. Watanabe, K. Sato, I. Motoyama, and H. Sano, *Chem. Lett.*, **1983**, 1775.

7) M. D. Raush, *J. Org. Chem.*, **26**, 1802 (1961).

8) H. Lenzner and W. H. Watts, *Tetrahedron*, **27**, 4343 (1971).

9) M. B. Laing and K. N. Trueblood, *Acta, Crystallogr.*, **19**, 373 (1965).

10) J. D. Dunitz, L. E. Orgel, and A. Rich, *Acta. Crystallogr.*, **9**, 373 (1956).

11) G. L. Herdgrove and D. H. Templeton, *Acta. Crystallogr.*, **12**, 28 (1959).

12) D. N. Hendrickson, Y. S. Sohn, W. H. Morrison, Jr., and H. B. Gray, *Inorg. Chem.*, **11**, 808 (1972).

13) T. Ito, Private communication.

14) J. E. O'Connor and E. R. Corey, *Inorg. Chem.*, **6**, 968 (1967).

15) J. W. Lauher and R. Hoffmann, *J. Amer. Chem. Soc.*, **98**, 1729 (1976).

The Syntheses, Properties, and Crystal and Molecular Structures of the Lanthanoid Mixed-Complexes of *O,O'*-Diisopropyl Dithiophosphate and Dimethyl Sulfoxide: $[Ln\{(C_3H_7O)_2PS_2\}_3\{(CH_3)_2SO\}_2]$ (Ln=La or Nd), and $[Eu\{(C_3H_7O)_2PS_2\}_2\{(CH_3)_2SO\}_3][Eu\{(C_3H_7O)_2PS_2\}_4]$

Takashi IMAI, Masao NAKAMURA, Kiyofumi NAGAI, Yoshiyuki OHKI,†
Yasuo SUZUKI,† Mamoru SHIMOI, and Akira OUCHI*
Department of Chemistry, College of Arts and Sciences, The University of Tokyo, Komaba, Meguro-ku, Tokyo 153
†Department of Industrial Chemistry, Faculty of Engineering, Meiji University, Higashi-Mita, Tama-ku, Kawasaki, Kanagawa 214
(Received January 6, 1986)

Two types of the mixed complexes indicated in the title have been synthesized, and their crystal and molecular structures of the lanthanum (**1**) and the europium (**2**) complexes have been determined by the X-ray diffraction method. Both **1** and **2** are monoclinic, space group $P2_1/n$, and $Z=4$. **1**, $a=17.354(7)$, $b=23.336(4)$, $c=10.955(2)$ Å, $\beta=96.04(2)°$, final R value calculated from 4870 reflections is 0.069; **2**, $a=29.846(7)$, $b=20.070(3)$, $c=14.057(3)$ Å, $\beta=92.13(2)°$, final R value calculated from 7811 reflections is 0.077. In **1**, the central metal atom is octa-coordinated, and is in a dodecahedral geometry, where all *O,O'*-diisopropyl dithiophosphato ligands (iPr_2dtp) span m-edges of the dodecahedron, chelating through both of the respective sulfur atoms. Dimethyl sulfoxide (dmso) ligands occupy the apexes of the other m-edge. In **2**, the europium(III) metal atom of the cationic species is hepta-coordinated and is in a pentagonal-bipyramidal geometry where two oxygen atoms of dmso ligate from respective ends of the axis and one oxygen atom of the remaining dmso from the equatorial direction. The central metal atom of the anion is octa-coordinated and is in a dodecahedron; where all m-edges are spanned by iPr_2dtp ligands. The solid and the acetonitrile solution of **2** is orange in color due to the charge-transfer band ($\lambda_{max}=415$ nm; $\varepsilon_{max}=1.5\times10^2$ dm^3 mol(Eu)$^{-1}$ cm^{-1}).

In previous papers, some of the present authors have reported on the syntheses and the structures of some mixed complexes of *O,O'*-diisopropyl dithiophosphate (iPr_2dtp), and benzamide (bza),[1,2] *N,N*-dimethylacetamide (dma),[3] or dibutyl sulfoxide.[4] Pinkerton has also published a study about the mixed complexes of *O,O'*-diethyl dithiophosphate (Et_2dtp) and triphenylphosphine oxide (Ph_3PO).[5] It is an interesting fact that, in these complexes sulfur atoms ligate to the central lanthanoid atom tightly in spite of the "hard acid" character of the metal.[6]

Moreover, in a series of the dialkyl dithiophosphates mixed complexes of lanthanoid elements, the molecular structures of the lighter and heavier elements are not the same. For example, in the case of the iPr_2dtp–bza mixed complexes, lanthanum(III), through gadolinium(III), form the $[M(iPr_2dtp)_3(bza)_2]$ types and gadolinium(III), through ytterbium(III), the $[M(iPr_2dtp)_2(bza)_3](ipr_2dtp)$ types.[1,2] In cases of the Et_2dtp–Ph_3PO mixed complexes, the former types are formed for lanthanum(III), through praseodymium(III), and the latter types for the rest of lanthanoid elements.[5]

In order to add such examples, we have tried to synthesize a series of the lanthanoid mixed complexes of iPr_2dtp and dimethyl sulfoxide (dmso) and obtained the two types of the complexes indicated in the title: Type **1** complexes were obtained for lanthanum and neodymium, and Type **2** complexes for europium. As shown in the title formula, a Type 2 complex includes an anionic complex, $[M(iPr_2dtp)_4]^-$, like the dibutyl sulfoxide adduct[4] in place of the free $(R_2dtp)^-$ ion (where R=ethyl or isopropyl), which is found in the R_2dtp–bza or Ph_3PO mixed complexes of the heavier lanthanoids.[2,5]

Another problem regarding the type of complex is the coordination sites of the oxygen atoms. As shown in a dodecahedral iPr_2dtp–dma[3] mixed complex, two oxygen atoms take neighbouring positions on one m-edge of the dodecahedron, which is expected to be the preferable situation because the same kind of the ligating atoms are apt to locate nearer,[7] if no steric hindrance occurs.[3] However, as no other example of the type of complex has been found yet, other than the iPr_2dtp–dma type, this time we tried to synthesize the iPr_2dtp–dmso mixed complexes of lanthanoid elements since dmso is relatively small in size and is polar.

To clarify the above-mentioned problems, we determined the structures of the title complexes by the X-ray diffraction technique using single crystals.

Experimental

Synthesis of Tris(*O,O'*-diisopropyl dithiophosphato)bis(dimethyl sulfoxide)lanthanum(III) (1). The $Na(iPr_2dtp)$ was obtained from phosphorus pentasulfide and 2-propanol by the Livingstone's method used to prepare $Na(Et_2dtp)$.[8] Lanthanum(III) chloride heptahydrate (0.49 g, 1.3 mmol) and $Na(iPr_2dtp)$ (1.27 g, 5.4 mmol) were mixed in 30 cm^3 of 2-propanol and refluxed for 30 min. After cooling, a deposited curdy matter was filtered off, and dmso (0.20 g, 2.6 mmol) was added to the filtrate. After being warmed to about 65 °C for 10 min, the solution was concentrated to about 10 cm^3 using a vacuum rotary

evaporator at about 60 °C. The solution, thus obtained, was left standing at about 5 °C overnight in a refrigerator; the crude product was precipitated. When more dmso was added in the process, no crystals were obtained by this method; even if the standing solution was more concentrated, the sirupy liquid did not become solidified. The crude product was dissolved in benzene (about 30 cm^3) and a little insoluble matter was filtered off. The filtrate was concentrated to about 5 cm^3 by a rotary vacuum evaporator at about 70 °C, and was left standing in a refrigerator (10 °C) for several days; pure crystals precipitated. They were washed with benzene, and dried in a vacuum desiccator on silica gel. Yield, 0.5 g (40%).

The neodymium(III) complex was obtained by the same way from its chloride. Yield from 0.45 g (1.3 mmol) of the metal chloride heptahydrate, 0.9 g (70%). Anal. ($MC_{22}H_{54}O_8P_3S_8$) M, C, H, S. (M=La or Nd).

The Synthesis of [Bis(*O,O'*-diisopropyl dithiophosphato)-tris(dimethyl sulfoxide)europium(III)][tetrakis(*O,O'*-diisopropyl dithiophosphato)europate(III)] (2). Europium(III) chloride hexahydrate (0.61 g, 1.7 mmol) and Na(iPr$_2$dtp) (1.6 g, 6.7 mmol) were dissolved in 25 cm^3 of 2-propanol and refluxed for 20 min. After cooling, the residue was filtered off and was added to the filtrate 0.31 g (0.40 mmol) of dmso. The solution was warmed to 65 °C for about 10 min to complete the reaction and was concentrated to about 5 cm^3 using a rotary vacuum evaporator at about 60 °C. The obtained solution was left standing overnight and the deposited curdy matter was filtered off. When the filtrate was kept in a refrigerator for several days, pure crystals were precipitated. These were separated, washed with 2-propanol, and dried in a vacuum desiccator. Yield, 0.65 g(43%). Anal. ($EuC_{42}H_{102}O_{15}P_6S_{15}$), Eu, C, H, S.

Intensity-Data Collection. Crystals with the dimensions of 0.4×0.3×0.3 mm^3 (all apexes were cut off) (**1**), and of 0.4 mm ϕ in sphere (**2**) were used for the respective measurements. The crystallographic data, some experimental conditions to obtain the intensity data, and the final R values[9] obtained by applying the anisotropic temperature factors are tabulated in Table 1. The reflections were collected on a Rigaku AFC-6A automated four-circle diffractometer with graphite-monochromated Mo $K\alpha$ radiation, the ω-scan technique being employed (scan speed 4° min^{-1}). The intensities were corrected for the Lorentz and polarization factors, but no correction was made for absorption and extinction.

Structure Determination. The structure was solved by the heavy-atom method. The positions of the metal, phosphorus, and sulfur atoms were deduced from a three-dimensional Patterson map; the other non-hydrogen atoms were located successively by the repeated Fourier syntheses. Their positional, isotropic and then anisotropic thermal parameters were refined by the block-diagonal least-squares method using the local version of the UNICS program.[10]

S(8), C(21), and C(22) of a dmso ligand of **1**, and S(17), C(17), C(18), and S(16) of the dmso ligand of **2** are found to be disordered, and are divided into two. Their positions and occupancy factors were refined with the fixed S–C bond length (1.799 Å). Most of the isopropyl groups of the both compounds showed quite large thermal parameters and gave some abnormal bond lengths if refined without any restrictions. We tried to divide them into disordered structures, but failed. Therefore, they were refined with a fixed geometry, assuming O–C, C–C, O···C, and C···C lengths to be 1.41, 1.53, 2.50, and 2.40 Å, respectively. These procedures were carried out by the blocked full-matrix least-squares method using the SHELX-76 program.[11]

Such ambiguity of positions of peripheral alkyl groups is often encountered in a structural determination of lanthanoid(III) O,O'-dialkyl dithiophosphato complexes.[1-5]

All the calculations were carried out on a HITAC M-280H computer at the Computer Center of the University of Tokyo. The atomic scattering factors were taken from the tables.[12]

Other Measurements. The infrared absorption spectra of the samples were obtained by means of a JASCO A202 grating infrared spectrophotometer, using Nujol and hexachloro-1,3-butadiene mull. The visible absorption spectra of the complexes were measured with a Hitachi 124 spectrophotometer.

Table 1. The Crystallographic Data of the Complexes **1** and **2**, as well as Some Experimental Conditions to Obtain Their Intensity Data

1. La(iPr$_2$dtp)$_3$(dmso)$_2$	
$LaC_{22}H_{54}O_8P_3S_8$	F.W. = 934.98
Monoclinic	Space group: $P2_1/n$
$Z=4$	μ(Mo $K\alpha$) = 1.49 mm^{-1}
$a=17.354(7)$ Å	$\beta=96.04(2)°$
$b=23.336(4)$ Å	$U=4412.0(15)$ Å^3
$c=10.955(2)$ Å	$D_m=1.40(3)$, $D_x=1.41$ Mg m^{-3}
Number of reflections measured: 10476	
Reflections used for the calculation: 4870	
Measured range (2θ/°): 3—55	
Scan width (ϕ/°): (1.40+0.5 tan θ)	
Final R value: 0.069	
2. [Eu(iPr$_2$dtp)$_2$(dmso)$_3$][Eu(iPr$_2$dtp)$_4$]	
$EuC_{42}H_{102}O_{15}P_6S_{15}$	F.W. = 1817.99
Monoclinic	Space group: P_{2_1}/n
$Z=4$	μ(Mo $K\alpha$) = 2.00 mm^{-1}
$a=29.846(7)$ Å	$\beta=92.13(2)°$
$b=20.070(3)$ Å	$U=8415(3)$ Å^3
$c=14.057(3)$ Å	$D_m=1.43(3)$, $D_x=1.44$ Mg m^{-3}
Number of reflections measured: 13413	
Reflections used for the calculation: 7811	
Measured range (2θ/°): 3—55	
Scan width (ϕ/°): (1.30+0.5 tan θ)	
Final R value: 0.077	

Results and Discussion

The final atomic parameters of the title complexes are listed in Table 2 (for **1**), and Table 3 (for **2**).[13] Selected bond lengths and bond angles of the complexes are shown in Table 4 (for **1**), and 5 (for **2**). A perspective drawings of the complexes around the respective central metal atoms and the numbering

Table 2. Final Atomic Coordinates ($\times 10^4$) of La(iPr_2dtp)$_3$-(pmso)$_2$ Together with the Equivalent Isotropic Temperature Factors with the Equivalent Isotropic or with the Isotropic Temperature Factors; Estimated Standard Deviations of Them are Shown in Parentheses

Atom	x	y	z	B_{eq}/Å^2 [a]
La	2986.7(3)	7671.6(3)	3058.3(5)	5.5
S(1)	3374(2)	7603(2)	5791(3)	8.0
S(2)	1593(2)	7661(2)	4482(3)	8.9
S(3)	2761(2)	6394(1)	3105(3)	8.2
S(4)	4483(2)	7005(1)	3269(3)	7.0
S(5)	2548(2)	8908(2)	2917(4)	10.5
S(6)	4351(2)	8475(1)	3354(3)	7.8
S(7)	4165(2)	7719(2)	497(3)	9.1
S(8A)[b]	1128(3)	7509(3)	799(4)	9.8
S(8B)[b]	1337(10)	7025(8)	1269(23)	18.5
P(1)	2274(2)	7656(2)	6034(3)	7.0
P(2)	3888(2)	6284(1)	3116(3)	7.1
P(3)	3639(2)	9123(2)	3179(4)	9.3
O(1)	2027(4)	7169(3)	6933(6)	7.5
O(3)	4111(4)	5972(3)	1913(7)	8.3
O(4)	4215(5)	5826(3)	4124(7)	9.0
O(7)	3371(4)	7684(4)	966(6)	7.8
O(8)	1829(4)	7594(4)	1675(7)	8.4
C(1)	1961(7)	6578(5)	6491(12)	8.7
C(2)	1119(7)	6385(7)	6407(15)	11.5
C(3)	2507(8)	6236(6)	7465(13)	10.4
C(7)	3707(7)	5437(5)	1502(12)	8.9
C(8)	4297(10)	4974(6)	1674(14)	12.2
C(9)	3467(14)	5524(7)	198(16)	17.4
C(10)	4100(10)	5880(7)	5429(13)	12.6
C(11)	4812(12)	6139(7)	6152(14)	14.7
C(12)	3941(10)	5247(7)	5799(15)	13.3
C(19)	4224(10)	7115(6)	−431(14)	12.0
C(20)	4045(10)	8261(7)	−699(14)	12.8
Atom	**x**	**y**	**z**	**B_{iso}/Å^2**
O(2)	2238(5)	8210(4)	6885(7)	9.42(2)
O(5)	3936(6)	9456(4)	2044(10)	12.67(3)
O(6)	3924(8)	9605(6)	4151(12)	17.09(4)
C(4)	1518(10)	8410(7)	7195(15)	12.52(5)
C(5)	1602(12)	8613(9)	8531(19)	16.75(7)
C(6)	1246(10)	8910(8)	6353(16)	13.62(5)
C(13)	3539(12)	9948(9)	1570(19)	15.95(6)
C(14)	4098(12)	10457(9)	1645(19)	17.24(7)
C(15)	3228(11)	9843(9)	230(18)	15.19(6)
C(16)	3586(12)	9646(9)	5262(19)	16.17(7)
C(17)	4003(14)	9239(10)	6207(21)	19.18(8)
C(18)	3663(15)	10262(12)	5740(23)	22.22(10)
C(21A)[b]	504(14)	7022(11)	1505(22)	12.64(7)
C(21B)[b]	408(23)	7365(18)	1296(38)	7.86(9)
C(22A)[b]	1385(22)	7024(17)	−369(34)	21.89(13)
C(22B)[b]	1365(29)	6976(23)	−366(46)	11.10(14)

a) The equivalent isotropic temperature factors were computed using the following expression; $B_{eq}=4/3(B_{11}a^2+B_{22}b^2+B_{33}c^2+B_{13}ac\cos\theta)$. The B_{ij}'s are defined by; $T=\exp[-(h^2B_{11}+k^2B_{22}+l^2B_{33}+2klB_{23}+2hlB_{13}+2hkB_{12})]$. b) The probability of the occupancy of each position was as follows: S(8A), C(21A), and C(22A), 70.4; S(8B), C(21B), and C(22B), 29.6%.

scheme of the atoms are shown in Figs. 1 (for **1**), 2, and 3 (for **2**). The schematic presentations to show the configurations of the ligating atoms around the respective metal atoms are shown in Figs. 4 (for **1**), and 5 (for **2**). The crystal packing diagrams of **1** and **2** are shown in Figs. 6 (for **1**), and 7 (for **2**).

Both of the crystals consist of discrete molecules or ions: No bridging is found between them.

In **1**, the lanthanum(III) atom is octa-coordinated and is in a dodecahedral geometry where each iPr_2dtp ligand spans m-edge forming a four-membered chelate ring. Two oxygen atoms of the dmso ligands occupy the apexes of the remaining m-edges. The average deviation of the central metal and the ligating atoms from the respective average trapezium planes is 0.063 Å (the maximum deviation (to O(8)) is 0.119 Å) and the dihedral angle between the two trapezia is 88.2°. The phosphorus atoms of the iPr_2dtp ligands as well as the sulfur atoms of the dmso ligands are also almost on the respective trapezium plane (average deviation of the six phosphorus and two sulfur atoms are 0.144 Å).

The average bond lengths of La–S and La–O of **1** are 3.01(1), and 2.42(3) Å, respectively. These values are comparable to those of La(iPr_2dtp)$_3$(dma)$_2$ (3.02(2), and 2.42(1) Å),[3] and to those of La(Et_2dtp)$_3$(Ph_3PO)$_2$ (3.05(4), and 2.44(2) Å).[5] The expected bond lengths of La–S and LaO are 3.00 and 2.51 Å, respectively, according to Shannon's ionic radii ($r_{La(III)}$ (octa coordinated), $r_{O(2-)}$, and $r_{S(2-)}$ are 1.160, 1.35, and 1.84 Å, respectively).[14] Therefore, compared with the calculated values, the La–S length of **1** is about the same; however, its La–O length is much shorter as was found in La(iPr_2dtp)$_3$(dma)$_2$.[3]

Complex **2** consists of a cationic and anionic species. All the metal atoms are almost on the (101) plane.

In the cation, the central europium(III) atom is hepta-coordinated and is in a pentagonal-bipyramidal geometry where four sulfur atoms of two iPr_2dtp ligands and one oxygen atom of a dmso molecule take the equatorial positions. The dmso oxygen atoms occupy both ends of the axis. The average positional deviations of the central metal and the five equatorially ligated atoms (from their average plane) is 0.069 Å (the maximum deviation is 0.126 Å for O(17)). The respective angles between the axial Eu(1)–O(15) or Eu(1)–O(16) bondings to the average pentagone plane are 88.2 and 88.3°. The average bond lengths of Eu–S and Eu–O are 2.880(8) and 2.249(8) Å, respectively. Although the former value is comparable to the calculated bond length, 2.85 Å, the latter is shorter by 0.11 Å than the sum of Shannon's ionic radii, 2.36 Å ($r_{Eu(III)}$ (hepta-coordinated) is 1.01 Å). The same tendency was observed in the average M–S and M–O bond lengths of the cationic complexes of the same type of geometry, [M(iPr_2dtp)$_2$(bza)$_3$](iPr_2dtp): 2.83(2) and 2.27(2) Å for M=Tb, and

Table 3. Final Atomic Coordinates ($\times 10^4$), and Equivalent Isotropic (above the Line) or Isotropic (below the Line) Temperature Factors of [Eu(iPr$_2$dtp)$_2$(dmso)$_3$][Eu(ipr$_2$dtp)$_4$], with Their Estimated Standard Deviations in Parentheses[a)]

Atom	x	y	z	B_{eq}/Å^2 [b)]	Atom	x	y	z	B_{eq}/Å^2 [b)]
Eu(1)	4197.0(2)	3314.7(4)	6156.5(6)	5.9	O(25)	2848(3)	11129(5)	7243(7)	7.7
S(11)	3894(2)	4546(2)	5293(4)	8.9	O(26)	2594(3)	11200(5)	5647(7)	7.8
S(12)	3877(2)	3118(2)	4210(4)	9.8	O(27)	3125(4)	7041(5)	5048(9)	11.4
S(13)	4310(2)	4383(2)	7504(4)	10.1					
S(14)	4566(2)	2829(2)	7943(4)	9.0	C(1)	2918(8)	3992(13)	3777(18)	15.0
S(15)	5225(2)	4072(2)	5472(4)	10.3	C(2)	2756(9)	3536(13)	2962(18)	15.0
S(16A)[b)]	3072(2)	3255(3)	7114(4)	7.5	C(3)	2582(9)	4558(13)	3895(18)	15.0
S(16B)[b)]	3036(6)	3323(10)	6214(14)	7.9	C(4)	4155(9)	4241(13)	2404(18)	15.0
S(17A)[b)]	4640(4)	1654(6)	5949(10)	15.0	C(5)	4629(9)	3993(13)	2217(18)	15.0
S(17B)[b)]	4440(3)	1697(4)	5121(7)	7.8	C(6)	4047(8)	4846(13)	1773(18)	15.0
P(11)	3795(2)	4081(2)	4084(4)	8.9	C(11)	3807(8)	2917(13)	10148(18)	15.0
P(12)	4534(2)	3747(2)	8455(4)	8.2	C(12)	3482(9)	4007(13)	9606(18)	15.0
O(11)	3339(5)	4261(7)	3567(12)	13.8	C(13)	5724(9)	3828(13)	6140(18)	15.0
O(12)	4131(6)	4426(7)	3369(9)	14.1	C(14)	5439(8)	3921(13)	4310(18)	15.0
O(13)	5009(4)	4032(5)	8854(8)	9.1	O(21)	4373(5)	8481(8)	8109(11)	14.0
O(14)	4256(3)	3741(6)	9396(7)	8.7	O(23)	3580(5)	10023(8)	2546(11)	14.0
O(15)	4883(3)	3527(5)	5628(9)	8.7	O(24)	3600(5)	8868(8)	2596(11)	14.0
O(16)	3495(3)	3146(5)	6621(8)	8.4	O(28)	3543(5)	7069(8)	6559(11)	14.0
O(17)	4366(3)	2239(4)	5858(7)	7.6	C(21)	4804(9)	8192(13)	8161(18)	15.0
C(7)	5249(6)	3706(9)	9624(13)	9.7	C(22)	4782(8)	7491(13)	7734(18)	15.0
C(8)	5654(7)	3374(11)	9133(18)	13.5	C(23)	4968(9)	8152(13)	9203(18)	15.0
C(9)	5403(7)	4281(11)	10312(14)	11.4	C(24)	4417(8)	10351(13)	8557(18)	15.0
C(10)	3822(7)	3463(11)	9390(15)	12.5	C(25)	4232(8)	10446(13)	9488(18)	15.0
C(15)	2658(6)	2797(11)	6520(16)	12.1	C(26)	4839(9)	10642(13)	8424(18)	15.0
C(16)	2916(7)	4080(9)	6779(15)	11.0	C(27)	3622(9)	10712(13)	2726(18)	15.0
C(17A)[b)]	5216(16)	1924(24)	5996(46)	19.0	C(28)	4097(9)	10938(13)	2514(18)	15.0
C(18A)[b)]	4599(21)	1197(25)	4848(42)	24.4	C(29)	3283(8)	11092(13)	2087(18)	15.0
C(17B)[b)]	4694(9)	1072(13)	5745(29)	8.3	C(30)	3937(8)	8627(13)	2008(18)	15.0
C(18B)[b)]	4852(10)	2006(15)	4759(47)	15.5	C(31)	3766(9)	8648(13)	968(18)	15.0
Eu(2)	3511.9(2)	9275.8(3)	5761.0(5)	5.5	C(32)	4052(8)	7909(13)	2287(18)	15.0
S(21)	3594(2)	9132(3)	7799(4)	10.7	C(33)	3153(8)	10979(13)	8123(18)	15.0
S(22)	4429(2)	9469(3)	6453(4)	9.7	C(34)	2839(9)	10722(13)	8827(18)	15.0
S(23)	4096(2)	9563(2)	4202(4)	8.1	C(35)	3356(9)	11671(13)	8361(19)	15.0
S(24)	3022(2)	9339(2)	3966(3)	8.2	C(36)	2540(9)	11110(13)	4655(18)	15.0
S(25)	3525(1)	10707(2)	5863(3)	7.2	C(37)	2641(9)	11765(13)	4149(18)	15.0
S(26)	2663(1)	9811(2)	6328(3)	7.7	C(38)	2058(9)	10896(13)	4408(18)	15.0
S(27)	2878(2)	8209(2)	6114(4)	10.7	C(39)	2969(8)	7226(13)	4127(18)	15.0
S(28)	3877(2)	7980(2)	5362(4)	9.3	C(40)	2456(9)	7216(13)	4081(18)	15.0
P(21)	4251(3)	9195(3)	7710(4)	12.6	C(41)	3146(9)	6735(13)	3400(18)	15.0
P(22)	3584(2)	9480(2)	3326(3)	8.5	C(42)	3302(9)	6709(13)	7233(19)	15.0
P(23)	2903(1)	10724(2)	6278(3)	6.2	C(43)	3456(9)	6926(13)	8237(18)	15.0
P(24)	3327(2)	7557(2)	5766(4)	9.8	C(44)	3391(9)	5963(13)	7110(18)	15.0
O(22)	4490(5)	9615(7)	8522(10)	13.2					

a) The isotropic temperature factors of the atoms below the line were fixed. The equivalent isotropic temperature factors were computed using the following expression: $B_{eq}=4/3(B_{11}a^2+B_{22}b^2+B_{33}c^2+B_{13}ac\cos\theta)$. The B_{ij}'s are defined by: $T=\exp[-(h^2B_{11}+k^2B_{22}+l^2B_{33}+2klB_{23}+2hlB_{13}+2hkB_{12})]$. b) The probability of the occupancy of each position was as follows: S(16A), 77.5; S(16B), 22.5; S(17A), C(17A), and C(18A), 54.4; S(17B), C(17B), and C(18B), 45.6%.

2.80(2) and 2.23(3) Å for M=Er,[2] whereas corresponding bond lengths calculated with Shannon's ionic radii are 2.82, 2.33, 2.78, and 2.29 Å, respectively ($r_{Tb(III)}$ and $r_{Er(III)}$ are 0.98 and 0.945 Å for hepta-coordination).

The equatorial Eu–O bond length (2.260(9) Å) is longer than both of the axial Eu–O ones (2.244(10) Å (both)) in this species, too, as in the case of the other same type of complexes above mentioned.[2]

In the anion, the central metal atom is octa-

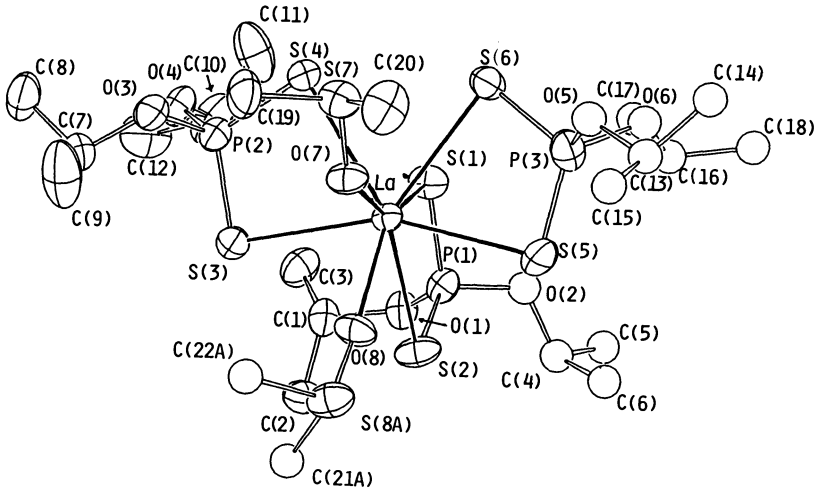

Fig. 1. A perspective drawing of $[La(iPr_2dtp)_3(dmso)_2]$ with the numbering scheme.

Table 4. Selected Bond Lengths and Bond Angles of $La(iPr_2dtp)_3(dmso)_2$ (**1**), with Estimated Standard Deviations in Parentheses

Bond length	l/Å	Bond length	l/Å
La-S(1)	3.002(3)	La-S(2)	3.014(4)
La-S(3)	3.008(3)	La-S(4)	3.014(3)
La-S(5)	2.984(4)	La-S(6)	3.011(3)
La-O(7)	2.454(8)	La-O(8)	2.392(7)
S(1)-P(1)	1.959(5)	S(2)-P(1)	1.966(5)
S(3)-P(2)	1.971(5)	S(4)-P(2)	1.973(5)
S(5)-P(3)	1.950(6)	S(6)-P(3)	1.948(5)
O(7)-S(7)	1.522(8)	O(8)-S(8A)	1.481(9)
O(8)-S(8B)	1.617(20)	P(1)-O(1)	1.592(8)
P(1)-O(2)	1.599(10)	P(2)-O(3)	1.589(9)
P(2)-O(4)	1.596(9)	P(3)-O(5)	1.597(12)
P(3)-O(6)	1.592(15)	S(7)-C(19)	1.747(16)
S(7)-C(20)	1.817(17)		
Bond angle	ϕ/°	**Bond angle**	ϕ/°
S(1)-La-S(2)	65.87(9)	S(1)-La-S(3)	86.91(9)
S(1)-La-S(4)	78.21(8)	S(1)-La-S(5)	97.61(10)
S(1)-La-S(6)	80.49(9)	S(1)-La-O(7)	151.4(2)
S(2)-La-S(3)	82.52(9)	S(2)-La-S(5)	79.67(10)
S(2)-La-O(8)	70.19(18)	S(3)-La-S(4)	66.43(8)
S(3)-La-S(5)	157.86(10)	S(3)-La-O(8)	80.40(18)
S(4)-La-S(6)	69.64(8)	S(5)-La-S(6)	66.20(9)
S(5)-La-O(7)	91.87(20)	S(5)-La-O(8)	81.25(19)
La-S(1)-P(1)	90.75(15)	La-S(2)-P(1)	90.29(14)
La-S(3)-P(2)	89.92(15)	La-S(4)-P(2)	89.70(14)
La-S(5)-P(3)	90.13(18)	La-S(6)-P(3)	89.38(16)
La-O(7)-S(7)	131.4(4)	La-O(8)-S(8A)	176.4(5)
S(1)-P(1)-S(2)	112.9(2)	La-O(8)-S(8B)	128.4(8)
S(3)-P(2)-S(4)	113.5(2)	S(5)-P(3)-S(6)	114.3(2)

coordinated, and is in a dodecahedral geometry, where four iPr_2dtp ligands span all m-edges. The positional deviation of the central metal and four

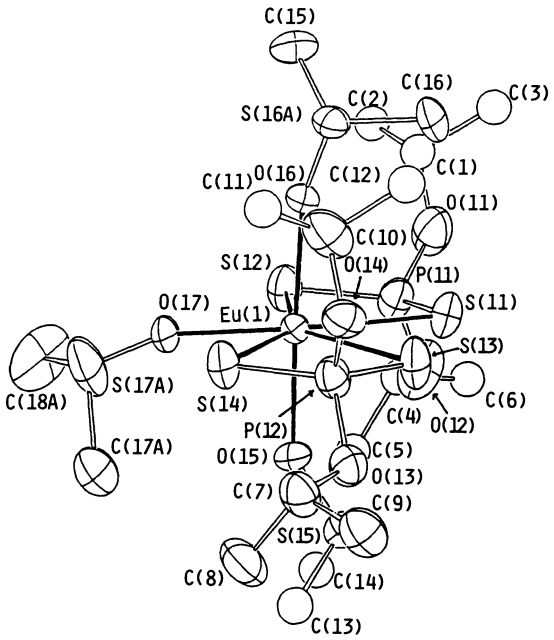

Fig. 2. A perspective drawing of $[Eu(iPr_2dtp)_2(dmso)_3]^+$ in **2** with numbering scheme.

ligating sulfur atoms from the respective plane is 0.025 Å on the average (maximum deviation is 0.045 Å, to S(26)). The dihedral angle between two trapezia is 89.4°. All phosphorus atoms of the iPr_2dtp ligands are also almost on the respective planes: The average deviation of the four phosphorus atom positions from the respective planes is 0.087 Å.

The average Eu-S bond length of this anionic complex is 2.888 Å, which is comparable to the sum of Shannon's ionic radii, 2.91 Å ($r_{Eu(III)}$ (octa-coordinated) is 1.066 Å).

As the pair of P-S bond lengths of each iPr_2dtp ligand are about the same in the anion, the P=S

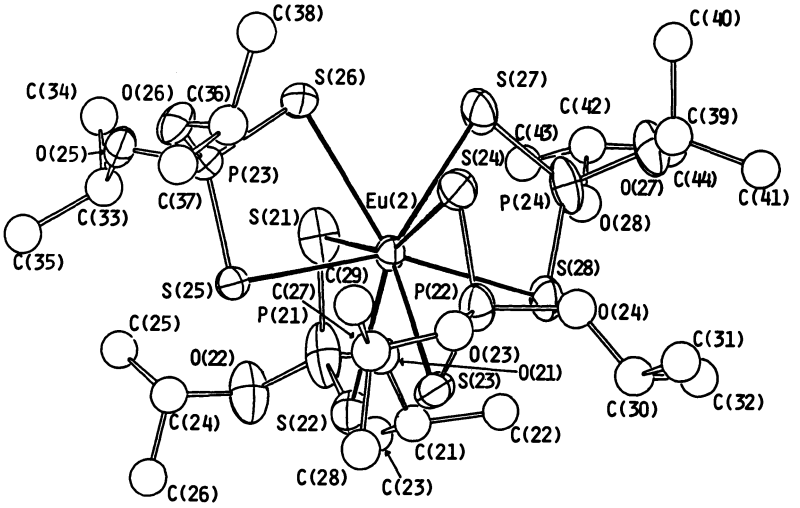

Fig. 3. A perspective drawing of $[Eu(iPr_2dtp_4)]^-$ in **2** with the numbering scheme.

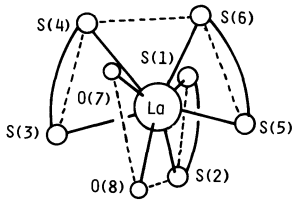

Fig. 4. The schematic presentation of the ligating atom positions around the central metal atom of **1**.

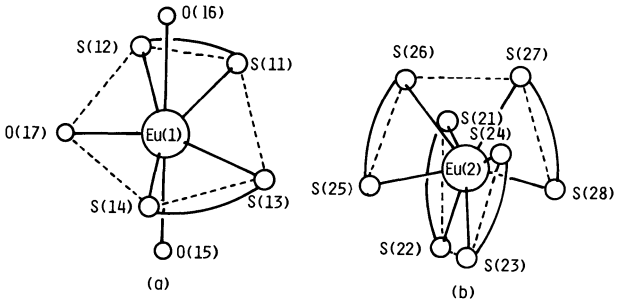

Fig. 5. The schematic presentation of the ligating atom positions around the central metal atoms of the cationic (a), and of anionic (b) complexes of **2**.

double bonds of the ligands are likely delocalized. The lengths of Eu–S of a pair of the sulfur atoms of each ligand are not much different from each other.

The infrared absorption spectral patterns of complexes **1** and **2**, together with those of some related compounds, are shown in Fig. 8. As shown in the figure, the ν(S–O) band of dmso in the 1000—1100 cm^{-1} region of the complex, which is red-shifted compared with that of the free ligand, splits into several peaks, probably due to the variety of the

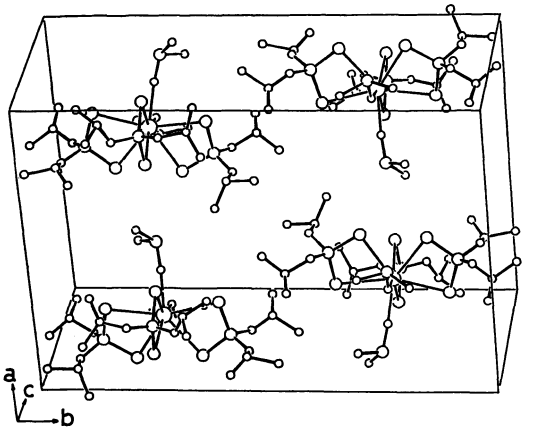

Fig. 6. The crystal packing diagram of **1**.

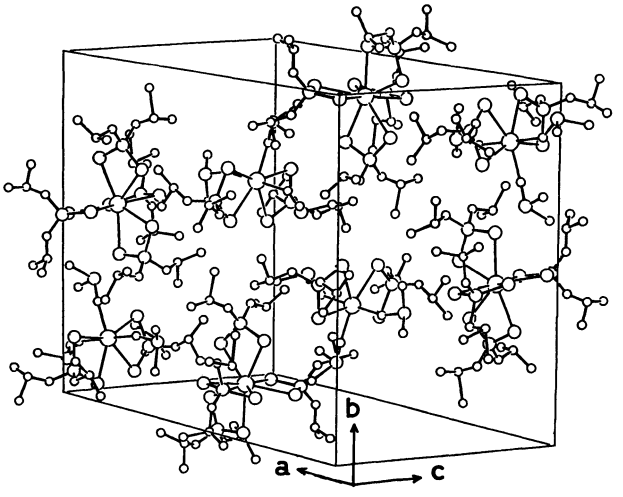

Fig. 7. The crystal packing diagram of **2**.

Table 5. Selected Bond Lengths and Bond Angles of $[Eu(iPr_2dtp)_2(dmso)_3][Eu(iPr_2dtp)_4]$ (**2**), with Estimated Standard Deviations in Parentheses

Bond length	l/Å	Bond length	l/Å
Eu(1)-S(11)	2.883(5)	Eu(1)-S(12)	2.891(6)
Eu(1)-S(13)	2.872(5)	Eu(1)-S(14)	2.874(6)
Eu(1)-O(15)	2.244(10)	Eu(1)-O(16)	2.244(10)
Eu(1)-O(17)	2.260(9)	S(11)-P(11)	1.952(8)
S(12)-P(11)	1.956(7)	S(13)-P(12)	1.948(8)
S(14)-P(12)	1.981(7)	S(15)-O(15)	1.520(11)
S(16A)-O(16)	1.478(12)	S(16B)-O(16)	1.51(2)
S(17A)-O(17)	1.433(15)	S(17B)-O(17)	1.523(15)
Eu(2)-S(21)	2.880(6)	Eu(2)-S(22)	2.898(5)
Eu(2)-S(23)	2.908(5)	Eu(2)-S(24)	2.872(5)
Eu(2)-S(25)	2.877(4)	Eu(2)-S(26)	2.890(4)
Eu(2)-S(27)	2.911(5)	Eu(2)-S(28)	2.882(5)
S(21)-P(21)	1.975(10)	S(22)-P(21)	1.942(10)
S(23)-P(22)	1.933(7)	S(24)-P(22)	1.955(8)
S(25)-P(23)	1.967(6)	S(26)-P(23)	1.968(6)
S(27)-P(24)	1.949(8)	S(28)-P(24)	1.949(8)
Bond angle	**ϕ/°**	**Bond angle**	**ϕ/°**
S(11)-Eu(1)-S(12)	68.37(15)	S(13)-Eu(1)-S(14)	69.21(15)
O(17)-Eu(1)-S(12)	76.2(3)	O(17)-Eu(1)-S(14)	76.0(3)
S(11)-Eu(1)-S(13)	70.44(14)	O(16)-Eu(1)-O(17)	97.3(3)
O(16)-Eu(1)-S(12)	88.6(3)	O(16)-Eu(1)-S(11)	88.3(3)
O(16)-Eu(1)-S(13)	90.5(3)	O(16)-Eu(1)-S(14)	91.5(3)
O(15)-Eu(1)-O(17)	84.7(4)	O(15)-Eu(1)-S(12)	89.2(3)
O(15)-Eu(1)-S(11)	88.5(3)	O(15)-Eu(1)-S(13)	89.5(3)
O(15)-Eu(1)-S(14)	91.7(3)	O(15)-Eu(1)-O(16)	176.6(4)
S(21)-Eu(2)-S(22)	68.60(16)	S(23)-Eu(2)-S(24)	68.22(15)
S(25)-Eu(2)-S(26)	67.98(11)	S(27)-Eu(2)-S(28)	67.81(14)
S(22)-Eu(2)-S(23)	68.98(14)	S(26)-Eu(2)-S(27)	69.21(14)
S(21)-Eu(2)-S(24)	154.13(17)	S(25)-Eu(2)-S(28)	154.99(12)
Eu(1)-S(11)-P(11)	89.6(2)	Eu(1)-S(12)-P(11)	89.3(2)
Eu(1)-S(13)-P(12)	89.6(2)	Eu(1)-S(14)-P(12)	88.9(2)
Eu(1)-O(15)-S(15)	144.3(7)	Eu(1)-O(16)-S(16A)	159.6(6)
Eu(1)-O(16)-S(16B)	134.4(10)	Eu(1)-O(17)-S(17A)	153.7(8)
Eu(1)-O(17)-S(17B)	147.9(7)	Eu(2)-S(21)-P(21)	88.8(3)
Eu(2)-S(22)P-(21)	88.9(3)	Eu(2)-S(23)-P(22)	89.0(2)
Eu(2)-S(24)-P(22)	89.6(2)	Eu(2)-S(25)-P(23)	91.20(18)
Eu(2)-S(26)-P(23)	90.78(19)	Eu(2)-S(27)-P(24)	89.6(3)
Eu(2)-S(28)-P(24)	90.5(3)		

coordination situations. The peak of **2** is broader than that of **1**. The ν_{as}(P-S) band appeared in 600—700 cm^{-1} region of **2**, splits into three peaks, while that of **1** into two peaks. The isostructural neodymium(III) complex shows almost the same infrared spectral pattern as that of **1**.

As in the case of $Eu(iPr_2dtp)_3(bza)_2$,[1] complex **2** is orange in color due to a charge-transfer band in both its solid and its acetonitrile-solution. The absorption spectra of the solution of **2**, as well as those of some other europium(III) complexes , are shown in Fig. 9. As shown in the figure, although the wavelength with maximum absorption of the band of **2** is about the same as that of $Na[Eu(iPr_2dtp)_4]$, or of $Eu(iPr_2dtp)_3(bza)_2$ (about 415 nm),[1] the absorpion coefficient of **2** at the wavelength, 1.5×10^2 dm^3 $mol(Eu)^{-1}$ cm^{-1}, is much smaller than those of the other europium complexes above mentioned.[1]

The authors are greatly obliged to the Shin-Etsu Chemical Ind. Co., Ltd., for aiding this study by presenting highly pure lanthanoid oxides. The

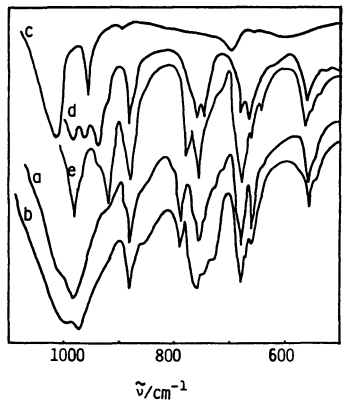

Fig. 8. Infrared absorption spectra of **1**, **2**, and some related compounds. (a), $[La(iPr_2dtp)_3(dmso)_2]$; (b), $[Eu(iPr_2dtp)_2(dmso)_3][Eu(iPr_2dtp)_4]$; (c), dmso; (d), $Na(iPr_2dtp)$; (e), $Na[La(iPr_2dtp)_4]$.

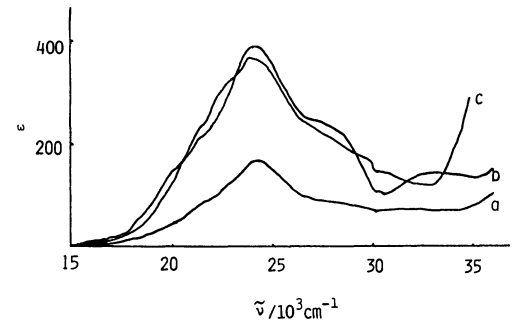

Fig. 9. The absorption spectra of **2** and some related complexes in acetonitrile solutions. (a), $[Eu(iPr_2dtp)_2(dmso)_3][Eu(iPr_2dtp)_4]$; (b), $Na[Eu(iPr_2dtp)_4]$; (c), $[Eu(iPr_2dtp)_3(bza)_2]$. The concentration of [Eu(III)] is 0.01—0.001 mol dm^{-3}.

present work was partially supported by a Grant-in-Aid for Scientific Research (No. 57430011) from the Ministry of Education, Sciences and Culture.

References

1) R. Nakamura, K. Nagai, M. Shimoi, and A. Ouchi, *Bull. Chem. Soc. Jpn.*, **57**, 2919 (1984).

2) K. Nagai, R. Nakamura, M. Shimoi, and A. Ouchi, *Bull. Chem. Soc. Jpn.*, **57**, 2725 (1984).

3) K. Nagai, Y. Sato, S. Kondo, and A. Ouchi, *Bull. Chem. Soc. Jpn.*, **56**, 2605 (1983).

4) Y. Ohki, M. Nakamura, Y. Suzuki, K. Nagai, M. Shimoi, and A. Ouchi, *Bull. Chem. Soc. Jpn.*, **58**, 1593 (1985).

5) A. A. Pinkerton and D. Schwarzenbach, *J. Chem. Soc., Dalton Trans.*, **1976**, 2466.

6) R. G. Pearson, *J. Chem. Educ.*, **45**, 581, 643 (1968).

7) M. E. Silver, H. K. Chun, and R. C. Fay, *Inorg. Chem.*, **21**, 3765 (1982).

8) S. E. Livingstone and A. E. Mihkelson, *Inorg. Chem.*, **9**, 2545 (1970).

9) $R=\Sigma||F_o|-|F_c||/\Sigma|F_o|$

10) "Universal Crystallographic Computation Program System (UNICS)," ed by T.Sakurai, Crystallographic Society of Japan, Tokyo (1967).

11) G. M. Sheldrick, "SHELX-76. A program for crystal structure determination," University of Cambridge, Cambridge, England, U.K. (1976).

12) "International Tables for Crystallography," Kynoch Press, Birmingham (1974), Vol. IV, pp. 72, 150.

13) The final thermal parameters and the final F_o-F_c table are deposited as Document No. 8628 at the Office of the Editor of Bull. Chem. Soc. Jpn.

14) R. D. Shannon, *Acta Crystallogr., Sect. A*, **32**, 751 (1976).

 © 1986 The Chemical Society of Japan Bull. Chem. Soc. Jpn., 59, 2123—2128 (1986)

Isomerism of the Metal Complexes Containing Multidentate Ligands. X. $[CoN_6]^{3+}$-Type Complexes Containing $H_2N(CH_2CH_2NH)_nH$ (n=0—4)

Yuzo Yoshikawa,* Nobuyuki Kato, Yuito Kimura, Shunji Utsuno,† and Gopal N. Natu††

Department of Chemistry, Faculty of Science, Nagoya University, Chikusa-ku Nagoya 464

†Department of Chemistry, Faculty of Science, Shizuoka University, Oya, Shizuoka 422

††Department of Chemistry, University of Poona, Pune 411 007, India

(Received January 7, 1986)

The preparation, separation, and characterization of isomeric complexes of type $[CoN_6]^{3+}$, containing one, two, or three molecules of NH_3, en, dien, trien, and tetren (n=0, 1, 2, 3, and 4, respectively for $H_2N(CH_2CH_2NH)_nH$) are reported. All the possible five stereoisomers for $[Co(NH_3)(en)(dien)]^{3+}$ and six stereoisomers for $[Co(en)(trien)]^{3+}$ have been successfully isolated, but only three of four possible geometrical isomers could be obtained for $[Co(NH_3)(tetren)]^{3+}$. These were characterized by electronic, circular dichroism (CD), and $^{13}C\{^1H\}$ NMR spectroscopy. Conformational analyses were, also, carried out and the stability, or formation of each isomer at the equilibrium state, is discussed from the calculated strain-energy data and experimental formation ratios.

Linear polyamines, $H_2N(CH_2CH_2NH)_nH$ (n=1—5)[1] coordinate to metal ions and the resulting coordination compounds contain only the five-membered chelate rings which are the most frequently found in metal complexes. Table 1 lists all the complexes of $[CoN_6]^{3+}$-type containing the polyamine ligand(s) and NH_3 (n=0).

Presently we are reporting the isomerism of the complexes, V, VI, IX, and X (Table 1). In the course of this study, the structures of both the geometrical isomers of $[Co(NH_3)_3(dien)]^{3+}$ have been determined by three-dimensional X-ray analysis.[6] The $^{13}C\{^1H\}$ NMR spectrum of the mer isomer was also reported.[12] The isomers of the complex, $[Co(NH_3)(en)(dien)]^{3+}$ are newly prepared in the present study. $[Co(NH_3)_2(trien)]^{3+}$ and $[Co(NH_3)(tetren)]^{3+}$ were prepared by Basolo[8] and Schlessinger,[13] respectively. $[Co(en)(trien)]^{3+}$ was studied by Schaefer and Brubaker.[10] However, all of their isomers were not isolated in these studies. Recently, we succeeded in isolating not only the six cis isomers, but also all of the three possible trans isomers of $[Co(NH_3)_2(trien)]^{3+}$.[9]

Isolation of each isomer was mainly performed by column chromatography on Sephadex ion exchanger.[14] The empirical elution rules that we reported,[15] were often effectively used for the assignment of geometrical isomers.

Experimental

Materials. The amines, $H_2N(CH_2CH_2NH)_nH$ (n=1—4) were obtained from Wako Pure Chemical Industries, LTD. and all other chemicals commercially available were used without further purification unless otherwise stated.

(i) $[Co(NH_3)_3(dien)]X_3$: To 25 cm^3 of a 3 M (=mol dm^{-3}) aqueous ammonia solution, 1.3 g of *mer*-$[CoCl_3(dien)]$,[16] 5 g of NH_4Cl, and 0.2 g of activated charcoal were added, and the mixture was stirred for 2 h. The activated charcoal

Table 1. Isomers of $[CoN_6]^{3+}$-Type Complexes Containing $H_2N(CH_2CH_2NH)_nH$ (n=0—5)

	Complexes	Number of Geometrical Isomers[a]	Number of Optical Isomers	Total Number of Isomers	Ref.
I.	$[Co(NH_3)_6]^{3+}$	1	0	1	2
II.	$[Co(NH_3)_4(en)]^{3+}$	1	0	1	3
III.	$[Co(NH_3)_2(en)_2]^{3+}$	2	1	3	4
IV.	$[Co(en)_3]^{3+}$	1	1	2	5
V.	$[Co(NH_3)_3(dien)]^{3+}$	2	0	2	6
VI.	$[Co(NH_3)(en)(dien)]^{3+}$	4	1	5	This work
VII.	$[Co(dien)_2]^{3+}$	3	2	5	7
VIII.	$[Co(NH_3)_2(trien)]^{3+}$	5	4	9	8, 9
IX.	$[Co(en)(trien)]^{3+}$	3	3	6	8, 10
X.	$[Co(NH_3)(tetren)]^{3+}$	8	7	15	This work
XI.	$[Co(linpen)]^{3+}$	8	8	16	11

a) All the possible existent conformational isomers, based on the configuration about a secondary amine nitrogen are included.

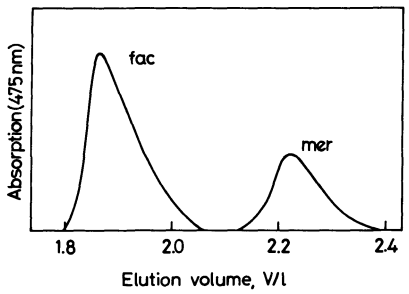

Fig. 1. Elution curve of $[Co(NH_3)_3(dien)]^{3+}$. ϕ2.7×140 cm SP-Sephadex (C-25); 0.18 M Na_2SO_4.

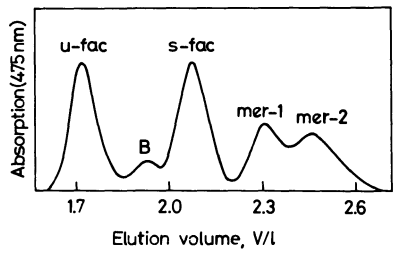

Fig. 2. Elution curve of $[Co(NH_3)(en)(dien)]^{3+}$. ϕ2.7×140 cm SP-Sephadex (C-25); 0.18 M Na_2SO_4.

was filtered off and the filtrate was acidified with hydrochloric acid. The resulting solution was diluted with a large amount of water and passed over a pre-column of SP-Sephadex (C-25).[14] A portion of the SP-Sephadex charged with the product was poured on the top of an SP-Sephadex column (ϕ2.7×140 cm) and the adsorbed complexes were eluted with 0.18 M Na_2SO_4. The elution curve is shown in Fig. 1. The effluents of two elution bands were separately collected and diluted with 0.01 M HCl about twenty times, and then each diluted solution was passed through a short column of SP-Sephadex previously conditioned with 1 M HCl and the complex was adsorbed on it. After the adsorbed column being washed with a large amount of 0.01 M HCl to remove sodium ions, the complex isomer was eluted with 1 M HCl. The chlorides of the complex were obtained by evaporating the eluate to dryness under reduced pressure, over P_2O_5 and NaOH.

(ii) $[Co(NH_3)(en)(dien)]X_3$: (*a*) To 25 cm^3 of a 0.5 M aqueous ammonia solution, 1.5 g of *s-fac*-$[CoCl(en)(dien)]Cl_2$,[17] 5 g of NH_4Cl, and 0.2 g of activated charcoal were added, and the suspension was stirred for 12 h.

(*b*) Using *mer*-$[CoCl_3(dien)]$ as a starting material: The mixture of 0.52 g of *mer*-$[CoCl_3(dien)]$, 0.26 g of en·2HCl, and 10 cm^3 of a 0.5 M aqueous ammonia solution was stirred for 48 h with 0.05 g of activated charcoal. The reaction products were processed in a similar manner a in (*i*). The resulting elution curves are shown in Fig. 2. The u-fac isomer was separated into two bands by elution with a 0.15 M sodium (+)tartratoantimonate(III) solution. The chlorides of each isomer were obtained as in (*i*). The B band is that of *fac*-$[Co(NH_3)_3(dien)]^{3+}$.

(iii) $[Co(en)(trien)]X_3$: $[Co(en)(trien)]Cl_3$ was prepared from $[CoCl_2(trien)]Cl$ and ethylenediamine, following the method of Schaefer and Brubaker.[10] The resulting

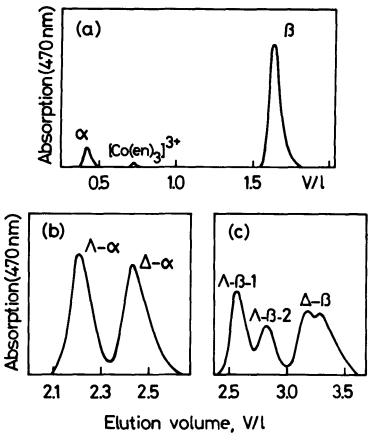

Fig. 3. Elution curves of $[Co(en)(trien)]^{3+}$. ϕ2.7×130 cm SP-Sephadex (C-25); (a) 0.1 M Na_3PO_4, (b) 0.18 M sodium (+)tartrate, (c) 0.13 M sodium (+)tartratoantimonate(III).

solution of the chloride mixture was subjected to SP-Sephadex chromatography (Fig. 3a). The α isomer easily isomerizes to the β isomers in an alkaline solution. Each isomer was resolved as shown in Fig. 3b and c. The two optically active β isomers could be more effectively isolated from each pure *racemic* β isomer, which was previously separated from each other by recycling chromatography using a mixture of 0.15 M Na_2SO_4 and 0.01 M HCl as eluent.

(iv) $[Co(NH_3)(tetren)]X_3$: (*a*) $[Co(NH_3)(tetren)]Cl_3$ was prepared from $[CoCl(NH_3)_5]Cl_2$ and tetren·5HCl, as described below. The ligand hydrochloride was purified twice by recrystallization from water. To 20 cm^3 of concentrated aqueous ammonia solution containing 2.5 g of $[CoCl(NH_3)_5]Cl_2$,[18] 4.3 g of tetren·5HCl and 0.5 g of activated charcoal were added, and the mixture was stirred for 15 h. The filtrate was diluted with 0.01 M HCl and passed through an SP-Sephadex column. The elution curve is shown in Fig. 4a, where the A, C-1, and C-2 bands were assigned to those of the isomers of $[Co(NH_3)(tetren)]^{3+}$ from their $^{13}C\{^1H\}$ NMR spectra and the others to those of impurities. These C-1 and C-2 bands were not separated by the elution with a neutral or basic eluent. The C-2 isomer formed also by the isomerization of the C-1 in an aqueous solution, but it was difficult to obtain purely because of its low formation ratio and low stability. The optical resolution of the C-1 isomer was attained by elution with 0.15 M sodium (+)tartratoantimonate(III) in a similar manner as in Fig. 3b.

(*b*) $[CoCl(tetren)](ClO_4)_2$[19] was allowed to react with liquid ammonia. Since only one geometrical isomer (C in the preceding (*a*)) could be obtained from "α-$[CoCl(tetren)](ClO_4)_2$,"[19] the following compound was used as starting material in order to get other isomers. The filtrate, in Method B of House and Garner,[19] after removing the first precipitated tetrachlorozincate(II) salt was allowed to stand for a month. The additionally formed tetrachlorozincate(II) crystals were changed to the perchlorate salt. To about 20 cm^3 of liquid ammonia, 1 g of the perchlorate was added. The excess ammonia was allowed to evaporate (slowly) at room temperature. An aqueous solution of the

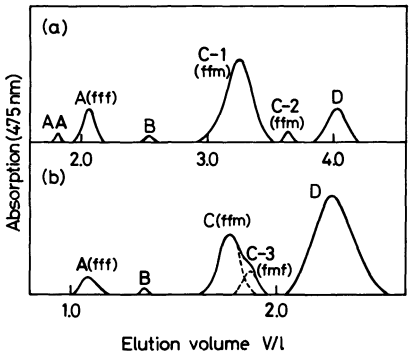

Fig. 4. Elution curves of $[Co(NH_3)(tetren)]^{3+}$ from different origin. $\phi 2.7 \times 140$ cm SP-Sephadex (C-25); (a) 0.15 M Na_2SO_4–0.01 M HCl, (b) 0.18 M Na_2SO_4.

orange residue was passed through an SP-Sephadex column (Fig. 4b). In Fig. 4b, the B and D bands are those of impurities. The C-3 isomer was completely separated into two portions by the elution with a 0.15 M sodium (+)tartratoantimonate(III) solution.

(*c*) The reaction of $[Co(NO_3)(NH_3)_5](NO_3)_2$ with tetren in DMSO (70—80 °C), and the reaction of $[CoCl(tetren)]ZnCl_4$ with ammonia in the presence of NH_4Cl and activated charcoal in an aqueous solution, were also used. Their chromatograms were similar to that in Fig. 4a.

Physical Measurements. Absorption spectra were obtained with a Union Giken SM 401 spectrophotometer equipped with a 1 cm quartz cell at 25 °C. The sample solutions contained the complex ions in 10^{-3}—10^{-2} M concentrations. CD spectra were measured for an approximately 10^{-3} M solution of each isomer in 0.01 M HCl, with a JASCO model J-20 or J-40 spectropolarimeter using a 1 cm cell. $^{13}C\{^1H\}$ NMR spectra were recorded on a JEOL JNM-FX60 spectrometer at a probe temperature of 35 °C. The solvent used was a 0.01 M HCl solution. Dioxane in D_2O in a coaxial inner tube was used as an external reference for all samples.[20]

Identification of Compositions. $^{13}C\{^1H\}$ NMR spectra were measured for the prepared metal complexes. The expected number of carbon atoms and/or the symmetry of the isomer was confirmed from their relative intensities of carbon signals. Elemental analyses were also performed for the hexacyanocobaltates of newly isolated isomers, which could be easily isolated from the solution due to their low solubilities. The agreement between the calculated and found values was within the usual limit of variation of elemental analysis.

Results and Discussion

Figures 5—8 show the possible geometrical and conformational isomers of the complexes, V, VI, IX, and X. The two isomers of $[Co(NH_3)_3(dien)]^{3+}$, the s-fac and two mer isomers of $[Co(NH_3)(en)(dien)]^{3+}$, and the fff isomer of $[Co(NH_3)(tetren)]^{3+}$ have plane-symmetric, that is, nonresolvable structures, but the others can be resolved into their optical isomers. As can be seen from Figs. 1—4, we could isolate all the

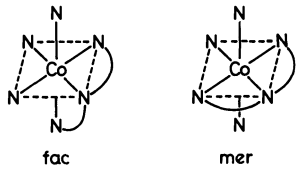

Fig. 5. Possible geometrical isomers of $[Co(NH_3)_3(dien)]^{3+}$.

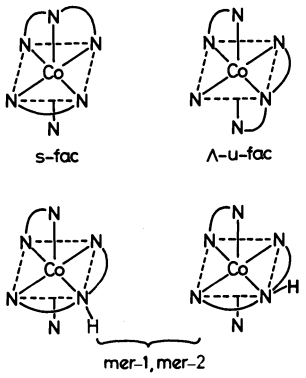

Fig. 6. Possible geometrical and conformational isomers of $[Co(NH_3)(en)(dien)]^{3+}$.

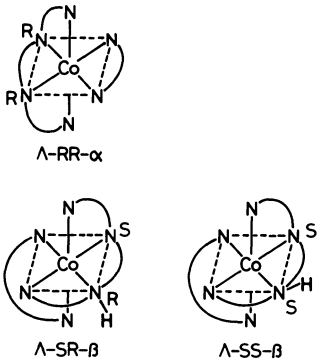

Fig. 7. Possible geometrical and conformational isomers of $[Co(en)(trien)]^{3+}$.

possible number of stereoisomers, i.e., 2, 5, and 6 for $[Co(NH_3)_3(dien)]^{3+}$, $[Co(NH_3)(en)(dien)]^{3+}$, and $[Co(en)(trien)]^{3+}$, respectively, but only three of four possible geometrical isomers of $[Co(NH_3)(tetren)]^{3+}$. All the four fmm conformational isomers, which were different in the configuration of two secondary nitrogen atoms in the center of the meridional structures, could not be isolated in the present study. The structure of each isomer was assigned mainly on the basis of the elution order[15] and $^{13}C\{^1H\}$ NMR spectrum.

The empirical elution rules predict that the complex isomer with higher ability to associate with eluent anions is eluted faster than the other(s).

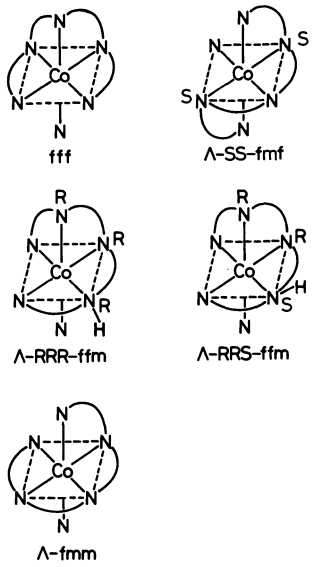

Fig. 8. Geometrical and conformational isomers of [Co(NH$_3$)(tetren)]$^{3+}$.
The absolute configuration, *R* or *S* of the central nitrogen atom of tetren in the ffm isomers, was determined assuming that the priority[24] of the *facial* structure as substituent is higher than that of the *meridional* structure. All the four possible existent conformational isomers were abbreviated for the fmm structure.

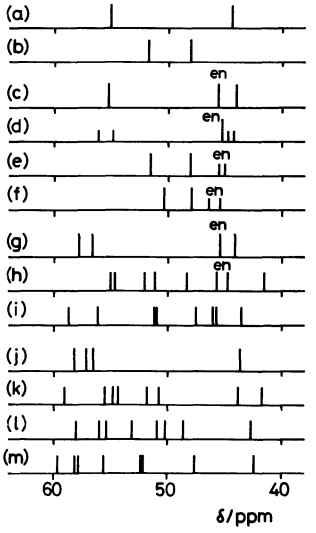

Fig. 9. Diagramatic representation of the $^{13}C\{^1H\}$ NMR spectra of $[CoN_6]^{3+}$-type complex isomers. (a) *fac*-; (b) *mer*-[Co(NH$_3$)$_3$(dien)]Cl$_3$; (c) *s-fac*-; (d) *u-fac*-; (e) *mer-1*-; (f) *mer-2*-[Co(NH$_3$)(en)(dien)]Cl$_3$; (g) α-; (h) β-1-; (i) β-*2*-[Co(en)(trien)]Cl$_3$; (j) *fff*-; (k) *fmf*-; (l) *ffm*(C-1)-; (m) *ffm*(C-2)-[Co(NH$_3$)(tetren)]Cl$_3$. The signals with "en" are those of ethylenediamine.

Therefore, it can be easily explained that the fac of [Co(NH$_3$)$_3$(dien)]$^{3+}$ (Fig. 1), the u-fac and then the s-fac of [Co(NH$_3$)(en)(dien)]$^{3+}$ (Fig. 2), the α of [Co(en)(trien)]$^{3+}$ (Fig. 3), and the fff isomer of [Co(NH$_3$)(tetren)]$^{3+}$ (Fig. 4), elute faster than the other isomers with meridional structures.

Figure 9 shows the diagramatic representation of $^{13}C\{^1H\}$ NMR spectra of all the present isomers. Since the aforementioned isomers including *mer*-[Co(NH$_3$)(en)(dien)]$^{3+}$ (C_s symmetry), and α-[Co(en)(trien)]$^{3+}$ (C_2 symmetry), have two equivalent carbons, the number of the NMR signals is reduced to one-half of that of the other asymmetric isomers. The two carbon atoms of ethylenediamine in *mer*-[Co(NH$_3$)(en)(dien)]$^{3+}$ are not equivalent and therefore show two different signals at the corresponding magnetic field. In general, the NMR signal of the carbon adjacent to a primary nitrogen atom appears at higher magnetic field than those adjacent to a secondary nitrogen atom.[21] This tendency is more pronounced in the fac configuration than in the mer, because of the less-strained valence angles about the secondary nitrogen atom of the former. Thus such isomeric structures are easily distinguished with each other in terms of the NMR signals.

The structures of the two β-[Co(en)(trien)]$^{3+}$ isomers, β-*1* and β-*2*, were assigned to (*Λ-SS,Δ-RR*) and (*Λ-SR,Δ-RS*), respectively, by comparison of their NMR signals with those of *cis*-β-[Co(NH$_3$)$_2$-(trien)]$^{3+}$.[8] The spectra of the C-1 isomer in Fig. 4a was very similar to that of (*Λ-RRS,Δ-SSR*)-*ffm*-[CoCl(tetren)](ClO$_4$)$_2$, the structure of which was determined by X-ray analysis.[22] Therefore, the C-1 was assigned to the above structure and the C-2 to (*Λ-RRR,Δ-SSS*)-ffm structure. The optical resolution of these isomers is consistent with assignment to the resolvable structures.

The data of absorption spectra in the visible region are summarized in Table 2 together with those of CD spectra (Fig. 10) of the optically active isomers. The positions of the first and second absorption maxima of the complexes are normal as those for the $[CoN_6]^{3+}$-type ones. The molar extinction coefficients, ε of the isomers with *meridional* structure are larger than those of the *facial* ones. It may be attributed to the distorsion from a regular octahedron in mer isomers. The absolute configurations of the optically active isomers were assigned according to the sign of the dominant CD component at the first absorption band region, that is, the plus sign to the *Λ* configuration.

Table 3 shows the results of the conformational analysis for all the possible isomers of the relevant complexes. The strain-energy minimization calculation was carried out by using a modification of the computer program of Boyd.[9b,23] A tendency, that fac isomers or structures are less-strained in angle bending and more-strained in torsional interaction

than mer ones, can be seen for the isomers except $[Co(NH_3)(tetren)]^{3+}$. Among the isolated isomers of each complex, there is a good correlation between the formation ratio and the strain energy, considering the statistical effects on some configurational structures. The strain-energy differences are rather small among the isomers of the complexes, the entire set of isomers of which could be isolated from the reaction mixtures.

Unambiguous assignment of the *mer*-$[Co(NH_3)(en)(dien)]^{3+}$ was difficult to make either from the conformational analysis, or from the elution order, or from the $^{13}C\{^1H\}$ NMR spectroscopy.

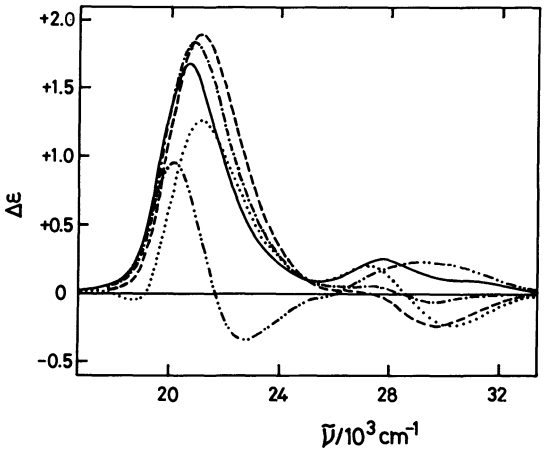

Fig. 10. Circular dichroism spectra of *Λ-u-fac*-$[Co(NH_3)(en)(dien)]^{3+}$(—··—), *Λ(SS)-β-1*-$[Co(en)(trien)]^{3+}$(—·—), *Λ(SR)-β-2*-$[Co(en)(trien)]^{3+}$(----), *Λ(SS)-fmf*-$[Co(NH_3)(tetren)]^{3+}$(——), and *Λ(RRS)-ffm*-$[Co(NH_3)(tetren)]^{3+}$(····).

Table 2. Absorption and CD Spectral Data

Complexes	Absorption		CD	
	$\tilde{\nu}$/cm^{-1}	ε	$\tilde{\nu}$/cm^{-1}	$\Delta\varepsilon$
fac-$[Co(NH_3)_3(dien)]^{3+}$	21140	82		
	29500	70		
mer-$[Co(NH_3)_3(dien)]^{3+}$	21190	105		
	29240	79		
s-fac-$[Co(NH_3)(en)(dien)]^{3+}$	21190	95		
	29540	85		
u-fac-$[Co(NH_3)(en)(dien)]^{3+}$	21410	75	20120	+0.96
(*Λ*)	29590	65	22680	−0.35
			29330	+0.22
mer-1-$[Co(NH_3)(en)(dien)]^{3+}$	21370	113		
	29370	86		
mer-2-$[Co(NH_3)(en)(dien)]^{3+}$	21280	111		
	29150	80		
α-$[Co(en)(trien)]^{3+}$	21370	88	20370	+2.42
(*Λ-RR*)	29590	82	22990	−0.53
			28330	+0.56
β-1-$[Co(en)(trien)]^{3+}$	21320	123	20880	+1.84
(*Λ-SS*)	29410	99	27170	+0.05
			29590	−0.06
β-2-$[Co(en)(trien)]^{3+}$	21140	135	21140	+1.81
(*Λ-SR*)	29330	113	29590	−0.23
fff-$[Co(NH_3)(tetren)]^{3+}$	21190	80		
	29410	61		
ffm-$[Co(NH_3)(tetren)]^{3+}$	21100	126	17120	+0.02
(*Λ-RRS*, C-1)	29100	88	18730	−0.05
			21140	+1.27
			27250	+0.20
			30210	−0.23
fmf-$[Co(NH_3)(tetren)]^{3+}$	21190	129	20700	+1.68
(*Λ-SS*)	29240	108	27700	+0.26

Table 3. Minimized Energy Terms (kJ mol^{-1}) for the Isomers of $[CoN_6]^{3+}$-Type Complexes

Complexes	Bond Stretching	Nonbonded Interaction	Angle Bending	Torsion	Total
fac-$[Co(NH_3)_3(dien)]^{3+}$	2.8	2.6	6.6	15.3	27.3
mer-$[Co(NH_3)_3(dien)]^{3+}$	3.2	4.7	12.5	10.6	31.0
s-fac-$[Co(NH_3)(en)(dien)]^{3+}$	3.5	4.2	8.7	16.9	33.3
u-fac-$[Co(NH_3)(en)(dien)]^{3+}$	2.9	3.1	7.8	19.7	33.5
mer-1-$[Co(NH_3)(en)(dien)]^{3+}$	3.4	3.7	13.0	13.8	33.9
mer-2-$[Co(NH_3)(en)(dien)]^{3+}$	3.2	3.0	12.7	14.2	33.1
α-$[Co(en)(trien)]^{3+}$	4.0	10.5	11.9	29.4	55.8
β-1-$[Co(en)(trien)]^{3+}$(*Λ-SS*)	4.0	6.5	14.5	22.9	47.9
β-2-$[Co(en)(trien)]^{3+}$(*Λ-SR*)	4.0	5.9	17.8	21.7	49.4
fff-$[Co(NH_3)(tetren)]^{3+}$	3.5	8.3	10.8	33.6	56.2
ffm-$[Co(NH_3)(tetren)]^{3+}$(*Λ-RRS*)	3.9	8.1	16.1	26.9	55.0
ffm-$[Co(NH_3)(tetren)]^{3+}$(*Λ-RRR*)	4.8	10.4	20.5	25.7	61.4
fmf-$[Co(NH_3)(tetren)]^{3+}$	4.3	12.7	15.6	31.1	63.7
fmm-1-$[Co(NH_3)(tetren)]^{3+}$(*Λ-SSS*)	4.5	14.1	17.6	33.8	70.0
fmm-2-$[Co(NH_3)(tetren)]^{3+}$(*Λ-SSR*)	4.4	12.0	27.0	23.6	67.0
fmm-3-$[Co(NH_3)(tetren)]^{3+}$(*Λ-SRS*)	4.3	10.4	28.3	24.3	67.3
fmm-4-$[Co(NH_3)(tetren)]^{3+}$(*Λ-SRR*)	4.3	11.0	20.6	33.9	69.8

The $[Co(NH_3)(tetren)]^{3+}$ complexes, the hitherto undetected fmm isomers will be much more strained than all the others from strain energy calculation. Even if the fmm isomers existed in the solution, it would be hard to detect or isolate them, because of their small content and low stability.

Thus, among the isomers of $[CoN_6]^{3+}$-type listed in Table 1, only those of fmm type of $[Co(NH_3)(tetren)]^{3+}$ remained to be detected and isolated.

References

1) The following abbreviations will be used in the present paper: en=ethylenediamine (n=1); dien=diethylenetriamine (n=2); trien=triethylenetetramine (n=3); tetren=tetraethylenepentamine (n=4); linpen=linear pentaethylenehexamine (n=5).

2) a) F. A. Genth, *vgl. C.*, **1851**, 417; b) E. Fremy, *C. r.*, **32**, 509, 808 (1851).

3) Y. Shimura, *Bull. Chem. Soc. Jpn.*, **31**, 311 (1958).

4) a) A. Werner and C. Kreutzer, *Lieb. Ann.*, **351**, 79 (1907); b) A. Werner, F. Bräunlich and E. Rogowina, *Ann.*, **351**, 71 (1907); c) A. Werner and Y. Shibata, *Ber.*, **45**, 3289 (1912).

5) a) S. M. Jörgensen, *J. Prakt. Chem.*, [2] **39**, 8 (1889); b) A. Werner, *Ber.*, **45**, 121 (1912).

6) a) I. F. Burstein, M. D. Mazus, V. N. Biyushkin, E. V. Popa, A. V. Ablov, T. I. Malinovski, N. V. Rannev, and B. M. Shedrin, *Koord. Khim.*, **4**, 282 (1978); b) A. V. Ablov, E. V. Popa, M. D. Mazus, V. N. Biyushkin, A. P. Gulya, T. I. Malinovski, *Koord. Khim.*, **5**, 287 (1979).

7) a) Y. Yoshikawa and K. Yamasaki, *Bull. Chem. Soc. Jpn.*, **45**, 179 (1972); b) F. R. Keene and G. H. Searle, *Inorg. Chem.*, **11**, 148 (1972).

8) F. Basolo, *J. Am. Chem. Soc.*, **70**, 2634 (1948).

9) a) S. Utsuno, Y. Sakai, Y. Yoshikawa, and H. Yamatera, *J. Am. Chem. Soc.*, **102**, 6903 (1980); b) S. Utsuno, Y. Yoshikawa, and Y. Tahata, *Inorg. Chem.*, **24**, 2724 (1985).

10) a) D. P. Schaefer and G. R. Brubaker, *Inorg. Chem.*, **8**, 1974 (1969); b) E. Kyuno and J. C. Bailar, Jr., *J. Am. Chem. Soc.*, **88**, 1125 (1966).

11) Y. Yoshikawa and K. Yamasaki, *Bull. Chem. Soc. Jpn.*, **46**, 3448 (1973).

12) J. W. Blunt, F. C. Ha, and D. A. House, *Inorg. Chim. Acta*, **32**, L5 (1979).

13) G. G. Sclessinger, *Gannon Coll. Chem. J.*, **1965**, 8.

14) Y. Yoshikawa and K. Yamasaki, *Coord. Chem. Rev.*, **28**, 205 (1979).

15) K. Sakakibara, Y. Yoshikawa, and H. Yamatera, *Bull. Chem. Soc. Jpn.*, **52**, 2725 (1979).

16) *Inorg. Synth.*, **7**, 211 (1963).

17) A. R. Gainsford and D. A. House, *Inorg. Chim. Acta*, **3**, 367 (1969).

18) The preparation, $[Co(NO_3)(NH_3)_5](NO_3)_2$, or $[Co(CO_3)(NH_3)_5]NO_3$ used as a starting material gave similar results.

19) D. A. House and C. S. Garner, *Inorg. Chem.*, **5**, 2097 (1966).

20) S. Ustuno, Y. Yoshikawa, A. Tatehata, and H. Yamatera, *Bull. Chem. Soc. Jpn.*, **54**, 1814 (1981).

21) a) F. D. Sancilio, L. F. Druding, and D. M. Lukaszewski, *Inorg. Chem.*, **15**, 1626 (1976); b) G. H. Searle, S. F. Lincoln, F. R. Keene, G. Teague, and D. G. Rowe, *Aust. J. Chem.*, **30**, 1221 (1977).

22) M. R. Snow, *J. Chem. Soc., Dalton Trans.*, **1972**, 1627.

23) R. H. Boyd, *J. Chem. Phys.*, **49**, 2574 (1968).

24) R. S. Cahn, C. K. Ingold, and V. Prelog, *Experientia*, **12**, 81 (1956).

Paramagnetic Shifts of DMF and DMA by Uranium(V)

Toshie HARAZONO and Hiroshi FUKUTOMI*
Research Laboratory for Nuclear Reactors, Tokyo Institute of Technology,
O-okayama, Meguro-ku, Tokyo 152
(Received January 11, 1986)

Paramagnetic shifts of DMF (*N,N*-dimethylformamide) and DMA (*N,N*-dimethylacetamide) induced by U(V) were studied by the ^1H and ^{13}C NMR spectroscopy. It was found that the ^1H and ^{13}C NMR signals of bulk DMF and DMA exhibited the paramagnetic shifts to the higher field by U(V). Positive pseudocontact shift and negative contact shift for both DMF and DMA are discussed on the basis of the electronic structure of U(V) complexes. The values of magnetic susceptibilities of U(V) complexes are also presented.

Paramagnetic shifts induced by lanthanoid compounds have been extensively studied since the pioneer work of Hinckley,[1-4] while a little of information are available for actinoid compounds. Some diketonato complexes of U(IV) having the electron configuration of $5f^2$ were found to induce the shift of ^1H and ^{13}C NMR signals of ligands,[5-8] and the ^1H signals of U(IV) $(allyl)_4$ were also found to shift to the higher field.[9,10] On the other hand, there are very few studies on the paramagnetic shift by U(V) which has the $5f^1$ electron configuration, since U(V) is extremely unstable in aqueous solution owing to its rapid disproportionation. We found that U(V) was formed by photoreduction of $[UO_2(dmf)_5]^{2+}$,[11,12] $[UO_2(dma)_5]^{2+}$,[13] and $[UO_2(dmso)_5]^{2+}$,[14] and the resulting U(V) was stable over several hours in acid-free organic solvents in the dark. This has enabled the determination of the paramagnetic shift by U(V) in solution reported in this paper. In the previous paper,[11] we reported briefly the result of paramagnetic shift of DMF owing to the fast exchange between the first coordination sphere of U(V) and the bulk solvent. It is the purpose of this paper to investigate the paramagnetic shifts of DMF and DMA by U(V) in more detail and to elucidate the mechanism of spin localization.

Experimental

The $[UO_2(dmf)_5](ClO_4)_2$ and $[UO_2(dma)_5](ClO_4)_2$ complexes were prepared by the same methods so far reported.[15] Elemental analysis was performed by using a Shimadzu CHN-1A analyzer. Calcd for $[UO_2(dmf)_5](ClO_4)_2$: C, 21.59; H, 4.23; N, 8.39%. Found: C, 20.98; H, 4.10; N, 8.39%. Calcd for $[UO_2(dma)_5](ClO_4)_2$: C, 26.56; H, 5.01; N, 7.74%. Found: C, 26.65; H, 5.00; N, 7.65%. Reagent grade DMF and DMA were distilled twice under vacuum and stored over 3A molecular sieves. Benzene and acetone-d_6 (CD_3COCD_3, Merck 99%) were of analytical grade and used without further purification. NMR shift reagents $Pr(fod)_3$ (fod=6,6,7,7,8,8,8-heptafluoro-2,2-dimethyl-3,5-octanedionate) and $Eu(fod)_3$ (Dojin) were dried in a vacuum dessicator over phosphorus pentoxide. $[UO_2(dmf)_5]^+$ and $[UO_2(dma)_5]^+$ solutions were prepared by irradiation of $[UO_2(dmf)_5](ClO_4)_2$ in DMF and $[UO_2(dma)_5](ClO_4)_2$ in DMA, respectively with the light of 365 nm from a 500 W ultrahigh-pressure mercury lamp (Ushio USH 500D). The U(V) concentration was determined spectrophotometrically by using a Shimadzu UV-210A spectrophotometer, where the values of 45.5 $M^{-1}cm^{-1}$ (M=mol dm^{-3}) at 755 nm and 45.4 $M^{-1}cm^{-1}$ at 760 nm were used for the molar extinction coefficients of the U(V)-DMF[12] and U(V)-DMA[13] complexes,respectively. NMR spectra were recorded on a JEOL JNMFX-100 FT NMR spectrometer equipped with a disc system NM-3974. Acetone-d_6 was used as an internal lock for the measurement of paramagnetic shifts. In the measurement of magnetic susceptibility, D_2O and benzene were used as an external lock and internal standard, respectively.

Results

The magnetic susceptibility of U(V) was determined by Evans' method,[16] the equation of which is given by

$$\frac{\Delta H}{H_0} = \frac{2\pi}{3}\Delta\kappa, \quad (1)$$

where H_0 is the external magnetic field, ΔH is the difference in chemical shift of the signal of benzene between reference and sample solutions containing benzene, and $\Delta\kappa$ is the difference in volume magnetic

Table 1. Molar Magnetic Susceptibilities of U(V) Complexes at 25 °C

U(VI) complex (concentration)	[V(V)] / 10^{-2} M	$\Delta\nu(C_6H_6)$[a] / Hz	$\Delta\nu(C_6H_6)$[b] / Hz	χ_M / 10^{-6} emu mol^{-1}
$[UO_2(dmf)_5](ClO_4)_2$ (0.277 M)	1.59	7.08	445	2140
$[UO_2(dma)_5](ClO_4)_2$ (0.307 M)	1.08	5.25	486	2330
	0.925	4.30	465	2230

a) Difference in chemical shift of benzene. b) Reduced values at [U(V)]=1 M.

susceptibility between reference and sample solutions. The results are shown in Table 1.

For the ^{1}H and ^{13}C NMR spectra of bulk DMF and DMA in the absence of U(V)–DMF and U(V)–DMA complexes respectively, assignments of DMF and DMA signals were performed by using $Pr(fod)_3$. In the following descriptions, hydrogen and carbon atoms with subscripts, e.g. H_1, C_3, correspond to the atoms of positions 1, 3, in Figs. 1 and 2. Since the pseudocontact term is a principal term for Pr(III),[17]

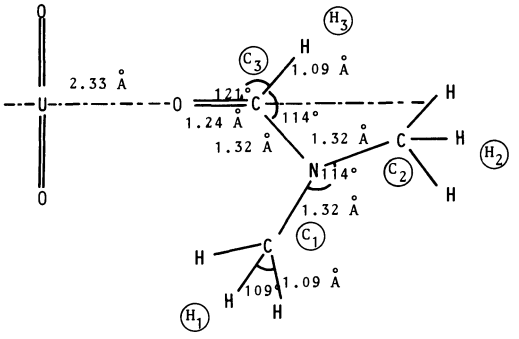

Fig. 1. Postulated structure of the U(V)–DMF complex.

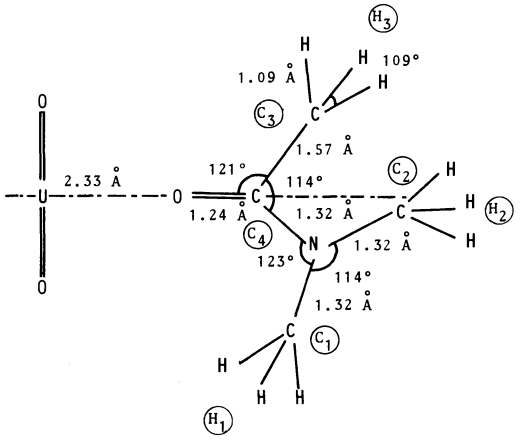

Fig. 2. Postulated structure of the U(V)–DMA complex.

Table 2. Relative Chemical Shifts of DMF Containing $Pr(fod)_3$

	Exptl	Calcd
H_1	0.47	0.43
H_2	0.26	0.35
H_3	1.00	1.00
C^1	0.40	0.30
C_2	0.20	0.23
C_3	1.00	1.00

The values indicated in Fig. 1 were used for the values of the bond lengths and angles.

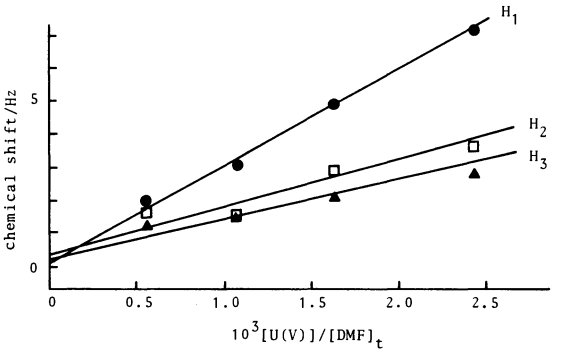

Fig. 3. Plots of ^{1}H chemical shifts of DMF vs. $[U(V)]/[DMF]_t$ at 25 °C. $[UO_2(dmf)_5^{3+}]=0.40$ M, $[DMF]_t=9.04$ M.

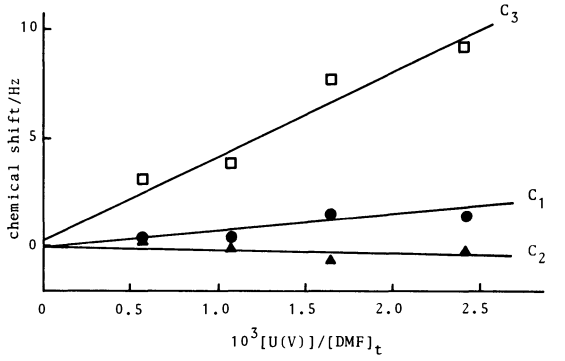

Fig. 4. Plots of ^{13}C chemical shifts of DMF vs. $[U(V)]/[DMF]_t$ at 25 °C. $[UO_2(dmf)_5^{3+}]=0.40$ M, $[DMF]_t=9.04$ M.

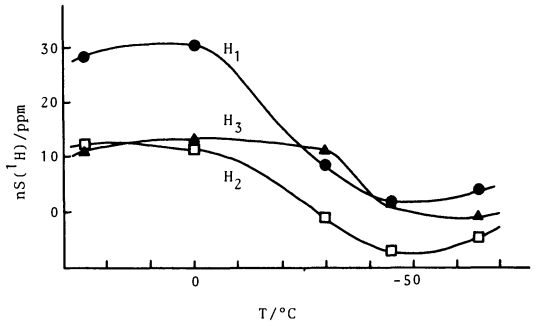

Fig. 5. Plots of $nS(^{1}H)$ of the U(V)–DMF complex as a function of temperature.

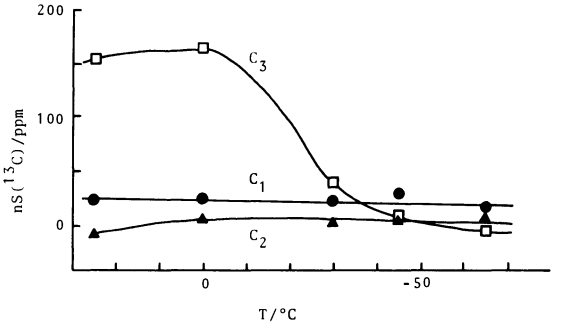

Fig. 6. Plots of $nS(^{13}C)$ of the U(V)–DMF complex as a function of temperature.

the chemical shifts of each atom, which are induced to the higher field by Pr(III), can be calculated by using the McConnell and Robertson equation[18] on the assumption that a principal axis passes through Pr···O=C. Experimental results of chemical shift of DMF are given in Table 2 and shows close agreement with the theoretical values. It was found that the NMR signals of bulk DMF exhibited the paramagnetic shift to the higher field by U(V), especially in signals of H_1 and C_3. Figures 3 and 4 show the plots of ^1H and ^{13}C chemical shifts of DMF vs. $[U(V)]/[DMF]_t$ at 25 °C, where $[DMF]_t$ denotes the total DMF concentration, and each plot gives a straight line. The value of the slope is expressed as nS, where n is the number of ligands coordinated to U(V). The number of coordinated dmf in the U(V)-DMF complex has not yet been determined, but 5 is most likely. In Figs. 5 and 6, the nS values of ^1H and ^{13}C signals are plotted as a function of temperature, respectively. With respect to the chemical shift of DMA, similar plots are given in Figs. 7 and 8, which also show the paramagnetic shift to the higher field by U(V), especially in the C_4 signal. The nS values were nearly constant at a temperature range from 25 to 0 °C.

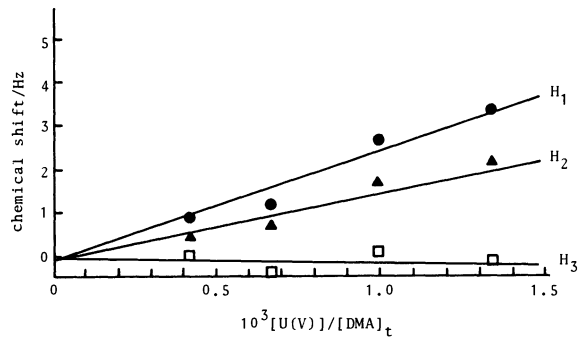

Fig. 7. Plots of ^1H chemical shifts of DMA vs. $[U(V)]/[DMA]_t$ at 25 °C. $[UO_2(dma)_5^{3+}]=0.40$ M, $[DMA]_t=7.53$ M.

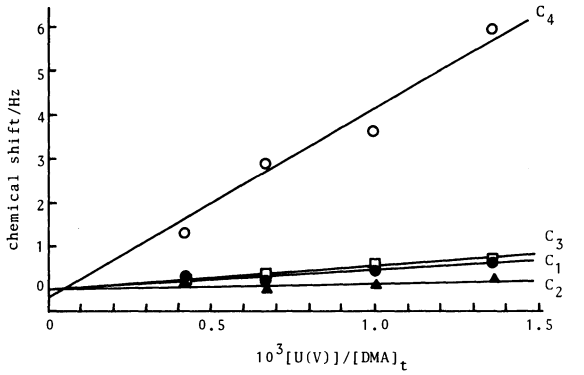

Fig. 8. Plots of ^{13}C chemical shifts of DMA vs. $[U(V)]/[DMA]_t$ at 25 °C. $[UO_2(dma)_5^{3+}]=0.40$ M, $[DMA]_t=7.53$ M.

Discussion

The values of magnetic susceptibilities of the U(V)-DMF and U(V)-DMA complexes are fairly large and are well consistent with that of the U(V)-TEP complex (2014×10^{-6}, TEP=triethyl phosphate).[19] The chemical shift induced by U(V) is expected to involve three terms, i. e. contact shift (CS), pseudocontact shift (PCS), and complex formation shift (CFS).[17] The CFS corrections for the U(V)-DMF and U(V)-DMA complexes were estimated by using $[UO_2(dmf)_5]^{2+}$ and $[UO_2(dma)_5]^{2+}$, respectively, which are diamagnetic complex ions having the $5f^0$ electron configuration. In the DMF complex, the CFS correction is negligibly small for H_1 and H_2 signals, and a small correction is required for H_3 signal (0.95 ppm for $[U(V)]/[DMF]_t=1$).[20] However, the information of CFS for ^{13}C is not available, and the CFS correction was neglected for ^{13}C on the basis of the fact that CFS is very small for aliphatic compounds.[17] As seen in Figs. 5 and 6, a fast ligand exchange region[21] appears at temperatures above 0 °C, and the ligand exchange comes gradually down below 0 °C. This was also confirmed by the temperature dependence of linewidths ($1/T_2-1/T_{2a}$), where T_2 and T_{2a} are the transverse relaxation times for the ^1H NMR signal (H_3 in Fig. 1) in the presence and the absence of U(V), respectively. The fact that the change in chemical shift with temperature is particularly large in C_3 signal as seen in Fig. 4 definitely indicates that the oxygen atom of DMF coordinates to U(V). Therefore, the structure of the U(V)-DMF complex shown in Fig. 1 seems to be most likely from the analogy to the Pr(III) complex.[22] On the assumption that the above structure is correct and the spin density (ρ) is the same in both methyl groups of DMF, the paramagnetic shift by U(V) is divided into CS and PCS terms. The results are listed in Table 3, where A represents a hyperfine coupling constant. The values of PCS are positive, and the nagative values of CS result in the positive

Table 3. Values of S, PCS, CS, A, and ρ for the U(V)-DMF Complex at 25° C

	n·S ppm	n·PCS ppm	n·CS ppm	n·A gauss	n·ρ
H_1	28.5	95.0	−66.5	0.896	
H_2	10.9	77.7	−66.5	0.896	
H_3	12.9	220	−207	2.79	
			(−206)	(2.78)	
C_1	26.7	140	−113	0.030	−0.039
C_2	−7.5	105	−113	0.030	−0.039
C_3	153	462	−309	0.081	−0.124
					(−0.123)

$A=\rho Q$. $Q=-22.5$ gauss. ( ): corrected value.

Table 4. Values of S, PCS, and CS for the $Eu(fod)_3$-DMF Complex at 25 °C

	S	PCS	CS
	ppm	ppm	ppm
H_1	−8.7	−23.1	14.4
H_2	−4.4	−18.8	14.4
H_3	−11.9	−53.8	41.9
C_1	−8.3	−24.0	15.7
C_2	−2.7	−18.4	15.7
C_3	0.20	−80.0	80.2

Table 5. Values of S, PCS, CS, A, and ρ for the U(V)-DMA Complex at 25 °C

	$n \cdot S$	$n \cdot PCS$	$n \cdot CS$	$n \cdot A$	$n \cdot \rho$
	ppm	ppm	ppm	gauss	
H_1	26.5	47.6	−21.1	0.206	
H_2	17.6	38.7	−21.1	0.206	
H_3	−1.9	66.4	−68.3	0.668	
C_1	19.6	55.1	−35.5	0.0093	−0.0092
C_2	6.1	41.6	−35.5	0.0093	−0.0092
C_3	22.1	75.7	−53.6	0.0140	−0.030
C_4	172	182	−10.4	0.0027	
	(180)		(−2.8)	(0.0007)	

$A = \rho Q$. $Q = -22.5$ gauss. ( ): corrected value.

hyperfine coupling constant and the negative spin density on the C atoms of DMF. It should be noted that the contact term has the largest absolute value at C_3 which is the nearest C atom to U(V). A DMF molecule is regarded as a conjugated system in which π orbitals of C=O and -N and pseudo π orbitals by hyperconjugation of two methyl groups are conjugated, and the unpaired electron of U(V) might be transferred to ^1H and ^{13}C of DMF through π electrons. Paramagnetic shifts of DMF by $Eu(fod)_3$ were also studied and divided into two terms as well as the U(V)-DMF complex. The results are listed in Table 4. Negative values of PCS and positive values of CS are just the opposite of the U(V)-DMF complex. This means that the anisotropy of manetic susceptibility or g tensor of U(V) ($\chi_{//} > \chi_{\perp}$, $g_{//} > g_{\perp}$) is the opposite of that of Eu(III).

Almost the same discussion can be applied to the U(V)-DMA complex. The CFS corrections are negligible for all the ^1H signals and are small for C_1, C_2, and C_3 signals. The C_4 signal requires the correction of 7.6 ppm for $[U[V)]/[DMA]_t = 1$.[23] As seen in Fig. 8, the change in chemical shift is most large in the C_4 signal, and this indicates that the oxygen atom of C=O coordinates to U(V). The proposed structure of the U(V)-DMA complex is illustrated in Fig. 2. The paramagnetic shift by U(V) consists of two terms, CS and PCS. The results are listed in Table 5. The signs of CS and PCS are the same as those of the U(V)-DMF complex. The absolute value of CS of C_4 is smaller than those of C_1, C_2, and C_3. If the bond length between U and O in U····O=C is slightly shorter than 2.33 Å which is the U····O bond length of U····O=C in $[UO_2(CF_3CO)_2CH]_2THF$ (THF= tetrahydrofuran),[24] the absolute value of CS of C_4 will become larger than those of CS of other carbon atoms as well as the case of U(V)-DMF. The results of the paramagnetic shifts of DMA by $Eu(fod)_3$ are given in Table 6.

Table 6. Values of S, PCS, and CS for the $Eu(fod)_3$-DMA Complex at 25 °C

	S	PCS	CS
	ppm	ppm	ppm
H_1	−11.0	−29.2	18.2
H_2	−5.4	−23.6	18.2
H_3	−11.8	−41.2	29.4
C_1	−11.9	−40.8	28.9
C_2	−1.9	−30.8	28.9
C_3	−20.5	−56.1	35.6
C_4	49.6	−135	185

It may be noted that the separation of paramagnetic shifts by U(V) into the CS and PCS terms was performed for the first time in this paper.

The present work was partially supported by a Grant-in-Aid for Scientific Research No. 57470035 from the Ministry of Education, Science and Culture.

References

1) C. C. Hinckley, *J. Am. Chem. Soc.*, **91**, 5160 (1969).
2) B. C. Mayo, *Chem. Soc. Rev.*, **2**, 49 (1973).
3) M. Hirayama, K. Akutsu, and K. Fukuzawa, *Bull. Chem. Soc. Jpn.*, **55**, 704 (1982).
4) L. F. Lindoy, *Coord. Chem. Rev.*, **48**, 83 (1983).
5) C. Wiedenheft, *Inorg. Chem.*, **8**, 1174 (1969).
6) T. H. Siddall, III, W. E. Stewart, and D. G. Karraker, *Chem. Phys. Lett.*, **3**, 498 (1969).
7) G. Folcher, J. Paris, P. Plurien, P. Rigny, and E. Soulié, *J. Chem. Soc., Chem. Commun.*, **1974**, 3.
8) G. M. Khvostik, V. N. Sokolov, G. K. Grebenshchikov, S. A. Toropov, and G. P. Kondratenkov, *Sov. J. Coord. Chem.*, **5**, 534 (1979).
9) N. Paladino, G. Lugli, U. Pedretti, and M. Brunelli *Chem. Phys. Lett.*, **5**, 15 (1970).
10) R. Von Ammon, B. Kanellakopulos, and R. D. Fisher, *Chem. Phys. Lett.*, **2**, 513 (1968).
11) T. Harazono, H. Tomiyasu, and H. Fukutomi. *Chem. Lett.*, **1983**, 1173.
12) H. Fukutomi, T. Harazono, and T. Kojima, *Bull. Chem. Soc. Jpn.*, (in press).
13) T. Harazono, T. Kojima, and H. Fukutomi. *Nippon Kagaku Kaishi*, **1984**, 213.
14) Unpublished data.
15) R. P. Bowen, S. F. Lincoln, and E. H. Williams. *Inorg*

Chem., **15**, 2125 (1976).
16) D. F. Evans, *J. Chem. Soc.*, **1959**, 2003.
17) K. Ajisaka and M. Kainosho, *J. Am. Chem. Soc.*, **97**, 330 (1975).
18) H. M. McConnell and R. E. Robertson, *J. Chem. Phys.*, **29**, 1361 (1958).
19) G. Cauzzo, G. Gennari. G. Giacometti, G. C. Agostini, and A. Gambaro, *Inorg. Chim. Acta*, **32**, 45 (1979).
20) Y. Ikeda, Ph. D. Thesis, Tokyo Institute of Technology, 1981.
21) T. W. Swift and R. E. Connick, *J. Chem. Phys.*, **37**, 307 (1962).
22) The values of bond lengths and angles are cited from the following reference. J. D. Roberts and M. C. Caserio, "Basic Principles of Organic Chemistry," Benjamin, New York (1964).
23) T. Harazono, Ph. D. Thesis, Tokyo Institute of Technology, 1983.
24) G. M. Kramer, M. B. Dines, R. B. Hall, A. Kaldor, A. J. Jacobson, and J. C. Scanlon, *Inorg. Chem.*, **19**, 1340 (1980).

Partial Molar Enthalpy of Solution for Tris(2,4-pentanedionato)cobalt(III) in Mixed Solvents of Water and Dimethyl Sulfoxide

Yasuki YOSHIMURA,* Nobuyoshi SATO, and Makoto KIKUCHI
Laboratory of Chemistry, College of Humanities and Social Sciences, Iwate University, Ueda, Morioka 020
(Received January 16, 1986)

The solubility (X_s) of tris(2,4-pentanedionato)cobalt(III) ([Co(acac)$_3$]) in mixed solvents of water and dimethyl sulfoxide (DMSO) with various compositions was determined over the temperature range 20—60 °C. It was found that the experimental values of X_s could be satisfactorily fitted to $\ln X_s = A(1/T) + B\ln T + C$ and the partial molar enthalpy of solution ($\Delta\bar{H}_s$) at 25 °C for [Co(acac)$_3$] was estimated from slopes of the solubility curves. When $\Delta\bar{H}_s$ was plotted against the mole fraction of DMSO (X_{DMSO}), a clear maximum was found at about X_{DMSO}=0.3. This composition profile of $\Delta\bar{H}_s$ is discussed in connection with the internal pressure of a mixture of water and DMSO. A method to estimate an approximate value of the partial molar enthalpy of hydrophobic hydration ($\Delta\bar{H}_h$) in an aqueous DMSO mixture of [Co(acac)$_3$] is also presented by using the solubility data in mixtures with a lower X_{DMSO} than 0.14.

In studies on the solvent extraction of various metal chelates, it has been found that the role of organic solvents can be successfully interpreted by the aid of the regular solution theory in terms of the solubility parameters of organic solvents.[1] However, an application of the regular solution theory to the aqueous phase in solvent-extraction systems is unreasonable because of strong interactions between solutes and water molecules such as the hydrogen bonding and association of water molecules due to hydrogen bonding among them.

Recently, Yamamoto applied a scaled particle theory to an interpretation of the thermodynamic properties of tris(2,4-pentanedionato)chromium(III) ([Cr(acac)$_3$]) in an aqueous solution.[2] Awano et al.[3] have found that the composition dependence of the partition coefficients of some tris(2,4-pentanedionato) chelates between heptane and mixed solvents of water and dimethyl sulfoxide (DMSO) can be explained in terms of the internal pressure of aqueous DMSO mixtures.

The thermodynamic properties of tetraalkylammonium salts[4—10] and some nonelectrolytes[11—14] in mixtures of water and aprotic solvents have been investigated rather extensively. Especially, Somsen et al.[7,9,10] have shown that the composition dependence of the enthalpy of solution for tetraalkylammonium salts in mixtures of water and aprotic solvents, such as DMSO and *N*,*N*-dimethylformamide (DMF), can be interpreted in terms of an effect of the organic solvents on the hydrophobic hydration of the solutes in the mixtures.

In tris(2,4-pentanedionato) chelates, central metal ions are octahedrally surrounded by three 2,4-pentanedionate anions and two oxygen atoms of the anion combine with the central metal ions. Since six methyl groups reside on the periphery of the chelates, these chelates may be expected to exhibit a hydrophobic property. In connection with the solvent extraction of metal chelates, it is interesting to examine the behavior of such chelates both in water and in mixtures of water and organic solvents such as DMSO.

Thus, in this study, tris(2,4-pentanedionato)cobalt(III) ([Co(acac)$_3$]), which is inert to exchange or substitution reactions of ligands and is fairly soluble in water,[15] was chosen as a model chelate and its solubility in water and in aqueous DMSO mixtures was determined over the temperature ranges 5—60 °C and 20—60 °C, respectively. From these data, the partial molar enthalpy of solution ($\Delta\bar{H}_s$) for [Co(acac)$_3$] was estimated and the effect of DMSO on $\Delta\bar{H}_s$ and on the hydrophobic hydration of [Co(acac)$_3$] is discussed.

Experimental

Materials. [Co(acac)$_3$] was obtained from Dojin Chemical Laboratories Ltd. and recrystallized from a water–acetone mixture (60% acetone by volume). The ultraviolet and visible absorption spectrum of the purified [Co(acac)$_3$] in ethanol agreed with values found in the literature.[16]

Commercial DMSO (spectrophotometric grade reagent, Dojin Chemical Laboratories Ltd.) was dried over calcium hydride for a week and distilled under reduced pressure. Middle fractions were collected and stored over a molecular sieve (type 4A). The water content in the purified DMSO, measured by Karl Fischer titration, was about 0.06% by weight. The purified DMSO was placed in a dry box whose humidity was kept below 20% with silica gel. Mixtures of water and DMSO were prepared by weight; preparations were carried out in the dry box. Redistilled water was used.

Solubility Measurement. The apparatus shown in Fig. 1 was used to saturate a given sample solution with [Co(acac)$_3$]. A sufficient amount of [Co(acac)$_3$] and about 50 cm^3 of a sample solution were placed in the apparatus, which was thermostated at the desired temperatures to within ±0.1 °C. The mixture was stirred with a magnetic stirrer for about 48—72 h at each temperature. At appropriate time intervals, the saturated solution was passed through an absorbent cotton filter by injecting dry air. A volume of the saturated solution suitable for subsequent spectroscopic measurements was transferred by

pipette into a 5 or 10 cm^3 volumetric flask which had been previously weighed. The total weight of the flask and the saturated solution was weighed. If $[Co(acac)_3]$ precipitated during weighing, 1 cm^3 of DMSO was added to the saturated solution in order to dissolve the precipitation. After letting the flask stand for 30 min in an incubator kept at 25±0.5 °C, water was added to the mark at 25 °C; this solution was further diluted with water to give an absorbance between 0.2 and 0.6 at 324 nm.

The concentration (C mol dm^{-3}) of $[Co(acac)_3]$ in the above final solution was calculated by using the absorbance at 324 nm (A) from

$$C = (A-0.0011)/\varepsilon d, \quad (1)$$

where εd was 8.37×10^3 mol^{-1} dm^3. The solubility in molality units (S_m mol kg^{-1}) was calculated from the weight of the saturated solution, the degree of dilution, and C.

The absorbance of $[Co(acac)_3]$ at 324 nm was not entirely affected by the presence of 5% DMSO by volume. Since in all cases, the volume fraction of DMSO in the final solution for measuring A was less than 1%, Eq. 1 settled in water was used throughout.

The temperature of the saturated solution was increased from 20 to 60 °C (from 5 to 60 °C for water) at 5 °C intervals. It was found that $[Co(acac)_3]$ attained equilibrium within 24 h at each temperature. Solubility measurements were carried out at least 3 times for equilibration times of 48—72 h at each temperature.

In solubility measurements for mixtures with a DMSO content of $X_{DMSO}\geq0.4$ (X_{DMSO} is mole fraction of DMSO), the saturated solution could not be passed rapidly through a cotton filter at the increased temperature because of the adhesion of a solid $[Co(acac)_3]$ to the cotton filter. In this case, a further measurement was not carried out.

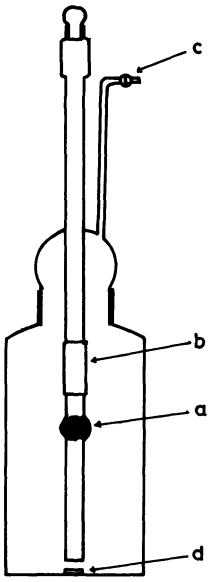

Fig. 1. Apparatus for solubility measurement. a: Filter filled with absorbent cotton, b: Silicone tube, c: Stop-cock for injecting air, d: Magnetic stirring bar.

Results

The S_m values of $[Co(acac)_3]$ in water are listed in Table 1. Errors denote deviations at a 95% confidence level and are less than 2%. In order to confirm whether $[Co(acac)_3]$ is hydrolyzed in water or not, independent measurements were carried out for two saturated solutions. The solubility was obtained from the absorbance at 324 nm in one measurement and from that at 593 nm in the other. The separately obtained S_m values closely agreed with each other (see Table 1). Furthermore, when the saturated solution equilibrated at 60 °C was allowed to attain equilibrium again at 25 °C, the solubility value at 25 °C was reproducible within the experimental error (see the lowest line in Table 1). These results show that $[Co(acac)_3]$ is not decomposed over the temperature range studied.

The S_m values in mixtures of water and DMSO are given in Table 2. The solubility data at 25 °C were reproducible within the experimental error when the solutions at the end of experiment at the highest temperature were allowed to attain equilibrium at 25 °C. This result shows that the evaporation of water or DMSO during the equilibration produced no detectable effect.

Discussion

Partial Molar Enthalpy of Solution of $[Co(acac)_3]$ ($\Delta\bar{H}_s$). The S_m values of $[Co(acac)_3]$ were converted to solubility in mole fraction (X_s) and then ln X_s was plotted against $1/T$. In Fig. 2 typical plots are

Table 1. Solubility of $[Co(acac)_3]$ in Water ($S_m\times10^3$/mol kg^{-1})[a]

Temperature/°C	S_m[b]	S_m[c]
5	6.93±0.05	6.85±0.02
10	5.70±0.04	5.64±0.02
15	4.86±0.03	4.82±0.03
20	4.27±0.02	4.25±0.01
25	3.82±0.05	3.83±0.01
30	3.52±0.02	3.53±0.01
35	3.29±0.04	3.32±0.02
40	3.13±0.01	3.09±0.02
45	3.04±0.02	3.02±0.01
50	3.02±0.02	2.97±0.02
55	3.00±0.02	2.99±0.01
60	3.06±0.02	3.05±0.01
25	3.79±0.02[d]	

a) Error denotes deviation at 95% confidence level. b, c) Solubility values obtained from absorbance at 324 nm and 593 nm, respectively. d) Value obtained by the experiment that the solution equilibrated at 60 °C is allowed to attain equilibrium again at 25 °C.

Table 2. Solubility of [Co(acac)$_3$] in Aqueous DMSO Mixtures ($S_m \times 10^3$/mol kg^{-1})[a)]

Temperature /°C	Mole Fraction of DMSO (X_{DMSO})						
	0.0160	0.0272	0.0587	0.0957	0.1400	0.1940	0.2644
20	3.81±0.02	3.43±0.06	2.62±0.02	2.00±0.01	1.50±0.01	1.25±0.01	1.32±0.01
25	3.50±0.01	3.25±0.07	2.67±0.02	2.13±0.01	1.68±0.01	1.45±0.01	1.58±0.01
30	3.29±0.05	3.16±0.03	2.72±0.01	2.28±0.03	1.90±0.01	1.70±0.01	1.89±0.01
35	3.18±0.01	3.12±0.01	2.83±0.02	2.45±0.01	2.18±0.01	2.01±0.02	2.28±0.01
40	3.13±0.02	3.12±0.02	2.97±0.02	2.69±0.03	2.47±0.04	2.38±0.04	2.74±0.02
45	3.13±0.01	3.17±0.01	3.15±0.01	2.97±0.03	2.82±0.02	2.80±0.01	3.31±0.01
50	3.17±0.01	3.28±0.02	3.37±0.01	3.29±0.04	3.26±0.01	3.31±0.02	3.99±0.05
55	3.25±0.02	3.44±0.04	3.66±0.01	3.64±0.04	3.72±0.02	3.91±0.07	4.83±0.02
60	3.33±0.02	3.64±0.03	3.96±0.07	4.11±0.08	4.32±0.07	4.62±0.07	5.76±0.17
	X_{DMSO}						
	0.3503	0.4309	0.4986	0.5690	0.6849	0.8555	1.0000
20	1.99±0.02	3.29±0.01	5.19±0.02	7.81±0.02	14.6±0.1	29.0±0.1	42.4±0.2
25	2.37±0.01	3.86±0.02	6.03±0.03	8.91±0.13	16.6±0.1	32.5±0.2	46.9±0.5
30	2.83±0.02	4.58±0.04	7.04±0.01	10.1±0.2	18.8±0.2	36.5±0.4	52.7±0.2
35	3.39±0.03	5.41±0.07	8.22±0.07	11.6±0.1	21.4±0.3	40.7±0.9	59.0±0.2
40	4.07±0.01	6.50±0.12	9.61±0.04	13.3±0.2	24.4±0.1	46.2±0.7	65.4±1.1
45	4.98±0.11	7.94±0.11	11.3±0.2	15.4±0.3	27.7±0.7	52.0±0.5	72.9±1.0
50	6.16±0.13	9.50±0.20	13.2±0.2	17.9±0.4	31.8±0.4	58.9±0.7	81.8±0.8
55	7.21±0.01		15.5±0.3	20.1±0.4	36.3±1.2	66.3±1.0	91.3±0.3
60	8.45±0.20						

a) Error denotes deviation at 95% confidence level.

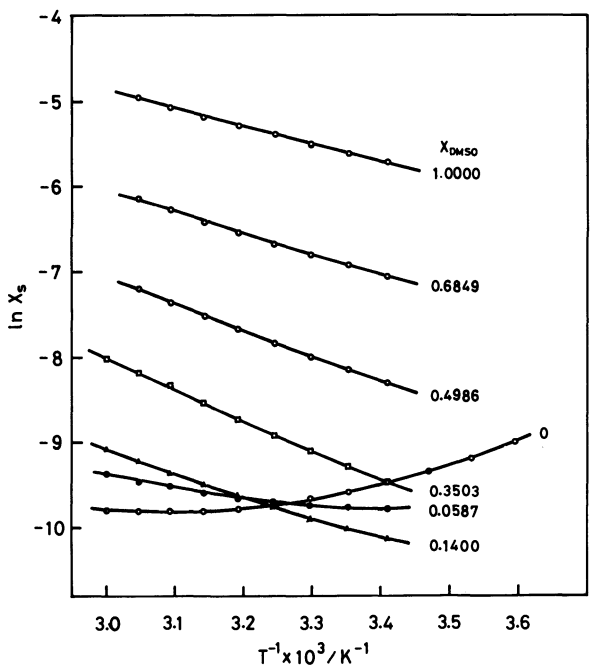

Fig. 2. Typical plot of ln X_s vs. $1/T$ for [Co(acac)$_3$] in water–DMSO mixture.
Solid lines are solubility curves calculated by Eq. 2.

shown. The solubility curve in water passed through a minimum at about 55 °C. Yamamoto has also found a similar minimum in the solubility curve of [Cr(acac)$_3$] in water.[2)]

The minima of the solubility curves in aqueous DMSO mixtures are obviously shifted to lower temperatures with increases in X_{DMSO} (40—45°C for X_{DMSO}=0.0160; 35 °C for X_{DMSO}=0.0272). In mixtures with a composition $X_{DMSO} \geq 0.0587$, the minimum was no longer distinct over the temperature range studied.

For representing solubility curves, all experimental values were fitted to

$$\ln X_s = A(1/T) + B \ln T + C, \quad (2)$$

where A, B, and C are fitting parameters. Equation 2 could reproduce the X_S values within errors of ±1% in all cases. In Table 3 the values of the fitting parameters in Eq. 2 are given. The values of $\Delta\bar{H}_s$ at 25 °C can be estimated by combining Eq. 2 with

$$\Delta\bar{H}_s = RT^2(d \ln X_s/dT). \quad (3)$$

The upward curvature in the low-temperature region of the solubility curves in water and in mixtures with a lower DMSO content might be related to the hydrophobic hydration of [Co(acac)$_3$]. (A discussion on hydrophobic hydration will be presented subsequently.) In order to confirm whether the solubility curves can be regarded as straight lines or not, an attempt was also made to fit the solubility data in mixtures of $X_{DMSO} \geq 0.1940$ to the

Table 3. Values of Fitting Parameters in Solubility Equation ($\ln X_s = A(1/T) + B \ln T + C$) of [Co(acac)$_3$]

X_{DMSO}	A/K	B	C
0	21073.338	64.845187	−449.72031
0.0160	18589.15	58.591129	−405.79352
0.0272	18278.294	59.000034	−407.11899
0.0587	12723.832	43.984506	−303.04912
0.0957	10944.5	40.641577	−278.15726
0.1400	6750.5504	29.867697	−202.83097
0.1940	4896.2513	25.950222	−174.32384
0.2644	4557.4002	26.138173	−174.04164
0.3503	3373.9398	22.317148	−147.75569
0.4309	9302.5399	41.138091	−274.26891
0.4986	4331.113	23.717577	−157.80623
0.5690	3225.146	18.900721	−126.17903
0.6849	3831.2347	20.375146	−135.86458
0.8555	3806.3492	19.595031	−130.50695
1.0000	2199.2121	13.871775	−92.01784

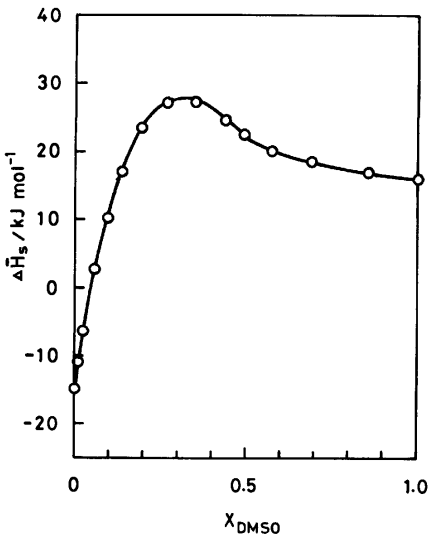

Fig. 3. Composition profile of $\Delta\bar{H}_s$ for [Co(acac)$_3$] in water–DMSO mixture.

Table 4. Partial Molar Enthalpy of Solution for [Co(acac)$_3$] at 25 °C[a]

X_{DMSO}	$\Delta\bar{H}_s$/kJ mol^{-1} [b]	$\Delta\bar{H}_s$/kJ mol^{-1} [c]
0	−14.5±0.4	
0.0160	−9.3±1.8	
0.0272	−5.7±1.6	
0.0587	3.2±1.2	
0.0957	9.8±1.2	
0.1400	17.9±1.0	
0.1940	23.6±0.9	26.7±1.2
0.2644	26.9±0.8	30.0±1.2
0.3503	27.3±2.3	29.9±1.3
0.4309	24.6±2.1	27.8±2.0
0.4986	22.8±0.9	25.1±1.1
0.5690	20.0±1.4	21.9±0.9
0.6849	18.7±0.7	20.6±0.9
0.8555	16.9±0.8	18.8±0.9
1.0000	16.1±0.7	17.7±0.6

a) Error was estimated from deviation at 95% confidence level of the fitting parameters in Eq. 2 or Eq. 4. b) Values estimated from slopes at 25 °C of curves obtained by fitting solubility data to Eq. 2. c) Values estimated from slopes of straight lines obtained by fitting solubility data to Eq. 4.

following equation over the whole temperature range studied.

$$\ln X_s = a(1/T) + b \quad (4)$$

The correlation coefficients (γ)** were higher than 0.998.

The values of $\Delta\bar{H}_s$ estimated by combining Eqs. 4 and 3 agreed fairly well with the values obtained using Eq. 2 (see Table 4). While this result shows that the solubility curves in these mixtures are practically straight, in the subsequent discussion, $\Delta\bar{H}_s$ estimated by Eq. 2 is used from the standpoint of consistency.

Effect of DMSO on $\Delta\bar{H}_s$ of [Co(acac)$_3$]. When $\Delta\bar{H}_s$ was plotted against X_{DMSO}, a clear maximum was observed at about X_{DMSO}=0.3 (Fig. 3). A similar maximum has been found for various properties of aqueous DMSO mixtures such as the enthalpy of mixing,[17] the viscosity,[18] and the internal pressure.[19] The maximization recognized for these properties has been interpreted in terms of a strong interaction between water and DMSO[18,19] or a marked rigidifying effect of DMSO on the water structure.[17,20,21] However, the cause of the maximization seems not to have been definitely established. Thus, in this discussion, an attempt is made to relate the composition profile of $\Delta\bar{H}_s$ to a certain property of the aqueous DMSO mixtures; also, the appearance of a maximum in Fig. 3 is not discussed in detail.

The composition dependence of the enthalpy of transfer of a hydrophobic solute from water to aqueous mixed solvents can be attributed to the enthalpy of cavity formation.[22] The partial molar enthalpy of cavity formation ($\bar{H}_c$) is related to the internal pressure (P_i) by[23]

$$\bar{H}_c = (\bar{V}_c - a^3 N\pi/6)(R/82.05)P_i, \quad (5)$$

where $\bar{V}_c$ and a are the partial molar volume of cavity formation and the hard-sphere diameter of the solute, respectively, N is Avogadro's number, and R is 8.314×10^{-3} kJ mol^{-1} K^{-1}.

Since data for P_i of aqueous DMSO mixtures are available,[19] it is significant to relate the composition

** The correlation coefficient is given by

$$\gamma = \Sigma\{(x_i-\bar{x})(y_i-\bar{y})\}/\sqrt{\Sigma(x_i-\bar{x})^2\Sigma(y_i-\bar{y})^2},$$

where $\bar{x}$ and $\bar{y}$ are means of x_i and y_i, respectively.

profile of $\Delta\bar{H}_s$ to that of P_i. First, the deviation of $\Delta\bar{H}_s$ from the ideal behavior in aqueous DMSO mixtures ($\delta\Delta\bar{H}_s$) can be defined as

$$\delta\Delta\bar{H}_s = \Delta\bar{H}_s - \{X_{DMSO}\Delta\bar{H}_s(DMSO) + (1-X_{DMSO})\Delta\bar{H}_s(H_2O)\}, \quad (6)$$

where (DMSO) and (H_2O) denote the values of $\Delta\bar{H}_s$ in DMSO and in water, respectively. Second, if it is assumed that $\bar{V}_c$ is approximately constant over the whole composition range, on the basis of Eq. 5, $\delta\Delta\bar{H}_s$ can be represented by

$$\delta\Delta\bar{H}_s = (\bar{V}_c - a^3N\pi/6)(R/82.05)\delta P_i, \quad (7)$$

where

$$\delta P_i = P_i - \{X_{DMSO}P_i(DMSO) + (1-X_{DMSO})P_i(H_2O)\}.$$

Figure 4 shows the good linear correlation between $\delta\Delta\bar{H}_s$ and δP_i which is expected from Eq. 7 (γ=0.980). Values of δP_i were calculated from values found in the literature for P_i[19] and $\delta\Delta\bar{H}_s$ values were read from a smooth curve of $\delta\Delta\bar{H}_s$ vs. X_{DMSO} which is not shown in the figure. Thus, the composition profile of $\Delta\bar{H}_s$ of [Co(acac)$_3$] can be linearly related to the composition dependence of P_i of aqueous DMSO mixtures. A definite explanation of the maximization observed in the composition profile of P_i can also be expected to clarify the cause of the maximum of $\Delta\bar{H}_s$.

The above assumption concerning $\bar{V}_c$ is not strictly valid since $\bar{V}_c$ is usually calculated using Eq. 5 with an $\bar{H}_c$ value estimated on the basis of the scaled particle theory.[23] However, the linear correlation between $\delta\Delta\bar{H}_s$ and δP_i in Fig. 4 shows that the influence of a change in $\bar{V}_c$ with the solvent composition on Eq. 7 is negligible.

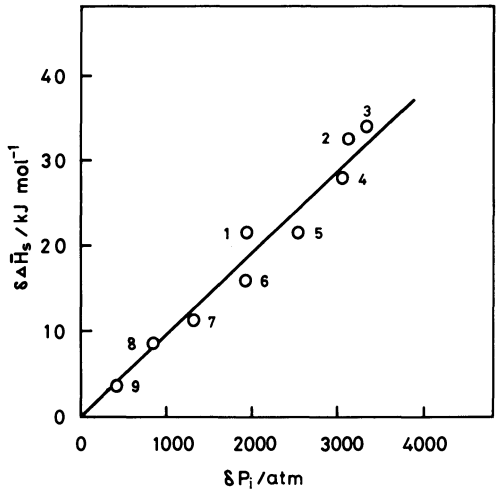

Fig. 4. Correlation between $\delta\Delta\bar{H}_s$ of [Co(acac)$_3$] and δP_i in water–DMSO mixture.
$\delta\Delta\bar{H}_s$ denotes deviation of $\Delta\bar{H}_s$ from ideal behavior defined by Eq. 6. X_{DMSO} is as follows: 1) 0.1; 2) 0.2; 3) 0.3; 4) 0.4; 5) 0.5; 6) 0.6; 7) 0.7; 8) 0.8; 9) 0.9.

In the derivation of Eq. 7, the partial molar enthalpy of interaction ($\bar{H}_i$) is not taken into account; that is, the contribution of $\delta\bar{H}_i$ to $\delta\Delta\bar{H}_s$ is ignored ($\delta\bar{H}_i$ is also defined by a similar equation to Eq. 6). The type of interaction between [Co(acac)$_3$] and water seems to differ from that between [Co(acac)$_3$] and DMSO. While an estimation of $\bar{H}_i$ is difficult, the result in Fig. 4 suggests that a change in $\bar{H}_i$ with solvent composition is approximately proportional to the solvent composition, that is, $\delta\bar{H}_i \fallingdotseq 0$.

Estimation of the Partial Molar Enthalpy of Hydrophobic Hydration ($\Delta\bar{H}_h$) for [Co(acac)$_3$]. The upward curvature at the low-temperature region of the solubility curves in Fig. 2 can be attributed to the hydrophobic hydration of [Co(acac)$_3$].[24] Shinoda has pointed out that the plot of ln X_s against $1/T$ for a hydrophobic solute in water gives a straight line at sufficiently high temperatures because of a disappearance of hydrophobic hydration.[24] The present observation that the minimum in the solubility curves is shifted to lower temperatures with increasing X_{DMSO} suggests that DMSO weakens the hydrophobic hydration of [Co(acac)$_3$].

In an attempt to estimate $\Delta\bar{H}_h$, the straightening of the solubility curve was regarded as an indication of the disappearance of hydrophobic hydration. Thus, the solubility data in aqueous DMSO mixtures with $X_{DMSO} \leq 0.14$ were fitted to Eq. 4 in limited temperature regions and the partial molar enthalpy of solution without hydrophobic hydration ($\Delta\bar{H}'_s$) was estimated from the slopes. The values of $\Delta\bar{H}_h$ were obtained by subtracting $\Delta\bar{H}'_s$ from $\Delta\bar{H}_s$.

In Table 5, $\Delta\bar{H}'_s$ and $\Delta\bar{H}_h$ are listed. For $X_{DMSO} \leq 0.0272$, errors of $\Delta\bar{H}'_s$ estimated from deviations at the 95% confidence level of the slopes in Eq. 4 were extremely large because of the narrow temperature region in which $\Delta\bar{H}'_s$ was estimated; hence, the $\Delta\bar{H}_h$ values should be regarded as being

Table 5. Partial Molar Enthalpy of Solution without Hydrophobic Hydration ($\Delta\bar{H}'_s$) and Partial Molar Enthalpy of Hydrophobic Hydration ($\Delta\bar{H}_h$) at 25 °C of [Co(acac)$_3$]

X_{DMSO}	$\Delta\bar{H}'_s$/kJ mol^{-1} a)	$\Delta\bar{H}_h$/kJ mol^{-1} b)
0.0160	4.4±2.8 (50—60 °C)	−13.7
0.0272	9.4±5.6 (50—60 °C)	−15.1
0.0587	13.5±1.8 (45—60 °C)	−10.3
0.0957	18.2±2.1 (40—60 °C)	−8.4
0.1400	23.3±1.5 (35—60 °C)	−5.4

a) Values were estimated from slopes of straight lines obtained by fitting solubility data to Eq. 4 in the temperature regions given in parentheses and errors were estimated from deviation at 95% confidence level of the slopes. b) $\Delta\bar{H}_h = \Delta\bar{H}_s - \Delta\bar{H}'_s$. The values of $\Delta\bar{H}_s$ are given in Table 4.

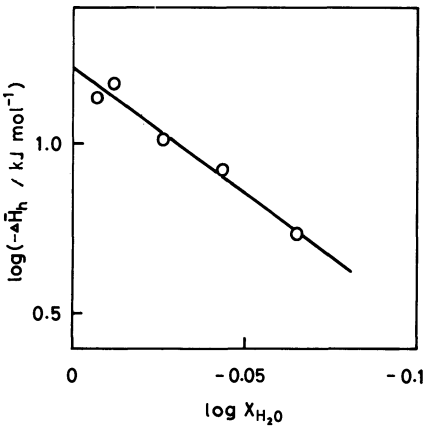

Fig. 5. Correlation between $\log(-\Delta\bar{H}_h)$ of $[Co(acac)_3]$ and $\log X_{H_2O}$ in water–DMSO mixture.

approximate. Nevertheless, it is worth noting that the differences between $\Delta\bar{H}_s$ and $\Delta\bar{H}'_s$ for mixtures with a lower X_{DMSO} than 0.14 are beyond the experimental errors. Therefore, the $\Delta\bar{H}_h$ values in Table 5 are significant.

According to Somsen et al.,[7,9,10] $\Delta\bar{H}_h$ in aqueous DMSO mixtures can be expressed by

$$\Delta\bar{H}_h = \Delta\bar{H}_h(H_2O)X^n_{H_2O}, \quad (8)$$

where $\Delta\bar{H}_h(H_2O)$ and X_{H_2O} are $\Delta\bar{H}_h$ in water and the mole fraction of water, respectively. In an earlier paper of Somsen et al.,[7] n was considered to denote the number of water molecules forming clathrate-like cages around hydrophobic sites or parts of a solute molecule. However, in a later paper, it was shown that n is not unambiguously defined by their model.[9] We consider that n is a measure of the magnitude of the decrease in $\Delta\bar{H}_h$ with X_{H_2O}. The values of $\log(-\Delta\bar{H}_h)$ are plotted against $\log X_{H_2O}$ in Fig. 5, which shows the validity of Eq. 8 (γ=0.984).

The value of $\Delta\bar{H}_h(H_2O)$ for $[Co(acac)_3]$, obtained from the intercept, is -16.7 ± 1.2 kJ mol^{-1}. Shinoda has estimated the $\Delta\bar{H}_h(H_2O)$ of benzene, methylbenzene, and ethylbenzene to be -31.5, -36.1, and -42.3 kJ mol^{-1}, respectively.[24] At present, the validity of $\Delta\bar{H}_h(H_2O)$ for $[Co(acac)_3]$ can not be discussed in terms of values from the literature for various compounds because of the difficulty in estimating $\Delta\bar{H}_h(H_2O)$. The present result suggests that the adoption of mixed solvents is useful for an estimation of $\Delta\bar{H}_h(H_2O)$. A further examination in mixed solvents of water and various organic solvents will be carried out.

The authors wish to thank Dr. Toshiki Wakabayashi for his valuable discussions and useful suggestions during this work.

References

1) For example, T. Wakabayashi, S. Oki, T. Omori, and N. Suzuki, *J. Inorg. Nucl. Chem.*, **26**, 2255 (1964); J. W. Mitchell and C. V. Banks, *ibid.*, **31**, 2105 (1969); H. Koshimura, *ibid.*, **39**, 148 (1977).
2) M. Yamamoto, *J. Phys. Chem.*, **88**, 3356 (1984).
3) H. Awano, H. Watarai, and N. Suzuki, *J. Inorg. Nucl. Chem.*, **41**, 124 (1979).
4) R. K. Mohanty, T. S. Sarma, S. Subramanian, and J. C. Ahluwalia, *Trans. Faraday Soc.*, **67**, 305 (1971).
5) M. Mastroianni, M. J. Pikal, and S. Lindenbaum, *J. Phys. Chem.*, **76**, 3050 (1972).
6) R. Fucks and C. P. Hagan, *J. Phys. Chem.*, **77**, 1797 (1973).
7) C. de Visser and G. Somsen, *J. Phys. Chem.*, **78**, 1719 (1974).
8) C. de Visser and G. Somsen, *J. Solution Chem.*, **3**, 847 (1974).
9) W. J. M. Heuvelsland, C. de Visser, and G. Somsen, *J. Phys. Chem.*, **82**, 29 (1978).
10) W. J. M. Heuvelsland, M. Bloemendal, C. de Visser, and G. Somsen, *J. Phys. Chem.*, **84**, 2391 (1980).
11) A. Ben-Naim and G. Moran, *Trans. Faraday Soc.*, **61**, 27 (1965).
12) B. G. Cox, *J. Chem. Soc., Perkin Trans. 2*, **1973**, 607.
13) S. Lindenbaum, D. Stevenson, and J. H. Rytting, *J. Solution Chem.*, **4**, 893 (1975).
14) K. Remerie and J. B. F. N. Engberts, *J. Phys. Chem.*, **87**, 5449 (1983).
15) E. Iwamoto, Y. Tanaka, H. Kimura, and Y. Yamamoto, *J. Solution Chem.*, **9**, 841 (1980).
16) D. W. Barnum, *J. Inorg. Nucl. Chem.*, **21**, 221 (1961).
17) F. Rallo, F. Rodante, and P. Silvestroni, *Thermochimica Acta*, **1**, 311 (1970).
18) J. M. G. Cowie and P. M. Toporowski, *Can. J. Chem.*, **39**, 2240 (1961).
19) D. D. Macdonald and J. B. Hyne, *Can. J. Chem.*, **49**, 611 (1971).
20) K. J. Packer and D. J. Tomlinson, *Trans. Faraday Soc.*, **67**, 1302 (1971).
21) G. J. Safford, P. C. Schaffer, P. S. Leung, G. F. Doebbler, G. W. Brady, and E. F. X. Lyden, *J. Chem. Phys.*, **50**, 2140 (1969).
22) N. Desrosiers and J. E. Desnoyers, *Can. J. Chem.*, **54**, 3800 (1976).
23) R. A. Pierotti, *J. Phys. Chem.*, **67**, 1840 (1963); *ibid.*, **69**, 281 (1965).
24) K. Shinoda, *J. Phys. Chem.*, **81**, 1300 (1977).

Organopalladium(II) Complexes Containing Carbon-Bonded Heterocycles as a Ligand

Kiyoshi ISOBE,* Kazuharu NANJO, Yukio NAKAMURA, and Shinichi KAWAGUCHI†
Department of Chemistry, Faculty of Science, Osaka City University,
Sumiyoshi-ku, Osaka 558
†School of Medicine(Premedical Building), Kinki University,
Sayama-cho, Minamikawachi-gun, Osaka 589
(Received January 18, 1986)

Oxidative addition reactions of 2-chloropyridine, 2,6-dichloropyridine, 2-chloropyrazine, and 2-chlorobenzothiazole with tetrakis(triphenylphosphine)palladium(0) gave [{PdCl(R)(PPh_3)}$_2$] or *trans*-[PdCl(R)(PPh_3)$_2$] depending on the nature of the carbon-bonded heterocycles R. They are all stable and the chloride ligand is readily replaced by other halides and pseudohalides. These novel organopalladium(II) complexes were characterized by the analytical and molecular-weight data together with IR, ^{1}H NMR and ^{13}C NMR spectra, and the 2-pyridyl-bridged dinuclear structure of [{PdBr(C_5H_4N-C^2)(PPh_3)}$_2$] was previously revealed by X-ray analysis. Both of the dinuclear and mononuclear 6-chloro-2-pyridylpalladium(II) complexes catalyze the cross coupling reaction between 2,6-dichloropyridine and methylmagnesium bromide to afford 2-methyl-6-chloropyridine selectively. The mononuclear 6-chloro-2-pyridylpalladium(II) complexes react with carbon monoxide to form the acyl complexes.

The σ-pyridyl complexes are of considerable current interest in connection with adsorption of pyridine on metal surfaces during the catalytic reactions,[1] and a fair number of these complexes have been prepared with cobalt(III),[2] gold(I),[3] titanium(III),[4] rhenium(I),[5] palladium(II),[6] and other metals.[7] We also have extensively developed σ-pyridyl nickel(II)[8] and palladium(II)[9] complexes. In the course of the studies, both the mononuclear and the dinuclear 2-pyridyl palladium(II) complexes were important starting materials for preparation of the mixed-ligand complexes containing both the pyridyl ligand and the *O,O'*-chelated or *O*-unidentate β-diketonate anion.[10] This paper describes more detailed results on the preparation, characterization and some reactivities of palladium(II) complexes containing the σ-carbon-bonded pyridyl as well as pyrazinyl and benzothiazolyl ligands. The molecular structure of a dinuclear complex [{PdBr(μ-C_5H_4N-C^2, N)(PPh_3)}$_2$] has previously been reported.[11]

Experimental

Air-sensitive materials were handled under a nitrogen atmosphere unless otherwise stated. Solvents were redistilled under nitrogen and other reagents purged with nitrogen before use. Tetrakis(triphenylphosphine)palladium(0), Pd(PPh_3)$_4$, was prepared by Coulson's method.[12] Tertiary phosphines, halopyridines, 2-chloropyrazine, 2-chlorobenzothiazole, and Grignard reagents were purchased and used without further purification.

Preparation of [{PdX(R)(PPh_3)}$_2$] (R=C_5H_4N-C^2, X=Cl (1a) or Br (1b), and R=$C_4H_3N_2$-C^2, X=Cl (7)) and *trans*-[PdCl(R)(PPh_3)$_2$] (R=C_5H_3(6-Cl)N-C^2 (2a) or C_7H_4SN-C^2 (6)) by the Oxidative Addition. To a solution of Pd(PPh_3)$_4$ (4.21 g, 3.63 mmol) in toluene (50 cm^3) was added ca. ten times molar amount of 2-chloropyridine (4.12 g), 2-bromopyridine (5.74 g), or 2-chloropyrazine (4.16 g) and the mixture was heated to 90 °C for 10, 3, and 10 h, respectively. After standing for 5h at room temperature, yellow precipitates of **1a**, **1b**, and **7** were obtained in 60, 55, and 79% yields, respectively. Complexes **2a** and **6** were obtained in a similar manner by using 2,6-dichloropyridine or 2-chlorobenzothiazole as alkyl halide. A refrigerator was utilized for depositing precipitates from the reaction mixture. The yields were 95 (**2a**) and 80% (**6**).

Preparation of [{PdX(R)(PPh_3)}$_2$] (R=C_5H_4N-C^2, X=I (1c), N_3 (8a), NCO (8b), NCS (8c), or NCSe (8d), R=C_5H_3(6-Cl)N-C^2, X=N_3 (10a), NCO (10b), or NCS (10c)) and *trans*-[PdX(C_5H_3(6-Cl)N-C^2)(PPh_3)$_2$] (X=Br (2b), I (2c), N_3 (9a), NCO (9b), or NCS (9c)) by the Halide Substitution Reactions. Compound **1a** (0.14 g, 0.15 mmol) was dissolved in dichloromethane (50 cm^3) and methanol (20 cm^3) was added to the solution. Then a methaol solution (20 cm^3) of sodium iodide (4.5 g, 30 mmol) was added and the mixture was heated to 40 °C for 2 h. Dichloromethane was evaporated under reduced pressure and yellow crystals separated were filtered. The yield of **1c** was 80%. In a similar manner yellow dinuclear complexes **8** and **10** and white mononuclear complexes **2** and **9** were obtained by the halide substitution reactions of **2a** or **3a** with sodium bromide, iodide, pseudohalides and potassium selenocyanate. Solubility of sodium cyanate is low in methanol and aqueous methanol (1:3 by volume) was used as solvent. Yields of the metathesis reactions were 73 (**8a**), 65 (**8b**), 83 (**8c**), 52 (**8d**), 53 (**10a**), 48 (**10b**), 59 (**10c**), 90 (**2b**), 85 (**2c**), 81 (**9a**), 79 (**9b**), and 63% (**9c**), respectively.

Preparation of [{PdX(C_5H_3(6-Cl)N-C^2)(PPh_3)}$_2$] (X=Cl (3a), Br (3b), or I (3c)). To a suspension of **2a** (0.18 g, 0.23 mmol) in acetone (30 cm^3) was added dropwise an 0.05 cm^3 portion of 30% aqueous solution of hydrogen peroxide (ca. 0.44 mmol) by means of micropipette and the mixture was stirred. The initially white suspension turned yellow gradually. Stirring was continued for 24 h and the yellow precipitate was filtered. The yield of **3a** was 96%. Complexes **3b** and **3c** were derived from **3a** by the halide substitution reactions in 90 and 87% yields, respectively.

Complexes **3a—c** were also prepared via an alternative route. The perchlorato complex[9a] [{$PdClO_4$(C_5H_3(6-Cl)N-C^2)(PPh_3)}$_2$](0.12 g, 0.10 mmol) was dissolved in dichloro-

methane (50 cm^3). To the solution was added methanol (20 cm^3) followed by a methanol solution (20 cm^3) of a large excess amount of sodium chloride (1.8 g), bromide (3.1 g) or iodide (4.5 g), and the mixture was heated to 40 °C for 2 h. Dichloromethane was then evaporated under reduced pressure to precipitate crystals of **3a**, **3b**, and **3c** in 32, 83, and 89% yields, respectively.

Preparation of *trans*-[PdCl(C_5H_3(6-Cl)N-C^2)(PEt_3)$_2$] (4a), *trans*-[PdCl(C_5H_3(6-Cl)N-C^2)($PPhMe_2$)$_2$] (4b), and *trans*-[PdNCO(C_5H_3(6-Cl)N-C^2)(PEt_3)$_2$] (11). In order to prevent oxidation of phosphines during long-time reactions by a trace of oxygen accompanied by cylinder nitrogen, an argon atmosphere was employed for preparation of these complexes. Triethylphosphine (0.07 g, 0.63 mmol) or phenyldimethylphosphine (0.09 g, 0.63 mmol) was added to a suspension of complex **2a** (0.16 g, 0.21 mmol) in diethyl ether (20 cm^3), and the mixture was stirred at room temperature for 20 h to result in a clear colorless solution. After addition of petroleum ether (20 cm^3), the solution was cooled in a Dry Ice–methanol bath for 3 h to precipitate white crystals, which were filtered promptly. The yields of **4a** and **4b** were 40 and 60%, respectively. In a similar manner **11** was obtained in a 14% yield by the reaction of **9b** with triethylphosphine.

Preparation of [{PdCl(C_5H_4N-C^2)(PEt_3)}$_2$] (5). Triethylphosphine (0.06 g, 0.52 mmol) was added to a suspension of **1a** (0.13 g, 0.13 mmol) in diethyl ether (20 cm^3) and the mixture was stirred under argon at room temperature for 20 h to obtain a clear colorless solution, which was concentrated to 3 cm^3 by evaporation under reduced pressure and poured onto a column (ϕ1.5 cm×30 cm) of Aluminiumoxid 60 PF_{254} (Type E by Merck). Petroleum ether (150 cm^3) was used as an eluent to remove free triethyl- and triphenylphosphines. The complex was eluted by dichloromethane (70 cm^3) and the yellow solution was concentrated. Complex **5** was obtained in a 50% yield by adding petroleum ether to the concentrate.

Preparation of *trans*-[PdX(C_5H_3(6-Cl)N-C^2-CO)(PPh_3)$_2$] (X=Cl (12a), Br (12b), I (12c), or NCS (12d)). Carbon monoxide was bubbled through a tetrahydrofuran solution (50 cm^3) at room temperature containing ca. 0.1 mmol of **2a** (0.078 g), **2b** (0.082 g), **2c** (0.087 g), or **9c** (0.108 g). The colorless solution turned yellow on reaction. After evaporation under reduced pressure, diethyl ether was added to the concentrate (10 cm^3) to separate out yellow crystals. The CO bubbling was continued for 1, 5, 48, and 170 h in the case of X=I, Br, Cl, and NCS to attain the 73 (**12a**), 85 (**12b**), 80 (**12c**), and 82% (**12d**) yields, respectively.

All of the newly-prepared complexes were purified by recrystallization from dichloromethane–methanol (for **1**, **2**, **3**, **6**, **7**, **8**, **9**, and **10**), diethyl ether–petroleum ether (for **4**, **5**, and **11**), chloroform–diethyl ether (for **12a**, **12b**, and **12d**), or dichloromethane–diethyl ether (for **12c**).

Reactions of 2a with Chlorine, Iodine, and Methyl Iodide. Gaseous chlorine was passed for 10 min through a solution of **2a** (0.11 g, 0.13 mmol) in dichloromethane (20 cm^3). The initially colorless solution turned red. A 10 cm^3 portion of the solution was poured onto a column of Kieselgel 60 F_{254} (Merck). Diethyl ether was used as an eluent to isolate 2,6-dichloropyridine, which was identified by IR and ultraviolet spectra and elemental analysis. Found: C, 40.36; H, 2.11; N, 9.31%. Calcd for $C_5H_3NCl_2$: C, 40.58; H, 2.04; N, 9.46%. To the other 10 cm^3 portion of the red solution was added diethyl ether (40 cm^3) and the mixture was left standing for 3 h to deposit red crystals, which were identified to be di-μ-chloro-dichlorobis(triphenylphosphine)dipalladium(II) on the basis of IR spectra and elemental analysis. Found: C, 49.51; H, 3.89%. Calcd for $C_{36}H_{30}P_2Cl_4Pd_2$: C, 49.18; H, 3.44%. The yield was 78%.

A dichloromethane solution (10 cm^3) containing **2a** (0.11 g, 0.13 mmol) and iodine (0.03 g, 0.12 mmol) was stirred for 4 h to deposit a yellow precipitate, which was identified as **3c** by IR spectral assay. The yield was 70%. When methyl iodide (0.02 g, 0.13 mmol) was added dropwise to a solution of **2a** in dichloromethane (20 cm^3), the initially colorless solution turned yellow. After 24 h standing, the solution was concentrated to 10 cm^3 by evaporation under reduced pressure. Methanol (30 cm^3) was added to the concentrate and the mixture was allowed to stand 2 h to separate out orange crystals, which were identified as **2c** by IR spectroscopy. The yield was 65%.

Reactions of 8a and 9a with Carbon Monoxide. Carbon monoxide was bubbled for 4 h through a solution of **8a** (0.14 g, 0.138 mmol) in a mixture (50 cm^3) of dichloromethane and THF (1:1 by volume) and the mixture was stirred for five days in a sealed vessel. The solution was then concentrated to 20 cm^3 by evaporation under reduced pressure to deposit a pale yellow crystalline precipitate in a 95% yield, which was identified as **8b** on the basis of IR spectra and elemental analysis. Found: C, 58.30; H, 3.87; N, 5.30%.

In a similar manner carbon monoxide was passed for 4 h through a solution of **9a** (0.20 g, 0.256 mmol) in THF (50 cm^3). The solvent was evaporated to 10 cm^3 and diethyl ether (20 cm^3) was added to the concentrate to deposit a brown precipitate, which was washed thoroughly with methanol and dried. Recrystallization from dichloromethane–methanol afforded white crystals which were identified as **9b**. Found: C, 64.05; H, 4.11; N, 3.12%. When carbon monoxide was passed through the solution of **9a** for more than 4 h, the solution turned red gradually. After 10 h passage, the mixture was stirred for 2 days in a stoppered vessel. Then the solution was concentrated to 10 cm^3 by evaporation under reduced pressure and diethyl ether (30 cm^3) was added to the concentrate to deposit red crystals of $Pd_3(PPh_3)_3(CO)_3$. Found: C, 57.43; H, 4.04%. Calcd for $C_{57}H_{45}O_3P_3Pd_3$: C, 57.53; H, 3.81%.

Reaction of 12b with Methanol to Afford an Ester. When methanol (10 cm^3) was added to a solution of **12b** (0.11 g, 0.123 mmol) in chloroform (20 cm^3), color of the solution turned from red to brown. After standing for 24 h, the solvent was evaporated to dryness under reduced pressure and the residue was extracted with diethyl ether. Methyl 6-chloropicolinate in ether solution was identified by ^1H NMR spectroscopy: $\delta(CH_3)$, 4.01 s; $\delta(H^4$ and $H^5)$, 7.40 m; $\delta(H^3)$, 8.00 m ppm. The yield was 60%. IR assay showed that the residue contained *trans*-dibromobis(triphenylphosphine)palladium(II) and free triphenylphosphine.

Cross Coupling Reactions of Methylmagnesium Bromide with 2-Chloropyridine and 2,6-Dichloropyridine Catalyzed by 1a, 2a, and 3a. A solution of methylmagnesium bromide (13 mmol) in THF (13 cm^3) was added dropwise to

Table 1. Analytical Data for the σ-Pyridyl and Related Palladium(II) Complexes

Complex		Found(Calcd)			
		C (%)	H (%)	N (%)	Mol wt
[{PdCl(C_5H_4N-C^2)(PPh_3)}$_2$]	**1a**	57.72 (57.29)	4.10 (3.97)	2.81 (2.91)	945 (964)
[{PdBr(C_5H_4N-C^2)(PPh_3)}$_2$]	**1b**	52.38 (52.45)	3.64 (3.64)	2.67 (2.66)	1028 (1053)
[{PdI(C_5H_4N-C^2)(PPh_3)}$_2$]	**1c**	47.37 (48.15)	3.47 (3.34)	2.38 (2.44)	890[a] (1147)
[PdCl(C_5H_3(6-Cl)N-C^2)(PPh_3)$_2$]	**2a**	63.18 (63.22)	4.24 (4.27)	1.80 (1.80)	782 (779)
[PdBr(C_5H_3(6-Cl)N-C^2)(PPh_3)$_2$]	**2b**	60.07 (59.81)	4.03 (4.04)	1.70 (1.70)	810 (823)
[PdI(C_5H_3(6-Cl)N-C^2)(PPh_3)$_2$]	**2c**	55.81 (56.58)	3.79 (3.82)	1.57 (1.61)	853 (870)
[{PdCl(C_5H_3(6-Cl)N-C^2)(PPh_3)}$_2$]	**3a**	53.19 (53.47)	3.40 (3.51)	2.60 (2.71)	1023 (1033)
[{PdBr(C_5H_3(6-Cl)N-C^2)(PPh_3)}$_2$]	**3b**	48.52 (49.23)	3.18 (3.23)	2.43 (2.50)	1097 (1122)
[{PdI(C_5H_3(6-Cl)N-C^2)(PPh_3)}$_2$]	**3c**	44.70 (45.43)	2.88 (2.98)	2.12 (2.30)	b)
[PdCl(C_5H_3(6-Cl)N-C^2)(PEt_3)$_2$]	**4a**	41.43 (41.61)	6.95 (6.78)	2.86 (2.85)	487 (491)
[PdCl(C_5H_3(6-Cl)N-C^2)($PPhMe_2$)$_2$]	**4b**	47.25 (47.53)	4.76 (4.71)	2.44 (2.64)	523 (531)
[PdCl(C_5H_4N-C^2)(PEt_3)}$_2$]	**5**	38.84 (39.08)	5.58 (5.66)	4.22 (4.14)	673 (676)
[PdCl(C_7H_4SN-C^2)(PPh_3)$_2$]	**6**	64.09 (64.51)	4.36 (4.28)	1.60 (1.75)	783 (801)
[{PdCl($C_4H_3N_2$-C^2)(PPh_3)}$_2$]	**7**	54.09 (54.68)	3.71 (3.76)	5.78 (5.80)	961 (967)
[{PdN_3(C_5H_4N-C^2)(PPh_3)}$_2$]	**8a**	55.81 (56.52)	3.86 (3.92)	10.90 (11.46)	905 (978)
[{PdNCO(C_5H_4N-C^2)(PPh_3)}$_2$]	**8b**	57.88 (58.97)	3.99 (3.92)	5.45 (5.73)	966 (978)
[{PdNCS(C_5H_4N-C^2)(PPh_3)}$_2$]	**8c**	56.80 (57.10)	3.61 (3.79)	5.11 (5.55)	967 (1010)
[{PdNCSe(C_5H_4N-C^2)(PPh_3)}$_2$]	**8d**	50.08 (52.24)	3.42 (3.47)	4.70 (5.08)	
[PdN_3(C_5H_3(6-Cl)N-C^2)(PPh_3)$_2$]	**9a**	62.73 (62.67)	4.31 (4.23)	6.89 (7.13)	687 (786)
[PdNCO(C_5H_3(6-Cl)N-C^2)(PPh_3)$_2$]	**9b**	64.08 (64.22)	4.30 (4.23)	3.33 (3.57)	695 (786)
[PdNCS(C_5H_3(6-Cl)N-C^2)(PPh_3)$_2$]	**9c**	62.76 (62.93)	4.12 (4.15)	3.61 (3.50)	703 (802)
[{PdN_3(C_5H_3(6-Cl)N-C^2)(PPh_3)}$_2$]	**10a**	52.45 (52.80)	3.50 (3.47)	10.83 (10.71)	1022 (1047)
[{PdNCO(C_5H_3(6-Cl)N-C^2)(PPh_3)}$_2$]	**10b**	54.70 (55.09)	3.50 (3.47)	5.01 (5.38)	1007 (1047)
[{PdNCS(C_5H_3(6-Cl)N-C^2)(PPh_3)}$_2$]	**10c**	53.30 (53.45)	3.37 (3.36)	5.21 (5.19)	1024 (1079)
[PdNCO(C_5H_3(6-Cl)N-C^2)(PEt_3)$_2$]	**11**	43.56 (43.48)	6.60 (6.69)	5.52 (5.63)	488 (497)
[PdCl(C_5H_3(6-Cl)N-C^2-CO)(PPh_3)$_2$]	**12a**	62.48 (62.51)	4.25 (4.12)	1.68 (1.74)	801[c] (807)
[PdBr(C_5H_3(6-Cl)N-C^2-CO)(PPh_3)$_2$]	**12b**	59.27 (59.25)	4.09 (3.91)	1.66 (1.65)	831[c] (851)
[PdI(C_5H_3(6-Cl)N-C^2-CO)(PPh_3)$_2$]	**12c**	55.81 (56.15)	3.70 (3.70)	1.56 (1.56)	827 (898)
[PdNCS(C_5H_3(6-Cl)N-C^2-CO)(PPh_3)$_2$]	**12d**	62.26 (62.25)	4.20 (4.01)	3.25 (3.38)	827[c] (830)

a) The value is unreliable due to low solubility. b) Undetermined because of poor solubility. c) Determined in chloroform.

a THF solution (50 cm^3) containing **1a** (0.10 g, 0.10 mmol) and 2-chloropyridine (1.14 g, 10 mmol), but the reaction did not occur at room temperature, the solution maintaining yellow color. When the solution was heated under reflux (about 66 °C), the reaction took place, color of the solution changing via reddish brown to deep green. After the reaction for 5 h, a 10 cm^3 aliquot was evaporated under reduced pressure and the residue was extracted with diethyl ether (20 cm^3). The ether solution was concentrated to 1 cm^3 and applied to the GLC analysis. 2-Methylpyridine was identified in a 13% yield accompanied by unreacted 2-chloropyridine. Prolonged refluxing did not improve the yield of 2-methylpyridine.

A mixed THF solution (55 cm^3) containing **2a** (0.14 g, 0.183 mmol), triphenylphosphine (4.81 g, 18.3 mmol), 2,6-dichloropyridine(2.96 g 20 mmol), and methylmagnesium bromide (25 mmol) was heated under reflux for 3 h. The resulting brown solution was concentrated and made up to 50 cm^3. 2-Methyl-6-chloropyridine was identified by GLC in a 53% yield accompanied by unreacted 2,6-dichloropyridine.

A mixed THF solution (55 cm^3) containing **3a** (0.09 g, 9.14×10^{-5} mol), 2,6-dichloropyridine (2.96 g, 20 mmol), and methylmagnesium bromide (25 mmol) was refluxed for 3 h. The resulting brown solution was concentrated and made up to 50 cm^3. 2,6-Dimethylpyridine was identified in a 4% yield in this case together with 2-methyl-6-chloropyridine (58% yield) and unreacted 2,6-dichloropyridine.

Measurements. IR spectra were recorded in Nujol on JASCO IR-E (4000-650 cm^{-1}), Hitachi EPI-L (700-200 cm^{-1}) and FIS-3 (400-30 cm^{-1}) spectrophotometers. ^1H NMR spectra were taken at 100 MHz with JEOL JNM MH-100 and PS-100 spectrometers using tetramethylsilane as internal reference. ^{13}C NMR spectra were obtained at 25.0 MHz by 6000 times scan on a JEOL JNM FX-100 instrument with tetramethylsilane as external reference. ^{15}N NMR spectra were recorded at 9.04 MHz by 3000 times scan on a JEOL JNM FX-90Q spectrometer with ammonium nitrate-^{15}N aqueous solution as external reference. Mass spectra were taken with a JEOL GC-mass spectrometer JMS D-300 and gas chromatography was performed on a Yanagimoto G-180 instrument with Silicone DC-550 and nitrogen gas, injection temperature being 200 °C. The decomposition temperatures of the newly-prepared compounds were determined in a capillary tube under nitrogen. The molecular weight was measured in dichloromethane at 25 °C by vapor pressure osmometry with an instrument manufactured by Knauer in Berline, West Germany.

Results and Discussion

Although tetrakis(triphenylphosphine)nickel(0) reacted readily with halopyridines in toluene at room temperature,[8] the reactions of $Pd(PPh_3)_4$ with halopyridines did not occur at room temperature, but heating for a long time, e.g. 3 h for 2-bromopyridine and 10 h for 2-chloropyridine at 90 °C, was necessary to afford the pyridylpalladium(II) complexes in high yields. 2-Chloropyrazine and 2-chlorobenzothiazole also reacted with $Pd(PPh_3)_4$ in toluene at 90 °C to produce the σ-carbon-bonded complexes in ca. 80% yields, although the 2-benzothiazolylnickel(II) complex could not be prepared.[8] Results of elemental analysis and molecular weight determination of newly-prepared complexes are collected in Table 1.

Properties of Halogeno 2-Pyridyl and Related Complexes. The analytical and molecular-weight data for compounds **1a—c**, **3a—c**, **5**, and **7** indicate that they are essentially dinuclear, although the observed molecular weight of **1c** in dichloromethane is appreciably lower than the calculated value. The dinuclear structure with bridging halide anions is quite common among palladium(II) complexes,[13] and is usually subject to cleavage by bonor ligands to give mononuclear species.

As is seen in Table 2, the ν(Pd-X) frequencies observed for **1a—c** are not unreasonable for the bridging halides. However the dinuclear structure in these complexes is very stable and is not cleaved by excess bases such as triphenylphosphine, pyridine, and thiourea. X-Ray analysis denied the halide-bridged structure and disclosed the bridging role of the 2-pyridyl ligand in **1b** (Fig. 1).[11] A similar μ-pyridyl(C^2,N) structure was also confirmed for (μ-H)$Re_2(CO)_8$(μ-C_5H_4N-C^2,N) and (μ-H)$Re_2(CO)_7$(μ-C_5H_4N-C^2,N)(Me_3NO).[5b] Basicity of the 2-pyridyl ligand coordinated to palladium(II) was reported to be 3700 times greater than that of free pyridine.[9b] This enhanced basicity enables the stable bridging of the 2-pyridyl ligand.*1 A similar bridged structure

Table 2. Decomposition Temperatures and Some FIR Data

Complex	Decomp temp[a] °C	ν(Pd-X) cm^{-1}	ν(Pd-P) cm^{-1}
1a	196	263 m	420 s
1b	185	196 m	420 m
1c	140	144 w	420 m
2a	250 (232)	295 s	351 m
2b	240 (230)	187 s	350 m
2c	205	172 s	346 s
3a	205	278 m	380 m
3b	197	221 m	379 m
3c	195	174 w	376 m
4a	249 (65)	300 s	350 m
4b	233 (117)	292 m	348 m
5		260 s	420 m
6	197	302 s	364 w
7	197	270 m	430 m

a) Numerals in parentheses give melting points in °C. s: strong, m: medium, w: weak.

*1 The reaction of $LPd_2(CH_3CO_2)$ (L=bridging benzenethiolate derivatives) with pyridines containing electron-donating substituents (X) at the 3-position also gave $LPd_2(C_5H_3XN$-C^2,$N)$ in low yields.[6]

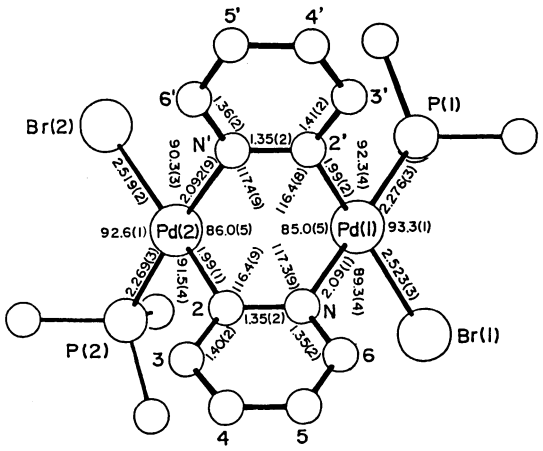

Fig. 1. Stereochemistry of *trans*-(*P*, *N*)-[{PdBr(μ-C_5H_4N-C^2,*N*)(PPh_3)}$_2$] (**1b**) viewed perpendicular to the plane containing C(2), N, C(2′), and N′. Phenyl groups are not shown for clarity, except the three carbon atoms bonded to each phosphorus atom. Important bond lengths (in Å) and angles (in degree) are also given with e.s.d.'s in parenthsses.[11]

has also been presumed for the 2-pyridyl group involved in triosmium clusters[7b] and a gold(I) complex[3] in which the 2-pyridyl ligand serves as a three-electron donor.

Complex **1a** was prepared under the same conditions as **1b**, and **1c** was derived from **1a** by the halide substitution. The patterns of ^{1}H NMR and IR spectra for **1a—c** are quite similar to each other. Furthermore, all of the IR absorption bands of these complexes in the region 1600—300 cm^{-1} are superimposable on each other within experimental errors. These facts suggest that **1a**, **1b**, and **1c** will have the identical structure. The ν(Pd–P) frequencies (in Table 2) are close to each other and the ν(Pd–Cl):ν(Pd–Br):ν(Pd–I) ratio (1:0.75:0.55) is similar to the value 1:0.75:0.61 observed for *trans*-$PdX_2(PEt_3)_2$ (X=Cl, Br, and I, respectively) and 1:0.73 for *cis*-$PdX_2(PMe_3)_2$ (X=Cl and Br).[14] Thus complexes **1a** and **1c** are considered to have the pyridyl-bridged structure analogous to **1b**. In each complex the halide anion occupies the coordination site trans to the pyridyl carbon, and the rather lower frequencies of the ν(Pd–X) vibrations are caused by the strong trans influence of the σ-carbon-bonded pyridyl ligand. Thermal stabilites of these complexes are in the sequence of **1a**>**1b**>**1c**. Stronger trans influence of the iodide anion compared with that of chloride may destabilize the Pd–C linkage.

When 2,6-dichloropyridine was used as a reagent, the mononuclear 6-chloro-2-pyridyl complexes **2a—c** were obtained. Complexes **4a** and **4b**, which were derived from **2a** by the phosphine exchange reactions, and the benzothiazolyl complex **6** are also mononuclear. When a dichloromethane solution of **2a** was allowed to stand at room temperature for a long time as weeks, one of the phosphine ligands was lost to form **3a**. A precipitate of **3a** thus produced was readily reconverted to **2a** on addition of excess triphenylphosphine, indicating that reaction (1) is reversible.

$$2[PdCl(C_5H_3(6\text{-}Cl)N\text{-}C^2)(PPh_3)_2] \rightleftarrows [\{PdCl(C_5H_3(6\text{-}Cl)N\text{-}C^2)(PPh_3)\}_2] + 2PPh_3 \quad (1)$$

By oxidizing the freed phosphine equilibrium (1) was shifted to right to obtain **3a** conveniently.[15] As was described in Experimental section, the reaction of $Pd(PPh_3)_4$ with 2,6-dichloropyridine gave **2a** exclusively without appreciable contamination with **3a** in spite of much lower solubility of the latter, indicating that the thermodynamic stability of **2a** is much higher than that of **3a**. A molecular model suggests that the dinuclear structure of **3a** analogous to **1b** is unfavorable because of the steric interaction between the chloro substituent on the pyridine ring and the benzene rings.

Mononuclear complexes **2a—c** are thermally more stable than the corresponding dinuclear complexes **3a—c**, the Cl>Br>I sequence holding again in either case, and **2a**, **2b**, **4a**, and **4b** showing clear melting points. The mononuclear complexes exhibit a single ν(Pd–X) band in the region reasonable for the terminal halide trans to the carbon-bonded organic ligand,[16] and a single ν(Pd–P) band at about 350 cm^{-1} in accordance with the trans structure. Data of ^{1}H NMR spectra included in Table 3 also support the trans structure. Thus the methyl protons of triethylphosphine in **4a** resonate at 1.11 ppm as a 1:4:6:4:1 quintet[17] with J=ca. 8.0 Hz and the methyl protons of phenyldimethylphosphine in **4b** at 1.53 ppm as a 1:2:1 triplet.[18]

As is shown in Table 3, the ring protons of triphenylphosphine in complex **1** through **7** resonate generally as two multiplets with the area ratio of 3:2 in the 7.33—7.42 and 7.45—7.86 ppm regions, respectively. The higher-field signal is assigned to the meta and para protons and the lower-field one to the ortho protons.[19] The pyridine-ring protons were assigned in a similar manner as those of the pyridylnickel(II) complexes.[8] In the case of the 2-benzothiazolyl complex **6**, signals of the hetero-ring protons overlapped with those of the benzene-ring protons.

The most remarkable feature of the ^{1}H NMR data for the 2-pyridyl complexes containing triphenylphosphine as the ancillary ligands is the up-field shift of the resonances of pyridine-ring protons at the 3, 4, and 5 positions as compared with those of uncoordinated pyridine (H^2 8.5, H^3 7.2, H^4 7.6 ppm), although the chemical shifts of pyridine-ring protons in **1a** and some other complexes such as **3a** and **4b** are so close to each other, exhibiting composite signals.

Table 3. Proton Chemical Shifts from Internal Me_4Si in CD_2Cl_2 (ppm)

Complex	Hetero-ring proton at the position 3	4	5	6	Benzene-ring proton at the position meta and para	ortho	Other protons
1a	———	(6.56 m)	———	8.47 m	7.36 m	7.86 m	
2a	6.13 d	6.29 t	6.64 d		7.42 m	7.65 m	
3a		(6.53 m)			7.33 m	7.45 m	
4a	6.72 d	7.05 t	7.13 d				1.11 quin (CH_3),[b] 1.57 m (CH_2)
4b	———	(6.70 m)	———		7.38 m	7.53 m	1.53 t (CH_3)
5	7.17 s	7.10 t	6.76 t	8.36 s			1.14 quin (CH_3),[c] 1.83 m (CH_2)
6					7.33 m	7.70 m	7.01 m (thiazolyl H)
7	8.40 m		———	(7.83 m) —	7.38 m	7.83 m	
8a	———	(6.64 m)	———	8.39 m	7.41 m	7.75 m	
8b	———	(6.63 m)	———	8.37 m	7.43 m	7.80 m	
8c	———	(6.60 m)	———	8.36 m	7.47 m	7.78 m	
9a	6.14 d	6.27 t	6.62 d		———	(7.39 m) ———	
9b	6.12 d	6.26 t	6.62 d		———	(7.42 m) ———	
9c	6.15 d	6.27 t	6.59 d		———	(7.44 m) ———	
10a	———	(6.70 m)	———		7.48 m	7.84 m	
10b	———	(6.66 m)	———		7.47 m	7.87 m	
10c	———	(6.67 m)	———		7.43 m	7.82 m	
11	7.13 m	6.79 m	7.13 m				1.09 quin (CH_3),[d] 1.50 m (CH_2)
12a[a]	— (6.90 m)	———		6.00 d	7.22 m	7.72 m	

a) In $CDCl_3$. b) 1 : 4 : 6 : 4 : 1 quintet with J=ca. 8.0 Hz. c) 1 : 2 : 2 : 2 : 1 quintet with ^3J(P-H)=ca. 17.0 Hz and ^3J(H-H)=ca. 8.5 Hz. d) 1 : 4 : 6 : 4 : 1 quintet with J=ca. 4.0 Hz. s: singlet, d: doublet, t: triplet, quin: quintet, m: multiplet.

Table 4. ^{13}C NMR Data for Complex **1b** and Uncoordinated Triphenylphosphine and Pyridine

Compound	Chemical shift (ppm)					Coupling constant (Hz)
$P(C_6H_5)_3$	C^1 138.3	C^2 134.4	C^3 129.2	C^4 129.3		J(P-C^1)=21, J(P-C^2)=20 J(P-C^3)=7, J(P-C^4)<1
C_5H_5N	C^2, C^6 149.7	C^3, C^5 123.6	C^4 135.5			
1b						
Phenyl carbon	C^1 138.6	C^2 143.0	C^3 135.3	C^4 139.7		J(P-C^1)=49, J(P-C^2)=11.7 J(P-C^3)=10.7, J(P-C^4)=0
Pyridyl carbon	C^2 200.5	C^3 124.5	C^4 140.3	C^5 124.4	C^6 161.7	

On the other hand, there was no significant up-field shift observed for the pyridine-ring proton resonances in the 2-pyridyl complexes containing triethylphosphine such as **5**, rhenium carbonyls,[5] and osmium clusters.[7b] Thus the up-field shift of pyridine-ring proton resonances seems to be caused by an anisotropic shielding effect of the triphenylphosphine ligand through space[20] as well as by the back-donation from palladium to the pyridine ring via the carbon atom. In fact, according to X-ray analysis of **1b**,[11] the pyridine-ring protons at the 3, 4, and 5 positions lie in the vicinity of a benzene ring of the triphenylphosphine ligand, whereas the proton at the 6 position is far from it.

Table 4 shows the ^{13}C NMR data for **1b** together with those for uncoordinated triphenylphosphine[21] and pyridine.[22] Assignment of the phenyl carbons in **1b** was readily made on the basis of J(P-C) values and also by reference to the data for the uncoordinated phosphine. It is worth noting that the J(P-C^1) value (49 Hz) is more than twice larger than the value (21 Hz) for the free ligand and that (20 Hz) for the corresponding nickel(II) complex.[8] Assignment of the pyridyl carbons in **1b** was based on

the results for *trans*-PdBr(C_5H_4N-C^2)(PEt_3)$_2$ which were obtained by the proton off-resonance and selective decoupling experiments.[9b] Pyridyl carbons are more or less deshielded on bonding to palladium(II) through C^2, and the down-field shift of C^2 is astonishingly large. The effect of coordination is quite different from the nickel(II) complexes where both the ^{13}C and ^1H signals showed up-field shifts probably due to the back donation from the metal atom. No reasonable rationalization of the palladium(II) case is possible at the present stage of investigation.

Characterization of the Pseudohalogeno σ-Pyridyl Complexes. The dinuclear pseudohalogeno complexes **8a—d** and **10a-c** were prepared by simple metathesis reactions of **1a** and **3a**, respectively, with the pseudohalides in good yields. It should be noted that the bridge-splitting reactions to give rise to anionic pyridyl complexes did not occur, but simple substitution of the halide ligands was resulted.

As is seen in Table 3, the patterns of ^1H NMR spectra for **8a—c** and the chemical shifts of pyridine and benzene-ring protons in these complexes are quite similar to each other. Compounds **10a—c** also exhibit a close resemblance to **8a—c** in the spectral patterns except for lacking of the pyridine H^6 resonance. These facts strongly suggest that all these complexes have a common bridging mode.

Complex **10c** containing the ^{15}NCS ligand (95% ^{15}N) was prepared and the ^{15}N NMR spectrum was measured in CD_2Cl_2. As Fig. 2 shows, a single doublet with J(P—N)=ca. 3.2 Hz is observed at −235.61 ppm up-field from external $NH_4{}^{15}NO_3$. The coupling constant of ^{15}N to ^{31}P situated at the trans position in *cis*-PtNCS(SCN){$P(OEt)_3$}$_2$[23] and PtNCS(SCN)($Ph_2PCH_2C(CF_3)$=CHPPh_2)[24] was found to be 91 and 53.71 Hz, respectively, whereas that of ^{15}N to the cis ^{31}P in either complex was too small to be detected. The small value of ^{31}P–^{15}N coupling constant in **10c** indicates that the N-bonded thiocyanate ligand occupies the coordination site cis to the phosphine.

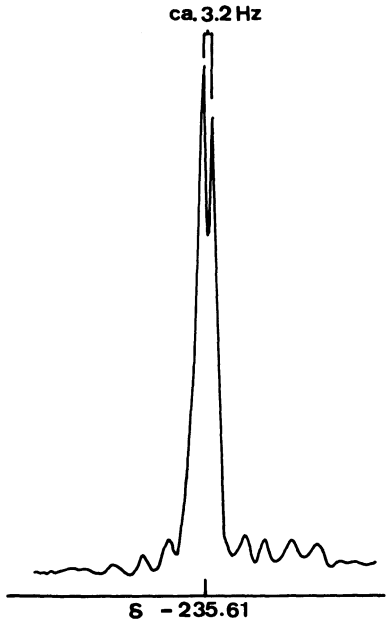

Fig. 2. ^{15}N NMR spectrum of diisothiocyanatobis(6-chloro-2-pyridyl)bis(triphenylphosphine)dipalladium(II) (**10c**) in CD_2Cl_2 by 3000 times scan at 9.04 MHz. The chemical shift is measured from external $NH_4{}^{15}NO_3$ (up-field negative).

Compounds **9a—c** were also prepared by the ligand substitution reactions of **2a**, and **11** was obtained from the reaction between **9b** and excess triethylphosphine. The trans mononuclear structure of these complexes is evidenced by the analytical and molecular-weight data in Table 1 and by the single ν(Pd-P) band around 350 cm^{-1} (Table 5). The quintet resonance at 1.09 ppm exhibited by the methyl protons of triethylphosphine in **11** (Table 3) also supports the trans structure of this complex.[17]

Infrared spectra are frequently useful in distinguishing the linkage mode of the pseudohalides in metal complexes.[25] Frequencies of the ν(CN) and ν(CS) vibrations observed for **8c**, **9c**, **10c**, and **12d** indicate that each NCS ligand in these complexes is N-bonded. Similarly the ν(CN), ν(CO), and δ(NCO) frequencies for the cyanate ligand in **8b**, **9b**, **10b**, and **11** (Table 5) are in the range assigned to N-bonding.[25] A related compound *trans*-PdNCS(C_5H_4N-C^3)(PPh_3)$_2$ was confirmed by X-ray analysis to have the N-bonded thiocyanato ligand.[26]

Reactions of the 2-Pyridylpalladium(II) Complexes. The pyridyl-palladium(II) bond is very strong and is not cleaved by methyl iodide and elementary iodine. Thus compound **2a** was merely

Table 5. Characteristic IR Data for the Pseudohalogeno Complexes[a]

Complex	ν(CN) or ν_a(NNN)	ν(CY) or ν_s(NNN)	δ(NCY) or δ(NNN)	ν(Pd-P)
8a	2044 s	1339 m	590 w	420 m
8b	2230 s	1330 m	605 m	425 m
8c	2090 s	810 w	b)	420 m
8d	2100 s	b)	b)	425 m
9a	2070 s	1337 m	597 w	347 m
9b	2220 s	1330 m	606 m	336 m
9c	2053 s	816 w	b)	353 w
10a	2050 s	1342 m	595 w	380 m
10b	2220 s	1336 m	604 m	381 m
10c	2053 s	815 w	b)	378 w
11	2240 s	1328 m	603 m	354 m
12d	2054 s	812 w	b)	b)

a) Y=O, S, or Se. b) Indiscernible.

converted to **2c** and **3c**, respectively. Iodine seems to have shifted the mononuclear-dinuclear equilibrium analogous to Eq. 1 to right by oxidizing the freed phosphine. Benzoyl chloride did not react with **2a** in dichloromethane at room temperature. On the other hand gaseous chlorine cleaved the Pd-C bond to afford 2,6-dichloropyridine.

Complexes **2a—c** and **9c** readily reacted with carbon monoxide to afford the pyridylcarbonyl complexes **12a—d**, which have the trans mononuclear structure as evidenced by the analytical and molecular-weight data as well as the existence of a single ν(Pd–P) band. Each of these complexes shows two ν(CO) bands in the frequency region reasonable for the acyl complex:[27] **12a**, 1661 and 1639 cm^{-1}; **12b**, 1663 and 1640 cm^{-1}; **12c**, 1672 and 1640 cm^{-1}, **12d**, 1673 and 1650 cm^{-1}. Compound **12b** reacted with methanol to produce methyl 6-chloropicolinate in a good yield. The reaction proceeded in the absence of base and the nucleophilic attack by the methanol molecule on the acyl carbon seems to have occurred. A proton must have been freed in this event, but the picolinate nitrogen is not protonated. Although ^{1}H NMR assay at low temperature (−40 to −60 °C) failed to detect a hydrido complex, the following sequence might be responsible for the overall reaction.

$$[PdBr(COR)(PPh_3)_2]+CH_3OH \rightarrow [PdBr(H)(PPh_3)_2]+RCOOCH_3$$

$$2[PdBr(H)(PPh_3)_2] \rightarrow [PdBr_2(PPh_3)_2]+Pd^0+2\,PPh_3+H_2.$$

The azide ligand in **8a** reacted with carbon monoxide to afford **8b**, which is the stable end product and did not react further with CO to give rise to an acyl complex, although carbonylation of the terminal azide ligand to isocyanate has been reported to occur readily for a number of metal complexes.[28] On the other hand, the mononuclear complex **9a** reacted with CO in two steps, a limited amount of CO converting the azide ligand to the isocyanate to result in **9b** and an additional amount of CO carbonylating the pyridyl ligand. The CO insertion into the Pd–pyridyl bond is appreciably slower than the reaction of the azide ligand with CO, and a small amount of $Pd_3(PPh_3)_3(CO)_3$[29] was produced by partial decomposition. Unfortunately, the product acyl complex analogous to **12d** could not be isolated in a satisfactory purity, but was characterized by the IR spectra (ν(CO)=1680 cm^{-1}).

It should be noted that only the pyridyl ligand in mononuclear complexes reacts with CO, while that in dinuclear complexes does not. The palladium–carbon bond in the latter complexes may be strengthened synergistically by the bridging of the pyridyl ligand to another metal atom through nitrogen so as to prevent CO insertion.

Cross Coupling Reactions. In recent years cross coupling reactions between organic halides and Grignard reagents have been found to be catalyzed by the nickel(II) and palladium(II) phosphine complexes.[30,31] Although $[\{NiCl(C_5H_4N\text{-}C^2)(PPh_3)\}_2]$ selectively catalyzes the cross coupling of 2-chloropyridine with methylmagnesium bromide in THF at room temperature,[8] the palladium(II) complex **1a** does not work as a catalyst under the same conditions. In refluxing THF, the catalytic coupling reaction does occur with **1a**, but the yield of 2-methylpyridine was as low as 13% when 1/100 molar amount of **1a** was added to 2-chloropyridine. Complex **3a** is more effective as a catalyst for the reaction of 2,6-dichloropyridine with methylmagnesium bromide in refluxing THF to give 2-methyl-6-chloropyridine in a 58% yield, reflecting the lability of **3a** compared with **1a**. In the presence of excess triphenylphosphine to prevent transformation of **2a** to **3a**, the mononuclear complex **2a** similarly attains the 53% yield of the product. On the other hand, the yield of 2,6-dimethylpyridine from 2,6-dichloropyridine was only 4% in the case of **3a** and was negligibly small when **2a** was used, although the nickel(II) catalyst was reported to promote the Grignard coupling of organo dihalides at both the reaction sites.[30] It is worth noting that the palladium(II) catalysts are less active but are more selective than the nickel(II) complexes for the synthesis of 2-methyl-6-chloropyridine. The selectivity of palladium(II) catalysts shown in the alkylation is analogous to that observed in the cross cou ling reactions of 2,6-dihalopyridines with $PhCH_2ZnBr$ in the presence of $Pd(PPh_3)_4$ as a catalyst.[32]

We wish to express our thanks to Mr. Junichi Gohda and Dr. Takamasa Kinoshita for elemental analyses and ^{13}C NMR measurements, respectively and to Mr. Tetsu Hinomoto of JEOL, Ltd. for ^{15}N NMR measurements.

References

1) R. M. Wexler, M.-C. Tsai, C. M. Friend, and E. L. Muetterties, *J. Am. Chem. Soc.*, **104**, 2034 (1982) and references cited therein.

2) J. Halpern and J. P. Maher, *J. Am. Chem. Soc.*, **87**, 5361 (1965).

3) L. G. Vaughan, *J. Am. Chem. Soc.*, **92**, 730 (1970).

4) E. Klei and J. H. Teuben, *J. Chem. Soc., Chem. Commun.*, **1978**, 659; *J. Organomet. Chem.*, **214**, 53 (1981).

5) a) D. R. Gard and T. L. Brown, *Organometallics*, **1** 1143 (1982); b) P. O. Nubel, S. R. Wilson, and T. L. Brown, *ibid.*, **2**, 515 (1983).

6) R. Robson, *Inorg. Chim. Acta*, **57**, 71 (1982).

7) a) J. Cooke, M. Green, and F. G. A. Stone, *J. Chem. Soc. (A)*, **1968**, 173; b) C. C. Yin and A. J. Deeming, *J. Chem. Soc., Dalton Trans.*, **1975**, 2091; c) A. Dormond, A. A. El Bouadili, and C. Moise, *J. Chem. Soc., Chem. Commun.*, **1985**, 914.

8) K. Isobe, Y. Nakamura, and S. Kawaguchi, *Bull. Chem. Soc. Jpn.*, **53**, 139 (1980).

9) a) K. Isobe, K. Nanjo, Y. Nakamura, and S.

Kawaguchi, *Chem. Lett.*, **1979**, 1193; b) K. Isobe, E. Kai, Y. Nakamura, K. Nishimoto, T. Miwa, S. Kawaguchi, K. Kinoshita, and K. Nakatsu, *J. Am. Chem. Soc.*, **102**, 2475 (1980); c) K. Isobe and S. Kawaguchi, *Heterocycles*, **16**, 1603 (1981).

10) H. Tanaka, K. Isobe, S. Kawaguchi, and S. Okeya, *Bull. Chem. Soc. Jpn.*, **57**, 456 (1984); H. Tanaka, K. Isobe, S. Kawaguchi, and S. Okeya, *ibid.*, **57**, 1850 (1984).

11) K. Nakatsu, K. Kinoshita, H. Kanda, K. Isobe, Y. Nakamura, and S. Kawaguchi, *Chem. Lett.*, **1980**, 913.

12) D. R. Coulson, *Inorg. Synth.*, **13**, 121 (1972).

13) F. A. Cotton and G. Wilkinson, "Advanced Inorganic Chemistry," 4th ed., Interscience, New York (1980), p. 952.

14) D. A. Duddell, P. L. Goggin, R. J. Goodfellow, M. G. Norton, and J. G. Smith, *J. Chem. Soc. (A)*, **1970**, 545.

15) e.g. R. Ros, M. Lenarda, T. Boschi, and R. Roulet, *Inorg. Chim. Acta*, **25**, 61 (1977).

16) For instance the ν(Pd-Cl) frequencies for *trans*-[PdCl(C_6H_4X)(PPh_3)$_2$] with various substituents X lie in the 284—309 cm^{-1} region: P. Fitton and E. A. Rick, *J. Organomet. Chem.*, **28**, 287 (1971).

17) G. W. Parshall, *J. Am. Chem. Soc.*, **88**, 704 (1966).

18) J. M. Jenkins and B. L. Shaw, *J. Chem. Soc. (A)*, **1966**, 770.

19) R. Keat, *Chem. Ind. (London)*, **1968**, 1362.

20) S. Baba, T. Ogura, and S. Kawaguchi, *Bull. Chem. Soc. Jpn.*, **47**, 665 (1974).

21) O. A. Gansow and B. Y. Kimura, *J. Chem. Soc., Chem. Commun.*, **1970**, 1621.

22) H. L. Retcofsky and R. A. Friedel, *J. Phys. Chem.*, **72**, 2619 (1968).

23) A. J. Carty and S. E. Jacobson, *J. Chem. Soc., Chem. Commun.*, **1975**, 175.

24) A. J. Carty, *Inorg. Chem.*, **15**, 1956 (1976).

25) R. A. Bailey, S. L. Kozak, T. W. Michelsen, and W. N. Mills, *Coord. Chem. Rev.*, **6**, 407 (1971); A. H. Norbury, *Advan. Inorg. Chem. Radiochem.*, **17**, 231 (1975).

26) K. Nakatsu and K. Kinoshita, private communication.

27) P. M. Maitlis, "The Organic Chemistry of Palladium," Academic Press, New York (1971), Vol. 2.

28) Z. Dori and R. F. Ziolo, *Chem. Rev.*, **73**, 247 (1973).

29) K. Kudo, M. Hidai, and Y. Uchida, *J. Organomet. Chem.*, **33**, 393 (1971).

30) K. Tamao, K. Sumitani, and M. Kumada, *J. Am. Chem. Soc.*, **94**, 4374 (1972); K. Tamao, S. Kodama, T. Nakatsuka, Y. Kiso, and M. Kumada, *ibid.*, **97**, 4405 (1975); K. Tamao, K. Sumitani, Y. Kiso, M. Zembayashi, A. Fujioka, S. Kodama, I. Nakajima, A. Minato, and M. Kumada, *Bull. Chem. Soc. Jpn.*, **49**, 1958 (1976).

31) A. Sekiya and N. Ishikawa, *J. Organomet. Chem.*, **118**, 349 (1976).

32) A. Minato, K. Tamao, T. Hayashi, K. Suzuki, and M. Kumada, *Tetrahedron Lett.*, **21**, 845 (1980).

Magnetic Circular Dichroism Spectra of Cobalt(III) Complexes in the Second d-d Absorption Band Region

Nobuko MATSUOKA
Department of Chemistry, Faculty of Science, Osaka University, Toyonaka, Osaka 560
(Received February 24, 1986)

The MCD spectra of seventeen cobalt(III) complexes were measured in the visible and near-ultraviolet regions. Their behavior in the second d-d absorption band region were compared with those of the [Co(ox)$_x$(gly)$_y$(en)$_z$] series comprising sixteen complexes (x, y, z=0, 1, 2, 3; and $x+y+z=3$), in which a positive band had been observed on the lower-energy side of the main negative band in this region. For the present work, the positive band was found in [Co(tn)$_3$]$^{3+}$, *cis*-[Co(ox)$_2$(NH$_3$)$_2$]$^-$, *cis*-[Co(OH$_2$)$_2$(en)$_2$]$^+$, *trans*-[Co(β-ala)$_2$(en)]$^+$, *mer*- and *fac*-[Co(picol)$_3$] (picol=picolinate(1−)), and [Co(acac)$_3$]. It is pointed out that all the complexes exhibiting a positive band were the tris(chelate) or *cis*-bis(chelate) types. Therefore the origin of this band is discussed in terms of the arrangement of two or three chelate rings. A positive band was not observed for complexes containing a CO_3^{2-} ligand, even if they were a tris(chelate) or *cis*-bis(chelate) type. This is explained from a structural basis. The two complexes which had a split second d-d absorption band, *mer-trans*(NH$_3$)-[CoCO$_3$(gly)(NH$_3$)$_2$] and [CoCO$_3$(picol)(NH$_3$)$_2$], showed two negative bands in the corresponding regions to both component absorption bands, in each complex.

In a previous paper,[1] the MCD (magnetic circular dichroism) spectra of [Co(ox)$_x$(gly)$_y$(en)$_z$] series comprising sixteen complexes were reported. All complexes, except [Co(en)$_3$]$^{3+}$, showed the same MCD-spectra pattern in the spin-allowed second d-d electronic-absorption band region ($^1A_{1g}\rightarrow{}^1T_{2g}(O_h)$), despite the fact that they had various types of ligand atom constitutions and geometrical structures. Some curves are shown in Fig. 1. The spectra were composed of two bands whose signs were positive and negative, from the lower-energy side to the higher. Because other cobalt(III) complexes reported earlier[2-5] did not show a positive band in the corresponding region, the MCD behavior of the series of complexes in the previous study were quite interesting. Only a vague explanation, however, was offered for the origin of the positive band at that time. Then, the MCD spectra of many more cobalt(III) complexes containing nitrogen and oxygen atoms, like in the [Co(ox)$_x$(gly)$_y$(en)$_z$] series complexes, have been measured in order to clarify the origin of this band.

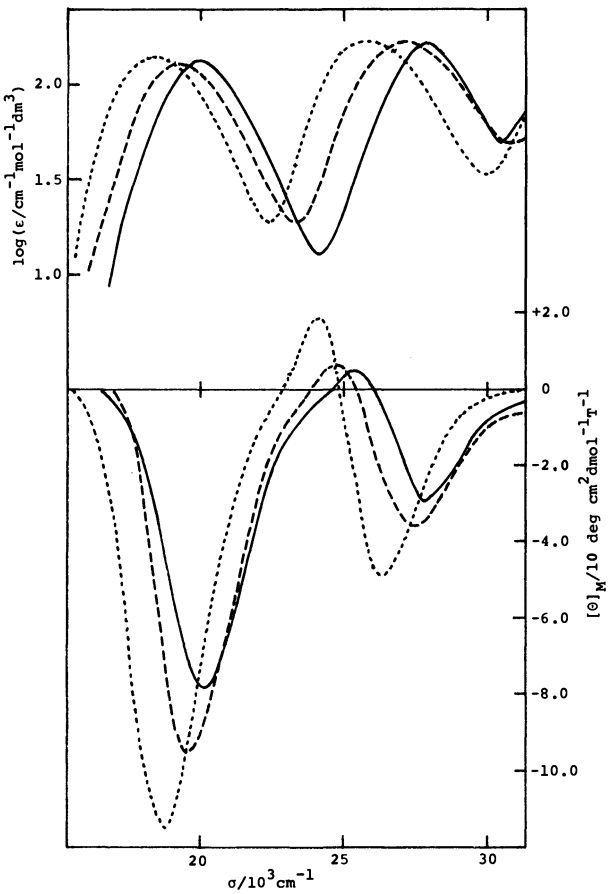

Fig. 1. Absorption and MCD spectra of C_1-*cis(O)*-[Co(gly)$_2$(en)]$^+$ (——), *fac*-[Co(ox)(gly)(en)] (— —), and C_1-*cis(N)*-[Co(ox)(gly)$_2$]$^-$ (----).

In addition, several cobalt(III) complexes, whose second d-d absorption bands were split, were reported by Shibata and his co-workers in the 1970's.[6-12] It is also interesting to know the MCD behavior of those complexes.

In the present paper, newly obtained MCD data regarding seventeen cobalt(III) complexes, including whose second d-d absorption bands are split, are described and discussed in terms of the origin of the positive MCD band.

Experimental

Materials. *mer-trans(NH$_3$)*-[CoCO$_3$(gly)(NH$_3$)$_2$], and *mer-trans(NH$_3$)*-, *mer-cis(NH$_3$)*- and *fac*-[CoCO$_3$(picol)(NH$_3$)$_2$] were prepared according to the method of Shibata et al.[6,11] All the other complexes described in this paper were synthesized by ordinary methods. The absorption and MCD data of *trans*- and *cis*-[Co(OH$_2$)$_2$(en)$_2$]$^+$ were obtained from a 10% HClO$_4$ solution of *trans*-[Co(OH)(OH$_2$)(en)$_2$](ClO$_4$)$_2$ which was provided by T. Komorita. When this solution was kept standing at room temperature for several hours, the absorption spectrum gradually changed with four isosbestic points(Fig. 2). After a week, the maximum data in the first and second d-d absorption bands of the solution approached the known data of *cis*-[Co(OH$_2$)$_2$-

$(en)_2]^{3+}$.[13,14] Then, the spectra found immediately after dissolving and measured after a week were regarded as the spectra of *trans*-$[Co(OH_2)_2(en)_2]^{3+}$ and *cis*-$[Co(OH_2)_2(en)_2]^{3+}$, respectively.

Measuremens. The electronic absorption spectra were measured by a Shimadzu UV-200 and a Hitachi 330 spectrophotometer. The MCD spectra were recorded in a magnetic field of 1.5 T with a JASCO MOE-1 spectropolarimeter. The MCD intensity is expressed in terms of molar ellipticity, $[\theta]_M$, which has the units of deg cm^2 dmol^{-1} T^{-1}. The data of $[Co(acac)_3]$ was obtained in an acetone solution, and *mer*- and *fac*-$[Co(picol)_3]$ were in a 30% $HClO_4$ solution, because they were insoluble or slightly soluble in water. The MCD and electronic absorption spectra of *trans*- and *cis*-$[Co(OH_2)_2(en)_2]^{3+}$ were recorded in a 10% $HClO_4$ solution, as mentioned above. All the other measurements were made in aqueous solutions at room temperature.

Results

The newly obtained MCD data of the seventeen cobalt(III) complexes are listed in Table 1, along with electronic absorption data. Some typical curves in the visible and near-ultraviolet regions are shown in Figs. 2—4.

As can be seen in these Figures, the shapes of the MCD spectra in the first absorption band region ($^1A_{1g}\rightarrow{}^1T_{1g}(O_h)$) are similar to those of the electronic absorption spectra, which indicates that the contribution of the B term is dominant in this region. Such a behavior has also been seen in other cobalt(III) complexes studied earlier.[1]

In the second d-d absorption-band region, however, the pattern of the MCD spectra for several complexes are different from those of the absorption spectra. The MCD behavior observed in the present work can be grouped roughly into the following three types.

In the first type, only a negative band is observed. This is, of course, the most simple pattern, and about half of the complexes listed in Table 1 belong to this type. They are $[Co(NH_3)_6]^{3+}$, $[Co(ox)(NH_3)_4]^+$, $[CoCO_3(en)_2]^+$, $[CoCO_3(NH_3)_4]^+$, *trans*-$[Co(OH_2)_2(en)_2]^{3+}$, *cis*-$[Co(OH_2)_2(NH_3)_4]^{3+}$, and *mer-cis(NH$_3$)*- and *fac*-$[CoCO_3(picol)(NH_3)_2]$.

The MCD spectra of the second type comprise two bands, a small positive band on the lower-energy side

Table 1. Absorption Maximum and MCD Extremum Data in d-d Absorption Band Region

Complex	First d-d band region		Second d-d band region	
	Absorption	MCD	Absorption	MCD
	σ[a] (log ε)[b]	σ[a] ($[\theta]_M$)[c]	σ[a] (log ε)[b]	σ[a] ($[\theta]_M$)[c]
$[Co(NH_3)_6]Cl_3$	21.0 (1.78)	21.0 (−2.1)	29.2 (1.68)	28.6 (−0.5)
$[Co(tn)_3]Cl_3$	20.5 (1.88)	20.5 (−2.4)	28.5 (1.87)	26.5 (−0.1)
				29.2 (+0.5)
$[Co(ox)(NH_3)_4]Cl$	19.7 (1.93)	20.0 (−6.6)	28.0 (2.15)	27.8 (−1.5)
cis-$NH_4[Co(ox)_2(NH_3)_2]$	18.1 (2.04)	18.5 (−10.6)	26.2 (2.31)	23.7 (+0.3)
				26.0 (−5.0)
$[CoCO_3(en)_2]Br$	19.6 (2.08)	20.0 (−9.8)	27.9 (2.04)	27.4 (−3.9)
$[CoCO_3(NH_3)_4](SO_4)_{1/2}$	19.1 (2.05)	19.6 (−8.0)	27.5 (2.14)	27.0 (−2.7)
trans-$[Co(OH_2)_2(en)_2](ClO_4)_3$	18.2 (1.50)	18.7 (−1.2)	28.7 (1.72)	28.2 (−0.8)
	22.9 (1.54)	22.4 (−1.0)		
cis-$[Co(OH_2)_2(en)_2](ClO_4)_3$	20.3 (1.86)	20.1 (−4.6)	27.9 (1.77)	26.2 (+0.5)
				29.2 (−0.7)
cis-$[Co(OH_2)_2(NH_3)_4](SO_4)_{3/2}$	19.7 (1.75)	19.0 (−3.2)	28.2 (1.65)	28.2 (−1.2)
trans-$[Co(\beta\text{-ala})_2(en)]ClO_4$	18.5 (2.02)	18.5 (−1.9)	27.5 (1.95)	25.6 (+0.2)
	21.8 (1.67)[d]	21.8 (−2.7)		28.0 (−0.8)
mer-$[Co(picol)_3]$	19.0 (2.00)	20.0 (−10.5)	26.4 (2.33)	24.6 (+0.8)
				27.0 (−6.7)
fac-$[Co(picol)_3]$	19.3 (2.17)	19.6 (−11.1)	26.4 (2.55)	24.4 (+0.5)
				27.0 (−6.2)
mer-trans(NH$_3$)-$[CoCO_3(gly)(NH_3)_2]$	18.7 (1.91)	18.7 (−4.1)	24.7 (1.71)[d]	24.7 (−2.2)
			27.3 (1.96)[d]	27.3 (−1.6)
mer-trans(NH$_3$)-$[CoCO_3(picol)(NH_3)_2]$	19.3 (1.96)	19.0 (−3.0)	24.7 (1.65)[d]	24.4 (−2.7)
			27.3 (1.86)[d]	26.7 (−1.5)[d]
mer-cis(NH$_3$)-$[CoCO_3(picol)(NH_3)_2]$	18.4 (2.04)	19.0 (−11.6)	26.8 (2.29)	26.2 (−7.3)
fac-$[CoCO_3(picol)(NH_3)_2]$	19.0 (2.11)	19.4 (−13.0)	27.0 (2.27)	27.0 (−7.8)
$[Co(acac)_3]$	16.8 (2.12)	16.7 (−11.7)	22.0 (2.25)[d]	22.0 (+1.0)
				23.8 (−1.3)

a) Wave numbers are given in 10^3 cm^{-1}. b) Logarithms of the molar absorption coefficients are given in log(ε/cm^{-1} mol^{-1} dm^3). c) Molar ellipticities are given in 10 deg cm^2 dmol^{-1} T^{-1}. d) Shoulders.

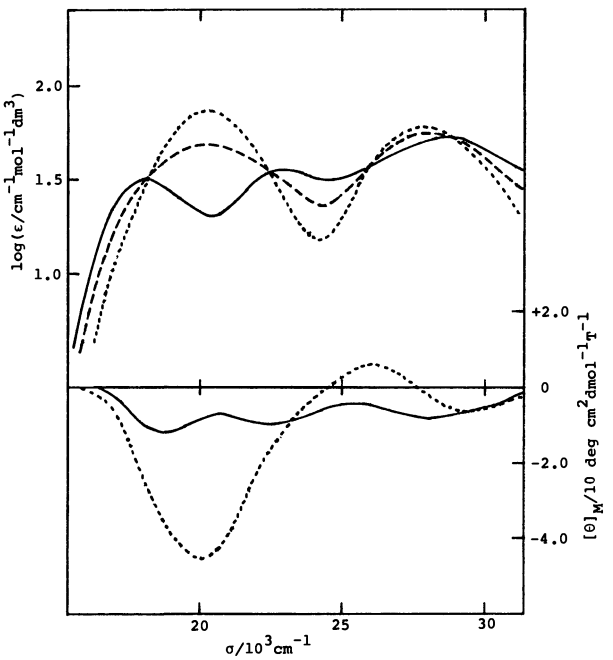

Fig. 2. Spectral change of *trans*-$[Co(OH)(OH_2)(en)_2]^{2+}$ in 10% $HClO_4$ with time: Within 1 h —— (*trans*-$[Co(OH_2)_2(en)_2]^{3+}$), after 2 d — —, and after one week ---- (*cis*-$[Co(OH_2)_2(en)_2]^{3+}$).

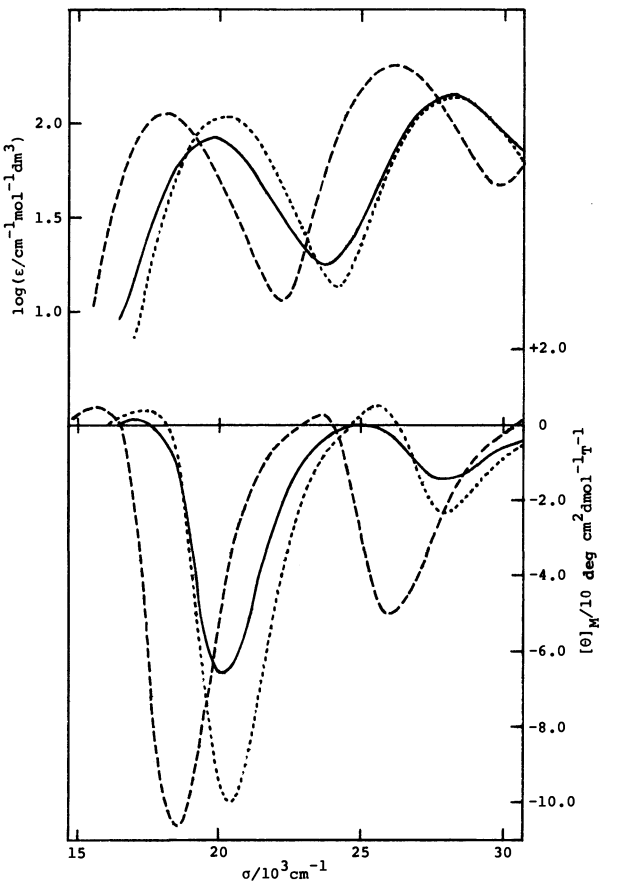

Fig. 3. Absorption and MCD spectra of $[Co(ox)(NH_3)_4]^+$ (——), $[Co(ox)_2(NH_3)_2]^-$ (— —), and $[Co(ox)(en)_2]^+$ (----).

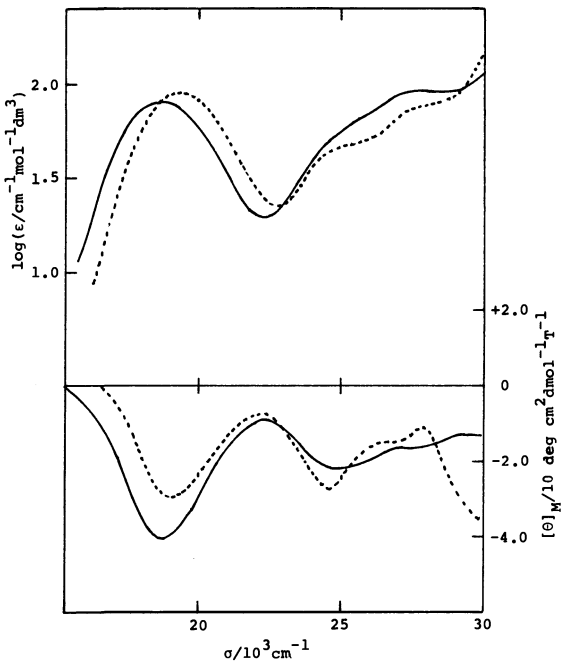

Fig. 4. Absorption and MCD spectra of *mer-trans(NH₃)*-$[CoCO_3(gly)(NH_3)_2]$ (——), and *mer-trans(NH₃)*-$[CoCO_3(picol)(NH_3)_2]$ (----).

and a large negative band on higher-energy side. This pattern is what has been seen in the $[Co(ox)_x(gly)_y(en)_z]$ series complexes.[1] In the present work, *cis*-$[Co(OH_2)_2(en)_2]^{3+}$, *trans(O)*-$[Co(\beta\text{-ala})_2(en)]^+$, *mer-* and *fac*-$[Co(picol)_3]$, *cis*-$[Co(ox)_2(NH_3)_2]^-$, and $[Co(acac)_3]$ show this type spectra.

The tris(trimethylenediamine) complexes, $[Co(tn)_3]^{3+}$, also exhibits two bands whose signs are opposite to each other. In this complex, however, the small band on the lower-energy side is negative and the dominant band on the higher-energy is positive. Since such a unique behavior of the sign of trimethylenediamine complexes has been reported elsewhere,[15] this complex is also included in the second group.

The two complexes which have a split second d–d absorption band, *mer-trans*(NH_3) form of $[CoCO_3(gly)(NH_3)_2]$ and $[CoCO_3(picol)(NH_3)_2]$, show the third type MCD behavior. They exhibit two negative bands in this region; each band is observed in a region corresponding to the component absorption band (Fig. 4).

Discussion

In the previous study on the MCD of $[Co(ox)_x(gly)_y(en)_z]$ series complexes,[1] the positive MCD band in the second d–d electronic absorption band region was suggested to be related to the presence of a coordinated carboxylato group. In the present work this assumption is also applicable for *trans(O)*-$[Co(\beta$-

ala)$_2$(en)]$^+$, *mer*- and *fac*-[Co(picol)$_3$], and *cis*-[Co(ox)$_2$(NH$_3$)$_2$]$^-$, which have coordinated carboxylato ligands and show a positive band. For [Co(ox)(NH$_3$)$_4$]$^+$, however, only a negative band is observed, in spite of the presence of two carboxylato groups. On the other hand, the two complexes which have no carboxylato ligands, [Co(tn)$_3$]$^{3+}$ and *cis*-[Co(OH$_2$)$_2$(en)$_2$]$^{3+}$, exhibit a positive band. From these facts, the previous suggestion that the origin of the positive band is connected with the presence of a coordinated carboxylato ligand will require reconsideration.

In the oxalato complexes, it is noticeable that the different types of MCD behavior is observed for a tetraammine-type complex of [Co(ox)(NH$_3$)$_4$]$^+$ (group 1), from a diammine-type complex of [Co(ox)$_2$(NH$_3$)$_2$]$^-$ and a bis(ethylenediamine)-type complex of [Co(ox)(en)$_2$]$^+$ (group 2), as can be seen in Fig. 3. The same aspect with the latter was also seen in another study on the MCD of (amino acidato)cobalt(III) complexes.[16] A positive band was observed in bis(ethylenediamine) complexes, [Co(amac)(en)$_2$]$^{2+}$, but not in tetraammine-type complexes, [Co(amac)(NH$_3$)$_4$]$^{2+}$, in which amac denotes glycinato and DL-alaninato ligands. Additionally, a positive band was not observed in the pentaammine-type complexes of [Co(Hamac)(NH$_3$)$_5$]$^{3+}$ either (Hamac=glycine, L-alanine, L-serine, L-phenylalanine and β-alanine).

In the three diaqua complexes, *trans*- and *cis*-[Co(OH$_2$)$_2$(en)$_2$]$^{3+}$ and *cis*-[Co(OH$_2$)$_2$(NH$_3$)$_4$]$^{3+}$, the positive band is observed only in *cis*-[Co(OH$_2$)$_2$(en)$_2$]$^{3+}$. Because other complexes studied to date have shown the same MCD-spectra pattern among their geometrical isomers, e.g., C_2-cis, C_1-cis and trans isomers of [Co(gly)$_2$(en)]$^+$ and [Co(ox)(gly)$_2$]$^-$ and mer and fac isomers of [Co(gly)$_3$], [Co(picol)$_3$], and [Co(ox)(gly)(en)], this difference in the MCD between the trans and cis isomers of [Co(OH$_2$)$_2$(en)$_2$]$^{3+}$ is interesting.[1]

As a result of these observations, it can be pointed out that the complexes exhibiting a positive band (group-2 complexes in the present work and the [Co(ox)$_x$(gly)$_y$(en)$_z$] series complexes in previous work) are all tris(chelate) or *cis*-bis(chelate) type. This fact leads us to a new assumption that the existence of the positive MCD band in question can be associated with a particular arrangement of two or three chelate rings.

It is reasonable to consider that the MCD behavior is affected by the arrangement of the chelate rings. For example, a D_3 or a pseudo D_3 symmetrical field would be produced around the central metal atom in tris(chelate)- and *cis*-bis(chelate)-type complexes. Then, the origin of the positive band might be associated with the electronic transition split in a D_3 (or pseudo D_3) symmetrical field caused in such a way. Namely, this band is assignable to one of the two component bands of E and A_1 in the T_{2g} (O_h) transition, which have opposite signs to each other. As an alternative explanation, it is also reasonable to consider that this band appears as a positive wing of the A term, which exhibits a dispersion-type curve, in a degenerated component of E in a D_3 (or pseudo D_3) symmetrical field. Although a full explanation can not be offered at the present stage, all experimental facts described above can be explained well from this assumption.

The tris(chelate)-type complex of [Co(en)$_3$]$^{3+}$ has not exhibited a positive band, as mentioned above. The MCD curve of this complex, however, is considerably asymmetrical and its shape suggests that a small positive band on the lower-energy side is hidden by a successive large negative band.[1]

The complexes containing a carbonato chelate ligand do not show a positive band either, even though they are the tris(chelate) or *cis*-bis(chelate) type. This might be explained in terms of distorted structures, which is brought about by a four-membered carbonato chelate ring. For example, it has been reported for [CoCO$_3$(NH$_3$)$_4$]$^+$ that the bite angle of the carbonato chelate ring is 70° and that the distance of the Co–N bond containing the nitrogen atom at a position trans to the carbonato oxygen atom is considerably longer (2.03 Å) than those containing the nitrogen atoms at the cis positions (1.93 and 1.95 Å).[17] Thus, the complexes containing a chelated carbonato ligand are inadequate for determining the MCD behavior in parallel with the other tris(chelate) or *cis*-bis(chelate) type complexes which have nearly octahedral structures.

The two complexes which have a split second d–d absorption band, *mer-trans(NH$_3$)*-[CoCO$_3$(gly)(NH$_3$)$_2$] and [CoCO$_3$(picol)(NH$_3$)$_2$], show two MCD bands in the corresponding regions (Fig. 4). Because their signs are both negative and their positions are almost the same as those of the component electronic absorption bands, each MCD band in both complexes is assignable to have a dominant B term character.

References

1) N. Matsuoka and Y. Shimura, *Bull. Chem. Soc. Jpn.*, **49**, 2118 (1976).
2) A. J. McCaffery, P. J. Stephens, and P. N. Schatz, *Inorg. Chem.*, **6**, 1614 (1967).
3) R. L. Russell and B. E. Douglas, *Inorg. Chim, Acta*, **3**, 426 (1969).
4) R. L. Russell and B. E. Douglas, *Inorg. Nucl. Chem, Lett.*, **9**, 1251 (1973).
5) H. Kato and J. Gohda, *Bull. Chem. Soc. Jpn.*, **46**, 636 (1973).
6) S. Kanazawa and M. Shibata, *Bull. Chem. Soc. Jpn.*, **44**, 2424 (1971).
7) S. Nakashima and M. Shibata, *Bull. Chem. Soc. Jpn.*, **47**, 2069 (1974).
8) S. Nakashima and M. Shibata, *Bull. Chem. Soc, Jpn.*,

48, 3128 (1975).
9) T. Ito and M. Shibata, *Inorg. Chem.*, **16**, 108 (1979).
10) Y. Ida, S. Fujinami, and M. Shibata, *Bull. Chem. Soc. Jpn.*, **50**, 2665 (1977).
11) Y. Ida, M. Sakai, S. Sakai, and M. Shibata, *Bull. Chem. Soc. Jpn.*, **50**, 2807 (1977).
12) K. Okazaki and M. Shibata, *Bull. Chem. Soc, Jpn,*, **52**, 1391 (1979).
13) F. Basolo, *J. Am. Chem. Soc.*, **72**, 4393 (1950).
14) J. Bjerrum and S. E. Rasmussen, *Acta Chem. Scand.*, **6**, 1265 (1952).
15) K. Nakayama, T. Komorita, and Y. Shimura, *Bull. Chem. Soc. Jpn.*, **57**, 2930 (1984).
16) E. Ueda, N. Matsuoka, and Y. Shimura, *Bull. Chem. Soc. Jpn.*, **51**, 1895 (1978).
17) G. A. Barclay and B. F, Hoskins, *J. Chem, Soc.*, **1962**, 586.

Spectroscopic and MO Study of Peptide Models for the M_{412} Intermediate of Bacteriorhodopsin. N^{ε}-Retinylidenelysyl Peptides Containing Aromatic Amino Acids

Minoru SAKURAI,* Satoshi TOMOMASA, Yûji SEIYA, Yoshio INOUE, and Riichirô CHÛJÔ
Department of Polymer Chemistry, Tokyo Institute of Technology, 12-1 Ookayama 2-Chome, Megro-ku, Tokyo 152
(Received April 30, 1985)

N^{ε}-Retinylidenelysyl peptides containing Tyr and Phe were prepared in order to investigate the effect of the surrounding microenvironment on the absorption maximum of the chromophore of bacteriorhodopsin. The absorption maximum of the retinylidene Schiff base of the lysyl peptide, Boc-Lys-Phe(or -Gly)-Tyr-OMe, was shifted to the red relative to the peptides lacking Tyr, Boc-Lys-Phe-Phe-OMe and Boc-Lys-Phe-OMe. UV and ^{13}C NMR studies on the Tyr-containing lysyl-peptide have confirmed an intramolecular interaction between Tyr and the retinylidene portion in low dielectric media. A hydrogen-bond formation of the Schiff base with a Tyr side chain is supported by a theoretical estimation of the transition energy and the shielding constants for some models of Tyr-Schiff base complexes. The side-chain conformation of the Tyr-contaning lysyl-peptide is discussed in terms of the ^{1}H NMR data. The hydrogen-bonding shift induced by Tyr was estimated as being no less than 10 nm.

Bacteriorhodopsin (bR) acts as a light-driven proton pump in the plasma membrane of halobacteria.[1] The chromophore of bR is a retinal Schiff base formed with Lys 216.[2,3] It is protonated in the initial state[4] and becomes deprotonated upon being illuminated (intermediate M_{412}).[5-7] The absorption maximum of the M_{412} is shifted considerably towards the red compared with an unprotonated retinal Schiff base, e.g., *N*-retinylidenebutylamine. This shift should be induced by neighboring amino acids of the chromophore.

Recent reports on the chemical modifications of bR[8-10] and the pH dependence of the M_{412} formation[11-14] have shown that tyrosine is one possible candidate near the Schiff base in bR. Following Engelman's model,[15] which was built on the basis of X-ray diffraction data of bR, helices A, B, and F were formed to lie close to helix G containing Lys 216 and involve several tyrosine residues. Therefore, it is interesting to study to what extent the absorption maximum is shifted by one tyrosine spatially arranged near a Schiff base using artificial pigments.

It has been demonstrated[16-18] that N^{ε}-retinylidenelysyl peptides are useful models to study specific interactions between a Schiff base and an amino acid. However, the mechanism of the spectral shift in such an artificial pigment has not been fully clarified. Preliminary consideration using the CPK model showed that several types of interactions involving a hydrogen bond are possible between Tyr and the Schiff base in tripeptide Lys(Ret)-X-Tyr, where Ret and X stand for the N^{ε}-retinylidene group and one of the common amino acids, respectively. We prepared Boc-Lys(Ret)-Phe-Tyr-OMe **1**, Boc-Lys(Ret)-Gly-Tyr-OMe **2**, Boc-Lys(Ret)-Phe-Phe-OMe **3**, Boc-Lys(Ret)-Phe-OMe **4**, where Boc is an abbreviation for a *t*-butoxycarbonyl group.

Here, we report that the absorption maximum of an unprotonated retinal Schiff base is shifted to the red by the perturbation of one tyrosine. Furthermore, we discuss the origin of the red shift on the basis of UV, ^{1}H and ^{13}C NMR spectra, and a MO calculation.

Theoretical

A ^{13}C NMR chemical shift was estimated according to a theory of Karplus and Pople[19] incorporated into the CNDO/S method.[20] The average excitation energy, ΔE, was taken as 10.0 eV. The details of the procedure were given in a previous paper.[21] The calculation of the π-π^* transition energy was carried out using the CNDO/S method. Some modifications have been proposed for the CNDO/S parameters from the originating laboratory.[22,23] According to these reports, coulomb integrals were estimated using the Nishimoto-Mataga formula and reevaluated values were used for core and bonding parameters. The lowest energy (60 configurations) of all single excitations were included in the configuration-interaction calculations.[23]

These calculations would have been computationally intractable if the entire framework of the retinylidene peptide was included. It has been shown that neglecting the C_9 and C_{13} methyl groups and the saturated carbon region of the β-ionylidene ring does not introduce any serious error to the results concerning the electronic structure.[24,25] We, therefore, approximate the retinal portion as *all-trans N*-undecapentylidenemethylamine (hereafter abbreviated as NUPM). The molecular geometry was derived from crystallographic data.[26] The other portion of the retinylidene peptide was represented by the phenol ring of Tyr. The orientation of the phenol ring to the polyene chain was determined based on a

CPK model of the peptide containing all atoms.

Experimental

All peptides were synthesized by conventional solution phase procedures, using dicyclohexylcarbodiimide as a coupling regent. The Boc group was used for α-amino group protection and methyl ester for the carboxyl group. The ε-amino group of the lysine residue was protected with a benzyloxycarbonyl group during the coupling reaction. The protecting group on the lysine side chain was removed in the final step by catalytic hydrogenation using palladium-charcoal in a methanol-acetic acid 1:1 solvent. The final products were recrystallized from ethyl acetate-hexane. All the intermediate and final products were identified by their ^{13}C NMR spectra and their purities were checked by TLC. Retinylidene peptides were prepared by keeping a mixture of *all-trans* retinal and the peptide (1:1 mole ratio) in ethanol with anhydrous potassium carbonate. The products were recrystallized from ethanol-hexane. *All-trans* retinal and *all-trans* *N*-retinylidenebutylamine-(NRB) were synthesized according to the procedure given in a previous paper.[27] All the Schiff bases were handled under a dim red light.

Absorption spectra were recorded on a Beckman model 25 spectrometer. ^{13}C NMR spectra were recorded on a JNM JEOL PS-100 spectrometer equipped with a PFT-Fourier transform system at 25.15 MHz. ^{1}H NMR spectra were recorded on a JEOL FX-400 spectrometer at 399.65 MHz. Unless otherwise noted, all spectroscopic measurments were made at 31±1 °C. Solvents (CCl_4, $CHCl_3$, and CH_3OH) used in absorption studies were spectral grade and were purchased from Tokyo Kasei Co., Tokyo. Perdeuterated dimethyl sulfoxide (DMSO-d_6), CD_3OD, and $CDCl_3$ were purchased from Merck Sharp & Dohme Canada, Ltd.

^{13}C NMR signals of the peptide portion of compounds **1**—**4** were assigned by comparisons with the spectra of their fragment peptides and the monomers.[28] The signals of the retinylidene portion were easily assigned by comparisons with the spectrum of NRB.[27,29] ^{1}H NMR resonances were assigned on the basis of their multiplet structure, selective homo-spin decoupling and a comparison with the literatures.[30,31]

The calculation was carried out with a HITAC M-200H computer system.

Results and Discussion

Identification of Retinylidenelysyl Peptides 1—4 by ^{13}C NMR and UV Spectroscopy. Figure 1 shows the ^{13}C NMR spectra of compund **1** together with that of NRB in CD_3OD. The signals corresponding to the peptide carbons (except the C_ε of Lys) were assigned by comparisons with the spectrum of compound **1'**, Boc-Lys-Phe-Tyr-OMe, under the assumption that the chemical shifts of these carbons are little changed by a Schiff base formation. The other signals were assigned by comparisons with the spectrum of NRB. As shown in Fig. 2, the signals corresponding to C_{10} and C_5 overlap with those of the $C_{2,6}$ of Tyr and Phe, respectively. There are no signals suggesting to the free retinal nor the C_ε of Lys having a free ε-amino group. This fact indicates the complete conversion of retinal to the Schiff base form. The chemical shifts of the retinylidene portion are in good agreement with those of the corresponding carbons for *all-trans* NRB. Therefore, the polyene chain was identified as an all-trans configuration. Similar results were also obtained for compounds **2**—**4**. The

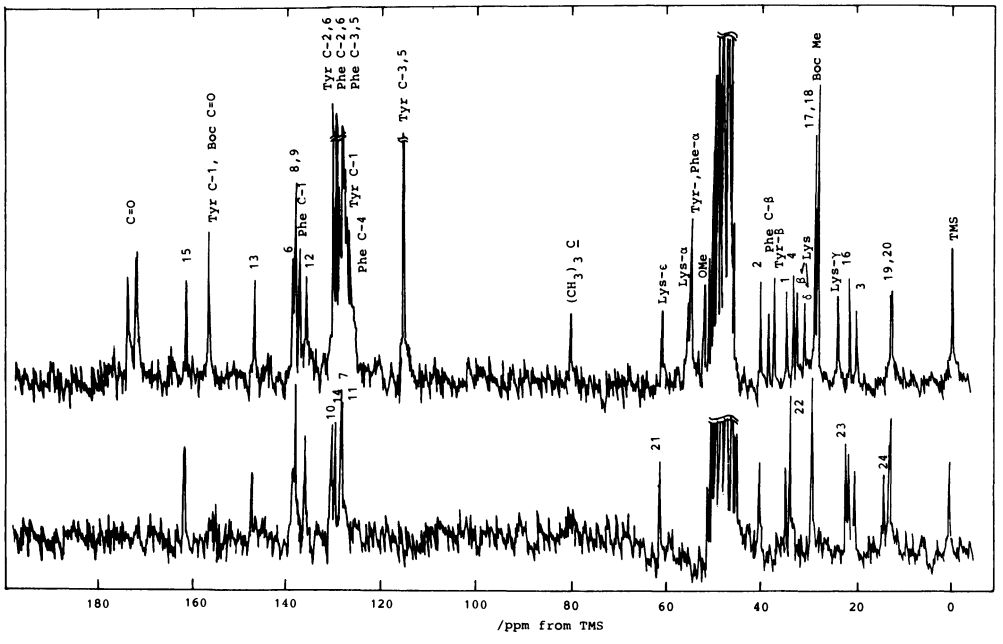

Fig. 1. ^{13}C NMR spectra of compound **1** and NRB at concd 0.1 mol dm^{-3} in CD_3OD.

peak assignments of compounds **1**—**4** are summarized in Table 1 together with those of compound **1'**, retinal and NRB.

Figure 3-a shows the absorption spectrum of compound **1** in methanol. The main peak is shifted to the blue by 15 nm compared with the *all-trans* retinal. This is consistent with the blue shift observed in the formation of NRB. The peak at 275 nm was assigned to the π-π^* transition of the aromatic rings by a comparison with the absorption spectrum of compound **1'**.

UV and ^{13}C NMR Spectra of the Retinylidene-lysyl Peptides in Low Dielectric Media. Table 2 summarizes the absorption maxima of compounds **1**—**4** and NRB in different solvents. In the halogenated solvents and in hexane, the absorption maxima of compounds **1** and **2** (which contain Tyr) were shifted to the red compared with other compounds. The concentration dependence of the absorption maximum of compound **1** was examined in carbon tetrachloride. There was no change in the band position in the observed concentration range(10^{-4}—10^{-5} mol dm^{-3}). Figure 4 shows the temperature dependence of the absorption maxima of compounds

Table 1. The Peak Assignments of Retinylidenelysyl Peptides **1**—**4**, *all-trans* NRB and *all-trans* Retinal in CD_3OD at 0.1 M[a)]

a. Retinylidene portion

Carbon No.[b)]	1	2	3	4	NRB[c)]	retinal[c)]
1	35.2	35.2	35.1	35.2	35.2	35.2
2	40.6	40.7	40.6	40.8	40.7	40.7
3	20.3	20.3	20.2	20.3	20.3	20.3
4	34.0	33.9	33.9	34.0	33.9	34.0
5	—[d)]	130.5			130.5	130.8
6	139.4	139.4	139.4	139.5	138.5	138.6
7	128.9	129.0	—[d)]	128.9	128.9	130.5
8	138.9	138.9	138.9	139.0	139.0	138.6
9	138.9	138.9	139.0	139.0	138.0	142.4
10	—[d)]	131.2	131.1	131.2	131.2	130.8
11	128.7	128.7	128.6	128.7	128.7	134.3
12	136.8	136.7	136.7	136.8	136.8	135.7
13	147.6	147.7	147.7	147.7	147.6	157.9
14	130.1	130.0	—[d)]	—[d)]	130.0	129.7
15	162.4	162.4	162.3	162.4	162.2	193.2
16	29.4	29.4	29.4	29.4	29.4	29.4
17	29.4	29.4	29.4	29.4	29.4	29.4
18	22.0	22.0	21.9	22.0	22.0	22.0
19[e)]	12.9	12.9	12.9	12.9	12.9	13.0
20[e)]	13.2	13.2	13.1	13.1	13.1	13.2
21					61.5	
22					33.9	
23					21.3	
24					14.1	

b. Peptide portion

Residue	atom	1	2	3	4	1'[f)]
Lys	α	56.0	56.3	56.2	55.9	55.5
	β	31.5	31.4	31.4	31.5	30.4
	γ	24.5	24.5	24.3	24.4	24.0
	δ	33.1	32.9	33.0	33.2	32.9
	ε	61.5	61.5	61.4	61.5	41.4
Phe	α	55.4		55.3[g)]	54.9	55.5
	β	39.1		38.9	38.4	39.0
				38.4		
	C-1	138.0		137.9	137.9	138.0
				137.7		
	C-4	127.6		127.8	127.8	127.7
				127.6		
	C-2, 6	130.4		130.1[g)]	130.3	130.4
	C-3, 5	129.3		129.3[g)]	129.4	129.4
Tyr	α	55.4	55.8			55.5
	β	37.7	37.9			37.7
	C-1	128.2	128.5			128.4
	C-4	157.5	157.8			157.3
	C-2, 6	131.2	130.8			131.2
	C-3, 5	116.3	116.6			116.2
Gly	α		43.2			
	C=O	174.6	175.6	174.6	174.8	174.7
		173.0	173.6	172.8[g)]	173.1	173.0
		172.8	171.1			172.8
	Boc C=O	157.5	157.9	157.6	157.4	157.3
	$(CH_3)_3\underline{C}$	80.6	80.6	80.6	80.6	80.7
	Ester Me	52.5	52.5	52.6	52.6	52.6
	Boc Me	28.7	28.7	28.7	28.7	28.8

a) Chemical shifts were measured as downfield shifts from internal tetramethylsilane (TMS) and are expressed in terms of ppm. The estimated error in the chemical shift is less than 0.1 ppm. b) The numbering of the carbons is given as shown in the following.

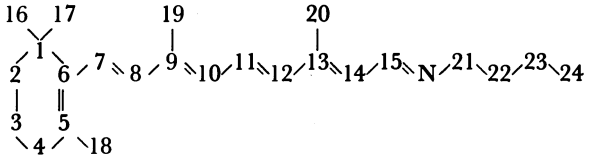

c) The assignments of these compounds were taken from Ref. 27 and 29. d) Overlapping with the peak of the aromatic carbons. e) The assignments to these carbons are tentative each other. f) Overlapping peak corresponding to two carbons in different residues.

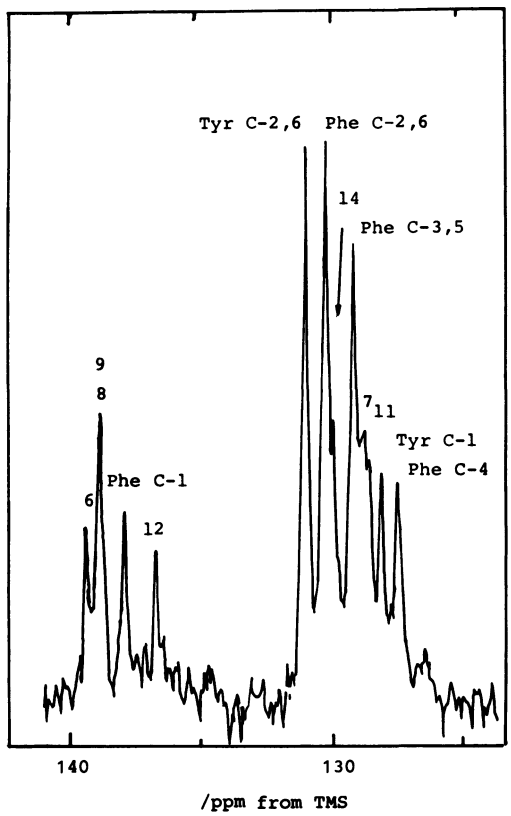

Fig. 2. Expanded spectrum of the 125—140 ppm region of compound **1**.

Table 2. Absorption Maxima (nm) of Retinylidenelysyl Peptides **1**—**4** and NRB in Different Solvents

Solvent	1	2	3	4	NRB
Carbon tetrachloride	375	370	368	363	365
Chloroform	375	372	367	366	367
Dichloromethane	375	370	366	365	363
Hexane	368	365	357	358	355
Methanol	365	364	365	364	365

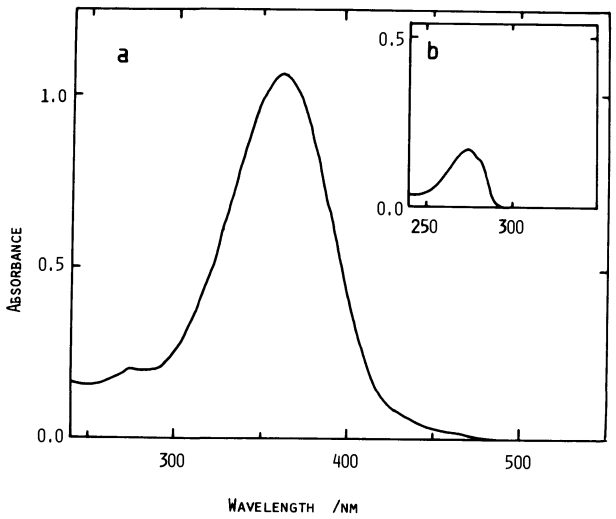

Fig. 3. (a) Absorption spectrum of compound **1** in methanol. (b) Absorption spectrum of the peptide, Boc-Lys-Phe-Tyr-OMe.

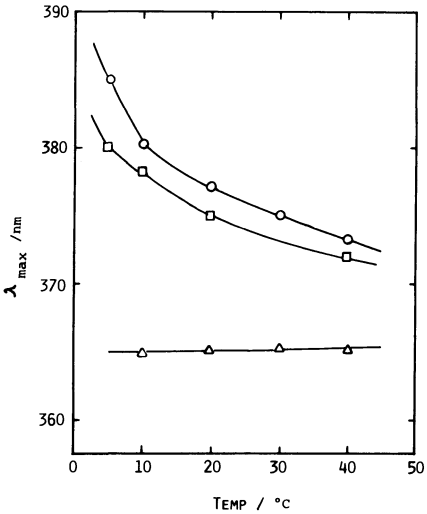

Fig. 4. Temperature dependence of the absorption maxima of compounds **1**, **2**, and **4** in carbon tetrachloride. ○: Compound **1**, □: compound **2**, △: compound **4**.

1, **2**, and **4** in carbon tetrachloride. Upon lowering the temperature from 40 to 5°, the absorption maxima of compounds **1** and **2** shifted to the red by 10 nm, but no apparent shift was detected for compound **4**. These results clearly indicate an intramolecular interaction between the retinylidene chromophore and Tyr in compounds **1** and **2**.

This interaction is also supported by the difference in the chemical shifts between compound **1** and NRB. Figure 5-a shows the chemical-shift difference($\Delta\delta$) along the polyene chain going from NRB to compound **1** in carbon tetrachloride. The magnitude of the chemical-shift difference alternates between odd- and even-numbered carbons, and the amplitude of the alternation decreases in going from the terminal nitrogen to the β-ionylidene ring. This behavior of the chemical shifts suggests an increase in the electronic polarization of the C=N bond going from NRB to compound **1**. There may be an electron-withdrawing group or a positive charge near the Schiff base nitrogen.

The absorption spectrum of a mixture of NRB and the protected tyrosine (Boc-Tyr-OMe) in carbon tetrachloride was observed. No apparent shift was detected within an observed molar ratio (Boc-Tyr-OMe/NRB) of 1—1000, with the concentration of NRB being kept constant at 3×10^{-5} mol dm^{-3}. This means that the intermolecular interaction is less

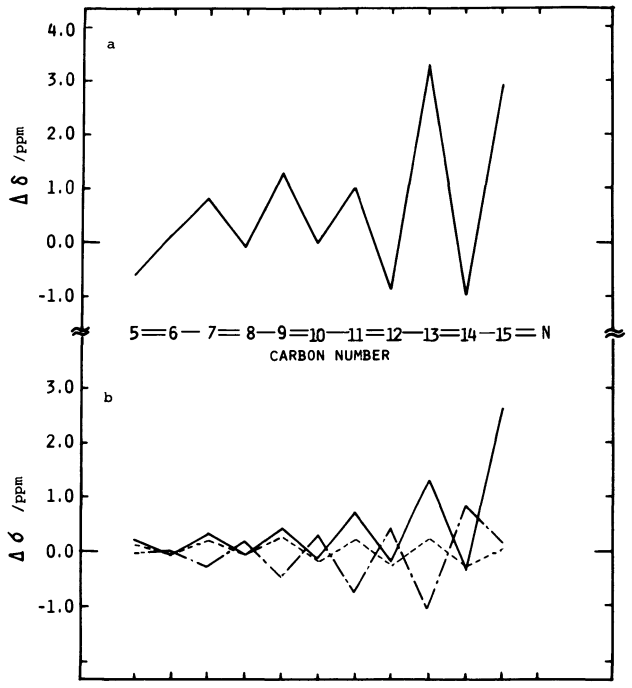

Fig. 5. Observed (a) and calculated (b) chemical shift differences of the polyene chain carbons going from the isolated Schiff base to each of the complexes as shown in Fig. 6.
(b) ——: Complex I, ——: complex II, ----: complex III.

important in a dilute solution, although a weak hydrogen-bond has been detected in more concentrated solutions (0.5 mol dm^{-3}) by IR spectra.[32] It is clear that in compounds **1** and **2** the peptide framework plays an essential role in the spatial arrangement of the tyrosine side chain to the Schiff base.

Theoretical Analysis of the UV and ^{13}C NMR Spectra of Retinylidenelysyl Peptides 1 and 2. CNDO/S calculations showed that the dipole moment of the unprotonated retinal Schiff base is directed perpendicular to the polyene axis on the polyene plane in the ground state. Bt upon excitation to the first excited state its direction becomes nearly parallel to the axis, and its magnitude increases from 2.7 to 3.7 D. Assming that a dipole-dipole type interaction is the main contributor to the spectral shift, this suggests that the π-π^* band of the Schiff base is effectively red-shifted by an electric dipole oriented antiparallel to the polyene axis. On the basis of CPK modeles of compounds **1** and **2**, three types of Tyr-Schiff base complexes were selected as association models. The geometrial configurations of these complexes are shown in Fig.6. Complexes I and II correspond to the models for a hydrogen-bond formation and stacking, respectively. In complex III, the C_1-O bond of the phenol ring is arranged parallel to the polyene axis. The phenol ring is coplanar to the polyene plane in complexes I and III.

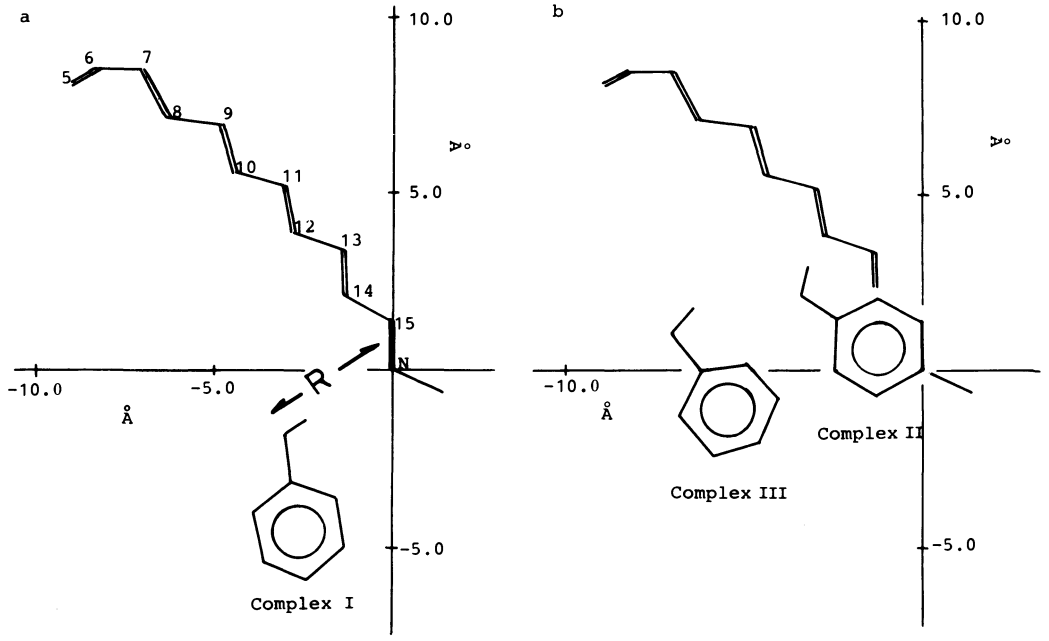

Fig. 6. The geometrical configurations of complexes between NUPM and the phenol ring assumed in the calculations.
(a) Complex I: hydrogen-bonding model. OH bond is placed on the extended line of the lone pair electron. (b) Complex II: stacking model. C_2, C_3, and C_4 of phenyl ring is placed 3 Å above C_{14}, C_{15} and N atoms, respectively. (c) Complex III: parallel model.
C_1-O bond of the phenol ring is arranged parallel to the polyene axis on the polyene plane.

Table 3. The Transition Energies, E_{tran}, of NUPM and the Complexes, and the Complex Formation Energies, ΔE_{compl}, in the Ground State

Compound	E_{tran}/eV(nm)	ΔE_{tran}/eV	ΔE_{compl}[c]/eV
NUPM	3.79(327.5)	0	—
Hydrogen bonding	3.73(331.6)	0.06	0.26
Stacking	3.69(335.7)	0.10	0.07
Parallel	3.78(328.3)	0.01	—
Compound **1**	3.31(375)[a]	0.09[b]	—

a) Observed in CCl_4 at room temperature. b) ΔE_{tran} was evaluated by subtracting E_{tran} of compound **1** from that of NRB. c) ΔE_{compl} means the energy change going from the isolated Tyr+isolated NUPM system to the complex. This was estimated by CNDO/2 method.

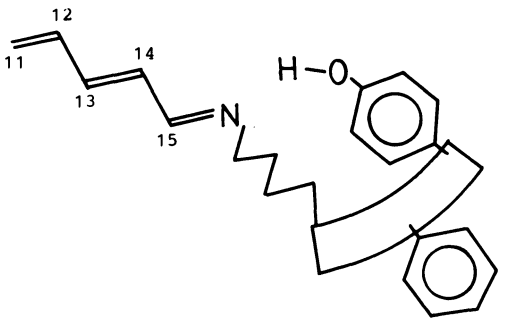

Fig. 7. Schematic representation of the overall conformation of compound **1** in low dielectric media based on CPK model considerations. The side chain of Tyr is oriented to the Schiff base. The steric hindrance about C_α–C_β bond of Phe is minimized.

Table 3 summarizes the transition energies (E_{tran}) of these complexes and NUPM, and also the complex formation energies (ΔE_{compl}) in the ground state. The complex formation energy is estimated as follows,

$$\Delta E_{compl} = E_s + E_t - E_{compl}$$

where E_s, E_t, and E_{compl} corresponds to the total energy of NUPM, the phenol ring and the respective complexes. The hydrogen bond length (R) and the O–H length were taken as 2.6 and 0.96 Å, respectively. The former value corresponds to the minimum energy structure in the ground state (determined by CNDO/2 calculations). In the other complexes, a van der Waals contact was assumed between the Schiff base and the phenol ring. The tyrosine+Schiff base system is stabilized by forming complex I or II. The transition energy decreases upon going from an isolated tyrosine (NUPM) to complex I or II. Figure 4-b shows the calculated chemical shift differences ($\Delta\delta$) going from NUPM to each of the complexes. The zigzag pattern (similar to Fig. 4-a) was reproduced in the formation of complex I. Consequently, the hydrogen-bonding model (complex I) is uniquely acceptable as an association model in compound **1**.

The hydrogen-bond length dependence was studied for the transition energy of complex I. Its values at R=2.8, 3.0 and 3.6 Å are 3.76, 3.77, and 3.79 eV, respectively. The transition energy rapidly approaches the value at an infinite bond length (3.79 eV). This explains the highly sensitive blue-shift of the absorption maxima of compounds **1** and **2** with a rise in temperature (Fig. 3). The second amino acid, Phe, of compound **1** is more bulky relative to Gly of compound **2**. The difference in the hydrogen-bond length, depending on the peptide framework, may induce a slight difference in the absorption maxima between these compounds.

NRB shows an absorption maximum at 376 nm in 2-chloroethanol,[33] which is a weaker hydrogen-bonding molecule (pK_a=14.3) relative to the tyrosine side chain (pK_a=11.1). Considering the case of NRB, a lower limit in the hydrogen-bond shift induced by a tyrosine side chain can be estimated as about 10 nm, according to the temperature dependence of the absorption maxima of compounds **1** and **2**.

Figure 7 shows a schematic representation of the overall conformation of compound **1** as predicted from the CPK model under the assumption of Tyr-Schiff base hydrogen bonding. The peptide backbone is folded to form the hydrogen bond. The side chain of Phe is exposed to the solvents.

The effect of a π-charge transfer interaction was examined in the above hydrogen-bonding system. A total charge transfer of 0.08 was found from the polyene part to the phenol ring in both the ground state and the first excited state, but the total π-charge density on the phenol ring was kept constant during hydrogen-bond formation. This means that the effect of a π-charge-transfer interaction is negligible in this system. This is in agreement with a report of Komatsu and Suzuki.[34] It seems that the hydrogen-bonding shift is chiefly induced by a dipole-dipole type of interaction between the Schiff base and Tyr.

Conformational Analysis of Retinylidenelysyl Peptide 1 by ^{1}H NMR. Table 4 summarizes the observed vicinal spin–spin coupling constants between α- and β-protons and the rotamer populations of compounds **1** and **1′**. Figure 8 shows the Newman projection of three staggered rotamers about the C_α–C_β bond of the side chain. Fractional populations P_I, P_{II}, and P_{III} were estimated by the following equations:

$$P_I = (J_{\alpha\beta A} - J_g)/(J_t - J_g) \quad (1)$$

$$P_{II} = (J_{\alpha\beta B} - J_g)/(J_t - J_g) \quad (2)$$

$$P_{III} = 1 - (P_I + P_{II}), \quad (3)$$

where $J_{\alpha\beta A(\text{or B})}$ represents the observed coupling

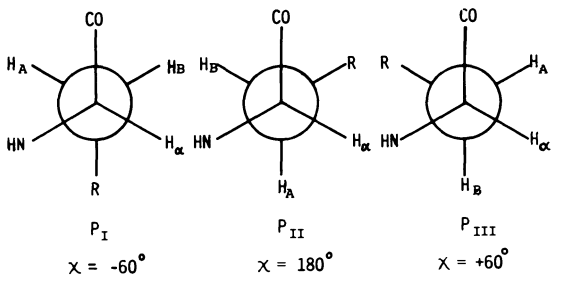

Fig. 8. Three stable rotamers about C_α–C_β bond and their notations.

Table 4. Proton Coupling Constants (Hz) and Rotamer Populations of Compounds **1** and **1′**

Compound	Residue	$J_{\alpha\beta A}$	$J_{\alpha\beta B}$	P_I	P_{II}	P_{III}
1′ a)	Phe	8.08	5.84	0.50	0.30	0.20
	Tyr	9.04	4.88	0.59	0.21	0.20
1′ b)	Phe	8.68	5.88	0.56	0.30	0.15
	Tyr	7.36	5.36	0.43	0.25	0.31
1 b)	Phe	6.60	6.00	0.37	0.31	0.33
	Tyr	8.04	5.88	0.50	0.30	0.21

a) Observed in DMSO-d_6. b) Observed in $CDCl_3$: DMSO-d_6=9 : 1.

constant between α- and βA (or βB)-protons, and J_t and J_g are the values of $^3J_{\alpha\beta}$ for the protons whose relative conformations are trans and gauche, respectively. The values of J_t and J_g are taken from Pachler's report:[35] J_t=13.56 Hz and J_g=2.60 Hz.

The relative rotamer populations of Phe in compound **1′** are almost independent of the solvent polarity. Accompanied by the formation of the Schiff base linkage, P_I decreases along with an increase in P_{III}, while P_{II} is kept constant. Consequently, three rotamers are equally populated in compound **1** in less polar solvents. This means that the side chain of Phe is randomly interconverted among the three rotamers during equilibrium. On the other hand, the rotamer population about the C_α-C_β bond of Tyr is non-random in compound **1**, with a prefered orientation of rotamer I. It seems that the conformational stability of each side chain based on a $^3J_{\alpha\beta}$ analysis is consistent with that predicted from the spatial arrangement of the side chains (Fig. 7).

In conclusion, a proximal tyrosine residue induces the red shift of the π-π^* band of an unprotonated retinal Schiff base through the hydrogen bond in a lower dielectric media. This hydrogen-bonding shift is estimated to be no less than 10 nm. The temperature coefficient, $d\lambda_{max}/dT$, was considerably large in the artificial pigments used. The hydrogen-bonding shift reached 20 nm at 5 °C. The absorption maximum of the M_{412} intermediate was shifted to the red by 47 nm compared with that of NRB in carbon tetrachloride at 30 °C. A significant part of the red shift in the M_{412} could be explained by the hydrogen-bond formation between the Schiff base and a proximal tyrosine.

The authors wish to express their thanks to Professor Isao Ando of Tokyo Institute of Technology for the use of the CNDO/2 program and his helpful discussions. We also would like to thank Dr. Shigetoshi Amiya of the Central Research Laboratories of Kuraray, Co. Ltd., Japan, for ^{1}H NMR spectra. We thank the Computer Center, Institute for Molecular Science, for the use of the HITAC M-200H computer.

References

1) W. Stoekenius and R. Bogomolni, *Annu. Rev. Biochem.*, **51**, 587 (1982).
2) H. D. Lemke and D. Oesterhelt, *FEBS Lett.*, **128**, 255 (1981).
3) H. Bayley, K. S. Huang, R. Radhakrishnan, A. H. Ross, Y. Takagi, and H. G. Khorana, *Proc. Natl. Acad. Sci. U.S.A.*, **78**, 2226 (1981).
4) M. A. Marcus, A. Lewis, *Science*, **195**, 1328 (1977).
5) A. Lewis, J. Spoonhower, R. A. Bogomolni, R. H. Lozier, and W. Stoeckenius, *Proc. Natl. Acad. Sci. U.S.A.*, **71**, 4462 (1974).
6) M. Braiman and R. Mathies, *Biochemistry*, **19**, 5412 (1980).
7) K. Bagley, G. Dollinger, L. Einstein, K. Singh, and L. Zimanyi, *Proc. Natl. Acad. Sci. U.S.A.*, **79**, 4972 (1982).
8) T. Konishi and L. Packer, *FEBS Lett.*, **92**, 1 (1978).
9) H. D. Lemke and D. Oesterhelt, *Eur. J. Biochem.*, **115**, 595 (1981).
10) T. Iwasa, T. Takeda, F. Tokunaga, P. S. Scherrer, and L. Packer, *Biosci, Rep.*, **2**, 949 (1982).
11) O. Kalisky, M. Ottolenghi, B. Honig, and R. Korenstein, *Biochemistry*, **17**, 1037 (1981).
12) V. Rosenbach, R, Goldberg, C. Gilon, and M. Ottolenghi, *Photochem. Photobiol.*, **36**, 197 (1982).
13) J. M. Fukumoto, J. H. Hanamoto, and M. A. EL-Sayed, *Photochem. Photobiol.*, **39**, 75 (1984).
14) J. H. Hanamoto, P. Dupus, and M. A. EL-Sayed, *Proc. Natl. Acad. Sci. U.S.A.*, **81**, 7083(1984).
15) D. Engelman, R. Henderson , A. D. Maclachlan, and B. A. Wallace, *Proc. Natl. Acad. Sci. U.S.A.*, **77**, 2023 (1980).
16) P. K. Das, R. S. Becker, D. Hannck, and E. Bayer, *J. Am. Chem. Soc.*, **101**, 239 (1979).
17) M. Engelhard and B. Hess, Proc. 7th American Peptide Symp. Univ. Wisconsin, June 14 (**1981**).
18) E. K. S. Vijayakuman and P. Balaram, *Photochem. Photobiol.*, **39**, 667 (1984).
19) M. Karplus and J. A. Pople, *J. Chem. Phys.*, **38**, 2803 (1963).
20) J. D. Bene and H. H. Jaffé, *J. Chem. Phys.*, **48**, 1807 (1968).
21) M. Sakurai, I. Ando, Y. Inoue, and R. Chûjô, *Photochem. Photobiol.*, **34**, 367 (1981).
22) R. L. Ellis, G. K. Kuehnlenz, and H. H. Jaffé, *Theoret.*

Chim. Acta, **26**, 131 (1972).
23) P. Jacques, J. Faure, O. Chalvet, and H. H. Jaffé, *J. Phys. Chem.*, **85**, 473 (1981).
24) R. R. Birge, J. A. Bennett, L. M. Hubburd, H. L. Fang, B. M. Pierce, D. S. Kliger, and J. E. Leroi, *J. Am. Chem. Soc.*, **104**, 2519 (1982).
25) P. Tavan, K. Shulten, and D. Oesterhelt, *Biophys. J.*, **47**, 415 (1985).
26) T. Hamanaka and T. Mistui, the 12 th Meeting of the Biophysical Society of Japan, Tokyo, Japan, Preprints, **1973**, 81.
27) Y. Inoue, Y. Tokito, R. Chûjô, and Y. Miyoshi, *J. Am. Chem. Soc.*, **99**, 5592 (1977).
28) J. B. Stothers, "Carbon-13 NMR Spectroscopy," Academic Press, New York (**1972**), Chap. 11.
29) Y. Inoue, Y. Tokito, S. Tomonoh, and R. Chûjô, *Bull. Chem. Soc. Jpn.*, **52**, 265 (1979).
30) J. Kobayashi, U. Nagai, T. Higashijima, and T. Miyazawa, *Biochim. Biophys. Acta*, **577**, 195 (1980).
31) J. Kobayashi, T. Higashijima, U. Nagai, and T. Miyazawa, *Biochem. Biophys. Acta*, **621**, 190 (1980).
32) P. P. Rastogi and G. Zundel, *Biochem. Biophys. Res. Commun.*, **99**, 804 (1981).
33) T. Suzuki and Y. Kito, *Photochem. Phtobiol.*, **15**, 275 (1972).
34) T. Komatsu and H. Suzuki, *J. Phys. Soc.Jpn.*, **40**, 1725 (1976).
35) K. G. R. Pachler, *Spectrochm. Acta*, **20**, 581 (1964).

^{13}C and ^{1}H NMR of α-Arylnitrones. Substituent Effects on the α-Position of α-(*p*-Substituted Phenyl)nitrones

Chino YIJIMA, Toshio TSUJIMOTO, Kohji SUDA,* and Masashige YAMAUCHI†
Department of Physical Chemistry, Meiji College of Pharmacy, 1-35-23, Nozawa, Setagaya-ku, Tokyo 154
†Faculty of Pharmaceutical Sciences, Josai University, Keyakidai, Sakado, Saitama 350-02
(Received November 26, 1985)

Substituent effects on the ^{13}C and ^{1}H NMR chemical shifts of the α-position of various α-(*p*-substituted phenyl)nitrones, α-phenyl-*N*-(1-cyano-2-methylpropyl)nitrones (**1**), α-phenyl-*N*-methylnitrones (**2**), and α-phenyl-*N*-phenylnitrones (**3**), have been investigated and the obtained results have been compared with data related to *N*-(*p*-substituted benzylidene)anilines (**4**) and reported data for *p*-substituted styrenes (**5**). The chemical shifts of the α-arylnitrones are well correlated with substituent constants by means of a linear combination of two empirical parameters, σ_I and σ_π. Inductive effects predominate at the α-carbon but resonance effects predominate at the α-hydrogen.

Much attention has been paid to the chemistry of nitrones because of their widely applicable reactivities.[1-3] 1,3-Dipolar cycloadditions of nitrones and their functionalizations at the α-position have great synthetic utilities.[3]

Nitrones have a positive charge on the nitrogen atom which can be delocalized between the nitrogen atom and the α-carbon atom.[1] The extent of the delocalization is naturally influenced by substituents on the α-carbon and the nitrogen. An understanding of the electronic behavior of the α-position is, therefore, one of the essential subjects in nitrone chemistry.

NMR spectroscopy is a powerfull tool for studying the electronic behavior of the nitrone function and a few attempts have been made to correlate electronic substituent constants with the chemical shifts of nitrones.[4] However, they are still lacking an adequate explanation regarding this subject. In a recent study of substituent effects on the ^{1}H and ^{13}C NMR spectra of α, *N*-diarylnitrones, Arumugam et al.[5] found a linear correlation between the chemical shifts of the α-proton ($^{1}H_\alpha$) and the Hammett σ_p parameters or the Swain-Lupton *F* and *R* parameters. Their analyses, however, have left some important problems, especially concerning the correlation with the chemical shifts of the α-carbon of a series of α-arylnitrones: the parameters they used showed no correlation with these chemical shifts which would give more direct information about the mechanisms of the transmission of substituent effects on the α-position. As a primary approach, it is necessary to decide whether this is due to the use of inappropriate parameters or to contributions from substituent effects other than inductive and resonance ones.

The present work is concerned with a systematic investigation of the effects of substituents in the phenyl ring on the α-position of various α-arylnitrones, α-(*p*-substituted phenyl)-*N*-(1-cyano-2-methylpropyl)nitrones (**1**), α-(*p*-substituted phenyl)-*N*-methylnitrones (**2**) and α-(*p*-substituted phenyl)-*N*-phenylnitrones (**3**), by means of ^{13}C and ^{1}H NMR spectroscopy. For a comparison, *N*-(*p*-substituted benzylidene)anilines (**4**) and *p*-substituted styrenes (**5**) have been investigated.

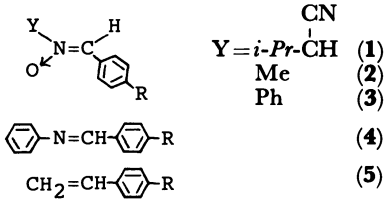

Experimental

Materials. 2-(Hydroxyamino)valeronitrile[6] and *N*-phenylhydroxylamine[7] were prepared and purified according to procedures described in the literature. *N*-Methylhydroxylamine was synthesized according to a reported method[8] with a little modification.

The nitrones used were generally prepared by the condensation of an apporopriate *N*-substituted hydroxylamine with *p*-substituted benzaldehydes in ethanol and purified by recrystallization from ethanol, ethanol-hexane or benzene-hexane.

N-(*p*-Substituted benzylidene)anilines were prepared by the literature method.[9]

Melting points (uncorrected, °C) of the compounds prepared are as follows. **1a**, 154.5—155.5; **1b**, 135—136; **1c**, 114—115; **1d**, 112.5—113.5; **1e**, 93—93.5; **1f**, 114—114.5; **1g**, 139; **1h**, 117.5—118.5; **1i**, 125—126; **2a**, 106—107 (lit, 105[10]); **2b**, 123.5—124, (lit, 120.5[11]); **2c**, 82.5—83; **2d**, 109—110; **2e**, 130—131, (lit, 127.5—128[11]); **2f**, 129.5—130; **2g**, 193—193.5 (lit, 187[11]); **2h**, 222—223, (lit, 206—207[11]); **3a**, 142—143; **3b**, 116—117; **3c**, 165—166; **3d**, 89—90, (lit, 95,[12] 85—87[4b]); **3e**, 105—106, (lit, 114,[12] 113—113.5[4b]); **3f**, 136—137; **3g**, 154—155; **3h**, 169—170, (lit, 165,[12] 161.5—162[4b]); **3i**, 133—134, (lit, 155.5—156[4b]); **3j**, 157—158, (lit, 147—149[4b]); **3k**, 193—194, (lit. 187,[12] 186—186.5[4b]); **4a**, 98—99; **4b**, 56—57, (lit, 63—64[13]); **4c**, 78—79; **4d**, 43.5—44.5, (lit, 146—147/3 mmHg[13] (1 mmHg=133.322 Pa)); **4e**, 50.5—51.5; **4f**, 42—43; **4g**, 64—65; **4h**, 73.5—74; **4i**, 76—77, (lit, 125.5—126.5[13]); **4j**, 97—98; **4k**, 91—92.

Compounds, **1a**, **1e**, **1g**, **2d**, **3c**, **3f**, **4c**, **4f**, and **4j** are new and their elemental analyses are as follows:

(**1a**) Found: C, 68.45; H, 8.01; N, 16.72%. Calcd for $C_{14}H_{19}N_3O$: C, 68.54; H, 7.81; N, 17.13%.

(**1e**) Found: C, 65.26 H, 5.95; N, 12.59%. Calcd for $C_{12}H_{13}FN_2O$: C, 65.43; H, 5.96; N, 12.72%.

(**1g**) Found: C, 51.22; H, 4.66; N, 9.91%. Calcd for $C_{12}H_{13}BrN_2O$: C, 51.25; H, 4.67; N, 9.96%.

(**2d**) Found: C, 63.01; H, 5.21; N, 9.21%. Calcd for C_8H_8FNO: C, 62.73; H, 5.28; N, 9.15%.

(**3c**) Found: C, 69.08; H, 5.20; N, 5.65%. Calcd for $C_{14}H_{13}NOS$: C, 69.11; H, 5.39; N, 5.75%.

(**3f**) Found: C, 72.58; H, 4.53; N, 6.48%. Calcd for $C_{13}H_{10}FNO$: C, 72.54; H, 4.68; N, 6.51%.

(**4c**) Found: C, 73.86; H, 5.65; N, 6.16%. Calcd for $C_{14}H_{13}NS$: C, 73.99; H, 5.77; N, 6.16%.

(**4f**) Found: C, 78.13; H, 4.79; N, 7.00%. Calcd for $C_{13}H_{10}FN$: C, 78.37; H, 5.06; N, 7.03%.

(**4j**) Found: C, 81.60; H, 4.70; N, 13.48%. Calcd for $C_{14}H_{10}N_2$: C, 81.53; H, 4.89; N, 13.58%.

NMR Measurement. The ^{13}C NMR spectra were measured at 67.8 MHz on a JEOL GX-270 spectrometer under a pulse Fourier transform mode. A spectral width of 17000—18000 Hz was used with 16K (resolution 2.4 Hz) data points. ^1H NMR spectra were obtained on a JEOL PS-100 NMR spectrometer operating at 100 MHz for **1**, at 270 MHz on a JEOL GX-270 NMR spectrometer for **2**, and at 90 MHz on a Hitachi Perkin Elmer R-22 NMR spectrometer for **3** and **4**. Sample solutions were prepared in a concentration of ca. 0.5 M (mol dm^{-3}) for ^{13}C NMR and 0.25 M for ^1H NMR spectra with $CDCl_3$ (99.8%, Merck) containing 1% TMS (tetramethylsilane) as an internal standard. Sample tubes with a 5-mm diameter were used and the probe was at room temperature.

$^{13}C_\alpha$ signals were assigned on the basis of their peak heights and the off-resonance decoupling method. $^1H_\alpha$ signals were either assigned on the basis of an integration of their peak areas or identified by a comparison of their chemical shifts with the spectral data of authentic samples.[4b,10,13]

Parametrizations of the simple HMO method were carried out on an NEC personal computer, PC-9801E, using a modified Tominaga's program.[14]

Results and Discussion

The observed ^{13}C and ^1H chemical shifts (δ) for the α-position of α-arylnitrones **1**—**3** and their substituent-induced chemical shifts (SCS) are summarized in Table 1 together with the corresponding chemical shifts and the SCS data for imines **4** and styrenes **5**.[15]

Although two geometrical isomers, *E* and *Z*, are known in several alkylnitrones,[1,16] all the nitrones used were exclusively in a *Z* configuration at room temperature and the two ortho hydrogens in the α-phenyl group situated syn to the nitrone oxygen appeared at a field lower than the rest of the aromatic hydrogens.

The chemical shifts were independent of the concentrations of the compounds used over a range of 0.1 to 2.0 M (with a smaller error than 0.05 ppm).

Table 1. $^{13}C_\alpha$ and $^1H_\alpha$ Chemical Shifts (δ) and SCS Values of α-Arylnitrones (**1**—**3**), Imines (**4**) and Styrenes (**5**)

Compound	R	^{13}C NMR		^1H NMR	
		δ[a]	SCS[b]	δ[a]	SCS[b]
1a	NMe_2	135.14	0.40	7.431	−0.195
b	OMe	134.46	−0.28	7.549	−0.077
c	Me	134.80	0.06	7.570	−0.056
d	H	134.74	0.0	7.626	0.0
e	F	133.61	−1.13	7.612	−0.014
f	Cl	133.64	−1.10	7.616	−0.010
g	Br	133.70	−1.04	7.597	−0.029
h	CN	133.09	−1.65	7.718	0.092
i	NO_2	132.48	−2.26	7.795	0.169
2a	SMe	134.90	−0.30	7.314	−0.057
b	Me	135.26	0.06	7.326	−0.045
c	H	135.20	0.0	7.371	0.0
d	F	134.04	−1.16	7.357	−0.014
e	Cl	134.10	−1.10	7.357	−0.014
f	Br	134.13	−1.07	7.344	−0.027
g	CN	133.52	−1.68	7.455	0.084
h	NO_2	133.15	−2.05	7.528	0.157
3a	NMe_2			7.772	−0.106
b	OMe	134.13	−0.46	7.823	−0.055
c	SMe	134.07	−0.52	7.850	−0.028
d	Me	134.59	0.00	7.864	−0.014
e	H	134.59	0.0	7.878	0.0
f	F	133.36	−1.22	7.874	−0.004
g	Cl	133.33	−1.25		
h	Br	133.42	−1.16	7.876	−0.011
i	COOMe	133.52	−1.07	7.890	0.012
j	CN	132.69	−1.90	7.997	0.119
k	NO_2	132.32	−2.26	8.033	0.155
4a	NMe_2	160.23	−0.12	8.297	−0.142
b	OMe	159.64	−0.71	8.366	−0.073
c	SMe	159.55	−0.80	8.371	−0.068
d	Me	160.29	−0.06	8.396	−0.043
e	H	160.35	0.0	8.439	0.0
f	F	158.76	−1.59	8.398	−0.041
g	Cl	158.73	−1.62	8.389	−0.050
h	Br	158.91	−1.44	8.443	0.004
i	COOMe	159.00	−1.35		
j	CN	157.80	−2.54	8.471	0.032
k	NO_2	157.32	−3.03	8.540	0.101
5a[c]	NMe_2	136.67	−0.29	6.503	−0.126
b	NH_2			6.494	−0.135
c	OMe	136.29	−0.67	6.561	−0.068
d	SMe			6.562	−0.067
e	Me	136.73	−0.23	6.574	−0.055
f	H	136.96	0.0	6.629	0.0
g	F	136.11	−0.85	6.591	−0.038
h	Cl	135.69	−1.27	6.582	−0.047
i	Br	135.76	−1.20	6.568	−0.061
j	I	135.84	−1.12	6.550	−0.079
k	COMe	136.07	−0.89	6.664	0.035
l	COOMe			6.655	0.026
m	CN	135.39	−1.57	6.630	0.001
n	NO_2	135.03	−1.93	6.701	0.072

a) δ: In ppm downfield from internal TMS. b) SCS $=\delta$(X-R)$-\delta$(X-H). c) Ref. 15.

The $^{13}C_\alpha$ signals of nitrones **1**—**3** appeared in a spectral region close to one another, and they were slightly upfield from the corresponding signals of styrenes **5** but more than 25 ppm upfield from those of imines **4**. Table 1 reveals that as the electron-withdrawing ability of substituents increases, the $^{13}C_\alpha$ signal of the nitrones moves upfield. The upfield shift caused by electron-donating *p*-substituents with a higher electronegative atom, such as OMe and SMe, is also noticeable. Such a behavior is, however, not a characteristic of nitrones alone and also observed in the corresponding chemical shifts of imines **4**[17] and styrenes **5**.[15,18]

In aromatic systems with a conjugated side chain, the range of the substituent chemical shift for the α-carbon, $^{13}C_\alpha$ SCS, is generally much narrower than that of the $^{13}C_\beta$ SCS. In the present investigation, the ranges of the $^{13}C_\alpha$ SCS for compounds **1**—**5** were all within a width of 3 ppm (Table 1).

The plots of the $^{13}C_\alpha$ SCS values of **1**—**4** against the values for styrenes exhibited good linear correlations (Fig. 1). The slopes are all larger than unity (Table 2). The magnitude of a slope should be a measure of the relative sensitivity of the α-carbon toward substituents.

The large slope for **4** may be explained by the participation of a lone pair on the nitrogen atom.

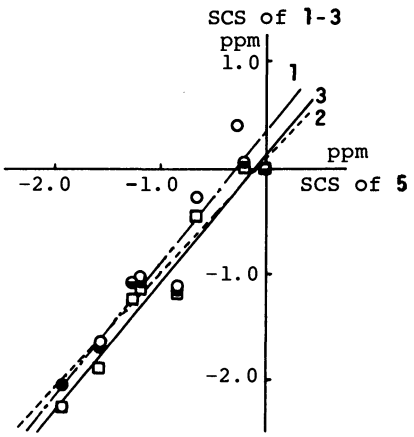

Fig. 1. Correlations of $^{13}C_\alpha$ SCS's of **1** (—○—), **2** (--●--), and **3** (—□—) with $^{13}C_\alpha$ SCS of **5**.

Table 2. Relative Susceptibility of **1**—**5** to Substituent Effects

X	SCS(X)/SCS(styrene)	
	^{13}C NMR	^1H NMR
1	1.28	1.78
2	1.09	1.47
3	1.23	1.34
4	1.64	1.17
5	1.00	1.00

The lone pair could shift the electron cloud around the C=N bond toward the α-carbon according to the requirement of the electron-withdrawing ability of *p*-substituents in the α-phenyl ring. The carbanionic character at the α-carbon increases with an increase in the electron-withdrawing ability of the substituent. The increased shielding at the α-carbon results in an upfield shift of the $^{13}C_\alpha$ signal.

Although nitrones are usually represented by a structure, **a** or **b**, the positive charge on the nitrogen atom is essentially delocalized between the nitrogen and the α-carbon atoms, as represented by an additional canonical structure **c**. However, the upfield shift of the $^{13}C_\alpha$ signals of nitrones **1**—**3**, which was caused by electron-withdrawing substituents, can not be rationalized by the structure of **c**. This behavior requires an explanation that the introduction of electron-withdrawing susbtituents and electron-donating substituents with an electronegative atom into the α-phenyl ring predominantly induces a "back polarized" structure **d** from **b**, or the concept of "π-polarization,"[19] in which an electron cloud around the C=N bond of **b** is withdrawn toward the α-carbon by electron-withdrawing substituents introduced in the α-phenyl group.

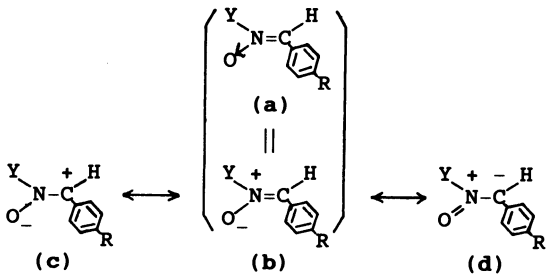

Although the net substituent effect at the α-carbon is smaller than that for imine **4**, this can be rationalized by the charge compensation between the normally-localized structure **c** and the "back polarized" structure **d**.

Table 3 shows the results of an HMO calculation. The Coulomb integral and the resonance integral values used for **3** and **4** are as follows: **3**[20]: h_N=0.6, h_O=1.0, k_{CN}=1.0, k_{NO}=1.5; **4**[21]: h_N=0.5, k_{CN}=1.0.

If these values used for pyridine *N*-oxides are truly applicable to a calculation for **3**, the order obtained for the α-carbon charge density, **3**>**5**>**4**, can explain

Table 3. Charge Densities and Bond Orders for **3**—**5**

	Charge density[a]	Bond order[a]	
	C_α	C_α=N or C_α=C	N→O
3	1.269	0.628	0.639
4	0.835	0.795	
5	1.000	0.911	

a) Calculated by the HMO method.

the largest upfield shift of the $^{13}C_\alpha$ chemical shift of **3**. On the other hand, the bond order for the C_α=N bond of **3** is smaller than those for the corresponding double bonds of **4** and **5**. These two estimations suggest a considerable contribution of the canonical form **d** in the structure of nitrones.

In Hammett plots of $^{13}C_\alpha$ chemical shifts vs. σ values, the slopes for α-arylnitrones **1**—**3** and imine **4** are larger than that of styrene **5** (Table 4), and the correlations are much better with σ_m than with σ_p. This and the order, $\rho_m > \rho_p$, obtained for all the compounds indicate that inductive effects are predominant at the α-carbon atom.

As shown in Table 4 and Figs. 2—4, the $^{13}C_\alpha$ SCS values for the nitrones are, expectedly, correlated much better with a linear combination of σ_i and σ_π, namely a correlation with $\rho_i\sigma_i+\rho_\pi\sigma_\pi$, than with σ_m. ρ_i and ρ_π represent empirical coefficients, and σ_π corresponds to resonance substituent constants, σ_π^+ and σ_π^-, presented by Yukawa and Tsuno,[22] having negative and positive signs for electron-donating groups and electron-withdrawing groups, respectively. The ρ_π values estimated for **1**—**5** were essentially equal to the arithmetic means of the corresponding coefficients of σ_π^+ and σ_π^- and, thus, the use of the linear combination of σ_i and σ_π is appropriate as a multivariate parameter analysis for the nitrones. Our dual-parameter analyses clealy show that inductive effects are the predominant factors in the $^{13}C_\alpha$ chemical shifts.

The relative importance of factors operating in the delocalization of the nitrone function can be estimated from the ratio, ρ_π/ρ_i (Table 5). The magnitude of the ratio, $\rho_\pi/\rho_i<0.5$, means that inductive effects are always stronger than resonance effects at the α-carbon.

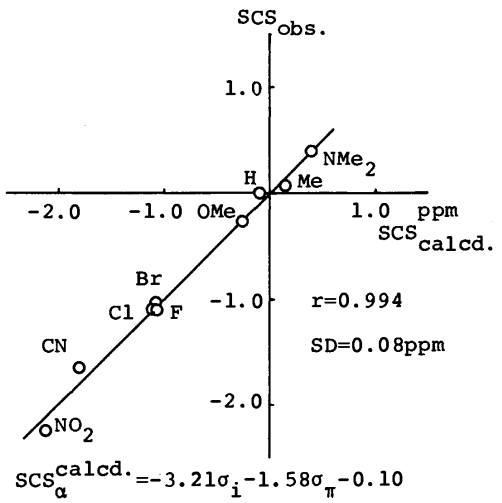

Fig. 2. Correlation between observed and calculated SCS_α for **1**.

Table 4. Correlation Analyses of SCS Values for Compounds **1**—**5**

		$SCS=\rho_p\sigma_p+C$				$SCS=\rho_m\sigma_m+C$				$SCS=\rho_i\sigma_i+\rho_\pi\sigma_\pi+C$				
	n[a]	ρ_p	C	SD[b]	r[c]	ρ_m	C	SD[b]	r[c]	ρ_i	ρ_π	C	SD[b]	r[c]
1 ^{13}C NMR	9	−1.92	−0.59	0.76	0.937	−2.69	−0.08	0.20	0.984	−3.21	−1.58	−0.10	0.08	0.994
		±0.64	±0.32			±0.44	±0.17			±0.61	±0.45	±0.19		
^{1}H NMR	9	0.23	−0.04	0.01	0.961	0.28	−0.08	0.02	0.871	0.09	0.36	−0.01	0.00	0.988
		±0.06	±0.02			±0.14	±0.06			±0.10	±0.07	±0.03		
2 ^{13}C NMR	8	−2.14	−0.46	0.62	0.922	−2.65	−0.06	0.12	0.986	−3.23	−1.23	−0.09	0.03	0.997
		±0.89	±0.34			±0.45	±0.19			±0.42	±0.41	±0.13		
^{1}H NMR	8	0.20	−0.03	0.01	0.942	0.20	−0.05	0.01	0.794	0.07	0.32	−0.01	0.00	0.967
		±0.08	±0.03			±0.15	±0.06			±0.13	±0.12	±0.04		
3 ^{13}C NMR	10	−1.88	−0.62	1.20	0.873	−2.85	−0.13	0.09	0.991	−3.57	−1.11	−0.12	0.09	0.991
		±0.85	±0.33			±0.31	±0.12			±0.57	±0.47	±0.17		
^{1}H NMR	10	0.16	−0.01	0.01	0.918	0.22	−0.05	0.01	0.881	0.12	0.22	−0.01	0.01	0.931
		±0.06	±0.02			±0.10	±0.04			±0.17	±0.11	±0.05		
4 ^{13}C NMR	11	−2.09	−0.95	2.52	0.862	−3.32	−0.37	0.52	0.973	−4.66	−1.25	−0.19	0.32	0.983
		±0.93	±0.38			±0.59	±0.22			±1.00	±0.66	±0.29		
^{1}H NMR	10	0.15	−0.04	0.11	0.922	0.17	−0.07	0.01	0.801	0.01	0.25	−0.01	0.00	0.966
		±0.05	±0.02			±0.11	±0.04			±0.01	±0.07	±0.03		
5 ^{13}C NMR	11	−1.18	−0.73	1.17	0.814	−1.92	−0.39	0.37	0.945	−2.95	−0.51	−0.20	0.30	0.956
		±0.63	±0.26			±0.50	±0.19			±0.96	±0.64	±0.28		
^{1}H NMR	14	0.12	−0.05	0.01	0.870	0.15	−0.07	0.02	0.692	−0.02	0.22	−0.02	0.01	0.943
		±0.04	±0.02			±0.10	±0.03			±0.10	±0.06	±0.03		

a) The number of data. b) Standard deviations. c) Correlation coefficients.

1) *i*-Pr-CH(CN)-N(→O)=CH-Ph-R 2) Me-N(→O)=CH-Ph-R 3) Ph-N(→O)=CH-Ph-R 4) Ph-N=CH-Ph-R 5) CH_2=CH-Ph-R

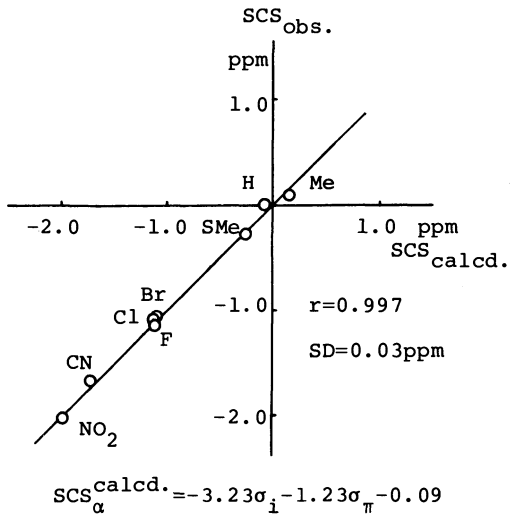

Fig. 3. Correlation between observed and calculated SCS_α for **2**.

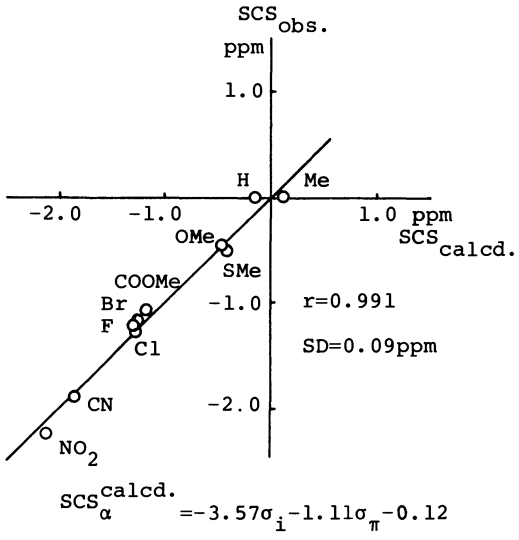

Fig. 4. Correlation between observed and calculated SCS_α for **3**.

The substituent effects of R on to the para and ipso positions, i.e. effects on to the ring carbons next and para to the C_α of nitrones, respectively, are essentially the same as those for monosubstituted benzenes.[23] The plots of SCS_1 vs. SCS_{Bz} showed a good linearity,

$$SCS_{1,para} = 0.96(SCS_{Bz}) - 0.24 \quad (r=0.996)$$
$$SCS_{1,ipso} = 0.92(SCS_{Bz}) + 0.21 \quad (r=0.997)$$

where SCS_1 and SCS_{Bz} represent the ^{13}C SCS of nitrones **1** and monosubstituted benzenes, respectively. On the other hand, no correlation was observed between $SCS_{1,ipso}$ and $SCS_{1,\alpha}$. These findings again support the above conclusion that resonance effects on the C_α through a conjugation system of a phenyl ring are minor. However, we do not suggest that the resonance effects are unimportant. The effects are rather important in nitrones, but the negative ρ_π values can not be rationalized by the canonical forms **c** and **d**. The negative ρ_π values probably result from resonance interactions of R with the nitrone function in structure **b**.

Table 5. Relative Contribution of Resonance Effects and Inductive Effects on the α-Position of **1**—**5**

X	ρ_π/ρ_i	
	^{13}C NMR	^1H NMR
1	0.49	4.0
2	0.38	4.6
3	0.31	1.8
4	0.27	25.0
5	0.17	11.0

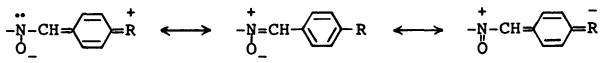

For nitrones with an electron-donating substituent, the charge transfer between the nitrogen atom and R (**b**↔**e**) results in a decrease in the net charge density of the shortened conjugation system. On the other hand, for nitrones with an electron-withdrawing substituent, the charge transfer between the oxygen atom and R (**b**↔**f**) increases the net charge density of the extended conjugation system. These interactions result in a relatively small negative ρ_π value at the C_α since it is a nonconjugating site. The resonance effects in nitrones **1**—**3** are, therefore, more important than those in imines **4** and styrenes **5**.

The region of $^1H_\alpha$ signals of nitrones **1**—**3** lies between the corresponding signal regions of **4** and **5**, i.e., in a lower field than that of **5** but in an upper field than that of **4**. The phenomenon also can be explained by the compensating contribution of structures **c** and **d**.

In contrast with the $^{13}C_\alpha$ chemical shifts, the $^1H_\alpha$ signals of compounds **1**—**5** normally move downfield as the electron-withdrawing ability of substituents increases. This opposite behavior results from a change in the causative factors of the ^{13}C and ^1H chemical shifts. It is well accepted that for a particular nucleus the total shielding constant, σ^t, can be approximated by a sum of three terms[24]: diamagnetic contribution (σ^d), paramagnetic contribution (σ^p), and the contribution from neighboring groups per nuclei (σ'). The first term, σ^p, has been shown to contribute to 90% of total screening of a ^{13}C nucleus, and the change in the chemical shift as a function of structure may be attributed to the change in σ^p. The second term, σ^d, on the other hand, dominates the proton chemical shift.

The correlations between $^1H_\alpha$ SCS and σ values

are much better with σ_p than with σ_m in all the compounds (Table 4). This suggests that resonance effects are stronger than inductive effects at the α-hydrogen. The slopes are, however, very small and nearly one-tenth of the Hammett slopes for the $^{13}C_\alpha$ chemical shifts, reflecting intervention of one carbon between the H_α and the α-phenyl ring. Correlation analyses with $\rho_i\sigma_i+\rho_\pi\sigma_\pi$ also suggest the predominance of resonance effects in $^1H_\alpha$ chemical shifts.

The observed substituent effects on the $^1H_\alpha$ chemical shifts of nitrones **1—3** are larger than those for imine **4** and styrene **5** (Table 2). A resonance measure ρ_π is nearly constant in all the compounds but the order of the magnitude of an inductive measure ρ_i is $\rho_{i\,\text{nitrone}}>\rho_{i\,\text{imine}}$ and $\rho_{i\,\text{styrene}}\simeq 0$. Thus, the ratio ρ_π/ρ_i for the nitrones is smaller than those for imine **4** and styrene **5** (Table 5).

In summary, the $^{13}C_\alpha$ signal of α-arylnitrones shifts upfield as the electron-withdrawing ability of substituents in the α-phenyl ring increases, but the $^1H_\alpha$ signal downfield. The $^{13}C_\alpha$ chemical shifts are well correlated with a linear combination of σ_i and σ_π. Inductive effects predominate at the α-carbon and the contribution of the canonical structure **d** is the largest although its contribution is known to be small in many chemical reactions. The importance of this structure will increase with the electron-withdrawing ability of the substituent R. For the α-hydrogen, resonance effects predominate instead of inductive effects.

The authors thank Professor Masami Sawada, Scientific and Industrial Research Institute, Osaka University, for helpful discussions, and Dr. Hitoshi Takai, Fuculty of Pharmaceutical Sciences, Osaka University, for the measurement of the ^1H spectra of **3** and **4**. Thanks are also due to Mr. Tatsuya Takagi for the use of his personal computer program package for multivariate analysis.

References

1) E. Breuer, "The Chemistry of Functional Groups," Supplement F (The Chemistry of Amino, Nitroso and Nitro Compounds and Their Derivatives Part 1), ed by S. Patai, John Wiley & Sons, New York (1982), Chap. 13.

2) A. Albini and M. Alpegiani, *Chem. Rev.*, **84**, 43 (1984).

3) D. St. C. Black, R. A. Crozier, and V. C. Davis, *Synthesis*, **1975**, 205.

4) a) K. Koyano and H. Suzuki, *Tetrahedron Lett.*, **1968**, 1859; b) *Bull. Chem. Soc. Jpn.*, **42**, 3306 (1969).

5) N. Arumugam, P. Manisankar, S. Sivasubramanian, and D. A. Wilson, *Org. Magn. Reson.*, **22**, 592 (1984).

6) L. Neelakantan and W. H. Hartung, *J. Org. Chem.*, **23**, 964 (1958).

7) L. Gattermann and T. Wieland, "Die Praxis des Organishen Chemikers," Walter de Gruyter and Co., Berlin (1961), p. 154.

8) E. Beckmann, *Ann.*, **365**, 201 (1909).

9) H. Gilman and A. H. Blatt, "Organic Syntheses," 2nd ed, John Wiley & Sons, New York (1961), Coll. Vol. I, p. 80.

10) V. I. Minkin, E. A. Medyantseva, I. M. Andreeva, and G. V. Gorshkova, *J. Org. Chem. USSR*, **9**, 148 (1973).

11) T. Kubota and H. Miyazaki, *Bull. Chem. Soc. Jpn.*, **40**, 245 (1967).

12) E. A. Medyantseva, I. M. Andreeva, and V. I. Minkin, *J. Org. Chem. USSR*, **8**, 149 (1972).

13) K. Tabei and E. Saitou, *Bull. Chem. Soc. Jpn.*, **42**, 1140 (1969).

14) N. Tominaga, *Kagaku No Ryoiki*, **36**, 724 (1982).

15) G. K. Hamer, I. R. Peat, and W. F. Reynolds, *Can. J. Chem.*, **51**, 897 (1973).

16) J. Bjorgo, D. R. Boyd, D. C. Niell, and W. B. Jennings, *J. Chem. Soc., Perkin Trans. 1*, **1977**, 254.

17) N. Inamoto, S. Masuda, K. Tokumaru, and M. Yoshida, *Tetrahedron Lett.*, **1975**, 3697.

18) D. A. R. Happer, *J. Chem. Soc., Perkin Trans. 2*, **1984**, 1637.

19) a) J. Bromilow, R. T. C. Brownlee, D. J. Craik, P. R. Fiske, J. E. Rowe, and M. J. Sadek, *J. Chem. Soc., Perkin Trans. 2*, **1981**, 753; b) D. J. Craik and R. T. C. Brownlee, "Progress in Physical Organic Chemistry," ed by R. W. Taft, John Wiley & Sons, New York (1983), Vol. 14, pp. 1—73.

20) R. A. Barnes, *J. Am. Chem. Soc.*, **81**, 1935 (1959).

21) a) A. Streitwieser, Jr., "Molecular Orbital Theory for Organic Chemists," John Willey & Sons, New York (1961), Chap. 5; b) T. Kubota and M. Yamakawa, *Bull. Chem. Soc. Jpn.*, **36**, 1564 (1963).

22) a) Y. Yukawa and Y. Tsuno, *Nippon Kagaku Zasshi*, **86**, 873 (1965); b) M. Sawada, M. Ichihara, Y. Yukawa, T. Nakachi, and Y. Tsuno, *Bull. Chem. Soc. Jpn.*, **53**, 2055 (1980).

We may analyze the substituent effects by the use of Linear Aromatic Substituent Reactivity (LArSR: $\log k/k_0=\rho_i\sigma_i+\rho_\pi^+\sigma_\pi^++\rho_\pi^-\sigma_\pi^-$) relationship, though the data have been treated as shown in the present text for the limited number of substituents. A part of the analyses is shown as follows, where substituent constants cited in ref. 22b have been used:

1: $^{13}C_\alpha$ SCS$=-3.14(\pm0.74)\sigma_i-1.47(\pm0.67)\sigma_\pi^+-1.82(\pm1.12)\sigma_\pi^--0.09(\pm0.22)$, $r=0.994$, SD=0.07 ppm, $n=9$

2: $^{13}C_\alpha$ SCS$=-3.15(\pm0.49)\sigma_i-0.93(\pm0.93)\sigma_\pi^+-1.48(\pm0.80)\sigma_\pi^--0.07(\pm0.15)$, $r=0.998$, SD=0.02 ppm, $n=8$

3: $^{13}C_\alpha$ SCS$=-3.43(\pm0.56)\sigma_i-0.58(\pm0.88)\sigma_\pi^+-1.64(\pm0.87)\sigma_\pi^--0.06(\pm0.17)$, $r=0.994$, SD=0.06 ppm, $n=10$

An alternative analysis of the $^{13}C_\alpha$ chemical shift of compounds **1—5** by means of Dual Substituent Parameter equation (DSP, $\log k/k_0=\rho_I\sigma_I+\rho_R\sigma_R$) paralleled the analysis done in the present text with comparable precisions. Some of the results are shown as follows:

1: $^{13}C_\alpha$ SCS$=-2.84(\pm0.46)\sigma_I-0.85(\pm0.36)\sigma_R-0.06(\pm0.22)$ $r=0.992$, SD=0.10 ppm, $n=9$.

2: $^{13}C_\alpha$ SCS$=-2.81(\pm0.37)\sigma_I-0.84(\pm0.43)\sigma_R-0.04(\pm0.17)$ $r=0.995$, SD=0.04 ppm, $n=8$

23) a) Miyajima, Y. Sasaki, and M. Suzuki, *Chem. Pharm. Bull. (Tokyo)*, **19**, 2301 (1971); b) D. F. Ewing, *Org. Magn. Reson.*, **12**, 499 (1979).

24) For example a) R. J. Abraham and P. Loftus, "Proton and Carbon-13 NMR Spectroscopy: An Integrated Approach," Heyden and Son, London (1978); b) G. C. Levy and R. L. Lichter, "Nitrogen-15 Nuclear Magnetic Resonance Spectroscopy," John Wiley & Sons, New York (1979); c) G. J. Martin and M. L. Martin, *Org. Magn. Reson.*, **7**, 2 (1975).

 © 1986 The Chemical Society of Japan Bull. Chem. Soc. Jpn., 59, 2171—2177 (1986)

Synthesis of Amides and Amidines by Reaction of Carboxylic Acids and Amines in the Presence of Polyphophoric Acid Trimethylsilyl Ester (PPSE)

Shin-ichi OGATA, Amane MOCHIZUKI, Masa-aki KAKIMOTO,* and Yoshio IMAI
Department of Textile and Polymeric Materials, Tokyo Institute of Technology, Meguro-ku, Tokyo 152
(Received January 14, 1986)

The reaction between amines and carboxylic aicds in the presence of polyphosphoric acid trimethylsilyl ester (PPSE) has been investigated from the view point of the synthesis of amides and amidines. Benzanilide was selectively prepared from benzoic acid and aniline in the presence of PPSE and pyridine at 100 °C, whereas a mixture of benzanilide and *N,N'*-diphenylbenzamidine was obtained without the use of pyridine. The reaction at 160 °C almost exclusively gave *N,N'*-diphenylbenzamidine. Various symmetrical amidines were obtained from combinations of carboxylic acids and aromatic amines in high yields by simply heating at 160 °C with four molar amounts of PPSE. The reactions of aliphatic and aromatic amines with *N*-monosubstituted and *N,N*-disubstituted amides also afforded corresponding unsymmetrical amidines under the same conditions. The reaction mechanism is discussed in some detail.

Polyphosphoric acid trimethylsilyl ester (PPSE) has been utilized extensively since its first preparation by Imamoto et al.[1] A PPSE-promoted synthesis of heterocyclic compounds[2] and nitriles from amides,[3] an unusual aldol reaction,[4] and the Beckmann,[1] pinacol-pinacolone,[5] and Pummerer rearrangements[6] have been reported. PPSE is readily prepared from diphosphorus pentaoxide and hexamethyldisiloxane, usually by heating in dichloromethane or chloroform for a short time.[1,4b] The structure of this reagent was confirmed to be a mixture of cyclotetraphosphate (**1**), isocyclotetraphosphate (**2**), linear tetraphosphate (**3**), and a small amount of pyrophosphate (**4**) on the basis of a ^{31}P NMR measurement[2a] (Scheme 1).

Although polyphosphoric acid (PPA), which has been well-known as a powerful reagent for dehydrative condensations,[7] is essentially insoluble in organic solvents, PPSE is readily soluble in various aprotic solvents such as benzene, chlorinated hydrocarbons, and sulfolane. Therefore, PPSE should be accepted as a very applicable reagent for an organic synthesis, compared with PPA. The structural and characteristic reactions of PPSE are similar to those of polyphosphoric acid ethyl ester (PPE),[8] of which a number of reactions have been presented mainly, from the view point of dehydration reactions.[9] In a comparison of these two polyphosphoric acid ester reagents, PPSE can be prepared much easier than PPE, whose preparation requires a few days from diphosphorus pentaoxide and diethyl ether.[8] Furthermore, PPSE was more reactive than PPE in some reactions.[2,4,7]

It has been demonstrated that a number of heterocyclic compounds can be easily prepared from appropriate amino compounds and carboxylic acids using PPA, PPE, and PPSE. On the other hand, the reactions of simple carboxylic acids with amines to afford acyclic compounds were only sparingly reported.[9a] Here, we wish to report on a novel synthesis of amides and amidines by a reaction of carboxylic acids and amines in the presence of PPSE.

Results and Discussion

Synthesis of Amides from Carboxylic Acids and

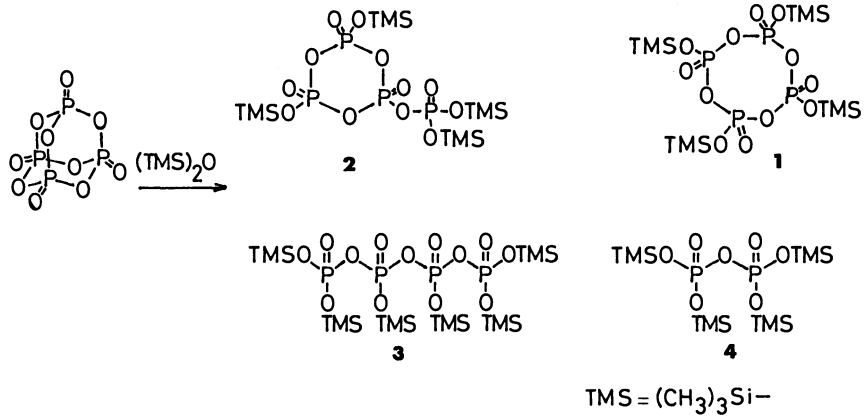

Scheme 1.

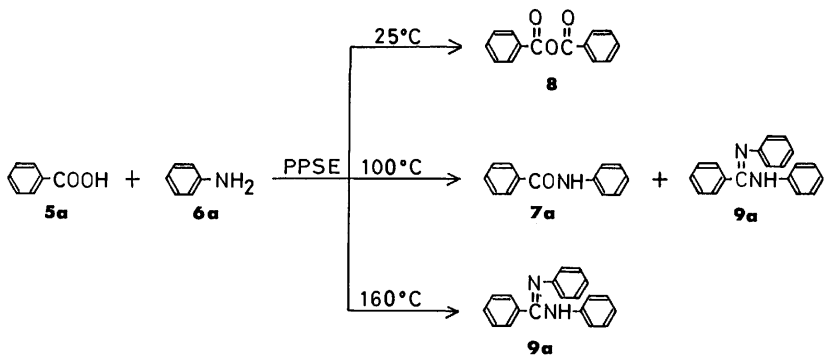

Scheme 2.

Amines. Our initial object was a synthesis of amides **7** by a direct condensation of carboxylic acids **5** and amines **6** using PPSE as condensing agent. In the beginning, the reaction between benzoic acid (**5a**) and aniline (**6a**) was conducted at the various temperatures as illustrated in Scheme 2. Results of the reactions are summarized as follows: 1) Benzoic anhydride (**8**) was the major product at 25 °C. 2) A mixture of almost the same amount of benzanilide (**7a**) and *N,N'*-diphenylbenzamidine (**9a**) was obtained at 100 °C. 3) Amidine **9a** was the only product at 160 °C.

The synthesis of amidines at a high temperature will be discussed later. For the purpose of a selective formation of amide **7a**, pyridine, which should increase the nucleophilicity of aniline (**6a**), was added to the reaction system. The procedure of the amide -forming reaction was examined. Thus, 1) an equimolar amount of benzoic acid (**5a**), aniline (**6a**), and pyridine were added to four-fold molar amounts of PPSE dissolved in sulfolane at 100 °C. 2) In the first step, **5a** was treated in a PPSE solution of sulfolane for 30 min at 100 °C, and then **6a** and pyridine were added to the solution. 3) A mixture of **5a** and pyridine in a small amount of 1,2-dichloroethane was added to PPSE solution in sulfolane at 100 °C, and then **6a** was added to the solution. The yields of amide **7a** by the each procedure were 80, 84, and 49%, respectively. The reaction was also carried out in various solvents such as sulfolane, anisole, dichloromethane, and *N,N*-dimethylacetamide, and sulfolane was found to be the best solvent for this reaction (Eq. 1).

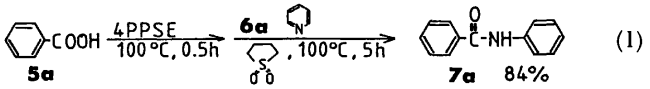

(1)

Although a detailed search was made to establish the optimum reaction conditions for amide formation, the suppression of the side reactions of amidine formation was fairly difficult. Therefore, it was concluded that this method was not so generally applicable compared with a direct synthesis of amides by the condensations of carboxylic acids with amines using some condensing agents.

Synthesis of Symmetrical Amidines from Carboxylic Acids and Amines.[10] The results of the high-temperature reaction described above have led to the suggestion that the reaction of carboxylic acids **5** with amines **6** in the presence of PPSE would be generalized to a direct synthesis of symmetrical amidines **9** as illustrated in Eq. 2. To our knowledge, the conversion of carboxylic acids and amines to amidines has been unknown except the case of cyclic amidines.[11]

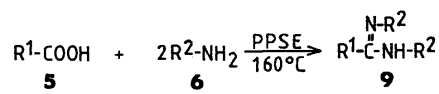

(2)

Various examples of the synthesis of symmetrical amidines are summarized in Table 1. From Entry 1 to 7, a variety of carboxylic acids **5** were treated with two equivalents of aniline (**6a**) at 160 °C for 5 h without solvent. From Entry 8 to 11, benzoic acid (**5a**) with aromatic amines **6** were examined. *N,N'*-Diphenylamidines were obtained by a reaction between aniline (**6a**) and various aromatic, aliphatic, and *α,β*-unsaturated carboxylic acids in high yields. *N,N'*-Bis(*p*-nitrophenyl)benzamidine (**9k**) was obtained from benzoic acid and *p*-nitroaniline having low nucleophilicity by use of PPSE prepared from two equivalents of hexamethyldisiloxane (Entry 11). When PPSE prepared from diphosphorus pentaoxide and three equivalents of hexamethyldisiloxane was used, the reaction of the same starting compounds did not afford the corresponding amidine **9k** but gave *N*-(*p*-nitrophenyl)benzamide in 59% yield. It was observed by a measurement of the ^{31}P NMR spectra that the PPSE prepared by the former method contained a large amount of isocyclotetraphosphate **2** having an active blanched unit structure.[2a] Thus, even from nitroaniline with a low nucleophilicity, amidine **9k** can be obtained using the active PPSE. Contrary to the successful synthesis of *N,N'*-diaryl-substituted amidines **9** from aromatic amines possessing electron-donating and -withdrowing groups,

Table 1. Preparation of Symmetrical Amidines

Entry	Carboxylic acid	Amine	Amidine		
			Code	Yield/%[a]	Mp(θ_m/°C) (lit,)[b]
1	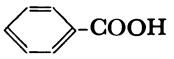	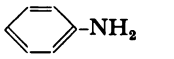	**9a**	83	143—144 (144[13])
2	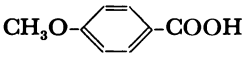	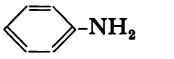	**9b**	87	115—116 (107—108[14])
3	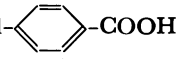	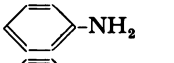	**9c**	88	149—150 (149[15])
4	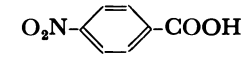	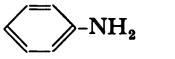	**9d**	84	151—153 (155[16])
5	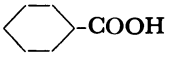	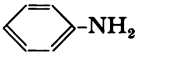	**9e**	81	110—111
6	$CH_3(CH_2)_4$-COOH	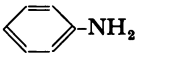	**9f**	79	91—92 (90[17])
7	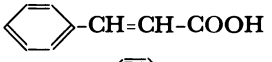	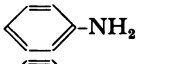	**9g**	65	115.5—116.5
8	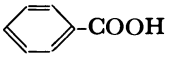	CH_3O- 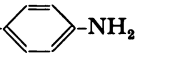	**9h**	88	120—122 (125[18])
9	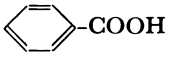	CH_3- 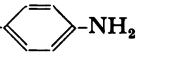	**9i**	87	131—131.5
10	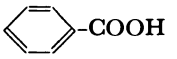	Cl- 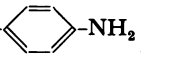	**9j**	69	140—141
11	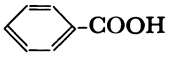	O_2N- 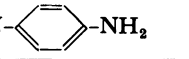	**9k**	82	193—194.5

a) Yields are after recrystallized from aqueous ethanol. b) Melting points are uncorrected.

highly nucleophilic aliphatic amines gave a mixture of amidines **9** and amides **7** in low yields.

Synthesis of Unsymmetrical Amidines from Amides and Amines. In the course of the reaction between carboxylic acids **5** and aromatic amines **6**, interesting phenomena were observed. When an equimolar amount of benzoic acid (**5a**) and aniline (**6a**) were reacted in the presence of PPSE at 160 °C for 5 h, amidine **9a** was obtained in 82% yield based on aniline, and benzanilide (**7a**) was not isolated from the reaction mixture. This result suggests that the rate of formation of amidine **9a** from **7a** should be greater than the rate of formation of benzanilide (**7a**), if the intermediate to give **9a** is **7a**. To prove the reaction pathway, the reaction of benzanilide (**7a**) and aniline (**6a**) was conducted. *N,N'*-Diphenylbenzamidine (**9a**) was also obtained in 90% yield under the same conditions for the amidine formation described above. Therefore, this reaction was successfully extended to an unsymmetrical amidine synthesis as illustrated in Eq. 3.

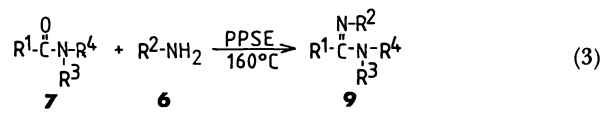

(3)

7 **6** **9**

As summarized in Table 2, various examples of the reaction were conducted. It is interesting to note that aliphatic amines, as well as aromatic amines could be applicable in this reaction, giving moderate to excellent yields of amidines **9**, whereas aliphatic amines did not give satisfactory results in a direct synthesis of the symmetrical amidines mentioned earlier. Primary, secondary, and tertiary aliphatic amines were examined in the reaction with benzanilide (**7a**). Amidine **9o** was obtained in moderate yield from cyclohexylamine, while the product of the reaction with hexylamine was a mixture of the desired amidine **9n** and *N,N'*-diphenylbenzamidine (**9a**). In the reaction with *t*-butylamine, the amine did not react with benzanilide (**7a**) and **9a** was obtained in 87% yield based on **7a**. Amide **7a** was expected to dimerize through the reaction to give amidine **9a**, similar to the reaction of amides with PPE.[9g] Indeed, amine **7a** afforded amidine **9a** in 90% yield by simply heating at 160 °C with excess of PPSE as depicted in Eq. 4.

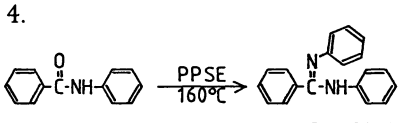

(4)

7a **9a** 90%

Furthermore, not only *N*-monosubstituted amides but also *N,N*-disubstituted amides could be used for this type of reaction. When the reaction of benzamide **7b** was conducted, it was found that **7b** reacted with PPSE predominantly to afford *p*-methoxybenzonitrile.[3]

Reaction Mechanism. When one discusses the mechanism of the present reaction, PPSE has two possible roles, where it acts as a silylating agent and a phosphorylating agent. Because tris(trimethylsilyl) orthophosphate, whose trimethylsilyl function seems

Table 2. Preparation of Unsymmetrical Amidines

Entry	Amide	Amine	Amidine		
			Code	Yield/%	Mp(Bp/Torr) /°C(lit,)
1	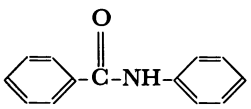	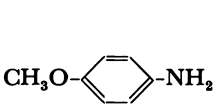	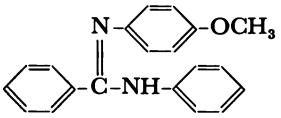 **9l**	97[a]	108—110[b] (120[19])
2	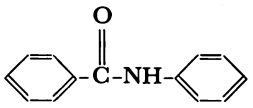	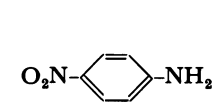	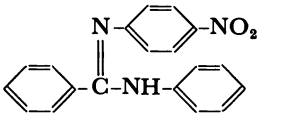 **9m**	91[a]	181—183[b] (184[20])
3	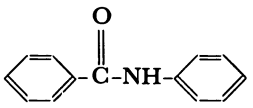		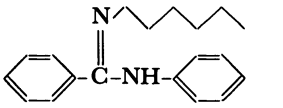 **9n**	23[d]	—
			+		
			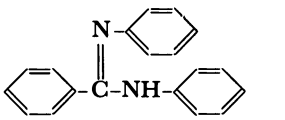 **9a**	53[d]	—
4	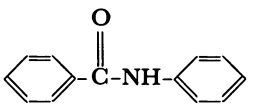	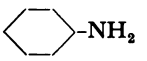	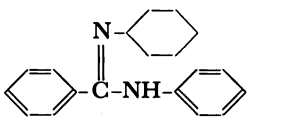 **9o**	54[a]	142—143.5[b]
5	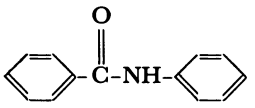		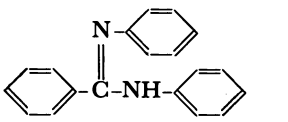 **9a**	87[a]	—
6	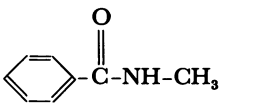	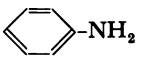	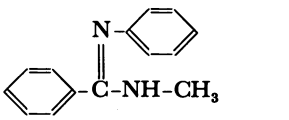 **9p**	94[a]	126—128[b] (135—136[21])
7	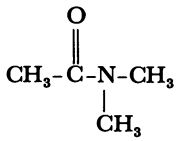	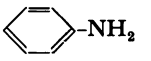	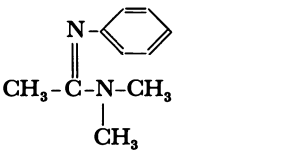 **9q**	89	(120/0.1)[c] (75—76/0.005[22])
8	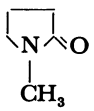	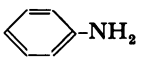	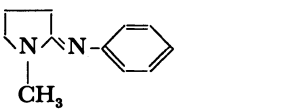 **9r**	85	(140/0.1)[c] (90/0.01[23])

a) Yields are after recrystallized from aqueous ethanol. b) Melting points are uncorrected. c) Boiling points refer to the bath temperature of bulb to bulb distillation. d) Yields are calculated from integration of ^{1}H NMR spectrum of the mixture of **9n** and **9a**. e) 1 Torr = 133.322 Pa.

to possess almost the same reactivity as PPSE was found to be ineffective for amidine synthesis, it is concluded that phosphorylation of carboxylic acid by PPSE is the initial reaction. The mechanism is presumed as illustrated in Scheme 3. In the beginning, carboxylic acid **5** reacts with PPSE to afford mixed anhydride **10**. Amide **7** is obtained by the action of pyridine through intermediate **11**, which is produced by the reaction of **10** and amine **6**. Intermediate **11** is then phosphorylated with PPSE to afford **12**. Imidate intermediate **13** is produced by the elimination of phosphoric function from **12**. Alternatively, amide **7** is converted to **13** by the reaction with PPSE. Finally, **13** reacts with amine **6** to afford amidine **9**. Although amine **6** can react with PPSE, the reaction product (phosphoric amide and/or phosphoric acid salt of **6**) should decompose at a high temperature to liberate amine **6**, and **6** may react with **13**. Since aromatic amine should be liberated more readily than aliphatic amine at a high temperature, the reaction proceeds predominantly with aromatic amine. The reaction between benzoic acid (**5a**) and an equimolar amount of aniline (**6a**) in the presence of PPSE afforded amidine **9a** in 82% yield

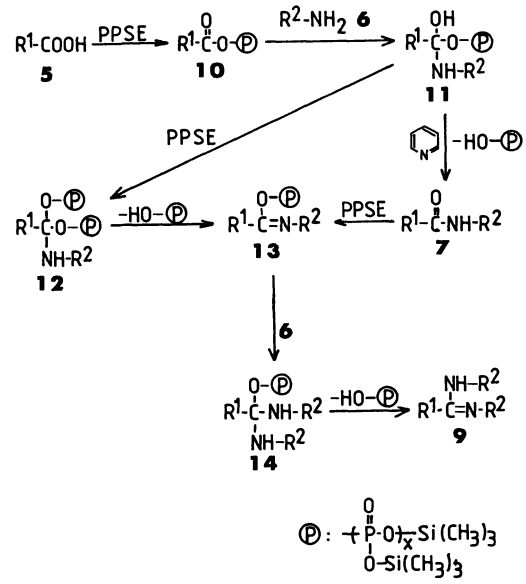

Scheme 3.

based on **6a**. This result suggests that the reaction from **13** to **9** was faster than the reaction from **10** to **13**. In the reaction of amide **7a** and aliphatic amine, the only successful example was the case of cyclohexylamine. Therein, hexylamine which has high nucleophilicity should competitively react with **13** and PPSE existing in the reaction mixture, and *t*-butylamine could not attack **13** because of the steric hindrance.

Conclusion

The conventional starting materials for amidine synthesis[11] are nitriles, imidates, imidohalides, and orthoesters etc., which are essentially derivatives of carboxylic acids and/or amines. The present method offers a convenient synthesis of amidines. Thus, symmetrical and unsymmetrical amidines were synthesized directly from reactant pairs of carboxylic acid-amine and amide-amine, respectively, in the presence of PPSE. Since PPSE possesses the characteristics of a Lewis acid as well as a dehydration agent, it should be accepted as a unique reagent for dehydrative condensation reactions.

Experimental

The ^{1}H NMR spectra were determined with a JEOL C-60 HL, and the chemical shifts are given in ppm based on tetramethylsilane. The ^{31}P NMR spectra were recorded with a JEOL FX-100. Solvents such as dichloromethane were purified by the usual procedures.

Preparation of Polyphosphoric Acid Trimethylsilyl Ester (PPSE). In a 50 mL round-bottom flask, a mixture of 1.42 g (5 mmol) of diphosphorus pentaoxide, 2.56 g (16 mmol) of hexamethyldisiloxane and 3 mL of dichloromethane was heated at refluxing temperature for 30 min under a thin stream of nitrogen. After a distillation apparatus was equipped on the flask, the mixture was gradually heated to 160 °C under nitrogen. During this period, volatile compounds such as dichloromethane and excess hexamethyldisiloxane were distilled away. The residual viscous syrup was used for the following reactions.

Preparation of Benzanilide (7a). To the syrup of PPSE which was prepared from 10 mmol of diphosphorus pentaoxide and 20 mmol of hexamethyldisiloxane, 5 mL of sulfolane and 0.305 g (2.5 mmol) of benzoic acid (**5a**) were added. After the solution was stirred for 30 min, 0.2 mL (2.5 mmol) of pyridine and 0.233 g (2.5 mmol) of aniline (**6a**) were added. The reaction mixture was stirred for 5 h at 100 °C under nitrogen. The benzanilide (**7a**) was obtained by pouring the mixture into cold 1 M† NaOH solution. Yields was 0.392 g (84%): Mp 160—161 °C (161 °C[12]); IR (KBr) 3300 cm^{-1} (N-H), 1650 cm^{-1} (C=O), 1594 and 1485 cm^{-1} (aromatic).

General Procedure for the Preparation of Symmetrical Amidines (9a—k). To the syrup of PPSE which was prepared from 5 mmol of diphosphorus pentaoxide and 16 mmol of hexamethyldisiloxane, 1.25 mmol of carboxylic acid and 2.50 mmol of amine were added at 160 °C, and the solution was stirred for 5 h at the temperature under nitrogen. The crude product was isolated by pouring the reaction mixture into a 1 M NaOH solution. Recrystallization from aqueous ethanol gave pure symmetrical amidine.

The yield and melting points of the products are summarized in Table 1. The IR and NMR data of the amidines are given in Table 3.

General Procedure for the Preparation of Amidines (9l—r) from Amides 7 and Amines 6. To the syrup of PPSE which was prepared from 10 mmol of diphosphorus pentaoxide and 20 mmol of hexamethyldisiloxane, 2.5 mmol of amide and 2.5 mmol of amine were added at 160 °C. The mixture was stirred for 2 h at that temperature under nitrogen. The product was isolated by pouring the reation mixture into a 1 M NaOH solution. The pure amidine was obtained by recrystallization from aqueous ethanol.

Yields and melting points are summarized in Table 2. The IR and NMR data of the products are also given in Table 3. Analytical data of new compounds are shown in Table 4.

Reaction of Benzanilide (7a) and Hexylamine. To the syrup of PPSE, 0.591 g (3 mmol) of benzanilide (**7a**) and 0.303 g (3 mmol) of hexylamine were added at 160 °C. After the reaction was carried out as described above, the reaction mixture was poured into a 1 M NaOH solution. The solution was extracted by dichloromethane, dried over $MgSO_4$, and the solvent was evapolated. Thin-layer chromatogram (aluminum oxide, ethyl acetate/hexane= 1/10) showed two spots at R_f 0.58 and 0.51. The latter spot was the same R_f value of amidine **9a**. The mixture of these two spots, collected by columm chromatography (aluminum oxide, ethyl acetate/hexane=1/10), weighed 0.414 g and shows the following spectra: IR (KBr) 1620 cm^{-1} (C=N), 1585 cm^{-1} (aromatic), and 1220 cm^{-1} (C-N), ^{1}H NMR ($CDCl_3$) δ=0.70—1.85 and 6.50—8.00 (integration

† 1 M=1 mol dm^{-3}.

Table 3. Spectral Data of Amidines

Amidine	IR C=N/cm^{-1}	^{1}H NMR/δ ppm ($CDCl_3$)
9a	1620	5.58(s, 1H), 6.68—7.55(m, 15H)
9b	1625	3.67(s, 3H), 5.70(s, 1H), 6.50—7.50(m, 14H)
9c	1625	6.63—7.53(m)
9d	1640	6.62—8.42(m)
9e	1635	0.86—2.90(m, 11H), 5.80(s, 1H), 6.75—7.49(m, 10H)
9f	1630	0.56—2.43(m, 11H), 6.62—7.47(m, 11H)
9g	1635	6.33(s, 1H), 6.60(s, 1H), 6.72—7.42(m, 16H)
9h	1625	3.63(s, 3H), 5.70(s, 1H), 6.34—7.42(m, 16H)
9i	1625	2.22(s, 3H), 6.13—7.79(m, 14H)
9j	1625	6.57—7.52(m)
9k	1635	6.64—8.31(m)
9l	1620	3.65(d, 3H), 6.33—7.87(m, 14H)
9m	1620	6.77—8.20(m)
9o	1620	0.93—2.22(m, 11H), 5.86(s, 1H), 6.55—7.85(m, 10H)
9p	1605	3.00(s, 3H), 4.61(s, 1H), 6.50—7.83(m, 10H)
9q	1615	1.83(s, 3H), 3.00(s, 6H), 6.65—7.52(m, 5H)
9r	1635	1.64—2.60(m, 4H), 2.85(s, 3H), 3.35(t, 2H), 6.63—7.57(m, 5H)

Table 4. Analytical Data of New Compounds

Code	Found/%	Calculated/%
9e	C: 82.31, H: 8.05, N: 9.94	$C_{19}H_{22}N_2$; C: 81.97, H: 7.97, N: 10.06
9g	C: 84.80, H: 6.10, N: 9.23	$C_{21}H_{18}N_2$; C: 84.53, H: 6.08, N: 9.39
9i	C: 83.67, H: 6.68, N: 9.05	$C_{21}H_{20}N_2$; C: 83.96, H: 6.71, N: 9.33
9j	C: 66.86, H: 4.02, N: 8.01, Cl: 20.70	$C_{19}H_{14}N_2Cl_2$; C: 66.88, H: 4.14, N: 8.21, Cl: 20.78
9k	C: 62.82, H: 3.96, N: 15.89	$C_{19}H_{14}N_4O_4$; C: 62.98, H: 3.89, N: 15.46
9o	C: 82.05, H: 8.07, N: 9.79	$C_{19}H_{22}N_2$; C: 81.97, H: 7.97, N: 10.06

ratio was 2.1:1). From these spectra data the product was the mixture of amidine **9n** and **9a** in the yield of 23 and 53%, respectively.

References

1) T. Imamoto, H. Yokoyama, and M. Yokoyama, *Tetrahedron Lett.*, **22**, 1803 (1981).

2) a) K. Yamamoto and H. Watanabe, *Chem. Lett.*, **1982**, 1225; b) Y. Imai, A. Mochizuki, and M. Kakimoto, *Synthesis*, **1983**, 851.

3) M. Yokoyama, S. Yoshida, and T. Imamoto, *Synthesis*, **1982**, 591.

4) a) T. Imamoto, H. Yokoyama, and M. Yokoyama, *Tetrahedron Lett.*, **23**, 1467 (1982); b) T. Imamoto, T. Matsumoto, H. Yokoyama, M. Yokoyama, and K. Yamaguchi, *J. Org. Chem.*, **49**, 1105 (1984).

5) M. Kakimoto, Y. Imai, unpublished data.

6) M. Kakimoto and Y. Imai, *Chem. Lett.*, **1984**, 1831.

7) For reviews, see: a) F. D. Popp and W. E. McEwen, *Chem. Rev.*, **58**, 321 (1958); b) F. Uhlig and H. R. Snyder, *Adv. Org. Chem.*, **1**, 35 (1960).

8) K. Langheld, *Chem. Ber.*, **43**, 1857 (1910).

9) a) Y. Kanaoka, O. Yonematsu, K. Tanizawa, and Y. Ban, *Chem. Pharm. Bull.*, **12**, 773 (1964); b) Y. Kanaoka, E. Sato, O. Yonemitsu, and Y. Ban, *Tetrahedron Lett.*, **1964**, 2419; c) Y. Kanaoka, M. Machida, O. Yonemitsu, and Y. Ban, *Chem. Pharm. Bull.*, **13**, 1065 (1965); d) Y. Kanaoka, Y. Ban, K. Miyashita, and K. Irie, *ibid*, **14**, 934 (1966); e) Y. Kanaoka, E. Sato, and Y. Ban, *ibid*, **15**, 101 (1967); f) Y. Kanaoka, K. Tanizawa, E. Sato, O. Yonemitsu, and Y. Ban, *ibid*, **15**, 593 (1967); g) Y. Kanaoka, O. Yonemitsu, and E. Sato, Y. Ban, *ibid*, **16**, 280 (1968); h) Y. Kanaoka, E. Sato, and O. Yonemitsu, *Tetrahedron*, **24**, 2591 (1968); i) Y. Kanaoka, O. Yonemitsu, and K. Tanizawa, *ibid*, **17**, 2381 (1969); j) O. Yonemitsu, K. Miyashita, Y. Ban, and Y. Kanaoka, *Tetrahedron*, **25**, 95 (1969); k) Y. Kanaoka, K. Miyashita, and O. Yonemitsu, *ibid*, **25**, 2757 (1969); l) M. P. Cava, M. V. Lakshmikantham, and M. J. Mitchell, *J. Org. Chem.*, **34**, 2665 (1969); m) Y. Kanaoka, T. Kuga, and K. Tanizawa, *Chem. Pharm. Bull.*, **18**, 397 (1970); n) J. H. Adams, J. R. Lewis, and J. G. Paul, *Synthesis*, **1979**, 429; o) M. Yokoyama, M. Nakamura, T. Imanoto, and K. Yamaguchi, *J. Chem. Soc., Chem. Commun.*, **1981**, 560; p) M. Yokoyama, M. Nakamura, H. Ohtaki, and T. Imamoto, *J. Org. Chem.*, **47**, 1090 (1982); q) T. Imamoto, M. Kodera, and M. Yokoyama, *Bull. Chem. Soc. Jpn.*, **55**, 2303 (1982); r) T. Imamoto, M. Kodera, and M. Yokoyama, *Synthesis*, **1982**, 134; s) T. Imamoto, T. Takaoka, and M. Yokoyama, *ibid*, **1983**, 142.

10) M. Kakimoto, S. Ogata, A. Mochizuki, and Y, Imai, *Chem. Lett.*, **1984**, 821.

11) A. Gautier, M. Miocque, C. C. Farnoux, "The Chemistry of Amidines and Imidates," ed by S. Patai, John

Wiley & Sons (1975), p. 283.
12) C. N. Webb, *Org. Syn.*, Coll. Vol. I., 82 (1941).
13) D. N. Shigotin and T. K. Syrkin, *Zh. Fiz. Khim.*, **23**, 241 (1949).
14) M. W. Parteidge, *J. Chem. Soc.*, **1949**, 3043.
15) S. A. Kulkarui and R. C. Shah, *J. Indian Chem. Soc.*, **27**, 111 (1950).
16) R. C. Shahm, *J. Univ. Bambay*, **1936**, 5, pt. 2, 62.
17) N. S. Drozdov and A. F. Bekhli, *J. Gen. Chem.*, **14**, 280 (1944).
18) N. J. Sintiv, J. S. Rodia, J. A. Tursich, H. L. Davis, and G. L. Webster, *J. Am. Chem. Soc.*, **71**, 3990 (1949).
19) T. B. Desai and R. C. Shah, *J. Indian Chem. Soc.*, **26**, 121 (1949).
20) C. Chew, F. L. Pyman, *J. Chem. Soc.*, **1927**, 2318.
21) E. L. Pyman, *J. Chem. Soc.*, **123**, 367 (1923).
22) H. Bredereck, R. Gompper, K. Klemm, and H. Rempfer, *Chem. Ber.*, **92**, 837 (1959).
23) H. Bredereck and K. Bredereck, *Chem. Ber.*, **94**, 2278 (1961).

Photochemical Reaction of 2-Aryl-1,2-benzisoselenazol-3(2*H*)-ones

Nobumasa KAMIGATA,* Hirokazu IIZUKA, Akira IZUOKA, and Michio KOBAYASHI
Department of Chemistry, Faculty of Science, Tokyo Metropolitan University,
Fukazawa, Setagaya-ku, Tokyo 158
(Received January 28, 1986)

The photochemical reaction of 2-aryl-1,2-benzisoselenazol-3(2*H*)-ones (**1**) in benzene was found to give dibenzo[*b*,*f*][1,4]selenazepin-11(10*H*)-ones (**2**). On the other hand, the photochemical reaction of **1** in *t*-butyl alcohol afforded 2-(2-hydroxy-2-methylpropylseleno)benzanilide, 2-(methylseleno)benzanilide, and 2-aryl-1,2-benzisoselenazol-3(2*H*)-one 1-oxides together with the photoisomer **2**. Mechanisms for these reactions are proposed.

Attention regarding the photochemistry of five-membered heterocyclic ring systems continues to be strong because of their use in heterocycle syntheses and studies concerning the reaction mechanisms.[1] Recently, we have reported a novel photoisomerization of 2-aryl-1,2-benzisothiazol-3(2*H*)-ones to dibenzo [*b*,*f*][1,4]thiazepin-11(10*H*)-ones.[2] In our systematic investigation of the photochemical reactions of benzisothiazolinones and their analogues, we have studied the photochemical reactions of 2-aryl-1,2-benzisoselenazol-3(2*H*)-ones, selenium analogues of 2-aryl-1,2-benzisothiazol-3(2*H*)-ones. The results are described herein.

When a solution containing 2-(4-methoxyphenyl)-1,2-benzisoselenazol-3(2*H*)-one (**1a**) in benzene was irradiated under argon with 300-nm light, a single photoproduct was obtained. The assignment of this material as 7-methoxydibenzo[*b*,*f*][1,4]selenazepin-11-(10*H*)-one (**2a**) was made on the basis of spectral data.

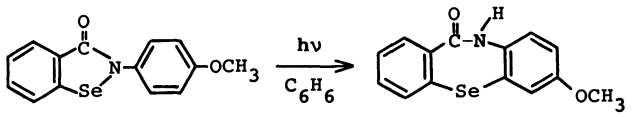

1a **2a**

Some related 2-aryl-1,2-benzisoselenazol-3(2*H*)-ones (**1**) were also irradiated under similar conditions to give dibenzo [*b*,*f*][1,4]selenazepin-11(10*H*)-ones (**2**) as the only isolable photoproducts. The results are summarized in Table 1.

The present results show a very similar feature to that of photochemical reactions of 2-aryl-1,2-benzisothiazol-3(2*H*)-ones.[2] Therefore, the reaction mechanism of **1** is similar to that proposed in the photoisomerization of 2-aryl-1,2-benzisothiazol-3(2*H*)-ones[2] and is outlined in Scheme 1. The photoexcited **1** undergoes a homolytic cleavage of the weakest bond (Se–N) in the molecule to give biradical (**3**). The initially formed biradical recombines at the ortho-position of the *N*-aryl group to give a cyclized product (**5**). A subsequent 1,7-hydrogen shift of the intermediate **5** leads to the final product **2**. The last step of the sequence can proceed by either a thermal or photochemical hydrogen shift.

Recently, Rokach, and Hammel reported that small amounts of a photo-ring expansion product were formed together with 3-phenyl-2(3*H*)-thiazolone upon irradiation of 2-phenyl-3(2*H*)-isothiazolone.[3] However, we could not detect the corresponding 3-aryl-

Table 1. Photochemical Reaction of **1** in Benzene[a]

X in **1**		Product	Yield/%[b]
1a	OCH_3	**2a**	55
1b	CH_3	**2b**	33
1c	H	**2c**	42

a) The irradiation was carried out on a 2.85×10^{-3} M ($1\ M = 1\ mol\ dm^{-3}$) solution of **1** in benzene under argon using a 450-W medium-pressure mercury lamp (Hanovia) through a Pyrex filter (>300 nm). b) The yields are based on the starting materials consumed.

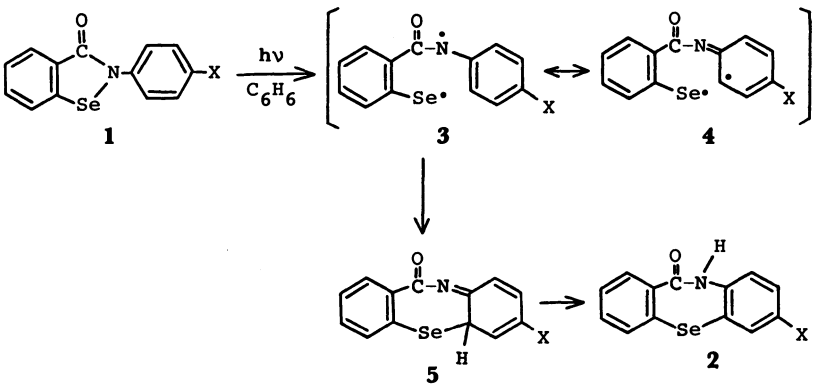

Scheme 1.

2(3*H*)-benzisoselenazolone in the reaction mixture, as in the case similar to the photochemical reaction of 2-aryl-1,2-benzisothiazol-3(2*H*)-one reported recently from our laboratory.[2)]

Irradiation of **1** in *t*-butyl alcohol was also carried out. When a solution containing 2-(4-methoxyphenyl)-1,2-benzisoselenazol-3(2*H*)-one (**1a**) in *t*-butyl alcohol was irradiated under argon with 300 nm light, the formation of four kinds of photoproducts was indicated by a TLC analysis. The products were separated by silica-gel chromatography and were assigned as **2a**, 4′-methoxy-2-(2-hydroxy-2-methylpropylseleno)benzanilide (**6a**), 4′-methoxy-2-(methylseleno)benzanilide (**7a**), and 2-(4-methoxyphenyl)-1,2-benzisoselenazol-3(2*H*)-one 1-oxide (**8a**) on the basis of their spectral data.

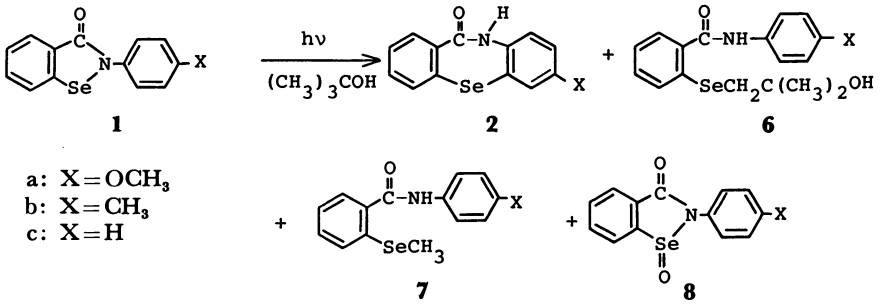

1 **2** **6** **7** **8**

a: X=OCH_3
b: X=CH_3
c: X=H

The irradiation of **1b** and **1c** was also carried out in *t*-butyl alcohol in a similar way and the corresponding four photoproducts **2**, **6**, **7**, and **8** were isolated. The results are summarized in Table 2.

The mechanism of the formation of **2** is the same as that proposed regarding the photochemical reaction of **1** in benzene (Scheme 1). Photoproduct **6** seems to be formed via a homolytic cleavage of the photoproduct **2** by the secondary photo-excitation, affording the biradical **9**. The phenyl radical in the biradical intermediate **9** abstracts a hydrogen atom from *t*-butyl alcohol to give a selenyl radical (**10**) and a 2-hydroxy-2-methylpropyl radical (**11**). The homolytic recombination of these radical intermediates, **10** and **11** affords **6** (Scheme 2).

Table 2. Photochemical Reaction of **1** in *t*-Butyl Alcohol

X in **1**		Product (Yield/%[a)])					
1a	OCH_3	**2a**	35	**6a**	17	**8a**	9
1b	CH_3	**2b**	24	**6b**	8	**8b**	3
1c	H	**2c**	19	**6c**	8	**8c**	4

a) The yields are based on the starting materials consumed.

In order to obtain supporting evidence for this mechanism, the isolated **2a** was irradiated in *t*-butyl alcohol, and **6a** was obtained in 47% yield. However, **2a** did not change to **6a** in *t*-butyl alcohol by refluxing the mixture for 3 h and all of the starting material of **2a** was recovered. These findings indicate a secondary photochemical reaction route from **2** to **6**.

We could not detect such a reaction product as **12a** in the photolysis of **1a** in *t*-butyl alcohol. This indicates that **2** does not cleave homolytically to **13** but to **9**. However at present we can not propose any explanation.

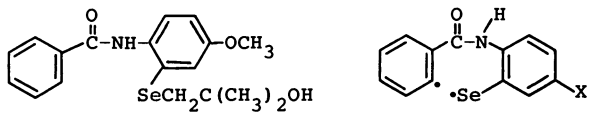

12a **13**

The photochemical cleavage of **2** to **9** suggests that the photochemical reaction of **1** in benzene has a

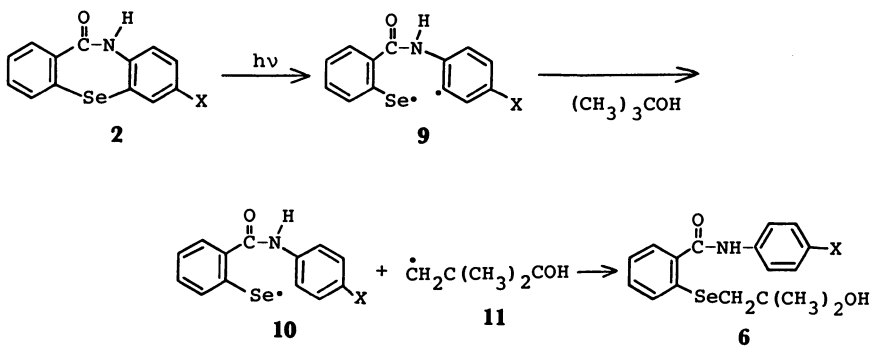

2 **9** **10** **11** **6**

Scheme 2.

possibility of affording such a compound as **14**.

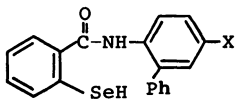

14

The absence of **14** in the photolysis of **1** in benzene means that **2** does not give **9** in a benzene solution or **9**, once formed, recombines to **2** again in a solvent cage faster than it reacts with the solvent benzene.

The formation of **7** is of considerable interest; however, it is very difficult to understand how the methyl group of compound **7** is introduced. It is certain that it comes from the methyl group of *t*-butyl alcohol, but the mechanism is not clear. One plausible interpretation is that formation of **7** is closely related to the formation of a photooxidized product **8**. The mechanism of the formation of **8** is a direct photooxidation, as we reported previously regarding the photochemical reaction of 2-aryl-1,2-benzisothiazolinones.[2] Another report was made by Tezuka et al.[4] The photooxidized product **8** was formed in spite of the fact that the photoreaction was carried out under argon gas. This means that a slight amount of oxygen was still present in *t*-butyl alcohol, and it oxidized **1** directly by irradiation, affording the peroxyl radical **15**. The intermediate **15** oxidized the solvent *t*-butyl alcohol and afforded selenoxide **7** and *t*-butoxyl radical. The *t*-butoxyl radical decomposed to a methyl radical and acetone, and the methyl radical attacked either the selenium atom of compound **1** to give a radical **16** or compound **2** to give a radical **17**. Either of these could abstract a hydrogen atom from *t*-butyl alcohol to give the final product **7**.

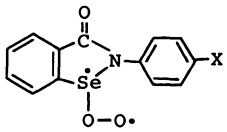

15

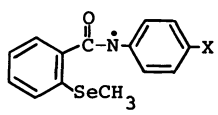

16

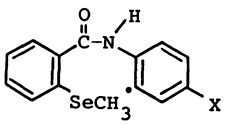

17

Experimental

Measurement. All melting points were uncorrected. IR and UV spectra were determined on a Hitachi EPI-G2 and a Hitachi 220A spectrometer. ^{1}H NMR spectra were recorded at 60 and 400 MHz using a JEOL JNM-PMX 60SI and a JEOL JNM-GX 400 spectrometer, respectively, using tetramethylsilane as an internal standard. Mass spectra were determined with a JEOL JMS-DX 300 high-resolution mass spectrometer with a JEOL JMA 5000 mass-data system with an ionization energy of 70 eV. Elemental analyses were carried out using a Perkin-Elmer 240 elemental analyzer.

Preparation of 2-Aryl-1,2-benzisoselenazol-3(2*H*)-ones (1). To a stirred solution containing 14.0 g of *o*-aminobenzoic acid and 20 cm^3 of concd hydrochloric acid in 20 cm^3 of water cooled with an ice bath under 5 °C was added dropwise to 9.0 g of sodium nitrite in 20 cm^3 of water. A solution of 2-carboxybenzenediazonium chloride resulted; this was added dropwise to a stirred solution containing sodium diselenide which was prepared in advance by the reaction of 8.8 g of selenium powder, 8.8 g of rongalite, and 4.4 g of sodium hydroxide in 60 cm^3 of water. The mixture was stirred for an additional 2 h after an initial evolution of nitrogen gas had been completed. It was confirmed that the solution was basic using litmus paper. The reaction mixture was acidified with hydrochloric acid and the precipitated solid was collected by filtration, washed with water, and dried in a desiccator to give 20.0 g (90% yield) of a crude solid of 2,2′-diselenobis[benzoic acid]; mp 293 °C (lit,[5] mp 295 °C).

A mixture of 3.0 g of 2,2′-diselenobis[benzoic acid] and 15 cm^3 of thionyl chloride was heated at reflux for 3 h. The excess thionyl chloride was removed under reduced pressure and the residual solid was recrystallized from hexane to give 3.1 g (81% yield) of pale-yellow crystals of pure 2-(chloroseleno)benzoyl chloride; mp 63—64 °C (lit,[6] mp 65 °C).

To a stirred solution containing 32 mmol of appropriate arylamine in 30 cm^3 of ether was added dropwise 3.0 g of 2-(chloroseleno)benzoyl chloride in 40 cm^3 of ether over a 30 min period, and the mixture was stirred for an additional 3 h. The solvent was removed under reduced pressure and the residue was subjected to chromatography on silica-gel using a 4:1 mixture of dichloromethane–ethyl acetate as the eluent to give pure **1**. The following compounds were prepared by this procedure.

2-(4-Methoxyphenyl)-1,2-benzisoselenazol-3(2*H*)-one (1a). Yield, 65%; mp 178—179 °C; IR (KBr) 1600 cm^{-1}(s, amide C=O); ^{1}H NMR ($CDCl_3$) δ=3.80 (3H, s), 6.90 (2H, d, J=8.4 Hz), 7.35 (2H, d, J=8.4 Hz), and 7.3—8.1 (4H, m); UV (methanol) 265 (log ε=4.57) and 325 nm (4.19); MS, *m/z* 305 (M^+), 274 225, and 184; HRMS, *m/z* 304.9924 ($C_{14}H_{11}NO_2Se$ requires 304.9954).

2-(*p*-Tolyl)-1,2-benzisoselenazol-3(2*H*)-one (1b). Yield, 65%; mp 169—170 °C; IR (KBr) 1620 cm^{-1} (s, amide C=O); ^{1}H NMR ($CDCl_3$) δ=2.37 (3H, s), 7.20 (2H, d, J=8.4 Hz), 7.52 (2H, d, J=8.4 Hz), and 7.3—8.2 (4H, m); UV (methanol) 265 (log ε=3.61) 325 nm (3.25); MS, *m/z* 289 (M^+), 274, and 209; HRMS, *m/z* 289.0017 ($C_{14}H_{11}NOSe$ requires 289.0005).

2-Phenyl-1,2-benzisoselenazol-3(2*H*)-one (1c). Yield, 86%; mp 179—180 °C; IR (KBr) 1600 cm^{-1} (s, amide C=O);

^{1}H NMR ($CDCl_3$) δ=7.20—8.13 (9H, m); UV (methanol) 260 (log ε=3.37) and 325 nm (3.30); MS, *m/z* 275 (M^+) and 195; HRMS, *m/z* 274.9845 ($C_{13}H_9NOSe$ requires 274.9849).

Photolysis of 2-Aryl-1,2-benzisoselenazol-3(2*H*)-one (1) in Benzene. A solution containing 0.65 mmol of 2-aryl-1,2-benzisoselenazol-3(2*H*)-one (**1**) in 230 cm^3 of benzene was irradiated under argon through a Pyrex filter sleeve using a 450-W Hanovia medium-pressure mercury lamp for 10 h. A removal of the solvent left a light-brown residue which was purified by silica-gel chromatography using chloroform as the eluent. Photoproduct **2** was isolated with the recovered starting material **1**. The physical, spectral data, and analyses of the photoproducts **2** are as follows:

7-Methoxydibenzo[*b,f*][1,4]selenazepin-11(10*H*)-one (2a). Mp 213 °C (from chloroform–hexane); IR (KBr) 2950—3200 (w, amide N–H) and 1650 cm^{-1} (s, amide C=O); ^{1}H NMR (DMSO-d_6) 400 MHz, δ=3.73 (3H, s), 6.92 (1H, dd, *J*=8.8 and 2.6 Hz), 7.14 (1H, d, *J*=8.4 Hz), 7.23 (1H, d, *J*=2.6 Hz), 7.37—7.64 (4H, m), and 10.39 (1H, s); MS, *m/z* 305 (M^+), 274, 225, and 210; HRMS, *m/z* 304.9951 ($C_{14}H_{11}NO_2Se$ requires 304.9954).

7-Methyldibenzo[*b,f*][1,4]selenazepin-11(10*H*)-one (2b). Mp 268—269 °C (from chloroform–hexane); IR (KBr) 2900—3200 (w, amide N–H) and 1650 cm^{-1} (s, amide C=O); ^{1}H NMR (DMSO-d_6) 400 MHz, δ=2.23 (3H, s), 7.12 (1H, d, *J*=8.4 Hz), 7.14 (1H, d, *J*=8.4 Hz), 7.39—7.41 (2H, m), 7.50 (1H, s), 7.59—7.62 (2H, m), and 10.48 (1H, s); MS, *m/z* 289 (M^+) and 209; HRMS, *m/z* 288.9991 ($C_{14}H_{11}NOSe$ requires 289.0005).

Dibenzo[*b,f*][1,4]selenazepin-11(10*H*)-one (2c). Mp 273.5 °C (from chloroform–hexane); IR (KBr) 2950—3200 (w, amide N–H) and 1650 cm^{-1} (s, amide C=O); ^{1}H NMR (DMSO-d_6) 400 MHz, δ=7.11 (1H, t, *J*=7.7 Hz), 7.22 (1H, d, *J*=7.7 Hz), 7.34 (1H, t, *J*=7.7 Hz), 7.40—7.43 (2H, m), 7.60—7.65 (2H, m), 7.68 (1H, d, *J*=7.7 Hz), and 10.59 (1H, s); MS, *m/z* 275 (M^+) and 195; HRMS, *m/z* 274.9854 ($C_{13}H_9NOSe$ requires 274.9849).

Photolysis of 2-Aryl-1,2-benzisoselenazol-3(2*H*)-one (1) in *t*-Butyl Alcohol. A solution containing 0.65 mmol of 2-aryl-1,2-benzisoselenazol-3(2*H*)-one (**1**) in 230 cm^3 of *t*-butyl alcohol was irradiated under argon through a Pyrex filter sleeve using a 450-W Hanovia medium-pressure mercury lamp for 10 h. A TLC analysis showed that four photoreaction products were formed. The solvent was removed under reduced pressure to give a light-brown residue which was purified by preparative TLC using chloroform as the eluent. Photoproducts **2**, **6**, **7**, and **8** were isolated, and the physical and spectral data of these products are as follows:

4′-Methoxy-2-(2-hydroxy-2-methylpropylseleno)benzanilide (6a). IR (neat) 2900—3000 (w, amide N–H and O–H) and 1650 cm^{-1} (s, amide C=O); ^{1}H NMR ($CDCl_3$) δ=1.33 (6H, s), 1.55 (1H, s), 3.21 (2H, s), 3.81 (3H, s), 6.90 (2H, d, *J*=9.0 Hz), 7.57 (2H, d, *J*=9.0 Hz), 7.2—8.3 (4H, m), and 8.13 (1H, s); MS, *m/z* 379 (M^+) and 306; HRMS, *m/z* 379.0700 ($C_{18}H_{21}NO_3Se$ requires 379.0684).

4′-Methoxy-2-(methylseleno)benzanilide (7a). Mp 266—267 °C (from benzene–hexane); IR (KBr) 3300 (s, amide N–H) and 1635 cm^{-1} (s, amide C=O); ^{1}H NMR ($CDCl_3$) δ=2.27 (3H, s), 3.73 (3H, s), 6.82 (2H, d, *J*=8.4 Hz), 7.42 (2H, d, *J*=8.4 Hz), 7.0—8.1 (4H, m); MS, *m/z* 321 (M^+), 306, 225, 199, and 122. Found: C, 56.24; H, 4.76; N, 3.99%. Calcd for $C_{15}H_{15}NO_2Se$: C, 56.25; H, 4.72; N, 4.37%.

2-(4-Methoxyphenyl)-1,2-benzisoselenazol-3(2*H*)-one 1-Oxide (8a). Mp 212—213 °C (from benzene); IR (KBr) 1690 (s, C=O) and 820 cm^{-1} (s, Se=O); ^{1}H NMR ($CDCl_3$) δ=3.80 (3H, s), 7.37 (2H, d, *J*=8.8 Hz), 7.50 (2H, d, *J*=8.8 Hz), 7.80—7.95 (3H, m), and 8.24 (1H, d, *J*=7.7 Hz); MS, *m/z* 321 (M^+), 305, 290, and 225; HRMS, *m/z* 320.9828 ($C_{14}H_{11}NO_3Se$ requires 320.9903).

4′-Methyl-2-(2-hydroxy-2-methylpropylseleno)benzanilide (6b). IR (neat) 3000—3500 (w, amide N–H and O–H) and 1650 cm^{-1} (s, amide C=O); ^{1}H NMR ($CDCl_3$) δ=2.00 (1H, s), 2.15 (1H, s), 2.36 (3H, s), 3.10 (2H, s), 7.12—7.95 (8H, m); MS, *m/z* 363 (M^+); HRMS, *m/z* 363.0031 ($C_{18}H_{21}NO_2Se$ requires 363.0681).

4′-Methyl-2-(methylseleno)benzanilide (7b). Mp 252.5—253.5 °C; IR (KBr) 3300 (s, amide N–H) and 1620 cm^{-1} (s, amide C=O); ^{1}H NMR ($CDCl_3$) δ=2.30 (3H, s), 2.74 (3H, s), 7.67—8.11 (8H, m), and 8.20 (1H, s); MS, *m/z* 305 (M^+) and 209; HRMS, *m/z* 305.0281 ($C_{15}H_{15}NOSe$ requires 305.0318).

2-(4-Methylphenyl)-1,2-benzisoselenazol-3(2*H*)-one 1-Oxide (8b). Mp 182—183 °C; IR (KBr) 1680 (s, C=O) and 810 cm^{-1} (s, S=O); ^{1}H NMR ($CDCl_3$) δ=2.26 (3H, s), 7.10—7.52 (8H, m); MS, *m/z* 305 (M^+); HRMS, *m/z* 305.0037 ($C_{14}H_{11}NO_2Se$ requires 304.9954).

2-(2-Hydroxy-2-methylpropylseleno)benzanilide (6c). IR (neat) 3000 (w, amide N–H and O–H) and 1650 cm^{-1} (s, amide C=O); ^{1}H NMR ($CDCl_3$) δ=1.31 (1H, s), 1.33 (6H, s), 3.13 (2H, s), 7.20—7.69 (9H, m), and 8.20 (1H, s); MS, *m/z* 349 (M^+); HRMS, *m/z* 349.0602 ($C_{17}H_{19}NO_2Se$ requires 349.0580).

2-(Methylseleno)benzanilide (7c). Mp 169—170 °C; IR (KBr) 3300 (s, amide N–H) and 1640 cm^{-1} (s, amide C=O); ^{1}H NMR ($CDCl_3$) δ=2.23 (3H, s), 7.00—7.79 (9H, m), and 7.97 (1H, s); MS, *m/z* 291 (M^+), 276, and 199; HRMS, *m/z* 291.0123 ($C_{14}H_{13}NOSe$ requires 291.0161).

2-Phenyl-1,2-benzisoselenazol-3(2*H*)-one 1-Oxide (8c). Mp 180—181 °C; IR (KBr) 1680 (s, C=O) and 810 cm^{-1} (s, Se=O); ^{1}H NMR ($CDCl_3$) δ=7.20—7.87 (10H, m); MS, *m/z* 291 (M^+); HRMS, *m/z* 291.0081 ($C_{13}H_9NO_2Se$ requires 290.9798).

Photolysis of 7-Methoxydibenzo[*b,f*][1,4]selenazepin-11-(10*H*)-one (2a). A solution containing 14 mg of 7-methoxydibenzo[*b,f*][1,4]selenazepin-11(10*H*)-one (**2a**) in 20 cm^3 of *t*-butyl alcohol was irradiated in a degassed sealed tube using a 450-W Hanovia medium-pressure mercury lamp through a Pyrex filter sleeve for 10 h. The solvent was removed under reduced pressure to give a residue which was subjected to the silica-gel preparative TLC using chloroform as the eluent. 4′-Methoxy-2-(2-hydroxy-2-methylpropylseleno)benzanilide (**6a**) 6.6 mg (47% yield) was isolated.

References

1) A. Padwa, "Rearrangement in Ground and Excited State," ed by P. de Mayo, Academic Press, New York, Vol. 3 (1980), p. 501; A. Lablache-Combier, "Photochemistry of Heterocyclic Compounds," ed by O. Buchardt, Wiley, New York (1976), p. 123.

2) N. Kamigata, S. Hashimoto, S. Fujie, and M. Kobayashi, *J. Chem. Soc., Chem. Commun.*, **1983**, 765; N. Kamigata, S. Hashimoto, M. Kobayashi, and H. Nakanishi,

Bull. Chem. Soc. Jpn., **58**, 3131 (1985); N. Kamigata, H. Iizuka, and M. Kobayashi, *Heterocycles*, **24**, 919 (1986); N. Kamigata, H. Iizuka, and M. Kobayashi, *Bull. Chem. Soc. Jpn.*, **59**, 1601 (1986).

3) J. Rokach and P. Hammel, *J. Chem. Soc., Chem. Commun.*, **1979**, 786.

4) T. Tezuka, H. Miyazaki, and H. Suzuki, *Tetrahedron Lett.*, **1978**, 1959.

5) A. Runet and M. Renson, *Bull. Soc. Chim. Belg.*, **75**, 157 (1966); L. B. Agenas, *Acta Chem. Scand.*, **16**, 1809 (1962); R. Lesser and R. Weiz, *Ber.*, **45**, 1835 (1912); R. Schoeller, *ibid* **52**, 1517 (1919).

6) R. Lesser and A. Schoeller, *Ber.*, **47**, 2505 (1914); R. Lesser and R. Weiz, *ibid* **57**, 1077 (1924).

 © 1986 The Chemical Society of Japan Bull. Chem. Soc. Jpn., 59, 2185—2189 (1986)

Syntheses of Althiomycin Analogs in Relation to Antibacterial Activities[1)]

Kaoru INAMI† and Tetsuo SHIBA*
Department of Chemistry, Faculty of Science, Osaka University,
Toyonaka, Osaka 560
(Received February 1, 1986)

Four analogs of an antibiotic althiomycin were synthesized in order to clarify the structure-activity relationships, especially with regard to two asymmetric centers and the aldoxime configuration. The antibiotic activity of de(hydroxymethyl) analog is comparable to that of the original antibiotic for Gram-positive bacteria.

Althiomycin (**1**), isolated from *Streptomyces althioticus*,[2)] inhibits the protein synthesis in both Gram-positive and negative bacteria. Recently, we achieved the total synthesis of this antibiotic.[3)] For investigation of the structure-reactivity relationships of althiomycin, we synthesized the following analogs (**2**—**5**) (Fig. 1).

First of all, the enantiomer of althiomycin, i.e., epialthiomycin (**2**), was synthesized according to the synthetic pathway of an original antibiotic (Fig. 2).

Secondly, de(hydroxymethyl) analog (**3**) was prepared from 1-[(*S*)-2-(benzyloxycarbonylaminomethyl)-2-thiazolin-4-yl-carbonyl]-4-methoxy-3-pyrrolin-2-one (**10**) which was the key intermediate of our synthetic study on althiomycin[3)] (Fig. 3). The

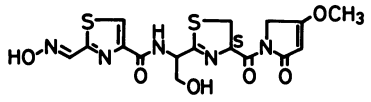
Althiomycin (1)

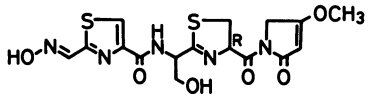
Epialthiomycin (2)

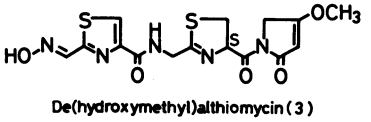
De(hydroxymethyl)althiomycin (3)

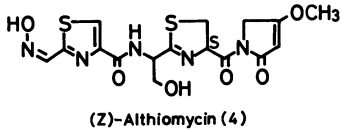
(Z)-Althiomycin (4)

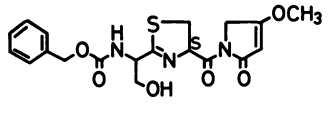
5

Fig. 1.

benzyloxycarbonyl (*Z*) group of this compound was removed with anhydrous hydrogen fluoride, followed by the coupling with the thiazole part by the azide method using potassium carbonate as the base.

Finally, we attempted to achieve the total synthesis of (*Z*)-althiomycin, which is the isomer of the natural (*E*)-althiomycin with respect to the aldoxime. (Fig. 4) The thiazole part of this compound was prepared from ethyl (*Z*)-2-(hydroxyiminomethyl)-4-thiazolecarboxylate (**11**) via successive procedures of conversion to the hydrazide with hydrazine and azidation with nitrite ester. The compound thus obtained was coupled with the thiazoline-pyrrolinone part (**5**)[3)] to give no desired product, but its bisanhydro derivative in very low yield. Therefore, we then tried to convert the natural althiomycin into its stereoisomer with anhydrous hydrogen fluoride at room temperature. Since this product was a mixture of (*E*)- and (*Z*)-althiomycins (about 1:1), the separation was performed with high-performance liquid chromatography (HPLC). The desired compound thus obtained gives two singlets at δ 8.59 and 8.09 which can be assigned as signals of the proton on C-5 in the thiazole ring and the methine proton of the aldoxime, while the original (*E*)-althiomycin gives the corresponding singlets at δ 8.37 and 8.35 in NMR respectively.[4)]

The antibacterial activities of these analogs, including the synthetic intermediate **5** of althiomycin, were shown in Table 1. This result suggests the following conclusions. The absence of the hydroxymethyl group attached to the adjacent carbon of C-2 in the thiazoline ring has no influence on the antibacterial activity of the parent antibiotic, while the inversion of the configuration of C-4 in the thiazoline ring or the aldoxime results in a significant decrease of the biological activity. The replacement of the thiazole part by benzyloxycarbonyl group gives the total loss of the antibiotic activity.

Experimental

All melting points are uncorrected. The ^{1}H NMR spectra were obtained with a Varian XL-100-15 NMR spectrometer, a JEOL FX-90Q NMR spectrometer, and a JEOL JNM-PMX 60 NMR spectrometer. The chemical shifts are given in δ, with tetramethylsilane (TMS) as the internal standard.

† Present address: Department of Chemistry, Faculty of Science, Yamaguchi University, Yamaguchi 753.

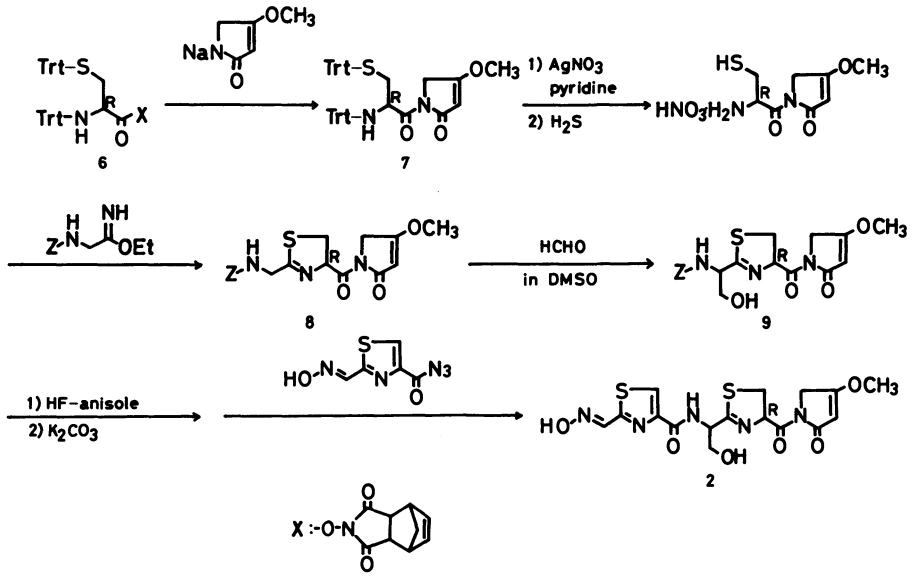

Fig. 2.

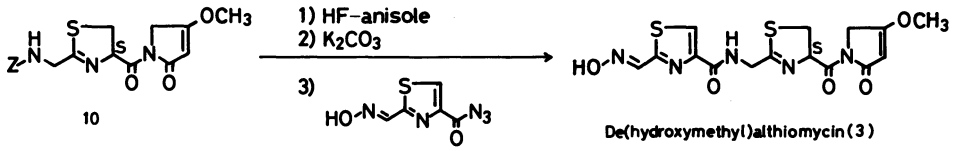

Fig. 3.

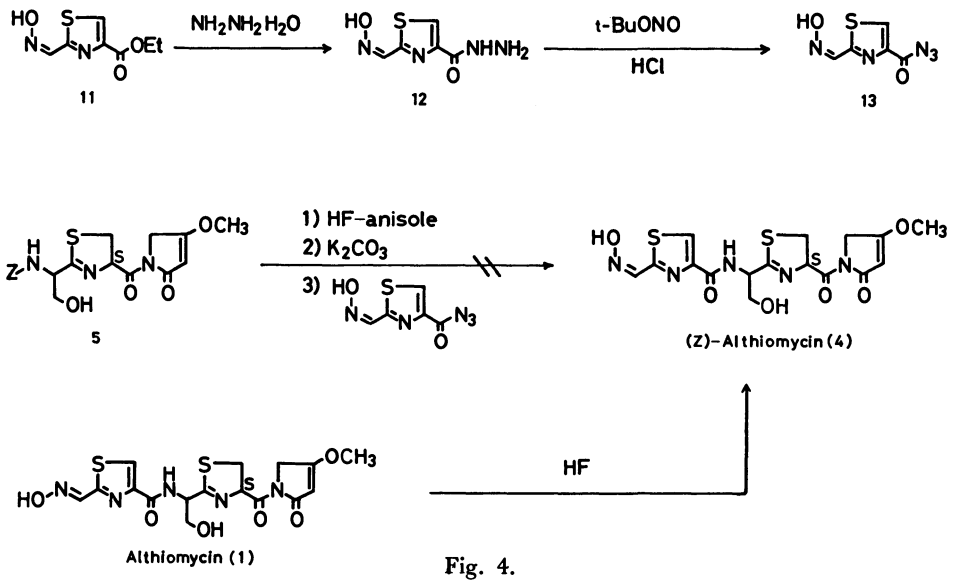

Fig. 4.

The UV spectra were obtained with a Hitachi 124 spectrophotometer. The specific rotations were obtained with a Perkin-Elmer 141 polarimeter. HPLC was performed with a Shimadzu LC-5A liquid chromatograph. TLC was carried out by the ascending method on a Merck Kieselgel 60 F_{254}.

***N,S*-Dititryl-L-cysteine 5-Norbornene-*endo*-2,3-dicarboximidyl Ester (6).** To a suspension of *N,S*-dititryl-L-cysteine diethylamine salt (10.0 g, 14.7 mmol) in 700 ml of ether, 1 M(1 M=1 mol dm^{-3}) aqueous citric acid (5 ml) was added and vigorously stirred for 30 min at 0 °C. The ethereal layer was washed with water and concentrated in vacuo. To the solution of the residual oil in 40 ml of THF, *N*-hydroxy-5-norbornene-*endo*-2,3-dicarboximide (3.95 g,

Table 1. Minimum Inhibitory Concentrations (mcg/ml) of Althiomycin Analogs

Test organism	**5**	Epialthiomycin	(*Z*)-Althiomycin	De(hydroxymethyl)-althiomycin	Natural althiomycin
Staph. aureus ATCC 6538P	>100	>100	>100	25	25
Staph. aureus MS353	>100	>100	>100	25	25
Staph. aureus MS353 C36	>100	>100	>100	25	25
Staph. aureus MS353 AO	>100	>100	>100	25	25
Staph. aureus 0116	>100	>100	>100	25	25
Staph. aureus 0119	>100	>100	>100	25	25
Staph. aureus 0126	>100	>100	>100	6.3	25
Staph. aureus 0127	>100	>100	>100	6.3	25
Staph. epidermidis sp-al-1	>100	>100	>100	25	25
Strept. pyogenes N.Y.5	>100	25	12.5	3.1	3.1
Strept. pyogenes 1022	>100	25	25	3.1	3.1
Strept. faecalis 1501	>100	>100	>100	50	100
Strept. agalactiae 1020	>100	50	25	12.5	6.3
Sarcina lutea ATCC 9341	>100	25	25	6.3	1.6
M. flavus ATCC 10240	>100	25	25	12.5	3.1
C. diphtheriae P.W.8	>100	12.5	12.5	3.1	0.8
Bac. subtilis ATCC 6633	>100	>100	>100	25	25
E. coli NIHJ-JC2	>100	>100	>100	>100	>100
E. coli B	>100	>100	>100	>100	50
K. pneumoniae ATCC 10031	>100	>100	50	25	6.3
Salm. typhosa H 901	>100	50	>100	>100	>100
Salm. entritidis Gaertner	>100	>100	>100	>100	>100
Shigella flexineri type 3a	>100	>100	>100	>100	25
Shigella sonnei E33	>100	>100	>100	>100	>100
Proteus vulgaris OX19	>100	>100	>100	>100	50
Serratia marcescens	>100	>100	>100	>100	>100
Ps. aeruginosa LAM1095	>100	>100	>100	>100	>100

22.1 mmol) and dicyclohexylcarbodiimide (3.63 g, 17.6 mmol) were added and stirred at 0 °C for 2 h. After additional stirring at room temperature for 10 h, the reaction mixture was concentrated in vacuo. The residual oil was dissolved in ethyl acetate, and the insoluble material was filtered off. The filtrate was washed with saturated aqueous sodium hydrogencarbonate and brine. The organic layer was dried over anhydrous magnesium sulfate and concentrated in vacuo. The residue was recrystallized from ethyl acetate and hexane; yield 9.43 g (83.5%). Mp 195—196 °C (decomp). $[\alpha]_D^{20}$ +74.0° (*c* 0.978, chloroform). Found: C, 77.88; H, 5.71; N, 3.56; S, 4.10%. Calcd for $C_{50}H_{42}N_2O_4S \cdot 0.3(C_2H_5)_2O$: C, 77.92; H, 5.75; N, 3.55; S, 4.06%.

1-(*N*,*S*-Dityrityl-L-cysteinyl)-4-methoxy-3-pyrrolin-2-one (7). To a solution of 4-methoxy-3-pyrrolin-2-one (3.63 g, 32.1 mmol) in 100 ml of anhydrous THF, 60% sodium hydride (1.03 g, 25.7 mmol) was added and heated under reflux for 10 min. To the solution, *N*,*S*-dityrityl-L-cysteine 5-norbornene-*endo*-2,3-dicarboximidyl ester (**6**) (15.6 g, 21.4 mmol) was added and vigorously stirred for 50 min at room temperature. Ethyl acetate was added to the reaction mixture, and the solution was washed with saturated aqueous sodium hydrogencarbonate and brine. The organic layer was dried over anhydrous magnesium sulfate and concentrated in vacuo. The residue was recrystallized from ethyl acetate and hexane; yield 14.1 g (94%). Mp 206—207 °C (decomp). $[\alpha]_D^{27}$ +23.1° (*c* 1.72, chloroform). 100 MHz ^{1}H NMR ($CDCl_3$) δ=7.0—7.6 (30H, m), 4.86(1H, s), 4.84(1H, br., s), 3.78(3H, s), 3.77(1H, d, *J*=18 Hz), 3.43(1H, br., t), 3.34(1H, d, *J*=18 Hz), 2.80(1H, dd, *J*=12 Hz, 6 Hz), 2.58(1H, dd, *J*=12 Hz, 4 Hz). Found: C, 78.56; H, 5.85; N, 3.97; S, 4.55%. Calcd for $C_{46}H_{40}N_2O_3S$: C, 78.83; H, 5.75; N, 4.00; S, 4.57%.

1-[(*R*)-2-(Benzyloxycarbonylaminomethyl)-2-thiazolin-4-yl-carbonyl]-4-methoxy-3-pyrrolin-2-one (8). To a suspension of 1-(*N*,*S*-dityrityl-L-cysteinyl)-4-methoxy-3-pyrrolin-2-one (**7**) (2.50 g, 3.57 mmol) in a mixture of 12.5 ml of methanol and 8.77 ml of benzene, pyridine (0.320 ml, 3.93 mmol) and silver nitrate (670 mg, 3.93 mmol) were added and stirred for 4 h at room temperature. Hydrogen sulfide was bubbled through the reaction mixture for 30 min at room temperature. Silver sulfide was filtered off and the solution was concentrated in vacuo. The residue was dissolved in 50 ml of anhydrous ethanol and ethyl benzyloxycarbonylaminoacetimidate (842 mg, 3.57 mmol) was added to the solution. After stirring for 20 h at room temperature, the reaction mixture was concentrated in vacuo. The residue was dissolved in ethyl acetate and washed with saturated aqueous sodium hydrogencarbonate and then brine. The organic layer was dried over anhydrous magnesium sulfate and concentrated in vacuo. The residue was recrystallized from ethyl acetate and hexane; yield 660 mg (47.5%). Mp 178—179 °C (decomp). $[\alpha]_D^{27}$ −16.4° (*c* 0.335, chloroform). 100 MHz ^{1}H NMR ($CDCl_3$) δ=7.34(5H, s), 6.24(1H, mt), 5.54(1H, br., s),

5.26(1H, s), 5.25(2H, s), 4.30(2H, s), 4.26(2H, dd, J=6 Hz, 2 Hz), 3.90(3H, s), 3.62(1H, dd, J=9 Hz, 6 Hz), 3.50(1H, dd, J=9 Hz, 6 Hz). Found: C, 55.12; H, 5.06; N, 10.41; S, 8.11%. Calcd for $C_{18}H_{19}N_3O_5S \cdot 0.25H_2O$: C, 54.88; H, 4.99; N, 10.67; S, 8.14%.

1-[(4*R*)-2-[1-(Benzyloxycarbonylamino)-2-hydroxyethyl]-2-thiazolin-4-ylcarbonyl]-4-methoxy-3-pyrrolin-2-one (9). A mixture of **8** (100 mg, 0.257 mmol) and pulverized paraformaldehyde (154 mg, 5.14 mmol) in 1 ml of degassed dimethyl sulfoxide was stirred at room temperature for 7 d. After the insoluble material was filtered off, the filtrate was diluted with ethyl acetate, and washed with water. The organic layer was dried over anhydrous magnesium sulfate. The solution was concentrated in vacuo and the residue was lyophilized; yield 108 mg (100%). Mp 72—73 °C (decomp). 100 MHz ^{1}H NMR ($CDCl_3$) δ=7.33 (5H, s), 6.30 (1H, m), 5.88 (1H, m), 5.16 (1H, s), 5.13 (2H, s), 4.28 (2H, s), 4.02 (1H, s), 3.91(2H, m), 3.90(3H, s), 3.47 (1H, d, J=6 Hz), 3.34 (1H, d, J=6 Hz).

Epialthiomycin (2). To a solution of **9** (83.3 mg, 0.199 mmol) in 215 μl of anisole, anhydrous hydrogen fluoride (ca. 1 ml) was introduced within 10 min at −78 °C and stirred at 0 °C for 20 min. Hydrogen fluoride was evaporated off at 0 °C under reduced pressure for 20 min. The residual oil was dissolved in 1 ml of DMF at −78 °C, and potassium carbonate (824 mg, 5.97 mmol) was added to the solution, and then the suspension was vigorously stirred for 5 min at room temperature. Under cooling with Dry Ice-methanol bath, (*E*)-2-(hydroxyiminomethyl)-4-thiazolecarbonyl azide[3] (39.2 mg, 0.199 mmol) was added and the suspension was stirred at 0 °C for 30 min. After additional stirring at room temperature for 2.5 h, the reaction mixture was diluted with ethyl acetate, and washed with 0.1 M potassium phosphate buffer (pH 7.15) and water. The organic layer was dried over anhydrous magnesium sulfate, and concentrated in vacuo. Purification by silica-gel preparative TLC using a developing solvent chloroform–methanol 7:1 gave colorless powder; yield 19.9 mg (22.7%). Mp 174—176 °C (decomp). $[\alpha]_D^{14}$ −20.5° (c 0.073, Methyl Cellosolve). UV_{max}(methanol): 223 nm (ε 34700), 240 nm (ε 26000), and 286 nm (ε 8590). 90 MHz ^{1}H NMR(DMSO-d_6) δ=8.40 (1H, br., s, NH), 8.38 (1H, s, CH of oxime), 8.35 (1H, s, 5-H of thiazole), 6.08 (1H, mt, 4-H of thiazoline), 5.43 (1H, s, 3-H of pyrrolinone), 4.93 (1H, br.,-C<u>H</u>-CH_2OH), 4.33(2H, s, 5-H of pyrrolinone), 3.89 (3H, s, OCH_3), 3.83 (2H, m, -CH-C<u>H_2</u>OH), 3.50 (2H, t, 5-H of thiazoline). Found: C, 44.42; H, 4.48; N, 13.84; S, 12.87%. Calcd for $C_{16}H_{17}N_5O_6S_2 \cdot 0.3H_2O \cdot 0.6C_4H_8O_2$: C, 44.40; H, 4.54; N, 14.07; S, 12.88%.

De(hydroxymethyl)althiomycin (3). To a solution of 1-[(*S*)-2-(benzyloxycarbonylaminomethyl)-2-thiazolin-4-yl-carbonyl]-4-methoxy-3-pyrrolin-2-one (**10**)[3] (100 mg, 0.257 mmol) in 278 μl of anisole, anhydrous hydrogen fluoride (ca. 1 ml) was introduced within 10 min at −78 °C. After stirring at 0 °C for 20 min, hydrogen fluoride was evaporated off under reduced pressure at 0 °C for 20 min. Under cooling with Dry Ice-methanol bath, the residual oil was dissolved in 1 ml of DMF, and the solution was stirred vigorously for 5 min at room temperature. To the suspension, (*E*)-2-(hydroxyiminomethyl)-4-thiazolecarbonyl azide (50.6 mg, 0.257 mmol) was added and stirred at room temperature for 2.5 h after stirring at 0 °C for 30 min. The reaction mixture was diluted with ethyl acetate, and washed with 0.1 M potassium phosphate buffer (pH 7.15) and water. The organic layer was dried over anhydrous magnesium sulfate and concentrated in vacuo. Purification by silica-gel preparative TLC (chloroform–methanol 9:1) gave colorless solid; yield 30.7 mg (29.2%). Mp 116—117 °C (decomp). $[\alpha]_D^{14}$ +11.6° (c 0.147, Methyl Cellosolve). 90 MHz ^{1}H NMR(DMSO-d_6) δ=9.00(1H, br., d, NH), 8.33 (2×1H, s, CH of oxime and 5-H of thiazole), 6.14 (1H, mt, 4-H of thiazoline), 5.42 (1H, s, 3-H of pyrrolinone), 4.33 (2H, s, 5-H of pyrrolinone), 4.25 (2H, m, $-CH_2-\overset{N-}{\overset{\|}{C}}-S-$), 3.88 (3H, s, OCH_3), 3.40 (2H, m, 5-H of thiazoline). Found: C, 43.97; H, 4.09; N, 15.24; S, 14.01%. Calcd for $C_{15}H_{15}N_5O_5S_2 \cdot 0.5H_2O \cdot 0.4C_4H_8O_2$: C, 43.96; H, 4.34; N, 15.22; S, 14.13%.

(*Z*)-2-(Hydroxyiminomethyl)-4-thiazolecarbohydrazide (12). Ethyl (*Z*)-2-(hydroxyiminomethyl)-4-thiazolecarboxylate (**11**)[3] (1.50 g 7.50 mmol) was dissolved in 13 ml of DMF. To the solution, 100% hydrazine hydrate (8.02 ml, 0.165 mol) was added and allowed to stand at 4 °C for 20 h. To the reaction mixture, 100 ml of methanol was added and the precipitates were collected; yield 1.17 g (83.6%). Mp >220 °C. Found: C, 32.45; H, 3.30; N, 29.93; S, 17.35%. Calcd for $C_5H_6N_4O_2S$: C, 32.35; H, 3.25; N, 30.09; S, 17.22%.

(*Z*)-2-(Hydroxyiminomethyl)-4-thiazolecarbonyl Azide (13). To a suspension of the hydrazide **12** (155 mg, 0.834 mmol) in 1.25 ml of DMF, *t*-butyl nitrite (109 μl, 0.918 mmol) and 4.35 M hydrogen chloride in THF (0.420 ml, 1.80 mmol) were added at −50 °C and stirred at −30 °C for 40 min. The reaction mixture was diluted with ethyl acetate and washed with water. The organic layer was dried over anhydrous magnesium sulfate and concentrated in vacuo to give colorless needles; yield 116 mg (70.7%). Mp 118—119 °C (decomp).

(*Z*)-Althiomycin (4). Althiomycin (**1**)(148 mg, 0.337 mmol) was dissolved in ca. 5 ml of anhydrous hydrogen fluoride and stirred at room temperature for 40 min. Hydrogen fluoride was evaporated off under reduced pressure and the residue was dissolved in 2 ml of DMF. Potassium carbonate (1.40 g, 10.1 mmol) was added to the solution and the suspension was vigorously stirred for 10 min at room temperature. The reaction mixture was diluted with ethyl acetate and washed with 0.1 M potassium phosphate buffer (pH 7.15) and water. The organic layer was dried over anhydrous magnesium sulfate and concentrated in vacuo to give colorless solid. Separation and purification by HPLC (Nagel Nucleosil 7C_{18} (8 mm×250 mm), 31% aqueous acetonitrile) gave colorless solid (retention time: 5.6 min); yield 13.1 mg (8.9%). Mp 170—172 °C (decomp). $[\alpha]_D^{14}$ +10.7° (c 0.197, Methyl Cellosolve). 90 MHz ^{1}H NMR (DMSO-d_6) δ=8.59 (1H, s, CH of oxime), 8.54 (1H, br., NH), 8.09 (1H, s, 5-H of thiazole), 6.27 (1H, mt, 4-H of thiazoline), 5.43 (1H, s, 3-H of pyrrolinone), 5.14 (1H, mt, OH), 4.90 (1H, m, -C<u>H</u>-CH_2OH), 4.33(2H, s, 5-H of pyrrolinone), 3.89 (3H, s, OCH_3), 3.85 (2H, m, -CH-C<u>H_2</u>OH), 3.59 (2H, t, 5-H of thiazoline). Found: C, 43.97; H, 4.52; N, 13.43; S, 12.27%. Calcd for $C_{16}H_{17}N_5O_6S_2 \cdot 0.75H_2O \cdot 0.75C_4H_8O_2$: C, 43.96; H, 4.76; N, 13.49; S, 12.36%.

We thank the Research Laboratories of Toyo Jozo Co., Ltd. for the measurements of the antibacterial spectra of all synthetic analogs.

References

1) This work was presented at the 9th International Congress of Heterocyclic Chemistry, Tokyo, August 1983.

2) H. Yamaguchi, Y. Nakayama, K. Takeda, K. Tawara, K. Maeda, and H. Umezawa, *J. Antibiot., Ser. A*, **10**, 195 (1957).

3) K. Inami and T. Shiba, *Bull. Chem. Soc. Jpn.*, **58**, 352 (1985).

4) The model compound of (*Z*)-aldoxime, ethyl (*Z*)-2-(hydroxyiminomethyl)thiazole-4-carboxylate, gives two doublets (J=1 Hz) at δ 8.67 and 8.10, see T. Shiba, K. Inami, K. Sawada, and Y. Hirotsu, *Heterocycles*, **13**, 175 (1979).

Palladium-Catalyzed Reaction of 2-Vinyl-2,3-dihydrobenzofurans and Chroman with Nucleophiles

Takahiro Hosokawa,* Takanori Kono, Toru Uno, and Shun-Ichi Murahashi*
Department of Chemistry, Faculty of Engineering Science, Osaka University,
Machikaneyama, Toyonaka, Osaka 560
(Received February 6, 1986)

Reaction of 2,3-dihydro-2-vinylbenzofuran with nucleophiles ($NaCH(COOEt)_2$ and $PhNHCH_3$) in the presence of palladium catalysts such as $Pd(PPh_3)_4$ and $PdCl_2(PR_3)_2$ (R=Ph and Et) gives 2-(2-butenyl)phenols (46—76% yields) in which nucleophiles are incorporated into the methyl group of the butenyl moiety. 2-Vinylchroman undergoes the same type of reaction where only the palladium complex bearing PEt_3 ligand is effective. The effectiveness of PEt_3 ligand is also observed in the reaction of 2,3-dihydro-2-isopropenylbenzofuran with diethyl sodiomalonate leading to 3-ethoxycarbonyl-4-(2-methyl-1-propenyl)-2-chromanone.

Palladium (II)-catalyzed cyclization of 2-(*trans*-2-butenyl)phenol(**1**) gives 2-vinyl-2,3-dihydrobenzofuran (**2**).[1] Since the vinyl compound has a structural unit of allylic ether, it is expected to react with nucleophiles in the presence of palladium(0) catalysts such as $Pd(PPh_3)_4$.[2] This will lead to functionalization of the methyl group in the butenyl moiety of **1** (Scheme 1). Described herein is the realization of the reduction of $PdCl_2$ complexes with excess diethyl sodiomalonate.[3] Diazopalladium(II) complex, $[PhC(N_2)]_2Pd(PEt_3)_2$ (**5**),[4] which upon heating generates $Pd(PEt_3)_2$, also serves as the catalyst to give **3a** (69%). Deethoxycarbonylation ($NaCN/LiI\cdot H_2O$/DMSO, 160 °C) of **3a** afford **6** (75%), resulting in two carbon homologation of the butenyl moiety of **1**.

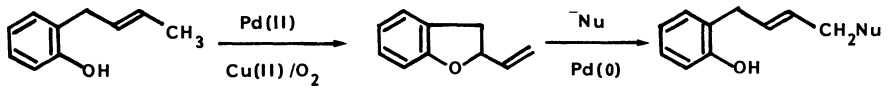

1 2 3

a; Nu=CH(COOEt)$_2$

b; Nu=NMePh

Scheme 1.

expectation, and an application of this procedure to 2-(*trans*-3-pentenyl)phenol (**8**) (Scheme 2).

The reaction of vinylbenzofuran **2** with diethyl sodiomalonate (1.2 equiv) in the presence of 3 mol% of $Pd(PPh_3)_4$ (THF-toluene, 110 °C, 4 h) gives a 76% yield of 4-substituted 2-butenylphenol **3a** along with its dimer **4** (10%). Palladium(II) complexes such as $PdCl_2(PR_3)_2$ (R=Ph and Et) are comparatively effective in promoting the reaction, in which palladium(0) species is generated in situ by the

Treatment of **2** with *N*-methylaniline (1.3 equiv) in the presence of $Pd(PPh_3)_4$ (3 mol%) in THF–toluene at 120 °C for 3 h gives **3b** in 46% yield (Scheme 1). The use of complex **5** bearing PEt_3 ligand affords a trace amount of **3b**. In this case, the substrate **2** largely rearranges into 2-methyl-2*H*-chromene (**7**) (46%).

2-Vinychroman (**9**), which is readily prepared by Pd(II)-catalyzed cyclization of 2-(*trans*-3-pentenyl)-phenol (**8**), undergoes the same type of alkylation with diethyl sodiomalonate (Scheme 2). In this case,

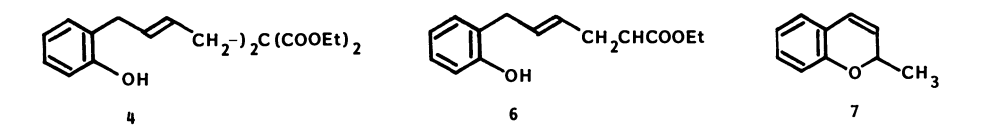

4 6 7

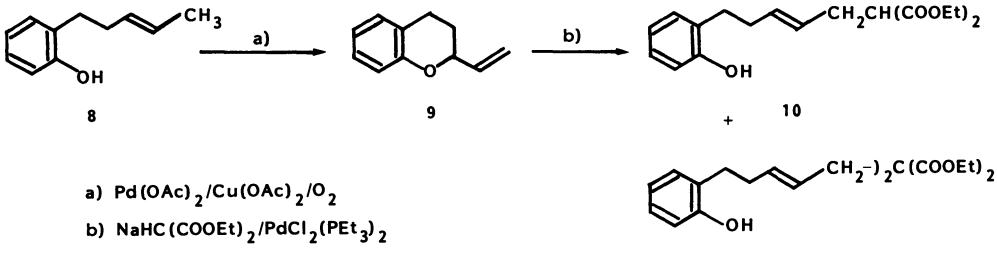

8 9 + 10 11

a) $Pd(OAc)_2/Cu(OAc)_2/O_2$

b) $NaHC(COOEt)_2/PdCl_2(PEt_3)_2$

Scheme 2.

however, only the palladium complex bearing PEt_3 is effective; no reaction takes place with $Pd(PPh_3)_4$ and $PdCl_2(PPh_3)_2$, while $PdCl_2(PEt_3)_2$ affords a 63% yield of **10** along with its dimer **11** (10%). Since PEt_3 complexes are more nucleophilic than PPh_3 complexes,[5] the oxidative addition of Pd(0) into the C–O bond must be the rate-determining step in this alkylation.[6] The effectiveness of PEt_3 ligand is also observed in the reaction of dihydrobenzofuran **12** with diethyl sodiomalonate leading to coumarin **13**.

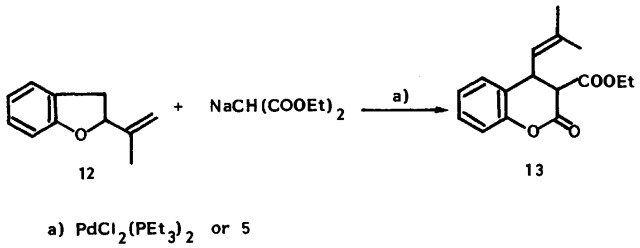

Thus, **13** is obtained in 54—64% yields with $PdCl_2(PEt_3)_2$ or **5**, while no reaction occurs with $Pd(PPh_3)_4$. In the reaction pathways shown in Scheme 3, **13** is assumed to be formed via isomerization of the intermediate π-allyl complex **14** to **15**.

Experimental

2-(*trans*-2-Butenyl)phenol (**1**) was prepared by C-alkylation of phenol with *trans*-1-chloro-2-butene (Tokyo Kasei).[1] 2-(*trans*-3-Pentenyl)phenol (**8**) was synthesized by the reaction of *o*-methoxybenzylmagnesium chloride with *trans*-2-butenyl diethyl phosphate[7] followed by demethylation.[8] The preparation of 2-isopropenyl-2,3-dihydrobenzofuran (**12**) was carried out by the reported procedure.[9]

Palladium(II)-Catalyzed Cyclization of 1 and 8. The reaction was performed by using substrate **1** or **8** (2.5 mmol), $Pd(OAc)_2$ (56.5 mg, 0.25 mmol), and $Cu(OAc)_2$ (45.0 mg, 0.25 mmol) in anhydrous MeOH (5 mL) under O_2 atmosphere (1 atm, balloon) at 36 °C. After usual workup,[1] the cyclized product was isolated by distillation followed by preparative TLC (SiO_2, hexane). **2**: Yield 62%; R_f=0.27. **9**:[10] Yield 57%; R_f=0.41.

Palladium-Catalyzed Alkylation of 2, 9, and 12 with Diethyl Sodiomalonate. Into a suspension of NaH (48 mg, 1.20 mmol) in dry THF (4 mL) was added diethyl sodiomalonate (240 mg, 1.50 mmol) at 0 °C, and the mixture was stirred for 1 h at room temperature. The resultant solution was then added by syringe to a solution of palladium catalyst (0.03 mmol) and vinyl compound **2**, **9**, or **12** (1 mmol) in dry toluene at room temperature, and the mixture was heated at 110 °C for 4 h. After cooling, the reaction was quenched by addition of water (10 mL) and ether (10 mL). The aqueous layer was neutralized by 2 M HCl(1 M=1 mol dm^{-3}) and extracted with ether (10 mL×3). The combined ethereal layer was washed with brine (20 mL×2) and dried over $MgSO_4$. Removal of the solvent followed by preparative TLC (SiO_2, hexane–EtOAc=7:3) gave the alkylated products. Their spectral and analytical data are listed below. The isolated yields of **3a** and **4** are 76 and 10% with $Pd(PPh_3)_4$, 56 and 19% with $PdCl_2(PPh_3)_2$, and 68 and 15% with $PdCl_2(PEt_3)_2$, respectively. Those of **10** and **11** are 63 and 10% with $PdCl_2(PEt_3)_2$ and 54 and 20% with $[PhC(N_2)]_2Pd(PEt_3)_2$ (**5**), respectively. The yield of **13** are 64 and 54%, with $PdCl_2(PEt_3)_2$ and **5**, respectively.

2-[*trans*-5,5-Bis(ethoxycarbonyl)-2-pentenyl]phenol (3a). R_f=0.34; bp 154—155 °C (1 mmHg); IR (neat) 3450, 3000, 1730 (C=O), 1600, 1040, and 965 (*trans* -CH=CH-) cm^{-1}; ^1H NMR (60 MHz, $CDCl_3$) δ=1.20 (6H, t, *J*=7 Hz, Me), 2.60 (2H, dd, *J*=8 and 6 Hz, $ArCH_2$-), 3.25—3.27 (3H, m, -CH- and $-CH_2C$=C), 4.14 (4H, q, *J*=7 Hz, $-OCH_2CH_3$), 5.17—6.00 (2H, m, -CH=CH-), 6.21—6.65 (1H, br s, OH), and 6.65—7.21 (4H, m, ArH). MS, *m/z* 306 (M^+). Deethoxycarbonylation of **3** by the reported procedure[11] gave 2-(*trans*-5-ethoxycarbonyl-2-pentenyl)phenol (**6**) in 75% yield;

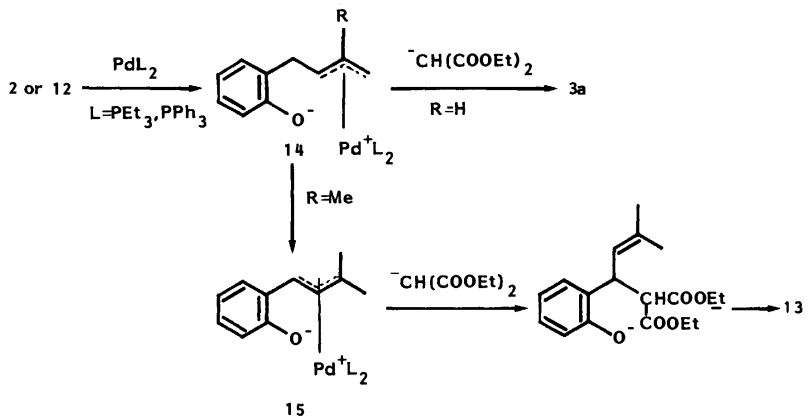

Scheme 3.

bp 115—116 °C (1 mmHg); IR (neat) 3400, 1730, 1710, 965 (*trans* -CH=CH-) cm^{-1}; ^1H NMR (60 MHz, $CDCl_3$) δ=1.16 (3H, t, J=7 Hz, Me), 2.32 (4H, m, $-CH_2CH_2-$), 3.63 (2H, d, J=5 Hz, $ArCH_2-$), 4.15 (2H, q, J=7 Hz, $-OCH_2CH_3$), 5.23—5.98 (2H, m, -CH=CH-). Found: C, 71.89; H, 7.69%. Calcd for $C_{14}H_{18}O_3$; C, 71.77; H, 7.74%.

(2*E*,7*E*)-1,9-Bis(2-hydroxyphenyl)-5,5-bis(ethoxycarbonyl)-2,7-nonadiene (4). R_f=0.17; IR (neat) 3450, 3000, 1725 (C=O). 1040, and 980 (*trans* -CH=CH-) cm^{-1}; ^1H NMR (60 MHz, $CDCl_3$) δ=1.16 (6H, t, J=7 Hz, Me), 2.60 (4H, d, J=6 Hz, $-CH_2C=C-$), 4.10 (4H, q, J=7 Hz, $-OCH_2CH_3$), 5.22 (2H, br s, OH), 5.12—5.91 (4H, m, -CH=CH-), and 6.33—6.86 (8H, m, ArH).

2-[*trans*-6,6-Bis(ethoxycarbonyl)-3-hexenyl]phenol (10). R_f=0.30; IR (neat) 3450, 3000, 1740 (C=O), 1240, and 980 (*trans* -CH=CH-) cm^{-1}; ^1H NMR (60 MHz, $CDCl_3$) δ=1.25 (6H, t, J=7 Hz, Me), 2.01—2.91 (6H, m, $-CH_2CH_2-$ and $-CH_2C=C$), 3.40 (1H, t, J=7 Hz, -CH-), 5.05 (1H, br s, OH), 5.15—5.88 (2H, m, -CH=CH-), 6.65—7.42 (4H, m, ArH).

Found: C, 67.60; H, 7.74%. Calcd for $C_{18}H_{24}O_5$: C, 67.48; H, 7.55%.

(3*E*,8*E*)-1,11-Bis(2-hydroxyphenyl)-6,6-bis(ethoxycarbonyl)-3,8-undecadiene (11). R_f=0.54; IR ($CHCl_3$), 3450, 2980, 1750, 1730, 1030, and 970 (trans -CH=CH-) cm^{-1}; ^1H NMR (60 MHz, $CDCl_3$) δ=1.21 (6H, t, J=7 Hz, Me), 2.08—2.86 (12H, m, $-CH_2CH_2-$ and $-CH_2C=C$), 4.14 (4H, q, J=7 Hz, $-OCH_2CH_3$), 4.98—5.80 (4H, m, -CH=CH-), and 6.60—7.34 (8H, m, ArH). The OH proton was unable to be assigned unambiguously. MS, m/z 481 (M^+).

3-Ethoxycarbonyl-4-(2-methyl-1-propenyl)coumarin (13). R_f=0.75; IR (neat) 1775 (C=O), 1740 (C=O), 1588, 1485, 1452, 1135, 1032, and 755 cm^{-1}; ^1H NMR (100 MHz, $CDCl_3$) δ=1.21 (3H, J=7 Hz, Me), 1.77 (3H, d, J=1.5 Hz, Me), 1.79 (3H, d, J=1.5 Hz, Me), 3.45 (1H, d, J=10 Hz, H-3), 4.17 (2H, q, J=7 Hz, $-OCH_2CH_3$), 4.35 (td, J=10 and ≈1 Hz, H-4), 4.95 (1H, dm, J=10 and 1—1.5 Hz, -CHC=C-), and 7.11 (4H, m, ArH). The coupling of $J_{3,4}$=10 Hz suggests the *trans* configuration between the H-3 and H-4 protons.

Found: C, 69.92; H, 6.52%, M^+, 274. Calcd for $C_{16}H_{18}O_4$: C, 70.06; H, 6.61%; M, 274.

Amination of 2 with *N*-Methylaniline. To a solution of $Pd(PPh_3)_4$ (39.5 mg, 0.034 mmol) in toluene (1 mL) were added successively **2** (173 mg, 1.2 mmol) and a solution of *N*-methylaniline (164 mg, 1.53 mmol) in dry THF (1 mL) at room temperature. The mixture was then heated at 120 °C with stirring for 3 h, and cooled to room temperature. Removal of the solvent followed by preparative TLC (SiO_2, $CHCl_3$-acetone=95:5) afforded **3b** in 46% yield. The same treatment of **2** with **5** gave **7** in 46% yield.

[*trans*-4-(*N*-Methylanilino)-2-butenyl]phenol (3b): R_f=0.45 (SiO_2, $CHCl_3$-acetone=19:1); IR (neat) 3380, 3035, 1920, 1800, 1700, 1600, 1500, 1232, 970, 745, 694 cm^{-1}; ^1H NMR (60 MHz, $CDCl_3$) δ=2.73 (3H, s, N-Me), 3.27 (2H, d, J=5.0 Hz, CH_2), 3.76 (2H, d, J=4.0 Hz, $N-CH_2-$), 4.86—5.14 (1H, br, OH), 5.06—5.98 (2H, m, -CH=CH-), 6.44—7.19 (9H, m, ArH).

Found: C, 80.70; H, 7.57; N, 5.59%. Calcd for $C_{17}H_{19}ON$: C, 80.57; H, 7.56; N, 5.53%.

The spectral properties of **7** have been already reported.[12]

References

1) T. Hosokawa, C. Okuda, and S.-I. Murahashi, *J. Org. Chem.*, **50**, 1282 (1985).

2) J. Tsuji, "Organic Synthesis with Palladium Compounds," Springer-Verlag, Berlin (1980); J. Tsuji, *Yuki Gosei Kagaku Kyokai Shi*, **41**, 619 (1983); B. M. Trost and T. R. Verhoeven, *Comp. Organomet. Chem.*, **8**, 799 (1982); J. Tsuji, I. Shimizu, I. Minami, Y. Ohashi, T. Sugiura, and K. Takahashi, *J. Org. Chem.*, **50**, 1523 (1985), and references cited therein.

3) Generation of palladium(0) species from $PdCl_2(PR_3)_2$ upon treatment with bases has been shown; see, S.-I. Murahashi, M. Yamamura, Y. Yanagisawa, N. Mita, and K. Kondo, *J. Org. Chem.*, **44**, 2408 (1979).

4) S.-I. Murahashi, Y. Kitani, T. Uno, T. Hosokawa, K. Miki, T. Yonezawa, and N. Kasai, *Organometallics*, **5**, 356 (1986).

5) R. G. Pearson and R. E. Figdore, *J. Am. Chem. Soc.*, **102**, 1541 (1980).

6) The difference in reactivity between 5- and 6-membered ring may reflect a stereoelectronic effect of the lone-pair electron of heterocyclic oxygen atom with respect to the p-orbital at the adjacent ring; see, G. W. Burton, L. Hughes, and K. U. Ingold, *J. Am. Chem. Soc.*, **105**, 5950 (1983); G. W. Burton, T. Doba, E. J. Gabe, L. Hughes, F. L. Lee, L. Prasad, and K. U. Ingold, *ibid.*, **107**, 7053 (1985).

7) S. Araki, T. Sato, and Y. Butsugan, *J. Chem. Soc., Chem. Commun.*, **1982**, 285.

8) G. I. Feutrill and R. N. Mirrington, *Aust. J. Chem.*, **25**, 1719 (1972).

9) S. Yamaguchi, S. Kondo, K. Shimokawa, O. Inoue, M. Sannomiya, and Y. Kawase, *Bull. Chem. Soc. Jpn.*, **55**, 2500 (1982).

10) The detail and related reactions will be reported in due course.

11) B. M. Trost, L. Weber, P. Strege, T. J. Fullerton, and T. J. Dietsche, *J. Am. Chem. Soc.*, **100**, 3426 (1978).

12) T. Hosokawa, S. Yamashita, S.-I. Murahashi, and A. Sonoda, *Bull. Chem. Soc. Jpn.*, **49**, 3666 (1976).

 © 1986 The Chemical Society of Japan Bull. Chem. Soc. Jpn., 59, 2195—2201 (1986)

Synthesis and Conformation of Aromatic Cyclic Dipeptides. Cyclo(phenylalanyl)$_2$, Cyclo(1-naphthylalanyl)$_2$, and Cyclo(2-naphthylalanyl)$_2$

Syun EGUSA,† Jun TAKAGI,† Masahiko SISIDO,*,†† and Yukio IMANISHI†
†Department of Polymer Chemistry, Faculty of Engineering, Kyoto University, Kyoto 606
††Research Center for Medical Polymers and Biomaterials, Kyoto University, Kyoto 606
(Received February 18, 1986)

Cyclic dipeptides of aromatic amino acids, cyclo(L-phenylalanyl)$_2$, cyclo(L-1-naphthylalanyl)$_2$, and cyclo(L-2-naphthylalanyl)$_2$ were synthesized and subjected to spectroscopic analyses using ^{1}H NMR, absorption, circular dichroism (CD), fluorescence, and fluorescence-detected circular dichroism (FDCD). The ^{1}H NMR data suggested that the 2,5-piperazinedione rings of the three cyclic dipeptides are in planar or nearly planar bowsplit boat-type conformation. The aromatic side groups of cyclo(1- and 2-naphthylalanyl)$_2$'s were found to take asymmetric configurations, one naphthyl group being folded onto the 2,5-piperazinedione ring, the other being unfolded. Strong exciton couplet was observed in CD spectra of the three compounds. The signs of the exciton splitting were opposite in the two naphthyl cyclic dipeptides. Fluorescence spectra of the two naphthyl cyclic dipeptides showed no excimer emission. The absence of strong interchromophoric interaction in the lowest excited state was also suggested by the virtual coincidence of CD spectrum with FDCD spectrum. From the above spectroscopic data, probable conformations were proposed for the naphthyl cyclic dipeptides.

Bichromophoric systems in which conformational freedom of the two chromophores are highly restricted, have been studied and basic information on electronic properties of spatially fixed chromophoric systems has been accumulated.[1] In this respect, cyclic compounds carrying aromatic groups are especially interesting because of the rigidity of the chromophore arrangement. Bichromophoric cyclophanes,[1] cyclobutanes,[2,3] and crown ethers[4] have been reported in the past. However, few *chiral* bichromophoric cyclic compound has been reported so far.[1] The chiral bichromophoric systems are advantageous, since chiroptical spectroscopy, such as circular dichroism (CD), circularly polarized fluorescence (CPF),[5,6] and fluorescence-detected circular dichroism (FDCD)[7] provides more information on the electronic properties than that from conventional spectroscopy.

In this study, syntheses of aromatic cyclic dipeptides carrying phenyl, 1-naphthyl, and 2-naphthyl chromophores were undertaken and their conformations in solution were investigated. Cyclic dipeptides consisting of natural amino acids i.e., phenylalanine (Phe), tyrosine (Tyr), histidine (His), and tryptophan (Trp) have been studied by ^{1}H NMR, ^{13}C NMR, CD, and X-ray crystallography.[8–15] However, the aromatic groups of the natural amino acids are not suited for photochemical and photophysical investigations. In this study, artificial aromatic amino acids carrying 1- or 2-naphthyl group, L-1- and L-2-naphthylalanine (1- or 2-napAla) are employed and their linear and cyclic dipeptides are prepared.

Experimental

Meterials. Linear and cyclic dipeptides of Phe, 1-napAla, and 2-napAla were prepared by the procedure shown in Scheme 1. Optically active 1- and 2-napAla's were prepared by the optical resolution of their acetyl derivatives with acylase,[16,17] which were synthesized by the acetamidomalonate ester method. In the following, syntheses of linear and cyclic dipeptides of 2-napAla are described as typical examples.

***N*-Benzyloxycarbonyl-L-2-naphthylalanine (*Z*-2-napAla).**

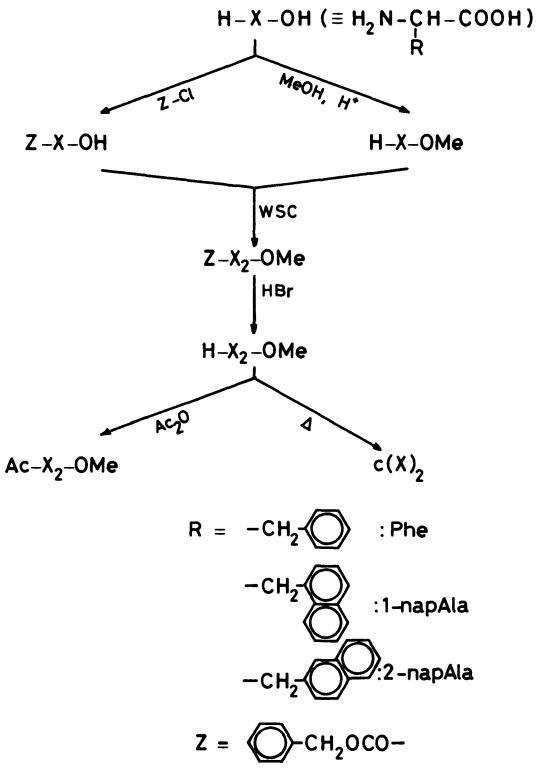

Scheme 1.

2-NapAla (200 mg) was dissolved in 1 M† NaOH aqueous solution (1 ml) and cooled by ice. Benzyloxycarbonyl chloride (0.15 ml) and 1 M NaOH were added dropwise concurrently under vigorous stirring. The stirring was continued overnight and then the pH of the solution was adjusted to about 3. The organic component was extracted with ethyl acetate and the extract was dried and evaporated. The crude crystals remained were recrystallized from an ether–hexane mixed solvent. Yield 90%, mp 165—170 °C. *Z*-l-napAla: Yield 95%, mp 150—152 °C. *Z*-Phe: Yield 71%, mp 86—89 °C.

L-2-Naphthylalanine Methyl Ester Hydrochloride (2-napAla-OMe·HCl). The amino acid (200 mg) was dissolved in methanol (20 ml) containing 2 ml of 1 M HCl and refluxed for 1 h. The solvent was evaporated and the residue was recrystallized from a methanol–ethyl acetate mixed solvent. Yield 87%, mp 165 °C (gradually sublimed above 130 °C). 1-NapAla-OMe·HCl: Yield 98%, mp 143—145 °C (partially sublimed). Phe-OMe·HCl: Yield 95%, mp 159—161 °C.

***N*-Benzyloxycarbonyl-L-2-naphthylalanyl-L-2-naphthylalanine Methyl Ester [*Z*-(2-napAla)$_2$-OMe].** *Z*-2-NapAla (133 mg) was dissolved in dichloromethane (2 ml) and 2-napAla-OMe·HCl (100 mg) and triethylamine (58 µl) were added. After cooling with an ice–water bath, water-soluble carbodiimide (WSC) [1-(3-dimethylaminopropyl)-3-ethylcarbodiimide hydrochloride] (80 mg) and 1-hydroxybenzotriazole (56 mg) were added. After stirring overnight the solvent was evaporated and ethyl acetate was added. The solution was washed with 10% citric acid, aq NaCl solution, 10% $NaHCO_3$, and water and dried over sodium sulfate. The residue remained after evaporation was recrystallized from an ethyl acetate–ether mixed solvent. Yield 83%, mp 163 °C. *Z*-(1-napAla)$_2$-OMe: Yield 73%, mp 136 °C. *Z*-(Phe)$_2$-OMe: Yield 40%, mp 106—109 °C.

Cyclo(L-2-naphthylalanyl-L-2-naphthylalanyl) [c(2-napAla)$_2$]. *Z*-(2-NapAla)$_2$-OMe (177 mg) was dissolved in 25% HBr–acetic acid (3 ml) and stirred for 30 min at room temperature. The solution was concentrated under reduced pressure and a small amount of acetic acid was added again. The solution was poured into ether and the precipitate was collected and dried under vacuum. The HBr salt was then dispersed in ethyl acetate and shaked with aqueous $NaHCO_3$ solution. The organic layer was dried over sodium sulfate and the solvent was evaporated. 1-Butanol (50 ml) was added to the residue remained and the solution was refluxed for 2 d. The crystal which appeared after cooling the reaction mixture in refrigerator, was collected and washed with methanol. The cyclic dipeptide was only slightly soluble in such polar aprotic solvents as *N*,*N*-dimethylformamide (DMF), dimethyl sulfoxide (DMSO), and trimethyl phosphate (TMP). No appropriate solvent was found for recrystallization. Yield 55%, mp>300 °C. Found: C, 79.39; H, 5.85; N, 7.22%. Calcd for $C_{26}H_{24}N_2O_2$: C, 79.17; H, 5.62; N, 7.10%. c(1-napAla)$_2$: Yield 47%, mp 272—274 °C. Anal. Found: C, 79.30; H, 5.58; N, 7.27%. c(Phe)$_2$: Yield 32%, mp>300 °C. Found: C, 73.61; H, 6.11; N, 9.43%. Calcd for $C_{18}H_{18}N_2O_2$: C, 73.45; H, 6.16; N, 9.52%.

† 1 M=1 mol dm^{-3}.

***N*-Acetyl-L-2-naphthylalanyl-L-2-naphthylalanine Methyl Ester [Ac-(2-napAla)$_2$-OMe].** The benzyloxycarbonyl group of *Z*-(2-napAla)$_2$-OMe was removed by 25% HBr–acetic acid. The HBr salt of the dipeptide methyl ester was dissolved in acetic anhydride–triethylamine (1:1) mixture and stirred overnight. The volatile component was removed under reduced pressure and the solid remained was dissolved in ethyl acetate. The solution was washed with 1 M HCl, 10% $NaHCO_3$, and water and dried over Na_2SO_4. Evaporation gave a crude crystal which was recrystallized from an ethyl acetate–hexane mixed solvent. Mp 200—205 °C. Found: C, 73.37; H, 5.96; N, 5.98%. Calcd for $C_{29}H_{28}N_2O_4$: C, 74.34; H, 6.02; N, 5.98%. Ac-(1-napAla)$_2$-OMe: Mp 208—212 °C. Found: C, 74.37; H, 5.99; N, 6.32%.

Measurements. ^{1}H NMR (90 MHz) was recorded on a JEOL FX90Q Fourier Transform spectrometer in *N*,*N*-dimethylformamide (DMF)-d_7 over the temperature range of 50—100 °C for c(Phe)$_2$ and c(2-napAla)$_2$ and over the temperature range of −40—100 °C for c(1-napAla)$_2$. Residual peaks of the solvent were eliminated by a 180°-τ-90° pulse sequence. The peak assignment reported by Kobayashi et al.[18] was adopted. The amide NH peaks of the naphthyl dipeptides overlapped with the peaks of aromatic protons. Therefore, the coupling parameter $J_{NH-C^{\alpha}H}$, was measured from the splitting of $C^{\alpha}H$ proton band under irradiating the $C^{\beta}H$ proton. Octets were observed in the region of $C^{\beta}H$ protons for the three cyclic dipeptides, indicating the two nonequivalent $C^{\beta}H$ protons [$C^{\beta}H$(S) and $C^{\beta}H$(R)] couple with each other and with the $C^{\alpha}H$ proton. The coupling constants, $J_{C^{\alpha}H-C^{\beta}H(S)}$ and $J_{C^{\alpha}H-C^{\beta}H(R)}$, were directly read from the peak separations of the octets.

Circular dichroism (CD) was recorded on a JASCO J-20 spectropolarimeter. Fluorescence-detected circular dichroism (FDCD) was also measured on the JASCO J-20 machine, equipped with a cutoff filter for excitation light, a Hamamatsu R268 photomultiplier tube, and a preamplifier.[7] Fluorescence spectra were recorded on a Hitachi MPF-4 instrument under an autocorrection mode. The dipeptides in DMF ([Aryl group]=1.0×10^{-5} mol l^{-1}) were put into a quartz tube of diameter 5 mm, and the tube was immersed into a Dewer vessel with quartz windows. The Dewer vessel was filled with a temperature-controlled methanol. The DMF solution was bubbled with nitrogen gas for 20 min before each measurement.

Results and Discussion

^{1}H NMR Spectra. The proton NMR spectra of the three cyclic dipeptides were measured in DMF-d_7. The spectra for c(1- and 2-napAla)$_2$ are shown in Fig. 1.

Coupling parameters obtained from the spectra are collected in Tables 1 and 2. They were virtually constant over the temperature range of 50—100 °C for c(Phe)$_2$ and c(2-napAla)$_2$ and −40—100 °C for c(1-napAla)$_2$, indicating a temperature independence of the skeletal conformations of the 2,5-piperazinedione rings and of the conformer populations of the side chains for the three cyclic dipeptides.

Table 1 lists the coupling constants $J_{NH-C^{\alpha}H}$, which are related to the dihedral angle $\theta_{NH-C^{\alpha}H}$ between C^{α}–N–H plane and H–C^{α}–N plane. $\theta_{NH-C^{\alpha}H}$ is approximately equal to $\phi(N-C^{\alpha})-60°$, where ϕ is the rotational angle around N–C^{α} bond as defined by the IUPAC-IUB nomenclature committee.[19] The dihedral angles were calculated from the coupling constants by using three different equations proposed by Bystrov et al.,[20] Ramachandran et al.,[21] and Chung et al.,[22] and are listed in the same table. It is seen that the angles estimated by using the three equations differ considerably.

Skeletal conformation of cyclic dipeptides in solution is often assumed to be symmetric and have planar amide bonds. Under these assumptions, the skeletal conformation is expressed by a single angle β, which is defined as a complementary angle between the two amide planes.[12,13] A skeletal conformation with positive β is called as a bowsplit boat-type one in which the two C^{β} atoms are in extended positions out of the 2,5-piperazinedione ring. The conformation of negative β is called as a flagpole boat-type one in which the two C^{β} atoms approach with each other above the 2,5-piperazinedione ring. β is zero for a planar 2,5-piperazinedione ring. The smallest β has been reported for cyclo(*N*-methyl-L-Val)$_2$[15] to be $-41°$, while the largest β has been found in cyclo(L-proline)$_2$[23] to be 38°. Larger or smaller β leads to unacceptably small bond angles at the C^{α} atom.

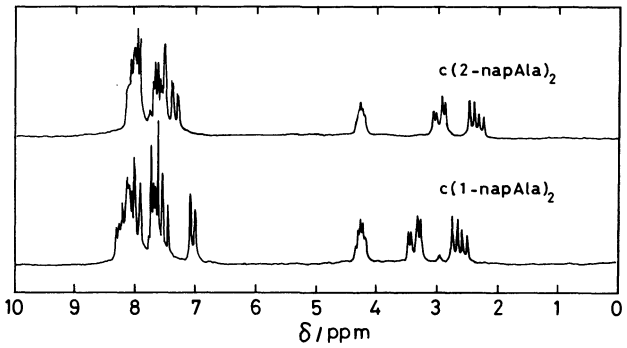

Fig. 1. Proton NMR spectra of c(1- and 2-napAla)$_2$ in DMF-d_7. Concentration=2.0 mg/0.4 ml. Temperature=30 °C for c(1-napAla)$_2$, 50 °C for c(2-napAla)$_2$.

If one allows a variation of β between ±45°, the allowed range of $\theta_{NH-C^{\alpha}H}$ is between $-20°$ and $-100°$. Hence, among the four values of $\theta_{NH-C^{\alpha}H}$ obtained as solutions of each equation of Table 1, only one is in the allowed range, which is indicated in the parentheses. If one adopts $\theta=-102°$ for c(Phe)$_2$, the bond angle $\angle$(N,C,C′) will be 97°. Similarly, if one takes $\theta=-115°$ for c(2-napAla)$_2$, the bond angle will be 85°. These small bond angles around C^{α} atom are unacceptable.

As the result of the above consideration, it was concluded that the $\theta_{NH-C^{\alpha}H}$ values lie between $-58°$ and $-39°$ for the two c(napAla)$_2$'s and between $-72°$ and $-57°$ for c(Phe)$_2$. These ranges of $\theta_{NH-C^{\alpha}H}$ correspond to the range of β between 0° and 20° for the two c(napAla)$_2$'s and between $-10°$ and 5° for c(Phe)$_2$. Therefore, the two c(napAla)$_2$'s have planar or nearly planar bowsplit boat-type skeletal conformations and c(Phe)$_2$ is in a planar conformation in DMF solution.

Little has been reported on the skeletal conformations of aromatic cyclic dipeptides. Snow and Hooker[13] calculated conformation energy and theoretical CD for c(Tyr)$_2$ and concluded that its β value was around 20°. This value is within the possible range of β for the two c(napAla)$_2$'s. On the other hand, Benedetti et al.[15] reported a result of X-ray crystallography of c(*N*-methyl-Phe)$_2$ and found that $\beta=-19°$. The large negative value may reflect the effect of *N*-methyl substituents and cannot be directly

Table 1. The Coupling Constant $J_{NH-C^{\alpha}H}$, and the Dihedral Angle $\theta_{NH-C^{\alpha}H}$, of Aromatic Cyclic Dipeptides in *N*,*N*-Dimethylformamide-d_7

Amino acid	$J_{NH-C^{\alpha}H}$[a]	$\theta_{NH-C^{\alpha}H}$/degree		
		Bystrov[c]	Ramachandran[d]	Chung[e]
Phe	≲1.0[b]	±102, ±72 (−72)[f]	[g]	±102, ±57 (−57)
1-napAla	2.9	±117, ±55 (−55)	±112, ±52 (−52)	±116, ±39 (−39)
2-napAla	2.5	±115, ±58 (−58)	±109, ±56 (−56)	±113, ±43 (−43)

a) Measured at 30 °C for c(1-napAla)$_2$ and at 50 °C for c(2-napAla)$_2$ and c(Phe)$_2$, ±0.2 Hz. b) Estimated from the linewidth of C^{α} proton signal under irradiating the C^{β} protons. c) $J_{NH-C^{\alpha}H}=9.4\cos^2\theta-1.1\cos\theta+0.4$. (Ref. 20). d) $J_{NH-C^{\alpha}H}=7.9\cos^2\theta-1.5\cos\theta+1.35\sin^2\theta$. (Ref. 21). e) $J_{NH-C^{\alpha}H}=4.3\cos^2\theta-2.9\cos\theta+4.3$. (Ref. 22). f) Value which corresponds to the allowed range of β(±45 °). g) The Ramachandran equation affords no solution.

compared with the present results.

Coupling constants $J_{C^{\alpha}H-C^{\beta}H(R)}$ and $J_{C^{\alpha}H-C^{\beta}H(S)}$ afford information on the rotamer population around $C^{\alpha}-C^{\beta}$ bond (χ_1), if the rotation is fast enough compared with the NMR time scale. Although the bulky aromatic groups is expected to retard the rotation considerably, no evidence for the restricted rotation was detected in the ^1H NMR spectra over the temperature range of −40—100 °C for c(1-napAla)$_2$ and 50—100 °C for c(2-napAla)$_2$ and c(Phe)$_2$. The coupling constants are listed in Table 2, together with the rotamer populations calculated according to the empirical equation reported by Pachler.[24]

The population of trans conformation is smaller than 20% for the three cyclic dipeptides. The small contribution of trans form is explained by a repulsive interaction between aromatic ring and the carbonyl oxygen. g^+ indicates a folded conformation in which the aromatic ring is overlapped onto the 2,5-piperazinedione ring. It should be noted that the population of the folded conformation is larger than 40% for the two c(napAla)$_2$'s and even larger for c(Phe)$_2$. The predominance of the folded conformation may be, at least partially, ascribed to an aromatic-amide interaction which has been detected by NMR spectroscopy.[25]

A CPK model examination and a preliminary result of empirical potential energy calculation for c(napAla)$_2$'s[26] suggested that the two side chains cannot take the folded conformation concurrently. Therefore, the high population of the folded conformation indicates that one side chain takes a folded conformation whereas the other is in unfolded conformations, t and g^- with a predominance of g^-. Incidentally, Benedetti et al.[15] reported that the side chains of c(*N*-methyl-L-Phe)$_2$ are in an asymmetric conformation, one being in a folded, the other in an unfolded conformation in the solid state.

To summarize the ^1H NMR results, the three aromatic cyclic dipeptides take similar skeletal and side-chain conformations. The skeletal conformation is planar ($\beta=0°$) or nearly planar bowsplit boat-type one ($\beta<20°$). The side-chains rotate rapidly within the NMR time scale and its rotamer population favors folded (g^+)-unfolded ($g^->t$) asymmetric conformations.

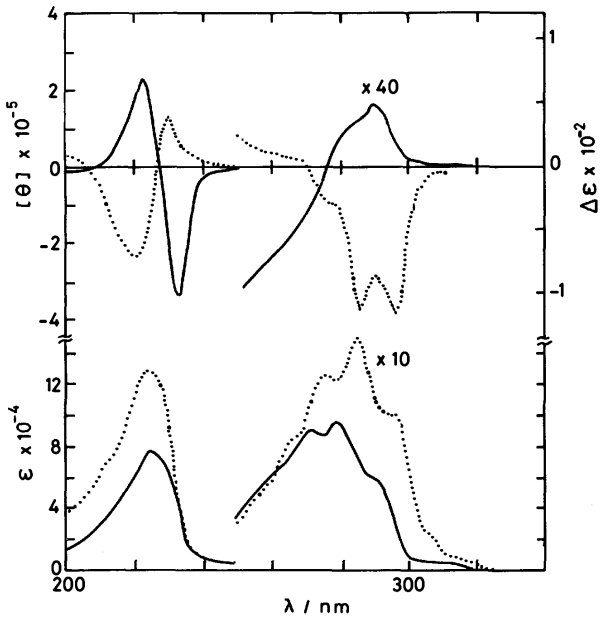

Fig. 2. CD (top) and absorption (bottom) spectra of c(1-napAla)$_2$ (·····) and c(2-napAla)$_2$ (——) in trimethyl phosphate at 25 °C. [θ] and ε are calculated with respect to two naphthyl chromophores.

Table 2. The Coupling Constant $J_{C^{\alpha}H-C^{\beta}H}$, and the Rotamer Populations around $C^{\alpha}-C^{\beta}$ Bond in *N,N*-Dimethylformamide-d_7

Amino acid	$J_{C^{\alpha}H-C^{\beta}H(S)}$	$J_{C^{\alpha}H-C^{\beta}H(R)}$[a]	Rotamer polulations[b]		
			t	g^-	g^+
Phe	4.1	6.9	0.14	0.39	0.47
1-napAla	4.5	7.2	0.17	0.42	0.41
2-napAla	4.6	7.1	0.18	0.41	0.41

a) These coupling parameters (in Hz) were constant over the temperature range of 30—100 °C. The estimated error is ±0.1 Hz for 1- and 2-napAla's and ±0.5 Hz for Phe. b) Calculated on the basis of the Pachler's empirical equation (Ref. 24): $J_{C^{\alpha}H-C^{\beta}H(S)}=10.96\,t+2.60$, $J_{C^{\alpha}H-C^{\beta}H(R)}=10.96\,g^-+2.60$. The configurations of the three rotamers are shown below.

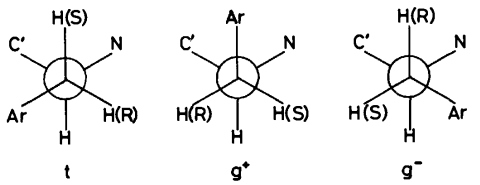

Absorption Spectra and Circular Dichroism. Figure 2 shows absorption and CD spectra of c(1- and 2-napAla)$_2$'s in TMP. The two cyclic dipeptides exhibit marked exciton couplets at the ^1B_b absorption band with opposite signs. The molar ellipticities are: $[\theta]_{229}=1.4\times10^5$, $[\theta]_{221}=-2.4\times10^5$ ($\Delta\tilde{\nu}=1581$ cm^{-1}) for c(1-napAla)$_2$ and $[\theta]_{233}=-3.5\times10^5$, $[\theta]_{222}=2.3\times10^5$ ($\Delta\tilde{\nu}=2127$ cm^{-1}) for c(2-napAla)$_2$. According to the exciton coupling rule,[27] the sign of exciton coupling in c(1-napAla)$_2$ indicates that the screw sense of the arrangement of ^1B_b absorption transition moment is right-handed in the conformation which contributes most significantly to the CD spectrum observed. The sign of exciton couplet in c(2-napAla)$_2$ indicates that the screw sense is left-handed in the most significant conformer.

The marked exciton couplet also suggests strong interchromophore interaction between naphthyl groups in the cyclic dipeptides. A preliminary conformational calculation[26] indicated that the center-to-center distances between two naphthyl groups in the two cyclic dipeptides are between 6—7 Å in the folded(g^+)-unfolded(g^-) side-chain conformations. The interchromophore distance is short enough to induce strong exciton couplet in the CD spectra.

The CD intensity at the ^1B_b absorption band is much more intense in the cyclic dipeptides than in the corresponding linear dipeptides which are shown in Fig. 3. No exciton couplet is seen in Ac-(1-napAla)$_2$-OMe and very weak CD is observed in Ac-(2-napAla)$_2$-OMe. The weak CD indicates a weaker interchromophore interaction in the linear dipeptides due to longer average interchromophore distances and/or an averaging of positive and negative CD spectra of a variety of conformations allowed for the linear dipeptides in solution. Absorption coefficients of the two cyclic dipeptides (Fig. 2) are smaller than those of the linear dipeptides (Fig. 3), especially for the 2-naphthyl derivatives. The hypochromicity indicates a stronger interchromophore interaction in the cyclic dipeptides than in the linear ones, suggesting that the weak CD of linear dipeptides is caused not by the averaging of positive and negative CD curves but by a weak interchromophore interaction in the linear dipeptides.

The weak chromophoric interaction in the linear dipeptides suggests that the dipeptides are in extended conformations in TMP. Rizzo and Jäckle[28] reported that linear aromatic dipeptides, such as Ac-(Trp)$_2$-NHMe, Ac-(Phe)$_2$-NHMe, and Ac-(Tyr)$_2$-NHMe, are in folded conformations in a protic solvent, 2,2,2-trifluoroethanol, and in extended ones in an aprotic solvent, tetrahydrofuran. Although it is impossible to test the above rule in the present case due to the limited solubility, the extended conformations suggested for the linear dipeptides of napAla's in TMP, which is an aprotic solvent, do not contradict the above rule.

Figure 4 shows absorption and CD spectra of c(Phe)$_2$ in TMP. A moderately strong exciton couplet is observed around 195 nm, which corresponds to the ^1B_b absorption band of the phenyl group. The interpretation of the sign of the exciton couplet of c(Phe)$_2$ is somewhat difficult due to the complexity in the direction of the ^1B_b transition moment.[29]

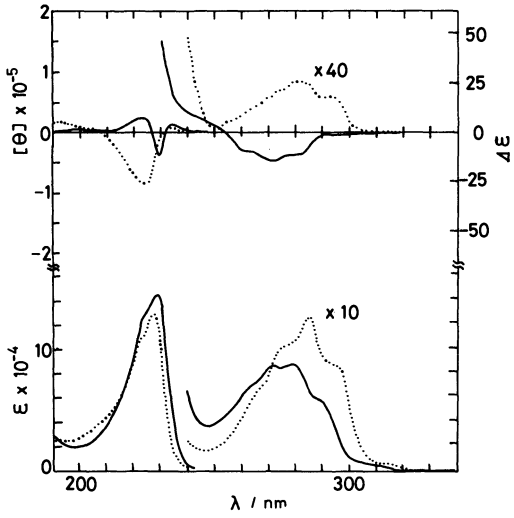

Fig. 3. CD (top) and absorption (bottom) spectra of Ac-(1-napAla)$_2$-OMe (·····) and Ac-(2-napAla)$_2$-OMe (——) in trimethyl phosphate at 25 °C. [θ] and ε are calculated with respect to two naphthyl chromophores.

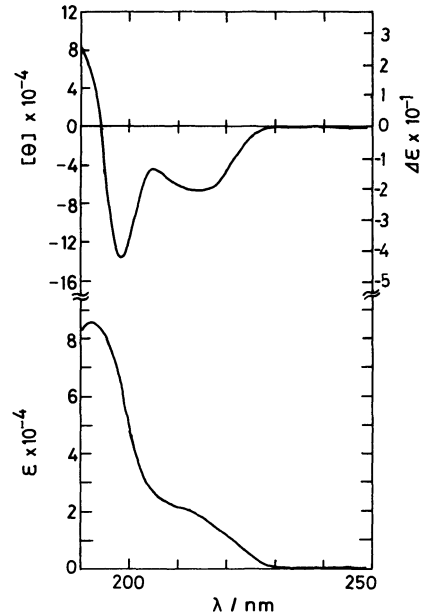

Fig. 4. CD (top) and absorption (bottom) spectra of c(Phe)$_2$ in trimethyl phosphate at 25 °C. [θ] and ε are calculated with respect to two phenyl chromophores.

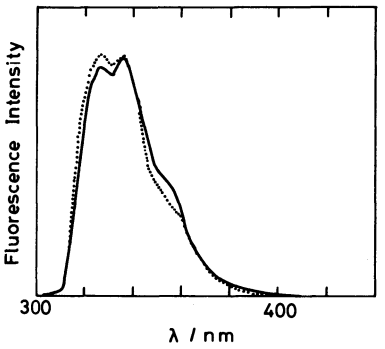

Fig. 5. Fluorescence spectra of c(l-napAla)$_2$ (·····) and c(2-napAla)$_2$ (——) in N_2-bubbled *N,N*-dimethylformamide at 25 °C. Excitation wavelength=285 nm.

Fluorescence Spectra and Fluorescence-Detected Circular Dichroism. Figure 5 shows fluorescence spectra of c(1- and 2-napAla)$_2$'s in DMF. No excimer emission was observed in the two cyclic dipeptides, indicating the inaccessibility of the two naphthyl groups connected to the 2,5-piperazinedione ring. Excimer emission was not detected even at low temperatures down to −50 °C for the two c(napAla)$_2$'s. This contrasts the case of *cis*-1,2-di(2-naphthyl)cyclobutane,[3] in which excimer emission has not been detected at room temperature, but observed at low temperatures (−20—−80 °C). The absence of excimer emission in the cyclic dipeptides indicates the rigidity of the skeletal and side-chain conformations and excludes the possibility of the folded(g$^+$)–folded(g$^+$) symmetrical side-chain conformation in the cyclic dipeptides.

No excimer was found also in linear dipeptides of 1- and 2-napAla's in DMF, suggesting, again, the extended conformation of the linear dipeptides in such aprotic solvents as TMP and DMF.

The absence of excimers in cyclic dipeptides does not contradict the observation of strong exciton couplet in CD spectra. In the latter case, one naphthyl group in the ^1B_b excited Franck-Condon state interacts with another naphthyl group, which is in the ground state, mainly by a dipole–dipole mechanism. In the case of excimer, one naphthyl group in the lowest ^1L_b excited state interacts with another naphthyl group by a mechanism including an electron-exchange interaction. The excimer formation requires a considerable distortion of molecular configuration to keep the two chromophores close to each other within ca. 3.5 Å.

The absence of strong interchromophore interaction in the lowest excited state is also evident from FDCD spectra shown in Fig. 6. FDCD spectroscopy measures a difference in fluorescence intensities (I_L^{ex}, I_R^{ex}) when excited by left- and right-circularly polarized lights, respectively, and are represented by the Kuhn's excitation dissymmetry factor g_{ex}.[7]

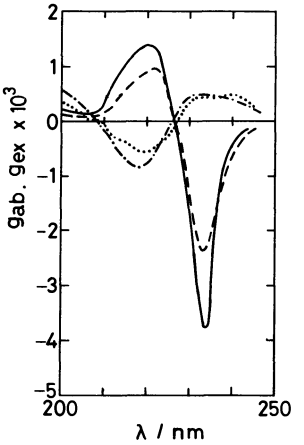

Fig. 6. FDCD spectra (g_{ex}) of c(l-napAla)$_2$ (·····) and c(2-napAla)$_2$ (----), and absorption CD spectra (g_{ab}) of c(l-napAla)$_2$ (—·—) and c(2-napAla)$_2$ (——) in trimethyl phosphate at 25 °C.

$$g_{ex} = 2(I_L^{ex} - I_R^{ex})/(I_L^{ex} + I_R^{ex})$$

The excitation dissymmetry factor should be compared with the absorption dissymmetry factor g_{ab}, calculated from CD and absorption spectra of the same sample.

$$g_{ab} = 2(\varepsilon_L - \varepsilon_R)/(\varepsilon_L + \varepsilon_R)$$

ε_L and ε_R are the absorption coefficients for left- and right-circularly polarized lights, respectively.

In Fig. 6, the absorption and the excitation dissymmetry factors of c(napAla)$_2$ coincides with each other within an experimental error, indicating the absence of any particular conformation which fluoresces predominantly. In other words, all conformers of c(l-napAla)$_2$ fluoresce equally. This, in turn, suggests the absence of any particular interaction between the naphthyl groups in the lowest excited state. The conclusion should be somewhat modified in the case of c(2-napAla)$_2$. In this case the excitation dissymmetry factor is a little smaller than the absorption dissymmetry factor, especially at the negative lobe. The smaller g_{ex} may indicate that the conformation which shows an intense CD, fluoresces less strongly than other conformers. Presumably, a conformation in which the two naphthyl groups are close to each other induces a strong exciton couplet but fluoresces little due to an enhanced nonradiative process caused by some interchromophoric interactions. However, the interaction is so small that the whole profile of the FDCD spectrum remains unchanged.

Conclusions

Possible conformations of c(1- and 2-napAla)$_2$'s are illustrated in Fig. 7. The folded(g$^+$)-unfolded(g$^-$)

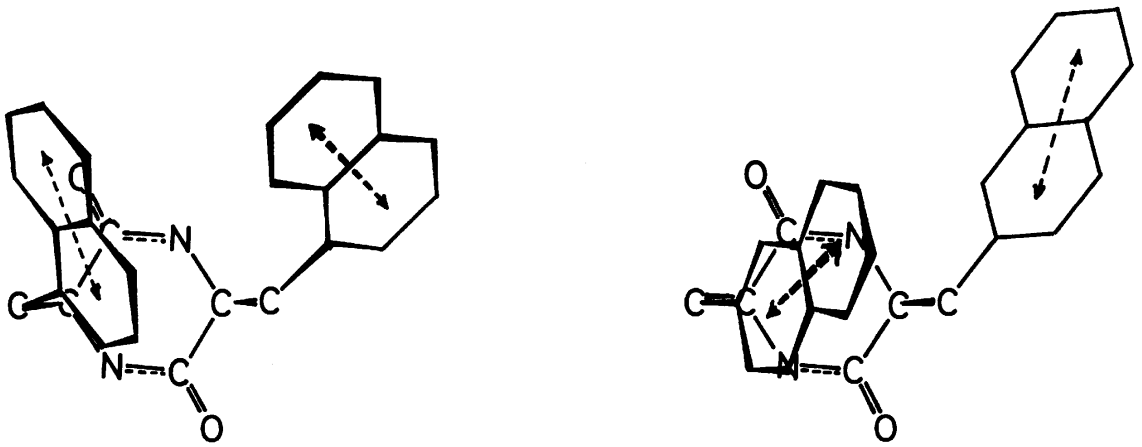

Fig. 7. Possible conformations of c(1-napAla)$_2$ (left) and c(2-napAla)$_2$ (right). The dashed arrows indicate directions of the ^1B_b transition moments.

asymmetric conformation is suggested by the ^1H NMR data and by the absence of excimer emission. The screw sense of the arrangement of the ^1B_b absorption transition moments of the two naphthyl groups is right-handed for c(1-napAla)$_2$ in a conformation which contributes most significantly to CD spectrum. It is left-handed for c(2-napAla)$_2$. The center-to-center interchromophoric distances are 6—7 Å. No particular interaction in the lowest excited state has been detected in the fluorescence and the FDCD spectra.

This work is partly supported by the Grant-in-Aid for Scientific Research No. 59550626, from the Ministry of Education, Science and Culture.

References

1) S. N. Semerak and C. W. Frank, *Adv. Polym. Sci.*, **54**, 31 (1983).
2) H. Masuhara, H. Shioyama, N. Mataga, T. Inoue, N. Kitamura, T. Tanabe, and S. Tazuke, *Macromolecules*, **14**, 1738 (1981).
3) S. Ito, M. Yamamoto, and Y. Nishijima, *Bull. Chem. Soc. Jpn.*, **57**, 3295 (1984).
4) P. Tundo and J. H. Fendler, *J. Am. Chem. Soc.*, **102**, 1760 (1980).
5) F. S. Richardson and J. P. Riehl, *Chem. Rev.*, **77**, 773 (1977).
6) M. Sisido, S. Egusa, A. Okamoto, and Y. Imanishi, *J. Am. Chem. Soc.*, **105**, 3351 (1983).
7) S. Egusa, M. Sisido, and Y. Imanishi, *Macromolecules*, **18**, 882 (1985).
8) K. D. Kopple and D. H. Murr, *J. Am. Chem. Soc.*, **89**, 6193 (1967).
9) K. D. Kopple and M. Ohnishi, *J. Am. Chem. Soc.*, **91**, 962 (1969).
10) H. Edelhoch and R. E. Lippoldt, *J. Biol. Chem.*, **243**, 4799 (1968).
11) E. H. Strickland, M. Wilchek, J. Horwitz, and C. J. Billups, *J. Biol. Chem.*, **245**, 4168 (1970).
12) P. E. Grebow, and T. M. Hooker, Jr., *Biopolymers*, **14**, 1863 (1975).
13) J. W. Snow and T. M. Hooker, Jr., *Biopolymers*, **16**, 121 (1977).
14) W. Radding, B. Donzel, N. Ueyama, and M. Goodman, *J. Am. Chem. Soc.*, **102**, 5999 (1980).
15) E. Benedetti, R. E. Marsh, and M. Goodman, *J. Am. Chem. Soc.*, **98**, 6676 (1976).
16) M. Sisido, S. Egusa, and Y. Imanishi, *J. Am. Chem. Soc.*, **105**, 1041 (1983).
17) M. Sisido, S. Egusa, and Y. Imanishi, *J. Am. Chem. Soc.*, **105**, 4077 (1983).
18) J. Kobayashi, T. Higashijima, S. Sekido, and T. Miyazawa, *Int. J. Pept. Protein Res.*, **17**, 486 (1981).
19) IUPAC-IUB Committee, *Biochemistry*, **18**, 3471 (1970).
20) V. F. Bystrov, V. T. Ivanov, S. L. Portonava, T. A. Balashova, and Y. A. Ovchinnikov, *Tetrahedron*, **29**, 873 (1973).
21) G. N. Ramachandran, R. Chandrasekaran, and K. D. Kopple, *Biopolymers*, **10**, 2113 (1971).
22) M. T. Chung, M. Marraud, and J. Neel, *Macromolecules*, **7**, 606 (1974).
23) E. Benedetti, M. Goodman, R. E. Marsh, H. Rapoport, and J. A. Musich, *Cryst. Struct. Commun.*, **4**, 641 (1975).
24) K. G. R. Pachler, *Spectrochim. Acta*, **20**, 581 (1964).
25) J. V. Hatton and R. E. Richards, *Mol. Phys.*, **3**, 253 (1960).
26) M. Sisido and Y. Imanishi, unpublished work.
27) N. Harada and K. Nakanishi, "Circular Dichroic Spectroscopy—Exciton Coupling in Organic Stereochemistry," University Sci. Books, N. Y. and Tokyo Kagaku Dojin, Tokyo (1982).
28) V. Rizzo and H. Jäckle, *J. Am. Chem. Soc.*, **105**, 4195 (1983).
29) K. Shingu, S. Imajo, H. Kuritani, S. Hagishita, and K. Kuriyama, *J. Am. Chem. Soc.*, **105**, 6966 (1983).

 © 1986 The Chemical Society of Japan Bull. Chem. Soc. Jpn., 59, 2203—2207 (1986)

Stereochemistry of Hydroxymethylations of *N*-Salicylideneglycyl Dipeptide Copper(II) Complexes. A Kinetically and Also Thermodynamically Controlled Reaction

Kaoru HARADA,* Shinnichiro SUZUKI,† Hideyuki NARITA, and Hiroshi WATANABE
Department of Chemistry, University of Tsukuba, Niihari-gun, Ibaraki 305
(Received February 18, 1986)

(*N*-Salicylideneglycyl-L-valinato)copper(II) or (*N*-salicylideneglycyl-L-isoleucinato)copper(II) was treated with formaldehyde in an aqueous solution under relatively mild conditions. It was found that the resulting seryl residue was D-configuration in the early stage of the reaction. However, the configuration was inverted from D- to L-form after prolonged reaction. The epimerization reactions of authentic (*N*-salicylideneglycyl-D- or L-seryl-L-isoleucinato)copper(II) were carried out under similar conditions. These results indicate that the reaction as a whole is controlled kinetically as well as thermodynamically.

Nonenzymatic pyridoxal-catalyzed reactions of amino acids have been studied.[1-7] These are transamination, decarboxylation, racemization, and α-β bond cleavage (or formation) of α-amino acids. In these reactions, the metal complexes of the Schiff bases of amino acids with pyridoxal have been considered to be the key compounds. The presence of metal ion contributes to the formation of the Schiff base, and the resulting metal complex which has a planar geometry, facilitates the various reactions in the molecule. Because of the electron-attracting property of the metal ion in the complex, the chemical bonds around the α-carbon atom of the amino acid are activated and therefore show various interesting chemical properties in the nonenzymatic pyridoxal-catalyzed reactions of amino acids (Scheme 1).

Several studies on the activation of the α-carbon of amino acids or peptides by the formation of metal complexes have been reported. The reaction of acetaldehyde with glycine copper(II) complex in alkaline aqueous solution resulted in the formation of threonine and allothreonine.[8-11] The reaction of formaldehyde with glycylglycine copper(II) complex gave serylglycine.[12] The reaction of acetaldehyde with triglycine copper(II) complex also occurred to form threonylglycylglycine and allothreonylglycylglycine.[13]

It has been known that the reactions of aldehydes with the copper(II) complex of the Schiff base of glycine with salicyl aldehyde [aqua(*N*-salicylideneglycinato)copper(II)] proceeded smoothly to form hydroxy amino acids.[14] Alkyl halides[15] and acrylonitrile[16] react with the complex to form α-amino acids. These results indicate that the methylene group adjacent to the azomethine group in the copper complex is activated as in the pyridoxal-catalyzed reactions.[17]

In this study employing the chemical properties of *N*-salicylidene amino acid copper(II) complex, an asymmetric synthesis of a seryl residue was carried out by the hydroxymethylation of (*N*-salicylideneglycyl-L-valinato)copper(II) complex (complex **1**) under relatively mild aqueous conditions (pH 8.5, 45—80 °C) (Scheme 2). The time courses of the reaction were studied. A part of the work was already published as a short communication.[18]

When glycyl-L-valine was used, the formation of D-seryl-L-valine was larger than the corresponding diastereomer in the beginning of the reaction. Prolonged reaction, however, resulted in the formation of L-seryl-L-valine in the reaction mixture. In the case of *N*-salicylideneglycyl-L-isoleucine copper(II) complex (complex **2**), D-seryl-L-isoleucine was formed in the initial stage of the reaction, but the amount of L-seryl-L-isoleucine increased with the reaction time. The formation of D-seryl-L-valine or D-seryl-L-isoleucine in the beginning of the reaction could be explained as a sterically controlled asymmetric Knoevenagel type reaction to the glycine residue. Formaldehyde attacked the methylene group of the copper(II) complex from the less bulky side of the

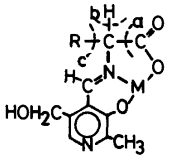

a: Decarboxylation
b: Racemization, transamination
c: α,β Bond cleavage (or formation)

Scheme 1.

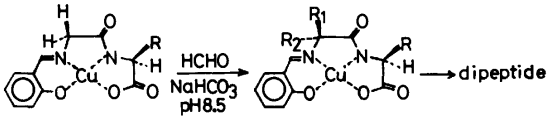

Complex 1
Cu(sal=Gly-L-Val),
R: -$CH(CH_3)_2$
Complex 2
Cu(sal=Gly-L-Ileu),
R: -$CH(CH_3)C_2H_5$

R_1=H, R_2=CH_2OH
Cu(sal=D-Ser-L-Val)
Cu(sal=D-Ser-L-Ileu)
R_1=CH_2OH, R_2=H
Cu(sal=L-Ser-L-Val)
Cu(sal=L-Ser-L-Ileu)

Scheme 2.

† Present address: Institute of Chemistry, College of General Education, Osaka University, Toyonaka, Osaka 560.

Table 1. Time Course of the Reaction of Complex **1** with Formaldehyde

Temp °C	Time h	Ser-L-Val/% D-L	Ser-L-Val/% L-L	Total yield/%	Optical purity of Ser[a]/%	HMSV[b] %	Recovery of Gly-L-Val/%
45	12	8.9	7.2	16.1	11 (D-L)	—	70.8
	25	17.7	14.4	32.1	10 (D-L)	—	26.4
	50	28.8	25.3	54.1	6.5 (D-L)	2	18.5
	75	29.3	26.3	55.6	5.4 (D-L)	2	10.3
	100	35.6	32.2	67.8	5.0 (D-L)	4	8.1
80	1	15.5	13.2	28.7	8.0 (D-L)	—	72.0
	2	24.6	22.7	47.3	4.0 (D-L)	0.7	51.8
	4	32.7	32.1	64.8	0.9 (D-L)	2	23.5
	6	39.1	39.2	78.3	0.1 (L-L)	4	13.7
	12	32.0	38.4	70.4	9.1 (L-L)	10	1.8
	25	16.0	22.4	38.4	16.7 (L-L)	20	Trace
	50	1.9	2.9	4.8	21 (L-L)	25	Trace

a) Optical purity $= |(\text{D-L}-\text{L-L})/(\text{D-L}+\text{L-L})| \times 100\%$. b) α-(Hydroxymethyl)seryl-L-valine.

planar molecule (from back side of the paper in Scheme 2).

Small amounts of the reaction mixture of Cu(sal=Gly-L-Val) and formaldehyde were withdrawn during the reaction, being treated with acid to decompose the copper complex. The resulting two diastereomers, D-seryl-L-valine and L-seryl-L-valine, and unchanged glycyl-L-valine were detected by an amino acid analyzer. The results are summarized in Table 1. The yields of seryl-L-valine increased up to 68% under the reaction conditions at 45 °C for 100 h, but the optical purities of D-serine residue decreased from 11 to 5%. At 80 °C, total yields of newly formed seryl-L-valine increase up to 78% after 6 h and then decrease gradually. In the early stage of the reaction, excess of D-seryl-L-valine was found in the reaction mixture. After 6 h, however, the content of L-seryl-L-valine increased. The increase of L-seryl-L-valine could be explained by the epimerization of the seryl residue in the dipeptide complex. The recovery of unchanged glycyl-L-valine decreased gradually and became trace amount after prolonged reaction at 80°C.

Table 2 shows the time course of the reaction of (*N*-salicylideneglycyl-L-isoleucinato)copper(II) (complex **2**) with formaldehyde at 60, 70, and 80 °C. At 60 °C, the yield of seryl-L-isoleucine reaches 63% after 15 h and the configuration of the newly formed seryl residue is D-form in the early stage of the reaction. Inversion of the configuration from D to L, however, takes place after 18 h as in the reaction of the glycyl-L-valine complex and the ratio of L-L-dipeptide to D-L-dipeptide increases gradually after longer reaction time. Similar behaviors were observed in the reactions at 70 and 80 °C. An unknown peak was detected in the reaction mixture on prolonged reaction by an amino acid analyzer. The hydrolysis of the reaction mixture showed the increase of the peak of α-(hydroxymethyl)serine. Therefore, the peak which is eluted more rapidly than the peaks of glycyl-amino acids and seryl-amino acids, was assumed to be due to α-(hydroxymethyl)seryl-L-valine (HMSV) and α-(hydroxymethyl)seryl-L-isoleucine (HMSI). Tables 1 and 2 show that the yields of HMSV and HMSI increase steadily depending on the reaction time, and the yield reaches about 20% at 80 °C. Small amounts of free amino acids such as serine, glycine, and valine or isoleucine were also found in the reaction mixtures. These amino acids formed by the hydrolysis of dipeptides during the reaction increased slowly with the reaction time. Thus the decrease of the total yield of seryl dipeptides could be caused by 1) hydrolysis of dipeptides, 2) formation of α-(hydroxymethyl)seryl dipeptides, and 3) decarboxylation, deamination, and other degradation of dipeptides.

After the reaction of complex **1** or **2** with formaldehyde, the reaction mixture was decomposed with acid and the resulting dipeptides were hydrolyzed. The amino acid mixtures were treated with 2,4-dinitroflouorobenzene and the resulting 2,4-dinitrophenyl derivatives of valine and isoleucine were separated by Celite column chromatography. The specific rotations showed that those derivatives were almost optically pure. The amino acid analysis of the hydrolyzed isoleucine exhibited no peak of alloisoleucine which would be generated by epimerization. These findings indicate that the epimerization of the dipeptide takes place only at the N-terminal amino acid and does not take place at the C-terminal of the dipeptide complex. The (D-L)-complex which is the major product of the asymmetric Knoevenagel type reaction in the early stage of the reaction, is epimerized to the (L-L)-complex under the conditions employed in the reaction, as shown in Scheme 3.

Table 2. Time Course of the Reaction of Complex **2** with Formaldehyde

Temp °C	Time h	Ser-L-Ileu/% D-L	Ser-L-Ileu/% L-L	Total yield/%	Optical purity of Ser[a]/%	HMSI[b]/%	Recovery of Gly-L-Ileu/%
60	1	5.6	5.2	10.8	3.7 (D-L)	—	89.1
	4	17.1	14.6	31.7	7.9 (D-L)	—	65.4
	8	26.0	24.2	50.2	3.6 (D-L)	0.7	43.4
	12	30.5	29.0	59.5	2.5 (D-L)	1.2	26.4
	15	31.5	31.1	62.6	<1 (D-L)	1.6	22.0
	18	29.4	30.2	59.6	1.3 (L-L)	1.9	17.2
	24	25.5	26.9	52.4	2.9 (L-L)	2.9	9.1
	48	21.8	25.3	47.1	8.4 (L-L)	4.1	Trace
	72	12.1	17.3	29.4	17.5 (L-L)	4.3	Trace
70	1	12.4	11.0	23.4	6.0 (D-L)	—	73.6
	2	21.6	18.5	40.1	7.7 (D-L)	—	52.9
	3	25.8	22.9	48.7	6.0 (D-L)	1.4	37.5
	6	30.7	29.0	59.7	2.8 (D-L)	2.9	15.2
	8	31.7	31.6	63.3	<1 (D-L)	3.1	8.8
	10	31.2	33.0	64.2	2.8 (L-L)	3.5	5.4
	12	27.4	33.0	60.4	9.3 (L-L)	4.3	2.9
	24	15.5	22.4	37.9	18.2 (L-L)	6.7	Trace
80	1	18.3	15.7	34.0	7.7 (D-L)	—	63.3
	2	35.1	31.2	66.3	5.9 (D-L)	1.0	25.8
	3	37.0	36.9	73.9	<1 (D-L)	1.5	16.4
	6	30.4	34.2	64.6	5.9 (L-L)	4.2	4.2
	12	14.3	19.5	33.8	15.4 (L-L)	14.7	Trace
	24	10.6	15.5	26.1	18.8 (L-L)	20.7	Trace

a) Optical purity = $|(\text{D-L}-\text{L-L})/(\text{D-L}+\text{L-L})| \times 100\%$. b) α-(Hydroxymethyl)seryl-L-isoleucine.

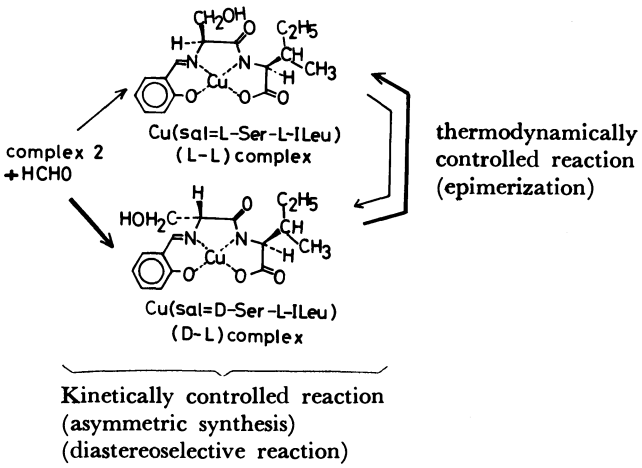

Scheme 3.

When the authentic *N*-salicylidene complexes composed of L-seryl-L-isoleucine and D-seryl-L-isoleucine were synthesized and treated at 80 °C in aqueous solution in the presence of sodium hydrogencarbonate, epimerization took place simultaneously. The time course of the reaction is shown in Table 3. Starting from (L-L)- or (D-L)-complex, epimerization reached an equilibrium after 24 h and the ratio of (L-L):(D-L) was about 6 : 4. Therefore it could be considered that the epimerization is a typical thermodynamically controlled reaction, and the first-order asymmetric transformation takes place between the two diastereomeric complexes in the reaction mixture.

The reason for the enrichment of (L-L)-complex in the equilibrium is unknown at the present stage, although the (L-L)-complex is usually considered to be less stable thermodynamically than the (D-L)-complex because of the steric repulsion between the two side chains of serine and isoleucine.

The asymmetric Knoevenagel type reaction of complex **1** or **2** with formaldehyde could be regarded as a kinetically controlled reaction. Therefore, the whole reaction is controlled by two different mechanisms, i.e. kinetically controlled reaction in the early stage of the reaction, which causes the formation of D-seryl dipeptides, and also thermodynamically controlled reaction which leads to the formation of L-seryl dipeptides in the later stage of the reaction.

Experimental

Preparation of Authentic Dipeptides. Glycyl-L-valine and glycyl-L-isoleucine were purchased from Sigma Chemical Company, St. Louis Mo. U.S.A. Authentic

Table 3. Epimerization of Diastereomeric Complexes

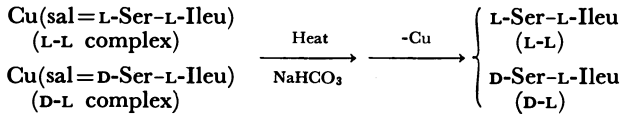

Temp/°C	Time/h	Cu(sal=L-Ser-L-Ileu)		Cu(sal=D-Ser-L-Ileu)	
		L-L/%	D-L/%	L-L/%	D-L/%
80	0.5	83.4	16.4	32.0	68.0
	1	81.0	19.0	44.5	55.5
	2	75.6	24.4	52.7	47.3
	3	72.7	27.3	53.5	46.5
	6	66.3	33.7	56.0	44.0
	12	58.0	42.0	57.9	42.1
	24	57.8	42.2	58.1	41.9

Table 4. Characterization of Dipeptides

Dipeptide	Mp(decomp) θ_m/°C	$[\alpha]_D$	Elemental analysis/%			
				C	H	N
L-Ser-L-Val	224—226	−1.4	Found	46.83	7.82	13.50
		(*c* 2.0, 1 M[a] HCl)	Calcd	47.04	7.89	13.71
D-Ser-L-Val	214—216	−28.3	Found	47.33	7.95	13.87
		(*c* 2.0, 1 M HCl)	Calcd	47.04	7.89	13.71
L-Ser-L-Ileu	202—203	−4.9	Found	49.82	8.19	12.88
		(*c* 1.0, Water)	Calcd	49.52	8.31	12.83
D-Ser-L-Ileu	212—213	−25.2	Found	49.74	8.16	12.83
		(*c* 1.0, Water)	Calcd	49.52	8.31	12.83

a) 1 M = 1 mol dm^{-3}.

seryl dipeptides were synthesized by coupling reactions of *N*-benzyloxycarbonyl-L- or D-serine and L-valine or L-isoleucine benzyl ester using dicyclohexylcarbodiimide. Coupled products were recrystallized from ethyl acetate and petroleum ether. The yields of the products are in a range of 75—87%. The *N*-benzyloxycarbonyl dipeptide ester (1.0 g) was dissolved in a mixture of *t*-butyl alcohol and water (7:3), and the solution was applied to catalytic hydrogenolysis with 5% palladium on charcoal (1.0 g) under 1 atmosphere of hydrogen at room temperature for 6 h. After the catalyst was removed by filtration, the filtrate was evaporated to dryness under reduced pressure, and the residue was recrystallized from water and ethanol. The properties of the synthesized dipeptides are listed in Table 4. These dipeptides are chromatographically pure and the retention times of glycyl and seryl dipeptides observed by an amino acid analyzer are summarized in Table 5.

Preparations of (*N*-Salicylideneglycyl-L-isoleucinato)copper(II) and (*N*-Salicylideneglycyl-L-valinato)copper(II). Glycyl-L-isoleucine (2.5 mmol) was dissolved in a mixture of water and ethanol (2:1). To this solution, freshly distilled salicylaldehyde (2.5 mmol) and copper(II) chloride (2.5 mmol) were added. Aqueous potassium hydroxide was added to the solution, and the pH was adjusted to about 10. The solution was stirred for 15 min at room temperature. After filtration, the filtrate was evaporated to dryness under reduced pressure and purplish needles were obtained. The product was recrystallized from hot water–ethanol. molecular formula: KCu(sal=Gly-L-Ileu)· 1.5H_2O; λ_{max} 558 nm(ε=185 M^{-1} cm^{-1}); Found: C, 42.66; H, 4.30; N, 6.77%; Calcd for $C_{15}H_{20}O_{5.5}N_2CuK$ C, 42.99; H, 4.82; N, 6.69%.

(*N*-Salicylideneglycyl-L-valinato)copper(II) was synthesized from glycyl-L-valine and bis(salicylaldehydato)copper(II) in a water–ethanol (2:1) mixture by adjusting the pH value to about 9, being isolated as barium salt. Found: C, 35.94; H, 4.52; N, 6.30%; Calcd for $C_{14}H_{22}O_{7.5}N_2CuBa_{0.5}$ C, 35.73; H, 4.72; N, 5.95%.

Hydroxymethylation of (*N*-Salicylideneglycyl-L-isoleucinato)copper(II) (Complex 2) The complex 2 (7.5×10^{-5} mol) was dissolved in 45 ml of water containing 1.5 mmol of $NaHCO_3$ and the pH of the solution was about 8.5. To this solution, 35% formaldehyde (9 mmol, 0.75 ml) was added and the reaction mixture was kept at a constant temperature under nitrogen atmosphere. During the reaction, small amounts of the sample was withdrawn from the reaction mixture, and the complex was decomposed with diluted hydrochloric acid. The resulting solution was applied to a Dowex 50 column. After the column was washed with water, peptides and amino acids were eluted with aqueous ammonia (1 mol dm^{-3}). The eluate was evaporated to dryness under reduce pressure. The residue was dissolved in water and an appropriate amount of the solution was applied to an amino acid analyzer to determine the diastereomeric ratio of the newly formed dipeptide and the amount of unchanged dipeptide. The

Table 5. Chromatographic Properties of Glycyl and Seryl Dipeptides[a)]

Dipeptide	Retention time/min	c-Value[b)]
Gly-L-Val	98	108
D-Ser-L-Val	78	106
L-Ser-L-Val	92	105
Gly-L-Ileu	128	114
D-Ser-L-Ileu	93	116
L-Ser-L-Ileu	120	118

a) Yanagimoto LC-5S amino acid analyzer; column, 0.8×50 cm; resin, cation-exchang resin SCX1001; elution buffer, pH 4.25 citrate buffer; temperature 53 °C. b) Observed constants for the integrations of peaks obtained by applying 1 μmol of each dipepeid.

hydroxymethylation of complex 1 was also carried out in a similar way.

Epimerization between (*N*-Salicylidene-L-seryl-L-isoleucinato)copper(II) and (*N*-Salicylidene-D-seryl-L-isoleucinato)-copper(II). *N*-Salicylidenedipeptide complexes were prepared by mixing of L- or D-seryl-L-isoleucine (7.5×10^{-5} mol), salicylaldehyde, and copper(II) chloride in an aqueous ethanol solvent with 45 ml of an aqueous solution of 1.5 mmol of $NaHCO_3$. The solution was kept at 80 °C for epimerization under nitrogen atmosphere. Small amounts of the reaction mixture were collected at varying times, being treated with a Dowex-50 column. The resulting peptides and amino acids were analyzed by an amino acid analyzer. The results are shown in Table 3.

References

1) R. H. Holm, "Inorganic Biochemistry," ed by G. L. Eichhorn, Elsevier Scientific Publishing Company, Amsterdam (1973), Vol. 2, Chap. 31.

2) H. Kuzuhara, T. Komatsu, and S. Emoto, *Tetrahedron Lett.*, **1978**, 3563.

3) Y. Tachibana, M. Ando, and H. Kuzuhara, *Chem. Lett.*, **1982**, 1765.

4) Y. Tachibana, M. Ando, and H. Kuzuhara, *Chem. Lett.*, **1982**, 1769.

5) K. Bernauer, R. Deschenaux, and T. Taura, *Helv. Chim. Acta*, **66**, 2049 (1983).

6) S. C. Zimmerman, A. W. Czarnik, and R. Breslow, *J. Am. Chem. Soc.*, **105**, 1694 (1983).

7) S. C. Zimmerman and R. Breslow, *J. Am. Chem. Soc.*, **106**, 1490 (1984).

8) M. Sato, K. Okawa, and S. Akabori, *Bull. Chem. Soc. Jpn.*, **30**, 937 (1957).

9) S. Akabori, T. T. Otani, R. Marshall, M. Winitz, and J. P. Greenstein, *Arch. Biochem. Biophys.*, **83**, 1 (1959).

10) J. A. Aune, P. Maldonado, G. Larcheres, and M. Pierrot, *J. Chem. Soc., Chem. Commun.*, **1970**, 1351.

11) L. Cassella, A. Pasini, R. Ugo, and M. Visca, *J. Chem. Soc., Dalton Trans.*, **1980**, 1655.

12) K. Noda, M. Bessho, T. kato, and N. Izumiya, *Bull. Chem. Soc. Jpn.*, **43**, 1834 (1970).

13) M. Fujioka, Y. Nakao, and A. Nakahara, *J. Inorg. Nucl. Chem.*, **39**, 1885 (1977).

14) K. Harada, and J. Ohashi, *J. Org. Chem.*, **32**, 1103 (1967).

15) A. Nakahara, S. Nishikawa, and J. Mitani, *Bull. Chem. Soc. Jpn.*, **40**, 2212 (1967).

16) T. Shono, Y. Yamashoji, and K. Shinra, *Bull. Chem. Soc. Jpn.*, **43**, 192 (1970).

17) T. Ichikawa, S. Maeda, T. Okamoto, Y. Araki, and Y. Ishido, *Bull. Chem. Soc. Jpn.*, **44**, 2779 (1971).

18) S. Suzuki, H. Narita, and K. Harada, *J. Chem. Soc., Chem. Commun.*, **1979**, 29.

The Synthesis of Dibenzo-Annelated Annulenes Using Reductive Coupling. Bisdehydrodibenzo[14]-, -[16]-, -[18]-, -[20]-, and -[22]annulene

Jūro Ojima,* Koji Yamamoto,†,* Tadahito Kato, Kazuyo Wada, Yoshiharu Yoneyama, and Emiko Ejiri
Department of Chemistry, Faculty of Science, Toyama University, Gofuku, Toyama 930
†Department of Chemistry, Faculty of Engineering Science, Osaka University, Toyonaka, Osaka 560
(Received February 19, 1986)

Bisdehydrodibenzo[14]-, -[16]-, -[18]-, -[20]-, and -[22]annulene were synthesized by intramolecular reductive couplings using a low-valent titanium reagent. These bisdehydrodibenzo-annulenes proved to be atropic from an examination of the ^{1}H NMR spectra.

The reductive coupling of carbonyl compounds with a low-valent titanium reagent, developed by McMurry[1] and modified by several workers,[2] provides a new synthetic tool for formation of carbon–carbon double bond, which enabled chemists synthesis of a vast variety of crowded[3] or twisted[4] olefines inaccessible by usual method. In 1977, McMurry and Kees showed the potential of the method in medium- and large-ring carbocyclic synthesis by preparing cycloalkenes.[5] This intrigued us for preparation of annulenes and dehydroannulenes which usually requires lengthy reaction steps. When we commenced the present study, there had been no reports of annulene synthesis by low-valent titanium reagent, although, recently, two reports of preparation of doubly bridged [16]-[6a] and [24]annulene[6b] have appeared. In this paper, we describe attempts to prepare annulenoannulene and annulenes, and a successful synthesis of dibenzo-annelated bisdehydro-[14]-, -[16]-, -[18]-, -[20]-, and -[22]annulenes, using reductive couplings of carbonyl compounds.

Results and Discussion

Firstly, we attempted an intramolecular reductive coupling of the cyclic diketone **5**, prepared as illustrated in Scheme 1, to obtain a tetrakisdehydro-[14]annuleno[14]annulene **6**, but this attempt was unsuccessful. Then, since we had it in mind that the [4*n*]annuleno[4*n*]annulenes have not yet been known[7] and one of the desired products should be the precursor **8** of tetrakisdehydro[16]annuleno[16]annulene, we tried an intramolecular reductive coupling of the acyclic ketone **7**,[8] but some attempts did not meet with success. Thus, since the couplings using **5** and **7** gave polymeric products, we used the dibenzo-fused acyclic ketones **9**[9] and **10**[10] which are more stable than the methylated ketones **5** and **7**. However, these attempts were also unsuccessful, which led us to use more reactive aldehydes than ketones. Then we attempted intramolecular couplings of the dialde-

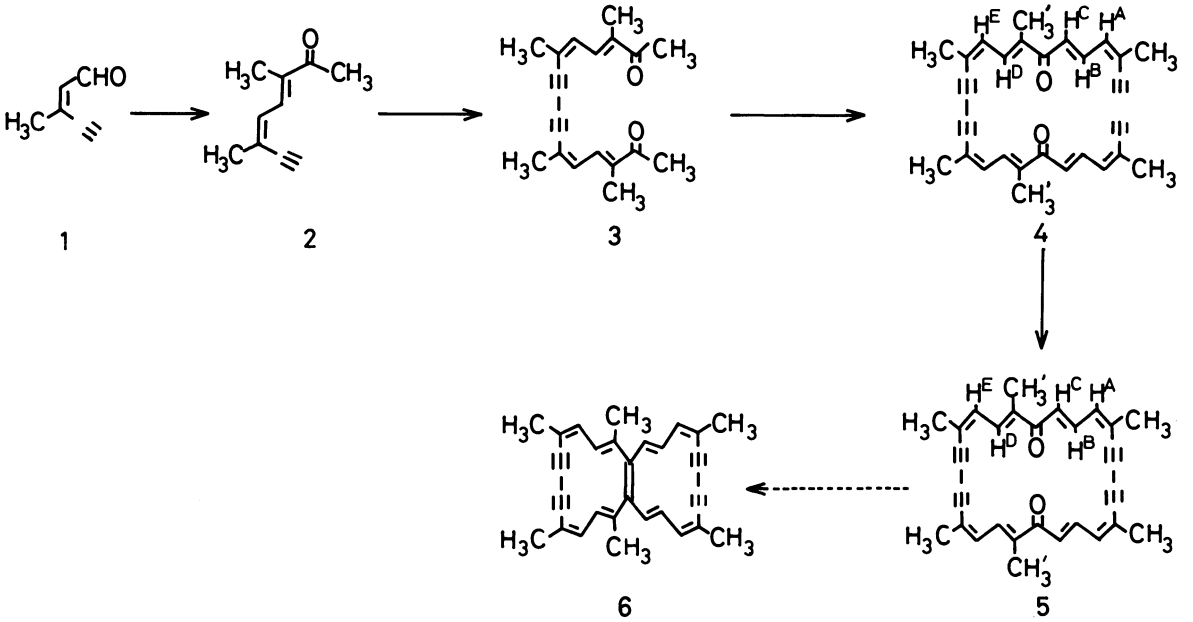

Scheme 1.

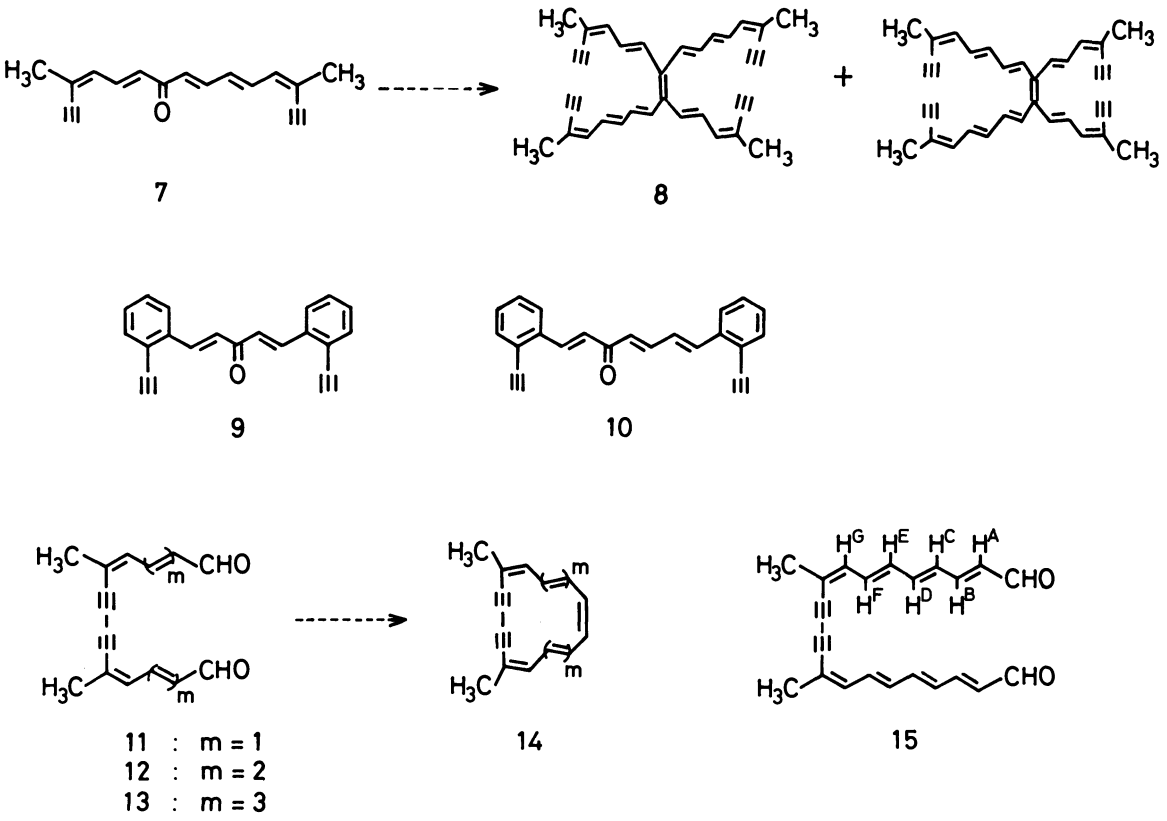

hydes **11**—**13**[11] to obtain the corresponding bisdehydroannulenes **14**; but the products of these reactions always gave only polymeric materials. Thus, since we learnd that these fully conjugated dialdehydes **11**—**13** or the products from them are insufferable against the reaction conditions employing $TiCl_3$ and $LiAlH_4$ in 1,2-dimethoxyethane, we tried to use the benzo-fused dialdehydes **20**, **22**—**26**. These dialdehydes were prepared by oxidative couplings of *o*-ethynylbenzaldehyde **16**[12] and/or its homologated aldehydes **17**—**19**.[13,14] The symmetrical dialdehydes **20**, **22**, **24**, and **26** were prepared from the corresponding monoaldehydes **16**—**18**, and **19**, respectively, in high yields, but the unsymmetrical dialdehydes **23** and **25** were obtained in moderate yields, since the symmetrical dialdehydes also formed. Rather surprisingly, we could not obtain the dialdehyde **21** by the oxidative coupling between **16** and **17** or by Wittig condensation with the dialdehyde **20** and 1.3 molar equivalent of [(1,3-dioxolan-2-yl)methyl]triphenylphosphonium bromide according to the procedure employed for the homologation of the aldehyde **16**.[13,14]

The intramolecular reductive couplings of these aldehydes **20**, **22**—**26** were carried out in the presence of $TiCl_3$ and $LiAlH_4$ in refluxing 1,2-dimethoxyethane under argon atmosphere, giving rise to the dibenzo-annelated bisdehydro[14]- **28**, -[16]- **29**, -[18]- **30**, -[20]- **31**, and -[22]annulene **32** in low yields. The didenzo[10]annulene **27** did not form from the dialdehyde **20**, presumably due to a severe steric strain expected for the structure.

The ^1H NMR chemical shifts of the dibenzoannulenes **28**—**32** thus obtained are listed in Table 1. The assignments of the resonances to the indiviual protons were made on the basis of multiplicities and coupling constants and the assumption that protons in a similar environment resonate at similar field, and were further clarified by the use of decoupling experiments where necessary. As we see from the Table 1, an examination of the chemical shifts suggests that these benzo-annelated annulenes **28**—**32** are atropic, since the high- or low-field shifts due to the olefinic inner or outer protons are not observed.

In conclusion, the results from this study indicate that the effectiveness of the reductive coupling in annulene synthesis greatly depends on the stability of the used conjugated carbonyl compounds and the products derived from them.

Experimental

All melting-points are uncorrected. IR spectra were measured on Hitachi 260-50 spectrophotometer as KBr disks; only significant maxima are reported. Electronic spectra were taken on Hitachi 220A spectrophotometer and recorded in nm. ε-Values are given in parentheses, shoulders being denoted by sh. Mass spectra were measured with JEOL JMS-D 200 spectrometer at 75 eV using a direct inlet system. ^1H NMR spectra were taken on JEOL FX-90Q (90 MHz) or Varian XL-200 (200 MHz) or

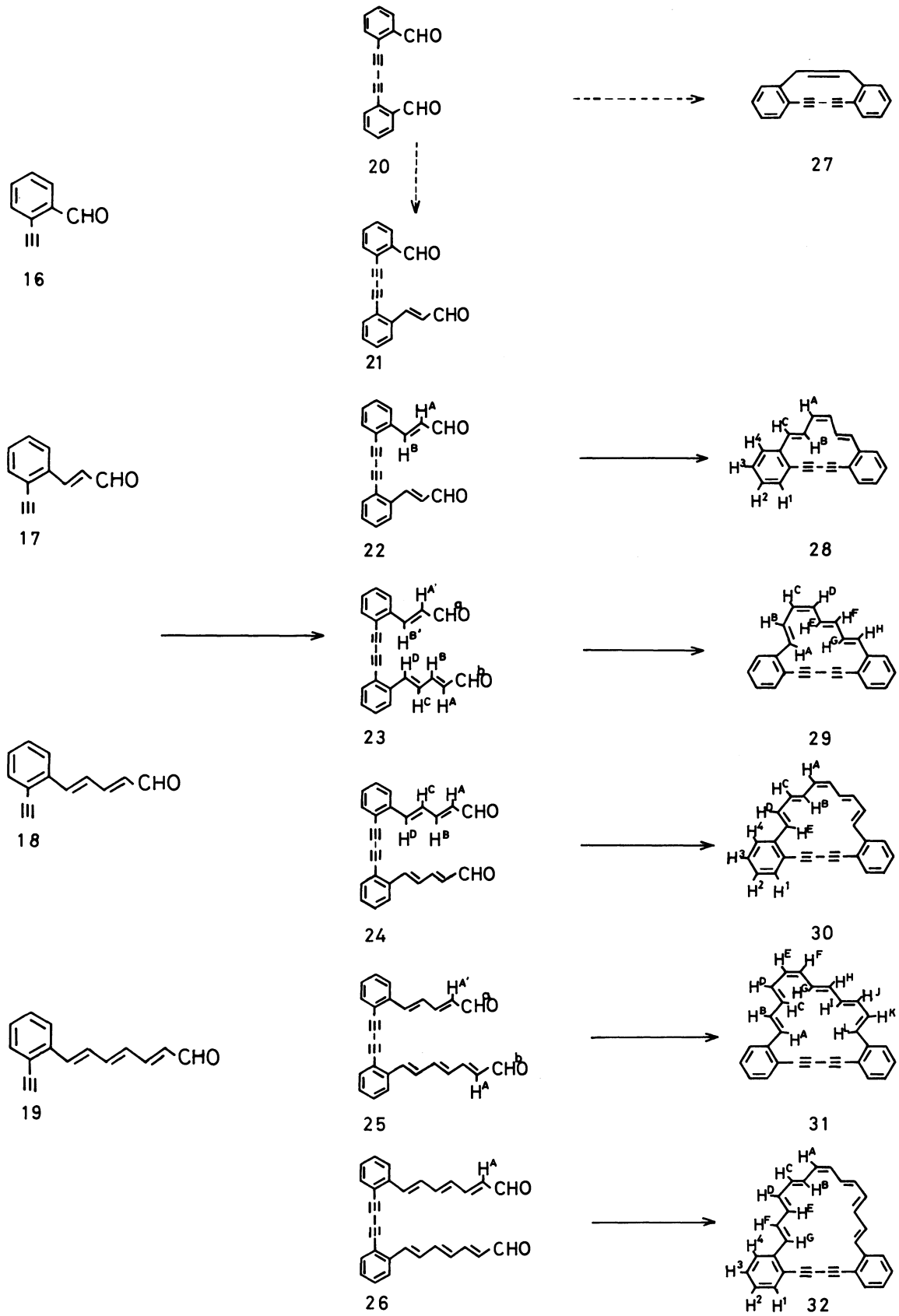
CHO
16
17
18
19
20
21
22
23
24
25
26
27
28
29
30
31
32

Table 1. ^{1}H NMR Chemical Shifts of Dibenzo-Annelated Annulenes **28**—**32** (in $CDCl_3$), Determined at 21 °C (τ Value; Internal Standard, Me_4Si)

Compd	H^A	H^B	H^C	H^D	H^E	H^F	H^G	H^H	H^I	H^J	H^K	H^L	Benzenoid H
[14]-**28**[a]	3.00—3.13	3.20—3.37	2.83										2.14—2.66
[16]-**29**[a]	1.63	(2.42—3.10)	4.18	3.99	1.08	3.96	1.11	(2.42—3.10)					(2.42—3.10)
[18]-**30**[b]	(3.26—3.34)	3.73	(3.26—3.34)	2.76	3.68								(2.01—2.62)
[20]-**31**[b]	1.75	(3.22—3.50)	2.28	(3.69—4.02)	4.30	(3.69—4.02)		(3.22—3.50)	1.54	(3.22—3.50)	(3.69—4.02)	1.52	2.61—2.98
[22]-**32**[a]	(3.30—3.54)	3.80	(3.30		3.52)	2.60	3.70						2.02—2.68

a) At 200 MHz. b) At 270 MHz.

JEOL GX-270 (270 MHz) spectrometer, and refer to solutions in $CDCl_3$, in τ-values with TMS as an internal standard. The coupling constants (J) are given in Hz. Alumina (II-III) or silica-gel (Merck) was used for column chromatography. Progress of most reactions was followed by TLC using Merck precoated silica-gel. Tetrahydrofuran (THF) and 1,2-dimethoxyethane (DME) were distilled from sodium benzophenone under nitrogen atmosphere before use. The organic extracts were dried over anhyd sodium sulfate or magnesium sulfate prior to solvent removal.

3,6-Dimethyl-3,5-octadien-7-yn-2-one (2). This compound was prepared from 3-methyl-2-penten-4-ynal (**1**)[15] and 2-butanone as reported.[16]

3,6,11,14-Tetramethyl-3,5,11,13-hexadecatetraene-7,9-diyne-2,5-dione (3). A soln of the ketone **2** (4.40 g, 30 mmol) in methanol (42 ml) was added dropwise to a stirred soln of copper(II) acetate monohydrate (12.2 g) in pyridine (142 ml) and methanol (142 ml) during 45 min at room temp. After stirring for a further 3.5 h at the same temp, the reaction mixture was poured into water and extracted with benzene. The extracts were washed with 7% hydrochloric acid until it turned acidic, and then with aq sodium hydrogencarbonate, and dried. The residual red liquid, after solvent removal, was chromatographed on alumina (4.0×6.0 cm). The fractions eluted with benzene gave the diketone **3** (3.51 g, 80%). Recrystallization from methanol afforded yellow needles: Mp 111—113 °C (lit,[16] mp 110—112 °C).

3,8,11,16,19,24-Hexamethyl-3,5,8,10,16,18,21,23-hexaicosaoctaene-1,12,14,25-tetrayne-7,20-dione (4). A soln of the aldehyde **1** (2.60 g, 27.6 mmol) in dry benzene (8 ml) was added dropwise during 10 min to an ice-cooled, stirred soln of the diketone **3** (2.00 g 6.80 mmol) in dry benzene (40 ml) containing ethanolic sodium ethoxide (11 ml), prepared from sodium (750 mg) and abs ethanol (50 ml). After stirring for a further 4.5 h under an ice-bath, the reaction was quenched by addition of acetic acid. Then the mixture was poured onto water and extracted with benzene. The extracts were washed with aq sodium hydrogencarbonate soln and brine, and dried. The residual dark red liquid, after solvent removal, was chromatographed on alumina (4.0×12.0 cm). The fractions eluted with hexane–ether (1:1) gave the diketone **4** (2.21 g, 72.8%). Recrystallization from hexane–benzene afforded yellow needles : Mp 114 °C (decomp); MS m/z 446 (M^+, 3%) and 78 (100); mol wt 446.5; IR 3300, 3240 (-C≡CH), 2200, 2100 (-C≡C-), 1640 (C=O), 1595 (C=C), and 995 cm^{-1} (trans C=C); UV_{max} (THF) 246 sh (24200), 258 sh (26700), 284 (27000), 302 sh (27300) 353 (35400), 385 (34500), 420 nm sh (19800); ^{1}H NMR (90 MHz) τ=2.25 (dd, 15, 12, 2H, H^B), 2.50 (d, 12, 2H, H^D), 3.15 (d, 15, 2H, H^C), 3.18 (d, 12, 2H, H^A or H^E), 3.53 (d, 12, 2H, H^A or H^E), 6.57 (s, 2H, -C≡CH), 7.90 (s, 6H, CH_3'), and 8.03 (s, 12H, CH_3).

Found: C, 85.13; H, 6.80%. Calcd for $C_{32}H_{30}O_2$:C, 86.06; H, 6.77%. Attempts to improve the elemental analysis failed.

2,5,10,13,18,23-Hexamethyl-2,4,10,12,15,17,23,25-cyclohexaicosaoctaene-6,8,19,21-tetrayne-1,14-dione (5). A soln of the acyclic diketone **4** (6.00 g, 13.4 mmol) in ether (80 ml), methanol (80 ml), and pyridine (200 ml) was added dropwise during 11 h to a stirred, refluxing mixture of anhyd copper(II) acetate (20 g) in ether (1200 ml), methanol (400 ml), and pyridine (1400 ml) at 50 °C, using high-dilution apparatus. After being refluxed for a further 1 h,

the mixture was allowed to stand overnight at room temp. Then the mixture was concentrated to ca. 400 ml under reduced pressure below 35 °C, and the concentrate was worked up as for the isolation of **3**. The residual dark red liquid, after solvent removal, was chromatographed on alumina (4.0×10.0 cm). The fractions eluted with ether–benzene (1:1) gave the cyclic diketone **5** (1.50 g, 25%). Recrystallization from chloroform–ethanol afforded yellow needles: Mp 120 °C (decomp); MS *m/z* 444 (M^+, 25%) and 178 (100); mol wt 444.5; IR 2180 (-C≡C-), 1635, 1610, 1590, 1570, (C=O, C=C), 985, and 970 cm^{-1} (trans C=C); UV_{max} (THF) 253 (29500), 291 (31900), 329 sh (43900), 350 (47900), and 403 nm sh (15800); ^1H NMR (200 MHz) τ=2.45 (d, 11, 2H, H^D), 2.47 (dd, 16, 11, 2H, H^B), 3.20 (d, 11, 2H, H^A or H^E), 3.43 (d, 11, 2H, H^A or H^E), 3.54 (d, 16, 2H, H^C), 7.94 (s, 6H, CH_3'), and 7.97 (s, 12H, CH_3).

Found: C, 86.23; H, 6.31%. Calcd for $C_{32}H_{28}O_2$:C, 86.45; H, 6.35%.

An Intramolecular Reductive Coupling of The Cyclic Diketone 5. The reaction was carried out under the same conditions as those described below for the dialdehyde **23**; however no monomeric product was obtained.

3,13-Dimethyl-3,5,8,10,12-pentadecapentaene-1,14-diyn-7-one (7). This compound was prepared as reported.[8]

1,5-Bis(*o*-ethynylphenyl)-1,4-dien-3-one (9) and 1,7-Bis(*o*-ethynylphenyl)-1,4,6-heptatrien-3-one (10). These compounds were prepared as reported.[9,10]

Intermolecular Reductive Couplings of The Ketones 9 and 10. These reactions were also carried out under the same conditions as those employed for the dialdehyde **22** (vide infra); however no dimeric product was obtained.

5,10-Dimethyl-2,4,10,12-tetradecatetraene-6,8-diynedial (11) and 7,12-Dimethyl-2,4,6,12,14,16-octadecahexaene-8,10-diynedial (12). The dialdehydes **11** and **12** were prepared as reported.[11]

9,14-Dimethyl-2,4,6,8,14,16,18,20-docosaoctaene-10,12-diynedial 15 (13: *m*=3). A soln of 9-methyl-2,4,6,8-undecatetraene-10-ynal[11] (2.47 g, 14.3 mmol) in pyridine (39 ml) and methanol (39 ml) was added dropwise during 40 min to a stirred soln of copper(II) acetate monohydrate (19.2 g) in pyridine (155 ml) and methanol (155 ml) at 16 °C. After stirring overnight at room temp, the reaction mixture was worked up as in the preparation of **3**. The residual red liquid, after solvent removal, was chromatoraphed on alumina (4.0×9 cm). The fractions eluted with ether gave the dialdehyde **15** (960 mg, 39.1%). Recrystallization from hexane–benzene afforded red cubes: Mp 164—166 °C; MS *m/z* 342 (M^+, 28%) and 81 (100); mol wt 342.4; IR 2170 (-C≡C-), 1675 (-CHO), 1610, 1590, 1570 (C=C), 1010, and 990 cm^{-1} (trans C=C); UV_{max} (THF) 254 sh (16300), 264 (18200), 290 sh (18900), 302 sh (22600), 315 sh (27100), 347 sh (50000), 364 (60200), 408 (52900), and 457 nm sh (30300); ^1H NMR (90 MHz) τ=0.42 (d, 8, 2H, CHO), 2.84 (dd, 15, 10.5, 2H, H^F), 2.94—3.78 (m, 6H, H^B, H^C, H^D), 3.35 (dd, 16, 10, 2H, H^E), 3.52 (d, 10, 2H, H^G), 3.83 (dd, 15, 8, 2H, H^A), and 7.97 (S, 6H, CH_3).

Found: C, 84.42; H, 6.53%. Calcd for $C_{24}H_{22}O_2$: C, 84.17; H, 6.47%.

Intramolecular Reductive Couplings of The Dialdehydes 11—13. These reactions were carried out under the similar conditions as described for the dialdehyde **22** (vide infra); however no monomeric product was obtained.

2,3:8,9-Dibenzodeca-4,6-diyndial (20). A soln of the dialdehyde **16**[12] (2.00 g 15.4 mmol) in pyridine (31 ml) was added dropwise during 1.5 h to a stirred soln of copper(II) acetate monohydrate (31 g) in pyridine (91 ml) at 47—49 °C. After stirring for a further 2 h at the same temp, the reaction mixture was worked up as in the isolation of **3**. The residual red liquid, after solvent removal, was chromatographed on alumina (3.7×6.5 cm). The fractions eluted with hexane–ether (2:3) gave the dialdehyde **20** (1.03 g, 52%). Recrystallization from benzene afforded yellow needles: Mp 163—164 °C; MS *m/z* 258 (M^+, 100%); mol wt 258.2; IR 2270, 2200 (-C≡C-), and 1700 cm^{-1} (-CHO); UV_{max} (THF) 227 sh (57000), 235 (61900), 244 sh (57100), 261 sh (35100), 270 sh (27200), 286 sh (14100), 308 (17900), 334 (23200), and 355 nm (20000); ^1H NMR (90 MHz) τ=—0.60 (s, 2H, CHO), 1.90—2.10 (m, 2H, benzenoid H), and 2.17—2.57 (m, 6H, benzenoid H).

Found: C, 83.51; H, 3.70%. Calcd for $C_{18}H_{10}O_2$: C, 83.71; H, 3.90%.

4,5: 10,11-Dibenzo-2,12-tetradecadiene-6,8-diynedial (22). A soln of the aldehyde **17**[13] (2.00 g, 12.8 mmol) in pyridine (25 ml) was added dropwise during 1 h to a stirred soln of copper(II) acetate monohydrate (24.6 g) in pyridine (75 ml) at 52—56 °C. After stirring for a further 3 h at the same temp, the reaction mixture was worked up as in the preparation of **3**. The residual dark brown liquid, after solvent removal, was chromatographed on alumina (3.7×9 cm). The fractions eluted with hexane–ether (1:4) gave the dialdehyde **22** (1.49 g, 60%). Recrystallization from hexane–benzene afforded yellow needles: Mp 203—204 °C; MS *m/z* 310 (M^+, 17%) and 254 (100); mol wt 310.3; IR 2200 (-C≡C-), 1680 (-CHO), and 980 cm^{-1} (trans C=C) UV_{max} (THF) 224 sh (18700), 254 (32200), 277 (28500), 294 sh (24000), 330 sh (12600), and 367 nm sh (8360); ^1H NMR (90 MHz) τ=0.10 (d, 8, 2H, CHO), 1.98 (d, 16, 2H, H^B), 2.13—2.65 (m, 8H, benzenoid H), and 3.15 (dd, 16, 8, 2H, H^A).

Found: C, 85.06; H, 4.26%. Calcd for $C_{22}H_{14}O_2$: C, 85.14; H, 4.55%.

4,5: 10,11-Dibenzo-2,12,14-hexadecatriene-6,8-diynedial (23). A soln of the aldehyde **17** (2.10 g, 14 mmol) and the aldehyde **18** (2.50 g, 14 mmol) in pyridine (45 ml) and methanol (45 ml) was added dropwise during 1 h to a stirred soln of copper(II) acetate monohydrate (22 g) in pyridine (170 ml) and methanol (170 ml) at room temp, and stirring was continued for a further 16 h at the same temp. Then the mixture was worked up as in the isolation of **3**. The residue, after solvent removal, was chromatoraphed on alumina (4.5×13 cm). The early fractions eluted with hexane–ether (2:3) gave the dialdehyde **22** (0.54 g, 13%). The following fractions eluted with benzene–chloroform (4:1) gave the dialdehyde **23** (2.03 g, 43%). Recrystallization from hexane–benzene afforded yellow cubes: Mp 176—177 °C; MS *m/z* 336 (M^+, 14%) and 252 (100); mol wt 336.3; IR 2240 (-C≡C-), 1680 (-CHO), and 990 cm^1 (trans C=C); UV_{max} (THF) 235 sh (32000), 261 (40900), 271 (38300), 285 (45700), 301 (39400), 313 (40600), and 338 nm sh (32700); ^1H NMR (90 MHz) τ=0.19 (d, 7.5, 1H, H^b), 0.35 (d, 7, 1H, H^a), 2.04 (d, 16, 1H, $H^{B'}$), 2.26—2.93 (m, 11H, H^B, H^C, H^D, and benzenoid H), 3.20 (dd, 16, 7.5, 1H, $H^{A'}$), and 3.71 (dd, 14, 8, 1H, H^A).

Found: C, 85.41; H, 4.99%. Calcd for $C_{24}H_{16}O_2$: C, 85.69; H, 4.79%.

The later fractions eluted with chloroform gave the

dialdehyde **24** (vide infra) (1.08 g, 21%).

6,7:12,13-Dibenzo-2,4,14,16-octadecatetraene-8,10-diynedial (24). A soln of the aldehyde **18**[14] (363 mg, 2.0 mmol) in pyridine (4 ml) was added dropwise during 20 min to a stirred soln of copper(II) acetate monohydrate (3.8 g) in pyridine (11 ml) at 50 °C. After stirring for a further 3 h at the same temp, the reaction mixture was worked up as in the preparation of **3**. The residual yellow solid, after solvent removal, was chromatographed on alumina (3.7×9 cm). The fractions eluted with hexane–ether (3:7) gave the dialdehyde **24** (257 mg, 71%). Recrystallization from benzene afforded yellow needles: Mp 170—171 °C; MS *m/z* 362 (M^+, 10%) and 289 (100); mol wt 362.4; IR 2270, 2210 (-C≡C-), 1680 (-CHO), 1620 (C=C), and 985 cm^{-1} (trans C=C); UV_{max} (THF) 227 (24600), 269 (32800), 283 sh (30800), 300 (42400), 327 (42600), and 355 nm sh (30100); ^1H NMR (90 MHz) τ=0.28 (d, 8, 2H, CHO), 2.22—3.03 (m, 14H, H^B, H^C, H^D, and benzenoid H), and 3.65 (dd, 14, 8, 2H, H^A).

Found: C, 86.42; H, 5.29%. Calcd for $C_{26}H_{18}O_2$: C, 86.16; H, 5.01%.

6,7:12,13-Dibenzo-2,4,14,16,18-icosapentaene-8,10-diynedial (25). A soln of the aldehyde **18**[14] (2.10 g, 11.5 mmol) and the aldehyde **19**[14] (2.42 g, 11.6 mmol) in pyridine (50 ml) was added dropwise during 20 min to a stirred soln of copper(II) acetate monohydrate (46 g) in pyridine (140 ml) at 50 °C. After stirring for a further 1 h at the same temp, the mixture was poured into water, and extracted with chloroform. The combined extracts were washed with 7% hydrochloric acid until it turned acidic, water, aq sodium hydrogencarbonate soln, and brine, successively, and dried over anhyd calcium chloride. The residue, after solvent removal, was chromatographed on alumina (4.2×5.0 cm). The early fractions eluted with ether–benzene (4:1) gave the dialdehyde **24** (260 mg, 6.0%). The following fractions eluted with ether–benzene (1:1) gave the dialdehyde **25** (560 mg, 12%). Recrystallization from hexane–chloroform afforded yellow microcrystals: Mp 156—157 °C; MS *m/z* 388 (M^+, 10%) and 289 (100); mol wt 388.4; IR 2200 (-C≡C-), 1680 (-CHO), and 990 cm^1 (trans C=C); UV_{max} (THF) 225 (26300), 240 sh (22900), 272 (28000), 284 sh (30300), 300 sh (36400), 310 sh (43800), and 340 nm (45800); ^1H NMR (90 MHz) τ=0.34 (d, 8, 1H, H^a), 0.41 (d, 7.7, 1H, H^b), 2.21—3.50 (m, 16H, olefinic and benzenoid H), 3.71 (dd, 14, 8, 1H, $H^{A'}$), and 3.85 (dd, 15, 7.7, 1H, H^A).

Found: C, 86.48; H, 5.54%. Calcd for $C_{28}H_{20}O_2$: C, 86.57; H, 5.19%.

The later fractions eluted with benzene–chloroform (1:1) gave the dialdehyde **26** (vide infra) (950 mg, 19%).

8,9:14,15-Dibenzo-2,4,6,16,18,20-docosahexaene-10,12-diynedial (26). A soln of the aldehyde **19**[14] (3.48 g, 16.7 mmol) in pyridine (33 ml) was added dropwise during 1.5 h to a stirred soln of copper(II) acetate monohydrate (32 g) in pyridine (98 ml) at 52—54 °C. After stirring for a further 1 h at the same temp, the reaction mixture was worked up as in the preparation of **3**. The residual red liquid, after solvent removal, was chromatographed on alumina (3.7×12 cm). The fractions eluted with benzene-chloroform (7:3) gave the dialdehyde **26** (1.97 g, 57%). Recrystallization from hexane–tetrahydrofuran afforded red cubes: Mp 186—188 °C; MS *m/z* 414 (M^+, 59%) and 396 (100); mol wt 414.4; IR 2200 (-C≡C-), 1670 (-CHO), 1620, 1600, 1580 (C=C), 1010, and 990 cm^{-1} (trans C=C); UV_{max} (THF) 241 (33700), 253 sh (23800), 283 (33000), 296 sh (35200), 321 (55400), 359 (66600), and 383 nm sh (59600); ^1H NMR (90 MHz) τ=0.41 (d, 9, 2H, CHO), 2.26—3.60 (m, 18H, olefinic and benzenoid H), and 3.79 (dd, 17, 9, 2H, H^A).

Found: C, 86.91; H, 5.55%. Calcd for $C_{30}H_{22}O_2$: C, 86.73; H, 5.35%.

Reductive Coupling of the dialdehyde **20** was carried out under the same conditions as those indicated for the dialdehyde **22**. But no monomeric compound was obtained.

3,5-Bisdehydro-1,2:7,8-dibenzo[14]annulene (28). $LiAlH_4$ (47 mg, 1.24 mmol) was added in one portion to titanium trichloride ($TiCl_3$) (327 mg, 2.12 mmol) in dry THF (20 ml) under argon. The resultant black mixture was heated under reflux for 15 min. To the mixture, a soln of the dialdehyde **22** (248 mg, 0.80 mmol) in dry THF (10 ml) was added dropwise during 10 h and then the mixture was stirred under reflux for a further 5 h. Then after addition of ethanol (5 ml), the mixture was filtered off to remove inorganic materials and the filtrate was concentrated under reduced pressure. The residue was chromatographed on alumina (10 g). The fractions eluted with hexane–benzene (1:1) gave the dibenzo[14]annulene **28** (60 mg, 27%). Recrystallization from hexane–benzene afforded yellow plates: Mp 193—195 °C; MS *m/z* 278 (M^+, 78%) and 276 (100); mol wt 278.3; IR 2150 (-C≡C-) and 950 cm^{-1} (trans C=C); UV_{max} (isooctane) 210 sh (64500), 236 sh (21000), 244 (23900), 289 (81000), 299 (82400), 307 (85300), 337 (20300), 372 (13700), and 414 nm sh (614); ^1H NMR (200 MHz) τ=2.14 (d, 8, 2H, H^4), 2.37—2.48 (m, 4H, H^1, H^2), 2.56—2.66 (m, 2H, H^3), 2.83 (d, 16, 2H, H^C), 3.00—3.13 (m, 2H, H^A), and 3.20—3.37 (m, 2H, H^B).

Found: C, 94.92; H, 4.92%. Calcd for $C_{22}H_{14}$:C, 95.14; H, 4.86%.

3,5-Bisdehydro-1,2:7,8-dibenzo[16]annulene (29). To a stirred, refluxed soln of $TiCl_3$ (0.61 g, 3.95 mmol) in 1,2-dimethoxyethane (DME) (40 ml) was added $LiAlH_4$ (90 mg, 2.38 mmol) in one portion under argon, and the mixture was refluxed for 30 min. To this mixture was added a soln of the dialdehyde **23** (0.50 g, 1.49 mmol) in DME (20 ml) during 8 h with stirring under reflux, and stirring was continued for a further 5 h under reflux. Then the reaction mixture was passed through Hyflo Super-Cel and washed with DME. The filtrate was concentrated, and the concentrate was extracted with benzene. The residue, after solvent removal, was chromatographed on silica-gel (20 g). The fractions eluted with hexane–benzene (4:1) gave the dibenzo[16]annulene **29** (90 mg, 20%). Recrystallization from hexane–benzene afforded red needles: Mp 159—161 °C; MS *m/z* 304 (M^+, 36%) and 306 (100); mol wt 304.3; IR 2200 (-C≡C-) and 960 cm^{-1} (trans C=C); UV_{max} (isooctane) 298 (77900), 308 sh (83900), 319 (93900), 390 (49700), 433 sh (24900), and 462 sh (16700); ^1H NMR (200 MHz) τ=1.08 (dd, 16, 10, 1H, H^E), 1.11 (dd, 16, 9, 1H, H^G), 1.69 (d, 16, 1H, H^A), 2.42—3.10 (m, 10H, H^B, H^H, and benzenoid H), 3.96 (dd, 15, 8, 1H, H^F), 3.99 (t, 10.5, 1H, H^D), and 4.18 (t, 10, 1H, H^C).

Found: C, 94.84; H, 5.17%. Calcd for $C_{24}H_{16}$:C, 94.70; H, 5.30%.

3,5-Bisdehydro-1,2:7,8-dibenzo[18]annulene (30). To the refluxing mixture of $LiAlH_4$ (47 mg, 1.24 mmol) and $TiCl_3$ (327 mg, 2.12 mmol) in dry DME (20 ml), prepared as described above, was added dropwise a soln of the dialdehyde **24** (290 mg, 0.80 mmol) in dry DME (10 ml)

during 6 h under argon and the mixture was stirred under reflux for a further 5 h. After work up as in the isolation of **29**, the residue was chromatographed on alumina (15 g). The fractions eluted with hexane-benzene (4:1) gave the dibenzo[18]annulene **30** (37 mg, 14%). Recrystallization from hexane-benzene afforded brown needles: Mp 261—263 °C; MS *m/z* 330 (M^+, 3%) and 302 (100); mol wt 330.4; IR 2200 (-C≡C-) and 960 cm^{-1} (trans C=C); UV_{max} (isooctane) 269 sh (22600), 284 sh (31400), 323 sh (70000), 342 (84300), 360 sh (33300), 417 (14800), 435 (14600), and 460 nm sh (8990); ^1H MNR (270 MHz) τ=2.01 (d, 8, 2H, H^4), 2.15 (d, 8, 2H, H^1), 2.48 (t, 8, 2H, H^3), 2.62 (t, 7.5, 2H, H^2), 2.76 (dd, 16.5, 6.5, 2H, H^D), 3.26—3.34 (m, 4H, H^A, H^C), 3.68 (d, 16.5, 2H, H^E), and 3.73 (dd, 16.5, 10, 2H, H^B).

Found: C, 94.42; H, 5.30%. Calcd for $C_{26}H_{18}$: C, 94.51; H, 5.49%.

3,5-Bisdehydro-1,2:7,8-dibenzo[20]annulene (31). To the black mixture of $TiCl_3$ (0.5 g, 3.3 mmol) and $LiAlH_4$ (75 mg, 2.0 mmol) in dry DME (40 ml), prepared as described above, a soln of the dialdehyde **25** (0.49 g, 1.26 mmol) in dry DME (20 ml) was added dropwise during 8 h and stirring was continued for a further 5 h under reflux. Then the mixture was worked up as in the isolation of **29**. The residue, after solvent removal, was chromatographed on silica-gel (20 g). The fractions eluted with hexane-benzene (2:1) gave the dibenzo[20]annulene **31** (40 mg, 8.7%). Recrystallization from hexane-dichloromethane afforded black cubes: Mp 300 °C (decomp); MS *m/z* 356 (M^+, 67%) and 339 (100); mol wt 356.4; IR 2200, 2150 (-C≡CH) and 990 cm^{-1} (trans C=C); UV_{max} (isooctane) 293 sh (46900), 320 sh (106000), 333 (121000), 413 sh (23300),435 (12600), 462 sh (19500), and 498 nm sh (14700); ^1H MNR (270 MHz) τ=1.52 (d, 16, 1H, H^L), 1.54 (dd, 16, 12, 1H, H^I), 1.75 (d, 16, 1H, H^A), 2.28 (dd, 16, 8, 1H, H^C), 2.61—2.98 (m, 8H, benzenoid H), 3.22—3.50 (m, 4H, H^B, H^J, H^G, H^H), 3.69—4.02 (m 3H, H^D, H^F, H^K), and 4.30 (dd, 12, 10, 1H, H^E).

Found: C, 94.24; H, 5.65%. Calcd for $C_{28}H_{20}$: C, 94.38; H, 5.66%.

3,5-Bisdehydro-1,2:7,8-dibenzo[22]annulene (32). To the refluxing mixture of $LiAlH_4$ (47 mg, 1.24 mmol) and $TiCl_3$ (327 mg, 2.12 mmol) in dry THF (20 ml), prepared as described above, was added dropwise a soln of the dialdehyde **26** (330 mg, 0.80 mmol) in dry THF (10 ml) during 10 h under argon and the mixture was stirred under reflux for a further 5 h. After work up as in the preparation of **28**, the residue, after solvent removal, was chromatographed on alumina (10 g). The fractions eluted with benzene gave the dibenzo[22]annulene **32** (12 mg, 4.0%). Recrystallization from hexane-benzene afforded brown needles: Mp ca. 300 °C (decomp); MS *m/z* 382 (M^+, 12%) and 57 (100); mol wt 382.4; IR 2200 (-C≡C-) and 980 cm^{-1} (trans C=C); UV_{max} (isooctane) 278 sh (28100), 297 (43200), 355 (113100), 420 sh (12600), 445 (15500), 464 (15100), and 501 nm sh (8200); ^1H NMR (200 MHz) τ=2.02 (d, 8, 2H, H^4), 2.18 (d. 8, 2H. H^1), 2.49 (t, 8, 2H, H^3), 2.60 (dd, 16, 11, 2H, H^F), 2.68 (t, 8, 2H, H^2), 3.30—3.54 (m, 8H, H^A, H^C, H^D, H^E), 3.70 (d, 16, 2H. H^G), and 3.80 (dd, 16, 10, 2H, H^B).

Found: C, 94.40; H, 5.69%. Calcd for $C_{30}H_{22}$: C, 94.20 H, 5.80%.

The present work was partially supported by a Grant-in-Aid for Scientific Research No. 60540324 from the Ministry of Education, Science and Culture.

References

1) J. E. McMurry, *Acc. Chem. Res.*, **7**, 281 (1974); **16**, 405 (1983).

2) For example, see A. L. Baumstark, C. J. McClosky and K. E. Witt., *J. Org. Chem.*, **43**, 3609 (1978).

3) G. A. Olah and G. K. Surya Prakash, *J. Org. Chem.*, **42**, 580 (1977).

4) J. A. Marshall, *Acc. Chem. Res.*, **13**, 213 (1980); M. Nakazaki, K. Yamamoto, and K. Naemura, *Top. Curr. Chem.*, **125**, 1 (1984).

5) J. E. McMurry and K. L. Kees, *J. Org. Chem.*, **42**, 2655 (1977).

6) a) D. Tanner, O. Wennerström, and E. Vogel, *Tetrahedron Lett.*, **23**, 1221 (1982); b) K. Yamamoto, M. Shibutani, S. Kuroda, E. Ejiri, and J. Ojima, *ibid.*, **27**, 975 (1986).

7) T. M. Cresp and F. Sondheimer, *J. Am. Chem. Soc.*, **99**, 194 (1977); M. Nakagawa, *Angew. Chem. Int. Ed. Engl.*, **18**, 202 (1974).

8) J. Ojima, Y. Shiroishi, K. Wada, and F. Sondheimer, *J. Org. Chem.*, **45**, 3564 (1980).

9) J. Ojima, Y. Yokoyama, and M. Enkaku, *Bull. Chem. Soc. Jpn.*, **50**, 1522 (1977).

10) R. T. Weavers, R. R. Jones, and F. Sondheimer, *Tetrahedron Lett.*, **1975**, 1043; see also, J. Ojima, K. Wada, K. Kanazawa, and Y. Nakagawa, *J. Chem. Soc., Perkin Trans. 1*, **1981**, 947.

11) J. Ojima, M. Kirita, Y. Murosawa, and T. Nakada, *Bull. Chem. Soc. Jpn.*, **56**, 1467 (1983).

12) J. Ojima, T. Yokomachi, and A. Kimura, *Bull. Chem. Soc. Jpn.*, **49**, 2840 (1976).

13) J. Ojima, A. Kimura, Y. Yokoyama, and T. Yokoyama, *Bull. Chem. Soc. Jpn.*, **48**, 367 (1975).

14) J. Ojima, M. Enkaku, and M. Ishiyama, *J. Chem. Soc., Perkin Trans. 1*, **1977**, 1548.

15) J. Ojima, T. Katakami, G. Nakaminami, and M. Nakagawa, *Bull. Chem. Soc. Jpn.*, **49**, 202 (1976).

16) T. M. Cresp, J. Ojima, and F. Sondheimer, *J. Org. Chem.*, **42**, 2130 (1977).

 © 1986 The Chemical Society of Japan Bull. Chem. Soc. Jpn., 59, 2217—2223 (1986)

Active Carbon-Supported Copper(I) Chloride as Solid Adsorbent for Carbon Monoxide[1)]

Hidefumi HIRAI,* Keiichiro WADA, and Makoto KOMIYAMA
Department of Industrial Chemistry, Faculty of Engineering, The University of Tokyo, Hongo, Bunkyo-ku, Tokyo 113
(Received January 7, 1986)

An active carbon-supported copper(I) chloride (CuCl) is prepared by stirring active carbon in aqueous hydrochloric acid solution of CuCl, followed by removal of the liquid phase under 6 mmHg at 100 °C. The resulting solid rapidly adsorbs carbon monoxide (CO) at 20 °C from 9:1 CO-N_2 mixture under 1 atm (the CO partial pressure 0.9 atm) and the equilibrium molar ratio of adsorbed CO to CuCl is 0.88. All of adsorbed CO is promptly desorbed either by reducing CO partial pressure to 0.4 mmHg at 20 °C or by elevating temperature from 20 °C to 120 °C under 1 atm (the CO partial pressure 0.9 atm). Reversible adsorption-desorption cycles are repeated four times without measurable decrease in the adsorbing capacity. The adsorbing capacity of the active carbon-supported CuCl is much larger than either that of CuCl solid or that of active carbon. Effective CO adsorption by the present adsorbent is attributed to formation of complex between CO and CuCl, which is highly dispersed on the surface of active carbon.

Efficient methods for separation of carbon monoxide (CO) from gas mixtures are important in industry, since almost all CO sources are gas mixtures with nitrogen, hydrogen, methane, and carbon dioxide.[2)] Many liquid absorbents for CO were proposed.[3-5)] However, reports on solid adsorbents for CO have been scanty. Solid adsorbents have an advantage over liquid absorbents that pressure-swing methods are available for separation of CO. In addition, CO separated from gas mixtures by use of solid adsorbents is free from contamination with solvent vapor.

Although a Y-type zeolite-supported copper(I) ion adsorbed CO,[6)] the interaction between CO and the copper(I) ion was so strong that adsorbed CO could not be sufficiently desorbed even at the CO partial pressure 10^{-4} mmHg (1.0 mmHg=1.33×10^2 Pa). A patent[7)] claimed that copper(I) ion supported on zeolites, which had high ratios of silica to alumina, had CO adsorbing abilities. The amount of adsorbed CO was rather independent of CO partial pressure at the partial pressure larger than 10 mmHg.

Previously, the authors reported that aluminium copper(I) chlorides supported both on polystyrene resin[8)] and on active carbon[9,10)] reversibly adsorbed CO under mild conditions.

In this paper, preparation of active carbon-supported copper(I) chloride (CuCl) as solid CO adsorbents is reported. Their CO adsorbing and desorbing abilities as well as effects of preparation solvent on the ability are shown. Pore size distribution, BET surface area, and distribution of CuCl of the adsorbents are also described. Mechanism of effective and reversible adsorption of CO is discussed on the basis of these results.

Experimental

Materials. Active carbon was obtained from Kureha Chemical Industry Co. (Petroleum pitch, BAC G-70R, Lot No. 810117, average diameter ca. 0.7 mm) and was subjected to a reduced pressure (6 mmHg) at 200 °C for 5 h. Copper(I) chloride (guaranteed grade) was purchased from Koso Chemical Co. All other metal salts and solvents were commercially obtained.

Carbon monoxide gas and nitrogen gas, which had purities of 99.95 and 99.999%, respectively, were passed through columns of molecular sieve 3 A immediately before use.

Preparation of CO Adsorbents. A predetermined amount of CuCl was magnetically stirred in 15 cm^3 of various solvents under dry nitrogen at room temperature for 1 h, and then 10 g of the active carbon was added to the mixture. After stirring the mixture for 1 h, the liquid phase was removed at 6 mmHg, 100 °C for 1 h.

Solid of CuCl without active carbon was prepared as white powder in the same way as described above except for the absence of the active carbon.

Determination of the Amount of CuCl in the Adsorbent. The adsorbent was thoroughly washed by stirring for 24 h at room temperature in four portions of aqueous hydrochloric acid solution (3 mol dm^{-3}, total volume 2000 cm^3). Total amount of copper atoms in the solution was determined by atomic absorption spectroscopy (Shimadzu Co., model AA-646).

Measurements of Pore Size Distribution and BET Surface Area. Pore size distribution in the adsorbent was determined from desorption isotherm of nitrogen at 77 K by the method of Dollimore.[11)] The method takes advantage of capillary condensation theory and is based on the assumption of cylindrical pores with radii r. The value $\Delta v/\Delta r$ is obtained as a function of r, where Δv is sum of volume for the pores having radii between r and $r+\Delta r$. Desorption isotherm of nitrogen at 77 K was measured on a Calroerba Co. Sorptomatic Series 1800.

The BET surface area was measured by nitrogen adsorption at 77 K with a Micromeritics Instrument Model 2200A Rapid Surface Area Analyzer.

Electron Microscopy and X-Ray Microanalysis. Scanning electron microscopy and X-ray microanalysis on the beads of the adsorbents were carried out by use of a Hitachi Micro Scanning X-ray Analyzer Model X-650, which had resolution ability of X-ray image around 100 Å. The beads

were embedded in epoxy resin, and the composites were cut with a stainless steel cutter and then were coated with gold so that cross-sections of the beads were irradiated by electron beam. The distributions of copper and chlorine atoms were evaluated from intensity of characteristic X-ray.

Measurement of CO Adsorption and Desorption. Adsorption of CO from CO–N_2 mixtures by the adsorbents was achieved at 20 °C under the atmospheric pressure using the apparatus depicted in Fig. 1. Uptake of CO was followed by a gas burette (3) using water as leveling liquid (5). The flask (2) containing the adsorbent (1) under nitrogen was connected with CO in the gas burette, and the adsorption was initiated by circulating the gases with the use of a gas pump (4). The circulation was effected for the first 10 min at a rate of 30 $cm^3 s^{-1}$ in order to mix the gas phase sufficiently.

Desorption of the adsorbed CO was carried out either by reducing the total pressure in the flask to 0.4 mmHg at 20 °C for 10 min or by heating the adsorbent to 120 °C under 1 atm for 10 min.

Results

Preparation of Active Carbon-Supported CuCl. Active carbon-supported CuCl adsorbents were obtained as black beads. The amount of CuCl supported on 10 g of the active carbon was 14.1 mmol, as determined by atomic absorption spectroscopy, when the charged amount of CuCl was 15.0 mmol and 15 cm^3 of aqueous hydrochloric acid solution (3 mol dm^{-3}) was used as preparation solvent. Thus, 94% of the charged CuCl was supported on the active carbon under these conditions.

BET surface area of the active carbon-supported CuCl composed of 14.1 mmol of CuCl and 10 g of the active carbon is 744 $m^2 g^{-1}$. This value is about 70% of the value (1044 $m^2 g^{-1}$) for the original active carbon.

Figure 2 depicts pore size distribution either in the present adsorbent (the solid line) or in the original active carbon (the broken line). The ordinate ($\Delta v/\Delta r$) approximately corresponds to number of pores. The number of pores with radii smaller than 10 Å for the present adsorbent is significantly smaller than the value for the original active carbon. In contrast, the number of pores with radii larger than 10 Å is almost identical with the value for the original active carbon.

Figure 3 shows scanning electron micrographs of a cross-section of a bead of the active carbon-supported CuCl. Waved white lines depict the distributions of copper atoms (a) and chlorine atoms (b) along the white straight lines on the cross-section. Both copper atoms and chlorine atoms are uniformly distributed in the bead. No deposition of CuCl is observed either on the surface of the bead or inside the bead.

Adsorption and Desorption of CO by the Active Carbon-Supported CuCl. Figure 4 shows repeated adsorption-desorption cycles using the active carbon-supported CuCl by temperature change. The adsorbent rapidly adsorbs CO on the contact with 9:1 CO–N_2 mixture at 20 °C under 1 atm (the region I-a), and the amount of CO adsorbed in 10 min is 11.8 mmol. An equilibrium is attained in 30 min, where the amount of adsorbed CO is 12.4 mmol. This value corresponds to molar ratio 0.88 of adsorbed CO to supported CuCl: 24 cm^3 (standard temperature and pressure) per 1 g of the adsorbent.

All of the adsorbed CO is desorbed in 10 min to the gas phase, as followed with the use of the gas burette, by heating the adsorbent to 120 °C at 1 atm (the region I-d in Fig. 4).

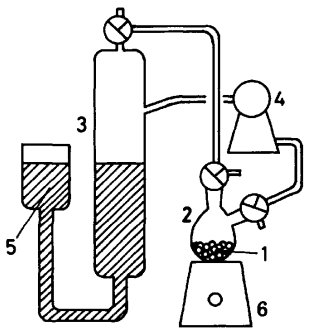

Fig. 1. Apparatus for measuring the amount of CO adsorbed by the adsorbents or desorbed from them. 1: adsorbent; 2: flask; 3: gas burette; 4: gas pump; 5: leveling liquid (water); 6: magnetic stirrer.

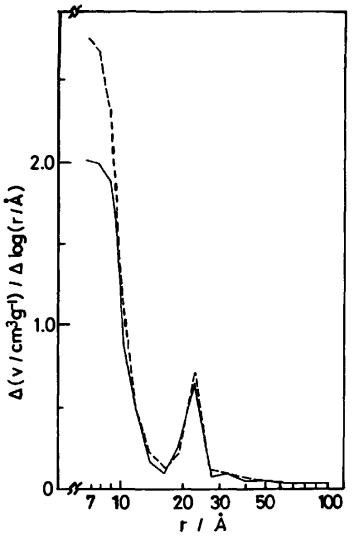

Fig. 2. Pore size distributions in the active carbon-supported CuCl (——) and the original active carbon (----): Δv is sum of volume for the pores having radii between r and $r+\Delta r$; the active carbon-supported CuCl was prepared from 15.0 mmol of CuCl and 10 g of the active carbon using 15 cm^3 of aqueous hydrochloric acid solution (3 mol dm^{-3}) as solvent, and contained 14.1 mmol of CuCl.

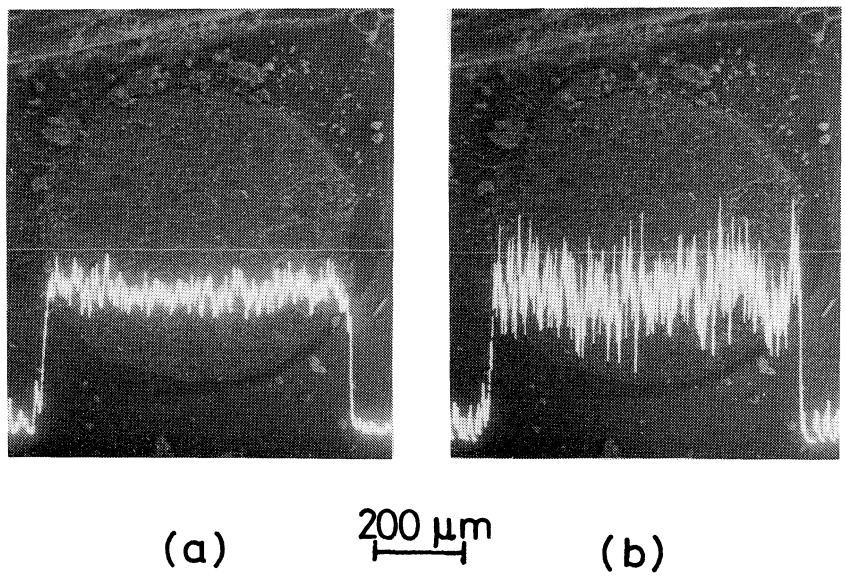

Fig. 3. Scanning electron micrographs for the cross-section of the active carbon-supported CuCl composed of 14.1 mmol of CuCl and 10 g of the active carbon: The waved white lines show distributions of copper atoms (a) and chlorine atoms (b) along the corresponding white straight lines.

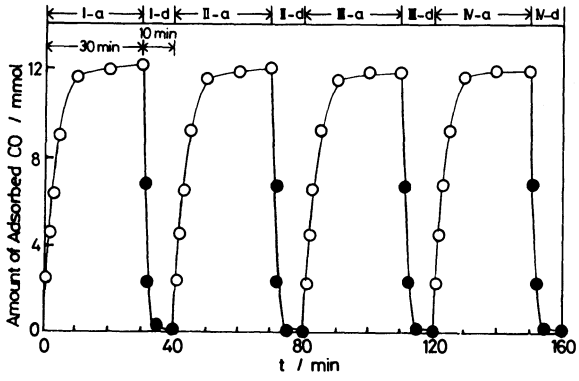

Fig. 4. Time courses of repeated CO adsorption-desorption cycles by the active carbon-supported CuCl using a change in temperature: CO adsorptions (○) from 9 : 1 $CO-N_2$ mixtures were carried out at 20 °C under 1 atm, and desorptions (●) of adsorbed CO were effected by heating the adsorbent to 120 °C under 1 atm for 10 min; the adsorbent was composed of 14.1 mmol of CuCl and 10 g of the active carbon.

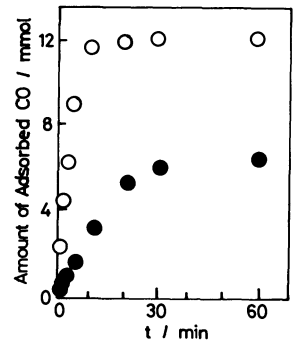

Fig. 5. CO adsorption and absorption from 9 : 1 $CO-N_2$ mixtures at 20 °C under 1 atm by the active carbon-supported CuCl (○) and by 2 mol dm^{-3} aqueous hydrochloric acid solution of CuCl (●): The charged amount of CuCl was 15.0 mmol.

On the next contact with 9:1 $CO-N_2$ mixture, the adsorbent rapidly adsorbs CO, as shown in the region II-a in Fig. 4, and the time course is almost identical with that in the first adsorption. The equilibrium amount of adsorbed CO is 12.4 mmol (24 cm^3 per 1 g of the adsorbent). The adsorption-desorption cycles are repeated four times without measurable deterioration.

Adsorption-desorption cycles for the present adsorbent were successfully carried out also by use of partial pressure change of CO in place of temperature change. Almost all of the adsorbed CO was rapidly desorbed by subjecting the adsorbent to a reduced pressure (0.4 mmHg) at 20 °C. In the following adsorptions, the time courses were virtually the same as the ones depicted by the open circles in Fig. 4. The cycles were repeated four times without measurable decrease in the adsorbing capacity.

As shown in Table 1, CO adsorbing capacity (12.4 mmol) of the active carbon-supported CuCl is much larger than either that (0.0 mmol) of the solid of CuCl or that (3.3 mmol) of the active carbon without CuCl. The capacity (6.5 mmol) of the aqueous hydrochloric acid solution of CuCl is about half of the value (12.4 mmol) of the active carbon-supported CuCl. The rate of adsorption for the active carbon-supported CuCl is much larger than that for the aqueous hydrochloric acid solution of CuCl, as depicted in Fig. 5.

Table 1. Adsorbing Capacities of the CO Adsorbents and Absorbent[a)]

Adsorbent or absorbent	Amount of CuCl / mmol	CO adsorbed in 60 min	
		Amount / mmol	Molar ratio to CuCl
Active carbon-supported CuCl[b)]	14.1	12.4	0.88
Solid of CuCl	15.0	0.0	0.00
Original active carbon[b)]	—	3.3[c)]	—
Hydrochloric acid solution of CuCl	15.0	6.5	0.43

a) At 20 °C; initial volume of gas mixture 1500 cm^3; initial partial pressures of CO and N_2, respectively, were 0.9 and 0.1 atm. b) Active carbon, 10 g. c) The value was measured using helium, in place of N_2, as balance, since the magnitudes of adsorptions of CO and N_2 to the active carbon were comparable with each other, and adsorption of helium was negligibly small.

Table 2. CO Adsorbing Capacities of Solid Adsorbents Composed of Various Copper(I) Halides and the Active Carbon[a)]

Copper(I) halide	Equilibrium amount of adsorbed CO / mmol
CuCl	12.4
CuBr	9.5
CuI	1.7

a) At 20 °C, under 1 atm; initial volume of gas mixture 1500 cm^3; initial partial pressures of CO and N_2, respectively, were 0.9 and 0.1 atm; the adsorbents were prepared from 15.0 mmol of copper(I) halide and 10 g of the active carbon using 15 cm^3 of 28% ammoniacal aqueous solution as solvent.

Table 2 lists CO adsorbing capacities of the adsorbents prepared from the active carbon and various copper(I) halides by use of 28% ammoniacal aqueous solution as solvent. The capacity decreases in the following order: CuCl>CuBr $\gg$ CuI. The adsorbing capacities (0.8, 0.9, and 0.9 mmol, respectively) for the adsorbents prepared from 10.0 g of the active carbon and 15.0 mmol of either sodium chloride, zinc chloride, or magnesium chloride were small.

Effect of Preparation Solvent on CO Adsorbing Capacity. Figure 6 depicts the dependence of the CO adsorbing capacity of the active carbon-supported CuCl on the concentration of aqueous hydrochloric acid solution used as preparation solvent. The concentration of CuCl in the solution is kept constant at 1.0 mol dm^{-3}. The adsorbing capacity of the active carbon-supported CuCl increases with increasing concentration of aqueous hydrochloric acid solution up to the concentration 1.0 mol dm^{-3}. At the concentration larger than 1.0 mol dm^{-3}, however, the capacity is constant irrespective of the concentration.

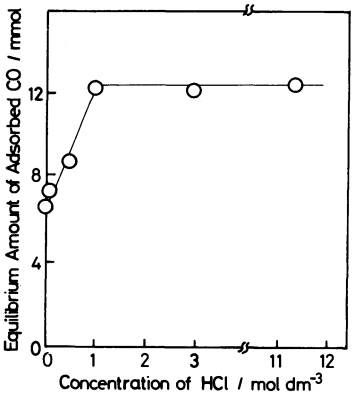

Fig. 6. Dependence of CO adsorbing capacity of the active carbon-supported CuCl on the concentration of aqueous hydrochloric acid solution used as preparation solvent; $[CuCl]_0 = 1.0$ mol dm^{-3}.

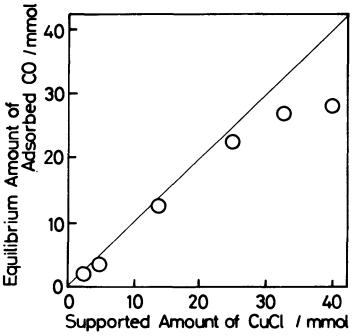

Fig. 7. Plot of CO adsorbing capacity of the active carbon-supported CuCl against the supported amount of CuCl.
Active carbon 10 g; the straight line is theoretical one calculated under the assumption that the supported CuCl forms 1 : 1 complex with CO.

Table 3 shows the CO adsorbing capacities of the active carbon-supported CuCl prepared by using various solvents. The adsorbent prepared using aqueous hydrochloric acid solution exhibits much larger adsorbing capacity and larger ratio of adsorbed CO to supported CuCl than those of the ones prepared using water, acetonitrile, and toluene.

Effect of Supported Amount of CuCl on CO Adsorbing Capacity. As shown in Table 4, both the ratio of the supported amount of CuCl to the charged amount and BET surface area of the active carbon-supported CuCl decrease with increasing charged amount of CuCl. Here, the amount of the active carbon is kept constant at 10 g.

Figure 7 depicts plot of CO adsorbing capacity of the active carbon-supported CuCl against the charged amount of CuCl. When the supported amount is smaller than 25 mmol, all the experimental points

Table 3. CO Adsorbing Capacities of the Active Carbon-Supported CuCl Prepared by Using Various Preparation Solvents[a)]

Solvent	Ratio of supported CuCl to charged CuCl	Amount of adsorbed CO / mmol	Molar ratio of adsorbed CO to supported CuCl
Aqueous hydrochloric acid solution (3 mol dm^{-3})	0.94	12.4	0.88
Water	0.70	5.6	0.64
Acetonitrile	0.87	6.1	0.47
Toluene	0.69	1.3	0.13

a) At 20 °C; initial volume of gas mixture 1500 cm^3; initial partial pressures of CO and N_2, respectively, were 0.9 and 0.1 atm; the adsorbents were prepared from 15.0 mmol of CuCl and 10 g of the active carbon using 15 cm^3 of one of the solvents.

Table 4. Supported Amounts of CuCl, Ratios of the Supported CuCl to the Charged CuCl, and BET Surface Areas for the Active Carbon-Supported CuCl Prepared from 10 g of the Active Carbon and Various Amounts of CuCl[a)]

Amount of CuCl / mmol		Ratio of supported CuCl to charged CuCl	BET surface area / $m^2 g^{-1}$
Charged	Supported		
0.0	0.0	—	1044
2.5	2.5	0.99	897
5.0	4.8	0.96	887
10.0	9.3	0.93	811
15.0	14.1	0.94	744
20.0	18.2	0.91	661
30.0	24.9	0.83	676
40.0	33.2	0.83	565
50.0	40.5	0.81	531

a) 15 cm^3 of 3 mol dm^{-3} aqueous hydrochloric acid solution was used as preparation solvent.

satisfactorily fit the theoretical line (the solid straight line) calculated under the assumption that the supported CuCl forms 1:1 complex with CO. At the supported amount larger than 25 mmol, however, CO adsorbing capacity is considerably smaller than the value estimated under the assumption.

Discussion

Preparation of the Active Carbon-Supported CuCl. Significant decrease of the BET surface area of the active carbon on the formation of the active carbon-supported CuCl adsorbents (Table 4) shows that CuCl is supported on the surface of the active carbon in the adsorbents. There, CuCl molecules probably exist in both monomeric and dimeric forms, resulting in effective adsorption of CO. Formation of large aggregates of CuCl is unlikely, since solid of CuCl shows no measurable adsorbing ability (Table 1) at 20 °C under the CO partial pressure 0.9 atm.

The proposed structure of the adsorbent involving CuCl in monomeric and dimeric forms is consistent with pore size distribution (Fig. 2) which indicates the presence of CuCl in the pores having radii smaller than 10 Å. The number of these micro-pores in the adsorbents is much smaller than that for the original active carbon, whereas the number of pores with radii larger than 10 Å is almost identical with each other. Molecular dimensions of monomeric form of CuCl and its dimeric form, respectively, are approximately 3.4 Å×3.4 Å×4.5 Å and 3.4 Å×3.9 Å×6.7 Å. These dimensions are evaluated from the bond length (2.05 Å)[12] of the Cu–Cl bond in solid of CuCl and the ionic radii (0.74 Å for copper(I) ion and 1.67 Å for chlorine anion).[12]

These arguments are further supported by the result of X-ray microanalysis (Fig. 3) showing uniform distribution of CuCl in the beads of the adsorbents without formation of any deposits of metal salts. Gradual decrease of BET surface area of the active carbon with increasing amount of supported CuCl (Table 4) is also consistent with them.

Rough estimation using the decrease (300 $m^2 g^{-1}$) of the BET surface area for the adsorbent composed of 10 g of the active carbon and 14.1 mmol of CuCl indicates that one molecule of CuCl occupies around 35 $Å^2$ of the surface area of the active carbon.

CO Adsorbing and Desorbing Ability of the Active Carbon-Supported CuCl. By use of the active carbon-supported CuCl, CO separation is successfully achieved both by temperature-swing method (Fig. 4) and by pressure-swing method. All the CO adsorbed at 20 °C under 1 atm (the CO partial pressure 0.9 atm) is desorbed both by heating the adsorbent to 120 °C under 1 atm and by reducing CO partial pressure to 0.4 mmHg at 20 °C. The amount of CO separated with the use of the present adsorbent for each of the cycles involving CO adsorption at 20 °C under 1 atm and desorption at 120 °C or for each of the cycles involving adsorption at 20 °C under 1 atm and desorption at 0.4 mmHg, 20 °C is

24 cm^3 (standard temperature and pressure) per 1 g of the adsorbent.

Complete desorption of adsorbed CO for the present adsorbent is highly in contrast with the fact that CO adsorbed by Y-type zeolite-supported copper(I) ion is not effectively desorbed even at 10^{-4} mmHg.[6] Desorption of CO, which is adsorbed by the adsorbent composed of copper(I) ion and zeolites having high SiO_2/Al_2O_3 ratios, is also difficult, as indicated by rather small dependence of the amount of adsorbed CO on CO partial pressure.[7]

The amount of CO adsorbed by 1 g of the active carbon-supported CuCl composed of 24.9 mmol of CuCl and 10 g of the active carbon is 38 cm^3 (standard temperature and pressure). The value is 2.4 times as large as the value (16 cm^3) for the adsorbent composed of copper(I) ion and high SiO_2/Al_2O_3 ratio zeolite.[7]

Mechanism of CO Adsorption by the Active Carbon-Supported CuCl. Much larger adsorbing capacity (12.4 mmol) of the active carbon-supported CuCl than both the value (0.0 mmol) for CuCl solid and that (3.3 mmol) for the active carbon (Table 1) shows that the presence of both of CuCl and active carbon is essential for the effective adsorption of CO by the active carbon-supported CuCl.

In the present adsorbent, CO is adsorbed by formation of 1:1 complex with the CuCl supported on the active carbon. This is clearly seen by the satisfactorily straight line with a slope unity for the plot between the CO adsorbing capacity and the supported amount of CuCl (Fig. 7). Deviation of the plot from the straight line at the supported amount 25 mmol or larger is ascribed to formation of small aggregates of CuCl at such large supported amounts. Furthermore, quite small capacities of the active carbon-supported sodium chloride, zinc chloride, and magnesium chloride confirm that the copper(I) ions are active species of CO adsorption by the present adsorbent. A possibility that surface of the active carbon treated with CuCl in aqueous hydrochloric acid solution has a CO adsorbing ability is ruled out by the independence of the capacity from the concentration of aqueous hydrochloric acid solution in the concentration range from 1.0 to 11.2 mol dm^{-3} (Fig. 6).

The order (CuCl>CuBr$\gg$CuI) in the CO adsorbing capacities of the active carbon-supported copper(I) halides (Table 2) is identical with that for copper(I) halides in various solvents.[13]

Effective adsorbing ability of the active carbon-supported CuCl is attributed to sufficient dispersion of CuCl on the surface of the active carbon, which produces vacant coordination sites at the copper(I) ions. Both the adsorbing capacity and the ratio of adsorbed CO to supported CuCl for the active carbon-supported CuCl prepared by use of aqueous hydrochloric acid solution are larger than the corresponding values for the ones prepared by use of acetonitrile, water, and toluene (Table 3). Aqueous hydrochloric acid solutions effectively dissolve CuCl in the form of $CuCl_2^-$,[14] whereas CuCl exhibits small solubility in acetonitrile or water, and virtually no solubility in toluene. When active carbon is stirred in hydrochloric acid solution of CuCl, most of the $CuCl_2^-$ ions, which are solvated with water, are supported on the surface of the active carbon due to mutual interactions. In the active carbon-supported CuCl obtained after evaporation of the liquid phase, CuCl molecules are satisfactorily dispersed on the surface of the active carbon. With the use of acetonitrile and water, however, the amount of CuCl supported on the active carbon is smaller due to small solubility of CuCl in them, and dispersion of CuCl molecules in the resultant adsorbents is poorer. The adsorbent prepared by use of toluene exhibits the smallest ability.

These arguments are further confirmed by the fact that the adsorbing capacity increases with increasing concentration of hydrochloric acid up to 1.0 mol dm^{-3}, when the charged amount of CuCl is 1.0 mol dm^{-3} (Fig. 6). One molecule of CuCl requires one molecule of hydrogen chloride for the formation of $CuCl_2^-$.

Adsorption of CO by the active carbon-supported CuCl is faster than that by a hydrochloric acid solution of CuCl (Fig. 5). This is due to the fact that diffusion of CO in liquid phase, which is rate-determining in the absorption by the solution, is not required for the present solid adsorbent to adsorb CO from gas phase.

In conclusion, the active carbon-supported CuCl is a solid adsorbent of CO having high abilities with respect to both adsorption and desorption. CO is efficiently adsorbed by the formation of complex with the CuCl, which is highly dispersed on the surface of the active carbon.

References

1) A preliminary communication: H. Hirai, K. Wada, and M. Komiyama, *Chem. Lett.*, **1983**, 361.

2) A. L. Kohl and F. C. Riesenfeld, "Gas Purification," 3rd ed., Gulf Publishing Co., Houston (1979).

3) A. T. Larson and C. S. Teitsworth, *J. Am. Chem. Soc.*, **44**, 2878 (1922).

4) H. Deringer, *Chimia*, **1**, 125 (1947).

5) D. J. Haase, *Chem. Eng. News*, **1975**, August 4, 52.

6) Y.-Y. Huang, *J. Catal.*, **30**, 187 (1973).

7) J. A. Rabo, J. N. Francis, and C. L. Angell, U.S. Patent 4019879 (1977).

8) H. Hirai, M. Komiyama, and S. Hara, *Chem. Lett.*, **1982**, 1685.

9) H. Hirai, M. Komiyama, and K. Wada, *Chem. Lett.*, **1982**, 1025.

10) H. Hirai, K. Wada, and M. Komiyama, *Bull. Chem. Soc. Jpn.*, **59**, 1043 (1986).
11) D. Dollimore and G. R. Heal, *J. Appl. Chem.* (London), **14**, 109 (1964).
12) "Kagaku Binran, Kiso-hen," ed by the Chemical Society of Japan, Maruzen, Tokyo (1984), pp. II-715 and II-718.
13) M. I. Bruce, *J. Organomet. Chem.*, **44**, 209 (1972).
14) D. D. Davis, K. L. Stevenson, and C. R. Davis, *J. Am. Chem. Soc.*, **100**, 5344 (1978).

 © 1986 The Chemical Society of Japan Bull. Chem. Soc. Jpn., 59, 2225—2232 (1986)

Recovery of Highly-Purified Rare Earth Elements Using Newly-Synthesized Chelating Resins

Kunihiko TAKEDA,* Minoru AKIYAMA, Fumiaki KAWAKAMI, and Mitsunaga SASAKI
Research & Development Administration, Asahi Chemical Industry Co., Ltd.,
1-3-2, Yako, Kawasaki-ku, Kawasaki 210
(Received June 22, 1985)

The chromatographic separation of rare earth elements was studied using newly-synthesized chelating resins which have EDTA (ethylenediaminetetraacetic acid) and DTTA (diethylenetriaminetetraacetic acid) pendant groups. The chromatography using EDTA- and DTTA-chelating resins gave excellent separation results, while the IDA-chelating resin was not satisfactory. The DTTA-type resin was especially effective, allowing highly purified rare earth elements to be recovered. The separation efficiency of each resin was attributed mainly to the difference in its complexing capability among rare earth ions. Prior to experimentation, the chromatographic conditions were assessed and optimized by computer simulation based on newly introduced equations. The simulation results were effective in the case of Pr^{3+}/Nd^{3+} for determining the experimental conditions. An analysis of the experimental results helped to elucidate the mechanism of the chromatographic separation while using the simulation results.

Lanthanum and cerium can be separated from other rare earth elements by a precipitation-filtration method; but the other 12 rare earth elements cannot be easily separated by such a simple chemical method. Many studies have been made on the separation of rare earth elements using solvent extraction and ion exchange.[1] In the field of analytical chemistry, it has been known that several organic ligands are capable of forming specific complexes with rare earth elements. Typical examples of such organic ligands are amine-*N*-polyacetic acids, such as NTA (nitrilotriacetic acid), EDTA (ethylenediaminetetraacetic acid) and DTPA (diethylenetriaminepentaacetic acid). Their stability constants are as high as 5 to 20 in terms of a logarithmic value (log *K*).

Differences in the values of their stability constants among the rare earth elements are expected to be sufficiently large for chromatographic separation. Several studies have been conducted on the separation of rare earth elements with such chelating resins as iminodiacetate resin,[2,3] *N*-methyliminodiacetate resin[4] and nitrilophosphonic resin.[5]

The authors have previously reported on results regarding studies of the selective bromination of *m*-divinylbenzene (*m*-DVB).[6] A bromination method was developed by referring to the selective addition reactions of various amines to *p*-DVB.[7] Follow-up and industrial application studies of that reaction have been made.[8] An attempt was also successfully made to synthesize chelating resins with pendant groups that are structurally similar to EDTA and DTTA (diethylenetriaminetetraacetic acid).[9] This paper describes the excellent results of our investigation on the chromatographic separation of rare earth elements using the newly-prepared resins, and comparing them with the obtained results using a known IDA (iminodiacetic acid)-chelating resin.

Prior to experimentation, the separation conditions of the chromatography were assessed and optimized by a computer simulation based on newly introduced equations. Although various simulation methods were known, the method introduced in this study is characterized by its easy procedure for finding a solution. The simulation results help to elucidate the chromatographic separation mechanism of rare earth elements.

Experimental

Synthesis of Chelating Resins. The procedures for synthesizing the resins followed that of previous reports.[9]

An IDA-chelating resin was synthesized from a copolymer of *m*-divinylbenzene (*m*-DVB) with vinylbenzyl chloride (VBC).[10,11] The backbone structure of a resin must be suitably designed in order to develop a greater chelate-forming capability. This capability of a resin is considered to depend primarily on the stability constant of the pendant group and secondarily on the crosslinking and rigidity of the polymer chain. Notably, there is a larger steric hindrance against pendant groups adjacent to DVB units in a resin. The monomer sequences of copolymers (VBC/*p*-DVB and VBC/*m*-DVB) were calculated based on the probability theory[12] of radical polymerization (Table 1). The formation of DVB–DVB chains in a polymer is most important from the standpoint of polymer-chain rigidity. The DVB–DVB and DVB–VBC sequences are

Table 1. Sequence Distributions in Copolymers of DVB(M_1) Isomers with VBC(M_2)

Copolymer	A[a]	B[a]
$P_2\{M_1M_1\}$	1.7	0.8
$P_2\{M_1M_2\}$[b]	41.6	18.2
$P_2\{M_2M_2\}$	56.7	80.9
$P_3\{M_1M_1M_1\}$	0.13	0.07
$P_3\{M_1M_1M_2\}$[b]	3.2	1.5
$P_3\{M_2M_1M_2\}$	19.2	8.4

a) A and B are copolymers of VBC with *p*-DVB and *m*-DVB, respectively, where $[M_1]/[M_2]=0.118$. b) $P_2\{M_1M_2\}$ consists of both diads M_1M_2 and M_2M_1, and $P_3\{M_1M_1M_2\}$ both triads $M_1M_1M_2$ and $M_2M_1M_1$.

believed to cause a steric hindrance against chelation. The probability of a DVB–DVB sequence is 0.8% for *m*-DVB and 1.7% for *p*-DVB. *m*-DVB also gives a lower probability (18.2%) for DVB–VBC chain formation than *p*-DVB (41.6%). Thus, *m*-DVB was selected as the crosslinking agent. IDA groups could be introduced into the resin by the reaction of a copolymer of *m*-DVB and VBC (*m*-DVB/VBC by wt.=1:10) with diethyl iminodiacetate (IDAE), followed by hydrolysis. It took approximately 8 h for the reaction to be completed. The resin produced had a cation-exchange capacity of 4.3 meq g^{-1}.

An EDTA-chelating resin was synthesized by the amination of a copolymer [**II**] of *m*-(1,2-dibromoethyl)-styrene (*m*-DBS) [**I**] and *m*-DVB (*m*-DVB/*m*-DBS by wt.=2.5:7.5) with IDAE, followed by hydrolysis (Fig. 1). Amination while synthesizing an EDTA-chelating resin [**IV**] was not as easy as during IDA-chelating resin synthesis. One side reaction was the elimination of HBr from the 1,2-dibromoethyl group of a DBS unit, resulting in the formation of a double bond. The obtained resin had a cation-exchange capacity of 3.9 meq g^{-1}.

DTTA-chelating resin synthesis was performed by the preparation of a copolymer [**VI**] consisting of a monomer [**V**] and *p*-DVB (*p*-DVB/monomer [V] by wt.=2:8), followed by the *N*-carboxymethylation of the amino groups with bromoacetic acid (Fig. 2). Copolymer [**VI**] had an anion-exchange capacity of 6.2 meq g^{-1}. If conversion rates for the monomer [V] and *p*-DVB were both 100%, the anion-exchange capacity of the copolymer [**VI**] should be 7.5 meq g^{-1} at its maximum. The chelating resin [**VII**] obtained after *N*-carboxymethylation had a cation-exchange capacity of 5.1 meq g^{-1}.[9]

Separation Studies. Chelating Resins: Each of the chelating resins was classified between 100-mesh and 200-mesh with sieves. The classified resins were washed (twice with a 0.1 mol dm^{-3} aqueous NaCl solution and then with 0.1 mol dm^{-3} hydrochloric acid).

Reagents: Salts of rare earth elements, rare earth chlorides, were of commercially available grade (purity: 99.9% or higher). Each salt was weighed and dissolved in deionized water. Other reagents were of commercially available guaranteed grade.

Analysis: The concentrations of rare earth elements in a solution were determined by an automatic-recording luminescence spectrophotometer, manufactured by Shimadzu Corporation. The pH values of the solutions were measured with a pH meter (model HM-18B) and a glass electrode (model GST-155C9 manufactured by Toa Elec-

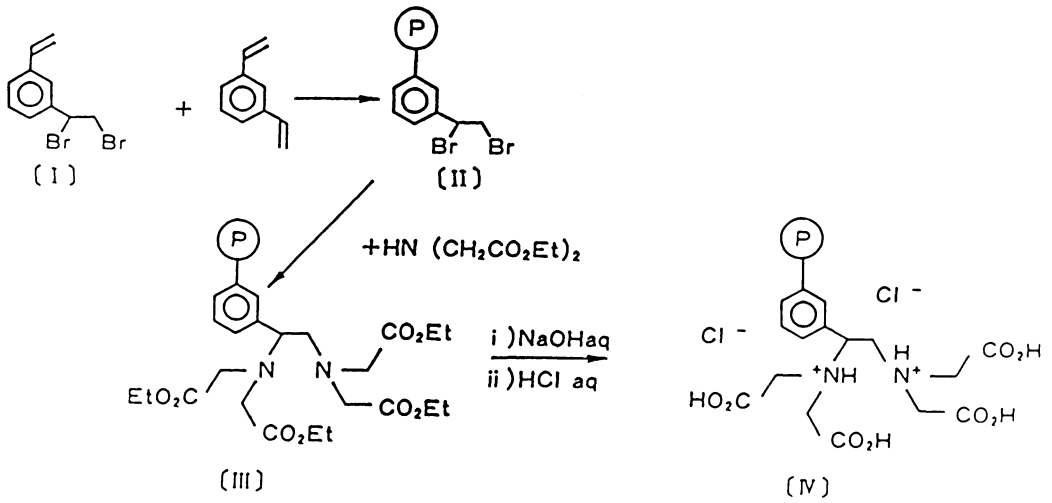

Fig. 1. Synthesis of EDTA-chelating resin.

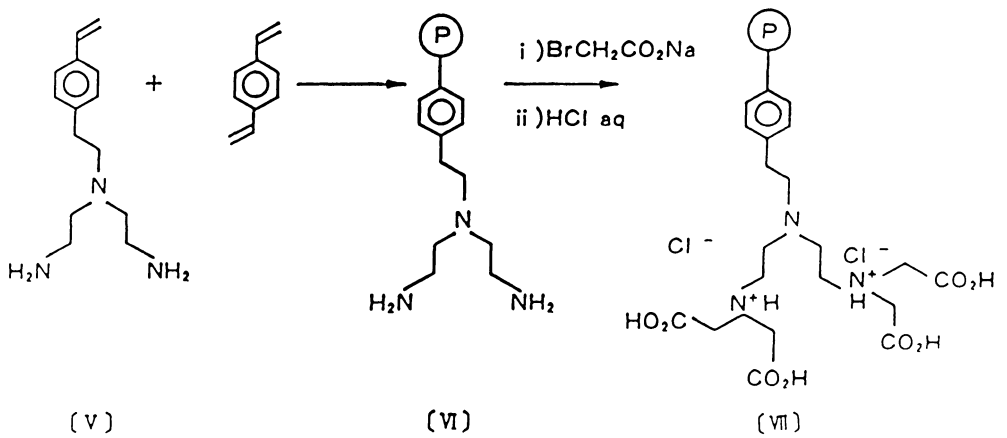

Fig. 2. Synthesis of DTTA-chelating resin.

Table 2. Rare Earth Ion Feed and Flow Rate for Each Separation Experiment

Figure No.	Rare earth feed		Flow rate
	Concentration (mol dm^{-3})	Amount (ml)	ml min^{-1}
5	44	125	14.6
6	34	106	17.3
7	29	120	14.1
8	19	120	12.7
9	19	120	12.5
10	25	120	12.7
11	25	347	9.32

tronics Ltd.).

Separation Procedure: Liquid chromatography was performed at 95 °C in a jacketed Pyrex column with an internal diameter of 10 mm and a length of 1 m (Figs. 5—10) or 2 m (Fig. 11). The concentration and amount of feed and the flow rate in each experiment are listed in Table 2. A chelating resin, which was converted to the OH^- form by an alkaline solution at pH=10, was embedded into this column. The resin bed was washed with de-ionized water to remove any remaining alkali from the column. A solution containing two rare earth elements at equal molar concentrations whose pH was adjusted using hydrochloric acid was fed into the column. Then, 0.1 mol dm^{-3} hydrochloric acid was added to the column and 2 cm^3 fractions of the eluate were collected by means of a fraction collector. The pH and concentrations of the rare earth elements were measured for each fraction.

Results and Discussion

Simulation of Separation for Determining the Experimental Conditions and Analyzing the Experimental Results. The equilibrium reactions involved in this chromatography consisted of the following two types: (i) Dissociation of amine-*N*-polyacetic acids fixed to a resin (acid-base reaction) and (ii) chelate formation of rare earth ions on the resin.

A well-known method for determining equilibrium is to introduce multidimensional equations using the equilibrium constant K. The equations give a plural of roots and it was generally hard to choose the correct root. An alternative method is to determine the concentrations in an equilibrium state by minimizing the Gibbs' free energy.[13,14] This method was more complicated, so both methods were unsuitable for the chromatography simulation.

Therefore, we devised a new method[15,16] in which each reaction was expressed as an addition reaction, and the "reduction potential strength" was used to evaluate the reaction thermodynamically. This method enabled the concentration of each chemical species to be readily determined for any equilibrium state of a system of plural reactions. Here, it is briefly explained.

In this study, a completely dissociated form of a resin-bound chelating group, denoted as R-$(COO^-)_n$, was adopted as an acceptor (Eq. 3) instead of a non-dissociated form, R-$(COOH)_n$. An addition of protons can generally be expressed as

$$\text{R-}(\text{COO}^-)_n + l\,\text{H}^+ \longrightarrow \text{R-}(\text{COO}^-)_{n-l}(\text{COOH})_l, \quad (1)$$

where n and l are integers safisfying $n \geqq l \geqq 1$. n=2 for an IDA type and n=4 for EDTA and DTTA types.

The addition of a rare earth ion to the acceptor can be expressed as

$$\{[\text{R-}(\text{COO})_n]^{n-}\}_m + \text{RE}^{3+} \longrightarrow \{[\text{R-}(\text{COO})_n]_m \cdot \text{RE}\}^- \quad (2)$$

where n=2 and m=2 for an IDA type. n=4 and m=1 for EDTA and DTTA types. The above two kinds of equations are referred to as individual reactions, where R-$(COO)_n^{n-}$ can be considered, apriori, to be suitable as an acceptor for both addends, H^+ and RE^{3+}, in the systems of this study. It was also reported[16] that amine-*N*-polyacetic acids such as EDTA complexed effectively with rare earth ions in an acceptor form as represented by Eq. 2. Taking advantage of the above expressions and reduction-potential strengths results in easier calculations and more definite determinations of the thermodynamics of a system involving plural exchange reactions, inclusive of the adsorption-desorption of rare earth ions and an acid-base reaction.

The protonation to a conjugate base and chelate formation are both generally expressed in a unified form:

$$\text{A} + \nu \cdot \text{X} \longrightarrow \text{D}. \quad (3)$$

where A is the acceptor of an addend X, D is an adduct and ν is the stoichiometric coefficient of an addend X. 'A' can refer to a carboxylate ion of an amine-*N*-polyacetic acid ligand; 'X' can refer to a rare earth ion or a proton and 'D' can be a complex of a rare earth ion with a carboxylate ion or a non-dissociated acid. The equilibrium relationship of Eq. 3 can be expressed as follows by using thermodynamic relations[17]:

$$\Delta\mu_x = \Delta\mu^\circ_{\text{D}} + \frac{RT}{\nu} \ln \frac{a_{\text{A}}}{a_{\text{D}}}. \quad (4)$$

Here, $\Delta\mu_x$ is termed the "reduction potential strength" and is defined by the chemical potential μ_x and standard chemical potential μ°_x as

$$\Delta\mu_x \equiv \mu^\circ_x - \mu_x. \quad (5)$$

$\Delta\mu^\circ_{\text{D}}$ is the "standard reduction potential strength" and is defined as

$$\Delta\mu^\circ_{\text{D}} \equiv \mu^\circ_x - \frac{(\mu^\circ_{\text{D}} - \mu^\circ_{\text{A}})}{\nu}. \quad (6)$$

Suppose that a system contains several kinds of

acceptor species A and N kinds of the addend X. The concentration ratio of an arbitrary adduct species D, which is a mixed-ligand complex of a given i-th species of A with L_j units of any j addend of X(j=1,2,…,N), to the remaining non-complexed i-th species can be expressed as Eq. 7[18]:

$$T_{i,Lj} = \exp\left(\frac{S_p - L_p}{RT}\right), \tag{7}$$

where

$$S_p = \sum_{j=1}^{N} \sum_{n_j=1}^{L_j} \nu_{i,n_j} \Delta\mu^\circ_{i,n_j} \tag{8}$$

and

$$L_p = \sum_{j=1}^{N} \sum_{n_j=1}^{L_j} \nu_{i,n_j} \Delta\mu_{i,n_j}. \tag{9}$$

Here, n_j is the stepwise number of additions of any addend j and L_j is the cumulative number of additions.

The introduced distribution function, Eq. 7, seems to be complicated, but it can be easily solved numerically since it always increases monotonously and leads to only one solution for any case.

Simulations were executed according to the following imaginary separation procedures: (1) An alkaline solution was supplied to a column packed with an EDTA-chelating resin, so as to dissociate amine-*N*-polyacetic acid groups of the resin; (2) An imaginary solution containing Nd^{3+} and Pr^{3+} was passed through the column and (3) the rare earth chelates were decomposed by supplying an acid solution. The first, second and third procedures are called "regeneration," "adsorption," and "development," respectively. Computations using an ECLIPS minicomputer manufactured by Data General Co., Ltd. were executed step-by-step for each imaginary plate formed by subdividing a packed column. In this procedure, Eq. 7 was repeatedly applied according to the reported treatment of multi-stage equilibrium.[19] The $\Delta\mu^\circ_{i,n_j}$ for rare earth ions and for H^+ are summarized in Tables 3(a)[20] and 3(c).[21] S_P for H^+ in Eq. 8 is shown in Table 3(b) and L_p is dependent on the concentrations of two addends (H^+ and RE^{3+}) in each plate of chromatography.

The results of simulated separation conditions in the chromatography can be summarized as follows:

1. A resin bed can be regenerated with an alkaline solution at pH>11.
2. A resin bed can be regenerated not only with a less alkaline solution but with a weakly acidic (pH>4) solution. It is hardly regenerated with a solution at pH<4.
3. Asorption bands can be developed at pH<2.
4. The concentrations of eluted rare earth ions are correlated positively with the acid concentration in the developing solution.

Table 3(a). $\Delta\mu^\circ_{i,n_j}$ for Protonation to the Conjugate Bases of Amine-*N*-polyacetic Acids

(kJ mol^{-1})

Amine-*N*-polyacetic acid	$\Delta\mu^\circ_{i,n_j}$[a]				
	n_j=1	n_j=2	n_j=3	n_j=4	n_j=5
IDA	44.0	14.3	—	—	—
EDTA	54.5	27.2	15.5	11.3	—
DTPA	59.9	49.0	20.4	15.0	10.8

a) The j refers to a proton and n_j to the stepwise number of the addition. Values of $\Delta\mu^\circ_{i,n_j}$ were calculated using the stepwise dissociation constants of the amine-*N*-polyacetic acids listed in Ref. 20.

Table 3(b). *S*-Potentials for Protonation to the Conjugate Base of Ethylenediaminetetraacetic Acid

(kJ mol^{-1})

L_j[a]	0	1	2	3	4
S_p	0	54.5	81.7	97.2	108.5

a) The j refers to a proton and L_j the cumulative number of additions.

Table 3(c). $\Delta\mu^\circ_{i,n_j}$[a] for a Complex Formation of Rare Earth Ions with Amine-*N*-polyacetic Acids

(kJ mol^{-1})

Rare earth ion	IDA	EDTA	DTPA
La^{3+}	33.5	88.4	114.0
Ce^{3+}	—	91.3	—
Pr^{3+}	39.4	93.9	124.9
Nd^{3+}	39.8	95.1	127.0
Sm^{3+}	40.6	98.0	130.7
Eu^{3+}	41.5	99.3	130.7
Gd^{3+}	40.2	99.3	131.6
Tb^{3+}	41.1	102.7	132.8
Dy^{3+}	41.9	104.8	134.1
Ho^{3+}	—	—	—
Er^{3+}	42.3	107.7	132.4
Tm^{3+}	42.7	110.6	131.1
Yb^{3+}	44.0	111.5	131.6
Lu^{3+}	—	113.1	—

a) The j refers to a rare earth ion. Values of $\Delta\mu^\circ_{i,n_j}$ were calculated using the stability constants of the rare earth ions listed in Ref. 21.

Examples of the simulation results, selected to determine a favorable experimental condition, are illustrated in Figs. 3 and 4.

When a solution has pH=10 (Fig. 3), the dissociation degree of EDTA groups within the resin is 83%. At pH=4 (Fig. 4) it is only 54%. In view of a reported observation,[16] it was originally expected that the rare earth ions could not be effectively adsorbed after a regeneration procedure at pH=4. However, it was predicted from simulation results that rare earth ions could be adsorbed when the solution was at pH=4 as well as at pH=10. At

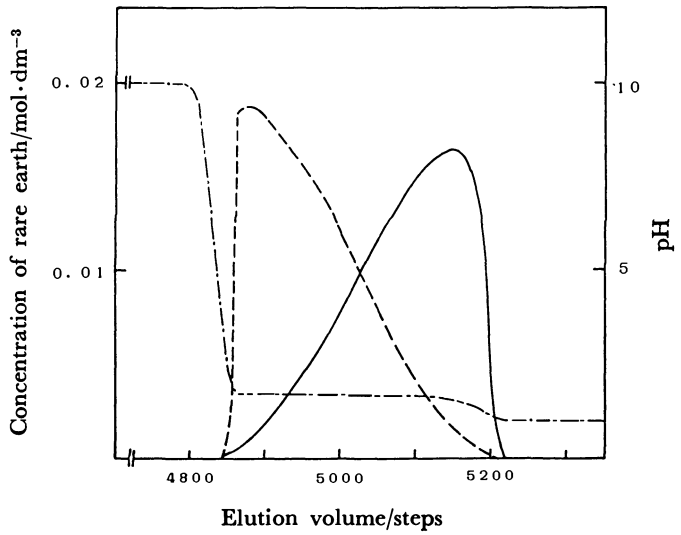

Fig. 3. Simulation of the separation of rare earth ions with EDTA-chelating resin. (The adsorption band is regenerated at pH=10 then developed with 0.1 mol dm^{-3} HCl.) ——: pH, ----: Pr^{3+}, ——: Nd^{3+}.

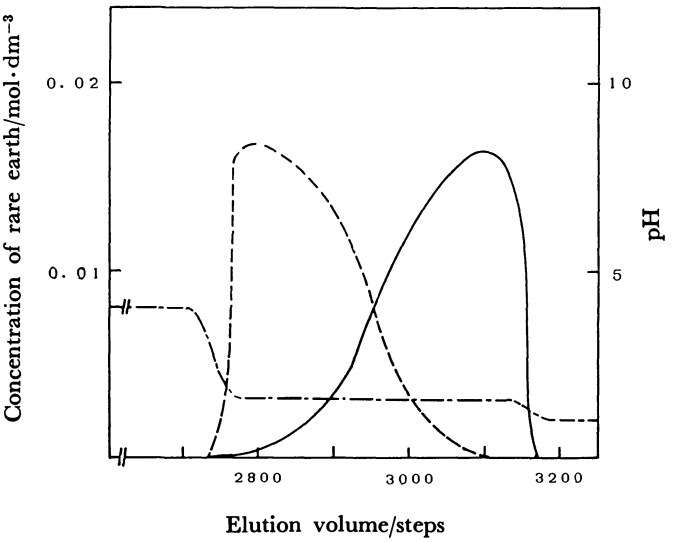

Fig. 4. Simulation of the separation of rare earth ions with EDTA-chelating resin. (The adsorption band is regenerated at pH=4 then developed with 0.1 mol dm^{-3} HCl.) ——: pH, ——: Pr^{3+}, ——: Nd^{3+}.

pH=4, two of the four carboxyl groups of an EDTA moiety were not dissociated. As a rare earth ion approaches the EDTA moiety, two nondissociated protons seem to be exchanged for a rare earth ion, allowing it to form a complex. The S_p of the second proton addition to the conjugate base of EDTA is 81.7 kJ mol^{-1} whereas the S_p of the complex formation of Pr^{3+} and Nd^{3+} with EDTA that are identical to the $\Delta\mu^{\circ}_{i,n_i}$ in these cases are as large as 93.9 and 95.1 kJ mol^{-1}. This might explain quantitatively why protons can be replaced by Pr^{3+} and Nd^{3+}.

The step number (the number of simulation calculations in which the imaginary solution phase is shifted downwards as the acid solution descends) at which rare earth ions begin to elute, is about 4840 when the adsorption band is initially regenerated at pH=10 (Fig. 3). The corresponding step number is 2750 when it is initially regenerated at pH=4(Fig. 4). It is noted that in the case of EDTA groups, the ratio of the dissociation degree at pH=10 to that at pH=4 is 1.5; also, the corresponding ratio of the step numbers for rare earth ions to start being eluted is 1.7. Thus, the former ratio does not agree with the latter ratio. It was then considered (on the basis of material balance) what determines the ratio of the step numbers for rare earth ions to start being eluted. The elution volume at the break-through point is defined by the resin volume and the rare earth ion concentrations in the solid and liquid phases.
That is,

$$V_f = \frac{C_{R,r}}{C_{R,s}} V_r \tag{10}$$

where V_f is the elution volume at the break-through point, V_r the resin volume, and $C_{R,r}$ and $C_{R,s}$ the rare earth ion concentrations in the solid and liquid phases. The ratio $C_{R,r}/C_{R,s}$ should be expressed by the proton concentrations in the respective regions as

$$\frac{C_{R,r}}{C_{R,s}} = \frac{[C_{H,r}]_B - [C_{H,r}]_F}{[C_{H,s}]_B}, \tag{11}$$

where $[C_{H,r}]_B$ and $[C_{H,s}]_B$ are the solid- and liquid-phase proton concentrations in the rare earth band and $[C_{H,r}]_F$ the solid-phase proton concentration in the front region. From Eqs. 10 and 11, the following equation is derived:

$$V_f = \frac{[C_{H,r}]_B - [C_{H,r}]_F}{[C_{H,s}]_B} V_r. \tag{12}$$

Calculations of V_f from Eq. 12 for regenerations at pH=10 and pH=4 give a value of 1.75 for the ratio of V_f. This value is almost equal to the value described above as the ratio of the step numbers for rare earth ions to start being eluted. The reason why the ratio of V_f at pH=10 to that at pH=4 is much larger than unity is that $[C_{H,r}]_F$ at pH=4 is almost three-times that at pH=10 while the $[C_{H,r}]_B$ at pH=4 is only two-times that at pH=10. $[C_{H,s}]_B$ does not change very much with the pH.

A rear boundary reaction is completed by bringing a sufficient amount of acid into contact with chelated rare earth ions. The acid concentration at the rear boundary is closely related to the liquid-phase concentration of rare earth ions in the adsorption band. The total concentration of the rare earth ions is about 110 mmol dm^{-3} when developed using 0.5 mol dm^{-3} hydrochloric acid whereas this concentration is about 20 mmol dm^{-3} with 0.1 mol dm^{-3} hydrochloric acid (Fig. 4).

The actual experimental conditions were set so that the pH of the regenerating solution was 10 and the acid concentration of the developing solution was 0.1 mol dm^{-3}.

Results of Experiments. A chromatographic separation of rare earth elements was carried out using each of the three different chelating resins under the computer-simulated conditions.

The result of a chromatographic separation of La^{3+} and Nd^{3+} with an IDA-chelating resin is shown in Fig. 5. The result was good, reflecting the large difference in the potential strengths of La^{3+} and Nd^{3+}, which is shown to be 6.3(kJ mol^{-1}) from Table 3(c). But Pr^{3+} and Nd^{3+} were slightly separated with IDA-chelating resin in Fig. 6. The result indicated that the difference $\Delta(\Delta\mu^\circ_{i,n_j})$ of the potential strengths $\Delta\mu^\circ_{i,n_j}$ between Pr^{3+} and Nd^{3+} with the IDA-chelating resin was small (see Table 4), as expected from the $\Delta(\Delta\mu^\circ_{i,n_j})$ with the corresponding acid (IDA) shown in Table 3(c).

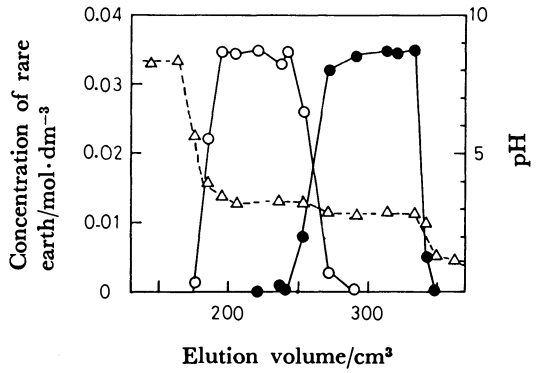

Fig. 5. Separation of La^{3+} and Nd^{3+} with IDA-chelating resin. △: pH, ○: La^{3+}, ●: Nd^{3+}.

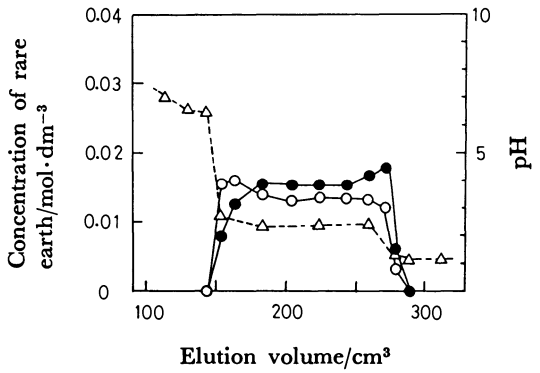

Fig. 6. Separation of Pr^{3+} and Nd^{3+} with IDA-chelating resin. △: pH, ○: Pr^{3+}, ●: Nd^{3+}.

Table 4. $\Delta(\Delta\mu^\circ_{i,n_j})$ for a Complex Formation of Rare Earth Ions with Chelating Resins

(kJ mol^{-1})

	IDA	EDTA	DTTA
Nd^{3+}/Pr^{3+}	0.17	0.88	0.92

Separation between Pr^{3+} and Nd^{3+} was more effectively attained with the EDTA-chelating resin prepared from m-DBS (Fig. 7). The potential difference $\Delta(\Delta\mu^\circ_{i,n_j})$ between both ions with the corresponding acid (EDTA) was 1.2 kJ mol^{-1}, larger than that of IDA (0.4 kJ mol^{-1}). Figure 8 shows even better separation result using the DTTA-chelating resin prepared from styrenetriamine monomer (**V**), than that using the EDTA-chelating resin. The potential difference of these ions with DTPA, whose structure is similar to DTTA, is 2.1 kJ mol^{-1} and is larger than that with EDTA. The potential-strength differences with the chelating resins observed in Fig. 6 to Fig. 8 (listed in Table 4) were all smaller than expected from the differences obtained with the corresponding amine-*N*-polyacetic acids. The reduction of the potential-strength differences is considered to be due to a steric hindrance of a polymer network to all the three acids and a chemical structure difference between DTPA and the resin-bound DTTA moiety. The other separation experiments for pairs of Eu^{3+}/Gd^{3+} and Ho^{3+}/Eu^{3+} with a DTTA-type resin gave the results shown in Figs. 9 and 10, respectively. The potential strength of Ho^{3+} is not

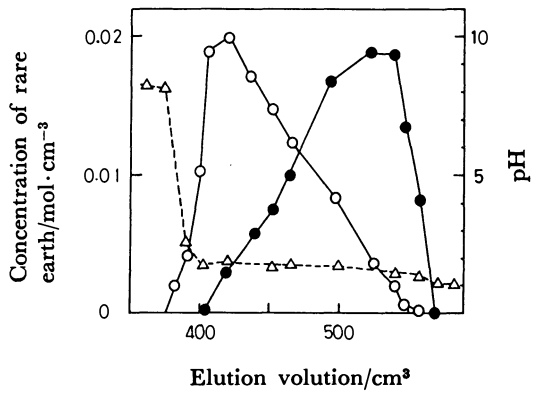

Fig. 7. Separation of Pr^{3+} and Nd^{3+} with EDTA-chelating resin. △: pH, ○: Pr^{3+}, ●: Nd^{3+}.

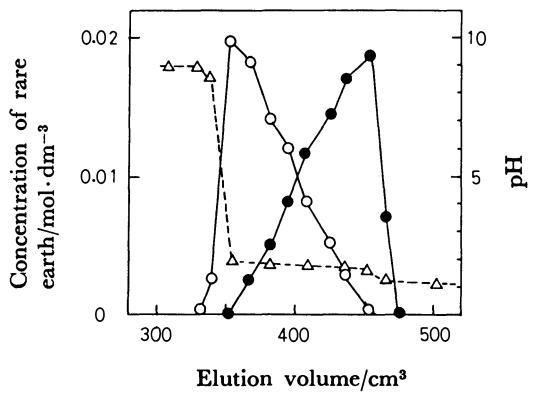

Fig. 8. Separation of Pr^{3+} and Nd^{3+} with DTTA-chelating resin. △: pH, ○: Pr^{3+}, ●: Nd^{3+}.

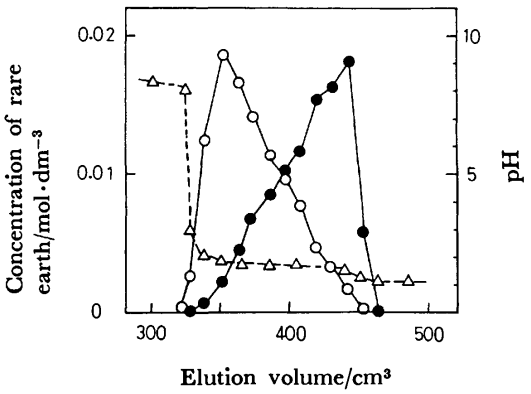

Fig. 9. Separation of Gd^{3+} and Eu^{3+} with DTTA-chelating resin. △: pH, ○: Gd^{3+}, ●: Eu^{3+}.

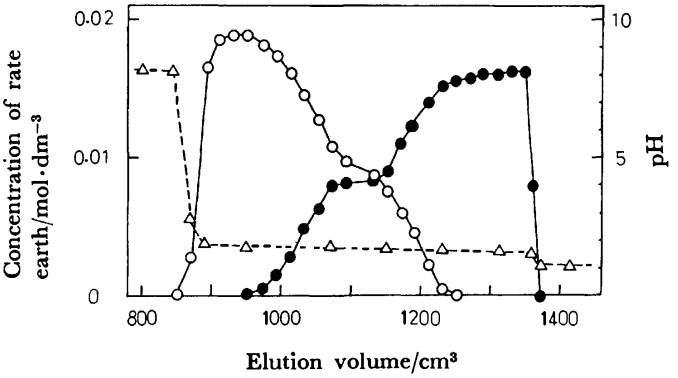

Fig. 11. Separation of Pr^{3+} and Nd^{3+} with DTTA-chelating resin. △: pH, ○: Pr^{3+}, ●: Nd^{3+}.

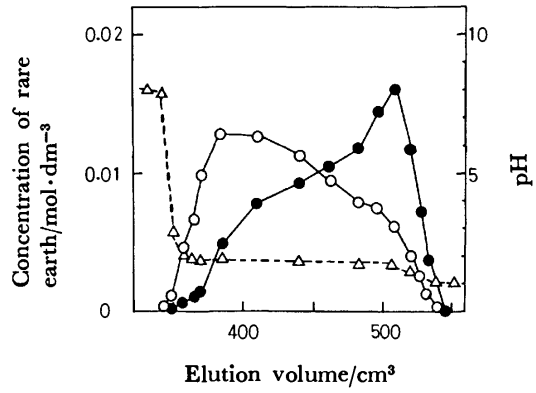

Fig. 10. Separation of Ho^{3+} and Eu^{3+} with DTTA-chelating resin. △: pH, ○: Ho^{3+}, ●: Eu^{3+}.

known and Fig. 10 is the first result of Ho^{3+} separation attempted with a DTTA-type chelate resin. The adsorbability of the Gd^{3+}/Eu^{3+} pair was contrary to that expected from the $\Delta(\Delta\mu^\circ)$ listed in the right column of Table 3(c). Several possible causes can be considered. The potential strengths of rare earth elements which have higher atomic numbers than Sm are similar to each other and no explicit tendency between the potential strengths and the atomic numbers has been observed for almost all amine-*N*-polyacetic acids. Moreover, structural distinction between DTPA and DTTA is necessary to be considered. Additional experimental results and theoretical considerations are necessary; these are presently being collected for our future reports.

Figure 11 shows the results using a longer separation column packed with a DTTA-chelating resin; the separation of Pr^{3+} and Nd^{3+} was further improved, compared with the shorter-column experiment shown in Fig. 8. Highly purified Pr^{3+} and Nd^{3+} could be recovered from almost half of the adsorption bands as well as from the neighborhoods of the front and rear boundaries. Comparing the results in Figs. 8 and 11, the volumes of the mixed-ion zone, where Pr^{3+} and Nd^{3+} were not fully (though partially) separated from each other, were not much different. It is, thus, recognized that with a longer separation column, more fractions containing highly-purified rare earth ions can be recovered. In elution chromatography the concentrations of separated materials in effluents generally decrease with an increasing length of the separation column. The concentration of rare earth ions recovered in Fig. 11 was nearly equal to that in Fig. 8 due to displacement chromatography. The fractions from 850 to 1370 cm^3 of the elution volume (Fig. 11) were analyzed by an Argon-plasma spectrometer to determine the purity of each constituent. Two fifths of the fractions had purity values ranging from 99.99 to 99.999%. Near the rear boundary, the purity of Nd^{3+} ions seemed to be higher than 99.999% since it tended to be higher in a later fraction; however, no accurate analytical value greater than 99.999% was obtained in the measurement. An analysis of kinetics is indispensable for any discussion of chromatography and results always strongly depend on the speed of adsorption-desorption or ligand exchange. In this study, the height of an imaginary plate used in the simulation was converted to the volume of the effluent under the experimental conditions by comparing the separation profiles.

Conclusion

The separation of rare earth ions was studied with synthesized amine-*N*-polyacetic acid type chelating resins.

(1) Satisfactory separation results were obtained in experiments by displacement chromatography using EDTA- and DTTA-chelating resins.

(2) Highly-purified rare earth ions could be recovered more efficiently using a longer separation column.

(3) Systems comprising five equilibrium reactions were analyzed using the concept of reduction potential strength and a novel distribution function. A prediction made on the basis of

simulation results matched the results of separation experiments in the case of Nd^{3+}/Pr^{3+} with good precision.

(4) The step number at which rare earth ions began to elute depended on the pH of the regenerating solution; the total concentration of the rare earth ions depended on the acid concentration of the developing solution.

(5) Several rare earth ions could be separated using a DTTA-chelating resin most efficiently. However, much remains to be done before quantitatively discussing the observed differences in $\Delta(\Delta\mu^\circ)$ between the chelating resins and the corresponding amine-*N*-polyacetic acids.

The authors would like to sincerely thank Prof. Teiji Tsuruta of the Science University of Tokyo for his instructions regarding the synthesis of the starting material and the polymer used in preparing the DTTA-chelating resin, and for his helpful suggestions regarding the characterization of the chelating resins. The authors also would like to thank Prof. Manabu Seno of the University of Tokyo for his suggestions regarding equilibrium and separations studies using chelating resins.

References

1) F. H. Spedding and A. H. Daane, "The Rare Earths," R. E. Krieger Publ. Co., New York (1971), pp. 38—70.

2) N. N. Matorina, S. M. Kagiyants, O. V. Kryuchkova, and K. V. Chmutov, *J. Phys. Chem.*, **52**, 1155 (1978).

3) R. Hering, *J. Inorg. Nucl. Chem.*, **24**, 1399 (1962).

4) G. J. Schrobilgen and C. E. Lang, *J. Inorg. Nucl. Chem.*, **30**, 3127 (1968).

5) K. V. Barsukova and N. Yu. Kremlyakova, *Radiokhimiya*, **23**, 306 (1981).

6) T. Yamamizu, M. Akiyama, and K. Takeda, *Reactive Polymers*, **3**, 173 (1985).

7) M. Maeda, Y. Nitadori, and T. Tsuruta, *Makromol. Chem.*, **181**, 2251 (1980).

8) a) T. Tsuruta and Y. Nitadori, Japanese Patent Publication (unexamined), 11523/1980, Jan. 26, (1980); b) T. Tsuruta, Y. Nitadori, and M. Maeda, Japanese Patent publication (unexamined), 13237/1980, Jan. 30, (1980).

9) K. Takeda, M. Akiyama, and T. Yamamizu, *Reactive Polymers*, **4**, 11 (1985).

10) E. B. Trostyanskaya, L. P. Losev, A. S. Tevlina, S. B. Makarova, G. Z. Nefedova, and L. J. Syan'-Zhao, *J. Polym. Sci.*, **59**, 379 (1962).

11) M. Okamura, Y. Komeda, and E. Imoto, *Koubunshi Kagaku*, **17**, 30 (1960).

12) a) K. Ito and Y. Yamashita, *J. Polym. Sci.*, **A3**, 2165 (1965); b) C. W. Pyun, *J. Polym. Sci.*, **A-2, 8**, 1111 (1970).

13) H. J. Kandiner and S. R. Brinkley, Jr., *Ind. Eng. Chem.* **42**, 850 (1950).

14) W. B. White, S. M. Johnson, and G. B. Dantzig, *J. Chem. Phys.*, **28**, 751 (1958).

15) K. Takeda, F. Kawakami, and M. Sasaki, *Denki Kagaku*, **53**, 8 (1985).

16) J. L. Hoard, B. Lee, and M. D. Lind, *J. Am. Chem. Soc.*, **87**, 1612 (1965).

17) K. Takeda, H. Obanawa, and M. Sasaki, *Denki Kagaku*, **53**, 794 (1985).

18) K. Takeda, M. Sasaki, I. Hataue, and H. Obanawa, *Denki Kagaku*, **53**, 685 (1985).

19) A. J. O. Martin and R. L. M. Synge, *Biochem. J.*, **35**, 1358 (1941).

20) L. G. Sillen and A. E. Martell (Compiled), Stability Constants of Metal-Ion Complexes, The Special Publication No. 17, The Chemical Society, London (1964).

21) P. Krumholz, Solution Chemistry, "Progress in the Science and Technology of the Rare Earths," ed by L. Eyring, Pergamon Press, Oxford, (1964), Vol. 1, pp. 110—138.

 © 1986 The Chemical Society of Japan Bull. Chem. Soc. Jpn., 59, 2233—2236 (1986)

Conformation of Condensed Polycyclic Aromatic Hydrocarbons. II. The Molecular and Crystal Structure of Violanthrene B (Dibenzo[*a, rst*]naphtho[8,1,2-*cde*]pentaphene)[1]

Isao Oonishi,* Shoji Fujisawa, Junji Aoki, Yuji Ohashi,† and Yoshio Sasada††
Department of Chemistry, Faculty of Science, Toho University, Funabashi, Chiba 274
†Department of Chemistry, Faculty of Science, Ochanomizu University, Otsuka, Bunkyo-ku, Tokyo 112
††Laboratory of Chemistry for Natural Products, Tokyo Institute of Technology, Nagatsuta, Midori-ku, Yokohama 227
(Received April 7, 1985)

The title compound, $C_{34}H_{18}$, has been obtained by reducing violanthrone B, a byproduct in the synthesis of violanthrone. Its structure has been determined by on X-ray analysis. The space group is $P2_1/c$, with unit-cell dimensions a=25.78(1), b=3.807(5), c=19.975(8) Å, β=96.55(3)°, and Z=4. The structure was solved by the direct method and refined by a block-diagonal least-squares method to an R value of 0.076 on the basis of 1242 independent reflections. The molecules are largely distorted from a planar structure owing to a steric repulsion between the intramolecular overcrowded hydrogen atoms. Also, they are stacked face-to-face to form a column structure along the b-axis.

The title hydrocarbon, violanthrene B, was obtained by reducing violanthrone B, a byproduct in the synthesis of violanthrone. Although its structure has been assumed to be I, a confirmation by X-ray analysis is still necessary to elucidate the reaction mechanism.[2-7] Futhermore, it is very interesting to examine the molecular deformations of such overcrowded hydrocarbons as I to IV, which have very short H···H contacts. The structure of II,[8] III,[9] and IV[10] have already been reported.

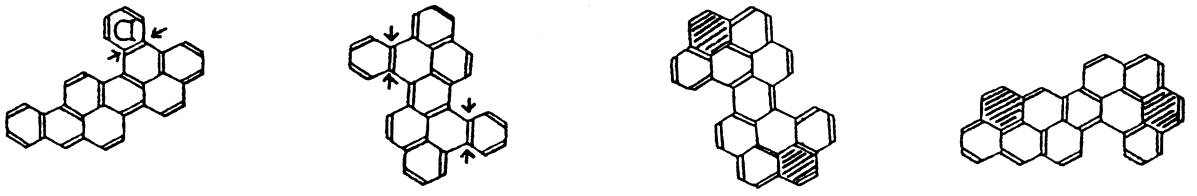

I II*1) III*2) IV*3)

*1) Tetrabenzo[*a,cd,j,lm*]perylene (TBP)
*2) Diphenanthro[5,4,3-*abcd*: 5′,4′,3′-*jklm*]perylene (DPP)
*3) Anthra[2,1,9,8-*hijkl*]benzo[*de*]naphtho[2,1,8,7-*stuv*]pentacene (1,11-BisoVEB)

Scheme

Experimental

The title compound was prepared by a previously reported conventional method.[11] The crystals used for X-ray work were grown from an *o*-dichlorobenzene solution. Crystal data are as follows: $C_{34}H_{18}$; M.W. 426.5; monoclinic; a=25.78(1), b=3.807(5), c=19.975(8) Å, β=96.55(3)°, and U=1948(3) Å^3; D_x=1.455 g cm^{-3}; Z=4; space group $P2_1/c$; μ(Cu $K\alpha$)=6.44 cm^{-1}. The intensity data were collected on a Rigaku automated four-circle diffractometer with the $\omega/2\theta$ scan technique, the scanning rate being 2°(2θ) min^{-1}. The dimensions of the crystal used for the data collection were 0.05×0.2×0.5 mm. A total of 2984 independent reflections were measured up to 2θ=125°, using graphite monochromated Cu $K\alpha$ radiation, of which 1242 reflections were ($|F_o|>3\sigma(|F_o|)$). Corrections for Lorentz and polarization factors were made, but not for absorption.

Structure Determination

Systematic absences of $h01$, $l=2n+1$, and $0k0$, $k=2n+1$ indicated the space group to be $P2_1/c$. The structure was solved by a direct method using the MULTAN 78 program.[12] Two disordered molecules with equal occupancies appeared on E-maps as shown in Fig. 1. The disordered structure was refined to R=0.162 by full-matrix least-squares with the SHELX 76 program,[13] but a further refinement based on this model was impossible. A new ordered model with a space group of Pc was constructed from the $P2_1/c$ structure by removing the crystallographic center of symmetry. The refinement was carried out by least-squares. The R value converged to 0.16. Another ordered model ($P2_1/c$) was constructed by

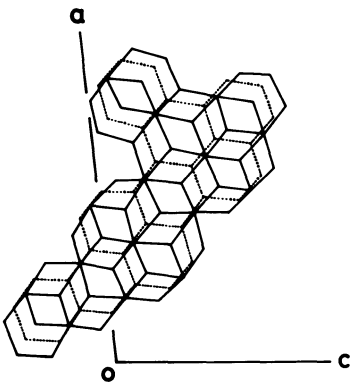

Fig. 1. The false disorderd structure (solid lines) found on the E-map and the true ordered one (dotted lines).

Table 1 Final Atomic Coordinates with Their Estimated Standard Deviations, Multiplied by 10^4 and 10 for B_{eq}

Atom	x	y	z	B_{eq}/Å$^{2a)}$
C(1)	1241(3)	2138(27)	−1452(5)	34(3)
C(2)	800(4)	2115(31)	−1900(5)	40(3)
C(3)	323(4)	849(29)	−1731(5)	43(3)
C(4)	291(4)	−558(29)	−1099(5)	42(3)
C(5)	746(4)	−517(27)	−613(5)	37(3)
C(6)	719(3)	−1932(29)	43(5)	39(3)
C(7)	1150(4)	−1843(26)	523(5)	34(3)
C(8)	1117(4)	−3256(28)	1205(5)	38(3)
C(9)	1540(4)	−3209(28)	1671(5)	38(3)
C(10)	2036(3)	−1904(26)	1537(5)	33(3)
C(11)	2474(3)	−1644(27)	2020(5)	33(3)
C(12)	2422(4)	−2480(29)	2739(5)	40(3)
C(13)	2838(4)	−1973(30)	3211(5)	38(3)
C(14)	3318(4)	−696(28)	3062(5)	38(3)
C(15)	3725(4)	12(32)	3570(5)	44(3)
C(16)	4183(4)	1410(35)	3408(5)	49(3)
C(17)	4275(4)	2043(32)	2732(5)	41(3)
C(18)	3878(3)	1253(29)	2218(5)	37(3)
C(19)	3977(3)	1447(27)	1499(5)	34(3)
C(20)	4474(4)	2186(33)	1328(5)	42(3)
C(21)	4586(4)	1827(32)	665(5)	43(3)
C(22)	4190(4)	617(30)	188(5)	39(3)
C(23)	3689(3)	41(30)	337(4)	35(3)
C(24)	3556(3)	700(25)	998(5)	30(3)
C(25)	3031(3)	176(26)	1166(5)	33(3)
C(26)	2578(3)	444(24)	699(5)	30(2)
C(27)	2592(3)	2116(26)	38(4)	32(3)
C(28)	2167(3)	2199(27)	−412(4)	32(3)
C(29)	1684(3)	778(24)	−288(5)	30(3)
C(30)	1227(3)	729(26)	−786(5)	31(3)
C(31)	1642(3)	−621(24)	366(5)	29(3)
C(32)	2089(3)	−671(23)	860(5)	27(2)
C(33)	2964(3)	−570(26)	1854(4)	30(3)
C(34)	3398(4)	−29(27)	2371(5)	33(3)

a) The equivalent isotropic temperature factors were computed using the following expression: $B_{eq}=1/3\sum_{i,j} a_i a_j a_i^* a_j^*$.

averaging two positions of the corresponding atoms of the disordered molecules as shown with dotted lines in Fig. 1; however, no peaks were found at the atomic positions. This model ($P2_1/c$) coincides to the Pc model if a slight difference between two crystallographically independent molecules is neglected and the origin in the Pc model is shifted so that the molecules are related by a center of symmetry. Six cycles of refinement on this model brought the value of R to 0.076, where the thermal parameters for the carbon atoms were assumed to be anisotropic and the unit weight was applied to F_o. No peaks higher than 0.3 eÅ^{-3} were found on the final defference map. The final R was 0.076 with a maximum Δ/δ of 0.5. The atomic-scattering factors were taken from the International Tables for X-ray Crystallography.[14] The final atomic parameters and their estimated standard deviations are listed in Table 1. Lists of the observed and calculated structure factors, parameters of the hydrogen atoms and anisotropic thermal parameters for non-hydrogen atoms are kept in the office of the Chemical Society (Document No. 8632). Computations were performed on the M-280H computer at the Computer Center of the University of Tokyo.

Results and Discussion

The present study has established the structure of I. Figure 2 illustrates the crystal structure viewed along the b axis. The numbering scheme is indicated in Fig. 3, together with the deviations of the atoms from the mean plane of the molecule. The bond lengths and angles are listed in Tables 2 and 3, respectively. The mean bond length of the outer bonds is slightly shorter than that of the inner lengths and the three bonds around each carbon atom are nearly coplanar. These facts have also been found for some polycyclic

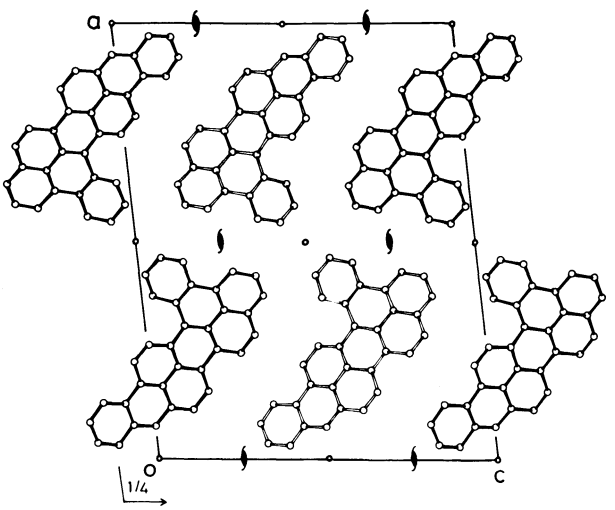

Fig. 2. A projection of the crystal structure along the b axis.

aromatic hydrocarbons.[8,9,10] Figure 4 shows a perspective drawing of the molecule. This molecule is greatly distorted from a planar conformation because of the repulsion betwen the crowded hydrogen atoms, known as an 1,7 interaction. The steric repulsion between H(23) and H(27) is mainly released by the enlargement of the C(24)–C(25)–C(26) angle and the twisting of the C(23)–C(24) and C(27)–C(26) bonds around the line C(24)···C(26) as defined in ref. 10. The angle of C(24)–C(25)–C(26) (α), the twisting angle of C(23)–C(24)···C(27)–C(26) (β) and the nonbonded C···C distances (C(24)···C(26))

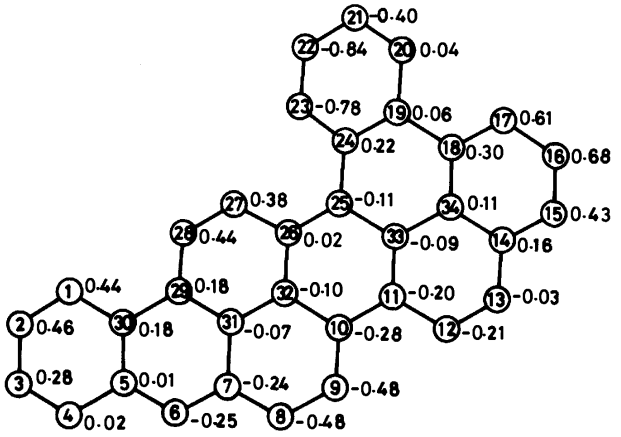

Fig. 3. The numbering scheme and displacements (l/Å) of atoms from the mean plane.

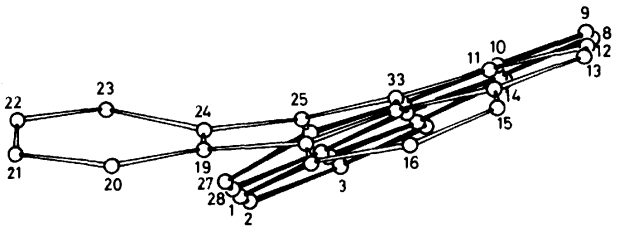

Fig. 4. A perspective drawing of the molecule.

Table 2. Bond Lengths (l/Å) with Their Estimated Standard Deviations

C(1)–C(2)	1.37(2)	C(16)–C(17)	1.42(2)
C(1)–C(30)	1.44(1)	C(17)–C(18)	1.40(2)
C(2)–C(3)	1.40(2)	C(18)–C(19)	1.48(2)
C(3)–C(4)	1.38(2)	C(18)–C(34)	1.39(2)
C(4)–C(5)	1.44(2)	C(19)–C(20)	1.39(2)
C(5)–C(6)	1.43(2)	C(19)–C(24)	1.42(1)
C(5)–C(30)	1.40(1)	C(20)–C(21)	1.39(2)
C(6)–C(7)	1.39(2)	C(21)–C(22)	1.40(2)
C(7)–C(8)	1.48(1)	C(22)–C(23)	1.37(2)
C(7)–C(31)	1.42(1)	C(23)–C(24)	1.42(2)
C(8)–C(9)	1.36(2)	C(24)–C(25)	1.44(1)
C(9)–C(10)	1.42(1)	C(25)–C(26)	1.42(1)
C(10)–C(11)	1.41(1)	C(25)–C(33)	1.43(1)
C(10)–C(32)	1.45(1)	C(26)–C(27)	1.47(1)
C(11)–C(12)	1.49(2)	C(26)–C(32)	1.40(1)
C(11)–C(33)	1.40(1)	C(27)–C(28)	1.34(1)
C(12)–C(13)	1.37(2)	C(28)–C(29)	1.40(1)
C(13)–C(14)	1.39(2)	C(29)–C(30)	1.46(1)
C(14)–C(15)	1.41(2)	C(29)–C(31)	1.43(1)
C(14)–C(34)	1.44(2)	C(31)–C(32)	1.43(1)
C(15)–C(16)	1.37(2)	C(33)–C(34)	1.45(1)

Table 3. Bond Angles (ϕ/°) with Their Estimated Standard Deviations

C(2)–C(1)–C(30)	120(1)	C(19)–C(20)–C(21)	121(1)
C(1)–C(2)–C(3)	122(1)	C(20)–C(21)–C(22)	118(1)
C(2)–C(3)–C(4)	120(1)	C(21)–C(22)–C(23)	122(1)
C(3)–C(4)–C(5)	119(1)	C(22)–C(23)–C(24)	120(1)
C(4)–C(5)–C(6)	119(1)	C(23)–C(24)–C(25)	122(1)
C(4)–C(5)–C(30)	121(1)	C(23)–C(24)–C(19)	116(1)
C(6)–C(5)–C(30)	120(1)	C(25)–C(24)–C(19)	122(1)
C(5)–C(6)–C(7)	120(1)	C(24)–C(25)–C(26)	124(1)
C(6)–C(7)–C(8)	120(1)	C(24)–C(25)–C(33)	118(1)
C(6)–C(7)–C(31)	122(1)	C(26)–C(25)–C(33)	118(1)
C(8)–C(7)–C(31)	118(1)	C(25)–C(26)–C(27)	121(1)
C(7)–C(8)–C(9)	120(1)	C(25)–C(26)–C(32)	121(1)
C(8)–C(9)–C(10)	123(1)	C(27)–C(26)–C(32)	117(1)
C(9)–C(10)–C(11)	124(1)	C(26)–C(27)–C(28)	121(1)
C(9)–C(10)–C(32)	119(1)	C(27)–C(28)–C(29)	123(1)
C(11)–C(10)–C(32)	117(1)	C(28)–C(29)–C(30)	123(1)
C(10)–C(11)–C(12)	119(1)	C(28)–C(29)–C(31)	118(1)
C(10)–C(11)–C(33)	122(1)	C(30)–C(29)–C(31)	119(1)
C(12)–C(11)–C(33)	119(1)	C(29)–C(30)–C(1)	121(1)
C(11)–C(12)–C(13)	119(1)	C(29)–C(30)–C(5)	120(1)
C(12)–C(13)–C(14)	123(1)	C(1)–C(30)–C(5)	118(1)
C(13)–C(14)–C(15)	121(1)	C(7)–C(31)–C(29)	119(1)
C(13)–C(14)–C(34)	120(1)	C(7)–C(31)–C(32)	121(1)
C(15)–C(14)–C(34)	119(1)	C(29)–C(31)–C(32)	120(1)
C(14)–C(15)–C(16)	120(1)	C(10)–C(32)–C(26)	120(1)
C(15)–C(16)–C(17)	122(1)	C(10)–C(32)–C(31)	119(1)
C(16)–C(17)–C(18)	118(1)	C(26)–C(32)–C(31)	121(1)
C(17)–C(18)–C(19)	120(1)	C(11)–C(33)–C(25)	120(1)
C(17)–C(18)–C(34)	120(1)	C(11)–C(33)–C(34)	121(1)
C(19)–C(18)–C(34)	119(1)	C(25)–C(33)–C(34)	119(1)
C(18)–C(19)–C(20)	121(1)	C(14)–C(34)–C(18)	120(1)
C(18)–C(19)–C(24)	118(1)	C(14)–C(34)–C(33)	118(1)
C(20)–C(19)–C(24)	121(1)	C(18)–C(34)–C(33)	122(1)

Table 4. Comparison of Steric Hindrance

Molecule		α/°	β/°	d(C···C)/Å
1. Benz[c]phenanthrene[15] (BPT)		124.6	31.4	3.03
2. VEB (This molecule)		124	37.3	2.93
3. 1,11-BisoVEB[a]	A)	128.7	30.1	2.94
	B)	120.9	37.6	2.96
4. TBP	1	123.5	41.0	2.971
	2	122.7	41.5	2.944
5. DPP[a,b]	A)	119	39	3.01
	B)	121	30	2.87

a) A and B indicate the crystallographically independent molecules. b) A and B molecules occupy the same site in a ratio of 2:1.

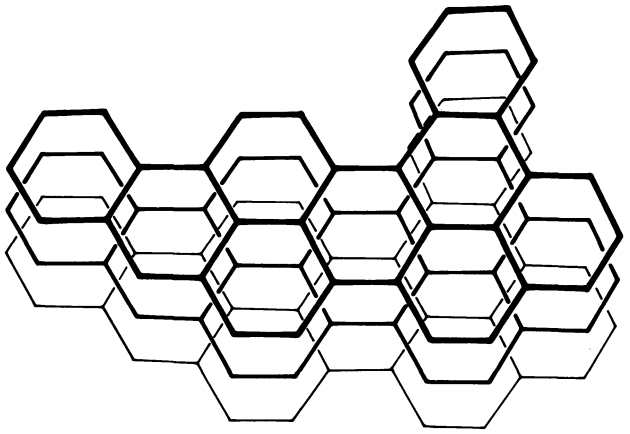

Fig. 5. Overlapping mode of the molecules.

are listed together with those of several related molecules in Table 4. Similar values were observed for the nonbonded C···C distances of the molecules. Although α in VEB is similar to that of the BPT, β resembles that of B molecules of 1,11-BisoVEB. In BPT, the expansions of the two C–C–C angles neighbouring the referred C–C–C angle also, somewhat, contributes to the relief of such a repulsion. Their angles are both 124° in BPT, whereas they are 121 and 122° in VEB. The twisting of C(23)–C(24) against the mean plane of the molecule is larger than that of C(26)–C(27) since terminal rings with C(23)–C(24) are easily bent at the bond of C(19)–C(24). The ring makes an angle of 21° to the mean molecular plane. Such bent rings are found in TBP(II),[8] where two benzene rings are bent at the bonds indicated by arrows in the scheme. On the other hand, additional (shaded) benzene rings prevent such bending in the cases of DPP (III) and 1,11-BisoVEB(IV).[9,10] The molecules are stacked face-to-face to make column structures along the *b*-axis. Figure 5 shows the overlapping mode of the molecules. The interplanar spacing (3.69 Å) is larger than the usual value. There is no unusual short contact between the molecules.

References

1) Part 5 of "Studies of Violanthrone B," Part 4. Ref. 11.
2) T. Maki, *Kogyo Kagaku Zasshi*, **35**, 1441 (1932).
3) T. Maki and Y. Nagai, *Kogyo Kagaku Zasshi*, **37**, 493 (1934).
4) J. Aoki, *Bull. Chem. Soc. Jpn.*, **34**, 1817 (1961).
5) J. Aoki, *Bull. Chem. Soc. Jpn.*, **34**, 1820 (1961).
6) J. Aoki, Dissertation, The University of Tokyo (1964).
7) Jan ho Li and (the late) N. Gotoh, *Yuki Gosei Kagaku Kyokai Shi*, **32**, 718 (1974).
8) Y. Kohno, M. Konno, Y. Saito, and H. Inokuchi, *Acta Crystallogr., Sect. B*, **31**, 2076 (1975).
9) I. Oonishi, S. Fujisawa, J. Aoki, and T. Danno, *Bull. Chem. Soc. Jpn.*, **51**, 2259 (1978).
10) S. Fujisawa, I. Oonishi, J. Aoki, Y. Ohashi, and Y. Sasada, *Bull. Chem. Soc. Jpn.*, **55**, 3424 (1982).
11) J. Aoki, M. Takekawa, S. Fujisawa, and S. Iwashima, *J. Org. Chem.*, **46**, 3922 (1981).
12) P. Main, L. Lesseiger, M. M. Woolfson, G. Germain, and J. P. Declercq, MULTAN78. A System of Computer Programs for the Automatic Solution of Crystal Structure from X-Ray Diffraction Data. Univs. of York, England and Louvain, Belgium (1978).
13) G. M. Scheldrick, SHELX. A program for crystal structure determination. Univ. of Cambridge, England (1976).
14) "International Tables for X-Ray Crystallographhy," Birmingham, Kynoch Press (1974), Vol. IV.
15) F. L. Hirshfeld, S. Sandler, and G. H. J. Schmidt, *J. Chem. Soc.*, **1962**, 2108.

 © 1986 The Chemical Society of Japan Bull. Chem. Soc. Jpn., 59, 2237—2239 (1986)

Reactivity of Electrons Produced in Gamma-Irradiated Zeolite Toward Several Electron Scavengers

Chiyoko NAKAZATO* and Takahiro MASUDA
Department of Chemistry, Faculty of Science, Tokyo Metropolitan University,
Fukasawa, Setagaya-ku, Tokyo 158
(Received December 19, 1985)

Relative rates of reaction of electrons produced in gamma-irradiated zeolite (Molecular Sieve 13X) with several electron scavengers were determined by competition kinetics using dinitrogen monoxide as a reference compound. A part of the electrons produced in irradiated zeolite have been disclosed to be quasi-free from the feature of their reactivity toward electron scavengers that the reactivity is similar to that of quasi-free electrons found in irradiated liquid 2,2-dimethylpropane. An analysis based on competition kinetics has provided a value 9.8×10^{12} dm^3 mol^{-1} s^{-1} as the lower limit on the rate constant for the reaction of quasi-free electrons with positive holes produced in irradiated zeolite.

A compound adsorbed on the surface of a solid is radiolyzed through a reaction induced by excitation energy transferred from an irradiated solid[1-6] and formation of electron and positive hole has been investigated by ESR or product analysis using electron or hole scavengers.[7-15] A synthesized zeolite, Molecular Sieve 13X, is an interesting adsorbent because of its highly ordered structure and large capacity of adsorption. The solid can be taken as an immobile solvent if the size of an adsorbate is small enough to enter a supercavity of zeolite. Reactions occurring in the system are considered approximately as those in solution, and kinetics used for reactions in solution will be applicable. The property of electrons produced in a solid insulator such as zeolite is interesting in connection with its reactivity. The present study was carried out to clarify the property and reactivity of electrons generated in irradiated zeolite. By using several electron scavengers and adopting kinetics for reactions in solution, it has been found that at least two kinds of electrons react with adsorbates, one showing a reactivity toward a series of electron scavengers similar to that of quasi-free electrons produced in liquid 2,2-dimethylpropane.[16,17]

Experimental

Zeolite (Molecular Sieve 13X; abbreviated to MS) was obtained from Nippon Kuromatokogyo K. K. The specific surface area is 1030 m^2 g^{-1}. Dinitrogen monoxide, sulfur hexafluoride, and methyl chloride were purchased from Takachiho Kagakukogyo K. K. Carbon tetrachloride and trichloroethylene were of spectrograde from Merck. Ethyl bromide was obtained from B. D. H.

About 12 g of MS was degassed in a quartz vessel at 600 °C for 24 h under a pressure below 10^{-3} Pa and divided to six ampules attached to the vessel in ca. 2 g each. A scavenger was introduced into the ampules through breakable seals with a vacuum line. After standing for 24 h, the ampules were irradiated by ^{60}Co gamma rays to a total dose of 1.34×10^4 Gy. The amount of molecular nitrogen formed from dinitrogen monoxide was determined by gas chromatography. Calculation for kinetic analysis was carried out with the aid of microcomputer PC-8001 (Nippon Electric Co.).

Results and Discussion

Formation of Molecular Nitrogen from MS-N_2O System. As shown in Fig. 1a, the G-value for formation of molecular nitrogen, $G(N_2)$, increases with increasing amount of N_2O introduced into an ampule and approaches a limiting value 2.8 at approximately 5×10^{-5} mol of N_2O per g of MS. The nitrogen formation is explained in terms of the reactions

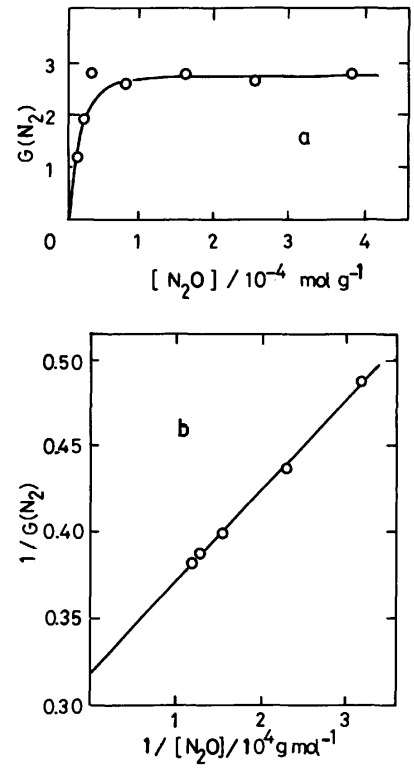

Fig. 1. a. Dependence of $G(N_2)$ on adsorbed amount of N_2O. Dose, 1.34×10^4 Gy. b. Competition plots of $1/G(N_2)$ vs. $1/[N_2O]$.

$$MS \rightsquigarrow MS^+ + e^-, \quad (1)$$

$$e^- + MS^+ \longrightarrow MS^*, \quad (2)$$

$$e^- + N_2O \longrightarrow N_2 + O^-_{ad}, \quad (3)$$

where MS^+ denotes a positive hole produced in γ-irradiated MS. From these reactions, we have

$$1/G(N_2) = 1/G_e(1+k_2[MS^+]/k_3[N_2O]). \quad (I)$$

Plotting $1/G(N_2)$ vs. $1/[N_2O]$ gave a straight line as shown in Fig. 1b, for which the observed values in Fig. 1a were not used for the plotting but the values obtained from the curve were used. Thus, a slope of 5.30×10^{-6} and an intercept of 0.32 were obtained with a correlation coefficient of 0.9988. G_e can be calculated from the intercept as 3.1, which agrees with the limiting $G(N_2)$, 2.8, within an experimental error. The slope will give k_2/k_3 if $[MS^+]$ can be estimated properly. Essentially the concentration of positive hole, $[MS^+]$, should be expressed by a steady state concentration but the estimation is very difficult. A lower limit of k_2/k_3, however, can be evaluated if the total concentration of positive hole produced in MS during irradiation is used as $[MS^+]$ instead of the steady state concentration. The total concentration of MS^+ can be calculated from G_e and the total dose by assuming $G_e=G(MS^+)$. In the present experimental conditions, it is 3.9×10^{-6} mol g^{-1} and hence 4.2 is obtained as k_2/k_3. If it is assumed that the rate constant for the reaction of quasi-free electron with N_2O in liquid 2,2-dimethylpropane, 2.3×10^{12} dm^3 mol^{-1} s^{-1}, is applicable to k_3, the lower limit of the rate constant for the reaction of electron with positive hole in MS is 9.8×10^{12} dm^3 $mol^{-1}s^{-1}$. Sulfur hexafluoride is known to react with quasi-free electron with the rate constant of 1.98×10^{14} dm^3 mol^{-1} s^{-1} in liquid 2,2-dimethylpropane[17] and the electron produced in γ-irradiated MS was found to react with SF_6 85 times as fast as with N_2O, as described below. The positive hole in MS is thought to have at least the same reactivity as SF_6. The steady state concentration of MS^+, therefore, would be less than 1.9×10^{-7} mol g^{-1}.

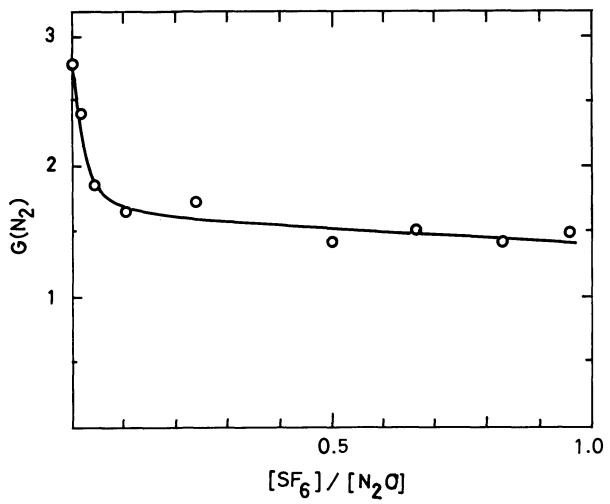

Fig. 2. Decrease in $G(N_2)$ in the presence of SF_6. $[N_2O]$, 4×10^{-4} mol g^{-1}.

Competition between N_2O and a Second Scavenger toward Electron Produced in MS. Addition of a second scavenger gives rise to decrease in the yield of molecular nitrogen formed from N_2O in irradiated MS. In Fig. 2, an effect of SF_6 on $G(N_2)$ is shown. The decrease in $G(N_2)$ is understood in terms of the competition between Reactions 3 and 4:

$$e^- + S \longrightarrow S^- \text{ or product(s)}, \quad (4)$$

where S denotes an electron scavenger added to the system as a competitor of N_2O such as SF_6. The competition kinetics is expressed by

$$1/\Delta G(N_2) = 1/G_e(1+k_3[N_2O]/k_4[S]), \quad (II)$$

where $\Delta G(N_2)$ is the difference of $G(N_2)$ between those observed in the absence and presence of the second scavenger, and G_e is the primary yield of electrons for which N_2O and the second scavenger compete with each other. As shown in Fig. 3, plots of $1/\Delta G(N_2)$ vs. $[N_2O]/[S]$ give a straight line. The relative reactivity of S to N_2O is obtained from the slope of the straight line. Results obtained for several electron scavengers are summarized in Table 1,

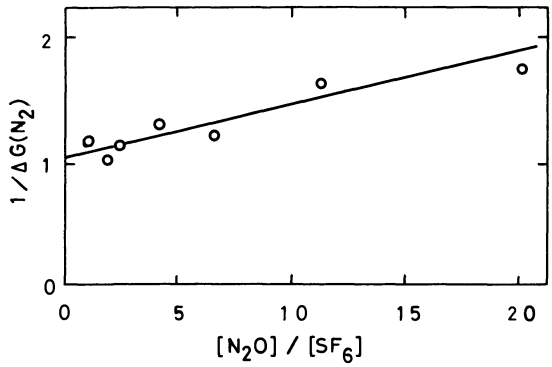

Fig. 3. Competition plots of $1/\Delta G(N_2)$ vs. $[N_2O]/[SF_6]$.

Table 1. Relative Rate Constants for Reactions of Electron with a Series of Electron Scavengers in Zeolite and Nonpolar Liquids

	k_4/k_3		
	MS	2,2-Dimethylpropane	Hexane
SF_6	85	86[a]	0.6[a]
C_2HCl_3	23	25.2[a]	1.3[a]
CCl_4	12.8	12.6[b]	0.7[a]
C_2H_5Br	0	0.1[b]	0.8[a]
CH_3Cl	0	0[c]	

a) Ref. 17. b) Ref. 16. c) Ref. 18.

together with values reported for electrons formed in irradiated nonpolar liquids. Accurate determination has failed for C_2H_5Br and CH_3Cl, because of their poor reactivity. A comparison of relative reactivities between MS and other systems indicates that the trend observed for MS is similar to that for 2,2-dimethylpropane. This suggests that the energy state of the elecron produced in MS is probaly very close to that of quasi-free electron generated in 2,2-dimethylpropane. The intercept of the straight line in Fig. 3 gives the initial yield of electrons witch react with N_2O or SF_6. Values from 0.85 to 1.1 were obtained by the experiments with SF_6, C_2HCl_3, and CCl_4. They are apparently inconsistent with the saturated $G(N_2)$, 2.8. As seen in Fig. 2, there remains a $G(N_2)$ which cannot effectively be depressed by the addition of SF_6. Similarly, a residual $G(N_2)$ was observed for the other scavengers. Since the size of the entrance to a supercavity of Molecular Sieve 13X allows the passage of a molecule below 0.8 nm in diameter, N_2O, SF_6, C_2HCl_3, and CCl_4 can enter the supercavity and hence the difference in molecular size does not explain the results. It will be explained on an assumption of two kinds of electrons, whose reactivities are different from each other. If it is assumed that the second electron, e_2^-, reacts with N_2O and SF_6 with a ratio of rate constants different from k_4/k_3, Eq. III is derived as follows:

$$e_2^- + N_2O \longrightarrow N_2 + O_{ad}^-, \quad (5)$$

$$e_2^- + SF_6 \longrightarrow \text{product(s)}, \quad (6)$$

$$G(N_2) = G_1\{k_3[N_2O]/(k_3[N_2O]+k_4[SF_6])\} + G_2\{k_5[N_2O]/(k_5[N_2O]+k_6[SF_6])\}, \quad (III)$$

where G_1 and G_2 denote the initial G-values of the first and the second electron, respectively. A computer simulation provides a curve shown in Fig. 2, by adopting $G_1=1.2$, $G_2=1.6$, $k_4/k_3=85$, and $k_6/k_5=6.7$. The curve appears to fit the experimental points fairly well. The first electron is considered to be quasi-free because its tendency in reactivity toward several electron scavengers is similar to that found in liquid 2,2-dimethylpropane by Allen et al.[16,17] The different reactivity of the second electron may be understood in terms of the different potential barriers at adsorption sites. Essentially the electrons generated in MS may be identical but the reactivity toward adsorbate is possibly affected by the potential barrier at adsorption site. The oxygen atoms of the SiO_2 network and Na^+ ions are considered as the possible candidates for the two kinds of adsorption sites where quasi-free electrons react with adsorbates. The reaction rate of the electron that reacts at the former site may be low due to its relatively high potential barrier, which is favorable for N_2O but not for the other scavengers. On the other hand, the potential barrier may be negligible at the latter site. However, further confirmation is indispensable for this speculation.

References

1) J. M. Cafrey, Jr. and A. O. Allen, *J. Phys. Chem.*, **62**, 33 (1958).
2) J. W. Sutherland and A. O. Allen, *J. Am. Chem. Soc.*, **83**, 1040 (1961).
3) J. G. Rabe, B. Rabe, and A. O. Allen, *J. Phys. Chem.*, **70**, 1098 (1966).
4) L. Abrams and A. O. Allen, *J. Phys. Chem.*, **73**, 2741 (1969).
5) G. R. Joppien and J. E. Willard, *J. Phys. Chem.*, **76**, 3158 (1972).
6) N. H. Sagert, J. A. Reid, and R. W. Robinson, *Can. J. Chem.*, **48**, 17 (1970).
7) J. W. Sutherland and R. Goodrich, *J. Am. Chem. Soc.*, **89**, 6779 (1967).
8) N. H. Sagert and R. W. Robinson, *Can. J. Chem.*, **46**, 207 (1968).
9) P-O. Kinell, T. Komatsu, A. Lund, T. Shiga, and A. Shimizu, *Acta Chem. Scand.*, **24**, 3265 (1970).
10) P. K. Wong, *J. Phys. Chem.*, **75**, 201 (1971).
11) K. Sogabe, A. Hasegawa, Y. Yamada, and M. Miura, *Bull. Chem. Soc. Jpn.*, **45**, 3362 (1972).
12) N. Kanzaki and I. Yasumori, *Bull. Chem. Soc. Jpn.*, **52**, 1923 (1979).
13) H. Ogura, Y. Tachika, Y. Suzuki, C. Nakazato, M. Kondo, T. Sawai, and T. Sawai, *J. Nucl. Sci. Technol.*, **12**, 167 (1975).
14) H. Ogura, M. Hinata, C. Nakazato, M. Kondo, T. Sawai, and T. Sawai, *J. Nucl. Sci. Technol.*, **15**, 433 (1978).
15) H. Ogura, C. Nakazato, M. Kondo, T. Sawai, and T. Sawai *J. Nucl. Sci. Technol.*, **16**, 57 (1979).
16) A. O. Allen and R. A. Holroyd, *J. Phys. Chem.*, **78**, 796 (1974).
17) A. O. Allen, T. E. Gangwer, and R. A. Holroyd, *J. Phys. Chem.*, **79**, 25 (1975).
18) K. Mori, K. Ito, and Y. Hatano, *J. Phys. Chem.*, **79**, 209 (1975).

 © 1986 The Chemical Society of Japan Bull. Chem. Soc. Jpn., 59, 2241—2245 (1986)

Infrared Multiple-Photon Decomposition of β-Propiolactone

Shunzo YAMAMOTO,† Yo-ichi ISHIKAWA,* and Shigeyoshi ARAI
†Department of Chemistry, School of Science, Okayama University,
3-1-1, Tsushima-naka, Okayama 700
The Institute of Physical and Chemical Research, Wako, Saitama 351-01
(Received February 3, 1986)

The infrared multiple-photon decomposition of β-propiolactone was found to give only ethylene and carbon dioxide with the same yield as the products, where the material balance was above 90%. This result suggests that the unimolecular decomposition into ethylene and carbon dioxide is a unique reaction channel of the compound at highly vibrationally excited states. It was shown that the decomposition probability was strongly dependent on the fluence but slightly dependent on the pressure.

It has been well-established in several studies that there are two nonradical unimolecular reaction modes in the thermal decomposition of cyclobutanone:

$$\longrightarrow C_2H_4 + CH_2CO, \quad (1)$$

$$\longrightarrow \triangle + CO. \quad (2)$$

The decomposition of this compound, induced by the intense infrared radiation from a CO_2 laser, has been widely investigated to obtain information on the energy distribution of highly vibrationally excited molecules, particularly, molecules whose energies are larger than either or both of the dissociation limits.[1-4]

It is possible for β-propiolactone to undergo three different ring cleavages, where each gives two stable molecules:

$$\longrightarrow C_2H_4 + CO_2, \quad (3)$$

$$\longrightarrow CH_3CHO + CO, \quad (4)$$

$$\longrightarrow CH_2CO + H_2CO. \quad (5)$$

The thermal decomposition of β-propiolactone in the temperature range of 205—255 °C has been found to be a first-order reaction and to yield only ethylene and carbon dioxide in equal amounts.[5] In the present study we have carried out the infrared multiple-photon decomposition of this compound in order to examine the possible contribution of Reaction (4) or (5) under the excitation conditions at high laser fluences.

Experimental

All the samples were irradiated with the R(20) line (1078.59 cm^{-1}) of the 9.6-μm CO_2 band from a Lumonics 103 TEA laser using and N_2-free lasing medium. The pulse profile showed a fwhm of about 80 ns without tailing. The laser-beam divergence was 2 mrad. The laser was operated in a multiple transverse mode; the intensity distribution across the beam was almost flat within a deviation of 10%.

The laser irradiation was performed in two beam geometries, i.e., mildly-focused and tightly-focused (Fig. 1). A cylindrical cell (2.5 cm diameter and 5 cm long) equipped with KBr windows at both ends was used in the former geometry. The laser beam was mildly focused by a BaF_2 lens with a focal length of 100 cm after passing through a Teflon iris with a 10-mm diameter. The irradiation fluence was controlled by setting the cell at a certain distance from the lens along the beam. The fluence inside the cell could be regarded as being nearly homogeneous along the beam. A cylindrical cell (2.5 cm diameter and 10 cm long) was used with the latter geometry, where the beam was tightly focused at the center of the cell by a BaF_2 lens with a focal length of 7.5 cm. The fluence was extremely inhomogeneous along the beam within the cell; the maximum fluence ϕ_f achieved at the focal point was three orders of magnitude greater than the fluences at both ends of the cell.

β-Propiolactone was purchased from Sigma Chemical Co. and purified by vacuum distillation at −98.5 °C. The sample pressure was controlled by changing the temperature of the sample reservoir connected directly to the cell, for example, 2.5 Torr (1 Torr=133.322 Pa) at the room temperature, 0.43 Torr at 0 °C, and 0.087 Torr at −22 °C.

After connecting the cell to a vacuum line, all samples were

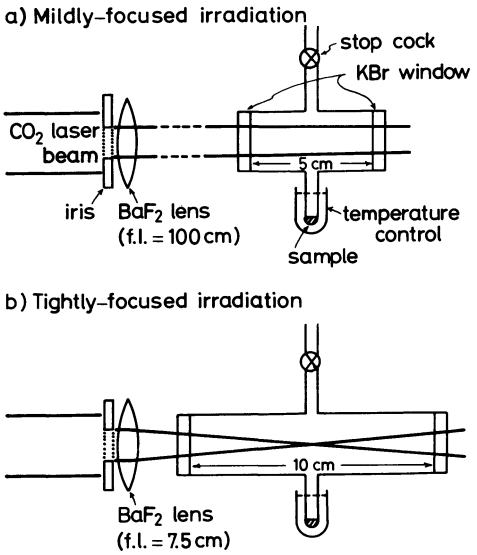

Fig. 1. Schematic diagram of the CO_2 laser irradiation geometry; mildly focused irradiation (a); tightly focused irradiation (b).

Table 1. Product Analysis of the CO_2 Lasers Irradiation of β-Propiolactone at Various Laser Fluences

Irradiation geometry	Reactant pressure / Torr	Fluence / J cm^{-2}	Product	C_2H_4/CO_2	Decomposition probability, (P_d)
MF[a]	0.43	0.34	none	—	0
TF[b]	0.43	<780	C_2H_4, CO_2	0.97	1.1×10^{-1}
MF	2.5	0.34	C_2H_4, CO_2	0.73	8.0×10^{-4}
MF	2.5	0.52	C_2H_4, CO_2	0.97	5.1×10^{-3}
MF	2.5	0.60	C_2H_4, CO_2	0.93	1.1×10^{-2}
MF	2.5	0.66	C_2H_4, CO_2	0.96	1.9×10^{-2}
MF	2.5	0.69	C_2H_4, CO_2	0.97	2.9×10^{-2}
MF	2.5	0.93	C_2H_4, CO_2	0.98	7.8×10^{-2}
MF	2.5	1.04	C_2H_4, CO_2	1.01	1.1×10^{-1}
MF	2.5	1.32	C_2H_4, CO_2	1.00	1.6×10^{-1}
MF	2.5	1.90	C_2H_4, CO_2	0.70	2.6×10^{-1}
TF	2.5	<350	C_2H_4, CO_2	0.98	1.6×10^{-1}
TF	2.5	<530	C_2H_4, CO_2	0.98	1.3×10^{-1}
TF	2.5	<640	C_2H_4, CO_2	0.99	0.9×10^{-1}
TF	2.5	<760	C_2H_4, CO_2	0.99	0.9×10^{-1}
Break down	2.5	<780	C_2H_4, CO_2	0.96	1.4×10^{-1}
			CH_3CHO, CO	—	1.6×10^{-2}

a) Mildly focused. b) Tightly focused.

passed through the two traps and cooled to −196 and −98.5 °C. Noncondensable gases such as H_2, CO, and CH_4 at −196 °C were not detected as products of the photolysis. A large fraction of unreacted β-propiolactone was captured by the trap at −98.5 °C. The condensable gases at −196 °C were analyzed by gas chromatography using a 3-m column of Porapak-Q at 50 °C.

Results and Discussion

The enthalpy changes of Reactions (3), (4), and (5) are −2.55, 12.95, and 36.7 kcal mol^{-1} (1 kcal=4.184 kJ), respectively.[5,6] Therefore, the activation energies of Reactions (4) and (5) are expected to be considerably larger than that of Reaction (3), i.e., 45.81 kcal mol^{-1}.[5] We checked the possible occurrence of Reaction (4) or (5) in the tightly-focused irradiation of β-propiolactone, although fluence homogeneity was sacrificed. At very high fluences a certain fraction of the molecules could be excited to much higher levels than the reaction thresholds. The experimental results are summarized in Table 1 for reactant pressure of 2.5 Torr. The decomposition probability P_d used in the table is meaningful only for irradiation with a homogeneous fluence, since it depends strongly on the fluence in IRMPD.[6]

$$P_d = (N_p/N_i) \times (1/t) \quad \text{(I)}$$

where N_p represents the number of product molecules, N_i the number of reactant molecules in the irradiation volume, and t the number of laser pulses. For tightly-focused irradiation, P_d is considered to be merely the average value over the decomposition in the inhomogeneous fluence region. The laser imput energy for the tightly-focused irradiation was controlled by changing the diameter of the iris during the experiment. Table 1 tabulates the results obtained through product analyses. The IRMPD of β-propiolactone gave only ethylene and carbon dioxide as products, being similar to the pyrolysis at 205—255 °C. There was no other product, even for photolysis at a high fluence of 760 J cm^{-2}. In general, an increase in the fluence causes shifts in the vibrational energy distribution of excited molecules to the higher-energy side.[7] However, the reaction channel of β-propiolactone involves only a decomposition into ethylene and carbon dioxide, even at fairly

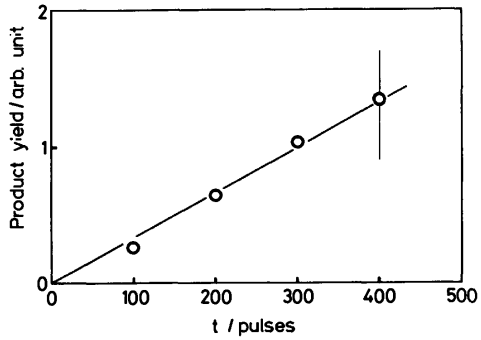

Fig. 2. Relation between product yield and laser pulse number t for multiple-photon decomposition of β-propiolactone. β-propiolactone, 2.5 Torr; fluence, 0.66 J cm^{-2}; irradiation laser wavenumber, R(20) (1078.59 cm^{-1}). The bar at 400 pulses indicates the experimental scatter.

high vibrational temperatures. When the focal fluence exceeded 760 J cm^{-2}, we observed an optical breakdown accompanied by the formation of a small amount of acetaldehyde and carbon monoxide in addition to the formation of ethylene and carbon dioxide. Acetaldehyde and carbon monoxide may be produced from electronically excited species or ionic species, because optical breakdown is essentially an electric discharge.[8]

Figure 2 shows the pulse-number dependence of the ethylene yield, where the laser fluence is 0.66 J cm^{-2}. The ethylene yield was always almost equal to the carbon dioxide yield and both yields increased linearly with the pulse number. Thus, these compounds can be produced directly from β-propiolactone. The decomposition probability was estimated to be 0.019±0.005 pulse^{-1}. Since β-propiolactone tends to be adsorbed on the walls, the adsorbed molecules on the front window might attenuate the laser intensity or decompose more efficiently than those in the gas phase. However, it may be concluded that there was no serious influence of adsorbed molecules in the present experiment. This is because the decomposition probability always remained constant throughout the irradiation period.

The material balance in the IRMPD of β-propiolactone was obtained from a comparison of the reactant consumption with the product yields. The experimental conditions were as follows: β-propiolactone pressure, 2.5 Torr; laser fluence, 0.66 J cm^{-2}; pulse number, 400 pulses. The consumption was measured with infrared absorption spectrophotometry, while the production yields of C_2H_4 and CO_2 were determined through gas chromatography. The consumption of β-propiolactone was 22.23 Torr ml, and the production yields of C_2H_4 and CO_2 were 20.25 and 21.57 Torr ml, respectively. The high material balance of 90% supports that β-propiolactone decomposes into only C_2H_4 and CO_2.

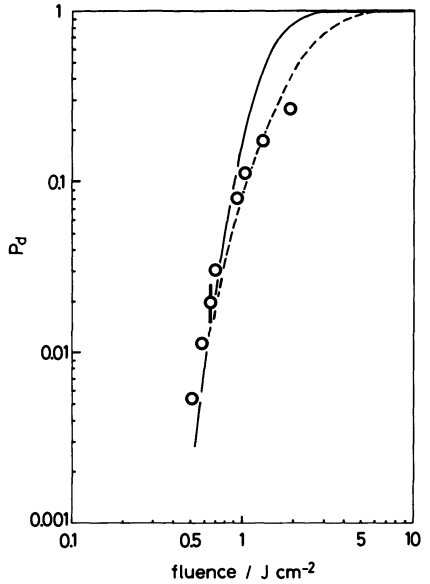

Fig. 3. Decomposition probability P_d(O) versus laser fluence observed for IRMPD of 2.5-Torr β-propiolactone. Solid curve shows the calculated P by assuming $\sigma_n=\sigma_0$. Dashed curve shows the calulated P_d by assuming $\sigma_n=\sigma_0$ ($E_n<E_a$) and $\sigma_n=\sigma_0\times n^{-0.5}$ ($E_n\geq E_a$).

The pressure effect on P_d was examined briefly in the irradiation of β-propiolactone at 2.5, 0.43, and 0.087 Torr, where the laser fluences were about 1.8 J cm^{-2}. The observed decomposition probabilities were 0.26 pulse^{-1} for 2.5 Torr, 0.18 pulse^{-1} for 0.43 Torr, and 0.17 pulse^{-1} for 0.087 Torr. Although the pressure variation was almost 30-fold, the probability changed from 0.26 to 0.17 pulse^{-1}. Thus, the pressure did not have a serious effect on the IRMPD of this compound. The slight decrease of P_d with decreasing pressure may be due to the so-called bottle-neck effect in a multiple-photon absorption process.[9]

The decomposition probability is plotted against laser fluence in Fig. 3, for a pressure of 2.5 Torr. P_d strongly depends on the laser fluence ϕ in a low fluence region, where P_d is approximately proportional to 7th power of ϕ. In a higher fluence region, however, the increase of P_d becomes much milder with increasing ϕ. Such a fluence dependence of P_d has been frequently observed for IRMPD.[10,11]

In order to obtain detailed information on infrared multiple-photon excitation (IRMPE), the absorption cross section σ_n and collisional deactivation rate $k_{d,n}$ were estimated from a simulation of the observed fluence dependence of P_d. Here, $k_{d,n}$ is a rate constant for a following collisional deactivation reaction:

$$A^*(v=n) + M \longrightarrow A^*(v=n-1) + M, \quad (6)$$

where A*(v=n) denotes the vibrationally excited molecule at level n. The method has been already reported elsewhere.[11,12] Briefly speaking, the stochastic calculation was carried out for the energy-grained master equations using assumed values of σ_n and $k_{d,n}$. The pulse was assumed to have a rectangular profile with a duration of 80 ns. The specific reaction rates during unimolecular decomposition were calculated using the QRRK theory.[13] Arrhenius parameters A=1.17×10^{16} s^{-1} and E_a=45.81 kcal mol^{-1} have been previously reported regarding a pyrolysis study of this compound.[5] The following vibrational frequencies were used for the activated complex: (100)^4 (300)^1 (500)^1 (800)^2 (1000)^1 (1200)^4 (1500)^2 (1700)^1 (3000)^4.[5] The best-fit simulation in a low fluence region was obtained for the following parameters: $k_{d,n}$=3.2×10^7×(E_n/E_a) s^{-1} and $\sigma_n=\sigma_0$=4×10^{-19} cm^{-2}. Rossi and Barker have reported that the average energy transfered per collision depends strongly on vibrational energy for azulene*.[14] This may support the assumption of the energy-dependent $k_{d,n}$ employed here. The calculated fluence depen-

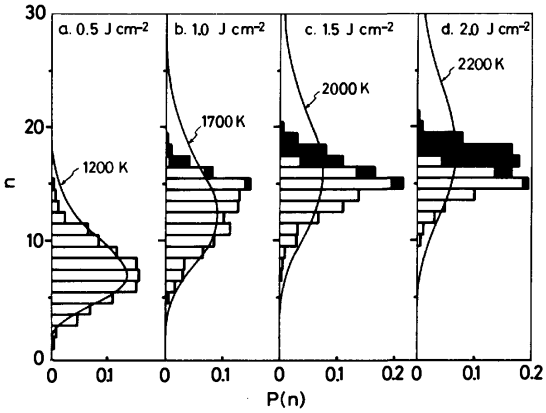

Fig. 4. Typical vibrational population distribution for β-propiolactone irradiated at various fluences. Filled areas indicate the fractions of decomposition. Solid lines show the Boltzmann distributions (Eq. II) by assuming cerain temperatures.

dence of P_d is represented by the solid curve in Fig. 3. Although the curve satisfactorily reproduces the observed dependence in the low-fluence region, there is a large discrepancy in the high-fluence region. The discrepancy may be explained in several different ways. One possible reason is that the volume irradiated in a high-fluence region is so small that the collisional quenching of excited molecules by unexcited molecules on the outer boundary of the reaction volume contributes more effectively to the reduction of P_d as compared with low fluence irradiation. Another possible reason is that a crude estimation of the absorption cross sections causes such a significant discrepancy. The absorption cross section is assumed to decrease with increasing internal energy in most of the IRMPD.[12] For example, we can improve the simulation by employing an energy-dependent absorption cross section, that is, for $E_n<E_a$, $\sigma_n=\sigma_o$; and for $E_n\geqq E_a$, $\sigma_n=\sigma_o\times n^{-0.5}$. The improved result is indicated by the dashed line in Fig. 3. At present, the simulations seem to have somewhat unavoidable uncertainties because of the lack of kinetic parameters for β-propiolactone together with an incomplete understanding of the multiple-photon absorption process. The simulation of the fluence dependence of P_d alone is thought to be insufficient to determine a unique parameter set, σ_n and $k_{n,d}$.[15]

Figure 4 shows the calculated vibrational energy distributions at various fluences, where the above-mentioned improved parameters were used. Filled areas represent the calculated decomposition fractions and solid curves represent the Boltzmann distribution $P(n)$ defined by the following equation:

$$P(n) = \frac{\rho(E_n)\exp(-E_n/kT)}{\sum\rho(E_n)\exp(-E_n/kT)} \qquad \text{(II)}$$

where $\rho(E_n)$ is the density of states at level n. The temperature was tentatively assumed as indicated in each distribution of Fig. 4. These values seem to be almost equal to the vibrational temperatures reported in IRMPD of polyatomic molecules.[16,17] The distribution estimated in the stochastic method agrees fairly well with the Boltzmann distribution in the low fluence region, where the decomposition hardly takes place. However, these two distributions do not agree with each other in the high-fluence region, where the docomposition of the molecules at vibrational levels above E_a (n=15) apparently disturbs the Boltzmann distribution. The vibrational temperature can not be defined exactly in the multiple-photon excitation, since the excitation is essentially regarded as a nonequilibrium process.

In conclusion, the reaction channel in the IRMPD of β-propiolactone is entirely a molecular decomposition into ethylene and carbon dioxide. Other decomposition channels with larger activation energies could not be observed at all during the irradiation of the compound at fluences as high as 700 J cm^{-2}. Since the pre-exponential factor A for the lowest channel has a large value of 10^{16} s^{-1}, the molecules excited to the levels above E_a (n=15) are thought to decompose rapidly before any further excitation due to light absorption.

The authors wish to express their thanks to Miss Kyoko Sugita for the computer calculations.

References

1) M. H. Back and R. A. Back, *Can. J. Chem.*, **57**, 1511 (1979); R. A. Back, *ibid.*, **60**, 2542 (1982).

2) R. G. Harrison, H. L. Hawkins, R. M. Leo, and P. John, *Chem. Phys. Lett.*, **70**, 555 (1980).

3) S. Koda, Y. Ohnuma, T. Ohkawa, and S. Tsuchiya, *Bull. Chem. Soc. Jpn.*, **53**, 3447 (1980).

4) V. Starov, N. Selamoglu, and C. Steel, *J. Phys. Chem.*, **85**, 320 (1981).

5) T. L. James and C. A. Welliagton, *J. Am. Chem. Soc.*, **91**, 7743 (1969).

6) S. W. Benson, "Thermochemical Kinetics," John Wiley & Sons, Inc., New York (1968).

7) R. V. Ambartzumian and V. S. Letokhov, "Chemical and Biochemical Applications of Lasers, Vol. III," ed by C. B. Moore, Academic Press, New York (1977).

8) Unpublished data. In the mercury-photosensitized decomposition of β-propiolactone, CO, acetaldehyde and ethyleneoxide were observed, besides CO_2 and ethylene.

9) V. S. Letokhov and C. B. Moore, "Chemical and Biochemical Applications of Lasers, Vol. III," ed by C. B. Moore, Academic Press, New York (1977).

10) J. C. Stephenson, S. E. Bialkowski, and D. S. King, *J. Chem. Phys.*, **72**, 1161 (1980); D. M. Golden, M. J. Rossi, A. C. Baldwin, and J. R. Barker, *Acc. Chem. Res.*, **14**, 56 (1981).

11) Y. Ishikawa and S. Arai, *Bull. Chem. Soc. Jpn.*, **57**, 681 (1984).

12) J. R. Barker, *J. Chem. Phys.*, **72**, 3686 (1980).
13) P. J. Robinson and K. A. Holbrook, "Unimolecular Reactions," Wiley-Interscience, London (1972).
14) M. J. Rossi and J. R. Barker, *Chem. Phys. Lett.*, **85**, 21 (1982).
15) S. Ruhman, O. Anner, and Y. Haas, *J. Phys. Chem.*, **88**, 6397 (1984).
16) R. N. Rosenfold, J. I. Brauman, J. R. Barker, and D. M. Golden, *J. Am. Chem. Soc.*, **99**, 8063 (1977).
17) R. E. Weston, Jr., *J. Phys. Chem.*, **86**, 4864 (1982).

Ion/Molecule Reactions in Gaseous Acetone

Kenzo HIRAOKA,* Hajime TAKIMOTO, Kazuya MORISE, Takashi SHODA, and Shizuo NAKAMURA†
Faculty of Engineering, Yamanashi University, Takeda 4, Kofu 400
†ULVAC Corporation, Hagizono 2500, Chigasaki 253
(Received February 10, 1986)

The ion/molecule reactions in acetone were investigated which were induced by the electron impact. It was found that the protonated acetone reacts with an acetone molecule to produce the protonated diacetone alcohol (4-hydroxy-4-methyl-2-pentanone) and the protonated mesityl oxide (4-methyl-3-penten-2-one) through the aldol condensation reaction. It was also found that the acetone molecule isomerizes from keto to enol form in the interaction with the chloride ion. The thermochemical data for the higher-order clustering reactions of the proton and chloride ion with acetone molecules were obtained.

In recent years a number of studies have been made of the gas-phase ion/molecule chemistry of acetone.[1–5] Through these experiments, the nature and rates of formation of several reaction products have become fairly well established. Like many ionic species, the ion/molecule chemistry of acetone centers around the formation of cluster ions. MacNeil and Futrell,[2] who ionized the acetone with an electron beam, as well as Sieck[3] and Wincel,[5] who employed photons as the ionizing agents, observed a number of cluster ions at relatively high pressures. Furthermore, the species corresponding to loss of a water molecule from $H^+(CH_3COCH_3)_n$ with $n \geqq 2$ have been observed.

Lau et al. measured the equilibria and van't Hoff plots for Reaction (1).[6]

$$H^+(CH_3COCH_3)_{n-1} + CH_3COCH_3 = H^+(CH_3COCH_3)_n \quad (n-1,\ n) \qquad (1)$$

They tried to measure the (2, 3) equilibria of Reaction (1). They found that the equilibrium "constants" were not independent of pressures but decreased when the pressure of third gas CH_4 and of acetone were increased. In our previous work,[7] we observed that the intensities of ions with m/z=157 and 175 increase gradually at the expense of the $H^+(CH_3COCH_3)_2$, m/z=117, ion. These results suggest the occurrence of some unique ion/molecule reactions in gaseous acetone. However, little information was obtained so far regarding the kinetics of ion/molecule reactions in gaseous acetone. In the present work, we made extensive kinetic measurements of ion/molecule reactions in gaseous acetone. We got some evidence that acid-catalysed keto-enol isomerization of the acetone molecule followed by the formation of diacetone alcohol (4-hydroxy-4-methyl-2-pentanone) and mesityl oxide (4-methyl-3-penten-2-one) take place in gaseous acetone. The keto-enol isomerization of the acetone molecule was also found to occur in the interaction of Cl^- with the acetone molecule.

Experimental

The measurements were made with the pulsed electron beam mass spectrometer which has been described previously.[7,8] The ion/molecule reactions observed in the gas mixtures of CH_3COCH_3/He, CH_3COCH_3/CH_4, CH_3COCH_3/CCl_4/He, and $CH_3COCH_3/CCl_4/CH_4$ were studied. Small amounts of CH_3COCH_3 and/or CCl_4 were introduced into the He or CH_4 carrier gas through stainless steel capillaries (0.1 mm×1 m). 2 keV electron beam (5×10^{-9} A) was pulsed on for 50 μs and off for 3 ms. The ions escaping from the field-free ion source into an evacuated region were mass analysed by a quadrupole mass spectrometer (ULVAC MSQ-400) and collected in a multichannel analyser as a function of their arrival time after the electron pulse. The ion counts collected in a multichannel analyser were transferred to the microcomputer and the time profile of the calculated per cent of total ionization of observed ions were recorded on the x—y plotter.

Two kinds of gases, He and CH_4, were used as carrier gases in order to examine the third-body dependence on the ion/molecule reactions (see the following section). The positive ions produced in CH_3COCH_3/He and CH_3COCH_3/CH_4 are more or less the same except that the $CH_3CO^+(CH_3COCH_3)_n$ and $C_2H_5^+(CH_3COCH_3)_n$ ions are only detected in CH_3COCH_3/He and CH_3COCH_3/CH_4, respectively. Negative ions could not be detected in CH_3COCH_3/He and CH_3COCH_3/CH_4. On the contrary, strong signals of Cl^- and its clusters were observed in CH_3COCH_3/CCl_4/He and $CH_3COCH_3/CCl_4/CH_4$. The Cl^- ion is yielded from the dissociative electron capture by CCl_4.

$$e + CCl_4 = Cl^- + CCl_3 \qquad (2)$$

No other negative ions originating from acetone could be detected.

Results and Discussion

1. Acetone Containing Mesityl Oxide and Diacetone Alcohol as Impurities. Positive Ions: Figure 1 shows the temporal profile of ions observed in 4.02 Torr (1 Torr=133.322 Pa) of He containing 86 mTorr of acetone at 33.7 °C.

The m/z=73, 131, and 189 ions correspond to

$CH_3^+(CH_3COCH_3)_n$ with n=1 to 3. The rapid decay of the m/z=73 ion is completely accounted for by the increase of m/z=131 and 189 ions.

The ions with m/z=159 and 217, which correspond to $CH_3CO^+(CH_3COCH_3)_n$ with n=2 and 3, decrease rapidly. The rapid consumption of these ions may be due to the reactions of CH_3CO^+ with acetone molecules.[2] The ions $CH_3CO^+(CH_3COCH_3)_n$ were not detected when methane is used as a carrier gas. This indicates that CH_3CO^+ is yielded by the reaction of the primary ion $He^{+\cdot}$ with acetone molecule.

The ions with m/z=155 and 213 may be the cluster ions of $C_3H_3^+$ with acetone molecules, $C_3H_3^+(CH_3COCH_3)_n$ with n=2 and 3. The mechanism for the formation of $C_3H_3^+$ ion is not clear.

The results described above indicate that acetone has an ability to form large cluster ions with onium ions R^+=CH_3^+, CH_3CO^+, and $C_3H_3^+$. The sequence for the formation of cluster ions may be described as follows:

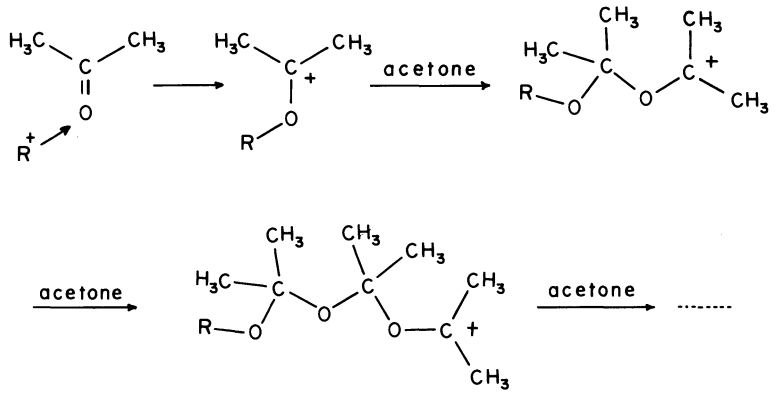

The reactions of onium ions with acetone molecules form polyethers. The reactions of onium ions with acetone molecules may be regarded as condensation reactions rather than clustering reactions.

The gradual increase of the ion $H_3O^+(CH_3COCH_3)_3$ with m/z=193 is observed which is yielded from water impurity. For aprotic solvent molecules B's such as acetone, acetonitrile, etc., the proton-held trimer ions $H^+(B)_3$ are known to be much less stable than the dimer ions $H^+(B)_2$.[9] Hence, the presence of a small amount of water impurity in aprotic solvents often yields quite a strong $H_3O^+(B)_3$ ion compared to $H^+(B)_3$ ion because H_3O^+ has three protic hydrogen atoms.

The gradual increase of ions with m/z=157 and 175 at the expense of the ion with m/z=117 is observed. It is evident that the ion $C_6H_{11}O^+(CH_3COCH_3)$ and some isomeric ion whose m/z is equal to the trimer ion $H^+(CH_3COCH_3)_3$ are formed from the dimer ion $H^+(CH_3COCH_3)_2$. In order to examine whether these ions are produced from acid (proton)-catalysed reactions of acetone or come from impurities contained in the acetone samples, we remeasured the ion/molecule reactions using the distilled and purified acetone samples. The apparent decrease in the growth rates of ions with m/z=157 and 175 were observed. This indicates that the gradual increase of ions with m/z=157 and 175 is due to the impurities present in the used acetone sample. It is known that under acidic or basic conditions, acetone produces diacetone alcohol and mesityl oxide by the aldol condensation reaction in the liquid phase.[10] The gradual increase in the intensities of ions with m/z=157 and 175 is likely to be due to the presence of mesityl oxide and diacetone alcohol contained in acetone as impurities.

Negative Ions: Figure 2 shows the temporal profile of negative ions observed in 4.09 Torr of He containing 0.790 Torr of acetone and 0.3 mTorr of CCl_4 at 38.9 °C.

The gradual decrease of Cl^- (m/z=35) and $Cl^-(CH_3COCH_3)$ (m/z=93) ions are observed. The decrease is compensated by the increase of m/z=151 and 209 ions. The used acetone sample contains diacetone alcohol as an impurity. As the diacetone alcohol molecule has a protic hydrogen atom, it can form a rather strong bond with Cl^- to yield $Cl^-\cdots HO(CH_3)_2CCH_2COCH_3$ (m/z=151) and its cluster with acetone (m/z=209). This explains the increase of m/z=151 and 209 ions at the expense of m/z=35 and 93 ions.

The cluster ion of Cl^- with mesityl oxide could not be detected under the present experimental conditions. This is because mesityl oxide does not have a protic hydrogen and it cannot form a strong bond with Cl^-.

The m/z=53, 111, and 169 ions correspond to $Cl^-(H_2O)(CH_3COCH_3)_n$ with n=0—2. In our previous paper,[8] we found that the third-order clustering reaction (3) with n=1 is particularly

$$Cl^-(H_2O)_{n-1} + H_2O + CH_4 = Cl^-(H_2O)_n + CH_4 \quad (3)$$

slow compared to higher order reactions ($n \geqq 2$). In

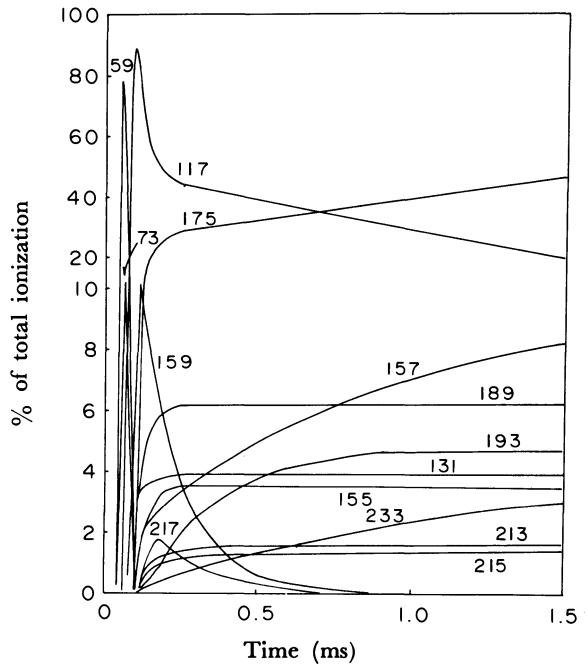

Fig. 1. Positive ions observed in a gas mixture containing 4.02 Torr of He and 86 m Torr of acetone at 33.7 °C. Acetone contains small amounts of mesityl oxide and diacetone alcohol as impurities. Mass 59 : $H^+(CH_3COCH_3)$, mass 117 : $H^+(CH_3COCH_3)_2$. The initial increase of mass 175 is due to the formation of $H^+(CH_3COCH_3)_3$. The gradual increase of mass 175 after 0.3 ms is due to the formation of $H^+(CH_3)_2C(OH)CH_2COCH_3)(CH_3COCH_3)$. Mass 233 : $H^+((CH_3)_2C(OH)CH_2COCH_3)_2$. Mass 159 : $CH_3CO^+(CH_3COCH_3)_2$, mass 217 : $CH_3CO^+(CH_3COCH_3)_3$. Mass 73 : $CH_3^+(CH_3COCH_3)$, mass 131 : $CH_3^+(CH_3COCH_3)_2$, mass 189 : $CH_3^+(CH_3COCH_3)_3$. Mass 157 : $H^+((CH_3)_2C{=}CHCOCH_3)(CH_3COCH_3)$, mass 215 : $H^+((CH_3)_2C{=}CHCOCH_3)(CH_3COCH_3)_2$. Mass 193 : $H_3O^+(CH_3COCH_3)_3$. Mass 155 : $C_3H_3^+(CH_3COCH_3)_2$, mass 213 : $C_3H_3^+(CH_3COCH_3)_3$.

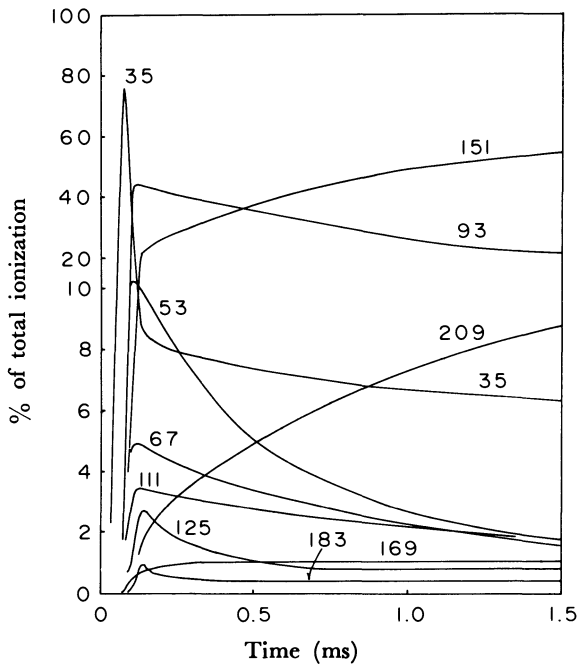

Fig. 2. Negative ions observed in a gas mixture containing 4.09 Torr of He, 0.79 Torr of acetone, and 0.3 mTorr of CCl_4 at 38.9 °C. Acetone contains small amounts of mesityl oxide and diacetone alcohol as impurities. Mass 35 : Cl^-, mass 93 : $Cl^-(CH_3COCH_3)$. The initial increase of mass 151 is due to $Cl^-(CH_3COCH_3)_2$. The gradual increase of mass 151 after 0.2 ms is due to the formation of $Cl^-((CH_3)_2C(OH)CH_2COCH_3)$. Mass 209 is mainly due to $Cl^-((CH_3)_2C(OH)CH_2COCH_3)(CH_3COCH_3)$. Mass 53 : $Cl^-(H_2O)$, mass 111 : $Cl^-(H_2O)(CH_3COCH_3)$, mass 169 : $Cl^-(H_2O)(CH_3COCH_3)_2$ and $Cl^-(H_2O)((CH_3)_2C(OH)CH_2COCH_3)$. Mass 67 : $Cl^-(CH_3OH)$, mass 125 : $Cl^-(CH_3OH)(CH_3COCH_3)$, mass 183 : $Cl^-(CH_3OH)(CH_3COCH_3)_2$ and $Cl^-(CH_3OH)((CH_3)_2C(OH)CH_2COCH_3)$.

Fig. 2, the rapid growth of $Cl^-(H_2O)$ is observed right after the electron pulse. Because the rate of reaction (3) with n=1 is slow, it is likely that $Cl^-(H_2O)$ is formed by switching Reaction (4).

$$Cl^-(CH_3COCH_3) + H_2O = Cl^-(H_2O) + CH_3COCH_3 \quad (4)$$

The ions $Cl^-(H_2O)$ and $Cl^-(H_2O)(CH_3COCH_3)$ are seen to be converted gradually to $Cl^-((CH_3)_2C(OH)CH_2COCH_3)(CH_3COCH_3)_n$ with n=0 and 1. This happens because the bond energy of $Cl^-(H_2O)$ is weaker than that of $Cl^-((CH_3)_2C(OH)CH_2COCH_3)$. The m/z=169 ion, whose intensity is independent on time, may be composed of not only $Cl^-(H_2O)(CH_3COCH_3)_2$ but also $Cl^-(H_2O)((CH_3)_2C(OH)CH_2COCH_3)$.

The m/z=67, 125, and 183 ions correspond to $Cl^-(CH_3OH)(CH_3COCH_3)_n$ with n=0—2. Methanol is a common impurity contained in acetone. The bond energies of $Cl^-\cdots CH_3OH$ and $Cl^-\cdots CH_3COCH_3$ are 17.4 and 12.4 kcal mol^{-1}(1 cal=4.184 J).[11] respectively, i.e., methanol has a greater chloride affinity than acetone. This is the reason why methanol can be readily detected by the present negative ion/molecule reactions. It should be noted that the methanol impurity could also be detected as the $CH_3OH_2^+(CH_3COCH_3)_2$ ion by the positive ion/molecule reactions when the ion source temperature was decreased. However, we found that the detection limit of methanol by positive ion/molecule reactions is about one order of magnitude lower than that by negative ion/molecule reactions under the present experimental conditions. This is because $H_3O^+(CH_3COCH_3)_3$ is thermochemically more stable than $CH_3OH_2^+(CH_3COCH_3)_2$ (i.e., the protic hydrogens of H_3O^+ are more acidic than those of $CH_3OH_2^+$) and the $H_3O^+(CH_3COCH_3)_3$ ion becomes dominant as an impurity ion under the present experimental conditions.

2. Ion/Molecule Reactions of Acetone. Positive Ions: As was described in the previous section, the used acetone contained diacetone alcohol and mesityl oxide as impurities. Although we tried to purify the sample by elaborate distillation, we could not decrease the contents of these impurities below the detection limit. We tried all available commercial acetone samples. We found that all samples measured contained detectable amounts of diacetone alcohol and mesityl oxide except the one purchased from Merck (Uvasol). The temporal profile of the positive ions observed in 4.16 Torr of CH_4 containing 0.259 Torr of acetone (Merck, Uvasol) at 46.7 °C is shown in Fig. 3. The intensities of m/z=157 and 175 ions are seen to be time-independent. This indicates that the contents of mesityl oxide and diacetone alcohol in the used acetone are below the detection limit.

The m/z=145 ion, which corresponds to $C_2H_5^+(CH_3COCH_3)_2$, is observed only when CH_4 is used as a carrier gas. The core ion $C_2H_5^+$ in the cluster may be the product ion from the ion/molecule reactions of methane.[12]

The m/z=157 ion may be the cluster ion of $C_6H_{11}O^+$ (m/z=99) with acetone. Since this ion is already produced right after the electron pulse, it may be yielded from the ion/molecule reactions induced by the primary electron irradiation. The core ion $C_6H_{11}O^+$ may have the structure $(CH_3)_2\overset{\oplus}{C}CH_2COCH_3$, which is different form that of the protonated mesityl oxide, $(CH_3)_2C{=}CHCO\overset{H\oplus}{C}H_3$ (see below).

When the ion source temperature was increased, the gradual growth of m/z=157 and 175 ions starts to be observed. Figure 4 shows the ions observed in 4.92 Torr of CH_4 containing 0.365 Torr of acetone at 104 °C. The m/z=157 and 175 ions grow gradually at the expense of the m/z=117 ion. The observed growth may not be due to the impurities because intensities of these ions are time-independent at room temperature as shown in Fig. 3. The ions seem to be produced by some ion/molecule reactions of acetone. The increase of the growth rates at higher temperature suggests the existence of energy barrier for the formation of m/z=157 and 175 ions. The growth rates increase with temperature up to ≈100 °C. Above ≈100 °C, they start to decrease and the intensities of m/z=157 and 175 ions become weaker.

It was also found that as shown in Fig. 5, the growth rates increased when the pressure of the carrier gas was decreased. This indicates that the formation of m/z=157 and 175 ions is suppressed by the third-body collision. In order to examine the

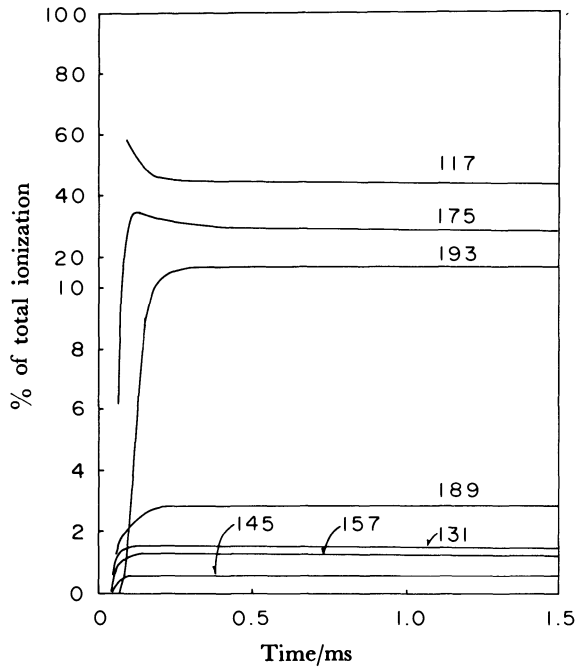

Fig. 3. Positive ions observed in a gas mixture containing 4.16 Torr of CH_4 and 0.259 Torr of acetone at 46.7 °C. Mass 117 : $H^+(CH_3COCH_3)_2$, mass 175 : $H^+(CH_3COCH_3)_3$. Mass 193 : $H_3O^+(CH_3COCH_3)_3$. Mass 131 : $CH_3^+(CH_3COCH_3)_2$, mass 189 : $CH_3^+(CH_3COCH_3)_3$. Mass 157 : $C_6H_{11}O^+(CH_3COCH_3)$. Mass 145 : $C_2H_5^+(CH_3COCH_3)_2$.

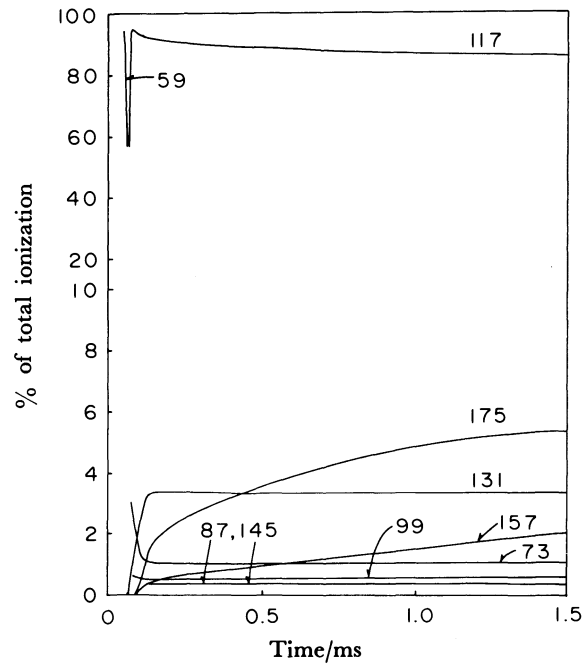

Fig. 4. Positive ions observed in a gas mixture contatining 4.92 Torr of CH_4 and 0.365 Torr of acetone at 104 °C. Mass 59 : $H^+(CH_3COCH_3)$, mass 117 : $H^+(CH_3COCH_3)_2$. Mass 73 : $CH_3^+(CH_3COCH_3)$, mass 131 : $CH_3^+(CH_3COCH_3)_2$. Mass 99 : $(CH_3)_2C^+CH_2COCH_3$. Mass 87 : $C_2H_5^+(CH_3COCH_3)$, mass 145 : $C_2H_5^+(CH_3COCH_3)_2$. The gradual increase of mass 157 and 175 may be due to the formation of $H^+((CH_3)_2C{=}CHCOCH_3)(CH_3COCH_3)$ and $H^+((CH_3)_2C(OH)CH_2COCH_3)(CH_3COCH_3)$, respectively, from the ion/molecule reactions of acetone (see text).

third-body dependence on the formation of these ions, the carrier gas was changed from CH_4 to He with keeping the ion source temperature and pressures of carrier gas and acetone constant. The apparent increase in the growth rates of these ions were observed. This may be due to the fact that helium is a less efficient third body than methane. It seems likely that m/z=157 and 175 ions are formed from the long-lived intermediate complex. The tentative reaction mechanisms for the formation of m/z=157 and 175 ions are given in Scheme 1, where M represents the third body. The clusters of species (IV) and (V) with acetone correspond to ions with m/z=175 and 157, respectively.

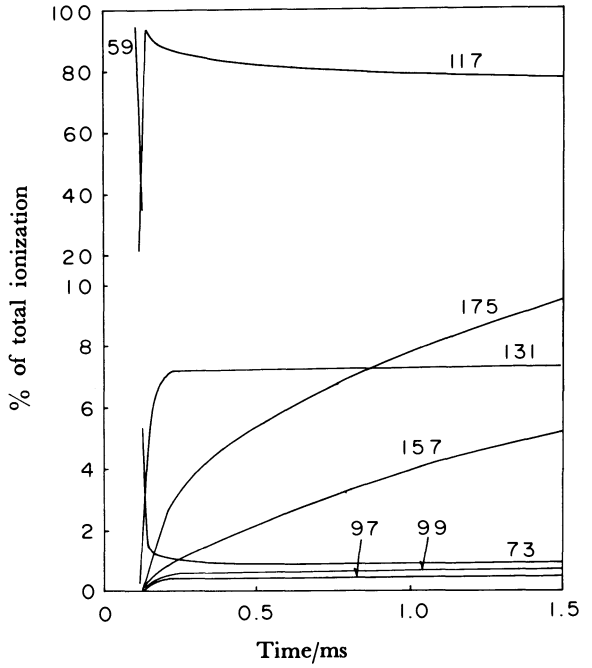

Fig. 5. Positive ions observed in a gas mixture containing 0.17 Torr of CH_4 and 0.33 Torr of acetone at 98 °C. Mass 59 : $H^+(CH_3COCH_3)$, mass 117 : $H^+(CH_3COCH_3)_2$. Mass 73 : $CH_3^+(CH_3COCH_3)$, mass 131 : $CH_3^+(CH_3COCH_3)_2$. Mass 99 : $(CH_3)_2C^+CH_2COCH_3$. Mass 97 : $C_3H_3^+(CH_3COCH_3)$. The increase of mass 157 and 175 are due to the formation of $H^+((CH_3)_2C{=}CHCOCH_3)(CH_3COCH_3)$ and $H^+((CH_3)_2C(OH)CH_2COCH_3)(CH_3COCH_3)$.

The bond energy of the proton-held acetone dimer ion is 29.6 kcal mol^{-1}.[13] Since the keto form of acetone is about 10 kcal mol^{-1} more stable than the enol form,[14] the complex (I) has more than enough internal energy for the isomerization of acetone from keto to enol form (Process (d)). The formation of the complex (III) may be followed by the formation of protonated diacetone alcohol (IV) or mesityl oxide (V). The formation of the latter species (V) is analogous to the aldol condensation reaction of acetone observed in the liquid phase.

With increase of ion source temperature ($\gtrsim$150 °C), the back dissociation reaction (b) of the intermediate complex (I) becomes prominent. This explains the decrease in the rate of the formation of m/z=157 (or 99) and 175 ions at high temperatures.

As shown in Figs. 4 and 5, the steady growth of m/z=157 ion is observed, while the intensity of m/z=99 ion is time-independent. As described in the reaction scheme given above, the m/z=157 ion is suggested to have the structure of the cluster of protonated mesityl oxide (m/z=99) with acetone. Since the protonated mesityl oxide has a protic

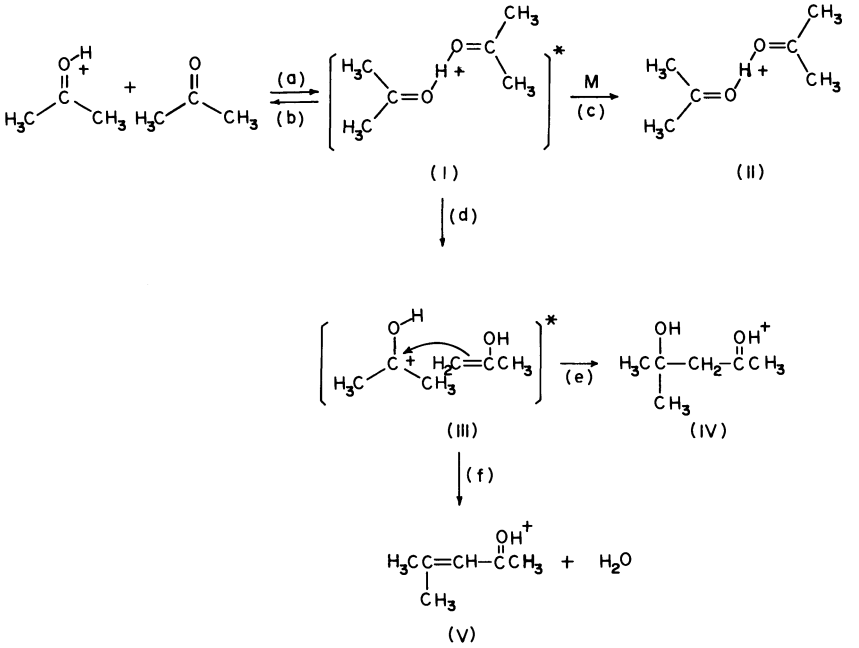

Scheme 1.

hydrogen atom, it can form a fairly strong hydrogen bond with acetone to give the m/z=157 ion. Since the intensity of the m/z=99 ion does not increase with time, this ion must have the different structure from the protonated mesityl oxide. We tentatively propose that the m/z=99 ion has the structure of $(CH_3)_2\overset{\oplus}{C}CH_2COCH_3$ which is produced during the primary electron irradiation. This ion is the tertiary carbonium ion and the bond of its cluster with acetone must be much weaker than that of protonated mesityl oxide with acetone.

Negative Ions: Figure 6 shows the negative ions observed in 4.07 Torr of CH_4 containing 0.287 Torr of acetone (Merck, Uvasol) and 0.2 mTorr of CCl_4. If the acetone sample contains diacetone alcohol as an impurity, the ion with m/z=151 (i.e. $Cl^-((CH_3)_2C(OH)CH_2COCH_3$) as well as its clusters with acetone molecules would be produced gradually with time. The steady intensity of ions observed in Fig. 6 indicates that the content of diacetone alcohol in the acetone sample is lower than the detection limit in the present experimental conditions.

When the ion source temperature is increased, the m/z=151 ion starts to increase as shown in Fig. 7. As described in the previous paper,[2] we think that solvent acetone molecule isomerizes from keto to enol form during the clustering reaction, as shown in Scheme 2. This reaction may be regarded as the base (Cl^- ion)-catalysed keto-enol isomerization reaction of acetone in the gas phase. In our previous work,[7] we observed that for higher order clustering Reactions (5),

$$Cl^-(CH_3COCH_3) + CH_3COCH_3 \rightleftharpoons [Cl^-(CH_3COCH_3)_2]^*$$

$$\rightarrow [CH_3COCH_3\cdots Cl^-\cdots HOC(CH_3)=CH_2]^* \xrightarrow{M} Cl^-(CH_3COCH_3)(HOC(CH_3)=CH_2)$$

Scheme 2.

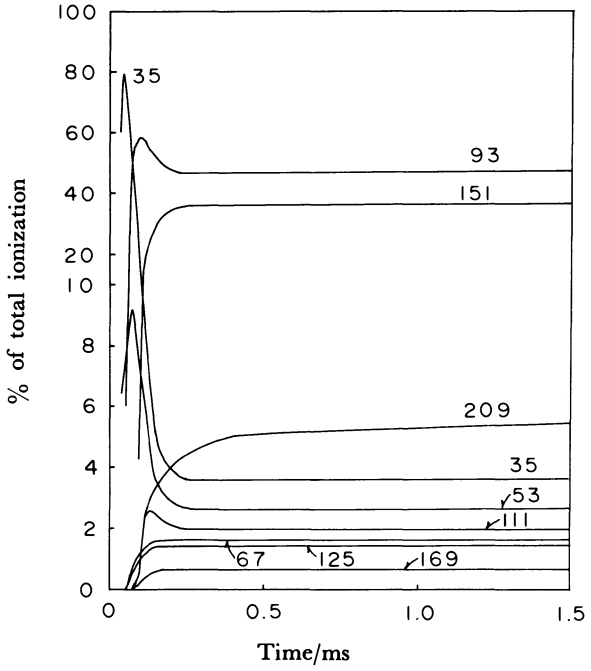

Fig. 6. Negative ions observed in a gas mixture containing 4.07 Torr of CH_4, 0.287 Torr of acetone, and 0.2 mTorr of CCl_4 at 30 °C. Mass 35 : Cl^-, mass 93 : $Cl^-(CH_3COCH_3)$, mass 151 : $Cl^-(CH_3COCH_3)_2$, mass 209 : $Cl^-(CH_3COCH_3)_3$. Mass 53 : $Cl^-(H_2O)$, mass 111 : $Cl^-(H_2O)(CH_3COCH_3)$, mass 169 : $Cl^-(H_2O)(CH_3COCH_3)_2$. Mass 67 : $Cl^-(CH_3OH)$, mass 125 : $Cl^-(CH_3OH)(CH_3COCH_3)$.

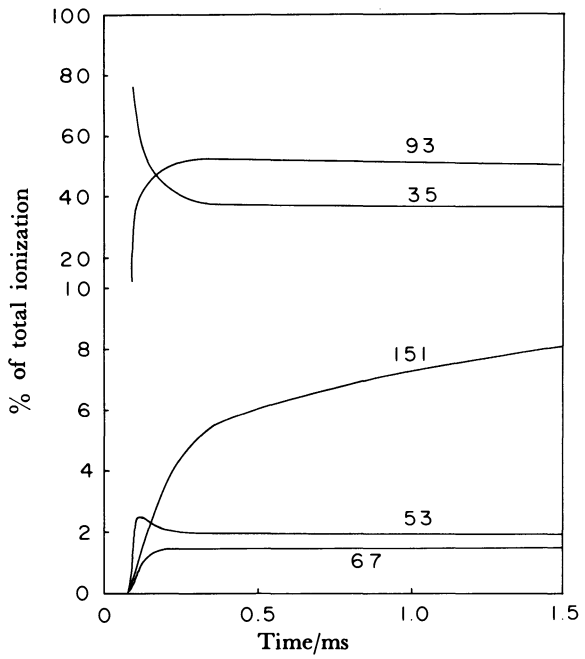

Fig. 7. Negative ions observed in a gas mixture containing 3.99 Torr of CH_4, 0.213 Torr of acetone, and 0.2 mTorr of CCl_4 at 80.5 °C. Mass 35 : Cl^-, mass 93 : $Cl^-(CH_3COCH_3)$. Mass 53 : $Cl^-(H_2O)$. Mass 67 : $Cl^-(CH_3OH)$. The initial increase of mass 151 is due to the formation of $Cl^-(CH_3COCH_3)_2$. The gradual increase of mass 151 after 0.3 ms may be due to the formation of $Cl^-(CH_3COCH_3)$ (CH_2=C(OH)-CH_3) by keto-enol isomerization of acetone.

$$Cl^-(CH_3COCH_3)_{n-1} + CH_3COCH_3 = Cl^-(CH_3COCH_3)_n \quad (5)$$

the decays of larger clusters were found to be slower at 15 °C (Fig. 8 in the Ref. 7). Since the gradual growth of larger clusters $Cl^-(CH_3COCH_3)_n$ were not observed at 30 °C in the present experiments (see Fig. 6), the acetone sample used in the previous work must contain diacetone alcohol as an impurity. We are now sure that the ions $Cl^-(CH_3COCH_3)_2$, $Cl^-(CH_3COCH_3)_3$, and $Cl^-(CH_3COCH_3)_4$ shown in Fig. 8 in Ref. 7 are more or less contaminated by $Cl^-((CH_3)_2C(OH)CH_2COCH_3)$, $Cl^-((CH_3)_2C(OH)CH_2COCH_3)(CH_3COCH_3)$, and $Cl^-((CH_3)_2C(OH)CH_2COCH_3)_2$, respectively.

The growth rate of m/z=151 ion becomes low at high ion source temperature (≈100 °C). The keto→enol isomerization reaction seems to be suppressed when the lifetime of the intermediate complex $[Cl^-(CH_3COCH_3)_2]^*$ gets short at high temperatures.

3. Equilibrium Measurements for Clustering Reactions of Proton and Chloride Ion with Acetone Molecules. Since the diacetone alcohol contained in the used acetone (Merck, Uvasol) is only a negligible amount, it was possible to measure clustering Reactions (1) and (5) without having the impurity problem. Figure 8 shows the van't Hoff plots for Reaction (1) with n=4 using the "pure" acetone sample. The van't Hoff plots of (1, 2) and (2, 3) were measured in our previous work.[7,13] The thermochemical data obtained from the van't Hoff plots are summarized in Table 1. There is a sudden decrease in the stabilities of clusters $H^+(CH_3COCH_3)_n$ between n=2 and 3. This indicates that the clusters $H^+(CH_3COCH_3)_n$ ($n \geqq 3$) are regarded as the shell $(CH_3)_2CO\cdots H^+\cdots OC(CH_3)_2$ plus surrounding ligand acetone molecules. Yamabe et al. studied the gas-phase solvation of acetone toward the proton theoretically.[9] They predicted the structure of $H^+(CH_3COCH_3)_3$ in which the proton in $(CH_3)_2CO\cdots H^+\cdots OC(CH_3)_2$ is attacked by the third molecule in the direction perpendicular to the shell plane.[9] This result suggests that the fourth acetone molecule may also approach to the proton perpendicularly from the other side of the shell plane.

Figure 9 shows the van't Hoff plots for Reaction (5) with n=2 and 3 obtained in the present work. The van't Hoff plots of (0, 1) was obtained in our previous work.[7] Contrary to the van't Hoff plots of reaction (1) (Fig. 8), the plots with n=1—3 are close with each other and the decrease in the enthalpy changes $-\Delta H^\circ_{n-1,n}$ is only gradual. This indicates that the interaction of Cl^- with ligand acetone molecules are

Table 1. Thermochemical Data for Clustering Reactions[a]

Reaction	$-\Delta H^\circ$	$-\Delta S^\circ$
$H^+(CH_3COCH_3)+CH_3COCH_3$ $=H^+(CH_3COCH_3)_2$	29.6[b]	29.3[b]
	30.1[c]	30.4[c]
$H^+(CH_3COCH_3)_2+CH_3COCH_3$ $=H^+(CH_3COCH_3)_3$	12.2[d]	23.0[d]
$H^+(CH_3COCH_3)_3+CH_3COCH_3$ $=H^+(CH_3COCH_3)_4$	8.5	17.0
$Cl^-+CH_3COCH_3=Cl^-(CH_3COCH_3)$	12.4[d]	17.1[d]
$Cl^-(CH_3COCH_3)+CH_3COCH_3$ $=Cl^-(CH_3COCH_3)_2$	11.5	20.3
$Cl^-(CH_3COCH_3)_2+CH_3COCH_3$ $=Cl^-(CH_3COCH_3)_3$	10.4	(22)[e]

a) $-\Delta H^\circ$ in kcal mol^{-1} and $-\Delta S^\circ$ in cal mol^{-1} K (standard state 1 atm). b) Ref. 9. c) Ref. 1. d) Ref. 2. e) Entropy value assumed.

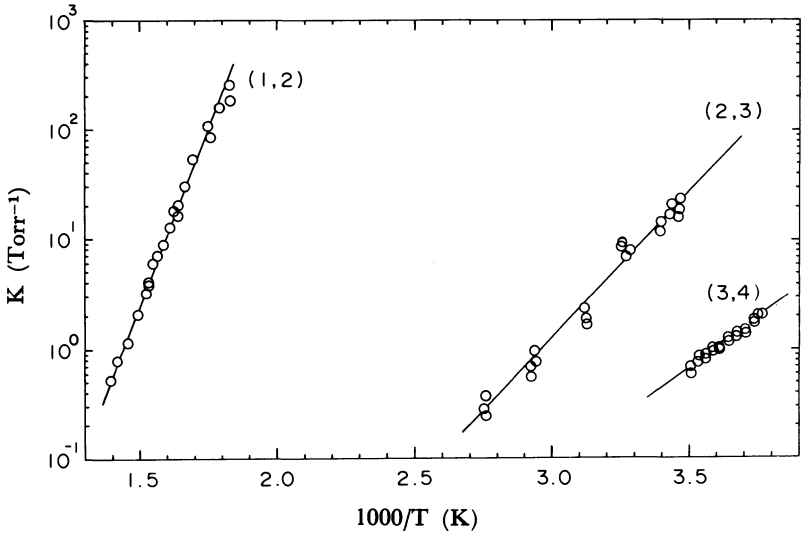

Fig. 8. The van't Hoff plots for clustering reactions: $H^+(CH_3COCH_3)_{n-1}+CH_3COCH_3=H^+(CH_3COCH_3)_n$, $(n-1, n)$.

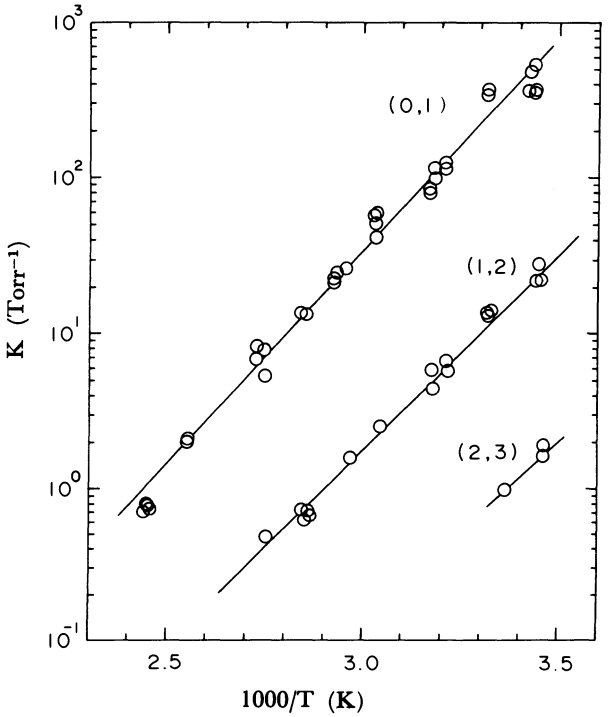

Fig. 9. The van't Hoff plots for clustering reactions: $Cl^-(CH_3COCH_3)_{n-1}+CH_3COCH_3=Cl^-(CH_3COCH_3)_n$, $(n-1, n)$.

mainly electrostatic.

Yamabe and Hirao investigated the stability and structure of the cluster $Cl^-\cdots CH_3CN$ by SCF computation.[15] They found that the most stable C_{3v} structure 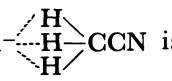 is more stable than the C_s structure $Cl^-\cdots H\text{-}CH_2CN$ by only$\leqq$1 kcal mol^{-1}. This suggests that the bond strength of the complex $Cl^-\cdots CH_3CN$ is less affected by the change of the angle for the bending motion of Cl^- and CH_3CN species. Thus the cluster would show a considerable flexibility in the bending motion of the bond between Cl^- and CH_3CN. By analogy with $Cl^-\cdots CH_3CN$, $Cl^-\cdots CH_3COCH_3$ would also be very flexible as already pointed out in our previous paper.[8] The great flexibility of the cluster $Cl^-\cdots CH_3COCH_3$ means that the species in the cluster have appreciable freedoms of motion. This may explain the small entropy change $-\Delta S^\circ_{0,1}$ for Reaction (5).

Concluding Remarks

The reactions of protonated acetone and chloride ion with acetone molecules were investigated. It was found that mesityl oxide and diacetone alcohol which are contained as impurities in commercial acetone samples spoil the studies of ion/molecule reactions in acetone seriously. Using the relatively pure acetone, detailed kinetic studies of the positive and negative ion/molecule reactions were done. In the reactions of protonated acetone with acetone molecule, the formation of protonated mesityl oxide and diacetone alcohol are suggested. For the clustering reactions of chloride ion with acetone molecules, the equilibria could not be observed at high temperatures. We tentatively concluded that this is due to a keto-enol isomerization of the acetone ligand molecules. However, we feel that the evidences obtained in this work are suggestive rather than compelling.

The author (Kenzo Hiraoka) is greatly indebted to Professor P. Kebarle of the University of Alberta for his help. The financial support of the Grant-in-Aid from the Ministry of Education is gratefully acknowledged.

References

1) M. S. B. Munson, *J. Am. Chem. Soc.*, **87**, 5313 (1965).
2) K. A. G. MacNeil and J. H. Futrell, *J. Phys. Chem.*, **76**, 409 (1972).
3) L. W. Sieck and P. Ausloos, *Radiat. Res.*, **52**, 47 (1972).
4) A. S. Blair and A. G. Harrison, *Can. J. Chem.*, **51**, 703 (1973).
5) Z. Luczynski and H. Wincel, *Int. J. Mass Spectrom. Ion Phys.*, **23**, 37 (1977).
6) Y. K. Lau, P. P. S. Saluja, and P. Kebarle, *J. Am. Chem. Soc.*, **102**, 7429 (1980).
7) K. Hiraoka, K. Morise, T. Nishijima, S. Nakamura, M. Nakazato, and K. Ohkuma, *Int. J. Mass Spectrom. Ion Process.*, **68**, 99 (1986).
8) K. Hiraoka, K. Morise, and T. Shoda, *Int. J. Mass Spectrom. Ion Process.*, **67**, 11 (1985).
9) S. Yamabe, T. Minato, and K. Hirao, *Can. J. Chem.*, **61**, 2827 (1983).
10) A. Streitwieser Jr. and C. H. Heathcock, "Introduction to Organic Chemistry," 2nd ed., Macmillan, New York (1976).
11) S. Yamabe, K. Hiraoka, K. Morise, and S. Nakamura, *Chem. Phys. Lett.*, to be submitted.
12) K. Hiraoka and P. Kebarle, *J. Chem. Phys.*, **63**, 394 (1975).
13) K. Hiraoka, H. Takimoto, and S. Yamabe, *J. Phys. Chem.*, 1986, in press.
14) J. L. Holmes and F. P. Lossing, *J. Am. Chem. Soc.*, **104**, 2648 (1982).
15) S. Yamabe and K. Hirao, *Chem. Phys. Lett.*, **84**, 598 (1981).

An Important Metal Complex in the Asymmetric Synthesis of α-Amino Acids. The Crystal and Molecular Structure of (−)$_{546}$-((*R*)-Alaninato)((6*R*,8*R*)-6,8-dimethyl-2,5,9,12-tetraazatridecane)cobalt(III) Bromide Trihydrate, (−)$_{546}$-[Co(*R*-ala)(1,5*R*,7*R*,11-Me$_4$-2,3,2-tet)]Br$_2$·3H$_2$O

Morio YASHIRO, Masanobu AJIOKA, Shigenobu YANO,* Koshiro TORIUMI,†
Tasuku ITO,† and Sadao YOSHIKAWA*
Department of Synthetic Chemistry, Faculty of Engineering, The University of Tokyo, Hongo, Bunkyo-ku, Tokyo 113
†Division of Applied Molecular Science, Institute for Molecular Science, Myodaiji, Okazaki 444
(Received December 19, 1985)

The crystal and molecular structures of (−)$_{546}$-((*R*)-alaninato)((6*R*,8*R*)-6,8-dimethyl-2,5,9,12-tetraazatridecane)cobalt(III) bromide trihydrate ((−)$_{546}$-[Co(*R*-ala)(1,5*R*,7*R*,11-Me$_4$-2,3,2-tet)]Br$_2$·3H$_2$O) (**1**), derived from (−)$_{546}$-[Co(AMM)(1,5*R*,7*R*,11-Me$_4$-2,3,2-tet)]$^+$ on decarboxylation, have been determined from three-dimensional X-ray counter data. In the above, AMM is an α-amino-α-methylmalonate ion. The compound crystallizes in an orthorhombic space group $P2_12_12_1$ with a=11.713 (1) Å, b=20.301 (2) Å, c=10.113 (2) Å, and Z=4. The structure was solved by the heavy-atom method followed by full-matrix least-squares and Fourier techniques. A refinement using 2168 reflections with $|F_o|>3[\sigma(F_o)]$ gave R=0.052. The absolute configuration of the complex cation is Λ in the β_2 form. The gauche conformations of two five-membered chelate rings for the tetramine are both δ, and the central six-membered chelate ring adopts a chair conformation with one methyl group axial and the other equatorial. All the secondary nitrogen atoms have S configurations except one of the terminal nitrogen atoms whose absolute configuration is R. The *N*-methyl group in an "out-of-plane" five-membered chelate ring is equatorial; however, the other in an "in-plane" five-membered chelate ring has an axial disposition. The alaninate ion coordinates to the cobalt via N and O atoms. The absolute configuration around the carbon center of the alanine was found to be R.

It is generally known that a chelated α-amino acidato ligand is not released from a cobalt(III) complex under mild basic conditions but results in epimerization of the α-carbon center.[1)]

When [Co(*R* or *S*-ala)(1,5*R*,7*R*,11-Me$_4$-2,3,2-tet)]$^{2+}$, derived from [Co(AMM)(1,5*R*,7*R*,11-Me$_4$-2,3,2-tet)]$^+$ on decarboxylation, was warmed under mild basic conditions, the release of alanine with a retention of the asymmetric carbon center from the cobalt(III) complex was unprecedentedly observed. In the above, ala is the alaninate ion, 1,5*R*,7*R*,11-Me$_4$-2,3,2-tet is (6*R*,8*R*)-6,8-dimethyl-2,5,9,12-tetraazatridecane, and AMM is an α-amino-α-methylmalonate ion. On the basis of this novel reaction, we have developed a new cyclic system for the asymmetric synthesis of α-amino acids by using cobalt(III) complexes containing 1,5*R*,7*R*,11-Me$_4$-2,3,2-tet as a ligand.[2)]

Some geometrical isomers, including the β_1 and β_2 modes,[3)] are possible for mixed cobalt(III) complexes of an α-amino acid and a tetramine. It is difficult to assign the geometry of these compounds by AB (electronic absorption), CD, or NMR spectra. We found that while trying to establish an asymmetric synthesis of α-amino acids using chiral cobalt(III) complexes, it is important to confirm the structure of the complex [Co(ala)(1,5*R*,7*R*,11-Me$_4$-2,3,2-tet)]$^{2+}$, which easily releases alanine under mild basic conditions. Our purpose in undertaking an X-ray structure determination was to examine whether any specific stereochemical features could be observed to which the labile feature of the complex could be ascribed.

Experimental

Measurements. The electronic absorption (AB) spectra were recorded on a Shimadzu UV-210 spectrophotometer. The circular dichroism (CD) spectra were measured with a JASCO J-20 recording spectropolarimeter. Microanalyses were performed by Shonan Bunseki Center Co., Ltd.

Materials. All the reagents were of the best commercial grade and were used without further purification. 1,5*R*,7*R*,11-Me$_4$-2,3,2-tet was prepared by the previously reported method.[4)]

Preparation of (−)$_{546}$-[Co(*R*-ala)(1,5*R*,7*R*,11-Me$_4$-2,3,2)](ClO$_4$)$_2$·H$_2$O (2). (−)$_{546}$-[Co(AMM)(1,5*R*,7*R*,11-Me$_4$-2,3,2-tet)]ClO$_4$·2.5H$_2$O[5)] (100 mg) was dissolved into 10 ml of 1 mol dm^{-3} hydrochloric acid and warmed on a water bath for 1 h at 60 °C. The reaction mixture was then cooled and allowed to stand overnight at room temperature. The resulting wine red crystals were collected, washed with ethanol and ether, and dried in vacuo. They were then recrystallized from a minimum amount of warm water; yield, 30 mg. Anal. Calcd for $C_{14}H_{36}N_5O_{11}Cl_2Co$: C, 29.0; H, 6.25; N, 12.1%. Found: C, 29.0; H, 6.6; N, 12.2%. ^{1}H NMR (400 MHz; solvent D_2O; standard DSS) δ=1.20 (3H, d, J 7.02 Hz, C*H*$_3$-CH), 1.45 (3H, d, J 6.41 Hz, C*H*$_3$-CH), 1.53 (3H, d, J 7.02 Hz, C*H*$_3$-CH of ala), 1.90 (3H, s, C*H*$_3$-N), 2.16 (3H, s, C*H*$_3$-N), 2.65—3.03, 3.16—3.22, 3.30—3.40 (multiplets), 3.86 (1H, q, C*H*-CH$_3$ of ala).

Crystal Data and Intensity Measurements for (−)$_{546}$-[Co(*R*-ala)(1,5*R*,7*R*,11-Me$_4$-2,3,2-tet)]Br$_2$·3H$_2$O (1). Since the perchlorate obtained above was unsuitable for the X-ray

Table 1. Crystal Data and Experimental Conditions

Formula	$C_{14}H_{40}N_5O_5Br_2Co$
Molecular wt	577.24
Crystal shape	sphere (0.34 mm ϕ)
Space group	$P2_12_12_1$
a	11.713(1) Å
b	20.301(2) Å
c	10.113(2) Å
V	2404.6(6) Å^3
d(obsd)	1.59 g cm^{-3}
d(calcd)	1.60 g cm^{-3}
Z	4
λ	0.7107 Å (Mo $K\alpha$)
Abs coeff	44.4 cm^{-1}
Monochromator	LiF
Take off angle	5°
Method	ω–2θ (θ–2θ, $2\theta \leq 30°$)
Scan speed	2° min^{-1}
Bkgd counts	10 s
Stds	3 every 50 reflections
2θ limits	70°
No. of data	2345
No. of obsd data	2168 ($F_o \geq 3\sigma(F_o)$)

crystallography, we have newly prepared the bromide as follows. The perchlorate obtained above was dissolved in water and converted to the bromide form by allowing it to pass through a Dowex 2-X8 anion-exchange-resin column (100—200 mesh, Br^- form). A pure bromide salt was obtained upon evaporation of the resultant solution to near-dryness. A wine-red powder was obtained, which yielded good wine-red crystals upon recrystallization from a minimum amount of an ethanol-water solution. Anal. Calcd for $C_{14}H_{40}N_5O_5Br_2Co$: C, 29.1; H, 7.0; N, 12.1; Br, 27.7%. Found: C, 30.0; H, 6.9; N, 12.6; Br, 28.5%. The AB and CD spectra of the bromide were almost identical with those of the perchlorate.

The crystal used in the data collection was shaped into a sphere of 0.34 mm in diameter. The crystallographic and experimental data are summarized in Table 1. The diffraction data were measured on a Rigaku AFC-5 diffractometer. Three standard reflections were monitored every 50 reflections and showed no variation in intensity, for which no correction was made. The standard Lorentz, polarization, and absorption corrections were applied.

Structure Solution and Refinement. The structure was solved by the heavy-atom method and refined by a block-diagonal least-squares method. Atomic scattering factors were taken from Ref. 6. Also, the weighting scheme

$$1/w = [\sigma(\text{count})]^2 + [0.015|F_o|]^2$$

was employed. Since the tetramine was derived from (*R*,*R*)-2,4-pentanediamine,[7] the known absolute configurations of the asymmetric carbon atoms were used as internal reference asymmetric centers to determine the absolute configuration of the complex ion. The effects of anomalous dispersion were included in F_c; values of f' and f'' for Br, Co, O, N, and C were taken from Ref. 8. One of the two Br atoms, Br(2), was located at two positions. A model structure postulating the disorder of that bromine atom was refined by a full-matrix least-squares method. The thermal parameters of the subsidiary bromine atom were assumed to be the same as those of the main bromine atom. The population of the main and subsidiary bromine atoms were refined to 0.817 (6) and 0.183 (6), respectively. All the hydrogen atoms, except for those of the methyl groups and waters of crystallization, were located by assuming a tetrahedral coordination; they were all included in the final refinement with the isotropic temperature factors (R=0.054 and R'=0.054), where $R=\sum||F_o|-|F_c||/\sum|F_o|$ and $R'=(\sum w(|F_o|-|F_c|)^2/\sum w|F_o|^2)^{1/2}$. Hydrogen atom scattering factors were taken from a compilation of Stewart et al.[9] The final positional parameters along with their standard deviations are listed in Table 2. Complications of the anisotropic thermal parameters as well as observed and calculated structure factors are deposited as Document No. 8638 at the office of the Editor of Bull. Chem. Soc. Jpn. The calculations were carried out on the Hitachi M-200H computer at the Computer Center of the Institute for Molecular Science with the Universal Crystallographic Computing Program System UNICS III.[10]

Table 2. Final Positional Parameters and Their Estimated Standard Deviations (in Parentheses)

Atom	x	y	z
Co	0.05931(10)	0.08529(5)	0.30307(11)
N(1)	−0.0386(7)	0.1189(4)	0.4506(8)
N(2)	−0.0851(6)	0.0494(3)	0.2268(8)
N(3)	0.0452(6)	0.1681(3)	0.1983(8)
N(4)	0.2023(7)	0.1258(3)	0.3805(8)
N(5)	0.0922(7)	0.0021(4)	0.3956(8)
O(1)	0.1496(4)	0.0490(2)	0.1658(5)
O(2)	0.2526(5)	−0.0372(2)	0.1082(6)
C(1)	−0.1416(9)	0.0761(6)	0.4521(12)
C(2)	−0.1796(9)	0.0722(5)	0.3133(17)
C(3)	−0.1158(9)	0.0587(5)	0.0849(13)
C(4)	−0.1028(11)	0.1320(6)	0.0443(13)
C(5)	0.0115(9)	0.1606(5)	0.0545(10)
C(6)	0.1532(10)	0.2041(5)	0.2119(12)
C(7)	0.1936(13)	0.1974(6)	0.3486(14)
C(8)	0.1409(7)	−0.0466(4)	0.3014(11)
C(9)	0.1866(7)	−0.0107(4)	0.1816(8)
C(N1)	0.0108(10)	0.1275(6)	0.5918(9)
C(N4)	0.3133(8)	0.0989(4)	0.3389(11)
C(C3)	−0.0495(10)	0.0131(5)	−0.0106(11)
C(C5)	0.0099(11)	0.2317(5)	−0.0135(12)
C(C8)	0.2224(8)	−0.0950(4)	0.3689(9)
Br(1)	0.17318(10)	0.39421(5)	0.21294(15)
Br(2)A[a]	0.32267(19)	0.24332(7)	0.65914(19)
Br(2)B	0.3853(9)	0.2264(3)	0.6158(9)
O(3)	0.0570(8)	0.4149(4)	0.9170(11)
O(4)	0.0778(9)	0.3216(5)	0.7087(14)
O(5)	0.0382(11)	0.3378(5)	0.4610(11)

a) Populations of Br(2)A and Br(2)B are 0.824(4) and 0.176(4), respectively.

Results and Discussion

Molecular Structure of $(-)_{546}$-β_2-[Co(*R*-ala)-(1,5*R*,7*R*,11-Me$_4$-2,3,2-tet)]Br$_2$·3H$_2$O (1). The present structure determination of the important intermediate complex in the asymmetric synthetic system of α-alanine could establish that the cobalt ion is a slightly distorted octahedral center to which alanine is coordinated as a bidentate.

A detailed view of the complex cation is given in Fig. 1, and the intramolecular distances and bond angles are given in Tables 3 and 4. The geometry of the tetramine ligand, 1,5*R*,7*R*,11-Me$_4$-2,3,2-tet, is *Λ*-cisβ. The alaninato coordinates to a cobalt atom with N(5) and O(1) atoms in the β_2 form; the configuration of the asymmetric carbon is R. Consequently, the complex ion is represented as *Λ*-β_2-[Co(*R*-ala)(1,5*R*,7*R*,11-Me$_4$-2,3,2-tet)]$^{2+}$.

The arrangement of the groups around the secondary nitrogen atoms, N(1), N(2), N(3), and N(4),

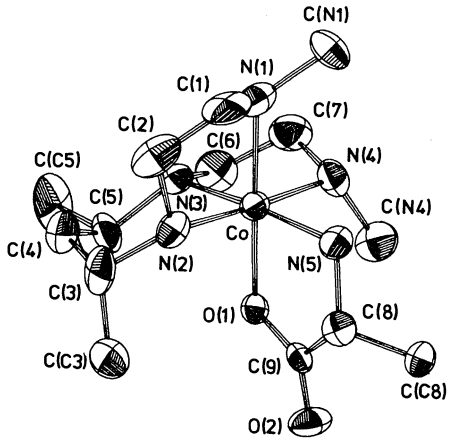

Fig. 1. ORTEP view of $(-)_{546}$-[Co(*R*-ala)(1,5*R*, 7*R*, 11-Me$_4$-2,3,2-tet)]$^{2+}$ ion with the atomic numbering scheme in an asymmetric unit.

Table 3. Bond Distances (*l*/Å) and Their Estimated Standard Deviations (in Parentheses)

Co-N(1)	2.002(15)
Co-N(2)	1.996(14)
Co-N(3)	1.995(13)
Co-N(4)	2.025(14)
Co-N(5)	1.969(14)
Co-O(1)	1.893(9)
N(1)-C(1)	1.486(27)
N(1)-C(N1)	1.552(25)
N(2)-C(2)	1.485(27)
N(2)-C(3)	1.491(24)
N(3)-C(5)	1.515(23)
N(3)-C(6)	1.467(24)
N(4)-C(7)	1.491(28)
N(4)-C(N4)	1.473(22)
N(5)-C(8)	1.488(22)
O(1)-C(9)	1.299(17)
O(2)-C(9)	1.199(18)
C(1)-C(2)	1.474(32)
C(3)-C(4)	1.550(30)
C(3)-C(C3)	1.549(28)
C(4)-C(5)	1.464(29)
C(5)-C(C5)	1.600(28)
C(6)-C(7)	1.468(32)
C(8)-C(9)	1.512(22)
C(8)-C(C8)	1.531(23)

Table 4. Bond Angles (ϕ/°) and Their Estimated Standard Deviations (in Parentheses)

N(1)-Co-N(2)	85.8(6)
N(1)-Co-N(3)	93.5(6)
N(1)-Co-N(4)	92.7(6)
N(1)-Co-N(5)	92.9(6)
N(1)-Co-O(1)	177.0(7)
N(2)-Co-N(3)	91.9(6)
N(2)-Co-N(4)	177.3(7)
N(2)-Co-N(5)	92.2(6)
N(2)-Co-O(1)	92.8(5)
N(3)-Co-N(4)	86.0(6)
N(3)-Co-N(5)	172.7(7)
N(3)-Co-O(1)	89.2(5)
N(4)-Co-N(5)	90.2(6)
N(4)-Co-O(1)	88.8(5)
N(5)-Co-O(1)	84.6(5)
Co-N(1)-C(1)	105.9(9)
Co-N(1)-C(N1)	120.7(8)
C(1)-N(1)-C(N1)	111.1(14)
Co-N(2)-C(2)	106.9(10)
Co-N(2)-C(3)	122.0(8)
C(2)-N(2)-C(3)	110.3(15)
Co-N(3)-C(5)	116.5(8)
Co-N(3)-C(6)	107.4(9)
C(5)-N(3)-C(6)	111.4(13)
Co-N(4)-C(7)	104.9(10)
Co-N(4)-C(N4)	118.0(8)
C(7)-N(4)-C(N4)	111.1(15)
Co-N(5)-C(8)	110.0(7)
Co-O(1)-C(9)	117.4(7)
N(1)-C(1)-C(2)	105.4(14)
N(2)-C(2)-C(1)	110.7(14)
N(2)-C(3)-C(4)	110.6(13)
N(2)-C(3)-C(C3)	113.9(13)
C(4)-C(3)-C(C3)	111.0(15)
C(3)-C(4)-C(5)	116.9(15)
N(3)-C(5)-C(4)	110.3(13)
N(3)-C(5)-C(C5)	109.0(12)
C(4)-C(5)-C(C5)	108.5(15)
N(3)-C(6)-C(7)	108.6(14)
N(4)-C(7)-C(6)	108.5(14)
N(5)-C(8)-C(9)	109.1(11)
N(5)-C(8)-C(C8)	112.4(11)
C(9)-C(8)-C(C8)	116.5(11)
O(1)-C(9)-O(2)	124.0(10)
O(1)-C(9)-C(8)	115.5(10)
O(2)-C(9)-C(8)	120.6(11)

are R, S, S, and S, respectively. The conformations of the three chelate rings of the tetramine are presented in Fig. 2-a,b,c. Both of the five-membered rings have a δ-gauche conformation with an equatorial methyl group on N(1) and an axial one on N(4). The central six-membered ring for the tetramine adopts a chair conformation with one methyl group axial, C(C3), and the other equatorial, C(C5).

The four Co–N distances of tetramine, Co–N(1), Co–N(2), Co–N(3), and Co–N(4), are not significantly different from one another, and the mean value (2.01 Å) is quite usual. The ring angles at the cobalt atom for the five-membered rings are 85.8 (6)° and 86.0 (6)° for N(1)–Co–N(2) and N(3)–Co–N(4), respectively. These are normal for cobalt(III) five-membered diamine chelate rings. The ring angle at the cobalt atom for a six-membered ring, N(2)–Co–N(3), is 91.9 (6)°. The average N–C and C–C distances of the membered nitrogen and carbon atoms are 1.49 and 1.48 Å, respectively.

The observed values of the Co–N(2)–C(3) and Co–N(3)–C(5) are 122.0 (8)° and 116.5 (8)°, significantly expanded from a tetrahedral configuration. This distortion is attributed to an interaction between the axial *C*-methyl group on C(3) and the apical O(1) atoms. The conformation of the six-membered chelate ring in the tetramine is represented diagrammatically in Fig. 3. The dihedral angles between the plane A and B (α), and B and C (β) are 35.8° and 59.0°, respectively. The value of α is considerably small, compared with a corresponding value of 40.6° in the [Co(ox)(*N*,*N'*-Me$_2$-*R*,*S*-2,3″,2-tet)]$^+$ ion,[11] which has no axial *C*-methyl group. However, it is similar to that of 36.4° in the [Co(ox)(5*R*,7*R*-Me$_2$-2,3,2-tet)]$^+$ ion,[12] which has an axial *C*-methyl group. This small α value indicates a flattened structure of the six-membered ring. The magnitude of the ring flattening of the two complexes containing axial *C*-methyl groups, [Co(ox)-(5*R*,7*R*-Me$_2$-2,3,2-tet)]$^+$ and [Co(*R*-ala)(1,5*R*,7*R*,11-Me$_4$-2,3,2-tet)]$^+$, is the same in spite of a difference in the bidentate ligands, oxalato or alaninato, and additional *N*-methyl groups. Thus, although the conformation of the tetramine is not much different

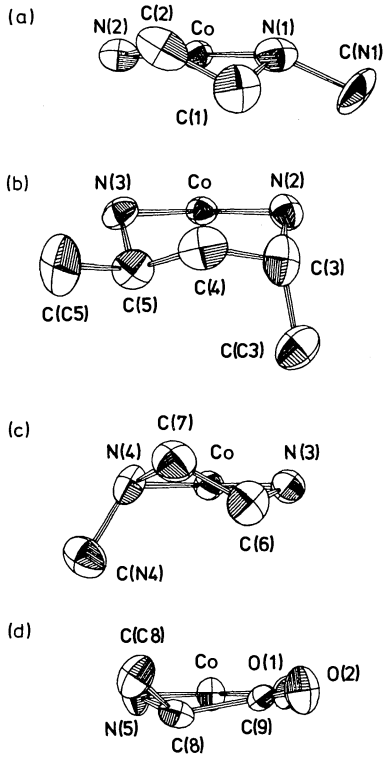

Fig. 2. A perspective drawing of the chelate rings. (a): The out-of-plane five-membered ring, (b): the central six-membered ring, (c): the in-plane five-membered ring, (d): the alaninato five-membered ring.

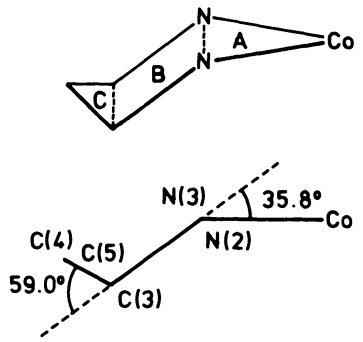

Fig. 3. The dihedral angles between the planes A and B, and between the planes B and C.

Table 5. Interatomic Nonbonded Distances (l/Å) between Methyl Groups and Other Atoms (Less than 3.5 Å) and Their Standard Deviations (in Parentheses)

C(N1)–Co	3.10(2)
C(N1)–N(4)	3.10(3)
C(N1)–N(5)	3.37(3)
C(N1)–C(1)	2.51(3)
C(N4)–Co	3.01(2)
C(N4)–N(5)	3.30(2)
C(N4)–O(1)	2.79(2)
C(N4)–C(6)	3.12(3)
C(N4)–C(7)	2.44(3)
C(N4)–C(9)	3.11(2)
C(C3)–N(2)	2.55(2)
C(C3)–O(1)	3.03(2)
C(C3)–C(4)	2.55(3)
C(C3)–C(5)	3.15(3)
C(C3)–C(9)	3.42(2)
C(C5)–N(3)	2.54(2)
C(C5)–C(4)	2.49(3)
C(C5)–C(6)	2.89(3)
C(C8)–N(5)	2.51(2)
C(C8)–O(2)	2.91(2)
C(C8)–C(9)	2.59(2)

from those of other analogous 2,3,2-tet complexes, the tetramine containing an *R,R*-2,4-pentanediamine unit is somewhat strained by nonbonded repulsions, including methyl substituents.

Close contacts between the *N*-methyl or *C*-methyl carbon atoms and other atoms in the complex (less than 3.5 Å) are listed in Table 5. Four close contacts between axial methyl groups and alaninato chelate ring, C(N4)–N(5) 3.30 (2) Å, C(N4)–C(9) 3.11 (2) Å, C(C3)–O(1) 3.03 (2) Å, and C(C3)–C(9) 3.42 (2) Å, were observed.

The conformation of the chelate ring for the alaninato is presented in Fig. 2-d. The five-membered ring has a slightly puckered pseudo-δ-gauche conformation (maximum deviation from the plane of best fit; N(5), 0.12 Å; C(8), 0.12 Å). In order to compare the structure of the alaninato chelate with those in reported alaninato-cobalt(III) complexes, the Cambridge Crystallographic Data File (XDC) was searched and alaninato-cobalt(III) complexes whose structures have been established on the basis of three-dimensional counter data were collected. Their selected distances, angles, and torsional angles are listed in Table 6. The bond lengths and angles in the present complex are normal compared with those in the reported complexes. The Co–N(5) distance is 1.969 (14) Å. This value is in the upper end of the reported range for the corresponding Co–N bonds (1.935—1.961 Å). The Co–O(1) distance is 1.893 (9) Å, which is normal for the Co–O bonds (the reported values are in the range 1.877—1.925 Å). The angle at the cobalt atom N(5)–Co–O(1) is 84.6 (5)°, while the reported values are in the range 83.4—86.3°. The angles Co–N(5)–C(8) and Co–O(1)–C(9) are 110.0 (7)° and 117.4 (7)°, while the reported values are in the range 106.1—110.8° and 114.3—116.8°, respectively. The torsional angle N(5)–C(8)–C(9)–O(1) is rather characteristic. The value is 17.6°; this is considerably smaller compared with those reported for the corresponding torsional angles (19.0—29.4°). This distortion is attributed to an interaction between the terminal *N*-methyl group in the tetramine part (C(N4)) and the carbon in the alanine part (C(9)). A similar distortion in the alaninato chelate has been observed in the *Λ*-*β*$_2$-[Co(*S*-ala)(*S,S*-pyht)]$^{2+}$ ion,[13] which has *N*-substituent on the terminal nitrogen of the tetramine that is similar to the present complex, whose torsional angle is 19.0°. We observed the release of alanine from the *Λ*-*β*$_2$-[Co(*S*-ala)(*S,S*-pyht)]$^{2+}$ ion when this complex was warmed under mild basic conditions; this is similar to the case of the [Co(*R*-ala)(1,5*R*,7*R*,11-Me$_4$-2,3,2-tet)]$^{2+}$ ion.

Thus, the present structure determination revealed that the important intermediate complex in the asymmetric synthetic system of α-alanine has the usual octahedral coordination geometry, although the conformation of the ligands are somewhat strained. The obtained results suggest that the labile feature of this complex should be ascribed to factors other than a stereochemical distortion of the alanine unit.

Description of the Unit Cell. The unit cell, Fig. 4, consists of four discrete complex cations, twelve bromine atoms (including eight disordered positions) and twelve waters of crystallization. In Table 7 are listed some of the important distances outside the

Table 6. Selected Distances, Angles, and Torsional Angles of Alaninato Chelates in Crystallographically Established Alaninato-Cobalt(III) Complexes

Complexes	Distances *d*/Å		Angles *θ*/°			Torsional Angles *φ*/°	*R*	Ref.
	Co–N	Co–O	N–Co–O	Co–N–C	Co–O–C	N–C–C–O		
(+)$_{589}$-[Co(*S*-ala)(NH$_3$)$_2$(NO$_2$)$_2$]	1.935[a]	1.919[a]	86.3[b]	108.8[b]	114.3[b]	27.2[b]	0.025	14
(−)-*mer*-[Co(*S*-ala)$_3$]·H$_2$O	1.942(10)	1.899(9)	85.2(4)	107.8(7)	114.4(8)	26.4(14)	0.075	15
	1.948(10)	1.880(8)	85.3(4)	108.2(8)	116.8(8)	23.7(16)		
	1.945(10)	1.877(9)	86.3(4)	109.2(8)	114.9(9)	29.4(15)		
[Co(*R*-ala)(NO$_2$)$_2$(tn)]	1.951[a]	1.910[a]	85.5[b]	109.5[b]	115.4[b]	24.1[b]	0.046	16
(+)$_{589}$-Ba[Co(*R*-ala)(glygly)(NO$_2$)]Cl·4H$_2$O	1.961[a]	1.925[a]	83.4[b]	106.1[b]	116.4[b]	29.1[b]	0.045	17
[Co(*S*-OHBH[c])(*S*-ala)·2H$_2$O	1.938(6)	1.912(5)	85.0(2)	108.2(4)	114.9(4)	19.1	0.059	18
Λ-*β*$_2$-[Co(*R*-ala)(*S,S*-pyht[d])](ClO$_4$)$_2$·2H$_2$O	1.96(2)	1.90(1)	85.8(6)	110.8(9)	115.4(10)	19.0	0.056	13
Λ-*β*$_2$-[Co(*R*-ala)(1,5*R*,7*R*,11-Me$_4$-2,3,2-tet)]Br$_2$·3H$_2$O	1.969(14)	1.893(9)	84.6(5)	110.0(7)	117.4(7)	17.6	0.054	This work

a) XDC data. b) Calculated on the basis of the XDC data. c) *α*-*N*-(*o*-hydroxybenzyl)-L-histidinato. d) 1,7-bis(2(*S*)-pyrrolidyl)-2,6-diazaheptane.

Table 7. Intermolecular Hydrogen Bonds (Less than 3.5 Å)

A-H···B	A···B	A-H···B	Symmetry of atom B		
N(1)-Br(2)A	3.42(2)A	138.3°	−1/2+X,	1/2−Y,	1−Z
N(1)-Br(2)B	3.33(2)	150.7	−1/2+X,	1/2−Y,	1−Z
N(2)-Br(1)	3.37(1)	131.3	−X,	−1/2+Y,	1/2−Z
N(3)-Br(2)A	3.48(1)	173.6	−1/2+X,	1/2−Y,	1−Z
N(3)-Br(2)B	3.41(2)	165.2	−1/2+X,	1/2−Y,	1−Z
N(4)-O(2)	2.97(2)	141.5	1/2−X,	−Y,	1/2+Z
N(5)-O(2)	2.90(2)	162.9	1/2−X,	−Y,	1/2+Z
N(5)-O(3)	3.13(2)	147.8	−X,	−1/2+Y,	3/2−Z
O(3)-Br(1)	3.31(2)		X,	Y,	1+Z
O(3)-O(4)	2.84(3)		X,	Y,	Z
O(4)-Br(2)A	3.32(2)		X,	Y,	Z
O(4)-O(5)	2.57(3)		X,	Y,	Z
O(5)-Br(1)	3.18(2)		X,	Y,	Z
O(5)-Br(2)A	3.25(2)		−1/2+X,	1/2−Y,	1−Z
O(5)-Br(2)B	2.35(3)		−1/2+X,	1/2−Y,	1−Z

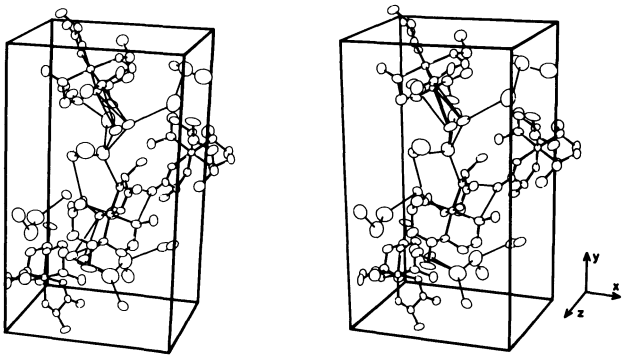

Fig. 4. Stereoscopic view of the unit cell contents showing the crystal packing.

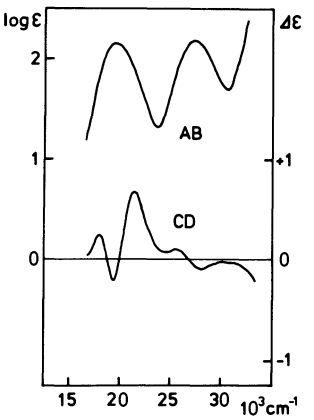

Fig. 5. Electronic absorption (AB) and circular dichroism (CD) spectra of $(-)_{546}$-[Co(*R*-ala) (1,5*R*, 7*R*,11-Me_4-2,3,2-tet)]$^{2+}$.

complex ion. Three water oxygen atoms, O(3), O(4), and O(5), and one bromide anion, Br(1), are aligned along the c-axis with distances of about 3 Å. O(4), O(5), and Br(2) (A or B) are aligned along the a-axis. There probably exists a network of hydrogen bonds between these water oxygens and the bromide anions. In addition of this network, there are N-H···Br and N-H···O hydrogen bonds between the complex ions and the water oxygen and bromide anion. An O(2) atom of the alaninato is linked to N(4) and N(5) by N-H···O hydrogen bonds at distances 2.97 (2) and 2.90 (2) Å, respectively.

Circular Dichroism and Absorption Spectra. The CD and AB spectra of $(-)_{546}$-*Λ*-β_2-[Co(*R*-ala)(1,5*R*,7*R*,11-Me_4-2,3,2-tet)]$^{2+}$ are shown in Fig. 5, and their spectral data are summarized in Table 8. It is often observed that the CD sign in the first absorption region is closely related to the absolute configurations for the dissymmetric cobalt complexes. For example, the sign of the dominant peak for the first absorption region is expected to be positive for a Λ configuration. However, the present complex has two positive and one negative cotton effects in the first absorption region. Therefore, it is difficult to assign the absolute configuration by means of CD spectroscopy.

Table 8. Electronic Absorption (AB) and Circular Dichroism (CD) Spectral Data of $(-)_{546}$-*Λ*-β_2-[Co(*R*-ala)(1,5*R*,7*R*,11-Me_4-2,3,2-tet)]$^{2+}$

AB $\tilde{\nu}/10^3$ cm^{-1} (log ε)	CD $\tilde{\nu}/10^3$ cm^{-1} (Δε)
19.5 (2.15)	17.9 (+0.24)
	19.3 (−0.20)
	21.0 (+0.67)
27.3 (2.18)	25.5 (+0.10)
	28.0 (−0.08)

The electronic absorption spectrum of the complex gives typical $[CoN_5O]^{2+}$ absorptions. The first absorption band of this complex is shifted by about 700 cm^{-1} to the lower-energy side compared to the alaninato complex of 2,3,2-tet. This indicates that an

alkyl group substitution on the tetramine nitrogen causes a weakening of the ligand field. Since the present crystal structure does not show any significant stereochemical features for the coordinated alanine part, we believe that the labile feature of this complex is closely related to the strength of the ligand field. Studies are now in progress to clarify the labile feature of amino acidato cobalt(III) complexes while hoping to establish metal-assisted asymmetric reactions.

This work was supported by the Joint Studies Program of the Institute for Molecular Science, and was partially supported by a Grant-in-Aid for Scientific Research from the Ministry of Education, Science and Culture.

References

1) D. H. Williams and D. H. Busch, *J. Am. Chem. Soc.*, **87**, 4644 (1965); M. Murakami and K. Takahashi, *Bull. Chem. Soc. Jpn.*, **32**, 303 (1956); D. A. Buckingham, L. G. Marzilli, and A. M. Sargeson, *J. Am. Chem. Soc.*, **89**, 5133 (1967); S. Yoshikawa, M. Saburi, and M. Yamaguchi, *Pure Appl. Chem.*, **915**, 50 (1978); M. Yamaguchi, S. Yamamatsu, T. Furusawa, S. Yano, M. Saburi, and S. Yoshikawa, *Inorg. Chem.*, **19**, 2010 (1980); M. Yamaguchi, S. Yano, M. Saburi, and S. Yoshikawa, *Bull. Chem. Soc. Jpn.*, **53**, 691 (1980).

2) M. Ajioka, K. Matsuda, S. Yano, and S. Yoshikawa, *J. Am. Chem. Soc.*, **103**, 2459 (1981).

3) β_1 and β_2 refer to the two configurational isomers obtained using different or unsymmetrical donor ligands in the remaining octahedral sites. For amino acidate, β_1 refers to the isomer with the amino group of amino acidato in a trans position to a terminal N atom of the tetramine, and β_2 refers to the isomer with the amino group trans to a secondary N atom of the quadridentate: D. A. Buckingham, L. G. Marzilli, *Inorg. Chem.*, **6**, 1042 (1967).

4) M. Ajioka, S. Yano, M. Saburi, and S. Yoshikawa, *Inorg. Chem.*, **20**, 884 (1981).

5) The preparation of this complex will be dealt in a subsequent paper.

6) 'International Tables for X-ray Crystallography,' Kynoch Press, Birmingham, England 1974, Vol. 4.

7) A. Kobayashi, F. Marumo, Y. Saito, J. Fujita, and F. Mizukami, *Inorg. Nucl. Chem. Lett.*, **7**, 777 (1971); A. Kobayashi, F. Marumo, and Y. Saito, *Acta Crystallogr., Sect. B*, **29**, 2443 (1973).

8) D. T. Cromer, *Acta Crystallogr.*, **18**, 17 (1965).

9) R. F. Stewart, E. R. Davison, and W. T. Simpson, *J. Chem. Phys.*, **42**, 3175 (1965).

10) T. Sakurai and K. Kobayashi, *Rikagaku Kenkyusho Hokoku*, **55**, 69 (1979).

11) S. Yano, K. Furuhashi, and S. Yoshikawa, *Bull. Chem. Soc. Jpn.*, **50**, 685 (1977).

12) S. Yano, M. Yamaguchi, A. Fujioka, and S. Yoshikawa, *Inorg. Chem.*, **17**, 14 (1978).

13) M. Yamaguchi, S. Yano, M. Saburi, and S. Yoshikawa, *Inorg. Chem.*, **19**, 2016 (1980).

14) R. Herak, K. W. Muir, L. Manojlovic-Muir, M. J. Malinar, and M. B. Celap, *Glas. Hem. Drus., Beograd*, **46**, 337 (1981). XDC, REFCODE: NALCOA10.

15) R. Herak, B. Prelesnik, and I. Krstanovic, *Acta. Crystallogr., Sect, B.* **34**, 91 (1978).

16) M. J. Malinar, R. Herak, M. B. Celap, N. Pavlovic, S. Milic, and D. Stojanov, *Glas. Hem. Drus., Beograd*, **46**, 303 (1981). XDC, REFCODE: BEMVIY.

17) R. Herak, L. Solujic, I. Krstanovic, B. Prelesnik, and M. B. Celap, *Rev. Chim. Miner.*, **19**, 282 (1982). XDC, REFCODE: BOVSOU.

18) K. E. Voss, R. J. Angelici, and R. A. Jacobson, *Inorg. Chem.*, **17**, 1922 (1978).

 © 1986 The Chemical Society of Japan Bull. Chem. Soc. Jpn., 59, 2263—2267 (1986)

X-Ray Photoelectron Spectroscopy of Rare Earth Halides

Yoshinori UWAMINO,* Akira TSUGE, Toshio ISHIZUKA, and Hideo YAMATERA†
Government Industrial Research Institute, Nagoya, Hirate-cho, Kita-ku, Nagoya 462
†Department of Chemistry, Faculty of Science, Nagoya University,
Furo-cho, Chikusa-ku, Nagoya 464
(Received January 22, 1986)

Rare earth (RE) halides (fluorides, chlorides, bromides, and iodides) have been studied by X-ray photoelectron spectroscopy. The binding energies (BE's) of the RE 3d and 4d peaks for the chlorides, bromides, and iodides are related to the atomic charge calculated on the basis of Pauling's scale of electronegativity (Pauling charge). Except for Y and Lu, the observed RE 3d and 4d BE's for the fluorides are lower than those expected. For Y and Lu, the observed RE 3d and 4d BE's for all halides are related to the Pauling charge. For the fluorides and chlorides, the BE's of the ligand peak show variations with increasing atomic number of RE's and a specific "tetrad effect" is observed in plots of BE versus RE atomic number and versus $1/R$ (where R is the mean distance from the ligand atom to the neighboring RE atom), except for the BE's of the F 1s peaks from the light RE fluorides. For the iodides and bromides, no or little characteristic variations are seen in the BE's of I and Br.

Rare earths (RE's) have been studied widely by X-ray photoelectron spectroscopy (XPS).[1-6] Satellite and multiplet peaks in the 3d and 4d spectra of RE compounds have been of paticular interest.[1,3-5] Although much attention has been devoted to the energy separations between the satellite and the main peak and between the multiplet components, there has been little consideration of absolute binding energies (BE's).

Jørgensen and Berthou measured absolute BE's of the inner and outer shells of RE elements and ligands in various RE compounds.[2] However, their calibrant (C 1s peak from mounting tape) is unsatisfactory for charge correction of nonconducting materials such as RE compounds.[7] Therefore, the BE values given by them may involve some uncertainty. To discuss chemical shifts for RE elements, it is necessary to measure absolute BE's with greater accuracy. Although the RE elements show a striking similarity to one another in their chemical properties, slight differences in these properties may influence the BE's of ligands in RE compounds. Therefore, it is worthwhile measuring the BE's of such ligands.

Thus, we systematically measured the absolute BE's of the RE elements and ligands in RE oxides, sulfates, and oxalates.[6] For the oxides, appreciable differences were found in the BE's of O 1s peaks, and a specific "inclined W" form was observed in plots of BE versus $1/R$ (where R is the mean distance from the oxygen atom to the neighboring RE atom) and versus the RE oxidation potential. In the present study, we examine whether the "inclined W" pattern appears or not for RE halides. In addition, we investigate the relation between the RE BE's and the electronegativities of halogen atoms. Thus we measured the BE's of the RE elements and ligands in a series of fluorides, chlorides, bromides, and iodides of RE's (including yttrium). The results of these measurements are discussed below.

Experimental

The photoelectron spectra of the RE compounds were obtained using a JEOL JESCA-4 photoelectron spectrometer equipped with an Al $K\alpha$ X-ray source ($h\nu$=1486.6 eV). The X-ray power supply was operated at 7 kV and 40 mA. The pressure inside the sample chamber was below 5×10^{-5} Pa during the measurements. The resolution of the analyzer was set to give a full width at half-maximum (FWHM) of 1.9 eV for the Au $4f_{7/2}$ peak. The XPS data were obtained by digital accumulation using a Texas Instruments 980B minicomputer. The digital data were processed with a Hewlett-Packard 9845B desk-top computer combined with the minicomputer. Data reduction consisted of smoothing of the raw data and curve synthesis using Gaussian peak shapes. The program was written in this laboratory.[8]

RE halide samples were prepared from 99.99% RE oxides (Shin-etsu Chemical Co.). The RE fluorides were precipitated from 1% nitric acid solutions by adding hydrofluoric acid and dried at 130 °C. The RE chlorides, bromides and iodides were prepared by dissolving the RE oxides in hydrochloric acid, hydrobromic acid, and hydroiodic acid, respectively, evaporating to dryness at 90 °C on a hot plate, and then drying in vacuum at room temperature for two days. Cerium iodide was not obtained by this method; therefore spectra are lacking on this compound.

All the powder samples were pressed at 200 kg cm^{-2} using a pellet die (Hitachi Ltd.) to give circular disks about 1 mm thick and 13 mm in diameter. All samples were fixed to the sample holder by means of double-sided adhesive tape.

Results and Discussion

The 3d spectra for Y and La through Gd were measured. The $3d_{5/2}$ spectra of Y, La, Nd, and Gd are shown in Fig. 1. The spectra for Ce, Pr, Sm, and Eu were similar to those for La, Nd, Gd, and Gd, respectively. The Y 3d spectra of YF_3, YCl_3, YBr_3, and YI_3 are very similar to one another. For each of the other RE's, the RE $3d_{5/2}$ spectra of the chloride, bromide, and iodide are similar to one another, but

Table 1. BE's (in eV) of RE 3d Peaks

	Fluoride				Chloride				Bromide				Iodide			
	$3d_{3/2}$			$3d_{5/2}$	$3d_{3/2}$			$3d_{5/2}$	$3d_{3/2}$			$3d_{5/2}$	$3d_{3/2}$			$3d_{5/2}$
Y		161.0		158.8		160.8		158.7		160.6		158.5		160.2		158.1
La	857.4[s]	853.3	840.7[s]	836.5	857.5[s]	853.8	840.6[s]	837.0	856.1[s]	852.5	839.3[s]	835.6	854.8[s]	851.6	838.1[s]	834.9
Ce	906.3	902.5[s]	887.8	884.0[s]	904.5	901.4[s]	886.8	882.8[s]	905.0	901.0[s]	886.5	882.4[s]		—[a]		—[a]
Pr		954.0		933.3	956.3	952.4[s]	935.8	931.7[s]	954.9	950.7[s]	934.5	930.4[s]	954.0	949.9[s]	933.7	929.9[s]
Nd		1006.1		982.9	1006.0	1002.1[s]	983.5	979.7[s]	1005.7	1001.5[s]	983.3	979.0[s]	1005.3	1000.9[s]	982.2	977.7[s]
Sm		1110.8		1083.5		1111.3		1084.2		1111.0		1083.9		1110.7		1083.8
Eu		1165.0		1135.0		1165.8		1136.0		1165.9		1135.4		1165.4		1134.9
Gd				1187.8				1188.6				1188.3				1187.7

s) Satellite peak. a) Cerium iodide sample was not obtained.

Table 2. BE's (in eV) of RE 4d Peaks

	Fluoride					Chloride			Bromide					Iodide	
La				106.9	104.0	109.5[s]	106.5	103.4	108.9[s]	106.3	103.4			106.8	103.7
Ce				113.7	110.1		112.4	108.9		113.5	110.1			—[a]	—[a]
Pr				120.3	115.9		119.4	115.4		119.5	115.4			119.3	115.1
Nd				125.7	121.5		125.3	121.3		124.8	121.0			124.9	120.8
Sm				136.6	131.8		137.1	132.3		136.8	132.0			136.3	131.5
Eu				142.5	137.2		142.8	137.4		142.4	136.9			142.1	136.5
Gd				148.4	143.3		149.0	143.7		148.9	143.5			148.4	143.1
Tb			178.7	154.8	149.9	177.9	155.0	149.8		154.8	149.5		176.9	154.7	149.6
Dy	211.0	183.4	173.1	163.3	157.4	180.3	158.0	154.8		157.6	154.5	209.5	185.1	178.5	157.4	154.2
Ho		190.5	177.8	168.9	163.1		177.7	163.1			162.5			187.5	166.3	162.1
Er		197.2	185.5	175.0	170.3	183.6	175.1	170.2			169.9		196.7	185.8	172.5	169.2
Tm			192.4	181.6	177.3		180.8	177.7			177.8		202.7	185.7	180.3	177.0
Yb		207.0	200.9	193.7	186.7			186.4	206.8	200.7	193.9	185.9		206.5	200.5	193.8	186.0
Lu				207.7	197.9		207.8	197.4			207.5	197.6				207.1	197.2

s) Satellite peak. a) Cerium iodide sample was not obtained.

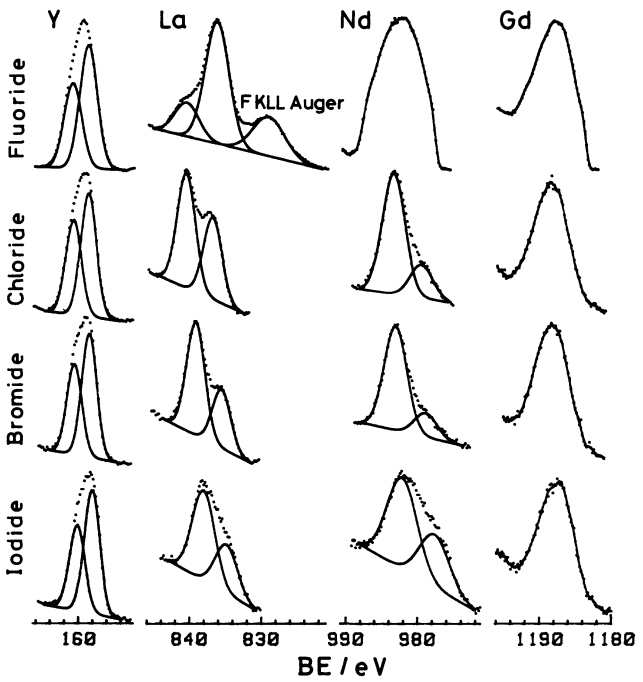

Fig. 1. Photoelectron spectra of the RE $3d_{5/2}$ level for RE halides (RE=Y, La, Nd, and Gd). Dotted lines show observed spectra. Solid lines give deconvolutions of the main and satellite peaks. Y $3d_{3/2}$ peak is shown at the higher BE site in each Y spectrum.

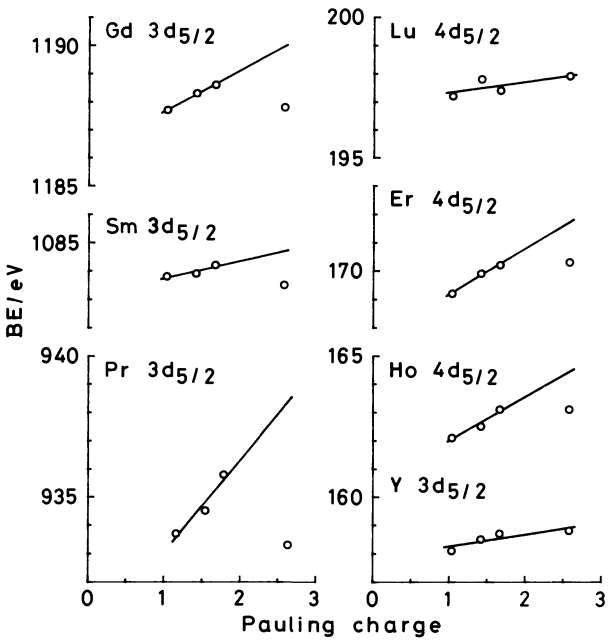

Fig. 2. Correlations of the BE's of the RE $3d_{5/2}$ and RE $4d_{5/2}$ (RE=Y, Pr, Sm, Gd, Ho, Er, and Lu) with Pauling charge for each RE halide.

rather different from that of the fluoride. The different shape of the fluoride spectra are due to the low intensity of the satellite arising from the charge-transfer transition from the ligand anion to the 4f level of RE ion.[4] Distinct satellite peaks are recognized in the Nd $3d_{5/2}$ spectra from the chloride, bromide, and iodide, but not in the spectra from the fluoride. For Gd, no distinct satellite peaks are recognized. For Nd and Gd, the FWHM's of the peaks from the fluorides are 1.3—2.0 times broader than those from the chlorides, bromides, and iodides.

The 4d spectra for all RE's were measured. The obtained spectra were similar to those given by Signorelli and Hayes[3] (the RE 4d spectra of several halides), and Suzuki et al.[4] (the RE 4d spectra of the fluorides, chlorides, and bromides of La and Ce). Satellite peaks were recognized in the La 4d spectra of the chloride and bromide. The RE 4d spectra for the halides of Tb through Yb were complex. Signorelli and Hayes have explained these complex structures by the electrostatic coupling of a 4d photohole with the unfilled 4f shell of RE.[3]

Tables 1 and 2 list the BE's of the 3d peaks and of the 4d peaks, respectively. Charging of the sample was corrected by regarding the C 1s peak from carbon contamination on the sample surface as located at 284.6 eV. The BE's of the measured satellite and multiplet peaks are also listed in Tables 1 and 2.

Jørgensen and Berthou[2] have reported the BE's of RE 3d and 4d peaks in a series of RE fluorides except for the fluorides of Dy, Ho, and Tm. The BE's of the RE 3d and 4d peaks listed in Tables 1 and 2 are 2.4—7.2 eV lower than those reported by them. The disagreement can be attributed to the difference in the calibrant used for charge correction.

In Tables 1 and 2, appreciable differences appear in the BE's of the RE 3d and 4d peaks for each RE element. Generally, chemical shifts in XPS are related to the atomic charge calculated on the basis of Pauling's scale of electronegativity (Pauling charge).[9] Figure 2 shows the dependence of the BE's of RE $3d_{5/2}$ or $4d_{5/2}$ peaks on the Pauling charge for Y, Pr, Sm, Gd, Ho, Er, and Lu (electronegativity values were quoted from Ref. 10). For Y with 4f levels far above the filled shell and Lu with a completely filled 4f shell, the BE's of Y $3d_{5/2}$ and Lu $4d_{5/2}$ peaks increase with an increase in Pauling charge for all compounds. For other RE's with a partly filled 4f shell, the BE's of RE $3d_{5/2}$ and $4d_{5/2}$ peaks increase in the order, iodide<bromide<chloride, but the peaks from the fluorides appear at lower BE's than expected. Why the solid lines in Fig. 2 show different slopes is a problem of further investigation.

The spectra of the ligands (F 1s, Cl 2s, Cl 2p, Br 3s, Br $3p_{1/2}$ and $_{3/2}$, Br 3d, I $3p_{1/2}$ and $_{3/2}$, I $3d_{3/2}$ and $_{5/2}$, and I 4d) in all RE halides were obtained. The spectrum for each RE was simple and no significant differences were observed between the ligand spectra of different RE's. Table 3 lists the BE's of the ligand peaks. The Br 3d and I 4d peaks were not resolved

Table 3. BE's (in eV) of F 1s, Cl 2s, Cl 2p, Br 3s, Br 3p, Br 3d, I 3p, I 3d, and I 4d Peaks

	Fluoride	Chloride		Bromide				Iodide				
	F 1s	Cl 2s	Cl 2p	Br 3s	Br $3p_{1/2}$	Br $3p_{3/2}$	Br 3d	I $3p_{1/2}$	I $3p_{3/2}$	I $3d_{3/2}$	I $3d_{5/2}$	I 4d
Y	684.8	269.6	199.0	256.1	189.1	182.3	69.1	930.3	874.4	630.5	619.0	49.5
La	684.6	269.5	198.8	255.8	188.8	182.0	68.8	930.2	874.2	630.4	618.9	49.4
Ce	684.6	269.5	199.0	255.7	188.7	181.9	68.7	—[a]	—[a]	—[a]	—[a]	—[a]
Pr	684.8	269.4	198.7	255.6	188.6	181.9	68.6	929.9	874.2	630.4	619.0	49.5
Nd	684.8	269.4	198.8	255.7	188.6	182.0	68.8	930.0	874.3	630.4	618.9	49.6
Sm	684.8	269.4	198.9	255.7	188.7	182.0	68.8	930.2	874.4	630.5	619.0	49.5
Eu	684.4	269.5	199.0	255.6	188.6	182.0	68.7	930.3	874.6	630.4	619.0	49.6
Gd	684.8	269.7	199.0	255.8	188.9	182.2	69.0	930.2	874.4	630.5	619.0	49.7
Tb	684.5	269.5	199.0	255.8	188.7	182.0	68.8	930.4	874.6	630.5	619.1	49.6
Dy	684.6	269.6	199.0	255.8	188.7	182.1	69.0	930.4	874.5	630.5	619.0	49.6
Ho	684.5	269.5	199.0	255.8	188.8	182.0	68.9	930.3	874.4	630.5	619.0	49.6
Er	684.6	269.5	199.0	255.8	188.7	182.2	68.9	930.4	874.6	630.5	619.0	49.3
Tm	684.6	269.6	199.1	255.9	188.9	182.1	69.0	930.0	874.3	630.4	618.9	49.5
Yb	684.9	269.7	199.1	255.8	188.8	181.9	68.8	930.2	874.4	630.4	618.9	49.6
Lu	685.0	269.8	199.2	256.0	188.9	182.3	69.1	930.1	874.5	630.5	619.0	49.5

a) Cerium iodide sample was not obtained.

into their $d_{3/2}$ and $d_{5/2}$ peaks. Jørgensen and Berthou[2] have reported the BE's of F 1s peaks for the fluorides of Y, La, Ce, Pr, Nd, Sm, Eu, Gd, Er, Yb, and Lu. The BE's of the F 1s peaks listed in Table 3 are 3.0—5.5 eV lower than those reported by Jørgensen and Berthou. The disagreement can be attributed to the difference in the calibrant used for charge correction.

For each RE halide, an intensity ratio of the halogen peak (F 1s, Cl 2s, Br $3p_{3/2}$, and I $3d_{5/2}$) to O 1s peak ranged from 27.0 to 8.2, after peak intensity was normalized with photoelectric cross sections,[11] mean free paths for photoelectron,[12] and efficiencies of detection of the electron. This demonstrates that the formation of halide oxides, if any, on our sample surface was not serious for the present XPS studies.

For the RE oxides, we have reported the "inclined W" pattern in the plots of the BE's of O 1s peaks versus $1/R$ and versus the RE oxidation potential.[6] The pattern is identical with the "tetrad effect"[13] that is the minute irregularity in the variation of complex formation constants[14] and unit cell volumes[15] as a function of lanthanoid atomic number. Figure 3 shows the relationships between the BE's of the F 1s, Cl 2s, Br $3p_{3/2}$, and I $3d_{5/2}$ peaks and the atomic number for lanthanoids. For the RE fluorides and chlorides, the solid lines connecting the points for La, Gd, and Lu (with spherical configurations) show that the BE of the F 1s and Cl 2s peak increases with an increase in RE atomic number. This result agrees with those shown for the BE's of O 1s peaks for the RE oxides.[6] The points for the other RE's deviate from the solid lines except for light RE fluorides. The pattern reflects electronic configurations of RE elements and is called "tetrad effect." We can not at present give a good reason for the absence of "tetrad

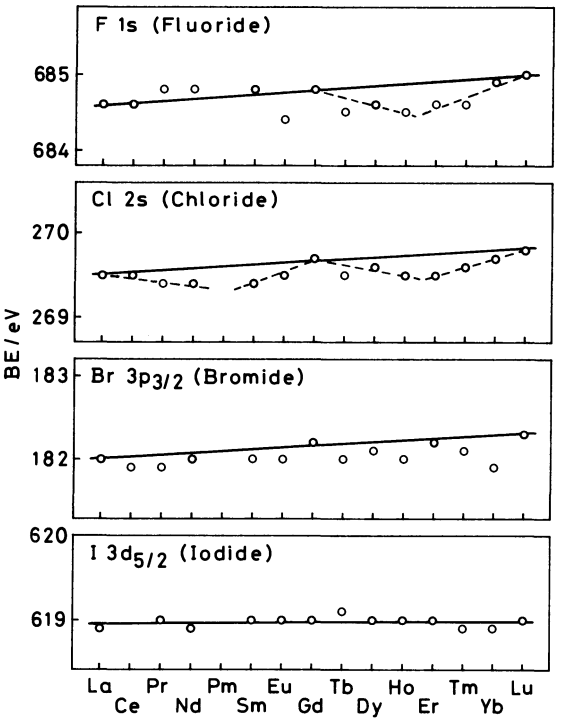

Fig. 3. BE's of the F 1s, Cl 2s, Br $3p_{3/2}$, and I $3d_{5/2}$ peaks as a function of the lanthanoid.

effect" for the fluorides of Ce through Eu. For the RE iodide and bromide, the BE's of the I $3d_{5/2}$ and Br $3p_{3/2}$ peaks show no or hardly meaningful dependence on the RE atomic number. It has been reported that the magnitude of the chemical shift for each element decreases with an increase in ionic radii.[16] The large radius of the bromide and iodide ion may be the reason for the very small chemical shift of iodine and bromine atom.

For the RE oxides, a correlation has been

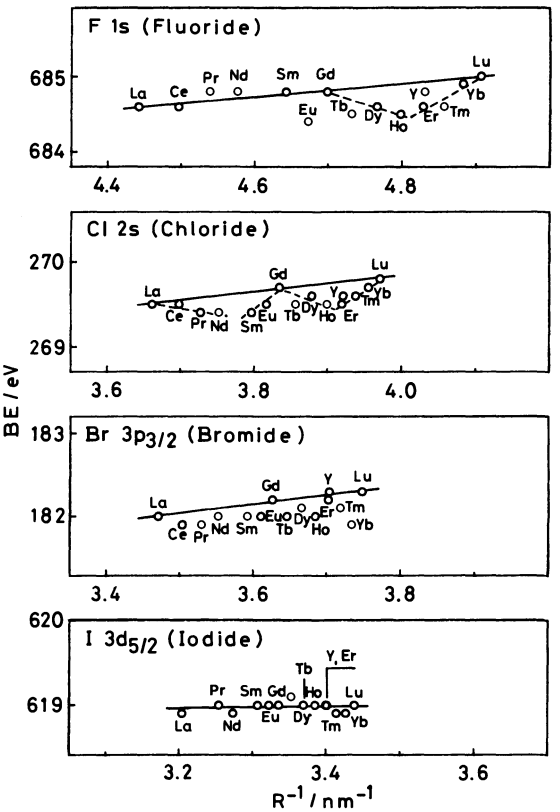

Fig. 4. Correlations of the BE's of the F 1s, Cl 2s, Br $3p_{3/2}$, and I $3d_{5/2}$ peaks with $1/R$ for each RE halide.

recognized between the BE of the O 1s peak and the mean distance from oxygen atom to the RE atom.[6] Figure 4 shows the relationships between the BE's of the F 1s, Cl 2s, Br $3p_{3/2}$, and I $3d_{5/2}$ peaks and $1/R$ for RE halides (R values quoted from Ref. 17). Solid lines were drawn so as to connect approximately the points for La, Gd, and Lu in the same manner as shown in Fig. 3. For the fluoride and the chloride, the BE's of the halogen peaks increase with an increase in $1/R$. This result agrees with those reported by Nefedov et al.[18] for the O 1s peaks for 37 kinds of oxides and the F 1s peaks for 20 kinds of fluorides. The plot for the BE's of the Cl 2s peaks show a "tetrad effect." The F 1s BE's of Gd through Lu show a similar trend. For the iodide, the BE's of the I $3d_{5/2}$ peaks show no meaningful dependence on the $1/R$. The Br $3p_{3/2}$ peaks of the bromide show a pattern intermediate between Cl 2s and I $3d_{5/2}$.

References

1) C. K. Jørgensen and H. Berthou, *Chem. Phys. Lett.*, **13**, 186 (1972).
2) C. K. Jørgensen and H. Berthou, *K. Dan. Vidensk. Selsk., Mat. Fys. Medd.*, **38**, 15 (1972).
3) A. J. Signorelli and R. G. Hayes, *Phys. Rev. B*, **8**, 81 (1973).
4) S. Suzuki, T. Ishii, and T. Sagawa, *J. Phys. Soc. Jpn.*, **37**, 1334 (1974).
5) Wei-Yean Howng and R. J. Thorn., *Chem. Phys. Lett.*, **56**, 463 (1978).
6) Y. Uwamino, T. Ishizuka, and H. Yamatera, *J. Electron Spectrosc. Relat. Phenom.*, **34**, 67 (1984).
7) S. Evans, "Handbook of X-Ray and Ultraviolet Photoelectron Spectroscopy," ed by D. Briggs, Heydon, London (1977), p. 121.
8) Y. Uwamino and T. Ishizuka, *Nagoya Kogyo Gijutsu Shikensho Houkoku*, **32**, 213 (1983).
9) K. Siegbahn, C. Nordling, A. Fahlman, R. Nordberg, K. Hamrin, J. Hedman, G. Johansson, T. Bergmark, S. E. Karlsson, I. Lindgren, and B. Lindberg, "ESCA: Atomic, Molecular, and Solid State Structure Studied by Means of Electron Spectroscopy," Nova Acta Regiac Soc. Sci. Upsaliensis Ser. IV, Upsala (1967), p. 20.
10) W. Gordy and W. J. O. Thomas, *J. Chem. Phys.*, **24**, 439 (1956).
11) J. H. Scofield, *J. Electron Spectrosc. Relat. Phenom.*, **8**, 129 (1976).
12) D. R. Penn, *J. Electron Spectrosc. Relat. Phenom.*, **9**, 29 (1976).
13) L. J. Nugent, *J. Inorg. Nucl. Chem.*, **32**, 3485 (1970).
14) D. F. Peppard, G. W. Mason, and S. Lewey, *J. Inorg. Nucl. Chem.*, **31**, 2271 (1969).
15) S. Siekierski, *J. Inorg. Nucl. Chem.*, **33**, 377 (1971).
16) T. A. Carlson, "Photoelectron and Auger Spectroscopy," Plenum, New York (1976).
17) L. C. Thompson, "Handbook on Physics and Chemistry of Rare Earths," ed by K. A. Gshneider, Jr. and L. Eyring, North-Holland, Amsterdam (1979), Vol. 3, p. 209.
18) V. I. Nefedov, N. P. Sergushin, and Ja. V. Salin, *J. Electron Spectrosc. Relat. Phenom.*, **8**, 81 (1976).

 © 1986 The Chemical Society of Japan Bull. Chem. Soc. Jpn., 59, 2269—2272 (1986)

Measurements of Association Constants of Iodine with Cyclodextrins and with Iodide or Bromide Ion in Aqueous Medium, Based on Volatilization Rate of Iodine from Aqueous into Gaseous Phase

Isao SANEMASA,* Yuko NISHIMOTO, Akira TANAKA, and Toshio DEGUCHI
Department of Chemistry, Faculty of Science, Kumamoto University,
Kurokami 2-39-1, Kumamoto 860
(Received January 23, 1986)

Iodine molecules, which are volatile, are expelled from an aqueous medium into the gaseous phase by introducing an inert gas at a constant flow rate into the aqueous phase, and the amount of the released iodine is measured as a function of aeration time. In the presence of a nonvolatile solute which associates with molecular iodine, the releasing rate of the volatile solute is reduced with increasing degree of the association between both the solutes in the aqueous medium. The method was applied to the case of association of iodine with α-, β-, or γ-cyclodextrin; the formation constants of the three 1:1 complexes are $(1.5\pm0.1)\times10^4$, $(1.5\pm0.2)\times10^2$, and 24 ± 3 dm^3 mol^{-1}, respectively, at 25.0 °C and low ionic strengths. The complexation of iodine with iodide or bromide ion was also studied; the I_3^- and I_2Br^- formation constants are $(6.5\pm0.1)\times10^2$ and 16 ± 1 dm^3 mol^{-1}, respectively, at 25.0 °C and I=0.1($NaClO_4$).

The complex formation of cyclodextrin (CyD) with molecular iodine in aqueous medium is well known and association constants have been measured by the spectrophotometric,[1,2] potentiometric,[3] and solubility[4] methods. There are, however, considerable disagreements among the literature values as seen in Table 1.

A simple method for measuring association constants between volatile and nonvolatile solutes in aqueous medium has been presented and successfully used to estimate 1:1 metal acetylactonate complex formation constants.[5] The method is based on the fact that a volatile solute present in an aqueous solution can readily be driven out of the aqueous phase by an inert gas stream and that the releasing rate depends on the extent to which the volatile and nonvolatile solutes associate with each other.

Here we have used the method to determine formation constants of 1:1 complexes of iodine with α-, β-, or γ-CyDs. In order to check the reliability of the estimated values, complex formation constants of iodine with iodide or bromide ion have also been determined by the same technique.

Experimental

Materials and Preparations of Sample Solutions. Solid iodine of analytical reagent grade and cyclodextrins (α-, β-, and γ-CyD from Nakarai Chemicals) of guaranteed grade were used without further purification (γ-CyD recrystallized from water was also used). An aqueous iodine solution in the order of 1×10^{-3} M (1 M=1 mol dm^{-3}), i.e., a nearly saturated solution, was prepared by adding an excess quantity of solid iodine to 1 dm^3 of 2×10^{-4} M $HClO_4$ solution and stirring in a thermostated bath at 25 °C for a few days. Suitable portions of this iodine solution were taken out successively, and one part was used to determine the I_2 concentration by titration with a 4×10^{-3} M $Na_2S_2O_3$ standard solution using starch as an indicator and the others were diluted with water to desired iodine concentrations ranging from 10^{-5} to 10^{-4} M to prepare CyD-free sample solutions. Into the aqueous iodine solution was dissolved a suitable amount of CyD, which had been dried over phosphorus pentaoxide under vacuum, to prepare sample solutions of known CyD concentrations. The $HClO_4$ concentration in the sample solution was as low as 2×10^{-6}—2×10^{-5} M.

In runs where formation constants were to be estimated for I_2–I^- and I_2–Br^- systems, sample solutions were prepared by adding a suitable volume of an iodide or bromide stock solution which had been prepared by dissolving a dried reagent (KI, NaBr) in water. The ionic strength of the sample solution was adjusted to 0.1 with $NaClO_4$.

Apparatus and Procedures. The apparatus used to expel molecular iodine was essentially the same as the one employed in a previous work.[5]

A 50 cm^3 portion of sample solution was transferred into a $2.5\phi\times25$ cm cylindrical glass tube with a ground glass joint, which was then immersed in a bath thermostated at 25.0±0.1 °C. A gas-inlet-type adaptor was mounted on the cylindrical tube and N_2 gas was dispersed through the solution via a capillary glass tube at a constant flow rate of 60.0 cm^3 min^{-1}. The N_2 gas flow rate was controlled by a Stec Type Sec 400 mass-flow controllor, which was donated by Standard Technology Co., Ltd. (Kyoto); an accuracy within ±1% is guaranteed for this device. The N_2 gas leaving the sample solution was dispersed via a sintered glass ball through an absorbent, 20 cm^3 of 5×10^{-4} M $Na_2S_2O_3$ solution, which was placed in a $15\phi\times18$ cm cylindrical glass tube with a ground glass joint. After a fixed time, the N_2 gas stream was interrupted, the absorption vessel was replaced by another one containing the same volume of the absorbent, and the introduction of N_2 gas was resumed. This operation was repeated at regular time intervals. The amount of iodine expelled from the sample solution during the fixed time, ΔQ_{I_2}, i.e., the amount of I_2 trapped in a single absorption vessel, was determined by measuring the discoloration degree of trisulfatocerium(IV) at 312 nm according to the flow injection analysis (FIA).

The principle of the analytical method is that the

reduction of Ce(IV) by As(III) will be promoted in the presence of iodide ion as a catalyst. The FIA manifold was the same as the one previously used,[6] but the temperature of the reaction coil where the catalytic reaction occurs was set at 30 °C and the absorbent, 5×10^{-4} M $Na_2S_2O_3$, was employed as a carrier stream into which portions of a sample solution were injected. Under these conditions, we could detect iodide ions down to 1×10^{-8} M.

Results and Discussion

Formation Constants of Molecular Iodine with Cyclodextrins. The stoichiometry of α-, β-, or γ-CyD complex with molecular iodine has been established to be 1:1,[4,7,8] and thus the reactions that should be taken into account are

$$CyD + I_2 \rightleftharpoons CyD\cdot I_2,\ K_{ass}, \quad (1)$$

$$I_2(aq) \longrightarrow I_2(gas),\ k, \quad (2)$$

where K_{ass} is the association constant and k is the rate constant for expulsion of iodine molecules from the aqueous into gaseous phase. Here we assume that the iodine present in the aqueous medium is in the molecular form, that is, the hydrolysis of iodine, $I_2+H_2O \rightleftharpoons HIO+H^++I^-$, is negligible, because of its small hydrolysis constant of the order of 10^{-13}.[9]

The iodine molecules expelled into the gaseous phase are trapped successively by the absorbent, and the total amount, Q_{I_2}, is measured as a function of aeration time, t. Here, we assume that the releasing rate of I_2 at a constant N_2 gas flow rate is of first-order dependence on the concentration of this species present in the solution, and thus

$$dQ_{I_2}V^{-1}/dt = k[I_2], \quad (3)$$

where V is the volume of the aqueous phase. We have the mass-balance equations

$$C_{CyD} = [CyD] + [CyD\cdot I_2], \quad (4)$$

$$C_{I_2} = [I_2] + Q_{I_2}V^{-1} + [CyD\cdot I_2] = [I_2] + Q_{I_2}V^{-1} + K_{ass}[CyD][I_2], \quad (5)$$

where C_{CyD} and C_{I_2} are the total concentration of CyD and that of iodine, respectively. Substitution of Eq. 5 into Eq. 3 yields

$$dQ_{I_2}V^{-1}/dt = k(C_{I_2} - Q_{I_2}V^{-1})/(1 + K_{ass}[CyD]), \quad (6)$$

which becomes, on integration and with $Q_{I_2}=0$ at $t=0$,

$$\ln(C_{I_2} - Q_{I_2}V^{-1}) = -kt/(1 + K_{ass}[CyD]) + \ln C_{I_2}. \quad (7)$$

Plots of $\ln(C_{I_2}-Q_{I_2}V^{-1})$ vs. t will give a straight line

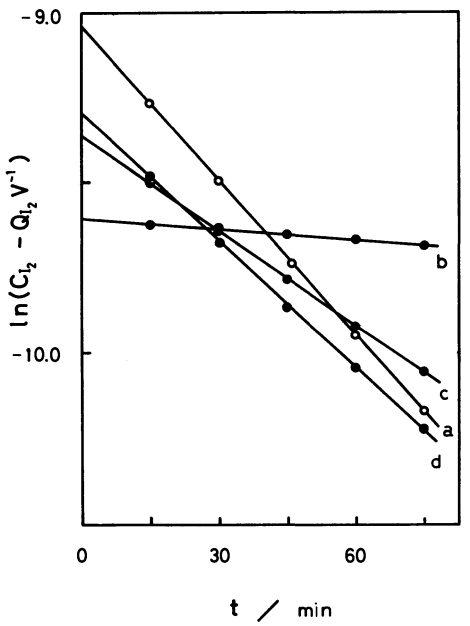

Fig. 1. The plots of $\ln(C_{I_2}-Q_{I_2}V^{-1})$ vs. t in the absence and presence of cyclodextrin. N_2 gas flow rate 60.0 cm³ min⁻¹; (a): $C_{CyD}=0$, $C_{I_2}=1.18\times10^{-4}$ M, (b): $C_{\alpha\text{-}CyD}=1.00\times10^{-3}$ M, $C_{I_2}=6.73\times10^{-5}$ M, (c): $C_{\beta\text{-}CyD}=5.00\times10^{-3}$ M, $C_{I_2}=8.70\times10^{-5}$ M, (d): $C_{\gamma\text{-}CyD}=1.00\times10^{-2}$ M, $C_{I_2}=9.20\times10^{-5}$ M.

Table 1. The α-, β-, γ-Cyclodexetrin-Iodine Association Constants at 25 °C Determined in This Work and the Literature Value

C_{CyD}[a]/mol dm⁻³	C_{I_2}[b]/mol dm⁻³	K_{ass}[c]/dm³ mol⁻¹
α-Cyclodextrin		
2.50×10^{-4}	1.06×10^{-5}	1.6×10^{4}
5.01×10^{-4}	1.99×10^{-5}	1.5×10^{4}
1.00×10^{-3}	6.73×10^{-5}	1.4×10^{4}
	Average:	$(1.5\pm0.1)\times10^{4}$
Literature K_{ass} Value: $(9.3\pm0.2)\times10^{3}$[d], $(2\pm1)\times10^{4}$[e], 2×10^{3}[f], 8.3×10^{3}[g]		
β-Cyclodextrin		
9.99×10^{-4}	4.61×10^{-5}	1.7×10^{2}
2.50×10^{-3}	2.23×10^{-5}	1.6×10^{2}
5.00×10^{-3}	8.70×10^{-5}	1.3×10^{2}
	Average:	$(1.5\pm0.2)\times10^{2}$
Literature K_{ass} Value: $(1.5\pm0.5)\times10^{3}$[e], 1.0×10^{2}[g], 1.85×10^{3}[h]		
γ-Cyclodextrin		
5.00×10^{-3}	1.45×10^{-4}	23
9.99×10^{-3}	1.04×10^{-4}	19
9.99×10^{-3}	3.92×10^{-5}	26
5.00×10^{-3}[i]	9.20×10^{-5}	28
1.00×10^{-2}[i]	9.20×10^{-5}	24
	Average:	24 ± 3
Literature K_{ass} Value: $(3.5\pm0.5)\times10^{2}$[e], 13[g]		

a) Total concentration of cyclodextrin. b) Total concentration of iodine. c) Association constant determined in this work (each value is an average of two measurements obtained under the same C_{CyD} and C_{I_2} concentrations. d) Ref. 1. e) Ref. 3. f) Cited in Ref. 3. g) Ref. 4. h) Ref. 2. i) The cyclodextrin used was recrystallized from water.

with a slope which corresponds to $-k/(1+K_{ass}[CyD])$ or to $-k$ in the absence of CyD solutes. Under the conditions that the total concentration of CyD is sufficiently large compared to the concentration of the associated complex formed, that is, $C_{CyD} \gg [CyD \cdot I_2]$, we can set [CyD] in Eq. 7 equal to C_{CyD}.

Figure 1 shows some plots constructed with the aid of Eq. 7. These plots give straight lines over the aeration time investigated, which indicates that the releasing rate of I_2 is of first-order dependence on the concentration of this species present in the solution. At a constant N_2 gas flow rate of 60.0 $cm^3\ min^{-1}$, the constant, k, was evaluated to be $(1.53\pm0.03)\times10^{-2}$ min^{-1} (an average from four replicated runs in the absence of CyD). The association constants derived for α-, β-, and γ-CyD complexes with iodine from the negative slopes of the straight lines are tabulated together with C_{CyD} and C_{I_2} in Table 1, where those reported so far in the literature are also listed.

With α-CyD, the cavity size of which is 4.7—5.2 Å, an iodine molecule can suitably be fitted with a van der Waals contact.[8] On the other hand, β- and γ-CyDs provide much less stable complexes with the guest owing to their large cavity sizes, 6.0—6.4 and 7.5—8.3 Å, respectively.

The association constants obtained by the present method are about 1.5 to 2 times as large as our previous ones[4] determined through solubility measurements. The disagreement, however, may be taken as rather small if we take it into consideration that quite different techniques were employed for the two works. The K_{ass} value determined in this work for the α-CyD complex is in reasonable agreement with that recently reported by Diard et al.[3] as a result of potentiometric measurements, while the values for β- and γ-complexes differ by one order of magnitude; their association constants decrease every one order of magnitude on going from α- to γ-CyD, while our values display a difference as much as two orders of magnitude between α- and β-CyD complexes.

It probably admits of no argument that the α-complex has the association constant as large as $1\times10^4\ M^{-1}$. The association constant for β- and γ-complexes, on the other hand, are still far from being generally acceptable. This is partially attributable to their relatively small association constants; the spectrophotometric, potentiometric, and solubility measurements are all desirable to be done under high CyD concentrations to get reliable values, β-CyD has a limited solubility in water (ca. 10^{-2} M). In view of its small association constant, some impurities which may be present in γ-CyD might cause serious errors in the estimatin of K_{ass} of γ-CyD-I_2. There is observed, however, no appreciable difference between the results obtained from purified (recrystallized from water) and untreated γ-CyD specimens, as can be seen from Table 1.

In order to make it clear whether the present method provides reasonable association constants as small as 10^2 or 10, I_2–I^- and I_2–Br^- systems were studied. The formation constant for the former system has been measured by many investigators and the latter is known for its small formation constant.

Formation Constants of Molecular Iodine with Iodide or Bromide Ion. The reactions that should be taken into account are

$$X^- + I_2 \rightleftarrows I_2X^-,\ K_{I_2X}, \tag{8}$$

$$I_2(aq) \longrightarrow I_2(gas),\ k, \tag{2}$$

where X^- denotes either I^- or Br^- and K_{I_2X} is the formation constant. An equation that allows estimation of the formation constant of I_2 with I^- or Br^- can be derived in the same way as described in the CyD–I_2 system:

$$\ln(C_{I_2} - Q_{I_2}V^{-1}) = -kt/(1 + K_{I_2X}[X^-]) + \ln C_{I_2}. \tag{9}$$

Experiments having been made under the condition that the total concentration of X^-, C_X, is sufficiently large compared to the concentration of the complex formed, we can set $[X^-]$ in Eq. 9 equal to C_X. Some examples of plots obtained with the aid of Eq. 9 are shown in Fig. 2. The plots also give straight lines

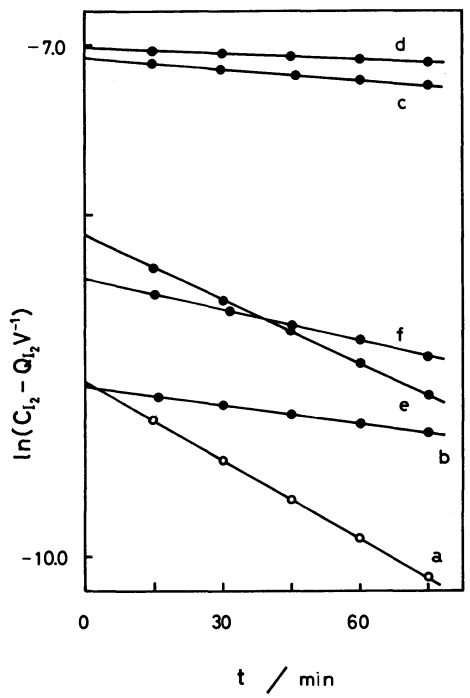

Fig. 2. The plots of $\ln(C_{I_2} - Q_{I_2}V^{-1})$ vs. t in the absence and presence of I^- or Br^-. N_2 gas flow rate 60.0 cm^3 min^{-1}; (a): $C_X=0$, $C_{I_2}=1.27\times10^{-4}$ M, (b): $C_I=5.00\times10^{-3}$ M, $C_{I_2}=1.23\times10^{-4}$ M, (c): $C_I=1.00\times10^{-2}$ M, $C_{I_2}=8.37\times10^{-4}$ M, (d) $C_I=2.00\times10^{-2}$ M, $C_{I_2}=9.01\times10^{-4}$ M, (e): $C_{Br}=2.00\times10^{-2}$ M, $C_{I_2}=2.96\times10^{-4}$ M, (f): $C_{Br}=1.00\times10^{-1}$ M, $C_{I_2}=2.31\times10^{-4}$ M.

Table 2. I_3^- and I_2Br^- Formation Constants Determined at 25 °C and I=0.1($NaClO_4$)

C_X[a] / mol dm^{-3}	C_{I_2}[b] / mol dm^{-3}	K_{I_2X}[c] / dm^3 mol^{-1}
$I^-+I_2 \rightleftarrows I_3^-$		
2.50×10^{-3}	1.20×10^{-4}	6.4×10^2
2.50×10^{-3}	1.26×10^{-4}	6.5×10^2
5.00×10^{-3}	1.23×10^{-4}	6.6×10^2
1.00×10^{-2}	8.37×10^{-4}	6.4×10^2
1.25×10^{-2}	1.25×10^{-4}	6.6×10^2
2.00×10^{-2}	9.01×10^{-4}	6.3×10^2
	Average:	$(6.5\pm0.1)\times10^2$
$Br^-+I_2 \rightleftarrows I_2Br^-$		
5.00×10^{-2}	2.91×10^{-4}	15
1.00×10^{-1}[d]	2.31×10^{-4}	16
	Average:	16±1

a) Total concentration of halide ion. b) Total concentration of iodine. c) Formation constant. d) $NaClO_4$ was not added; I=0.1(NaBr).

over the aeration time investigated. Formation constants calculated from the slopes of the straight lines for I_3^- and I_2Br^- by using the k value 1.54×10^{-2} min^{-1} determined with 0.1 M $NaClO_4$ are listed in Table 2, together with C_{I_2} and C_X.

To our knowledge, only three K_{I_2Br} values have been reported; 14.9 M^{-1} by spectrophotometry,[10] 12.2 M^{-1} from solubility,[11] and 8.35 M^{-1} through solvent extraction.[12] The present result, 16 M^{-1}, is in reasonable agreement with the first one cited; because of the lack of available literature values, it is difficult at present to judge whether the agreement is accidental or not.

With respect to K_{I_3}, on the other hand, abundant literature data are available which have been obtained by spectrophotometric,[13,14] potentiometric,[9,15] distribution,[12,16] solubility,[17,18] and conductimetric[19] methods. Some representative values are arranged in decreasing order of magnitude as follows: 768,[16] 761,[17] 7.3×10^2,[14] 725,[9] 723,[13] 714,[15] 680,[12] and 654[17] M^{-1}. If we choose 723 M^{-1} as the most reliable K_{I_3} value in accord with the recommendation by Ramette and Sandford,[20] the present result, 6.5×10^2 M^{-1}, is about 10% lower. As has been pointed out by many investigators, the I_3^- formation constant should be determined under as low iodine and/or iodide concentrations as possible. The observed K_{I_3} tends to increase with increasing iodine and/or iodide concentrations due to significant formation of higher polyiodide species such as I_5^- and I_6^{2-} in addition to I_3^-.[16,20] From this point of view, the present method, which employs very low I_2 and I^- concentrations, seems to provide rather a small I_3^- formation constant.

After all, the method proposed here can be used to determine association constants with molecular iodine, magnitudes of which are as small as the order of 10^2 or 10.

The present work was partially supported by a Grant-in Aid for Scientific Research No. 6054037 from the Ministry of Education, Science and Calture.

References

1) J. A. Thoma and D. French, *J. Phys. Chem.*, **62**, 1603 (1958).
2) Y. Miyazaki, *Saga Daigaku Nogaku Iho*, **31**, 49 (1971).
3) J. P. Diard, E. Saint-Aman, and D. Serve, *J. Electroanal. Chem. Interfacial Electrochem.*, **189**, 113 (1985).
4) I. Sanemasa, T. Kobayashi, and T. Deguchi, *Bull. Chem. Soc. Jpn.*, **58**. 1033 (1985).
5) I. Sanemasa, Y. Nishimoto, A. Tanaka, and T. Deguchi, *Bull. Chem. Soc. Jpn.*, **59**, 1459 (1986).
6) T. Deguchi, A. Tanaka, I. Sanemasa, and H. Nagai, *Bunseki Kagaku*, **32**, 23 (1983).
7) J. A. Thoma and D. French, *J. Am. Chem. Soc.*, **80**, 6142 (1958).
8) R. K. McMullan, W. Saenger, J. Fayos, and D. Mootz, *Carbohydr. Res.*, **31**, 37 (1973).
9) J. D. Burger and H. A. Liebhafsky, *Anal. Chem.*, **45**, 600 (1973).
10) Daniele, *Gazz. Chim. Ital.*, **90**, 1082 (1960).
11) V. K. LaMer and M. H. Lewinsohn, *J. Phys. Chem.*, **38**, 171 (1934).
12) L. S. Sowers and S. A. Katz, *Rev. Latinoamer. Quim.*, **5**, 80 (1974): *Chem. Abstr.*, **81**, 54951b (1974).
13) G. Daniele, *Gazz. Chim. Ital.*, **90**, 1068 (1960).
14) K. Hayakawa and S. Nakamura, *Bull. Chem. Soc. Jpn.*, **50**, 566 (1977).
15) G. Jones and B. B. Kaplan, *J. Am. Chem. Soc.*, **50**, 1845 (1928).
16) M. Davies and E. Gwynne, *J. Am. Chem. Soc.*, **74**, 2748 (1952).
17) L. I. Katzin and E. Gebert, *J. Am. Chem. Soc.*, **77**, 5814 (1955).
18) J. S. Carter, *J. Chem. Soc.*, **130**, 2227 (1928).
19) W. C. Bray and C. M. MacKay, *J. Am. Chem. Soc.*, **32**, 914 (1910).
20) R. W. Ramette and R. W. Sandford, Jr., *J. Am. Chem. Soc.*, **87**, 5001 (1965).

 © 1986 The Chemical Society of Japan Bull. Chem. Soc. Jpn., 59, 2273—2278 (1986)

Vertical Concentration Distributions of Arsenic in a Reservoir and Its Sediment

Yuzo TAMARI,* Kimio NISHIMURA, Haruo TSUJI, and Yuzuru KUSAKA
Department of Chemistry, Faculty of Science, Konan University,
Higashinada-ku, Kobe 658
(Received January 24, 1986)

Vertical concentration distributions of arsenite and arsenate in a reservoir (depth, ≈31 m) and its bottom sediment (core depth, ≈18 cm) have been investigated. The concentrations of arsenite and arsenate in the water were determined by a spectrophotometric method, and those in the sediment were also determined by the same method after the following leaching-treatments of the sediment. The leaching of arsenic from the sediment was carried out by using three solutions; (1) 0.1 M† hydrochloric acid (acid-soluble fraction), (2) 1 M sodium hydroxide solution (alkali-soluble fraction), and (3) hydrofluoric and perchloric acid mixture (silicate fraction). It was found that arsenic was rich in the surface layer of the sediment, and most of it existed as arsenite fixed with iron hydroxide. Based on the analytical and leaching results of arsenic, iron, manganese, zinc, copper, and others in the reservoir and in its sediment respectively, the sedimentation process of arsenic from the reservoir and its dissolution process from the sediment have been discussed.

Arsenic is one of the most widely distributed elements in the earth's crust and in the biosphere. Arsenic is commonly considered to be intrinsically toxic to life. However, it has been recognized to be one of the essential trace elements in living organisms since 1975,[1] and has become significant for men and animals as an important element in their nutrition.[2,3] Thus, it is our concern to know the concentration of arsenic contained in drinking water or in its original reservoir.[4]

Arsenic generally exists as the following chemical species; arsine [As(−III)], elemental arsenic [As(0)], arsenite [As(III)], arsenate [As(V)], and organically-complexed arsenic. For the detailed researches of arsenic in natural water, reservoir water, and its bottom sediment, this chemical state analysis of arsenic is important. In this work, a reservoir, which is located in Hyogo Prefecture and has been used for drinking water supplies, was selected as one of the geochemical researches of arsenic. The vertical distributions of arsenite, arsenate, and organic arsenic in the reservoir and its sediment have been investigated. The concentrations of arsenite and arsenate in the water were determined by spectrophotometry.[5] The inorganic and organic arsenic in the sediment were analyzed for the solutions prepared by a chemical leaching method,[6–8] by which arsenic was released from the sediment to a solution.

Experimental

Sediment and Water Samples. A sediment sample was collected from the bottom of the reservoir of a 17.5-cm depth core, using a core sampler (Rigo Co., Ltd., model 2010). The core sample was taken in a plastic cylinder and was immediately cooled in an ice-box. It was then taken back to the laboratory within 1h. The wet core (17.5-cm length) was cut into sections, 1.5-cm in depth, and each of the divided wet core samples was then subjected to a leaching experiment without drying.

Water samples were collected from the surface to a 30.5-m depth of the reservoir. The water samples were collected in a plastic-made sampler (Rigo Co., Ltd., model 22046) and were immediately analyzed for temperature, pH, conductivity, turbidity, dissolved oxygen (D.O.), and oxidation reduction potential (O.R.P.). They were then transferred to a 2000-cm^3 polyethylene bottle after adding 33 cm^3 of 6 M hydrochloric acid to avoid the precipitation of iron (III) hydroxide. However, for the analyses of nitrate, nitrite, and ammonium ions, a part of the water sample in the sampler was transferred to a glass bottle without the addition of 6 M hydrochloric acid.

Analytical Methods. Arsenite and arsenate were determined by spectrophotometry with silver diethyldithiocarbamate, after converting the arsenic into arsine with sodium tetrahydroborate.[5] Calcium, magnesium, iron, manganese, copper, and zinc were determined by atomic absorption spectrometry. Sodium and potassium were determined by flamephotometry. Sulfide was determined by iodatimetry after converting the sulfur into hydrogen sulfide with hydrochloric acid. The other chemical species dissolved in water samples were determined by ordinary spectrophotometry and other conventional methods.[9]

Chemical Leaching Methods. The following solutions were used for fractionation into acid-soluble, alkali-soluble, and silicate fractions: (1) 0.1 M Hydrochloric acid solution[7,10,11] to dissolve sulfide, hydroxide, and some ions loosely adsorbed with sediments, but not to dissolve both lithogeneous materials derived from rocks and organically-complexed ions such as copper. (2) 1 M Sodium hydroxide solution[8] to leach some organically-bound elements or organic compounds such as humic acids. (3) Hydrofluoric and perchloric acid mixture[11,12] to decompose residual silicates and their lattice constituent elements. The preparing procedure of each fraction was as follows.

Acid-soluble fraction: Accurately weighed 2—3 g of a wet core-sediment (e.g., 2.17 g corresponds to 1.00 g of the sediment on dry basis) was placed in a 50-cm^3 centrifugal tube. Into the tube, 25 cm^3 of 0.1 M hydrochloric acid was added. The tube was then set in a hot water-bath thermostatically controlled at 40 °C, and ultrasonic waves were irradiated into the bath in order to mix and suspend the sediment particles into the acid solution. The

† 1 M=1 mol dm^{-3}.

irradiation time was for 20 min. After centrifuging the tube, the supernatant solution was filtered (filter pore size: 0.45 μm). This filtrate was saved for later analyses. Another aliquot (25 cm^3) of the fresh hydrochloric acid was then added to the residue in the tube. The mixture was again subjected to ultrasonic irradiations. This procedure was repeated five times to perfectly dissolve arsenic and other ions from the sediment.[6]

Alkali-soluble fraction: The alkali-soluble fraction was collected in a similar manner to the acid-soluble fraction. This fractionation procedure was carried out on the residue after the acid leaching.

Silicate fraction: Finally, the residue, after the alkali leaching, was transferred to a Teflon beaker, and decomposed with the mixture of 10 cm^3 of 46% hydrofluoric acid and 2 cm^3 of 60% perchloric acid. The resulting mixture was concentrated under heating until white fumes of the perchloric acid appeared. To decompose some organic compounds in the mixture, 4 cm^3 of 61% nitric acid and 2 cm^3 of 60% perchloric acid were also added, and the new mixture was again concentrated in a similar manner. The resultant solution was diluted to 50 cm^3 with 0.1 M hydrochloric acid.

Results and Discussion

Effect of Leaching Numbers on the Dissolution of Arsenic from Sediments. Figure 1 shows one of the leaching patterns of arsenic by acid- and alkali-leaching. Each shape of the patterns was a log-normal distribution, and so were those of calcium, magnesium, iron, and zinc. Therefore, it was found that these elements were effectively dissolved in the leaching solutions up to No.5.

Vertical Distribution Profiles of Several Sedimental Elements in Acid-Soluble, Alkali-Soluble, and Silicate Fractions. Table 1 summarizes the amount of each element leached out from one gram of dry sediments in each fraction. The value in parentheses represents a dissolved percentage of the element in the sediment (see the calculation formula in the footnotes in Table 1). It is noted in Table 1 that about 63—73% of total calcium went into the acid-soluble fraction throughout the entire core depth, whereas the other alkaline earth metal magnesium, alkali metals sodium and potassium (from other measurements) were poorly dissolved, e.g., 4—7% for magnesium, 0—3% for sodium and potassium. The much dissolution of calcium from the sediment can be explained from a result that the sediment is derived from detritus of rhyolite rocks which surround the reservoir of interest, because the dissolved percentages of calcium and the other elements by acid leaching of the rocks were almost same as those of the sediment.

Figure 2 is drawn from the data of Table 1, and shows the depth distribution pofiles of typical elements, arsenic and metal ions, in the core sediment. It is worth noting that arsenic, copper, zinc, and iron dissolved by the acid leaching were rich in the surface layer of the sediment and were poor in the deeper layers. A similar tendency was found in sulfide content of the sediment (this data is listed in Appendix 1).

Alkali-soluble fractions occupied considerable portions of dissolved percentages of total arsenic, copper, and zinc in the sediment. The percentages for each element were nearly constant for the entire core depth, e.g., at 11—19 μg for arsenic, 11—20 μg for copper, and 10—20 μg for zinc. It is pointed out that arsenic in the alkali-soluble fraction could not be volatilized directly as arsine from the acidified determining solution of the fraction by the addition of tetrahydroborate. Accordingly, the arsenic was determined after wet-ashing with nitric and perchloric acid mixture (see the procedure in silicate fraction of this paper). Thus the arsenic leached in the alkaline solution is probably in some form of organically-complexed arsenic, but not a simple inorganic arsenic.

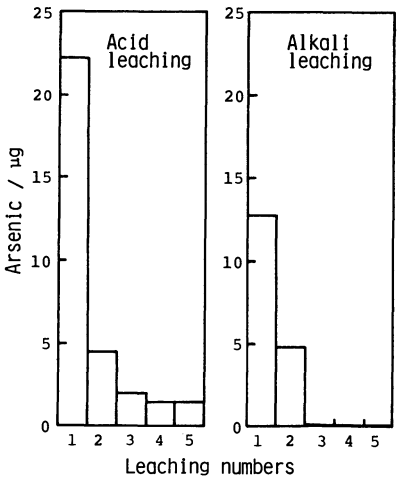

Fig. 1. Leaching patterns of arsenic by acid- and alkali-leaching treatments.
Amounts of arsenic (arsenite + arsenate) indicate to be leached from one gram of dry sediments (the core depth: 1.5—3.5 cm from sediment surface).

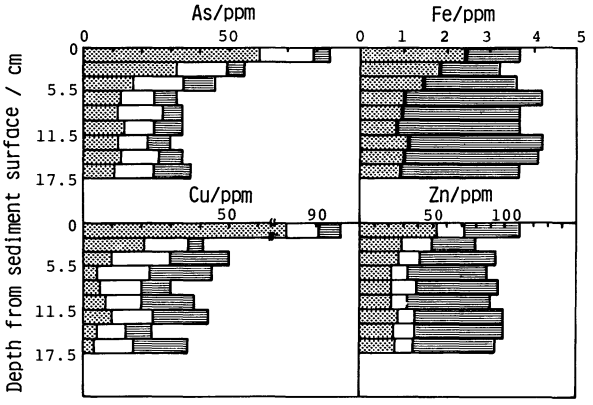

Fig. 2. Vertical distributions of concentrations of arsenic and several elements in sediments.
▨: Acid-soluble fraction, □: Alkali-soluble fraction, ▤: Silicate fraction.
Concentrations of elements in dry sediments.

In silicate fractions, the dissolved percentages of calcium and magnesium were almost constant regardless of the core depth, while those of arsenic, copper, zinc, iron, and manganese increased with the core depth.

Chemical Oxidation State of Arsenic in the Sediment. Figure 3 shows the vertical concentration distributions of arsenate and arsenite in the acid-

Table 1. Arsenic and Several Elements Dissolved in Acid-Soluble, Alkali-Soluble, and Silicate Fractions from One Gram of Dry Sediments

Core depth of sediment (cm from surface)	Ca/mg Fraction			Mg/mg Fraction			Fe/mg Fraction			Mn/mg Fraction		
	Acid	Alk.	Sil.	Acid	Alk.	Sil.	Acid	Alk.	Sil.	Acid	Alk.	Sil.
0— 1.5	0.91	0.11	0.33	0.20	0.020	2.4	24	0.38	13	1.3	0.006	0.11
	(67)	(9)	(24)	(7)	(1)	(92)	(64)	(1)	(35)	(92)	(1)	(7)
1.5— 3.5	0.71	0.064	0.31	0.12	0.012	2.0	18	0.36	14	0.91	0.013	0.10
	(66)	(5)	(29)	(5)	(1)	(94)	(56)	(1)	(43)	(89)	(1)	(10)
3.5— 5.5	0.85	0.062	0.42	0.18	0.011	3.8	14	0.24	22	0.67	0.015	0.18
	(64)	(4)	(32)	(4)	(1)	(95)	(39)	(1)	(60)	(77)	(2)	(21)
5.5— 7.5	0.96	0.029	0.40	0.27	0.014	4.4	10	0.14	33	0.60	0.008	0.20
	(69)	(2)	(29)	(5)	(1)	(94)	(23)	(1)	(76)	(74)	(1)	(25)
7.5— 9.5	0.89	0.058	0.51	0.24	0.011	4.0	9.8	0.24	27	0.49	0.012	0.16
	(61)	(4)	(35)	(5)	(1)	(94)	(26)	(1)	(73)	(74)	(2)	(24)
9.5—11.5	0.89	0.036	0.49	0.18	0.009	3.8	8.2	0.22	29	0.58	0.010	0.24
	(63)	(2)	(35)	(4)	(1)	(95)	(22)	(1)	(77)	(70)	(1)	(29)
11.5—13.5	1.3	0.033	0.44	0.31	0.009	4.2	11	0.22	31	0.89	0.012	0.19
	(73)	(2)	(25)	(6)	(1)	(93)	(26)	(1)	(73)	(82)	(1)	(17)
13.5—15.5	1.1	0.044	0.51	0.27	0.008	4.6	9.8	0.16	31	0.84	0.007	0.18
	(67)	(2)	(31)	(5)	(1)	(94)	(24)	(1)	(75)	(82)	(1)	(17)
15.5—17.5	1.1	0.042	0.38	0.27	0.016	4.0	9.3	0.16	27	0.73	0.009	0.17
	(72)	(3)	(25)	(6)	(1)	(93)	(25)	(1)	(74)	(80)	(1)	(19)

Core depth of sediment (cm from surface)	Cu/μg Fraction			Zn/μg Fraction			As(III+V)/μg Fraction		
	Acid	Alk.	Sil.	Acid	Alk.	Sil.	Acid	Alk.	Sil.
0— 1.5	80	11	7.8	53	20	40	60	19	6.0
	(81)	(11)	(8)	(47)	(18)	(35)	(71)	(22)	(7)
1.5— 3.5	21	15	4.7	29	20	31	33	18	5.3
	(52)	(36)	(12)	(36)	(25)	(39)	(58)	(32)	(10)
3.5— 5.5	9.8	20	20	27	14	53	18	17	11
	(20)	(40)	(40)	(29)	(15)	(56)	(38)	(38)	(24)
5.5— 7.5	4.7	18	21	22	9.6	56	13	11	8.0
	(11)	(41)	(48)	(25)	(11)	(64)	(41)	(34)	(25)
7.5— 9.5	5.8	14	10	22	17	56	12	16	6.4
	(19)	(47)	(34)	(23)	(18)	(59)	(35)	(46)	(19)
9.5—11.5	8.2	12	18	22	10	58	14	10	10
	(21)	(32)	(47)	(24)	(12)	(64)	(42)	(29)	(29)
11.5—13.5	9.6	14	19	27	12	64	12	9.6	8.7
	(23)	(32)	(45)	(26)	(12)	(62)	(40)	(32)	(28)
13.5—15.5	5.3	9.8	8.9	24	16	62	13	14	7.8
	(22)	(41)	(37)	(24)	(15)	(61)	(36)	(41)	(23)
15.5—17.7	3.8	13	19	24	13	56	11	13	10
	(11)	(36)	(53)	(26)	(14)	(60)	(38)	(35)	(27)

Acid: 0.1 M Hydrochloric acid.
Alk. : 1 M Sodium hydroxide solution.
Sil. : Conc. Hydrofluoric and perchloric acid mixture.
Values in parentheses: Dissolved percentages $\left(\frac{\text{amounts of an element dissolved from 1 g of sediments} \times 100}{\text{total amounts of an element in 1 g of sediments}}\right)$.

Appendix 1. Total Concentrations of Arsenic and Several Elements Dissolved in Sum of Acid-Soluble, Alkali-Soluble, and Silicate Fractions

Core depth of a sediment (cm)	Na %	K %	Ca %	Mg %	Fe %	Mn %	Cu ppm	Zn ppm	S[a] ppm	As[b] ppm
0— 1.5	0.33	2.0	0.14	0.26	3.7	0.14	99	110	190	85
1.5— 3.5	0.38	2.2	0.11	0.21	3.2	0.10	41	80	110	56
3.5— 5.5	0.37	2.1	0.13	0.40	3.6	0.087	50	94	70	46
5.5— 7.5	0.35	1.8	0.14	0.47	4.3	0.081	44	88	38	32
7.5— 9.5	0.39	1.9	0.15	0.43	3.7	0.066	30	95	39	34
9.5—11.5	0.33	1.8	0.14	0.40	3.7	0.083	38	90	51	34
11.5—13.5	0.39	1.9	0.18	0.45	4.2	0.11	43	100	25	30
13.5—15.5	0.32	2.0	0.17	0.49	4.1	0.10	24	100	70	35
15.5—17.5	0.27	1.9	0.15	0.43	3.7	0.091	36	93	—	34

a) Sulfide. b) Total of As(III) and As(V). All values are on dry basis.

Appendix 2. Arsenite and Arsenate Leached in Acid-Soluble Fraction from One Gram of Dry Sediments

Core depth of sediment (cm from surface)	As(III) μg	As(V) μg	As(III+V) μg	As(III)/As(V) ratio
0— 1.5	55.1	5.1	60.2	10.8
1.5— 3.5	28.0	4.7	32.7	6.0
3.5— 5.5	11.1	6.7	17.8	1.7
5.5— 7.5	8.4	4.4	12.8	1.9
7.5— 9.5	7.3	4.4	11.8	1.7
9.5—11.5	6.9	6.7	13.6	1.0
11.5—13.5	7.1	5.3	12.4	1.3
13.5—15.5	6.7	5.8	12.5	1.1
15.5—17.7	6.2	5.1	11.3	1.2

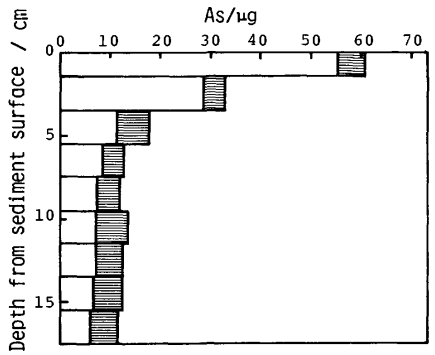

Fig. 3. Vertical distributions of concentrations of arsenite and arsenate in acid-soluble fractions leached from one gram of dry sediments.
□: Arsenite, ▨: Arsenate.

soluble fraction of the core sediment. Original data are tabulated in Appendix 2. As shown in Fig. 3, arsenite exists predominantly in the surface layer of the sediment, whereas the amounts of arsenate was almost constant throughout the entire core depth.

Table 2 presents the correlations between arsenic and the other elements in the sediment. In the acid-soluble fraction, good correlations were found for

Table 2. Coefficients of Correlations between Arsenic and Other Elements in Sediments

	Total As (Acid-soluble fraction)	As(III) (Acid-soluble fraction)	As(V) (Acid-soluble fraction)	Total As (Alkali-soluble fraction)	Total As (Silicate fraction)
Ca	−0.40	−0.39	0.007	0.86	0.33
Mg	−0.49	−0.46	−0.23	0.46	0.022
Fe	0.97	0.97	−0.15	0.73	0.48
Mn	0.45	0.84	−0.09	0.11	0.74
Cu	0.97	0.97	−0.11	0.042	0.85
Zn	0.97	0.96	−0.06	0.04	0.86
S[a]	0.97	0.96	−0.06		

a) Sulfide determined as hydrogen sulfide from the sediment.

arsenite but not for arsenate. For example, the coefficients of correlation are 0.96—0.97 for Fe/As (III), Cu/As(III), and S/As(III). From these results the following discussions are made on the chemical oxidation state of arsenic in sediment.

(1) Arsenic exists rich in the surface of the sediment mainly as an arsenite species. This trace arsenite is considered to be fixed with large amounts of iron hydroxide from the following experimental results. (I) There was a good correlation between trace arsenite and large amounts of iron (see Table 2). (II) The vertical distribution curve of arsenite in the acid-soluble fraction was nearly same as that of iron (see Figs. 2 and 3). (III) Arsenite and iron were easily dissolved in the acid-soluble fraction (see Table 1). (IV) Trace arsenite is usually coprecipitated from a neutral solution with iron (III) hydroxide but not with manganese hydroxide. All the manganese in the reservoir was in the form of soluble species and not in colloidal ones such as manganese hydroxide, because the concentration of manganese determined in the water with the addition of hydrochloric acid was equal to that in the same water sample without

Appendix 3. Concentrations of Major and Minor Species in the Reservoir
(Sampling Date: Nov. 1983)

Water depth	Temp.	pH	Cond. at 18 °C	O.R.P. vs. N.H.E.	D.O.	Turb.	E.R.	Ca	Mg	Na	K	HCO_3	Cl	SO_4
m	°C		μs/cm	mV	ppm									
0	14.6	6.6	66	137	8.2	6	80.8	7.1	1.1	4.0	1.5	22	6.0	3.0
5	13.7	6.5	64	145	8.5	10	73.1	7.1	1.1	5.0	1.5	22	6.3	3.0
10	13.6	6.5	61	139	9.2	10	85.8	7.0	1.0	4.0	1.5	22	5.0	N.D.
15	13.2	6.6	61	142	8.3	10	80.5	7.3	1.1	4.0	1.4	24	4.4	N.D.
20	12.8	6.6	62	135	3.1	10	86.5	7.4	1.1	4.0	1.4	24	4.5	N.D.
25	9.0	6.4	96	121	2.3	10	114	11	1.6	5.5	1.5	54	5.6	N.D.
27	7.6	6.2	195	80	3.2	10	191	15	2.1	6.0	2.3	120	5.8	N.D.
29	7.7	6.3	327	72	4.4	24	160	17	2.6	6.5	2.8	200	6.5	N.D.
30	7.4	6.5	438	52	3.8		168	19	2.9	6.5	2.9	240	7.1	N.D.

Water depth	PO_4	SiO_2	C.O.D.	NO_3-N	NO_2-N	NH_4-N	Fe	Mn	Cu	Zn	Al	As(III)	As(V)
m	ppm				ppb								
0	N.D.	10	1.1	2.0	26	300	72	70	4.0	6.6	66	N.D.	0.7
5	N.D.	8.4	1.2	12	16	220	78	97	3.2	16	63	N.D.	0.7
10	N.D.	9.7	1.3	11	14	220	72	92	4.4	11	46	N.D.	0.7
15	N.D.	11	1.4	1.0	23	440	94	280	2.4	6.6	100	N.D.	0.7
20	N.D.	9.4	1.3	0.5	23	390	130	410	2.8	7.6	58	N.D.	0.9
25	N.D.	9.4	1.3	0.4	N.D.	1400	130	3700	3.4	10	58	N.D.	0.7
27	N.D.	11	5.7	1.3	N.D.	4300	15000	9000	4.4	14	97	9.9	5.0
29	N.D.	21	5.4	0.4	N.D.	13000	56000	11000	4.8	19	150	100	15
30	N.D.	40	13	0.4	N.D.	14000	88000	14000	19	40	810	240	28

Temp: Temperature. Cond: Conductivity. O.R.P.: Oxidation reduction potential. D.O.: Dissolved oxygen. Turb.: Turbidity. E.R.: Evaporated residue. C.O.D.: Chemical oxygen demand.

the additin of the acid. (V) It is not expected that the trace arsenic is coprecipitated by the formation of aluminum hydroxide, because the concentration of aluminum in the reservoir was extremely lower than that of iron (see Appendix 3).

(2) In deep layers of the sediment, arsenite fixed with iron (III) hydroxide is released from the iron by the reductive dissolution reaction of iron (III) to iron (II). This reaction is considered from the data of a good correlation between arsenite and iron dissolved from the core sediment, shown in Table 2. Similar idea on the dissolution of arsenic from lake sediments has been reported by Nakashima et al.[11] With the dissolution of the iron hydroxide, arsenite will be released from the deeper layer of the sediment to an aqueous phase, and diffuse up to the surface layer of the sediment.

(3) There is another arsenic species leached in alkali-soluble fractions. The color of the alkaline solution was light-brown, and the maximum wavelength in the absorption and fluorescence of the solution were measured respectively to be 470 and 540 nm, which correspond to probably humic acids

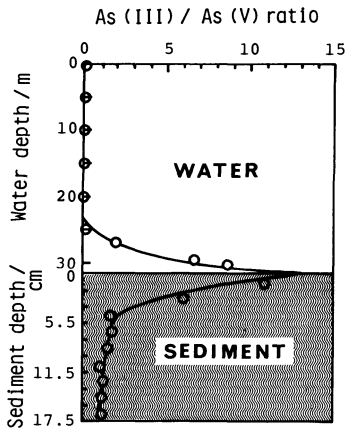

Fig. 4. Concentration ratios of arsenite to arsenate in the reservoir and its bottom sediment.
Data for sedimental arsenic are obtained from acid-soluble fractions.

or derivatives of chlorophylls. The arsenic was not vollatilized directly as arsine from the acidified alkaline solution, as already mentioned above. It can be, therefore, pointed out that the arsenic in the alkaline solution is chemically stable, and is probably organically-complexed or -bonded with

humic acids and their further decompositional products. It is worth noting that a considerable 30—40% of total arsenic content was leached out from the sediment by the alkali leaching.

Arsenite to Arsenate Ratio in Reservoir Water and Its Sediment. Figure 4 shows the ratio of As(III)/As(V) in the reservoir water and its bottom sediment. The concentrations of arsenite and arsenate in the water were quoted from Appendix 3, and those in the sediment were from the acid-soluble fraction shown in Appendix 2. As is seen in Fig. 4, the As(III)/As(V) ratio increased from the water depth of 25 m toward the bottom, which is in line with the decreasing O. R. P. values (see Appendix 3). The As(III)/As(V) in the water and in the sediment indicate a common feature that they reached maxima in the boundary layers between the two phases. On the other hand, the concentration ratio of Fe/As(III) in the bottom water, 370, was nearly equal to that in the surface sediment by acid leaching, 440. It is, therefore, considered that the formation and dissolution of the iron hydroxide coprecipitating arsenite are taking place repeatedly at the boundary layer between the water and the sediment.

References

1) S. Maeda, *Kagaku No Ryoiki.* **37**, 606 (1983).
2) M. Anke, "Trace Element-Analytical Chemistry in Medicine and Biology," Walter de Gruyter & Co. (1984), Vol. 3, p. 421.
3) S. Toda and A. Yamasaki, *Kagaku To Kogyo,* **38**, 324 (1985).
4) S. D. Faust and O. M. Aly, "Chemistry of Natural Waters," Ann Arbor Science Publishers Inc., (1981), p. 320.
5) H. Tsuji, K. Nishimura, Y. Tamari, and Y. Kusaka, *Bunseki Kagaku,* **33**, 43 (1984).
6) Y. Tamari, Y. Inoue, H. Tsuji, and Y. Kusaka, *Bunseki Kagaku,* **31**, E409 (1982).
7) Y. Tamari, Y. Inoue, H. Tsuji, and Y. Kusaka, *Bull. Chem. Soc. Jpn.*, **55**, 3760 (1982).
8) Y. Tamari, K. Hiraki, and Y. Nishikawa, *Chikyu Kagaku,* **12**, 37 (1978).
9) Nihon Bunseki Kagakukai Hokkaidoshibu, "Mizu no Bunseki," Kagakudozin Co. Ltd., (1985), p. 173.
10) D. Z. Piper, *Geochim. Cosmochim. Acta,* **35**, 531 (1971).
11) S. Nakashima and F. Morii, *Nogaku Kenkyu,* **59**, 189 (1982).
12) Y. Kitano and R. Fujiyoshi, *Geochem. J.*, **14**, 113 (1980).

The Effect of Tetraalkylammonium Ions on the Distribution of the Silicate Anions in Aqueous Solutions

Isao HASEGAWA, Kazuyuki KURODA, and Chuzo KATO*
Department of Applied Chemistry, School of Science and Engineering, Waseda University, Ohkubo, Shinjuku-ku, Tokyo 160
(Received January 30, 1986)

The effect of the addition of tetramethylammonium, (2-hydroxyethyl)trimethylammonium and benzyltrimethylammonium ions on the distribution of the silicate anions arising from the hydrolysis of tetraethoxysilane was studied by using the trimethylsilylation method. The selective formation of the octameric silicate anion with a double four-membered cage was confirmed in these solutions. It was found that tetraalkylammonium ions with three methyl groups, whether or not the other group was a methyl group, contributed to the formation of a double four-membered cage octamer.

Tetraalkylammonium ions play an important role in the structure formation involved in zeolite syntheses and constitute one of the principal factors controlling the structure of zeolite.[1] These ions also affect the distribution of soluble silicate anions in aqueous solutions. Generally, silicate anions polymerize at random in aqueous solutions; this makes the distribution of the anions very complicated. By adding tetraalkylammonium ions to the systems under appropriate conditions, however, silicate anions with specific structures are formed. In this manner, the formation of silicate species with a double three-membered cage ($Si_6O_{15}^{6-}$), a double four-membered cage ($Si_8O_{20}^{8-}$) and a double five-membered cage ($Si_{10}O_{25}^{10-}$) have been reported.[2-15]

However, several reports have described the effect of the addition of tetraalkylammonium ions with different alkyl groups or other organic cations such as pyridinium ions.[11-15] In those papers, for example, it has been described that the (2-hydroxyethyl)trimethylammonium ion ($N^+(CH_3)_3C_2H_4OH$) contributes to the formation of the double four-membered cage silicate anion (cubic octamer)[11] as well as the tetramethylammonium ion ($N^+(CH_3)_4$). However, it remains obscure why these two tetraalkylammonium ions contribute to the formation of the cubic octamer similarly.

In order to clarify the interaction between tetramethylammonium ions and silicate anions, it is necessary to study the ratio of controlled silicate species quantitatively. Previous studies by Scheler et al.[11-15] only reported the results of the selective formation of silicate anions at a few SiO_2 concentrations and cation/Si ratios by means of ^{29}Si NMR. Therefore, the purpose of this study is to investigate the effect of tetraalkylammonium ions on the silicate anions over a broader range of variable factors (SiO_2 concentration and tetraalkylammonium ion/Si ratio) by means of trimethylsilylation.

Trimethylsilylation, originally applied to silicate minerals and solutions by Lentz,[16] is an effective chemical method for the structure study of silicates[17] as well as ^{29}Si NMR spectroscopy.[18-24] ^{29}Si NMR is an extremely powerful analytical procedure for the study of silicate structure. However, some doubts remain in its quantitative analysis.[24] Trimethylsilylation has the advantage of making it easy to perform quantitative analysis by means of gas chromatography in spite of the limits imposed by the side reactions upon silylation. Although several methods are available according to the silicate samples, the Lentz method is reported to be most favorable for the trimethylsilylation of aqueous silicate solutions;[25] thus, the Lentz method was used in this study.

Experimental

Materials. Tetraethoxysilane (reagent-grade) was used as a silica source. A 10% tetramethylammonium hydroxide aqueous solution, a 50% (2-hydroxyethyl)trimethylammonium hydroxide aqueous solution, and a 40% benzyltrimethylammonium ($N^+(CH_3)_3CH_2C_6H_5$) hydroxide aqueous solution were used as the tetraalkylammonium ions. The sodium hydroxide, concentrated hydrochloric acid, and 2-propanol were all reagent grade. The hexamethyldisiloxane was obtained by the hydrolysis of chlorotrimethylsilane and was distilled once (bp 100—101 °C).

Preparation of Sample Solutions. A fixed amount of tetraethoxysilane was added to a tetraalkylammonium hydroxide solution whose concentration had been adjusted by adding deionized water. The mixture was stirred for 2 d at room temperature to complete the hydrolysis of tetraethoxysilane. In this manner, two series of sample solutions were prepared --- samples with different SiO_2 concentrations at a constant N/Si ratio (molar ratio of tetraalkylammonium ion against silica), which was 1.0, and samples with different N/Si ratios at a constant SiO_2 concentration (1.0 mol dm^{-3}). In the case of the addition of the tetramethylammonium ion, sample solutions of only the former series were prepared because of the low concentration of the tetramethylammonium hydroxide aqueous solution.

In order to compare the effects of tetraalkylammonium ions and those of alkali metal ions, sample solutions with different SiO_2 concentrations at the Na/Si ratio of 1.0, solutions to which the sodium ion had been added, were prepared in the same described above by using a 4 mol dm^{-3} aqueous sodium hydroxide solution.

Trimethylsilylation by the Lentz Method. A 2 cm^3 portion of a sample solution was added to a mixture of concentrated hydrochloric acid (6 cm^3), water (5 cm^3), 2-propanol (12 cm^3), and hexamethyldisiloxane (8 cm^3) which had been stirred for 1 h at room temperature. After the silylation had been completed by stirring the reaction mixture for 1 h at room temperature, the siloxane phase was separated and Amberlyst-15 (cation-exchange resin) was added to complete the trimethylsilylation.

Analytical Procedure. The trimethylsilylated derivatives were analyzed by means of gas-liquid chromatography. Quantitative analysis was performed with respect to SiO_4^{4-}, $Si_2O_7^{6-}$, $Si_3O_{10}^{8-}$, $Si_4O_{12}^{8-}$, and $Si_8O_{20}^{8-}$ by using tetradecane as the internal-standard substance.[26] The results are shown as SiO_2 recovery, which was the proportion of SiO_2 recovered as trimethylsilylated derivatives converted from the SiO_2 component in the starting material. (The ionic charge was omitted for the sake of simplicity in the figures of this report.) The peaks on the chromatograms were identified for the trimethylsilylated derivatives of the monomer, dimer, linear trimer, cyclic tetramer and cubic octamer by means of mass spectrometry. The chromatographic conditions were as follows: Shimadzu GC-8A apparatus, equipped with a hydrogen FID; stainless steel column (length: 6 m, internal diameter: 2.6 mm), packed with OV-17 2% Chromosorb W for 3 m and SE-30 5% Shimalite W for 3 m; oven temperature: 80 °C to 270 °C at 8 °C min^{-1}; injection temperature: 300 °C; carrier gas (nitrogen) flow rate: 50 cm^3 min^{-1}.

Results and Discussion

1. Gas Chromatograms and the Effect of Sodium Ions. Figure 1 shows typical gas chromatograms of trimethylsilylated derivatives of soluble silicate anions in (a) a sodium silicate solution and (b) a tetramethylammonium silicate solution. In the case of the sodium ion, it was found that low-molecular species such as the monomer, dimer, linear trimer, and cyclic tetramer, and also unidentified species with relatively higher molecular weights existed. This means that a random polymerization of the silicate anions occurred in the system. After adding the tetramethylammonium ion under proper conditions, however, a considerably large peak appeared, as is shown in Fig. 1(b). This peak was identified as the cubic octamer. In this way, the selective structure formation of silicate anions in the system is shown on a gas chromatogram, for almost always only one peak appeared: peaks of other species hardly ever appeared.

Figure 2 shows the variation in the silicate-anion distribution with the variation in the SiO_2 concentration at the Na/Si ratio of 1.0. With the increase in the SiO_2 concentration, the recovery of low-molecular species from the monomer to the cyclic tetramer was reduced gradually. This means that these low-molecular species polymerized and that higher molecular species were formed in the system. Although the cubic octamer existed in a small amount (the maximum recovery was 1.3% at the SiO_2 concentration of 0.7 mol dm^{-3}), it occurred in the course of the polymerization of the silicate anions because its recovery was relatively low and its lower recovery was observed in the region of higher SiO_2 concentrations, where polymerization proceeded. Therefore, in the sodium-coexisting system, silicate anions polymerize at random and there is no selective structure formation.

2. Addition of Tetramethylammonium Ions. When tetramethylammonium ions were present in a

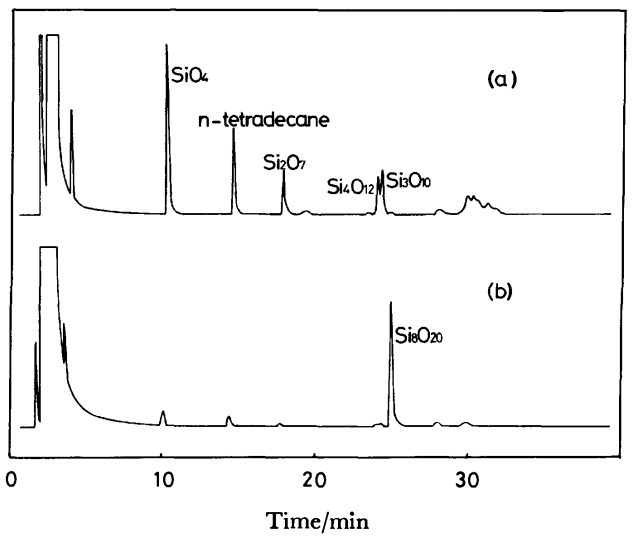

Fig. 1. Gas chromatograms of the trimethylsilylated derivatives of silicate species in (a) sodium silicate solution (Na/Si=1.0, SiO_2 concentration: 0.4 mol dm^{-3}) and (b) tetramethylammonium silicate solution N/Si=1.0, SiO_2 concentration: 0.88 mol dm^{-3}).

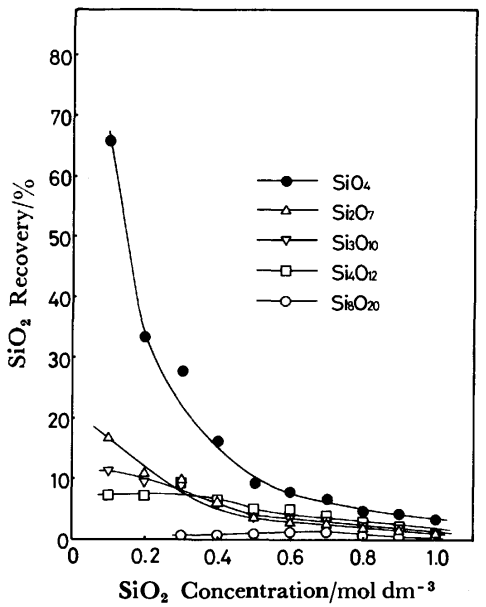

Fig. 2. Variation in the silicate-anion distribution with the SiO_2 concentration (Na/Si=1.0) in sodium silicate solution.

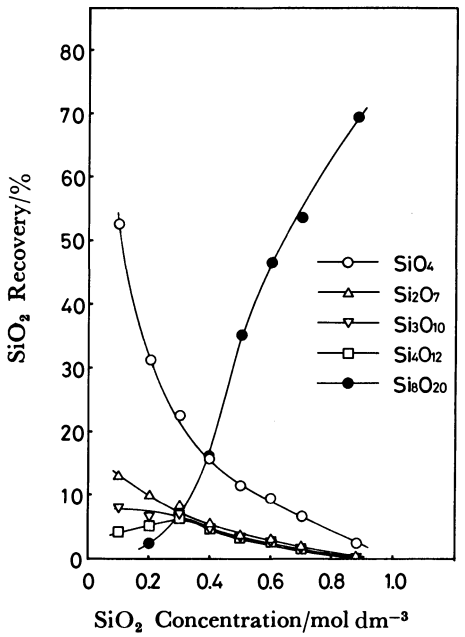

Fig. 3. Variation in the silicate-anion distribution with the SiO_2 concentration (N/Si=1.0) in tetramethylammonium silicate solution.

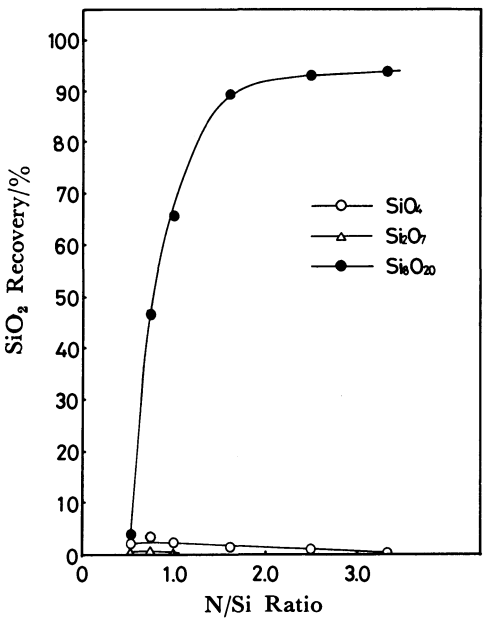

Fig. 4. Variation in the silicate-anion distribution with the N/Si ratio in 1.0 mol dm^{-3} (2-hydroxyethyl)-trimethylammonium silicate solution.

silicate solution, the silicate-anion distribution varied in a different way with the variation in the SiO_2 concentration at the N/Si ratio of 1.0, as is shown in Fig. 3. As the SiO_2 concentration increased, the recovery of low-molecular species from the monomer to the cyclic tetramer decreased. On the other hand, the recovery of the cubic octamer increased rapidly. In comparison with the results obtained from the Na_2O–SiO_2 system, shown in Fig. 2, the behavior of low-molecular species showed a similar tendency. As for the formation of the cubic octamer, however, the behavior was obviously different. This was evidently caused by the difference in the added cations. The selective formation of the cubic octamer has also been observed by Hoebbel et al., who used another silica source,[4] and a similar tendency was confirmed in this study. Thus, upon the addition of tetramethylammonium ions to aqueous silicate solutions, random polymerization did not occur, but a specified silicate skeleton was selectively formed.

3. Addition of (2-Hydroxyethyl)trimethylammonium Ions. In order to clarify the effect of another tetraalkylammonium ion, the (2-hydroxyethyl)trimethylammonium ion was employed initially. When the N/Si ratio was varied in a 1.0 mol dm^{-3} SiO_2 sample solution, the variation in the silicate-anion distribution indicated a highly selective formation of a silicate framework. As Fig. 4 shows, the low-molecular species decreased, and only the cubic octamer was formed singularly, with an increase in the N/Si ratio.

The variation in the silicate-anion distribution with the SiO_2 concentration at the N/Si ratio of 1.0 is

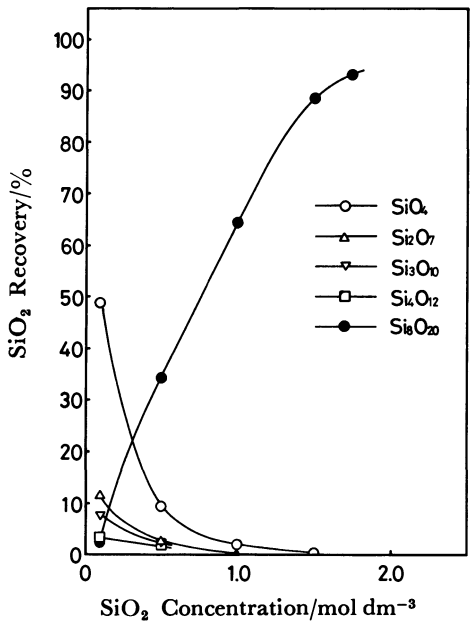

Fig. 5. Variation in the silicate-anion distribution with the SiO_2 concentration (N/Si=1.0) in (2-hydroxyethyl)trimethylammonium silicate solution.

shown in Fig. 5. The cubic octamer was formed singularly at higher SiO_2 concentrations, as was previously shown in the case of the addition of the tetramethylammonium ion. In (2-hydroxyethyl)trimethylammonium silicate solutions whose N/Si ratios were 1.0 and 2.0, the singular formation of the cubic octamer in both solutions was confirmed by Scheler et al.[11] using ^{29}Si NMR. Although the SiO_2 concentration in this work was different from that in

the earlier report, there was yet a pronounced difference in the recovery of the cubic octamer between the N/Si ratios of 1.0 and 2.0. When trimethylsilylation is used as an analytical tool, it is impossible to obtain trimethylsilylated derivatives which reflect the original distribution of the silicate anions completely, as side reactions necessarily occur. Nevertheless, the fact that the cubic octamer was recovered in a yield of ca. 90% means that virtually only the cubic octamer existed.

4. Addition of Benzyltrimethylammonium Ions. The effect of tetraalkylammonium ions with a different alkyl group was investigated by the use of benzyltrimethylammonium ion as well as (2-hydroxyethyl)trimethylammonium ions. Figure 6 shows the variation in the silicate-anion distribution with the N/Si ratio in a 1.0 mol dm^{-3} sample solution, while Fig. 7 shows the variation in the SiO_2 concentration at the N/Si ratio of 1.0. In the two cases, similar tendencies were recognized, and in both, singularly the cubic octamer was also formed. Thus, it was found that benzyltrimethylammonium ions also contributed to the formation of the cubic octamer.

From these results, it was obvious that a tetraalkylammonium ion with three methyl groups could contribute to the selective formation of the cubic octamer, even if one of the four alkyl groups was not a methyl group but was either hydrophilic or hydrophobic.

As for the structure of crystalline tetramethylammonium silicate ($Si_8O_{20}(N(CH_3)_4)_8$), a detailed structure study by means of X-ray diffraction analysis was performed by Smolin et al.[27] It remains obscure, however, how the tetramethylammonium ion contributes to the selective formation of the cubic octamer in an aqueous silicate solution. Also, several investigators have reported that the formation of silicate species with cage-like structures was affected by the structure of the tetraalkylammonium ions.[2-9] As compared with those reports, we ourselves have found that the interaction of silicate anions and tetraalkylammonium ions is not influenced by a bulky group such as the benzyl group during the selective formation and that only three methyl groups are essential for the formation of the cubic octamer, even if the other alkyl group was hydrophilic or hydrophobic. From the results in this study, it was concluded that not all four methyl groups in a tetramethylammonium ion always contribute to the selective structure formation.

The application of the trimethylsilylation technique to the early stages of the hydrolysis of tetraethoxysilane would be useful for a better understanding of this system, which requires further study.

This work was supported by the Yazaki Memorial Foundation for Science And Technology, for which help grateful acknowledgement was made.

References

1) B. M. Lok, T. R. Cannan, and C. A. Messina, *Zeolites*, **3**, 282 (1983).
2) D. Hoebbel and W. Wieker, *Z. Anorg. Allg. Chem.*, **384**, 43 (1971).
3) O. Rademacher, M. Zschuppe, and H. Scheler, *Z.*

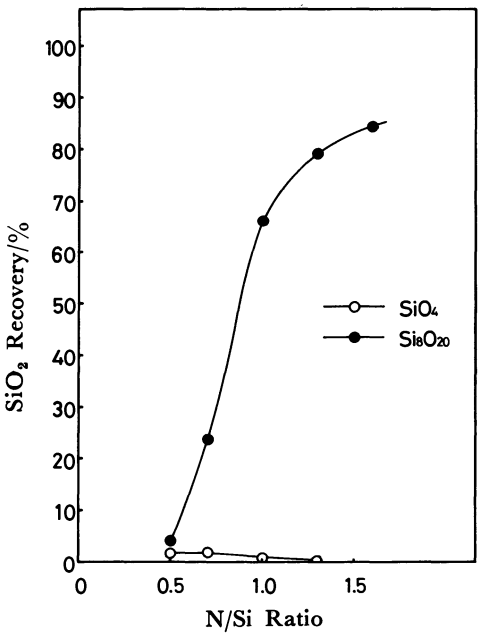

Fig. 6. Variation in the silicate-anion distribution with the N/Si ratio in 1.0 mol dm^{-3} benzyltrimethylammonium silicate solution.

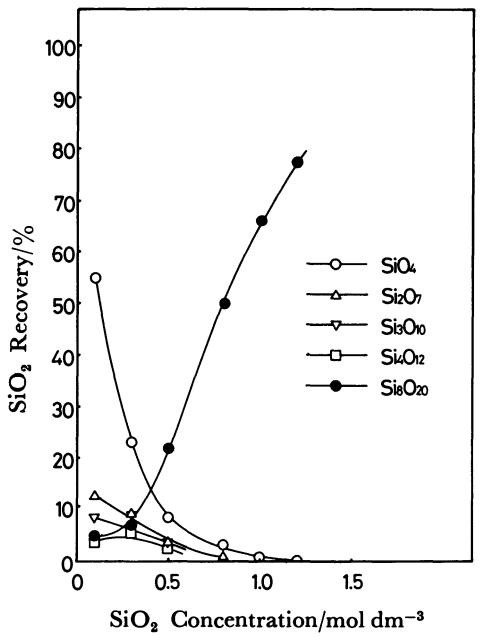

Fig. 7. Variation in the silicate-anion distribution with the SiO_2 concentration (N/Si=1.0) in benzyltrimethylammonium silicate solution.

Chem., **18**, 341 (1978).
4) D. Hoebbel, G. Garzó, G. Engelhardt, and A. Vargha, *Z. Anorg. Allg. Chem.*, **494**, 31 (1982).
5) D. Hoebbel, G. Garzó, G. Engelhardt, R. Ebert, E. Lippmaa, and M. Alla, *Z. Anorg. Allg. Chem.*, **465**, 15 (1980).
6) D. Hoebbel, A. Vargha, B. Fahlke, and G. Engelhardt, *Z. Anorg. Allg. Chem.*, **521**, 61 (1985).
7) D. Hoebbel, W. Wieker, P. Franke, and A. Otto, *Z. Anorg. Allg. Chem.*, **418**, 35 (1975).
8) D. Hoebbel, A. Vargha, G. Engelhardt, and K. Újszászy, *Z. Anorg. Allg. Chem.*, **509**, 85 (1984).
9) R. K. Harris and C. T. G. Knight, *J. Mol. Struct.*, **78**, 273 (1982).
10) N. H. Ray and R. J. Plaisted, *J. Chem. Soc., Dalton Trans.*, **1983**, 475.
11) F. Schlenkrich, E. Beit, O. Rademacher, and H. Scheler, *Z. Anorg. Allg. Chem.*, **511**, 41 (1984).
12) F. Schlenkrich, O. Ziemens, O. Rademacher, and H. Scheler, *Z. Chem.*, **24**, 130 (1984).
13) O. Ziemens, F. Schlenkrich, O. Rademacher, and H. Scheler, *Z. Chem.*, **24**, 130 (1984).
14) O. Rademacher, F. Schlenkrich, O. Ziemens, and H. Scheler, *Z. Chem.*, **24**, 131 (1984).
15) O. Rademacher, O. Ziemens, and H. Scheler, *Z. Anorg. Allg. Chem.*, **519**, 165 (1984).
16) C. W. Lentz, *Inorg. Chem.*, **3**, 574 (1964).
17) B. R. Currell and J. R. Parsonage, *J. Macromol. Sci., Chem.*, **A16**, 141 (1981).
18) G. Engelhardt, H. Jancke, D. Hoebbel, and W. Wieker, *Z. Chem.*, **14**, 109 (1974).
19) G. Engelhardt, D. Zeigan, H. Jancke, D. Hoebbel, and W. Wieker, *Z. Anorg. Allg. Chem.*, **418**, 17 (1975).
20) R. K. Harris and R. H. Newman, *J. Chem. Soc., Faraday Trans. 2*, **73**, 1204 (1977).
21) R. K. Harris, J. Jones, C. T. G. Knight, and D. Pawson, *J. Mol. Struct.*, **69**, 95 (1980).
22) R. K. Harris, C. T. G. Knight, and W. E. Hull, *J. Am. Chem. Soc.*, **103**, 1577 (1981).
23) R. K. Harris and C. T. G. Knight, *J. Chem. Soc., Faraday Trans. 2*, **79**, 1525 (1983).
24) R. K. Harris and C. T. G. Knight, *J. Chem. Soc., Faraday Trans. 2*, **79**, 1539 (1983).
25) L. S. D. Glasser and S. K. Sharma, *Br. Polym. J.*, **6**, 283 (1974).
26) T. Shimono, T. Isobe, and T. Tarutani, *J. Chromatogr.*, **205**, 49 (1981).
27) Yu. I. Smolin, Yu. F. Shepelev, R. Pomes, D. Hoebbel, and W. Wieker, *Kristallografiya*, **24**, 38 (1979). <*Sov. Phys. Crystallogr.*, **24**, 19 (1979)>.

An EXAFS Investigation of the Coordination Structure of Copper(II) Ions in Aqueous $Cu(ClO_4)_2$ and Methanolic $CuCl_2$ Solutions

Yoshichika TAJIRI and Hisanobu WAKITA*
Department of Chemistry, Faculty of Science, Fukuoka University,
8-19-1, Nanakuma, Jonan-ku, Fukuoka 814-01
(Received February 5, 1986)

The coordination structure of copper(II) ions in aqueous and methanolic solutions was investigated by means of EXAFS spectroscopy. The hexaaquacopper(II) complex in the aqueous $Cu(ClO_4)_2$ solution had an elongated octahedral structure, with four equatorial distances of 2.00 Å and two axial distances of 2.28 Å. Scarcely no axial interaction has been seen in the radial-distribution curve after the Fourier transform of the EXAFS spectrum, for the real and imaginary parts of the Fourier transformed function for the axial interactions are diminished by the interference of those for the equatorial interactions. Two distances for the equatorial interactions of the mixed-ligand chlorocopper(II) complexes in the methanolic $CuCl_2$ solution were clearly resolvable in the radial-distribution curve; they were 2.00 Å and 2.22 Å for the Cu–O and Cu–Cl interactions respectively.

Both EXAFS and X-ray diffraction methods have been used in the structural studies of metal complexes in solution.[1–10] A number of X-ray-diffraction studies have established the elongated octahedral structure of six-coordinated copper(II) complexes in solution.[1–3,7–9] However, only a few EXAFS studies[4,5] have been performed to determine the axial interaction of the octahedral structure in solution.

X-Ray-diffraction investigations have shown that the hexaaquacopper(II) complex in 1.94—3.55 mol dm^{-3} aqueous $Cu(ClO_4)_2$[1,2] and 1.386 mol dm^{-3} aqueous $CuSO_4$[3] solutions has an elongated octahedral structure with four equatorial bonds of 1.94—1.98 Å and two axial bonds of 2.34—2.43 Å, because there exist peaks caused by the $Cu-O_{eq}$ (equatorial) and $Cu-O_{ax}$ (axial) bonds in the radial-distribution function, $D(r)$.

According to Sham et al.,[4] who analyzed the EXAFS spectrum of the K-edge of copper in a 1 mol dm^{-3} aqueous $Cu(ClO_4)_2$ solution, the extremely large values of the axial distance (2.60 Å) and the Debye–Waller factor (0.12 Å) suggested that the axial ligands were loosly bonded. Sano et al.[5] mentioned, in their EXAFS study of a 0.32 mol dm^{-3} aqueous $Cu(ClO_4)_2$ solution, but without detailed analysis, that the second peak appearing at 2.46 Å in the radial-distribution curve corresponds to the $Cu-O_{ax}$ interaction.

X-Ray-diffraction studies of a 2.952 mol dm^{-3} aqueous $CuCl_2$ solution[7] and a 1.016—4.364 mol dm^{-3} aqueous $CuBr_2$ solution[8] disclosed that mixed-ligand six-coordinated aquahalogenocopper(II) complexes had elongated octahedral structures with four bonds including both $Cu-X_{eq}$ (X=Cl,Br) and $Cu-O_{eq}$ and two $Cu-O_{ax}$ bonds, although the peak due to the $Cu-O_{ax}$ bonds did not appear as a separate one. Moreover, 1.055—2.350 mol dm^{-3} methanolic $CuCl_2$ solutions[9] included nearly equivalent amounts of three copper(II) complexes, $[CuCl_n(CH_3OH)_{6-n}]$, where n=1, 2, and 3, although the peaks caused by the $Cu-O_{eq}$, $Cu-Cl_{eq}$, and $Cu-O_{ax}$ bonds overlapped with each other.

Thus far no elongated octahedral structure of aquahalogenocopper(II) complexes in solution has been reported on the basis of EXAFS spectroscopy.[10]

From the consideration of the investigations described above, it seemed that it would be of interest to examine whether or not the EXAFS spectroscopy is able to "see" the axial interaction of the six-coordinated octahedral copper(II) complexes in solution. In the present paper, we attempt to analyze the structures of the copper(II) complexes in 1.019 mol dm^{-3} aqueous $Cu(ClO_4)_2$ and 0.996 mol dm^{-3} methanolic $CuCl_2$ solutions for the purpose of seeing the axial interaction by means of EXAFS spectroscopy. In order to obtain detailed information on the structure, the EXAFS data were analyzed by using not only a conventional curve-fitting method, but also the radial-distribution method to be described in the following Experimental section. The radial-distribution method used in an EXAFS study of a rhodium catalyst by Koningsberger et al.[11] seemed suitable for the analysis of the present EXAFS data, where the interatomic distances are close to each other.

Experimental

EXAFS Measurements. The EXAFS measurements were carried out by the use of synchrotron radiation using the EXAFS facilities at BL-10B of the Photon Factory in the National Laboratory for High-Energy Physics (KEK-PF). The data were collected in the range from ca. 400 eV on the lower-energy side of the Cu absorption K-edge of 8981.83 eV (λ=1.3804 Å) to ca. 1600 eV on the higher-energy side; the time for the data collection was fixed at 1 s at each measuring point.

The reference compounds, bis(acetylacetonato)copper(II) and tetramethylammonium tetrachlorocuprate(II), were prepared by the conventional methods, powdered with an agate mortar, and pressed with polyethylene powder into

films.

An 1.019 mol dm^{-3} aqueous copper(II) perchlorate solution was prepared by dissolving the copper(II) perchlorate in distilled water, which had been obtained by the reaction of copper(II) oxide with a hot perchloric acid solution and recrystallized three times from distilled water. A 0.996 mol dm^{-3} methanolic copper(II) chloride solution was prepared by dissolving copper(II) chloride crystals in absolute methanol. The concentrations of the copper(II) ion in the sample solutions were determined by the EDTA titration method. Each solution sample was put into a polyethylene pouch sandwiched by a polyacrylate holder.

Data Reduction Procedure. The EXAFS spectrum which is extracted from the observed absorption spectrum is expressed by:

$$\chi_{obsd}(k) = [\mu_{obsd}(k) - \mu_0(k)]/\mu_0(k), \quad (1)$$

where $\mu_{obsd}(k)$ is the absorption coefficient, attributed only to the K-edge of the absorption atom and where $\mu_0(k)$ is the smoothly varying background absorption coefficient, approximated by a cubic spline function.[12] k is the photoelectron wave-number and is given as $\sqrt{2m(E-E_0-\Delta E)/h^2}$, where E denotes the energy of the incident X-ray; E_0 is the theoretical energy at the absorption edge for the absorption atom, and ΔE is the correction value for the E_0 value at the absorption edge.

Analysis by the Curve-Fitting Method. The EXAFS spectrum, weighted by k^3, is converted by the Fourier transform into the Fourier transformed function, $F(r)$, in the r-space as:

$$F(r) = \int_{k_{min}}^{k_{max}} k^3 \cdot \chi_{obsd}(k) \cdot \exp(2ikr)dk = ReF(r) + iImF(r). \quad (2)$$

Moreover, the radial distribution function, $|F(r)|$, is given as:

$$|F(r)| = [ReF(r)^2 + ImF(r)^2]^{1/2}, \quad (3)$$

where $ReF(r)$ and $ImF(r)$ are the real and imaginary parts of the $F(r)$ function respectively. The structure parameters (interatomic distances, mean-square displacements, and coordination numbers) are obtained by comparing the Fourier filtered EXAFS spectrum, $\overline{\chi}(k)$, with the calculated EXAFS spectrum, $\chi_{calcd}(k)$. $\overline{\chi}(k)$ is obtained by performing the Fourier backfiltering of the peak in the $|F(r)|$ curve into the EXAFS spectrum in the k-space, while $\chi_{calcd}(k)$ is given by the single-scattering theory[13] as:

$$\chi_{calcd}(k) = \sum_j [N_j/(k \cdot R_j^2)] \cdot |f_j(\pi, k)| \cdot \sin(2kR_j + \phi_j(k)) \cdot \exp(-2R_j/\gamma) \cdot \exp(-2\sigma_j^2 k^2), \quad (4)$$

where R_j and N_j are the distance from the absorbing atom to the j-th coordination shell and the number of atoms at R_j respectively, where σ_j^2 is the mean square displacement[14] of R_j, and γ is the mean free path. $|f_j(\pi,k)|$ and $\phi_j(k)$ are the backscattering amplitude and the phase shift of the atoms in the j-th backscattering shell respectively. A curve fitting is applied to minimize the error-square sum, U ($=\sum[k^3 \cdot \overline{\chi}(k) - k^3 \cdot \chi_{calcd}(k)]^2$).

Analysis by the Radial-Distribution Method. The analysis of this method[11] is performed by using the Fourier transformed function, $F'(r)$, which is corrected for the phase shift and the backscattering amplitude as:

$$F'(r) = \int_{k_{min}}^{k_{max}} [k \cdot \chi(k)/|f(\pi, k)|] \cdot \exp(2ikr + \phi(k))dk = ReF'(r) + iImF'(r), \quad (5)$$

and using the radial-distribution function, $|F'(r)|$, given as:

$$|F'(r)| = [ReF'(r)^2 + ImF'(r)^2]^{1/2}. \quad (6)$$

The optimal values of the structure parameters are obtained by comparing the peak in the calculated $|F'(r)|$ curve with that in the observed $|F'(r)|$ curve in order to minimize the disagreement of the peak-height, -width, and -position. The calculated $|F'(r)|$ curve is obtained from $\chi_{calcd}(k)$ by the Fourier transform according to Eqs. 5 and 6, where $\chi_{calcd}(k)$ is given by substituting j (=1), γ (the initial value in the present paper, 5.0), and the initial values of the structure parameters (taken from the literature) in Eq. 4. The γ, N, R, and σ^2 parameters are allowed to vary at intervals of 0.02, 0.01, 0.001 Å, and 0.0001 Å^2 respectively.

If the EXAFS spectrum comes from one interaction, the peak in the $|F'(r)|$ curve as corrected for the phase shift and backscattering amplitude of the interaction, should coincide in position with the maximum peak in the $ImF'(r)$ oscillation.[12,15] In addition, the main peak in the $|F'(r)|$ curve and the $ImF'(r)$ oscillation should be almost symmetrical with respect to the ordinate at the position of the coincidence.[15] On the other hand, if the $|F'(r)|$ curve is inappropriately corrected for the phase shift and backscattering amplitude by taking an improper interaction into consideration, the maximum peak in the $ImF'(r)$ oscillation can not coincide in position with that in the $|F'(r)|$ curve. If the EXAFS spectrum arises from two interactions or more, the $ImF'(r)$ oscillation can be asymmetrical with respect to the ordinate around the maximum peak. The analysis of the peaks in the $|F'(r)|$ curve is as follows. The first step is to estimate the values of the structure parameters of one interaction which peaks more clearly than the other interactions in the $|F'(r)|$ curve. The next step is to subtract the $\chi_{calcd}(k)$ spectrum from the $\chi_{obsd}(k)$ spectrum. This subtraction gives the residual EXAFS spectrum, $\chi_{res}(k)$, in which the contribution of other interactions is included. Then, the third step is to analyze the peak in the $|F'(r)|$ curve of the $\chi_{res}(k)$ in a way similar to that described above by but using another set of structural parameters for an additional interaction in order to obtain the best-fit function of $\chi'_{calcd}(k)$. If a difference between the peak in the $|F'(r)|$ of the $\chi_{res}(k)$ and that of the $\chi'_{calcd}(k)$ still remains, the analysis should be repeated in a similar way by assuming further interactions.

The curve-fitting method is carried out by comparing the $\overline{\chi}(k)$ with the $\chi_{calcd}(k)$ spectra in the k-space; it needs an additional Fourier backfiltering of the peak in the $|F(r)|$ curve. On the other hand, the radial-distribution method compares the observed $|F'(r)|$ value with the calculated $|F'(r)|$ curves in the r-space and necessitates a Fourier transform of the $\chi_{calcd}(k)$. Theoretically, therefore, the two methods should give equivalent results.

Results and Discussion

Reference Compounds. The analysis of the EXAFS data makes it necessary to estimate the phase shift and the backscattering amplitude. In the present study, the phase shift and the backscattering amplitude are determined experimentally by the use of approximated equations.[16,17] The EXAFS spectra of two reference compounds, powdered $Cu(acac)_2$ (acac = acetylacetonate ion) and $[(CH_3)_4N]_2[CuCl_4]$ crystals, with known structures[18,19] were measured in order to estimate the phase shifts and backscattering amplitudes of the copper-oxygen and copper-chlorine interactions. The EXAFS spectrum, $k^3 \cdot \chi_{obsd}(k)$, and the radial distribution curve, $|F(r)|$, for the $Cu(acac)_2$ crystal are shown in Figs. 1-A and 1-B, and those for the $[(CH_3)_4N]_2[CuCl_4]$ crystal, in Figs. 1-C and 1-D. Judging from the crystal structures of these two reference compounds, we considered that the first peak in Figs. 1-B and 1-D corresponds to the first backscattering shell around the Cu^{2+} ion. Therefore, the first peak at 1.56 Å in Fig. 1-B is attributed to the interaction between copper and oxygen atoms within coordinated acetylacetonate ions,[18] while the first peak at 1.86 Å in Fig. 1-D is ascribed to the interaction between copper and chlorine atoms.[19] Performing the Fourier backfiltering over the region of the first peak in each $|F(r)|$ curve, we carried out the curve-fitting in order to obtain the phase shifts and backscattering amplitudes, using known coordination numbers and bond distances. The ΔE and γ values were fixed at 0.0 eV and 5.0 respectively, while σ^2 was allowed to vary. The crystallographic data and Fourier transform range of the reference compounds are summarized in Table 1.

Aqueous $Cu(ClO_4)_2$ Solution. The $k^3 \cdot \chi_{obsd}(k)$ spectrum and the $|F(r)|$ curve for the aqueous $Cu(ClO_4)_2$ solution are depicted in Figs. 2-A and 2-B respectively. The clear peak at 1.6 Å in the $|F(r)|$ curve can be attributed to the interaction between copper and water oxygen atoms at the equatorial site, for the first shell around the Cu^{2+} ion in this solution corresponds to the $Cu-O_{eq}$ interaction, judging from the results of X-ray diffraction.[1,2] The difference in value between the peak position in the $|F(r)|$ curve and the bond distance of the $Cu-O_{eq}$ obtained by X-ray diffraction[1] (1.94 Å) is −0.34 Å. If we use this value as the correction value for the peak position in the $|F(r)|$ curve, a peak due to the interaction between copper and water oxygen atoms at the axial site (2.43 Å, from X-ray diffraction[1]) should appear at 2.09 Å in the $|F(r)|$ curve. However, the peak found at ca. 2.1 Å is too small to be attributed to the $Cu-O_{ax}$ interaction. If the peak due to the $Cu-O_{ax}$ interaction

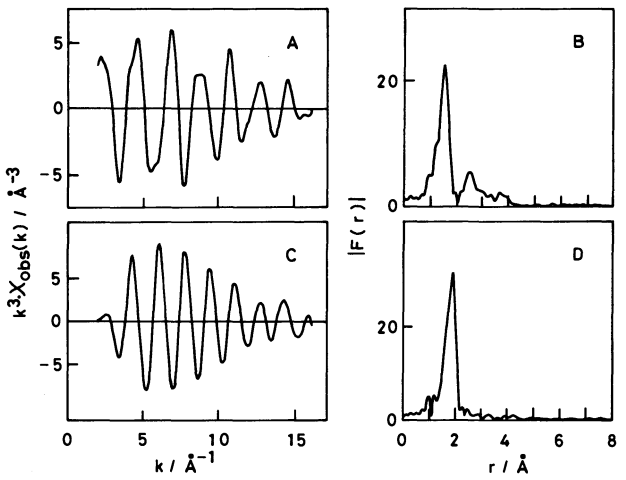

Fig. 1. The EXAFS spectra, $k^3 \cdot \chi_{obsd}(k)$ and the radial distribution curves, $|F(r)|$ for the reference compounds. A, C: $k^3 \cdot \chi_{obsd}(k)$. B, D: $|F(r)|$. A, B: $[Cu(acac)_2]$ crystal. C, D: $[(CH_3)_4N]_2[CuCl_4]$ crystal.

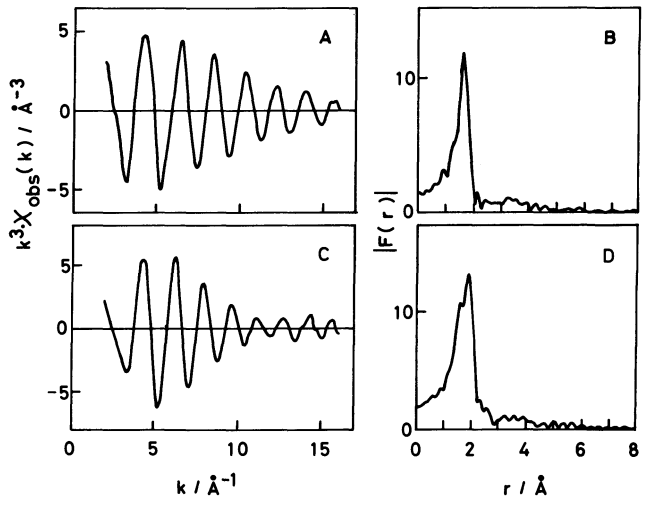

Fig. 2. The EXAFS spectra, $k^3 \cdot \chi_{obsd}(k)$ and the radial distribution curves, $|F(r)|$ for the solution samples. A, C: $k^3 \cdot \chi_{obsd}(k)$. B, D: $|F(r)|$. A, B: aqueous $Cu(ClO_4)_2$ solution. C, D: methanolic $CuCl_2$ solution.

Table 1. Crystallographic Data and Ranges of Fourier Transforms of the Reference Compounds

Sample	k_1-range	r-range	k_2-range	N_{ref}	R_{ref}
$Cu(acac)_2$	3.0—17.0	0.80—1.90	4.5—16.0	4.0	1.95
$[(CH_3)_4N]_2[CuCl_4]$	3.0—18.0	1.11—2.22	4.5—15.0	4.0	2.22

k_1-range: the range of the Fourier transform, $Å^{-1}$; r-range: the range of the Fourier backfiltering, Å; k_2-range: the range of the curve-fitting, $Å^{-1}$; N_{ref}: coordination number; R_{ref}: interatomic distance, Å.

is small and widespread in the r-space, the peaks caused by the Cu–O_{eq} and Cu–O_{ax} interactions might not be clearly resolvable in the $|F(r)|$ curve because the bond distances of the two interactions are too close to each other. On the basis of this consideration, the curve-fitting analysis of the EXAFS data of this solution was carried out in the following way.

Performing the Fourier backfiltering over the region around the first peak (from 0.93 Å to 2.69 Å) in the $|F(r)|$ curve, we carried out the curve-fitting analysis by assuming two models; one corresponds to a two-shell model which has a six-coordinated elongated octahedral structure, as has been proposed on the basis of the results of X-ray diffraction,[1,2] while the other corresponds to a one-shell model which has a square-planar structure with four Cu–O_{eq} interatomic distances. In the course of the curve-fitting analysis, the coordination numbers were fixed at 4 for the one-shell model and at 6 (N_{eq}=4, N_{ax}=2) for the two-shell model; ΔE was also fixed at 0.0 eV. On the other hand, the γ value was allowed to vary. The γ value thus obtained changed from 5.0 (which was initially determined by the use of the $Cu(acac)_2$ crystal) to 5.4. The results of the curve-fitting analysis are listed in Table 2. The value of the error-square sum obtained from the two-shell model (7.74) is smaller than that from the one-shell model (24.08). As seen in Table 2, the interatomic distances for the Cu–O_{eq} and Cu–O_{ax} interactions obtained from the two-shell model are 2.00 Å and 2.28 Å respectively; these values are slightly different from those of the results reported by Ohtaki et al.,[1] but almost identical with those reported by Magini.[2] The difference in interatomic distance between the X-ray diffraction studies and our EXAFS data analysis may result from the uncertainties in the backscattering amplitude and phase shift used and those in the EXAFS data. The σ^2 values of the Cu–O_{eq} and Cu–O_{ax} interactions obtained are 0.0036 Å^2 and 0.0105 Å^2 respectively; they are in good agreement with the results obtained by the X-ray diffraction method.[1,14] According to the results reported by Sham et al.,[4] the interatomic distance of the Cu–O_{ax} interaction and the $[\sigma_{ax}^2/\sigma_{eq}^2]$ ratio are 2.60 Å and ca. 10 respectively. These values may be too large compared to the maxima values of the X-ray-diffraction studies (2.5 Å for the interatomic distance of the Cu–O_{ax} interaction[20] and ca. 6.5 for the $[b_{ax}/b_{eq}]$ ratio).[2,14] If the structure parameters obtained by the EXAFS method have the same quality as those obtained by the X-ray-diffraction method, the values obtained by the two methods should be close to each other.

By the theoretical calculation of the $|F(r)|$ curve for the Cu–O_{ax} interaction, which was performed independently of that for the Cu–O_{eq} interaction, the Cu–O_{ax} interaction gave a clear peak in the $|F(r)|$ curve different from that in the observed $|F(r)|$ curve. In the next step, therefore, we performed the radial-distribution analysis of the peaks in the radial-distribution curve in order to examine why the peak due to the Cu–O_{ax} interaction is scarcely seen in the curve and to reconfirm the presence of the peak. Instead of the $|F(r)|$ curve, the $|F'(r)|$ curve was used for the radial-distribution method, which was corrected for the phase shift and the backscattering amplitude. In the course of the radial-distribution analysis, the N_{eq} of the Cu–O_{eq} interaction was fixed at 4, while the γ, R_{eq}, and σ_{eq}^2 values of the Cu–O_{eq} interaction were allowed to vary simultaneously. The optimal γ value thus obtained was 5.4, in good agreement with that obtained by the curve-fitting method. The initial values of the Cu–O_{eq} interaction were 1.94 Å for R_{eq} and 0.004 Å^2 for σ_{eq}^2.

In Figs. 3-A and 3-B, the solid lines show the $|F'(r)|$ curve and the $ImF'(r)$ oscillation respectively. The peak caused by the Cu–O_{ax} interaction is scarcely seen at all in Fig. 3-A. In Fig. 3-B, the $ImF'(r)$ oscillation is slightly asymmetrical along the axis passing through the maximum peak at ca. 2.0 Å; that is, the

Table 2. Structure Parameters Obtained by the Analysis of the EXAFS Data of Solution Samples

Sample	Structure model	U	Interaction	Curve-Fitting			Radial-Distribution		
				N	R	σ^2	N	R	σ^2
1.019 mol dm^{-3} aqueous $Cu(ClO_4)_2$ solution	one-shell	24.08	Cu–O_{eq}	4.0[a]	2.00±0.001	0.0037±0.0002			
	two-shell	7.74	Cu–O_{eq}	4.0[a]	2.00±0.001	0.0036±0.0002	4.0[a]	2.00	0.0037
			Cu–O_{ax}	2.0[a]	2.28±0.005	0.0105±0.0007	1.8	2.28	0.0090
0.996 mol dm^{-3} methanolic $CuCl_2$ solution	two-shell	5.93	Cu–O_{eq}	2.0[a]	2.01±0.001	0.0047±0.0003			
			Cu–Cl_{eq}	2.0[a]	2.22±0.001	0.0059±0.0002			
	three-shell	5.92	Cu–O_{eq}	2.0[a]	2.01±0.001	0.0047±0.0003	2.0[a]	2.00	0.0047
			Cu–Cl_{eq}	2.0[a]	2.22±0.001	0.0059±0.0002	2.0[a]	2.22	0.0059
			Cu–O_{ax}	2.0[a]	2.28±0.711	0.0872±0.2672			

a) Fixed, N: coordination number, R: interatomic distance; Å, σ^2: mean square displacement of R; Å^2, U: error square sum ($=\Sigma[k^3\cdot\bar{\chi}(k)-k^3\cdot\chi_{calcd}(k)]^2$); Å^{-6}.

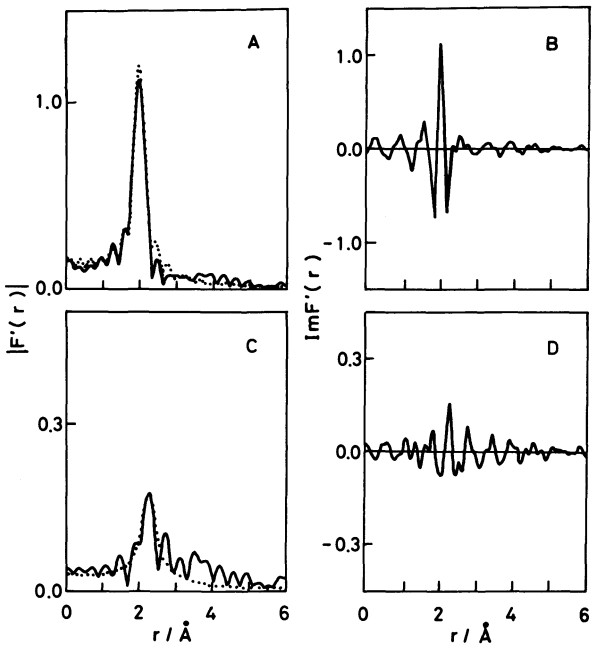

Fig. 3. The corrected radial distribution curves, $|F'(r)|$ and the imaginary parts, $ImF'(r)$ for the aqueous $Cu(ClO_4)_2$ solution. A: $|F'(r)|$ of the $\chi_{obsd}(k)$ (solid line), the $\chi_{calcd}(k)$ of the $Cu-O_{eq}$ interaction (dotted line). B: $ImF'(r)$ of the $\chi_{obsd}(k)$. C: $|F'(r)|$ of the $\chi_{res}(k)$ (solid line), the $\chi_{calcd}(k)$ of the $Cu-O_{ax}$ interaction (dotted line). D: $ImF'(r)$ of the $\chi_{res}(k)$.

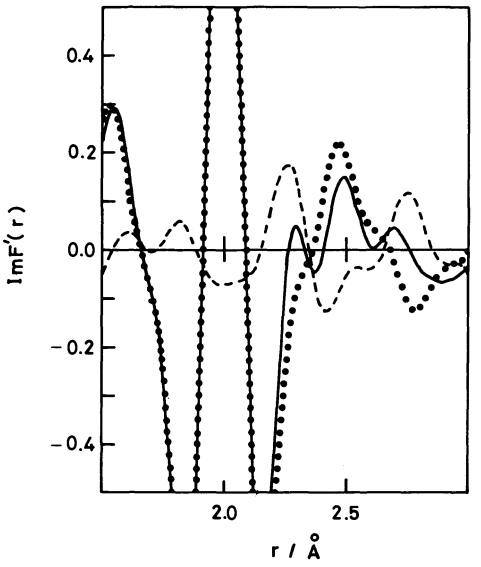

Fig. 4. The imaginary part, $ImF'(r)$ of the corrected Fourier transformed function for the aqueous $Cu(ClO_4)_2$ solution. The $ImF'(r)$ of the $\chi_{obsd}(k)$ (solid line), the $\chi_{calcd}(k)$ of the $Cu-O_{eq}$ interaction (dotted line), and the $\chi_{res}(k)$ (dashed line).

height of the peak at ca. 2.3 Å is lower than that of the peak at ca. 1.6 Å. In Fig. 3-A, the dotted line depicts the $|F'(r)|$ curve of the $\chi_{calcd}(k)$ calculated from the optimal values of the structure parameters of the $Cu-O_{eq}$ interaction. These optimal values were obtained in the r-range below about 2.0 Å in the way described in the Experimental section. When the $|F'(r)|$ curve of the $\chi_{obsd}(k)$ is compared with that of the $\chi_{calcd}(k)$, a small but clear difference is seen at ca. 2.3 Å. To analyze this difference, the residual EXAFS spectrum, $\chi_{res}(k)$, was obtained by subtracting the $\chi_{calcd}(k)$ due to the $Cu-O_{eq}$ interaction from the $\chi_{obsd}(k)$. In Figs. 3-C and 3-D, the solid lines show the $|F'(r)|$ curve and the $ImF'(r)$ oscillation of the $\chi_{res}(k)$ respectively. As the maximum peak of the $ImF'(r)$ oscillation in Fig. 3-D coincided in position with the peak in the $|F'(r)|$ curve in Fig. 3-C, the peak at ca. 2.3 Å can be ascribed to the copper-oxygen interaction. Moreover, from the analysis of this peak, we concluded that this peak was caused by the $Cu-O_{ax}$ interaction, for the coordination number obtained was about 2. Here, the initial values for N_{ax}, R_{ax}, and σ_{ax}^2 were 2, 2.43 Å, and 0.01 Å^2 respectively; they were allowed to vary simultaneously, while γ was fixed at 5.4. In Fig. 3-C, the dotted line shows the $|F'(r)|$ curve of the $\chi_{calcd}(k)$ of the $Cu-O_{ax}$ interaction. The parameter values of this interaction were obtained in the r-range below about 3.0 Å. The results of the radial-distribution method are listed in Table 2. The structure parameters obtained by this method are in good agreement with those obtained by means of the curve-fitting method.

The results of the radial-distribution method were as follows: in the case of the EXAFS spectrum corresponding to two interactions or more, the observed $ImF'(r)$ (or $ReF'(r)$) is the sum of all the $ImF'(r)$ (or $ReF'(r)$) values. If an EXAFS spectrum comes from two interactions, and if the $ImF'(r)$ oscillation due to one interaction has a sign opposite from that of the other interaction at the position of the maximum peak in the latter $ImF'(r)$ oscillation, the latter $ImF'(r)$ oscillation is reduced by the former one. Figure 4 shows the $ImF'(r)$ oscillations of the $\chi_{obsd}(k)$ (solid line), the $\chi_{calcd}(k)$ of the $Cu-O_{eq}$ interaction (dotted line),[15] and the $\chi_{res}(k)$ (dashed line). At ca. 2.3 Å, the dashed line depicts a larger positive peak than that of the solid line, for the dashed line was obtained by subtracting the dotted line (largely negative) from the solid line (barely positive). From a comparison of the $ImF'(r)$ oscillations, we can conclude that the $ImF'(r)$ oscillation due to the $Cu-O_{ax}$ interaction is diminished at the position of the peak due to the $Cu-O_{ax}$ interaction in the radial-distribution curve by the interference of the $ImF'(r)$ oscillation due to the $Cu-O_{eq}$ interaction; consequently, the peak caused by the $Cu-O_{ax}$ interaction can scarcely be seen in the radial-distribution curve.

Methanolic $CuCl_2$ Solution. The $k^3 \cdot \chi_{obsd}(k)$ value and the $|F(r)|$ curve for the 0.996 mol dm^{-3} methanolic $CuCl_2$ solution are shown in Figs. 2-C and 2-D

respectively. According to the results of an X-ray-diffraction study of the methanolic $CuCl_2$ solution,[9] the interatomic distances of the Cu–O_{eq}, Cu–Cl_{eq}, and Cu–O_{ax} interactions are very similar; hence, the corresponding peaks overlap with one another in the radial-distribution function, $D(r)$. However, the $|F(r)|$ curve for the methanolic $CuCl_2$ solution seems to show a double peak in Fig. 2-D. When two back-scattering shells consist of the same number of atoms, but of different kinds, these two distinct absorber-scatterer distances should be resolvable in the $|F(r)|$ curve as separate peaks. Therefore, the peak at ca. 1.9 Å can be attributed to the Cu–Cl interaction, because the position of this peak is close to that in the reference $[(CH_3)_4N]_2[CuCl_4]$ crystal (1.86 Å). Moreover, the shoulder at ca. 1.6 Å of this double peak may be ascribed to the interaction between copper and methanol oxygen atoms at the equatorial site, because the position of this shoulder is close to that in the reference $Cu(acac)_2$ crystal. Similarly to the aqueous $Cu(ClO_4)_2$ solution, the peak due to the Cu–O_{ax} interaction in this solution could scarcely be seen in the $|F(r)|$ curve as a separate peak. Therefore, performing the Fourier backfiltering over the region around this double peak (from 0.95 Å to 3.00 Å), we carried out the curve-fitting analysis by assuming two models; one was a three-shell model which had the same six-coordinated elongated octahedral structure as the results of the X-ray diffraction investigation,[9] while the other was a two-shell model which had a four-coordinated structure with two Cu–O and two Cu–Cl interatomic distances. In the course of the curve fitting, the coordination numbers for those interactions were fixed at 2. The results of the curve-fitting analysis are listed in Table 2. As may be seen in Table 2, the curve-fitting analysis of these two models gave similar error-square sums. Therefore, at this step, we could not conclude whether or not the average structure of the mixed-ligand copper(II) complexes in this solution was an elongated octahedron. The radial-distribution method was, therefore, used for the analysis of this solution.

In the course of the radial-distribution analysis, the coordination numbers for both Cu–O_{eq} and Cu–Cl_{eq} interactions were fixed at 2, while the γ, R, and σ^2 values for each interaction were allowed to vary. The initial values of the Cu–Cl_{eq} interaction were 2.22 Å for R and 0.006 Å^2 for σ^2. In Figs. 5-A and 5-B, the solid lines show the $|F'(r)|$ curve and the $ImF'(r)$ oscillation of the $\chi_{obsd}(k)$ value respectively. The γ value changed from 5.0 (initially determined by the $[(CH_3)_4N]_2[CuCl_4]$ crystal) to 5.4. The Cu–O_{eq} bond length may differ by only ca. 0.2 Å from the Cu–Cl_{eq} one, and the Cu–Cl_{eq} and Cu–O_{ax} interatomic distances are very close to each other; therefore, we first estimated the structure parameters for the Cu–Cl_{eq} interaction because the peak due to the

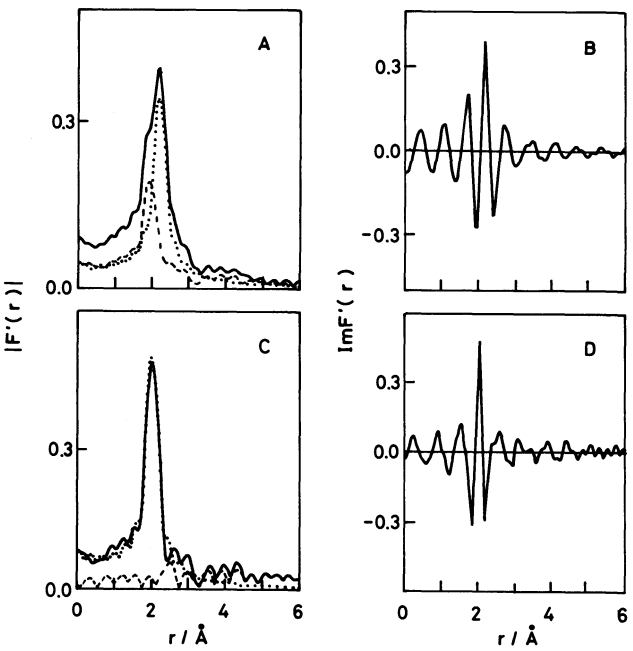

Fig. 5. The corrected radial distribution curves, $|F'(r)|$ and the imaginary parts, $ImF'(r)$ for the methanolic $CuCl_2$ solution. A: $|F'(r)|$ of the $\chi_{obsd}(k)$ (solid line), the $\chi_{calcd}(k)$ of the Cu–Cl_{eq} interaction (dotted line), and the $\chi_{res}(k)$ (dashed line). B: $ImF'(r)$ of the $\chi_{obsd}(k)$. C: $|F'(r)|$ of the $\chi_{res}(k)$ (solid line), the $\chi_{calcd}(k)$ of the Cu–O_{eq} interaction (dotted line), and the $\chi_{rem}(k)$ (dashed line). D: $ImF'(r)$ of the $\chi_{res}(k)$.

Cu–Cl_{eq} interaction was larger and clearer than those due to other interactions. Figure 5-A shows the $|F'(r)|$ curves of the $\chi_{calcd}(k)$ of Cu–Cl_{eq} interaction (dotted line) and the $\chi_{res}(k)$ (dashed line). The structural parameter values of the Cu–Cl_{eq} interaction were obtained in the r-range from ca. 2.0 Å to ca. 3.0 Å. In the $|F'(r)|$ curve of the $\chi_{res}(k)$, there existed a clear peak at ca. 2.0 Å (dashed line). From the value of this peak-position, the main contribution to this peak can be attributed to the Cu–O_{eq} interaction. Therefore, the initial values for the analysis of this peak were 1.95 Å for R and 0.004 Å^2 for σ^2. The γ value was fixed at 5.4, while R and σ^2 were allowed to vary. Figures 5-C and 5-D depict the $|F'(r)|$ curve (solid line) and the $ImF'(r)$ oscillation of the $\chi_{res}(k)$ value respectively. In Fig. 5-C, the dotted line shows the $|F'(r)|$ curve of the $\chi_{calcd}(k)$ of Cu–O_{eq} interaction, while the dashed line shows that of the remaining EXAFS spectrum, $\chi_{rem}(k)$, which is yielded by subtracting the $\chi_{calcd}(k)$ of the Cu–O_{eq} interaction from the $\chi_{res}(k)$ value. The parameter values of the Cu–O_{eq} interaction were obtained in the r-range below about 2.0 Å. A small peak around 2.4 Å in the $|F'(r)|$ curve of the $\chi_{rem}(k)$ was analyzed using the initial values of N(=2), R(=2.4 Å), and σ^2(=0.01 Å^2), where γ was fixed at 5.4, while N, R, and σ^2 were allowed to vary. The coordination number obtained

from this analysis (in the r-range from 2.2 Å to 2.6 Å) was not more than 0.3; therefore, we could not conclude that this small peak is caused by the $Cu-O_{ax}$ interaction. The results of the radial-distribution method are listed in Table 2, without the values of the $Cu-O_{ax}$ interaction.

The results obtained by the use of this method for the equatorial interactions are in good agreement with those obtained by the use of the curve-fitting method, and the values of the structure parameters obtained from both methods support well those of the X-ray diffraction study.[9] However, neither method showed any clear evidence of the $Cu-O_{ax}$ interactions of the mixed-ligand chlorocopper(II) complexes in this solution, in contrast to that of the hexaaquacopper(II) complex in the aqueous $Cu(ClO_4)_2$ solution; therefore, we could not determine whether or not the average structure of the copper(II) complexes in this solution is an elongated octahedron. Presumably, this fact results from the $Cu-Cl_{eq}$ bond length in this solution, which is very close to the $Cu-O_{ax}$ bond length, also, the former bond contributes to a large extent to the EXAFS spectrum, while the $Cu-O_{ax}$ interactions in this solution contribute to the spectrum to only a small extent. Accordingly, it might be difficult to analyze such a small contribution as that of the $Cu-O_{ax}$ interaction in this solution by means of the radial-distribution method, because the estimated errors for the structure parameters, i.e., N, R, and σ^2, of an interaction increase with an increase in the number of peaks caused by other interactions which should be subtracted.

The present EXAFS data analyses by using both methods gave similar results. The radial-distribution method is able to show an anticipated and clear peak in the $|F'(r)|$ curve as evidence of the interaction, which is diminished by the interference of other interactions. Consequently, a combined use of these two methods seems useful for further EXAFS analysis.

Sham et al.[4] explained that the diminishment of the peak due to the $Cu-O_{ax}$ interaction in an aqueous $Cu(ClO_4)_2$ solution results from the interaction having a large σ value. However, a preferable explanation may be that the diminishment of the peak due to the $Cu-O_{ax}$ interaction is caused by the interference between the imaginary and real parts of the Fourier-transformed function of the $Cu-O_{ax}$ interaction and those of the $Cu-O_{eq}$ interaction.

The authors are grateful to Professor Hitoshi Ohtaki and Dr. Toshio Yamaguchi for their valuable discussion and advice. The authors also wish to thank to Dr. Masaharu Nomura for his help and advice in the EXAFS measurements.

References

1) H. Ohtaki and M. Maeda, *Bull. Chem. Soc. Jpn.*, **47**, 2197 (1974).
2) M. Magini, *Inorg. Chem.*, **21**, 1535 (1982).
3) H. Ohtaki, T. Yamaguchi, and M. Maeda, *Bull. Chem. Soc. Jpn.*, **49**, 701 (1976).
4) T. K. Sham, J. B. Hastings, and M. L. Perlman, *Chem. Phys. Lett.*, **83**, 391 (1981).
5) M. Sano, K. Taniguchi, and H. Yamatera, *Chem. Lett.*, **1980**, 1285.
6) M. Sano, T. Maruo, and H. Yamatera, *Bull. Chem. Soc. Jpn.*, **56**, 3287 (1983).
7) M. Magini, *J. Chem, Phys.*, **74**, 2523 (1981).
8) M. Ichihashi, H. Wakita, T. Mibuchi, and I. Masuda, *Bull. Chem. Soc. Jpn.*, **55**, 3160 (1982).
9) M. Ichihashi, H. Wakita, and I. Masuda, *Bull. Chem. Soc. Jpn.*, **56**, 3761 (1983).
10) G. Galli, G. Maisano, P. Migliardo, C. Vasi, F. Wanderlingh, and M. P. Fontana, *Solid State Commun.*, **42**, 213 (1982).
11) This method was not named in their papers, but one of the authors, J. B. A. D. van Zon, called this "modelling" in his Ph. D. Thesis. From the classification of the analytical methods of the EXAFS spectra, we call this method the "radial-distribution method" in this paper; T. Yokoyama, *Kagaku To Kogyo*, **38**, 631 (1985); H. F. J. van't Blik, J. B. A. D. van Zon, T. Huizinga, J. C. Vis, D. C. Koningsberger, and R. Prins, *J. Phys. Chem.*, **87**, 2264 (1983); J. B. A. D. van Zon, D. C. Konigsberger, H. F. J. van't Blik, R. Prins, and D. E. Sayers, *J. Chem. Phys.*, **80**, 3914 (1984); H. F. J. van't Blik, J. B. A. D. van Zon, D. C. Koningsberger, and R. Prins, *J. Mol. Catal.*, **25**, 379 (1984); J. B. A. D. van Zon, Ph. D. Thesis, Eindhoven University of Technology, Eindhoven, The Netherlands (1984).
12) For details of the data treatments, refer to the following literature: I. Masuda, H. Wakita, Y. Tajiri, and M. Ichihashi, *Fukuoka Univ. Sci. Rep.*, **13**, 63 (1983); H. Wakita, Y. Tajiri, and S. Yamashita, *Fukuoka Univ. Sci. Rep.*, **15**, 109 (1985).
13) D. E. Sayers, E. A. Stern, and F. W. Lytle, *Phys. Rev. Lett.*, **27**, 1204 (1971); E. A. Stern, *Phys. Rev.*, **B10**, 3027 (1974).
14) We assumed that the σ value is equivalent to the root mean-square-amplitude, $\langle\Delta r\rangle$, of the X-ray diffraction method, as $\sigma=\langle\Delta r\rangle$ and $b=\sigma^2/2$, where b is the temperature factor of the X-ray diffraction method.
15) Strictly speaking, the symmetry of the main peak in the $|F'(r)|$ curve and that of the $ImF'(r)$ oscillation had been slightly broken by the truncation effect of the Fourier transform; P. A. Lee and G. Beni, *Phys. Rev.*, **B15**, 2862 (1977).
16) B. K. Teo, P. A. Lee, A. L. Simons, P. Eisenberger, and B. M. Kincaid, *J. Am. Chem. Soc.*, **99**, 3854 (1977).
17) P. A. Lee, B. K. Teo, and A. L. Simons, *J. Am. Chem. Soc.*, **99**, 3856 (1977).
18) H. Koyama, Y. Saito, and H. Kuroya, *J. Inst. Polytech. Osaka City Univ.*, **C4**, 43 (1953).
19) B. Morosin and E. C. Lingafelter, *J. Phys. Chem.*, **65**, 50 (1961).
20) H. Ohtaki, "Youeki Kagaku," Shokabo, Tokyo (1985), p. 143.

 © 1986 The Chemical Society of Japan Bull. Chem. Soc. Jpn., 59, 2293—2297 (1986)

Kinetics and Mechanism of the Extraction of Nickel(II) with 3-Mercapto-1,5-Diphenylformazan in the Presence of 1,10-Phenanthroline or Pyridine

Kousaburo OHASHI,* Hidetoshi SHOJI, and Katsumi YAMAMOTO
Department of Chemistry, Faculty of Science, Ibaraki University, Mito 310
(Received February 7, 1986)

The kinetics and mechanism of the extraction of nickel(II) with 3-mercapto-1,5-diphenylformazan (dithizone, Hdz) into chloroform in the presence of 1,10-phenanthroline (phen) or pyridine (py) were studied in the presence of 0.1 mol dm^{-3} or 0.2 mol dm^{-3} $NaNO_3$ at 25 °C. For the nickel(II)–dithizone–1,10-phenanthroline system, the rate-determining steps were the competitive reactions of nickel(II) with dithizonate and with 1,10-phenanthroline in an aqueous phase. The second-order rate constants for the formation of $[Ni(dz)]^+$ and of $[Ni(phen)]^{2+}$ were determined to be $(6.0\pm0.4)\times10^3$ mol^{-1} dm^3 s^{-1} and $(3.4\pm0.2)\times10^3$ mol^{-1} dm^3 s^{-1} respectively. It was suggested that $[Ni(phen)]^{2+}$ is more reactive toward dithizonate than toward 1,10-phenanthroline in an aqueous phase. The formation of $[Ni(phen)_2]^{2+}$ retards the extraction of nickel(II) with dithizone. For the nickel(II)–dithizone–pyridine system, the rate-determining step is probably the reaction of $[Ni(py)]^{2+}$ with dithizonate in an aqueous phase. The second-order rate constant for this reaction was determined to be $(1.7\pm0.3)\times10^5$ mol^{-1} dm^3 s^{-1}.

From the point of view of a selective separation and sensitive determination of metal ions, the synergistic extraction is a remarkably interesting method.[1–4]

Dithizone reacts with many metal ions to give solvent-extractable and highly colored metal complexes, whereas this extractant is less selective for metal ions. The selectivity for the extraction of metal ions with dithizone was improved by the addition of pyridine or 1,10-phenanthroline. For example, cadmium(II) was predominantly separated and determined from a mixture of cadmium(II) and zinc(II) with dithizone in the presence of 1,10-phenanthroline.[5] The extraction of nickel(II) with dithizone in the presence of 1,10-phenanthroline gave an intensely pink adduct, $[Ni(dz)_2(phen)]$, absorbing strongly in the visible range around 520 nm with a molar extinction coefficient of about 5×10^4 mol^{-1} dm^3 cm^{-1}. The above development was utilized for the sensitive determination of nickel(II).[6,7] At a pH lower than 6.0, the extraction rate of $[Ni(dz)_2]$ into chloroform is very small, but it is remarkably accelerated by the addition of 1,10-phenanthroline. In order to clarify the mechanism of the synergistic extraction of the nickel(II) ion with dithizone in the presence of 1,10-phenanthroline or of pyridine, kinetic studies of this method were carried out. The rate-determining step of the extraction of nickel(II) with dithizone was the formation of $[Ni(dz)]^+$ in an aqueous phase.[8–10] On the other hand, the rate-determining steps of synergistic extraction were found to be the competitive extraction of nickel(II) with dithizonate and that with 1,10-phenanthroline in an aqueous phase.

Experimental

Apparatus. For the determinations of the rates of the extraction reactions, the high-stirring apparatus was used.[11] An Iwaki KM shaker was used for shaking a solution in order to study the extraction equilibrium. A Hitachi 170-30 atomic absorption spectrophotometer was used for the determination of the nickel(II) ion in an aqueous phase. A Hitachi 101 spectrophotometer was used for the measurements of the absorbances of $[Ni(dz)_2(phen)]$. All the pH measurements were carried out with a Hitachi-Horiba F-7 pH meter.

Reagents. A 3-mercapto-1,5-diphenylformazan (dithizone) (Kanto Chemical Co., Inc.) was purified according to the method described in a preceding paper.[12] The chloroform solution of dithizone was prepared by dissolving a weighed amount of dithizone into chloroform just before use.

The nickel(II) stock solution was prepared by dissolving a given amount of nickel(II) nitrate hexahydrate in water. A stock solution of 1,10-phenanthroline was prepared by dissolving the weighed amount of reagent-grade 1,10-phenanthroline (Kanto Kagaku) in chloroform. Spectrophotometric-grade pyridine (Kanto Kagaku) was used without purification.

The chloroform was distilled and treated with $NH_2OH\cdot2HCl$ at pH 8 just before use.

All the other chemicals used were of a reagent-grade quality. Sodium nitrate was used to adjust the ionic strength to 0.10 mol dm^{-3} and 0.20 mol dm^{-3} for the nickel(II)–dithizone–1,10-phenanthroline and nickel(II)–dithizone–pyridine systems respectively. A potassium dihydrogenphosphate–sodium hydroxide buffer solution was used to adjust the pH of the aqueous solution. The concentration of potassium dihydrogenphosphate for the nickel(II)–dithizone–1,10-phenanthroline and nickel(II)–dithizone–pyridine systems were adjusted to 0.01 mol dm^{-3} and 0.1 mol dm^{-3} respectively.

Procedure for the Kinetics of the Extraction. The kinetics was carried out under the pseudo-first order conditions, in which dithizone is present in a large excess with respect to the nickel(II) ion. One hundred-cm^3 portions of an aqueous solution containing nickel(II) and of a phosphate buffer solution were placed in a three-necked flask. Then, a 100-cm^3 portion of a chloroform solution of dithizone containing 1,10-phenanthroline or of

pyridine was added carefully using a funnel. Before mixing, both of the solutions were thermostated at 25 °C. The solutions were vigorously stirred, and then equal volumes of two phases were removed in a test tube for a definite time interval. Each sample was centrifuged to separate the phases. The nickel(II) ion in an aqueous phase was determined by means of atomic-absorption spectrophotometry. After stirring, the pH value of an aqueous phase was measured. For the nickel(II)–dithizone–1,10-phenanthroline system, the change of the pH in an aqueous phase during the extraction reaction was within ±0.01 pH unit. The extractions were done at a constant stirring speed of 1500 rpm, because the extraction rate was independent of the stirring speed in the range greater than 1500 rpm.

Procedure for the Extraction Equilibrium. A 25-cm^3 portion of an aqueous phase containing the nickel(II) ion and a 25-cm^3 portion of a chloroform solution containing dithizone and 1,10-phenanthroline were placed in a separatory funnel. The solutions were then shaken vigorously by using an automatic shaker. After phase-separation, the nickel(II) ion remaining in an aqueous phase was determined. For nickel(II)–dithizone–pyridine, we used almost the same procedure as for nickel(II)–dithizone–1,10-phenanthroline.

Distribution Constant of 1,10-Phenanthroline. The distribution constant of 1,10-phenanthroline, K_D between chloroform and water was determined to be (1.1±0.08)×10^3 at 25 °C and I=0.10 mol dm^{-3} ($NaNO_3$) by using the same procedure as was used for dithizone.[9]

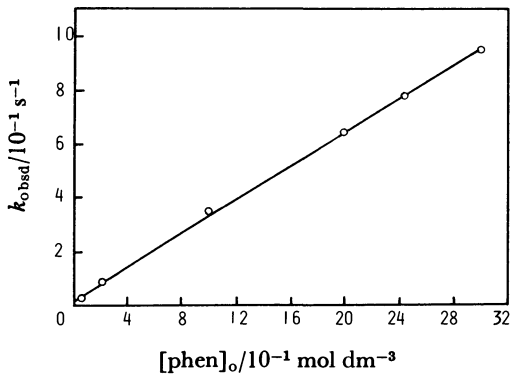

Fig. 1. Relationship between k_{obsd} and 1,10-phenanthroline concentration in the organic phase. [Ni^{2+}]: 1.90×10^{-5} mol dm^{-3}; [Hdz]: 4.80×10^{-4} mol dm^{-3}; pH: 6.0; 25 °C; I: 0.1 mol dm^{-3} ($NaNO_3$).

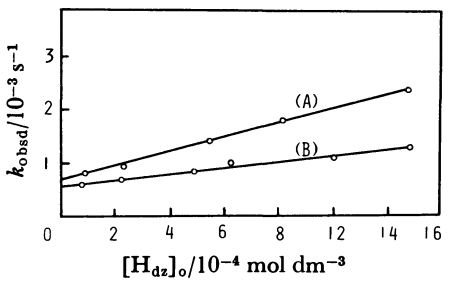

Fig. 2. Relationship between k_{obsd} and dithizone concentration. [phen]: 2.00×10^{-4} mol dm^{-3}; I: 0.1 mol dm^{-3} ($NaNO_3$); (A): pH 6.5; (B): pH 6.0.

The Kinetics of the Extraction of [Ni(dz)$_2$(phen)]. The relationship between log [Ni^{2+}]$_t$ and the extracting time appeared linear. The rate of the extraction of nickel(II) with dithizone in the presence of 1,10-phenanthroline was found to be first-order with respect to the nickel(II) ion. The pseudo first-order rate constant, k_{obsd}, was obtained by plotting log [Ni^{2+}]$_t$ vs. the time, where [Ni^{2+}]$_t$ represents the nickel(II) ion in the aqueous phase at a given time.

As is shown in Fig. 1, a plot of k_{obsd} vs. [phen]$_o$ in the chloroform phase gives a straight line with an intercept. In addition, the value of k_{obsd}, as is shown in Fig. 2, increases linearly with an increase in the dithizone concentration at a given 1,10-phenanthroline concentration. These findings suggest that the rate-determining reactions proceed through two parallel paths in an aqueous phase. One is the reaction between nickel(II) and 1,10-phenanthroline. The other is the reaction of nickel(II) with dithizone.

The rate-determining step for the extraction reaction of nickel(II) with dithizone is the reaction of nickel(II) with dithizonate, dz$^-$, in an aqueous phase. The second-order rate constant, k (rate=k [Ni^{2+}] [dz$^-$]), has been reported to be 6.1×10^3 mol^{-1} dm^3 s^{-1} at 25 °C and I=0.10 mol dm^{-3}.[9]

If they are similar to the extraction of nickel(II) with dithizone, the rate-determining reactions of the synergistic extraction occur in an aqueous phase, and the rate law for the extraction of nickel(II) with dithizone–1,10-phenanthroline system can be expressed by:

$$\frac{-d[Ni^{2+}]}{dt} = k_{phen}[Ni^{2+}][phen]_w + k_{Hdz}[Ni^{2+}][dz^-]_w. \quad (1)$$

The pseudo first-order rate constant, k_{obsd}, is represented by:

$$k_{obsd} = k_{phen}K_D{}^{phen\text{-}1}[phen]_o + k_{Hdz}K_a{}^{Hdz}[Hdz]_o[H^+]^{-1} \quad (2)$$

where k_{phen} and k_{Hdz} are the second-order rate constant, and where $K_D{}^{phen}$ (=1.1×10^3 at 25 °C) is the distribution constant of 1,10-phenanthroline between chloroform and water. A 1,10-phenanthroline species distributed into water at pH 6.0 should be predominantly present as a neutral form because of the pK_a of 4.92.[13] The value of k_{Hdz} was determined to be (6.0±0.4)×10^3 mol^{-1} dm^3 s^{-1} by using the value of the intercept in Fig. 1 and the following constants: $K_a{}^{Hdz}$=4.90×10^{-5} mol dm^{-3} [12] and $K_D{}^{Hdz}$=7.94×10^5 mol dm^{-3}.[12] The k_{Hdz} value thus obtained is approximately equal to that obtained in the previous work within the limits of experimental error.[9] The k_{phen} value was calculated to be (3.4±0.2)×10^3 mol^{-1} dm^3 s^{-1} by using $K_D{}^{phen}$=1.1×10^3 and the slope of a plot of log k_{obsd} vs. [phen]$_o$ (Fig. 1). The k_{phen} value thus obtained agrees satisfactorily with the second-order rate constant for the formation of [Ni(phen)]$^{2+}$ in an aqueous phase in the absence of dithizone.[14] The k_{Hdz} and k_{phen} values calculated from the intercept and the slope in Fig. 2 were in good agreement with the k_{Hdz} and k_{phen} values respectively obtained from the data shown in Fig. 1. Judging from these results, the first reaction of the synergistic extraction should take place in an aqueous phase. When 1,10-phenanthroline is present in a large excess to dithizone at pH 6.0, the reaction schemes in an aqueous phase are represented as follows:

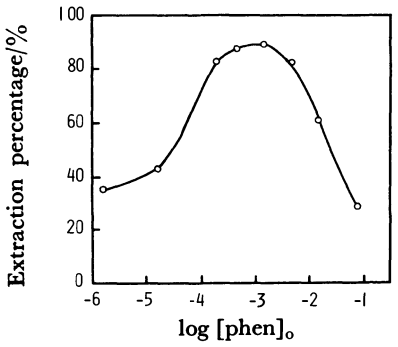

Fig. 3. Relationship between extraction percentage and 1,10-phenanthroline concentration in the presence of dithizone. [Ni^{2+}]: 1.90×10^{-5} mol dm^{-3}; [Hdz]: 4.80×10^{-4} mol dm^{-3}; pH 6.0; Shaking time: 30 min; I: 0.1 mol dm^{-3} ($NaNO_3$).

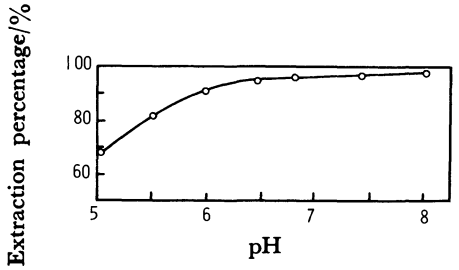

Fig. 4. Relationship between extraction percentage and pH. [Ni^{2+}]: 1.90×10^{-5} mol dm^{-3}; [Hdz]: 4.80×10^{-4} mol dm^{-3}; [phen]: 1.60×10^{-3} mol dm^{-3}; 25 °C; Shaking time: 30 min; I: 0.1 mol dm^{-3} ($NaNO_3$).

$$Ni^{2+} + phen \xrightarrow{slow} [Ni(phen)]^{2+} \quad (3)$$

$$[Ni(phen)]^{2+} + dz^- \xrightarrow{fast} [Ni(phen)(dz)]^+ \quad (4)$$

$$[Ni(phen)(dz)]^+ + dz^- \xrightarrow{fast} [Ni(phen)(dz)_2] \quad (5)$$

The reaction of $[Ni(phen)]^{2+}$ with 1,10-phenanthroline should not occur in the presence of dithizone, because $[Ni(phen)_2]^{2+}$ does not react with dithizone. The extraction of nickel(II) with dithizone takes place at a lower pH range in the presence of 1,10-phenanthroline. The acceleration effect of 1,10-phenanthroline was ascribed to the rapid formation of $[Ni(phen)]^{2+}$, based on the small K_D^{phen} value compared with the K_D^{Hdz} value, and on the lower reactivity of $[Ni(phen)]^{2+}$ toward 1,10-phenanthroline than toward dithizonate. When dithizone is in excess to 1,10-phenanthroline at pH 6.0, the following reactions should be added to Reactions (3)—(5):

$$Ni^{2+} + dz^- \xrightarrow{slow} [Ni(dz)]^+ \quad (6)$$

$$[Ni(dz)]^+ + dz^- \xrightarrow{fast} [Ni(dz)_2] \quad (7)$$

$$[Ni(dz)]^+ + phen \xrightarrow{fast} [Ni(dz)(phen)]^+ \quad (8)$$

$$[Ni(dz)_2] + phen \xrightarrow{fast} [Ni(dz)_2(phen)] \quad (9)$$

At pH 8.0, the predominant reaction path may be Reaction (6) because of the high concentration of the dithizonate distributed into an aqueous phase, even when an excess of 1,10-phenanthroline is present.

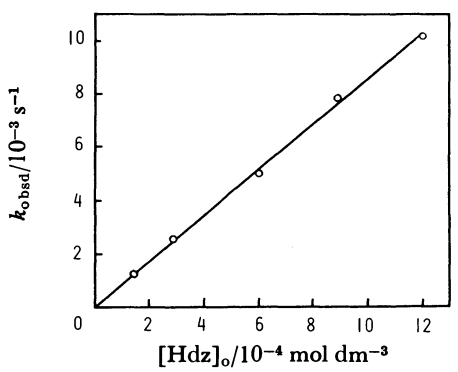

Fig. 5. Relationship between k_{obsd} and dithizone concentration. [Ni^{2+}]: 1.90×10^{-5} mol dm^{-3}; [py]: 0.20 mol dm^{-3}; pH: 6.0; 25 °C, I: 0.20 mol dm^{-3} ($NaNO_3$).

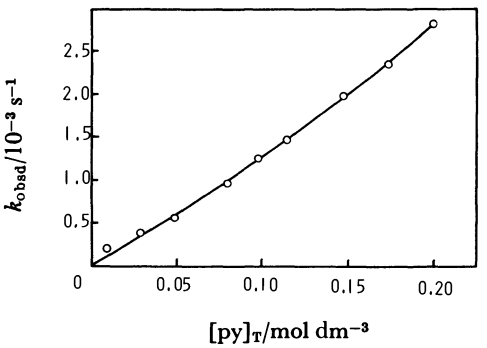

Fig. 6. Relationship between k_{obsd} and pyridine concentration. [Ni^{2+}]: 1.90×10^{-5} mol dm^{-3}; [py]: 0.2 mol dm^{-3}; pH: 6.0; 25 °C; I: 0.20 mol dm^{-3} ($NaNO_3$).

Reactions (6)—(8) should take place in an aqueous phase. The formation reaction of $[Ni(dz)_2(phen)]$ may occur in an aqueous phase and/or in an organic phase.

The effect of the 1,10-phenanthroline concentration and of the pH on the extraction of nickel(II) are shown in Figs. 3 and 4 respectively. The extraction percentage increases with an increase in the 1,10-phenanthroline concentration and the pH. In the presence of more than 1×10^{-3} mol dm^{-3} of 1,10-phenanthroline at pH 6.0, the extraction percentage decreases with an increase in the concentration of 1,10-phenanthroline. The small extraction percentage is probably to be ascribed to the formation of $[Ni(phen)_2]^{2+}$.

The Kinetics of the Extraction of $[Ni(dz)_2(py)]$. The relationship between the pseudo first-order rate constant, k_{obsd}, and the concentration of dithizone, as shown in Fig. 5, gives a straight line without an intercept, indicating that the extraction rate is first-order with respect to the concentration of dithizone. Though a plot of k_{obsd} vs. the concentration of pyridine does not give a straight line, the extraction rate increases with an increase in the concentration of pyridine (Fig. 6).

The effect of the pH on the rate for the extraction reaction of nickel(II) with dithizone in the presence of pyridine is represented by Curve (A) of Fig. 7. The dotted line (Curve (B) in Fig. 7) shows the theoretical line calculated by assuming that the rate-determining step of the extraction of nickel(II) with dithizone in the absence of pyridine is the reaction of nickel(II) with dithizonate in an

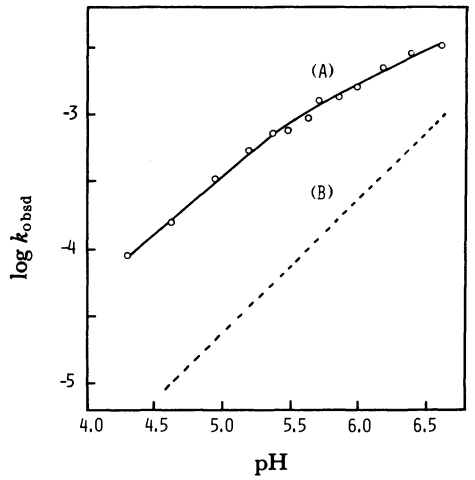

Fig. 7. Relationship between k_{obsd} and pH. [Ni^{2+}]: 1.90×10^{-5} mol dm^{-3}; [Hdz]: 8.90×10^{-4} mol dm^{-3}; [py]: 0.10 mol dm^{-3}; 25 °C; I: 0.20 mol dm^{-3} ($NaNO_3$). (A): Experimental curve; (B): Theoretical curve.

aqueous phase reacts with nickel(II) to form a nickel(II)-pyridine complex, $Ni(py)_n^{2+}$, prior to the extraction of nickel(II) with dithizone. The step-by-step stability constants of $Ni(py)_n^{2+}$ have been reported to be K_1= 8.32×10,[15] K_2=7.08,[15] K_3=3.98,[15] and K_4=1.35.[15] The K_5 and K_6 values, which are unavailable, must be very small. If the rate-determining reaction is the reaction of dithizonate with $[Ni(py)_n]^{2+}$ (n=0—4) in an aqueous phase, the rate equation can be represented by Eq. 10:

$$\frac{-d[Ni^{2+}]}{dt} = \{k_0[Ni^{2+}]+k_1[Ni(py)^{2+}]+k_2[Ni(py)_2^{2+}] + k_3[Ni(py)_3^{2+}]+k_4[Ni(py)_4^{2+}]\}[dz^-] \quad (10)$$

where k_0, k_1, k_2, k_3, and k_4 are the second-order rate constants. The pseudo first-order rate constant is represented as follows:

$$k_{obsd} = \{k_0+k_1K_1\beta+k_2K_1K_2\beta^2+k_3K_1K_2K_3\beta^3+k_4K_1K_2K_3K_4\beta^4\} \times \left\{\frac{K_a^{Hdz}\cdot[Hdz]_0}{A\cdot[H^+]\cdot K_D^{Hdz}}\right\} \quad (11)$$

where $A=1+K_1\beta+K_1K_2\beta^2+K_1K_2K_3\beta^3+K_1K_2K_3K_4\beta^4$, $\beta=[py]_T\{1+K_D^{py}+[H^+]/K_a^{py}\}^{-1}$. The values of $K_a^{Hdz}/A[H^+]$, $K_1\beta K_a^{Hdz}/A\cdot[H^+]$, $K_1K_2\beta^2K_a^{Hdz}/A\cdot[H^+]$, $K_1K_2K_3\beta^3K_a^{Hdz}/A\cdot[H^+]$, and $K_1K_2K_3K_4\beta^4K_a^{Hdz}/A\cdot[H^+]$ were calculated by introducing the following constants: K_D^{py}=0.80,[16] K_a^{py}= 5.89×10^{-6},[17] K_a^{Hdz}=4.90×10^{-5},[12] and K_D^{Hdz}=7.94×10^5,[12] Equation 11 shows that a plot of k_{obsd} vs. $[Hdz]_0$ should provide a straight line and that the rate is not first-order with respect to pyridine and the hydrogen-ion concentration. As is shown in Figs. 6 and 7, the results satisfy the above conditions. The value of k_1 which best fitted the log k_{obsd}-pH curve was found to be $(1.7\pm0.3)\times10^5$ mol^{-1} dm^3 s^{-1} at 25 °C. The value of k_0 was independently determined to be $(3.0\pm0.2)\times10^3$ mol^{-1} dm^3 s^{-1} at 0.1 mol dm^{-3} potassium dihydrogenphosphate. The value of k_2 is estimated to be $(1\pm0.8)\times10^4$ mol^{-1} dm^3 s^{-1}. It is safe to conclude that the values of k_3 and k_4 are negligibly smaller than the k_2 value. Also, the paths of the reactions of $[Ni(py)_5]^{2+}$ and

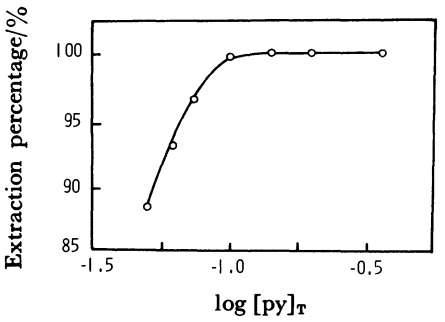

Fig. 8. Relationship between extraction percentage and pyridine concentration. [Ni^{2+}]: 1.90×10^{-5} mol dm^{-3}; [Hdz]: 4.80×10^{-4} mol dm^{-3}; pH 6.9; Shaking time: 30 min.

$[Ni(py)_6]^{2+}$ with dz^- should be omitted. On the base of these results, the reaction scheme for the synergistic extraction of nickel(II) with dithizone-pyridine can be represented by:

$$Ni^{2+} + py \xrightarrow{fast} [Ni(py)]^{2+} \quad (12)$$

$$[Ni(py)]^{2+} + dz^- \xrightarrow{slow} [Ni(dz)(py)]^+ \quad (13)$$

$$[Ni(dz)(py)]^+ + dz^- \xrightarrow{fast} [Ni(dz)_2(py)] \quad (14)$$

As the reactivity of $[Ni(py)]^{2+}$ toward dz^- was found to be about 60 times larger than that of aqua Ni^{2+} toward dz^-, the acceleration effect of pyridine on the extraction of nickel(II) with dithizone was ascribed to the formation of $[Ni(py)_n]^{2+}$.[3] It was suggested that the rate-determining step for the extraction of nickel(II) with thenoyltrifluoroacetone (tta) in the presence of pyridine was the reaction of tta with aqua Ni^{2+} and $[Ni(py)]^{2+}$ in the pH range from 1.5 to 3.9.[18] These facts further support the mechanism proposed for the extraction of nickel(II) with dithizone-pyridine.

Figure 8 represents the effect of the pyridine concentration on the extraction percentage of nickel(II) with dithizone into chloroform. In the presence of more than 0.1 mol dm^{-3} of pyridine, the complete extraction of nickel(II) was achieved with 4.8×10^{-4} mol dm^{-3} of dithizone at pH 6.9. Pyridine does not mask the extraction of nickel(II) with dithizone, even when pyridine is present in a large excess to dithizone.

As has been shown above, the rate-determining steps for the nickel(II)-dithizone-1,10-phenanthroline and nickel(II)-dithizone-pyridine systems are different from each other. This difference should result in a difference in the distribution constant between pyridine and 1,10-phenanthroline. The coordination of pyridine or 1,10-phenanthroline to the aqua nickel(II) ion probably facilitates the removal of water molecules from the central nickel(II) ion, hence accelerating the extraction rate of nickel(II) with dithizone in the presence of 1,10-phenanthroline or pyridine.

1,10-Phenanthroline behaves as a masking reagent for the extraction of zinc(II) with dithizone.[11] On the other hand, nickel(II),[1] cobalt(II),[19] and manganese(II)[20] are extracted as an adduct, $[M(dz)_2(phen)]$, with dithizone in the presence of 1,10-phenanthroline. The phenomenon

that zinc(II) does not form an adduct can not be reasonably explained by considering the difference in the softness of these metal ions as a Lewis acid. Manganese(II), cadmium(II), and zinc(II) are classified as hard, soft, and middle-class acids respectively.[21,22] Furthermore, there seems to be no relationship between the capability of the adduct formation of metal ions and the stability constants of the metal complex of dithizone and 1,10-phenanthroline. A systematical study of the kinetics of a synergistic extraction of metal ions would perhaps give more valuable guidelines for the development of a new synergistic extraction system.

The authors would like to thank Prof. Henry Freiser of the University of Arizona and Prof. Kenji Nakamura of Ibaraki University for their valuable comments and their encouragement for this work.

References

1) K. S. Math and H. Freiser, *Anal. Chem.*, **41**, 1682 (1969).
2) T. Honjyo and T. Shigematsu, *Chemistry*, **23**, 708 (1968).
3) H. Akaiwa, K. Kawamoto, and M. Hara, *Nippon Kagaku Zasshi*, **90**, 186 (1969).
4) T. Sekine and Y. Hasegawa, "Solvent Extraction Chemistry," Fundamentals and Application, (1977) (Marcel Dekker, New York).
5) H. Akaiwa, H. Kawamoto, and E. Yoshimatsu, *Chem. Lett.*, **1978**, 421.
6) K. S. Math, K. S. Bhatki, and H. Freiser, *Talanta*, **16**, 412 (1969).
7) H. Akaiwa, H. Kawamoto, and M. Konishi, *Bunseki Kagaku*, **28**, 690 (1979).
8) J. S. Oh and H. Freiser, *Anal. Chem.*, **39**, 295 (1967).
9) K. Ohashi and H. Freiser, *Anal. Chem.*, **52**, 767 (1980).
10) H. Watarai and H. Freiser, *J. Am. Chem. Soc.*, **105**, 189 (1983).
11) S. P. Carter and H. Freiser, *Anal. Chem.*, **51**, 1100 (1979).
12) K. S. Math, Q. Fernando, and H. Freiser, *Anal. Chem.*, **36**, 1762 (1964).
13) M. Yasuda and K. Yamasaki, *J. Am. Chem. Soc.*, **78**, 1234 (1956).
14) G. Colovos, A. Yokoyama, and H. Freiser, *Anal. Chem.*, **47**, 2441 (1975).
15) L. G. Sillén and A. E. Martell, "Stability Constants," Spec. Pub. No. 17, The Chemical Society, London (1964).
16) J. Bjerrum, *Chem. Rev.*, **46**, 381 (1950).
17) L. Sacconi, G. Lombardo, and P. Paoletti, *J. Chem. Soc.*, **1958**, 848.
18) H. Akaiwa, H. Kawamoto, and T. Ishii, *J. Inorg. Nucl. Chem.*, **36**, 2077 (1974).
19) H. Kawamoto and H. Akaiwa, *Anal. Chim. Acta*, **40**, 407 (1968).
20) H. Akaiwa, H. Kawamoto, and E. Hiyamuta, *Nippon Kagaku Kaishi*, **1979**, 1716.
21) R. G. Pearson, *J. Am. Chem. Soc.*, **85**, 3533 (1963).
22) R. G. Pearson, *J. Chem. Educ.*, **45**, 581, 643 (1968).

 © 1986 The Chemical Society of Japan Bull. Chem. Soc. Jpn., 59, 2299—2302 (1986)

The Crystal and Molecular Structure of Bis(4-methylpyridine)-bis(thiocyanato)cadmium(II) in Polymeric Form, $[Cd(SCN)_2(CH_3C_5H_4N)_2]_n$

Masahiro TANIGUCHI, Mamoru SHIMOI, and Akira OUCHI*
Department of Chemistry, College of Arts and Sciences, The University of Tokyo, Komaba, Meguro-ku, Tokyo 153
(Received February 7, 1986)

The crystal and molecular structure of the title complex was determined by a single-crystal X-ray diffraction technique. The crystal is triclinic with a space group $P\bar{1}$, a=11.323(4), b=18.383(10), c=9.284(5) Å, α=104.62(4), β=114.26(3), γ=77.71(4)°, Z=4; the final R value obtained was 0.034. All cadmium atoms are lined approximately along the [111] axis and each pair of metal atoms are bridged by two thiocyanate ions (SCN), one of which is *S*-coordinated and the other is *N*-coordinated to the same side metal atom. Also bonded with two nitrogen atoms of 4-methylpyridine (pic) ligands, the metal atom is 4*N*2*S*-hexa-coordinated and is in an octahedral geometry. The cadmium atoms, where the ligated respective pairs of N(SCN), N(pic), and S(SCN) atoms are all in a trans configuration, and the metal atoms where the ligated respective pairs of N(pic) and S(SCN) are in cis, while the pair of the N(SCN) in trans configuration, appear alternatively in the polymer chain.

A variety of polymeric structures of the metal thiocyanates and of their Lewis-base adducts are one of the interesting themes of structural chemistry, and several reports have already been published.[1] According to the soft-hard acid-base theory, cadmium is a rather soft metal, though its softness is less than that of mercury or lead.[2] Therefore, it is expected that the nitrogen as well as the sulfur atoms of a thiocyanate (SCN) ion are able to bond with cadmium easily, and that SCN-bridged polymeric complexes are stable. In fact, the cadmium(II) thiocyanate has a three-dimensional polymeric structure bridged by SCN ions,[3] and some Lewis-base adducts of cadmium(II) thiocyanate are in a variety of linear polymeric forms. For example, in *N,N'*-ethylenethiourea (2-imidazolidinethione) (etu) adduct, $Cd(SCN)_2(etu)_2$(**1**),[4] the 1*H*-1,2,4-triazole (trz) adduct, $Cd(SCN)_2(trz)_2$(**2**),[5] and the tri-*m*-tolylphosphine (tl_3P) adduct, $Cd(SCN)_2(tl_3P)$ (**3**),[6] each pair of the metal atoms, which are lined linearly, are doubly bridged by SCN ions. On the other hand, in the case of bis(2-aminoethyl)amine (ben) adduct, $Cd(SCN)_2(ben)_2$[7] each pair of metal atoms are bridged by one SCN as well as one ben ligand. In the case of 4-*t*-butyl-4*H*-1,2,4-triazole (btrz) adduct, $Cd(SCN)_2(btrz)_2$,[8] metal atoms are bridged by two N-bonded SCN ions and by three btrz ligands (alternatively) on the line.

This paper reports on the crystal and molecular structures of the title complex, $Cd(SCN)_2(pic)_2$ (pic=4-methylpyridine), determined by a single-crystal X-ray diffraction technique.

Experimental

Synthesis of Bis(4-methylpyridine)bis(thiocyanato)cadmium(II). The complex was obtained in almost the same way as that of Ahuja[9] and was recrystallized from methanol. Anal. Found: Cd, 26.99; C, 40.28; H, 3.31; N, 13.45%. Calcd for $CdC_{14}H_{14}N_4S_2$: Cd, 27.10; C, 40.54; H, 3.40; N, 13.51%. The wavenumbers of its infrared spectral bands almost coincide with the respective values of the reference.[9]

Intensity-Data Collection. A crystal with the dimension of 0.3×0.3×0.1 mm³ was used for the measurements. The crystallographic data are: $CdC_{14}H_{14}N_4S_2$, F.W. 414.82, triclinic, space group $P\bar{1}$, a=11.323(4), b=18.383(10), c=9.284(5)Å, α=104.62(4), β=114.26(3), γ=77.71(4)°, Z=4, U=1691.7(15) Å³, D_m=1.62(3), D_x=1.63 Mg m^{-3}, μ(Mo $K\alpha$)= 1.52 mm^{-1}. Reflections within a range of $3°<2\theta<50°$ were collected on a Rigaku AFC-6A automated four-circle X-ray diffractometer with graphite monochromated Mo $K\alpha$ radiation, the ω—2θ scan technique being employed (scan speed 4° min^{-1} (θ), scan width (1.10+0.5tanθ)°). The crystal was stable during exposure to X-rays. Of the 5983 reflections measured, 4652 with $|F_o|>3\sigma(|F_o|)$ were used for the structure determination. The intensities were corrected for the Lorentz and polarization factors, but no correction was made for absorption and extinction.

Structure Determination. The structure was solved by the heavy-atom method. The positions of the cadmium, and some sulfur atoms, were deduced from a three-dimensional Patterson map; other non-hydrogen atoms were located by means of successive Fourier syntheses. Their positional, isotropic and anisotropic thermal parameters were refined by a block-diagonal least-squares method. All the hydrogen atoms were at respective calculated positions, assuming their B_{iso}'s to be 8.0 Å², and C–H bond lengths to be 1.08 Å. The final R value obtained was 0.034.[10]

All the calculations were carried out on a HITAC M-280H computer at the Computer Center of the University of Tokyo using a local version of the UNICS program.[11] The atomic scattering factors were taken from Ref. 12.

Results and Discussion

The final atomic parameters of non-hydrogen atoms are listed in Table 1; the selected bond lengths and bond angles are tabulated in Table 2.[13] A perspective drawing of the skeleton of the polymeric chain of the complex, together with the numbering scheme of the atoms, is shown in Fig. 1, the crystal

Table 1. Final Atomic Coordinates ($\times 10^4$) of the Non-Hydrogen Atoms and Their Equivalent Isotropic Temperature Factors of the Complex (Estimated Standard Deviations in Parentheses)

Atom	x	y	z	B_{eq}/Å^{2} a)
Cd(1)	0	0	0	3.90
Cd(2)	5000	5000	5000	3.84
Cd(3)	2500.7(3)	2499.8(2)	316.4(4)	4.09
S(1)	2023(1)	−267(1)	−1002(2)	5.15
S(2)	605(2)	2730(1)	1529(2)	6.26
S(3)	4397(2)	2269(1)	3191(2)	5.89
S(4)	2979(1)	5267(1)	2240(1)	4.69
N(1)	2669(4)	1195(2)	−255(5)	5.27
N(2)	−157(4)	1291(2)	341(5)	5.15
N(3)	5162(4)	3707(2)	4207(4)	4.88
N(4)	2342(4)	3803(2)	879(4)	4.91
C(1)	2391(4)	598(2)	−568(5)	3.82
C(2)	165(4)	1881(2)	823(5)	4.14
C(3)	4823(4)	3118(2)	3775(5)	4.06
C(4)	2616(4)	4398(2)	1446(5)	3.67
N(11)	4088(4)	2510(2)	−695(4)	4.72
C(11)	5076(5)	1952(3)	−596(6)	4.97
C(12)	6039(4)	1946(3)	−1144(6)	4.93
C(13)	6022(4)	2545(3)	−1806(5)	4.52
C(14)	5009(5)	3114(3)	−1887(7)	6.99
C(15)	4072(5)	3082(3)	−1345(7)	6.82
C(16)	7087(5)	2582(3)	−2354(7)	6.52
N(21)	904(4)	2493(2)	−2295(4)	4.50
C(21)	−74(5)	3047(3)	−2624(6)	4.96
C(22)	−1038(5)	3052(3)	−4133(5)	4.94
C(23)	−1026(4)	2455(3)	−5366(5)	4.56
C(24)	0(5)	1879(3)	−5011(6)	5.95
C(25)	932(5)	1916(3)	−3503(6)	6.13
C(26)	−2077(5)	2420(4)	−7004(6)	6.22
N(31)	3497(4)	4940(2)	6124(4)	4.53
C(31)	2638(5)	4448(3)	5476(6)	5.02
C(32)	1659(5)	4470(3)	6022(6)	5.47
C(33)	1555(4)	5024(3)	7310(5)	4.97
C(34)	2481(6)	5518(3)	8001(6)	6.30
C(35)	3426(5)	5454(3)	7391(6)	6.12
C(36)	502(5)	5098(4)	7936(7)	6.67
N(41)	1502(4)	61(2)	2691(4)	4.55
C(41)	2364(5)	555(3)	3396(6)	5.14
C(42)	3341(5)	527(3)	4893(6)	5.31
C(43)	3448(4)	−28(3)	5741(5)	4.95
C(44)	2522(6)	−517(3)	5007(6)	6.04
C(45)	1582(5)	−458(3)	3505(6)	5.84
C(46)	4508(5)	−98(4)	7344(6)	6.24

a) The equivalent isotropic temperature factors were computed using the following expression; $B_{eq}=4/3\text{-}(B_{11}a^2+B_{22}b^2+B_{33}c^2+B_{12}ab\cos\gamma+B_{13}ac\cos\beta+B_{23}bc\cos\alpha)$. The B_{ij}'s are defined by; $T=\exp[-(h^2B_{11}+k^2B_{22}+l^2B_{33}+2klB_{12}+2hlB_{13}+2hkB_{12})]$.

Table 2. Selected Bond Lengths and Bond Angles of the Complex

Bond length	l/Å	Bond length	l/Å
Cd(1)-S(1)	2.719(2)	Cd(2)-S(4)	2.717(2)
Cd(3)-S(2)	2.722(2)	Cd(3)-S(3)	2.718(2)
Cd(1)-N(2)	2.291(4)	Cd(2)-N(3)	2.295(4)
Cd(3)-N(1)	2.306(4)	Cd(3)-N(4)	2.304(4)
Cd(1)-N(41)	2.365(4)	Cd(2)-N(31)	2.366(5)
Cd(3)-N(11)	2.350(5)	Cd(3)-N(21)	3.353(4)
S(1)-C(1)	1.637(5)	S(2)-C(2)	1.631(5)
S(3)-C(3)	1.625(5)	S(4)-C(4)	1.644(4)
N(1)-C(1)	1.141(6)	N(2)-C(2)	1.141(6)
N(3)-C(3)	1.145(6)	N(4)-C(4)	1.135(5)
Bond angle	ϕ/°	**Bond angle**	ϕ/°
S(1)-Cd(1)-N(2)	94.21(10)	S(1)-Cd(1)-N(41)	89.75(9)
N(2)-Cd(1)-N(41)	89.32(12)	S(4)-Cd(2)-N(3)	94.32(9)
S(4)-Cd(2)-N(31)	89.72(12)	N(3)-Cd(2)-N(31)	89.45(15)
S(2)-Cd(3)-S(3)	91.56(5)	S(2)-Cd(3)-N(1)	96.64(10)
S(2)-Cd(3)-N(4)	83.72(10)	S(2)-Cd(3)-N(21)	90.44(9)
S(3)-Cd(3)-N(1)	83.45(10)	S(3)-Cd(3)-N(4)	96.60(9)
S(3)-Cd(3)-N(11)	90.56(13)	N(1)-Cd(3)-N(11)	92.34(15)
N(1)-Cd(3)-N(21)	87.65(12)	N(4)-Cd(3)-N(11)	87.30(15)
N(4)-Cd(3)-N(21)	92.30(12)	N(11)-Cd(3)-N(21)	88.81(15)
Cd(1)-S(1)-C(1)	99.50(16)	Cd(3)-S(2)-C(2)	96.55(17)
Cd(3)-S(3)-C(3)	96.38(17)	Cd(2)-S(4)-C(4)	99.19(15)
Cd(3)-N(1)-C(1)	160.3(4)	Cd(1)-N(2)-C(2)	158.2(3)
Cd(2)-N(3)-C(3)	157.2(3)	Cd(3)-N(4)-C(4)	160.5(3)
S(1)-C(1)-N(1)	178.9(4)	S(2)-C(2)-N(2)	179.0(4)
S(3)-C(3)-N(3)	177.9(4)	S(4)-C(4)-N(4)	178.6(4)
Cd(3)-N(11)-C(11)	121.4(4)	Cd(3)-N(11)-C(15)	121.7(4)
Cd(3)-N(21)-C(21)	121.6(3)	Cd(3)-N(21)-C(25)	121.1(3)
Cd(2)-N(31)-C(31)	122.9(4)	Cd(2)-N(31)-C(35)	119.7(4)
Cd(1)-N(41)-C(41)	122.8(3)	Cd(1)-N(41)-C(45)	119.7(4)

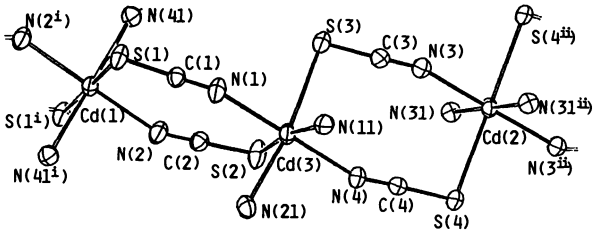

Fig. 1. A perspective drawing of the structure of the title complex with the numbering scheme. The symmetry operations are: i, $-x$, $-y$, $-z$; ii, $1-x$, $1-y$, $1-z$.

packing diagram in Fig. 2, and the numbering scheme of the pic ligand atoms in Fig. 3.

Crystallographically, there are three kinds of cadmium atoms; two of them (Cd(1) and Cd(2)) are located at the centers of symmetry (0,0,0 and 0.5,0.5,0.5), while the other one (Cd(3)) takes a position near their midpoint. All cadmium atoms are lined approximately along the [1 1 1] axis.

Along this direction, neighboring cadmium atoms are bridged by two SCN ions, one of them is *S*-coordinated and the other one is *N*-coordinated to the same side metal atom, thus forming a polymeric linear chain structure.

As two pic nitrogen atoms are also coordinated to each metal atom, the respective cadmium atoms are totally 4*N*2*S*-hexa-coordinated and are in a slightly deformed octahedral geometry. Around the Cd(1) and Cd(2) atoms, respective pairs of N(SCN), S(SCN), and N(pic) are in trans and their geometries are almost the same. Around Cd(3), respective pairs of

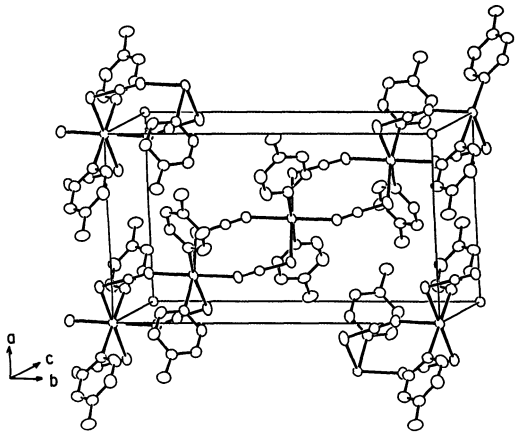

Fig. 2. Crystal packing diagram of the complex.

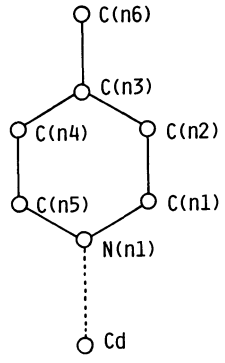

Fig. 3. Schematic presentation of the 4-methylpyridine ligand with the numbering scheme (n=1,2,3, and 4).

S(SCN) and N(pic) are in cis, while the pair of N(SCN) are in a trans configuration. Such a variation of the configuration around the cadmium atoms on the polymer chain has not been found yet for the Lewis-base adducts of cadmium thiocyanate.

The atoms of doubly bridging SCN ios, as well as the cadmium atoms on both sides, make a eight-membered ring.

They are almost on a plane: the average deviations of the atomic positions from the average plane of Cd(1), Cd(3), S(1), C(1), N(1), S(2), C(2), N(2), is 0.111 Å (maximum deviation is to S(2), 0.212 Å), while that from the average plane of Cd(2), Cd(3), S(3), C(3), N(3), S(4), C(4), N(4), is 0.100 Å (maximum deviation is to N(3), 0.244 Å). The dihedral angle between the two planes is 74.3.°.

The Cd-N(SCN) as well as Cd-N(pic) bond lengths around all cadmium atoms are not much different from each other, respectively. However, the bond length Cd-N(SCN) (2.297 Å av.[a]) is significantly shorter than that of Cd-N (pic) (2.361 Å av.). All bond lengths Cd-S are not much different from each other (2.719 Å av.), and the average bond angles of Cd-N-C(SCN) and Cd-S-C(SCN) are 158.6 and 98.4°, respectively.

As the Shannon's ionic radii of cadmium (valence (Val), 2+; and coordination number (CN), 6), sulfur (Val, 2−; CN, 6), nitrogen (Val, 3−; CN, 4) are 0.95, 1.84, and 1.46 Å, respectively, the calculated bond lengths of Cd-S and Cd-N are 2.79 and 2.41 Å.[14] Observed Cd-S lengths are not much different from the calculated one, but the observed Cd-N lengths are shorter than the calculated value. The discrepancy is probably due to the assumed Val of the nitrogen atom, which is not appropriate for atoms where the charge is significantly delocalized; the nitrogen atom in the thiocyanate ion is expected to be less negatively charged, and its ionic radius is likely to be shorter than 1.46 Å.

The bond lengths of Cd-N(SCN) and Cd-S(SCN), as well as the bond angles Cd-N-C(SCN) and Cd-S-C(SCN) in the related other cadmium thiocyanate complexes, are as follows: **1**, 2.53, 2.73 Å; 143, 109.1°; **2** , 2.330, 2.754 Å; 143.4, 96.3°; **3**, 2.28, 2.7 Å; 159, 97°.

For the title complex and **3**, the angles of Cd-N-C(SCN) are approximately 160°, Cd-N(SCN) lengths are relatively short, 2.2—2.3 Å, and Cd-S(SCN) lengths are about 2.69—2.71 Å. On the other hand, for **1** and **2**, the angle is about 140°, and Cd-N(SCN) lengths are longer than 2.3 Å, while the Cd-S(SCN) lengths are a little longer than that of the title complex. The Lewis base of **2** is coordinated to the metal atom by a nitrogen atom as the title complex, and the Cd-N(base) of **2** is shorter than that of the title complex (2.317 vs. 2.361 Å av.). From these data, the SCN bridgings of **3** and the title complex are likely to be stronger than those of **1** and **2**, and the bonding of the Lewis base with the metal atom of the title complex is weaker than that of **2**.

[a] av. means the average value. In cases of the average of the all Cd-N or S lengths, as each Cd(1 or 2)-N or S bond length shown in the table is equivalent with the one which is trans to it, the value was doubled and added to obtain the sum.

References

1) A. F. Wells, "Structural Inorganic Chemistry," 5th ed, Clarendon, Oxford, U. K. (1984), pp. 126, 935, 1159.

2) R. G. Pearson, *Science*, **151**, 172 (1966).

3) M. Cannas, G. Carta, A. Cristini, and G. Marongiu, *J. Chem. Soc. Dalton Trans.*, **1976**, 300.

4) L. Cavalca, M. Nardelli, and G. Fava, *Acta Crystallogr.*, **13**, 125 (1960).

5) J. G. Haasnoot, G. C. M. de Keyzer, and G. C. Verschoor, *Acta Crystallogr., Sect C*, **39**, 1207 (1983).

6) R. G. Goel, W. P. Henry, M. J. Oliver, and A. L. Beauchamp, *Inorg. Chem.*, **20**, 3924 (1981).

7) M. Cannas, G. Carta, A. Cristini, and G. Marongiu, *Inorg. Chem.*, **16**, 228 (1977).

8) L. R. Groeneveld, G. Vos, G. C. Verschoor, and J. Reedijk, *J. Chem. Soc., Chem. Commun.*, **1982**, 620.

9) I. S. Ahuja and A. Garg, *J. Inorg. Nucl. Chem.*, **34**, 1929

(1972).
10) $R=\sum||F_o|-|F_c||/\sum|F_o|$
11) "Universal Crystallographic Computation Program System (UNICS)," ed by T. Sakurai, Crystallographic Society of Japan, Tokyo (1967).
12) "International Tables for X-Ray Crystallography," Kynoch Press, Birmingham (1974), Vol. IV, pp. 72, 150.
13) The positions of hydrogen atoms, the final thermal parameters, the final F_o—F_c table, and some additional bond-length and angle data are deposited as Document No. 8635 at the office of the Bull. Chem. Soc. Jpn.
14) R. D. Shannon, *Acta Crystallogr., Sect A*, **32**, 751 (1976).

Kinetics of Ligand-Exchange Reactions in Tetrakis(acetylacetonato)-uranium(IV) in Organic Solvents

Hiroshi FUKUTOMI,* Hideki OHNO, and Hiroshi TOMIYASU
Research Laboratory for Nuclear Reactors, Tokyo Institute of Technology,
O-okayama, Meguro-ku, Tokyo 152
(Received February 10, 1986)

The kinetics of ligand-exchange reactions between tetrakis(acetylacetonato)uranium(IV) [U(acac)$_4$] (acac= acetylacetonate) and free acetylacetone Hacac in various organic solvents, $CDCl_3$, C_6D_6, and CD_3CN has been studied by ^1H NMR. The rate laws were found to change remarkably with these solvents used. The observed first-order rate constant k_{obsd} in $CDCl_3$ depended linearly on the concentration of free Hacac in the enol form as $k_{obsd}=k_s[Hacac]_{enol}$, while the plots of k_{obsd} vs. $[Hacac]_{enol}$ in C_6D_6 deviated from straight lines in higher concentrations of $Hacac_{enol}$. The exchange rate was much slower in CD_3CN than in $CDCl_3$ and C_6D_6, and k_{obsd} increased only slightly with $[Hacac]_{enol}$. Addition of dimethyl sulfoxide (DMSO) in C_6D_6 yielded the retardation of exchange rate giving a rate law $k_{obsd}^{-1}=p+q[DMSO]$, where p and q are constants. From the results obtained in these solvents, a mechanism passing through nine-coordinate intermediates was proposed.

Among quadrivalent metal ions which form eight-coordinate complexes with β-diketones, uranium(IV) has been studied most extensively. Earlier studies were much concerned with the solvent extractions of a variety of U(IV) β-diketonato complexes, [U(acac)$_4$], [U(hfaa)$_4$], [U(tta)$_4$], and [U(ba)$_4$], where hfaa=hexafluoroacetylacetonate, tta=2-thenoyltrifluoroacetonate and ba=benzoylacetonate, since the solvent extraction method has been of particular importance in the separation of actinoid elements. Despite a large number of studies little has been known with respect to the kinetics of ligand exchange reactions in the above complexes.[1,2]

Recently, we reported the kinetic results of ligand-exchange reactions in tetrakis(β-diketonato) complexes of thorium(IV), [Th(acac)$_4$],[3,4] and [Th(tta)$_4$],[5] and proposed a mechanism passing through nine-coordinate intermediates. This paper presents the results of kinetic experiments on the acac exchange between [U(acac)$_4$] and free Hacac, and the results are compared with those of earlier studies. A similar mechanism in the reactions of [Th(β-diketonate)$_4$] is also proposed in the present study.

Experimental

The [U(acac)$_4$] complex was synthesized by the same procedure as described in a earlier paper.[6] The solution of uranium(IV) chloride which was prepared by electrolytic reduction of uranyl(VI) chloride solution in 0.1 M HCl (M=mol dm^{-3}), was stirred with 0.1 M acetylacetone and the pH of the mixture was adjusted to about 4 with 0.1 M NaOH solution. A green precipitate was dried in vacuo for two days, and then recrystallized from benzene in a glove box filled with dried nitrogen. Identification of the complex was made by measurements of UV-visible and NMR spectra. Both the UV-visible and NMR spectra agreed well with those reported in a earlier paper.[7] Acetylacetone was dried over anhydrous calcium sulfate and distilled twice. Chloroform-*d* $CDCl_3$ (Merck 99%) was distilled. Acetonitrile-d_3 CD_3CN (Merck 99.95%) was dried over 4A molecular sieves and distilled. Benzene-d_6 C_6D_6 (Merck 99.6%) was dried over 4A molecular sieves and distilled. Dimethyl sulfoxide was distilled under reduced pressure. The UV-visible spectra were measured by using a Shimadzu 210 spectrophotometer with 10 mm quartz cells. The NMR spectra were recorded on a JEOL JNM-FX 100 NMR spectrometer equipped with a JNM-VT-3B temperature controller. The fraction of keto and enol isomers of Hacac in C_6D_6 were determined by area measurements of methyl proton NMR signals for keto and enol isomers in the temperature regions in which kinetic experiments were carried out.

Results

The ^1H NMR spectra of the mixture of [U(acac)$_4$] and Hacac in C_6D_6 were measured at various temperatures (Fig. 1), where the signals were assigned as follows: A and C are methine proton signals of [U(acac)$_4$] and $Hacac_{enol}$, respectively, G and F methyl proton signals of [U(acac)$_4$] and $Hacac_{enol}$, respectively, D and E methylene and methyl proton signals of $Hacac_{keto}$, and B refers to the signal of C_6D_5H involved in C_6D_6. The methyl proton signal (G) of [U(acac)$_4$] shifted to the upfield, while the methine proton signal (A) shifted to the downfield. These results agree well with those of earlier studies[8,9] suggesting that $\chi_{\parallel}$ is greater than $\chi_{\perp}$ in [U(acac)$_4$].

It can be seen in Fig. 1 that signals A, C, F, and G exhibit the broadening of line widths as the temperature goes up from 4 to 64 °C. This is attributed to the exchange of acac between [U(acac)$_4$] and $Hacac_{enol}$ as follows:

$$[U(acac)_4] + Hacac^*_{enol} \rightleftharpoons [U(acac)_3(acac^*)] + Hacac_{enol}, \quad (1)$$

where an asterisk denotes the exchanging species. Since signal G is isolated from other signals and reveals the most clear broadening, the kinetic data were determined from the line-shape analysis of signal G.

In the case of the slow exchange region,[10] the lifetime τ of the ligand at the coordination site is related with the transverse relaxation time of the exchanging nucleus by

$$1/\tau = 1/T_2 - 1/T_{2a}. \quad (2)$$

In the present study T_2 refers to the relaxation time of signal G in the reaction mixture, where acac exchanges between $[U(acac)_4]$ and $Hacac_{enol}$, and T_{2a} refers to the relaxation time of signal G in the absence of free Hacac. The first-order rate constant k_{obsd} for reaction 1 is given by the following equation.

$$k_{obsd} = 4/\tau \quad (3)$$

Application of the slow exchange region was tested by plotting k_{obsd} thus determined as a function of temperature, where the plot should obey an Arrhenius type relationship. A typical plot is shown in Fig. 2 indicating that the relaxation process is controlled by the chemical exchange at temperatures studied.

From the plots of k_{obsd} vs. the concentration of the complex (Fig. 3), the exchange reaction is found to be first-order with respect to $[U(acac)_4]$ in C_6D_6, i.e. rate$=k_{obsd}[U(acac)_4]$. In Fig. 4, the plots of k_{obsd} determined in $CDCl_3$ vs. $[Hacac]_{enol}$ give straight lines passing through the origin, which are expressed by

$$k_{obsd} = k_s[Hacac]_{enol}, \quad (4)$$

where k_s denotes the second-order rate constant. The values of k_s ($s^{-1}\,mol^{-1}\,kg$) were determined as: $(1.57\pm0.15)\times10^3$, $(2.66\pm0.30)\times10^3$ and $(4.21\pm0.55)\times10^3$ at 30, 40, and 50 °C, respectively. The corresponding plots with $[Hacac]_{enol}$ in C_6D_6 deviate from a linear relationship, but the plots of k_{obsd}^{-1} vs. $[Hacac]_{enol}^{-1}$ yield straight lines (Fig. 5) giving the following rate law.

$$k_{obsd}^{-1} = a + b[Hacac]_{enol}^{-1} \quad (5)$$

In CD_3CN, k_{obsd} changes only slightly with $[Hacac]_{enol}$

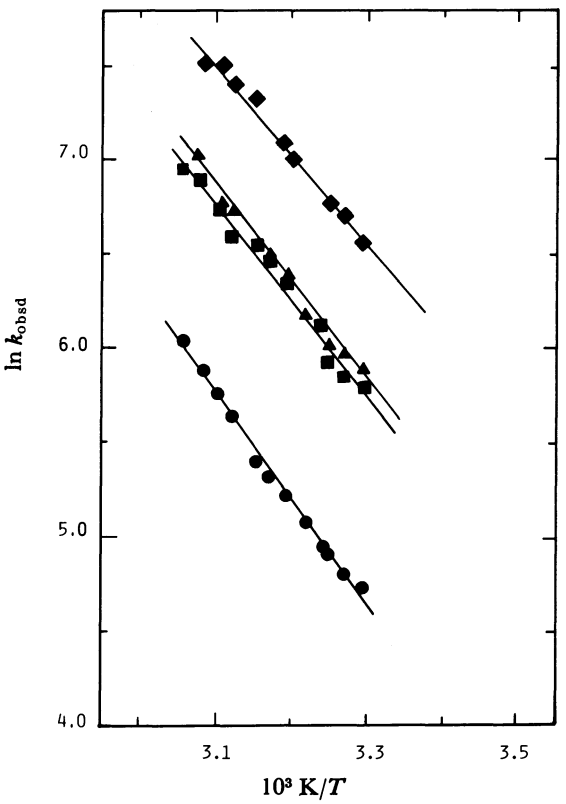

Fig. 2. Typical plots of k_{obsd} as a function of reciprocal temperature in $CDCl_3$. The concentrations of $[U(acac)_4]$ and $Hacac_{total}$ (mol kg^{-1}) are as follows: ●: 0.0317, 0.0693; ■: 0.0319, 0.182; ▲: 0.0325, 0.264; ◆: 0.0324, 0.500.

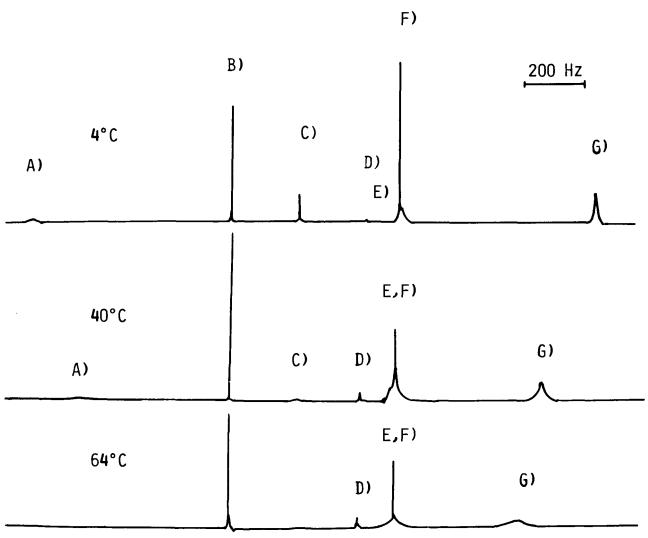

Fig. 1. ^1H NMR spectra of the mixture of $[U(acac)_4]$ and free Hacac in C_6D_6 at 4, 40 and 64 °C under the following conditions: $[U(acac)_4]=0.0496$ mol kg^{-1}, $[Hacac]=0.0128$ mol kg^{-1}.

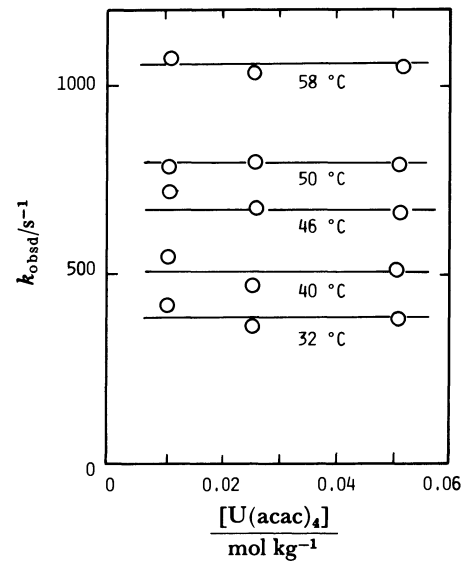

Fig. 3. The dependence of k_{obsd} on the concentration of $[U(acac)_4]$ in C_6D_6 at various temperatures. The concentration of total Hacac was kept at 0.545 mol kg^{-1}.

as is illustrated in Fig. 6.

Addition of DMSO to C_6D_6 solutions retarded remarkably the exchange rates (Fig. 7). Under the conditions [DMSO]<0.15 mol kg^{-1} in C_6D_6, plots of k_{obsd}^{-1} vs. [DMSO] are fitted to straight lines (Fig. 8) and the rate law at constant $[Hacac]_{enol}$ is expressed by

$$k_{obsd}^{-1} = p + q[DMSO]. \quad (6)$$

In the presence of high concentration of DMSO ([DMSO]≧0.5 mol kg^{-1}), k_{obsd} (s^{-1}) reaches constant values as follows: 113±14, 179±11, 241±9, and 412±16, at 40, 50, 60, and 70 °C, respectively. The concentrations of $Hacac_{enol}$ in C_6D_6 at various temperatures were calculated by using values of $\Delta H°$ (kJ mol^{-1}) and $\Delta S°$ (J K^{-1} mol^{-1}) for the equilibrium in Hacac, which were determined by the NMR method as above-described. The values obtained are −7.16±0.44 for $\Delta H°$ and −4.35±1.4 for $\Delta S°$. The $\Delta H°$ and $\Delta S°$ values used for calculation in other solvents[4] are as follows: −7.5±0.5 and 10.3±0.2 in $CDCl_3$; −1.6±0.08 and 1.38±0.30 in CD_3CN, respectively.

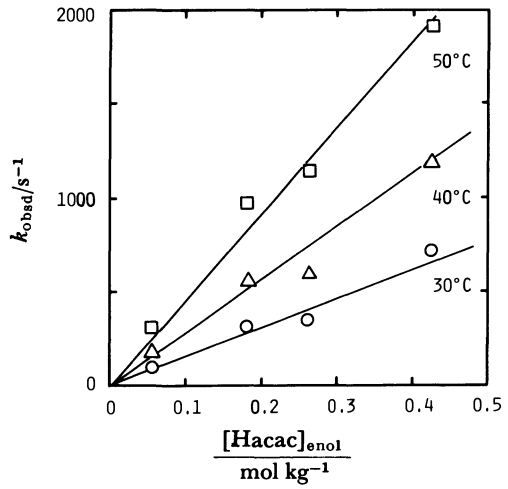

Fig. 4. Plots of k_{obsd} vs. $[Hacac]_{enol}$ in $CDCl_3$ at various temperatures. $[U(acac)_4]=0.0321$ mol kg^{-1}.

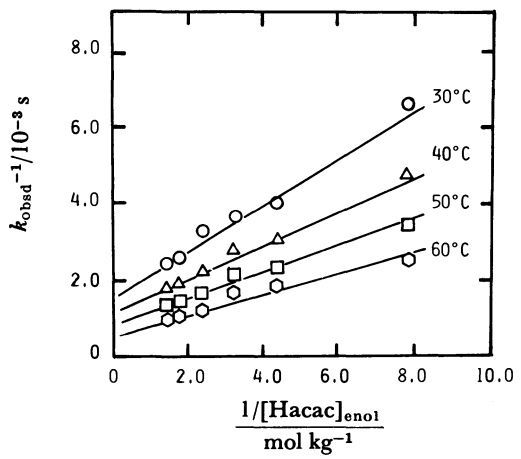

Fig. 5. Plots of k_{obsd}^{-1} vs. $1/[Hacac]_{enol}$ in C_6D_6.

Discussion

The rate laws (Eqs. 4 and 5) can be well explained by assuming the presence of a preequilibrium between $[U(acac)_4]$ and free $Hacac^*_{enol}$ prior to the acac exchange as follows:

$$[U(acac)_4] + Hacac^*_{enol} \overset{K_1}{\rightleftharpoons} [U(acac)_4 \cdots Hacac^*_{enol}], \quad (7)$$

where K_1 is the equilibrium constant and [U-

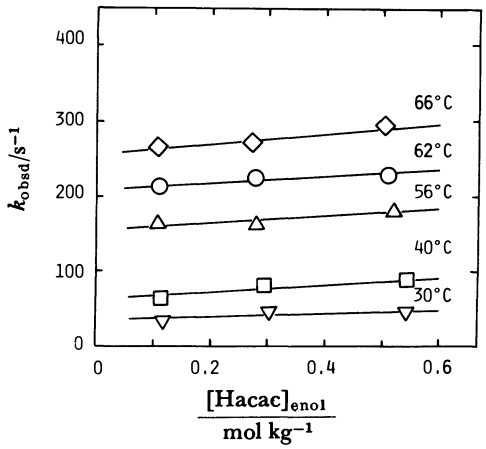

Fig. 6. Plots of k_{obsd} vs. $[Hacac]_{enol}$ in CD_3CN at various temperatures. $[U(acac)_4]=0.0521$ mol kg^{-1}.

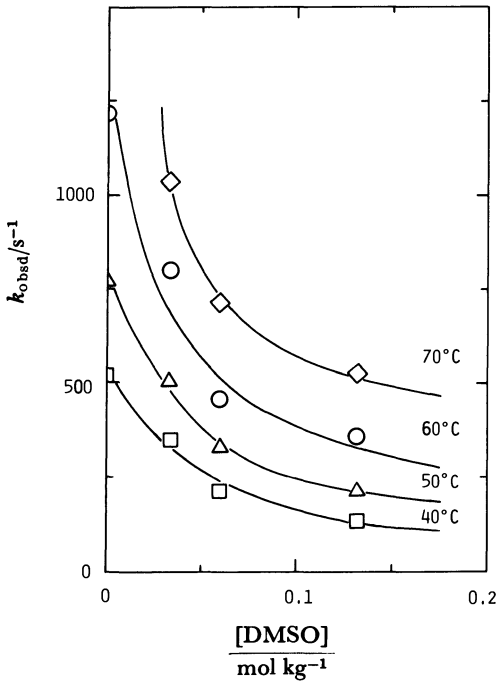

Fig. 7. Effect of added DMSO on the exchange rate in C_6D_6 at various temperatures. $[U(acac)_4]=0.0485$ mol kg^{-1}, $[Hacac]_{total}=0.556$ mol kg^{-1}.

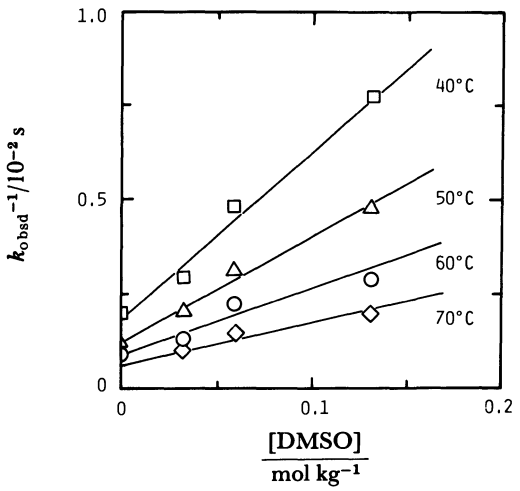

Fig. 8. Plots of k_{obsd}^{-1} vs. [DMSO] in C_6D_6 at various temperatures.

Table 1. Values of K_1, K_3, and k_2 at Various Temperatures in C_6D_6

Temperature °C	K_1 kg mol^{-1}	K_3 kg mol^{-1}	k_2 $s^{-1}\times 10^3$
40	2.72	63.8	0.901
50	2.68	40.0	1.24
60	2.69	36.6	1.69

$(acac)_4\cdots Hacac^*_{enol}]$ denotes an intermediate complex. If the acac exchange takes place only through the intermediate, k_{obsd} can be expressed by

$$k_{obsd} = \frac{k_2K_1[Hacac]_{enol}}{1+K_1[Hacac]_{enol}} \quad (8a)$$

or

$$k_{obsd}^{-1} = 1/k_2 + 1/(k_2K_1[Hacac]_{enol}), \quad (8b)$$

where k_2 refers to the rate constant for acac exchange in the intermediate, which is accompanied by a proton transfer from $Hacac^*_{enol}$ to one of the coordinated acac.

If K_1 is small enough to apply the condition $K_1[Hacac]_{enol} \ll 1$, Eq. 8 is simplified as

$$k_{obsd} = k_2K_1[Hacac]_{enol}. \quad (9)$$

Equation 9 is essentially the same as Eq. 4. This is the case for the reaction in $CDCl_3$, where $k_s=k_2K_1$, and k_2 and K_1 can not be determined independently. Under the conditions $K_1[Hacac]_{enol}\simeq 1$ with relatively large values of K_1, a linear relationship is no longer expected for the plot of k_{obsd} vs. $[Hacac]_{enol}$. On the other hand, Eq. 8b shows that the plot should be linear if k_{obsd}^{-1} is plotted against $[Hacac]^{-1}_{enol}$. This is the case for the reaction in C_6D_6, where Eq. 5 coincides with Eq. 8b, and the values of K_1 and k_2 can

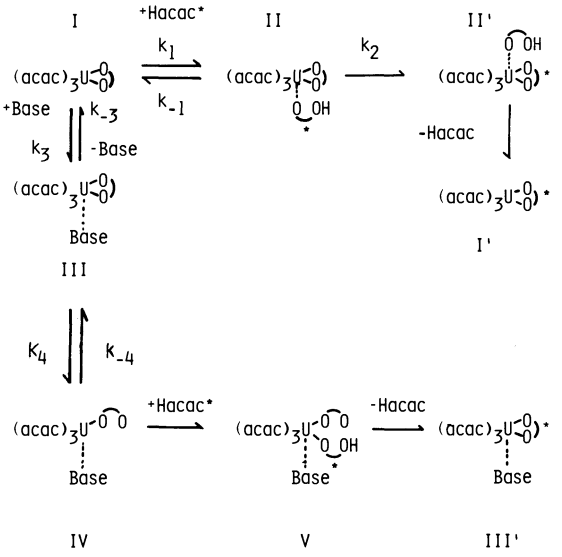

Fig. 9. Possible mechanism for the exchange of acac between $[U(acac)_4]$ and $Hacac^*_{enol}$. $\widehat{OO}$ and $\widehat{OOH}$ represent acac and $Hacac_{enol}$, respectively.

be determined. The results are listed in Table 1.

From the rate analysis, K_1 is expected to be smaller in $CDCl_3$ than in C_6D_6. This might be attributed to the difference in dielectric constant of these solvents, because K_1 is supposed to be smaller in the solvent with a larger dielectric constant, if the electrostatic interaction is responsible for the nine-coordinate adduct formation.[12]

Khvostik et al.[1] studied the kinetics of the same reaction in benzene. Although their results were not quantitative, the following data were reported: $k_2=1\times10^3$ s^{-1} and $K_1=0.4$ M^{-1} (no description of temperature was given). Compared with the present study, k_2 has the same order, but K_1 is much smaller than the values in Table 1. Since they determined the values of K_1 and k_2 from a plot of k_{obsd} vs. [Hacac] under the condition $K_1[Hacac] \ll 1$, where [Hacac] includes both keto and enol isomers, the K_1 and k_2 values obtained seem not to be correct.

We studied the ligand-exchange reactions in tetrakis(β-diketonato)thorium(IV) [Th(β-diketonate)$_4$] and proposed a mechanism passing through a nine-coordinate intermediate.[3-5] On the basis of the kinetic data and structures of Th(IV) and U(IV) β-diketonato complexes, a mechanism similar to that in Th(IV) complexes is proposed in the present study as is illustrated in Fig. 9. Addition of free $Hacac^*_{enol}$ to $[U(acac)_4]$ leads to the formation of a nine-coordinate complex (I $\rightarrow$ II), and a proton is transferred from $Hacac^*_{enol}$ to one of the coordinated acac (II$\rightarrow$II'), followed by rapid dissociation of $Hacac_{enol}$ from the coordination sphere (II' $\rightarrow$ I'). In $CDCl_3$ and C_6D_6 the pathway I $\rightarrow$ II $\rightarrow$ II' $\rightarrow$ I', which is consistent with a mechanism reported by Folcher et al. for the ligand exchange in $[U(fod)_4]$,[2] appears to be the principal

exchange pathway.

In the presence of such a free base as DMSO, another nine-coordinate complex (III) might be formed. On the assumption that complexes I, II, and III are in equilibrium and that only the pathway I → II → II′ → I′ contributes to the exchange of acac, k_{obsd} can be expressed by

$$k_{obsd} = \frac{k_2K_1[\text{Hacac}]_{enol}}{1+K_1[\text{Hacac}]_{enol}+K_3[\text{Base}]} \quad (10a)$$

or

$$k_{obsd}^{-1} = \frac{1+K_1[\text{Hacac}]_{enol}}{k_2K_1[\text{Hacac}]_{enol}} + \frac{K_3[\text{Base}]}{k_2K_1[\text{Hacac}]_{enol}}, \quad (10b)$$

where K_3 refers to the equilibrium constant for the reaction, I+Base ⇌ III. In Eq. 10b, k_{obsd}^{-1} is a linear function of the concentration of the base at constant $[\text{Hacac}]_{enol}$, and consistent with Eq. 6 obtained experimentally. In other words, the retardation effect of DMSO can be accounted for by the adduct complex formation. Additional evidence for the adduct formation came from the solvent extraction study[11] and the NMR chemical shift measurement.[2]

It should be noted, however, that k_{obsd} approaches constant values as [DMSO] increases over 0.5 mol kg^{-1}. The results suggest an alternative exchange pathway, which corresponds to the pathway I → III → IV → V → III′. The existence of two exchange processes is demonstrated clearly by the exchange reaction in CD_3CN, where k_{obsd} changes only slightly with $[\text{Hacac}]_{enol}$ (Fig. 6) giving an observed rate law

$$k_{obsd} = k_{AN} + k'_{AN}[\text{Hacac}]_{enol}. \quad (11)$$

Since CD_3CN acts as a base even though its basicity is not so strong as DMSO, the reaction might proceed via both the pathways. In the pathway I → III → IV → V → III′ the rate determining step is expected to be the bond breaking of an acac chelate ring (III → IV), because the rates of paths IV → V (coordination of Hacac^*_{enol}) and V → III′ (proton transfer) should be comparable with those of paths I → II and II → II′, respectively and hence are much faster than the observed rates in Fig. 6. Therefore, k_{obsd} can be written by

$$k_{obsd} = \frac{k_2K_1[\text{Hacac}]_{enol}+k_4K_3[CD_3CN]}{1+K_1[\text{Hacac}]_{enol}+K_3[CD_3CN]}. \quad (12)$$

If $K_3[CD_3CN] \gg (1+K_1[\text{Hacac}]_{enol})$ is assumed in CD_3CN, Eq. 12 can be simplified as

$$k_{obsd} = k_4 + \frac{k_2K_1[\text{Hacac}]_{enol}}{K_3[CD_3CN]}. \quad (13)$$

Equation 13 is consistent with Eq. 11, where

$$k_{AN} = k_4$$

and

$$k'_{AN} = k_2K_1/K_3[CD_3CN]. \quad (14)$$

The fact that the values of $k'_{AN} \approx 50$ kg mol^{-1} at 56 °C, which was determined from the plots in Fig. 6, are about hundred times smaller than those of k_2K_1 in $CDCl_3$ supports the above assumption, $K_3[CD_3CN] \gg (1+K_1[\text{Hacac}]_{enol})$. The values of k_{AN} in Fig. 6 are comparable with those of k_{obsd} obtained in the presence of high DMSO concentration in benzene, though the latter is slightly larger than the former. This fact also supports that the path III → IV controls the rates. The larger values of k_{obsd} in the presence of DMSO, as compared with k_{AN}, might be attributed to the stronger affinity of DMSO than CD_3CN toward $[U(acac)_4]$, because the adduct formation with the strong base in complex III may contribute to weaken the U(IV)–acac bonds and hence accelerate the rate in the k_4 path.

The activation parameters for the ligand-exchange reactions in $[U(acac)_4]$ are summarized in Table 2 together with those of $[Th(acac)_4]$. Similar values, particularly the large negative values of ΔS^*, suggest the similarlity in mechanism for the ligand exchange reactions in both U(IV) and Th(IV) complexes, although the pathway III → IV → V → III′ was not observed in the latter complex. In the case of ligand exchange in $[Th(acac)_4]$, the rate law was expressed by Eq. 4 under the condition $K_1[\text{Hacac}]_{enol} \ll 1$ in solvents $CDCl_3$ and CD_3CN. As compared with the results of the present study, K_1 appears relatively smaller for $[Th(acac)_4]$ than for $[U(acac)_4]$. Since the exchange rate in $[Th(acac)_4]$ is faster than in $[U(acac)_4]$ and the values of k_2K_1 for $[Th(acac)_4]$ and $[U(acac)_4]$ are 4.5×10^2 and 1.0×10^2 kg s^{-1} mol^{-1} at 20 °C in $CDCl_3$ respectively, k_2 for $[Th(acac)_4]$ is expected to be much larger than for $[U(acac)_4]$. This fact may account for that the pathway III → IV → V → III′ is observed only in $[U(acac)_4]$, because the pathway I → II → II′ → I′, whose rate is controlled by the k_2 path, is so fast in $[Th(acac)_4]$ that the probability of taking pathway III→IV→V→III′ becomes negligible. A marked difference in k_2 value might be attributed to a difference in size of these complexes: the distance between Hacac* and acac in complex II is presumed to be more favorable for the proton transfer in Th(IV) complex than in U(IV) complex.

Table 2. Activation Parameters of acac Exchange in $[U(acac)_4]$ and $[Th(acac)_4]$

Complex	Solvent	Rate constant	ΔH^* / kJ mol^{-1}	ΔS^* / J mol^{-1} K^{-1}
$[U(acac)_4]$	$CDCl_3$	$k_s(=k_2K_1)$	37.6±0.9	−69.8±3.0
$[U(acac)_4]$	C_6D_6	k_2	40.4±6.6	−62.6±2.1
$[U(acac)_4]$	CD_3CN	$k_4(=k_{AN})$	46.4±0.1	−63.6±3.5
$[Th(acac)_4]$	$CDCl_3$	k_2K_1	30.8±0.7	−81.3±2.5
$[Th(acac)_4]$	CD_3CN	k_2K_1	30.2±1.0	−97.3±3.5

The authors wish to thank Dr. Naoshi Fujiwara, Department of Medicine, Niigata University, for his helpful advice.

References

1) G. M. Khvostik, V. N. Sokolov, G. K. Grebenshchikev, S. A. Tropov, and G. P. Kondratenkov, *Koord. Khim.*, **5**, 680 (1979).

2) G. Folcher, N. Keller, C. Kiener, and J. Paris, *Can. J. Chem.*, **55**, 3559 (1977).

3) N. Fujiwara, H. Tomiyasu, and H. Fukutomi, *Chem. Lett.*, **1983**, 377.

4) N. Fujiwara, H. Tomiyasu, and H. Fukutomi, *Bull. Chem. Soc. Jpn.*, **57**, 1576 (1984).

5) N. Fujiwara, H. Tomiyasu, and H. Fukutomi, *Bull. Chem. Soc. Jpn.*, **58**, 1386 (1985).

6) A. C. Adams and E. M. Larsen, *Inorg. Chem.*, **5**, 814 (1966).

7) S. Sostero, O. Traverso, and L. Magon, *J. Chem. Soc., Dalton Trans.*, **1980**, 1324.

8) R. C. Fay and J. K. Howie, *J. Am Chem. Soc.*, **99**, 8110 (1977).

9) R. C. Fay and J. K. Howie, *J. Am. Chem. Soc.*, **101**, 1115 (1979).

10) T. J. Swift and R. E. Connick, *J. Chem. Phys.*, **37**, 307 (1962).

11) J. I. Bullock and A. J. Sweatman, *Inorg. Chim. Acta*, **64**, L1 (1982).

12) R. M. Fuoss and C. A. Kraus, *J. Am. Chem. Soc.*, **80**, 5059 (1958).

Preparation and Thermal Square Planar–Octahedral Transformation of Nickel(II) Complexes Containing 1,2-Butanediamine or 3,3-Dimethyl-1,2-butanediamine in Solid Phase

Yoshinori IHARA,* Akiko WADA, Yutaka FUKUDA,† and Kozo SONE†
Laboratory of Chemistry, Faculty of Education, Kanazawa University, Marunouchi, Kanazawa 920
†Department of Chemistry, Faculty of Science, Ochanomizu University, Otsuka, Bunkyo-ku, Tokyo 112
(Received February 22, 1986)

Nickel(II) complexes of 1,2-butanediamine(1,2-bn) and 3,3-dimethyl-1,2-butanediamine(dmbn), were prepared, and their thermal behavior was investigated in solid phase. The original complexes were all violet, octahedral diaquabis(diamine) complexes($[Ni(H_2O)_2(1,2\text{-bn/dmbn})_2]X_2$; X=Cl, Br, NO_3, or ClO_4). The 1,2-bn complexes with Cl^- or Br^- and the dmbn complex with NO_3^- showed a two-step thermochromism, violet→yellow→violet blue, upon heating. These steps correspond to structural changes to a square planar anhydride, and then to an octahedral dianiono complex. The complexes of both ligands with ClO_4^- underwent only thermal deaquation, changing into orange square planar anhydride. Other salts, the 1,2-bn complex with NO_3^- and the dmbn complexes with Cl^- or Br^-, were converted into octahedral dianiono complexes by thermal deaquation-anation which occurs in one step. The differences among the thermal reactivities of the complexes with different diamines can be understood on the basis of steric hindrance caused by the substituent groups on the diamine.

It has been well-known that the bis(*N*- or *C*-substituted ethylenediamine) complexes of Ni(II) have either an octahedral structure, $[Ni(A)_2(diamine)_2]X_2$ or $[NiX_2(diamine)_2]$(A: neutral unidentate ligand, X: univalent anion), or a square planar one, $[Ni(diamine)_2]X_2$, depending upon the structure of the diamines and the nature of X^- ions. Among the alkyl-substituted ethylenediamine complexes, in particular, two effects due to the substituent groups on the diamines seem to influence the coordination structure of the complexes. One is their inductive effect, and another is their steric hindrance. The former tends to raise the ligand field strength(l.f.s.) in the octahedral complex,[1] whereas the latter disturbs the coordination of A and X^- and thus favors the formation of square planar structure.

Both of these effects are reflected in the modes of the thermal reactions of these complexes in solid phase.[2–4] Such reactions are, in general, accompanied by distinct color changes, and can be classified into the following four types.

a) $[Ni(H_2O)_2(diamine)_2]X_2$ (Oh) $\xrightarrow[\Delta]{-2H_2O}$ $[NiX_2(diamine)_2]$ (Oh')

b) $[Ni(H_2O)_2(diamine)_2]X_2$ (Oh) $\xrightarrow[\Delta]{-2H_2O}$ $[Ni(diamine)_2]X_2$ (Sp)

c) $[Ni(H_2O)_2(diamine)_2]X_2$ (Oh) $\xrightarrow[\Delta]{-2H_2O}$ $[Ni(diamine)_2]X_2$ (Sp) $\xrightarrow[\Delta]{}$ $[NiX_2(diamine)_2]$ (Oh')

d) $[Ni(diamine)_2]X_2$ (Sp) $\xrightarrow[\Delta]{}$ $[NiX_2(diamine)_2]$ (Oh')

Here, Oh(or Oh') and Sp represent an octahedral diaqua(or dianiono) species and a square planar one, respectively.

In the case of the *N*-substituted ethylenediamine complexes, only reactions of the type (a) or (b) are observed on heating; in certain instances, no diaqua complex can be prepared at room temperature, and the square planar complex obtained scarcely show any structural change until it decomposes on strong heating. Thus it is comparatively easy to see which kind of structure(Oh, Oh', or Sp) is favored by a particular ligand. This situation is probably due to the fact that, in these complexes, the substituent groups are bound directly to the donor N atom(s) of diamines, so that they can excert highly selective influence on the stabilities of the complexes.

On the other hand, in the case of the *C*-substituted ethylenediamine complexes, thermal reactions of the type (c) or (d) often take place,[5] which include the transformation of a square planar species into an octahedral ones on heating, in addition to those of the pattern (a) or (b), so that the correlation between structure and reactivity becomes much more complicated.[7–9] In these complexes, the substituent groups are bound somewhat apart from the donor N atoms, often forming specific conformations; the mode of the thermal reaction thus seems to depend on more delicate structural factors than in the case of the *N*-substituted diamine complexes.

In continuation of these studies, thermal reactions of the nickel(II) complexes with 1,2-butanediamine or 3,3-dimethyl-1,2-butanediamine in solid phase were investigated. The obtained results will be reported in this paper.

Experimental

Materials. 1,2-Butanediamine(1,2-bn)[10] was prepared

by the reaction of 2-ethylaziridine[11] with liquid ammonia. 3,3-Dimethyl-1,2-butanediamine(dmbn)[12] was obtained by reducing 3,3-dimethyl-1,2-butanedione dioxime[13] with Raney nickel.

The complexes with these ligands were prepared by the following method. To an ethanolic solution of a nickel(II) salt, $NiX_2 \cdot nH_2O$ (X=Cl, Br, NO_3, or ClO_4), an ethanolic solution of 1,2-bn or dmbn was added in the molar ratio of 1:2.[14] The solutions were allowed to stand for several days to precipitate the desired bis-type complexes. The violet crystals obtained were collected by filtration and washed with ethanol and/or diethyl ether.

The products of the thermal reactions of these complexes were obtained by isothermal heating at the temperatures of the respective DTA peaks, using an electric furnace in static air. They were studied directly after preparation, or in carefully dried atmosphere, to avoid the occurrence of backward reactions towards the original complexes(see later).

Visual Observations of Thermochromic Changes. The mode of thermochromic color change of each complex, which usually occurs within a temperature range of several degrees, was observed by putting a small amount of finely powdered sample on the bulb of a spiral-formed thermometer, and heating it on a hot plate with a rate of ca. 5 °C min^{-1}.

Measurements. Simultaneous TG-DTA or TG-DSC measurements were carried out with a Sinku Riko TGD-3000M or a Rigaku Denki standard TG-DSC apparatus. The conditions of the runs are given in the captions of Figs. 3 and 4.

The electronic spectra in solid phase were measured by the diffuse reflectance method with a Hitachi 340 spectrophotometer equipped by reflection attachments for the visible(850—300 nm) and near IR(1400—850 nm) parts of the spectrum. The spectra at elevated temperatures were obtained by using a powder cell attached to a heating block.[15] The IR spectra were measured with a JASCO IR-A3 spectrophotometer in Nujol mulls.

Magnetic susceptibility measurements were performed with a Shimadzu Torsion Magnetometer MB-100 at room temperature.

Results and Discussion

Structure of the Original Complexes. The analytical data and magnetic moments in Table 1 show that all the complexes prepared are of the composition, $NiX_2 \cdot 2(\text{diamine}) \cdot nH_2O$ (n is 2.5 for perchlorate with 1,2-bn or 2 for others), and are high spin. The spectrum of one of them, the 1,2-bn complex with Br^-, is shown in Fig. 1 (together with those of its thermal reaction products; see later). The number of observed bands and their modes of splitting clearly indicate that the original complex has a *trans*-octahedral structure.[16,17] The spectra of the other 1,2-bn complexes and all the dmbn complexes are all similar, leading to the formulas of these complexes given in Table 1.

Thermochromism of the Complexes. Figure 2 shows the results of visual observations on the solid phase thermochromism of the complexes. All the complexes except for *trans*-$[Ni(H_2O)_2(1,2\text{-bn})_2](NO_3)_2$ change their color from violet to yellow, orange, or violet blue at a relatively low temperature (ca. 100 °C or lower). Among them, the changes observed in the 1,2-bn complexes with Cl^- and Br^- and in the dmbn complex with NO_3^- are especially remarkable, since they show a second color change from yellow to violet blue upon continued heating, leading to a two-step thermochromism(violet→yellow→violet blue).

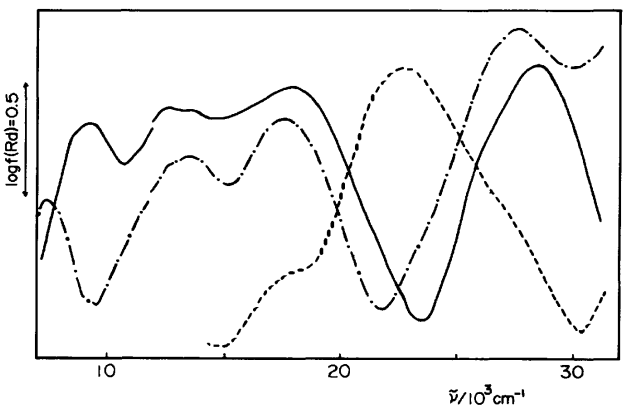

Fig. 1. Electronic spectra of *trans*-$[Ni(H_2O)_2(1,2\text{-bn})_2]Br_2$ at room temperature(——), at 100 °C(----), and at 160 °C(—·—).

Table 1. Data on the Elemental Analyses, Electronic Spectra, and Magnetic Moments of the Original Complexes

Complexes	Analytical data[a]			Absorption maxima $\tilde{\nu}/10^3$ cm^{-1}					μ_{eff} B. M.
	H (%)	C (%)	N (%)						
trans-$[Ni(H_2O)_2(1,2\text{-bn})_2]Cl_2$	8.43(8.25)	27.65(28.10)	16.12(16.38)	9.3	12.5	13.5	17.4	28.1	3.12
trans-$[Ni(H_2O)_2(1,2\text{-bn})_2]Br_2$	6.68(6.55)	21.97(22.30)	12.58(13.00)	9.3	12.5	13.5	17.9	28.4	3.13
trans-$[Ni(H_2O)_2(1,2\text{-bn})_2](NO_3)_2$	7.37(7.16)	24.33(24.32)	21.70(21.27)	8.8	12.8	13.5	18.2	28.4	3.17
trans-$[Ni(H_2O)_2(1,2\text{-bn})_2](ClO_4)_2 \cdot 0.5H_2O$	5.98(6.11)	19.65(20.01)	11.08(11.70)	8.8	12.8	13.5	18.2	28.4	3.27
trans-$[Ni(H_2O)_2(dmbn)_2]Cl_2$	8.98(9.12)	35.92(36.21)	14.16(14.08)	8.8	12.8	13.5	18.5	28.4	3.29
trans-$[Ni(H_2O)_2(dmbn)_2]Br_2$	7.34(7.45)	29.16(29.60)	11.42(11.51)	9.3	12.8	13.5	18.5	29.1	3.18
trans-$[Ni(H_2O)_2(dmbn)_2](NO_3)_2$	7.87(8.04)	31.98(31.95)	18.64(18.63)	9.3	12.8	13.5	18.2	28.4	3.22
trans-$[Ni(H_2O)_2(dmbn)_2](ClO_4)_2$	6.42(6.90)	27.25(27.40)	10.66(11.43)	8.5	12.8	13.8	18.2	28.7	3.15

a) Calculated values are in parentheses.

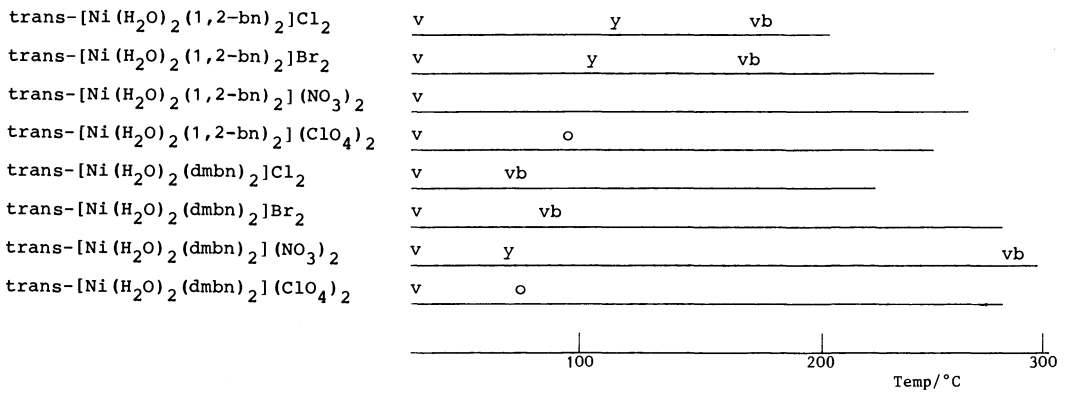

Fig. 2. Results of visual observations on the thermochromic changes of the complexes. v: violet, vb: violet blue, y: yellow, o: orange. The high-temperature colors are shown at the spots on the temperature scale(horizontal lines) where they begin to appear; the right-hand ends of the lines correspond to the decomposition points.

These color changes are reversible; in particular, the violet blue product of the dmbn complex with NO_3^- returns to yellow immeadiately on cooling. Also in the case of the 1,2-bn complexes with Cl^- and Br^-, reverse changes from violet blue or yellow to an original violet are observed on cooling for a few minutes. The violet blue product of the former complex and the yellow and violet blue products of the latter ones are thus stable only at the correspondingly elevated temperatures. The yellow product of the dmbn complex with NO_3^- could be cooled to room temperature and identified; however, it also returned to the original violet complex on standing for some days in open air. The violet blue products of the dmbn complexes with Cl^- and Br^-, and the violet one of the 1,2-bn complex with NO_3^- (anhydrous salt; see later) also revert to the original diaqua species more or less gradually.

Thermal Analyses. The results of simultaneous TG-DTA analyses for the 1,2-bn complexes with Cl^- and Br^- are shown in Fig. 3. The abrupt weight losses observed in both TG curves before 100 °C, and the corresponding endothermic DTA peaks, are due to the liberation of two moles of coordinated water, which is responsible for the color change from violet to yellow. The endothermic peaks near 160 °C(Cl^-) and 150 °C(Br^-), on the other hand, apparently correspond to the second color changes from yellow to violet blue, in which the TG curves remain flat.

Figure 4 depicts the results of TG-DTA analysis of *trans*-$[Ni(H_2O)_2(dmbn)_2](NO_3)_2$, as another example of the complexes showing the two-step thermochromism. The DTA curve at the heating rate of 2 °C min^{-1} gives no peak for the second color change (yellow→violet blue), until the complex decomposes exothermically near 260 °C. When the heating rate is increased to 8 °C min^{-1}, however, the endothermic peak begins to appear, and becomes very apparent at 10 °C min^{-1}, as can be seen in the same Figure. It is considered that this endothermic peak corresponds to the color change (yellow→violet blue).

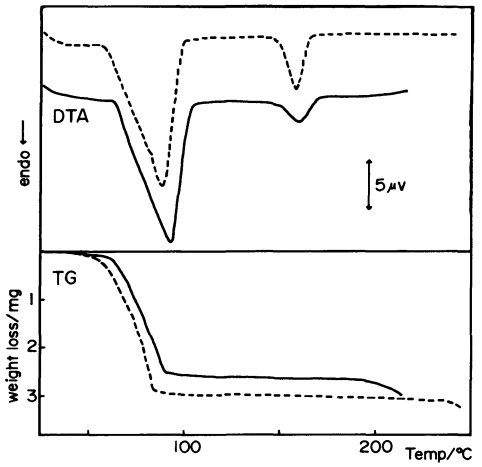

Fig. 3. TG-DTA patterns of *trans*-$[Ni(H_2O)_2(1,2\text{-bn})_2]Cl_2$(——) and *trans*-$[Ni(H_2O)_2(1,2\text{-bn})_2]Br_2$(----). Heating rate: 2 °C min^{-1}; DTA sensitivity: ±25 μV with Pt–Rh thermocouple; gas flow: N_2 at 20 ml min^{-1}; amounts of samples: 24.8 mg for chloride and 34.8 mg for bromide.

The features of TG-DTA curves of the remaining five complexes are quite similar to those of the complexes in Figs. 3 and 4, except for that the second endothermic peak does not appear. The results obtained by TG-DTA analyses of all the complexes studied are summarized in Table 2. The enthalpy changes for the reactions of the type (yellow→violet blue), also shown in Table 2, were estimated from the DSC measurements carried out separately.

Spectral Changes of the Complexes on Heating. The spectra of the 1,2-bn complexes with NO_3^- and ClO_4^- after dehydration are shown in Fig. 5. In the former case, the spectral pattern remains nearly unchanged after dehydration, showing that the *trans*-octahedral configuration is retained. In the latter case, however, there is a drastic spectral change, and a broad band characteristic to the spectrum of a square

planar Ni(II) complex appears. It is thus clear that the reactions of types (a) and (b) take place in these two cases, respectively; the reason why a distinct change in color does not occur in the former case can also be understood, since the ligands exchanged (H_2O and NO_3^-) are both O-ligands with nearly the same ligand field strength.

Figure 1 gives a comparison of the spectra of the yellow and violet blue species of the 1,2-bn complex with Br^- with that of the original violet one. The spectra of both products were measured at the elevated temperatures where the respective species form, because they change rapidly into the original complex on cooling (see above). As shown in the Figure, it is clear that the yellow product formed by dehydration has a square planar structure and the violet blue product has a *trans*-octahedral one, which is similar to that of the original violet specimen. The spectral data on the same color change, violet→yellow→violet blue, of the 1,2-bn complex with Cl^-, which are not shown, are quite similar to those in Fig. 1. In these cases, the reactions which take place are clearly of type (c).

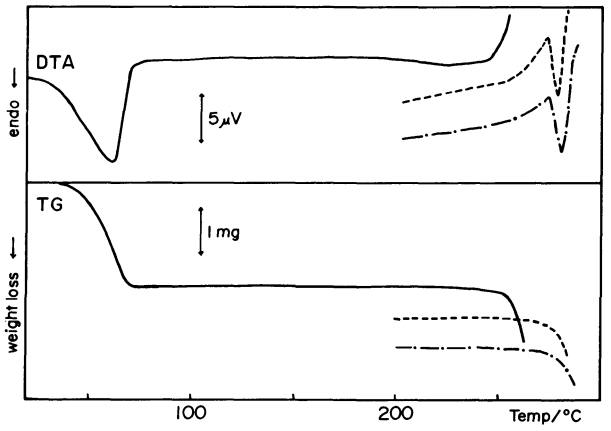

Fig. 4. TG-DTA patterns of *trans*-$[Ni(H_2O)_2(dmbn)_2](NO_3)_2$. Heating rate: 2 °C min^{-1}(run 1, ——), 8 °C min^{-1}(run 2, ----), and 10 °C min^{-1}(run 3, —·—). DTA sensitivity: ±25 μV with Pt–Rh thermocouple; gas flow: N_2 at 20 ml min^{-1}; amounts of samples: 26.5 mg for run 1, 25.8 mg for 2, and 26.3 mg for 3, respectively. The first(dehydration) step observed in run 2 and run 3 is essentially the same as that in run 1, except for a gradual shift to higher temperature like that observed with the second step.

Confirmation of the Structures of the Thermal Reaction Products. It was also tried to isolate the products of the thermal reactions and to confirm their structures separately. Although they readily revert to the original diaqua species on cooling, such reverse changes are sometimes slow enough to allow rapid measurements. In addition, they (except those of the Oh′→Sp type) can be stopped by operating in extremely dry air to avoid the reaquation of the dehydrated species. The data in Table 3 were obtained by making use of these facts; some of the spectra were obtained at high temperatures. It can be seen that all these data, and the structures deduced from them are compatible with the modes of the formation of these complexes proposed above.

The mode of coordination in the nitrato complex(Oh′) with 1,2-bn was also studied by means of its IR spectrum. In general, NO_3^- ion in a metallic complex gives rise to a weak combination band in the range of 1700—1800 cm^{-1}. When it is coordinat-

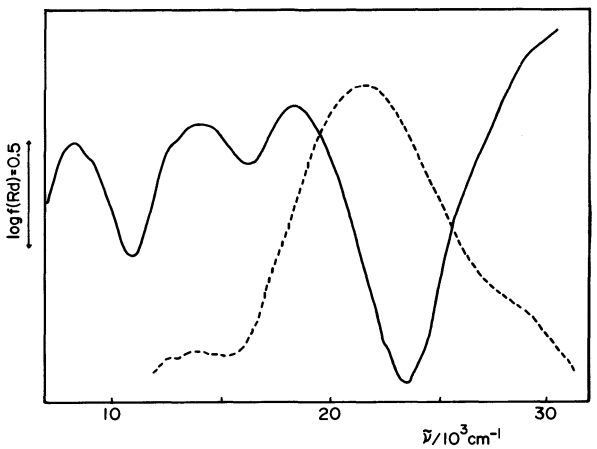

Fig. 5. Electronic spectra of *trans*-$[Ni(NO_3)_2(1,2\text{-bn})_2]$ (——) and $[Ni(1,2\text{-bn})_2](ClO_4)_2$ (----).

Table 2. The Results of Thermal Analyses

Complexes	Dehydration		Sp→Oh′ Transformation	
	Temp/°C	Weight loss/%[a]	Temp/°C	ΔH/kJ mol^{-1}
trans-$[Ni(H_2O)_2(1,2\text{-bn})_2]Cl_2$	65—95	11.0(10.5)	148—170	21.3
trans-$[Ni(H_2O)_2(1,2\text{-bn})_2]Br_2$	50—85	8.6(8.4)	140—160	8.02
trans-$[Ni(H_2O)_2(1,2\text{-bn})_2](NO_3)_2$	60—90	9.2(9.1)		
trans-$[Ni(H_2O)_2(1,2\text{-bn})_2](ClO_4)_2\cdot 0.5H_2O$	35—75	8.7(9.4)		
trans-$[Ni(H_2O)_2(dmbn)_2]Cl_2$	RT—53	9.0(9.1)		
trans-$[Ni(H_2O)_2(dmbn)_2]Br_2$	RT—70	7.4(7.4)		
trans-$[Ni(H_2O)_2(dmbn)_2](NO_3)_2$	RT—48	7.6(8.0)	280—290	—
trans-$[Ni(H_2O)_2(dmbn)_2](ClO_4)_2$	RT—62	6.5(6.8)		

a) Calculated values are in parentheses.

Table 3. Data on the Elemental Analyses, Electronic Spectra, and Magnetic Moments of the Complexes Obtained by Heating the Complexes in Table 1

Complexes	Color	Analytical data[a]			Absorption maxima[b] $\bar{\nu}/10^3$ cm^{-1}					μ_{eff} B. M.
		H (%)	C (%)	N (%)						
$[Ni(1,2\text{-bn})_2]Cl_2$	Yellow						22.8			Diamag.
trans-$[NiCl_2(1,2\text{-bn})_2]$	Violet blue	7.65 (7.92)	30.86 (31.40)	17.84 (18.32)	8.3*	12.5 sh*	13.9*	17.2*	27.5*	3.15
$[Ni(1,2\text{-bn})_2]Br_2$	Yellow						22.6			Diamag.
trans-$[NiBr_2(1,2\text{-bn})_2]$	Violet blue	6.29 (6.14)	24.39 (24.33)	13.88 (14.19)	7.3*	12.0 sh*	13.5*	17.5*	27.5*	3.15
trans-$[Ni(NO_3)_2(1,2\text{-bn})_2]$	Violet	6.67 (6.75)	26.70 (26.76)	23.26 (23.41)	8.3	12.8 sh	13.9	18.5	28.5 sh	3.18
$[Ni(1,2\text{-bn})_2](ClO_4)_2$	Orange	5.40 (5.59)	21.43 (22.14)	12.53 (12.91)			21.6			Diamag.
trans-$[NiCl_2(dmbn)_2]$	Violet blue	9.29 (8.91)	39.33 (39.81)	15.26 (15.48)	8.4	13.2 sh	13.9	18.2	27.8	3.21
trans-$[NiBr_2(dmbn)_2]$	Violet blue	7.42 (7.15)	31.57 (31.96)	12.49 (12.43)	7.5	12.8 sh	13.9	18.2	27.8	3.17
$[Ni(dmbn)_2](NO_3)_2$	Yellow	7.35 (7.77)	34.61 (34.72)	20.14 (20.24)				22.5		Diamag.
$[Ni(dmbn)_2](ClO_4)_2$	Orange	6.56 (6.58)	29.41 (29.41)	11.52 (11.43)				21.8		Diamag.

a) Calculated values are in parentheses. b) The data obtained at high temperatures are marked with.*

ed as a monodentate ion, a small splitting into two components (less than 25 cm^{-1}) takes place. When it acts as a bidentate ligand, the splitting becomes much larger(20—50 cm^{-1}).[18,19] The band at 1768 cm^{-1} in the original complex is found to split into two bands at 1752 cm^{-1} and 1773 cm^{-1} with a separation of 21 cm^{-1} after heating. This is compatible with the view that the two NO_3^- ions are coordinated at the axial positions as unidentate ligands to form the *trans*-octahedral complex.

The thermochemical changes of all the complexes observed can thus be represented by the following equations, and classified into the types (a), (b), and (c) mentioned above:

(a) *trans*-$[Ni(H_2O)_2(1,2\text{-bn})_2](NO_3)_2 \xrightarrow[\Delta]{-2H_2O}$ *trans*-$[Ni(NO_3)_2(1,2\text{-bn})_2]$

trans-$[Ni(H_2O)_2(dmbn)_2]X_2 \xrightarrow[\Delta]{-2H_2O}$ *trans*-$[NiX_2(dmbn)_2]$ (X=Cl or Br)

(b) *trans*-$[Ni(H_2O)_2(1,2\text{-bn or dmbn})_2](ClO_4)_2 \xrightarrow[\Delta]{-2H_2O} [Ni(1,2\text{-bn or dmbn})_2](ClO_4)_2$

(c) *trans*-$[Ni(H_2O)_2(1,2\text{-bn})_2]X_2 \xrightarrow[\Delta]{-2H_2O}$ $[Ni(1,2\text{-bn})_2]X_2 \xrightarrow[\Delta]{}$ *trans*-$[NiX_2(1,2\text{-bn})_2]$ (X=Cl or Br)

The data for the violet blue product of the dmbn complex with NO_3^- are lacking in Table 3, because it reverts so easily to the yellow species on cooling, at a temperature which is quite close to the decomposition point (see above and Figs. 2 and 4). The first step, violet→yellow, of its formation is, however, clearly a structural change to a square planar anhydrous complex (Table 3), and the general features of the second steps, yellow→violet blue, indicates that a type (c) reaction also takes place here.

Effects of Structures of Diamines upon Thermal Reactions. Table 4 summarizes the results on the thermal reactions of 1,2-bn and dmbn complexes, and those of 1-phenyl-1,2-ethanediamine(phenen) complexes already studied.[9] When heated, they change in one of the three ways, Oh→Oh′(type (a)), Oh→Sp(type (b)), and Oh→Sp→Oh′(type (c)). On the other hand, when the original species are square planar, they remain unchanged upon heating until decomposition; only one such example is shown in the Table, i. e., $[Ni(phenen)_2](ClO_4)_2$.

It can be seen that both 1,2-bn and dmbn complexes easily undergo deaquation-anation either in one step or in two, producing aniono complexes, retaining their octahedral configuration. Perchlorates are exceptions, undergoing deaquation to Sp only, because of the poor coordination ability of ClO_4^- ions.

The tendency of favoring an octahedral configuration observed in *C*-monosubstituted ethylenediamine complexes, such as those in Table 4, is more remarkable than that in 1,1-di- or 1,2-disubstituted ethylenediamine complexes.[3,7,20] The main reason for such a differences can be found in the magnitudes of steric hindrance caused by the substituent groups on the diamines. From NMR studies on Co(III),[21] Pt(II),[22,23] and Ni(II)[24,25] complexes with several *C*-substituted ethylenediamines, it is known that, when there is only one substituent group on the diamine, it almost always occupies the equatorial position on

Table 4. Classification of Thermal Reactions of Nickel(II) Complexes Containing *C*-Mono Substituted Ethylenediamines

	Cl	Br	NO_3	ClO_4
1,2-bn	Oh→Sp→Oh′	Oh→Sp→Oh′	Oh→Oh′	Oh→Sp
dmbn	Oh→Oh′	Oh→Oh′	Oh→Sp→Oh′	Oh→Sp
phenen[9]	Oh→Oh′	Oh→Oh′	Oh→Sp→Oh′	Sp

the plane containing two diamines at room temperature. It is clear that, in such a case, there is enough space above and below to permit the approach of the additional ligands such as water molecules and counter anions. On the other hand, in the complexes with 1,1-di- or *meso*-1,2-disubstituted ethylenediamines, at least one of the substituents in each diamine ligand is forced to occupy the axial positions.[26,27] Such a configuration generates a larger steric hindrance, preventing the approach of other ligands from the axial direction and stabilizing the square planar structure.

For the square planar species to occur in the *C*-monosubstituted ethylenediamine complexes, therefore, it is tempting to suppose that the substituent group in the diamine protruding on the equatorial plane should be so bulky that they can influence the axial coordination to some extent. In fact, except for the case of perchlorates, such a species is formed in the 1,2-bn complexes with Cl^- and Br^-, and in the dmbn complex with NO_3^-. However, since the substituent group in dmbn(i.e., $(CH_3)_3C$–) is much larger than that in 1,2-bn(C_2H_5–), the tendency observed in the complex halides is rather unexpected.

A possible explanation for this apparent anomaly is as follows. At high temperature, the conformation of the diamine chelate ring will not be rigid, and a conformational equilibrium will finally be brought about by thermal agitation, in which the equatorial group(R) on the ligand temporarily "stands up" as the axial one.[28,29] Such a "stand up" motion will occur more easily when R is small, hindering the coordination of X^- at trans positions of Ni(II), but when R is as large as $(CH_3)_3C$–, it will be hard to move in crystals, so that dianiono complexes can be formed more easily.[30] It seems probable that the occurence of such thermal deformation of the ligands is complicating the observed situations also in the case of related complexes.

The authors wish to express their thanks to Professor Eishin Kyuno and his colleagues of Hokuriku University for their kind aid in TG-DSC measurements. This work was partially supported by a Grant-in-Aid for Scientific Reseach No. 59430009 from the Ministry of Education, Science, and Culture.

References

1) If the l.f.s. is raised strongly, it is also conceivable that a crossover into the square planar(i.e., low spin) structure is brought about by this effect. In the present case, however, it seems that the steric effect is more important when the square planar structure is favored.

2) R. Tsuchiya, S. Joba, A. Uehara, and E. Kyuno, *Bull. Chem. Soc. Jpn.*, **46**, 1454 (1973).

3) H. Nishimoto, T. Yoshikuni, A. Uehara, E. Kyuno, and R. Tsuchiya, *Bull. Chem. Soc. Jpn.*, **51**, 1068 (1978).

4) Y. Ihara, E. Izumi, A. Uehara, R. Tsuchiya, S. Nakagawa, and E. Kyuno, *Bull. Chem. Soc. Jpn.*, **55**, 1028 (1982).

5) Such kind of thermal transformation was first observed by Tsuchiya et al.[6] with tetrakis(benzimidazole)-nickel(II) nitrate, but our studies on the complexes of *C*-substituted ethylenediamines added a number of new examples.[7–9]

6) R. Tsuchiya, E. Kyuno, A. Uehara, S. Joba, and S. Ohba, *Chem. Lett.*, **1976**, 911.

7) Y. Ihara, T. Kamishima, and R. Tsuchiya, *Thermochim. Acta*, **67**, 23 (1983).

8) Y. Ihara and R. Tsuchiya, *Bull. Chem. Soc. Jpn*, **57**, 2829 (1984).

9) Y. Ihara, *Bull. Chem. Soc. Jpn.*, **58**, 3248 (1985).

10) L. B. Clapp, *J. Am. Chem. Soc.*, **70**, 184 (1948).

11) H. Wenker, *J. Am. Chem. Soc.*, **57**, 2328 (1935).

12) C. J. Hawkins and R. M. Peachey, *Aust. J. Chem.*, **29**, 33 (1976).

13) R. C. Fuson, H. Gray, and J. J. Gouza, *J. Am. Chem. Soc.*, **61**, 1937 (1939).

14) In the preparation of the 1,2-bn complex with ClO_4^-, the ratio of $Ni(ClO_4)_2$: 1,2-bn was modified to 1:1.5, to prevent the contamination by the tris complex which can form easily when the ligand concentration is high.

15) S. Yamaki and Y. Fukuda, *Hitachi Scientific Instrument News*, **24**, 9 (1981).

16) A. B. P. Lever, *Coord. Chem. Rev.*, **43**, 63 (1982).

17) Y. Ihara, Y. Fukuda, and K. Sone, *Bull. Chem. Soc. Jpn.*, **59**, 1825 (1986).

18) A. B. P. Lever, E. Mantovani, and B. S. Ramaswamy, *Can. J. Chem.*, **49**, 1957 (1971).

19) Y. Fukuda, R. Morishita, and K. Sone, *Bull. Chem. Soc. Jpn.*, **49**, 1017 (1976).

20) L. D. Pettit and J. L. M. Swash, *J. Chem. Soc., Dalton Trans.*, **1977**, 697.

21) S. Yano, T. Tsukada, M. Saburi, and S. Yoshikawa, *Inorg. Chem.*, **17**, 2520 (1978).

22) S. Bagger, *Acta Chim. Scand., A*, **28**, 467 (1974).

23) Y. Nakayama, K. Matsumoto, S. Ooi, and H.

Kuroya, *Bull. Chem. Soc. Jpn.*, **50**, 2304 (1977).
24) R. J. Fitzgerald and R. S. Drago, *Inorg. Chem.*, **8**, 2254 (1969).
25) R. F. Evilia, D. C. Young, and C. N. Reilley, *Inorg. Chem.*, **10**, 433 (1971).
26) J. I. Zink and R. S. Drago, *J. Am. Chem. Soc.*, **92**, 5339 (1970).
27) S. C. Nyburg and J. S. Wood, *Inorg. Chem.*, **3**, 468 (1964).
28) C. J. Hawkins and J. A. Palmer, *Coord. Chem. Rev.*, **44**, 1 (1982).
29) C. J. Hawkins and R. M. Peachey, *Acta Chim. Scand., A*, **32**, 815 (1978).
30) T. W. Hambley, C. J. Hawkins, J. Martin, J. A. Palmer, and M. R. Snow, *Aust. J. Chem.*, **34**, 2505 (1981); according to these authors, the energies needed for such a "stand up" motion in $[Co(NH_3)_4(pn)]^{3+}$ and $[Co(NH_3)_4(dmbn)]^{3+}$ are 4.64 kJ mol^{-1} and 18.25 kJ mol^{-1}, respectively. They show that dmbn favors the equatorial conformation much more strongly than pn.

Synthesis of the 3*H*-Azepines Utilizing the Thermolysis of Substituted Aryl Azides

Yoshihiro OHBA,* Shinji KUBO, Masaaki NAKAI, Atsunori NAGAI, and Masayo YOSHIMOTO
Department of Chemistry, Faculty of Sciences, Yamaguchi University, Yamaguchi 753
(Received October 18, 1985)

Thermolysis of several *p*-substituted aryl azides (*p*-R-$C_6H_4N_3$; R=$COCH_3$, CO_2CH_3, COPh) in methanol gave 5-substituted 2-methoxy-3*H*-azepines in moderate yields. Thermolysis of *m*-substituted aryl azides (*m*-R-$C_6H_4N_3$; R=$COCH_3$, CO_2CH_3, COPh, NO_2) gave 4-substituted 2-methoxy-3*H*-azepines and 6-substituted 2-methoxy-3*H*-azepines in good yields. In contrast, thermolysis of *p*-azidoacetophenone in piperidine gave 5-acetyl-2-piperidino-3*H*-azepine and an unusual product, 6-acetyl-2-piperidino-3*H*-azepine, and *p*-aminoacetophenone.

Formation of 3*H*-azepines by the thermolysis and photolysis of aryl azides in methanol is well documented.[1-3]

In general, however, many attempts at the synthesis of 3*H*-azepines by the thermolysis or photolysis of aryl azides have failed or given low yields of 3*H*-azepines. Only succeeded experiment was the photolysis of o-azidobenzoic acids[4a-c] in alcohols. It has been considered that an electron-withdrawing substituent at *m*-or *p*-position of azidobenzene apparently prevents the azepine formation by decreasing the electron density on the carbon center at which the electrophilic single nitrene attacks.[4a]

We have investigated the thermolysis of *m*-azidoacetophenone (**2a**) and *p*-azidoacetophenone (**1a**), and in a preliminary communication[5] we have shown that the thermolysis of these azides in methanol gives ring-expansion products, 3*H*-azepines, in excellent yields. We now report the thermolysis of *p*-substituted aryl azides (**1**; R=$COCH_3$, CO_2CH_3, COPh, NO_2) and *m*-substituted aryl azides (**2**; R=$COCH_3$, CO_2CH_3, COPh, NO_2) in methanol and the thermolysis of **1a** and **1c** in piperidine and morpholine.

Results and Discussion

The thermolysis of methanol solution of **1a—c** in a sealed Pyrex tube at 170 °C gave 5-substituted 2-methoxy-3*H*-azepines (**3a—c**) in moderate yields. The results are shown in Table 1. The structure of all azepines (**3a—c**) was confirmed by ^1H NMR spectroscopy. The thermolysis of 1-azido-4-nitrobenzene (**1d**) at 190 °C for 2 h gave only tar.

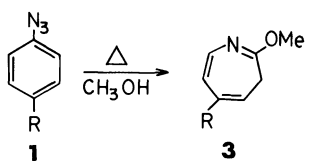

1 **3**

a: R=$COCH_3$
b: R=CO_2CH_3
c: R=COPh
d: R=NO_2

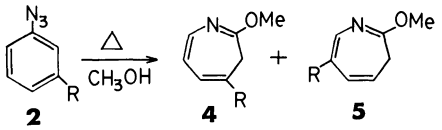

2 **4** **5**

a: R=$COCH_3$
b: R=CO_2CH_3
c: R=COPh
d: R=NO_2

Thermolysis of *m*-substituted aryl azides (**2a—d**) under the similar conditions also gave 6-substituted 3*H*-azepines (**5a—d**) and 4-substituted 3*H*-azepines (**4a—d**). These results are also shown in Table 1. The observed ratio of **5a—c** to **4a—c** shows that electron-withdrawing *m*-substituent ($COCH_3$. CO_2CH_3, COPh) favor an intramolecular cycloaddition of nitrene (**N**) at C-2 position to give **5a—c**. It is

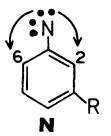

N

suggested from the failure to give 2-methoxy-3*H*-azepine in the thermolysis of azidobenzene in methanol that electron-withdrawing *m*- and *p*-substituents accelerate cycloaddition of singlet nitrene (**A**) to give azirne (**B**) and facilitate ring-expansion of (**C**) to 1*H*-azepine (**D**), which by prototropic migration yields 3*H*-azepine (**E**)(Scheme 1). In contrast with the thermolysis, the photolysis of **1a** and **2a** in methanol gave a low yields of 3*H*-azepines (**3a, 4a, 5a**). These results show that the thermolysis is superior to the photolysis for the formation of 3*H*-azepines from *m*-

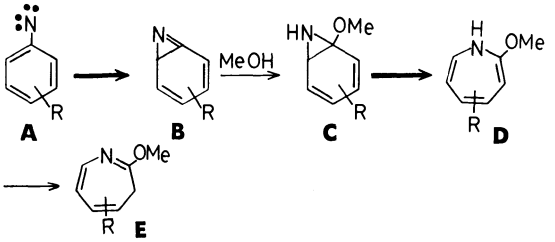

Scheme 1.

Table 1. Yieldes of 3*H*-Azepines

AZIDE	R[a]	Reaction Conditions Temp/°C	Time/h	Yield of Product/% 3	4	5
1a	*p*-$COCH_3$	170	4	60		
1b	*p*-CO_2CH_3	170	1.5	47		
1c	*p*-COPh	170	4	32		
1d	*p*-NO_2	190	2	—		
2a	*m*-$COCH_3$	170	4		25	58
2b	*m*-CO_2CH_3	170	2		35	63
2c	*m*-COPh	170	4		24	62
2d	*m*-NO_2	180	2		15	5

a) 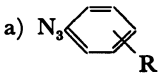

and *p*-substituted azidobenzenes.

The thermolysis of **1a** in piperidine at 170 °C for 2 h gave 5-acetyl-2-piperidino-3*H*-azepine (**6a**) (10%) and unexpected product, 6-acetyl-2-piperidino-3*H*-azepine (**7a**) (13%) and a triplet product,[7] *p*-aminoacetophenone (**8a**) (22%). The thermolysis of **1c** in piperidine at 170°C for 2 h gave 6-benozyl-2-piperidino-3*H*-azepine (**7c**) (18%) and *p*-aminobenzophenone (**8c**) (27%). The thermolysis of **1a** in morpholine at 170 °C for 2 h gave 5-acetyl-2-morpholino-3*H*-azepine (**13a**) (30%), 6-acetyl-2-morpholino-3*H*-azepine (**14a**) (22%) and *p*-aminoacetophenone (**8a**) (32%). The thermolysis of **1c** in morpholine at 170 °C for 6 h gave 6-benzoyl-2-

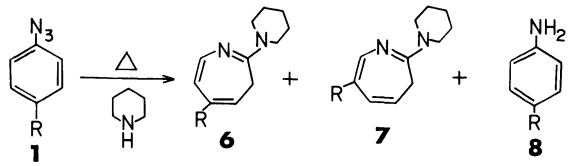

1 **6** **7** **8**

a: R=$COCH_3$
c: R=COPh

morpholino-3*H*-azepine (**14c**) (7%) and tar. The pathway to 6-acetyl-3*H*-azepine (**7a**) must involve the bicyclic valence isomers **10** and **11** (Scheme 2). Analogous step has been postulaed[8] for the formation of 1,3-diazepine by the thermal isomerzation of 1,2-diazepine. In support of the above mechanism, the thermal isomerzation of **6a** in piperidine at 170 °C for 6 h gave **7a** (85%). The thermal isomerization of **13a** in morpholine at 170 °C for 6 h gave **14a** in 75% yield. But the thermal isomerzation of **6a** in xylene at 170 °C for 6 h gave no **7a**, and **6a** was recovered in 91% yield. These results can be explained by the existence of the dipolar transition state or intermediae (**11**) for the formation of **7a** from **6a** in piperidine. Rate constant for this valence isomerization[9] was found to be 9.45×10^{-5} s^{-1}.

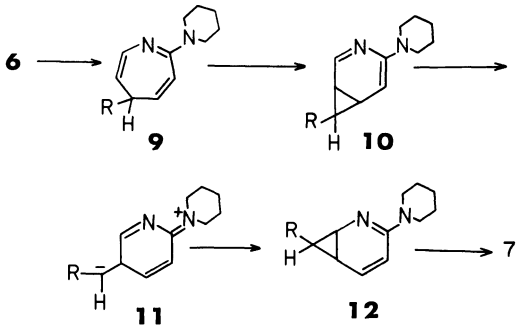

Scheme 2.

Experimental

Melting points were determined in a capillary tube. IR spectra were recorded for liquids as thin films and solids as KBr discs on a Japan Spectroscopic IR-G spectrometer. UV spectra were recorded in ethanol on a Hitachi 220A spectrophotometer. ^1H NMR spectra were recorded in $CDCl_3$ at 60 MHz using a Hitachi R24-B spectrometer (Me_4Si as internal standard). Mass spectra were determined with a JEOL JMS-01SG-2 spectrometer (75 eV). Unless otherwise stated recorded yields are based on the material after separation by medium-pressure liquid chromatography (Silica-gel Woelm 32—63 μm or aluminium oxide 200—300 mesh).

Preparation of Azidobenzenes. All azides were prepared from the corresponding amines by diazotization, followed by azidation with sodium azide. Azidobenzenes (**1b, 1d, 2b,** and **2d**) were prepared according to literature.[11a-c]

***p*-Azidoacetophenone (1a)** To a solution of *p*-aminoacetophenoe (1.00 g, 7.41 mmol) in acetic acid (10 ml), concd sulfulic acid (3 ml) was added under cooling (0—5 °C), and a solution of sodium nitrite (3.00 g, 43 mmol) in water (15 ml) was added over 15 min and stirrd at 0—5 °C for 2 h. A solution of sodium azide (5.00 g, 77 mmol) in water (23 ml) was added over 2 h and stirred at 0—5 °C for 1 h and extracted with ether. The extract was washed with water and dried over Na_2SO_4. Evaporation of the extract to dryness and chromatography of residue with hexane/ethyl acetate=3:1 on silica-gel (Wako Q-22) gave 879 mg (75%) of *p*-azidoacetophenone (**1a**); Yellow needles; mp 43—44 C(lit,[11a] mp 44 °C); Anal. ($C_8H_7O_1N_3$) C, H, N. IR(KBr) 3030, 2929, 2130, 2100, 1670, and 1598 cm^{-1}; ^1H NMR ($CDCl_3$) δ=2.58 (3H, s), 7.10 (2H d, J=8 H), and 7.95 (2H, d, J=8 Hz).

Following azides were prepared similarly:

***p*-Azidobenzophenone (1c)** (90%): Yellow needles; Anal. ($C_{13}H_9O_1N_3$) C, H, N.; mp 73—74 °C(lit,[12] mp 74 °C); IR(KBr) 3040, 2900, 2130, 2100, 1658, and 1592 cm^{-1}; ^1H NMR ($CDCl_3$) δ=7.0—7.8 (9H, m).

***m*-Azidoacetophenone (2a)** (86%): Yellow oil; Anal. ($C_8H_7O_1N_3$) C, H, N.; IR(oil) 3050, 2910, 2125, 2120, 1685, and 1585 cm^{-1}: ^1H NMR ($CDCl_3$) δ=2.58 (3H, s), and 7.05—7.80 (4H, m).

***m*-Azidobenzophenone (2c)** (93%): Yellow oil; Anal.

($C_{13}H_9O_1N_3$) C, H, N.); IR(oil) 3040, 2150, 2110, 1658, 1598, and 1580 cm^{-1}; ^1H NMR ($CDCl_3$) δ=7.10—7.90 (9H, m).

Thermolysis of *p*-Azidoacetophenone (1a). General procedure. A solution of 319 mg (1.98 mmol) of **1a** in methanol (10 ml) was sealed in a Pyrex tube and heated at 170 °C for 2 h. Evaporation of the solution to dryness gave dark brown oil which was chromatographed on silica-gel (Wako-gel Q-22) with benzene:ethyl acetate=3:1 to give 196 mg(60%) of 5-acetyl-2-methoxy-3*H*-azepine (**3a**) as yellow oil; Anal. ($C_9H_{11}O_2N_1$) C, H, N.; UV (95% C_2H_5OH) 220.0 (ε 15400) and 290 nm (sh, 1960); IR (oil) 2980, 2930, 2840, 1670, and 1620 cm^{-1}; ^1H NMR ($CDCl_3$) δ=2.38 (3H, s), 2.79 (2H, d, J=7.5 Hz), 3.73 (3H, s), 6.22 (1H, t, J=7.5 Hz), 6.52 (1H, d, J=8 Hz), 7.10 (1H, d, J=8 Hz), and 61 mg (23%) of *p*-aminoacetophenone.

Thermolysis of Methyl *p*-Azidobenzoate (1b). A solution of 102 mg (0.68 mmol) of **1b** in methanol (20 ml) was heated at 170 °C for 2 h to give 101 mg (97%) of methyl 2-methoxy-3*H*-azepine-5-carboxylate (**3b**)[4b] as yellow oil; Anal. ($C_9H_{11}O_3N_1$) C, H, N.; UV (95% C_2H_5OH) 285.0 nm (ε 2970); IR (oil) 2095, 2840, 1723, and 1627 cm^{-1}; ^1H NMR ($CDCl_3$) δ=2.74 (2H, d, J=7 Hz), 3.72 (3H, s), 3.79 (3H, s), 6.36 (1H, t, J=7 Hz), 6.48 (1H, d, J=8 Hz), 7.09 (1H, d, J=8 Hz).

Thermolysis of *p*-Azidobenzophenone (1c). Thermolysis of 256 mg (1.16 mmol) of **1c** in methanol (39 ml) at 170 °C for 4 h gave 84 mg of 5-benzoyl-2-methoxy-3*H*-azepine (**3c**) as yellow oil; Anal. ($C_{14}H_{13}O_2N_1$) C, H, N.; UV (95% C_2H_5OH) 251.0 nm (ε 15000); IR (oil) 3050, 2950, 2840, 1645, 1620, and 1595 cm^{-1}; ^1H NMR ($CDCl_3$) δ=2.76 (2H, d, J=7 Hz), 3.76 (3H, s) 5.83 (1H, t, J=7 Hz), 6.47 (1H, d, J=8 Hz), 7.06 (1H, d, J=8 Hz), 7.24—7.75 (5H, m).

Thermolysis of 1-Azido-4-nitrobenzene (1d). A solution of 360 mg (2.20 mmol) of **1d** in methanol (20 ml) was heated at 190 °C for 2 h to give no 3*H*-azepine and some tar.

Thermolysis of *m*-Azidoacetophenone (2a). A solution of 530 mg of **2a** in methanol (20 ml) was heated at 170 °C for 2 h. After the similar procedure, described for the thermolysis of **1a**, a mixture of 330 mg (61%) of 6-acetyl-2-methoxy-3*H*-azepine (**5a**) and 122 mg (22%) of 4-acetyl-2-mehoxy-3*H*-azepine (**4a**) was obtained. The yields of **5a** and **4a** were determined by ^1H NMR. The analytical samples of **4a** and **5a** were obtained by HPLC (Dupont Zorbax ODS, 15.0 cm×4.6 mm; solvent, MeOH/H_2O=1:1), giving **5a** as yellow oil; Anal. ($C_9H_{11}O_2N_1$) C, H, N.; UV (95% C_2H_5OH) 217.0 (ε 18300) and 288.5 nm (13900); IR (oil) 2990, 2940, 2840, 1658, and 1615 cm^{-1}; ^1H NMR ($CDCl_3$) δ=2.43 (3H, s), 2.66 (2H, d, J=7 Hz), 3.73 (3H, s), 5.47 (1H, dt, J=9 and 7 Hz), 6.79 (1H, dd, J=9 and 1 Hz), 7.94 (1H, d, J=1 Hz) and **4a** as yellow; oil Anal. ($C_9H_{11}O_2N_1$) C, H, N.; UV (95% C_2H_5OH) 221.0 (ε 12800) and 313.0 nm (6400); IR (oil) 2990, 2940, 2840, 1658, and 1615 cm^{-1}; ^1H NMR ($CDCl_3$) δ=2.37 (3H, s). 2.98 (2H, s), 3.70 (3H, s), 6.09 (1H, dd, J=8 and 6 Hz), 7.14 (1H, dd, J=6 and 1 H), 7.22 (1H, dd, J=8 and 1 Hz).

Thermolysis of Methyl *m*-Azidobenzoate (2b). A solution of 640 mg (3.62 mmol) of **2b** in methanol (20 ml) was heated a 170 °C for 2 h to give a mixture of 396 mg (60%) of methyl 2-methoxy-3*H*-azepine-6-carboxylate (**5b**) and 222 mg (34%) of methyl 2-methoxy-3*H*-azepine-4-carboxylate (**4b**). Analytical samples were obtained by HPLC under the same conditions used for **4a** and **5a**, giving **5b** as yellow oil; Anal. ($C_9H_{11}O_3N_1$) C, H, N.; UV (C_2H_5OH) 280.0 nm, (ε 6650); IR (oil) 2960, 2940, 2820, 1708, and 1605 cm^{-1}; ^1H NMR ($CDCl_3$) δ=2.60 (2H, d, J=7 Hz), 3.75 (3H, s), 3.80 (3H, s), 5.40 (1H, dt, J=9 and 7 Hz), 6.74 (3H, s), 3.80 (3H, s), 5.40 (1H, dt, J=9 and 7 Hz), 6.74 (1H, dd, J=9 and 2 Hz), 8.05 (1H, d J=2 Hz) and **4b** as yellow oil; Anal. ($C_9H_{11}O_3N_1$) C, H, N.; UV (95% C_2H_5OH) 213.5 (ε 6610) and 308.0 nm (5430); IR (oil) 2960, 2910, 2825, 1704, and 1615 cm^{-1}; ^1H NMR ($CDCl_3$) δ=3.01 (2H, s), 3.73 (3H, s), 3.80 (3H, s), 6.03 (1H, dd, J=6 and 8 Hz), 7.20 (1H, dd, J=8 and 1 Hz), 7.27 (1H, dd, J=6 and 1 Hz).

Thermolysis of *m*-Azidobenzophenone (2c). A solution of 241 mg (1.08 mmol) of **2c** in methanol (10 ml) was heated at 170 °C for 4 h to give the mixture of 152 mg (62%) of 6-benzoyl-2-methoxy-3*H*-azepine (**5c**) and 58 mg (24%) of 4-benzoyl-2-methoxy-3*H*-azepine (**4c**). Analytical samples were obtained similarly. **5c**; yellow oil; Anal. ($C_{14}H_{13}O_2N_1$) C, H, N.; UV (C_2H_5OH) 245.0 (ε 9300) and 296.0 nm (9620); IR (oil) 3050, 3000, 2940, 1640, and 1605 cm^{-1}; ^1H NMR ($CDCl_3$) δ=2.80 (2H, d, J=6 Hz), 3.80 (3H, s), 5.60 (1H, dt, J=9 and 6 Hz), 6.94 (1H, dd, J=9 and 1 Hz), 7.70 (1H, d, J=1 Hz). **4c**; yellow oil; Anal. ($C_{14}H_{13}O_2N_1$) C, H, N.; UV (C_2H_5OH) ca. 240 (sh, ε 7430) and 318.0 nm (5330); IR (oil) 3020, 2930, 2850, 1640, and 1618 cm^{-1}; ^1H NMR ($CDCl_3$) δ=3.16 (2H, s), 3.58 (3H, s), 6.06 (1H, dd, J=8 and 6 Hz), 6.94 (1H, d, J=6 Hz), 7.20 (1H, d, J=8 Hz), 7.3—7.8 (5H, m).

Thermolysis of 1-Azido-3-nitrobenzene (2d). A solution of 231 mg (1.41 mmol) of **2d** in methanol (20 ml) was heated at 180 °C for 2 h to give the mixture of 11 mg (5%) of 6-nitro-2-methoxy-3*H*-azepine (**5d**) and 36 mg (15%) of 4-nitro-2-methoxy-3*H*-azepine (**4d**). 5d; colorless oil; Anal. ($C_7H_8O_3N_2$) C, H, N.; UV (95% C_2H_5OH) 224.0 (ε 7030) and 323.0 nm (5990); IR (oil) 2980, 2940, 2850, and 1605 cm^{-1}; ^1H NMR ($CDCl_3$) δ=2.75 (2H, d, J=7 Hz), 3.73 (3H, s), 5.48 (1H, dt, J=9 and 7 Hz), 7.00 (1H, dd, J=9 and 2 Hz), 8.43 (1H, d, J=2 Hz). **4d**; yellow oil; Anal. ($C_7H_8O_3N_2$) C, H, N.; UV (95% C_2H_5OH) 231.5 (ε 9900) and 347.5 nm (4910); IR (oil) 2980, 2930, 2840, and 1623 cm^{-1}; ^1H NMR ($CDCl_3$) δ=3.33 (2H, s), 3.76 (3H, s), 6.00 (1H, dd, J=8 and 6 Hz), 7.31 (1H, dd, J=8 and 1 Hz), 7.64 (1H, dd, J=8 and 1 Hz).

Phtolysis of *p*-Azidoacetophenone (1a) in Methanol. A solution of 500 mg (3.11 mmol) of **1a** in methanol (400 ml) was irradiated (Ushio 100 W high pressure Hg lamp with Pyrex filter) for 5 h under nitrogen to give 40 mg (8%) of **3a** and intractable tar. The reaction was monitored using HPLC,[6] and **1a** was consumed completely.

Photolysis of *m*-Azidoacetophenone (2a) in Methanol. A solution of 425 mg (2.64 mmol) of **2a** in methanol (400 ml) was irradiated under the similar conditions to give 26 mg (8%) of the mixture of **4a** (2%) and **5a** (6%). An intractable tar was also obtained, and **2a** was consumed completely.

Thermolysis of *p*-Azidoacetophenone (1a) in Piperidine. A solution of 300 mg (1.86 mmol) of **1a** in piperidine (20 ml) was heated at 170 °C for 2 h. The reaction mixture was chromatographed by medium-pressure liquid chromatography (aluminium oxide 200—300 mesh) with ethyl acetate/hexane=1:3 to give 53 mg (13%) of 6-acetyl-2-piperidino-3*H*-azepine (**7a**) as brown oil; Found: M^+, 218.1395. Calcd for $C_{13}H_{18}O_1N_2$: M^+, 218.1418.[10] UV (95%

C_2H_5OH) 231.5 (ε 13400) and 335.0 nm (22700); IR (oil) 2980, 2920, 2850, 1638, and 1602 cm^{-1}; ^1H NMR ($CDCl_3$) δ=1.46—1.78 (6H, m), 2.39 (3H, s), 2.70 (2H. d. J=7 Hz), 3.37—3.73 (4H, m), 5.23 (1H, dt, J=8 and 7 Hz), 6.88 (1H dd, J=8 and 1.5 Hz), 8.07 (1H, d, J=1.5 Hz) and 41 mg (10%) of 5-acetyl-2-piperidino-3*H*-azepine (**6a**) as brown oil; Found: N, 12.94%; Calcd for $C_{13}H_{18}O_1N_2$: N, 12.83%; UV (95% C_2H_5OH) 230.0 (sh, ε 15600) and 325.0 nm (4350); IR (oil) 2980, 2920, 2850, 1705, and 1668 cm^{-1}; ^1H NMR ($CDCl_3$) δ=1.51—1.84 (6H, m), 2.36 (3H, s), 2.77 (2H, d, J=7.5 Hz), 3.34—3.70 (4H m), 5.93 (1H, dt, J=1 and 7.5 Hz), 6.23 (1H, dd, J=8 and 1 Hz), 7.20 (1H, d, J=8 Hz), and 54 mg (22%) of **8a**.

Thermolysis of 1a in Morpholine. Thermolysis of 272 mg (1.69 mmol) of **1a** in morpholine (20 ml) a 170 °C for 2 h gave 82 mg (22%) of 6-acetyl-2-morpholino-3*H*-azepine (**14a**) as yellow oil; Found: N, 12.94%; Calcd for $C_{12}H_{16}O_2N_2$; N, 12.72%; UV (95% C_2H_5OH) 231.5 (ε 6000) and 330.5 nm (9190); IR (oil) 2940, 2890, 2840, 1636, and 1600 cm^{-1}; ^1H NMR ($CDCl_3$) δ=2.42 (3H, s), 2.72 (2H, d, J=7 Hz), 3.25—4.11 (8H, m), 5.24 (1H, dt, J=9 and 7 Hz), 6.89 (1H, dd, J=9 and 1 Hz), 8.09 (1H, d, J=1 Hz), and 110 mg (30%) of 5-acetyl-2-morpholino-3*H*-azepine (**13a**) as yellow oil; Found: M^+, 220.1218. Calcd for $C_{12}H_{16}O_2N_2$: M^+, 220.1211.[10]; UV (95% C_2H_5OH) 233.0 (ε 7780) and 274.5 nm (6250); IR (oil) 2950, 2880, 2840, 1668, and 1563 cm^{-1}; ^1H NMR ($CDCl_3$) δ=2.37 (3H, s), 2.75 (2H, d, J=7 Hz), 3.23—3.79 (8H, m), 5.99 (1H, td, J=7 and 1 Hz), 6.32 (1H, dd, J=9 and 1 Hz), 7.22 (1H, d, J=9 Hz), and 72 mg (32%) of **8a**.

Thermolysis of 1c in Piperidine. A solution of 270 mg (1.21 mmol) of **1c** in piperidine (20 ml) was heated at 170 °C for 2 h to give 61 mg (18%) of 6-benzoyl-2-piperidino-3*H*-azepine (**7c**) as yellow oil; Found: M^+, 280.1577. Calcd for $C_{18}H_{20}O_1N_2$: M^+, 280.1575.[10]; UV (95% C_2H_5OH) 235.5 (ε 9270) and 347.0 nm (12200); IR (oil) 3010, 2930, 2850, 1625, and 1600 cm^{-1}; ^1H NMR ($CDCl_3$) δ=1.01—1.92 (6H, m), 2.81 (2H, d, J=7 Hz), 3.23—3.95 (4H, m), 5.27 (1H, dt, J=9 and 7 Hz), 7.04 (1H, dd, J=9 and 1.5 Hz), 7.23—7.85 (5H, m), 7.89 (1H, d, J=1.5 Hz), and 64 mg (27%) of **8c**.

Thermolysis of 1c in Morpholine. Thermolysis of 191 mg (0.86 mmol) of **1c** in morpholine (10 ml) at 170 °C for 2 h gave 16 mg (7%) of 6-benzoyl-2-morpholino-3*H*-azepine (**14c**) as brown oil; Found: M^+, 282.1361. Calcd for $C_{17}H_{18}O_2N_2$: M^+, 282.1367.[10]; UV (95% C_2H_5OH) 340.5 (ε 15100) and 237.0 nm (12200); IR (oil) 2940, 2890, 2840, 1626, and 1595 cm^{-1}; ^1H NMR ($CDCl_3$) δ=2.79 (2H, d, J=7 Hz), 3.63 (8H m) 5.29 (1H, dt, J=9 and 7 Hz), 7.02 (1H, dd, J=9 and 1 Hz), 7.20—7.80 (5H, m), 7.85 (1H, d, J=1 Hz).

Thermolysis of 5-Acetyl-2-piperidino-3*H*-azepine (6a) in Piperidine. A solution of 44 mg (0.2 mmol) of **6a** in piperidine (4 ml) was heated at 170 °C for 6 h. The solution was evaporated and the residue was chromatographed by medium-pressure liquid chromatography (aluminium oxide 200—300 mesh, hexane/ethyl acetate=3:1) to give 35 mg (80%) of **7a** and no **6a**.

Thermolysis of 5-Acetyl-2-piperidino-3*H*-azepine (6a) in Xylene. A solution of 44 mg (0.2 mmol) of **6a** in xylene (4 ml) was heated at 170 °C for 6 h and the similar procedure gave 36 mg (82%) of recovered **6a** and no other products.

Thermolysis of 5-Acetyl-2-morpholino-3*H*-azepine (13a) in Morpholine. A solution of 54 mg (0.25 mmol) of **13a** in morpholine (4 ml) was heated at 170 °C for 6 h and the similar procedures described above gave 40 mg (74%) of 6-acetyl-2-morpholino-3*H*-azepine (**14a**).

The authors wish to express their thanks to Dr. Nobuo Kato of Kyushu University for mass spectral determination.

References

1) A. C. Mair and M. F. G. Steven, *J. Chem. Soc. (C)*, **1971**, 2317.

2) R. J. Sundberg and R. H. Smith, Jun., *J. Org. Chem.*, **36**, 295 (1971).

3) M. A. Berwirck, *J. Am. Chem. Soc.*, **93**, 5780 (1971).

4) a) R. Purvis, R. K. Smalley, W. A. Strachan, and H. Suschitzky, *J. Chem. Soc., Perkin Trans. 1*, **1978**, 191; b) R. Purvis, R. K. Smalley, H. Suschitzky, and M. A. Alkhader, *J. Chem. Soc., Perkin Trans. 1*, **1984**, 249; c) M. A. Ardakani, S. M. Salem, R. K. Smalley, and D. I. Patel, *J. Chem. Soc., Perkin Trans. 1*, **1985**, 1121.

5) Y. Ohba, S. Kubo, T. Nishiwaki, and N. Aratani, *Heterocycles*, **22**, 457 (1984).

6) HPLC; Column conditions: Dupont Zorbax ODS, 15.0 cm×4.6 mm; solvent, MeOH/H_2O=1:1.

7) D. S. Breslow and E. I. Edwards, *Tetrahedron Lett.*, **1967**, 2123.

8) J. A. Moore, W. J. Freeman, R. C. Gearhart, and H. B. Yokelson, *J. Org. Chem.*, **43**, 787 (1978).

9) A solution of **6a** in piperidine was sealed in a Pyrex tube and heated at 170 °C. Disappearance rate of **6a** was obtained from recovered yield of **6a** obtained by ^1H NMR spectra.

10) Some of 2-piperidino- or 2-morpholino-3*H*-azepines are not fully stable. These structures are confirmed by high resoluton mass spectra.

11) a) M. Apple and R. Huisgen, *Chem. Ber.*, **92**, 2951 (1959); b) P. A. S. Smith and J. H. Hall, *J. Am. Chem. Soc.* **84**, 480 (1962); c) H. Rupe and K. Majewski, *Ber.*, **33**, 3401 (1900).

12) O. Dimroth and K. Pfister, *Ber.*, **43**, 2757 (1910).

The Synthesis of Dihydro-2(3*H*)-thiophenone Derivatives

Yoichi TAGUCHI* and Yasuo SUHARA
National Chemical Laboratory for Industry, Higashi 1-1, Yatabe, Tsukuba, Ibaraki 305
(Received January 22, 1986)

The reaction of 2,2-dimethylthiirane (**4**) with diethyl malonate (**5**) in the presence of sodium ethoxide gave 3-ethoxycarbonyl-5,5-dimethyl-dihydro-2(3*H*)-thiophenone (**6**) and a polymer. The yield of **6** could be increased to 65%. The reaction of thiirane, 2-methylthiirane, 2-butylthiirane, 2-hexylthiirane, 1,2-epithiocyclohexane, and 2-phenylthiirane with **5** also gave corresponding dihydro-2(3*H*)-thiophenone derivatives. Although the reaction of an alkyl-substituted thiirane with **5** selectively gave a product formed by an attack of a carbanion at the less-hindered carbon of the thiirane ring, the major product of the reaction of 2-phenylthiirane with **5** was an isomer formed by an attack at the more hindered carbon of the thiirane ring. The reaction of **4** with ethyl acetoacetate gave 3-acetyl-5,5-dimethyl-dihydro-2(3*H*)-thiophenone selectively. A product **6** was also obtained by a reaction of **4** with **5** by using sodium hydride instead of sodium ethoxide.

It was reported that a reaction of thiiranes with ethyl cyanoacetate[1] and malononitrile[2] in the presence of a base catalyst has dihydrothiophene derivatives (**3**). The first step of these reactions was considered to be the formation of an intermediate **1** by an attack of carbanion to the thiirane ring, and a following ring closure by the reaction of thiol **1** with

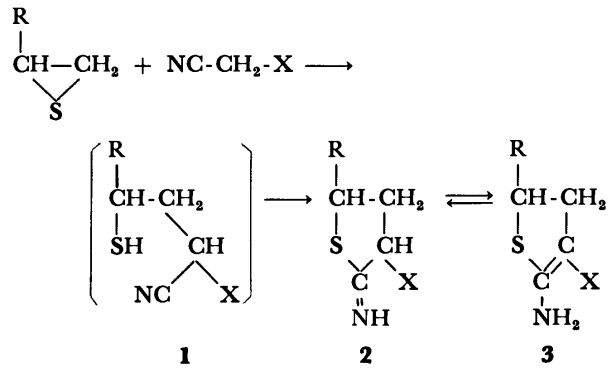

1 **2** **3**

the cyano group. This ring closure was considered to inhibit the polymerization of **1** with thiirane. Though it was reported[1] that the reaction of thiiranes with other active methylene compounds with cyano groups attached to the methylene gave only polymers, we expected that a ring closure similar to the condensation of **1** occured in the reaction of thiiranes with β-oxo-esters.

In this work, we found that the reaction of thiiranes with diethyl malonate (**5**) and ethyl acetoacetate gave dihydro-2(3*H*)-thiophene derivatives. The direction of the attack of carbanions to the thiirane rings, the effect of the structures of the thiiranes and the active methylene compounds, and the effect of the reaction conditions were studied.

Results and Discussion

The reaction of **4** with **5** in the presence of sodium ethoxide gave 3-ethoxycarbonyl-5,5-dimethyl-dihydro-2(3*H*)-thiophenone (**6**) selectively and did not give it's isomer, 3-ethoxycarbonyl-4,4-dimethyl-dihydro-2(3*H*)-thiophenone (**7**). This shows that the carbanion formed from **5** selectively attacked the sterically less-hindered terminal carbon of the thiirane; this selectivety is similar to that in a reaction of thiiranes with ethyl cyanoacetate,[1] malononitrile,[2] and the secondary amine.[6]

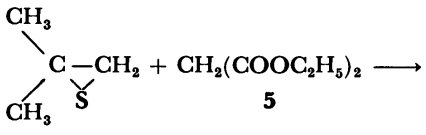

4 **5**

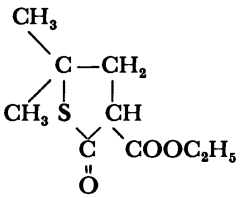

6

Table 1 shows the effects of the reaction conditions on a reaction of **4** with **5**. A product which was insoluble in water and ether was obtained, and the ^{1}H NMR and IR spectra of this product showed that it was a polymer of **4** with a few carbonyl groups. The yield of **6** decreased and the ratio of the polymer to **6** increased at lower temperatures or by using more ethanol. By using less ethanol and a great exess of **5**, the yield of **6** increased to 65% (Run 7).

Table 2 shows the products and their yields in the reactions of various thiiranes with **5**. Thiiranes have a tendency to easily polymerize such molecules as thiirane, 2-methylthiirane and 1,2-epithiocyclohexane reacted with **5** to give corresponding dihydro-2(3*H*)-thiophenones in low yield. Although a reaction of alkyl-substituted thiiranes with **5** gave a product corresponding to **6**, selectively, the major product of a reaction of 2-phenylthiirane with **5** was 3-ethoxycarbonyl-4-phenyl-dihydro-2(3*H*)-thiophenone, corresponding to **7**. The different reactivity of 2-phenylthiirane from alkyl-substituted thiiranes was cosidered to be due to a polymerization of 2-phenylthiirane by the phenyl group.

Table 1. Effect of Reaction Conditions on the Reaction of 2,2-Dimethylthiirane with Diethyl Malonate[a)]

Run	Sulfide mmol	Malonate mmol	Sodium mmol	EtOH ml	Temp °C	Time h	Yield %	Solid[b)] g
1	10	20	15	50	Reflux	1	17	0.51
2	10	20	15	50	30	1	4	0.41
3	10	20	15	50	30	5	6	0.52
4	10	20	15	200	Reflux	1	2	0.24
5	10	20	15	10	Reflux	1	34	0.63
6	5	20	15	10	Reflux	1	46	0.11
7	5	40	30	20	Reflux	1	65	0.02

a) Nitrogen atmosphere. b) Polymer of 2,2-dimethylthiirane.

Table 2. The Reaction of Various Thiiranes with 5[a)]

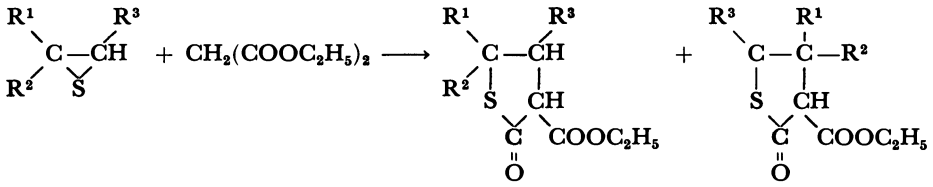

R^1	R^2	R^3	Yield/% (A)	Yield/% (B)
H	H	H	38	
CH_3	H	H	48	—
CH_3	CH_3	H	65	—
n-C_4H_9	H	H	59	—
n-C_6H_{13}	H	H	58	—
H	$-(CH_2)_4-$		40	
C_6H_5	H	H	18	45

a) Same reaction conditions to Run 7 in Table 1 were used.

Table 3 shows the products and their yields in the reaction of **4** with malononitrile, ethyl cyanoacetate, and ethyl acetoacetate under the same reaction conditions as that of reaction of **4** with **5** (Run 1 and Run 7 in Table 1). The reaction of **4** with diethyl methylmalonate scarcely gave the corresponding dihydro-2(3*H*)-thiophenone. In the reaction of thiiranes with ethyl cyanoacetate, Snyder and Alexander[1)] could not determine the ratio of the tautomers, **2** and **3**. It was found that the equilibrium was shifted to **3** on the basis of a ^1H NMR analysis. It was also observed that the product of the reaction of **4** with ethyl acetoacetate was a tautomeric mixture, and the ratio of the tautomers **8** and **9** was about 6:4 from an analysis of the 400-MHz ^1H NMR and ^{13}C NMR.

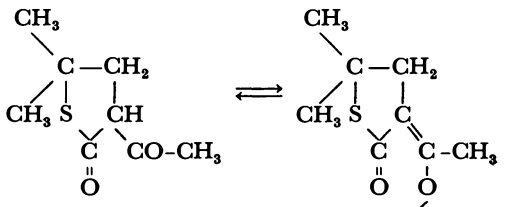

8 **9**

A pronounced increase in the yield was observed in a reaction of **4** with active methylene compounds having ester groups (such as **5** and ethyl acetoacetate) when an active methylene compound was used in great exess (Yield II in Table 3).

Table 3. The Reaction of **4** with Active Methylene Compounds

Reactant		Yield/% I[a]	Yield/% II[b]
$CH_2(CN)_2$	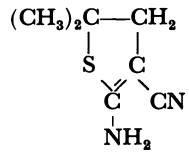	50	62
$NCCH_2COOC_2H_5$	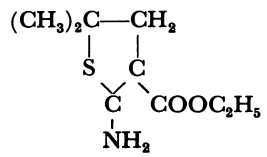	43	70
$CH_2(COOC_2H_5)_2$	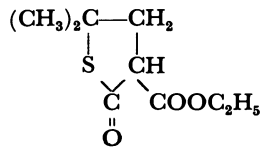	17	65
$CH_3COCH_2COOC_2H_5$	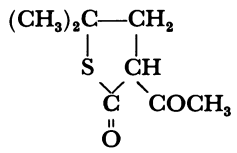	8	27

a) Same reaction conditions to Run 1 in Table 1 were used. b) Same reaction conditions to Run 7 in Table 1 were used.

Table 4. Solvent Effect on the Reaction of **4** with **5**[a]

Solvent	Yield %	**5**[b] %	Solid[c] g
CH_3CN	16	38	0.36
DMSO	5	65	0.82
DMF	9	58	0.71
THF	21	38	—

a) Solvent, 15 ml; NaH, 15 mmol; **4**, 10 mmol; **5**, 20 mmol; reaction temperature, 80 °C; time, 3 h. b) Recovered after the reaction. c) Polymer of **4**.

Compound **6** could be obtained by using sodium hydride instead of sodium ethoxide. Table 4 shows the effects of a solvent on the reaction of **4** with **5** in the presence of sodium hydride. Polar solvents, such as DMF and DMSO, make the yield of **6** low, and make that of the polymer high. A better result was obtained when acetonitrile or THF was used as a solvent. The use of nonpolar solvents did not produce a good result since it could not dissolve the sodium salt of **5**. The yield in a reaction using sodium hydride was lower than that using sodium ethoxide.

The reaction of **4** with **5** was considered to involve three different reactions; 1) the polymerization of thiirane by sodium ethoxide (Eq. 2), 2) the polymerization of **8** with **4** (Eq. 3) and 3) the formation of **6** by a ring-closure reaction (Eq. 4). An intermediate **10** was very reactive and could not be detected through an analysis after the reaction. Although it was

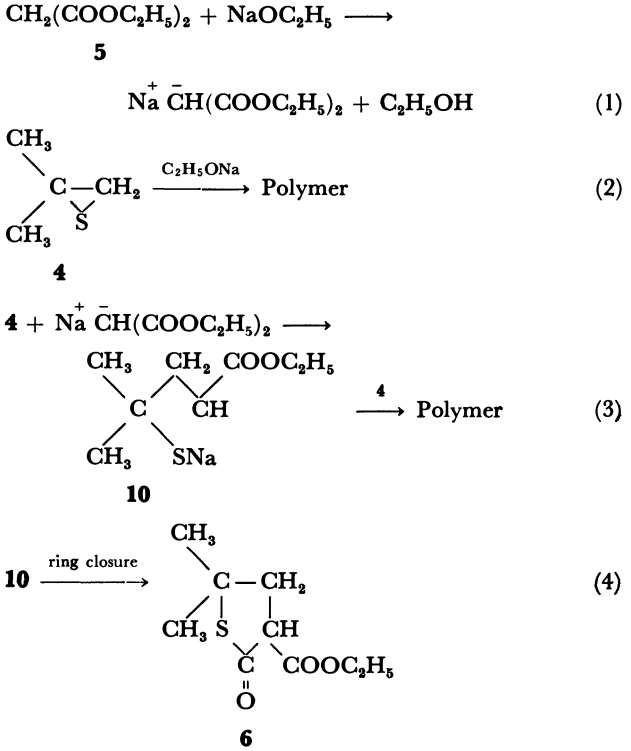

presumed that a large amount of ethanol was favorable for an intramolecular condensation and

increased the yield of **6**, an opposite result occurred since the polymerization of **4** was accerelated by the sodium ethoxide (Eqs. 1, 2). When a large amount of active methylene compounds was used, higher effect was observed in the reaction of **4** with **5** or ethyl acetoacetate than these in the reaction of **4** with malononitrile and ethyl cyanoacetate. This was attributed to the fact that dihydro-2(3*H*)-thiophenone derivatives were more stable than dihydrothiophene derivatives having amino groups. Though **6** had active methine, and could possibly react with thiirane, its high steric hinderance was expected to disturb the reaction, because the reaction of **4** with diethyl methylmalonate scarcely gave the dihydro-2(3*H*)-thiophenone derivative.

Experimental

Measurement. GLC was carried out with a JEOL 20KF chromatograph equiped with 20% SE-30 columns. ^{1}H NMR spectra were measured with a Hitachi R-40 spectrometer. Mass spectra were measured with a JEOL D-300 GC-MS spectrometer using the CI(chemical ion) method with isobutane. IR spectra were obtained on a JASCO A302 spectrophotometer.

Materials. 2-Butylthiirane and 2-hexylthiirane were prepared as previously described.[3] 2,2-Dimethylthiirane-(4)[4], 1,2-epithiocyclohexane[4] and 2-phenylthiirane[5] were prepared according to a procedure described in the literature.

Reaction of Thiirane with 5. A typical procedure is as follows: To a solution prepared by disolving 0.70 g of sodium in 20 ml of absolute ethanol was added 6.40 g of **5** under a nitrogen atmosphere. This mixture was refluxed while 0.44 g of **4** was added dropwise over a period of one hour. Refluxing continued for more than one hour; then, the solution was poured into ice-cold water. The solution was acidified with dilute hydrochloric acid and extracted with ether. An insoluble polymeric material was filtered off and dried in vacuo. An organic layer was dried over anhydrous sodium sulfate and after the evaporation of solvent the residue was distilled in vacuo. This distillate was purified to give 3-ethoxycarbonyl-5,5-dimethyl-dihydro-2(3*H*)-thiophenone (**6**) by column chromatography on silica gel using a mixture of petroleum benzine (bp 50—90 °C) and ethyl acetate (100:1 v/v) as an eluent. IR: 1730 cm^{-1}, 1687 cm^{-1}, ^{1}H NMR δ=1.30 (t, 3H, CH_3), 1.57 (s, 3H, CH_3), 1.64 (s, 3H, CH_3), 2.17—2.76 (m, 2H, CH_2), 3.75—4.05 (quar, 1H, CH), 4.25 (quar, 2H, CH_2); QM$^+$: 203.

Thiirane, 2-methylthiirane, 2-butylthiirane, 2-hexylthiirane, 1,2-epithiocyclohexane, and 2-phenylthiirane were treated with **5**. The spectral data of these products are as follows:

3-Ethoxycarbonyl-dihydro-2(3*H*)-thiophenone. IR: 1740 cm^{-1}, ^{1}H NMR δ=1.29 (t, 3H, CH_3), 2.42—2.75 (m, 2H, CH_2), 3.20—3.70 (m, 3H, CH, SCH_2); QM$^+$: 175.

3-Ethoxycarbonyl-5-methyl-dihydro-2(3*H*)-thiophenone. IR, 1739 cm^{-1}, 1700 cm^{-1}, ^{1}H NMR δ=1.28 (t, 3H, CH_3), 1.47 (d, 1.5H, CH_3), 1.54 (d, 1.5H, CH_3), 1.80—2.95 (m, 2H, CHCO, CHS), 4.25 (quar, 2H, OCH_2); QM$^+$: 189.

5-Butyl-3-ethoxycarbonyl-2(3*H*)-thiophenone. IR: 1732 cm^{-1}, 1693 cm^{-1}, ^{1}H NMR δ=0.94 (t, 3H, CH_3), 1.30—2.00 (m, 6H, $(-CH_2-)_3$), 2.03—2.93 (m, 2H, CH_2), 3.47—3.80 (m, 1H, CHS), 3.75—4.10 (m, 1H, CHCO), 4.22 (quar, 2H, CH_2O); QM$^+$; 231.

9-Ethoxycarbonyl-7-thiabicyclo[4,3,0]nonane-8-one. IR: 1740 cm^{-1}, 1700 cm^{-1}, ^{1}H NMR δ=1.28 (t, 3H, CH_3), 1.05—2.70 (m, 9H, $(-CH_2-)_4$, CH), 3.05—3.65 (m, 2H, SCH, CHCO), 4.25 (quar, 2H, CH_2); QM$^+$: 229.

3-Ethoxycarbonyl-4-phenyl-2(3*H*)-thiophenone. IR: 1727 cm^{-1}, 1688 cm^{-1}, ^{1}H NMR δ=1.18 (t, 3H, CH_3), 3.40—4.40 (m, 4H, PhCH, CH_2S, CH_2), 7.33 (s, 5H, C_6H_5); QM$^+$: 251.

3-Ethoxycarbonyl-5-phenyl-2(3*H*)-thiophenone. IR: 1740 cm^{-1}, 1700 cm^{-1}, ^{1}H NMR δ=1.30 (t, 3H, CH_3), 2.25—3.15 (m, 2H, CH_2), 3.40—4.00 (m, 1H, CHCO), 4.25 (quar, 2H, CH_2), 4.80—5.10, 5.17—5.40 (m, 1H, PhCH), 7.25—7.60 (m, 5H, C_6H_5); QM$^+$: 251.

Reaction of 4 with Other Active Methylene Compounds. Compound **4** was reacted with ethyl cyanoacetate, malononitrile, and ethyl acetoacetate in a similar way to that for the reaction with **5**. The spectral data of these products are as follows:

2-Amino-3-ethoxycarbonyl-5,5-dimethyl-4,5-dihydrothiophene. IR: 3392 cm^{-1}, 1644 cm^{-1}, 1616 cm^{-1}, ^{1}H NMR δ=1.26 (t, 3H, CH_3), 1.51 (s, 6H, $2CH_3$), 2.83 (s, 2H, CH_2), 4.14 (quar, 2H, OCH_2), 6.00 (s, 2H, NH_2); QM$^+$: 155.

2-Amino-3-cyano-5,5-dimethyl-4,5-dihydrothiophene. IR: 3416 cm^{-1}, 1630 cm^{-1}, ^{1}H NMR δ=1.52 (s, 6H, $2CH_3$), 2.73 (s, 2H, CH_2), 4.80 (s, 2H, NH_2); QM$^+$: 202.

3-Acetyl-5,5-dimethyl-dihydro-2(3*H*)-thiophenone. IR: 1718 cm^{-1}, 1680 cm^{-1}, 1641 cm^{-1}, 1586 cm^{-1}, ^{1}H NMR (400 MHz): (keto type) δ=1.58 (s, 3H, CH_3), 1.62 (s, 3H, CH_3), 2.38 (s, 3H, $COCH_3$), 1.90—2.90 (m, 2H, CH_2), 3.90—4.20 (dd, 1H, CH). (enol type) δ=1.56 (s, 6H, $2CH_3$), 1.96 (s, 3H, CH_3-), 2.73 (s, 2H, CH_2); ^{13}C NMR: (keto type) δ=30.23, 31.25, 31.19, 42.23, 52.91, 65.77, 201.21, 202.07. (enol type) δ=19.91, 30.77(2C), 43.72, 52.63, 109.45, 166.11, 202.79; QM$^+$: 173.

The authors wish to express their thanks to Dr. Hiroshi Nakanishi and Dr. Yoshinobu Nagawa for the analysis of 3-acetyl-5,5-dimethyl-dihydro-2(3*H*)-thiophenone by 400 MHz ^{1}H NMR and ^{13}C NMR.

References

1) H. R. Snyder and W. Alexander, *J. Am. Chem. Soc.*, **70**, 217 (1948).
2) Hisamitsu Pharmceutical Co. Ltd., Japan Patent, 13164 (1974).
3) Y. Suhara and Y. Taguchi, *Yukagaku*, **25**, 848 (1976).
4) H. R. Snyder, J. M. Stewart, and J. B. Ziegler, *J. Am. Chem. Soc.*, **69**, 2672 (1947).
5) J. M. Stewart, *J. Org. Chem.*, **28**, 596 (1963).
6) Y. Taguchi and Y. Suhara, *Yukagaku*, **33**, 280 (1984).

ESR Study of Radical Halogen Abstractions. Participation of Electron-Transfer Mechanism in the Radical Halogen Abstractions

Yoko KUWAE, Mikiharu KAMACHI,* Koichiro HAYASHI,† and Heinz G. VIEHE††
Department of Macromolecular Science, Faculty of Science, Osaka University, Toyonaka, Osaka 560
†Institute of Science and Industrial Research, Osaka University, Mihogaoka, Ibaraki, Osaka 567
††Laboratory of Organic Chemistry, University of Louvain, Place L. Pasteul, 1, B-1348 Louvain-la-Neuve, Belgium
(Received January 24, 1986)

The halogen-abstraction reactions of carbon radicals were investigated as a model of the chain-transfer reaction in the radical polymerization of vinyl compounds. The kinetics of the halogen-abstraction reaction of carbon radicals ($(CH_3)_2\dot{C}X$, X=OC_6H_5, $OCOCH_3$, SC_6H_5, C_6H_5, and CN) from tetrahalomethanes(CBr_4, $CBrCl_3$, CCl_4) were studied in toluene at 80 °C by the ESR method using 2-(*t*-butyl)thioacrylonitrile as a spin-trapping reagent. The reactivity of these radicals for each halomethane decreased in the order X: OC_6H_5>$OCOCH_3$>SC_6H_5>C_6H_5>CN The reactivity of tetrahalomethanes for each radical decreased in the order CBr_4>$CBrCl_3$>CCl_4. Results are explained by taking into account the electron-transfer process from carbon radicals to tetrahalomethanes. Absolute rate constants of the halogen abstraction of $(CH_3)_2\dot{C}CN$ and $(CH_3)_2\dot{C}C_6H_5$ from CBr_4 and $CBrCl_3$, and of their additions to 2-(*t*-butylthio)acrylonitrile were estimated by the spin-trapping method, and they were compared with available data for similar reactions.

It has been reported that the solvent effect on the propagation rate constant k_p of vinyl esters, which have negative e values, is opposite in trend to that of methacrylates, which have positive e values. A proposal was made that the solvent effect could be explained in terms of donor-acceptor complexes of the propagating radicals with aromatic solvents[1-5] In these cases, the propagating radicals of methacrylates(e>0) were considered to be electron acceptors to the aromatic solvents and those of vinyl esters(e<0) to be electron donors to the solvents. This opposite trend in the reactivity of the propagating radicals between methyl methacrylate(MMA) and vinyl acetate(VAc) was also found in chain-transfer reactions to CCl_4 and triethylamine:[6-9] CCl_4 showed higher reactivity to the propagating radical of VAc and triethylamine to that of MMA. These facts suggest that the reactions proceed through a donor-acceptor complex formation or an electron-transfer process.

Recently, the participation of the electron-transfer process in radical reactions was pointed out in ESR studies on the reaction of the hydroxymethyl radical with CCl_4,[10,11] and in a flash photolysis on the reaction of the triethylsilyl radical with tetrahalomethanes.[12] Other examples supporting the electron-transfer process might be the chain-transfer reaction to strong transfer reagents in the radical polymerization. Since the occurrance of a net electron transfer indicates that a free radical can be converted to an ion, the finding of such a reaction seems to afford a new possibility for the reaction control of the radical polymerization. In order to investigate the possibility of the electron transfer of free radicals, we studied the reaction of free radicals with electron-accepting chain-transfer reagents, such as CBr_4 and $CBrCl_3$.

In this paper, we will repoprt an ESR study on the chain-transfer reactions of model radicals of the propagating end to tetrahalomethanes and discuss the participation of the electron-transfer process in the radical reactions. The radicals obtained by the chain-transfer reaction were trapped by 2-(*t*-butylthio)acrylonitrile which was found by Viehe as a strong radical scavenger.[13] Moreover, a new method for a determination of the rate constant of the chain transfer will be proposed.

Experimental

ESR spectra were recorded on a Japan Electron Optics Laboratory Model JES-FE 1X ESR spectrometer with a variable temperature accesory (ES-VT-3A) under irradiation with a 500 w high-pressure mercury lamp (Ushio 500) at 80 °C. A solution of azo compound 5×10^{-2} M, trapping reagent 6.4×10^{-1}—3.9×10^{-3} M, and tetrahalomethane 1.1×10^{-1}—9.8×10^{-4} M in toluene (1 ml) in a quartz sample tube (3 mmϕ) was degassed by repeated melting and freezing under vacuum and then sealed.

UV spectra were measured on a Hitachi 124 UV-visible spectrometer.

2,2′-Azobisisobutyronitrile(AIBN) was recrystallized from ethanol. 2,2′-Diacetoxy-2,2′-azopropane, 2,2′-bis(phenylthio)-2,2′-azopropane, and 2,2′-diphenoxy-2,2′-azopropane were prepared by the method of Benzing et al.[14] Azocumene was prepared from α-cumenamine and IF_5 by the method of Bartlet et al.[15] 2-(*t*-Butylthio)acrylonitrile was prepared according to the method of Viehe et al.[16]

CBr_4 was recrystallized from hexane. $CBrCl_3$(104 °C/760 mmHg(1 mmHg=133.322 Pa)) and CCl_4 (76.6 °C/760 mmHg) were purified by distillation. Hexamethylbenzene for the measurement of the electron affinity was sublimed twice. Toluene was dried and distilled by the conventional method. 2,2,6,6-Tetramethyl-1-piperidinyloxyl (Tempol)[17] was purified by recrystallization from cyclohexane.

An estimation of the kinetic parameter was carried out by a computer calculation using a nonlinear least-squares

method, computer program of which was Sals II written by Nakagawa and Koyanagi(Tokyo University Program). The simulation for the overlap of two adducts was carried out by a JEOL ESR simulation program 0398.

Results

Addition Reaction of Carbon Radicals to 2-(*t*-Butyl)thioacrylonitrile. Figure 1 shows the ESR spectrum observed under irradiation of a mixture of AIBN and 2-(*t*-butylthio)acrylonitrile, a spin-trapping reagent(T). The ESR spectrum of a triplet of triplets with hyperfine splitting constants of 0.88 and 0.28 mT due to nitrogen and two equivalent protons, respectively, was assigned to the adduct of $(CH_3)_2\dot{C}CN$ to T. Similar spectra were observed in the systems of other azo compounds and T. The hyperfine splitting constants of the adducts are shown in Table 1. The change in the ESR spectrum with reaction time shows that the concentration of the adduct became stationary within several minutes after irradiation. The signal due to the radicals (M·) of azo compounds (Eq. 1) could not be detected, indicating that the stationary concentration of M· was negligibly small compared with the adduct(MT·). Therefore, the bimolecular self-termination of M· was not taken into account in the kinetic treatment. Thus, the reactions are shown in Eqs. 1 to 4.

$$\text{M-N=N-M} \xrightarrow{I} \text{M}\cdot, \qquad I\text{: Rate} \tag{1}$$

$$\text{M}\cdot + \text{T} \xrightarrow{k_1} \text{MT}\cdot, \tag{2}$$

$$\text{MT}\cdot + \text{M}\cdot \xrightarrow{k_2} \text{Product}, \tag{3}$$

$$\text{MT}\cdot + \text{MT}\cdot \xrightarrow{k_3} \text{Product}. \tag{4}$$

The assumption of the steady state for the concentrations of M· and MT· leads to Eq. 5:

$$[\text{T}] = \frac{(k_2/k_1)[\text{MT}\cdot](1+k_3/I[\text{MT}\cdot]^2)}{1-k_3/I[\text{MT}\cdot]^2} \tag{5}$$

The relation between the stationary concentrations of MT· and T is shown in Fig. 2. The ratios, k_2/k_1 and k_3/I, were determined from Eq. 5 by a computation using the data shown in Fig. 2. The obtained ratios are shown in Table 2. The k_1/k_2 were influenced by substituents at the α-position, decreasing in the order:

$$-OC_6H_5 > -OCOCH_3 > -SC_6H_5 > -C_6H_5 > -CN.$$

The values of k_3/I changed remakably with the substituents.

Halogen Abstraction Reaction of Carbon Radicals from Tetrahalomethane. The intensity of the ESR spectra of the mixture of $CBrCl_3$, AIBN, and T was not large enough to perform a kinetic study in the absence of UV irradiation at 80 °C. Figure 3 shows the ESR spectrum observed upon irradiating the mixture. The spectrum (Fig. 3) was an overlap of two kinds of triplets of triplets, which were assigned

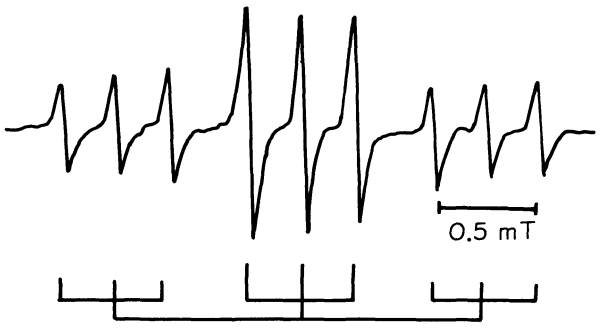

Fig. 1. ESR Spectrum observed on irradiation of a mixture of AIBN and 2-(*t*-butylthio)acrylonitrile(T) in toluene at 80 °C.
[AIBN]=5×10⁻²M, and [T]=0.64 M.

Table 1. Hyperfine Splitting Constants for Adducts Obtained by Reaction of Carbon Radicals with 2-(*t*-Butylthio)acrylonitrile[a)]

Radicals		a_H/mT	a_N/mT
$(CH_3)_2\dot{C}X$	X=-CN	0.88	0.28
	$-C_6H_5$	0.93	0.28
	$-OCOC_6H_5$	0.94	0.28
	$-SC_6H_5$	0.92	0.28
	$-OC_6H_5$	0.95	0.27
$\dot{C}Cl_3$		0.80	0.26
$\dot{C}Br_3$		0.77	0.26

a) 80 °C in toluene.

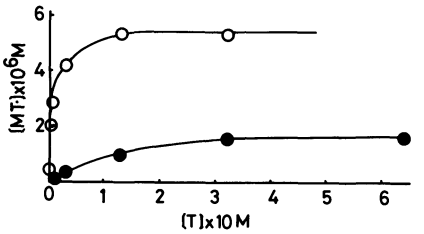

Fig. 2. Relation between MT· and T Concentrations.
○: 2,2'-Diacetoxy-2,2'-azobispropane, ●: AIBN.
[AIBN]=5×10⁻² M.

Table 2. Kinetic Data in Addition Reaction of Free Radicals $(CH_3)_2\dot{C}X$ to 2-(*t*-Butylthio)acrylonitrile[a,b)]

X	$k_1/k_2/10^{-4}$	$k_3/I/10^{10}$ M^{-2}
-CN	0.10	39
$-C_6H_5$	0.38	43
$-OCOCH_3$	3.6	450
$-SC_6H_5$	3.1	2.6
$-OC_6H_5$	4.4	2.2

a) 80 °C in toluene, [M-N=N-M]=5×10⁻² M. b) Average values of 3—5 runs(mean deviation ±50%).

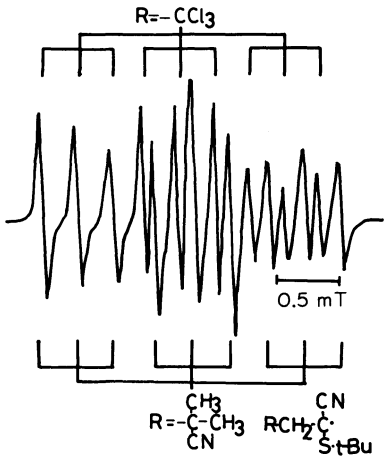

Fig. 3. ESR Spectrum observed on the UV irradiation of a mixture of $CBrCl_3$, AIBN, and 2-(*t*-buthylthio) acrylonitrile in toluene at 80 °C.
$[CBrCl_3]=8.8\times10^{-2}$ M, $[AIBN]=10^{-2}$ M, and [T]= 0.32 M.

to the adducts of the 1-cyano-1-methylethyl radical and of the trichloromethyl radical produced from AIBN and by bromine abstraction from $CBrCl_3$, respectively. Similar spectra were observed in other systems of tetrahalomethanes, azo compounds, and T. The hyperfine-splitting constants of the adducts are shown in Table 1. The reactions are illustrated in the following equations.

$$M\text{-}N{=}N\text{-}M \xrightarrow{I} M\cdot, \quad (1)$$

$$M\cdot + T \xrightarrow{k_1} MT\cdot, \quad (2)$$

$$M\cdot + RX \xrightarrow{k_x} MX + R\cdot, \quad (6)$$

$$R\cdot + T \xrightarrow{k_{1x}} RT\cdot, \quad (7)$$

$$RT\cdot + RT\cdot \xrightarrow{k_3} RTTR, \quad (8)$$

$$RT\cdot + MT\cdot \xrightarrow{k_3} MTTR, \quad (9)$$

$$MT\cdot + MT\cdot \xrightarrow{k_3} MTTM. \quad (10)$$

Since M· and R· were not observed in the ESR spectra, the self-coupling reactions of these radicals were not taken into account. A stationary state treatment on R·, RT·, and MT· gives

$$\frac{[RT\cdot]}{[MT\cdot]} = \frac{k_{1x}}{k_1}\frac{[R\cdot][T]}{[M\cdot][T]} = \frac{k_x}{k_1}\frac{[RX]}{[T]}. \quad (11)$$

Two examples of a plot of [RT·]/[MT·] vs. [RX] are shown in Fig. 4. Linear relations were observed, the ratios, k_X/k_1, being calculated from the slopes. Results are shown in Table 3. Since the signal MT· was not observed in the reactions of the radicals X=–CN, $-C_6H_5$, and $-OCOCH_3$ with CCl_4, the ratios could not be estimated. This fact indicates that k_x is too small for the ESR spectrum to be detected. From

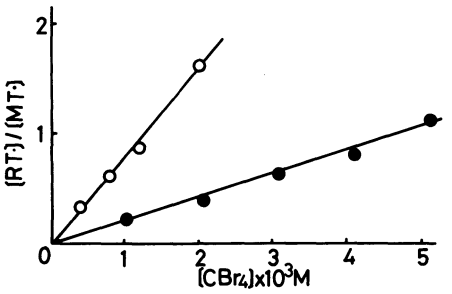

Fig. 4. Plot of [RT·]/[MT·] versus [CBr_4] in the stationary concentrations of RT· and MT·.
○: 2,2'-Phenoxy-2,2'-azopropane, ●: 2,2'-phenylthio-2,2'-azopropane.
$[M\text{-}N{=}N\text{-}M]=5\times10^{-2}$ M, and [T]=0.32 M.

Table 3. Relative Rate Constants for Radicals $(CH_3)_2\dot{C}X$ in Halogen Abstraction[a,b]

X	k_x/k_1		
	CBr_4	$CBrCl_3$	CCl_4
-CN	4.9	0.21	—
$-C_6H_5$	2.4	0.61	—
$-OCOCH_3$	200	15	—
$-SC_6H_5$	56	5.3	0.0075
$-OC_6H_5$	210	89	2.2

a) 80 °C in toluene, $[M\text{-}N{=}N\text{-}M]=5\times10^{-2}$ M. b) Average value of 3—5 runs(mean deviation ±10%).

a comparison of k_x/k_1 for the reactions of a given radical with CBr_4, $CBrCl_3$, and CCl_4, it is concluded that rate constants for the halogen abstraction decrease in the order, $CBr_4>CCl_3Br>CCl_4$, in all reaction systems.

A remarkable difference in k_x/k_1 was found in the reactions of different radicals with a given tetrahalomethane. However, since k_1 are not considered to be constant, no information regarding k_x could be obtained from k_x/k_1.

Absolute Rate Constants for Elementary Steps. Since the kinetic parameters obtained so far were k_x/k_1, k_2/k_1, k_x/k_2 and k_3/I, absolute rate constants of each elementary processes could not be directly estimated. If the k_2 could be evaluated, k_1 and k_x could be estimated. It is difficult to directly measure k_2. However, if the self-coupling constants of M· and MT· are determined, rate constants of the cross-coupling reactions can generally be estimated as the geometrical mean of the self-coupling rate constants:[18]

$$k_2 = (k_3k_M)^{1/2} \quad (12)$$

where k_M and k_3 are the rate constants for the self-coupling reactions.

In order to estimate k_3 from k_3/I, I for each azo compound was estimated by the following method. Carbon radicals are known to be quantitatively

trapped by *N*-oxyl radical such as 2,2,6,6-tetramethyl-1-piperidinyloxyl(Tempol).[19] Accordingly, I for all azo compounds were determined from measurements of the decreasing rates of Tempol which were added to the reaction system. The rates were estimated from the change in the signal intensity of the ESR spectrum with time. The values of k_3 were calculated from k_3/I and I was thus obtained. I and k_3 are shown in Table 4. The k_3 values obtained are of the same order for all systems; this indicates that this method leads to reasonable data because k_3, which is the reaction rate constant of a diffusion-controlled reaction, should be constant, at least regarding the order of magnitude in all systems. I changed remarkably with the substituent. This change might be due to a difference in the light intensity, the molecular extinction coefficients of the azo compounds, the extent of the contribution of thermal decomposition, or the efficiency of Eq. 2.

The values of k_M for $(CH_3)_2\dot{C}C_6H_5$ and $(CH_3)_2\dot{C}CN$ have been reported in the literature.[20,21] The k_2 values for these radicals were estimated from Eq. 12 using k_3 and k_M (Table 6). Since k_M for the other radicals has not yet been reported, k_1 and k_x for only two radicals were estimated by a substitution of k_2 for k_1/k_2 and k_x/k_2 and are shown in Tables 5 and 6.

Table 4. Rate Constants of the Coupling Reaction of the Adduct and Rates of Formation of Radicals ($(CH_3)_2\dot{C}X$)[a,b]

X	$k_3/10^8$ / $M^{-1}s^{-1}$	I[b] / $M\,s^{-1}$
-CN	3.5	9.0×10^{-4}
$-C_6H_5$	7.0	1.6×10^{-3}
$-OCOCH_3$	6.6	1.5×10^{-4}
$-SC_6H_5$	8.7	3.5×10^{-2}
$-OC_6H_5$	7.0	1.6×10^{-3}

a) 80 °C in toluene, $[M\text{-}N{=}N\text{-}M]=5.0\times10^{-2}$ M. b) b) Average values of 3—5 runs(mean deviation ±30%).

Table 5. Rate Constants of the Addition Reaction and Coupling Reactions[a]

$(CH_3)_2\dot{C}X$	$k_1/10^4$ $M^{-1}s^{-1}$	$k_2/10^8$ $M^{-1}s^{-1}$
X=CN	0.84	8.4
C_6H_5	1.2	24

a) 80 °C in toluene.

Table 6. Rate Constants of the Halogen Abstraction of $(CH_3)_2\dot{C}X$ from tetrahalomethanes[a]

X	$k_x/10^5$ $M^{-1}s^{-1}$		
	CBr_4	$CBrCl_3$	CCl_4
-CN	4.1	0.17	—
$-C_6H_5$	22	5.5	—

a) 80 °C in toluene.

Discussion

Reactivity of Model Radicals in Addition Reaction to 2-(*t*-Butylthio)acrylonitrile and Halogen Abstraction. Since the absolute rate constants for an addition reaction(k_1) and a halogen abstraction(k_x) were determined for only two kinds of radicals, it is difficult to discuss the mechanism of the addition reaction and a chain-transfer reaction by a comparison of k_1 and k_x. However, since the bimolecular reactions between M· and MT· are diffusion-controlled in all reaction systems, k_2 are reasonably assumed to be constant, at least regarding the order of magnitude, in all reaction systems. Therefore, k_1/k_2 is considered to represent the reactivity of M· in Eq. 2. The reactivities of the radicals were influenced by substituents at the α-position; these decreased in the order:

$$-OC_6H_5 > -OCOCH_3 > -SC_6H_5 > -C_6H_5 > -CN.$$

This order shows that the radicals binding to heteroatoms have a larger reactivity than those stabilized by a phenyl or cyano group. The difference in the reactivity between $-OC_6H_5$ and $-OCOCH_3$, or between the phenyl and cyano groups, seems to be explained by the polarity of the substituent: the radicals binding to more electrodonating substituent have a higher reactivity.

Any information concerning the reactivity of model radicals in a halogen-abstraction reaction could not be obtained from k_x/k_1. However, it is possible to discuss the reactivity of a given radical with k_x/k_2 (Table 7), because k_2 is considered not to be influenced by the halomethanes used. Therefore, k_x/k_2 ratios were estimated from the k_x/k_1 and k_1/k_2 obtained in the last section. The values of k_x/k_2 are shown in Table 7, and decrease in the following order:

$$-OC_6H_5 > -OCOCH_3 > -SC_6H_5 > -C_6H_5 > -CN.$$

Table 7. Relative Rate Constants of Radicals $(CH_3)_2\dot{C}X$ in Halogen Abstractions[a]

X	k_x/k_2		
	CBr_4	$CBrCl_3$	CCl_4
-CN	0.49	0.02	—
$-C_6H_5$	0.91	0.23	—
$-OCOCH_3$	720	54	—
$-SC_6H_5$	170	16	0.0075
$-OC_6H_5$	920	390	9.7

a) 80 °C in toluene, $[M\text{-}N{=}N\text{-}M]=5\times10^{-2}$ M.

This order shows that the carbon radicals binding to heteroatoms have a larger reactivity for halogen abstraction than radicals stabilized by phenyl or cyano groups. From Table 7, it is concluded that the rate constants for reaction between a given radical and tetrahalomethanes increase in the order CCl_4< $CBrCl_3$<CBr_4. For example, the reaction rate of $(CH_3)_2\dot{C}OC_6H_5$ and $(CH_3)_2\dot{C}SC_6H_5$ with CBr_4 was 10^2—10^3 times as large as that with CCl_4.

It has been reported that the activation energy of the halogen abstraction of free radicals from halomethane can be estimated from their bond dissociation energies(BDE) by the following relation[22]:

$$E = 0.055 \times [\text{BDE}] \quad (13)$$

If the preexponential factors are assumed to be the same in halogen-abstraction reactions of a given radical from tetrahalomethanes, k_x/k_1 for CBr_4 is calculated to be less than 10-times as large as that for CCl_4(C-Cl 67.9 kcal mol^{-1}(1 cal=4.184 J), and C-Br 45—57 kcal mol^{-1}),[23] the difference being much smaller than that observed. If the reaction mechanism is the same in all halogen-abstraction reactions, the preexponential factor is considered to be in the same order of magnitude[24] because tetrahalomethanes are composed of the same number of atoms. This large difference in k_x among halomethanes may be due to a difference in the reaction mechanism. Accordingly, we investigated the possibility of an electron-transfer mechanism in halogen-abstraction reactions of carbon radicals from tetrahalomethanes.

Electron-Transfer Mechanism. First, the electron affinities(EA) were estimated from the absorption spectra of their complexes with hexamethylbenzene by the method of Hatano et al.[25] Results are shown in Table 8, indicating that EA decreases in the order

$$CBr_4 > CCl_3Br > CCl_4.$$

This order is in agreement with the order of rates for halogen abstraction.

The reactivity of each radical with a given tetrahalomethanes was estimated by k_x/k_2 (Table 7), decreasing with the α-substituents in the following order:

$$\text{-}OC_6H_5 > \text{-}OCOCH_3 > \text{-}SC_6H_5 \gg \text{-}C_6H_5 > \text{-}CN.$$

The ratio for CBr_4 and $(CH_3)_2\dot{C}OC_6H_5$ which has an electron-donating group is about 2000 times as large as that for CBr_4 and $(CH_3)_2\dot{C}CN$, which has an electron-accepting group. Therefore, the electron-donating power of free radicals is considered to be an important factor for the halogen-abstraction reaction. The fact that the electron-donating character of radicals and the electron-accepting character of tetrahalomethanes seem to be important in halogen abstraction shows that this reaction might proceed through the electron-transfer process when electron-transfer from free radicals to tetrahalomethanes is thermodynamically favorable.

Table 8. Electron Affinity/eV

CBr_4	$CBrCl_3$	CCl_4
1.2	0.68	0.15

For more quantitative information on the possibility of the electron-transfer reaction, an estimation of the difference in the redox potential between halomethanes and radicals would be helpful. The reduction potentials of CCl_4 and CBr_4 are reported to be −0.78 V and −0.30 V, respectively.[26,27] Although the redox potentials of the radicals formed by a decomposition of the azo compound are not available, the oxidation potential of the hydroxymethyl radical was used which was reported to be −0.98 V.[28] The redox potentials of the radicals with an electron-donating substituent, $-OC_6H_5$, $-OCOCH_3$, and $-SC_6H_5$ are considered close to that of the hydroxymethyl radical. This value suggests that the electron transfer from these radicals to tetrahalomethane, especially CBr_4, is thermodynamically possible(ΔG=−0.6 eV for CBr_4 and ΔG=−0.2 eV for CCl_4).

Although k_x of the reaction of $(CH_3)_2\dot{C}CN$ and $(CH_3)_2\dot{C}C_6H_5$ with CBr_4 and CCl_3Br have been succesfully determined, k_x with CCl_4 was not determined, because the concentration of the adduct of $CCl_3\cdot$ was so small that the rate constants of the Cl-abstraction of these radicals could not be determined by the ESR measurement. The rate constants with CCl_4 are presumed to be less than k_x for $(CH_3)_2\dot{C}CN$ and $CBrCl_3$, being less than 10^3 M^{-1} s^{-1}. Really, k_x for the reaction of $CH_3\cdot$ with CCl_4 has been reported to be 3.3×10^2 M^{-1} s^{-1} at 65 °C.[29,30] Therefore, it is concluded that the rate constant for the halogen abstraction of these radicals from CBr_4 is more than 100 times as large as that from CCl_4. The large difference in the absolute rate constants between CBr_4 and CCl_4 is probably explained by participation of electron transfer from these radicals to CBr_4 in the halogen-abstraction reaction.

Next, we investigated the difference in k_x's for each radical between CCl_4 and $CBrCl_3$. In the $(CH_3)_2\dot{C}CN$ radical, k_x for Br abstraction from CBr_4 was 24-times larger than that for $CBrCl_3$, while in the $(CH_3)_2\dot{C}C_6H_5$ radical k_x from CBr_4 was four times larger than that from $CBrCl_3$. The ionization potential of the $(CH_3)_2\dot{C}C_6H_5$ radical is considered to be smaller than that of the $(CH_3)_2\dot{C}CN$ radical, because the cyano group is more electron-accepting than the phenyl group. Therefore, these results suggest that the electron transfer from the $(CH_3)_2\dot{C}CN$ radical to $CBrCl_3$ might be thermodynamically difficult and, that in the other three cases, electron-transfer reactions are thermodynamically favorable. This

presumption reasonably explains the smaller difference in k_x for $(CH_3)_2\dot{C}C_6H_5$ between CBr_4 and $CBrCl_3$ because in this radical the rate constants are considered to be mainly controlled by the difference in the dissociation energy of the C–Br bond between radical anions obtained by an electron-transfer reaction.

Reliability of Rate Constants. Let us discuss the reliability of k_1 and k_3. The k_1 values are $10—10^3$ times larger than the propagation rate constants of vinyl compounds.[31] This fact is reasonably explained by the fact that 2-*t*-(butylthio)acrylonitrile is a strong radical scavenger due to its stabilizing effect of captodative substituent.[13] The k_3 values are one order of magnitude smaller than those of the self-coupling reaction of carbon radicals such as $(CH_3)_2\dot{C}CN$ and $(CH_3)_2\dot{C}C_6H_5$.[20,21] This result can be reasonably explained by the stabilization of the adduct due to the capto-dative substituent effect.[13]

There are only a little available data regarding the elementary rate constants for the halogen-abstraction of carbon radicals from tetrahalomethanes, except for CCl_4:[10,11,30] k_x of the halogen abstraction reaction of $CH_3\cdot$ from $CBrCl_3$ was reported to be 2.2×10^6 M^{-1} s^{-1} at 65 °C.[30] On the assumption that the activation energy for the reaction is 5—10 kcal mol^{-1},[32] k_x at 80 °C are calculated to be the range of 3.0×10^6—4.2×10^6 M^{-1} s^{-1}. The k_x value for $(CH_3)_2\dot{C}C_6H_5$ obtained by our experiments are one order of magnitude less than the calculated values, which can be reasonably explained by the difference in the steric factor.

Thus, the spin-trapping method is considered to be applicable to a determination of the rate constants for a halogen-abstraction reaction and the chain-transfer reaction in radical polymerizations.

We thank Professor S. Nozakura for his helpful discussions and numerous suggestions for the manuscript, and Daikin Kogyo Ltd for providing IF_5.

References

1) M. Kamachi, J. Satoh, D. J. Liaw, and S. Nozakura, *Macromolecules*, **10**, 501 (1977).
2) M. Kamachi, D. J. Liaw, and S. Nozakura, *Polymer J.*, **9**, 307 (1977).
3) M. Kamachi, J. Satoh, and S. Nozakura, *J. Polym. Sci., Polym. Chem. Ed.*, **16**, 1789 (1978).
4) M. Kamachi, D. J. Liaw, and S. Nozakura, *Polym. J.*, **11**, 921 (1979).
5) M. Kamachi, D. J. Liaw, and S. Nozakura, *Polym. J.*, **13**, 41 (1981).
6) G. Odian, "Principles of Polymerization" 2nd Ed. McGraw-Hill, New York (1970), p. 237.
7) C. H. Bamford A. D. Jenkins, and R. Johnston, *Trans. Faraday Soc.*, **59**, 530 (1963).
8) C. H. Bamford, and A. D. Jenkins, *J. Polym. Sci.*, **53**, 149 (1961).
9) C. H. Bamford, A. D. Jenkins, and R. Johnston, *Trans Faraday Soc.*, **59**, 530 (1963).
10) H. Paul, Int. *J. Chem. Kinet.*, **11**, 495 (1979).
11) R. Koster, K. D. Asmus, *Z. Naturforsch.*, **226**, 1104 (1971).
12) C. Chatigilialoglu, K. U. Ingold, and J. C. Scaiano, *J. Am. Chem. Soc.*, **104**, 5123 (1982).
13) V. H. C. Viehe, R. Merenyl, L. Stella, and M. Janousek, *Angew. Chem.*, **91**, 982 (1979).
14) E. Benzing, *Ann*, **631**, 1 (1960).
15) S. F. Nelson and P. D. Bartlett, *J. Am. Chem. Soc.*, **88**, 137 (1966).
16) I. Stella, R. Merenyi, Z. Janousek, H. G. Viehe, P. Tordo, and A. Munoz, *J. Phys. Chem.*, **84**, 304 (1980).
17) T. Kurosaki, K. W. Lee, and M. Okamura, *J. Polym. Soc., Polym. Chem. Ed.*, **10**, 3295 (1972).
18) H. Schuh, E. J. Hamilton, Jr., H. Paul, and H. Fischer, *Helv. Chim. Acta*, **57**, 2011 (1974).
19) P. G. Grifiths, E. Rizzardo, and D. H. Solomon, *J. Macromol. Sci.*, **A17**, 45 (1982).
20) S. A. Weiner and G. Hammond, *J. Am. Chem. Soc.*, **91**, 986 (1969).
21) K. U. Ingold, "Free Radicals," ed by J. K. Kochi, Wiley-Interscience, New York (1973), Vol. 1, p. 43.
22) J. Hirshfelder, *J. Chem. Phys.*, **9**, 645 (1941).
23) C. T. Mortimer, "Reaction Heats and Bond Strength," Pergamon Press, London (1962), p. 133; *J. Phys. Chem.*, **64**, 1031 (1960).
24) K. J. Laidler, "Theory of Chemical Reaction Rates," McGraw-Hill, New York (1969), pp. 80—99.
25) H. Hatano and O, Ito, *Bull. Chem. Soc., Jpn.*, **44**, 916 (1971).
26) J. C. McGowan and T. Powell, *Rec Trav. Chim.*, **81**, 1061 (1962).
27) J. W. Timberlake, M. L. Hidges, *Tetrahedron Lett.*, **1970**, 4147.
28) J. Lilie, G. Beck, and A. Henglein, *Ber. Bunsenges. Phys. Chem.*, **75**, 458 (1971).
29) F. G. Edwards and F. Mayo, *J. Am. Chem. Soc.*, **72**, 1265 (1950).
30) K. U. Ingold, "Free Radicals," ed by J. K. Kochi, Wiley-Interscience, New York (1973), Vol. 1, p. 85.
31) K. U. Ingold, "Free Radicals," ed by J. K. Kochi, Wiley-Interscience, New York (1973), p. 92.
32) I. Matheson and J. Tedder, Int. *J. Chem. Kinet.*, **14**, 1033 (1982).

 © 1986 The Chemical Society of Japan Bull. Chem. Soc. Jpn., 59, 2331—2334 (1986)

Racemic Structures and Optical Resolutions by Preferential Crystallization of Organic Ammonium Salts of *N*-Formyl-DL-phenylalanine

Tadashi SHIRAIWA,* Hideya MIYAZAKI, Yoshihiro SAKAMOTO, and Hidemoto KUROKAWA
Faculty of Engineering, Kansai University, Yamate-cho, Suita, Osaka 564
(Received January 24, 1986)

Racemic structures of the butylammonium salt, pentylammonium salt, benzylammonium salt, dicyclohexylammonium salt (DL-DCH salt), and 4-methylpiperidinium salt (DL-4-MP salt) of *N*-formyl-DL-phenylalanine were studied to explore the possibility of optical resolution by preferential crystallization. Free energies of formation of racemate (ΔG^F) of the DL-salts and data at eutectic points in binary phase diagrams of melting points indicate that the DL-salts form racemic compounds in the vicinity of the melting points. However, according to ΔG^F of DL-DCH and 4-MP salts and infrared spectra and solubilities of the DL- and L-salts, these DL-salts transform into conglomerates around room temperature. It is possible to resolve DL-DCH and 4-MP salts by preferential crystallization at 10 °C. Successive preferential crystallization of DL-4-MP salt at 10 °C in 1-butanol gives the D- and L-salts with optical purities of 95—100%.

DL-Phenylalanine (abbreviated as DL-Phe) has been optically resolved by emzymatic, diastereomeric, and preferential crystallization procedures. Of these procedures, the preferential crystallization procedure is useful for industrial operation, since the optical resolution can easily be achieved by providing a small amount of one enantiomer as seed crystals in a supersaturated solution of racemic modifications. Optical resolutions by this procedure have been reported on the ammonium salt,[1] ethylammonium salt,[2] isopropylammonium salt,[3] butylammonium salt,[3] 1,1,3,3-tetramethylbutylammonium salt,[2] and cyclohexylammonium salt[4] of *N*-acetyl-DL-phenylalanine. It is expected that the hydrolysis of *N*-formylphenylalanine (FrPhe) is easier than that of *N*-acetylphenylalanine. However, no optical resolution of DL-FrPhe by preferential crystallization has been reported, though DL-FrPhe has been optically resolved through its diastereomeric salts with (−)-fenchylamine.[5] This paper describes an attempt to resolve organic ammonium salts of DL-FrPhe by preferential crystallization.

The racemic structures of the butylammonium salt (DL-BA salt), pentylammonium salt (DL-PTA salt), benzylammonium salt (DL-BZA salt), dicyclohexylammonium salt (DL-DCH salt), and 4-methylpiperidinium salt (DL-4-MP salt) of DL-FrPhe were determined on the basis of free energies of racemates (ΔG^F)[2,6,7] and data at eutectic points in binary phase diagrams of melting points. The results indicated that the DL-salts form racemic compounds in the vicinity of the melting points. However, the ΔG^F values of DL-DCH and 4-MP salts suggested that the DL-salts are transformed into conglomerates at lower temperatures. This was supported by a comparison of solubilities and infrared spectra of the DL-salts with those of the corresponding L-salts. Optical resolutions of DL-DCH and 4-MP salts were attempted by preferential crystallization at 10 °C.

Experimental

Materials. DL-Phe and L-Phe were purchased from Sigma Chemicals Co., and amines from Wako Pure Chemicals Ind.

***N*-Formylation.** DL- and L-FrPhe were obtained, respectively, by formylating DL- and L-Phe in the usual way.[8] DL-FrPhe: Mp 168 °C (lit,[5] 165—166 °C). L-FrPhe: Mp 168 °C (lit,[5] 167.0 °C); $[\alpha]_D^{20}$ +75.1° (*c* 1.00, ethanol) (specific rotation of D-FrPhe[5]: $[\alpha]_D^{20}$ −75.2° (ethanol)).

Preparation of Organic Ammonium Salts. DL- or L-FrPhe (0.01 mol) and 0.01 mol of an amine were dissolved in 30 cm³ of methanol. To the solution was added 30 cm³ of diethyl ether and the salt formed was collected by filtration.

Elemental analysis and specific rotation of L-DCH salt: C, 70.32; H, 9.15; N, 7.44%; $[\alpha]_D^{20}$ +36.1° (*c* 1.00, methanol). DL-DCH salt: C, 70.35; H, 9.15; N, 7.44% (calcd for $C_{22}H_{34}N_2O_3$: C, 70.55; H, 9.15; N, 7.48%). L-4-MP salt: C, 65.55; H, 8.27; N, 9.59%; $[\alpha]_D^{20}$ +45.7° (*c* 1.00, methanol). DL-4-MP salt: C, 65.46; H, 8.27; N, 9.60% (Calcd for $C_{16}H_{24}N_2O_3$: C, 65.73; H, 8.27; N, 9.58%).

The D-4-MP salt (3.00 g) obtained from the mother liquor in the optical resolution of the DL-salt was dissolved in 15 cm³ of 1-butanol at an elevated temperature. After standing overnight around 5 °C, the salt crystallized was collected by filtration, washed with a small amount of diethyl ether, and dried; yield, 2.57 g. The recrystallization was repeated twice: Mp 167 °C; $[\alpha]_D^{20}$ −45.7° (*c* 1.00, methanol).

Optical Resolution. DL-Dicyclohexylammonium Salt: DL-DCH salt (1.221 g) was dissolved in 100 cm³ of ethanol around 40 °C to give a racemic solution with a degree of supersaturation of 161% at 10 °C. The solution was slowly cooled to 10 °C and seeded with 0.020 g of L-DCH salt. After stirring for 60—180 min at 10 °C, the salt precipitated was collected by filtration and washed with a small amount of diethyl ether. The optical purity, the yield of the optically pure modification (YOPM), and the degree of resolution of the salt obtained were determined by the equations in our previous paper.[9]

DL-4-Methylpiperidinium Salt: DL-4-MP salt (2.631 g) was dissolved in 50 cm³ of 1-butanol around 40 °C to give a racemic solution with a degree of supersaturation of 160% at 10 °C. The optical resolution of DL-4-MP salt was

carried out with this solution similarly to that of DL-DCH salt.

Successive Preferential Crystallization: DL-4-MP salt (10.560 g) was dissolved in 200 cm^3 of 1-butanol around 40 °C. The solution was slowly cooled to 10 °C and seeded with 0.050 g of L-4-MP salt. After stirring for 70 min at 10 °C, the salt precipitated was collected by filtration, and washed with a small amount of diethyl ether. DL-4-MP salt (1.268 g) was added to the filtrate, and dissolved around 40 °C. The solution was cooled to 10 °C and seeded with 0.050 g of D-4-MP salt. After stirring for 80 min, the salt precipitated was collected by filtration. The filtrate was treated similarly to above.

Preparation of Optically Active Phenylalanine: The D- or L-4-MP salt obtained by successive preferential crystallization (4.83 g) was added in 25 cm^3 of 1 mol dm^{-3} hydrochloric acid without recrystallization, and the mixture was stirred for 40 min at 5 °C. The FrPhe was collected by filtration, washed with a small amount of water, and dried: yield of each of D- and L-FrPhe 3.09 g; for D-FrPhe $[\alpha]_D^{20}$ −75.2° (*c* 1.00, ethanol); for L-FrPhe $[\alpha]_D^{20}$ +74.5° (*c* 1.00, ethanol). The D- or L-FrPhe (2.50 g) was added in 20 cm^3 of 1 mol dm^{-3} hydrochloric acid. After refluxing for 2 h, the solution was evaporated to dryness under reduced pressure around 50 °C. The residue was dissolved in 70 cm^3 of methanol, and the pH was adjusted to around 6 with ammonium hydroxide. The Phe crystallized was collected by filtration, washed with small amounts of water and methanol, and dried. D-Phe: yield 1.36 g; $[\alpha]_D^{20}$ +34.4° (*c*. 1.00, water). L-Phe: Yield 1.32 g; $[\alpha]_D^{20}$ −33.5° (*c* 1.00, water) (lit,[10] $[\alpha]_D$ −34.5° (water)).

Measurements. Specific rotations were measured with a Union Giken high sensitivity PM-101 digital polarimeter using a 0.5 dm path length quartz cell. Infrared spectra were obtained in the range 4000—400 cm^{-1} with a JASCO A-102 infrared spectrophotometer by the KBr disk method. Solubilities of DL- and L-DCH salts in ethanol and those of DL- and L-4-MP salts in 1-butanol were measured at 10 °C in a similar manner as described in our previous paper.[2] These solubilities are given in Table 1. Enthalpies of fusion and melting points were determined by use of a differential scanning calorimeter (Rigaku Denki DSC-8230). Benzoic acid, potassium nitrate, and sodium nitrate were used as standard samples to obtain enthalpies of fusion.

Table 1. Solubilities of Dicyclohexylammonium and 4-Methylpiperidinium Salts of *N*-Formylphenylalanine

Salt	Solvent	Solubility at 10 °C g/(100 cm^3 solvent)
DCH[a]	Ethanol	DL : 0.758 L : 0.561
4-MP[b]	1-Butanol	DL : 3.289 L : 1.628

a) DCH: Dicyclohexylammonium salt. b) 4-MP: 4-Methylpiperidinium salt.

Results and Discussion

Recemic Structures at Melting Piont. Racemic structures of the organic ammonium salts of DL-FrPhe were examined, since the optical resolution by preferential crystallization requires that the racemic modification is a conglomerate. The free energies of formation of racemate at melting point (ΔG^F_{mp}) of the DL-salts were calculated on the basis of the enthalpies of fusion (ΔH^f) and melting points of the DL- or L-salts.[2,6,7] These thermodynamic data are given in Table 2.

Since the ΔG^F_{mp} values of these DL-salts are negative (−2.8—−0.5 kJ mol^{-1}), it was suggested that the DL-salts would be racemic compounds or racemic solid solutions in the vicinity of the melting points and not conglomerates.[2,6]

If the DL-salts form racemic compounds, the eutectic points must be found in the mole fraction range of 0.5 to 1 in the binary phase diagrams of melting points and it is possible to calculate the mole fractions of the L-salts and temperatures for the eutectic points from the Schröder-Van Laar and Prigogine-Defay equations on the basis of the ΔH^f and melting points of the DL- and L-salts.[11] The mixtures with the mole fractions of the L-salts calculated (0.58—0.85) were prepared, and the melting points were compared with the eutectic temperatures calculated. These results are given in Table 3.

The melting points obtained agreed very closely with the eutectic temperatures calculated, and the mixtures melted at the temperatures and not over a wide range. Although the mole fractions of L-DCH and 4-MP salts at the eutectic points (about 0.5) are relatively close to 0.5 and the melting points are equal to those of their respective DL-salts, the binary phase diagrams of melting points (Figs. 1 and 2) show that the eutectic mixtures consist of the D- and L-salts in the molar ratio of about 4:6. The above results indicate that BA, PTA, BZA, DCH, and 4-MP salts have the eutectic mixtures consisting of the D-

Table 2. Thermodynamic Data for Organic Ammonium Salts of *N*-Formyl-phenylalanine

Salt	Mp/K		$\Delta H^{f\,a)}$/kJ mol^{-1}		$\Delta G^{F\,b)}_{mp}$
	DL-Salt	L-Salt	DL-Salt	L-Salt	kJ mol^{-1}
BA[c]	417	412	32.9	30.4	−2.73
PTA[d]	398	392	36.9	32.8	−2.78
BZA[e]	415	428	39.0	31.4	−1.43
DCH	483	499	63.2	61.1	−0.82
4-MP	420	440	39.5	41.3	−0.59

a) ΔH^f: Enthalpy of fusion. b) ΔG^F_{mp}: Free energy of formation of recemate at melting point. c) BA: Butylammonium salt. d) PTA: Pentylammonium salt. e) BZA: Benzylammonium salt.

and L-salts in the molar ratios calculated, which leads to a clear conclusion that these DL-salts form racemic compounds in the vicinity of the melting points.

However, the mole fractions of L-DCH and 4-MP salts at the eutectic points and the absolute values of ΔG^{F}_{mp} of the DL-salts are smaller than those of the other salts. Therefore, it is suggested that the DL-DCH and 4-MP salts are unstable racemic compounds in the vicinity of the melting points.[2,7] Such an unstable racemic compound has a possibility of transformation to a conglomerate at a lower temperature,[2,7] though stable ones in the vicinity of the melting points exist in racemic compounds even around room temperature.

Table 3. Mole Fractions and Temperatures at Eutectic Points for Organic Ammonium Salts of *N*-Formylphenylalanine

Salt	Mole fraction of L-salt[a]	Temperature/K	
		Found	Calcd[a]
BA	0.84	403	404
PTA	0.85	387	386
BZA	0.70	412	412
DCH	0.60	483	483
4-MP	0.58	420	420

a) These values were calculated from the Schröder-Van Laar and Prigogine-Defay equations.

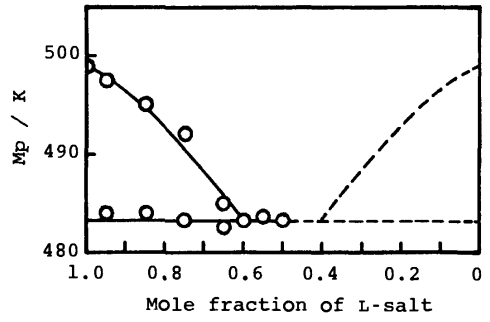

Fig. 1. Binary phase diagram of melting point of dicyclohexylammonium salt of *N*-formylphenylalanine.

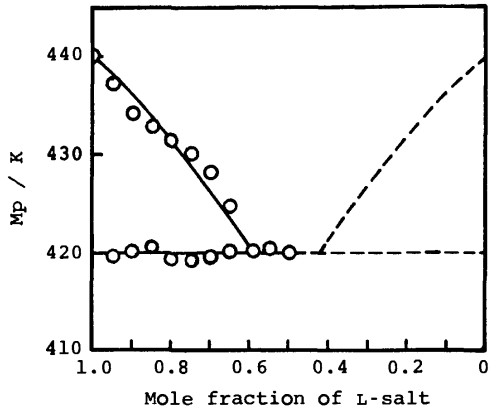

Fig. 2. Binary phase diagram of melting point of 4-methylpiperidinium salt of *N*-formylphenylalanine.

Racemic Structures Around Room Temperature. The above results suggest that DL-DCH and 4-MP salts have a possibility of existing in conglomerate around room temperature. Therefore, the transition temperatures (T_0) of DL-DCH and 4-MP salts were estimated according to previous papers;[2,7] the ΔG^{F} is zero at T_0. The T_0 obtained was 314 K for DL-DCH salt and 324 K for DL-4-MP salt. The T_0 values indicate that DL-DCH and 4-MP salts do not form racemic compounds around room temperature, since the ΔG^{F} values are positive at temperatures below T_0. The results are supported by the infrared spectra and solubilities of these DL- and L-salts; DL-DCH and 4-MP salts show infrared spectra identical with those of the corresponding L-salts, and are more soluble than the L-salts as shown in Table 1. The above results indicate that DL-DCH and 4-MP salts exist in conglomerate around room temperature, though the DL-salts form racemic compounds in the vicinity of the melting points.

Since the T_0 values estimated for DL-BA, PTA, and BZA salts are lower than 0 K and the infrared spectra of these DL-salts are different form those of the L-salts, it may be concluded that these DL-salts form also racemic compounds around room temperature.

Optical Resolution by Preferential Crystallization. Optical resolutions of DL-DCH and 4-MP salts have been attempted at 10 °C for racemic solutions with a degree of supersaturation of about 160%. The results are given in Tables 4 and 5.

It was possible to obtain the L-salts with high optical purity (93—97%) by preferential crystallization. Although the L-DCH salt obtained at resolution times of 60 and 90 min had an optical purity of over 90%, the degrees of resolution were low (22—29%). On the other hand, in the optical resolution of DL-4-MP salt, L-salt with an optical purity of 96.8% was obtained in a relatively high

Table 4. Optical Resolution of Dicyclohexylammonium Salt of *N*-Formyl-DL-phenylalanine[a]

Resolution time / min	Yield / g	Optical purity / %	YOPM[b] / g	Degree of resolution / %
60	0.076	96.1	0.053	22.9
90	0.095	93.0	0.068	29.4
120	0.186	74.5	0.119	51.5
150	0.234	60.4	0.121	52.4
180	0.274	40.8	0.092	39.8

a) Solvent: 100 cm^3 of ethanol. Degree of supersaturation of racemic solution: 161%. Seed crystals: 0.020 g of L-salt. Temperature: 10 °C. b) YOPM: Yield of optically pure modification.

Table 5. Optical Resolution of 4-Methylpiperidinium Salt of *N*-Formyl-DL-phenylalanine[a]

Resolution time / min	Yield / g	Optical purity / %	YOPM[b] / g	Degree of resolution / %
30	0.280	95.1	0.246	49.9
60	0.332	96.8	0.301	61.0
90	0.339	87.2	0.276	56.0
120	0.551	25.8	0.122	24.7
180	0.602	15.8	0.075	15.2

a) Solvent: 50 cm³ of 1-butanol. Degree of supersaturation of racemic solution: 160%. Seed crystals: 0.020 g of L-salt. Temperature: 10 °C. b) See note in Table 4.

Table 6. Successive Preferential Crystallization of 4-Methylpiperidinium Salt of *N*-Formyl-DL-phenylalanine[a]

Run	Added amount of DL-salt / g	Resolution time / min	Salt obtained: Configuration	Salt obtained: Yield / g	Salt obtained: Optical purity / %
1	10.560	70	L	1.226	97.1
2	1.268	80	D	1.877	99.4
3	1.901	80	L	1.496	95.4
4	1.500	120	D	1.143	99.8

a) Solvent: 200 cm³ of 1-butanol. Seed crystals: 0.050 g of D- or L-salt. Temperature: 10 °C.

degree of resolution (61.0%) at time 60 min. The L-4-MP salt partially resolved is easily purified to the L-salt with high optical purity by recrystallization. For example, the L-salt with an optical purity of 84.8% ($[\alpha]_D^{20}$ +38.8° (*c* 1.00, methanol)) was recrystallized once from 1-butanol to give L-salt with purity of 100% ($[\alpha]_D^{20}$ +45.7° (*c* 1.00, methanol)) similarly to the D-4-MP salt described in the experimental section. The L-salt obtained was treated with hydrochloric acid in the usual way to give L-Phe with an optical purity of 100% ($[\alpha]_D^{20}$ −34.5° (*c* 1.00, water)). These results indicate that the optical resolution of DL-4-MP salt is more favorable for obtaining the optically active Phe than that of DL-DCH salt. The optical resolution by successive preferential crystallization of DL-4-MP salt was found to give D- and L-Phe with high optical purity. The result is given in Table 6.

The D-4-MP salts obtained had optical purities of about 100%, and the L-salts those of over 95%. These D- and L-salts gave D-Phe with an optical purity of 99.8% and L-Phe with 97.0%, respectively.

It was found from the above results that DL-DCH and 4-MP salts are conglomerates around room temperature though the DL-salts form racemic compounds in the vicinity of the melting points, and that the optical resolution by successive preferential crystallization of DL-4-MP salt gives D- and L-Phe with optical purities of obout 100%.

References

1) M. Miyoshi and T. Harano, Japan Patent, 5013 (1964); *Chem. Abstr.*, **61**, 7097 (1964).
2) T. Shiraiwa, H. Miyazaki, A. Ikawa, and H. Kurokawa, *Nippon Kagaku Kaishi*, **1984**, 1425.
3) T. Shiraiwa, S. Taniguchi, A. Ikawa, K. Iwafuji, and H. Kurokawa, *Nippon Kagaku Kaishi*, **1983**, 1189.
4) K. Toi and T. Ugetsu, and N. Sato, Japan Patent, 8821 (1977); *Chem. Abstr.*, **88**, 62609 (1978).
5) L. R. Overby and A. W. Ingersoll, *J. Am. Chem. Soc.*, **73**, 3363 (1951).
6) M. Leclercq, A. Collet, and J. Jacques, *Tetrahedron*, **32**, 821 (1976).
7) J. Jacques, A. Collet, and S. H. Wilen, "Enantiomers, Racemates, and Resolutions," John Wiley and Sons, New York (1981), Section 2.5.
8) J. C. Sheehan and D. H. Yang, *J. Am. Chem. Soc.*, **80**, 1154 (1958).
9) T. Shiraiwa, S. Taniguchi, A. Ikawa, Y. Kashima, and H. Kurokawa, *Nippon Kagaku Kaishi*, **1983**, 1617.
10) "Seikagaku Data Bukku," ed by the Japanese Biochemical Society, Tokyo Kagaku Dojin, Tokyo (1982), Vol. I, p. 31.
11) S. H. Wilen, A. Collet, and J. Jacques, *Tetrahedron*, **33**, 2725 (1977).

A Study of the Color of Coal Liquids. II. Involvement of Light, Oxygen, Phenols, and Aromatic Amines in Formation of Colored Materials from Wandoan-Coal-Derived Liquids

Shigeru FUTAMURA* and Yoshio KAMIYA
Department of Reaction Chemistry, Faculty of Engineering, The University of Tokyo, Hongo, Bunkyo-ku, Tokyo 113
(Received January 31, 1986)

Triggering materials responsible for coloring of coal liquids have been searched by comparing the structures of the colored materials derived from the neutrals, acids, and bases of the coal liquid and the nitrogenous model compounds. Basic constituents of the coal liquid are most prone to photooxidation and afford colored materials of higher molecular weight and stronger absorption in the visible region. Model compound studies suggest that they are predominantly formed in the photoinduced oxidative coupling of aromatic amines.

It has already been reported in our preceding paper that a 10 to 20-fold increase is observed in the contents of nitrogen and oxygen for the colored materials separated from the degraded Wandoan-Coal-derived liquids, compared with those of the fresh sample oils.[1] It has also been shown that they have wider absorption range from the UV to visible region and abound in the constituents of large molecular sizes.

These results further prompted us to separate neutrals, acids, and bases from the fresh sample oils and to investigate their reactivities toward oxygen and/or light. Model compounds were also photooxidized in order to disclose triggering materials responsible for coloring of the coal liquids. The structures of their photooxygenated products were compared with those derived from the constituents of the coal liquids.

In this paper, we present that the above colored materials are principally formed in the oxidative coupling of aromatic amines, minor components of coal liquids.

Experimental

The coal liquid samples used were the kerosene (bp 180—240 °C) and light oil (bp 240—340 °C) fractions of the coal liquid produced from Wandoan-Coal in the 1 t/d PDU of Sumitomo Metal Corporation's. The kerosene and light oil fractions were separated into neutrals, acids, and bases according to the procedure shown in Fig. 1 after the removal of the colored materials by vacuum distillation. The colored materials with the strongest absorption in the visible region were prepared as the methanol-eluted fractions in chromatographing through a silica-gel column the residues obtained in the vacuum distillation (2 mmHg (1 mmHg=133.322 Pa)) of the above degraded kerosene fraction (≈75 °C) and the light oil fraction (≈145 °C), respectively. The colored materials obtained in the photooxidation of the coal liquid constituents and the model compounds were treated and prepared as well as those derived from the original coal liquids.

All the solvents and the model compounds were commercially purchased. Ethanol and tetrahydrofuran of spectrograde were used as received. The following model compounds were further purified by distillation or recrystallization (purity >99%): *p*-toluidine, 2-aminobiphenyl, 1-naphthylamine, 1,2,3,4-tetrahydroquinoline, diphenylamine, isoquinoline, 1-methylindole, and 2,3-dimethylindole.

In order to trace the structural change of the coal liquid constituents or model compounds caused by aerobic irradiation, light from a 200W super-high-pressure mercury arc (Shimadzu-Bausch-Lomb) through a Toshiba glass filter (λ>310 nm) was irradiated externally to ethanol solutions (2.5×10^{-3}% v/v) of the coal liquid constituents or the model compounds in Pyrex cells. For preparation of

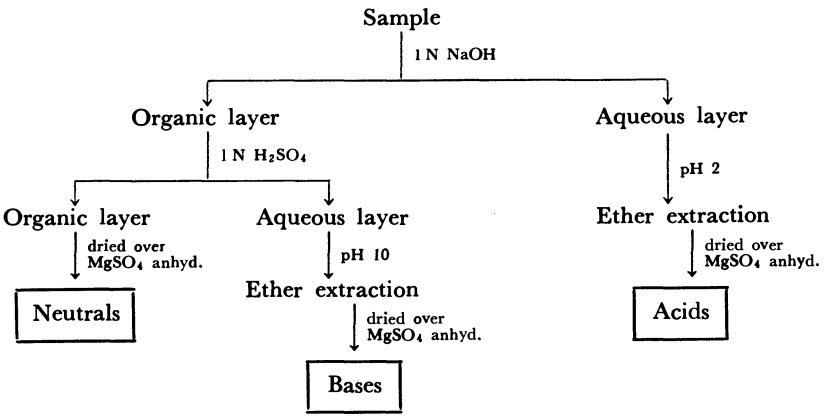

Fig. 1. Scheme for separation of coal liquids.

Table 1. Abbreviations of Coal Liquid Components and Colored Materials

K	Kerosene fraction.	NK	Neutrals of K.
Ak	Acids of K.	BK	Bases of K.
CK	Colored materials derived from K.		
CAK	Colored materials derived from AK.		
L	Light oil fraction	NL	Neutrals of L.
AL	Acids of L.	BL	Bases of L.
CL	Colored materials derived from L.		
NA	Colored materials derived from 1-naphthylamine.		
TOL	Colored materials derived from *p*-toluidine.		
THQ	Colored materials derived from 1,2,3,4-tetrahydroquinoline.		
MI	Colored materials derived from 1-methylindole.		
DMI	Colored materials derived from 2,3-dimethylindole.		

Table 2. Composition of Kerosene and Light Oil Fractions

Component	Kerosene	Light oil
Neutrals	83.6%	85.7%
Acids	14.8	11.2
Bases	1.6	3.1

Table 3. Elemental Analyses of Kerosene and Light Oil Components

	C	H	N	O(diff.)
K	88.2%	9.2%	0.21%	1.9%
NK	90.07	9.52	<0.1	0.41
AK	78.34	8.10	0.14	13.42
BK	81.09	8.26	8.93	1.72
L	89.2	8.3	0.47	1.7
NL	88.76	8.67	<0.1	2.57
AL	80.97	8.68	0	10.35
BL	82.04	8.20	8.06	1.70

the photooxygenated products, light from a 400W high-pressure mercury arc (Riko Kagaku) through a 75% aqueous $NaNO_2$ solution was irradiated externally to the above sample solutions (λ>400 nm).

The UV spectra were recorded on a JASCO RC-200. Ethanol was used as solvent. The gel permeation chromatograms were obtained on a Dupont 830 liquid chromatograph equipped with a column of HSG 15+20. Tetrahydrofuran was used as carrier. The IR spectra were taken on a Shimadzu IR-420 infrared spectrophotometer.

Results and Discussion

Table 1 summarizes the abbreviations of the coal liquid components and the colored materials. Table 2 shows the chemical compositions of the kerosene and light oil fractions. Both oils contain almost the same amounts of neutrals and acids. Bases occupy only 1.6 and 3.1 weight% of each oil. Table 3 shows the elemental analyses of the kerosene fraction and the light oil fraction. These data show that nitrogen and oxygen in coal liquids are concentrated into bases and acids, respectively. Comparison of the two bases by IR confirmed that the absorption ascribed to the pyrrolic N-H stretching band can be observed at 3480 cm^{-1} for BK,[2] while the absorption of basic N-H are stronger for BL. Difference in the chemical compositions between BK and BL affects the amounts and chemical structures of the colored materials. This point will be discussed later. Absorptions ascribed to the phenolic O-H stretching band can be observed at around 3600 cm^{-1} for both of AK and AL, and they cannot be differentiated by IR.

Mechanism for Coloring of Coal Liquids. Mechanisms for oxidative degradation of coal liquids can be classified into two reaction modes as shown in Fig. 2. One is oxygen incorporation, and the other is oxidative coupling. The former reaction can be exemplified as the decomposition of hydroperoxides produced in the autoxidation of hydrocarbons, affording carbonyl compounds and alcohols. This reaction proceeds under ordinary storage conditions since the colored materials obtained contain much oxygen.[1] However, it is improbable that this reaction is responsible for formation of the colored materials with strong absorption in the visible region. On the other hand, the latter reaction affords compounds with extended conjugated systems from phenolics and aromatic amines. For example, oxidative dimerization of substituted phenols give diphenoquinones. These compounds absorb at longer wavelengths (λ_{max}=420 nm) with stronger absorption (ε=70800 M^{-1} cm^{-1}) than benzoquinones (λ_{max}=400 nm).[3] Photooxidation of 2-naphthylamine affords dibenzophenazine,[4] which can be expected to absorb at longer wavelengths than phenazine ($\lambda_{abs}\approx$440 nm). The colored materials of large molecular sizes occupy only a little less than 1 weight% of the degraded coal liquids, and these colored materials could be formed in the oxidative coupling of polar compounds at room temperature.

Structural Change Accompanied by Photooxidation of the Coal Liquid. Seven samples such as L, NL, AL, BL, (NL+AL) (5.6:1.0 weight ratio), (NL+BL) (50:1.0 weight ratio), (AL+BL) (9.3:1.0 weight ratio) were stored in the dark under oxygen at room temperature for 5 d, but all the samples were colorless and no change was observed in their UV spectra. These results show that each component of the coal liquid is rather stable under oxygen without light. Then, all the above samples were irradiated under air. Figure 3a shows that the absorption of NL at longer than 300 nm grows with irradiation time

and it levels off after 8 h. The original light oil fraction showed almost the same UV spectral change as NL. As Fig. 3b shows, increase in the absorbance in the visible region was only small on irradiating AL under air. On the other hand, BL was extremely unstable under the photooxidation conditions. As Fig. 3c shows, aerobic irradiation decreased its absorption at 280—320 nm and increased that at longer than 320 nm. The increasing rate for the absorption at 400 nm is 4 to 8 times larger for BL than for NL and AL. The UV spectrum obtained by irradiating BL under argon for 7 h (dotted line in Fig. 3c) shows that BL is sensitive to anaerobic irradiation while the absorption at longer wavelengths is much weaker than under air. These results reveal that BL is most prone to structural change induced by irradiation and that oxygen promotes the formation of chromophores with the absorption from the UV to visible region. Furthermore, on 6 h irradiation, BL comes to take almost the same spectral pattern as that of CL(Fig. 3c). All of these results suggest that BL is predominantly involved in formation of colored materials with stronger absorption in the visible region. Mixing of AL and BL had no synergistic effect on increasing the rate of the absorbance at 400 nm. This finding suggests that acid-base interaction is negligible in photoinduced formation of colored materials.

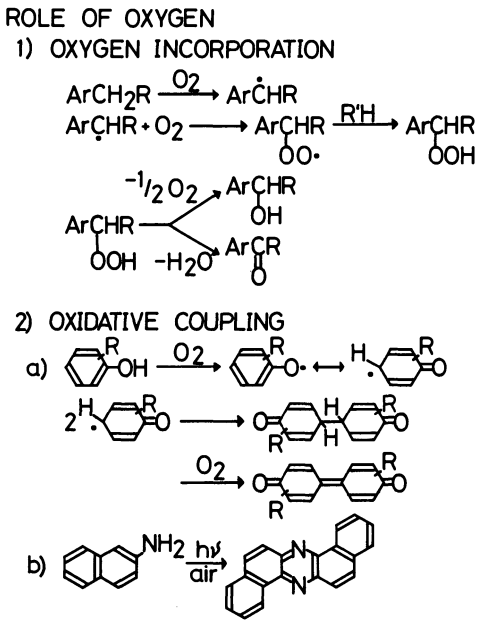

Fig. 2. Reaction modes for oxidation of coal liquids.

Comparison of Kerosene and Light Oil Fractions. The UV spectrum of the kerosene fraction remained unchanged on aerobic irradiation for 20 h. This fact coincides well with the fact that the kerosene fraction is more stable than the light oil fraction under ordinary storage conditions. NK and AK showed a similar UV spectral change on aerobic irradiation, but their absorption range did not extend to wavelengths longer than 350 nm. Aerobic irradiation of BK shifted the absorption range up to visible region, but the increasing rate of the absorbance at 400 nm was only 1/5 of that for BL. In this case, oxygen did not promote formation of colored materials. It is interesting that such difference was observed in the increasing rate of the absorption at 400 nm for pyrrole-rich BK and amine-rich BL.

Structural Change Accompanied by Photooxidation of Nitrogen Compounds. Predominant involvement of nitrogen compounds has been suggested in coloring of coal liquids, and the following model compounds have been chosen and subjected to photooxidation by taking account of the GC-MS analyses of the coal liquids used and the product analyses of the polar compounds contained in the SRC-II coal liquids.[5]: *p*-toluidine, 1-naphthylamine, 1,2,3,4-tetrahydroquinoline, diphenylamine, and iso-

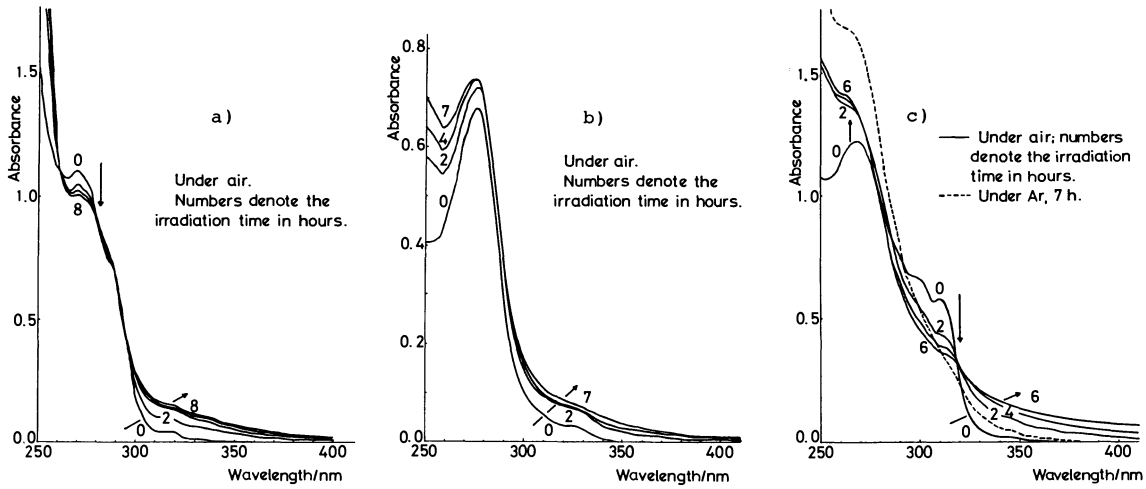

Fig. 3. UV spectral change induced by aerobic irradiation in ethanol.
a): NL, b): AL, c): BL.

quinoline. As to pyrrole-type nitrogen heterocycles, 2,3-dimethylindole and 1-methylindole have been chosen. The former compound has been reported to be deleterious in deposit formation in oil shale.[6] 1-Methylindole has been chosen as one of the *N*-alkylindoles for comparison of its reactivity toward photooxidation with that of 2,3-dimethylindole. Figure 4 shows the UV spectral changes of isoquinoline, diphenylamine, 1-naphthylamine, and 2,3-dimethylindole induced by aerobic irradiation, respectively. Any of them disappeared within 6 h, but the pattern of UV spectral change is quite different from each other. In the case of isoquinoline, no absorption can be observed at longer wavelengths. The increasing rate of the absorbance at 400 nm is 6 times larger for 1-naphthylamine and 2,3-dimethylindole than for diphenylamine. It is also interesting to note that aerobic irradiation of 1-naphthylamine for 3 h gives almost the same UV spectral pattern as that of CL.

Wright et al.[7] have alreadv pointed out that under air at 100 °C, anilines and indoles are the most reactive among the nitrogen compounds contained in the SRC-II coal liquid, and that their concentrations decrease to 1.4 and 11% after 112 d, respectively. Our results clearly show that the above compounds are photosensitive even at room temperature, forming colored materials more rapidly than aromatic secondary and tertiary amines under air.

Table 4. Weight Ratio of Colored Materials(CM)[a] to Substrate

Substrate	CM/Subst.
AK	0.16
BK	0.43
p-Toluidine	0.15
1-Naphthylamine	0.50
1,2,3,4-Tetrahydroquinoline	0.24
1-Methylindole	0.43
2,3-Dimethylindole	1.42

a) Prepared as the residue in the vacuum distillation of the reaction mixture obtained in the photooxidation of each sample in EtOH for 5 h.

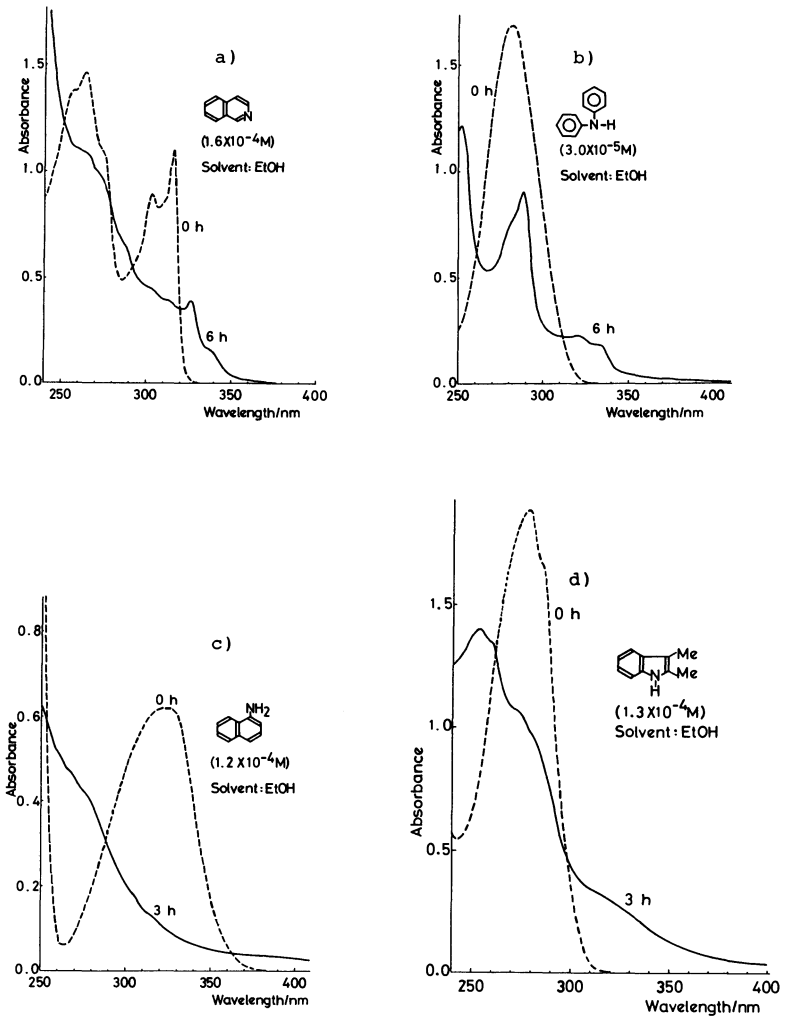

Fig. 4. UV spectral change induced by aerobic irradiation in ethanol(1 M = 1 mol dm^{-3}).
a): Isoquinoline, b): diphenylamine, c): 1-naphthylamine, d): 2,3-dimethylindole.

Gravimetrical Analysis of the Colored Materials. Next, the structures of the colored materials were compared, taking AK, BK, *p*-toluidine, 1-naphthylamine, 1-methylindole, 2,3-dimethylindole, and 1,2,3,4-tetrahydroquinoline as substrate. Table 4 summarizes the gravimetrical analyses of the colored materials. Minor component BK affords more colored materials than AK. Among the model compounds, an unusually large amount of colored materials is obtained from 2,3-dimethylindole, suggesting considerable oxygen uptake. Among the primary amines, 1-naphthylamine seems to give more colored materials than *p*-toluidine. It may reflect their different reactivities toward oxidative coupling. Figure 5 shows the UV spectra of the colored materials obtained in the photooxidations of AK, BK, and the model compounds. CBK is stronger in absorption in the visible region than CAK, and the UV spectrum of the former is more similar to that of CK. Absorption intensity at 400 nm of the colored materials derived from the model compounds decreases in the order of NA>TOL>THQ>DMI>MI.

Comparison of Figs. 4 and 5 indicates that among the nitrogen compounds, aromatic primary amines are most responsible for coloring of coal liquids.

Elemental Analysis of the Colored Materials. Table 5 shows the results of the elemental analyses of the colored materials. CAK contains almost no nitrogen, indicating that acids contribute to a lesser extent for coloring of coal liquids. The oxygen content of CK is larger than that of CL by about 10%. It is most likely that this was induced by the different chemical compositions of pyrrole-rich BK and amine-rich BL. In fact, the colored materials derived from the indoles tend to contain more oxygen than those from the amines by 4.6—15%.

IR Analysis. Figure 6 shows the IR spectra of the colored materials. Absorption of conjugated carbonyls can be observed at around 1680 cm^{-1} for CBK and its spectral pattern coincides well with that of CK.

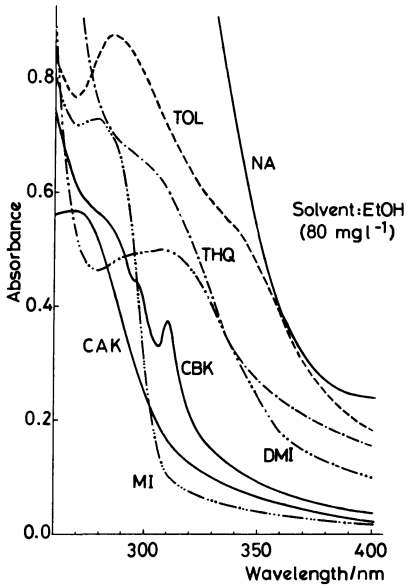

Fig. 5. UV spectra of the colored materials (concn: 80 mg l^{-1}).

Table 5. Elemental Analyses of Colored Materials(CM)[a)]

CM	C	H	N	O(diff.)
CK	60.66%	7.54%	4.91%	26.89%
CAK	61.13	6.83	0	32.04
CBK	69.53	6.91	7.72	15.84
CL	68.65	8.82	5.57	16.96
TOL	73.48	7.04	9.30	10.18
NA	79.81	4.73	7.45	8.01
THQ	75.76	6.85	8.54	8.85
MI	70.60	6.69	7.97	14.74
DMI	64.26	5.93	6.78	23.03

a) Dried in vacuo at room temperature for 6 h.

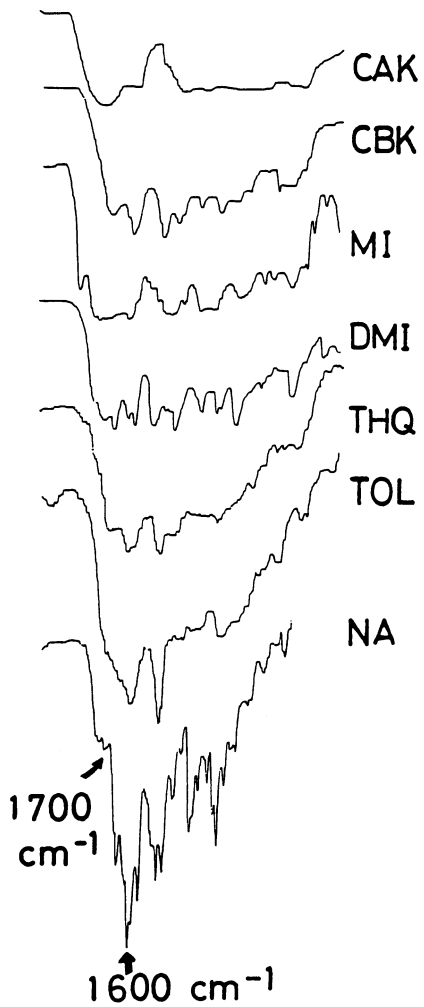

Fig. 6. IR spectra of the colored materials.

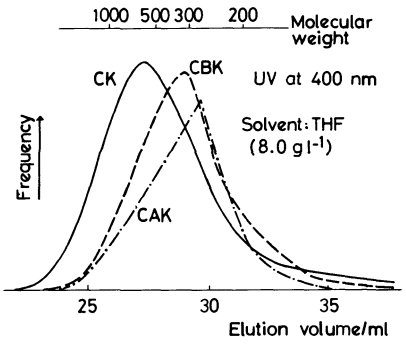

Fig. 7. GPC profiles of the colored materials derived from the kerosene fraction (concn: 8.0 g l^{-1}, detected with UV at 400 nm).

On the other hand, the carbonylic absorption of CAK shifts to higher wavenumbers. As to the model compounds, relative intensity of the absorption at 1680 cm^{-1} to that at 1600 cm^{-1} decreases in the order of MI>DMI>THQ>TOL>NA. This order is reversed against that of the UV absorption intensity at 400 nm (see Fig. 5). This fact clearly shows that the degree of photooxygenation does not parallel formation of chromophores with absorption at longer wavelengths. Therefore, it is most likely that oxidative coupling of aromatic primary amines afford colored materials of higher molecular weight with stronger absorption in the visible region.

GPC Analysis. Figures 7 and 8 show the GPC profiles of the colored materials. As to the colored materials derived from the coal liquids, nominal peak molecular weights of CK, CBK, and CAK are 580, 330, and 250, respectively (polystyrene standards). CBK is more similar to CK than CAK in molecular weight distribution. Among the colored materials derived from the model compounds, the scan of DMI extends to an area of the most highest molecular weight with a shoulder at nominal molecular weight 600. Oxidative trimers and tetramers could be formed. The molecular weight distributions of NA and TOL also suggest the formation of the constituents with higher molecular weight in the cases of 1-naphthylamine and *p*-toluidine. The scan of THQ has a wide molecular weight distribution with two peaks in the area of lower molecular weight. MI is considered to contain only a small amount of high molecular weight compounds.

All of these results show that the colored materials with the stronger absorption in the visible region tends to be of higher molecular weight.

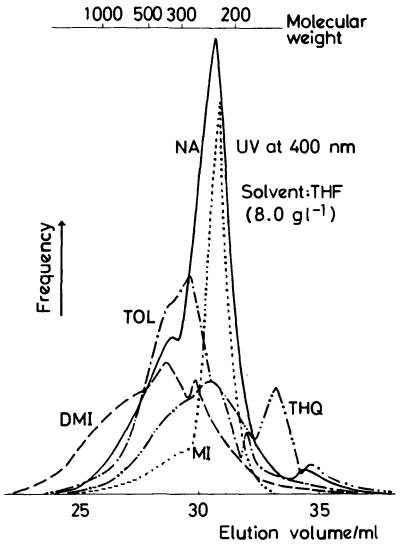

Fig. 8. GPC profiles of the colored materials derived from the model compounds (concn: 8.0 g l^{-1}, detected with UV at 400 nm).

In this paper, we have shown that coloring of coal liquids is induced by light and greatly promoted by oxygen. Bases in coal liquids are most liable to photooxidation and affords colored materials of higher molecular weight and stronger absorption in the visible region than neutrals and acids. Among the nitrogen compounds, aromatic primary amines are most deleterious and the above colored materials could be afforded predominantly in their oxidative coupling although they are only minor components in coal liquids.

This research has been entrusted by NEDO and the sample coal liquids were offered by Sumitomo Metal Corporation. The authors are very grateful to both of them.

References

1) S. Futamura and Y. Kamiya, *Fuel*, in press.
2) R. B. Thompson, J. A. Chenicek, L. W. Druge, and T. Symon, *Ind. Eng. Chem.*, **43**, 935 (1951).
3) W. J. Detroit and H. Hart, *J. Am. Chem. Soc.*, **74**, 5215 (1952).
4) G. R. Clemo and E. C. Dawson, *J. Chem. Soc.*, **1939**, 1114.
5) D. W. Lafer, M. L. Lee, K. D. Bartle, R. C. Kong, and D. L. Vassilros, *Anal. Chem.*, **53**, 1612 (1981).
6) J. W. Frankenfeld and W. F. Taylor, *Ind. Eng. Chem., Prod. Res. Dev.*, **22**, 608, 615, 622 (1983).
7) C. W. Wright, E. K. Chess, D. L. Stewart, and W. C. Weimer, *Fuel*, **64**, 443 (1985).

 © 1986 The Chemical Society of Japan Bull. Chem. Soc. Jpn., 59, 2341—2345 (1986)

Microheterogeniety in Aqueous Mixtures of Hydrophobic Solutes through Viscosity Studies

M. V. RAMANAMURTI, P. V. S. S. PRABHU,* and S. L. BAHADUR
Electrochemical Research Laboratories, Department of Chemistry, Banaras Hindu University, Varanasi-221 005, India
(Received May 21, 1985)

Precise viscosity data for aqueous binary mixtures of ethylene glycol (EG), 2-methoxyethanol (ME), and 1,2-dimethoxyethane (DME) at different mole fractions and at various temperatures are presented. EG behaves as a structure breaker showing negative deviation in viscosity-composition curve. Hydrophobic solutes ME and DME showed typical maximum in viscosity-composition curve in water rich region; attributed to the existence of "microheterogeniety" in these mixtures.

In order to explicate the structural arrangements at molecular level, the study of physicochemical properties of solutions would be of considerable help. With the notion to gain an insight into the molecular orientations and interactions occurring between the components of the binary mixtures, viscosities at different mole fractions of ethylene glycol (EG), 2-methoxyethanol (ME), and 1,2-dimethoxyethane (DME) in water at five different temperatures, namely 25, 30, 35, 40, and 45 °C, have been determined. Of these three solutes, EG exhibits protic character due to the two hydrogen atoms of hydroxyl groups. Obviously, in the remaining two solutes, ME and DME, succinct replacement of two hydrogen atoms of EG by electron donating methyl groups, renders them to impart quasiaprotic and aprotic characters, respectively. Also IR studies indicated that intramolecular hydrogen bonding exists in EG[1,2] and ME[2,3] molecules in the liquid state. However, it is apparent that no intramolecular hydrogen bonding is feasible in pure DME. Keeping the bifunctional nature especially of these solutes, EG, ME, and DME in view, viscosity studies of their binary mixtures with water would be of interest to elucidate the structural arrangements and molecular interactions. Although the viscosity data for these aqueous binary mixtures at 25 °C were already reported,[4-6] a thorough study on the structural details has not been dealt with.

This communication presents the viscosities of aqueous binary mixtures of EG, ME, and DME at five different temperatures viz., 25, 30, 35, 40, and 45 °C.

Experimental

Materials. Ethylene glycol, (B. D. H., AnalaR) was fractionally distilled under reduced pressure; dried over anhydrous sodium sulfate for two days and decanted. This was fractionally distilled under reduced pressure and the middle cut was collected.[7]

2-Methoxyethanol (A. R.) was treated with lithium hydride until the evolution of hydrogen gas ceased. Then it was distilled twice and the middle fraction was collected.[8]

1,2-Dimethoxyethane (Riedel-De-Haenag) was kept two days over KOH and then refluxed for 24 h. This was distilled over sodium and refluxed again for 24 h. Then the sample was distilled and middle fraction was directly used for measurements.[9]

Since these three solvents are highly hygroscopic in nature, they were kept under dry nitrogen atmosphere in order to minimize atmospheric contamination before use. Aqueous mixtures of these solvents were prepared with conductivity water (κ=0.2—0.5×10^{-6} Ω^{-1} cm^{-1}) obtained by triple distillation of water in the presence of alkaline $KMnO_4$.

Apparatus. Two Cannon-Ubbelohde viscometers, with flow times approximately 200 and 500 s, for water at room temperature, were calibrated[10] using pure water, methanol, carbon tetrachloride, benzene, and toluene. Viscosities of pure EG, ME, and DME so obtained at 25 °C are in excellent agreement with the literature values.[4,6,11] Thus e.g., at 25 °C η_{EG}[4]=16.84×10^{-3}, η_{ME}[5]=1.60×10^{-3}, and η_{DME}[11]=0.455×10^{-3} kg m^{-1} s^{-1}. Our values at 25 °C are η_{EG}=16.63×10^{-3}, η_{ME}=1.59×10^{-3}, and η_{DME}=0.451×10^{-3} kg m^{-1} s^{-1}.

During the course of measurements temperature constancy was ensured within ±0.01 °C. There was no need to incorporate corrections due to kinetic energy effects in the viscosity values calculated.[12]

Results and Discussion

Viscosity (η) values determined for aqueous binary mixtures of EG, ME, and DME, covering the whole range of composition, at 25, 30, 35, 40, and 45 °C are given in Tables 1, 2, and 3, respectively.

The monotonious increase in viscosity with the increase of EG content in the EG+water mixture (cf. Fig. 1) shows negative deviation from the ideal behavior indicating the structure breaking effect of the components on one another. Water has a well defined characteristic geometric structure.[13] However, EG, despite possessing a high degree of self-association through hydrogen bonding, does not have a defined geometric structure.[14,15] The autoprotolysis constant studies in these mixtures have also shown the absence of defined geometric structure in EG.[16] Therefore, the incompatibility which arises due to the dissimilarity in the basic geometric structures, as well as the differences in hydrogen bond energies results in the breakage of the

Table 1. Viscosities of Ethylene Glycol + Water Mixtures at Different Temperatures

No.	Mole fraction of EG	$\eta/10^{-3}$ kg m^{-1} s^{-1}				
		25 °C	30 °C	35 °C	40 °C	45 °C
1.	0.0000	0.890	0.801	0.723	0.656	0.598
2.	0.1000	1.714	1.481	1.313	1.175	1.040
3.	0.1985	2.764	2.409	2.107	1.846	1.627
4.	0.2998	4.084	3.701	2.903	2.535	2.201
5.	0.3999	5.490	4.370	3.844	3.326	2.900
6.	0.5002	6.904	5.689	4.761	4.051	3.550
7.	0.6000	8.666	7.320	5.955	5.037	4.240
8.	0.6999	10.200	8.589	6.831	5.897	4.822
9.	0.8003	11.880	9.375	7.958	6.552	5.730
10.	0.9027	13.460	11.170	9.235	7.942	6.444
11.	1.0000	16.630	13.250	10.766	9.236	7.444

Table 2. Viscosities of 2-Methoxyethanol + Water Mixtures at Different Temperatures

No.	Mole fraction of ME	$\eta/10^{-3}$ kg m^{-1} s^{-1}				
		25 °C	30 °C	35 °C	40 °C	45 °C
1.	0.0000	0.890	0.801	0.723	0.656	0.598
2.	0.1098	1.969	1.682	1.473	1.305	1.145
3.	0.2001	2.645	2.241	1.947	1.699	1.494
4.	0.3005	2.950	2.449	2.119	1.858	1.634
5.	0.4013	2.877	2.415	2.102	1.858	1.650
6.	0.5002	2.659	2.277	2.008	1.769	1.582
7.	0.5985	2.422	2.097	1.842	1.641	1.479
8.	0.7004	2.133	1.959	1.723	1.553	1.401
9.	0.7999	1.987	1.791	1.584	1.452	1.309
10.	0.9003	1.789	1.666	1.468	1.350	1.232
11.	1.0000	1.590	1.388	1.259	1.147	1.002

Table 3. Viscosities of 1,2-Dimethoxyethane + Water Mixtures at Different Temperatures

No.	Mole fraction of DME	$\eta/10^{-3}$ kg m^{-1} s^{-1}				
		25 °C	30 °C	35 °C	40 °C	45 °C
1.	0.0000	0.890	0.801	0.723	0.656	0.598
2.	0.0999	1.986	1.595	1.457	1.282	1.126
3.	0.1998	1.990	1.608	1.469	1.291	1.141
4.	0.2997	1.563	1.352	1.219	1.073	0.988
5.	0.3999	1.216	1.013	0.978	0.881	0.845
6.	0.5001	0.950	0.842	0.799	0.777	0.724
7.	0.5997	0.772	0.700	0.688	0.614	0.585
8.	0.6999	0.679	0.592	0.570	0.523	0.494
9.	0.8002	0.555	0.499	0.484	0.445	0.427
10.	0.9001	0.491	0.459	0.441	0.416	0.401
11.	1.0000	0.451	0.421	0.389	0.376	0.369

structural integrities of EG and water. Subsequently the individual water molecules will get themselves loosely associated with ethylene glycol molecules through hydrogen bonding resulting in an overall less structured solvent mixture than that expected from ideal behavior.

In case of aqueous mixtures of ME or DME, viscosity increases rapidly with the increase of solute content (ME or DME) in the mixture and reaches a maximum at a particular composition in the water-

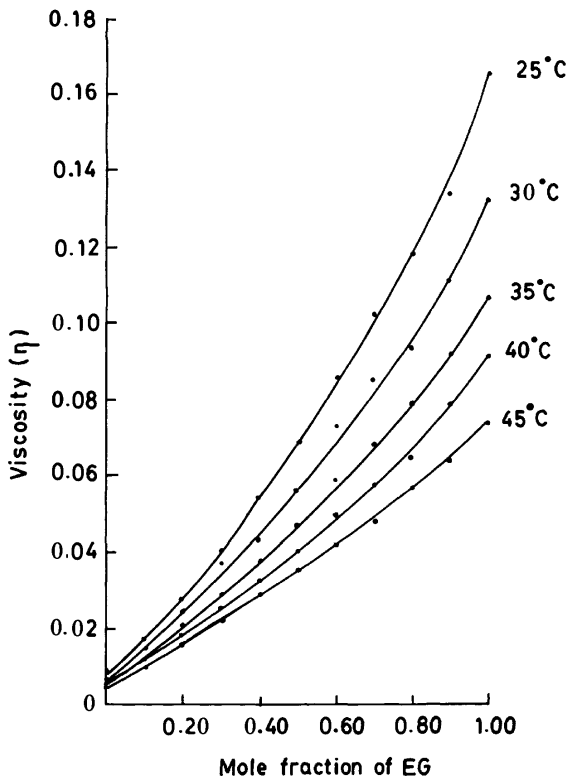

Fig. 1. Variation of viscosity (η) with the mole fraction of ethylene glycol at different temperatures.

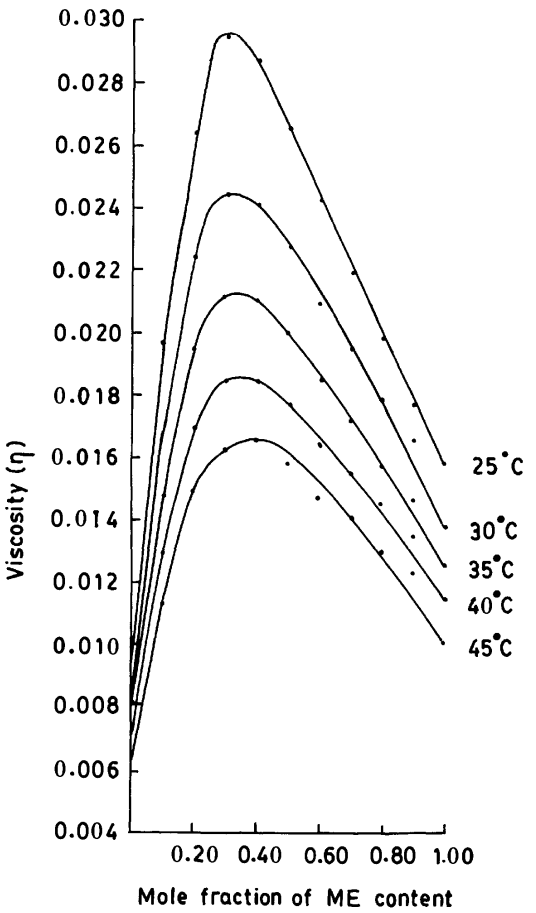

Fig. 2. Variation of viscosity (η) with the mole fraction of 2-methoxyethanol at different temperatures.

rich region (cf. Figs. 2 and 3). The viscosity maxima are nearly 2.9 and 2.0 times viscosity of water and appear around 0.30 and 0.20 mole fractions of ME and DME, respectively. Although, such a maximum, observed for aqueous mixtures of different organic solvents was attributed to the formation of an association complex,[17–20] an appropriate explanation may be given as follows. The ascending part of viscosity–composition curve (water-rich region in Figs. 2 and 3) represents structural promotion in the mixture by gradual formation of clusters of associated species. These clusters[21–27] may be formed in three different possible ways such as the association between (a) the same species (b) different species, and (c) the same species and different species simultaneously. A gradual aggregation of these different types of clusters would obviously lead to an increase in the viscosity and approach to a maximum value when aggregation is maximum. So viscosity maximum is an indication of maximum structuredness. However, the participation of different types of associated molecular species in aggregation at viscosity maximum apparently brings heterogeniety in the system (mixture). Therefore, since the observed maximum in viscosity is a consequence of aggregation of heterogeneous associated species at molecular level, this phenomenon may be termed as "microheterogeniety". The shift of viscosity maximum (Figs. 2 and 3) towards water-rich region with the addition of methyl group e.g. 0.30 mole fraction ME to 0.20 mole fraction DME in respective aqueous mixtures suggests the solvation of water into organic solute (interstitial solvation) in agreement with findings of Rohdewald and Moldner.[28]

Franks[29] has explained the structure promotion and destruction effects on the basis of the variation in $d\eta/dx$ with x (i.e. rate of change of viscosity with the change in solute content) instead of variation in η with x. The solutes, ME and DME, may be brought under the category of "structure promoters" for water-rich region, following Franks. Structural promotion 'effect' decreases with the increase in solute content and it passes through "zero structural promotion" effect (i.e. $d\eta/dx=0$) at mole fraction value corresponding to η_{max} (Fig. 4). This implies that at viscosity maximum no further structural promotion is possible. Further addition of solute decreases $d\eta/dx$ to a minimum value which indicates "structure breaking" in solute rich mixtures due to excess presence of solute. The mole fraction value corresponding to $d\eta/dx=0$ remains unaltered with change in temperature (Fig. 4).

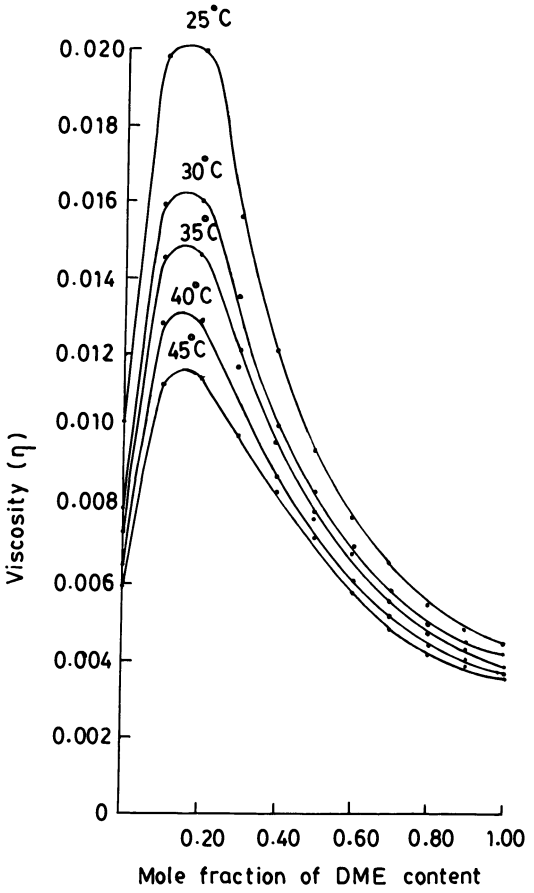

Fig. 3. Variation of viscosity (η) with the mole fraction of 1,2-dimethoxyethane at different temperatures.

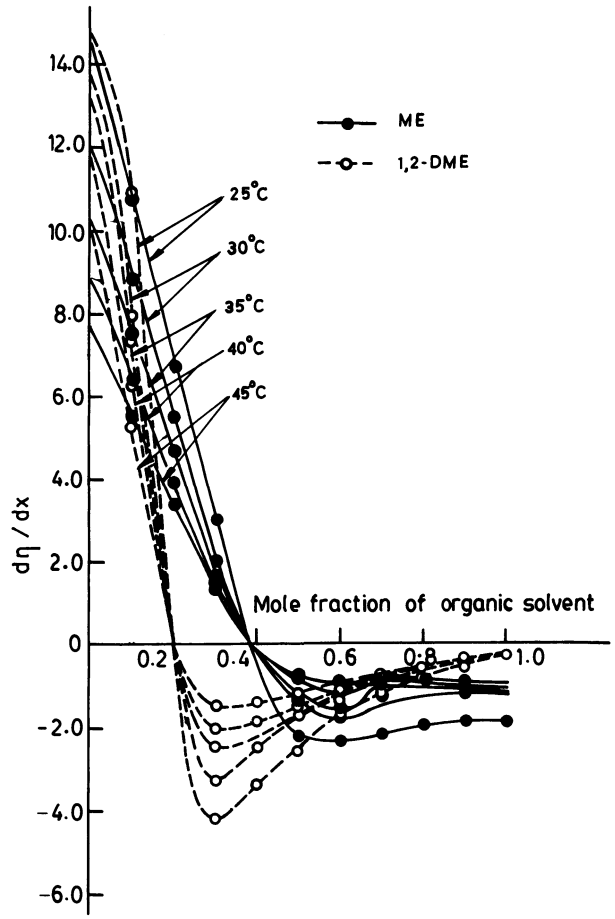

Fig. 4. Variation of first derivative ($d\eta/dx$) with mole fraction (x) of organic solvent.

These three systems have followed fairly closely the Andrade's relation[30]

$$\eta = Ae^{B/RT},$$

where B is called the "activation energy for viscous flow" and A is system specific parameter. A representative plot of variation of log η with $1/T$ for EG+water mixtures is illustrated in the Fig. 5, which clearly shows the applicability of Andrade's relation. Various other workers[31–33] also have showed that this equation is fairly applicable for several other systems.

A consideration of molecular size (S) of pure EG, ME, and DME (viz., $S_{EG}<S_{ME}<S_{DME}$) suggests that, if molecular association were not to be present the same should have been the trend in viscosity values also. A decrease in viscosity values as observed viz., $\eta_{EG}(16.63\times10^{-3}$ Kg m^{-1} s$^{-1}) > \eta_{ME}(1.59\times10^{-3}$ Kg m^{-1} s$^{-1}) > \eta_{DME}(0.0451$ Kg m^{-1} s^{-1}) can be explained on the basis of the gradual reduction of inter- and intramolecular association because of successive replacement of hydrogen atoms of hydroxyl groups in EG by methyl group.

Authors thank UGC (Government of India) for the financial support, and Head, Department of Chemistry,

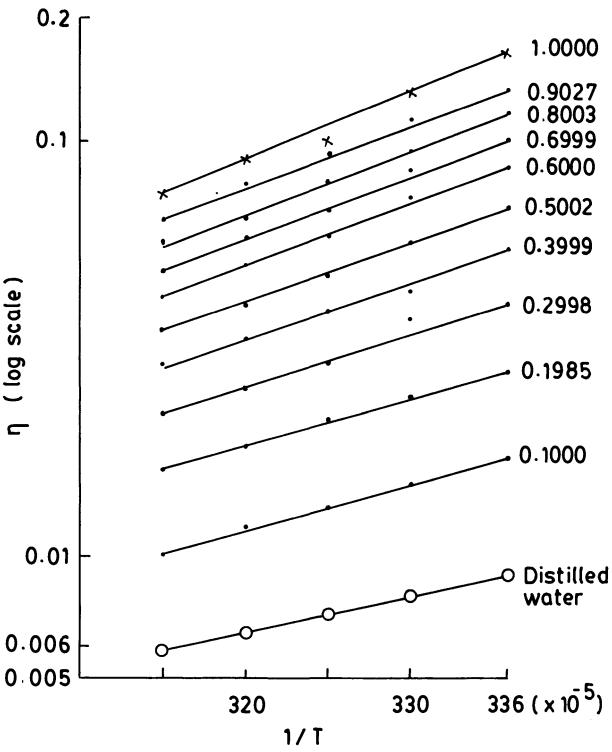

Fig. 5. log η vs. $1/T$ at different mole fractions of ethylene glycol in water.

Faculty of Science, Banaras Hindu University for facilities. Authors' thanks are also due to one of the referees for his valuable critical comments.

References

1) P. Buckley and I. A. Guguere, *Can, J. Chem.*, **45**, 397 (1967).
2) R. Iwamoto, *Spectrochim. Acta*, **27**, 2385 (1971).
3) L. P. Kuhn and R. A. Wires, *J. Am. Chem. Soc.*, **86**, 2161 (1964).
4) F. Accascina and S. Petrucci, *Ric. Sci.*, **30**, 808 (1960).
5) F. Accascina, P. D'Angelo, and S. Schiavo, *Sci. Tec.*, **4**, 32 (1960).
6) E. Renard and J.-C. Justice, *J. Solution Chem.*, **3**, 633 (1974).
7) N. Koizumi and T. Hanai, *J. Phys. Chem.*, **60**, 1496 (1956).
8) Chu, K-Yu and A. R. Thompson, *J. Chem., Eng. Data*, **5**, 147 (1960).
9) W. J. Wallace and A. L. Mathews, *J. Chem. Eng. Data*, **8**, 496 (1963).
10) "Handbook of Chemistry and Physics," 52nd Edition, CRC Press Inc., USA (1978).
11) J. A. Riddick and W. B. Bunger, "Organic Solvents," Wiley-Inter Science Publishers, Inc., USA, (1970).
12) M. R. Cannon, R. E. Manning, and J. D. Bell., *Anal. Chem.* **32**, 355 (1960).
13) N. Ohtomo, K. Tokiwano, and K. Arakawa., *Bull. Chem. Soc. Jpn.*, **54** 1802 (1981).
14) M. N. Das and K. K. Kundu, *J. Indian Chem. Soc.*, **51**, 266 (1974).
15) K. K. Kundu and A. K. Das, *Indian J. Chem.* **16(A)**, 467 (1978).
16) K. K. Kundu, P. K. Chattopadhyay, D. Jana, and M. N. Das., *J. Phys. Chem.* **74**, 2633 (1970).
17) P. Assarsson and F. R. Eirich, *J. Phys. Chem.* **72**, 2710 (1968); M. V. Ramanamurti and L. Bahadur, *Electrochim. Acta*, **25**, 601 (1980); *J. Solution Chem.*, **6**, 703 (1977); *J. Chem. Soc., Faraday Trans. 1*, **76**, 1409 (1980).
18) R. L. Kay and T. L. Broadwater, *J. Solution. Chem.*, **5**, 57 (1976).
19) R. L. Kay and T. L. Broadwater, *Electrochim. Acta*, **16**, 667 (1971).
20) J. M. G. Cowie and P. M. Toporowski, *Can. J. Chem.*, **39**, 2240 (1961).
21) D. N. Glew, H. D. Mak, and N. S. Rath, "Hydrogen-Bonded Solvent System," ed by A. K. Covington and P. Jones, Taylor and Francis, London (1968), p. 195.
22) M. J. Blandamer, D. E. Clark, N. J. Hidden, and M. C. R. Symons, *Trans. Faraday Soc.*, **64**, 2691 (1968).
23) R. J. Fanning and P. Kruus, *Can. J. Chem.*, **48**, 2052 (1970); K. Tamura, M. Maekawa, and T. Yasunaga., *J. Phys. Chem.*, **81**, 2122 (1977).
24) N. Muller, *J. Magn. Reson.*, **28**, 203 (1977).
25) K. Iwasaki and T. Fujiyama, *J. Phys. Chem.*, **81**, 1988 (1977).
26) G. Roux, G. Perron, and J. E. Desnoyers, *J. Solution Chem.*, **7**, 639 (1978).
27) G. Roux, D. Roberts, G. Perron, and J. E. Desnoyers, *J. Solution Chem.*, **9**, 629 (1980).
28) P. Rohdewald and L. Moldener, *J. Phys. Chem.*, **77**, 373 (1973).
29) Physico-Chemical Process in Mixed Aqueous Solvents," ed by F. Franks Heinemann Educational Books, London (1967), pp. 66—67.
30) "Findlays Practical Physical Chemistry," 9th Edition, Longman Group Limited, London (1973), p. 90.
31) A. S. C. Lawrance, M. P. MacDonald, and J. V. Stevens, *Trans. Faraday Soc.*, **85**, 3231 (1969).
32) B. X. Lippold and M. S. Adel, *Arch. Pharm. (Weinheim Ger.)* **305**, 418 (1979).
33) A. D'Aprano, L. D. Donato, E. Caponetti, and V. Agrigento, *J. Solution Chem.*, **8**, 793 (1979).

Solvent Effect on Lifetime of Triplet Exciplex between Chloranil and Durene

Harumichi KOBASHI,* Tomoyuki KONDO, and Masa-aki FUNABASHI
Department of Chemistry, Faculty of Engineering, Gunma University,
Kiryu, Gunma 376
(Received January 9, 1986)

Synopsis. The triplet exciplex between chloranil (CA) and durene (DH) shows a decay which is associated with solvent viscosity rather than polarity, in spite of having a full charge-transfer (CT) character.

A strong dependence of the photophysical and photochemical processes of exciplexes upon solvent polarity is well-known for singlet states. However, solvent effects on the dynamic behavior of triplet exciplexes have not yet been fully investigated. The triplet exciplex with a nearly complete CT nature (CT-type triplet exciplex) or an ion pair between CA and DH has previously been reported by us for the solvent 1,2-dichloroethane (DCE).[1] Here, we report on the lifetimes of this triplet exciplex in various solvents, while paying attention to the effects of the solvent polarity and viscosity.

Experimental

The transient spectra and lifetimes of the exciplex were measured by means of nanosecond laser photolysis using a Q-switched frequency-doubled ruby laser at room temperature (20±1 °C).[1] The method used for photocurrent measurements was the same as that used before.[1] Solvents used were 1,4-dioxane (DO), benzene (BZ), diethyl ether (EE), ethyl acetate (EAC), dichloromethane (DCM), acetone (ACT), and acetonitrile (ACN). DCM was purified as follows: shaken with concd. H_2SO_4, water, aq 5% NaOH, and again water, it was then distilled twice over P_2O_5 after being pre-dried with $CaCl_2$ and stored in a brown bottle with molecular sieves (Zeolite 4A). After these treatments, it was fractionally distilled just before use. Other solvents of spectrograde (Dotite) were distilled after being dried with Zeolite 4A.

Results and Discussion

In DO, BZ, EE, EAC, and DCM (nonpolar and moderately polar solvents) the quenching of triplet chloranil (^{3}CA) by DH led to the formation of a short-lived triplet exciplex, $^3(CA^{\cdot-}\cdots DH^{\cdot+})$, having an absorption band around 450 nm, similar to that in DCE.[1] After a lapse of time, a long-lived chloranil semiquinone radical (CAH·) was observed at 435 and 365 nm in these solvents as well as in DCE.[1] Figure 1 shows the transient spectra observed in DCM as a representative of such spectral features. The first-order decay rate constants of $^3(CA^{\cdot-}\cdots DH^{\cdot+})$ were analyzed at 448 nm in the same manner as that used for the case of a DCE solution.[1]

In ACT and ACN (polar solvents) ^{3}CA quenching also led to a rapid appearance of an absorption band around 450 nm due to a $CA^{\cdot-}$ unit. However, its decay was very slow and did not obey first- or second-order kinetics. Figure 2 gives an example of the spectral change together with an oscillogram of the absorption band at 448 nm observed in ACN. Absorbance at a later stage of the time trace decays with a second-order kinetics resulting from a recombination between free $CA^{\cdot-}$ and $DH^{\cdot+}$ produced through the ionic dissociation of a relaxed and/or nonrelaxed exciplex. A fast formation of free ions and their decays (obeying second-order kinetics) were also observed through transient photocurrent measurements.[2] The decay curve at 448 nm consists of at least two components, first- and second-order decays in both solvents. However, a further detailed analysis of the decay in the polar solvents was not performed during the present stage of the investigation.

Table 1 summarized the data for the lifetimes of the triplet exciplex in various solvents. The values of $\tau_{1/e}$ in ACT and ACN are the apparent decay times of both ion pairs and free ions superposing each other. These values have only qualitative meanings for a comparison purpose with those of true exciplexes in

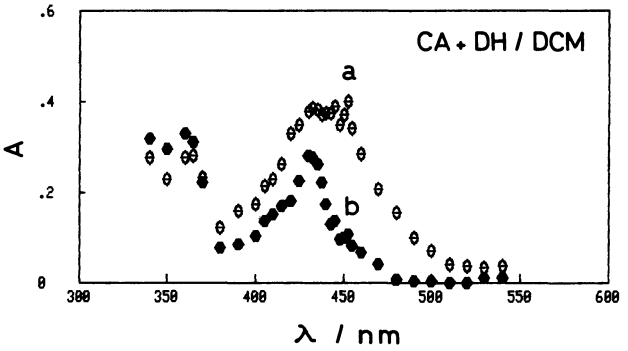

Fig. 1. Transient absorption spectra for the system of CA (2.0×10^{-3} mol dm^{-3}) and DH (0.20 mol dm^{-3}) in DCM. The delay time after the start of laser oscillation. a): 60 ns, b): 540 ns.

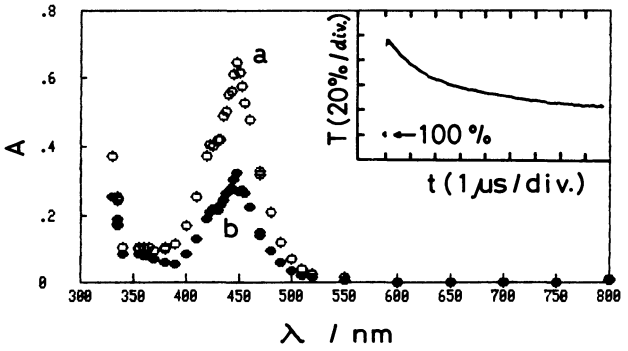

Fig. 2. Transient absorption spectra for the system of CA (2.5×10^{-3} mol cm^{-3}) and DH (0.19 mol dm^{-3}) in ACN. The delay time. a): 60 ns, b): 1.54 μs.

Table 1. Lifetimes of the Triplet Exciplex τ (in ns) in Various Solvents of Dielectric Constant ε and Viscosity Coefficient η (in cp; 1cp=10^{-3} Pas)

Solvent	ε	η	τ[a]
DO	2.3	1.31	60
BZ	2.3	0.64	45
EE	4.3	0.24	25
EAC	6.4	0.45	47
DCM	9.1	0.43	47
DCE	10.7	0.83	49[b]
ACT	21.4	0.32	(1250)[c]
ACN	37.5	0.36	(2600)[c]

a) Experimental errors were within 6% in the standard deviation. b) Ref. 1. c) The apparent decay time ($\tau_{1/e}$) of the band at 448 nm on changing from the initial absorbance (ca. 0.6) to $1/e$ of it.

other solvents. It has been found that the lifetime of $^3(CA^{\mp}\cdots DH^{\pm})$ does not depend on the polarity of the solvent in a range of ε from 2.3 to 10.7, while it depends weakly upon the viscosity of the solvent. A linear correlation (factor γ=0.87) between the decay rate τ^{-1} and the parameter T/η (here, T=293 K) of the diffusion coefficient seems to indicate that τ^{-1} is affected by the easiness of the vibrational and/or reorientational motion of the exciplex associated with solvent molecules. It is known that the escape probability of the triplet exciplex, between fluorenone and 1,4-diazabicyclo[2.2.2]octane, into dissociated ions depends on the solvent viscosity.[3] In our case, however, the ionic dissociation is not involved in the exciplex decay since no transient photocurrent was gained in DO, BZ, EE, and EAC.[4] Kuz'min et al. have reported that the lifetimes of the triplet exciplexes of 2,6-diphenyl-*p*-benzoquinone with diphenylamine and triphenylamine tend to decrease with increasing ε, ranging from 2.4 to 7.3.[5] The polarity dependence of the present exciplex differs from those of the exciplexes cited above, though they are exciplexes of quinones with a full CT character. This difference in decay behavior can be attributed to a difference in the chemical species constructing the exciplex. Although there is a small difference, such a small (or no) effect of the solvent polarity seems to be consistent with the result that the intersystem crossing (ISC) or back electron transfer of CT-type triplet exciplexes is only weakly dependent on the polarity of the medium.[6]

The relaxation of our exciplex consists of two processes, ISC and a proton transfer, except for cases involving a slight ionic dissociation.[4] Then, if the rate constant of ISC can be regarded as almost constant while changing ε,[7] the dependence on η in the present exciplex might mainly reflect a change in the rate of the proton transfer (k_p). This expectation would not contradict the supposition that $^3(CA^{\mp}\cdots DH^{\pm})$ is necessary for changing its conformation through a diffusive movement upon going from the relaxed state to a state favorable for causing a proton transfer.[1] Recently, Manring and Peters have also pointed out the requirement of molecular reorientation in a triplet ion pair prior to causing a proton transfer (k_p) for the benzophenone and *N*-methyldiphenylamine system.[8] They have additionally shown in the same system that the rate constant corresponding to k_p decreases upon increasing the solvent polarity. Thus, the decay behavior of triplet exciplexes exhibits various dependences on solvents. A further study of the solvent effect on the single process of a proton transfer in our exicplex is in progress now.

We with to thank Prof. Haruo Shizuka for his interest and encouragement.

References

1) H. Kobashi, M. Funabashi, T. Kondo, T. Morita, T. Okada, and N. Mataga, *Bull. Chem. Soc. Jpn.*, **57**, 3557 (1984).
2) An example of photocurrent for the system in ACN has been given in Fig. 11 of Ref. 1.
3) N. Periasamy and H. Linschitz, *Chem. Phys. Lett.*, **64**, 281 (1979).
4) A weak photocurrent was observed in DCM as well as in DCE.[1] Accordingly, ionic dissociation contributes a little to the decay of $^3(CA^{\mp}\cdots DH^{\pm})$ in these two solvents.
5) V. A. Kuz'min, A. P. Darmanyan, and P. P. Levin, *Chem. Phys. Lett.*, **63**, 509 (1979).
6) P. P. Levin and T. A. Kokrashvili, *Bull. Akad. Sci. USSR, Div. Chem. Sci.*, **30**, 971 (1981); P. P. Levin, A. M. Vinogradov, A. P. Darmanyan, and V. A. Kuz'min, *Dokl. Akad. Nauk SSSR*, **254**, 1158 (1980).
7) P. P. Levin, T. A. Kokrashvili, and V. A. Kuz'min, *Bull. Acad. Sci. USSR, Div. Chem. Sci.*, **31**, 466 (1982).
8) L. E. Manring and K. S. Peters, *J. Am. Chem. Soc.*, **107**, 6452 (1985).

Temperature Effect on the Rhodium-Catalyzed Direct Synthesis of Ethylene Glycol from Carbon Monoxide and Hydrogen in Several Solvents

Takashi MASUDA,* Kazuhisa MURATA, Toshiaki KOBAYASHI, and Akio MATSUDA
National Chemical Laboratory for Industry, Higashi, Yatabe, Tsukuba-gun, Ibaraki 305
(Received December 26, 1985)

Synopsis. The $Rh_4(CO)_{12}$/*N*-methyl-2-pyrrolidone system is featured in that the rate of ethylene glycol (EG) formation is significantly accelerated with increasing reaction temperature. The turnover frequency of EG at 300 °C and 2000 kg/cm² ($H_2/CO=1$) is about 2000 h^{-1}. The $Rh_4(CO)_{12}$/tributylamine system also has a high catalytic activity at a high temperature.

The direct synthesis of ethylene glycol (EG) from carbon monoxide and hydrogen is interesting from the fundamental and industrial points of view. Much attention has been paid on this direct synthesis and a number of patents have appeared.[1] Clusters and complexes of group VIII elements of the periodic table such as Co,[2a] Rh, Ru, and Ir[2b] are used as catalysts. Most noteworthy is the work of Union Carbide Corporation which describes the direct synthesis of EG with rhodium catalysts. Union Carbide workers also carried out bench-scale experiments in a continuous flow unit capable of catalyst recycle.[3] Fahey[4] has reported of a Rh-catalyzed direct synthesis in tetraglyme solvent with promoters at about 2000 atm of synthesis gas. The highest turnover frequency of EG including ethylene glycol monoformate in his results was 248 h^{-1}, which is, to our knowledge, the highest rate to EG in the literature.[1-4] However, little is known about the influence of temperature on the glycol producing activity of rhodium catalyst. In the present paper, we report of remarkable temperature effects on the Rh-catalyzed formation of EG from carbon monoxide and hydrogen in nitrogen-containing solvents.

Experimental

All reagents were commercially available. All experiments were carried out in a 20 ml rocking batch reactor made of Inconel Alloy under a constant pressure. Oxygenated compounds such as methyl alcohol (MeOH), ethylene glycol (EG), methyl formate (MF), ethyl alcohol (EtOH), and ethylene glycol monoformate (EGMOF) were formed as products. The products were analyzed by gas chromatography using a Chromosorb 102 column. Sulfolane was used as an internal standard. Rates to products were given in terms of turnover frequency, defined as the number of moles of the product formed per gram-atom of metal per hour. The turnover frequency of EG, N(EG), is obtained by

$$N(EG) = \text{mol}(EG+EGMOF)/(\text{g-atom Rh})h$$

Product selectivity is defined as the carbon efficiency on the basis of reduced carbon monoxide in a product obtained. The selectivity value of EG, Sel.(EG), is obtained by

$$\text{Sel.}(EG) = \frac{2(EG+EGMOF)\times 100}{MeOH+MF+2(EtOH+EG+EGMOF)}$$

Results and Discussion

The results are summarized in Table 1. The $Rh_4(CO)_{12}$/tributylamine system has a high catalytic activity at 290 °C (Run 1). In intial patents, a number of amines have been used as promoters. Optimum EG productivities have generally been achieved at relatively low amine/rhodium ratios of 0.1—2.3.[1b] However, there have been no precedents

Table 1. Influence of Temperature on the Direct Synthesis of Ethylene Glycol[a]

Run No.	Solvent (7 ml)	Temp °C	Press. kg/cm²	$Rh_4(CO)_{12}$ mg-atom	Products/mmol MeOH	MF	EtOH	EG	EGMOF	N (EG)	Sel. (EG)	Color[b]
1	Tributylamine[c]	290	1800	0.025	8.56	1.06	0.77	10.06	—[e]	402	64.3	Colorless
2	NMP	230	1800	0.1	1.26	0.03	0.04	4.00	0.18	41.8	85.9	Colorless
3	NMP	250	1800	0.1	2.85	0.17	0.20	10.17	1.01	111.8	86.7	Colorless
4	NMP	290	1800	0.01	8.37	1.38	0.31	10.81	1.66	1247	70.6	Colorless
5	NMP	300	2000	0.01	11.06	2.24	2.43	17.40	3.29	2069	69.5	Colorless
6	Toluene[d]	230	1800	0.1	7.55	3.15	0	0.14	—[e]	1.4	2.6	Yellowish brown
7	Tetraglyme	230	1800	0.1	6.40	1.14	0.09	0.91	0	9.1	19.1	Wine red
8	Tetraglyme	250	1800	0.1	4.79	0.32	0.30	0.14	0	1.4	4.7	Purplish brown
9	γ-Butyrolactone	230	1800	0.1	1.83	0.17	0.07	0.24	0	2.4	18.3	Wine red
10	γ-Butyrolactone	250	1800	0.1	7.37	0.97	0.13	0.40	0	4.0	8.5	Wine red
11	γ-Butyrolactone	290	1800	0.01	9.82	1.78	0.06	0.03	0	3.0	1.0	Pale purple

a) Reaction conditions: $P_{H_2}/P_{CO}=1$; Reaction time 1 h. b) The color of product solution at ambient temperature and pressure. c) The reaction mixture (tributylamine+products) was homogenized by adding pyridine before analysis. d) The reaction mixture (toluene+products) was homogenized by adding tetrahydrofuran before analysis. e) Not determined.

in which reactions in amine solvents give as high a catalytic activity as the N(EG) of Run 1.

The $Rh_4(CO)_{12}$/*N*-methyl-2-pyrrolidone (NMP) system shows a remarkable temperature effect on the formation of EG. Keim et al.[5] reported that the $Rh(CO)_2acac$/NMP system yielded EG in the hydrogenation of carbon monoxide, but without giving no rates to EG. As can be seen from Runs 2—5, the rate of EG formation is significantly accelerated by increase in reaction temperature. The N(EG) at 300 °C and 2000 kg/cm^2 of synthesis gas is about 2000 h^{-1} (Run 5). The Sel.(EG) of Run 5 is about 70%. This value of N(EG) is the highest that has ever been found with rhodium catalysts. This value is interesting from the standpoint of the cost and availability of rhodium.

The result obtained for the $Rh_4(CO)_{12}$/toluene solvent system is given in Run 6. The rate of EG formation is significantly lower than that of the $Rh_4(CO)_{12}$/NMP system (Run 2), though the rate of MeOH formation is higher than that of Run 2. This reaction in toluene at 230 °C caused precipitation of rhodium metal, which suggests that the catalyst stability in toluene is low.

Although tetraglyme and γ-butyrolactone have been used as effective solvents in the presence of promoters in the literature,[1,4] little is known about their catalytic effectiveness in the absence of promoters. The results obtained for the $Rh_4(CO)_{12}$/tetraglyme solvent system are given in Runs 7 and 8. This catalyst system also gives lower rates to EG than the $Rh_4(CO)_{12}$/NMP system (Runs 2 and 3). The reaction in tetraglyme at 250 °C gives rise to precipitates of rhodium metal.

The results obtained for the $Rh_4(CO)_{12}$/γ-butyrolactone solvent system are shown in Runs 9—11. In contrast to the results of the nitrogen-containing solvents (Runs 1—5), increase in temperature has only a small effect on the rate of EG formation, though there was no visible evidence for the formation of rhodium metal at the end of the reaction.

For γ-butyrolactone, tetraglyme, and toluene, the effectiveness order for catalyst stability is γ-butyrolactone>tetraglyme>toluene. It appears that solvents having high dielectric constants enhance the stability of the rhodium catalyst. On the other hand, a comparison of Run 1 with Runs 6 and 7 shows that tributylamine improves the catalyst stability, though the dielectric constant of tributylamine is low (2.33 at 20 °C).[6] The nitrogen atom in NMP seems to contribute to the enhancement of the catalyst activity for the EG formation, as is evident from a comparison of Run 4 with Run 11.

As shown in Table 1, the reactions in toluene, tetraglyme, and γ-butyrolactone which show low turnover frequencies of EG give colored solutions at the end of reaction. On the other hand, the reactions in nitrogen-containing solvents which show high turnover frequencies of EG give colorless solution. Watanabe et al.[7] reported that the reaction with the $Rh(CO)_2acac$/NMP system under about 500 kg/cm^2 of synthesis gas gives a colorless solution. These results are interesting in connection with the active species and the role of solvent.

This work is a part of "C_1-Chemistry Project," a National Research and Development Program of Agency of Industrial Science and Technology, Ministry of International Trade and Industry (M.I.T.I.), Japan. The authors thank Drs. Ken-ichro Bando and Ikuei Ogata for their valuable suggestions.

References

1) For reviews, see: a) T. Deguchi, T. Takano, M. Ishino, S. Nakamura, *Shokubai (Catalyst)*, **23**, 18 (1981); b) D. D. Dombek, *Advan. Catal.*, **32**, 325 (1983).

2) a) T. Masuda, K. Murata, T. Kobayashi, and A. Matsuda, *Nippon Kagaku Kaishi*, **1986**, 171; b) W. Keim, M. Anstock, M. Roper, and J. Schlupp, *C_1 Mol. Chem.*, **1**, 21 (1984).

3) Union Carbide Corp., Japan Kokai 55-79045 (1979).

4) D. R. Fahey; *J. Am. Chem Soc.*, **103**, 136 (1981).

5) W. Keim, M. Berger, and J. Schlupp, *J. Catal.*, **61**, 359 (1980).

6) C. Klofutar, Š. Paljk, and R. Malneršič, *J. Chem. Soc., Faraday Trans. 1*, **78**, 3693 (1982).

7) E. Watanabe, K. Murayama, Y. Hara, Y. Kobayashi, K. Wada, and T. Onoda, *J. Chem. Soc., Chem. Commun.*, **1986**, 227.

The Direct Preparation of Flavones from 2′-Hydroxychalcones Using Disulfides

Yukio HOSHINO,* Toshinori OOHINATA,†† and Noboru TAKENO†
Department of Natural Science, Muroran Institute of Technology, Mizumoto-cho, Muroran 050
†Department of Industrial Chemistry, Muroran Institute of Technology, Mizumoto-cho, Muroran 050
(Received December 19, 1985)

Synopsis. Flavone was obtained by a reaction of 2′-hydroxychalcone with disulfides in good yield. Among several disulfides, diphenyl disulfide gave the best result. Under the same conditions, some flavones were obtained from the corresponding 2′-hydroxychalcones in satisfactory yields.

A synthesis of flavones(**2**), which are the main materials of naturally occurring flavonoids, is usually based on the dehydrogenation of flavanones obtained by the cyclization of 2′-hydroxychalcones(**1**).[1] Flavones can also be obtained directly from **1** by use of selenium dioxide,[2] Pd-black[3] or Pd(II).[4] In a previous paper,[5] we reported that **2** could be obtained by a reaction of **1** with sulfur in *N,N*-dimethylformamide (DMF) in good yields.

We now report the new synthesis of **2** from **1** using disulfides. In this reaction a mixture of **1a** and disulfides was heated at 260—290 °C under a nitrogen atmosphere.

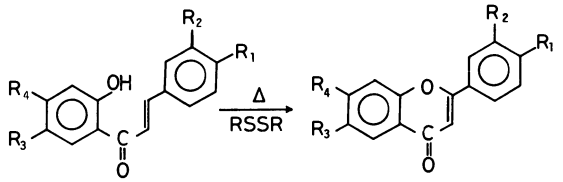

1 2

a $R_1=R_2=R_3=R_4=H$
b $R_1=Ph$, $R_2=R_3=R_4=H$
c $R_1=R_2=R_4=H$, $R_3=CH_3$
d $R_1=R_2=R_3=H$, $R_4=CH_3$
e $R_1=R_3=R_4=H$, $R_2=CH_3$
f $R_1=OCH_3$, $R_2=R_3=R_4=H$
g $R_1=R_3=R_4=H$, $R_2=OCH_3$
h $R_1=R_2=R_3=H$, $R_4=OCH_3$
i $R_1=Cl$, $R_2=R_3=R_4=H$
j $R_1=NO_2$, $R_2=R_3=R_4=H$

The effects of the disulfides on the formation of **2a** are shown in Table 1. Among four disulfides, diphenyl disulfide gave the best result. In the case of aliphatic disulfides, the low yields of **2a** may be due to the bulky carbon chains of thiyl radicals which are presumed to be formed in the course of the reaction.

Using diphenyl disulfide, nine flavone derivatives(**2b—j**) were prepared from the corresponding chalcones(**1b—j**) under the same conditions in various yields. The results are summarized in Table 2. In this and the above tables, the yields of **2** were determined by means of HPLC or GLC analyses using an absolute calibration method. For a comparison, the results of a run using flavanone(**3a**) as the starting material is also shown in Table 2.

In all cases, the conversions were complete and there was no isolable material in addition to the flavones. Table 2 shows that substituents having an electron-withdrawing effect tend to decrease the yields to a large extent. The nitroderivative(**1j** or **2j**) resinated considerably in these reaction conditions, and resulted in the lowest yield of **2j**. Although a slight increase in the yield of **2a** was observed in the case of **3a**, it can not be concluded in view of the

Table 1. Comparison of Reactivities of Disulfides for the Formation of flavone **2a** at 260—290 °C

Disulfide	Reaction time / h	Yield / %
$(CH_3-\overset{CH_3}{\underset{CH_3}{C}}-CH_2-S-)_2$	5	37[a]
$(CH_3-\underset{CH_3}{CH}-CH_2-CH_2-S-)_2$	5	40[a]
$(CH_3-CH_2-CH_2-CH_2-CH_2-S-)_2$	5	47[a]
$(C_6H_5-S-)_2$	2.5	80[b]

a) GLC analysis. b) HPLC analysis.

Table 2. Yields of Flavones(**2a—j**) in the Reaction of 2′-Hydroxychalcones(**1a—j**) with Diphenyl Disulfide at 260—290 °C

Compound No.	Reaction time / h	Product	Yield[a] / %
1a	2.5	**2a**	80
1b	2.5	**2b**	82
1c	3	**2c**	79[b]
1d	3	**2d**	74[b]
1e	3	**2e**	69[b]
1f	1.5	**2f**	63
1g	3	**2g**	52
1h	2.5	**2h**	40
1i	2.5	**2i**	31
1j	3	**2j**	19
flavanone (3a)	2.75	**2a**	87

a) HPLC analysis. b) GLC analysis.

†† Present address: Sohka Factory, Kantoh Chemical Co. Inc., Inari-cho, Sohka 340.

reaction time that there is the difference in the reactivity between **1a** and **3a**. Eventually, the varieties of the yields of **2** may depend on the stabilities or the presence of secondary decompositions of the substrates and/or the products.

Although the mechanism of this reaction is not clear at present, we believe that the reaction provides a useful route to a one-step synthesis of flavones.

Experimental

Materials and Instruments. Disulfides were of a commercial grade and were used without further purification. 2′-Hydroxychalcones were prepared according to known procedures[6] from the corresponding 2′-hydroxyacetophenones and benzaldehydes. Those physical data have already been reported,[5] except **1b**, **1g**, and **1i**. All melting points are uncorrected and ^{1}H NMR spectra were obtained with a Hitachi R-22(90 MHz) spectrometer using tetramethylsilane as an internal standard.

4-Phenyl-2′-hydroxychalcone(1b): Mp 149.5—151.0 °C, ^{1}H NMR (CCl_4) δ=6.74—7.98 (15H, m, Olefin and Aromatic), 12.60 (1H, s, 2′-OH); Found: C, 84.20; H, 5.37%. Calcd for $C_{21}H_{16}O_2$: C, 83.98; H, 5.37%.

3-Methoxy-2′-hydroxychalcone(1g): Mp 91.5—92.5 °C, ^{1}H NMR (CCl_4) δ=3.81 (3H, s, 3-OCH_3), 6.73—7.88 (10H, m, Olefin and Aromatic), 12.59 (1H, s, 2′-OH); Found: C, 75.79; H, 5.42%. Calcd for $C_{16}H_{14}O_3$: C, 75.57; H, 5.55%.

4-Chloro-2′-hydroxychalcone(1i): Mp 155—156 °C, ^{1}H NMR (CCl_4) δ=6.73—7.91 (10H, m, Olefin and Aromatic), 12.48 (1H, s, 2′-OH); Found: C, 69.26; H, 4.15; Cl, 13.64%. Calcd for $C_{15}H_{11}O_2Cl$: C, 69.64; H, 4.29; Cl, 13.70%. Flavones as authentic samples were also obtained by known procedures[1] and those physical data have already been reported.[7]

HPLC and GLC analyses were conducted using instruments by Yanagimoto High Speed Liquid Chromatograph L-2000 and Shimazu Gas Chromatograph GC-3BT, respectively.

General Reaction and Purification Procedure. In a 50 ml three-necked round-bottom flask equipped with nitrogen inlet and outlet tubes at both side necks, a mixture of chalcones(4.46 mmol) and disulfides(4.66 mmol) was placed and the center neck was sealded by a Uni-stopper. The flask was then dipped into a silicone oil bath and heated at 260—290 °C under a nitrogen atmosphere until the distilling of the formed thiols through the outlet tube ceased. The reaction mixture was then cooled at room temperature and solved in 50 ml chloroform. The yields of the flavones were determined by HPLC or GLC analyses. Then, the solvent was removed and the residue was purified by silica-gel column chromatography using dichloromethane as an eluent and crystallized from ligroin or benzene. All flavones were identified by a comparison of melting points and the IR and ^{1}H NMR spectra with those of authentic samples.

References

1) a) S. Matsuura and T. Kunii, *Yakugaku Zasshi*, **94**, 645 (1974); b) F. Cramer and G. H. Elshnig, *Chem. Ber.*, **89**, 1 (1956); c) S. Matsuura, M. Iinuma, and K. Ishikawa, *Chem. Pharm. Bull.*, **26**, 305 (1978).

2) a) N. R. Bannerjee and T. R. Seshadri, *Current Sci.*, **25**, 143 (1956); b) A. Schiavello and C. Sebastiani, *Gazz. Chim. Ital.*, **79**, 909 (1949).

3) J. Massicot, *Compt. Rend.*, **240**, 94 (1955).

4) A. Kasahara, T. Izumi, and M. Ooshima, *Bull. Chem. Soc. Jpn.*, **47**, 2526 (1974).

5) Y. Hoshino, T. Oohinata, and N. Takeno, *Nippon Kagaku Kaishi*, **1985**, 2104.

6) N. S. Poonia, K. Chhabra, C. Kumer, and V. W. Bhagwat, *J. Org. Chem.*, **42**, 3311 (1977).

7) Y. Hoshino, S. Takeda, M. Hamada, and N. Takeno, *Nippon Kagaku Kaishi*, **1982**, 1564.

New Piperidinic Synthons via Ring Contraction. Formal Synthesis of (±)-Perhydrohistrionicotoxin

Pierre DUHAMEL,* Mitsuharu KOTERA, and Thierry MONTEIL
U.A.464 Laboratoire de Chimie Organique,
Faculté des Sciences et des Techniques de Rouen,
76130 Mont Saint Aignan, France
(Received February 10, 1986)

Synopsis. The 2,2-bifunctionalized piperidines **6** and **10** were obtained via ring contraction of the seven-membered heterocyclic enamino aldehyde **5** in nearly quantitative yield. The synthesis of 1-benzyl-1-azaspiro[5.5]undec-7-en-9-one **9** (a formal precursor of perhydrohistrionicotoxin **1b**) in 3 steps from the piperidinedialdehyde monoacetal **6**, is reported.

The histrionicotoxins, a group of unique spiropiperidinol alkaloids isolated from skin extracts of the Colombian poisonous frog "Dendrobates histrionicus," have been the subject of current synthetic investigation because of their important neurophysiological activity.[1] In particular, several successful syntheses of dodecahydro derivative **1b**, commonly named perhydrohistrionicotoxin or H_{12}-HTX, have been reported as have a number of approaches to similar compounds[2–4]. Recently a total synthesis of (±)-histrionicotoxin **1a** ((±)-HTX), the parent alkaloid of this family has been reported[5].

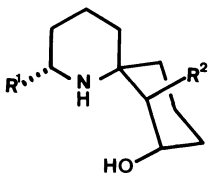

1a R^1 = $-CH_2CH=CH-C\equiv CH$, R^2 = $-CH=CH-C\equiv CH$

1b R^1 = C_5H_{11}, R^2 = C_4H_9

1c R^1 = $-(CH_2)_3-CH=CH_2$, R^2 = $-(CH_2)_2-CH=CH_2$

1d R^1 = H, R^2 = C_4H_9

Having developed a new strategy for the preparation of 2,2-bifunctionalized pyrrolidines and piperidines via ring contraction of heterocyclic enamines[6], we sought to further demonstrate its utility by applying it in a synthesis of **9** which is reported to be a flexible synthon for the H_{12}-HTX.[4g] We selected the heterocyclic enamino aldehyde **5**, which is available in 3 steps from the thiolactame **2**,[7] as starting material.

Formylation of **2** was carried out by Bredereck's reagent followed by hydrolysis.[8] Methylation and deprotonation of **3** afford the methylthiotetrahydroazepinecarbaldehyde **4**. Reductive desulfurization of **4** to the enamino aldehyde **5** was accomplished by deactivated Raney nickel (64% overall yield from **2**).

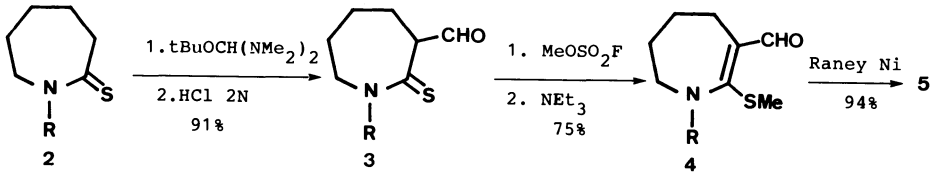

Upon treatment with bromine followed by triethylamine-methanol[6], the tetrahydroazepine **5** was easily transformed to the piperidinedicarbaldehyde monoacetal **6** in 98% yield. The same reaction using triethylamine-water lead to the dicarbaldehyde **10** in quantitative yield.

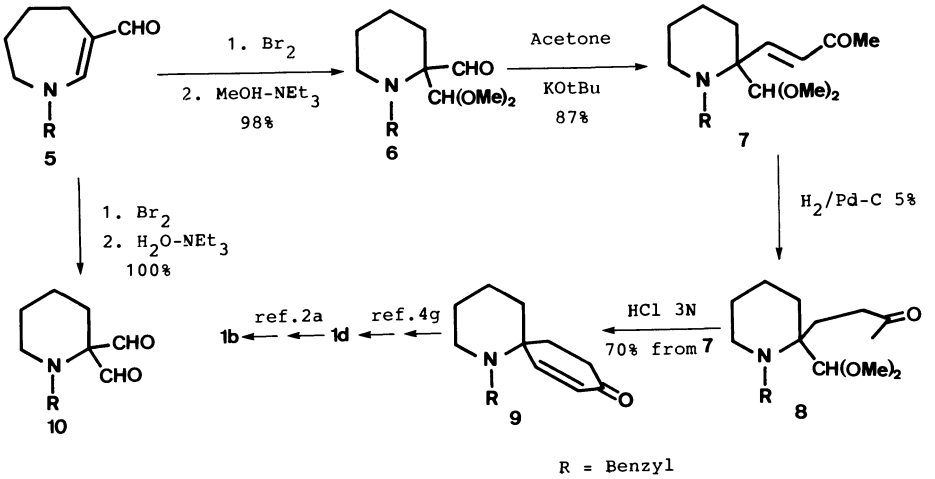

This ring contraction affords us a direct and effective method for the synthesis of azaspiranic enone **9**. Thus the monoacetal **6** was condensed with acetone to give the unsaturated keto acetal **7** which was hydrogenated in the presence of 5% Pd-C. The resulting saturated keto acetal **8** was hydrolyzed without isolation and spontaneously cyclized by acid work-up (3 M HCl)[9] to the azaspirannic enone **9** (60% overall yield from **5**). The same enone **9** has been converted by others[4g,2a] into depentyl H_{12}-HTX **1d** and thence H_{12}-HTX **1b**.

Experimental

General Procedure. All melting points are uncorrected. Infrared spectra (IR) were recorded on a Perkin Elmer 337 spectrophotometer and are reported in cm^{-1}. ^1H NMR spectra were taken on a Perkin Elmer R 12. ^{13}C NMR spectra were taken on a Varian CFT20. The chemical shifts (δ values) are given in parts per million relative to TMS as an internal standard in $CDCl_3$ solutions and coupling constants in hertz. Splitting patterns are designated as follows: s, singlet; d, doublet; t, triplet; q, quartet; m, multiplet; br, broad.

1-Benzyl-2-thioxohexahydroazepine-3-carbaldehyde 3. A mixture of **2** (35.0 g, 0.16 mol) and *t*-BuOCH(NMe_2)$_2$ (44.3 g, 0.25 mol) was heated at 140 °C for 3 h until most of *t*-BuOH had been removed by distillation. After cooling, the reaction mixture was poured into 2 M HCl (500 ml (1 M=1 mol dm^{-1})) and stirred for 2 h at room temperature. The resulting solid was collected by filtration, washed with cold water and dried on P_2O_5, providing 36.0 g (91%) of **3** which was utilized without further purification: IR (nujol) 1730; ^1H NMR 9.80 (d, J=2 Hz, 1H), 7.35 (s, 5H), 5.44, 5.88 (ABq, J=15 Hz, 2H), 3.5—3.8 (m, 3H), 1.2—2.5 (m, 6H); ^{13}C NMR 202.1, 192.3, 135.2, 128.6, 128.0, 127.7, 60.6, 56.6, 52.4, 27.3, 26.0, 23.6.

1-Benzyl-2-methylthio-4,5,6,7-tetrahydro-1H-azepine-3-carbaldehyde 4. Methyl fluorosulfate (24 g, 0.21 mol) was rapidly added to a solution of **3** (35.6 g, 0.14 mol) in CH_2Cl_2 (350 ml). The mixture was stirred overnight at room temperature. To this mixture, triethylamine (73 g, 0.72 mol) was added slowly with stirring and after 1 h, the dichloromethane was removed in vacuo. The oily residue was continuously extracted with hot hexane. **4** crystallized out on cooling (28.5 g, 75%) and was utilized without further purification: mp 88—89 °C; IR (nujol) 1610, 1510; ^1H NMR 9.92 (s, 1H), 7.30 (s, 5H), 4.73 (s, 2H), 3.15—3.4 (m, 2H), 2.2—2.5 (m, 2H), 2.25 (s, 3H), 1.25—1.6 (m, 4H); ^{13}C NMR 190.2, 168.3, 137.6, 128.7, 127.9, 127.8, 118.7, 56.5, 52.7, 25.1, 24.7, 23.2, 19.1; Anal. ($C_{15}H_{19}NOS$) C, H, N.

1-Benzyl-4,5,6,7-tetrahydro-1*H*-azepine-3-carbaldehyde 5. To about 20 g of W2 Raney nickel previously refluxed in acetone (100 ml) for 2 h was added a solution of **4** (3.9 g, 14.9 mmol) in acetone (30 ml), and the mixture was refluxed for 3 h. After cooling, the solution was decanted and the catalyst was washed six times with acetone. The decanted solution and washings were together filtered and concentrated. The resulting solid was purified by flash chromatography on silica gel with ethyl acetate as the eluant to give 3.0 g (94%) of **5**: Mp 69—70 °C (ethyl acetate); IR (nujol) 1600; ^1H NMR 8.98 (s, 1H), 7.3 (m, 5H), 6.90 (s, 1H), 4.40 (s, 2H), 3.1—3.4 (m, 2H), 2.3—2.6 (m, 2H), 1.5—1.9 (m, 4H); ^{13}C NMR 190.5, 160.3, 136.6, 128.9, 128.1, 127.3, 115.4, 63.1, 52.5, 28.2, 26.2, 23.6; Anal. ($C_{14}H_{17}NO$) C, H, N.

1-Benzyl-2-dimethoxymethylpiperidine-2-carbaldehyde 6. To a suspension of **5** (3.23 g, 15.0 mmol) in anhydrous ether (420 ml) were added at −70 °C 2.6 g (16.2 mmol) of bromine in 25 ml of cold (about −30 °C) anhydrous ether. After completion of the addition, the resulting yellow suspension of the iminium salt was stirred at this temperature for 30 min. To this suspension, a mixture of methanol (12.7 g, 0.39 mol) and triethylamine (4.55 g, 45.0 mmol) was added at −70 °C and the reaction mixture was allowed to warm to room temperature, stirred for 24 h, and filtered. The filtrate was concentrated under reduced pressure, and cold anhydrous ether (50 ml) added to the residue. The triethylamine hydrobromide was filtered and the solvent was evaporated under reduced pressure to give 4.08 g (98%) of **6** which was utilized without further purification. An analytical sample was obtained by flash chromatography on silica gel with petroleum ether/ether (9:1) as the eluant: Mp 38—39 °C (pentane); IR (nujol) 1730; ^1H NMR 9.69 (s, 1H), 7.2—7.6 (m, 5H), 4.72 (s, 1H), 3.93 (s, 2H), 3.59 (s, 6H), 2.6—2.8 (m, 2H), 1.4—2.0 (m, 6H); ^{13}C NMR 201.3, 138.5, 126.0, 125.9, 124.5, 107.1, 67.7, 56.3, 56.0, 53.6, 44.8, 24.5, 23.0, 17.9; Anal. ($C_{16}H_{23}NO_3$) C, H, N.

1-Benzylpiperidine-2,2-dicarbaldehyde 10. To a suspension of the iminium salt (1.0 mmol) in 35 ml of anhydrous ether, prepared from 213 mg of **5** and 0.17 g of bromine as above, was added at −70 °C a mixture of water (38 mg, 2.1 mmol) and triethylamine (0.5 g, 5 mmol). The reaction mixture was allowed to warm to room temperature and stirred for 3 h. The triethylamine hydrobromide was filtered and washed with a solution of triethylamine (0.5 g) in 50 ml of ether. After removal of the solvent, 25 ml of ether were added and the precipitated salt was removed by filtration. The filtrate was concentrated in vacuo to give **10** (220 mg, 100%) as a colorless oil which became discoloured with decomposition on standing at room temperature: IR (neat) 1720; ^1H NMR 9.72 (s, 2H), 7.0—7.4 (m, 5H), 3.80 (s, 2H), 2.5—2.8 (m, 2H), 1.2—1.9 (m, 6H); ^{13}C NMR 202.1, 138.9, 128.3, 128.0, 127.3, 76.2, 58.1, 46.6, 27.6, 24.9, 19.4.

(*E*)-4-(1-Benzyl-2-dimethoxymethylpiperidin-2-yl)-3-buten-2-one 7. To a suspension of *t*-BuOK (2.55 g, 22.7 mmol) in anhydrous THF (50 ml) was rapidly added at −5 °C a solution of acetone (0.95 g, 16.3 mmol) in THF (5 ml). After cooling to −10 °C a solution of **6** (1.25 g, 4, 50 mmol) in THF (10 ml) was added. The reaction mixture was allowed to warm to room temperature, stirred for 1 h and then poured into 2 M HCl (200 ml). After neutralization with Na_2CO_3, the aqueous solution was extracted with ether, dried over Na_2CO_3 and concentrated. The resulting solid was recrystallized from hexane to yield 1.24 g (87%) of **7**: Mp 117—118 °C; IR (nujol) 1670; ^1H NMR 7.2—7.5 (m, 5H), 7.18, 6.45 (ABq, J=17 Hz, 2H), 4.66 (s, 1H), 3.88, 3.71 (ABq, J=15 Hz, 2H), 3.57 (5s, 3H), 3.55 (s, 3H) 2.5—2.7 (m, 2H), 2.23 (s, 3H), 1.4—2.2 (m, 6H); ^{13}C NMR 198.2, 149.6, 140.7, 130.7, 127.7, 127.1, 125.9, 106.8, 64.5, 58.0, 57.2, 55.2, 46.5, 33.1, 26.4, 25.1, 20.3; Anal. ($C_{19}H_{27}NO_3$) C, H, N.

1-Benzyl-1-azaspiro[5.5]undec-7-en-9-one 9. A suspension of 0.22 g of 5% Pd-C in 0.3 M ethanolic KOH (20 ml) was saturated with hydrogen. A solution of enone **7** (1.58 g, 5.0 mmol) in a mixture of 0.3 M ethanolic KOH (20 ml) and ethyl acetate (25 ml) was added and the mixture hydrogenated at room temperature and atmospheric pressure until 1 equiv of hydrogen (120 ml) was absorbed (about 20 min). After filtration of the catalyst, the filtrate was concentrated at reduced pressure to about 20 ml, acidified with 3 M HCl (20 ml), concentrated again to about 20 ml. Then 3 M HCl (30 ml) was added and the mixture refluxed for 16 h. After cooling, the mixture was basified with Na_2CO_3, extracted with ether, dried over Na_2CO_3 and concentrated. The residue was purified by

flash chromatography on silica gel with petroleum ether/ether (1:1) as the eluant to yield 0.89 g (70%): Mp 57—59 °C (methanol-water); IR (neat) 1680; ^{1}H NMR 7.2—7.6 (m, 5H), 6.95 (d, br, J=10 Hz, 1H), 6.03 (d, J=10 Hz, 1H), 3.73, 3.33 (ABq, J=15 Hz, 2H), 2.0—2.8 (m, 6H), 1.3—1.9 (m, 6H); ^{13}C NMR 198.8, 160.1, 139.9, 128.8, 127.9, 127.6, 126.5, 57.3, 55.9, 45.3, 34.3, 32.2, 25.6, 21.0, 20.4; Anal. ($C_{17}H_{21}NO$) C, H, N.

References

1) a) J. W. Daly, "Progress in the Chemistry of Organic Natural Products," ed by W. Herz, H. Grisebach, and G. W. Kirby, Springer-Verlag, Wien-New York (1982), Vol. 41, p. 247; b) K. Takahashi, A. E. Jacobson, C.-P. Mak, B. Witkop, A. Brossi, E. X. Albuquerque, J. E. Warnick, M. A. Maleque, A. Bavoso, and J. V. Silverton, *J. Med. Chem.*, **25**, 919 (1982); c) K. Takahashi, B. Witkop, A. Brossi, M. A. Maleque, and E. X. Albuquerque, *Helv. Chim. Acta.*, **65**, 252 (1982).

2) The first total syntheses: a) E. J. Corey, J. F. Arnett, and G. N. Widiger, *J. Amer. Chem. Soc.*, **97**, 430 (1975); b) E. J. Corey, M. Petrzilka, and Y. Ueda, *Tetrahedron Lett.*, **1975**, 4343; c) M. Aratani, L. V. Dunkerton, T. Fukuyama, Y. Kishi, H. Kakoi, S. Sugiura, and S. Inoue, *J. Org. Chem.*, **40**, 2009 (1975); d) T. Fukuyama, L. V. Dunkerton, M. Aratani, Y. Kishi, *J. Org. Chem.*, **40**, 2011 (1975).

3) For reviews on synthetic studies until 1981 see: a) Y. Inubushi and T. Ibuka, *Heterocycles*, **17**, 507 (1982); b) B. Witkop and E. Gössinger, "The Alkaloids," ed by A. Brossi, Academic Press, New York (1983), Vol. 21, p. 168. c) G. Quinkert, F.-P. Montforts, M. Ockenfeld, and D. Rehm, *Synform* **1984**, 1.

4) Recent syntheses and approaches: a) M. Glanzmann, C. Karalai, B. Ostersehlt, U. Schön, C. Frese, and E. Winterfeldt, *Tetrahedron*, **38**, 2805 (1982); b) G. E. Keck and J. B. Yates, *J. Org. Chem.*, **47**, 3590 (1982); c) W. Carruthers and S. A. Cumming, *J. Chem. Soc., Chem. Commun.* **1983**, 360; d) W. Carruthers and S. A. Cumming, *J. Chem. Soc., Perkin Trans. I*, **1983**, 2383; e) A. B. Holmes, P. R. Raithby, M. J. Rosales, K. Russell, E. S. Stern, and M. E. Stubbs, *Tetrahedron Lett.*, **25**, 5705 (1984); f) A. B. Holmes, K. Russell, E. S. Stern, M. E. Stubbs, and N. K. Wellard, *Tetrahedron Lett.*, **25**, 4163 (1984); g) A. J. Pearson and P. Ham, *J. Chem. Soc., Perkin Trans. 1*, **1983**, 1421; h) S. A. Godleski, D. J. Heacock, J. D. Meinhart, and S. V. Wallendael, *J. Org. Chem.*, **48**, 2101 (1983); i) S. A. Godleski and D. J. Heacock, *J. Org. Chem.*, **47**, 4820 (1982); j) E. R. Koft and A. B. Smith, III., *J. Org. Chem.*, **49**, 832 (1984); k) M. Harris, D.-S. Grierson, and H.-P. Husson, *Tetrahedron Lett.*, **22**, 1511 (1981); l) W. Gessner, K. Takahashi, B. Witkop, and A. Brossi, *Helv. Chim. Acta.*, **68**, 49 (1985); m) D. Tanner and P. Somfai, *Tetrahedron Lett.*, **26**, 3883 (1985).

5) S. C. Carey, M. Aratani, and Y. Kishi, *Tetrahedron Lett.*, **26**, 5887 (1985).

6) P. Duhamel and M. Kotera, *J. Org. Chem.*, **47**, 1688 (1982).

7) S. Scheibye, B. S. Pedersen, and S.-O. Lawesson, *Bull. Soc. Chim. Belg.*, **87**, 229 (1978).

8) H. Bredereck, G. Simchen, and B. Funke, *Chem. Ber.*, **104**, 2709 (1971).

9) An azacycle opening phenol ($PhCH_2NH(CH_2)_4C_6H_4p$-OH) was isolated (about 15% yield) in this step.

Electron-Transfer Reactions between Cobalt(III) Complexes and Polymer-Bound Ferrous Chelate

Yoshimi KURIMURA,* Kiyomi TAKATO, and Norihisa SUZUKI
Department of Chemistry, Ibaraki University,
Bunkyo, Mito, Ibaraki 310
(Received January 24, 1986)

Synopsis. The reductions of some cobalt(III) complexes having overall charges of −1 to +3 by the polymer-bound ferrous chelate, Fe(II)-PBDA (PBDA=vinylbenzylamine-*N,N*-diacetate-co-4-styrenesulfonate), and the effect of sodium chloride on the reduction rate have been investigated. The specific rate increases sharply with the positive charge on the Co(III) complexes by electrostatic interactions between reactant species.

In previous papers,[1-4] the reductions of macromolecular cobalt(III) complexes by some low-molecular-weight ferrous chelates have been reported. The results of kinetic studies, i.e., the acceleration and retardation of the rates of electron-transfer reactions relative to the corresponding low-molecular-weight systems, have been interpreted, essentially, by the effects of the electrostatic, steric, and hydrophobic interactions between the reactant species in the macromolecular domains.

Experimental

The preparation of (vinylbenzyl)amine-*N,N*-diacetic acid (VBDA) and a method for the copolymerization of VBDA with sodium 4-styrenesulfonate (NaSS) have been described elsewhere.[5,6] To the reaction mixture after copolymerization, dilute sodium hydoxide solution was added. The mixture was dialyzed in water for 3 d with cellulose dialyzer tubing (Nakarai Chemicals Co., MW cutoff 8,000), evapolated to dryness, grained with a mortar, and dried in vacuo at 80 °C. The sodium salt of VBDA-co-NaSS (PBDA) was obtained as a white powder. The intrinsic viscosity of an aqueous solution of PBDA was 1.3 dl g^{-1} at 25 °C. (Ethylbenzyl)amine-*N,N*-diacetic acid (EBDA) was prepared according to a similar method described elsewhere.[5] Sodium chloro[ethylenediaminetetraacetato(3−)]-cobaltate(III) (Na[CoCl(Hedta)]),[7] bis(ethylenediamine)oxalatocobalt(III) chloride ([Co(ox)(en)$_2$]Cl),[8] pentaamminechlorocobalt(III) chloride ([CoCl(NH$_3$)$_5$]Cl$_2$),[9] hexaamminecobalt(III) chloride ([Co(NH$_3$)$_6$]Cl$_3$),[10] and tris(ethylenediamine)cobalt(III) chloride ([Co(en)$_3$]Cl$_3$)[11] were prepared by the reported methods. The concentration of PBDA is represented by the monomer unit of the VBDA in the copolymer and the unit of the concentration is expressed by mol dm^{-3}. Solutions of Fe(II)-PBDA and Fe(II)-EBDA were prepared by mixing a deoxygenated buffer solution of the chelating agent with equivalent amounts of deoxygenated ammonium iron(II) sulfate solution under an atmosphere of argon. The viscosities were measured in aqueous solutions, using Ubbelohde-type viscometer at 25±0.1 °C.

The kinetic experiments were undertaken at pH 7.5—8.5 (phosphate buffer), I=0.03 (I; ionic strength), and 25±0.2 °C. The reactions were followed under pseudo-first-order conditions with a large excess of the ferrous chelate by observing the decay of the absorbances of the cobalt(III) complexes at 350—600 nm using a Yanagimoto Model SPS-1 stopped-flow spectrophotometer. The concentrations of Co(III) and Fe(II) in the reaction solutions were 1.0×10^{-4} and 1.0×10^{-3} mol dm^{-3}, respectively. The rate constants were determined from the slopes of the log (A_t-A_∞) vs time. Absorption spectra were recorded on a Hithachi Model 320 recording spectrophotometer.

Results and Discussion

The chemical structure and composition of the sodium salt of PBDA prepared is illustrated in Fig. 1. The content of the VBDA moieties on the polymer chain was also ascertained spectrometrically: e.g., examinations of the method of continuous variation and the absorption spectra for a VBDA-co-NaSS-Ni^{2+} solution were carried out. The molecular weight of this polymer-bound chelating agent was estimated to be at least 8000 since a dialysis of the copolymer solution was carried out using cellulose dialyzer tubing of MW cutoff through 8000. This molecular weight corresponds to about 4 monomer units of the chelating agent and about 33 units of the sulfonate groups on a polymer chain. This indicates that this polymer has a great number of negatively charged sulfonato groups on the polymer backbone.

In all cases for the polymer and the low-molecular-weight systems, plots of log (A_t-A_∞) vs time gave

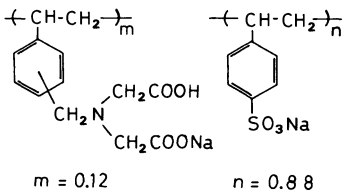

Fig. 1. Chemical structure of PBDA.

Table Pseudo-First-Order Rate Constants for the Reductions of Co(III) Complexes with the Ferrous Chelates at pH 8.0, I=0.03, and 25 °C[a]

Co(III) complex ion	Reductant	
	Fe(II)-PBDA k_p/s^{-1}	Fe(II)-EBDA k_m/s^{-1}
[CoCl(Hedta)]$^-$	1.75±0.04	1.40±0.30
[Co(ox)(en)$_2$]$^+$	42.7±2.2	17.6±0.6
[CoCl(NH$_3$)$_5$]$^{2+}$	7.6±0.4	2.1±0.04
	7.4±0.4[b]	2.2±0.1[b]
	7.6±0.8[c]	2.0±0.07[c]
[Co(en)$_3$]$^{3+}$	41.9±0.5	3.5±0.1
[Co(NH$_3$)$_6$]$^{3+}$	60.4±0.5	8.8±0.1

a) Initial concentrations are 1.0×10^{-4} mol dm^{-3} Co(III) and 1.0×10^{-3} mol dm^{-3} Fe(II). b) pH 7.5. c) pH 8.5.

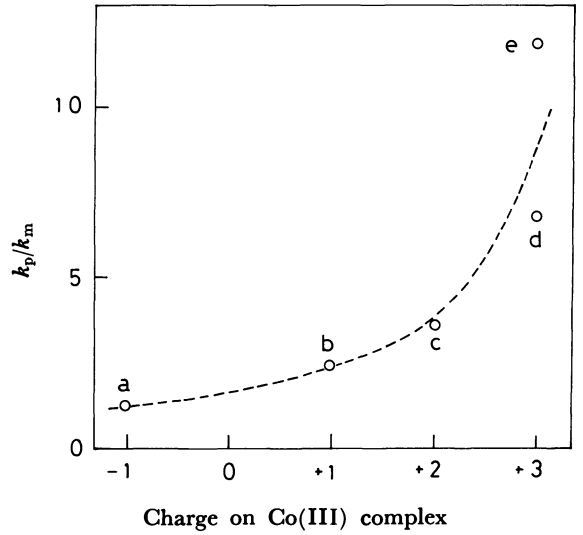

Fig. 2. Relationship between acceleration factor and the charges on the Co(III) complexes.
a: $[CoCl(Hedta)]^-$, b: $[Co(ox)(en)_2]^+$, c: $[CoCl(NH_3)_5]^{2+}$, d: $[Co(en)_3]^{3+}$, e: $[Co(NH_3)_6]^{3+}$.

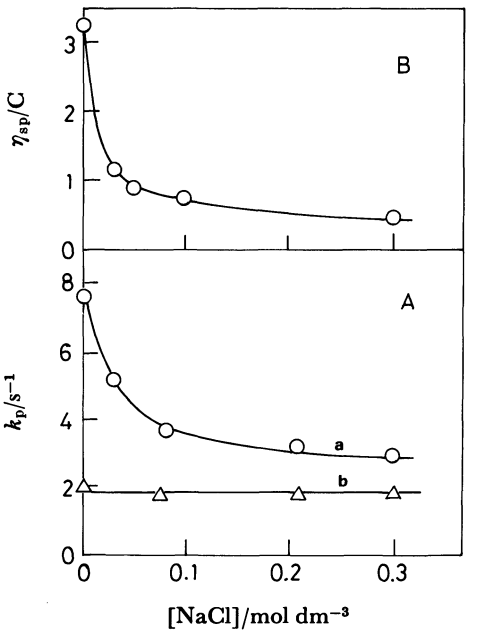

Fig. 3. Dependences of k_p on [NaCl] (A) and η_{sp}/C on [NaCl] (B).
(A): 1.0×10^{-4} mol dm^{-3} $[CoCl(NH_3)_5]^{2+}$, $I=0.03$, pH 8.0, and 25 °C. (a) 1.0×10^{-3} mol dm^{-3} Fe(II)-PBDA. (b) 1.0×10^{-3} mol dm^{-3} Fe(II)-EBDA (B): 1.0×10^{-3} mol dm^{-3} Ni(II)-PBDA, $I=0.03$, pH 8.0, and 25 °C.

straight lines for at least two-times the half-life of the reactions, indicating a first-order dependency of the rates with respect to Co(III). The pseudo-first-order rate constant for the reductions of the Co(III) complexes with a polymer-bound Fe(II)-chelate and those with a low-molecular-weight Fe(II)-chelate, k_p and k_m, respectively, are summerized in the Table. The rate constant for the reduction of $[CoCl(NH_3)_5]^{2+}$ was independent on pH in the region of pH 7.5—8.5. This suggests that no appreciable change in the chemical species of the polymer and the low-molecular-weight Fe(II)-chelates occur in this pH region. The results show explicitly that the overall charges of the Co(III) complexes are of great importance in controling the rate of the electron-transfer reactions in the polymer system; the rate constant for the negatively charged Co(III) complex with Fe(II)-PBDA was of the same order as that with Fe(II)-EBDA, whereas the rate constants for the positively-charged Co(III) complexes with Fe(II)-PBDA were greater than that of the corresponding Co(III) with Fe(II)-EBDA. The ratio of the rate constants, k_p/k_m (represented by acceleration factor) where k_p is the pseudo-first-order rate constant for a given Co(III) complex for the polymer system and k_m is that for the corresponding low-molecular-weight system, is introduced as a measure of the degree of the acceleration. The relationship between the acceleration factor and the overall charge of the Co(III) complex is represented in Fig. 2. The results show that the acceleration factor increases sharply with the positive charges on the Co(III) complexes, i.e., in the domains of the polymeric metal complex anions, a great enhancement of the specific reduction rate occurs with an increase in the positive charge on the low-molecular-weight metal complex ions. Such a charge effect might be ascribed to a large negative charge density in the domains of the Fe(II)-PBDA polymers. Namely, positively-charged inorganic Co(III) complex ions tend to concentrate within the polymer domain with an increase in their positive charge due to an electrostatic attraction between these, leading to an enhancement of the collision frequency between the reactant species. However, no appreciable decrease in the enhancement factor was observed for a reduction of the negatively charged species of $[CoCl(Hedta)]^-$ by a polymeric ferrous chelate relative to that of the monopositively charged species, $[Co(ox)(en)_2]^+$. This seems to indicate that the effect of the coulombic repulsion between the negatively charged polymer domain and a mono-negatively charged Co(III) complex is quite small or can be ignored.

The pseudo-first-order rate constant for the reduction of $[CoCl(NH_3)_5]^{2+}$ by Fe(II)-PBDA decreased rapidly with the addition of NaCl in the concentration region below 0.1 mol dm^{-3}. However, the rate constant for the low-molecular-weight system was little affected by the presence of 0—0.3 mol dm^{-3} NaCl (Fig. 3A). It is known that the local charge density in the polyion domains is greatly affected by the presence of inorganic salts.[12] For example, an addition of sodium chloride to a dilute solution of sodium 4-styrenesulfonate containing $[Ru(bpy)_3]^{2+}$ (bpy=2,2′-bipyridine), which was concentrated in the domains of the poly(4-styrenesulfonate), tended to replace by the sodium ions with an increase in the concentration of sodium chloride.[6] The results of the salt effect on the reduced viscosity of the polymer-bound Ni(II) chelate solution (Fig. 3B) also seems to account for the salt effect on the rate. For a lower salt

concentration than 0.1 mol dm^{-3}, a sharp decrease in the viscosity of the Ni(II)–PBDA solution was observed along with an increase in the salt concentration, indicating a shrinkage of the polymer chain by the shielding of the negative charge in the domains by counter ions. The explanation for the acceleration of the rate is quite similar to that for the reduction of the polymeric Co(III) complexes with low-molecular-weight Fe(II) species.

References

1) Y. Kurimura, K. Yamada, M. Kaneko, and E. Tsuchida, *J. Polym. Sci.*, **9**, 3521 (1971).
2) Y. Kurimura, I. Sekine, E. Tsuchida, and Y. Karino, *Bull. Chem. Soc. Jpn.*, **47**, 1823 (1974).
3) E. Tsuchida, Y. Karino, H. Nishide, and Y. Kurimura, *Macromol. Chem.*, **175**, 161 (1974).
4) E. Tsuchida, K. Shigehara, and Y. Kurimura, *J. Polym. Sci.*, **13**, 1457 (1975).
5) A. Uehara, E. Kyuno, and R. Tsuchiya, *Bull. Chem. Soc. Jpn.*, **43**, 1394 (1970).
6) Y. Kurimura, K. Takato, M. Takeda, and N. Ohtsuka, *J. Phys. Chem.*, **89**, 1023 (1985).
7) M. L. Morris and D. H. Bush, *J. Am. Chem. Soc.*, **78**, 5179 (1956).
8) E. P. Dwyer, I. K. Reid, and F. L. Garvon, *J. Am. Chem. Soc.*, **83**, 1285 (1967).
9) R. Mitzner, P. Blankenburg, and W. Depkat, *Z. Chem.*, **9**, 68 (1960).
10) R. N. Keller and W. C. Fernelius, *Inorg. Synth.* **2**, 216 (1946).
11) R. N. Keller and W. C. Fernelius, *Inorg. Synth.* **2**, 218 (1946).
12) B. Vogel and H. Morawetz, *J. Am. Chem. Soc.*, **90**, 1368 (1968).

Photochemical Reaction of Tricarbonyl(η-methylcyclopentadienyl)manganese(I), [Mn(CO)$_3$(MeCp)], with 1,1′-Bis(diphenylphosphino)ferrocene, (dppfe), and X-Ray Molecular Structure Analysis of [Mn(CO)(MeCp)(dppfe)]

Satoru ONAKA
Department of Chemistry, Nagoya Institute of Technology,
Gokiso-cho, Showa-ku, Nagoya 466
(Received February 4, 1986)

Synopsis. Photochemical reaction of MeCpMn(CO)$_3$ with (Ph$_2$PC$_5$H$_4$)$_2$Fe, (dppfe), was conducted in benzene. From the reaction mixture, the title compound [Mn(CO)(MeCp)(dppfe)] was isolated and its molecular structure was solved by X-ray analysis. ν(CO) peak at 1810 cm^{-1} of the title compound was clarified to be originated from the terminal carbonyl. Temperature-dependent ^{1}H NMR spectra were also measured for the title compound.

It is well-established that tricarbonyl(η-cyclopentadienyl)manganese(I), [Mn(CO)$_3$Cp], dissociates CO quite easily upon photolysis to yield CpMn(CO)$_2$, which, on treatment with various nucleophiles to yield CpMn(CO)$_2$L,[1] where L is phosphines, nitriles, alkadienes, and alkynes. However, the reaction with bidentate phosphine ligands has not yet been well-explored except PR$_2$(CH$_2$)$_n$PR$_2$ type ligands (n=1 and 2; R=CH$_3$ and C$_6$H$_5$) to our knowledge.[2] Recently, it was demonstrated that the dppfe-palladium complex, PdCl$_2$(dppfe), exhibits selective catalytic activity toward cross-coupling of Grignard and organozinc reagents.[3] Therefore, the reaction of **dppfe**, which is a new type of enticing bindentate ligand, with tricarbonyl(η-methylcyclopentadienyl)manganese(I)(**1**), which is a cheaper congener of CpMn(CO)$_3$, under UV irradiation was attempted with the hope of obtaining a new bimetallic compound which may exhibit intriguing reactivity.

From the photolysis of **1** with **dppfe** in benzene, two components were isolated by column chromatography. The second component eluted with benzene afforded orange-red crystals **2** by recrystallization from chloroform–hexane, which showed a strong IR peak at 1810 cm^{-1}. This peak is 24 cm^{-1} lower than that of CpMn(CO)(Ph$_2$PCH$_2$CH$_2$PPh$_2$) and 44 cm^{-1} lower than that of CpMn(CO)(Ph$_2$PCH$_2$PPh$_2$).[2] The observation posed some expectation that the CO group in **2** might be located in a bridging or semi-bridging position. ^{1}H NMR spectrum of **2** showed a broad feature in the methyl proton region at room temperature; the observation suggested some kind of dynamic process such as exchange among the conformers. These lines of structural interest motivated us to carry out X-ray molecular structure analysis of **2**.

Figure 1 shows an ORTEP view of the complex **2**, (CH$_3$C$_5$H$_4$)Mn(CO){(C$_6$H$_5$)$_2$PC$_5$H$_4$}$_2$Fe, and the atom numbering system; **dppfe** functions as a bidentate ligand. Important bond lengths and angles are listed in Table 1. The separation between Mn and Fe is 4.231(2)—4.308(2) Å, which is too far to expect any strong interaction between these two metal atoms. The distances between the carbon atom in CO and Fe atom are 3.89(1)—3.91(1) Å. This range of distance falsifies our expectation that the CO group may occupy a bridging position or a semi-bridging position rather than a terminal position. Therefore, occurance of the absorption of the carbonyl group as low as 1810 cm^{-1} for a terminal carbonyl should be originated from the strong electron-donating nature of **dppfe**. Another interesting feature of the structure of **2** is that the methyl substituent in CH$_3$C$_5$H$_4$ group extends to the same direction as that of CO in solid state, that is, the methyl and CO groups form an eclipsed conformation. Two Ph$_2$PC$_5$H$_4$ groups in **dppfe** moiety also compose an eclipsed conformation. Two C$_5$H$_4$ planes in **dppfe** moiety are almost parallel for each other and perpendicular to the C$_5$H$_4$ plane in (CH$_3$C$_5$H$_4$)Mn(CO) moiety. Mn–P distances are in

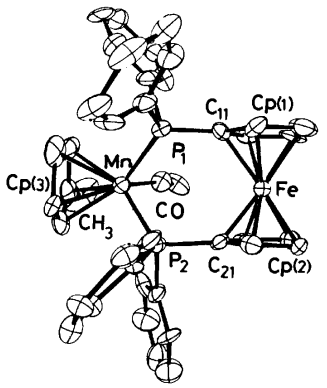

Fig. 1. An ORTEP view of MeCpMn(CO)·dppfe. Thermal elipsoids are drawn at 50% probability level.

Table 1. Important Bond Lengths and Angles

Bond, Angle	Molecule 1	Molecule 2
Mn···Fe	4.308(2) Å	4.231(2) Å
Mn–P$_1$	2.233(3)	2.209(3)
Mn–P$_2$	2.222(3)	2.214(3)
Mn–CO	1.85(1)	1.68(1)
C–O	1.12(2)	1.24(2)
Fe···CO	3.89(1)	3.91(1)
P$_1$–C$_{11}$	1.76(1)	1.94(1)
P$_2$–C$_{21}$	1.85(1)	1.82(1)
Mn···Cp(3) plane	1.80	1.76
Fe···Cp(1) plane	1.60	1.58
Fe···Cp(2) plane	1.70	1.69
CH$_3$-Cp(3)	1.57(3)	1.51(2)
∠P$_1$–Mn–P$_2$	99.5(1)°	98.2(1)°

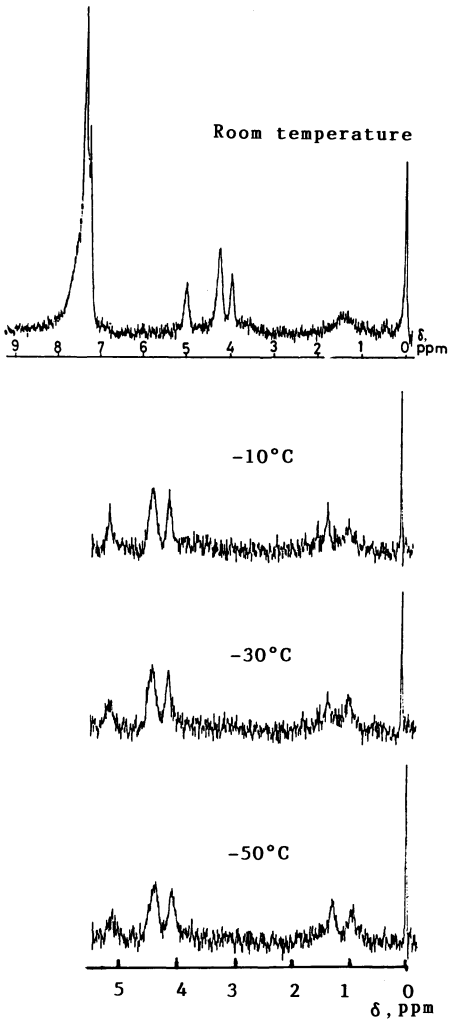

Fig. 2. Temperature-dependent ^{1}H NMR spectra of MeCpMn(CO)·dppfe in $CDCl_3$.

the range of 2.209(3)—2.233(3) Å, which are shorter than Pd–P distances in $PdCl_2$(dppfe) and the bond angle, ∠P–Mn–P, is 99.5(1)—98.2(1)°, which is close to 99.07° for ∠P–Pd–P in $PdCl_2$(dppfe).[3]

Figure 2 shows a temperature-dependent ^{1}H NMR spectra of **2** in $CDCl_3$; the broad feature at around δ 1.4 ppm observed at room temperature splits into two peaks with lowering the temperature. This observation clearly indicates the existence of exchange between two structures. The most plausible explanation for this dynamic process is that **2** exchanges between two conformers in solution such as shown in the Scheme.

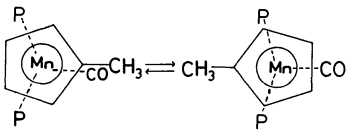

Scheme

Experimental

Syntheses. 1.11 g (2 mmol) of **dppfe** and 410 mg (2 mmol) of **1**, which were both purchased from Strem Chemicals, Inc., were dissolved into 75 ml of benzene and this orange solution was photolyzed for 3.5 h under Ar atmosphere with a Riko 100 W high-pressure Hg lamp. The resulting yellow brown precipitate was filtered off and the solvent was vacuum-stripped from the filtrate to leave orange-red semisolid. This semisolid was dissolved into minimum amount of chloroform and was loaded on a Florisil column. First, an orange band was eluted with petroleum ether and then second orange band was eluted with benzene. From the first orange band, yellow microcrystalline product **3** was isolated by recrystallization from dichloromethane–hexane, which showed two strong ν(CO) peaks at 1920 and 1845 cm^{-1} (a Nujol mull). IR data suggest that **dppfe** functions as a monodentate ligand in **3**. Anal. Calcd for [Mn(CO)$_2$($CH_3C_5H_4$)(dppfe)], $C_{42}H_{35}FeMnO_2P_2$: C, 67.76; H, 4.74%. Found: C, 67.53; H, 4.91%. The orange-red product from the benzene eluent was recrystallized from chloroform–hexane to yield orange-red crystals **2** from which a good crystal for X-ray analysis was selected. X-Ray analysis showed that one chloroform molecule is contained for one [Mn(CO)($CH_3C_5H_4$)(dppfe)] molecule in the crystal of **2**. Anal. Calcd for $FeMnC_{41}H_{35}OP_2 \cdot CHCl_3$: C, 60.35; H, 4.34%. Found: C, 60.79; H, 4.45%. IR spectra were measured with a Jasco 701G spectrometer for Nujol mull samples and proton NMR spectra were recorded with a Hitachi-Perkin-Elmer R-20B and R-24A spectrometers (60 MHz) for $CDCl_3$ solutions.

X-Ray Analysis. A single crystal of Mn(CO)($CH_3C_5H_4$)($Ph_2PC_5H_4$)$_2$Fe·$CHCl_3$ with approximate dimensions 0.25×0.35×0.60 mm^3 was mounted on a Rigaku AFC-5 diffractometer with graphite monochromatized Mo $K\alpha$ radiation. Crystal data: monoclinic, $P2_1$, a=18.589(3), b=20.574(3), c=9.785(1) Å, β=91.46(1)°, V=3741(1) Å^3, Z=4 and μ(Mo $K\alpha$)=10.5 cm^{-1}. The structure was solved by direct method with MULTAN 78 and refined by block-diagonal least-squares method. Two independent molecules of Mn(CO)($CH_3C_5H_4$)($Ph_2PC_5H_4$)$_2$Fe and $CHCl_3$ were contained in an asymmetric unit. The final R indices were 0.057 and R_w=0.072 for 100 non-hydrogen atoms with anisotropic temperature factors based on 4838 independent reflections (2θ<50° and $|F_o|>3\sigma(|F_o|)$), which were collected by 2θ—ω scan method.[4,5] Calculations were made on the HITAC M-200H computer at the Computation Center of the Institute for Molecular Science by use of the Universal Crystallographic Computation Program System, UNICS III.[6]

The present study was supported by Grant-in-Aid for Scientific Research No. 57470036 from the Ministry of Education, Science and Culture. Thanks are also due to the Institute for Molecular Science for permission to use the AFC-5 automated X-ray diffractometer (the Instrument Center) and the computer (the Computation Center).

References

1) a) M. L. Ziegler and R. K. Sheline, *Inorg. Chem.*, 4, 1230 (1965); b) I. B. Benson, S. A. R. Knox, R. F. D. Stansfield, and P. Woodward, *J. Chem. Soc., Chem. Commun.*, **1977**, 404; c) P. J. Giordano and M. S. Wrighton, *Inorg. Chem.*, **16**, 160 (1977); d) M. F. Neumann and F. Brion, *Angew. Chem. Int. Ed.*, **18**, 688 (1979); e) K. Folting, J. C. Huffman, L. N. Lewis, and K. G. Caulton, *Inorg. Chem.*, **18**,

3483 (1979); f) A. M. Rosan, *J. Chem. Soc., Chem. Commun.*, **1981**, 311; g) P. L. Gaus, N. Marsinek, and M. O. Funk, *Inorg. Chem.*, **23**, 3269 (1984).

2) R. G. Hayter and L. W. Williams, *J. Inorg. Nucl. Chem.*, **26**, 1977 (1964).

3) T. Hayashi, M. Konishi, Y. Kobori, M. Kumada, T. Higuchi, and K. Hirotsu, *J. Am. Chem. Soc.*, **106**, 158 (1984).

4) Chloroform molecules were so severely disordered that it was difficult to locate exact positions of atoms in $CHCl_3$.

5) Tables of atom coordinates, anisotropic thermal parameters, and observed and calculated structure factors are kept in the office of the Chemical Society of Japan (Document No. 8636).

6) T. Sakurai and K. Kobayashi, *Rikagaku Kenkyusho Hokoku*, **55**, 69 (1979).

NMR Spectra of Dimethyl 1-Acetyl-1,2-dihydro-2-quinolyl-phosphonate and Related Compounds

Hiroko SUEZAWA,* Minoru HIROTA, Yasuhiro SHIBATA,† Isao TAKEUCHI,† and Yoshiki HAMADA†

Department of Applied Chemistry, Faculty of Engineering, Yokohama National University, Tokiwadai, Hodogaya-ku, Yokohama 240

†Faculty of Pharmacy, Meijo University, Tempakucho, Tempaku-ku, Nagoya 468

(Received February 20, 1986)

Synopsis. ^{1}H, ^{13}C, and ^{31}P NMR spectra of the products from the Reissert type reactions using acyl halides and trimethyl phosphite were measured and correlated with their structures. ^{31}P Chemical shift of dimethoxyphosphinyl group and ^{13}C chemical shift of the α-carbon atom, as well as $^{1}J_{CP}$ and $^{2}J_{PH}$, can be criteria to differentiate the 1,2- and the 1,4-adducts from each other. Thus, there NMR parameters can be a clue to elucidate the regioselectivity of the reactions.

Pyridine and similar heterocycles containing six-membered azaaromatic ring were shown to react with acyl halides and trimethyl phosphite to give the corresponding 1-acyl-1,2-dihydro-1-azaaromatic phosphonates by Akiba and co-workers.[1] In some instances, the formation of 1,4-adducts was also reported.[2,3] In relation to our recent studies[4] on the Reissert type reactions of some azaheterocycles, some diazanaphthalenes and mono- and diazaphenanthrenes were allowed to react with similar reagents and the structures of the products were elucidated by means of ^{1}H, ^{13}C, and ^{31}P NMR spectroscopy.

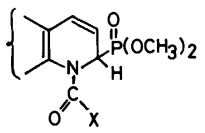

1,2-Adduct

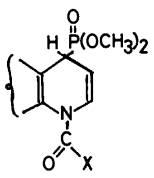

1,4-Adduct

Results and Discussion

1-Azaphenanthrene (**1**), 1,5-diazaphenanthrene (**2**), and 1,8-diazanaphthalene (**3**) were allowed to react with trimethyl phosphite in the presence of several acyl and sulfonyl chlorides. The structures of the products were determined by NMR spectroscopy in view of examining the regioselectivity (1,2- vs. 1,4-addition) of the reactions. In order to have unambiguous knowledge on the NMR spectral characteristics of the 1,2- and the 1,4- adducts, the adducts were also prepared from phthalazine (**4**), 9-azaphenanthrene (**5**), and acridine (**6**). The adducts thus obtained were used as the reference compounds of known regioselectivity. Only the 1,2-adducts are expected to be formed in the cases of (**4**) and (**5**). In contrast, acridine (**6**) should give the 1,4-adduct.

The ^{1}H, ^{13}C, and ^{31}P chemical shifts, as well as $^{1}J_{CP}$ and $^{2}J_{PH}$ spin-spin coupling constants, of these *N*-acyl-dihydroazaaromatic phosphonates are given in Table 1. The structural feature of the adducts is reflected in the NMR spectral parameters of the phosphonate parts of the molecules, i.e. ^{31}P chemical shift of dimethoxyphosphinyl group, ^{13}C chemical shift of the carbon atom directly bonded to the phosphorus atom (named α-carbon atom, hereafter), ^{1}H chemical shift of the proton on the α-carbon atom, one bond ^{13}C–^{31}P coupling constant, and two bond ^{1}H–^{31}P coupling constant.

The Chemical Shifts. In the 1,2-adducts which have the *N*-acylated nitrogen atom on the α-carbon atom, ^{31}P and α-^{13}C chemical shifts fall in the ranges of 19 to 21 ppm and 48 to 54 ppm, respectively. The ^{13}C chemical shift differences among the 1,2-adducts are relatively small. The ^{13}C chemical shift is affected far more significantly by the substituent on the nitrogen atom than the skeletal structure of the heterocycle. When the substituent on the nitrogen atom (COX) was changed from acetyl ($COCH_3$) to benzoyl (COC_6H_5), a low field shift of 1 to 1.5 ppm is generally induced.[5] Considerably larger low field shift was observed when the substituent COX was ethoxycarbonyl ($COOC_2H_5$) or diphenylcarbamoyl ($CON(C_6H_5)_2$).

Chemical shifts of the hydrogen atom on the α-carbon atom (named α-hydrogen atom, hereafter) are renging between 5.6 and 6.5 ppm in the series of the 1,2-adducts. Small but definite deviation dependent on the structure of the parent heterocyle was observed among them. Thus the ^{1}H chemical shifts of the 1,2-adducts of 1,8-diazanaphthalene (**3**) appear at a little higher fields, while those of 9-azaphenanthrene (**5**) at lower fields, than the average. As a whole, the chemical shift of α-hydrogen is more sensitive to the skeletal structure of the heterocycle than that of α-carbon. When the substituent COX was changed from acetyl to benzoyl, the ^{1}H chemical shift generally moves towards a high field in contrast to the low field shift of the ^{13}C signal of α-carbon caused by the same structural modification.[5]

The corresponding ^{31}P ^{13}C, and ^{1}H chemical shifts of the 1,4-adducts fall in the range of 23—24 ppm, 34—45 ppm, and 4.4—4.9 ppm, respectively. The ranges of the chemical shifts overlap to each other in neither cases. Therefore, the chemical shift values can be good criteria to differentiate the 1,2- and the 1,4-adducts.

The Spin-Spin Coupling Constant. The ^{1}H-decoupled spectrum of α-carbon atom is split into a doublet by the coupling with the phosphorus nucleus from which $^{1}J_{CP}$ was determined. The $^{1}J_{CP}$ values of the 1,2-adducts fall within a relatively narrow range between 149 and 154 Hz, again the difference among the 1,2-adducts not being large.

Table 1. NMR Spectra of Fused Dimethyl 1-Acyl-1,2-dihydro-2-pyridylphosphonates and -1,4-Dihydro-4-pyridylphosphonates
(solvent: $CDCl_3$, concentration ca. 0.3 mol/l)

Starting compound		Acyl	Orientation of addition	Chemical shift/ppm						Coupling constant/Hz		
				^{31}P	$^{13}C(\alpha)$	$^{13}C(OCH)$	$^{13}C(C{=}O)$	$^{1}H(\alpha)$	$^{1}H(OCH)$	$^{1}J_{CP}$	$^{2}J_{HP}$	$^{3}J_{POCH}$
(1)	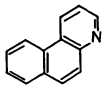	CH_3CO	1, 2	20.43	48.46	53.34	170.30	6.3	3.49	153.8	—	10.7
		C_2H_5CO	1, 2	20.63	48.71	53.34	174.17	6.3	3.48	153.8	—	10.7
		C_6H_5CO	1, 2	20.63	50.14	53.42	169.83	6.01	3.53	151.4	20.7	10.8
		C_2H_5OCO	1, 2	20.39	50.98	53.47	154.10	5.75	3.48	152.6	22.0	13.2
		CH_3CO	1, 4	23.79	35.31	53.57	168.37	4.74	3.57	146.6	24.2	10.7
		C_2H_5CO	1, 4	23.73	35.33	53.70	171.82	4.76	3.57	144.0	24.2	10.7
		C_6H_5CO	1, 4	24.23	35.77	53.81	168.04	4.83	3.68	146.5	24.4	10.7
(2)	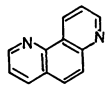	CH_3CO	1, 2	20.16	48.93	53.21	169.95	6.35	3.53	148.9	19.8	10.7
		C_6H_5CO	1, 2	20.33	50.68	53.69	169.46	6.03	3.58	151.4	21.0	10.6
		C_6H_5CO	1, 4	25.41	33.80	53.65	168.26	5.59	3.75	141.6	21.5	10.7
(3)		CH_3CO	1, 2	19.76	49.08	53.42	170.54	6.06	3.69	151.4	17.3	10.8
		C_6H_5CO	1, 2	19.45	51.09	53.69	168.37	5.91	3.64	148.9	20.5	10.7
		CH_3SO_2	1, 2	19.42	52.50	53.82	—	5.73	3.64	153.8	19.0	10.6
(4)		CH_3CO	1, 2	19.59	48.16	53.53	171.52	6.35	3.65	153.8	16.1	10.7
		C_6H_5CO	1, 2	19.65	49.19	53.66	169.78	6.52	3.69	151.4	16.3	10.8
		$(Ph)_2NCO$	1, 2	20.39	50.71	53.12	156.46	6.19	3.69	151.4	15.3	10.8
		CH_3SO_2	1, 2	19.08	51.41	53.63	—	5.85	3.67	153.8	12.4	10.6
		$C_6H_5SO_2$	1, 2	18.04	51.74	53.79	—	5.98	3.65	158.7	15.6	10.7
(5)	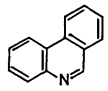	CH_3CO	1, 2	21.24	51.03	52.75	168.92	6.57	3.43	151.4	20.3	10.4
		C_6H_5CO	1, 2	21.14	52.82	52.82	167.94	6.47	3.46	148.9	19.7	10.7
		C_2H_5OCO	1, 2	21.20	53.58	52.50	153.10	6.12	3.37	153.8	20.3	10.7
(6)	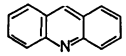	CH_3CO	1, 4	23.36	45.13	53.74	169.57	4.41	3.56	139.2	25.9	10.7
(7)		CH_3CO	1, 2	20.36	48.43	53.26	169.89	6.13	3.56	151.4	—	10.6
		C_6H_5CO	1, 2	20.43	50.44	53.42	169.35	5.94	3.61	148.9	20.3	10.7
(8)		CH_3CO	1, 2	21.27	50.93	53.39	168.16	6.29	3.60	151.4	17.6	10.6
		C_6H_5CO	1, 2	21.44	51.97	53.22	168.28	6.39	3.63	148.9	20.7	10.4
		$(Ph)_2NCO$	1, 2	21.88	54.55	53.74	156.56	5.89	3.59	148.9	16.4	9.0

Table 2. Summary of the Characteristic Differences in NMR Spectra of 1,2- and 1,4-Adducts

NMR	1,2-Adduct	1,4-Adduct
^{31}P	19—21 ppm	23—24 ppm
$^{13}C(\alpha)$	48—54 ppm	35—45 ppm
$^{1}H(\alpha)$	5.9—6.5 ppm	4.4—4.9 ppm
$^{1}J_{CP}$	148—154 Hz	139—146 Hz
$^{2}J_{HP}$	16—21 Hz	21—26 Hz

$^{1}J_{CP}$ becomes 2—3 Hz smaller when *N*-acyl substituent is changed from acetyl to benzoyl. The $^{2}J_{PH}$ of the 1,2-adducts are ranging from 15 to 21 Hz and are considerably smaller than those of the 1,4-adducts. Those of phthalazine (**4**) adducts is around 16 Hz, being considerably smaller than the average. The $^{1}J_{CP}$'s and $^{2}J_{PH}$'s of the 1,4-adducts are 139—146 Hz and 21—26 Hz, respectively. These ranges do not overlap with the corresponding ranges for the 1,2-adducts. Therefore, the coupling constants will provide an additional clue to characterize the isomeric 1,2- and the 1,4-adducts by NMR spectroscopy.

Other NMR Parameters. The chemical shifts and the spin-spin coupling constants of other ^{1}H and ^{13}C nuclei are rather insensitive to the mode of addition. The ^{1}H and ^{13}C chemical shifts of dimethoxyphosphinyl group are almost unaffected by the change of *N*-acyl group and by the modification of ring structure, ranging 3.3 to 3.8 ppm (two lines) and 52.8 to 53.8 ppm (two lines usually), respectively. The $^{3}J_{POCH}$ values are rather insensitive to the structure of the adducts and not versatile to the discrimination of the two isomeric adducts. As expected, the carbonyl chemical shifts of the acyl groups are determined by the nature of acyl groups, i.e. 168 to 171 ppm for acetyl, 168 to 170 for benzoyl, around 157 ppm for diphenylcarbamoyl, and around 153 ppm for ethoxycarbonyl.

Experimental

Preparation of Materials. Fused 1-acyl-1,2-dihydro-2-pyridylphosphonates from **1—5** were newly prepared by the present authors by the following procedures: To an ice-cooled solution of the azaaromatic compound (9.6 mmol) dissolved in 40 ml of acetonitrile, slightly excess (10.6 mmol) of acyl chloride was added dropwise under stirring, and the whole was kept stirring for 20 min after the completion of addition. Then trimetyl phosphite (10.6 mmol) and sodium iodide (14 mmol) were added successively. The mixture was warmed to 50 °C and left standing for additional 30 min. The solvent was distilled off, and 30 ml of 5% aqueous Na_2CO_3 solution was added to the residue. The crude *N*-acyldihydroazaaromatic phosphonate(s) obtained by extracting the aqueous solution with dichloromethane. In cases when isomeric (1,2- and 1,4-) adducts were formed, they were separated by column chromatography on silica gel.

Measurement of NMR Spectra. All NMR spectra were measured on a JEOL JNM FX-90Q spectrometer in chloroform-*d* solutions at room temperature (26 °C in the probe) unless otherwise remarked. ^{1}H and ^{13}C chemical shifts were determined in reference to the signal of TMS added in the solution, and ^{31}P chemical shifts in reference to the external phosphoric acid standard.

References

1) K. Akiba, Y. Negishi, and N. Inamoto, *Synthesis*, **1979**, 55.

2) K. Akiba, H. Matsuoka, and M. Wada, *Tetrahedron Lett.*, **22**, 4093 (1981).

3) K. Akiba, T. Kasai, and M. Wada, *Tetrahedron Lett.*, **23**, 1709 (1982).

4) a) I. Takeuchi, Y. Shibata, and Y. Hamada, *Yakugaku Zasshi*, **104**, 1133 (1984); b) I. Takeuchi, Y. Shibata, and Y. Hamada, 9th International Congress on Heterocyclic Chemistry, Tokyo, August 1983, Abstr., p. 101.

5) In the case of the 1,2-adducts derived from isoquinoline, both the ^{1}H and the ^{13}C chemical shifts of α-carbon and the hydrogen attached on it tend to move towards low fields by the change from acetyl to benzoyl in *N*-acyl group. Thus, the quinoline- and isoquinoline-derived adducts were shown to behave apparently different from each other towards the same structural modification, and their behaviors could be explained by the difference in preferred conformation between these two series of adducts. The *N*-benzoyl-1,2-dihydroquinoline-2-phosphonateds are expected to take a favorable conformation in which the aromatic ring of the benzoyl group orient itself towards the α-carbon atom (antiperiplanar about the C(carbonyl)–N bond) to avoid the steric hindrance between the phenyl and the peri-hydrogen atom. On the contrary, a synperiplanar conformation might be favorable in the adducts of isoquinoline-like heterocycles. The fact that the C(3) and C(4) chemical shifts of the latter adducts shift towards high fields by the same change in the *N*-acyl substituent supports the preference of synperiplanar conformation.

Metal Carbonyl-Induced N-O Bond Cleavage of the Oxime Group

Makoto NITTA* and Yukio IINO
Department of Chemistry, School of Science and Engineering, Waseda University, Shinjuku-ku, Tokyo 160
(Received December 26, 1985)

Synopsis. The reaction of $[Mo(CO)_6]$ or $[Fe_2(CO)_9]$ with oxime *O*-acetate of 1,3-diphenyl-2-propen-1-one undergoes a reductive N-O bond cleavage to give an imine which dimerises and/or is hydrolyzed to ketones. The dimer, so formed, undergoes fragmentations to give pyridine and pyrimidine derivatives. Similarly, the reaction of $[Mo(CO)_6]$ with several oxime *O*-acetates, oximes, and an oxime ether were shown to give the corresponding ketones. A reaction of oxime *O*-acetates with $[Cr(CO)_6]$ or with $[W(CO)_6]$ to give the corresponding ketones was also shown to proceed very slowly.

In relation to the synthetic and mechanistic interests of a $[Mo(CO)_6]$-, $[Fe_2(CO)_9]$-, or $[Fe(CO)_5]$-induced reductive N-O bond cleavage of isoxazoles[1] and 2-isoxazolines,[2,3] we previously showed that oxime *O*-acetates, oximes, and oxime ethers can be converted to the corresponding ketones in the presence of $[Fe_2(CO)_9]$ or $[Fe(CO)_5]$ under thermal conditions or under photoirradiations.[4] The postulated mechanism involves the imine intermediate. In connection with this study, we report here that a $[Mo(CO)_6]$-induced reaction of oxime *O*-acetate of 1,3-diphenyl-2-propen-1-one gives the imine intermediate. The deoximation of several oxime derivatives using group VI metal carbonyls $[M(CO)_6]$: M=Mo, Cr, and W] are described.

The thermal reaction of oxime *O*-acetates **1** with $[Mo(CO)_6]$ in ethanol or in mosit acetonitrile under reflux afforded 1,3-diphenyl-3-propen-1-one (**2**), 1,3-diphenyl-1-propanone (**3**), 2,4,6-triphenylpyridine (**4**),[5] 2,4,6-triphenylpyrimidine (**5**),[6] (Table 1, Entries 1 and 2). The detailed reaction conditions and the yields of the products, all of which are known compounds, are summarized in Table 1.

The present reaction can be explained by the mechanism shown in Scheme 1. From an analogy of the $[Mo(CO)_6]$-induced N-O bond cleavage of isoxazoles[1] and 2-isoxazolines,[3] and the $[Fe_2(CO)_9]$-induced deoximation reaction of oxime derivatives,[4] the initial step of the reaction was shown to be a complexation of **1** to give **7**.[4] The subsequent N-O bond cleavage gives complex **8**, the nitrogen moiety of which would be reduced by the central molybdenum followed by protonation to give the imine **9** in a protic media.[4] The hydrolysis of **9** would result in the formation of **2** even by stray water. Under the present conditions, **2** was reduced to give **3** (see Experimental).

The imine **9** has been known to dimerise to give a bicyclic dimer **6**, the thermal reaction of which at 190 °C gives **4** and **5** in the presence of sulfur.[7] The thermal reaction of **6** in ethanol under reflux for 24 h afforded **4** (5%) and a trace of **5**; the starting material **6** was recovered in 95% yield. However, the

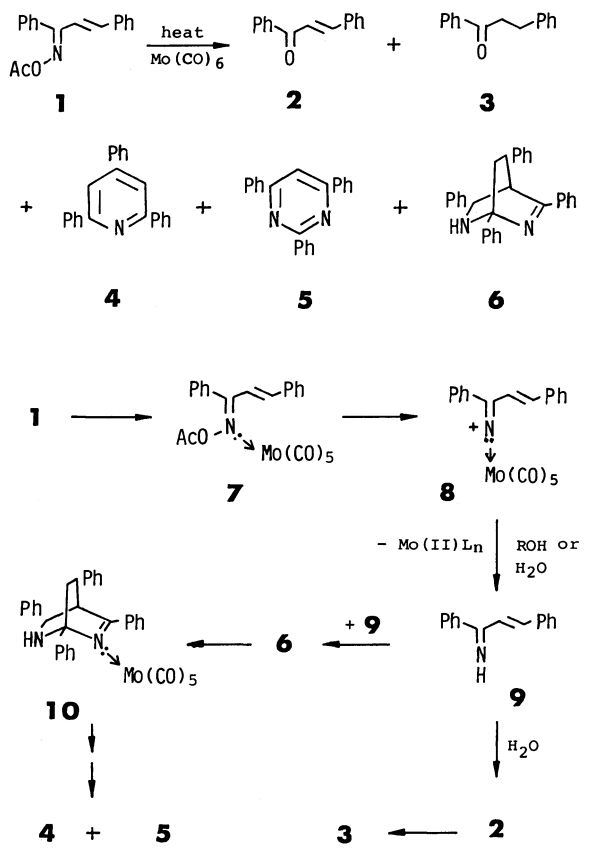

Scheme 1.

Table 1. Experimental Results Obtained in the Reaction of **1**

Entry	Solvent	Reaction Conditions[a]	Reaction Time/h	Product (yield/%) 2	3	4	5	6
1	EtOH	A	24	0	7	31	6	15
2	MeCN-H_2O	A	7	5	6	39	1	9
3	EtOH	B	1.5	6	0	2	0	29

a) A: A molar equivalent amount of $[Mo(CO)_6]$ was used, being heated under reflux. B: 1.2 Molar equivalent amount of $[Fe_2(CO)_9]$ was used, being heated under reflux.

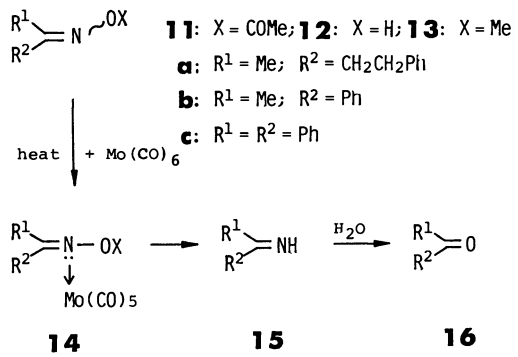

Scheme 2.

fragmentation reaction of **6** was accelerated in the presence of [$Mo(CO)_6$], resulting in the formation of **4** (42%), **5** (1%), and **6** (48%) under reflux in ethanol for 24 h. A possible explanation of this fact is a complexation of the [$Mo(CO)_5$] species to the nitrogen atom of **6** to give **10**. Previously, it was suggested that [$Mo(CO)_5$] and [$Fe(CO)_4$] species can coordinate to the oxygen atom of an epoxide ring to facilitate a C–O bond cleavage.[8] The metal carbonyl species also seems to exhibit the nature of a Lewis acid. In a similar fashion, [$Mo(CO)_5$] in a possible intermediate **10** might facilitate the elimination of styrene or benzaldimine from **6**, followed by dehydrogenation to give **4** and **5**.

In relation to a previous study,[4] a reaction of **1** with [$Fe_2(CO)_9$] in ethanol was carried out. The reaction proceeded very fast compared to an [$Mo(CO)_6$]-induced reaction, and **2**, **4**, and **6** were obtained in rather low yields (Table 1, Entry 3). Thus, the reaction is very similar to an [$Mo(CO)_6$]-induced reaction (Scheme 1). The reduction of **2** to give **3** was not observed in this case.

Thermal reactions of oxime O-acetates **11a—c**, oximes **12a—c**, and an oxime ether **13c** in the presence of [$Mo(CO)_6$] afforded the corresponding ketones **16a—c**. Reaction pathways similar to that in Scheme 1 are depicted in Scheme 2. The reaction conditions and yields of the products are summarized in Table 2. The reactions of oxime *O*-acetates **11a—c** proceeded fast and the starting materials were completely consumed to give **16a—c** in good yields (Table 2, Entries 1—3). However, the reaction of the oximes and the oxime ether generally proceeded slowly and the starting materials were recovered (Entries 5—7). Thus, oxime *O*-acetates are labile compared to oximes and the oxime ether.[4] On the other hand, the reaction of **11a** with [$W(CO)_6$] or with [$Cr(CO)_6$] did not occur and **11a** was recovered (Table 2, Entry 8 or 10). Similarly, the reaction of **11c** proceeded very slowly and the corresponding ketone **16c** was obtained in low yield in addition to **11c** (Table 2, Entries 9 and 11). In the deoximation reactions of oxime derivatives, [$Mo(CO)_6$] was shown to be effective compared to [$W(CO)_6$] and [$Cr(CO)_6$] under the present conditions.

Ketimine and aldimine complexes of pentacarbonylchromium have been synthesized.[9] Furthermore, recent work by Shvo et al. clarified that ketimine and aldimine complexes of pentacarbonyltungsten can be obtained in yields ranging from 10 to 20% from a reaction of [$W(CO)_5$THF] with ketoximes and aldoximes.[10] Under the present reaction conditions, no ketimine complex of the group VI metal carbonyls was obtained.

Table 2. Deoximation of **11a—c**, **12a—c**, and **13c**[a]

Entry	Compound	Reaction Time/h	Product yield/%	Recovery/%
1	**11a**	24	**16a** (77)	0
2	**11b**	20	**16b** (60)	0
3	**11c**	10	**16c** (85)	0
4	**12a**	22	**16a** (77)	0
5	**12b**	48	**16b** (55)	13
6	**12c**	144	**16c** (81)	16
7	**13c**	27	**16c** (56)	32
8[b]	**11a**	24	**16a** (0)	90
9[b]	**11c**	14	**16c** (5)	94
10[c]	**11a**	24	**16a** (0)	98
11[c]	**11c**	14	**16c** (2)	96

a) The reactions were carried out in moist acetonitrile under reflux by using an equivalent amount of [$Mo(CO)_6$]. b) The reactions were carried out by using an equivalent amount of [$W(CO)_6$]. C) The reactions were carried out by using an equivalent amount of [$Cr(CO)_6$].

Experimental

General Procedure for the Reaction of 1,3-Diphenyl-2-propen-1-one Oxime O-Acetate 1 with [$Mo(CO)_6$] or with [$Fe_2(CO)_9$]. A solution of **1** (265 mg, 1 mmol) with [$Mo(CO)_6$] (264 mg, 1 mmol) or with [$Fe_2(CO)_9$] (437 mg, 1.2 mmol) in ethanol (3 cm^3) or in acetonitrile (3 cm^3) containing water (ca. 1 mmol) was heated under reflux until **1** was completely consumed. After removing the solvent, the residue was dissolved in benzene (10 cm^3) and filtered through Celite to remove any insoluble material. The filtrate was concentrated and the resulting residue was separated by TLC on silica gel using benzene–hexane (1/1) as a developer to give the products. The results are summarized in Table 1.

Reduction of 1,3-Diphenyl-2-propen-1-one 2 with [$Mo(CO)_6$]. A solution of **2** (104 mg, 0.5 mmol and [$Mo(CO)_6$] (264 mg, 1 mmol) in ethanol (2 cm^3) was heated under reflux for 24 h under a nitrogen atmosphere. After hexane was added to the reaction mixture, it was filtered through Celite to remove any insoluble material. The filtrate was concentrated and the resulting residue was separated by TLC on silica gel using benzene-hexane (1/1) as a developer to give **3** (58 mg, 55%) and **2** (15 mg, 14%).

Thermal Reaction of 6. A solution of **6** (42 mg, 0.1 mmol) in ethanol (1 cm^3) was heated under reflux for 24 h. After the solvent was evaporated, the residue was separated by TLC on silica gel using benzene–dichloromethane (1/1) as a developer to give **2** (2 mg, 5%), a trace of **3**, and **6** (40 mg, 95%).

Thermal Reaction of 6 in the Presence of [$Mo(CO)_6$]. A solution of **6** (42 mg, 0.1 mmol) and [$Mo(CO)_6$] (27 mg, 0.1 mmol) in ethanol (1 cm^3) was heated under reflux for

24 h. After the solvent was evaporated, the resulting residue was separated by TLC on silica gel using benzene–dichloromethane as a developer to give **2** (13 mg, 42%), **3** (1 mg, 2%), and **6** (20 mg, 48%).

General Procedure for the Deoximation Reaction of Oxime *O*-Acetates 11a—c, Oximes 12a—c, and Oxime Ehter 13c with [Mo(CO)$_6$]. A solution of oxime derivatives **11a—c**, **12a—c**, or **13c** (1 mmol) with [Mo(CO)$_6$] (264 mg, 1 mmol) in acetonitrile (2 cm^3) containing water (ca. 1 mmol) was heated under reflux for various periods of time. After the solvent was evaporated, the residue was dissolved in benzene (10 cm^3) and filtered through Celitė to remove any insoluble material. The filtrate was concentrated and the resulting residue was separated by TLC on silica gel using benzene–dichloromethane (1/1) as a developer to give the products. The reaction conditions and the yields of the products are summarized in Table 2 (Entries 1—7).

General Procedure for the Deoximation Reaction of Oxime *O*-Acetate 11a,c with [W(CO)$_6$] or with [Cr(CO)$_6$]. A solution of oxime *O*-acetate **11a,c** (1 mmol) with [W(CO)$_6$] (352 mg, 1 mmol) or with [Cr(CO)$_6$] (220 mg, 1 mmol) in acetonitrile (2 cm^3) containing water (ca. 1 mmol) was heated under reflux for various periods of time. After the solvent was evaporated, the residue was dissolved in benzene (10 cm^3) and filtered through Celite to remove a insoluble material. The filtrate was concentrated and the resulting residue was separated by TLC on silica gel using benzene-dichloromethane as any developer to give the products. The reaction conditions and the yields of the products are summarized in Table 2 (Entries 8—11).

References

1) M. Nitta and T. Kobayashi, *J. Chem. Soc., Perkin Trans. 1*, **1985**, 1401.
2) M. Nitta and T. Kobayashi, *J. Chem. Soc., Perkin Trans. 1*, **1984**, 2103.
3) M. Nitta, A. Yi, and T. Kobayashi, *Bull. Chem. Soc. Jpn.*, **58**, 991 (1985).
4) M. Nitta, I. Sasaki, H. Miyano, and T. Kobayashi, *Bull. Chem. Soc. Jpn.*, **57**, 3358 (1984).
5) O. Tsuge, M. Tashiro, and K. Yamada, *Kogyo Kagaku Zasshi*, **71**, 1667 (1968).
6) A. L. Weis and V. Rosenbach, *Tetrahedron Lett.*, **22**, 1453 (1981).
7) A. R. Forrester, M. Gill, and R. H. Thomson, *J. Chem. Soc., Perkin Trans. 1*, **1979**, 616.
8) H. Alper, D. D. Roches, J. Durst, and R. Legault, *J. Org. Chem.*, **41**, 3611 (1976); T. Kobayashi and M. Nitta, *Chem. Lett.*, **1982**, 325; M. Nitta and T. Kobayashi, *Chem. Lett.*, **1985**, 877.
9) E. O. Fisher and I. Knaus, *Chem. Ber.*, **103**, 1262 (1970).
10) D. Czarkie and Y. Shvo, *J. Organomet. Chem.*, **280**, 123 (1985).

The Determination of a Small Amount of Biological Constituent by the Use of Chemiluminescence. VII. An Attempt of Cyclic Immunoaffinity Chromatography

Tadashi HARA,* Motohiro TORIYAMA,† Takashi EBUCHI, and Masakatsu IMAKI††
Department of Chemical Engineering, Faculty of Engineering, Doshisha University, Karasuma Imadegawa, Kamigyo-ku, Kyoto 602
†Government Industrial Reserch Instituent, Nagoya, Hirate-machi, Kita-ku, Nagoya 462
††Horiba Ltd., Kisshoin, Minami-ku, Kyoto 601
(Received February 4, 1986)

Synopsis. An immunoaffinity chromatography has been established by combining a chemiluminescence detector developed by the authors with two kinds of immunoaffinity columns connected in series. According to the present method, human serum albumin and ovalbumin in the range of 100 ng to 15 μg in their mixtures could be continuously and selectively determined.

It has been desired to develop an analytical technique for a sensitive, continuous, and selective determination of the desired constituents in serum.

Through immunoassay, used as a labeling reagent, a synthesized metal-complex compound having catalytic activity for a chemiluminescence(CL) reaction, was continuously carried out by the sandwich method mentioned in a previous paper. It required six operating steps and tedious labeling.[1]

So far, there have been several reports[2-5] in which the desired constituent was specially separated on an affinity column based on a biological reaction analyzed by means of a suitable detector. However, the detector used for such a measurment was not always very sensitive.

The method for a flow-injection analysis of protein was established by the authors on the basis of the phenomenon that the catalytic activity of copper(II) against a CL reaction between 5-amino-2,3-dihydro-1,4-phtalazinedione (luminol) and hydrogen peroxide(H_2O_2) is lowered in the presence of protein. According to this method, 2×10^{-4}—1×10^{-1} g dm^{-3} of protein could be sensitively determined with a detection limit of 10 ng.[6,7] A highly sensitive detector for the HPLC of protein was manufactured by making use of the same phenomenon that is described above, and the detector was shown to be also useful for the post-column detection of protein in HPLC.[7]

It was therefore expected that an immunoaffinity chromatography for the sensitive, continuous and selective determination of the desired constituents in a sample without labeling might be established by combining the CL detector with the affinity columns used for an immune reaction.

Experimental

All the reagents used were of a commercially available special grade. A 2.0×10^{-6} mol dm^{-3} copper(II) solution was prepared by diluting a 2.0×10^{-2} mol dm^{-3} copper(II) stock solution[8] with a buffer solution (pH 12.8) consisting of a 0.20 mol dm^{-3} boric acid (H_3BO_3) solution and a 0.25 mol dm^{-3} potassium hydroxide (KOH) solution. A 1.0×10^{-4} mol dm^{-3} luminol solution was prepared by use of a buffer solution (pH 10.2)(0.20 mol dm^{-3} H_3BO_3–0.20 mol dm^{-3} KOH buffer solution). A 5.0×10^{-4} mol dm^{-3} H_2O_2 solution was prepared in a manner similar to that described in a previous paper.[7] These reagents were used for the CL detector developed by the authors. Human serum albumin(HSA)(Miles Labolatolies, Inc.), bovine serum albumin(BSA)(Nakarai Chemicals, Ltd.), ovalbumin (Ova)(Sigma Chemical Co.), human serum γ-globuline-(HγG)(Sigma Chemical Co.), bovine serum γ-globulin-(BγG)(Sigma Chemical Co.), bovine serum α-globulin-(BαG)(ICN Pharmaceuticals, Inc.), and control serum(Q-PAK-Chemistry Control Serum I; Hyland) were diluted with a 8.34×10^{-3} mol dm^{-3} phosphate buffer solution(Buff-A; pH 7.3) consisting of a 2.78×10^{-3} mol dm^{-3} potassium dihydrogenphosphate solution and a 5.56×10^{-3} mol dm^{-3} disodium hydrogenphosphate solution.

Rabbit anti-HSA(DAKO) and goat anti-Ova(Cappel), respectively, were immobilized onto 2 g of porous glass beads (CPG-3000, 200/400 mesh, 29260 nm mean pore diameter, ELECTRO-NUCLEONICS, INC.) by a periodate method.[1] Each amount of anti-HSA and anti-Ova immobilized onto a gram of support was 18.5 and 3.10 mg, as determined by the CL detector developed by the authors.

A flow diagram of the immunoaffinity chromatography system equipped with the CL detector devised by the authors is shown in Fig. 1, and its operating procedure is shown in Scheme 1. Buff-A(a) was fed at a flow rate of 1.8 cm^3 min^{-1} by the pump(d)(Atto, SJ 1211) and an elluent(b)(pH 2.5; 4.2×10^{-3} mol dm^{-3} hydrochloric acid –2.5×10^{-2} mol dm^{-3} potassium chloride buffer solution) (Buff-B) was fed at a flow rate of 1.0 cm^3 min^{-1} by the pump(e)(Pharmacia High-precision Pump P-500). The porous glass beads immobilized with anti-HSA and anti-Ova were packed in a column 1(Col. 1)(15×1 mm i.d.) and a column 2(Col. 2)(15×1 mm i.d.), respectively.

A 50-mm^3 mixed solution containing HSA and Ova was

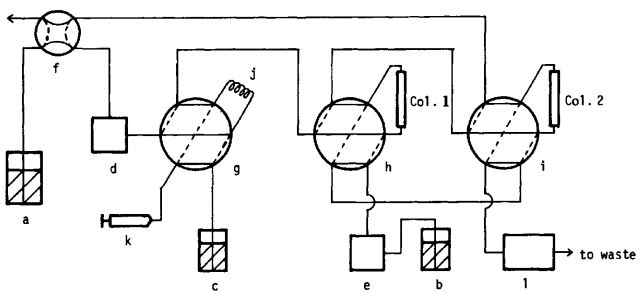

Fig. 1. Schematic flow diagram of the immunoaffinity chromatography system equipped with a CL detector. a: Buffer solution (Buff-A), b: eluent(Buff-B), c: sample solution, d and e: pump, f: four-way cock, g,h, and i: six-way cock, j: sampling loop, k: syringe, and l : CL detector.

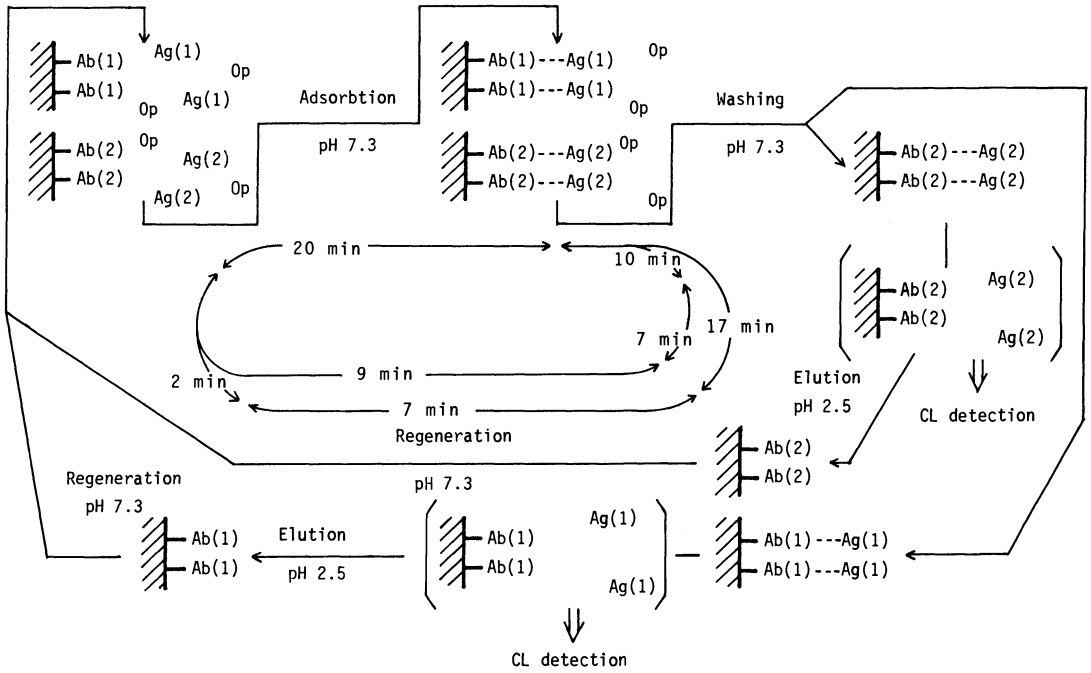

Scheme 1. Operating procedure for the immunoaffinity chromatography. Ab: Antibody, Ag: antigen, and Op: other protein.

injected into the Buff-A line through the sampling loop(j) and a six-way cock(g). A sample flaction was repeatedly passed through columns 1 and 2 for 20 min by operating a four-way cock(f). Here, HSA and Ova were collected on columns 1 and 2, respectively, by an immune reaction. Then Buff-A was fed to columns 1 and 2 for 10 min by operating a four-way cock(f) to wash out coexisting constituents. Ova was eluted from column 2 by operating a six-way cock(i); then cock(i) was again operated to feed Buff-A. HSA was eluted from column 1 by operating a six-way cock(h) and then cock(h) was again operated to feed Buff-A. Ova and HSA in each eluate was detected by a CL detector(1) as mentioned in a previous paper.[7] Columns 1 and 2 were regenerated by operating the six-way cocks and by feeding Buff-A.

Results and Discussion

Four steps consisting of adsorption, washing, elution (CL detection), and regeneration were developed for optimum operation as follows: both the flow rate and the feeding time of Buff-A for adsorption and regeneration were chosen so that each analytical value of a mixed sample containing 500 ng HSA and 500 ng Ova might give a definite value; both the flow rate and the feeding time of Buff-A for washing were also chosen so that the analytical value of 500 ng BSA, as a coexisting constituent, might give a minimum value; HSA and Ova, less than 500 ng, could almost be completely eluted in 7 min from affinity columns. The chosen experimental conditions are shown in Scheme 1.

A chromatogram for the mixture consisting of 500 ng of both HSA and Ova is shown in Fig. 2. The selectivities of affinity columns 1 and 2 are indicated on the basis of the analytical values of HSA and Ova, respectively (Table 1). Each 500 ng of protein was

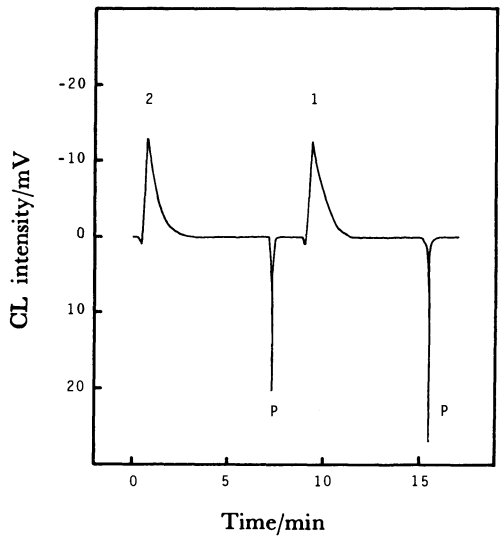

Fig. 2. Chromatogram of the mixture of HSA and Ova. 1: HSA, 2: Ova, and P: shock peak appeared owing to the exchange between the two cylinders in the pump.

Table 1. Selectivity of the Affinity Columns

Proteins (500 ng)	Column 1 (anti-HSA)	Column 2 (ati-Ova)
HSA	1.00	0.00
Ova	0.00	1.00
BSA	0.58	0.00
HγG	0.18	0.07
BγG	0.63	0.23
BαG	0.40	0.15

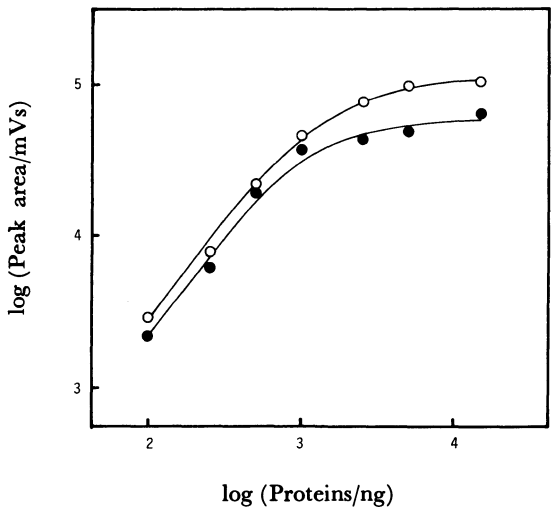

Fig. 3. Analysis of the mixture of HSA and Ova.
○: HSA and ●: Ova.

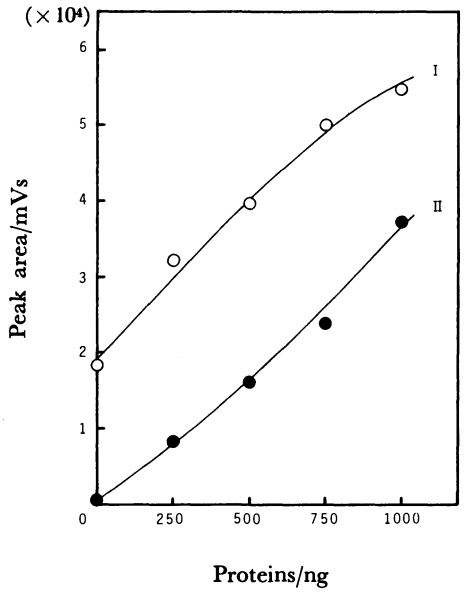

Fig. 4. Relationship between protein concentration and peak area.
○: Analytical value obtained by use of column 1 and
●: analytical value obtained by use of column 2.

used throughout this experiment. As can be seen from Table 1, the selectivity of column 1 (immobilized with anti-Ova) was fairly good. Porous glass beads were subjected to the immobilization treatment described in a previous paper[1] in the absence of antibodies. It was charged in a column to analyze HγG. According to the obtained result, no nonspecific adsorption was obtained. This suggests that nonspecific adsorption of HγG onto an affinity column is based on a cross reaction due to the use of inpure antibodies and HγG.

The present method was applied to a mixture of HSA and Ova, and each in the range of 100 ng—15 μg could be successfully determined (Fig. 3). The difference between two calibration curves seemed to result from a difference between the amounts of immobilized antibodies. The coefficient of variation for five analyses of a mixture containing each 500 ng HSA and Ova were 5.7% for HSA and 9.3% for Ova. The time necessary for an analysis was 46 min and the affinity columns were durable for about 20 replicate analyses. The beads immobilized with antibodies were stable and available for about 3 months after their preparation. By assuming the following (1)—(3): (1) 2 g of beads are immobilized with antibodies at a time, (2) 5.9 mg of beads are charged in a column, and (3) an affinity column is durable for about 20 replicate analyses, therefore, about 6800 analyses are feasible. Thus, the present method is sufficiently economical.

To examine the applicability of the present method to a practical sample, a control serum was diluted 5000 times and to it a definit amount of HSA and Ova was added. This was followed by an analysis of the resulting three mixtures (Fig. 4). Curves I and II in Fig. 4 were obtained from columns 1 and 2, respectively. Curve I showed the sum of albumin and non-specifically adsorbed protein in the control serum and of the added HSA. Curve II passed through an original point. This meant that the added Ova alone could be selectively analyzed without being affected by the serum matrix.

Judging from these results, the present method is sufficiently applicable to a practical sample if a selective column immobilized with antibodies is available.

References

1) T. Hara, M. Toriyama, and M. Imaki, *Bull. Chem. Soc. Jpn.*, **58**, 1299 (1985).
2) S. Ohlson, L. Hansson, P. Larsson, and K. Mosbach, *FEBS Lett.*, **93**, 5 (1978).
3) J. R. Sportsman and G. S. Wilson, *Anal. Chem.*, **52**, 2013 (1980).
4) R. R. Walters, *Anal. Chem.*, **55**, 1395 (1983).
5) S. C. Crowley and R. R. Walters, *J. Chromatogr.*, **266**, 157 (1983).
6) T. Hara, M. Toriyama, and K. Tsukagoshi, *Bull. Chem. Soc. Jpn.*, **57**, 1551 (1984).
7) T. Hara, M. Toriyama, and T. Ebuchi, *Bull. Chem. Soc. Jpn.*, **58**, 109 (1985).
8) T. Hara, M. Toriyama, and K. Tsukagoshi, *Bull. Chem. Soc. Jpn.*, **56**, 1382 (1983).

A New Phase-Transfer Porphyrin Catalyst for the Olefin Epoxidation

Shigeru TAKAGI, T. Ken MIYAMOTO,* and Yukiyoshi SASAKI
Department of Chemistry, Faculty of Science, The University of Tokyo,
Hongo, Bunkyo-ku, Tokyo 113
(Received December 24, 1985)

Synopsis. A new type of amphiphilic porphyrin has been synthesized and its manganese(III) complex has been used as a catalyst for the epoxidation of olefin. Catalytic oxygenation in a two-phase (CH_2Cl_2/H_2O) system has been undertaken in the absence of a phase-transfer reagent, such as benzyldimethyltetradecylammonium chloride.

During the last several years, efficient catalytic systems for the epoxidation of olefin in a two-phase (CH_2Cl_2/H_2O) system have been reported.[1,2] These synthetic model systems for the cytochrome P-450 have had several constituent elements. These elements included a hydrophobic Mn(III) porphyrin, an imidazole (or pyridine), a hypochlorite solution as an oxidant, and a phase-transfer reagent which catalyzed the transfer of an oxygen atom from hypochlorite to olefin (See Fig. 1).[3] In order to simplify the two-phase catalytic system, we developed a porphyrin catalyst toward a new amphiphilic manganese(III) salt (abb. Mn srf. **6**, Fig. 2) which had the function of a phase-transfer reagent as well as an epoxidation capability. We report here on the preparation of a new phase-transfer porphyrin catalyst (Mn srf. **6**) and its epoxidation of styrene and cyclohexene.

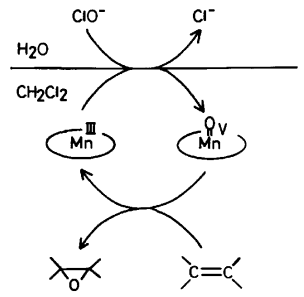

Fig. 1. The two-phase (CH_2Cl_2/H_2O) catalytic system for the olefin epoxidation.

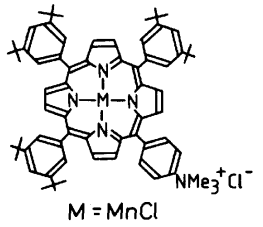

Fig. 2. Mn srf. **6**.

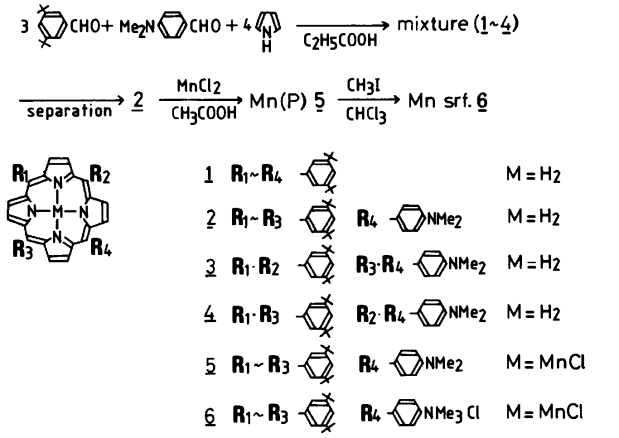

Scheme. The synthetic procedure to Mn srf. **6**.

Exprimental

The synthetic procedure to Mn srf. **6** followed that of previous work[4] and is shown in the scheme.

5,10,15-Tris(3,5-di-*t*-butylphenyl)-20-(4-dimethylaminophenyl)-21*H*,23*H*-porphyrin 2. The porphyrin **2** was synthesized by Rothemund condensation. 3,5-di-*t*-butylbenzaldehyde (76 g, 0.35 mol), 4-dimethylaminobenzaldehyde (18 g, 0.12 mol), and pyrrole (33 g, 0.49 mol) in propionic acid (1 dm^3) were heated under reflux for 2 h. Propionic acid was removed by distillation to give a mixture of porphyrins **1**—**4**. The crude mixture was dissolved in chloroform and chromatographed on an alumina (Merck Alumina 90) column with chloroform as an eluent. The porphyrins **1**—**4** were eluted and other by-products tended to be absorbed on the alumina. After the solvent was removed, the mixture of porphyrins was redissolved in benzene/hexane (1:4). The solution was poured onto a silica gel (Wako gel C-200) column prepared as a slurry in hexane. After all the material was loaded, 1:2 benzene/hexane was added. The porphyrin **1** was eluted, and the mixed solvent was passed through the column until the eluate became very pale. Then, benzene was added and the desired porphyrin **2** was eluted. The solvent was removed and dried in vacuo. Yield: 15.5 g (13%). Anal. Calcd for $C_{70}H_{83}N_5$: C, 84.54; H, 8.41; N, 7.04. Found: C, 84.24; H, 8.24; N, 7.27. ^{1}H NMR ($CDCl_3$) δ=−2.5 (2H, s, internal pyrrole H), 1.4 (54H, s, *t*-butyl H), 3.1 (6H, s, N-CH_3), 6.9—7.9 (21H, m, phenyl H), 8.7 (8H, s, β-pyrrole H).

Mn Insertion to Porphyrin 2. The porphyrin **2** (2.0 g, 2.2 mol), anhydrous $MnCl_2$ (2.0 g), CH_3COONa (2.0 g), and pyridine (20 cm^3) were dissolved in 260 cm^3 of mixed solvent ($CHCl_3/CH_3COOH$ 3:10). The solution was heated under reflux for 4 h. A Mn (III) complex **5** was extracted with $CHCl_3$ and the crude material was purified by alumina column ($CHCl_3$). The eluate was stirred with 10% hydrochloric acid. The solvent was then evaporated. Yield: 2.1 g (91%).

Preparation of the Mn srf. 6. Mn porphyrin **5** (1.0 g) was treated with methyl iodide (30 cm^3) in $CHCl_3$ under reflux for 5 h. The product was purified by chromatography as an alumina column ($CHCl_3$) eluting with 2:1 $CHCl_3/CH_3OH$. After the eluate was stirred with 10% hydrochloric acid, the solvent was removed by the evaporator. Yield: 0.4 g (37%): Anal. Calcd for $C_{71}H_{84}N_5MnCl_2$: C, 75.25; H, 7.47; N, 6.18. Found: C, 75.40; H, 7.46; N, 6.09. UV-vis. ($CHCl_3$) λ/nm ($\varepsilon/M^{-1}cm^{-1}$)[5]: 381 ($4.9\times10^4$),

Table 1. Products of a Styrene Oxidation Reaction

Product	Yield/%[15]	(Yield/turnover)
Styrene oxide	44	(64)
Phenylacetaldehyde	24	(37)
Benzaldehyde	2	(5)
Total	70	(106)

Table 2. Products of a Cyclohexene Oxidation Reaction

Product	Yield/%[15]	(Yield/turnover)
Cyclohexene oxide	58	(90)
2-Cyclohexen-1-one	6	(9)
2-Cyclohexen-1-ol	4	(6)
Total	68	(105)

406 (4.4×10⁴), 482 (7.9×10⁴), 589 (9.1×10³), 627 (1.3×10⁴).

Epoxidation Reaction. All experiments were carried out as follows. Mn srf. **6** (0.018 mmol), 4′-(imidazol-1-yl) acetophenone (65 times as many as mol of Mn srf. **6**), styrene (8 mmol, or cyclohexene), and *p*-dichlorobenzene (or cyclohexanone) as an internal standard were dissolved in 50 cm³ of dichloromethane. Then 50 cm³ of the sodium hypochlorite solution (2.9 mmol) was layed over the organic phase. The epoxidation reaction was initiated by stirring vigorously, and was carried out in an ice bath. The products were monitored by gas chromatography. A dependence of the reaction rate on the olefin concentration or on the Mn srf. **6** concentration was evidenced by control experiments. In an analysis of the kinetic experiments, the olefin concentration or the concentration of **6** was changed as listed in Table 3 or 4. Other conditions were maintained as mentioned above.

Results and Discussion

Mn srf. **6** was soluble in most organic solvents such as benzene, chloroform, *N*,*N*-dimethylformamide, ethanol and acetone etc. Mn srf. **6** was not soluble in water, but was soluble in an ethanol/water (1:5) mixed solvent. Soret bands were blue-shifted about 10 nm in methanol and ethanol/water compared with those in $CHCl_3$.[6]

The results of 2 h-oxidation of styrene and of cyclohexene are listed in Tables 1 and 2. In each reaction, epoxides were the main products. A certain amount of phenylacetaldehyde and a small amount of benzaldehyde[7] were also detected during styrene oxidation.[8] Styrene oxidation using Mn srf. **6** reached a maximum turnover number of 1200,[9] compared with that of 240[10] using a Mn complex of **1** and a phase-transfer reagent (benzyldimethyltetradecylammonium chloride). This result shows that Mn srf. **6** is superior to the Mn complex of **1** as a stable catalyst in an oxygenation reaction.[11,12]

The dependence of the reaction rate on the styrene concentration showed that a higher concentration led to a lower reaction rate (See Table 3). The catalyst concentration dependence indicated that the reaction rate changed from 8[13] (under a higher concentration, such as 0.27 and 0.37 mM) to 1.2 (under a lower concentration, such as 0.19 mM (See Table 4)).

Table 3. Dependence of the Reaction Rate on the Olefin Concentration

Styrene concentration/M[5]	Reaction rate[13]
0.06	5.6
0.24	3.7
0.41	1.8

Table 4. Dependence of the Reaction Rate on the Catalyst Concentration

Mn srf. **6** concentration/mM[5]	Reaction rate[13]
0.19	1.2
0.27	8.0
0.37	8.0

This catalytic system using Mn srf. **6** showed a unique behavior regarding the dependence of the reaction rate on the substrate concentration or on the catalyst concentration in comparison with those of other Mn(III) porphyrin catalytic systems.[2,14] The kinetic behavior of an epoxidation reaction using Mn srf. **6** could not be completely fitted by a Michaels-Menten equation, which was proposed by Collman et al.[2] At the present stage, we cannot rationalize these characteristic concentration dependencies of the reaction rate. However, our Mn srf. **6** system efficiently put olefin epoxidation into practice without using a phase-transfer reagent.

References

1) E. Guilmet and B. Meunier, *Nouv. J. Chim.*, **6**, 511 (1982).

2) J. P. Collman, J. I. Brauman, B. Meunier, T. Hayashi, T. Kodadek, and S. A. Raybuck, *J. Am. Chem. Soc.*, **107**, 2000 (1985).

3) The catalytic epoxidation reaction was capable of using other oxidants such as iodosylbenzene and dioxygen. a) J. T. Groves, T. E. Nemo, and R. S. Myers, *J. Am. Chem. Soc.*, **101**, 1032 (1979). b) J. P. Collman, T. Kodadek, S. A. Raybuck, J. I. Brauman, and L. M. Papazian, *J. Am. Chem. Soc.*, **107**, 5537 (1985). c) T. G. Traylor, J. C. Marsters Jr., T. Nakano, and B. E. Dunlap, *J. Am. Chem. Soc.*, **107**, 4343 (1985). d) C. K. Chang and F. Ebina, *J. Chem. Soc., Chem. Commun.*, **1981**, 778. e) I. Tabushi, M. Kodera, and M. Yokoyama, *J. Am. Chem. Soc.*, **107**, 4466 (1985). f) Y. Matsuda, S. Sakamoto, H. Koshima, and Y. Murakami, *J. Am. Chem. Soc.*, **107**, 6415 (1985).

4) S. Takagi, T. Yamamura, M. Nakajima, K. Ishiguro, Y. Kawanishi, S. Nihojima, H. Tsuchiya, T. Saito, and Y. Sasaki, *Bull. Chem. Soc. Jpn.*, **54**, 3879 (1981).

5) M=mol dm^{-3}.

6) UV-vis (CH_3OH) λ/nm (ε/M^{-1}cm^{-1}): 384 (5.1×10⁴), 402 (5.2×10⁴), 422 (4.8×10⁴), 471 (7.2×10⁴), 572 (1.0×10⁴), 610 (1.0×10⁴). (C_2H_5OH/H_2O 1:5): 378 (4.0×10⁴), 398 (4.0×10⁴), 469 (4.7×10⁴), 588 (7.0×10³), 630 (8.8×10³).

7) Benzaldehyde was identified by gas chromatography

and ^{1}H NMR.

8) Styrene oxidation using MnTPP and a phase-transfer reagent produced less amount of phenylacetaldehyde (11%) than using Mn srf. **6** (24%).

9) Mn srf. **6** was not bleached in this reaction.

10) Mn complex of **1** was almost bleached.

11) We ascertained that the reaction rate of styrene oxidation using Mn srf. **6** was more than ten times as large as that using a Mn complex of **1** and a phase-transfer reagent.

12) The reaction rates of epoxidation at 22 °C using Mn srf. **6** or MnTPP are as follows: styrene, 18 (Mn srf. **6**), 220 (MnTPP); cyclohexene, 2.0 (Mn srf. **6**), 2.2 (MnTPP); cyclooctene, 7.8 (Mn srf. **6**), 8.4 (MnTPP). All experiments were carried out as follows. Mn porphyrin (0.0081 mmol), 1-triphenylmethylimidazole (0.46 mmol), substrate (7.8 mmol), and a internal standard were dissolved in 20 cm^3 of CH_2Cl_2. In case of MnTPP, a phase-transfer reagent was added in CH_2Cl_2. Then, 15 cm^3 of the sodium hypochlorite solution (8.7 mmol) was added and the reaction was started by stirring.

13) The reaction rates are represented by the turnover numbers per minute.

14) M. W. Nee and T. C. Bruice, *J. Am. Chem. Soc.*, **104**, 6123 (1981).

15) Yields are based on the sodium hypochlorite consumed.

 © 1986 The Chemical Society of Japan Bull. Chem. Soc. Jpn., 59, 2375—2379 (1986)

Electrochemistry of the Redox-Active Langmuir-Blodgett Films Coated on Glassy Carbon Electrodes

Masamichi FUJIHIRA* and Toshinari ARAKI
Department of Chemical Engineering, Tokyo Institute of Technology, Ookayama, Meguro-ku, Tokyo 152
(Received January 6, 1986)

In order to study the electrochemical behavior of a redox species in the Langmuir-Blodgett (LB) film on a glassy carbon (GC) electrode, three kinds of amphiphilic redox compounds, each carrying an anthraquinone, a viologen, and a ferrocene moiety, were confined on the electrode surfaces. Prior to the deposition of the film on the electrode, surface pressure-area isotherms for a number of mixed films of the redox-active amphiphiles and arachidic acid were recorded and the stability of the monolayers was discussed. Finally, the cyclic voltammetric behavior of the LB film-modified electrodes was discussed in terms of the changes in the structure and the nature of the LB film caused by the redox reactions.

In the course of the development of the modified electrodes,[1,2] a high density of the immobilized functional species,[1] a regularity in the molecular organization,[3,4] and an ultrathinness of the coated film on the electrode surface[2,5] are of crucial importance. The LB method, the technological possibilities of which have been widely appreciated in connection with molecular engineering,[6,7] was utilized to fulfill these requirements. This technique not only ensures the molecular electrochemical devices,[3,4] but also gives some insights into the structure of the electrical double-layer.[8]

In the present work, we confined redox-active amphiphiles, such as an anthraquinone (AQS), a viologen (VS), and a ferrocene surfactant derivative (FcS), on a GC electrode by the use of the LB method, thereby organizing the desired film structure in which electroactive and electroinactive layers were assembled in a deliberate way. Arachidic acid (AA) was used to form the stable electroactive mixed layers with each redox-active amphiphile and also to build the electroinactive layers. The cyclic voltammetry of these LB modified electrodes and some of the unexpected findings therefrom are discussed in terms of i) the charge on, or in the vicinity of, the redox moieties; ii) the environment and location of the redox moieties, and iii) the change in some of these characteristics by the redox reaction and its effect on the structure and nature of the LB multilayer film.

Experimental

Materials. The redox-active amphiphiles used in the present work are shown in Fig. 1. The AQS was prepared according to the following procedure: dodecylamine was transformed into *N,N*-didodecylmethylamine by the method of Ralston et al.[9]; 2-methylanthraquinone was treated with *N*-bromosuccinimide in the presence of benzoyl peroxide in carbon tetrachloride,[10] and the resulting 2-(bromomethyl)-anthraquinone was reacted with *N,N*-didodecylmethylamine in 1,4-dioxane to yield AQS. For the preparation of FcS, the method of Ohkawara[11] for amide formation from 1,1′-ferrocenedicarboxylic acid was used, as previously.[4] The VS was synthesized according to the method of Fendler et al.[12]

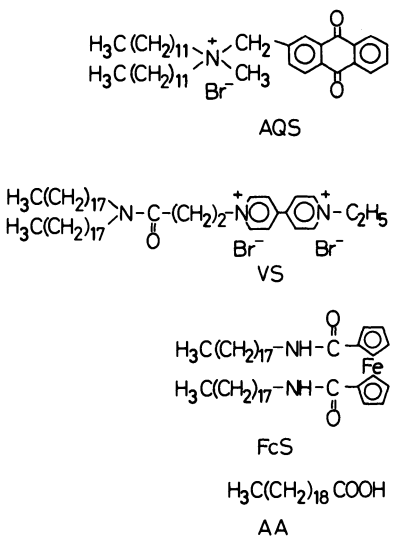

Fig. 1. The structures of the redox-active amphiphiles and a fatty acid used in this work.

Monolayer Preparation and Surface Pressure-Area Isotherms. The surface pressure-area isotherms were studied by using a commercially available Langmuir trough equipped with a film balance (Kyowa Kaimenkagaku Co.). Monolayers were obtained by spreading chloroform solutions of amphiphiles on the air-water interface of the trough and by then compressing the surface at 2 Å^2 molecule^{-1} min^{-1}. Doubly distilled water was used as the subphase; it contained no salt unless otherwise stated. The surface pressure-area isotherms were measured at 24°C.

Film Deposition on the Electrode Surface. The monolayer formed at the air-water interface was deposited at 40 mN m^{-1} on the GC disk electrode (diameter: 0.3 cm) at a dipping rate of 3 mm min^{-1}, except in the case of the pure monolayer of AQS or VS, which was deposited at 35 mN m^{-1}. Since the surface of GC is hydrophilic, little material was deposited on the first insertion of the electrode surface into the subphase, but a good coverage was obtained on the withdrawal of the electrode surface through the film. With repetitive strokes, the multilayer structure of a typical Y film was formed on the GC electrode. For the sake of accuracy, the transfer ratio was determined independently with a GC plate possessing a larger area (6 cm^2). In every case, the apparent transfer ratios for both downward and upward strokes were between 0.8 and 1.1.

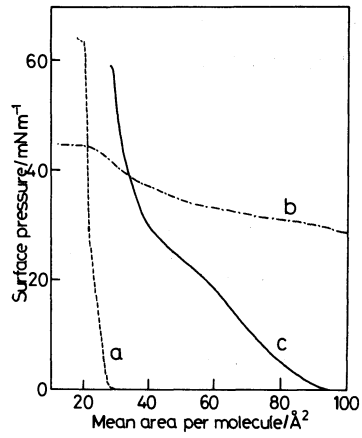

Fig. 2. Surface pressure-area isotherms of (a) AA, (b) AQS, and (c) a mixture of AQS and AA (1:3), on pure water at 24°C.

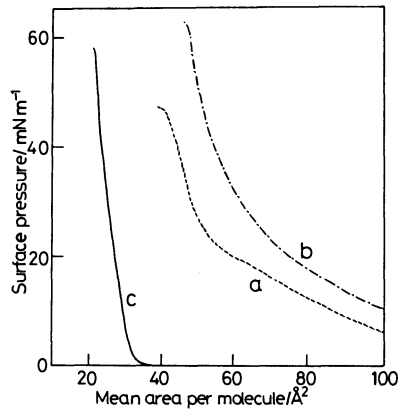

Fig. 3. Surface pressure-area isotherms of (a) VS on pure water, (b) on 0.3 mM Na_2CO_3, and (c) a mixture of VS and AA (1:3) on pure water, at 24°C.

Cyclic Voltammetry. The electrochemical characteristics of the LB film-modified GC electrodes were examined by means of cyclic voltammetry. A three-electrode configuration was employed: an SCE was used as the reference, and a platinum wire as the counter electrode, in addition to the LB film-modified working electrode. Measurements were carried out at room temperature (24°C). An aqueous solution of 0.5 M† KCl was used as the electrolyte. For the AQS-modified electrode, hydrochloric acid was added also to make the pH of the solution two, for in an acidic solution, although there are kinetic complications due to proton addition during the electron transfer, the anthraquinone derivative attached to the GC electrodes exhibits a clear two-electron and two-proton reduction peak to hydroanthraquinone.[8]

Results and Discussion

Stability of the Mixed Monolayers. The isotherms were compared between the mixed monolayer and the monolayer that contained only a redox surfactant, as is shown in Figs. 2—4. For a pure AQS monolayer, only a liquid-expanded film was formed (Fig. 2b). The mixed film of AQS and AA in the molar mixing ratio of 1:3, however, exhibited a condensed state at high surface pressures (Fig. 2c). A pure VS monolayer was unstable on the pure-water subphase (Fig. 3a). The stability was improved on an aqueous solution of 0.3 mM Na_2CO_3 (Fig. 3b). A remarkable stability was achieved by mixing with AA (Fig. 3c). A pure FcS monolayer collapsed at a low surface pressure (Fig. 4a). When mixed with AA, the film was stabilized (Fig. 4b). In all the cases mentioned above, the mixed monolayer, when compressed, formed an extremely stable monolayer, with no appreciable collapse being evident over a period of many hours. The molar mixing ratio of the

† 1 M=1 mol dm^{-3}.

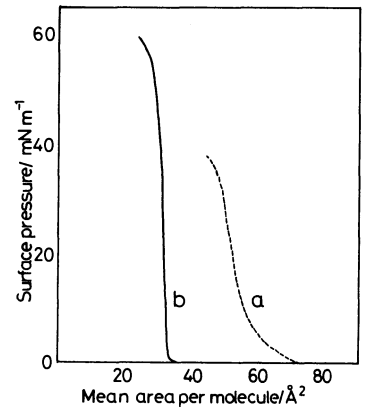

Fig. 4. Surface pressure-area isotherms of (a) FcS and (b) a mixture of FcS and AA (1:3), on pure water at 24°C.

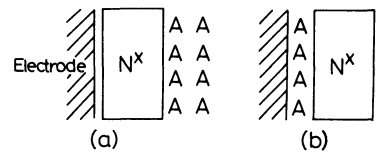

Fig. 5. Schematic structures of multilayer-deposited electrodes. (a): N^xA^2, (b): AN^x.

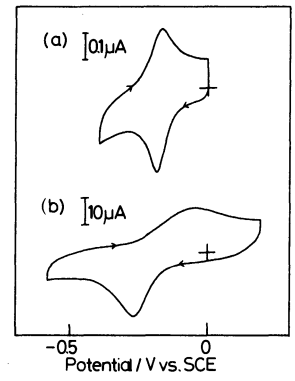

Fig. 6. Cyclic voltammograms for an N^3A^2 type of the AQS modified electrode in 0.1 M KCl solution containing 0.01 M HCl. Scan rate. (a): 0.01 Vs^{-1}, (b): 1 Vs^{-1}. A: a mixed monolayer of AQS and AA (1:3). N: a pure AA monolayer.

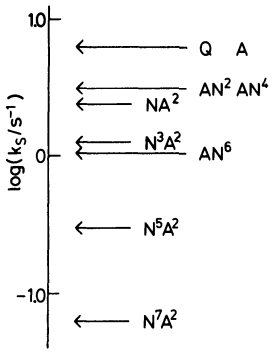

Fig. 7. Comparison of the apparent surface reaction rates of N^xA^2 and AN^x types of the AQS modified electrodes. Q: a pure AQS monolayer. A: a mixed monolayer of AQS and AA (1:3).

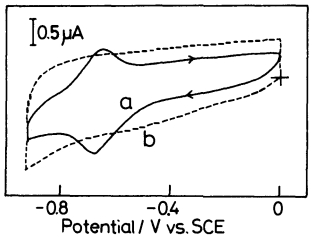

Fig. 8. Cyclic voltammograms for (a) an N^3A^2 type of the VS modified electrode and (b) the naked electrode, in 0.1 M KCl. Scan rate: 0.05 V s^{-1}. A: a mixed monolayer of VS and AA (1:3).

redox surfactant and AA (1:3) was chosen in view of both the film stability and the accuracy required for the electrochemical measurements.

Electrochemistry of the LB Film-Modified GC Electrode. We have concentrated our attention on two types of multilayer-deposited electrodes: in one, some AA layers as an electroinactive matrix were sandwiched between the electrode surface and the AA-redox surfactant mixed bilayer, while in the other the relative locations of the AA layers and the AA-redox surfactant monolayer were reversed. The former system is termed an N^xA^2 type, and the latter AN^x, where A, N, and x signify the electroactive AA-redox surfactant mixed layer, the electroinactive AA layer, and the number of the AA layers respectively (Fig. 5).

Figure 6 shows cyclic voltamograms for an N^3A^2 type of AQS modified electrode.* The peak separation became significant as the sweep rate increased. This irreversibility of the electrode process observed on the cyclic voltammogram makes possible the calculation of an apparent surface-reaction rate, k_s.[8,13-15] Figure 7 shows a comparison of the k's for various kinds of N^xA^2

* The electroreactivity of the redox-surfactant in N^xA^2 may need mediators in the N^x matrix, since the direct electron transfer from the electrode to the A layers through the N^x matrix seems to be impossible. As candidates for the mediators, the redox-surfactant itself diffusing into the N^x matrix and redox-active impurities such as a trace of oxygen are considered.

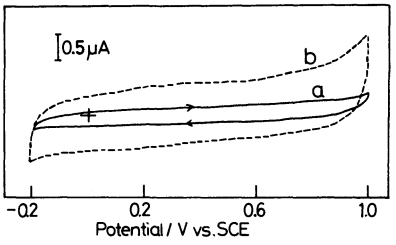

Fig. 9. Cyclic voltammograms for (a) an N^3A^2 type of the FcS modified electrode and (b) the naked electrode, in 0.1 M KCl. Scan rate: 0.05 V s^{-1}. A: a mixed monolayer of FcS and AA (1:3).

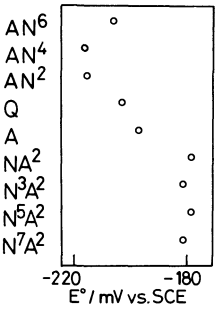

Fig. 10. The formal reversible peak potentials of the AQS modified electrodes. Q: a pure AQS monolayer. A: a mixed monolayer of AQS and AA (1:3).

and AN^x electrodes. It should be noted that, in the series of N^xA^2 electrodes, k_s becomes smaller as x increases.

The VS modified electrodes behaved reversibly as long as the potential range was limited to between 0 and −0.9 V vs. SCE. The only peak observed in this region corresponds to $V^{2+}+e=V^+$ (Fig. 8). For the FcS modified electrodes, an unexpected result was obtained: no peak for ferrocene site oxidation was observed in any N^xA^2 and AN^x structure (Fig. 9). The decrease in the charging current compared with the background current for the naked GC electrode (a dashed line in Fig. 9), however, suggests a compact structure of the FcS–AA mixed film. A similar decrease in the charging current was also observed for the VS–AA mixed film (Fig. 8), but the decrease is not so enormous as that of the FcS–AA mixed film.

The formal reversible peak potential, $E°$, was estimated by the extrapolation of the E_{pa}, E_{pc} vs. v plots to v=0, where the E's are peak potentials for the anodic and cathodic sweeps and where v is the sweep rate. The definition of the formal reversible peak potential is available in the literature.[15] Figures 10 and 11 show the formal potentials of the AQS and the VS modified electrodes respectively. On the AQS modified electrodes, the $E°$ values are classified roughly according to the structure of the film: on the N^xA^2-type electrodes, whatever the number of the AA layer was, the $E°$'s were concentrated at values around −0.18 V, whereas on the AN^x-type electrodes the $E°$'s were distributed between −0.22 and −0.20 V. In Fig. 10, Q

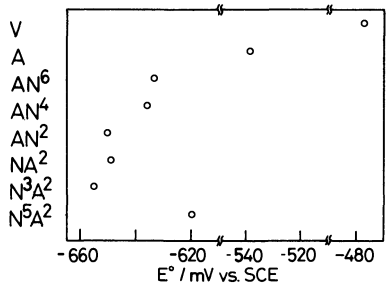

Fig. 11. The formal reversible peak potentials of the VS modified electrodes. V: a pure VS monolayer. A: a mixed monolayer of VS and AA (1:3).

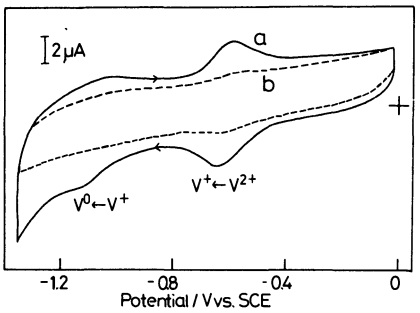

Fig. 12. Cyclic voltammograms for an AN^4 type of the VS modified electrode in 0.1 M KCl. (a): the first cycling, (b): after several cyclings. Scan rate: 0.5 $V\,s^{-1}$. A: a mixed monolayer of VS and AA (1:3).

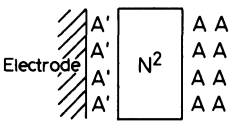

Fig. 13. A schematic structure of the multilayer-deposited electrode possessing both AQS and VS layers. A': a mixed monolayer of AQS and AA (1:3). A: a mixed monolayer of VS and AA (1:3).

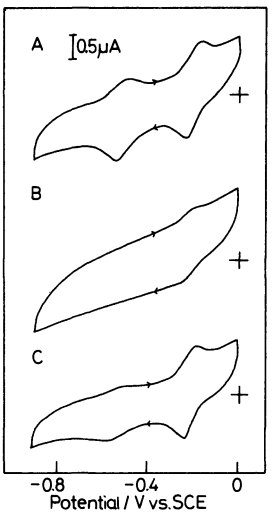

Fig. 14. Cyclic voltammograms for the electrode schematically shown in Fig. 13 in 0.1 M KCl. Scan rate: 0.05 $V\,s^{-1}$. A: the potential range is limited between 0 and −0.9 V. B: after holding the potential at −1.5 V for 1 min. C: after holding the potential at 0 V for 5 min. subsequently to B.

denotes the pure AQS layer. The difference in the $E°$'s may be attributed to the electrical potential difference between the film and the solution phases. As the AA layers act as a cation-exchange membrane, the negative bias may be created between these two phases and may be effective for the shift of $E°$ for AN^x.

On the VS electrodes, however, no such regular effect of the film structure on the $E°$ in the multilayer system was observed (Fig. 11). Rather, we found a different kind of shift in $E°$ that was not encountered in the AQS modified electrodes. On the pure VS monolayer modified electrode (denoted by V), $E°=-0.48$ V, whereas on the mixed monolayer modified electrode (denoted by A), $E°=-0.54$ V. The mixing of VS with AA thus resulted in a shift of $E°$ to a more negative value. A further negative shift was observed in any type of multilayer modified electrode (−0.62 — −0.66 V). One possible interpretation for the large negative shift up to 180 mV may be an ion-pair formation of the viologen moiety with the carboxylate anion of AA rather than the membrane potential effect. The ion-pair interaction increases in a more hydrophobic environment,[16,17] such as N^xA^2 and AN^x, than in A. The ion-pair may also be formed between cationic AQS and AA, but in this case the neutral anthraquinone redox moiety does not interact directly with the carboxylate anion; therefore, the effect of the ion-pair formation on $E°$ is not so obvious as that for the VS–AA mixed film. Alternatively, the negative shift may be attributed to the less preferable dimer formation between the viologen monocation radicals resulting from the dilution of VS by mixing with AA and from the decrease in polarity[18] in the multilayer films.

An Ion-Gate Function of the VS-Modified Electrode. Figure 12 shows by the solid line, a cyclic voltammogram for an AN^4 type of VS-modified electrode over the potential range from 0 to −1.3 V for the first cycling. At ca. −1.1 V, appeared the second redox peaks corresponding to $V^+ + e = V^0$. The two pairs of peaks for viologen gradually diminished as the sweep was repeated, until finally the shape represented by the dashed line was obtained. This diminution was not observed when the potential was limited to the region with di/monovalent viologens. The disappearance of the peaks was common to any N^xA^{2-} and AN^x-type electrode except for the monolayer-modified electrodes. This phenomenon indicates that VS, when reduced to an electrically neutral state, forms a compact structure with AA in the multilayer and also makes the film more hydrophobic, so that the reoxidation of V^0 is hindered by blocking the supporting electrolyte. If this is taken into account, the inactivity of the electrically neutral FcS film described above becomes very reasonable. Recently, Tokuda, Matsuda, and their co-workers[19]

have found that the electrochemical reactivity of the LB film of a surface-active nitroxide radical deposited on an SnO_2 electrode was affected by the kinds and concentrations of ions in the solution and was diminished strongly under some conditions. Such an effect has been ascribed to the change in the structure of the LB film caused by the "salt-out" effect. Consequently, if the ion-blocking ability is controlled by changing the charge of the head group of the redox-active surfactants electrochemically, a novel function, i.e., an ion gate,[20] can be expected in the LB-modified electrode.

Taking these findings into consideration, a multilayer possessing both AQS and VS layers was fabricated on the electrode, as is shown schematically in Fig. 13. An AQS layer as the electrochemical probe was inserted between the electrode and an N^2A^2-type VS multilayer. Cyclic voltammograms of this electrode are shown in Fig. 14. In Fig. 14A, two cathodic peaks due to the AQS reduction and the first reduction of VS and the corresponding anodic peaks appeared. After the potential had been held at −1.5 V for one minute instead of the negative sweep, the first wave of viologen completely disappeared, and that of anthraquinone showed a remarkable decrease in the peak current as well (Fig. 14B). Here again, the V^0 formation in the multilayer made the viologen site itself and the anthraquinone site electrochemically inactive. The neutral compact structure and the hydrophobicity of the completely reduced N^2A^2-type VS multilayer film possibly obstructs the approach of various ions to the proximity of the anthraquinone site and therefore hinders the ions from establishing an electrochemical neutrality or an electrochemical double-layer in the LB film. If the latter effect is true, the anthraquinone site lies in a potential inadequate for the electron transfer. The further decrease in the capacitive current shown in Fig. 12 after the complete reduction of V^{2+} to V^0 and the comparison with the background current of the naked GC electrode in Fig. 8 may support this interpretation. When the electrode potential was kept at 0 V for five minutes afterwards, a total recovery of the AQS wave and a partial recovery of the VS wave were observed (Fig. 14C). One possible explanation of this observation is that a partial amount of neutral viologen is reoxidized to the initial cationic states and that the resulting partial breakdown of the compactness and hydrophobicity allows the electrochemical response of the anthraquinone site.

The authors are deeply grateful to Professors Hiroaki Matsuda and Koichi Tokuda of Tokyo Institute of Technology for their fruitful discussions and for the use of the Kyowa Kaimenkagaku Langmuir trough. We are also grateful to Mr. Katsuhiko Nishiyama and Dr. Tetsuo Saji for their gifts of FcS and VS respectively. This work was partially supported by Grant-in-Aid for Scientific Research No. 60040051 and No. 59470067 from the Ministry of Education, Science and Culture.

References

1) R. W. Murray, "Electroanalytical Chemistry," ed by A. J. Bard, Marcel Dekker, New York (1984), Vol. 13, p. 191.
2) M. Fujihira, "Topics in Organic Electrochemistry," ed by A. J. Fry and W. E. Britton, Plenum Publishing Corp., New York (1985), Chap. 6, p. 255.
3) P. Fromherz and W. Arden, *J. Am. Chem. Soc.*, **102**, 6211 (1980).
4) M. Fujihira, K. Nishiyama, and H. Yamada, *Thin Solid Films*, **132**, 77 (1985).
5) M. Fujihira and S. Poosittisak, *Chem. Lett.*, **1986**, 251.
6) "Molecular Electronic Devices," ed by F. L. Carter, Marcel Dekker, New York (1982).
7) H. Kuhn, *Thin Solid Films*, **99**, 1 (1983).
8) M. Fujihira and T. Araki, *J. Electroanal. Chem. Interfacial Electrochem.*, in press.
9) A. W. Ralston, D. N. Eggenberger, and P. L. Du Brow, *J. Am. Chem. Soc.*, **70**, 977 (1948).
10) M. Fujihira, S. Tasaki, T. Osa, and T. Kuwana, *J. Electroanal. Chem. Interfacial Electrochem.*, **150**, 665 (1983).
11) M. Ohkawara, Y. Takemoto, H. Kitaoka, E. Haruki, and E. Imoto, *Kogyo Kagaku Zasshi*, **65**, 685 (1962).
12) P. Tundo, D. J. Kippenberger, M. J. Politi, P. Klahn, and J. H. Fendler, *J. Am. Chem. Soc.*, **104**, 5352 (1982).
13) E. Laviron, *J. Electroanal. Chem. Interfacial Electrochem.*, **101**, 19 (1979).
14) M. Sharp, M. Petersson, and K. Edstrom, *J. Electroanal. Chem. Interfacial Electrochem.*, **95**, 123 (1979).
15) M. Sharp and M. Petersson, *J. Electroanal. Chem. Interfacial Electrochem.*, **122**, 409 (1981).
16) S. Hayano and M. Fujihira, *Bull. Chem. Soc. Jpn.*, **44**, 2051 (1971).
17) M. E. Peover, "Electroanalytical Chemistry," ed by A. J. Bard, Marcel Dekker, New York (1967), Vol. 2, p. 1.
18) E. M. Kosower and J. L. Cotter, *J. Am. Chem. Soc.*, **86**, 5524 (1964).
19) S. G. Park, K. Aoki, K. Tokuda, and H. Matsuda, *J. Electroanal. Chem. Interfacial Elechrochem.*, **195**, 157 (1985).
20) P. Burgmayer and R. W. Murray, *J. Am. Chem. Soc.*, **104**, 6139 (1982); *J. Phys. Chem.*, **88**, 2515 (1984).

 © 1986 The Chemical Society of Japan Bull. Chem. Soc. Jpn., 59, 2381—2386 (1986)

Solvent Effects on the $n\pi^*$ and $\pi\pi^*$ Absorption Intensities of Some Organic Molecules

Takehiro ABE* and Idowu IWEIBO†

College of General Education, Tohoku University, Kawauchi, Sendai 980

(Received March 6, 1986)

Recently proposed experimental and theoretical expressions for the molecular electronic oscillator strength in a solution (*J. Chem. Phys.*, **83**, 1546 (1985)) have been succesfully applied to the spectral data of some nonpolar and polar organic molecules (benzoquinones, ketones, nitroalkanes, β-carotene, and substituted benzenes). In an application of the theoretical expression, the transition moment of a nonpolar solute molecule in various solvents was assumed to be approximately constant, while that of a polar solute molecule was developed on the assumptions of a first-order perturbation of the wave function and a Block-Walker reaction field. The ratio of the oscillator strength in a solution to that either in a vapor or a specified solvent was computed from both experimental data and theoretically from the transition moments. The results of the two computational modes are, generally, in good agreement for the range of compounds studied.

For an electronic transition from the ground state to the ith excited state in a solute molecule, we have recently proposed the following equations[1] for the experimental and theoretical oscillator strengths in a solution:

$$f^{\mathrm{exp}}(\mathrm{soln}) = \frac{4n}{(1+n)^2} \times \frac{10^3(\ln 10)m_e c^2}{\pi e^2 L}\int \varepsilon(\tilde{\nu})\mathrm{d}\tilde{\nu} \qquad (1)$$

and

$$f^{\mathrm{theor}}(\mathrm{soln}) = \frac{36n^4}{(1+n)^2(2n+1)^2} \times \frac{8\pi^2 m_e c}{3he^2} \times \tilde{\nu}_{0i}|\mu_{0i}(\mathrm{soln})|^2, \qquad (2)$$

where n is the refractive index of the solvent, c the speed of light in a vacuum, h the Planck constant, e the charge of a proton, m_e the mass of an electron, and L Avogadro's constant. Here, $\tilde{\nu}_{0i}$ is the wave number of the transition, $\varepsilon(\tilde{\nu})$ the molar absorption coefficient at a wave number $\tilde{\nu}$, and $\mu_{0i}(\mathrm{soln})$ the transition moment of a solute molecule in a solution. Then, the ratio of the oscillator strength in, for example, two solvents (denoted by subscripts 1 and 2), i.e., $f^{\mathrm{exp}}(\mathrm{soln}\ 2)/f^{\mathrm{exp}}(\mathrm{soln}\ 1)$, gives a ratio of the energies absorbed per unit time by the transitions, as described in a previous paper.[1]

Here, by either assuming a constant value for $\mu_{0i}(\mathrm{soln})$ or using first-order perturbation theory to find an approximate expression for $\mu_{0i}(\mathrm{soln})$, we apply Eqs. 1 and 2 to the $n\pi^*$- and $\pi\pi^*$-absorption spectral data which are available for several compounds and demonstrate that our previously proposed expressions for the oscillator strength of a molecule in a solution give fairly good results.

Theory

We can write the oscillator strength of a gaseous absorbing system as $f(\mathrm{vap})$, and the usual experimental oscillator strength in a solution (n=1) as $\bar{f}^{\mathrm{exp}}(\mathrm{soln})$. Then, from Eqs. 1 and 2 the following equations can be derived:

$$\frac{f^{\mathrm{exp}}(\mathrm{soln})}{f^{\mathrm{exp}}(\mathrm{vap})} = \frac{4n}{(1+n)^2} \times \frac{\bar{f}^{\mathrm{exp}}(\mathrm{soln})}{f^{\mathrm{exp}}(\mathrm{vap})} \qquad (3)$$

and

$$\frac{f^{\mathrm{theor}}(\mathrm{soln})}{f^{\mathrm{theor}}(\mathrm{vap})} = \frac{36n^4}{(1+n)^2(2n^2+1)^2} \times \frac{\tilde{\nu}_{0i}|\mu_{0i}(\mathrm{soln})|^2}{\tilde{\nu}^0_{0i}|\mu^0_{0i}|^2}, \qquad (4)$$

where $\tilde{\nu}^0_i$ and μ^0_i are the transition energy (in cm^{-1}) and the transition moment, respectively, of the isolated solute molecule. In a case where there are no data in the literature for $f^{\mathrm{exp}}(\mathrm{vap})$, we used equations corresponding to $f^{\mathrm{exp}}(\mathrm{soln}\ 2)/f^{\mathrm{exp}}(\mathrm{soln}\ 1)$ and $f^{\mathrm{theor}}(\mathrm{soln}\ 2)/f^{\mathrm{theor}}(\mathrm{soln}\ 1)$ instead of Eqs. 3 and 4, respectively.

In the present analysis, $\mu_{0i}(\mathrm{soln})$ are not transition moments like those formulated by Weigang[2] and Myers and Birge[3] for a system that includes a solute and many solvent molecules, but rather for a single solute molecule in a solution. Even Liptay's generalized expression[4] for $\mu_{0i}(\mathrm{soln})$ is still difficult to apply practically. We have, however, found an approximate expression for $\mu_{0i}(\mathrm{soln})$ in the following two ways:

Approximation of $\mu_{0i}(\mathrm{soln})$ for Nonpolar Solute Molecules. Since, in this case, there is usually no data in the literature for $f^{\mathrm{exp}}(\mathrm{vap})$, we have adopted an equation corresponding to the expression $f^{\mathrm{theor}}(\mathrm{soln}\ 2)/f^{\mathrm{theor}}(\mathrm{soln}\ 1)$ instead of Eq. 4. Further, for a nonpolar solute molecule, we assumed that the values of $\mu_{0i}(\mathrm{soln})$ in various solvents are approximately constant, since a solute molecule has no dipole moment. From this assumption, it follows from Eq. 2 that

$$\frac{f^{\mathrm{theor}}(\mathrm{soln}\ 2)}{f^{\mathrm{theor}}(\mathrm{soln}\ 1)} = \frac{F(\mathrm{soln}\ 2)\tilde{\nu}_{0i}(\mathrm{soln}\ 2)}{F(\mathrm{soln}\ 1)\tilde{\nu}_{0i}(\mathrm{soln}\ 1)}, \qquad (5)$$

where $F(\mathrm{soln}\ i)=36n^4/(1+n)^2(2n^2+1)^2$ and $\tilde{\nu}_{0i}(\mathrm{soln}\ i)$ are, respectively, the solvent correction factor and the transition wave number for the ith solvent. By using

†Present address: Department of Chemistry, University of Ibadan, Ibadan, Nigeria.

Eq. 3, we obtained experimental values for f^{exp}(soln 2)/f^{exp}(soln 1); these results could be compared with those of Eq. 5.

Approximation of μ_{0i}(soln) for Polar Solute Molecules. For a polar solute molecule, we formulated an approximate expression for μ_{0i}(soln) by using the Block–Walker reaction field.[5]

The ground and ith excited state of a neutral solute molecule are denoted by the wave functions Ψ_0 and Ψ_i, respectively. According to first-order perturbation theory, Ψ_i, for example, can be written as

$$\Psi_i = \Psi_i^\circ + \sum_{k\neq i} \frac{(\Psi_k^{\circ *}|H'|\Psi_i^\circ)}{E_i^\circ - E_k^\circ}\Psi_k^\circ, \tag{6}$$

where E_k° is the energy of the kth excited state (Ψ_k°) for an isolated solute molecule. The perturbation operator H' is written as[6,7]

$$H' = -\sum_j e_j \boldsymbol{R}\cdot\boldsymbol{r}_j. \tag{7}$$

Here, e_j and $\boldsymbol{r}_j$ are the charge and position vector of the jth charged particle in the solute molecule, and $\boldsymbol{R}$ is the reaction field. The expression Ψ_0 is similarly obtained by replacing i with 0 in Eq. 6. We denote, for example, the average of all values of $(E_k^\circ - E_i^\circ)$ by ΔE_i and assume that $\Delta E_i = \Delta E_0 = I_0$, as was done in a previous paper,[8] where I_0 denotes the ionization potential of the ground state of an isolated solute molecule. We then obtain the following approximate expression for μ_{0i}(soln):

$$\begin{aligned}
\mu_{0i}(\text{soln}) &= (\Psi_i^*|\Sigma e_j\boldsymbol{r}_j|\Psi_0) \\
&\approx \mu_{0i}^\circ - \frac{1}{I_0}\{\sum_{k\neq 0}(\Psi_0^{\circ *}|H'|\Psi_k^\circ)(\Psi_k^{\circ *}|\Sigma e_j\boldsymbol{r}_j|\Psi_i^\circ) \\
&\quad + \sum_{k\neq i}(\Psi_i^{\circ *}|H'|\Psi_k^\circ)(\Psi_k^{\circ *}|\Sigma e_j\boldsymbol{r}_j|\Psi_0^\circ)\} \\
&\quad + \frac{1}{I_0^2}\sum_{i\neq}\sum_{k\neq 0}(\Psi_0^{\circ *}|H'|\Psi_k^\circ)(\Psi_i^{\circ *}|H'|\Psi_i^\circ)(\Psi_i^{\circ *}|\Sigma e_j\boldsymbol{r}_j|\Psi_k^\circ) \\
&= \mu_{0i}^\circ + \frac{\boldsymbol{R}}{I_0}[\{\sum_k^{all}(\Psi_0^{\circ *}|\Sigma e_j\boldsymbol{r}_j|\Psi_k^\circ)(\Psi_k^{\circ *}|\Sigma e_j\boldsymbol{r}_j|\Psi_i^\circ) \\
&\quad - (\Psi_0^{\circ *}|\Sigma e_j\boldsymbol{r}_j|\Psi_0^\circ)(\Psi_0^{\circ *}|\Sigma e_j\boldsymbol{r}_j|\Psi_i^\circ)\} \\
&\quad + \{\sum_k^{all}(\Psi_i^{\circ *}|\Sigma e_j\boldsymbol{r}_j|\Psi_k^\circ)(\Psi_k^{\circ *}|\Sigma e_j\boldsymbol{r}_j|\Psi_0^\circ) \\
&\quad - (\Psi_i^{\circ *}|\Sigma e_j\boldsymbol{r}_j|\Psi_i^\circ)(\Psi_i^{\circ *}|\Sigma e_j\boldsymbol{r}_j|\Psi_0^\circ)\}] \\
&\quad + \frac{R^2}{I_0^2}\sum_{i\neq}\sum_{k\neq 0}\left\{\frac{\boldsymbol{R}}{R}(\Psi_0^{\circ *}|\Sigma e_j\boldsymbol{r}_j|\Psi_k^\circ)\right\} \\
&\quad \times \left\{\frac{\boldsymbol{R}}{R}(\Psi_i^{\circ *}|\Sigma e_j\boldsymbol{r}_j|\Psi_i^\circ)\right\} \times (\Psi_i^{\circ *}|\Sigma e_j\boldsymbol{r}_j|\Psi_k^\circ) \\
&= \mu_{0i}^\circ + \frac{\boldsymbol{R}}{I_0}\times(2Q_{0i}^\circ - \mu_{0i}^\circ\boldsymbol{p}_0^\circ - \mu_{0i}^\circ\boldsymbol{p}_i^\circ) + \frac{R^2}{I_0^2}\times\boldsymbol{R}_{0k,il}^\circ,
\end{aligned} \tag{8}$$

where $\boldsymbol{p}_0^\circ$ and $\boldsymbol{p}_i^\circ$ are the ground- and ith-excited-state electric dipole moments, respectively, of the isolated solute molecule and

$$Q_{0i}^\circ = \sum_k^{all}(\Psi_0^{\circ *}|\Sigma e_j\boldsymbol{r}_j|\Psi_k^\circ)(\Psi_k^{\circ *}|\Sigma e_j\boldsymbol{r}_j|\Psi_i^\circ) = (\Psi_i^{\circ *}|(\Sigma e_j\boldsymbol{r}_j)^2|\Psi_0^\circ) \tag{9}$$

and

$$\boldsymbol{R}_{0k,il}^\circ = \sum_{i\neq}\sum_{k\neq 0}\left\{\frac{\boldsymbol{p}_0^\circ}{p_0^\circ}(\Psi_0^{\circ *}|\Sigma e_j\boldsymbol{r}_j|\Psi_k^\circ)\right\} \times \left\{\frac{\boldsymbol{p}_0^\circ}{p_0^\circ}(\Psi_i^{\circ *}|\Sigma e_j\boldsymbol{r}_j|\Psi_i^\circ)\right\} \times (\Psi_i^{\circ *}|\Sigma e_j\boldsymbol{r}_j|\Psi_k^\circ). \tag{10}$$

If the Block-Walker reaction field[5] is written as

$$\boldsymbol{R} = \frac{\theta(\varepsilon_r)}{a^3}\boldsymbol{p}_0^\circ, \tag{11}$$

where

$$\theta(\varepsilon_r) = \frac{3\varepsilon_r \ln\varepsilon_r}{\varepsilon_r\ln\varepsilon_r - \varepsilon_r + 1} - \frac{6}{\ln\varepsilon_r} - 2 \tag{12}$$

and a and ε_r are the cavity radius of the solute molecule and the relative permittivity of the solvent, respectively, the following expression for μ_{0i}(soln) is obtained from Eq. 8:

$$\mu_{0i}(\text{soln}) = \mu_{0i}^\circ\{1 + \theta(\varepsilon_r)\times A + \theta^2(\varepsilon_r)\times B\}. \tag{13}$$

Here, A and B are characteristic of a solute molecule and are expressed as

$$A = \frac{\boldsymbol{p}_0^\circ}{a^3 I_0}\left\{\frac{2\mu_{0i}^\circ Q_{0i}^\circ}{(\mu_{0i}^\circ)^2} - \boldsymbol{p}_0^\circ - \boldsymbol{p}_i^\circ\right\} \tag{14}$$

and

$$B = \frac{(p_0^\circ)^2\mu_{0i}^\circ \boldsymbol{R}_{0k,il}^\circ}{a^6 I_0^2(\mu_{0i}^\circ)^2}. \tag{15}$$

Substituting Eq. 13 into Eq. 4 makes f^{theor}(soln)/f^{theor}(vap) a determinable quantity from experimental data, i.e., f^{theor}(soln)/f^{theor}(vap)=f^{exp}(soln)/f^{exp}(vap), so that alternatively

$$\frac{f^{exp}(\text{soln})}{f^{exp}(\text{vap})} = F(\text{soln})\times\frac{\tilde{\nu}_{0i}}{\tilde{\nu}_{0i}^\circ}\times\{1+\theta(\varepsilon_r)\times A + \theta^2(\varepsilon_r)\times B\}^2. \tag{16}$$

For relative f values in two solvents, Eq. 16 can be transformed into

$$\frac{f^{exp}(\text{soln 2})}{f^{exp}(\text{soln 1})} = \frac{F(\text{soln 2})}{F(\text{soln 1})}\times\frac{\tilde{\nu}_{0i}(\text{soln 2})}{\tilde{\nu}_{0i}(\text{soln 1})} \times \frac{\{1+\theta(\varepsilon_r\ 2)\times A+\theta^2(\varepsilon_r\ 2)\times B\}^2}{\{1+\theta(\varepsilon_r\ 1)\times A+\theta^2(\varepsilon_r\ 1)\times B\}^2}, \tag{17}$$

where $\theta(\varepsilon_r\ i)$ and $\tilde{\nu}_{0i}$ (soln i) are the Block–Walker parameter for the ith solvent and the transition energy (cm^{-1}) in the ith solvent. The squared, bracketed term $\{1+\theta(\varepsilon_r)\times A+\theta^2(\varepsilon_r)\times B\}^2$ in Eq. 16 comes from the calculation of $|\mu_{0i}(\text{soln})|^2/|\mu_{0i}^\circ|^2$ ($=|\mu_{0i}^\circ|^2|1+\theta(\varepsilon_r)\times A+\theta^2(\varepsilon_r)\times B|^2/|\mu_{0i}^\circ|^2$) in the derivation of Eq. 16. As should be clear from Eq. 13, the second and third terms in the brackets are due to the perturbation of the transition moment by the solvent. Accordingly, on

the assumption that the perturbation is small, we assume that $|\theta(\varepsilon_r)\times A+\theta^2(\varepsilon_r)\times B|<1$, i.e., that the bracketed term is always positive. Thus, a data analysis of the square roots of both sides of Eq. 16 by a multiple linear regression permits an evaluation of the constants A and B. A similar simultaneous solution of A and B in Eq. 17 also follows from the substitution of experimental values of f^{exp}(soln 2)/f^{exp}(soln 1) and of the refractive indices in the square roots of both sides of Eq. 17.

As has already been pointed out in a previous paper,[6] the present treatment neglects dispersion effects. Consequently, Eqs. 16 and 17 cannot be applied to solute molecules with no electric dipole moments.

In applying Eqs. 5, 16, and 17, we always assumed a temperature of 20°C and excluded data of solvents which were capable of forming hydrogen bonds or complexes with solutes, since such specific interactions were not considered in the derivations of these equations. Moreover, we used the spectral data reported for a solute by the same authors, since experimental values of oscillator strengths considerably vary with different authors.

Results and Discussion

nπ* Transitions. We first test the applicability of Eqs. 5, 16, and 17 from the data of some compounds whose weak electronic spectral bands are assigned to nπ* transitions. These bands are advantageous in the present consideration because of their relatively small overlaps with bands of other transitions in the spectral profiles of these compounds.

(i) *p*-Benzoquinone, 2,5-Di-*t*-butyl-*p*-benzoquinone and 4,5,5-Trimehtyl-4-phenyl-1,3-dithiolane-2-thione: Obviously 4,5,5-trimethyl-4-phenyl-1,3-dithiolane-2-thione ought to have a dipole moment owing to its molecular structure. A small experimental dipole moment of 0.81 D[9] (1 D=3.333×10^{-30} Cm) has been reported for 2,5-di-*t*-butyl-*p*-benzoquinone. This value can be predicted from a resolution of the bond moments of the substituents. Experimentally, *p*-benzoquinone does not have a dipole moment in the vapor phase but has small dipole moments (0.63—0.69 D) in a solution; it varies slightly in such solvents as hexane, dioxane, carbon tetrachloride and benzene.[10] The small and slightly varying dipole moment of *p*-benzoquinone in solvents is probably due to its molecular structure, which is not strictly planar but has a slightly chair form.[11] Accordingly, Eq. 17 was applied to the oscillator strength data of Kuboyama and his coworkers[12] on these compounds. The results are shown in Fig. 1. For each compound, the ratios of the oscillator strengths calculated to that of the standard value in a solvent are in good agreement with those observed.

(ii) Pyrazine: The experimental dipole moment of pyrazine has been reported as 0.66 D[13] in dioxane, 0.15 D[14] in carbon tetrachloride, and 0.34 D[14] in cyclohexane. Both Eqs. 5 and 17 were, therefore, applied to the reported data[3] for the nπ* absorption intensities of pyrazine. The results are shown in Fig. 2. The figure shows that calculations with Eq. 17 give a good correlation between the experimental and

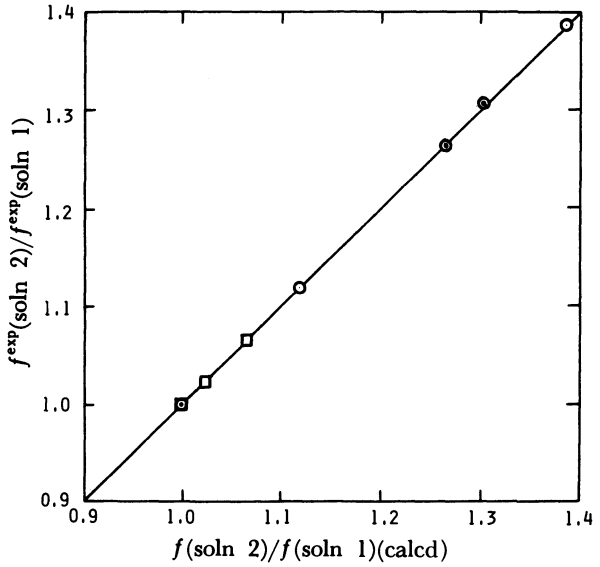

Fig. 1. Correlations between the observed and calculated values of f(soln 2)/f(soln 1) for *p*-benzoquinone (○) with heptane as the standard solvent (A=−8.584 and B=44.939), 2,5-*t*-butyl-*p*-benzoquinone (□) with cyclohexane as the standard solvent (A=−4.955 and B=−23.903) and 4,5,5-trimethyl-4-phenyl-1,3-dithiolane-2-thione (⊙) with cyclohexane as the standard solvent (A=4.153 and B=60.873).

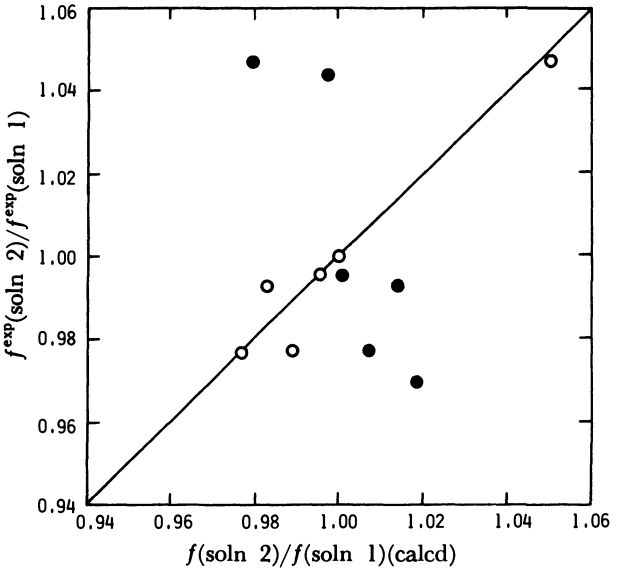

Fig. 2. Correlations between the observed and calculated values of f(soln 2)/f(soln 1) for pyrazine with cyclohexane as the standard solvent. The plots (○) denote those obtained according to Eq. 17 (A=−2.107 and B=16.989). The plots (●) denote those obtained according to Eq. 5.

Table 1. Values of f(soln)/f(vap) for Ketones

Ketone	Solvent							A	B
	Heptane	2,2,4-trimethyl-pentane	Cyclohexane	Carbon tetrachloride	Chloroform	Dichloro-methane	Diethyl ether		
Acetone									
Obsd	1.19	1.10	0.991	1.27	—	1.17	1.26		
Calcd	1.15	1.15	1.14	1.14	—	1.18	1.23	0.984	−2.23
Ethyl methyl ketone									
Obsd	1.20	1.17	1.24	1.25	—	1.29	1.03		
Calcd	1.17	1.17	1.16	1.17	—	1.20	1.25	1.05	−2.40
Diethyl ketone									
Obsd	1.18	1.07	1.00	1.23	1.10	1.15	1.08		
Calcd	1.11	1.11	1.09	1.09	1.13	1.12	1.16	0.648	−1.48
Methyl propyl ketone									
Obsd	1.06	1.09	1.03	1.24	—	1.18	1.03		
Calcd	1.08	1.08	1.08	1.07	—	1.14	1.15	0.517	−0.917
Dipropyl ketone									
Obsd	1.17	1.10	1.09	1.22	1.30	1.36	1.16		
Calcd	1.14	1.13	1.13	1.13	1.26	1.34	1.27	0.628	−0.390
Diisopropyl ketone									
Obsd	1.14	1.21	1.19	1.27	1.29	1.41	1.15		
Calcd	1.16	1.16	1.16	1.17	1.30	1.34	1.31	0.974	−1.36
Dibutyl ketone									
Obsd	1.19	1.18	1.24	1.44	1.29	1.34	1.21		
Calcd	1.23	1.23	1.23	1.23	1.31	1.28	1.34	1.32	−2.86
Diisobutyl ketone									
Obsd	1.13	1.16	1.11	1.32	1.22	1.39	1.15		
Calcd	1.14	1.15	1.14	1.15	1.26	1.32	1.28	0.778	−0.857
Cyclohexanone									
Obsd	1.35	1.43	1.35	1.77	1.73	1.53	1.51		
Calcd	1.45	1.45	1.46	1.48	1.63	1.53	1.66	2.59	−5.94

calculated ratios of the oscillator strengths to the value selected as a standard; calculations with Eq. 5 give a poor correlation. Thus, it seems that the pyrazine molecule in solution does have a small dipole moment.

(iii) Ketones: In applying the equations developed in this paper to the data of Bayliss and Wills-Johnson[15] on the effects of solvents on the usual oscillator strengths of $n\pi^*$ bands of ketones and nitroalkanes, we have selectively avoided solute-solvent systems with strong tendencies to form a hydrogen bond (e.g., acetone-chloroform, water, and alcohol systems[16]) or a weak donor-acceptor complex (e.g., acetone-benzene complex[17]). Moreover, Nakashima et al.[18] have pointed out that their data for benzene were likely to contain large errors. Accordingly, for the ketones we have chosen data for 6 or 7 solvents out of a reported total of 11. By applying Eq. 16 to the data, we obtained values for A and B (Table 1) from which we calculated the ratios of f(soln)/f(vap) (Table 1) together with the observed ratios. Considering the difficulties that may attend a determination of the oscillator strengths from the experimental estimates of the values of the integral, $\int\varepsilon(\bar{\nu})d\bar{\nu}$, and the inherent approximations in the development of the present treatment, we found that all of the correlations between the observed and calculated ratios of f(soln)/f(vap) in the case of these ketones were good.

(iv) Nitroalkanes: For computations of the nitroalkanes, we chose 6 data points from a total of 11 found by Bayliss and Wills-Johnson.[15] The data gathered for benzene as a solvent were excluded since benzene forms donor-acceptor complexes with nitromethane and nitroethane.[17] The results of calculations by means of Eq. 16 are shown in Table 2. Correlations between the observed and calculated ratios of f(soln)/f(vap) are reasonably good, but are generally worse than those for the ketones. This may be due to the relatively large overlaps with bands of other transitions in the spectral profiles of these nitroalkanes.

$\pi\pi^*$ Transitions. There are only a few advantageous examples of the bands assigned to the $\pi\pi^*$ transitions because of their relatively large overlaps with bands of other $\pi\pi^*$ and/or $n\pi^*$ transitions.

(i) β-Carotene: Myers and Birge[3] have reported relative oscillator-strength values for β-carotene in various solvents. From their total of 21 data points we chose 19, excluding data points of hexadecane and decalin (mixed isomers). The relative permittivity for hexadecane is unknown. We applied Eq. 5 to these selected data points and obtained the results shown in Fig. 3. This figure shows that the correlation between the observed and calculated ratios of oscillator strengths to those for the benzene solvent is fairly good. However, all the points in Fig. 3 have a tendency to fit a steeper line. This may be due to a neglect of the dispersion effect and the solute-induced dipole (solvent dipole interaction) in the derivation of Eq. 5.

(ii) Benzene: Considering that benzene is a weak hydrogen-bonding acceptor,[16] we chose 11 data points from Macovei's total[19] of 17 for the solvent effects on

Table 2. Values of f(soln)/f(vap) for Nitroalkanes

Nitroalkane	Solvent						A	B
	Heptane	2,2,4-trimethyl-pentane	Cyclohexane	Carbon tetrachloride	Dichloro-methane	Diethyl ether		
Nitromethane								
Obsd	1.56	1.65	1.68	2.11	1.95	1.97		
Calcd	1.70	1.70	1.72	1.78	1.91	2.09	3.96	−8.66
Nitroethane								
Obsd	1.68	1.59	1.69	1.91	1.98	1.92		
Calcd	1.66	1.67	1.69	1.74	1.94	2.06	3.68	−7.75
1-Nitropropane								
Obsd	1.86	2.07	1.73	2.03	2.09	1.87		
Calcd	1.82	1.83	1.84	1.91	1.96	2.21	4.48	−10.25
2-Nitropropane								
Obsd	1.45	1.62	1.59	1.77	1.81	1.44		
Calcd	1.52	1.52	1.53	1.56	1.68	1.79	2.93	−6.33
2-Nitro-2-methylpropane								
Obsd	1.51	1.68	1.59	1.93	1.75	1.67		
Calcd	1.61	1.61	1.62	1.67	1.68	1.89	3.49	−8.12

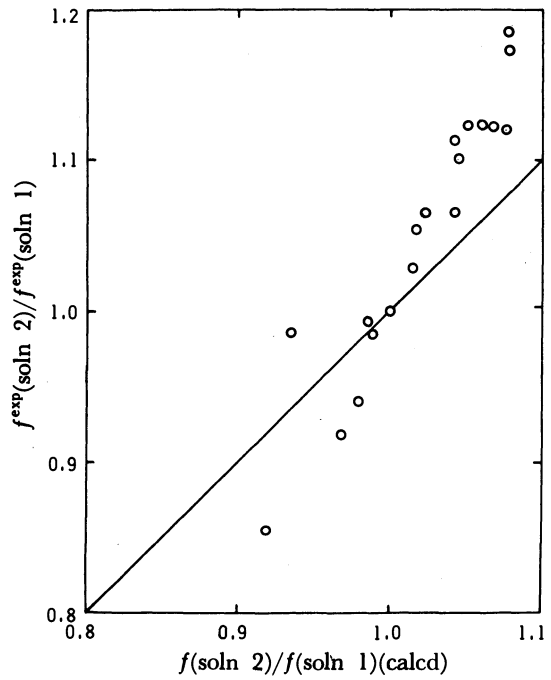

Fig. 3. Correlation between the observed and calculated values of f(soln 2)/f(soln 1) for β-carotene with benzene as the standard solvent.

Table 3. Values of f(soln 2)/f(soln 1) for Benzene

Solvent	f(soln 2)/f(soln 1)[a]	
	Obsd	Calcd
Cyclopentane	1.03	1.00
Pentane	0.780	1.02
Cyclohexane	1.00	1.00
Hexane	0.980	1.01
Heptane	1.03	1.01
Octane	1.02	1.01
Decane	1.07	1.00
Dodecane	1.04	1.00
Diethyl ether	0.833	1.02
Acetonitrile	1.07	1.02
1,4-Dioxane	1.14	1.00

a) The oscillator strength in cyclohexane is selected as f(soln 1).

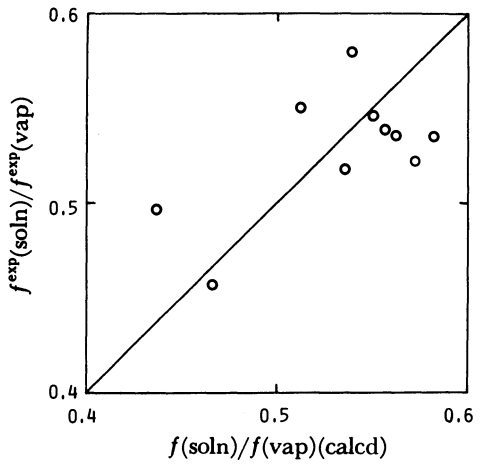

Fig. 4. Correlation between the observed and calculated values of f(soln)/f(vap) for chlorobenzene (A=−3.108 and B=7.154).

the electronic spectra of benzene and applied Eq. 5 to these data points. Values for the experimental and calculated ratios of oscillator strengths to those for the cyclohexane solvent are given in Table 3. The calculated ratios agree to a gross approximation with the corresponding observed values.

(iii) Chlorobenzene: Since chlorobenzene is a weak hydrogen-bonding acceptor,[16] we chose 10 data points from Macovei's total[20] of 19 for solvent effects on the spectral intensities of this molecule. Using f^{exp}(vap)=5×10^{-3} for chlorobenzene,[21] we applied Eq. 16 to these selected data points. The results of the calculations are summarized in Fig. 4. The figure shows that the correlation between the observed and calculated values for f(soln)/f(vap) is also fairly good.

(iv) Nitrobenzene: Macovei[22] has reported the effects of a solvent on the oscillator strength of the principal band of nitrobenzene in the near-ultraviolet region. Of his total of 22 data points, we chose only 9;

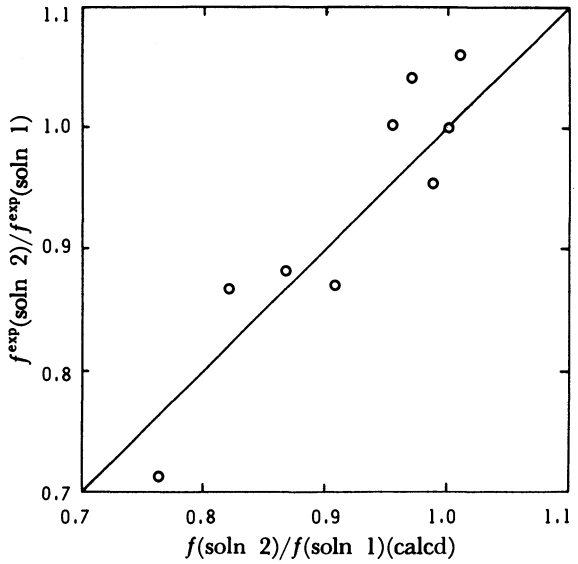

Fig. 5. Correlation between the observed and calculated values of f(soln 2)/f(soln 1) for nitrobenzene (A=−1.584 and B=2.654).

the excluded data being those of nonpolar solvents whose molecular shapes are too much long and plane. The principal band of nitrobenzene at 240 nm overlaps a weak band at 288 nm and a strong band at 193 nm.[23,24] In particular, a weak band of nitrobenzene in a solution is hidden in the principal band (Fig. 1 of Ref. 24). Macovei's data for the oscillator strengths in a solution seem not to have been corrected for a contribution from such an overlaps with the weak band. The application of Eq. 17, therefore, to Macovei's data yields the results shown in Fig. 5. The correlation between the observed and calculated values of f(soln 2)/f(soln 1) is good.

References

1) T. Abe and I. Iweibo, *J. Chem. Phys.*, **83**, 1546 (1985).
2) O. E. Weigang, Jr., *J. Chem. Phys.*, **41**, 1435 (1964).
3) A. B. Myers and R. R. Birge, *J. Chem. Phys.*, **73**, 5314 (1980).
4) W. Liptay, *Z. Naturforsch.*, **21a**, 1605 (1966).
5) M. Block and S. M. Walker, *Chem. Phys. Lett.*, **19**, 363 (1973).
6) T. Abe, S. Tero-Kubota, and Y. Ikegami, *J. Phys. Chem.*, **86**, 1358 (1982).
7) T. Abe, *Bull. Chem. Soc. Jpn.*, **56**, 1206 (1983).
8) T. Abe and I. Iweibo, *Bull. Chem. Soc. Jpn.*, **58**, 3415 (1985).
9) H. Kolod, *Acta Chem. Scand.*, **7**, 928 (1953).
10) T. Shimozawa, "Yudenritsu no Kaishaku (Interpretation of Relative Permittivities)," Kyoritsu Publishing Co., Tokyo (1967), p. 83.
11) F. Van Bolhuis and C. T. Kiers, *Acta Crystallogr., Sect. B*, **34**, 1015 (1978).
12) Y. Jinnouchi, M. Kohno, and A. Kuboyama, *Bull. Chem. Soc. Jpn.*, **57**, 1147 (1984). According to a private communication from Dr. A. Kuboyama, the experimental refractive-index correction factor of $1/n^2$ should be read for the factor of $1/n$ in their paper. Thus, we used their data regarding them as being corrected by the factor of $1/n^2$.
13) W. C. Schneider, *J. Am. Chem. Soc.*, **70**, 627 (1948).
14) M. A. A. de Molina, M. N. Loncharich, J. J. G. de Paez, and Y. P. W. Lobo, *An. Asoc. Quim. Argent.*, **70**, 1043 (1982); *Chem. Abstr.*, **98**, 215112x (1983).
15) N. S. Bayliss and G. Wills-Johnson, *Spectrochim. Acta*, **24A**, 551 (1968).
16) M. J. Kamlet and R. W. Taft, *J. Am. Chem. Soc.*, **98**, 377 (1976).
17) C. N. R. Rao, S. N. Bhat, and P. C. Dwivedi, *Appl. Spectrosc. Rev.*, **5**, 1 (1972).
18) K. Nakashima, K. Uchida-Kai, M. Koyanagi, and Y. Kanda, *Bull. Chem. Soc. Jpn.*, **55**, 415 (1982).
19) V. Macovei, *Rev. Roum. Chim.*, **20**, 1413 (1975).
20) V. Macovei, *Rev. Roum. Chim.*, **21**, 193 (1976).
21) K. Kimura and S. Nagakura, *Mol. Phys.*, **9**, 117 (1965).
22) V. Macovei, *Rev. Roum. Chim.*, **21**, 1137 (1976).
23) J. Tanaka, *Nippon Kagaku Zasshi*, **79**, 1114 (1958).
24) S. Nagakura, M. Kojima, and Y. Maruyama, *J. Mol. Spectrosc.*, **13**, 174 (1964).

Photochemical Reactions of Pentakis(*N,N*-dimethylformamide)-dioxouranium(VI) Ions in Nonaqueous Solutions

Hiroshi FUKUTOMI,* Toshie HARAZONO, and Takashi KOJIMA
Research Laboratory for Nuclear Reactors, Tokyo Institute of Technology, O-okayama, Meguro-ku, Tokyo 152
(Received November 29, 1985)

Photochemical reactions of $[UO_2(dmf)_5]^{2+}$ (dmf=*N,N*-dimethylformamide) ions were investigated in DMF and acetone solutions. The photolysis product of $[UO_2(dmf)_5]^{2+}$ at the initial stage was U(V), which was so stable in acid-free organic solvents in the dark that the absorption spectrum of U(V) was easily obtained in DMF. The molar extinction coefficient of U(V) was determined to be 45.5±1.5 M^{-1} cm^{-1} (M=mol dm^{-3}) at 755 nm. The formation of U(V) seems to proceed through the intramolecular reaction (k_i) and the lower limit of k_i was determined to be about 10^7 s^{-1} from the lifetime of excited uranyl ions by using a laser flash photolysis.

With respect to photochemical reactions of uranyl ions (UO_2^{2+})[1] with organic substrates in aqueous acidic solutions, a large number of investigations were performed, especially with alcohols,[2-4] acetaldehyde,[5] and acetone.[6] In aqueous acidic solutions, the uranyl ion is reduced giving UO_2^+ as an intermediate, which immediately disproportionates to U^{4+} and UO_2^{2+}.[7,8] On the other hand, a limited number of studies were carried out in nonaqueous solutions. It was reported that U(V) was formed on irradiation of $[UO_2(tbp)_2](NO_3)_2$ in TBP (tributyl phosphate)[9] and of UO_2(18-crown-6)$(ClO_4)_2$ in acetonitrile.[10] Cauzzo et al. studied the photochemical reaction mechanism of $UO_2(NO_3)_2 \cdot 2TEP$ in TEP (triethyl phosphate),[11] and reported that U(V) formed was stable in the dark. The reaction of $[UO_2(hfac)_2]$thf (hfac=hexafluoroacetylacetonate, thf=tetrahydrofuran) was studied in hydrocarbon solvents, and the final product was considered to be U^{4+}, where the appearance of U(V) was proposed as an intermediate.[12] In order to elucidate photochemical reaction mechanisms of uranyl ions in nonaqueous solvents, the photochemical reactions of $[UO_2(dmf)_5](ClO_4)_2$ in DMF and acetone were studied, and a possible reaction mechanism including the formation of U(V) is proposed.

Experimental

Materials. The $[UO_2(dmf)_5](ClO_4)_2$ complex was prepared by the same method as reported by Lincoln et al.[12] Dimethyl sulfoxide (DMSO) and DMF were distilled twice in vacuo and stored over 3A molecular sieves. Aceone was distilled after refluxing over potassium permanganate, followed by distillation with calcium chloride, then treated with phosphorus pentaoxide, and fractionally distilled. The distillate was stored over 4A molecular sieves. ^{13}C-enriched DMF ($H^{13}CON(CH_3)_2$, Merck 90%) and acetone-d_6 (CD_3COCD_3, Merck 90%) were used without further purification. Preparation of $[U(dmso)_8](ClO_4)_4$ was performed by adding DMSO into aqueous U^{4+} solution[14] which was prepared by electrolytic reduction of uranyl perchlorate solution. Brownish green crystals were filtered and washed with diethyl ether. All other chemicals were of analytical grade and used without further purification.

Apparatus and Procedures. Elemental analysis of the complexes was carried out by using a Shimadzu CHN-1A analyzer. Calcd for $[UO_2(dmf)_5](ClO_4)_2$: U, 28.53; C, 21.59; H, 4.22; N, 8.39. Found: U, 28.50; C, 20.98; H, 4.10; N, 8.39. Calcd for $[U(dmso)_8](ClO_4)_4$: U, 18.88 C, 15.24; H, 3.84. Found: U, 18.79; C, 15.67; H, 3.65. Luminescence spectra and intensities of excited uranyl ions were measured by using a JASCO FP-550A fluorescence spectrophotometer at room temperature. Uranyl ions were excited with light of 430 nm and the luminescence intensity was measured at 522 nm. Other spectrophotometric measurements were carried on a Shimadzu UV-210A spectrophotometer. The lifetimes of excited uranyl ions were measured by using a pulsed dye laser (420 nm) with a pulse width of 6.7 ns. Sample solutions for the measurement of quantum yields were degassed under vacuum and irradiated at 25±0.1 °C with a 500 W ultrahigh pressure mercury lamp (Ushio USH-500D) at various wavelengths by using a set of appropriate filters. Sample solutions for ESR measurements were degassed in vacuo and ESR spectra were recorded on a JEOL- JES-FX3 spectrometer. All the ESR measurements were carried out during the light irradiation.

Results

Absorption Spectra of Uranium Species and a Luminescence Spectrum of the Excited Uranyl Ion. Absorption spectra of $[UO_2(dmf)_5]^{2+}$ in DMF and acetone, and a luminescence spectrum of the excited uranyl ion in acetone are illustrated in Fig. 1. The molar extinction coefficient (ε_{VI}) of the uranyl ion in

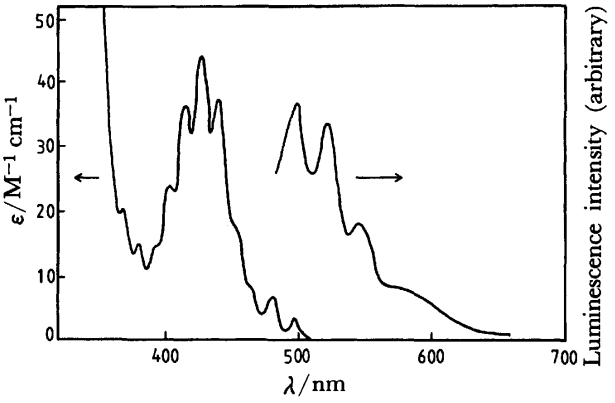

Fig. 1. Absorption spectrum of $[UO_2(dmf)_5](ClO_4)_2$ in DMF and acetone, and its luminescence spectrum in acetone.

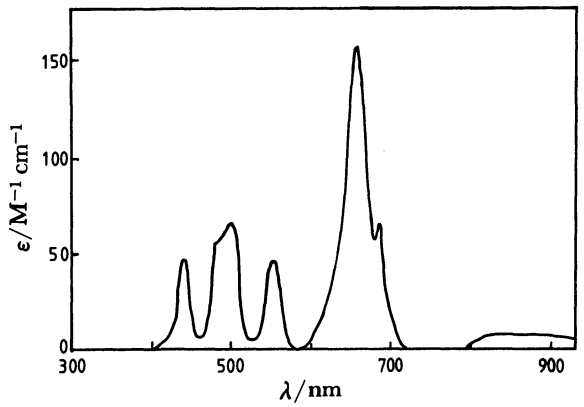

Fig. 2. Absorption spectrum of the DMF solution containing $[UO_2(dmf)_5](ClO_4)_2$ and $HClO_4$ after long-time irradiation.

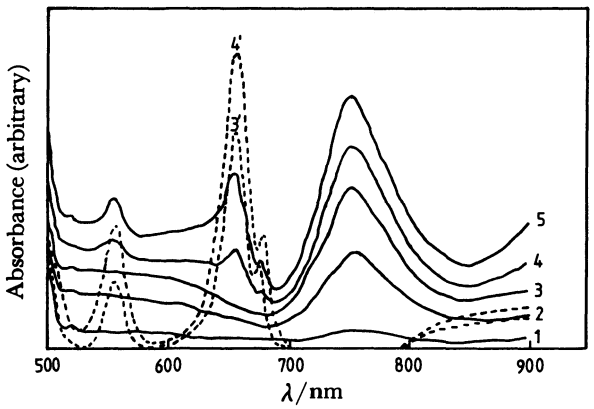

Fig. 3. Spectral changes of 0.1 M $[UO_2(dmf)_5]^{2+}$ in DMF irradiated with 365 nm light. (1): 2 min, (2): 13 min, (3): 23 min, (4): 30 min, (5): 40 min. Spectra 3′ and 4′ were obtained on addition of $HClO_4$ to solutions 3 and 4, respectively.

DMF and acetone at 426 nm was 44.4 $M^{-1}cm^{-1}$. The luminescence of the excited uranyl ion was not observed in DMF at room temperature, but observed in acetone. Figure 2 shows an absorption spectrum which was obtained after long-time irradiation of the DMF solution containing $[UO_2(dmf)_5](ClO_4)_2$ and a small amount of perchloric acid. This spectrum is well-consistent with that of the U(IV)–DMF complex (ε_{IV}= 155.7±1.5 $M^{-1}cm^{-1}$ at 657 nm) which was prepared by dissolving $[U(dmso)_8](ClO_4)_4$ into DMF or by dissolving U^{4+} into DMF (H_2O: DMF=1:99).[15] Therefore, the spectrum was identified as that of the U(IV)–DMF complex. Figure 3 shows changes in absorption spectrum of 0.1 M $[UO_2(dmf)_5](ClO_4)_2$ in DMF irradiated with 365 nm light. The appearance of a different absorption peak at 755 nm indicates the formation of a new complex (A), and then the absorption spectrum after further irradiation shows the formation of another compound (U^{IV}) which has two peaks at 558 and 657 nm. These two peaks are consistent with those of the U(IV)–DMF complex, but the peak heights are quite different. Addition of

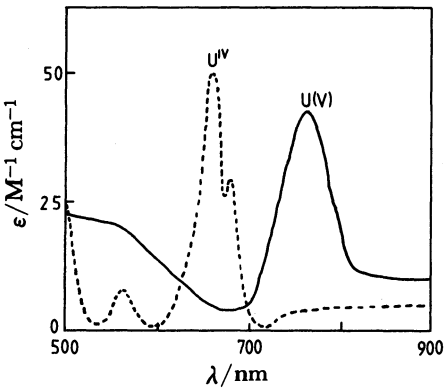

Fig. 4. Absorption spectra of U(V) and U^{IV} in DMF.

perchloric acid to the complex A solution under nitrogen atmosphere caused the rapid disappearance of complex A and the formation of U(VI)- and U(IV)–DMF complexes. Therefore, complex A was identified as the U(V)–DMF complex which disproportionated as follows:[7,8]

$$2UO_2^+ + 4H^+ \longrightarrow UO_2^{2+} + U^{4+} + 2H_2O \quad (1)$$

The concentration of U(V) was determined spectrophotometrically in the following way. An appropriate quantity of perchloric acid was added to the U(V) solution and the concentration of the resulting U(IV) was used for the determination of the U(V) concentration using the relation of 2[U(IV)]=[U(V)]. The molar extinction coefficient of U(V) at 755 nm was determined to be 45.5±1.5 $M^{-1}cm^{-1}$. The spectrum of U(V) was obtained as follows. The molar extinction coefficient of U(V) at wavelength λ, $\varepsilon_V(\lambda)$, can be evaluated by

$$\varepsilon_V(\lambda) = \varepsilon_{VI}(\lambda) + \frac{\Delta A(\lambda,t)}{\Delta C_V(t)}, \quad (2)$$

where $\Delta A(\lambda, t)$ is the absorbance change of the solution at the wavelength of λ after irradiation time t, and $\Delta C_V(t)$ is the concentration change of U(V) after t. The U(V) spectrum obtained is shown in Fig. 4.

The spectrum of U^{IV}, which is discussed later, was obtained by adding perchloric acid to the solution containing U(V) and U^{IV}, and using Eq. 3.

$$\varepsilon^{IV}(\lambda) = \varepsilon_{VI}(\lambda) + \frac{\Delta A(\lambda,t) + \{\varepsilon_{VI}(\lambda) - \varepsilon_V(\lambda)\}\Delta C_V(t)}{\Delta C^{IV}(t)}, \quad (3)$$

where $\varepsilon^{IV}(\lambda)$ and ΔC^{IV} denote the molar extinction coefficient at λ and the concentration change of U^{IV}, respectively. The absorption spectrum of U^{IV} is also shown in Fig. 4.

ESR Spectrum. Figure 5 shows the ESR spectrum of photolysis products of $[UO_2(dmf)_5](ClO_4)_2$ in the rigid DMF matrix at −170°C, where ESR measurements were carried out during the light irradiation. The ESR measurement was also carried out for $[UO_2$-

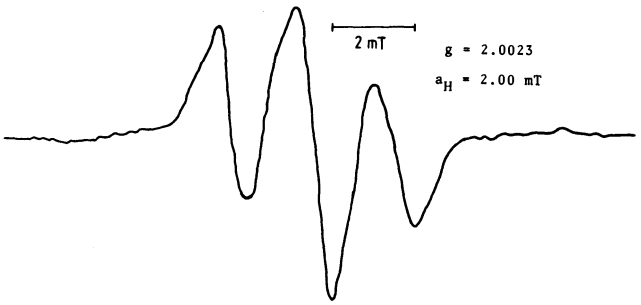

Fig. 5. ESR spectrum of the sample containing $[UO_2(dmf)_5]^{2+}$ in DMF during the irradiation at 365 nm and −170 °C. Symbols g and a_H are the g-factor (reference: Mn^{2+}) and hyperfine coupling constant, respectively.

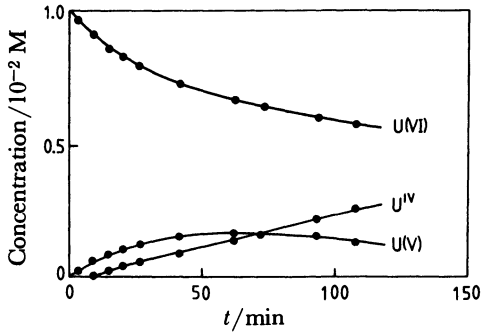

Fig. 6. Changes in the concentrations of reactant and products on irradiation of $[UO_2(dmf)_5]^{2+}$ in DMF with light of 313 nm. $[UO_2(dmf)_5^{2+}]$=0.01 M, T=25 °C.

$(dmf)_5](ClO_4)_2$ dissolved in $H^{13}CON(CH_3)_2$ at −170 °C, which shows the same ESR spectrum given in Fig. 5, and the radical species was assigned to $HCON(CH_3)$-CH_2·.[16,17] In addition, $[UO_2(dmf)_5](ClO_4)_2$ in the rigid acetone-d_6 matrix yielded the same radical.

Changes in Concentration of Uranium Species. Figure 6 shows the changes in concentration of U^{IV}, U(V) and U(VI) resulted from the irradiation of 0.01 M $[UO_2(dmf)_5](ClO_4)_2$ in DMF at 313 nm. The U(VI) concentration was estimated by subtracting ([U(V)]+[U^{IV}]) from the initial concentration of U(VI). The U(V) concentration has a maximum, and U^{IV} appears somewhat later during the irradiation, and gradually increases. These changes occur irrespective of λ of the light and the initial concentration of U(VI). The ratio of the maximum U(V) concentration to the initial U(VI) concentration is about 0.16—0.19 in the initial U(VI) concentration range of 2×10^{-3}—2×10^{-1} M. The plot of log[U(VI)] vs. irradiation time before the appearance of U^{IV} gives a first-order decay as shown in Fig. 7.

Quantum Yields. The quantum yield of U(V), Φ_V, was measured to elucidate the photochemical reaction mechanism of $[UO_2(dmf)_5](ClO_4)_2$ in DMF and acetone. Table 1 shows the dependence of quantum yields on the absorbed light intensities, and indicates

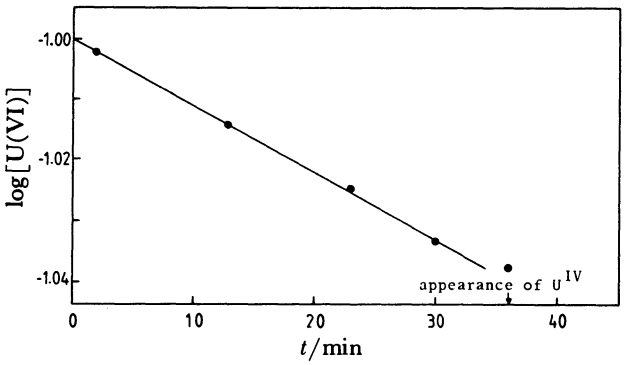

Fig. 7. Plot of log [U(VI)] vs. irradiation time. $[UO_2(dmf)_5^{2+}]$=0.10 M, λ_{irr}(wavelength of irradiating light)= 365 nm, T=25 °C.

Table 1. Dependence of the Quantum Yield of U(V) on the Absorbed Light Intensity[a]

I_a / 10^{-7} einstein min^{-1}		Φ_V
0.56		0.31
1.55		0.31
1.62		0.34
3.66		0.31
4.62		0.32
4.65		0.29
4.99		0.32
5.13		0.31
	average	0.31±0.01

a) $[UO_2(dmf)_5^{2+}]$=0.020 M, λ_{irr}=365 nm, T=25 °C.

Table 2. Dependence of the Quantum Yield of U(V) on the Initial Concentration of U(VI)

$[UO_2(dmf)_5^{2+}]$ / M	Φ_V
0.010	0.31±0.01[a]
0.020	0.31±0.01[b]
0.100	0.30±0.03[b]
0.202	0.32±0.01[b]

a) λ_{irr}=436 nm, T=25 °C. b) λ_{irr}=365 nm, T=25 °C.

that the quantum yield does not depend on the absorbed light intensity. The quantum yield is also independent of the initial U(VI) concentration (Table 2). Additional experiments were carried out to investigate the depencence of the quantum yield on the DMF concentration, where the solution of $[UO_2(dmf)_5](ClO_4)_2$ dissolved in the mixture of acetone and DMF was used. As a milky precipitate which was readily soluble in perchloric acid was observed with irradiation and was supposed to be hydrolysis products or polymers of U(IV), perchloric acid was added to the solution in these experiments prior to irradiation. In the acetone-DMF mixture, where the concentration of DMF was over three times higher than that of the uranyl ion, the number of coordinated DMF molecules was determined to be five by the NMR method at −50 °C. As the

Table 3. Quantum Yield of U(IV) as a Function of DMF Concentration[a)]

[DMF] / M	Φ_{IV}
0.126	0.11±0.01
0.319	0.10±0.00
0.642	0.12±0.01
1.261	0.12±0.00

a) $[UO_2(dmf)_5^{2+}]=0.010$ M, $[H^+]=0.023$ M, $\lambda_{irr}=365$ nm, $T=25$ °C.

Table 4. Quantum Yield of U(V) as a Function of Wavelength of Irradiating Light[a)]

λ_{irr} / nm	Φ_V
313	0.26±0.01
334	0.28±0.02
365	0.31±0.01
436	0.31±0.01

a) $[UO_2(dmf)_5^{2+}]=0.010$ M, $T=25$ °C.

donicity of DMF is larger than those of acetone and water on the basis of Gutmann's donor number,[18,19] the first-coordination sphere of the uranyl ion might be fully occupied by DMF even at 25 °C. The results are given as the quantum yield of U(IV) in Table 3. As the quantum yield of U(IV) in the photochemical reaction of the uranyl ion in acetone is less than 10^{-3} in this acid concentration range (ca. 0.02 M),[6] the chemical path of the excited uranyl ion with acetone can be neglected. As is seen in Table 3, the quantum yield was independent of the DMF concentration. Table 4 shows the dependence of the quantum yield of U(V) on the wavelength of light.

Luminescence Lifetime. Measurements of the luminescence lifetime of 0.01 M $[UO_2(dmf)_5](ClO_4)_2$ in acetone containing 0.18 M DMF were not successful because the decay of luminescence was faster than the time resolution of the instrument (50 ns), and hence the lifetime of the excited uranyl complex was estimated to be less than 50 ns.

Discussion

The absorption spectrum of U(V) obtained in this work is very similar to those produced by electrolysis of U(VI) in DMSO,[20] and by reduction of U(VI) with Eu(II) in aqueous solution.[21] However, it is very different in shape and peak position from the spectrum of U(V) in triethyl phosphate.[11] The U(V) formed by photolysis of $[UO_2(dmf)_5](ClO_4)_2$ in DMF is very stable in oxygen- and acid-free solution in the dark, and did not disproportionate. Therefore, it is considered that U^{IV} is produced by the light absorption of U(V). As no change occurs when U(V) is irradiated with light of $\lambda>520$ nm, U(V) presumably absorbs light of the charge-transfer band with short wavelength and is reduced to U^{IV}. The molar extinction coefficient of U^{IV} at 657 nm was 50.0 $M^{-1}cm^{-1}$ when U^{IV} is assumed to be a single species. The absorption spectrum of U^{IV} is very similar to that of U(IV) except for its value of the molar extinction coefficient, which is about one third of U(IV). Long irradiation of the sample solution caused a remarkable increase in base line of the absorption spectrum, especially at a short-wavelength region. This might be due to the light scattering from colloidal particles. Cauzzo et al. suggested that U(V) was in a UO_2^+ form and U^{IV} was in a UO_2 form in TEP.[11] Gritzner and Selbin reported that a brown colloidal precipitate was UO_2 in DMSO.[20] The U^{IV} formed in DMF seems similar to those so far reported. Unfortunately, the colloidal precipitate could not be isolated by centrifugation.

Mechanism. The primary photochemical reactions can be expressed as follows:

$$UO_2L_5^{2+} \xrightarrow{h\nu} (UO_2L_5^{2+})^*, \quad (4)$$

$$(UO_2L_5^{2+})^* \longrightarrow UO_2L_4^+ + \cdot L + H^+, \quad (5)$$

or

$$(UO_2L_5^{2+})^* + L \longrightarrow UO_2L_5^+ + \cdot L + H^+, \quad (6)$$

where L and ·L represent DMF and $HCON(CH_3)CH_2\cdot$, respectively. Figure 7 supports the reaction path of Eqs. 5 or 6, and means that the following reaction path, if any, in which the excited uranyl ion reacts with a product (P), can be ignored.

$$(UO_2L_5^{2+})^* + P \longrightarrow UO_2L_n^+ + P' \quad (7)$$

As the quantum yield of U(V) is independent of the absorbed light intensity, it is reasonable to assume that U(V) is formed from $(UO_2L_5^{2+})^*$, which is represented by Eqs. 5 or 6. In addition, the following reaction seems to be negligible because the quantum yield of U(V) is less than unity.

$$UO_2L_5^{2+} + \cdot L \longrightarrow UO_2L_5^+ + \cdot L^+ \quad (8)$$

The ·L radical may disappear by radical recombination or self-decomposition.

On the assumption that the formation of U(V) occurs from $(UO_2L_5^{2+})^*$, and from the fact that the quantum yield is less than unity, one would expect that the deactivation path expressed by Eq. 9 would be operative.

$$(UO_2L_5^{2+})^* \xrightarrow{k_d} UO_2L_5^{2+} \quad (9)$$

This path may include the recombination in the solvent "cage".

$$(UO_2L_5^{2+})^* \xrightarrow{k_r} (UO_2L_4^+ \cdots \cdot L \cdots H^+) \longrightarrow UO_2L_5^{2+} \quad (10)$$

The results in Table 2 suggest that the self-quenching of $(UO_2L_5^{2+})^*$, which was observed in TEP,[11] is negligible.

$$(UO_2L_5^{2+})^* + UO_2L_5^{2+} \longrightarrow 2UO_2L_5^{2+} \quad (11)$$

It is of great interest to clarify which path (Eqs. 5 or 6) being operative. As seen in Table 3, the quantum yield of U(IV) is independent of the DMF concentration, and the ESR spectrum of $[UO_2(dmf)_5](ClO_4)_2$ in acetone-d_6 irradiated at $-170°C$ gives the signal of $HCON(CH_3)CH_2\cdot$. These results might indicate that the uranyl ion directly reacts with the coordinated dmf, i.e. the photochemical reaction occurs by intramolecular reaction (Eq. 5). Miyake et al.[22] observed the ESR spectrum of U(V) in both photo- and electrolytic-reduction processes of $[UO_2(dmf)_5]^{2+}$ in DMF and found the stronger bond between uranium and oxygen in the equatorial plane than in the axial direction. This fact also supports the formation mechanism of U(V) by the intramolecular reaction.

As is shown in Fig. 1, the uranyl ion has a triplet state (T_1) around 426 nm and a charge transfer band (CT) at shorter wavelengths. The wavelength dependence of the quantum yield of U(V) indicates that the excitation to the triplet state of the uranyl ion gives better yield than that to the charge transfer band. This implies that the photochemical reaction occurs from the triplet state of the excited uranyl ion.

Since the recombination in the solvent cage usually decreases as the irradiation wavelength becomes shorter, it is expected that the quantum yield of U(V) increases. The results in Table 4 are not in accord with this expectation, and consequently suggest no appreciable recombination in the solvent cage.

The decrease in quantum yield at the charge transfer band suggests the presence of a nonradiative deactivation from the charge-transfer band, which results in a lowering of the quantum yield of intersystem crossing from CT to T_1.

From the above discussion, the photochemical reaction mechanism is described as follows:

$$UO_2(dmf)_5^{2+} \xrightarrow{h\nu} (UO_2(dmf)_5^{2+})^*, \quad (4')$$

$$(UO_2(dmf)_5^{2+})^* \xrightarrow{k_i} UO_2(dmf)_4^{+} + HCON(CH_3)CH_2\cdot + H^+, \quad (5')$$

$$\longrightarrow UO_2(dmf)_n^{+} + P,$$

$$(UO_2(dmf)_5^{2+})^* \xrightarrow{k_d} UO_2(dmf)_5^{2+}, \quad (9')$$

where n is the number of coordinated dmf. The average value of the quantum yields in Table 1 and the relation, $\Phi_V = k_i/(k_i+k_d)$, give the value of $k_d/k_i = 2.2$. The energy level diagram is shown in Fig. 8, where ISC denotes the intersystem crossing ($\Phi < 1$) and k_{dCT} is the deactivation rate constant from CT. In

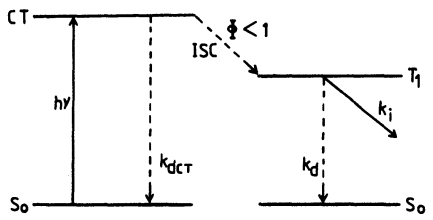

Fig. 8. Energy level diagram.

the photochemical reaction of $UO_2(NO_3)_2\cdot 2TEP$ in TEP, the ratio of the maximum concentration of U(V) to the initial concentration of U(VI) decreased as the initial U(VI) concentration increased, and it was suggested that the photoexcited U(V) disproportionated to give U^{IV} and U(VI)[11]. However, the ratio is about constant at any initial concentration of U(VI) in DMF, and no disproportionation was observed.

The photochemical reaction mechanism of $[UO_2(dmf)_5](ClO_4)_2$ in acetone is essentially the same as that in DMF except for the presence of the following luminescence path.

$$(UO_2(dmf)_5^{2+})^* \xrightarrow{k_l} UO_2(dmf)_5^{2+} + h\nu' \quad (12)$$

This might lead to the result that the quantum yield of U(V) in DMF is larger than that in acetone containing perchloric acid as is shown in Table 3, where $2\Phi_{IV}$ corresponds to Φ_V. Since the lifetime of the excited uranyl complex ion was less than 50 ns as described above, the lower limit of the k_i value is estimated to be $\approx 10^7\ s^{-1}$.

The authors wish to thank Professor Ikuzo Tanaka of the Tokyo Institute of Technology for providing a laser flash photolysis instrument. The present work was partially supported by a Grant-in-Aid for Scientific Research No. 57470035 from the Ministry of Education, Science and Culture.

References

1) For the sake of simplicity, the symbols of U(IV), U(V), and U(VI) are used for U^{4+}, UO_2^+, and UO_2^{2+} respectively, unless otherwise noted, and U^{IV} represents unidentified chemical species with 4+ oxidation state.

2) S. Sakuraba and R. Matsushima, *Bull. Chem. Soc. Jpn.*, **43**, 2359 (1970).

3) G. I. Sergeeva, A. K. Chibisov, L. V. Levshin, and A. V. Karyakin, *J. Photochem.*, **5**, 253 (1976).

4) R. J. Hill, T. J. Kemp, D. M. Allen, and A. Cox, *J. Chem. Soc., Faraday Trans. 1*, **68**, 847 (1972).

5) S. Sakuraba and R. Matsushima, *Chem. Lett.*, **1972**, 919.

6) T. Harazono, S. Nakamura, T. Kojima, and H. Fukutomi, *Bull. Res. Lab. Nucl. Reactor (Tokyo Inst. Tech.)*, **8**, 1 (1983).

7) T. W. Newton and F. B. Baker, *Inorg. Chem.*, **4**, 1166 (1965).

8) H. Kaneki and H. Fukutomi, *Bull. Res. Lab. Nucl. Reactor (Tokyo Inst. Tech.)*, **5**, 27 (1980).

9) C. K. Rofer-Depoorter and G. L. Depoorter, *J. Inorg. Nucl. Chem.*, **41**, 215 (1979).
10) G. Folcher, L. Lambard, and G. C. De Vilardi, *Inorg. Chim. Acta*, **45**, 159 (1980).
11) G. Cauzzo, G. Gennari, G. Giacometti, G. C. Agostini, and A. Gambaro, *Inorg. Chim. Acta*, **32**, 45 (1979).
12) G. M. Kramer, M. B. Dines, A. Kaldor, R. Hall, and D. McClure, *Inorg. Chem.*, **20**, 1421 (1981).
13) R. P. Bowen, S. F. Lincoln, and E. H. Williams, *Inorg. Chem.*, **15**, 2126 (1976).
14) T. Harazono, T. Kojima, and H. Fukutomi, *Nippon Kagaku Kaishi*, **1984**, 213.
15) T. Harazono, Ph. D. Thesis, Tokyo Institute of Technology, 1983.
16) A. Cox and T. J. Kemp, *J. Chem. Soc., Faraday Trans. 1*, **71**, 2490 (1975).
17) D. Greatorex, R. J. Hill, T. J. Kemp, and T. J. Stone, *J. Chem. Soc., Faraday Trans. 1*, **68**, 2059 (1972).
18) V. Gutmann and R. Schmid, *Coord. Chem. Rev.*, **12**, 263 (1974).
19) T. R. Griffiths and D. C. Pugh, *Coord. Chem. Rev.*, **29**, 129 (1979).
20) G. Gritzner and J. Selbin, *J. Inorg. Nucl. Chem.*, **30**, 1799 (1968).
21) A. Ekstrom, *Inorg. Chem.*, **13**, 2237 (1974).
22) C. Miyake, Y. Yamana, S. Imoto, and H. Ohya-Nishiguchi, *Inorg. Chim. Acta*, **95**, 17 (1984).

 © 1986 The Chemical Society of Japan Bull. Chem. Soc. Jpn., 59, 2393—2400 (1986)

Raman Spectral Characteristics of $[Co(ida)_n(dien)_{2-n}]$-Type and Related Complexes

Tatsuya KAWAMOTO,* Toshihide F. MARUYAMA,† Takaji YASUI,†† Ken-ichi OKAMOTO, Jinsai HIDAKA, and Hisahiko EINAGA†

Department of Chemistry, University of Tsukuba, Sakura, Ibaraki 305
†Institute of Materials Science, University of Tsukuba, Sakura, Ibaraki 305
††Department of Chemistry, Faculty of Science, Kochi University, Akebono-cho, Kochi 780

(Received December 27, 1985)

The Raman spectra of $[Co(ida)_n(dien)_{2-n}]^{(3-2n)+}$ (n=0, 1, and 2), where ida and dien denote iminodiacetate and diethylenetriamine respectively, and related complexes in the skeletal vibration region were measured in order to deduce the relation between their spectra and their geometrical structures. The Raman bands could be classified into five vibration modes: Totally symmetric stretching vibration modes (polarized bands in the 510—625 cm^{-1} region); Co-O and Co-N stretching vibration modes (depolarized bands in the 430—525 cm^{-1} region); metal-ligand skeletal breathing vibration modes (polarized bands in the 360—480 cm^{-1} region); skeletal bending deformation modes (depolarized bands in the 290—405 cm^{-1} region), and chelate ring deformation modes (polarized bands in the 220—260 cm^{-1} region). The polarized bands around 400 cm^{-1} were regarded as characteristic of the mono and bis(terdentate)cobalt(III) complexes. The mer isomers of each complex gave Raman spectra clearly different from those of the fac isomers in the stretching vibration region.

It has been accepted[1] that vibrational spectra are one of the most useful means for investigating the stereochemistry of transition metal complexes. Especially, the Raman spectra of the complexes in the skeletal vibration region, which appear in the low frequency region, reflect their structural characteristics.

The Raman spectra in the skeletal vibration region of $[Co(a)(b)(en)_2]$,[2] $[Co(a)(b)(NH_3)_4]$,[3] $[Co(a)(b)(tn)_2]$,[4] and $[Co(a)_2(NH_3)_2(en)]$,[5] where a and b stand for unidentate ligands and where en and tn denote ethylenediamine and trimethylenediamine respectively, have been measured in order to find the vibrational criteria for differentiating their geometrical configurations. Recently, the Raman spectra of the nitroammine series[6] and the complete series of the $[Co(gly)_x(ox)_y(en)_z]$-type complexes ($x+y+z=3$),[7] where gly and ox denote glycinate and oxalate respectively, have been systematically investigated in order to establish the relation between the spectra and geometrical structures among their isomers. In particular, it has been concluded that the Raman bands of the $[Co(gly)_x(ox)_y(en)_z]$-type complexes could be treated in terms of the effective symmetry, which was mainly determined by the arrangement of coordinated atoms around the cobalt(III), and could be classified into several vibration modes.

The present investigation aims at finding more general information as to the relation between the geometrical structures and the Raman spectra in the skeletal vibration region of the cobalt(III) complexes. For this purpose, the Raman spectra of $[Co(ida)_n(dien)_{2-n}]^{(3-2n)+}$ (n=0, 1, and 2), $[Co(NH_3)_3(dien)]^{3+}$, and $[Co(ida)(NH_3)_3]^+$ were measured in the low frequency region (200—800 cm^{-1}) in an aqueous solution and were compared with those of the $[Co(gly)_x(ox)_y(en)_z]$-type complexes. Furthermore, the Raman spectra of $[Co(ida)(mida)]^-$, $[Co(mida)_2]^-$, and $[Co(mida)(mdien)]^+$, where mida and mdien denote *N*-methyliminodiacetate and *N,N*-bis(2-aminoethyl)methylamine respectively, were measured and compared with those of the $[Co(ida)_n(dien)_{2-n}]$-type complexes.

Experimental

Complexes. The complexes were prepared and characterized according to the literature procedures except for $[Co(NH_3)_3(dien)]Cl_3$ (vide infra): *sym-fac*-$[Co(dien)_2]Br_3$,[8] *unsym-fac*-$[Co(dien)_2]Cl_3$,[8] *mer*-$[Co(dien)_2]Cl_3$,[8] *sym-fac*-$[Co(ida)(dien)]ClO_4$,[9] *unsym-fac*-$[Co(ida)(dien)]ClO_4$,[9] *mer*-$[Co(ida)(dien)]ClO_4$,[9] *sym-fac*-$K[Co(ida)_2]$,[10] *unsym-fac*-$K[Co(ida)_2]$,[10] *fac*-$[Co(ida)(NH_3)_3]ClO_4$,[11] *sym-fac*-Na-$[Co(ida)(mida)]$,[12] *unsym-fac*-$K[Co(ida)(mida)]$,[12] *mer*-K-$[Co(ida)(mida)]$,[13] *sym-fac*-$K[Co(mida)_2]$,[14] *unsym-fac*-$K[Co(mida)_2]$,[14] *mer*-$K[Co(mida)_2]$,[14] *sym-fac*-$[Co(mida)(mdien)]$-Cl,[15] and *mer*-$[Co(mida)(mdien)]Cl$.[15]

$[Co(NH_3)_3(dien)]Cl_3$. Two grams of $[CoCl_3(dien)]$ were dissolved in 50 cm^3 of 28% aqueous ammonia, and the solution was evaporated to dryness on a steam bath. The precipitate was then dissolved in a small amount of water and poured onto a column (40 mmϕ×600 mm) containing strong acid cation exchange resin (SP-Sephadex, C-25, Na^+ form). Having been swept with water, the band adsorbed on the column was eluted with a 0.3 mol dm^{-3} aqueous sodium chloride solution. A yellow band of the desired complex was then eluted and fractionated. It was found, from the absorption spectra of the fractions, that the middle eluates contained $[Co(NH_3)_3(dien)]^{3+}$. Then the middle fractions were combined and concentrated to a small volume, and the Raman spectrum was measured. This

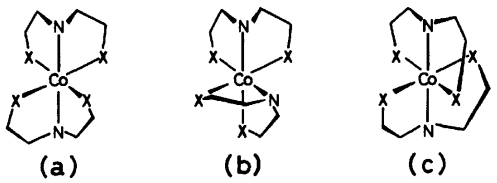

Fig. 1. Three geometrical isomers of [Co(terdentate-X,N,X)$_2$] (X=O or N). (a): sym-fac, (b): unsym-fac, (c): mer.

complex was characterized on the basis of the electronic absorption spectrum and elemental analysis.

Measurements. The Raman spectra were recorded on a JASCO Laser Raman Spectrometer, which had been constructed specially with a double monochromator, model CT-25, a He-Ne Laser, model NEC GLS-8500, and a data processor, model DP-500 as the main components. The sample solution was excited at 632.8 nm, and the Raman spectra were calibrated with indene.

Results and Discussion

General Aspect. For the present bis(terdentate-X,N,X)cobalt(III)(X=O or N) complexes, these are three geometrical isomers, sym-fac, unsym-fac, and mer, as may be seen in Fig. 1.[8-15] Their Raman spectral data, obtained in the skeletal vibration region, are summarized in Table 1, together with those of such related complexes as $[Co(NH_3)_3(dien)]^{3+}$ and $[Co(ida)(NH_3)_3]^{+}$.

Figure 2 shows the Raman spectrum of *unsym-fac*-$[Co(dien)_2]^{3+}$ as a typical example of the bis(terdentate)cobalt(III) complexes, together with those of $[Co(NH_3)_6]^{3+}$ and $[Co(en)_3]^{3+}$;[7] these three complexes equally have O_h symmetry for the coordinated atoms. Their Raman frequencies, intensities, and depolarization ratios indicate that *unsym-fac*-$[Co(dien)_2]^{3+}$ has the same spectral characteristics as $[Co(NH_3)_6]^{3+}$ and $[Co(en)_3]^{3+}$ except for a polarized band at 409 cm^{-1}. That is, the Raman bands at 546, 430—485, and 321 cm^{-1} of the unsym-fac isomer correspond to those at 495, 440, and 320 cm^{-1} of $[Co(NH_3)_6]^{3+}$ and to those at 525, 440, and 378 cm^{-1} of $[Co(en)_3]^{3+}$

Table 1. Observed Raman Bands and Their Assignments for $[Co(ida)_n(dien)_{2-n}]^{(3-2n)+}$ (n=0, 1, and 2) and Related Complexes

No.	Complex	Raman frequency/cm^{-1}[a]				
1	*sym-fac*-$[Co(dien)_2]^{3+}$	549 s(0)	478 m(dp) 448 vw(—) 437 m(dp)	401 m(0.36)		260 vw(—) 230 vw(—)
2	*unsym-fac*-$[Co(dien)_2]^{3+}$	546 s(0)	485 m(dp) 444 m(dp) 434 m(dp)	409 w(0)	321 m(dp)	255 vw(—)
3	*mer*-$[Co(dien)_2]^{3+}$	579 m(0) 546 vw(—) 514 s(0.15)		480 s(0) 442 s(0.37)	402 m(dp) 381 vw(dp) 323 m(dp)	222 m(0)
4	*sym-fac*-$[Co(ida)(dien)]^{+}$	609 m(0) 546 s(0)	510 w(dp) 472 w(dp) 461 sh(dp)	418 w(—) 387 s(0.22)		235 s(0)
5	*unsym-fac*-$[Co(ida)(dien)]^{+}$	610 m(0) 546 s(0)	504 m(dp) 470 vw(dp) 453 vw(dp)	410 m(0.27) 401 m(0.36)	301 w(dp)	235 w(0)
6	*mer*-$[Co(ida)(dien)]^{+}$	614 vw(0) 585 w(0) 524 s(0.12)		476 m(0.18) 451 s(0.31) 436 w(—) 390 s(0)	346 w(dp) 302 vw(dp)	
7	*sym-fac*-$[Co(ida)_2]^{-}$	610 s(0) 569 m(0)	522 vw(dp)	394 w(—) 372 m(0.29)		229 m(0)
8	*unsym-fac*-$[Co(ida)_2]^{-}$	621 s(0) 562 m(0)	446 vw(—)	398 m(0.39) 382 vw(—)	291 w(—)	
9	$[Co(NH_3)_3(dien)]^{3+}$[b]	547 s(0)	486 m(dp) 469 m(dp) 454 w(dp)	422 s(0.39)		
10	*fac*-$[Co(ida)(NH_3)_3]^{+}$	614 w(0) 514 m(0.24)	505 sh(dp) 457 vw(dp)	417 m(0.18) 403 m(0.27)	339 vw(dp)	
11	*sym-fac*-$[Co(ida)(mida)]^{-}$	611 m(0) 546 m(0.23)	497 w(dp) 450 w(—)	407 w(—) 382 w(—) 361 w(—)		246 m(0)
12	*unsym-fac*-$[Co(ida)(mida)]^{-}$	622 w(0) 547 m(0.35)	495 vw(—) 450 vw(—)	409 w(0) 386 vw(—)	354 vw(dp)	

Table 1. (Continued)

No.	Complex	Raman frequency/cm^{-1}[a]				
13	*mer*-[Co(ida)(mida)]$^-$	533 m(0)	455 vw(—)	407 m(0)		
14	*sym-fac*-[Co(mida)$_2$]$^-$	541 vw(0)	501 vw(dp)			
15	*unsym-fac*-[Co(mida)$_2$]$^-$	545 vw(—)	506 vw(—)			
16	*mer*-[Co(mida)$_2$]$^-$	563 s(0.22)	504 vw(dp) 465 w(dp)	404 m(0.32)		259 vw(—)
17	*sym-fac*-[Co(mida)(mdien)]$^+$	531 s(0.05)	505 w(0.67) 451 vw(—)	405 w(0.15) 397 w(0.30) 370 w(0.25) 361 w(0.57)		224 m(—)
18	*mer*-[Co(mida)(mdien)]$^+$	546 sh(0.15) 535 s(0.14)	487 w(—)	440 m(0.24) 392 m(0.35) 377 sh(0.32)		254 vw(0)
19	[Co(NH$_3$)$_6$]$^{3+}$[c]	495 s(p)	440 m(dp)		320 w(dp)	
20	[Co(en)$_3$]$^{3+}$[c]	525 s(p)	440 m(dp)		378 w(dp)	283 s(p)
	Assignment[d]	ν_{ts}(Co-L)	ν(Co-L)	ν_{br}	δ_{sbd}(L-Co-L)	δ_{crd}(Co$\overset{L}{<}_{L}$)

a) The following abbreviations are used: s, strong; m, medium; w, weak; vw, very weak; sh, shoulder; p, polarized; dp, depolarized. Numerals in the parentheses show the polarization ratio. b) This isomer seems to be facial, judging from the Raman spectral behavior. c) Ref. 7. d) ν_{ts} denotes the totally symmetric stretching vibration mode; ν, the stretching vibration mode excluding the totally symmetric one; ν_{br}, the skeletal breathing vibration mode; δ_{sbd}, the metal-ligand skeletal bending deformation mode; δ_{crd}, the chelate ring deformation mode, and L, the donor atom (N and/or O).

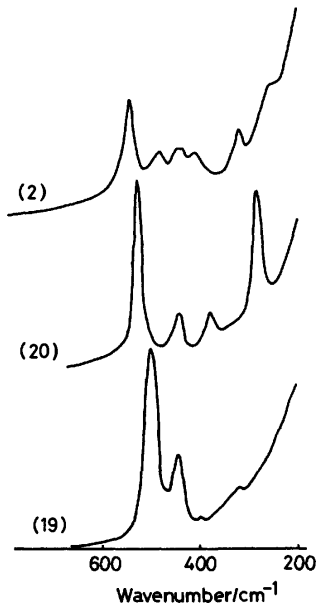

Fig. 2. Raman spectra of *unsym-fac*-[Co(dien)$_2$]$^{3+}$, [Co(en)$_3$]$^{3+}$, and [Co(NH$_3$)$_6$]$^{3+}$ (Ref. 7). Numbers in parentheses correspond to those in Table 1.

respectively, while the Raman band at 255 cm^{-1} of the unsym-fac isomer corresponds to that at 283 cm^{-1} of [Co(en)$_3$]$^{3+}$. Hence, the polarized band at 546 cm^{-1}, the depolarized bands in the 430—485 cm^{-1} region, the depolarized band at 321 cm^{-1}, and the polarized band at 255 cm^{-1} of *unsym-fac*-[Co(dien)$_2$]$^{3+}$ can be assigned to the totally symmetric metal-ligand stretching, the Co-N stretching, the metal-ligand skeletal bending deformation, and the chelate ring deformation modes respectively. The polarized band at 409 cm^{-1} of *unsym-fac*-[Co(dien)$_2$]$^{3+}$ is regarded as a band characteristic of the bis(terdentate)cobalt(III) complexes, for we could not find the corresponding band in the spectra of [Co(NH$_3$)$_6$]$^{3+}$ and [Co(en)$_3$]$^{3+}$, but could find it uniquely in the spectra of the [Co(ida)$_n$(dien)$_{2-n}$]-type complexes (Table 1). On the basis of the Raman frequency and polarization characteristics, the polarized band at 409 cm^{-1} of *unsym-fac*-[Co(dien)$_2$]$^{3+}$ is tentatively assigned to the breathing mode, which corresponds to the symmetric vibration of the overall structure of the complexes, i.e., the coupled vibration of the totally symmetric metal-ligand stretching and the chelate ring deformation. Furthermore, the good correlation between the vibration modes of *unsym-fac*-[Co(dien)$_2$]$^{3+}$ (C_2 symmetry) with those of [Co(NH$_3$)$_6$]$^{3+}$ (O_h symmetry) and [Co(en)$_3$]$^{3+}$ (D_3 symmetry)[7] suggests that the Raman spectra of the bis(terdentate)cobalt(III) complexes with linked five-membered chelate rings can be treated as a first approximation on the basis of the effective symmetry, which is mainly determined by the arrangement of the coordinated atoms around the central metal ion, as in the case of the tris-(bidentate)cobalt(III) complexes with the five-membered chelate rings.[7]

Figure 3 shows the Raman spectra of the three geometrical isomers of [Co(dien)$_2$]$^{3+}$ and [Co(ida)-

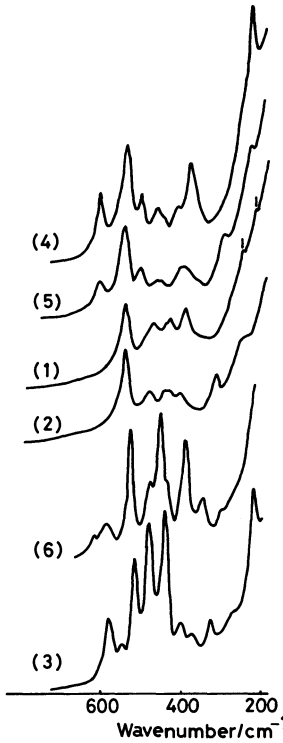

Fig. 3. Raman spectra of three geometrical isomers of $[Co(ida)(dien)]^+$ and $[Co(dien)_2]^{3+}$. Numbers in parentheses correspond to those in Table 1.

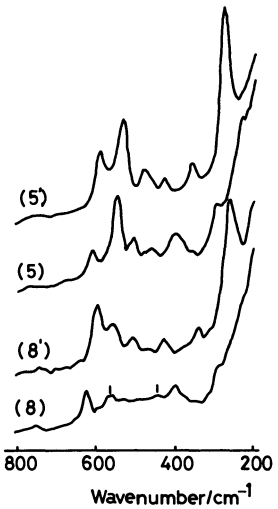

Fig. 4. Raman spectra of *unsym-fac*-$[Co(ida)(dien)]^+$ and $[Co(ida)_2]^-$. Raman spectra of C_2-*cis(O)*-$[Co(gly)_2(en)]^+$(5') and C_2-*cis(N)*-$[Co(gly)_2(ox)]^-$(8') were also shown (Ref. 7).

$(dien)]^+$. It is evident from Fig. 3 and Table 1 that the unsym-fac and sym-fac isomers of $[Co(dien)_2]^{3+}$ of the $[Co(N)_6]$-type have the same spectral characteristics except for minor differences in the low frequency region. The same thing is observed for the unsym-fac and sym-fac isomers of $[Co(ida)(dien)]^+$ of the $[Co(N)_4(O)_2]$-type (Fig. 3 and Table 1) and $[Co(ida)_2]^-$ of the $[Co(N)_2(O)_4]$-type (Table 1). Hence, we may expect that, so far as the skeletal vibrations of the fac isomers for the bis(terdentate)cobalt(III) complexes with the two linked five-membered chelate rings are concerned, the Raman spectral characteristics are predominantly determined by the arrangement of the coordinated atoms. The predominant contribution of the arrangement of the coordinated atoms to the Raman spectral characteristics is further supported by the Raman spectral characteristics of *unsym-fac*-$[Co(ida)_2]^-$ and C_2-*cis(N)*-$[Co(gly)_2(ox)]^-$ and of *unsym-fac*-$[Co(ida)(dien)]^+$ and C_2-*cis(O)*-$[Co(gly)_2(en)]^+$ (Fig. 4). Figure 4 and Table 1 show that the Raman bands at 560—625, 446, and 291 cm^{-1} of *unsym-fac*-$[Co(ida)_2]^-$ correspond to those at 560—605, 430—510, and 348 cm^{-1} of C_2-*cis(N)*-$[Co(gly)_2(ox)]^-$, while the Raman bands at 545—610, 450—505, 301, and 235 cm^{-1} of *unsym-fac*-$[Co(ida)(dien)]^+$ correspond to those of 535—600, 430—490, 360, and 276 cm^{-1} of C_2-*cis(O)*-$[Co(gly)_2(en)]^+$ respectively, irrespective of the chelate ring structure. On the other hand, the mer isomer shows Raman spectral characteristics quite different from those of the fac isomers. Figure 3 and Table 1 demonstrate that the Raman spectra of the mer isomers of $[Co(dien)_2]^{3+}$ and $[Co(ida)(dien)]^+$ exhibit several polarized bands, but no depolarized bands, in the 390—615 cm^{-1} region, while those of the fac isomers of $[Co(dien)_2]^{3+}$ and $[Co(ida)(dien)]^+$ exhibit both polarized and depolarized bands in this region. This striking difference in the Raman spectral characteristics in the stretching vibration region can be ascribed to the difference in the stretching vibration mode depending on the coordination mode whether the linked two five-membered chelate rings take the mer coordination or the fac one.

On the basis of the above discussion and the Raman spectral characteristics summarized in Table 1, the Raman spectra of the bis(terdentate)cobalt(III) complexes can be classified into five categories: Polarized bands in the 510—625 cm^{-1} region, depolarized ones in the 430—525 cm^{-1} region, polarized ones in the 360—480 cm^{-1} region, depolarized ones in the 290—405 cm^{-1} region, and polarized ones in the 220—260 cm^{-1} region which can be assigned to the totally symmetric metal-ligand stretching, the Co–N and Co–O stretching except for the totally symmetric stretching character, the metal-ligand skeletal breathing, the skeletal bending deformation, and chelate ring deformation modes respectively.

Figure 5 shows the Raman spectra of the triamminecobalt(III)-type complexes, $[Co(NH_3)_3(dien)]^{3+}$ and $[Co(ida)(NH_3)_3]^+$, together with those of related complexes. The Raman spectrum of $[Co(NH_3)_3(dien)]^{3+}$ can be better correlated to that of *sym-fac*-$[Co(dien)_2]^{3+}$ than to that of $[Co(NH_3)_6]^{3+}$. That is, the character of the linked chelate rings appears similarly in the spectra of the mono(terdentate)cobalt(III)-type complexes. Further, Fig. 5 and Table 1 demonstrate that the Raman spectral characteristics of *fac*-$[Co(ida)(NH_3)_3]^+$

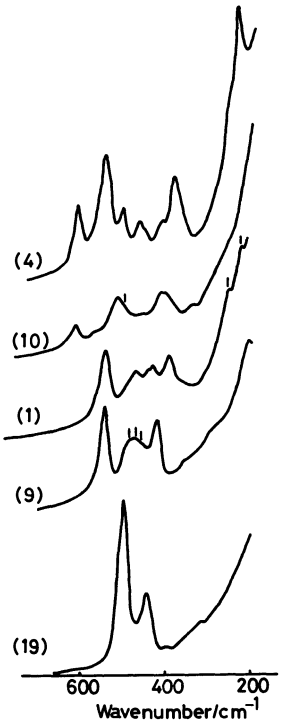

Fig. 5. Raman spectra of *sym-fac*-[Co(ida)(dien)]$^+$, *fac*-[Co(ida)$(NH_3)_3$]$^+$, *sym-fac*-[Co$(dien)_2$]$^{3+}$, [Co$(NH_3)_3$(dien)]$^{3+}$, and [Co$(NH_3)_6$]$^{3+}$ (Ref. 7). Numbers in parentheses correspond to those in Table 1.

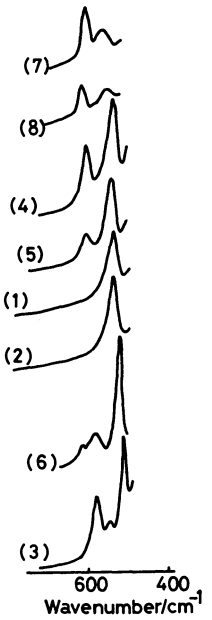

Fig. 6. Raman spectra of [Co$(ida)_n(dien)_{2-n}$]$^{(3-2n)+}$ (n= 0, 1, and 2) in the totally symmetric stretching vibration region. Numbers in parentheses correspond to those in Table 1.

are superimposed on those of the sym-fac and unsym-fac isomers of [Co(ida)(dien)]$^+$. It is interesting to note in Table 1 that the Raman spectral characteristics of [Co$(NH_3)_3$(dien)]$^{3+}$ can be correlated to those of the fac isomers of [Co$(dien)_2$]$^{3+}$ rather than to those of the mer isomer. Hence, we can expect that the dien in [Co$(NH_3)_3$(dien)]$^{3+}$ takes the facial coordination.

Finally, it should be noted that *sym-fac*-[Co$(dien)_2$]$^{3+}$ has more Raman bands than those expected from C_{2h} symmetry ($4A_g+2B_g$) because of the splitting of the chelate ring deformation mode. In crystal, *sym-fac*-[Co$(dien)_2$]Br_3 has been reported to have an "approximate" C_{2h} symmetry as a result of X-ray crystal structure analysis.[8,16] This Raman spectrum evidence implies that the sym-fac isomer is somewhat distorted structurally from C_{2h} molecular symmetry in an aqueous solution so far as the skeletal vibration characteristics are concerned.

Polarized Bands in the 510—625 cm^{-1} Region. Figure 6 shows the Raman spectra in the totally symmetric stretching vibration region. The mer isomers of [Co$(ida)_n(dien)_{2-n}$]-type complexes exhibit characteristic Raman spectra in this region. That is, each of the mer isomers of [Co$(dien)_2$]$^{3+}$ and [Co(ida)(dien)]$^+$ exhibits three polarized bands and no depolarized bands in the vibration region of lower frequencies. This is in contrast to the fac isomers, which exhibit both polarized and depolarized bands in the vibration region. The change of the depolarized bands to the polarized ones, together with the shift to the higher frequency region on going from the fac isomers to the mer ones, can be explained in terms of the strengthening of the harmonic stretching vibration characteristic of the totally symmetric stretching mode because of the diagonally connected chelate rings; in fact, the mer isomers are distorted from the regular octahedral structure, for the Co–N(imino nitrogen) bond in the mer isomers is appreciably stronger than the others.[8,17] Hence, the Raman spectral characteristics in this region can be used for the differentiation of the fac and mer isomers.

In the fac isomers, [Co$(dien)_2$]$^{3+}$ exhibits only one Raman band, whereas [Co(ida)(dien)]$^+$ and [Co$(ida)_2$]$^-$ give doublets. It is evident from the Raman frequencies of the cobalt(III) complexes with the fac coodination (Table 1) that the Raman bands can be classified into two categories: Those above 605 cm^{-1} and those below 570 cm^{-1}, and that the former can be assigned to the ν_{ts}(Co–O) mode, and the latter, to the ν_{ts}(Co–N) mode. This assignment was supported by the isotopic shift; the polarized bands near 545 cm^{-1} of the fac isomers of [Co(ida)(dien)]$^+$ and [Co$(dien)_2$]$^{3+}$ exhibited a shift to a lower frequency upon the deuteration of the amino protons.

Depolarized Bands in the 430—525 cm^{-1} Region. In this region, the Raman spectra exhibit from one to three depolarized bands, except for *mer*-[Co$(dien)_2$]$^{3+}$ and [Co(ida)(dien)]$^+$, which give no depolarized bands at all (Fig. 7). These Raman bands can be assigned to the stretching mode, excluding the totally symmetric one, by comparison with the Raman spectra of the tris(bidentate)cobalt(III) complexes.[7] Furthermore,

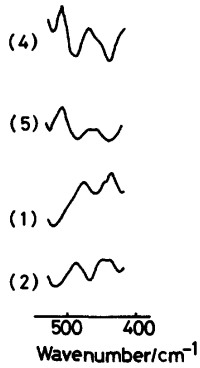

Fig. 7. Raman spectra of the fac isomers of [Co(ida)(dien)]$^+$ and [Co(dien)$_2$]$^{3+}$ in the stretching vibration region excluding the totally symmetric one. Numbers in parentheses correspond to those in Table 1.

the depolarized bands of *sym-fac*-[Co(dien)$_2$]$^{3+}$ are assigned to ν(Co–N), because the bands exhibit a large spectral shift (about 15 cm^{-1}) upon deuteration. As a whole, the Raman bands of *fac*-[Co(ida)(dien)]$^+$ and [Co(ida)$_2$]$^-$ are observed at higher frequencies (445—525 cm^{-1}) than those of *fac*-[Co(dien)$_2$]$^{3+}$ (430—485 cm^{-1}). This result implies that the Raman bands of [Co(ida)(dien)]$^+$ and [Co(ida)$_2$]$^-$ may be greatly influenced by the Co–O stretching vibration mode, for the Raman spectra of the tris(bidentate)cobalt(III) complexes have shown that the Raman bands of the ν(Co–O) mode appear at a higher frequency than those of the ν(Co–N) mode.[7]

Polarized Bands in the 360—480 cm^{-1} Region. The Raman spectra of the [Co(ida)$_n$(dien)$_{2-n}$]-type complexes in this region exhibit some unique polarized bands, as is shown in Table 1. These sorts of polarized bands have not been found in the Raman spectra of the tris(bidentate)cobalt(III) complexes;[7] they may be characteristic of the octahedral mono and bis(terdentate)cobalt(III) complexes. As has been mentioned before, these bands can be assigned to the skeletal breathing mode in the sense of the totally symmetric stretching, to which the chelate ring deformation is coupled, because the Raman bands in this region have totally symmetric vibration characteristics.

Depolarized Bands in the 290—405 cm^{-1} Region. From a comparison with the data of the tris(bidentate)-cobalt(III) complexes,[7] the Raman bands in this region have been assigned to the metal-ligand skeletal bending deformation mode. Figure 8 shows the relation between the Raman spectra of the sym-fac and unsym-fac isomers of [Co(dien)$_2$]$^{3+}$, [Co(ida)(dien)]$^+$, and [Co(ida)$_2$]$^-$ and their geometrical structures. The Raman spectra reflect the chelate ring structure (Fig. 8 and Table 1): The unsym-fac isomers have a depolarized band, the sym-fac isomers have no bands, and the mer isomers have a few bands. That is, it can be said that the combination of the chelate rings changes the metal-ligand skeletal bending deformation characteristics. This result is quite unlike that for the [Co(gly)$_x$(ox)$_y$(en)$_z$]-type complexes, each of which gives a Raman band, irrespective of the chelate ring structure, except for the [Co(ox)$_y$(en)$_z$]-type complexes, which have a major band accompanied by a very weak one.[7]

Fig. 8. Raman spectra of [Co(ida)$_n$(dien)$_{2-n}$]$^{(3-2n)+}$ (n=0, 1, and 2) in the skeletal bending deformation and the chelate ring deformation regions. Numbers in parentheses correspond to those in Table 1.

It seems to indicate that tha Raman bands in this region can be used for the differentiation of the sym-fac and unsym-fac isomers of the [Co(ida)$_n$(dien)$_{2-n}$]-type complexes.

Polarized Bands in the 220—260 cm^{-1} Region. Polarized Raman bands of the [Co(ida)$_n$(dien)$_{2-n}$]-type complexes in this region have been assigned to the chelate ring deformation mode of the coordinated terdentate ligands, because they correspond well to a sharp band near 270 cm^{-1} of the [Co(a)(b)(en)$_2$]-type complexes.[2] Unlike those in the 290—405 cm^{-1} region, the Raman bands of the [Co(ida)$_n$(dien)$_{2-n}$]-type complexes in this region do not reflect the chelate ring structure (Table 1 and Fig. 8). Rather, they belong to the same skeletal vibration modes as those of the tris(bidentate)cobalt(III) complexes with the five-membered chelate rings. A shift to the lower frequency side was noticed for the polarized band by the linkage of the chelate rings (Table 1[7]).

No polarized bands were observed on the Raman spectra of [Co(ida)(NH$_3$)$_3$]$^+$ and [Co(NH$_3$)$_3$(dien)]$^{3+}$, both of which have one linked chelate ring.

Raman Spectra of [Co(ida)$_n$(mida)$_{2-n}$]$^-$(n=0 and 1)

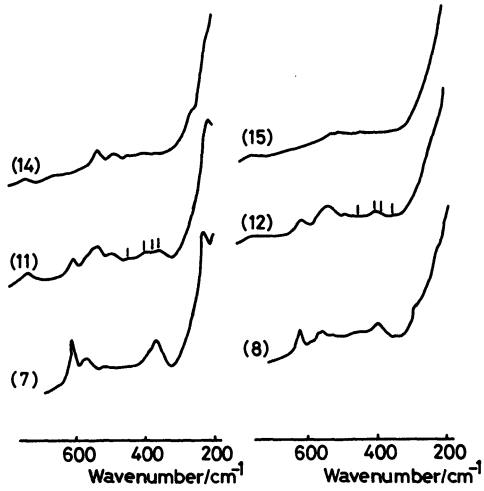

Fig. 9. Raman spectra of the fac isomers of $[Co(ida)_n(mida)_{2-n}]^-$ (n=0, 1, and 2). Numbers in parentheses correspond to those in Table 1.

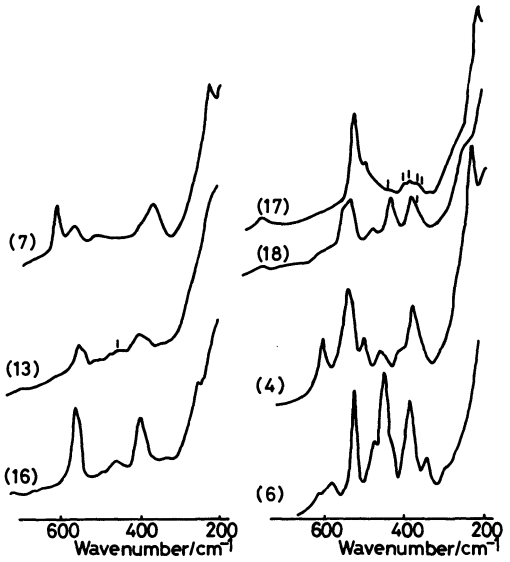

Fig. 10. Raman spectra of *sym-fac*-$[Co(ida)_2]^-$, *mer*-$[Co(ida)(mida)]^-$, *mer*-$[Co(mida)_2]^-$, *sym-fac*-$[Co(mida)(mdien)]^+$, *mer*-$[Co(mida)(mdien)]^+$, *sym-fac*-$[Co(ida)(dien)]^+$, and *mer*-$[Co(ida)(dien)]^+$. Numbers in parentheses correspond to those in Table 1.

and $[Co(mida)(mdien)]^+$ Complexes. The Raman spectra of the $[Co(ida)_n(mida)_{2-n}]^-$($n$=0 and 1) and $[Co(mida)(mdien)]^+$ complexes were measured in the skeletal vibration region as an extension of the $[Co(ida)_n(dien)_{2-n}]$-type complexes; those spectral data are also summarized in Table 1. The coordinated mida and mdien ligands are characteristic in that their conformations are somewhat restricted by the methyl group on imino nitrogen.

The Raman bands of the $[Co(ida)_n(mida)_{2-n}]$-type and $[Co(mida)(mdien)]^+$ complexes can be classified into five vibration modes as in the case of the $[Co(ida)_n(dien)_{2-n}]$-type ones.

Figure 9 shows the Raman spectra of the $[Co(ida)_n(mida)_{2-n}]$-type complexes. The replacement of a hydrogen on the imino nitrogen by a methyl group causes a marked change in the Raman spectral characteristics rather than the spectral shift anticipated in the case of the deuteration of the amino protons. At the same time, the Raman spectra become less well defined with an increase in the numbers of the methyl group in the complexes.

The Raman spectra of the sym-fac and mer isomers of the $[Co(ida)_n(mida)_{2-n}]$-type and $[Co(mida)(mdien)]^+$ complexes are shown in Fig. 10, together with those of the $[Co(ida)_n(dien)_{2-n}]$-type complexes. The Raman spectra in the stretching vibration region of the mer isomers for $[Co(ida)(mida)]^-$, $[Co(mida)_2]^-$, and $[Co(mida)(mdien)]^+$ exhibit depolarized bands. These spectral characteristics differ somewhat from the Raman spectra of the mer isomers for the $[Co(ida)_n(dien)_{2-n}]$-type complexes, which give only polarized bands. These findings suggest that the skeletal vibration characteristics of the mer isomers for the mida or mdien cobalt(III) complexes are mainly regulated by the linked chelate rings, which are folded by the restriction imposed by the methyl group on the imino nitrogen.

Finally, it should be pointed out that the two fac isomers of $[Co(mida)_2]^-$ exhibit no intense bands around 400 cm^{-1}. This may be due to the two methyl groups on the imino nitrogen atoms, which change the normal vibrations of the fac isomers by means of the fixed conformation of all of the chelate rings.

References

1) K. Nakamoto, "Infrared and Raman Spectra of Inorganic and Coordination Compounds," 3rd ed, Wiley-Interscience, New York (1977), Part III.

2) K. Kanamori and K. Kawai, *Bull. Chem. Soc. Jpn.*, **53**, 2520 (1980).

3) K. Kanamori and K. Kawai, *Bull. Chem. Soc. Jpn.*, **55**, 764 (1982).

4) K. Kanamori, H. Ichinose, and K. Kawai, *Bull. Chem. Soc. Jpn.*, **55**, 1315 (1982).

5) K. Kanamori, I. Bansho, K. Kawai, K. Akamatsu, and Y. Shimura, *Bull. Chem. Soc. Jpn.*, **58**, 943 (1985).

6) K. Kanamori, T. Morikawa, and K. Kawai, *Bull. Chem. Soc. Jpn.*, **53**, 2787 (1980).

7) T. F. Maruyama, K. Okamoto, J. Hidaka, and H. Einaga, *Bull. Chem. Soc. Jpn.*, **56**, 2610 (1983).

8) Y. Yoshikawa and K. Yamasaki, *Bull. Chem. Soc. Jpn.*, **45**, 179 (1972); F. R. Keene and G. H. Searle, *Inorg. Chem.*, **11**, 148 (1972).

9) K. Okamoto, J. Hidaka, and Y. Shimura, *Bull. Chem. Soc. Jpn.*, **48**, 2456 (1975). The prefixes sym-fac, unsym-fac, and mer in the present paper correspond to sym-cis(O), unsym-cis(O), and trans(O) respectively.

10) J. Hidaka, Y. Shimura, and R. Tsuchida, *Bull. Chem. Soc. Jpn.*, **35**, 567 (1962). The prefixes sym-fac and unsym-fac in the present paper correspond to trans(N) and cis(N) respectively.

11) K. Okamoto, J. Hidaka, and Y. Shimura, *Bull. Chem. Soc. Jpn.*, **46**, 3134 (1973). The prefix fac in the present paper corresponds to cis(O).
12) T. Yasui, H. Kawaguchi, N. Koine, and T. Ama, *Bull. Chem. Soc. Jpn.*, **56**, 127 (1983).
13) H. Kawaguchi, T. Ama, and T. Yasui, *Bull. Chem. Soc. Jpn.*, **57**, 2422 (1984).
14) T. Ama, H. Kawaguchi, and T. Yasui, *Chem. Lett.*, **1981**, 323.
15) Presented at the Symposium by the Chemical Society of Japan, Kochi, 1984, Abstr., p. 91.
16) M. Kobayashi, F. Marumo, and Y. Saito, *Acta Crystallogr., Sect. B*, **28**, 470 (1972).
17) K. Okiyama, S. Sato, and Y. Saito, *Acta Crystallogr., Sect. B*, **35**, 2389 (1979).

 © 1986 The Chemical Society of Japan Bull. Chem. Soc. Jpn., 59, 2401—2405 (1986)

Mössbauer and DTA Studies of Superionic Conducting $AgCl$-Ag_2O-B_2O_3 Glasses

Tetsuaki NISHIDA,* Michiko OGATA, and Yoshimasa TAKASHIMA
Department of Chemistry, Faculty of Science, Kyushu University 33, Hakozaki, Higashiku, Fukuoka 812
(Received January 6, 1986)

A structural study of silver borate glasses containing 20 or 30 mol% AgCl and 1 mol% Fe_2O_3 has been performed by means of Mössbauer spectroscopy. The distinct decreases in the Mössbauer parameters observed in the borate glasses with Ag_2O contents higher than about 10 mol% suggest that chloride ions are covalently bonded with tetrahedral iron or boron atoms as nonbridging chlorine. On the other hand, chloride ions are considered to be ionically bonded with Ag^+ ions at the interstitial sites of the three-dimensional network composed of BO_3, BO_4, and FeO_4 units when the Ag_2O content is lower than 10 mol%. Measurements of the glass transition temperatures and the electric conductivity show a good agreement with the Mössbauer results, suggesting that mobile and electric conducting Ag^+ ions change their configurational sites from the interstitial sites which are close to Cl^- ions to different interstitial sites which are close to the nonbridging chlorine atom.

Superionic conducting glasses containing Ag^+ ions have attracted much attention because of the scientific interest in the conduction mechanism as well as their technological applications.[1-13] The high electric conductivity of these glasses, amounting to the order of 10^{-2} S cm^{-1}, has been reported to be brought about by a cation conduction due to mobile Ag^+ ions which are considered to be present at interstitial sites of the glass-network structure. (The electric conductivity of ordinary alkali oxide glasses is known to be lower than 10^{-13} or 10^{-14} S cm^{-1}.) Minami et al.[1,5,6] suggested that mobile Ag^+ ions originate from AgX (X=Cl, Br, and I) molecules and that the nature of the chemical bond between the mobile Ag^+ ion and the neighboring halide ion is completely ionic. They also suggested that the nature of the chemical bond between the Ag^+ ion originating from Ag_2O and the oxygen atom constituting the skeleton of the glass network is partially covalent. This is different from the ionic bond between the alkali metal ion and the oxygen in ordinary alkali oxide glasses. In the light of this suggestion, the latter type of Ag^+ ion has been considered to be essentially immobile. Raman and EXAFS studies of the superionic conducting glasses revealed that the mobile Ag^+ ion is tetrahedrally surrounded by four halide ions at the interstitial site, forming a microdomain or a distorted sublattice of the α-AgI phase which itself has a high electric conductivity.[9,10,12] On the other hand, Chiodelli et al.[13] ruled out the presence of a high electric-conducting α-AgI phase dispersed in the glass network, for the electric conductivity of silver borate glasses containing AgI also shows a marked increase with the Ag_2O content when the AgI content is constant, and also the conductivity of binary Ag_2O-B_2O_3 glasses is much higher than that of ordinary alkali borate glasses. The electric conductivity measurements of binary Ag_2O-B_2O_3 glasses performed by Matusita and Sakka[14] and by Tsuchiya et al.[15] revealed that the conductivity of $30Ag_2O \cdot 70B_2O_3$ glass is about 10^{-6} S cm^{-1} at 100 °C and that it is higher than 10^{-8} S cm^{-1} at room temperature. These experimental results seem to lead to the tentative conclusion that at least a part of the Ag^+ ions originating from Ag_2O also participate in the electric conduction. One possible explanation of the high electric conductivity of binary silver borate glasses is the electron hopping from the colloidal Ag^0 to the Ag^+ ions originating from Ag_2O.[15]

Mössbauer spectroscopy has been successfully used for the structural study of several glasses, such as borate,[16-20] borosilicate,[21,22] phosphate,[23,24] borophosphate,[25] germanate,[26,27] KCl-$ZnCl_2$,[28] and BaF_2-ZrF_4[29] glasses. Mössbauer and ESR studies of potassium borate glasses containing a small amount of KCl or KBr revealed that chloride and bromide ions are ionically present at interstitial sites of the three-dimensional network composed of BO_3 and BO_4 units when the alkali oxide (K_2O) content is lower than 15 mol%.[19,20] On the other hand, the chloride and bromide ions proved to be covalently bonded with tetrahedal boron or iron (Fe^{3+}), as nonbridging chlorine (-Cl) and bromine (-Br) atoms respectively, when the K_2O content is higher than 15 mol%.[19,20] These results are almost entirely consistent with the optical absorption results reported by Maekawa et al.[30]

The present Mössbauer study was carried out in order to elucidate the local structure of superionic conducting $AgCl$-Ag_2O-B_2O_3 glasses, for Mössbauer spectroscopy is a very useful method for the structural study of amorphous materials, the structural study of which is very difficult by means of ordinary diffraction methods. The differential thermal analysis (DTA) of these glasses was performed because any change in the local structure of glasses, such as a change in the coordination number of network-forming atoms or the formation of nonbridging atoms, is known to be well reflected in the glass transition temperature (T_g).[26,29,31-35]

Experimental

Silver borate glasses containing 20, 30, and 40 mol% AgCl and 1 mol% Fe_2O_3 were prepared by fusing the individual mixtures of AgCl, Ag_2O, B_2O_3, and $^{57}Fe_2O_3$, of a guaranteed

reagent grade, at 1020 °C for 3 h using an electric muffle furnace. After the fusion, each melt in a platinum crucible was quenched with ice-cold water. The yellowish brown to reddish brown glasses obtained in this way were pulverized for the Mössbauer, DTA, and electric-conductivity measurements. Mössbauer measurements were performed by means of a constant-acceleration method at room temperature. Cobalt-57 (10 mCi) diffused into a palladium foil and a metallic iron foil enriched with iron-57 were used as the Mössbauer source and the reference for the isomer shift respectively. The velocity of the spectrometer was calibrated with the spectrum of metallic iron foil. Using a least-squares method, each Mössbauer spectrum was analyzed into a quadrupole doublet with the same width and the same intensity. DTA measurements were performed at a heating rate of 5 °C min^{-1} over the range from room temperature to 700 °C, and Al_2O_3 powder was used as the standard material. Electric-conductivity measurements for each glass sample (600 mg), pressed at a net pressure of 2.6×10^6 g cm^{-2}, were performed at room temperature by applying a DC voltage of 3 V.

Results and Discussion

The Mössbauer measurements of AgCl–Ag_2O–B_2O_3 glasses containing 1 mol% Fe_2O_3 revealed that iron is present only in the Fe^{3+} state, as is shown in Fig. 1. It may also be seen from Fig. 1 that the spectrum consists of a quadrupole doublet caused by the electric field gradient at the iron nucleus. Quadrupole doublets are often observed in the Mössbauer spectra of borate glasses,[16–20] and the increase in the quadrupole splitting of Fe^{3+} suggests the decreased symmetry of FeO_4 tetrahedra, because high-spin Fe^{3+} species have a symmetric $3d^5$ electron configuration in the outermost orbital. Therefore, only the electric field gradient brought about by the neighboring atoms or ions, i.e., oxygen atoms in the oxide glasses, affects the quadrupole splitting values. The symmetry of the BO_4 tetrahedra will also be reflected in the magnitude of the quadrupole splitting, for all the Fe^{3+} ions are considered to be present at the substitutional sites of the boron atoms constituting the BO_4 tetrahedra. (The isomer shifts smaller than ca. 0.4 mm s^{-1} mean that each Fe^{3+} ion is surrounded by four oxygen atoms, just as in the case of the boron atoms constituting the BO_4 tetrahedra.) It may be seen from Fig. 1 that the linewidth (FWHM) of the Fe^{3+} absorption is much larger than those of the Fe^{2+} or Fe^{3+} absorptions in the ordinary crystalline compounds, which is usually smaller than ca. 0.4 mm s^{-1} in the case of ^{57}Fe-Mössbauer spectroscopy. The large linewidth of the Fe^{3+} absorption in the borate glasses suggests that the Fe–O (and B–O) bond lengths and also the O–Fe–O (and O–B–O) bond angles are distributed. These distributions can be described as characteristic of amorphous materials. All the Mössbauer parameters obtained in the present study are summarized in Table 1, in which the isomer shifts of Fe^{3+} are in the range of 0.27 to 0.33 mm s^{-1} and show a slight decrease with an increase in the Ag_2O content. Table 1 indicates that quadrupole splitting also decreases with an increase in the Ag_2O content. (The experimental error for the isomer shift is estimated to be ±0.01 mm s^{-1}, and the errors for the quadrupole splitting and the linewidth are estimated to be ±0.02 mm s^{-1}.) The changes in the isomer shift and the quadrupole splitting with the Ag_2O content are also shown in Figs. 2 and 3 respectively.

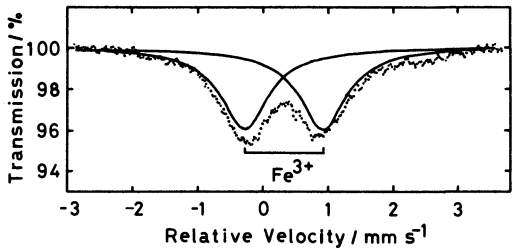

Fig. 1. Mössbauer spectrum for $20AgCl\cdot10Ag_2O\cdot69B_2O_3\cdot Fe_2O_3$ glass.

Table 1. Mössbauer Parameters for AgCl–Ag_2O–B_2O_3 Glasses

Composition	δ[a]	Δ[b]	Γ[c]
	mm s^{-1}	mm s^{-1}	mm s^{-1}
$20AgCl\cdot5Ag_2O\cdot74B_2O_3\cdot Fe_2O_3$	0.33	1.28	0.88
$20AgCl\cdot10Ag_2O\cdot69B_2O_3\cdot Fe_2O_3$	0.32	1.19	0.91
$20AgCl\cdot15Ag_2O\cdot64B_2O_3\cdot Fe_2O_3$	0.30	1.15	0.92
$20AgCl\cdot20Ag_2O\cdot59B_2O_3\cdot Fe_2O_3$	0.30	1.11	0.88
$20AgCl\cdot25Ag_2O\cdot54B_2O_3\cdot Fe_2O_3$	0.30	1.09	0.84
$20AgCl\cdot30Ag_2O\cdot49B_2O_3\cdot Fe_2O_3$	0.30	1.09	0.87
$30AgCl\cdot5Ag_2O\cdot64B_2O_3\cdot Fe_2O_3$	0.30	1.28	0.91
$30AgCl\cdot10Ag_2O\cdot59B_2O_3\cdot Fe_2O_3$	0.28	1.08	0.86
$30AgCl\cdot15Ag_2O\cdot54B_2O_3\cdot Fe_2O_3$	0.27	1.09	0.86
$30AgCl\cdot20Ag_2O\cdot49B_2O_3\cdot Fe_2O_3$	0.28	1.09	0.84
$30AgCl\cdot25Ag_2O\cdot44B_2O_3\cdot Fe_2O_3$	0.27	1.09	0.82

a) Isomer shift. b) Quadrupole splitting. c) Linewidth (FWHM).

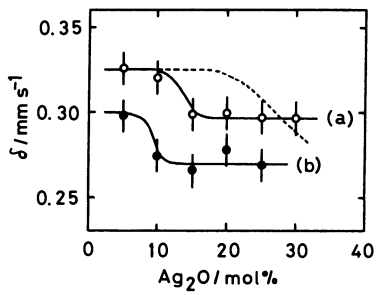

Fig. 2. Isomer shifts of Fe^{3+} in silver borate glasses containing (a) 20 mol% and (b) 30 mol% AgCl. A broken line refers to the change in the isomer shift of Fe^{3+} in K_2O–B_2O_3 glasses.[16,18]

Figure 2 demonstrates distinct decreases in the isomer shift of Fe^{3+} when the Ag_2O contents are in the ranges of 10—15 mol% and 5—10 mol% in the borate glasses containing 20 and 30 mol% AgCl respectively. The broken line shown in Fig. 2 refers to a change in the

isomer shift of Fe^{3+} in the K_2O–B_2O_3 glasses, from which the formation of a nonbridging oxygen (NBO) atom in BO_4 and FeO_4 units can be deduced when the K_2O content is equal to or higher than 20 mol%.[16,18] In the Mössbauer and ESR studies of K_2O–B_2O_3 glasses containing a small amount of KCl or KBr, the formation of nonbridging chlorine or bromine atoms was concluded on the basis of the distinct decreases in the isomer shift of Fe^{3+} and the ESR absorption intensity of Cl_2^- and Br_2^- when the K_2O content is equal to or higher than 15 mol%.[19,20] These results suggest that the formation of nonbridging chlorine atom starts when the Ag_2O content is higher than about 10 mol% in the case of silver borate glasses containing 20 or 30 mol% AgCl. The critical composition of the ternary AgCl–Ag_2O–B_2O_3 glass, where a distinct change in the isomer shift is observed, is found to be almost identical with the composition of the binary K_2O–B_2O_3 glass containing only 0.63 mol% KCl[19,20] when the Ag_2O/B_2O_3 molar ratio is compared to the K_2O/B_2O_3 ratio. That is, the molar ratio of 15/85 (=0.18) in the K_2O–B_2O_3 glass,[19,20] where it was concluded that the formation of the nonbridging chlorine atom starts, corresponds to the Ag_2O contents of about 12 and 10.5 mol% in the AgCl–Ag_2O–B_2O_3 glasses containing 20 and 30 mol% AgCl respectively. These conclusions are consistent with the results of the quadrupole splitting shown in Fig. 3, from which it is obvious that the quadrupole splitting shows a drastic decrease when the Ag_2O content is equal to or higher than 10 mol%. The broken line shown in Fig. 3 refers to a change in the quadrupole splitting of Fe^{3+} in the K_2O–B_2O_3 glasses;[16] the distinct decrease in the quadrupole splitting when the K_2O content is higher than 20 mol% is ascribed to the formation of a nonbridging oxygen atom in BO_4 and FeO_4 tetrahedral units, as has been described above. The increased quadrupole splittings of Fe^{3+} in the AgCl–Ag_2O–B_2O_3 glasses are ascribed to the substitution of the chloride ion for one of the oxygen atoms constituting the BO_4 or FeO_4 tetrahedra, or to the decreased symmetry of FeO_4 when the Ag_2O content is very low. Similar overall increases in the quadrupole splitting of Fe^{3+} have been observed in K_2O–B_2O_3 glasses containing a small number of chloride ions.[19]

DTA measurements were performed for all the glass samples prepared in the present study. The DTA curve consists of a broad exothermic peak, followed by an endothermic peak and a few exothermic peaks due to crystallization (Fig. 4). As is shown in Fig. 4, the glass transition temperature (T_g) is generally obtained from the intersection of the tangent to the broad exothermic peak and that to the following endothermic peak. All the glass transition temperatures obtained in this way are shown in Fig. 5, in which T_g shows a maximum when the Ag_2O content is about 10 mol%. It is already known that the increased coordination number of network-forming boron and germanium, in borate and germanate glasses respectively, is well reflected in the gradual increase in T_g.[26,31–35] This is probably due to the increased degree of bridging in the glass skeleton as a result of the step-by-step structural changes from BO_3 to BO_4 units and from GeO_4 to GeO_6 units in borate and germanate glasses respectively. On the other hand, the formation of nonbridging oxygen atom, i.e., a decreased degree of bridging in the glass skeleton, is known to result in a decrease in T_g.[26,34,35] Therefore, the gradual decrease in the T_g observed in the silver borate glasses with the Ag_2O contents higher than about 10 mol% is concluded to be due to the formation of a nonbridging chlorine atom in BO_4 or FeO_4 units, i.e., the formation of BO_3Cl or FeO_3Cl units.

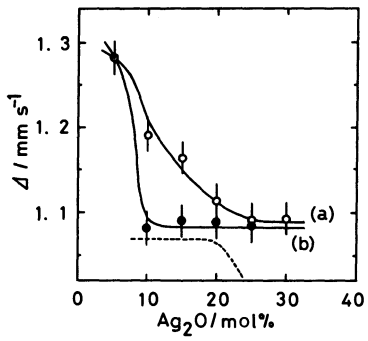

Fig. 3. Quadrupole splittings of Fe^{3+} in silver borate glasses containing (a) 20 mol% and (b) 30 mol% AgCl. A broken line refers to the change in the quadrupole splitting of Fe^{3+} in K_2O–B_2O_3 glasses.[16]

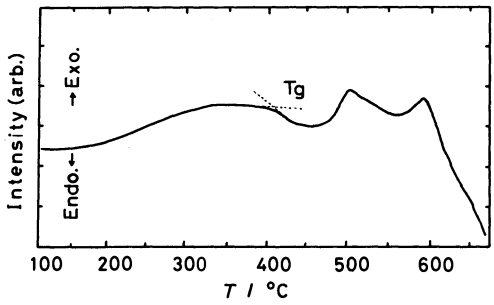

Fig. 4. DTA curve for $20AgCl \cdot 10Ag_2O \cdot 69B_2O_3 \cdot Fe_2O_3$ glass.

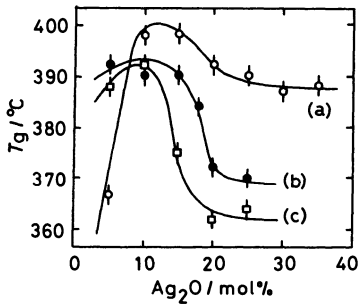

Fig. 5. Glass transition temperatures of silver borate glasses containing (a) 20 mol%, (b) 30 mol%, and (c) 40 mol% AgCl.

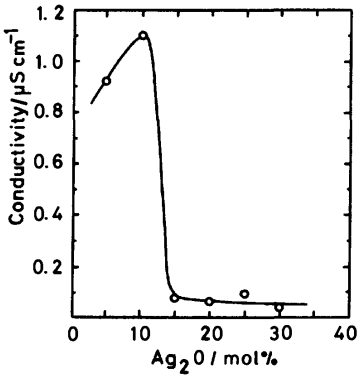

Fig. 6. Electric conductivities of silver borate glasses containing 20 mol% AgCl.

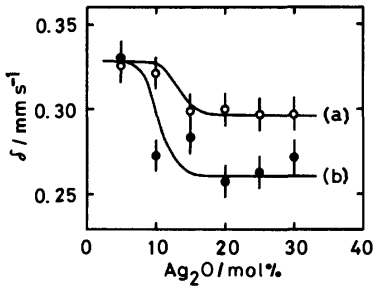

Fig. 7. Isomer shifts of Fe^{3+} in silver borate glasses containing 20 mol% AgCl. (a): Non-irrad., (b): irrad. with ^{60}Co-γ rays of 10^8 R.

This conclusion is consistent with the Mössbauer results presented above. An overall decrease in T_g with an increase in the AgCl content also supports this conclusion, because the number of nonbridging chlorine atoms will, to some extent, be proportional to the concentration of chloride ions in glasses.

The composition dependency of electric conductivity for silver borate glasses containing 20 mol% AgCl is shown in Fig. 6, which also shows a drastic change when the Ag_2O content exceeds about 10 mol%. Considering the experimental findings that the electric conductivity for binary Ag_2O–B_2O_3 glasses shows a drastic and almost linear increase with an increase in the Ag_2O content,[13–15] the remarkable decrease in the electric conductivity shown in Fig. 6 is concluded to be caused by AgCl. The drastic decrease in the electric conductivity suggests that the number of mobile Ag^+ ions decreases abruptly when the Ag_2O content exceeds about 10 mol% in the case of silver borate glasses containing 20 mol% AgCl. Considering the Mössbauer (Figs. 2 and 3) and DTA (Fig. 5) results presented above, this phenomenon can be correlated with the formation of nonbridging chlorine atoms in the silver borate glasses with an Ag_2O content higher than about 10 mol%. The number of mobile Ag^+ ions will be reduced because most of the Ag^+ ions, which were present with Cl^- ions at the interstitial sites of the three-dimensional network structure, follow the nonbridging chlorine atoms. As a result, such Ag^+ ions will become less mobile, just like the Ag^+ ions originating from Ag_2O molecules. These results are consistent with the prediction made by Minami et al.[1,5,6] that the electric conduction in AgX–Ag_2O–B_2O_3 glasses is primarily made by Ag^+ ions originating from AgX molecules. (X indicates Cl, Br, and I, as has been described above.) Their prediction will be especially valid in an Ag_2O content region in which most chloride ions are present at the interstitial sites of the three-dimensional network structure, i.e., when the Ag_2O content is lower than about 12 and 10.5 mol% in the cases of the silver borate glasses containing 20 and 30 mol% AgCl respectively. In the case of AgI–Ag_2O–B_2O_3 glasses, somewhat different results will be obtained, because the structural behavior of the I^- ion has been reported to be independent of the Ag_2O content of the glasses,[30] being contrary to the behavior of the Cl^- or Br^- ions.

Gamma-Ray irradiation experiments with silver borate glasses containing 20 mol% AgCl were performed in order to confirm the presence of nonbridging chlorine atoms in the silver borate glasses when the Ag_2O content is higher than about 10 mol%. According to the Mössbauer studies of γ-ray irradiated borate or borosilicate glasses, the irradiation is known to result in a decrease in the isomer shift of Fe^{3+} when a nonbridging oxygen atom is present in FeO_4 or BO_4 tetrahedral units.[21,36] Figure 7 shows the irradiation-induced changes in the isomer shift of Fe^{3+} in silver borate glasses containing 20 mol% AgCl. Gamma-Ray irradiations of 10^6 and 10^7 R result in gradual decreases in the isomer shifts, which are intermediate between the (a) and (b) curves. The gamma-ray irradiation of borate glasses is known to result in a reduction of Fe^{3+} to Fe^{2+} when the total iron content of the glasses is very low.[11,36] The decrease in the isomer shift shown in Fig. 7 is, therefore, ascribed to an increased *s*-electron density at the iron nucleus as a result of the charge transfer from a nonbridging chlorine atom to the neighboring iron atom constituting a FeO_3Cl tetrahedral unit. This will also be the case for a tetrahedral BO_3Cl unit.

All the experimental results obtained in the present study lead to the following conclusions. Chloride ions in AgCl–Ag_2O–B_2O_3 glasses are ionically bonded with Ag^+ ions at the interstitial sites of the three-dimensional network composed of BO_3 and BO_4 (and FeO_4) units when the Ag_2O content is lower than about 10 mol%, i.e., when the Ag_2O/B_2O_3 ratio is smaller than 15/85. On the other hand, chloride ions are covalently bonded with tetrahedral boron (or iron) atoms as nonbridging chlorine when the Ag_2O content exceeds about 10 mol%. These structural changes are concluded to affect the steric configuration of the Ag^+ ion, which is a cation conductor. That is, Ag^+ ions are considered to change their structural sites from the interstitial sites which are close to the Cl^- ions to different interstitial

sites which are close to the nonbridging chlorine atoms. The latter type of Ag^+ ions seems to be less mobile than the former, because a drastic decrease in the electric conductivity is observed when the Ag_2O content exceeds about 10 mol%.

The authors are indebted to Mr. Toshiharu Hirai of Chemical and Catalysis Industrial Corporation for his kind help in the electric-conductivity measurements. The present study was partially supported by the Itoh Science Foundation and by a Grant-in-Aid for Scientific Research (No. 60740234) from the Ministry of Education, Science, and Culture.

References

1) T. Minami, Y. Takura, and M. Tanaka, *J. Electrochem. Soc.*, **124**, 1659 (1977).
2) J. P. Malugani, A. Wasniewski, M. Doreau, G. Robert, and A. Rikabi, *Mater. Res. Bull.*, **13**, 427 (1978).
3) T. Minami and M. Tanaka, *Rev. Chim. Miner.*, **16**, 283 (1979).
4) A. Magistris, G. Chiodelli, and A. Schiraldi, *Electrochim. Acta*, **24**, 203 (1979).
5) T. Minami and M. Tanaka, *J. Non-Cryst. Solids*, **38**, **39**, 289 (1980).
6) T. Minami, K. Imazawa, and M. Tanaka, *J. Non-Cryst. Solids*, **42**, 469 (1980).
7) J. P. Malugani, G. Robert, and R. Mercier, *Mater. Res. Bull.*, **15**, 715 (1980).
8) G. Chiodelli, A. Magistris, M. Villa, and J. L. Bjorkstam, *Mater. Res. Bull.*, **17**, 1 (1982).
9) A. Fontana, G. Mariotto, E. Cazzanelli, G. Carini, M. Cutroni, and M. Federico, *Phys. Lett.*, **93A**, 209 (1983).
10) G. Dalba, A. Fontana, P. Fornasini, G. Mariotto, M. R. Masullo, and F. Rocca, *Solid State Ionics*, **9**, **10**, 597 (1983).
11) J. P. Malugani, R. Mercier, B. Fahys, and G. Robert, *J. Solid State Chem.*, **45**, 309 (1982).
12) J. P. Malugani and R. Mercier, *Solid State Ionics*, **13**, 293 (1984).
13) G. Chiodelli, G. Campariviganо, G. Flor, A. Magistris, and M. Villa, *Solid State Ionics*, **8**, 311 (1983).
14) K. Matusita and S. Sakka, *Yogyo Kyokai Shi*, **84**, 496 (1976).
15) T. Tsuchiya, T. Horiuchi, and T. Moriya, *Yogyo Kyokai Shi*, **87**, 223 (1979).
16) T. Nishida and Y. Takashima, *J. Non-Cryst. Solids*, **37**, 37 (1980).
17) T. Nishida, T. Shiotsuki, and Y. Takashima, *J. Non-Cryst. Solids*, **41**, 161 (1980).
18) T. Nishida, T. Hirai, and Y. Takashima, *J. Non-Cryst. Solids*, **43**, 221 (1981).
19) T. Nishida, N. Kai, and Y. Takashima, *Phys. Chem. Glasses*, **22**, 107 (1981).
20) T. Nishida, T. Nonaka, T. Isobe, and Y. Takashima, *Phys. Chem. Glasses*, **24**, 88 (1983).
21) T. Nishida, T. Hirai, and Y. Takashima, *Phys. Chem. Glasses*, **22**, 94 (1981).
22) T. Nishida, T. Hirai, and Y. Takashima, *Bull. Chem. Soc. Jpn.*, **54**, 3735 (1981).
23) T. Nishida, T. Shiotsuki, and Y. Takashima, *J. Non-Cryst. Solids*, **43**, 115 (1981).
24) T. Nishida, T. Shiotsuki, and Y. Takashima, *J. Non-Cryst. Solids*, **43**, 123 (1981).
25) T. Nishida, Y. Miyamoto, and Y. Takashima, *Bull. Chem. Soc. Jpn.*, **56**, 439 (1983).
26) T. Nishida, M. Katada, and Y. Takashima, *Bull. Chem. Soc. Jpn.*, **57**, 3566 (1984).
27) T. Nishida, M. Katada, and Y. Takashima, *Bull. Chem. Soc. Jpn.*, **58**,1745 (1985).
28) T. Nishida, A. Nakamura, and Y. Takashima, *Chem. Lett.*, **1984**, 1683.
29) T. Nishida, T. Nonaka, and Y. Takashima, *Bull. Chem. Soc. Jpn.*, **58**, 2255 (1985)
30) T.Maekawa, S. Satoh, and T. Yokokawa, *Yogyo Kyokai Shi*, **93**, 20 (1985).
31) R. M. Almeida and J. D. Mackenzie, *J. Chem. Phys.*, **74**, 5954 (1981).
32) E. N. Boulos and N. J. Kreidl, *J. Am. Ceram. Soc.*, **54**, 368 (1971).
33) J. L. Piguet and J. E. Shelby, *J. Am. Ceram. Soc.*, **68**, 450 (1985).
34) J. E. Shelby, *J. Am. Ceram. Soc.*, **57**, 436 (1974).
35) J. E. Shelby, *J. Appl. Phys.*, **46**, 193 (1975).
36) T. Nishida, Y. Takashima, and Y. Nakayama, *J. Solid State Chem.*, **33**, 141 (1980).

 © 1986 The Chemical Society of Japan Bull. Chem. Soc. Jpn., 59, 2407—2413 (1986)

Calorimetric and Spectrophotometric Studies of Copper(II) Chloro Complexes in Dimethyl Sulfoxide

Shin-ichi Ishiguro, Honoh Suzuki, Bojana G. Jeliazkova,† and Hitoshi Ohtaki*
Department of Electronic Chemistry, Tokyo Institute of Technology at Nagatsuta, 4259, Nagatsuta-cho, Midori-ku, Yokohama 227
†Department of Analytical Chemistry, Sofia University, Anton Ivanov 1, Sofia, Bulgaria
(Received March 5, 1986)

Complex formation equilibria between copper(II) and chloride ions have been studied by calorimetric and spectrophotometric titrations in dimethyl sulfoxide (DMSO) containing 0.2 mol dm^{-3} $(C_2H_5)_4NClO_4$ or 1 mol dm^{-3} $LiClO_4$ as a constant ionic medium at 25 °C. Both calorimetric and spectrophotometric data obtained were well explained in terms of formation of $[CuCl_n]^{(2-n)+}$ (n=1—4) in each solution, and their formation constants, enthalpies and entropies were determined. It was found that the complexation at each step was appreciably suppressed in the $LiClO_4$ DMSO solution compared to that in the $(C_2H_5)_4NClO_4$ one, which was ascribed to the extensive formation of LiCl ion-pairs in the former solution. As well as in *N,N*-dimethylformamide (DMF),[1] positive values of stepwise ΔH_n° and ΔS_n° (n=1—3) and negative ΔH_4° values were observed in DMSO. However, the ΔS_n° (n=1, 2, and 4) values in DMSO were appreciably smaller than the corresponding ones in DMF. The result was interpreted in terms of stronger intermolecular interactions in the bulk DMSO than those in DMF. The entropies of transfer of $[CuCl_n]^{(2-n)+}$ (n=0—4) from DMF to DMSO were significantly positive. This result also suggested that DMSO is a highly associated solvent. Electronic spectra of individual copper(II) chloro complexes were extracted from the spectra measured by varying molar ratios of chloride to copper(II) ions in solution. In contrast to the electronic spectra of Cu^{2+}, $[CuCl]^+$ and $[CuCl_2]$, the spectra of $[CuCl_3]^-$ and $[CuCl_4]^{2-}$ in DMSO were not appreciably different from those in DMF, indicating that solvation of these complexes are rather weak in both solvents.

The complexation of copper(II) with chloride ions in dimethyl sulfoxide (DMSO) has so far been studied by spectrophotometry,[2,3] potentiometry,[3-5] and conductometry.[5] These works elucidated the formation of mononuclear copper(II) chloro complexes in the solvent. Although the formation constants of these complexes have been obtained, their enthalpies and entropies have not been determined in DMSO yet.

We previously reported the complex formation equilibria between copper(II) and chloride ions in *N,N*-dimethylformamide (DMF),[1] in acetonitrile[6] and in their mixtures[7] by calorimetric and spectrophotometric measurements. A large difference was found in the enthalpies of complexation in these solvents, so that the difference in the metal-solvent bonding energies was indicated to play a dominant role for solvent effect on the complexation. In this respect, the donicity of DMSO is only slightly larger than that of DMF.[8] However, DMSO is expected to be a highly associated liquid,[9] while DMF has so weak intermolecular interactions that it shows practically random distribution in the bulk.[10]

In this work, therefore, we investigated the complexation of copper(II) with chloride ions in DMSO and compared the thermodynamic quantities of complexation thus obtained with those in DMF. The thermodynamic quantities were determined in 0.2 mol dm^{-3} $(C_2H_5)_4NClO_4$ and 1 mol dm^{-3} $LiClO_4$ DMSO solutions by the same methods as used in previous works.[1,6] In order to evaluate the enthalpies of transfer of each $[CuCl_n]^{(2-n)+}$ (n=0—4) complex from DMF to DMSO, the enthalpy of solution of neutral $CuCl_2$ was determined in DMSO, as well as in DMF. Similarly, the corresponding Gibbs energies of transfer ΔG_t° of each complex were evaluated on the basis of the ΔG_t° values of copper(II) and chloride ions from the literature.[11,12] Electronic spectra of individual copper(II) chloro complexes were extracted by resolving the spectra measured in DMSO by varying molar ratios of chloride to metal ions.

Experimental

Reagents. *Copper(II) Perchlorate* was prepared from copper(II) oxide and perchloric acid of super special reagent grade. The copper(II) perchlorate thus prepared were recrystallized three times from water, and $Cu(ClO_4)_2 \cdot 6H_2O$ crystals were then dried in a vacuum oven at 70 °C. *Copper(II) perchlorate DMSO solvates*, $Cu(ClO_4)_2 \cdot x$DMSO, were prepared from $Cu(ClO_4)_2 \cdot 6H_2O$ by dissolving in an ethanol-diethyl ether mixture of equal volume fractions, followed by adding DMSO to yield the DMSO solvate crystals. The crystals thus obtained were washed with acetone, recrystallized from acetone and dried in vacuum at 50 °C for several days. An electrogravimetrical analysis showed that the value of x within the crystals finally obtained was close to 5.

Dimethyl sulfoxide was refluxed over CaH_2 for about one day, then distilled twice over CaH_2 at 50 °C under a reduced pressure (260 Pa) and kept over molecular sieves 4A 1/16 in a dark bottle with a P_2O_5 drying-tube.

Other chemicals used were prepared and dried by usual procedures as described elsewhere.[1] All test solutions were prepared in a dry box over P_2O_5 under an atmosphere of nitrogen gas.

Measurements. Calorimetric and spectrophotometric measurements were carried out in a room thermostated at (25.0±0.2) °C. All test solutions prepared contained 0.2 mol dm^{-3} $(C_2H_5)_4NClO_4$ or 1 mol dm^{-3} $LiClO_4$ as a constant ionic medium.

Calorimetric measurements were performed in a thermostated water-bath at (25.000±0.007) °C. 100 cm^3 of a cop-

per(II) perchlorate solution was placed in a Dewar vessel, which was filled with nitrogen gas and prevented from moisture with a P_2O_5 drying-tube, and then was titrated with either 0.2 mol dm^{-3} $(C_2H_5)_4NCl$ or 1 mol dm^{-3} LiCl DMSO solution. The concentration of copper(II) ion in the initial test solutions was varied in the range 8—40 mmol dm^{-3}. Heats of complexation at each point of titration were ranged 1—5 J with a certainty ±0.05 J and were corrected for heats of dilution of the titrant separately determined by titrating either 0.2 mol dm^{-3} $(C_2H_5)_4NClO_4$ or 1 mol dm^{-3} $LiClO_4$ DMSO solution with relevant titrant solutions in advance. Details of the data treatment have been described previously.[1,13]

Electronic spectra were measured with a HITACHI 340 spectrophotometer (HITACHI) equipped with a JEC 6 electronic computer (JEOL) which recorded data at selected wavelengths. A flow cell with a light-pass length of 0.5 cm was connected with a titration vessel through teflon and glass tubes. 15 cm^3 of a $Cu(ClO_4)_2$ DMSO solution was placed in a vessel under a nitrogen atmosphere and then was titrated with either the $(C_2H_5)_4NCl$ or LiCl DMSO solution.

Analysis of Calorimetric and Spectrophotometric Data. Calorimetric data obtained were analyzed by assuming the formation of mononuclear $[CuCl_n]^{(2-n)+}$, and their formation constants and enthalpies were simultaneously determined by the least-squares method as described previously.[1,6,7,13]

The absorbance data obtained at thirty different wavelengths in the range 250—500 nm were analyzed by the same procedure as that used previously,[1,6] and the formation constants of $[CuCl_n]^{(2-n)+}$ (n=1—4) were determined together with the molar extinction coefficents of the complexes at each relevant wavelength.

Results and Discussion

Calorimetric titration curves obtained in 0.2 mol dm^{-3} $(C_2H_5)_4NClO_4$ and 1 mol dm^{-3} $LiClO_4$ DMSO solutions are depicted in Figs. 1 and 2, respectively. In each solution, enthalpies $\Delta H^\circ = -q/(\delta v C_{X,tit})$ were plotted against C_X/C_M, where q, δv, C_X and C_M stand for the heat evolved, the volume of an aliquot of the titrant added and the total concentrations of chloride and copper(II) ions in a solution, respectively, at each titration point, and $C_{X,tit}$ denotes the concentration of chloride ion in the titrant solution.

The trend of variation of the titration curves was similar in both $(C_2H_5)_4NClO_4$ and $LiClO_4$ DMSO solutions over the whole range of C_X/C_M examined. In both solutions, the ΔH° values at lower $C_X/C_M<0.5$ were kept constant and were independent of the metal concentration in solutions, the $[CuCl]^+$ complex being indicated to solely form in the range. With increasing C_X/C_M up to 2, the ΔH° value then increased and changed depending on the metal concentration, so that $[CuCl_2]$ was expected to form with a more endothermicity than $[CuCl]^+$. In the range $C_X/C_M>2$, the ΔH° value gradually decreased to approach $\Delta H^\circ=0$ with an increase in C_X/C_M, the higher $[CuCl_3]^-$ and $[CuCl_4]^{2-}$ complexes being expected to form over the range.

The result of the least-squares refinement of the calorimetric and spectrophotometric data in the $(C_2H_5)_4NClO_4$ DMSO solution are summarized in Table 1.

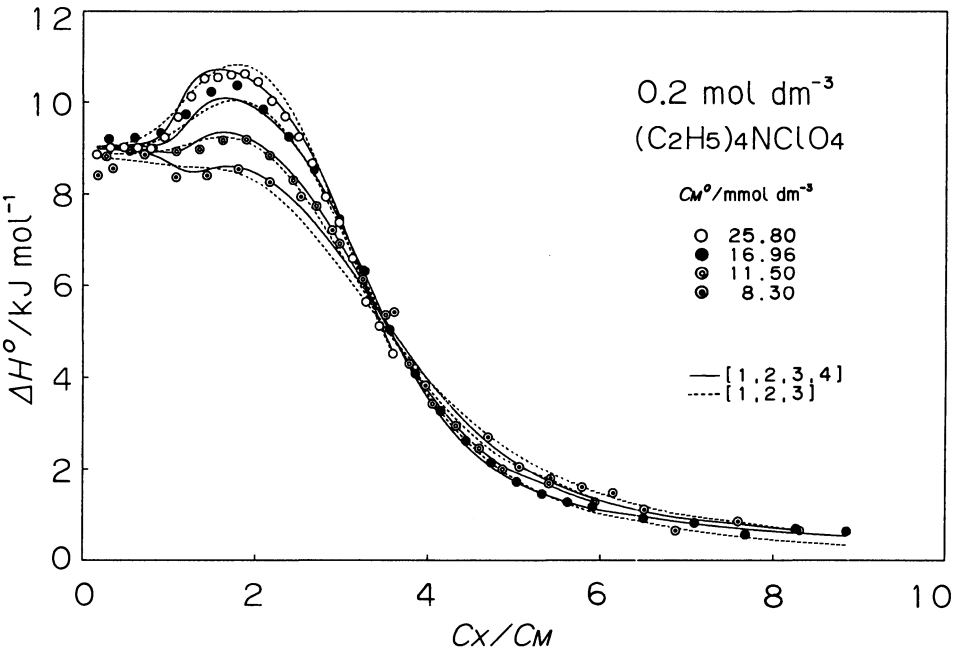

Fig. 1. Calorimetric titration curves of copper(II) chloride DMSO solutions containing 0.2 mol dm^{-3} $(C_2H_5)_4NClO_4$ at 25 °C. Initial concentrations of copper(II) perchlorate (C_M°/mmol dm^{-3}) are given in the figure. The solid and broken lines show the theoretical curves calculated by using the constants of the sets (1—4) and (1—3), respectively, in Table 1.

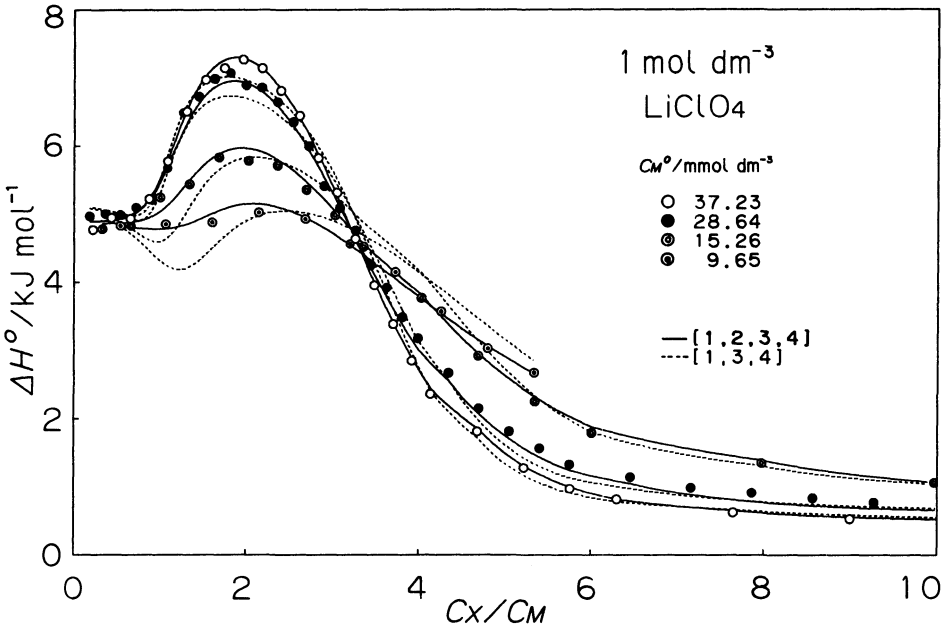

Fig. 2. Calorimetric titration curves of copper(II) chloride DMSO solutions containing 1 mol dm^{-3} $LiClO_4$ at 25 °C. Initial concentrations of copper(II) perchlorate (C°_M/mmol dm^{-3}) are given in the figure. The solid and broken lines show the theoretical curves calculated by using the constants of the sets (1—4) in Table 2 and the set (1, 3, 4), respectively.

Table 1. The Least-Squares Refinement of Overall Formation Constants, β_n/mol^{-n} dm^{3n}, and Enthalpies, $\Delta H^{\circ}_{\beta n}$/kJ mol^{-1}, of Formaion of Copper(II) Chloro Complexes in Dimethyl Sulfoxide Containing 0.2 mol dm^{-3} $(C_2H_5)_4ClO_4$ as a Constant Ionic Medium at 25 °C

	Cal (1—3)[a]	Cal (1—4)[a]	Spec (1—4)[a]
$\log\beta_1$	3.61(0.19)	4.23(0.23)	4.66(0.08)
$\log\beta_2$	6.07(0.19)	6.48(0.25)	7.30(0.11)
$\log\beta_3$	8.13(0.19)	8.95(0.26)	9.56(0.10)
$\log\beta_4$	—	9.55(0.46)	10.59(0.12)
$\Delta H^{\circ}_{\beta 1}$	9.08(0.09)	9.06(0.05)	—
$\Delta H^{\circ}_{\beta 2}$	20.4(0.3)	21.4(0.4)	—
$\Delta H^{\circ}_{\beta 3}$	39.9(0.3)	34.9(0.5)	—
$\Delta H^{\circ}_{\beta 4}$	—	55(9)	—
N[b]	90	90	2370
U[c]	0.728	0.348	0.114
R[d]	0.0323	0.0223	0.0099

Values in parentheses refer to standard deviations. a) The numbers indicate the n values of the $[CuCl_n]^{(2-n)+}$ complexes assumed in the course of the refinements. b) The number of data points. c) The error-square sum. d) The Hamilton R-factor.

The calorimetric data were analyzed by assuming several sets of mononuclear complexes. Among these sets examined, the set (1—4) assuming the formation of $[CuCl_n]^{(2-n)+}$ (n=1, 2, 3, and 4) gave the minimum error-square sum. However, since the $\Delta H^{\circ}_{\beta 4}$ value showed a rather large standard deviation, the $[CuCl_4]^{2-}$ complex may not appreciably form in the solution. Therefore, the set (1—3) eliminating $[CuCl_4]^{2-}$ was also examined for comparison. As seen in Fig. 1 by the broken lines, the theoretical curves calculated by using the constants of the set (1—3) in Table 1 ill fitted the experimental points, and thus it was concluded that the $[CuCl_4]^{2-}$ complex must not be neglected. In fact, as seen in Fig. 1 by the solid lines, the experimental points well fell on the theoretical curves when the four $[CuCl_n]^{(2-n)+}$ (n=1—4) complexes were taken into account. Electronic spectra measured in the solution were also indicated the formation of the four complexes and their formation constants evaluated were similar to those obtained by calorimetry.

The result of the least-squares refinement of the calorimetric and spectrophotometric data in the $LiClO_4$ DMSO solution are summarized in Table 2. In the solution, the formation constants and enthalpies of all the $[CuCl_n]^{(2-n)+}$ (n=1—4) complexes were determined with sufficient accuracy by both calorimetry and spectrophotometry. According to the result obtained by Elleb et al.[2] in the same solution by spectrophotometry, the formation of $[CuCl_2]$ was not conclusive. In fact, the distribution of species calculated by using the formation constants of the complexes in Table 2 indicated that the degree of formation of $[CuCl_2]$ was rather small. Thus, the refinement of the calorimetric data was also carried out for the set (1, 3, and 4) by eliminating the neutral complex. However, as seen in Fig. 2, the theoretical curves for the set (1—4) given by the solid lines well reproduced the experimental points, while those for the set (1, 3, and 4) shown by the broken lines ill

Table 2. The Least-Squares Refinement of Overall Formation Constants, β_n/mol^{-n}dm^{3n}, Enthalpies, $\Delta H^\circ_{\beta n}$/kJ mol^{-1}, of Formation of Copper(II) Chloro Complexes in Dimethyl Sulfoxide Containing 1 mol dm^{-3} $LiClO_4$ as a Constant Ionic Medium at 25 °C

	Cal	Spec	Cal[a]	Spec[a]
$\log\beta_1$	3.63(0.16)	3.35(0.02)	4.11(0.17)	3.79(0.02)
$\log\beta_2$	5.67(0.19)	5.11(0.08)	6.56(0.19)	6.01(0.08)
$\log\beta_3$	7.49(0.17)	7.21(0.07)	8.85(0.17)	8.55(0.07)
$\log\beta_4$	8.19(0.20)	7.78(0.09)	9.64(0.19)	9.59(0.09)
$\Delta H^\circ_{\beta 1}$	3.56(0.06)	—	8.99(0.06)	—
$\Delta H^\circ_{\beta 2}$	9.6(0.2)	—	20.5(0.2)	—
$\Delta H^\circ_{\beta 3}$	22.5(0.5)	—	37.9(0.4)	—
$\Delta H^\circ_{\beta 4}$	11.9(0.6)	—	23.5(1.1)	—
N[b]	104	2160	104	2160
U[c]	1.16	0.113	1.09	0.113
R[d]	0.0503	0.0126	0.0332	0.0126

Values in parentheses refer to standard deviations. a) The formation of LiCl ion-pairs is taken into consideration: $\log K_{ip}=0.25$, $\Delta H^\circ_{ip}=8.5$ kJ mol^{-1}. b) The number of data points. The formation constants by spectrophotometry were obtained by using absorbance data at 30 different wavelengths. c) The error-square sum. d) The Hamilton R-factor.

fitted the experimental points, implying that the $[CuCl_2]$ complex should not be neglected. The formation constants were also evaluated from the spectrophotometric data, which were similar to those obtained by calorimetry as well.

As seen in Tables 1 and 2, a significant difference was found between the corresponding quantities in the $(C_2H_5)_4NClO_4$ and $LiClO_4$ solutions. It has been so far suggested that lithium chloride forms contact ion-pairs in DMSO,[14-16] although it is ambiguous.[17] Besides, in contrast to the $(C_2H_5)_4NClO_4$ DMSO solution, significant heats of dilution were observed when the LiCl DMSO solution was added to a DMSO solution of the relevant ionic medium. Therefore, it was expected that the LiCl contact ion-pairs appreciably formed in the LiCl titrant solution, and its formation constant and enthalpy, $\log(K_{ip}/\text{mol}^{-1}\text{dm}^3)=(0.25\pm0.07)$ and $\Delta H^\circ_{ip}=(8.5\pm0.6)$ kJ mol^{-1} (the uncertainties refer to standard deviations), respectively, were estimated by analyzing the heats of dilution of the LiCl titrant solution. Then, a further analysis of the calorimetric and spectrophotometric data obtained in the $LiClO_4$ DMSO solution was performed by knowing amount of LiCl ion-pairs formed in the solution. The formation constants and enthalpies of formation of $[CuCl_n]^{(2-n)+}$ (n=1—4) thus corrected for the formation of LiCl ion pairs are also listed in Table 2, the stepwise $\log(\beta_n/\beta_{n-1})$ values being practically the same as the corresponding values in the $(C_2H_5)_4NClO_4$ DMSO solution. Thus, it is concluded that an extensive formation of LiCl ion-pairs reduces the concentration of free chloride ions, which reflects on the unfavorable complexation of copper(II) with chloride ions in the $LiClO_4$ DMSO solution compared to that in the $(C_2H_5)_4NClO_4$ DMSO solution.

Figure 3 shows the distribution of species of the copper(II) chloro complexes in the 0.2 mol dm^{-3} $(C_2H_5)_4NClO_4$ DMSO solution (the upper figure by the solid lines) and 1 mol dm^{-3} $LiClO_4$ DMSO solution (the lower figure). The distribution of species corrected for the formation of LiCl ion-pairs in the $LiClO_4$ solution is also depicted (the upper figure by the broken lines), which is similar to that in the $(C_2H_5)_4NClO_4$ solution.

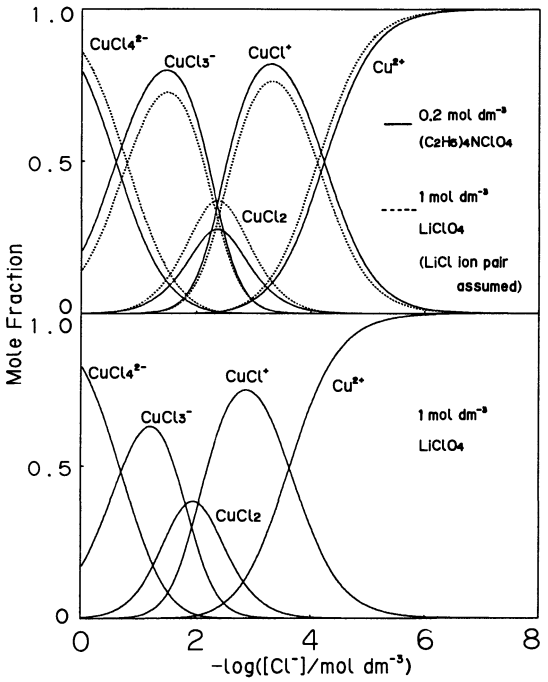

Fig. 3. Distribution of species of the copper(II) chloro complexes in the 0.2 mol dm^{-3} $(C_2H_5)_4NClO_4$ and 1 mol dm^{-3} $LiClO_4$ DMSO solutions. The distribution of species in the $LiClO_4$ DMSO solution corrected for the formation of LiCl ion-pairs is depicted by the broken lines.

Thermodynamic quantities, $\log(K_n/\text{mol}^{-1}\text{dm}^3)$, ΔG°_n/kJ mol^{-1}, ΔH°_n/kJ mol^{-1} and ΔS°_n/J K^{-1} mol^{-1}, for the stepwise formation of $[CuCl_n]^{(2-n)+}$ in DMSO are summarized in Table 3, together with those in DMF for comparison.[1]

Table 3. Thermodynamic Quantities, $\log(K_n/\mathrm{mol^{-1}\,dm^3})$, $\Delta G_n^\circ/\mathrm{kJ\,mol^{-1}}$, $\Delta H_n^\circ/\mathrm{kJ\,mol^{-1}}$, and $\Delta S_n^\circ/\mathrm{J\,K^{-1}\,mol^{-1}}$, for the Stepwise Formation of $[CuCl_n]^{(2-n)+}$ in Dimethyl Sulfoxide at 25 °C

	Dimethyl Sulfoxide			*N,N*-Dimethylformamide
	0.2 mol dm^{-3} $(C_2H_5)_4NClO_4$	1 mol dm^{-3} $LiClO_4$	1 mol dm^{-3} $LiClO_4$[a]	0.2 mol dm^{-3} $(C_2H_5)_4NClO_4$[c]
$\log K_1$	4.23	3.63	4.11	6.79
$\log K_2$	2.25	2.04	2.45	4.54
$\log K_3$	2.47	1.82	2.29	4.00
$\log K_4$	0.60	0.70	0.79	1.52
ΔG_1°	−24.1	−20.7	−23.5	−38.8
ΔG_2°	−12.8	−11.6	−14.0	−25.9
ΔG_3°	−14.1	−10.4	−13.1	−22.8
ΔG_4°	−3.4	−4.0	−4.5	−8.7
ΔH_1°	9.1	3.6	9.0	10.3
ΔH_2°	12.3	6.0	11.5	9.7
ΔH_3°	13.5	13.0	17.5	7.3
ΔH_4°		−10.6	−14.5	−8.1
ΔS_1°	111	81	109	165
ΔS_2°	84	59	85	120
ΔS_3°	93	78	103	101
ΔS_4°		−22	−33	2
$\Delta G_{\beta 4}^\circ$[b]		−46.7	−55.0	−96.2
$\Delta H_{\beta 4}^\circ$[b]		11.9	23.5	19.2
$\Delta S_{\beta 4}^\circ$[b]		197	263	387

a) The formation of LiCl ion-pairs was taken into account. b) For the overall formation of $[CuCl_4]^{2-}$. c) Ref. 1.

Formation of Copper(II) Chloro Complexes. As seen in Table 3, the thermodynamic quantities of formation of the copper(II) chloro complexes in DMSO are, in general, similar to those in DMF, as expected from strong donicities and relatively weak acceptor abilities of both solvents.[8] As well as in DMF, the positive ΔH_n° (n=1—3) values were observed in DMSO, indicating that copper(II) ion is strongly solvated in these solvents. It was found that the ΔH_n° (n=1—3) values changed in the sequence $\Delta H_1^\circ<\Delta H_2^\circ<\Delta H_3^\circ$ in DMSO but in the sequence $\Delta H_1^\circ>\Delta H_2^\circ>\Delta H_3^\circ$ in DMF. The Cu–Cl bonds are weaken within a higher $[CuCl_n]^{(2-n)+}$ complex and solvation energies of $[CuCl_n]^{(2-n)+}$ (n=1—3) become weaker with n due to an electron donation from chloride ions to the metal ion. The different trend of ΔH_n° (n=1—3) in DMSO and DMF suggests that weakening of the metal-solvent bonds within $[CuCl_n]^{(2-n)+}$ (n=1—3) with n occurs in a different manner in these solvents. The negative ΔH_4° value observed in DMSO suggests that the metal-solvent bond is very weak within $[CuCl_3(dmso)]^-$, and $[CuCl_4]^{2-}$ is not solvated in the first coordination sphere of the metal ion, the structure of the complexes being discussed in the later section.

In previous papers,[1,6] we discussed the entropies of formation of the copper(II) chloro complexes in DMF and acetonitrile in relation to the solvent-solvent interactions in the bulk. The positive and large ΔS_n° (n=1—3) values observed in DMSO suggests that DMSO molecules solvating copper(II) and chloride ions are liberated from the coordination shells of the ions, and enter the bulk solvent with a relatively high freedom.[18] However, comparing the entropy changes in DMSO (corrected for the formation of LiCl ion-pairs) with those in DMF, the ΔS_n° (n=1 and 2) values, as well as $\Delta S_{\beta 4}^\circ$, in DMSO are appreciably smaller than the corresponding ones in DMF. This suggests that the solvent-solvent interaction in DMSO is significantly different from that in DMF. It has been so far pointed out that DMSO is a highly associated liquid,[9] and DMSO oligomers are formed even in dilute DMSO solutions of benzene,[19] while DMF has only weak intermolecular interactions in the liquid state.[10] Therefore, less entropies of formation of the complexes in DMSO are attributable to larger entropy losses of the solvent molecules at entering the structured bulk phase from the coordination sphere as compared with the case of DMF which has a random intermolecular structure in the bulk. In contrast to large difference in $\Delta S_{\beta 4}^\circ$ in DMSO and DMF, the $\Delta H_{\beta 4}^\circ$ value in DMSO was even more positive than that in DMF. Thus, we propose that the effect of solvent-solvent interactions in the bulk on the thermodynamic quantities of formation of complexes in aprotic solvents reflects mainly on the entropy changes.

Thermodynamic Quantities of Transfer from *N,N*-Dimethylformamide to Dimethyl Sulfoxide. By measuring heats of solution of anhydrous $CuCl_2$ in DMSO, the enthalpies of solution for the following processes were evaluated:[6]

$$CuCl_2(c) = Cu^{2+}(s) + 2Cl^-(s);\ \Delta H_s^\circ(Cu^{2+}, 2Cl^-), \quad (1)$$

$$CuCl_2(c) = CuCl_2(s);\ \Delta H_s^\circ([CuCl_2]), \quad (2)$$

where c and s stand for the crystalline and solution states, respectively. Since the $\Delta H_s^\circ(Cu^{2+}, 2Cl^-)$ and $\Delta H_s^\circ([CuCl_2])$ values have been determined in DMF,[6] the enthalpy of transfer of copper(II) ion from DMF to DMSO, $\Delta H_t^\circ(Cu^{2+})$, was evaluated by knowing the $\Delta H_t^\circ(Cl^-)$ value from the literature:[20]

$$\Delta H^\circ_{s,DMSO}(Cu^{2+},2Cl^-) - \Delta H^\circ_{s,DMF}(Cu^{2+},2Cl^-) = \Delta H_t^\circ(Cu^{2+}) + 2\Delta H_t^\circ(Cl^-). \quad (3)$$

Similarly, the enthalpies of transfer of $[CuCl_n]^{(2-n)+}$ from DMF to DMSO, $\Delta H_t^\circ([CuCl_n]^{(2-n)+})$, were obtained from the relation:

$$\Delta H^\circ_{\beta n,DMSO} - \Delta H^\circ_{\beta n,DMF} = \Delta H_t^\circ([CuCl_n]^{(2-n)+}) - \Delta H_t^\circ(Cu^{2+}) - n\Delta H_t^\circ(Cl^-), \quad (4)$$

since all the values except for $\Delta H_t^\circ([CuCl_n]^{(2-n)+})$ have been known.

The Gibbs energies of transfer, $\Delta G_t^\circ([CuCl_n]^{(2-n)+})$ from DMF to DMSO were calculated by using the relation similar to Eq. 4 on the basis of the known $\Delta G_t^\circ(Cu^{2+})$ and $\Delta G_t^\circ(Cl^-)$ values from the literature.[11,12] The results are summarized in Table 4, together with the corresponding ΔS_t° values calculated from the ΔG_t° and ΔH_t° values.

The negative $\Delta H_t^\circ(Cu^{2+})$ value from DMF to DMSO may be attributable to the slightly larger donicity of DMSO than that of DMF.[8] Since the $\Delta H_t^\circ(Cl^-)$ value is also negative, the negative $\Delta H_t^\circ([CuCl_n]^{(2-n)+})$ values are expected from the view-point of both metal-solvent and ligand-solvent interactions of each complex.

The $\Delta G_t^\circ(Cu^{2+})$ value is more negative than $\Delta H_t^\circ(Cu^{2+})$ due to the largely positive $\Delta S_t^\circ(Cu^{2+})$ value. The ΔS_t° values of all the $[CuCl_n]^{(2-n)+}$ (n=1—4) complexes are positive. However, such positive ΔS_t° value from DMF to DMSO can hardly be explained in terms of the solely different donicities of these solvents, because the ΔS_t° values of the $[CuCl_n]^{(2-n)+}$ complex from acetonitrile to DMF, these solvents having largely different donicities, are close to zero.[6] The significantly positive $\Delta S_t^\circ([CuCl_n]^{(2-n)+})$ (n=1—4) values from DMF to DMSO may be ascribed to the difference in their intermolecular interactions in the bulk. When we consider the process of solvation of an ion which is transferred from vacuum to a solvent, the entropy of solvation of an ion, ΔS°_{solv}, should be negative as the result of formation of the solvation sphere. The stronger the metal-solvent bonds, the more negative value of ΔS°_{solv} may result. However, at the formation of solvation shell, solvent-solvent interactions in the bulk must be partially broken, and this process gives a positive value of entropy change. The more the association of solvent molecules in the bulk, the larger the positive entropy change is at the breaking of intermolecular interactions. Accordingly, the ΔS_t° value of an ion may be largely positive when the ion is transferred from a solvent randomly distributed to that associated, as such a case of transferring ions from acetonitrile to water.[21] Since DMSO has a long range intermolecular interactions,[9] and easily associates,[19] the large and positive ΔS_t° values of transfer of $[CuCl_n]^{(2-n)+}$ (n=0—4), as well as $\Delta S_t^\circ(Cl^-)$, from DMF to DMSO can be explained in terms of the different intermolecular interactions in the bulk phase.

Table 4. Thermodynamic Quantities of Transfer, ΔG_t°/kJ mol^{-1}, ΔH_t°/kJ mol^{-1} and ΔS_t°/J K^{-1} mol^{-1}, of $[CuCl_n]^{(2-n)+}$ from *N,N*-Dimethylformamide to Dimethyl Sulfoxide at 25 °C

	ΔG_t°	ΔH_t°	ΔS_t°
Cu^{2+}	−30.5[a]	−3.6	90
$[CuCl]^+$	−21.2	−7.4	46
$[CuCl_2]$	−15.3	−8.1	24
$[CuCl_3]^-$	−11.6	−0.4	38
$[CuCl_4]^{2-}$	−13.4	−9.3	14
Cl^-	−6.0[b]	−2.5[c]	12

a) Ref. 11. b) Ref. 12. c) Ref. 20.

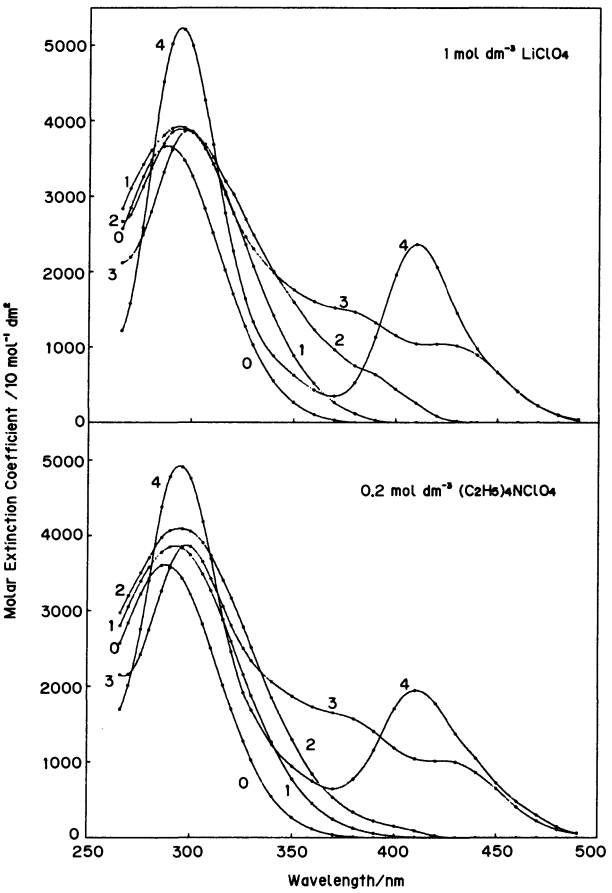

Fig. 4. Electronic spectra of individual copper(II) chloro complexes in the range 250—500 nm obtained in the 0.2 mol dm^{-3} $(C_2H_5)_4NClO_4$ and 1 mol dm^{-3} $LiClO_4$ DMSO solutions. The numbers represent n within $[CuCl_n]^{(2-n)+}$.

Electronic Spectra of Copper(II) Chloro Complexes. Together with the formation constants, electronic spectra of individual copper(II) chloro complex-

es were extracted by resolving the spectra measured at various C_X/C_M ratios in the 0.2 mol dm^{-3} $(C_2H_5)_4NClO_4$ and 1 mol dm^{-3} $LiClO_4$ DMSO solutions and represented in Fig. 4 over the range 250—500 nm.

As well as in DMF,[1] electronic spectra of each $[CuCl_n]^{(2-n)+}$ complex obtained are practically independent of ionic media, indicating that the structures of each complex obtained are not influenced by the medium salts.

As to Cu^{2+}, $[CuCl]^+$ and $[CuCl_2]$, the absorption maximum of each species in DMSO is appreciably shifted to a longer wavelength than that in DMF, suggesting that these species are differently solvated with DMSO and with DMF. In contrast, the electronic spectra of $[CuCl_3]^-$ and $[CuCl_4]^{2-}$ in DMSO are very similar to those of relevant species in DMF,[1] and thus the metal-solvent interaction in these solvent may be very weak. According to X-ray diffraction measurements for DMF solutions of copper(II) chloride,[22] the $[CuCl_4]^{2-}$ complex has a distorted tetrahedral structure and no solvent molecule is directly coordinated to the central metal ion, and the $[CuCl_3]^-$ complex has an additional DMF molecule to form a distorted tetrahedral structure and thus the complex should be described as $[CuCl_3(dmf)]^-$. The Cu–dmf bond within $[CuCl_3(dmf)]^-$ is weaker as indicated by its longer bond-length (230 pm) than the Cu–dmf(eq) bond (201 pm) within $[Cu(dmf)_6]^{2+}$. The similar electronic spectra of $[CuCl_3]^-$ and $[CuCl_4]^{2-}$ in DMSO and in DMF suggest that these complexes have practically the same structures in both solvents and the Cu–dmso bond within $[CuCl_3(dmso)]^-$ may be as weak as the Cu–dmf bond within $[CuCl_3(dmf)]^-$.

The present work has been financially supported by the Grant-in-Aid for Special Project Research No. 60129031 and partly by the Grant-in-Aid for Scientific Research No. 60540389 from the Ministry of Education, Science and Culture.

References

1) S.Ishiguro, B. G. Jeliazkova, and H. Ohtaki, *Bull. Chem. Soc. Jpn.*, **58**, 1143 (1985).
2) M. Elleb, J. Meullemeestre, M. J. Schwing-Weill, and F. Vierling, *Inorg. Chem.*, **21**, 1477 (1982).
3) T. E. Suares, R. T. Iwamoto, and J. Kleinberg, *Inorg. Chim. Acta*, **7**, 292 (1973).
4) A. Foll, M. Le Démezet, and J. Courtot-Coupez, *J. Electroanal. Chem.*, **35** (1972).
5) W.Libuś, M. Pilarczyk, and T. Szuchnicka, *Electrochim. Acta*, **25**, 1033 (1980).
6) S. Ishiguro, B. G. Jeliazkova, and H. Ohtaki, *Bull. Chem. Soc. Jpn.*, **58**, 1749 (1985).
7) S. Ishiguro, B. G. Jeliazkova, and H. Ohtaki, *Bull. Chem. Soc. Jpn.*, **59**, 1073 (1986).
8) V. Gutmann, "The Donor-Acceptor Approach to Molecular Interactions," Prenum, New York and London (1978).
9) H. H. Szmant, "Dimethyl Sulfoxide," ed by S. W. Jacob, E. E. Rosenbaum, and C. D. Wood, Marcel Dekker, New York (1971).
10) H. Ohtaki, S. Itoh, T. Yamaguchi, S. Ishiguro, and B. M. Rode, *Bull. Chem. Soc. Jpn.*, **56**, 3406 (1983).
11) J. F. Coetzee and W. K. Istone, *Anal. Chem.*, **52**, 53 (1980).
12) A. J. Parker, U. Mayer, R. Schmid, and V. Gutmann, *J. Org. Chem.*, **43**, 1843 (1978).
13) S. Ishiguro, K. Yamamoto, and H. Ohtaki, *Anal. Sci.*, **1**, 263 (1985).
14) R. Garnsey and J. E. Prue, *Trans. Faraday Soc.*, **64**, 1206 (1967).
15) J. S. Dunnett and R. P. H. Gasser, *Trans. Faraday Soc.*, **61**, 922 (1965).
16) W. H. Smyrl and C. W. Tobias, *J. Electrochem. Soc.*, **115**, 33 (1968).
17) G. Holleck, D. R. Cogley, and J. N. Butler, *J. Electrochem. Soc.*, **116**, 952 (1969).
18) S. Ahrland, *Pure Appl. Chem.*, **51**, 2019 (1979).
19) J. J. Kenttamaa and J. J. Lindberg, *Suomen Kemistilehti*, **33B**, 189 (1960).
20) B. G. Cox, G. R. Hedwig, A. J. Parker, and D. W. Watts, *Aust. J. Chem.*, **27**, 477 (1974).
21) Y. Marcus, *Pure Appl. Chem.*, **57**, 1103 (1985).
22) K. Ozutsumi, S. Ishiguro, and H. Ohtaki, to be published.

 © 1986 The Chemical Society of Japan Bull. Chem. Soc. Jpn., 59, 2415—2419 (1986)

Crystal Structure and Molecular Motion of Tetramethylammonium Hexaiodotellurate(IV)-Iodine (1/1) Compound

Hideko KIRIYAMA* and Kyoko NISHIZAKI
Department of Chemistry, Faculty of Science, Kobe University, Nada, Kobe 657
(Received March 31, 1986)

The crystal structure of the title compound was determined by means of X-ray diffraction. The crystal data and the final R value are: $[(CH_3)_4N]_2TeI_6 \cdot I_2$, tetragonal $I4_1/acd$, a=20.356 (3) and c=27.571 (5) Å, V=11,424 (3) Å^3, Z=16, R=0.082 for 1562 observed unique reflections. The structure consists of discrete $[TeI_6]^{2-}$ anions and Me_4N^+ cations in an arrangement analogous to the K_2PtCl_6 structure and of additional I_2 molecules bridging adjacent complex anions. The TeI_6 octahedron is considerably distorted with Te-I distances of 2.933 (2), 3.017 (2), and 2.857 (2) Å, owing to different interaction with the surrounding I_2 molecules. Two of three independent Me_4N^+ cations are orientationally disordered and distributed over each two positions. A phase transition was found at 234 K from DTA and its molar enthalpy was estimated to be approximately 2.4 kJ mol^{-1} from DSC. Proton NMR studies offered direct evidences for threefold reorientation of CH_3 groups and overall rotation of Me_4N^+ cations taking place consecutively far below room temperatures. At 234 K the spin-lattice relaxation time T_1 changes discontinuously by about one order of magnitude, suggesting the first order of transition. The activation energies of such composite reorientation in the fast regions ($\omega\tau_c \ll 1$) are 5.4 and 14.2 kJ mol^{-1} in the high- and low-temperature phases, respectively.

A large family of methylammonium hexahalometallate(IV) complexes, $[(CH_3)_nNH_{4-n}]_2MX_6$ where M=Pd, Pt, Sn, Te, X=Cl, Br, I, and n=1, 2, 3, 4 exhibit one or more phase transitions associated with molecular motion of cation groups or complex anions.[1,2] Most of them have the typical K_2PtCl_6 type structure, but some tellurate complexes of the series, especially their iodo analogues, are characterized by the unique structures different from the others.[3,4] In order to develop our study on methylammonium hexaiodotellurate(IV), $[(CH_3)_nNH_{4-n}]_2TeI_6$, the complex for n=4 was tried to prepare, but the obtained crystals did include extra iodine atoms, as encountered in $(Me_3NH)_2TeI_7$.[4] The crystal structure of the resulting octaiodotellurate complex was determined by X-ray diffraction methods to elucidate the role of extra iodine atoms and the dynamic process of cations was revealed by ^{1}H NMR experiments to connect with the phase transition newly found.

Experimental

Preparation. A saturated aqueous solution of tetramethylammonium iodide added dropwise with stirring into a hydrogen iodide solution of tellurium dioxide in a stoichiometric molar ratio yielded black precipitates. The product showed broad X-ray powder patterns because of its poor crystallinity. Most of the reflections could be roughly indexed on the basis of a cubic K_2PtCl_6 cell (space group $Fm3m$) with a=14.2 Å, but some of them remained unindexed. In order to obtain single crystals suitable for X-ray use, the precipitate was dissolved into a hot, dilute (ca. 3%) HI solution and black cubooctahedron-like crystals were grown from the filtrate. These crystals were identified with the source material from the X-ray powder patterns and confirmed to be $(Me_4N)_2TeI_8$ by chemical analyses. Unlike $(Me_3NH)_2TeI_7$, the recrystallization from an HI solution did not change the chemical constitution, therefore the original precipitate also being not hexaiodide but octaiodide.

X-Ray Structure Determination. The density was measured by pycnometry with o-xylene at 20°C; the lattice parameters and the space group were previously determined with a Weissenberg camera, reflection conditions hkl: $h+k+l=2n$, $hk0$: $h,k=2n$, $0kl$: $k,l=2n$, hhl: $2h+l=4n$, $00l$: $l=4n$ leading to $I4_1/acd$; crystal 0.2×0.2×0.25 mm^3 in size was mounted with c coincident with the goniostat axis; Rigaku AFC-4 diffractometer, graphite-monochromated Mo $K\alpha$ radiation (λ=0.7107 Å), 40 kV-200mA; unit cell parameters were refined by least-squares method using 25 2θ values ($20° < 2\theta < 24°$); intensity measurement was made up to 2θ =55° ($0 \le h \le 18$, $0 \le k \le 26$, $0 \le l \le 34$), ω—2θ scan technique, all intensities monitored by three standard reflections (0, 0, 16; 6, 4, 10; 800) every 50 reflections throughout experiments; 3629 unique reflections were measured. 1569 reflections classified as observed [$|F_o| > 3\sigma(F_o)$] used for the structure determination; Lorentz-polarization factors and absorption were corrected, empirical correction factors on F 0.996—1.091;[5] the possible positions of Te and I deduced from the E map were confirmed by the Patterson function, starting with these positions the other non-hydrogen atoms located on electron density maps, the structure refined by full-matrix least-squares on F with anisotropic thermal parameters for Te and I, and isotropic ones for N and C; H atoms were not found in difference maps and omitted in refinement, $\sum w(|F_o| - |F_c|)^2$ minimized for 72 parameters, seven reflections with low angles and strong intensities removed to avoid possible extinction effects, $w = [\sigma^2(F_o)]^{-1}$; final R=0.082, R_w=0.056 and goodness of fit S=1.86 for unique 1562 reflections, $(\Delta/\sigma)_{max}$=0.48 for Te and I, but 2.28 for C and N, maximum positive and negative electron densities, $(\Delta\rho)_{max}$ and $(\Delta\rho)_{min}$, in final difference fourier syntheses 1.90 and −2.52 e Å^{-3}, respectively.

Neutral atom scattering factors and anomalous dispersion terms were taken from International Tables for X-Ray Crystallography.[6] UNICS Program System,[7] Finger Computing System,[8] and their modifications were used for calculations at the Computation Center, Osaka University and later at the Information Processing Center, Kobe University.

Crystal Data: $[(CH_3)_4N]_2TeI_6 \cdot I_2$, F.W.=1291, tetragonal, space group $I4_1/acd$, a=20.356(3), c=27.571(5) Å, V=11,

424 Å^3, D_m(20°C)=3.01, D_x(20°C)=3.00 Mg m^{-3}, Z=16, F(000)=8992, μ(Mo $K\alpha$)=9.6 mm^{-1}.

Proton NMR Experiments. For NMR measurements, the polycrystalline sample was sealed in a glass tube with a small amount of helium gas for heat exchange. The continuous wave (CW) absorption spectrum was observed with a bridge-type spectrometer (homemade) operated at 19.4 MHz, while the spin-lattice relaxation time T_1 was measured by an induction type of pulse spectrometer (homemade) adjusted at 10.5 MHz. A conventional pulse sequence of $90°_{comb}$-τ-90° or 180°-τ-90° was selectively used. The temperature of the specimen was kept constant within ±0.5 K for the CW experiments and ±1 K for the pulse one. It was measured with a Chromel-Constantan thermocouple above 15 K and with a germanium resistance thermometer or an Au(Fe)-Chromel thermocouple below 15 K.

Thermal Analyses. Differential thermal analysis (DTA) and differential scanning calorimetry (DSC) were carried out with a Rigaku DTA & DSC apparatus. Carbontetrachloride CCl_4 of "extra pure" grade was used as a standard to calibrate the DSC scale.

Table 1. Fractional Coordinates and Equivalent or Isotropic Thermal Parameters (Å^2) with Their e.s.d.'s in Parentheses

Atom	x	y	z	B_{eq}[a)]/B_{iso}
Te	0.03057(8)	0	0.25	2.74(2)[a)]
I(1)	0.02912(9)	0.00119(16)	0.35637(5)	6.47(2)[a)]
I(2)	0.14876(9)	0.17235(10)	0.49773(13)	7.21(5)[a)]
I(3)	0.14760(7)	0.12349(8)	0.00229(11)	5.58(4)[a)]
I(4)	0.04410(7)	0.05109(7)	0.49947(8)	3.83(2)[a)]
N(1)	0	0.25	0.125	1.9(13)
N(2)	0.271(1)	0.021(1)	0.375	4.1(7)
N(3)	0	0.25	0.375	7.9(26)
C(11)	0.029(5)	0.196(5)	0.098(4)	13.9(30)
C(12)	0.025(6)	0.297(6)	0.093(4)	17.8(36)
C(21)	0.266(4)	0.018(4)	0.168(3)	10.0(23)
C(22)	0.253(4)	0.089(3)	0.373(2)	8.8(16)
C(23)	0.200(4)	0.005(6)	0.116(4)	13.9(31)
C(24)	0.282(5)	0.083(5)	0.359(4)	8.8(34)
C(3)	0.059(3)	0.231(3)	0.346(2)	12.2(17)

a) $B_{eq}=(4/3)\sum_i\sum_j\beta_{ij}\boldsymbol{a}_i\cdot\boldsymbol{a}_j$.

Results and Discussion

Crystal Structure. The fractional coordinates and isotropic thermal parameters for non-hydrogen atoms are listed in Table 1.[9] The stereoscopic drawing viewed along $\boldsymbol{a}$ and the (001) projection with the atom numbering scheme of the structure are shown in Figs. 1 and 2, respectively.[10] Selected interatomic distances and angles are given in Table 2.

The crystal consists of octahedral anions $[TeI_6]^{2-}$, cation group Me_4N^+ and iodine molecules. The large unit cell as well as the large Z number causes the structure to appear much complicated. However, the principle of the structure is rather simple and adequately described in terms of the K_2PtCl_6 structure, when the tetragonal deformation arising from the inclusion of dumbbell like I_2 molecules and also slight displacements of all constituents are neglected. As shown in Fig. 2, the tetragonal subcell with $\boldsymbol{a}_s=(\boldsymbol{a}+\boldsymbol{b})/2$(=14.39 Å), $c_s=c/2$ (=13.79 Å) and Z_s=4 is closely related to the antifluorite structure. Octahedral $[TeI_6]^{2-}$

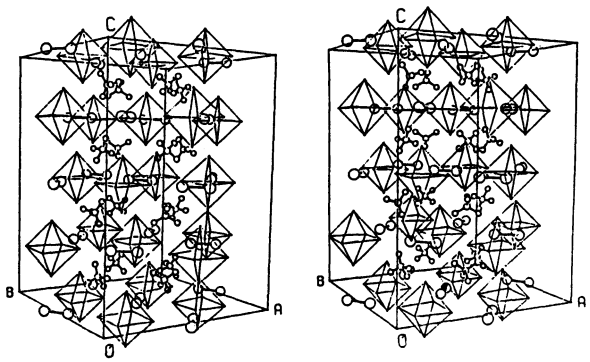

Fig. 1. The *ORTEP* drawing of the structure. Only one of two configurations for each disordered $[(Me)_4N]^+$ cation is given for simplicity.

Table 2. Interatomic Distances (l/Å) and Angles (ϕ/°)

(a) $[TeI_6]^{2-}$ anion

Te-I(1)	2.933(2)	I(1)-Te-I(2)	88.07(9),	91.09(9)
Te-I(2)	3.017(2)	I(1)-Te-I(3)	89.47(8).	91.32(8)
Te-I(3)	2.857(2)	I(2)-Te-I(2)	86.21(8)	
		I(2)-Te-I(3)	90.07(5),	175.50(7)
I(1)···I(4)	4.085(3), 4.376(3)			
I(2)···I(4)	3.261(2)			
I(3)···I(4)	4.132(2), 4.172(2)			

(b) $[(CH_3)_4N]^+$ cation (mean values)

(i) N(1)-C(1) 1.43(6) C(1)-N(1)-C(1) 109(3)

(ii) configuration A: N(2)-C(21′), C(21″), C(22), C(24‴)
N(2)-C(2) 1.41(3) C(2)-N(2)-C(2) 108(2)
configuration B: N(2)-C(22‴), C(23′), C(23″), C(24)
N(2)-C(2) 1.47(5) C(2)-N(2)-C(2) 110(3)

(iii) N(3)-C(3) 1.49(3) C(3)-N(3)-C(3) 109(1)

symmetry code: none, (x, y, z); (′), (x, $-y$, 1/2−z); (″), (1/4−y, 3/4+x, 1/4+z); (‴), (1/4+y, 3/4+z, 3/4−z).

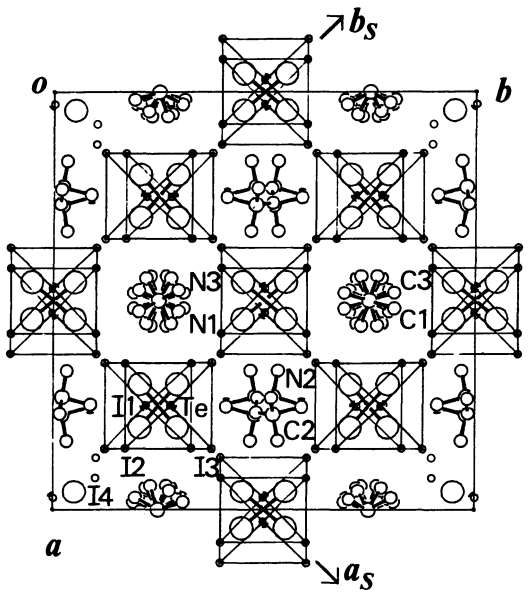

Fig. 2. The projection of the structure along [001] with the atom numbering scheme. Only one orientation for each disordered cation is shown. Atom symbols, for example, I1 denotes I(11) and C2 represents C(21), C(22) and C(24) as listed in Tables 1 and 2.

anions form a tetragonally deformed, face-centered lattice and Me_4N^+ cations occupy the eight tetrahedral holes. The subcell further contains I_2 molecules aligned parallel to a_s or b_s axis at the interstitial sites of twelve edge-centers (1/2, 0, 0) etc. and one body-center (1/2, 1/2, 1/2). Thus, the iodine molecule bridges adjacent complex anions.

Each Te^{IV} atom is coordinated octahedrally by six iodine atoms with Te–I distances of 2.933(2), 3.017(2), and 2.857(2) Å. The average value 2.94 Å is close to the typical one of 2.952(2) Å found in $(Me_3NH)_2TeI_6$.[4] The individual Te–I distances, however, are significantly different from one another, reflecting a variety of interactions with the surroundings. The arrangement of six iodine molecules around a central TeI_6 octahedron is illustrated in Fig. 3. The Te–I(2) bond is parallel to the axis of the neighboring I_2 molecule, while the other two Te–I(1) and Te–I(3) bonds are perpendicular to them. The axial I(1) atom is surrounded by two I(4) atoms with distances of 4.085(3) and 4.376(3) Å. The equatorial I(2) is close to only one I(4) atom with the shortest intermolecular I···I distance 3.261(2) Å, this being much shorter than the corresponding one (3.57 Å) in iodine crystal.[11] The remaining equatorial I(3) has also two I(4) neighbors at distances of 4.132(2) and 4.172(2) Å. A comparison of these I···I separations with the van der Waals contact 4.3 Å suggests that a remarkable interaction such as charge transfer occurs between I(2) and I(4). For this reason the Te–I(2) distance is lengthened than the normal 2.95 Å and consequently the Te–(3) bond may be shortened by some trans effect.

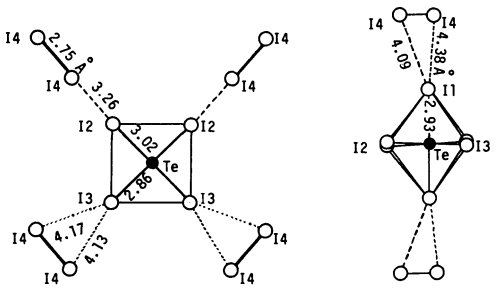

Fig. 3. The arrangement of six I_2 molecules around a central TeI_6 octahedron, (a) viewed along *c*, and (b) viewed along *b* (=*a*).

On the other hand, the intramolecular I–I length 2.748(3) Å is longer than 2.68 Å found in solid iodine. All these facts indicate that the intermolecular I···I interaction is fairly strong in the octaiodo complex relative to iodine crystals. The present X-ray analysis showed that excess iodine atoms are included as iodine molecules in contrast to $(Me_3NH)_2TeI_7$ complex where excess iodine atoms are held together as infinite linear chains.[4] To the best of our knowledge the present complex is the first example for inclusion of iodine molecules in the series of hexaiodometallate(IV) complexes.

There are three kinds of Me_4N^+ cations which are denoted by their central nitrogen atoms in Fig. 2. The N(1), N(2), and N(3) atoms are located at **8b**(222), **16f**(2), and **8a**(4) positions of $I4_1/acd$, respectively. The cation of N(3) is ordered, whereas those of N(1) and N(2) are orientationally disordered and distributed over each two configurations with the equal probability 0.5. Thus, the occupancy factors of their methyl carbons are 1 for C(3) and 0.5 for the other six from C(11) to C(24). Although the positional parameters of such disordered methyl carbons are less reliable than the ordered ones, the assigned geometry for each cation group appears to be reasonable. The mean C–N distances and the mean C–N–C bond angles around N(1), N(2), and N(3) are 1.43, 1.45, 1.49 Å and 109, 109, 112°, respectively, in agreement with 1.47 Å and the tetrahedral angle in the literature.

Phase Transition. The DTA and NMR results showed that the crystal undergoes a phase transition at 234 K, like some other members of the family. The transition enthalpy was determined approximately to be 2.4 kJ mol^{-1} from DSC. Recently, Matsuo et al. reported the transition enthalpy 1.78 kJ mol^{-1} for $(CH_3NH_3)_2SnCl_6$,[12] where no structural change was disclosed except for slight discontinuities in some lattice parameters.[13] Accordingly, the structural change caused by the transition would not be so much in the octaiodo complex also.

Dynamic Behavior of Me_4N^+ Cation Groups. The ^1H NMR spectra at the lowest temperatures of measurement showed a fine structure characteristic of the static array of nuclei, and it remained fairly well

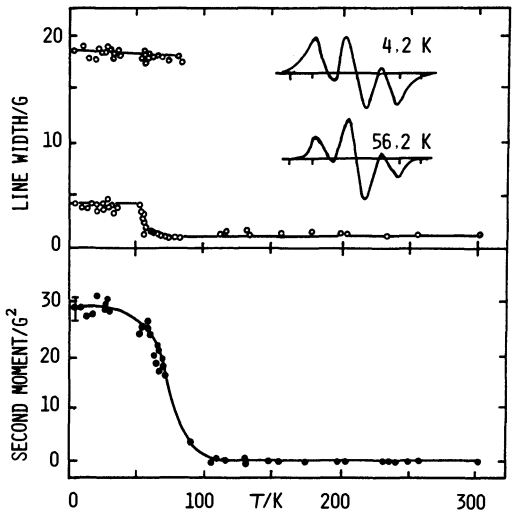

Fig. 4. The temperature dependences of ^{1}H NMR line width and second moment observed for $[(CH_3)_4N]_2TeI_8$.

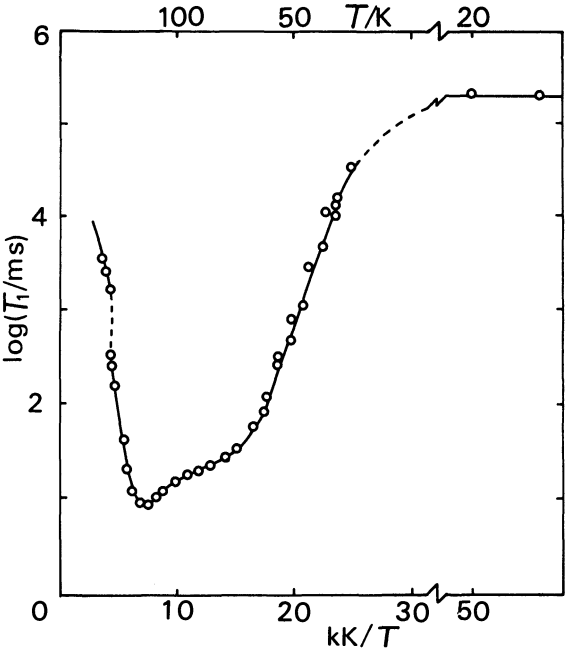

Fig. 5. The temperature variation of proton T_1 measured at 10.5 MHz for $[(CH_3)_4N]_2TeI_8$.

up to about 50 K. The line width δH_{msl} measured on the absorption derivative and the observed second moment M_2 are plotted against temperature in Fig. 4. From liquid helium temperature to 30 K δH_{msl} were 18.4±0.1(outer) and 4.0±0.1 G(inner), and M_2 was 29±2 G^2, these being close to the rigid lattice values expected for Me_4N^+ cations.[14] The spectrum was narrowed strongly between 50 and 100 K, above which the line width and the second moment were again constant at 1.5±0.1 G and 0.5±0.1 G^2, respectively. The M_2 values for various dynamic models of Me_4N^+ cations were calculated in the usual manner based on Van Vleck formula: M_2=30 G^2 for the rigid lattice; M_2=9 G^2 for the threefold reorientation of all CH_3 groups; M_2=0.5 G^2 for the isotropic reorientation of whole cations. In these calculations, the geometry of the cation was taken to be tetrahedral 109°28′ for all the bond angles, 1.47 Å for the C–N bond length and 1.10 Å for the C–H length in all-staggered conformation.[15] A comparison of these calculated values with the experimental ones indicates that all the Me_4N^+ cations reorient rapidly and isotropically far below room temperatures. As seen in Fig. 4, the narrowing process occurs in only a single step, suggesting the three fold reorientation of methyl groups consecutively followed by the overall reorientation of the cations itself.

The spin-lattice relaxation times are plotted in Fig. 5 against reciprocal temperatures. As described previously, the T_1 value changed discontinuously by one order of magnitude at 234 K, indicating the presence of a phase transition which was confirmed by thermal analyses. The T_1 vs. T^{-1} curve exhibits a deep and very broad minimum with a value of 8.5 ms at 133 K. The appearance of a shoulder on the low temperature side of the T_1 minimum may be due to reorientation of methyl groups. However, the T_1 value of the shoulder is longer than that of T_1 minimum in contrast with the usual behavior of methylammonium groups.[16] It is therefore supposed that three or more nonequivalent Me_4N^+ cations set in motion with slightly different motional parameters in the low temperature phase, causing the T_1 minimum to be shallow and consequently to be quite broad. Such a T_1 behavior seems too complicated to analyze, because of many unknown parameters included. Therefore, the activation energy for the threefold (C_3) reorientation of CH_3 groups was tentatively deduced from the positive slope ($\omega\tau_c \gg 1$) in the low temperature side of the T_1 minimum, while the value for the overall reorientation of whole cations from the negative slope ($\omega\tau_c \ll 1$): These are 6.3 and 14.2 kJ mol^{-1}, respectively. The similar T_1 minima were observed in analogous complexes of $(Me_4N)_2MX_6$ (M=Pt, Te, Sn, X=Cl, Br), and each shallow minimum in the low temperature side was successfully explained in terms of a small-angle reorientation of methyl groups of the cations.[17,18] It is not clear whether or not this is the case in the present complex, because of no sufficient evidence for it and also of unusual breadth of the T_1 minimum in comparison with those for the other analogues.

Above T_{tr} (234K), the negative slope of the T_1 curve gives the activation energy 5.4 kJ mol^{-1} for the composite reorientation of cations, which is much smaller than the corresponding value 14.2 kJ mol^{-1} below T_{tr}, reflecting more loose packing in the high temperature phase. This finding together with the discontinuity of T_1 at T_{tr} suggests that the reorientational motion of the cations is associated with the phase transition more or less.

The authors wish to express their thanks to Dr. Yuriko Yamagata for her help in part of the X-ray work and also to Dr. Taisei Yamanoto for the CW NMR data collection.

The present work was supported by a Grant-in-Aid for Scientific Research No. 593700350 from the Ministry of Education, Science and Culture.

References

1) H. Ishida, R. Ikeda, and D. Nakamura, *Ber. Bunsenges. Phys. Chem.*, **88**, 546 (1984).

2) H. Kiriyama and T. Yamamoto, Molecular Structure Symposium of the Chemical Society of Japan, Sendai, September 1983, Abstr., No. 3P23.

3) K. Kitahama and H. Kiriyama, *Acta Crystallogr. Sect. A.*, **34**, S302 (1978).

4) H. Kiriyama, Y. Mizuhashi, and J. Ootani, *Bull. Chem. Soc. Jpn.*, **59**, 581 (1986).

5) A. C. North, D. C. Phillips, and F. S. Mathews, *Acta Crystallogr., Sect. A*, **24**, 351 (1968).

6) "International Tables for X-Ray Crystallography," Birmingham (1974), Vol. IV, Knoch Press (Present Distributor D. Reidel, Dordrecht.).

7) UNICS (1967). "Universal Crystallographic Computation Program System," ed by T. Sakurai, Tokyo; Crystallographic Society of Japan.

8) L. W. Finger, *Carnegie Institute Washington Yearb.*, **67**, 216 (1969).

9) Lists of structure factors and anisotropic thermal parameters are deposited as Document No. 8639 at the office of the editor of *Bull. Chem. Soc. Jpn.*

10) C. K. Johnson, *ORTEP* II. Report ORNL-5138. Oak Ridge National Laboratory, Tennessee (1976).

11) F. van Bolhuis, P. S. Koster, and T. MiGchelsen, *Acta Crystallogr.*, **23**, 90 (1967).

12) T. Matsuo, M. Ueda, H. Suga, *Chem. Phys. Lett.*, **82**, 577 (1981).

13) K. Kitahama, H. Kiriyama, and Y. Baba, *Bull. Chem. Soc. Jpn.*, **52**, 324 (1979).

14) $1G=1\times10^{-4}T$.

15) E. R. Andrew and P. C. Canepa, *J. Magn. Reson.*, **7**, 429 (1972).

16) H. Roger and A. Weiss, *Ber. Bunsenges. Phys. Chem.*, **80**, 138 (1976).

17) L. S. Prabhumirashi, R. Ikeda, and D. Nakamura, *Ber. Bunsenges. Phys. Chem.*, **85**, 1142 (1981).

18) S. Sato, R. Ikeda, and D. Nakamura, *Ber. Bunsenges. Phys. Chem.*, **86**, 936 (1982).

N-Hydroxy Amides. IV.[1] Synthesis and Properties of a Trihydroxamic Acid Anilide as a Model for Ferrioxamines

Kazuyuki SHIMIZU, Kazuyuki NAKAYAMA, and Masayasu AKIYAMA*
Department of Applied Chemistry for Resources, Tokyo University of Agriculture and Technology, Koganei, Tokyo 184
(Received October 11, 1985)

A trihydroxamic acid having a 6-aminohexanoyl-3-(hydroxyamino)propanoyl sequence has been synthesized in a stepwise manner, starting with glycinanilide. The trihydroxamic acid anilide bears a good structural resemblance with *N*-benzoyl-deferriferrioxamine B (Benzoyl-DFB). A plot of the absorbance vs. the molar ratio of iron(III) to the hydroxamate group indicates the formation of a 1 : 1 intramolecular iron(III) complex for the trihydroxamic acid anilide and Benzoyl-DFB. Cyclic voltammetry also shows that the iron complexes of both compounds have similar electrochemical properties. A solid iron(III) complex was obtained when the trihydroxamic acid anilide was mixed with tris(2,4-pentanedionato)iron(III) in methanol.

There is a growing interest in natural and synthetic iron sequestering agents.[2-6] Ferrioxamines, an important class of microbial iron-transporting compounds (siderophores), are stable octahedral iron(III) complexes of linear and cyclic trihydroxamic acids (deferriferrioxamines). They show unique biological activities, such as antibiotics and growth factors.[2,4,7-9] A characteristic structural feature for these trihydroxamic acids is a repeating unit comprising 5-hydroxyamino-1-pentanamine and succinic acid.[2,8] Deferriferrioxamine B (DFB) is used as a drug for the treatment of an iron-overload disease in humans.[4,5,8,10] In this respect, it is of interest for designing and synthesizing trihydroxamic acids of a similar nature but of different molecular compositions as a model and for comparing the important properties, such as iron(III) complex formation and the electrochemical behavior between these synthetic and natural compounds.

A previous paper reported on a synthesis of an *N*-hydroxy hexapeptide anilide containing three hydroxamic acid units in the chain.[11] The hexapeptide anilide showed a rather weak iron(III) bond, owing to the close spacing between hydroxamate groups. In an attempt to provide compounds that firmly hold iron(III), the synthesis of a linear oligoamide having a 6-aminohexanoyl-3-(hydroxylamino)propanoyl sequence has been made. This paper describes the results together with an examination of iron(III) binding properties.

Results and Discussion

Synthesis. A trihydroxamic acid carrying an anilide terminal was synthesized by the reactions shown in Scheme 1. The anilide derivative was chosen in order to obtain a series of compounds as crystals. Thus, glycinanilide was coupled with *p*-nitrophenyl 3-(benzyloxyamino)propanoate H-(BzlO)Apr-ONp[12] to give *N*-[3-(benzyloxyamino)propanoyl]glycinanilide (**1**). The terminal *N*-benzyloxyamino group of **1** was acylated with 6-(Boc-amino)hexanoic acid (Boc-Ahe-OH) by a mixed anhydride procedure to give compound (**2**). The low nucleophilicity of the benzyloxyamino group allowed us to use a *p*-nitrophenyl ester without *N*-protection;[11] yet, the same benzyloxyamino group had a sufficient activity to attack a mixed anhydride. A repeated-acylation technique, needed to couple *N*-benzyloxy α-amino acid derivatives,[11] was unnecessary for the benzyloxy-β-alanyl unit. The ease of acylation is ascribed to less steric constraint around the nitrogen atom, relative to

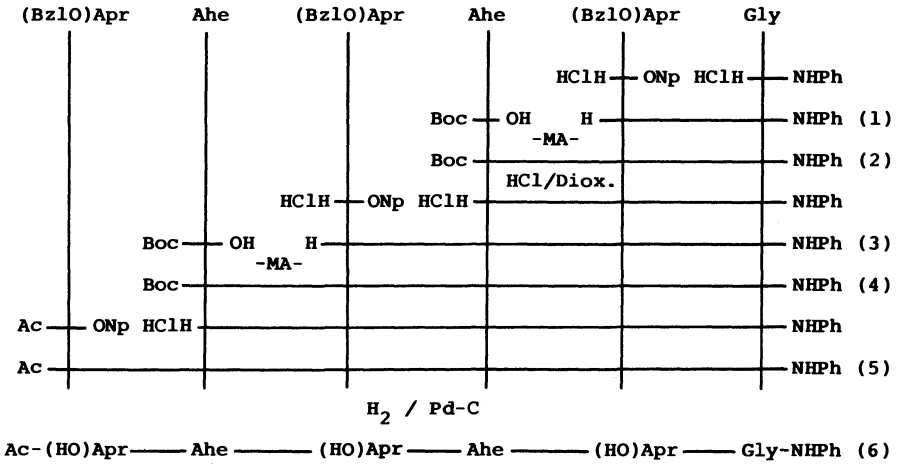

Scheme 1.

CH_3-CON(OH)-$(CH_2)_2$CONH$(CH_2)_5$-CON(OH)-$(CH_2)_2$CONH$(CH_2)_5$-CON(OH)-$(CH_2)_2$CONHCH$_2$CONH-Ph

Compound 6

CH_3-CON(OH)-$(CH_2)_5$NHCO$(CH_2)_2$-CON(OH)-$(CH_2)_5$NHCO$(CH_2)_2$-CON(OH)-$(CH_2)_5$NHCO-Ph

Benzoyl-DFB

that of *N*-benzyloxy α-amino acid derivatives.[11]

A reaction cycle involving the acylation of the benzyloxyamino group with a mixed anhydride of Boc-Ahe-OH and a subsequent deprotection of the Boc-group, followed by another acylation with H-(BzlO)Apr-ONp, gave compounds **1**, **2**, **3**, **4**, and **5** in good yields. The cycle was terminated at the hexamer stage by use of Ac-(BzlO)Apr-ONp. Column chromatography at each stage provided a pure product. The desired trihydroxamic acid anilide (**6**) was obtained by catalytic hydrogenation[1,13] with Pd-C, followed by column chromatography. IR absorptions for the carbonyl groups were 1670 (sh) (-CONH-) and 1630 cm^{-1} -CON(OH)-, the latter of which is ascribed to the cis configuration.[14] ^1H NMR peaks were observed in the expected regions (Experimental). The compound was soluble in aqueous DMF but insoluble in water and methanol.

As a reference, compound Benzoyl-DFB was prepared according to a method described in the literature.[15] Molecular models reveal that there is a good structural analogy between compound **6** and Benzoyl-DFB; both compounds have a 9-atom spacing between the hydroxamic acid groups[8] and the same 7 atoms exist in the sequence between the phenyl group and the nearest hydroxamic acid moiety. These two compounds show similar solubilities.

Iron(III) Binding. DFB itself has a great affinity for iron(III), forming a 1:1 intramolecular iron(III) complex by the three hydroxamate groups.[8,15] Benzoyl-DFB was reported to form a stable iron(III) complex.[15] The formation constant of a similar complex of Acetyl-DFB[16] is as high as 10^{30}.

The complex-forming tendency of compound **6** was examined in a 50% aqueous DMF solution[17,18] using DFB as a reference compound. Plots of absorbance vs. the molar ratio of iron(III) to the hydroxamic acid groups are shown in Fig. 1. Both compound **6** and Benzoyl-DFB show a sharp inflection at a ratio of 1/3 as DFB does,[17,18] indicating the formation of the expected complex. The complex formation is also supported by its λ_{max} 435 nm and ε 2700, which are close to those of iron(III)-DFB.[16] From these results, the 9-atom spacing seems to be satisfactory for the formation of a stable complex, regardless of the position of the amide groups. In an aqueous DMF solution, a slight increase in the absorbance and a bathochromic shift of λ_{max} were observed in the iron(III) excess region (Fig. 1). Although the reason is still obscure, one explanation is that the spectral

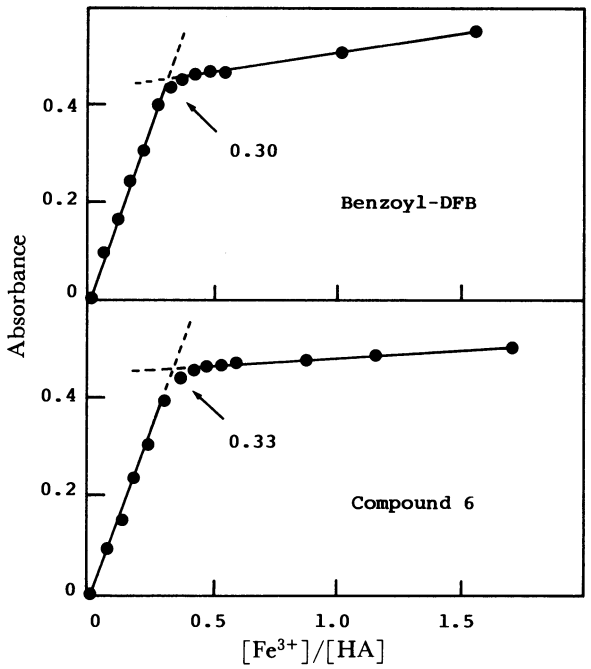

Fig. 1. Absorbance vs. the ratio of iron(III) to the hydroxamic acid (HA) units in 50% aqueous DMF solution at apparent pH=3.0 and 25 °C, ionic strength 0.1 with KNO_3. Absorbance of λ_{max} was determined for Benzoyl-DFB at 430—470 nm and for compound **6** at 423—445 nm.

changes are due to a weak interaction between free, or free and complexed iron(III) and solvent amide groups.[19]

An examination of CPK molecular models of the iron(III) complexes reveals that there are several molecular arrangements leading to a stable complex.[15] When compound **6** was mixed with tris(2,4-pentanedionato)iron(III) in methanol, the compound dissolved readily and an iron(III) complex was formed as a solid when the solvent was evaporated. The complex, soluble in water, showed a visible spectrum similar to that of ferrioxamine B.[16]

Cyclic Voltammetry. In order to determine the usefulness of compound **6** as a siderophore model, it was worthwhile to determine the electrochemical properties of the iron(III) complex. To this end, the cyclic voltammetry was carried out at a neutral pH in an aqueous solution. The results are summarized in Table 1 and some details are given in Table 2. It has been reported that DFB with iron(III) (ferrioxamine B) exhibits a reversible one-electron oxidation-reduction wave at pH 8 when a mercury electrode is used.[20]

Table 1. Results of Cyclic Voltammetry[a]

Ligand	$E_{1/2}$ vs. SCE[b]	ΔE
	mV	mV
DFB	−698[c]	60[c]
	−705	65[d]
Benzoyl-DFB	−710	35
Compound **6**	−703	35

a) Conditions: 0.05 M sodium borate-0.05 M sodium phosphate buffer, pH 8.0; ionic strength 0.5 with 1 M KCl. b) Saturated calomel electrode. c) Ref. 20. d) $i_{pc}/i_{pa}=1.00$.

Table 2. Cyclic Voltammetry Data[a]

Ligand	Scan rate	i_{pc}	i_{pa}	i_{pc}/i_{pa}
	mVs^{-1}	A	A	
Benzoyl-DFB	500	42	29	1.44
	200	21	15	1.40
	100	14	10	1.40
	50	8.5	6.0	1.40
	20	5.5	4.0	1.37
Compound **6**	500	51	38	1.34
	200	26	20	1.30
	100	17	13	1.30
	50	11	8.5	1.29
	20	6	5	1.20

a) Details of the data in Table 1.

Under present conditions with a carbon electrode at pH8, the same compound showed a slightly different value of the peak-to-peak separation (ΔE). The data may be interpreted as indicating a similar reversible redox process since $i_{pa}/i_{pc}=1.0$ and $i_{pc}\propto v^{1/2}$.[21] Half-wave potentials ($E_{1/2}$) obtained for iron(III) with compound **6** and Benzoyl-DFB are very close to that of DFB, as expected from the similar 9-atom spacing; however, the value of the peak-to-peak separation is different from that of DFB. Although a value 35 mV for both compound **6** and Benzoyl-DFB may correspond to a two-electron transfer process, it is improbable that the introduction of a phenyl group in the remote position can change the electron-transfer mode, that is, from a one-electron-transfer to a two-electron transfer. The observed small separation and the deviation of i_{pa}/i_{pc} values from unity for both compound **6** and Benzoyl-DFB are considered rather to be due to a weak adsorption of these ligands to the carbon electrode through phenyl groups; a case of weak adsorption of both reactant and product. A plot of i_{pc} vs. either v or $v^{1/2}$ from the data in Table 2 does not necessarily yield a straight line. A situation is known in which as adsorption occurs the peak separation narrows.[22]

In short, compound **6** and Benzoyl-DFB behave similarly during the formation of an iron(III) complex. Also, the complexes formed show a quasi-reversible redox wave in an electrochemical determination.

Experimental

All the melting points are uncorrected. IR spectra were obtained with a JASCO model A-302 spectrophotometer and ^{1}H NMR spectra were recorded on a JEOL JNM-FX 200 spectrometer with TMS as internal standard. HPLC was carried out with a JASCO model TWINCLE apparatus by using a column packed with a Finepak SIL C_{18}. A microanalysis was performed in the Analytical Section, Institute of Physical and Chemical Research, Saitama. TLC was carried out by using Merck precoated silica gel $60F_{254}$ plates: R_f^1, THF-hexane (5:1); R_f^2, $CHCl_3$-MeOH-C_6H_6 (6:1:3); R_f^3, $CHCl_3$-MeOH (3:1).

The iron(III) complex molar ratio was determined with a Hitachi model 320 spectrophotometer in a 50% aqueous DMF solution, as before.[17,18] 1 M=1 mol dm^{-3}.

H-(BzlO)Apr-Gly-NHPh (1). A solution containing *p*-nitrophenyl 3-(benzyloxyamino)propanoate hydrochloride[12] (2.22 g, 6.3 mmol) and Et_3N (0.64 g, 6.3 mmol) in $CHCl_3$ (15 mL) was added to a solution of glycinanilide hydrochloride (1.18 g, 6.3 mmol) and Et_3N (0.64 g, 6.3 mmol) in $CHCl_3$ (25 mL); the mixture was stirred at 30°C for 48 h. Chloroform (100 mL) was added to this and the $CHCl_3$ layer was washed with aqueous Na_2CO_3 and water, and dried (Na_2SO_4). Evaporation of the solvent gave a crude product (1.91 g, 93%). Purification by column chromatography (Wako gel C-300 with THF-hexane, 3:2 v/v) and reprecipitation from EtOAc-hexane gave a solid, 1.62 g (78%). The hydrochloride of **1** was obtained as crystals by a treatment of the solid with 3.6 M HCl in dioxane, mp 147—148°C: R_f^1=0.54, R_f^2=0.46, R_f^3=0.90. Found: C, 59.23; H, 6.12; N, 11.55%. Calcd for $C_{18}H_{21}N_3O_3$·HCl: C, 59.42; H, 6.10; N, 11.55%.

Boc-Ahe-(BzlO)Apr-Gly-NHPh (2). A mixture of Boc-Ahe-OH (0.783 g, 3.39 mmol) and Et_3N (0.342 g, 3.39 mmol) in THF (20 mL) was chilled at −12°C, and Bu^{t}OCOCl (0.442 g, 3.25 mmol) in THF (5 mL) was added and the mixture was kept at −15°C for 15 min. To this were slowly added HCl·H-(BzlO)Apr-Gly-NHPh (0.986 g, 2.71 mmol) and Et_3N (0.274 g, 2.71 mmol) in $CHCl_3$ (15 mL); the mixture kept for 3 h at −15°C and for 20 h at room temperature. After evaporation of the solvent, the residue was extracted with EtOAc (100 mL), washed with 5% $NaHCO_3$, 5% citric acid, and water, and dried (Na_2SO_4). Evaporation of the solvent gave a crude product, which was purified by chromatography (Wako gel C-300 with $CHCl_3$-MeOH). Recrystallization from THF-Et_2O- petroleum ether gave 1.03 g (70%) of **2**, mp 105—106°C: R_f^1=0.73, R_f^2=0.49, R_f^3=0.94. Found: C, 64.39; H, 7.55; N, 10.30%. Calcd for $C_{29}H_{40}N_4O_6$: C, 64.42; H, 7.46; N, 10.36%.

H-(BzlO)Apr-Ahe-(BzlO)Apr-Gly-NHPh (3). HCl·H-Ahe-(BzlO)Apr-Gly-NHPh was obtained by deprotection of **2** with 3.6 M HCl in dioxane.

A mixture of HCl·H-(BzlO)Apr-ONp (0.12 g, 0.34 mmol) and Et_3N (0.034 g, 0.34 mmol) in DMF (5 mL) was added to a solution containing HCl·H-Ahe-(BzlO)Apr-Gly-NHPh (0.161 g, 0.34 mmol) and Et_3N (0.034 g, 0.34 mmol) in DMF (10 mL); the mixture was stirred for 48 h at 30°C, and evaporated. An extraction of the residue with EtOAc, washing (aqueous Na_2CO_3 and water), drying (Na_2SO_4), solvent evaporation, and column chromatography (Wako gel C-300 with THF-hexane) afforded 0.191 g (92%) of **3** as an oil. The oily product was converted into the hydrochloride of **3** (syrup) with 3.6 M HCl in dioxane: R_f^1=0.40, R_f^2=0.39, R_f^3=0.92.

Boc-Ahe-(BzlO)Apr-Ahe-(BzlO)Apr-Gly-NHPh (4). To a mixed anhydride solution of Boc-Ahe-OH prepared as

above, was slowly added a solution of HCl·H-(BzlO)Apr-Ahe-(BzlO)Apr-Gly-NHPh (0.884 g, 1.35 mmol) and Et_3N (1.37 g, 1.35 mmol) in DMF; the mixture was kept at −16°C for 4 h, and at room temperature for 20 h. Concentration of the solution, extraction with EtOAc, washing (5% $NaHCO_3$, 5% citric acid, and H_2O), and drying (Na_2SO_4) gave a crude product (1.05 g, 94%) of **4**, which was purified by chromatography (LH-20 with MeOH) to give **4** as an oil, 0.955 g (85%): R_f^1=0.54, R_f^2=0.42, R_f^3= 0.92.

Ac-(BzlO)Apr-ONp. *O*-Benzylhydroxylamine (1.97 g, 16 mmol) in Et_2O (40 mL) was added to a solution of *p*-nitrophenyl acrylate (2.90 g, 15 mmol) in Et_2O (40 mL); the mixture stirred for 15 h at room temperature and concentrated to give an oil. The oil was acetylated with Ac_2O (10 mL) in THF (20 mL) at 70°C for 1 h and evaporated. The resulting residue was crystallized on addition of Et_2O-petroleum ether, 2.90 g (54%). Recrystallization from Et_2O- petroleum ether gave the product, 1.67 g (36%); mp 73—74°C. Found: C, 60.33; H, 5.06; N, 7.82%. Calcd for $C_{18}H_{19}N_2O_6$: C, 60.16; H, 5.33; N, 7.80%.

Ac-(BzlO)Apr-[Ahe-(BzlO)Apr]$_2$-Gly-NHPh (5). HCl·H-Ahe-(BzlO)Apr-Ahe-(BzlO)Apr-Gly-NHPh (**4'**) was obtained by deprotection of **4** with 3.6 M HCl in dioxane.

Ac-(BzlO)Apr-ONp (0.455 g, 1.27 mmol) was added to a solution of the hydrochloride (0.813 g, 1.06 mmol) and Et_3N (0.107 g, 1.06 mmol) in DMF (20 mL). The solution was stirred for 48 h at 30°C, and the solvent was evaporated to give a residue. Extraction of the residue with EtOAc, washing (aqueous Na_2CO_3 and water), drying (Na_2SO_4), and evaporation of the solvent gave a crude product of **5**. Column chromatography (Wako gel C-300 with THF-hexane) afforded 0.855 g (85%) of **5**, mp 99—101°C; R_f^1= 0.23, R_f^2=0.35, R_f^3=0.94. Found: C, 65.49; H, 7.30; N, 10.00%. Calcd for $C_{52}H_{67}N_7O_{10}$; C, 65.73; H, 7.11; N, 10.32%.

Ac-(HO)Apr-[Ahe-(HO)Apr]$_2$-Gly-NHPh (6). A mixture containing the hexaamide (**5**) (0.60 g, 0.63 mmol) and 10% Pd-C (0.12 g) in MeOH (30 mL) was subjected to hydrogenation with H_2 at 35°C for 40 h. DMF (30 mL) was added; the hot suspension was filtered. Concentration of the filtrate and column chromatography (Toyo pearl HW-40 with DMF) afforded 0.35 g (82%) of **6**, mp 175—176°C (decomp); R_f^2=0.03, R_f^3=0.44; IR, $\nu_{C=O}$ 1670 (sh) and 1630 cm^{-1}; ^1H NMR (DMSO-d_6) δ=1.35 (12H, m, $-CH_2-CH_2-CH_2-$), 2.00 (3H, s, CH_3-), 2.30 (8H, m, N-CH_2- and $-CH_2-$CO in -Ahe-), 3.00 (6H, m, $-CH_2-$CO in -Apr-), 3.70 (6H, m, N-CH_2- in -Apr-), 3.85 (2H, d, N-CH_2-CO), 7.30 (5H, m, $-C_6H_5$), 7.78 (3H, -NH-CO), 8.20 (1H, -NH-Ph), and 9.6—9.8 (3H, N-OH). Found: C, 54.62; H, 7.42; N, 14.31%. Calcd for $C_{31}H_{49}N_7O_{10}$: C, 54.77; H, 7.27; N, 14.43%.

Iron(III) Complex of 6. Tris(2,4-pentanedionato)iron-(III) (13 mg) was added to a methanolic suspension (5 mL) of **6** (26 mg). The suspension became a clear solution. The mixture was left at room temperature for 1 d, and concentrated to give a crude product, 25 mg (64%). Reprecipitation from MeOH to ether and drying under vaccum (60 °C, 1 d) gave a sample; λ_{max} 420 nm, ε=2590 (in water). Found: C, 50.38; H, 6.63; N, 11.25; Fe, 7.37%. Calcd for $C_{31}H_{46}N_7O_{10}\cdot Fe\cdot CH_3OH$: C, 50.26; H, 6.59; N, 12.82; Fe, 7.30%.

Cyclic Voltammetry. To a DMF solution containing a trihydroxamic acid ligand was added 0.90 equivalent of an aqueous $Fe(NO_3)_3$ solution. The solvent was then evaporated. To this was added a phosphate buffer solution (pH 8.2 and ionic strength 0.50 with KCl). This was filtered and adjusted to pH 8.00 with 1 M HCl.

Cyclic voltammetry was carried out for solutions, thus obtained, by generating triangular waves at an ambient temperature. A carbon electrode was used for measurements with a saturated calomel electrode as a reference and a platinum wire as an auxiliary electrode. Current-voltage curves were recorded on an X-Y recorder.

We are grateful to Prof. Noboru Oyama and Dr. Yukio Ohnuki for discussion and cyclic-voltammetry measurements.

References

1) Part 3: M. Akiyama, K. Shimizu, S. Aiba, and H. Katoh, *Bull. Chem. Soc. Jpn.*, **58**, 1421 (1985).

2) J. B. Neilands, *Science*, **156**, 1443 (1967); "Inorganic Biochemistry," ed by G. Eichhorn, Elsevier, New York (1973), p. 167; *Ann. Rev. Biochem.*, **50**, 715 (1981).

3) K. N. Raymond and C. J. Carrano, *Acc. Chem. Res.*, **12** 183 (1979); K. N. Raymond, *Adv. Chem. Ser.*, American Chemical Society, Washigton D. C. (1977), No. 162, p. 33.

4) T. Emery, *Adv. Enzymol. Relat. Areas Mol. Biol.*, **33**, 135 (1971); *Am. Sci.*, **70**, 626 (1982).

5) R. L. Rawls, *Chem. Eng. News*, **55** (18), 24 (1977); **58** (39), 42 (1980).

6) H. Maehr, *Pure Appl. Chem.*, **28**, 603 (1971).

7) H. Bickel, R. Bossharrdt, E. Gäumann, P. Reusser, E. Vischer, W. Voser, A. Wettstein, and H, Zähner, *Helv. Chim. Acta*, **43**, 2118 (1960).

8) W. Keller-Schierlein, V. Prelog, and H. Zähner, *Fortschr. Chem. Org. Naturst.*, **22**, 279 (1964).

9) H. Zähner, R. Hütter, and E. Bachmann, *Arch. Mikrobiol.*, **36**, 325 (1960).

10) "Inorganic Chemistry in Biology and Medicine," ed by A. E. Martell, American Chemical Society, Washington D. C. (1973).

11) K. Shimizu, K. Nakayama, and M. Akiyama, *Bull. Chem. Soc. Jpn.*, **57**, 2456 (1984).

12) M. Narita, T. Teramoto, and M. Okawara, *Bull. Chem. Soc. Jpn.*, **45**, 3149 (1972).

13) T. Kolasa and A. Chimiak, *Tetrahedron*, **33**, 3285 (1977).

14) W. L. Smith and K. N. Raymond, *J. Am. Chem. Soc.*, **102**, 1252 (1980).

15) H. Bickel, G. E. Hall, W. Keller-Schierlein, V. Prelog, E. Vischer, and A. Wettstein, *Helv. Chim. Acta*, **43**, 2129 (1960).

16) G. Anderegg, F. L'Eplattenier, and G. Schwarzenbach, *Helv. Chim. Acta*, **46**, 1409 (1963).

17) K. Shimizu, M. Hasegawa, and M. Akiyama, *Bull. Chem. Soc. Jpn.*, **57**, 495 (1984).

18) A. Winston and E. T. Mazza, *J. Polym. Sci., Polym. Chem. Ed.*, **13**, 2019 (1975).

19) P. Desaraju and A. Winston, *J. Polym. Sci., Polym. Lett. Ed.*, **23**, 75 (1985).

20) S. R. Cooper, J. V. McArdle, and K. N. Raymond, *Proc. Natl. Acad. Sci. U.S.A*, **75**, 3551 (1978).

21) R. S. Nicholson and I. Shain, *Anal. Chem.*, **36**, 706 (1964).

22) R. H. Wopschall and I. Shain, *Anal. Chem.*, **39**, 1514 (1967).

Preparation and Complexing Properties of Crown Ether Compounds Incorporating a Ferrocene Unit at 1,2- or 1,3-Positions

Taeko IZUMI,* Katsuo SAITOU, Shigeki MATSUNAGA, and Akira KASAHARA
Department of Applied Chemistry, Faculty of Engineering, Yamagata University, Yonezawa 992
(Received December 16, 1985)

Ten new crown ethers incorporating a ferrocene unit at 1,2- or 1,3-positions are reported. These crown ethers were synthesized by the reaction of 1,2- or 1,3-bis(hydroxymethyl)ferrocene with oligoethylene glycol ditosylate (n=1—5) with potassium t-butoxide by a high-dilution method. These new types of ferrocene crown ethers were examined for complexation behavior with alkali, alkaline earth, and transition-metal cations by solvent extraction. It was found to extract thallium ions most effectively.

Crown compounds with a ferrocene unit incorporated into a macrocyclic ring have recently received considerable attention. Polyoxaferrocenophanes,[1] polythiaferrocenophanes,[2] polyoxathiaferrocenophanes[3] and ferrocene cryptands[4] have been synthesized and their functions have been investigated. Before, we reported on the synthesis and the cation-complexing ability of ferrocene-containing oxo crown ethers.[5] Most of these ferrocenophanes and cryptands exhibit rather weak binding toward alkali metal cations, but better complexation toward silver and thallium ions. Furthermore, all of these ferrocenophanes and cryptands formed a macrocycle at the 1,1′-positions of a ferrocene ring. In this work we considered the effects of a ferrocene structure on the complexing ability of a macrocycle. We now report on the synthesis and give a survey of the complexing properties of new ferrocenophanes which contain crown-ether type units connected at the 1,2- or 1,3-positions of a ferrocene ring.

Results and Discussion

Synthesis. The following reactions were carried out in order to obtain 1,2-bis(hydroxymethyl)ferrocene (**1**) and 1,3-bis(hydroxymethyl)ferrocene (**2**) as starting materials. In connection with the synthesis of the ferrocenophanes (**4b—e**, **5a**, **6b—e**, and **7a**), it became desirable to synthesize 1,2- and 1,3-bis(hydroxymethyl)-ferrocenes (**1** and **2**) in quantity. 2-Lithio[(dimethylamino)methyl]ferrocene, which was prepared by the reaction of [(dimethylamino)methyl]ferrocene with t-buthyllithium, was condensed with paraformaldehyde to give 2-[(dimethylamino)methyl]ferrocenemethanol. The amino alcohol was quaternized by methyl iodide, this ammonium iodide was converted to ferrocene-1,2-dimethanol (**1**) by boiling with an aqueous alkali. A treatment of 1,3-diacetylferrocene with sodium hypobromite in dioxane–H_2O below 10°C led to the formation of 1,3-ferrocenedicarboxylic acid. Then, ferrocene-1,3-dimethanol (**2**) was synthesized by the usual $LiAlH_4$ reduction of the dimethyl ester, which was prepared by an acid-catalyzed esterification of 1,3-diacid. A new series of "crowned" ferrocenophanes were prepared by the synthetic sequence shown in Fig. 1.

We used a facile modification of the Williamson ether synthesis which was performed in aprotic solvents using tosylate as the leaving group, the potassium cation improved the yields by forming a template

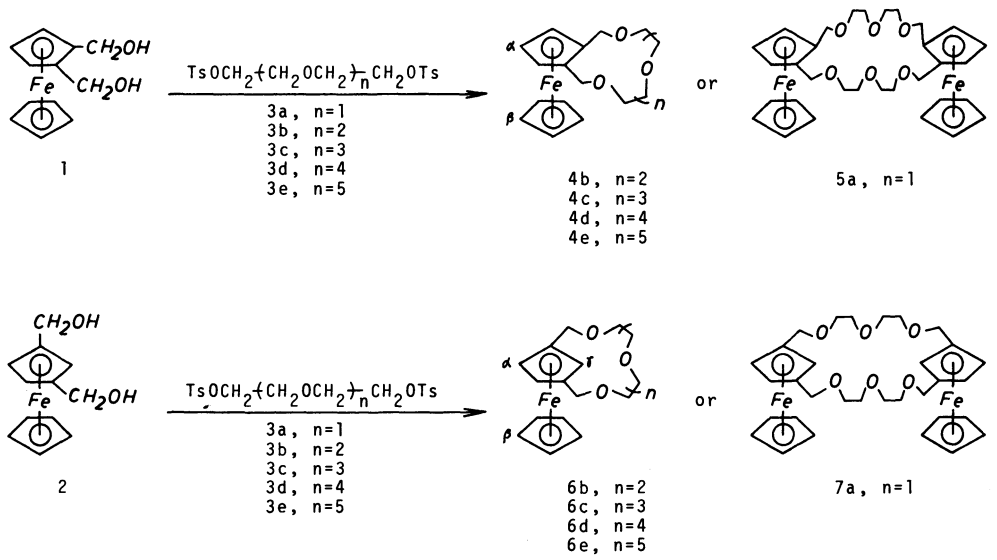

Fig. 1.

Table 1. Reaction of 1,2-Bis(hydroxymethyl)ferrocene and 1,3-Bis(hydroxymethyl)-ferrocene with Oligoethylene Glycole Ditosylates

Starting materials		Product	Yield/%	Mp θ_m/°C	Color
Ferrocene dialcohol	$TsOCH_2$-$(CH_2OCH_2)_n$-CH_2OTs				
1	n=1	**5a**	5.8	109—110	Yellow
1	n=2	**4b**	10.8	66—67	Yellow
1	n=3	**4c**	6.1	48—49	Yellow
1	n=4	**4d**	8.2	Oil	Orange
1	n=5	**4e**	7.6	Oil	Orange
2	n=1	**7a**	4.0	144—145	Yellow
2	n=2	**6b**	6.9	92—93	Yellow
2	n=3	**6c**	12.2	Oil	Orange
2	n=4	**6d**	17.3	Oil	Orange
2	n=5	**6e**	15.8	Oil	Orange

about which molecules could cyclize.[6] The reaction of diol (**1** or **2**) with the ditosylates of oligoethylene glycols (**3b—e**) in dry benzene in the presence of potassium *t*-butoxide gave crowned ferrocenophanes (**4b—e** and **6b—e**) in 5.8—10.8% yields for 1,2-ferrocenophanes or 4.0—17.3% yields for 1,3-ferrocenophanes, respectively, as yellow crystals or orange oils, along with unexpected polymeric materials (5—8 weight %). The starting materials (**1** and **2**) were recovered in every case in 40—60% yields. We tried to improve the product yields, but this could not be done by changing the reaction conditions (reaction time and solvent). Binuclear ferrocenophanes (**5a** and **7a**) were formed in the reaction of diethylene glycol ditosylate (**3a**) with **1** and **2**. This might indicate that the diethylene glycol chain (n=1) is too short to cyclize on the same cyclopentadienyl ring (1,2- or 1,3-positions). The results are summarized in Table 1. The structures of all ferrocenophanes, thus prepared, were determined on the bases of their IR, ^{1}H NMR, mass spectra and elemental analyses. The IR spectra of the ferrocenophanes showed bands caused by ether a linkage at 1090 or near 1127 cm^{-1}, by homoannular disubstituted ferrocene in 3105—3095, 1100, 1020—1000, and 820 cm^{-1} regions, and by methylene group in 2980—2920, 2880—2870, 1460—1420, and 1380—1360 cm^{-1} regions. In the ^{1}H NMR spectra, all the ferrocenophanes showed a similar pattern: methylene protons as a broad singlet at about 3.6 ppm, protons of methylene groups adjacent to the ferrocene ring at 4.26—4.39 ppm, unsubstituted cyclopentadienyl protons at 4.08—4.10 ppm as sharp singlets and substituted cyclopentadienyl protons as multiplets at 4.22—4.42 ppm. The mass spectra and the elemental analyses also confirmed the structures.

Extraction Ability. The complexing ability between synthesized polyoxaferrocenophanes (**4b—e**, **6b—e**, **5a**, and **7a**) and alkali, alkalin earths, and transition metal cations could be established by Pedersen's solvent extraction method.[7] The data are summarized in Table 2. These results indicate little or no extractability toward alkali metal cations (Li^+ and Na^+) for almost all of polyoxaferrocenophanes, except **4c** which exhibits selectivity toward the thallium cation.

Table 2. Extraction Data (Water-Dichloromethane)[a]

Compound	Extracted/%					
	Li^+	Na^+	K^+	Ba^{2+}	Tl^+	Ag^+
4b	0	2.9	0.7	5.3	14.9	Oxidation
4c	0.9	32.9	19.3	14.2	67.6	86.1
4d	4.3	4.3	13.4	19.2	66.4	Oxidation
4e	2.9	2.9	24.3	53.6	77.9	Oxidation
6b	0	0	0	10.0	4.4	Oxidation
6c	0	0	4.0	8.3	56.3	Oxidation
6d	0	0	11.4	0.7	66.3	25.7
6e	1.4	1.8	6.7	4.0	60.8	42.1
5a	0	1.8	9.0	6.4	56.2	Oxidation
7a	0	0	0	9.1	34.2	Oxidation

a) Equal volumes of water and dichloromethane, and picric acid at 7.0×10^{-5}M (1M=1 mol dm^{-3}). Concentration of ferrocenophane: 7.0×10^{-4}M. Concentration of metal nitrate: 0.1 M.

Furthermore, the extraction efficiency toward others cations (K^+, Ba^{2+}, and Tl^+) is dependent on the size of the crown ether ring in the polyoxaferrocenophanes, especially in the cases of **4b—e**. It is interesting that **4b—e** (1,2-ferrocenophanes) shows a high complexing ability compared with **6b—e** (1,3-ferrocenophanes), even though the latter has a large ring size, and even though these ferrocenophanes have similar structures. This can be explained by assuming that the proton at the 2-position of the substituted cyclopentadienyl ring of **6b—e** is more sterically hindered in the process of complexation. On the other hand, the attached position of ferrocene to the crown ether seems to influence the complexing ability. For example, 1,2-polyoxaferrocenophanes (**4b—e**) show a high complexing ability, except toward silver ions, compared with 1,1′-polyoxaferrocenophanes which were reported by Akabori et al.[1c] It should be emphasized that **4c** (n=3) has a high complexing ability toward sodium, thallium, and silver ions. It is also interesting that the extraction ability toward thallium ion shows a remarkable dependence on the cavity size in the macrocycle of **4b—e**. Binuclear polyoxaferrocenophanes (**5a** and **7a**) show a low extractability to-

ward metal cations (Li^+, Na^+, K^+, and Ba^{2+}), but show an appreciable selectivity toward thallium cations. A similar trend of affinity toward transition metal cations have been observed in hitherto reported "crowned" ferrocenophanes and these synthesized polyoxaferrocenophanes; this suggests that the iron atom of the ferrocene nucleus participates in the process of complexation. This means that the metal cation is drawn into the crown ether ring from the iron-atom side of ferrocene, even though the opposite side of the ring has less hindrance. In the case of a silver ion, the ferrocene nucleus changed to a ferricenium ion, which showed blue color in solution, upon oxidation with $AgNO_3$ (except **4c**, **6d**, and **6e**). This oxidation seems very sensitive to the crown-ring member since **4c** showed an 86.1% extractability and almost all cases showed oxidation reaction. These facts indicate that the distance between the iron atom of ferrocene and the incorporated silver cation influences the oxidation of ferrocene. A similar result was also observed in polyoxa-[1c] or polyoxathiaferrocenophanes.[3e,3f]

Experimental

Materials and Measurements. All melting points are uncorrected. Diethylene glycol, triethylene glycol and tetraethylene glycol were commercial products, pentaethylene glycol and hexaethylene glycol were prepared by reactions of tri- and diethylene glycol ditosylates with the sodium salt of ethylene glycol and diethylene glycol, respectively.[8] 1,2-Bis(hydroxymethyl)ferrocene[9] and 1,3-bis(hydroxymethyl)-ferrocene[10] were prepared as described in the literature. The other reagents employed were commercial materials or were prepared by the usual method. All inorganic compounds were reagents grade. The IR, ^1H NMR, mass, and electronic spectra were recorded on Hitachi 260-10, Hitachi R-22, Hitachi RMU-6M, and Hitachi 200-10 spectrometers, respectively.

General Procedure for Polyoxa[*n*](1,2)ferrocenophanes (5a and 4b—e) and polyoxa[*n*](1,3)ferrocenophanes (7a and 6b—e). A mixture of 1,2-bis(hydroxymethyl)ferrocene (**1**) (2.00 g, 0.0081 mol) or 1,3-bis(hydroxymethyl)ferrocene (**2**) (2.00 g, 0.0081 mol) and oligoethylene glycol ditosylate (n=1—5) (0.0081 mol) in 160 ml of dry benzene was added dropwise to a benzene solution (20 ml) of potassium *t*-butoxide (K: 0.8 g, 0.020 mol) over a period of 7 h at a refluxing temperature under nitrogen, and then further stirred for 20 h. After the solution has been cooled to room temperature, precipitated potassium tosylate was filtered off and washed with warm chloroform. Evaporation of the solvent left crude products as viscous oils; these were purified by silica-gel column chromatography. The first fraction eluted with benzene–ether (10:1) gave ferrocenophane (**5a**, **4b—e**, **7a**, and **6b—e**); the second fraction eluted with chloroform–methanol (5:1) recovered the starting dialcohol (**1** or **2**); and the last fraction eluted with chloroform–methanol (2:1) gave polymeric materials. The crude product was recrystallized from hexane. The results are summarized in Table 1.

2,5,8,22,25,28-Hexaoxa[9.9](1,2)ferrocenophane (5a). IR (KBr): 3080, 2950—2860, 1460, 1360, 1100, 1090, 1000, 820 cm^{-1}. ^1H NMR ($CDCl_3$) δ=3.53 (br-s, 16H, $-OC\underline{H_2}C\underline{H_2}O-$), 4.04 (s, 10H, Fc–$H_\beta$), 4.26 (m, 6H, Fc–$H_\alpha$), 4.36 (s, 8H, Fc–$C\underline{H_2}O-$) ppm. MS (70 eV) m/z 632 [M^+]. Found: C, 60.66; H, 6.30%. Calcd for $C_{32}H_{40}Fe_2O_6$: C, 60.78; H, 6.38%; M, 632.36.

2,5,8,11-Tetraoxa[12](1,2)ferrocenophane (4b). IR (KBr): 3080, 2920—2850, 1450, 1360, 1100, 1080, 1000, 820 cm^{-1}. ^1H NMR ($CDCl_3$) δ=3.62 (br-s, 12H, $-OC\underline{H_2}C\underline{H_2}O-$), 4.08 (s, 5H, Fc–$H_\beta$), 4.28 (m, 3H, Fc–$H_\alpha$), 4.36 (br-s, 4H, Fc–$C\underline{H_2}O-$) ppm. MS (70 eV) m/z 360 [M^+]. Found: C, 59.73; H, 6.66%. Calcd for $C_{18}H_{24}FeO_4$: C, 60.02; H, 6.72%; M, 360.23.

2,5,8,11,14-Pentaoxa[15](1,2)ferrocenophane (4c). IR (KBr): 3090, 2920—2850, 1460, 1355, 1100, 1085, 1020, 830 cm^{-1}. ^1H NMR ($CDCl_3$) δ=3.61 (s, 16H, $-OC\underline{H_2}C\underline{H_2}O-$), 4.09 (s, 5H, Fc–$H_\beta$), 4.28 (m, 3H, Fc–$H_\alpha$), 4.34 (s, 4H, Fc–$C\underline{H_2}O-$) ppm. MS (70 eV) m/z 404 [M^+]. Found: C, 59.49; H, 6.89%. Calcd for $C_{20}H_{28}FeO_5$: C, 59.42; H, 6.98%; M, 404.29.

2,5,8,11,14,17-Hexaoxa[18](1,2)ferrocenophane (4d). IR (neat): 3090, 2950—2860, 1465, 1350, 1125, 1100, 1000, 820 cm^{-1}. ^1H NMR ($CDCl_3$) δ=3.53 (s, 20H, $-OC\underline{H_2}C\underline{H_2}O-$), 4.04 (s, 5H, Fc–$H_\beta$), 4.26 (m, 3H, Fc–$H_\alpha$), 4.36 (s, 4H, Fc–$C\underline{H_2}O-$) ppm. MS (70 eV) m/z 448 [M^+]. Found: C, 59.06; H, 7.23%. Calcd for $C_{22}H_{32}FeO_6$: C, 58.94; H, 7.19%; M, 448.34.

2,5,8,11,14,17,20-Heptaoxa[21](1,2)ferrocenophane (4e). IR (neat): 3100, 2950—2860, 1460, 1360, 1100, 1000, 820 cm^{-1}. ^1H NMR ($CDCl_3$) δ=3.62 (s, 24H, $-OC\underline{H_2}C\underline{H_2}O-$), 4.09 (s, 5H, Fc–$H_\beta$), 4.28 (br-s, 3H, Fc–$H_\alpha$), 4.39 (br-s, 4H, Fc–$C\underline{H_2}O-$) ppm. MS (70 eV) m/z 492 [M^+]. Found: C, 58.46; H, 7.40%. Calcd for $C_{24}H_{36}FeO_7$: C, 58.54; H, 7.37%; M, 492.39.

2,5,8,22,25,28-Hexaoxa[9.9](1,3)ferrocenophane (7a). IR (KBr): 3080, 2950—2850, 1460, 1350, 1100, 1090, 1000, 820 cm^{-1}. ^1H NMR ($CDCl_3$) δ=3.52 (s, 16H, $-OC\underline{H_2}C\underline{H_2}O-$), 4.08 (s, 10H, Fc–$H_\beta$), 4.22 (s, 6H, Fc–$H_\alpha$), 4.27 (s, 8H, Fc–$C\underline{H_2}O-$), 4.44 (s, 2H, Fc–$H_\gamma$) ppm. MS (70 eV) m/z 632 [M^+]. Found: C, 60.52; H, 6.22%. Calcd for $C_{32}H_{40}Fe_2O_6$: C, 60.78; H, 6.38%; M, 632.36.

2,5,8,11-Tetraoxa[12](1,3)ferrocenophane (6b). IR (KBr): 3080, 2940—2850, 1450, 1350, 1100, 1090, 1010, 820 cm^{-1}. ^1H NMR ($CDCl_3$) δ=3.43 (br-s, 12H, $-OC\underline{H_2}C\underline{H_2}O-$), 4.10 (s, 5H, Fc–$H_\beta$), 4.15 (s, 2H, Fc–$H_\alpha$), 4.23 (br-s, 4H, Fc–$C\underline{H_2}O-$), 4.58 (s, 1H, Fc–$H_\gamma$) ppm. MS (70 eV) m/z 360 [M^+]. Found: C, 60.13; H, 6.68%. Calcd for $C_{18}H_{24}FeO_4$: C, 60.02; H, 6.72%; M, 360.23.

2,5,8,11,14-Pentaoxa[15](1,3)ferrocenophane (6c). IR (neat): 3080, 2940—2850, 1450, 1350, 1120, 1100, 1000, 820 cm^{-1}. ^1H NMR ($CDCl_3$) δ=3.51 (s, 16H, $-OC\underline{H_2}C\underline{H_2}O-$), 4.12 (s, 5H, Fc–$H_\beta$), 4.18 (m, 2H, Fc–$H_\alpha$), 4.26 (s, 4H, Fc–$C\underline{H_2}O-$), 4.46 (s, 1H, Fc–$H_\gamma$) ppm. MS (70 eV) m/z 404 [M^+]. Found: C, 59.33, H, 6.87%. Calcd for $C_{20}H_{28}FeO_5$: C, 59.42; H, 6.98%; M, 404.29.

2,5,8,11,14,17-Hexaoxa[18](1,3)ferrocenophane (6d). IR (neat): 3080, 2940—2850, 1460, 1360, 1125, 1100, 1000, 820 cm^{-1}. ^1H NMR ($CDCl_3$) δ=3.56 (s, 20H, $-OC\underline{H_2}C\underline{H_2}O-$), 4.08 (s, 5H, Fc–$H_\beta$), 4.18 (m, 2H, Fc–$H_\alpha$), 4.30 (s, 4H, Fc–$C\underline{H_2}O-$), 4.44 (s, 1H, Fc–$H_\gamma$) ppm. MS (70 eV) m/z 448 [M^+]. Found: C, 58.90; H, 7.02%. Calcd for $C_{22}H_{32}FeO_6$: C, 58.94; H, 7.19%; M, 448.34.

2,5,8,11,14,17,20-Heptaoxa[21](1,3)ferrocenophane (6e). IR (neat): 3080, 2940—2850, 1460, 1360, 1125, 1100, 1000, 820 cm^{-1}. ^1H NMR ($CDCl_3$) δ=3.60 (s, 24H, $-OC\underline{H_2}C\underline{H_2}O-$), 4.10 (s, 5H, Fc–$H_\beta$), 4.24 (m, 2H, Fc–$H_\alpha$), 4.33 (s, 4H, Fc–$C\underline{H_2}O-$), 4.51 (s, 1H, Fc–$H_\gamma$) ppm. MS (70 eV) m/z 492

[M^+]. Found: C, 58.46; H, 7.32%. Calcd for $C_{24}H_{36}FeO_7$: C, 58.54; H, 7.37%; M, 492.39.

Solvent Extraction Experiments of Metal Ions. The extraction ability of synthesized polyoxaferrocenophanes with metal picrates was examined by a method described in a previous paper.[5]

References

1) a) J. F. Biernat and T. Wilczewski, *Tetrahedron*, **36**, 2521 (1980); b) S. Akabori, H. Fukuda, Y. Habata, M. Sato, and S. Ebine, *Chem. Lett.*, **1982**, 1393; c) S. Akabori, Y. Habata, Y. Sakamoto, M. Sato, and S. Ebine, *Bull. Chem. Soc. Jpn.*, **56**, 537 (1983).

2) a) M. Sato, H. Watanabe, S. Ebine, and S. Akabori, *Chem. Lett.*, **1982**, 1753; b) M. Sato, S. Tanaka, S. Ebine, and S. Akabori, *Bull. Chem. Soc. Jpn.*, **57**, 1929 (1984).

3) a) G. Oepen and F. Vögtle, *Liebigs Ann. Chem.*, **1979**, 1094; b) B. Czech and A. Ratajczak, *Polish J. Chem.*, **54**, 767 (1980); c) B. Czech, A. Ratajczak, and K. Nagraba, *Monatsh. Chem.*, **113**, 965 (1982); d) M. Sato, M. Kubo, S. Ebine, and S. Akabori, *Tetrahedron Lett.*, **23**, 185 (1982); e) S. Akabori, Y. Habata, M. Sato, and S. Ebine, *Bull. Chem. Soc. Jpn.*, **56**, 1459 (1983); f) S. Akabori, S. Shibahara, Y. Habata, and M. Sato, *ibid.*, **57**, 63 (1984); g) M. Sato, M. Kubo, S. Ebine, and S. Akabori, *ibid.*, **57**, 421 (1984).

4) a) 3e), b); A. P. Bell and C. D. Hall, *J. Chem. Soc., Chem. Commun.*, **1980**, 163; c) P. J. Hammond, A. P. Bell, and C. D. Hall, *J. Chem. Soc., Perkin Trans. 1*, **1983**, 707.

5) T. Izumi, T. Tezuka, S. Yusa, and A. Kasahara, *Bull. Chem. Soc. Jpn.*, **57**, 2433 (1984).

6) J. Dale and P. Kristiansen, *Acta. Chem. Scand.*, **26**, 1471 (1972).

7) C. J. Pedersen, *Federation Proceeding*, **27**, 1305 (1968).

8) N. Newcomb, S. S. Moore, and D. J. Cram, *J. Am. Chem. Soc.*, **99**, 6405 (1977).

9) G. Marr, B. W. Rockett, and A. Rushworth, *J. Organometal. Chem.*, **16**, 141 (1969).

10) A. Kasahara, T. Izumi, Y. Yoshida, and I. Shimizu, *Bull. Chem. Soc. Jpn.*, **55**, 1901 (1982).

 © 1986 The Chemical Society of Japan Bull. Chem. Soc. Jpn., 59, 2429—2432 (1986)

Thermal Racemization of Thiaheterohelicenes

Koh-ichi YAMADA, Hiroko NAKAGAWA, and Hiroshi KAWAZURA*
Faculty of Pharmaceutical Sciences, Josai University, Sakado, Saitama 350-02
(Received January 27, 1986)

Thermal racemizations of four thiaheterohelicenes (TH) with alternant thiophene and benzene rings were examined and compared with those of carbohelicenes (CH). The racemization rate of [5]TH was very fast at room temperature, and the rates of [7]TH and [9]TH were found to be 1/5 to 1/50 times slower than the corresponding CH having a similar internal angle. The $\Delta S^{\ddagger}$ values obtained by temperature-variable experiments showed a large difference between [7]TH (-103.9 ± 4.8 JK^{-1} mol^{-1}) and [9]TH (-66.3 ± 4.0), suggesting different conformations in the transition state. CNDO calculations on the transitional conformations of [5]TH demonstrated that a geometry, such as that distorting the benzene rings, has a lower energy than a geometry such as that twisting the thiophene ring. Based upon these results, the conformations in the transition states for the THs are inferred.

Reports on the racemization of carbohelicenes (CH) were very surprising in view of the flexibility of the angularly fused benzene rings.[1] Despite their structural overcrowding, the free energies of the activation ($\Delta G^{\ddagger}$) for the reactions did not seem to be too large to override a severe transition path: [8]CH, 181.9; [9]CH, 188.3kJ mol^{-1} at 543 K. Thus, the racemization is thought to occur via an achiral transition state in which the deformations spread over the entire molecule so as to prevent a local severe strain, accompanied by much motional freedom. Lindner calculated the energy differences between the ground state and some assumed transition states for a [6]CH molecule by the π-SCF-force-field method, and argued that the most plausible geometry for a transition state is that in which the terminal portions of the molecule are in a face-to-face position with each other (Figure).[2] So far, only a few heterohelicenes, partially composed of heteroaromatics, were investigated regarding racemizations.[3] However, they were confined to hexa homologs which do not complete a full turn and, hence, do not reveal the distinct effect of heteroaromatics on the reaction.

As a part of the study on the properties and structures of thiaheterohelicene (TH), we examined the thermal racemizations of TH containing alternant thiophene and benzene rings. We wish to describe here the kinetic results of the reactions and to discuss their transition states by referring to our CNDO calculation on the transition state models. A comparison of CH with TH in the transition states is also made while focusing on the influence of the heteroaromatics.

Experimental

Syntheses[4] and optical resolutions[5] of the thiaheterohelicenes studied have been reported in the foregoing publications. Optical rotations were measured on a JASCO DIP-180 digital polarimeter or a JASCO J-20A automatic recording spectropolarimeter. Chromatograms of THs were recorded on a Waters Model 204 HPLC system. CNDO calculations[6] were performed on a FACOM M-160F computer.

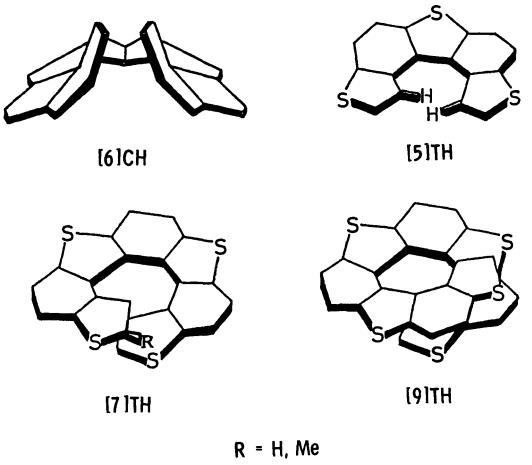

Racemization reactions of chiral TH were carried out in a mesitylene solution in a tube sealed under a nitrogen atmosphere. Tubes of the solution were thermostated in an oil bath and the reaction progress was pursued by measuring the optical rotation at given time intervals. The reactions were also followed by measuring changes in the absorption spectra and HPLC peaks.

Results and Discussion

The ease of racemization depends on the winding degree of the helix, i.e. the extent of the intramolecular overlap, which can be estimated with the internal angle (IA) of the TH molecules[3] studied here: [9]TH, 465; [7]TH and 2-methyl[7]TH, 360; and [5]TH, 255°.[7] Thus, it is expected that [5]TH should racemize rapidly in solution, although the structure in crystals retains a rigid helix.[8] In fact, HPLC using a column containing (+)TAPA-bonded silica gel (TAPA: 2-(2,4,5,7-tetranitro-9-fluorenylideneaminooxy)-propionic acid) could not be used to separate the enantiomers of [5]TH at −14°C. Several recyclings or a lowering of the temperature to −24°C caused a slight separation between *P* and *M* enantiomers[9] (Fig. 1). All attempts to isolate the enantiomers were, however, unsuccessful, even at lowered temperatures, suggesting a low activation energy for the racemization of [5]TH.

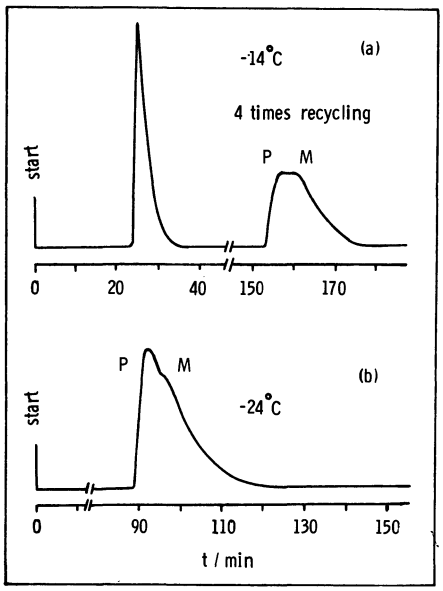

Fig. 1. Resolutions of the enantiomers of [5]TH by HPLC. (+)TAPA-bonded silica-gel column, CH_2Cl_2/n-C_6H_{14}=4/1, monitored at 254 nm, (a) flow rate 2 ml min^{-1}, and (b) 1 ml min^{-1}.

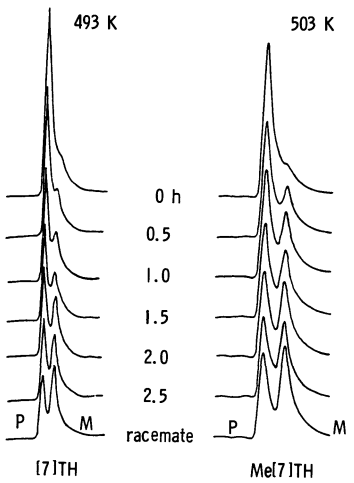

Fig. 2. Time course of HPLC peaks of [7]TH and 2-Me[7]TH. (+)TAPA-bonded silica-gel column, CH_2Cl_2/n-C_6H_{14}=1/1, flow rate 1 ml min^{-1}, and monitored at 254 nm.

Figure 2 illustrates the time course of the HPLC peaks for reactions of [7]TH and 2-Me[7]TH. During every reaction time, no peak except for those illustrated was observed, indicating that no meaningful side reaction took place and that all the changes in the optical rotations could be regarded as racemization processes.

The first-order rate constant k_r and the activation parameters were obtained from the following equations by least-squares treatments,

$$k_r = 1/2\,t \ln(\alpha_0/\alpha_t),$$
$$\Delta G^* = RT[\ln(k/h) - \ln(k_r/T)],$$
$$\Delta G^* = \Delta H^* - T\Delta S^*,$$

Table 1. k_r and ΔG^* of Racemization at 500 K

	Internal angle	$k_r \times 10^6$	ΔG^*
	deg.	s^{-1}	kJ mol^{-1}
[7]TH	360	124	162.0
Me[7]TH	360	113	162.4
[9]TH	465	0.021	198.1
[6]CH[a)]	360	668	154.3
[8]CH[a)]	480	1.10	181.9

a) The values are cited from Ref. 1.

Table 2. Activation Parameters of Racemization

	ΔH^*	$-\Delta S^*$
	kJ mol^{-1}	JK^{-1} mol^{-1}
[7]TH	110.0±2.8	103.9±4.8
Me[7]TH	120.7±2.8	83.3±4.6
[9]TH	164.9±2.2	66.3±4.0
[6]CH[a)]	146.4	17.6
[8]CH[a)]	171.5	19.2

a) The values are cited from Ref. 1.

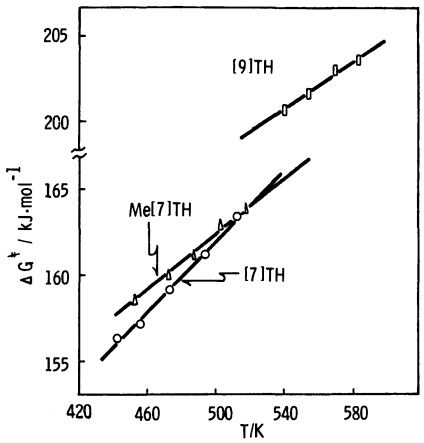

Fig. 3. Temperature dependence of ΔG^*.

where α_0 and α_t are the optical rotation at time 0 and t, respectively. The k_r's and the free energies of the activation (ΔG^*) at 500 K are tabulated in Table 1, together with the calculated IA values. The effect of a methyl substituent at the 2-position in a [7]TH molecule seems to be relatively small. It is notable that the rate of [9]TH becomes much smaller than that of [7]TH by about 1/5900 times with a large ΔG^* value by 36.1 kJ mol^{-1}. Compared with the k_r of carbohelicene having a similar IA value, the k_r of [7]TH is 1/5.4 times smaller than that of [6]CH, and [9]TH (which possesses the smaller IA than [8]CH) shows a k_r that is 1/52 times slower as a result of the larger ΔG^* by 16.2 kJ mol^{-1}. These results demonstrate that TH molecules hold more rigid skeleton than CH molecules.

The temperature dependences of ΔG^* are depicted in Fig. 3 and the activation enthalpies (ΔH^*) and entropies (ΔS^*) are listed in Table 2. As is apparent

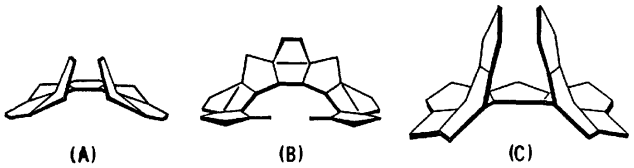

Fig. 4. The possible transitional geometries of [7]TH ((A) and (B)), and the plausible transitional geometry of [9]TH ((C)).

from the Table, a comparison between the two CHs exhibits an increasing $-\Delta S^*$ with an increasing ΔH^*. This relationship between ΔH^* and ΔS^* is generally observed in such a case as a series of homologs whose racemization could occur through the same kind of transitional geometries. On the other hand, the trend of $-\Delta S^*$ against ΔH^* in the TH series was found to be opposite; this might imply that [9]TH should take a different transitional geometry from that of [7]THs. Moreover, the most striking feature is the large difference of $-\Delta S^*$ values between CH and TH. In the racemization of a TH molecule, the entropy term contributes greatly to the free energy of the activation, suggesting a great loss of motional freedom in the transition state.

As for the transitional geometry of [7]TH racemization two conformations, (A) and (B), are thought possibly to exist (Fig. 4), as speculated in the literature.[2] Form (A) is produced by a distortion of the terminal thiophene rings, while (B) is formed by a distortion of the benzene portions. The kinetic results indicate that type (B) is more plausible since in this form the distortion should occur synchronously at the three sites to provide a greater entropy change than at the two sites in form (A). Regarding the [9]TH transition state, it may be no longer possible to hold form (B) on account of its larger extent of winding. Figure 4 (C) illustrates the plausible transitional geometry of the [9]TH racemization. In this geometry the number of the mainly distorted sites is two; this is more related to the smaller $-\Delta S^*$ value than that of [7]TH.

Finally, we attempted to obtain CNDO-calculational support for the geometries mentioned above. However, the [7]TH and [9]TH molecules are so big that the energies could not converge to definite values. For the [5]TH molecule, the total energies were attained with iterative methods for the ground-state geometry determined by an X-ray analysis, and for a planar geometry having the same bond lengths, in which the terminal hydrogens are brought into close proximity with each other: 1.36 Å (Table 3, (a) and (b)). Interestingly, the energies of both conformations were found to be close; the increase in the conjugation energy, due to the planarity, would counteract the repulsion energy between the terminal hydrogens. Thus, the transition state of the [5]TH racemization

Table 3. Total Energies (E_T) of Some Conformations of the [5]TH Molecule. Refer to Fig. 5.

Conformation	r	E_T
	Å	eV
(a) Ground State	2.11	−4141.17
(b) Plane	1.36	−4140.94
Distorted Ring		
(c) Thiophene	1.55	−4139.28
(d) Benzene	1.56	−4139.74

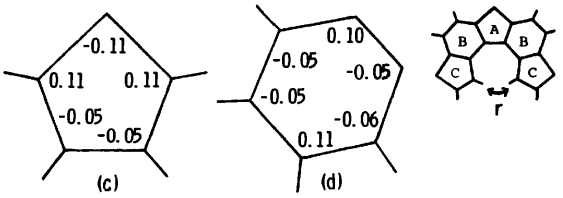

Fig. 5. Distorted conformations of [5]TH molecule. Distorted sites are (c) thiophene A ring and (d) benzene B rings. The figures in the rings are deviations (Å) from the least-squares plane.

can be supposed to be like a planar geometry.

Furthermore, a series of tentative calculations of the total energies of the [5]TH molecules was carried out using various hypothetical models in which only thiophene or benzene rings were distorted from the planar geometry. Figure 5 and Table 3 ((c) and (d)) show an example where two kinds of distorted molecules are chosen as being equal at a distance (r) between the terminal hydrogens. In every case, it was found that the energy obtained for the molecule with a distorted benzene became smaller than that of a molecule with a distorted thiophene. This implies that in order to hold the terminal moieties in the same separation, the distortion of the five-membered ring thiophene needs to have a higher energy than that of the six-membered ring benzene. This difference in the rigidity between thiophene and benzene ring might play a role in the transitional geometry of the [7]TH racemization.

In conclusion, thiaheterohelicenes manifest fairly different behaviors in thermal racemization reactions from carbohelicenes, presumably because of the existence of the heteroaromatics thiophene.

References

1) R. H. Martin and M. J. Marchant, *Tetrahedron Lett.*, **1972**, 3707; C. Goedicke and H. Stegemeyer, *ibid*, **1970**, 937; R. H. Martin and M. J. Marchant, *Tetrahedron*, **30**, 347 (1974); J. H. Borkent and W. H. Laarhoven, *ibid*, **34**, 2565 (1978); R. H. Martin, *Angew. Chem., Int. Ed. Engl.*, **13**, 649 (1974); W. H. Laarhoven and W. J. C. Prinsen, *Topics in Current Chemistry*, **125**, 63 (1984).

2) H. J. Lindner, *Tetrahedron*, **31**, 281 (1975).

3) H. Wynberg and M. B. Groen, *J. Chem. Soc.*, **D1969**, 964; H. Wynberg, *Acc. Chem. Res.*, **4**, 65 (1971).

4) K. Yamada, S. Ogashiwa, H. Tanaka, H. Nakagawa, and H. Kawazura, *Chem. Lett.*, **1981**, 343.

5) H. Nakagawa, S. Ogashiwa, H. Tanaka, K. Yamada, and H. Kawazura, *Bull. Chem. Soc. Jpn.*, **54**, 1903 (1981).

6) J. A. Pople and G. A. Segal, *J. Chem. Phys.*, **44**, 3289 (1966).

7) IUPAC nomenclatures of the compounds studied are as follows; [5]TH thieno[3,2-*e*:4,5-*e'*]di[1]benzothiophene, [7]TH bisthieno[3',2':4,5]benzo[1,2-*b*:4,3-*b'*]di[1]benzothiophene, [9]TH bis[1]benzothieno[5',4':2,3]thieno[3,2-*e*:4,5-*e'*]di[1]benzothiophene.

8) H. Nakagawa, K. Yamada, H. Kawazura, and H. Miyamae, *Acta Crystallogr., Sect. C*, **40**, 1039 (1984).

9) K. P. Meurer and F. Vögtle, *Topics in Current Chemistry*, **127**, 10 (1986).

Design of the Synthetic Route for Peptides and Proteins Based on the Solubility Prediction Method. I. Synthesis and Solubility Properties of Human Proinsulin C-Peptide Fragments[1)]

Mitsuaki NARITA,* Toshihiko OGURA, Kazuhiro SATO, and Shinya HONDA
Department of Industrial Chemistry, Faculty of Technology, Tokyo University of Agriculture and Technology, Koganei 184
(Received February 25, 1986)

The usefulness of the solubility prediction method is demonstrated using relatively small peptide fragments of human proinsulin C-peptide. The propriety of the solubility prediction method for peptides having polar side chains is also examined in the following respects: (1) Peptide intermediates smaller than a heptapeptide have high solubility regardless of their $\langle P_c \rangle$ values; (2) the $\langle P_c \rangle$ values of peptide intermediates are useful for judging solubility of peptide intermediates equal to or larger than an octapeptide level; (3) the Pro residue in a central position of a peptide chain is effective for increasing peptide solubility; and (4) there is critical chain length for peptide insolubility caused by a β-sheet aggregation. A strategy suitable for the design of the synthetic route for human proinsulin C-peptide is subsequently discussed on the basis of the solubility prediction of peptide intermediates.

To achieve total synthesis of large peptides and proteins, all of the components must be soluble in coupling solvents. In many cases of protein syntheses, indeed, avoidance of insolubility of peptide intermediates in coupling solvents is claimed to be a problem of utmost importance to achieve the protein syntheses favorably.[2)] Thus, the proper design of the synthetic route based on the solubility prediction of peptide intermediates is greatly required to avoid erroneous synthetic routes. Following this concept, we are pursuing the scope of the design of the synthetic routes for peptides and proteins based on a solubility prediction method.[3)]

So far, however, it has been widely recognized that the solubility prediction of protected peptide intermediates is difficult due to the diverse individuality of their amino acid sequences since their solubility is primarily dependent on their amino acid sequences. In our recent papers,[3-10)] however, we have demonstrated that insolubility of peptide intermediates is caused by a β-sheet aggregation of peptide intermediates equal to or larger than an octapeptide level and that the temporary protection of a N-H peptide bond in a central position of a peptide chain helps improve solubility to a remarkable extent.[4)] Furthermore, we have also demonstrated that, in hydrophobic sequences found in proteins, the β-sheet aggregation plays an important role in insolubility of hydrophobic peptides and that, contrary to the general recognition that solubility of peptide intermediates is primarily dependent on their amino acid sequences, their solubility is independent on their amino acid sequences.[10)] On the basis of these results, the solubility prediction of peptide intermediates was successfully performed by making use of both the randomness of peptide structures in the solid state and the existence of tertiary peptide bonds, that is, the disturbance of a β-sheet structure.[3)] The correctness of the concept of this solubility prediction method was furthermore verified by another evidence, that is, solubility improvement by promotion of helical folding in oligopeptides based on the restriction of the values of the backbone dihedral angles ϕ and ψ of the α-aminoisobutyric acid residue.[10-12)]

The usefulness of the solubility prediction method has been previously confirmed in hydrophobic oligopeptides.[3-12)] We here demonstrate its usefulness also for relatively small peptide fragments of human proinsulin C-peptide having polar side chains and we then propose a strategy suitable for the design of the synthetic routes for the C-peptide on the basis of the solubility prediction of peptide intermediates.

Experimental

General. The uncorrected capillary melting points will be reported. The amino acid compositions of acid hydrolysates were determined with a Shimadzu HPLC LC-3A all amino acid analysis system. The acid hydrolyses of the peptides containing the Ser residue were carried out with 3M† *p*-toluenesulfonic acid[13)] for 3 d at 115 °C in evacuated, sealed tubes, and those of other peptides, with propionic acid/12M HCl (vol. ratio, 2/1)[14)] for 2 d at 115°C. Other analytical instruments and conditions were described in the previous paper.[11)]

General Procedure for Removal of the Boc Group. Boc-amino acid Pac esters (10 mmol) and Boc-peptide Pac esters (10 mmol) in 3 M HCl/AcOEt (60 ml) were stirred in an ice-chilled bath for 1.5—3 h. Then, the mixture was concentrated in vacuo, followed by the repetition of the addition and removal in vacuo of dichloromethane. The residual amino component HCl salt was used for a subsequent coupling reaction without further purification.

General Procedure for Stepwise Elongation of Peptide Chains Using DCC Activation (Preparation of the Peptides 1—6 and 10). DCC (1.2 equiv) was added to an ice-chilled, stirred mixture of a carboxyl component (1.2 equiv) and an amino component (10 mmol) in dichloromethane, a mixture of dichloromethane and DMF, or DMF (100 ml). The amino components were obtained from the corresponding HCl salt with an equivalent of NMM. For incorpora-

† 1 M=1 mol dm^{-3}.

tion of the Gln residue, instead of DCC activation, Boc-Gln-ONp (1.5 equiv) was used for chain elongation. The reaction mixture was stirred in an ice-chilled bath for 3 h, at room temperature overnight, and then subjected to ninhydrin test. When the test was positive, double and triple couplings were carried out using the carboxyl component and DCC (each 0.3 equiv). After completion of the reaction, the reaction mixture was filtered. The subsequent work-up procedure was essentially the same as those described before.[11] The synthetic results and analytical data are shown in Tables 1—3.

General Procedure for Fragment Condensation Using DCC Activation in the Presence of HOBt (Preparation of the Peptides 7—9, 11, and 12). Assembly of peptide chains by fragment condensation was carried out in DMF or a mixture of DMF and NMP. DCC (1.2 equiv) was added to an ice-chilled, stirred mixture of a carboxyl component (1.2 equiv), HOBt (1.2 equiv), and an amino component (10 mmol) in solvent (100 ml). The amino components were obtained from the corresponding HCl salts with an equivalent of NMM. The reaction mixture was stirred in an ice-chilled bath for 3 h, at room temperature for 2 d, and then subjected to ninhydrin test. When the test was positive, double and triple couplings were carried out using the carboxyl component and DCC (each 0.3 equiv). After completion of the reaction, the reaction mixture was filtered. The subsequent work-up procedure was essentially the same as those described before.[11] The synthetic results and analytical data are also shown in Tables 1—3.

General Procedure for Removal of the Pac Group. Boc-peptide Pac esters were stirred in a mixture of AcOH using a several-fold molar excess of Zn dust at room temperature for several days. After removal of Zn residues, the filtrate was concentrated in vacuo. The residue was treated with aqueous citric acid, followed by washing with water and hexane. Completion of the reaction was examined by TLC. The residue was used for a subsequent coupling reaction without further purification.

Results

Fragmentation of Human Proinsulin C-Peptide Based on the Solubility Prediction Method. One of our purposes in this paper is to examine the propriety of the solubility prediction method for peptide intermediates having polar side chains in the following respects: (1) Peptide intermediates smaller than heptapeptides have high solubility regardless of their $<P_c>$ values; (2) the $<P_c>$ values of peptide intermediates are useful for judging solubility of peptide intermediates equal to or larger than an octapeptide level; (3) the Pro residue in a central position of a peptide chain is effective for increasing peptide solubility; and (4) there is critical chain length for peptide insolubility caused by a β-sheet aggregation.

To investigate these points, the primary structure[15] of human proinsulin C-peptide was divided into seven fragments at the points indicated by arrows in Fig. 1, where the primary structure includes side-chain-protecting Bzl groups in the Asp, Glu, and Ser residues. Figure 1 also illustrates the N- and C-terminal-protected peptide fragments **1—12** used in this study. The solubility properties of the peptides **1—12** will be discussed later on the basis of the solubility prediction method.[3]

Synthesis and Solubility Properties of Each Peptide Fragment. Starting from the Pac ester of each C-terminal amino acid residue as the amino component, the peptide fragments **1—6** and **10** were prepared by the usual stepwise elongation of the peptide chain using Boc-amino acids[16] as the acid components. The following side-chain-protected amino acids were used for the synthesis: Glu(OBzl), Asp(OBzl),

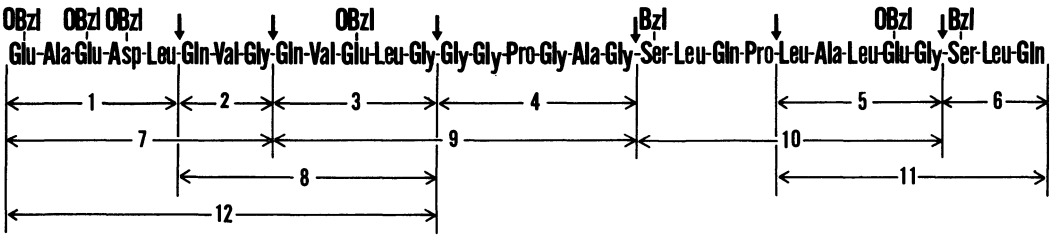

1. Boc-Glu(OBzl)Ala Glu(OBzl)Asp(OBzl)Leu-OPac
2. Boc-Gln Val Gly-OPac
3. Boc-Gln Val Glu(OBzl)Leu Gly-OPac
4. Boc-Gly Gly Pro Gly Ala Gly-OPac
5. Boc-Leu Ala Leu Glu(OBzl)Gly-OPac
6. Boc-Ser(Bzl)Leu Gln-OPac
7. Boc-Glu(OBzl)Ala Glu(OBzl)Asp(OBzl)Leu Gln Val Gly-OPac
8. Boc-Gln Val Gly Gln Val Glu(OBzl)Leu Gly-OPac
9. Boc-Gln Val Glu(OBzl)Leu Gly Gly Gly Pro Gly Ala Gly-OPac
10. Boc-Ser(Bzl)Leu Gln Pro Leu Ala Leu Glu(OBzl)Gly-OPac
11. Boc-Leu Ala Leu Gln(OBzl)Gly Ser(Bzl)Leu Gln-OPac
12. Boc-Glu(OBzl)Ala Glu(OBzl)Asp(OBzl)Leu Gln Val Gly Gln Val Glu(OBzl)Leu Gly-OPac

Fig. 1. The amino acid sequence of human proinsulin C-peptide and the N- and C-terminal protected peptide fragments **1—12** used in this study.

and Ser(Bzl).[17,18] The coupling reactions were mediated by DCC[19] throughout except for the Gln residue, which was incorporated by the active ester method[20] using Boc-Gln-ONp. Use of the Pac ester[21] at the C-terminus should have the advantage that Boc-peptide Pac ester thus prepared can be used not only as an amino component, but also as a carboxyl component since the stability of the side-chain-protecting Bzl group under removal conditions of Boc- and Pac groups has been well established.[17] Liberation of the amino groups from Boc-peptide Pac esters was performed by treatment with 3 M HCl/AcOEt, followed by treatment with NMM. Removal of the Pac group from the Boc-peptide Pac esters was performed by hydrogenolysis using Zn dust in AcOH.[22] The larger peptide fragments **7**—**9**, **11**, and **12** were subsequently prepared by the fragment condensation method after removal of the C- or N-terminal-protecting

Table 1. Synthetic Results and Physical Properties of the Peptides **1**—**12**

Compound	Yield/%[a]	Recrystallization solvent	Mp θ_m/°C	$[\alpha]_D^{19°}$ (c=1.0, DMF)	Retention time time/min
1	67	AcOEt/Hexane	102—104	−21.2	13.1
2	77	MeOH/Water	203—205	−21.0	13.5
3	95	EtOH/Water	216—220	−23.2	13.2
4	52	AcOEt/Hexane	104—109	−28.0	13.6
5	86	AcOEt/Hexane	179—183	−27.0	13.4
6	90	AcOEt/Hexane	157—160	−20.2	13.5
7	86	b)	235—237	−47.0[d]	13.0
8	56	b)	235—236	−41.0[d]	13.0
9	60	b)	203—205	−31.4	12.8
10	57	THF/Hexane	175—179	−37.8	13.1
11	92	c)	210—213	−25.9	13.0
12	72	b)	Over 250	e)	e)

a) Coupling yields in final steps. b) Purified by washing with hot MeOH. c) Purified by washing with hot EtOH. d) Measured in AcOH. e) Not obtained due to insolubility in DMF.

Table 2. Elemental Analyses of the Peptides **1**—**12**

Compound	Formula	Found (Calcd) (%)		
		C	H	N
1	$C_{57}H_{69}N_5O_{15}\cdot H_2O$	63.47 (63.26)	6.70 (6.61)	6.78 (6.47)
2	$C_{25}H_{36}N_4O_8$	57.95 (57.68)	7.11 (6.97)	10.72 (10.76)
3	$C_{43}H_{60}N_6O_{12}\cdot 0.5H_2O$	59.75 (59.92)	6.92 (7.13)	9.73 (9.75)
4	$C_{29}H_{40}N_6O_{10}$	55.43 (55.06)	6.60 (6.37)	12.88 (13.28)
5	$C_{42}H_{59}N_5O_{11}$	62.41 (62.28)	7.44 (7.34)	8.69 (8.65)
6	$C_{34}H_{46}N_4O_9\cdot 0.5H_2O$	61.69 (61.52)	6.91 (7.14)	8.57 (8.44)
7	$C_{69}H_{89}N_9O_{19}$	61.28 (61.46)	6.80 (6.65)	9.50 (9.35)
8	$C_{55}H_{80}N_{10}O_{16}\cdot H_2O$	57.41 (57.18)	7.15 (7.15)	12.07 (12.12)
9	$C_{59}H_{84}N_{12}O_{18}\cdot 2H_2O$	55.09 (55.13)	7.14 (6.90)	12.96 (13.08)
10	$C_{68}H_{96}N_{10}O_{17}\cdot 0.5H_2O$	61.19 (61.20)	7.42 (7.33)	10.52 (10.50)
11	$C_{63}H_{89}N_9O_{16}\cdot 2.5H_2O$	59.15 (59.42)	7.17 (7.44)	9.78 (9.90)
12	$C_{99}H_{133}N_{15}O_{27}\cdot 3H_2O\cdot 3DMF$	57.93 (57.95)	6.88 (7.20)	11.35 (11.26)

Table 3. Amino Acid Analyses of the Peptides **1**—**12**

Compound	Found (Calcd)							
	Gly	Ala	Val	Leu	Ser	Pro	Asp	Glu[a]
1	—	1.05 (1)	—	0.85 (1)	—	—	1.15 (1)	2.00 (2)
2	1.05 (1)	—	1.00 (1)	—	—	—	—	0.90 (1)
3	1.08 (1)	—	1.05 (1)	1.00 (1)	—	—	—	1.80 (2)
4	4.44 (4)	1.03 (1)	—	—	—	1.00 (1)	—	—
5	1.00 (1)	0.89 (1)	—	2.04 (2)	—	—	—	0.98 (1)
6	—	—	—	1.00 (1)	0.98 (1)	—	—	1.02 (1)
7	1.00 (1)	1.10 (1)	1.00 (1)	0.95 (1)	—	—	1.21 (1)	2.92 (3)
8	2.08 (2)	—	2.00 (2)	0.99 (1)	—	—	—	2.70 (3)
9	4.58 (5)	0.89 (1)	1.05 (1)	1.00 (1)	—	1.21 (1)	—	2.05 (2)
10	1.06 (1)	1.09 (1)	—	2.98 (3)	0.94 (1)	1.00 (1)	—	1.89 (2)
11	1.05 (1)	1.00 (1)	—	3.03 (3)	0.91 (1)	—	—	1.93 (2)
12	2.12 (2)	0.93 (1)	2.08 (2)	2.00 (2)	—	—	1.02 (1)	4.51 (5)

a) Included Gln.

Table 4. Solubility Properties[a] of the Peptides **1**—**12** (c=1.0 g/dl)

Compound ( )[c]	$<P_c>$	Solvent[b]								
		High-polar solvent[d]	AcOH	MeOH EtOH	DCM	Dioxane, THF, $CHCl_3$	AC	AN	AcOEt	Benzene CCl_4
1 (5)	0.85	A	A	A	A	A	A	B	B	B
2 (3)	0.82	A	A	B	C	C	C	C	D	D
3 (5)	0.80	A	A	B	B	C	D	C	D	D
4 (6)	1.22	A	A	A	A	A	A	A	B	C
5 (5)	0.78	A	A	A	A	A	A	A	B	B
6 (3)	0.95	A	A	A	A	A	A	B	B	D
7 (8)	0.84	A	A	C	C	C	D	D	D	D
8 (8)	0.88	A	A	D	D	D	D	D	D	D
9 (11)	1.12	A	A	B	D	D	D	D	D	D
10 (9)	0.93	A	A	A	A	A	B	A	D	D, B[e]
11 (8)	0.91	A	A	B	C	D	C	D	D	D
12 (13)	0.86	D	C	D	D	D	D	D	D	D

a) Solubility: A, soluble at room temperature; B, soluble at 80° or refluxing temperature; C, partially soluble at 80° or refluxing temperature; D, practically insoluble at 80° or refluxing temperature. b) Abbreviations: DCM, dichloromethane; THF, tetrahydrofuran; AC, acetone; AN, acetonitrile. Others, see Ref. 1). c) Number of amino acid residues of the peptide. d) DMF, NMP, DMA, DMSO, and HMPA. e) Solubility in benzene.

group of the corresponding fragment. Each fragment was coupled mainly in DMF with least danger of racemization using DCC activation in the presence of HOBt.[23] Completion of every coupling reaction was monitored by checking the reaction product with the sensitive ninhydrin test.

All of the soluble peptides were purified by repeated recrystallization, and, as a result of this purification process, each peptide gave a single peak on HPLC. The peptides **7**, **8**, and **12** which were insoluble in MeOH were purified by repeated washing with hot MeOH. Synthetic and analytical results of the peptides **1**—**12** are assembled in Tables 1—3. The amino acid and elemental analyses of the peptides shown in Tables 2 and 3 are in good agreement with the calculated values.

Solubility properties of the peptides **1**—**12** in organic solvents are also summarized in Table 4. The $<P_c>$ values of peptides shown in Table 4 indicate the randomness of each peptide fragment and they are obtained using P_c value for each amino acid residue.[3] For example, a peptide intermediate with the $<P_c>$ value above 1.00 is predicted to have a random structure in the polar solvents such as DMA, DMF, DMSO, NMP, and HMPA. According to the rule 1 of the solubility prediction method,[3] regardless of its peptide chain length, it is soluble in the polar solvents sufficiently enough to be susceptible to subsequent coupling reactions. In fact, the undecapeptide **9** has high solubility in the polar solvents, while the tridecapeptide **12** having the $<P_c>$ value of 0.86, as expected on the basis of the rule 3 of the solubility prediction method,[3] is extraordinarily less soluble in the solvents such as DMA, DMF, DMSO, NMP, HMPA, MeOH, and AcOH. With respect to the oligopeptides smaller than a heptapeptide, except for the peptides **2** and **3** containing the Gln residue, the oligopeptides **1** and **4**—**6** are easily soluble even in the moderate-polar solvents such as dichloromethane, chloroform, dioxane, and THF.

Conformations of Each Peptide Fragment in the Solid State. Conformational analysis of each peptide fragment in the solid state is interesting for the purpose of elucidating the relationship between the conformation and solubility of peptides having polar side chains. All of the peptides show strong bands at 3290—3270 cm^{-1} and 1635—1625 cm^{-1}, assigned to a typical β-sheet structure.[24] The IR absorption spectra of the peptides **4**, **9**, and **10**, which contain the Pro residue in central positions of the peptides, have strong broad shoulders at 1700—1650 cm^{-1}, indicating the disturbance of the β-sheet structure by rotation of the tertiary peptide bond plane as reported in previous papers.[3-9] The peptides **10** and **11** happen to have the very close amino acid sequences except for the Pro residue and the peptide **10** clearly shows the effect of the Pro residue in a central position of the peptide chain on the disturbance of the β-sheet structure. Analytical details will be reported elsewhere.[25,26]

Discussion

As expected from the solubility prediction of peptide intermediates, all peptide fragments **1**—**12** of human proinsulin C-peptide were prepared without difficulty by the usual stepwise elongation and fragment condensation methods, and, during the formation of the peptide fragments **8** and **12**, gelation eventually took place in a mixture of DMF and NMP along with the coupling reaction.

Regardless of the $<P_c>$ values of peptide fragments, in actuality, the peptide fragments **1**—**6** smaller than a heptapeptide are readily soluble in the polar solvents (Table 4). Most of them, except for the peptides **2** and **3** containing the Gln residue, have high solubility even in moderate-polar solvents. As reported

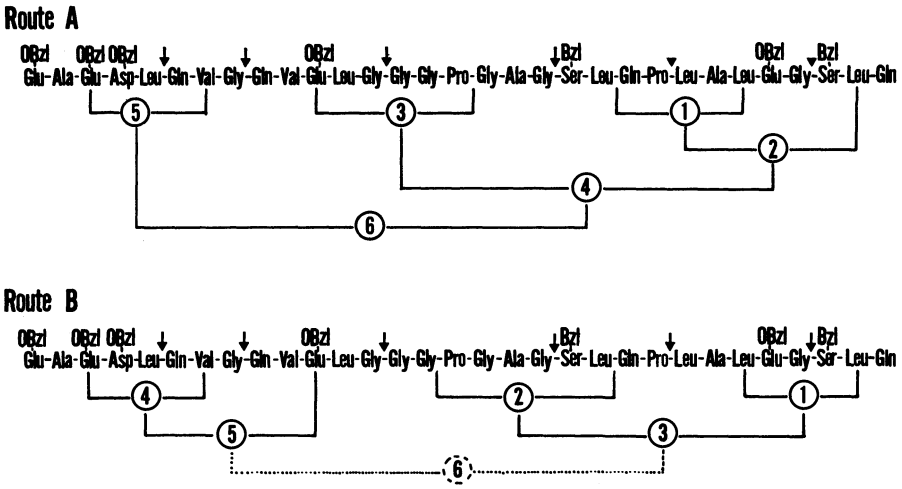

Fig. 2. Design of the synthetic routes for human proinsulin C-peptide. The number in a circle represents the order of each fragment condensation reaction.

for oligopeptides containing the Asn residue,[27] the peptides **2** and **3** have low solubility in the moderate-polar solvents probably due to hydrogen bonds through the Gln side-chain amide. The hexapeptide **4** and nonapeptide **10** are readily soluble even in the moderate-polar solvents such as dichloromethane, chloroform, dioxane, THF, and acetonitrile. The result apparently indicates that the tertiary peptide bonds (X–Pro) cause the disturbance of the β-sheet structures by the rotation of the tertiary peptide bond planes, bringing about their high solubility. The disturbance of the β-sheet structures is clearly verified by broadening of IR absorption bands in the amide I region. The solubility difference between the peptides **10** and **11** also conspicuously exhibits the effect of the Pro residue in a central position of the peptide chain on increasing peptide solubility (Table 4). Actually both the peptides have the very close amino acid sequences except for the Pro residue. On the other hand, solubility properties of the octapeptides **7**, **8**, and **11** are on a boundary. Although the peptides **7**, **8**, and **11** are soluble in the polar solvents, the peptides **7** and **8** are practically insoluble in MeOH and EtOH, and the peptide **11** is soluble only in the hot alcohols. These solubility behaviors indicate that, for the peptides containing polar side chains, critical chain length for peptide insolubility caused by the β-sheet aggregation is larger than an octapeptide level. With respect to larger peptides, the undecapeptide **9** is sufficiently soluble in the polar solvents due to the presence of the Pro residue in a central position of the peptide chain, while the tridecapeptide **12** has the $<P_c>$ value of 0.89, indicating that it is extraordinarily less soluble in the polar solvents. The peptide **12**, indeed, is actually insoluble in the polar solvents shown in Table 4 and difficult to remove the Pac group using Zn dust in AcOH. In terms of the relationship between the conformation and solubility of the peptides **7**, **8**, **11**, and **12**, the β-sheet aggregation clearly plays an important role in reducing these solubility properties.

The results and discussion mentioned above thoroughly make clear that the solubility prediction of peptide intermediates is very useful for the design of the synthetic routes for peptides and proteins. In general, assembly of the target structure by fragment condensation allows for great flexibility in the choice of the synthetic routes. In most cases of peptide and protein syntheses, for example, the Gly and Pro residues are recommended to be placed at C-termini of peptide intermediates since they are free from racemization in fragment condensation reactions. Our results clearly show that, for solving the insolubility problem of the peptide intermediates, the Pro residue should be placed in central positions of peptide intermediates. Thus, on the basis of the solubility prediction method, principally, we can design the proper synthetic route A of human proinsulin C-peptide as shown in Fig. 2. Assembled peptide intermediates in the route A are predicted to be sufficiently soluble in the polar solvents and to be susceptible to the subsequent fragment condensations **1**—**6**. All acid component candidates are also predicted to be sufficiently soluble in AcOH and to be converted to the corresponding acid components by removal of the Pac group from the peptide esters using Zn dust in AcOH. Contrary to the proper route A, if we choose the erroneous route B in Fig. 2, the acid component candidate obtained by the fragment condensation **5** is confronted with the insolubility problem on removal of the Pac group from the peptide ester using Zn dust in AcOH.

References

1) The abbreviations for amino acids are those recommended by the IUPAC-IUB Commission on Biochemical Nomenclature *J. Biol. Chem.*, **247**, 977 (1972). Amino acid symbols except for Gly denote the L-configuration. Addi-

tional abbreviations used are the following: Boc, *t*-butoxycarbonyl; Pac, phenacyl; AcOEt, ethyl acetate; DCC, dicyclohexylcarbodiimide; DMF, *N*,*N*-dimethylformamide; NMM, *N*-methylmorpholine; ONp, *p*-nitrophenyl ester; HOBt, *1*-hydroxy-1*H*-benzotriazole; NMP, *N*-methylpyrrolidone; AcOH, acetic acid; TLC, thin-layer chromatography; Bzl, benzyl; DMA, *N*,*N*-dimethylacetamide; DMSO, dimethyl sulfoxide; HMPA, hexamethylphosphoric triamide; HPLC, high-performance liquid chromatography; MeOH, methanol; THF, tetrahydrofuran; EtOH, ethanol; IR, infrared.

2) T. Kimura, Y. Takai, Y. Masui, T. Morikawa, and S. Sakakibara, *Biopolymers*, **20**, 1823 (1981); T. Kimura, M. Takai, K. Yoshizawa, and S. Sakakibara, *Biochem. Biophys. Res. Commun.*, **114**, 493 (1983).

3) M. Narita, K. Ishikawa, J.-Y. Chen, and Y. Kim, *Int. J. Peptide Protein Res.*, **24**, 580 (1984).

4) M. Narita, T. Fukunaga, A. Wakabayashi, K. Ishikawa, and H. Nakano, *Int. J. Peptide Protein Res.*, **23**, 306 (1984).

5) M. Narita, S. Nagasawa, J.-Y. Chen, H. Sato, and Y. Tanaka, *Makromol. Chem.*, **185**, 1069 (1984).

6) M. Narita, K. Ishikawa, H. Nakano, and S. Isokawa, *Int. J. Peptide Protein Res.*, **24**, 14 (1984).

7) M. Narita, N. Ohkawa, S. Nagasawa, and S. Isokawa, *Int. J. Peptide Protein Res.*, **24**, 129 (1984).

8) S. Isokawa, T. Asakura, and M. Narita, *Macromolecules*, **18**, 871 (1985).

9) S. Isokawa, I. Tominaga, T. Asakura, and M. Narita, *Macromolecules*, **18**, 878 (1985).

10) M. Narita, J.-Y. Chen, H. Sato, and Y. Kim, *Bull. Chem. Soc. Jpn.*, **58**, 2494 (1985).

11) M. Narita, M. Doi, H. Sugasawa, and K. Ishikawa, *Bull. Chem. Soc. Jpn.*, **58**, 1473 (1985).

12) M. Narita, K. Ishikawa, H. Sugasawa, and M. Doi, *Bull. Chem. Soc. Jpn.*, **58**, 1731 (1985).

13) T. Y. Liu and Y. H. Chang, *J. Biol. Chem.*, **246**, 2842 (1971).

14) F. C. Westall, J. Scotchler, and A. B. Robinson, *J. Org. Chem.*, **37**, 3363 (1972).

15) P. E. Oyer, S. Cho, J. D. Peterson, and D. F. Steiner, *J. Biol. Chem.*, **246**, 1375 (1971).

16) F. C. McKay and W. F. Albertson, *J. Am. Chem. Soc.*, **79**, 4686 (1957).

17) R. Schwyzer and P. Sieber, *Helv. Chim. Acta*, **42**, 972 (1959).

18) K. Okawa, *Bull. Chem. Soc. Jpn.*, **29**, 486 (1956).

19) J. C. Sheehan and G. P. Hess, *J. Am. Chem. Soc.*, **77**, 1067 (1955); H. G. Khorana, *Chem. Rev.*, **53**, 145 (1953).

20) M. Bodanszky and V. du Vigneaud, *J. Am. Chem. Soc.*, **81**, 5688 (1959).

21) G. C. Stelakatos, A. Paganov, and L. Zervas, *J. Chem. Soc.*, **1966**, 1191.

22) J. B. Hendrickson and C. Kandall, *Tetrahedron Lett.*, **1970**, 343.

23) W. König and R. Geiger, *Chem. Ber.*, **103**, 788 (1970).

24) T. Miyazawa and E. J. Blout, *J. Am. Chem. Soc.*, **83**, 712 (1961).

25) M. Narita, T. Ogura, K. Sato, and S. Honda, *Bull. Chem. Soc. Jpn.*, **59**, 2439 (1986).

26) M. Narita, T. Ogura, K. Sato, and S. Honda, *Bull. Chem. Soc. Jpn.*, **59**, 2445 (1986).

27) T. Toniolo, G. M. Bonora, and W. M. M. Schaaper, *Int. J. Peptide Protein Res.*, **23**, 389 (1984).

Infrared Absorption Study of Human Proinsulin C-Peptide Fragments in the Solid State[1)]

Mitsuaki NARITA,* Toshihiko OGURA, Kazuhiro SATO, and Shinya HONDA
Department of Industrial Chemistry, Faculty of Technology, Tokyo University of Agriculture and Technology, Koganei 184
(Received March 15, 1986)

In order to evaluate the propriety of the solubility prediction method for peptide intermediates having polar side chains, IR absorption spectroscopic analysis of human proinsulin C-peptide fragments was performed in the solid state. The polar amino acid residues involved in the peptide fragments are in the following: Glu(OBzl), Asp(OBzl), Gln, and Ser(Bzl). All peptide fragments except for ones containing the Pro residue exhibit a high potential for the formation of a β-sheet structure, indicating that, even when the polar side chains of the Glu, Asp, and Ser residues are protected by the Bzl group, the coil conformation parameter P_c for each amino acid residue is useful for estimating the potential for the formation of a β-sheet structure of peptide fragments smaller than critical size for development of α-helical structure in the solid state. As in the case of hydrophobic peptides, the β-sheet aggregation clearly plays an important role in reducing solubility of the peptide fragments having polar side chains. The effect of the Pro residue on the disturbance of the β-sheet structure was also observed. The ability of the short-range (polar side chain-backbone) or intraresidue interactions due to the low flexibility of the pyrrolidine ring of the Pro residue to promote helical folding in peptide fragments in the solid state was not observed for the peptide fragments corresponding to helical regions of human proinsulin.

In a previous paper,[2)] the usefulness of the solubility prediction method proposed previously by us[3)] was demonstrated taking the synthesis of human proinsulin C-peptide fragments as an example. On the basis of the solubility prediction of peptide intermediates, subsequently, a strategy suitable for the design of the synthetic route for peptides and proteins was proposed. Insolubility of peptide intermediates is essentially caused by a β-sheet aggregation formed by peptides equal to or larger than an octapeptide sequence level and their solubility is independent on their amino acid sequences and compositions.[4)] Thus, the solubility prediction method is principally based on both the randomness of peptide intermediates in the solid state and the existence of tertiary peptide bond, that is, the disturbance of the β-sheet structure by the rotation of the tertiary peptide bond plane. In order to evaluate the structural randomness of peptide chains, we have used the coil conformation parameter, P_c, for each intact amino acid residue which is determined according to the definition of Chou and Fasman.[5)] One of our purposes in this study is to examine the propriety of evaluation of the structural randomness of peptide fragments with protected polar side chains using the coil conformation parameter, P_c, obtained for each intact amino acid residue.[3)]

The correctness of the concept of the solubility prediction method was moreover verified by the another evidence that solubility improvement on oligopeptides was easily achieved by a β-sheet → helix conformational transition using the ability of the Aib residue to promote helical folding in oligopeptides.[4,6)] The ability of the Aib residue to promote helical folding was distinctly demonstrated using oligo(Leu)s and was clearly attributed to the restriction of the values of the backbone dihedral angles ϕ and ψ of the Aib residue to helical regions due to steric hindrance.[6)] These result also suggested that the restriction of the values of the backbone dihedral angles ϕ and ψ of an amino acid residue to the right-handed α-helical region (ϕ=−57° and ψ=−47°) was one of important initiation mechanisms of α-helical folding in natural proteins.[6)] In connection with the results, it is quite interesting to investigate the ability of the short-range (polar side chain-backbone) or intraresidue interactions due to the low flexibility of the pyrrolidine ring of the Pro residue to promote helical folding in peptide fragments since two helical regions of human proinsulin are included in fragments of the C-peptide.

In this paper, we report IR absorption spectroscopic analysis of human proinsulin C-peptide fragments with protecting groups in the solid state and investigate the points described above.

Experimental

Materials. Samples of human proinsulin C-peptide fragments are those prepared in the previous paper.[2)] The solid samples of the peptides **1** and **5—9** were obtained by repeated recrystallization from appropriate solvents.[2)] Those of the peptides **2—4** and **10** were obtained by repeated washing with hot methanol or ethanol. The purity of the peptides **1—10** was confirmed by the amino acid and elemental analyses. The peptides **1—3** and **5—10** which were soluble in *N,N*-dimethylformamide also gave a single peak on HPLC.

IR Measurements. The IR absorption spectra of the solid samples were recorded with a Jasco Model DS-701G spectrometer in a nujol mull.

Results

IR Absorption Spectroscopic Analysis of Each Peptide Fragment in the Solid State. The peptide fragments **1—10**, investigated in this study are shown in Fig. 1, which are corresponding to the C-peptide (1-5), (1-8), (6-13), (1-13), (14-19), (9-19), (20-22), (24-28), (20-28), and (24-31), respectively.[2)] The numbers in

1. Boc-Glu(OBzl)Ala Glu(OBzl) Asp(OBzl)Leu-OPac
2. Boc-Glu(OBzl) Ala Glu(OBzl) Asp(OBzl)Leu Gln Val Gly-OPac
3. Boc-Gln Val Gly Gln Val Glu(OBzl) Leu Gly-OPac
4. Boc-Glu(OBzl) Ala Glu(OBzl) Asp(OBzl) Leu Gln Val Gly-Gln Val Glu(OBzl) Leu Gly-OPac
5. Boc-Gly Gly Pro Gly Ala Gly-OPac
6. Boc-Gln Val Glu(OBzl) Leu Gly Gly Gly Pro Gly Ala Gly-OPac
7. Boc-Ser(Bzl) Leu Gln-OPac
8. Boc-Leu Ala Leu Glu(OBzl) Gly-OPac
9. Boc-Ser(Bzl) Leu Gln Pro Leu Ala Leu Glu(OBzl) Gly-OPac
10. Boc-Leu Ala Leu Glu(OBzl) Gly Ser(Bzl Leu Gln-OPac

Fig. 1. The peptides **1**—**10** used in this study.

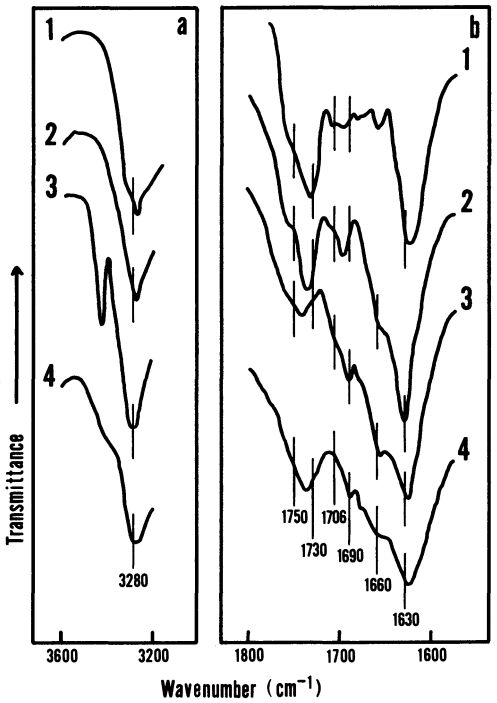

Fig. 2. IR absorption spectra in the solid state of the peptides **1**—**4**. a: The amide A region; b: the amide I region.

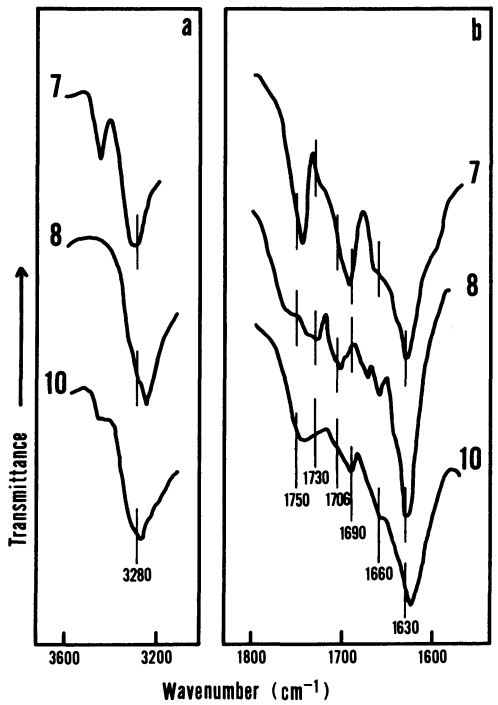

Fig. 3. IR absorption spectra in the solid state of the peptides **7**, **8**, and **10**. a: The amide A region; b: the amide I region.

parentheses in the following C-peptide represent the positions of the first and last amino acids from the N-terminal in the C-peptide. Figures 2 and 3 show the IR absorption spectra of the peptides **1**—**4**, **7**, **8**, and **10** in the solid state in the most significant spectral regions for the conformational assignments (3600—3200 cm^{-1}, amide A; 1800—1600 cm^{-1}, amide I). All of the peptides show strong bands at 3290—3270 cm^{-1} and 1635—1625 cm^{-1}, assigned to a typical β-sheet structure.[7] The absorption band at 1690 cm^{-1} of the peptides **3**, **4**, and **10** also suggests the antiparrallel β-sheet structure. The absorption band or shoulder around 1750 cm^{-1} is assigned to the Pac ester carbonyl group, while the bands around 1730, and 1706 cm^{-1} are assigned to the Bzl ester- and Boc urethane-carbonyl groups, respectively. These absorption bands were assigned by IR measurement in dichloromethane of the peptides **1**, **7**, and **8**. The Pac ketone carbonyl group is estimated to show the band around 1685 cm^{-1}, overlapped with the amide carbonyl group. Although the absorption band characteristic to the Gln side-chain amide can not clearly be assigned, the band at 1660—1655 cm^{-1} of the peptide **2**—**4**, **7**, and **10** is incidentally assigned to the Gln side-chain amide. Similar assignment was reported for the Asn side-chain amide.[8] Figure 4 represents the IR absorption spectra in the solid state of the peptides **5**, **6**, and **9**, which contain the Pro residue in central positions of the peptide chains. These IR absorption spectra are accompanied by additional strong broad shoulders at 1680—1650 cm^{-1}, indicating the disturbance of β-sheet structures by the rotation of the tertiary peptide bond planes (Gly-Pro and Gln-Pro) as reported in previous papers.[9-13] The peptide **9** happens to have, except for the Pro residue, the very close amino acid sequence with the peptide **10**, clearly showing the effect of the Pro residue in a central position of the peptide chain on the disturbance of the β-sheet structure in the peptide

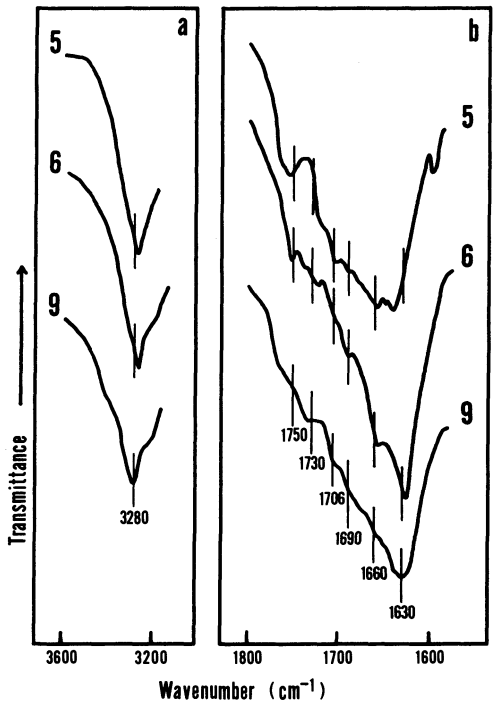

Fig. 4. IR absorption spectra in the solid state of the peptides **5**, **6**, and **9**. a: The amide A region; b: the amide I region.

9.

Discussion

All peptide fragments **1**—**4**, **7**, **8**, and **10**, except for the peptides **5**, **6**, and **9** containing the Pro residue, exhibit a high potential for the formation of the β-sheet structure. Their chain lengths range from a tripeptide to a tridecapeptide. The results indicate that, with respect to peptides having protected or intact polar amino acid residues such as the Glu(OBzl), Asp(OBzl), Gln, and Ser(Bzl) residues, the polar side chain-backbone (short-range) interactions within neighboring residues can not give rise to the disturbance of the formation of the β-sheet structure of the peptides in the solid state. The typical β-sheet structure of the higher oligopeptides **2**—**4** and **10** is also supported by the fact that these peptides have low solubility as reported previously.[2] If the short-range interactions play an important role in determing the conformation of the peptides, it is estimated that they conduct the peptides to random coil, turn, or helical structure, resulting in high solubility of the peptides.

In Table 1, the conformational parameters $\langle P_c \rangle$, $\langle P_\alpha \rangle$, and $\langle P_\beta \rangle$ of each peptide fragment are summarized. The values of $\langle P_c \rangle$,[3] $\langle P_\alpha \rangle$,[5] and $\langle P_\beta \rangle$[5] were determined according to the literatures. The low values of average coil conformation parameters, $\langle P_c \rangle$, of the peptide fragments **1**—**4** and **7**—**10** suggest that these peptides are highly structured. In actuality, all of the peptide fragments **1**—**4**, **7**, **8**, and **10**, except for the peptide **9** containing the Pro residue, exhibit the high potential for the formation of the β-sheet structure (Figs. 2 and 3). The conformational behaviors of the peptides **1**—**4**, **7**, **8**, and **10** indicate that, even when the polar side chains of the Glu, Asp, and Ser residues are protected by the Bzl group, the coil conformational parameters, P_c, obtained for each intact amino acid residue are useful for estimating the potential for the formation of a β-sheet structure of peptides smaller than critical size for development of α-helical structure in the solid state. On the contrary, the $\langle P_\beta \rangle$ values of the peptides except for **3** and **7** are very low, indicating a low potential for the formation of the β-sheet structure of these peptides. In the case of the peptides **1**, **2**, **4**, and **8**—**10** which are smaller than a critical size for development of α-helical structure in the solid state, their high $\langle P_\alpha \rangle$ values indicate a high potential for the formation of the β-sheet structure. Eventually, we can easily estimate the potential for the formation of the β-sheet structure of peptide intermediates only using their $\langle P_c \rangle$ values.

Table 1. The Values of Average Conformational Parameters $\langle P_c \rangle$, $\langle P_\alpha \rangle$, and $\langle P_\beta \rangle$ of the Peptides **1**—**10**

Peptide	$\langle P_c \rangle$	$\langle P_\alpha \rangle$	$\langle P_\beta \rangle$
1	0.85	1.37	0.70
2	0.84	1.33	0.46
3	0.88	1.07	1.03
4	0.86	1.26	0.68
5	1.22	0.69	0.81
6	1.12	0.90	0.91
7	0.95	1.10	1.06
8	0.78	1.24	0.90
9	0.93	1.12	0.92
10	0.91	1.19	0.96

The β-sheet→helix conformational transition is provoked by the change of intermolecular hydrogen bonds to intramolecular hydrogen bonds, providing high solubility of peptides. In fact, we previously showed a dramatic solubility change of oligo(Leu)s by the complete β-sheet→helix conformational transition using the great ability of the Aib residue to promote helical folding in peptides.[4,6] As well known, the β-sheet→helix conformation transition is dependent on a peptide chain length, and the critical chain length for α-helix formation in the solid state in oligopeptides is not lower than n=10 although it depends on the nature of the constituent amino acid residues.[14] On the other hand, we have demonstrated that the restriction of the values of the backbone dihedral angles ϕ and ψ of the Aib residue to helical regions is an important initiation and stabilization mechanisms of helical folding in peptides.[4,6] In this case, the restriction of the values ϕ and ψ of the Aib residue is apparently attributed to the intraresidue interactions due to steric hindrance,[15] being favorable

to helical folding in peptides. Therefore, if nucleation sites for helical folding in peptide fragments is able to predict as in the case of the Aib residue, it is useful for predicting their solubility. In certain cases, turn structures, which are mainly promoted by backbone-backbone interactions within neighboring residues, are suggested to be nucleation sites for helix formation in proteins.[16] Therefore, the polar side chain-backbone interactions within neighboring residues have the possibility to promote helical folding in oligopeptides. However, unfortunately, the octapeptides **2**, **3**, and **10** having high $<P_\alpha>$ values show the β-sheet structure in the solid state, and no ability of the short-range interactions to promote helical folding in each peptide was observed.

The estimated structure of human proinsulin indicates that the protein contains three short helices, and two of them are included in the part of human proinsulin C-peptide.[17] These helical regions are also included in the peptides **4** and **9**. However, the tridecapeptide **4** also has the β-sheet structure in the solid state, indicating no ability of the short-range interactions to promote helical folding in the peptide **4**. In the sequence analysis of helical regions in proteins, several authors[18-21] have pointed out the tendency of charged side chains to cluster at the ends of helices. Blagdon and Goodman[16] have also suggested that the proper arrangement of charged side chains stabilize helices and they have denoted the route to helix formation as a polar mechanism of initiating helices. Therefore, one of causes of no ability of the peptide **4** to promote helical folding may be attributed to the negation of negative charges at the Glu and Asp residues by their protection with the Bzl group.

In connection with the fact that the most frequently observed conformations for the Pro residue lie in the region of the backbone dihedral angles $\phi=-60°\pm10°$ and $\psi=-30°\pm20°$, and $\phi=-60°\pm10°$, $\psi=-120\pm20°$ due to the low flexibility of the pyrrolidine ring in the Pro residue,[22] in which the former is corresponding to the helical region, it is quite interesting to investigate the ability of the Pro residue to promote helical folding in the peptide **9** due to the low flexibility of the pyrrolidine ring of the Pro residue, which is one of intraresidue interactions as in the case of the Aib residue. Unfortunately, the sample of the peptide **9** in the solid state mainly shows the β-sheet structure, accompanied by an unordered structure which is caused by the rotation of the tertiary peptide bond plane (Gln-Pro) due to steric hindrance. On the other hand, IR conformational analysis of the peptide **9** in dichloromethane solution clearly indicates that the peptide **9** has successive-intramolecular hydrogen bonds, probably corresponding to a stable α-helix in solution.[23] Therefore, another procedure for the preparation of the solid sample of the peptide **9** was examined. But IR conformational behaviors of the sample obtained by reprecipitation by pouring the dichloromethane solution into hexane were essentially the same with the sample before, indicating that the α-helical structure of the peptide **9** in dichloromethane solution was not so stable enough to tolerate the phase transformation from solution into the solid state.

References

1) This paper forms Part II of "Design of the Synthetic Route for Peptides and Proteins Based on the Solubility Prediction Method" series. For part I of this series, see M. Narita, T. Ogura, K. Sato, and S. Honda, *Bull. Chem. Soc. Jpn.*, **59**, 2433 (1986). The abbreviations for amino acids are those recommended by the IUPAC-IUB Commission on Biochemical Nomenclature, *J. Biol. Chem.*, **247**, 977 (1972). Amino acid symbols except for Gly denote the L-configuration. Additional abbreviations used are the following: Aib, α-aminoisobutyric acid residue; Bzl, benzyl; Boc, *t*-butoxycarbonyl; Pac, phenacyl.

2) M. Narita, T. Ogura, K. Sato, and S. Honda, *Bull. Chem. Soc. Jpn.*, **59**, 2433 (1986).

3) M. Narita, K. Ishikawa, J.-Y. Chen, and Y. Kim, *Int. J. Peptide Protein Res.*, **24**, 580 (1984).

4) M. Narita, J.-Y. Chen, H. Sato, and Y. Kim, *Bull. Chem. Soc. Jpn.*, **58**, 2494 (1985).

5) P. Y. Chou and G. D. Fasman, *Biochemistry*, **13**, 211 (1974).

6) M. Narita, M. Doi, H. Sugasawa, and K. Ishikawa, *Bull. Chem. Soc. Jpn.*, **58**, 1473 (1985); M. Narita, K. Ishikawa, H. Sugasawa, and M. Doi, *Bull. Chem. Soc. Jpn.*, **58**, 1731 (1985).

7) T. Miyazawa and E. J. Blout, *J. Am. Chem. Soc.*, **83**, 712 (1961); Yu. N. Chirgadze and N. A. Nevskaya, *Biopolymers*, **15**, 627 (1976); M. Narita, S. Isokawa, Y. Tomotake, and S. Nagasawa, *Polymer J.*, **15**, 25 (1983), and references cited therein.

8) T. Toniolo, G. M. Bonora, and W. M. M. Schaaper, *Int. J. Peptide Protein Res.*, **23**, 389 (1984).

9) M. Narita, T. Fukunaga, A. Wakabayashi, K. Ishikawa, and H. Nakano, *Int. J. Peptide Protein Res.*, **23**, 306 (1984).

10) M. Narita, K. Ishikawa, H. Nakano, and S. Isokawa, *Int. J. Peptide Protein Res.*, **24**, 14 (1984).

11) M. Narita, N. Ohkawa, S. Nagasawa, and S. Isokawa, *Int. J. Peptide Protein Res.*, **24**, 129 (1984).

12) S. Isokawa, T. Asakura, and M. Narita, *Macromolecules*, **18**, 871 (1985).

13) S. Isokawa, I. Tominaga, T. Asakura, and M. Narita, *Macromolecules*, **18**, 878 (1985).

14) R. Katakai and Y. Nakayama, *J. Chem. Soc. Chem. Commun.*, **1977**, 805; C. Toniolo, G. M. Bonora, and M. Mutter, *Int. J. Biolog. Macromolecules*, **1**, 188 (1979) and references cited therein.

15) G. R. Marshall, "*Intra-Science Chemistry Report*," Vol. **5**, Ed. by N. Kharasch, Gordon and Breach, New York, pp. 305—316 (1971); A. W. Burgess and S. J. Leach, *Biopolymers*, **12**, 2599 (1973); Y. Paterson, S. M. Rumsey, E. Benedetti, G. Nemethy, and H. A. Scheraga, *J. Am. Chem. Soc.*, **103**, 2947 (1981) and references cited therein.

16) D. E. Blagdon and M. Goodman, *Biopolymers*, **14**, 241 (1975).

17) C. R. Snell and P. G. Smyth, *J. Biol. Chem.*, **250**, 6291 (1975).

18) P. Y. Chou and G. D. Fasman, *Biochemistry*, **13**, 222

(1974).
19) P. N. Lewis, F. A. Momany, and H. A. Scheraga, *Proc. Nat. Acad. Sci. U.S.A.*, **68**, 2293 (1971).
20) J. L. Crawford, W. N. Lipscomb, and C. G. Schellman, *Proc. Nat. Acad. Sci. U.S.A.*, **70**, 538 (1971).
21) E. Ralston and J.-L. deCoen, *J. Mol. Biol.*, **83**, 393 (1974).
22) D. F. De Tar and N. Luthra, *J. Am. Chem. Soc.*, **99**, 1232 (1977); V. Madison, *Biopolymers*, **16**, 2671 (1977); B. V. V. Prasad, H. Balaram, and P. Balaram, *Biopolymers*, **21**, 1261 (1982).
23) M. Narita, T. Ogura, K. Sato, and S. Honda, *Bull. Chem. Soc. Jpn.*, **59**, 2445 (1986).

Infrared Absorption Study of Human Proinsulin C-Peptide Fragments in Dichloromethane[1)]

Mitsuaki NARITA,* Toshihiko OGURA, Kazuhiro SATO, and Shinya HONDA
Department of Industrial Chemistry, Faculty of Technology, Tokyo University of Agriculture and Technology, Koganei 184
(Received March 20, 1986)

In connection with the relationship between the conformation and solubility of peptide intermediates having polar side chains, IR spectroscopic conformational analysis of human proinsulin C-peptide fragments was performed in dichloromethane. The polar amino acid residues involved in the peptide fragments are Glu(OBzl), Asp(OBzl), Gln, and Ser(Bzl). Especially, the N-H stretching absorption spectra have been explored over a wide range of concentration. Based on the concentration dependence of the N-H stretching bands, it has been shown that the characteristic N-H stretching band around 3330 cm^{-1} is due to the intramolecular hydrogen bond. Intermolecular hydrogen bonding also occurs to a small extent in these peptides, giving rise to a slight concentration dependence of the N-H stretching bands. Conformational behaviors of oligopeptides having protected polar side chains of the Glu(OBzl) and Asp(OBzl) residues are just the same as those of the corresponding homooligo(Leu)s, indicating that the protected polar side chains do not disturb conformational behaviors of the oligopeptides. Conformational analysis of the peptide in dichloromethane, which contains the Pro residue and has a high potential for the formation of an α-helical structure, distinctly suggests that the Pro residue near the N-terminal in the peptide has the great ability to promote successive intramolecular hydrogen bonds, probably corresponding to the α-helical structure of the peptide.

In connection with the design of the synthetic route for peptides and proteins based on the solubility prediction method,[2-4)] it is quite interesting to investigate conformational behaviors of peptide intermediates in solution since the investigation offers useful information for the solubility prediction of peptide intermediates. In the previous paper,[4)] we reported IR spectroscopic conformational analysis in the solid state of human proinsulin C-peptide fragments. Here, we report their IR spectroscopic conformational analysis in dichloromethane, which is commonly used in conventional solid-phase peptide synthesis.[5,6)] Especially, in this paper, we give attention to the role of the Pro residue in solubility improvement of peptide fragments containing the Pro residue.

The Pro residue is well recognized to a strong helix and β-sheet breaker and plays an important role in stopping the development of helix and β-sheet structures in peptides and proteins.[7-10)] In fact, the insertion of the Pro residue into oligo(Leu)s caused "the peptide segment separation" in the solid state and achieved remarkable solubility improvement of peptides in a variety of organic solvents.[11-13)] The effect of the Pro residue on increasing solubility of peptide intermediates was also confirmed in human proinsulin C-peptide fragments.[2)]

On the other hand, the values of the backbone dihedral angles ϕ and ψ of the Pro residue are severely restricted to be $\phi=-60°\pm10°$, $\psi=-30°\pm20°$, and $\phi=-60°\pm10°$, $\psi=-120°\pm20°$ due to the low flexibility of the pyrrolidine ring in the Pro residue.[14)] In our recent papers,[15,16)] we demonstrated the great ability of the Aib residue to promote helical folding in peptides due to the short-range interactions by van der Waals repulsions and subsequently proposed that the restriction of the dihedral angles was one of important initiation mechanisms of helical folding in the natural proteins. One of our purposes in this paper is also to investigate the ability of the Pro residue to promote helical folding in oligopeptides in solution.

Experimental

Materials. Samples of human proinsulin C-peptide fragments are those prepared in the previous papers.[2)] The purity of the peptides was confirmed by the amino acid and elemental analyses. The peptides also gave a single peak on HPLC. The peptide fragments used in this study are in the following: Boc-Glu(OBzl)-Ala-Glu(OBzl)-Asp(OBzl)-Leu-OPac (**1**), Boc-Leu-Ala-Leu-Glu(OBzl)-Gly-OPac (**2**), Boc-Gly-Gly-Pro-Gly-Ala-Gly-OPac (**3**), Boc-Ser(Bzl)-Leu-Gln-Pro-Leu-Ala-Leu-Glu(OBzl)-Gly-OPac (**4**), and Boc-Ser(Bzl)-Leu-Gln-OPac (**5**).

IR Measurements. The IR absorption spectra of the samples in dichloromethane were recorded at room temperature with a JEOL Model JIR-100 FT-IR spectrometer by employing 0.5 mm- and 5 mm-path length cells with potassium bromide windows.

Results

IR Absorption Study of the Pentapeptide Fragments 1 and 2 in Dichloromethane. Conformational analysis of peptide fragments having polar side chains is quite interesting in order to elucidate the role of protected polar amino acid residues in conformational behaviors of peptide fragments in dichloromethane. As reported in the previous paper,[2)] the pentapeptides **1** and **2** are easily soluble in dichloromethane, and their IR absorption spectra are easily obtained over a wide range of concentration (1.0×10^{-4}—10^{-2} M[†]). In Fig. 1, we show the N-H stretching bands of both peptides in dichloromethane and

[†] 1 M=1 mol dm^{-3}.

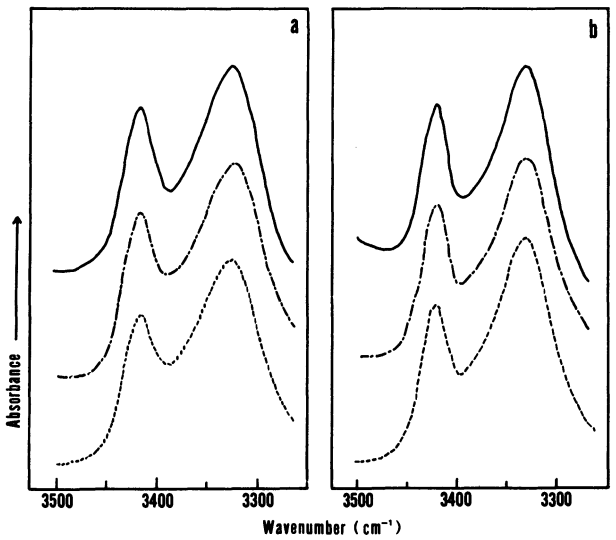

Fig. 1. Concentration dependence of the N-H stretching bands in the IR absorption spectra of the peptides **1** and **2** in dichloromethane. -----: 1.0×10^{-2} M, —·—·—: 1.0×10^{-3} M, ——: 1.0×10^{-4} M. a: The peptide **1**; b: the peptide **2**.

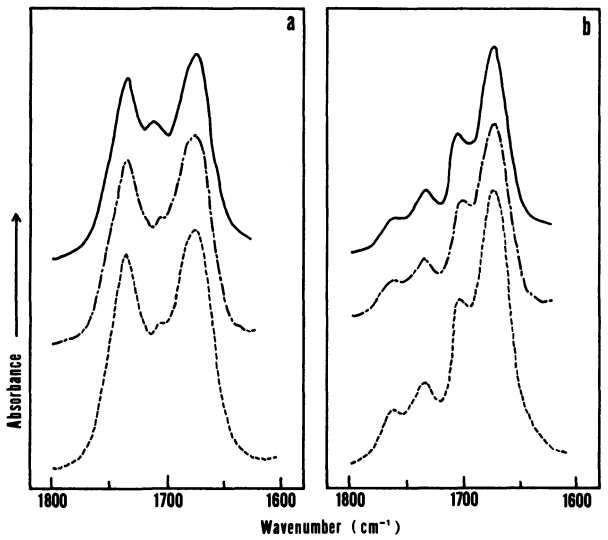

Fig. 2. Concentration dependence of the IR absorption bands in the amide I region of the peptides **1** and **2** in dichloromethane. -----: 1.0×10^{-2} M, —·—·—: 1.0×10^{-3} M, ——: 1.0×10^{-4} M. a: The peptide **1**; b: the peptide **2**.

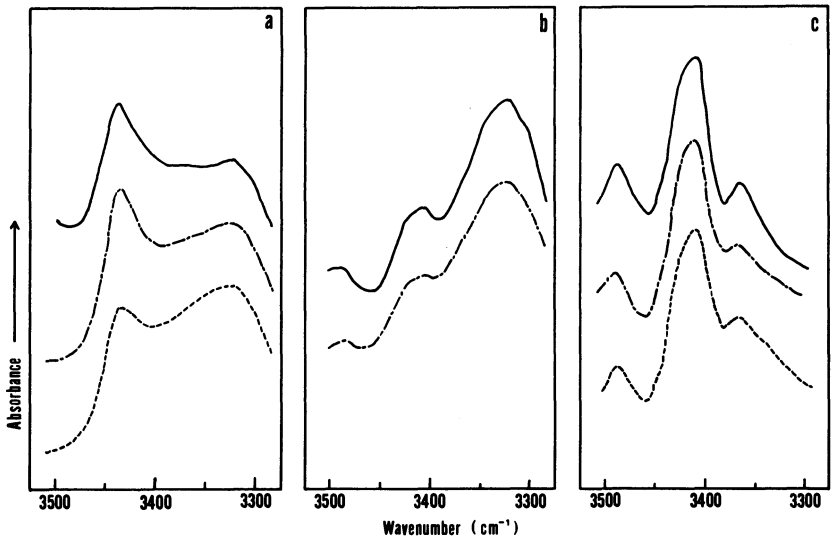

Fig. 3. Concentration dependence of the N-H stretching bands in the IR absorption spectra of the peptides **3**—**5** in dichloromethane. -----: 1.0×10^{-2} M, —·—·—: 1.0×10^{-3} M, ——: 1.0×10^{-4} M. a: The peptide **3**; b: the peptide **4**; c: the peptide **5**.

clearly see two distinct bands at 3420 and 3330 cm^{-1} over the entire concentration range. The 3420 cm^{-1} band is clearly due to the free N-H stretching vibration, while the 3330 cm^{-1} band is due to a hydrogen-bonded species.[17-19] Since the intensities of these two bands show little dependence on concentrations, the 3330 cm^{-1} band is attributed mainly to the intramolecular hydrogen-bonded species, accompanied by a slight contribution from intermolecular hydrogen bonding. The IR absorption spectra in the amide I region of the peptides **1** and **2** in dichloromethane are also illustrated in Fig. 2. The IR spectra of both peptides measured over the wide range of concentrations show the bands around 1760, 1733, 1706, and 1675 cm^{-1}, corresponding to the Pac ester carbonyl, Bzl ester carbonyl, Boc urethane carbonyl, and amide carbonyl groups, respectively. The Pac ketone carbonyl group is estimated to have the absorption band around 1685 cm^{-1}, overlapped with the amide carbonyl group. The amide carbonyl band also showed little dependence on concentration (1.0×10^{-4}—10^{-2} M).

IR Absorption Study of the Hexapeptide 3, Nonapeptide 4, and Tripeptide 5 in Dichloromethane. The IR absorption spectra in the N-H stretching region of the peptides **3**—**5** in dichloromethane (1.0×10^{-4}—10^{-2} M) are shown in Fig. 3. We also see two

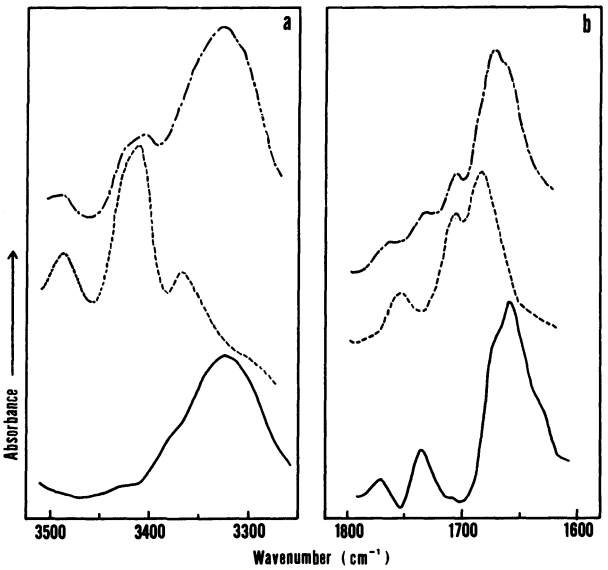

Fig. 4. IR absorption spectra in the amide A and amide I regions of the peptides **4** and **5** in dichloromethane (1.0×10^{-4} M). —·—·—: The peptide **4**, ------: the peptide **5**, ——: IR difference spectra for the peptides **4** and **5**. a: The amide A region; b; the amide I region.

distinct bands at 3435—3425 cm^{-1} and around 3370 or 3330 cm^{-1} over the entire concentration range. The peptides **4** and **5** have the additional absorption band at 3487 cm^{-1} corresponding to the side-chain amide group, which is free from hydrogen bonding. Again, the 3430 cm^{-1} band is due to the free N-H stretching vibration, while the bands around 3370—3330 cm^{-1} are due to hydrogen-bonded species. The intensities of the hydrogen-bonded band of the peptide **3** (Fig. 3a) are more dependent on concentration than the intensities of the band at 3330 cm^{-1} of the peptides **1**, **2**, **4**, and **5** (Figs. 1, 3b, and 3c), indicating that the peptide **3** is accompanied by more contribution from intermolecular hydrogen bonding than the peptides **1**, **2**, **4**, and **5**. Figures 4a and 4b show the IR absorption spectra in the amide A and amide I regions of the peptides **4** and **5** in dichloromethane (1.0×10^{-4} M). The amide carbonyl band also showed little dependence on concentration (1.0×10^{-4}—10^{-2} M) (not shown). Assignment of each band in the amide I region of the peptides **4** and **5** is essentially the same with that of the peptides **1** and **2**. In Figs. 4a and 4b, the IR difference spectra for both peptides are also represented. The spectra indicate the disappearance of the free N-H stretching vibration and clear-cut features of absorption bands at 3323 $^{-1}$ and 1658 cm^{-1}, probably assigned to the α-helical structure.[17-19]

Discussion

Contrary to the fact that the pentapeptides **1** and **2** in the solid state have the β-sheet structure,[4] in dichloromethane, the clear conformational transformation from intermolecular to intramolecular hydrogen bonding takes place in both peptides. The N-H stretching absorption band at 3330 cm^{-1} of the peptides **1** and **2** shows little dependence on concentration, indicating a slight contribution from inter molecular hydrogen bonds, which are apparently different from the intermolecular hydrogen bonds in the solid state assigned by the band at 3270 cm^{-1} (β-sheet). Their conformational behaviors both in the solid state and in dichloromethane are just the same as those of Boc-Leu_4-OBzl and Boc-Leu_5-OBzl,[20] indicating that the protected polar side chains of the Glu(OBzl) and Asp(OBzl) residues do not disturb the conformational behaviors of the pentapeptides **1** and **2** both in the solid state and in dichloromethane. Since the IR difference spectrum in dichloromethane for Boc-Leu_5-OBzl and Boc-Leu_3-OBzl suggests that the conformation formed by the intramolecular hydrogen bonds of Boc-Leu_5-OBzl appears to be a helical structure in dichloromethane,[20] the conformation of the peptides **1** and **2** is assumed to be the helical structure in dichloromethane. A little concentration dependence of the peptides **1** and **2** is assumed to be mainly due to intermolecular hydrogen bonds between the free N-H and C=O groups in the helical structure. On the other hand, Boc-Gln-Val-Glu(OBzl)-Leu-Gly-OPac **6**, which is also the partial sequence of the C-peptide, has the β-sheet structure in the solid state and it is insoluble in dichloromethane.[2,4] The insolubility represents that, in dichloromethane, the conformational transformation from intermolecular to intramolecular hydrogen bonding does not take place in the pentapeptide **6**. The insolubility is probably due to intermolecular hydrogen bonds through the Gln side-chain amide as reported for oligopeptides containing the Asn residue,[21] and the intermolecular hydrogen bonds may interrupt the conformational transformation from intermolecular to intramolecular hydrogen bonding in dichloromethane.

With respect to the role of the Pro residue in conformational behaviors of peptides containing the Pro residue, as reported in the previous papers,[2,4] the peptides **3** and **4** in the solid state, which contain the Pro residue in central positions in the peptide chains, have strong bands at 3290—3270 and 1635—1630 cm^{-1}, accompanied by strong broad shoulders at 1700—1650 cm^{-1} in the amide I region, indicating the disturbance of the β-sheet structure by the rotation of the tertiary peptide bond planes (Gly-Pro and Gln-Pro). In the solid state, the role of the Pro residue in conformational behaviors of the peptides **3** and **4** is just the same as that of oligo(Leu)s as reported in previous papers.[11-13] In dichloromethane, each Pro residue in the hexapeptide **3** and the nonapeptide **4** clearly plays a different role in conformational behaviors of both peptides. When we compare

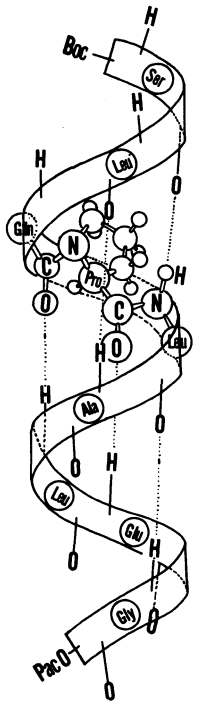

Fig. 5. α-Helical structure of the peptide **4**. Circles containing abbreviations for amino acids represent C^{α} atoms for each amino acid.

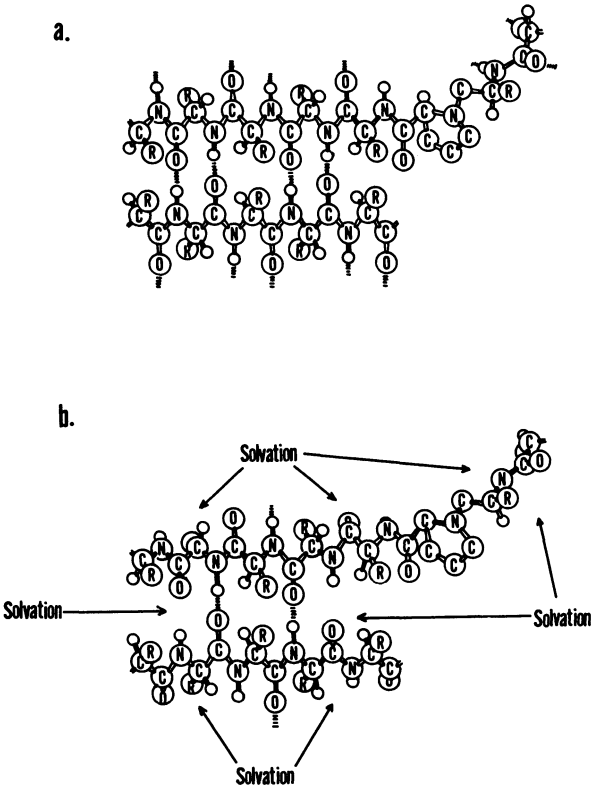

Fig. 6. Role of the Pro residue in dissolving process of the peptide **4**. a: In the solid state; b: solvating process.

solubility of the peptide **3** with that of Boc-Gly_6-OBzl,[22] the solubility improvement in the peptide **3** by the Pro residue is quite significant. The Pro residue in the peptide **3** clearly disturbs the development of the β-sheet structure in dichloromethane. The peptide **3** contains the four Gly residues, and each Gly residue can explore a large conformational space,[22,23] thus inducing a high flexibility to the peptide chain. Actually, the wide range of hydrogen bonded N-H stretching band and concentration dependence of the peptide **3** indicate that the peptide **3** in dichloromethane contains many kinds of intermolecular and intramolecular hydrogen bonds and exists in more than one conformation. On the other hand, the conformational behaviors of the peptide **4** in dichloromethane, which has polar side chains, are just the same as those of Boc-Leu_3-Pro-Leu_4-OBzl (**7**),[20] and the IR difference spectrum for the peptides **4** and **5** (Fig. 4) suggests that the peptide **4** appears to have successive-intramolecular hydrogen bonds, probably corresponding to the α-helical structure as shown in Fig. 5. This is in remarkable contrast with the fact that Boc-Leu-Ala-Leu-Glu(OBzl)-Gly-Ser(Bzl)-Leu-Gln-OPac (**8**), which is also the partial sequence of the C-peptide and has the very close amino acid sequence with the peptide **4**, has the β-sheet structure in the solid state and is insoluble in dichloromethane.[2,4] The peptides **4** and **7** have high parameters for α-helix formation, and their $<P_{\alpha}>$ values[24] are 1.12 and 1.25, respectively. In fact, the peptide **4** is included in one of helical regions in human proinsulin.[25] In comparison with the conformational behaviors of the peptide **8**, the IR difference spectra for the peptides **4** and **5** in dichloromethane clearly suggest that the Pro residue, which exists in near the N-terminal portion in the peptide having a high potential for the formation of the α-helical structure, plays an important role in helical folding in the peptide. Figure 6 represents the role of the Pro residue in dissolving process of the peptide **4**. The Pro residue in the peptide **4** clearly disturbs the development of the β-sheet aggregation in the solid state by the rotation of the tertiary peptide bond plane (Gln-Pro) and facilitates solvation of the peptide chain. Thus, the restriction of the values of the backbone dihedral angles ϕ and ψ of the Pro residue appears to promote helical folding in dichloromethane of the peptide **4**.

References

1) This paper forms Part III of "Design of the Synthetic Route for Peptides and Proteins Based on the Solubility Prediction Method" series. For part II of this series, see M. Narita, T. Ogura, K. Sato, and S. Honda, *Bull. Chem. Soc. Jpn.*, **59**, 2439 (1986). The abbreviations for amino acids are those recommended by the IUPAC-IUB Commission on Biochemical Nomenclature, *J. Biol. Chem.*, **247**, 977 (1972). Amino acid symbols except for Gly denote the L-configuration. Additional abbreviations used are the following: IR, infrared; OBzl, benzyl ester; Bzl, benzyl; Aib, α-aminoisobutyric acid residue; HPLC, high-performance liquid

chromatography; Boc, *t*-butoxycarbonyl; Pac, phenacyl.

2) M. Narita, T. Ogura, K. Sato, and S. Honda, *Bull. Chem. Soc.* **59**, 2433 (1986).

3) M. Narita, K. Ishikawa, J.-Y. Chen, and Y. Kim, *Int. J. Peptide Protein Res.*, **24**, 580 (1984).

4) M. Narita, T. Ogura, K. Sato, and S. Honda, *Bull. Chem. Soc. Jpn.*, **59**, 2439 (1986).

5) R. B. Merrifield, *J. Am. Chem. Soc.*, **85**, 2149 (1963).

6) M. Narita, Y. Tomotake, S. Isokawa, T. Matsuzawa, and T. Miyauchi, *Macromolecules*, **17**, 1903 (1984).

7) P. Y. Chou and G. D. Fasman, *Biochemistry*, **13**, 211 (1974); *ibid.*, **13**, 222 (1974); P. Y. Chou and G. D. Fasman, *Advan. Enzymol.*, **47**, 45 (1978).

8) S. Lifson and C. Sander, *Nature*, **282**, 109 (1979).

9) K. Nagano, *Kagakunoryoiki*, **36**, 120 (1982).

10) C. Toniolo, G. M. Bonora, M. Mutter, and V. N. R. Pillai, *Makromol. Chem.*, **182**, 1997 (1981); *ibid.*, **182**, 2007 (1981).

11) M. Narita, T. Fukunaga, A. Wakabayashi, K. Ishikawa, and H. Nakano, *Int. J. Peptide Protein Res.*, **23**, 306 (1984); M. Narita, K. Ishikawa, H. Nakano, and S. Isokawa, *ibid.*, **24**, 14 (1984).

12) M. Narita, S. Nagasawa, J.-Y. Chen, H. Sato, and Y. Tanaka, *Makromol. Chem.*, **185**, 1069 (1984); M. Narita, N. Ohkawa, S. Nagasawa, and S. Isokawa, *Int. J. Peptide Protein Res.*, **24**, 129 (1984).

13) S. Isokawa, T. Asakura, and M. Narita, *Macromolecules*, **18**, 871 (1985); S. Isokawa, I. Tominaga, T. Asakura, and M. Narita, *ibid.*, **18**, 878 (1985).

14) D. F. De Tar and N. Luthra, *J. Am. Chem. Soc.*, **99**, 1232 (1977); V. Madison, *Biopolymers*, **16**, 2671 (1977); B. V. V. Prasad, H. Balaram, and P. Balaram, *ibid.*, **21**, 1261 (1982).

15) M. Narita, M. Doi, H. Sugasawa, and K. Ishikawa, *Bull. Chem. Soc. Jpn.*, **58**, 1473 (1985); M. Narita, K. Ishikawa, H. Sugasawa, and M. Doi, *ibid.*, **58**, 1731 (1985).

16) M. Narita, J.-Y. Chen, H. Sato, and Y. Kim, *Bull. Chem. Soc. Jpn.*, **58**, 2494 (1985).

17) T. Miyazawa and E. J. Blout, *J. Am. Chem. Soc.*, **83**, 712 (1961); Yu. N. Chirgadze and N. A. Nevskaya, *Biopolymers*, **15**, 627 (1976); M. Narita, Y. Tomotake, S. Isokawa, T. Matsuzawa, and T. Miyauchi, *Macromolecules*, **17**, 1903 (1984); M. Narita, S. Isokawa, Y. Tomotake, and S. Nagasawa, *Polymer J.*, **15**, 25 (1983), and references cited therein.

18) C. H. P. Rao, P. Balaram, and C. N. R. Rao, *Biopolymers*, **22**, 2091 (1983) and references cited therein.

19) G. Boussard and M. Marraud, *J. Am. Chem. Soc.*, **107**, 1825 (1985); C. Toniolo, G. M. Bonora, V. Borone, A. Bavoso, E. Benedetti, B. D. Blasio, P. Grimaldi, F. Lelj, V. Pavone, and C. Pedone, *Macromolecules*, **18**, 895 (1985).

20) M. Narita, M. Doi, R. Wakita, and S. Isokawa, *Bull. Chem. Soc. Jpn.*, in press.

21) T. Toniolo, G. M. Bonora, and W. M. M. Schaaper, *Int. J. Peptide Protein Res.*, **23**, 389 (1984).

22) M. Narita, M. Doi, K. Kudo, and Y. Terauchi, *Bull. Chem. Soc. Jpn.*, in press.

23) D. A. Brant, W. G. Miller, and P. J. Flory, *J. Mol. Biol.*, **23**, 47 (1967); R. T. Ingwall, E. A. Crurylo, and P. J. Flory, *Biopolymers*, **12**, 1137 (1973).

24) P. Y. Chou and G. D. Fasman, *Biochemistry*, **13**, 211 (1974).

25) C. R. Snell and P. G. Smyth, *J. Biol. Chem.*, **250**, 6291 (1975).

 © 1986 The Chemical Society of Japan Bull. Chem. Soc. Jpn., 59, 2451—2458 (1986)

A Diels-Alder Cycloaddition and Electrocyclization Sequence as a New [6.5] Annelation Method to Benzene Ring

Eiji WADA, Shuji KANEMASA, and Otohiko TSUGE*
Research Institute of Industrial Science, and Department of Molecular Science and Technology, Interdisciplinary Graduate School of Engineering Sciences, Kyushu University, Kasugakoen, Kasuga 816
(Received February 27, 1986)

The Diels-Alder reactions of 1-aryl-2-methylene-3-buten-1-ols, readily available from chloroprene and aryl ketones, with olefinic dienophiles and subsequent electrocyclic reactions of the cycloadducts offer a new method of [6.5] annelation to benzene ring. By this way, tetrahydrofluorene skeletons bearing functional groups can be prepared. Stereochemical aspect of this sequence is also discussed.

The Diels-Alder reaction involves the interaction between diene and dienophile forming six-membered ring with an endo double bond. Therefore, two rings annelation including a six-membered ring will be established when another ring-forming reaction is performed across this unsaturated bond. Such sequential ring formation is quite limited,[1] while the double Diels-Alder cycloaddition of cross-conjugated trienes offers an annelation method of this category.[2] It is important that the sequential ring formation is to be initiated by Diels-Alder cycloaddition since this cycloaddition takes place in a highly stereoselective and stereospecific manner. The second ring formation is expected to occur also in a selective way to afford stereochemically defined fused ring systems.[3]

Our method for sequential [6.5] annelation consists of the initial Diels-Alder reactions on 1-aryl-2-methylene-3-buten-1-ols and the subsequent acid-catalized electrocyclic reactions of the cycloadducts. In the Diels-Alder steps, dimethyl maleate, fumarate, and *N*-methylmaleimide are employed as representatives for cis, trans, and cyclic olefinic dienophiles, respectively. It should be emphasized that the present method permits the introduction of several functional groups onto tetrahydrofluorene skeletons.[4]

Results and Discussion

Diene alcohols **1a—c** as starting materials in the present [6.5] annelation can be prepared from the reaction of 2-lithio-1,3-butadiene with aryl ketones.[5] Without separation of isomeric allene alcohols as side products, the Diels-Alder reaction with dimethyl maleate (**2**), fumarate (**3**), or *N*-methylmaleimide (**4**) was carried out under reflux in benzene to give the corresponding cycloadducts **5a—c**, **6a—c**, or **7a—c**, in excellent yields (Table 1). These cycloadducts were separated from the unreacted allene alcohols through column chromatography. Then, acid-catalyzed electrocyclic reaction of these cycloadducts was investigated under various conditions.[6]

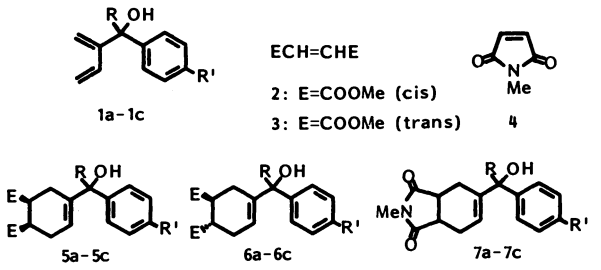

a: R=Ph, R'=H; b: R=Me, R'=H; c: R=Me, R'=OMe

The maleate cycloadduct **5a** derived from benzophenone adduct **1a** was found to undergo ready cyclization, in the presence of trifluoroacetic acid (TFA) or zinc chloride, to afford a mixture of two stereoisomeric tetrahydrofluorene derivatives **8a** and **9a** together with a trace amount of diene **10a** (Entries 1—3 in Table 2). Structures of the major product **8a** and the minor one **9a** were assigned to be 3,4a-cis and 3,4a-trans isomers on the basis of coupling constants J_{3-4}, and J_{4-4a}, and also by comparison with their

Table 1. The Diels-Alder Cycloaddition of **1** with **2—4**

Dienophile (equiv)	Diene	Reaction time/h[a]	Product	Yield/%[b]
2 (2)	**1a**	48	**5a**	82
2 (2)	**1b**	48	**5b**	86
2 (2)	**1c**	48	**5c**	80
3 (2)	**1a**	12	**6a**	86
3 (1.1)	**1b**	16	**6b**	100
3 (1.02)	**1c**	10	**6c**	100
4 (1.2)	**1a**	5	**7a**	86
4 (1)	**1b**	2	**7b**	94
4 (1)	**1c**	5	**7c**	91

a) Under reflux in benzene. b) Isolated yield based on **1**.

Table 2. Electrocyclic Reaction of Maleate **5** and Fumarate Cycloadducts **6**

Entry	Cyclo-adduct	Reaction conditions[a]				Total yield/%	Product (isolated yield/%)	3,4a-cis:trans
		Solvent	Catalyst	Temp/°C	Time/h			
1	**5a**	DCM	TFA	−78→0	3	95	**8a** (82), **9a** (11), **10a** (2)	88:12
2		DCM	TFA	rt	8	91	**8a** (83), **9a** (6), **10a** (2)	93: 7
3		DCM	$ZnCl_2$	rt	2.25	91	**8a** (80), **9a** (9), **10a** (2)	90:10
4		BZ	MS	rt	17	93	**8a** (85), **9a** (4), **10a** (4)	95: 5
5	**5b**	DCM	TFA	rt	5 min	89	**8b** (75), **9b** (13), **10b** (1)	85:15
6		THF	6M†-HCl	rt	12	77	**10b** (12), **11** (65)	—
7	**5c**	DCM	TFA	rt	3 min	79	**8c** (68), **9c** (10), **10c** (1)	87:13
8		THF	4M-HCl	rt	24	68	**10c** (14), **12** (54)	—
9	**6a**	DCM	TFA	−78→0	4.5	96	**13a** (41), **14a** (54), **15a** (1)	43:57
10		DCM	TFA	rt	140	74	**13a** (44), **14a** (30)	54:46
11		DCM	$ZnCl_2$	rt	5	93	**13a** (52), **14a** (39), **15a** (2)	57:43
12		BZ	MS	rt	15	93	**13a** (53), **14a** (36), **15a** (4)	60:40
13	**6b**	DCM	TFA	rt	10 min	86	**13b** (56), **14b** (29), **15b** (1)	66:34
14		DCM	TFA[b]	rt	2	79	**13b** (6), **14b** (4), **16** (69)	—
15		BZ	MS	rt	12	98	**13b** (43), **14b** (33), **16** (22)	56:44
16		THF	3M-HCl	rt	68	52	**16** (52)	—
17	**6c**	DMC	TFA	rt	3 min	69	**13c** (40), **14c** (29)	58:42
18		BZ	MS	rt	40	78	**13c** (21), **14c** (38), **17** (19)	36:64
19		THF	1M-HCl	rt	60	71	**17** (71)	—

a) Solvent: DCM: dichloromethane; BZ: benzene; THF: tetrahydrofuran. Catalyst: TFA: trifluoroacetic acid; MS: molecular sieves 5A. Unless otherwise stated, the catalyst was used in large excess. b) In the presence of an equimolar amount of TFA. † 1M=1 mol dm^{-3}.

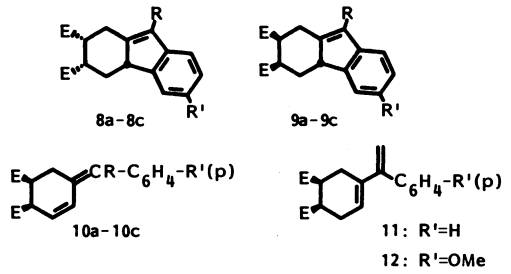

a: R=Ph, R'=H; b: R=Me, R'=H; c: R=Me, R'=OMe

isomers **13a** and **14a** obtained from similar cyclization of fumarate cycloadduct **6a**.[7] No isomerization between **8a** and **9a** was observed under conditions of the cyclization, indicating that one of two possible conrotatory rotations has predominantly occurred to lead to this high stereoselectivity. This will be discussed later. The highest selectivity in favor for the 3,4a-cis isomer **8a** was obtained (**8a**:**9a**=95:5) when cyclization was carried out in benzene at room temperature in the presence of molecular sieves 5A (Entry 4). Although some examples for the dehydration of tertiary alcohols with molecular sieves are already known,[8] this example might be the first case in which molecular sieves are utilized in cationic cyclization reactions.

Other maleate cycloadducts **5b** and **5c** derived from acetophenone adducts **1b** and **1c** similarly cyclized within 5 min at room temperature in the presence of TFA, to give two stereoisomeric tetrahydrofluorenes **8b**+**9b** and **8c**+**9c** (Entries 5 and 7 in Table 2). However, no cyclized product was obtained when **5b** or **5c** was treated with aqueous HCl (Entries 6 and 8). 1-(1-Arylvinyl)cyclohexene **11** or **12** as a major product in this reaction was found to be a kinetically controlled product since **11** or **12** gradually isomerized into 3-methylenecyclohexene **10b** or **10c** under conditions of the dehydration. Although **10b** or **10c** underwent no cyclization, **11** or **12** cyclized on treatment with TFA leading to quantitative yield of **8b**+**9b** or **8c**+**9c**, respectively.[9]

Fumarate cycloadducts **6a**—**c** underwent cyclizations into the corresponding tetrahydrofluorene derivatives **13a**—**c** and **14a**—**c** under similar conditions (Entries 9—19 in Table 2). However, stereoselectivity between **13** and **14** was found extremely low under all the conditions employed for cyclization. This makes a striking contrast with the stereoselective cyclization of maleate cycloadducts **5a**—**c**. Formation of 3-methylenecyclohexenes **15** as side products was not critical, and 1-(1-arylvinyl)cyclohexene **16** or **17** was the only product when acetophenone adduct **6b** or **6c** was treated with aqueous HCl, respectively.

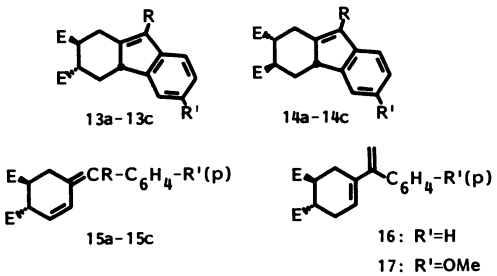

R=Ph, R'=H; b: R=Me, R'=H; c: R=Me, R'=OMe

Maleimide cycloadducts **7a**—**c** underwent similar cyclizations in the presence of TFA or molecular sieves

Table 3. Electrocyclic Reaction of Maleimide Cycloadducts **7**

Entry	Cyclo-adduct	Reaction conditions[a]				Total yield/%	Product (isolated yield/%)	3a,4a-cis:trans
		Solvent	Catalyst	Temp/°C	Time/h			
1	**7a**	DCM	TFA	−78→−10	3	93	**18a** (15), **19a** (78)	16:84
2		DCM	TFA	rt	10 min	95	**18a** (29), **19a** (66)	31:69
3		BZ	TFA	rt	20 min	86	**18a** (12), **19a** (74)	14:86
4		BZ	MS	rt	24	97	**18a** (69), **19a** (28)	71:29
5		DCM	MS	rt	20	96	**18a** (51), **19a** (45)	53:47
6	**7b**	DCM	TFA	−78→0	2	75	**18b** (25), **19b** (50)	33:67
7		DCM	TFA	rt	10 min	84	**18b** (36), **19b** (48)	43:57
8		BZ	MS	rt	24	100	**18b** (67), **19b** (17), **20** (16)[b]	80:20
9		DCM	MS	rt	36	100	**18b** (39), **19b** (28), **20** (33)[b]	58:42
10	**7c**	DCM	TFA	rt	5 min	51	**18c** (18), **19c** (33)	35:65
11		BZ	MS	rt	16	100	**18c** (75), **19c** (13), **21** (12)[b]	85:15
12		DCM	MS	rt	16	100	**18c** (59), **19c** (24), **21** (17)[b]	71:29

a) Solvent: DCM: dichloromethane; BZ: benzene. Catalyst: TFA: trifluoroacetic acid; MS: molecular sieves 5A. The catalyst was used in large excess in all cases. b) The ratio was determined by GLC.

5A to give two stereoisomeric octahydroindeno[1,2-*f*]isoindoles **18a—c** and **19a—c** (Table 3). Surprising is that the isomer ratio is very much dependent on the reaction conditions. The reactions in benzene in the presence of molecular sieves 5A preferentially produced 3a,4a-cis isomers **18** (**18**:**19**=71—85:29—15, Entries 4, 8, and 11). On the other hand, the reactions in the presence of TFA favored 3a,4a-trans isomers **19** rather than **18** (**18**:**19**=14—43:86—57, Entries 1—3, 6, 7, and 10). When acetophenone adduct **7b** or **7c** was treated with molecular sieves, noncyclized dehydration product **20** or **21** was formed as a side product, respectively.

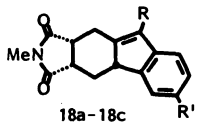

18a-18c

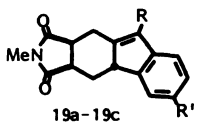

19a-19c

a: R=Ph, R'=H; b: R=Me, R'=H; c: R=Me, R'=OMe

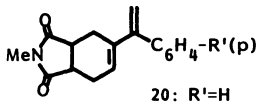

20: R'=H
21: R'=OMe

On the basis of the above results, such difference of stereoselectivity of these electrocyclic reactions may be explained as follows: as it is quite certain that the cyclization involves an aryl-substituted allyl cationic intermediate, the stereochemistry of cyclized products must have been determined at the stage of irreversible cyclization of this cation by either of two possible conrotatory rotations, clockwise and counterclockwise conrotatory rotations. Two half-chair conformations **A** and **B** (X=COOMe, Y=H) are possible for cationic intermediates from the maleate cycloadducts **5**, and they should have almost equal stability. Counterclockwise rotation of **A** leads to 3,4a-cis cyclization product **C**, while clockwise rotation of **B** forms sterically unfavorable 3,4a-trans isomer **D** whose quasi-chair six-membered ring carries an axial ester substituent at the 3-position causing considerable steric repulsion toward axial 4a-H.[10] Consequently, cyclization of **5** has predominantly occurred through counterclockwise rotation of **A** giving **8** as far major product.

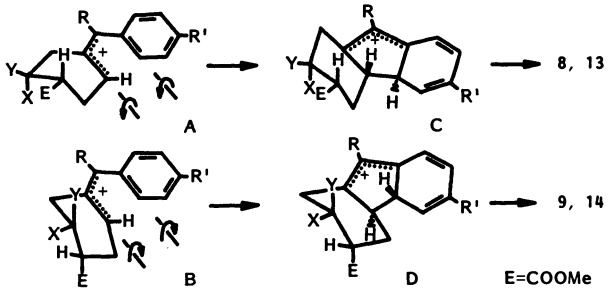

On the other hand, stability of two cationic intermediates **A** and **B** (X=H, Y=COOMe) from the fumarate cycloadducts **6** is not identical. Conformer **A** bearing two ester groups at adjacent equatorial positions may be less stable than **B** with two axial ester substituents.[11] The less stable cation **A** undergoes cyclization through a transition state leading to more stable cyclization product **C**, and the more stable cation **B** to less stable product **D**. As a result, stereoselectivity between **13** and **14** was lowered.

In the case of electrocyclization of the maleimide cycloadducts **7**, cationic intermediates **E** and **F** are expected to cyclize into cyclization products **G** and **H**, respectively. During this transformation, conformation of the six-membered ring changes from a folded conformation into an envelope shape.[12] Relative stabilities should be **F**>**E** and **G**>**H**, and this situation resembles to the case of electrocyclization of fumarate cycloadducts **6**. However, difference of stability between **E** and **F** and between **G** and **H** may be relatively smaller.[13] This might be the main reason for the high dependence of stereoselectivity upon reaction conditions. Cyclization under less polar con-

ditions (e.g. use of molecular sieves in benzene) has favored the route going through more stable transition state (**E→G→18**). On the other hand, cyclization under more polar conditions (e.g. TFA in dichloromethane) has selected the route starting from more stable ionic intermediate (**F→H→19**).

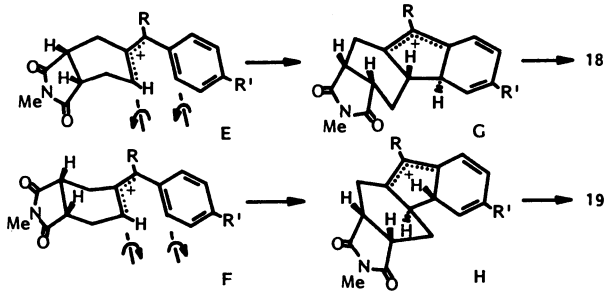

Thus, the sequence of Diels–Alder reaction and electrocyclization of 1-aryl-2-methylene-3-buten-1-ols works well as a new method of [6.5] annelation. Stereoselectivity in the second electrocyclization step mainly depends upon the structure of dienophiles used in the initial Diels–Alder cycloaddition.

Experimental

General. Melting points were determined on a Yanagimoto micro melting point apparatus and are uncorrected. IR spectra were taken with a JASCO IRA-1 or a JASCO A-702 spectrometer. ^{1}H-NMR spectra were recorded on a Hitachi R-40 (90 MHz) or a JEOL FX-100 instrument (100 MHz) and ^{13}C-NMR spectra on a JEOL FX-100 spectrometer at 25.05 MHz. Chemical shifts are expressed in parts per million downfield from tetramethylsilane as internal standard. Mass spectra were measured with a JEOL JMS-01SG-2 spectrometer at 70 eV of ionization energy. Elemental analyses were performed on a Hitachi 026 CHN micro analyzer. Thin-layer chromatography (TLC) was accomplished on 0.2 mm precoated plates of silica gel 60 F-254 (Merck) or of aluminum oxide 60 F-254 type-E (Merck). Visualization was made with ultraviolet light (254 and 365 nm), iodine, molybdophosphoric acid (5% in ethanol), or *p*-anisaldehyde (5% in ethanol containing 5% of sulfuric acid). For preparative column chromatography, Wakogel C-200, C-300 (Wako), or Kieselgel 60 (230—400 mesh, Merck) was used. Flash chromatography was carried out on an EYELA EF-10 apparatus using a column (20×180 mm) packed with Silicagel 60 (Merck, size: 0.04—0.063 mm). Gas liquid chromatography (GLC) was accomplished on a Yanaco G-2800 gas chromatography (Yanagimoto) with an ionization detector using a glass column (SE-30, 3×2000 mm). Solvents were evaporated with a Tokyo Rikakikai rotary evaporator type-V at about 50 °C unless otherwise stated.

Materials and Solvents. Benzene and dichloromethane were distilled over sodium wire and calcium hydride, respectively, prior to their use. Zinc chloride was purified by crystallization from anhydrous dioxane and dried over phosphorus pentaoxide under vacuum. 1-Aryl-2-methylene-3-buten-1-ols **1a—c** were prepared according to the method previously reported.[5] They are available as mixtures with the corresponding allene alcohols (purity: **1a**: 50%; **1b**: 90%; **1c**: 95%). No separation of **1** from these mixtures is needed, but these mixtures were submitted to the following Diels–Alder cycloadditions. Other solvents such as THF, hexane, and ethyl acetate and olefins **2—4** are commercially available, and were used without further purification.

General Procedure for the Diels–Alder Reactions of 1 with 2—4 Leading to 5—7. Diene alcohols **1a—c** with the purity shown above and olefins **2—4** were heated under reflux in dry benzene (2—5 ml for 1 mmol of **1**) under the conditions listed in Table 1. The crude mixtures were condensed in vacuo and chromatographed over silica gel with hexane–ethyl acetate to give cycloadducts **5—7**. The results are summarized in Table 1.

5a: Colorless prisms (ethyl acetate–hexane); mp 113—115 °C; IR (KBr) 3500, 1725, and 1705 cm^{-1}; ^{1}H-NMR ($CDCl_3$) δ=2.2—2.6 (4H, m, CH_2), 2.8—3.2 (3H, m, CH and OH), 3.58, 3.64 (each 3H, s, COOMe), 5.34 (1H, m, 2-H), 7.23, and 7.25 (each 5H, br s, Ph); ^{13}C-NMR ($CDCl_3$) δ=25.71, 26.36 (each t, 3- and 6-C), 39.51, 40.16 (each d, 4- and 5-C), 51.73 (2×C, q, COOMe), 82.49 (s, q-C), 124.64, 127.05, 127.46, 127.58, 127.75 (each d), 140.26, 144.60, 144.95 (each s), and 173.43 (2×C, s, COOMe); MS *m/z* (rel. intensity, %) 363 (M^+−17, 23), 362 (87), 303 (25), 302 (72), 244 (23), 243 (80), 183 (23), 165 (55), and 105 (base peak). Found: C, 72.73; H, 6.51%. Calcd for $C_{23}H_{24}O_5$: C, 72.61; H, 6.36%.

5b: (Mixture of two diastereomers): Colorless viscous oil; IR (neat) 3500 and 1725 cm^{-1}; ^{1}H-NMR ($CDCl_3$) δ=1.61 (3H, s, Me), 2.0—3.1 (7H, m, CH_2, CH, and OH), 3.47, 3.49 (each 3H, s, COOMe), 5.86 (1H, m, 2-H), and 7.0—7.5 (5H, m, Ph); ^{13}C-NMR ($CDCl_3$) δ=25.58 (t, CH_2), 28.46, 28.80 (each q, Me), 39.52, 39.67, 39.96, 40.15 (each d, CH), 51.61, 51.80 (each q, COOMe), 76.12, 76.51 (each s, q-C), 119.24, 119.49, 125.24, 126.65, 127.92 (each d), 140.73, 140.93, 146.09 (each s), 173.33, 173.48, and 173.68 (each s, COOMe); MS *m/z* (rel. intensity, %) 301 (M^+−17, 31), 241 (50), 181 (base peak), and 105 (29). Found: C, 67.80; H, 6.91%. Calcd for $C_{18}H_{12}O_5$: C, 67.91; H, 6.97%.

5c: (Mixture of two diastereomers): Colorless viscous oil; IR (neat) 3500 and 1725 cm^{-1}; ^{1}H-NMR ($CDCl_3$) δ= 1.60 (3H, s, Me), 2.0—3.2 (7H, m, CH_2, CH, and OH), 3.51, 3.53, 3.62 (6H, each s, COOMe), 3.74 (3H, s, OMe), 5.85 (1H, m, 2-H), 6.79, and 7.24 (each 2H, br d, Ar); ^{13}C-NMR ($CDCl_3$) δ=25.58 (t, CH_2), 28.31, 28.65 (each q, Me), 39.47, 40.01, 40.10 (each d, CH), 51.56, 51.75 (each q, COOMe), 55.11 (q, OMe), 76.12 (s, q-C), 113.20, 119.05, 126.41 (each d), 138.25, 140.93, 158.22 (each s), 173.33, and 173.57 (each s, COOMe); MS *m/z* (rel. intensity, %) 348 (M^+, 13), 331 (21), 330 (base peak), 273 (21), 271 (29), 270 (61), 213 (28), 211 (91), 152 (48), and 135 (57). Found: C, 65.22; H, 7.02%. Calcd for $C_{19}H_{24}O_6$: C, 65.50; H, 6.94%.

6a: Colorless prisms (diethyl ether–hexane); mp 126—128 °C; IR (KBr) 3520, 3480, and 1720 cm^{-1}; ^{1}H-NMR ($CDCl_3$) δ=2.0—2.6 (4H, m, CH_2), 2.7—3.0 (3H, m, CH and OH), 3.57, 3.63 (each 3H, s, COOMe), 5.34 (1H, m, 2-H), 7.22, and 7.26 (each 5H, br s, Ph); ^{13}C-NMR ($CDCl_3$) δ=27.83, 28.00 (each t, 3-and 6-C), 40.86, 41.57 (each d, 4- and 5-C), 51.72 (2×C, q, COOMe), 82.37 (s, q-C), 123.88, 127.17, 127.46, 127.81 (each d), 140.49, 144.48, 144.66 (each s), 174.84, and 175.01 (each s, COOMe); MS *m/z* (rel. intensity, %) 363 (M^+−17, 0.3), 302 (34), 243 (43), 183 (55), 165 (71), 155 (25), 105 (61), and 59 (base peak). Found: C, 72.52; H, 6.36%. Calcd for $C_{23}H_{22}O_5$: C, 72.61; H, 6.36%.

6b: (Mixture of two diastereomers): Colorless viscous

oil; IR (neat) 3500 and 1730 cm^{-1}; ^{1}H-NMR ($CDCl_3$) δ=1.61, 1.62 (3H, each, s, Me), 2.0—3.0 (7H, m, CH_2, CH, and OH), 3.54, 3.61 (6H, each s, COOMe), 5.7—6.0 (1H, m, 2-H), and 7.0—7.5 (5H, m, Ph); ^{13}C-NMR ($CDCl_3$) δ=26.95, 27.53 (each t, CH_2), 28.24, 28.77 (each q, Me), 40.80, 41.33 (each d, CH), 51.67 (2×C, q, COOMe), 75.50, 76.15 (each s, q-C), 118.36, 118.95, 124.88, 124.99, 126.52, 127.81 (each d), 141.02, 145.60, 145.89 (each s), 174.89, and 175.07 (s). Found: C, 68.04; H, 7.07%. Calcd for $C_{18}H_{22}O_5$: C, 67.91; H, 6.97%.

6c: (Mixture of two diastereomers): Colorless viscous oil; IR (neat) 3500 and 1725 cm^{-1}; ^{1}H-NMR ($CDCl_3$) δ=1.62 (3H, s, Me), 1.9—3.0 (7H, m, CH_2, CH, and OH), 3.55, 3.65 (each 3H, s, COOMe), 3.77 (3H, s, OMe), 5.86 (1H, m, 2-H), 6.81, and 7.26 (each 2H, br d, Ar); ^{13}C-NMR ($CDCl_3$) δ=27.30, 27.83 (each t, CH_2), 28.36, 28.94 (each q, Me), 40.98, 41.10, 41.63 (each d, CH), 51.84 (2×C, q, COOMe), 55.19 (q, OMe), 75.62, 76.21 (each s, q-C), 113.43, 118.36, 119.00, 126.35, 126.46, 128.22 (each d), 137.73, 138.09, 141.26, 158.40 (each s), and 175.07 (2×C, s, COOMe). MS *m/z* (rel. intensity, %) 348 (M^+, 16), 333 (32), 330 (55), 298 (37), 273 (26), 271 (29), 270 (85), 213 (21), 211 (base peak), 152 (54), 135 (72), and 133 (27). Found: C, 65.41; H, 7.05%. Calcd for $C_{19}H_{24}O_6$: C, 65.50; H, 6.94%.

7a: Colorless prisms (diethyl ether-hexane); mp 125—126 °C; IR (KBr) 3450, 1770, 1660, and 1600 cm^{-1}; ^{1}H-NMR ($CDCl_3$) δ=1.9—2.7 (4H, m, CH_2), 2.86 (3H, s, NMe), 2.96 (2H, m, CH), 5.41 (1H, m, 6-H), and 7.2—7.3 (10H, m, Ph); ^{13}C-NMR ($CDCl_3$) δ=24.02 (t, 7-C), 24.85 (q, NMe), 25.39 (t, 4-C), 39.23, 39.96 (each d, 3a- and 7a-C), 81.62 (s, q-C), 124.95, 127.09, 127.09, 127.33, 127.62, 127.87 (each d), 143.90, 144.14, 145.07 (each s), 179.77, and 179.91(each s, CON); MS *m/z* (rel. intensity, %) 347 (M^+, 19), 329 (38), 165 (34), 112 (30), 105 (base peak), 80 (22), 78 (55), and 77 (91). Found: C, 76.08; H, 6.05; N, 4.18%. Calcd for $C_{22}H_{21}NO_3$: C, 76.06; H, 6.09; N, 4.03%.

7b: (Mixture of two diastereomers): Colorless viscous oil; IR (neat) 3420, 1770, and 1700 cm^{-1}; ^{1}H-NMR ($CDCl_3$) δ=1.56, 1.58 (3H, each s, Me), 1.8—4.1 (7H, m, CH_2, CH, and OH), 2.79, 2.83 (3H, each s, NMe), 5.96 (1H, m, 6-H), and 7.23 (5H, m, Ph); ^{13}C-NMR ($CDCl_3$) δ=23.63, 23.93, 24.41 (each t, CH_2), 24.66 (q, NMe), 24.85 (t, 4-C), 27.68 (q, Me), 39.37, 39.62, 39.81 (d, CH), 75.87 (s, q-C), 119.49, 119.92, 125.24, 126.94, 128.01 (each d), 144.97, 145.31, 145.55 (each s), 179.27, 179.91, and 180.01 (each s, CON); MS *m/z* (rel. intensity, %) 285 (M^+, 5), 270 (19), 79 (36), 78 (30), 77 (69), and 43 (base peak). Found: C, 71.80; H, 6.70; N, 5.07%. Calcd for $C_{17}H_{19}NO_3$: C, 71.56; H, 6.71; N, 4.91%.

7c: (Mixture of two diastereomers): Colorless viscous oil; IR (neat) 3450, 1770, and 1690 cm^{-1}; ^{1}H-NMR ($CDCl_3$) δ=1.54, 1.56 (3H, each s, Me), 1.8—3.2 (7H, m, CH_2, CH, and OH), 2.82, 2.85 (3H, each 3H, NMe), 3.75 (3H, s, OMe), 5.97 (1H, m, 6-H), 6.78, and 7.19 (each 2H, m, Ar); ^{13}C-NMR ($CDCl_3$) δ=23.68, 23.98 (each t, CH_2), 24.46, 24.85 (each q, Me), 24.90 (t, 4-C), 27.48, 27.87 (each q, NMe), 39.37, 39.42, 39.67, 39.86 (each d, CH), 55.21 (q, OMe), 75.29, 75.58 (each s, q-C), 113.35, 113.39, 119.14, 119.73, 126.45, 126.55 (each d), 137.12, 137.66, 145.55, 145.57, 158.42, 158.52 (each s), 179.42, 179.96, and 180.00 (each s, CON); MS *m/z* (rel. intensity, %) 315 (M^+, base peak), 300 (91), 272 (31), 192 (65), 151 (80), 135 (25), 121 (53), and 79 (23). Found: C, 68.60; H, 6.67; N, 4.55%. Calcd for $C_{18}H_{21}NO_4$: C, 68.55; H, 6.71; N, 4.44%.

General Procedure for the Acid-Catalyzed Electrocyclization of 5—7 Leading to 8—21. The Diels-Alder cycloadducts **5—7** were treated with a catalyst such as TFA, $ZnCl_2$, aqeous HCl, and molecular sieves 5A under the conditions shown in Tables 2 and 3. The amounts of catalyst and reaction solvent used for 1 mmol of **5—7** are as follows: TFA: 7—15 mmol in 6—10 ml of dichloromethane or benzene; $ZnCl_2$: 1.5—2 g in 10 ml of dichloromethane; aqeous HCl: 5 ml in 5 ml of THF. After the reaction was over, the mixture was poured into ice water and extracted with diethyl ether twice. The combined extracts were washed with aqueous sodium hydrogencarbonate, with water, dried over anhydrous magnesium sulfate, and finally evaporated in vacuo. The residue was subjected to ^{1}H-NMR and GLC analysis to know the ratio of products, and chromatographed over silica gel with ethyl acetate-hexane. All results were summarized in Tables 2 and 3.

8a: Colorless prisms (diethyl ether-hexane); mp 124—125 °C; IR (KBr) 1720 cm^{-1}; ^{1}H-NMR ($CDCl_3$) δ=1.67 (1H, q, J=13.1 Hz, one of 4-H), 2.61 (1H, dd, J=14.8 and 6.0 Hz, one of 1-H), 2.7—3.0 (2H, m, the other of 1- and 4-H), 3.1—3.6 (3H, m, CH), 3.35 (3H, s, 2-COOMe), 3.67 (3H, s, 3-COOMe), and 7.0—7.6 (9H, m, Ar); ^{13}C-NMR ($CDCl_3$) δ=28.21, 29.58 (each t, 1- and 4-C), 43.27, 43.52 (each d, 2- and 3-C), 48.78 (d, 4a-C), 51.41, 51.90 (each q, COOMe), 119.88, 122.56, 124.56, 126.65, 127.19, 128.31, 128.79 (each d), 134.50, 137.62, 141.85, 144.92, 146.24 (each s), 172.36, and 173.29 (each s, COOMe); MS *m/z* (rel. intensity, %) 362 (M^+, 64), 303 (28), 302 (base peak), 243 (40), 242 (25), 203 (22), 202 (21), and 165 (82). Found: C, 76.36; H, 6.15%. Calcd for $C_{23}H_{22}O_4$: C, 76.22; H, 6.12%.

8b: Colorless prisms (dichloromethane-hexane); mp 188—189 °C; IR (KBr) 1725 cm^{-1}; ^{1}H-NMR ($CDCl_3$) δ=1.39 (1H, dt, J=13.1, 13.1, and 12.2 Hz, one of 4-H), 2.01 (3H, t, J=1.8 Hz, 9-Me), 2.48 (1H, br dd, J=14.0 and 5.5 Hz, one of 1-H), 2.6—3.6 (5H, m, CH_2 and CH), 3.52, 3.68 (each 3H, s, COOMe), and 7.0—7.4 (4H, m, Ar); ^{13}C-NMR ($CDCl_3$) δ=9.69 (q, 9-Me), 27.83, 29.71 (each t, 1- and 4-C), 43.50, 43.62 (each d, 2- and 3-C), 48.32 (d, 4a-C), 51.61, 51.84 (each q, COOMe), 118.60, 122.17, 124.17, 126.52 (each d), 131.39, 139.43, 146.19 (each s), 172.43, and 173.43 (each s, COOMe); MS *m/z* (rel. intensity, %) 300 (M^+, 21), 240 (88), 182 (22), 181 (base peak), 166 (20), 165 (32), and 141 (26). Found: C, 72.07; H, 6.72%. Calcd for $C_{18}H_{26}O_4$: C, 71.98; H, 6.71%.

8c: Colorless needles (dichloromethane-hexane); mp 182—183 °C; IR (KBr) 1725 cm^{-1}; ^{1}H-NMR ($CDCl_3$) δ=1.40 (1H, dt, J=13.0, 13.0, and 12.0 Hz, one of 4-H), 1.97 (3H, t, J=1.6 Hz, 9-Me), 2.46 (1H, br dd, J=14.0 and 5.8 Hz, one of 1-H), 2.3—3.6 (5H, m, CH_2 and CH), 3.30 (1H, dd, J=14.0 and 2.3 Hz, the other of 1-H), 3.52, 3.67 (each 3H, s, COOMe), 3.77 (3H, s, OMe), 6.74 (1H, dd, J=8.2 and 2.5 Hz, 7-H), 6.95 (1H, d, J=2.5 Hz, 5-H), and 7.07 (1H, d, J=8.2 Hz, 8-H); ^{13}C-NMR ($CDCl_3$) δ=9.70 (q, 9-Me), 27.78, 29.68 (each t, 1- and 4-C), 43.52 (2×C, d, 2- and 3-C), 48.15 (d, 4a-C), 51.51, 51.75 (each q, COOMe), 55.46 (q, OMe), 109.16, 111.64, 118.75 (each d), 130.79, 137.42, 139.17, 147.84, 157.54 (each s), 172.41, and 173.33 (each s, COOMe); MS *m/z* (rel. intensity, %) 330 (M^+, 55), 271 (27), 270 (78), 212 (31), 211 (base peak), 197 (22), 195 (20), 172 (24), 165 (29), 129 (26), and 128 (21). Found: C, 69.21; H, 6.73%. Calcd for $C_{19}H_{22}O_5$: C, 69.07; H, 6.71%.

9a: Colorless prisms (diethyl ether-hexane); mp 134—136 °C; IR (KBr) 1720 cm^{-1}; ^{1}H-NMR ($CDCl_3$) δ=1.32 (1H, dt, J=13.0, 13.0, and 4.7 Hz, one of 4-H), 2.25 (1H, ddd, J=11.7,

5.8, 4.2 Hz, 2-H), 2.94 (1H, dd, J=13.0 and 11.7 Hz, one of 1-H), 3.13 (1H, ddd, J=13.0, 5.8, and 2.8 Hz, the other of 4-H), 3.02 (1H, dd, J=13.0 and 5.8 Hz, the other of 1-H), 3.32 (1H, dd, J=13.0 and 5.8 Hz, 4a-H), 3.47 (1H, ddd, J=4.7, 4.2, and 2.8 Hz, 3-H), 3.67, 3.78 (each 3H, s, COOMe), and 7.0—7.6 (9H, m, Ar); MS m/z (rel. intensity, %) 362 (M^+, 76), 331 (29), 330 (66), 303 (26), 302 (89), 243 (56), 242 (84), 241 (32), 217 (63), 215 (24), 203 (32), 202 (31), and 165 (base peak). Found: C, 75.98; H, 6.16%. Calcd for $C_{23}H_{22}O_4$: C, 76.22; H, 6.12%.

9b: Colorless solid; mp 120—122 °C; IR (KBr) 1720 cm^{-1}; ^{1}H-NMR ($CDCl_3$) δ=1.13 (1H, dt, J=12.7, 12.7, and 4.5 Hz, one of 4-H), 2.03 (3H, t, J=1.6 Hz, 9-Me), 2.40 (1H, ddd, J=12.0, 5.0, and 4.0 Hz, 2-H), 2.6—3.3 (4H, m, CH_2 and CH), 3.40 (1H, m, 4a-H), 3.72, 3.76 (each 3H, s, COOMe), and 6.9—7.4 (4H, m, Ar); ^{13}C-NMR ($CDCl_3$) δ=9.89 (q, 9-Me), 24.71 (t, 4-C), 32.70 (t, 1-C), 41.81, 44.83, 45.42 (each d, CH), 51.90 (2×C, q, COOMe), 118.56, 122.22, 124.02, 126.65 (each d), 130.21, 142.04, 145.94, 146.39 (each s), 173.33, and 173.48 (each s, COOMe); MS m/z (rel. intensity, %) 300 (M^+, 13), 240 (37), 182 (26), 181 (base peak), 180 (57), 179 (25), 178 (23), 167 (36), 166 (45), 165 (85), 155 (31), 153 (27), 142 (28), 141 (46), and 115 (30). Found: C, 72.16; H, 6.80%. Calcd for $C_{18}H_{20}O_4$: C, 71.98; H, 6.71%.

9c: This product was not separated in pure form from the mixture with **8c**. ^{1}H-NMR ($CDCl_3$, only major signals are given): δ=1.15 (1H, dt, J=12.7, 12.7, and 4.7 Hz, one of 4-H), 2.00 (3H, t, J=1.7 Hz, 9-Me), 2.40 (1H, ddd, J=12.0, 4.9, and 4.2 Hz, one of 2-H), 3.71, 3.74, 3.78 (each 3H, s, COOMe and OMe), 6.77 (1H, dd, J=8.2 and 2.5 Hz, 7-H), 6.93 (1H, d, J=2.5 Hz, 5-H), and 7.09 (1H, d, J=8.2 Hz, 8-H); ^{13}C-NMR ($CDCl_3$) δ=9.94 (q, 9-Me), 24.71 (t, 4-C), 32.84 (t, 1-C), 41.86, 44.93, 45.32 (each d, CH), 51.90 (2×C, q, COOMe), 55.55 (q, OMe), 109.35, 111.73, 118.75, 125.67, 129.867 (each d), 139.51, 139.81, 147.65, 157.50 (each s), 173.38, and 173.57 (each s, COOMe); MS m/z 330 (M^+). Found: C, 68.95; H, 6.82%. Calcd for $C_{19}H_{22}O_5$: C, 69.07; H, 6.71%.

10a—c: These products were not fully characterized because of too poor yields and unsuccessful separation from the major products. Their formation was deduced only on the basis of ^{1}H-NMR ($CDCl_3$) of crude reaction mixtures and the yields were determined by GLC analysis. **10a**: δ=5.90 (dd, J=10 and 5 Hz, 2-H) and 6.34 (dd, J=10 and 3 Hz, 1-H); **10b**: δ= 2.08 (s, Me), 5.55 (dd, J=10 and 5 Hz, 2-H), and 6.16 (br d, J=10 Hz, 1-H); **10c**: δ=2.06 (s, Me), 5.60 (dd, J=10 and 5 Hz, 2-H), and 6.18 (br d, J=10 Hz, 1-H).

11: Colorless viscous oil; IR (neat) 1730 cm^{-1} ; ^{1}H-NMR ($CDCl_3$) δ=2.2—3.2 (6H, m, CH_2 and CH), 3.67, 3.68 (each 3H, s, COOMe), 5.04, 5.22 (each 1H, s, $=CH_2$), 5.59 (1H, m, 2-H), and 7.23 (5H, br s, Ph); ^{13}C-NMR ($CDCl_3$) δ=26.37, 27.20 (each t, 3- and 6-C), 39.45, 40.23 (each d, 4- and 5-C), 51.90 (2×C, q, COOMe), 112.40 (t, $=CH_2$), 126.22, 127.39, 128.12, 128.71 (each d), 135.84, 141.55, 150.78 (each s), and 173.73 (2×C, s, COOMe); MS m/z (rel. intensity, %) 300 (M^+, 51), 269 (24), 240 (base peak), 181 (93), 180 (50), 103 (93), and 42 (20). Found: C, 71.97; H, 6.74%. Calcd for $C_{18}H_{20}O_4$: C, 71.98; H, 6.71%.

12: Colorless viscous oil; IR (neat) 1725 cm^{-1}; ^{1}H-NMR ($CDCl_3$) δ=2.3—3.2 (6H, m, CH_2 and CH), 3.67, 3.69 (each 3H, s, COOMe), 3.73 (3H, s, OMe), 5.00, 5.14 (each 1H, d, J=1.1 Hz, $=CH_2$), 5.62 (1H, m, 2-H), 6.81, and 7.13 (each br d, Ar); ^{13}C-NMR ($CDCl_3$) δ=26.30, 27.36 (each t, 3- and 6-C), 39.45, 40.22 (each d, 4- and 5-C), 51.84 (2×C, q, COOMe), 55.19 (q, OMe), 113.37 (t, $=CH_2$), 113.31, 125.70, 129.52 (each d), 133.63, 135.91, 150.00, 158.92 (each s), and 173.48 (2×C, s, COOMe); MS m/z (rel. intensity, %) 330 (M^+, 23), 270 (29), 211 (46), 210 (22), 133 (45), and 59 (base peak). Found: C, 68.81; H, 6.67%. Calcd for $C_{19}H_{22}O_5$: C, 69.07; H, 6.71%.

13a: Colorless prisms (diethyl ether–hexane); mp 112—113 °C; IR (KBr) 1725 cm^{-1}; ^{1}H-NMR ($CDCl_3$) δ=1.20 (1H, q, J=12.5 Hz, one of 4-H), 2.48 (1H, t, J=12.3 Hz, one of 1-H), 2.72 (1H, ddd, J=12.3, 9.3, and 3.2 Hz, 2-H), 2.82 (1H, ddd, J=12.5, 5.8, and 2.8 Hz, the other of 4-H), 2.95 (1H, ddd, J=12.5, 9.3, and 2.8 Hz, 3-H), 3.19 (1H, dd, J= 12.3 and 3.2 Hz, the other of 1-H), 3.31 (1H, dd, J=12.5 and 5.8 Hz, 4a-H), 3.64, 3.66 (each 3H, s, COOMe), and 7.0—7.6 (9H, m, Ar); ^{13}C-NMR ($CDCl_3$) δ=28.75 (t, 4-C), 33.62 (t, 1-C), 44.88, 46.34, 48.39 (each d, CH), 51.90 (2×C, q, COOMe), 119.97, 122.61, 124.65, 126.84, 127.43, 128.55, 128.94 (each d), 134.01, 136.88, 142.43, 144.63, 145.512 (each s), 174.26, and 174.40 (each s, COOMe); MS m/z (rel. intensity, %) 362 (M^+, 15), 302 (20), 243 (46), 242 (42), 241 (25), 215 (36), 204 (22), 203 (47), 202 (47), 166 (22), and 165 (base peak). Found: C, 76.35; H, 6.14%. Calcd for $C_{23}H_{22}O_4$: C, 76.22; H, 6.12%.

13b: Colorless prisms (diethyl ether–hexane); mp 107—108 °C; IR (KBr) 1720 cm^{-1}; ^{1}H-NMR ($CDCl_3$) δ=1.00 (1H, q, J=12.5 Hz, one of 4-H), 2.03 (3H, t, J=1.5 Hz, 9-Me), 2.33 (1H, br t, J=12.5 Hz, one of 1-H), 2.4—3.3 (5H, m, CH_2 and CH), 3.66, 3.71 (each 3H, s, COOMe), and 7.0—7.4 (4H, m, Ar); ^{13}C-NMR ($CDCl_3$) δ=9.65 (q, 9-Me), 28.06 (t, 4-C), 33.36 (t, 1-C), 44.77, 46.00, 47.77 (each d, CH), 51.77 (2×C, q, COOMe), 118.65, 122.18, 124.30, 126.77 (each d), 130.77, 140.25, 145.36, 146.07 (each s), 174.54, and 174.77 (each s, COOMe); MS m/z (rel. intensity, %) 300 (M^+, 13), 240 (34), 182 (20), 181 (63), 180 (37), 167 (28), 166 (30), 165 (47), 142 (24), 141 (48), 115 (26), and 59 (base peak). Found: C, 72.13; H, 6.75%. Calcd for $C_{18}H_{20}O_4$: C, 71.98; H, 6.71%.

13c: Colorless prisms (diethyl ether–hexane); mp 112—114 °C; IR (KBr) 1725 cm^{-1}; ^{1}H-NMR ($CDCl_3$) δ=1.02 (1H, q, J=12.5 Hz, one of 4-H), 2.00 (3H, q, J=1.6 Hz, 9-Me), 2.30 (1H, br t, J=12.5 Hz, one of 1-H), 2.4—3.2 (5H, m, CH_2 and CH), 3.66, 3.70 (each 3H, s, COOMe), 3.77 (3H, s, COOMe), 6.77 (1H, dd, J=8.3 and 2.4 Hz, 7-H), 6.91 (1H, d, J=2.4 Hz, 5-H), and 7.21 (1H, d, J=8.3 Hz, 8-H); ^{13}C-NMR ($CDCl_3$) δ=10.00 (q, 9-Me), 28.35 (t, 4-C), 33.77, (t, 1-C), 45.06, 46.36, 47.94 (each d CH), 52.00 (2×C, q, COOMe), 55.59 (q, OMe), 109.60, 112.01, 119.19 (each d), 130.60, 138.30, 139.42, 147.36, 158.01 (each s), 174.89, and 175.07 (each s, COOMe); MS m/z (rel. intensity, %) 330 (M^+, 73), 271 (28), 270 (87), 212 (31), 211 (base peak), 210 (26), 195 (28), 185 (31), 172 (27), 165 (23), 129 (31), and 128 (24). Found: C, 69.04; H, 6.73%. Calcd for $C_{19}H_{22}O_5$: C, 69.07; H, 6.71%.

14a: Colorless prisms (diethyl ether–hexane); mp 130—132 °C; IR (KBr) 1725 cm^{-1}; ^{1}H-NMR ($CDCl_3$) δ=1.44 (1H, dt, J=13.0, 13.0, and 4.4 Hz, one of 4-H), 2.71 (1H, dd, J= 14.8 and 5.8 Hz, one of 1-H), 2.9—3.5 (5H, m, CH_2 and CH), 3.39, 3.79 (each 3H, s, COOMe), and 7.0—7.6 (9H, m, Ar); ^{13}C-NMR ($CDCl_3$) δ=25.14 (t, 4-C), 29.92 (t, 1-C), 40.93, 42.69 (each d, 2- and 3-C), 45.95 (d, 4a-C), 51.56, 52.04 (each q, COOMe), 119.78, 122.46, 124.17, 126.45, 127.00, 128.16, 128.74 (each d), 134.54, 136.88, 142.53, 144.92, 146.63 (each s), 172.90, and 173.72 (each s, COOMe); MS m/z (rel. intensity, %) 362 (M^+, 53), 302 (66), 243 (49), 242 (63), 241 (24), 215 (26), 203 (27), 202 (31), and 165 (base peak). Found:

C, 76.22; H, 6.12%. Calcd for $C_{23}H_{22}O_4$: C, 76.22; H, 6.12%.

14b: Colorless viscous oil; IR (neat) 1730 cm^{-1}; ^{1}H-NMR ($CDCl_3$) δ=1.19 (1H, dt, J=13.0, 13.0, and 4.7 Hz, one of 4-H), 2.03 (3H, t, J=1.6 Hz, 9-Me), 2.4—3.6 (5H, m, CH_2 and CH), 2.56 (1H, br dd, J=14.0 and 5.8 Hz, one of 1-H), 3.55, 3.77 (each 3H, s, COOMe), and 7.0—7.4 (4H, m, Ar); ^{13}C-NMR ($CDCl_3$) δ=9.59 (q, 9-Me), 24.65 (t, 4-C), 30.18, (t, 1-C), 41.12, 42.83 (each d, 2- and 3-C), 45.53 (d, 4a-C), 51.83, 52.12 (each q, COOMe), 118.65, 122.30, 124.01, 126.54 (each d), 130.89, 140.60, 146.48, 146.83 (each s), 173.25, and 174.13 (each s, COOMe); MS m/z (rel. intensity, %) 300 (M^+, 34), 240 (55), 182 (22), 181 (base peak), 180 (49), 167 (24), 166 (37), 165 (65), 142 (22), 141 (36), 115 (22), and 59 (35). Found: C, 72.16; H, 6.83%. Calcd for $C_{18}H_{20}O_4$: C, 71.98; H, 6.71%.

14c: Colorless prisms (diethyl ether–hexane); mp 107—108 °C; IR (KBr) 1720 cm^{-1}; ^{1}H-NMR ($CDCl_3$) δ=1.21 (1H, dt, J=13.0, 13.0, and 4.7 Hz, one of 4-H), 2.00 (3H, t, J=1.6 Hz, 9-Me), 2.34 (1H, br dd, J=14.5 and 5.4 Hz, one of 1-H), 2.4—3.5 (5H, m, CH_2 and CH), 3.57, 3.77, 3.79 (each 3H, s, COOMe and OMe), 6.79 (1H, dd, J=8.2 and 2.4 Hz, 7-H), 6.95 (1H, d, J=2.4 Hz, 5-H), and 7.09 (1H, d, J=8.2 Hz, 8-H); ^{13}C-NMR ($CDCl_3$) δ=9.80 (q, 9-Me), 24.83 (t, 4-C), 30.47 (t, 1-C), 41.27, 43.03, 45.62 (each d, CH), 51.90, 52.19 (each q, COOMe), 55.60 (q, OMe), 109.38, 111.67, 118.83 (each d), 130.28, 138.26, 139.50, 148.48, 157.51 (each s), 173.19, and 173.95 (each s COOMe); MS m/z (rel. intensity, %) 330 (M^+, base peak), 271 (29), 270 (96), 211 (76), 210 (22), 195 (21), and 185 (32). Found: C, 69.30; H, 6.74%. Calcd for $C_{19}H_{22}O_5$: C, 69.07; H, 6.71%.

15a: Colorless prisms (diethyl ether–hexane); mp 120—121 °C; IR (KBr) 1725 cm^{-1}; ^{1}H-NMR ($CDCl_3$) δ=2.50 (1H, dd, J=14.5 and 11.0 Hz, one of 5-H), 2.85 (1H, dd, J=14.5 and 4.0 Hz, the other of 5-H), 3.08 (1H, ddd, J=11.0, 9.0, and 4.0 Hz, 4-H), 3.61, 3.69 (each 3H, s, COOMe), 3.6—3.8 (1H, m, 3-H), 5.79 (1H, dd, J=10.1 and 3.1 Hz, 2-H), 6.33 (1H, dd, J=10.1 and 2.9 Hz, 1-H), and 7.0—7.5 (9H, m, Ar); ^{13}C-NMR ($CDCl_3$) δ=30.53 (t, 5-C), 42.24, 44.65 (each d, 3- and 4-C), 52.06, 52.30 (each q, COOMe), 124.89, 127.30, 128.01, 128.18, 129.24, 129.54, 130.25, 130.95 (each d), 140.83, 141.54, 141.66 (each s), 173.12, and 174.77 (each s, COOMe); MS m/z (rel. intensity, %) 362 (M^+, 5), 243 (base peak), 165 (72), and 59 (31). Found: C, 76.36; H, 6.15%. Calcd for $C_{23}H_{22}O_4$: C, 76.22; H, 6.12%.

16: Colorless viscous oil; IR (neat) 1730 cm^{-1}; ^{1}H-NMR ($CDCl_3$) δ=2.0—3.3 (6H, m, CH_2 and CH), 3.66, 3.67 (each 3H, s, COOMe), 5.05, 5.19 (each 1H, br s, $=CH_2$), 5.60 (1H, m, 2-H), and 7.24 (5H, br s, Ph); ^{13}C-NMR ($CDCl_3$) δ=28.36, 29.06 (each t, 3- and 6-C), 40.86, 41.57 (each d, 4- and 5-C), 51.72 (2×C, q, COOMe), 112.25 (t, $=CH_2$), 125.64, 127.11, 127.81, 128.28 (each d), 135.33, 140.91, 149.83 (each s), and 174.84 (2×C, s, COOMe); MS m/z (rel. intensity, %) 300 (M^+, 19), 269 (20), 268 (27), 240 (65), 182 (23), 181 (base peak), 180 (53), 165 (26), 103 (84), and 77 (26). Found: C, 72.07; H, 6.78%. Calcd for $C_{18}H_{20}O_4$: C, 71.98; H, 6.71%.

17: Colorless viscous oil; IR (neat) 1730 cm^{-1}; ^{1}H-NMR ($CDCl_3$) δ=2.1—3.1 (6H, m, CH_2 and CH), 3.67, 3.68 (each 3H, s, COOMe), 3.77 (3H, s, OMe), 5.01, 5.11 (each 1H, s, $=CH_2$), 5.62 (1H, m, 2-H), 6.82, and 7.14 (each 2H, br d, Ar); ^{13}C-NMR ($CDCl_3$) δ=28.35, 29.30 (each t, 3- and 6-C), 40.89, 41.65 (each d, 4- and 5-C), 51.83 (2×C, q, COOMe), 55.12 (q, OMe), 111.66 (t, $=CH_2$), 113.42, 125.48, 129.54 (each d), 133.42, 135.89, 149.60, 159.01 (each s), and 175.19 (2×C, s, COOMe); MS m/z (rel. intensity, %) 330 (M^+, 25), 270 (63), 212 (23), 211 (base peak), 210 (49), 195 (20), 165 (26), 133 (91), 115 (20), 103 (36), and 77 (29). Found: C, 68.54; H, 6.75%. Calcd for $C_{19}H_{22}O_5$: C, 69.07; H, 6.71%.

18a: Colorless prisms (diethyl ether–hexane); mp 202—204 °C; IR (KBr) 1770 and 1680 cm^{-1}; ^{1}H-NMR ($CDCl_3$) δ=1.33 (1H, dt, J=14.6, 14.6, and 6.7 Hz, one of 4-H), 2.62 (1H, dd, J=14.8 and 6.5 Hz, one of 10-H), 2.8—3.4 (4H, m, CH_2 and CH), 3.04 (3H, s, NMe), 3.29 (1H, dd, J=14.8 and 7.5 Hz, the other of 10-H), and 7.6—7.0 (9H, m, Ar); ^{13}C-NMR ($CDCl_3$) δ=24.95 (q, NMe), 25.83 (t, 4-C), 27.78 (t, 10-C), 40.28, 40.48 (each d, 3a- and 10a-C), 45.56 (d, 4a-C), 120.31, 123.19, 124.90, 127.15, 127.73, 128.80, 128.91 (each d), 134.23, 137.25, 141.55, 144.87, 146.43 (each s), 179.05, and 179.73 (each s, CON); MS m/z (rel. intensity, %) 329 (M^+, base peak), 218 (37), 217 (54), 202 (23), and 165 (25). Found: C, 80.28; H, 5.83; N, 4.46%. Calcd for $C_{22}H_{19}NO_2$: C, 80.22; H, 5.81; N, 4.25%.

18b: Colorless needles (diethyl ether–hexane); mp 64—67 °C; IR (KBr) 1765 and 1685 cm^{-1}; ^{1}H-NMR ($CDCl_3$) δ=0.73 (1H, dt, J=12.8, 12.8, and 11.2 Hz, one of 4-H), 2.04 (3H, t, J=1.7 Hz, 9-Me), 2.3—3.3 (5H, m, CH_2 and CH), 2.81 (3H, s, NMe), 3.46 (1H, br d, J=15.2 Hz, one of 10-H), and 7.0—7.4 (4H, m, Ar); ^{13}C-NMR ($CDCl_3$) δ=9.99 (q, 9-Me), 21.00 (t, 4-C), 24.56 (q, NMe), 32.75 (t, 10-C), 40.64, 41.27 (each d, 3a- and 10a-C), 46.05 (d, 4a-C), 118.75, 122.36, 124.36, 126.89 (each d), 131.77, 138.98, 145.70, 146.0 (each s), 178.25, and 179.03 (each s, CON); MS m/z (rel. intensity, %) 267 (M^+, base peak), 181 (32), 167 (50), 166 (39), 165 (71), 156 (78), 155 (81), 153 (21), 152 (40), 141 (68), 115 (45), and 58 (23). HRMS Found: m/z 267.1256. Calcd for $C_{18}H_{19}NO_3$: M, 267.1257.

18c: Colorless prisms (diethyl ether–hexane); mp 143—145 °C; IR (KBr) 1770 and 1700 cm^{-1}; ^{1}H-NMR ($CDCl_3$) δ=0.80 (1H, dt, J=12.7, 12.7, and 11.2 Hz, one of 4-H), 2.04 (3H, t, J=1.7 Hz, 9-Me), 2.4—3.3 (5H, m, CH_2 and CH), 2.90 (3H, s, NMe), 3.48 (1H, br d, J=15.6 Hz, one of 10-H), 3.79 (3H, s, OMe), 6.80 (1H, dd, J=8.2 and 2.3 Hz, 7-H), 6.93 (1H, d, J=2.3 Hz, 5-H), and 7.13 (1H, d, J=8.2 Hz, 8-H); MS m/z (rel. intensity, %) 297 (M^+, 98), 186 (27), and 185 (base peak). Found: C, 73.19; H, 6.48; N, 4.91%. Calcd for $C_{18}H_{19}NO_3$: C, 72.70; H, 6.44; N, 4.71%.

19a: Colorless plates (diethyl ether–hexane); mp 180—181 °C; IR (KBr) 1760 and 1675 cm^{-1}; ^{1}H-NMR ($CDCl_3$) δ=0.92 (1H, dt, J=12.6, 12.6, and 11.2 Hz, one of 4-H), 2.65 (1H, dd, J=15.5 and 8.2 Hz, one of 10-H), 2.5—3.4 (5H, m, CH_2 and CH), 2.83 (3H, s, NMe), 3.60 (1H, d, J=15.5 Hz, the other of 10-H), and 7.0—7.6 (9H, m, Ar); ^{13}C-NMR ($CDCl_3$) δ=21.48 (t, 4-C), 24.61 (q, NMe), 32.86 (t, 10-C), 40.72, 41.55 (each d, 3a- and 10a-C), 46.63 (d, 4a-C), 120.31, 122.95, 124.90, 127.20, 127.64, 128.76, 129.00 (each d), 134.08, 137.64, 141.16, 145.02, 145.90 (each s), 178.17, and 179.05 (each s, CON); MS m/z (rel. intensity, %) 329 (M^+, 44), 243 (21), 217 (32), 215 (29), 202 (30), 167 (29), 166 (42), and 165 (base peak). Found: C, 80.26; H, 5.86; N, 4.43%. Calcd for $C_{22}H_{19}NO_2$: C, 80.22; H, 5.81; N, 4.25%.

19b: Colorless prisms (diethyl ether–hexane); mp 92—94 °C; IR (KBr) 1770 and 1685 cm^{-1}; ^{1}H-NMR ($CDCl_3$) δ=1.22 (1H, dt, J=15.0, 15.0, and 6.8 Hz, one of 4-H), 2.03 (3H, t, J=1.8 Hz, 9-Me), 2.67 (1H, br d, J=12.9 Hz, one of 10-H), 2.7—3.4 (5H, m, CH_2 and CH), 3.05 (3H, s, NMe), and 7.0—7.6 (5H, m, Ph); ^{13}C-NMR ($CDCl_3$) δ=10.09 (q, 9-Me), 24.95 (q, NMe), 24.95 (t, 4-C), 27.68 (t, 10-C), 40.10, 40.54 (each d, 3a-

and 10a-C), 44.98 (d, 4a-C), 118.71, 122.56, 124.36, 126.89 (each d), 131.37, 138.98, 145.94, 146.09 (each s), 179.03, and 179.77 (each s, CON); MS *m/z* (rel. intensity, %) 267 (M^+, base peak), 181 (22), 167 (62), 166 (22), 165 (48), 156 (76), 155 (80), 153 (20), 141 (37), 116 (20), and 113 (27). Found: C, 76.19; H, 6.42; N, 5.27%. Calcd for $C_{17}H_{17}NO_2$: C, 76.38; H, 6.41; N, 5.24%.

19c: Colorless needles (diethyl ether–hexane); mp 149—151 °C; IR (KBr) 1765 and 1685 cm^{-1}; ^{1}H-NMR ($CDCl_3$) δ=1.22 (1H, ddd, J=16.0, 14.0, and 6.5 Hz, one of 4-H), 1.3—3.4 (6H, m, CH_2 and CH), 2.00 (3H, t, J=1.6 Hz, 9-Me), 3.05 (3H, s, NMe), 3.79 (3H, s, OMe), 6.79 (1H, dd, J=8.2 and 2.3 Hz, 7-H), 6.92 (1H, d, J=2.3 Hz, 5-H), and 7.10 (1H, d, J=8.2 Hz, 8-H); ^{13}C-NMR ($CDCl_3$) δ=10.14 (q, 9-Me), 24.99 (q, NMe), 24.99 (t, 4-C), 27.78 (10-C), 40.20, 40.59 (each d, 3a- and 10a-C), 44.88 (d, 4a-C), 55.50 (q, OMe), 109.40, 112.13, 119.00 (each d), 130.84, 136.59, 139.12, 147.70, 157.64 (each s), 179.03, and 179.77 (each s, CON). Found: C, 72.97; H, 6.47; N, 4.92%. Calcd for $C_{18}H_{19}NO_3$: C, 72.70; H, 6.44; N, 4.71%.

20: Colorless viscous oil; IR (neat) 1775 and 1700 cm^{-1}; ^{1}H-NMR ($CDCl_3$) δ=2.0—3.3 (6H, m, CH_2 and CH), 2.94 (3H, s, NMe), 5.08, 5.26 (each 1H, s, $=CH_2$), 5.70 (1H, m, 6-H), and 7.0—7.4 (5H, m, Ph); ^{13}C-NMR ($CDCl_3$) δ=24.61 (t, 4- or 7-C), 24.90 (q, NMe), 25.63 (t, 4- or 7-C), 38.94, 39.76 (each d, 3a- and 7a-C), 113.15 (t, $=CH_2$), 126.36, 127.43, 127.96, 128.35 (each d), 139.51, 140.59 (each s), 179.47, and 179.86 (each s, CON); MS *m/z* (rel. intensity, %) 267 (M^+, base peak), 181 (28), 167 (40), 165 (33), 156 (73), 155 (62), 141 (34), 128 (21), 115 (26), 112 (27), 103 (59), 78 (25), and 77 (67). Found: C, 76.28; H, 6.62; N, 5.20%. Calcd for $C_{17}H_{17}NO_2$: C, 76.38; H, 6.41; N, 5.24%.

21: Colorless needles (diethyl ether–hexane); mp 102—103 °C; IR (KBr) 1765 and 1690 cm^{-1}; ^{1}H-NMR ($CDCl_3$) δ=2.1—3.2 (6H, m, CH_2 and CH), 2.96 (3H, s, NMe), 3.77 (3H, s, OMe), 5.05, 5.17 (each s, $=CH_2$), 5.74 (1H, m, 6-H), 6.89, and 7.06 (each 2H, br d, Ar); ^{13}C-NMR ($CDCl_3$) δ= 24.51 (t, 4- or 7-C), 24.80 (q, NMe), 25.78 (t, 4- or 7-C), 38.84, 39.67 (each d, 3a- and 7a-C), 55.07 (q, OMe), 112.13 (t, $=CH_2$), 113.25, 125.92, 129.28 (each d), 132.84, 139.70, 148.62, 158.91 (each s), 179.38, and 179.77 (each s, CON); MS *m/z* (rel. intensity, %) 297 (M^+, base peak), 186 (21), 185 (50), and 133 (22). Found: C, 72.85; H, 6.55; N, 4.88%. Calcd for $C_{18}H_{19}NO_3$: C, 72.70; H, 6.44; N, 4.71%.

References

1) B. M. Trost and M. Shimizu, *J. Am. Chem. Soc.*, **104**, 4299 (1982); T. Minami, Y. Taniguchi, and I. Hirao, *J. Chem. Soc., Chem. Commun.*, **1984**, 1046.

2) O. Tsuge, E. Wada, S. Kanemasa, and H. Sakoh, *Bull. Chem. Soc. Jpn.*, **57**, 3221 (1984); O. Tsuge, S. Kanemasa, H. Sakoh, and E. Wada, *ibid.*, **57**, 3234 (1984); S. Kanemasa, H. Sakoh, E. Wada, and O. Tsuge, *ibid.*, **58**, 3312 (1985); S. Kanemasa, H. Sakoh, E. Wada, and O. Tsuge, *ibid.*, **59**, 1869 (1986).

3) Recent reviews on Diels–Alder reactions: W. Oppolzer, *Angew. Chem. Int. Ed. Engl.*, **16**, 10 (1977); W. Oppolzer, *Synthesis*, **1978**, 793; G. Brieger and J. N. Bennett, *Chem. Rev.*, **80**, 63 (1980); T. Wagner-Jauregg, *Synthesis*, **1980**, 165; J. Sauer and R. Sustmann, *Angew. Chem. Int. Ed. Engl.*, **19**, 779 (1980); S. Danishefsky, *Acc. Chem. Res.*, **14**, 400 (1981); M. Petrzilka and J. I. Grayson, *Synthesis*, **1981**, 753; D. L. Boger, *Tetrahedron*, **39**, 2869 (1983).

4) Although some electrocyclic reactions on 1-aryl-2-propen-1-ols and diarylmethanols are known (Ref. 6), there have been reported only a few extensions to the functionalized systems (S. K. Dasgupta, R. Dasgupta, S. R. Ghosh, and U. R. Ghatak, *J. Chem. Soc., Chem. Commun.*, **1969**, 498; F. A. Neugebauer and W. R. Groh, *Chem. Ber.*, **107**, 1903 (1974)).

5) E. Wada, S. Kanemasa, I. Fujiwara, and O. Tsuge, *Bull. Chem. Soc. Jpn.*, **58**, 1942 (1985).

6) C. U. Pittman, Jr., and W. G. Miller, *J. Am. Chem. Soc.*, **95**, 2947 (1973); W. G. Miller and C. U. Pittman, Jr., *J. Org. Chem.*, **39**, 1955 (1974); L. M. Tolbert, *ibid.*, **44**, 4584 (1979).

7) The axial hydrogen at the 4-position of **8a** is antiparallel to both 3-H and 4a-H so that it couples with them with large coupling constants of 13.1 Hz, while the corresponding hydrogen of **9a** which is cis and trans to 3-H and 4a-H, respectively, couples with them with coupling constants of 4.7 and 13.0 Hz.

8) O. Makabe, Y. Murai, and S. Fukatsu, *Heterocycles*, **13**, 239 (1979); H. Narkgraf, E. W. Greeno, M. D. Miller, and W. J. Zaks, *Tetrahedron Lett.*, **24**, 241 (1983); O. Tsuge, E. Wada, S. Kanemasa, and H. Sakoh, *Chem. Lett.*, **1984**, 469 and 709.

9) Protonation of **11** or **12** leads to the cationic intermediate which is the same to that involved in the electrocyclization of **5** forming **8** and **9**.

10) Both clockwise rotation of **A** and counterclockwise rotation of **B** lead to boat conformations, therefore these rotations were excluded.

11) It is known that, in 4,5-disubstituted cyclohexene series, 4,5-diequatorial conformer is always more stable than 4,5-diaxial isomer (N. S. Zefirov, V. N. Chekulaeva, and A. I. Belozerov, *Tetrahedron*, **25**, 1997 (1969)). However, the conformer **B** with two axial ester groups is expected to be more stable than the conformer **A** with two equatorial esters because only the axial esters can interact with the cationic centers stabilizing these centers. As a similar interaction, see G. P. Kugatova-Shemyakina and G. M. Nikolaev, *Tetrahedron*, **23**, 2987 (1967).

12) The envelope conformation can be replaced by another name, twisted half-chair conformation.

13) As the six-membered ring of **H** takes twisted half-chair conformation, the 1,3-steric repulsion between 3a-carbonyl and 4a-H is insignificant. Accordingly, the energy difference between **G** and **H** should be smaller that between **C** and **D** (X=H, Y=COOMe).

 © 1986 The Chemical Society of Japan Bull. Chem. Soc. Jpn., 59, 2459—2462 (1986)

Novel Regioselective Iodination of Estradiol 17β-Acetate[1)]

C. Akira Horiuchi,* Akinori Haga, and J. Yasuo Satoh
Department of Chemistry, Rikkyo (St. Paul's) University, Nishi-Ikebukuro, Toshima-ku, Tokyo 171
(Received March 1, 1986)

Direct iodination of estradiol 17β-acetate (**3**) using iodine–copper(II) acetate in acetic acid afforded the 2-iodo derivative regioselectively in high yield. The iodination of **3** using several methods was discussed. On the other hand, the reaction of **3** with iodine–copper(II) bromide gave the 4-bromo derivative (**7**), not the 2-iodo compound. The reaction of 3-methoxy-17β-acetoxy-1,3,5(10)-estratriene (**4**) with iodine–copper(II) chloride–iron(III) chloride in acetic acid gave the 2- (**10**) and 4-iodo (**11**) derivative.

2-Iodoestradiols are important as synthethic intermediates and as possessors of biological activity, and also in making highly radioactive iodine isotopes. They are usually prepared either from diazotization of the corresponding 2- or 4-amino-3-methoxyestrone derivative, reduction with sodium borohydride, and then demethylation using boron tribromide,[2)] or from the reaction of estradiol (**1**) with mercury(II) acetate and iodine.[3)] However, recently the synthesis of 2-iodoestradiol (**5**) by the reaction of **1** with mercury(II) acetate and iodine in acetic acid has been questioned.[3)] More recently, Santaniello and Ferrabschi[4)] reported that the reaction of 3-methoxy-17β-acetoxy-1,3,5(10)-estratriene with mercury(II) acetate in dry acetonitrile gave the 2-iodo derivative. However, since these methods involve many steps and the demethylation results in low yield, we wished to find a method for the direct regioselective iodination of estradiol (**1**).

We have been investigating a novel iodination using iodine–copper(II) acetate, and as a first step in this research project, we reported earlier the α-iodination of ketone,[5)] the iodination of electron-rich aromatic compound,[6)] and synthesis of α-iodo carboxylic acid.[7)] Earlier, we described a novel regioselective iodination of estradiol, estriol, and estrone using iodine–copper(II) acetate to afford the 2-iodo derivative.[8)] In the present paper, we would like to report the details of this iodination. We have been now also investigated the reaction of estradiol (**1**) with iodine and some other copper(II) salts.

The reaction of **1** with iodine (1.5 mol equiv)–copper(II) chloride dihydrate (1.5 mol equiv) in acetic acid at 55°C for 35 h gave the diiodo compound **8** (mp 190—193°C) and the monoiodo compound **6** (mp 175—177°C). Compound **8** showed absorption at 1708 (C=O) and 1264 cm^{-1} (C–O) in its IR spectrum. The NMR spectrum showed a singlet at δ 7.60 (C_1–H) and a singlet at δ 2.06 ($C_{17\beta}$–OAc). Therefore, compound **8** was presumed to be 2,4-diiodoestradiol 17β-acetate. The IR spectrum of **6** showed absorption at 1708 (C=O), 1268 (C–O), and 880 cm^{-1} (–CH). This product **6** was presumed to be 2-iodoestradiol 17β-acetate, identification being based on the presence of two singlets in the NMR spectrum at δ 6.70 (C_4–H) and δ 7.50 (C_1–H), and a singlet at δ 2.06 ($C_{17\beta}$–OAc). In the case of the reaction using iodine (1.5 mol equiv)–copper(II) bromide (1.5 mol equiv), the bromo estrogen derivative **7**, mp 140—142°C was obtained. This product was presumed to be 4-bromoestradiol 17β-acetate, identification being based on the presence of two doublets in the NMR spectrum at δ 6.62 and δ 7.16. These results are summarized in Table 1 for the iodination of **1**.

On the basis of these results, it was found that (i) copper(II) acetate and copper(II) chloride were the best reagents for C_2–iodination, (ii) copper(II) chloride was more active than copper(II) acetate, and (iii) in the case of copper(II) bromide, bromination occurred at the C_4-position, not iodination at the C_2-position. Also, these results showed that copper(II) salts acted as a catalyst of acetylation of 17β-hydroxyl group.

Hence, we attempted acetylation of the hydroxyl group using copper(II) acetate-acetic acid. The reaction of **1** or **2** with copper(II) acetate in acetic acid under refluxing for 2 h gave 17β-acetoxy derivative (**3** or **4**) in good yield. The treatment of **3** with iodine–copper(II) acetate at 60°C for 10 h yielded the 2-iodo derivative **6** (89%). Moreover, the reaction of **3** with iodine–copper(II) chloride, iodine–copper(I) acetate, iodine–copper(I) chloride, iodine–thallium(I) acetate, iodine monochloride, iodine–morpholine complex, or iodine–copper(II) chloride–iron(III) chloride was carried out in a similar manner to the procedure mentioned above, and the results are presented in Table 2.

From these results, it was concluded that iodine–copper(II) acetate and iodine–copper(II) chloride are efficient and regioselective iodinating agents in com-

Table 1. Products and Isolated Yields (%) in the Iodination of Estradiol (**1**) at 60°C

Reagents (molar equiv)	Time/h	Products	Isolated yield/%
I_2–$CuCl_2 \cdot 2H_2O$	35	**6**	50
(1.5) (1.5)		**8**	11
I_2–$CuCl_2 \cdot 2H_2O$	20	**3**	39
(0.5) (1.0)			
I_2–$CuBr_2$	10	**3**	20
(1.5) (1.5)		**7**	45
$CuBr_2$	10	**3**	41
(2.0)		**7**	42
I_2–$Cu(OAc)_2 \cdot H_2O$	22	**5**	64
(1.5) (1.5)			

Table 2. Products and Isolated Yields (%) in the Iodination of Estradiol 17β-Acetate (**3**) at 60°C

Reagents (molar equiv)	Time/h	Products	Isolated yield/%
I_2–$Cu(OAc)_2 \cdot H_2O$ (1.5) (1.5)	10	**6**	89
I_2–$CuCl_2 \cdot 2H_2O$ (1.5) (1.5)	52	**6**	52
		8	6
		9	22
I_2–CuOAc (1.2) (1.2)	27	**6**	36
I_2–CuCl (1.2) (1.2)	65	**6**	25
I_2–TlOAc (1.2) (1.2)	8	**6**	30
$CuBr_2$ (2.0)	6	**7**	62
$CuCl_2 \cdot 2H_2O$ (2.0)	50	[no reaction]	
ICl (1.0)	1	**6**	50
		9	29
I_2–Morpholine/MeOH (1.0)	3	**6**	17
		8	27
		9	21
I_2–$CuCl_2 \cdot 2H_2O$– (1.5) (1.5) $FeCl_3 \cdot 6H_2O$ (1.5)	3	**6**	30
		8	35
		9	14

parison with the other reagents. Moreover, it was found that the iodination of estradiol 17β-acetate (**3**) gave 2-iodoestradiol 17β-acetate (**6**) in good yield (80—90%). This results is also supported by our earlier finding that the iodination using iodine–copper(II) acetate of phenol occurred at the ortho-position.[6]

Thus, it is considered that in the reaction of **3** using iodine–copper(II) acetate, the copper is coordinated to the oxygen of the phenolic hydroxyl group, and then attacks at the less hindered C_2-position than the corresponding C_4-position.

We attempted the iodination of 3-methoxy-17β-acetoxy-1,3,5(10)-estratriene (**4**) with affecting the coordinating ability of the oxygen atom using iodine–copper(II) acetate or iodine–copper(II) chloride in acetic acid. The reaction resulted in the recovery of the starting material. The reaction of **4** with iodine–copper(II) chloride–iron(III) chloride in acetic acid gave the 2- (**10**) (56%) and the 4-iodo derivative (**11**) (18%).

From these results, it is considered that the iodination using iodine–copper(II) chloride–iron(III) chloride of the 3-methoxyestrogen (**4**) proceeds by an initial π-complex of iodine with the aryl ring and the more powerful Lewis acid, iron(III) chloride is no doubt attributable to the roles as a potent catalyst.

Experimental

All the melting points are uncorrected. The IR spectra were measured using a Hitachi Model 215 grating infrared spectrometer. The NMR spectra were measured using either Hitachi Model R-900 or JEOL FX200 Model Spectrometer in deuteriochloroform with TMS as an internal standard.

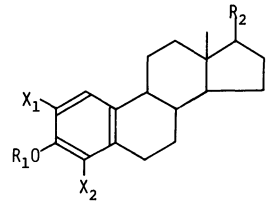

1 : $X_1=X_2=R_1=H$, $R_2=OH$
2 : $X_1=X_2=H$, $R_1=Me$, $R_2=OH$
3 : $X_1=X_2=R_1=H$, $R_2=OAc$
4 : $X_1=X_2=H$, $R_1=Me$, $R_2=OAc$
5 : $X_1=I$, $X_2=R_1=H$, $R_2=OH$
6 : $X_1=I$, $X_2=R_1=H$, $R_2=OAc$
7 : $X_1=R_1=H$, $X_2=Br$, $R_2=OAc$
8 : $X_1=X_2=I$, $R_1=H$, $R_2=OAc$
9 : $X_1=R_1=H$, $X_2=I$, $R_2=OAc$
10 : $X_1=I$, $X_2=H$, $R_1=Me$, $R_2=OAc$
11 : $X_1=H$, $X_2=I$, $R_1=Me$, $R_2=OAc$

The high-resolution mass spectra were recorded at 75 eV on a JEOL JMS-O1SG-2 instrument with a direct inlet.

Estradiol 17β-Acetate (3). A mixture of estradiol (**1**) (3.0 g) and copper(II) acetate monohydrate (0.2 mol equiv) in acetic acid (80 ml) was stirred under refluxing for 4 h. The solvent was then removed under reduced pressure, and the residue was poured into water and extracted with ether. The ethereal solution was washed successively with aqueous sodium hydrogencarbonate and with water, dried, and concentrated. Crystallization of the residue from methanol gave plates of **3** (3.02 g, 87%), mp 216—218°C (lit,[9] 217—218°C). The IR and ^1H NMR spectra were identical with those of an authentic sample.

3-Methoxy-17β-acetoxy-1,3,5(10)-estratriene (4). A mixture of 3-methoxyestradiol (**2**) (1.0 g) and copper(II) acetate mono-

hydrate (0.2 mol equiv) in acetic acid (30 ml) was stirred under refluxing for 12 h. After a similar work-up, the resulting oil, on crystallization from methanol, gave **4** as plates (1.05 g, 92%), mp 102—103 °C (lit,[10] 103.5—104.5 °C). The IR and ^{1}H NMR spectra were identical with those of an authentic sample.

Reaction of Estradiol with Iodine and Copper(II) Chloride in Acetic Acid. Estradiol (**1**) (200 mg) in acetic acid (20 ml) was treated with iodine (280 mg) and copper(II) chloride dihydrate (188 mg) at 60 °C for 35 h. After a similar work-up, the resulting oil (322 mg) was purified by preparative TLC on silica-gel plates (2 mm layer) (Merck). Developement with benzene–ether (2:1) gave 2,4-diiodoestradiol 17β-acetate (**8**) as plates (44 mg) from methanol, mp 190—193 °C; IR (KBr): 3450, 1708, 1530, 1264, and 750 cm^{-1}; ^{1}H NMR ($CDCl_3$, 90 MHz) δ=0.82 (3H, s, C_{18}–H_3), 2.07 (3H, s, $C_{17\beta}$–$OCOCH_3$), 4.70 (1H, t, J=7.5 Hz, $C_{17\alpha}$–H), and 7.60 (1H, s, C_1–H).

Found: C, 42.51; H, 4.40%. HRMS m/z 565.9770. Calcd for $C_{20}H_{24}O_3I_2$: C, 42.43; H, 4.27%; M, 565.9816.

The less polar fraction on crystallization from methanol gave 2-iodoestradiol 17β-acetate (**6**) as needles (162 mg), mp 175—177 °C; IR (KBr): 3450, 1708, 1594, 1268, 880, and 865 cm^{-1}; ^{1}H NMR ($CDCl_3$, 90 MHz) δ=0.82 (3H, s, C_{18}–H_3), 2.06 (3H, s, $C_{17\beta}$–$OCOCH_3$), 4.68 (1H, t, J=7.5 Hz, $C_{17\alpha}$–H), 6.70 (1H, s, C_4–H), and 7.50 (1H, s, C_1–H).

Found: C, 54.74; H, 5.76%. HRMS m/z 440.0892. Calcd for $C_{20}H_{25}O_3I$: C, 54.56; H, 5.72%; M, 440.0850.

Reaction of Estradiol 17β-Acetate with Copper(II) Bromide in Acetic Acid. Estradiol (**1**) (100 mg) in acetic acid (10 ml) was treated with copper(II) bromide (82 mg) at 60 °C for 10 h. After a similar work-up, the resulting oil (127 mg) was purified by preparative TLC on silica-gel plates (2 mm layer) (Merck). Developement with benzene–ether (2:1) gave 4-bromoestradiol 17β-acetate (**7**) as needles (61 mg) from acetone, mp 213—215 °C; IR (KBr): 3430, 1705, 1605, 1561, 1274, and 793 cm^{-1}; ^{1}H NMR ($CDCl_3$, 90 MHz) δ=0.82 (3H, s, C_{18}–H_3), 2.07 (3H, s, $C_{17\beta}$–$OCOCH_3$), 4.71 (1H, t, J=7.5 Hz, $C_{17\alpha}$–H), 6.62 (1H, d, J=8.0 Hz, C_2–H), and 7.16 (1H, d, J=8.0 Hz, C_1–H).

Found: m/z 392.1019 (M^+); 394.0926 $(M+2)^+$. Calcd for $C_{20}H_{25}O_3Br$: M, 392.0986; M+2, 394.0966.

Reaction of Estradiol 17β-Acetate with Iodine–Copper(II) Acetate in Acetic Acid. A mixture of estradiol 17β-acetate (**13**) (200 mg), iodine (242 mg), and copper(II) acetate (116 mg) in acetic acid (20 ml) was stirred at 60 °C for 10 h. The precipitated copper(I) iodide was removed by filtration, and the filtrate was poured into water and extracted with ether. After a similar work-up, the resulting oil, on crystallization from methanol, gave **6** as needles (250 mg), mp 175—177 °C.

Reaction of Estradiol 17β-Acetate with Iodine–Copper(II) Chloride in Acetic Acid. A mixture of estradiol 17β-acetate (**3**) (200 mg), iodine (242 mg), and copper(II) chloride (163 mg) in acetic acid (20 ml) was stirred at 60 °C for 50 h. After a similar work-up, the resultant oil was chromatographed on silica gel (30 g). Elution with benzene (250 ml) gave 2,4-diiodoestradiol 17β-acetate (**8**) as plates (23 mg) from methanol, mp 190—193 °C. The next fraction, eluted by the same solvent (30 ml), on crystallization from methanol gave plates of **6** (146 mg), mp 175—177 °C. The third fraction, eluted by the same solvent (30 ml), on crystallization from methanol gave plates of 4-iodoestradiol 17β-acetate (**9**) (61 mg), mp 161—164 °C; IR (KBr): 3430, 1705, 1595, 1557, 1267, and 790 cm^{-1}; ^{1}H NMR ($CDCl_3$, 200 MHz) δ=0.82 (3H, s, C_{18}–H_3), 2.06 (3H, s, $OCOCH_3$), 4.69 (1H, t, J=8.9 Hz, $C_{17\alpha}$–H), 7.20 (1H, d, J=8.8 Hz, C_1–H), and 6.84 (1H, d, J=8.8Hz, C_2–H).

Found: C, 54.24; H, 5.72%; HRMS m/z 440.0840. Calcd for $C_{20}H_{25}O_3I$: C, 54.56; H, 5.72%; M, 440.0850.

Reaction of Estradiol 17β-Acetate with Iodine Monochloride. A mixture of estradiol 17β-acetate (**3**) (200 mg) and iodine monochloride (103 mg) in acetic acid (20 ml) was stirred at 60 °C for 1 h. After a similar work-up, crystallization from methanol afforded plates of **9** (81 mg), mp 161—164 °C. From the mother liquor, recrystallization from methanol gave plates of **6** (139 mg), mp 175—177 °C.

Reaction of Estradiol 17β-Acetate with Iodine–Morpholine. A mixture of estradiol 17β-acetate (**3**) (200 mg), iodine (161 mg), and morpholine (166 mg) in methanol (40 ml) was stirred at 0 °C for 2 h. After a similar work-up, the resultant oil was chromatographed on silica gel (30 g). Elution with benzene–ether (10:1) (60 ml) gave 2,4-diiodoestradiol 17β-acetate (**8**) as plates (99 mg) from methanol, mp 190—193 °C. The second fraction, eluted by the same solvent (24 ml), on crystallization from methanol gave plates of **6** (48 mg), mp 175—177 °C. The third fraction, eluted by the same solvent (8 ml), on crystallization from methanol gave plates of **9** as plates (59 mg), mp 161—164 °C.

Reaction of 3-Methoxy-17β-acetoxy-1,3,5(10)-estratriene with Iodine, Copper(II) Chloride Dihydrate, and Iron(III) Chloride Hexahydrate. Estradiol 17β-acetate 3-methyl ether (**4**) (200 mg) in acetic acid (20 ml) was treated with iodine (232 mg), copper(II) chloride dihydrate (156 mg), and iron(III) chloride hexahydrate (247 mg) under stirring at 60 °C for 5 h. After a similar work-up, the resultant oil was chromatographed on silica gel (30 g). Elution with benzene (130 ml) gave 2-iodoestradiol 17β-acetate 3-methyl ether (**10**) as plates (154 mg) from methanol, mp 138—141 °C; IR (KBr): 1738, 1590, 1240, 878, and 860 cm^{-1}; ^{1}H NMR ($CDCl_3$, 200 MHz) δ=0.82 (3H, s, C_{18}–H_3), 2.06 (3H, s, $C_{17\beta}$–$OCOCH_3$), 3.83 (3H, s, OCH_3), 4.69 (1H, t, J=9.4 Hz, $C_{17\alpha}$–H), 6.54 (1H, s, C_4–H), and 7.64 (1H, s, C_1–H).

Found: C, 55.35; H, 5.97%; HRMS: m/z 454.1003. Calcd for $C_{21}H_{27}O_3I$: C, 55.52; H, 5.99%; M, 454.1006. The second fraction, eluted by the same solvent (40 ml) gave 4-iodoestradiol 17β-acetate 3-methyl ether (**11**) as plates (51 mg) from methanol, mp 165—167 °C; IR (KBr): 1734, 1590, 1556, 1260, 1245, and 786 cm^{-1}; ^{1}H NMR ($CDCl_3$, 200 MHz) δ=0.82 (3H, s, C_{18}–H_3), 2.06 (3H, s, $C_{17\beta}$–$OCOCH_3$), 3.87 (3H, s, OCH_3), 4.69 (1H, t, J=7.6 Hz, $C_{17\alpha}$–H), 7.25 (1H, d, J=8.50 Hz, C_1–H), and 6.66 (1H, d, J=8.50 Hz, C_2–H).

Found: C, 55.80; H, 6.12%; HRMS: m/z 454.1008. Calcd for $C_{21}H_{27}O_3I$: C, 55.52; H, 5.99%; M, 454.1006.

We are indebted to Associate Professor Sukekatsu Nozaki, Josai University, for his measurement of the high resolution mass spectra and Research Laboratories of Toyo Jozo Co., Ltd. for the elemental analyses. Thanks are also due to Associate Professor Yoshio Koike and Mr. Toshio Takayama, Kanagawa University, for the measurement of FT-NMR spectra.

References

1) A preliminary report on this work was presented at the 1984 International Chemical Congress of Pacific Basin Societies, Honolulu, Hawai, December 1984.

2) W. Sweet, T. B. Patrick, and J. M. Mudd, *J. Org. Chem.*, **44**, 2296 (1979).
3) A. Hillmann-Elies, G. Hillmann, and U. Schiedt, *Z. Naturforsch. Teil B.*, **8**, 436 (1953).
4) E. Santaniello and P. Ferraboschi, *J. Chem. Soc., Chem. Commun.*, **1981**, 217; E. Santaniello, A. Fiecchi, P. Frraboschi, and M. Ravasi, *J. Chem. Soc., Perkin Trans. 1*, **1983**, 2765.
5) C. A. Horiuchi and J. Y. Satoh, *Synthesis*, **1981**, 312.
6) C. A. Horiuchi and J. Y. Satoh, *Bull. Chem. Soc. Jpn.*, **57**, 2691 (1984).
7) C. A. Horiuchi and J. Y. Satoh, *Chem. Lett.*, **1984**, 1509.
8) C. A. Horiuchi and J. Y. Satoh, *J. Chem. Soc., Chem. Commun.*, **1982**, 671.
9) E. Hecker, *Chem. Ber.*, **92**, 1386 (1959).
10) Y. Urushibara and T. Nitta, *Bull. Chem. Soc. Jpn.*, **16**, 179 (1941).

Stereospecific Desulfinylation of α,β-Epoxy Sulfoxides with Butyllithium. A New Synthesis of Epoxides and Allylic Alcohols from Carbonyl Compounds[1)]

Tsuyoshi SATOH, Youhei KANEKO, and Koji YAMAKAWA*
Faculty of Pharmaceutical Sciences, Science University of Tokyo,
Ichigaya-funagawara-machi, Shinjuku-ku, Tokyo 162
(Received March 8, 1986)

Desulfinylation of α,β-epoxy sulfoxides, easily prepared from carbonyl compounds and 1-chloroalkyl phenyl sulfoxide, with 1 equivalent of butyllithium at low temperature gave epoxides in good yields. The similar α,β-epoxy sulfoxides having an arylmethyl group at the α-position gave 3-aryl-allylic alcohols upon treatment with excess butyllithium at −70 °C. These reactions offer a simple and useful approach to the synthesis of epoxides and 3-aryl-allylic alcohols from a carbonyl compound.

Epoxides have received considerable attention in recent years with interest concerning their synthesis, including asymmetric synthesis,[2)] their use as versatile intermediates in organic synthesis,[3)] and their use in the total synthesis of complex natural products.[4)] The preparation of epoxides are usually classified into two categories. One is the oxidation of a double bond with peroxy acids[2a,5)] or peroxides[2b)] or with NBS in the presence of water followed by a treatment with an alkali.[6)] The other is the method from ketones *via* Darzens-type condensation[7)] including sulfur ylides[8)] or arsonium ylides.[9)] The most important characteristic of the latter method is that the reaction gives epoxides with carbon–carbon bond formation.

α,β-Epoxy sulfoxides (**4**) are very easily prepared in high yields and on a large scale from carbonyl compounds (**1**) and 1-chloroalkyl phenyl sulfoxide (**2**) by the Darzens-type condensation.[10)] We have reported that the β-carbon of α,β-epoxy sulfoxides (**4**) is highly reactive toward nucleophiles such as selenolates, thiolates, amines, and acetate giving dialkyl ketones,[11a)] α-sulfenylated ketones,[11b)] α-amino ketones,[11c)] and α-acetoxy ketones,[11d)] respectively, in good yields.

In the course of studies on the new synthetic methods from carbonyl compounds through α,β-epoxy sulfoxides, we found that the phenylsulfinyl group of the α,β-epoxy sulfoxides (**4**) could be easily cleaved with butyllithium (*n*-BuLi), even at −100 °C, to give epoxides (**5**) in quite good yields. This reaction leads to a novel synthetic method for the synthesis of epoxides from carbonyl compounds via α,β-epoxy sulfoxides. We also found that the α,β-epoxy sulfoxides (**4**) having an arylmethyl group at the α-position afforded 3-aryl-allylic alcohols (**6**) upon treatment with excess *n*-BuLi at −70 °C. These procedures are given in Scheme 1.

In this paper we describe details and the mechanistic aspects of these reactions.

Results and Discussion

A Synthesis of Epoxides from Carbonyl Compounds

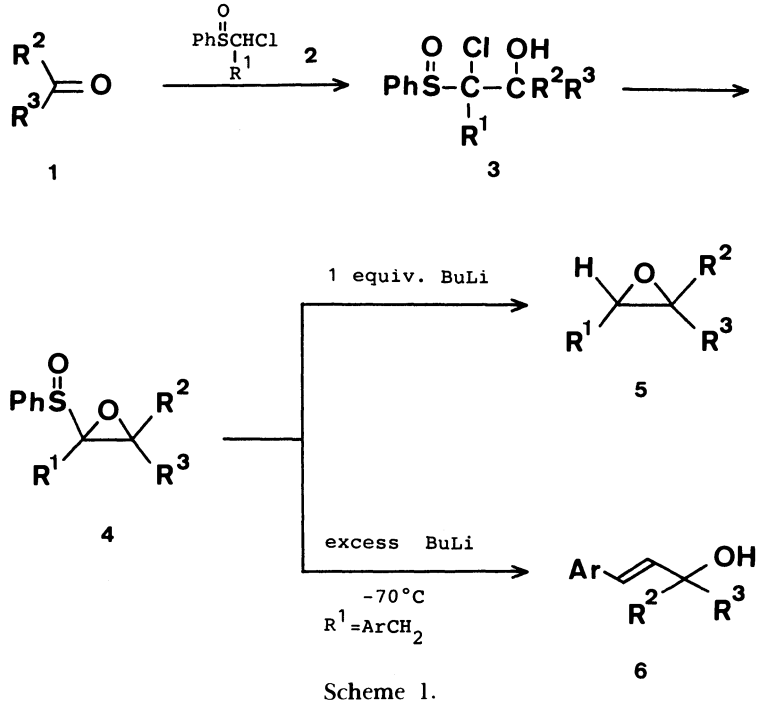

Scheme 1.

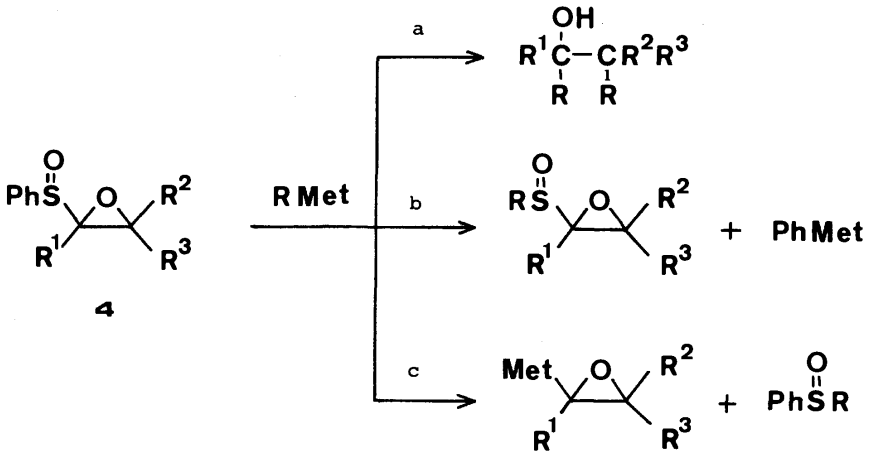

Scheme 2.

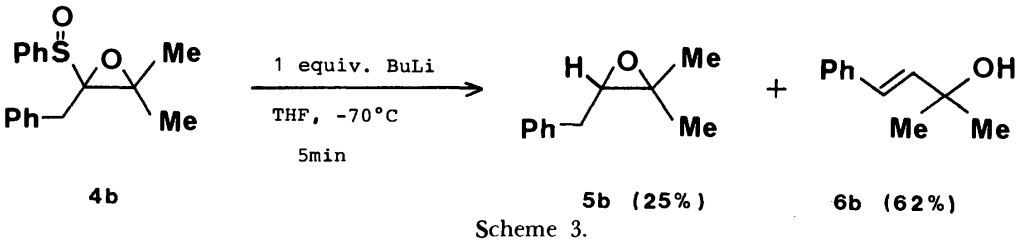

Scheme 3.

Through α,β-Epoxy Sulfoxides. If the phenylsulfinyl group of the α,β-epoxy sulfoxides (**4**) can be easily exchanged with hydrogen; this reaction offers a novel method for the epoxidation of carbonyl compounds. It has been reported that a treatment of sulfoxides with alkylmetal takes place carbon–sulfur bond cleavage.[12] In the treatment of α,β-epoxy sulfoxides (**4**) with alkylmetal, three types of reactions could be expected to take place: 1) A nucleophilic attack of a carbanion to the β-carbon of α,β-epoxy sulfoxides (**4**) (route a in Scheme 2); 2) the addition of a carbanion to the sulfinyl group leading to phenyl-alkyl exchange (route b); and 3) the addition of a carbanion to the sulfinyl group leading to the cleavage of the bond between sulfur and epoxide (route c). On the basis of this consideration α,β-epoxy sulfoxide (**4a**) was treated with 1 equivalent of *n*-BuLi in THF at −70°C. In this reaction all the starting materials disappeared within 5 min, and an 89% yield of the epoxide (**5a**) along with trace amounts of by-products and reasonable amount (about 50%) of butyl phenyl sulfoxide were obtained. This result clearly indicates that the reaction proceeded along route c shown in Scheme 2.

A search was made to find the most effective alkylmetal for this reaction. Table 1 shows the results for a treatment of α,β-epoxy sulfoxide (**4a**) with various alkylmetals, including lithium diisopropylamide (LDA) in THF at −70°C for 5 min. From these results, we decided to use *n*-BuLi throughout the study.

Next, α,β-epoxy sulfoxide (**4b**) was treated with 1 equivalent of *n*-BuLi under the same conditions as above. In this reaction a 62% yield of unexpected 3-phenyl-allylic alcohol (**6b**) along with the expected epoxide (**5b**) (25% yield) was obtained as shown in Scheme 3. The allylic alcohol (**6b**) was thought to form from the epoxide (**5b**) by isomerization with bases. When the reaction was carried out at −100°C for 5 min it was found that the desired epoxide (**5b**) was obtained in 71% yield with almost no allylic alcohol (**6b**).

Table 1. Treatment of the α,β-Epoxy Sulfoxide (**4a**) with 1 Equivalent of Alkylmetal (RMet) in THF at −70°C for 5 min

RMet	**5a** (%)	Recovered (**4a**)/%
n-BuLi	89	0
CH_3Li	43	30[a]
t-BuLi	28	Trace[a]
EtMgBr	Trace	47[a]
LDA	0	88

a) The product other than **5a** was a complex mixture.

Representative results of the treatment of α,β-epoxy sulfoxides (**4**) with 1 equivalent of *n*-BuLi are listed in Table 2. As shown in Table 2, quite good results were obtained, except for Entry 12. It should be noted that in Entries 5 and 6, diastereomers (**4e-L**) and (**4e-P**)[13] afforded (*Z*)-epoxide (**5e-L**) and (*E*)-epoxide (**5e-P**),[14] respectively, without any contamination of their isomers. In previous studies the configuration of the diastereomers of the α,β-epoxy sulfoxides (**4**) was not determined but in this study, in order to clarify the stereochemistry of this reaction, we needed to determine the configuration of **4e**.

Table 2. Synthesis of Epoxides from α,β-Epoxy Sulfoxides and 1 Equivalent of Butyllithium[19]

Entry	α,β-Epoxy sulfoxide (4)				Temp	Epoxide (5)		Yield[a]
	R^1	R^2	R^3		°C			%
1	$CH_3(CH_2)_5$	— $(CH_2)_5$ —		(**4a**)	−70	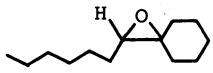	(**5a**)	89
2	$PhCH_2$	CH_3	CH_3	(**4b**)	−100	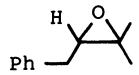	(**5b**)	71
3		$CH_3(CH_2)_4$ or H		(**4c-L**)[b] (**4c-P**)[b]	−70 −70	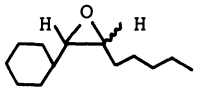	(**5c-L**)[b] (**5c-P**)[b]	86 97
4	$PhCH_2$	— $(CH_2)_5$ —		(**4d**)	−100	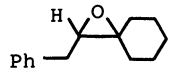	(**5d**)	65(91)
5	$PhCH_2$	H	Ph	(**4e-L**)[c]	−100	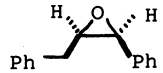	(**5e-L**)	79
6	$PhCH_2$	Ph	H	(**4e-P**)[c]	−100	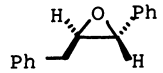	(**5e-P**)	90
7	MeO- -CH_2	CH_3	CH_3	(**4f**)	−100	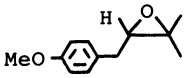	(**5f**)	69
8	MeO- -CH_2	— $(CH_2)_5$ —		(**4g**)	−100	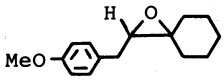	(**5g**)	78
9		CH_3	CH_3	(**4h**)	−100	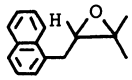	(**5h**)	49(62)
10	CH_2=$CHCH_2$	Ph	Ph	(**4i**)	−100	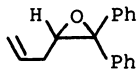	(**5i**)	85
11	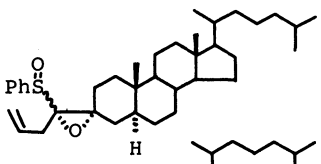			(**4j**)[b]	−100	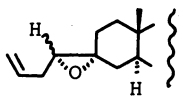	(**5j**)[b]	83
12	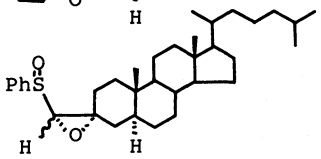			(**4k**)[b]	−100	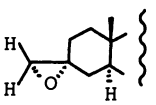	(**5k**)[17]	27

a) Isolated yields after silica-gel column chromatography. The yields in parenthesis are calculated from consumed starting material. b) The configuration was not determined. c) The configuration see Fig. 1.

The structures of these α,β-epoxy sulfoxides (**4e-L**) and (**4e-P**) were determined by the lanthanoid-induced shift[15] of their NMR spectra using tris[(heptafuluorobutanoyl)pivaloylmetanato]europium as a NMR shift reagent. Figure 1 shows the shift curves of the hydrogen on the β-carbon of the α,β-epoxy sulfoxides (**4e**), in which the differences of the chemical shift between original ones (**4e-L**:δ 4.87, **4e-P**:δ 3.79) and shifted ones (Δδ) are scaled on a vertical line and amounts (mole equivalents) of the shift reagent added are scaled on a horizontal line. From the results shown in Fig. 1, the structure of **4e-L** and **4e-P** were unambiguously determined as *E*- and *Z*-configurations, respectively. As already described, **4e-L** (*E*) and **4e-P** (*Z*) gave *Z*-epoxide (**5e-L**) and *E*-epoxide (**5e-P**); this reaction is stereospecific and the configuration of the carbon bearing the sulfinyl group was retained.

A Synthesis of 3-Aryl- and 3-Vinyl-Allylic Alcohols from Carbonyl Compounds Through α,β-Epoxy Sulfoxides. As mentioned above, a treatment of α,β-epoxy sulfoxide having a benzyl group as R^1 (**4b**) with 1 equivalent of *n*-BuLi gave 3-phenyl-allylic alcohol (**6b**) along with the epoxide (**5b**). The supposed mechanism of this reaction is shown in Scheme 4. The attack

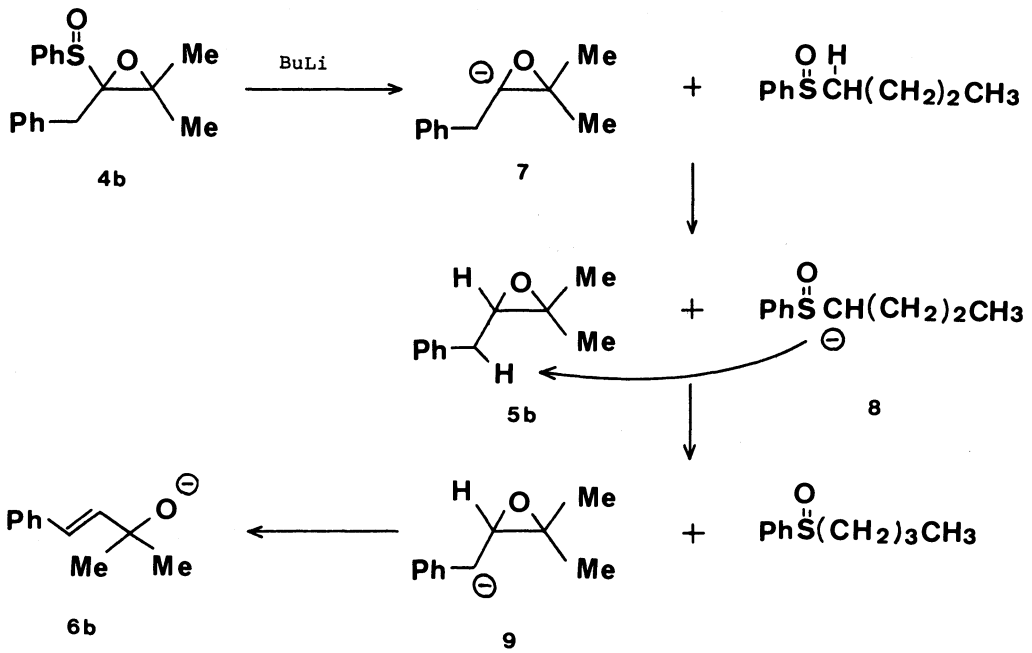

Scheme 4.

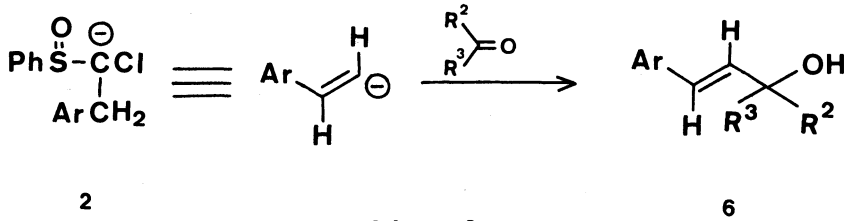

Scheme 5.

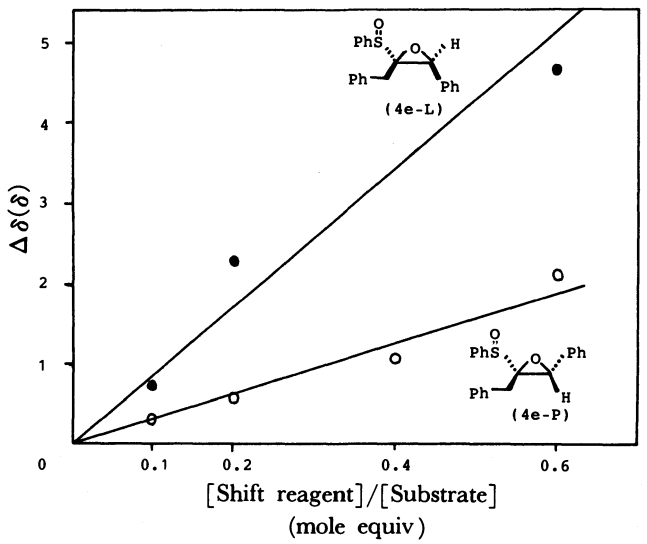

Fig. 1.

of *n*-BuLi on the sulfinyl group of **4b** leads to a carbon–sulfur bond cleavage, giving the carbanion (**7**) and butyl phenyl sulfoxide. Then, a proton transfer from the sulfoxide to **7** takes place to afford **5b** and the α-carbanion of butyl phenyl sulfoxide (**8**). As **5b** has acidic hydrogens on benzyl methylene carbon, the hydrogen is eliminated by the carbanion (**8**) giving **9**. This is isomerized to the allylic alcohol (**6b**). To make sure that the carbanion (**8**) acted as a base to isomerize the epoxide (**5**) into the allylic alcohol (**6**), the following experiment was carried out by using **5e-P** as an epoxide. To a solution of **5e-P** in THF at −70°C was added a solution of 1 equivalent of the carbanion (**8**), prepared from butyl phenyl sulfoxide and LDA. The reaction mixture was stirred for 5 min. After the usual work-up, the allylic alcohol (**6e**) and the starting material (**5e-P**) were obtained in 25 and 75% yields, respectively. From these facts it was predicted that excess bases and the higher temperature cause an acceleration of the epoxide-allylic alcohol isomerization. In fact, a treatment of **4b** with 3 equivalents of *n*-BuLi at −70°C for 5 min gave the allylic alcohol (**6b**) in 76% yield without the epoxide (**5b**).

Table 3 shows the results of the treatment of α,β-epoxy sulfoxides with excess *n*-BuLi (3—5 equivalents) in THF at −70°C for 5 min. All α,β-epoxy sulfoxides having an arylmethyl group, including an allyl group at the α-position, afforded 3-aryl-allylic alcohols (**6**) in good yields (except Entry 3). In this reaction the α,β-epoxy sulfoxides having a simple alkyl group as R^1 gave only epoxides (**5**) and no allylic alcohol was observed. The configuration of the double bond of **6** was confirmed as E by the NMR spectra.[16] It is

Table 3. Synthesis of Allylic Alcohols from α,β-Eoxy Sulfoxides and Excess Butyllithium at −70 °C[19]

Entry	α,β-Epoxy sulfoxide (4)	BuLi (eq)	Allylic alcohol (6)		Yield[a] %
1	**4b**	3	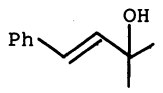	(**6b**)	76
2	**4d**	3	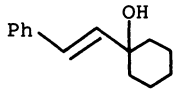	(**6d**)	87
3	**4e-L**	3	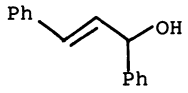	(**6e**)[18]	16
4	**4e-P**	3	**6e**		58
5	**4f**	3	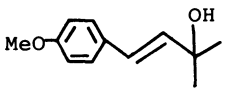	(**6f**)	72
6	**4g**	3	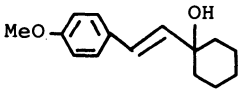	(**6g**)	71
7	**4h**	3	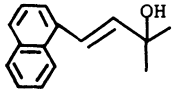	(**6h**)	69
8	**4i**	5	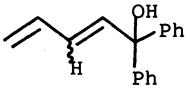	(**6i**)[b]	85
9	**4j**	3	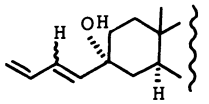	(**6j**)[b]	68

a) Isolated yields after silica-gel column chromatography. b) The product is single isomer. The configuration of the double bond is not determined.

noteworthy that in this reaction the carbanion of 1-chloroalkyl phenyl sulfoxide (**2**; $R^1=CH_2Ar$) acted as a β-arylvinyl carbanion equivalent as shown in Scheme 5.

In conclusion, a novel and versatile procedure for the synthesis of epoxides and 3-aryl-allylic alcohols has been developed from carbonyl compounds with carbon–carbon bond formation through α,β-epoxy sulfoxides. In regard to the accessibility of the starting materials, the simplicity and mildness of the operation, and high overall yields, the present procedure offers a simple and useful approach to the synthesis of epoxides and 3-aryl-allylic alcohols from carbonyl compounds.

Experimental

All melting points are uncorrected. Infrared (IR) spectra were measured directly on a NaCl plate or in KBr disks with a Hitachi 215 spectrometer. ^1H Nuclear magnetic resonance (NMR) spectra were measured in a $CDCl_3$ solution with a JEOL FX-100 spectrometer using Me_4Si as an internal standard. Electron-impact mass spectra (MS) were obtained on a Hitachi M-80 double-focusing spectrometer at 70 eV by direct insertion. Silica gel BW-127ZH (Fuji-Devison) containing 2% fluorescence reagent 254 and quartz column were used for column chromatography and the products having ultraviolet (UV) absorption were detected by UV irradiation.

Materials. All α,β-epoxy sulfoxides (**4**) except **4f—j** were reported in the references IIa and 11b.

Preparation of 1-Chloro-2-(4-methoxyphenyl)ethyl Phenyl Sulfoxide, 1-Chloro-2-(1-naphthyl)ethyl Phenyl Sulfoxide, and 1-Chloro-3-butenyl Phenyl Sulfoxide. These sulfoxides were prepared from chloromethyl phenyl sulfoxide with 4-methoxybenzyl chloride, 1-(chloromethyl)naphthalene, and allyl bromide according to the procedure reported previously.[11a] 1-Chloro-2-(4-methoxyphenyl)ethyl phenyl sulfoxide: Diastereomeric mixture; colorless oil; 87% yield; IR (neat): 1090, 1040 (SO) cm^{-1}; ^1H NMR δ=2.76 (dd, *J*=9, 14 Hz), 3.18 (dd, *J*=9.5, 14.5 Hz), 3.53 (dd, *J*=3, 14.5 Hz), 3.58 (dd, *J*=5, 14 Hz), 3.79 (s), 4.55 (dd, *J*=3, 9 Hz), 4.67 (dd, *J*=5, 9 Hz), 6.8—7.3 (m), 7.5—7.9 (m); MS *m/z* (%): 179 ([M−PhSO]$^+$, 100), 178 ([M−PhSOH]$^+$, 84), 134 (43), 121 (26). 1-Chloro-2-(1-naphthyl)ethyl phenyl sulfoxide: Diastereomeric mixture; colorless crystals; mp 127—129 °C (AcOEt–hexane); 40% yield; IR (KBr): 1085, 1040 (SO) cm^{-1}; ^1H NMR δ=3.06 (dd, *J*=9, 14.5 Hz), 3.36 (dd, *J*=11, 15 Hz), 4.27 (dd, *J*=4.5, 15 Hz), 4.34 (dd, *J*=2, 14.5 Hz), 4.70 (dd, *J*=2, 11 Hz), 4.93 (dd, *J*=4.5, 9 Hz), 7.3—8.1 (m); MS *m/z* (%): 314 (M$^+$, trace),

188 ([M−PhSOH]$^+$, 23), 153 (100). 1-Chloro-3-butenyl phenyl sulfoxide: Diastereomeric mixture; colorless oil; 72% yield; IR (neat): 1090, 1050 (SO) cm^{-1}; ^{1}H NMR δ=2.1—2.5 (m), 2.6—3.2 (m), 4.48 (dd, J=4, 8 Hz), 4.60 (dd, J=4.5, 8.5 Hz), 5.1—5.3 (m), 5.6—6.1 (m), 7.5—7.9 (m); MS m/z (%): 214 (M$^+$, 2), 126 ([M−C_4H_4Cl]$^+$, 100), 89 ([M−PhSO]$^+$, 26), 78 (79).

General Procedure for the Preparation of α,β-Epoxy Sulfoxide (4): The synthesis of 2,3-epoxy-1-(4-methoxyphenyl)-3-methyl-2-(phenylsulfinyl)butane (**4f**) is described. To a solution of LDA (2.2 mmol) in dry THF (3 ml) at −70 °C under N_2 was added a solution of 1-chloro-2-(4-methoxyphenyl)-ethyl phenyl sulfoxide (2 mmol) in 2 ml of dry THF dropwise through a syringe with stirring. The solution was stirred at −40 °C for 20 min and then acetone (3 mmol) was added through a syringe and the reaction mixture was stirred for additional 10 min. The reaction was quenched with sat. aq NH_4Cl and the whole was extracted with ethyl acetate. The product was separated by silica-gel column chromatography to give chlorohydrin (**3**) and recovered starting material in 49 and 37% yield, respectively. Chlorohydrin: Mp 103—105 °C (AcOEt-hexane); IR (KBr): 3400 (OH), 1035 (SO) cm^{-1}; ^{1}H NMR δ=1.26, 1.58 (each 3H, s), 3.30, 3.48 (each 1H, d, J=15 Hz), 3.83 (3H, s), 6.88, 7.30 (each 2H, d, J=9 Hz), 7.4—7.8 (5H, m); MS m/z (%): 226 ([M−PhSOH]$^+$, 29), 211 (67), 125 (40), 78 (76), 43 (100).

To a solution of the chlorohydrin (1.47 mmol) in 7 ml of MeOH and 4 ml of THF was added 30% aq KOH (6 ml) dropwise with stirring and the mixture was stirred at room temperature for 2 h. The reaction mixture was neutralized by adding NH_4Cl and the MeOH was evaporated. The residue was extracted with ethyl acetate and the product was purified by silica-gel column chromatography to give **4f** in quantitative yield. Mp 70—72 °C (AcOEt-hexane); IR (KBr): 1080, 1050 (SO) cm^{-1}; ^{1}H NMR δ=1.29, 1.83 (each 3H, s), 3.23 (2H, s), 3.73 (3H, s), 6.64, 6.72 (each 2H, d, J=10 Hz), 7.4—7.8 (5H, m); MS m/z (%): 316 (M$^+$, trace), 191 ([M−PhSO]$^+$, 31), 163 (8), 121 (100); Found: C, 68.22; H, 6.37; S, 9.95%. Calcd for $C_{18}H_{20}O_3S$: C, 68.33; H, 6.37; S, 10.13%.

3′-(4-methoxybenzyl)-3′-(phenylsulfinyl)spiro[cyclohexane-1,2′-oxirane] (4g). Chlorohydrin (**3**); colorless oil; 65% yield; IR (neat): 3400 (OH), 1080, 1035 (SO) cm^{-1}; ^{1}H NMR δ=1.0—2.4 (10H, m), 3.32, 3.44 (each 1H, d, J=15 Hz), 3.82 (3H, s), 6.7—7.0 (2H, m), 7.2—7.4 (2H, m), 7.4—7.8 (5H, m); MS m/z (%): 266 ([M−PhSOH]$^+$, 22), 209 (40), 126 (57), 78 (100). Epoxy sulfoxide (**4g**); 88% yield; colorless oil; IR (neat): 1080, 1050, 1035 (SO) cm^{-1}; ^{1}H NMR δ=1.3—2.3 (10H, m), 3.21 (2H, s), 3.73 (3H, s), 6.64, 6.77 (each 2H, d, J=10 Hz), 7.4—7.8 (5H, m); MS m/z (%): 231 ([M−PhSO]$^+$, 11), 202 (2), 121 (100).

2,3-Epoxy-3-methyl-1-(1-naphthyl)-2-(phenylsulfinyl)butane (4h). Chlorohydrin (**3**); mp 101—103 °C (AcOEt-hexane); 52% yield; IR (KBr): 3380 (OH), 1080, 1040, 1020 (SO) cm^{-1}; ^{1}H NMR δ=1.45, 1.60 (each, 3H, s), 4.02, 4.40 (each 1H, d, J=15 Hz), 7.3—8.3 (12H, m); MS m/z (%): 246 ([M−PhSOH]$^+$, 68), 231 (18), 213 (80), 141 (28), 110 (87), 43 (100). Epoxy sulfoxide (**4h**); 93% yield; colorless oil; IR (neat): 1090, 1055, 1045 (SO) cm^{-1}; ^{1}H NMR δ=1.07, 1.89 (each 3H, s), 3.50, 3.87 (each 1H, d, J=17 Hz), 7.2—7.9 (12H, m); MS m/z (%): 336 (M$^+$, trace), 211 ([M−PhSO]$^+$, 22), 169 (68), 141 (100).

5,5-Diphenyl-4,5-epoxy-4-phenylsulfinyl-1-pentene (4i). In this case alkylation of 1-chloro-3-butenyl phenyl sulfoxide with benzophenone directly gave the α,β-epoxy sulfoxide (**4i**) in 92% yield. Mp 121—123 °C (AcOEt-hexane); IR (KBr): 1640 (C=C), 1085, 1045 (SO) cm^{-1}; ^{1}H NMR δ=2.20, 2.90 (each 1H, dddd, J=1.2, 1.2, 6.5, 16 Hz), 4.36 (1H, m, $W/2$=20 Hz), 4.62 (1H, m, $W/2$=11 Hz), 4.96 (1H, dddd, J=6.5, 6.5, 10, 17 Hz), 7.2—7.8 (15 H, m); MS m/z (%): 234 ([M−PhSOH]$^+$, 41), 194 (46), 167 (71), 165 (100), 129 (80); Found: C, 75.95; H, 5.50; S, 8.90%. Calcd for $C_{23}H_{20}O_2S$: C, 76.64; H, 5.59; S, 8.89%.

3′-Allyl-3′-(phenylsulfinyl)spiro[5α-cholestane-3,2′-oxirane] (4j). Chlorohydrin (**3**); mp 107—108 °C (AcOEt-hexane); 88% yield; IR (KBr): 3450 (OH), 1085, 1060, 1025 (SO) cm^{-1}; ^{1}H NMR δ=0.65 (3H, s), 0.87 (6H, d, J=7 Hz), 0.91 (3H, d, J=7 Hz), 0.97 (3H, s), 2.66 (2H, d, J=6.5 Hz), 5.08—5.50 (1H, m), 5.71—6.13 (1H, m), 6.44—6.94 (1H, m), 7.3—7.9 (5H, m); MS m/z (%): 474 ([M−PhSOH]$^+$, trace), 456 (4), 438 (9), 421 (5), 43 (100). Epoxy sulfoxide (**4j**); 88% yield; mp 114—116 °C (MeOH-H_2O); IR (KBr): 1095, 1060 (SO) cm^{-1}; ^{1}H NMR δ=0.68 (3H, s), 0.88 (6H, d, J=7 Hz), 0.92 (3H, d, J=7 Hz), 1.03 (3H, s), 4.60—5.50 (3H, m), 7.4—7.8 (5H, m); MS m/z (%): 438 ([M−PhSOH]$^+$, 100), 397 (44), 369 (9); Found: C, 78.70; H, 9.93; S, 5.62%. Calcd for $C_{37}H_{56}O_2S$: C, 78.67; H, 9.99; S, 5.68%.

General Procedure for the Preparation of Epoxide (5) from α,β-Epoxy Sulfoxide (4): The synthesis of 3′-hexylspiro[cyclohexane-1,2′-oxirane] (**5a**) is described. To a solution of n-BuLi (0.1 mmol) in 0.2 ml of dry THF at −70 °C under N_2 was added a solution of **4a** (0.1 mmol) in 0.2 ml of dry THF through a syringe with stirring. The reaction mixture was stirred for 5 min, then the reaction was quenched by adding sat. aq NH_4Cl and the whole was extracted with ethyl acetate. The organic layer was washed with sat. aq NH_4Cl and dried over Na_2SO_4. The product was purified by silica-gel column chromatography to give **5a** as a colorless oil in 89% yield. IR (neat): 2970, 2940, 2860, 1470, 1445, 910 cm^{-1}; ^{1}H NMR δ=0.90 (3H, t, J=6 Hz), 1.0—2.2 (20H, m), 2.73 (1H, t, J=6 Hz); MS m/z (%): 196 (M$^+$, 1), 153 (4), 125 (19), 98 (100).

2,3-Epoxy-3-methyl-1-phenylbutane (5b). Colorless oil; IR (neat): 1260, 1035 cm^{-1}; ^{1}H NMR δ=1.34, 1.41 (each 3H, s), 2.92 (3H, m), 7.30 (5H, m); MS m/z (%): 162 (M$^+$, 6), 147 ([M−CH_3]$^+$, 35), 119 (52), 91 (100).

1-Cyclohexyl-1,2-epoxyheptane (5c). 5c-L: Colorless oil; IR (neat): 2960, 2940, 2870, 1470, 1450, 1390, 1260, 885, 855, 830, 820, 790 cm^{-1}; ^{1}H NMR δ=0.91 (3H, t, J=6 Hz), 1.0—2.1 (19H, m), 2.64 (1H, m, $W/2$=13 Hz) 2.93 (1H, m, $W/2$=12 Hz); MS m/z (%): 196 (M$^+$, 2), 113 (44), 95 (58), 81 (100); Found: m/z 196.1818. Calcd for $C_{13}H_{24}O$: M, 196.1825. **5c-P:** Colorless oil; IR (neat): 2970, 2940, 2870, 1470, 1450, 925, 900, 890, 875 cm^{-1}; ^{1}H NMR δ=0.90 (3H, t, J=6 Hz), 1.2—2.0 (19H, m), 2.47 (1H, m, $W/2$=10 Hz), 2.75 (1H, m, $W/2$=10 Hz); MS m/z (%): 196 (M$^+$, 2), 113 (44), 95 (58), 81 (100); Found: m/z 196.1831. Calcd for $C_{13}H_{24}O$: M, 196.1826.

3′-Benzylspiro[cyclohexane-1,2′-oxirane] (5d). Colorless oil; IR (neat): 3040, 2940, 2860, 1610, 1495, 1450, 740, 695 cm^{-1}; ^{1}H NMR δ=1.2—1.9 (10H, m), 2.94 (3H, m, $W/2$=14 Hz), 7.31 (5H, m, $W/2$=3 Hz); MS m/z (%): 202 (M$^+$, 7), 173 (20), 159 (35), 105 (100), 91 (73); Found: m/z 202.1345. Calcd for $C_{14}H_{18}O$: M, 202.1355.

2,3-Epoxy-1-(4-methoxyphenyl)-3-methylbutane (5f). Colorless oil; IR (neat): 1255, 1040 cm^{-1}; ^{1}H NMR δ=1.33, 1.40 (each 3H, s), 2.85 (3H, m), 3.82 (3H, s), 6.88, 7.18 (each 2H, d, J=9 Hz); MS m/z (%): 192 (M$^+$, 43), 177 ([M−CH_3]$^+$, 8),

163 (32), 149 (77), 121 (100); Found: *m/z* 192.1130. Calcd for $C_{12}H_{16}O_2$: M, 192.1149.

3′-(4-Methoxybenzyl)spiro[cyclohexane-1,2′-oxirane] (5g). Colorless oil; IR (neat): 1250, 1040 cm^{-1}; ^1H NMR δ=1.3—1.9 (10H, m), 2.88 (3H, m), 3.83 (3H, s), 6.88, 7.20 (each 2H, d, J=8 Hz); MS *m/z* (%): 232 (M^+, 20), 203 (23), 189 (34), 121 (100); Found: *m/z* 232.1463. Calcd for $C_{15}H_{20}O_2$: M, 232.1462.

2,3-Epoxy-3-methyl-1-(1-naphthyl)butane (5h). Colorless oil; IR (neat): 1260, 1030 cm^{-1}; ^1H NMR δ=1.36, 1.48 (each 3H, s), 3.06—3.56 (3H, m), 7.4—8.2 (7H, m); MS *m/z* (%): 212 (M^+, 33), 197 ($[M-CH_3]^+$, 7), 183 (17), 153 (83), 141 (100); Found: *m/z* 212.1196. Calcd for $C_{15}H_{16}O$: M, 212.1199.

5,5-Diphenyl-4,5-epoxy-1-pentene (5i). Colorless oil; IR (neat): 1270, 1030 cm^{-1}; ^1H NMR δ=2.16 (2H, bt, J=6.5 Hz), 3.51 (1H, t, J=6.5 Hz), 5.06 (1H, m, $W/2$=9 Hz), 5.19 (1H, m, $W/2$=6 Hz), 5.77—6.08 (1H, m), 7.2—7.6 (10H, m); MS *m/z* (%): 236 (M^+, 7), 207 (7), 194 (34), 165 (100); Found: *m/z* 236.1203. Calcd for $C_{17}H_{16}O$: M, 236.1200.

3′-Allylspiro[5α-cholestane-3,2′-oxirane] (5j). Colorless oil; IR (neat): 1650, 1265 cm^{-1}; ^1H NMR δ=0.67 (3H, s), 0.87 (6H, d, J=7 Hz), 0.92 (3H, d, J=7 Hz), 1.00 (3H, s), 2.2—2.4 (2H, m), 2.85 (1H, t, J=6 Hz), 5.0—5.3 (2H, m), 5.88 (1H, dddd, J=6.5, 6.5, 10, 17.5 Hz); MS *m/z* (%): 440 (M^+, 6), 400 (83), 381 (41), 55 (100), 43 (100); Found: *m/z* 440.4009. Calcd for $C_{31}H_{52}O$: M, 440.4014.

General Procedure for the Preparation of Allylic Alcohols (6) from α,β-Epoxy Sulfoxides (4): The synthesis of (*E*)-2-methyl-4-phenyl-3-buten-2-ol (**6b**) is described. To a solution of *n*-BuLi (0.6 mmol) in 0.3 ml of dry THF at −70 °C under N_2 was added a solution of epoxy sulfoxide (**4b**) (0.2 mmol) in 0.3 ml of dry THF with stirring. The reaction mixture was stirred for 5 min; then the reaction was quenched by adding sat. aq NH_4Cl. The whole was extracted with ethyl acetate and after the usual work-up, the product was purified by silica-gel column chromatography to give **6b** as a colorless oil in 76% yield. IR (neat): 3360 (OH) cm^{-1}; ^1H NMR δ=1.44 (6H, s), 6.37 (1H, d, J=16 Hz), 6.62 (1H, d, J=16 Hz), 7.2—7.5 (5H, m); MS *m/z* (%): 161 ($[M-H]^+$, 30), 126 (32), 91 (100).

(*E*)-1-Styryl-1-cyclohexanol (6d). Mp 65—66 °C (hexane); IR (KBr): 3400 (OH) cm^{-1}; ^1H NMR δ=1.1—2.0 (10H, m), 6.36 (1H, d, J=16 Hz), 6.67 (1H, d, J=16 Hz), 7.1—7.6 (5H, m); MS *m/z* (%): 202 (M^+, 69), 184 ($[M-H_2O]^+$, 24), 159 (100); Found: C, 83.09; H, 9.00%; *m/z* 202.1353. Calcd for $C_{14}H_{18}O$: C, 83.12; H, 8.79%; M, 202.1356.

(*E*)-4-(4-Methoxyphenyl)-2-methyl-3-buten-2-ol (6f). Mp 57—59 °C (hexane); IR (KBr): 3370 (OH) cm^{-1}; ^1H NMR δ=1.42 (6H, s), 3.83 (3H, s), 6.24 (1H, d, J=16.5 Hz), 6.54 (1H, d, J=16.5 Hz), 6.88, 7.33 (each 2H, d, J=8 Hz) MS *m/z* (%): 192 (M^+, 42), 177 ($[M-CH_3]^+$, 100), 159 (24), 121 (90); Found: C, 75.07; H, 8.28%. Calcd for $C_{12}H_{16}O_2$: C, 74.97; H, 8.39%.

(*E*)-1-(4-Methoxystyryl)-1-cyclohexanol (6g). Colorless oil; IR (neat): 3400 (OH) cm^{-1}; ^1H NMR δ=1.0—1.8 (10H, m), 3.82 (3H, s), 6.22 (1H, d, J=16 Hz), 6.58 (1H, d, J=16 Hz), 6.87, 7.33 (each 2H, d, J=9 Hz); MS *m/z* (%): 232 (M^+, 46), 214 ($[M-H_2O]^+$, 7), 189 (54), 121 (100); Found: *m/z* 232.1466. Calcd for $C_{15}H_{20}O_2$: M, 232.1462.

(*E*)-2-Methyl-4-(1-naphthyl)-3-buten-2-ol (6h). Colorless oil; IR (neat): 3370 (OH) cm^{-1}; ^1H NMR δ=1.49 (6H, s), 6.40 (1H, d, J=16 Hz), 7.2—8.2 (8H, m); MS *m/z* (%): 212 (M^+, 52), 197 ($[M-CH_3]^+$, 26), 179 (77), 152 (34), 141 (100); Found: *m/z* 212.1204. Calcd for $C_{15}H_{16}O$: M, 212.1200.

1,1-Diphenyl-2,5-pentadien-1-ol (6i). Mp 52—54 °C (MeOH-H_2O); IR (KBr): 3380 (OH) cm^{-1}; ^1H NMR δ= 5.08—5.37 (2H, m), 6.23—6.68 (3H, m), 7.1—7.5 (10H, m); MS *m/z* (%): 236 (M^+, 8), 218 ($[M-H_2O]^+$, 1), 183 (5), 165 (4), 105 (100); Found: *m/z* 236.1192. Calcd for $C_{17}H_{16}O$: M, 236.1200.

3β-(1,3-Butadienyl)-5α-cholestan-3α-ol (6j). Mp 84—86 °C (MeOH-H_2O); IR (KBr): 3500 (OH) cm^{-1}; ^1H NMR δ=0.66 (3H, s), 0.87 (6H, d, J=6.5 Hz), 0.90 (3H, d, J=6.5 Hz), 0.99 (3H, s), 5.0—5.4 (2H, m), 5.7—6.0 (1H, m), 6.1—6.6 (2H, m); MS *m/z* (%): 440 (M^+, 12), 422 ($[M-H_2O]^+$, 16), 407 (10), 43 (100); Found: *m/z* 440.3999. Calcd for $C_{31}H_{52}O$: M, 440.4014.

Isomerization of the Epoxide (5e-P) into Allylic Alcohol (6e). To a solution of LDA (0.2 mmol) in 0.2 ml of dry THF was added a solution of butyl phenyl sulfoxide (0.2 mmol) in 0.2 ml of dry THF under N_2 at −70 °C. After 10 min, a solution of **5e-P** (0.2 mmol) in 0.4 ml of dry THF was added to the mixture and stirred at −70 °C for 5 min. The reaction was quenched with sat. aq NH_4Cl. After the usual work-up, the allylic alcohol (**6e**) and the starting material (**5e-P**) were obtained in 25 and 75% yield, respectively.

The authors are grateful to Dr. S. Saito, Tanabe Seiyaku Co., Ltd., for the elemental analysis and Miss Sawabe, Mrs. Yamatani and Miss Ohne of this laboratory for NMR and MS measurements.

References

1) α,β-Epoxy sulfoxides as useful intermediates in organic synthesis VIII. Part VII. T. Satoh, S. Motohashi, and K. Yamakawa, *Tetrahedron Lett.*, **27**, 2889 (1986).

2) a) H. O. House "Modern Synthetic Reactions," W. A. Benjamine, Inc. Menlo Park, California (1982), pp. 292—352; b) K. B. Sharpless and T. R. Verhoeven, *Aldrichmica Acta*, **12**, 63 (1979); c) T. Katsuki and K. B. Sharpless, *J. Am. Chem. Soc.*, **102**, 5974 (1980).

3) C. H. Behrens and K. B. Sharpless, *Aldrichmica Acta*, **16**, 67 (1983); J. G. Smith, *Synthesis*, **1983**, 629.

4) Y. Kishi, *Aldrichimica Acta*, **13**, 23 (1980); S. Masamune and W. Choy, *ibid.*, **15**, 47 (1982).

5) D. Swern, *Org. React.*, **7**, 378 (1953).

6) J. P. Pizey "Synthetic Reagents," John Wiley & Sons, Inc., 2, pp. 1—66 (1974).

7) M. S. Newmann and B. J. Mogerlein, *Org. React.*, **5**, 413 (1949); M. Ballester, *Chem. Rev.*, **55**, 283 (1955).

8) E. J. Corey and M. Chaykovsky, *J. Am. Chem. Soc.*, **87**, 1353 (1965); B. M. Trost and L. S. Melvin, Jr., "Sulfur Ylides," Academic Press, New York (1975).

9) W. C. Still and V. J. Novack, *J. Am. Chem. Soc.*, **103**, 1283 (1981).

10) T. Durst, *J. Am. Chem. Soc.*, **91**, 1034 (1969); T. Durst, K.-C. Tin, F. de Reinach-Hirtzbach, J. M. Decesare, and M. D. Ryan, *Can. J. Chem.*, **57**, 258 (1979).

11) a) T. Satoh, Y. Kaneko, T. Izawa, K. Sakata, and K. Yamakawa, *Bull. Chem. Soc. Jpn.*, **58**, 1983 (1985); b) T. Satoh, T. Kumagawa, and K. Yamakawa, *ibid.*, **58**, 2849 (1985); c) T. Satoh, Y. Kaneko, K. Sakata, and K. Yamakawa, *ibid.*, **59**, 457 (1986); d) T. Satoh, S. Motohashi, and K. Yamakawa, *ibid.*, **59**, 946 (1986).

12) J. P. lockard, C. W. Schroeck, and C. R. Johnson, *Synthesis*, **1973**, 485; T. Durst, M. J. LeBelle, R. Van den Elzen, and K.-C. Tin, *Can. J. Chem.*, **52**, 761 (1974); K. Ogura, K. Arai, and G. Tsuchihashi, *Bull. Chem. Soc. Jpn.*, **55**, 3669 (1982).

13) The diastereomers of the α,β-epoxy sulfoxides (**4**) are expressed as L- and P-, respectively. Details see references lla and llb.

14) Y. Tamura, S. M. Bayomi, K. Sumoto, and M. Ikeda, *Synthesis*, **1977**, 693.

15) A. Gaudemer, M. Golfier, A. Mandelbaum, and R. Parthasarathy "Stereochemistry Fundamentals and Methods" H. B. Kagan, Ed., Georg Thieme Publishers Stuttgart, Vol. 1. pp. 51—53 (1977).

16) A. C. Cope and J. K. Heeren, *J. Am. Chem. Soc.*, **87**, 3125 (1965); H. Nozaki, T. Mori, and R. Noyori, *Tetrahedron*, **22**, 1207 (1966).

17) J. D. Ballantine and P. J. Sykes, *J. Chem. Soc.*, (C) **1970**, 731; C. Fleischmann and E. Zbiral, *Tetrahedron*, **34**, 317 (1978).

18) H. Neumann and D. Seebach, *Chem. Ber.*, **111**, 2785 (1978).

19) In the preliminary communication (T. Satoh, Y. Kaneko, and K. Yamakawa, *Tetrahedron Lett.*, **27**, 2379 (1986)) of this study, the configuration of 3-position of cholestanone derivatives (**4j**, **4k**, **5j**, **5k**, and **6j**) were erroneously described as β-epoxides and β-hydroxy compound.

Regioselective Carboxylation of Silicon-Stabilized Allylic Carbanions and the Synthetic Utility of 2-Silyl-3-butenoates

Hidemitsu UNO
Advanced Instrumentation Center for Chemical Analysis, Ehime University, Bunkyo-cho 2-5, Matsuyama 790
(Received March 10, 1986)

Carbanions of allylic dimethylphenylsilanes show remarkable regioselectivity toward both carboxylation with carbon dioxide and methylation with methyl iodide. Methylation of these compounds occurred preferentialy at α position, although allyltrimethylsilane and allyltriphenylsilane are known to give γ selectivity toward the same electrophiles. Moreover, their aluminum "ate" complexes react with carbon dioxide regioselectively at the α position irrespective of methyl substitution pattern of the allylic moieties. The α-carboxylated allylic silanes proved to be useful synthons of 3-(methoxycarbonyl)allyl anions after esterification.

Regioselectivity in the reaction of unsymmetrical allylic carbanions with electrophiles has been discussed from both theoretical and synthetic points of view by numerous investigators[1] and is still subtle because it depends upon not only inherent characters of allylic carbanions, i.e. charge densities and HOMO coefficients, but also counter metal cations, solvation, steric effects, and transition states. Many efforts have been made to attain preferable regiochemistry. For example, predominant location of the counter cations was successfully achieved by charge repulsion,[2] intramolecular chelation,[3] and transmetallation[4] including "ate" complexation.[5] Accessibility of electrophiles to the carbanionic centers was well controlled by "hard-soft" interaction,[6] steric effects,[7] and transition state.[7] Although similar methodologies could be generally applied for the regiochemical control of silicon-stabilized allylic carbanions, γ-regioselectivity was frequently realized mainly because of steric factors.[8] Tsai and Matteson[9] have reported an exclusive α selectivity in reactions of 3-trimethylsilyl-2-propenyl-boronate. Similar results[10] have been reported in the reaction of η^3-trimethylsilylallyltitanium(III) compound, [Ti(η^5-cp)$_2$(η^3-1-trimethylsilylallyl)]. Success of these reactions may be ascribed to location of very bulky counter cations on the γ carbon. While the effects of counter cations at the transition state have been frequently discussed,[8] the roles of substituents on silicon atom have never been considered. We have already reported that aluminates of dimethylphenylsilyl-stabilized allylic carbanions reacted with carbon dioxide regioselectively at α position.[11] In this report, we describe the further results about the effects of substituents on a silicon atom.

Results and Discussion

Regioselectivity in Nucleophilic Reaction of Silyl-Stabilized Allylic Carbanions. Alkylation of silyl-stabilized carbanions bearing alkali metals as counter cations has been reported to occur preferably at γ position because of the steric hindrance and the large γ charge densities. For example, lithiated allyltriphenylsilane (**1b**) reacted with methyl iodide exclusively at γ position as well as the corresponding trimethylsilyl derivatives.[8a,8f,8l] The lithiated derivative of allyldimethylphenylsilane (**1c**), however, was found to react predominantly at α position to give a mixture of (1-methyl-2-propenyl)dimethylphenylsilane (**1h**) and (1-butenyl)dimethylphenylsilane (**2c**) (**1h**/**2c** =80/20) (Eq. 1). Also, moderate α selectivity was observed in 1-methyl-2-propenylsilane **1h** (**1l**/**2h**= 64/36). Allylmethyldiphenylsilane (**1d**), of which α position could be more hindered than **1c**, still showed α selectivity (**1m**/**2d**=73/27).

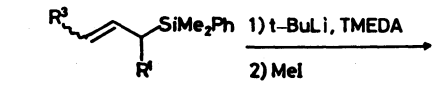

1c $R^1=R^3=H$
1h $R^1=Me, R^3=H$

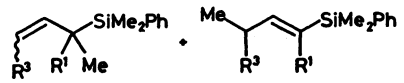

(1)

1h $R^1=R^3=H$ **2c**
1l $R^1=Me, R^3=H$ **2h**

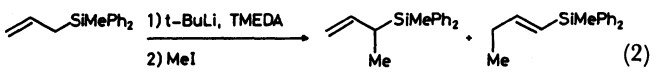

(2)

1d **1m** **2d**

According to MINDO/3 calculation for a carbanion of allylsilane,[12] α selectivity was predicted under orbital control conditions, while γ selectivity under charge control conditions. From orbital cosideration, stabilization of an adjacent carbanion by a silyl group is attributable to p-σ* hyperconjugation.[13] In allyldimethylphenylsilane (**1c**), the energy level of the σ*

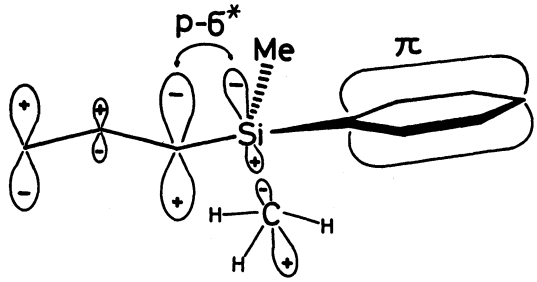

Fig. 1. Proposed orbital interaction of 1c.

Table 1. Carboxylation of Allylic Carbanions

Entry	Silane 1						3/4 Ratio (Yield/%)[a]	
	R_3	R^1	R^2	R^3	R^4		M^+=Li^+	M^+=$AlEt_3 \cdot Li^+$
1	Me_3	H	H	H	H	(**1a**)	12/88	75 (35)/25
2	Ph_3	H	H	H	H	(**1b**)	20/80 (60)[b]	70 (55)/30
3	Me_2Ph	H	H	H	H	(**1c**)	20/80 (59)[c]	100 (85)/—
4	$MePh_2$	H	H	H	H	(**1d**)	23/77 (91)[c]	100 (60)/—
5	$Me_2(CH{=}CH_2)$	H	H	H	H	(**1e**)	29/71 (29)[c]	100 (46)/—
6	Me_2(*p*-Tol)	H	H	H	H	(**1f**)	22/78 (53)[c]	100 (50)/—
7	Me_2(*t*-Bu)	H	H	H	H	(**1g**)	—[d]	100 (20)/—
8	Me_2Ph	Me	H	H	H	(**1h**)	45 (35)/55 (44)	100 (75)/—
9	Me_2Ph	H	Me	H	H	(**1i**)	20/80 (50)[c]	100 (70)/—
10	Me_2Ph	H	H	Me	H	(**1j**)	—/100 (79)	100 (65)/—[e]
11	Me_2Ph	H	H	Me	Me	(**1k**)	—/100 (25)	—

a) Isolated yield. b) Ref. 8b. c) Isolated yield of the regioisomeric mixture. d) Not determined. e) Stereoisomeric ratio was determined to be Z/E=>10/1 by the ^1H NMR (400 MHz) analysis after methylation with diazomethane.

orbital of Si-Me bond would be lowered by the conjugation with a phenyl group (Fig. 1).[14] Therefore, the interaction between p orbitals of an allylic carbanion moiety and the σ^* antibonding orbital might be increased and larger HOMO coefficient at α carbon was expected than that of allyltrimethylsilane (**1a**). Moreover, the charge density at the α carbon might be increased according to the electron-attracting character of a phenyl group. Allyltriphenylsilane (**1b**) would show the reverse selectivity because of not only large steric hindrance but the lack of the low lying sp^3-σ^* orbital. Indeed, it was reported that methylation of **1b** occurred exclusively at the γ carbon[8a] and that moderate γ selectivity (α/γ=35/65) was observed in the alkylation of **1a** with alkyl iodides. On the other hand, preferential α methylation was observed if the silicon atom had both methyl and phenyl groups (**1c**: α/γ=80/20, **1d**: α/γ=73/27). Allylic carbanions stabilized by a dimethylphenylsilyl or methyldiphenylsilyl group were no longer γ selective in the reaction with methyl iodide, a "soft" electrophile. In the next, we will focus the discussion on the regioselectivity in the carboxylation of silyl-substituted allylic carbanions with carbon dioxide, which is classified to a "hard" electrophile.

Carboxylation of the lithiated derivatives of allyltriorganosilanes was carried out at −78 °C by reverse addition of the carbanion solution to give a regioisomeric mixture in moderate to good yields (Eq 3 and Table 1). In Entries 1—6, moderate γ regio-

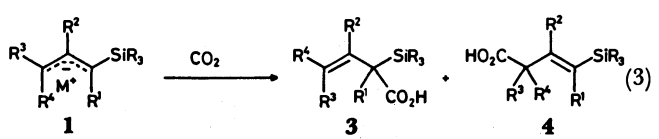

1 3 4 (3)

selectivity (**3**/**4**=12/88—29/71) was observed. The γ selectivity could be well explained in terms of the 6-membered cyclic transition state if the equilibrium between the α-lithio allylic silanes and γ-lithio vinylic silanes was assumed to lie to the formers (Eq. 4).

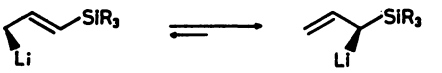

(4)

This assumption was supported by the fact that carboxylation of butenylsilane **1j** occurred preferably at the carbanion center bearing a methyl substituent to give exclusively γ carboxylated compounds **4j** in good yield, although this position is sterically disadvantageous (Entry 10). On the other hand, the reaction of (1-methyl-2-propenyl)dimethylphenylsilane (**1h**) showed lower regioselectivity (Entry 8, **3h**/**4h**=45/55).[15] It is known that a methyl substituent increases the charge density on the γ carbon to the methyl group because of its electron-donating character. Therefore, lithium counter cation would tend to be localized at the γ position to the methyl group. Opposite effects between methyl and dimethylphenylsilyl groups described above would be the reason for the low selectivity in 1-methyl-2-propenylsilane **1h**. On the other hand, cooperative effects of both substituents to give the high γ regioselectivity in **1j** and **1k**.

We turned our attention to effects of counter cations. Corriu and his co-workers[8b] reported that α-carboxylated compound **3b** was preferably obtained (**3b**/**4b**=85/15) in the reaction of the Grignard reagent prepared from 3-bromo-1-triphenylsilylpropene. The similar result (**3c**/**4c**=83/17) was obtained in the carboxylation of the Grignard reagent prepared from 3-bromo-1-(dimethylphenylsilyl)propene.[8b] As the carboxylation of the Grignard reagents would also be thought to proceed via 6-membered cyclic transition state, the different selectivity between lithio and magnesio derivatives might be interpreted if we would assume that the magnesium counter cation would be localized mainly at the γ position by the electronic repulsion with the silyl group. Though the respective electronegativity values of magnesium and lithium were given as 1.2 and 1.0, a magnesium counter cation might be more positive than a lithium counter cation

because the former had another highly polarized magnesium-halogen bond.[16]

In order to obtain the α-carboxylated products in high selectivity, we examined the effects of additives to lithio derivatives of allylic silanes. As high α selectivity was reported in the reaction of lithiated allyltrimethylsilane with acetophenone in the presence of $MgBr_2$,[8f] carboxylation was carried out according to the similar manner to give a regioisomeric mixture (**3a**/**4a**=83/17). In the course of the reaction, it was ambigous whether the actual intermediate was a magnesio derivative or a magnesium "ate" complex, because the magnesium-bromine bond was accounted to undergo transmetallation reaction with alkyllithiums.

As aluminum "ate" complexes were reported to show marked regioselectivity in the reaction with various electrophiles,[5] we attempted to utilize this method to the carboxylation. The allylic aluminum "ate" complex, which was generated in situ by adding triethylaluminum to the lithiated allyltrimethylsilane, reacted smoothly with CO_2 to give a regioisomeric mixture which consisted of **3a** and **4a** (**3a**/**4a**=75/25). By chromatographic separation, pure α-carboxylated compound **3a** was obtained in 35% yield (Table 1). The low isolated yield seemed to be attributable to instability of **3a**. During the isolation and purification, **3a** slowly decomposed to give 2- and 3-butenoic acid. Once **3a** was isolated as solids, it could be stored in a freezer without decomposition for several weeks. Allyltriphenylsilane (**1b**) gave a mixture of α- and γ-carboxylated compounds (**3b**/**4b**=70/30). On the other hand, carboxylation of dimethylphenylsilyl derivative **1c** occurred exclusively at the α position to give 2-(dimethylphenylsilyl)-3-butenoic acid (**3c**) in good yield (Entry 3). Similar high α selectivity was realized in the reaction of "hybrid" allylsilanes (Entries 4—7). Low yields obtained in the reaction of **1e** and **1g** (Entries 5 and 7) could be ascribed to anionic polymerization and poor metallation. A methyl substituent on the allyl moiety proved to have no influence on the regioselectivity if the dimethylphenylsilyl group was employed as an anion-stabilizing group. Silanes **1h**, **1i**, and **1j** were carboxylated regioselectively at α position to give α-silyl β,γ-unsaturated carboxylic acids in good yields (Entries 8, 9, and 10). It is noteworthy that 2-butenylsilane **1j** gave *Z*-isomer of 2-(dimethylphenylsilyl)-3-pentenoic acid (**3j**) in good selectivity (*Z*/*E*=>10/1) (Entry 10). 3-Methyl-2-butenylsilane **1k** (Entry 11) did not show the existence of any carboxylated compounds. Similar results were also obtained in the reactions of (1,2-dimethyl-2-propenyl)-, (2-methyl-2-butenyl)-, and (1-methyl-2-butenyl)dimethylphenylsilanes of which lithiation seemed to occur insufficiently. Though there is some limitation that this method could not be applied for highly-substituted allylic silanes, this method is very useful for the preparation of α-silyl β,γ-unsaturated carboxylic acids.

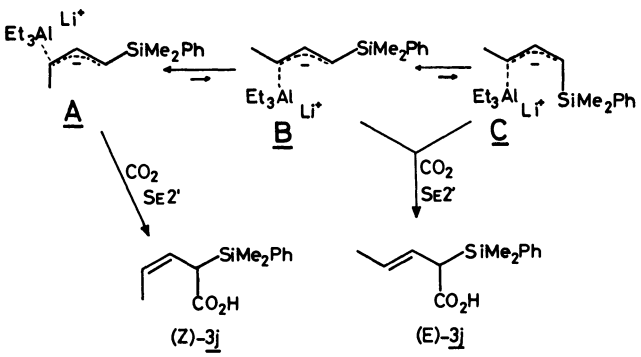

Fig. 2. Proposed carboxylation mechanism.

The remarkable α regioselectivity and stereoselectivity may be interpreted by applying the similar postulation described in the alkylation except for the case of **1g**. The reaction mechanism is discussed about 2-butenyldimethylphenylsilane (**1j**) as a representative case including both problems. There might be a conformational equilibrium of the allylic aluminate generated by adding Et_3Al to the lithiated derivative of 2-butenylsilane **1j** (Fig. 2). In the equilibrium, triethylaluminum would be localized at γ position by steric and/or electrostatic repulsions with the silyl group. Since 2-butenyllithium was reported to exist preferably as an "S"-shape comformer in a THF solution,[17] the conformer **A** would be more faborable than the "W"-shape conformer **B**. Another "S"-shape conformer **C** seemed to be disadvantageous because of the steric interaction between the bulky silyl group and a γ-allylic proton. Indeed, all vinylic silanes obtained in the reaction at γ position had trans geometry and no generation of cis vinylic silanes was observed in all cases irrespective of the species of counter cations. As aluminum "ate" complexes were considered to be in a saturated coordination state, 6-membered cyclic transition state might not participate even in the reaction of carbon dioxide. Therefore, it is suitable to consider that S_E2' type reaction via the conformer **A** would occur on the α carbon which had the large HOMO coefficient to afford *cis*-2-(dimethylphenylsilyl)-3-pentenoic acid (**3j**).

By treatment with CH_2N_2, α-carboxylated allylic silanes were converted to the corresponding methyl esters which proved to be useful for introduction of 3-(methoxycarbonyl)allyl groups.[11] We have demonstrated the utility of methyl 2-(dimethylphenylsilyl)-

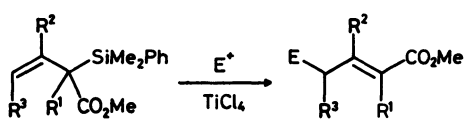

(5)

5c $R^1=R^2=R^3=H$
5h $R^1=Me$, $R^2=R^3=H$
5i $R^1=R^3=H$, $R^2=Me$
5j $R^1=R^2=H$, $R^3=Me$

Table 2. Reaction of Allylic Silanes **5** with Electrophiles

Entry	Electrophile	Silane	Conditions	Product	Yield/%[a]
1	$MeOCH_2Cl$	**5h**	−78 °C, 1 h	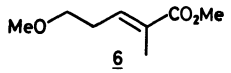 **6**	77[b]
2		**5j**	−78 °C, 1 h	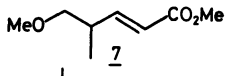 **7**	66
3	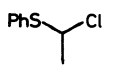	**5h**	−78 ~ −10 °C, 1 h	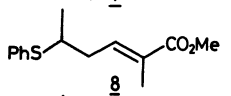 **8**	73[b]
4		**5j**	−78 ~ −10 °C, 1 h	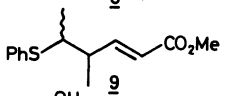 **9**	66[c]
5		**5h**	−78 °C ~ r.t., 2 h	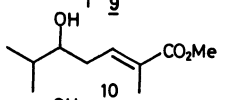 **10**	48[b]
6		**5j**	−78 °C ~ r.t., 2 h	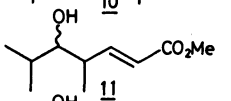 **11**	70[c]
7	$MeCOCO_2Me$	**5h**	−78 °C ~ r.t., 3 h	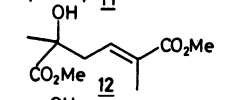 **12**	96[b]
8		**5j**	−78 °C ~ r.t., 2 h	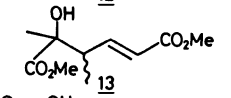 **13**	–[d]
9	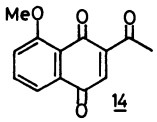 **14**	**5h**	−78 ~ −10 °C, 1 h[e]	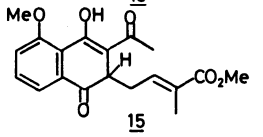 **15**	70[f]
10		**5j**	−78 ~ −10 °C, 1 h[e]	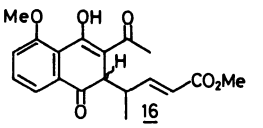 **16**	72[f]
11		**5h**	−78 °C ~ r.t., 1 h	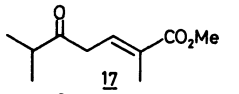 **17**	54
12		**5j**	−78 °C ~ r.t., 1 h	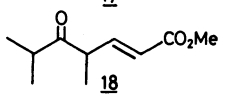 **18**	77[g]
				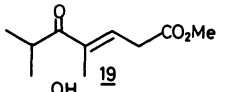 **19**	
13	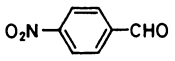	**5h**	−78 °C ~ r.t., 1 h	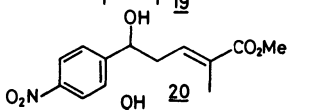 **20**	53
14		**5j**	−78 °C ~ r.t., 1 h	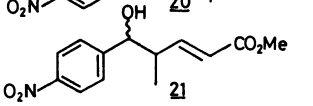 **21**	69[h]

a) Isolated yield. b) Only E isomer. c) Diastereomeric mixture (ca. 1:1). d) Cyclic trimers of methyl pyruvate was obtained and **5j** was recovered in a 57% yield. e) Tin tetrachloride was employed instead of $TiCl_4$. f) Isolated yield of the corresponding hydroquinone diacetate after treatment with pyridine and acetic anhydride. g) During the purification by column chromatography the double bond of **18** migrated to give a mixture (**18**/**19**=1/5.8). h) The diastereomeric ratio was estimated to be 73:27 by the NMR analysis.

3-butenoate (**5c**) in the total syntheses of 1*H*-3,4-dihydronaphtho[2,3-*c*]pyran-5,10-dione antibiotics[18] and anthracyclinones.[19] α-Silyl β,γ-unsaturated esters (**5h** and **5j**) can be prepared only by our method[20] and are synthetically more valuable.

Lewis Acid-Mediated Reaction of Allylic Silanes 5 with Electrophiles. In the presence of $TiCl_4$, **5h** prepared from **3h** in quantitative yield reacted smoothly with electrophiles at γ position as expected[21] (Table 2). The reaction with chloromethoxymethane was

carried out in the presence of $TiCl_4$ (1 equiv) at −78°C to give a crude mixture which consisted of almost only (*E*)-**7**. After column chromatography, pure (*E*)-**7** was obtained in 77% yield. α-Chloroethyl phenyl sulfide, isobutyraldehyde, and methyl pyruvate were also reacted smoothly to give trans α,β-unsaturated esters (**8**; 73%, **10**; 48%, and **12**; 96%). The reaction of acetylquinone **14** occurred at the quinone nucleus to afford **15**, which was isolated as the corresponding hydroquinone diacetate **15a** after treatment with acetic anhydride and pyridine. In this reaction $SnCl_4$, as a milder Lewis acid than $TiCl_4$, was employed instead of $TiCl_4$ because the quinone **14** was a very good Michael acceptor. Isobutyryl chloride was also employed to give δ-oxo, α,β-unsaturated ester **17** which was isolated by column chromatography in a 54% yield without the double bond migration. Similarly, (*Z*)-**5j** also reacted with various electrophiles at γ position in the presence of a Lewis acid to give 3-substituted *trans*-pentenoates in good yields (Table 2). Pure (*Z*)-**5j** employed in this reaction was readily prepared from the corresponding (*Z*)-carboxylic acid **3j** which was purified by recrystallization. It is noteworthy that isobutyryl chloride reacted with **5j** to give only α,β-unsaturated ester **18**. During the isolation by column chromatography the double bond of **18** mostly migrated to give a mixture (**18**/**19** = 1/5.8). In Entry 8, **5j** was recoverd in a 57% yield instead of the expected compound **13**. Under the applied reaction conditions methyl pyruvate reacted with itself to give a cyclic trimer. The remarkable contrast between the reaction of **5h** and **5j** (Entries 7 and 8) could be attributed to the steric difference at their γ carbons. In any reactions of **5j**, diastereoselectivity could not be observed in spite of all our efforts. The lack of high selectivity might be considered as follows. The reaction of (2-butenyl)trimethylsilane probably proceeds via acyclic transition state to exibit the selectivity whereas in that of **5j**, cyclic transition state might participate since the reagent has a carbonyl group which could coordinate the Lewis acid.

In both reactions of **5h** and **5j**, only (*E*)-olefins were obtained. This *E* selectivity could be easily interpreted if we assumed **5h** and **5j** would take the similar conformation as that of **5c** described in the preliminary report (Scheme 1).[11]

Experimental

All melting points were measured with a Yanagimoto micromelting point apparatus and are uncorrected. ^1H NMR spectra were observed with Hitachi R-600 (60 MHz), JEOL-PS-100 (100 MHz), and/or JEOL-GX-400 (400 MHz) spectrometers with TMS as an internal standard. IR spectra were measured with a JASCO IRA-1 and/or Hitachi 270-30 spectrometers. Mass spectra were measured with Hitachi M-80B spectrometer. Column chromatography was performed using Wakogel C-200. Diethyl ether and THF were distilled from sodium benzophenone ketyl and stored over sodium wire. Dichloromethane was distilled from calcium hydride and stored over 4A molecular sieves. Other solvents were used after simple distillation otherwise noted. Allylic silanes; **1c** (bp 93°C/2.27 kPa), **1d** (bp 85°C/27 Pa), **1e** (bp 112°C), **1f** (bp 80—84°C/667 Pa), **1g** (bp, 147°C), **1h**[22] (bp 106°C/2.67 kPa), and **1i** (bp 110°C/3.07 kPa), were prepared from chlorosilanes and the Grignard reagents. 2-Butenylsilane **1j** (bp 106°C/2.67 kPa) and 3-methyl-2-butenylsilane **1k**[22] (bp 115—118°C/2.00 kPa) were prepared from the silyllithium and allylic halides.

Lithiation of Allylic Silanes. Following methods A and B are applicable for almost cases except for **1e**, and give similar results. For the lithiation of **1e** method C was employed to privent from Michael addition to a vinyl group.

Method A: An allylic silane (1 equiv) and *N,N,N',N'*-tetramethylethylenediamine (TMEDA, 1.5 equiv) were placed in a three-necked flask fitted with a stopcock, a rubber serum cap, and a thermometer. The vessel was filled with nitrogen. After addition of THF (3 ml/1 mmol) the mixture was cooled to −78°C by Dry Ice acetone bath and then *t*-BuLi (pentane solution, 1.5 equiv) was added dropwise. After the addition the mixture was gradually warmed to −40°C and stirred at −40—−30°C for 1 h.

Method B: To a THF solution (3 ml/1 mmol) of an allylic silane (1 equiv) and TMEDA (1.5 equiv) was added *n*-BuLi (hexane solution, 1.5 equiv) under −70°C. The mixture was gradually warmed up to −15°C and allowed to stand for 2 d in a freezer (−15°C).

Method C: To a THF solution (3 ml/1 mmol) of an allylic silane (1 equiv) and TMEDA (1.5 equiv) was added MeLi (ether solution, 1.5 equiv) at −20°C. The mixture was allowed to stand for 3 d in a freezer (−15°C).

Methylation of Allyldimethylphenylsilane 1c. To an orange yellow solution of lithiated **1c** prepared by method A (**1c**, 880 mg, 5 mmol) was added MeI (1.42 g, 10 mmol) at −78°C. The resulted white suspension was allowed to warm to 0°C and then aq NH_4Cl was added. The reaction mixture was extracted with ether. The ethereal phase was wash-

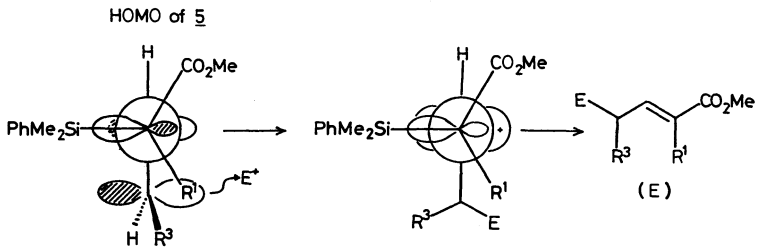

Scheme 1.

ed with brine and dried over Na_2SO_4. After the solvent was evaporated, the residue was simply purified by being passed through a short silica-gel column (hexane–ether). From the ^1H NMR spectrum (400 MHz), the mixture was proved to consist of the starting silane **1c** (32%), **1h** (53%), and **2c** (15%). Separation of the methylated compounds from **1c** was achieved by preparative GPC (Japan Analytical Industry, LC-08, JAI-1H (20 mmID × 60 cm) +JAI-2H (20 mmID× 60 cm)) using $CHCl_3$ as a carrier solvent to give 672 mg (65%) of **1h** (80%) and **2c** (20%). Isomer ratio of the purified products was almost unchanged from the crude one. **1h**: ^1H NMR ($CDCl_3$, 400 MHz) δ=0.30 (6H, s), 1.08 (3H, d, J=17.3 Hz), 1.87 (1H, t-quintet, J=7.3, 1.6 Hz), 4.83 (1H, dt, J=17.1, 1.8 Hz), 4.89 (1H, dt, J=10.4, 1.5 Hz), 5.89 (1H, ddd, J=17.1, 10.4, 7.3 Hz), 7.39 (3H, m), and 7.54 (2H, m). **2c**: ^1H NMR ($CDCl_3$, 400 MHz) δ=0.35 (6H, s), 1.04 (3H, t, J=7.3 Hz), 2.19 (2H, m), 5.80 (1H, d, J=18.3 Hz), 6.21 (1H, dt, J=18.3, 5.6 Hz), 7.39 (3H, m), and 7.54 (2H, m).

Methylation of (1-Methyl-2-propenyl)dimethylphenylsilane (1h). The reaction of **1h** (380 mg, 2 mmol) was carried out in the similar manner as described above. By the NMR analysis of the reaction mixture, it was estimated to consist of **1h** (67%), **1l** (21%), and **2h** (12%). **1l**: ^1H NMR ($CDCl_3$, 400 MHz) δ=0.29 (6H, s), 1.02 (6H, s), 4.73 (1H, dd, J=17.4, 1.5 Hz), 4.91 (1H, dd, J=10.7, 1.5 Hz), 5.84 (1H, dd, J=17.4, 10.7 Hz), 7.38 (3H, m), and 7.53 (2H, m). **2h**: ^1H NMR ($CDCl_3$, 400 MHz) δ=0.35 (6H, s), 1.02 (3H, t, J=7 Hz), 1.68 (3H, m), 2.16 (2H, quintet, J=7 Hz), 5.40 (1H, m), 7.38 (3H, m), and 7.53 (2H, m).

Methylation of Allylmethyldiphenylsilane (1d). The reaction of **1d** (476 mg, 2 mmol) was carried out in the similar manner. By the NMR analysis of the reaction mixture, it was proved to consist of **1d** (65%), **1m** (18%), and **2d** (7%). **1m**: ^1H NMR ($CDCl_3$, 400 MHz) δ=0.58 (3H, s), 1.19 (3H, d, J=7.3 Hz), 2.34 (1H, m), 4.95 (2H, m), 5.98 (1H, ddd, J=17.1, 10.4, 7.0 Hz), 7.40 (6H, m), and 7.57 (4H, m). **2d**: ^1H NMR ($CDCl_3$, 400 MHz) δ=0.65 (3H, s), 1.08 (3H, t, J=7.5 Hz), 2.25 (2H, m), 6.00 (1H, d, J=18.6 Hz), 6.28 (1H, dt, J=18.6, 5.6 Hz), 7.40 (6H, m), and 7.57 (4H, m).

Carboxylation of Lithiated Allylic Silanes. General Procedure: Dry CO_2 gas (through a $CaCl_2$ column) was bubbled into THF (5 ml/1 mmol) at −78°C under argon. A solution of the lithiated allylic silane was slowly introduced into the THF solution absorbing CO_2 at −78°C by a stainless steel transfer tube. The color of the lithiated allylic silane (yellow or orange yellow) rapidly faded to give a clear colorless solution. The reaction was quenched by adding an aqueous NH_4Cl solution and acidified by 5% HCl. The reaction mixture was extracted with ether. The ethereal phase was washed with brine and dried over Na_2SO_4. After the solvent was evaporated in vacuo at room temperature, the residue was chromatographed on silica gel (hexane/CH_2Cl_2/ether=1/1/0—1/1/0.1).

Carboxylation of Allylic Aluminates. General Procedure: A hexane solution of triethylaluminum (ca. 1.4 M[†]) was slowly added to the solution of the lithiated allylic silane at −78° C untill the color of the solution became almost colorless. The mixture was stirred for additional 10 min and then dry CO_2 gas was slowly introduced to the solution at −78° C. After a large excess amount of CO_2 was absorbed, the solution was gradually warmed to 0° C and stirred for 15 min. After being recooled to −30° C, the reaction mixture was poured into a cold aq NH_4Cl solution (ca. −10° C) and then ether was added. The mixture was acidified by cold 5% aq HCl until both phases became clear. The organic phase was separated and the aqeous phase was extracted twice with ether. The combined organic phase was washed twice with cold 5% aq HCl and brine and dried over Na_2SO_4. After the solvent was evaporated in vacuo at ambient temperature, the residue was chromatographed on silica gel (hexane/CH_2Cl_2/ether=1/1/0—1/1/0.1).

2-(Trimethylsilyl)-3-butenoic Acid (3a): Colorless crystals (ether/hexane); mp 72—73° C; ^1H NMR ($CDCl_3$) δ=0.13 (9H, s), 2.95 (1H, d, J=10 Hz), 4.76—5.08 (2H, m), 6.00 (1H, dt, J=16, 10 Hz), and 9.02 (1H, broad s). Found: C, 53.31; H, 8.97%. Calcd for $C_7H_{14}O_2Si$: C, 53.12; H, 8.92%.

4-(Trimethylsilyl)-3-butenoic Acid (4a): A colorless oil; ^1H NMR ($CDCl_3$) δ=0.08 (9H, s), 3.13 (2H, d, J=6 Hz), 5.76 (1H, d, J=19 Hz), 6.09 (1H, dt, J=19, 6 Hz), and 10.90 (1H, broad s); IR (neat) 2960 (broad s), 1714 (vs), 1616 (m), 1418 (m), 1250 (s), 862 (s), and 840 cm^{-1} (s).

2-(Triphenylsilyl)-3-butenoic Acid (3b):[8b] Colorless prisms (benzene/hexane); mp 179—180° C; ^1H NMR ($CDCl_3$) δ=3.75 (1H, d, J=10 Hz), 4.80—5.10 (2H, m), 6.02 (1H, dt, J=16, 10 Hz), 7.20—7.80 (15H, m), and 10.0 (1H, broad s); IR (KBr) 300 (broad s), 1675 (vs), 1425 (vs), 1200 (s), and 1115 cm^{-1} (vs).

4-(Triphenylsilyl)-3-butenoic Acid (4b):[8b] Colorless crystals (benzene/hexane); mp 157—158° C; ^1H NMR ($CDCl_3$) δ=3.31 (2H, d, J=5 Hz), 6.10 (1H, dt, J=16, 5 Hz), 6.36 (1H, d, J=16 Hz), 7.2—7.7 (15H, m), and 10.30 (1H, broad s).

2-(Dimethylphenylsilyl)-3-butenoic Acid (3c): Colorless crystals (ether/hexane); mp 48—49.5° C; ^1H NMR ($CDCl_3$) δ=0.42 (6H, s), 3.04 (1H, d, J=10 Hz), 4.56—4.96 (2H, m), 5.87 (1H, dt, J=17, 10 Hz), 7.16—7.50 (5H, m), and 10.58 (1H, broad s); IR (neat) 3200 (broad m), 1690 (vs), 1430 (s), 1255 (s), and 1120 cm^{-1} (s). Found: C, 65.47; H, 7.44%. Calcd for $C_{12}H_{16}O_2Si$: C, 65.41; H, 7.31%.

4-(Dimethylphenylsilyl)-3-butenoic Acid (4c): A colorless oil; ^1H NMR ($CDCl_3$) δ=0.35 (6H, s), 3.14 (2H, d, J=5 Hz), 5.83 (1H, d, J=19 Hz), 6.10 (1H, dt, J=19, 5 Hz), 7.20 (5H, m), and 11.35 (1H, broad s); IR (neat) 3000 (broad s), 1700 (vs), 1420 (s), 1245 (s), and 1100 cm^{-1} (s).

2-(Methyldiphenylsilyl)-3-butenoic Acid (3d): Colorless crystals (ether/hexane); mp 65—68 °C; ^1H NMR (CCl_4) δ=0.65 (3H, s), 3.35 (1H, d, J=10 Hz), 4.45—4.85 (2H, m), 5.75 (1H, dt, J=16, 10 Hz), 6.9—7.5 (10H, m), and 10.53 (1H, s); IR (KBr) 3000 (broad s), 1680 (vs), 1430 (s), 1315 (s), 1200 (s), and 1100 cm^{-1} (s). Found: C, 71.97; H, 6.43%. Calcd for $C_{17}H_{18}O_2Si$: C, 72.30; H, 6.42%.

4-(Methyldiphenylsilyl)-3-butenoic Acid (4d): Colorless crystals (ether/hexane); mp 93—96° C; ^1H NMR ($CDCl_3$) δ=0.62 (3H, s), 3.21 (2H, m), 6.09 (2H, m), 7.1—7.6 (10H, m), and 10.56 (1H, broad s); IR (KBr) 2900 (broad m), 1700 (vs), 1420 (vs), 1245 (vs), 1220 (vs), and 1110 cm^{-1} (s). Found: C, 72.42; H, 6.56%. Calcd for $C_{17}H_{18}O_2Si$: C, 72.30; H, 6.42%.

2-(Dimethylvinylsilyl)-3-butenoic Acid (3e): A colorless oil; ^1H NMR ($CDCl_3$) δ=(6H, s), 2.92 (1H, d, J=10 Hz), 4.9 (2H, m), 5.9 (4H, m), and 9.0 (1H, broad s); IR (neat) 2950 (broad s), 1685 (vs), 1405 (s), 1250 (s), 905 (s), and 840 cm^{-1} (vs).

4-(Dimethylvinylsilyl)-3-butenoic Acid (4e): ^1H NMR ($CDCl_3$) δ=0.20 (6H, s), 3.18 (2H, d, J=5 Hz), 5.3—6.4 (5H, m), and 9.4 (1H, broad s); IR (neat) 2950 (broad s), 1700 (vs), 1610

[†] 1 M=1 mol dm^{-3}.

(s), 1405 (s), 1250 (vs), and 840 cm^{-1} (vs).

2-(Dimethyl-*p*-tolylsilyl)-3-butenoic Acid (3f): Colorless crystals (ether/hexane); mp 50—51 °C; ^1H NMR ($CDCl_3$) δ=0.39 (6H, s), 2.32 (3H, s), 3.06 (1H, d, J=10 Hz), 4.6—5.0 (2H, m), 5.85 (1H, dt, J=16, 10 Hz), 7.10 (2H, d, J=8 Hz), 7.34 (2H, d, J=8 Hz), and 9.46 (1H, broad s); IR (CCl_4) 2960 (broad s), 1690 (vs), 1250 (s), and 1110 cm^{-1} (vs). Found: C, 66.44; H, 7.77%. Calcd for $C_{13}H_{18}O_2Si$: C, 66.62; H, 7.74%.

2-(*t*-Butyldimethylsilyl)-3-butenoic Acid (3g): A colorless oil; ^1H NMR ($CDCl_3$) δ=0.08 (6H, s), 0.95 (9H, s), 2.93 (1H, d, J=10 Hz), 4.70—4.92 (2H, m), 5.84 (1H, dt, J=16, 10 Hz), and 10.98 (1H, broad s); IR (neat) 3080 (broad s), 1690 (vs), 1630 (m), 1405 (m), 1250 (m), 1200 (m), 1075 (m), 835 (m), and 815 cm^{-1} (m).

2-Methyl-2-(dimethylphenylsilyl)-3-butenoic Acid (3h): Colorless crystals (ether/hexane); mp 103—105° C; ^1H NMR ($CDCl_3$) δ=0.39 (6H, s), 1.20 (3H, s), 4.59 (1H, d, J=17 Hz), 4.84 (1H, d, J=10 Hz), 6.20 (1H, dd, J=17, 10 Hz), 7.0—7.3 (5H, m), and 11.65 (1H, broad s); IR (KBr) 2960 (broad m), 1680 (vs), 1628 (m), 1430 (m), 1410 (m), 1280 (vs), 1260 (s), 1112 (s), 914 (s), 832 (m), 812 (vs), 738 (m), and 700 cm^{-1} (s). Found: C, 66.40; H, 7.93%. Calcd for $C_{13}H_{18}O_2Si$: C, 66.62; H, 7.74%.

4-(Dimethylphenylsilyl)-3-pentenoic Acid (4h): A colorless oil; ^1H NMR ($CDCl_3$) δ=0.40 (6H, s), 1.67 (3H, m), 3.15 (2H, d, J=7 Hz), 5.92 (1H, m), 7.1—7.5 (5H, m), and 10.08 (1H, broad s); IR 2960 (broad s), 1712 (vs), 1620 (m), 1430 (s), 1250 (s), 1216 (m), 1114 (s), 910 (m), 834 (s), 816 (s), 776 (s), 732 (s), and 702 cm^{-1} (s).

3-Methyl-2-(dimethylphenylsilyl)-3-butenoic Acid (3i): Colorless crystals (ether/hexane); mp 65—67° C; ^1H NMR ($CDCl_3$) δ=0.48 (6H, s), 1.62 (3H, s), 3.04 (1H, s), 4.74 (1H, m), 4.84 (1H, m), 7.20—7.35 (3H, m), 7.35—7.55 (2H, m), and 10.5 (1H, broad s); IR (KBr) 2900 (broad s), 1680 (vs), 1425 (s), 1250 (vs), 1115 (vs), 810 (vs), and 700 cm^{-1} (vs). Found: C, 66.33; H, 7.86%. Calcd for $C_{13}H_{18}O_2Si$: C, 66.62; H, 7.74%.

3-Methyl-4-(dimethylphenylsilyl)-3-butenoic Acid (4i): ^1H NMR ($CDCl_3$) δ=0.39 (6H, s), 1.80 (3H, s), 3.12 (2H, s), 5.51 (1H, s), 7.1—7.6 (5H, m), and 8.27 (1H, broad s); IR (neat) 2960 (broad s) 1710 (vs), 1622 (m), 1430 (m), 1252 (s), 1114 (m), 836 (s), 730 (s), and 702 cm^{-1} (s).

***cis*-2-(Dimethylphenylsilyl)-3-pentenoic Acid (3j):** Colorless crystals (ether/hexane); mp 84—88° C; ^1H NMR ($CDCl_3$) δ=0.43 (6H, s), 1.27 (3H, d, J=6 Hz), 3.37 (1H, d, J=10 Hz), 5.40 (1H, dq, J=10, 6 Hz), 5.59 (1H, t, J=7 Hz), 7.2—7.6 (5H, m), and 8.40 (1H, broad s); IR (KBr) 2900 (broad m), 1675 (vs), 1430 (s), 1310 (vs), 1250 (s), 1195 (s), 1120 (s), 820 (s), and 725 cm^{-1} (vs). Found: C, 66.38; H, 7.87%. Calcd for $C_{13}H_{18}O_2Si$: C, 66.62; H, 7.74%.

2-Methyl-4-(dimethylphenylsilyl)-3-butenoic Acid (4j): A colorless oil; ^1H NMR ($CDCl_3$) δ=0.36 (6H, s), 1.29 (3H, d, J=7 Hz), 3.20 (1H, m), 5.88 (1H, d, J=19 Hz), 6.10 (1H, dd, J=19, 6 Hz), 7.3 (5H, m), and 10.5 (1H, broad s); IR (neat) 2960 (broad s), 1710 (vs), 1614 (m), 1430 (s), 1250 (s), 116 (s), 824 (s), 732 (s), and 700 cm^{-1} (s).

2,2-Dimethyl-4-(dimethylphenylsilyl)-3-butenoic Acid (4k): Colorless crystals (ether/hexane); mp 62—64 °C; ^1H NMR ($CDCl_3$) δ=0.40 (6H, s), 1.35 (6H, s), 5.84 (1H, d, J=19 Hz), 6.20 (1H, d, J=19 Hz), 7.25 (m, 5H), and 11.1 (1H, broad s); IR (KBr) 2900 (broad s), 1685 (vs), 1295 (s), 1250 (s), 1110 (s), 995 (s), 840 (vs), 730 (vs), and 700 cm^{-1} (vs). Found: C, 68.01; H, 8.47%. Calcd for $C_{14}H_{20}O_2Si$: C, 67.70; H, 8.12%.

Methyl 2-(Dimethylphenylsilyl)-3-butenoate (5c). To a solution (ether) of **3c** (3.749 g, 17 mmol) was added an ethereal solution of CH_2N_2 under 0° C until the solution became slightly yellow. After ether was evaporated in vacuo, the residue was chromatographed on silica gel (CH_2Cl_2/hexane) to give 2.952 g (74%) of **5c** as a colorless oil; ^1H NMR ($CDCl_3$) δ=0.38 (6H, s), 3.10 (1H, d, J=10 Hz), 3.48 (3H, s), 4.64—5.00 (2H, m), 5.93 (1H, dt, J=17, 10 Hz), and 7.25—7.5 (5H, m); IR (neat) 2950 (m), 1630 (m), 1430 (s), 1315 (s), 1250 (s), 1165 (vs), 1135 (s), 1115 (vs), 835 (vs), 810 (s), and 695 cm^{-1} (s); MS (20 eV) m/z (rel intensity) 234 (M^+, 15), 203 (4), 151 (19), 135 (81), and 68 (100).

Methyl 2-Methyl-2-(dimethylphenylsilyl)-3-butenoate (5h): A colorless oil; ^1H NMR (CCl_4) δ=0.31 (6H, s), 1.19 (3H, s), 3.41 (3H, s), 4.60 (1H, dd, J=17, ≈1 Hz), 4.81 (1H, dd, J=11, ≈1 Hz), 6.16 (1H, dd, J=17, 11 Hz), and 7.13 (5H, m); IR (neat) 2960 (m), 1720 (vs), 1635 (m), 1440 (s), 1245 (vs), 1120 (vs), 905 (s), 840 (s), 820 (s), 790 (s), 745 (s), and 710 cm^{-1} (s); MS (20 eV) m/z (rel intensity) 248 (M^+, 21), 233 (6), 217 (7), 151 (13), 135 (69), and 82 (100).

Methyl 3-Methyl-2-(dimethylphenylsilyl)-3-butenoate (5i): A colorless oil; ^1H NMR ($CDCl_3$) δ=0.43 (6H, s), 1.66 (3H, s), 3.08 (1H, s), 3.54 (3H, s), 4.88 (2H, m), and 7.40 (5H, m); IR (neat) 2956 (m), 1724 (vs), 1638 (m), 1434 (s), 1250 (s), 1152 (vs), 1118 (s), 838 (s), 816 (s), 734 (m), and 702 cm^{-1} (s); MS (20 eV) m/z (rel intensity) 248 (M^+, 8), 233 (5), 217 (4), 151 (9), 135 (69), and 82 (100).

Methyl *cis*-2-(Dimethylphenylsilyl)-3-pentenoate (5j): A colorless oil; ^1H NMR ($CDCl_3$) δ=0.39 (6H, s), 1.32 (3H, d, J=7 Hz), 3.39 (1H, d, J=11 Hz), 3.52 (3H, s), 5.40 (1H, dq, J=11, 7 Hz), 5.65 (1H, t, J=11 Hz), 7.36 (3H, m), and 7.49 (2H, m); IR (neat) 2950 (m), 1720 (vs), 1430 (s), 1305 (vs), 1250 (vs), 1150 (vs), 1115 (s), 835 (s), 810 (s), 725 (s), and 695 cm^{-1} (vs); MS (20 eV) m/z (rel intensity) 248 (M^+, 12), 217 (3), 151 (6), 135 (55), and 82 (100).

Methyl *trans*-2-(Dimethylphenylsilyl)-3-butenoate: Typical ^1H NMR signals: δ=5.21 (1H, dq, J=15, 6 Hz) and 5.59 (1H, ddq, J=15, 9, 2 Hz).

Reaction of 5. General Procedure: To a CH_2Cl_2 solution (20 ml/1 mmol) of **5** (1 equiv) and an electrophile (1.2 equiv) was added a CH_2Cl_2 solution of $TiCl_4$ (1 M solution, 2.4 equiv) at −78° C with stirring. The reaction was continued under the conditions listed in Table 2. The reaction mixture was quenched with water and extracted with ether or CH_2Cl_2. The organic phase was washed with brine, and dried over Na_2SO_4. After the solvent was removed, the residue was chromatographed on silica gel (hexane/ether or hexane/CH_2Cl_2).

Methyl 5-Methoxy-2-methyl-2-pentenoate (6): A colorless oil; ^1H NMR (CCl_4) δ=1.76 (3H, s), 2.32 (2H, q, J=7 Hz), 3.20 (3H, s), 3.30 (2H, t, J=7 Hz), 3.59 (3H, s), and 6.50 (1H, t, J=7 Hz); IR (neat) 2952 (m), 1720 (vs), 1652 (m), 1438 (m), 1228 (s), 1152 (s), and 1118 cm^{-1} (s); MS (20 eV) m/z (rel intensity) 158 (M^+, 1), 127 (37), 126 (93), 113 (17), 111 (15), 95 (18), and 82 (100).

Methyl 5-Methoxy-4-methyl-2-pentenoate (7): A colorless oil; ^1H NMR (CCl_4) δ=0.74 (3H, d, J=7 Hz), 2.19 (1H, m), 2.85 (2H, d, J=7 Hz), 2.89 (3H, s), 3.26 (3H, s), 5.30 (1H, d, J=16 Hz), and 6.35 (1H, dd, J=16, 7 Hz); IR (neat) 1726 (vs), 1660 (m), 1438 (m), 1276 (s), 1198 (s), 1178 (s), and 1150 cm^{-1} (s); MS (70 eV) m/z (rel intensity) 158 (M^+, 1), 137 (8), 127 (13), 113 (7), and 82 (100).

Methyl 2-Methyl-5-phenylthio-2-hexenoate (8): A colorless oil; ^1H NMR ($CDCl_3$) δ=1.24 (3H, d, J=7 Hz), 2.13 (3H,

d, J=1 Hz), 2.35 (2H, m), 3.35 (1H, m), 3.67 (3H, s), 5.70 (1H, m), and 7.35 (5H, m); IR (neat) 1720 (vs), 1650 (s), 1440 (s), 1226 (vs), 1150 (vs), 748 (s), and 694 cm^{-1} (s); MS (70 eV) m/z (rel intensity) 250 (M^+, 10), 219 (2), 141 (38), and 137 (100).

Methyl 4-Methyl-5-phenylthio-2-hexenoate (9): A diastereomeric mixture; a colorless oil; ^1H NMR (CCl_4) δ= 1.12 (3H, m), 1.16 (3H, m), 2.25 (1H, m), 3.23 (1H, m), 3.62 (3H, s), 5.70 (1H, d, J=16 Hz), 6.82 (1H, m), and 7.18 (5H, m); IR (neat) 2972 (m), 1724 (vs), 1656 (s), 1440 (s), 1276 (s), 1196 (s), 1178 (s), 748 (m), and 694 cm^{-1} (m); MS (70 eV) m/z (rel intensity) 250 (M^+, 7), 219 (2), 141 (3), and 137 (100).

Methyl 5-Hydroxy-2,6-dimethyl-2-heptenoate (10): A colorless oil; ^1H NMR ($CDCl_3$) δ=0.95 (6H, m), 1.80 (1H, m), 1.95 (1H, broad), 2.20 (3H, m), 2.30 (2H, m), 3.60 (1H, m), 3.69 (3H, s), and 5.80 (1H, m); IR (neat) 3468 (broad m), 2964 (s), 1720 (vs), 1648 (m), 1440 (m), 1230 (s), 1154 cm^{-1} (s); MS (20 eV) m/z (rel intensity) 154 (M^+−MeOH, 3), 126 (5), 111 (100), and 82 (31).

Methyl 5-Hydroxy-4,6-dimethyl-2-heptenoate (11): A diastereomeric mixture; a colorless oil; ^1H NMR ($CDCl_3$) δ=0.90 (6H, d, J=6 Hz), 1.08 (3H, d, J=7 Hz), 1.65 (1H, m), 2.45 (1H, broad s), 2.48 (1H, m), 3.16 (1H, m), 3.62 (3H, s), 5.72 (1H, d, J=16 Hz), and 6.80 (1H, m); IR (neat) 3476 (broad s), 2964 (s), 1724 (vs), 1658 (m), 1440 (m), 1282 (s), 1198 (m), 1178 (m), 1156 (m), and 994 cm^{-1} (m); MS (70 eV) m/z (rel intensity) 186 (M^+, 0.2), 155 (1), 114 (100), and 82 (41).

Dimethyl 5-Hydroxy-2,5-dimethyl-2-hexenedioate (12): A colorless oil; ^1H NMR ($CDCl_3$) δ=1.36 (3H, s), 1.76 (3H, s), 2.46 (2H, d, J=7 Hz), 3.30 (1H, broad), 3.61 (3H, s), 3.68 (3H, s), and 6.47 (1H, t, J=7 Hz); IR (neat) 3500 (broad m), 2956 (m), 1722 (vs), 1648 (s), 1440 (s), 1224 (vs), 1154 (vs), and 1120 cm^{-1} (s); MS (20 eV) m/z (rel intensity) 216 (M^+, 0.2), 185 (7), 184 (3), 157 (5), 125 (42), and 114 (100).

Methyl 4-(3-Acetyl-4-hydroxy-5-methoxy-1-oxo-1,2-dihydro-2-naphthyl)-2-methyl-2-butenoate (15): ^1H NMR ($CDCl_3$) δ=2.20 (3H, broad s), 2.23 (3H, s), 2.50 (2H, m), 3.55 (1H, m), 3.65 (3H, s), 3.98 (3H, s), 6.90 (1H, m), 7.4 (3H, m), and 17.05 (1H, s).

Methyl 4-(1,4-Acetoxy-3-acetyl-5-methoxy-2-naphthyl)-2-methyl-2-butenoate (15a): Colorless crystals (CH_2Cl_2/ether); mp 149—151° C; ^1H NMR ($CDCl_3$) δ=2.15 (3H, broad s), 2.31 (3H, s), 2.39 (3H, s), 2.47 (3H, s), 3.49 (2H, m), 3.62 (3H, s), 3.87 (3H, s), 5.50 (1H, m), 6.85 (1H, m), and 7.35 (2H, m); IR (KBr) 1764 (vs), 1714 (vs), 1652 (m), 1574 (s), 1440 (s), 1366 (s), 1270 (s), 1212 (vs), 1186 (vs), 1144 (s), and 1070 cm^{-1} (m); MS (70 eV) m/z (rel intensity) 429 (M^++1, 2), 428 (M^+, 8), 344 (52), 326 (20), and 270 (100). Found: C, 64.21; H, 5.70%. Calcd for $C_{23}H_{24}O_8$: C, 64.48; H, 5.64%.

Methyl 4-(3-Acetyl-4-hydroxy-5-methoxy-1-oxo-1,2-dihydro-2-naphthyl)-2-pentenoate (16): A diastereomeric mixture; ^1H NMR ($CDCl_3$) δ=0.75 (3H of one diastereomer, d, J= 7 Hz), 1.15 (3H of another, d, J=7 Hz), 2.2 (3H, m), 2.5 (1H, m), 3.1 (4H, m), 3.98 (3H, m), 5.5 (1H, d, J=16 Hz), 6.5 (1H, m), 7.4 (3H, m), 17.15 (1H of one diastereomer, s), and 17.24 (1H of another, s).

Methyl 4-(1,4-Diacetoxy-3-acetyl-5-methoxy-2-naphthyl)-2-pentenoate (16a): Colorless crystals (CH_2Cl_2/ether); mp 146—148° C; ^1H NMR ($CDCl_3$) δ=1.45 (3H, d, J=7 Hz), 2.25 (3H, s), 2.33 (3H, s), 2.49 (3H, s), 3.63 (1H, m), 3.66 (3H, s), 3.80 (3H, s), 5.88 (1H, d, J=16 Hz), 6.80 (1H, m), and 7.2 (3H, m); IR (KBr) 1764 (vs), 1722 (vs), 1704 (vs), 1650 (m), 1574 (s), 1368 (vs), 1270 (vs), 1198 (vs), and 1064 cm^{-1} (s); MS (70 eV) m/z (rel intensity) 429 (M^++1, 9), 428 (M^+, 32), 386 (80), 344 (97), 326 (78), 312 (52), 270 (100), and 267 (99). Found: C, 64.34; H, 5.75%. Calcd for $C_{23}H_{24}O_8$: C, 64.48; H, 5.64%.

Methyl 2,6-Dimethyl-5-oxo-2-heptenoate (17): A colorless oil; ^1H NMR ($CDCl_3$) δ=1.12 (6H, d, J=7 Hz), 1.86 (3H, s), 2.65 (1H, m), 3.44 (2H, d, J=7 Hz), 3.73 (3H, s), and 6.97 (1H, t, J=7 Hz); IR (neat) 2968 (m), 1712 (vs), 1652 (m), 1440 (s), 1256 (vs), 1122 (s), 1092 (vs), and 1038 cm^{-1} (s); MS (20 eV) m/z (rel intensity) 184 (M^+, 3), 153 (10), 152 (5), 141 (35), 114 (41), 113 (52), 109 (24), 82 (44), and 71 (100).

Methyl 4,6-Dimethyl-5-oxo-2-heptenoate (18): ^1H NMR ($CDCl_3$) δ=1.2 (9H, m), 2.70 (1H, m), 3.55 (1H, m), 3.75 (3H, s), 5.95 (1H, d, J=15 Hz), and 6.95 (1H, dd, J=15, 8 Hz).

Methyl 4,6-Dimethyl-5-oxo-3-heptenoate (19): (19/18=5.8/1); ^1H NMR ($CDCl_3$) δ=1.10 (6H, d, J=7 Hz), 1.70 (3H, s), 3.30 (2H, d, J=7 Hz), 3.4 (1H, m), 3.75 (3H, s), and 6.80 (1H, t, J=7 Hz); IR (neat) 2972 (m), 1742 (vs), 1672 (vs), 1440 (m), 1236 (m), 1200 (s), 1172 (s), and 1046 cm^{-1} (m); MS (20 eV) m/z (rel intensity) 184 (M^+, 1.4), 153 (3), 152 (3), 141 (100), and 113 (42).

Methyl 5-Hydroxy-2-methyl-5-(4-nitrophenyl)-2-pentenoate (20): A pale yellow oil; ^1H NMR ($CDCl_3$) δ=1.80 (3H, s), 2.65 (3H, m), 3.74 (3H, s), 5.00 (1H, t, J=6 Hz), 6.80 (1H, t, J=7 Hz), 7.57 (2H, d, J=9 Hz), and 8.23 (2H, d, J=9 Hz); IR (neat) 3464 (broad m), 2950 (m), 1710 (vs), 1650 (m), 1604 (m), 1522 (vs), 1440 (s), 1348 (vs), 1282 (vs), 1064 (s), 856 (s), 734 (s), and 702 cm^{-1} (m); MS (20 eV) m/z (rel intensity) 234 (M^+-MeO, 22), 217 (45), 158 (51), 152 (88), 122 (85), 115 (81), and 114 (100).

Methyl 5-Hydroxy-4-methyl-5-(4-nitrophenyl)-2-pentenoate (21): A diastereomeric mixture (73/27); a pale yellow oil; ^1H NMR ($CDCl_3$) δ=1.01 (3H of major isomer, d, J=6.6 Hz), 1.04 (3H of minor isomer, d, J=7.0 Hz), 2.66 (1H, m), 2.75 (1H, m), 3.70 (3H of minor isomer, s), 3.71 (3H of major isomer, s), 4.70 (1H of major isomer, d, J=6.6 Hz), 4.85 (1H of minor isomer, d, J=5.1 Hz), 5.79 (1H of minor isomer, dd, J=15.7, 1.1 Hz), 5.81 (1H of major isomer, dd, J=15.7, 1.1 Hz), 6.96 (1H, dd, J=15.7, 8.0 Hz), 7.49 (2H, d, J=9 Hz), and 8.18 (2H, d, J=9 Hz); IR (neat) 3460 (broad m), 2976 (m), 1722 (vs), 1658 (m), 1606 (m), 1522 (vs), 1440 (m), 1348 (vs), 1282 (s), 1200 (m), 1178 (m), 1034 (m), and 862 cm^{-1} (m); MS (20 eV) m/z (rel intensity) 234 (M^+−MeO, 11) 217 (14), 188 (17), 158 (26), 152 (100).

The author wishes to thank Prof. Kazuhiro Maruyama, Prof. Yoshinori Yamamoto, Dr. Yoshinori Naruta, and Prof. Hitomi Suzuki for their guidance and valuable discussions. The author also wishes to thank Dr. Hiroyuki Furuta for the measurement of 400 MHz NMR. Gifts of chlorosilanes from Shin-etsu Chemical Co. are greatly appreciated.

References

1) For recent reviews, see: a) J. C. Stowell, *Chem. Rev.*, **84**, 409 (1984); b) S. F. Martin, *Synthesis*, **1979**, 633; c) G. Courtois and L. Maginiac, *J. Organomet. Chem.*, **69**, 1 (1974); d) D. A. Evans and G. C. Andrews, *Acc. Chem. Res.*, **7**, 147 (1974).

2) a) K. H. Geiss, B. Seuring, R. Piefer, and D. Seebach, *Angew. Chem. Int. Ed. Engl.*, **13**, 479 (1974); b) D. Seebach, K. H. Geiss, and M. Pohmakotor, *ibid.*, **15**, 437 (1976); c) K. H. Geiss, D. Seebach, and B. Seuring, *Chem. Ber.*, **110**, 1833 (1977); d) M. Pohmakotor, K. H. Geiss, and D. Seebach, *ibid.*,

112, 1420 (1979); e) S. F. Martin, and M. T. DuPrest, *Tetrahedron Lett.*, **1977**, 3925; f) H. Ahlbrecht and J. Eicher, *Synthesis*, **1974**, 672; g) M. Julia, A. Schouteeten, and M. M. Baillarge, *Tetrahedron Lett.*, **1974**, 3433.

3) a) K. Narasaka, H. Hayashi, and T. Mukaiyama, *Chem. Lett.*, **1972**, 259; b) T. Mukaiyama and M. Yamaguchi, *ibid.*, **1979**, 657; c) J. Hartmann, M. Stahle, and M. Schlosser, *Synthesis*, **1974**, 888; d) J. Hartmann, R. Muthukrishnan, and M. Schlosser, *Helv. Chim. Acta*, **57**, 77 (1977); e) K. Hirai and Y. Kishida, *Org. Synth.*, **56**, 77 (1977); f) D. A. Evans, G. C. Andrews, and B. Buckwalter, *J. Am. Chem. Soc.*, **96**, 5560 (1974); g) W. C. Still and T. L. MacDonald, *ibid.*, **96**, 5561 (1974); h) T. Hassel and D. Seebach, *Angew. Chem. Int. Ed. Engl.*, **18**, 399 (1979); i) R. Kow and M. Rathke, *J. Am. Chem. Soc.*, **95**, 2715 (1973); j) E. Dziadulewicz and T. Gallagher, *Tetrahedron Lett.*, **26**, 4547 (1985).

4) a) K. Ohshima, H. Yamamoto, and H. Nozaki, *Bull. Chem. Soc. Jpn.*, **48**, 1567 (1975); b) F. E. Ziegler and C. C. Tam, *J. Org. Chem.*, **44**, 3428 (1979); c) D. A. Evans, D. J. Baillargeon, and J. V. Nelson, *J. Am. Chem. Soc.*, **100**, 2242 (1978); d) P. Brownbrige and S. Warren, *J. Chem. Soc., Perkin Trans. 1*, **1977**, 1131; e) A. P. Kozikowski and K. Isobe, *Tetrahedron Lett.*, **20**, 833 (1979); and also see Ref. 2e, 3f, and 3h.

5) a) Y. Yamamoto, H. Yatagai, and K. Maruyama, *J. Org. Chem.*, **45**, 195 (1980); b) Y. Yamamoto, H. Yatagai, and K. Maruyama, *Chem. Lett.*, **1979**, 385; c) Y. Yamamoto, H. Yatagai, and K. Maruyama, *J. Chem. Soc., Chem. Commun.*, **1979**, 157.

6) a) S. Torii, H. Tanaka, and Y. Tomotaki, *Chem. Lett.*, **1974**, 1541; For a discussion of hard-soft behavior, see: b) T.-L. Ho, "Hard and Soft Acids and Bases Principle in Organic Chemistry," Academic Press, Inc., New York (1977); c) I. Fleming "Frontier Orbitals and Organic Chemical Reactions," John Wiley & Sons, London.

7) See Ref. 2—6.

8) a) R. J. P. Corriu and J. Masse, *J. Organomet. Chem.*, **57**, C5 (1973); b) R. J. P. Corriu, J. Masse, and D. Samate, *ibid.*, **93**, 71 (1975); c) R. J. P. Corriu, G. F. Lanneau, J. P. Masse, and D. Samate, *ibid.*, **127**, 281 (1977); d) R. J. P. Corriu, G. F. Lanneau, D. Leclercq, and D. Sammate, *ibid.*, **144**, 155 (1978); e) R. J. P. Corriu, C. Guerin, and J. M'Boula, *Tetrahedron Lett.*, **22**, 2985 (1981); f) P. W. K. Lau and T. H. Chan, *ibid.*, **19**, 2383, (1978); g) K. Koumaglo and T. H. Chan, *ibid.*, **25**, 717 (1984); h) E. Ehlinger and P. Magnus, *J. Chem. Soc., Chem. Commun.*, **1979**, 421; i) E. Ehlinger and P. Magnus, *J. Am. Chem. Soc.*, **102**, 5004 (1980); j) K. S. Kyler and D. S. Watt, *J. Org. Chem.*, **46**, 5182 (1981); k) P. E. Bauer, K. S. Kyler, and D. S. Watt, *J. Org. Chem.*, **48**, 34 (1983); l) K. S. Kyler, M. A. Netzel, S. Arsenigadis, and D. S. Watt, *ibid.*, **48**, 383 (1983); m) J. M. Muchowski, R. Naef, and M. L. Maddox, *Tetrahedron Lett.*, **26**, 5375 (1985); n) N. Ryu, H. Yamamoto, S. Murai, and N. Sonoda, 50th Japan Chem. Soc. Meeting, Koen Yokoshu II, **1985**, 2V34, p. 1483.

9) D. J. S. Tsai and D. S. Matteson, *Tetrahedron Lett.*, **22**, 2751 (1981).

10) F. Sato, Y. Suzuki, and M. Sato, *Tetrahedron Lett.*, **23**, 4589 (1982).

11) Y. Naruta, H. Uno, and K. Maruyama, *Chem. Lett.*, **1982**, 961.

12) D. Kempf; personal communication to Prof. Y. Yamamoto about his presentation at the university of Illinois Seminar Series in Organic Chemistry (December 3, 1979). Results of MINDO/3 caluculation about hetero-substituted allylic carbanions were included in the abstract accompanying his presentation. According to them, charge densities of α and γ positions for a carbanion of allylsilane were -0.4167 and -0.4416, and HOMO coefficients of α and γ positions were -0.69729 and $+0.66642$, respectively.

13) E. Colvin, "Silicon in Organic Synthesis," Butterworth, London (1981), Chap. 2.

14) For a qualitative discussion in terms of PMO theory, see ref. 7c.

15) Carboxylation of (1,2-dimethyl-2-propenyl)dimethylphenylsilane and (2-methyl-2-butenyl)dimethylphenylsilane did not occur sufficiently, though generation of γ-carboxylated compounds could only be detected. In the case of (1-methyl-2-butenyl)dimethylphenylsilane, any carboxylated compounds were not obtained in detectable amounts.

16) L. Pauling, "The nature of the Chemical Bond," 3rd ed., Cornell University Press. Ithaca, New York (1960).

17) V. Rautenstrauch, *Helv. Chim. Acta*, **57**, 496 (1974).

18) a) Y. Naruta, H. Uno, and K. Maruyama, *Chem. Lett.*, **1982**, 609; b) H. Uno, *J. Org. Chem.*, **51**, 350 (1986).

19) a) K. Maruyama, H. Uno, and Y. Naruta, *Chem. Lett.*, **1983**, 1767; b) H. Uno, Y. Naruta, and K. Maruyama, *Tetrahedron*, **40**, 4725 (1984).

20) Katzenellenbogen reported the synthesis of 3-methyl-2-trimethylsilyl-3-butenoate, but this method does not have wide applicability for the preparation of α-silyl β,γ-unsaturated esters, such as **5h** and **5j**: see P. Albaugh-Robertson and J. A. Katzenellenborgen, *Tetrahedron Lett.*, **1982**, 723; P. Albaugh-Robertson and J. A. Katzenellenbogen, *J. Org. Chem.*, **48**, 5288 (1983); and also see Y. Morizawa, S. Kanemoto, K. Ohshima, and H. Nozaki, *Tetrahedron Lett.*, **23**, 2953 (1982).

21) H. Sakurai, K. Sasaki, and A. Hosomi, *Tetrahedron Lett.*, **22**, 745 (1981), and references cited therein.

22) a) J. Slutsky and H. Kwart, *J. Am. Chem. Soc.*, **95**, 8678 (1973); b) I. Fleming and D. Waterson, *J. Chem. Soc., Perkin Trans. 1*, **1984**, 1809.

 © 1986 The Chemical Society of Japan Bull. Chem. Soc. Jpn., 59, 2481—2483 (1986)

Methylation of Alcohols, Phenols, and Carboxylic Acids, and Selective Monomethylation of Diols and Dicarboxylic Acids with Dimethyl Sulfate by Use of Alumina

Haruo OGAWA,* Youko ICHIMURA, Teiji CHIHARA,† Shousuke TERATANI, and Kazuo TAYA
Department of Chemistry, Tokyo Gakugei University, Koganei, Tokyo 184
†The Institute of Physical and Chemical Research, Wako, Saitama 351-01
(Received March 12, 1986)

Alcohols in cyclohexane give their methyl ethers in high yields by the use of a combination of dimethyl sulfate and alumina. Some diols and dicarboxylic acids adsorbed on alumina react with dimethyl sulfate and produce the corresponding monomethyl ethers and esters in high selectivities.

The utilization of solid adsorbents such as alumina and silica gel as a reaction media represents one of the recent advances of organic syntheses.[1-3] The use of solid adsorbents is advantageous to milder reaction conditions, simpler work-ups and higher selectivities. We have successfully applied solid adsorbents to the acetylation of alcohols and phenols,[4] the selective monomethyl esterification of dicarboxylic acids,[5] and the selective reduction of dicarbonyl compounds.[6] We then extended this approach to the methylation of various compounds containining hydroxyl groups.

Alcohols, phenols and carboxylic acids are methylated with dimethyl sulfate in the presence of alkali. Sodium hydroxide is used for the methylation of glucose,[7,8] 1-(2,5-dihydroxyphenyl)ethanone,[9] *m*-hydroxybenzaldehyde[10] and gallic acid.[11] Potassium hydroxide and potassium carbonate are also used for the methylation of benzoic acid derivatives.[12,13] We report here the successful methylation of alcohols with dimethyl sulfate in which the alcohols were converted to the ethers in high yields by the addition of alumina instead of alkali to the reaction system. Diols and dicarboxylic acids were selectively monomethylated by a modified method. Details of these reactions are described in this paper.

Results and Discussion

Methylation of Alcohols, Phenols and Carboxylic Acids. Primary, secondary and tertiary alcohols were quantitatively converted to the corresponding methyl ethers as shown in Table 1. Phenols were converted in lower yields, and further low yields were found for carboxylic acids. The yields of methylated compounds of phenols and carboxylic acids hardly increased even though a large amount of dimethyl sulfate was used. In the absence of alumina alcohols, phenols, and carboxylic acids were not methylated with dimethyl sulfate at all.

In the methylation of benzyl alcohol Merck's neutral aluminum oxide and silica alumina (28.6% Al_2O_3) were also effective, and gave benzyl methyl ether in yields of 52 and 41%, respectively, under the same reaction conditions described in Table 1.

Selective Monomethylation of Diols and Dicarboxylic Acids. Table 2 shows the reactions that proceeded to give, selectively, monomethylated compounds in high yields. It was confirmed that no reactions took place in the absence of alumina. In the conventional method using potassium carbonate,[13] 55% methyl hydrogen terephthalate and 24% dimethyl terephthalate were formed at the point of a 79% conversion of terephthalic acid. It shows a typical example of a two-stage reaction proceeding via the intermediate methyl hydrogen terephthalate.

It is reasonable to assume that dicarboxylic acids are chemisorbed on alumina as monocarboxylate anions and that there carboxyl groups are left in positions

Table 1. Methylation of Alcohols, Phenols, and Carboxylic Acids[a]

Substrate	Me_2SO_4/mol eq	Yield/%[b]	Substrate	Me_2SO_4/mol eq	Yield/%[b]
1-Heptanol	1.5	66	o-*t*-Butylphenol	1.5	7.1
1-Heptanol	3	85	2,6-Dimethylphenol	1.5	10
1-Heptanol	6	95	2,6-Diisopropylphenol	1.5	0.1
1-Heptanol	12	99	2,6-Di-*t*-butylphenol	1.5	0.1
1-Decanol	12	92	1-Naphthol	1.5	38
Benzyl alcohol	12	99	2-Naphthol	1.5	44
2-Heptanol	12	76	Benzoic acid	1.5	12
Cyclohexanol	12	75	Benzoic acid	10	13
2-Methyl-2-hexanol	12	97	Heptanoic acid	1.5	8.0
Phenol	1.5	36	Undecanoic acid	1.5	7.0
Phenol	12	36			

a) Substrate (0.467 mmol), alumina (1.0 g), and cyclohexane (8 mL) were refluxed for 2 h. b) Determined by GLC, GSC, and/or HPLC.

Table 2. Selective Monomethylation of Diols and Dicarboxylic Acids[a)]

Substrate	Yield of methylated compound/%[b)]	
	mono-	di-
1,4-Benzenedimethanol	73	9.2
1,4-Benzenedimethanol[e)]	0.0	0.0
1,10-Decanediol	86	13
Terephthalic acid	72	12
Terephthalic acid[c)]	6.5	0.0
Terephthalic acid[d)]	4.1	0.2
Terephthalic acid[e)]	0.0	0.0
Terephthalic acid[f)]	55	24
Isophthalic acid	63	19
Phthalic acid	80	8.0
Adipic acid	93	6.7
Suberic acid	99	0.0
Suberic acid[e)]	0.0	0.0
1,12-Dodecanedioic acid	97	3.2

a) Each experiment was carried out at room temperature in cyclohexane (8 mL) using the adsorbed sample (1 g), which held diol (0.467 mmol/g-alumina) or diarboxylic acid (0.400—0.467 mmol/g-alumina). In the case of diols 12 mol eq of dimethyl sulfate, and in the case of dicarboxylic acid 1.5 mol eq of dimethyl sulfate was used. b) Determined by GLC, GSC, and/or HPLC. c) In 1,4-dioxane. d) In formamide. e) In DMF solution in the absence of alumina. f) Using potassium carbonate according to the usual method[13)] in the absence of alumina.

remote from the alumina surface.[5)] A low yield (12%; see Table 1) for methyl esterification of benzoic acid, which is strongly adsorbed on alumina,[14)] indicates that the carboxylate anion has a very low reactivity toward dimethyl sulfate. The high selectivities for monomethyl esterification of dicarboxylic acids adsorbed on alumina might be due to the much higher reactivities of free carboxyl groups than those of carboxylate anions.

Experimental results suggested that the adsorbed molecules of aliphatic dicarboxylic acids align with their axis perpendicular to the adsorbent surface in a closed-packed rigid array.[5)] Selective monomethyl esterification of aliphatic dicarboxylic acids is attributable to the characteristic adsorption mode which protects the carboxyl groups being adsorbed on alumina, but not those in the free state, from the attack of dimethyl sulfate. With the aid of this protecting effect, the terminal chlorination of octanoic acid adsorbed on alumina was attained.[15)]

In contrast to the carboxylic acids, mono-alcohols adsorbed on alumina were methylated with dimethyl sulfate to produce the corresponding ethers almost quantitatively as shown in Table 1. This result means that the hydroxyl group became reactive with dimethyl sulfate by adsorption on alumina. IR and inelastic electron tunneling spectroscopy proved that alcohols are chemisorbed on alumina as alkoxides or the species in which O–H bonds are strongly polarized.[16,17)] The selective monomethylation of diols is attributable to their adsorption states in which the hydroxyl groups at one end of the molecule are activated through chemisorption on alumina to react with dimethyl sulfate, and suggests that there free hydroxyl groups are left in positions remote from alumina surface.

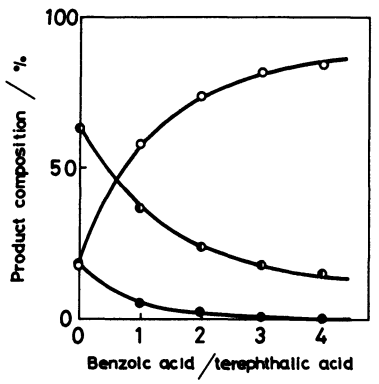

Fig. 1. Effect of benzoic acid addition on methylation of terephthalic acid on alumina. (○): Terephthalic acid, (◐): methyl hydrogen terephthalate, (●): dimethyl terephthalate. Dimethyl sulfate: Terephthalic acid=3:1 (mole).

Effect of Benzoic Acid Addition on Reactivity of Terephthalic Acid. Benzoic acid was added to cyclohexane suspension of alumina adsorbing terephthalic acid. The reactivity of terephthalic acid toward dimethyl sulfate decreased with increasing amounts of benzoic acid, as shown in Fig. 1. A desorption of terephthalic acid into cyclohexane was not detected.

Carboxylic acids exist stably in a dimer state in a solution as well as in a crystal. Benzoic acid in cyclohexane (98 mmol L^{-1}) was confirmed to be in a dimer state on the basis of the IR absorption spectrum, which has only a band at 1695 cm^{-1} assignable to dimeric acid in the reagion of C=O streching vibration. Benzoic acid added to the reaction system probably forms acid dimers by using the free carboxyl groups of terephthalic acid adsorbed on alumina. This gives rise to the decrease in the reactivities of terephthalic

acid.

In 1,4-dioxane or formamide, the adsorbed terephthalic acid was hardly converted to methyl hydrogen terephthalate (see Table 2). This is, perhaps, due to the solvation of free carboxyl groups which impedes the attack of dimethyl sulfate.

Experimental

Materials. Alumina (the reference catalyst of the Catalysis Society of Japan; JRC-ALO-5), Merck's neutral aluminum oxide 90 for column chromatography and silica alumina (28.6% Al_2O_3: JRC-SAH-1) were dried at 110 °C for a day and stored in a desiccator. Cyclohexane was dried by refluxing with calcium hydride and distilled. Other materials were commercially available and used without further purification.

Preparation of Adsorbed Sample. Diols were adsorbed on alumina by the following procedure: One gram of alumina was added to an ether solution of diol in which 0.467 mmol of diol was contained; then, ether was eliminated under a reduced pressure.

Dicarboxylic acids were adsorbed on alumina according to a previously reported procedure: One gram of alumina powder was added to 10 mL of a 1% solution of acid in DMF, the mixture was allowed to stand for 8 h; then, the alumina was filtered off and dried.[5]

Reaction Procedure. Alcoholes, phenols, and benzoic acid: Typically, 1.0 g of alumina, 54.3 mg (0.467 mmol) of 1-heptanol and 706 mg (5.60 mmol) of dimethyl sulfate was added to 8 mL of cyclohexane, and refluxed for 2 h. Then, the alumina was filtered off and eluted with ethyl acetate. After the eluate was concentrated, the product was analyzed by GLC. The analysis showed that a 1-methoxyheptane product was obtained at about 99% yield.

Diols and Dicarboxylic Acids: About 6.4 mL (5 g) of cyclohexane and 0.5 g of the adsorbed sample were placed in a reaction vessel. A calculated amount of dimethyl sulfate was introduced and the reaction was started with vigorous stirring at room temperature. Subsequent procedures were the same as those for mono-alcohols, except for washing the eluate with an alkali solution. The products were analyzed by GLC, GSC and/or HPLC.

References

1) A. McKillop and D. W. Young, *Synthesis*, **1979**, 401; **1979**, 481.

2) G. H. Posner, *Angew. Chem. Int. Ed. Engl.*, **17**, 487 (1978).

3) M. Hojo, *Yuki Gousei Kagaku Kyoukai Shi*, **42**, 635 (1984).

4) T. Chihara, S. Teratani, and H. Ogawa, *J. Chem. Soc., Chem. Commun.*, **1981**, 1120; T. Chihara, Y. Takagi, S. Teratani, and H. Ogawa, *Chem. Lett.*, **1982**, 60.

5) H. Ogawa, T. Chihara, and K. Taya, *J. Am. Chem. Soc.*, **107**, 1365 (1985).

6) T. Chihara, E. Waniguchi, T. Wakabayashi, and K. Taya, *Bull. Chem. Soc. Jpn.*, **57**, 2479 (1984).

7) E. S. West and R. F. Holden, *Org. Synth.* Coll. Vol. III, 800 (1955).

8) K. Wallenfels, G. Bechtler, R. Kuhn, H. Trischmann, and H. Egge, *Angew. Chem. Int. Ed.*, **2**, 515 (1963).

9) G. N. Vyas and N. M. Shah, *Org. Synth.* Coll. Vol. IV, 836 (1963).

10) R. N. Icke, C. E. Redemann, B. B. Wisegarver, and G. A. Alles, *Org. Synth.*, **3**, 564 (1955).

11) F. Mauthner, *Org. Synth.* Coll. Vol. I, 537 (1941).

12) J. Grundy, B. G. James, and G. Pattenden, *Tetrahedron Lett.*, **1972**, 757.

13) K. Sabih, C. D. Klaassen, and K. Sabih, *J. Pharm. Sci.*, **60**, 745 (1971).

14) J. T. Hall and P. K. Hansma, *Surf. Sci.*, **76**, 61 (1978).

15) N. C. Deno, R. Fishbein, and C. Pierson, *J. Am. Chem. Soc.*, **92**, 1451 (1970).

16) S. D. Williams and K. W. Hipps, *J. Catal.*, **78**, 96 (1982).

17) H. Jeziorowski, H. Knözinger, W. Meye, and H. D. Müller, *J. Chem. Soc., Faraday Trans. 1*, **69**, 1744 (1973).

[2+4] and [6+4] Type Cycloaddition Reactions of 1-Ethoxycarbonyl-1*H*-azepine and 1-Ethoxycarbonyl-1*H*-1,2-diazepine with 3,4,5,6-Tetrachloro-1,2-benzoquinone

Katsuhiro Saito,* Toshio Mukai,† and Shigenori Iida†
Department of Chemistry, Nagoya Institute of Technology, Gokiso-cho, Showa-ku, Nagoya 466
†Department of Chemistry, Faculty of Science, Tohoku University, Aoba, Aramaki, Sendai 980
(Received March 14, 1986)

The reaction of 1-ethoxycarbonyl-1*H*-azepine with 3,4,5,6-tetrachloro-1,2-benzoquinone at room temperature gave a [6+4]-type cycloadduct as the major product and two kinds of [2+4]-type cycloadducts. In this reaction the diketone moiety of the benzoquinone derivative was used as the 4π component to form ether linkages. The [6+4]-type cycloadduct became rearranged to one of the [2+4]-type cycloadducts by heating at 90 °C. The same reaction, but using 1-ethoxycarbonyl-1*H*-1,2-diazepine, afforded two kinds of [2+4]-type cycloadducts. An electronic attraction between the oxygen atoms of the benzoquinone derivative and the carbons in the 2 and 7-positions of the azepine derivative is considered to be one of the driving force of the [6+4]-type cycloaddition reaction. The [2+4]-type cycloadducts are regarded to be formed via inverse electron demand Diels–Alder reactions.

Unsaturated heterocyclic compounds have attracted the attention of chemists from the viewpoint of their synthetic utility and an elucidation of their electronic nature. Five-membered unsaturated heterocyclic compounds such as furan, pyrrole, or thiophene derivatives are known to have aromaticity due to the contributions of lone-pair electrons of the heteroatoms to construct a 6 π-electron aromatic structure.[1] On the other hand, seven-membered unsaturated heterocyclic compounds such as oxepine, azepine, or diazepine derivatives are olefinic compounds because of a lack of the above-type contribution.[2] The five-membered unsaturated heterocyclic compounds proceed substitution and addition reactions,[3] but the seven-membered unsaturated heterocyclic compounds proceed mainly valence isomerization[4] and addition reactions[5] as olefinic compounds.[3]

While a lot of details have been published in connection with the reactions of five-membered unsaturated heterocyclic compounds,[3] reports concerning the addition reactions of seven-membered unsaturated heterocyclic compounds are relatively few in number. One of the reasons is considered to be the instability of these seven-membered unsaturated heterocyclic compounds; and also, the stable derivatives of these heterocyclic compounds are limited to only a few kinds.[4,5]

Azepine and diazepine derivatives are known to react with olefins possessing electron-withdrawing groups to give [2+4], [4+2], and [4+6]-types of cycloadducts.[5] The reaction positions of azepine and diazepines in a [2+4]-type cycloaddition is limited to their 4 and 5 positions; the yields of a [4+6]-type cycloaddition reaction is low. Exceptional cases are the dimerization reactions.[5a,b,c] The authors have investigated addition reactions of azepine and diazepine derivatives with variable olefins and organosilane compounds.[5i,j,k] Also studied were the addition reactions of azepine and diazepine derivatives with 3,4,5,6-tetrachlo-1,2-benzoquinone (**3**), typical of the class of dienes displaying a reverse electron demand in Diels–Alder reactions.[6] The cycloaddition reactions proceeded not through the olefinic part but through the diketone moiety of **3** to give [2+4]- and [6+4]-type cycloadduts forming the ether linkages. Here, we wish to report on the results of these reactions.

Result

1-Ethoxycarbonyl-1*H*-azepine (**1**) was allowed to react with one molar equivalent of 3,4,5,6-tetrachloro-1,2-benzoquinone (**3**) in benzene at room temperature for 70 min to give three kinds of colorles crystals **4**, **5**, and **6** in the yields of 46, 16, and 8%, respectively. The same reaction, but using 1-ethoxycarbonyl-1*H*-1,2-diazepine (**2**) at room temperature for 3.5 h, afforded two kinds of colorless crystals **7** and **8** in yields of 10 and 4%, respectively, along with an intractable black oily material. Products **5** and **6** were stable during heating and recovered completely even after being heated at 180° C for 24 h in benzene in a sealed tube. On the other hand, product **4** rearranged to **6** in a 63% yield upon being heated at 90° C for 4 h in benzene. Products **7** and **8** did not changed at all upon being heated at 130° C for 15 h in benzene in a sealed tube, but turned to black intractable materials upon heating at 180 °C for 10 h.

Reaction of **1** with 1,2-naphthoquinone (**9**) at room temperature for 4 d resulted in a quantitative recovery of **1**. Reactions of **1** and **9** at elevated temperatures of 70 and 110° C for 5 d gave the recovery of **1** in 30 and 0% yields, respectively, along with balck intractable materials. The same reaction of **2** with **9** gave almost the same results as the above.

The structures of the products were deduced on the basis of their spectral properties as follows. The elemental analyses and the molecular-ion peaks in the mass spectra showed that all of the products were 1:1 addition products of **1** or **2** with **3**. The fact that the IR spectra of these products showed no absorption of carbonyl group, except those due to the ester groups, indicates that **1** and **2** reacted with **3** at its oxygen atoms to form the ether linkages.

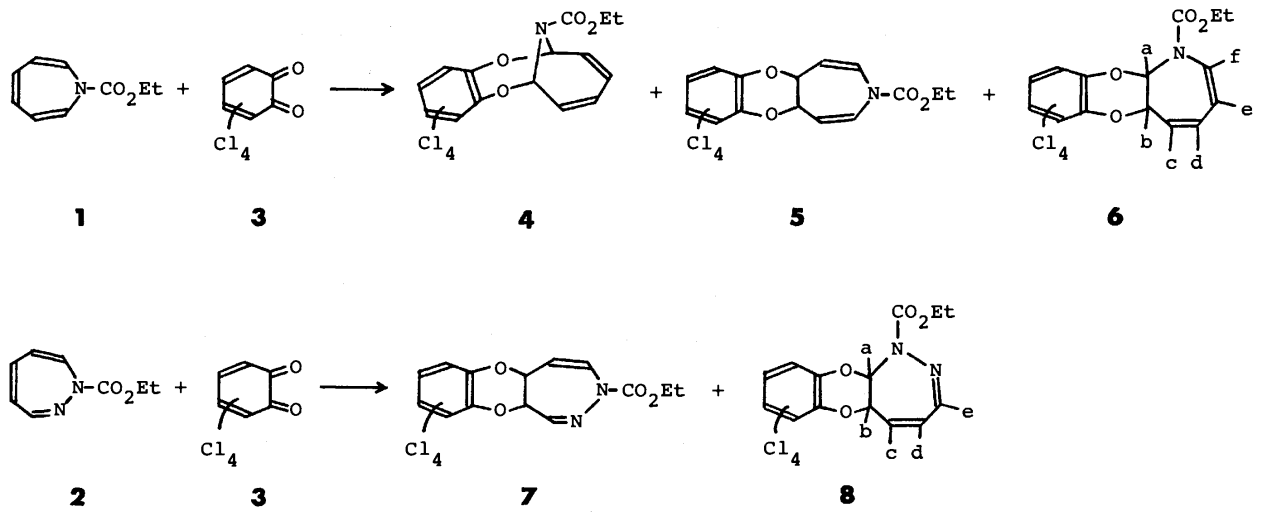

Fig. 1.

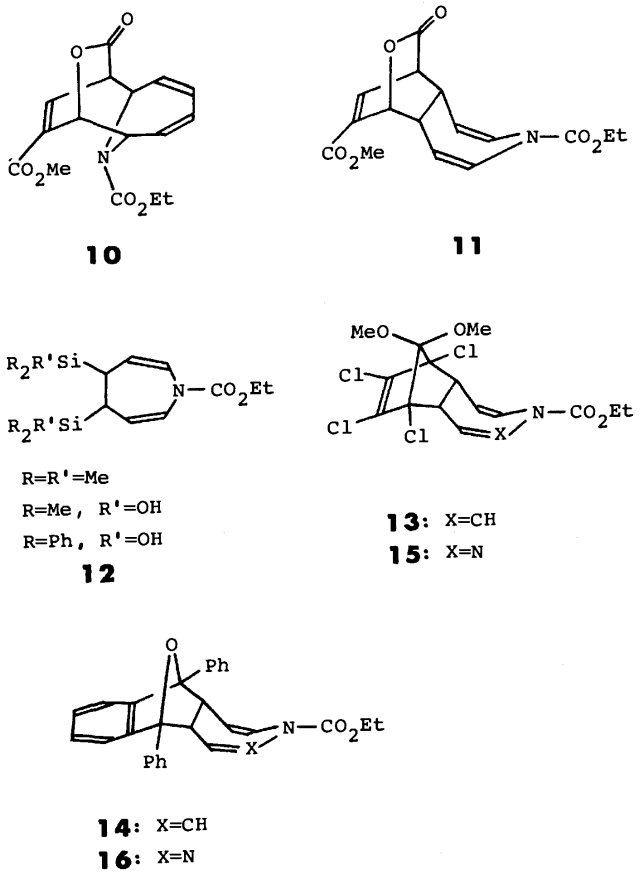

Fig. 2.

The structures of **4** and **5** were determined mainly on the basis of their NMR spectral properties, which show that these adducts are symmetric compounds. This suggests that the 2 and 7 positions or the 4 and 5 positions of **1** were involved in these reactions. The chemical shift (δ=6.04) and the broad singlet nature of the olefinic protons of **4** closely resembled those features of the olefinic protons of the skeletary analogous compound (**10**)[5i,j] and the azepine dimers. Similarly, the chemical shift (δ=7.06) and the coupling constant (9.0 Hz) of the olefinic protons of **5** had a likeness to those parameters of a similar compound (**10**,[5i,j] **11**,[5i,j] **12**,[5k] **13**,[5i,j,l] **14**[5f,m]). The broad singlet peak at δ 4.97 of **5** was considered to contain absorptions due to the other two olefinic protons and the two methine protons. On the basis of this spectroscopic data, the structures of **4** and **5** were determined as shown in the figure. The electronegativity of the oxygen atoms accounts for the observed lower field resonance of the bridgehead protons of **4** and **5** compared to **10**, **11**, **12**, **13**, and **14**.

The structure of **6** was assigned mainly on the basis of its NMR spectral properties, employing the double-resonance technique. The two continued methine protons (H_a, H_b) and four olefinic protons (H_c–H_f) and the coupling constants between these olefinic protons suggested that **6** contains a seven-membered ring.[5k,7] Dreiding models demonstrate that the diheadral angle between H_a and H_b should be approximately 60° for a cis-configuration and 170° for a trans-configuration. The small coupling constant between H_a and H_b (ca. 2 Hz) indicates that **6** is a cis-adduct of **1** with **3**.[7] The structure of **6** was confirmed by the formation of **6** from **4**, since the transformation of **4** to **6** can be quite reasonably attributed to a thermally allowed 1,5-carbon migration.[8]

The structures of **7** and **8** were also determined mainly on the basis of their NMR spectral properties and were confirmed by a comparison of these data with those of analogous compounds such as **15**,[5i,j] **16**,[5i,j] and **6**. The low field shift of the bridgehead protons of **7** and **8** in their NMR spectra compared to **15** and **16** can be explained using the same reason as that proposed for **5** and **6**.

Discussion

Adduct **6** can be regarded as a secondary product, thermally derived from **4**. However, the fact that the

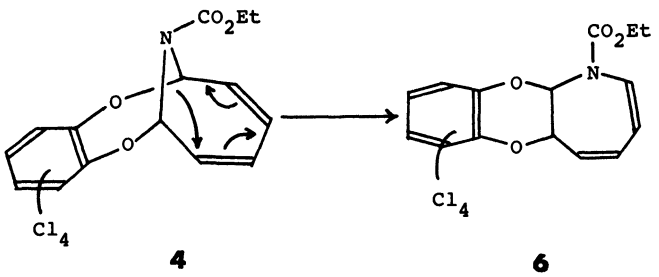

4 6

Fig. 3.

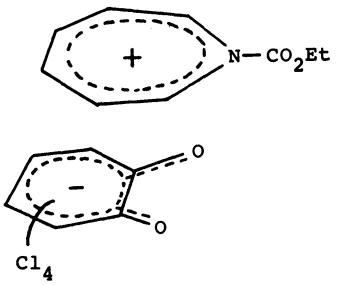

17

Fig. 4.

addition reaction of **1** with **3** proceeded at room temperature and that the isomerization of **4** to **6** required prolonged heating, seem to prove that **6** was the primary product of a [2+4]-type cycloaddition reaction of **1** with **3**.

The major adduct **4** was formed via a [6+4]-type cycloaddition of **1** with **3**. As previously mentioned, azepine derivatives are known to proceed a [6+4]-type addition reactions in low yields.[5] Furthermore, to our knowledge, no example can be found for [6+4]-type cycloadditions, in which **3** reacts as a **4** π-component. The possibility of a participation of a charge-transfer complex such as **17** can be proposed. The above possibility seems to be negated by the fact that no absorption due to a charge-transfer complex could not be observed in the UV spectrum of a mixture of **1** and **3**.

The major formation of the [6+4]-type cycloaddition product can be regarded as the result of an elctronic attraction between the oxygen atoms of **3** and the carbon atoms in the 2 and 7 positions of **1** as shown in Fig. 5.[8] It is well-known that oxygen atoms of carbonyl groups are negatively charged and a molecular orbital calculation has shown that the azepine has the lowest electron density at the carbons in the 2 and 7 positions.[9]

The adducts **5**, **6**, **7**, and **8** are considered to be formed via reverse electron demand [4+2]-type cycloaddition reactions,[8] in which the HOMO of **1** or **2** interact with the LUMO of **3**. The low energy level of the LUMO of **3** promotes an interaction with the HOMO of **1** or **2**; as a result, it stimulates the addition reactions.[10]

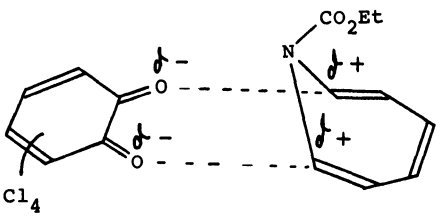

18

Fig. 5.

Experimental

All melting points were uncorrected. NMR spectra were measured with a Varian HA-100 or Hitachi R-20B spectrometer with tetramethylsilane as an internal standard. UV and IR spectra were measured with Hitachi 220A and DS-701G spectrometers, respectively. Mass spectra were measured with a Hitachi M-52 spectrometer. Wako Gel C-200 and Wako Gel B5F were used for column and thin-layer chromatography, respectively.

Reaction of 1 with 3. A mixture of **1** (1650 mg, 10 mmol) and **3** (2460 mg, 10 mmol) in benzene (10 ml) was stirred at room temperature for 70 min. After evaporating of the solvent, the crystals **4** (1860 mg, 46%) were separated by filtration and the filtrate was chromatographed on silica gel to give crystals **5** (637 mg, 16%) and crystals **6** (315 mg, 8%) in this order by the use of pet ether–benzene (2:3). The crystals were recrystallized from cyclohexane to give pure crystals.

4: Mp 156—157°C. Found: C, 43.55; H, 2.67; N, 3.27%. Calcd for $C_{15}H_{11}O_4NCl_4$: C, 43.82; H, 2.70; N, 3.41%. Mass *m/z* (rel intensity): 411 (M^+, 9), 165 (100), 92 (82). IR (KBr): 3030, 2980, 1720 cm^{-1}. ^1H NMR ($CDCl_3$) δ=1.29 (t, CH_3, J=7.0 Hz), 4.20 (d, CH_2, J=7.0 Hz), 6.04 (bs, 4H), 6.83 (d, 2H, J=4.5 Hz).

5: Mp 165—166°C. Found: C, 43.78; H, 2.54; N, 3.40%. Calcd for $C_{15}H_{11}O_4NCl_4$: C, 43.82; H, 2.70; N, 3.41%. Mass *m/z* (rel intensity): 411 (M^+, 1), 165 (31), 152 (98), 80 (100). IR (KBr): 3030, 2980, 1735 cm^{-1}. ^1H NMR ($CDCl_3$) δ=1.36 (t, CH_3, J=7.0 Hz), 4.30 (q, CH_2, J=7.0 Hz), 4.97 (bs, 4H), 7.06 (d, 2H, J=9.0 Hz).

6: Mp 200—202°C. Found: C, 43.93; H, 2.62; N, 3.31%. Calcd for $C_{15}H_{11}O_4NCl_4$: C, 43.82; H, 2.70, N, 3.41%. Mass *m/z* (rel intensity): 411 (M^+, 8), 165 (100), 152 (48), 92 (84). IR (KBr): 3030, 2980, 1730 cm^{-1}. ^1H NMR ($CDCl_3$) δ=1.36 (t, CH_3, J=7.0 Hz), 4.31 (q, CH_2, J=7.0 Hz), 5.11 (narrow m, H_b), 5.28 (dd, H_e, J_{de}=7.5, J_{ef}=8.6 Hz), 5.39 (bd, H_c, J_{bc}= 2.1, J_{cd}=11.9 Hz), 5.91 (ddd, H_d, J_{cd}=11.9, J_{de}=7.5, J_{bd}=2.1 Hz), 6.63 (narrow m, H_a), 6.87 (d, H_f, J_{ef}=8.6 Hz).

Reaction of 2 with 3. A mixture of **2** (1660 mg, 10 mmol) and **3** (2460 mg, 10 mmol) in benzene (10 ml) was stirred at room temperature for 3.5 h. After evaporating of the solvent, the residue was chromatographed on silica gel to give crystals of **7** (415 mg, 10%) and **8** (165 mg, 4%), in this order, by the use of benzene–ether (4:1). The crystals were recrystallized from benzene to give pure crystals.

7: Mp 183—184°C. Found: C, 40.67; H, 2.56; N, 6.73%. Calcd for $C_{14}H_{10}O_4N_2Cl_4$: C, 40, 81; H, 2.45; N, 6.80%. Mass *m/z* (rel intensity): 412 (M^+, 11), 166 (65), 107 (50), 94 (100), 81 (71). IR (KBr): 3030, 2980, 1740 cm^{-1}. ^1H NMR ($CDCl_3$)

δ=1.40 (t, CH_3, J=7.0 Hz), 4.40 (q, CH_2, J=7.0 Hz), 4.93 (ddd, H_c, J_{ac}=2.5, J_{ac}=2.1, J_{cd}=6.5 Hz), 5.22 (dd, H_b, J_{ab}=2.5, J_{bc}=3.1 Hz), 5.30 (dd, H_d, J_{cd}=6.5, J_{de}=10.3 Hz), 7.07 (dd, H_a, J_{ab}=2.5, J_{ac}=2.5 Hz), 7.49 (d, H_e, J_{de}=10.3 Hz).

8: Mp 209—211 °C. Found: C, 41.03; H, 2.41; N, 6.86%. Calcd for $C_{14}H_{10}O_4N_2Cl_4$: C, 40.81; H, 2.41; N, 6.80%. Mass *m/z* (rel intensity): 412 (M^+, 14), 166 (50), 107 (44), 94 (83), 81 (100). IR (KBr): 3030, 2980, 1720 cm^{-1}. ^1H NMR ($CDCl_3$) δ=1.41 (t, CH_3, J=7.0 Hz), 4.45 (q, CH_2, J=7.0 Hz), 5.08 (narrow m, H_b, J_{bc}=2.1 Hz), 5.90 (ddd, H_d, J_{dc}=11.2, J_{db}=2.0, J_{de}=5.5 Hz), 5.98 (dd, H_c, J_{cb}=2.0, J_{cd}=11.2, J_{ce}=2.0 Hz), 6.88 (narrow m, H_a), 7.25 (dd, J_{de}=5.5, J_{ec}=2.0 Hz).

Thermal Rearrangement of 4 to Form 6. A solution of **4** (40 mg) in benzene-d_6 (0.3 ml) was heated at 90 °C for 4 h and subjected to preparative thin layer chromatography on silica gel using pet ether–benzene 1:1 as a developing solvent to give crystals **6** (R_f=0.65, 25 mg, 63%).

The authors are indebted to Honorable Professor Tadashi Sasaki of Nagoya University for his kind suggestions.

References

1) D. S. Sappenfield and M. Kreevoy, *Tetrahedron*, **19**, 157 (1963); D. T. Clark, *ibid.*, **24**, 3285 and 4689 (1968): G. M. Marino, *J. Heterocycl. Chem.*, **9**, 817 (1972); T. J. Barton, R. W. Roth, and J. G. Verkade, *J. Am. Chem. Soc.*, **94**, 8854 (1972); R. M. Acheson, "An Introduction to the Heterocyclic Compounds," John Willey & Sons, Inc., New York (1976), Chap. 3.

2) A. Streitwieser, "Molecular Orbital Theory for Organic Chemists," John Willey & Sons, Inc., New York (1961), Chap. 10; M. Cook, Jr., A. R. Katritzky, and P. Linda, *Adv. Heterocyclic Chem.*, **17**, 255 (1974).

3) A. P. Terent'ev, L. I. Belen'kii, and L. A. Yanovskaya, *Chem. Abstr.*, **49**, 12327d (1955); F. A. Annet, *Tetrahedron Lett.*, **1962**, 1219; A. W. McCulloch, D. G. Smith, and A. G. MacInnes, *Can. J. Chem.*, **51**, 4125 (1973); A. R. Butler and A. P. Sanderson, *J. Chem. Soc., Perkin Trans. 2*, **1974**, 1214; R. Helder and H, Wynberg, *Tetrahedron Lett.*, **1972**, 605; D. D. Callander. P. L. Coe, and J. C. Tatlow, *J. Chem. Soc., Chem. Commun.*, **1966**, 143; A. R. Cooksey, K. J. Morgan, and D. P. Morrey, *Tetrahedron*, **26**, 5101 (1970); V. Bocchi, L. Chierici, and G. P. Gardini, *ibid.*, **26**, 4073 (1970); M. G. Barlow, R. N. Hazeldine, and R. Hubbrad, *J. Chem. Soc., Chem. Commun.*, **1969**, 301; R. C. Bansal, A. W. McCulloch, and A. G. McInnes, *Can. J. Chem.*, **48**, 1472 (1970).

4) J. A. Moore, W. J. Freeman, R. C. Gearhart, and H. B. Yokelson, *J. Org. Chem.*, **43**, 787 (1978); J. M. Holovka and P. D. Gardner, *J. Am. Chem. Soc.*, **89**, 6390 (1967); H. Hofmann, and P. Hofmann, *Tetrahedron Lett.*, **1971**, 4055; L. A. Paquette and D. E. Kuhla, *J. Org. Chem.* **34**, 2885 (1969); R. A. Odum and B. Shmall, *J. Chem. Soc., Chem. Commun.*, **1969**, 1299; E. Lerner, R. A. Odum, and B. Schmall., *ibid.*, **1973**, 327; J. Streith, J..P. Luttringer, M. Nastasi, *J. Org. Chem.*, **36**, 2962 (1971).

5) a) K. Hafner and J. Mondt, *Angew. Chem. Int. Ed. Engl.*, **5**, 839 (1966); b) A. L. Johnson and H. E. Simmons, *J. Am. Chem. Soc.*, **88**, 2591 (1966); c) L. A. Paquette and J. H. Barrett, *ibid.*, **88**, 2590 (1966); d) E. Vogel, W. A. Boll, and H. Gunther, *Tetrahedron Lett.*, **1965**, 609; e) W. H. Rastetter, *J. Am. Chem. Soc.*, **97**, 210 (1975); f) L. A. Paquette, D. E. Kuhla, J. H. Barrett, and C. M. Leichter, *J. Org. Chem.*, **34**, 2888 (1969); g) A. G. Annastassiou, E. Reichmanis, S. J. Girgenti, M. S. Ridder, *ibid.*, **43**, 315 (1978); h) J. M. Photis, *J. Heterocycl. Chem.*, **8**, 729 (1971); i) S. Iida, T. Mukai, and K. Saito, *Heterocycles*, **11**, 401 (1978); j) K. Saito, S. Iida, and T. Mukai, *Bull. Chem. Soc. Jpn.*, **57**, 3483 (1984); k) K. Saito, S. Kojima, T. Okudaira, and K. Takahashi, *ibid.*, **56**, 175 (1983); l) T. Imagawa, N. Sueda, and M. Kawanishi, *Tetrahedron*, **30**, 2227 (1974); m) J. R. Wiseman and B. P. Chong, *Tetrahedron Lett.*, **1969**, 1619; n) K. Harano, T. Ban, M. Yasuda, and K. Kanematsu, *ibid.*, **1979**, 1599; o) M. Yasuda, H. Harano, and K. Kanematsu, *J. Org. Chem.*, **45**, 4455 (1980); p) U. Gockel, U. Hartmannsgruber, A. Steigel, and J. Sauer, *Tetrahedron Lett.*, **21**, 599 (1980); q) W. S. Murphy and K. P. Raman, *ibid.*, **21**, 319 (1980).

6) S. Sauer, *Angew. Chem. Int. Ed. Engl.*, **6**, 16 (1967); E. E. Numann, W. S. Wilson, and R. N. Warrener, *Tetrahedron Lett.*, **1972**, 175; R. Allmann, T. Debaerdemaeker, W. Friedrichsen, H. J. Jurgens, and M. Betz, *Tetrahedron*, **32**, 147 (1976); R. N. Warrener, E. E. Numann, and M. N. Paddon-Row, *Tetrahedron Lett.*, **1976**, 2355; W. Pritschins and W. Grimme, *ibid.*, **1979**, 4545; E. Buldt, T. Debaerdemaeker, and W. Friedrichsen, *Tetrahedron*, **36**, 267 (1980).

7) O. L. Chapman, *J. Am. Chem. Soc.*, **85**, 2014 (1963); M. Karplus, *ibid.*, **85**, 2870 (1963).

8) R. B. Woodward and R. Hoffman, *Angew. Chem. Int. Ed. Engl.*, **8**, 781 (1969).

9) R. W. Shmidt, *Helv. Chim. Acta*, **45**, 1982 (1962).

10) The energy level of the LUMO of **9** is considered to be higher than that of **3**. The bigger energy difference between the HOMO of **1** and the LUMO of **9** (ΔE_2) comparing to that between the HOMO of **1** and the LUMO of **3** (ΔE_1) explains the inertness of **9** to **1**. The same explanation can be applied to the [6+4] type cycloaddition reaction as shown below.

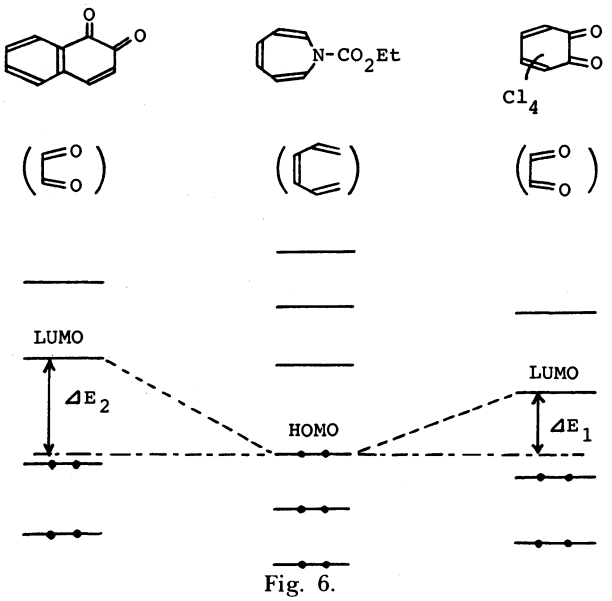

Fig. 6.

Formation and Reaction of Carbonyl Ylides. Production of 2:1-Cycloadducts of 2-Benzopyrylium-4-olates with Carbonyl Compounds

Toshikazu IBATA* and Jiro TOYODA
Institute of Chemistry, College of General Education, Osaka University, Toyonaka, Osaka 560
(Received March 22, 1986)

The $Cu(acac)_2$-catalyzed decomposition of *o*-(diazoacetyl)benzoates in the presence of carbonyl compounds such as benzaldehydes, acetophenones, acetone, fluorenone, and anthraquinone gave 2:1-adducts of the corresponding 2-benzopyrylium-4-olate (**3**) and the carbonyl compound, together with 1:1-adducts. The 2:1-adducts were confirmed to be produced by the cycloaddition of **3** toward the carbonyl group of the 1:1-adducts which have bulky aryl groups on exo-direction. The product ratios of the 2:1-adducts were explained according to the MNDO calculation.

In recent years the chemistry of carbonyl ylide has been studied extensively from the theoretical and synthetic interests.[1] The authors have developed the formation of carbonyl ylide through the carbene-carbonyl reaction[2,3] and reported the 1,3-dipolar cycloaddition with ethylenic,[3,4] and acetylenic compounds.[3,5] In the previous paper of this series, we have reported the $Cu(acac)_2$-catalyzed decomposition of *o*-(diazoacetyl)-benzoates (**1**) in the presence of carbonyl compounds to give not **4B** but **4A** type of cycloadducts of the carbonyl ylide intermediate, 1-(*p*-methoxyphenoxy)-2-benzopyrylium-4-olate (**3a**: R=*p*-$CH_3OC_6H_4$) and 1-methoxy-2-benzopyrylium-4-olate (**3b**: R=CH_3), with carbonyl compounds.[6] The reactions with carbonyl compounds of medium reactivity were found to yield 2:1-adducts containing two molecules of **3** and a molecule of carbonyl compound besides usual 1:1-adducts. In this paper the structure of the 2:1-adducts of **3** with various carbonyl compounds and the substituent effect on the yield of the 2:1-adducts in the reactions of substituted benzaldehydes and acetophenones were discussed.

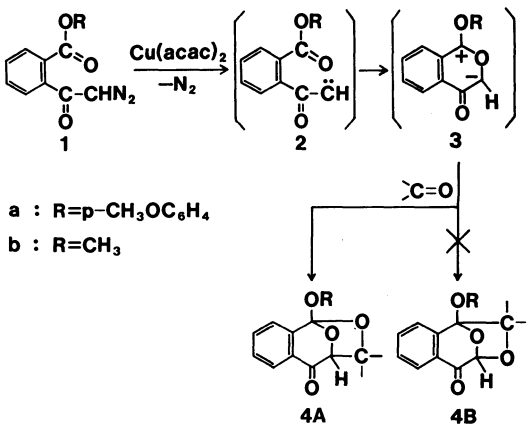

Results and Discussion

The $Cu(acac)_2$-catalyzed decomposition of *p*-methoxyphenyl *o*-(diazoacethyl)benzoate (**1a**) in the presence of two molar equivalents of *p*-anisaldehyde (**5a**) in benzene solution at 80°C gave a 2:1-adduct of 1-(*p*-methoxyphenoxy)-2-benzopyrylium-4-olate (**3a**) and **5a** in 25% yield together with the corresponding *endo*- and *exo*-1:1-adducts. The 2:1-adduct (**8a**) has three methine proton signals at δ 4.04 (d, Ha), 4.65 (d, Hb=R′), and 5.25 (s, Hc) in which the two doublet signals are shown to couple each other. The similarity of the coupling pattern of two doublets of the 2:1-adduct (**8a**) with that of the *exo*-1:1-adduct (**7a**)[7] suggests that in **8a** and **7a** these methine protons (Ha and Hb) have the same configuration. That is, small coupling constants *J*ab, 1.5 Hz for **8a** and 1.3 Hz for **7a**, and their chemical shifts of Hb, δ 4.65 for **8a** and δ 4.63 for **7a** are quite similar. But the chemical shifts of Ha are separated by 0.5 ppm in **7a** and **8a**. This indicates that the magnetic environment of Ha are different in these two compounds. This suggests that the 2:1-adduct is produced by the second attack of **3a** on the carbonyl group of the *exo*-1:1-adduct (**7a**). The position of the second attack is inferred from the usual behavior of carbonyl compounds toward **3**.[6] In fact a similar 2:1-adduct (**9**) was observed in the reaction of **3b** (R=CH_3) with acenaphthylene.[8] In this case the second attack of **3b** has been confirmed to occur on the carbonyl group of a 1:1-adduct of **3b** and acenaphthylene, on the basis of the X-ray crystallography of **9**. Benzaldehyde was also found to give 2:1-adduct (**8b**) having an *exo*-phenyl group on bicyclic dioxolane ring system together with the corresponding 1:1-adducts (Table 1, Run b).

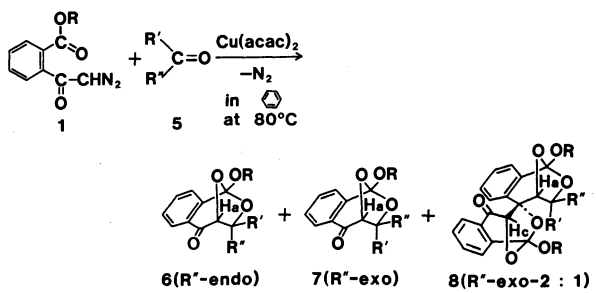

In order to explain the absence of *endo*-2:1-adduct in these reaction products, the MNDO calculation[9] for the *endo*-1:1-adduct (**6b**) and *exo*-1:1-adduct (**7b**)

Table 1. Yields of 1:1-Adduct and 2:1-Adduct between **3** and Carbonyl Compounds

Run	**1** R	**5** R′	**5** R″	Yield of 1:1-Adduct/% R″-endo **6**	Yield of 1:1-Adduct/% R″-exo **7**	Yield of 2:1-Adduct/% **8**	Total Yield/%	Ratio 2:1/1:1
a	*p*-$CH_3OC_6H_4$	H	*p*-$CH_3OC_6H_4$	35	21	25	81	0.45
b	*p*-$CH_3OC_6H_4$	H	C_6H_5	43	38	11	92	0.12
c	*p*-$CH_3OC_6H_4$	H	*p*-$NO_2C_6H_4$	60	36	0.6	97	0.006
d	*p*-$CH_3OC_6H_4$	CH_3	*p*-$CH_3OC_6H_4$	4	0	1	5[a]	(0.25)
e	*p*-$CH_3OC_6H_4$	CH_3	C_6H_5	13	8	5	26[a]	0.24
f	*p*-$CH_3OC_6H_4$	CH_3	*p*-$NO_2C_6H_4$	29	54	11	94	0.13
g	*p*-$CH_3OC_6H_4$	9-Fluorenone		53		37	90	0.41
h	CH_3	Anthraquinone		17		12	29[a]	0.41
i	CH_3	CH_3	CH_3	75		12	87	0.16

a) Intractable tarry products were obtained.

Table 2. Spectroscopic Data of the 2:1-Adducts (**8**)

Adduct	IR/cm^{-1} C=O	^1H NMR/δ OCH_3[a]		CH Ha	CH Hb	CH Hc	CH_3[a]	Others[b]
8a	1711	3.47	3.73	4.04 (d) J=1.5 Hz	4.65 (d)	5.25 (s)		6.27
8b	1710	3.47	3.76	4.09 (d) J=1.4 Hz	4.71 (d)	5.26 (s)		6.34
8c	1710	3.46	3.71	4.08 (s)	4.68 (s)	5.27 (s)		6.40
8d	1715	3.70 3.81	3.77	4.20 (s)	5.35 (s)		1.53	6.20
8e	1711	3.78	3.82	4.27 (s)	5.36 (s)		1.26	6.10
8f	1711	3.80	3.87	4.15 (s)	5.34 (s)		1.22	6.27
8g	1704	3.47	3.77	4.08 (s)	5.33 (s)			c)
8h	1710	3.30	4.00	4.45 (s)	5.10 (s)			5.80
8i	1714	3.63	3.71	4.38 (s)	5.26 (s)		1.26 1.57	6.22

a) Signals are all singlet. b) Only high field signals of aryl protons (Hd) are shown. c) Complex multiplets were observed together with other aromatic proton signals.

was undertaken. From the previous work, these cycloadditions were found to proceed through the interaction controlled by carbonyl ylide-HOMO and carbonyl compound-LUMO.[6b,10] In this cycloaddition the interacting molecular orbitals of carbonyl compounds are C=O π^*. The energy levels and atomic orbital coefficients of the C=O π^* do not show significant difference for the *endo*- (**6b**) and *exo*-1:1-adduct (**7b**) as is seen in Fig. 1. Therefore, difference in the reactivity of two 1:1-adducts can not be explained in this aspect. The small reactivity of **6b** possibly be attributed to the steric factor. The *endo*-adduct (**6b**) has a phenyl group in the vicinity of the carbonyl group which is the reaction center of the second cycloaddition. The free rotation of the phenyl group of the *endo*-adduct (**6b**) hinders the developement of sp^3 orbital of C-O bond during the approach of the second **3a** to the C=O double bond, and presumably suppresses the reactivity of **6b**.

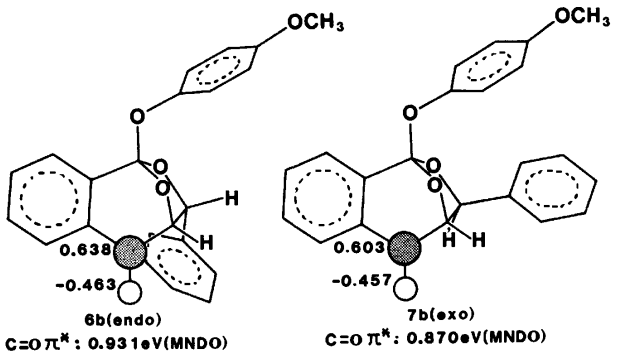

Fig. 1. The energy levels and atomic orbital coefficients of C=O π^* of **6b** and **7b**.

The substituted acetophenones also gave 2:1-adducts besides the corresponding two types of 1:1-adducts in the reactions with 2-benzopyrylium-4-olate (**3a**) (Table 1, Run d, e, f). For example, acetophenone gave *endo*-Ph-1:1-adduct (**6e**), *exo*-Ph-1:1-adduct (**7e**), and 2:1-adduct (**8e**) in 13, 8, and 5% yields, respectively. The structural determination of the bicyclic dioxolane ring system of **8e** was done as follows. The 2:1-adduct (**8e**) shows a singlet signal of CH_3(=R′) at δ 1.26 which is closer to the methyl signal of *exo*-Ph-1:1-adduct (**7e**)

at δ 1.31 than to the signal of *endo*-Ph-1:1-adduct (**6e**) at δ 1.90. This indicates that the methyl group in the 2:1-adduct has *endo* configuration in the same manner as that of *exo*-Ph-1:1-adduct. In other words, phenyl group has *exo* configuration in **7e** and **8e**. These facts suggest that the 1:1-adducts (**6**) having bulky aryl groups in *endo*-direction exhibit no reactivity of cycloaddition toward **3a** depending upon the steric hindrance.

The reaction of **3a** with fluorenone also gave a 2:1-adduct in 37% yield together with a 1:1-adduct in 53% yield. In this case the CPK model shows that the fluorene ring of the 1:1-adduct does not deter the second approach of **3a** from the side of bridged oxygen of the 1:1-adduct, because the fluorene ring is fixed not to rotate like the phenyl group of **6b** described above. The reaction of 1-methoxy-2-benzopyrylium-4-olate (**3b**) with anthraquinone also gave a 2:1-adduct in 12% yield. However the structure of the 2:1-adduct is not determined yet because the 1:1-adduct have two carbonyl groups to be attacked by the second molecule of **3b** and the spectroscopic data do not characterize the structure. Acetone also gave a 1:1-adduct and a 2:1-adduct in the yields of 75 and 12%, respectively.

Stereochemistry of the Second Cycloaddition of 3. The stereochemistry of the second cycloaddition of the 2-benzopyrylium-4-olate (**3**) to the *exo*-1:1-adduct (**7**) is the next question. From the results of the previous works of this series, the regiochemistry of the second cycloaddition may be concluded to proceed in the same manner as the first cycloaddition.[6] That is, the C_1 of the benzopyryliumolate bound to the carbonyl oxygen of the 1:1-adduct. Concerning the stereochemistry of the second cycloaddition, there are four possible structures **8iA(RRR)**, **8iB(RRS)**, **8iC(RSR)**, and **8iD(RSS)** and their mirror image structures in the 2:1-adduct (**8i**) of **3b** and acetone. The CPK model inspection of these isomers reveals that the **8iB(RRS)** structure is free from the steric repulsion in the molecule. This indicates that the **8iB** is sterically the most stable one and then the most probable structure of the four possible ones.

The coupling constant $^3J(^{13}C, H)$ has been reported to be useful for the determination of configuration of rigid cyclic system,[11] and to be calculated using the dihedral angle according to the equation (Eq. 1).[12] The calculation of torsion angles of C_9–C_4–C_5–Ha and C_5–C_4–C_9–Hc, using the observed coupling constants $^3J(^{13}C_9$–Ha)=2.35 and $^3J(^{13}C_5$–Hc)=3.18 Hz of **8f** are 56 and 48°, respectively. These values are consistent with the values of torsion angles, 50° and 30°, estimated by the Dreiding model inspection for **RRS** structure in the possible four structures cited above.

$$^3J(^{13}C, H) = 4.26 - 1.00\cos\theta + 3.56\cos 2\theta \quad (1)$$

It also supports the above conclusion that the 2:1-adduct of **3b** and acenaphthylene has the same **RRS** structure.[8] The 2:1-adduct (**8iB**) of acetone shows a doublet signal of an aromatic proton at δ 6.19 which is at higher field by 1 ppm than the usual ones. This high field shift can not be expected from the other three structures than **8iB**. In the structure **8iB(RRS)** Hd attached to benzene ring A locates above the benzene ring B. The ring current anisotropy effect may shift the signal of Hd at higher field than usual.[8] A similar high field shift has been observed in the 2:1-adduct (**9**) of acenaphthylene and **3b** which has the same **RRS** structure.[8] This also supports the above assignment. Other 2:1-adducts of benzaldehydes and acetophenones also have similar aromatic proton signals at higher field (Table 2). From these results the stereochemistry at the C_5, C_4, and C_9 of the 2:1-adducts was confirmed to have **RRS** structure.

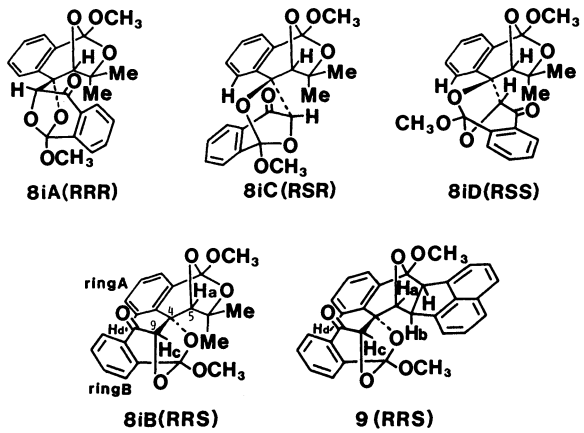

Reactivity of the Substituted Benzaldehydes and Acetophenones. In the reactions of **3a** with benzaldehydes, electron-attracting group like *p*-NO_2 decreases the yields of the 2:1-adducts. For example, the ratios of the yield of 2:1-adduct/1:1-adduct decreased from 0.45 (*p*-CH_3O), to 0.12 (H), and 0.006 (*p*-NO_2). On the other hand, *p*-anisaldehyde is concluded less reactive than benzaldehyde or *p*-nitrobenzaldehyde from the results of competitive reactions.[13] Similar result is also observed in the reactions of acetophenones. The reactivity of acetophenones is lower than that of benzaldehydes having the same substituent. For example, *p*-methoxyacetophenone and acetophenone gave 1:1- and 2:1-adducts in small total yields (5 and 26%) accompanying a lot of intractable tarry products. The product ratio seems to be explained by the competitive reaction between initially formed *exo*-Ar-1:1-adduct (**7**) and starting carbonyl compounds (**5**). Once a small amount of **7** is produced in the reaction system, **3** reacts with **7** or **5** competitively. The substituent effect on the reactivity of the 1:1-adducts is smaller than the effect on the reactivity of benzaldehydes and acetophenones. When electron-attracting *p*-NO_2 group is attached, benzaldehyde and acetophenone have larger reactivity than the corresponding 1:1-adduct, and then the ratios

Table 3. Melting Points and Results of Elemental Analysis of the 2:1-Adducts

Adduct	Mp	Found(%)			Calcd(%)			Molecular formula
	θ_m/°C	C	H	N	C	H	N	
8a	246—247	71.85	4.88		71.42	4.79		$C_{40}H_{32}O_{10}$
8b	241—243	73.06	4.92		72.89	4.70		$C_{39}H_{30}O_9$
8d	248—250	70.76	5.17		71.71	4.99		$C_{41}H_{34}O_{10}$
8e	214—216	72.74	4.84		73.16	4.91		$C_{40}H_{32}O_9$
8f	253—255	68.61	4.48	2.08	68.47	4.45	2.00	$C_{40}H_{31}O_{11}N$
8g	265—267	73.41	4.38		75.41	4.50		$C_{45}H_{32}O_9$
8h	>300	73.07	4.45		72.85	4.32		$C_{34}H_{24}O_8$
8i	184—185	67.71	5.47		67.31	5.40		$C_{23}H_{22}O_7$

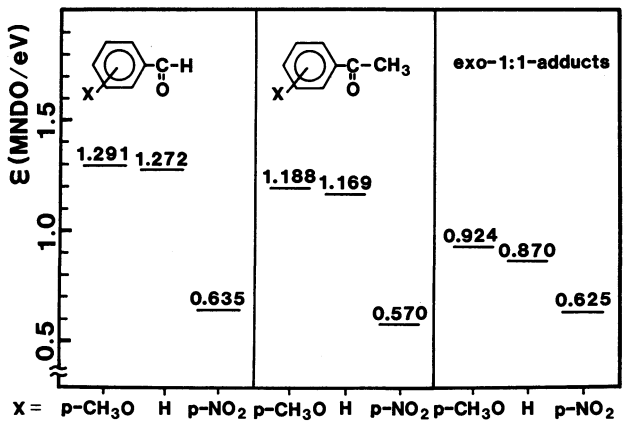

Fig. 2. The ε values of substituted benzaldehydes, acetophenones, and *exo*-1:1-adducts (**7a—c**).

of 2:1-adduct/1:1-adduct come to small. On the other hand, electron-releasing *p*-CH_3O group lowers the reactivity of the starting carbonyl compounds, and then the reactivity of anisaldehyde and the 1:1-adduct becomes comparable to give large 2:1/1:1 ratio.

The MNDO Calculation on the Energy Levels of Carbonyl Compounds. The results of MNDO calculation[9] supports the above assumption. As described previously,[6b] these cycloadditions proceed through the concerted process controlled by the carbonyl ylide-HOMO and carbonyl compound-LUMO (C=O π^*). Therefore, we can conclude that the carbonyl compound of the lower C=O π^* level have higher reactivity by decreasing the values of E(C=O π^*)−E(**3**-HOMO).[6b,10]

The C=O π^* energy levels (ε, eV) of 1,3-dipolarophiles, such as benzaldehydes, acetophenones, and *exo*-1:1-adducts (**7**), are shown in Fig. 2. The C=O π^* energy levels (ε) of benzaldehydes and acetophenones are stabilized largely by the substitution of electron-attracting *p*-NO_2 group, and are destabilized by electron-releasing *p*-CH_3O group (Fig. 2). On the other hand, the *exo*-1:1-adducts (**7a—c**) receive similar but much smaller substituent effect than benzaldehydes and acetophenones. When we compare the ε values of **7a—c** and benzaldehydes (**5a—c**), compounds (**7c** and **5c**) with *p*-NO_2 group have almost same ε values. However, the values for unsubstituted and *p*-CH_3O-substituted compounds are much smaller for **7** than for aldehydes. When we assume that the energy difference between carbonyl compound-LUMO (C=O π^*) and **3**-HOMO is the most effective factor on the reaction rate, *p*-nitrobenzaldehyde and *p*-NO_2-1:1-adduct (**7c**) should have comparable rate. However, the reaction of *p*-nitrobenzaldehyde with **3a** actually gave only 0.6% of expected 2:1-adduct (**8c**). This indicates that *p*-nitrobenzaldehyde is much more reactive than **7c**.

Other possible factors to affect the reactivity of **5c** and **7c** are as follows: (1) The atomic coefficient values of C=O π^* of **7c** and **5c**; (2) the extent of dipole-dipole interaction between **3a** and dipolarophiles, **7c** or **5c**;[10] (3) steric depression on the rate of the reaction of **7c**. In this case the factors (1) and (2) seem to be less effective than (3). The CPK model inspection reveals the large crowdedness around carbonyl group of the 1:1-adduct. Therefore, the steric depression is thought to be the most effective one. In the case of unsubstituted or *p*-CH_3O-substituted compounds, *exo*-1:1-adduct have smaller ε values than aldehydes by 0.40 eV for unsubstituted and 0.37 eV for *p*-CH_3O. The reactivity of **7a** or **7b** becomes comparable to **5a** or **5b**, under consideration of deactivation on **7** according to steric effect. Hence **3a** reacts competitively with **5** or **7** to give large values of 2:1-adduct/1:1-adduct.

Substituent effect on ε values of acetophenones is quite similar to benzaldehydes. However the small reactivities of acetophenones in comparison with those of benzaldehydes are probably caused by the steric hindrance on acetophenones, which lowers the total yields of the adducts except the case of *p*-nitroacetophenone.

Experimental

All melting points were measured on a Yanagimoto Melting Piont Apparatus and recorded without correction. The IR spectra were taken on a Perkin Elmer, model 983 in KBr pellet. The ^{1}H NMR spectra were recorded on a Varian Spectrometer, model EM390 in a $CDCl_3$ solution using TMS as an internal standard. The ^{13}C NMR spectra were measured on a Brucker NMR spectrometer, model AM360 in $CDCl_3$.

Materials. *p*-Methoxyphenyl *o*-(diazoacetyl)benzoate (**1a**)

and methyl *o*-(diazoacetyl)benzoate (**1b**) were prepared by the procedure described in the previous paper.[6b] Benzaldehydes, acetophenones, fluorenone, and anthraquinone were purified just before use by vacuum distillation or recrystallization of the commercial reagents. Benzene was purified by distillation over lithium aluminum hydride.

General Procedure of the Reaction of 3 and Carbonyl Compounds. The $Cu(acac)_2$-catalyzed decomposition of **1** was carried out according to the method described in the previous paper[6b]: A benzene solution of **1** was added drop by drop into a magnetically stirred benzene solution of 2 molar equivalents of carbonyl compound and catalytic amount (1/10 equivalent) of $Cu(acac)_2$ under reflux of benzene at 80°C in N_2 atmosphere. The reaction mixture was heated until no more N_2 was evolved (about one hour) and then the reaction products were separated by silica-gel column chromatography using benzene as an eluent. The reaction with acetone was carried out using large excess acetone because of its high volatility.

The authors express their sincere thanks to Dr. Masami Sawada and Mr. Yoshio Takai of ISIR, Osaka University for measurement and fruitful discussion on ^{13}CNMR spectra.

References

1) R. Huisgen, *Angew. Chem, Int. Ed. Engl.*, **16**, 572 (1977); M. Bêkhazi and J. Warkentin, *J. Am. Chem. Soc.*, **105**, 1289 (1983); and references cited therein.

2) M. Takebayashi, T. Ibata, and K. Ueda, *Bull. Chem. Soc. Jpn.*, **43**, 1500 (1970).

3) K. Ueda, T. Ibata, and M. Takebayashi, *Bull. Chem. Soc. Jpn.*, **45**, 2779 (1972).

4) T. Ibata, K. Jitsuhiro, and Y. Tsubokura, *Bull. Chem. Soc. Jpn.*, **54**, 240 (1981).

5) T. Ibata and K. Jitsuhiro, *Bull. Chem. Soc. Jpn.*, **52**, 3582 (1979).

6) a) T. Ibata and J. Toyoda, *Chem. Lett.*, **1983**, 1453; b) T. Ibata and J. Toyoda, *Bull. Chem. Soc. Jpn.*, **58**, 1787 (1985).

7) ^1H NMR ($CDCl_3$) of **7a**: δ3.69 (s, OCH_3), 3.79 (s, OCH_3), 4.70 (d, Ha, J=1.3 Hz), 4.63 (d, Hb, J=1.3 Hz) and multiplet signals of aromatic protons.

8) J. Toyoda, T. Ibata, H. Tamura, and K. Ogawa, *Bull. Chem. Soc. Jpn.*, **58**, 2212 (1985).

9) W. Thiel, *QCPE*, **11**, 353 (1978); Y. Beppu and I. Ninomiya, *QCPE*, **14**, 409 (1981); Y. Sasaki, T. Takagi, A. Tanaka, and R. Tokura, *Bulletin of Computation Center Osaka University*, **14**, 103 (1985).

10) K. N. Houk, J. Sims, C. R. Watts, and L. J. Luskus, *J. Am. Chem. Soc.*, **95**, 7301 (1973).

11) S. Takeuchi, J. Uzawa, H. Seto, and H. Yonehara, *Tetrahedron Lett.*, **1977**, 2943.

12) R. Wasylishen and T. Schaefer, *Can. J. Chem.*, **50**, 2710 (1972).

13) Details on the competitive reactions will be published elsewhere.

Structures of Agelasines, Diterpenes Having a 9-Methyladeninium Chromophore Isolated from the Okinawan Marine Sponge *Agelas nakamurai* Hoshino[1)]

Houming Wu,[2)] Hideshi Nakamura,* Jun'ichi Kobayashi, Masaki Kobayashi, Yasushi Ohizumi, and Yoshimasa Hirata†
Mitsubishi-Kasei Institute of Life Sciences, 11 Minamiooya, Machida, Tokyo 194
†Faculty of Pharmacy, Meijo University, Tempa-ku, Nagoya 468
(Received March 5, 1986)

Novel diterpenes, agelasine-A, -B, -C, -D, -E, and -F were isolated from the Okinawan marine sponge *Agelas nakamurai* Hoshino and their structures were established to be monocyclic and bicyclic diterpenes having a 9-methyladeninium unit by spectral analyses and chemical transformations.

Since Cullen and Devlin reported the isolation of agelasine, a quaternary 9-methyladenine derivative of an unidentified diterpene as a constituent of the marine sponge *Agelas dispar* in 1975,[3)] a variety of novel compounds having a polar functionality attached to a terpenoid moiety, the latter varying from acyclic sesqui to a mono or bicyclic diterpene skeleton have been isolated from marine sponges of the genus *Agelas* as bioactive metabolites. Included among these were terpenoid derivatives of hypotaurocyamine, agelasidine-A, -B and -C (**1**, **2**, and **3**)[4,5)] and seven diterpene derivatives of quaternary 9-methyladenine, agelasine-A, -B, -C, -D, and -E (**4**, **5**, **6**, **7**, **8**), agelasine-F (ageline-A, **9**), and ageline-B (**10**) isolated from the Okinawan marine sponge *Agelas nakamurai* by us[6,7)] and from a Pacific marine sponge *Agelas* sp. by Capon and Faulkner[8)] (Fig. 1). These compounds exhibited interesting bioactivities: Inhibitory effects on growth of microorganisms, contractive responses of smooth muscles and enzymic reactions of Na,K-ATPase. We

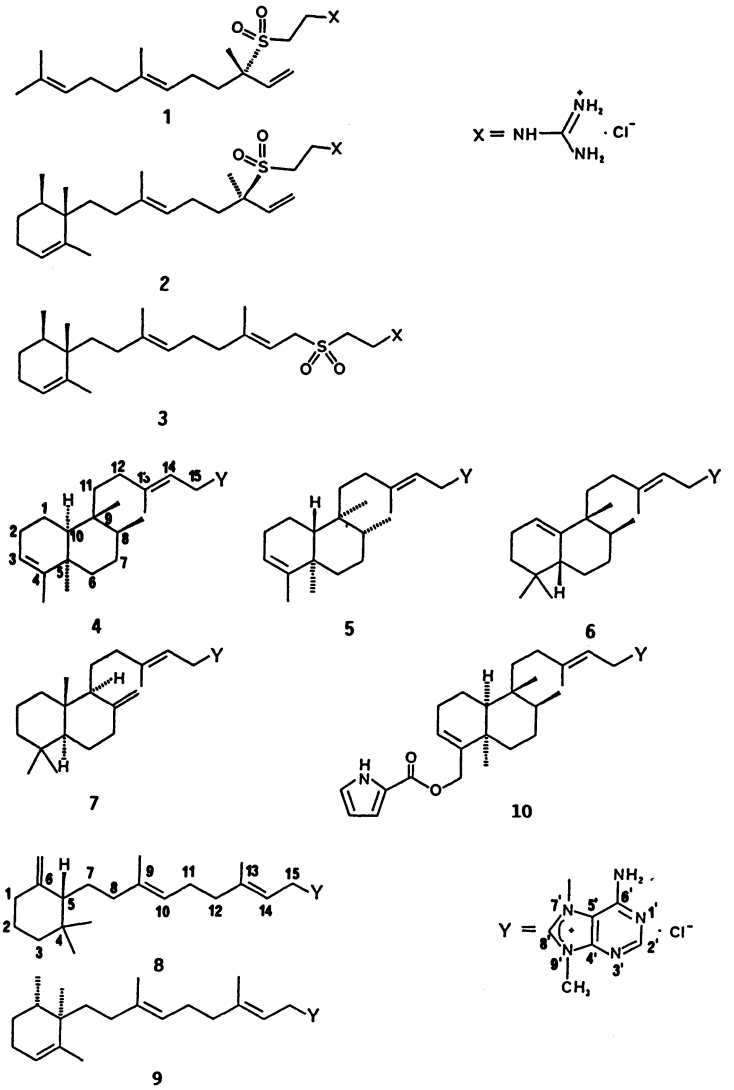

Fig. 1.

Table 1. ^{13}C NMR Data for Agelasine-A (**4**), -B (**5**), -C (**6**), -D (**7**), -E (**8**), -F (**9**), 7,9-Dimethyladeninium Perchlorate (**16**), and Methyl Kolavenate (**24**)[a)]

Carbon	4	5	6	7	8	9	16	24
1	17.6t	18.3t	121.0d	39.4t	38.0t	25.2t		18.4t
2	24.0t	27.5t	23.9t	20.3t	23.5t	26.8t		27.5t
3	123.1d	120.3d	38.2t	43.2t	36.1t	122.4d		120.5d
4	139.7s	144.3s	32.1s	34.4s	34.6s	139.3s		144.4s
5	40.2s	38.7s	44.5d	56.8d	53.5d	40.1s		38.8s
6	36.1t	36.3t	24.5t	25.5t	149.0s	33.0d		36.4t
7	28.8t	26.9t	29.9t	40.2t	24.6t	34.0t		26.9t
8	37.4d	36.3d	40.2d	149.0s	32.3t	35.0t		36.4d
9	37.7s	38.2s	43.8s	57.4d	136.2s	136.5s		38.3t
10	44.7d	46.4d	142.5s	40.6s	122.7d	123.7d		46.6d
11	33.0t	33.1t	34.2t	39.4t	26.0t	26.1t		34.7t
12	36.9t	36.8t	35.4t	22.5t	39.4t	39.4t		36.9t
13	147.9s	147.5s	149.3s	149.5s	146.8s	146.8s		161.6s
14	115.7d	115.7d	115.4d	115.9d	115.2d	115.2d		114.9d
15	48.7t	48.7t	48.8t	48.8t	48.4t	48.4t		162.3s
4-CH_3	19.7q	18.3q	22.6q	22.1q	26.0q	18.9q		19.2q
			28.6q	34.0q	28.2q			
5-CH_3	33.0q	19.9q				15.6q		20.0q
6-CH_3						20.8q		
6-=CH_2					108.6t			
8-CH_3	16.0q	16.0q	16.0q					16.0q
8-=CH_2				106.9t				
9-CH_3	17.8q	17.9q	26.3q		15.9q	16.0q		18.1q
10-CH_3				15.0q				
13-CH_3	17.3q	17.5q	17.3q	17.1q	17.2q	17.2q		18.4q
2′	155.8d	156.0d	156.7d	156.9d	155.2d	155.7d	155.4d	
4′	149.4s	149.5s	150.5s	150.7s	149.2s	149.2s	148.6s	
5′	109.7s	109.7s	110.8s	111.0s	109.5s	109.5s	109.7s	
6′	152.4s	152.5s	153.8s	153.9s	152.2s	152.2s	152.4s	
8′	141.7d	141.7d	142.0d	142.6d	141.2d	141.2d	141.9d	
9′-NCH_3	32.0q	32.0q	32.1q	32.0q	31.7q	31.7q	31.3q	
7′-NCH_3							36.2q	

a) δ in ppm, **4**—**9** and **24** in $CDCl_3$ and **16** in DMSO-d_6.

have recently reported the isolation and structures of agelasine-A—F briefly. In this paper, we describe the structural elucidation of the compounds in detail.

Specimens of *Agelas nakamurai* were collected at Zanpa Cape, Okinawa using SCUBA (−10—−20m), frozen shortly for transportation and stored at −20° C until workup. The chloroform-soluble material of methanolic extract of the sponge was chromatographed on a silica-gel column with 3:12:2:2 chloroform–1-butanol–acetic acid–water as eluent to give two fractions. The less polar fraction was repeatedly fractionated by HPLC on a C_{18} column using a methanol–water solvent system containing 0.2 M† sodium chloride to give agelasine-A, agelasine-E and agelasine-F (ageline-A), and a mixture of agelasine-B, -C, and -D. The mixture was further repeatedly chromatographed by HPLC using a C_8 column with methanol–water containing 0.2 M sodium chloride as a mobile phase to yield agelasine-B, -C, and -D. Agelasine-A—F are ammonium salts and isolated as chloride forms. The isolation yields were 0.037, 0.1, 0.01, 0.0056, 0.031, and 0.08% for agelasine-A—F respectively, from the wet weight of the sponge.

Agelasine-A—F (**4**—**9**) showed a number of spectral features in common: Their field desorption mass spectra (FDMS) contained identical principal ions at *m/z* 422 (M^+—Cl) and their high-resolution EI mass spectra (HREIMS) exhibited the principal ions at *m/z* 421.3216, 421.3204, 421.3177, 421.3182, 421.3202, and 421.3201 (M^+—HCl), respectively, revealing the same molecular formula, $C_{26}H_{40}N_5Cl$ (Calcd for $C_{26}H_{39}N_5$: M—HCl 421.3202). Their UV spectra showed alike absorption maxima at 272 nm with very similar ε values, indicating the presence of a same UV absorbing chromophore in these components. The presence of a common main fragment ion at *m/z* 149 in their electron impact mass spectra suggested that the chromophore was composed of $C_6H_7N_5$ (HREIMS *m/z* 149.0722, Calcd for $C_6H_7N_5$: 149.0709). This was supported by the facts that their ^1H NMR spectra contained four common signals corresponding seven protons assignable to NH_2 (δ=6.76—6.98), N-CH_3 (δ=4.10) and two aromatic protons (δ=8.48—8.50, 2′-H and δ=10.91—10.94, 8′-H) and their ^{13}C NMR spectra (Table 1) possessed six common signals due to a heteroaromatic ring. The common chromophore was assigned as a

† 1 M=1 mol dm^{-3}.

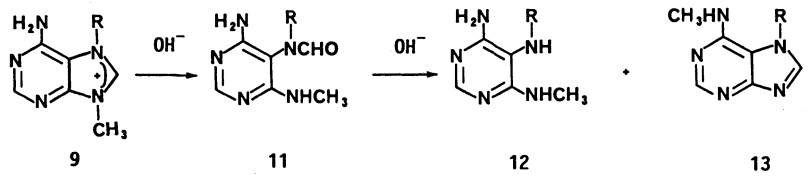

9 11 12 13

Fig. 2.

quaternary 9-methyladenine moiety on the basis of above spectral data and their following chemical behavior.

Agelasines were quite stable under acidic conditions, whereas the compounds were very unstable under basic conditions, even on a alumina column these compounds decomposed to yield less polar materials (Fig. 2). Agelasine-F (**9**), upon treatment with a base, was converted to the corresponding formamide **11**, whose ^{1}H NMR spectrum for the nitrogen-containing portion showed signals at δ 2.97 (d, 3H, J=5 Hz) for N-CH_3, 4.80 (brs, 2H) due to NH_2, and 7.96, and 8.14 (s, each 1H) assignable to the formamide group and 2′-H, respectively. Its electron impact mass spectrum (EIMS) exhibited a molecular ion at m/z 439 corresponding to a molecular formula $C_{26}H_{41}N_5O$. These data were in good agreement with literature values.[3] Furthermore, **9** was heated with 40% KOH at 110° C in a sealed tube to give two products. The less polar product was a white powder; UV absorption maximum at 272 nm (ε 8350); its ^{1}H NMR spectrum contained signals at δ 2.99 (d, 3H, J=5 Hz) for N-CH_3, 3.40 (d, 2H, J=7.5 Hz) due to N-methylene and 7.99 (s, 1H) arising from 2′-H. Lack of the signal for the formamide and the molecular ion at m/z 411 encouraged us to formulate the nitrogenous portion of the molecule as **12**. The polar product was identified as 6-N-methyl-7-alkyladenine derivative (**13**) which had been obtained by Cullen and Devlin from the cyclization of a relevant formamide with sodium hydride in N,N-dimethylacetamide. The structure was confirmed by comparing the spectral data of **13** with those of 6-N-methyl-7-prenyladenine (**14**) and 6-N-methyl-9-prenyladenine (**15**). During these chemical conversions no notable change could be found for the structure of its alkyl moiety.

The other components demonstrated identical behavior on treating with a base. The structure of nitrogenous portion of agelasines was resultantly confirmed by the comparison of the spectral data with those of 7,9-dimethyladeninium perchlorate (**16**).[9a] Above results established that agelasines contained a common polar group, quaternary 9-methyladeninium, and differed only in hydrocarbon portion which was composed of $C_{20}H_{33}$, a diterpene moiety. Further examination of the ^{1}H and ^{13}C NMR spectra of agelasines made it apparent that agelasines contained a common terminal grouping -C(CH_3)=CH-CH_2-Y, whereby the hydrocarbon portion of the molecule connected to 7-N atom of the 9-methyladenine. The E geometry of the double bond was established by their

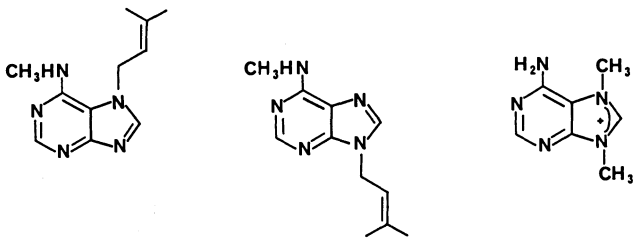

14 15 16

Fig. 3.

high field ^{13}C NMR signals for vinyl methyls (δ=17.1—17.5). The elucidation of the structures of remaining parts for each component was performed as follows.

Agelasine-A and -B (**4**, **5**), both exhibited one vinyl proton signal, two singlet, one doublet and one vinyl methyl signals at δ 5.28 (brs), 0.79 (s), 1.02 (s), 0.73 (d, J=5.8 Hz) and 1.67 (brs) for **4** and δ 5.17 (brs), 0.70 (s), 0.97 (s), 0.76 (d, J=5.2 Hz) and 1.57 (brs) for **5**, respectively, in their ^{1}H NMR spectra and the ^{13}C NMR signals for a trisubstituted double bond at δ 123.1 (d) and 139.7 (s) for **4** and 120.3 (d), 144.3 (s) for **5**, respectively. This spectral feature is consistent with a clerodane skeleton, a bicyclic ring system. For clerodane type compounds, the ^{13}C NMR chemical shift of 5-methyl usually provides particularly valuable piece of structural evidence for the mode of ring fusion: That of the trans-isomer occurs ca. 11—12 ppm upfield from that of the cis-isomer.[10] Indeed, on inspection of their ^{13}C NMR data, it was found that **4** exhibited a diagnostic low field signal (δ=33.4) due to the angular methyl while **5** showed a high field signal for the angular methyl (δ=19.9). Therefore cis and trans fused clerodane skeleton were assigned to **4** and **5**, respectively.

Since there are four asymmetric centers for clerodane ring system, for the gross structure there are sixteen stereochemical variations, wherein only six have been reported. However **4** on treating with a mixture of hydrochloric acid and acetic acid, converted to **17a** (Fig. 4), leaving only two asymmetric centers at 8 and 9 positions. **17a** can be correlated to **18a**, **18b**, and **18c**. For **18a**[11] having *trans*-8,9-dimethyl, the three singlet methyl signals occurred at δ 0.98, while for **18b**[11] and **18c**[12] having *cis*-8,9-dimethyl, two singlet methyl signals appeared at low field (δ=0.98 for **18b**, and 0.97 and 0.98 for **18c**, respectively), the other was at somewhat high field (δ=0.78 for **18b** and 0.84 for **18c**). The similarity of chemical shifts for three methyl signals in **17a** (δ=0.79, 0.94, and 0.96) clearly favored

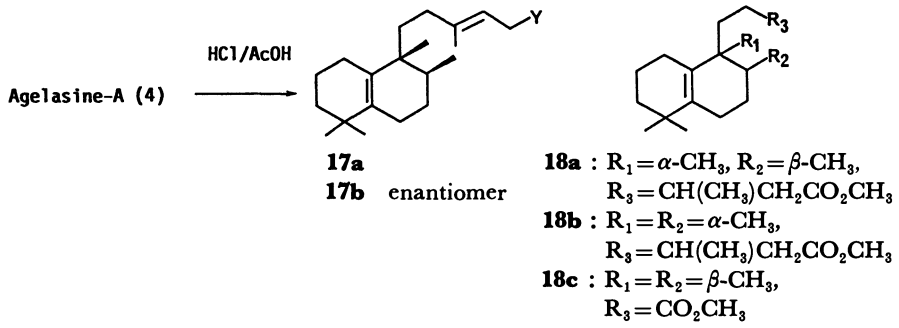

Fig. 4.

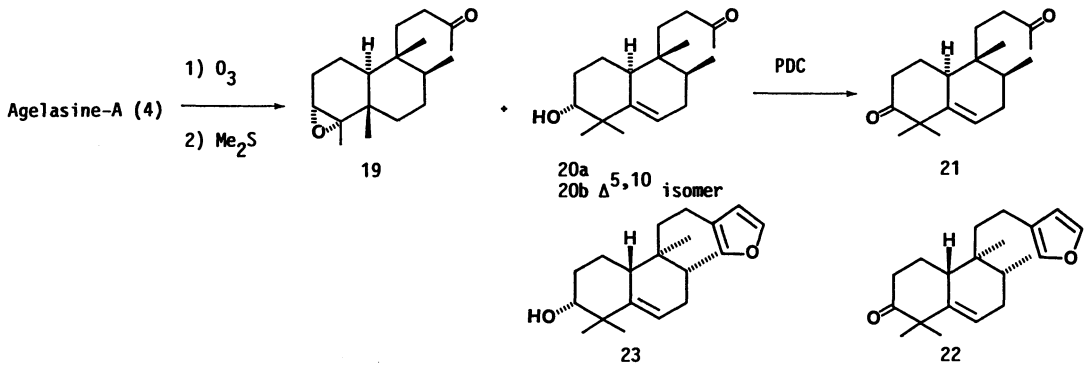

Fig. 5.

the relative stereochemistry of **18b** and **18c** over that of **18a**. Since the specific rotation of **17a** ($[\alpha]_D$ −14.7°) was same in sign to that of **18c** ($[\alpha]_D$ −52.9°), the absolute configuration of **17a** is probably identical to that of **18c**. It was confirmed by comparing **17a** with the enantiomeric **17b** which was obtained from agelasine-B (**5**). For agelasine-A, the remaining problem involved the deduction of the configuration of C-5 or C-10. Ozonolysis of **4** followed by reduction with dimethyl sulfide furnished an epoxide **19** and two olefinic alcohols **20a** and **20b** (Fig. 5), whose structures were assigned on the basis of their spectral data: **20a** showed an olefinic proton signal at δ 5.55 (m, 1H) and two ^{13}C NMR signals at δ 144.8 (s) and 118.4 (d) for a trisubstituted vinyl group while **20b** showed no olefinic proton signal and two ^{13}C NMR signals at δ 131.3 (s) and 135.1 (s) for a tetrasubstituted double bond. **20a** was oxidized with pyridinium dichromate (PDC) to yield a diketone **21**, which can be correlated to **22** obtained from a solidago diterpene via **23** by McCrindle et al.[13] The comparison of the ^1H NMR spectral data between **21** and **22** revealed close similarity. But **21** showed negative Cotton effect ($[\theta]_{293}$ −3480), which was opposit to that of **22** ($[\theta]_{291}$ +3320) suggesting that the absolute configuration of C-10 in **21** is reversed to that of **22**. Since **4** had a cis-fused decalin skeleton, absolute configurations for all asymmetric centers in **4** thus were well established. On the other hand, there were some differences in chemical shifts for methyls between **20a** and **23**; δ=0.65 (s), 0.81 (d, J=6.5 Hz), 0.94 (s), and 1.13 (s) for **20a** and 0.72 (s), 0.87 (d, J=6 Hz), 1.06 (s),

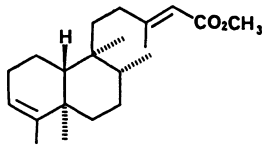

24

Fig. 6.

and 1.17 (s) for **23** respectively. This may be explained by different orientation of the hydroxyl group with respect to 10-H between them. In **23**, the hydroxyl group was situated anti and oriented axially, but in **20a** the hydroxyl group must be situated syn and adopted equatorial orientation, which was indicated by the coupling constants of 3-H proton signal at δ 3.23 (dd, J=4 and 11 Hz). This revealed that the epoxy group in **19** and the hydroxyl group in **20b** were also α-oriented.

Treatment of agelasine-B with a mixture of hydrochloric acid and acetic acid as well as agelasine-A furnished a tetrasubstituted olefinic compound. As **17b** was identical to **17a** in all respects except the sign of optical rotation ($[\alpha]_D$ +17.1°), it must be an antipode with α-dimethyl groups at 8 and 9 positions. Since agelasine-B has a trans-fused clerodane skeleton, there were only two stereochemical alternatives: 5β-methyl and 10α-proton or 5α-methyl and 10β-proton. The latter was present in methyl kolavenate (**24**)[14] (Fig. 6). The chemical shifts of four methyl signals in **5**, δ=0.70 (s), 0.76 (d, J=5.2 Hz), 0.97 (s) and 1.57 (s), were closely parallel to those of **24**, δ=0.76 (s), 0.85 (d),1.02 (s) and

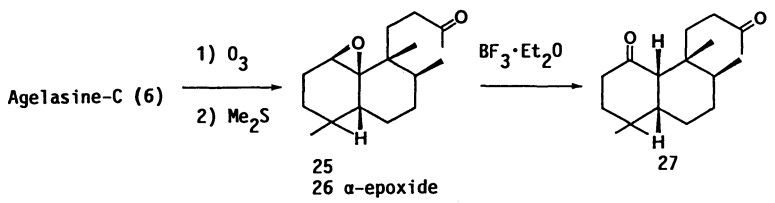

Fig. 7.

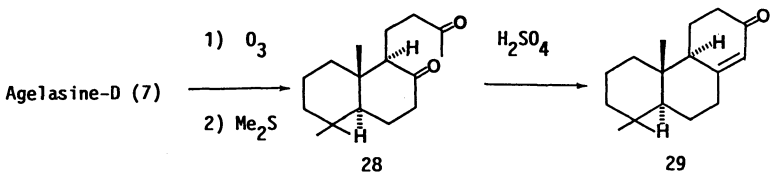

Fig. 8.

1.60 (s), and comparison of ^{13}CNMR spectrum of **5** with that of **24** revealed an excellent correlation for the relevant signals (Table 1). Since the optical rotation of **5** ($[\alpha]_D$ −21.5°) is same in sign to that of **24** ($[\delta]_D$ −58°), the absolute configuration of **5** must be identical to that of **24** at all asymmetric centers. Recently, the structure of agelasine-B (**5**) was confirmed by the synthesis of **5** from **24** by Iio et al.[15]

The ^{1}HNMR spectrum of agelasine-C (**6**) showed a vinyl proton signal at δ 5.31, three singlet methyl signals at δ 0.82, 0.84, and 0.87 and one doublet methyl signal at δ 0.79 (J=6.8 Hz). Thus a rearranged labdane skeleton with 1, 10- or 5,6-double bond was assumed for its gross structure. However, lack of a high field methyl signal, which had been observed for 9-methyl in **20a** (δ=0.65), favored the double bond arrangement at 1,10-position. An acid catalyzed rearrangement of **6** as well as **4** yielded **17a**, indicating the stereochemistry of C-8 and C-9 as illustrated in **6**. Furthermore, reductive ozonolysis workup of **6** (ozone and dimethyl sulfide) gave two epoxides **25** and **26** (Fig. 7). Both epoxides were very hindered and the attempt to reduce them with lithium triethylhydroborate was failed. Then **26** was treated with boron trifluoride etherate to yield a diketone **27** whose ^{1}HNMR spectrum contained signals for α-protons to the carbonyl group at 1-position, δ=2.12 (2-H, ddd, 1H, J=2.3, 4.4, and 13.5 Hz), 2.42 (2-H, dt, 1H, J=6.3 and 13.5 Hz) and 2.48 (10-H, d, 1H, J=5.0 Hz) besides four methyl signals at δ=0.97 (s), 1.03 (d, J=6.9 Hz), 1.17 (s) and 1.23 (s). On irradiation at δ=1.44 (8-H), the doublet methyl signal for C-8 methyl was collapsed to a singlet, whereas the α-proton signals were not affected. This result companied with the small J-value of 10-H signal (5.0 Hz) provided valid evidence for that **27** has a cis-fused decalin skeleton with a carbonyl group at **1** position. In addition, the observation of nuclear Overhauser effects between both the two singlet methyl signals at C-4 and C-9 (δ=0.97 and 1.23) and the 10-H signal (δ=2.48) required a non-steroid-like conformation for **27** which exhibited negative

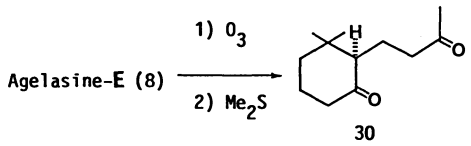

Fig. 9.

Cotton effect ($[\theta]_{298}$ −2370). On the basis of the octant rule, the absolute configuration of **27** was determined as illustrated. Since **27** might be formed from the α-epoxide **26** via a trans antiparallel hydride shift from C-1 to an incipient cationic center at 10-position and the configuration of C-5 was uneffected by the rearrangement conditions employed, the epoxy groups in **25** and **26** might be β- and α-oriented and the stereochemistry of **6** should be as illustrated.

Agelasine-D (**7**) showed three singlet methyl signals at δ 0.65, 0.79, and 0.87 and two vinyl proton signals at δ 4.43 (brs) and 4.81 (brs) for an exomethylene group which was further suggested by the ^{13}CNMR signals at δ 106.9 (t) and 149.0 (s). These data are compatible with a labdane ring system, a well studied skeleton. The stereochemistry of **7** was established by following chemical conversion (Fig. 8). Ozonolysis of **7** followed by reduction with dimethyl sulfide afforded a diketone **28**, which was treated with sulfuric acid to yield an enone **29**. Its spectral data and optical properties were identical with those of an authentic enone.[16,17]

The ^{13}CNMR spectrum of agelasine-E (**8**) showed six olefinic carbon signals at δ 108.3 (t), 115.2 (d), 122.7 (d), 136.2 (s), 146.8 (s), and 149.0 (s) due to its hydrocarbon portion, indicating the presence of three double bonds and a ring. In addition, its ^{1}HNMR spectrum contained signals at δ 5.00 (brs, 1H) and 1.57 (s, 3H) for additional group $-C(CH_3)=CH-CH_2-$, in which the geometry of the double bond was assigned to be *E* on the basis of a high field resonace of an olefinic methyl carbon (δ=15.9), leaving a terminal monocyclic moiety. The remaining ^{1}HNMR data showed two singlet methyl signals at δ 0.82 and 0.90 and an exomethylene proton signals at δ 4.53 (brd,

J=1.5 Hz) and 4.76 (brd, J=1.5 Hz) due to the terminal cyclic part. A 1-alkyl-2-methylene-6,6-dimethylcyclohexane ring system was assigned for the terminal residue. The structure of the diterpene portion in **8** was confirmed by ozonolysis results (Fig. 9). **8** was treated with ozone and worked up with dimethyl sulfide to give a diketone **30** and an unidentified compound **31** arising from the linear polyisoprenyl chain. The CD spectrum of **30** showed a negative Cotton effect ($\Delta\varepsilon_{292}$ −1.57) which was opposite to that of a known diketone having a 5*S* configuration ($\Delta\varepsilon_{296}$ +1.57),[18] indicating the absolute configuration of **8** to be 5*S*. The reduction of **31** with sodium borohydride followed by acetylation with acetic anhydride and pyridine to give 1,4-diacetoxypentane.

The spectral data of agelasine-F (**9**) was in good agreement with those of ageline-A and an identical structure was proposed for it.[8] However, the absolute configuration of **9** was independently established by a successive chemical conversions outlined as following (Fig. 10). The ozonolysis of **9** followed by reductive workup (ozone at −78° C and sodium borohydride) furnished an epoxide **32** and 1,4-pentanediol. **32** was further reduced with lithium triethylhydroborate to give a diol **33**, which was acetylated and then was submitted to dehydration with thionyl chloride/pyridine to yield a 2:1 mixture of an exocyclic olefin **35** and its endo-isomer. The mixture without separation was deacetylated with sodium methoxide to give olefinic alcohol **36**, which then was oxidized with pyridinium dichromate to yield a mixture containing a compound **37**. The mixture was treated with ozone, reduced with dimethyl sulfide and cyclized in methanolic KOH under an argon atmosphere to yield a cis-octalone **38**, which was identical in all respects with an authentic sample.[19] The CD spectrum of **38** exhibited a positive Cotton effect at 236 nm ([θ] +5800) and a negative one at 335 nm ([θ] −390) in hexane, indicating the absolute configuration of the ring junction methyl group as illustrated. On the other hand, ozonolysis of **9** (reductive workup with dimethyl sulfide) furnished an enol ether **39** and a ketone **40**. **39** may be formed via a trans-opening of an epoxide and was characterized by the carbon signals at δ 92.8 (d) and 146.9 (s). It then was treated with *p*-bromobenzoyl chloride and triethylamine to yield **41**. The structure of **41** was elucidated by the interpretation of its ^{1}HNMR spectrum and extensive homodecoupling experiments run at 400 MHz. The axial orientation of *p*-bromobenzoyloxy group and equatorial orientation of 1-methyl were indicated by the coupling constants of the proton signals at 1 and 4 position (J_{1-2a}=13 Hz and J_{3a-4}=J_{3b-4}=3 Hz). Therefore the downfield shift of the signal for 10-methyl (δ=0.93) by the benzoylation ($\Delta\delta$ 0.12) revealed that the *p*-bromobenzoyloxy group i.e. the epoxy group and 10-methyl group in **32** were situated syn. The CD spectrum of compound **40** showed a positive Cotton effect ([θ]$_{295}$ +131). Hence it could in turn be used as a standard to deduce the stereochemistry of agelasidine-B and -C.[5]

Experimental

General. All mp's were obtained on a Yanagimoto micro melting point apparatus and uncorrected. Optical rotations were measured on a Union automatic polarimeter PM-201. IR spectra were recorded on a Hitachi 260-50 spectrophotometer. ^{1}HNMR spectra were taken on JEOL FX-90Q (90 MHz), Bruker WH-270 (270 MHz), or Bruker AM-400 (400 MHz) instruments. ^{13}CNMR spectra were recorded with a JEOL FX-90Q (22.5 MHz) spectrometer. FD mass spectra and HREI mass spectra were measured on a Hitachi M-80A mass spectrometer. CD spectra were obtained on a JASCO J-40A spectrophotometer. UV spectra were taken on a Varian Cary-17 instrument.

Collection, Extraction, and Separation. The marine sponge *Agelas nakamurai* Hoshino (5 Kg, wet weight) was collected at Zampa Cape, Okinawa in 1981 using SCUBA

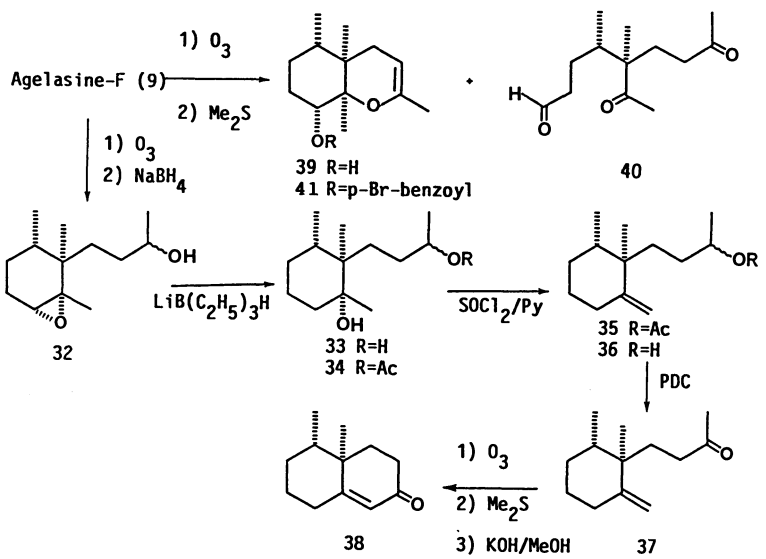

Fig. 10.

(−10—−20 m), shortly frozen and shipped via air to Tokyo, then stored at −20° C until workup. The sponge was cut into small pieces and extracted with methanol (3×40 l). The solvent was evaporated under reduced pressure to give a crude extract (195 g), which was dissolved in methanol. The methanol-soluble material (125 g) was partitioned between chloroform and water. Each 12 g of chloroform-soluble material (60 g) was chromatographed on a silica-gel column (Wako gel C-300, Wako Chemical, 50×600 mm) with 3:12:2:2 chloroform–1-butanol–acetic acid–water as eluent, monitered by TLC. The less polar fraction contained agelasidines (positive coloration with Sakaguchi reagent) and the polar fractions were consisted of agelasines (slightly positive coloration with Sakaguchi reagent and strong UV absorption). The polar fraction was purified by preparative HPLC on a C_{18} column (Nomura Chemical Co. Ltd. Develosil ODS 15/30, 21×250 mm×3) with 8:2 methanol–water containing 0.2 M sodium chloride (flow rate 28 ml min^{-1}) to give a mixture of agelasines (22 g). A part (2 g) of the mixture was separated on a C_{18} column (Develosil ODS-5, 10×250 mm) with 8:2 methanol–water containing 0.2 M sodium chloride (flow rate 4 ml min^{-1}) to yield agelasine-A (**4**, t_R=17.3 min, 170 mg), a mixture of agelasine-B, -C, and -D (t_R=18 min, 822 mg), and agelasine-E (**8**, t_R=19.8 min, 255 mg) and agelasine-F (**9**, t_R=21 min, 368 mg). The mixture was chromatographed on a C_8 column (Develosil C_8-5, 10×250 mm) using methanol–water (73:27) containing 0.2 M sodium chloride as eluent to give a mixture of agelasine-B and -D (t_R=32.3 min, 643 mg), and agelasine-C (**6**, t_R=39 min, 143 mg). The former was further separated by HPLC on a C_8 column (Develosil C_8-5, 10×250 mm) with 7:3 methanol–water containing 0.2 M sodium chloride to furnish agelasine-B (**5**, t_R=53.5 min, 220 mg) and agelasine-D (**7**, t_R=56.3 min, 24 mg).

Agelasine-A (4). Amorphous solid; mp 173—174° C; $[\alpha]_D$ −31.3° (*c* 0.59, CH_3OH); UV (CH_3OH) 272 nm (ε 8910); IR ($CHCl_3$) 3320, 3150, 2950, 1640, 1610, 1455, 1380, 1300, 1230, 1190, 1090 cm^{-1}; ^{1}H NMR ($CDCl_3$, 400 MHz) δ=0.73 (d, 3H, *J*=5.8 Hz), 0.79 (s, 3H), 1.02 (s, 3H), 1.67 (brs, 3H), 1.88 (brs, 3H), 1.0—2.1 (m, 14H), 4.10 (s, 3H), 5.26 (brs, 1H), 5.41 (brt, 1H, *J*=6.5 Hz), 5.71 (brd, 2H, *J*=6.5 Hz), 6.98 (brs, 2H, exch), 8.48 (s, 1H), 10.81 (s, 1H); EIMS *m/z* 421 (M^+−HCl), 149, 150, 81, 41, 69, 55, 216, 217, 163, 298, 406; FDMS *m/z* 422 (M^+−Cl); Found: *m/z* 421.3216. Calcd for $C_{26}H_{39}N_5$: M−HCl 421.3202.

Agelasine-B (5). Amorphous solid; mp 167—170° C; $[\alpha]_D$ −21.5° (*c* 1.0, CH_3OH); UV (CH_3OH) 272 nm (ε 8240); IR ($CHCl_3$) 3370, 3160, 2960, 1640, 1610, 1590, 1460, 1385, 1300, 1240, 1195, 1090 cm^{-1}; ^{1}H NMR ($CDCl_3$, 400 MHz) δ=0.70 (s, 3H), 0.76 (d, 3H, *J*=5.2 Hz), 0.97 (s, 3H), 1.57 (s, 3H), 1.86 (brs, 3H), 0.7—2.2 (m, 14H), 4.10 (s, 3H), 5.17 (brs, 1H), 5.41 (brt, 1H, *J*=6.5 Hz), 5.71 (brd, 2H, *J*=6.5 Hz), 6.84 (brs, 2H, exch), 8.50 (s, 1H), 10.89 (s, 1H); EIMS *m/z* 421 (M^+−HCl), 149, 95, 121, 107, 189, 163; FDMS *m/z* 422 (M^+−Cl); Found: *m/z* 421.3204. Calcd for $C_{26}H_{39}N_5$: M−HCl 421.3202.

Agelasine-C (6). Amorphous solid; mp 176—179° C; $[\alpha]_D$ −55.1° (*c* 2.04, CH_3OH); UV (CH_3OH) 272 nm (ε 8340); IR (KBr) 3300, 3140, 2965, 1645, 1615, 1470, 1380, 1360, 1230, 1180 cm^{-1}; ^{1}H NMR ($CDCl_3$, 400 MHz) δ=0.79 (d, 3H, *J*=6.8 Hz), 0.82 (s, 3H), 0.84 (s, 3H), 0.87 (s, 3H), 0.7—2.2 (m, 14H), 4.10 (s, 3H), 5.31 (brt, 1H, *J*=6.2 Hz), 5.41 (brt, 1H, *J*=6.5 Hz), 5.70 (brd, 2H, *J*=6.5 Hz), 6.84 (brs, 2H, exch), 8.50 (s, 1H), 10.88 (s, 1H); EIMS *m/z* 421 (M^+−HCl), 149, 191, 177, 135, 122, 95, 107; FDMS *m/z* 422 (M^+−Cl); Found: *m/z* 421.3177. Calcd for $C_{26}H_{39}N_5$: M−HCl 421.3202.

Agelasine-D (7). Amorphous solid; mp 175—176° C; $[\alpha]_D$ +10.4° (*c* 1.05, CH_3OH); UV (CH_3OH) 272 nm (ε 9180); IR ($CHCl_3$) 3300, 3150, 2950, 1640, 1610, 1590, 1455, 1390, 1300, 1090, 895 cm^{-1}; ^{1}H NMR ($CDCl_3$, 400 MHz) δ=0.65 (s, 3H), 0.79 (s, 3H), 0.87 (s, 3H), 0.6—2.4 (m, 16H), 1.86 (s, 3H), 4.10 (s, 3H), 4.43 (brs, 1H), 4.81 (brs, 1H), 5.41 (brt, 1H, *J*=6.5 Hz), 5.72 (brd, 2H, *J*=6.5 Hz), 6.75 (brs, 2H, exch), 8.50 (s, 1H), 10.94 (s, 1H); EIMS *m/z* 421 (M^+−HCl), 149, 81, 95, 69, 137, 109, 121, 217, 293; FDMS *m/z* 422 (M^+−Cl); Found: *m/z* 421.3182. Calcd for $C_{26}H_{39}N_5$: M−HCl 421.3202.

Agelasine-E (8). Amorphous solid; mp 180—182° C; $[\alpha]_D$ −17.1° (*c* 1.88, CH_3OH); UV (CH_3OH) 272 nm (ε 9720); IR ($CHCl_3$) 3330, 3150, 2950, 1640, 1610, 1590, 1455, 1405, 1380, 1365, 1300, 1235, 1190, 1090 cm^{-1}; ^{1}H NMR ($CDCl_3$, 400 MHz) δ=0.82 (s, 3H), 0.90 (s, 3H), 1.56 (s, 3H), 1.86 (s, 3H), 0.7—2.2 (m, 15H), 4.10 (s, 3H), 4.53 (brd, 1H, *J*=1.5 Hz), 4.76 (brd, 1H, *J*=1.5 Hz), 5.00 (brs, 1H), 5.46 (brt, 1H, *J*=6.5 Hz), 5.72 (brd, 2H, *J*=6.5 Hz), 6.87 (brs, 2H, exch), 8.50 (s, 1H), 10.83 (s, 1H); EIMS *m/z* 421 (M^+−HCl), 149, 216, 81, 95, 69, 109; FDMS *m/z* 422 (M^+−Cl); Found: *m/z* 421.3202. Calcd for $C_{26}H_{39}N_5$: M−HCl 421.3202.

Agelasine-F (9). Amorphous solid; mp 178—180° C; $[\alpha]_D$ −5.5° (*c* 2.55, CH_3OH); UV (CH_3OH) 272 nm (ε 7700); IR ($CHCl_3$) 3300, 3150, 2970, 1640, 1590, 1455, 1380, 1300, 1235, 1090 cm^{-1}; ^{1}H NMR ($CDCl_3$, 400 MHz) δ=0.84 (s, 3H), 0.85 (d, 3H, *J*=7 Hz), 1.57 (s, 3H), 1.59 (s, 3H), 1.86 (s, 3H), 1.0—2.2 (m, 13H), 4.10 (s, 3H), 5.02 (brs, 1H), 5.42 (brs, 1H), 5.47 (brt, 1H, *J*=7 Hz), 5.72 (brd, 2H, *J*=7 Hz), 6.87 (brs, 2H, exch), 8.50 (s, 1H), 10.83 (s, 1H); EIMS *m/z* 421 (M^+−HCl), 149, 150, 216, 217, 298, 123, 121; FDMS *m/z* 422 (M^+−Cl); Found: *m/z* 421.3201, 149.0722. Calcd for $C_{26}H_{39}N_5$ and $C_6H_7N_5$: M−HCl 421.3202 and 149.0709.

Acid Catalyzed Rearrangement of Agelasine-A (4). **4** (10 mg, 0.022 mmol) was treated with a solution of acetic acid (0.4 ml) and 12 M HCl (0.1 ml) at room temperature using HPLC to follow the reaction. After 30 min the starting meterial was converted completely to give single product. The reagents were removed in vacuo and 1 M NaCl solution (7 ml) was added. The solution was extracted with ethyl acetate (2×15 ml). The extract was concentrated to yield **17a** (10 mg, 100% theoretical). **17a**: Colorless crystals; ^{1}H NMR ($CDCl_3$, 270 MHz) δ=0.79 (s, 3H), 0.80 (d, 3H, *J*=6 Hz), 0.94 (s, 3H), 0.96 (s, 3H), 1.86 (brs, 3H), 1.0—2.0 (m, 15H), 4.08 (brs, 3H), 5.40 (brt, 1H, *J*=6 Hz), 5.67 (brd, 2H, *J*=6 Hz), 7.04 (brs, 2H exch), 8.46 (brs, 1H), 10.70 (s, 1H); ^{13}C NMR ($CDCl_3$, 67.5 MHz) δ=16.3 (q), 17.6 (q), 20.0 (t), 21.2 (q), 25.2 (t), 25.8 (t), 27.2 (t), 27.8 (q), 29.3 (q), 32.0 (q), 33.7 (d), 34.4 (t), 34.6 (s), 40.0 (t), 40.7 (s), 48.8 (t), 109.9 (s), 115.5 (d), 132.0 (s), 137.5 (s), 141.9 (d), 147.8 (s), 149.6 (s), 152.5 (s), 156.0 (d); $[\alpha]_D$ −14.7° (*c* 0.42, CH_3OH).

Ozonolysis of Agelasine-A (4). A solution of **4** (30 mg, 0.066 mmol) in methanol (3 ml) was saturated with ozone for 30 min at −78° C. The excess ozone was removed by a N_2 stream and dimethyl sulfide (0.055 ml) was added. The solution was stirred at 0° C for 30 min and room temperature overnight. The solvent was removed under reduced pressure and the residue was separated by HPLC on a C_{18} column (Develosil ODS-5, 10×250 mm) with methanol–water (8:2) to give the olefinic alcohol **20a** (4 mg, t_R=13.38 min, 22% theoretical), the epoxide **19** (1.5 mg, t_R=20.63 min, 8.3% theoretical) and the olefinic alcohol **20b** (3 mg, t_R=23.85 min, 16.6% theoretical). **20a**: A colorless syrup; ^{1}H NMR ($CDCl_3$,

90 MHz) δ=0.65 (s, 3H), 0.81 (d, 3H, J=6.5 Hz), 0.94 (s, 3H), 1.13 (s, 3H), 2.16 (s, 3H), 3.23 (dd, 1H, J=4, 11 Hz), 5.55 (m, 1H); EIMS m/z 278 (M^+), 189, 187, 119, 207, 227, 161, 224, 260. **19**: A colorless syrup; ^{1}H NMR ($CDCl_3$, 90 MHz) δ=0.81 (d, 3H, J=6 Hz), 0.87 (s, 3H), 1.09 (s, 3H), 1.32 (s, 3H), 2.15 (s, 3H), 2.98 (brd, 1H, J=3.5 Hz); EIMS m/z 278 (M^+), 207, 189, 149, 121, 123, 119, 109, 107, 95, 249, 221. **20b**: A colorless syrup; ^{1}H NMR ($CDCl_3$, 90 MHz) δ=0.83 (d, 3H, J=4.8 Hz), 0.85 (s, 3H), 1.01 (s, 3H), 1.02 (s, 3H), 2.12 (s, 3H), 3.52 (m, 1H); EIMS m/z 278 (M^+), 189, 207, 119, 135, 187, 105, 227, 260, 244, 242.

Oxidation of Olefinic Alcohol (20a). To a solution of **20a** (2.4 mg, 0.0086 mmol) in CH_2Cl_2 (1 ml), pyridinium dichromate (13 mg) was added. The reaction mixture was stirred at room temperature overnight. Diethyl ether (5 ml) was added, and then the reaction mixture was filtrated to remove the solid and concentrated under reduced pressure. The residue was purified by a short silica-gel column (hexane–ethyl acetate 17:3) to yield the olefinic diketone **21** (2 mg, 80% theoretical). **21**: A colorless syrup; ^{1}H NMR ($CDCl_3$, 90 MHz) δ=0.69 (s, 3H), 0.83 (d, 3H, J=6 Hz), 1.24 (s, 6H), 2.18 (s, 3H), 5.26 (m, 1H); EIMS m/z 276 (M^+), 205, 206, 163, 187, 93, 119, 121, 203, 191, 107; CD $[\theta]_{293}$ −3480.

Acid Catalyzed Rearrangement of Agelasine-B (5). **5** (10 mg, 0.022 mmol) was treated with a solution of acetic acid (0.4 ml) and 12 M HCl (0.1 ml) at room temperature for 3 h. The reaction mixture was dried in vacuo and the residue was separated by HPLC on a C_8 column (Develosil C_8-5 packed column, 10×250 mm) using methanol–water (8:2) containing 0.2 M sodium chloride as a mobile phase. The main fraction was concentrated under reduced pressure and the resultant water layer was extracted with ethyl acetate. Concentration of the extract gave **17b** (7 mg, 70% theoretical). **17b**, amorphous solid, was identical with **17a** in all respects except $[\alpha]_D^{25}$ +17.4° (*c* 0.35, CH_3OH).

Acid Catalyzed Rearrangement of Agelasine-C (6). **6** (12 mg, 0.026 mmol) was treated with a solution of acetic acid (0.48 ml) and 12 M HCl (0.32 ml) at room temperature for 3 h and worked up as above to yield **17a** (8.8 mg, 73% theoretical), which was identical with that obtained from agelasine-A, and showed $[\alpha]_D$ −15.9° (*c* 0.44, CH_3OH).

Ozonolysis of Agelasine-C (6). Ozone was bubbled in the solution of **6** (70 mg, 0.15 mmol) in methanol (50 ml) at −78° C for 1 h. The excess ozone was removed by N_2 flow. Dimethyl sulfide (1 ml) was added, then the solution was allowed to warm up to 0° C and then room temperature (in 30 min each). The reaction mixture was dried under reduced pressure and the residue was submitted to silica-gel column chromatography (hexane–ethyl acetate 95:5) to furnish two epoxides **25** and **26** (9 mg, 21% and 13 mg, 31% theoretical, respectively). **25**: A colorless syrup; ^{1}H NMR ($CDCl_3$, 90 MHz) δ=0.68 (s, 3H), 0.79 (s, 3H), 0.93 (d, 3H, J=7.2 Hz), 1.06 (s, 3H), 2.15 (s, 3H), 3.04 (brd, 1H, J=4 Hz), 1.0—2.7 (m, 14H); EIMS m/z 278 (M^+), 207, 263, 189, 137, 119; $[\alpha]_D^{25}$ −36.7° (*c* 0.60, CH_3OH). **26**: A colorless syrup; ^{1}H NMR ($CDCl_3$, 90 MHz) δ=0.64 (s, 3H), 0.86 (s, 6H), 1.03 (d, 3H, J=7.2 Hz), 2.16 (s, 3H), 2.91 (brd, 1H, J=4 Hz), 1.0—2.6 (m, 14H); EIMS m/z 278 (M^+), 207, 163, 137, 83, 55, 67, 95, 105, 119, 121; $[\alpha]_D^{25}$ +6.5° (*c* 1.85, CH_3OH).

Reaction of 26 with Boron Trifluoride Etherate. A solution of **26** (3.5 mg, 0.013 mmol) in anhydrous benzene (1.5 ml) was treated with boron trifluoride etherate (0.1 ml) for 10 min at room temperature. The solution was diluted with ethyl acetate (5 ml) and extracted with aqueous sodium hydrogencarbonate (10%, 10 ml), then washed with brine (10 ml), and dried under anhydrous sodium sulfate. Evaporation left a residue, which was submitted to silica-gel column chromatography (hexane–ethyl acetate 85:15) to yield the diketone **27** (1.5 mg, 43% theoretical). **27**: A colorless syrup; ^{1}H NMR ($CDCl_3$, 400 MHz) δ=0.97 (s, 3H), 1.03 (d, 3H, J=6.9 Hz), 1.13 (s, 3H), 1.23 (s, 3H), 2.12 (ddd, 1H, J=2.3, 4.4, 13.5 Hz), 2.17 (s, 3H), 2.26 (m, 2H), 2.42 (dt, 1H, J=6.3, 13.5 Hz), 2.48 (d, 1H, J=5 Hz); EIMS m/z 278 (M^+), 207, 125, 151, 208, 95, 109, 152, 119, 161, 189; CD $[\theta]_{298}$ −2370.

Ozonolysis of Agelasine-D (7). A solution of **7** (5 mg, 0.011 mmol) in methanol (0.5 ml) was treated with ozone at −78° C for 30 min. After removing excess ozone, dimethyl sulfide (0.03 ml) was added, then the solution was kept at 0° C for 30 min and at room temperature for 3 h. Evaporation of the solvent left a residue, which was submitted to silica-gel column chromatography (hexane–ethyl acetate 85:15) to afford the diketone **28** (1.5 mg, 52% theoretical). An additional amount (ca. 18 mg) was obtained from the ozonolysis of the mixture of agelasines. **28**: A colorless syrup; ^{1}H NMR ($CDCl_3$, 90 MHz) δ=0.72 (s, 3H), 0.84 (s, 3H), 0.95 (s, 3H), 2.08 (s, 3H), 1.0—2.8 (m, 16H); ^{13}C NMR ($CDCl_3$, 22.5 MHz) δ=14.6 (q), 16.3 (q), 19.0 (t), 21.7 (q), 24.0 (t), 29.9 (q), 33.6 (q), 33.7 (t), 39.2 (t), 42.0 (t), 42.6 (t), 42.7 (s), 42.8 (t), 54.2 (d), 63.2 (d), 208.9 (s), 211.9 (s); IR ($CHCl_3$) 1710 cm^{-1}; EIMS m/z 264 (M^+), 249, 81, 95, 67, 55, 121, 139, 231; $[\alpha]_D^{25}$ −28.5° (*c* 1.5, CH_3OH).

Conversion of 28 to the Enone (29). Concentrated sulfuric acid (0.13 ml) was added dropwise to the solution of **28** (16 mg, 0.061 mmol) in methanol (2.4 ml). The solution was heated to boiling, then cooled, diluted with water (15 ml) and extracted with diethyl ether (2×15 ml). Evaporation of the solvent left a residue, which was submitted to silica-gel column chromatography (hexane–ethyl acetate 9:1) to give the enone **29** (12.2 mg, 76.2% theoretical): Colorless crystals; ^{1}H NMR ($CDCl_3$, 90 MHz) δ=0.80 (s, 3H), 0.87 (s, 3H), 0.92 (s, 3H), 5.88 (brs, 1H); ^{13}C NMR ($CDCl_3$, 22.5 MHz) δ=15.1 (q), 18.6 (t), 20.4 (t), 21.9 (q), 21.9 (t), 33.3 (s), 33.5 (q), 36.7 (t), 38.9 (s), 39.2 (t), 41.7 (t), 51.5 (d), 53.9 (d), 125.7 (d), 165.7 (s), 199.4 (s); IR ($CHCl_3$) 1680 cm^{-1}; EIMS m/z 246 (M^+), 110, 137, 123, 231; $[\alpha]_D^{25}$ +36.0° (*c* 0.5, CH_3OH); UV (CH_3OH) 242 (ε 20050), 310 nm (360); CD $[\theta]_{242}$ +38460, $[\theta]_{317}$ −8720.

Ozonolysis of Agelasine-E (8). A solution of **8** (26 mg, 0.057 mmol) in methanol (3 ml) was saturated with ozone at −78 °C for 30 min. After removing the excess ozone dimethyl sulfide (0.075 ml) was added, then the solution was allowed to warm up to 0° C (30 min) and room temperature overnight. The reaction mixture was dried under reduced pressure and the residue was submitted to silica-gel column chromatography (hexane–ethyl acetate 85:15) to yield the diketone **30** (10 mg, 90% theoretical) and the compound **31** (5.1 mg). **30**: A colorless syrup; ^{1}H NMR ($CDCl_3$, 270 MHz) δ=0.79 (s, 3H), 1.09 (s, 3H), 2.12 (s, 3H), 1.5—2.6 (m, 11H); ^{13}C NMR ($CDCl_3$, 22.5 MHz) δ=18.3 (t), 21.8 (q), 23.1 (t), 29.5 (q), 39.5 (t), 39.7 (s), 41.4 (t), 42.6 (t), 60.1 (d), 208.6 (s), 213.0 (s); IR ($CHCl_3$) 1710 cm^{-1}: EIMS m/z 196 (M^+), 181, 111, 163, 139, 121, 95; CD $[\theta]_{292}$ −5174, $\Delta\varepsilon_{292}$ −1.57.

Reduction and Acetylation of 31. **31** (5 mg) was reduced with sodium borohydride (10 mg) in methanol (1.5 ml), workup in usual way to give a crude product, which was purified by silica-gel column chromatography (chloroform–methanol 9:1) to yield 1,4-pentanediol (4.5 mg), which was acetylated with acetic anhydride (0.1 ml) and pyridine

(0.1 ml) to give 1,4-diacetoxypentane.

Ozonolysis of Agelasine-F (9) with Sodium Borohydride Reduction. A solution of **9** (50 mg, 0.11 mmol) in methanol (3 ml) was treated with ozone at −78° C for 15 min. After removing the excess ozone, sodium borohydride (105 mg, in three portions) was added. The reaction mixture was stirred and allowed to warm up to 0° C and room temperature (in 30 min each), then was neutralized with acetic acid. Removing solvent left a residue, which was submitted to silica-gel column chromatography (chloroform–methanol 95:5) to furnish the epoxide **32** (13.8 mg, 54% theoretical) and 1,4-pentanediol (3 mg). **32**: A colorless syrup; ^{1}H NMR ($CDCl_3$, 90 MHz) δ=0.77 (d, 3H, J=6 Hz), 0.88 (s, 3H), 1.20 (d, 3H, J=5 Hz), 1.24 (s, 3H), 2.98 (brs, 1H), 3.76 (brq, 1H, J=7 Hz); ^{13}C NMR ($CDCl_3$, 22.5 MHz) δ=15.9 (q), 18.1 (q), 20.8 (q), 23.5 (q), 24.2 (t), 25.9 (t), 33.3 (d), 33.6 (t), 34.4 (t), 38.4 (s), 62.5 (d), 62.8 (s), 68.8 (d); EIMS m/z 212 (M^+), 197, 126, 109, 153, 167, 179.

Reduction of the Epoxide 32. A solution of **32** (13 mg, 0.061 mmol) in anhydrous THF (1 ml) was treated with lithium triethylhydroborate (1 M, 0.5 ml) under nitrogen atmosphere and the reaction mixture was stirred at room temperature overnight. The solvent was evaporated and the residue was dissolved in a solution of chloroform and methanol (15 ml, 95:5). The solution was passed through a short silica-gel column to give the pure diol **33** (11 mg, 84% theoretical): Amorphous solid; mp 121.5—123 °C; ^{1}H NMR ($CDCl_3$, 90 MHz) δ=0.88 (d, 3H, J=6 Hz), 0.90 (s, 3H), 1.22 (d, 3H, J=6.5 Hz), 1.26 (s, 3H), 3.68 (m, 1H); EIMS m/z 214 (M^+), 196, 181, 178, 170, 163, 138, 96, 149.

Acetylation of 33. A mixture of **33** (8 mg, 0.037 mmol), acetic anhydride (0.1 ml), triethylamine (0.1 ml) and 4-dimethylaminopyridine (1 mg) was stirred at room temperature for 1 h. The product was purified by silica-gel column chromatography (ethyl acetate–hexane 15:85) to yield the monoacetate **34** (8.5 mg, 88% theoretical): A colorless syrup; ^{1}H NMR ($CDCl_3$, 90 MHz) δ=0.85 (d, 3H, J=6 Hz), 0.88 (s, 3H), 1.21 (d, 3H, J=6.5 Hz), 1.25 (s, 3H), 2.02 (s, 3H), 4.78 (hexalet, 1H, J=6 Hz); EIMS m/z 256 (M^+), 239, 196, 181, 178, 163, 154, 149, 136, 138.

Dehydration of 34. A solution of **34** (8 mg, 0.031 mmol) in pyridine (1 ml) was treated with thionyl chloride (0.1 ml) at −5° C for 15 min. The reaction mixture was diluted with diethyl ether (5 ml), quenched with water (5 ml) and then separated. The aqueous layer was extracted with diethyl ether (5 ml). The combined ether layer was dried over anhydrous sodium sulfate and concentrated to give a residue, which was chromatographed on a silica-gel column (hexane–ethyl acetate 85:15) to give a mixture of the *exo*-olefin 35 and its *endo*-isomer with a ratio 2:1 (total 7.5 mg): A colorless syrup; ^{1}H NMR ($CDCl_3$, 90 MHz) δ=0.84 (d, 3H, J=6 Hz), 0.85 (s, 3H×1/3), 0.91 (s, 3H×2/3), 1.20 (d, 3H, J=6.5 Hz), 2.01 (s, 3H), 4.54 (d, 1H×2/3, J=2 Hz), 4.78 (brd, 1H×2/3, J=2 Hz), 4.84 (hexalet, 1H, J=6 Hz), 5.40 (brs, 1H×1/3); EIMS m/z 239 (M^++1), 123, 178, 149, 136.

Deacetylation of 35. A solution of **35** and its isomer (7 mg, 0.029 mmol) in methanol (1 ml) was treated with 1 M sodium methoxide (0.5 ml in three portion) under nitrogen atmosphere, then silica-gel column chromatography of the product gave a mixture of **36** and its *endo*-olefin isomer (5 mg): A colorless syrup; ^{1}H NMR ($CDCl_3$, 90 MHz) δ=3.73 (hexalet, 1H, J=6 Hz), 4.54 (d, 1H×2/3, J=2 Hz), 4.78 (brs, 1H×2/3), 5.40 (brs, 1H×1/3); EIMS m/z 196 (M^+), 123, 178, 163, 121.

Oxidation of 36. To a solution of **36** and its *endo*-olefin isomer (5 mg, 0.026 mmol) in anhydrous dichloromethane (1 ml) pyridinium dichromate (10 mg) was added and the reaction mixture was stirred under nitrogen atmosphere for 6 h, then it was diluted with diethyl ether (5 ml) and filtrated to remove the solid. The filtrate was passed through a short silica-gel column and concentrated to yield the olefinic ketone **37** and its *endo*-olefin isomer (3 mg): A syrup; ^{1}H NMR ($CDCl_3$, 90 MHz) δ=0.84 (d, 3H, J=6 Hz), 0.88 (s, 3H×1/3), 0.90 (s, 3H×2/3), 2.12 (s, 3H), 4.54 (d, 1H×2/3, J=2 Hz), 4.79 (brs, 1H×2/3), 5.40 (brs, 1H×1/3); EIMS m/z 194 (M^+), 123, 176, 161.

Conversion of 37 to the Octalone 38. A solution of **37** and its isomer (3 mg, 0.015 mmol) in methanol (1 ml) was saturated with ozone at −78° C for 5 min. After removing the excess ozone, dimethyl sulfide (0.007 ml) was added, then the reaction mixture was allowed to warm up to 0° C and room temperature (in 30 min each). After removing the solvent and excess reagent under reduced pressure, 5% KOH aqueous solution (0.1 ml) and methanol (1 ml) were added. The solution was refluxed for 3 h under argon atmosphere, then cooled to room temperature. Evaporation left a residue, which was chromatographed on a silica-gel column (hexane–ethyl acetate 85:15) to yield the octalone **38** (1 mg), which was further purified by TLC (hexane–ethyl acetate 85:15). ^{1}H NMR ($CDCl_3$, 90 MHz) δ=0.91 (brs, 3H, J=6Hz), 1.11 (s, 3H), 5.74 (brs, 1H); EIMS m/z 178 (M^+), 136, 163, 121, 107; CD $[\theta]_{335}$ −390, $[\theta]_{236}$ +5800.

Ozonolysis of Agelasine-F (9) with Dimethyl Sulfide Reduction. Ozone was bubbled in a solution of **9** (59 mg, 0.11 mmol) in methanol (3 ml) at −78° C for 30 min. After removing the excess ozone, dimethyl sulfide (0.5 ml) was added, then the solution was allowed to warm up to 0° C and room temperature (in 30 min each) and stirred overnight. Usual workup and HPLC separation (Develosil 60-3, 10× 250 mm, benzene–acetone 90:10) furnished the enol ether **39** (7.6 mg) and the aldehyde **40**. **39**: A colorless syrup; ^{1}H NMR ($CDCl_3$, 90 MHz) δ=0.80 (d, 3H, J=6.5 Hz), 0.93 (s, 3H), 1.24 (s, 3H), 1.67 (d, 3H, J=1.5 Hz), 3.68 (brs, 1H), 4.32 (m, 1H); ^{13}C NMR ($CDCl_3$, 22.5 MHz) δ=16.2 (q), 18.0 (q), 18.8 (q), 20.0 (q), 25.2 (t), 29.0 (t), 30.3 (t), 32.1 (d), 35.7 (s), 74.8 (d), 79.6 (s), 92.8 (d), 146.9 (s); EIMS m/z 210 (M^+), 149, 125, 123, 109. **40**: A colorless syrup; ^{1}H NMR ($CDCl_3$, 90 MHz) δ=0.85 (d, 3H, J=7 Hz), 1.03 (s, 3H), 2.11 (s, 6H), 9.75 (t, 1H, J=2 Hz); EIMS m/z 226 (M^+), 107, 123, 121, 142, 147, 165, 183; CD $[\theta]_{296}$ +130.

***p*-Bromobenzoylation of 39.** A mixutre of **39** (5 mg, 0.024 mmol), triethylamine, *p*-bromobenzoylchloride (20 mg) and anhydrous benzene (0.5 ml) was stirred at room temperature overnight. Usual workup and silica-gel column chromatography (hexane–ethyl acetate 96:4) yield the ester **41** (2.5 mg), a colorless syrup; ^{1}H NMR ($CDCl_3$, 400 MHz) δ=0.83 (d, 3H, J=6.6 Hz), 1.05 (s, 3H), 1.18 (s, 3H), 1.35 (dm, 1H, J= 13 Hz), 1.53 (dq, 1H, J=13, 4 Hz), 1.70 (s, 3H), 1.73 (dm, 1H, J=13 Hz), 1.78 (dm, 1H, J=17 Hz), 1.82 (m, 1H), 1.96 (dd, 1H, J=17, 5 Hz), 2.13 (tt, 1H, J=13 and 3 Hz), 4.19 (brd, 1H, J=5 Hz), 5.06 (brt, 1H, J=3 Hz).

Treatment of 9 with Sodium Carbonate. A solution of **9** (5 mg, 0.0011 mmol) in water (2 ml) was treated with 2 M sodium carbonate aqueous solution (0.01 ml) for 2 h, and then it was extracted with ethyl acetate. Concentration of the extracts gave the formamide **11** (5 mg, 100% yield): Amor-

phous solid; UV (CH_3OH) 260 (ε 4360), 270 (pH 2, 9160), 260 nm (pH 11, 8930); ^1HNMR ($CDCl_3$, 90 MHz) δ=2.97 (d, J=5 Hz), 4.14 (d, 3H, J=7 Hz), 4.80 (brs, 2H), 7.96 (s, 1H), 8.14 (s, 1H); EIMS m/z 439 (M^+), 396.

Hydrolysis of 9 with KOH. A mixture of **9** (10 mg, 0.0022 mmol), methanol (2 ml) and 40% KOH aqueous solution (1 ml) was heated in a sealed tube at 115° C for 3 h. The reaction mixture was dried under reduced pressure to give a residue, which was submitted to TLC separation (chloroform–methanol 95:5) to yield the less polar product **12** (0.5 mg, 6% yield) and the polar product **13** (4 mg). **12**: Amorphous solid; UV (CH_3OH) 272 nm (ε 8350); ^1HNMR ($CDCl_3$, 90 MHz) δ=2.99 (d, 3H, J=5 Hz), 3.40 (d, 2H, J=7.5 Hz), 7.99 (s, 1H); EIMS m/z 411 (M^+), 396, 139. **13**: UV (CH_3OH) 272 nm (ε 8520), 277 (8360), 282 (pH 2); ^1HNMR ($CDCl_3$, 90 MHz) δ=3.10 (d, 3H, J=5 Hz), 4.87 (d, 2H, J=7 Hz), 7.85 (s, 1H), 8.55 (s, 1H); EIMS m/z 421 (M^+), 406, 298, 149.

Preparation of 6-*N*-Methyl-7-prenyladenine (14), 6-*N*-Methyl-9-prenyladenine (15), and 7,9-Dimethyladeninium Perchlorate (16). Compounds **14**, **15**, and **16** were prepared by the methods described in literatures.[9] **14**: Amorphous solid; mp 157—158° C; UV (CH_3OH) 272 (sh, ε 12300), 277 nm (12600); IR (KBr) 1670, 1615, 1580, 1480, 1460, 1390, 1350 cm^{-1}; ^1HNMR ($CDCl_3$) δ=1.84 (s, 3H), 1.85 (s, 3H), 3.08 (d, 3H, J=4.8 Hz, NMe), 4.85 (d, 2H, J=6.2 Hz, NCH_2), 5.30 (brs, 1H, NH), 5.40 (t, 1H, J=6.2 Hz, =CH), 7.80 (s, 1H, 8-H), 8.48 (s, 1H, 2-H); ^{13}CNMR ($CDCl_3$) δ=18.2 (q), 25.6 (q), 28.1 (q, NMe), 45.8 (t, NCH_2), 112.2 (s, C-5), 119.0 (d, =CH), 139.6 (s, =C), 143.6 (d, C-8), 151.6 (s, C-6), 153.0 (d, C-2), 159.6 (s, C-4); EIMS m/z 217 (M^+). **15**: Crystals; mp 110—111° C; UV (CH_3OH) 267 nm (ε 16300); IR (KBr) 3280, 2920, 1615, 1580, 1400, 1330, 1305, 1225 cm^{-1}; ^1HNMR ($CDCl_3$) δ=1.80 (s, 6H), 3.19 (d, 3H, J=4.9 Hz, NMe), 4.73 (d, 2H, J=6.0 Hz, NCH_2), 5.42 (t, 1H, J=6.0 Hz, =CH), 6.12 (brs, 1H, NH), 7.69 (s, 8-H), 8.42 (s, 2-H); ^{13}CNMR ($CDCl_3$) δ=17.7 (q), 25.3 (q), 27.4 (q, NMe), 40.2 (t, NCH_2), 117.8 (d, =CH), 119.6 (s, C-5), 138.3 (s, =C), 138.7 (d, C-8), 148.7 (s, C-6), 152.8 (d, C-2), 155.3 (s, C-4); EIMS m/z 217 (M^+). **16**: Rods; mp 293—294° C; UV (CH_3OH) 212 (ε 12900), 272 nm (8080); IR (KBr) 3410, 3100, 1675, 1620, 1140, 1110, 1080, 620 cm^{-1}; ^1HNMR (DMSO-d_6) δ=3.86 (s, 3-H, 9-NMe), 4.17 (s, 3H, 7-NMe), 7.93 (brs, 2H, NH_2), 8.40 (s, 1H, 2-H), 9.59 (s, 1H, 8-H); EIMS m/z 163 (M^+-HClO_4).

The authors acknowledge Dr. Takaharu Hoshino of Mukaishima Biological Station, Hiroshima University for his kind identification of the marine sponge, Professor Tatsuo Miyazawa and Mr. Kaoru Wakamatsu of The University of Tokyo for 400 MHz ^1HNMR measurements, and Professor Takashi Tokoroyama of Osaka City University for ^{13}CNMR data of methyl kolavenate. We also thank Mr. Zengo Nagahama for his assistance to collect the sponges and Miss Reiko Abe for her technical assistance.

References

1) Physiologically active marine natural products from Porifera XII. Preceding paper: H. Nakamura, J. Kobayashi, Y. Ohizumi, Y. Hirata, *J. Chem. Soc., Perkin Trans. 1*, in press.

2) Present address: Shanghai Institute of Organic Chemistry, Academia Sinica, 345 Linglin Lu, Shanghai, China.

3) E. Cullen, and J. P. Devlin, *Can. J. Chem.*, **53**, 1690 (1975).

4) H. Nakamura, H. Wu, J. Kobayashi, Y. Ohizumi, and Y. Hirata, *Tetrahedron Lett.*, **24**, 4105 (1983).

5) H. Nakamura, H. Wu, J. Kobayashi, M. Kobayashi, Y. Ohizumi, and Y. Hirata, *J. Org. Chem.*, **50**, 2949 (1985).

6) H. Nakamura, H. Wu, Y. Ohizumi, and Y. Hirata, *Tetrahedron Lett.*, **25**, 2989 (1984).

7) H. Wu, H. Nakamura, J. Kobayashi, Y. Ohizumi, and Y. Hirata, *Tetrahedron Lett.*, **25**, 3719 (1984).

8) R. J. Capon, and D. J. Faulkner, *J. Am. Chem. Soc.*, **106**, 1819 (1984).

9) a) J. A. Montgomery and C. Temple, Jr., *J. Am. Chem. Soc.*, **83**, 630 (1964); b) T. Fujii, F. Tanaka, T. Mohri, T. Itaya, and T. Saito, *Tetrahedron Lett.*, **1973**, 4873; T. Fujii, T. Sato, T. Sakuma, M. Minami, and I. Inoue, *Heterocycles*, **16**, 215 (1981); T. Fujii, T. Itaya, F. Tanaka, T. Saito, K. Mohri, and K. Yamamoto, *Chem. Pharm. Bull.*, **31**, 3149 (1983).

10) S. de Rosa, L. Minale, R. Riccio, G. Sodano, *J. Chem. Soc., Perkin Trans. 1*, **1976**, 1408.

11) J. De Pasucual Teresa, J. G. Urones, I. S. Marcos, F. Bermejo, and P. Basabe, *Phytochemistry*, **22**, 2783 (1983).

12) R. P. Walker and D. J. Faulkner, *J. Org. Chem.*, **46**, 1098 (1981).

13) R. McCrindle, E. Nakamura, and A. B. Anderson, *J. Chem. Soc., Perkin Trans. 1*, **1976**, 1590.

14) A. Ohsuka, S. Kusumoto, and M. Kotake, *Nippon Kagaku Kaishi*, **1973**, 631.

15) H. Iio, K. Asao, and T. Tokoroyama, *J. Chem. Soc., Chem. Commun.*, **1985**, 774.

16) C. W. L. Bevan, D. E. V. Ekong, and J. I. Okogun, *J. Chem. Soc., Chem. Commun.*, **1968**, 1067.

17) B. L. Buckwalter, I. R. Burfitt, H. Felkin, M. J-. Goudket, K. Naemura, M. F. Salomom, E. Wenkert, and P. M. Wovkulich, *J. Am. Chem. Soc.*, **100**, 6445 (1978).

18) J. De Pascual Teresa, E. Caballero, C. Caballero, M. Medarde, A. F. Barrero, and M. Grade, *Tetrahedron Lett.*, **1978**, 3491.

19) *cis*- and *trans*-octalones were prepared by the method of P. A. Zoretic, J. A. Golen, and M. D. Saltzman, *J. Org. Chem.*, **46**, 3554 (1981). The ^1HNMR spectrum of the *trans*-octalone showed signals at δ 0.93 (d, 3H, J=7 Hz), 1.31 (s, 3H) and 5.81 (d, 1H, J=1.5 Hz).

Synthetic Study on Peptide Antibiotic Nisin. II. The Synthesis of Ring B[1)]

Koichi FUKASE, Tateaki WAKAMIYA, and Tetsuo SHIBA*
Department of Chemistry, Faculty of Science, Osaka University, Toyonaka, Osaka 560
(Received March 5, 1986)

Synthesis of a cyclic sulfide moiety ring B in peptide antibiotic nisin was successfully achieved by desulfurization from a corresponding disulfide peptide with tris(diethylamino)phosphine. The configuration on β-carbon atom of *threo*-3-methyl-D-cysteine residue in the disulfide peptide was retained through the reaction to give a desired natural *threo* form of methyllanthionine.

Peptide antibiotic nisin was isolated from culture broth of *Streptococcus lactis* by Mattick and Hirsh in 1947,[2)] and Berridge et al. in 1952.[3)] Nisin shows several biological activities such as antibacterial activity against Gram-positive microorganisms, particularly *Clostridium botulinum*, as well as antimalarial activity, and so on.[4)] Nisin is now in practical use widely in European countries as an important food preservative but not as a chemotherapeutic agent because of low solubility at physiological pH value.

In 1971, quite unique and complicated structure of nisin was proposed by Gross and Morell as shown in Fig. 1.[5)] It is composed of thirty-four amino acid residues including three dehydroamino acids and five lanthionines which construct cyclic moieties via sulfide bond. These five ring parts were named A, B, C, D, and E respectively from *N*-terminal in the molecule.

From the standpoint of a synthetic interest in such a complicated peptide as well as an elucidation on structure-activity relationship of nisin, we started the synthetic study of this antibiotic, and have already accomplished the synthesis of ring A.[6)]

In the synthetic study of ring A, we could establish an advantageous preparative method of cyclic lanthionine peptide by an elimination of one sulfur atom from a corresponding cystine peptide using tris(diethylamino)phosphine [$P(NEt_2)_3$] as desulfurization reagent[7)] (Fig. 2). According to the application of this procedure, synthesis of ring B (Fig. 3) was now carried out as shown in Fig. 4.

threo-3-Methyl-D-cysteine required for this synthesis was prepared from D-threonine by use of our novel method via 2-aziridinecarboxylic acid derivative.[8)] Mercapto groups on L-cysteine and *threo*-3-methyl-D-cysteine residues were protected with acetamidomethyl (Acm) and trityl (Trt) groups, respectively as in ring A synthesis. These protecting groups can be readily removed with I_2 oxidation in methanol to form a cyclic disulfide compound directly.[9)] Since *S*-tritylation is better than *S*-acetamidomethylation in convenience on manipulation and in yield on reaction, the mercapto group of precious *threo*-3-methyl-D-cysteine residue was protected with trityl group. The protected linear tetrapeptide **7** was first prepared successively from the *C*-terminal by stepwise elongation with either a mixed anhydride method or an active ester method. The peptide **7** thus obtained was then subjected to I_2 oxidation. The monomeric disulfide **8** was satisfactorily obtained by high dilution method. In order to confirm the formation of monomer, the molecular weight of the compound **8** was measured by mass spectrometry (*m/z* 504; calcd 504).

In the synthetic study of ring A, the desulfurization reaction was successfully carried out in *N*,*N*-dimethylformamide (DMF). Thus the desulfurization reaction of disulfide **8** was first performed in DMF. Although we could obtain the desired monomeric sulfide peptide **9**, whose molecular weight was confirmed by mass spectrometry (*m/z* 472; calcd 472), the yield did not exceed 30% even though under the

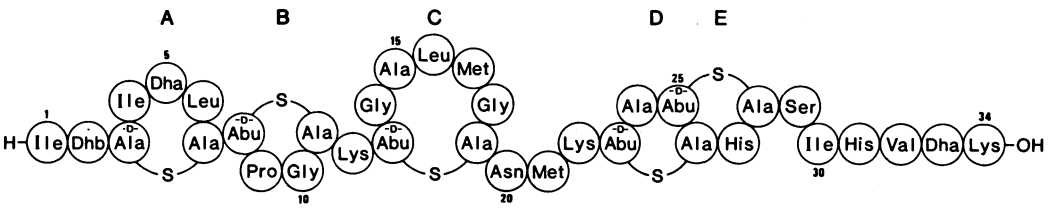

Fig. 1. The structure of nisin. Abu: 2-aminobutyric acid; Dha: dehydroalanine; Dha: dehydrobutyrine (=3-methyldehydroalanine); Ala Ala: lanthionine; Abu Ala: methyllanthionine.

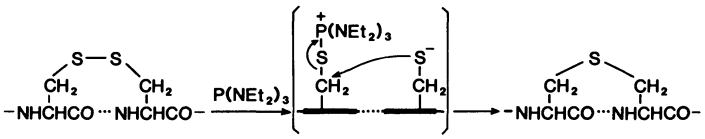

Fig. 2. The reaction mechanism of the desulfurization.

optimum conditions used in the case of ring A synthesis (Table 1). In order to improve the reaction conditions in the present case, we examined effects of the solvent, reaction temperature, amount of $P(NEt_2)_3$, and concentration of the substrate (Table 1). Among general organic solvents tested, benzene and DMF can be utilized while other solvents such as dioxane, THF, $CHCl_3$, ethyl acetate, CH_3CN, and so on were not suitable because of considerable occurrence of undesirable side reactions.

In view of reproducibility in yield, easiness in purification of the reaction product, and readiness of preparation of absolute solvent, benzene is better than DMF as reaction solvent in the present study. The yield was improved when desulfurization reaction was performed under higher dilution as far as it reached to the optimum at 0.62 mM (1 M=1 mol dm^{-3}) at room temperature as shown in Table 1. Thus, the cyclic sulfide peptide **9** was satisfactorily obtained in a 57% yield.

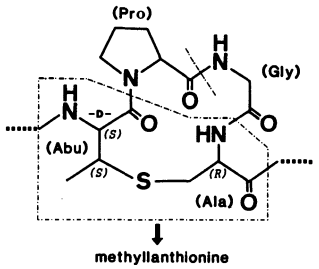

Fig. 3. The chemical structure of the ring B part in nisin.

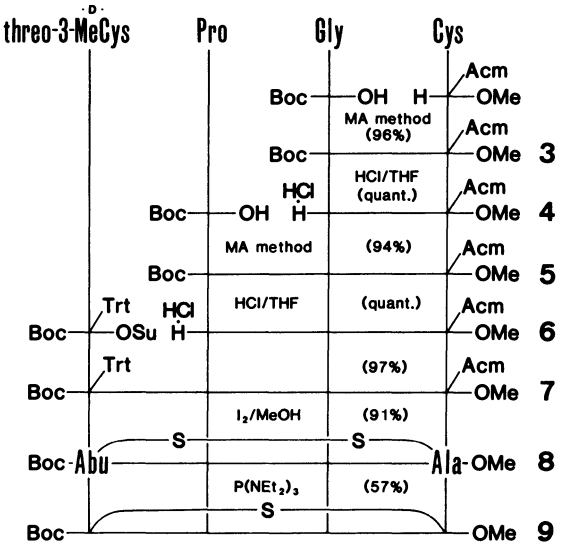

Fig. 4. The synthetic scheme of the protected ring B.

In the case of ring B preparation, it is very important to investigate about two possible desulfurization pathways (Fig. 5). When the reaction proceeds via path (a), the configuration on β-carbon atom of *threo*-3-methyl-D-cysteine is retained to give a *threo* form of methyllanthionine i.e., natural form in nisin. On the other hand, the reaction via path (b) will cause an inversion of the configuration on the β-carbon of 3-methylcysteine residue to form *erythro*-methyllanthionine.

Amino acid analysis of the hydrolyzate of the final product **9** clearly indicated the sole formation of desirable *threo*-methyllanthionine[10] residue via path (a) (Fig. 6). This result can be explained by following two plausible reasons; i) because of steric hindrance of 3-methyl group in *threo*-3-methyl-D-cysteine residue, the nucleophilic attack took place selectively at the sulfur atom of L-cysteine residue, ii) thiolate anion of 3-methylcysteine residue is more stable than that of cysteine residue.

Thus, ring B in nisin was successfully synthesized, verifying a possibility for preparation of *threo*-methyllanthionine peptide from a disulfide peptide composed of *threo*-3-methyl-D-cysteine and L-cysteine by the desulfurization with $P(NEt_2)_3$. Based on the synthetic studies of rings A and B, we could confirm that the desulfurization is very versatile method for the preparation of lanthionine peptide in general. In fact, we recently applied this method successfully to the synthesis of ring C as well as conjunctive ring D–E moiety in nisin, whose results will be reported soon elsewhere.

Experimental

All melting points are uncorrected. The FD-MS spectra were obtained with a JEOL JMS-01SG-2 spectrometer on silicone emitter. Specific rotations were obtained with a Perkin-Elmer 141 polarimeter. Amino acid analyses were carried out with a Hitachi KLA-5 analyzer. Sample for the amino acid analysis was hydrolyzed with constant boiling

Table 1. Yields of Compound **9** on Various Reaction Conditions

Solvent	Concn/mM	$P(NEt_2)_3$	Temp/°C	Reaction time/h	Yield/%
DMF	2.3	40 eq	50	96	28
DMF[a)]	2.4	20 eq	50	96	24
C_6H_6	2.5	40 eq	50	1	12
C_6H_6	2.5	40 eq	25	24	34
C_6H_6	2.5	10 eq	25	24	31
C_6H_6	1.3	40 eq	25	24	43
C_6H_6	0.62	40 eq	25	48	57
C_6H_6	0.31	40 eq	25	48	53

a) The optimum conditions in the case of ring A synthesis.

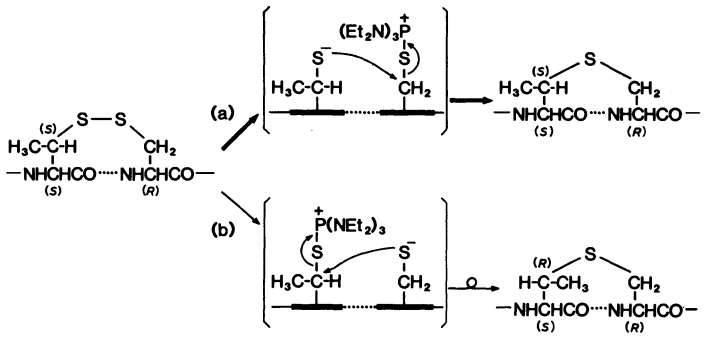

Fig. 5. Plausible desulfurization pathways in ring B preparation.

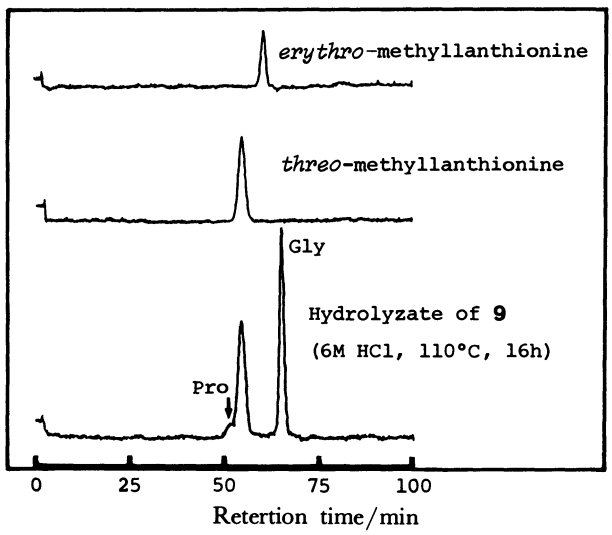

Fig. 6. Amino acid analysis of compound **9**. Column: Hitachi #2618 resin (0.9×25 cm, 55°C), buffer: 0.20 M sodium citrate (pH 3.0).

6 M HCl in a sealed tube at 110°C for 16 h.

H-3-Me-D-Cys(Trt)-OH (1). *threo*-3-Methyl-D-cysteine[8] (11.6 g, 85.9 mmol) and triphenylmethanol (22.3 g, 85.9 mmol) were dissolved in 150 ml of trifluoroacetic acid. The clear solution was allowed to stand at room temperature for 15 min and then trifluoroacetic acid was removed in vacuo. To an ether solution of the residue was added 10% aqueous sodium acetate until pH of the aqueous layer became 5 to precipitate H-3-Me-D-Cys(Trt)-OH (**1**). The precipitate collected was washed with water and ether: Yield 31.7 g (97.8%). A part of the product was recrystallized from ethanol and ether to obtain an analytical sample: Mp 163—164°C; $[\alpha]_D^{17}$ −28.9°(*c* 1.00, MeOH).

Found: C, 69.98; H, 6.23; N, 3.55; S, 8.16%. Calcd for $C_{23}H_{23}NO_2S \cdot H_2O$: C, 69.85; H, 6.37; N, 3.54; S, 8.11%.

Boc-3-Me-D-Cys(Trt)-OH·DCHA (2). To a suspension of the compound **1** (3.07 g, 8.14 mmol) in 60 ml of methanol were added di-*t*-butyl dicarbonate (2.10 g, 9.80 mmol) and triethylamine (0.906 g, 8.95 mmol). After stirring at room temperature overnight, the reaction mixture was concentrated in vacuo and the residue was dissolved in ethyl acetate. The solution was washed with 10% aqueous citric acid and saturated sodium chloride solutions. The organic layer was dried over $MgSO_4$ and then concentrated in vacuo. An oily residue thus obtained was dissolved in hexane to which dicyclohexylamine (1.77 g, 9.76 mmol) was added. After the reaction mixture was cooled in an ice bath, the precipitate was filtered: Yield 5.10 g (95.1%). A part of the product was recrystallized from ethyl acetate and hexane to obtain an analytical sample: Mp 186.5—187°C; $[\alpha]_D^{23}$ −83.0° (*c* 1.07, MeOH).

Found: C, 72.72; H, 8.29; N, 4.27; S, 4.81%. Calcd for $C_{40}H_{54}N_2O_4S$: C, 72.91; H, 8.26; N, 4.25; S, 4.87%.

Boc-Gly-Cys(Acm)-OMe (3). To a solution of Boc-Gly-OH (20.0 g, 114 mmol) in 80 ml of DMF were added ethoxycarbonyl chloride (12.4 g, 114 mmol) and triethylamine (11.5 g, 114 mmol) under cooling in an ice-salt bath. After the reaction mixture was stirred in the chilled bath for 50 min, a solution of HCl·H-Cys(Acm)-OMe[13] (23.1 g, 95.2 mmol) and triethylamine (9.63 g, 95.2 mmol) in 200 ml of DMF was added. The solution was stirred under cooling in an ice bath for additional 20 min and then kept at room temperature overnight. The reaction mixture was concentrated in vacuo to the residue, which was dissolved in chloroform, and washed with 10% aqueous citric acid, saturated sodium hydrogencarbonate, and saturated sodium chloride solutions. The organic layer was dried over $MgSO_4$ and then concentrated in vacuo to give an oily product: Yield 33.3 g (96.2%); $[\alpha]_D^{18}$ −9.50° (*c* 2.78, $CHCl_3$).

Found: C, 45.30; H, 6.94; N, 11.21; S, 8.72%. Calcd for $C_{14}H_{25}N_3O_6S \cdot 1/2H_2O$: C, 45.15; H, 7.04; N, 11.28; S, 8.61%.

HCl·H-Gly-Cys(Acm)-OMe (4). Protected dipeptide **3** (33.3 g, 91.6 mmol) was dissolved in 290 ml of 4.67 M hydrogen chloride in THF. The solution was allowed to stand at room temperature for 1 h, and then diluted with 2 l of ether. After cooling in an ice-salt bath for 1 h, the supernatant was decanted to separate dipeptide hydrochloride precipitated. The hydrochloride **4** thus obtained was dried over NaOH in vacuum desiccator and then subjected to the following reaction without purification.

Boc-Pro-Gly-Cys(Acm)-OMe (5). Ethoxycarbonyl chloride (11.0 g, 101 mmol) and triethylamine (10.2 g, 101 mmol) were added to a solution of Boc-Pro-OH (21.7 g, 101 mmol) in 70 ml of DMF under cooling in an ice-salt bath. To the mixture stirred in the chilled bath for 15 min was added a solution of dipeptide hydrochloride **4** (91.6 mmol) and triethylamine (9.27 g, 91.6 mmol) in 210 ml of DMF. The reaction mixture was stirred for 1 h and then concentrated in vacuo. The residue was dissolved in chloroform and the solution was washed with 10% aqueous citric acid, saturated sodium hydrogencarbonate, and saturated sodium chloride solutions. The organic layer was dried over $MgSO_4$ and then concentrated in vacuo to give an oily product: Yield

39.6 g (93.8%); $[\alpha]_D^{18}$ −55.1° (*c* 1.04, $CHCl_3$).

Found: C, 48.47; H, 7.26; N, 11.70; S, 6.75%. Calcd for $C_{19}H_{32}N_4O_7S \cdot 1/2H_2O$: C, 48.60; H, 7.08; N, 11.93; S, 6.83%.

HCl·H–Pro–Gly–Cys(Acm)–OMe (6). Protected tripeptide **5** (15.3 g, 33.2 mmol) was dissolved in 110 ml of 4.67 M hydrogen chloride in THF to give tripeptide hydrochloride which was obtained in a quantitative yield after the same treatment as mentioned in the preparation of **4**.

Boc-3-Me-D-Cys(Trt)–Pro–Gly–Cys(Acm)–OMe (7). Boc-3-Me-D-Cys(Trt)-OH·DCHA (**2**) (20.0 g, 30.4 mmol) was treated with ethyl acetate and 10% aqueous citric acid. Ethyl acetate layer separated from the aqueous layer was washed with water and dried over $MgSO_4$. The oily residue obtained by vacuum concentration was dissolved in 120 ml of THF. To the solution were added *N*-hydroxysuccinimide (3.50 g, 30.4 mmol) and dicyclohexylcarbodiimide (6.26 g, 30.4 mmol) under ice cooling. The mixture was stirred at 0°C for 40 min and then at room temperature for 2 h. *N,N'*-Dicyclohexylurea precipitated was filtered off and the filtrate was concentrated in vacuo. The oily residue dissolved in 30 ml of chloroform was added to a solution of tripeptide hydrochloride **6** (33.2 mmol) and triethylamine (3.36 g, 33.2 mmol) in 60 ml of chloroform. After stirring at room temperature overnight, the mixture was concentrated in vacuo. Ethyl acetate was added to the residue and an insoluble material was filtered off. The filtrate was washed with 10% aqueous citric acid, saturated sodium hydrogencarbonate, and saturated sodium chloride solutions. The organic layer dried over $MgSO_4$ was concentrated in vacuo. The oily residue was washed by trituration with hexane several times to remove off unreacted Boc-3-Me-D-Cys(Trt)-OH and then precipitated from ethyl acetate and hexane: Yield 24.2 g (97.2%); mp 76—80°C; $[\alpha]_D^{28}$ −39.5° (*c* 1.03, $CHCl_3$).

Found: C, 60.91; H, 6.52; N, 8.38; S, 7.61%. Calcd for $C_{42}H_{53}N_5O_8S_2 \cdot 1/2H_2O$: C, 60.85; H, 6.57; N, 8.45; S, 7.73%.

Boc–3-Me-D–Cys–Pro–Gly–Cys–OMe (8). To a solution of protected linear tetrapeptide **7** (620 mg, 0.757 mmol) in 150 ml of methanol was added I_2 (576 mg, 2.27 mmol) in 23 ml of methanol under vigorous stirring. The oxidation was carried out at room temperature for 1 h and stopped by an addition of 0.2 M sodium thiosulfate solution until the color of I_2 disappeared. The reaction mixture was concentrated in vacuo and the residue was suspended in water. Extraction with chloroform was repeated three times and the extract was concentrated in vacuo after drying over $MgSO_4$. The oily residue thus obtained was crystallized from ethyl acetate and hexane: Yield 345 mg (90.3%); mp 177—179°C; $[\alpha]_D^{28}$ +38.1° (*c* 0.950, $CHCl_3$); FD-MS, *m/z* 504 (M^+).

Found: C, 46.49; H, 6.33; N, 10.71; S, 12.12%. Calcd for $C_{20}H_{32}N_4O_7S_2 \cdot 1/2H_2O$: C, 46.77; H, 6.48; N, 10.91; S, 12.48%.

Boc–D–Abu–Pro–Gly–Ala–OMe (9). To a solution of **8** (100 mg, 0.198 mmol) in 320 ml of anhydrous benzene was added tris(diethylamino)phosphine[7] (1.96 g, 7.94 mmol). The reaction mixture was stirred at room temperature for 2 d and then concentrated in vacuo. The residue was dissolved in ethyl acetate and washed with 10% aqueous citric acid and saturated sodium chloride solutions three times, respectively. Organic layer was dried over $MgSO_4$ and concentrated in vacuo. An oily residue obtained was applied to Sephadex LH-20 column (1.8×56 cm) and eluted with DMF. The column-chromatographic purification was repeated twice to give the product **9** as powder: Yield 53 mg (57%). A part of the product was recrystallized from ethyl acetate to obtain an analytical sample: Mp 206—207.5°C (decomp); $[\alpha]_D^{16}$ +62.8° (*c* 0.931, DMF); FD-MS, *m/z* 472 (M^+). Amino acid analysis: Melan (0.92), Pro (1.01), Gly (1.00).

Found: C, 49.09; H, 7.05; N, 11.18; S, 6.39%. Calcd for $C_{20}H_{32}N_4O_7S \cdot H_2O$: C, 48.97; H, 6.99; N, 11.42; S, 6.54%.

The present work was partially supported by a Grant-in-Aid for Scientific Research No. 57540305 from the Ministry of Education, Science and Culture.

References

1) T. Wakamiya, K. Shimbo, A. Sano, K. Fukase, H. Yasuda, and T. Shiba, "Peptide Chemistry 1982," ed by S. Sakakibara, Peptide Institute, Protein Research Foundation, Osaka (1983), p. 149.

2) A. T. R. Mattick and A. Hirsh, *Lancet*, ii, 5 (1947).

3) N. J. Berridge, G. G. F. Newton, and E. P. Abraham, *Biochem. J.*, **52**, 529 (1952).

4) E. Gross and J. L. Morell, *J. Am. Chem. Soc.*, **89**, 2791 (1967).

5) E. Gross and J. L. Morell, *J. Am. Chem. Soc.*, **93**, 4634 (1971).

6) T. Wakamiya, K. Shimbo, A. Sano, K. Fukase, and T. Shiba, *Bull. Chem. Soc. Jpn.*, **56**, 2044 (1983).

7) D. N. Harpp and J. G. Gleason, *J. Org. Chem.*, **35**, 3259 (1970); **36**, 73 (1971).

8) T. Wakamiya, K. Shimbo, T. Shiba, K. Nakajima, M. Neya, and K. Okawa, *Bull. Chem. Soc. Jpn.*, **55**, 3878 (1982); T. Wakamiya, K. Fukase, K. Shimbo, and T. Shiba, *ibid.*, **56**, 1559 (1983).

9) B. Kamber, A. Hartmann, K. Eisler, B. Riniker, H. Rink, P. Sieber, and W. Rittel, *Helv. Chim. Acta*, **63**, 899 (1980).

10) We have synthesized four stereoisomers of methyllanthionine. ^1H NMR analysis and amino acid analysis of them were studied. T. Wakamiya, Y. Oda, K. Fukase, and T. Shiba, *Bull. Chem. Soc. Jpn.*, **58**, 536 (1985).

11) B. Kamber, *Helv. Chim. Acta*, **54**, 927 (1971); P. Sieber, B. Kamber, K. Eisler, A. Hartmann, B. Riniker, and W. Rittel, *ibid.*, **59**, 1489 (1976).

The Synthesis of Macrocyclic Diaza *n*-*n'*-Fulvadiene Derivatives

Jūro Ojima,* Emiko Ejiri, Sumio Manaka, Noboru Morita,† and Toyonobu Asao†,*
Department of Chemistry, Faculty of Science, Toyama University, Gofuku, Toyama 930
†Department of Chemistry, College of General Education, Tohoku University, Kawauchi, Sendai 980
(Received March 7, 1986)

The diaza analogs of 7-13-, 7-15-, 7-17-, 13-13-, 13-15-, 15-15-, and 19-19-fulvadiene derivatives were synthesized through the reaction of 2,4,6-cycloheptatrienone and the corresponding bisdehydroannulenones with hydrazine dihydrochloride. The ^{1}H NMR and electronic spectra of these compounds are discussed in connection with tropicity.

Bicyclic polyenes containing a cyclic cross-conjugated π-electron system of the fulvalenes of type 1 have been extensively investigated.[1] The convenient synthesis of the bisdehydroannulenones of type **2**[2] in satisfactory yield made it possible to prepare the heptafulvalenes[3] and the pentafulvalenes[4,5] using **2** as the starting material.

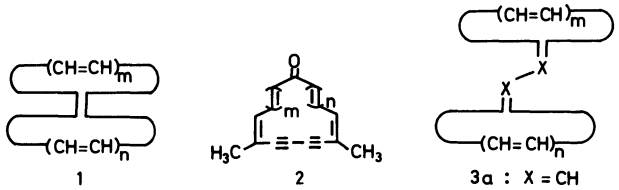

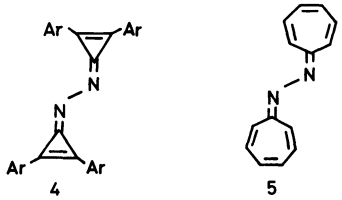

Recently, a number of vinylogous fulvalenes (fulvadienes) of type **3a** have been studied.[6] We were interested in a synthesis of the diaza analogs **3b** of the system; only known examples are the diaza analogs **4**[7] and **5**[8] of the triatriafulvadiene and the heptaheptafulvadiene, respectively, in which both rings are the same.

We considered that the diazafulvadienes containing different-membered rings might cause π-electron polarization across the azine group. For example, the diaza 7-13- **9**[9] and 13-15-fulvadiene **13** will be expected to exhibit π-electron polarization from 7- and 15-membered ring to 13-membered rings to form zwitterionic forms **9a** and **13a**, respectively, in which all rings are [4n+2]π-electron systems and are potentially diatropic. To examine this, preparation of the diazafulvadienes having inner ring protons as marks would be desirable. In this paper, we describe synthesis

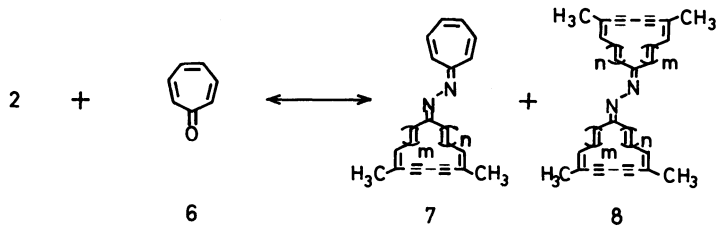

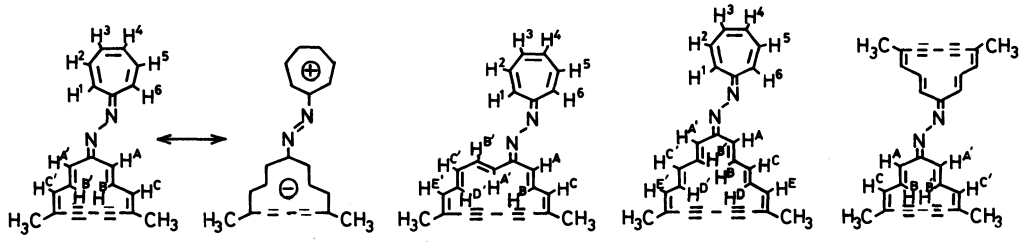

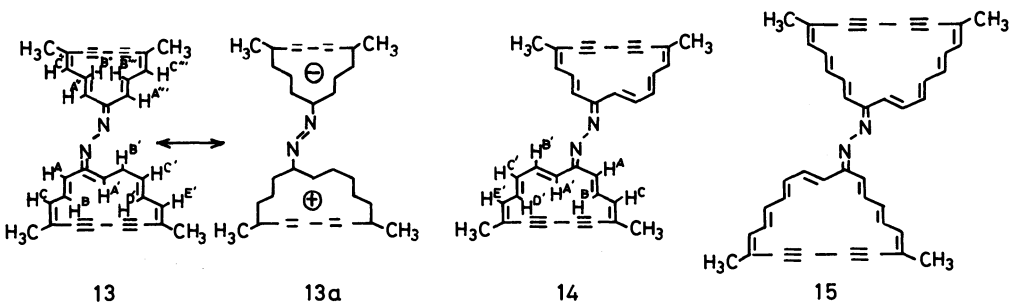

Table 1. Electronic Absorption Maxima of Diazafulvadienes **9**—**15** in Tetrahydrofuran
λ_{max}/nm (ε_{max})

9		**10**		**11**		**12**		**13**		**14**		**15**	
276	(32200)	293	(31700)	222	(23400)	255	(33000)	265	(35500)	278	(37000)	231 sh	(25000)
442	(28200)	375	(20700)	264 sh	(26400)	264 sh	(32500)	318	(31300)	323	(31000)	313	(47500)
		444	(26300)	281 sh	(52900)	290	(26000)	465	(25300)	466	(22100)	404 sh	(26600)
				298	(83700)	420	(28000)					495	(23800)
				306	(85400)								
				422	(7240)								

a) All the spectra showed tailing to ≃600 nm.

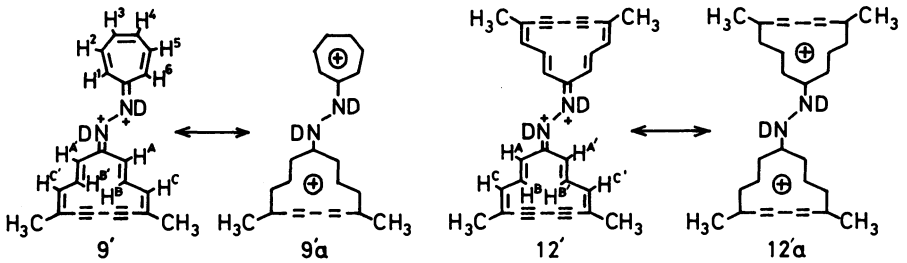

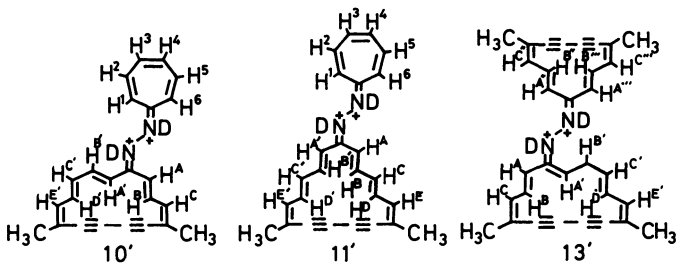

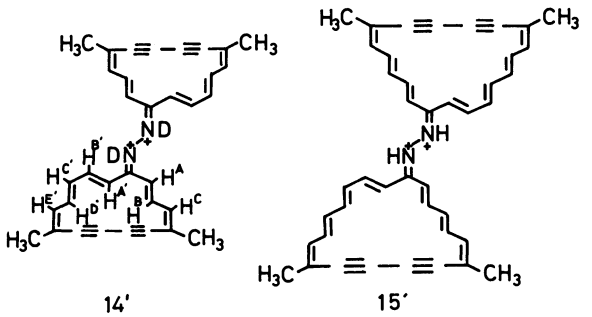

and properties of some of the hepta-derivatives **7** (**9**—**11**) and the large-ring ones **8** (**12**—**15**).

Results and Discussion

Synthesis. The synthesis was accomplished by the reaction of the bisdehydroannulenones **2** with hydrazine dihydrochloride in the presence of 2,4,6-cycloheptatrienone (**6**), usually giving rise to the diaza hepta- **7** and large-ring derivatives **8**. Thus, the reaction of a mixture of the ketone **6** and one of the following annulenones, 5,10-dimethyl-6,8-bisdehydro[13]annuleone,[2a] 5,10-dimethyl-6,8-bisdehydro[15]annulenone,[2b] and 7,12-dimethyl-8,10-bisdehydro[17]annulenone[2b] with hydrazine dihydrochloride in methanol–tetrahydrofuran at room temperature gave the diaza 7-13- **9** (5.0%), 7-15- **10** (3.0%), and 7-17-fulvadiene **11** (6.6%), respectively. In the first two cases, bis-condensation products, the diaza 13-13- **12** (24%) and 15-15-fulvadiene **14** (3.6%) were formed, but rather surprisingly, the diaza 7-7-fulvadiene was not obtained in any above reactions. The diaza analog **13** of 13-15-fulvadiene was obtained (2.9%) by the reaction of a mixture of [13]- and [15]-annulenones with hydrazine dihydrochloride. Compounds **12** and **14** were also prepared by the reaction of [13]- and [15]annulenones with hydrazine, respectively. The diaza 19-19-fulvadiene **15** (1.4%) was obtained by the reaction of 7,12-dimethyl-8,10-bisdehydro[19]annulenone[2b] with hydrazine in the presence of **6**; however the diaza 7-19-fulvadiene was not detected in the reaction mixture. The diaza 17-17-fulvadiene also was not detected in the reaction mixtures of the [17]annulenone with hydrazine in the presence of **6** or in the absence of **6**. These diazafulvadienes **9**—**15** thus obtained were recrystallized from hexane–benzene or hexane–chloroform to afford

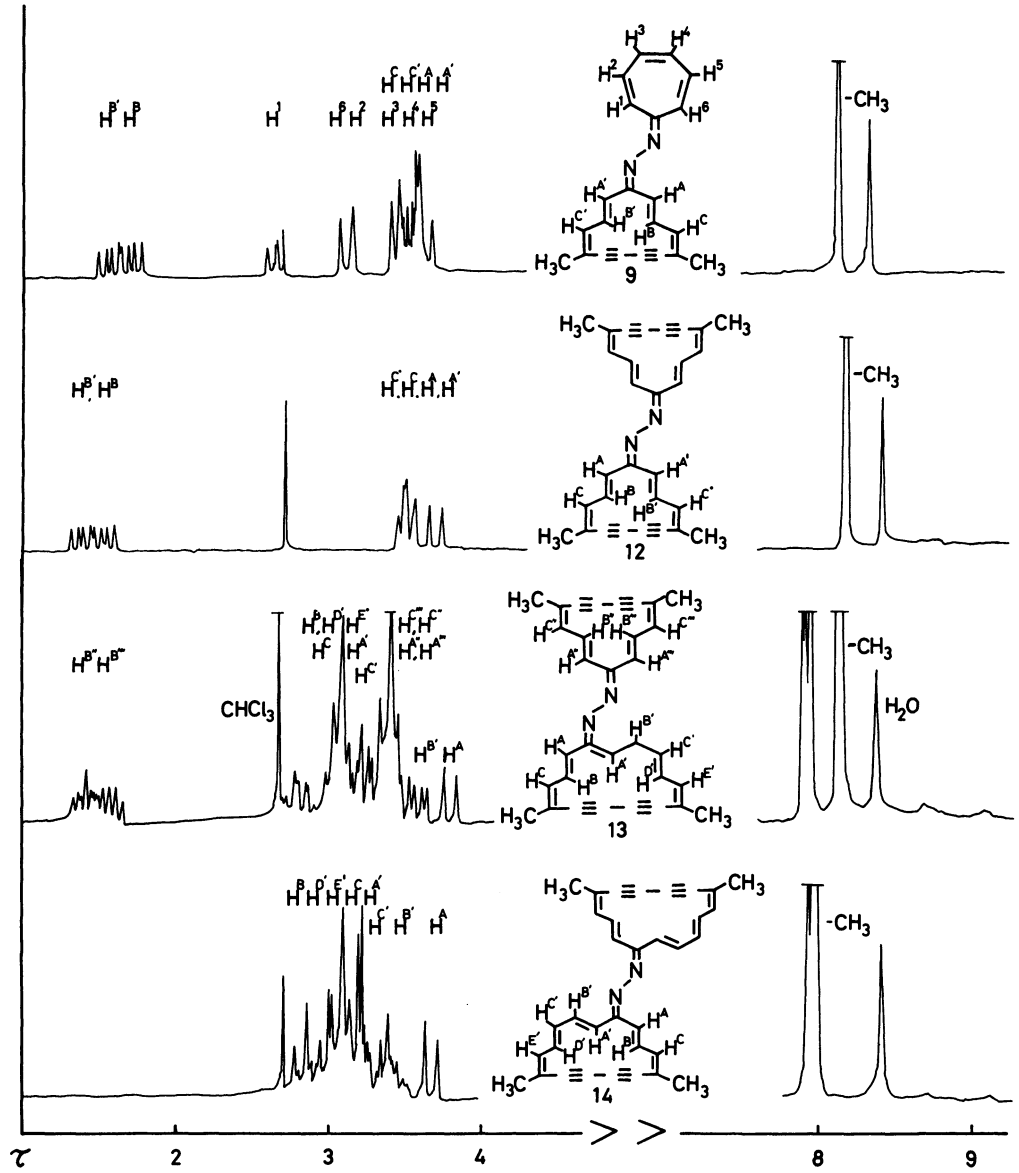

Fig. 1. The 200 MHz ^{1}H NMR spectra of the diazafulvadienes **9**, **12**, **13**, and **14** in $CDCl_3$.

deep colored (dark reddish or dark purple), unstable crystals, which were gradually decomposed at room temperature to diffused light under air.

Electronic Spectra. The electronic absorption maxima (in tetrahydrofuran) of these diazafulvadienes **9**—**15** are listed in Table 1. In two series compounds, hepta-derivatives **9**—**11** and large-ones **12**—**15**, it is clear that the most intensive maxima exhibit an almost regular bathochromic shift as the ring size increases. Thus, the occurrence of the same sort of alternation along with increasing ring size between the maxima of [$4n$−2] and of [$4n$]systems, as has been observed for annulenes and dehydroannulenes [($4n$−2)π-systems absorbing at longer wavelengths than the ($4n$)π-systems],[10] is not observed, suggesting that these diazafulvadienes are atropic, as revealed by examination of ^{1}H NMR spectra (vide infra).

The electronic absorption maxima of these diazafulvadienes **9**—**15** in trifluoroacetic acid (TFA) are listed in Table 2. It is evident that protonation with this acid causes the shift of the maxima to longer wavelength in every case and gives the corresponding protonated (or deuteronated when TFA-d_1 is used) specics **9'**—**15'**, in which **9'** was brown in color, **10'** blue, **11'** green, **12'** brown, **13'** reddish purple, **14'** blue, and **15'** brown. Neutralization of the protonated large-ring species **12'**—**15'** with aqueous sodium hydrogencarbonate resulted in regeneration of **12**—**15**, respectively. However, standing the solutions of the protonated hepta-species **9'**—**11'** resulted in a change, and the diazafulvadiene **9**—**11** were not recovered from them on quenching.

^{1}H NMR Spectra. The ^{1}H NMR chemical shifts of olefinic and methyl protons of these diazafulvadienes

Table 2. Electronic Absorption Maxima of Diazafulvadienes **9**—**15** in Trifluoroacetic Acid
λ_{max}/nm (Relative extinction coefficient)[a)]

9	**10**	**11**	**12**	**13**	**14**	**15**
261 sh (0.66)	258 (0.47)	264 (0.33)	271 (0.78)	258 sh (0.64)	258 (0.37)	275 sh (0.93)
284 (0.85)	367 (0.98)	308 sh (0.58)	289 (0.79)	274 (0.76)	277 sh (0.28)	285 (1.00)
417 (1.00)	378 (1.00)	326 (1.00)	445 (1.00)	293 (0.69)	366 (1.00)	306 (0.93)
526 (0.21)	461 sh (0.14)	358 (0.67)	580 sh (0.19)	346 sh (0.73)	375 sh (0.99)	423 (0.90)
	491 sh (0.20)	437 (0.68)		382 (1.00)	429 (0.36)	447 sh (0.86)
	542 (0.36)	671 (0.03)		593 (0.95)	529 sh (0.20)	464 sh (0.74)
	579 (0.66)			608 sh (0.92)	598 (0.82)	628 (0.56)
					634 sh (0.54)	701 sh (0.47)

a) All the spectra showed tailing to ≃800 nm.

Table 3. ^{1}H NMR Chemical Shifts of Diaazafulvadienes **9**—**14** (in $CDCl_3$) and Deuterated Species **9′**—**14′** (CF_3COOD in $CDCl_3$) at 200 MHz, Determined at 21 °C (τ Value; Standard, Me_4Si)

Compd	H^A	$H^{A'}$	$H^{A''}$	$H^{A'''}$	H^B	$H^{B'}$	$H^{B''}$	$H^{B'''}$	H^C	$H^{C'}$	$H^{C''}$	$H^{C'''}$
9	3.53	3.66			1.73	1.58			3.45	3.46		
9′	3.77	3.79			1.07	0.87			3.67	3.58		
10	3.64	2.74			2.95	3.66			3.20	3.55		
10′	3.06	6.06			4.11	(1.76—2.39)			2.83	(1.76—2.39)		
11	3.46	3.76			2.38	2.42			(3.34 — 3.77)			
11′	3.98	3.98			1.44	1.44			3.87[a)]	3.93[a)]		
12	3.71	3.54			1.54	1.39			3.49	3.50		
12′	3.91	3.77			−0.76	−0.67			3.84	3.85		
13	3.83	(2.72 — 3.51)				3.61	(1.45 — 1.64)		(2.72 — 3.51)			
13′	(1.98—2.35)	(3.11 — 3.81)				1.28	0.50[b)]	0.70[b)]	(1.98—2.35)	2.44	(3.11 — 3.81)	
14	3.70	3.20			2.91	3.50			3.19	3.31		
14′[c)]	(2.16—2.96)	(4.82—5.60)			(4.82—5.60)	(2.16—2.96)			(2.16 — 2.96)			

Compd	H^D	$H^{D'}$	H^E	$H^{E'}$	H^1	H^6	H^2	H^5	H^3	H^4	CH_3
9					2.59—2.68	(3.10 — 3.19)	(3.49 —		— 3.63)		8.18
9′					1.50—1.56	(1.98—2.13)	2.24 —	2.38	(1.98 —	2.13)	8.20
10		2.97		3.15	2.49—2.59	2.86—2.91	3.50 —	3.71	3.17 —	3.24	7.99, 8.02
10′		4.31		(1.76—2.39)	1.50—1.67	(1.76 —				2.39)	7.47, 7.54
11	2.56	2.56	(3.34—3.77)		2.57—2.60	3.16—3.22	(3.34 —			3.77)	8.14
11′	1.25	1.25	3.63	3.63	1.69—1.75	(2.04—2.20)	2.32 —	2.42	(2.04 —	2.20)	8.20
12											8.19, 8.20
12′											8.28
13		(2.72—3.51)		(2.72—3.51)							7.96, 7.99, 8.12, 8.17
13′		(3.11—3.81)		(1.98—2.35)							7.42, 7.67, 8.21
14		3.04		3.15							7.96, 8.01
14′[c)]		(4.82—5.60)		(2.16—2.96)							7.64, 7.71

a), b) Assignments may be reversed in each group (see Experimental). c) At 270 MHz.

9—**14** are listed in Table 3, together with those of their deuteronated species **9′**—**14′**, obtained in deuteriochloroform solution admixed with a few drops of TFA-d_1. Individual assignments, some of which are tentative, were made on the basis of multiplicities, coupling constants, and the assumption that protons in a similar environment resonate at similar field, and were clarified by decoupling experiments where necessary. The ^{1}H NMR spectra of only the diaza 7-13- **9**, 13-13- **12**, 13-15- **13**, and 15-15-fulvadiene **14** are illustrated in Fig. 1. As we see from Table 3 and Fig. 1, the downfield and upfield shifts of the olefinic protons as well as the methyl protons are not observed in the spectrum of the diaza 7-13-fulvadiene **9**, as compared with the resonances of the corresponding protons in the spectrum of the diaza 13-13-fulvadiene **12**, which is not expected to polarize since both rings are the same. Similarly, the olefinic and methyl protons of **13** resonate at the almost same field as those of the resonances of the corresponding protons of the diaza 13-13- **12** and 15-15-fulvadiene **14**. These facts show that both **9** and **13** do not exhibit π-electron polarization across the azine group to form polar structures **9a** and **13a**. On the other hand, the spectra of the deuteronated species **9′** and **12′**, which are illustrated in Fig. 2, show the downfield or upfield shifts of olefinic resonances. In the spectrum of **9′**, the proton resonances of the 7-membered ring appear in lower field (Δ−0.6 ppm), and the outer proton resonances of the 13-membered ring in higher field (Δ+1 ppm), as compared with the resonances of the corresponding olefinic protons of **9**. In the spectrum of **12′**, the much larger downfield shift (Δ−1.5 ppm) of the inner proton resonances, as compared with the resonances of the corresponding protons of **12**, is seen. These facts suggest that the 7-membered ring in **9′** is diatropic, while the 13-membered ring in both **9′** and **12′** is paratropic, and the dicationic forms **9a′** and **12a′** contribute to the structures **9′** and **12′** as resonance hybrid to some extent, respectively.

As we can see from Table 3, the upfield and downfield shifts of the proton resonances of the large ring are not seen in the spectrum of the diaza 7-15-fulvadiene **10**, as compared with the resonances of the corresponding protons of the diaza 15-15-fulvadiene **14**.

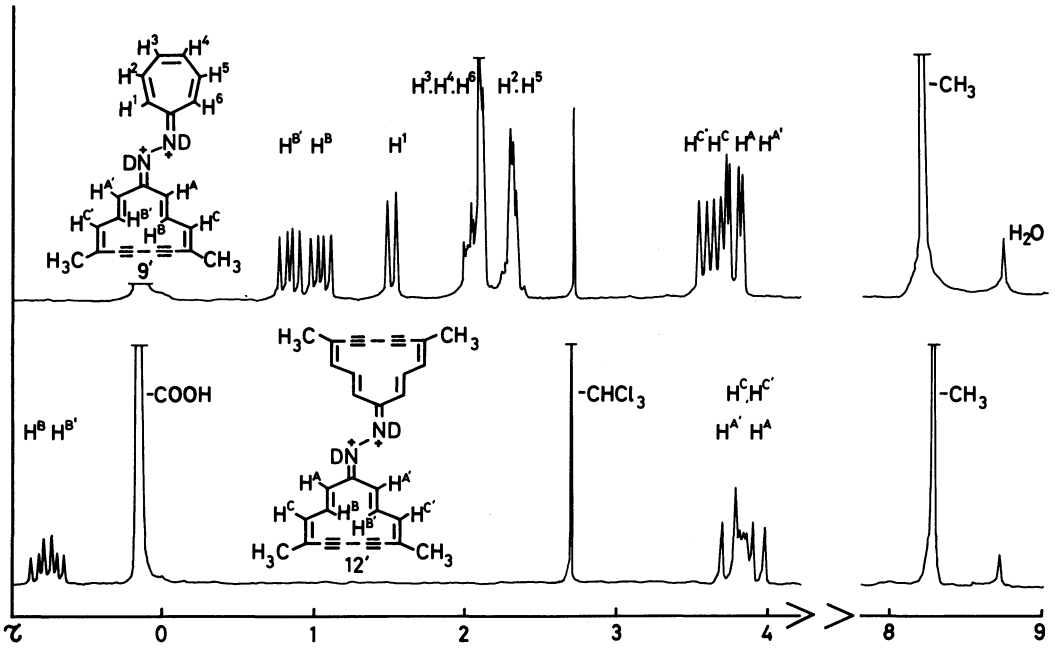

Fig. 2. The 200 MHz ^{1}H NMR spectra of the deuterated species **9'** and **12'**.

Thus, the compound **10** also does not exhibit π-electron polarization. The olefinic protons of both the diaza 7-17- **11** (Table 3) and the diaza 19-19-fulvadiene **15** (see Experimental) resonate in normal region, and these are also polyolefinic molecules. On the other hand, the deuteronated species, **10'**, **11'**, **13'**, and **14'** show that the downfield or upfield shifts of the olefinic proton resonances as well as the methyl proton resonances, as compared with the corresponding proton resonances of the respective diazafulvadienes **10**, **11**, **13**, and **14** (Table 3). In the spectra of the deuteronated species **10'** and **11'**, the protons of the 7-membered ring resonate at low field, indicating that the ring is diatropic. In **10'**, **13'**, **14'**, the inner protons of the 15-membered ring resonate at high field, and the outer and methyl protons at low field, indicating the 15-membered ring in **10'**, **13'**, and **14'** being diatropic. Conversely, the inner protons of the 13- and 17-membered rings in **11'** and **13'** resonate at low field, and the outer and methyl protons at high field, indicating the 13- and 17-membered rings in **11'** and **13'** being paratropic. These results also suggest that the similar dicationic forms as those (**9a'** and **12a'**) depicted for **9'** and **12'**, contribute to the structures of the species **10'**, **11'**, **13'**, and **14'**.

Experimental

Melting points are uncorrected. IR spectra were measured on Hitachi 260-50 spectrophotometer as KBr disk; only significant maxima are reported. Electronic spectra were recorded on Hitachi 220-A spectrophotometer in nm, in tetrahydrofuran solution. Mass spectra were measured with JMS-D 200 spectrometer at 75 eV using a direct inlet system or JMS-D spectrometer equipped with field desorption system. ^{1}H NMR spectra were taken on Varian XL-200 (200 MHz) or JEOL GX-270 (270 MHz) spectrometer, and refer to solution in $CDCl_3$, unless otherwise stated, in τ-values with TMS as an internal standard. The coupling constants (J) are given in Hz. The individual assignments were made on the basis of multiplicities and coupling constants, and were further clarified by decoupling experiments where necessary. Alumina (II—III) was used for column chromatography. Progress of most reactions was monitored by TLC using precoated Merck silica-gel plates. Preparative plate chromatography was carried out on 20×20 cm silica-gel plates (Merck, 0.5 or 2 mm thick). Evaporation of solvents was performed under water aspirator pressure, and sodium sulfate was used as drying agent.

1-(2,4,6-Cycloheptatrienylidene)-2-(5,10-dimethyl-2,4,10,12-tridecatetraene-6,8-diynylidene)hydrazine (9) and 1,2-Bis(5,10-dimethyl-2,4,10,12-tridecatetraene-6,8-diynylidene)hydrazine (12). A soln of hydrazine dihydrochloride (170 mg, 1.62 mmol) in water (2 ml) was added in one portion to a stirred soln of 2,4,6-cycloheptatrienone (**6**) (170 mg, 1.60 mmol) and 5,10-dimethyl-6,8-bisdehydro[13]annulenone[2a] (300 mg, 1.44 mmol) in methanol (80 ml) and tetrahydrofuran (THF) (20 ml) at 40 °C, and stirring was continued overnight at the same temperature. After an aqueous 10% sodium hydrogencarbonate soln was added (pH 7—8), the mixture was poured onto water and extracted with chloroform. The combined extracts were washed with brine, and dried. After solvent removal, the residual dark red liquid was chromatographed on alumina (4.0×7.0 cm). The early fractions eluted with hexane–chloroform (3:2) gave a red solid, which was purified by preparative plate chromatography (4 times, benzene–chloroform as eluent). The fast-moving, first band gave the diaza 13-13-fulvadiene **12** (140 mg, 24%). Recrystallization from hexane–tetrahydrofuran afforded purple needles: Mp 189—190 °C (decomp); MS m/z 412 (M^+, 16%) and 32 (100); mol wt 412.5; ^{1}H NMR (200 MHz) τ=1.39 (dd, 16, 10, 2H, $H^{B'}$), 1.54 (dd, 17, 10, 2H, H^B), 3.49 (d, 10,

2H, H^C), 3.50 (d, 10, 2H, $H^{C'}$), 3.54 (d, 16, 2H, $H^{A'}$), 3.71 (d, 17, 2H, H^A), 8.19 (s, 6H, CH_3), 8.20 (s, 6H, CH_3), and see Fig. 1; (CF_3COOD in $CDCl_3$, 200 MHz) τ=−0.76 (dd, 16.5, 10, 2H, H^B), −0.67 (dd, 16.5, 10, 2H, $H^{B'}$), 3.77 (d, 16.5, 2H, $H^{A'}$), 3.84 (d, 10, 2H, H^C), 3.85 (d, 10, 2H, $H^{C'}$), 3.91 (d, 16.5, 2H, H^A), 8.28 (s, 12H, CH_3), and see Fig. 2.

Found: C, 87.16; H, 5.95; N, 6.81%. Calcd for $C_{30}H_{24}N_2$: C, 87.34; H, 5.87; N, 6.79%.

The later fractions eluted with hexane–chloroform (2:3) gave a red liquid, which was purified by preparative plate chromatography (4 times, benzene–chloroform as eluent). The fast-moving, second band gave the diaza 7-13-fulvadiene **9** (23 mg, 5.0%). Recrystallization from hexane afforded red cubes: Mp 141—142 °C; MS *m/z* 310 (M^+, 41%) and 190 (100); mol wt 310.3; IR 2170 (–C≡C–) and 975 cm^{-1} (trans C=C); UV: see Tables 1 and 2; ^1H NMR (200 MHz) τ=1.58 (dd, 17, 10, 1H, $H^{B'}$), 1.73 (dd, 17, 10, 1H, H^B), 2.59—2.68 (m, 1H, H^1), 3.10—3.19 (m, 2H, H^2, H^6), 3.45 (d, 10, 1H, H^C), 3.46 (d, 10, 1H, $H^{C'}$), 3.49—3.63 (m, 3H, H^3, H^4, H^5), 3.53 (d, 17, 1H, H^A), 3.66 (d, 17, 1H, $H^{A'}$), 8.18 (s, 6H, CH_3), and see Fig. 1; (CF_3COOD in $CDCl_3$, 200 MHz) τ=0.87 (dd, 16, 10, 1H, $H^{B'}$), 1.07 (dd, 16, 10, 1H, H^B), 1.50—1.56 (m, 1H, H^1), 1.98—2.13 (m, 3H, H^3, H^4, H^6), 2.24—2.38 (m, 2H, H^2, H^5), 3.58 (d, 10, 1H, $H^{C'}$), 3.67 (d, 10, 1H, H^C), 3.77 (d, 16, 1H, H^A), 3.79 (d, 16, 1H, $H^{A'}$), 8.20 (s, 6H, CH_3), and see Fig. 2.

Found: C, 85.30; H, 5.90; N, 9.01%. Calcd for $C_{22}H_{18}N_2$: C, 85.13; H, 5.85; N, 9.03%.

The Diaza 13-13-Fulvadiene 12 from Bisdehydro[13]annulenone. A soln of hydrazine dihydrochloride (50 mg, 0.48 mmol) in water (1 ml) was added in one portion to a stirred soln of bisdehydro[13]annulenone[2a] (152 mg, 0.73 mmol) in methanol (100 ml) and THF (17 ml) at room temperature and stirring was continued overnight. The mixture was worked up as described above. The residue, after solvent removal, was chromatographed on alumina (3.7×7.5 cm). The fractions eluted with benzene gave the diaza 13-13-fulvadiene **12** (110 mg, 73%).

1-(2,4,6-Cycloheptatrienylidene)-2-(5,10-dimethyl-2,4,10,12,-14-pentadecapentaene-6,8-diynylidene)hydrazine (10) and 1,2-Bis(5,10-dimethyl-2,4,10,12,14-pentadecapentaene-6,8-diynylidene)hydrazine (14). A soln of hydrazine dihydrochloride (260 mg, 2.48 mmol) in water (2 ml) was added in one portion to a stirred soln of the ketone **6** (255 mg, 2.40 mmol) and the bisdehydro[15]annulenone[2b] (563 mg, 2.40 mmol) in methanol (180 ml) and THF (50 ml) at room temperature and stirring was continued overnight. The mixture was worked up as in the isolation of **9** and **12**. The residual red liquid, after solvent removal, was chromatographed on alumina (3.7×12.5 cm). The fractions eluted with hexane–benzene (1:4—1:9) gave a red solid, which was further purified by preparative plate chromatography (5 times, benzene as eluent). The fast moving, purple band gave the diaza 15-15-fulvadiene **14** (20 mg, 3.6%). Recrystallization from hexane–benzene afforded purple needles: Mp 171—172 °C (decomp); MS (field desorption method) *m/z* 464 (M^+); mol wt 464.6; IR 2170 (–C≡C–) and 975 cm^{-1} (trans C=C); UV: see Tables 1 and 2; ^1H NMR (200 MHz) τ=2.91 (dd, 16, 11, 2H, H^B), 3.04 (dd, 16, 11, 2H, $H^{D'}$), 3.15 (d, 11, 2H, $H^{E'}$), 3.19 (d, 11, 2H, H^C), 3.20 (d, 15.5, 2H, $H^{A'}$), 3.31 (dd, 16, 5, 2H, $H^{C'}$), 3.50 (dd, 15.5, 5, 2H, $H^{B'}$), 3.70 (d, 16, 2H, H^A), 7.96 (s, 6H, CH_3), 8.01 (s, 6H, CH_3), and see Fig. 1; (CF_3COOD in $CDCl_3$, 270 MHz) τ=2.16—2.96 (m, 10H, H^A, $H^{B'}$, H^C, $H^{C'}$, $H^{E'}$), 4.82—5.60 (m, 6H, $H^{A'}$, H^B, $H^{D'}$), 7.64 (s, 6H, CH_3), and 7.71 (s, 6H, CH_3).

Found: C, 87.04; H, 5.86; N, 6.15%. Calcd for $C_{34}H_{28}N_2$: C, 87.89; H, 6.08; N, 6.03%. Attempts to improve the elemental analysis failed.

The following fractions eluted with benzene gave a semi-solid, which was further purified by preparative plate chromatography (5 times, benzene as eluent). The fast-moving, second band gave the diaza 7-15-fulvadiene **10** (24 mg, 3.0%). Recrystallization from hexane afforded red cubes: Mp 130—131 °C; MS *m/z* 336 (M^+, 100%); mol wt 336.4; IR 2170 (–C≡C–), 1640 (C=N), and 975 cm^{-1} (trans C=C); UV: see Tables 1 and 2; ^1H NMR (270 MHz) τ=2.49—2.59 (m, 1H, H^1), 2.74 (d, 16, 1H, $H^{A'}$), 2.86—2.91 (m, 1H, H^6), 2.95 (dd, 16, 11, 1H, H^B), 2.97 (dd, 15.5, 10, 1H, $H^{D'}$), 3.15 (d, 10, 1H, $H^{E'}$), 3.17—3.24 (m, 2H, H^3, H^4), 3.20 (d, 11, 1H, H^C), 3.50—3.71 (m, 2H, H^2, H^5), 3.55 (dd, 15.5, 5, 1H, $H^{C'}$), 3.64 (d, 16, 1H, H^A), 3.66 (dd, 16, 5, 1H, $H^{B'}$), 7.99 (s, 3H, CH_3), and 8.02 (s, 3H, CH_3); (CF_3COOD in $CDCl_3$, 200 MHz) τ=1.50—1.67 (m, 1H, H^1), 1.76—2.39 (m, 8H, $H^{B'}$, $H^{C'}$, $H^{E'}$, H^2, H^3, H^4, H^5, H^6), 2.83 (d, 11, 1H, H^C), 3.06 (d, 16, 1H, H^A), 4.11 (dd, 16, 11, 1H, H^B), 4.31 (dd, 16, 11, 1H, $H^{D'}$), 6.06 (d, 16, 1H, $H^{A'}$), 7.47 (s, 3H, CH_3), and 7.54 (s, 3H, CH_3).

Found: C, 85.44; H, 6.07; N, 8.36%. Calcd for $C_{24}H_{20}N_2$: C, 85.68; H, 5.99; N, 8.33%.

The Diaza 15-15-Fulvadiene 14 from Bisdehydro[15]annulenone. A soln of hydrazine dihydrochloride (93 mg, 0.86 mmol) in water (2 ml) was added in one portion to a soln of [15]annulenone[2b] (413 mg, 1.76 mmol) in methanol (120 ml) and THF (60 ml). After stirring overnight at room temperature, the mixture was worked up as in the isolation of **9** and **12**. The residual dark red liquid, after solvent removal, was chromatographed on alumina (4.2×13 cm). The fractions eluted with hexane–benzene (1:4) gave a red solid, which was further purified by preparative plate chromatography (5 times, benzene–chloroform as eluent). The fast-moving, second red band gave the diaza 15-15-fulvadiene **14** (28 mg, 6.9%).

1-(2,4,6-Cycloheptatrienylidene)-2-(7,12-dimethyl-2,4,6,12,14,16-heptadecahexaene-8,10-diynylidene)hydrazine (11). A soln of hydrazine dihydrochloride (210 mg, 2.00 mmol) in water (2 ml) was added in one portion to a stirred soln of the ketone **6** (215 mg, 2.03 mmol) and bisdehydro[17]-annulenone[2b] (496 mg, 1.91 mmol) in methanol (200 ml) and THF (80 ml) at room temperature and stirring was continued overnight at the same temperature. Then a further quantity of the ketone **6** (80 mg) in methanol (5 ml) was added and the mixture was stirred for further 8 h. The mixture was worked up as in the isolation of **9** and **12**. The residual red liquid, after solvent removal, was chromatographed on alumina (4.0×12.5 cm). The fractions eluted with benzene–chloroform (4:1—2:3) gave a brown solid, which was further purified by preparative plate chromatography (6 times, chloroform as eluent). The fast moving, second band gave the diaza 7-17-fulvadiene **11** (46 mg, 6.6%). Recrystallization from hexane–chloroform afforded purple needles: Mp 209 °C (decomp); MS *m/z* 362 (M^+, 100%); mol wt 362.4; IR 2190 (–C≡C–), 1620 (C=N), and 1000 cm^{-1} (trans C=C); UV: see Tables 1 and 2; ^1H NMR (200 MHz) τ=2.38 (dd, 15, 11, 1H, H^B), 2.42 (dd, 16, 11, 1H, $H^{B'}$), 2.56 (dd, 16, 11, 2H, H^D, $H^{D'}$), 2.57—2.60 (m, 1H, H^1), 3.16—3.22 (m, 1H, H^6), 3.34—3.77 (m, 8H, H^C, $H^{C'}$, H^E, $H^{E'}$, H^2, H^3, H^4, H^5), 3.46 (d, 15, 1H, H^A), 3.76 (d, 16, 1H, $H^{A'}$), and 8.14 (s, 6H, CH_3); (CF_3COOD in $CDCl_3$, 200 MHz)

τ=1.25 (dd, 15.5, 10, 2H, H^D, $H^{D'}$), 1.44 (dd, 15.5, 11, 2H, H^B, $H^{B'}$), 1.69—1.75 (m, 1H, H^1), 2.04—2.20 (m, 3H, H^3, H^4, H^6), 2.32—2.42 (m, 2H, H^2, H^5), 3.63 (d, 10, 2H, H^E, $H^{E'}$), 3.87 (dd, 15.5, 11, 1H, H^C or $H^{C'}$), 3.93 (dd, 15.5, 10, 1H, H^C or $H^{C'}$), 3.98 (d, 15.5, 2H, H^A, $H^{A'}$), and 8.20 (s, 6H, CH_3).

Found: C, 85.88; H, 6.20; N, 8.04%. Calcd for $C_{26}H_{22}N_2$: C, 86.16; H, 6.12; N, 7.73%.

The Reaction of Bisdehydro[17]annulenone with Hydrazine Dihydrochloride. The reaction of the bisdehydro[17]-annulenone with hydrazine dihydrochloride was carried out under the exactly same conditions as those for the preparation of the diaza 13-13-fulvadiene **12**; however the diaza 17-17-fulvadiene was not obtained.

1,2-Bis(7,12-dimethyl-2,4,6,12,14,16,18-nonadecaheptaene-8,10-diynylidene)hydrazine (15). A soln of hydrazine dihydrochloride (225 mg, 2.14 mmol) in water (3 ml) was added in one portion to a stirred soln of the ketone **6** (230 mg, 2.17 mmol) and bisdehydro[19]annulenone[2b] (606 mg, 2.11 mmol) in methanol (150 ml) and THF (80 ml), and stirring was continued for 7 h at the room temperature. Then a further quantity of the ketone **6** (50 mg) in methanol (5 ml) was added and the mixture was stirred for further 15 h. Then the mixture was worked up as in the isolation of **9** and **12**. The residual red liquid, after solvent removal, was chromatographed on alumina (4.0×12 cm). The fractions eluted with benzene–chloroform (9:1—3:7) gave a red solid, which was further purified by preparative plate chromatography (5 times, chloroform as eluent). The fast-moving, second band gave the diaza 19-19-fulvadiene **15** (16 mg, 1.4%). Recrystallization from hexane–benzene afforded purple microcrystals: Mp 146—147 °C (decomp); MS (field desorption method) *m/z* 568 (M^+); mol wt 568.7; IR 2175 (-C≡C-), 995, and 970 cm^{-1} (trans C=C); UV: see Tables 1 and 2; ^1H NMR (200 MHz) τ ca. 2.50—3.08 (m, 4H, olefinic H), 3.10—3.76 (m, 20H, olefinic H), 7.82 (s, 3H, CH_3), 7.90 (s, 3H, CH_3), 7.96 (s, 3H, CH_3), and 8.00 (s, 3H, CH_3). In this reaction the diaza 7-19-fulvadiene was not obtained.

1-(5,10-Dimethyl-2,4,10,12-tridecatetraene-6,8-diynylidene)-2-(5,10-dimethyl-2,4,10,12,14-pentadecapentaene-6,8-diynylidene)hydrazine (13). A soln of hydrazine dihydrochloride (220 mg, 2.10 mmol) in water (2 ml) was added in one portion to a stirred soln of bisdehydro[13]annulenone (421 mg, 2.02 mmol) and bisdehydro[15]annulenone (642 mg, 2.74 mmol) in methanol (160 ml) and THF (80 ml) at room temperature and the mixture was stirred for 6 h. After a further quantity of hydrazine dihydrochloride (100 mg) in water (2 ml) was added, stirring was continued for further 19 h at room temperature. Then the mixture was worked up as in the isolation of **9** and **12**. The residual dark red liquid, after solvent removal, was chromatographed on alumina (4.0× 12.5 cm). The early fractions eluted with hexane–benzene (2:3) gave the diaza 13-13-fulvadiene **12** (70 mg, 17%). The following fractions eluted with hexane–benzene (3:7) gave a red solid, which was further purified by preparative plate chromatography (6 times, benzene as eluent). The fast moving, second band gave the diaza 13-15-fulvadiene **13** (26 mg, 2.9%). Recrystallization from hexane–benzene afforded purple plates: Mp 160—161 °C (decomp); MS (field desorption method) *m/z* 439 (M^+); mol wt 438.5; IR 2160 (-C≡C-) and 980 cm^{-1} (trans C=C); UV: see Tables 1 and 2; ^1H NMR (200 MHz) τ=1.45—1.64 (m, 2H, $H^{B''}$, $H^{B'''}$), 2.72—3.51 (m, 10H, $H^{A'}$, $H^{A''}$, $H^{A'''}$, H^B, H^C, $H^{C'}$, $H^{C''}$, $H^{C'''}$, $H^{D'}$, $H^{E'}$), 3.61 (dd, 16.5, 7, 1H, $H^{B'}$), 3.83 (d, 16.5, 1H, H^A), 7.96 (s, 3H, CH_3), 7.99 (s, 3H, CH_3), 8.12 (s, 3H, CH_3), 8.17 (s, 3H, CH_3), and see Fig. 1; (CF_3COOD in $CDCl_3$, 200 MHz) τ=0.50 (dd, 15.5, 11, 1H, $H^{B''}$ or $H^{B'''}$), 0.70 (dd, 15.5, 11, 1H, $H^{B''}$ or $H^{B'''}$), 1.28 (dd, 15, 7, 1H, $H^{B'}$), 1.98—2.35 (m, 3H, H^A, H^C, $H^{E'}$), 2.44 (dd, 15.5, 7, 1H, $H^{C'}$), 3.11—3.81 (m, 7H, $H^{A'}$, $H^{A''}$, $H^{A'''}$, H^B, $H^{C''}$, $H^{C'''}$, $H^{D'}$), 7.42 (s, 3H, CH_3), 7.67 (s, 3H, CH_3), and 8.21 (s, 6H, CH_3).

Found: C, 87.36; H, 6.14; N, 6.65%. Calcd for $C_{32}H_{26}N_2$: C, 87.64; H, 5.98; N, 6.39%.

The later fractions eluted with hexane–benzene (1:4—1:9) gave the diaza 15-15-fulvadiene **14** (29 mg, 3.0%).

The present work was partially supported by a Grant-in-Aid for Scientific Research No. 60540321, from the Ministry of Education, Science and Culture.

References

1) For reviews, see E. D. Bergmann, *Chem. Rev.*, **68**, 41 (1968); F. Pietra, *ibid.*, **73**, 293 (1973); G. Becker, *Methoden Org. Chem.* (Houben-Weyl), **5**, 697 (1985).

2) a) T. M. Cresp, J. Ojima, and F. Sondheimer, *J. Org. Chem.*, **42**, 2130 (1977); b) J. Ojima, Y. Shiroishi, K. Wada, and F. Sondheimer, *ibid.*, **45**, 3564 (1980).

3) T. Asao, N. Morita, J. Ojima, and M. Fujiyoshi, *Tetrahedron Lett.*, **1978**, 2795; N. Morita, T. Asao, J. Ojima, and K. Wada, *Chem. Lett.*, **1981**, 57.

4) J. Ojima, K. Itagawa, and T. Nakada, *Tetrahedron Lett.*, **24**, 5273 (1983); *Bull. Chem. Soc. Jpn.*, **59**, 1723 (1986).

5) N. Morita, T. Asao, J. Ojima, and S. Hamai, *Chem. Lett.*, **1983**, 1887.

6) Inter alia, A. Beck, L. Knothe, D. Hunkler, and H. Prinzbach, *Tetrahedron Lett.*, **25**, 1785 (1984), and the references cited therein.

7) W. M. Jones, M. E. Stowe, E. E. Wells, Jr., and E. W. Lester, *J. Am. Chem. Soc.*, **90**, 1849 (1968).

8) A. Beck, H. Bingmann, S. Kagabu, L. Knothe, E. Hädicke, and H. Prinzbach, *Chem. Ber.*, **116**, 1963 (1983).

9) In this paper, for example, we used abbreviation such as 7-13- and 13-15-fulvadiene for heptatridecafulvadiene and tridecapentadecafulvadiene, respectively.

10) P. J. Garratt and K. Grohmann, *Methoden Org. Chem.* (Houben-Weyl), **5**, 533 (1972).

Insertion of Sulfur Trioxide into the N-Si Bond of Anilinotrimethylsilane. An Improved Method for the Preparation of Free Phenylamidosulfuric Acid[1)]

Fujio KANETANI,* Eiji OKADA, and Kenji NEGORO
Department of Applied Chemistry, Faculty of Engineering, Hiroshima University, Saijo, Higashi-Hiroshima 724
(Received March 13, 1986)

The reaction between anilinotrimethylsilane (**1**) and a variety of sulfonating agents [SO_3, $ClSO_3H$, trimethylsilyl chlorosulfate (**5**), dioxane-sulfur trioxide complex, ethyl chlorosulfate (**10**)] has been studied. With SO_3, **5**, or a dioxane-sulfur trioxide complex a sulfur trioxide molecule was inserted selectively into the N-Si bond of **1** to yield trimethylsilyl phenylamidosulfate (**2**), which on treatment with acetic acid, trifluoroacetic acid, or methanol gave free phenylamidosulfuric acid (**3**). The reaction of **1** with $ClSO_3H$ afforded **3** directly, but the product was contaminated with slight amounts of anilinium hydrogensulfate and anilinium chloride. The reaction of **1** with **10** yielded a mixture containing dianilinium (4-sulfonatophenylamido)sulfate, 4-aminobenzenesulfonic acid, and ethyl phenylamidosulfate as major products (after desilylation). The reaction of **1** with **5** has been found to provide an improved method for preparing **3**.

Arylamidosulfuric acids ($ArR^1R^2N^+SO_3^-$) have long been believed, but not yet proved, to be intermediates in the sulfonation of aromatic amines.[2-5)] In a previous paper,[6)] one of us (F. K.) has reported the first definite preparation and characterization of some arylamidosulfuric acids. The method of preparation used simply involves the addition of ice-cold concentrated hydrochloric acid to a saturated aqueous solution of an appropriate ammonium arylamidosulfate, followed by filtration and drying of the product. This method, however, rather requires technical skillfulness for obtaining the product of high purity; therefore, it is desirable to develop a more convenient method for preparing free arylamidosulfuric acids.

In view of their great tendency to undergo thermal rearrangement and reactions with Lewis bases, such as water, alcohols, amines, etc., it is highly desirable that arylamidosulfuric acids should be generated in an inert organic medium under mild conditions and isolated in a high purity without any purification. We considered that the silyl esters ($ArR^1NSO_3SiR^2_3$) would meet such requirements and be the most promising precursor of the free arylamidosulfuric acids.

To our knowledge, there is no report on the silyl esters of arylamidosulfuric acids, although several reports[7-9)] have appeared on the aliphatic counterparts. We, therefore, decided to examine the reation of anilinotrimethylsilane (**1**) with several sulfonating agents with the aim of preparing trimethylsilyl phenylamidsosulfate (**2**) and have found that a sulfur trioxide molecule is inserted into the N-Si bond of **1** to yield the desired silyl ester **2**, which, on treatment with an appropriate desilylating agent such as trifluoroacetic acid, directly gives pure phenylamidosulfuric acid (**3**) very easily.

Results and Discussion

Reaction of Anilinotrimethylsilane (1) with Sulfur Trioxide. The reaction of **1** with sulfur trioxide at −15°C for 8 h, followed by the treatment with trifluoroacetic acid gave the desired phenylamidosulfuric acid (**3**). HPLC analysis revealed that sulfur trioxide was inserted exclusively into the N-Si bond; the ring-sulfonation products were detected but in traces. In contrast, the same reaction at room temperature (17°C) for 4 h led to the formation of 4-aminobenzenesulfonic acid and (4-sulfophenylamido)sulfuric acid in addition to **3**.

$$\underset{\mathbf{1}}{C_6H_5NHSi(CH_3)_3} + SO_3 \xrightarrow[-15^\circ C]{} \underset{\mathbf{2}}{[C_6H_5\overset{+}{N}HSi(CH_3)_3]\,SO_3^-} \xrightarrow{CF_3COOH} \underset{\mathbf{3}}{C_6H_5NH_2{}^+SO_3^-}$$

Reaction of 1 with Chlorosulfuric Acid. When chlorosulfuric acid was added dropwise to a solution of **1** in 1,2-dichloroethane at −20°C, **3** separated out directly. This product, however, was contaminated with slight amounts of anilinium hydrogensulfate and anilinium chloride as indicated by HPLC and IR spectroscopy, and also by tests for sulfate and chloride ions. The anilinium hydrogensulfate arose probably

$$\mathbf{1} + ClSO_3H \xrightarrow[-20^\circ C]{} \mathbf{3} + \underset{\mathbf{4}}{(CH_3)_3SiCl}$$

from aniline and sulfuric acid, which are commonly present as contaminants in **1** and chlorosulfuric acid, respectively. Great difficulty in obtaining very pure starting materials and the lack of methods for purifying **3** make this reaction less valuable for the preparation of pure **3**.

Reaction of 1 with Trimethylsilyl Chlorosulfate (5). Sundermeyer and his collaborators[10)] have prepared several trimethylsilyl esters of alkylamidosulfuric acids in yields of 70—90% by the reaction of (alkylamino)trimethylsilane with **5**. Our preliminary experiments showed that, with anilinotrimethylsilane (**1**), the use of much lower temperature is essential, or else

$$R^1R^2NSi(CH_3)_3 + \underset{\mathbf{5}}{ClSO_3Si(CH_3)_3} \xrightarrow[r.t.]{CH_2Cl_2} R^1R^2NSO_3Si(CH_3)_3 + \mathbf{4}$$

ring sulfonation occurs appreciably. Thus, a solution of **5** in dichloromethane was added dropwise to a solution of **1** in the same solvent at −10—−15 °C and the mixture was stirred at −10—−15 °C for 7 h; after removal of insoluble material,[11] the filtrate was treated with trifluoroacetic acid to give analytically pure phenylamidosulfuric acid (**3**) in yields of 62—71%. When the desilylating process was omitted, trimethylsilyl phenylamidosulfate (**2**)[12] was isolated from the reaction mixture.

$$\underset{\mathbf{1}}{C_6H_5NHSi(CH_3)_3} + \underset{\mathbf{5}}{ClSO_3Si(CH_3)_3} \xrightarrow[-10\ -\ -15°C]{} \underset{\mathbf{2}}{C_6H_5NHSO_3Si(CH_3)_3} + \mathbf{4}$$

Acetic acid and methanol, as well as trifluoroacetic acid, can be used as a desilylating agent. As for methanol, however, its use in excess must be avoided; otherwise phenylamidosulfuric acid first formed will react with the excess methanol at room temperature to yield anilinium methyl sulfate (**6**).

$$\underset{\mathbf{3}}{C_6H_5NH_2{}^+SO_3{}^-} + CH_3OH \xrightarrow[r.t.]{} \underset{\mathbf{6}}{C_6H_5NH_3{}^+CH_3OSO_3{}^-}$$

Reaction of Aniline with Trimethylsilyl Chlorosulfate (5). The reaction of aniline with **5** in a 1:1 molar ratio produced a mixture consisting of trimethylsilyl phenylamidosulfate (**2**) (16%), phenylamidosulfuric acid (**3**) (51%), anilinium hydrogensulfate, and anilinium chloride. The latter two anilinium salts arose probably from the hydrolysis of **5** by adventitious water during the reaction. Simchen and his

$$C_6H_5NH_2 + \mathbf{5} \longrightarrow \left[\ C_6H_5\overset{H}{\overset{|}{N}}\!\!-\!\!\overset{O}{\overset{\|}{S}}\!\!-\!\!Cl \quad (O\text{–}Si(CH_3)_3)\ \right] \longrightarrow$$

$$C_6H_5NH_2{}^+SO_3Si(CH_3)_3 + Cl^- \begin{cases} \xrightarrow{} \underset{\mathbf{2}}{C_6H_5NHSO_3Si(CH_3)_3} + HCl \\ \xrightarrow{} \underset{\mathbf{3}}{C_6H_5NH_2{}^+SO_3{}^-} + \mathbf{4} \end{cases}$$

collaborator have repoted[13] that the action of **5** on *N,N*-diethylaniline with ice-cooling gives an *N,N*-diethylanilinesulfur trioxide adduct (**7**), which rearranges to 4-(diethylamino)benzenesulfonic acid at room temperature.

$$C_6H_5N(C_2H_5)_2 + \mathbf{5} \longrightarrow \underset{\mathbf{7}}{C_6H_5N(C_2H_5)_2{}^+SO_3{}^-} + \mathbf{4}$$

$$\mathbf{7} \xrightarrow[r.t.]{} 4\text{-}(C_2H_5)_2NH^+C_6H_4SO_3{}^-$$

The reaction of aniline with **5** in a 2:1 molar ratio at −10—−15 °C yielded anilinium phenylamidosulfate (**8**) in a 87% yield; the same result was obtained when the direction of addition of both reagents was inverted. HPLC analysis showed the absence of the ring sulfonation; in addition, tests with acidic aqueous silver nitrate and barium nitrate solutions were practically negative. These facts indicate that the reaction proceeds probably as follows.

$$2\ C_6H_5NH_2 + \underset{\mathbf{5}}{ClSO_3Si(CH_3)_3} \longrightarrow \left[\ C_6H_5NH_2 \rightarrow C_6H_5\overset{H}{\overset{|}{N}}\!\!-\!\!\overset{O}{\overset{\|}{S}}\!\!-\!\!Cl \quad (O\text{–}Si(CH_3)_3)\ \right]$$

$$\longrightarrow \underset{\mathbf{8}}{C_6H_5NHSO_3{}^-C_6H_5NH_3{}^+} + \mathbf{4}$$

Reaction of 1 with Dioxane–Sulfur Trioxide Complex. Kricheldorf and his collaborator[8] have prepared trimethylsilyl *N*-methylbenzylamidosulfate in 77% yield by reaction of *N*-methyl-*N*-(trimethylsilyl)-benzylamine[9] with dioxane–sulfur trioxide. In our case, the reaction of **1** with dioxane–sulfur trioxide (−20 °C, 2 h) in 1,2-dichloroethane and subsequent desilylation with trifluoroacetic acid gave a mixture consisting of the desired product **3**, 4-aminobenzenesulfonic acid, and anilinium hydrogensulfate. The sulfate salt arose undoubtedly from the hydrolysis of unconverted **1** and the dioxane–sulfur trioxide in the course of workup; therefore, lengthening of the reaction time would lead to an increase in the yield of **3**, and removal of the insoluble by-products from the reaction mixture before the desilylation would permit the isolation of **3** in a pure state without any additional purification.

$$C_6H_5NHSi(CH_3)_3 + \text{dioxane–}SO_3 \rightleftharpoons C_6H_5\overset{+}{N}HSi(CH_3)_3 \quad (SO_3^-) + \text{dioxane}$$

$$\underset{\mathbf{2}}{C_6H_5NHSO_3Si(CH_3)_3} \xrightarrow{H^+} \underset{\mathbf{3}}{C_6H_5NH_2{}^+SO_3{}^-}$$

Reaction of 1 with Ethyl Chlorosulfate (10). The reactions between aromatic as well as aliphatic amines and alkyl chlorosulfates have been studied by several investigators.[14,15] It has been found that, for example, in the reaction of aniline with **10**, *N*-ethyl- and *N,N*-diethylaniline, phenylamidosulfate, *N*-ethylphenylamidosulfate, and 4-aminobenzenesulfonic acid are formed in varying proportions, which depend on the reaction conditions used. Yaguzhinskii and Berlin[15] have investigated the reaction of anilines with alkyl chlorosulfates in some detail and found that the corresponding alkyl *N*-alkylphenylamidosulfates were also formed.

By analogy with these findings, the reaction of anilinotrimethylsilane **1** with **10** had been expected to yield the desired product **3**; actually, however, **3** was formed in only a trace. Thus, treatment of **1** with **10** in

dichloromethane at −10—−15 °C for 1 h and at reflux for 3 h yielded a solid product, which was identified as dianilinium (4-sulfonatophenylamido)sulfate; treatment of the filtrate with acetic acid gave another precipitate, which was found to be 4-aminobenzenesulfonic acid contaminated with slight amounts of 2-aminobenzenesulfonic acid and a disulfonic acid, and a trace of **3**. In addition, ethyl phenylamidosulfate and its *N*-ethyl derivative were isolated from the desilylation mixture.

Experimental

All reactions were carried out in oven-dried glassware under a dry nitrogen atmosphere by use of Schlenk-tube techniques. All solvents were dried over appropriate drying agents. Aniline was dried over KOH pellets and distilled under reduced pressure. Triethylamine was dried over KOH and distilled. Chlorotrimethylsilane was distilled (bp 57.0—57.5 °C). Trifluoroacetic acid and chlorosulfuric acid were of reagent grade and used as purchased. Sulfur trioxide was obtained from 60—65% fuming sulfuric acid by distillation. IR spectra were recorded on a Hitachi 215 spectrophotometer; ^{1}H NMR spectra were obtained on a JNM-PMX 60 instrument. High-performance liquid chromatography (HPLC) was carried out on a Toyo Soda HPLC-803D instrument by using a TSK-GEL ODS-120T (4.6 mm ×25 cm)column and a 0.05 M Na_2HPO_4 (pH 7.0) aqueous solution containing 1% of CH_3CN as the eluant; peaks were monitored at 240 nm on a UVIDEC-100-IV. TLC was performed on Cellulose mikrokristallin (E Merck) plates by using dioxane–water (3 : 1 v/v) as a developing solvent; spots were visualized by diazotization with nitrous gases and spraying with 1% sodium 1-naphthol-4-sulfonate and subsequent exposure to ammonia. Samples for HPLC and TLC analyses were prepared by dissolving the products in aqueous NaOH.

Preparation of Anilinotrimethylsilane (1). To a stirred solution of chlorotrimethylsilane (24.0 g, 0.220 mol) in cyclohexane (100 ml) was added at 5 °C over 10 min a solution of triethylamine (22.2 g, 0.220 mol) in cyclohexane (15 ml). After the mixture had been stirred for 1 h, aniline (20.5 g, 0.220 mol) was added at 5—6 °C over 30 min, and stirring was continued for further 7 h. The mixture was filtered and evaporated. The residue was fractionally distilled under reduced pressure to give **1** (23.5 g, 65%): Bp 103.7—104.5 °C/21 Torr† (lit, 106-107 °C/24 Torr);[16] 95% purity as determined by GLC;IR (neat) 3405, 1605, 1503, 1388, 1295, 1253, 900, 838, and 690 cm^{-1}.

Preparation of Trimethylsilyl Chlorosulfate (5). Sulfur trioxide (71.0 g, 0.89 mol) was added with stirring to chlorotrimethylsilane (96.3 g, 0.89 mol) at −35 °C. The mixture was then allowed to warm to room temperature, heated at 50 °C for 10 min, and distilled in vacuo to yield **5** (145.8 g, 87%): Bp 73.0—74.0 °C/18 Torr (lit, [17] 66 °C/12 Torr).

Reaction of 1 with Sulfur Trioxide. To a stirred solution of **1** (2.50 g, 15.1 mmol) in 1,2-dichloroethane (55 ml) was added at −15 °C over 30 min a solution of SO_3 (1.21 g, 15.1 mmol) in 1,2-dichloroethane (15 ml). After being stirred for 8 h at −15 °C, the mixture was filtered and the filtrate was treated with CF_3COOH (1.72 g, 15.1 mmol) at −15 °C for 2 h. The solid produced (1.19 g, 45.5%) was collected by filtration, washed with 1,2-dichloroethane, and dried in vacuo. The product was identified as phenylamidosulfuric acid (**3**) by comparison of its IR spectrum and HPLC data with those of the authentic sample prepared in previous work.[6]

Reaction of 1 with Chlorosulfuric Acid. To a stirred solution of **1** (2.56 g, 15.5 mmol) in 1,2-dichloroethane (55 ml) was added at −20 °C over 30 min chlorosulfuric acid (1.81 g, 15.5 mmol). The mixture was then stirred for 8 h at −20 °C. A precipitate produced was collected by filtration under dry nitrogen, washed with 1,2-dichloroethane, and dried in vacuo to give **3** (2.55 g, 95%). HPLC analysis and tests with acidic aqueous $Ba(NO_3)_2$ and 0.05 M $AgNO_3$ solutions indicated the contamination with slight amounts of anilinium hydrogensulfate and anilinium chloride.

Reaction of 1 with 5. Trimethylsilyl chlorosulfate (**5**) was redistilled directly into a dropping funnel under reduced pressure (bp 75.0—75.5 °C/23 Torr). A solution of this ester (3.43 g, 18 mmol) in CH_2Cl_2 (5 ml) was added with stirring to freshly distilled anilinotrimethylsilane (**1**) (bp 104.5—106.0 °C/22 Torr) (2.97 g, 18 mmol) in CH_2Cl_2 (20 ml) at −10—−15 °C over 30 min. The mixture was stirred at this temperature for further 7 h and filtered. The filtrate was then treated at −10—−15 °C for 3 h with CF_3COOH (2.00 g, 18 mmol) to give a white solid, which was collected by filtration, washed with CH_2Cl_2, and dried in vacuo to yield pure phenylamidosulfuric acid **3** (2.0 g, 64%); IR (KBr) 1545 (NH_2^+), 1497, 1480, 1360 (SO_3^-), 1302, 1256 (SO_3^-), 1050 (SO_3^-), 875, 765, and 685 cm^{-1}. Found: C, 41.63; H, 4.17; N, 8.26%. Calcd for $C_6H_7O_3NS$: C, 41.61; H, 4.07; N, 8.09%. This product gave no turbidity with aqueous $Ba(NO_3)_2$; its homogeneity was proved by HPLC analysis.

Isolation of Trimethylsilyl Phenylamidosulfate (2). The reaction of **1** with **5** was carried out as described above. The reaction mixture was filtered and evaporated in vacuo. Distillation of the residue yielded **2** as a colorless liquid boiling at 119 °C/ca. 1 Torr; IR (film) 3285 (NH), 2965, 2900, 1605, 1503, 1345 (SO_2), 1258 ($Si(CH_3)_3$), 1175 (SO_2), 950 (SiOSi), 845, 765, and 698 cm^{-1}; treatment of this compound with CF_3COOH yielded phenylamidosulfuric acid **3**.

Formation of Anilinium Methyl Sulfate (6) on Treatment of 2 with Excess of Methanol. The reaction between **1** (2.60 g, 15.7 mmol) and **5** (2.29 g, 15.7 mmol) was carried out as described above. After removal of a white precipitate (0.85 g), the filtrate was treated with methanol (1.00 g, 31.4 mmol) at −10—−15 °C. A white solid rapidly separated out, as the methanol was added.[18] While the mixture was stirred for further 1.5 h, the solid gradually disappeared and colorless crystals, in turn, separated out as thin plates; this compound (1.26 g, 39%) was identified as **6** by comparison of its melting point (130—131 °C) and IR spectrum with those of an authentic sample.[19] Found: C, 41.09; H, 5.04; N, 6.65%. Calcd for $C_7H_{11}O_4NS$: C, 40.97; H, 5.40; N, 6.83%.

Reaction of Aniline with 5 in a 1 : 1 Molar Ratio. To a stirred solution of **5** (2.14 g, 11.3 mmol) in CCl_4 (20 ml) was added a solution of aniline (1.06 g, 11.3 mmol) in CCl_4 (20 ml) at −10—−15 °C over 30 min. After the mixture had been stirred for 7 h at −10—−15 °C, a precipitate (**A**) thus formed (1.26 g) was collected by filtration. Treatment of the filtrate with acetic acid (0.68 g; 11.3 mmol) for 3 h at −10—−15 °C yielded another precipitate (**B**) (0.34 g).

Precipitate **A**: Neutralization of this material with aqueous NaOH gave sodium phenylamidosulfate; its identity was verified by HPLC analysis and by comparison of its IR

†Torr=133.322Pa.

spectrum with that of an authentic sample; tests with aqueous $Ba(NO_3)_2$ and $AgNO_3$ indicated the contamination with anilinium hydrogensulfate and anilinium chloride.

Precipitate **B**: Its IR spectrum was identical with that of an authentic sample of **2** and its HPLC showed a single peak ascribable to **2**.

Reaction of Aniline with 5 in a 2:1 Molar Ratio. To a stirred solution of aniline (1.69 g, 18.2 mmol) in CCl_4 was added a solution of **5** (1.72 g, 9.1 mmol) in the same solvent (5 ml) over 30 min at −10—−15 °C. After the mixture had been stirred for 3 h at −10—−15 °C, the resulting precipitate was collected, washed with CCl_4, and dried in vacuo to give anilinium phenylamidosulfate (**8**) (2.12 g, 87%). Recrystallization from water gave the pure salt; its IR spectrum was identical with that of an authentic sample. Found: C, 54.33; H, 5.24; N, 10.27%. Calcd for $C_{12}H_{14}O_3N_2S$: C, 54.12; H, 5.30; N, 10.52%.

Reaction of 1 with Dioxane–Sulfur Trioxide. To a stirred solution of 1,4-dioxane (1.00 g, 11.4 mmol) in 1,2-dichloroethane (20 ml) was added a solution of SO_3 (0.78 g; 9.74 mmol) in 1,2-dichloroethane (20 ml) over 1 h at −10 °C. To this mixture was added with stirring a solution of **1** (1.61 g; 9.74 mmol) in 1,2-dichloroethane (20 ml) over 30 min at −20 °C. After having been stirred for an additional 2 h at −20 °C, the mixture was filtered. The filtrate was then treated with CF_3COOH (1.50 g, 13 mmol) at −5 °C for 3 h; the solid thus formed was collected, washed with 1,2-dichloroethane, and dried in vacuo, giving phenylamidosulfuric acid (**3**) (1.1 g; 65%).

Reaction of 1 with Ethyl Chlorosulfate (10). To a stirred solution of **1** (2.28 g; 13.8 mmol) in CH_2Cl_2 (20 ml) was added a solution of **10** (2.00 g; 13.8 mmol) in CH_2Cl_2 (10 ml) at −10—−15 °C over 30 min. After having been stirred for an additional 2 h, the mixture was allowed to warm to room temperature, and then refluxed for 3 h. A white solid (**A**) (0.45 g) was collected, washed with CH_2Cl_2, and dried; the combined filtrate and washings were treated with CH_3COOH at −10—−15 °C for 3 h to yield a solid (**B**). After the solid (**B**) had been filtered off, the filtrate was washed with water repeatedly, dried over Na_2SO_4, and evaporated to give a semi-solid (**C**), which probably is a mixture of ethyl phenylamidosulfate and ethyl *N*-ethyl-*N*-phenylamidosulfate.

Solid **A**: IR (KBr) 3270 (NH), 1601, 1501, 1230 (SO_3^-), 1162 (SO_3^-), 1125, 1033 (SO_3^-), 900, 835, 740, and 682 cm^{-1}; the IR spectrum of its sodium salt was identical with that of an authentic sample of disodium (4-sulfonatophenylamido)-sulfate.[20]

Solid **B**: The IR and NMR spectra of its sodium salt agreed with those of an authentic sample of sodium 4-aminobenzenesulfonate; HPLC analysis revealed the contamination with slight amounts of 2-aminobenzenesulfonic acid and aminobenzenedisulfonic acid, and with a trace of **3**.

Residue **C**: IR (KBr) 1603, 1503, 1360 (SO_2), 1165 (SO_2), 1008, 915, 752, and 695 cm^{-1}. ^1H NMR (DMSO-d_6) δ=1.0 (t, CH_3), 1.23 (t, CH_3), 3.65 (q, OCH_2), 4.08 (q, NCH_2), and 7.48 (m, ArH).

One of the authors (F. K.) thanks Prof. Dr. H. Schmidbaur for the laboratory facilities during his stay at Anorganisch-Chemisches Institut der Technischen Universität München on sabbatical leave.

References

1) Studies of Reactions of Amines with Sulfur Trioxide. Part 8. Part 7: F. Kanetani, *Bull. Chem. Soc. Jpn.*, **59**, 952 (1986).

2) E. R. Alexander, *J. Am. Chem. Soc.*, **69**, 1599 (1947).

3) P. K. Maarsen and H. Cerfontain, *J. Chem. Soc., Perkin 2*, **1977**, 1008 and references cited therein.

4) A. Junghahn, *Chem. Ind. (Berlin)*, **26**, 57 (1903).

5) W. Huber, *Helv. Chem. Acta*, **15**, 1372 (1932).

6) Fujio Kanetani, *Chem. Lett.*, **1980**, 965.

7) M. Schmidt and H. Schmidbaur, *Angew. Chem.*, **70**, 657 (1958).

8) H. R. Kricheldorf and E. Leppert, *Synthesis*, **1975**, 49.

9) *N*-Methyl-*N*-(trimethylsilyl)benzylamine and *N*-methylbenzylamidosulfuric acid trimethylsilyl ester have been written in the text mistakenly as *N*-methyl-*N*-phenyl-*N*-trimethylsilylamine and *N*-methyl-*N*-phenylsulfamidic acid trimethylsilyl ester, respectively (Personal communication from Prof. Dr. H. R. Kricheldorf, Universität Hamburg).

10) W. Buss, H.-J. Krannich, and W. Sundermeyer, *Z. Naturforsch.*, **30b**, 842 (1975).

11) HPLC and IR sepctroscopic analysis showed that this material consisted of anilinium hydrogen sulfate and minor amounts of anilinium phenylamidosulfate and 4-aminobenzenesulfonic acid.

12) To our knowledge, this compound is the first silyl ester of arylamidosulfuric acids.

13) K. Hofmann and G. Simchen, *Justus Liebigs Ann. Chem.*, **1982**, 282.

14) For reviews on esters of chlorosulfuric acid see F. Sinn and K. Schimmelschmidt, "Methoden der Organischen Chemie," Georg Thieme Verlag, Stuttgart (1963), 4. Aufl., Bd. VI/2, pp. 472—473; E. Buncel, *Chem. Revs.*, **70**, 323 (1970).

15) L. S. Yaguzhinskii and A. Ya. Berlin, *Zhur. Obshch. Khim.*, **33**, 3087 (1963).

16) R. C. Osthoff and S. W. Kantor, *Inorg. Syntheses*, **5**, 55 (1957).

17) M. Schmidt and H. Schmidbaur, *Chem. Ber.*, **95**, 47 (1962).

18) The use of an equimolar amount of methanol and immediate filtration permit the isolation of phenylamidosulfuric acid.

19) F. Kanetani and K. Negoro, unpublished data.

20) F. Kanetani and H.Yamaguchi, *Bull. Chem. Soc. Jpn.*, **54**, 3048 (1981).

Rearrangement Approaches to Cyclic Skeletons. IV. The Total Synthesis of (±)-Pinguisone and (±)-Deoxopinguisone Based on Photochemical [1,3] Acyl Migration of a Bicyclo[3.2.2]non-6-en-2-one[1]

Tadao UYEHARA,* Yasuhiro KABASAWA, and Tadahiro KATO
Department of Chemistry, Faculty of Science, Tohoku University, Aramaki-Aoba, Sendai 980
(Received March 14, 1986)

The total synthesis of (±)-Pinguisone (**2**) and (±)-deoxopinguisone (**3**), [5—6] fused-ring sesquiterpenes, has been achieved starting from 1-methoxy-3,4,5-trimethylbenzene. 1-Methoxy-4,5,*endo*-8-trimethylbicyclo[2.2.2]-non-5-en-2-one (**9**) was prepared selectively via facial selective Diels–Alder reaction of the diene derived from the benzene and 2-chloroacrylonitrile. Ring enlargement of **9** using $(CH_3)_3SiCHN_2$ and BF_3 etherate gave the corresponding bicyclo[3.2.2]oct-6-en-2-one (**8**). The photochemical [1,3] acyl migration of **8** gave the [5—6] fused-ring compound (**7**). The fourth methyl was introduced selectively by the conjugate addition of $(CH_3)_2CuLi$ to the spiro[bicyclo[4.3.0]non-8-ene-3,2′-[1,3]dioxolan]-7-one prepared from **7**. Each furan ring of **2** and **3** was constructed via the corresponding butenolide derived from the γ-keto acid by acid-catalyzed dehydration.

Pinguisane-type sesquiterpenes, possessing the unusual terpene skeleton (**1**),[3] have been found from various kinds of liverworts; such as pinguisone (**2**)[4] from *Aneura pinguis* (L.) Dum.[4b] and deoxopinguisone (**3**)[5] from *Ptilidium ciliare* (L.) Nees.[5a] These compounds are of particular interest in the total synthesis[6] since they have novel tricyclic furan skeletons with a cis-junction between the five- and six-membered rings and four adjacent cis-located methyl groups. Already it has been found that such polymethylated compounds do not belong to the simple cis-fused ring system whose convex and concave sides are predictable with ease.[6]

In connection with our program to develop methods for stereoselective syntheses of [*m*—*n*] fused-ring terpenoids from bridged bicyclic systems,[7] we have explored the photochemical reactions of bicyclo[3.2.2]-non-6-en-2-ones (**4**) and found a practical route to *cis*-bicyclo[4.3.0]non-4-en-7-ones (**5**) based on [1,3] acyl migration.[2] In this paper we describe the total synthesis of (±)-pinguisone (**2**) and (±)-deoxopinguisone (**3**), as the first application of this photochemical transformation to natural product syntheses.

Results and Discussion

Our synthetic plan is outlined in Scheme 1. The diketone **6**, possessing four adjacent cis methyl groups, should be an important precursor of the natural products. A key step in this plan is photochemical transformation of the bicyclo[3.2.2]non-6-en-2-one (**8**) to give the [5—6] fused ring system (**7**). The ketone **8** would be derived from the bridged bicyclooctenone **9** by ring enlargement. The stereochemistry of the 8-methyl of **9** should be controlled at the stage of cycloaddition to give the precursor of **9** by the approach of a ketene equivalent from the less hindered side to the diene **10**.

1-Methoxy-3,4,5-trimethyl-1,4-cyclohexadiene (**11**) was prepared from the corresponding anisole by dissolved metal reduction.[8] When **11** was heated with

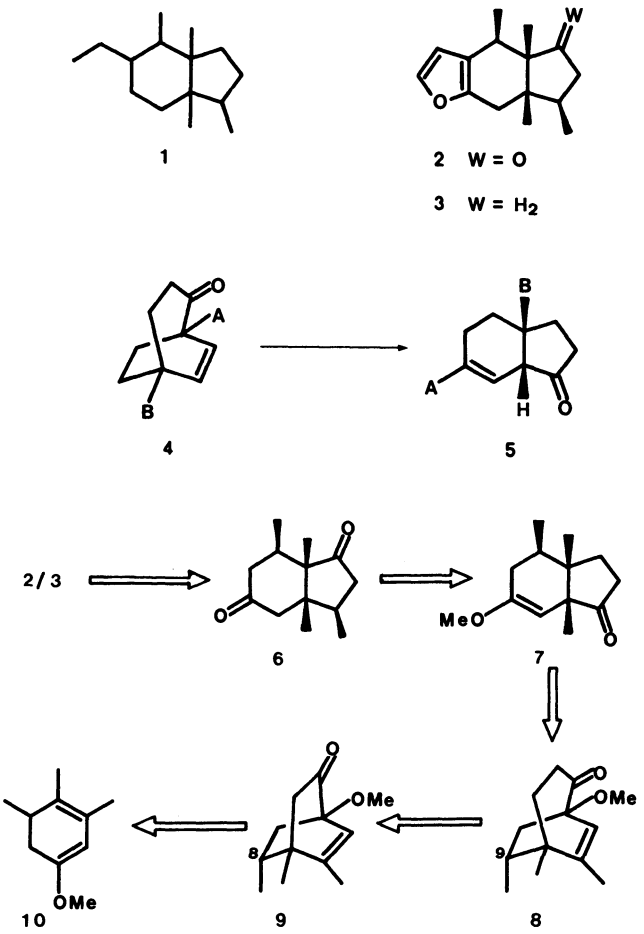

Scheme 1.

2-chloroacrylonitrile at 90°C in toluene, the 1,3-diene **10** was generated in situ and a mixture of the 1,4-addition products was obtained in 77% yield. Treating of the mixture with ethanolic sodium sulfide and potassium hydroxide[9] followed by Collins oxidation gave a ca. 10 to 1 mixture of **9** and **9a** in 57% yield. Prolongation of the treatment with sodium sulfide gave a large amount of the alcohols derived from **9** and **9a**. ^1H NMR spectrum of **9**, purified by HPLC,

shows the signals due to the 8-methyl at δ 0.89, whereas that of the isomer **9a** exhibits the corresponding signals at δ 1.01. This high-field shift of the former means that **9** is the 8-*endo*-methyl isomer. Their ^{13}C NMR spectra are also informative; that of **9** shows representative signals at δ 144.7 (5-C, s) and 47.7 (3-C, t) while those of **9a** are the singlet at δ 149.0 (5-C) and the triplet at 41.1 (3-C). These difference should be caused by the steric repulsion between the 5-carbon and the 8-*endo*-methyl in **9** and that between the 3-methylene and the 8-*exo*-methyl in **9a**.

Treatment of **9** with trimethylsilyldiazomethane and boron trifluoride etherate[10] in dichloromethane at −78 °C followed by desilylation with potassium carbonate in aqueous methanol gave the ring-enlargement product **8** in 79% yield. At higher temperature than −73 °C, the yield of **8** decreased definitely.

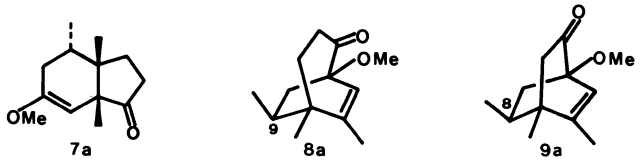

Photochemical transformation of **8** to give the cis [5—6] fused-ring system **7** was carried out in 59% yield by irradiation of its tetrahydrofuran (THF) solution using a high-pressure mercury lamp through a Pyrex filter. In practice, the mixture of **9** and **9a** was converted into a mixture of **7** and **7a** and then the desired ketone **7** was isolated by silica-gel column chromatography.

The enol methyl ether **7** underwent disproportionation slowly upon standing at ambient temperature. Terefore, **7** was treated with 2-ethyl-2-methyl-1,3-dioxolane and *p*-toluenesulfonic acid (TsOH) in benzene to give the acetal **12**, a remarkably stable compound.

In order to introduce the fourth methyl group stereoselectively, we first attempted the dissolved metal reduction route as shown in Scheme 2. The ketone **12** was converted into the α,β-unsaturated carbonyl compound **13** in 61% yield by successive treatment with 1) lithium diisopropylamide (LDA) and *S*-phenyl benzenethiosulfonate[11] and 2) sodium periodate in aqueous methanol, followed by 3) pyrolysis with calcium carbonate in toluene at 90 °C. Treatment of **13** with methyllitium and then with pyridinium chlorochromate (PCC)[12] gave the oxidative rearrangement product **14** in 79% yield. Reduction of **14** with lithium and *t*-butyl alcohol in liquid ammonia–THF gave the mixtures of the isomeric alcohols (**15** and **16**) in 33 and 58% yields, respectively. Each of them was converted quantitatively into the corresponding ketone by PCC oxidation in the presence of sodium acetate.

Stereochemistry of the fourth methyl group of the ketones **17** and **18** were determined on the basis of their ^{1}H NMR spectra. The spectrum of **17** shows the signals

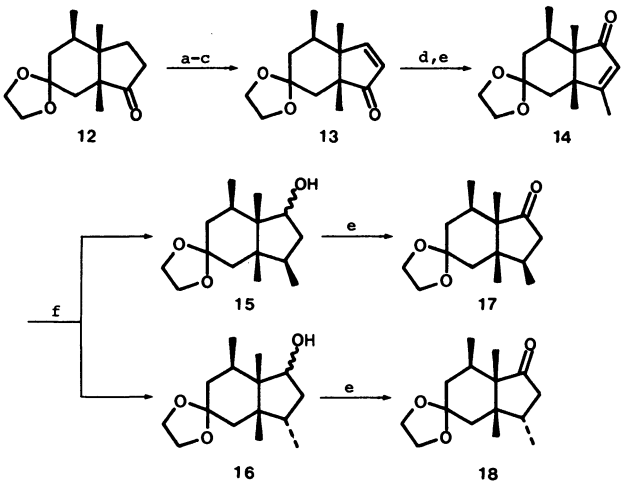

Scheme 2. Preparation of the *cis*-tetramethyl-*cis*-perhydroindanone (**17**).[a)]
a) (a): LDA, $PhSSO_2Ph$, THF, (b): $NaIO_4$, MeOH–H_2O, (c): $CaCO_3$, PhMe, 90 °C, (d): MeLi, ether, (e): PCC, NaOAc, CH_2Cl_2, (f): Li, NH_3, *t*-BuOH, THF.

due to the 9-methine proton at δ 3.04. On the other hand, the signals due to the corresponding proton of **18** appear at the higher field than δ 2.5. This remarkable difference means the presence of large deshielding effect to the proton of **17**.

The 200 MHz NMR spectrum of **17** suggests that its presumable conformation is **17a**, as depicted. The coupling pattern of the 5-methine proton (δ=2.07, $J_{5,4}$= 13.0 and 3.8 Hz) reflects that this is an axial proton of a chair cyclohexane ring. The spin–spin coupling between one of the 4-protons (δ=1.49, $J_{4,5}$=3.8 Hz and $J_{4,2}$=2.3 Hz) and one of the 2-protons (δ=1.75, $J_{2,4}$= 2.3 Hz) should be the "W"-shape long-range coupling. This means both of the protons are present at the equatrial positions of a chair six-membered ring. Thus, the C_1–C_9 bond should be axial-like and the 9-proton approaches to the axial-like oxygen of the acetal part. The nonbonding distance between this oxygen and the 9-proton is estimated to be ca. 1.9 Å based on Dreiding model study. The low-field shift of the 9-methine proton signals should be caused by this steric compression. The isomer **18** may have a different conformation from that of **17**. The ^{13}C NMR spectrum of **17** shows the signals due to the methine carbons

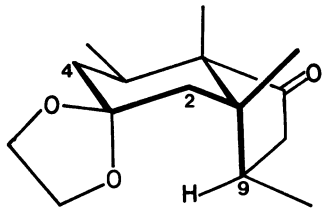

17a

at δ 30.3 and 29.2 while that of **18** exhibits the corresponding ones at δ 36.9 and 32.2. These remarkable

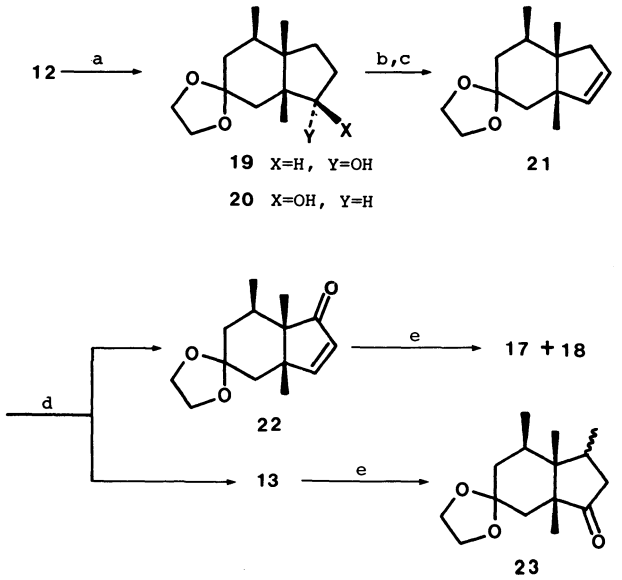

Scheme 3. An alternative route to the *cis*-tetramethyl-*cis*-perhydroindanone (**17**).[a)]
a) (a): $LiAlH_4$, ether, (b): MsCl, Py, (c): *t*-BuOK, DMSO, (d): CrO_3-3,5-DMP, CH_2Cl_2, (e): $(CH_3)_2CuLi$, ether.

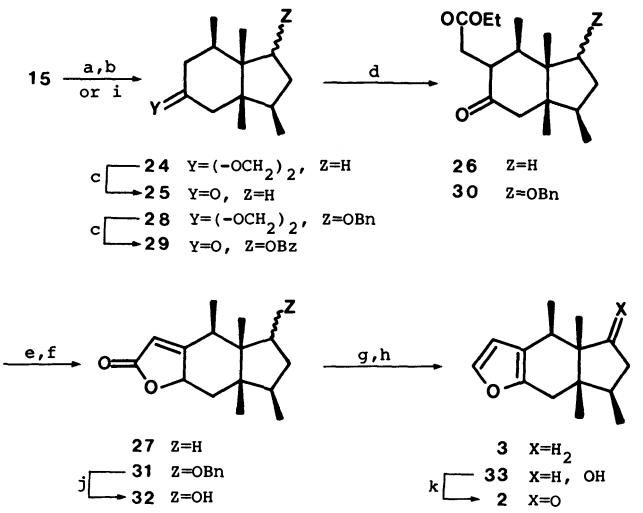

Scheme 4. Completion of the synthesis of (±)-pinguisone (**2**) and (±)-deoxopinguisone (**3**).[a)]
a) (a): NaH, CS_2, THF, then MeI, (b): $(n\text{-Bu})_3SnH$, PhMe, reflux, (c): HCl, H_2O-acetone, (d): LDA, ICH_2CO_2Et, THF-HMPA, (e): K_2CO_3, MeOH-H_2O, (f): TsOH, PhH, reflux, (g): DIBAH, THF, (h): 1 M H_2SO_4, (i): NaH, $PhCH_2Br$, $(n\text{-Bu})_4NI$, DME, (j): BBr_3, CH_2Cl_2, (k): $(Ac)_2O$, DMSO.

differences also suggest the conformational difference between **17** and **18** and the presence of the large steric compression in the former.

Catalytic hydrogenation of **14** using 5% palladium on charcoal in ethanol gave a 1 to 1 mixture of **17** and **18**.

In order to prepare the ketone **17** selectively, an alternative route was examined (Scheme 3). Reduction of **12** with $LiAlH_4$ gave the alcohols **19** and **20** in 82 and 17% yields, respectively. Treatment of the methanesulfonate (mesylate) of **19** with potassium *t*-butoxide in DMSO gave the olefin **21** in 95% yield (from **19**), whereas **21** was not derived from the mesylate of **20**. Allylic oxidation of **21** with chromium trioxide-3,5-dimethylpyrazole complex[13] at −20 °C gave a 9 to 2 mixture of the ketones **22** and **13** in 79% yield. Reaction of this mixture with lithium dimethylcuprate(I) formed a mixture of **17** and **18**, in a ratio of 94 to 6, in 76% yield and **23**, derived from **13**, in 17% yield. Remarkable stereoselectivity of the conjugate addition to **22** is caused by steric approach control due to the steric bulk of the acetal. Reduction of the mixture of **17** and **18** by $LiAlH_4$ gave the alcohols (**15** and **16**) quantitatively.

The final stages of the (±)-deoxopinguisone (**3**) synthesis is shown in Scheme 4. The alcohols **15** were converted into the xanthates.[14] Treatment of them with tributyltin hydride in toluene gave the deoxo derivative **24** in 84% yield from **15**. Cleavage of the acetal yielded the ketone **25** (97%). The kinetic enolate of **25** generated by treating with LDA was reacted with ethyl iodoacetate in THF–hexamethylphosphoric triamide (HMPA)[15] to produce **26**, alkylated at the appropriate position, in 63% yield and 26% recovery of **25**. Hydrolysis of **26** and then heating under reflux with TsOH in benzene[16] gave the butenolide **27** in 72% yield. Reduction of **27** with diisobutylaluminium hydride (DIBAH) followed by an acid work-up produced a colorless oil, in 69% yield, whose ^1H NMR was identical with that of natural deoxopinguisone (**3**).

In order to prepare (±)-pinguisone (**2**) from **15**, the hydroxyl group was protected as a benzyl ether (**28**, 92%), and the synthetic route of (±)-deoxopinguisone was traced as shown in Scheme 4. The 1,3-dioxolane was cleaved by hydrochloric acid in acetone to yield **29** in 91% yield. Selective alkylation of **29** by treating with LDA and ethyl iodoacetate gave **30** in 68% yield and 24% recovery of **29**. Hydrolysis of **30** followed by the treatment with TsOH provided the butenolide **31** in 52% yield. Cleavage of the benzyl ether by boron tribromide[17] in dichloromethane at 0 °C gave **32** in 82% yield. DIBAH reduction of **32** follwed by an acid work-up gave the furan **33** in 66% yield. Oxidation of **33** with DMSO–acetic anhydride[18] provided the ketone, as a colorless oil (62%), whose spectral characteristics were identical with those of natural pinguisone ((+)-**2**, lit[4a,6b] mp 63 °C).

Thus, we have demonstrated that the photochemical [1,3] acyl migration of the bicyclo[3.2.2]nonenone system is incorporated into the synthetic route of the [5—6] fused-ring sesquiterpenes.

Experimental

General. Boiling points are uncorrected. Melting points were determined with a Yamato MP-21 capillary melting point apparatus and are uncorrected. UV and IR spectra (in CCl_4, unless otherwise mentioned) were recorded on Hitachi

Model 323 and 215 spectrometers, respectively. ^{1}H NMR spectra (in CCl_4, unless otherwise noted) were obtained on JEOL JNM-PMX60, Varian EM-390 90 MHz, and/or Varian XL-200 NMR specrometers, using tetramethylsilane as an internal standared. ^{13}C NMR spectra (in $CDCl_3$) were recorded on a JEOL FX 90Q NMR spectrometer. The mass spectral studies were conducted using a Hitachi M-52 spectrometer. THF and ether were distilled from benzophenone ketyl under argon, immediately prior to use. 1,2-Dimethoxyethane (DME) was distilled from lithium aluminium hydride under argon immediately prior to use. Dichloromethane was distilled from P_2O_5 and stored on 4A molecular sieves. Benzene and toluene were distilled from P_2O_5 and stored over sodium wire. *S*-Phenyl benzenethiosulfonate,[11] *N*-nitroso-*N*-trimethylsilylmetylurea,[19] and PCC[20] were prepared by using literature procedures. All reactions were monitored by analytical TLC using E. Merck precoated silica gel $60F_{254}$ plates. Column chromatography was carried out with E. Merck silica gel 60 (70—230 mesh ASTM). HPLC was performed on a Warters Associates Model R-401 liquid chromatograph using a 25 cm×8 mm stainless-steel column packed with Lichrosorb SI 100. Analytical VPC was carried out using a Hitachi 663-50 gas chromatograph, outfitted with a 3 m×3 mm stainless-steel column packed with 10% FFAP on 60/80 Uniport B.

1-Methoxy-4,5,*endo*-8-trimethylbicyclo[2.2.2]oct-5-en-2-one (9). To a solution of 9.85 g (62.9 mmol) of 1-methoxy-3,4,5-trimethyl-1,4-cyclohexadiene (**11**)[8] in 10 ml of toluene were added 11.0 g (125.7 mmol) of 2-chloroacrylonitrile and 0.23 g (2.1 mmol) of hydroquinone. The mixture was heated at 90 °C overnight, cooled, and concentrated. Distillation of the residue (bp 118 °C/0.1 Torr (1 Torr=133.322 Pa)) yielded 11.55 g (48.2 mmol, 77%) of a mixture of the isomeric addition products as a pale yellow oil which solidified upon standing.

A solution of 4.52 g (18.8 mmol) of the adducts was added to a mixture of 6.8 g (28.3 mmol) of sodium sulfide, 3.9 g (56.5 mmol) of potassium hydroxide, and 9.4 ml of water. After heated under reflux for 8 h, the reaction mixture was diluted with water, and extracted with three portions of ether. The extracts were combined, washed with water and saturated brine, and dried over $MgSO_4$. Evaporation of the solvent, followed by chromatography of the residue (2.83 g) using 100 g of silica gel (8:1 then 3:1hexane–ethyl acetate) gave 1.84 g (9.47 mmol, 50%) of a mixture of **9** and the *exo*-8-methyl isomer **9a** and 0.24 g (1.22 mmol, 7%) of the alcohols, which were converted quantitatively into **9** and **9a** by Collins oxidation. The ratio of **9** and **9a**, 10 to 1, was determined by VPC (200 °C). Pure **9** and **9a** were obtained by repeated HPLC (10:1 hexane–ethyl acetate). **9**: Colorless oil; IR 1740 (s) cm^{-1}; ^{1}H NMR δ=0.89 (3H, d, J=6.9 Hz), 1.06 (1H, dd, J=12.4 and 4.5 Hz), 1.17 (3H, s), 1.6—2.0 (1H, m), 1.81 (3H, d, J=1.5 Hz), 1.87 (2H, broad s), 2.19 (1H, dd, J=12.2 and 9.8 Hz), 3.40 (3H, s), and 5.82 (1H, broad s); ^{13}C NMR δ=209.8 (s), 144.7 (s), 122.1 (d), 84.3 (s), 52.9 (q), 47.7 (t), 42.1 (s), 38.3 (d), 37.1 (t), 19.5 (q), 19.3 (q), and 19.1 (q); MS (25 eV) m/z (rel intensity) 194 (M$^+$, 1), 166 (8), and 137 (100). Found: C, 74.11; H, 9.52%. Calcd for $C_{12}H_{18}O_2$: C, 74.19, H, 9.34%. **9a**: Colorless oil; IR 1745 (s) cm^{-1}; ^{1}H NMR δ=1.01 (3H, d, J=6.9 Hz), 1.10 (3H, s), 1.35 (1H, dd, J=10.5 and 4.4 Hz), 1.5—1.9 (3H, m), 1.80 (3H, d, J=1.5 Hz), 2.12 (1H, d, J=18.3 Hz), 3.83 (3H, s), and 5.75 (1H, broad s); ^{13}C NMR δ=209.2 (s), 149.0 (s), 122.3 (d), 84.1 (s), 52.9 (q), 41.3 (s), 41.1 (t), 36.9 (t), 35.9 (d), 18.8 (q), 17.5 (q), and 16.0 (q); MS (25 eV) m/z (rel intensity) 194 (M$^+$, 21) and 103 (100).

Ring Enlargement of 9 Using $TMSCHN_2$ and BF_3 Etherate. Preparation of 1-Methoxy-5,endo-6,9-trimethylbicyclo-[3.2.2]non-6-en-2-one (8). In a flask equipped with a Dry Ice condenser were placed 4.59 g (25.67 mmol) of *N*-nitroso-*N*-trimethylsilylmethylurea and 5 ml of pentane. To the mixture was added 2.0 ml of 20% aqueous potassium hydroxide solution at 0 °C. After 1.5 h stirring at 0 °C, the organic layer was diluted with pentane, separated, washed with water, and dried over Na_2SO_4. This solution was concentrated carefully to ca. 2 ml, and diluted with 6.6 ml of dichloromethane. To a solution of 446.6 mg (2.3 mmol) of **9** in 8.9 ml dichloromethane was added 0.41 ml (3.45 mmol) of BF_3 etherate at −78 °C under argon and the mixture was stirred for 5 min. To this reaction mixture was added that $TMSCHN_2$ solution over a period of 30 min. After 1 h stirring, to the solution was added 20 ml of saturated aqueous $NaHCO_3$ solution. The mixture was allowed to warm to room temperature with stirring. After 2 h stirring the organic layer was separated, washed with saturated brine, dried over $MgSO_4$, and concentrated in vacuo. The residual oil was a mixture of **8** and its α-silylated derivatives. This mixture was diluted with 4.5 ml of methanol and treated with 0.3 g of K_2CO_3 and 1.5 ml of water for 2 h at room temperature. After dilution with water, the mixture was extracted with ether. The extracts were combined, washed with water and brine, and dried over $MgSO_4$. Evaporation of the solvent, followed by silica-gel chromatography (20 g; 8:1 hexane–ethyl acetate) of the residue (611.3 mg) gave 378.3 mg (1.82 mmol, 79%) of **8**: Colorless oil; UV (cyclohexane) 302 nm (ε 186); IR 1725 cm^{-1};^{1}H NMR δ=0.93 (3H, d, J=6.5 Hz), 1.06 (3H, s), 1.1—2.1 (4H, m), 1.75 (3H, d, J=1.5 Hz), 2.2—2.8 (3H, m), 3.15 (3H, s), and 5.47 (1H, broad s); ^{13}C NMR δ=205.0 (s), 144.6 (s), 124.3 (d), 82.4 (s), 51.3 (q), 40.7 (t), 40.4 (s), 38.6 (t), 37.9 (t), 35.2 (d), 24.1 (q), 21.7 (q), and 20.0 (q); MS (25 eV) m/z (rel intensiity) 208 (M$^+$, 13) and 147 (100). The 2,4-DNP derivative: Mp 146.5—147 °C. Found: C, 58.74, H, 6.37; N, 14.45%. Calcd for $C_{19}H_{24}N_4O_5$: C, 58.75; H, 6.23; N, 14.42%.

Photochemical Transformation of 8 into 4-Methoxy-*r*-1,*c*-2,*c*-6-trimethylbicyclo[4.3.0]non-4-en-7-one (7). A solution of 203.9 mg (1.15 mmol) of **8** in 100 ml of THF was placed in an immersion well equipped with a Pyrex filter and degassed by sonication. The solution under nitrogen was irradiated using a 100-W Rikou high pressure Hg lamp for 4 h. From the crude photolysate (208.6 mg), 120.0 mg (0.58 mmol, 59%) of **7** was isolated by column chromatography (15 g of SiO_2; 20:1 hexane–ethyl acetate). **7**: Colorless oil; IR 1740 (s) and 1675 (m) cm^{-1}; ^{1}H NMR δ=0.89 (3H, s), 0.98 (3H, s), 1.02 (3H, d, J=6.3 Hz), 1.4—2.3 (7H, m), 3.49 (3H, s), and 4.27 (1H, broad s); MS (25 eV) m/z (rel intensity) 208 (M$^+$, 30) and 137 (100).

***r*-1,*c*-5,*c*-6-Trimethylspiro[bicyclo[4.3.0]nonane-3,2′-[1,3]-dioxolan]-9-one (12).** A mixture of 38.1 mg (0.19 mmol) of **7**, 0.5 ml each of 2-ethyl-2-methyl-1,3-dioxolane and benzene, and 3 mg of TsOH was allowed to stand at room temperature for 2 d. This reaction mixture was diluted with ether, washed successively with saturated aqueous $NaHCO_3$ and NaCl solutions, and dried over $MgSO_4$. Concentration followed by chromatography (1.5 g of SiO_2; 5:1 hexane–ethyl acetate) gave 43.3 mg (99%) of **12** as colorless prisms. **12**: Mp 66.5—67.5 °C; IR 1745 (s) cm^{-1}; ^{1}H NMR δ=0.83 (3H, s), 0.90 (3H, s), 0.93 (3H, d, J=1.5 Hz), 1.1—1.3 (9H, m), and 3.4—4.0 (4H, m); ^{13}C NMR δ=220.6 (s), 107.5 (s), 64.2

(t), 63.7 (t), 54.1 (s), 40.8 (s), 38.9 (t), 37.2 (t), 33.5 (t), 33.3 (d), 28.6 (t), 22.9 (q), 168. (q), and 14.0 (q); MS (25 eV) *m/z* (rel intensity) 238 (M^+, 18) and 113 (100). Found: C, 70.61; H, 9.47%. Calcd for $C_{14}H_{22}O_3$: C, 70.56; H, 9.47%.

***r*-1,*c*-5,*c*-6-Trimethylspiro[bicyclo[4.3.0]non-7-ene-3,2'-[1,3]dioxolan]-9-one (13).** To a solution of 0.11 ml (2.5 mmol) of diisopropylamine in 2 ml of dry THF, prepared under argon, was added 0.47 ml (0.78 mmol) of 1.56 M† hexane solution of *n*-BuLi at 0°C, stirred for 10 min, and cooled to −78°C. To this LDA solution was added a solution of 166.5 mg (0.70 mmol) of **12** in 2 ml of THF via a double-ended needle, and kept at −78°C for 15 min. To the enolate solution was added a solution of 175.0 mg (0.70 mmol) of *S*-phenyl benzenethiosulfonate in 2 ml of THF. After stirring at −78°C for 1 h and then at room temperature for an additional hour, the reaction was quenched by addition of saturated aqueous ammonium chloride, and extracted with three portions of ether. The ethereal extracts were combined, washed with saturated aqueous $NaHCO_3$ and saturated brine, and dried over $MgSO_4$. Evaporation of the solvent, followed by chromatography (5 g of SiO_2; 30:1 benzene–ethyl acetate) of the residue (256.6 mg) gave 199.1 mg (0.57 mmol, 82%) of the α-phenylthio ketone as a colorless oil. This ketone was dissolved in a mixture of 11 ml of methanol and 1.4 ml of water and treated with 134 mg (0.63 mmol) of sodium periodate at room temperature overnight. The reaction mixture was poured into saturated aqueous $NaHCO_3$ solution, and extracted with three portions of dichloromethane. The combined extracts were washed with saturated brine and dried over $MgSO_4$. After removal of the solvent, the residue (249.5 mg) was purified by chromatography (10:1 benzene–ethyl acetate) to give 196.5 g (0.54 mmol, 95%) of a mixture of the sulfoxides. To a solution of the sulfoxides in 6 ml of toluene was added 0.1 g of $CaCO_3$. The mixture was heated at 90°C for 12 h and then under reflux for 6 h. After filtration through an alumina layer, concentration of the filtrate gave 174.1 mg of a colorless oil. Chromatography on silica gel (5 g; 5:1 hexane–ethyl acetate) gave 99 mg (0.42 mmol, 78%) of **13**: Colorless needles; mp 58—60°C; IR 1720 (s) cm^{-1}; ^1H NMR δ=0.95 (3H, s), 0.97 (3H, d, *J*=6.0 Hz), 1.00 (3H, s), 1.37 (1H, d, *J*=14.1 Hz), 1.3—1.8 (3H, m), 2.00 (1H, dd, *J*=14.1 and 1.0 Hz), 3.8 (4H, m), 5.89 (1H, d, *J*=5.7 Hz), and 7.35 (1H, d, *J*=5.7 Hz); MS (25 eV) *m/z* (rel intensity) 236 (M^+, 16) and 113 (100). Found: C, 71.45; H, 8.45%. Calcd for $C_{14}H_{20}O_3$: C, 71.16; H, 8.53%.

***r*-1,*c*-5,*c*-6,9-Tetramethylspiro[bicyclo[4.3.0]non-8-ene-3,2'-[1,3]dioxolan]-9-one (14).** To a solution of 99 mg (0.42 mmol) of **13** in 10 ml of dry ether was added 0.49 ml (0.63 mmol) of 1.3 M methyllithium solution in ether at 0°C under argon and stirred for 30 min. To the reaction mixture was added saturated aqueous ammonium chloride solution and extracted with three portions of ether. The combined extracts were washed with water and saturated brine, and dried over $MgSO_4$. After removal of the solvent, the remaining oil (97.2 mg) was chromatographed on silica gel (3 g; 5:1 then 2:1 hexane–ethyl acetate) to yield 94.8 mg (0.38 mmol, 90%) of the allylic alcohols. To a solution of these alcohols in 3 ml of dichloromethane were added 62 mg of sodium acetate and 164 mg (0.76 mmol) of PCC at room temperature, and the mixture was stirred for 2.5 h. After addition of 4 ml of ether, the solution was decanted from the black solid. The residue was washed in turn with several portions of ether. The combined ethereal extracts were passed through a silica-gel layer to give 92.8 mg of a colorless oil. Chromatography (3 g of silica gel; 5:1 hexane–ethyl acetate) of the oil gave 83.5 mg (0.33 mmol, 87%) of **14**: Colorless oil; IR 1715 (s) and 1625 (m) cm^{-1}; ^1H NMR δ=0.86 (3H, d, *J*=7.1 Hz), 0.89 (3H, s), 0.99 (3H, s), 1.2—1.6 (3H, m), 1.7—2.1 (2H, m), 2.01 (3H, d, *J*=1.5 Hz), 3.83 (4H, m), and 5.51 (1H, brosd s).

***r*-1,*c*-5,*c*-6,*c*-9- and *r*-1,*c*-5,*c*-6,*t*-9-Tetramethylspiro[bicyclo[4.3.0]nonane-3,2'-[1,3]dioxolan]-7-ols (15 and 16, Respectively).** To a flask containing 60.1 mg (0.24 mmol) of **14** were added ca. 30 ml of ammonia, distilled from sodium, 0.5 ml (5.3 mmol) of *t*-butyl alcohol, 5 ml of THF, and 16 mg (2.4 mmol) of litium at −78°C under argon. The mixture was allowed to warm to room temperature very slowly, and treated with water. This mixture was extracted with ether, and the extracts were combined, washed with water and saturated brine, and dried over $MgSO_4$. After evaporation of the solvent, silica-gel chromatography (8 g; 5:1 hexane–ethyl acetate) of the residue (83 mg) gave 20.3 mg (0.08 mmol, 33%) of the less polar alcohols (**15**) and 35.9 mg (0.14 mmol, 58%) of the more polar alcohols (**16**).

***r*-1,*c*-5,*c*-6,*c*-9-Tetramethylspiro[bicyclo[4.3.0]nonane-3,2'-[1,3]dioxolan]-7-one (17).** To a solution of 5.2 mg (0.02 mmol) of **15** in 0.5 ml of dichloromethane were added 40 mg (1.32 mmol) of PCC and 10 mg of sodium acetate. After 11 h stirring, to the reaction mixture was added 3 ml of ether and the ethereal solution was filtered through a silica-gel layer. Concentration of the filtrate gave 8.3 mg of an oil. Chromatography on silica gel (1 g; 10:1 hexane–ethyl acetate) gave 5.1 mg (0.02 mmol, 100%) of **17**: Mp 58.5—59°C; IR 1735 (s) cm^{-1}; ^1H NMR δ=0.60 (3H, s), 0.73 (3H, d, *J*=6.9 Hz), 0.76 (3H, s), 0.88 (3H, d, *J*=6.8 Hz), 1.31 (1H, d, *J*=14.9 Hz), 1.35 (1H, dd, *J*=13.8 and 13.0 Hz), 1.49 (1H, ddd, *J*=13.8, 3.8, and 2.3 Hz), 1.73 (1H, dd, *J*=19.3 and 11.0 Hz), 1.75 (1H, dd, *J*=14.9 and 2.3 Hz), 2.07 (1H, ddd, *J*=13.0, 6.9, and 3.8 Hz), 2.47 (1H, dd, *J*=19.3 and 9.0 Hz), 3.04 (1H, ddq, *J*=11.0, 9.0, and 6.8 Hz), 3.8—4.6 (4H, m); ^{13}C NMR δ=219.8 (s), 108.4 (s), 64.7 (t), 63.4 (t), 55.9 (s), 45.7 (s), 41.8 (t), 38.3 (t), 38.1 (t), 30.3 (d), 29.2 (d), 19.2 (q), 15.7 (q), 13.8 (q), and 8.2 (q); MS (25 eV) *m/z* (rel intensity) 252 (M^+, 2) and 113 (100). Found: C, 71.59; H, 9.70%. Calcd for $C_{15}H_{24}O_3$: C, 71.39; H, 9.59%.

***r*-1,*c*-5,*c*-6,*t*-9-Tetramethylspiro[bicyclo[4.3.0]nonane-3,2'-[1,3]dioxolan]-7-one (18).** Alcohols **16** (7.8 mg, 0.03 mmol) was treated with PCC (40 mg) and sodium acetate (10 mg) dry CH_2Cl_2 (0.5 ml) at room temperature for 11 h. A workup similar to that employed for the synthesis of **17** gave a colorless oil (8.1 mg). Chromatography on silica gel (1.4 g; 10:1 hexane–ethyl acetate) gave 7.8 mg (0.03 mmol, 100%) of pure **18**: Colorless needles; mp 63—64°C; IR 1740 (s) cm^{-1}; ^1H NMR δ=0.89 (3H, s), 0.97 (3H, d, *J*=6.6 Hz), 1.10 (3H, d, *J*=7.5 Hz), 1.17 (3H, s), 1.1—1.6 (4H, m), 1.6—2.5 (4H, m), and 3.6—4.0 (4H, m); ^{13}C NMR δ=220.6 (s), 109.3 (s), 64.6 (t), 62.9 (t), 55.2 (s), 44.3 (s), 41.1 (t), 38.1 (t), 37.6 (t), 36.9 (d), 32.2 (d), 20.2 (q), 17.4 (q), 16.1 (q), and 12.5 (q); MS (25 eV) *m/z* (rel intensity) 252 (M^+, 4) and 113 (100).

Reduction of 12. Preparation of *t*-1,*t*-5,*t*-6-Trimethylspiro[bicyclo[4.3.0]nonane-3,2'-[1,3]dioxolan]-*r*-8-ol (19). To a suspension of 92 mg (2.42 mmol) of $LiAlH_4$ in 4 ml of dry ether was added a solution of 577.2 mg (2.42 mmol) of **12** in 3 ml of ether at 0°C. After 5 min stirring, to the reaction mixture were added successively 0.09 ml of water, 0.09 ml of 15% aq NaOH, and 0.27 ml of water. After stirring

† 1 M=1 mol dm^{-3}.

until a granular precipitate was formed, $MgSO_4$ was added to the mixture and filtered. Concentration of the filtrate gave 578.5 mg of a colorless oil. Chromatography on silica gel (20 g; 3:1 hexane–ethyl acetate) gave 475.1 mg (1.98 mmol, 82%) of **19** and 101.9 mg (0.42 mmol, 17%) of the C-9 isomer (**20**). **19**: Colorless oil; IR 3480 (m), 2980 (s), and 2890 (m) cm^{-1}; ^1H NMR δ=0.81 (3H, s), 0.84 (3H, s), 0.88 (3H, d, J=6.8 Hz), 1.0—2.3 (9H, m), 3.62 (1H, dd, J=6.0 and 3.5 Hz), 3.74 (1H, broad s), and 3.8—4.0 (4H, m); ^{13}C NMR δ=108.9 (s), 83.0 (d), 64.4 (t), 64.0 (t), 49.5 (s), 44.6 (s), 40.1 (t), 38.8 (t), 33.7 (t), 33.7 (d), 32.2 (t), 27.4 (q), 17.0 (q), and 15.4 (q); MS (25 eV) m/z (rel intensity) 240 (M^+, 19) and 113 (100). Found: C, 69.96; H, 10.24%. Calcd for $C_{14}H_{24}O_3$: C, 69.96; H, 10.07%. **20**: IR 3640 (w) and 3500 (w) cm^{-1}; ^1H NMR δ=0.6—2.0 (10H, m), 0.73 (3H, s), 0.79 (3H, s), 0.82 (3H, d, J=6.3 Hz), 3.7—4.0 (4H, m), and 4.6 (1H, m), ^{13}C NMR δ= 108.8 (s), 74.5 (d), 64.6 (t), 63.3 (t), 47.7 (s), 44.3 (s), 38.8 (t), 33.4 (d), 31.7 (t), 28.8 (t), 17.8 (q), and 14.2 (q); MS (25 eV) m/z (rel intensity) 240 (M^+, 13) and 113 (100).

r-1,c-5,c-6-Trimethylspiro[bicyclo[4.3.0]non-8-ene-3,2′[1,3]-dioxolane] (21). To a solution of 475.0 mg (1.98 mmol) of **19** in 10 ml of pyridine was added 0.18 ml (2.37 mmol) of methanesulfonyl chloride at 0 °C, and the mixture was allowed to warm to room temperature. After stirring overnight, the mixture was diluted with saturated aqueous NH_4Cl solution and extracted with ether. The ethereal solution was washed successively with water and saturated brine, dried over $MgSO_4$, and then concentrated to give 632.6 mg of the crude mesylate as a pale yellow oil.

To a solution of this oil in 10 ml DMSO was added 490 mg (4.37 mmol) of potassium t-butoxide under a nitrogen atmosphere, and the mixture was stirred overnight at room temperature. After addition of 20 ml of saturated aqueous NH_4Cl, the mixture was extracted with three portions of ether. The ethereal extracts were combined, washed with water and saturated brine, and dried over $MgSO_4$. Evaporation of the solvent gave 436.8 mg of a yellow oil. Silica-gel column chromatography (10 g; 15:1 hexane–ethyl acetate) of the oil gave 418.8 mg (1.88 mmol, 95%) of **21**: Colorless oil; IR 3070 (w) and 1090 (s) cm^{-1}; ^1H NMR δ=0.82 (3H, s), 0.84 (3H, d, J=6.0 Hz), 0.88 (3H, s), 1.2—2.0 (5H, m), 2.12 (2H, m), 3.8 (4H, m), 5.30 (1H, dt, J=6.0 and 2.2 Hz), and 5.52 (1H, dm, J=6.0 Hz); MS (25 eV) m/z (rel intensity) 222 (M^+, 95) and 113 (100). Found: C, 75.74; H, 10.16%. Calcd for $C_{14}H_{22}O_2$: C, 75.63; H, 9.97%.

Allylic Oxidation of 21. Preparation of r-1,c-5,c-6-Trimethylspiro[bicyclo[4.3.0]non-8-ene-3,2′-[1,3]dioxolan]-7-one (22). Chromium trioxide (3.76 g, 37.6 mmol) was placed in a reaction flask, dried at 40 °C in vacuo (0.2 Torr) overnight, and dissolved in 32 ml of dry CH_2Cl_2. To this solution was added 3.64 g (37.6 mmol) of 3,5-dimethylpyrazole bellow −20 °C (ice–methanol bath) and stirred for 15 min. A solution of **21** (418.8 mg, 1.88 mmol) in dichloromethane (1 ml) was added to the solution of the complex and stirred for 4 h at −20 °C. Into the reaction flask was poured 16 ml of 5 M aqueous sodium hydroxide solution and the mixture was stirred for 1 h at 0 °C. To the mixture was added 100 ml of ether, and the organic layer was separeted. The ethereal solution was washed with three portions of water, two portions of 0.5 M hydrochloric acid, and a portion of saturated brine, and then dried over $MgSO_4$. Removal of the solvent under reduced pressure gave 1.38 g of white solids. Silica-gel chromatography (30 g; 5:1 hexane–ethyl acetate) gave 305.5 mg (1.29 mmol, 69%) of a 9 to 2 mixture of **22** and **13**. Repeated HPLC (10:1 hexane–ethyl acetate) gave pure **22** as colorless needles. **22**: Mp 74.0—75.0 °C; IR 1715 (s) cm^{-1}; ^1H NMR δ=0.85 (3H, d, J=6.8 Hz), 0.90 (3H, s), 0.97 (3H, s), 1.2—1.5 (2H, m), 1.6—1.8 (2H, m), 1.92 (1H, dq, J=8.3 and 6.8 Hz), 3.83 (4H, m), 5.74 (1H, d, J=5.9 Hz), and 7.22 (1H, d, J=5.9 Hz); MS (25 eV) m/z (rel intensity) 236 (M^+, 51) and 221 (100). Found: C, 71.36; H, 8.62%. Calcd for $C_{14}H_{20}O_3$: C, 71.16; H, 8.53%.

Reaction of 22 and Lithium Dimethylcuprate(I). An Alternative Route to 17. To a suspension of 1.47 g (7.69 mmol) of copper(I) iodide in 25 ml of ether was added dropwise 10.5 ml (1.42 M, 14.88 mmol) of ethereal methyllithium at 0 °C under argon, and the mixture was stirred for 5 min. To this clear solution was added a solution of the 9 to 2 mixture of **22** and **13** (294.1 mg, 1.24 mmol) in ether (2 ml). After stirring 2 h at 0 °C, this reaction mixture was poured into 60 ml of saturated aqueous NH_4Cl solution and extracted with ether. The extracts were combined, washed successively with water and saturated brine, and dried over $MgSO_4$. Evaporation of the solvent gave 309.9 mg of a colorless oil. Chromatography (10 g of silica gel; 10:1 hexane–ethyl acetate) of the oil gave 238.6 mg (0.95 mmol, 76%) of a mixture of **17** and **18**, in a ratio of 94 to 6, and 54.3 mg (0.22 mmol, 17%) of **23**.

Lithium Aluminium Hydride Reduction of a Mixture of 17 and 18. An Alternative Route to 15. To a suspension of 50 mg (1.32 mmol) of $LiAlH_4$ in 5 ml of dry ether was added a solution of 238.6 mg (0.95 mmol) of the mixture of **17** and **18** derived from **22**, in 5 ml of ether at 0 °C. After 5 min stirring, to the reaction mixture were added successively 0.05 ml of water, 0.05 ml of 15% aq NaOH, and 0.15 ml of water. After stirring for 30 min, to the mixture was added $MgSO_4$ and filtered through a Celite layer. Concentration of the filtrate gave 239.3 mg of colorless needles. Chromatography (14 g of silica gel; 5:1 hexane ethyl acetate) of the products gave 225.9 mg (0.89 mmol, 94%) of **15**, as a ca. 1:1 mixture of the C-7 epimers, and 14.4 mg (0.06 mmol, 6%) of **16**.

r-1,c-5,c-6,c-9-Tetramethylspiro[bicyclo[4.3.0]nonane-3,2′-[1,3]dioxolane] (24). Sodium hydride (50% dispersion in mineral oil, 64 mg, 1.34 mmol) was washed with three portions of THF under argon, and suspended in 2 ml of THF. To this mixture was added a solution of 225.9 mg (0.89 mmol) of **15** and 20 mg of imidazole in 3 ml of THF, and heated under reflux for 30 min. After addition of 0.27 ml (4.49 mmol) of carbon disulfide, the mixture was heated under reflux for 2 h and then cooled to room temperature. To the resulting yellow solution was added 0.27 ml (4.34 mmol) of iodomethane, and the mixture was stirred for 5 min. Saturated aqueous NH_4Cl solution was added, and extracted with three portions of ether. The extracts were combined, washed with water and saturated brine, and then dried over $MgSO_4$. Removal of the solvent gave 350 mg of a yellow oil. Chromatography (10 g of silica gel; 10:1 hexane–ethyl acetate) of this oil gave 300.4 mg (0.87 mmol, 98 %) of the xanthates as a colorless oil.

To a boiling solution of 0.25 ml (0.92 mmol) of tributyltin hydride in 5 ml of toluene was added a solution of 244.2 mg (0.71 mmol) of the xanthates in 3 ml of toluene and the reaction was continued for 6 h. The reaction mixture was concentrated in vacuo and then the residue was chromatographed on 10 g of silica gel (10:1 then 5:1 hexane–

ethyl acetate) to give 145.4 mg (0.61 mmol, 86%) of **24**: Colorless oil; IR 1105 (s) cm^{-1}; ^1H NMR δ=0.62 (3H, s), 0.78 (3H, d, J=7.1 Hz), 0.79 (3H, s), 0.84 (3H, d, J=6.5 Hz), 1.0—2.0 (9H, m), 2.65 (1H, m), and 3.6—3.9 (4H, m); MS (25 eV) m/z (rel intensity) 238 (M^+, 2) and 113 (100). Found: C, 75.76; H, 11.22%. Calcd for $C_{15}H_{26}O_2$: C, 75.58; H, 10.99%.

***r*-1,*c*-5,*c*-6,*c*-9-Tetramethylbicyclo[4.3.0]nonan-3-one (25).** To a solution of 127.6 mg (0.54 mmol) of **24** in 2 ml of acetone was added 0.5 ml (4.34 mmol) of 1 M hydrochloric acid at room temperature, and the mixture was allowed to stand for 4 h. To the solution was added 30 ml of ether, the aqueous layer was removed. The organic layer was washed successively with saturated aqueous $NaHCO_3$ and NaCl solutions and then dried over $MgSO_4$. The solvent was removed carefully, and the residue was chromatographed (10 g of silica gel; 10:1 hexane–ethyl aetate) to yield 100.4 mg (0.52 mmol, 97%) of **25** as a volatile oil. **25**: IR 1710 (s) cm^{-1}; ^1H NMR δ=0.74 (3H, s), 0.89 (3H, d, J=6.2 Hz), 0.93 (3H, d, J=6.0 Hz), 0.96 (3H, s), and 1.0—2.0 (10H, m); MS (25 eV) m/z (rel intensity) 194 (M^+, 2) and 109 (100). The 2,4-DNP derivative of **25**: Mp 159.0—160.0° C. Found: C, 60.89; H, 7.21; N, 14.91%. Calcd for $C_{19}H_{26}N_4O_4$: C, 60.95; H, 7.00; N, 14.96%.

Ethyl *r*-1,*c*-2,*c*-6,*c*-7-Tetramethyl-4-oxobicyclo[4.3.0]non-3-yl Acetate (26). LDA was generated from 0.18 ml (1.30 mmol) of diisopropylamine and 0.18 ml (1.04 mmol) of 1.5 M butyllithium in 4 ml of THF at −78° C. To this solution were added 0.5 ml of hexamethylphosphoric triamide (HMPA) and a solution of 100.4 mg (0.52 mmol) of **25** in 2 ml of THF at 0° C, and the mixture was stirred for 30 min at 0° C. To the enolate solution was added 0.12 ml (1.04 mmol) of ethyl iodoacetate, and the mixture was allowed to stand at 0° C for 4 h. Saturated aqueous NH_4Cl solution was added, and the mixture was extracted with three potions of ether. The extracts were combined washed with two portions of water and a portion of saturated brine, and then dried over $MgSO_4$. Concentration of the solution gave 183.4 mg of a yellow oil. Silica-gel chromatography (12 g; 10:1 then 5:1 hexane–ethyl acetate) gave 92.3 mg (0.33 mmol, 63%) of **26** and 13.4 mg (0.07 mmol, 13%) of **25**. **26**: Colorless oil; IR 1735 (s), and 1715 (s) cm^{-1}; ^1H NMR δ=0.7—3.0 (11H, m), 0.77 (3H, s), 0.88 (3H, d, J=6.5 Hz), 1.05 (3H, s), 1.25 (3H, t, J=6.5 Hz), and 4.04 (2H, q, J=6.5 Hz).

Preparation of *r*-4,*c*-4a,*c*-7,*c*-7a-Tetramethyl-4,4a,5,6,7,7a,-8,8a-octahydroindeno[5,6-*b*]furan-2-one (27). Into a flask containing 22.9 mg (0.082 mmol) of **26** were added 3 ml of methanol, 0.7 ml of water, and 60 mg of K_2CO_3. This mixture was stirred at room temperature overnight, and then acidifed with 6 M HCl. The aqueous solution was extracted with three portions of ether. The ethereal extracts were combined, washed with saturated brine, dried over $MgSO_4$, and then concentrated to give 18.3 mg of a colorless oil. A solution of the oil and a small amount of TsOH in benzene (20 ml) was placed in a flask equipped with a Soxhlet extracter containing 3A Molecular sieves and heated under reflux for 2 d. The benzene solution was washed with saturated aqueous $NaHCO_3$ and NaCl solutions, and dried over $MgSO_4$. Evaporation of the solvent gave 21.0 mg of a yellow oil. Column chromatography (3 g of silica gel; 10:1 then 5:1 hexane–ethyl acetate) gave 13.8 mg (0.059 mmol, 72%) of **27**: Colorless needles; mp 89—90°C; IR 1800 (m) and 1765 (s) cm^{-1}; ^1H NMR ($CDCl_3$) δ=0.72 (3H, s), 0.73 (3H, s), 0.97 (3H, d, J=7 Hz, 7-Me), 1.16 (3H, d, J=6.7 Hz, 4-Me), 1.18 (1H, dd, J=13.7 and 10.4 Hz), 1.2—2.05 (4H, m), 2.28 (2H, m), 2.39 (1H, dd, J=13.7 and 6.5 Hz), 4.93 (1H, dddd, J=11.2, 6.7, 1.3 and 1 Hz), and 5.69 (1H, dd, J=2.0 and 1.3 Hz); MS (25 eV) m/z (rel intensity) 234 (M^+, 42) and 109 (100). Found: C, 76.58; H, 9.36%. Calcd for $C_{15}H_{22}O_2$: C, 76.88; H, 9.46%.

(±)-Deoxopinguisone (3). A 1.5 M solution of DIBAH in hexane (0.06 ml) was added to a solution of 13.8 mg (0.059 mmol) of the butenolide **27** in 2 ml of THF at −20°C under an argon atmosphere, and the mixture was stirred for 5 min. To the solution was added 1 M sulfuric acid and the mixture was stirred at 0°C for 30 min. The reaction mixture was diluted with water and extracted with ether. The ethereal extracts were washed with saturated aqueous $NaHCO_3$ and NaCl solutions, and dried over $MgSO_4$. Evaporation of the solvent gave 11.8 mg of a colorless oil. Column chromatography (2 g of silica gel; hexane) of the oil gave 8.9 mg (0.041 mmol, 69%) of (±)-**3**: Colorless oil; IR 2960 (s), 2885 (s), 1645 (w), 1510 (w), 1475 (m), 1460 (m), 1388 (sh), 1385 (m), 1165 (w), 1142 (m), 1045 (m), 903 (m), and 725 (s); ^1H NMR ($CDCl_3$) δ=0.73 (3H, s), 0.82 (3H, s), 0.85 (3H, d, J=6.5 Hz), 1.12 (3H, d, J=7.2), 1.3—2.7 (8H, s), 6.16 (1H, d, J=1.8 Hz), and 7.20 (1H, dd, J=1.8 and 1.0 Hz); ^1H NMR (CCl_4) δ=0.74 (3H, s), 0.83 (3H, s), 0.89 (3H, d, J=6.5 Hz), 1.12 (3H, d, J=7.2 Hz), 1.0—2.7 (8H, m), 6.02 (1H, d, J=1.8 Hz), and 7.06 (1H, dd, J=1.8 and 1.0 Hz). MS (25 eV) m/z (rel intensity) 218 (M^+, 11), 161 (7), 119 (17), and 118 (100).

7-Bezyloxy-*r*-1,c-5,*c*-6,*c*-9-tetramethylbicyclo[4.3.0]nonan-3-ones (29). Sodium hydride (50% dispersion in mineral oil, 50 mg, 1.08 mmol) was washed with dry DME under argon and then suspended in 2 ml of DME. To this suspension was added a solution of 22.9 mg (0.09 mmol) of **15**, 166.6 mg (0.45 mmol) of tetrabutylammonium iodide and 0.05 ml (0.45 mmol) of α-bromotoluene in 3 ml of DME and the mixture was heated under reflux overnight. To this solution was added saturated aqueous NH_4Cl solution, and the mixture was extraced with three portions of ether. Combined extracts were washed with water and saturated brine, and then dried over $MgSO_4$. Concentration of the solution followed by chromatography (3 g of silica gel; 20:1 hexane–ethyl acetate) of the residue (55 mg) gave 28.6 mg of the isomeric mixture of the benzyl ethers (**28**) as a colorless oil.

A mixture of 28.6 mg (0.083 mmol) of **28**, 1 ml of acetone, and 0.3 ml of 1 M HCl was allowed to stand at room temperature for 2 h. The mixture was diluted with 20 ml of ether, washed with saturated $NaHCO_3$ and NaCl solutions, and then dried over $MgSO_4$. Concentration of the solution gave 25.8 mg of a colorless oil. Chromatography of (3 g of silica gel, 20:1 then 10:1 hexane–ethyl acetate) the oil gave 22.7 mg (0.076 mmol, 91%) of **29** as the 1:1 mixture of the C-7 epimers. Each of the stereoisomers was separated by repeated HPLC (20:1 hexane–ethyl acetate). **29a**: Colorless oil: IR 1720 (s) cm^{-1}; ^1H NMR δ=0.72 (3H, s), 0.88 (3H, d, J=6.8 Hz), 1.01 (3H, s), 1.04 (3H, d, J=6.8 Hz), 1.2—2.8 (8H, m), 3.70 (1H, dd, J=6.8 and 4.5 Hz), 4.38 (1H, d, J=12.0 Hz), 4.42 (1H, d, J=12.0 Hz), and 7.18 (5H, broad s); MS (25 eV) m/z (rel intensity) 209 ($M^+-C_7H_7$, 28) and 161 (100). **29b**: Colorless oil: IR 1725 (m) cm^{-1}; ^1H NMR δ=0.88 (3H, d, J=6.0 Hz), 0.90 (3H, s), 0.91 (3H, d, J=6.0 Hz), 1.06 (3H, s), 1.2—2.5 (8H, m), 3.49 (1H, dd, J=7.7 and 3.5 Hz), 4.40 (1H, d, J=12.0 Hz), 4.42 (1H, d, J=12.0 Hz), and 7.21 (5H, broad s); MS (25 eV) m/z (rel intensity) 300 (M^+, 2), 209 ($M^+-C_7H_7$, 28) and 161 (100).

(±)-Pinguisone (2). In order to prepare 5-benzyloxy deriv-

atives of **27** (**31**), we adopted a similar procedure to that used for the synthesis of **27** from **25**. A reaction of the enolates derived from 80.2 mg (27 mmol) of **29** with ethyl iodoacetate gave 69.8 mg (0.18 mmol, 68%) of keto esters **30** as a colorless oil and 8.8 mg (11%) of the recovery. Hydrolysis of **30** (69.8 mg) followed by acid-catalyzed dehydration gave 32.0 mg (0.094 mmol, 52%) of a mixture of the butenolides (**31**). **31a**: Colorless oil; IR 1805 (s) and 1770 (s) cm^{-1}. **31b**: Colorless oil; IR 1798 (s) and 1760 (s) cm^{-1}; ^1H NMR δ=0.80 (3H, s), 0.89 (3H, s), 1.03 (3H, d, J=6.5 Hz), 1.08 (3H, d, J=6.8 Hz), 1.0—2.6 (6H, m), 3.53 (1H, dd, J=7.5 and 3.0 Hz), 4.26 (1H, d, J=12.0 Hz), 4.54 (1H, d, J=12.0 Hz), 4.68 (1H, broad dd, J=11.5 and 8.0 Hz), 5.52 (1H, dd, J=1.8 and 1 Hz), and 7.19 (5H, s).

To a solution of 12.9 mg (0.038 mmol) of **31** in 0.5 ml of CH_2Cl_2 was added 0.64 ml of 0.22 M BBr_3 solution in CH_2Cl_2 at 0°C. After 5 min stirring at 0°C, to the reaction mixture were added 0.5 ml of saturated aqueous $NaHCO_3$ solution and 20 ml of ether. The organic layer was separated, washed with saturated brine, and then dried over $MgSO_4$. Concentration of the solution gave 9.6 mg of a yellow oil. Chromatography (1.5 g of silica gel; 5:1 then 1:1 hexane–ethyl acetate) of the oil gave 7.9 mg (0.032 mmol, 83%) of a mixture of hydroxy lactones **32**. **32a**: Colorless oil: IR 3630 (w), 3450 (broad w), 1798 (m), 1760 (s), and 1750 (sh) cm^{-1}; ^1H NMR δ=0.75 (3H, s), 0.86 (3H, s), 0.96 (3H, d, J=7.0 Hz), 1.40 (3H, d, J=6.5 Hz), 4.16 (1H, dd, J=9.0 and 6.5 Hz), 4.83 (1H, broad dd, J=11.0 and 6.5 Hz), and 5.57 (1H, dd, J=1.5 and 1.5 Hz).

In a procedure similar to that employed for the synthesis of (±)-deoxopinguisone, **32** (7.9 mg, 0.032 mmol) was transformed into **33** (4.9 mg, 0.021 mmol, 66%) which was purified by silica-gel chromatography (1.5 g; 5:1 hexane–ethyl acetate). A mixture of 4.9 mg of **33**, 0.5 ml of DMSO, and 0.5 ml of acetic anhydride, was stirred overnight at room temperature. This reaction mixture was diluted with 20 ml of ether, washed with two portions of saturated aqueous $NaHCO_3$ and with a portion of saturated brine, and then dried over $MgSO_4$. Concentration of the solution followed by purification using a silica-gel column (2 g; 20:1 hexane–ethyl acetate) gave 3.0 mg (0.013 mmol, 62%) of a colorless oil (**3**) whose spectral characteristics are identical with those of natural pinguisone. (±)-**3**: IR 2980 (m), 1745 (s), 1460 (m), 1390 (m), 1152 (w), 1138 (w), 1075 (w), 1050 (w), 908 (w), and 832 (s) cm^{-1}; ^1H NMR ($CDCl_3$) δ=0.82 (3H, s), 0.88 (3H, s), 1.06 (3H, d, J=6.8 Hz, 6-Me), 1.10 (3H, J=7.0 Hz, 3-Me), 1.90 (1H, dd, J=19.2 and 11.0 Hz, 5-H), 2.33 (1H, ddd, J= 18.2, 3.2, and 1.0 Hz, 7-H), 2.39 (1H, ddq, J=10.0, 8.0, and 6.8 Hz, 6-H), 2.71 (1H, dd, J=19.2 and 8.6 Hz, 5-H), 2.78 (1H, dd, J=18.2 and 2.0 Hz, 7-H), 2.80 (1H, broad, 3-H), 6.27 (1H, d, J=2.0 Hz, 2-H), and 7.31 (1H, J=2.0 and 0.8 Hz, 1-H).

We are grateful to Professor Yoshinori Asakawa of Tokushima Bunri University for kindly providing a copy of the ^1H NMR spectrum of natural deoxopinguisone.

References

1) A portion of this work has been published as a preliminary communication: T. Uyehara, Y. Kabasawa, T. Kato, and T. Furuta, *Tetrahedron Lett.*, **26**, 2343 (1985). Part III in this series is Ref. 2.

2) T. Uyehara, Y. Kabasawa, T. Furuta, and T. Kato, *Bull. Chem. Soc. Jpn.*, **59**, 539 (1986).

3) V. Herout. "Aspects of Terpenoid Chemisty and Biology," ed by T. W. Goodwin, Academic Press, London and New York (1971), p. 68.

4) a) V. Benesova, Z. Samek, V. Herout, and F. Sorm, *Collect. Czech. Chem. Commun.*, **34**, 582 (1969); b) V. Benesova, V. Herout, and F. Sorm, *ibid.*, **34**, 1810 (1969); Y. Asakawa, T. Takemoto, M. Toyota, and T. Aratani, *Tetrahedron Lett.*, **1977**, 1407.

5) a) S. M. Krutov, Z. Samek, V. Benesova, and Herout, *Phytochemistry*, **12**, 1405 (1973); b) Y. Asakawa, M. Toyota, M. Kano, and T. Takemoto, *ibid.*, **19**, 2651 (1980) and the references cited therein.

6) a) S. Bernasconi, M. Ferrari, P. Gariboldi, G. Jommi, M. Sisti, and R. Destro, *J. Chem. Soc., Perkin Trans. 1*, **1981**, 1994; b) S. Bernasconi, P. Gariboldi, G. Jommi, S. Montanari, and M. Sisti, *ibid.*, **1981**, 2394.

7) T. Uyehara, J. Yamada, T. Kato, and F. Bohlmann, *Bull. Chem. Soc. Jpn.*, **58**, 861 (1985); T. Uyehara, J. Yamada, K. Ogata, and T. Kato, *ibid.*, **58**, 211 (1985) and the references cited therein.

8) K. P. Dastur, *J. Am. Chem. Soc.*, **96**, 2605 (1975).

9) S. A. Monti, S. C. Chen, Y. L. Yang, S. S. Yuan, and O. P. Bourgeois, *J. Org. Chem.*, **43**, 4062 (1978); D. A. Evans, W. L. Scott, and L. K. Truesdale, *Tetrahedron Lett.*, **1972**, 121.

10) N. Hashimoto, T. Aoyama, and T. Shioiri, *Chem. Pharm. Bull.*, **30**, 119 (1982).

11) B. M. Trost and G. S. Massiot, *J. Am. Chem. Soc.*, **99**, 4405 (1977).

12) W. G. Dauben and Z. Goldschmidt, *J. Am. Chem. Soc.*, **102**, 7926 (1980).

13) W. G. Solmond, M. A. Barta, and J. L. Havens, *J. Org. Chem.*, **43**, 2057 (1978).

14) D. H. R. Barton and S. W. McCombie, *J. Chem. Soc., Perkin Trans., 1*, **1975**, 1574.

15) For example, see: E. Piers, M. B. Geraghty, and R. D. Smille, *Chem. Commun.*, **1971**, 614.

16) S. Czenecki, C. Georgoulis, and C. Provelenghiou, *Tetrahedron Lett.*, **1976**, 3535.

17) J. P. Kutney, N. Abdurahman, P. Le Quesne, E. Piers, and I. Vlattas, *J. Am. Chem. Soc.*, **88**, 3656 (1966).

18) J. D. Albright and L. Doldman, *J. Am. Chem. Soc.*, **87**, 4214 (1965).

19) D. Seyferth, H. Menzel, A. W. Dow, and T. C. Flood, *J. Organomet. Chem.*, **44**, 279 (1972).

20) E. J. Corey and J. W. Suggs, *Tetrahedron Lett.*, **1975**, 2647.

Reactions of 2,4,6-Tri-*t*-butylphenyllithium with *O*-Alkyl Selenoformates: Intermediate Formation of 2,4,6-Tri-*t*-butylselenobenzaldehyde

Akihiko Ishii, Renji Okazaki,* and Naoki Inamoto
Department of Chemistry, The University of Tokyo, Hongo, Bunkyo-ku, Tokyo 113
(Received March 19, 1986)

2,4,6-Tri-*t*-butylphenyllithium reacts with *O*-alkyl selenoformates (**1**) at three different sites (i. e., the selenoformyl carbon, the selenoformyl hydrogen, and the selenium) to give 1,3,5-tri-*t*-butylbenzene, 2,4,6-tri-*t*-butylbenzaldehyde, 6,8-di-*t*-butyl-3,4-dihydro-4,4-dimethyl-1*H*-2-benzoselenin(**11**), bis(2,4,6-tri-*t*-butylphenylmethyl) di(and tri) selenides, bis(2,4,6-tri-*t*-butylphenyl) diselenide, and dibutyl diselenide depending on the reaction conditions and the alkyl group in **1**. The formation of **11** is explained in terms of the intermediacy of 2,4,6-tri-*t*-butylselenobenzaldehyde, which is trapped by condensation reaction with butylamine leading to *N*-(2,4,6-tri-*t*-butylbenzylidene)butylamine. Mechanism for the formation of these products is also discussed.

Recently much attention has been paid to the chemistry of the compounds having a multiple bond containing the third or fourth period elements. Among them are the selenocarbonyl compounds. Although sterically crowded selenoketones have been recently synthesized,[1] only a few have been reported for the selenoformyl compound. For example, selenoformaldehyde was generated by flash pyrolysis and characterized by photoelectron spectroscopy,[2] absorption,[3] or phosphorescence spectrum.[4] Selenoacetaldehyde was also characterized by microwave spectrum.[5] However, these selenoaldehydes are extremely unstable and can not exist in the monomeric form under normal conditions,[6] though selenoformaldehyde[7a] and selenobenzaldehyde[7b] have been reported to be stabilized by complexation with transition metals.

There have been isolated the compounds owning a selenoformyl group such as selenoformates **1**,[8] selenoformamide **2**,[9] and their vinylogs like indolizine-1-carboselenaldehyde **3**.[10] The selenoformyl group in these compounds, however, is stabilized by the mesomeric effect due to the lone-pair electrons on heteroatom.

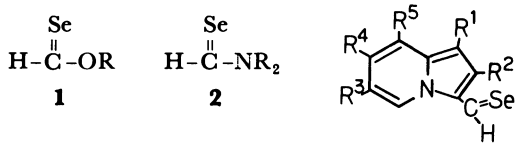

1 **2** **3**

Although the thioaldehyde had also been known too unstable to be isolated, we recently reported the synthesis of 2,4,6-tri-*t*-butylthiobenzaldehyde (**4**) by reaction of 2,4,6-tri-*t*-butylphenyllithium (**5**) with *O*-ethyl thioformate.[11] Compound **4** was the first stable thioaldehyde without above-mentioned electronic stabilization by heteroatoms. In **4**, the highly reactive thioformyl group is protected by two bulky *o*-*t*-butyl groups from oligomerization and from attack by other reagents.

We undertook an investigation on the reaction of **5** with *O*-alkyl selenoformates **1** in the hope that it would also give stable 2,4,6-tri-*t*-butylselenobenzaldehyde (**6**).[12]

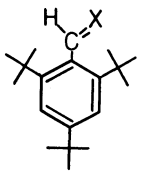

4 : X = S
6 : X = Se

Results and Discussion

Synthesis of Selenoformates. *O*-Cholesteryl (**1a**), *O*-*t*-butyl (**1b**),and *O*-(1,1-diethylpropyl) selenoformates (**1c**) were prepared by the Barton's method (Eq. 1)[8] in 70, 22, and 6.5% yields, respectively, the latter two being new compounds.

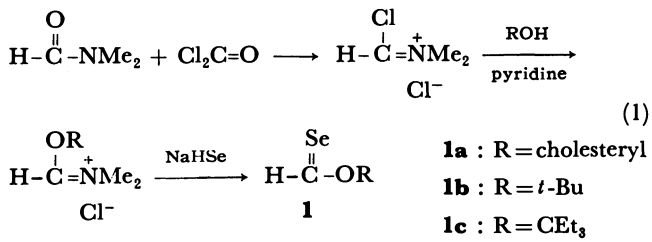

(1)

1a : R=cholesteryl
1b : R=*t*-Bu
1c : R=CEt_3

We also tried to prepare selenoformates derived from primary alcohols (**1d**: R=ethyl; **1e**: R=2,2-dimethylpropyl). Although they existed in a reaction solution, as judged from the presence of characteristic ^{1}H NMR signals due to the selenoformyl proton at ca. δ 12 (cf., δ 12.07, 12.20, and 12.14 for **1a**, **1b**, and **1c**, respectively), they polymerized during concentration to give orange and pale orange jelly for **1d** and **1e**, respectively. The former jellied material was insoluble in organic solvents, while the latter was slightly soluble and showed a small peak due to the selenoformyl group.

The synthesis of *O*-aryl selenoformates (**1f**: R=phenyl; **1g**: R=*p*-methoxyphenyl) was also attempted, but only *N*,*N*-dimethylselenoformamide was obtained in 85 and 74% yields, respectively.

Reactions of Selenoformates 1 with 2,4,6-Tri-*t*-butylphenyllithium (ArLi, 5).† A tetrahydrofuran (THF) solution of **1** was added dropwise to **5**, prepared from

†Throughout this paper, Ar denotes 2,4,6-tri-*t*-butylphenyl.

Table 1. Reaction Products of **1a** and **1b** with **5** Prepared from **7** and Butyllithium

R	Yield/%			
	9	**10**	(n-BuSe)$_2$	**8**
Cholesteryl (**1a**)	48	4.5	62	29
t-Butyl (**1b**)	45	15	55	18

1-bromo-2,4,6-tri-t-butylbenzene (**7**) and butyllithium in THF at −78 °C, and then the reaction mixture was warmed to room temperature. The ^{1}H NMR spectrum of the reaction mixture showed the formation of 1,3,5-tri-t-butylbenzene (**8**) and a small amount of 2,4,6-tri-t-butylbenzaldehyde (**9**). ^{77}Se NMR spectra of the mixture gave signals at δ 360 and 364 for **1a** and δ 442 for **1b**. Appearance of these signals in the region of chemical shifts of selenides suggested the existence of relatively stable selenides in the crude reaction mixture. Chromatography of the reaction mixture on silica gel gave aldehyde **9**, butyl 2,4,6-tri-t-butylphenyl selenide (**10**), dibutyl diselenide, and **8** (Eq. 2, Table 1).

$$\mathrm{H\text{-}\overset{\overset{\mathrm{Se}}{\|}}{C}\text{-}OR + ArLi \xrightarrow{THF\ SiO_2} ArCHO\ (\mathbf{9}) + ArSeBu^n\ (\mathbf{10}) + (n\text{-}BuSe)_2 + ArH\ (\mathbf{8})} \quad (2)$$

Ar = 2, 4, 6-(t-Bu)$_3$C$_6$H$_2$

The fact that the amounts of aldehyde **9** and dibutyl diselenide were much increased than that before the chromatography indicates the presence of an intermediate which afforded **9** and dibutyl diselenide by hydrolysis on silica gel. The intermediate is considered to be monoselenoacetal **I** formed from the reaction of initial adduct **II** with 1-bromobutane generated in the preparation of **5** (Eq. 3). The formation

$$\mathbf{1} + \mathbf{5} \longrightarrow \underset{\mathbf{II}}{\mathrm{Ar\text{-}\overset{\overset{H}{|}}{\underset{\underset{SeLi}{|}}{C}}\text{-}OR}} \xrightarrow{n\text{-}BuBr} \underset{\mathbf{I}}{\mathrm{Ar\text{-}\overset{\overset{H}{|}}{\underset{\underset{SeBu^n}{|}}{C}}\text{-}OR}} \quad (3)$$

a : R = cholesteryl

b : R = t-Bu

of **II** is reasonable by analogy with known reactivity of formates and thioformic O-esters. The appearance in ^{77}Se NMR of two signals with similar chemical shift and intensity in the reaction of **1a** also gives support to the structure of **I**, for two diastereomers due to chiral centers adjacent to the ether oxygen should exist in **Ia**. Since some monoselenoacetals have been isolated,[8b,13] the instability of monoselenoacetal **I** is probably due to its benzylic structure with high reactivity.

Since the above results suggested that **II** reacted with 1-bromobutane before it was cleaved into selenoaldehyde **6** and ROLi, **5** was next prepared by the reaction of **7** with two equivalents of t-butyllithium in order to avoid the coexistence of an alkyl halide. Reactions of selenoformates **1** with **5** prepared in this way afforded results shown in Eq. 4 and Table 2.

Table 2. Reaction Products of **1a**, **1b**, and **1c** with **5** Prepared from **7** and t-Butyllithium

Run	**1**	Temp/°C	Yield/%				
			11	**9**	**12** (n=2,3)	**13**	**8**
1	**1a**	R.t.	—	52	—	2	37
2	**1a**	60	12	5	17, 10	Trace	35
3	**1b**	R.t.	32	13	—	2	35
4	**1b**	40	44	7	—	5	28
5	**1c**	Reflux	Trace	16	Trace	8	60

$$\mathbf{1} + \mathbf{5} \xrightarrow[THF]{-78\,^\circ C} \xrightarrow[\text{in Table 2}]{Temp.} \underset{\mathbf{11}}{\text{Se-ring}} + ArCHO\ (\mathbf{9}) + ArCH_2Se_nCH_2Ar\ (\mathbf{12}, n=2,3) + (ArSe)_2\ (\mathbf{13}) + ArH\ (\mathbf{8}) \quad (4)$$

After the reaction was conducted at −78 °C, the temperature of the reaction mixture was allowed to rise as indicated in Table 2. Although the intermediate **IIa** was stable at room temperature to give aldehyde **9** by hydrolysis (Run 1), the reaction of **1a** at 60 °C gave a new product, 6,8-di-t-butyl-3,4-dihydro-4,4-dimethyl-1H-2-benzoselenin (**11**) (Run 2). In the case of **1b**, **11** was obtained even at room temperature (Runs 3 and 4). This unusual formation of dihydrobenzoselenin **11** is very interesting since it strongly suggests the intermediacy of selenoaldehyde **6**. We previously observed that thioaldehyde **4** was very stable at room temperature, but it isomerized into dihydrobenzothiopyran **14** when heated at about 200 °C.[14] In view of this reactivity of **4**, the formation of **11** in the present

$$\underset{\mathbf{4}}{ArCHS} \xrightarrow{200\,^\circ C} \underset{\mathbf{14}}{\text{S-ring}}$$

reaction is most probably explicable in terms of intermediacy of **6**. The collapse of **IIb** occurred at a lower temperature than that of **IIa**, which indicated that t-BuO$^-$ anion was a more effective leaving group than cholesteryloxyl group. Since this is most likely explained in terms of steric acceleration, we next employed **1c** with the expectation that **IIc** could release Et$_3$CO$^-$ anion at a lower temperature than **IIb**. However, **IIc** was considerably stable and required reflux temper-

ature for cleavage, giving only a trace amount of **11**. This is probably because steric acceleration cannot overcome the intrinsic poor reactvity of Et_3CO^- anion as a leaving group.

Since the tetrahedral intermediate **II** is more stable than a similar intermediate in the reaction of **5** with *O*-ethyl thioformate which is found to be collapsed into the thioaldehyde **4** below −30°C, the conversion of **II** into the selenoaldehyde **6** seems to require higher temperatures where **6** can not exist as such and is isomerized to the dihydrobenzoselenin **11**. In order to collapse **II** into **6** at lower temperatures, hexamethylphosphoric triamide, dry HCl gas, or trimethylsilyl trifluoromethanesulfonate was added to the reaction mixture, but all of them were ineffective, the product in each case being aldehyde **9**.

Trapping of 6. Since selenoaldehyde **6** seemed to be too unstable to be isolated at ordinary temperature, some attempts to trap it were made. Since some thioketones[15a] and thioaldehydes[15b] are known to undergo the Diels-Alder reaction with dienes, 2,3-dimethylbutadiene was added to the reaction mixture with **1b** at 0°C and the resulting mixture was allowed to warm to room temperature. However, no [4+2] adduct was obtained probably because of steric congestion by Ar group; the products were dihydrobenzoselenin **11** (18%), aldehyde **9** (17%), **12** (trace), diselenide **13** (9%), and **8** (10%).

Reactions with 1,1-dimethylhydrazine were also attempted in the hope that selenoaldehyde **6** would be reactive enough to undergo condensation with the hydrazine as it was formed. Reaction in the presence of the hydrazine, however, gave no expected hydrazone **15** but ether **16** was obtained in a reasonable yield (25%).

$ArCH{=}NNMe_2$ **15** $ArCH_2OBu^t$ **16** $ArCH{=}NBu^n$ **17**

Since the ether **16** is considered to be formed by reductive cleavage of **II** by 1,1-dimethylhydrazine, the reaction with butylamine, which is a weaker reducing agent than the hydrazine, was next carried out. In this case imine **17** was obtained, though in a low yield (1.3%), along with **16** (25%).

The formation of imine **17** suggests the existence of selenoaldehyde **6** in the reaction solution, in view of similar reactivities of the corresponding thioaldehyde **4**, which reacts with butylamine at 70°C to give **17** quantitatively.[16] Furthermore this indicates that **6** has much greater reactivity toward amines than **4**, since **4** does not react with butylamine at room temperature.[17]

We consider that the formation of dihydrobenzoselenin **11** and the condensation product **17** is strong evidence for the intermediacy of selenoaldehyde **6**.

Mechanism. Since the reaction products of **5** with selenoformates **1** depend on the preparative method of **5** as described above, we classify the reactions into Case I and Case II for the convenience of the following disccussion. Case I is reactions with butyllithium as lithiating agent (Table 1) and Case II is those with *t*-buytllithium (Table 2).

Though the reactions of selenoformate **1** with **5** afford several kinds of compounds, the formation of them can be explained by three reaction paths (A)—(C) as shown in Scheme 1. These paths correspond to reac-

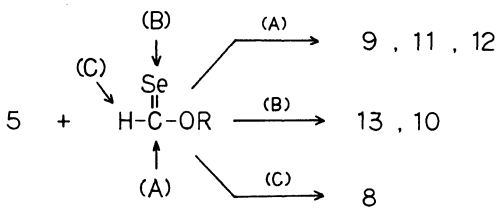

Scheme 1.

tions at the selenocarbonyl carbon, the selenium, and the selenoformyl hydrogen, respectively, and the products in these paths are as follows: (A): aldehyde **9** (Cases I, II), dihydrobenzoselenin **11** (Case II), polyselenide **12** (Case II); (B): diselenide **13** (Case II), selenide **10** (Case II); (C): hydrocarbon **8** (Cases I, II). We next discuss the details of each path.

(1) Path (A). Path (A), leading to initial adduct **II**, is desirable for the formation of selenoaldehyde **6**. The fact that the reaction of **5** with *O*-ethyl thioformate gives thioaldehyde **4** at −30°C, while that with *O*-alkyl selenoformates **1** does not afford selenoaldehyde **6** under similar conditions, indicates that the initial adduct **II** in the later reaction is thermally more stable than a similar adduct **III** in the former reaction. In

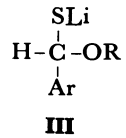

III

Case I reaction, therefore, **II** is quenched by 1-bromobutane to give selenoacetal **I**, whose hydrolysis on silica gel leads to aldehyde **9** and *n*-BuSeH. Case II reactions afford dihydrobenzoselenin **11**, aldehyde **9**, and selenides **12** depending on the reaction temperature. The formation of **11** can be explained in terms of intermediacy of **6** as mentioned previously. The diselenide **12** (n=2) probably results from oxidative dimerization of selenol $ArCH_2SeH$ which is formed by reduction of **6** with RO^- anion (R=cholesteryl) having α-hydrogen. Similar reduction with an alkoxide ion having α-hydrogen has been reported for thioketones.[18] The triselenide **12** (n=3) would be an oxidative coupling product between $ArCH_2SeH$ and $ArCH_2SeSeH$ which is formed by the reaction of $ArCH_2Se^-$ anion with selenium.[19] Aldehyde **9** is thought to be formed by hydrolysis of unreacted **II** and/or by a process as shown below.

(2) Path (B). When the addition of **5** occurs on selenium of the selenocarbonyl group, adduct **IV** is

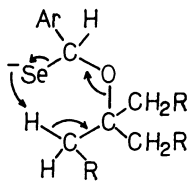

formed (Eq. 5). The intermediate **IV** is not so stable

$$\underset{\text{IV}}{\text{H-C(SeAr)(Li}^+\text{)-OR}} \longrightarrow \text{ArSeLi} + \underset{\text{V}}{\text{H-C-OR}} \qquad (5)$$

and decomposes to ArSeLi and alkoxycarbene **V**. ArSeLi thus formed is quenched by 1-bromobutane to yield **10** (Case I) or protonated to give ArSeH (Case II). ArSeH is gradually oxidized to **13** during workup. Though alkoxycarbenes have been reported to dimerize,[20] the dimer of **V** could not be found.

Such heterophilic additions of organolithium or organomagnesium reagents have been reported for thioketones and selenoketones. In the reaction of bulky 2,6-dimethylphenyllithium with di-*t*-butyl thioketone, similar decomposition of an initial adduct leading to carbenes has been observed.[21] We also reported similar formation of carbene in the reaction of 1,1,3,3-tetramethyl-2-indanselone with some Grignard reagents.[22] The bulkiness of Ar group is considered to make the decomposition even easier in the present case.

When the reaction of **1b** with **5** was carried out at −98 °C, the ratio of Se-addition/C-addition was 15/40 (Case I) or 17/26 (Case II) while the ratio of 1/10—1/20 at −78 °C. Thus the ratio of Se-addition was increased at lower temperatures. This is in keeping with the observation reported for the reaction of di-*t*-butyl thioketone with phenyllithium that the thiophilic addition is more advantageous at lower temperatures.[21]

(3) Path (C). In order to obtain direct evidence for abstraction of a selenoformyl proton of **1** by **5**, **5** was allowed to react with *O*-cholesteryl selenoformate-*d* (**1a-*d***) having a deuterated selenoformyl group. 1,3,5-Tri-*t*-butylbenzene (**8**) thus obtained (35% yield) was analyzed for deuterium content by mass spectrometry to be 6%, providing conclusive evidence for the abstraction of the selenoformyl proton. This is, to our knowledge, the first demonstration of the proton abstraction from a selenoformyl group although formyl proton abstraction from *O*-ethyl formate[23] and that from formamides and thioformamides[24] have been reported.

Although the reason for the formation of protium species ArH is not clear at the present stage, it is probably due to proton abstraction from the solvent (THF) by unreacted **5** and/or to hydrogen abstraction by 2,4,6-tri-*t*-butylphenyl radical generated by single electron transfer from **5** to **1**.

Experimental

Melting points are uncorrected. ^{1}H (90 MHz) and ^{13}C (22.49 MHz) NMR spectra were measured in $CDCl_3$ with a JEOL FX-90Q spectrometer using tetramethylsilane as an internal standard. ^{77}Se NMR spectra were recorded at 17.03 MHz with a JEOL FX-90Q spectrometer, whose chemical shifts were measured in $CDCl_3$ with dimethyl selenide as an external standard. The mass spectra were recorded with a JEOL JMS-D300 mass spectrometer. Preparative liquid chromatography (PLC) was carried out using JAI Gel 1H columm (Japan Analytical Industry) with chloroform as solvent. All reactions were carried out under argon.

Preparation of Selenoformate 1. Selenoformates (**1a**, **b**, and **c**) were prepared by the Barton's method.[8]

O-Cholesteryl selenoformate (**1a**) was obtained in 70%; mp 128—131 °C; ^{1}H NMR δ=12.07 (HC=Se) (δ=12.15 in Ref. 8); ^{77}Se NMR δ=1006. *O*-*t*-Butyl selenoformate (**1b**) (22%) was recrystallized from hexane at −30 °C; mp 50.5—51.5 °C; ^{1}H NMR δ=1.57 (9H, s, *t*-Bu) and 12.20 (1H, s, HC=Se); ^{13}C NMR δ=28.4 [C($\underline{C}H_3)_3$], 89.5 [$\underline{C}(CH_3)_3$], and 215.0 (C=Se); ^{77}Se NMR δ=1052; MS *m/z* (rel intensity) 166 (M^+, 12) and 57 (100). Found *m/z* 165.9903. Calcd for $C_5H_{10}O^{80}Se$: M, 165.9897. *O*-(1,1-Diethylpropyl) selenoformate (**1c**) (6.5%) was obtained as an orange oil after Kugelrohr distillation (70 °C, 0.05 mmHg).# ^{1}H NMR δ=0.92 (9H, t, *J*=7 Hz), 1.84 (6H, q, *J*=7 Hz), and 12.14 (1H, s, $\underline{H}C$=Se); MS *m/z* (rel intensity) 208 (M^+, 2), 99 (50), 69 (76), 57 (100), and 55 (59). Found *m/z* 208.0371. Calcd for $C_8H_{16}O^{80}Se$: M, 208.0366.

Preparation of ArLi (5). I) *n*-BuLi (1 equiv) was added to a solution of ArBr (**7**)[25] (1 equiv) in THF at −78 °C and the resulting mixture was stirred for 15 min at −78 °C before use. **5** prepared in this way is denoted as ArLi(I). II) *t*-BuLi (2 equiv) was added to the solution of **7** (1 equiv) in THF at −78 °C and the resulting yellow solution was stirred at −78 °C till the yellow color disappeared (ca. 1 h). **5** prepared by this method is denoted as ArLi(II).

Reactions of 1 with ArLi(I). (a) A solution of **1a** (0.331 g, 0.693 mmol) in THF (3 ml) was added to ArLi(I) (0.631 mmol) in THF (5 ml) at −78 °C during 5 min. The mixture was stirred at this temperature for 30 min. The yellow reaction mixture was warmed to room temperature to give an orange red solution. After stirring for 30 min at this temperature, water and ether were added. The ethereal extract was washed with water and dried ($MgSO_4$). Removal of the solvent under reduced pressure left 0.497 g of an orange solid, whose ^{77}Se NMR showed major peaks at δ 360 and 364, and other small peaks at δ 224 (ArSeBu^n, **10**), 313 (*n*-BuSe)$_2$, and 345, 349, 491, and 498 (unknown). This crude reaction mixture was subjected to chromatography (silica gel, hexane–dichloromethane 10:1). The first yellow fraction was separated again by PLC to afford ArH (**8**) (44.9 mg, 29%), dibutyl diselenide[26] (53.2 mg, 62%), and ArSeBu^n **10** (10.9 mg, 4.5%). **10** was recrystallized from ethanol giving colorless crystals. They once melted at 67.5—68.0 °C and crystallized again. These second crystals melted at 77.5—78.0 °C. ^{1}H NMR δ=0.80—1.61 [34H, m; 18H for *o*-*t*-Bu (δ=1.61), 9H for *p*-*t*-Bu (δ=1.30), 3H for ArSe(CH$_2$)$_3$-$\underline{C}H_3$ (δ=0.87, t, *J*=7 Hz), and 4H for ArSeCH$_2\underline{C}H_2\underline{C}H_2CH_3$ (m)], 2.46 (2H, t, *J*=8 Hz, ArSe$\underline{C}H_2$CH$_2$CH$_2$CH$_3$), 7.37 (2H, s, aromatic); MS *m/z* (rel intensity) 382 (M^+, 25), 367 (4), 336

1 mmHg=133.322 Pa.

(2), 311 (4), and 57 (100). Found: C, 69.08; H, 10.29%. Calcd for $C_{22}H_{38}Se$: C, 69.26; H, 10.04%. The second fraction was purified by PLC to give ArCHO (**9**)[27] (83.4 mg, 48%): Mp 189.5—190.5 °C after recystallization from methanol. ^1H NMR δ=1.32 (9H, s, *p*-*t*-Bu), 1.36 (18H, s, *o*-*t*-Bu), 7.37 (2H, s, aromatic), and 11.11 (1H, s, CHO); ^{13}C NMR δ=202.7 (CHO), 150.8, 147.4, 137.2, 36.6, 35.1, 32.6, and 31.3; MS *m*/*z* (rel intensity) 274 (M^+, 22), 259 (100), 241 (45), 217 (42), and 57 (72). Found: C, 82.94; H, 10.97%. Calcd for $C_{19}H_{30}O$: C, 83.15; H, 11.02%.

(b) A solution of **1b** (0.133 g, 0.803 mmol) in THF (1 ml) was added to ArLi(I) (0.804 mmol) in THF (5 ml) at −98 °C. The reaction mixture was stirred for 20 min at −98 °C and warmed to room temperature and to this was added aqueous ammonium chloride and ether. The ethereal extract was washed with water and dried ($MgSO_4$). Removal of the solvent gave 0.358 g of an orange oil, whose ^{77}Se NMR showed a peak at δ 442. This reaction mixture was subjected to chromatography (silica gel, hexane–dichloromethane, 10:1). The first fraction contained **8**, **10**, and dibutyl diselenide, whose yields were determined by ^1H NMR to be 18, 15, and 55%, respectively. The second fraction was **9** (87.1 mg, 40%).

Reactions of 1 with ArLi(II). (a) A THF solution of **1a** (0.474 g, 0.992 mmol) in THF (5 ml) was added to ArLi(II) (0.902 mmol) in THF (10 ml) at −78 °C during 10 min. The resulting reaction mixture was stirred for 20 min at this temperature and warmed to room temperature. To the red solution was added aqueous ammonium chloride and ether, when much red selenium was precipitated. The organic layer was washed with water and dried ($MgSO_4$). After removal of the solvent, the residue was subjected to chromatography (silica gel, hexane–dichloromethane 10:1) and PLC to give **9** (129 mg, 52%), **8** (81.2 mg, 37%), and $(ArSe)_2$ (**13**)[28] (5.2 mg, 2%). **13** was recrystallized from ethanol giving an orange crystal: Mp 251.2—253.2 °C. ^1H NMR δ=1.28 (36H, s, *o*-*t*-Bu), 1.32 (18H, bs, *p*-*t*-Bu), and 7.25 (4H, s, aromatic); ^{77}Se NMR δ=521; MS *m*/*z* (rel intensity) 650 (M^+, 7), 326 (8), and 57 (100). Found: *m*/*z* 650.2887. Calcd for $C_{36}H_{58}{}^{80}Se_2$: M, 650.2867.

The following reactions were carried out in a similar way.

(b) **1a** (0.447 g, 1.00 mmol) was reacted with ArLi(II) (1.00 mmol). The resulting reaction mixture was heated to 60 °C and stirred at this temperature for 12 h. Products were dihydrobenzoselenin **11** (40 mg, 12%), $ArCH_2Se_nCH_2Ar$ (**12**, 130 mg, from ^1H NMR *n*=2, 17%; *n*=3, 10%), **9** (14.8 mg, 5%), **13** (trace), and **8** (85.5 mg, 35%). **11** was recrystallized from ethanol to give colorless needles: Mp 180.5—181.0 °C; ^1H NMR δ=1.32 (9H, s, *t*-Bu), 1.47 (9H, s, *t*-Bu), 1.53 [6H, s, $SeCH_2C(CH_3)_2$], 2.76 [2H, s, $SeCH_2C(CH_3)_2$], 4.04 (2H, s, benzyl), and 7.35 (2H, s, aromatic); ^{13}C NMR δ=147.8, 145.9, 145.9, 131.8, 121.2, 121.3, 38.0, 35.9, 34.9, 32.8, 31.9, 31.5, 30.6, and 18.2; ^{77}Se NMR δ=89.3; MS *m*/*z* (rel intensity) 338 (M^+, 34), 323 (13), 281 (18), 229 (14), and 57 (100). Found: C, 67.36; H, 9.07%. Calcd for $C_{19}H_{30}Se$: C, 67.64; H, 8.96%. Found: *m*/*z* 338.1500. Calcd for $C_{19}H_{30}{}^{80}Se$: M, 338.1511. **12**, a mixture of selenides, was dissolved in methanol. Insoluble orange solid contained triselenide (**12**, *n*=3) as judged by mass spectroscopy and showed peaks at δ 512, 521, 619, and 719 in ^{77}Se NMR. From the filtrate was obtained diselenide (**12**, *n*=2) after repetitive recrystallization from ethanol–hexane: Yellow crystals, mp 150.0—152.0 °C. ^1H NMR δ=1.58 (36H, s, *o*-*t*-Bu), 1.30 (18H, s, *p*-*t*-Bu), 5.05 (4H, s, benzyl), and 7.33 (4H, s, aromatic); ^{77}Se NMR δ=412; MS *m*/*z* (rel intensity) 678 (M^+, 0.1), 259 (38), 243 (100), 149 (19), and 57 (93). Found: C, 67.51; H, 9.53%. Calcd for $C_{38}H_{62}Se_2$: C, 67.43; H, 9.23%.

(c) **1b** (0.113 g, 0.684 mmol) in THF (2 ml) was added to ArLi(II) (0.683 mmol) in THF (5 ml) at −78 °C. The resulting reaction mixture was warmed to room temperature and stirred at this temperature for 1 h. Products were **11** (74.5 mg, 32%), **9** (32.5 mg, 13%), **13** (5.4 mg, 2%), and **8** (58.6 mg, 35%).

(d) **1b** (0.111 g, 0.670 mmol) in THF (2 ml) was added to ArLi(II) (0.699 mmol) in THF (5 ml) at −78 °C. The resulting red reaction mixture was heated to 40 °C and stirred at this temperature for 30 min. Products were **11** (100 mg, 44%), **9** (13.6 mg, 7%), **13** (11.3 mg, 5%), and **8** (61.0 mg, 28%).

(e) **1b** (0.083 g, 0.50 mmol) in THF (1 ml) was added to ArLi(II) (0.50 mmol) at −98 °C. The reaction mixture was heated to 60 °C and to this was added water. **11** was obtained in 26% (43 mg). **8** was obtained as a mixture with **13** and ArSeH. This mixture was stirred with KOH (1 grain) in dichloromethane and methanol in order to convert ArSeH to **13**. Separation by PLC yielded **8** (30 mg, 25%) and **13** (27 mg, 17%).

(f) **1c** (0.104 g, 0.500 mmol) in THF (0.5 ml) was added to ArLi(II) (0.503 mmol) in THF (5 ml) at −78 °C. The resulting orange reaction mixture was stirred at room temperature for 12 h and at reflux for 16 h. Products were **11** (trace), **9** (22 mg, 16%), **12** (trace), **13** (13 mg, 7.8%), and **8** (74 mg, 60%).

Reaction of 1 and 5 with Hexamethylphosphoric Triamide (HMPA). (a) A solution of **1a** (0.400 g, 0.838 mmol) in THF (5 ml) was added to ArLi(II) (0.757 mmol) in THF (5 ml) at −78 °C. The yellow reaction mixture was stirred at this temperature for 1 h and was added HMPA (1.44 g, 8.00 mmol) at −78 °C. The orange reaction mixture was warmed to room temperature and stirred at room temperature for 2 d. TLC of the reaction mixture showed that **11** was not formed. Silica-gel chromatography and PLC gave **9** (76.2 mg, 37%), **12** (trace), **13** (trace), and **8** (89.7 mg, 48%).

(b) A solution of **1b** (0.172 g, 0.680 mmol) in THF (2 ml) was added to ArLi(II) (0.680 mmol) at −78 °C. The reaction mixture was warmed to 0 °C and again cooled to −78 °C. To the red orange reaction mixture was added HMPA (0.72 g, 4.0 mmol). The temperature of the resulting mixture was allowed to rise to −30 °C and stirred at this temperature for 1 h, and to this was added water. Silica-gel chromatography and PLC afforded **9** (59.9 mg, 36%), **13** (11.4 mg, 5%), and **8** (81.8 mg, 49%).

Reaction of 1a and 5 with Dry HCl Gas. A solution of **1a** (0.321 g, 0.673 mmol) in THF (5 ml) was added to ArLi(II) (0.619 mmol) in THF (5 ml) at −78 °C. The reaction mixture was allowed to rise to room temperature. The solvent was removed in vacuo and dichloromethane (15 ml) was added. The resulting reaction mixture was cooled to −78 °C and excess dry HCl gas was bubbled into it. The yellow suspension was warmed to room temperature. When dichloromethane was removed in vacuo, a gas of unpleasant smell was detected (probably hydrogen selenide, absorbed by KOH). Products were **9** (70.0 mg, 41%), **13** (trace), and **8** (83.0 mg, 54%).

Reaction of 1b and 5 with Trimethylsilyl Trifluoromethanesulfonate (TMSOTf). A solution of **1b** (0.106 g, 0.643 mmol) in THF (2 ml) was added to ArLi(II) (0.643 mmol) in THF (5 ml) at −78 °C. The reaction mixture was warmed to 0 °C. The solvent was removed in vacuo and dichloromethane (10 ml) was added. The yellow suspension

was warmed to room temperature and stirred for 18 h. TLC showed no **11**. Additional TMSOTf (0.146 g, 0.657 mmol) was added at 0 °C and the mixture was stirred for 10 h at room temperature. **9** (62.1 mg, 35%), **13** (7.8 mg, 4%), and **8** (84.2 mg, 53%) were obtained.

Trapping Reaction of 6 with Butylamine. A solution of **1b** (95.8 mg, 0.58 mmol) in THF (1 ml) was added to ArLi(II) (0.579 mmol) in THF (5 ml) at −78 °C. The reaction mixture was warmed to 0 °C and to this was added butylamine (0.422 g, 5.77 mmol) in THF (1 ml). The resulting reaction mixture was stirred for 2 h at room temperature. After the addition of water and ether, the separated ethereal layer was washed successively with dil HCl, dil aqueous sodium carbonate, and water, and dried ($MgSO_4$). After chromatographic separation, there were obtained imine **17** (2.5 mg, 1.3%), ether **16** (47.8 mg, 25%), **9** (16.2 mg, 10%), **12** (trace), **13** (12.9 mg, 7%), and **8** (62.3 mg, 48%). **17** was identified by comparing its ^{1}H NMR spectrum with that of an authentic sample.[16] **16** was recrystallized from ethanol–water to give colorless crystals: Mp 94.8—95.4 °C; ^{1}H NMR δ=1.29 (9H, s),1.34 (9H, s), 1.52 (18H, s), 4.86 (2H, s, benzyl), and 7.41 (2H, s, aromatic); MS *m/z* (rel intensity) 332 (M^+, 7.6), 259 (7.6), 247 (18), 219 (56), and 57 (100). Found: *m/z* 332.3076. Calcd for $C_{23}H_{40}O$: M, 332.3077.

An Attempt to Trap 6 with 2,3-Dimethyl-1,3-Butadiene. A solution of **1b** (0.100 g, 0.608 mmol) in THF (1 ml) was added to ArLi(II) (0.607 mmol) in THF (5 ml) at −78 °C. The reaction mixture was stirred at this temperature for 30 min and warmed to 0 °C. 2,3-Dimethyl-1,3-butadiene (0.508 g, 6.3 mmol) in THF (1 ml) was added and the resulting mixture was stirred for 2 h at room temperature. Chromatographic purification gave **11** (37.8 mg, 18%), **9** (28.4 mg, 17%), **12** (trace), **13** (8.6 mg, 9%), and **8** (69.8 mg, 47%).

An Attempt to Condense 6 with 1,1-Dimethylhydrazine. A solution of **1b** (94.4 mg, 0.602 mmol) in THF (1 ml) was added to ArLi(II) (0.602 mmol) in THF (5 ml) at −78 °C. The reaction mixture was stirred for 30 min at this temperature and warmed to 0 °C. 1,1-Dimethylhydrazine (0.364 g, 6.05 mmol) in THF (1 ml) was added and the resulting reaction mixture was stirred for 1.5 h at room temperature. Products obtained were **16** (50.7 mg, 25%), **9** (19.9 mg, 12%), **13** (16.1 mg, 18%), and **8** (80.0 mg, 54%).

O*-Cholesteryl Selenoformate-*d* (1a-*d*).** **1a-*d was prepared in 67% yield by the Barton's method, using *N,N*-dimethylformamide-d_7 (99%, Merck) instead of *N,N*-dimethylformamide in preparation of imidoyl chloride: Mp 135—137 °C (after recrystallization from hexane); ^{1}H NMR δ= 0.69—2.28 (43H, m), 2.50—2.60 (2H, bd), and 5.30—5.78 (2H, m). Selenoformyl proton was observed at δ=12.06 but negligibly small. ^{77}Se NMR δ=1000.

Reaction of *O*-Cholesteryl Selenoformate-*d* (1a-*d*) with 5. A solution of **1a-*d*** (0.319 g, 0.666 mmol) in THF (3 ml) was added to ArLi(II) (0.619 mmol) in THF (10 ml) at −78 °C. The reaction mixture was heated to 60 °C and stirred at this temperature for 20 h. Chromatographic purification afforded a mixture of ArH (**8**) and ArD (**8-*d***) (53.7 mg, 35%). The ratio of **8**/**8-*d*** was 94/6 (by mass spectrum).

References

1) T. G. Back, D. H. R. Barton, M. R. Britten-Kelly, and F. S. Guziec, Jr., *J. Chem. Soc., Chem. Commun.*, **1975**, 539; *J. Chem. Soc., Perkin Trans. 1*, **1976**, 2079; C.-P. Klages and J. Voß, *Chem. Ber.*, **113**, 2255 (1980); F. S. Guziec, Jr. and C. J. Murphy, *J. Org. Chem.*, **45**, 2890 (1980); E. R. Cullen, F. S. Guziec, Jr., and C. J. Murphy, *ibid.*, **47**, 3563 (1982); T. C. Wong, F. S. Guziec, Jr., and C. A. Moustakis, *J. Chem. Soc., Perkin Trans. 2*, **1983**, 1471; R. Okazaki, A. Ishii, and N. Inamoto, *J. Chem. Soc., Chem. Commun.*, **1983**, 1429; F. S. Guziec, Jr. and C. A. Moustakis, *J. Org. Chem.*, **49**, 189 (1984).

2) H. Bock, S. Aygen, P. Rosmus, B. Solouki, and E. Weißflog, *Chem. Ber.*, **117**, 187 (1984).

3) R. H. Judge and D. C. Moule, *J. Am. Chem. Soc.*, **106**, 5406 (1984).

4) R. J. Glinski, E. A. Mishalanie and J. W. Birks, *J. Am. Chem. Soc.*, **108**, 531 (1986).

5) H. Hutchinson and H. W. Kroto, *J. Mol. Spectrosc.*, **70**, 347 (1978).

6) L. Vanino and A. Schinner, *J. Prakt. Chem.*, **91**, 116 (1915); T. G. Pearson, R. H. Purcell, and G. S. Saigh, *J. Chem. Soc.*, **1938**, 409; H. J. Bridger and R. W. Pittman, *ibid.*, **1950**, 1371; M. Russo and L. Credali, *J. Macromol. Sci., Part A*, **1**, 387 (1967).

7) a) L. Hofmann and H. Werner, *J. Organomet. Chem.*, **255**, C41 (1983); C. E. L. Headford and W. R. Roper, *ibid.*, **244**, C53 (1983); A. F. Hill, W. R. Roper, J. M. Waters, and A. H. Wright, *J. Am. Chem. Soc.*, **105**, 5939 (1983); W. A. Herrmann, J. Weichmann, R. Serrano, K. Blechschmitt, H. Pfisterer, and M. L. Ziegler, *Angew. Chem. Int. Ed. Engl.*, **22**, 314 (1983); M. Herberhold, W. Ehrenreich, and W. Bühlmeyer, *ibid.*, **22**, 315 (1983); W. Paul and H. Werner, *ibid.*, **22**, 316 (1983); H. Werner and W. Paul, *ibid.*, **23**, 58 (1984); W. A. Herrmann, J. Rohrmann, and A. Schäfer, *J. Organomet. Chem.*, **265**, C1 (1984); b) H. Fisher, S. Zeuner, and J. Riede, *Angew. Chem. Int. Ed. Engl.*, **23**, 726 (1984).

8) a) D. H. R. Barton and S. W. McCombie, *J. Chem. Soc., Perkin Trans. 1*, **1975**, 1574; b) D. H. R. Barton, P.-E. Hansen, and K. Picker, *J. Chem. Soc., Perkin Trans. 1*, **1977**, 1723.

9) C. Collard-Charon and M. Renson, *Bull. Soc. Chim. Belg.*, **72**, 304 (1963); H. Hartmann, *Z. Chem.*, **11**, 60 (1971); L. Henriksen, *Synthesis*, **1974**, 501; K. Geisler, H. Below, A. Moeller, and E. Bulka, *Z. Chem.*, **24**, 99 (1984).

10) D. H. Reid, R. G. Webster, and S. McKenzie, *J. Chem. Soc., Perkin Trans. 1*, **1979**, 2334.

11) R. Okazaki, A. Ishii, N. Fukuda, H. Oyama, and N. Inamoto, *J. Chem. Soc., Chem. Commun.*, **1982**, 1187.

12) A part of this work was reported in a preliminary form: R. Okazaki, A. Ishii, N. Inamoto, *J. Chem. Soc., Chem. Commun.*, **1986**, 71.

13) A. Anciaux, A. Eman, W. Dumont, D. van Ende, and A. Krief, *Tetrahedron Lett.*, **1975**, 1613; W. Dumont and A. Krief, *Angew. Chem. Int. Ed. Engl.*, **16**, 540 (1977); D. L. J. Clive and S. M. Menchen, *J. Org. Chem.*, **44**, 1883 (1979).

14) R. Okazaki, A. Ishii, N. Fukuda, H. Oyama, and N. Inamoto, *Tetrahedron Lett.*, **25**, 849 (1984).

15) a) Y. Omote, M. Yoshioka, K. Yamada, and N. Sugiyama, *J. Org. Chem.*, **32**, 3676 (1967); K. Yamada, M. Yoshioka, and N. Sugiyama, *ibid.*, **33**, 1240 (1968); A. Ohno, Y. Ohnishi, and G. Tsuchihashi, *Tetrahedron*, **25**, 871 (1969); W. J. Middleton, *J. Org. Chem.*, **30**, 1390 (1965); b) D. R. Dice and R. P. Steer, *Can. J. Chem.*, **52**, 3518 (1974); A. G. Anastassiou, J. C. Wetzel, and B. Chao, *J. Am. Chem. Soc.*, **98**, 6405 (1976); J. E. Baldwin and R. C. G. Lopez, *J. Chem. Soc., Chem. Commun.*, **1982**, 1029; *Tetrahedron*, **39**, 1487 (1983); E. Vedejs and D. A. Perry, K. N. Houk, and N. G. Rondan, *J.*

Am. Chem. Soc., **105**, 6999 (1983); E. Vedejs and D. A. Perry, *ibid.*, **105**, 1683 (1983); G. W. Kirby, A. W. Lochead, and G. N. Sheldrake, *J. Chem. Soc., Chem. Commun.*, **1984**, 1469; G. A. Krafft and P. T. Meinke, *Tetrahedron Lett.*, **26**, 1947 (1985); E. Schaumann and G. Rühter, *ibid.*, **26**, 5265 (1985).

16) A full account of the reactivities of **4** will be published eleswhere.

17) Aldehyde **9** and dihydrobenzoselenin **11** are also totally inactive toward butylamine at room temperature.

18) A. Ohno, K. Nakamura, M. Uohama, S. Oka, T. Yamabe, and S. Nagata, *Bull. Chem. Soc. Jpn.*, **48**, 3718 (1975).

19) A small amount of polyselenides $(ArCH_2)_2Se_n$ $(n>4)$ were also formed as judged by the presence of some minor peaks in selenide region of ^{77}Se NMR although they could not be isolated.

20) Y. Fukuda, T. Negoro, K. Kimura, and Y. Odaira, *J. Org. Chem.*, **45**, 177 (1980).

21) A. Ohno, K. Nakamura, Y. Shizume, and S. Oka, *Bull. Chem. Soc. Jpn.*, **50**, 1003 (1977).

22) R. Okazaki, A. Ishii, and N. Inamoto, *Tetrahedron Lett.*, **25**, 5147 (1984).

23) F. Adickes and G. Schäfer, *Ber.*, **65B**, 950 (1932); F. Adickes and P. P. Peckelhoff, *Ber.*, **68B**, 1138 (1935).

24) B. Bánhidai and U. Schöllkopf, *Angew. Chem., Int. Ed. Engl.*, **12**, 836 (1973); R. R. Fraser and P. R. Hubert, *Can. J. Chem.*, **52**, 185 (1974); A. S. Fletcher, K. Smith, and K. Swaminathan, *J. Chem. Soc., Perkin Trans. 1*, **1977**, 1881; D. Seebach, W. Lubosch, and D. Enders, *Chem. Ber.*, **109**, 1309 (1976).

25) D. E. Pearson, M. G. Frazer, V. S. Frazer, and L. C. Washburn, *Synthesis*, **1976**, 621.

26) L. Syper and J. Młochowski, *Synthesis*, **1984**, 439.

27) This compound has been reported in the literature; W. A. Gibbons and V. M. S. Gil, *Mol. Phys.*, **9**, 163 (1965). However, there is no description other than chemical shifts of ^1H NMR of ortho and para *t*-butyl groups and aromatic protons.

28) Detailed data on this compound are not known although temperature dependent ^1H NMR study has been reported; H. Kessler and W. Rundel, *Chem. Ber.*, **101**, 3350 (1968).

Synthetic Versatility of *N*-(Silylmethyl)imines: Water-Induced Generation of *N*-Protonated Azomethine Ylides of Nonstabilized Type and Fluoride-Induced Generation of 2-Azaallyl Anions

Otohiko TSUGE,* Shuji KANEMASA, Akira HATADA, and Koyo MATSUDA
Research Institute of Industrial Science, and Department of Molecular Science and Technology, Interdisciplinary Graduate School of Engineering Sciences, Kyushu University, Kasugakoen, Kasuga 816
(Received March 19, 1986)

N-(Silylmethyl)imines generate *N*-protonated azomethine ylides of nonstabilized type when treated with water in HMPA, which undergo stereospecific and regioselective cycloadditions with electron-poor olefins affording *N*-unsubstituted pyrrolidines. On the other hand, fluoride-induced desilylation of the imines leads to 2-azaallyl anions which are found to be synthetic equivalents of aminomethyl anion in the Michael additions with electron-poor olefins and nucleophilic additions with carbonyl compounds.

Since Vedejs and Martinez reported the first generation of azomethine ylides from *N*-(trimethylsilylmethyl)iminium salts,[1] this reaction has been applied to organic synthesis more frequently than any other methods known for the generation of azomethine ylide 1,3-dipoles. A variety of methodologies for the preparation of *N*-(silylmethyl)iminium salts were devised,[2] and this generation method has been successfully utilized as a key reaction in the synthesis of some natural products.[3]

To be noteworthy is that this method generates nonstabilized azomethine ylides which carry no substituents capable of stabilizing the ylide centers. Even the azomethine ylides carrying no substituents at the carbons are available according to the related reactions.[4] A variety of substituents such as alkyl,[5] acyl,[6] and silyl[7] can be introduced on the nitrogen.

After our recent discovery of the general and convenient synthesis of *N*-(trimethylsilylmethyl)imines,[8] we have engaged in a research aiming at opening the synthetic utility of these imines. One attracting utilization is the generation of azomethine ylide 1,3-dipoles, and another is the generation of 2-azaallyl anions. So far there is no report available on the direct desilylation of *N*-(silylmethyl)imines leading to 2-azaallyl anions.[9]

The present article describes the water-induced generation of *N*-protonated azomethine ylides from *N*-(silylmethyl)imines,[10] and the desilylation of the imines without quaterization on the nitrogen leading to 2-azaallyl anions.

Results and Discussion

N-(Trimethylsilylmethyl)imines **1—5** derived from aldehydes are readily available by reactions of trimethylsilylmethyl azide with aldehydes in the presence of triphenylphosphine (Scheme 1).[8] As a good yield of trimethylsilylmethylamine is obtained from the reaction of the azide with triphenylphosphine and subsequent hydrolysis, condensations of this silylmethylamine with aldehydes can be also a convenient route to the *N*-(silylmethyl)imines **1—5**.

The azide method directly leads to *N*-(silylmethyl)imines by a simple one-flask procedure, but the imines have to be separated from triphenylphosphine oxide. This route can be conveniently applied to the synthesis of low-boiling or water-sensitive imines. On the other hand, the condensation method using trimethylsilylmethyamine needs one more step, in which the amine is separated from triphenylphosphine oxide by vacuum distillation. Accordingly, this condensation is favored when the imines can be hardly separated from triphenylphosphine oxide. Although benzophenone could not be converted into its imine **6** by either of the above two methods, **6** was successfully prepared by condensation of the silylmethylamine with benzophenone in the presence of triethylaluminum.

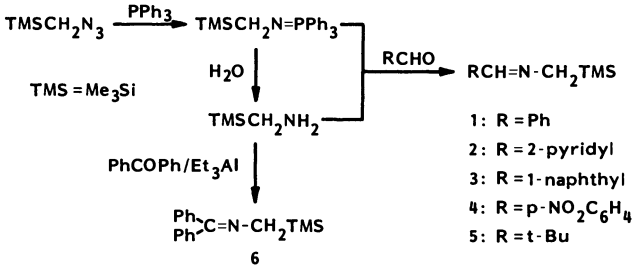

Scheme 1.

Water-Induced Generation of *N*-Protonated Azomethine Ylides of Nonstabilized Type. *N*-(Silylmethyl)imines react with water, slowly but cleanly at room temperature, in such a polar solvent as HMPA or DMF to generate *N*-protonated azomethine ylide 1,3-dipoles **A**. If electron-poor olefins are present, these ylides are captured as cycloadducts, *N*-unsubstituted pyrrolidines (Scheme 2).

N-(Benzylidene)trimethylsilylmethylamine **1** as an example was allowed to react with a variety of olefinic dipolarophiles, in HMPA in the presence of water and acetic acid for 12—24 h at room temperature, to give cycloadducts **7a—g** (Scheme 2 and Table 1). Water can be used in excess, but the use of more than five equivalents produces *N*-(benzylidene)methylamine as a tautomeric isomer of the corresponding *N*-protonated azomethine ylide. Less than one equivalent of acetic acid was employed, since acid catalyst was found to facilitate the ylide generation. Water, in this case,

Table 1. Water-Induced Cycloaddition of *N*-(Silylmethyl)imines with Olefins[a]

Imine	Olefin	Solvent	Time/h	Conditions[b]	Product	Yield/%[c]	2,3-cis/2,3-trans[d]
1	*N*-Methylmaleimide	HMPA	24	A	**7a**	100	1/2[e]
1	Dimethyl fumarate	HMPA	24	A	**7b**	100	1/1
1	Fumaronitrile	HMPA	24	A	**7c**	80	7/5
1	Methyl cinnamate	HMPA	24	A	**7d**	72	3/1
1	Methyl crotonate	HMPA	24	A	**7e**	65	2/1
1	Dimethyl maleate	HMPA	24	A	**7f**	100	3/7
1	Methyl methacrylate	HMPA	24	A	**7g**	75	4/3[f]
2	Dimethyl fumarate	THF	12	B	**8**	78	1/3
2	Dimethyl fumarate	HMPA	12	B	**12**	73	—
3	Dimethyl fumarate	HMPA	12	B	**9**	74	4/5
5	Dimethyl fumarate	HMPA	24	A	**10**	78	1/1
6	Dimethyl fumarate	HMPA	12	B	**11**	95	—

a) All reactions were carried out under nitrogen at room temperature. b) Each 1 mmol amounts of imines and olefins in 2 ml of solvent were allowed to react in the presence of: A: each 1 mmole of water and acetic acid or B: 1 mmol of water and a catalytic amount of acetic acid. c) Isolated yield. d) Determined by ^{1}H NMR. e) 3a,4-cis/3a,4-trans. f) 2,3-cis Isomer bears 3-ester cis to 2-phenyl.

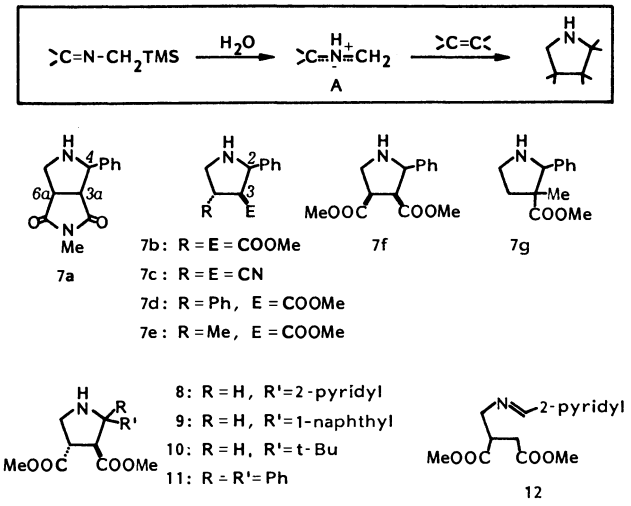

Scheme 2.

is not only a reagent neccessary for the generation of the ylide but also an inhibitor of polymerization of the dipolarophiles. When **1** is treated with *N*-methylmaleimide in very dry HMPA under nitrogen, the maleimide suffers from complete polymerization and **1** is quantitatively recovered.

Other *N*-(silylmethyl)imines **3** and **5**—**6** reacted with dimethyl fumarate under similar conditions to give the corresponding cycloadducts **9**—**11** (Scheme 2 and Table 1). Smooth generation of *N*-protonated azomethine ylide from **5** is quite interesting because this ylide is carrying no substituents which are capable of stabilizing the dipole centers.[11] Although similar reaction of the *N*-(silylmethyl)imine **2** bearing a 2-pyridyl substituent with dimethyl fumarate produced cycloadduct **8** when carried out in THF, the same reaction in HMPA afforded a Michael type product **12**. This difference will be discussed later.

The cycloadditions shown in Scheme 2 are exclusively stereospecific and regioselective, but awfully poor in stereoselectivity. In every case was formed an unseparable mixture of two stereoisomeric cycloadducts, endo and exo cycloadducts. Assignment of the stereostructures was based on $J_{3a\text{-}4}$ for **7a** or magnetic shielding of ester methyls by the adjacent phenyl moiety at the 2-position for **7b**, **7d**—**g**, and **8**—**9**. The 2-H of exo isomer (2,3-trans) of **7c** appeared in a lower field than that of endo isomer. Two isomers of **10** could not be assigned, but anyhow the isomer ratio was 1:1.

Two geometries are possible for the *N*-protonated azomethine ylide **A**, but *E*-isomer (*E*)-**A** should be much more stable than *Z*-isomer (*Z*)-**A** (Scheme 3).[12] Accordingly, two stereoisomers mentioned above are most likely to have been formed through endo and exo approaches of (*E*)-**A**.[13] Although the reason for such poor stereoselectivity can not be explained so far, there are some examples known for poor *endo*-selectivity of nonstabilized azomethine ylides.[14]

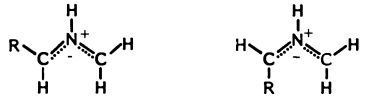

(*E*)-azomethine ylide ≫ (*Z*)-azomethine ylide

Scheme 3.

Fluoride-Induced Generation of 2-Azaallyl Anions. *N*-(Silylmethyl)imines are desilylated by a fluoride ion to generate 2-azaallyl anions **B**, which undergo cycloadditions with unactivated olefins, nucleophilic additions to carbonyl groups, or Michael additions to electron-deficient olefins (Scheme 4). Through these reactions, the anions **B** become synthetic equivalents of aminomethyl anion.

N-(Silylmethyl)imine **1** was treated with *trans*-stilbene in dry HMPA in the presence of cesium fluoride, at 80 °C for 3 d under nitrogen, to give 80% yield of 2,3,4-triphenylpyrrolidine **13** as single stereoisomer. On the basis of the very poor stereospecificity and stereoselectivity in a similar reaction of **1** with *cis*-stilbene,[15] its structure was tentatively assigned to be all-*trans*

Table 2. Nucleophilic Addition of 2-Azaallyl Anions Generated from *N*-(Silylmethyl)imines[a)]

Imine	Electrophile	Conditions[b)]	Product	Yield/%[c)]	Subsequent work-up[d)]
1	PhCHO	A	**16**	100	—
1	PhCHO	A	**17a**	88	A
1	2-Furancarbaldehyde	A	**17b**	73	A
1	3-Pyridinecarbaldehyde	A	**17c**	51	A
1	PhCOMe	A	**17d**	60	A
1	Fluorenone	A	**17e**	88	A
1	Dimethyl fumarate	B	**19a**	97	—
1	Dimethyl fumarate	B	**22a**	51	B
1	Methyl cinnamate	B	**22b**	60	B
1	Methyl methacrylate	B	**22c**	48	B
3	Benzylideneacetone	C	**23**	60	A
4	Dimethyl fumarate	C	**24**	100	—
6	Benzylideneacetone	D	**23**	77	A
6	Methyl acrylate	D	**25**	55	C

a) All reactions were carried out with equivalents of imines and electrophiles in the presence of TBAF (10 mol%). b) A: At room temperature for 48 h in DMF; B: At room temperature for 36 h in DMF in the presence of one equivalent of water; C: At 0 °C for 30 min in THF; D: At room temperature for 12 h in DMF in the presence of one equivalent of water. c) Isolated yield. d) A: Chromatographed over silica gel with MeOH–EtOAc (1:3); B: Reduced with $NaBH_4$ in MeOH at room temperature; C: Hydrolyzed with concd HCl in MeOH at room temperature and then acetylated with Ac_2O in the presence of pyridine at room temperature.

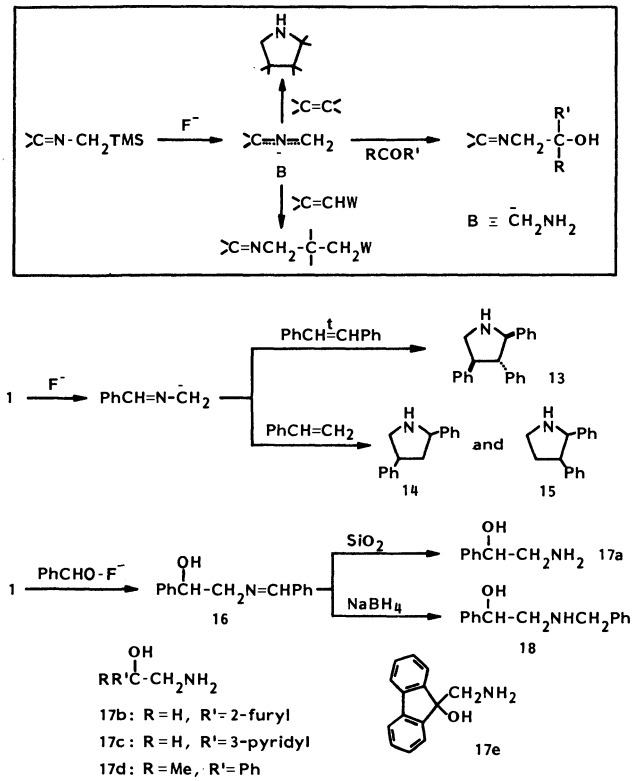

Scheme 4.

isomer that is thermodynamically most stable. Two regioisomeric cycloadducts **14** and **15** were obtained in the reaction of **1** with styrene under similar conditions, but their stereostructures could not be determined. In these reactions, a catalytic amount (0.1 equivalent) of cesium fluoride was sufficient.

As the imine **1** is inactive toward such unactivated olefins as stilbene and styrene in the presence of water, it is apparent that the reaction in the presence of cesium fluoride involves a reactive species other than *N*-protonated azomethine ylide **A**. 2-Azaallyl anion **B** will be the species involved. So we tried to capture **B** with aldehydes.

When **1** was treated with benzaldehyde in dry DMF in the presence of cesium fluoride at room temperature, a quantitative yield of 2-benzylideneamino-1-phenylethanol **16** was obtained (Scheme 4 and Table 2). This imine **16** was readily hydrolyzed into 2-amino-1-phenylethanol **17a** or reduced with sodium borohydride into its *N*-benzyl derivative **18**. The exclusive formation of **16** indicates that the 2-azaallyl anion from **1** undergoes highly regioselective nucleophilic addition with aldehydes at the carbon which was substituted with the silyl moiety. Thus, *N*-(silylmethyl)imine **1** can be a good reagent for nucleophilic aminomethylation. Therefore, similar reactions with some other carbonyl compounds were carried out. After the reactions were over, the crude reaction mixtures were subjected to column chromatography over silica gel to give hydrolyzed products, 2-aminoethanols **17b**—**e**.

Although some examples are known for the Michael addition reaction using ester-stabilized 2-azaallyl anion,[16] no nucleophilic aminomethylation using nonstabilized 2-azaallyl anion **B** has been reported so far.[17]

The 2-azaallyl anion generated from **1** and tetrabutylammonium fluoride was trapped with dimethyl fumarate at room temperature to give a regioselective Michael adduct **19a** in a quantitative yield (Scheme 5 and Table 2). One equivalent amount of water was used in this reaction, since otherwise the fumarate as a Michael acceptor readily polymerized. The adduct **19a** was hydrolyzed providing amino diester **20** which then cyclized into 2-pyrrolidinone **21** when treated with triethylamine, or it was reduced with sodium borohydride to give *N*-benzyl-2-pyrrolidinone **22a**

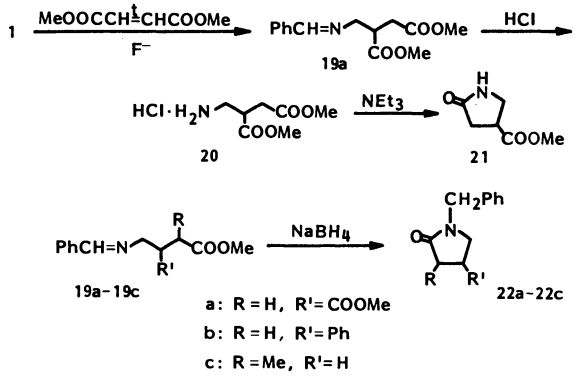

Scheme 5.

after spontaneous cyclization. Among these two sequences which look promising as a new synthetic method of 2-pyrrolidinones, the latter sequence seems more useful because all the procedures can be performed in the same flask. So the one-flask reaction was applied to some other Michael acceptors such as methyl cinnamate and methyl methacrylate to afford the corresponding *N*-benzyl-2-pyrrolidinones **22b** and **22c** (Table 2).[18]

One serious limitation is that olefins such as acrylates and methyl vinyl ketone polymerize under the reaction conditions even if water is present as an inhibitor. Such ready polymerization of olefins presumably results from the lack of stability of the 2-azaallyl anion from **1**. Therefore, several *N*-(silylmethyl)imines **3**, **4**, and **6** carrying anion-stabilizing substituents other than phenyl were examined.

The imine **3** with a 1-naphthyl moiety was easily desilylated under very mild conditions. The anion generated underwent the Michael addition to benzylideneacetone followed by subsequent hydrolysis and cyclization providing 1-pyrroline **23** (Scheme 6 and Table 2). In this reaction, no water was needed. The 2-azaallyl anion generated from **4** also under mild conditions added to dimethyl fumarate in the absence of water to give a quantitative yield of **24**. However, the Michael addition using **3** is not highly regioselective,[19] and the anion from **4** undergoes ready oxidative coupling reaction especially if the Michael acceptor employed is not highly reactive.[20]

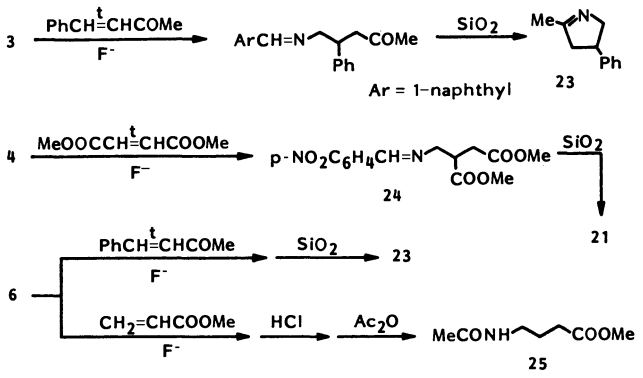

Scheme. 6.

So far the 2-azaallyl anion from **6** is most promising. With benzylideneacetone, 1-pyrroline **23** was obtained in 77% yield. The reaction with methyl acrylate produced 55% of methyl 4-acetamidopropanoate **25** after subsequent hydrolysis and acetylation (Scheme 6 and Table 2).

Thus, *N*-(silylmethyl)imines generate azomethine ylide 1,3-dipoles if desilylated after *N*-protonation and 2-azaallyl anions if directly desilylated. Although *N*-protonated azomethine ylides **A** and 2-azaallyl anions **B** are isoelectronic to each other, they show completely different chemical properties. Only structural difference is that the nonbonding electron pair on the nitrogen of **B** is used for the N–H bond in **A** (Scheme 7). This means that *N*-protonated azomethine ylides

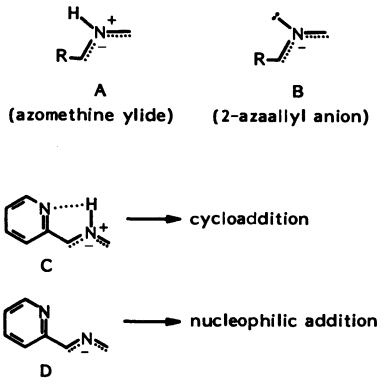

Scheme 7.

A and 2-azaallyl anions **B** would be interconvertible to each other by protonation and deprotonation procedure. As described above, the reaction of imine **2** with dimethyl fumarate in THF in the presence of water produced pyrrolidine **8** which is a product expected from azomethine ylide **C**, whereas the same reaction in HMPA provided imine **12** expected from 2-azaallyl anion **D**. Probably the NH hydrogen of **C** is coordinating with the pyridine nitrogen so that the N–H bond may be weakened. In less polar solvent, THF, the hydrogen will be still sitting on the imine nitrogen, allowing the cycloaddition as azomethine ylide **C**. In highly polar HMPA, this hydrogen no longer stays on the imine nitrogen and hence the species involved is no longer azomethine ylide **C** but 2-azaallyl anion **D**. Nucleophilic addition is the reaction which actually took place.

Experimental

General. Melting points were determined on a Yanagimoto micro melting point apparatus and are uncorrected. IR spectra were taken with a JASCO IRA-1 or a JASCO A-702 spectrometer. ^{1}H NMR spectra were recorded on a Hitachi R-40 (90 MHz) or a JEOL FX-100 instrument (100 MHz) and ^{13}C NMR spectra on a JEOL FX-100 spectrometer at 25.05 MHz. Chemical shifts are expressed in parts per million downfield from tetramethylsilane as internal standard. Mass spectra were measured with a JEOL JMS-01SG-2 spectrometer at 70 eV of ionization energy. Ele-

mental analyses were performed on a Hitachi 026 CHN micro analyzer. Thin-layer chromatography (TLC) was accomplished on 0.2 mm precoated plates of silica gel 60F-254 (Merck) or of aluminum oxide 60 F-254 type-E (Merck). Visualization was made with ultraviolet light (254 and 365 nm) and iodine. For preparative column chromatography, Wakogel C-200, C-300 (Wako), or Kieselgel 60 (230—400 mesh, Merck) was used. Flash chromatography was carried out on an EYELA EF-10 apparatus using a column (20×180 mm) packed with Silicagel 60 (Merck, size: 0.04—0.063 mm). Gas liquid chromatography (GLC) was accomplished on a Yanaco G-2800 gas chromatography (Yanagimoto) with an ionization detector using a glass column (SE-30, 3×2000 mm). Micro vacuum distillation was performed with a Sibata GTO-250R Kugelrohr distilling apparatus. Solvents were evaporated with a Tokyo Rikakikai rotary evaporator type-V at about 50°C unless otherwise stated.

Preparation of *N*-(Silylmethyl)imines 1—6. The imines were prepared according to either of the following three methods: A: Imines **1**, **2**, and **5** were prepared according to the known method using trimethylsilylmethyl azide, triphenylphosphine, and the corresponding aldehydes.[8] B: A mixture of trimethylsilylmethylamine (40 mmol) and an aldehyde (44 mmol) was stirred in ethanol (10 ml) at room temperature. The ethanol was evaporated in vacuo and the residue was dissolved in dichloromethane (20 ml). The solution was dried on magnesium sulfate and evaporated in vacuo. Crude imines **2**—**4** thus obtained all in quantitative yields were purified through vacuum distillation. C: To a solution of Et_3Al (16% in hexane, 30 ml, 30 mmol) in dry benzene (40 ml) was added trimethylsilylmethylamine (3.09 g, 30 mmol) at room temperature. The mixture was heated under reflux under nitrogen for 0.5 h. The mixture was refluxed with benzophenone (3.64 g, 20 mmol) for 1.5 h, treated with ethanol (5 ml), and poured into an aqueous solution of sodium tartrate (10%). Organic materials were extracted with dichloromethane (100 ml), the extract was dried over magnesium sulfate, and evaporated in vacuo to give almost pure **6** (5.30 g, 99%, purity 99% (GLC)).

Imines **1** (89%), **2** (72% by method A; 88% by method B), and **5** (58%) are all known compounds.[8]

3: Colorless liquid; yield 82%; bp 115—118°C/27 Pa; IR (neat) 1630, 1245, and 850 cm^{-1}; ^1H NMR ($CDCl_3$) δ=0.12 (9H, s, TMS), 3.47 (2H, d, J=1.5 Hz, CH_2), 7.2—7.5 (3H, m, Ar), 7.6—7.9 (3H, m, Ar), 8.64 (1H, t, J=1.5 Hz, N=CH), and 8.7—8.9 (1H, m, Ar); MS m/z (rel intensity, %) 241 (M^+, 51), 240 (base peak), 168 (35), 167 (23), 141 (21), and 73 (99). HRMS Found: m/z 241.1212. Calcd for $C_{15}H_{19}NSi$: M, 241.1286.

4: Colorless liquid; yield 100%; bp 107—110°C/107 Pa; IR (neat) 1600, 1250, and 840 cm^{-1}; ^1H NMR ($CDCl_3$) δ=0.08 (9H, s, TMS), 3.44 (2H, d, J=1, 3 Hz, CH_2), 7.70, 8.12 (each 2H, br d, Ar), and 8.08 (1H, t, J=1.3 Hz, N=CH); MS m/z (rel intensity, %) 236 (M^+, 34), 235 (74), 219 (41), 189 (22), 117 (37), and 73 (base peak). HRMS Found: m/z 236.1021. Calcd for $C_{11}H_{16}N_2O_2Si$: M, 236.0976.

6: Colorless liquid; IR (neat) 1610, 1250, and 840 cm^{-1}; ^1H NMR ($CDCl_3$) δ=0.03 (9H, s, TMS), 3.26 (2H, s, CH_2), and 6.9—7.6 (10H, m, Ph); MS m/z (rel intensity, %) 267 (M^+, base peak), 165 (20), 91 (29), and 73 (38). HRMS Found: m/z 267.1503. Calcd for $C_{17}H_{21}NSi$: M, 267.1442.

General Procedure for the Water-Induced Cycloadditions of *N*-(Silylmethyl)imines with Olefins Leading to 7—11. A mixture of *N*-(silylmethyl)imine and olefin (each 1 mmol) in HMPA or THF (2 ml) was stirred, under nitrogen at room temperature, in the presence of water and acetic acid. Reaction conditions are listed in Tabel 1. After the reaction was completed, the mixture was poured into aqueous sodium hydroxide and extracted with dichloromethane (15 ml×2). The combined extracts were washed with water, dried over magnesium sulfate, and evaporated in vacuo. The residue was chromatographed over silica gel with benzene-ether. All the cycloadducts were obtained as mixtures of two stereoisomers, whose separation was unsuccessful. The results are summarized in Table 1.

7a: Colorless liquid; IR (neat) 3400, 1775, and 1700 cm^{-1}; ^1H NMR ($CDCl_3$) δ=2.11 (1H, s, NH), 2.7—3.8 (4H, m, 3a-, 6-, and 6a-H), 2.85 (1/3×3H, s, NMe), 2.98 (2/3×3H, s, NMe), 4.32 (1/3H, d, J=8.0 Hz, 4-H), 4.60 (2/3H, d, J=2.0 Hz, 4-H), and 7.1—7.5 (5H, m, Ph); ^{13}C NMR ($CDCl_3$) δ=24.78, 25.07 (each q, NMe), 45.91, 46.62 (each d), 48.79, 48.96 (each t, 6-C), 49.32, 53.13 (each d), 64.76, 65.52 (each d, 4-C), 126.11, 126.59, 127.28, 127.75, 128.11 128.58 (each d), 137.79, 141.31 (each s), 175.66, 178.30, 178.77, and 179.18 (each s, CON); MS m/z (rel intensity, %) 230 (M^+, 50), 119 (56), 118 (base peak), and 106 (20). HRMS Found: m/z 230.1059. Calcd for $C_{13}H_{14}N_2O_2$: M, 230.1054.

7b: Colorless liquid; IR (neat) 3400 and 1730 cm^{-1}; ^1H NMR ($CDCl_3$) δ=2.32 (1H, br s, NH), 3.0—3.9 (4H, m, 3-, 4-, and 5-H), 3.15 (1/2×3H, s, 3-COOMe), 3.63 (1/2×3H, s, COOMe), 3.70 (3H, s, COOMe), 4.27 (1/2H, d, J=7.0 Hz, 2-H), 4.50 (1/2H, d, J=8.0 Hz, 2-H), and 7.1—7.5 (5H, m, Ph); ^{13}C NMR ($CDCl_3$) δ=47.14, 48.67, 50.20, 50.43, 50.90, 51.67, 51.78, 52.66, 54.89 (d), 65.87, 67.34 (each d, 2-C), 126.40, 127.05, 127.28, 127.64, 128.11 (each d), 138.37, 140.61 (each s), 172.31, 173.19, and 173.78 (each s, COOMe); MS m/z (rel intensity, %) 263 (M^+, 80), 232 (40), 204 (30), 177 (47), 144 (26), 119 (91), and 118 (base peak). Found: C, 63.89; H, 6.60; N, 5.15%. Calcd for $C_{14}H_{17}NO_4$: C, 63.87; H, 6.51; N, 5.32%.

7c: Colorless liquid; bp 150°C/400 Pa; IR (neat) 3350 and 2240 cm^{-1}; ^1H NMR ($CDCl_3$) δ=2.29 (1H, br, NH), 2.9—3.8 (4H, m, 3-, 4-, and 5-H), 4.25 (7/12H, d, J=9.0 Hz, 2-H), 4.46 (5/12H, d, J=7.0 Hz, 2-H), and 7.2—7.5 (5H, m, Ph); ^{13}C NMR (DMSO-d_6) δ=33.02, 33.09 (each d), 50.26, (t, 5-C), 63.94, 66.99 (each, d, 2-C), 118.48, 118.77, 119.71, 120.06 (each, s, CN), 126.81, 127. 05, 127.74, 128.11, 128.52 (each, d), 137.97, and 138.26 (each s); MS m/z (rel intensity, %) 197 (M^+, 28), 119 (36), 118 (base peak), 91 (40), 89 (31), and 77 (37). Found: C, 73.23; H, 5.70; N, 21.28%. Calcd for $C_{12}H_{11}N_3$: C, 73.07; H, 5.62; N, 21.31%.

7d: Colorless liquid; IR (neat) 3320 and 1720 cm^{-1}; ^1H NMR ($CDCl_3$) δ=2.60 (1H, br, NH), 2.9—4.0 (4H, m, 3-, 4-, and 5-H), 3.11 (3/4×3H, s, COOMe), 3.55 (1/4×3H, s, COOMe), 4.55 (1/4H, d, J=9.0 Hz, 2-H), 4.70 (3/4H, d, J=9.0 Hz, 2-H), and 7.0—7.5 (10H, m, Ph); MS m/z (rel intensity, %) 281 (M^+, 9), 131 (24), 119 (72), 118 (base peak), 117 (38), 115 (37), 103 (32), 91 (40), and 77 (30). Found: C, 77.04; H, 7.06; N, 4.72%. Calcd for $C_{18}H_{19}NO_2$: C, 76.84; H, 6.81; N, 4.98%.

7e: Colorless liquid; IR (neat) 3310 and 1725 cm^{-1}; ^1H NMR ($CDCl_3$) δ=1.10, 1.13 (3H, each d, J=6.0 Hz, 4-Me), 2.30 (1H, s, NH), 2.4—3.6 (4H, m, 3-, 4-, and 5-H), 3.16 (2/3×3H, s, COOMe), 3.61 (1/3×3H, s, COOMe), 4.44 (1/3H, d, J=8.0 Hz, 2-H), 4.46 (2/3H, d, J=8.0 Hz, 2-H), and 7.1—7.4 (5H, m, Ph); ^{13}C NMR ($CDCl_3$) δ=18.14, 18.32 (each q, 4-Me), 37.40, 40.39 (each d, 4-C), 50.78, 51.55 (each q, COOMe), 54.25, 54.78 (each t, 5-C), 57.71, 60.35 (each d, 3-C),

65.17, 66.40 (each d, 2-C), 126.28, 126.64, 126.93, 127.40, 127.75, 128.05, 128.22 (each d), 140.08, 142.67 (each d), 173.31, and 174.37 (each s, COOMe); MS *m/z* (rel intensity, %) 219 (M^+, 40), 119 (76), and 118 (base peak); HRMS Found: *m/z* 219.1273. Calcd for $C_{13}H_{17}NO_2$: M, 219.1258.

7f: Colorless liquid; IR (neat) 3400 and 1740 cm^{-1}; ^1H NMR ($CDCl_3$) δ=2.33 (1H, s, NH), 3.1—3.5 (4H, m, 3-, 4-, and 5-H), 3.20 (3/10×3H, s, COOMe), 3.62, 3.63 (3H+7/10×3H, each s, COOMe), 4.39 (3/10H, d, *J*=6.0 Hz, 2-H), 4.59 (7/10H, d, *J*=6.0 Hz, 2-H), and 7.1—7.5 (5H, m, Ph); ^{13}C NMR ($CDCl_3$) δ=47.67, 49.85, 51.08, 51.90, 55.07, 64.76, 67.28, 126.34, 126.46, 127.22, 127.40, 128.11, 128.40, 142.84, 172.14, 172.31, 172.61, and 172.84; MS *m/z* (rel intensity, %) 263 (M^+, 8), 144 (59), 143 (21), 119 (51), 118 (base peak), 117 (32), 115 (50), 104 (25), 91 (49), and 77 (31). Found:, C, 64.14; H, 6.58; N, 5.24%. Calcd for $C_{14}H_{17}NO$: C, 63.87; H, 6.51; N, 5.32%.

7g: Colorless liquid; bp 95 °C/532 Pa; IR (neat) 3320 and 1725 cm^{-1}; ^1H NMR ($CDCl_3$) δ=0.84 (3/7×3H, s, 3-Me), 1.37 (4/7×3H, s, 3-Me), 1.5—1.9 (1H, m), 2.2—2.7 (1H, m), 2.35 (1H, br s, NH), 2.9—3.5 (2H, m), 3.17 (4/7×3H, s, COOMe), 3.66 (3/7×3H, s, COOMe), 3.84 (4/7H, s, 2-H), 4.55 (3/7H, s, 2-H), and 7.1—7.3 (5H, m, Ph); ^{13}C NMR ($CDCl_3$) δ=19.96, 22.90 (each q, 3-Me), 38.16, 38.75 (each t, 4-C), 44.74, 45.62 (each t, 5-C), 51.20, 51.96 (each q, COOMe), 54.89 (s, 3-C), 68.57, 74.15 (each d, 2-C), 126.58, 127.05, 127.28, 127.46, 127.87 (each d), 139.14, 140.20 (each s), 175.60, and 177.48 (each s, COOMe); MS *m/z* (rel intensity, %) 219 (M^+, 32), 119 (79), and 118 (base peak). Found: C, 71.46; H, 8.08; N, 6.64%. Calcd for $C_{13}H_{17}NO_2$: C, 71.20; H, 7.82; N, 6.39%.

8: Colorless liquid; IR (neat) 3400, 1730, and 1600 cm^{-1}; ^1H NMR ($CDCl_3$) δ=3.0—3.8 (4H, m, 3-, 4-, and 5-H), 3.20 (3/4×3H, s, COOMe), 3.32 (1H, s, NH), 3.66 (3H+3/4H, s, COOMe), 4.34 (1/4H, d, *J*=7.0 Hz, 2-H), 4.57 (3/4H, d, *J*=7.0 Hz, 2-H), 7.4—7.7 (3H, m, Py), and 8.40 (1H, br d, Py); MS *m/z* (rel intensity, %) 264 (M^+, 10), 145 (91), 132 (28), 126 (23), 120 (21), 119 (65), 118 (43), 117 (55), 105 (23), 92 (49), 79 (54), 78 (74), and 59 (base peak). Found: C, 59.93; H, 6.11; N, 10.32%. Calcd for $C_{13}H_{16}N_2O_4$: C, 59.08; H, 6.10; N, 10.60%.

9: Colorless liquid; IR (neat) 3400 and 1730 cm^{-1}; ^1H NMR ($CDCl_3$) δ=2.28 (1H, br s, NH), 2.80 (4/9×3H, s, COOMe), 3.0—3.9 (4H, m, 3-, 4-, and 5-H), 3.56, 3.68 (each 5/9×3H, s, COOMe), 3.74 (4/9×3H, s, COOMe), 5.10 (4/9H, d, *J*=7.0 Hz, 2-H), 5.20 (5/9H, d, *J*=8.0 Hz, 2-H), and 7.3—8.2 (7H, m, Ar); MS *m/z* (rel intensity, %) 313 (M^+, 24), 194 (39), 193 (20), 169 (43), 168 (base peak), 167 (52), 166 (29), 165 (57), 154 (37), 153 (24), 141 (25), 139 (23), 128 (24), 127 (38), 115 (22), and 113 (22). Found: C, 69.05; H, 6.15; N, 4.68%. Calcd for $C_{18}H_{19}NO_4$: C, 68.99; H, 6.11; N, 4.47%.

10: Colorless liquid; IR (neat) 3400 and 1730 cm^{-1}; ^1H NMR ($CDCl_3$) δ=0.93, 0.98 (each 1/2×9H, s, *t*-Bu), 1.96 (1H, br s, NH), 2.8—3.4 (6H, m, 2-, 3-, 4-, and 5-H), 3.65 and 3.67 (6H, each s, COOMe); ^{13}C NMR ($CDCl_3$) δ=26.54, 27.42 (each q, *t*-Bu), 32.41, 33.64 (each s, *q*-C), 48.55, 48.79, 49.14, 50.31, 51.02, 51.67, 52.02, 73.74 (d, 2-C), 74.50 (d, 2-C), 173.84, 174.25, 175.01, and 175.48 (each s, COOMe); MS *m/z* (rel intensity, %) 243 (M^+, 7), 186 (33), 154 (base peak), 126 (78), and 68 (38). Found: C, 59.01; H, 8.91; N, 5.81%. Calcd for $C_{12}H_{21}NO_4$: C, 59.24; H, 8.70; N, 5.76%.

11: Colorless needles; mp 140.5 °C; IR (KBr) 3400 and 1720 cm^{-1}; ^1H NMR ($CDCl_3$) δ=2.74 (1H, br, NH), 3.0—3.7 (3H, m, 4- and 5-H), 3.24, 3.47 (each 3H, s, COOMe), 4.35 (1H, d, *J*=5.0 Hz, 3-H), and 7.0—7.6 (10H, m, Ph); MS *m/z* (rel intensity, %) 339 (M^+, 5), 220 (25), 202 (49), 195 (34), 194 (base peak), 191 (21), 170 (36), 165 (55), 144 (46), 143 (49), 117 (21), 115 (43), 104 (29), 91 (36), and 77 (53). Found: C, 70.96; H, 6.28; N, 4.21%. Calcd for $C_{20}H_{21}NO_4$: C, 70.78; H, 6.24; N, 4.13%.

12: Colorless liquid; IR (neat) 1740 and 1590 cm^{-1}; ^1H NMR ($CDCl_3$) δ=2.72 (1H, t, *J*=6.5 Hz), 3.1—3.5 (2H, m), 3.62, 3.66 (each 3H, s, COOMe), 3.87 (2H, d, *J*=7.0 Hz, NCH_2), 7.0—7.9 (3H, m, Py), 8.25 (1H, br s, CH=N), and 8.50 (1H, br d, Py); MS *m/z* 264 (M^+). Found: C, 59.23; H, 6.12; N, 10.35%. Calcd for $C_{13}H_{16}N_2O_4$: C, 59.08; H, 6.10; N, 10.60%.

Reaction of 1 with *trans*-Stilbene Leading to 13. A mixture of **1** (191 mg, 1 mmol), *trans*-stilbene (180 mg, 1 mmol), and cesium fluoride (CsF, 15 mg, 0.1 mmol) in dry HMPA (2 ml) was heated under nitrogen at 80 °C for 3 d. The mixture was poured into aqueous sodium hydrogencarbonate and extracted with dichloromethane (15 ml×2). The dichloromethane was washed with water, dried over magnesium sulfate, and evaporated in vacuo. The residue was chromatographed over silica gel with hexane–ethyl acetate (2:1) to give **13** (239 mg, 80%): Colorless prisms; mp 64—67 °C; IR (KBr) 3340 cm^{-1}; ^1H NMR ($CDCl_3$) δ=2.20 (1H, s, NH), 3.1—3.8 (4H, m, 3-, 4-, and 5-H), 4.35 (1H, d, 2-H), and 6.8—7.4 (15H, m, Ph); ^{13}C NMR ($CDCl_3$) δ=54.19 (d, 4-C), 54.60 (t, 5-C), 63.06 (d, 3-C), 71.04 (d, 2-C), 126.28, 126.64, 126.99, 127.28, 127.87, 128.22, 128.34, 128.87 (each d), 140.44, 142.55, and 143.02 (each s); MS *m/z* (rel intensity, %) 299 (M^+, base peak), 180 (21), 179 (25), 178 (25), 119 (25), 118 (27), and 91 (35). Found: C, 88.27; H, 7.11; N, 4.51%. Calcd for $C_{22}H_{21}N$: C, 88.25; H, 7.07; N, 4.68%.

Reaction of 1 with Styrene Leading to 14 and 15. A mixture of **1** (382 mg, 2 mmol), styrene (416 mg, 4 mmol), and CsF (30 mg, 0.2 mmol) was heated under nitrogen at 80 °C for 3 h. The same work-up as above gave **14** (152 mg, 34%) and **15** (71 mg, 16%).

14: Colorless prisms; mp 61—63.5 °C; IR (KBr) 3300 cm^{-1}; ^1H NMR ($CDCl_3$) δ=2.1—2.4 (2H, m, 3-H), 2.32 (1H, s, NH), 2.9—3.7 (3H, m, 4- and 5-H), 4.39 (1H, t, *J*=7.5 Hz, 2-H), and 7.1—7.5 (10H, m, Ph); ^{13}C NMR ($CDCl_3$) δ=42.51 (t, 3-C), 44.80 (d, 4-C), 55.54 (t, 5-C), 62.47 (d, 2-C), 126.23, 126.46, 126.87, 127.28, 128.40 (each d), 144.01, and 144.90 (each s); MS *m/z* (rel intensity, %) 223 (M^+, 21), 119 (56), 118 (base peak), 115 (21), 91 (31), and 77 (24). Found: C, 86.05; H, 7.69; N, 6.32%. Calcd for $C_{16}H_{17}N$: C, 86.05; H, 7.67; N, 6.27%.

15: Colorless liquid; IR (neat) 3300 cm^{-1}; ^1H NMR ($CDCl_3$) δ=1.9—2.5 (2H, m, 4-H), 2.40 (1H, br s, NH), 2.9—3.5 (3H, m, 3- and 5-H), 4.05 (1H, d, *J*=8.5 Hz, 2-H), and 7.0—7.3 (10H, m, Ph); ^{13}C NMR ($CDCl_3$) δ=35.13 (t, 4-C), 46.49 (t, 5-C), 53.94 (d, 3-C), 70.71 (d, 2-C), 126.21, 126.70, 126.94, 127.56, 128.16, 128.26 (each d), 142.63, and 142.78 (each s); MS *m/z* (rel intensity, %) 223 (M^+, 29), 119 (80), and 118 (base peak). Found: C, 86.18; H, 7.72; N, 6.45%. Calcd for $C_{16}H_{17}N$: C, 86.05; H, 7.67; N, 6.27%.

Reaction of 1 with Benzaldehyde Leading to 16. To a mixture of **1** (191 mg, 1 mmol) and benzaldehyde (106 mg, 1 mmol) in dry DMF (2 ml) was added at 0 °C tetrabutylammonium fluoride (TBAF, 1M solution in THF, 0.1 ml, 0.1 mmol). The mixture was stirred under nitrogen at room temperature for 2 d, poured into aqueous sodium hydrogencarbonate, and extracted with dichloromethane (15 ml×2). The conbined extracts were dried over magnesium sulfate and evaporated in vacuo to give crude **16** (195 mg, 100%): Colorless prisms (hexane); mp 114.5 °C; IR (KBr) 3400

and 1640 cm^{-1}; ^1H NMR ($CDCl_3$) δ=3.00 (1H, br, OH, exchanged with D_2O), 3.4—4.0 (2H, m, NCH_2), 4.95 (1H, dd, J=8.5 and 4.0 Hz, CH), 7.1—7.8 (10H, m, Ph), and 8.20 (1H, br s, CH=N); MS *m/z* (rel intensity, %) 194 (M^+, base peak), 91 (25), 89 (22), and 77 (31). Found: C, 80.10; H, 6.64; N, 6.15%. Calcd for $C_{15}H_{15}NO$: C, 79.97; H, 6.71; N, 6.22%.

General Procedure for the One-Pot Synthesis of 17. To a mixture of **1** (382 mg, 2 mmol) and carbonyl compounds (2 mmol) in dry DMF (4 ml) was added TBAF (1M in THF (1M=1 mol dm^{-3}), 0.2 ml) at 0°C. The mixture was allowed to stir under nitrogen at room temperature for 2 d, treated with aqueous sodium hydrogencarbonate, and extracted with dichloromethane (20 ml×2). The combined extracts were dried over magnesium sulfate and evaporated in vacuo. The residue was filtered through a long column packed with silica gel using ethyl acetate-methanol (3:1) to give **17**. The results are summarized in Table 2.

17a: Colorless prisms; mp 54—56°C (lit,[21] mp 57°C); IR (KBr) 3200—3600 cm^{-1}; ^1H NMR ($CDCl_3$) δ=2.50 (3H, br s, OH and NH_2), 2.78 (2H, m, CH_2), 4.50 (1H, dd, J=7.2 and 4.6 Hz, CH), and 7.2—7.3 (5H, br s, Ph); MS *m/z* (rel intensity, %) 118 (23), 117 (16), 107 (19), 105 (30), 91 (47), 90 (13), 89 (18), 79 (75), 78 (37), and 77 (base peak).

17b: Colorless needles; mp 85—87.5°C; IR (KBr) 2700—3300 cm^{-1}; ^1H NMR ($CDCl_3$) δ=2.70 (3H, br s, OH and NH_2), 2.88 (2H, d, J=6.0 Hz, CH_2), 4.51 (1H, t, J=6.0 Hz, CH), 6.12, 6.22, and 7.22 (each 1H, dd, 2-Furyl); MS *m/z* (rel intensity, %) 127 (M^+, 23), 98 (37), 97 (70), 69 (30), and 41 (base peak). Found: C, 56.84; H, 7.11; N, 10.95%. Calcd for $C_6H_9NO_2$: C, 56.68; H, 7.14; N, 11.02%.

17c: Colorless liquid; bp 140°C/107 Pa; IR (neat) 2800—3400 cm^{-1}; ^1H NMR (DMSO-d_6) δ=2.67 (2H, d, J=5.5 Hz, CH_2), 3.10 (3H, br, OH and NH_2), 4.55 (1H, t, J=5.5 Hz, CH), 7.30, 7.70, 8.42, and 8.49 (each 1H, dd, dt, dd, and d, respectively, 3-Py); MS *m/z* (rel intensity, %) 109 (base peak), 108 (61), 80 (13), and 53 (10). HRMS Found: *m/z* 138.0793. Calcd for $C_7H_{10}N_2O$: M, 138.0788.

17d: Colorless liquid; bp 95°C/13 Pa; IR (neat) 2800—3400 cm^{-1}; ^1H NMR ($CDCl_3$) δ=1.44 (3H, s, Me), 2.12 (3H, s, OH and NH_2), 2.75, 3.06 (each 1H, d, J=10.5 Hz, CH_2), and 7.1—7.5 (5H, m, Ph); MS *m/z* (rel intensity, %) 151 (M^+, 1), 121 (32), 105 (51), 91 (28), 78 (49), 77 (99), 51 (33), and 43 (base peak). HRMS Found: *m/z* 151.0999. Calcd for $C_9H_{13}NO$: M, 151.0996.

17e: Colorless needles; mp 134.5—135.5°C; IR (KBr) 2700—3400 cm^{-1}; ^1H NMR ($CDCl_3$) δ=2.03 (3H, br, OH and NH_2), 2.74 (2H, s, CH_2), and 7.1—7.6 (8H, m, Ar); MS *m/z* (rel intensity, %) 211 (M^+, 9), 182 (24), 181 (82), 180 (25), 153 (base peak), 152 (35), and 151 (19). Found: C, 79.66; H, 6.25; N, 6.61%. Calcd for $C_{14}H_{13}NO$: C, 79.59; H, 6.20; N, 6.63%.

Reduction of 16 with Sodium Borohydride Leading to 18. To a solution of **16** (225 mg, 1mmol) in methanol (2 ml) was added little by little sodium borohydride (38 mg, 1 mmol) under cooling with ice. After 10 min, acetone (10 ml) was added and the mixture was evaporated in vacuo. The residue was treated with water (10 ml) and extracted with dichloromethane (20 ml). The extract was dried over magnesium sulfate and evaporated in vacuo to give **18** (159 mg, 70%): Colorless needles (hexane); mp 100—101°C; IR (KBr) 2700—3200 and 1430 cm^{-1}; ^1H NMR ($CDCl_3$) δ=2.70 (2H, two d, J=7.4 and 5.2 Hz, CH_2), 3.28 (2H, br, OH and NH), 3.64 (2H, s, $PhCH_2$), 4.69 (1H, dd, J=7.4 and 5.2 Hz, CH), and 7.1—7.3 (10H, m, Ph); ^{13}C NMR ($CDCl_3$) δ=53.41 (t, CH_2), 56.53 (t, $PhCH_2$), 71.83 (d, CH), 125.77, 126.99, 127.28, 128.06, 128.20, 128.35 (each d), 139.56, and 142.92 (each s); MS *m/z* (rel intensity, %) 227 (M^+, 5), 121 (base peak), 118 (23), 107 (28), 92 (70), 79 (40), and 77 (49). Found: C, 79.40; H, 7.54; N, 6.21%. Calcd for $C_{15}H_{17}NO$: C, 79.26; H, 7.54; N, 6.16%.

Reaction of 1 with Dimethyl Fumarate Leading to 19a. To a solution of **1** (382 mg, 2 mmol), dimethyl fumarate (288 mg, 2 mmol), and water (32 mg, 2 mmol) in DMF (2 ml) was added TBAF (1M in THF, 0.2 ml, 0.2 mmol) at 0°C. The mixture was stirred at room temperature for 36 h and evaporated in vacuo. The residue was dissolved in dichloromethane, the dichloromethane was washed with water, dried over magnesium sulfate, and evaporated in vacuo to give **19a** (518 mg, 98%, purity: 99% by GLC): Colorless liquid; bp 145°C/53 Pa; IR (neat) 1730 and 1640 cm^{-1}; ^1H NMR ($CDCl_3$) δ=2.72 (2H, m, CH_2), 3.27 (1H, m, CH), 3.63, 3.68 (each 3H, s, COOMe), 3.84 (2H, dd, J=6.5 and 1.5 Hz, NCH_2), 7.2—7.8 (5H, m, Ph), and 8.23 (1H, d, J=1.5 Hz, CH=N); MS *m/z* (rel intensity, %) 263 (M^+, 59), 232 (66), 204 (64), 203 (30), 195 (25), 190 (56), 158 (36), 118 (60), and 91 (base peak). Found: C, 63.73; H, 6.56; N, 5.49%. Calcd for $C_{14}H_{17}NO_4$: C, 63.86; H, 6.51; N, 5.32%.

Hydrolysis of 19a into 20 and Cyclization of 20 Leading to 21. To a solution of **19a** (616 mg, 2.3 mmol) in methanol (1 ml) was added a few drops of conc HCl. After 5 min at room temperature, diethyl ether (50 ml) was added to give colorless precipitate of **20** (331 mg, 68%). This hydrochloride **20** (300 mg, 1.4 mmol) was dissolved in methanol (5 ml) and triethylamine (1 ml) was added. The mixture was heated under reflux for 2 h. The methanol was evaporated in vacuo. To the resude was added dry diethyl ether (20 ml). The ether was dried over magnesium sulfate and evaporated in vacuo to give **21** (191 mg, 94%).

20: Colorless prisms (ethyl acetate-methanol); mp 178—179.5°C; IR (KBr) 2800—3200, 1730, and 1595 cm^{-1}; ^1H NMR (DMSO-d_6) δ=2.4—3.3 (5H, m, CH_2 and CH), 3.58, 3.62 (each 3H, s, COOMe), and 8.35 (2H, br, NH); MS *m/z* (rel intensity, %) 176 (M^++1, 2), 144 (15), 115 (13), 114 (14), 102 (32), 70 (24), 56 (20), 55 (25), and 30 (base peak). Found: C, 39.84; H, 6.66; N, 6.64%. Calcd for $C_7H_{14}NO_4Cl$: C, 39.73; H, 6.67; N, 6.62%.

21: Colorless liquid; IR (neat) 3300 and 1800—1650 cm^{-1}; ^1H NMR ($CDCl_3$) δ=2.55 (2H, two d, J=8.5 and 7.0 Hz, 3-H), 3.0—3.8 (3H, m, 4- and 5-H), 3.72 (3H, s, COOMe), and 7.50 (1H, br, NH); MS *m/z* (rel intensity, %) 143 (M^+, 10), 116 (85), 113 (20), 101 (73), 100 (21), 87 (25), 84 (50), 83 (69), 70 (31), 59 (30), and 55 (base peak). HRMS Found: *m/z* 143.0599. Calcd for $C_6H_9NO_3$: M, 143.0582.

General Procedure for the One-Pot Synthesis of 22. To a mixture of **1** (382 mg, 2 mmol), electron-poor olefins (2 mmol), and water (2 mmol) was added TBAF (0.2 mmol) at 0°C. The mixture was stirred at room temperature for 36 h and evaporated in vacuo. The residue was dissolved in methanol (4 ml) and sodium borohydride (76 mg, 2 mmol) was added. After 10 min, acetone was added and the mixture was evaporated in vacuo. The residue was treated with water (2 ml) and extracted with dichloromethane (20 ml×2). The combined extracts were dried over magnesium sulfate and evaporated in vacuo. The residue was heated under reflux in methanol for 0.5 h and the methanol was evaporated in vacuo. The crude product was chromatographed over silica gel with hexane-ethyl acetate (3:1) to give **22**. The results are summarized in Table 2.

22a: Colorless liquid; bp 150°C/267 Pa; IR (neat) 1740 and

1680 cm^{-1}; ^{1}H NMR ($CDCl_3$) δ=2.75 (2H, two d, J=9.3 and 6.7 Hz, 3-H), 3.0—3.4 (1H, m, 4-H), 3.46 (2H, two d, J=7.9 and 6.3 Hz, 5-H), 3.64 (3H, s, COOMe), 4.44 (2H, s, $PhCH_2$), and 7.1—7.4 (5H, m, Ph); ^{13}C NMR ($CDCl_3$) δ=33.70 (t, 3-C), 35.52 (d, 4-C), 46.15, 48.12 (each t, 5-C and $PhCH_2$), 52.02 (q, COOMe), 127.34, 127.75, 128.34 (each d), 135.56 (s), 171.96, and 172.78 (each s, COOMe and CON); MS m/z (rel intensity, %) 233 (M^+, 47), 91 (base peak), 65 (34), and 55 (27). Found: C, 66.60; H, 6.64; N, 5.97%. Calcd for $C_{13}H_{15}NO_3$: C, 66.93; H, 6.48; N, 6.01%.

22b: Colorless liquid; bp 160°C/107 Pa; IR (neat) 1690 cm^{-1}; ^{1}H NMR ($CDCl_3$) δ=2.57, 2.89 (each 1H, dd, J=16.7 and 8.3 Hz, 3-H), 3.2—3.7 (3H, m, 4- and 5-H), 4.42, 4.56 (each 1H, d, J=14.5 Hz, $PhCH_2$), and 7.0—7.4 (10H, m, Ph); MS m/z (rel intensity, %) 251 (M^+, 78), 160 (24), 146 (22), 120 (21), 105 (98), and 91 (base peak). Found: C, 81.00; H, 6.79; N, 5.41%. Calcd for $C_{17}H_{17}NO$: C, 81.24; H, 6.82; N, 5.57%.

22c: Colorless liquid; bp 100°C/107 Pa; IR (neat) 1680 cm^{-1}; ^{1}H NMR ($CDCl_3$) δ=1.23 (3H, d, J=6.0 Hz, 3-Me), 1.58 (1H, dq, J=12.3, 8.5, 8.5, and 8.5 Hz, one of 4-H), 2.0—2.7 (2H, m, 3-H and the other of 4-H), 3.14, 3.19 (each 2H, d, J=8.5 Hz, 5-H), 4.42 (2H, s, $PhCH_2$), and 7.1—7.4 (5H, m, Ph); MS m/z (rel intensity, %) 189 (M^+, 85), 107 (27), 98 (42), 92 (22), and 91 (base peak). Found: C, 76.38; H, 7.84; N, 7.25%. Calcd for $C_{12}H_{15}NO$: C, 76.15; H, 7.99; N, 7.40%.

Reaction of 3 with Benzylideneacetone Leading to 23. To a mixture of **3** (482 mg, 1 mmol) and benzylideneacetone (292 mg, 2 mmol) in dry THF (2 ml) was added TBAF (1M in THF, 0.2 ml, 0.2 mmol) at 0°C. The mixture was stirred at 0°C for 30 min and poured into aqueous sodium hydrogencarbonate. Organic products were collected in dichloromethane, the dichloromethane was dried over magnesium sulfate, and evaporated in vacuo. The residue was chromatographed through a long column packed with silica gel using ethyl acetate–methanol (3:1) to give **23** (191 mg, 60%): Colorless liquid; IR (neat) 1650 cm^{-1}; ^{1}H NMR ($CDCl_3$) δ=2.05 (3H, s, 2-Me), 2.54 (1H, dd, J=17.5 and 7.5 Hz, one of 3-H), 2.96 (1H, m, the other of 3-H), 3.48 (1H, m, 4-H), 3.77, 4.24 (each 1H, m, 5-H), and 7.0—7.4 (5H, m, Ph); MS m/z (rel intensity, %) 159 (M^+, 28) and 55 (base peak). HRMS Found: m/z 159.1029. Calcd for $C_{11}H_{13}N$: M, 159.1047.

Reaction of 4 with Dimethyl Fumarate Leading to 24 and Then to 21. A mixture of **4** (572 mg, 2 mmol), dimethyl fumarate (288 mg, 2 mmol), and TBAF (1M in THF, 0.2 mmol) in dry THF (3 ml) was stirred at 0°C for 30 min, or the same mixture in ethanol (2 ml) was stirred at 0°C for 1 h. The resulting mixture was poured into aqueous sodium hydrogencarbonate and extracted with dichloromethane (15 ml×2). The combined extracts were dried over magnesium sulfate and evaporated in vacuo to give **24** in quantitative yields in both cases (^{1}H NMR ($CDCl_3$) δ=2.73 (2H, m, CH_2), 3.25 (1H, m, CH), 3.63, 3.68 (each 3H, s, COOMe), 3.89 (2H, dd, J=5.5 and 1.5 Hz, NCH_2), 7.78, 8.14 (each 2H, d, Ar), and 8.28 (1H, d, J=1.5 Hz, CH=N)). Crude **24** was chromatographed through a long column packed with silica gel using ethyl acetate–methanol (5:1) to give **21** (63% yield).

Reaction of 6 with Benzylideneacetone Leading to 23. A mixture of **6** (267 mg, 1 mmol), benzylideneacetone (146 mg, 1 mmol), TBAF (0.1 mmol), and water (18 mg, 1 mmol) in DMF (2 ml) was stirred at room temperature for 12 h. The same chromatographic work-up as above gave **23** (123 mg, 77%).

Reaction of 6 with Methyl Acrylate and Subsequent Hydrolysis and Acetylation Leading to 25. A mixture of **6** (267 mg, 1 mmol), methyl acrylate (86 mg, 1 mmol), TBAF (0.1 mmol), and water (1 mmol) in DMF (2 ml) was stirred at room temperature for 12 h. The mixture was poured into aqueous sodium hydrogencarbonate and extracted with dichloromethane (15 ml×2). The combined extracts were dried over magnesium sulfate and evaporated in vacuo. To the residue dissolved in methanol (2 ml) was added concentrated HCl (0.5 ml). The mixture was stirred at room temperature for 10 min, neutralized with aqueous sodium carbonate, and extracted with dichloromethane (20 ml). The dichloromethane was dried and evaporated in vacuo. The residue was dissolved in acetic anhydride (2 ml). After pyridine (1 ml) was added, the mixture was stirred at room temperature for 2 h and poured into ice water. Organic products were extracted with dichloromethane (15 ml), the extract was dried, and evaporated in vacuo. The residue was chromatographed over silica gel with ethyl acetate–ethanol (30:1) to give **25** (88 mg, 55%): Colorless liquid; IR (neat) 3300, 1725, and 1650 cm^{-1}; ^{1}H NMR ($CDCl_3$) δ=1.83 (1H, m, CH_2), 1.96 (3H, s, MeCO), 2.37 (2H, t, J=6.5 Hz, CH_2COOMe), 3.29 (2H, t, J=6.0 Hz, NCH_2), 3.67 (3H, s, COOMe), and 5.90 (1H, br, NH, exchanged with D_2O); MS m/z (rel intensity, %) 159 (M^+, 11), 116 (34), 86 (71), and 43 (base peak). HRMS Found: m/z 159.0874. Calcd for $C_7H_{13}NO_3$: M, 159.0895.

References

1) E. Vedejs and G. R. Martinez, *J. Am. Chem. Soc.*, **101**, 6452 (1979).

2) *N*-Silylmethylation of imines: E. Vedejs and G. R. Martinez, *J. Am. Chem. Soc.*, **102**, 7993 (1980); A. Padwa, G. Haffmann, and M. Tomas, *Tetrahedron Lett.*, **24**, 4303 (1983); O. Tsuge, S. Kanemasa, S. Kuraoka, and S. Takenaka, *Chem. Lett.*, **1984**, 279; O. Tsuge, S. Kanemasa, and S. Kuraoka, *Bull. Chem. Soc. Jpn.*, **58**, 1570 (1985). *O*-, *S*-, or *N'*-Alkylation of *N*-(silylmethyl)amides, -thioamides, or -amidines: E. Vedejs and F. G. West, *J. Org. Chem.*, **48**, 4773 (1983); O. Tsuge, S. Kanemasa, and K. Matsuda, *Chem. Lett.*, **1985**, 1411; O. Tsuge, S. Kanemasa, and K. Matsuda, *J. Org. Chem.*, **51**, 1997 (1986). *N*-Protonation of *N*-(silylmethyl)imines: O. Tsuge, S. Kanemasa, T. Yamada, and K. Matsuda, *Heterocycles*, **23**, 2489 (1985). As *N*-alkylation, *N*-acylation, and *N*-silylation of *N*-(silylmethyl)imines, see Refs. 5, 6, and 7, respectively.

3) E. Vedejs, S. Larsen, and F. G. West, *J. Org. Chem.*, **50**, 2170 (1985); R. Smith and T. Livinghouse, *ibid.*, **48**, 1554 (1983); Y. Terao, N. Imai, K. Achiwa, and M. Sekiya, *Chem. Pharm. Bull.*, **30**, 3167 (1982).

4) A. Padwa and Y.-Y. Chen, *Tetrahedron Lett.*, **24**, 3447 (1983); A. Hosomi, Y. Sakata, and H. Sakurai, *Chem. Lett.*, **1984**, 1117; A. Padwa, Y.-Y. Chen, U. Chiacchio, and W. Dent, *Tetrahedron*, **41**, 3529 (1985); A. Padwa, Y.-Y. Chen, W. Dent, and H. Nimmesgern, *J. Org. Chem.*, **50**, 4006 (1985).

5) K. Achiwa, N. Imai, T. Inaoka, and M. Sekiya, *Chem. Pharm. Bull.*, **32**, 2878 (1984); R. Smith and T. Livinghouse, *Tetrahedron*, **41**, 3559 (1985).

6) K. Achiwa and M. Sekiya, *Chem. Lett.*, **1981**, 1213; K. Achiwa, T. Motoyama, and M. Sekiya, *Chem. Pharm. Bull.*, **31**, 3939 (1983); T. Livinghouse and R. Smith, *J. Chem. Soc., Chem. Commun.*, **1983**, 210.

7) K. Achiwa and M. Sekiya, *Tetrahedron Lett.*, **23**, 2589 (1982).

8) O. Tsuge, S. Kanemasa, and K. Matsuda, *Chem., Lett.*,

1983, 1131; O. Tsuge, S. Kanemasa, and K. Matsuda, *J. Org. Chem.*, **49**, 2688 (1984).

9) K. Achiwa, N. Imai, T. Motoyama, and M. Sekiya, *Chem. Lett.*, **1984**, 2041

10) A part of the present work was already reported as a preliminary communication (O. Tsuge, S. Kanemasa, A. Hatada, and K. Matsuda, *Chem. Lett.*, **1984**, 801).

11) Azomethine ylides carrying an alkyl substituent other than *t*-butyl could not be generated by this procedure.

12) As *N*-protonated azomethine ylides **A** are carrying a sterically negligible hydrogen on the ylide nitrogen, relative stability between (*E*)-**A** and (*Z*)-**A** may be estimated by use of their imine tautomers as models. *N*-Benzylidenemethylamine as a model for the azomethine ylide derived from **1** is known to exist predominantly in an *E*-form in solution (C. G. McCarty, "syn-anti Isomerizations and Rearrangements," in "The Chemistry of the Carbon-Nitrogen Double Bond," ed by S. Patai, Interscience Publishers, London, New York, Sydney, Toronto (1970), Chap. 9, pp. 363—464).

13) The poor stereoselectivity in cycloaddition of the *N*-protonated azomethine ylide generated from **1** makes a striking contrast with the exclusively *endo*-selective cycloaddition of the *N*-protonated azomethine ylide generated from *N*-(benzylidene)cyanomethylamine (O. Tsuge, S. Kanemasa, K. Yorozu, and K. Ueno, *Chem. Lett.*, **1985**, 1601; O. Tsuge, S. Kanemasa, K. Ueno, and K. Yorozu, *Bull. Chem. Soc. Jpn.*, **59**, 1809 (1986).

14) N. Imai, Y. Terao, and K. Achiwa, *Yuki Gosei Kagaku Kyokai Shi*, **43**, 862 (1985).

15) The reaction of **1** with *cis*-stilbene under the same conditions gave a mixture of three stereoisomeric cycloadducts (73% of total yield), one of which was identical to **13**.

16) G. Stork, A. Y. W. Leong, and A. M. Touzin, *J. Org. Chem.*, **41**, 3491 (1976); P. Bey and J. P. Vevert, *Tetrahedron Lett.*, **1977**, 1455; J. J. Fitt and H. W. Gschwend, *J. Org. Chem.*, **42**, 2639 (1977); R. Grigg, J. Kemp, J. Malone, and A. Tangthongkum, *J. Chem. Soc., Chem. Commun.*, **1980**, 648; A. H. Schulthess and H.-J. Hansen, *Helv. Chim. Acta*, **64**, 1322 (1981).

17) A few examples are known for the Michael addition of 1,3-diphenyl-2-azaallyl anion: T. Kauffmann, H. Ahlers, A. Hamsen, H. Schulz, H.-J. Tilhard, and A. Vahrenhorst, *Angew. Chem.* **89**, 107 (1977); S. Sinbandhit and J. Hamelin, *J. Chem. Soc., Chem. Commun.*, **1977**, 768; V. Dryanska, K. Popandova-Yambolieva, and C. Ivanov, *Tetrahedron Lett.*, **1979**, 443; L. V. Quang, H. Gaessler, and Y. V. Quang, *Angew. Chem. Int. Ed. Engl.*, **20**, 880 (1981); T. Kauffmann, H. Ahlers, K.-J. Echsler, H. Schulz, and H.-J. Tilhard, *Chem. Ber.*, **118**, 4496 (1985).

18) The corresponding Michael adducts **19b** and **19c** can be obtained if the reduction with sodium borohydride is omitted. **19b**: Yield 97%; colorless liquid; bp 150—160 °C/80 Pa; IR (neat) 1730 and 1640 cm^{-1}; ^1H NMR ($CDCl_3$) δ=2.5—3.1 (2H, m, CH_2COOMe), 3.4—4.0 (3H, m, NCH_2 and CH), 3.49 (3H, s, COOMe), 7.0—7.8 (10H, m, Ph), and 8.07 (1H, t, J=1.5 Hz, CH=N); MS m/z 281 (M^+). **19c**: Yield 77%; IR (neat) 1730 and 1640 cm^{-1}; ^1H NMR ($CDCl_3$) δ=1.20 (3H, d, J=7.0 Hz Me), 1.6—2.9 (3H, m, CH_2COOMe and CH), 3.4—3.75 (2H, m, NCH_2), 3.62 (3H, s, COOMe), 7.2—7.8 (5H, m, Ph), and 8.19 (1H, t, J=1.5 Hz, CH=N); MS m/z 219 (M^+).

19) 2-Methyl-5-(1-naphthyl)-4-phenyl-1-pyrroline was formed in 10% yield together with **23** in the reaction of **3** with benzylideneacetone, indicating that the 2-azaallyl anion generated from **3** can react at the both carbons.

20) The coupling product is quantitatively obtained in the reaction of **4** with TBAF in the absence of olefins, and was tentatively assigned as 1,2-bis(*p*-nitrobenzylideneamino)ethane (^1H NMR ($CDCl_3$) δ=4.00 (4H, s, CH_2), 7.75, 8.09 (each 2H, d, Ar), and 8.25 (2H, s, CH=N)).

21) K. Kindler and W. Peschke, *Arch. Pharm.*, **269**, 581 (1931).

Bromochlorination of Alkenes with Dichlorobromate (1−) Ion. IV.[1,2] Regiochemistry of Bromochlorinations of Alkenes with Molecular Bromine Chloride and Dichlorobromate (1−) Ion

Takeshi NEGORO* and Yoshitsugu IKEDA
Department of Chemistry, Faculty of Education, Wakayama University, Sakaedani, Wakayama 640
(Received March 25, 1986)

The regioselectivity of the addition of molecular bromine chloride to alkenes is dependent on both the steric and electronic effects of the alkyl substituent. In contrast, the regioselectivity of the addition of dichlorobromate (1−) ion to alkenes is controlled mainly by the steric effect of the substituent.

The regioselectivity of bromochlorination of phenyl- and vinyl-substituted alkenes has been shown to be markedly dependent both on the bromochlorinating agent and on the structure of alkene employed.[1-3] There have been a few investigations on the regiochemistry of bromochlorination of alkyl-substituted ethylenes with molecular bromine chloride and dichlorobromate(1−) ion, and the addition of BrCl to such alkenes as propene, 3-chloro-1-propene, and 1-hexene has been reported to give both Markownikoff and *anti*- Markownikoff adducts.[2,5] We have also reported that dichlorobromate(1−) ion reacted with propene and 3-chloro-1-propene to give two regioisomers.[1] However, no systematic study has been carried out on the bromochlorination reaction of alkyl-substituted ethylenes. As a continuation of our studies[1-3] we have carried out a study on the regiochemical effect of the alkyl substituent in the addition of molecular bromine chloride and dichlorobromate (1−) ion to various alkenes.

Results and Discussion

Reactions of a series of alkenes **3a-l** with tetrabutylammonium dichlorobromate(1−) (**1**) in dichloromethane gave the corresponding bromo chloro compounds **4a—l** and **5a—l** in good yields (Table 1 and Scheme 1). Similar reactions of methylenecycloalkanes **3m—n** with **1** also gave the corresponding bromo chloro compounds **4m—n** and **5m—n** in good yields (Table 1 and Scheme 2).

The orientation of halogen atoms in all the addition products was elucidated mainly on the basis of chemical shifts of the carbon bearing bromine and chlorine atoms in ^{13}C NMR spectra, since it has been observed that the carbon atom bearing a chlorine atom is deshielded relative to the one bearing a bromine atom.[6] Meanwhile, the structures of two regioisomers **4** and **5** have been determined by comparison of their ^{13}C NMR spectra with those of the corresponding

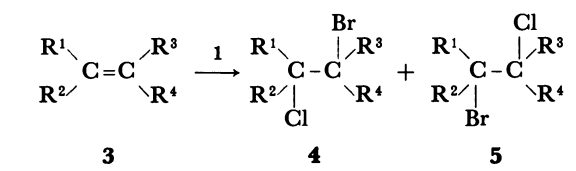

3 **4** **5**

	R^1	R^2	R^3	R^4		R^1	R^2	R^3	R^4
a	Et	H	H	H	**g**	Et	H	Me	H
b	*n*-Pr	H	H	H	**h**	Me	Me	H	H
c	*n*-Bu	H	H	H	**i**	Et	Et	H	H
d	*i*-Pr	H	H	H	**j**	Me	Me	Me	H
e	*t*-Bu	H	H	H	**k**	Et	Me	H	Me
f	Et	H	H	Me	**l**	Et	Me	Me	H

Scheme 1.

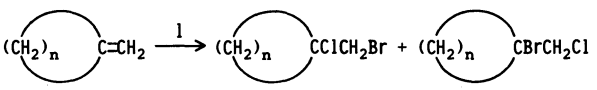

n = 4: **3m** **4m** **5m**
n = 5: **3n** **4n** **5n**

Scheme 2.

Table 1. Bromochlorination of Alkenes with **1** in CH_2Cl_2[a]

Alkenes 3	Product composition/%[b] 4	5	Yield/%[c]	Alkenes 3	Product composition/%[b] 4	5	Yield/%[c]
3a	44	56	80	**3h**	69 (66)	31 (34)	78
3b	43	57	82	**3i**	67 (68)	33 (32)	76
3c	41	59	83	**3j**	71	29	79
3d	24	76	78	**3k**	68[f]	32[f]	81
3e	0	100	74	**3l**	47[g]	53[g]	80
3f	40[d]	60[d]	82	**3m**	92 (89)	8 (11)	75
3g	33[e]	67[e]	81	**3n**	26 (25)	74 (75)	79

a) Reactions were carried out with 30 mmol of **1**, 36 mmol of alkene, and 50 ml of CH_2Cl_2 at 0 °C. b) Percentages are normalized to 100%. Determined by ^{13}C NMR analysis. The figures in parentheses represent product distributions determined by ^1H NMR analysis. c) Isolated yield based on **1**. d) *erythro*. e) *threo*. f) (*RS,SR*). g) (*RS,RS*).

Table 2. Bromochlorination of Alkenes with **2** in CH_2Cl_2[a]

Alkenes	Product composition/%[b]		Yield/%[c]	Alkenes	Product composition/%[b]		Yield/%[c]
3	**4**	**5**		**3**	**4**	**5**	
3a	58	42	61	**3h**	86	14	72
3b	55	45	72	**3i**	87	13	70
3c	58	42	65	**3j**	86	14	71
3d	41	59	69	**3k**	84[f]	16[f]	70
3e	11	89	68	**3l**	68[g]	32[g]	69
3f	48[d]	52[d]	72	**3m**	100	0	11
3g	36[e]	64[e]	69	**3n**	82	18	55

a) Reactions were carried out with 10 mmol of **2**, 12 mmol of alkene,and 50 ml of CH_2Cl_2 at 0°C. b) Percentages are normalized to 100%. Determined by ^{13}C NMR analysis. c) Determined by GLC analysis. d) *erythro*. e) *threo*. f) (*RS,SR*). g) (*RS,RS*).

dibromo and dichloro compounds. Control experiments revealed that all the bromo chloro compounds are stable under the reaction conditions.

Treatments of a series of alkenes **3a—l** with molecular bromine chloride (**2**) in CH_2Cl_2 also gave the corresponding bromo chloro compounds **4a—l** and **5a—l** (Table 2). The yields are lower than those in the reaction with **1** due to formation of dibromo- and dichloroalkanes. The formation of these by-products in the reaction is undoubtedly due to the attack of both Br_2 and Cl_2, which are formed from and in equilibrium with **2**, on alkenes.[7]

On the other hand, the reaction of methylenecyclopentane (**3m**) with **2** gave a mixture of 2-bromo-1-chloro- and 1-bromo-2-chloro-1-methylcyclopentanes (**4o** and **5o**, 54.5% yield by GLC analysis) as the major products. The expected bromo chloro compound **4m** (11.0% yield by GLC analysis) was a minor component (Scheme 3 and Table 2). The formation of

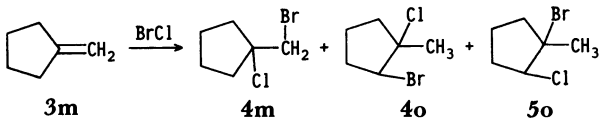

3m **4m** **4o** **5o**

Scheme 3.

both **4o** and **5o** may be due to the competing allylic halogenation which produces hydrogen halide. The hydrogen halide thus formed is considered to isomerize the terminal alkene **3m** into a more stable internal alkene **3o** (1-methylcyclopentene), to which **2** is then presumed to add. In fact, the presence of **3o** was confirmed by ^1H NMR analysis of the reaction mixture. Furthermore, the ratio of the two regioisomers (**4o**:**5o**=86:14) is the same as that observed for the reaction of **3o** with **2**. A similar reaction has been reported for the addition of bromine to **3m**.[8] Similarly, the reaction of methylenecyclohexane (**3n**) also gave a small amount of 2-bromo-1-chloro- and 1-bromo-2-chloro-1-methylcyclohexane (**4p** and **5p**).

An inspection of the data in Tables 1 and 2 clearly reveals that the regiochemistry of the addition of **1** to alkenes is strikingly different from that of the reaction of **2**. Therefore, the product-determining step must be different in these two reactions.

Regioselectivity of the Reaction of 3 with 2. The reaction with **2** can best be explained by the AdE_{C_1}-type mechanism involving the attack of chloride ion to a bridged bromonium ion intermediate **6**:[5,9] a similar intermediate has also been suggested for the bromination of alkenes with molecular bromine.[10]

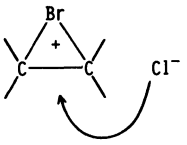

(6)

As shown in Table 2, the bromochlorination of the unsymmetrical alkenes, 1,2-dialkyl- **3f** and **3g** and 1,1,2-trialkylethylenes **3k** and **3l**, with **2** gave completely *anti* stereospecific adducts. This supports further the assumption that the intermediate in the bromochlorination of alkyl-substituted ethylenes with **2** resembles the bridged ion **6**. These results are in marked contrast to the stereoselective addition of **2** to phenyl- or vinyl-substituted alkenes, which involves a very weakly bridged ion intermediate.[2,3] Thus, the *anti* stereospecific addition of **2** to **3k** and **3l** would rule out the possibility of carbonium ion-like intermediate which is considered to be involved in the bromination of these alkenes with bromine.[10]

Both the steric and the electronic effect of the alkyl substituent on ethylene linkage would play a major role in the orientation of the approach of chloride ion on the bromonium ion intermediate **6**. As shown in Table 2, nearly the same ratio of regioisomers is given for the reactions of 1-butene (**3a**), 1-pentene (**3b**), and 1-hexene (**3c**) with **2**, which indicates the effects of linear alkyl substituents to be nearly the same. Meanwhile, the replacement of the hydrogen on ethylene by isopropyl (**3d**) or *t*-butyl (**3e**) results in the formation of an increasing amount of the *anti*-Markownikoff adduct **5d** or **5e**. This reveals clearly that the addition of **2** can be influenced by steric factors of the bulky groups.

On the other hand, the additions of **2** to 1,1-disubstituted **3h** and **3i** and 1,1,2-trisubstituted ethylenes **3j**, **3k**, and **3l** or methylenecycloalkanes **3m** and **3n** gave regioselective Markownikoff adducts **4** (Table 2).

These results imply that the attack of chloride ion on the bromonium ion intermediate **6** occurs at the more substituted carbon atom. Thus, the orientation of bromochlorination with **2** would be due to the electronic effect of the 1,1-dialkyl substituent which stabilizes the developed cationic character on the more substituted carbon atom in the intermediate **6**. A similar accumulative electronic effect of dialkyl substituent groups on the regiochemistry has previously been observed in the bromination of these alkenes in methanol.[11]

Regioselectivity of the Reaction of 3 with 1. We have previously suggested that the reaction of alkenes with **1** can be best explained by the $AdEC_2$-type mechanism involving the attack of chloride ion on the three-centered π-complex intermediate **7** with a very little charge development on the unsaturated carbon.[2,3]

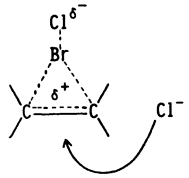

(7)

Therefore, there would be a relatively small demand for electronic stabilization of the reaction center by alkyl substituents on the intermediate **7**. As expected, the amount of the *anti*-Markownikoff adduct **5** in the addition with **1** (Table 1) is generally larger than that in the addition with **2** (Table 2). Thus, the addition of **1** to linear alkyl-substituted ethylenes **3a**, **3b**, and **3c** was found to be slightly more regioselective in an *anti*-Markownikoff manner than that in the addition of **2**. Meanwhile, the replacement of the hydrogen on ethylene by an isopropyl (**3d**) or a *t*-butyl group (**3e**) results in the formation of a larger amount of the *anti*-Markownikoff adduct **5** than that in the addition of **2**. It is interesting to note that only the *anti*-Markownikoff adduct **5e** is obtained in the reaction of 3,3-dimethyl-1-butene (**3e**), as anticipated from the greater steric requirement of *t*-butyl group. The reaction of methylenecyclohexane (**3n**) with **1** also gives a regioselective *anti*-Markownikoff adduct **5n**, where the opposite orientation results from that of the reaction with **2**. All these results support that the steric effect outweighs the electronic effect of the alkyl substituent in the reaction with **1**.

However, the reaction of **1** to 1,1-dialkyl- **3h** and **3i** and 1,1,2-trialkylethylenes **3j** and **3k** or methylenecyclopentane (**3m**) gave the regioselective Markownikoff adduct **4** (Table 1). As in the reaction with **2**, the electronic effect of the 1,1-dialkyl groups would overcome partially the steric influence.

Experimental

NMR spectra were recorded on a JEOL JNM FX-60Q and a JEOL C-60HL spectrometer using TMS as the internal standard. Mass spectra were recorded on a JMS-D-300 mass spectrometer. GLC analyses were performed on a Yanako G-180 gas chromatograph with a Silicone SE-30 (5%)-Chromosorb WAW DMCS (2 m) column with helium as the carrier gas. Tetrabutylammonium dichlorobromate(1−) (**1**) was prepared by the known procedure.[12] All the organic starting materials, including the solvents, were distilled before use. Bromine chloride (**2**) was prepared by adding an equimolar amount of bromine to chlorine-carbon tetrachloride solution. 1,2-Dibromoalkanes **8a—n** were prepared by bromination of alkenes **3a—n** with bromine, respectively. 1,2-Dichloroalkanes **9a—n** were prepared by chlorination of alkenes **3a—n** with chlorine, respectively.

Reaction of Alkenes 3a—n with 1. Details of the reaction have previously been reported.[1,2] To a solution of **3** (36 mmol) in CH_2Cl_2 (50 ml) was added **1** (11.8 g, 30 mmol) at 0°C over 20 min with stirring. After the usual work-up, the products were purified by distillation. Although attempts to separate **4** and **5** were unsuccessful, these structures were determined by comparison of their ^{13}C NMR spectra with those of the corresponding dibromo and dichloro analogs.

A Mixture of 1-Bromo-2-chloro- and 2-Bromo-1-chlorobutanes (4a and 5a) from 1-Butene (3a): Bp 82°C/110 mmHg (1 mmHg=133.322 Pa); MS M^+ *m/z* (rel intensity) 170, 172, and 174 (100:135:32); ^1H NMR ($CDCl_3$) δ=1.04 (3H, t, J=6.5 Hz), 1.40—2.30 (2H, m), and 3.50—4.30 (3H, m); ^{13}C NMR ($CDCl_3$) (the asterisk indicates **5a**) δ=10.1, 11.1,* 28.4,* 28.8, 35.8, 47.6,* 54.9,* and 62.1. Although attempts to separate **4a** and **5a** were unsuccessful, these assignments were supported for dibromo and dichloro analogs as follows: 1,2-dibromobutane (**8a**), ^{13}C NMR ($CDCl_3$) δ= 11.0, 29.0, 35.6, and 54.3; 1,2-dichlorobutane (**9a**), ^{13}C NMR ($CDCl_3$) δ=10.2, 28.2, 47.8, and 62.6.

A Mixture of 1-Bromo-2-chloro- and 2-Bromo-1-chloropentanes (4b and 5b) from 1-Pentene (3b): Bp 70—72°C/ 50 mmHg; MS M^+ *m/z* (rel intensity) 184, 186, and 188 (100:134:36); ^1H NMR ($CDCl_3$) δ=0.83—2.30 (7H, m) and 3.33—4.35 (3H, m); ^{13}C NMR ($CDCl_3$) (the asterisk indicates **5b**) δ=13.3,* 13.4, 19.2, 20.2,* 36.5, 37.4,* 37.8, 48.3,* 53.2,* and 60.6. These assignments were supported for dibromo and dichloro analogs as follows: 1,2-dibromopentane (**8b**), ^{13}C NMR ($CDCl_3$) δ=13.3, 20.1, 36.3, 38.0, and 52.7; 1,2-dichloropentane (**9b**), ^{13}C NMR ($CDCl_3$) δ=13.5, 19.2, 37.1, 48.3, and 60.9.

A Mixture of 1-Bromo-2-chloro- and 2-Bromo-1-chlorohexanes (4c and 5c) from 1-Hexene (3c): Bp 95—96°C/ 50 mmHg; MS M^+ *m/z* (rel intensity) 198, 200, and 202 (100:129:31); ^1H NMR ($CDCl_3$) δ=0.93—2.40 (9H, m) and 3.50—4.30 (3H, m); ^{13}C NMR ($CDCl_3$) (the asterisk indicates **5c**) δ=13.9, 22.0,* 22.1, 28.0, 28.9,* 35.1,* 35.5, 36.5, 48.2,* 53.5,* and 60.8. These assignments were supported for dibromo and dichloro analogs as follows: 1,2-dibromohexane (**8c**), ^{13}C NMR ($CDCl_3$) δ=13.9, 21.9, 28.8, 35.7, 36.3, and 53.0; 1,2-dichlorohexane (**9c**), ^{13}C NMR ($CDCl_3$) δ= 13.9, 22.1, 27.9, 34.7, 48.2, and 61.2.

A Mixture of 1-Bromo-2-chloro- and 2-Bromo-1-chloro-3-methylbutanes (4d and 5d) from 3-Methyl-1-butene (3d): Bp 68—70°C/50 mmHg; MS M^+ *m/z* (rel intensity) 184, 186, and 188 (100:130:35); ^1H NMR ($CDCl_3$) δ=0.99 (6H, t, J=6.6 Hz), 2.00—2.57 (1H, m), and 3.63—4.33 (3H, m); ^{13}C NMR ($CDCl_3$) (the asterisk indicates **5d**) δ=15.1, 16.1,* 20.4, 21.4,* 29.6,* 30.8, 34.4, 46.1,* 61.8,* and 67.2. These assignments were supported for dibromo and dichloro analogs as follows:

1,2-dibromo-3-methylbutane (**8d**), ^{13}C NMR ($CDCl_3$) δ=15.5, 21.7, 29.9, 34.1, and 61.5; 1,2-dichloro-3-methylbutane (**9d**), ^{13}C NMR ($CDCl_3$) δ=15.6, 20.2, 30.3, 46.3, and 67.6.

2-Bromo-1-chloro-3,3-dimethylbutane (5e) from 3,3-Dimethyl-1-butene (3e): Bp 95—100°C/50 mmHg; MS M$^+$ *m/z* (rel intensity) 198, 200, and 202 (100:129:31); ^{1}H NMR ($CDCl_3$) δ=1.12 (9H, s) and 3.52—4.13 (3H, m); ^{13}C NMR ($CDCl_3$) δ=27.6, 36.3, 47.6, and 68.8. ^{13}C NMR spectra for dibromo and dichloro analogs are as follows: 1,2-dibromo-3,3-dimethylbutane (**8e**), ^{13}C NMR ($CDCl_3$) δ=27.6, 35.8, 37.0, and 69.0; 1,2-dichloro-3,3-dimethylbutane (**9e**), ^{13}C NMR ($CDCl_3$) δ=26.7, 36.2, 47.1, and 73.7.

A Mixture of *erythro*-2-Bromo-3-chloro- and 3-Bromo-2-chloropentanes (4f and 5f) from *trans*-2-Pentene (3f): Bp 71—72°C/50 mmHg; MS M$^+$ *m/z* (rel intensity) 184, 186, and 188 (100:128:32); ^{1}H NMR ($CDCl_3$) δ=1.07 (3H, t, J=6.8 Hz), 1.33—2.26 (5H, m), and 3.78—4.40 (2H, m); ^{13}C NMR ($CDCl_3$) (the asterisk indicates **5f**) δ=10.5, 11.6,* 23.4, 23.5,* 29.1,* 29.4, 51.8, 59.7,* 63.0,* and 69.0. These assignments were supported for dibromo and dichloro analogs as follows: *erythro*-2,3-dibromopentane (**8f**), ^{13}C NMR ($CDCl_3$) δ=11.4, 25.2, 30.5, 51.8, and 63.2; *erythro*-2,3-dichloropentane (**9f**), ^{13}C NMR ($CDCl_3$) δ=10.4, 22.2, 28.3, 59.5, and 68.6.

A Mixture of *threo*-2-Bromo-3-chloro- and 3-Bromo-2-chloropentanes (4g and 5g) from *cis*-2-Pentene (3g): Bp 72—73°C/50 mmHg; MS M$^+$ *m/z* (rel intensity) 184, 186, and 188 (100:132:35); ^{1}H NMR ($CDCl_3$) δ=1.07 (3H, t, J=6.9 Hz), 1.34—2.24 (5H, m), and 3.77—4.57 (2H, m); ^{13}C NMR ($CDCl_3$) (the asterisk indicates **5g**) δ=11.5, 12.6,* 21.3,* 21.5, 27.3,* 27.7, 52.2, 59.9,* 62.1,* and 68.2. These assignments were supported for dibromo and dichloro analogs as follows: *threo*-2,3-dibromopentane (**8g**), ^{13}C NMR ($CDCl_3$) δ=12.7, 21.6, 27.5, 52.2, and 62.1; *threo*-2,3-dichloropentane (**9g**), ^{13}C NMR ($CDCl_3$) δ=11.4, 20.8, 27.1, 59.7, and 67.9.

A Mixture of 1-Bromo-2-chloro- and 2-Bromo-1-chloro-2-methylpropanes (4h and 5h) from 2-Methylpropene (3h): Bp 79—82°C/90 mmHg; MS M$^+$ *m/z* (rel intensity) 170, 172, and 174 (100:132:34); ^{1}H NMR ($CDCl_3$) (the asterisk indicates **5h**) δ=1.69, 1.83* (6H, 2s), 3.63, and 3.83* (2H, 2s); ^{13}C NMR ($CDCl_3$) (the asterisk indicates **5h**) δ=30.4, 31.0,* 43.7, 55.3,* 62.3,* and 67.1. These assignments were supported for dibromo and dichloro analogs as follows: 1,2-dibromo-2-methylpropane (**8h**), ^{13}C NMR ($CDCl_3$) δ=31.9, 44.7, and 62.1; 1,2-dichloro-2-methylpropane (**9h**), ^{13}C NMR ($CDCl_3$) δ=29.6, 54.6, and 67.6.

A Mixture of 1-Bromo-2-chloro- and 2-Bromo-1-chloro-2-ethylbutanes (4i and 5i) from 2-Ethyl-1-butene (3i): Bp 65—66°C/19 mmHg; MS M$^+$ *m/z* (rel intensity) 198, 200, and 202 (100:130:35); ^{1}H NMR ($CDCl_3$) (the asterisk indicates **5i**) δ=0.90—1.14 (6H, m), 1.66—2.11 (4H, m), 3.63, and 3.87* (2H, 2s); ^{13}C NMR ($CDCl_3$) (the asterisk indicates **5i**) δ=8.2, 9.4,* 32.6, 32.9,* 37.7, 48.8,* 75.4,* and 75.8. These assignments were supported for dibromo and dichloro analogs as follows: 1,2-dibromo-2-ethylbutane (**8i**), ^{13}C NMR ($CDCl_3$) δ=9.5, 33.8, 38.2, and 75.3; 1,2-dichloro-2-ethylbutane (**9i**), ^{13}C NMR ($CDCl_3$) δ=8.2, 31.8, 48.5, and 76.1.

A Mixture of 3-Bromo-2-chloro- and 2-Bromo-3-chloro-2-methylbutanes (4j and 5j) from 2-Methyl-2-butene (3j): Bp 80—81°C/70 mmHg; MS M$^+$ *m/z* (rel intensity) 184, 186, and 188 (100:134:35); ^{1}H NMR ($CDCl_3$) δ=1.67—1.98 (9H, m) and 4.13—4.46 (1H, m); ^{13}C NMR ($CDCl_3$) (the asterisk indicates **5j**) δ=21.9,* 22.1, 27.0, 27.9,* 32.5, 33.2,* 58.4, 66.1,* 67.9,* and 71.6. These assignments were supported for dibromo and dichloro analogs as follows: 2,3-dibromo-2-methylbutane (**8j**), ^{13}C NMR ($CDCl_3$) δ=23.5, 28.0, 34.9, 59.4, and 68.2; 2,3-dichloro-2-methylbutane (**9j**), ^{13}C NMR ($CDCl_3$) δ=20.6, 26.5, 31.1, 65.2, and 71.3.

A Mixture of (*RS,SR*)-2-Bromo-3-chloro- and 3-Bromo-2-chloro-3-methylpentanes (4k and 5k) from (*E*)-3-Methyl-2-pentene (3k): Bp 68—69°C/48 mmHg; MS M$^+$ *m/z* (rel intensity) 198, 200, and 202 (100:134:28); ^{1}H NMR ($CDCl_3$) δ=0.93—1.18 (3H, m), 1.63—2.03 (8H, m), and 4.31 (1H, q, J=6.7 Hz); ^{13}C NMR ($CDCl_3$) (the asterisk indicates **5k**) δ=8.6, 9.8,* 21.7, 21.8,* 24.6, 25.2,* 36.6, 36.9,* 55.6, 63.0,* 74.4,* and 76.1. These assignments were supported for dibromo and dichloro analogs as follows: (*RS,SR*)-2,3-dibromo-3-methylpentane (**8k**), ^{13}C NMR ($CDCl_3$) δ=9.8, 23.2, 25.9, 38.4, 56.2, and 74.9; (*RS,SR*)-2,3-dichloro-3-methylpentane (**9k**), ^{13}C NMR ($CDCl_3$) δ=8.4, 20.3, 23.8, 35.2, 62.5, and 75.8.

A Mixture of (*RS,RS*)-2-Bromo-3-chloro- and 3-Bromo-2-chloro-3-methylpentanes (4l and 5l) from (*Z*)-3-Methyl-2-pentene (3l): Bp 70—71°C/48 mmHg; MS M$^+$ *m/z* (rel intensity) 198, 200, and 202 (100:132:35); ^{1}H NMR ($CDCl_3$) δ=0.93—1.18 (3H, m), 1.61—2.20 (8H, m), and 4.08—4.52 (1H, m); ^{13}C NMR ($CDCl_3$) (the asterisk indicates **5l**) δ=8.8, 9.9,* 21.5,* 21.8, 27.8, 28.7*, 32.3, 32.7,* 58.8, 66.0,* 74.7,* and 76.1. These assignments were supported for dibromo and dichloro analogs as follows: (*RS,RS*)-2,3-dibromo-3-methylpentane (**8l**), ^{13}C NMR ($CDCl_3$) δ=10.0, 23.0, 30.3, 32.4, 59.8, and 75.0; (*RS,RS*)-2,3-dichloro-3-methylpentane (**9l**), ^{13}C NMR ($CDCl_3$) δ=8.7, 20.4, 26.7, 31.8, 65.2, and 76.0.

A Mixture of 1-Bromomethyl-1-chloro- and 1-Bromo-1-(chloromethyl)cyclopentanes (4m and 5m) from Methylenecyclopentane (3m): Bp 42—43°C/5 mmHg; MS M$^+$ *m/z* (rel intensity) 196, 198, and 200 (100:132:34); ^{1}H NMR ($CDCl_3$) (the asterisk indicates **5m**) δ=1.52—2.26 (8H, m), 3.80, and 4.01* (2H, 2s); ^{13}C NMR ($CDCl_3$) (the asterisk indicates **5m**) δ=23.8, 40.6, 41.2, 52.2,* 74.9,* and 79.2. These assignments were supported for dibromo and dichloro analogs as follows: 1-bromo-1-(bromomethyl)cyclopentane (**8m**), ^{13}C NMR ($CDCl_3$) δ=23.9, 41.3, 41.4, and 74.9; 1-chloro-1-(chloromethyl)cyclopentane (**9m**), ^{13}C NMR ($CDCl_3$) δ=23.6, 39.8, 51.9, and 79.0.

A Mixture of 1-Bromomethyl-1-chloro- and 1-Bromo-1-(chloromethyl)cyclohexane (4n and 5n) from Methylenecyclohexane (3n): Bp 41—42°C/2 mmHg; MS M$^+$ *m/z* (rel intensity) 210, 212, and 214 (100:130:35); ^{1}H NMR ($CDCl_3$) (the asterisk indicates **5n**) δ=1.40—2.00 (10H, m), 3.68, and 3.92* (2H, 2s); ^{13}C NMR ($CDCl_3$) (the asterisk indicates **5n**) δ=22.1, 22.8,* 24.9, 37.3, 44.3, 55.2,* 72.5,* and 72.7. These assignments were supported for dibromo and dichloro analogs as follows: 1-bromo-1-(bromomethyl)cyclohexane (**8n**), ^{13}C NMR ($CDCl_3$) δ=23.0, 24.8, 38.0, 44.7, and 72.3; 1-chloro-1-(chloromethyl)cyclohexane (**9n**), ^{13}C NMR ($CDCl_3$) δ=21.8, 24.9, 36.4, 54.6, and 73.2.

Reaction of Alkenes 3a—n with 2. To a solution of **3** (12 mmol) in CH_2Cl_2 (50 ml) was added 5.5 ml of BrCl solution in CCl_4 (1.8 mol dm^{-3}) at 0°C over 5 min with stirring. After the solvent was removed under reduced pressure, the residues were analyzed by GLC and ^{13}C NMR. The results are given in Table 2. In all cases, GLC analyses showed the presence of 11—16% of dichloro adduct **9** and 13—19% of dibromo adduct **8** as by-products.

The reaction of 3,3-dimethyl-1-butene (**3e**) with **2** gave a

mixture of 1-bromo-2-chloro- and 2-bromo-1-chloro-3,3-dimethylbutane (**4e** and **5e**). The product composition of **4e** and **5e** was determined by ^{13}C NMR analysis: ^{13}C NMR ($CDCl_3$) (the asterisk indicates **5e**) δ=26.8, 27.6,* 35.2, 36.3,* 37.0, 47.6,* 68.8,* and 74.6. These assignments were supported for the ^{13}C NMR data of dibromo and dichloro adducts **8e** and **9e** as described above.

The reaction of methylenecyclopentane (**3m**) with **2** gave a mixture of 2-bromo-1-chloro- and 1-bromo-2-chloro-1-methylcyclopentane (**4o** and **5o**, 54.5%), 1-bromomethyl-1-chlorocyclopentane (**4m**, 11.0%), dichloro and dibromo adducts (25.5%), and unidentified products (9.0%), as determined by GLC analysis. Although no isolation of **4o** and **5o** was carried out, the retention time of GLC agreed with that of the sample prepared by the reaction of 1-methylcyclopentene (**3o**) with **1** as follows: Bp 42—43°C/5 mmHg; MS M^+ *m/z* (rel intensity) 196, 198, and 200 (100:131:32); ^1H NMR ($CDCl_3$) (the asterisk indicates **5o**) δ=1.90, 1.96* (2s), 1.70—3.10 (m), and 4.44—4.62 (m); ^{13}C NMR ($CDCl_3$) (the asterisk indicates **5o**) δ=20.8, 21.0,* 28.5,* 28.6, 34.9,* 35.4, 39.3, 40.6,* 62.6, 70.9,* 75.1,* and 79.5. The ratio of **4o** and **5o** was shown to be 86:14 by ^{13}C NMR analysis. This product ratio is close to the product ratio (**4o**:**5o**=83:17) for the reaction of **3o** with **2** under the same reaction conditions.

^1H NMR analysis of the recovered alkenes from the reaction of **3m** (20 mmol) with **2** (10 mmol) gave 67% of 1-methylcyclopentene (**3o**) and 33% of methylenecyclopentane (**3m**) as based on the relative areas of the signals at δ=5.30 and 4.83 for the olefinic protons, respectively.

The reaction of methylenecyclohexane (**3n**) with **2** also gave a mixture of 2-bromo-1-chloro- and 1-bromo-2-chloro-1-methylcyclohexanes (**4p** and **5p**, 7.5%), **4n** and **5n** (55.2%), and dichloro and dibromo adducts (37.3%), as determined by GLC analysis. Although no isolation of **4p** and **5p** was carried out, the retention time agreed with that of the sample prepared by the reaction of 1-methylcyclohexene (**3p**) with **1** as follows: Bp 41—42°C/2 mmHg; MS M^+ *m/z* (rel intensity) 210, 212, and 214 (100:134:34); ^1H NMR ($CDCl_3$) (the asterisk indicates **5p**) δ=1.75, 1.91* (2s), 1.56—2.60 (m), and 4.35—4.70 (m).

The authors sincerely wish to thank Professor Shigeru Oae of Okayama University of Science for his kind guidance.

References

1) T. Negoro and Y. Ikeda, *Bull. Chem. Soc. Jpn.*, **57**, 2111 (1984).

2) T. Negoro and Y. Ikeda, *Bull. Chem. Soc. Jpn.*, **57**, 2116 (1984).

3) T. Negoro and Y. Ikeda, *Bull. Chem. Soc. Jpn.*, **58**, 3655 (1985).

4) R. E. Buckles, J. L. Forrester, R. L. Burham, and T. W. McGee, *J. Org. Chem.*, **25**, 24 (1960).

5) V. L. Heasley, D. F. Shellhamer, J. A. Iskikian, D. L. Street, and G. E. Heasley, *J. Org. Chem.*, **43**, 3139 (1978).

6) P. Crews, S. Naylor, F. J. Hanke, E. R. Hogue, E. Kho, and R. Braslau, *J. Org. Chem.*, **49**, 1371 (1984).

7) A. I. Popov and J. J. Mannion, *J. Am. Chem. Soc.*, **74**, 222 (1952).

8) J. Wolinsky, R. W. Novak, and K. L. Erickson, *J. Org. Chem.*, **34**, 490 (1969).

9) V. L. Heasley, D. W. Spaite, D. L. Shellhamer, and G. E. Heasley, *J. Org. Chem.*, **44**, 2608 (1979).

10) G. H. Schmid and D. G. Garratt, "The Chemistry of Double-Bonded Functional Groups," ed by S. Patai, John Wiley and Sons, London (1977), Supplement A, part 2, pp. 764—771.

11) J. E. Dubois and J. R. Chretien, *J. Am. Chem. Soc.*, **100**, 3506 (1978).

12) A. I. Popov and R. L. Buckles, *Inorg. Synth.*, Vol. V. 172 (1957).

 © 1986 The Chemical Society of Japan Bull. Chem. Soc. Jpn., 59, 2553—2558 (1986)

Carbon Monoxide Adsorbent Composed of Copper(I) Chloride and Polystyrene Resin Having Amino Groups

Hidefumi HIRAI,* Keiichiro WADA, Kazunori KURIMA, and Makoto KOMIYAMA
Department of Industrial Chemistry, Faculty of Engineering, The University of Tokyo, Hongo, Tokyo 113
(Received March 13, 1986)

A novel adsorbent of carbon monoxide (CO) is prepared by stirring copper(I) chloride and a macroreticular type polystyrene resin having amino groups in acetonitrile, followed by removal of the liquid phase at 5 mmHg, 80 °C. The adsorbent rapidly adsorbs carbon monoxide from 9 : 1 carbon monoxide–nitrogen mixture at 20 °C under 1 atm. The adsorbed carbon monoxide is readily desorbed by heating the adsorbent to 80 °C under 1 atm or by reducing the partial pressure of carbon monoxide to 5 mmHg at 20 °C. The CO adsorbing capacity (15.9 mmol) of the adsorbent composed of 10.0 g of the resin and 70 mmol of copper(I) chloride is 5.7 times as large as the carbon dioxide adsorbing capacity (2.8 mmol). The efficient adsorption of carbon monoxide by the present adsorbents is attributed to coordination of carbon monoxide to the copper(I) ions which coordinate the amino residues in the resin. The carbon dioxide adsorbing capacity (2.8 mmol) of the adsorbent is much smaller than that (8.3 mmol) of the resin without copper(I) chloride. The present adsorbent exhibits no measurable adsorptions of methane, nitrogen, and hydrogen at 20 °C under 1 atm, and thus is applicable to selective separation of carbon monoxide from gas mixtures containing these gases and carbon dioxide.

Carbon monoxide (CO), an important raw material in industry, is usually obtained as gas mixtures with carbon dioxide (CO_2), methane, nitrogen, and hydrogen.[1] Thus, separation of CO from gas mixtures is required for efficient utilization of CO. Considerable number of liquid absorbents of CO have been proposed.[2] However, solid adsorbents of CO have been rather few.

Active carbon exhibits adsorbing ability of CO. The adsorbing capacity for CO, however, is smaller than those for CO_2 and methane.[3] As a result, selective separation of CO from gas mixtures containing CO_2 and methane is difficult by using active carbon as adsorbent. Zeolite-supported copper(I) ions adsorbed both CO and CO_2.[4,5]

Previously, the authors reported that polystyrene resin-supported aluminium copper(I) chloride,[6,7] active carbon-supported aluminium copper(I) chloride,[8,9] and active carbon-supported copper(I) chloride[10] adsorbed CO reversibly and selectively under mild conditions.

This paper describes preparation of solid CO adsorbents composed of copper(I) chloride (CuCl) and a macroreticular type polystyrene resin having amino groups. The CO adsorbing and desorbing abilities of the adsorbents are reported. The selectivity of CO adsorption with respect to adsorptions of CO_2, methane, hydrogen, and nitrogen is presented. In addition, the results of X-ray photoelectron spectroscopy on the adsorbents are shown. The mechanism of selective adsorption of CO by the present adsorbents is discussed in terms of these results.

Experimental

Materials. A macroreticular type polystyrene resin having primary and secondary amino groups was purchased from Mitsubishi Chemical Industries (DIAION WA20; pale yellow beads of diameter 0.35—0.55 mm; ion-exchange capacity 2.5 equiv dm^{-3}; apparent density 650 g dm^{-3}). A macroreticular type polystyrene resin having carboxylate residues, a macroreticular type polystyrene resin having sulfonate residues, and a macroreticular type polystyrene resin having no functional groups were obtained also from Mitsubishi Chemical Industries: DIAION WK20 (white beads of diameter 0.35—0.55 mm; ion-exchange capacity 3.5 equiv dm^{-3}; apparent density 690 g dm^{-3}), DIAION PK208 (pale yellow beads of diameter 0.40—0.55 mm; ion-exchange capacity 1.2 equiv dm^{-3}; apparent density 745 g dm^{-3}), and DIAION HP30 (white beads of diameter 0.20—0.30 mm; surface area 570 $m^2\ g^{-1}$), respectively.

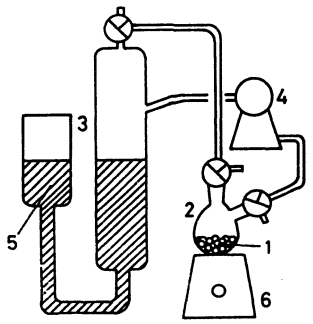

Fig. 1. Apparatus for measuring the amount of CO adsorbed by the adsorbents or desorbed from them; 1: Adsorbent, 2: flask, 3: gas burette, 4: gas pump, 5: leveling liquid (water), 6: magnetic stirrer.

Preparation of Adsorbent. 10.0 g of the polystyrene resin having amino groups and various amounts of CuCl were stirred in 80 cm^3 of solvents at 20° C for 5 h, and then the liquid phase was removed at 5 mmHg (1 mmHg=1.33×10² Pa), 80° C. In the present study, acetonitrile was used as a preparation solvent unless otherwise noted.

Adsorption and Desorption of Carbon Monoxide by the Adsorbent. Adsorption of CO by the adsorbents was carried out at 20° C under 1 atm using the apparatus depicted in Fig. 1. A flask (2) containing the adsorbent (1) under nitrogen (N_2) was connected with CO in the gas burette (3), and the adsorption was initiated by circulating the CO–N_2 mixture with the use of a gas pump (4). The uptake of CO was followed by the gas burette (3) using water as leveling liquid (5). The desorption of adsorbed CO was effected either by heating the adsorbents to 80° C under 1 atm for 10 min or by subjecting the adsorbents to a reduced pressure (5 mmHg) at

20° C for 10 min.

Adsorbing abilities of the adsorbents on carbon dioxide, methane, nitrogen, and hydrogen were measured in similar ways.

Determination of the Amounts of Copper(I) Chloride in the Adsorbents. The adsorbents were thoroughly washed with 100 cm^3 of aqueous nitric acid solution (11.8 mol dm^{-3}). The amounts of copper atoms in the resultant solutions were determined by atomic absorption spectroscopy (Shimadzu Model AA-646 spectrometer).

X-Ray Photoelectron Spectroscopy. X-Ray photoelectron spectra of the adsorbents were measured on a Shimadzu Electron Spectrometer ESCA 750 with Mg X-ray anode (8 kV, 30 mA) under a pressure smaller than 1.5×10^{-7} mmHg. Chemical shifts were determined using the $4f_{7/2}$ band of metallic gold at 84.0 eV as reference.

Results

Preparation of Carbon Monoxide Adsorbents Composed of Copper(I) Chloride and Polystyrene Resin Having Amino Groups. The adsorbents composed of CuCl and the macroreticular type polystyrene resin having amino groups were obtained as green beads. The amount of CuCl supported on the resin was 64 mmol, when the charged amounts of the resin and CuCl, respectively, were 10.0 g and 9.9 g (100 mmol), and acetonitrile was used as a preparation solvent.

Figure 2 shows a plot of the amount of CuCl supported on the polystyrene resin against the charged amount of CuCl. The charged amount of the resin is kept constant at 10.0 g. The supported amount of CuCl increases proportionally with increasing charged amount of CuCl up to the charged amount 50 mmol. Here almost all of the charged CuCl is supported on the resin. Above the charged amount 50 mmol, the supported amount is considerably smaller than the charged amount, being almost constant irrespective of the charged amount.

Adsorption and Desorption of Carbon Monoxide by the Adsorbents Composed of Copper(I) Chloride and Polystyrene Resin Having Amino Groups. Figures 3 and 4 show repeated adsorptions of CO by the adsorbents, which have been prepared from 10.0 g of the resin and 9.9 g (100 mmol) of CuCl, containing 64 mmol of CuCl. In Fig. 3 the desorption of adsorbed CO is carried out by heating the adsorbent to 80° C under 1 atm for 10 min, whereas in Fig. 4 it is achieved by subjecting the adsorbent to a reduced pressure (5 mmHg) at 20° C for 10 min.

The open circles in Fig. 3 depict the first adsorption of CO by the adsorbent from 9:1 $CO-N_2$ mixture at 20° C under 1 atm. The adsorption is rapid and the equilibrium amount of adsorbed CO is 15.2 mmol. Thus, 21 cm^3 (standard temperature and pressure) of CO is adsorbed by 1 g of the adsorbent.

The adsorbed CO is desorbed by heating the adsorbent to 80° C under 1 atm for 10 min. In the second adsorption (the closed circles), the adsorption of CO is rapid and the equilibrium amount of adsorbed CO is 9.1 mmol. In the third and the fourth adsorptions, both the rate of adsorption and the equilibrium amount of adsorbed CO are almost identical with the corresponding values in the second adsorption.

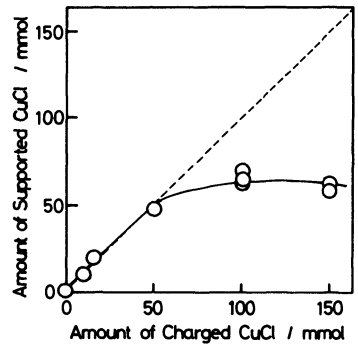

Fig. 2. Plot of the amount of CuCl supported on the polystyrene resin having amino groups against the charged amount of CuCl for the adsorbent prepared from CuCl and the resin by use of 80 cm^3 of acetonitrile as solvent: The charged amount of the resin was kept constant at 10.0 g.

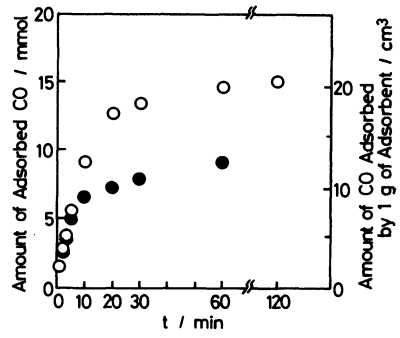

Fig. 3. Repeated adsorptions of CO from 9:1 $CO-N_2$ mixtures at 20 °C under 1 atm by the adsorbent composed of 64 mmol of CuCl and 10.0 g of the polystyrene resin having amino groups: The desorption of adsorbed CO was carried out at 80 °C under 1 atm for 10 min; the first (○) and the second (●) adsorptions.

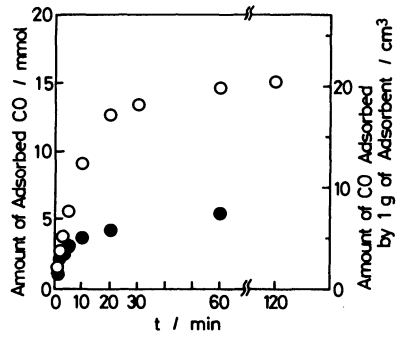

Fig. 4. Repeated adsorptions of CO from 9:1 $CO-N_2$ mixtures at 20 °C under 1 atm by the adsorbent composed of 64 mmol of CuCl and 10.0 g of the polystyrene resin having amino groups: The desorption of adsorbed CO was carried out at 5 mmHg, 20 °C; the first (○) and the second (●) adsorptions.

Table 1. Adsorbing Capacities of the CO Adsorbents Prepared from Copper(I) Chloride and Macroreticular Type Polystyrene Resins Having Various Functional Groups[a,b]

Functional group in the polystyrene resin	CO adsorbing capacity / mmol
Amino residue	15.9
Carboxylate residue	1.2
Sulfonate residue	0.8
None	2.2

a) Adsorption from 9:1 $CO-N_2$ mixture was carried out at 20°C under 1 atm. b) The adsorbents were prepared from 9.9 g (100 mmol) of CuCl and 10.0 g of the resins by use of 80 cm^3 of acetonitrile as solvent.

Table 2. Adsorbing Capacities on Various Gases for the Adsorbent Composed of 70 mmol of Copper(I) Chloride and 10.0 g of the Polystyrene Resin having Amino Groups[a]

Gas	Capacity/mmol	Amount of gas adsorbed by 1 g of adsorbent/cm^3[b]
CO	15.9	21.0
CO_2	2.8	3.7
Methane	0.0	0.0
Hydrogen	0.0	0.0
Nitrogen	0.0	0.0

a) Adsorption from 9:1 $CO-N_2$ mixture was carried out at 20°C under 1 atm. b) Standard temperature and pressure.

The open circles in Fig. 4 show the first adsorption of CO by the adsorbent, which is separately prepared. The equilibrium amount of adsorbed CO is 15.2 mmol. The adsorbed CO is desorbed by subjecting the adsorbent to a reduced pressure (5 mmHg) at 20° C for 10 min. In the second adsorption (the closed circles), the adsorption is rapid and the equilibrium amount of adsorbed CO is 5.4 mmol. Both the time courses and the equilibrium amounts of adsorbed CO in the third and the fourth adsorptions are identical with those in the second adsorption.

Adsorbing Capacities of Carbon Monoxide Adsorbents Composed of Copper(I) Chloride and Polystyrene Resins Having Various Functional Groups. Table 1 shows the CO adsorbing capacities of the adsorbents prepared from 100 mmol of CuCl and 10.0 g of the polystyrene resins having various functional groups. The capacity (15.9 mmol) of the adsorbent prepared with the use of the polystyrene resin having amino groups is much larger than the value (1.2 mmol) for the adsorbent with the resin having carboxylate residues, that (0.8 mmol) for the adsorbent with the resin having sulfonate residues, and that (2.2 mmol) for the adsorbent with the resin having no functional groups.

Selectivity of Carbon Monoxide Adsorption. Table 2 lists the adsorbing capacities of the adsorbent, composed of 10.0 g of the polystyrene resin having amino groups and 70 mmol of CuCl for various gases. The capacity (15.9 mmol) of the adsorbent for CO is 5.7 times as large as the value (2.8 mmol) for CO_2. The adsorbent exhibits no measurable adsorbing ability for methane, hydrogen, and nitrogen.

Figure 5 shows the plots of the adsorbing capacity for CO (the open circles) and the adsorbing capacity for CO_2 (the closed circles) against the amount of CuCl supported on 10.0 g of the polystyrene resin having amino groups. At the amount 0.0 mmol of supported CuCl, the resin does not adsorb CO in a measurable amount, and the adsorbing capacity for CO_2 is 8.3 mmol. The adsorbing capacity for CO largely increases with increasing amount of the supported CuCl, whereas the adsorbing capacity for CO_2 monotonously decreases. Consequently, the selectivity of CO adsorption, which is defined by the ratio of the adsorbing capacity for CO to the value for CO_2, significantly increases with increase in the supported amount of CuCl, as shown by the open squares. A selectivity 5.7 is attained at the supported amount 70 mmol of CuCl.

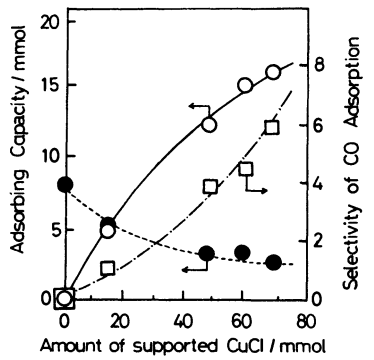

Fig. 5. Plots of adsorbing capacity (○) for CO, adsorbing capacity (●) for CO_2, and the selectivity (□) of CO adsorption against the amount of CuCl supported on the polystyrene resin having amino groups for the adsorbent prepared from CuCl and the resin by use of acetonitrile as preparation solvent: The selectivity of CO adsorption is defined by the ratio of the capacity for CO to the value for CO_2; the amount of the resin is kept constant at 10.0 g.

Effect of Preparation Solvent on the Adsorbing Capacity of the Adsorbent. Table 3 lists the CO adsorbing capacities of the adsorbents prepared with the use of various solvents. The adsorbent prepared using acetonitrile exhibits much larger capacity than the ones prepared using acetone, water, and the aqueous hydrochloric acid solution.

X-Ray Photoelectron Spectroscopy. Figure 6 shows the X-ray photoelectron spectra in the Cu_{2p} region of (a) the adsorbent composed of 65 mmol of CuCl and 10.0 g of the polystyrene resin having amino groups, (b) solid of CuCl, and (c) solid of $CuCl_2$. For the adsorbent, two bands are observed at 933 and 953 eV. The solid of CuCl also exhibits two bands at 933 and 953 eV. The spectrum for the solid of $CuCl_2$ con-

Table 3. CO Adsorbing Capacities of the Adsorbents Prepared by Use of Various Solvents[a,b]

Preparation solvent	Adsorbing capacity/mmol
Acetonitrile	15.9
Acetone	7.2
Water	6.3
Aqueous hydrochloric acid solution (1 mol dm^{-3})	5.6

a) Adsorbents were prepared from 9.9 g (100 mmol) of CuCl and 10.0 g of the polystyrene resin having amino groups with the use of 80 cm^3 of solvents. b) Adsorption from 9:1 CO–N_2 mixture was carried out at 20 °C under 1 atm.

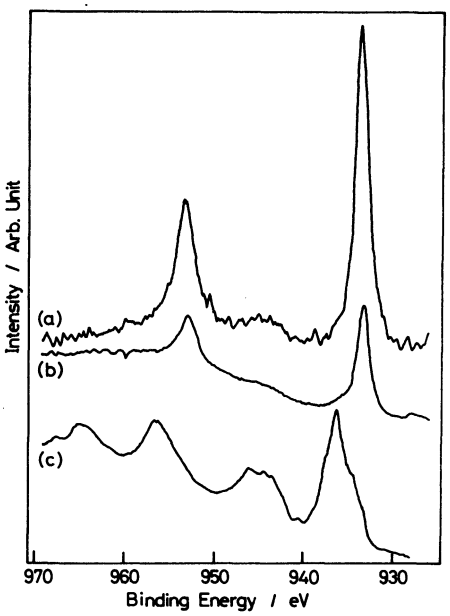

Fig. 6. X-Ray photoelectron spectra in the Cu_{2p} region for (a) the adsorbent composed of 65 mmol of CuCl and 10.0 g of the polystyrene resin having amino groups, (b) solid of CuCl, and (c) solid of $CuCl_2$.

sists of four bands at 937, 944, 957, and 964 eV.

Figure 7 depicts the X-ray photoelectron spectra in the Cl_{2p} region for (a) the adsorbent and (b) solid of CuCl. Both spectra are almost identical with each other, and are composed of a band at 200 eV and a shoulder peak around 201 eV.

Discussion

Adsorption and Desorption of Carbon Monoxide by the Adsorbents Composed of Copper(I) Chloride and Polystyrene Resin Having Amino Groups. The adsorptions of CO by the present adsorbents are ascribed to coordinations of CO to the copper(I) ions, which are complexing with the amino residues of the resin. Thus, the amount of adsorbed CO increases with increasing amount of the CuCl supported on the resin, as shown by open circles in Fig. 5.

Significance of the complexes between CuCl and the

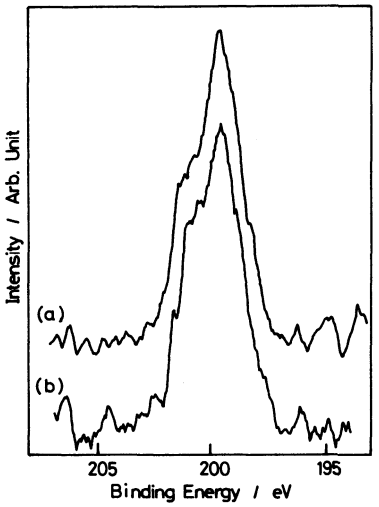

Fig. 7. X-Ray photoelectron spectra in the Cl_{2p} region for (a) the adsorbent composed of 65 mmol of CuCl and 10.0 g of the polystyrene resin having amino groups, and (b) solid of CuCl.

amino residues of the resin as the active species for the CO adsorption by the present adsorbents is definitely shown by the fact that the adsorbing capacity (15.9 mmol) of the adsorbent, prepared by use of the macroreticular type polystyrene resin having amino groups, is much larger than those (0.8—2.2 mmol) of the adsorbents prepared by use of the macroreticular type polystyrene resin having carboxylate residues, the polystyrene resin having sulfonate residues, and the polystyrene resin having no functional groups (Table 1). A methanol solution of CuCl–ethylenediamine complex absorbs CO,[11] whereas a solid of CuCl shows no measurable adsorption of CO at 20° C under 1 atm.[12]

Larger adsorbing capacity (15.9 mmol) of the adsorbent prepared by use of acetonitrile as solvent than the values (7.2 and 6.3 mmol) of the ones prepared by use of acetone and water (Table 3) is also consistent with the important role of the CuCl–amine complexes for the CO adsorption. The solubility of CuCl in acetonitrile is larger than that in acetone or in water, due to complex formation between copper(I) ion and acetonitrile.[13] Consequently, the formation of complex between CuCl and the amino residues of the resin proceeds more efficiently in acetonitrile than in acetone or in water. The small capacity (5.6 mmol) of the adsorbent obtained with the use of aqueous hydrochloric acid solution is associated with poor complex formation between CuCl and the amino residues of the polystyrene resin. In the aqueous hydrochloric acid solution, CuCl molecules dissolve in forms of $CuCl_2^-$[14] and the amino residues are present in their protonated forms. Both of these ionic species are highly stabilized by solvation with water molecules, which is unfavorable for the formations of the CuCl–amine complexes in the adsorbents.

Univalent states of virtually all the copper atoms in the adsorbents are confirmed by the fact that the

X-ray photoelectron spectrum in the Cu_{2p} region (Fig. 6 (a)) showing two bands at 953 and 933 eV is almost identical with that (Fig. 6 (b)) for the solid of CuCl. The solid of $CuCl_2$, however, exhibits satellite bands at 964 and 944 eV in addition to main bands at 937 and 957 eV (Fig. 6 (c)). Spectra in the Cu_{2p} region can be used for distinction between copper(I) species and copper(II) species.[15]

The differences (6.1 mmol and 9.8 mmol, respectively, for Figs. 3 and 4) between the equilibrium amounts of adsorbed CO in the first adsorption by the adsorbent and the values in the second and the later adsorptions correspond to the amounts of CO, which are not desorbed under the desorption conditions employed (80° C under 1 atm for 10 min and 5 mmHg at 20° C for 10 min, respectively).

When cycles involving adsorption of CO at 20° C under 1 atm and desorption of CO at 80° C under 1 atm for 10 min are repeated using the adsorbent composed of 10.0 g of the resin and 64 mmol of CuCl, 9.1 mmol of CO is separated for each of the cycles. For the cycles involving adsorption of CO at 20° C under 1 atm and desorption of CO at 5 mmHg, 20° C for 10 min, the amount of CO separated by one cycle is 5.4 mmol. In these repeated cycles, the amounts of CO separated by 1 g of the adsorbent for one cycle are 12 and 7.4 cm^3 (standard temperature and pressure), respectively.

Selectivity of Carbon Monoxide Adsorption for the Adsorbent Composed of Copper(I) Chloride and Polystyrene Resin Having Amino Groups. Much larger adsorbing capacity (15.9 mmol) on CO for the adsorbent composed of 10.0 g of the resin having amino groups and 70 mmol of CuCl than that (2.8 mmol) on CO_2 (Table 2) is highly in contrast with the adsorbing abilities of the resin itself: The adsorbing capacities of the resin on CO and on CO_2, respectively, are 0.0 and 8.3 mmol. The CuCl molecules supported on the resin are predominantly important for high selectivities of the present CO adsorbents. The adsorbents show no measurable adsorption on methane, hydrogen, and nitrogen.

The amounts of CuCl supported on the polystyrene resin having amino groups in the present adsorbents are larger than the ion-exchange capacity (38 mmol) of 10.0 g of the resin. The capacity is estimated by use of both the ion-exchange capacity per volume (2.5 equiv dm^{-3}) and the apparent density (650 g dm^{-3}) of the resin. Thus, considerable amounts of CuCl are supported on the resin without formation of complexes with the amino residues of the resin. These CuCl molecules are connected by chloride bridges with each other and with the CuCl molecules, which are complexing with the amino residues of the resin. In solids of CuCl, tetrahedrally coordinated copper(I) ions are bound by chloride bridges.[16] Consequently, layers composed of CuCl molecules are probably formed on the surface of the micropores of the resin. Even within the ion-exchange capacity of the resin, some portion of the supported CuCl is probably bound to the resin without complex formation with the amino groups, resulting in monotonous increase of adsorbing capacity with increasing amount of supported CuCl up to the amount 70 mmol (Fig. 5).

The present adsorbents efficiently adsorb CO by coordination of CO to the copper(I) ions in the complexes between CuCl and the amino residues of the polystyrene resin. In contrast, physical adsorption of CO_2 to the surface of the resin is suppressed by the layers of CuCl formed on the surface of the micropores. Chemical adsorption of CO_2 due to interactions with the amino groups of the resin is also inhibited by the complex formation between the amino groups and CuCl.

The arguments are confirmed both by the increase in the adsorbing capacity on CO and by the decrease in the adsorbing capacity on CO_2 with increasing amount of CuCl supported on the resin (Fig. 5). For the resin without CuCl, chemical and physical adsorptions of CO_2 to the resin are predominant, and the amount of adsorbed CO is zero.

The X-ray photoelectron spectroscopy on the adsorbent (Fig. 7) is consistent with formation of layers of CuCl in the adsorbents. The spectrum (a) for the chlorine atoms in the adsorbent is similar to the one (b) for a solid of CuCl. The CuCl molecules, which form layers on the surface of micropores of the resin by mutual chloride bridges, are arranged in almost the same way as those in a solid of CuCl.

The proposed mechanism of the selective adsorption of CO by the present adsorbents is supported by the fact that the adsorbents selectively adsorb ethylene with minimal adsorption of ethane.[17] There, ethylene is effectively adsorbed by the coordination to the copper(I) ions complexing with the amino groups of the macroreticular type polystyrene resin. In contrast, physical adsorption of ethane to the resin is suppressed by the layer of CuCl formed on the surface of the micropores.

In conclusion, selective carbon monoxide adsorbents are prepared from copper(I) chloride and a macroreticular type polystyrene resin having amino groups. The adsorbents are applicable to selective separation of carbon monoxide from gas mixtures containing carbon dioxide, methane, hydrogen, and nitrogen.

The authors would like to thank Dr. Yasuhiko Yoshida at Toyo University for kind assistance in the X-ray photoelectron spectroscopy.

References

1) "Kirk-Othmer Encyclopedia of Chemical Technology," 3rd ed, ed by H. F. Mark, D. F. Othmer, C. G. Overberger, and G. T. Seaborg, John-Wiley & Sons, New York (1978), Vol. 4, p. 772.

2) L. Kohl and F. C. Riesenfeld, "Gas Purification," 3rd

ed, Gulf Publishing Co., Houston (1979).
3) K. Wada, M. Komiyama, and H. Hirai, 51st National Meeting of Chemical Society of Japan, Kanazawa, October 1985, Abstr., No. 2M08.
4) Y.-Y. Huang, *J. Catal.*, **30**, 187 (1973).
5) J. A. Rabo, J. N. Francis, and C. L. Angell, U. S. Patent 4019879 (1977).
6) H. Hirai, M. Komiyama, and S. Hara, *Chem. Lett.*, **1982**, 1685.
7) H. Hirai, S. Hara, and M. Komiyama, *Bull. Chem. Soc. Jpn.*, **59**, 109 (1986).
8) H. Hirai, K. Wada, and M. Komiyama, *Chem. Lett.*, **1982**, 1025.
9) H. Hirai, K. Wada, and M. Komiyama, *Bull. Chem. Soc. Jpn.*, **59**, 1043 (1986).
10) H. Hirai, K. Wada, and M. Komiyama, *Chem. Lett.*, **1983**, 361.
11) M. Pasquali, C. Floriani, and A. Gaetani-Manfredotti, *Inorg. Chem.*, **19**, 1191 (1980).
12) H. Hirai, K. Wada, and M. Komiyama, *Bull. Chem. Soc. Jpn.*, **59**, 2217 (1986).
13) P. Kroneck, J. Kodweiss, O. Lutz, A. Nolle, and D. Zepf, *Z. Naturforsch.*, **A**, **37A**, 186 (1982).
14) D. D. Davis, K. L. Stevenson, and C. R. Davis, *J. Am. Chem. Soc.*, **100**, 5344 (1978).
15) D. C. Frost, A. Ishitani, and C. A. McDowell, *Mol. Phys.*, **24**, 861 (1972).
16) F. A. Cotton and G. Wilkinson, "Advanced Inorganic Chemistry," 4th ed, John Wiley & Sons, New York (1980), p. 802.
17) H. Hirai, K. Kurima, K. Wada, and M. Komiyama, *Chem. Lett.*, **1985**, 1513.

Mercury- and Cadmium-Photosensitized Reactions of β-Propiolactone

Shunzo YAMAMOTO,* Rinko GOHDA, Rie MORIKAWA, Hiroshi TAKAHOSO, Yoshimi SUEISHI, and Norio NISHIMURA
Department of Chemistry, School of Science, Okayama University, 3-1-1, Tsushima-naka, Okayama 700
(Received February 20, 1986)

The mercury- and cadmium-photosensitized reactions of β-propiolactone (PL) have been investigated. The gaseous products from the mercury-photosensitized reaction were carbon dioxide, ethylene, carbon monoxide, ethylene oxide, acetaldehyde, and methane, while the products obtained in the cadmium-photosensitized reaction were carbon monoxide, ethylene oxide, and acetaldehyde. In the mercury-photosensitized reaction, the quantum yields of the products were independent of the lactone pressure at pressures higher than 1500 Pa, while in the cadmium-photosensitized reaction, the quantum yields of the products decreased with the increase in the lactone pressure. Several possible reaction schemes have been proposed to explain the above kinetic behavior. The mercury- and cadmium-photosensitized reactions proceed through different intermediates, that is, a triplet lactone in the former and an excited complex between an excited cadmium atom and a lactone molecule in the latter.

Recently we have studied the mercury- and cadmium-photosensitized reactions of γ-butyrolactone(BL) and found that the mercury-photosensitized reaction gives carbon dioxide, cyclopropane, and propylene, while the cadmium-photosensitized reaction gives carbon monoxide, and ethylene.[1] We concluded that the mercury-photosensitized reaction proceeds through a lactone triplet state, while the cadmium-photosensitized reaction proceeds through an excited complex between an excited cadmium atom and a lactone molecule.

The present study was undertaken to see whether other simple lactones behave similarly.

Experimental

The mercury-photosensitized reaction was carried out at 100° C in a conventional cylindrical quartz vessel, 10 cm long and 4 cm in diameter, fitted with plane quartz windows at each end. A low pressure mercury lamp (Toshiba Electric Co., germicidal lamp) made from a quartz tube was used. The 184.9 nm resonance line was filtered out by means of a Vicor filter. The light intensity absorbed by mercury atoms at 253.7 nm was determined by means of *cis*-2-butene actinometry.[2]

The cadmium-photosensitized reaction was carried out at 235° C in a cylindrical Pyrex cell, 2 cm in diameter and 20 cm long. A U-shaped cadmium discharge lamp made of Pyrex, filled with 670 Pa Ar, was used. The light intensity absorbed by cadmium atoms at 326.1 nm was determined by means of *cis*-2-butene actinometry.[3]

Product analysis was done by fractionation at −196 and −89° C, and messurement by gas buret and gas chromatography. The first portion, non-condensable at −196° C, was collected by the use of a Toepler pump. This portion consisted of carbon monoxide and methane, and it was analyzed by combustion over copper oxide at 250° C. The products in the second portion, which was not condensable at −89° C, were analyzed by means of gas chromatography, using a 6-m column of Gasukuro-pack 55 (Gasukuro Kogyo Co., LTD) at 100°C. The third portion, which was condensable at −89 °C, contained a large amount of PL; it was not analyzed.

β-Propiolsctone(PL)(Sigms Chem. Co., Grade II) was dried over a molecular sieve 4A and purified by means of trap-to-trap distillation. A known amount of liquid propiolactone was injected into a capillary by the use of a microsyringe, fully degassed by many careful freeze-pump cycles, and completely transfered to the cell. The pressure of PL in the cell was calculated by means of the perfect-gas equation.

Results and Discussion

The Mercury-Photosensitized Reaction. Since the vapor pressure of PL is low at room temperature, it is necessary to elevate the reaction temperature in order to obtain sufficient vapor pressure. As was been mentioned above, the mercury-photosensitized reaction was studied at 100° C. The thermal decomposition at this temperature and the direct photolysis at 253.7 nm were found to be negligible. The major volatile products observed in the mercury-photosensitized reaction of PL were carbon dioxide, ethylene, carbon monoxide, acetaldehyde, ethylene oxide, and methane. The yields of these products increased linearly with increase in the resction time and the light intensity, showing that they are primary products. The quantum yields of all products except for carbon monoxide and methane increase with the increase in the lactone pressure up to 1500 Pa, while they are independent of the lactone pressure above 1500 Pa. The increase in the rate of product formation with the increase in the lactone pressure at pressures below 1500 Pa may be explained in terms of the increase in the rate of the energy transfer from $Hg(^3P_1)$ to lactone with the increase in the lactone pressure and/or in terms of the increase in the absorption intensity by mercury atoms as a results of the pressure broadening of the absorption line. The relative yields of products are shown in Fig. 1 as a function of the lactone pressure. Ethylene is always formed in amounts equimolar with carbon dioxide. The relative yields of ethylne oxide and acetaldehyde reach a constant value of about 0.12 above 1500 Pa, and fall slightly at lower pressures, while that of carbon monoxide decreased rapidly with the increase in the lactone pressure below 1500 Pa and reaches an almost constant value of at pressures higher than 1500 Pa. (Methane was found at pressures lower than 5000 Pa. The yield of methane decrease with the increase in the

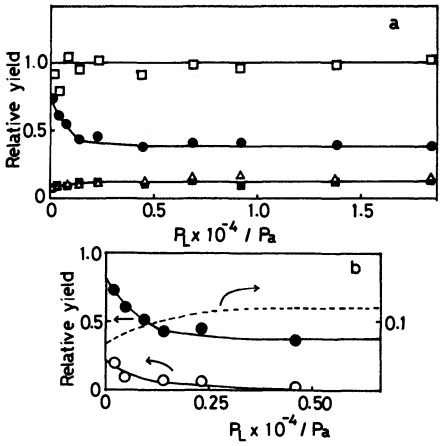

Fig. 1. Pressure dependence of relative quantum yields of products in the mercury-photosensitized reaction of PL.
a; ethylene (□), CO (●), ethylene oxide (△), and acetaldehyde (■). b; CO (●) and methane (○).
Dashed line in b shows pressure dependence for ethylene oxide and acetaldehyde.

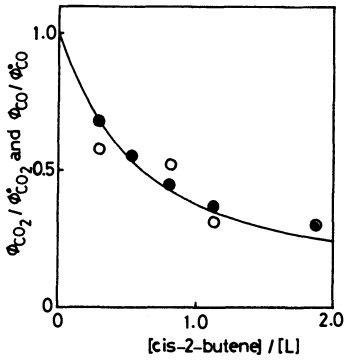

Fig. 2. Quantum yields of CO_2 (●) and CO (○) in the mercury-photosensitized reaction of PL in the presence of *cis*-2-butene.

lactone pressure and reached zero at about 5000 Pa)

When *cis*-2-butene was added to lactone, the quantum yields of carbon dioxide and carbon monoxide decreased as the quantum yield of *trans*-2-butene formation increased with the increase in the *cis*-2-butene pressure. From the slope of the reciprocal plot of the quantum yield of *trans*-2-butene vs. the lactone/*cis*-2-butene ratio, the quenching efficiency of lactone relative to that of *cis*-2-butene was estimated to be 0.62. Figure 2 shows the effect of *cis*-2-butene on the yields of carbon dioxide and carbon monoxide. The solid line shows the relative quantum yields calculated using the relative quenching efficiency of lactone obtained above. As Fig. 2 shows, the decrease in the quantum yields observed in the presence of *cis*-2-butene can be explained by the competitive quenching of the triplet mercury atom by lactone and *cis*-2-butene.

When oxygen was added to lactone, the quantum yields of the products decreased. For example, when 1333.3 Pa of oxygen was added to 4000 Pa of lactone, the following ratios of yields were obtained:

ϕ/ϕ°=0.87 (carbon dioxide), 0.75 (ethylene), 0.82 (ethylene oxide), and 0.85 (acetaldehyde). Here, ϕ° is the quantum yield in the absence of oxygen. These values are in good agreement with the ratio (0.81) calculated using the following relative quanching efficiencies of lactone and oxygen:

$$\sigma(\text{lactone})/\sigma(\textit{cis}\text{-2-butene}) = 0.62$$
$$\sigma(\text{oxygen})/\sigma(\textit{cis}\text{-2-butene}) = 0.45^{4)}$$

The decrease in the quantum yields can again be explained by the Competitive quenching of the triplet mercury atoms by lactone and oxygen. These findings show that the nature of the formation of these products was not affected by the addition of *cis*-2-butene and oxygen.

In order to explain the experimental results, the following set of reactions is proposed:

$$Hg(^1S_0) + h\nu(253.7\text{ nm}) \longrightarrow Hg(^3P_1), \quad (1)$$
$$Hg(^3P_1) \longrightarrow Hg(^1S_0) + h\nu(253.7\text{ nm}), \quad (2)$$
$$Hg(^3P_1) + L \longrightarrow Hg(^1S_0) + {}^3L, \quad (3)$$
$${}^3L \longrightarrow CO_2 + C_2H_4, \quad (4)$$
$${}^3L \longrightarrow CO + C_2H_4O^*, \quad (5)$$
$$C_2H_4O^* \longrightarrow CH_4 + CO, \quad (6)$$
$$C_2H_4O^* + L \longrightarrow \triangle_O + L, \quad (7)$$
$$C_2H_4O^* + L \longrightarrow CH_3CHO + L, \quad (8)$$
$$C_2H_4O^* + L \longrightarrow \text{other products}. \quad (9)$$

Here, ^3L denotes triplet lactone, while $C_2H_2O^*$ is an energy-rich intermediate. From this mechanism, the following equations can be derived:

$$\frac{\phi C_2H_4}{\phi CO_2} = 1.0, \quad (10)$$
$$\frac{\phi\triangle_O}{\phi CO_2} = \frac{k_5}{k_4}\frac{k_7[L]}{k_6+(k_7+k_8+k_9)[L]}, \quad (11)$$
$$\frac{\phi CH_3CHO}{\phi CO_2} = \frac{k_5}{k_4}\frac{k_8[L]}{k_6+(k_7+k_8+k_9)[L]}, \quad (12)$$
$$\frac{\phi CO}{\phi CO_2} = \frac{k_5}{k_4}\left(1+\frac{k_6}{k_6+(k_7+k_8+k_9)[L]}\right). \quad (13)$$

These equations show that the yield of ethylene is equal to that of carbon dioxide, and that the relative yields of acetaldehyde and ethylene oxide increase with the increase in the lactone pressure and reach a constant value at higher pressures, while the relative yield of carbon monoxide decreases with the increase in the lactone pressure and becomes constant (k_5/k_4) at higher pressures. These pressure dependences are consistent with those observed (Fig. 1). The decrease in the yield of methane observed (Fig. 1) is parallel to that of carbon monoxide at lower pressures, as was predicted by the above reaction mechanism. From the constant values of the relative yields at higher pressures, some ratios of

Table 1. Ratios of Rate Constants

$k_5/k_4=0.38$
$k_7/(k_7+k_8+k_9)=k_8/(k_7+k_8+k_9)=0.33$
$k_7:k_8:k_9=1:1:1$

rate constants are obtained; they are listed in Table 1.

The fate of the $C_2H_4O^*$ formed in Reaction (5) at high pressures requires some comment. Reactions (7) and (8), simple rearrangements (or stabilizations) to acetaldehyde and ethylene oxide, are suggested as the sources of these products, and because the sum of ethylene oxide and acetaldehyde was always less than carbon monoxide, Reaction (9) is suggested.

One possibility for Reaction (9) is a reaction with lactone to give higher products which were not observed.

Another possibility is the formation of vinyl alcohol, CH_2=CHOH, which would probably have been lost by polymerization before or during analysis. Although vinyl alcohol is about 84 kJ mol^{-1} less stable thermodynamically than acetaldehyde, the formation of either compound through the biradical($\cdot CH_2CH_2O\cdot$) which is considered to be formed from $C_2H_4O^*$ before formation of acetaldehyde in the thermal decomposition of ethylene oxide[5] should be quite exothermic; both would require hydrogen transfer through three-membered transition states, which might be about equally probable:

$$\overset{\cdot\cdot}{CH_2}CH\text{–}O \longrightarrow CH_3CHO, \quad (14)$$
$$\overset{\cdot\cdot}{H}$$

$$CH_2\text{–}CH\text{—}O \longrightarrow CH_2{=}CHOH. \quad (15)$$
$$\overset{\cdot\cdot}{H}$$

As Table 1 shows, the rate of Reaction (9) is equal to that of Reaction (8). This seems to show that the second case is more possible, although the existence of vinyl alcohol has not been reported in the reaction of ethylene with the oxygen atom,[6] the mercury-photosensitized reaction of ethylene oxide,[7] etc.[8,9]

From the above mechanism, the following relationship can be derived:

$$\frac{\phi CO}{\phi\Delta_0+\phi CH_3CHO}=\frac{k_7+k_8+k_9}{k_7+k_8}+\frac{2k_6}{k_7+k_8}\frac{1}{[L]}. \quad (16)$$

From the slope of the line shown in Fig. 3, $2k_6/(k_7+k_8)$=906 Pa was obtained. As is shown in Table 1, $k_7=k_8$. Therefore, $k_6/k_7=k_6/k_8$=906 Pa. The experimental value of k_6/k_7 gives $k_6=7.14\times10^7$ s^{-1} when 7.9×10^4 s^{-1} is adopted as the kinetic collision frequency at 1 Pa snd 100° C and when a collision deactivation efficiency of unity is assumed for lactone.

The excess energy of energized intermediate ($C_2H_4O^*$) can be estimated using

$$k_6(E)=A\left(1-\frac{E_a}{E}\right)^{s-1}, \quad (17)$$

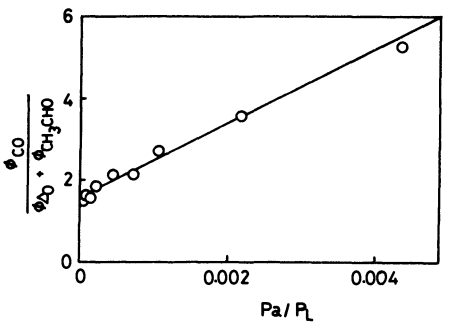

Fig. 3. Plots of $\phi_{CO}/(\phi_{\Delta_0}+\phi_{CH_3CHO})$ against the reciprocal of lactone pressure.

Here, k (E) is the rate constant for the decomposition of $C_2H_4O^*$ when the excess energy is E; A is the frequency factor, E_a is the critical energy, and s is the number of effective oscillators in the molecule. Using the experimental value of k_6 and substituting $A=10^{14.34}$ S^{-1} and E_a=240.2 kJ mol^{-1} (taken from the experiment of Mueller and Walters[8]) and s=8 (about half of the number of the modes of vibration of ethylene oxide), the value of E was found to be 272 kJ mol^{-1}. This excess energy corresponds to about 78% of the enthalpy change for the following reaction, which is estimated to be 351 kJ mol^{-1} by using the standard enthalpies of formation (ΔH_f°=−282.8 (propiolactone), −52.7 (CO), and −110.0 kJ mol^{-1} (ethylene oxide) and the excitation energy of mercury (E_T=469 kJ mol^{-1});

(18)

A comparison of the vibrational energy distribution in different systems is given in Table 2. It is evident that the major portion of the excess energy goes to the product with the most vibrational degree of freedom.

The reactions of oxygen atoms with ethylene in the gas phase[6] and in a liquid nitrogen solution[10] have been reported, and it was concluded that the primary step of the reactions involves the direct addition of an oxygen atom to the double bond to form an energy-rich intermediate ($C_2H_4O^*$) which then undergoes further reactions.

Cvetanovic pointed out[6] that there is a significant similarity among the following different modes of the decomposition of ethylene oxide: The thermal,[8] photolitic,[9] mercury-photosensitized decompositions,[7] and the decomposition of the energy-rich molecule formed in the reaction of oxygen atoms with ethylene in the gas phase.[6] As Table 3 shows, the product distribution in the present case is much simpler than those in the other cases mentioned above, and it is rather similar to that for the reaction of oxygen atoms with ethylene in a liquid nitrogen solution. It seems to be interesting that the fate of $C_2H_4O^*$ in the present case is very similar to that in the reaction of oxygen atoms with ethylene in the liquid phase.[10]

Table 2. Comparison of Excess Energy in Primary Products

Reaction	Energy carried over from primary process (kJ)	% of Energy entering complex product	Ref.
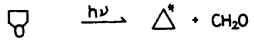	481	75	a
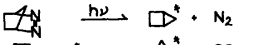	418	77	b
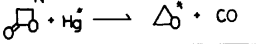	351	78	This work

a) B. C. Roquitte, *J. Am. Chem. Soc.*, **91**, 7664 (1969). b) T. F. Thomas, C. I. Suita, and C. Steel, *J. Am. Chem. Soc.*, **89**, 5107 (1967).

Table 3. Comparison of Product Distribution in the Reactions of Energy-rich Molecule, $C_2H_4O^*$

Reaction	Ref.	Products
Reaction of oxygen atoms with ethylene in the gas phase	6	CO, H_2, CH_4, C_2H_6, C_3H_8, Ethylene oxide, CH_2O, Aldehydes
Mercury-photosensitized reaction of ethylene oxide	7	CO, H_2, CH_4, C_2H_6, C_3H_8, CH_2CO, C_2H_4, Aldehydes
Thermal decomposition of ethylene oxide at 400°C	8	CO, H_2, CH_4, CH_3CHO, CH_2O, CH_2CO
Photolysis of ethylene oxide at wavelengths below 200 nm	9	CO, H_2, CH_4, C_2H_6, CH_2O, CH_3CHO
Reaction of oxygen atoms with ethylene in liquid nitrogen solution	10	Ethylene oxide, CH_3CHO (CH_2O, cyclopropane)
Mercury-photosensitized reaction of β-propiolactone	This work	Ethylene oxide, CH_3CHO (CO, CH_4)

The Cadmium-Photosensitized Reaction. The cadmium-photosensitized reaction was carried out at 235°C to get a sufficient vapor pressure of cadmium. The thermal decomposition of PL occurred at this temperature and gave carbon dioxide and ethylene. Under the irradiation of the cadmium-resonance line, we obtained carbon monoxide, ethylene oxide, and acetaldehyde besides carbon dioxide and ethylene. The amounts of carbon dioxide and ethylene were almost the same as those obtained from the thermal decomposition. We checked the influence of carbon dioxide and/or ethylene on the cadmium-photosensitized reaction, and found that the quantum yields of carbon monoxide, ethylene oxide, and acetaldehyde are independent of the pressure of the carbon dioxide (and/or ethylene) added, if the competitive quenching of the triplet cadmium atoms by lactone and carbon dioxide (and/or ethylene) is taken into account. Therefore, the influence of the thermal decomposition on the results of the cadmium-photosensitized reaction was regarded as negligible. The rate of the cadmium-photosensitized reaction decreases more rapidly than that of the thermal decomposition with a decrease in the reaction temperature. Therefore, the cadmium-photosensitized reaction was difficult to study at temperature lower than 235°C.

The major products obtained in the cadmium-photosensitized reaction of PL were carbon monoxide, ethylene oxide, and acetaldehyde. The yields of these products increased linearly with the reaction time,

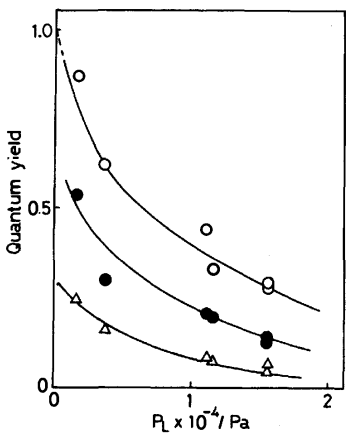

Fig. 4. Pressure dependence of quantum yields of CO (○), ethylene oxide (△), and acetaldehyde (●) in the cadmium-photosensitized reaction of PL.

showing that these are primary products. The quantum yields of these products are shown in Fig. 4 as a function of the lactone pressure. All of them decrease with an increase in the lactone pressure, showing the operation of the collisional deactivation process. This pressure dependence is quite different from that in the mercury-photosensitized reaction. Furthermore, in contrast with the mercury-photosensitized reaction, carbon dioxide and ethylene were not obtained, and the sum of ethylene oxide and acetaldehyde yields almost equals the carbon monoxide yield at low pressures (methane was not obtained even at low pressures).

These findings indicate that the cadmium-photosensitized reaction of PL proceeds through a different intermediate from that in the mercury-photosensitized reaction.

As has been mentioned previously,[1] the triplet state of BL seems to lie at about 440 kJ mol^{-1} above the ground state. If the energy of the triplet state of PL is similar to that of BL, the triplet state of PL is formed in the mercury-photosensitized reaction, as has been mentioned above ($Hg(^3P_1)$ has an energy of 469 kJ mol^{-1}), but it can not be formed by reaction with $Cd(^3P_1)$, which has an energy of only 367 kJ mol^{-1}. This probably accounts for the difference between the mercury- and cadmium-photosensitized reactions of PL.

In order to explain the experimental results, the following set of reactions is proposed:

$$Cd(^1S_0) + h\nu(326.1\ nm) \longrightarrow Cd(^3P_1), \quad (19)$$

$$Cd(^3P_1) \longrightarrow Cd(^1S_0) + h\nu(326.1\ nm), \quad (20)$$

$$Cd(^3P_1) + L \longrightarrow CdL^*, \quad (21)$$

$$CdL^* \longrightarrow Cd(^1S_0) + CO + C_2H_4O^*, \quad (22)$$

$$CdL^* + L \longrightarrow Cd(^1S_0) + 2L, \quad (23)$$

$$C_2H_4O^* \longrightarrow \triangle O, \quad (24)$$

$$C_2H_4O^* \longrightarrow CH_3CHO, \quad (25)$$

$$C_2H_4O^* + L \longrightarrow \text{other products}. \quad (26)$$

Here, CdL* stands for a transient complex between an excited cadmium atom and a lactone molecule, and $C_2H_4O^*$ is an energy-rich intermediate. The large pressure dependence of the quantum yields for the product formation is explained by Reaction (23). This mechanism is almost the same as that proposed for the cadmium-photosensitized reaction of γ-butyrolactone,[1] and of γ-valerolactone and α-methyl-γ-butyrolactone.[11]

From the above mechanism, the following equations can be derived:

$$\frac{\phi CO}{\phi\triangle_O} = \left(1+\frac{k_{25}}{k_{24}}\right) + \frac{k_{26}}{k_{24}}[L], \quad (27)$$

$$\frac{\phi CO}{\phi CH_3CHO} = \left(1+\frac{k_{24}}{k_{25}}\right) + \frac{k_{26}}{k_{25}}[L]. \quad (28)$$

Plots of $\phi_{CO}/\phi_{\triangle O}$ and ϕ_{CO}/ϕ_{CH_3CHO} vs. the lactone pressure are presented in Fig. 5. The values of k_{25}/k_{24} obtained from the intercepts and the slopes of the straight lines in Fig. 5 are in good agreement with one another within the limits of experimental error

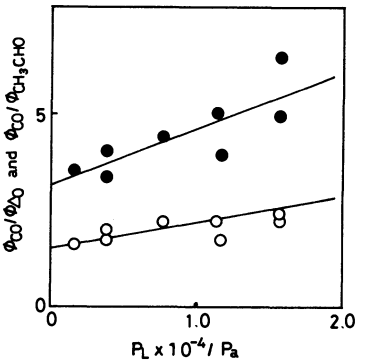

Fig. 5. Plots of $\phi_{CO}/\phi\triangle_O$ (●) and ϕ_{CO}/ϕ_{CH_3CHO} (○) against lactone pressure.

(2.1±0.1). This demonstrates that the above scheme is reasonable.

The intermediate, $C_2H_4O^*$, is similar to that in the mercury-photosensitized reaction. Since methane was not found even at low pressures, as has been mentioned above, the excess energy of $C_2H_4O^*$ in the cadmium-photosensitized reaction seems to be considerably smaller than that in the mercury-photosensitized reaction. As has been described above, the cadmium-photosensitized reaction are always accompanied by a rapid thermal decomposition at 235°C. Therefore, we could not obtain more detailed data, and further quantitative discussion of the cadmium-photosensitized reaction does not seem to be justified.

References

1) S. Yamamoto, S. Matsuda, C. Ozaki, H. Takahoso, and N. Nishimura, *Bull. Chem. Soc. Jpn.*, **57**, 3408 (1984).

2) R. B. Cundall and T. F. Palmer, *Trans. Faraday Soc.*, **56**, 1211 (1960).

3) S. Tsunashima and S. Sato, *Bull. Chem. Soc. Jpn.*, **41**, 284 (1968).

4) R. J. Cvetanovic, "Mercury Photosensitized Reactions," Progress in Reaction Kinertics, Vol. 2, ed. by G. Porter, The Macmillan Co., New York (1964), p. 39.

5) S. W. Benson, *J. Chem. Phys.*, **40**, 105 (1964).

6) R. J. Cvetanovic, *J. Chem. Phys.*, **23**, 1375 (1955).

7) R. J. Cvetanovic, *Can. J. Chem.*, **33**, 1684 (1955).

8) K. H. Mueller and W. D. Walters, *J. Am. Chem. Soc.*, **73**, 1485 (1951); **76**, 330 (1954).

9) R. Gomer and W. A. Noyes, Jr., *J. Am. Chem. Soc.*, **72**, 101 (1950).

10) S. Hirokami and R. J. Cvetanovic, *Can. J. Chem.*, **51**, 373 (1973).

11) S. Yamamoto, H. Takahoso, Y. Sueishi, and N. Nishimura, *Bull. Chem. Soc. Jpn.*, **58**, 2038 (1985).

 © 1986 The Chemical Society of Japan Bull. Chem. Soc. Jpn., 59, 2565—2570 (1986)

Selective Formation of 2-Phenylethanol in the Homologation of Benzyl Alcohol

Kazuhiro WATANABE,* Kiyoshi KUDO, Sadayuki MORI, and Nobuyuki SUGITA
Institute for Chemical Research, Kyoto University, Gokanosho, Uji, Kyoto 611
(Received March 8, 1986)

High selectivity of 2-phenylethanol (87%) in the homologation of benzyl alcohol was obtained with cobalt-ruthenium mixed catalyst. The formation of toluene as the major by-product was suppressed by adding water at low reaction temperature. Bromide as promoter was more effective for the homologation than chloride or iodide. From in situ IR observation, $[Co(CO)_4]^-$, which was active species for the homologation, was found to be produced by the dissociation of $[CoH(CO)_4]$ but not by the disproportionation of $[Co_2(CO)_8]$ under the reaction temperature employed (120 °C). It was also revealed that ruthenium chloride as precatalyst was converted into a bromocarbonyl complex of ruthenium under the homologation conditions.

The homologation of benzyl alcohol to 2-phenylethanol is an important reaction because the latter can be dehydrated to styrene. This reaction was first reported by Wender and his co-workers.[1] Their results showed that the hydrocarbon, toluene, and the homologous alcohol, 2-phenylethanol, were formed in a ratio of about 2:1. Based on the effects of substituents on aromatic ring, they postulated[2] that the homologation (Eq. 1) and the reduction (Eq. 2)

$$C_6H_5CH_2OH + CO + 2H_2 \longrightarrow C_6H_5CH_2CH_2OH + H_2O, \quad (1)$$

$$C_6H_5CH_2OH + H_2 \longrightarrow C_6H_5CH_3 + H_2O, \quad (2)$$

proceeded via the same intermediate. In spite of their studies, the selectivity of the homologation products were insufficient and toluene derivatives were major products. Up to now, higher molar ratio of 2-phenylethanol to toluene in this homologation was only reported in a patent.[3] Thus the main aim of this work is to improve the selectivity of the homologation step.

It has been known[4] that cobalt-catalyzed methanol homologation is promoted by iodide such as methyl iodide and by the addition of ruthenium as co-catalyst. So, we explored optimum reaction conditions for the homologation of benzyl alcohol with this mixed catalyst and halides as promoters. We also discussed the reaction mechanism.

Experimental

All materials other than solvent were commercially available and used without further purification. Solvent, 1,4-dioxane, was distilled over a Na-Pb alloy under nitrogen atmosphere. Hydrogen was commercial material (purity: above 99%) and carbon monoxide was prepared in our laboratory (purity: above 98%). Apparatus and procedure were similar to those used previously.[5,6]

Result and Discussion

Preliminary Experiments. At first, we investigated the effect of various halides as promoters on the homologation of benzyl alcohol. By the use of hydriodic acid as promoter at high temperature (180 °C), toluene was obtained preferentially and 2-phenylethanol in much lower yield under the reaction conditions employed (Run 1 in Table 1). Wender and his co-workers suggested[2] that toluene was formed through the radical mechanism involving benzyl radical. Carbon-metal bond is generally weak, for instance, 105 kJ mol^{-1} in $[C_6H_5CH_2Mn(CO)_6]$[7] and 92 kJ mol^{-1} in $[C_6H_5CH_2Co(Saloph)(py)]$,[8] so that this bond in

Table 1. The Homologation of Benzyl Alcohol[a]

Run	Temp/°C	Promoter (M)[b]		Benzyl Alcohol Conversion/%	Yield/%	
					Homologous Comp.[c]	Toluene
1	180	HI	(0.2)	95	8.2 (8.6)	78
2	120	—	(—)	10	5.0 (50)	1.8
3	120	HCl	(0.3)	14	8.1 (57)	0.8
4	120	HI	(0.2)	59	13 (22)	44
5	120	HBr	(0.2)	30	21 (70)	2.9
6	180	HBr	(0.2)	80	16 (20)	57
7	150	HBr	(0.2)	47	30 (64)	14
8	100	HBr	(0.2)	20	9.0 (45)	1.2
9[d]	120	$C_6H_5CH_2Br$	(0.2)	29	20 (69)	3.8

a) Reaction conditions: Total pressure, 300 kg cm^{-2} at room temp ($H_2/CO=2/1$); benzyl alcohol, 7 M; $Co(AcO)_2$, 0.23 M; $RuCl_3$, 0.023 M; 1,4-dioxane, 2 ml; reaction time, 4 h. b) Added as its aqueous solution, 1 M = 1 mol dm^{-3}. c) Total yield of 2-phenylethanol and phenylacetaldehyde. The selectivity of homologous compounds is shown in the parentheses. d) H_2O was added at the same concentration as that of hydrobromic acid used in Runs 5 to 8.

$[C_6H_5CH_2Co(CO)_4]$ is considered to be weak. Thus, the benzyl radical is supposed to be formed by homolysis of benzylcobalt complex and the reaction mechanism of toluene formation is considered as Eq. 3 to Eq. 7. On the other hand, if benzylcobalt complex (**1**)

$$C_6H_5CH_2OH + HX \rightleftharpoons C_6H_5CH_2X + H_2O \quad (3)$$
X : halogen atom

$$C_6H_5CH_2X + [Co(CO)_4]^- \rightleftharpoons [C_6H_5CH_2Co(CO)_4] + X^- \quad (4)$$
1

$$\mathbf{1} \rightleftharpoons C_6H_5CH_2\cdot + \cdot Co(CO)_4 \quad (5)$$
2 **3**

$$\mathbf{2} + [CoH(CO)_4] \rightleftharpoons C_6H_5CH_3 + \mathbf{3} \quad (6)$$

$$\mathbf{2}\ \mathbf{3} \rightleftharpoons [Co_2(CO)_8] \quad (7)$$

undergoes CO insertion followed by hydrogenolysis (Eqs. 8 and 9), phenylacetaldehyde is produced which

$$\mathbf{1} + CO \rightleftharpoons [(C_6H_5CH_2CO)Co(CO)_4] \quad (8)$$
4

$$\mathbf{4} + H_2 \rightleftharpoons C_6H_5CH_2CHO + [CoH(CO)_4] \quad (9)$$

is rapidly converted into 2-phenylethanol by ruthenium catalyst as shown later. 2-Phenylethanol and toluene are produced via the same intermediate, that is, benzylcobalt complex. Therefore, the suppression of homolytic cleavage (Eq. 5) or of the hydrogen abstraction reaction (Eq. 6) should improve the selectivity of 2-phenylethanol. Benzyl radical may also be formed by homolysis of benzyl iodide (Eq. 10).

$$C_6H_5CH_2I \rightleftharpoons C_6H_5CH_2\cdot + \cdot I \quad (10)$$

In order to suppress the radical cleavage such as Eq. 5 or Eq. 10, the reaction was carried out without iodide at low temperature (120 °C). Under these reaction conditions, 2-phenylethanol was a major product (Run 2 in Table 1) but its selectivity was not sufficient. By-products other than toluene were dibenzyl ether, ethylbenzene and benzyl acetate. The yield of dibenzyl ether was about 2% and that of ethylbenzene about 0.1% through the all runs. Benzyl acetate was formed by the reaction of benzyl alcohol with acetate anion originating in a precatalyst, cobalt(II) acetate, since benzyl acetate could not be detected by using octacarbonyldicobalt instead of cobalt(II) acetate. 1,2-Diphenylethane, the coupling product of benzyl radical, was also obtained in small amount through all runs. This result suggests the existance of benzyl radical.

Table 1 shows the effect of halides as promoters at low reaction temperature (Runs 3—5). Hydrobromic acid was more effective than hydrochloric acid for both the yield and selectivity of 2-phenylethanol. Hydriodic acid enhanced the conversion of benzyl alcohol but toluene was preferentially obtained. This implies that homolysis of benzyl iodide occurs to produce benzyl radical. From above results, we chose bromide as promoter and examined the effects of other reaction variables on the homologation.

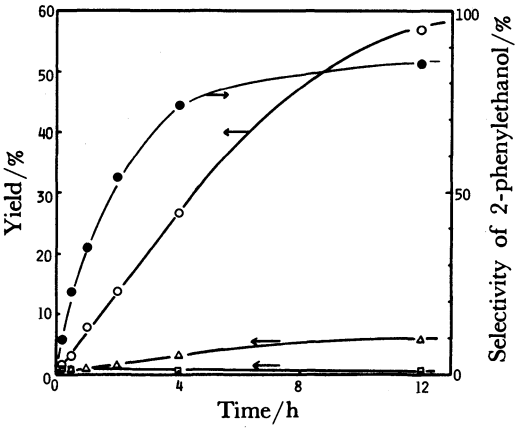

Fig. 1. Time dependent products yield in benzyl alcohol homologation. Reaction temp, 120 °C, total pressure, 320 kg cm^{-2} at 120 °C, (H_2/CO=2/1); benzyl alcohol, 7 M; HBr, 0.2 M as aqueous solution; $Co(AcO)_2$, 0.23 M; $RuCl_3$, 0.023 M; 1,4-dioxane, 10 ml. Total pressure was kept constant during the reaction. ○: 2-Phenylethanol, △: toluene, □: phenylacetaldehyde and ●: selectivity of 2-phenylethanol.

Effects of Temperature. Table 1 also shows that the yield of toluene decreases and the selectivity of 2-phenylethanol increases as the reaction temperature decreases from 180 °C to 120 °C (Runs 5—7). At 100 °C, the activity of catalyst for the homologation fell down and dibenzyl ether was obtained as the major by-product (yield: 4%). Thus, the optimum temperature for the high selectivity of the homologation step was about 120 °C.

The time-yield curves of 2-phenylethanol, phenylacetaldehyde and toluene at 120 °C are shown in Fig. 1. From these curves, it is suggested that phenylacetaldehyde is the intermediate for the formation of 2-phenylethanol (Eqs. 11 and 12). Figure 1 also shows

$$C_6H_5CH_2OH + CO + H_2 \longrightarrow C_6H_5CH_2CHO + H_2O \quad (11)$$

$$C_6H_5CH_2CHO + H_2 \longrightarrow C_6H_5CH_2CH_2OH \quad (12)$$

that the selectivity of 2-phenylethanol increases with the reaction time. As discussed later, this phenomenon is explained by the increase in the concentration of water which is produced by the reaction of benzyl alcohol with hydrogen bromide (Eq. 3, X=Br).

Effect of Ruthenium Concentration. The addition of ruthenium is known[4] to improve the selectivity of ethanol in methanol homologation and we proved[5] that its effectiveness was ascribed to the high reactivity on the hydrogenation of acetaldehyde. Figure 2 shows that ruthenium is also effective for improving the selectivity of 2-phenylethanol on account of the fast hydrogenation of phenylacetaldehyde. This fast hydrogenation of phenylacetaldehyde implies that the decarbonylation of phenylacetaldehyde affording toluene

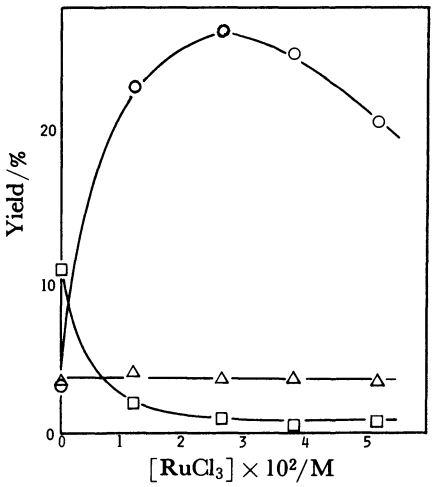

Fig. 2. Effect of ruthenium concentration on benzyl alcohol homologation. Reaction conditions were the same as those of Fig. 1, except ruthenium concentration and reaction time (4 h). ○: 2-Phenylethanol, △: toluene, □: phenylacetaldehyde.

is ruled out.

An optimum concentration of ruthenium existed and the yield of 2-phenylethanol decreased by the addition of ruthenium in large excess. This phenomenon was also observed in the case of methanol homologation.[6] As in the previous report,[5] this phenomenon is interpreted as resulting from the consumption of halogens which coordinate to ruthenium species (see later).

Effect of H_2O. As shown earlier, the concentration of water had an effect on the selectivity of 2-phenylethanol. In order to examine the effect of water in detail, we employed $C_6H_5CH_2Br$ as promoter instead of hydrobromic acid in this and the following experiments. The effect of $C_6H_5CH_2Br$ on the homologation was similar to that of HBr (Runs 5 and 9 in Table 1). [$Co_2(CO)_8$] was employed as catalyst precursor to avoid the formation of benzyl acetate.

From the results of in situ IR observation as shown later, water enhances the dissociation of [$CoH(CO)_4$] (Eq. 13). (An oxonium ion reacts rapidly with bromide anion which is produced by Eq. 4 affording water and hydrogen bromide as shown in Eq. 14).

$$[CoH(CO)_4] + H_2O \rightleftharpoons [H_3O]^+ + [Co(CO)_4]^- \quad (13)$$

$$[H_3O]^+ + Br^- \rightleftharpoons H_2O + HBr \quad (14)$$

When the initial concentration of water was lower than 2.0 M, both the yield and selectivity of 2-phenylethanol increased with the water concentration but the total yield of 2-phenylethanol and toluene was independent of it (Fig. 3 and Runs 1—3 in Table 2). Water inhibits the hydrogen abstraction reaction of benzyl radical from [$CoH(CO)_4$] (Eq. 6) because the concentration of [$CoH(CO)_4$] decreases with the initial concentration of water on account of the shift of equilibrium 13 to the right. On the other hand, addition of water in excess (higher than 2.0 M) diminished the total yield of 2-phenylethanol and toluene (Fig. 3) due to the shift of equilibrium 3 to the left. The selectivity of 2-phenylethanol, however, became not to be affected by the initial concentration of water (Runs 4, 6, and 7 in Table 2). Therefore, equilibrium 13 lies far to the right.

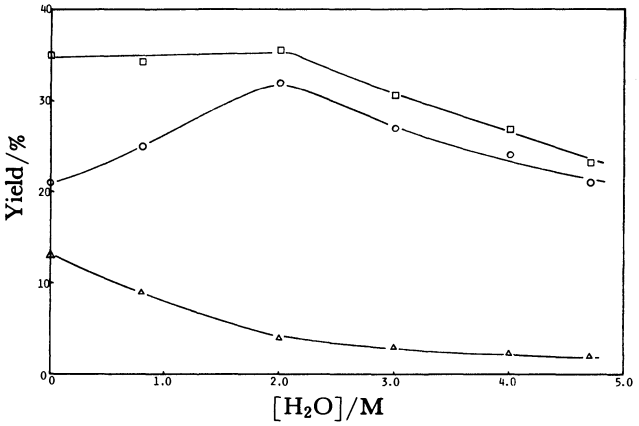

Fig. 3. Effect of H_2O concentration on toluene formation. Reaction conditions were the same as those of Table 2. ○: 2-Phenylethanol, △: toluene, □: total yield of 2-phenylethanol and toluene.

Table 2. The Effect of H_2O

Run	[H_2O]/M	Yield/%	
		$C_6H_5CH_2CH_2OH$[a]	$C_6H_5CH_3$
1	0[b]	22 (59)	13
2	0.8	25 (67)	9.2
3	2.0	32 (83)	4.1
4	3.0	27 (85)	3.1
5[c]	3.0	41 (87)	4.0
6	4.0	24 (84)	2.6
7	4.7	21 (85)	2.3

Reaction conditions: Reaction temp., 120 °C; total pressure, 320 kg cm^{-2} at 120 °C (H_2/CO=2/1); benzyl alcohol, 7 M; $Co_2(CO)_8$, 0.11 M; $RuCl_3$, 0.029 M; benzyl bromide, 0.21 M; 1,4-dioxane, 10 ml; reaction time, 4 h; the consumed gas was supplied during the reaction. a) The selectivity of 2-phenylethanol is shown in the parentheses. b) $Ru_3(CO)_{12}$, 8.8×10^{-3} M. c) Reaction time, 8 h.

As the reaction proceeded, the concentration of water increased by Eq. 3 and the selectivity of 2-phenylethanol increased as shown in Fig. 1. When the reaction was carried out for long period (12 h), one of the minor by-products, dibenzyl ether, was obtained in lower yield (0.5%) than that obtained for 4 h (1.4%). This result is due to the progress of the reverse reaction in equilibrium 15 since the concentration of water

$$2\,C_6H_5CH_2OH \rightleftharpoons C_6H_5CH_2OCH_2C_6H_5 + H_2O \quad (15)$$

increases and that of benzyl alcohol decreases with proceeding of the reaction. Thus the highest selectivity of 2-phenylethanol (87%, Run 5 in Table 2) was achieved, when the homologation was carried out for

Table 3. The Effect of $C_6H_5CH_2Br$

Run	$[C_6H_5CH_2Br]$/M	Yield/%		
		$C_6H_5CH_2CH_2OH$[a)]	$C_6H_5CH_2CHO$	$C_6H_5CH_3$
1	0	14 (49)	5.3	2.8
2	0.1	26 (78)	1.2	3.1
3	0.2	32 (83)	1.3	4.1
4	0.3	26 (63)	1.0	4.6
5	0.4	17 (49)	1.7	7.4

Reaction conditions: H_2O, 2.0 M; other reaction conditions were the same as those of Table 2. a) The selectivity of 2-phenylethanol is shown in the parentheses.

Table 4. Effect of Partial Pressure

Run	CO/H_2[a)]	Yield/%		
		$C_6H_5CH_2CH_2OH$[b)]	$C_6H_5CH_2CHO$	$C_6H_5CH_3$
1	1/3.5	25 (80)	0.7	5.3
2	1/2	32 (82)	1.3	4.1
3	1/1	28 (78)	1.6	5.3
4	2/1	19 (55)	3.0	7.0

Reaction conditions: Total pressure, 320 kg cm^{-2} at 120 °C; H_2O, 2.0 M; other reaction conditions were the same as those of Table 2. a) Partial pressure ratio. b) The selectivity of 2-phenylethanol is shown in the parentheses.

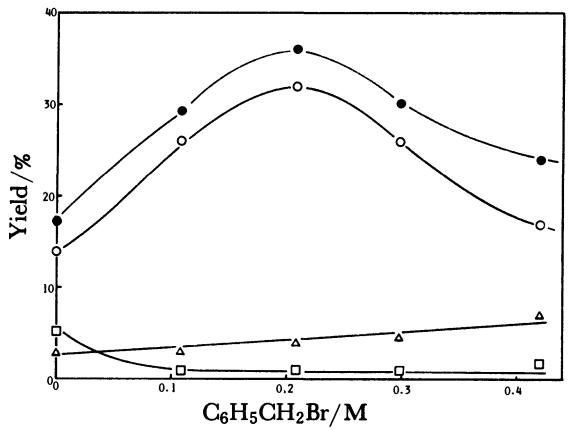

Fig. 4. Effect of benzyl bromide concentration on benzyl alcohol homologation. Reaction conditions were the same as those of Table 3. ○: 2-Phenylethanol, △: toluene, □: phenylacetaldehyde, ●: total yield of 2-phenylethanol and toluene.

long period under the optimum reaction conditions for its selectivity.

Effect of Benzyl Bromide and Partial Pressure of CO to H_2. Benzyl bromide promoted both the reactions of the homologation (Eq. 1) and the reduction (Eq. 2), when the initial concentration of benzyl bromide was lower than 0.2 M (Runs 1—3 in Table 3). The total yield of 2-phenylethanol and toluene, however, decreased with the initial concentration of benzyl bromide higher than 0.2 M (Fig. 4). These results indicate that the rate of benzylcobalt complex formation is retarded when the benzyl bromide is added in large excess. This is due to the suppression of the forward reaction of Eq. 4 by the high concentration of bromide anion. Although suppressing the forward reaction of Eq. 4 should lead to repression of the yield of toluene, that of toluene increased with the initial concentration of benzyl bromide. This implies that toluene is also produced via homolysis of benzyl bromide.

Figure 4 also shows that the hydrogenation of phenylacetaldehyde is slower in the absence of bromide than in the presence of it. As shown later, under the reaction conditions, ruthenium chloride as precatalyst was converted into chlorocarbonyl complex in the absence of bromide and into bromocarbonyl complex in the presence of it. Consequently, the former is supposed to be less reactive for the hydrogenation of phenylacetaldehyde than the latter.

Concerning the partial pressure ratio of CO to H_2, the highest yield and selectivity of 2-phenylethanol were found by using a CO to H_2 ratio of about 1:2 (Table 4). High partial pressure of H_2 increased the yield of toluene (Run 1 in Table 4) on account of high concentration of $[CoH(CO)_4]$ by equilibrium 16.

$$[Co_2(CO)_8] + H_2 \rightleftharpoons 2[CoH(CO)_4] \quad (16)$$

While low partial pressure of H_2 retarded the rate of hydrogenation of phenylacetaldehyde (Run 4 in Table 4) and also retards the formation of $[CoH(CO)_4]$ in equilibrium 16. In this case, homolysis of Co–Co bond in $[Co_2(CO)_8]$, the bond energy of which is very low (61 kJ mol^{-1}),[9] may occur to form cobalt carbonyl radical (Eq. 17). This radical abstracts $[Co(CO)_4]$ from

$$[Co_2(CO)_8] \rightleftharpoons 2\cdot Co(CO)_4 \quad (17)$$

benzylcobalt complex to afford benzyl radical (Eq. 18)

$$[C_6H_5CH_2Co(CO)_4] + \cdot Co(CO)_4 \rightleftharpoons C_6H_5CH_2\cdot + [Co_2(CO)_8] \quad (18)$$

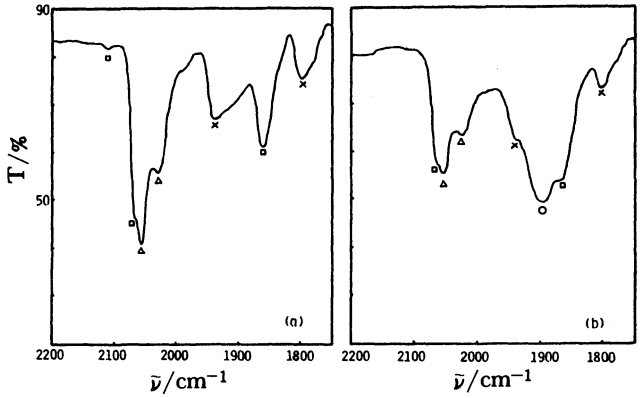

Fig. 5. IR spectra of $[Co_2(CO)_8]$, $[CoH(CO)_4]$ and $[Co(CO)_4]^-$ under high pressure of syngas. Conditions: total pressure, 125 kg cm^{-2} at 120°C (H_2/CO=2/1). Peaks ascribed to O: $[Co(CO)_4]^-$, □: $[Co_2(CO)_8]$, Δ: $[CoH(CO)_4]$, ×: benzyl alcohol. (a) solvent: benzyl alcohol, (b) solvent: benzyl alcohol-H_2O-1,4-dioxane (50:1:0.5 volume ratio).

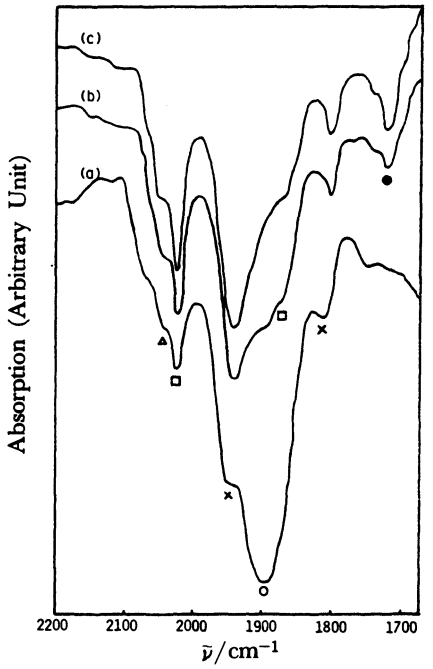

Fig. 6. IR spectra of $[Co_2(CO)_8]$ with benzyl bromide under high pressure of syngas in benzyl alcohol-H_2O-1,4-dioxane (50:1:0.5 volume ratio). Conditions: benzyl bromide, 0.04 M (bromide/Co=0.5). Peaks ascribed to O: $[Co(CO)_4]^-$, □: $[Co_2(CO)_8]$, Δ: $[CoH(CO)_4]$, ●: phenylacetaldehyde, ×: benzyl alcohol. Spectra were observed under (a) 120 kg cm^{-2} (H_2/CO=2/1) at 25°C, (b) 125 kg cm^{-2} at 100°C and (c) 127 kg cm^{-2} at 120°C.

because the yield of toluene increases, although very little, with decreasing partial pressure of H_2 (Runs 3 and 4 in Table 4).

In Situ IR Observation. The respective infrared spectral changes of $[Co_2(CO)_8]$ and $RuCl_3$ as catalyst precursors were followed under high pressure of syngas (H_2/CO=2/1) from room temperature (25°C) to

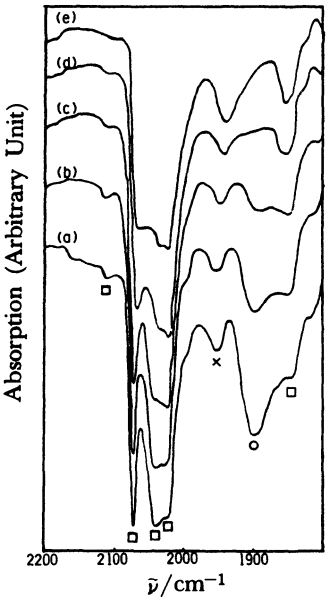

Fig. 7. IR spectra of $[Co_2(CO)_8]$ under high pressure of CO. Conditions: solvent: benzyl alcohol-H_2O-1,4-dioxane. Peaks ascribed to O: $[Co(CO)_4]^-$, □: $[Co_2(CO)_8]$, ×: benzyl alcohol. Spectra were observed under (a) 30 kg cm^{-2} of CO at 25°C, (b) 32 kg cm^{-2} at 50°C, (c) 33 kg cm^{-2} at 70°C, (d) 34 kg cm^{-2} at 100°C and (e) 35 kg cm^{-2} at 120°C.

optimum reaction temperature (120°C). Typical spectra are shown in Figs. 5—7. Figure 5 illustrates that, at 120°C, the characteristic absorption of $[Co(CO)_4]^-$, **5**, at 1890 cm^{-1} [10] is not observed without adding water (Fig. 5-(a)) but observed with adding water (Fig. 5-(b)), with the characteristic bands of $[Co_2(CO)_8]$, **6**, (2105, 2068, 2024, and 1860 cm^{-1})[11] and those of $[CoH(CO)_4]$, **7**, (2053 and 2030 cm^{-1}).[11] When benzyl bromide and water were added to this system, the absorption of **5** diminished as temperature was raised (Figs. 6-(a) and (b)) and ultimately disappeared at 120°C (Fig. 6-(c)). On the other hand, the absorption of phenylacetaldehyde (at 1700 cm^{-1}) increased (Fig. 6-(a) to (c)). This result indicates that **5** is active species for the homologation as reported previously.[5]

It is known that $[Co_2(CO)_8]$ reacts with water to afford **5** and Co(II) ion by disproportionation (Eq. 19).[12] This disproportionation occurred at low tem-

$$3[Co_2(CO)_8] + 12H_2O \rightleftharpoons 2\{[Co(H_2O)_6]^{2+}[Co(CO)_4]_2^-\} + 8CO \quad (19)$$

perature (25—75°C, Figs. 7-(a) to (c)) but did not at high temperature (100—120°C, Figs. 7-(d) and (e)). From above results, under the homologation conditions, **5** is deduced to be formed by the dissociation of **7** (Eq. 13), that is, the addition of water causes the large dissociation of **7** to produce **5**. Hence, the homologation is accelerated and formation of toluene is suppressed.

It was found from in situ IR observation that

$RuCl_3$ was converted into dichlorodicarbonylruthenium (absorption bands: 2150, 2070, and 2030 cm^{-1})[13] without adding hydrobromic acid and into dibromodicarbonylruthenium (absorption bands: 2135 and 2165 cm^{-1})[13] with adding it (HBr/Ru=2) at 120°C under syngas pressure. Although the number of bromide coordinating to ruthenium is obscure under the homologation conditions, bromoruthenium complex is more active for the hydrogenation of 2-phenylacetaldehyde than chlororuthenium complex (see Fig. 4). When ruthenium is added in excess to the homologation system, the concentration of bromide (HBr or $C_6H_5CH_2Br$) significantly decreases by the coordination to ruthenium and consequently the rate of phenylacetaldehyde formation promoted by bromide is retarded.

The authors wish to thank Messers. Yukio Ichikawa and Mitsuo Yasumoto for the contribution of manufacturing in situ high-pressure IR cell and assembling the high-pressure experimental equipments.

References

1) I. Wender, R. Levine, and M. Orchin, *J. Am. Chem. Soc.*, **71**, 4160 (1949).

2) I. Wender, R. Levine, and M. Orchin, *J. Am. Chem. Soc.*, **74**, 4079 (1952).

3) M. B. Sherwin, U. K. Patent 2007652 (1979); *Chem. Abstr.*, **92**, 58423f (1980).

4) M. Röper, and H. Loevenich, "Catalysis in C_1 Chemistry," ed by W. Keim, D. Reidel Publishing Company, Dordrecht, Lancaster (1983), p. 462.

5) K. Watanabe, K. Kudo, and N. Sugita, *Bull. Chem. Soc. Jpn.*, **58**, 2029 (1985).

6) K. Kudo, and N. Sugita, *Nippon Kagaku Kaishi*, **1982**, 462.

7) M. Nappa, R. Santi, and J. Halpern, *Organometallics*, **4**, 34 (1985).

8) T. T. Tsou, M. Loots, and J. Halpern, *J. Am. Chem. Soc.*, **104**, 623 (1982).

9) O. R. Bidinstosti, and N. S. McIntyre, *Can. J. Chem.*, **48**, 593 (1970).

10) J. E. Ellis, and E. A. Flom, *J. Organomet. Chem.*, **99**, 263 (1975).

11) R. A. Friedel, I. Wender, S. L. Shufler, and H. W. Sternberg, *J. Am. Chem. Soc.*, **77**, 3951 (1955).

12) I. Wender, H. W. Sternberg, and M. Orchin, *J. Am. Chem. Soc.*, **74**, 1216 (1952).

13) R. Colton, and R. H. Farthing, *Aust. J. Chem.*, **20**, 1283 (1967); R. Colton, and R. H. Farthing, *ibid*, **24**, 903 (1971).

 © 1986 The Chemical Society of Japan Bull. Chem. Soc. Jpn., 59, 2571—2575 (1986)

Relationship between Donor and Acceptor Numbers and Intrinsic Molecular Properties from Gas-Phase Ion Equilibria

Kenzo HIRAOKA
Faculty of Engineering, Yamanashi University, Takeda 4, Kofu 400
(Received March 12, 1986)

Molecular and bulk solvent properties of protic and aprotic solvent molecules were discussed in the respects of donor numbers (DN) and acceptor numbers (AN) proposed recently by Gutmann, and the intrinsic molecular properties obtained from gas-phase ion equilibria measurements. For aprotic solvent molecules, good correlations are generally found between the gas-phase thermochemical data and both of DN and AN. This indicates that DN and AN for aprotic solvents well reflect the intrinsic molecular properties. On the other hand, the correlations for H_2O and lower alcohols are not good. This is due to the more effective enhancement effect in the intermolecular interactions for protic solvents than for aprotic solvents.

Several empirical parameters have been proposed for characterizing the solvent properties. Grunwald and Winstein proposed the Y value as a scale for the ionizing properties of solvents.[1] This was based on a comparison of the rate constant for the solvolysis of t-butyl chloride in one solvent with that in the reference solvent mixture of 80% ethanol and 20% water.

Kosower introduced the Z value which characterizes the ionizing property of solvent.[2-4] This value is based on the UV spectra of 1-ethyl-4(methoxycarbonyl)-pyridinium iodide. The charge-transfer energy of this compound in a particular solvent was considered as an empirical measure of the ionizing property.

The E_t values proposed by Dimroth and Reichhardt[5,6] are based on the solvent sensitivity of optical absorption of a 4-(1-pyridinio)phenolate due to the intramolecular charge-transfer transition. All these parameters, Y, Z, and E_t, are known to be a good measure for the acceptor properties of solvents.[7]

In order to obtain a solvent-independent representation for the donor ability of a molecule, the donor numbers (DN) were introduced by Gutmann and Wychera.[8] The donor number is defined as a molar enthalpy value for the reaction of the donor (D) with $SbCl_5$ as a reference acceptor in a 10^{-3} M† solution of 1,2-dichloroethane.[7]

$$D + SbCl_5 = D\cdot SbCl_5 \qquad (1)$$
$$(-\Delta H_{D\cdot SbCl_5} = DN)$$

Recently, an empirical parameter for the acceptor properties of solvents has been proposed by Mayer et al.[9,10] which is based on the ^{31}P NMR chemical shift in triethylphosphine oxide in the respective pure solvent. In constrast to classical solvent parameters such as dielectric constant, dipole moment, or polarizability, the acceptor number (AN) allows the interpretation of numerous solvent dependent NMR-, IR, Raman-, UV-spectroscopic, and kinetic data.

The extended donor-acceptor concept presented by Gutmann[7] can be applied to very weak (electrostatic) as well as to strong (covalent or coordinate) interactions, because in both cases rearrangement of the charges in the interacting species takes place. The objective of this work is to investigate the molecular and solvent properties of protic and aprotic solvent molecules by examining the relations between the donor and acceptor numbers and gas-phase thermochemical data which represent the intrinsic molecular properties.

† 1 M=1 mol dm^{-3}.

Discussion

DN's vs. Gas-Phase Proton Affinities. In the determination of DN's, the adducts of $D\cdot SbCl_5$ are formed in a 1:1 molar ratio with all donor molecules.[7] Thus DN's represent molecular donicities rather than donicities for bulk solvents.

The gas-phase proton affinity (PA) is defined as the negative of the enthalpy change for the protonation Reaction (2).

$$A + H^+ = AH^+, \quad -\Delta H^\circ = PA(A) \qquad (2)$$

Namely, the proton affinity is a measure of the Brönsted basicity. On the protonation, a sort of coordinate bond is formed between A and H^+, i.e., $A\rightarrow H^+$. Thus the proton affinity may also be regarded as a scale of the gas-phase Lewis basicity.

Figure 1 shows the relationship between the gas-phase PA's[11] and DN's[7] for protic and aprotic solvent molecules. A fair correlation is seen between these two parameters for aprotic solvent molecules. This indicates that PA's could be a measure of molecular donicity for aprotic solvents.

Contrary to the aprotic solvent molecules, the correlation is not good for protic solvent molecules. The H_2O, CH_3OH, and C_2H_5OH molecules have about the same DN's. This means that the bond energies of D–$SbCl_5$ is more or less the same for D= C_2H_5OH, CH_3OH, and H_2O. On the contrary, proton affinities for these compounds are quite different. The smallest value of the PA for H_2O is due to the localization of positive charge in three protic hydrogens in H_3O^+. Almlöf and Wahlgren examined the electronic structure of H_3O^+ by ab initio MO calculations.[12] They deduced an HOH angle of 117° and net positive charges on H and O of 0.328 and 0.015, re-

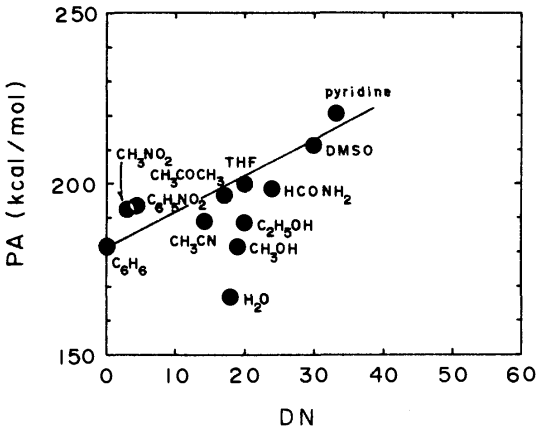

Fig. 1. Relationship between donor numbers (DN's) and gas-phase proton affinities (PA's) for protic and aprotic solvents. THF: tetrahydrofuran, DMSO: dimethyl sulfoxide.

spectively. Nearly all the positive charge in H_3O^+ is on three hydrogen atoms. In the protonated alcohols, the positive charge can be more delocalized owing to the electron-donating ability of the alkyl, making the value of PA larger than H_2O. As shown in Fig. 1, alcohols are seen to approach to the correlation curve for aprotic solvents as the alkyl gets larger. Thus the gas-phase proton affinities may be used for the measure of the molecular donicities for aprotic solvents and higher alcohols. However, PA's cannot be the measure of the molecular donicities for water and lower alcohols, and may be not for ammonia and lower amines, either.

DN's vs. Bond Energies of L_i^+ and K^+ with Solvent Molecules Measured in the Gas Phase. Figure 2 shows the relationship between DN's and the bond energies ($-\Delta H°$'s) of the complexes L_i^+·D and K^+·D for D=various protic and aprotic solvents.[13]

Since L_i^+ and K^+ have inert closed shells, they refuse the acceptance of electrons from the solvent molecule, D. Thus the stabilization of the clusters of L_i^+·D and K^+·D comes from electrostatic and polarization interactions.[14]

As shown in Fig. 2, a fair correlation is found between DN and $-\Delta H°$ for aprotic solvents, except for pyridine.

For the complex of the alkali ion M^+ with pyridine, the two stable structures may exist as shown below.

(I) (II)

The structure (I) assumes the importance of the ion-dipole interaction. The relatively large dipole moment of pyridine (μ_D=2.2 D) is mainly due to the large size of

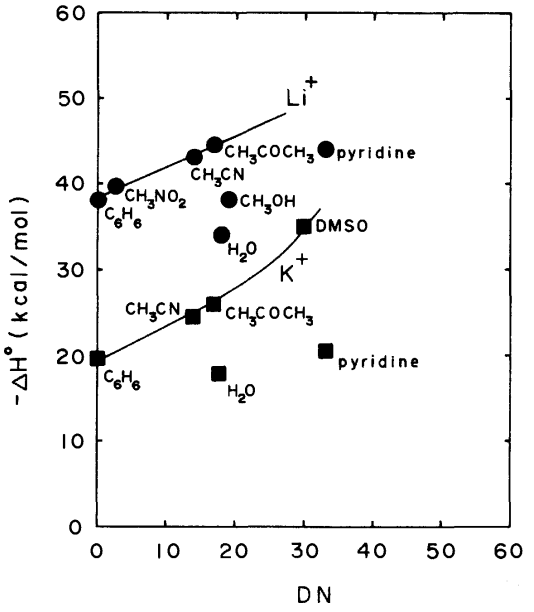

Fig. 2. Relationship between donor numbers (DN's) and enthalpy changes ($\Delta H°$'s) for reaction: M^++ solvent=M^+(solvent), measured in the gas phase. M^+=L_i^+ and K^+. $-\Delta H°$ corresponds to the bond energy of the cluster M^+---solvent. DMSO: dimethyl sulfoxide.

the molecule, i.e., pyridine is a rather soft Lewis base. Thus the interaction of the molecule with hard Lewis acids such as L_i^+ and K^+ could not be so strong as would be expected from the large μ_D of pyridine. In addition, the exchange repulsion between the closed shells of alkali ions and the lone pair plus diffuse π electrons of the pyridine molecule would make the interaction of the structure (I) less favorable. This might explain the deviation of pyridine from the correlation curve.

If the bond energy of the structure (I) is small, the complex may prefer the structure (II), in which the stabilization is due to the ion-quadrupole interaction. Such a structure is found to be most stable for the complex of K^+ with benzene.[15,16]

As the case of PA vs. DN, the protic solvents deviate from the correlation curve for aprotic solvents. In Fig. 2, the deviation of H_2O is larger than CH_3OH. This suggests that the ion-induced dipole moment interaction plays an important role for the stabilization of the bonds of M^+·D. The polarizability of CH_3OH(3.25 Å^3) is larger than that of H_2O(1.45 Å^3) while the dipole moment of CH_3OH(1.70 D) is smaller than that of H_2O(1.84 D). Although the data points are rather scarce, it may be worthwhile nothing that the DN's which represent the measure of the mainly covalent (or coordinate) bond strengths can also be a good measure for the electrostatic bond strengths for aprotic solvents.

AN's vs. Gas-Phase Acidities. The gas-phase acidity scale may be given by the enthalpy change $-\Delta H°_{acid}$ of Reaction (3),

$$AH = A^- + H^+ \qquad (3)$$

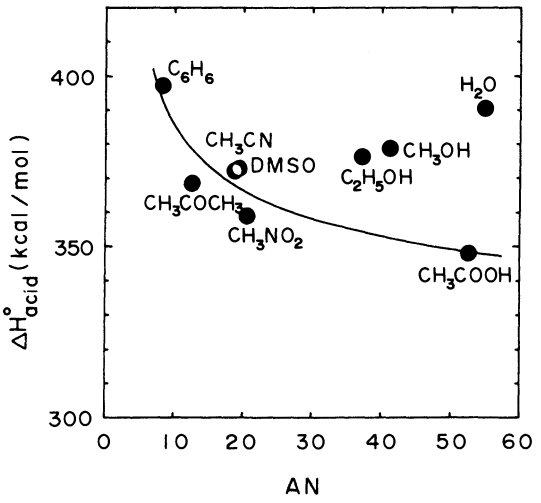

Fig. 3. Relationship between acceptor numbers (AN's) and gas-phase acidities ($-\Delta H^\circ_{acid}$) for protic and aprotic solvents. DMSO: dimethyl sulfoxide.

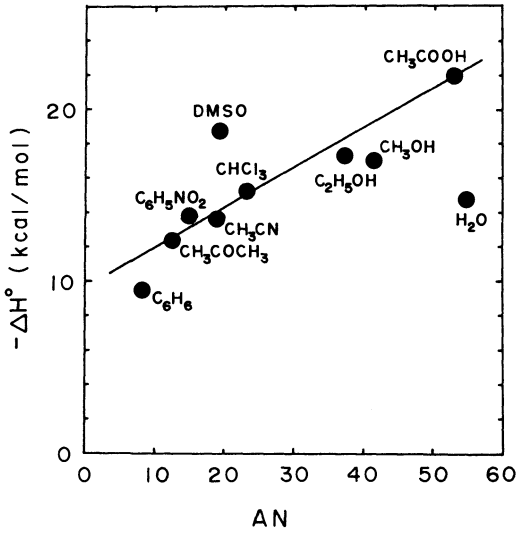

Fig. 4. Relationship between acceptor numbers (AN's) and enthalpy changes (ΔH°'s) for reaction: Cl^-+solvent=Cl^----solvent, measured in the gas phase. $-\Delta H^\circ$ corresponds to the bond energy of the cluster Cl^----solvent.

$-\Delta H^\circ_{acid}$=DH°(A-H)+IP(H)−EA(A) where DH°(A-H) is the bond energy of A-H, IP(H) is the ionization energy of the hydrogen atom, and EA(A) is the electron affinity of the radical A. Any molecule containing a hydrogen atom is potentially a proton donor, or Brönsted acid. For the complex of an acceptor AH and a donor D, $A\text{-}\overset{\delta-}{H}\cdots\overset{\delta+}{D}$, the stronger interaction may be expected for AH which has a larger gas-phase acidity (smaller value of $-\Delta H^\circ_{acid}$).

Figure 3 shows the relationship between $-\Delta H^\circ_{acid}$[17] and AN's for protic and aprotic solvents. A fair correlation exists between these two parameters for aprotic solvents, i.e., $-\Delta H^\circ_{acid}$ decreases with an increase of AN. However, just the opposite correlation is found for protic solvents, i.e., $-\Delta H^\circ_{acid}$ *increases* with an increase of AN in the order $C_2H_5OH \rightarrow CH_3OH \rightarrow H_2O$. This is ascribed to the fact that AN is a measure of the acceptor ability for the bulk solvent rather than that for a free molecule (see the following section).

AN's vs. Bond Energies of Cl^- with Solvent Molecules Measured in the Gas Phase. Figure 4 shows the relationship between AN's and bond energies of Cl^- with protic and aprotic solvents.[13]

A good correlation is seen for aprotic solvents and acetic acid as the case of gas-phase acidities vs. AN's. These results suggest that there is some correlation between the gas-phase acidity and the bond strength of the complex AH···Cl^-. Actually it is already pointed out that the bond strength of AH···X^- increases with the acidity of AH where X^- corresponds to halide or O_2^- ion.[18,19,20] An approximate correlation of the bond strength with the gas-phase acidity can be expected on the grounds that the bond strength of the bond AH···X^- should be related to D($A^-\cdots H^+$) since the bridging H atom in the complex must carry appreciable positive charge induced by the negative ion X^-.

Contrary to a good correlation observed for aprotic solvents, just the opposite correlation is found for protic solvents, i.e., $-\Delta H^\circ$ *decreases* with an increase of AN in the order $C_2H_5OH \rightarrow CH_3OH \rightarrow H_2O$. The H_2O molecule which has the largest AN as a solvent has the least $-\Delta H^\circ$. This is somewhat puzzling because the larger AN suggests the stronger bond of AH···Cl^- as is observed for aprotic solvents. This must be due to the characteristic solvent properties which arise from the intrinsic molecular properties. The stepwise solvation enthalpies $\Delta H^\circ_{n-1,n}$ for Reaction (4),

$$\text{Ion(solvent)}_{n-1} + \text{solvent} = \text{Ion(solvent)}_n \qquad (4)$$

and the heats of solvation ΔH°_s are related as

$$\Delta H^\circ_S = \sum_{n=1}^{n=N} \Delta H^\circ_{n-1,n}(\text{Ion(solvent)}_n) - \sum_{n=2}^{n=N} \Delta H^\circ_{n-1,n}(\text{solvent})_n \qquad (5)$$

The value of $\Delta H^\circ_{n-1,n}$ (Ion(solvent)$_n$) and $\Delta H^\circ_{n-1,n}$ (solvent)$_n$ converge at $n=N$. It may be reasonable to assume that the solvent of large AN is a good solvent for negative ions, namely, AN and $-\Delta H^\circ_s$ correlate with each other. The large value of AN for H_2O suggests that the value of $-\Delta H^\circ_s$ is also large. The small value of $-\Delta H^\circ$ for H_2O (Fig. 4) is understandable because of the low gas-phase acidity of the H_2O molecule. When the H_2O molecule interacts with the ion, the H_2O molecule is polarized. The polarized H_2O molecule would enhance the further hydrogen bonding with the H_2O molecule in the outer shell. This enhancement effect would extend from inner ligands to outer ligands in the shells surrounding the core ion and thus make the value of $-\Delta H^\circ_s$ ultimately large. This kind of enhancement effect may be envisaged more clearly by the donor-acceptor concept, i.e., the spillover effect of the acceptor and the pileup

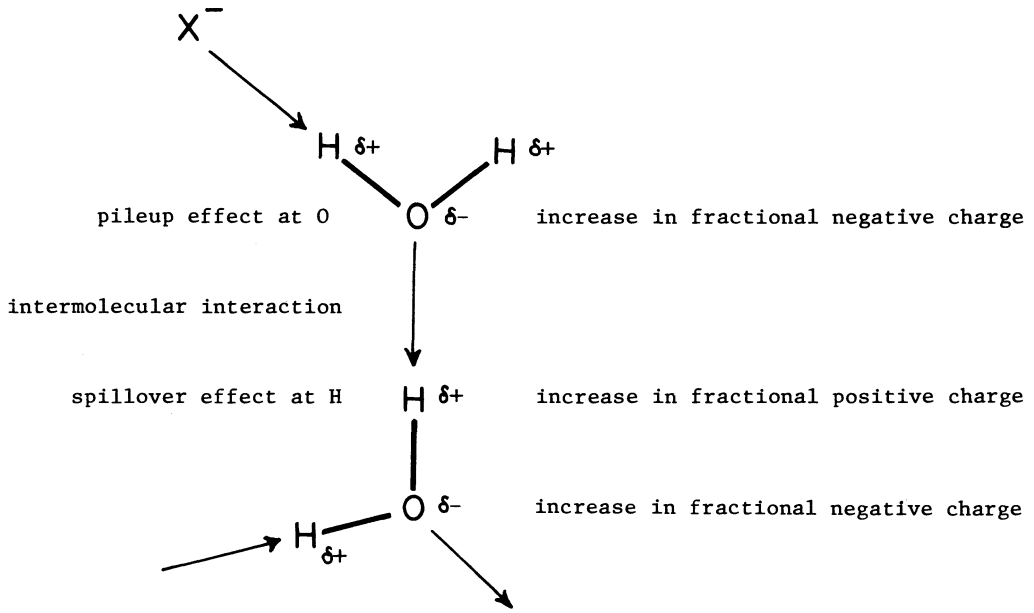

effect of the donor.[7] As an example, the interaction between a negative ion X^- and water molecules is shown above in a version of pileup and spillover effects.

A donor-acceptor interaction leads to increasing polarities of the bonds originating from the donor and acceptor atoms, respectively. Increasing polarity is related to an increase in fractional positive charge at the acceptor atom and an increase in fractional negative charge at the donor atom. The original decrease of fractional positive charge at the acceptor atom due to both the charge-transfer and polarization effects is overcompensated by passing over the negative charges, including part of those originally situated at the accepter atom to other areas of the acceptor molecule. In this way the fractional negative charges of other nuclei in the acceptor component are increased, in particular those terminating the acceptor molecule. This has been described as the spillover effect of negative charge from the acceptor atom. The original loss of negative charge at the donor atom by charge transfer toward the acceptor molecule is overcompensated by attracting electronic charge from other parts of the donor molecule to the donor atom. In this way the electron density at the donor atom is increased with appropriate changes of fractional nuclear charges in other areas of the donor component. This has been termed by the pileup effect of negative charges at the donor atom.

The enhancement effect for alcohols may be weaker than that for H_2O. The induced charge in the alcohol molecule is more or less dispersed in the alkyl, and this makes the net negative charge on the oxygen atom smaller. The charge dispersion leads to the weaker intermolecular interactions for alcohols. Thus the value of $-\Delta H_s^\circ$ or $-\sum_{n=1}^{n=N}\Delta H_{n-1,n}^\circ$ (Ion(solvent)$_n$) for alcohol may be expected to be smaller than that for H_2O. In fact, a positive enthalpy change (2.0 kcal mol^{-1}) is found for the transfer of Cl^- from H_2O to CH_3OH.[23] Figure 5 shows the n dependence of the sum of the stepwise solvation of the Cl^- ion $-\Delta H_{0,n}^\circ$ (i.e. $-\sum_{n=1}^{n=n}\Delta H_{n-1,n}^\circ$ (Cl^-(solvent)$_n$) for solvents=H_2O and CH_3OH up to n=4 or 5.[14,24] The value of $-\Delta H_{0,n}^\circ$ for CH_3OH is larger than that for H_2O up to n=5. This is reasonable because the first solvation shell around the Cl^- ion is composed of more than 5 solvent molecules[20,25] and the interaction of Cl^- with ligand molecules in the first shell is stronger (or nearly equal) for CH_3OH than for H_2O mainly due to the larger gas-phase acidity of CH_3OH than that of H_2O. In the cluster ion which is composed of several solvation shells, the strength of the intermolecular interactions between molecules belonging to the neighboring solvation shells would become stronger for H_2O than for alcohols, because of the greater enhancement effect for H_2O than for alcohols. This effect would make the ultimate value of $-\Delta H_s^\circ$ for H_2O larger than that for alcohols. The

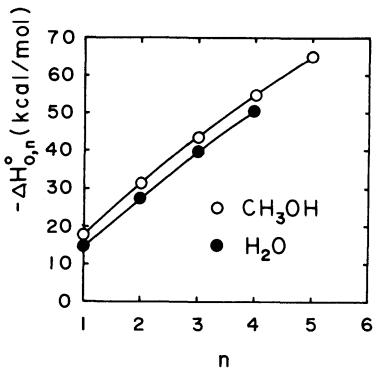

Fig. 5. The n dependence of the sum of the stepwise solvation enthalpies $\Delta H_{n-1,n}^\circ$ for reaction: Cl^-(solvent)$_{n-1}$+solvent=Cl^-(solvent)$_n$. $\Delta H_{0,n}^\circ=\sum_{n=1}^{n=n}\Delta H_{n-1,n}^\circ$ (Cl^-(solvent)$_n$). Solvents=H_2O and CH_3OH.

strong and extensive enhancement effect expected for H_2O suggests that the number N in Eq. 5 for H_2O is larger than that for alcohols.

The relatively small values of AN for aprotic solvents compared to protic solvents may partly due to the less effective enhancement effect. The positive charge in the aprotic solvent molecule can be well dispersed in the hydrophobic groups and the electrostatic intermolecular interactions must be weaker than those for protic solvents. Thus the solvation shells surrounding the core ion may not grow so large as the case of protic solvents, i.e., the number N for the aprotic solvent may be generally smaller than those for the protic solvents.

Concluding Remarks

The relationships between DN's and AN's and intrinsic molecular properties from gas-phase ion equilibria are studied.

For aprotic solvents, good correlations are generally found between DN's and AN's and intrinsic molecular properties. Since DN's represent the molecular properties, good correlations between DN's and intrinsic molecular properties are reasonable. It is of interest that there are also good correlations between intrinsic molecular properties and AN's which represent the bulk solvent properties. This indicates that AN's for aprotic solvents reflect more or less the molecular properties. From the observed good correlations and relatively small values of AN's, it is tentatively concluded that the negative ions in aprotic solvents are solvated by only a restricted number of ligands. We think that the negative ion in aprotic solvents is composed of rather tight single solvation shell which is further solvated by sorrounding solvent molecules only weakly. In such a case, the molecular properties of solvent molecules would be reflected on the AN's.

For protic solvents, just the opposite correlations between AN's and intrinsic molecular properties are found compared to those for aprotic solvents. This may be mainly due to the extensive solvation of ions in protic solvents owing to the enhancement effects in the intermolecular interactions, i.e., the formation of multiple solvation shells which is realized by the pileup and spillover effects of protic solvent molecules. The enhancement effects are the most prominent for H_2O.

Stimulating discussions with Professors H. Ohtaki and S. Ishiguro of the Tokyo Institute of Technology are gratefully acknowledged.

References

1) E. Grunwald and S. Winstein, *J. Am. Chem. Soc.*, **70**, 846 (1948).
2) E. M. Kosower, *J. Am. Chem. Soc.*, **78**, 5700 (1956).
3) E. M. Kosower and E. P. Klinedinst, *J. Am. Chem. Soc.*, **78**, 3483 (1956).
4) E. M. Kosower, *J. Am. Chem. Soc.*, **80**, 3253, 3261, 3267 (1958).
5) K. Dimroth, C. Reichlardt, T. Siepmann, and F. Bohlmann, *Ann. Chem.*, **661**, 1 (1963).
6) C. Reichhardt, "Lösungsmitteleffekte in der Organischen Chemie," Verlag Chemie, Weinheim (1969).
7) V. Gutmann, "The Donor-Acceptor Approach to Molecular Interactions," Plenum, New York (1978).
8) V. Gutmann and E. Wychera, *Inorg. Nucl. Chem. Lett.*, **2**, 257 (1966).
9) U. Mayer and V. Gutmann, *Adv. Inorg. Chem. Radiochem.*, **17**, 189 (1975).
10) U. Mayer, V. Gutmann, and W. Gerger, *Mh. Chem.*, **106**, 1235 (1975).
11) S. Lias, J. F. Liebman, and R. D. Levin, *J. Phys. Chem. Ref. Data*, **13**, 695 (1984).
12) J. Almlöf and V. Wahlgren, *Theoret. Chim. Acta*, **28**, 161 (1973).
13) R. G. Keesee and A. W. Castleman, Jr., *J. Phys. Chem., Ref. Data*, in press.
14) K. Hirao, S. Yamabe, and M. Sano, *J. Phys. Chem.*, **86**, 2626 (1982).
15) H. Tatewaki and S. Huzinaga, *J. Comput. Chem.*, **1**, 205 (1980).
16) J. Sunner, K. Nishizawa, and P. Kebarle, *J. Phys. Chem.*, **85**, 1814 (1981).
17) J. E. Bartmess and R. T. McIver, Jr., "Gas phase Ion Chemistry," ed by M. T. Bowers, Academic Press, New York (1979), Vol. 2.
18) J. D. Payzant, R. Yamdagni and P. Kebarle, *Can. J. Chem.*, **49**, 3308 (1971).
19) R. Yamdagni and P. Kebarle, *J. Am. Chem. Soc.*, **93**, 7139 (1971).
20) R. Yamdagni, J. D. Payzant, and P. Kebarle, *Can. J. Chem.*, **51**, 2507 (1973).
21) Y. K. Lau, P. P. S. Saluja, and P. Kebarle, *J. Am. Chem. Soc.*, **102**, 7429 (1980).
22) C. E. Klots, *J. Phys. Chem.*, **85**, 3585 (1981).
23) Y. Marcus, *Pure Appl. Chem.*, **57**, 1103 (1985).
24) K. Hiraoka, K. Morise, and S. Yamabe, to be submitted.
25) G. Pálinskás, W. O. Riede, and K. Heinzinger, *Naturforsch.*, **32a**, 1137 (1977).

Production of Cyclohexene and Reactive Sulfur Species in Vapor-Phase Catalytic Oxidative Dehydrogenation of Cyclohexane with Carbonyl Sulfide

Masamichi AKIMOTO,* Yoshinori KASHITA, and Hiroo NIIYAMA
Department of Chemical Engineering, Tokyo Institute of Technology, Ookayama, Meguro-ku, Tokyo 152
(Received March 12, 1986)

The vapor-phase catalytic oxidative dehydrogenation of cyclohexane with COS over SiO_2 and Al_2O_3 catalysts (e.g., $C_6H_{12}+COS \rightarrow C_6H_{10}+CO+H_2S$) has been investigated with respect to the production of cyclohexene and cyclohexadiene as well as the mechanism of the dehydrogenation reaction. The representative value of the combined yield of cyclohexene+cyclohexadiene is 8.0% and the combined selectivity to these two products at this yield obtained is 34.0%. These values are comparable to the values 8.0 and 30.8% reported in a recent Japanese patent. The comparison of the catalytic performance between two types of flow fixed-bed reactors demonstrates that the role of solid catalysts is to decompose COS into CO and sulfur, which then dehydrogenates hydrocarbons through a homogeneous mechanism. The results of the kinetic analysis of these reactions, together with the simulation of the overall catalytic reaction system, suggest a contribution of atomic sulfur to the oxidative dehydrogenation of cyclohexane in a conventional flow fixed-bed reactor.

The vapor-phase catalytic oxidative dehydrogenation of cyclohexane (C_6H_{12}) to cyclohexene (C_6H_{10}) is of industrial importance for the production of adipic acid and ε-caprolactam. A number of challenging works have been reported on the production of C_6H_{10} through the oxidative dehydrogenation with gaseous oxygen: Cr_2O_3–CeO_2–K_2O/Al_2O_3,[1] SiO_2–TiO_2–CeO_2,[2] native zeolites,[3] metal ion-exchanged zeolites,[4,5] group 2 metal silicates,[6] and polyquinones[7] have been employed as catalysts. A recent Japanese patent[8] also proposed the production of C_6H_{10} through a similar catalytic oxidative dehydrogenation, but the yield and selectivity to C_6H_{10} reported are as low as 8.0 and 30.8%, respectively, although a noble bimetallic catalyst Ru–Rh/SiO_2 is employed at 773K.

We have investigated the vapor-phase catalytic oxidative dehydrogenation of lower paraffinic hydrocarbons and arylalkyl compounds with COS.[9,10] In this oxidative dehydrogenation, COS is catalytically decomposed to CO and sulfur, which then abstracts hydrogen atoms from these hydrocarbons to give unsaturated hydrocarbons and H_2S.[10]

$$COS \longrightarrow CO + S \qquad xS \longrightarrow S_x (x = 2, 4, 6, \cdots) \quad (1)$$

$$C_nH_{2n+2} + 1/xS_x \longrightarrow C_nH_{2n} + H_2S \quad (2)$$

One of the characteristic features of this dehydrogenation, compared with the conventional oxidative dehydrogenation with gaseous oxygen, is that the difference in reactivity of hydrocarbons is small between paraffinic and olefinic hydrocarbons, as shown by the reaction of butane and *trans*-2-butene over SiO_2 at 873K (e.g., conversion: butane 30% and *trans*-2-butene 48%).[9] Hence we expected to produce C_6H_{10} with high yield and selectivity by the vapor-phase catalytic oxidative dehydrogenation of C_6H_{12} with COS. In the present work, we have tried to find the best reaction conditions for the selective production of C_6H_{10} and have then elucidated the nature of sulfur species responsible for the oxidative dehydrogenation through kinetic analysis of the reactions involved, and by simulation of the overall catalytic reaction system.

Experimental

Reaction and Catalysts. Vapor-phase oxidative dehydrogenation of C_6H_{12} was carried out with a conventional flow fixed-bed reactor at atmospheric pressure (1 Torr= 133.322 Pa). The reactor system comprised a 15-mm-i.d. quartz tube, 470-mm long, and a concentric thermowell. The reactor was heated with a cylindrical electric furnace. Raschig rings (2×2 mm) were added above and below the catalyst bed. Guaranteed reagent grade C_6H_{12} and commercially available COS of greater than 97.5 vol% purity (Matheson Co., CO_2 1.4 vol%, N_2+CO 0.6 vol%, CS_2 0.19 vol%, O_2 0.10 vol% and H_2O 0.01 vol%) were used without further purification. Nitrogen (purity>99.99 vol%) was used as the diluent. The standard total feed rate was held constant at 150 (NTP) $cm^3 min^{-1}$; the standard feed composition was 10 vol% each of C_6H_{12} and COS. The catalysts employed are SiO_2 (20—40 mesh) and the referenced Al_2O_3 catalysts of the Catalysis Society of Japan (JRC-ALO-1 and -4). SiO_2 catalyst was prepared by the calcination of hydrated silica gel at 1073K in air for 5 h. Silica sol (Snowtex-O, Nissan Chemical Industries Ltd.) was used as the catalyst source. The BET surface area is 182 $m^2 g^{-1}$ (SiO_2), 176 $m^2 g^{-1}$ (JRC-ALO-1),[11] and 174 $m^2 g^{-1}$ (JRC-ALO-4),[11] respectively.

Analysis. The reaction products were analyzed by gas chromatography with helium as the carrier gas. Two columns in series, 2.0 m of Porapak R (50—80 mesh, 358K) and 2.0 m of molecular sieve 13X (60—80 mesh, room temperature), were used for the analysis of the gaseous reaction products (N_2, COS, CO_2, CO, CS_2, and H_2S). The liquid products (C_6H_{12}, C_6H_{10}, cyclohexadienes, and benzene) were analyzed with 6.0 m of PEG 6000 (20 wt% on Celite 545, 60—80 mesh, 338K). The yield of H_2S was always calculated on the basis of COS fed.

Results

Production of Cyclohexene. Table 1 summarizes the results of catalytic oxidative dehydrogenation of C_6H_{12} with COS over SiO_2 at different reaction temperatures. Preliminary studies indicated that the yields of C_6H_{10} and benzene (C_6H_6) are not restricted by the equilibrium of these reactions (e.g., K_p=661 and 2.61×

Table 1. Results of the Catalytic Oxidative Dehydrogenation of Cyclohexane with COS over SiO_2

Reaction temperature	Conversion of C_6H_{12}	Yield/%			Selectivity to $C_6H_{10}+C_6H_8$	Conversion of COS[a]	Conversion to CO+S	Yield of H_2S
K	%	C_6H_{10}	C_6H_8	C_6H_6	%	%	%	%
673	Neg[b]	Neg	Neg	Neg	—	17.6	Neg	Neg
723	0.4	0.4	Neg	Neg	100	27.9	0.2	0.2
773	1.1	0.7	Neg	0.4	63.6	36.2	2.3	2.1
823	2.4	1.5	Neg	0.9	62.5	39.8	4.8	4.3
873	6.0	3.3	0.1[c]	2.6	56.7	45.2	11.6	11.0

Catalyst: 2.0 g. Total feed rate: 150 (NTP) $cm^3\,min^{-1}$ (C_6H_{12} 10 vol%, COS 10 vol%, N_2 80 vol%). a) The conversion to the side reaction ($2COS \rightarrow CO_2+CS_2$) is included. b) Negligible. c) 1,3-Cyclohexadiene.

Table 2. Effect of the COS/C_6H_{12} Feed Ratio on the Catalytic Oxidative Dehydrogenation of Cyclohexane

COS/C_6H_{12} feed ratio	Conversion of C_6H_{12}	Yield/%			Selectivity to $C_6H_{10}+C_6H_8$	Conversion of COS[a]	Conversion to CO+S	Yield of H_2S
v/v	%	C_6H_{10}	C_6H_8	C_6H_6	%	%	%	%
5/10	20.7	5.4	0.3	15.0	27.5	82.3	69.7	62.8 (102.0)[b]
10/10	38.0[c]	8.2	0.2	29.3	22.1	78.8	59.3	57.9 (96.5)[b]
15/10	34.0[c]	5.1	Neg[d]	28.4	15.0	72.1	52.8	51.3 (60.2)[b]

Catalyst: JRC-ALO-4 Al_2O_3 1.0 g. Total feed rate: 150 (NTP) $cm^3\,min^{-1}$ (C_6H_{12} 10 vol% fixed). a) The conversion to the side reaction ($2COS \rightarrow CO_2+CS_2$) is included. b) Yield of H_2S calculated from the yields of C_6H_{10}, C_6H_8, and C_6H_6. c) A small amount of CH_4 (yield=0.3—0.5%) was formed.

10^{12} for C_6H_{10} and C_6H_6 formations, respectively, at 900K[12]). Preliminary experiments showed that no significant change with time in the catalytic activity or selectivity took place during the reaction over SiO_2 and Al_2O_3 catalysts at 723—923K. The conversion of C_6H_{12} was negligibly small at 673K: the conversion of COS to CO+S was nearly 0%, but the oxidative dehydrogenation took place at 723K, at which temperature the catalytic conversion of COS to CO+S was initiated (Table 1). The olefinic product in the oxidative dehydrogenation at 723K was only C_6H_{10}, but the formation of C_6H_6 was seen at 773K and the yields of these two products increased with further rise in reaction temperature. The formation of 1,3-cyclohexadiene (C_6H_8) was seen only at 873K, but its yield was as low as 0.1%.

Figure 1 shows the variation of the conversion of C_6H_{12}, the yields of $C_6H_{10}+C_6H_8$ and C_6H_6 and the combined selectivity to $C_6H_{10}+C_6H_8$ as a function of the conversion of COS to CO+S at 873K. The conversion of C_6H_{12} and the yield of C_6H_6 were 4.4 and 1.7% at a conversion to CO+S of 7.4%, but they increased markedly at higher conversions and reached 44.5 and 38.5%, respectively, at 80.8%. In contrast, the combined selectivity to $C_6H_{10}+C_6H_8$ decreased from 61.4% to 12.1% with such an increase in the conversion to CO+S. The combined yield of $C_6H_{10}+C_6H_8$ showed a maximum at ca. 50% (Fig. 1). The combined yield and selectivity to $C_6H_{10}+C_6H_8$ at the conversions to CO+S of 40.0 and 59.3% were 8.0 and 34.0% and 8.4 and 22.1%, respectively (Fig. 1). It should be noted that the conversion of C_6H_{12}, the yields of $C_6H_{10}+C_6H_8$ and C_6H_6 and the combined selectivity to $C_6H_{10}+C_6H_8$

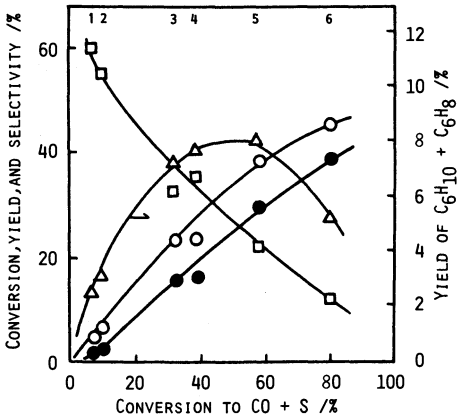

Fig. 1. Variation of the conversion of cyclohexane, the yields of cyclohexene+cyclohexadiene and benzene, and the selectivity to cyclohexene+cyclohexadiene as a function of the conversion of COS to CO+S.
Reaction temperature: 873 K. Total feed rate: 150 (NTP) $cm^3\,min^{-1}$ (C_6H_{12} 10 vol%, COS 10 vol%, N_2 80 vol%).
○: Conversion of C_6H_{12}, △: Yield of $C_6H_{10}+C_6H_8$, ●: Yield of C_6H_6, □: Selectivity to $C_6H_{10}+C_6H_8$.
1: SiO_2 1.0 g, 2: SiO_2 2.0 g, 3: JRC-ALO-4 Al_2O_3 0.5 g, 4: JRC-ALO-1 Al_2O_3 1.0 g, 5: JRC-ALO-4 Al_2O_3 1.0 g, 6: JRC-ALO-4 Al_2O_3 2.0 g. The yield of C_6H_8 is 0.1—0.5%.

are determined by the conversion of COS to CO+S, regardless of the catalysts employed (Fig. 1).

The catalytic oxidative dehydrogenation of C_6H_{12} was carried out at 873K with JRC-ALO-4 Al_2O_3 at various COS/C_6H_{12} feed ratios (Table 2). When the COS/C_6H_{12} volumetric feed ratio was 5/10, the con-

Table 3. Results of the Vapor-Phase Homogeneous Reaction of Sulfur with Cyclohexane[a)]

Reaction temperature	Conversion of C_6H_{12}	Yield/%			Selectivity to $C_6H_{10}+C_6H_8$	Conversion of COS[b)]	Conversion to CO+S	Yield of H_2S
K	%	C_6H_{10}	C_6H_8	C_6H_6	%	%	%	%
823	4.7	3.0	Neg[c)]	1.7	63.8	39.1	9.5	8.4 (8.1)[d)]
873	8.1[e)]	3.9	0.3	3.7	51.9	44.2	14.3	13.4 (15.6)[d)]

a) The reactor shown in Fig. 2 was employed. Catalyst: JRC-ALO-4 Al_2O_3 2.0 g. Feed-1: COS 15 (NTP) $cm^3\,min^{-1}$+N_2 80 (NTP) $cm^3\,min^{-1}$. Feed-2: C_6H_{12} 15 (NTP) $cm^3\,min^{-1}$+N_2 40 (NTP) $cm^3\,min^{-1}$. b) The conversion to the side reaction ($2COS \rightarrow CO_2+CS_2$) is included. c) Negligible. d) Yield of H_2S calculated from the yields of C_6H_{10}, C_6H_8, and C_6H_6. e) Yield of CH_4 is 0.2%.

version of C_6H_{12} was 20.7% and the combined yield of $C_6H_{10}+C_6H_8$ was 5.7%. But, they increased to 38.0 and 8.4% at a COS/C_6H_{12} feed ratio of 10/10 and then decreased to 34.0 and 5.1%, respectively, at 15/10. The yield of C_6H_6 showed a similar behavior. In contrast, the combined selectivity to $C_6H_{10}+C_6H_8$ decreased from 27.5% to 15.0% with such a change in the COS/C_6H_{12} feed ratio (Table 2). For the selective production of C_6H_{10}, the COS/C_6H_{12} volumetric feed ratio of 10/10 seems to be optimum at 873K. The observed values of the yields of H_2S (Table 2) give us some information about the mechanism of the oxidative dehydrogenation of C_6H_{12}. That is, the yields of H_2S calculated from the yields of dehydrogenation products (C_6H_{10}, C_6H_8, and C_6H_6) are always greater than the experimentally observed yields of H_2S, although the latter yields of H_2S are always comparable to the values of the conversion of COS to CO+S (Table 2). Similar results were obtained over JRC-ALO-1 and -4 Al_2O_3 at 873K (Fig. 1), but not over SiO_2 at 723—873K (Table 1). These results indicate that a large portion of the C_6H_8 formed, but not C_6H_{12} or C_6H_{10}, was thermally dehydrogenated to C_6H_6 when the amount of sulfur evolved was smaller than that of hydrocarbons.

Mechanistic Studies. In order to elucidate the role of solid catalysts and the mechanism of oxidative dehydrogenation, the catalytic oxidative dehydrogenation of C_6H_{12} with COS was carried out with a special reactor shown in Fig. 2. In this reactor, only the mixture of COS and N_2 is allowed to come into contact with solid catalyst and the resulting gaseous product containing sulfur is then mixed with another gaseous mixture ($C_6H_{12}+N_2$) in the absence of catalyst. The temperature of the reactor in which the homogeneous reaction of sulfur with C_6H_{12} takes place is always kept to nearly equal to that for the catalytic decomposition of COS. The results obtained at 823 and 873K over JRC-ALO-4 Al_2O_3 are summarized in Table 3. At these two reaction temperatures, the oxidative dehydrogenation of C_6H_{12} always took place to produce C_6H_{10}, C_6H_8, and C_6H_6 with formation of H_2S. Moreover, the values of the conversion of C_6H_{12}, the yields of $C_6H_{10}+C_6H_8$ and C_6H_6, and the combined selectivity to $C_6H_{10}+C_6H_8$ at 873K (Table 3) are nearly equal to the values (8.3, 4.2, 4.1, and 50.6%, respectively) expected from the conversion of COS to CO+S (14.3%)

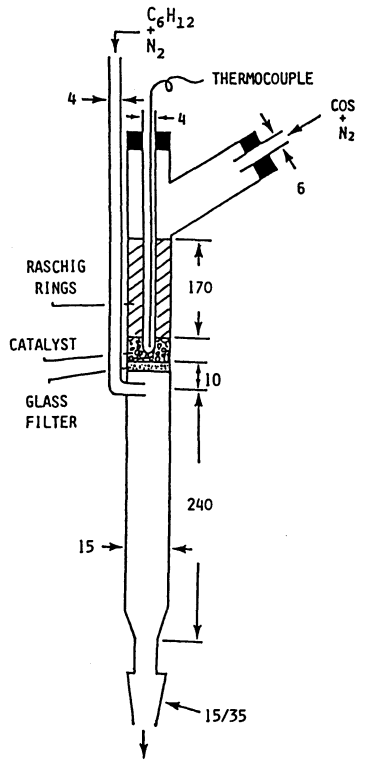

Fig. 2. A schematic figure of the reactor employed in the vapor-phase homogeneous reaction of sulfur with cyclohexane. The dimensions of the reactor are given in millimeters.

in Fig. 1. As discussed later, these results support the view that the role of solid catalyst is to decompose COS into CO and sulfur, which then dehydrogenates hydrocarbons through a homogeneous mechanism. The yield of H_2S at 823K (8.4%) is nearly the same as that calculated from the yields of C_6H_{10}, C_6H_8, and C_6H_6 (8.1%) (Table 3). This indicates that no thermal dehydrogenation of C_6H_8 to C_6H_6 took place during the oxidative dehydrogenation of C_6H_{12} at 823K.

Kinetic Studies. We estimated the rate constants for the catalytic decomposition of COS to CO+S and for the dehydrogenation of C_6H_{12} and C_6H_{10} with S_2 and then predicted the nature of sulfur species responsible for the dehydrogenation by simulation of the overall catalytic reaction system. Based on the present mechanistic findings, we propose the following reactions for the catalytic oxidative dehydrogenation of

C_6H_{12} with COS at 823K.

$$COS \longrightarrow CO + S \quad xS \longrightarrow S_x (x=2, 4, 6, \cdots) \quad (1)$$
$$2COS \longrightarrow CO_2 + CS_2 \quad (3)$$
$$C_6H_{12} + 1/xS_x \longrightarrow C_6H_{10} + H_2S \quad (4)$$
$$C_6H_{10} + 2/xS_x \longrightarrow C_6H_6 + 2H_2S \quad (5)$$

We use Reaction 5 instead of two consecutive reactions ($C_6H_{10}+1/xS_x \rightarrow C_6H_8+H_2S$, $C_6H_8+1/xS_x \rightarrow C_6H_6+H_2S$) since the yield of C_6H_8 was always negligible at 823K (Tables 1 and 3). In a conventional fixed-bed reactor, Reactions 1 and 3 take place at the surface of solid catalysts, whereas Reactions 4 and 5 occur homogeneously. In these kinetic studies, we employed JRC-ALO-4 Al_2O_3 catalyst. The reaction order with respect to COS in Reaction 1 was approximately 0.8 at 823K and the chemical equilibrium was always established for Reaction 3, as shown later. Thus, the rate equations derived for these reaction steps are as follows:

$$d[COS]/d(W/F) = -k_{01}[COS] \quad (6)$$
$$K_{p1} = [CO_2][CS_2]/[COS]^2 \quad (7)$$
$$d[C_6H_{12}]/d(V/F) = -k_1[C_6H_{12}][S_x] \quad (8)$$
$$d[C_6H_{10}]/d(V/F) = k_1[C_6H_{12}][S_x] - k_2[C_6H_{10}][S_x] \quad (9)$$
$$d[C_6H_6]/d(V/F) = k_2[C_6H_{10}][S_x] \quad (10)$$

Here k_{01}, k_1, and k_2 are rate constants for Reactions 1, 4, and 5, respectively, and K_{p1}, W, V, and F are equilibrium constant of Reaction 3, weight of catalyst, void volume in the catalyst bed, and total feed rate of reactant mixture. The parentheses in Equations 6, 7, 8, 9, and 10 denote the concentration of reactant species in mol fraction units. The density of JRC-ALO-4 Al_2O_3 was determined with liquid C_6H_{12} and a measuring cylinder: the relation V/F(min)=8.03×10^{-5} W/F(g-catalyst·min·g-mol^{-1}) was obtained at 823K. Equation 10 shows that the rate-controlling step for the formation of C_6H_6 from C_6H_{10} is the oxidative dehydrogenation of C_6H_{10} to C_6H_8, not that of C_6H_8 to C_6H_6.

Estimation of k_{01} and K_{p1}. Figure 3 shows the effect of the contact time on the conversion of COS over JRC-ALO-4 Al_2O_3 at 823K. At a contact time of 15.0 g-catalyst·min·g-mol^{-1}, the conversion to CO+S was 5.8%, but it increased for longer contact times of the reaction and levelled off at 15.0% between 150 and 300 g-catalyst·min·g-mol^{-1}. In contrast, the conversion to CO_2+CS_2 was nearly constant at 30.3—30.8% between 15.0 and 300.0 g-catalyst·min·g-mol^{-1}. Hence one could say that the chemical equilibrium for the catalytic decomposition of COS to CO_2+CS_2 is readily established even at very short contact times of the reaction, whereas that for the decomposition to CO+S is established only above 150 g-catalyst·min·g-mol^{-1}. At these reaction conditions, the sulfur species formed at equilibrium is of S_2 type (Reaction 11).[13] Using the composition of the gaseous product at 300 g-catalyst·min·g-mol^{-1}, the equilibrium constants for Reactions 3 and 11 were calculated to be 8.07×10^{-2}

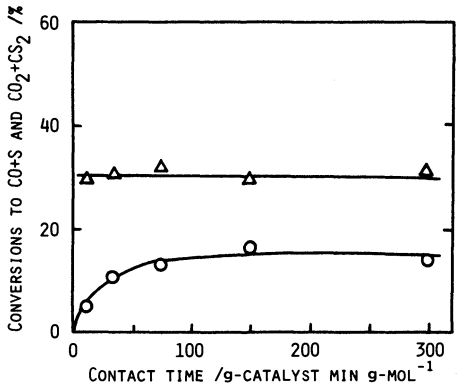

Fig. 3. Effect of contact time on the catalytic conversion of COS.
Catalyst: JRC-ALO-4 Al_2O_3. Reaction temperature: 823K. Total feed rate: 150 (NTP) cm^{-3} min^{-1} (COS 10 vol%, N_2 90 vol%).
○: Conversion to CO+S, △: Conversion to CO_2+CS_2.

$$COS \underset{}{\overset{K_{p2}}{\rightleftharpoons}} CO + 1/2S_2 \quad (11)$$

and 2.40×10^{-2}, respectively. These values agree well with the thermodynamically calculated values (K_{p1} =2.29×10^{-1}, K_{p2}=2.21×10^{-2}).[12] At a contact time of 15.0 g-catalyst·min·g-mol^{-1}, the conversions to CO+S and CO_2+CS_2 and rate of the conversion to CO+S were 5.8 and 30.5% and 3.87×10^{-4} g-mol·g-catalyst^{-1}·min^{-1}, respectively. With these values and Equation 12, the rate constants k_{01} and k_{02} were

$$d[CO]/d(W/F) = k_{01}[COS] - k_{02}[CO][S_2] \quad (K_{p2}=k_{01}/k_{02}) \quad (12)$$

estimated to be 6.14×10^{-3} and 2.56×10^{-1} g-mol·g-catalyst^{-1}·min^{-1} at 823K.

Estimation of k_1 and k_2. The rate constants for the oxidative dehydrogenation of C_6H_{12} and C_6H_{10} with S_2 were estimated at 823K by the kinetic analysis of these reactions by using the reactor shown in Fig. 2. Here COS was decomposed at 467.3 g-catalyst·min·g-mol^{-1} over JRC-ALO-4 Al_2O_3 at 823K and the evolved sulfur (S_2) was reacted with C_6H_{12} at 823K (Table 4). From Equations 8 and 9, the following equation can be derived; here x, y, and k are the fractional conversion of C_6H_{12}, the fractional yield of C_6H_{10}, and k_2/k_1, respectively:

$$y = \frac{1}{(k-1)}[(1-x) - (1-x)^k] \quad (13)$$

The averaged value of k was thus estimated to be 27.1 at 823K (Table 4).

The value of k_1 for the reaction of C_6H_{12} with S_2 was estimated by the kinetic analysis of the reaction by using the same reactor (Fig. 2). By integration of Equation 8, the following equation is obtained:

Table 4. Determination of k

$v/F^{a)}$/min	Conversion of C_6H_{12}/%	Yield/%[b]			k/—
		C_6H_{10}	C_6H_6	H_2S	
4.67×10^{-2}	5.1	2.8	2.3	9.2	26.0
2.32×10^{-2}	4.8	2.9	1.9	8.4	23.1
1.74×10^{-2}	3.3	2.1	1.2	4.9	29.1
0.83×10^{-2}	1.9	1.4	0.5	3.2	30.0

a) Reaction temperature: 823K. Catalyst: JRC-ALO-4 Al_2O_3 2.0 g. Feed-1 : COS 15 (NTP) $cm^3\,min^{-1}$+N_2 80 (NTP) $cm^3\,min^{-1}$ (W/F=467.3 g-catalyst·min·g-mol^{-1}). Feed-2 : C_6H_{12} 15 (NTP) $cm^3\,min^{-1}$+N_2 40 (NTP) $cm^3\,min^{-1}$. The conversion of COS to CO+S is 9.5%. a) v is the volume of reactor below the catalyst bed. This volume was changed by adding Rasching rings (2×2 mm). b) Yield of C_6H_8 is negligible.

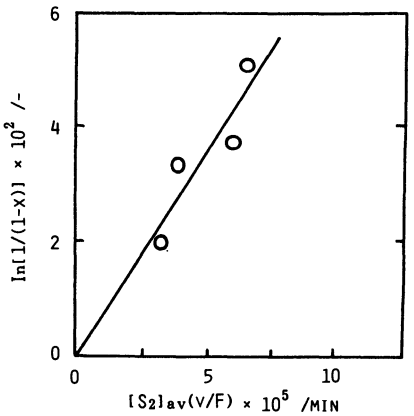

Fig. 4. Determination of k_1 based on Equation 14. Catalyst: JRC-ALO-4 Al_2O_3 2.0—10.0 g. Reaction temperature: 823K. Feed-1: 95—475 (NTP) $cm^3\,min^{-1}$ (COS/N_2=3/16, fixed. W/F=467.3 g-catalyst·min·g-mol^{-1}). Feed-2: 55—275 (NTP) $cm^3\,min^{-1}$ (C_6H_{12}/N_2=1/3, fixed). v: 17.10—32.92 cm^3.

$$k_1 = \frac{\ln[1/(1-x)]}{[S_2]_{av}(v/F)} \qquad (14)$$

Here $[S_2]_{av}$ is the logarithmically averaged value of the concentration of diatomic sulfur throughout the homogeneous reaction zone and v is its volume. By changing the amount of catalyst, the volume of the homogeneous reaction zone, and the feed rates of the respective gaseous mixtures at the fixed concentration of C_6H_{12} at the inlet of the homogeneous reaction zone (10 vol%), the relation between $\ln[1/(1-x)]$ and $[S_2]_{av}(v/F)$ at 823K was determined (Fig. 4). From the slope of the straight line in Fig. 4, k_1 for the dehydrogenation of C_6H_{12} with S_2 was estimated to be 7.38×10^2 min^{-1} at 823K. With this value of k_1 and k=27.1, k_2 for the dehydrogenation of C_6H_{10} with S_2 was calculated to be 2.00×10^4 min^{-1} at 823K.

Simulation of Catalytic Reaction System. Assuming the participation of S_2 in the oxidative dehydrogenation and no gaseous volume change during the reaction, we simulated the catalytic oxidative dehydrogenation of C_6H_{12} with COS over JRC-ALO-4 Al_2O_3

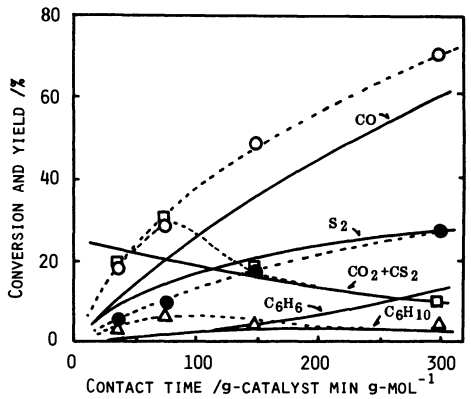

Fig. 5. Simulation of the catalytic oxidative dehydrogenation system.
Catalyst: JRC-ALO-4 Al_2O_3. Reaction temperature: 823K. Feed composition: C_6H_{12} 10 vol%, COS 10 vol%, N_2 80 vol%.
Dotted lines-observed values. Solid lines-simulated values.
$k_0=6.14\times10^{-3}$ g-mol·g-catalyst^{-1}·min^{-1}, $K_{p1}=8.07\times10^{-2}$, $k_1=7.38\times10^2$ min^{-1}, $k_2=2.00\times10^4$ min^{-1}.
○: Conversion of COS to CO+S, □: Conversion of COS to CO_2+CS_2, △: Yield of C_6H_{10}, ●: Yield of C_6H_6.

at 823K in the conventional fixed-bed reactor using Equations 6, 7, 8, 9, and 10 and the values of k_{01}, K_{p1}, k_1, and k_2 obtained above. The calculation was made by the Runge-Kutta Gill method. The calculated catalytic performance versus the contact time of the reaction is shown in Fig. 5. The calculated values of the conversion of COS to CO_2+CS_2 and the yield of C_6H_{10} are nearly equal to the experimentally observed values, especially at the contact time of 150—300 g-catalyst·min·g-mol^{-1}. However, there is a big difference between the calculated and observed values of the conversion of COS to CO+S and the yield of C_6H_6 although these two kinds of values similarly increase with increasing the contact time of the reaction. For example, the calculated (observed) values of the yield of C_6H_6 are 1.7 (9.1), 5.7 (17.0), and 14.2% (27.4%), respectively, at the contact time of 75,150, and 300 g-catalyst·min·g-mol^{-1}, and those of the conversion of COS to CO+S at these contact times are 19.6 (28.4), 36.3 (48.3), and 60.1% (70.5%), respectively (Fig. 5). The most striking difference between the calculated and observed values is the much greater yields of sulfur (2.0—24.0% at W/F=10—300 g-catalyst·min·g-mol^{-1}) in the calculated result (Fig. 5). In this oxidative dehydrogenation, the yield of sulfur was always negligible, as shown by the nearly stoichiometric formation of H_2S (Tables 1, 2, and 3).

Assuming the participation of atomic sulfur in the oxidative dehydrogenation, we have again simulated the catalytic reaction system at 823K, in which, however, only the values of k_1 and k_2 are increased to nearly 36 times k_1 and k_2 values employed in Fig. 5. In agreement with the experimental observation, the

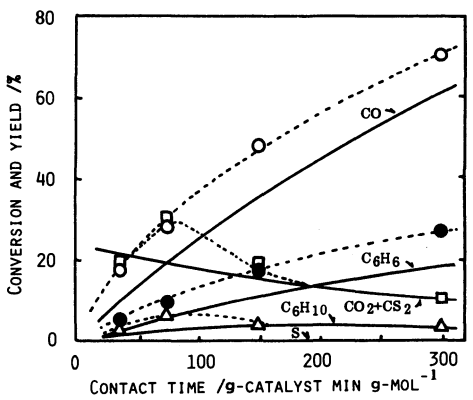

Fig. 6. Simulation of the catalytic oxidative dehydrogenation system.
Reaction conditions and symbols used are the same as those in Fig. 5.
$k_0=6.14\times10^{-3}$ g-mol·g-catalyst^{-1}·min^{-1}, $K_{p1}=8.07\times10^{-2}$, $k_1=2.66\times10^4$ min^{-1}, $k_2=7.20\times10^5$ min^{-1}.

yield of sulfur in this calculation is always negligible within the contact time of the reaction studied (Fig. 6). Both the calculated values of the yields of C_6H_{10} and C_6H_6 increased to be nearer to the observed values than the case in Fig. 5: the calculated values of the yield of C_6H_6 at the contact time of 75, 150, and 300 g-catalyst·min·g-mol^{-1} are 7.1, 10.8, and 18.8%, respectively. In contrast, the values of the conversions of COS to CO+S and CO_2+CS_2 remained unchanged in this calculation (Fig. 6).

Discussion

We first discuss the role of solid catalyst and the mechanism of the oxidative dehydrogenation of C_6H_{12} with COS. But, we do not refer here to the mechanism of the catalytic decomposition of COS since it was already reported.[14] Although the yield of C_6H_8 over SiO_2 was negligibly small between 723 and 823K, the observed behavior of the yields of C_6H_{10} and C_6H_6 with rising reaction temperature, i.e., formation of C_6H_{10} at 723K, that of C_6H_{10} and C_6H_6 at 773K, and the increase in the yields of these two products with further rise in reaction temperature (Table 1) suggest that the oxidative dehydrogenation of C_6H_{12} with COS proceeds through the following consecutive reaction steps.

$$C_6H_{12} \xrightarrow{-2H\cdot} C_6H_{10} \xrightarrow{-2H\cdot} C_6H_8 \xrightarrow{-2H\cdot} C_6H_6 \qquad (15)$$

Both the convex behavior of the yield of $C_6H_{10}+C_6H_8$ against the conversion of C_6H_{12} and the decrease in the selectivity to these two products with increasing conversion of C_6H_{12} (Fig. 1) support this reaction scheme.

The occurrence of the catalytic oxidative dehydrogenation of C_6H_{12} with COS in the special reactor, in which only COS contacts with the catalyst and the evolved gaseous sulfur reacts with C_6H_{12} in the absence of solid catalyst (Table 3, Fig. 2), indicates that the role of solid catalysts is to decompose COS into CO+S and that the evolved sulfur can dehydrogenate C_6H_{12}, C_6H_{10}, and C_6H_8 even in the absence of solid catalysts. Since the values of the conversion of C_6H_{12}, the yields of $C_6H_{10}+C_6H_8$ and C_6H_6, and the combined selectivity to $C_6H_{10}+C_6H_8$ at 873K obtained with the special type reactor were nearly equal to the values at 873K obtained with the conventional fixed-bed reactor (Table 3, Fig. 1), we believe that the oxidative dehydrogenation of C_6H_{12} with sulfur proceeded homogeneously also in the conventional fixed-bed reactor. The decisive effect observed of the conversion of COS to CO+S on the conversion of C_6H_{12} and the product distributions (Fig. 1) supports this view. The heterogeneous-homogeneous reaction mechanism for the catalytic oxidative dehydrogenation of C_6H_{12} with COS proposed in the present work agrees with the reaction mechanism for the cases of ethylbenzene and paraffinic hydrocarbons reported.[9,10] The representative values of the combined yield and selectivity to $C_6H_{10}+C_6H_8$, 8.0 and 34.0%, obtained in the present work (Fig. 1) are comparable to those, 8.0 and 30.8%, reported in a recent Japanese patent.[8]

Next we discuss the nature of sulfur species responsible for the oxidative dehydrogenation of C_6H_{12}. Although the calculated values of the conversion of COS to CO+S and CO_2+CS_2 and the yields of C_6H_{10} and C_6H_6 in the simulation at 823K did not always agree with the experimentally observed values, the behavior of these calculated values versus the contact time of the reaction is similar to that of the observed values (Figs. 5 and 6), thus supporting the reasonability of the simulation method employed in the present work. The big difference between the calculated and observed values of the conversion of COS to CO+S at 823K (Figs. 5 and 6) must have been caused by the low estimation of the value of the rate constant k_{01} for the catalytic decomposition of COS to CO+S at 823K. We believe that by the use of a larger value of k_{01} ($>6.14\times10^{-3}$ g-mol·g-catalyst^{-1}·min^{-1}) not only the calculated value of the conversion of COS to CO+S but also that of the yields of C_6H_{10} and C_6H_6 can be increased to be much nearer to the observed values than those in Fig. 6.

The most important implication suggested by the results of simulation concerns the nature of sulfur species responsible for the oxidative dehydrogenation of C_6H_{12}. The agreement of the negligibly small yields of sulfur between the calculated and observed values caused by the assumption of the participation of atomic sulfur and the rise of the values of the rate constants for the dehydrogenation of C_6H_{12} and C_6H_{10} with sulfur (k_1 and k_2) by 36 times (Figs. 5 and 6) suggests that the sulfur species responsible for the oxidative dehydrogenation in the conventional fixed-bed reactor is mainly of atomic type, although some degree of the contribution of diatomic sulfur to

the reaction can not be rejected. This view can be supported by the following discussion based on the Evans & Polanyi rule (Equation 16).[15]

$$\Delta E = -\alpha\Delta Q \quad (\alpha=0.25) \tag{16}$$

Where ΔE and ΔQ are the differences in activation energy and heat of reaction, respectively. The heat of formation of S_2 from atomic sulfur ($S \rightarrow 1/2S_2$) is ca. 40 kcal[†]·atom^{-1}.[16] When we assume that ΔQ is equal to 40 kcal·atom^{-1}, the value of $e^{-\Delta E/RT}$ at 823K is calculated to be 417. This means that the reactivity of atomic sulfur is at the greatest nearly 400 times greater than that of diatomic one in exothermal reactions. The value of the relative reactivity to C_6H_{12} and C_6H_{10} of atomic sulfur to diatomic sulfur employed in the present work, 36, is smaller than the calculated one, 417. This supports our view concerning the nature of the sulfur species responsible for the dehydrogenation reactions. In the present work, the relative degree of contribution of atomic and diatomic sulfurs to the oxidative dehydrogenation of C_6H_{12} was not determined.

[†]1 cal=4.184J.

References

1) A. Uchida, T. Nakazawa, K. Oh-uchi, and S. Matsuda, *Ind. Eng. Chem., Prod. Res. Dev.*, **10**,153 (1971).

2) T. Hayakawa, S. V. Martinez, G. M. Carrizales, K. Takehira, and T. Ishikawa, Proceeding of 49th National Meeting of the Chemical Society of Japan, Tokyo, April 1984, Abstr., No 2P18.

3) Kh. M. Minachev, D. B. Tagiev, Z. G. Zulfugarov, and V. V. Kharlamov, *J. Appl. Chem., USSR*, **52**, 2475 (1979).

4) T. Kubo, T. Hino, H. Tominaga, and T. Kunugi, *Nippon Kagaku Kaishi*, **1973**, 2257.

5) Kh. M. Minachev, D. B. Tagiev, Z. G. Zulfugarov, and V. V. Kharlamov, *Kinet. Katal.*, **20**, 399 (1979).

6) D. B. Tagiev, *J. Appl. Chem., USSR*, **53**, 1070 (1980).

7) K. Uehara, Y. Taketomi, and T.Kunugi, *Sekiyu Gakkai Shi*, **22**, 203 (1979).

8) Mitsubishi Chemical Industry, Japan Patent 57-51364 (1982).

9) M. Akimoto, T. Sakatani, and E. Echigoya, *Bull. Chem. Soc. Jpn.*, **56**, 3503 (1983).

10) M. Akimoto, K. Yamagami, and E. Echigoya, *J. Catal.*, **86**, 205 (1984).

11) *Shokubai (Catalyst)*, **22**, 115 (1980): Data for 5th Conference on Referenced Catalysts of the Catalysis Society of Japan, 1983, p. 56.

12) D. R. Stull, E. F. Westrum, Jr., and G. C. Sinke, "The Chemical Thermodynamics of Organic Compounds," John Wiley & Sons Inc. (1969).

13) M. Wakihara, J. Nii, T. Uchida, and M. Taniguchi, *Chem. Lett.*, **1977**, 621.

14) M. Akimoto, H. Suto, and H. Niiyama, *Bull. Chem. Soc. Jpn.*, **59**, 683 (1986).

15) M. G. Evans and M. Polanyi, *Trans. Faraday Soc.*, **32**, 1933 (1936); **34**, 22 (1938).

16) D. R. Stull and G. C. Sinke, "Thermodynamic Properties of the Elements," American Chemical Society, Washington, D. C., (1956).

 © 1986 The Chemical Society of Japan Bull. Chem. Soc. Jpn., 59, 2585—2588 (1986)

Spectrophotometric Determination of Gentamicin by Using a Membrane Filter Preconcentration Technique with *o*-Hydroxyhydroquinonephthalein and Uranium(VI)

Itsuo MORI,* Yoshikazu FUJITA, Kinuko FUJITA, Takeshi TANAKA, Hiroshi KAWABE, and Yozo KOSHIYAMA
Osaka University of Pharmaceutical Sciences, 2-10-65, Kawai, Matsubara, Osaka 580
(Received January 8, 1986)

Color reactions among amino glycoside antibiotics such as gentamicin (GM), a metal ion such as uranium(VI), and *o*-hydroxyhydroquinonephthalein (Qnph) as a xanthene dye were studied by using a preconcentration technique based on membrane filtration. A simple, new, and highly sensitive spectrophotometric determination of GM has been established by using a preconcentration to collect Qnph–uranium(VI)–GM ternary complex. Beer's law is obeyed over the range 0—5.4 μg of GM in 5 cm^3 of dimethyl sulfoxide at 565 nm, and the apparent molar absorptivity for GM is 4.2×10^5 dm^3 cm^{-1} mol^{-1} with a Sandell sensitivity of 0.0013 μg cm^{-2} GM at 565 nm. The procedure is about 2.5-fold as sensitive as the method employing aqueous medium, and is applicable to determination of GM in calf serum.

We have already reported a simple and highly sensitive spectrophotometric determination of antibiotics such as neomycin, toburamycin (TOB),[1] streptomycin (SM),[2] cephalexin, ampicillin,[3] and minocycline[4] which uses *o*-hydroxyhydroquinonephthalein (Qnph) and uranium(VI), manganese(II), palladium(II), or zirconium(IV) in the presence of surfactants without solvent extraction. Alykov[5] reported a determination of amino glycoside antibiotics which uses Pyrocatechol Violet (PV), aluminium(III), and amino glycoside antibiotics ternary complex in water–ethanol (7:3) medium. But, most of these methods are somewhat unsatisfactory for gentamicin (GM) in respect of sensitivity and selectivity, and thus their application to biological samples has scarcely been carried out.

On the other hand, we have already reported[6] a new and sensitive spectrophotometry of micro quantities of papaverine hydrochloride as organic bases which resorts to a preconcentration technique based on membrane filtration of the 2,4,5,7-tetrachlorofluorescein (T.Cl.fl.)–palladium(II)–papaverine hydrochloride ternary complex.

In this research, a color reaction was studied of amino glycoside antibiotics by utilizing the Qnph–metal ion–amino glycoside colored formation with a metal ion and Qnph, and suitable conditions were established for the spectrophotometric determination of microquantities of GM by using a preconcentration technique based on the use of membrane filter to collect the Qnph–uranium(VI)–GM ternary complex. The proposed method was applied to an assay of GM in calf serum.

Experimental

Reagents and Materials. GM (Shionogi Co., Ltd.; manifested potency 612 μg mg^{-1}) and uranium(VI) solutions (5.0×10^{-4} mol dm^{-3}) were prepared as described in our previous report.[1] Qnph methanol solution (5.0×10^{-4} mol dm^{-3}) and Walpole buffer solution (sodium acetate–acetic acid) were prepared according to our previous reports,[1,6] and 0.05% methyl cellulose (MC, 1500 cps, Kishida Chemical Co., Ltd.) solution was prepared by dissolving MC in water. All the other materials and reagents were of analytical grade and were used without further purification. Doubly deionized water was used.

Apparatus. A Shimadzu model UV-160 or 240 recording spectrophotometer with 1.0 cm silica cells was used to record absorption spectra and for absorbance measurements. A Hitachi-Horiba F-7AD glass electrode pH meter was used for pH measurements. A Toyo TM 4 membrane filter (nitrocellulose membrane, 25 mm in diameter and 0.2 μm in pore size) and a Toyo KGS-25 filter holder were used.

Standard Procedure. A GM solution containing 0—5.4 μg of GM was placed in a 10 cm^3 volumetric flask; to this were added 0.5 cm^3 of 0.05% MC solution, 2.0 cm^3 of acetate buffer solution (pH 5.0), 2.0 cm^3 of 5.0×10^{-4} mol dm^{-3} uranium(VI) solution, and 1.0 cm^3 of 5.0×10^{-4} mol dm^{-3} Qnph solution. The mixture was diluted to the mark with water, agitated well (aqueous solution A), and kept at 20—25 °C for 10 min together with a reference solution (Qnph–uranium(VI) solution, aqueous solution B). Aqueous solutions A and B were each filtered with a membrane filter, and then the filtered substances were washed with about 10 cm^3 of water. The membrane filters were dissolved in 5 cm^3 of dimethyl sulfoxide (DMSO), and then the absorbance of DMSO solution A was measured at 565 nm against DMSO solution B as a reference. The concentration of GM was determined by using a calibration curve.

Results and Discussion

Color Reaction, Absorption Spectra, and Effects of Dyes and Metal Ions. The absorption spectra of Qnph solution (DMSO solution C), Qnph–uranium(VI) binary complex solution (DMSO solution B), and Qnph–uranium(VI)–GM ternary complex solution (DMSO solution A) are shown in Fig. 1. The absorption maximum of DMSO solution A is around 565 nm, and the magnitude of absorbance at 565 nm is proportional to the concentration of GM.

Application of Xanthene Derivatives for Analytical Chemistry, Part LVI. Part LV, Y. Fujita, I. Mori, K. Fujita, T. Tanaka, Y. Koshiyama, H. Kawabe, *Chem. Pharm. Bull.*, **34**, 2236 (1986).

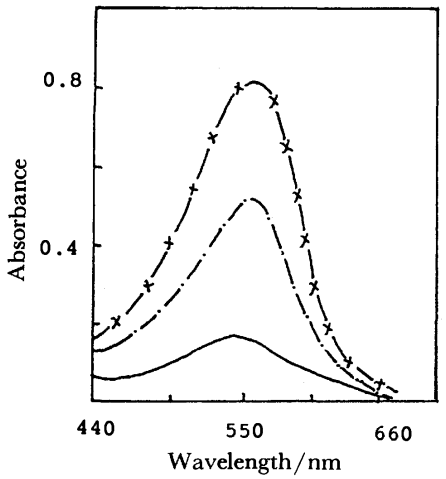

Fig. 1. Absorption spectra of Quph-uranium(VI)-GM DMSO solution (DMSO solution A), Quph-uranium(VI) DMSO solution (DMSO solution B) and Qnph DMSO solution (DMSO solution C). Uranium(VI): 1.0×10^{-4} mol dm^{-3}; Qnph: 5.0×10^{-5} mol dm^{-3}; Reference: DMSO.
——: DMSO solution C, —·—·—: DMSO solution B, —×—: DMSO solution A.

The effects of xanthene dyes and metal ions in this reaction system were also examined by measuring the absorbance of xanthene dye-metal ion-GM DMSO solution against the xanthene dye-metal ion DMSO solution. In respect of sensitivity, stability, and selectivity, Qnph as a xanthene dye and uranium(VI) as a metal ion are superior to the other xanthene dyes-salicylfluorone (Sal.fl), phenylfluorone (Phfl), *o*-hydroxyhydroquinonesulfophthalein (Qn.sul.ph), Gallein (Gall), Xylenol Orange (XO), and PV- and the other metal ions such as molybdenum(VI), tungstic acid (W(VI)), palladium(II), and lanthanum(III). These results are given in Tables 1 and 2. Next, color reactions between the Qnph-uranium(VI) solution and various amino glycoside antibiotics were compared by measuring the absorbance at 565 nm against DMSO solution B. Of the various amino glycoside antibiotics tested, the color reactions for GM and TOB are most sensitive. The results are given in Table 3.

On the basis of these results, GM was chosen for the purpose of fundamental investigations on the determination of amino glycoside antibiotics using Qnph and uranium(VI).

Effect of pH. A constant and maximum difference of absorbance between DMSO solutions A and B was obtained in the pH range from 4.8 to 5.2 when the final solution was adjusted with 2.0 cm^3 of 2.0×10^{-1} mol dm^{-3} sodium acetate-acetic acid buffer solution.

Effect of Surfactants. The effect of surfactant on the preconcentration technique using a membrane filter was examined for various surfactants. Although DMSO solutions A and B in the absence of surfactant are lacking in reproducibility and sensitivity, the presence of a small amount of MC (1500 cps), a nonionic surfactant, is most effective of the various surfactants: poly(*N*-vinylpyrrolidone) (PVP, K-15), poly(vinyl alcohol) (PVA, n=2000), MC, and sodium dodecyl sulfate (SDS). A maximum and constant absorbance of DMSO solution A was observed addition of 0.4—0.6 cm^3 of 0.05% MC solution in a final volume of 10 cm^3.

Table 1. Effect of Dyes[a]

Dye	λ_{max}/nm	Absorbance
Qnph	565	0.420
Sal.fl	565	0.357
Phfl	570	0.129
Qn.sul.ph	550	0.079
Gall	560	0.068
PV	555	0.004
XO	—	—

a) GM taken: 2.7 μg/5 cm^3; uranium(VI): 1.0×10^{-4} mol dm^{-3}; dyes: 5.0×10^{-5} mol dm^{-3}; MC: 0.5 cm^3 of 0.05% MC solution/10 cm^3; pH: 5.0; reference: dye-uranium(VI) DMSO solution.

Table 2. Effect of Metal Ions[a]

Metal ion	λ_{max}/nm	Absorbance
U(VI) (UO_2^{2+})	565	0.420
Mo(VI) (MoO_4^{2-})	565	0.156
W(VI) (WO_4^{2-})	495	0.039
V(V) (VO_3^-)	530	0.111
Pd(II)	545	0.379
La(III)	530	0.063

a) GM taken: 2.7 μg/5 cm^3; metal ions: 1.0×10^{-4} mol dm^{-3}; Qnph: 5.0×10^{-5} mol dm^{-3}; MC: 0.5 cm^3 of 0.05% MC solution/10 cm^3; pH: 5.0; reference: Quph-metal ion DMSO solution.

Table 3. The Apparent Molar Absorptivities of Amino Glycoside Antibiotics Obtained by the Present Method[a]

Compound	Apparent molar absorptivity at 565 nm ε/dm^3 mol^{-1} cm^{-1}
Gentamicin (GM)	4.2×10^5
Toburamycin (TOB)	2.6×10^5
Kanamycin	1.0×10^5
Viomycin	0.5×10^5
Streptomycin (SM)	4.9×10^3

a) Uranium(VI): 1.0×10^{-4} mol dm^{-3}; Qnph: 5.0×10^{-5} mol dm^{-3}; MC: 0.5 cm^3 of 0.05% MC solution; pH: 5.0; reference: Qnph-uranium(VI) DMSO solution.

Table 4. Effect of Foreign Substances[a)]

Substance	Added		Absorbance at 565 nm	Recovery
	μg	mole ratio		%
—	—	—	0.420	100.0
Iron(III) (Sulfate)	4.2	15	0.503	119.8
Magnesium (Nitrate)	48.6	400	0.429	102.1
Calcium (Chloride)	80.2	400	0.400	95.2
Phosphate (Sodium)	0.5	1	0.359	85.5
Oxalic Acid	6.3	10	0.386	91.9
Oleic Acid	211.8	150	0.543	129.3
Citric Acid	28.8	30	0.247	58.8
Uric Acid	126.0	150	0.242	57.6
Glutamic Acid	220.0	300	0.420	100.0
Deoxyribonucleic Acid	3.0	—	0.320	76.2
Trichloroacetic Acid	122.5	150	0.934	222.4
D-Glucose	2702.4	3000	0.420	100.0
Glycine	1126.1	3000	0.420	100.0
Thiamine (Hydrochloride)	13.3	10	0.688	163.8
Human albumin	10.0	—	0.565	134.5
Caffeine	29.1	30	0.336	80.0
Minocycline (Hydrochloride)	6.9	3	0.770	183.3
Ampicillin	610.0	350	0.420	100.0
Adenosine Triphosphate	380.0	150	0.163	38.8
Chondroitin Sulfate (Sodium)	500.0	—	0.488	116.2
N-Hexadecylpyridinium (Chloride)	3.0	2	0.580	138.1
Sulfisomidin	139.2	100	0.450	107.1

a) GM taken: 2.7 μg/5 cm^3; uranium(VI): 1.0×10^{-4} mol dm^{-3}; Qnph: 5.0×10^{-5} mol dm^{-3}; MC: 0.5 cm^3 of 0.05% MC solution/10 cm^3; pH: 5.0; reference: Qnph–uranium(VI) DMSO solution (DMSO solution B).

Effects of Qnph and Uranium(VI) Concentrations. The effect of Qnph and uranium(VI) concentrations on the standard procedure was examined by varying the molar ratio of Qnph to uranium(VI) and measuring the absorbance at 565 nm with the amounts of uranium(VI) and GM kept constant. The molar ratio of uranium(VI) 2 to Qnph 1 is most effective for the determination of GM. Accordingly, all further works were carried out with 1.0×10^{-4} mol dm^{-3} uranium(VI) and 5.0×10^{-5} mol dm^{-3} Qnph in the final volume of 10 cm^3.

Effects of Membrane Filters and Organic Solvents. Effects of organic solvent-soluble membrane filters and water miscible organic solvents in this reaction system were examined according to our previous report.[6] Nitrocellulose of 0.20 μm pore size is most effective of the pore sizes tested: 0.10, 0.20, 0.30, 0.45, 0.65, and 0.80 μm. DMSO is the best in respect of sensitivity and reproducibility.

Calibration Curve and Reproducibilty. Beer's law holds in the concentration range up to 5.4 μg of GM in the final volume of 5 cm^3 DMSO. The sensitivity, according to Sandell's scale, is 0.0013 μg cm^{-2} for GM at 565 nm, and the apparent molar absorptivity was calculated to be 4.2×10^5 dm^3 mol^{-1} cm^{-1}. The coefficient of variation (CV) for 5 replicate determinations was 1.6% for 2.7 μg of GM.

Interference of Foreign Substances. The interference of various ions and substances was examined for the determination of 2.7 μg 5 cm^{-3} of GM. Coexistence of a metal ion such as iron(III) or copper(II) causes positive errors, though the interference can be suppressed by addition of nitrilotriacetic acid (NTA) as a masking agent. Coexistence of oxalate, or phosphate, or fluoride ion, or protein interferes with carrying out the reaction. Glycine, D-glucose, glutamic acid, salicylic acid, or ampicillin does not interfere when present in 300- to 3000-fold excess over GM. These results are summarized in Table 4.

The effect of various agents was investigated to suppress the interference of protein in this proposed method using membrane filter. Sulfosalicylic acid is most suitable, because pH adjustment of sample solution is easy and because the effect of metal ions is partially masked by its addition, of the agents tested: methanol, trichloroacetic acid, sulfosalicylic acid, tungstic acid, perchloric acid, etc.

Composition of Complex. The molar ratio of GM to uranium(VI) in the Qnph–uranium(VI)–GM ternary complex was estimated to be 1:2 by the molar ratio method. The molar ratio of the Qnph–uranium(VI) complex mixture in the presence of GM was 1:2 as determined by the continuous variation and molar ratio methods. Thus, though further investigation is necessary, the colored ternary complex formed in this reaction system appears to be a ternary complex with a ratio Qnph 1: uranium(VI) 2: GM 1 in DMSO solution.

Recovery of GM Added to Calf Serum. Recovery of GM added to calf serum (Nakarai Chemical Co., Ltd.) was examined by the proposed method. A satisfactory result was obtained in the following way: Exactly 0.5 cm^3 of calf serum containing up to 0—54 μg of GM was taken, 2.0 cm^3 of 3.0% sulfosalicylic acid

Table 5. Analytical Results of GM or TOB Added to Calf Serum[a]

	Amounts of antibiotics		Recovery/%[b]
	Added/μg	Found/μg[b]	
Gentamicin (GM)	1.36	1.44	105.6
	2.72	2.90	106.6
Toburamycin (TOB)	1.46	1.48	101.4
	2.92	3.04	104.1

a) Calf serum taken: 0.5 cm³. b) Average from 5 determinations.

solution was added to this solution, and the mixture was filtered by using a membrane filter. The filtrate was diluted to 10 cm³ with water, and 1.0 cm³ of this diluted solution was taken, and then the GM content was determined according to the standard procedure. The results are given in Table 5. The experimental results were in good agreement with these given in our previous report[4] and those obtained according to other methods.[7,8]

In conclusion, this proposed spectrophotometric determination of GM by the membrane filter preconcentration technique is more than 2.5-fold as sensitive as the method employing aqueous medium,[3] and 30-fold as sensitive as the method using PV–aluminium(III) complex.[5] The proposed method is simple, rapid, sensitive, and reproducible as compared with the Qnph–uranium(VI) aqueous method,[1] the PV–aluminium(III) method,[5] and other methods.[7,8]

Although further investigation is necessary, this preconcentration method using membrane filter may be available as a new, highly sensitive, and simple analytical procedure for various pharmaceutical and biological samples.

Presented at the 106th Annual Meeting of the Pharmaceutical Society of Japan, Chiba, April (1986).

The authors are grateful to Dr. T. Nishino of this university for supplying gentamicin.

References

1) Y. Fujita, I. Mori, and S. Kitano, *Chem. Pharm. Bull.*, **32**, 1214 (1984).
2) Y. Fujita, I. Mori, and S. Kitano, *Chem. Pharm. Bull.*, **31**, 1289 (1983).
3) I. Mori, Y. Fujita, and S. Kitano, *Chem. Pharm. Bull.*, **30**, 2599 (1982).
4) Y. Fujita, I. Mori, and S. Kitano, *Chem. Pharm. Bull.*, **31**, 4016 (1983).
5) N. M. Alykov, *Zh. Anal. Khim.*, **39**, 1130 (1985).
6) I. Mori, Y. Fujita, H. Kawabe, and K. Fujita, *Chem. Pharm. Bull.*, **34**, 902 (1986).
7) D. W. Huges, A. Villim, and W. L. Wilson, *Can. J. Pharm. Sci.*, **13**, 21 (1978).
8) J. E. Fairbrother, *Pharm. J.*, **218**, 237, 509 (1977).

 © 1986 The Chemical Society of Japan Bull. Chem. Soc. Jpn., 59, 2589—2594 (1986)

Comparison of ESR Signal Intensities of Some Binuclear Copper Complexes

Kunio NAKANO,* Hiroshi TADANO, So OSHIGE, Nobuaki WADA, Mari YAMAGUCHI, and Heijiro OJIMA†
Department of Chemistry, College of Science, Rikkyo University, Nishi-Ikebukuro 3, Toshima-ku, Tokyo 171
†Aichi Kyoiku University, Igaya-cho, Kariya 448
(Received February 13, 1986)

ESR signal intensities of two kinds of binuclear copper complex were measured by the two-step integral method with a multi-mode resonator cavity. The intensities standardized with $CuSO_4 \cdot 5H_2O$ are the proper values for these substances, and can be compared with each other. The intensities of oxamide type complexes (A-group) were a few tens of percent of the intensity of $CuSO_4 \cdot 5H_2O$, while the intensities of binuclear complexes having a bridge of two oxygens (B-group) were less than one percent. This suggests that the two coppers in each binuclear molecule interact, and that the magnitude of the interaction of the B-group can be considered to be much greater than that of the A-group.

Although the electron spin resonance (ESR) spectra of many substances have been determined, there are not so many examples of quantitative measurements of ESR signal intensity. An ESR signal is usually recorded in derivative shape of an absorption curve, and there are some instances of quantitative analysis by using the peak-to-peak height of the signal.[1–15] However, the peak-to-peak height method cannot be used except in the case of sharp and symmetrical signals. Hence, the two-step integration method was attempted for quantitative measurements and gave good results for general signals.[16,17] After this, a few instances of the integration method have been seen.[18–21] The wave height of a two-step integral curve, however, varies with changes in the measuring conditions; and it cannot be normalized for the microwave output power, although normalization for the other measuring conditions is possible.[22] Moreover, the Q-value of a sample varies in its signal intensity, and thus the signal intensities of samples having different Q-values cannot be compared with each other even if determined under the same measuring conditions. To make such comparison between different species possible two-step integral method using a multi-mode resonator (double cavity) was devices.[23]

A sample and a standard substance were put into each hole of two sample holes of the double cavity, and the wave heights of two-step integral were measured under same-phase and anti-phase of magnetic modulation. This method made it possible to obtain the proper ESR signal intensities of various substances. These proper values can be considered to have the same sort of significance as that of such properties as molar absorption coefficient, magnetic moment and molar heat. The ESR signal intensities of some binuclear copper complexes are reported in the present paper.

Experimental

Apparatus. The ESR apparatus used was a JES-ME3X (Japan Electron Optics Laboratory Co. Ltd.) which had been partially modified in its phase sensitive detector circuit.[24] The multi-mode cavity resonator was a TE_{105} mode type (JES-MCX-1, JEOL). Its cavity had two sample holes and in each hole was set a quartz adapter to minimize the variation of sample position by reinsertion.[24] Into one of two holes was inserted a sample and into the other a standard. Magnetic modulation applied to the two holes could be switched to the same-phase or to the anti-phase.

A signal was integrated by a hand-made integrator in which two operational amplifiers were employed.[16] The wave height of the two-step integral curve was measured by a process similar to the method for measuring limiting current in polarography. Quartz tubes of 5 mm outside diameter to just fit the adapter were used for the sample tube.

Materials. The binuclear copper complexes were synthesized by one of the present authors.[25–30] The complexes measured and their symbols are listed in Table 1. From a few mg to about 20 mg of $CuSO_4 \cdot 5H_2O$ were used as standards. Mononuclear copper complexes measured for comparison were extra pure grade or were prepared from extra pure reagents. The samples used for measurements were fine grain or powder.

Measurements. Figure 1 shows each signal example of A-group and B-group. They were measured with a single cavity. As B-4 was measured under ten-fold greater sensitivity than A-6, the signal of B-4 was much smaller than that of A-6.

The method of calculation was as follows. Sample a and sample b are inserted into the two holes, hole 1 and hole 2, of the double cavity, respectively. When the magnetic modulation of the two holes is in the same phase, the wave heights of the two-step integral curve is represented as h_s, and when in the anti phase, it is represented as h_a, then,

$$h_s = I_a + \alpha I_b \quad (1)$$

$$h_a = \beta(I_a - \alpha I_b) \quad (2)$$

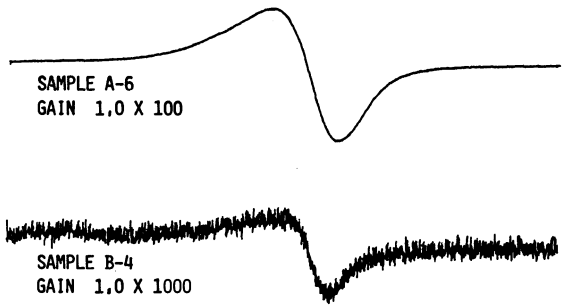

Fig. 1. Examples of ESR signal of binuclear copper complexes. Magnetic field: 3100±1000 gauss, magnetic moduration width: 6.06 gauss, microwave frequency: 9.42 GHz, microwave output power: 6.0 mW, crystal current: 0.4 mA, sweep time: 10 min, at room temperature.

Table 1. Binuclear Copper Complexes and Their Symbols

Symbol	Complex	Lit.
A- 1	μ-[*N*,*N*′-Bis(2-pyridylmethyl)oxamido]dichlorodicopper(II)	25)
A- 2	μ-[*N*,*N*′-Bis(3-dimethylaminopropyl)oxamido]dichlorodicopper(II)	26)
A- 3	μ-[*N*,*N*′-Bis(2-pyridylethyl)oxamido]dichlorodicopper(II)	25)
A- 4	μ-[*N*,*N*′-Bis[2-(2-pyridyl)ethyl]oxamido]-(1,10-phenanthroline)dicopper(II) nitrate	a)
A- 5	μ-[*N*,*N*′-Bis[2-(2-pyridyl)ethyl]oxamido]-(2,2′-bipyridine)dicopper(II) nitrate	27)
A- 6	μ-[*N*,*N*′-Bis(2-pyridylethyl)oxamido]-(2,2′-bipyridine)dicopper(II) nitrate	b)
A-10	μ-[*N*,*N*′-Bis(2-pyridylmethyl)oxamido]-bis(γ-picoline)dicopper(II) nitrate	b)
A-16	μ-[*N*,*N*′-Bis(2-pyridylmethyl)oxamido]-(2,2′-bipyridine)dicopper(II) nitrate	27)
A-18	μ-[*N*,*N*′-Bis[2-(2-pyridyl)ethyl]oxamido]-bis(γ-picoline)dicopper(II) nitrate	b)
A-33	μ-[*N*,*N*′-Bis(2-dimethylaminoethyl)oxamido]dicopper(II) chloride	26)
A-34	μ-[*N*,*N*′-Bis[2-(3-dimethylaminopropylamino)ethyl]oxamido]dicopper(II) chloride	26)
A-35	μ-[*N*,*N*′-Bis[3-(2-dimethylaminoethylamino)propyl]oxamido]dicopper(II) chloride	26)
A-36	μ-[*N*,*N*′-Bis[3-(3-dimethylaminopropylamino)propyl]oxamido]dicopper(II) chloride	26)
A-37	μ-[*N*,*N*′-Bis[4-(2-dimethylaminoethylamino)butyl]oxamido]dicopper(II) chloride	26)
A-38	μ-[*N*,*N*′-Bis[4-(3-dimethylaminopropylamino)butyl]oxamido]dicopper(II) chloride	26)
A-39	μ-[*N*,*N*′-Bis[6-(2-dimethylaminoethylamino)hexyl]oxamido]dicopper(II) chloride	26)
A-40	μ-[*N*,*N*′-Bis[6-(3-dimethylaminopropylamino)hexyl]oxamido]dicopper(II) chloride	26)
A-41	μ-[*N*,*N*′-Bis[2-(2-dimethylaminoethylamino)ethyl]oxamido]dicopper(II) perchlorate	26)
A-42	μ-[*N*,*N*′-Bis[2-(3-dimethylaminopropylamino)ethyl]oxamido]dicopper(II) perchlorate	26)
A-43	μ-[*N*,*N*′-Bis[3-(2-dimethylaminoethylamino)propyl]oxamido]dicopper(II) perchlorate	26)
A-44	μ-[*N*,*N*′-Bis[3-(3-dimethylaminopropylamino)propyl]oxamido]dicopper(II) perchlorate	26)
A-45	μ-[*N*,*N*′-Bis[4-(2-dimethylaminoethylamino)butyl]oxamido]dicopper(II) perchlorate	26)
A-46	μ-[*N*,*N*′-Bis[4-(3-dimethylaminopropylamino)butyl]oxamido]dicopper(II) perchlorate	26)
A-47	μ-[*N*,*N*′-Bis[6-(2-dimethylaminoethylamino)hexyl]oxamido]dicopper(II) perchlorate	26)
B- 1	μ-Bis[*N*-(3-hydroxopropyl)-*N*′-methylglycinamido]dicopper(II)	28)
B- 2	μ-Bis[*N*-(3-hydroxopropyl)-*N*′,*N*′-dimethylglycinamido]dicopper(II)	28)
B- 3	μ-Bis[*N*-(3-hydroxopropyl)glycinamido]dicopper(II)	28)
B- 4	μ-Bis[*N*-(3-hydroxopropyl)picolinamido]dicopper(II)	29)
B- 6	μ-Bis[*N*-(3-methylaminopropyl)hydroxoacetamido]dicopper(II)	30)
B- 7	μ-Bis[*N*-(3-dimethylaminopropyl)hydroxoacetamido]dicopper(II)	30)
B- 8	μ-Bis[*N*-(2-pyridylethyl)hydroxoacetamido]dicopper(II)	26)
B- 9	μ-Bis[*N*-(2-pyridylmethyl)hydroxoacetamido]dicopper(II)	26)

a) Obtained similarly to the complex A-5 using 1,10-phenanthroline instead of 2,2′-bipyridine in the complex A-5. b) Derived from the complex A-1 or A-3 using pyridine- or 4-methylpyridine.

while I_a and I_b are respectively the wave heights of sample a and sample b in hole 1 in the same phase, α is the ratio of the wave heights in hole 1 and hole 2, and β is the ratio of the wave heights of the same sample in the same phase and in the anti phase. Figure 2 shows an example of an original curve (1), the 1st step integral curve (2), and the 2nd step integral curve (3), and the determination of h_s and h_a are also shown in the figure.

The following equation is obtained from Eqs. 1 and 2.

$$\frac{I_a}{I_b} = \frac{\alpha(h_s + h_a/\beta)}{h_s - h_a/\beta} \tag{3}$$

I_a and I_b vary considerably with changes in the measuring conditions and in the Q-value of the sample; however, the ratio I_a/I_b is maintained almost constant. Therefore, if sample b is a standard, the signal intensity of sample a can be obtained by Eq. 3.

$CuSO_4 \cdot 5H_2O$ was employed as the standard substance in the present experiments. If n mg of $CuSO_4 \cdot 5H_2O$ are taken as a standard and m mg of binuclear complex are taken as a sample, the ratio γ of copper atoms to those in the standard is

$$\gamma = \frac{2m}{M} \cdot \frac{249.7}{n} \tag{4}$$

M: molecular weight of the binuclear complex.

The ESR signal intensity of copper in the sample is given by

$$I = \frac{1}{\gamma} \cdot \frac{I_a}{I_b} \tag{5}$$

All measurements were carried out at room temperature. Measuring conditions of the spectrometer were as follows: Sweep width of the magnetic field was 3100±1000 gauss, sweep time was 1 min, magnetic modulation width was 6.06 gauss, the microwave frequency was 9.4 GHz and its output power was 6.0 mW, and the crystal current was 0.4 mA. The cavity constants, α and β, were revaluated when the cavity and the adapters were reset.

The relative standard deviation of repeated measurements of a sample was generally within a few %, when the shape of the signal was favorable. However, when the signal was very small, as in the B-type complex, the number of significant figures of the intensity I was only one. Moreover, when the two wings of a signal curve did not coincide with the base line, the precision decreased. However, noise with short periods scarcely affected the precision, since it was canceled out by integration. The relative standard deviations of the signal intensities obtained in the present work except for the B-group were within a few %, and even the maximum deviation was less than 10%.

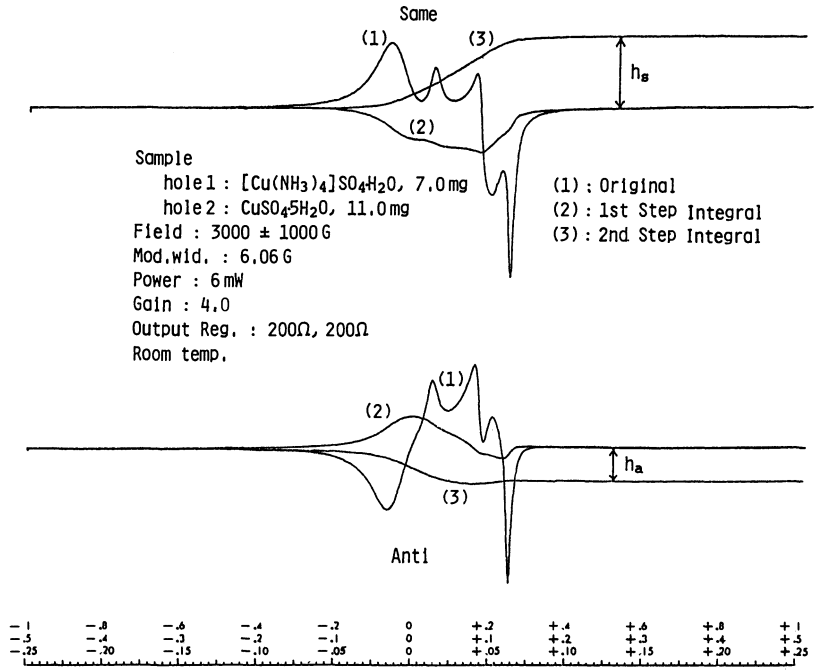

Fig. 2. An example of integrated curves of ESR signal with double cavity.
h_s: Wave height in same phase. h_a: Wave height in anti phase.

Results and Discussion

The results obtained for the ESR signal intensities I standardized with $CuSO_4 \cdot 5H_2O$ are tabulated in Table 2. The table also includes the magnetic moment μ measured previously by one of the present authors. In addition, the signal intensities of a few mononuclear copper complexes are also listed. The data are compiled and presented in Fig. 3; and when roughly classified, they show that, although the intensities of mononuclear complexes are almost 1, those of the A-group are a few tens of % and those of B-group under 1% of the copper sulfate crystals. This suggests that the two unpaired electrons of the two copper atoms in a molecule partly make a pair through bridging atoms. The interaction can be considered to be stronger in the B-group (two-oxygen bridge) than in the A-group (oxamide bridge).

With respect to the compounds A-1 to A-18, those whose chelate ring adjacent to the bridging ring has fine members have about half the I value of those having six members. Thus, it can be considered that the copper–copper interaction of a five-membered ring is stronger than that of a six-membered ring, since the larger strain of the six-membered ring more strongly affects the delocalization of π-electrons through the bridging atoms. The same tendency can be seen in the compounds from A-33 to A-47, that is, the I values of the compounds of l=2 (five-membered ring) are smaller than those of l=3 (six-membered ring). However, that the values of l=6 (nine-membered ring) are smaller than those of l=3 may suggest that the structural strain is

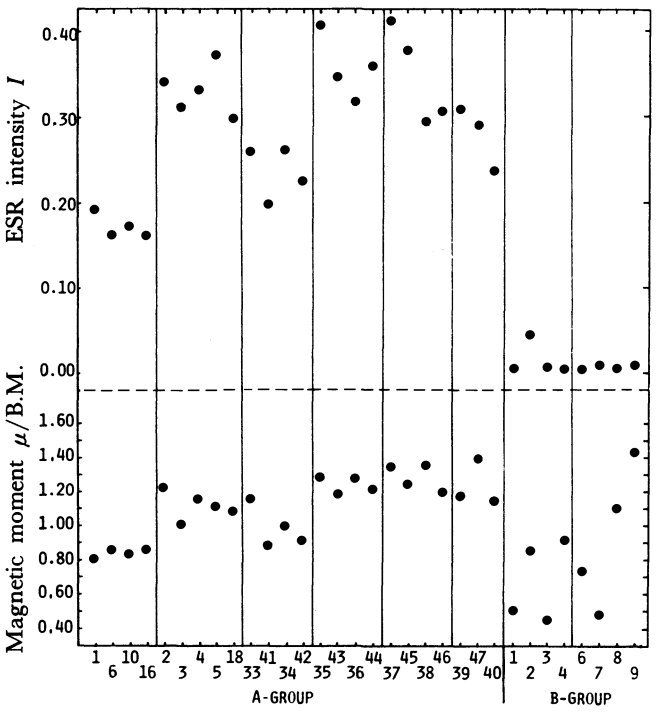

Fig. 3. ESR signal intensities and magnetic moments of binuclear copper complexes.

rather smaller than in the six-membered ring. The number of members of the chelate ring on the opposite side of the bridging ring does not seem to have obvious effect on its signal intensity.

The values of magnetic moment μ of binuclear complexes shown in Fig. 3 are smaller than the value of

Table 2. ESR Signal Intensities and Magnetic Moments of Binuclear Cu Complexes

Complex	$CuCl_2 \cdot 2H_2O$	$[Cu(NH_3)_4] \cdot (NO_3)_2$	$[Cu(acac)_2]$	$[Na_2Cu(edta)] \cdot 4H_2O$
Intensity	0.945	1.017	0.932	1.025

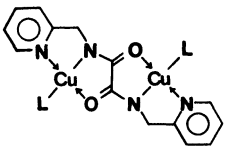

	A-1	A-6	A-10	A-16
2L	2Cl trans	2N⟨⬡⟩ trans	2N⟨⬡⟩CH_3 trans	bipy cis
Anion	—	$(NO_3)_2$	$(NO_3)_2$	$(NO_3)_2$
H_2O	—	—	—	—
I	0.190	0.158	0.171	0.159
μ(B.M.)	0.81	0.87	0.84	0.87

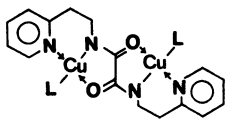

	A-3	A-4	A-5	A-18
2L	2Cl trans	phen cis	bipy cis	2N⟨⬡⟩CH_3 trans
Anion	—	$(NO_3)_2$	$(NO_3)_2$	$(NO_3)_2$
H_2O	0.5	2	3	—
I	0.309	0.329	0.369	0.291
μ(B.M.)	1.21	1.01	1.16	1.12

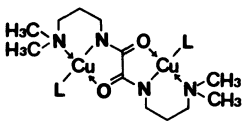

	A-2
2L	2Cl trans
Anion	—
H_2O	—
I	0.388
μ(B.M.)	1.23

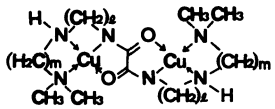

No.	A-33	A-41	A-34	A-42	A-35	A-43
ℓ	2	2	2	2	3	3
m	2	2	3	3	2	2
Anion	Cl	ClO_4	Cl	ClO_4	Cl	ClO_4
H_2O	5/2	—	1	2	1/4	—
I	0.258	0.198	0.259	0.213	0.404	0.345
μ	1.16	0.89	1.00	0.92	1.29	1.19

No.	A-36	A-44	A-37	A-45	A-38	A-46	A-39	A-47	A-40
ℓ	3	3	4	4	4	4	6	6	6
m	3	3	2	2	3	3	2	2	3
Anion	Cl	ClO_4	Cl	ClO_4	Cl	ClO_4	Cl	ClO_4	Cl
H_2O	1/2	2	2	1/4	1/2	1	5/4	2	—
I	0.315	0.358	0.410	0.376	0.293	0.304	0.306	0.287	0.235
μ	1.28	1.22	1.35	1.25	1.36	1.20	1.18	1.40	1.15

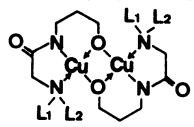

	B-1	B-2	B-3
L_1	H	CH_3	H
L_2	CH_3	CH_3	H
I	0.005	0.043	0.007
μ	0.51	0.86	0.46

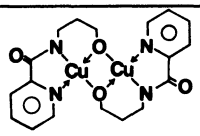

	B-4
I	0.003
μ	0.78

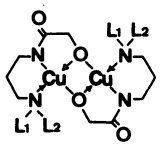

	B-6	B-7
L_1	H	CH_3
L_2	CH_3	CH_3
I	0.003	0.006
μ	0.74	0.49

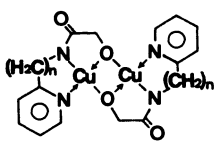

	B-8	B-9
n	2	1
I	0.004	0.007
μ	1.11	1.44

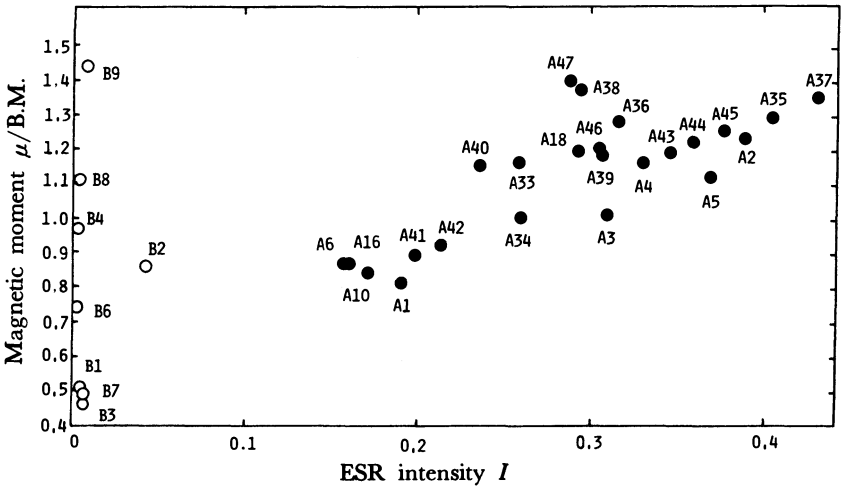

Fig. 4. Relationship between the ESR signal intensities and the magnetic moments of binuclear copper complexes.

the general mononuclear copper complex, which is about 1.9. Although the values of five-membered rings are smaller than those of six-membered rings as in the relationship in the case of ESR signal intensity, no significant difference between six or seven-membered ring and nine-membered rings can be seen. Moreover, although the ESR intensities of the B-group are much smaller than those of the A-group, there is no great difference in the magnetic moments of the A-group and B-group. The relationship between the signal intensities and magnetic moments is shown in Fig. 4. A considerable correlation is exhibited between I and μ in the A-group, but such correlation cannot be seen in the B-group. The reason for this is not yet understood.

Conclusion

The two-step integral method using a multimode cavity made it possible to obtain the intensities of ESR signals of samples relative to a standard substance, regardless of the measuring conditions and the Q-values of the samples. It can be considered that the accurate determination of an ESR signal intensity as a proper value of a species is very important. In the present work the ESR signal intensities of some binuclear copper complexes were measured as the first examples. The results showed that the intensities of the binuclear copper complexes of the A-group (oxamide type) were a few tens of percent of the intensity of copper sulfate crystals, while those of B-group (binuclear complexes bridged with two oxygen atoms) were less than one percent of copper sulfate. This difference may have been caused by the magnitude of interaction between the two copper atoms in binuclear molecule. On the other hand, the difference in the magnetic moments between the A-group and B-group was not notable. However, as the interaction between the two copper atoms of a B-group compound is generally supposed to be stronger than that of an A-group compound due to their structures, the ESR signal intensity can be considered to be more useful than the magnetic moment for estimating the interaction between these atoms.

References

1) S. Fujiwara, K. Nagashima, and M. Codell, *Bull. Chem. Soc. Jpn.*, **37**, 773 (1964).
2) G. G. Guilbault and T. Meisel, *Anal. Chem.*, **41**, 1100 (1969).
3) E. F. Moyer and W. J. McCarthy, *Anal. Chim. Acta*, **48**, 79 (1969).
4) G. G. Guilbault and E. S. Moyer, *Anal Chem.*, **42**, 441 (1970).
5) T. Meisel and G. G. Guilbault, *Anal. Chim. Acta*, **50**, 143 (1970).
6) S. Fujiwara, H. Tadano, and M. Nakajima, *Bull. Chem. Soc. Jpn.*, **43**, 3023 (1970).
7) D. Yamamoto, T. Fukumoto, and N. Ikawa, *Bull. Chem. Soc. Jpn.*, **45**, 1403 (1972).
8) D. Yamamoto and N. Ikawa, *Bull Chem. Soc. Jpn.*, **45**, 1405 (1972).
9) D. Yamamoto and F. Ozaki, *Bull. Chem. Soc. Jpn.*, **45**, 1408 (1972).
10) W. G. Bryson, D. P. Hubbard, B. M. Peake, and J. Simpson, *Anal. Chim. Acta*, **77**, 107 (1975).
11) D. C. Warren and J. M. Fitzgerald, *Anal. Chem.*, **49**, 250 (1977).
12) G. Hanson, A. Szabo, and N. D. Chasteen, *Anal. Chem.*, **49**, 461 (1977).
13) W. G. Bryson, D. P. Hubbard, B. M. Peake, and J. Simpson, *Anal. Chim. Acta*, **96**, 99 (1978).
14) W. G. Bryson, D. P. Hubbard, B. M. Peake, and J. Simpson, *Anal. Chim. Acta*, **116**, 353 (1980).
15) Y. Sakane, K. Saito, K. Matsumoto, and Y. Osajima, *Bunseki Kagaku*, **30**, 715 (1981).
16) K. Nakano, H. Tadano, and M. Oshima, *Nippon Kagaku Kaishi*, **1972**, 2453.
17) K. Nakano, H. Tadano, and S. Sugimoto, *Bunseki Kagaku*, **27**, 256 (1978).
18) Ira B. Goldberg, H. R. Crown, and W. M. Robertson,

Anal. Chem., **49**, 962 (1977).
19) Ira B. Goldberg and H. R. Crown, *Anal. Chem.*, **49**, 1353 (1977).
20) Ira B. Goldberg, *J. Magn. Reson.*, **32**, 233 (1978).
21) J. L. Gerlock, *Anal Chem.*, **55**, 1520 (1983).
22) K. Nakano, H. Tadano, and S. Sugimoto, *Nippon Kagaku Kaishi*, **1979**, 885.
23) K. Nakano, H. Tadano, and S. Takahashi, *Anal. Chem.*, **54**, 1850 (1982).
24) K. Nakano, H. Tadano, S. Mitsuhashi, and H. Suzuki, *Bunseki Kagaku*, **32**, T11 (1983).
25) H. Ojima and K. Nonoyama, *Z. Anorg. Allg. Chem.*, **401**, 195 (1973).
26) Unpublished.
27) H. Ojima and K. Yamada, "Proceedings Symposium on Coordination Chemistry," Debrecen Hungary (1970), Vol. 1, p. 281.
28) H. Ojima and K. Nonoyama, *Z. Anorg. Allg. Chem.*, **379**, 322 (1970).
29) H. Ojima, *Nippon Kagaku Zasshi*, **88**, 1056 (1967).
30) K. Nonoyama and H. Ojima, *Nippon Kagaku Zasshi*, **92**, 297 (1971).

Syntheses and Properties of Copper(II) Triperchlorates with *N,N',N'',N'''*-Tetrakis(2-aminoethyl)-1,4,8,11-tetraazacyclotetradecane and an Anion

Sigeo KIDA,* Ichiro MURASE, Chizu HARADA, Liao DAIZENG, and Masahiro MIKURIYA
Department of Chemistry, Faculty of Science, Kyushu University 33, Hakozaki, Higashi-ku, Fukuoka 812
Laboratory of Chemistry, College of General Education, Kyushu University 01, Ropponmatsu, Fukuoka 810
(Received February 14, 1986)

Copper complexes of the title ligand (taec) of the general formula $Cu_2(taec)X(ClO_4)_3$ (X=F, Cl, Br, I, HCOO, CH_3COO, NO_2) were prepared and characterized. The formation constants for $[Cu_2(taec)]^{4+}+X^-=[Cu_2(taec)X]^{3+}$(X=F, Cl, Br, I) were determined spectrophotometrically in aqueous solution. The stabilities of the halogen-copper bonds were greatly enhanced relative to those of ordinary halogenocopper complexes, the order of the formation constants being Cl>Br>I>F. This result can be explained as that the anion is trapped in a cavity formed by two copper ions and the methylene chains of taec molecule, thereby the stability of the bound anion is enhanced and the fitness of the size of anion to the cavity is the most important factor for the formation constant.

A number of tetraazamacrocycles with pendant arms on the nitrogen atoms were synthesized and characterized in recent several years because of their specific complexation behavior and structural interest of their metal complexes.[1-6] In the preceding papers,[7,8] we reported the synthesis and characterization of dicopper(II) complexes of taec(*N,N',N'',N'''*-tetrakis(2-aminoethyl)cyclam). The crystal structure analyses revealed that in $Cu_2(taec)(ClO_4)_4$ and $Cu_2(taec)Br(ClO_4)_3$ each copper ion is coordinated by the two ring nitrogens and the two pendant nitrogens forming a nearly square planar coordination entity, but the coordination modes of ligand are entirely different between these complexes as depicted in Fig. 1. In both cases one of the axial sites is open for coordination on each copper, but the other site is hindered with ligand methylene groups. In $Cu_2(taec)(ClO_4)_4$ both axial coordination sites are open toward the outside of the molecule in opposite direction so that perchlorate oxygen weakly coordinates to each copper, whereas in $Cu_2(taec)Br(ClO_4)_3$ the axial coordination sites face to each other allowing the bromide ion to be bound by both coppers. This structure is in good harmony with the facts that the addition of excess sodium perchlorate to a concentrated solution of $Cu_2(taec)Br_4$ does not yield the tetrakis(perchlorate) but invariably precipitated the bromide tris(perchlorate) and the Cu-Br bond is very stable toward hydrolysis relative to ordinary Cu-Br bonds. Being interested in these results, in this study we have newly prepared a series of complexes of the formula, $Cu_2(taec)X(ClO_4)_3$ (X=F, Cl, I, HCOO, CH_3COO, NO_2), and discussed the nature of Cu-X bonds in terms of stability constants and electronic spectra.

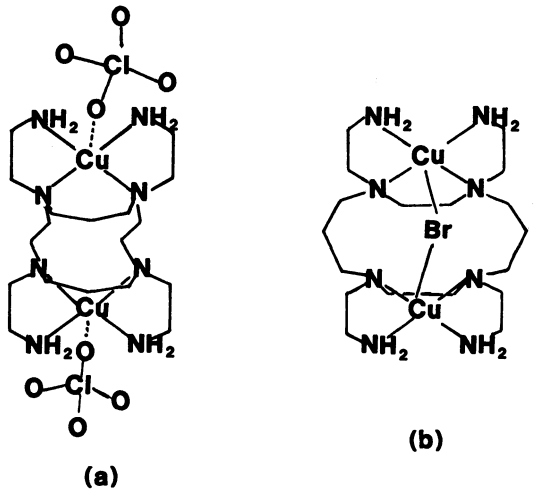

Fig. 1. Schematic drawing of the molecular structures of (a) $Cu_2(taec)(ClO_4)_4$ and (b) $Cu_2(taec)Br(ClO_4)_3$, where uncoordinated perchlorate ions are omitted.

Experimental

Preparation. The preparative methods for taec and $Cu_2(taec)Br(ClO_4)_3$ were already reported in the preceding papers.[7,8]

Complexes, $Cu_2(taec)X(CLO_4)_3$ (X=F, Cl, I, HCOO, CH_3COO, NO_2), were prepared by similar procedures from $Cu(ClO_4)_2\cdot 6H_2O$, taec, and NaX. The procedure for $Cu_2(taec)F(ClO_4)_3\cdot 2H_2O$ is shown below as an example.

$Cu_2(taec)F(ClO_4)_3\cdot 2H_2O$. To an aqueous solution of $Cu(ClO_4)_2\cdot 6H_2O$ (185 mg, 0.5 mmol) and taec (93 mg, 0.25 mmol) was added NaF (82 mg, 2 mmol), and the mixture was heated at 80 °C for 20 min. The resulting blue solution was filtered. When the filtrate was allowed to stand for about 6 h, blue needles were separated. Leaving the mixture for longer period may result in contamination of purple crystals ($Cu_2(taec)(ClO_4)_4$). The crude product was recrystallized from aqueous solution by adding NaF (≈ 50 mg). The crystals were collected, washed with methanol, and desiccated over P_2O_5. Yield; 175 mg (85%). Found: C, 25.60; H, 5.73; N, 13.23; Cu, 14.87%. Calcd for $C_{18}H_{48}N_8O_{14}Cl_3FCu_2$: C, 25.35; H, 5.67; N, 13.14; Cu, 14.90%

$Cu_2(taec)Cl(ClO_4)_3\cdot H_2O$. Blue fine crystals. Yield; 177 mg (85%). Found: C, 25.37; H, 5.25; N, 13.25; Cu, 14.87%. Calcd for $C_{18}H_{46}N_8O_{13}Cl_4Cu_2$: C, 25.39; H, 5.44; N, 13.16; Cu, 14.93%.

$Cu_2(taec)I(ClO_4)_3$. Violet needles. Yield; 210 mg (91%). Found: C, 23.32; H, 4.69; N, 11.95; Cu, 13.48%. Calcd for $C_{18}H_{44}N_8O_{12}Cl_3ICu_2$: C, 23.37; H, 4.79; N, 12.11; Cu, 13.74%.

$Cu_2(taec)(HCOO)(ClO_4)_3$. Blue needles. Yield; 196 mg (93%). Found: C, 26.73; H, 5.43; N, 13.15; Cu, 15.07%. Calcd for

Table 1. Magnetic, Spectral, and Stability Data

Compounds	μ_{eff} (290K)	μ_{eff} (88K)	θ/K	$\nu_{max}/10^3\,cm^{-1}$ Nujol	$\nu_{max}/10^3\,cm^{-1}$ H_2O (ε)	log$K$
$Cu_2(taec)F(ClO_4)_3\cdot 2H_2O$	1.85	1.78	−10	15.3	16.9(160)	3.93±0.13
$Cu_2(taec)Cl(ClO_4)_3\cdot H_2O$	1.76	1.70	−8	16.1	16.3(220)	5.14±0.08
$Cu_2(taec)Br(ClO_4)_3$	1.80	1.77	−5	16.2	16.3(230)	4.78±0.12
$Cu_2(taec)I(ClO_4)_3$	1.75	1.71	−4	16.2	16.3(230)	4.46±0.17
$Cu_2(taec)(NO_2)(ClO_4)_3$	1.79	1.77	−3	16.7	17.0(170)	
$Cu_2(taec)(HCOO)(ClO_4)_3$	1.78	1.75	−4	15.9	17.3(150)	
$Cu_2(taec)(CH_3COO)(ClO_4)_3\cdot 2H_2O$	1.78	1.74	−5	15.7	17.4(150)	
$Cu_2(taec)(ClO_4)_4$	1.81	1.67	−20	19.2	17.7(165)	

$K=[Cu_2(taec)X^{3+}]/[Cu_2(taec)^{4+}][X^-]$ at 30°C in the presence of 0.01 M $NaClO_4$.

$C_{19}H_{45}N_8O_{14}Cl_3Cu_2$: C, 27.07; H, 5.38; N, 13.29; Cu, 15.08%.

$Cu_2(taec)(CH_3COO)(ClO_4)_3\cdot 2H_2O$. Blue needles. Yield; 161 mg (89%). Found: C, 26.86; H, 5.78; N, 12.35; Cu, 14.82%. Calcd for $C_{20}H_{51}N_8O_{16}Cl_3Cu_2$: C, 26.90; H, 5.76; N, 12.55; Cu, 14.23%.

$Cu_2(taec)(NO_2)(ClO_4)_3$. Fine indigo-blue crystals. Yield; 200 mg (95%). Found: C, 26.86; H, 5.78; N, 12.35; Cu, 14.82%. Calcd for $C_{18}H_{44}N_9Cl_3O_{14}Cu_2$: C, 26.90; H, 5.76; N, 12.55; Cu, 14.23%.

Measurements. Electronic spectra were measured with a Shimazu MPS-5000 Multipurpose Spectrophotometer.

Infrared spectra were obtained with a Hitachi Grating Infrared Spectrophotometer Model 215 on KBr disk.

Magnetic susceptibilities were measured by the Faraday method. The apparatus was calibrated by use of $[Ni(en)_3]S_2O_3$. The susceptibilities were corrected for the diamagnetism of constituent atoms by use of Pascal's constants. Effective magnetic moments were calculated from the equation, $\mu_{eff}=2\sqrt{2(\chi-N\alpha)T}$, where χ is atomic magnetic susceptibility, and $N\alpha=60\times10^{-6}$ cgs emu.

Determination of stability constants. The equilibrium constants for $[Cu_2(taec)]^{4+}+X^- \leftrightarrows [Cu_2(taec)X]^{3+}$ (X=F, Cl, Br, I) were determined by a spectrophotometric method.[9] Absorbances of aqueous solutions containing $Cu_2(taec)X(ClO_4)_3$ (2×10^{-3}, 1×10^{-3}, 4×10^{-4}, 2×10^{-4}, 1×10^{-4}, and 5×10^{-5} M) and $NaClO_4$ (1×10^{-2} M) were measured in 1 cm or 10 cm cell at 30°C, where M=mol dm^{-3}. The spectrum of $Cu_2(taec)(ClO_4)_4$ (1×10^{-3} M) was also measured to determine its molar extinction coefficients at the same condition as the above. The constants K were obtained by exploiting the relations,

$$\varepsilon_a(a-x) + \varepsilon_b x = D$$
$$(a-x)/x^2 = K,$$

where a and $a-x$ are initial and equilibrium concentrations of $[Cu_2(taec)X]^{3+}$, respectively; D is optical density of the solution; and ε_a and ε_b are molar extinction coefficients of $[Cu_2(taec)X]^{3+}$ and $[Cu_2(taec)]^{4+}$, respectively, the former of which were determined by measuring the absorbances of solutions containing $[Cu_2(taec)X]^{3+}$ (1×10^{-3} M) and the excess of X^- (10^{-2}—10^{-3}). Reasonable K values were obtained from the data in the range 600—640 nm, and those at 620 nm were chosen as the best values, which are listed in Table 1.

Results and Discussion

The binuclear structure of the present complexes is obvious judging from the elemental analyses and the crystal structures of $Cu_2(taec)Br(ClO_4)_3$ and $Cu_2(taec)(ClO_4)_4$.[8] However, as seen in Table 1 magnetic moments are not subnormal, and obey Curie-Weiss law in 80—300 K with very small negative Weiss constants, implying that there is no significant magnetic interaction between the copper ions.

Infrared spectra of all the complexes showed bands at 3400—3200, 3000—2900, 1580—1500, and 1050—1150 cm^{-1} whcih can be assigned to the ν(NH), ν(CH), $\delta(NH_2)$, $\delta(CH_2)$, and $\nu(ClO_4^-)$, respectively,[10] and many small bands in the 1400—650 cm^{-1} region forming a complicated pattern. The spectra of the F^-, Cl^-, Br^-, and I^- complexes closely resemble each other, suggesting similar molecular structures. The spectra of the NO_2 and RCOO (R=CH_3, H) complexes differ from each other and from those of the halogeno complexes in detail in the 1400—650 cm^{-1} region, and the bands due to the axial ligands overlapped with those of the equatorial ligand (taec), hence no definite assignments were feasible.

As shown in Table 1 the ligand field bands of $Cu_2(taec)X(ClO_4)_3$ are generally lower in wave number than that of $Cu_2(taec)(ClO_4)_4$ in nujol mull spectra. When the complexes are dissolved in water, the bands of tris(perchlorate) complexes are blue-shifted in more or less degree, whereas that of the tetrakis(perchlorate) is red-shifted though it still maintains the highest ν_{max} values among those complexes. These shifts should be due to the hydrolysis of the axial ligands. Judging from the degree of the blue-shift, it seems that the halogeno complexes are hydrolyzed very little in spite of the general view that halogeno copper(II) complexes are readily hydrolized in water.[11] On the other hand, the other complexes of $Cu_2(taec)X(ClO_4)_3$ are considerably hydrolized. In the case of tetrakis(perchlorate) it is most likely that the weakly coordinated perchlorate ions in crystal[7] are fully replaced by water molecules.

In order to make the above view quantitative we have determined the formation constants K of the halogeno complexes spectrophotometrically, and the results are listed in Table 1.[12]

$$K = [Cu_2(taec)X^{3+}]/[Cu_2(taec)^{4+}][X^-]$$

Chung et al. determined the complexation constants between mononegative ions and some macrocyclic tetraamine copper(II) complexes, and found that they fell in the range of 1—10 for the cases of Cl^- and Br^- ions.[13] These values are comparable to the first formation constants (k_1) of Cl^- and Br^- ions with Cu^{2+} (log k_1=0.08 and −0.055 respectively). Thus, the presently obtained K values are larger than those values by a factor of 10^4—10^5 (cf. Table 1). Such an amazing stability should be attributed to a special steric arrangement of the coordination site. In fact, the X-ray analysis of Cu_2(taec)Br$(ClO_4)_3$ demonstrated that the bromide ion is linked by the two copper ions and hedged by nondonating atoms of taec molecule like being trapped in a cavity.[8] Thus, the environment around the coordinated halide ion will become somewhat similar to that in a nonpolar solvent so that the copper-halide bond is greatly stabilized. It is also to be noted that the K values decrease in the order, Cl>Br>I>F. This can also be rationalized in terms of the fitness of the anion to the cavity. In the present case fluoride ion seems to be too small for the cavity to get the largest enhancement of stability. In view of the above results the present complexes may be a model for active sites of some metal enzymes possessing specific selectivity and reactivity which are not found in ordinary synthetic metal complexes.

References

1) E. K. Barefield and F. Wagner, *Inorg. Chem.*, **12**, 2435 (1973); M. J. D'amiello, M. T. Mocella, F. Wagner, E. K. Barefield, and I. C. Paul, *J. Am. Chem. Soc.*, **97**, 192 (1975); F. Wagner and E. K. Barefield, *Inorg. Chem.*, **15**, 408 (1976); A. K. Basak and T. A. Kaden, *Helv. Chim. Acta*, **1983**, 2086; T. A. Kaden, *Top. Curr. Chem.*, **1984**, 121, and references therein.

2) H. Stetter and W. Frank, *Angew. Chem., Int. Ed. Engl.*, **15**, 686 (1976).

3) C. M. Madeski, J. P. Michael, and R. D. Hancock, *Inorg. Chem.*, **23**, 1487 (1984).

4) K. P. Wainwright, *J. Chem. Soc., Dalton Trans.*, **1980**, 2117.

5) K. P. Wainwright, *J. Chem. Soc., Dalton Trans.*, **1983**, 1149.

6) G. M. Freeman, E. K. Barefield, and D. G. Van Derveer, *Inorg. Chem.*, **23**, 3092 (1984).

7) I. Murase, M. Mikuriya, H. Sonoda, and S. Kida, *J. Chem. Soc., Chem. Commun.*, **1984**, 692.

8) I. Murase, M. Mikuriya, H. Sonoda, Y. Fukuda, and S. Kida, *J. Chem. Soc., Dalton Trans.*, **1986**, 953.

9) The constants for the NO_2^-, $HCOO^-$, and CH_3COO^- complexes could not be determined because of the low solubility or low stability in aqueous solution under the present condition.

10) K. Nakamoto, "Infrared and Raman Spectra of Inorganic and Coordination Compounds," 3rd ed., John Willey & Sons, New York (1978).

11) "Stability Constants," ed by L. G. Sillen and A. E. Martell, The Chemical Society, London (1978).

12) Although the interconversion between $[Cu_2(taec)]^{4+}$ + X^- and $[Cu_2(taec)X]^{3+}$ involves a substantial change in ligand configuration, we have confirmed that the solution readily reaches equilibrium under these experimental conditions. Because the spectra of the solutions were entirely time-independent, and $Cu_2(taec)(ClO_4)_4$ can be readily converted into $Cu_2(taec)X(ClO_4)_3$ in aqueous solution by adding NaX and vice versa by adding $AgClO_4$ instead of NaX.

13) S.-Y. Wu, C.-S. Lee, and C.-S. Chung, *Inorg. Chem.*, **23**, 2548 (1984); B.-F. Liang, T.-H. Peng, C.-S. Chung, *J. Inorg. Nucl. Chem.*, **43**, 1671 (1981).

 © 1986 The Chemical Society of Japan Bull. Chem. Soc. Jpn., 59, 2599—2606 (1986)

Thermodynamic Quantities of Transfer of Glycinato and β-Alaninato Complexes of Silver(I) and Related Species from Water to an Aqueous Dioxane Solution

Shin-ichi Ishiguro, Honoh Suzuki, Masayuki Zama, Arup K. Basak,† and Hitoshi Ohtaki*
Department of Electronic Chemistry, Tokyo Institute of Technology at Nagatsuta, 4259, Nagatsuta-cho, Midori-ku, Yokohama 227
(Received January 31, 1986)

Complexation of silver(I) with glycinate (gly^-) and β-alaninate (β-ala^-) ions have been studied by potentiometry and calorimetry in 0.2 mole fraction (55.0%w/w) dioxane-water mixture containing 3 mol dm^{-3} $LiClO_4$ as a constant ionic medium at 25 °C. Potentiometric titration curves obtained were well-explained in terms of formation of [AgL], $[AgL_2]^-$, and $[AgHL]^+$ (L^-=gly^- or β-ala^-) in both systems, together with $[Ag(OH)L]^-$ in the Ag(I)-β-alanine system, and their formation constants were determined. Enthalpies of formation of the complexes in the mixed solvent, as well as in water containing the same ionic medium, were calorimetrically determined on the basis of the formation constants potentiometrically determined. Solubilities and enthalpies of solution of the neutral [AgL] (L^-=gly^- and β-ala^-) complexes and some related compounds were determined in water and the mixture, the Gibbs energies of transfer, ΔG_t°, of silver(I) ion and proton from water to the mixture being also determined by potentiometry. By combining the thermodynamic quantities thus obtained, thermodynamic quantities of transfer of single species from water to the mixture were evaluated. Compared to the enthalpy, ΔH_t°, and entropy, ΔS_t°, of transfer of a neutral species, the ΔH_t° and ΔS_t° values of any charged species were significantly large with the negative sign for cations and positive one for anions. As to neutral species, [HL] and [AgL], the relation, $\Delta G_t^\circ > \Delta H_t^\circ \cong 0$ and $\Delta S_t^\circ < 0$, was found, suggesting that the [AgL] complexes have a similar zwitterionic structure to that of glycine and β-alanine zwitterions.

Complex formation equilibria between silver(I) ion and amino acids have so far been studied in water.[1] In a previous paper,[2] we also reported the formation of glycinato (gly^-) and β-alaninato (β-ala^-) complexes of Ag(I) in water, and suggested that the metal ion was coordinated with the amino nitrogen atom within [AgL] and $[AgL_2]^-$ (L^-=gly^- and β-ala^-) but with the carboxylato oxygen atom within $[AgHL]^+$.

In water-rich dioxane-water mixtures, although metal ions and ligands are expected to be preferentially solvated with water, complexation in some metal-ligand systems, such as nickel(II)-ethylenediamine,[3] nickel(II)-glycinate[4] and copper(II)-ethylenediamine systems,[5] are appreciably different from those in water, due perhaps to a partially destroyed hydrogen-bonding structure of bulk water in the mixture compared to that in water.

Silver(I) ion which tends to have a linear coordination structure with ligands may show a different solvent effect on complexation from that of the bivalent transition metal ions having an octahedral coordination structure.

In this work, therefore, we investigated the complexation of silver(I) ion with glycinate and β-alaninate ions by potentiometry and calorimetry in water and in 0.2 mole fraction dioxane-water mixture, and solvent effects on the thermodynamic quantities of formation of the metal complexes in these solvents are discussed. Solubilities and enthalpies of solution of the [AgL] (L^-=gly^- and β-ala^-) complexes and some related compounds were also determined in these solvents. The Gibbs energies of transfer of Ag^+ and H^+ from water to various dioxane-water mixtures were potentiometrically determined. By combining the thermodynamic quantities thus obtained, thermodynamic quantities of transfer of single species from water to the 0.2 mole fraction dioxane-water mixture were evaluated.

†Present address: Department of Chemistry, Texas A & M University, Colledge Station, Texas 77840, U.S.A.

Experimental

Reagents. All chemicals used were of reagent grade. *Lithium glycinate* and *lithium β-alaninate* were prepared by mixing equimolar amounts of glycine or β-alanine and lithium hydroxide in methanol and recrystallized twice from methanol, and then dried at 100 °C in a vacuum oven. *Sodium β-alaninate* was prepared with sodium methoxide by a similar procedure to that used for lithium β-alaninate. *Silver(I) glycinate* and *silver(I) β-alaninate* were prepared by dissolving silver(I) nitrate in aqueous glycine or β-alanine solution, and then by adding sodium hydroxide in the solution. The silver(I) glycinate and silver(I) β-alaninate crystals thus prepared were filtered, washed with methanol and ether, and then dried in vacuum in a dark desiccator at room temperature.

Other chemicals were prepared and purified as described elsewhere.[2,6,7]

Measurements. Potentiometric and calorimetric measurements were carried out in a room thermostated at (25.0±0.2) °C. All test solutions prepared for the measurements contained 3 mol dm^{-3} $LiClO_4$ as a constant ionic medium.

Formation constants were determined by potentiometric measurements which were carried out in a liquid paraffin bath controlled at (25.00±0.02) °C. A test solution containing metal, ligand and hydrogen ions was titrated with a lithium hydroxide solution, and pH of the test solution was determined by using a glass electrode in combination with an Ag-AgCl electrode as a reference. The method of measurements was the same as that described in previous papers.[2-7]

Enthalpies of complexation were calorimetrically determined by measuring in a water bath thermostated at

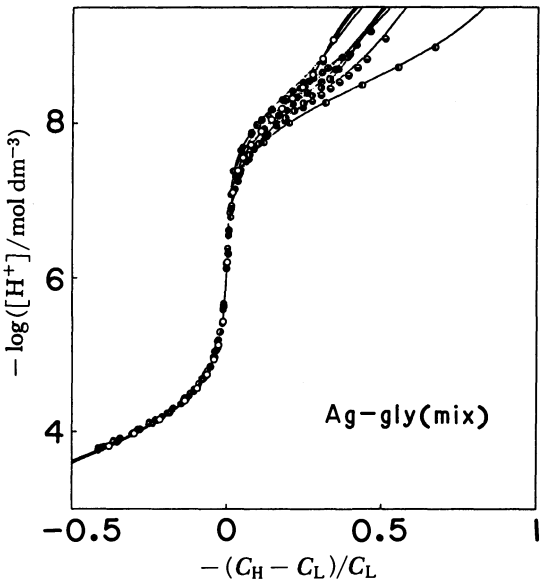

Fig. 1. Potentiometric titration curves for the silver(I)-glycinate system in the 0.2 mole fraction dioxane-water mixture. Initial concentrations of the metal and ligand ions, C_M/mmol dm^{-3} and C_L/mmol dm^{-3}: 2.385, 10.10 (⊙); 2.387, 13.99 (●); 2.926, 13.44 (◕); 3.763, 17.29 (⊕); 3.773, 23.94 (○); 4.741, 18.14 (◒); 5.611, 26.90 (◑); 5.626, 37.25 (◎); 5.801, 11.08 (◐).
The concentrations of the metal and ligand ions were changed by dilution during the titrations. The solid lines show the curves calculated by using the constants in Table 1.

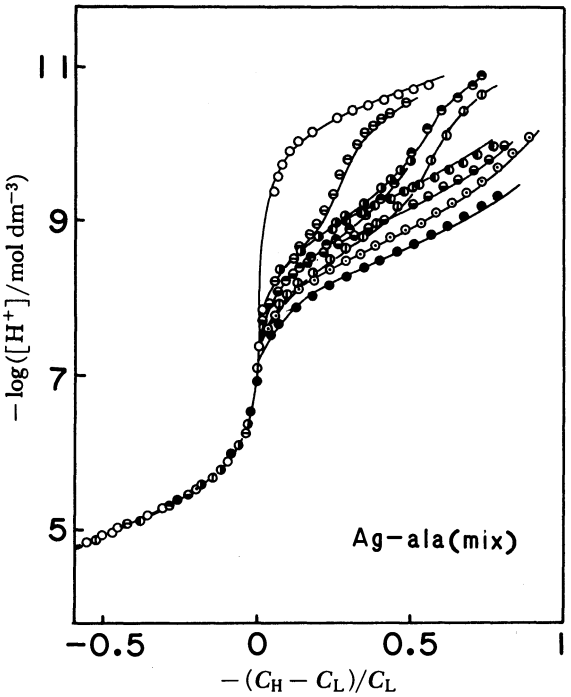

Fig. 2. Potentiometric titration curves for the silver(I)-β-alaninate system in the 0.2 mole fraction dioxane-water mixture. Initial concentrations of the metal and ligand ions, C_M/mmol dm^{-3} and C_L/mmol dm^{-3}: 0.0, 10.03 (○); 2.559, 5.246 (◐); 2.559, 10.12 (◑); 2.559, 20.15 (⊖); 4.997, 10.12 (◒); 4.997, 20.15 (◓); 4.997, 40.90 (Φ); 10.07, 20.15 (⊙); 10.07, 40.90 (●).
The concentrations of the metal and ligand ions were changed by dilution during the titrations. The solid lines show the curves calculated by using the constants in Table 1.

(25.000±0.007)°C. An initial test solution contained silver(I) and ligand ions, and hydrogen ions of relatively low concentration, and was titrated with a perchloric acid solution. Details of measurements were described elsewhere.[3-5,8,9]

The Gibbs energies of transfer of silver(I) ion and proton from water to dioxane-water mixtures were potentiometrically determined by using an Ag-AgCl and a glass electrodes, respectively, in combination with an Ag-AgCl electrode as a reference, and the total concentrations of the relevant ions were kept constant with varying solvent composition in a test solution.

Solubilities of the mono(glycinato)- and mono(β-alaninato)silver(I) complexes were determined in water and in the 0.2 mole fraction dioxane-water mixture, each solution containing 3 mol dm^{-3} $LiClO_4$ and a small amount of glycine or β-alanine in order to prevent hydrolysis of the metal ion, after the solution was equilibrated for more than two weeks in a thermostated room at (25.0±0.2)°C. Concentrations of silver(I) ion in these solution at equilibrium were gravimetrically determined as AgCl. Net concentrations of the [AgL] (L^-=gly$^-$ and β-ala$^-$) complexes in the solutions were calculated by taking into account the distribution of the glycinato and β-alaninato complexes of silver(I) in each solvent.

Enthalpies of solution of the mono(glycinato)- and mono(β-alaninato)silver(I) complexes and related species were measured by dissolving a given amount of crystals of the relevant species in water and in the mixture, each containing 3 mol dm^{-3} $LiClO_4$. Procedures of the measurements and analysis of data were described in a previous paper.[9]

Determination of Formation Constants and Enthalpies. In advance of determining formation constants and enthalpies of complexation of metal ion with ligands, protonation constants and enthalpies of protonation of each ligand had been determined by potentiometry and calorimetry, respectively. The thermodynamic quantities thus obtained were kept constant in the course of the analysis of the formation constants and enthalpies of formation of the glycinato and β-alaninato complexes of Ag(I). Details of the analysis of potentiometric and calorimetric data were described previously.[3-5]

Results and Discussion

Potentiometric titration curves obtained for silver(I) glycinate and β-alaninate systems in the 0.2 mole fraction dioxane-water mixture are depicted in Figs. 1 and 2, respectively. The potentiometric data were first analyzed by the same graphical procedure as that used in a previous work.[2] For both systems, the graphical analysis indicated the formation of [AgL], $[AgL_2]^-$, and $[AgHL]^+$ over the pH range 3—10. In the silver(I)-β-alaninate system, the formation of $[Ag(OH)L]^-$ was also indicated at pH>8. Formation constants of these complexes were refined by the least-squares method, the

Table 1. The Least-Squares Refinements of Overall Formation Constants, $\log\beta_{pqr}$, of the $[Ag_pH_qL_r]^{(p+q-r)+}$ (L^-=gly$^-$ or β-ala$^-$) Complexes in the 0.2 Mole Fraction Dioxane-Water Mixture Containing 3 mol dm^{-3} $LiClO_4$ as a Constant Ionic Medium at 25 °C
$\beta_{pqr}=[Ag_pH_qL_r^{(p+q-r)+}]/[Ag^+]^p[H^+]^q[L^-]^r$

	Species	Glycinate	β-Alaninate
$\log\beta_{011}$	$[HL]^{a)}$	10.22[b)]	10.86(0.03)
$\log\beta_{021}$	$[H_2L]^+$	13.81[b)]	15.84(0.03)
$\log\beta_{111}$	$[AgHL]^+$	10.93(0.04)	11.63(0.03)
$\log\beta_{101}$	$[AgL]$	3.77(0.01)	4.02(0.22)
$\log\beta_{102}$	$[AgL_2]^-$	7.76(0.01)	8.31(0.03)
$\log\beta_{1-11}$	$[Ag(OH)L]^-$	—	−6.97(0.3)

Values in parentheses refer to 3σ where σ denotes a standard deviation. a) Zwitterion: $^+H_3NCH_2COO^-$ or $^+H_3NCH_2CH_2COO^-$. b) Ref. 4.

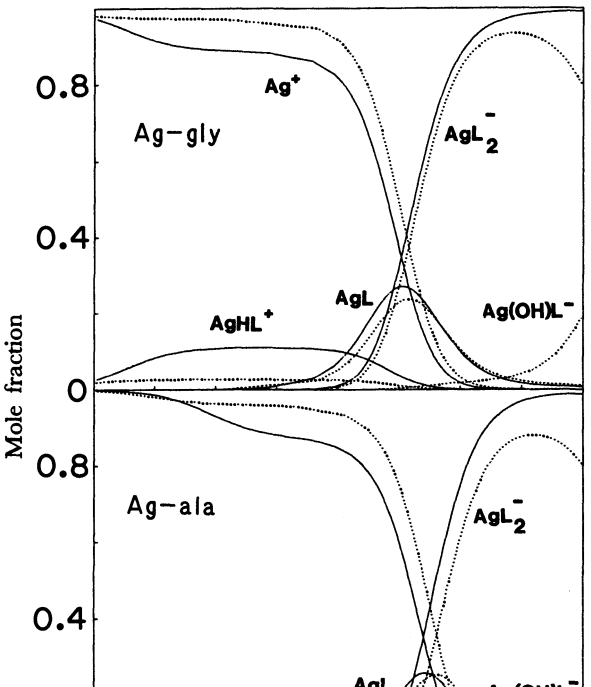

Fig. 3. Distribution of species for the silver(I) glycinate and β-alaninate systems in the 0.2 mole fraction dioxane-water mixture (the solid lines) and in water (the broken lines), both solutions containing 5 and 25 mmol dm^{-3} of silver and ligand ions, respectively, in each system.

results being summarized in Table 1, together with the protonation constants of the ligands. As seen in Figs. 1 and 2 by the solid lines, the theoretical titration curves calculated by using the formation constants in Table 1 well fitted the experimental points over the whole pH range examined in each metal-ligand system. The distribution of species of the silver(I) glycinate and β-alaninate systems in the mixture is shown in Fig. 3.

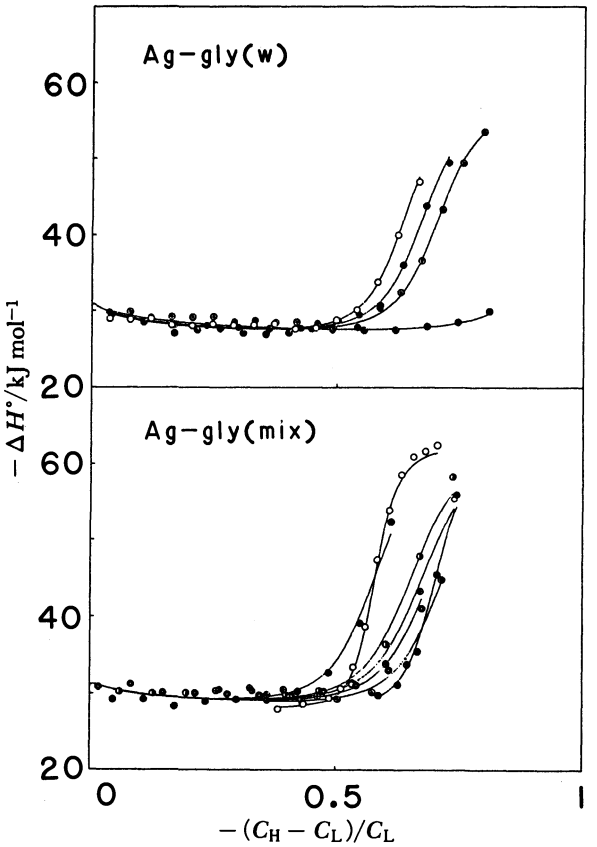

Fig. 4. Calorimetric titration curves of the silver(I)-glycinate system in water and in the 0.2 mole fraction dioxane-water mixture. Initial concentrations of the metal and ligand ions, C_M/mmol dm^{-3} and C_L/mmol dm^{-3}: 15.57, 31.81 (◎); 15.28, 43.09 (⊙); 14.77, 43.46 (●) and 15.21, 47.44 (○) in water and 5.098, 14.64 (⊕); 5.019, 14.91 (◑); 5.476, 15.40 (◉); 4.779, 15.98 (◎); 6.355, 17.18 (⊙); 12.56, 35.21 (●) and 16.41, 56.09 (○) in the mixture.
The solid lines show the calculated curves obtained by using the constants in Tables 1 and 2.

Calorimetric titration curves obtained for the silver(I) glycinate and β-alaninate systems are depicted in Figs. 4 and 5, respectively. Enthalpies $-\Delta H°$/kJ mol^{-1} ($=q/(\delta v C_{H,tit})$, where q and δv denote the heat evolved and the volume of an aliquot of the titrant added, respectively, at each titration point and $C_{H,tit}$ stands for the concentration of $HClO_4$ in the titrant solution) were plotted against the degree of neutralization X ($=-(C_H-C_L)/C_L$, where C_L and C_H denote the total concentration of glycine or β-alanine and hydrogen ion, respectively) of ligand in a solution. The calorimetric data in water were analyzed by using the formation constants of the complexes determined in a previous work.[2)]

As seen in Fig. 3, the formation of $[AgHL]^+$ is weak, so that the enthalpy of formation of the complex was not determined with a sufficient accuracy in each system. The enthalpy of formation of $[Ag(OH)L]^-$ was not also obtained with a reasonable reliability under the present experimental conditions.

The enthalpies of protonation of glycinate and β-alaninate ions and of complex formation of Ag(I) with glycinate and β-alaninate ions in water (w) and in the 0.2 mole fraction dioxane-water mixture (mix) obtained by the least-squares method are summarized in Table 2. The theoretical titration curves calculated by using the formation constants and enthalpies of complexes in Tables 1 and 2 are drawn by the solid lines in Figs. 4 and 5, respectively, which well reproduced the experimental points in each system.

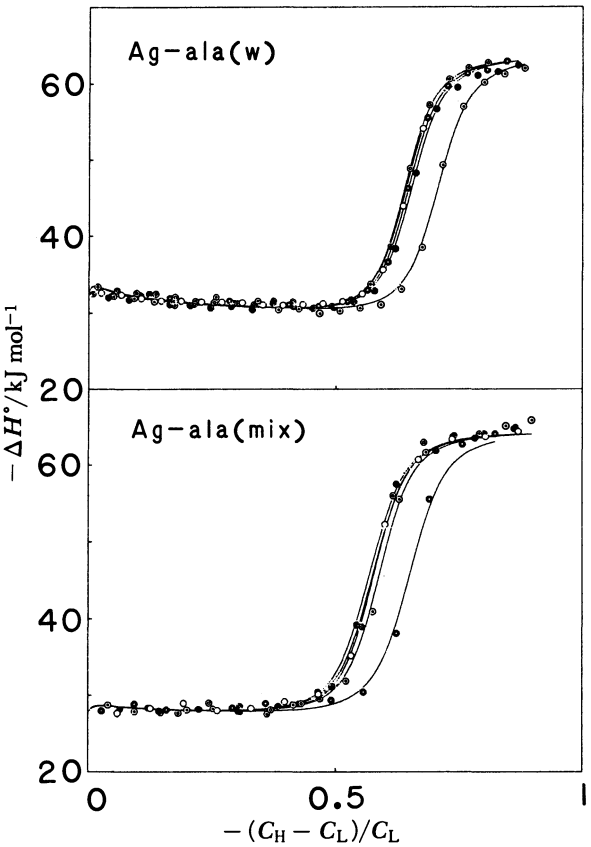

Fig. 5. Calorimetric titration curves of the silver(I)-β-alaninate system in water and in the 0.2 mole fraction dioxane-water mixture. Initial concentrations of the metal and ligand ions, C_M/mmol dm^{-3} and C_L/mmol dm^{-3}: 14.32, 43.82 (○); 15.96, 44.45 (⊙); 14.80, 44.51 (●); 14.97, 45.48 (◉) and 15.02, 46.17 (◎) in water, and 4.558, 15.13 (○); 5.203, 15.40 (◉); 4.690, 15.59 (●); 4.777, 15.70 (⊙) and 4.979, 16.55 (◎) in the mixture.
The solid lines show the calculated curves obtained by using the constants in Tables 1 and 2.

Thermodynamic quantities, $\log(K_n/\text{mol}^{-1}\,\text{dm}^3)$, ΔG_n°/kJ mol^{-1}, ΔH_n°/kJ mol^{-1} and ΔS_n°/J K^{-1} mol^{-1}, for the stepwise formation of $[H_nL]^{(n-1)+}$ (L^-=β-ala$^-$) and $[AgL_n]^{(1-n)+}$ (L^-=gly$^-$ and β-ala$^-$) are listed in Table 3, together with the difference, P_n(mix)−P_n(w) (P=log K, $\Delta G°$, $\Delta H°$, and $\Delta S°$), between the relevant quantities in water and in the mixture.

Gibbs Energies and Enthalpies of Transfer of Proton, and Silver(I), Glycinate and β-Alaninate Ions from Water to the 0.2 Mole Fraction Dioxane-Water Mixture. Changes in activities of proton and silver(I) ion in dioxane-water mixtures relative to those in water were determined by measuring emfs of a cell constructed with a glass and an Ag-AgCl electrodes in combination with an Ag-AgCl electrode as a reference, in which the total concentrations of relevant ions were kept constant with varying solvent composition. In each case of proton and silver(I) ion, the difference in emfs, ΔE=E(mix)−E(w), was obtained as a function of the concentration of dioxane in the mixtures, the result being shown in Fig. 6. As seen in Fig. 6, the ΔE values were independent of the concentrations of relevant ions, but depended on the solvent composition. Thus, ΔE is represented by Eq. 1:

$$\Delta E = (RT/F)\ln\{y(\text{mix})/y(\text{w})\} + \{E_j(\text{mix}) - E_j(\text{w})\}, \quad (1)$$

where y and E_j stand for the activity coefficient and the liquid junction potential of a species at the interface between a test solution and a salt bridge (an aqueous solution or 0.2 mole fraction dioxane-water mixture containing 3 mol dm^{-3} $LiClO_4$ as an ionic medium) and F denotes the Faraday constant. Since the difference in emfs was not influenced by the change of the composition of the salt bridge, the term $\{E_j(\text{mix})-E_j(\text{w})\}$ should be negligibly small. In these measurements, therefore, the ΔE values observed for proton and silver(I) ion could be attributed to the Gibbs energy of transfer of a relevant ion from water to the mixture:

$$\Delta G_t^\circ = RT\ln\{y(\text{mix})/y(\text{w})\} = F\Delta E. \quad (2)$$

The ΔG_t° values of proton and silver(I) ion from water to the 0.2 mole fraction dioxane-water mixture were thus obtained to be 1.9 and 3.1 kJ mol^{-1}, respectively.

Solubilities of the mono(glycinato)- and mono(β-

Table 2. The Least-Squares Refinements of Overall Enthalpies, $\Delta H_{\beta pqr}^\circ$/kJ mol^{-1}, of Formation of $[Ag_pH_qL_r]^{(p+q-r)+}$ (L^-=gly$^-$ or β-ala$^-$) in Water(w) and in the 0.2 Mole Fraction Dioxane-Water Mixture (mix), Each Solution Containing 3 mol dm^{-3} $LiClO_4$ as a Constant Ionic Medium at 25 °C

	Species	Gly$^-$(w)	Gly$^-$(mix)	β-Ala$^-$(w)	β-Ala$^-$(mix)
$\Delta H_{\beta 011}^\circ$	[HL][a)]	−57.9[b)]	−62.7[b)]	−63.8(0.5)	−64.5(0.3)
$\Delta H_{\beta 021}^\circ$	$[H_2L]^+$	−63.4[b)]	−73.0[b)]	−73.0(0.5)	−78.8(0.4)
$\Delta H_{\beta 101}^\circ$	[AgL]	−25.7(1.1)	−30.3(1.6)	−28.2(0.8)	−34.5(1.4)
$\Delta H_{\beta 102}^\circ$	$[AgL_2]^-$	−62.2(0.5)	−69.4(0.8)	−67.1(0.4)	−74.6(0.7)

Values in parentheses refer to 3σ where σ denotes a standard deviation. a) Zwitterion: $^+H_3NCH_2COO^-$ or $^+H_3NCH_2CH_2COO^-$. b) Ref. 4.

Table 3. Thermodynamic Quantities, $\log(K_n/\text{mol}^{-1}\,\text{dm}^3)$, $\Delta G_n^\circ/\text{kJ mol}^{-1}$, $\Delta H_n^\circ/\text{kJ mol}^{-1}$, and $\Delta S_n^\circ/\text{J K}^{-1}\,\text{mol}^{-1}$, for the Stepwise Formation of $[H_nL]^{(n-1)+}$ (L^-=β-ala$^-$) and $[AgL_n]^{(1-n)+}$ (L^-=gly$^-$ or β-ala$^-$) in Water and in the 0.2 Mole Fraction Dioxane-Water Mixture, and Their Differences in the Solvents

	Water	0.2 Mole Fraction Dioxane-Water Mixture	Difference
H^+–β-ala$^-$ system			
$\log K_1$	10.65	10.86	0.21
$\log K_2$	4.03	4.98	0.96
ΔG_1°	−60.9	−62.1	−1.2
ΔG_2°	−23.0	−28.5	−5.5
ΔH_1°	−63.8	−64.5	−0.7
ΔH_2°	−9.2	−14.3	−5.1
ΔS_1°	−10	−8	2
ΔS_2°	46	48	2
Ag^+–gly$^-$ system			
$\log K_1$	3.28	3.77	0.51
$\log K_2$	3.68	3.99	0.36
ΔG_1°	−18.7	−21.6	−2.9
ΔG_2°	−21.0	−22.8	−1.8
ΔH_1°	−25.7	−30.3	−4.6
ΔH_2°	−36.5	−39.1	−2.6
ΔS_1°	−23	−29	−6
ΔS_2°	−52	−55	−3
Ag^+–β-ala$^-$ system			
$\log K_1$	3.58	4.02	0.44
$\log K_2$	3.88	4.29	0.41
ΔG_1°	−20.4	−23.0	−2.6
ΔG_2°	−22.2	−24.5	−2.3
ΔH_1°	−28.2	−34.5	−6.3
ΔH_2°	−38.9	−40.1	−1.2
ΔS_1°	−26	−39	−13
ΔS_2°	−56	−52	4

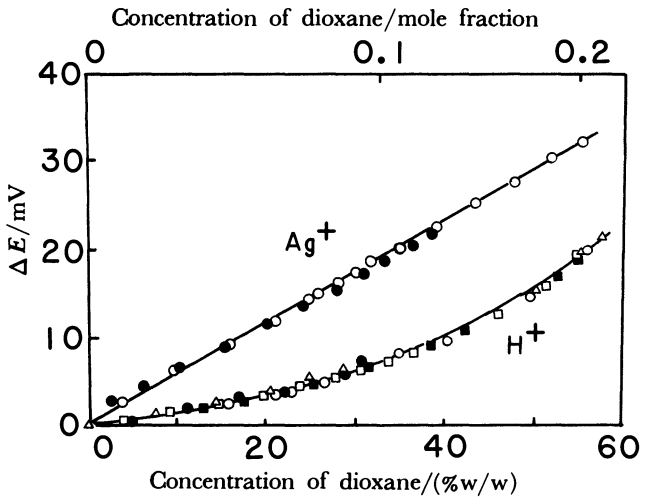

Fig. 6. Emfs obtained as a function of the dioxane concentration in dioxane-water mixtures. An aqueous solution (w) and the 0.2 mole fraction dioxane-water mixture (mix), each containing 3 mol dm^{-3} $LiClO_4$, were used as the salt-bridge solutions. Emfs measured in solutions of the same concentration of Ag^+ or H^+ ion (5—20 mmol dm^{-3}) are plotted with the same symbol.

alaninato)silver(I) complexes were determined in water and in the 0.2 mole fraction dioxane-water mixture. The net solubilities (Γ/mol dm^{-3}) of the complexes were evaluated by taking into account the distribution of species in each solution, the result being given in Table 4. The Gibbs energy of transfer of [AgL], $\Delta G_t^\circ([AgL])$, from water to the mixture was calculated:

$$\Delta G_t^\circ([AgL]) = -RT\ln\{\Gamma_{mix}([AgL])/\Gamma_w([AgL])\}, \quad (3)$$

which is related to the Gibbs energies of transfer of relevant ions, $\Delta G_t^\circ(Ag^+)$ and $\Delta G_t^\circ(L^-)$, and the Gibbs energies of formation of [AgL], ΔG_1°, in water and in the mixture given in Table 3:

$$\Delta G_1^\circ(\text{mix}) - \Delta G_1^\circ(\text{w}) = \Delta G_t^\circ([AgL]) - \Delta G_t^\circ(Ag^+) - \Delta G_t^\circ(L^-). \quad (4)$$

Since all the values except for $\Delta G_t^\circ(L^-)$ have been determined, the $\Delta G_t^\circ(L^-)$ values for glycinate and β-alaninate ions were determined.

Crystals of silver(I) glycinate and β-alaninate which were in equilibrium with the solution may involve some water molecules such as $Aggly\cdot(1/2)H_2O$.[10] In this case, the $\Delta G_t^\circ([AgL])$ value involves the contribution of the Gibbs energy of transfer of a half mole of water from water to the mixture. However, the $\Delta G_t^\circ(H_2O)$ value is about −0.4 kJ mol^{-1},[11] and thus, the contribution of water was neglected.

The enthalpies of solution of $AgClO_4$, β-alanine, sodium β-alaninate, and silver(I) glycinate and β-alaninate in water and in the 0.2 mole fraction

Table 4. Solubilities, Γ/mol dm^{-3}, and Enthalpies of Solution, ΔH_s°/kJ mol^{-1}, of the Mono(glycinato)- and Mono(β-alaninato)silver(I) Complexes and Some Related Species in Water and in the 0.2 Mole Fraction Dioxane-Water Mixture at 25 °C, and the Enthalpies of Transfer, ΔH_t°/kJ mol^{-1}, of the Species from Water to the Mixure

	Water	0.2 Mole Fraction Dioxane-Water Mixture	ΔH_t°
Γ([Aggly])[a]	7.37×10^{-3}	6.10×10^{-4}	
Γ([Agala])[a]	9.24×10^{-3}	6.55×10^{-4}	
ΔH_s°([Aggly])[b]	33.2	36.3	3.1
ΔH_s°([Agala])[b]	25.6	24.8	−0.8
ΔH_s°($AgClO_4$)	8.6	−17.9	−26.6
ΔH_s°([Hala])	9.5	16.3	6.8
ΔH_s°(Naala)[c]	−19.4	−9.2	10.2

a) Concentration of [AgL] corrected by taking into account the distribution of species in each solution. b) Dissolved in solutions containing excess ligand ions to yield $[AgL_2]^-$, and the measured enthalpy of solution was corrected for the enthalpy for the reaction, $[AgL]+L^-=[AgL_2]^-$. c) Dissolved in solutions containing 0.01 mol dm^{-3} NaOH.

dioxane-water mixture are summarized in Table 4.

As to silver(I) glycinate and β-alaninate, the solubilities were too low in both solutions to directly measure the enthalpies of solution of the salts. Therefore, silver(I) glycinate (or silver(I) β-alaninate) was dissolved in a solution containing appropriate concentrations of glycine and lithium glycinate (or β-alanine and lithiun β-alaninate) in order to fully convert the species to $[AgL_2]^-$ in the solution. Thus, the measured enthalpy of solution is represented as the sum of the enthalpy of solution of [AgL], ΔH_s°([AgL]), and the enthalpy of reaction, $[AgL]+L^-=[AgL_2]^-$. Since the latter value is known, the ΔH_s°([AgL]) value was evaluated. Although the reliability of the ΔH_s°([AgL]) is low due to a low solublility of the complex in each solution, the value may account for the corresponding one calculated from the related thermodynamic quantities as will be discussed in a later section.

Since the $\Delta H_t^\circ(AgClO_4)$ and ΔH_t°(Naala) values are represented as the sum of the enthalpies of transfer of relevant ions, the $\Delta H_t^\circ(Ag^+)$ and $\Delta H_t^\circ(\beta\text{-ala}^-)$ values were obtained by subtracting the known $\Delta H_t^\circ(ClO_4^-)$ and $\Delta H_t^\circ(Na^+)$ values[9] from the $\Delta H_t^\circ(AgClO_4)$ and ΔH_t°(Naala) values, respectively.

β-Alanine exists as the zwitterion in the aqueous solutions, and thus the difference in the ΔH_s° values in these solutions corresponds to the enthalpy of transfer of the zwitterionic β-alanine.

The thermodynamic quantities of transfer of complex species were then evaluated in a following section.

Thermodynamic Quantities of Transfer of Complexes from Water to the 0.2 Mole Fraction Dioxane-Water Mixture. The Gibbs energies of protonation of β-alaninate ion in water, ΔG_{HL}°(w), and in the mixture, ΔG_{HL}°(mix), are related to the Gibbs energies of transfer of β-alanine zwitterion, ΔG_t°([HL]), proton, $\Delta G_t^\circ(H^+)$, and β-alaninate ion, $\Delta G_t^\circ(L^-)$, from water to the mixture as follows:

$$\Delta G_{HL}^\circ(\text{mix}) - \Delta G_{HL}^\circ(\text{w}) = \Delta G_t^\circ([HL]) - \Delta G_t^\circ(H^+) - \Delta G_t^\circ(L^-). \quad (5)$$

Since all the values except for ΔG_t°([HL]) have been determined, the ΔG_t°([HL]) value was evaluated. Then, the Gibbs energy of transfer of $[H_2L]^+$, $\Delta G_t^\circ([H_2L]^+)$, was successively obtained by using the corresponding relationship similar to that in Eq. 5.

Similarly, the stepwise Gibbs energies of formation of the bis(glycinato)- and bis(β-alaninato)silver(I) complexes in water, ΔG_2°(w), and in the mixture, ΔG_2°(mix), are related to the Gibbs energies of transfer of the related species in Eq. 6:

$$\Delta G_2^\circ(\text{mix}) - \Delta G_2^\circ(\text{w}) = \Delta G_t^\circ([AgL_2]^-) - \Delta G_t^\circ([AgL]) - \Delta G_t^\circ(L^-). \quad (6)$$

Since the ΔG_t°([AgL]) value has been determined by solubility measurements and the $\Delta G_t^\circ(L^-)$, ΔG_2°(w), and ΔG_2°(mix) values were also known as described in a preceding section, the $\Delta G_t^\circ([AgL_2]^-)$ (L^-=gly$^-$ and β-ala$^-$) values were evaluated.

A similar procedure was applicable for evaluation of the enthalpies of transfer of complex species. In the enthalpy relationship corresponding to Eq. 5, all the values except for $\Delta H_t^\circ(H^+)$ in the β-alanine system have been determined, thus, the $\Delta H_t^\circ(H^+)$ value was evaluated to be −22.5 kJ mol^{-1}, which is in good agreement with that (−22.7 kJ mol^{-1}) determined in the glycine system. Since the $\Delta H_t^\circ(H^+)$, ΔH_t°([HL]), $\Delta H_t^\circ(Ag^+)$, and $\Delta H_t^\circ(L^-)$ have been determined, the ΔH_t° values of $[H_2L]^+$ and $[AgL_n]^{(1-n)+}$ (n=1 and 2) were calculated. The results are summarized in Table 5, together with the corresponding entropies of transfer of species calculated from the ΔG_t° and ΔH_t° values.

Solvation Structure around Ionic Species in Dioxane-Water Mixtures. Thermodynamic quantities of transfer of ions from water to a dioxane-water mixture reflect the differences in both ion-solvent (solvation of ion) and solvent-solvent interactions in the solvents. In water, water molecules are hydrogen-bonded with each other in the bulk, and ions introduced from the gas phase to water first destroy the hydrogen-bonding water-water bonds and then are coordinated with the water molecules liberated from the structure of water

Table 5. Thermodynamic Quantities of Transfer, ΔG_t° / kJ mol^{-1}, ΔH_t° / kJ mol^{-1}, and ΔS_t° / J K^{-1} mol^{-1}, of Single Species from Water to the 0.2 Mole Fraction Dioxane-Water Mixture at 25 °C

Species	ΔG_t°	ΔH_t°	ΔS_t°
H^+	1.9	−22.7[a]	−83
gly^-	6.0	28.7[a]	76
β-ala^-	6.0	30.0	81
[Hgly][b]	6.3	1.2[a]	−17
$[H_2gly]^+$	4.1	−26.3[a]	−100
[Hala][b]	7.3	6.8	−2
$[H_2ala]^+$	3.5	−20.8	−82
Ag^+	3.1	−21.9	−84
[Aggly]	6.2	2.4	−13
$[Ag(gly)_2]^-$	10.1	28.6	62
[Agala]	6.6	1.8	−16
$[Ag(ala)_2]^-$	10.3	30.6	68

a) Ref. 9. b) Zwitterion: $^+H_3NCH_2COO^-$ or $^+H_3NCH_2CH_2COO^-$.

in the bulk. Similarly, ions introduced to a dioxane-water mixture may destroy both dioxane-water and water-water bonds. The bonding energies between solvent molecules in a dioxane-water mixture may be different from those in pure water, but the difference is not appreciable in the 0.2 mole fraction dioxane-water mixture because the ΔH_t° value of one mole of water molecules from water to the mixture is not significant (−0.6 kJ mol^{-1}) as compared with the corresponding ΔH_t° values of ions.[9,12] Consequently, it is postulated that thermodynamic quantities of transfer of ions from water to the dioxane-water mixture mainly reflect the change in the ion-solvent interaction in the solvents.

As seen in Table 5, compared to the ΔH_t° and ΔS_t° values of neutral species, the ΔH_t° and ΔS_t° values of cationic species, Ag^+, H^+ and $[H_2L]^+$, are significantly negative, while the ΔH_t° and ΔS_t° values of anionic species, L^- and $[AgL_2]^-$, are remarkably positive.

Negative ΔH_t° values of Ag^+, H^+, and $[H_2L]^+$ from water to the dioxane-water mixture imply that solvation energies of the ions are increased in the mixture compared to those in water. Corresponding negative ΔS_t° values of the cations suggest that solvent molecules solvating the cations are more ordered, i.e., the solvation structure is enhanced, in the dioxane-water mixture than in water. The reverse is the case for anions, L^- and $[AgL_2]^-$, which have positive ΔH_t° and ΔS_t° values. It is expected that solvation energies of the anions are decreased and solvent molecules solvating the anions are less ordered, i.e., the solvation structure is weakened, in the mixture than in water. The enhancement or weakening of solvation structure around ions may occur at the secondary or higher solvation shells because, since both donor and acceptor properties of dioxane are weaker than those of water, metal ions and ligands are expected to be preferentially solvated with water molecules in the primary solvation shell.[9]

The reason why solvation energies of cations are increased and those of anions are decreased by the addition of dioxane to water may be explained by a following consideration:

A water molecule has an oxygen atom as the electron donor (D_w) and two protons as the electron acceptor (A_w). They interact to form hydrogen-bonds in the bulk water and the equilibrium as the following equation may hold:

$$D_w + A_w = D_w\text{-}A_w, \quad (7)$$

where D_w-A_w denotes the formation of a hydrogen-bond between D_w and A_w of water molecules. It should be noted that free D_w or A_w means not only a free water molecule but also a terminal oxygen or hydrogen atom of water within a hydrogen-bonded network chain of water. The equilibrium in Eq. 7 is largely shifted toward the right hand side in pure water at room temperature.

A basic dioxane molecule may act as a donor (D_d) with a comparable donicity with water, because the donor number of dioxane (D_N=14.8) is not largely different from that of water (D_N=18.0).[13] On the other hand, the acceptor ability of dioxane (the acceptor number A_N=10.8) is much smaller than that of water (A_N=54.8).[13] Therefore, when dioxane is introduced in water, a dioxane molecule may interact with water molecules to form hydrogen-bonds through its etherial oxygen atoms as represented by D_d-A_w:

$$D_d + A_w = D_d - A_w \quad (8)$$

Thus, the formation of hydrogen-bonds between dioxane and water molecules will shift the equilibrium in Eq. 7 to result in an increase of the concentration of D_w, while the concentration of A_w decreases with decreasing mole fraction of water in the mixture.

In water-rich dioxane-water mixtures, metal ions and anionic ligands may be preferentially solvated with water molecules. Metal ions thus interact with oxygen donor atoms (D_w) and anionic ligands interact with protons (A_w) of water molecules, and thus, solvated metal ions and anionic ligands are in equilibrium with free D_w and A_w, respectively, of water. In the water-rich 0.2 mole fraction dioxane-water mixture compared to pure water, an increase of the concentration of D_w may therefore lead to an enhanced hydration structure around metal ions, while a decrease of the concentration of A_w may lead to a weakened hydration structure around anions.

In the case of glycine and β-alanine zwitterions in contrast to simple ions, the ΔH_t° value is smaller than the ΔG_t° value, so that the ΔS_t° value is negative. The same trend in the thermodynamic quantities of transfer has been observed for the [AgL] (L^-=gly^- and β-ala^-) complexes in Table 5. Therefore, we propose that [AgL] (L^-=gly^- and β-ala^-) complexes have simi-

lar zwitterionic structures, $^{+}AgNH_2CH_2COO^{-}$ and $^{+}AgNH_2CH_2CH_2COO^{-}$, to those of glycine ($^{+}H_3NCH_2COO^{-}$) and β-alanine ($^{+}H_3NCH_2CH_2COO^{-}$) zwitterions, respectively, both in water and in the dioxane–water mixture examined.

The present work has been financially supported by the Grant-in-Aid for special Project Research No. 60129031 from the Ministry of Education, Science and Calture.

References

1) D. D. Perrin, "Stability Constants of Metal-Ion Complexes: Part B, Organic Ligands," Pergamon Press (1979) and L. G. Sillén and A. E. Martell, "Stability Constants," The Chemical Society, London (1964) and (1971), *Spec. Publ. No.* **17** and *Supplement No.* **1**, *Spec. Publ. No.* **25**.

2) H. Ohtaki, M. Zama, H. Koyama, and S. Ishiguro, *Bull. Chem. Soc. Jpn.*, **53**, 2865 (1980).

3) S. Ishiguro, Y. Oka, and H. Ohtaki, *Bull. Chem. Soc. Jpn.*, **56**, 2426 (1983).

4) S. Ishiguro, T. Pithprecha, and H. Ohtaki, *Bull. Chem. Soc. Jpn.*, **59**, 1487 (1986).

5) S. Ishiguro, Y. Oka, and H. Ohtaki, *Bull. Chem. Soc. Jpn.*, **57**, 391 (1984).

6) H. Ohtaki and Y. Ito, *J. Coord. Chem.*, **3**, 131 (1973).

7) H. Ohtaki and K. Cho, *Bull. Chem. Soc. Jpn.*, **50**, 2674 (1974).

8) S. Ishiguro, K. Yamamoto, and H. Ohtaki, *Anal. Sci.*, **1**, 263 (1985).

9) S. Ishiguro and H. Ohtaki, *Bull. Chem. Soc. Jpn.*, **57**, 2622 (1984).

10) C. B. Acland and H. C. Freeman, *J. Chem. Soc. Dalton Trans.*, **1971**, 1016.

11) J. R. Goates and R. J. Sullivan, *J. Phys. Chem.*, **62**, 188 (1958).

12) S. Ishiguro and H. Ohtaki, *J. Coord. Chem., Sect. B*, in press.

13) V. Gutmann, "The Donor-Acceptor Approach to Molecular Interactions," Prenum, New York and London (1978).

 © 1986 The Chemical Society of Japan Bull. Chem. Soc. Jpn., 59, 2607—2610 (1986)

Synthesis of Kaolinite-Lactam Intercalation Compounds

Yoshiyuki SUGAHARA, Shuichi KITANO, Shigeo SATOKAWA, Kazuyuki KURODA, and Chuzo KATO*
Department of Applied Chemistry, School of Science and Engineering, Waseda University,
Ohkubo, Shinjuku-ku, Tokyo 160
(Received February 21, 1986)

Intercalation compounds of kaolinite with 2-pyrrolidone and 2-piperidone have been prepared for the first time by displacing other intercalates. 2-Pyrrolidone expanded the lattice of kaolinite to 11.9 Å, while d_{001} of 12.7 Å was observed with the kaolinite-2-piperidone intercalation compound. Their IR spectra indicated the formation of a hydrogen bond between the C=O of the lactams and the OH of kaolinite. Nevertheless, their interactions were different between these two intercalation compounds. By a comparison of their behaviors, it has been concluded that the kaolinite-2-pyrrolidone intercalation compound is thermally more stable than the kaolinite-2-piperidone intercalation compound.

It is well-known that some clay minerals with a layer structure form intercalation compounds. Kaolinite can form intercalation compounds only with a limited number of polar molecules, whereas smectite reacts with a variety of molecules. Though some of them can react with kaolinite directly, others form intercalation compounds only in the presence of an "entraining agent" or by displacement of other intercalates.[1]

Intercalated polar molecules form hydrogen bonds with hydroxyl groups of kaolinite on the surface of the sheet. The hydroxyl groups of kaolinite show four sharp IR absorption bands at approximately 3690, 3670, 3650, and 3620 cm^{-1}. With the formation of a hydrogen bond, only the absorption bands at 3690, 3670, and 3650 cm^{-1} are perturbed, since these bands are ascribed to the vibration of the hydroxyls on the surface of the sheet and the 3620 cm^{-1} band is assigned to the inner-sheet hydroxyl.[1]

Amides are typical polar organic molecules, and some of them can be intercalated into the interlayer space of kaolinite. Many investigations were reported on the intercalation compounds with formamide (FA),[2-8] *N*-methylformamide (NMF),[4,5,8-10] *N*,*N*-dimethylformamide (DMF),[4,5,8] acetamide,[5,8,11] *N*-methylacetamide (NMA),[5,8,11] and *N*,*N*-dimethylacetamide (DMA).[5,8,11]

In their IR spectra, Ledoux and White[3] and Cruz et al.[4] observed the intensity decrease of the bands at 3690, 3670, and 3650 cm^{-1} for the hydroxyls in the intercalation compounds with FA, NMF, and DMF, while Oljenik et al.[6,11] reported that all of six amides perturbed a pair of hydroxyl bands; those at 3690 and 3670 cm^{-1} or those at 3690 and 3650 cm^{-1}. In other regions, the results showed a similar tendency; that is, an amide I band was observed at the same or a slightly higher wavenumber than liquid, and the NH stretching band was shifted to a higher wavenumber.

Lactams have NHCO group in their structures, so they can be regarded as "cyclic amides." Therefore, it is expected that an investigation of kaolinite-lactam intercalation compounds contributes to a series of studies on intercalation chemistry between kaolinite and organic molecules. In this study, 2-pyrrolidone and 2-piperidone were selected as lactams to synthesize the kaolinite-lactam intercalation compounds by a direct reaction or displacement method.

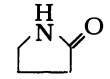
2-pyrrolidone

2-piperidone

Experimental

The kaolinite used was the API standard clay mineral No. 9 (Nesa Alta, New Mexico). The X-ray diffraction (XRD) pattern of kaolinite showed no obvious peaks due to impurities.

(1) **Direct Reaction.** A lactam was added to kaolinite at a ratio of 20 ml/1 g kaolinite. The suspension was then stirred for 72 h. The reaction was performed at two different temperatures to study the effect of the increase in the reaction temperature. One was just above the melting points of the lactams, that is, 30 °C for 2-pyrrolidone and 50 °C for 2-piperidone; the other temperature was 70 °C.

(2) **Displacement Method.** Intercalation compounds with FA, NMF, or dimethyl sulfoxide (DMSO) were used as starting materials. The lactam was added to a preformed complex with the same ratio as that in the direct reaction. The suspension was stirred for 10 min, and centrifuged. Then, the lactam was added again with the same ratio and the suspension was stirred between 0 and 96 h. The reaction temperatures were varied from 30 to 90 °C for 2-pyrrolidone and from 50 to 90 °C for 2-piperidone.

Products were analyzed by XRD (Shimadzu VD-11). The yield was calculated approximately from the proportion of the (001) peak heights of the intercalation compound, the preformed complex and the nonexpanded kaolinite.[1] The IR spectra of the products were also measured with a Shimadzu IR-435 (wavenumbers were calibrated using indene and polystyrene) using the KBr method (ca. 0.5%) after drying the products at 110 °C. Also, the IR spectra of the lactams were measured in CCl_4 (0.05 mol dm^{-3}).

Results and Discussion

In syntheses of the intercalation compounds with a direct reaction, no peaks due to intercalation compounds were observed in their XRD patterns. This indicated that lactams could not form intercalation

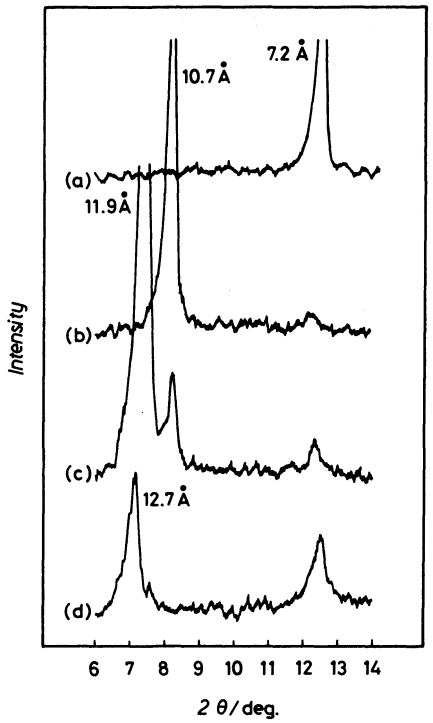

Fig. 1. X-ray diffraction patterns of (a) kaolinite, (b) kaolinite-NMF complex, (c) kaolinite-NMF complex treated with 2-pyrrolidone for 72 h, and (d) kaolinite-NMF complex treated with 2-piperidone for 72 h.

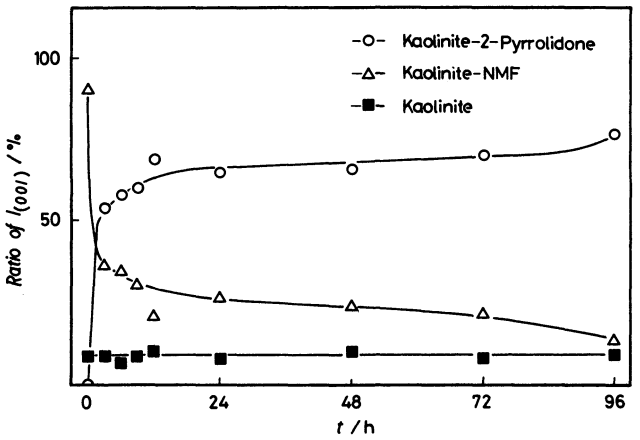

Fig. 2. The variation of the composition of the products with reaction time (t) at 30°C (kaolinite-NMF complex reacted with 2-pyrrolidone).

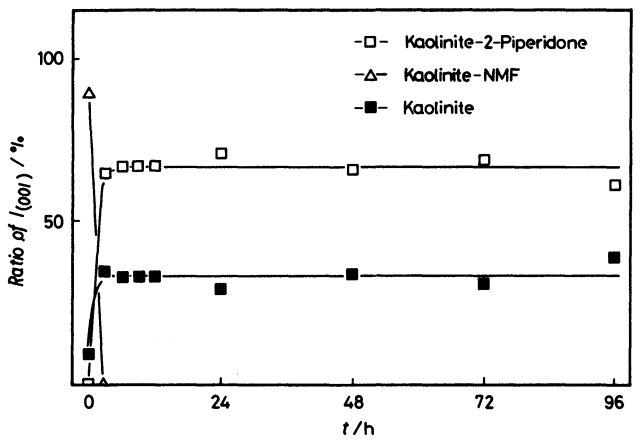

Fig. 3. The variation of the composition of the products with reaction time (t) at 50°C (kaolinite-NMF complex reacted with 2-piperidone).

compounds under these conditions. However, the possibility of intercalation with a direct reaction could not be excluded, since a relatively large molecule like DMF was intercalated directly after a long reaction period.[5]

On the other hand, intercalation compounds with 2-pyrrolidone and 2-piperidone were easily formed by a displacement reaction. The reaction temperatures were 30°C for 2-pyrrolidone and 50°C for 2-piperidone, and the reaction time was 72 h. Figure 1 shows the XRD patterns of products prepared from a kaolinite-NMF complex. In the case of 2-pyrrolidone, a new peak due to a (001) diffraction line appeared at d=11.9 Å, whereas 2-piperidone expanded the lattice of kaolinite to 12.7 Å.

It was hard to assume the orientation of lactams from their basal spacings since the conformations of their monomeric species could not be determined; 2-pyrrolidone can not be in a planner conformation, and 2-piperidone can show a few structures without strain.[12] Pyridine *N*-oxide had a six-membered ring in its structure and could be intercalated into a kaolinite lattice with a basal spacing of 12.5 Å.[5] Its orientation was assumed to be perpendicular to the plane of kaolinite. Therefore, the similar basal spacing of a kaolinite-2-piperidone intercalation compound (12.9 Å) might imply the possibility of a perpendicular orientation of lactams in the interlayer space of kaolinite. However, further work, such as neutron diffraction, is needed for a precise discussion.

Figures 2 and 3 reveal the variation of the approximate composition of the products with the reaction time. In a reaction with 2-pyrrolidone, the yield of the kaolinite-2-pyrrolidone intercalation compound was gradually augmented with an increase in the reaction time. A corresponding decrease in that of the kaolinite-NMF complex was observed during the reaction. The ratio of nonexpanded kaolinite was the same, indicating no collapse from both the preformed complex and the kaolinite-2-pyrrolidone intercalation compound to kaolinite during the reaction.

In the case of 2-piperidone, an increase in the reaction rate was observed; the X-ray diffraction line due to the kaolinite-NMF complex disappeared within 3 h and the yield of the kaolinite-2-piperidone intercalation compound did not change after 3 h. This increase of the reaction rate was ascribed to a high reaction temperature of 50°C. The ratio of the nonexpanded kaolinite increased at the beginning of the reaction.

Table 1. Effect of Reaction Temperature on the Yield of the Kaolinite-Lactam Intercalation Compounds[a)]

Lactam	Reaction Temperature			
	30°C	50°C	70°C	90°C
2-Pyrrolidone	70%	90%	93%	92%
2-Piperidone		69%	62%	30%

a) Reaction time was 72 h, and starting complex was kaolinite-NMF complex.

Since the composition was constant after 3 h, the kaolinite-2-piperidone intercalation compound was thermally stable at 50°C. Therefore, this indicates that the NMF complex partly collapsed to kaolinite during the reaction.

The effect of the reaction temperature is given in Table 1. The yield of the kaolinite-2-pyrrolidone intercalation compound increased when the reaction temperature was increased from 30 to 50°C. However, similar yields were obtained above 50°C. Since the yield of the kaolinite-NMF complex was about 90%, the kaolinite-NMF complex was completely converted to the kaolinite-2-pyrrolidone intercalation compound above 50°C during a reaction for 72 h.

In the case of 2-piperidone, yields of around 65% were obtained at 50 and 70°C. The yield was 30% at 90°C, while no differences were observed in the temperature range from 50 to 90°C with the kaolinite-2-pyrrolidone intercalation compound. A decrease in the yield at 90°C implied that the kaolinite-2-piperidone intercalation compound was thermally less stable than the kaolinite-2-pyrrolidone intercalation compound.

In addition, preparations from various preformed complexes were attempted. 2-pyrrolidone could form the intercalation compound from all of the starting complexes at 30°C. However, the formation of the kaolinite-2-piperidone intercalation compound was observed only from the FA and NMF complexes, in spite of a reaction temperature of 50°C; the DMSO complex was not converted to the intercalation compound and did not collapse to kaolinite. This fact suggested that the kaolinite-DMSO complex was much more stable than the kaolinite-2-piperidone intercalation compound at 50°C.

For measuring the IR spectra, the excess lactams adsorbed on the external surface of the particles must be removed. It is well known that intercalation compounds of kaolinite are generally unstable against washing. Therefore, the removal of the excess lactams by evaporation seemed to be suitable. Thus, the effect of the drying time on the yields of the kaolinite-lactam intercalation compounds at 110°C was initially investigated to clarify the thermal behavior of the compounds.

Figure 4 shows the results of drying the intercalation compounds at 110°C. The kaolinite-2-pyrrolidone intercalation compound used was prepared at 70°C, while the sample prepared at 50°C was used for the

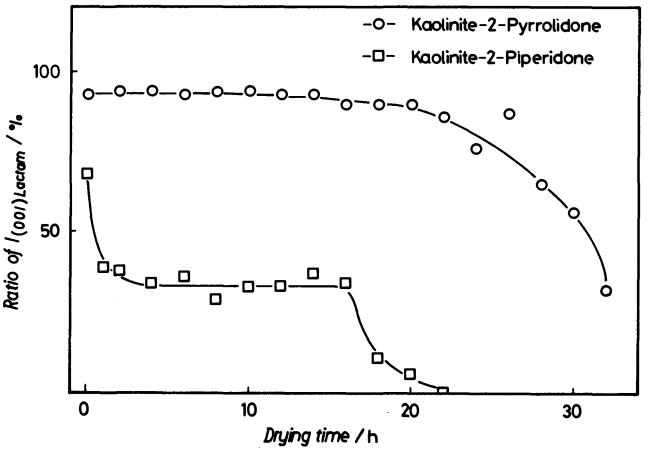

Fig. 4. The variation of the yield of the kaolinite-lactam intercalation compounds with drying time at 110°C.

kaolinite-2-piperidone intercalation compound. In the case of the kaolinite-2-pyrrolidone intercalation compound, the initial yield was retained. After 20 h, the yield of the compound began to decrease gradually.

On the other hand, the kaolinite-2-piperidone intercalation compound showed a different behavior; the yield decreased to about 30% within 1 h. Then, the compound showed the same yield for 15 h. After 18 h, the compound began to collapse again; the X-ray diffraction line of the compound disappeared after 22 h.

The difference in the initial period suggested that the kaolinite-2-piperidone intercalation compound contained at least two different kinds of arrangements of 2-piperidone in the interlayer space; 2-piperidone was present in different ways with the same d_{001} value. Also, weakly bonded 2-piperidone was unstable at a higher temperature and was deintercalated. This assumption was supported by the fact that the product prepared at 90°C showed the similar yield of 30%.

In both intercalation compounds, the products changed to a dried state during the periods, with a plateau as shown in Fig. 4. It seems that most of the lactams adsorbed on the external surface vaporize before those in interlayer spaces were deintercalated. Thus, the samples just after the plateau periods were used for IR measurements; the kaolinite-2-pyrrolidone intercalation compound was dried for 26 h (yield= 87%) and the kaolinite-2-piperidone intercalation compound was dried for 16 h (yield=34%).

Figure 5 shows the IR spectra of the products. In the case of the kaolinite-2-pyrrolidone intercalation compound (Fig. 5-c), amide I bands were observed at 1698 and 1666 cm^{-1}. The position of the 1666 cm^{-1} band was at a lower wavenumber than that of 2-pyrrolidone (Fig. 5-b). This indicated that a part of the C=O groups formed hydrogen bonds. Since the other band showed similar wavenumbers to that of 2-pyrrolidone monomer, this band was assigned to the C=O

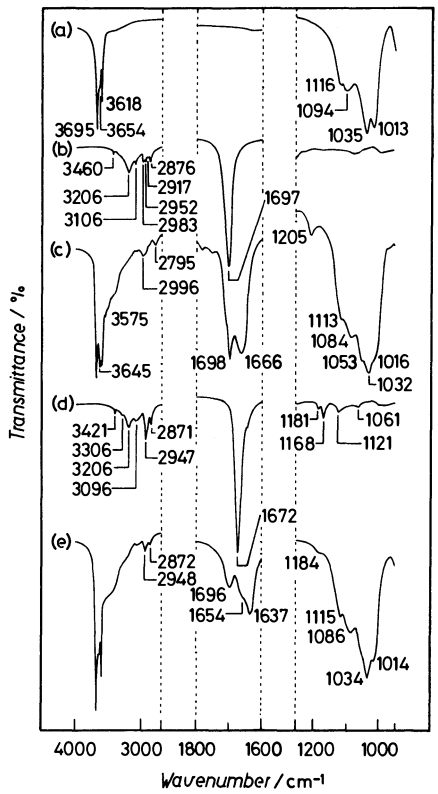

Fig. 5. IR spectra of (a) kaolinite, (b) 2-pyrrolidone (in CCl_4), (c) kaolinite-2-pyrrolidone intercalation compound dried for 26 h, (d) 2-piperidone (in CCl_4), and (e) kaolinite-2-piperidone intercalation compound dried for 16 h.

group having no hydrogen bonds with OH groups of kaolinite. In the OH region, new bands were observed at 3645 and 3575 cm^{-1}; these were ascribed to the shifted OH groups involved in the hydrogen bond. Also, a corresponding decrease of the original hydroxyl bands of kaolinite was observed; the 3695 cm^{-1} band was perturbed by 2-pyrrolidone (Fig. 5-a, c).

In terms of an Si–O stretching vibration, the spectrum (Fig. 5-c) showed a different profile from that of nonexpanded kaolinite; an intensity decrease of the 1013 cm^{-1} band and some additional shoulder bands (at 1084 and 1053 cm^{-1}) were observed. This suggested the presence of an interaction between 2-pyrrolidone and the SiO_2 surface of kaolinite.

For a measurement of the kaolinite–2-piperidone intercalation compound, a sample with a relatively lower yield (34%) was used. It should be noted that the weakly bonded 2-piperidone which was present before drying had already been deintercalated from the sample and the spectrum must have been different from that of a sample with the higher yield before drying.

The IR spectrum of a kaolinite–2-piperidone intercalation compound differed from that of a kaolinite–2-pyrrolidone intercalation compound (Fig. 5-e). The amide I band became more complicated; they split into three bands, two of which were shifted to lower frequencies than that of 2-piperidone in CCl_4 (Fig. 5-d). This implied the presence of different kinds of hydrogen bonds in the intercalation compound. In the OH region, no bands due to hydrogen-bonded OH were observed. Also, no original OH bands were clearly perturbed. This was ascribed to the low yield of the compound.

The Si–O stretching mode was slightly different from that of the kaolinite–2-pyrrolidone intercalation compound; a new band at about 1050 cm^{-1} was not clearly observed. This implied that the effect of intercalation of 2-piperidone on the Si–O stretching was similar to that of 2-pyrrolidone.

Though some similarities were observed in their IR spectra, the profiles of the bands due to C=O stretching, the yields of the compounds and their thermal stabilities were quite different between these two intercalation compounds. These facts suggest that structural differences in the lactams considerably influence the hydrogen bonds. Between two lactams, 2-pyrrolidone seems more preferable for forming an intercalation compound.

This work was supported by the Grant-in-Aid for Special Project Research on the Properties of Molecular Assemblies (No. 58218033, 60104004) from the Ministry of Education, Science and Culture.

References

1) B. K. G. Theng, "The Chemistry of Clay-Organic Reactions," Adam Hilger, London (1974), p. 243.
2) A. Weiss, W. Thielepare, G. Gornig, W. Ritter, and H. Schafer, *Proc. Inter. Clay Conf., Stockholm*, **1**, 287 (1963).
3) R. L. Ledoux and J. L. White, *J. Colloid Interface Sci.*, **21**, 127 (1966).
4) M. Cruz, A. Laycock, and J. L. White, *Proc. Inter. Clay Conf., Tokyo*, **1**, 775 (1969).
5) S. Olejnik, A. M. Posner, and J. P. Quirk, *Clay Minerals*, **8**, 421 (1970).
6) S. Olejnik, A. M. Posner, and J. P. Quirk, *Clays Clay Miner.*, **19**, 83 (1971).
7) J. M. Adams, P. I. Ried, J. M. Thomas, and M. J. Walters, *Clays Clay Miner.*, **24**, 267 (1976).
8) J.M. Adams, *Clays Clay Miner.*, **26**, 291 (1978).
9) A. Weiss, W. Thielepape, and H. Ohth, *Proc. Inter. Clay Conf., Jerusalem*, **1**, 277 (1966).
10) J. M. Adams, *Clays Clay Miner.*, **26**, 169 (1978).
11) S. Olejnik, A. M. Posner, and J. P. Quirk, *J, Colloid Interface Sci.*, **37**, 536 (1971).
12) H. E. Hallam and C. M. Jones, *J. Mol. Struc.*, **1**, 413 (1967-68).

Adsorption of Phosphorus Oxoacid on Hydrous Titanium(IV) Oxide in an Aqueous Solution

Satoshi FUJII,* Yosohiro SUGIE, and Chiaki SAKAMOTO
Department of Applied Chemistry, Himeji Institute of Technology, Shosha, Himeji 671-22
(Received March 15, 1986)

The adsorption behavior of phosphorus oxoacid, such as phosphinate, phosphonate, and phosphate, on hydrous titanium(IV) oxide in an aqueous solution was studied in detail. Hydrous titanium(IV) oxide has a pronounced activity for the adsorption of phosphonate and phosphate ions. However, phosphinate ion is little adsorbed on hydrous titanium(IV) oxide. The pH of aqueous solution remarkably affects the adsorption. Amounts of adsorbed phosphonate or phosphate ion from solutions of 500 mg l^{-1} concentration are about 0.5 mmol g^{-1} near pH 2. The Langmuir equation, applicable to the adsorption of phosphonate ion, has evaluated the maximum adsorption as being about 0.9 and 0.3 mmol g^{-1} at pHs 2 and 7, respectively. The heat of adsorption of phosphonate is −5.9 kJ mol^{-1} at pH 2. The adsorptive activity of hydrous titanium(IV) oxide for phosphonate is suppressed by coexisting ions, such as phosphate and anionic nickel(II) complexes.

In recent years, the industrial use of electroless plating has expanded rapidly. Literature data for conventional waste water treatment methods and their applicability to spent electroless nickel solution are reviewed.[1] However, most of these treatment methods are related to uptake of Ni(II). Phosphinates have been extensively used as reducing agents in the electroless plating of nickel and cobalt. During the normal plating bath operation, the concentration of phosphonate ion increases with the number of wafers plated. Nickel phosphonate has a low solubility and can precipitate under the typical bath operating conditions in solution, and the insoluble salt provides nucleation sites for spontaneous bath decomposition.[2] A commercial nickel plating bath contains nickel ion-complexing reagents, such as citrate, which serve to delay the onset of precipitation and bath decomposition. Removal of phosphonate ion from the plating solution is required for recycling use and waste water treatment on the solution.

Titanium(IV) oxide and its hydrate have been found to be excellent adsorbents for uranium in sea water[3] as well as for nickel and cobalt in aqueous citrate solution.[4] However, no studies dealing with the adsorption of phosphonate by hydrous titanium(IV) oxide have been reported.

In this paper, we report the activity of hydrous titanium(IV) oxide for the adsorption of phosphonate and other phosphorus oxoacid in aqueous solution.

Experimental

Preparation of Hydrous Titanium(IV) Oxide. Hydrous titanium(IV) oxide was prepared by the hydrolysis of titanium tetraisopropoxide at room temperature. The precipitate was filtered, washed several times with water, and dried in air at 60 °C for 20 h. The dried sample was crushed and sieved, a portion of 100 mesh pass being used in the experiment. The water content of the dried sample was determined by measuring the ignition loss at 800 °C and found to be about 18%, which corresponds to that of $TiO(OH)_2$.

The alumina and activated carbon used were commercial products of the Woelm Co. (N, Akt.I) and Takeda Yakuhin Kogyo K.K. (wH2c).

Table 1. Adsorption Activities of Adsorbents for Phosphorus Oxoacid

Adsorbate[b]	Degree of adsorption/mmol g^{-1} (%)[a]		
	Alumina	Hydrous titanium (IV) oxide	Activated carbon
Phosphinate ($H_2PO_2^-$)	0.01 (0.5)	0 (0)	0.01 (0.5)
Phosphonate ($H_2PO_3^-$)	0.55 (45)	0.79 (64)	0.26 (21)
Phosphate ($H_2PO_4^-$)	0.34 (33)	0.44 (43)	0.02 (1.6)

a) Adsorption temperature, 25 °C; time, 20 h; initial concentration of phosphorus oxoacid, 1000 mg l^{-1}. b) pH of solution: 6.60 ($H_2PO_2^-$), 2.21 ($H_2PO_3^-$), 5.00 ($H_2PO_4^-$).

Method of Adsorption. In the phosphorus oxoacid adsorption experiment, 1 g hydrous titanium(IV) oxide was put into 100 ml of a solution containing 50—1000 mg l^{-1} of phosphorus oxoacid, and then the mixture was continuously shaken for 8 h at 25 °C with a shaker. After adsorption equilibrium was attained, the solution was filtered and the phosphorus oxoacid concentration was measured. The pH of the solution was adjusted in the range 2—11 with HCl or NaOH solution.

Analysis. The analysis of phosphorus oxoacid and anions was carried out by ion-chromatography using a conductometric detector Shodex IC CD-2 (Showa Denko K.K.). Ni(II) was determined by the EDTA titration method.

Results and Discussion

Comparison of Adsorptive Activities of Adsorbents for Phosphorus Oxoacid. The results obtained for the adsorption of phosphorus oxoacid are listed in Table 1. Adsorptive activities of other adsorbents, such as alumina and activated carbon, were also examined, but their activities were considerably lower than that of hydrous titanium(IV) oxide.

As shown in Table 1, hydrous titanium(IV) oxide exhibits the highest activity for the adsorption of phosphonate and phosphate. Phosphinate is little adsorbed on the adsorbents.

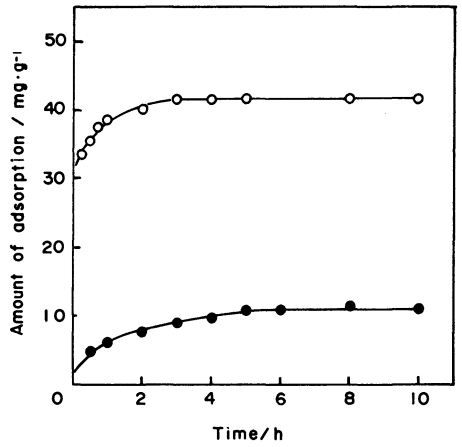

Fig. 1. Adsorbed amounts of phosphonate as a function of adsorption time.
Temperature, 25°C; phosphonate, 500 mg l^{-1}; Initial pH 2 (○), pH 8 (●).

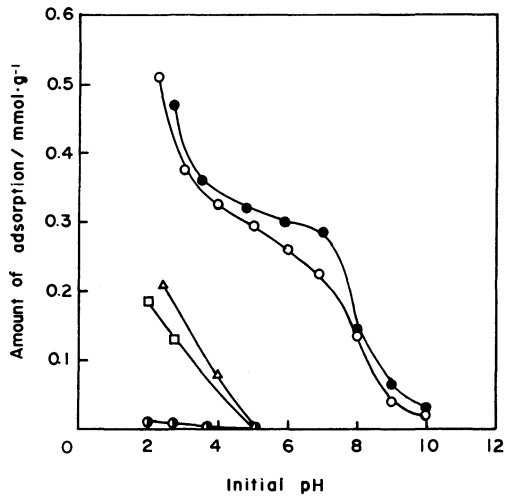

Fig. 2. Effect of pH on phosphorus oxoacid, Cl^- and SO_4^{2-} adsorption.
Adsorption time, 8 h; temperature, 25°C; phosphorus oxoacid, 500 mg l^{-1}; Cl^- and SO_4^{2-} 250 mg l^{-1}, ○: Phosphonate, ○: phosphinate, ●: phosphate, □: Cl^-, △: SO_4^{2-}.

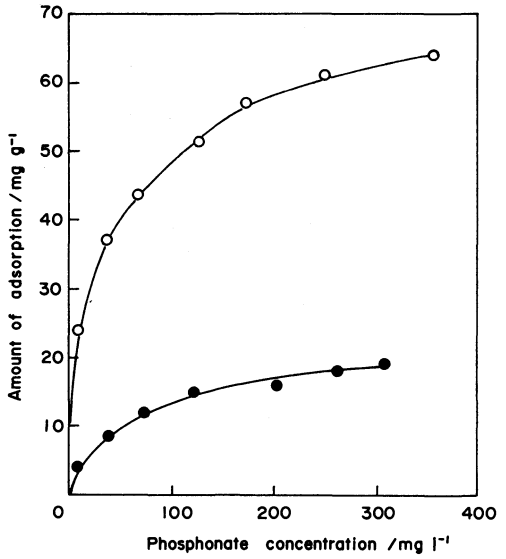

Fig. 3. Adsorption isotherm of phosphonate.
Adsorption time, 8 h; temperature, 25°C; phosphonate 500 mg l^{-1}; Initial pH 2 (○), pH 7 (●).

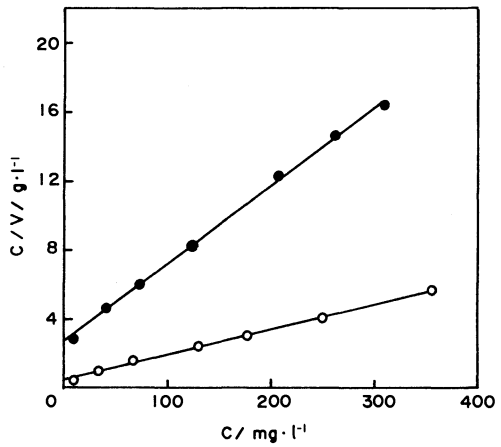

Fig. 4. Application of Langmuir equation to the adsorption shown in Fig. 3.
Initial pH 2 (○), pH 7 (●).
C is the concentration of phosphonate in solution.
V is the concentration of adsorbed phosphonate in the adsorbent at equilibrium.

Adsorption Equilibrium. The phosphonate adsorption as a function of adsorption time with hydrous titanium(IV) oxide at different pHs is shown in Fig. 1. Considerable change in the pH of solution occurs during the course of adsorption. The rate of phosphonate adsorption is faster at low pH than at high pH. Adsorption equilibrium is attained within 5 h at pH 8. The adsorption time of 8 h was chosen for subsequent experiments.

Effect of pH on Adsorption. The effect of pH on the phosphorus oxoacid adsorption by hydrous titanium(IV) oxide is shown in Fig. 2. Phosphinate is little adsorbed on hydrous titanium(IV) oxide. The adsorption of phosphonate and phosphate is much more efficient than that of Cl^- and SO_4^{2-} and remarkably dependent on the pH of solution; the amounts of adsorbed phosphonate and phosphate are both about 0.5 mmol/g-adsorbent near pH 2, decreasing with rise in pH. Hydrous titanium(IV) oxide possesses the property of amphoteric ion exchange.[5] The isoelectric point of hydrous titanium(IV) oxide, lies around pH 6[6] and it does not adsorb at higher pH than that; considerable amounts of phosphonate and phosphate are adsorbed even at the isoelectric point. The distribution of ionic species in aqueous solution was calculated for phosphonate and phosphate at various pH values.[7] With phosphonate, $H_2PO_3^-$ and HPO_3^{2-} are predominant species at pHs 5.5 and 8, respectively. With phosphate, $H_2PO_4^-$ and HPO_4^{2-} are predominant species at pHs 4.5 and 10, respectively.

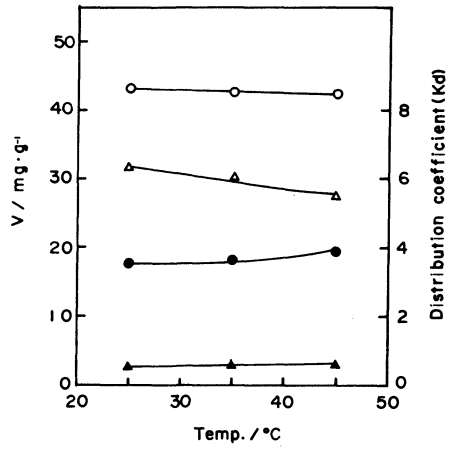

Fig. 5. Effect of temperature on phosphonate adsorption.
Adsorption time, 8h; phosphonate, 500 mg l^{-1}; Initial pH 2 (○, △), pH 7 (●, ▲).
Phosphonate adsorption (○, ●), K_d (△, ▲). V is the same as shown in Fig. 4.

The adsorption behavior of phosphonate is significantly close to that of phosphate.

Adsorption Isotherms. Figure 3 shows that adsorption of phosphonate in pHs 2 and 7. The main species of phosphonate are $H_2PO_3^-$ at pH 2 and HPO_3^{2-} at pH 7. As shown in Fig. 4, a linear relation holds between C (the concentration of phosphonate in solution) and C/V (V: the concentration of adsorbed phosphonate in the adsorption in equilibrium). This indicates that the Langmuir adsorption equation is applicable at both pHs 2 and 7. The monomolecular adsorption of phosphonate or maxmum adsorption, V_m, was calculated to be 0.88 (at pH 2) and 0.28 mmol g^{-1} (at pH 7) from the reciprocal of the slope $\Delta C/\Delta(C/V)$.

Effect of Temperature. The effect of temperature on the phosphonate adsorption by hydrous titanium(IV) oxide is shown in Fig. 5. The amount of phosphonate adsorbed is little changed with the adsorption temperature at pHs 2 and 7 in the solution. A linear relation was obtained between $1/T$ and the logarithm of the distribution coefficient (log K_d, $K_d=V/C$). The enthalpy of adsorption (ΔH_a) was calculated to be −5.9 (pH 2) and 6.8 kJ mol^{-1} (pH 7) by using the van't Hoff equation. The former value suggests that the phosphonate adsorption at pH 2 is due either to physical adsorption or ion exchange reaction. The latter value suggests that the adsorption at pH 7 does not relate to ion exchange reaction. The enthalpy change of ion exchange reaction is said to be −8.4—−12.6 kJ mol^{-1},[8] and physical adsorption is ordinaily exothermic. Anyhow, the interaction of phosphonate with hydrous titanium(IV) oxide surface is rather weak.

Effects of Coexisting Ions. Various ions such as chloride, sulfate, phosphinate, phosphate, borate, citrate, and nickel(II) citrate complexes coexist in an electroless plating solution.[9] In order to investigate

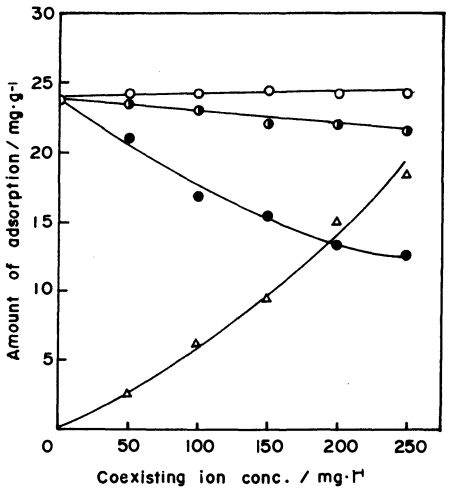

Fig. 6. Effects of coexisting ions on phosphonate adsorption.
Adsorption time, 8h; temperature, 25 °C; phosphonate, 250 mg l^{-1}; Initial pH 3. Phosphate adsorption △.
Coexisting ion ○: Cl^-, BO_3^{3-}, phosphinate, ◑: SO_4^{2-}, citrate, ●: phosphate.

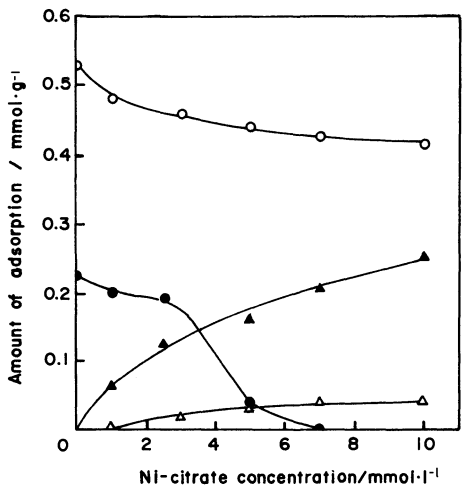

Fig. 7. Effect of nickel(II) citrate on phosphonate adsorption.
Adsorption time, 8h; temperature, 25 °C; phosphonate, 500 mg l^{-1}; Ni(II)/citrate=1(molar ratio).
Initial pH 2 (○, △), pH 7 (●, ▲).
Phosphonate adsorption (○, ●), Ni(II) adsorption (△, ▲).

the effect of coexisting ions, the phosphonate adsorption was measured for a solution containing 250 mg l^{-1} phosphonate ion and 0—250 mg l^{-1} coexisting foreign ions at pH 3. The results are shown in Fig. 6. The phosphonate adsorption is little affected by the coexisting ions except for phosphate. This fact suggests that phosphonate and phosphate are adsorbed on the same adsorption sites. Thus, it appears that the adsorption of phosphonate would proceeded in competition with phosphate. The phosphonate adsorption was measured with a solution containing 500 mg l^{-1} phosphonate and 0—10 mmol l^{-1} of nickel(II)

citrate (molar ratio of Ni/citrate=1) at pHs 2 and 7. The results are shown in Fig. 7. At pH 2, the phosphonate adsorption decreases slightly with increase in the nickel(II) citrate species in aqueous solution indicates that the predominant species at pH 2 is $[Ni(H_2citH)]^0$. At pH 7, both $[Ni(HcitH)]^-$ and $[Ni(citH)]^{2-}$ exist. It is found from Fig. 7 that the phosphonate adsorption decreases slightly with increase in amount of nickel(II) citrate is acidic solution, whereas it decreases remarkably in neutral solution. It may, therefore, be considerd that phosphonate and nickel(II) citrate compete for the same adsorption sites.

In conclusion, if hydrous titanium(IV) oxide is to be used for the removal of phosphonate in electroless plating solution, the process should be operated in acidic solution, and also, the oxidation of phosphinate to phosphonate or phosphate is necessary for removing residual phosphinate is spent electroless plating solution.

References

1) K. Parker, *Plating Surface Fin.*, **70**, 52 (1983).
2) S. Ishibashi, "Mudenkai Mekki," Asakura-shoten, Tokyo (1971), p. 28.
3) H. Yamashita, Y. Ozawa, F. Nakajima, and T. Murata, *Nippon Kagaku Kaishi*, **1978**, 1057.
4) S. Fujii, H. Kakuno, Y. Sugie, and C. Sakamoto, *Nippon Kagaku Kaishi*, **1985**, 1635.
5) M. Abe and T. Ito, *Nippon Kagaku Zasshi*, **86**, 1259 (1965).
6) J.P. Bonsack, *J. Colloid Interface Sci.*, **44**, 430 (1973).
7) N. Tanaka and H. Sugi, "Sakukeisei Hannō," ed by A. Rinqbom, Sangyo Tosho, Tokyo (1966), p. 268.
8) F. Heifferich, "Ion Exchange," McGraw-Hill, New York (1962), p. 166.
9) Ref. 2, p. 16.

Magnetism, Electronic State, and Local Structure of Iron-Containing Organometallic Polymers

Tadashi SUGANO, Masaharu NOMURA,† Kunio AWAGA, POH Lee Kieng,††
Toshiaki OHTA,† and Minoru KINOSHITA*
The Institute for Solid State Physics, The University of Tokyo, Roppongi, Minato-ku, Tokyo 106
†Photon Factory, National Laboratory for High Energy Physics, Ooho-machi, Tsukuba, Ibaraki 305
(Received March 10, 1986)

Schiff-base polymers were synthesized by the reaction of 2,6-pyridinedicarbaldehyde with 1,4-butane-, 1,6-hexane-, 1,8-octane-, and 1,12-dodecanediamine. Each of the polymers, when combined with iron(II) sulfate or iron(II) chloride, exhibited anomalously large magnetization and a nonlinear relation of the magnetization curve at room temperature. These iron-containing solids were found to be amorphous and, hence, the local structures around the iron atoms in the compounds were determined by the measurements of Fe K-edge X-ray absorption spectra. It was found that the iron atoms were each surrounded by six nitrogen atoms with the almost equivalent distance of 1.93±0.02Å. This was consistent with a possible geometry in which the tridentate ligand moieties of the polymers were coordinated with the iron atoms in a ratio 2 : 1. It was also found from the results of X-ray photoelectron and Mössbauer spectroscopies that the iron atoms in the solid obtained from the reaction between poly(2,6-pyridinediylmethylidynenitrilohexamethylenenitrilomethylidyne) and iron(II) sulfate were in two valence states consisted of the high spin (S=5/2) irons(III) which were responsible for the observed magnetism and the low-spin (S=0) irons(II) which gave no contribution to the magnetism.

It is of great interest to study the magnetism due to the transition-metal ions coordinated with organic ligands, because there are several organometallic compounds exhibiting ferromagnetic behavior: Bis(diethyldithiocarbamato)iron(III) chloride, T_C=4.5 K;[1,2] bis(diethyldithiocarbamato)iron(III) bromide, T_C= 1.52 K;[3] and manganese(II) phthalocyanine, T_C= 8.6 K,[4,5] where T_C is the Curie temperature. Since the magnetic interactions among metal ions are expected to be controlled by varying the structure of ligands, the length of the repeating unit of polymer chains and the kind of metal ions, there may be a possibility of finding ferromagnetic organometallic compounds with a higher T_C.

Previously, we have shown that, when the organic polymer poly(2,6-pyridinediylmethylidynenitrilohexamethylenenitrilomethylidyne) $(C_{13}H_{17}N_3)_n$ is combined with iron(II) sulfate, a solid (abbreviated as **6**-SO_4) of which the chemical composition is approximately $[Fe(C_{13}H_{17}N_3)_2]SO_4 \cdot 6H_2O$ is obtained.[6,7] This solid shows an anomalously large magnetization over the whole temperature range from 1.9 to 300 K and S-shaped magnetization curves below about 50 K.[7] In order to obtain a further insight into this magnetism, we have synthesized new compounds in which the structure of the ligand moiety and the length of the methylene chain of the polymer are varied systematically from **6**-SO_4. In addition, since all the iron-containing solids obtained have been found to be amorphous, we have measured X-ray absorption spectra in order to determine the local structure around the iron atoms in the solids. Furthermore, to reveal the valence and spin states of the iron ions in the solids, we have examined the X-ray photoelectron and ^{57}Fe Mössbauer spectra of **6**-SO_4 and found that the iron ions in this solid contribute only partially to the magnetism.

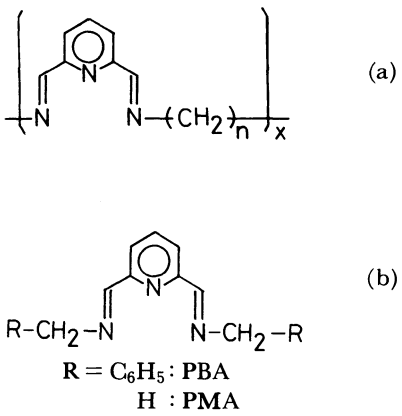

Fig. 1. Molecular structure of polymeric (a) and monomeric (b) ligands.

The present paper describes the applied field dependence of the magnetization of the iron-containing solids, the bond length and the coordination number around the iron atoms as well as their valences and spin states. The magnetic behavior of the solids will be discussed in relation to the structural and electronic properties derived from the results of X-ray absorption, X-ray photoelectron, and ^{57}Fe Mössbauer spectroscopies.

Experimental

The polymers shown in Fig. 1(a) were synthesized by the reaction of 2,6-pyridinedicarbaldehyde with 1,4-butane-, 1,6-hexane-, 1,8-octane-, and 1,12-dodecanediamine as described in the literature[6] and are abbreviated, respectively, as **4**, **6**, **8**, and **12**, according to the number of methylene groups, n. The obtained polymers were white powders and had a tendency to become fibrous upon increasing the length, n, of the methylene chain. When the polymers were treated with iron(II) sulfate or iron(II) chloride in an aqueous solution

††On leave of absence from Department of Physics, University of Agriculture Malaysia, Serdang, Salangor, Malaysia.

under a nitrogen stream, dark-violet solids were obtained. The solids were filtered off and dried over diphosphorus pentaoxide and sodium hydroxide in a vacuum desiccator. The solids are given abbreviated names: For instance, **4**-SO_4 and **8**-Cl_2 denote, respectively, solids prepared by combining polymer **4** with iron(II) sulfate and polymer **8** with iron(II) chloride. Typical results for elemental analyses are as follows; Found: C, 45.31; H, 6.57; N, 12.55; S, 5.49; Fe, 8.52%; Calcd for $[\{Fe(C_{13}H_{17}N_3)_2\}(SO_4)_{1.15}\cdot 5H_2O]_n$ (**6**-SO_4): C, 45.46; H, 6.46; N, 12.33; S, 5.37; Fe, 8.13%. Found: C, 50.40; H, 7.13; N, 11.92; Cl, 12.22; Fe, 7.81%; Calcd for $[\{Fe(C_{15}H_{21}N_3)_2Cl_{2.4}5H_2O]_n$(**8**-$Cl_2$): C, 50.21; H, 7.30; N, 11.71; Cl, 11.86; Fe, 7.78%. The water content varied to a small extent from sample to sample and the molar ratio of the sulfate or chloride ions was a little larger than the stoichiometry expected for bivalent iron ions. The latter modification of the chemical composition will be discussed below in relation to the valence state of the iron atoms.

As a reference compound for X-ray absorption measurements, two iron(II) complexes of the ligands shown in Fig. 1(b) were prepared and two ferrites γ-Fe_2O_3 (maghemite) and Fe_3O_4 (magnetite) were freshly prepared and identified by means of powder X-ray diffraction. The two complexes, [2,6-bis(benzyliminomethylene)pyridine]iron(II) bromide and [2,6-bis(methyliminomethylene)pyridine]iron(II) iodide, are abbreviated as PBA-$FeBr_2$ and PMA-FeI_2, respectively.

Fe K-edge X-ray absorption spectra were measured on powder samples sandwiched between adhesive tapes by using the EXAFS facilities installed at the beam-line 10B in Photon Factory. Extended X-ray absorption fine structure (EXAFS) oscillations were extracted by removing a cubic spline background with four sections. Bond distances and coordination numbers were determined by a single-shell curve-fitting analysis with the theoretically evaluated phase shifts.[8-10]

The infrared spectra were measured with a Perkin-Elmer PE684 infrared spectrometer. X-Ray photoelectron spectra were measured with a McPherson ESCA36 electron spectrometer by employing Mg$K\alpha$ (1253.6 eV) as the stimulating radiation. The X-ray photoelectron spectra were measured on a powder sample mounted onto an aluminum plate using a double-sided adhesive tape. The binding energies of photoelectron peaks were calibrated against that of the Au $4f_{7/2}$ peak (83.8 eV) of a thin gold film evaporated onto a sample surface in the spectrometer.

Mössbauer spectra were measured with a Shimazu MEG-2 Mössbauer spectrometer on powder samples at 77 and 300 K. Isomer shifts, quadrupole splittings and internal fields were calibrated against the six hyperfine splitting peaks of an iron metal separately measured as a reference.

The magnetization was measured with a Faraday-type susceptometer constructed in combination with a JEOL electromagnet and a Cahn 2000 electromicrobalance in the field range 0.1—0.4 T at room temperature.

Local Structure around the Iron Atoms

It is difficult to determine the molecular structure of these iron-containing solids by means of X-ray diffraction because they are found to be amorphous. Therefore, we have attempted to determine particularly the molecular structure around the iron atoms which are responsible for the magnetism, using X-ray absorption spectroscopy. Figure 2 shows the first derivative curves of the Fe K X-ray absorption near-edge structure (XANES) spectra of the solids, an iron foil, the two ferrites, and the monomeric iron(II) complexes. The spectra of the solids resemble those of monomeric complexes; this indicates that the local structures of iron-containing solids and the complexes are similar to each other. On the other hand, structures denoted by B or C split into two peaks in the spectra of the ferrites. Structure A, appearing in the pre-edge region, is attributed to quadrupolar-allowed 1s→3d transitions.[11] Its relative intensity is known to be weak for six-coordinated iron compounds, whereas it is strong for four-coordinated iron compounds.[12] The relative intensities of structure A of the iron-containing solids and complexes are similarly weaker than those of ferrites having four- and six-coordinated iron sites. Therefore, taking the chemical structure of the ligands into account, we could suggest that the iron atoms in the solids as well as those in the complexes are surrounded by six nitrogen atoms.

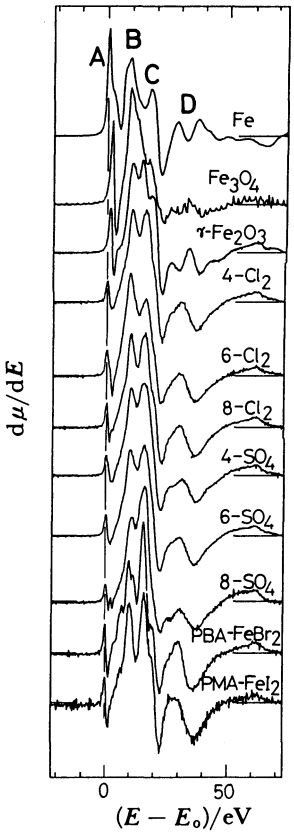

Fig. 2. First derivative $d\mu/dE$ curves of XANES spectra of an iron foil, ferrites the iron-containing solids, and the iron(II) complexes, where E is the photon energy and E_0 is the photon energy at the first maximum for the iron foil. The substances are given in abbreviated names (see the text).

Figure 3 shows a comparison among the EXAFS oscillations of iron, maghemite γ-Fe_2O_3, the iron-containing solids **6**-SO_4 and **6**-Cl_2, and the complex PBA-$FeBr_2$. It can be clearly seen that the EXAFS

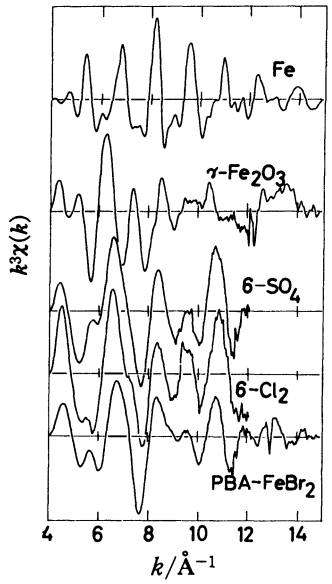

Fig. 3. EXAFS oscillations $k^3\chi(k)$ of the iron-containing solids and the iron(II) complexes.

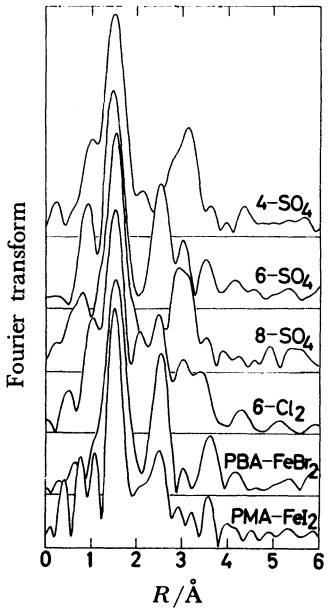

Fig. 4. Fourier transforms of EXAFS oscillations of the iron-containing solids and the iron(II) complexes.

oscillations of the solids are nearly identical to those of the complex, while they are very different from those of iron and maghemite. This behavior is quite similar to that observed in XANES spectra.

The Fourier transforms of the EXAFS oscillations, $k^3\chi(k)$ are shown in Fig. 4. The transforms for the iron-containing solids also resemble those for the complexes. The most prominent peak for the solids is located at about 1.5 Å (phase shift has not yet been corrected) and is coincident with the peak position for the complexes. This indicates that the peak corresponds to Fe–N bonds. From the chemical structure of the ligands, the peak at 2.5—3 Å could be due to Fe–C bonds.

We carried out a least-squares curve-fitting analysis by making a back-Fourier transformation of the region around the most prominent peak since it was difficult to construct reasonable structural models for second- and third-nearest neighbor atoms. The obtained bond distances are summarized in Table 1. The bond distances of the iron-containing solids are very similar to each other and are equal to those of the reference complexes within the experimental errors. Since the Fe–N bond distances in the six-nitrogen coordinated iron(II) complexes with ligands of similar molecular structure are known to be 1.9—2.0 Å,[13,14] the bond distance of 1.93±0.02 Å obtained for the iron-containing solids and the reference complexes are quite consistent with the Fe–N bond formation as expected from the molecular structure of the ligand moieties of the polymers.

The coordination number was shown to be about six for the reference complexes, although the estimated errors are somewhat large. This indicates that the present analysis which utilizes theoretical values of the phase shift instead of the experimental values is not

Table 1. The Fe–N bond Distance R and the Coordination Number N Derived from the Analysis of Fe K-edge EXAFS

Compound	R/Å (±0.02)	N (±1.0)
Monomer		
PBA-$FeBr_2$	1.93	5.9
PMA-FeI_2	1.90	5.8
Polymer		
4-SO_4	1.93	6.0
6-SO_4	1.94	5.3
8-SO_4	1.93	6.0
4-Cl_2	1.94	5.1
6-Cl_2	1.92	4.8
8-Cl_2	1.93	4.5

unreasonable for a determination of the coordination numbers for the compounds studied here. As shown in Table 1, the coordination numbers for the iron-containing SO_4-solids were found to be in the range from five to six. Although those for the Cl_2-solids are in the vicinity of five, these values seem to be underestimated to some extent in view of the similarity of the XANES and EXAFS spectra observed with all the solids and with the reference complexes. Therefore, it may be reasonable to conclude that the coordination numbers for these solids are six.

The above conclusion is further supported by the following fact. We have synthesized a polymer by reacting 1,6-hexanediamine with 1,3-benzenedicarbaldehyde instead of 2,6-pyridinedicarbaldehyde. This polymer is obtained as transparent soft lumps. We have tried to make a chelate compound of this polymer with iron(II) sulfate and chloride, but it turns out that the

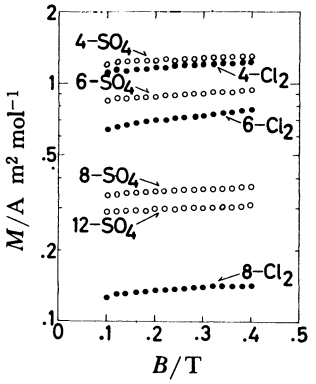

Fig. 5. Molar magnetization M of the iron-containing solids as a function of applied field strength B at room temperature.

polymer does not react with either sulfate or chloride. This implies that the tridentate structure of the ligand moiety is necessary for the polymer to form a chelate compound like **6**-SO_4; that is, the coordination number for the solids is six rather than four.

From the results mentioned above, it is concluded that the iron atoms in the solids are each surrounded by six nitrogen atoms with an almost equal distance of 1.93±0.02 Å, as observed for the iron(II) complexes in which one iron(II) ion is coordinated with two tridentate ligands. This conclusion is consistent with the 1:2 stoichiometry of Fe and the repeating units of the polymeric ligands determined by an elemental analysis. It is to be noted, at least from the results of X-ray absorption spectra, that there is no evidence for the presence of ferrite or metallic iron which would cause the ferromagnetism.

Effect of Chemical Modification of Polymers on the Magnetism

Since a magnetic interaction among the transition metal atoms is expected to be influenced by the chemical environment, particulary by the interatomic distances, we have examined the effect of chemical modifications of the length of the methylene chain and/or the anion on the magnetism of the iron-containing solids by comparing the magnetization curves at room temperature.

The length of the methylene chain does not qualitatively affect the magnetism. As shown in Fig. 5, all the iron-containing solids obtained by reacting polymers **4**, **6**, **8**, and **12** with iron(II) sulfate and iron(II) chloride exhibit magnetization curves similar to those of **6**-SO_4, i.e., a nonlinear relation to an applied field with a large magnetization, while the magnetization tends to decrease upon increasing the length, n, of the methylene chain. This indicates that only the tridentate structure is related to the large magnetization and its nonlinear relationship to the applied field.

The anions, sulfate and chloride, do not affect the magnetic behavior. Table 2 summarizes the molar magnetization of the iron-containing solids at 0.4 T. There seems to be a tendency to decrease the magnetization with a substitution of sulfate for a chloride ion. However, the magnitude of the magnetization still remains on the same order. The infrared spectra indicates that sulfate anions are only weakly or indirectly bound to the iron atoms. As shown in Fig. 6, the infrared spectrum of **6**-SO_4 exhibits the four bands attributable to sulfate ions at about 1100 cm^{-1} (ν_3) and at 610 cm^{-1} (ν_4) which are relatively strong in intensity and at 960 cm^{-1} (ν_1) and at 430 cm^{-1} (ν_2) which are very weak. Quite similar results have been obtained for all the solids containing sulfate ions. Since a free sulfate ion has a T_d symmetry, only a stretching mode (ν_3) and a bending mode (ν_4) are allowed for dipole transitions. This selection rule may be relaxed upon complex formation and the ν_1 and ν_2 modes appear with intensity, depending on the nature of the bonds formed. Simultaneously, each of bands due to ν_3 and ν_4 modes splits into two or three bands according to the occurrence of a symmetry lowering. The spectral feature observed is, therefore, characteristics of a sulfate ion that is very weakly bound to a metal ion.[15] On the other hand, a similar discussion may not be possible for monoatomic chloride anions.

Table 2. Molar Magnetization $M/A\,m^2\,mol^{-1}$ at 0.4 T and at 295 K of the Iron-Containing Solids Obtained by Reaction of the Polymers with $Fe^{II}SO_4$ or $Fe^{II}Cl_2$ (1 $A\,M^2\,mol^{-1} = 10^3$ Oe emu mol^{-1})

Polymer	Anion	
	SO_4^{2-}	Cl^-
4	1.3 ±0.2	1.2 ±0.2
6	1.0 ±0.3	0.8 ±0.2
8	0.37±0.04	0.14±0.04
12	0.31±0.04	—

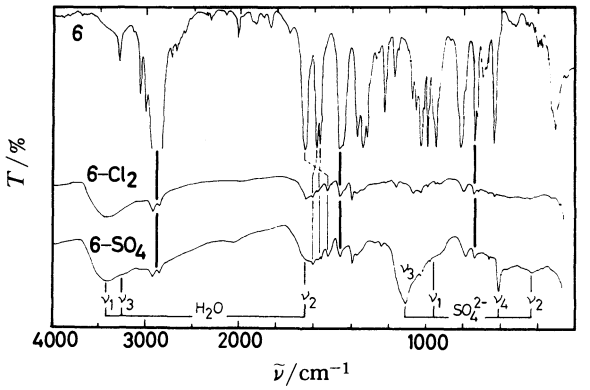

Fig. 6. Infrared spectra of **6**, **6**-SO_4, and **6**-Cl_2. The thick lines indicates the absorption bands assigned to the vibrational modes of the hexamethylene group of the polymer and the thin lines indicate those due to the tridentate moiety of the polymer. The vibrational modes of H_2O and those of SO_4^{2-} ion are also indicated. Similar results were obtained for the other polymers.

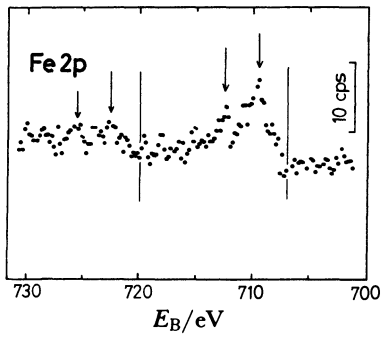

Fig. 7. Fe2p photoelectron spectrum of **6**-SO_4. Background is subtracted. The peak positions are indicated by arrows. Vertical lines represent the Fe2p peak position in metallic iron.

However, as shown in Fig. 6, a close similarity of the infrared spectra due to tridentate moieties would exclude a strong coordination of the chloride ion with the iron. Therefore, the sulfate and chloride anions in the iron-containing solids are almost isolated from iron ions and, consequently, they do not affect the magnetism.

Valence and Spin States of the Iron Atoms

Since it is important to know the valence state of the iron species in the iron-containing solids in order to discuss their magnetic behavior, we have measured the X-ray photoelectron spectra of **6** and **6**-SO_4. Figure 7 shows the X-ray photoelectron spectrum of **6**-SO_4 in the Fe2p region. The signal-to-noise ratio is not very good since the atomic fraction of the iron in **6**-SO_4 is only one-ninetieth. However, two peaks can be recognized in the $Fe2p_{3/2}$ region; also, there seem to be two peaks in the $Fe2p_{1/2}$ region. The binding energies are listed in Table 3. The binding energies of all the peaks observed shift to the higher-energy side from those of metallic iron (Fig. 7). This suggests that the iron atoms are ionized in **6**-SO_4.

The lower energy side peak in the $Fe2p_{3/2}$ region is attributed to iron(II) since its bindigng energy is close to that of tris(2,2′-bipyridine)iron(II) sulfate[16] where the iron(II) ion is associated with the six nitrogen atoms and the SO_4^{2-} ion is separated from the iron(II) ion in good agreement to that of **6**-SO_4. The binding energy of the higher energy side peak is located between the binding energies[16] of $(NH_4)_3[Fe^{III}F_6]$ and tris(8-quinolinolato)iron(III), which are six-coordinate iron(III) complexes. Therefore, this peak can be ascribed to iron(III).

It is known that the photoelectron peaks of magnetic transition-metal compounds often accompany strong satellites at positions with binding energies higher by 4 to 6 eV.[18] The energy difference between the two peaks attributed to iron(II) and iron(III) is only 3 eV. Therefore, the high energy peak can not be regarded as a satellite of the low-energy peak. In addition, the results of Mössbauer measurements described below also suggest the presence of iron(III). Thus, it is quite reasonable to attribute the high-energy peak to iron(III).

Table 3. Binding Energies of the Fe2p and N1s Core Electron Peaks in eV

Compound	$Fe2p_{1/2}$	$Fe2p_{3/2}$	N1s (fwhm)
6			399.3 (1.6)
6-SO_4	726	712.4	399.7 (2.3)
	723	709.5	
Fe-metal	720[b]	706.9[a]	
$Fe^{II}SO_4 \cdot 7H_2O$	723[b]	710.5[a]	
$[Fe^{II}(bpy)_3]SO_4$[c]	721.6[a]	709.2[a]	
$[Fe^{III}(oxinat)_3]$[d]		711.5[a]	
$(NH_4)_3[Fe^{III}F_6]$		713.8[a]	

a) Ref. 16. b) Ref. 17. c) Tris(2,2′-bipyridine)iron(II) sulfate. d) Tris(8-quinolinolato)iron(III).

Therefore, the irons in **6**-SO_4 are in the valence states of iron(II) and iron(III). **6**-SO_4 has been prepared by reacting **6** with iron(II) sulfate under a nitrogen stream to prevent the oxidation of the bivalent iron. It should be noted that **6**-SO_4 can not be obtained by a reaction between **6** and iron(III) sulfate. Therefore, the partial oxidation seems to occur after the iron(II) has been included in the polymer chains.

The presence of two valence states explains the nonstoichiometry of the sulfate ion in **6**-SO_4 described in the experimental section. It follows from the ratio of observed intensities of the peaks that about 70% of the iron ions is in the bivalent state and about 30% is in the tervalent state. To keep charge neutrality of **6**-SO_4, the chemical composition of the relevant part is written as $(Fe^{II}SO_4)_{0.7}[Fe^{III}(SO_4)_{1.5}]_{0.3}=Fe(SO_4)_{1.15}$. This composition agrees well with that obtained by an elemental analysis.

The N1s photoelectron spectra (not shown) of **6** and **6**-SO_4 exhibit a single peak without satellite. The binding energy shifts to the higher energy in **6**-SO_4. This energy shift implies that the formal charges on the nitrogen atoms become more positive in **6**-SO_4 than in **6**. This is consistent with the coordination of the iron with nitrogen. In addition, the full-width at half-maximum (fwhm) of the N1s peak is 1.6 eV for **6** and 2.3 eV for **6**-SO_4. The line broadening observed in the latter compounds would be related to the difference in the chemical nature of the nitrogen atoms which are coordinated with the iron.

The results discussed above clearly indicate that the irons in **6**-SO_4 are in the two valence states consisting of iron(II) and iron(III). Since no evidence has been found for the presence of a magnetic moment on the organic species in **6**-SO_4, it is natural to consider that the magnetic moment in **6**-SO_4 is associated with the iron ions.

Figure 8 shows the ^{57}Fe Mössbauer spectrum of **6**-SO_4 at 77 K. It is found from a Lorentzian least-squares curve fitting analysis that the experimental

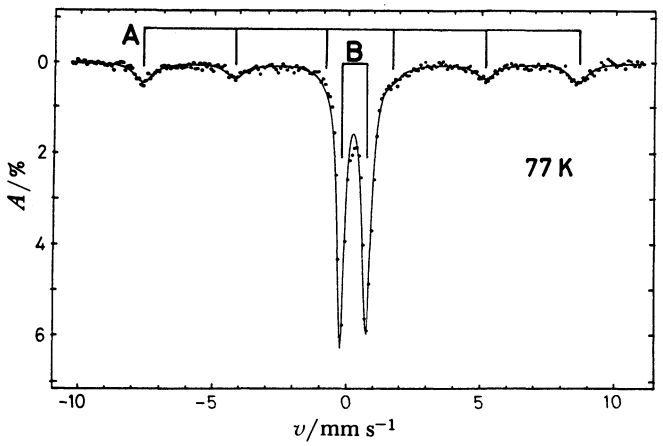

Fig. 8. Mössbauer spectrum of **6**-SO_4 at 77 K. Experimental points are shown by closed circles and the results of a Lorentzian least-squares fit is indicated by the solid line. The spectrum is composed of two subspectra denoted A and B. Stick diagrams indicate the peak positions of each subspectrum obtained by the analysis.

spectrum can well be reproduced by superimposing the subspectrum A which consists of six peaks of hyperfine splitting due to an internal field and the subspectrum B which consists of two peaks of quadrupole splitting. The absorption intensity of the Mössbauer spectra is markedly reduced at 300 K, probably due to a reduction of the recoil-free fraction. However, subspectra A and B still remain. The obtained parameters of the isomer shift δ, quadrupole splitting ΔE_q, and internal field H_i at 77 and 300 K are summarized in Table 4.

The subspectrum B can be attributed to the low-spin iron(II). The high-spin state (S=2) and the low-spin state (S=0) are possible for six-coordinate iron(II). The former possibility could be excluded on the basis of the values of the isomer shift. The isomer shift is known to be larger than 0.7 mm s^{-1} for a high-spin iron(II). Therefore, the iron(II) ions present in **6**-SO_4 have been concluded to be in a low-spin state. The iron(II) ions have no unpaired electrons in the low-spin state and, hence, does not cause an internal field. Therefore, subspectrum B should correspond to the low-spin iron(II). The quadrupole splitting of 0.96 mm s^{-1} obtained for the subspectrum B indicates the presence of an electric-field gradient induced by distortion from the octahedral symmetry, as is usually observed in low-spin iron(II) complexes with nitrogen donor ligands.[19]

On the other hand, the subspectrum A would be attributed to the high-spin state of iron(III). The presence of a hyperfine splitting in this subspectrum clearly indicates that the iron ion species have unpaired electrons. As discussed above, the possibility of high-spin iron(II) has already been eliminated. The remaining possibilities are, therefore, high-spin (S= 5/2) and low-spin (S=1/2) iron(III). These are not distinguishable from a difference in the isomer shift since the isomer shift is known to be comparable for

Table 4. Isomer Shift δ (relative to iron-metal film), Electric-Quadrupole Splittings ΔE_q, and Internal Field H_i Obtained from the Analysis of the Mössbauer Spectrum of **6**-SO_4 by the Lorentzian Least-Squares Curve Fitting

	77 K	300 K
Subspectrum A (Fe^{3+})		
δ/mm s^{-1}	0.46	0.46
ΔE_q/mm s^{-1}	−0.016	0
H_i/T	50.5±0.5	46±2
Subspectrum B (Fe^{2+})		
δ/mm s^{-1}	0.27	0.27
ΔE_q/mm s^{-1}	0.96	0.96

both states.[18] However, the internal field of 50.5±0.5 T is comparable with that of Fe_3O_4[20] and γ-Fe_2O_3[21] where iron(III) ions are in the high-spin state. In addition, this value is in good agreement with the internal field of 55 T expected for the $|M_S|$=5/2 state from the empirical relation for iron(III) ions in corundum, H_i=22$\langle S_z \rangle$.[22] Therefore, the assignment of the subspectrum A to the high-spin iron(III) is quite reasonable.

The fact that the quadrupole splitting observed for the subspectrum A is very close to zero also supports the above assignment. In the high spin-iron(III), the five d-electrons are separately distributed over the five d-orbitals so that the electron cloud becomes almost symmetric and the electric field gradient vanishes. It is known that the electron transfer between an iron atom and ligands is negligible in a high-spin iron compound[19] and that the electric field gradient is not affected very much by ligands.

The internal field is reduced to 46±2 T at 300 K, while the quadrupole splittings and the isomer shifts do not change. The reduction of internal field is quite natural, because the saturation magnetization decreases with increasing temperature.[7] A considerably large internal field, even at 300 K, indicates that the magnetic ordering would be maintained, even to a temperature higher than room temperature.

Concluding Remarks

From the discussion on the results of the X-ray photoelectron and Mössbauer spectroscopies, it is suggested that the iron atoms in **6**-SO_4 are in two valence states, consisting of the high-spin iron(III) which is responsible for the magnetism and the low-spin iron(II) which has no contribution to the magnetism. That is, only a fraction of the iron ions contributes to the observed magnetism in the iron-containing solids.

The large magnetization and its nonlinear relationship to an applied field was not only observed for **6**-SO_4 but also for the other iron-containing solids examined here. It was found that the length of the methylene chain of the polymer as well as the anions accompanying the iron ions hardly affect the

magnetism. Only the presence of the tridentate ligand moiety causes the formation of the iron-containing solids and, hence, the magnetism. This implies that the magnetic behavior observed for the iron-containing solids is not very much affected by the distance between the iron atoms coordinated with the tridentate moieties of the polymers, while the change in the length of the methylene chain may cause a variation of the distance.

This is somewhat peculiar for the large magnetization since magnetic interaction among the transition-metal ions may be influenced by their interatomic distances. X-Ray absorption measurements suggest that each of the iron ions in the solid is coordinated with two tridentate moieties of the polymers, as is expected for the stoichiometry determined by the elemental analyses. However, there remains a possibility of the presence of a small amount of iron ions which have different coordination characteristics and have escaped from observation because of limitations in the sensitivity of X-ray absorption spectroscopy for minor substances, including the same element.

The authors are greatful to Professor Takeshi Tominaga, Dr. Haruo Sato, and Dr. Motoyuki Matsuo for the measurements of the Mössbauer spectra. The authors also thank Professor Haruo Kuroda and Professor Isao Ikemoto for the use of the X-ray photoelectron spectrometer, and Professor Koichi Ohno for his valuable suggestions regarding this work.

This work was in part supported by the Grant-in-Aid for Scientific Research from the Ministry of Education, Science and Culture.

References

1) H. H. Wickman, A. M. Trozzolo, H. J. Williams, G. W. Hull, and F. R. Merritt, *Phys. Rev.*, **155**, 563 (1967).

2) G. E. Chapps, S. W. McCann, H. H. Wickman, and R. C. Sherwood, *J. Chem. Phys.*, **60**, 990 (1974).

3) S. Decurtins, F. V. Wells, K. C.-P. Sun, and H. H. Wickman, *Chem. Phys. Lett.*, **89**, 79 (1982).

4) C. G. Barraclough, R. L. Martin, S. Mitra, and R. C. Sherwood, *J. Chem. Phys.*, **53**, 1638 (1970).

5) H. Miyoshi, H. Ohya-Nishiguchi, and Y. Deguchi, *Bull. Chem. Soc. Jpn.*, **46**, 2724 (1973).

6) F. Lions and K. V. Martin, *J. Am. Chem. Soc.*, **79**, 2733 (1957).

7) T. Sugano, M. Kinoshita, I. Shirotani, and K. Ohno, *Solid State Commun.*, **45**, 99 (1983).

8) B. K. Teo, P. A. Lee, A. L. Simons, P. Eisenberger, and B. M. Kincaid, *J. Am. Chem. Soc.*, **99**, 3854 (1977).

9) P. A. Lee, B. K. Teo, and A. L. Simons, *J. Am. Chem. Soc.*, **99**, 3856 (1977).

10) M. Nomura, K. Asakura, U. Kaminaga, T. Matsushita, K. Kohra, and H. Kuroda, *Bull. Chem. Soc. Jpn.*, **55**, 3911 (1982).

11) A. Bianconi, "EXAFS for Inorganic Systems," Daresbury Laboratory, SERC DL/SCI/R17, 13 (1981).

12) G. Cales and J. Petieu, *Solid State Commun.*, **48**, 625 (1983).

13) V. L. Goedken, Y. Park, S.-M. Peng, and J. M. Norris, *J. Am. Chem. Soc.*, **96**, 7693 (1974).

14) A. Zalkin, D. H. Templeton, and T. Ueki, *Inorg. Chem.*, **12**, 1641 (1973).

15) K. Nakamoto, "Infrared and Raman Spectra of Inorganic and Coordination Compounds," 3rd ed John Wiley & Sons Inc., New York (1978).

16) L. Y. Johansson, R. Larsson, J. Blomquist, C. Cederstrom, S. Grapengiesser, U. Helgeson, L. C. Moberg, and M. Sundbom, *Chem. Phys. Lett.*, **24**, 508 (1974).

17) T. Tsang, G. J. Coyle, I. Adler, and L. Yin, *J. Electron Spectrosc. Relat. Phenom.*, **16**, 389 (1979).

18) L. Yin, I. Adler, T. Tsang, L. J. Matienzo, and S. O. Grim, *Chem. Phys. Lett.*, **24**, 81 (1974).

19) For example, N. N. Greenwood and T. C. Gibb, "Mössbauer Spectroscopy," Chappman and Hall Ltd., London (1971); H. Sano, "Mössubauer Spectroscopy: Application to Chemistry," (in Japanese) Kodansha Ltd., Tokyo (1972).

20) H. Weber and S. S. Hafner, *Z. Krist.*, **133**, 331 (1971).

21) J. M. Coey and D. Khalafalla, *Phys. Status Solidi A*, **11**, 229 (1972).

22) G. K. Wertheim and J. P. Remeika, *Phys. Lett.*, **10**, 14 (1964).

Determination of the Solvation Number of Sodium Anion in Hexamethylphosphoric Triamide

Tetsuo SAJI,* Katsunori AOKI, Kosaku SUGA, Masamichi FUJIHIRA,* and Shigeru AOYAGUI
Department of Chemical Engineering, Tokyo Institute of Technology, Ohokayama, Meguro-ku, Tokyo 152
(Received October 25, 1985)

Synopsis. Electronic absorption spectra for saturated solutions of Na in HMPA–THF mixtures with HMPA mole fractions 0.39—0.061 exhibit only a band for Na^-. A log–log plot of maximum absorbance vs. HMPA concentration has led to a numerical value 3 for the number of HMPA molecules solvating a Na^- ion.

Of stable solvated-electron species existing in solutions of alkali metals in certain amines, amides, or ethers, (free) solvated electron (e_s^-) and metal anion (M^-) have been identified by electronic spectroscopy[1] and investigated on their physicochemical properties. The solvation number of e_s^- has been determined with an interest in the nature of this specific chemical species.[2] No paper has, however, dealt with the solvation number of electron-excess species, M^-. This paper presents an indirect determination of the solvation number of Na^- in hexamethylphosphoric triamide (HMPA) from the known solvation number of Na^+ with the aid of electronic and NMR spectroscopies.

Experimental

HMPA and tetrahydrofuran (THF) were purified by the usual method in which sodium anthracenide was used to remove trace impurities.[3] Commercial sodium tetraphenylborate (NaTPB) was dried in vacuo at 60 °C for 24 h and used as a ^{23}Na source in NMR measurements. The other chemicals were commercially obtained and used without further purification. Mixing HMPA with THF at various HMPA mole fractions (x) and addition of sodium metal to pure HMPA or mixed solvents were carried out under nitrogen atmosphere. The electronic absorption spectrum of a supernatant solution was recorded after stirring the solution with excess sodium metal overnight. After additional one hour stirring of this solution, the absorbance at λ_{max} decreased slowly after stirring was stopped. However, when this absorbance for the solution was reproduced after the additional stirring of the solution, this solution was considered as a saturated solution of sodium. Mixed solvents are denoted by HMPA(x)–THF.

Electronic absorption spectra in the visible and near-IR regions were recorded at 25 °C on a Hitachi 220 and a Shimadzu MPS-50L double-beam spectrophotometers, respectively, by using a cell of 1 *mm* path length and a reference solution of THF. ^{23}Na NMR spectra were recorded at 23 °C on a Bruker CXP-300 spectrometer operating at 83.08 MHz. The chemical shifts reported are relative to external 0.1 M (1M=1 mol dm^{-3}) NaCl in D_2O, with positive sign representing a downfield shift. No signal locks were used because of broad line width.

Results and Discussion

Solvation of Na^- in HMPA–THF. The two bands at 750 and 2250 nm in the absorption spectrum of a solution of Na in HMPA have been assigned to Na^- and e_s^-, respectively.[4] Each of the spectra for the saturated solutions of Na in HMPA(0.039)–THF and HMPA(0.061)–THF exhibits only a band at 750 nm, which indicates that of the two electron-excess species only Na^- should be considered in saturated solutions of Na in HMPA(x)–THF with $0.039<x<0.061$. In view of the facts that the peak wavelengths λ_{max} for Na^- in pure HMPA and these HMPA–THF mixtures agree with one another and not with that in pure THF in the presence of cryptand (680 nm),[5] it may be safe to conclude that Na^- is solvated exclusively by HMPA molecules in solutions with $0.039<x<1$.

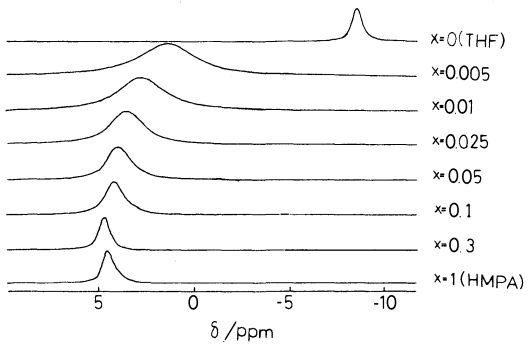

Fig. 1. ^{23}Na NMR spectra of 0.01 M sodium tetraphenylborate in HMPA–THF mixtures with varying HMPA mole fractions (x). Chemical shifts (δ) are referred to an external standard of 0.1 M NaCl in D_2O. Temperature: 23 °C.

Solvation of Na^+ in HMPA–THF. Figure 1 shows ^{23}Na NMR spectra for 0.01 M NaTPB in HMPA–THF of varying HMPA contents. An Addition of even a small amount of HMPA to THF, e.g., to x=0.005, is enough to cause a drastic change in ^{23}Na chemical shift δ, while this is not the case with the addition of THF to HMPA. These features may indicate that HMPA molecules solvate Na^+ much more strongly than THF molecules. The change in ^{23}Na chemical shift caused by a change in x may be attributed to the replacement of the THF molecules solvating Na^+ by HMPA molecules, since the observed chemical shift δ is related to the intrinsic shifts of each species i by[10]

$$\delta = \sum x_i \delta_i,$$

where x_i is the molar fraction of species i. The following discussion is based on the approximation that Na^+ is solvated selectively by HMPA molecules in HMPA(x)–THF mixtures with $0.039<x<1$.

The Sovation Number of Na^+ and Na^-. In view of the bulk dielectric constants of THF (7.4) and HMPA (30), bulk dielectric constants of HMPA(x)–THF mixtures ($0.039<x<0.061$) are expected to be 8.5—9.7 based on the volume average. A calculation with the Fuoss equation[6] for ion pair formation for a closest approach distance of about 12 Å (center to center

distance) has led to an ion pair formation constant of 2×10^2 M^{-1} at concentration 2.5×10^{-4} M for both Na^+ and Na^-, where the closest approach distance was estimated by assuming that both Na^+ and Na^- are solvated only by HMPA. The degree of ion pairing is expected to be less than 0.07, so small that ion pairing may be negligible. The following equilibrium is established in an HMPA–THF mixture saturated by Na:

$$2Na(solid) + nL \overset{K}{\rightleftharpoons} Na^+L_k + Na^-L_{n-k}, \quad (1)$$

where K is the equilibrium constant, k the solvation number of Na^+, and L stands for HMPA. The equilibrium constant is written as

$$K = [Na^+][Na^-]/[L]^n = c^2/[L]^n, \quad (2)$$

where brackets mean the concentration in molarity and $c=[Na^+]=[Na^-]$. The absorbance at λ_{max} for Na^-, A, can then be expressed by the following equation in terms of the molar absorptivity ε, the optical path length l, n, $[L]$, and K:

$$\ln A = (n/2)\ln[L] + \ln(\varepsilon l K^{1/2}). \quad (3)$$

When the total HMPA concentration $[HMPA]_0$ is much higher than c, the plot of ln A vs. $\ln[HMPA]_0$ should give a straight line whose slope and intercept on the ln A axis are $n/2$ and $\ln(\varepsilon l K^{1/2})$, respectively.[7]

Figure 2 shows that the experimental points within the concentration range of $[HMPA]_0=0.46$—0.71 M or $x=0.039$—0.061 are well fit to the following straight line obtained by the least-squares method:

$$\ln A = [(5.8\pm0.3)/2]\ln[HMPA]_0 + 2.0. \quad (4)$$

The slope of this straight line gives a round number of 6 as n, i.e., the sum of the solvation numbers for Na^+ and Na^-. This n value combined with the literature k value[8–10] of 3 leads to a numerical value of 3 for the number of HMPA molecules solvated to a Na^- ion in HMPA–THF mixtures with HMPA mole fractions ranging from 0.039 to 0.061. It is very likely that this solvation number is also valid for Na^- in pure HMPA, since the λ_{max} value for Na^- and solvation number of HMPA to a Na^+ in the HMPA–THF mixtures of the above composition are, respectively, equal and nearly equal to those in pure HMPA.

We are grateful to Mr. Yoshiharu Toida, Bruker Japan Co. for furnishing NMR spectra and to Professor Makoto Okamoto of our Institute and his group for optical providing spectra. Facilities for preliminary NMR experiments were offered by Professor Hiroshi Fukutomi of our Institute and his group.

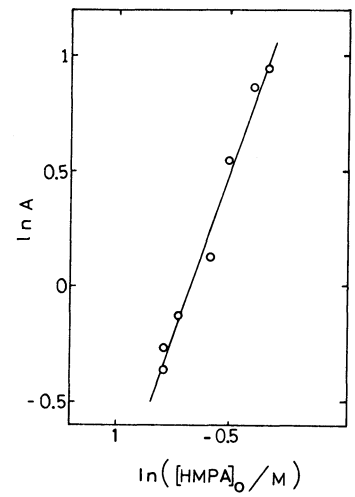

Fig. 2. A plot of the logarithmus of the absorbance at λ_{max} for Na^- (A) against the logarithmus of the total concentration of HMPA in HMPA–THF ($[HMPA]_0$). Temperature: 25 °C.

References

1) W. A. Seddon and H. W. Fletcher, *J. Phys. Chem.*, **84**, 1104 (1980).
2) J. J. Lagowski, "Electrons in Fluids," ed by J. Jortner and N. R. Kestner, Proceedings of Colloque Weyl III, Springer-Verlag, Berlin (1973), pp. 29—38.
3) K. Suga and S. Aoyagui, *Bull. Chem. Soc. Jpn.*, **45**, 1375 (1972).
4) E. I. Mal'tsev and A. V. Vannikov, *Radiat. Phys. Chem.*, **10**, 99 (1977).
5) J. Lacoste and F. Schue, *J. Organomet. Chem.*, **231**, 279 (1982).
6) R. M. Fuoss, *J. Am. Chem. Soc.*, **80**, 5059 (1958).
7) Our final result will show that the condition of $[HMPA]_0 \gg c$ is fulfilled. When calculated from the experimental values of $n=6$ and intercept=2.0 and the literature value[4] of 4×10^4 M^{-1} cm^{-1}, the c value of the order of 10^{-4} M and hence is negligible compared with the $[HMPA]_0$ values of the order of 10^{-1} M.
8) W. Martir, A. E. Alegria, and G. R. Stevenson, *J. Am. Chem. Soc.*, **98**, 7955 (1976).
9) K. Izutsu, T. Nomura, T. Nakamura, H. Kazama, and S. Nakajima, *Bull. Chem. Soc. Jpn.*, **47**, 1657 (1974).
10) The change in δ in Fig. 1 gives an average value ca. 10^2 for the equilibrium constants of the successive formation of solvated Na^+ ions with $k=1$, 2, and 3, if one makes a similar assumption as was made in the paper dealing with the ^{23}Na chemical shift in H_2O_2–H_2O mixtures: A. K. Convington, T. H. Lilley, K. E. Newman, and G. A. Porthouse, *J. Chem. Soc. Faraday Trans. 1*, **69**, 963 (1973). If viscosity data of the HMPA–THF mixtures are available, the change in line width may give the T_2 values for the intermediate species with $k=1$ and 2, in a similar way as in C. Detellier, A Gerstmans, and P. Laszlo, *Inorg. Nucl. Chem. Lett.*, **15**, 93 (1979).

Nonsteroidal Antiinflammatory Drugs. V. The Crystal and Molecular Structure of (±)-(2S*)-2-[4-((1S*,2R*)-2-hydroxycyclopentylmethyl)-phenyl]propionic Acid

Tadashi HATA,* Sadao SATO, and Chihiro TAMURA
Analytical and Metabolic Research Laboratories, Sankyo Co. Ltd., 1-2-58 Hiromachi, Shinagawa-ku, Tokyo 140
(Received March 25, 1986)

Synopsis. The crystal structure of the title compound was determined by X-ray diffraction techniques and was refined to a final R index of 0.094 for 1249 reflections. The cyclopentane ring takes a half-chair conformation in which the two substituents are attached at equatorial positions. The molecules form centrosymmetric tetramers by the two hydrogen bonds through the carboxyl and hydroxyl groups.

A new antiinflammatory agent, sodium (±)-2-[4-(2-oxocyclopentylmethyl)phenyl]propionate (loxoprofen sodium) (**1**), may exhibit the inhibitory activity for prostaglandin synthesis after the conversion to an active metabolite of (+)-(2S)-2-[4-((1R,2S)-2-hydroxycyclopentylmethyl)phenyl]propionic acid.[1] Since the molecule of this metabolite has three asymmetric carbons, the eight optical isomers can be theoretically considered, wherein the above metabolite is found to be the most active. Since the structure of (±)-(2S*)-2-[4-((1R*,2R*)-2-hydroxycyclopentylmethyl)phenyl]propionic acid (cis-OH isomer) has been determined,[2] the structure determination of the title compound **2**, racemic trans-OH isomer, has been performed for comparison with the isomers and related compounds.

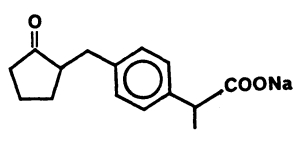

1

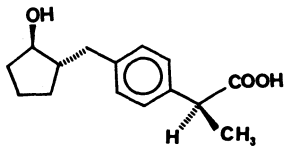

2

Experimental

Colorless prisms were grown by slow evaporation of a solution of the substance in a mixture of ether and hexane at room temperature. The lattice parameters and intensity data were collected from a 0.1×0.1×0.6 mm crystal on a Rigaku AFC-5 diffractometer with monochromated Cu$K\alpha$ radiation. Twenty reflections with $32° < 2\theta < 49°$ were used to determine the cell parameters. Space group was assigned from systematic absences. The crystal data were as follows; $C_{15}H_{20}O_3$, M=248.3, monoclinic, $P2_1/n$, a=20.275(1), b=5.479(1), c=12.005(1)Å, β=94.43(1)°, V=1329.6(3)Å^3, Z=4, D_c=1.24 gcm^{-3}, μ(Cu$K\alpha$) 6.9cm^{-1}. An ω—2θ scanning mode was employed up to 2θ=130° and 2270 reflections were measured. For the structure solution and refinement 1249 unique measurements with $F > 3\sigma(F)$ were used. No significant variation in the intensities of the three standard reflections was found. The intensities were corrected for the Lorentz and polarization factors, but not for absorptoion. The structure was solved by the direct method using MULTAN78,[3] and refined by the full-matrix least-squares method with anisotropic thermal parameters. H atom positions, except for two H atoms at C(16), were determined from a difference Fourier synthesis and refined with isotropic thermal parameters. The two remaining H atoms were placed geometrically and included in the refinements with fixed contributions to Fc. The final refinement converged at R=0.094 and R_w=0.037. The weighing sheme in the final stage was $w = 1/\sigma^2(F)$. Atomic scattering factors were taken from Ref. 4. The final fractional atomic coordinates and equivalent isotropic thermal parameters are given in Table 1.[5]

Results and Discussion

The atom labelling and the anisotropic thermal ellipsoids are shown in Fig. 1. Bond lengths and angles are given in Table 2. The C(1)–C(2) bond length of 1.354(8)Å is shorter than the normal bond length of the benzene ring due to some structural requirement and the others are all normal within the limits of experimental error.

The torsional angles of C(2)–C(1)–C(7)–C(9) and C(1)–C(7)–C(9)–O(10) of the propionic acid side chain are 122.0(6) and 126.5(7)°, respectively. These values are larger than those of 96.4 and 89.3° in ibuprofen,[6] 107.7 and 77.3° in flurbiprofen,[7] 111.7 and 90.2° in naproxen,[8] and 114.7 and 94.9° in one of the two independent molecules in the cis-OH isomer.[2] Another molecule in the cis-OH isomer has angles of 162.6

Table 1. Fractional Atomic Coordinates and Equivalent Isotropic Thermal Parameters, with e.s.d.'s in Parentheses

Atom	10^4x	10^4y	10^4z	B_{eq}/Å^2	Atom	10^4x	10^4y	10^4z	B_{eq}/Å^2
C(1)	2448(2)	6230(11)	125(4)	2.5(2)	O(10)	4047(2)	4333(8)	−385(3)	4.8(2)
C(2)	2022(3)	8138(11)	98(5)	3.1(2)	O(11)	3789(2)	7837(10)	362(5)	6.0(2)
C(3)	1546(3)	8405(12)	863(5)	2.9(2)	C(12)	987(3)	6988(14)	2541(5)	3.4(2)
C(4)	1507(2)	6719(11)	1707(4)	2.3(2)	C(13)	327(2)	5820(13)	2114(5)	3.2(2)
C(5)	1952(3)	4788(12)	1760(5)	3.5(2)	C(14)	−140(3)	5348(14)	2993(5)	3.8(2)
C(6)	2411(3)	4532(13)	959(5)	3.3(2)	C(15)	−815(3)	5110(18)	2355(7)	5.4(3)
C(7)	2952(2)	5956(12)	−775(5)	3.0(2)	C(16)	−793(3)	6753(14)	1354(5)	6.6(3)
C(8)	2804(3)	3739(15)	−1507(6)	4.1(2)	C(17)	−77(3)	7491(18)	1259(7)	5.1(3)
C(9)	3653(3)	5882(13)	−239(5)	3.2(2)	O(18)	38(2)	3218(11)	3601(4)	5.3(2)

Table 2. Bond Lengths (l/Å) and Bond Angles (θ/°), with e.s.d.'s in Parentheses

C(1)	-C(2)	1.354(8)	C(14)	-C(15)	1.522(8)	C(1)	-C(7)	-C(9)	110.7(4)
C(1)	-C(6)	1.372(9)	C(14)	-O(18)	1.408(9)	C(8)	-C(7)	-C(9)	111.3(5)
C(1)	-C(7)	1.552(8)	C(15)	-C(16)	1.505(11)	C(7)	-C(9)	-O(10)	125.2(6)
C(2)	-C(3)	1.390(8)	C(16)	-C(17)	1.520(9)	C(7)	-C(9)	-O(11)	111.4(5)
C(3)	-C(4)	1.377(8)	C(2)	-C(1)	-C(6) 118.0(5)	O(10)	-C(9)	-O(11)	123.3(5)
C(4)	-C(5)	1.389(8)	C(2)	-C(1)	-C(7) 120.7(5)	C(4)	-C(12)	-C(13)	111.8(5)
C(4)	-C(12)	1.517(8)	C(6)	-C(1)	-C(7) 121.3(5)	C(12)	-C(13)	-C(14)	114.9(5)
C(5)	-C(6)	1.396(9)	C(1)	-C(2)	-C(3) 122.6(6)	C(12)	-C(13)	-C(17)	112.1(6)
C(7)	-C(8)	1.515(10)	C(2)	-C(3)	-C(4) 119.8(5)	C(14)	-C(13)	-C(17)	103.6(5)
C(7)	-C(9)	1.514(7)	C(3)	-C(4)	-C(5) 118.1(5)	C(13)	-C(14)	-C(15)	104.8(5)
C(9)	-O(10)	1.189(8)	C(3)	-C(4)	-C(12) 120.2(5)	C(13)	-C(14)	-O(18)	110.9(5)
C(9)	-O(11)	1.310(9)	C(5)	-C(4)	-C(12) 121.7(5)	C(15)	-C(14)	-O(18)	112.0(6)
C(12)	-C(13)	1.535(8)	C(4)	-C(5)	-C(6) 120.6(6)	C(14)	-C(15)	-C(16)	105.6(6)
C(13)	-C(14)	1.495(8)	C(1)	-C(6)	-C(5) 120.8(6)	C(15)	-C(16)	-C(17)	107.9(5)
C(13)	-C(17)	1.560(10)	C(1)	-C(7)	-C(8) 111.7(5)	C(13)	-C(17)	-C(16)	104.6(6)

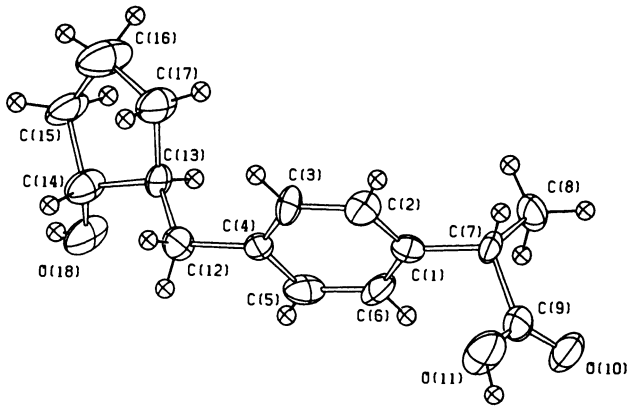

Fig. 1. ORTEP plot of the title compound with thermal ellipsoids at the 50% probability level.

and 96.2°. The former angle is larger than that in the title compound and the latter is smaller.

The cyclopentane ring adopts half-chair conformations with the two equatorial hydroxyl and methylphenyl groups, in which the C(13) and C(14) atoms are displaced by −0.27(1) and 0.31(1)Å from the plane through C(15)–C(16)–C(17). The two independent molecules of the cis-OH isomer also take half-chair forms, however, both hydroxyl groups in these molecules are attached at axial positions. The rotational angle of C(3)–C(4)–C(12)–C(13) is 86.1(8)°, compared with 100.7 and 76.6° in the two independent molecules of the cis-OH isomer. In these molecules, the steric hindrances between the benzene and cyclopentane rings are avoided in such a way that the arrangement of C(3)–C(4)–C(12)–C(13) is nearly perpendicular. The torsional angle of C(4)–C(12)–C(13)–C(14) is 162.8(5)° and the two hydrogen atoms attached at the methylene C(12) atom straddle the H(C14) atom. On the other hand, in the cis-OH isomer, the two corresponding hydrogen atoms straddle the hydroxyl oxygen atom instead of the hydrogen atom, since the oxygen atom is located on the same side of the plane through the cyclopentane ring as the H(C14) atom in the title compound.

The molecules form centrosymmetric tetramers by the two hydrogen-bonds between the carboxyl and hydroxyl groups. The O(18) atom donates the hydogen to O(10^{i}) and accepts one from O(11^{ii}) [(i) $-1/2-x$, $1/2-y$, $1/2-z$; (ii) $1/2-x$, $-1/2+y$, $1/2-z$]. The distances of these hydrogen bonds are 2.801(6) and 2.606(6)Å, respectively.

We would like to thank Dr. Atusuke Terada of The Chemical Research Laboratories of our company for providing samples.

References

1) K. Matsuda, Y. Tanaka, S. Ushiyama, K. Ohnishi, and M. Yamazaki, *Biochem. Pharmacol.*, **33**, 2473 (1984).

2) T. Hata, S. Sato, and C. Tamura, *Acta Crystallogr.*, in press.

3) P. Main, S. E. Hull, L. Lessinger, G. Germain, J.-P. Declercq, and M. M. Woolfson, "MULTAN78, A System of Computer Programs for the Automatic Solution of Crystal Structures from X-ray Diffraction Data," Univs. of York, England, and Louvain, Belgium (1978).

4) "International Tables for X-ray Crystallography," Kynoch Press, Birmingham (1974), Vol. IV.

5) Lists of structure factors, anisotropic thermal parameters and atomic parameters for hydrogen atoms have been deposited as Document No. 8640 at the Office of the Chemical Society of Japan.

6) J. F. McConnell, *Cryst. Struct. Comm.*, **3**, 73 (1974).

7) J. L. Flippen and R. D. Gilardi, *Acta Crystallogr., Sect. B*, **31**, 926 (1975)

8) K. Ravikumar, S. S. Rajan, V. Pattabhi, and E. J. Gabe, *Acta Crystallogr., Sect. C*, **41**, 280 (1985).

Synthesis of β-ZrClN by Thermal Decomposition of Zirconium(IV) Amide Trichloride

Masao OHASHI,* Shoji YAMANAKA, and Makoto HATTORI
Department of Applied Chemistry, Faculty of Engineering, Hiroshima University, Higashi-Hiroshima 724
(Received February 20, 1986)

Synopsis. The zirconium amide trichloride $ZrCl_3(NH_2)\cdot 7NH_3$ was prepared by the reaction of $ZrCl_4$ with liquid ammonia. On heating up to 600 °C in flowing ammonia gas, the amide was efficiently converted into β-ZrClN, whereas under vacuum it was decomposed to a different product. The decomposition processes were followed by using a quartz spring balance.

In a preceding study, we showed that a layer structured crystal β-ZrClN could be a promising candidate for electrochromic electrode, since the crystal forms a lithium intercalation compound, and exhibits reversible color changes between pale yellow green and black.[1,2]

The powder sample of β-ZrClN for the study was prepared according to a similar procedure reported by Juza and Heners:[3] Anhydrous zirconium tetrachloride was subjected to react with a dry ammonia in a silica glass tube installed horizontally in an electric furnace. The disadvantage of this procedure is that the yield of β-ZrClN is as low as 20—30%. The low yield is mainly due to the formation of the additional compound of ammonia $ZrCl_4\cdot 2NH_3$ which is easily vaporized above 400 °C[4] and physically transported to the cooler parts outside the heating zone before being decomposed to β-ZrClN.

In the present study, a new preparation method has been developed by thermal decomposition of the zirconium(IV) amide trichloride $ZrCl_3(NH_2)\cdot 7NH_3$ in an ammonia stream.

Experimental

Preparation of Zirconium Amide Chloride. Drake and Fowles[5] revealed that $ZrCl_4$ was subjected to ammonolysis to only one Zr–Cl bond in liquid ammonia, giving the zirconium amide chloride:

$$ZrCl_4 + (n+2)NH_3 \longrightarrow ZrCl_3(NH_2)\cdot nNH_3 + NH_4Cl$$

They removed the resulting ammonium chloride by washing the separated solid with liquid ammonia repeatedly. In this study, a glass apparatus was used, which was so designed that the ammonium chloride could be continuously leached out with liquid ammonia, as shown in Fig. 1. The apparatus works essentially as a Soxhlet extraction unit. Under a dry nitrogen atmosphere, about 4 g of zirconium tetrachloride purified by sublimation was placed on the glass filter E in the reaction tube D, the upper end of which is connected to a Dry Ice–methanol condenser B by a ground joint. Dry ammonia gas (99.999%) was introduced into the apparatus through the valve A and liquefied by the condenser. The liquefied ammonia comes down and reacts with the $ZrCl_4$ on the glass filter. The ammonium chloride formed by the reaction was dissolved in the liquid ammonia and leached out into the flask F connected below by a ground joint. The ammonia gas rising from the flask through the bypass C can also be liquefied by the condenser. After

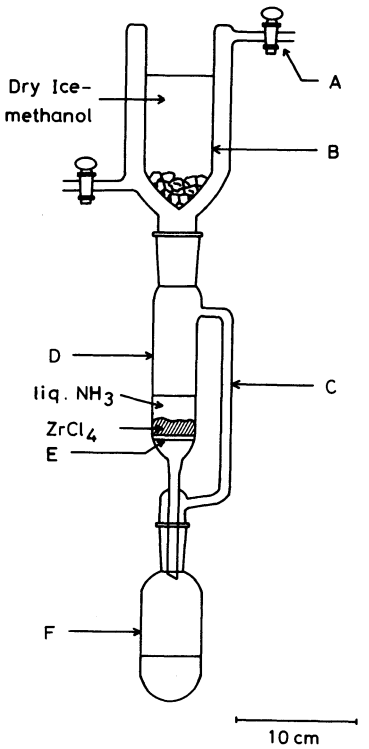

Fig. 1. Soxhlet type glass apparatus used for the preparation of zirconium amide trichloride.

refluxing for 3 h, the liquid ammonia was removed and the apparatus was purged with dry nitrogen. The amide was left on the glass filter in the form of white flocculent.

Analyses. A weighed amount of the reaction product was dissolved in 2 mol dm^{-3} sulfuric acid, and the zirconium content was determined gravimetrically as ZrO_2 after precipitation with sodium hydroxide. Nitrogen and chlorine contents were analyzed on the sulfuric acid solution by Kjeldahl and Fajans' methods, respectively.

The thermogravimetric analysis of the zirconium amide chloride was carried out by using a quartz spring balance in a vacuum and in an ammonia stream for a heating rate of 3 °C min^{-1}. The flow rate of the ammonia was 50 ml min^{-1}.

Results and Discussion

The chemical analysis of the product showed that the contents of Zr, N, and Cl were 28.1, 33.6, and 31.5%, respectively. This analytical result corresponds to the atomic ratio Zr:N:Cl=1.00:7.8:2.9, indicating that only one of the Zr–Cl bonds was subjected to ammonolysis and that the zirconium amide chloride with an approximately stoichiometric composition $ZrCl_3(NH_2)\cdot 7NH_3$ was obtained.

The thermogravimetric analysis (TG) curves of the zirconium amide chloride are shown in Fig. 2. On evacuation at room temperature for 3 h, the amide

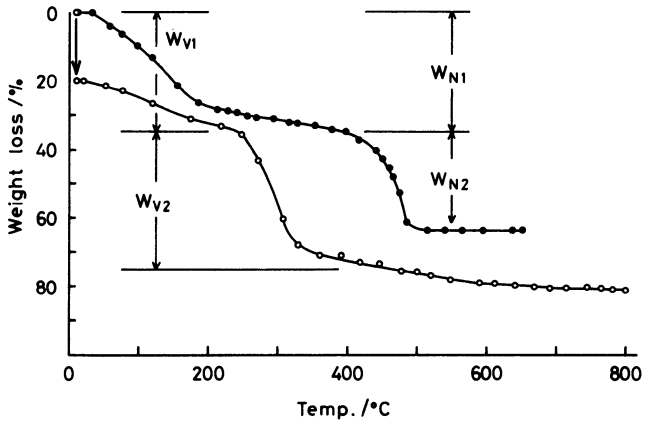

Fig. 2. Thermogravimetric curves for zirconium amide trichloride $ZrCl_3(NH_2)\cdot 7NH_3$ measured in a vacuum (○) and in an ammonia stream (●).

lost about 4 moles of ammonia, and then 3 moles of ammonia are gradually removed up to 240°C.

$$ZrCl_3(NH_2)\cdot 7NH_3 \longrightarrow ZrCl_3(NH_2)\cdot 3NH_3 + 4NH_3$$

$$ZrCl_3(NH_2)\cdot 3NH_3 \longrightarrow ZrCl_3(NH_2) + 3NH_3$$

In the second decomposition stage accompanied by a steep weight loss beginning from 280°C, white sublimate consisting of $ZrCl_4$ and NH_4Cl appeared on the cooler parts of the glass walls. Probably, the following decomposition occurs in this heating stage:

$$2ZrCl_3(NH_2) \longrightarrow ZrClN + ZrCl_4 + NH_4Cl$$

The amount of the weight loss for this reaction was calculated to be 67%. On the ammoniate formula ($ZrCl_3(NH_2)\cdot 7NH_3$) basis, this amount is reduced to 43%, which is in good agreement with the amount of the loss W_{V2} (40%). Yellow solid having the atomic ratio $Zr_{1.0}Cl_{1.0}N_{0.8}$ was obtained when the decomposition was interrupted at 450°C. The solid was very reactive and took fire when dropped into water. Irrespective of the similarity of the atomic ratio, it is apparent that the solid is different from our desired β-ZrClN which is stable in water. Similar unkown yellow solid was also found by Fowles and Pollard[6] in the course of the preliminary study of the decomposition of the zirconium amide trichloride. On further heating up to 800°C, the sample lost the weight gradually and gave black powder, which was found to be ZrN by X-ray powder diffraction analysis.

Even in an ammonia stream, the amount of the first weight loss (W_{N1}) corresponded almost to the first weight loss (W_{V1}) observed in a vacuum. However, the second weight loss began at the temperature higher by about 150°C than that of the decomposition in a vacuum. The residue obtained after the decomposition at 650°C was identified to be β-ZrClN by X-ray powder diffraction analysis. The amount of the weight loss (ammoniate formula basis) calculated on the basis of the following reaction was 22%:

$$ZrCl_3(NH_2) + 2NH_3 \longrightarrow ZrClN + 2NH_4Cl$$

Although the amount of the weight loss W_{N2} (29%) was a little larger than the calculated amount, it is apparent that the zirconium amide trichloride could be effficiently converted into β-ZrClN. It should be noted that in the ammonia stream, the decomposition temperature of $ZrCl_3(NH_2)$ is much higher than the temperature in a vacuum. It seems likely that the ammonia suppresses the decomposition of the amide, and that no sooner the $ZrCl_4$ is evolved at the higher decomposition temperature than it reacts with ammonia, forming β-ZrClN.

The resulting β-ZrClN formed lithium intercalation compound and showed changes in color from pale yellow green to black by soaking into butyl lithium solution in hexane.

This work was supported in part by a Grant-in-Aid for Special Project Research from the Ministry of Education, Science and Culture.

References

1) S. Yamanaka, M. Ohashi, M. Sumihara, and M. Hattori, *Chem. Lett.*, **1984**, 1403.
2) M. Ohashi, S. Yamanaka, M. Sumihara, and M. Hattori, *J. Inclusion Phenomena*, **2**, 289 (1984).
3) R. Juza and J. Heners, *Z. Anorg. Allg. Chem.*, **332**, 159 (1964).
4) A. Yajima, Y. Segawa, R. Matsuzaki, and Y. Saeki, *Bull. Chem. Soc. Jpn.*, **56**, 2638 (1983).
5) J. E. Drake and G W. A. Fowles, *J. Less-Common Met.*, **2**, 401 (1960).
6) G. W. A. Fowles and F. H. Pollard, *J. Chem. Soc.*, **1953**, 4128.

Direct Evidence for the Peroxo Substitution of the Oxo Group in the Oxotitanium(IV) Porphyrin Complex in the Aqueous Solution

Masahiko INAMO, Shigenobu FUNAHASHI,† and Motoharu TANAKA†,*
Department of Chemistry, Faculty of Education, Aichi University of Education, Kariya 448
†Laboratory of Analytical Chemistry, Faculty of Science, Nagoya University, Chikusa-ku, Nagoya 464
(Received March 8, 1986)

Synopsis. Labeling experiments for IR and NMR spectra of oxo- and peroxotitanium(IV) complexes show that the oxo group of oxotitanium(IV) porphyrin is fully substituted by a peroxo group in the course of the reaction with hydrogen peroxide in the aqueous solution, i.e. the O–O bond of H_2O_2 remains intact in the peroxo complex.

In recent years interests have been focused on dioxygen complexes of transition metals for their interesting features as catalysts, reagents, or key intermediates of selective oxidation involving molecular oxygen, hydrogen peroxide, or alkyl hydroperoxide.[1] Of the high valent d^0 transition metal complexes, those of molybdenum(VI), vanadium(V), and titanium(IV) complexes are especially known to play an important role in the oxidation by peroxide species.[2] The exchange of oxygen atoms bound to the central metal ion has been investigated in order to elucidate the mechanisms of the catalytic action of these metal complexes. Modena et al. have reported that the oxygen exchange between the oxo and peroxo groups occurs in complexes containing both oxo and peroxo moiety,[3] while controversy still surrounds the mechanisms of these reactions.[4]

We have been interested in the formation of peroxo complexes in the aqueous solution and studied the kinetics of these reactions.[5] Oxo complexes of early transition metal ions react with hydrogen peroxide to give rise to the corresponding peroxo compounds with release of a water molecule:

$$\text{—M(=O)—} + H_2O_2 \longrightarrow \text{—M(O–O)—} + H_2O \qquad (1)$$

In these oxo-peroxo substitution reactions there are two possibilities: (1) The oxo group in the reactant is fully substituted by the peroxo group in hydrogen peroxide, i.e. the O–O bond of H_2O_2 remains intact in the peroxo compound, and (2) the peroxo group in the product results from both the oxo complex and hydrogen peroxide. There is, however, no direct evidence to distinguish whether the oxo group in the reactant or the oxygen atom in hydrogen peroxide is released as a water molecule. In general, oxygen exchange between the oxo complex and water in aqueous solution, i.e. oxo-oxo substitution, is very slow in comparison with the oxo-peroxo substitution[6] and mostly their rates are dependent on hydrogen ion concentration.[7,8] The latter substitution reaction has been studied on the titanium(IV) porphyrins in the organic solvent.[9] Little is known, however, about the mechanisms of this type of reaction in the aqueous solution. In this paper we will discuss the mechanism

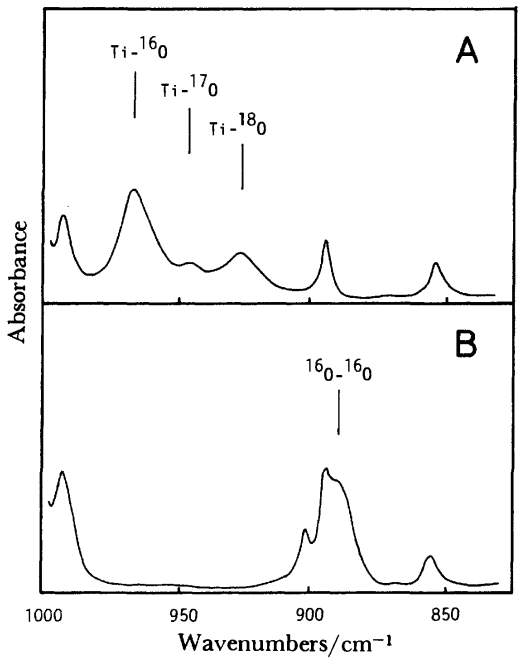

Fig. 1. Infrared spectra of ^{17}O- and ^{18}O-enriched TiO(tpyp) (A) and its peroxo derivative, Ti(O_2)(tpyp) (B), both recorded in absorbance mode. Scales of the ordinate are in arbitrary unit. The IR spectra were obtained by subtracting the spectrum of chloroform from that of the chloroform solution of each complex.

of the oxo-peroxo substitution reaction of titanium(IV) porphyrin in the aqueous solution.

Oxotitanium(IV) porphyrin, TiO(tpyp) (tpyp:5,10,15,20-tetra-4-pyridylporphine) was prepared according to the method described previously.[5c] Isotopically enriched water was purchased from C.E.A.-C.E.N.-Saclay: 35.8 wt% $^{16}OH_2$, 20.2 wt% $^{17}OH_2$, 44.0 wt% $^{18}OH_2$. The mixture involving 10 g of 0.012 mol kg^{-1} chloroform solution of TiO(tpyp) and 0.2 g of isotopically enriched water stood for ten days at 100°C in a sealed glass tube. The infrared spectrum of ^{17}O and ^{18}O labeled complex TiO*(tpyp) in chloroform, measured on a Nicolet MX-1 FT-IR spectrometer, shows three peaks due to titanium–oxygen stretching vibration (Fig. 1A); 966.5 cm^{-1} (Ti–^{16}O), 945.5 cm^{-1} (Ti–^{17}O), and 927.1 cm^{-1} (Ti–^{18}O). The measured IR spectrum was simulated to estimate the isotopic composition of the oxygen atom in TiO(tpyp) on the assumption that the absorption bands are Lorentzian and that the band widths are the same for these three peaks. The oxo group consists of 67.2% of ^{16}O, 9.2% of ^{17}O, and 23.4% of ^{18}O. Therefore 50% of oxygen

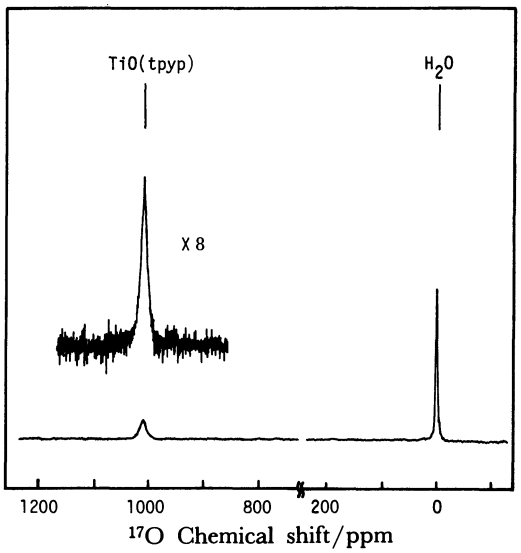

Fig. 2. 13.51-MHz ^{17}O NMR spectrum of TiO(tpyp). Chemical shifts were measured relative to the internal water. In the area of water is seen only one peak because of the proton noise decoupling.

atom of TiO(tpyp) exchanged with that of labeled water present in large excess over the complex under the present experimental conditions. Figure 2 shows the ^{17}O NMR spectrum of Ti^{17}O(tpyp) in a 2.7×10^{-2} mol kg^{-1} chloroform solution at room temperature, recorded on a JEOL FX-100 spectrometer (δ=1010 ppm, $\nu_{1/2}$=186 Hz). The extent of the oxygen exchange estimated by the integration of the ^{17}O NMR spectrum is consistent with that evaluated from the IR spectrum.

The oxo–peroxo substitution reaction in aqueous solution was accomplished by the following procedure. The titanium(IV) porphyrin complex, TiO(tpyp), is soluble in acidic aqueous solution as $[TiO(H_4tpyp)]^{4+}$, where H_4tpyp represents porphyrin ligand of which four pyridyl groups are protonated. The isotopically labeled complex was extracted from the chloroform solution to the aqueous phase at pH 1.7, and then hydrogen peroxide was added to the aqueous phase to perform the oxo–peroxo substitution. As soon as the reaction proceeded completely (<1 min),[10] the produced peroxo complex, $Ti(O_2)$(tpyp), was again extracted into the chloroform phase by neutralizing the acidic aqueous solution with sodium carbonate. This procedure can be carried out within 15 min. Addition of diethyl ether to the chloroform solution yielded the $Ti(O_2)$(tpyp) crystals. The infrared spectrum of the peroxo complex thus obtained is the same as that synthesized from nonlabeled TiO(tpyp) (See Fig. 1B). This fact indicates that this procedure afforded the nonlabeled peroxo complex. On the other hand, the control experiment showed that both oxygen exchange reactions between $[TiO^*(H_4tpyp)]^{4+}$ and bulk water and between $[Ti(O_2)(H_4tpyp)]^{4+}$ and bulk H_2O^* in acidic aqueous solution do not occur to a significant extent (<10%) for a period of 15 min under the present experimental conditions. Consequently it is concluded that the oxo group of $[TiO(H_4tpyp)]^{4+}$ is fully substituted by hydrogen peroxide to give the peroxo complex in which the oxygen atoms come entirely from H_2O_2 as shown by Eq. 2.

$$[TiO^*(H_4tpyp)]^{4+} + H_2O_2 \longrightarrow [Ti(O_2)(H_4tpyp)]^{4+} + H_2O^* \quad (2)$$

This substitution process includes both the entering of hydrogen peroxide into the inner sphere of the central titanium(IV) ion and the leaving of the oxo group which should be expelled as water or hydroxide ion. Since the titanium(IV) atom lies about 0.6 Å above the mean plane of the porphyrin skeleton toward the oxo group in the case of oxotitanium(IV) octaethylporphine in the crystalline state,[11] the similar situation will prevail in solution. In our previous paper,[5a] the associative mode of activation has been proposed for the reaction of titanium(IV) porphyrin with hydrogen peroxide on the basis of the kinetic feature, and we have put forward the acid-base catalyzed mechanism for the oxo-peroxo substitution which would include some assistance of hydrogen bonding between the oxo group of the complex and the hydrogen atom of hydrogen peroxide in the transition state. Such a mechanism is now strongly supported by the present work.

Financial support from the Ministry of Education, Science, and Culture through a Grant-in-Aid for Scientific Research (Grant No. 59430010) and a Grant-in-Aid for Special Project Research (Grant No. 60129031) is gratefully acknowledged.

References

1) N. N. Greenwood and A. Earnshow, "Chemistry of the Elements," Pergamon Press, Oxford (1984).
2) R. D. Bach, G. J. Wolber, and B. A. Coddens, *J. Am. Chem. Soc.*, **106**, 6098 (1984).
3) O. Bortolini, F. Di Furia, and G. Modena, *J. Am. Chem. Soc.*, **103**, 3924 (1981).
4) M. Postel, C. Brevard, H. Arzoumanian, and J. G. Riess, *J. Am. Chem. Soc.*, **105**, 4922 (1983).
5) a) M. Inamo, S. Funahashi, and M. Tanaka, *Inorg. Chem.*, **24**, 2475 (1985); b) M. Inamo, S. Funahashi, Y. Ito, Y. Hamada, and M. Tanaka, *ibid.*, **24**, 2468 (1985); c) M. Inamo, S. Funahashi, and M. Tanaka, *ibid.*, **22**, 3734 (1983); d) S. Funahashi, S. Funada, M. Inamo, R. Kurita, and M. Tanaka, *ibid.*, **21**, 2202 (1982).
6) R. K. Murmann, *Inorg. Chem.*, **16**, 46 (1977).
7) H. Gamsjäger and R. K. Murmann, "Advances in Inorganic and Bioinorganic Mechanisms," ed by A. G. Sykes, Academic Press, London (1983), Vol. 2, p. 317.
8) R. H. Betts and R. H. Voss, *Can. J. Chem.*, **48**, 2035 (1970).
9) J.-M. Latour, B. Galland, and J.-C. Marchon, *J. Chem. Soc., Chem. Commun.*, **1979**, 570.
10) According to the results of Ref. 5c, the value of the conditional second-order rate constant is 1 mol^{-1} dm^3 s^{-1} at pH 1.7. Thus the reaction should be complete within 1 min under the present experimental conditions.
11) R. Guilard, J.-M. Latour, C. Lecomte, J.-C. Marchon, J. Protas, and D. Ripoll, *Inorg. Chem.*, **17**, 1228 (1978).

Reactions of Trifluoroacetonitrile Oxide or -nitrilimines with β-Diketones and β-Keto Esters

Kiyoshi TANAKA,* Munehisa KISHIDA, Seiji MAENO, and Keiryo MITSUHASHI
Department of Industrial Chemistry, College of Technology, Seikei University, Kichijoji-Kitamachi, Musashino, Tokyo 180
(Received March 3, 1986)

Synopsis. *N*-Phenyl-*C*-(trifluoromethyl)nitrilimine cyclized with β-diketones or β-keto esters under alkaline conditions to give the corresponding 3-trifluoromethylpyrazoles with acyl or alkoxycarbonyl group at the 4-position of the ring, respectively. While trifluoroacetonitrile oxide with β-diketones provided the corresponding trifluoromethylisoxazoles, its reactions with β-keto esters gave 4-acyl-5-hydroxy-3-trifluoromethylisoxazoles as well as the expected isoxazoles without the regioselectivity.

The reaction of nitrile oxides or nitrilimines with the doubly activated methylene compounds provides a regiospecific synthesis of isoxazoles or pyrazoles with a wide variety of substituents.[1] For example, acyl group attached to methylene group is regarded as a functional group for an introduction of alkyl group into the 5-position of the azole ring. In the course of our program researching on the reactivity of the fluorinated 1,3-dipolar compounds, we now wish to describe the synthesis of 3-trifluoromethylpyrazoles or -isoxazoles having carbonyl functions through the reactions of *N*-phenyl-*C*-(trifluoromethyl)nitrilimine (**2**) or trifluoroacetonitrile oxide (**6**) with various β-diketones or β-keto esters and also to report the regioselectivity of the cycloaddition.[2]

The nitrilimine **2**, derived in situ from *N*-phenyltrifluoroacetohydrazonoyl bromide (**1**), reacted with methyl acetoacetate under alkaline conditions in methanol to give 4-methoxycarbonyl-5-methyl-1-phenyl-3-trifluoromethylpyrazole (**3a**) in fairly good yield. The pyrazole **3a** was easily transformed into 5-methyl-1-phenyl-3-trifluoromethylpyrazole (**4**) by hydrolysis followed by decarboxylation. This transformation confirmed the structure of **3a** having methoxycarbonyl group at the 4-position of the ring, indicating that cycloaddition proceeds with high regioselectivity. Similarly, **2** reacted with 2,4-pentanedione, giving rise to the corresponding acetylpyrazole **3b**. The reactions of **6**, generated in situ from trifluoroacetohydroximoyl bromide etherate (**5**), are also related to the synthesis of the acylisoxazoles **7a**, **b**, **c** from 2,4-pentanedione, dibenzoylmethane, and 1,3-cyclohexanedione,[3] respectively (Table 1). However, methyl acetoacetate produced 4-acetyl-5-hydroxy-3-trifluoromethylisoxazole (**9**), disturbing the high regioselectivity, in substantial quantity together with the expected isoxazole **8a** which was also converted into 5-methyl-3-trifluoromethylisoxazole (**10**). Although ethyl acetoacetate also produced **9** in as low as 7% yield besides **8b**, methyl benzoylacetate afforded only **8c**, accompanied by no corresponding hydroxyisoxazole.

The formation of **9** can be reasonably explained by the stepwise path involving electrophilic substitution of **6** toward the anion **11** of β-keto ester followed by intramolecular cyclization of thus formed anion **12** with the ester moiety. These ionic or hard properties are characteristic of **6** and seem to be caused by the strong electron-withdrawing effects of trifluoromethyl group.[4] On the other hand, intramolecular cyclization of the anion **12** with the acetyl group may produce the expected isoxazole **8**[5] and , however, the alternative direct formation of **8** by a concerted cycloaddition of **6** with **11** can not be still ruled out.

Experimental

All melting and boiling points are uncorrected. The IR spectra were recorded on a JASCO A-100 spectrometer. The

Table 1. Preparation of Trifluoromethylpyrazoles (**3**) and -isoxazoles (**7** and **8**)

Compound	Yield %	Mp(θ_m/°C) [Bp(θ_b/°C/mmHg)]	Formula	Calcd(Found)/% C	H	N	IRν/cm^{-1} C=O	^{1}H NMR δ[a]
3a	92	73—75[b]	$C_{13}H_{11}F_3N_2O_2$	54.93 (55.12)	3.90 (3.89)	9.86 (9.87)	1727	2.55(s, 3H), 3.89(s, 3H) 7.2—7.7(m, 5H)
3b	88	91—93[b]	$C_{13}H_{11}F_3N_2O$	58.21 (58.35)	4.13 (4.12)	10.44 (10.48)	1668	2.51(s, 3H), 2.58(s, 3H) 7.3—7.7(m, 5H)
7a	54	[60—62/10]	$C_7H_6F_3NO_2$	43.54 (43.35)	3.13 (2.80)	7.25 (7.35)	1700	2.50(s, 3H), 2.76(s, 3H)
7b	25	66—67[b]	$C_{17}H_{10}F_3NO_2$	64.36 (64.21)	3.18 (3.01)	4.41 (4.37)	1655	7.1—8.0(m)
7c	29	44—45[c]	$C_8H_6F_3NO_2$	46.84 (46.61)	2.95 (2.83)	6.83 (6.87)	1702	2.1—2.8(m, 4H), 3.10(t, 2H)
8a	24[d]	Oil	$C_7H_6F_3NO_3$	40.20 (40.12)	2.89 (2.90)	6.70 (6.83)	1740	2.75(s, 3H), 3.90(s, 3H)
8b	61[e]	Oil	$C_8H_8F_3NO_3$	43.06 (43.21)	3.61 (3.75)	6.28 (6.16)	1740	1.36(t, 3H), 2.76(s, 3H) 4.33(q, 2H)
8c	23	69—70[f]	$C_{12}H_8F_3NO_3$	53.15 (52.87)	2.97 (2.82)	5.16 (5.21)	1740	3.90(s, 3H), 7.4—8.0(m, 5H)

a) Measured in $CDCl_3$. b) Recrystallized from hexane. c) Recrystallized from hexane–diethyl ether. d) Other than **8a**, **9** was isolated in 16% yield. e) Other than **8b**, **9** was isolated in 7% yield. f) Recrystallized from chloroform.

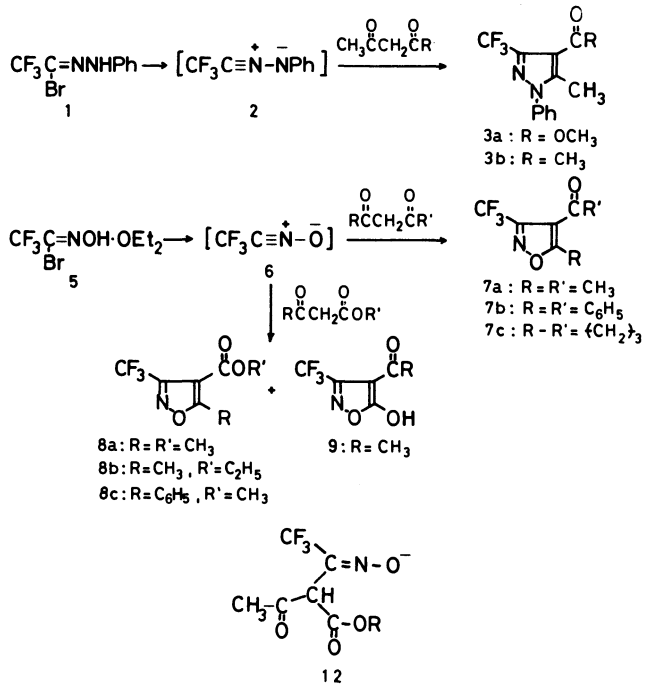

^{1}HNMR spectra were measured with JEOL JNM-PMX 60 spectrometer, using tetramethylsilane as an internal standard, the chemical shifts being given in δ ppm downfield. The MS spectra were obtained on a Finnigan 4023 GC-MS DS spectrometer. The bromides **1** and **5** were prepared by the methods reported in our previous papers.[6]

Preparations of 3 and 7. General Procedure. A solution of **1** (4.5 mmol) in 10 cm^3 of methanol was added dropwise to a solution of sodium methoxide (9.0 mmol) and 13.5 mmol of methyl acetoacetate or 2,4-pentanedione in 20 cm^3 of methanol. After stirring at room temperature for 2 h, 100 cm^3 of diethyl ether was added to the reaction mixture. The mixture was washed with water and brine, dried over magnesium sulfate, and evaporated to leave a residue which was placed on a column (silica gel) and eluted to give the pyrazole **3**. Product was further purified by recrystallization. The isoxazoles **7** were similarly prepared from **5** and β-diketones.

Decarboxylation of 3a and 8a. A mixture of **3a** (1.59 g, 5.6 mmol) in ethanol (25 cm^3) and 10% aqueous sodium carbonate (50 cm^3) was refluxed for 12 h. After the solvent was removed, the resulting mixture was washed with diethyl ether and dissolved in water. The aqueous solution was acidified with concd hydrochloric acid, extracted with diethyl ether, and dried over magnesium sulfate. Removal of the solvent left a solid (1.03 g). A mixture of thus obtained solid and 0.1 g of copper powder in 3 cm^3 of quinoline was heated at 190°C for 3 h and evaporated under reduced pressure to leave a residue. The residue was chromatographed on silica gel and eluted with hexane–ethyl acetate (5:1) to give 0.41 g (32%) of **4** which was further purified by preparative GLC; ^{1}HNMR ($CDCl_3$) δ=2.30 (s, 3H), 6.37 (s, 1H), 7.4 (s, 5H), IR (neat) 1590 (Ph), 1170,1130 cm^{-1} (CF_3).

Found: C, 58.57; H, 3.96; N, 12.37%. Calcd for $C_{11}H_9F_3N_2$: C, 58.41; H, 4.01; N, 12.38%.

Similar treatment of **8a** provided **10** which was collected by distillation (64%) and purified by preparative GLC. ^{1}H NMR ($CDCl_3$) δ=2.52 (s, 3H), 6.25 (s, 1H), IR (neat) 3150 (CH), 1185, 1145 cm^{-1} (CF_3).

Found: C, 39.72; H, 2.31; N, 9.28%. Calcd for $C_5H_4F_3NO$: C, 39.75; H, 2.67; N, 9.27%.

Reaction of 5 with Methyl Acetoacetate. After the similar procedures to the above using **5** (5.00 g, 18.8 mmol), methyl acetoacetate (5.95 g, 51.3 mmol), and sodium methoxide (2.77 g, 51.3 mmol), the solvent was removed to leave a residue. The residue was extracted with chloroform and then with ethyl acetate. The chloroform layer was washed with water, dried over magnesium sulfate, and evaporated. The resulting residue was distilled to give 3.44 g of a mixture of **8a** (24% yield) and methyl acetoacetate in the ratio of 17:83 (boiling range, 74—76°C/25 mmHg, 1 mmHg=133.322 Pa). The isoxazole **8a** was further separated by preparative GLC. On the other hand, the ethyl acetate layer was evaporated to give a residue which was dissolved in water. The aqueous solution was acidified with concd hydrochloric acid and extracted with diethyl ether. The extracts were dried over magnesium sulfate and evaporated to leave an oily matter which was sublimed under reduced pressure to give 0.57 g (16%) of **9**; mp 96—98°C (recrystallized from chloroform), ^{1}HNMR ($CDCl_3$–DMSO-d_6) δ=2.53 (s), 9.3 (br. s), IR(KBr) 3340 (OH), 1730 (C=O), 1150 cm^{-1} (CF_3), MS (CI, *m/z*) 196 $(M+H)^+$, 224 $(M+Et)^+$.

Found: C, 32.91; H, 2.60; N, 6.34%. Calcd for $C_6H_4F_3NO_3 \cdot 1.3H_2O$[7]: C, 32.98; H, 3.04; N, 6.41%.

In a similar manner, the reaction with ethyl acetoacetate or methyl benzoylacetate was performed and the results are summarized in Table 1.

References

1) S. A. Lang, Jr. and Y. -i Lin, "Isoxazoles and their Benzo Derivatives," in "Comprehensive Heterocyclic Chemistry," ed by A. Katritzky and C. W. Rees, Pergamon Press, Oxford (1984), Vol. 6; A. S. Shawali and C. Párkányi, *J. Heterocyclic Chem.*, **17**, 833 (1980).

2) This paper constitutes part IX in "Applications of the fluorinated 1,3-dipolar compounds as building blocks of the heterocycles with fluorine groups." Part VIII: K. Tanaka, T. Suzuki, S. Maeno, and K. Mitsuhashi, *J. Heterocyclic Chem.*, in press.

3) A. A. Akhrem, F. A. Lakhvich, V. A. Khripach, and A. G. Pozdeyev, *Synthesis*, **1978**, 43.

4) For the ionic behavior of **6**, see K. Tanaka, H. Masuda, and K. Mitsuhashi, *Bull. Chem. Soc. Jpn.*, **58**, 2061 (1985).

5) P. Bravo and P. P. Ponti, *J. Heterocyclic Chem.*, **10**, 669 (1973).

6) K. Tanaka, S. Maeno, and K. Mitsuhashi, *J. Heterocyclic Chem.*, **22**, 565 (1985); K. Tanaka, H. Masuda, and K. Mitsuhashi, *Bull. Chem. Soc. Jpn.*, **57**, 2184 (1984).

7) Since the isoxazole **9** is hygroscopic and easily sublimed under reduced pressure, the complete drying was impossible.

Preparation of Organocalcium Halides Using Calcium Ultrafine Particle

Kunio MOCHIDA,* Sei-ichi OGURA, and Takayuki YAMANISHI
Department of Chemistry, Faculty of Sciences, Gakushuin University, 1-5-1 Mejiro, Toshima-ku, Tokyo 171
(Received March 11, 1986)

Synopsis. Organocalcium halides were prepared from organic halides and calcium ultrafine particle in good yields.

In contrast to the organomagnesium halides (Grignard reagents), the preparations and chemical reactivities of organocalcium halides have been little studied.[1] This slow progress could be due to the lack of a useful method to prepare organocalcium halides.

The formation of organocalcium halides from organic halides and calcium metal has been reported. An important problem in the preparation of organocalcium halides is the impurities in the calcium metal. Various efforts to activate calcium metal have been described.[2-4] Kawabata and co-workers have reported the preparation of organocalcium iodides and bromides by using higher-purity calcium metal than was previously available.[5-7] The reactivities of organocalcium halides, thus prepared, seem to resemble those of organolithium reagents than Grignard reagents.[7] Recently, we have reported the preparation of solvent-free organocalcium halides using calcium atoms.[1] Solvent-free organocalcium halides are highly reactive solids.

On the other hand, there are many articles in the literature concerning the unusual reactivity and chemistry of ultrafine particles (UFP).[8] These active UFP have been easily produced using a heated tungsten basket. Therefore, calcium UFP is expected to be useful for the preparation of various organocalcium halides which are unobtainable by other methods, or which can be prepared only in low yields.

In this paper, we report on a new method for the preparation of organocalcium halides from the corresponding organic halides and calcium UFP produced by a heated tungsten basket.

Results and Discussion

Calcium UFP was conveniently produced by a heated tungsten-wire basket (ca. 900 °C) in an evacuated vessel (ca. 10^{-2}—10^{-3} Torr, 1 Torr=133.322 Pa).[9] After the preparation of the calcium UFP, a desired amount of the calcium UFP was transfered to a reaction flask in an argon-filled glove box. To this reaction flask, organic halides and solvents were syringed in. All manipulations were carried out under an argon atmosphere.

The hydrolysis of the products from the reactions of calcium UFP with organic halides (RX) gave reduction products (RH) and coupling products (R-R) as the main products. These results are summarized in Table 1. It is known that the reduction product is formed quantitatively by the hydrolysis of organocalcium halides.[10,11] Therefore, the yield of the reduction product can be regarded as that of organocalcium halides.

The calcium UFP produced by a heated tungsten-wire basket is useful for the preparation of organocalcium halides in tetrahydrofuran (THF) shown in Table 1. The reaction proceeded smoothly, even at low temperatures, and the Wurtz-type coupling was relatively less important under these conditions. Yields of organocalcium halides were better than those described in the literature.[1]

The reactions of calcium UFP with octyl iodide and bromide, respectively, afforded the corresponding organocalcium halides in high yields (Runs 1 and 3). On the other hand, the reaction was restricted to octyl chloride (Run 5). The ease of reaction with calcium UFP follows the order octyl iodide>octyl bromide≫octyl chloride. The reactivity of octyl halides shown in Table 1 is consistent with that published by Bryce-Smith and Skinner,[2] and Kawabata and coworkers.[5] As shown in Table 1, the preparation of octylcalcium bromide using calcium UFP in the absence of THF was extremely difficult (Run 4). Thus, the reaction of calcium UFP with octyl bromide in toluene at 100 °C for 2 h resulted in a poorer yield. This result is clearly different from that of Kawabata and co-workers.[5-7] These authors described the reactions of alkyl halides with higher-purity calcium metal as proceeding smoothly in toluene. An initiation of the reaction was not necessarily when calcium UFP was used. Thus, calcium UFP reacted with octyl bromide in THF at −5 °C to give a 41.0% yield of octylcalcium bromide in 2 h (Run 2). This reaction started immediately at −5 °C, and was even produced at temperature as low as −78 °C in a 6.4% yield. The yields of the products from reactions of calcium UFP with octyl halides are almost constant within the temperature range examined (10—50 °C).

Calcium UFP easily reacted with cyclohexyl halides (Table 1), but the yields of cyclohexylcalcium halides were lower, as expected, than those of octylcalcium halides (Runs 6—8).

The reactions of calcium UFP with aryl iodides and bromides, respectively, afforded the corresponding arylcalcium halides in high yields (Runs 9, 10, and 14). A higher reaction temperature (50 °C) was necessary to obtain arylcalcium halides in high yields. Calcium UFP reacted selectively with the bromo substituent of *p*-dibromobenzene and *p*-bromochlorobenzene to give bromobenzene and chlorobenzene, respectively (Runs 11 and 12). No reactions of calcium UFP with chlorobenzene and 1-chloronaphthalene took place (Runs 13 and 15).

The reaction of calcium UFP with benzyl bromide gave the corresponding organocalcium halide in low yield on account of a Wurtz-type coupling as a side reaction (Run 16). The reaction was restricted to benzyl chloride (Run 17).

Although organocalcium halides are useful reagents for alkylation and arylation, the following points can be made about the usefulness of the calcium UFP method.

Table 1. Products from the Reactions of Calcium UFP with Organic Halides[a)]

Run	R-X	Solvent	Conditions	Products, Yield/%[b)]	
				R-H	R-R
1	n-$C_8H_{17}I$	THF	10°C, 2h	95.3	
2	n-$C_8H_{17}Br$	THF	−5°C, 2h	41.0	
3	n-$C_8H_{17}Br$	THF	10°C, 2h	70.2	
4	n-$C_8H_{17}Br$	Toluene	100°C, 2h	0.5	
5	n-$C_8H_{17}Cl$	THF	50°C, 2h	0.4	
6	c-$C_6H_{11}I$	THF	10°C, 2h	39.4	
7	c-$C_6H_{11}Br$	THF	10°C, 2h	44.9	
8	c-$C_6H_{11}Cl$	THF	50°C, 2h	5.1	
9		THF	50°C, 2h	65.6	6.7
10		THF	50°C, 2h	58.7	7.8
11	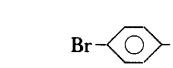	THF	10°C, 2h	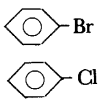 26.7	
12	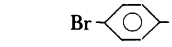	THF	10°C, 2h	20.0	
13		THF	50°C, 2h	no reaction	
14		THF	50°C, 2h	69.9	
15		THF	50°C, 2h	no reaction	
16	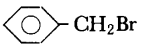	THF	50°C, 2h	3.0	42.0
17	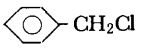	THF	50°C, 2h		trace

a) Typical reaction conditions: Organic halides, 30 mmol, Ca UFP, 10.0 mmol; THF as solvent, 20 cm³. b) Based on the calcium UFP.

(a)Reactions of calcium UFP with various organic iodides and bromides proceed smoothly under an argon atmosphere.

(b) Yields of organocalcium halides are better than those published by other workers.

(c) Low temperatures and short times are required in these reactions.

Experimental

GLC analyses were performed on a Shimadzu GC-6A or 8A gas chromatograph. NMR spectra were obtained with a Varian FT-80 A spectrometer using $CDCl_3$ as the solvent and TMS as the internal standard.

Materials. Calcium metal (granules, 99% pure, Wako Chemicals), organic halides, and other chemicals were commercially available. THF was distilled from benzophenone ketyl immediately prior to use.

Preparation of Calcium UFP. In a typical calcium UFP preparation, calcium metal (300 mg, 7.5 mmol) was vaporized in 30 min, from an aluminum oxide crucible in a tungsten filament (ca. 900°C). This apparatus was contained in a vacuum vessel (ca. 10^{-2}—10^{-3} Torr). The calcium UFP was deposited (vessel immersed in liquid nitrogen). Upon completion of a deposition, the vessel was isolated from the vacuum pump and allowed to become room temperature. The calcium UFP was weighed in an argon-filled glove box.

Reactions of Calcium UFP with Organic Halides. As a typical example, the reaction of calcium UFP with octyl bromide is described. Calcium UFP (9.0 mmol) was transferred to two-necked 50 cm³ flask equipped with a serum cap and reflux condenser. Then, THF (20 cm³) and octyl bromide (27.0 mmol) were syringed in. The reaction mixture was stirred at 10°C for 2 h under argon. After hydrolysis of the reaction mixture with dilute HCl, the organic layer was extracted with ether.

References

1) K. Mochida and H. Ogawa, *J. Organomet. Chem.*, **243**, 131 (1983) and references cited therein.
2) D. Bryce Smith and A. C. Skinner, *J. Chem. Soc.*, **1963**, 577.
3) E. Beckman, *Chem. Ber.*, **38**, 904 (1905).
4) Z. C. Glacet, *Bull. Soc. Chim. Fr*, **5**, 895 (1938).
5) N. Kawabata, A. Matsuura, and S. Yamashita, *Tetrahedron*, **29**, 1069 (1973).
6) N. Kawabata, A. Matsuura, and S. Yamashita, *J. Org. Chem.*, **38**, 4268 (1973).
7) N. Kawabata, H. Kawamura, and S. Yamashita, *J. Org. Chem.*, **38**, 3403 (1973).
8) For examples; K. J. Klabunde, "Chemistry of Free Atoms and Particles," Academic Press, New York (1980); T. Hayashi and Y. Saito, *Kagaku*, **36**, 667 (1984); A. V. Kavaliunas, A. Taylor, and R. D. Rieke, *Organometallics*, **2**, 377 (1983).
9) The diameter of calcium particle produced by a heated tungsten-wire basket was 70—100 nm.
10) M. A. Zemlyanichenko, N. I. Shverdina, I. M. Viktorova, V. A. Chernoplekova, N. P. Bariminova, and K. A. Kocheskov, *Dokl. Akad. Nauk SSSR*, **1970**, 197. *Chem. Abstr.*, **74**, 22932k (1971).
11) B. G. Gowenlock, W. E. Lindsell, and B. Singh, *J. Chem. Soc., Dalton Trans.*, **1978**, 657.

Synthesis of 2-Pyrrolidinylideneacetates by Means of a Reaction of Magnesium Ester Enolate with γ-Cyanoalkyl Tosylates

Kazuhiro KOBAYASHI* and Hiroshi SUGINOME
Organic Synthesis Division, Department of Chemical Process Engineering, Faculty of Engineering, Hokkaido University, Sapporo 060
(Received March 13, 1986)

Synopsis. We describe a new and efficient synthesis of *t*-butyl 2-pyrrolidinylideneacetate and its 3-substituted derivatives from a reaction of the magnesium enolate of *t*-butyl acetate with γ-cyanoalkyl tosylates.

In our revious paper,[1] one of the present authors reported the synthesis of 3-amino-2-alkenoates by means of a reaction of magnesium ester enolates with nitriles. It has been successfully applied to the synthesis of amino sugars such as acosamine[2] and daunosamine.[3] We now wish to report a new method for the synthesis of 2-pyrrolidinylideneacetate (**2**),[4] which is a useful intermediate for the synthesis of several biologically important natural products,[5] by the addition-cyclization sequence from the reaction of the magnesium enolate of *t*-butyl acetate with γ-cyanoalkyl tosylates (**1**).

The magnesium enolate was generated by treatment of *t*-butyl acetate with magnesium bis(diisopropylamide)[6] that had been derived from diisopropylamine and ethylmagnesium bromide (2:1) at 0 °C in diethyl ether; it was then allowed to react with **1** at that temperature. After being warmed up to room temperature, an aqueous work-up followed by distillation or chromatography on silica gel afforded *t*-butyl 2-pyrrolidinylideneacetates (**2**) in fair yields (Scheme 1).[7] We found that 4-bromobutanenitrile can also be used instead of tosylate **1a**.

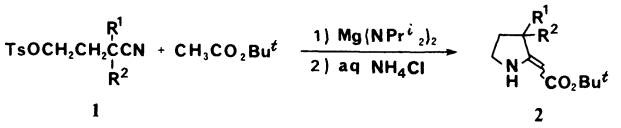

1 2

Scheme 1.

The yields and the stereochemistry of **2** in the reaction of the magnesium ester enolate with various nitriles **1** are summarized in Table 1. The table indicates that the *E*/*Z* ratio of the products **2** depends on the alkyl substituents attached to the carbon atom adjacent to the cyano group of the nitrile **1**. The assignment of their configuration is based on an ^{1}HNMR analysis. The NH proton of the *Z*-form of 2 appears at around δ 7.8,[4a] owing to the intramolecular hydrogen bonding, whereas that of the *E*-form appears at around δ 6.2.

The cyclization of an ambident species **4**, which is the tautomer of the initial adduct **3** in the present reaction, may take place either at the nitrogen or at the carbon center adjacent to the *t*-butoxycarbonyl group to give **2** or an aminocyclopentene **5**, respectively (Scheme 2). The product was, however, found to be an exclusively pyrrolidine derivative **2** and no aminocyclopentene was detected.

Table 1. The Synthesis of *t*-Butyl 2-Pyrrolidinylideneacetates (**2**)

	R^1	R^2	Yield of 2[a]/%	*Z*:*E*[b]
a	H	H	52 (55)[c]	62:38[d]
b	H	Me	60	73:27
c	H	*n*-Bu	56	85:15
d	Me	Me	47	>99: 1
e	Me	Ph	74	>99: 1

a) Isolated Yields. b) Determined by the separation of each isomer by preparative TLC on silica gel. c) 4-Bromobutanenitrile was employed instead of **1a**. d) Determined by the ^{1}H-NMR of an isolated *Z*/*E* mixture.

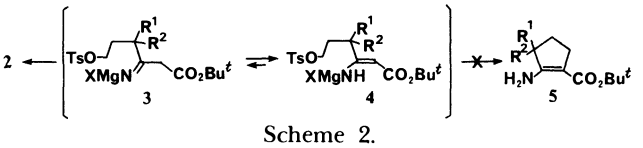

Scheme 2.

Attempts to obtain 2-piperidinylideneacetates from a reaction of the enolate with δ-cyanoalkyl tosylates were unsuccessful.

Experimental

The IR spectra were recorded on a Hitachi 285 spectrometer. The NMR spectra were recorded on a Hitachi R-90B spectrometer in $CDCl_3$ with TMS as an internal standard. Thin-layer chromatography was performed using Merck Silica Gel 60 GF_{254}. All solvents were used after having been dried over appropriate drying agents and distilled under nitrogen.

Preparation of the Cyanoalkyl Tosylate **1**. The cyanoalkyl tosylates **1** were prepared from the corresponding nitriles in three steps. α-Lithiated nitriles[8] were treated with 2-(1-ethoxyethoxy)ethyl bromide[9] to give alkylated nitriles, which were then deprotected with pyridinium *p*-toluenesulfonate (PPTS) in methanol. The resulting hydroxy nitriles were converted into **1** by treatment with *p*-toluenesulfonyl chloride in pyridine. The physical, spectal, and analytical data for **1** are as follows.

3-Cyanopropyl 4-Methylbenzenesulfonate (1a): R_f=0.58 (1:1 AcOEt–hexane); IR (neat) 2230, 1595, 1355, 1175 cm^{-1}; ^{1}HNMR δ=1.8—2.2 (m, 2H), 2.3—2.5 and 2.46 (m and s, combined 5H), 4.14 (t, *J*=5.7 Hz, 2H), 7.36 (d, *J*=8.1 Hz, 2H), 7.80 (d, *J*=8.1 Hz, 2H). Found: *m*/*z* 239.0609. Calcd for $C_{11}H_{13}NO_3S$: M, 239.0617.

3-Cyanobutyl 4-Methylbenzenesulfonate (1b): R_f=0.67 (diethyl ether); IR (neat) 2240, 1600, 1360, 1180 cm^{-1}; ^{1}HNMR δ=1.31 (d, *J*=7.3 Hz, 3H), 1.94 (q, *J*=6.8 Hz, 2H), 2.46 (s, 3H), 2.8 (m, 1H), 4.16 (t, *J*=6.8 Hz, 2H), 7.36 (d, *J*=8.1 Hz, 2H), 7.80 (d, *J*=8.1 Hz, 2H). Found: *m*/*z* 253.0773. Calcd for $C_{12}H_{15}NO_3S$: M, 253.0773.

3-Cyanoheptyl 4-Methylbenzenesulfonate (1c): R_f=0.68 (CH_2Cl_2); IR (neat) 2230, 1595, 1360, 1180 cm^{-1}; ^{1}HNMR

δ=0.92 (t, *J*=6.8 Hz, 3H), 1.2—2.1 (m, 8H), 2.59 (s, 3H), 2.7 (m, 1H), 4.2 (m, 2H), 7.42 (d, *J*=8.1 Hz, 2H), 7.87 (d, *J*=8.1 Hz, 2H). Found: *m/z* 295.1245. Calcd for $C_{15}H_{21}NO_3S$: M, 295.1243.

3-Cyano-3-methylbutyl 4-Methylbenzenesulfonate (1d): R_f=0.36 (1:3 AcOEt-hexane); IR (neat) 2240, 1600, 1365, 1180 cm^{-1}; ^{1}HNMR δ=1.36 (s, 6H), 1.95 (t, *J*=6.6 Hz, 2H), 2.46 (s, 3H), 4.22 (t, *J*=6.6 Hz, 2H), 7.36 (d, *J*=8.2 Hz, 2H), 7.81 (d, *J*=8.2 Hz, 2H). Found: *m/z* 267.0934. Calcd for $C_{13}H_{17}NO_3S$: M, 267.0930.

3-Cyano-3-phenylbutyl 4-Methylbenzenesulfonate (1e): Mp 51—52°C (diethyl ether-hexane); IR (KBr disk) 2240, 1600, 1365, 1180 cm^{-1}; ^{1}HNMR δ=1.72 (s, 3H), 2.34 (t, *J*=7.3 Hz, 2H), 2.45 (s, 3H), 4.1 (m, 2H), 7.3 (m, 7H), 7.71 (d, *J*=8.4 Hz, 2H). Found: *m/z* 329.1082. Calcd for $C_{18}H_{19}NO_3S$: M, 329.1086.

***t*-Butyl (*Z*)- and (*E*)-3-Methyl-2-pyrrolidinylideneacetate (2b). General Procedure.** Diisopropylamine (1.21 g, 12 mmol) was added to an etherial solution (9 ml) of ethylmagnesium bromide (6 mmol) at 0°C and the mixture was stirred for 1 h at the same temperature. To the resulting turbid solution was successively added *t*-butyl acetate (0.36 g, 3 mmol) and **1b** (0.76 g, 3 mmol) in THF (3 ml) and the mixture was allowed to warm up to room temperature. After 30 min the reaction mixture was quenched with aqueous ammonium chloride and extracted with diethyl ether. The extract was washed with brine, dried over anhydrous magnesium sulfate, filtered, and concentrated in vacuo. The oily residue was chromatographed on silica gel (1:3 AcOEt-hexane) to give (*Z*)-**2b** (R_f=0.67, 0.26 g, 44%) and (*E*)-**2b** (R_f=0.58, 0.096 g, 16%). (*Z*)-**2b**: IR (neat) 3370, 1655, 1605 cm^{-1}; ^{1}HNMR δ=1.16 (d, *J*=6.8 Hz, 3H), 1.47 (s, 9H), 1.5—2.1 (m, 2H), 2.7 (m, 1H), 3.5—3.9 (m, 2H), 4.43 (s, 1H), 7.8 (br, 1H). Found: *m/z* 197.1422. Calcd for $C_{11}H_{19}NO_2$: M, 197.1416. (*E*)-**2b**: IR (neat) 3450, 3320 (w), 1660, 1625 cm^{-1}; ^{1}HNMR δ=1.14 (d, *J*=6.8 Hz, 3H), 1.47 (s, 9H), 1.8—2.5 (m, 2H), 3.4—3.7 (m, 3H), 4.48 (s, 1H), 6.2 (br, 1H). Found: *m/z* 197.1403. Calcd for $C_{11}H_{19}NO_2$: M, 197.1416.

***t*-Butyl 2-Pyrrolidinylideneacetate (2a):** A mixture of isomers: Bp 130°C/0.3 Torr†; IR (neat) 3450, 3320, 1645, 1605 cm^{-1}; ^{1}HNMR δ=1.46 (s, 9H), 1.7—2.6 (m, 4H), 3.45 and 3.52 (2t, combined 2H), 4.41 and 4.48 (2s, combined 1H), 6.2 and 7.8 (2br, combined 1H). Found: *m/z* 183.1250. Calcd for $C_{10}H_{17}NO_2$: M, 183.1258.

***t*-Butyl 3-Butyl-2-pyrrolidinylideneacetate (2c):** (*Z*)-**2c**: R_f=0.59 (1:5 AcOEt-hexane); IR (neat) 3360, 1655, 1600 cm^{-1}; ^{1}HNMR δ=0.91 (t, *J*=6.8 Hz, 3H), 1.2—2.8 and 1.48 (m and s, combined 18H), 3.4—3.7 (m, 2H), 4.46 (s, 1H), 7.8 (br, 1H). Found: *m/z* 239.1896. Calcd for $C_{14}H_{25}NO_2$: M, 239.1886.

†1 Torr=133.322 Pa.

(*E*)-**2c**: R_f=0.48 (1:5 AcOEt-hexane); IR (neat) 3450, 3300 (w), 1655, 1620 cm^{-1}; ^{1}HNMR δ=0.91 (t, *J*=6.8 Hz, 3H), 1.2—2.6 and 1.48 (m and s, combined 17H), 3.3—3.6 (m, 3H), 4.51 (s, 1H), 6.2 (br, 1H). Found: *m/z* 239.1888. Calcd for $C_{14}H_{25}NO_2$: M, 239.1886.

***t*-Butyl (*Z*)-3,3-Dimethyl-2-pyrrolidinylideneacetate (2d):** R_f=0.88 (1:1 AcOEt-hexane); IR (neat) 3360, 1655, 1600 cm^{-1}; ^{1}HNMR δ=1.15 (s, 6H), 1.47 (s, 9H), 1.77 (t, *J*=6.8 Hz, 2H), 3.43 (t, *J*=6.8 Hz, 2H), 4.40 (s, 1H), 7.8 (br, 1H). Found: *m/z* 211.1585. Calcd for $C_{12}H_{21}NO_2$: M, 211.1573.

***t*-Butyl (*Z*)-3-Methyl-3-phenyl-2-pyrrolidinylideneacetate (2e):** Mp 116—118°C (hexane); IR (KBr disk) 3380, 1655, 1615 cm^{-1}; ^{1}HNMR 1.46 (s, 9H), 1.56 (s, 3H), 2.0—2.3 (m, 2H), 3.46 (t, *J*=6.2 Hz, 2H), 4.28 (s, 1H), 7.2—7.4 (m, 5H), 7.9—8.2 (br, 1H). Found: *m/z* 273.1718. Calcd for $C_{17}H_{23}NO_2$: M, 273.1728.

References

1) T. Hiyama and K. Kobayashi, *Tetrahedron Lett.*, **23**, 1597 (1982).

2) T. Hiyama, K. Nishide, and K. Kobayashi, *Tetrahedron Lett.*, **25**, 569 (1984).

3) T. Hiyama, K. Nishide, and K. Kobayashi, *Chem. Lett.*, **1984**, 361.

4) Previous general syntheses: a) M. Roth, P. Dubs, E. Goetschi, and A. Eschenmoser, *Helv. Chim. Acta*, **54**, 710 (1971); b) M. M. Gugelchuk, D. J. Hart, and Y. -M. Tsai, *J. Org. Chem.*, **46**, 3671 (1981); c) S. M. Hannick and Y. Kishi, *ibid.*, **48**, 3833 (1983); d) J. P. Celerier, M. G. Richard, and G. Lhomet, *Synthesis*, **1983**, 195, e) M. Yamaguchi and I. Hirao, *J. Org. Chem.*, **50**, 1975 (1985).

5) R. E. Ireland and F. R. Brown, Jr., *J. Org. Chem.*, **45**, 1868 (1980); D. J. Hart and Y. -M. Tsai, *ibid.*, **47**, 4403 (1982); G. Buchanan, G. Singh, and R. H. Wightman, *J. Chem. Soc., Chem. Commun.*, **1984**, 1299; J. S. Peterson, G. Fels, and H. Rapoport, *J. Am. Chem. Soc.*, **106**, 4539 (1984); see also Ref. 4c.

6) F. Korte and K. H. Buchel, *Chem. Ber.*, **93**, 1025 (1960); H. Kukertz and U. Wannagat, *Angew. Chem. Int. Ed. Engl.*, **2**, 47 (1963).

7) Hannick and Kishi (Ref. 4c) have reported a similar addition of zinc ester enolates to γ-cyanoalkyl mesylates and the subsequent cyclization of the adducts using potassium carbonate. The reaction, however, needs a large excess of activated zinc and α-bromo esters.

8) E. M. Kaiser and C. R. Hauser, *J. Org. Chem.*, **33**, 3402 (1968); K. Kobayashi and T. Hiyama, *Tetrahedron Lett.*, **24**, 3509 (1983).

9) C. G. M. Janssen and E. F. Godefroi, *Org. Prep. Proced. Int.*, **13**, 209 (1981); *Chem. Abstr.*, **95**, 61359e (1983).

Oxidation of Cyclopentene by $RuCl_3$-NaOCl Catalyst

Hideo ORITA,* Takashi HAYAKAWA, and Katsuomi TAKEHIRA
National Chemical Laboratory for Industry, Yatabe, Ibaraki 305
(Received October 15, 1985)

Synopsis. Oxidation of cyclopentene by $RuCl_3$-NaOCl catalyst in an aqueous-organic two phase system was investigated by changing compositions of solvent system and additives to the aqueous solution. Use of acetonitrile as a cosolvent enhanced the reaction rate greatly, and addition of NaOH improved the yield of glutaric acid up to 80%.

Ruthenium tetraoxide is one of the most powerful oxidants of various organic compounds under mild condition.[1] Berkowitz and Rylander[2] reported the oxidation of various organic compounds by using ruthenium tetraoxide as a stoichiometric oxidant. In 1970, Wolfe et al.[3] reported that cyclohexene was oxidized to adipic acid (86—95%) with RuO_4 generated in situ from $RuCl_3$ and sodium hypochlorite. Foglia et al.[4] reexamined the work of Wolfe et al., and found that this procedure gave good yield of cleavage products from *acyclic* alkenes only when the oxidations were carried out with added sodium hydroxide and a *phase transfer catalyst*. Furthermore, the direct oxidation of cyclic olefines to corresponding dicarboxylic acids with RuO_2 (or $RuCl_3$)-hypochlorite oxidant was scarcely investigated.

Sharpless et al.[5] reported an improved procedure for traditional $RuCl_3 \cdot xH_2O$-IO_4^-/CCl_4-H_2O catalytic oxidation system by adding acetonitrile as a cosolvent. The effects of acetonitrile are speculated to disrupt the inactive lower valent ruthenium complexes and return the ruthenium to the catalytic cycle. Although this method is convenient, it also has several drawbacks owing to using periodate as a reoxidant; the relative high cost and high molecular weight of periodate; the precipitation of voluminous quantities of iodate as the reaction proceeds. We describe herein a convenient and effective procedure of the oxidation of cyclopentene to glutaric acid by using readily available sodium hypochlorite in the presence of a catalytic amount of $RuCl_3 \cdot xH_2O$.

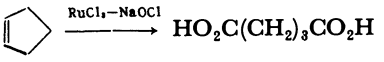

Experimental

The reaction was carried out in a three necked flask equipped with a magnetic stirrer, addition funnel, and condenser. The typical experiment is as follows. The flask was charged with 90 ml of CCl_4, 10 ml of H_2O, 3.2 g of cyclopentene (47 mmol), and 0.15 g of $RuCl_3 \cdot xH_2O$ (the molar ratio of $RuCl_3$ to cyclopentene was 0.014 on calculations based on x=1). Aqueous sodium hypochlorite (100 g of 21 wt% solution, 282 mmol) with added 4 g of NaOH was added to the stirred CCl_4 solution dropwise for about 2 h while the flask was cooled by means of an ice bath. The vigorous stirring was continued until the color of the reaction solution turned black, at which time the starch iodide test for active chlorine was negative. The reaction mixture was filtered through a Celite pad in order to remove the precipitated RuO_2. After the separation of organic layer, the aqueous phase was washed with CH_2Cl_2, acidified to a pH of one with concd HCl and the solvent was removed under reduced pressure. The residual solid was extracted with ether, and the solvent was removed under reduced pressure to give 4.7 g of white powder. After esterification by BF_3-methanol reagent, gas chromatography showed that 4.4 g of glutaric acid (71 mol% yield based on charged cyclopentene) was produced. The products were also identified by IR.

Results and Discussion

Oxidation of cyclopentene by $RuCl_3$-NaOCl catalyst was investigated under various conditions and the results are shown in Table 1. The reaction time and the yield of glutaric acid were very dependent on the compositions of the organic solvent and the addtion of alkali to the aqueous solution. In the absence of alkali (Runs 1 and 2, the reaction conditions were similar to the work of Wolfe et al.[3]), or when sodium

Table 1. Oxidation of Cyclopentene by $RuCl_3$-NaOCl Catalysts[a]

Run	Solvent / ml	Alkali / g	Reaction time/h	Products		
				total amount / g	glutaric acid / g	yield / mol%
1	CCl_4, 90 H_2O, 10	—	8	3.1	2.3	37
2	CH_2Cl_2, 90 H_2O, 10	—	8.5	3.0	2.1	34
3	CCl_4, 90 H_2O, 10	NaOH, 4	8	4.7	4.4	71
4	CCl_4, 90 CH_3CN, 10	NaOH, 4	6.5	5.0	4.9	79
5	CCl_4, 70 CH_3CN, 30	NaOH, 4	2	4.1	4.1	66
6	CCl_4, 50 CH_3CN, 50	NaOH, 4	2	5.2	5.1	82
7	CH_3CN, 90 H_2O, 10	NaOH, 4	2	4.3	4.3	69
8	CCl_4, 90 CH_3CN, 10	$Na_2CO_3 \cdot 10H_2O$, 14	3.5	3.9	2.9	47

a) Cyclopentene 3.2 g, NaOCl aqueous solution 100 g (21 wt%, 282 mmol), $RuCl_3 \cdot xH_2O$ 0.15 g.

carbonate was used instead of NaOH (Run 8), the yield and selectivity of glutaric acid were relatively low. Determination by gas chromatography indicated that a considerable amount of succinic acid (about 10 mol% yield) was produced. This result indicated that the further oxidation of glutaric acid occurred. Furthermore, all of ruthenium catalyst could not be recovered as RuO_2 by means of filtration of the reaction mixture and the aqueous solution remained black even after the filtration.

The addition of NaOH (the molar ratio of NaOH to cyclopentene is 2) improved the yield of glutaric acid considerably. In these cases, all of the ruthenium catalyst could be recovered by filtration and reused easily. The effects of added NaOH are considered to depress the formation of hypochlorous acid, which often leads to the formation of chlorinated byproducts by addition to the double bond,[6] to prevent glutaric acid from the consecutive oxidation in organic layer by extraction to the aqueous layer as sodium salt, and to promote the precipitation of RuO_2 after all the consumption of charged sodium hypochlorite. Under alkaline conditions, RuO_4 is readily reduced to RuO_4^- and further to RuO_4^{2-}.[7] It was found that the molar ratio of about 2:1 NaOH to cyclopentene gave the good yield of glutaric acid. The further addition of NaOH promoted reduction of RuO_4 to RuO_4^{2-}, which is a good oxidant for alcohols but not for alkenes,[8] and then led to slower reaction and poorer yield.

When acetonitrile was used as a cosolvent of cyclopentene, the reaction rate increased greatly, and the yield of glutaric acid improved up to 82 mol% (Run 6). Although the effect of acetonitrile is not understood well in the present stage, we also speculate that acetonitrile disrupts the inactive lower valent ruthenium carboxylate complexes and makes the regeneration of RuO_4 much easier. In the work of Sharpless et al.,[5] the third solvent component, CCl_4, was necessary for the reaction. However, the solvent system which consisted of acetonitrile and water alone gave the fairly good yield of glutaric acid (Run 7) in the present work.

Although the addtion of propionitrile to the reaction mixture in place of acetonitrile also enhanced the reaction rate, the yield of glutaric acid decreased 80% of that when acetonitrile was used. Adiponitrile was not an effective cosolvent, and rather made the reaction very slow and/or incomplete. This might be due to inactivation of the catalyst owing to its strong bonding to the ruthenium.

The oxidation of other cycloalkenes with $RuCl_3$–NaOCl catalysts was also examined (the reaction conditions were the same as those of run 6 in Table 1). Cyclohexene was oxidized to adipic acid in 56 mol%, and cyclooctene to suberic acid in 36 mol%, pimeric acid in 5 mol%, and adipic acid in 5 mol%. As the ring size of cyclic olefins became bigger, and the reaction took longer time (7 h for cyclohexene and overnight for cyclooctene) and the yield of corresponding dicarboxylic acids decreased. Extention of this catalytic system to cyclododecene oxidation proved impractical, since soap formation seriously complicated reaction procedure. Cyclohexanone was oxidized under similar conditions to adipic acid in 45 mol%, glutaric acid in 1 mol%, and succinic acid in 1 mol%.

Table 2. Ruthenium-Catalyzed Oxidation of Cyclopentene with Various Reoxidants[a]

Reoxidant	Reaction time	Yield of glutaric acid/%[b]
NaOCl[c]	2 h	82
$NaClO_2$[d]	8.5 h	53
$NaClO_3$[e]	1 d	—[i]
$NaBrO_2$[f]	1 d	32
$NaBrO_3$[g]	1 d	21
$NaIO_4$[h]	1 d	68

a) Cyclopentene 3.2 g, $RuCl_3 \cdot xH_2O$ 0.15 g, CCl_4 50 ml, CH_3CN 50 ml. b) Determined by GC after esterification. c) 21 wt% NaOCl aqueous solution 100 g, NaOH 4 g. d) $NaClO_2$ 9 g in H_2O 100 ml, NaOH 2 g. e) $NaClO_3$ 7 g in H_2O 100 ml. f) $NaBrO_2 \cdot 3H_2O$ 18 g in H_2O 100 ml, NaOH 2 g. g) $NaBrO_3$ 9.5 g in H_2O 100 ml. h) Cyclopentene 1 g, $RuCl_3 \cdot xH_2O$ 0.05 g, $NaIO_4$ 15 g in H_2O 100 ml. i) Not reacted.

The ruthenium catalyzed oxidation of cyclopentene with various reoxidants was investigated and the results are tabulated in Table 2. The reaction conditions were slightly different from one to another, but not optimized. Among the reoxidants investigated, NaOCl gave the best yield of glutaric acid. Although $NaIO_4$ gave the fairly good result, reaction took longer time and the precipitation of the voluminous amounts of iodate during the reaction made the reaction system complicated.

References

1) E. S. Gore, *Platinum Metal Rev.*, **27**, 111 (1983).
2) L. M. Berkowitz and P. N. Rylander, *J. Am. Chem. Soc.*, **80**, 6682 (1958).
3) S. Wolfe, S. K. Hasan, and J. R. Campbell, *J. Chem. Soc.,Chem. Commum.*, **1970**, 1420.
4) T. A. Foglia, P. A. Barr, and A. J. Malloy, *J. Am. Oil Chem. Soc.*, **54**, 858A (1977); T. A. Foglia, P. A. Barr, A. J. Malloy, and M. J. Costanzo, *ibid.*, **54**, 870A (1977).
5) P. H. J. Carlsen, T. Katsuki, V. S. Martin, and K. B. Sharpless, *J. Org. Chem.*, **46**, 3936 (1981).
6) S. G. Hegde, M. K. Vogel, J. Saddler, T. Hrinyo, N. Rockwell, R. Haynes, M. Oliver, and J. Wolinsky, *Tetrahedron Lett.*, **21**, 441 (1980).
7) Y. Nakano and T. A. Foglia, *J. Am. Oil Chem. Soc.*, **59**, 163 (1982).
8) D. G. Lee, D. T. Hall, and J. H. Cleland, *Can. J. Chem.*, **50**, 3741 (1972); M. Schröder and W. P. Griffith, *J. Chem. Soc., Chem. Commun.*, **1979**, 58; G. Green, W. P. Griffith, D. M. Hollinshead, S. V. Ley, and M. Schröder, *J. Chem. Soc., Perkin Trans. 1*, **1984**, 681.

Temperature Dependence of ^{35}Cl Nuclear Quadrupole Resonance Frequencies and Hydrogen Bonding in Some Metal(II) Hexachlorostannate(IV) Hexahydrates

Keizo HORIUCHI, Akinobu SASANE, Yoshihiro MORI, Tetsuo ASAJI,† and Daiyu NAKAMURA†,*
Department of Chemistry, Faculty of Science, Shinshu University, Matsumoto 390
†Department of Chemistry, Faculty of Science, Nagoya University, Chikusa-ku, Nagoya 464
(Received March 20, 1986)

Synopsis. The temperature dependences of ^{35}Cl NQR frequencies were observed over a fairly wide range of temperature for $MSnCl_6 \cdot 6H_2O$ [M(II)=Mg, Ca, Mn, Co, Ni] forming isomorphous crystals ($R\bar{3}$) at room temperature. These complexes yielded unusual ^{35}Cl NQR temperature dependence curves showing a positive temperature coefficient. This can be attributed to the existence of Cl···H-O type weak hydrogen bonds.

The ^{35}Cl NQR frequencies of $MSnCl_6 \cdot 6H_2O$ [M(II)= Mg, Ca, Zn, Cd, Mn, Co, Ni] were reported by Graybeal et al.[1] and independently by Brill et al.[2] For the Ca(II) and Mg(II) salts, the temperature dependence of ^{35}Cl NQR frequencies was studied and the positive temperature coefficients were found. Although Graybeal et al.[1] attributed the unusual positive temperature coefficient to the π bond character of Sn-Cl bonds,[3] their explanation seems to be implausible because no positive temperature coefficients were observed for several R_2SnCl_6 type complexes.[4] As already suggested by one of the present authors,[5] the observed positive coefficient is attributable to hydrogen bonds formed between chloride ligands and water molecules.

Recently, Kitazume et al.[6] determined the crystal structure of $CaSnCl_6 \cdot 6H_2O$ by single-crystal X-ray diffraction and NQR Zeeman effect measurements. From these studies, they concluded that the anomalous temperature dependence of ^{35}Cl NQR frequencies is due to the hydrogen bonding effect as already pointed out.[5] In order to obtain further information about the suggested mechanism which gives rise to the positive temperature coefficient, the temperature dependence study of ^{35}Cl NQR frequencies was carried out for some hexachlorostannates(IV) crystallized with hexahydrated divalent counter cations.

Experimental

Measurements of ^{35}Cl NQR frequencies were performed above 77 K by use of a modified Dean-type spectrometer described elsewhere.[7] For $NiSnCl_6 \cdot 6H_2O$, the measurements were extended down to 4.2 K by employing a homemade cryostat. Temperatures were determined using a chromel vs. alumel and a chromel vs. gold (0.03% iron) thermocouple above and below 77 K, respectively, within the accuracy of ±1 K.

The all complexes studied were prepared according to the method described in literature.[2] Deuterated compounds, $CaSnCl_6 \cdot 6D_2O$, $CoSnCl_6 \cdot 6D_2O$, and $NiSnCl_6 \cdot 6D_2O$, were synthesized in a dry box using deuterated hydrochloric acid and $SnCl_4$. The extent of deuteration (>95%) was checked by means of Hitachi EPI-G and 345 infrared spectrometers.

Results and Discussion

X-Ray powder patterns recorded for the complexes studied could be well interpreted by use of the reported lattice constants with the space group of $R\bar{3}$.[6,8] Only one ^{35}Cl NQR line was found in each complex studied in agreement with the crystal structure already reported. The frequencies determined at four temperatures are listed in Table 1.

The NQR frequencies observed at room temperature for the present complexes except for the Ni(II) salt agree well with the reported values.[1,2] For the Ni(II) salt, Graybeal et al.[1] reported two very closely spaced ^{35}Cl NQR frequencies. The appearance of multiplet structure for the resonance line of the Mg(II) and Ca(II) salts at lower temperatures was also pointed out by the same authors. However, only a broad single line could be observed for the Ni(II) salt at all temperatures studied and for the Mg(II) and Ca(II) salts even at lower temperatures. Although the existence of phase transitions above room temperature had been reported for the Ca(II) salt,[6] no heat anomaly was observed in the present DTA measurements up to the fade-out temperature of the NQR signal (≈390 K).

The Mg(II) and Ca(II) salts gave a very broad signal at 77 K. With increasing temperature, the signals became gradually sharp. A broad and intense ^{35}Cl NQR signal was observed for the remaining complexes at 77 K and for the Ni(II) salt even at 4.2 K. This means that no saturation effect was observed for the Ni(II) salt because of the presence of paramagnetic ions in the crystal. With increasing temperature, the resonance frequencies of these paramagnetic com-

Table 1. ^{35}Cl Nuclear Quadrupole Resonance Frequencies in Some Hexachlorostannates(IV) Crystallized with Hexahydrated Divalent Cations Observed at Several Temperatures

Compound	Frequency(±0.002)/MHz			
	77 K	193 K	293 K	382 K
$MgSnCl_6 \cdot 6H_2O$	15.82_4[b]	15.820[a]	15.834	15.861
$CaSnCl_6 \cdot 6H_2O$	15.94_1[b]	15.902[a]	15.902	15.90_6[b]
$CaSnCl_6 \cdot 6D_2O$	15.906[a]	15.897[a]	15.903	15.90_9[b]
$MnSnCl_6 \cdot 6H_2O$	15.733[a]	15.739	15.770	15.813
$CoSnCl_6 \cdot 6H_2O$	15.694[a]	15.706	15.750	15.808
$CoSnCl_6 \cdot 6D_2O$	15.670[a]	15.697	15.750	15.813
$NiSnCl_6 \cdot 6H_2O$	15.670[a] (15.675[a])[c]	15.681	15.720	15.773
$NiSnCl_6 \cdot 6D_2O$	15.648[a]	15.671	15.718	15.781

a) ±0.005 MHz. b) ±0.010 MHz. c) at 4.2 K.

plexes increased rather rapidly.

For $CoSnCl_6 \cdot 6D_2O$, two ^{35}Cl resonance lines in place of a single line could be observed at first. The complex freshly prepared yielded two broad resonance lines at 15.75 and 15.90 MHz at room temperature. Immediately after the first annealing at ca. 450 K, only the high frequency line could be observed. However, no resonance could be detected with the above same sample after six months. The crystals which gave only the strong and sharp low-frequency line was obtained by the second annealing at ca. 410 K. This crystalline state showing the low-frequency line was stable and the high-frequency line could not be detected any more throughout the measurements of the temperature dependence of NQR frequencies as well as even after six months. For $CoSnCl_6 \cdot 6D_2O$, the data of this crystalline state are indicated in Table 1 and in Fig. 1. No such anomaly due to annealing could be observed for $CoSnCl_6 \cdot 6H_2O$ and the other complexes studied. A similar phenomenon has been also observed for $MnPtCl_6 \cdot 6D_2O$.[7]

It is interesting to note that the resonance frequency observed at 77 K for these complexes decreases in the order of Ca(II), Mg(II), Mn(II), Co(II), and Ni(II), which approximately coincides with the order of increasing electronegativities.[9,10] According to the X-ray analysis of $CaSnCl_6 \cdot 6H_2O$, each chloride ion has three neighboring hydrogens which exist nearly on the plane including the chloride ion and perpendicular to the Sn–Cl bond axis. Let the bond axis be the z axis. Then, the three hydrogens are nearly on the xy plane. Since each hydrogen of water molecules is polarized positively, the hydrogen bearing a fractional positive charge will draw out the $3p_x$ or $3p_y$ electrons of the chloride ligand to the higher orbitals. This means that the $3p_x$ and/or $3p_y$ electron cloud will be expanded and the unbalanced p electrons of the chloride ligand decrease leading to a decrease of the ^{35}Cl NQR frequency. The lone-pair electrons of water molecules attached to a more electronegative divalent cation may be drawn out more strongly to the cation resulting in an increase of a fractional positive charge on the hydrogens. In other words, those water molecules form stronger hydrogen bonds with the chloride ligands at lower temperatures, where the motion of water molecules and/or complex anions can be neglected. This is an explanation of the correlation between the ^{35}Cl NQR frequencies observed at 77 K and the electronegativity of the divalent cations in these complexes.

With increasing the temperature from ca. 100 K, the ^{35}Cl NQR frequency of the all complexes except for the Mg(II) and Ca(II) salts increased and also its temperature coefficient became larger. This effect is remarkable especially for the Mn(II), Co(II), and Ni(II) salts which yield lower NQR frequencies at lower temperatures as can be seen in Fig. 1. The Mg(II) salt showed a maximum of the NQR frequency at ca. 450 K, above which temperature the frequency decreased with increasing temperature. The NQR frequency of the Ca(II) salts decreased with increasing temperature above 77 K. However, $CaSnCl_6 \cdot 6H_2O$ yielded a broad minimum and a maximum at ca. 250 and ca. 380 K,

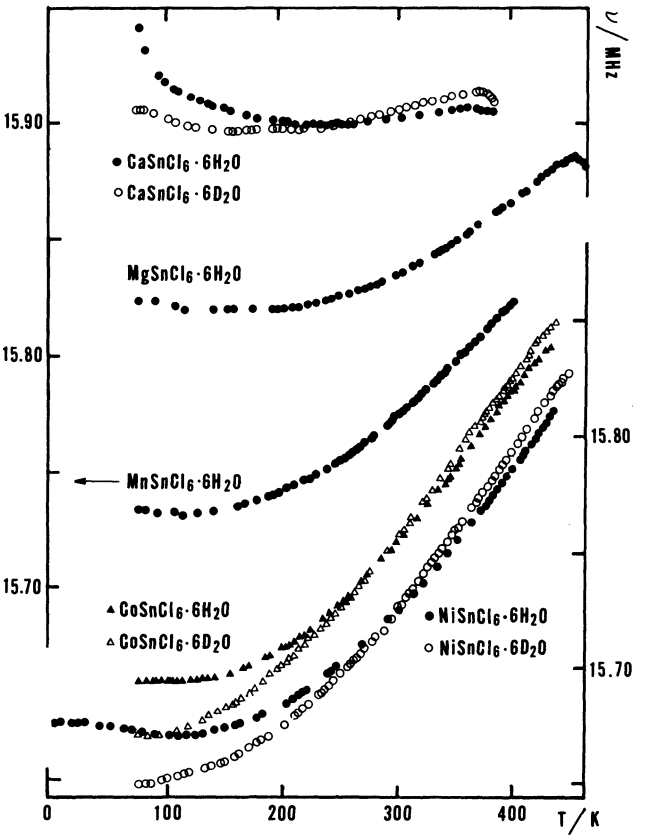

Fig. 1. Temperature dependence of ^{35}Cl NQR frequencies in the crystals of $MSnCl_6 \cdot 6H_2O$ [M(II): Mg, Ca, Mn, Co, Ni] and $MSnCl_6 \cdot 6D_2O$ [M(II): Ca, Co, Ni] observed above 77 K. For $NiSnCl_6 \cdot 6H_2O$, measurements were extended down to 4.2 K.

respectively, while $CaSnCl_6 \cdot 6D_2O$ yielded them at ca. 170 and 385 K, respectively. These results can be explained as follows.

At first, we discuss about the above results only on the usual ^1H hydrated complexes. With increasing temperature, the motions of water molecules, which are mainly librational motions are thought to be excited and the hydrogen bonding can be considered to be weakened gradually. This leads to an increase of the NQR frequency for the present type of hydrogen bonding.[5,11] For the Mn(II), Co(II), and Ni(II) complexes, the effect due to the weakening of hydrogen bonding prevails over the normal Bayer effect[12] yielding a positive temperature coefficient up to each fade-out temperature of the NQR frequencies. For the Mg(II) salt, the former effect dominates against the latter below the maximum temperature whereas the latter does above the temperature. The Ca(II) salts probably having the weakest hydrogen bonds among the present complexes show the smallest contribution to the temperature dependence from the hydrogen-bond effect. At high temperatures, the resonance frequencies of these complexes seem to converge upon ca. 15.85 MHz. This is considerably large among various complexes having $[SnCl_6]^{2-}$ ions ever studied at room temperature[2,4] and may be the resonance frequency of the complex anion crystallized with large cations. The cation size effect in complexes was already

discussed.[13]

For the deuterated analogs of the Ca(II), Co(II), and Ni(II) complexes, the temperature dependence of ^{35}Cl NQR frequencies was also studied. In these complexes, it was commonly observed that the resonance frequencies determined for each deuterated analog at lower temperatures were smaller than those of the corresponding protonated complex. However, each deuterated analog showed slightly larger NQR frequencies at higher temperatures than the corresponding protonated one. At 77 K, the frequency difference between the deuterated and protonated analogs of each kind is fairly large amounting to 20—30 kHz. The above isotope effect detected on the ^{35}Cl NQR frequencies of these complexes can be understood as described below.

Since the amplitude of the librations and/or the frequency of the reorientational motions of coordinated water molecules can be expected to be reduced by deuteration, the motionally averaged distance $\langle r_{H\cdots Cl}\rangle$ may become longer than the $\langle r_{D\cdots Cl}\rangle$.[14] Therefore, the ^{35}Cl NQR frequency in crystals having hydrogen bonds of the present type decreases by deuteration at lower temperatures where only low-frequency vibrations such as librations are considered to affect the NQR frequency. At higher temperatures where librations are well excited, however, the anharmonicity of the stretching vibration of water molecules appears as the most important origin of the isotope effect. Owing to the anharmonicity of the interatomic potential, the distance $r_{X\cdots Y}$ is assumed to be elongated by deuteration in a hydrogen bond system X–H···Y.[15] For this case, the NQR frequency of the present complexes is expected to increase by deuteration as really observed at high temperatures. This isotope effect was already pointed out from the ^{35}Cl NQR study to exist in some compounds involving O–H···Cl type hydrogen bonds.[16]

The authors are grateful to Mr. Hitoshi Ota for his help in preparing some complexes.

References

1) J. D. Graybeal, R. J. McKown, and S. D. Ing, *J. Phys. Chem.*, **74**, 1814 (1970).
2) T. B. Brill, Z. Z. Hugus, Jr., and A. F. Schreiner, *J. Phys. Chem.*, **74**, 2999 (1970).
3) R. Ikeda, D. Nakamura, and M. Kubo, *J. Phys. Chem.*, **69**, 2101 (1965); *Bull. Chem. Soc. Jpn.*, **36**, 1056 (1963).
4) D. Nakamura, *Bull. Chem. Soc. Jpn.*, **36**, 1662 (1963); A. Sasane, D. Nakamura, and M. Kubo, *J. Magn. Reson.*, **3**, 76 (1970).
5) D. Nakamura, R. Ikeda, and M. Kubo, *Coord. Chem. Rev.*, **17**, 281 (1975).
6) T. Kitazume, M. Sekizaki, and M. Suhara, *J. Mol. Struct.*, **58**, 161 (1980).
7) A. Sasane, H. Shinohara, Y. Mori, Y. Kume, T. Asaji, and D. Nakamura, to be published.
8) "Crystal Data Determinative Tables," 3rd ed., Vol. 2, Inorg. Compds., U. S. Dept. of Commerce, N. B. S., and the Joint Committee on Powder Diffraction Standards, USA, 1973.
9) M. C. Day, Jr. and J. Selbin, "Theoretical Inorganic Chemistry," 2nd ed., Reinhold Book Co., New York (1968), p. 132.
10) W. Gordy and R. L. Cook, "Microwave Molecular Spectra," 3rd ed., John Wiley & Sons, Inc., New York (1984), p. 875.
11) A. Sasane, T. Matsuo, D. Nakamura, and M. Kubo, *J. Magn. Reson.*, **4**, 257 (1971).
12) H. Bayer, *Z. Physik*, **130**, 227 (1951).
13) D. Nakamura and M. Kubo, *J. Phys. Chem.*, **68**, 2986 (1964).
14) L. V. Jones, M. Sabir, and J. A. S. Smith, *J. Chem. Soc., Dalton Trans.*, **1979**, 703.
15) I. Olovsson and P. G. Jönsson, "The Hydrogen Bond," ed by P. Schuster et al., North Holland, Amsterdam (1976), Vol. II.
16) W. Pies and A. Weiss, *Adv. Nucl. Quadrupole Reson.*, **1**, 57 (1974); *J. Magn. Reson.*, **30**, 469 (1978); *Bull. Chem. Soc. Jpn.*, **51**, 1051 (1978).

An ^{1}H NMR Study on the Motion of Guanidinium Cations in Some Crystals Formed with Tetrahedral or Octahedral Complex Anions Having Halide Ions as Ligands

Yoshihiro FURUKAWA and Daiyu NAKAMURA*
Department of Chemistry, Faculty of Science, Nagoya University, Chikusa-ku, Nagoya 464
(Received March 25, 1986)

Synopsis. The temperature dependences of ^{1}H NMR spin-lattice relaxation times were determined at 20 MHz for $[C(NH_2)_3]_2ZnX_4$ (X=Cl, Br), $[C(NH_2)_3]_2MCl_6$ (M=Sn, Te, Pt), and $[C(NH_2)_3]_2PtBr_6$. Above room temperature, the D_{3h} cation undergoes reorientational motion by 120° about the cationic C_3 axis. For $[C(NH_2)_3]_2TeCl_6$ crystals, two phase transitions were located at 312 and 373 K.

Recently, we studied the temperature dependences of ^{1}H NMR second moments and ^{1}H spin-lattice relaxation times (T_1) in various guanidinium (guH^+) salts involving simple salts such as guanidinium halides and the salts with D_{4h} tetrahalo complexes, such as tetrahaloaurates(III), and obtained information about the motion of the cation in solids.[1-3] From these investigations, it becomes apparent that with increasing temperature the cation undergoes 120° reorientations as a whole, i.e., the C_3 reorientation, about the principal axis of the D_{3h} cation. The observed activation energies (E_a) for this motion are distributed in a fairly wide range from 78 kJ mol^{-1} for (guH)Cl to 20 kJ mol^{-1} for the high-temperature phase and its supercooled state of (guH)$AuBr_4$. This is presumably due to the following reasons. The strength of hydrogen bonding formed between the cation and the counter anion is considered to vary to a large extent from salt to salt. Furthermore, steric hindrance to perform the C_3 reorientation may be largely determined by the loosely or densely packed crystal structure, where the size and/or the shape of the counter anion might play a crucial role. To clarify which is the most important factor, the accumulation of much more data is required. Therefore, the present investigation of ^{1}H T_1 has been undertaken for some guanidinium salts containing tetrahalo T_d and hexahalo O_h complex anions.

Experimental

$(guH)_2ZnCl_4$ and $(guH)_2ZnBr_4$ were prepared by adding the corresponding guanidinium halide to a hydrohalogenic acid solution of $ZnCl_2$ and $ZnBr_2$, respectively. Colorless crystals were obtained for both complexes. Colorless $(guH)_2SnCl_6$ and yellow $(guH)_2TeCl_6$ crystals were obtained by mixing a concd aqueous solution of (guH)Cl with concd hydrochloric acid solutions of $SnCl_4 \cdot xH_2O$ and TeO_2, respectively.[4,5] Orange colored crystals of $(guH)_2PtCl_6$ were obtained from $(guH)_2PtCl_4$ which had been synthesized in the previous work[1] by oxidizing it with chlorine gas in a concd hydrochloric acid solution. Reddish brown $(guH)_2PtBr_6$ crystals were prepared by adding a concd aqueous solution of (guH)Br to a concd hydrobromic acid solution of hexabromoplatinic(IV) acid. All samples prepared were identified by usual chemical analysis. Anal. Calcd for $[C(NH_2)_3]_2ZnCl_4$: N, 25.7; Cl, 43.3%. Found: N, 26.0; Cl, 43.6%. Calcd for $[C(NH_2)_3]_2ZnBr_4$: N, 16.6; Br, 63.3%. Found: N, 16.8; Br, 63.5%. Calcd for $[C(NH_2)_3]_2SnCl_6$: N, 18.6%. Found: N, 18.9%. Calcd for $[C(NH_2)_3]TeCl_6$: N, 18.3; Cl, 46.2%. Found: N, 18.5; Cl, 46.0%. Calcd for $[C(NH_2)_3]_2PtCl_6$: N, 15.9; Cl, 40.3%. Found: N, 16.2; Cl, 40.2%. Calcd for $[C(NH_2)_3]_2PtBr_6$: N, 10.6; Br, 60.3%. Found: N, 10.7; Br, 60.2%.

A pulsed NMR spectrometer[6] was employed for the measurements of the temperature dependence of ^{1}H T_1 observed at 20 MHz. A usual π-τ-$\pi/2$ pulse sequence was used for the determination of T_1. Differential thermal analysis (DTA) curves for $(guH)_2TeCl_6$ were recorded by use of a homemade apparatus.[7] Sample temperatures were determined within the accuracy of ±1 K using copper-constantan thermocouples.

Results and Discussion

The temperature dependences of ^{1}H T_1 observed at 20 MHz are shown in Fig. 1 for $(guH)_2ZnCl_4$ and $(guH)_2ZnBr_4$, and in Fig. 2 for $(guH)_2SnCl_6$, $(guH)_2TeCl_6$, $(guH)_2PtCl_6$, and $(guH)_2PtBr_6$. All of these complexes showed a single ^{1}H T_1 minimum above room temperature having approximately the same T_1 minimum value. The present complexes except $(guH)_2TeCl_6$ yielded usual T_1 curves explainable by the simple BPP theory.[8] The ^{1}H T_1 curve of $(guH)_2TeCl_6$ showed anomalies suggesting the presence of phase transitions.

When $(guH)_2TeCl_6$ was heated from room temperature, ^{1}H T_1 observed decreased monotonously up to ca. 315 K where it increased discontinuously. With further increasing temperature, $\log T_1$ again decreased linearly with decreasing T^{-1} although it decreased discontinuously at 373 K. Above this temperature, $(guH)_2TeCl_6$ yielded a usual BPP curve.

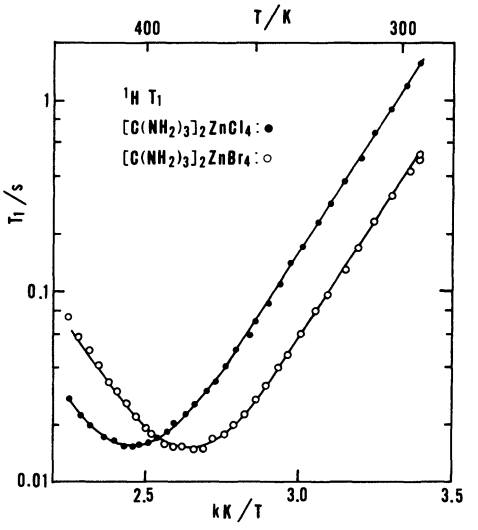

Fig. 1. Temperature dependences of ^{1}H T_1 determined at 20 MHz for guanidinium tetrachloro- and tetrabromozincate(II). Best-fitted BPP curves are depicted by solid line.

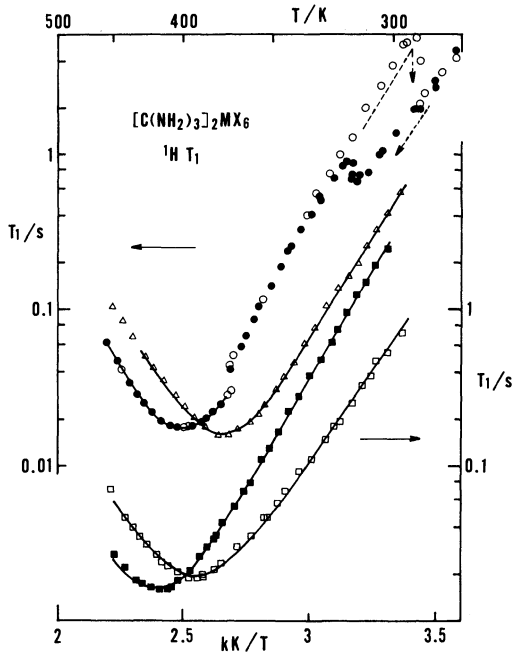

Fig. 2. Temperature dependences of ^1H T_1 determined at 20 MHz for $[C(NH_2)_3]_2SnCl_6$ (△), $[C(NH_2)_3]_2PtCl_6$ (■), and $[C(NH_2)_3]_2PtBr_6$ (□). The data of $[C(NH_2)_3]_2TeCl_6$ are also plotted by ● and ○ for the heating and cooling runs, respectively. Best-fitted curves are indicated by solid line. Broken lines with arrows show heating and cooling processes.

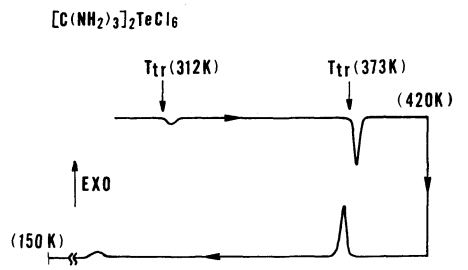

Fig. 3. DTA curves recorded for guanidinium hexachlorotellurate(IV).

When the temperature was lowered from ca. 450 K, the ^1H T_1 value observed followed the same curve down to ca. 330 K as that obtained on the heating run. Below this temperature, $\log T_1$ values obtained deviated from the curve observed on the heating run and increased almost linearly against T^{-1} down to ca. 290 K. Around this temperature, ^1H T_1 shortened drastically to the value which was observed on the heating run. Below this temperature, $\log T_1$ increased linearly with increasing T^{-1}.

To confirm the occurrence of phase transitions and to determine the phase-transition temperature, T_{tr}, DTA experiments were carried out for $(guH)_2TeCl_6$ (see Fig. 3). When the sample was heated, small and large endothermic peaks appeared at 312 and 373 K, respectively. With decreasing temperature, exothermic anomalies corresponding to the above ones were detected at 372 and near 290 K. Since the latter heat anomaly was weak and broad, a definite transition temperature could not be located on the cooling run. However, it can be said that this phase transition shows marked hysteresis phenomenon as was also observed in the foregoing T_1 experiments. Thermal hysteresis could also be detected for the high-temperature phase transition. Accordingly, it is concluded from the DTA experiments that $(guH)_2TeCl_6$ crystals undergo two first-order phase transitions at 312 and 373 K.

Table 1. ^1H T_1 Minimum Value, $T_{1\,min}$, Observed at 20 MHz, Activation Energy, E_a, and Correlation Time, τ_0, Obtained from T_1 Measurements for the C_3 Reorientation of Guanidinium Ions in the Crystals of Several Complexes

Compound (phase)	$T_{1\,min}$/ms	E_a/kJ mol^{-1}	τ_0/s
$[C(NH_2)_3]_2ZnCl_4$	16	48	3.2×10^{-15}
$[C(NH_2)_3]_2ZnBr_4$	15	48	1.0×10^{-15}
$[C(NH_2)_3]_2PtCl_6$	16	53	1.2×10^{-15}
$[C(NH_2)_3]_2PtBr_6$	19	45	5.2×10^{-15}
$[C(NH_2)_3]_2SnCl_6$	16	52	3.9×10^{-16}
$[C(NH_2)_3]_2TeCl_6$ (highest-temp.)	17	57	2.2×10^{-16}

The all complexes investigated yielded a single T_1 minimum, the values of which were in the range of 15—19 ms. These values are approximately the same as those found for various guanidinium salts already studied.[1-3,9,10] In the preceding works, those T_1 minima could be attributed to the C_3 reorientation of the cation as a whole about its principal axis on the basis of the theoretical value calculated for the cation using the geometrical values obtained by the X-ray analysis of $(guH)ClO_4$.[2,3,9,10] Therefore, each T_1 minimum detected in the present complexes can be assigned to the magnetic dipolar relaxation due to the cationic C_3 reorientations.

Since guH^+ cations include $-NH_2$ groups in which two kinds of magnetic nuclei, ^1H and ^{14}N, exist although ^{14}N nuclei have a small magnetic moment, we should take into account two kinds of magnetic dipolar interactions, ^1H-^1H and ^1H-^{14}N, to calculate motionally averaging ^1H T_1. Therefore, the observed ^1H T_1 can be written for the present complexes as,[2,8]

$$T_1^{-1} = C\left(\frac{\tau}{1+\omega_H^2\tau^2} + \frac{4\tau}{1+4\omega_H^2\tau^2}\right) + C'\left[\frac{\tau}{1+(\omega_H-\omega_N)^2\tau^2} + \frac{3\tau}{1+\omega_H^2\tau^2} + \frac{6\tau}{1+(\omega_H+\omega_N)^2\tau^2}\right]. \quad (1)$$

Here, ω_H and ω_N denote the Larmor frequencies of a proton and a ^{14}N nucleus, respectively. The motional constants, C and C', are determined by the dipolar interactions operative between protons and between the hetero nuclear spins, respectively. The correlation time, τ, of the motion is assumed to obey the Arrhenius relationship,

$$\tau = \tau_0 \exp(E_a/RT), \quad (2)$$

where E_a and τ_0 are the activation energy for the motion of the cation and its correlation time at the limit of infinite temperature.

The ^1H T_1 values observed at various temperatures for each complex except $(guH)_2TeCl_6$ were fitted to Eqs. 1 and 2 by changing the values of E_a and τ_0 as adjustable parameters. The calculation was performed using a personal computer Model PC-9801 from NEC by the least-squares method using a program written by us. For $(guH)_2TeCl_6$, the same method of fitting calculation was used for the ^1H T_1 values obtained in the highest-temperature phase. However, only the E_a values of this complex were roughly estimated from the gradient of each linear portion of $\log T_1$ vs. T^{-1} curves observed in the middle- and low-temperature phases as 60 and 42 kJ mol^{-1}, respectively. It is interesting to note that the low-temperature phase of $(guH)_2TeCl_6$, which is stable below room temperature, has the considerably smaller E_a than those estimated for the higher-temperature phases. This suggests that $(guH)_2TeCl_6$ forms more loosely packed crystals in the low-temperature phase as compared with those at the other high-temperature phases.

The best-fitted curves calculated by the least-squares method are shown by solid lines in Figs. 1 and 2. The most probable values of E_a and τ_0 are listed in Table 1 along with the observed T_1 minimum values.

For the C_3 reorientation of the cation in the crystal of $(guH)_2ZnCl_4$ and $(guH)_2ZnBr_4$, the same E_a value was observed as 48 kJ mol^{-1}. Although the anionic size of the former is smaller than the latter and the ionic characters of halide ligands estimated from the NQR frequencies reported are fairly small,[11] both complexes exhibit rather small and the same E_a value. This suggests that the size difference of the complex anions and the formation of hydrogen bonding between the cations and halide ligands give negligible effect on the hindering barrier of the cationic C_3 reorientation. Among octahedral complexes, only $(guH)_2PtBr_6$ gave fairly small E_a. This suggests that the cations placed in the large openings surrounded by the bulky anions which practically determine the lattice, can be reoriented more easily than those in the crystals of the hexachloro complexes. Hindering barrier for the C_3 reorientation of the cation due to hydrogen bonding between $-NH_2$ groups and the ligands may be neglected because $(guH)_2SnCl_6$ having more ionic ligands than $(guH)_2PtCl_6$[12] gives lower E_a. Since no information about the crystal structure of the present complexes is available, no further discussion can be made.

References

1) S. Gima, Y. Furukawa, R. Ikeda, and D. Nakamura, *J. Mol. Struct.*, **111**, 189 (1983).
2) S. Gima, Y. Furukawa, and D. Nakamura, *Ber. Bunsenges. Phys. Chem.*, **88**, 939 (1984).
3) Y. Furukawa, S. Gima, and D. Nakamura, *Ber. Bunsenges. Phys. Chem.*, **89**, 863 (1985).
4) J. W. Mellor, "A Comprehensive Treatise on Inorganic and Theoretical Chemistry," Longmans, Green and Co., London (1937), Vol. 16, p. 376.
5) R. Kadel, Diplomarbeit, TH Darmstadt, 1974.
6) L. S. Prabhumirashi, R. Ikeda, and D. Nakamura, *Ber. Bunsenges. Phys. Chem.*, **85**, 1142 (1981).
7) Y. Kume, R. Ikeda, and D. Nakamura, *J. Magn. Reson.*, **33**, 331 (1979).
8) A. Abragam, "The Principles of Nuclear Magnetism," Clarendon Press, Oxford (1961), Chap. 8.
9) Z. Pajak, M. Grottel, and A. E. Koziol, *J. Chem. Soc., Faraday Trans. 2*, **78**, 1529 (1982).
10) M. Grottel and Z. Pajak, *J. Chem. Soc., Faraday Trans., 2*, **80**, 553 (1984).
11) D. E. Scaife, *Aust. J. Chem.*, **24**, 1316 (1971).
12) M. Kubo and D. Nakamura, *Adv. Inorg. Chem. Radiochem.*, **8**, 257 (1966).

Vacuum Sublimation Behavior of Iron(III), Cobalt(II), Nickel(II), Copper(II), and Palladium(II) Chelates with Tetradentate *N,N'*-Disalicylideneethylenediamine and *N,N'*-Bis(1-methyl-3-oxobutylidene)ethylenediamine

Takaharu Honjo* and Kazuhiko Nukui
Department of Chemistry, Faculty of Science, Kanazawa University, Marunouchi, Kanazawa 920
(Received February 10, 1986)

Synopsis. A vacuum sublimation apparatus with a continuous temperature gradient (25—200°C) along the tube (50—0cm) at 2×10^{-2} Torr (1 Torr=133.322 Pa) was used. *N,N'*-disalicylideneethylenediamine, *N,N'*-bis(1-methyl-3-oxobutylidene)ethylenediamine and its metal chelates (Fe^{III}, Co^{II}, Ni^{II}, Cu^{II}, and Pd^{II}) were sublimed without thermal decomposition, while the chelates of Fe^{III}, Co^{II}, Ni^{II}, Cu^{II}, and Pd^{II} with *N,N'*-disalicylideneethylenediamine were thermally stable, but did not sublime completely.

The vacuum sublimation method is useful for the purification and separation of metal chelates of 4-anilino-3-penten-2-one, 2,4-pentanedione, dithiocarbamates, 8-quinolinol and its derivatives, dimethylglyoxime, diphenylthiocarbazone, 1-(2-pyridylazo)-2-naphthol, 5,10,15,20-tetraphenylporphyrin, and 1,1,1-trifluoro-4-(2-thienyl)-4-mercapto-3-buten-2-one.[1-3] Of the metal chelates described above, bidentate shiff base chelates of β-imino ketones, such as 4-anilino-3-penten-2-one, were accompanied by remarkable thermal decompositions during the sublimation process; however, the sublimation-recrystallization temperatures of these chelates were found in the lower-temperature region of all the chelates studied. The present research aims to investigate the tetradentate ligands of *N,N'*-disalicylideneethylenediamine and *N,N'*-bis(1-methyl-3-oxobutylidene)ethylenediamine for the purification of metals in milligram amounts (as their chelates) by a vacuum sublimator with a continuous temperature gradient under low pressure. Some of these chelates in nanogram amounts have already been evaluated by gas chromatography, mainly for Cu^{II}, Ni^{II}, and Pd^{II}.[4]

Experimental

Materials. The shiff bases of *N,N'*-disalicylideneethylenediamine and *N,N'*-bis(1-methyl-3-oxobutylidene)ethylenediamine were easily prepared by the condensation of ethylenediamine with salicylaldehyde in ethanol or with 2,4-pentanedione (directly), as described previously.[5]

Metal chelate compounds with these ligands were generally prepared by the addition of an ethanolic solution of the corresponding chelating reagent to an aqueous ammonia solution of each metal salt at room temperature, or by heating if necessary. This has been previously mentioned.[5,6] These materials were purified by recrystallization from ethanol or by vacuum sublimation before use.

Sublimation Procedure. A vacuum sublimation apparatus which provided a continuous temperature gradient (25—200°C) along the tube (50—0cm) at 2×10^{-2} Torr was used, as previously described.[1] The temperature gradient along the sublimator is shown in Fig. 1; this was obtained after thermal equilibrium for 4 h. These patterns were obtained by supplying the following electric power through the heating mantle, 16V, 8V, and 3V at 1.0A. Metal chelates were placed inside the apparatus for 5.5 h after establishing thermal equilibrium. The sublimate zone along the sublimation tube was decided from the color of the chelate and its deposition position. The thermal conditions of the sublimator were always checked from the sublimation zone of a definite amount of copper(II) acetylacetonate after sublimating it by another sublimation tube with the metal chelates to be investigated. The sublimation-recrystallization zone temperatures of copper(II) acetylacetonate (in 12-mg amounts) were 89—60°C at 0.02 Torr, 120—66°C at 0.1 Torr, and 162—158°C at 7 Torr, respectively.

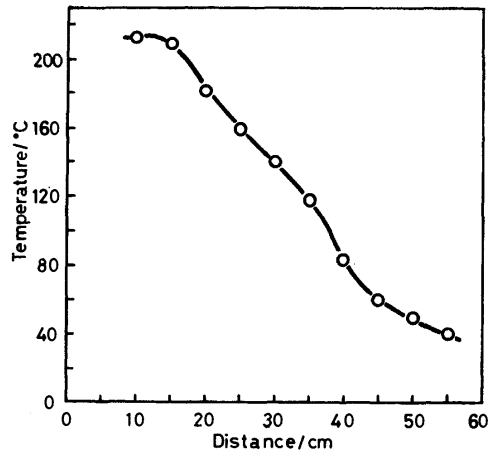

Fig. 1. Continuous temperature gradient along vacuum sublimator.

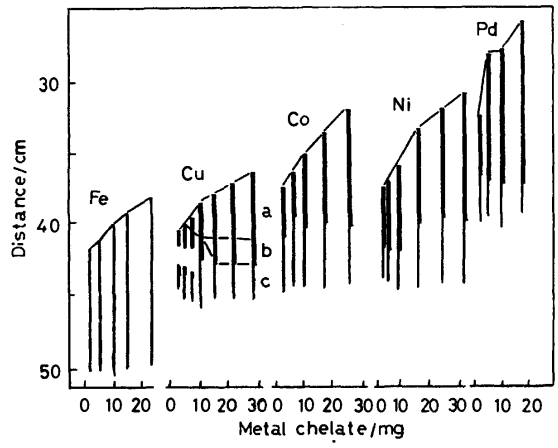

Fig. 2. Sublimation-recrystallization zone of metal chelate compounds of *N,N'*-bis(1-methyl-3-oxobutylidene) ethylenediamine in various quantities. Color of copper chelate: a green, b green and purple mixture, c purple.

Table 1. Sublimation-Recrystallization Zone Temperatures, Amounts Remaining, and Colors of Various Metal Chelates with *N,N'*-Disalicylideneethylenediamine and *N,N'*-Bis(1-methyl-3-oxobutylidene)ethylenediamine after Sublimation at 2×10^{-2} Torr

Metal chelates	Recrystallization zone temperature/°C	Color	Chelate taken / mg	Metal Compound remaining[a)]
N,N'-Disalicylidene-ethylenediamine	90—55	Yellow	6.8	None
Fe^{III}	About 200	Brown	3.4	Much
Co^{II}	171—160	Brown	1.8	Much
Ni^{II}	178—160	Dark red	10.9	Much
Cu^{II}	172—160	Grayish green	3.9	Much
Pd^{II}	171—158	Pale yellow	6.0	Much
N,N'-Bis(1-methyl-3-oxo-butylidene)ethylenediamine	105—60	White	7.0	None
Fe^{III}	83—46	Red	10.0	None
Co^{II}	118—60	Orange yellow	10.0	None
Ni^{II}	116—60	Dark red	10.0	None
Cu^{II}	94—78 78—58	Green Purple	10.0	None
Pd^{II}	150—80	Yellow	10.0	None

a) None, 0—10%; much, >30%.

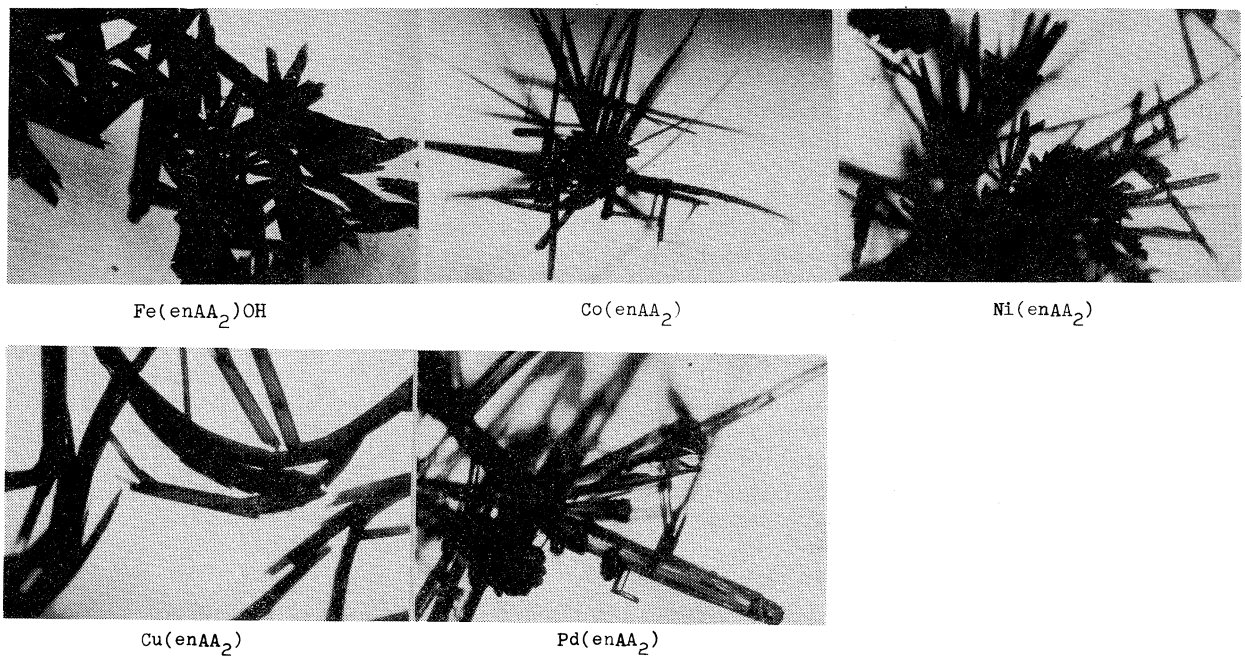

Fig. 3. Microphotographs of metal chelates.
H_2 (en AA_2): *N,N'*-Bis(1-methyl-3-oxobutylidene)ethylenediamine.
Photograph: 40 times.

Results and Discussion

The temperature range of the deposited zones, the recovery, and the colors of the various metal chelates after sublimation are summarized in Table 1.

N,N'-Disalicylideneethylenediamine, and *N,N'*-bis(1-methyl-3-oxobutylidene)ethylenediamine and its metal chelates (Fe^{III}, Co^{II}, Ni^{II}, Cu^{II}, and Pd^{II}) were sublimed without any thermal decomposition, while the chelates of Fe^{III}, Co^{II}, Ni^{II}, Cu^{II}, and Pd^{II} with *N,N'*-disalicylideneethylenediamine were thermally stable, but did not sublime completely. This fact may have been caused by the rate of sublimation of the chelate compounds, which depends upon the temperature established at the high-temperature end of the sublimator. The sublimation-recrystallization temperature of individual chelates generally increased in the following order: $Fe^{III}<Cu^{II}<Ni^{II}$, $Co^{II}<Pd^{II}$. The sublimation-recrystallization zones for metal chelates of Fe^{III}, Cu^{II}, Co^{II}, Ni^{II}, and Pd^{II} with *N,N'*-bis(1-methyl-3-oxobutylidene)ethylenediamine in varying quantities are graphically presented in Fig. 2. In general, the sublimation-recrystallization distance gave shorter values with an increase in quantity of the chelates. In cases where the recrystallization-zone pattern was not uniform, the deposition zones (where over 90% of the chelates were

found) are indicated by a thicker lines.

Representative photomicrographs of metal chelates with *N,N'*-bis(1-methyl-3-oxobutylidene)ethylenediamine deposited on the glass wall inside the sublimation tube are given in Fig. 3. Metal chelates of Co^{II}, Ni^{II}, and Pd^{II} form stereoradial needle-like crystals, and Fe^{III} chelate forms hexahedral crystals. A copper chelate forms two kinds of crystals; a purple planar needle-like crystal at the lower-temperature side, and a green plate crystal at the higher-temperature side, when sublimating it in more than 5 mg amount. Both crystals are purple in their powder states. Therefore, it is clear that sublimation is useful for the purification of milligram amounts of each metal chelate since large-sized crystals can be obtained.

References

1) T. Honjo, H. Imura, S. Shima, and T. Kiba, *Anal Chem.*, **50**, 1545 (1978).
2) T. Honjo and S. Shima, *DOJIN News*, **1980**, 1.
3) T. Honjo and S. Shima, *Bull. Chem. Soc. Jpn.*, **57**, 293 (1984).
4) P. C. Uden and D. E. Henderson, *Analyst (London)*, **102**, 889 (1977).
5) J. V. Dubsky and A. Sokol, *Collect. Czech. Chem. Commun.*, **3**, 548 (1931).
6) R. Belcher, K. Blessel, T. Cardwell, M. Pravica, W. I. Stephen, and P. C. Uden, *J. Inorg. Nucl. Chem.*, **35**, 1127 (1973).

Preparation and Characterization of Nickel(II) Complexes with Diethyl *N,N'*-Ethylenebis(2-hydroxyimino-3-iminobutanoate) and Its Analogue

Soo Han KIM,† Ken-ichi OKAMOTO,* Hisahiko EINAGA,†† and Jinsai HIDAKA
Department of Chemistry, University of Tsukuba, Sakura, Ibaraki 305
(Received March 1, 1986)

Synopsis. The reaction of nickel(II) chloride hexahydrate and ethyl α-(hydroxyimino)acetoacetate with ethylenediamine or (*R*)-propylenediamine gives [diethyl *N,N'*-ethylenebis(2-hydroxyimino-3-iminobutanoato)]nickel(II) or {diethyl *N,N'*-[(*R*)-1-methylethylene]bis(2-hydroxyimino-3-iminobutanoato)}nickel(II). The nickel(II) complexes with Schiff base ligands were characterized by their electronic absorption, ^{13}CNMR, infrared, and CD spectra.

In the metal complexes with α-hydroxyimino β-diketone or its derivatives, it has been known that two coordination modes are possible for the hydroxyimino group.[1-8] Namely, the ligands coordinate to a metal ion through the nitrogen of the hydroxyimino group to form a five-membered ring or through the oxygen of the group to form a six-membered one. In the previous paper,[9] we reported some properties of the palladium(II) complexes with diethyl *N,N'*-ethylenebis(2-hydroxyimino-3-iminobutanoate), (ieaa)$_2$-en, and ethyl 3-[(*R*)-2-aminopropylimino]-2-hydroxyiminobutanoate, (ieaa)-(*R*)-pn,[10] in which the hydroxyimino group coordinates to palladium(II) ion through the nitrogens. It is of interest that the (ieaa)$_2$-en was formed as a quadridentate ligand and the (ieaa)-(*R*)-pn as a terdentate one, though a similar reaction was adopted.[9] In order to examine the difference in formation, the preparation of the nickel(II) complexes with Schiff base ligands, which are derived from the reaction of ethyl α-(hydroxyimino)acetoacetate, ieaa, with the ethylenediamine or (*R*)-propylenediamine, was attempted. The resulting nickel(II) complexes are characterized by the electronic absorption, ^{13}CNMR, infrared, and CD spectra.

Experimental

Materials. Ethyl α-(hydroxyimino)acetoacetate was prepared by nitrosation of ethyl acetoacetate with sodium nitrite according to the method of Adams.[11] Nickel(II) chloride hexahydrate and the other reagents used were obtained from the Wako Pure Chemicals Ind. Co., Ltd.

Preparation of Complexes. 1) [Diethyl *N,N'*-Ethylenebis(2-hydroxyimino-3-iminobutanoato)]nickel(II): [Ni{(ieaa)$_2$-en}]. Nickel(II) chloride hexahydrate (0.65 g, 0.005 mol) and ieaa (3.2 g, 0.02 mol) were dissolved in 70 cm^3 of 1-propanol, and 0.7 cm^3 of ethylenediamine was added to it. After reflux for 45 min, the red precipitate which appeared was collected by filtration. The crude product was recrystallized from chloroform and dried in a vacuum desiccator. The orange red needle crystals obtained were insoluble in water, but soluble in methanol, dimethyl sulfoxide (DMSO), and chloroform. Found: C, 41.97; H, 5.02; N, 14.03%. Calcd for $NiC_{14}H_{20}N_4O_6$: C, 42.14; H, 5.05; N, 14.04%.

2) {Diethyl *N,N'*-[(*R*)-1-Methylethylene]bis(2-hydroxyimino-3-iminobutanoato)}nickel(II): [Ni{(ieaa)$_2$-(*R*)-pn}]. Nickel(II) chloride hexahydrate (0.65 g, 0.005 mol) and ieaa (3.2 g, 0.02 mol) were dissolved in 80 cm^3 of absolute ethanol, and 0.8 cm^3 of (*R*)-propylenediamine and 10 drops of 28% aqueous ammonia were added to it. After reflux for 72 h, the reaction mixture was stood in a refrigerator for 48 h. The crystals which appeared were collected by filtration, washed three times with small amounts of cold ethanol, and dried in a vacuum desiccator. The red fine crystals obtained were also insoluble in water, but soluble in methanol, DMSO, and chloroform. Found: C, 43.60; H, 5.35; N, 13.70%. Calcd for $NiC_{15}H_{22}N_4O_6$: C, 43.61; H, 5.36; N, 13.56%.

Measurements. The electronic absorption spectra were recorded with JASCO UVIDEC-1 and UVIDEC-610 spectrophotometers and the CD spectra with a JASCO J-20 and J-500 spectropolarimeters. All measurements were carried out at room temperature. The ^{13}CNMR spectra were recorded in $CDCl_3$ with a JEOL JNM-FX-100 or -FX-90Q NMR spectrometer at the probe temperature. Tetramethylsilane was used as an internal reference. The infrared spectra were recorded with a Hitachi 260-50 infrared spectrophotometer using the KBr disk method. The elemental analyses were carried out in the Analysis Center of the University of Tsukuba.

Results and Discussion

Only an orange red needle crystalline complex was formed by the reaction of nickel(II) chloride hexahydrate and ieaa with ethylenediamine in 1-propanol. The elemental analytical result suggests the formation of the nickel(II) complex containing (ieaa)$_2$-en type Schiff base as a quadridentate ligand, [Ni{(ieaa)$_2$-en}], as in the case of [Pd{(ieaa)$_2$-en}].[9] Although two kinds of structure, square planar and tetrahedral, are possible for this nickel(II) complex, the ^{1}H and ^{13}CNMR spectral behaviors seem to prefer the former to the latter (vide infra). This is supported by the fact that the present nickel(II) complex exhibits a quite similar absorption spectral behavior to the square planar nickel(II) complexes with Schiff base ligands such as 3-hydroxyimino-4-imino-2-pentanone (iaa-NH),[5] 2-hydroxyimino-3-imino-1-phenyl-1-butanone (iba-NH),[6] ethyl 2-hydroxyimino-3-iminobutanoate (ieaa-NH),[12] their *N*-alkyl derivatives (iaa-NR, iba-NR, and ieaa-NR; R=CH_3, C_2H_5, *n*-C_3H_7, and so on),[5,6,12] (*R*)-*N,N'*-disalicylidene-1,2-propanediamine, and its derivatives (Fig. 1).[13,14]

For the square planar nickel(II) complex, three geometrical isomers with respect to the coordination modes of the hydroxyimino groups of the ieaa moieties are possible as shown in Fig. 2. The ^{13}CNMR spectrum of [Ni{(ieaa)$_2$-en}] exhibits eight resonance lines for the four methyl (14.1, 14.2, 17.4, and 18.5 ppm) and four

†Present address: Department of Chemistry, The 3rd Military Academy, Youngchun, 671-09, Korea.
††Present address: Institute of Materials Science, University of Tsukuba, Sakura, Ibarski 305.

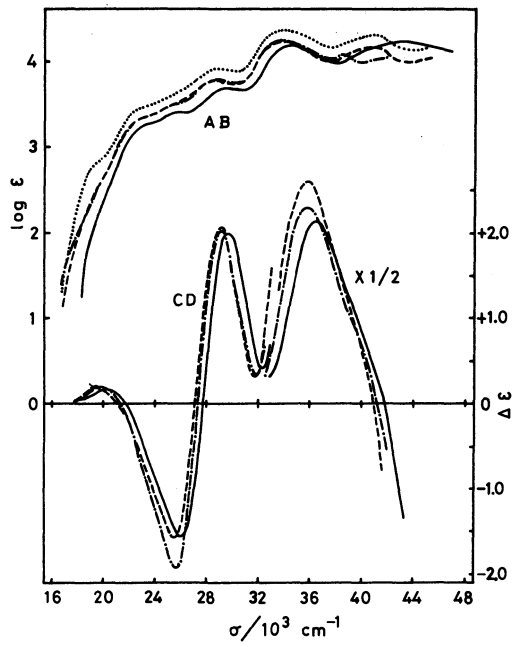

Fig. 1. Absorption spectrum of [Ni{(ieaa)$_2$-en}] in chloroform (·····), and absorption and CD spectra of [Ni{(ieaa)$_2$-(*R*)-pn}] in chloroform (------), in DMSO (—·—·—·—), and in methanol (———).

methylene carbon atoms (48.6, 59.4, 60.4, and 61.7 ppm). As seen in Fig. 2, eight resonance lines for the methyl and methylene carbon atoms are expected for the ^{13}CNMR spectrum of (b) and four resonance lines for the carbon atoms are expected for that of (a) or (c), since (b) is C_1 symmetry and (a) or (c) C_2 one. The infrared spectrum of this complex exhibits the stretching vibration bands, $\nu_{N\text{-}O}$=1260 cm^{-1}, $\nu_{C=O}$=1688 and 1706 cm^{-1}, $\nu_{Ni\text{-}N}$=503 and 541 cm^{-1}, and $\nu_{Ni\text{-}O}$=ca. 315 cm^{-1}. The infrared spectral characteristics coincide well with those of [Ni(iaa-NH)(iaa-NR)][5] or [Ni(ieaa-NR)$_2$][12] (R; H and alkyl groups), in which one ligand coordinates through the nitrogen of the hydroxyimino group and the other through the oxygen. These ^{13}CNMR and infrared spectral characteristics indicate that the present nickel(II) complex takes the form (b) in Fig. 2, namely, one of the two hydroxyimino groups coordinates to nickel(II) ion through the nitrogen to form a five-membered chelate ring and the other through the oxygen to form a six-membered one.

Nickel(II) chloride hexahydrate reacted with ieaa and (*R*)-propylenediamine in basic ethanol to give one product as in the case of [Ni{(ieaa)$_2$-en}]. The analytical result of this complex suggests that one diethyl *N,N'*-[(*R*)-1-methylethylene]bis(2-hydroxyimino-3-iminobutanoate) ligand, (ieaa)$_2$-(*R*)-pn, coordinates to a nickel(II) ion, and the nickel(II) complex exhibits a quite similar absorption spectrum to [Ni{(ieaa)$_2$-en}] (Fig. 1). Further, its infrared spectral bands also agree well with those of the (ieaa)$_2$-en complex; $\nu_{N\text{-}O}$=1255 cm^{-1}, $\nu_{C=O}$=1673 and 1710 cm^{-1}, $\nu_{Ni\text{-}N}$=506 and 538 cm^{-1}, and $\nu_{Ni\text{-}O}$=ca. 325 cm^{-1} (stretching vibrations). These facts suggest that the quadridentate ligand in [Ni{(ieaa)$_2$-(*R*)-pn}] takes a similar coordination mode to that in [Ni{(ieaa)$_2$-en}] ((b) in Fig. 2). The ^{13}CNMR spectrum

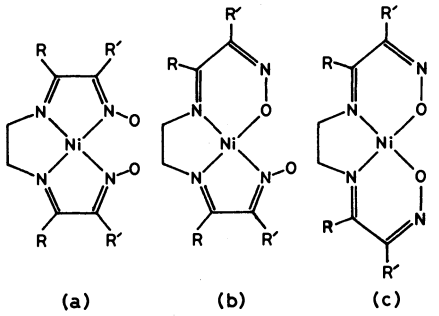

Fig. 2. Possible geometrical isomers of the square planar configuration for [Ni{(ieaa)$_2$-en}]; R=CH_3 and R'=$CO_2C_2H_5$.

of [Ni{(ieaa)$_2$-(*R*)-pn}] exhibits seven resonance lines due to the methyl carbon atoms and eight resonance ones due to the methylene carbon atoms. This ^{13}CNMR spectral behavior seems to indicate that the nickel(II) complex is a composite of two possible isomers, which are caused by the configuration due to the methyl group of the (*R*)-propylenediamine moiety of (b) in Fig. 2.

When the absorption and/or CD spectra of [Ni{(ieaa)$_2$-en}] and [Ni{(ieaa)$_2$-(*R*)-pn}] are compared with those of the square planar nickel(II) complexes with the quadridentate Schiff base ligands such as (*R*)-*N,N'*-disalicylidene-1,2-propanediamine (sal-(*R*)-pn),[10,13,14] their absorption bands are assigned as follows; the intense bands at ca. 34 and 40×10^3 cm^{-1} originate from the π-π* transitions due to the coordinated (ieaa)$_2$-en or (ieaa)$_2$-(*R*)-pn, other three intense bands at 22—29×10^3 cm^{-1} from the charge transfer, and the shoulder at ca. 19.5×10^3 cm^{-1} from the d-d transition. In the region of 18—38×10^3 cm^{-1}, the absorption and/or CD spectral patterns of [Ni{(ieaa)$_2$-en}] and [Ni{(ieaa)$_2$-(*R*)-pn}] were almost unaffected by nature of the solvents such as chloroform, dimethyl sulfoxide, methanol, and pyridine (Fig. 1).

In contrast to [Ni{(ieaa)$_2$-(*R*)-pn}], the corresponding palladium(II) complex, [Pd{(ieaa)$_2$-(*R*)-pn}], could not be formed by a reaction similar to that for the nickel(II) complex, but the palladium(II) complex with a terdentate Schiff base ligand, [Pd(Cl){(ieaa)-(*R*)-pn}], was formed.[9] This difference in the formation of the (*R*)-pn Schiff base ligand between the palladium(II) and nickel(II) complexes is presumably related to the affinity of chloride,[15] which is lower to nickel(II) ion than to palladium(II) ion, and to the adaptability of the strained quadridentate Schiff base ligand with (*R*)-propylenediamine backbone ring, which coordinates more easily to nickel(II) ion capable of taking distorted square planar structure than to palladium(II) ion.

References

1) T. W. J. Taylor and E. K. Ewbank, *J. Chem. Soc.*, **1926**, 2818.

2) N. J. Patel and B. C. Haldar, *J. Inorg. Nucl. Chem.*, **29**, 1037 (1967).

3) U. B. Talwer and B. C. Haldar, *J. Inorg. Nucl. Chem.*, **32**, 213 (1970).

4) M. J. Lacey, C. C. Macdonald, J. S. Shannon, and P. J. Collin, *Aust. J. Chem.*, **23**, 2279 (1970).

5) K. S. Bose, B. C. Sharma, and C. C. Patel, *Inorg. Chem.*, **12**, 120 (1973).
6) M. H. Lee, D. S. Oh, and K. W. Lee, *J. Kor. Chem. Soc.*, **22**, 19 (1978).
7) M. H. Lee, D. S. Oh, and S. H. Kim, *J. Kor. Chem. Soc.*, **24**, 121 (1980).
8) T. S. Oh, M. H. Lee, S. H. Kim, J. H. Park, and K. W. Lee, *J. Kor. Chem. Soc.*, **26**, 31 (1982).
9) S. H. Kim, K. Okamoto, H. Einaga, and J. Hidaka, *J. Kor. Chem. Soc.*, **29**, 490 (1985).
10) (*R*)-Propylenediamine, $(-)_{589}$-l-pn, and its moiety in the compounds are abbreviated to (*R*)-pn in this paper.
11) R. Adams, "Organic Reaction," 2nd. ed., John Wiley & Sons, Inc. (1960), Vol VII, pp. 353—354.
12) S. H. Kim, Ph. D. Thesis, Kyungpook National University, Taegu 635, Korea (1983).
13) B. Bosnich, *J. Am. Chem. Soc.*, **90**, 627 (1968).
14) R. S. Downing and F. L. Urbach, *J. Am. Chem. Soc.*, **92**, 5861 (1970).
15) R. M. Smith and A. E. Martell, ed., "Critical Stability Constants," Plenum Press, New York (1976), Vol 4, pp. 105—107.

Cyclic Peptides. XXIII.[1] Synthesis of Retro-Enantio-AM-Toxin I

Hisakazu MIHARA,* Haruhiko AOYAGI, Tamio UENO,† Tetsuo KATO, and Nobuo IZUMIYA
Laboratory of Biochemistry, Faculty of Science, Kyushu University 33, Higashi-ku, Fukuoka 812
† Pesticide Research Institute, College of Agriculture, Kyoto University, Sakyo-ku, Kyoto 606
(Received March 15, 1986)

Synopsis. To characterize a receptive substance in an apple leaf of phytotoxic AM-toxin I, retro-enantiomer of the toxin was synthesized by the solution method. This analog showed no toxic activity, indicating that the specific backbone conformation of the toxin is essential for the activity.

AM-toxins are host-specific phytotoxic metabolites produced by *Alternaria mali*, which cause spot disease on apple leaves. The structure of AM-toxin I is a cyclic tetradepsipeptide as shown in Fig. 1.[2] We have synthesized various analogs of AM-toxin I and examined their necrotic activities on apple leaves in order to study the relationships between structure and activity of the toxin. We have found that the following factors are important for the induction of the full toxic activity: i) the specific ring conformation,[3] ii) bulkiness of the isopropyl side chain of the L-Hmb[4] residue at position 2,[5] iii) the exact side chain length of the L-Amp residue at position 3,[6] iv) the presence of the ΔAla residue at position 4.[7] The size of side chain of the L-Ala residue at position 1 is not critical to the toxic activity.[8] Thus, AM-toxin I holds a unique structure which can not be easily handled by chemical modifications without loss of the activity. Previously, we illustrated a scheme on interaction between AM-toxin I and a possible receptive substance in the sensitive apple leaf.[6] In this connection, we attempted to design a compound which could characterize the receptive substance.

The cycloretro-enantiomer is a cycloisomer which has unique topochemical relations to the parent cyclic peptide as follows: both are equivalent in the spatial arrangement of various side chains, but reversed in the chirality of each center and the direction of the amide bonds. As the first step of receptor study, we tried to synthesize retro-enantio-AM-toxin I (**1**, Fig. 1) and examined its necrotic activity on an apple leaf. Compared with the sequence of AM-toxin I, the retro-enantio-AM-toxin I (**1**) should have inversed chirality of each center and reversed direction of amide and ester bonds. Therefore, the retro-enantiomer contains D-Val and D-Lac instead of L-Hmb and L-Ala, respectively, in AM-toxin I. Topochemical arrangement of each side chain in **1** is equivalent to that in AM-toxin I.

The synthetic route for retro-enantiomer (**1**) is shown in Fig. 2. In a preliminary study, according to the successful synthesis of AM-toxin I—III and AM-toxin analogs,[5-8] a linear tetradepsipeptide H-D-Amp-D-Val-D-Lac-D-Dpr(Z)-ONSu (**11**), in which the ester bond was placed at the center was selected for cyclization. Cyclization of **11**, however, gave the desired cyclic tetradepsipeptide 9 in a very low yield (4%). Main product of this reaction was a 2,5-piperazinedione *cyclo*(-D-Amp-D-Val-) identified with mass spectrum and

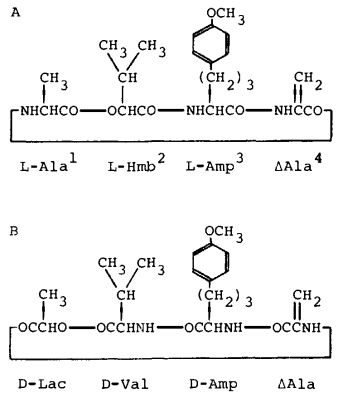

Fig. 1. Structure of AM-toxin I (A) and its retro-enantiomer (**1**, B).

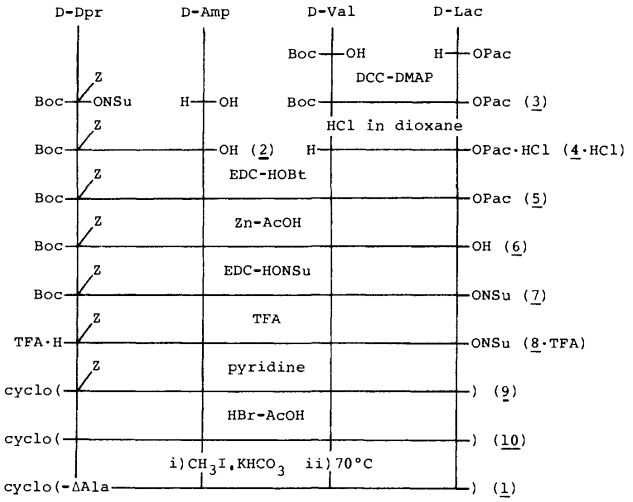

Fig. 2. Synthesis of retro-enantio-AM-toxin I.

elemental analysis. This may be due to preferential ability to form the 2,5-piperazinedione from H-D-Amp-D-Val-OR. In the previous studies,[5-8] such a by-product was not found in cyclization of linear tetradepsipeptide, e.g., H-D-Dpr(Z)-L-Ala-L-Hmb-L-Amp-ONSu.

Therefore, the sequence of a linear tetradepsipeptide as the precursor of 9 was changed to H-D-Dpr(Z)-D-Amp-D-Val-D-Lac-ONSu (**8**), in which the D-Lac residue was placed at the C-terminal to avoid the 2,5-piperazinedione formation, as shown in Fig. 2. Boc-D-Dpr(Z)-ONSu was coupled with D-Amp to give Boc-D-Dpr(Z)-D-Amp-OH (**2**). Boc-D-Val-D-Lac-OPac (**3**) was prepared from Boc-D-Val-OH and D-Lac-OPac with DCC-DMAP.[9] Boc group in **3** was removed with HCl followed by condensation with **2** to give Boc-tetradepsipeptide-OPac (**5**). After Pac group was removed with Zn-AcOH, the resulting acid (**6**) was

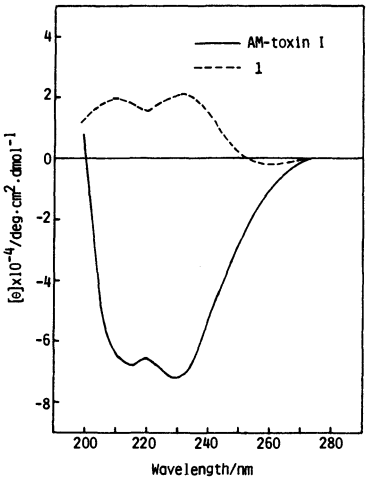

Fig. 3. CD spectra of AM-toxin I and its retro-enantiomer (**1**) in MeOH.

converted to the corresponding active ester (**7**) and its Boc group was removed with TFA to give the active ester trifluoroacetate (**8**·TFA). Cyclization of **8** at a concentration of 3 mM in pyridine gave the cyclic peptide **9** in a yield of 37% from **7**. After deprotection of Z group in **9** with HBr–AcOH, the resulting HBr salt was treated with CH_3I and $KHCO_3$[10] to give the desired **1**. The yield of **1** from **9** was 17% comparable to the yields in previous syntheses of AM-toxins.[5-8]

CD spectra of the retro-enantiomer **1** and AM-toxin I in MeOH are shown in Fig. 3. Although AM-toxin I showed double minima of negative molar ellipticities at 210 and 230 nm, **1** showed positive ones at similar wavelengths. The enantiomer of AM-toxin I, *cyclo*-(-D-Ala-D-Hmb-D-Amp-ΔAla-), should show positive bands with the same ellipticities at the same wavelengths as AM-toxin I. When the spectrum of the retro-enantiomer **1** was compared with that of the enantiomer, wavelengths of minima were similar each other but ellipticities of **1** were much smaller than those of the enantiomer. These results indicate that the conformation of **1** differs from that of AM-toxin I which should have the same conformation as the enantiomer, or the content of the common conformation is low in **1**.

Minimum toxic activity of AM-toxin I for the induction of necrosis on an apple leaf (Indo) was 0.001 μg ml^{-1}, while the retro-enantiomer **1** did not show any toxicity at the high concentration up to 100 μg ml^{-1}. The retro-enantiomer **1** contains each side chain topo-equivalently arranged to that of AM-toxin I, but the chirality of each center and the direction of the amide and ester bonds in **1** were reversed. Combined with the previous results,[3,5-8] the presence of each side chain in AM-toxin I is very important, but the direction of the amide and ester bonds, i.e., backbone conformation, also is essential to induce the toxic activity. This specific conformation[3] of AM-toxin I may confirm the exact orientation of each side chain, and then can reveal the full toxic activity.

Experimental

Thin layer chromatography was carried out on Merck silica gel G with the following solvent system: R_f^1, $CHCl_3$–MeOH (5:1); R_f^2, $CHCl_3$–MeOH (9:1); R_f^3, $CHCl_3$–MeOH–AcOH (95:5:1); R_f^4, *n*-BuOH–AcOH–pyridine–H_2O (4:1:1:2). Optical rotations were measured with a Union high sensitivity polarimeter PM-71. Mass spectra were taken on a Nihondenshi mass spectrometer Model JMS-01SG-2 with a direct inlet system operating at 75 eV, and CD on a JASCO J-40A spectropolarimeter.

Boc-D-Dpr(Z)-D-Amp-OH (2). To a solution of H-D-Amp-OH (810 mg, 3.3 mmol) and NEt_3 (0.46 ml, 3.3 mmol) in DMF (30 ml) was added a solution of Boc-D-Dpr(Z)-ONSu (1.3 g; 3.0 mmol) in DMF (5 ml). The mixture was stirred at room temperature overnight. After evaporation, 10% citric acid was added to the residue. The separated oil was extracted with EtOAc, and the solution was washed with water and dried over Na_2SO_4. After evaporation, the residue was recrystallized from EtOAc–ether–petroleum ether: yield, 1.2 g (73%); mp 141—143°C; $[\alpha]_D^{20}$ +7.9° (*c* 1, DMF); R_f^1=0.57, R_f^3=0.46. Found: C, 61.78; H, 6.86; N, 7.71%. Calcd for $C_{28}H_{37}N_3O_8$: C, 61.86; H, 6.86; N, 7.73%.

Boc-D-Val-D-Lac-OPac (3). To a chilled solution of Boc-D-Val-OH (2.2 g, 10 mmol), D-Lac-OPac[11] (2.1 g, 10 mmol) and DMAP[9] (1.2 g, 10 mmol) in CH_2Cl_2 (30 ml) was added DCC (2.1 g, 10 mmol). The mixture was stirred at 0°C for 3 h and at room temperature overnight. After evaporation, the residue was dissolved in EtOAc, washed with 10% citric acid, 4% $NaHCO_3$ and water, and dried over Na_2SO_4. After evaporation, **3** was obtained as an oil: yield, 3.4 g (83%); R_f^2=0.87, R_f^3=0.36.

H-D-Val-D-Lac-OPac·HCl (4·HCl). Compound **3** (2.9 g, 7.0 mmol) was dissolved in 4 M (1M=1 mol dm^{-3}) HCl in dioxane (20 ml). The solution was allowed to stand at room temperature for 2 h. After removal of the solvent, the evaporation was repeated several times by the addition of dioxane. The residue was crystallized by the addition of ether: yield, 2.0 g (92%); R_f^1=0.52.

Boc-D-Dpr(Z)-D-Amp-D-Val-D-Lac-OPac (5). To a chilled solution of **2** (1.2 g, 2.2 mmol), **4**·HCl (670 mg, 2.2 mmol), HOBt (450 mg, 3.3 mmol) and NEt_3 (0.31 ml, 2.2 mmol) in DMF (20 ml) was added EDC·HCl (630 mg, 3.3 mmol). The mixture was stirred at 0°C overnight. After evaporation, the residue was dissolved in EtOAc, washed with 10% citric acid, 4% $NaHCO_3$ and water, and dried over Na_2SO_4. After evaporation, the residue was recrystallized from EtOAc–ether–petroleum ether: yield, 1.5 g (83%); mp 108—110°C; $[\alpha]_D^{20}$ +35.1° (*c* 0.5, DMF); R_f^2=0.45, R_f^3=0.40. Found: C, 63.39; H, 6.79; N, 6.71%. Calcd for $C_{44}H_{56}N_4O_{12}$: C, 63.45; H, 6.78; N, 6.73%.

Boc-D-Dpr(Z)-D-Amp-D-Val-D-Lac-OH (6). To a solution of **5** (1.5 g, 1.8 mmol) in 90% AcOH (20 ml) was added Zn powder (0.5 g) at room temperature. The mixture was stirred at room temperature for 8 h. The insoluble Zn was filtered off and the filtrate was evaporated. Ten per cent citric acid was added to the residue. The separated oil was extracted with EtOAc, washed with water, and dried over Na_2SO_4. After evaporation, the residue was recrystallized from EtOAc–ether–petroleum ether: yield, 1.17 g (91%); mp 115—118°C; $[\alpha]_D^{20}$ +26.9° (*c* 0.5, DMF); R_f^1=0.55, R_f^3=0.33. Found: C, 60.64; H, 6.91; N, 7.61%. Calcd for $C_{36}H_{50}N_4O_{11}$: C, 60.49; H, 7.05; N, 7.84%.

Boc-D-Dpr(Z)-D-Amp-D-Val-D-Lac-ONSu (7). To a chilled solution of **6** (1.1 g, 1.5 mmol) and HONSu (345 mg, 3.0 mmol) in DMF (10 ml) was added EDC·HCl (575 mg, 3.0 mmol). The mixture was stirred at 0°C overnight. After evaporation, the residual solid was collected with the aid of cold water and dried in vacuo: yield, 1.2 g (98%); R_f^2= 0.53. This was used to the next step without purification.

***Cyclo*(-D-Dpr(Z)-D-Amp-D-Val-D-Lac-) (9).** A solution of **7** (1.2 g, 1.5 mmol) in TFA (5 ml) was allowed to stand

at 0°C for 30 min. After evaporation, the residual oil was solidified by the addition of ether. The powder was washed several times with ether by decantation to give H-D-Dpr(Z)-D-Amp-D-Val-D-Lac-ONSu·TFA (**8**·TFA). The powder was dissolved in DMF (10 ml) and the solution was added dropwise into pyridine (500 ml) with stirring at room temperature. The stirring was continued for 3 d and the reaction mixture was evaporated. The residue was collected with the aid of cold water, and washed with 10% citric acid and water. This was recrystallized from EtOAc-ether: yield, 330 mg (37%); mp 224—226°C (decomp); $[\alpha]_D^{20}$ +155° (*c* 0.3, DMF); MS *m/z* 596 (M^+); R_f^2=0.45, R_f^3=0.29. Found: C, 62.30; H, 6.87; N, 9.40%. Calcd for $C_{31}H_{40}N_4O_8$: C, 62.40; H, 6.76; N, 9.39%.

***Cyclo*(-ΔAla-D-Amp-D-Val-D-Lac-) (1).** Compound **9** (120 mg, 0.2 mmol) in 25% HBr in AcOH (5 ml) was allowed to stand at room temperature for 2 h. After evaporation, the residue was solidified by the addition of ether to give a powder of cyclo (-D-Dpr-D-Amp-D-Val-D-Lac-)·HBr (**10**·HBr). To a suspension of **10**·HBr in EtOAc (30 ml) were added CH_3I (2 ml) and $KHCO_3$ (400 mg), and the mixture was stirred in the dark at room temperature. The same amounts of CH_3I and $KHCO_3$ were added again 2 d later, the stirring being continued for 4 d. After removal of solvent and excess CH_3I in vacuo, the residue was suspended in EtOAc (30 ml) and the suspension was stirred at 70°C for 2 h. Insoluble material was filtered off and the filtrate was evaporated to give a crude product. The crude product was purified by silica gel column (1.1×20 cm) chromatography using $CHCl_3$-acetone (4:1) followed by recrystallization from EtOAc-ether-petroleum ether: yield, 15 mg (17%); mp 158—160°C; MS *m/z* 445 (M^+); R_f^2=0.48, R_f^3=0.36. Found: C, 61.83; H, 7.07; N, 9.01%. Calcd for $C_{23}H_{31}N_3O_6$: C, 62.01; H, 7.01; N, 9.43%.

Biological Assay. Biological assay on apple leaves (susceptible cultivar, Indo) was carried out as described previously.[6]

We thank Dr. S. Lee of this laboratory for his helpful discussion during this work, and Dr. H. Nishikawa, Fukuoka University, for the measurement of CD spectra.

References

1) Part XXII of this series: H. Mihara, H. Aoyagi, T. Ueno, T. Kato, and N. Izumiya, *Bull. Chem. Soc. Jpn.*, **59**, 2041 (1986).
2) T. Ueno, T. Nakashima, Y. Hayashi, and H. Fukami, *Agric. Biol. Chem.*, **39**, 1115 (1975).
3) T. Higashijima, Y. Shimohigashi, T. Kato, N. Izumiya, T. Ueno, and T. Miyazawa, *Biopolymers*, **22**, 1167 (1983).
4) Abbreviations: Amp, 2-amino-5-(*p*-methoxyphenyl)-pentanoic acid; ΔAla, 2,3-dehydroalanine; DMAP, 4-dimethylaminopyridine; DMF, *N*,*N*-dimethylformamide; EDC, 1-ethyl-3-(3-dimethylaminopropyl)carbodiimide; Hmb, 2-hydroxy-3-methylbutanoic acid; HOBt, 1-hydroxybenzotriazole; HONSu, *N*-hydroxysuccinimide; Lac, lactic acid; -OPac, phenacyloxy; TFA, trifluoroacetic acid.
5) H. Mihara, K. Ikesue, S. Lee, H. Aoyagi, T. Kato, T. Ueno, and N. Izumiya, *Int. J. Pept. Protein Res.*, in press.
6) H. Mihara, H. Aoyagi, S. Lee, M. Waki, T. Kato, and N. Izumiya, *Int. J. Pept. Protein Res.*, **23**, 447 (1984).
7) Y. Shimohigashi, S. Lee, T. Kato, and N. Izumiya, *Bull. Chem. Soc. Jpn.*, **51**, 584 (1978).
8) H. Aoyagi, H. Mihara, S. Lee, T. Kato, T. Ueno, and N. Izumiya, *Int. J. Pept. Protein Res.*, **25**, 144 (1985).
9) C. Gilon, Y. Klausner, and A. Hassner, *Tetrahedron Lett.*, **1979**, 3811.
10) S. Nomoto, A. Sano, and T. Shiba, *Tetrahedron Lett.*, **1979**, 521.
11) G. C. Stelakatos, A. Paganou, and L. Zervas, *J. Chem. Soc. C*, **1966**, 1191.

Optical Resolution of Asymmetric Selenoxides by High-Performance Liquid Chromatography Using Optically Active Column

Toshio SHIMIZU and Michio KOBAYASHI*
Department of Chemistry, Faculty of Science, Tokyo Metropolitan University, Fukazawa, Setagaya-ku, Tokyo 158
(Received March 6, 1986)

Synopsis. The optical resolution of asymmetric diaryl selenoxides and the determination of the enantiomeric excess of the partially active selenoxides were found to be possible by HPLC using an optically active column.

Although optically active sulfoxides have been known for a long time, the synthesis of an optically active pure selenoxide has so far been unsuccessful. The reason for the difficulty in isolating the enantiomer of selenoxides has been attributed to either a facile racemization due to the formation of a hydrate or to a rapid pyramidal inversion of the conformation around the selenium atom. In 1983, the preparation of partially optically active selenoxides was reported for the first time, but their optical purities were only 5—11%.[1] Recently, we described a synthesis of the optically pure diastereomeric selenoxide as well as the enantiomeric selenoxide with a high optical activity.[2] The determination of the enantiomeric excess has a vital importance in studies on optical resolution. We have discovered that asymmetric diaryl selenoxides can be resolved into the antipodes and also that the optical purities of the selenoxides, in which optical rotation is unknown, can be determined by HPLC using an optically active column. Details are described in this paper.

Results and Discussion

Selenides were prepared according to published methods.[3-6] The oxidation of selenides to selenoxides was carried out with *t*-butyl hypochlorite in the presence of methanol and pyridine.[7]

An example of the general procedure is shown for the case of *p*-tolyl 2,4,6-triisopropylphenyl selenoxide (**1**). A chromatographic separation of the racemic selenoxides was performed with a Bakerbond chiral phase HPLC column RP 7103-O (250×4.6 mm) packed with DNBPG/aminopropylsilica (particle size 5 μm), similar to those which have been used for the separation of various optically active compounds,[8] using hexane containing 5 vol% of 2-propanol as the mobile phase at a flow rate of 1.0 ml min^{-1} (Fig. 1). The chromatographic separability factor of the enantiomers, α was calculated to be 1.10. The R_S value was also calculated as 1.46. The integration ratio (lower R_f/higher R_f) was 1.01. This integration value over 1.00 could be attributed to the tailing of higher R_f enantiomer.

Several diaryl and alkyl aryl selenoxides were subjected to HPLC in a similar way using an optically active column; the results are summarized in Table 1. The R_S value and the integration ratio are a measure of the capability for a chromatographic separation of the optical isomers. The R_S values of the selenoxides **1**—**6** were 1.00—1.86 and integration ratios were 1.01—1.05.

In order to investigate the effect of bulky ortho substituents to retard the rate of racemization through a conformational inversion, the separabilities of phenyl 2,4,6-trimethylphenyl selenoxide (**8**), triethyl derivative **7**, triisopropyl derivative **2**, and tri-*t*-butyl derivative **5** in the HPLC with optical active column were compared with each other. All selenoxides were found to be separable into optical isomers; however, as can be seen in Table 1, compared to selenoxides **2** and **5**, the R_S values of selenoxides **7** and **8**, which possess less bulky substituents than isopropyl or *t*-butyl groups, were small. The integration ratios of selenoxides **7** and **8** increased by over 1.00. The decrease of the chromatographic separability of latter selenoxides might be attributed to a decrease in the conformational stability. We have also attempted a resolution of alkyl aryl selenoxide **9** and benzyl aryl selenoxide **10**, which possess bulky ortho substituents. However, contrary to

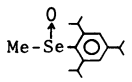

9

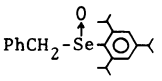

10

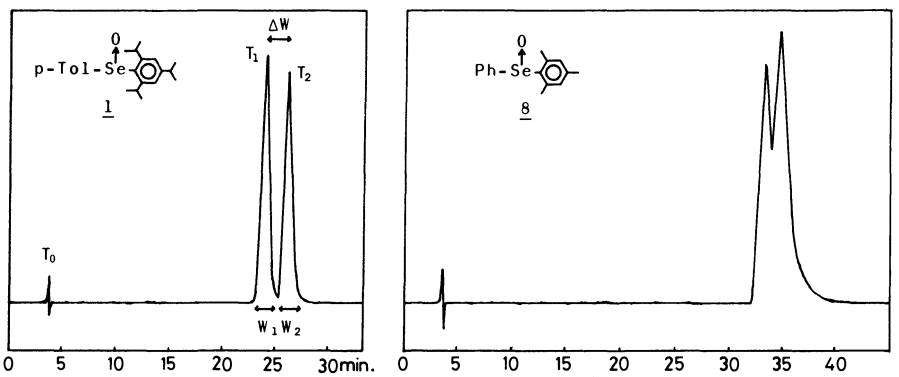

Fig. 1. Chromatographic resolution of enantiomers.

Table 1. Chromatographic Resolution of Selenoxide

	Selenoxide	2-Propanol[c] %	k_1'[d]	α[e]	R_s[f]	Integration ratio[g]
(1)	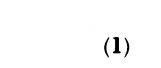	5	5.17	1.10	1.46	1.01
(2)	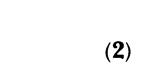	5	4.15	1.09	1.35	1.02
(3)	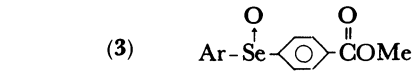	5	7.79	1.12	1.83	1.02
(4)	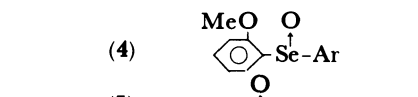	5	11.8	1.10	1.86	1.02
(5)	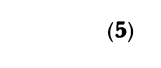	3	3.01	1.06	1.00	1.05
(6)	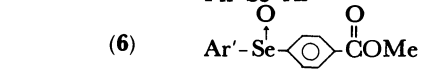	3	4.43	1.07	1.25	1.03
(7)	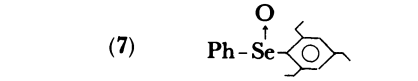	5	9.33	1.06	0.77	1.18
(8)	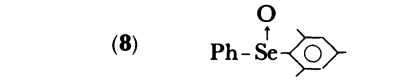	10	7.43	1.05	0.51	1.83

a) Ar is 2,4,6-triisopropylphenyl group. b) Ar′ is 2,4,6-tri-*t*-butylphenyl group. c) The volume percentage of 2-propanol in hexane used as a mobile phase. d) k_1' is the capacity ratio for the initially eluted enantiomer; $k_1'=(T_1-T_0)/T_0$. e) The chromatographic separability factor of the enantiomers, α, is the ratio of the capacity ratios of the two enantiomers; $\alpha=k_2'/k_1'$. f) R_s is the peak resolution of the two enantiomers; $R_s=2\Delta W/(W_1+W_2)$. g) The integration ratio of the two enantiomers; lower R_f/higher R_f.

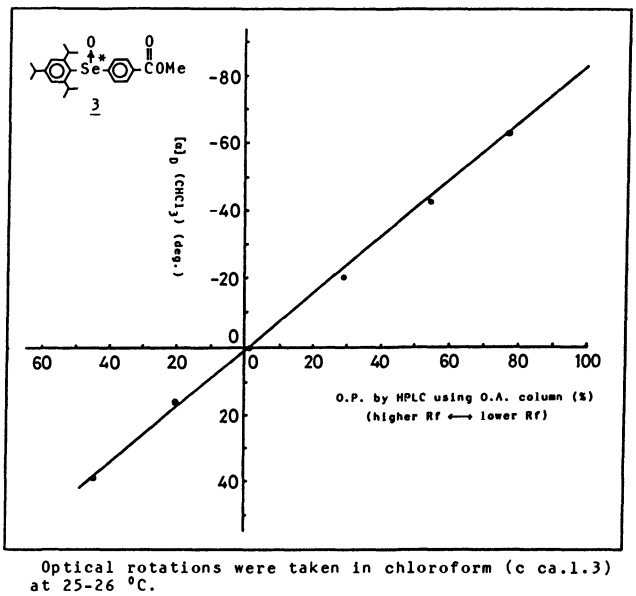

Optical rotations were taken in chloroform (c ca.1.3) at 25-26 °C.

Fig. 2. Correlation of optical rotations and optical purities by HPLC using optically active column.

the diaryl selenoxides, we found that these alkyl aryl selenoxides could not be separated by HPLC using an optically active column.

A plot of the optical rotations $[\alpha]_D$ and the optical purities estimated by HPLC gave a good straight line (Fig. 2) in the case of selenoxide **3**.

In conclusion, HPLC with an optical active column is useful for indicating which selenoxide can be separable into optical antipodes and to determine their optical purities.

Experimental

All melting points were determined on a Yamato MP-21 and were uncorrected. The IR spectra were recorded on a Hitachi 260-10 Spectrometer, ^{1}HNMR spectra with TMS as an internal standard on a JEOL JNM-PMX 60, and mass spectra on a JEOL JMS-DX300 Mass Spectrometer. The optical rotations were measured on a JASCO DIP-140 digital polarimeter. Silica-gel TLC and column chromatography were performed with a Merck Kieselgel 60F_{254} and a Wako Wakogel C-200, respectively. The HPLC system consisted of a Hitachi 655 Liquid Chromatograph equipped with a Rheodyne 7125 sample injector. Elutions were monitored at 265 nm using a Hitachi 638-41 variable-wavelength UV monitor. A Hewlett-Packard 3390A reporting integrator was used to obtain accurate retention times and integration areas at a chart speed of 5 mm min^{-1}.

Materials. Selenoxides (**1**, **3**, **5**, and **9**) were the known compounds.[1,2,7]

Phenyl 2,4,6-Triisopropylphenyl Selenoxide (2): Selenide was prepared from bis(2,4,6-triisopropylphenyl) diselenide and phenylmagnesium bromide.[3] The oxidation of this selenide to selenoxide **2** was accomplished according to our published method.[7] Mp 148.5—149.5 °C (hexane). IR (KBr) ν=815 cm^{-1} (Se=O). ^{1}HNMR ($CDCl_3$) δ=0.90, 1.24, 1.30 (18H, d, J=6.8 Hz), 2.86 (1H, m), 3.73 (2H, hep, J=6.8 Hz), 6.98 (2H, s), 7.2—7.7 (5H, m). Exact MS, Found: m/z 376.1217 (^{80}Se), Calcd for $C_{21}H_{28}O^{80}Se$: 376.1305.

2-Methoxyphenyl 2,4,6-Triisopropylphenyl Selenoxide (4): Starting selenide was prepared from bis(2-methoxyphenyl) diselenide and 2,4,6-triisopropylphenylmagnesium bromide[3]

and oxidized to selenoxide **4** by *t*-butyl hypochlorite.[7] Mp 154.5—155 °C (benzene–hexane). IR (KBr) ν=825 cm^{-1} (Se=O). ^{1}H NMR ($CDCl_3$) δ=0.86, 1.18, 1.29 (18H, d, J=6.6 Hz), 2.80 (1H, hep, J=6.6 Hz), 3.56 (3H, s), 3.84 (2H, hep, J=6.6 Hz), 6.93 (2H, s), 6.7—8.1 (4H, m). Exact MS, Found: *m/z* 406.1459, Calcd for $C_{22}H_{30}O_2{}^{80}Se$: 406.1411.

4-(Methoxycarbonyl)phenyl 2,4,6-Tri-*t*-butylphenyl Selenoxide (6): A starting selenide was prepared from *p*-ethoxycarbonylphenyl selenocyanate and 2,4,6-tri-*t*-butylphenyllithium in THF[5] followed by the hydrolysis and methylation. The oxidation of the selenide to the selenoxide **6** was performed in a similar method as **4**. Mp 129—129.5 °C. IR (KBr) ν=840 (Se=O) and 1725 (C=O) cm^{-1}. ^{1}H NMR ($CDCl_3$) δ=1.36 (9H, s), 1.45 (18H, s), 3.86 (3H, s), 6.97 and 7.87 (4H, ABq, J=8.6 Hz), 7.49 (2H, s). Mass, M$^+$ 476 (^{80}Se). Exact MS, Found: *m/z* 460.1916 (^{80}Se)(lack of one oxygen, Calcd for $C_{26}H_{36}O_2{}^{80}Se$: 460.1880.

Phenyl 2,4,6-Triethylphenyl Selenoxide (7): Selenide prepared from diphenyl diselenide and 2,4,6-triethylphenylmagnesium bromide[3] was oxidized to the selenoxide **7** as in the case of **4**. Mp 50.5—51.5 °C. IR (KBr) ν=820 cm^{-1} (Se=O). ^{1}H NMR ($CDCl_3$) δ=1.06 (6H, t, J=7.8 Hz), 1.18 (3H, t, J=7.8 Hz), 2.60 (2H, q, J=7.8 Hz), 2.91 (4H, q, J=7.8 Hz), 6.89 (2H, s), 7.2—7.7 (5H, m). Exact MS, Found: *m/z* 334.0841 (^{80}Se), Calcd for $C_{18}H_{22}O^{80}Se$: 334.0836.

Phenyl 2,4,6-Trimethylphenyl Selenoxide (8): Oxidation of the selenide prepared from diphenyl diselenide and 2,4,6-trimethylphenylmagnesium bromide[3] with our published method[7] gave the selenoxide **8** in good yield. Mp 82—82.5 °C. IR (KBr) ν=805 cm^{-1} (Se=O). ^{1}H NMR ($CDCl_3$) δ=2.25 (3H, s), 2.44 (6H, s), 6.81 (2H, s), 7.2—7.7 (5H, m). Exact MS, Found: 292.0287, Calcd for $C_{15}H_{16}O^{80}Se$: 292.0366

Benzyl 2,4,6-Triisopropylphenyl Selenoxide (10): Selenide prepared from bis(2,4,6-triisopropylphenyl) diselenide and benzyl magnesium bromide[3] was oxidized to the selenoxide **10** according to the published method.[7] Mp 132.5—134 °C (hexane). IR (KBr) ν=820 cm^{-1} (Se=O). ^{1}H NMR ($CDCl_3$) δ=1.04, 1.26, 1.27 (18H, d, J=6.8 Hz), 2.88 (1H, m), 3.94 (2H, hep, J=6.8 Hz), 4.38 (2H, s), 6.98 (2H, s), 6.8—7.3 (5H, m).

Optically Active 4-(Methoxycarbonyl)phenyl 2,4,6-Triisopropylphenyl Selenoxide (3): The optically active selenoxide (**3**) was synthesized by the method described in our previous paper.[2] The selenoxide samples with lower enantiomeric excess were prepared by mixing of (+) selenoxide and (−) selenoxide.

References

1) F. A. Davis, J. M. Billmers, and O. D. Stringer, *Tetrahedron Lett.*, **24**, 3191 (1983).
2) T. Shimizu and M. Kobayashi, *Chem. Lett.*, **1986**, 161.
3) T. W. Campbell and J. D. McCullough, *J. Am. Chem. Soc.*, **67**, 1965 (1945).
4) K. Šindelář, E. Svátek, J. Metyšová, J. Metyš, and M. Protiva, *Collect. Czech. Chem. Commun.*, **34**, 3792 (1969).
5) B. Greenberg, E. S. Gould, and W. Burlant, *J. Am. Chem. Soc.*, **78**, 4028 (1956).
6) A. M. C. Bava and L. Chierici, *Boll. Chim. Pharm.*, **89**, 397 (1950).
7) M. Kobayashi, H. Ohkubo, and T. Shimizu, *Bull. Chem. Soc. Jpn.*, **59**, 503 (1986).
8) W. H. Pirkle, J. M. Finn, J. L. Schreiner, and B. C. Hamper, *J. Am. Chem. Soc.*, **103**, 3964 (1981).

S-Alkyl-4-oxothianium Ions for the Synthesis of Cyclopentenones. Acid-Catalyzed Cyclization of Divinyl Ketones

Haruo MATSUYAMA,* Yuji TAKEI, and Michio KOBAYASHI
Department of Chemistry, Faculty of Science, Tokyo Metropolitan University, Fukazawa, Setagaya-ku, Tokyo 158
(Received March 4, 1986)

Synopsis. A new approach to 2-cyclopentenones via an acidic cyclization of divinyl ketones by the use of S-alkyl-4-oxothianium ions as key compounds is described.

Considerable attention has been focused in recent years on cyclic sulfur compounds for the synthesis of interesting organic compounds. 4-Thianone (**1**) (R=H) is constituted of 5 carbon units and a sulfur atom as an active functional group for a ring transformation. Recently, we reported a general synthesis of 2-alkyl-3-cyclopentenones via a Ramberg-Bäcklund reaction starting from **1** (R=alkyl) as a 5 C synthon.[1] In connection with the use of **1** for the synthesis of cyclopentenones, we examined the possible route to 2-cyclopentenones (**6**) from S-alkyl-4-oxothianium ions (**2**) as shown in Scheme 1.[2] Cardwell reported that S-methyl-4-oxothianium iodide reacted with a carbon nucleophile, such as sodium diethyl malonate, to give a ring-substitution product in good yield (Eq. 1).[3]

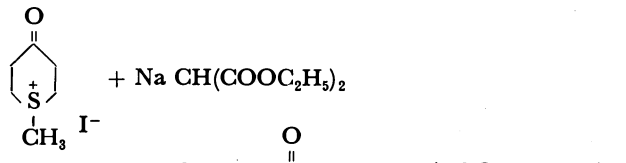

(1)

We found that sulfonium ions (**2**) reacted smoothly with sodium ethanethiolate to give **3** in good yield (Scheme 1). In this note we illustrate the utility of S-ethyl-4-oxothianium ions (**2**) for the synthesis of 2-alkyl-2-cyclopentenones (**6**). The starting materials, 3-alkyl-4-thianones (**1**) (R=alkyl), were prepared by the alkylation of 3-methoxycarbonyl-4-thianone with alkyl halides (R-X, NaH, *N*,*N*-dimethylformamide (DMF)), followed by demethoxycarbonylation (NaCl, wet dimethyl sulfoxide (DMSO), 150 °C) (Eq. 2).[4] S-

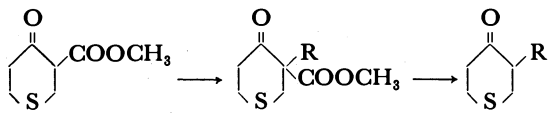

(2)

1

a : R=*n*-C_5H_{11}

b : R=$C_6H_5CH_2$

Ethyl-4-oxothianium tetrafluoroborate (**2**) was readily prepared from **1** with Meerwein's reagent (triethyloxonium tetrafluoroborate) in dichloromethane at room temperature. It underwent a clean substitution reaction with sodium ethanethiolate in methanol (room temperature for 20 h) to form 2-alkyl-1,5-bis(ethylthio)-3-pentanone **3** (**3a**: 89%; **3b**: 69%). **3** was oxidized with sodium periodate (2.2 equiv) in methanol (room temperature for 20 h) to give 2-alkyl-1,5-bis(ethylsulfinyl)-3-pentanone (**4**) (**4a**: 82%; **4b**: 80%). Divinyl ketone (**5**) was formed by refluxing a benzene solution of **4** in the presence of calcium carbonate (3 equiv). The IR spectrum of the benzene solution showed a strong absorp-

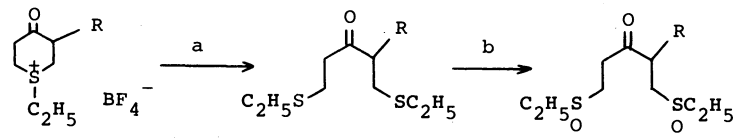

2 **3** **4**

a: R = *n*-C_5H_{11}
b: R = $C_6H_5CH_2$

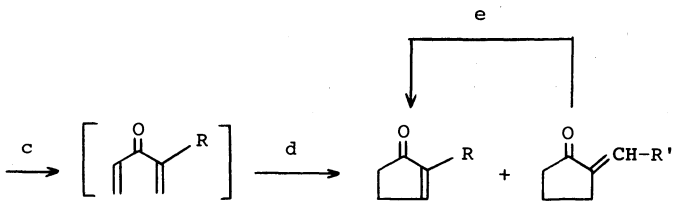

5 **6** **7**

a: R = *n*-C_5H_{11} **a**: R′ = *n*-C_4H_9
b: R = $C_6H_5CH_2$ **b**: R′ = C_6H_5

a: C_2H_5SH-CH_3ONa-CH_3OH, **b**: $NaIO_4$-CH_3OH,
c: $CaCO_3$-C_6H_6, **d**: H_3PO_4-HCOOH (1:1),
e: HCl-1-C_4H_9OH

Scheme 1.

tion band of the carbonyl group at 1680 cm^{-1}, corresponding to the vinyl ketone. An acid-catalyzed cyclization (phosphoric acid–formic acid (1:1), reflux)[5] of the divinyl ketone (**5**) gave 2-alkyl-2-cyclopentenone (**6**) (**6a**: 34%; **6b**: 22%) and its *exo*-enone isomer (**7**) (**7a**: 20%; **7b**: 10%). In our reaction system, a chemical yield of 2-cyclopentenones can be 32 to 54% because the isomerization of **7** to **6** could be accomplished by heating **7** in HCl/1-butanol at 90 °C.[6]

In conclusion, as shown in Scheme 1, S-alkyl-4-oxothianium ions (**2**) are very interesting compounds for a ring transformation of a six-membered ketone (4-thianone, **1**) to a five-membered ketone (2-cyclopentenone, **6**).

Experimental

The IR spectra were determined on a Hitachi 260-10 spectrometer. The NMR spectra were recorded on Hitachi R-20B and JEOL FX-60 spectrometers, using TMS (tetramethylsilane) as an internal standard. The mass spectra were recorded with a JEOL DMX-300 mass spectrometer. Column chromatography was performed with silica gel Wakogel C-200 and preparative TLC was carried out using silica gel $60F_{254}$ PLC plates (Merck 5717).

3-Pentyl-4-thianone (1a). Granular sodium hydride (0.36 g, 15 mmol) was added to a solution of 3-methoxycarbonyl-4-thianone[3] (1.74 g, 10 mmol) and pentyl iodide (2.97 g, 15 mmol) in dry DMF (60 ml) under an atmosphere of dry nitrogen. The mixture was stirred at ambient temperature for 20 h and then poured into water (100 ml). A normal ether work-up followed by column chromatography (hexane: ether=5:1) gave 3-pentyl-3-methoxycarbonyl-4-thianone as a colourless oil (1.76 g, 72%); Bp 138 °C/2.5 mmHg (1 mmHg=133.322 Pa); IR (neat) 1740 and 1710 cm^{-1}; ^{1}H NMR ($CDCl_3$) δ=0.97 (3H, t), 1.00—1.50 (8H, m), and 2.84—3.46 (6H, m), 3.77 (3H, s); MS: *m/z* 244 (M^+).

A mixture of the β-keto ester (1.25 g, 5.1 mmol), anhydrous sodium chloride (0.33 g, 5.6 mmol) and water (0.3 ml) in DMSO (20 ml) was heated (oil bath temperature, 150 °C) for 20 h. After cooling the solution to room temperature, a normal ether work-up followed by column chromatography (hexane:ether=9:1) gave the ketone (**1a**) as a colourless oil (442 mg, 46%); IR (neat) 1705 cm^{-1}; ^{1}H NMR ($CDCl_3$) δ=0.90 (3H, br t), 1.29—1.33 (8H, m), 2.60—3.10 (7H, m); MS: *m/z* 186 (M^+).

3-Benzyl-4-thianone (1b). Granular sodium hydride (0.36 g, 15 mmol) was added to a solution of 3-methoxycarbonyl-4-thianone (1.74 g, 10 mmol) and benzyl bromide (1.88 g, 11 mmol) in dry DMF (60 ml) under an atmosphere of dry nitrogen. The mixture was stirred at ambient temperature for 2.5 h and then poured into water (100 ml). A normal ether work-up followed by column chromatography (hexane:ether=5:1) gave 3-benzyl-3-methoxycarbony-4-thianone as solids (2.16 g, 82%); Mp 64.5—65.3 °C; IR (KBr) 1750 and 1710 cm^{-1}; ^{1}H NMR ($CDCl_3$) δ=2.90 (5H, br s), 3.20—3.30 (3H, m), 3.69 (3H, s), 7.23 (5H, br s); ^{13}C NMR ($CDCl_3$) δ= 30.6, 37.9, 39.7, 43.4, 52.3, 64.2 (OCH_3), 126.9, 128.1, 130.4, 135.6, 170.5 (ester C=O), 204.7 (keto C=O); MS: *m/z* 264 (M^+). Anal. ($C_{14}H_{16}O_3S$) C, H.

A mixture of the β-keto ester (1.10 g, 4 mmol), anhydrous sodium chloride (0.26 g, 4.4 mmol) and water (0.22 ml) in DMSO (5 ml) was heated (oil bath temperature, 150 °C) for 20 h. After cooling the solution to room temperature, a normal ether work-up followed by column chromatography gave the ketone (**1b**) as a colourless oil (0.49 g, 60%); Bp 149 °C/2 mmHg; IR (neat) 1705 (C=O) and 1490 cm^{-1} (aryl); ^{1}H NMR ($CDCl_3$) δ=2.40—3.30 (9H, m), 7.24 (5H, br s); ^{13}C NMR ($CDCl_3$) δ=30.8, 35.0, 35.2, 43.9, 54.5, 126.3, 128.4, 129.0, 138.8, 205.5 (C=O); MS: *m/z* 206 (M^+).

2-Pentyl-1,5-bis(ethylthio)-3-pentanone (3a). A dichloromethane solution (20 ml) of 3-pentyl-4-thianone (**1a**) (408 mg, 2.2 mmol) and triethyloxonium tetrafluoroborate (500 mg, 2.6 mmol) was stirred for 20 h at room temperature. After the reaction solution was concentrated in vacuo, the residual oil was dissolved in dry methanol (10 ml). To a methanol solution (20 ml) of sodium ethanethiolate (2.8 mmol; 1.3 equiv) was added the above methanol solution of sulfonium salt (**2a**) and the mixture was stirred at room temperature for 21 h. After the removal of methanol in vacuo, a normal dichloromethane work-up to give an oil (**3a**) which was homogeneous on silica gel TLC (539 mg, 89%); IR (neat) 1710 cm^{-1}; ^{1}H NMR ($CDCl_3$) δ=0.90 (3H, t), 1.00—1.80 (14H, m containing t at 1.26 (J=7.2 Hz)), 2.30—3.00 (11H, m containing s at 2.76).

2-Benzyl-1,5-bis(ethylthio)-3-pentanone (3b). A dichloromethane solution (20 ml) of 3-benzyl-4-thianone (**1b**) (734 mg, 3.6 mmol) and triethyloxonium tetrafluoroborate (820 mg, 4.3 mmol) was stirred for 19 h at room temperature. After the dichloromethane solution was concentrated in vacuo, the residual oil was dissolved in dry methanol (10 ml). To a methanol solution (20 ml) of sodium ethanethiolate, which was prepared by the reaction between sodium metal (4.8 mmol) and ethanethiol (330 mg, 5.3 mmol), was added the above methanol solution of sulfonium salt (**2b**) and the mixture was stirred at room temperature for 22 h. After the methanol solution was concentrated in vacuo, a normal dichloromethane work-up to give an oil (**3b**) which was homogeneous on silica gel TLC (726 mg, 69%); IR (neat) 1705 cm^{-1}; ^{1}H NMR ($CDCl_3$) δ=1.20 (6H, t, J=6.6 Hz), 2.24—2.97 (3H, m), 7.19—7.21 (5H, m); ^{13}C NMR ($CDCl_3$) δ=14.67, 24.67, 25.97, 26.75, 32.86, 38.18; 44.80, 53.89, 126.49, 128.56, 128.81, 138.56, 210.89 (C=O).

2-Pentyl-1,5-bis(ethylsulfinyl)-3-pentanone (4a). 2-Pentyl-1,5-bis(ethylthio)-3-pentanone (**3a**) (539 mg, 2 mmol) was treated with sodium periodate (940 mg, 4.4 mmol) in methanol at room temperature for 21 h. After removal of insoluble solids, methanol solution was concentrated in vacuo and the residue was dissolved in chloroform to give **4a** (492 mg, 82%); IR (neat) 1710 (C=O), 1050 and 1020 cm^{-1} (S=O); ^{1}H NMR ($CDCl_3$) δ=0.90 (3H, br t), 1.20—1.90 (14H, m containing t at 1.35 (J=7.2 Hz)), 2.56—3.30 (11H, m containing t at 2.68 (J=7.2 Hz)).

2-Benzyl-1,5-bis(ethylsulfinyl)-3-pentanone (4b). 2-Benzyl-1,5-bis(ethylthio)-3-pentanone (**3b**) (193 mg, 0.56 mmol) was oxidized with sodium periodate (310 mg, 1.45 mmol) in methanol at room temperature for 20 h. After filtration of insoluble solids, methanol solution was concentrated in vacuo and the product was extracted with chloroform to give **4b** (151 mg, 71%); IR (neat) 1715 (C=O), 1050 and 1020 cm^{-1} (S=O).

2-Pentyl-2-cyclopentenone (6a). A benzene solution (10 ml) of **4a** (492 mg, 1.6 mmol) and calcium carbonate (480 mg, 4.8 mmol) was refluxed for 17 h. After filtration of the above solution, its IR spectrum showed a strong absorption band at 1680 cm^{-1} corresponding to vinyl ketone. After removal of benzene, phosphoric acid (8 ml) and formic acid (8 ml) were added to the residual oil and the solution was refluxed for 20 h (oil bath temperature, 100 °C). After cooling the solution to room temperature, a normal benzene work-up, followed by preparative TLC (hexane:ether=5:1) to give **6a** (83 mg, 34%) and its *exo*-enone isomer **7a** (48 mg, 20%); **6a**:[5] IR (neat) 1700 (C=O) and 1625 cm^{-1} (C=C); ^{1}H NMR ($CDCl_3$) δ=0.90 (3H, br t), 1.00—1.70 (6H, m), 2.00—2.26 (6H, m), 7.31 (1H, m); MS: *m/z* 152 (M^+). **7a**: IR (neat) 1715 (C=O) and 1645 (C=C) cm^{-1}; ^{1}H NMR ($CDCl_3$) δ=0.95 (3H, br t), 1.10—1.60 (4H, m), 1.60—2.73 (8H, m), 6.16—6.60 (1H, m). Authentic **7a** was also

prepared by cross-aldol reaction between enol silyl ether of cyclopentanone (2.60 g, 16.7 mmol) and pentanal (1.59 g, 18.5 mmol) in the presence of titanium tetrachloride (1.85 ml, 16.7 mmol) in dichloromethane at −78 °C for 4.5 h in 59% yield;[7] IR (neat) 1720 (C=O) and 1645 (C=C) cm^{-1}. **6a** was obtained by heating **7a** (1.496 g, 9.87 mmol) in HCl (1 ml)/1-butanol (40 ml) at 90 °C for 19 h in 87% yield;[6] Bp 79.5—82.0 °C/5 mmHg; IR (neat) 1700 and 1630 cm^{-1}; ^1H NMR ($CDCl_3$) δ=0.85 (3H, br t), 1.00—1.74 (6H, m), 1.86—2.66 (6H, m), 7.25 (1H, m).

2-Benzyl-2-cyclopentanone (6b). A benzene solution (5 ml) of **4b** (445 mg, 1.4 mmol) and calcium carbonate (410 mg, 4.1 mmol) was refluxed for 21 h. After filtration of the above solution, its IR spectrum showed a strong absorption band at 1680 cm^{-1} corresponding to vinyl ketone. After the removal of benzene, phosphoric acid (6 ml) and formic acid (6 ml) were added to the residual oil and the solution was refluxed for 23 h (oil bath temperature, 100 °C). After cooling the solution to room temperature, a normal benzene work-up, followed by preparative TLC (hexane:ether=1:1) to give **6b** (76 mg, 22%) and its *exo*-enone isomer **7b** (34 mg, 10%); **6b**: IR (neat) 1690 and 1630 cm^{-1}; ^1H NMR ($CDCl_3$) δ=2.40—2.60 (4H, m), 3.40—3.60 (2H, m), 7.10—7.30 (6H, m containing s at 7.25); MS: *m/z* 172 (M^+). **7b**: IR (CCl_4) 1710 and 1620 cm^{-1}; ^1H NMR ($CDCl_3$) δ=1.79—2.50 (4H, m), 2.85 (2H, t, d, *J*=6.6 and 3 Hz), 7.31—7.56 (6H, m). **7b** was prepared by aldol reaction between cyclopentanone (8.4 g, 0.10 mol) and benzaldehyde (3.56 g, 0.03 mol) in sodium hydroxide solution (sodium hydroxide (2.0 g, 0.05 mol) in 463 ml of water) at room temperature for 22 h in 53% yield;[8] Bp 115—117 °C/2 mmHg; IR (CCl_4) 1710 and 1620 cm^{-1}.

References

1) H. Matsuyama, Y. Miyazawa, Y. Takei, and M. Kobayashi, *Chem. Lett.*, **1984**, 833.

2) H. Matsuyama, Y. Miyazawa, Y. Takei, and M. Kobayashi, the abstracts of the 12th Symposium on Organic Sulfur and Phosphorus Chemistry, Osaka, January, 1984, Abstr., p. 83, 20.

3) H. M. E. Cardwell, *J. Chem. Soc.*, **1949**, 715.

4) 3-Alkyl-4-thianones (R=CH_3, C_2H_5): T. Takemura and J. B. Jones, *J. Org. Chem.*, **48**, 791 (1983); 2,3-dialkylated 4-thianones: S. Lane, S. J. Quick, and R. J. K. Taylor, *J. Chem. Soc.*, **1985**, 893.

5) S. Hirano, S. Takagi, T. Hiyama, and H. Nozaki, *Bull. Chem. Soc. Jpn.*, **53**, 169 (1980).

6) D. Liotta, C. S. Barnum, and M. Saindane, *J. Org. Chem.*, **46**, 4301 (1981).

7) T. Mukaiyama, K. Banno, and K. Narasaka, *J. Am. Chem. Soc.*, **96**, 7503 (1974).

8) W. S. Emerson, G. H. Birum, and R. I. Longley, Jr., *J. Am. Chem. Soc.*, **75**, 1312 (1953); A. Hassner and T. C. Mead, *Tetrahedron*, **20**, 2201 (1964).

Proton Inventory of Carboxypeptidase Y-Catalyzed Reactions

Shigeru KUNUGI,* Kazuo TANABE, and Mitsuhiro FUKUDA†
Department of Applied Chemistry, Fukui University, Fukui 910
†Department of Practical Life Studies, Hyogo University of Teacher Education, Yashiro-cho, Hyogo 673-14
(Received February 13, 1986)

Synopsis. The partial solvent isotope effect of D_2O on the carboxypeptidase Y-catalyzed hydrolysis of a peptide (3-(2-furyl)acryloyl-L-phenylalanyl-L-phenylalanine) and an ester (3-(2-furyl)acryloyl-L-phenylalanine ethyl ester) was investigated. The peptide hydrolysis showed a smaller kinetic isotope effect regarding the catalytic rate constant (k_{cat}) and the second-order rate constant (k_{cat}/K_m). k_{cat} Varied linearly on the heavy-water content, indicating that one proton is essentially transferred during the rate-determining step. On the other hand, an ester hydrolysis showed a larger, nonlinear effect, indicating the possibility of a transfer of two or more protons in the rate-determining step of the ester hydrolysis, possibly the deacylation step.

Serine carboxypeptidase [EC.3.4.16.1] is a group of *exo*-protease which have a crucial serine residue in the active site.[1] It is found in tissues from mold and yeast to plants and animals as an intercellular protease.[2] Some of the enzymes of this group are now commercially available, and are largely utilized in peptide sequencing. They are also useful for peptide syntheses through an enzymatic condensation reaction.[3]

One of the characteristics of enzymes of this class is that they often show esterase and/or amidase activities besides the intrinsic peptidase activity.[4-7] This is in contrast to carboxypeptidase A,[8] a well-known metallo-carboxypeptidase from mammalian. This endopeptidase-like activity of serine carboxypeptidase raises questions about the reaction mechanism, especially for the substrate binding to this enzyme.

We have investigated some of the details of reactions of these enzymes,[6,7,9,10] including the pressure dependence of the reaction rate, and found that the two different types of activities show contrasting characters: In a neutral pH region, the apparent activity of amidase or esterase increases with the pH while that of the peptidase increases with a decreasing pH. The latter is very sensitive to pressure.

For an enzyme isolated from yeast (carboxypeptidase Y), Douglas et al.[11] observed a burst process in a the reaction with a non-specific acylating reagent, trimethylacetyl *p*-nitrophenolate. Lobb and Auld[12] reported a presteady-state process in a reaction of this enzyme with a fluorescent depsipeptide substrate. Our preliminary study[13] on a chromophoric amino acid ester substrate using a stopped-flow method also indicated the existence of a presteady-state process. Coupled with the results of a trans-peptidation study catalyzed by this enzyme,[14] these results led us to postulate a so-called three-step mechanism including the acylated enzyme (Eq.1), just as in the case of the serine protease reactions, such as α-chymotrypsin or trypsin.

However, the rates of acylation (k_2) and the deacylation (k_3) are comparable in the case of carboxypeptidase Y-catalyzed hydrolysis of the peptide.[6] Under certain conditions a burst process has been observed,

$$E + S \underset{k_{-1}}{\overset{k_1}{\rightleftharpoons}} ES \xrightarrow{k_2} ES' + P_1 \xrightarrow{k_3} E + P_2 \qquad (1)$$

(E, enzyme; S, substrate; E S, enzyme-substrate complex; ES′, acyl-enzyme; P_1, product; k_1, respective rate constant)

even for the peptide substrate.[13] These are fairly different from serine protease. To find more details regarding these constituent reaction steps, we studied the partial solvent isotope effect of deuterium oxide, known as a proton inventory technique that is useful for determining the behavior of protons during reaction pocesses.[15]

Experimental

Three types of serine carboxypeptidases (carboxypeptidase Y from yeast, W from wheat and P from penicillium) were studied. They were obtained from Oriental Yeast Co., (Osaka; Lot. 21003001), Pentel Co., (Tokyo; Lot. 6930606) and the Protein Research Foundation, (Osaka; Lot. 099201), respectively. Chromophoric substrates, 3-(2-furyl)acryloyl-L-phenylalanyl-L-phenylalanine (Fua-Phe-Phe) and 3-(2-furyl)acryloyl-L-phenylalanine ethyl ester (Fua-Phe-OEt), were used as before.[6] Benzoyl-L-tyrosine-*p*-nitroanilide (Bz-Tyr-*p*NA) was from the Protein Research Foundation. 2-morpholinoethanesulfonic acid (MES) and 2-[4-(2-hydroxyethyl)-1-piperazinyl]ethanesulfonic acid (HEPES) were from the Dohjindo Laboratories (Kumamoto, Japan). Deuterium oxide (99.85%) and sodium deuterium oxide solution in D_2O were purchased from CEA (France). The absorbance spectrum was measured using a Uvidec type-650 spectrophotometer (Nippon Bunkou Co.). The pH was measured with a Hitachi-Horiba pH meter (F-7LC) and the pD value for a D_2O solution was calculated by adding 0.4 to the value read on the meter.[15] Most of the preparation of D_2O-containing solutions was carried out under a stream of dry nitrogen gas. The atom fraction of deuterium in an H_2O-D_2O mixture was calculated on the basis of weight. For a very low content, a NMR apparatus (JEOL GX-270) was also used.

Results

Figure 1 shows the pH or pD dependence of k_{cat} on the carboxypeptidase Y-catalyzed hydrolysis of Fua-Phe-Phe (**a**) and Fua-Phe-OEt (**b**). When the optimum values were compared, the kinetic deuterium-isotope effect ((k_{cat} in H_2O)/(k_{cat} in D_2O)=k_H/k_D) for the peptide substrate was found to be about 1.6, and that for the ester substrate was about 3.5. These values are somewhat larger than those for Z-Phe-Leu and Ac-Phe-OEt reported by Hayashi's group.[16] The K_m parameter was largely unaffected by the solvent D_2O, though not shown here. Thus a comparison of the second-order rate constant (k_{cat}/K_m) can also show the approximate effect on the catalytic process; for

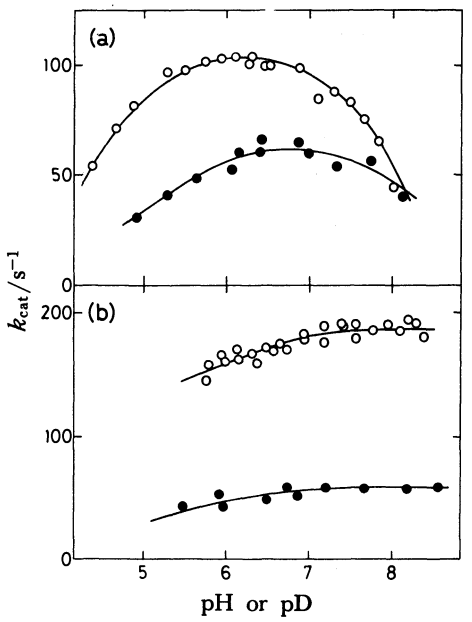

Fig. 1. The pH* dependence of k_{cat} for the carboxypeptidase Y-catalyzed hydrolysis of Fua-Phe-Phe (a) and of Fua-Phe-OEt (b). (○) in H_2O and (●) in D_2O, at 25°C.
(a) [Fua-Phe-Phe]=0.46 mM, [E]=0.17 μM in H_2O and 0.21 μM in D_2O, containing 2.5% (v/v) CH_3CN.
(b) [Fua-Phe-OEt]=0.50 mM, [E]=0.10 μM in H_2O and 0.16 μM in D_2O, containing 2.0% (v/v) CH_3CN.

carboxypeptidase W, k_H/k_D of k_{cat}/K_m was 2.44 for Fua-Phe-OEt hydrolysis (at pH=7.60 and pD=8.01) and 1.13 for Fua-Phe-Phe hydrolysis (at pH=3.95 and pD=4.35). For carboxypeptidase P, only the peptide hydrolysis could be practically measurable and the k_H/k_D of k_{cat}/K_m was 1.11 (at pH=3.87 and pD=4.46). The effect was always small for a peptide hydrolysis.

When measured in an H_2O–D_2O mixture, the k_{cat} value changed as shown in Fig. 2. In the peptide hydrolysis (**a**) the rate constant varied almost linearly with a change in the D_2O content, while the rate of ester hydrolysis (**b**) varied considerably in a concave manner. According to a simplified theoretical treatment of the proton inventory, the rate constant in an H_2O–D_2O mixture can be expressed, provided that all the protons contribute to the total effect in equal amounts,[15] as

$$k = k_{H_2O}(1-n+n\phi)^{\nu}, \quad (2)$$

where n and ν indicate the D_2O content and the number of protons concerning the rate-determining step, respectively. ϕ is a deuterium isotope effect in an elementary step. A nonlinear regression of the data showed us that the ester hydrolysis can be represented by a ϕ value of 0.54 for ν=2 (two-proton assumption) and 0.66 for ν=3 (three-proton assumption). We can mention that at least two protons take part in the rate-determining process of ester hydrolysis while only one proton is apparently concerned in the rate-determining step of the peptide hydrolysis.

Discussion

A proton inventory technique has been successfully

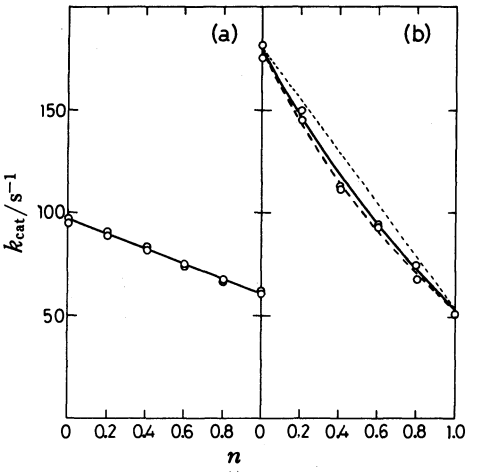

Fig. 2. The partial solvent isotope effect as a function of atom fraction of deuterium (n) for the k_{cat} of the carboxypeptidase Y-catalyzed hydrolysis of Fua-Phe-Phe (a) and of Fua-Phe-OEt (b), at 25°C. [E]=0.11 μM, containing 2.5% (v/v) CH_3CN.
(a) [Fua-Phe-Phe]=0.40 mM. (——) ν=1, ϕ=0.63.
(b) [Fua-Phe-OEt]=0.52 mM.
(——) ν=2, ϕ=0.54, (-----) ν=3, ϕ=0.66 for Eq. 2.
(----) ν=1, ϕ=0.29.

applied to the analysis of an enzyme reaction, especially for the reaction involving serine proteases. In the cases of a serine proteases such as α-chymotrypsin or elastase, a coupled movement of protons was reported for the hydrolysis of specific peptide anilide substrates,[15,17] largely related to the character of the acylation step, while most of the deacylation processes gave a very simple partial isotope effect.[15,18] The coupled movement of the protons during the acylation step of these enzymes was explained based on the so-called charge-relay mechanism involving a concerted proton movement within the Ser–His–Asp residues. This was originally postulated by Blows's group[19] on the basis of their X-ray crystallographical studies, though this mechanism (especially the existence of a very week carbonic acid side chain of Asp 102) has been recently questioned.[20]

Compared to these serine proteases, we know far less about the active site of serine carboxypeptidase. Hayashi et al.[21] showed that a His residue was crucial for the catalytic activity of carboxypeptidase Y. This gives us a picture of an active site similar to that of serine protease; a cooperative function of the Ser and His residues. We have reported after a systematic study of the steady-state kinetics of this enzyme that the peptide hydrolysis by serine carboxypeptidase is partly rate-controlled by the acylation step and that the ester hydrolysis is mostly deacylation-controlled.[6] The present results involving proton inventory indicates that the acylation reaction for these enzymes involves a transfer of one proton, probably between Ser and His residues. On the other hand, the deacylation process is more or less cooperative and a coupled movement of proton(s), in addition to the one between the hydration water and the His residue, is to be considered. Based on a new understanding of the proton movement of the serine protease reaction,[20] a mechanism including the

relaying of ptotons (not a charge) is still considered to be meaningful, especially when the substrate is bound to the active site. Therefore, the present result for carboxypeptidase Y might be explained by a coupled proton transfer occurring when the acyl part of the substrate is co-valently attached to the active site of the enzyme. However, the possibility of other mechanisms, such as a structural change of the protein or a change in the hydration state, might also be considered.

We gratefully acknowledge the advice and encouragement of Professors Norio Ise (Kyoto University) and Yoshiharu Nakamura (Fukui University) throughout the study.

References

1) R. Hayashi, S. Moore, and W. H. Stein, *J. Biol. Chem.*, **248**, 8366 (1973).
2) R. Hayashi, in "Koso Handbook," ed by Y. Kajiro, M. Tokushige, T. Yagi, and E. Ichishima, Asakura Shoten, Tokyo (1982), p. 541.
3) K. Breddam, J. T. Johansen, and M. Ottesen, *Carlsberg Res. Commun.*, **49**, 457 (1984).
4) R. Hayashi, Y. Bai, and T. Hata, *J. Biochem. (Tokyo)*, **77**, 69 (1975).
5) Y. Bai, R. Hayashi, and T. Hata, *J. Biochem. (Tokyo)*, **77**, 81 (1975).
6) M. Fukuda and S. Kunugi, *Eur. J. Biochem.*, **149**, 657 (1985).
7) M. Fukuda, Doctoral Dissertation, Kyoto University (1985).
8) H. Neurath and W. G. Schwert, *Chem. Rev.*, **46**, 69 (1950).
9) M. Fukuda, H. Shima, and S. Kunugi, *J. Biochem. (Tokyo)*, **98**, 517 (1985).
10) S. Kunugi, M. Fukuda, and R. Hayashi, *Eur. J. Biochem.*, **153**, 37 (1985).
11) K. T. Douglas, Y. Nakagawa, and E. T. Kaiser, *J. Am. Chem. Soc.*, **98**, 8231 (1985).
12) R. R. Lobb and D. S. Auld, *Proc. Natl. Acad. Sci. U.S.A.*, **76**, 2684 (1979).
13) S. Kunugi and M. Fukuda, 30th IUPAC Congress (Manchester), 5P-55, Sep. (1985).
14) K. Breddam, F. Widmer, and J. T. Johansen, *Carlsberg Res. Commun.*, **45**, 237 (1980).
15) R. L. Schowen, "Isotope Effects on Enzyme-Catalyzed Reactions," ed by W. W. Cleland, Univ. Park. Press, Baltimore (1977), p. 64.
16) Y. Bai, R. Hayashi, and T. Hata, *J. Biochem. (Tokyo)*, **78**, 617 (1975).
17) M. W. Hunkapiller, M. D. Forgac, and J. H. Richards, *Biochemistry*, **15**, 5581 (1976); J. P. Elrod, J. L. Hogg, D. M. Quinn, K. S. Venkatasubban, and R. L. Schowen, *J. Am. Chem. Soc.*, **102**, 3917 (1980); R. L. Stein, *J. Am. Chem. Soc.*, **105**, 5111 (1983).
18) R. L. Stein, J. P. Elrod, and R. L. Schowen, *J. Am. Chem. Soc.*, **105**, 2446 (1983).
19) D. M. Blow, J. J. Birktoff, and B. S. Hartley, *Nature*, **221**, 337 (1969).
20) T. A. Steitz and R. G. Shulman, *Ann. Rev. Biophys. Bioeng.*, **11**, 419 (1982); F. Sakiyama, *Seikagaku*, **55**, 166 (1983).
21) R. Hayashi, Y. Bai, and T. Hata, *J. Biol. Chem.*, **250**, 5221 (1975).

Stereoselective Reduction of Symmetrical Diketones with Biological Methods. Microbial Reduction of *cis*-2,7-Decalindione

Hiroaki CHIKAMATSU,* Masatoshi TANIGUCHI, and Takamasa KANEMITSU
Department of Chemistry, Faculty of Engineering Science, Osaka University, Toyonaka, Osaka 560
(Received March 22, 1986)

Synopsis. The *pro-S* group of two enantiotopic carbonyl groups in *cis*-2,7-decalindione was preferentially reduced with *Rhodotorula rubra* to give (−)-(7*S*,9*R*,10*S*)-7-hydroxy-*cis*-2-decalone of high optical purity.

In the course of our investigations of the stereo-differentiating reduction of various carbonyl compounds with biological systems, two completely opposite enantiomer selectivities toward C_2-ketones,[1] which were found in a microbial reduction and a horse liver alcohol dehydrogenase (HLADH)-mediated reduction, have led us to propose the microbial "*P*-C_2-ketone rule"[2] and the HLADH "*M*-C_2-ketone rule"[3] to summarize their respective stereochemical behaviors.

Among our further studies on the symmetrical diketones,[4,5] we found that one of two enantiotopic carbonyl groups was preferentially reduced and the hydrogen attack occurred from the *Re*-face of its carbonyl plane.[5] These findings encouraged us to develop a useful methodology for asymmetric syntheses.[6] For instance, it is theoretically possible by utilizing biological stereoselectivity toward prochiral diketone, *cis*-2,7-decalindione (**1**),[7] to transfer the total amount of starting material into one chiral isomer of four molecules, enantiomers of *cis,trans*-ketol **2**[8] and of *cis,cis*-ketol **3**.[8] The HLADH-mediated reduction of **1** did indeed show differentiations between enantiotopic *pro-R* and *pro-S* carbonyl groups,[9] and diastereotopic faces of the carbonyl plane affording (−)-(7*S*,9*S*,10*R*)-7-hydroxy-*cis*-2-decalone (**2**)[10] with a good yield and high optical purity. Starting from **2**, optically pure (+)-twistane was synthesized in short steps.[5b,11]

Coupled with the opposite enantiomer selectivities toward C_2-ketone, we expected to find the opposite enantiotopic group selectivities toward the diketone **1** in the HLADH-mediated reduction and the microbial reduction.

Results and Discussion

Microbial Reduction of Diketone 1. The preliminary test incubation of **1** both with *Rhodotorula rubra* and *Curvularia lunata* revealed that these microbes rapidly reduced **1** giving a ketol as the major product and sluggishly reduced it into diol(s) during further incubation. Monitoring by means of GLC indicated that the metabolite ketol was found to be *cis,cis*-ketol **3**, one of the diastereomers of (−)-*cis,trans*-ketol **2** obtained from an HLADH-mediated reduction.

Preparative-scale incubation with *R. rubra* was carried out for 68 h at 30°C. During this period, 85% of the diketone was consumed. After an extraction of the metabolite, alumina chromatography provided a 59% yield of crystalline (−)-ketol **3**, $[\alpha]_D^{25}$ −2.3°. Contrary to *R. rubra*, *C. lunata* was found to show a poor enantiotopic group selectivity, affording a 21% yield of optically inactive ketol **3**.[12]

In the ^{1}HNMR spectrum, a singlet signal at δ 3.0 ppm due to methyl protons of $-OSO_2CH_3$ exhibited by the (±)-keto mesylate **4** of (±)-ketol **3**, was clearly separated ($\Delta\Delta\delta$ 0.04 ppm) with an addition of a chiral shift reagent, Eu(facam)$_3$.[13] In case of (−)-**4** prepared from (−)-ketol **3**, such an enantiomer differential shift was not observed to give any information about the optical purity of (−)-ketol **3** as to be 100% within experimental error.

To secure information on the absolute configuration of (−)-ketol **3**, we attempted to relate it to (−)-ketol **2**, whose absolute configuration had been established as being (7*S*,9*S*,10*R*) in our labolatory.[5b]

By the method of Mitsunobu,[14] an inversion of the configuration at C-7 of (−)-ketol **2** using triphenylphosphine, diethyl azodicarboxylate, and acetic acid in tetrahydrofuran, gave (+)-keto acetate **5**, $[\alpha]_D^{24}$ +41°. This was found to be an enantiomer of (−)-**5**, $[\alpha]_D^{24}$ −40°, prepared from (−)-ketol **3** by a treatment with acetic anhydride in pyridine. Thus, the absolute configuration of (−)-ketol **3** was determined as being a (7*S*,9*R*,10*S*)-configuration.[15]

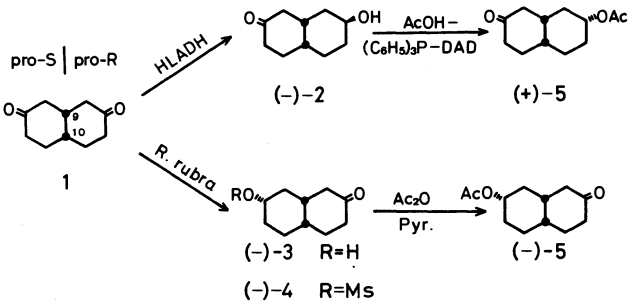

These results clearly show that *R. rubra* preferentially catches the *pro-S* carbonyl group and the hydrogen attack occurs from the *Re*-face of the carbonyl plane. The demonstrated enantiotopic group selectivity of *R. rubra* is completely opposite to that found in the HLADH-mediated process which selectively reduced the *pro-R* carbonyl group.

Experimental

Melting points are uncorrected. ^{1}HNMR spectra were determined on a JNM-60-HL and JNM-NH-100 with Me_4Si as an internal standard (δ=0). Optical rotations were measured with a JASCO-DIP-140 polarimeter. CD spectra were determined on a JASCO-J-40 spectropolarimer. GLC analyses were performed on a JGC-20K equipped with a FID using a 1 m×3 mm inside diameter column of 10% Carbowax 20M on Chromosorb W. Column-chromatography was carried out with Woelm active alumina (neutral, activity III).

Preparation of 1. The diketone **1** was prepared by the method of Anderson and Barlow,[16] mp 63—64°C (lit,[16] mp 62—64°C).

Cultured Broth. *(a). Microbe Culture*: The cultures of *R. rubra* (IFO 0889) and *C. lunata* (IFO 6288) were obtained from the Institute of Fermentation, Osaka, Japan. *(b). Culture medium*:[17] The culture medium was prepared by dissolving glucose (30 g), KH_2PO_4 (1 g), corn-steep liquor (10 g), $MgSO_4 \cdot 7H_2O$ (0.5 g), $NaNO_3$ (2 g), $FeSO_4 \cdot 7H_2O$ (0.02 g), K_2HPO_4 (2 g), and KCl (0.5 g) in 1 L of tap water and was sterillized at 123 °C for 15 min. *(c). Growth of Microbes*: 25 mL of the culture medium in a 100-mL Erlenmeyer flask was inoculated with spores of the microbe on Difco MY agar slants and was shaken for 48 h at 30 °C on a shaker. The culture was transferred into a 500 mL Erlenmeyer flask containing 200 mL of the culture medium, incubation was maintained for another 48 h at 30 °C until a sufficient mass of mycelium had developed.

Microbial Reduction of 1 with *R. rubra*. An aquous solution (40 mL) containing 1.5 g (9 mmol) of **1** was divided into eight batches of the culture broth of *R. rubra* (each 200 mL) and the mixture was incubated at 30 °C for 68 h. After the mycelium was collected by filtration through the layer of Hyflo Super Cel and extracted with chloroform, the beer filtrate was also extracted with the same solvent. The combined extracts were washed with water and dried over anhydrous magnesium sulfate. The removal of the solvent in vacuo left a metabolite mixture (1.4 g) which was analyzed by GLC to reveal that it was a 15:5:78:2 mixture of **1**, **2**, **3**, and diol(s).

The mixture was taken up in benzene and chromatographed upon 50 g of alumina. Elution with 200 mL of benzene–chloroform (10:1) afforded 50 mg of **1**. Further elution with 200 mL of benzene–chloroform (1:1), followed by 600 mL of chloroform, gave 880 mg (59% yield) of (−)-ketol **3**; mp 88—89 °C (from pentane); $[\alpha]_D^{25}$ −2.3 ° (*c* 1.6, $CHCl_3$); CD (*c* 2.4×10^{-3} mol dm^{-3}, MeOH) $[\theta]$ 290 nm −380; IR (KBr) 3400, 1690, 1060 cm^{-1}; ^{1}H NMR (100 MHz, $CDCl_3$) δ= 3.6 (m, 1H, 1/2*W* 24Hz, C-7-H).

Found: C, 71.45; H, 9.57%. Calcd for $C_{10}H_{16}O_2$: C, 71.39; H, 9.39%.

(−)-Keto Mesylate 4. To a solution of (−)-ketol **3** (460 mg, 2.7 mmol) in pyridine (5 mL) was added methanesulfonyl chloride (600 mg, 5.2 mmol) at 0 °C. The mixture was allowed to stand overnight in a refrigerator. The reaction mixture was diluted with ice-water and extracted with dichloromethane. The extract was washed with dil hydrochloric acid and water, then dried over anhydrous magnesium sulfate. After the removal of the solvent in vacuo, the residue (620 mg) was recrystallized from pentane-dichloromethane to give 420 mg (62% yield) of (−)-keto mesylate **4** as flaks; mp 99—100 °C; $[\alpha]_D^{25}$ −24.4 ° (*c* 1.7, $CHCl_3$); IR (KBr) 1700, 1350, 1170, 938 cm^{-1}: ^{1}H NMR (60 MHz, $CDCl_3$) δ=4.65 (m, 1H, 1/2*W* 23Hz, C-7-H), 3.0 (s, 3H, S-CH_3).

Found: C, 53.57; H, 7.39; S, 12.98%. Calcd for $C_{11}H_{18}O_4S$: C, 53.64; H, 7.37; S, 13.02%.

(−)-Keto Acetate 5. To a solution of (−)-ketol **3** (103 mg, 0.6 mmol) in pyridine (1 mL) was added acetic anhydride (0.1 mL). The mixture was allowed to stand overnight. The reaction mixture was poured into ice-water and extracted with ether. The ethereal layer was washed with 5% hydrochloric acid and water followed by drying over anhydrous magnesium sulfate. The removal of the solvent gave 110 mg (90% yield) of (−)-keto acetate **5**; mp 82—83 °C (from pentane); $[\alpha]_D^{22}$ −40.0 ° (*c* 0.54, $CHCl_3$); IR (KBr) 1730, 1705, 1250, 1050 cm^{-1}; ^{1}H NMR (60 MHz $CDCl_3$) δ=4.75 (m, 1/2*W* 22 Hz, C-7-H), 2.0 (s, 3H, O-CH_3).

Found: C, 68.52; H, 8.69%. Calcd for $C_{12}H_{18}O_3$: C, 68.54; H, 8.63%.

Microbial Reduction of 1 with *C. lunata*. The diketone **1** (total 1.5 g, 9 mmol) was incubated for 68 h at 30 °C in eight batches. The metabolite mixture containing **1**, **2**, **3**, and diol(s) in a ratio of 8:9:80:3 was worked up according to the procedure described on the *R. rubra* reduction to afford 317 mg (21% yield) of (±)-ketol **3**; mp 101.5—102.5 °C (from pentane); $[\alpha]_D^{23.5}$ ±0 ° (*c* 1.33, $CHCl_3$).

Found: C, 71.51; H, 9.58%. Calcd for $C_{10}H_{16}O_2$: C, 71.39; H, 9.59%.

The (±)-keto mesylate **4**; mp 78—79 °C (from pentane–dichloromethane); $[\alpha]_D^{24}$ ±0 ° (*c* 1.2, $CHCl_3$).

Found: C, 53.57; H, 7.39%. Calcd for $C_{11}H_{18}O_4S$: C, 53.64; H, 7.37%.

(+)-Keto Acetate 5. To a solution of (−)-ketol **2** obtained from HLADH mediated reduction ($[\alpha]_D^{24}$−16.4 °,[5b] 170 mg, 1 mmol), triphenylphosphine (510 mg, 2 mmol), and acetic acid (120 mg, 1 mmol) in dry THF (4 mL) was added dropwise a solution of diethyl azodicarboxylate (340 mg, 2 mmol) in dry THF (2 mL). After being stirred at room temperature for 48 h, the reaction mixture was analyzed by GLC to reveal that 76% of **2** was inverted into keto acetate **5**. The solvent was removed under reduced pressure to afford a syrupy product which was taken up into ether (50 mL). An insoluble material was filtered off and the filtrate was concentrated. The resultant residue was taken up into pentane (150 mL) and a soluble portion was washed with aq sodium hydrogencarbonate. It was then chromatographed over alumina (5 g). Elution with pentane–ether (10:1) (250 mL) gave 55 mg (26% yield) of (+)-keto acetate **5**; mp 82—83 °C (from pentane); $[\alpha]_D^{24}$ +41 ° (*c* 0.73, $CHCl_3$).

Found: C, 68.58; H, 8.72%. Calcd for $C_{12}H_{18}O_3$: C, 68.54; H, 8.63%.

This work was partially supported by grants from the Ministry of Education, Science and Culture (57470024), and Suntory Institute for Bioorganic Research, for which the authors' thanks are due.

References

1) Proposed name for ketones which belong to C_2 point group and have the C_2 axis coincident with the carbonyl axis.

2) a) M. Nakazaki, H. Chikamatsu, K. Naemura, M. Nishino, H. Murakami, and M. Asao, *J. Chem. Soc., Chem. Commun.*, **1978**, 667; b) M. Nakazaki, H. Chikamatsu, K. Naemura, M. Nishino, H. Murakami, and M. Asao, *J. Org. Chem.*, **44**, 4588 (1979).

3) a) M. Nakazaki, H. Chikamatsu, K. Naemura, Y. Sasaki, and T. Fujii, *J. Chem. Soc., Chem. Commun.*, **1980**, 626; b) M. Nakazaki, H. Chikamatsu, K. Naemura, T. Suzuki, M. Iwasaki, Y. Sasaki, and T. Fujii, *J. Org. Chem.*, **46**, 2726 (1981).

4) Stereo-differentiating reduction of homotopic carbonyl groups in symmetrical diketones: a) M. Nakazaki, H. Chikamatsu, and M. Asao, *J. Org. Chem.*, **46**, 1147 (1981); b) M. Nakazaki, H. Chikamatsu, M. Nishino, and H. Murakami, *ibid.*, **46**, 1151 (1981).

5) Stereo-differentiating reduction of enantiotopic carbonyl groups in symmetrical diketones: a) M. Nakazaki, H. Chikamatsu, Y. Hirose, and T. Shimizu, *J. Org. Chem.*, **44**, 1043 (1979); b) M. Nakazaki, H. Chikamatsu, and M. Taniguchi, *Chem. Lett.*, **1982**, 1761.

6) For a review see: J. B. Jones, "Enzymes in Organic Synthesis," ed by R. Porter and S. Clark, Pitman, London (1985), pp. 3—21.

7) IUPAC nomenclature; 4,4aβ,5,6,8,8aβ-hexahydro-2,7(1*H*,3*H*)-naphthalenedione.

8) According to the stereochemical naming of decalols, we named these ketols *cis,cis* and *cis,trans*. First *cis* means a *cis* relationship between C-9 and C-10 hydrogens, and second *cis* or *trans* means a *cis* or *trans* relationship between C-7 and C-9 hydrogens. See, a) T. Cohen, M. Malaiyandi, and J. L.

Pinkus, *J. Org. Chem.*, **29**, 3393 (1964); b) T. Oritani, M. Ichimura, Y. Hanyu, and K. Yamashita, *Agric. Biol. Chem.*, **47**, 2613 (1983); c) T. Oritani and K. Yamashita, *J. Org. Chem.*, **49**, 3689 (1984).

9) *Pro-R* and *pro-S* carbonyl groups can be specified respsct to prochiral C-9.

10) IUPAC nomenclature; (4a*R*,7*S*,8a*S*)-7β-hydroxy-3,4,4aβ,5,6,7,8,8aβ-octahydro-2(1*H*)-naphthalenone.

11) D. R. Dodds and J. B. Jones, *J. Chem. Soc., Chem. Commun.*, **1982**, 1080.

12) Bec, Durand, and Huet prepared the racemic modification of ketol **3** by LiAlH(t-C_4H_9)$_3$ reduction of **1**; mp 92°C. Their stereochemical naming for ketol **2** and **3** are as *cis,cis* and *cis,trans* respectively; J.-M. Bec, J. Durand, and J. Huet, *Bull. Soc. Chim. Fr.*, **1972**, 4344.

13) Eu(facam)$_3$; tris(3-trifluoroacetyl-*d*-camphorato)europium (III).

14) O. Mitsunobu and M. Eguchi, *Bull. Chem. Soc. Jpn.*, **44**, 3472 (1971).

15) IUPAC nomenclature of (—)-ketol **3**; (4a*S*,7*S*,8a*R*)-7α-hydroxy-3,4,4aβ,5,6,7,8,8aβ-octahydro-2(1*H*)-naphthalenone.

16) A. G. Anderson Jr. and D. O Barlow, *J. Am. Chem. Soc.*, **77**, 5165 (1955).

17) K. Kieslich, *Synthesis*, **1969**, 120.

Tertiary Amine-Catalyzed Acyl Group-Exchange Reactions of *N,O*-Diacyl-*o*-aminophenols

Tadamitsu SAKURAI,* Shuichi YAMADA, and Hiroyasu INOUE
Department of Applied Chemistry, Faculty of Technology, Kanagawa University, Kanagawa-ku, Yokohama 221
(Received January 27, 1986)

Synopsis. A kinetic study on the base-catalyzed acyl group-exchange reactions of *N,O*-diacyl-*o*-aminophenols was undertaken to show that the formation of the amidate ion should be the rate-determining step in these intramolecular acyl-exchange reactions, and that the electron-withdrawing power of acyl group becomes an important factor to control the relative stabilities of a pair of *N,O*-diacyl-*o*-aminophenols.

The acyl group-exchange reactions of *N,O*-diacyl derivatives of *o*-aminophenol have been extensively studied in the past because these exchange reactions have attracted attention of both theoretical and synthetic organic chemists.[1] The use of HPLC made it possible to separate and analyze quantitatively labile acyl-exchanged products and thus allowed Smith and Elrod to propose the hypothesis that the inductive effects of acyl groups attached to nitrogen or oxygen in the molecule determine the relative stabilities of a pair of *N,O*-diacyl-*o*-aminophenols.[1,2] The failure of this hypothesis to explain the relative stabilities of a pair of *N,O*-acyl-alkoxycarbonyl-*o*-aminophenols[3] prompted us to study the acyl-migration reactions whose mechanism still remains obscure.

We chose *N,O*-(*p*-substituted benzoyl)-(1-naphthoyl) derivatives of *o*-aminophenol as a new system and investigated the solvent, base (tertiary amine), and substituent effects on the rate and equilibrium constants for acyl-exchange reactions, hoping to shed light on the mechanism of these reactions.

The tertiary amine-catalyzed acyl-exchange reactions shown in Scheme 1 follow first-order kinetics in **1** ($2.5—3.3\times10^{-3}$ M, 1 M=1 mol dm^{-3}) at the amine concentration 8.6×10^{-4}—1.2 M at 30 °C (correlation coefficient r=0.990—0.999). In addition, the pseudo-first-order rate constants (k), observed typically for **1a**—**2a** pair, increase linearly in proportion to the amine concentration (r=0.996), suggesting that the reaction is first-order in both **1** and the amine. The acyl exchange was not observed in benzene and 1,2-dichloroethane without the amines, whereas the reaction proceeded to a minor extent in acetonitrile containing no amines. However, such a solvent(acetonitrile)-catalyzed reaction ($k\approx3\times10^{-5}$ min^{-1}) was shown to have a negligible effect on the observed rate constants, e.g., k=0.40 min^{-1} for the triethylamine(1.65×10^{-3} M)-catalyzed reaction of **1a** in acetonitrile. On the other hand, no HPLC peaks attributable to the conceivable intermediates could be detected during the course of the reaction under any conditions. The equilibrium constants (K) were estimated from the concentration ratios [**2**]/[**1**] at equilibrium state and the second-order rate constants (k_1) were obtained by dividing the k values by the amine concentration used. The rate and equilibrium constants thus evaluated are collected in Table 1.

First we discuss the solvent, base, and substituent effects on the rate of the acyl-migration reaction. The increased solvent polarity was found to greatly accelerate the reaction. In addition, the reaction rates have a tendency to increase with increasing the basicity of the amines and the electron-withdrawing power of the

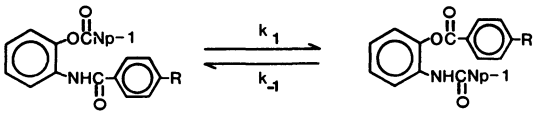

1a: R=Me
1b: R=Cl
1c: R=NO$_2$

2a: R=Me
2b: R=Cl
2c: R=NO$_2$

1-Np = 1-naphthyl

Scheme 1.

Table 1. Rate and Equilibrium Constants for the Base-Catalyzed Acyl Migration of *N,O*-Diacyl-*o*-aminophenols at 30 °C

1 M=1 mol dm^{-3}

System	Solvent(ε)[a]	Base(pK_a)	$K=k_1/k_{-1}$	k_1/M^{-1} min^{-1}	k_{-1}[b]/M^{-1} min^{-1}
1a—2a	CH_2ClCH_2Cl (10.36)	Triethylamine (11.01[c], 10.75[d])	4.6	0.76	0.17
1b—2b	CH_2ClCH_2Cl	Triethylamine	3.4	2.9	0.85
1c—2c	CH_2ClCH_2Cl	Triethylamine	1.3	11	8.5
1a—2a	CH_2ClCH_2Cl	Tributylamine (10.89[e], 9.93[d])	4.9	0.54	0.11
1a—2a	CH_2ClCH_2Cl	*N*-Methylpiperidine (10.08)[c,d]	5.0	0.15	0.030
1a—2a	CH_2ClCH_2Cl	*N*-Methylmorpholine (7.38)[d]	5.3	0.0018	0.00034
1a—2a	CH_2ClCH_2Cl	Pyridine (5.25)[c,d]	4.6	1.2×10^{-5}	0.26×10^{-5}
1a—2a	CH_3CN (37.5)	Triethylamine	5.1	240	47
1a—2a	Benzene (2.275)	Triethylamine	3.9	0.019	0.0049
7—8	$CDCl_3$	Triethylamine	1.0	0.049	0.049

a) Dielectric constants which were taken from J. A. Riddick and W. B. Bunger, "Organic Solvents," 3rd ed, Wiley-Interscience, New York (1970). b) Determined by using the equation $k_{-1}=k_1/K$. c) "Handbook of Chemistry and Physics," 51st ed, CRC Press (1970). d) "Handbook of Tables for Organic Compound Identification," 3rd ed, CRC Press (1967). e) "Handbook of Biochemistry, Selected Data for Molecular Biology," 2nd ed, CRC Press (1970).

substituents R. All these observations can be nicely explained in terms of the rate-determining formation of the amidate ion. Thus we propose the mechanism shown in Scheme 2 to explain the observed acyl-exchange reactions of *N,O*-diacyl-*o*-aminophenol derivatives. Amundsen and Ambrosio[4] have previously proposed a similar mechanism but they have presented no kinetic evidence in support of their mechanism. The facts that both **1a** in acetic acid and the *N*-methyl derivative **3** in acetonitrile containing triethylamine do not undergo the acyl-exchange reaction to any extent support this mechanism. To ascertain the intra- or intermolecularity of this acyl-exchange reaction, an equimolar mixture of **1a** and **2a** was allowed to react with triethylamine in acetonitrile until the equilibrium is established. Careful HPLC analysis of the mixture indicates no formation of the crossover products **4** and **5**. In addition to the fact that the para-isomer **6** is not subject to the base-catalyzed exchange reaction in acetonitrile the result of this crossover experiment allows us to conclude that the observed acyl-migration is exclusively intramolecular reaction. Furthermore, definitive evidence for the occurrence of acyl-group migration comes from the observation of triethylamine-catalyzed exchange of ^{13}C-labeled benzoyl group between **7** and **8**. No migration of the benzoyl group was observed without the amine also in this case.

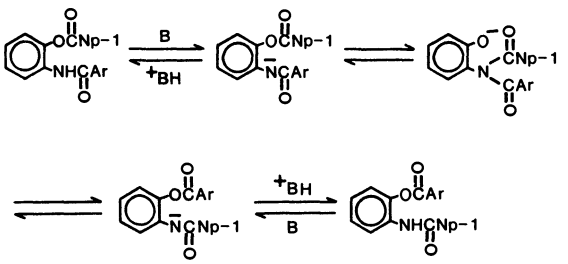

Scheme 2.

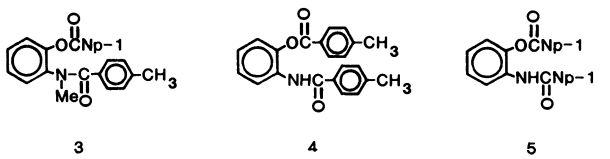

3 4 5

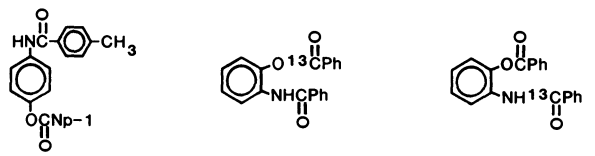

6 7 8

The equilibrium constants obtained for **1—2** pairs were found to decrease as the electron-withdrawing ability of the substituents R is increased. Smith and Elrod[2] have suggested that the more stable isomer should be the one with the stronger electron-withdrawing acyl group bonded to nitrogen. Because the electron-withdrawing ability of acyl groups in our system should have the following order on the basis of the p*K*a values of the corresponding carboxylic acids: *p*-$NO_2C_6H_4CO$ > 1-naphthoyl > *p*-ClC_6H_4CO > *p*-$CH_3C_6H_4CO$, only the relative stabilities of **1c—2c** pair do not conform to their proposal. We felt that the solvent polarity also plays a role in determining the relative stabilities of **1** and its isomer **2**. For this purpose **1a—2a** pair was chosen and the solvent effects on the magnitude of *K* were examined. Although there is a tendency that the increased solvent polarity shifts the equilibrium slightly to the direction of **2**, the equilibrium is not much affected by a change in solvent polarity. On the other hand, the magnitude of *K* is neither very sensitive to a change in the amine bases nor correlate with the basicity of tertiary amines used.

Although in *N,O*-acetyl-chloroacetyl-,[5] *N,O*-(1-naphthoyl)-(*p*-toluoyl)-, and *N,O*-(1-naphthoyl)-(*p*-chlorobenzoyl)-*o*-aminophenols the more stable isomer is the one with the stronger electron-withdrawing acyl group attached to nitrogen as proposed by Smith and Elrod, their hypothesis cannot predict the more stable isomer in acetyl-aroyl,[2] acetyl-alkoxycarbonyl,[3] and 1-naphthoyl-(*p*-nitrobenzoyl) derivatives of *o*-aminophenol, indicating that the inductive effects of acyl groups are not the only factor to determine which isomer is more stable. As mentioned above, however, the results of substituent effects on the magnitude of *K* demonstrate that the electron-withdrawing ability of acyl group plays a crucial role in controlling the relative stabilities of **1—2** pairs.

We expect that the equilibrium constant for the reaction of *N,O*-diacyl-*o*-aminophenol wherein the two acyl groups are the same becomes practically unity. As expected, it was estimated to be unity for **7—8** pair within the limits of experimental accuracy.

Experimental

Materials. *N*-(*p*-Substituted benzoyl)-*o*-aminophenol and *N*-(1-naphthoyl)-*o*-aminophenol were prepared by *N*-aroylation of two equiv of *o*-aminophenol with *p*-substituted benzoyl and 1-naphthoyl chlorides in dichloromethane, respectively. Recrystallization of the crude products from aqueous ethanol gave pure samples whose physical properties are the followings. *N*-Benzoyl-*o*-aminophenol, mp 167.5—168.5 °C; IR (KBr) 3400, 3000 (broad), 1640 cm^{-1}. *N*-(*p*-Toluoyl)-*o*-aminophenol, mp 157.5—158.5 °C; IR (KBr) 3410, 3080 (broad), 1640 cm^{-1}. *N*-(*p*-Chlorobenzoyl)-*o*-aminophenol, mp 180.5—181.5 °C; IR (KBr) 3200 (broad), 1630 cm^{-1}. *N*-(*p*-Nitrobenzoyl)-*o*-aminophenol, mp 206—207 °C; IR (KBr) 3280, 3120 (broad), 1650, 1520, 1350 cm^{-1}. *N*-(1-Naphthoyl)-*o*-aminophenol, mp 194.5—195.5 °C; IR (KBr) 3400, 3100 (broad), 1640 cm^{-1}.

N-Methyl-*N*-(*p*-toluoyl)-*o*-aminophenol was prepared according to the following reaction steps. The crude product obtained was recrystallized from aqueous ethanol and then from benzene-hexane affording colorless crystals, mp 140—141 °C; IR (KBr) 3100 (broad), 1620 cm^{-1}.

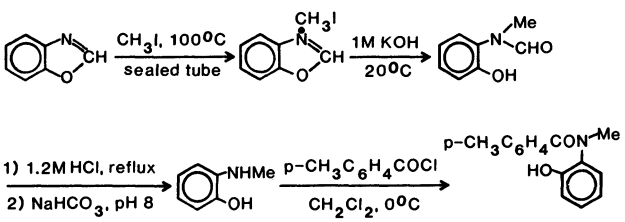

Table 2. Physical Properties of **1a—c**, **2a—c**, and **3—7**

Compd	Mp	IR(KBr)/cm^{-1}			Anal/%, Found(Calcd)		
	θ_m/°C	Ester C=O	Amido C=O	Amido NH	C	H	N
1a	137—138	1735	1675	3430	78.87(78.74),	4.92(4.99),	3.67(3.67)
1b	156—157	1710	1680	3340	71.92(71.73),	4.00(4.01),	3.42(3.49)
1c	177—178	1710	1675	3310	69.88(69.90),	3.85(3.91),	6.82(6.79)
2a	168—170	1730	1650	3180	79.02(78.74),	4.96(4.99),	3.65(3.67)
2b	177.5—179.5	1735	1655	3200	72.10(71.73),	3.95(4.01),	3.47(3.49)
2c	201—203	1735	1650	3200	69.65(69.90),	3.83(3.91),	6.74(6.79)
3	130.5—131.5	1730	1640	—	79.34(78.99),	5.31(5.32),	3.58(3.54)
4	108.5—109.5	1735	1640	3270	76.58(76.52),	5.53(5.51),	4.07(4.06)
5	177.5—178.5	1730	1640	3200	80.95(80.58),	4.54(4.56),	3.36(3.36)
6	235.5—236.5	1730	1650	3300	78.95(78.74),	4.98(4.99),	3.67(3.67)
7	181—182	1690	1655	3270	75.63(75.77),	4.71(4.75),	4.34(4.40)

N,O-Diacyl-*o*-aminophenols (**1a—c**, **2a—c**, **3—5**, and **7**) were derived from the reactions between *N*-acyl-*o*-aminophenols (1 mol) and the corresponding acyl chlorides (1 mol) in the presence of triethylamine (0.9 mol) in dichloromethane. The usual work-up gave the crude products which were purified by column chromatography on silica gel (70—230 mesh, Merck) with chloroform as eluent, followed by recrystallization from benzene–hexane yielding analytical samples whose physical properties are listed in Table 2. IR and HPLC analyses of these diacyl derivatives showed them to be pure samples containing negligible amounts of the opposite isomers. Benzoyl-*carbonyl*-^{13}C chloride (99+ atom% ^{13}C, Aldrich) was employed as acylating agent to synthesize **7**.

N-(*p*-Toluoyl)-*o*-(1-naphthoyl)-*p*-aminophenol (**6**) was prepared by treatment of *N*-(*p*-toluoyl)-*p*-aminophenol (mp 212.5—214 °C, 1 mol), which was obtained from the reaction of two equiv of *p*-aminophenol with *p*-toluoyl chloride, with 1-naphthoyl chloride (1.1 mol) in the presence of triethylamine (1.1 mol) in dichloromethane. Analytical sample, listed in Table 2, was obtained by recrystallizing the crude product from ethyl acetate.

Kinetic Methods. The rate of appearance of **2a—c** or disappearance of **1a—c** was followed with a JASCO twincle HPLC apparatus equipped with an UV detector (254 nm) and a 25 cm×4.6 mm (i.d.) ODS column at 30 °C. Carefully purified acetonitrile containing 35% (by volume) distilled water was used as the developing solvent in all cases. In this developing solvent the acyl-exchange reaction proceeds to a negligible extent. Each kinetic run was carried out by analyzing 2-μl aliquots of the solutions at suitable time intervals. The concentrations of **1** and **2** were determined by employing the linear calibration curves made for each compound under the same analytical conditions.

All the pseudo-first-order rate constants (k) were determined from the following rate equation and the extent of the reaction studied was more than two half-lives, allowing us to get reliable rate constants.

$$\ln\{[\mathbf{2}]_e/([\mathbf{2}]_e-[\mathbf{2}]_t)\} = [\mathbf{1}]_0 kt/[\mathbf{2}]_e$$

where $[\mathbf{1}]_0$, $[\mathbf{2}]_t$, and $[\mathbf{2}]_e$ refer to initial concentration of **1**, concentration of **2** at time t and at equilibrium state, respectively. The acyl-exchange rate of ^{13}C-labeled **7** was determined with a JEOL FX-200 spectrometer (200 MHz) in $CDCl_3$ at 30 °C. Tetramethylsilane was used as an internal standard. Increasing concentration of **8** or decreasing concentration of **7** was estimated from the area ratio of the two signals arising from the ester (164.5 ppm) and amido (165.3 ppm) carbonyl carbons. The migration reaction of ^{13}C-labeled benzoyl group also follows first-order kinetics (r=0.997). The experimental errors in the estimated rate and equilibrium constants are of the order of about 10%.

References

1) A. L. LeRosen and E. D. Smith, *J. Am. Chem. Soc.*, **70**, 2705 (1948); *ibid.*, **71**, 2815 (1949) and references cited therein.

2) E. D. Smith and L. Elrod, Jr., *J. Org. Chem.*, **42**, 652 (1977).

3) E. D. Smith and L. Elrod, Jr., *J. Org. Chem.*, **43**, 775 (1978).

4) L. H. Amundsen and C. Ambrosio, *J. Org. Chem.*, **36**, 3130 (1971).

5) E. D. Smith and V. S. Mayasandra, *J. Org. Chem.*, **45**, 1715 (1980).

Racemic Structures and Optical Resolution by Preferential Crystallization of Organic Ammonium Salts of (±)-Mandelic Acid

Tadashi SHIRAIWA,* Mitsuhiro NAKAMURA, Masanobu NOBEOKA, and Hidemoto KUROKAWA
Faculty of Engineering, Kansai University, Yamate-cho, Suita, Osaka 564
(Received March 24, 1986)

Synopsis. According to a thermodynamic analysis the 4-methylpiperidinium salt of (±)-mandelic acid is a conglomerate around room temperature, though the salt forms a racemic compound in the vicinity of the melting point. A successive preferential crystallization in ethanol at 10°C yields both the (+)- and (−)-salts with optical purities of over 95%.

Mandelic acid (abbreviated as MAN) is very useful as medicines and intermediate materials, such as phenyramidol, a centrally axting muscle relaxant.[1] Optically active MAN has also been used as a resolving agent in optical resolution of racemic organic bases.[2] (±)-MAN has been optically resolved by the diastereomeric procedure using L-phenylalanine[3] and cinchonine[4] as resolving agents. However, the diastereomeric procedure requires a relatively large quantity of resolving agents. On the other hand, the preferential crystallization procedure is more useful on the industrial scale than the diastereomeric one, since optical resolution can easily be achieved by providing a small amount of one enantiomer as seed crystals in a supersaturated racemic solution. However, the optical resolution by this procedure has scarcely been reported on (±)-MAN.[5] This note describes an attempt to resolve optically organic ammonium salts of (±)-MAN by preferential crystallization.

Racemic structures of propylammonium salt ((±)-PA salt), isopropylammonium salt ((±)-IPA salt), isobutylammonium salt ((±)-IBA salt), benzylammonium salt ((±)-BZA salt), and 4-methylpiperidinium salt ((±)-4-MP salt) of (±)-MAN were determined on the basis of thermodynamic analysis,[6,7] with the results that all of these (±)-salts form racemic compounds in the vicinity of their melting points and that (±)-4-MP salt exists in a conglomerate around room temperature. An optical resolution of (±)-4-MP salt has been achieved by successive preferential crystallization in ethanol at 10°C.

Experimental

Materials. (±)- and (+)-MAN were purchased from Sigma Chemicals Co., and amines from Wako Pure Chemicals Ind.

Preparation of Organic Ammonium Salts. (±)- or (+)-MAN (0.01 mol) was dissolved in diethyl ether. After adding 0.01 mol of amine and stirring for 10 min in an ice bath, the salt formed was collected by filtration, washed with a small amount of diethyl ether, and dried. The salts obtained were recrystallized from an appropriate solvent.

(±)- and (+)-4-MP salts were recrystallized from ethanol. Elemental analysis, specific rotation, and solubility of (±)-4-MP salt: C, 66.73; H, 8.42; N, 5.56% (calcd for $C_{14}H_{21}NO_3$: C, 66.91; H, 8.42; N, 5.57%); $[\alpha]_D^{20}$ +56.0° (*c* 0.50, ethanol); 4.470 g/(100 cm³ ethanol). (±)-4-MP salt: C, 66.73; H, 8.42; N, 5.57%; 11.578 g/(100 cm³ ethanol). (−)-4-MP salt was obtained from mother liquor in the optical resolution by preferential crystallization and was recrystallized twice from ethanol: Mp 136°C; $[\alpha]_D^{20}$ −56.0° (*c* 0.50, ethanol).

Optical Resolution. (±)-4-MP salt (3.184 g) was dissolved in 25 cm³ of ethanol around 40°C to give a racemic solution with a degree of supersaturation of 110% at 10°C. The solution was slowly cooled to 10°C and seeded with 0.010 g of (+)-salt. After stirring for 20 min at 10°C, the salt precipitated was collected by filtration and washed with a small amount of diethyl ether. (±)-4-MP salt (0.112 g) was dissolved in the filtrate around 40°C. The solution was cooled to 10°C and seeded with 0.010 g of (−)-salt. After stirring for 30 min, the salt precipitated was collected by filtration. The filtrate was treated in a similar manner as above. The degrees of resolution of (+)- and (−)-salts were calculated by

$$\text{Degree of resolution}/\% = [\text{YOPM/g} \times 100]/[(\text{Operation amount of (+)- or (−)-salt/g}) - 1.447], \quad (1)$$

where YOPM is the yield of optically pure modification.[8]

Preparation of Optically Pure Mandelic Acid. The (+)- and (−)-4-MP salts (about 0.85 g) obtained in the successive resolution were treated as aqueous solutions through a 1×10 cm column of Amberlite IR-120 in the H^+ form by eluting with water; the initial (+)-salt had an optical purity of 96.5% and the (−)-salt that of 98.2%. The eluents were evaporated to dryness under reduced pressure around 40°C to give (+)- and (−)-MAN. (+)-MAN: yield 95.8%; $[\alpha]_D^{20}$ +154° (*c* 1.00, ethanol). (−)-MAN: yield 94.6%; $[\alpha]_D^{20}$ −157° (*c* 1.00, ethanol) (lit,[9] $[\alpha]_D^{20}$ −159.7° (ethanol)).

Measurements. Specific rotations were measured with a Union Giken high sensitivity PM-101 digital polarimeter using a 0.5 dm path length quarz cell. Infrared spectra were obtained in the range 4000—400 cm^{-1} with a JASCO A-102 infrared spectrophotometer by the KBr disk method. Enthalpies of fusion and melting points were determined with a Rigaku Denki DSC-8230. The solubilities of (±)- and (+)-4-MP salts and the ternary phase diagram were obtained in a similar manner as described in our previous paper.[10]

Results and Discussion

Racemic Structures. Racemic Structures at Melting Point: Free energies of formation of racemates at melting point, ΔG_{mp}^F, were calculated on the basis of

Table 1. Thermodynamic Data for Organic Ammonium Salts of Mandelic Acid

Salts	Mp/K		ΔH^{f} a)/kJ mol^{-1}		ΔG^{F}_{mp} b)	Eutectic point		
	(±)	(+)	(±)	(+)	kJ mol^{-1}	Mole fraction of (+)-salt c)	Temperature Found	Calcd c)
PA d)	374	373	35.9	26.6	−2.28	0.83	364	365
IPA e)	435	431	43.1	38.5	−2.88	0.84	426	424
IBA f)	404	399	32.6	27.4	−2.77	0.85	390	391
BZA g)	472	449	54.0	48.6	−5.18	0.94	448	447
4-MP h)	394	409	31.8	33.5	−1.01	0.65	393	392

a) ΔH^{f}; Enthalpy of fusion. b) ΔG^{F}_{mp}: Free energy of formation of racemate at melting point. c) These values were calculated by the Schröder-Van Laar and Prigogine-Defay equations. d) PA: Propylammonium salt. e) IPA: Isopropylammonium salt. f) IBA: Isobutylammonium salt. g) BZA: Benzylammonium salt. h) 4-MP: 4-Methylpiperidinium salt.

the enthalpies of fusion, ΔH^{f}, and melting points of (±)- and (+)-salts.[6,7] The thermodynamic data are given in Table 1.

The ΔG^{F}_{mp} values suggest that these (±)-salts are racemic compounds or racemic solid solutions in the vicinity of their melting points, since the values are negative.[6,7,10] The mole fractions and temperatures at the eutectic points were calculated from the Schröder-Van Laar and Prigogine-Defay equations.[11] Mixtures with mole fractions calculated were prepared and their melting points were compared with the eutectic temperatures calculated (Table 1). The melting points obtained agreed closely with the eutectic temperatures calculated. The mixtures melted at their respective temperatures and not over wide ranges. It is concluded from the above results that these (±)-salts form racemic compounds in the vicinity of their melting points.

The mole fractions of (+)-PA, -IPA, -IBA, and -BZA salts at their eutectic points (0.83—0.94) are close to 1, and the absolute values of ΔG^{F}_{mp} are more than 2 kJ mol^{-1}. Therefore, the above (±)-salts form stable racemic compounds.[6,7] However, (±)-4-MP salt may be an unstable racemic compound, since the mole fraction (0.65) is relatively close to 0.5 and the ΔG^{F}_{mp} is −1.01 kJ mol^{-1}.[6,7]

Racemic Structures Around Room Temperature: Unstable racemic compounds such as 4-MP salt have a possibility of transformation to conglomerate at a lower temperature.[6,7] The ΔG^{F}_{283} at 283 K of (±)-4-MP salt was calculated to examine this possibility,[6,7] a positive value (+0.26 kJ mole^{-1}) being obtained. This value indicates that (±)-4-MP salt will form no racemic compounds at 283 K. (±)-4-MP salt shows a infrared spectrum identical with that of its (+)-salt and is more soluble than the (+)-salt at 10 °C. The ternary phase diagram of solubility of 4-MP salt at 10 °C displays the pattern of a conglomerate as shown in Fig. 1.[12] The above results clearly indicated that (±)-4-MP salt exists in a conglomerate around room temperature.

The infrared spectra of (±)-PA, -IPA, -IBA, and -BZA salts are different from those of respective (+)-salts, and the ΔG^{F}_{283} values are negative. Therefore, these (±)-salts also form racemic compounds around room temperature.

Optical Resolution of (±)-4-Methylpiperidinium Salt. The optical resolution of (±)-4-MP salt by successive preferential crystallization has been carried out for a racemic solution with a degree of supersaturation of 110% in ethanol at 10 °C. The result is given in Table 2.

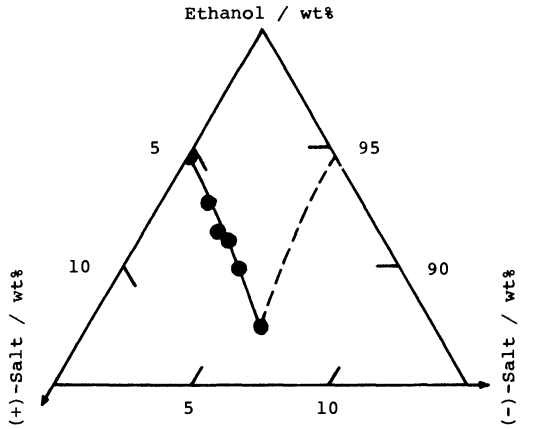

Fig. 1. Ternary phase diagram of solubility of 4-methylpiperidinium salt of mandelic acid. Solvent: Ethanol. Temperature: 10 °C.

It was possible to obtain the (+)- and (−)-salts with an optical purity of 95—100% in a degree of resolution of 62—81%. The (+)- and (−)-salts obtained gave (+)-MAN with an optical purity of 96.4% and (−)-MAN with that of 98.3%, respectively.

The optical resolution has also been carried out for a racemic solution with a degree of supersaturation of 138% to give the (+)-salt with an optical purity of around 90% at a resolution time of 5—10 min. However, the optical purity of the (+)-salt obtained at a resolution time beyond 10 min rapidly decreased with resolution time. The salt with a low optical purity is easily purified by recrystallization. The phase diagram of solubility or the solubility of the (±)-salt gives the optimum amount of ethanol which permits one to obtain the maximum yield of the optically pure salt.[13] The amount of ethanol Ws/wt% is expressed by

$$W_s = 100\, W_E \cdot W/[5000 - W_E \cdot (50 - W)], \quad (2)$$

where W_E/wt% is the amount of ethanol at the eutectic point at 10° ((+)-4-MP salt, 6.34; (−)-salt, 6.34; ethanol, 87.33 wt%) and W/wt% is the amount of the (−)-salt contained in the crystalline salt having an abundance

Table 2. Successive Preferential Crystallization of 4-Methylpiperidinium Salt of (±)-Mandelic Acid[a)]

Run	Added amount of (±)-salt	Operation amount[b)]/g		Resolution time	Salt obtained			
					Yield	Optical purity	YOPM[c)]	Degree of resolution[d)]
	g	(+)-Salt	(−)-Salt	min	g	%	g	%
1	3.184	1.592	1.592	20	0.122	(+) 95.7	0.107	73.8
2	0.112	1.538	1.645	30	0.168	(−)100	0.158	79.8
3	0.158	1.617	1.566	40	0.151	(+) 96.8	0.137	80.6
4	0.141	1.549	1.634	40	0.132	(−) 95.5	0.116	62.0

a) Solvent: 25 cm³ of ethanol. Degree of supersaturation of initial racemic solution: 110%. Seed crystals: 0.010 g of (+)- or (−)-salt. Temperature: 10°C. b) The operation amounts of the (+)- and (−)-salts in solutions were calculated on the basis of the analyses of the salts obtained in Run 1—3. c) YOPM: Yield of optically pure modification. d) Degree of resolution/%=[YOPM/g×100]/[(Operation amount of (+)- or (−)-salt/g)−1.447/g].

of the (+)-salt.

A (+)-4-MP salt with an optical purity of 28.0% (4.00 g) was recrystallized from 25 cm³ of ethanol; the amount calculated is 25.07 cm³. After dissolving the salt at an elevated temperature, the solution was stirred for 30 min at 10°C to crystallize 1.05 g of the (+)-salt with an optical purity of 99.6%; the theoretical yield of the optically pure (+)-salt is 1.12 g. An approximate (±)-salt ($[\alpha]_D^{20}$ +0.7°) was recovered in 2.89 g from the filtrate. (+)-MAN with an optical purity of 99.6% was obtained from the (+)-salt recrystallized.

The above result indicates that (±)-4-MP salt exists in a conglomerate around room temperature, though the (±)-salt forms a racemic compound in the vicinity of the melting point. It was possible to obtain the (+)- and (−)-MAN with a high optical purity by successive preferential crystallization of the (±)-4-MP salt.

References

1) K. Tsuda, S. Yoshida, and A. Kubo, "Iyakuhin Gosei Kagaku," Nankodo, Tokyo (1983), p. 245.
2) J. Jacques, A. Collet, and S. H. Wilen, "Enantiomers, Racemates, and Resolutions," John Wily & Sons, New York, Chichester, Brisbane, Toronto (1981), p. 254.
3) J. Koga, Y. Ihara, T. Ikura, and N. Kuroki, *Nippon Kagaku Zasshi*, **92**, 999 (1972).
4) J. L. Norula and J. Kenyon, *Curr. Sci.*, **32**, 260 (1963); P. Newman, "Optical Resolution Procedures for Chemical Compounds," Optical Resolution Information Center, New York (1981), Vol. 2, p. 304.
5) Y. Ohmichi and H. Kurokawa, *Nippon Kagaku Kaishi*, **1979**, 1092.
6) M. Leclercq, A. Collet, and J. Jacques, *Tetrahedron*, **32**, 821 (1976).
7) T. Shiraiwa, H. Miyazaki, A. Ikawa, and H. Kurokawa, *Nippon Kagaku Kaishi*, **1984**, 1425.
8) T. Shiraiwa, S. Taniguchi, A. Ikawa, Y. Kashima, and H. Kurokawa, *Nippon Kagaku Kaishi*, **1983**, 1617.
9) "Kagaku Daijiten," ed by Kagaku Daijiten Hensyu Iinkai, Kyoritsu Shuppan, Tokyo (1971), Vol. 8, p. 920.
10) T. Shiraiwa, M. Nakamura, H. Nakagawa, N. Seike, S. Taniguchi, and H. Kurokawa, *Nippon Kagaku Kaishi*, **1985**, 1549.
11) S. H. Wilen, A. Collet, and J. Jacques, *Tetrahedron*, **33**, 2725 (1977).
12) A. Collet, M. J. Brienne, and J. Jacques, *Chem. Rev.*, **80**, 215 (1980).
13) Ref. 2, p. 389.

Dehydrogenation of Ethylbenzene on Potassium-Promoted Iron Oxide Catalyst Containing Magnesium Oxide

Takenori HIRANO
Kasukabe Laboratory, Nissan Girdler Catalyst Co. Ltd., Ushijima 573, Kasukabe, Saitama 344
(Received March 26, 1986)

Synopsis. Among potassium-promoted iron oxide catalysts containing a minor chromia and a series of alkaline earth oxides, i.e., MgO, CaO, SrO, and BaO, the MgO-containing catalyst showed the best performance with respect to the dehydrogenation activity and the stability even at a steam-to-ethylbenzene molar ratio (H_2O/EB ratio) as low as 6.

The styrene monomer has commercially been produced by the dehydrogenation of ethylbenzene over potassium-promoted iron oxide catalysts in the presence of steam; the usual industrial catalysts consist of iron oxide, potassium carbonate and chromia:[1] known as Shell 105 or G-64A. Nowadays, styrene producers are making efforts to reduce steam consumption from a standpoint of saving energy, that is, lowering the H_2O/EB ratio has the advantage of reducing cost of styrene. Therefore, a more active and stable catalyst is desired in order to obtain an appreciable styrene yield at a low steam condition.[2] In order to modify the catalytic properties of the potassium-promoted iron oxide containing a minor chromia, various alkaline earth oxides were added to the system and the effects of these additives, especially of magnesium oxide, upon the catalytic properties were investigated. Although some patents on dehydrogenation catalysts containing alkaline earth oxides have been published,[3] few basic studies on the catalysts have been carried out.

Experimental

All the catalysts examined were prepared as follows: iron oxide (α-Fe_2O_3, 23 m^2g^{-1}), chromia (Cr_2O_3) and suitable amounts of potassium carbonate (K_2CO_3) and alkaline earth carbonate were mixed and extruded to pellets of 3.2 mm dia. and 4—6 mm length. These were crushed into 16/20 mesh granulates for activity tests at a high H_2O/EB ratio of 11.8, and were used without crushing for long-run tests at a low H_2O/EB ratio of 6. The pellets were dried at 120 °C overnight followed by calcination at 600 °C for 4 h in a muffle furnace. The reactor made of stainless steel (20 mm i.d.) was used for the activity tests at atmospheric pressure. The products were analyzed by gas-chromatography. The surface areas were measured by the BET method. The amounts of carbonaceous deposits, including polymers, were determined by trapping the CO_2 released during oxidation at 450 °C in a closed system (138 cm^3) after vacuum treatments at 250 °C for 30 min. XRD measurements were carried out on a Rigaku X-ray diffractometer with Co $K\alpha$ radiation. The pore volumes and their distributions were measured on an Amco Hg-porosimeter.

Results and Discussion

In order to evaluate the intrinsic activities of catalysts whose compositions are listed in Table 1, dehydrogenation tests on granulated (16/20 mesh) catalysts were carried out at a low conversion region, a high H_2O/EB ratio of 11.8 and in the temperature range 550—620 °C. Since the catalysts were granulated and the H_2O/EB ratio was high, the influences of the pore structure and the deposited carbon on the activity could be eliminated; all the activities reached a steady state within about 20 h after starting a run. The rates and selectivities for styrene formation at 580 °C, and the activation energies for styrene, benzene and toluene formations over various catalysts are listed in Table 1. Among the alkaline earth oxides added, only MgO enhanced the dehydrogenation activity of the potassium-promoted iron oxide without decreasing the selectivity, and CaO enhanced the selectivity although the activity was decreased. The order of promoting effect on the activity was as follows: MgO > SrO > CaO > BaO.

Changing the magnesium content in the Fe_2O_3-K_2CO_3-Cr_2O_3-MgO system, the rate and selectivity for the styrene formation were investigated as functions of the magnesium contents. The results are shown in Fig. 1, where the rate and the selectivity are plotted against the content. A plot of the rate shows a folded straight line, in which the rate increases with an increase in the content at low levels (0—4 wt%). It is almost independent of the content at high levels (4—12 wt%), although the selectivity does not show any significant change with the content. X-ray diffraction analyses of the Mg catalyst indicated that a part of the magnesium oxide was contained as a form of magnesium ferrite ($MgFe_2O_4$), the XRD patterns being shown in Fig. 2. When the MgO content was changed, as depicted in Fig. 3, the XRD peak intensity of the magnesium ferrite (d: 2.97 Å) increased with an

Table 1. The Dehydrogenation Activities,[a] Selectivities and Activation Energies on Various Granulated[b] Catalysts at High H_2O/EB Ratio

Catalys designation	Composition/wt%				r_{ST}[c]	Selec. to ST/%	Ea/kcal mol^{-1}		
	Fe_2O_3	K_2CO_3	Cr_2O_3	Others			ST	BZ	TOL
K	65	32	3	—	26.8	95.1	26.6	31.6	51.3
Mg	52	33	3	12 MgO	33.8	95.4	27.8	32.0	50.6
Ca	52	33	3	12 CaO	14.6	96.4	34.2	28.8	56.4
Sr	50	32	3	15 SrO	21.0	95.6	32.4	28.4	53.3
Ba	50	32	3	15 BaO	8.0	92.9	36.2	30.8	58.8

a) Test conditions: H_2O/EB ratio = 11.8, SV = 39100 ml g^{-1} h^{-1}, 3 g cat. b) 16/20 mesh. c) Rate of styrene formation (mol g^{-1} min^{-1}, $\times 10^5$) at 580 °C.

increase in the content below 4 wt%. It then changed little in the content range 4—12 wt%; this behavior of the peak intensity of the magnesium ferrite with the magnesium content is similar to that of the activity with the content. On the other hand, the XRD peak intensity of magnesium oxide (MgO, d: 2. 11 Å) increased linearly with the content (Fig. 3). From these results, it is guessed that the formation of magnesium ferrite on iron oxide can participate in the effect of the magunesium addition on the activity of the potassium-promoted iron oxide catalyst.

For the ethylbenzene dehydrogenation catalyst, a stable activity is required under reaction conditions as well as the activity since the catalyst is used for one or two years at any styrene plant. In order to examine the stability of the Mg catalyst, the change in activity (% EB conversion) with time was investigated at a H_2O/EB ratio as low as 6 and 620 °C. It was then compared with the changes of the K and Ca catalysts; all the catalysts (3.2 mm dia. and 4—6 mm length) were used to investigate the pore structure in addition to the activity. As shown in Fig. 4, the Mg catalyst exhibited an appreciable activity and stability under such severe conditions, while other catalysts, i.e., K and Ca, showed a significant deterioration of the activity with time.

The physical properties of the catalysts in fresh and used states are listed in Table 2; increases in both surface area and pore volume were found on the Mg catalyst after a reaction, whereas those properties of other catalysts were decreased. The mean pore diameter of the Mg catalyst was not greatly altered after a reaction, compared to those of the K and Ca catalysts. These showed remarkable enlargements of the mean pore diameter; the mean pore diameters (*mPD*) were defined by the value at the midpoint of the cumulative pore distribution curve, because all the catalysts showed nallow distributions. Since the mean pore diameter can be determined from the size of the skeletons forming the pore structure of a pellet, the extent of pore destruction under reaction conditions can be expressed by the change in the mean pore diameter. The mean pore diameters of the K and Ca

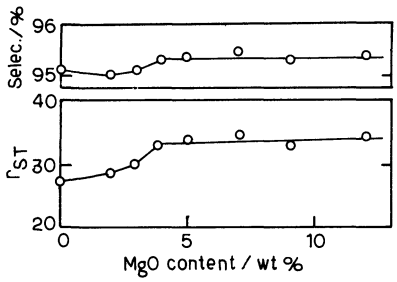

Fig. 1. Plots of the styrene formation rate (r_{ST}/mol $g^{-1}min^{-1}$, $\times 10^5$) and the selectivity to styrene at 580 °C vs. MgO content in the potassium-promoted iron oxide catalyst.

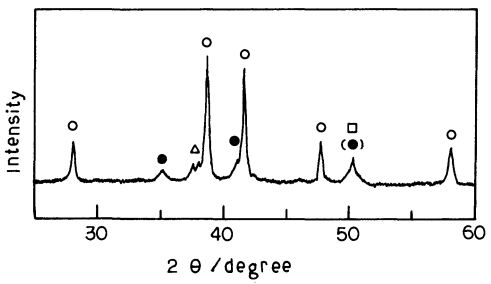

Fig. 2. X-Ray diffraction pattern of the Mg catalyst; ○: α-Fe_2O_3, △: K_2CO_3, ●: $MgFe_2O_4$, □: MgO.

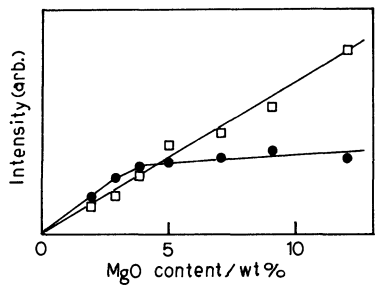

Fig. 3. Plots of the XRD peak intensities of $MgFe_2O_4$ (●; d: 2.97 Å) and MgO (□; d: 2.11 Å) vs. MgO content in the potassium-promoted iron oxide catalyst.

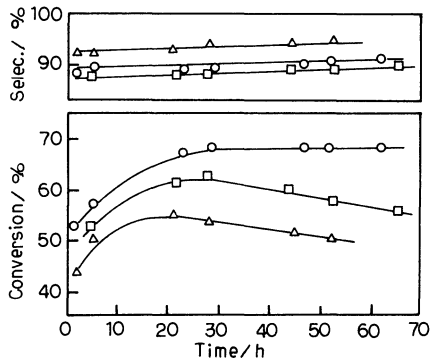

Fig. 4. Changes in the EB conversion and the selectivity with time over the K(□), Mg(○), and Ca(△) catalysts; reaction conditions: H_2O/EB ratio=6, SV=1280 h^{-1}, 620 °C.

Table 2. The Physical Properties and the Deposited Amounts of Carbon on the K, Mg, and Ca Catalysts[a] in Fresh and Used[b] States

Catalyst designation	SA/m^2g^{-1}		PV/cm^3g^{-1}		mPD/nm		Deposited carbon/wt%
	Fresh	Used	Fresh	Used	Fresh	Used	
K	4.8	3.8	0.27	0.24	266	412	0.117
Mg	3.4	4.4	0.39	0.47	457	430	0.127
Ca	4.0	2.7	0.28	0.27	282	397	0.039

a) Pellets of 3.2 mm dia. and 4—6 mm length. b) Reaction conditions; H_2O/EB ratio=6, SV=1280 h^{-1}, 50 cm^3 cat.

catalysts were enlarged and their surface areas were reduced; therefore, the pore skeletons, which may be constituted by iron oxide particles, of both catalysts might grow under the reaction conditions. On the other hand, the MgO catalyst exhibited little change in the mean pore diameter; hence, it is considered that the magnesium addition might prevent the pore destruction of the potassium-promoted iron oxide catalyst. From these results, it is suspected that the stability of the pore structure of the Mg catalyst might be associated with the observed stability of the activity at a low H_2O/EB condition.

The carbonaceous deposit on the catalyst was sometimes considered to deactivate the catalysts;[4] however, such a deactivating effect was not observed in this study because the deposited amounts on the K and Ca catalysts, which showed a deterioration in the long-run test, were not so large as that on the Mg catalyst, which showed little deterioration. Then, it can be presumed that the carbonaceous deposit does not exist on the active sites to inhibit the activities.

In earlier commercial dehydrogenation catalysts, MgO and CaO were used as a support.[5] Lee[6] investigated a binaly system of the iron oxide-alkaline earth oxide to find a relationship between the intrinsic activity and the first ionization energy for an alkaline earth atom. The order of the promoting effects of various alkaline earth oxides on iron oxide was as follows: BaO>SrO>CaO>MgO. This is different from the order obtained in this study. Accordingly, the promoting effect of MgO in the potassium-promoted iron oxide might be different from that in a binaly catalyst. From the results obtained in this study, the formation of magnesium ferrite in potassium-promoted iron oxide is considered to take part in the effects of a magnesium addition upon the activity and the stability of the catalyst.

References

1) W. R. Gutmann, U. S, Patent 3361683 (1968); K. K. Kearby, U. S. Patent 2426829 (1947); C. L. Gutzeil, U. S. Patent 2408140 (1946).

2) G. R. Germaine and J. P. Darnanville, U. S. Patent 4395579 (1983).

3) C. C. Chu, U. S. Patent 4496662 (1985), U. S. Patent 4503163 (1985).

4) J. Mason and B. Delmon, Proc. 5th Int. Cong. Catal., Amsterdam, 1972, Paper 6-1.

5) H. M. Stanly and F. E. Salt, U. S. Patent 2342980 (1944), H. M. Stanley, F. E. Salt, and T. Weier, French Patent 947371 (1947).

6) E. H. Lee, *Catal. Rev.*, **8**, 285 (1973).

Studies on the Valence State of Iron Atoms in the Mixed-Valence Binuclear Ferrocenes by X-Ray Absorption Near Edge Structure (XANES) and by X-Ray Photoelectron Spectroscopy (XPS)

Kumiko Iwai,* Makoto Iwai, Kyoko Suto, Satoru Nakashima,
Izumi Motoyama, Hirotoshi Sano,* Isao Ikemoto,
Nobuhiro Kosugi,† and Haruo Kuroda†
Department of Chemistry, Faculty of Science, Tokyo Metropolitan University,
Fukasawa, Setagaya-ku, Tokyo 158
†Department of Chemistry, Faculty of Science, The University of Tokyo,
Hongo, Bunkyo-ku, Tokyo 113
(Received September 12, 1985)

In order to study the valence state in the mixed-valence binuclear ferrocenes, X-ray absorption spectra near the Fe K-edge were measured using synchrotron radiation. Well-resolved lines in the spectra obtained for ferrocene derivatives were assigned to the 1s→3d, 1s→Cp(π^*), and 1s→4p transitions, respectively, based on the molecular orbitals. There is an apparent difference in the 1s→3d transitions between trapped-valence compounds and averaged-valence compounds in the I_3^- salts of the monocation of binuclear ferrocenes. The valence states of the mixed-valence binuclear ferrocenes were also studied by X-ray photoelectron spectroscopy.

Among polynuclear organometallic mixed-valence compounds, there exist metal ions having different formal oxidation states in their individual chemical species. A growing interest has been paid to such compounds in connection with studies of superconductive materials and of biological "mixed-valence" systems.[1] The present authors have studied by Mössbauer spectroscopy the valence state for the salts of mono-oxidized binuclear ferrocene cations, in which two kinds of iron atoms, formally in the Fe(II) and Fe(III) states, are simultaneously present.[2-4]

Mössbauer spectra of the salts of mono-oxidized binuclear ferrocene cations are classified into two types; one is the trapped-valence type which contains ferrocene-like bivalent and ferrocenium-like tervalent atoms, as found in the case of triiodide salts of biferrocene[5] and 1′,1‴-dichlorobiferrocene,[4] and the other is the averaged-valence type which contains two equivalent iron atoms, as in the case of triiodide salts of 1,1″:1′,1‴-biferrocenylene,[6] 1′,1‴-dibromo- and 1′,1‴-diiodobiferrocene.[4] It has been also reported that 1′,1‴-diethyl- and 1′,1‴-dipropylbiferrocenium$^+I_3^-$ salts give rise to a transition from the averaged-valence state of iron atoms to the trapped-valence state as the temperature is lowered.[7] Although Mössbauer spectroscopy can distinguish whether or not the rate of the thermal electron transfer between two iron atoms is higher than ca. 10^{-7} s, no additional information from Mössbauer spectroscopy is available about the thermal electron transfer between the two atoms with a time scale faster than 10^{-7} s.

In the present study, X-ray absorption spectra near the edge structure (XANES) and X-ray photoelectron spectroscopy (XPS), both of which have a time scale of ca. 10^{-16} s, were measured at room temperature and at 80 K. The detailed electronic states of the iron atoms in the mixed-valence binuclear ferrocene salts are discussed by comparing the results with those obtained in Mössbauer spectroscopy of the same compounds which has a time scale of ca. 10^{-7} s.

Experimental

Commercially available ferrocene was purified by sublimation for the measurements. Other compounds were synthesized following the methods described in Refs. 4—7. The confirmed purities were >99% by means of the melting point, elemental analysis, IR, NMR, and Mössbauer spectroscopy.

Fe K-edge XANES spectra were measured at the National Synchrotron Radiation Research Facility (Photon Factory) affiliated to the National Laboratory for High Energy Physics (KEK-PF). Synchrotron radiation emitted from a storage ring, working at 2.5 GeV and ≈160 mA, was monochromated by a Si(311) channel-cut single crystal. The powdery samples were placed between two thin sheets transparent to the X-rays.[8]

XPS spectra were obtained by using Mg $K\alpha$ radiation with a Shimazu ESCA 750 spectrometer. Binding energy data were calibrated by using the binding energy of Cls photoelectron as the standard (285.5 eV). The experimental error for the binding energy was estimated within ±0.1 eV.

Results and Discussion

XANES Spectra. Ferrocene and Ferrocenium Triiodide. In the solid state, the molecular symmetry of ferrocene is known to be D_{5d}. Sohn et al. reported that the π orbitals in cyclopentadienyl (Cp) can be classified into the symmetries with the energy levels shown in Fig. 1.[9] The valence orbitals in iron atoms consist of $e_{2g}(3d)$, $a_{1g}(3d)$, $e_{1g}(3d)$, $a_{1g}(4s)$, $a_{2u}(4p)$, and $e_{1u}(4p)$. The ground state of ferrocene is also known to be $^1A_{1g}(1e_{2g})^4(2a_{1g})^2$. The ground state of the ferrocenium ion is shown to be $^2E_{2g}(1e_{2g})^3(2a_{1g})^2$ by ESR,[10] and by magnetic susceptibility measure-

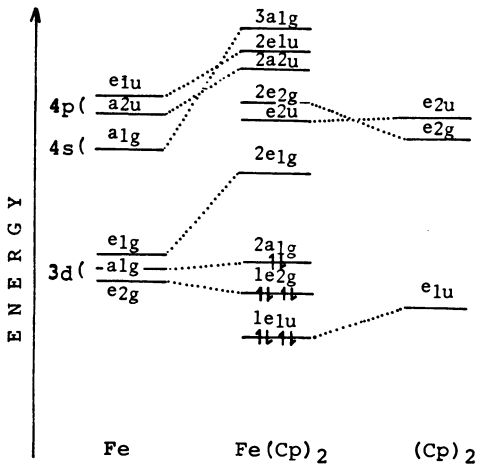

Fig. 1. The estimated relative energy for the molecular orbitals in ferrocene.[9]

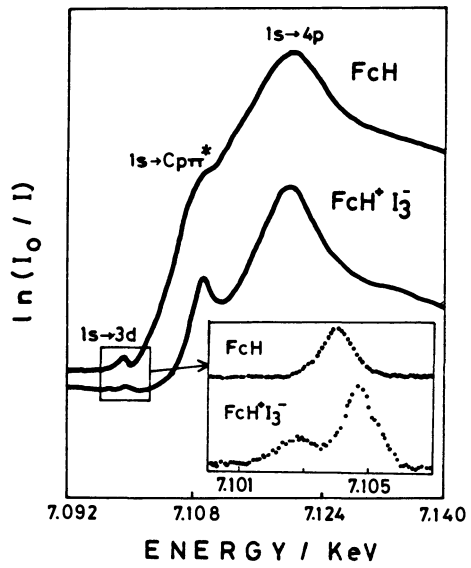

Fig. 2. The XANES spectra of ferrocene and ferrocenium$^+I_3^-$. The 1s→3d transitions are given under magnification. The pre-edge continuum background has been subtracted by smoothing the foot of the main peak.

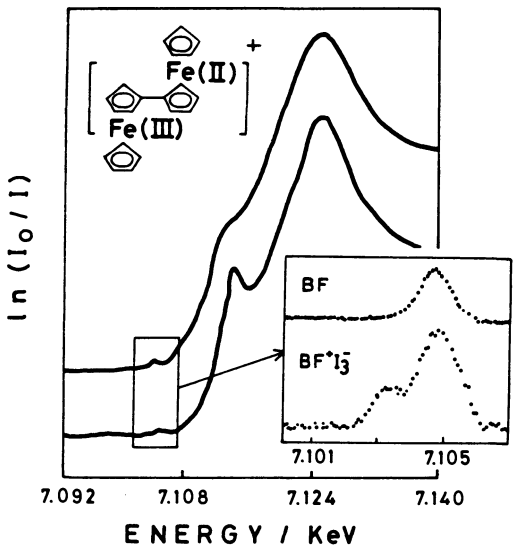

Fig. 3. The XANES spectra of BF and BF$^+I_3^-$. The weak 1s→3d transition in BF consists of a single peak, while the splitting of 1.57eV in the 1s→3d transition of BF$^+I_3^-$ is observed.

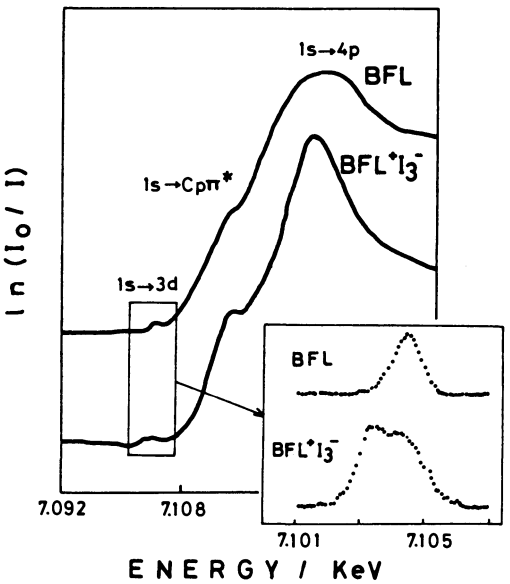

Fig. 4. The XANES spectra of BFL and BFL$^+I_3^-$. For BFL$^+I_3^-$ the splitting in the 1s→3d transition is small and the intensity of the lower energy peak is strong.

ments.[11] This state is slightly split into two Kramers doublets by spin-orbit coupling, indicating a crystal field with a symmetry lower than D_{5d}. However, since the splitting of the two Kramers doublets is estimated to be much smaller than the relevant transition energy, it is neglected in the present investigation.

Figure 2 shows the Fe K-edge XANES spectra of ferrocene and ferrocenium triiodide salt. There is a weak absorption peak below the Fe K-edge ionization threshold, followed by a shoulder on a rising absorption curve which culminates in a strong peak. In the XANES spectrum of ferrocene, the strong peak can be ascribed to the allowed transitions 1s→4p e_{1u} or a_{2u}, the lower-energy shoulder to the 1s→Cp(π^*), and the weak pre-edge peak to the dipole-forbidden (quadrupole-allowed or vibronically allowed) transition 1s→3d e_{1g}, respectively, based on the relative energy estimated in the molecular orbitals in ferrocene shown in Fig. 1.[9]

The XANES spectrum of ferrocenium ion has been compared with that of ferrocene. In Fig. 2, no energy difference is observed in the intense 1s→4p transitions between ferrocene and ferrocenium$^+I_3^-$. On the other hand, there exists a significant difference in the forbidden transition 1s→3d between ferrocene and

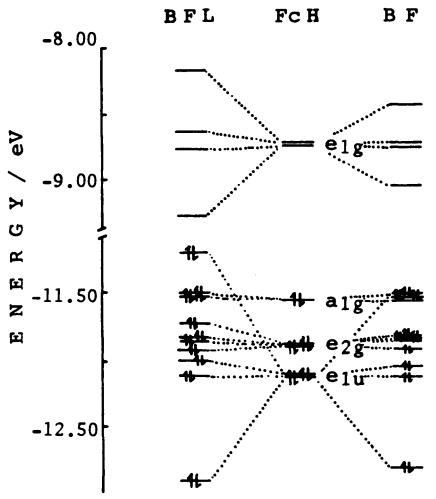

Fig. 5. The total ground-state configuration in the trans (C_{2h}) conformation of BF and in the D_{2h} point group of BFL.[12]

ferrocenium$^+I_3^-$. The weak 1s→3d transition in ferrocene consists of a single peak, while a splitting of ca. 2 eV is observed in the 1s→3d transition of ferrocenium ion. These results are explained in terms of the crystal field splitting of the ground state. The electronic ground states of the ferrocene and ferrocenium ion are $^1A_{1g}$ and $^2E_{2g}$ consisting of the $a_{1g}^2e_{2g}^4$ and $a_{1g}^2e_{2g}^3$ configurations, respectively. The 1s→3d transition of ferrocene is assigned to the transition from the 1s orbital to the unoccupied e_{1g} state; in ferrocenium ion, there are two possibilities for the 1s→3d transitions from the 1s to the unoccupied valence state e_{1g} and e_{2g}. The value of the splitting (ca. 2 eV) in the 1s→3d transitions of ferrocenium ion is roughly comparable with the crystal field splitting observed in the electronic absorption data assigned to the d-d transition which corresponds to about 25000 cm^{-1} (ca. 3 eV).[12]

Biferrocene, 1,1″:1′,1‴-Biferrocenylene and Their Triiodide Salts. Figures 3 and 4 show the XANES spectra of biferrocene (BF) and 1,1″:1′,1‴-biferrocenylene (BFL) compared with their triiodide salts, respectively. The features in the XANES spectra for the neutral species are similar to the spectral feature for ferrocene. Kirchner et al. reported on the molecular orbitals calculated for BF in the trans (C_{2h}) conformation that the net charge on the iron atom and total electron density in each d orbital of BF are similar to those of ferrocene, as shown in Fig. 5.[12] This result is consistent with the data that the isomer shift and quadrupole splitting in Mössbauer spectra of BF and BFL agree with those of ferrocene.

There is an apparent difference in the 1s→3d transition between biferrocenium$^+I_3^-$ (BF$^+I_3^-$) and 1,1″:1′,1‴-biferrocenylenium$^+I_3^-$(BFL$^+I_3^-$), as seen in Figs. 3 and 4 under magnification. The pre-edge continuum background has been subtracted by

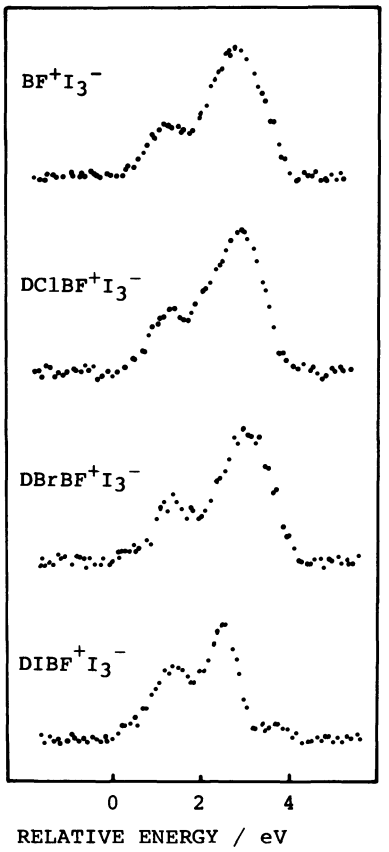

Fig. 6. The 1s→3d transition in the XANES spectra for the salts.

smoothing the foot of the main peak. BF$^+I_3^-$, which shows a trapped-valence state in the Mössbauer spectrum, exhibits an asymmetric splitting of 1.57 eV in the 1s→3d transition, while BFL$^+I_3^-$, which shows an averaged-valence state in the Mössbauer spectrum, gives a nearly symmetric splitting of 0.89 eV. These transitions are assigned to the transitions from 1s to unoccupied molecular orbitals which are mainly ascribed to the 3d orbitals corresponding to e_{1g} and e_{2g} in ferrocene.

The splitting in the 3d orbital for averaged-valence type, BFL$^+I_3^-$, is found to be smaller than that for trapped-valence type, BF$^+I_3^-$, and the intensity of the lower-energy peak in the 1s→3d transition for BFL$^+I_3^-$ is stronger than that for BF$^+I_3^-$. These results are consistent with those obtained in Mössbauer spectroscopy, suggesting that the molecular orbital of BF$^+I_3^-$ differs from that of BFL$^+I_3^-$.

Halogenated Biferrocene Derivatives and Their Triiodide Salts. The features of the XANES spectra for halogenated biferrocenes are also similar to the spectral feature for ferrocene. Figure 6 shows the 1s→3d transitions in the XANES spectra for the salts of monooxidized biferrocene (BF$^+I_3^-$), 1′,1‴-dichlorobiferrocene (DClBF$^+I_3^-$), 1′,1‴-dibromobiferrocene (DBrBF$^+I_3^-$) and 1′,1‴-diiodobiferrocene (DIBF$^+I_3^-$).

The Mössbauer spectrum of $DClBF^+I_3^-$ shows a trapped-valence state, while the Mössbauer spectra of $DBrBF^+I_3^-$ and $DIBF^+I_3^-$ show averaged-valence states. The XANES spectrum of $DIBF^+I_3^-$ is distinguishable from the others by the ratio of the peak intensities and by the separation of the split peaks. Although it is difficult to interpret the XANES spectrum quantitatively for the averaged-valence state, the peculiar XANES spectrum for $DIBF^+I_3^-$ can be qualitatively interpreted as a fully delocalized system on two equivalent iron atoms. On the other hand, the XANES spectrum for $DBrBF^+I_3^-$ is similar to those of $BF^+I_3^-$ and $DClBF^+I_3^-$, which indicate trapped-valence states in the Mössbauer spectra. The inconsistensy of the results obtained from XANES spectra and Mössbauer spectra is explained by assuming that the rate of the thermal electron transfer between the two iron atoms in $DIBF^+I_3^-$ is higher than ca. 10^{16} s^{-1} and the rate in $DBrBF^+I_3^-$ is higher than ca. 10^7 s^{-1} but lower than ca. 10^{16} s^{-1}.

X-Ray Photoelectron Spectroscopy. Since the time scale of XPS is ca. 10^{-16} s comparable with that of XANES, XPS also affords the possibility of distinguishing the localized electronic systems from delocalized ones in the mixed-valence binuclear ferrocenes.[13] Although the XPS for ferrocene itself and ferrocenium salts has been studied for many years, there are few reports concerning the XPS for the mixed-valence binuclear ferrocenes. In the present studies, attempts were also made to interpret the XPS spectra of the mixed-valence binuclear ferrocene derivatives in comparison with those of ferrocene and ferrocenium salts.

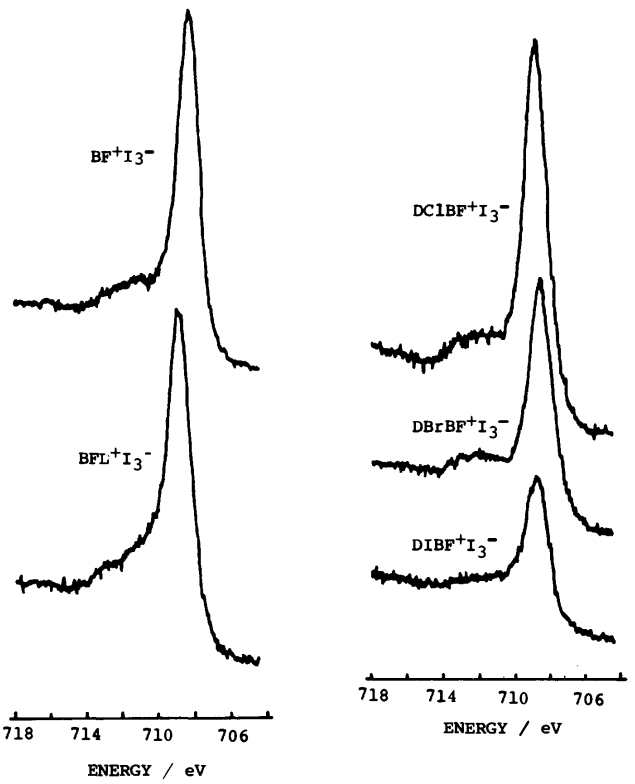

Fig. 7. The $Fe2p_{3/2}$ XPS spectra of the triiodide salts for binuclear ferrocenes.

For ferrocene a sharp band $Fe2p_{3/2}$ is observed at a binding energy of ca. 708 eV, while ferrocenium triiodide has much broader $Fe2p_{3/2}$ lines at 771 eV due to the exchange interaction of the core electrons with the unpaired valence electrons.[14] In addition, the satellite band with the broad line for ferrocenium ion is observed at 713 eV and is ascribed to the shake-up from the highest occupied orbital to the lowest unoccupied orbital.[14]

As shown in Fig. 7, the XPS spectra of the I_3^- salts of monocation of binuclear ferrocenes are found to consist of a single $Fe2p_{3/2}$ transition peak with a satellite peak. In the XPS spectra for mixed-valence binuclear ferrocenes, it is difficult to distinguish completely a sharp Fe(II) band from an Fe(III) band broadened by the exchange interaction of the core electrons with the valence electrons.

The XPS spectra of $BF^+I_3^-$, which indicates a trapped-valence state in Mössbauer spectra, are characterized by the main peak in the high energy state and the satellite peak in the low energy state. On the other hand, the satellite band in the spectrum of $BFL^+I_3^-$ which shows an averaged-valence state in Mössbauer spectra becomes broader and of lower energy than that of $BF^+I_3^-$. The fact that the position of the shake-up satellite band shifts to lower energy indicates that the splitting in the 3d orbitals for averaged-valence compounds is smaller than that for trapped-valence compounds.

Figure 7 shows the XPS spectra for halogenated compounds. In the XPS spectra of $DBrBF^+I_3^-$ and $DClBF^+I_3^-$, the satellite bands are clearly observed at the high-energy region as in the case of $BF^+I_3^-$. On the other hand, the XPS spectrum of $DIBF^+I_3^-$ is similar to that of $BFL^+I_3^-$, although the satellite band is not definitely characterized in the spectrum. These results indicate that two iron atoms of $DIBF^+I_3^-$ are equivalent in a delocalized system in the range of the time scale of 10^{-16} s and that the electrons are hopping thermally between the two unequivalent iron atoms in the rate from 10^{-7} s to 10^{-16} s in the case of $DBrBF^+I_3^-$.

In the temperature range from 80 K to 298 K, Mössbauer spectra show the trapped-valence states for $BF^+I_3^-$ and $DClBF^+I_3^-$ and the averaged-valence states for $BFL^+I_3^-$, $DBrBF^+I_3^-$ and $DIBF^+I_3^-$. The latter are known to give the averaged-valence states even at 4.2 K, whereas $BF^+I_3^-$ becomes an averaged-valence state above 298 K. From the results of Mössbauer, XANES, and XPS data, it can be concluded that the trapped-valence state becomes more stable in the order $DClBF^+I_3^- > BF^+I_3^- > DBrBF^+I_3^- > DIBF^+I_3^-$. This order can neither be explained by the order of electronega-

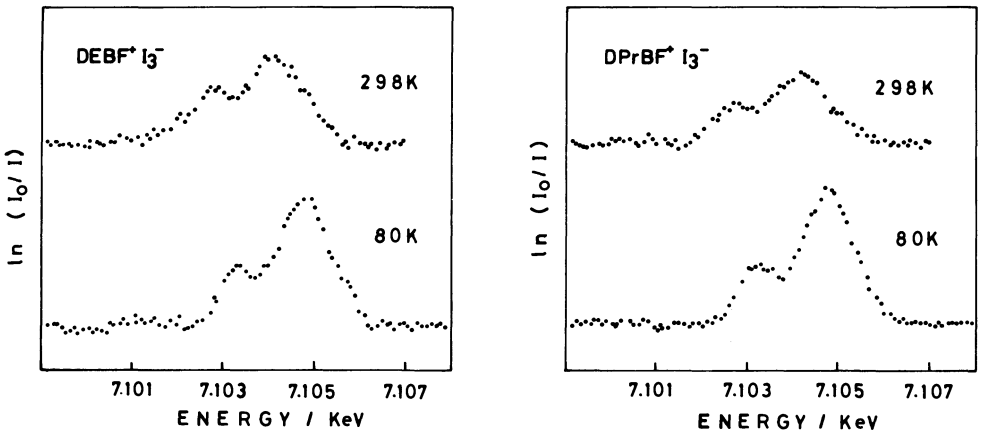

Fig. 8. The temperature dependence of the 1s→3d transition in the XANES spectra for $DEBF^+I_3^-$ and $DPrBF^+I_3^-$.

tivity for the substituted halogen atoms nor by the order of the ionic radii. It can, therefore, be presumed that the difference in electronic state between the two iron atoms is caused by the structual effect of substituents, rather than by their electronic effect.

The most prominent features of the infrared spectra are similar in binuclear ferrocenium ions because of the similarity of the molecular structures. However, there appears to be a difference in the band near 680 cm^{-1} band associated with the fulvalene moiety.[15] The disappearance of the 680 cm^{-1} band in $DIBF^+I_3^-$ reveals that the fulvalene moiety has a symmetric structure and the others, whose spectra give strong peaks at ca. 680 cm^{-1}, have an asymmetric fulvalene moiety. Although further structual studies need to be carried out, it would appear that a symmetric molecular structure is indispensable for yielding the averaged-valence state of the iron atoms.

1′,1‴-Diethyl- and Dipropylbiferrocene and their Triiodide Salts. It is found that Mössbauer spectra in 1′,1‴-diethylbiferrocenium$^+I_3^-$ ($DEBF^+I_3^-$) and 1′,1‴-dipropylbiferrocenium$^+I_3^-$ ($DPrBF^+I_3^-$) are temperature dependent, since a trapped-valence state of the iron atoms is observed at low temperatures and an averaged-valence state at room temperature.[7] The mechanism of this temperature dependence of the Mössbauer spectra has been interpreted by a change of the molecular orbitals accompanying a change in the crystal structure. This is because no-broadening cannot be ascribed to a relaxation effect adopted to the temperature dependence of the Mössbauer spectrum found in *trans*-μ-(as-indacene)bis(cyclopentadienyliron).[7,16] This interpretation was later supported by the X-ray crystal-structure determination of 1′,1‴-dipropylbiferrocenium triiodide at different temperatures.[15] The structural data indicate that the molecular orbitals are influenced more directly by the interaction between the triiodide ion and the ferrocene moiety rather by the intramolecular structural change, especially in the case of the mixed-valence compounds.

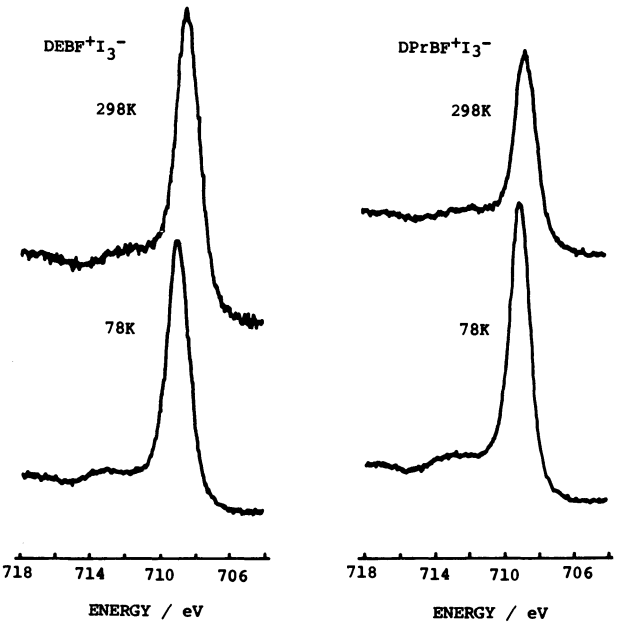

Fig. 9. The temperature dependence of the $Fe2p_{3/2}$ XPS spectra for $DEBF^+I_3^-$ and $DPrBF^+I_3^-$.

The temperature dependence of the XANES spectra for $DEBF^+I_3^-$ and $DPrBF^+I_3^-$ is shown in Fig. 8. The XANES spectra at 80 K resemble those of the trapped-valence type compounds, while the spectra at room temperature are similar to those of the averaged-valence type compounds. As shown in Fig. 9, there seems to be a slight temperature dependence of the peak assigned to $Fe2p_{3/2}$ in XPS spectra for $DEBF^+I_3^-$ and $DPrBF^+I_3^-$, that is, the satellite peaks are likely to appear at lower temperatures. This dependence is not inconsistent with the results obtained in XANES. These results lead to the conclusion that the temperature dependence of the electronic states for $DEBF^+I_3^-$ and $DPrBF^+I_3^-$ is explained by assuming a substantial change in the molecular orbital caused by the change of the crystal structure.[15]

It is concluded that there are two types of electronic states in the mixed-valence compounds. One is satisfactorily explained by a thermal electron tranfer between the two iron atoms in $DBrBF^+I_3^-$, because the Mössbauer spectra show the averaged-valence state at the studied temperature, while the feature of XANES and XPS spectra are similar to those for the trapped-valence compounds. The other is interpreted in terms of the substantial change of the molecular orbital caused by the change of the crystal structure at higher temperatures.

The XPS spectra of $I3d_{5/2}$ for mixed-valence binuclear ferrocenes are shown in Fig. 10. The XPS spectrum of $BF^+I_3^-$ consists of a single $I3d_{5/2}$ transition peak with a shoulder whose intensity is one half that of the main peak. The main peak is assigned to two negatively charged iodine atoms in the terminal position of I_3^- and the shoulder is assigned to an iodine atom at the central position of I_3^-. The charge on the triiodide ion is highly localized and the negatively charged iodine atoms in the terminal position seem to have a significant effect on the electronic states of the ferrocene moiety.

This speculation is supported by the study of the crystal structure for an analogous trapped-valence compound determined by single-crystal X-ray diffraction.[2,3] The crystal structure for 1′,1‴-dibutylbiferrocenium triiodide at 150 K, whose Mössbauer spectrum shows a trapped-valence state, reveals that one of the negatively charged iodine atoms in the terminal position in a triiodide ion is situated near the ferrocenium-like moiety. It can be presumed that the localization of the molecular orbitals should be caused by such an asymmetric structure between the triiodide ion and the ferrocene moiety.

On the other hand, the XPS spectrum of $I3d_{5/2}$ for $BFL^+I_3^-$, whose Mössbauer spectrum shows the averaged-valence state, gives an apparently symmetric peak. Since this peak broadens, it can be interpreted as a splitting between the main peak and the side peak in the XPS spectrum of $BFL^+I_3^-$ which is smaller than that of $BF^+I_3^-$. It can be presumed that the shift of the negative charge on I_3^- in $BFL^+I_3^-$ is insignificant and then the electronic effect of the counter anion on the ferrocene moiety is symmetric, which seems to be favorable to the averaged-valence state.

The XPS spectra of $I3d_{5/2}$ for halogenated derivatives are also given in Fig. 10. The spectra for $DClBF^+I_3^-$ and $DBrBF^+I_3^-$ are characterized by the broad bands, indicating that there exist various kinds of iodine atoms with different electronic states in the crystal. Unfortunately, the spectra of $DIBF^+I_3^-$ cannot be readily interpreted because of the overlap of the spectral components of the iodine atoms of I_3^- and those attached to the Cp rings.

Figure 11 shows the XPS spectra of $I3d_{5/2}$ for $DEBF^+I_3^-$ and $DPrBF^+I_3^-$. These spectra also show broad single peaks both at 78 K and 298 K. It can, therefore, be presumed that a slight difference of the interaction between the triiodide ion and the ferrocene moiety at an increased temperature gives rise to a valence fluctuation in $DEBF^+I_3^-$ and $DPrBF^+I_3^-$.

The authors are indebted to Dr. Sei'ichiro Iijima, at Research Institute for Polymers and Textiles, for his kind preparation of diethyl- and dipropylbiferrocenium triiodides, and to Professor Takaharu Ohnishi and Dr. Kazunari Domen at Research Laboratory of Resources Utilization, Tokyo Institute of Technology, for their kind help with the use of the X-ray photoelectron spectrometer and the discussion of the results. The authors are grateful to Dr. Masaharu Nomura at National Laboratory for High Energy Physics, and Messrs. Toshihiko Yokoyama, Kiyotaka

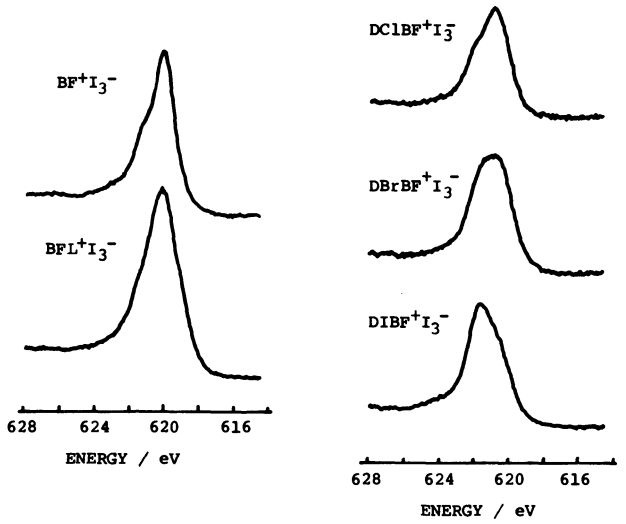

Fig. 10. The XPS spectra of $I3d_{5/2}$ for mixed-valence binuclear ferrocenes.

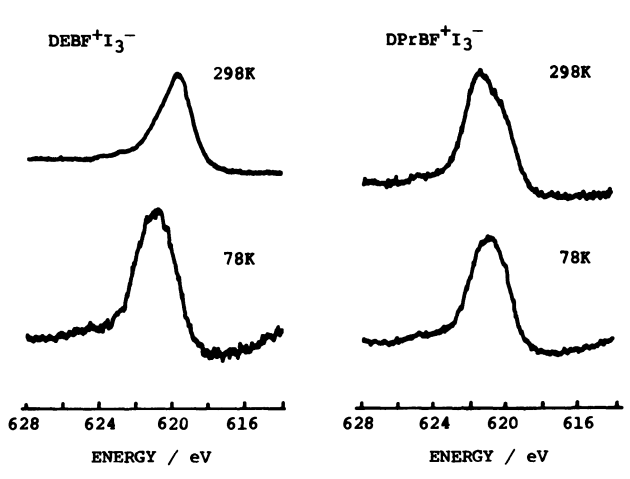

Fig. 11. The temperature dependence of the XPS spectra $I3d_{5/2}$ for $DEBF^+I_3^-$ and $DPrBF^+I_3^-$.

Asakura, and Hiromu Ishii at The University of Tokyo for their help in the experiments at KEK-PF.

References

1) I. F. Schegolev, Phy. Status Solid A, 12, 9 (1972); R. H. Holm and J. A. Ibers, "Iron-Sulfer Proteins," ed by W. Lovenberg, Academic Press, New York (1977) Vol. 3, Chap. 7; J. Cambray, R. W. Lane, A. G. Wedd, R. W. Johnson, and R. H. Folm, *Inorg. Chem.*, **16**, 2565 (1977).

2) K. Sato, S. Nakashima, M. Watanabe, I. Motoyama, and H. Sano, *Nippon Kagaku Kaishi*, **1985**, 580.

3) T-Y. Dong, D. N. Hendrickson, K. Iwai, M. J. Cohn, S. J. Geib, A. L. Rheingold, H. Sano, I. Motoyama, and S. Nakashima, *J. Am. Chem. Soc.*, **107**, 7996 (1985).

4) I. Motoyama, K. Suto, M. Katada, and H. Sano, *Chem. Lett.*, **1983**, 1215.

5) F. Kaufman and D. O. Cowan, *J. Am. Chem. Soc.*, **92**, 6198 (1976); D. O. Cowan, R. L. Collins, and F. Kaufman, *J. Phys. Chem.*, **75**, 2025 (1971); D. O. Cowan, G. A. Candela, and F. Kaufman, *J. Am. Chem. Soc.*, **93**, 3889 (1971); D. O. Cowan and J. Park, *Chem. Commn.*, **1971**, 1444.

6) W. H. Morrison, Jr. and D. N. Hendrickson, *Inorg. Chem.*, **14**, 2331 (1975); C. LeVanda, K. Bechggard, D. O. Cowan, U. T. Mueller-Westerhoff, P. Eilbrachat, G. A. Candela, and R. L. Collins, *J. Am. Chem. Soc.*, **98**, 3181 (1976).

7) S. Iijima, R. Saida, I. Motoyama, and H. Sano, *Bull. Chem. Soc. Jpn.*, **54**, 1375 (1981).

8) H. Oyanagi, T. Matsushita, M. Ito, and H. Kuroda, KEK Report, KEK83 (1984).

9) Y. S. Sohn, D. N. Hendrickson, and H. B. Gray, *J. Am. Chem. Soc.*, **92**, 3233 (1970).

10) R. Prins and F. J. Reinders, *J. Am. Chem. Soc.*, **91**, 4929 (1969); A. H. Maki and T. E. Berry, *ibid.*, **87**, 4437 (1965).

11) D. O. Cowan, C. LeVanda, R. L. Collins, G. A. Candela, U. T. Mueller-Westerhoff, and P. Eilbrachat, *J. Chem. Soc., Chem. Commun.*, **1973**, 329.

12) P. F. Kirchner, G. H. Loew, and U. T. Mueller-Westerhoff, *Inorg. Chem.*, **15**, 2665 (1976).

13) C. LeVanda, K. Bechgaard, D. O. Cowan, U. T. Mueller-Westerhoff, P. Eilbrachat, G. A. Candela, and R. L. Collins, *J. Am. Chem. Soc.*, **98**, 3181 (1976).

14) P. C. Healy and A. H. White, *Chem. Commun.*, **1971**, 1444.

15) M. Konno, S. Hyodo, and S. Iijima, *Bull. Chem. Soc. Jpn.*, **55**, 2327 (1982).

16) S. Iijima, I. Motoyama, and H. Sano, *Bull. Chem. Soc. Jpn.*, **53**, 3130 (1980).

 © 1986 The Chemical Society of Japan Bull. Chem. Soc. Jpn., 59, 2683—2687 (1986)

The Point of Zero Charge and the Isoelectric Point of γ-Fe_2O_3 and α-Fe_2O_3

Haruo WATANABE and Jun'etsu SETO*
Sony Corporation Research Center, 174 Fujitsuka-cho, Hodogaya-ku, Yokohama 240
(Received October 1, 1985)

The difference of the point of zero charge (PZC) and isoelectric point (IEP) values for γ- and α-Fe_2O_3 were measured and are quantitatively explained by the difference in crystal structure. Great care was taken to assure the purity of the samples and that measurements were taken under identical conditions. The PZC and the IEP for the "unhydrated" samples, were the same for each crystal structure, with the values for γ-Fe_2O_3 being more acidic, by 1.1 or 1.2 pH units, than for α-Fe_2O_3. This difference can be quantitatively explained by Parks' equation, in terms of the difference in the coordinations of the Fe^{3+} ions in the two crystal structures.

γ-Fe_2O_3 is a ferrimagnetic inverse-spinel type iron oxide, which is widely used for making magnetic recording tapes. Its surface properties have a large influence on its dispersibility in the paint, and thus on the output and noise characteristics of the tape.[1] Although the PZC and the IEP are important parameters which characterize the surface of the γ-Fe_2O_3, little work has been reported on this subject. Iwasaki et al.[2] reported an IEP at pH 6.7 for a sample with a γ-FeOOH phase. Parks' review[3] of the work on α-Fe_2O_3 shows a wide scattering of the reported values of IEP and PZC, ranging from 1.9 to 9.04. This can be attributed to variations, in the level of surface impurities, the hydration states, and in the conditions and methods of measurement.

The dependence of the IEP value on the crystal structure was reported for manganese[4] and aluminum oxides.[5] Kittaka and Morimoto[6] reported that the IEP in inverse-spinel type oxides is lower than that in normal-spinel type oxides. They explained this in terms of the coordination between the hydroxyl group and the metal ions at the surface.

The aim of the present work is to measure the inherent PZC and IEP values of acicular γ- and α-Fe_2O_3, and to provide a quantitative explanation for the difference between them. In order to obtain reliable values, care was taken to assure both the purity of the samples and the reproducibility of the measurement conditions. The control of the measurement conditions is especially important in measurements involving the state of hydration of the samples.

Experimental

Samples. The γ-Fe_2O_3 sample was prepared by the dehydration reduction of synthetic acicular α-FeOOH, followed by an oxidation. The α-FeOOH was prepared by the oxidation of the precipitate, formed by adding a NaOH aqueous solution to an iron (II) sulfate aqueous solution. The α-FeOOH was subjected to dehydration reduction at 350 °C under a hydrogen flow for 1 h, and then, oxidized at 250 °C under an air flow for 1 h. The product was confirmed to be spinel latticed γ-Fe_2O_3 by X-ray diffraction and had a magnetization of 73.0 emu g^{-1} as measured at room temperature by a vibrating sample magnetometer (Princeton Applied Research, Model-155). An electron micrograph of the γ-Fe_2O_3 particles is shown in Fig. 1a. The specific surface area of the γ-Fe_2O_3 particles was established as 18.6 $m^2 g^{-1}$ by the BET method of nitrogen adsorption at liquid nitrogen temperature. The atomic absorption spectrum of the γ-Fe_2O_3 particles revealed no significant metallic ion impurity, although a small amount of sulfate ion was detected. The sulfate ion content was determined from the amount of $BaSO_4$ precipitate, formed on the addition of $BaCl_2$ to a HCl solution of the γ-Fe_2O_3 particles, and was found to be 0.96 wt.%.

The α-Fe_2O_3 sample was prepared by heat treating the γ-Fe_2O_3 sample at 550 °C for 2 h in air.[7] Examination of the sample by X-ray diffraction verified it to be rhombohedral hematite. The α-Fe_2O_3 particles' specific surface area was 16.0 $m^2 g^{-1}$, which is a little smaller than that of the parent γ-Fe_2O_3 particles. Electron microscopic observation of α-Fe_2O_3 particles in Fig. 1b indicated that they retained the shape of the γ-Fe_2O_3 particles. The sulfate ion content in these samples was 0.85 wt%.

Cleaning the Samples. The samples were cleaned in 150 g batches using the following procedure. First, a water rinse in which the sample is decanted ten times with 5L of doubly-distilled water. Second, an alkali wash where the sample is decanted 3 times with 5L of KOH solution (pH 9), followed by a second water rinse. Third, the batches were electrodialized for one week, after which they were then filtered, dried at 100 °C for 24 h in an oven, and then stored in a desiccator.

Potentiometric Titration Method.[8] Batches of both samples, corresponding to 100 m^2 of total surface area, were

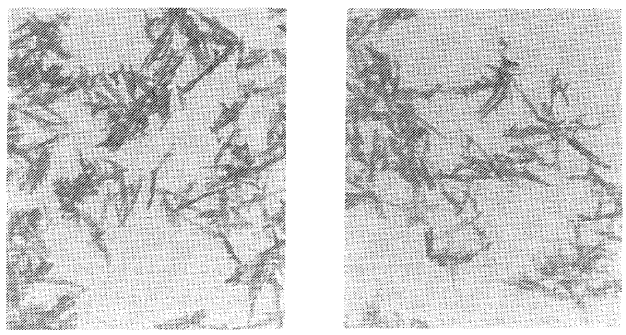

γ-Fe_2O_3 18.6 $m^2 g^{-1}$ (a) α-Fe_2O_3 16.0 $m^2 g^{-1}$ (b)

Fig. 1. Electron micrograph of γ-Fe_2O_3 sample (a) and α-Fe_2O_3 sample (b).

dispersed into 150 ml of about 0.01 M† KOH solution and adjusted to various values of ionic strength by the addition of KCl. The solution was then titrated potentiometrically. The titration cell was a 500 ml Pyrex flask, with a water jacket through which thermostated water was circulated to maintain the cell temperature at 20 °C. Glass and calomel electrodes, a thermometer, a microburet, and an inlet and outlet for purified nitrogen gas, were inserted into the cell through rubber gaskets. A Teflon stirring rod with Teflon blades, was also inserted into the center of the cell, through a Teflon greaseless seal. The amount of titrant added and the pH of the suspension were recorded by a Recording Auto Titrator (Hiranuma Sangyo Co., Ltd.). The titration was started at about pH 12, and 0.1 ml of the titrant, HCl standard solution, was added at 3 min intervals (because equilibrium was reached in 3 min.) The measurement was repeated 3 times and the pH values differed by less than ± 0.1 pH unit which is equivalent to an adsorption density of ± 1.0 $\mu C\,cm^{-2}$. The measurment was also carried out for solutions of different ionic strength.

Microelectrophoretic Method A lateral quartz cell with plane-parallel walls was used in the microelectrophoretic measurement. The 40 mm long cell had a rectangular cross-section whose inside dimensions were 1.0×10 mm. The electric field strength (E) was about 10 $V\,cm^{-1}$. The migration speed (u) of the particles was measured and the ζ-potential was calculated by the following formula by Smoluchowski.[9]

$$\zeta = 4\pi\eta u/\varepsilon E,$$

where ε is the dielectric constant, and η is the vicosity.

The suspension was prepared by dispersing 5 mg of the sample ultrasonically in 100 ml of aqueous solution, the pH of which was adjusted by KOH and HCl, and the ionic strength of which was adjusted to 4.0×10^{-5} M by KCl. This suspension was stored in tightly stoppered glass vessel and handled under a nitrogen atmosphere. The pH value of the suspension did not change for 20 h, which is quite adequate for measuring the IEP.

The hydration time hereafter mentioned is the time taken from the preparation of the dispersion to the measurement, that is the time during which the samples were in contact, at room temperature, with the aqueous media.

Results

The γ-Fe_2O_3 sample after washing with water contained 0.56 wt% of sulfate ions, and the α-Fe_2O_3 sample contained 0.55 wt% of sulfate ions. The γ-Fe_2O_3 sample after electrodialysis contained 0.06 wt% of sulfate ions and the α-Fe_2O_3 sample contained 0.25 wt%. The higher content of sulfate ions in the α-Fe_2O_3 sample can be explained by the migration of sulfate ions from the surface into the bulk during the heat treatment. Contamination by potassium ions, possibly introduced during the alkali washing, was found to be less than 5 ppm by the atomic absorption method. The adsorption density of the γ-Fe_2O_3 sample at the three stages of cleaning is plotted against pH in Fig. 2. The PZC is the pH value when the surface charge density is zero, and was found to be more basic after cleaning. The PZC value of the sample after alkali washing and electrodialysis, was 5.5.

Figure 3 shows the results of the potentiometric titration of the α-Fe_2O_3 sample. The PZC value of the α-Fe_2O_3, as with the γ-Fe_2O_3 sample, shifted in the basic direction during cleaning. The PZC value of the α-Fe_2O_3 sample after alkali washing and electrodialysis was 6.7.

Figures 4 and 5 show the plots of adsorption density versus pH taken at various ionic strengths, for the γ- and α-Fe_2O_3 respectively. As can be seen for an ionic strength of 1.0 M or less the curves have the same intersection point. Thus, the absence of a shift in the PZC value with variation of ionic strength was ascertained for both samples.

The ζ-potential increased with the hydration time, as shown in Figs. 6 and 7, for the γ-Fe_2O_3 and α-Fe_2O_3 samples respectively. Constant ζ-potential values were observed for both the γ- and α-Fe_2O_3 samples, for hydration times of 15 h and over, with no significant change being observed even after one week's hydration. The ζ-potentials at 0.5 h hydration are plotted

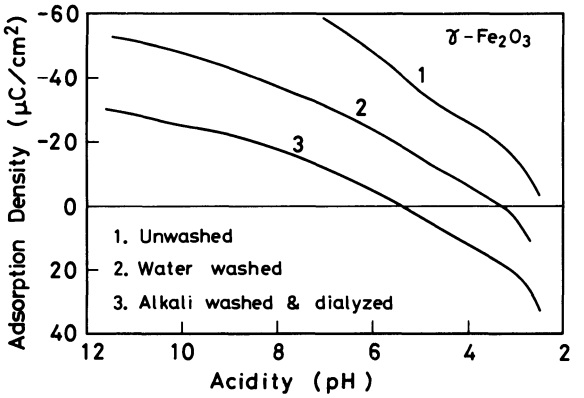

Fig. 2. Surface charge density on γ-Fe_2O_3 as a function of pH: ionic strength, 0.1 M: temperature, 20 °C.

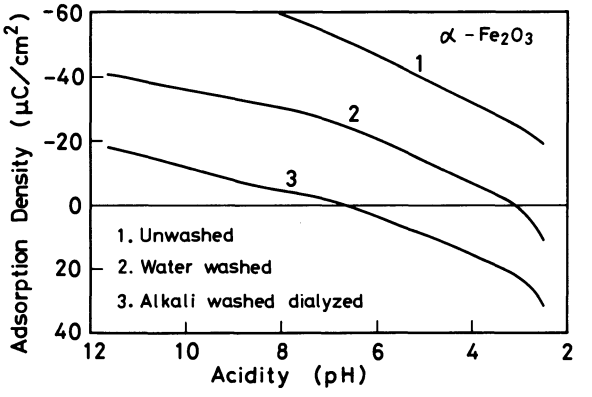

Fig. 3. Surface charge density of α-Fe_2O_3 as a function of pH: ionic strength, 0.1 M: temperature, 20 °C.

† 1 M=1 mol dm^{-3}.

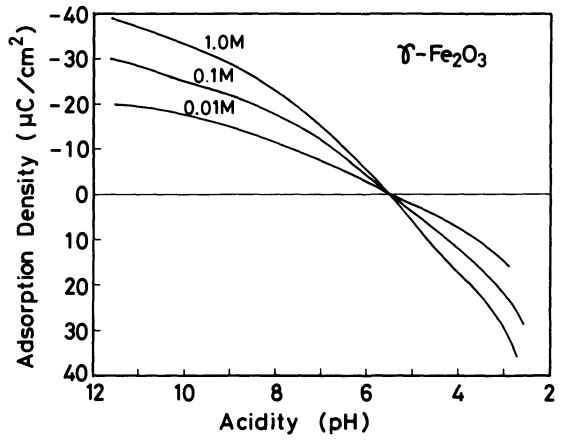

Fig. 4. Surface charge density of γ-Fe_2O_3 as a function of pH: ionic strength, 0.01 M, 0.1 M, 1.0 M: temperature, 20 °C.

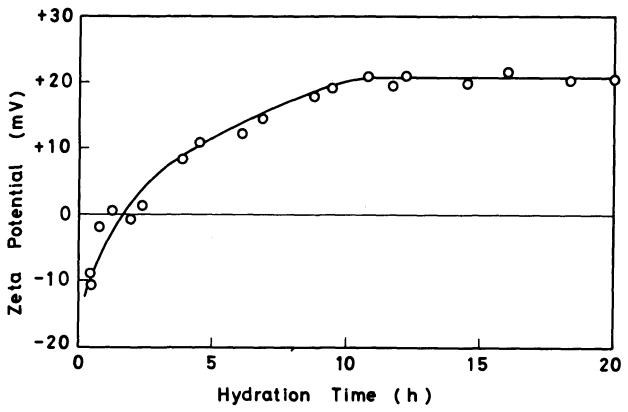

Fig. 7. Zeta potential of α-Fe_2O_3 at pH 7.05 as a function of the hydration time.

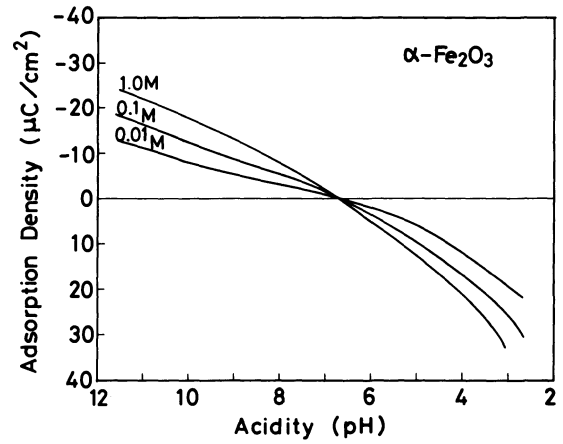

Fig. 5. Surface charge density of α-Fe_2O_3 as a function of pH: ionic strength, 0.01 M, 0.1 M, 1.0 M: temperature, 20 °C.

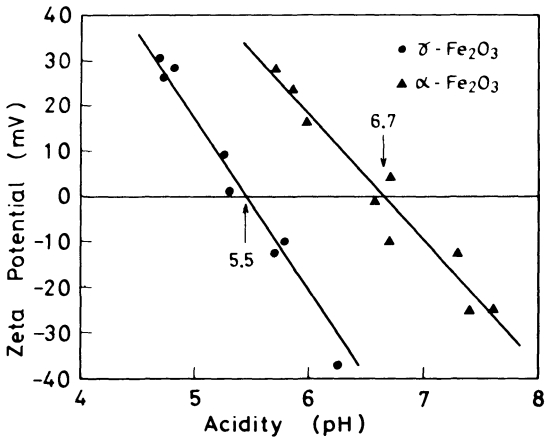

Fig. 8. Zeta potentials of γ-Fe_2O_3 hydrated up to 30 min as a function of pH: ionic strength, 4×10^{-5} M.

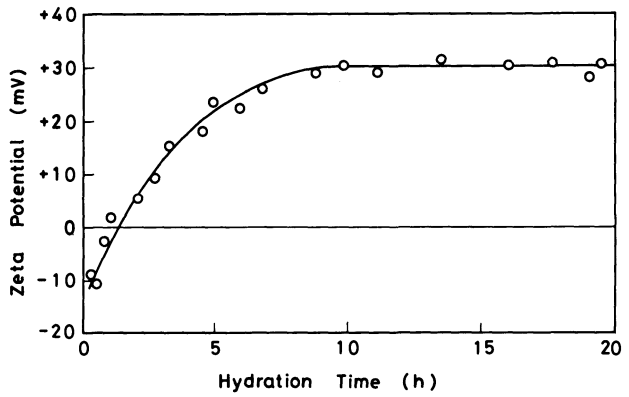

Fig. 6. Zeta potential of γ-Fe_2O_3 at pH 5.70 as a function of the hydration time.

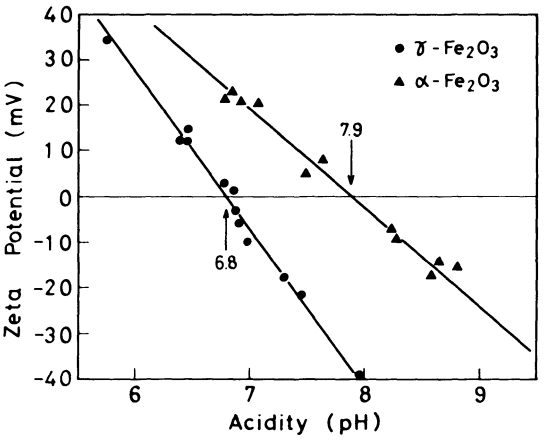

Fig. 9. Zeta potentials of γ- and α-Fe_2O_3 hydrated for 20 h as a function of pH: ionic strength, 4×10^{-5} M.

against the pH in Fig. 8. The zero point of the ζ-potential of the γ-Fe_2O_3 sample, that is its IEP, is 5.5±0.2 and that of the α-Fe_2O_3 sample is 6.7±0.2. These values, for the low hydration state, agree with the PZC values measured by potentiometric titration.

The ζ-potential of the γ- and α-Fe_2O_3 sample after 20 h hydration are plotted in Fig. 9. After 20 h hydration, the IEP of the γ-Fe_2O_3 sample was 6.8±0.2, and that of the α-Fe_2O_3 sample was 7.9±0.2. The IEPs of the γ- and α-Fe_2O_3 samples move in the basic direction by 1.3 and 1.2 pH units, respectively.

Discussion

Effect of Sulfate Ions. The PZC of the γ- and α-Fe_2O_3 samples shifts to higher values as the sulfate ion content decreases. These results correspond to those reviewed by Parks on α-Fe_2O_3[3].

The adsorption equilibrium of sulfate ions on iron oxide is represented as follows,

$$O\begin{matrix}\rangle Fe\text{-}OH \\ \rangle Fe\text{-}OH\end{matrix} + SO_4^{2-} \rightleftharpoons O\begin{matrix}\rangle Fe\text{-}O \\ \rangle Fe\text{-}O\end{matrix}\rangle S\begin{matrix}\langle O \\ \langle O\end{matrix} + 2OH^-$$

Parfitt and Smart[10] showed that this adsorption occurs at pH values less than 8. Therefore, the desorption of sulfate ions from the surface is not negligible around the pH values corresponding to the IEP and PZC of the iron oxides. The desorption of sulfate ions causes the adsorption of hydroxide ions, which results in a lowering of the pH of the suspension and thus shifts the PZC value in the acidic direction.

The PZCs obtained by potentiometric titration of the γ- and α-Fe_2O_3 samples after alkali washing and electrodialysis, coincide with the IEPs measured by the electrophoretic method for the short hydration time of 0.5 h. This suggests that the influence of the specific adsorption of ions on the particles' surface has been eliminated.

Effect of Hydration. The value of the PZC and IEP of γ-Fe_2O_3 hydrated for 0.5 h is 5.5, and the value for α-Fe_2O_3 hydrated for 0.5 h is 6.7. This value of 6.7 for α-Fe_2O_3 is nearly equal to the values reported, on natural hematite and ignited α-Fe_2O_3 by Johansen and Buchanan[11] and Iwasaki et al.[12]

The value of the IEPs of γ- and α-Fe_2O_3 increases with increasing hydration time. The IEP of hydrated γ-Fe_2O_3 is 6.8, and that of hydrated α-Fe_2O_3 is 7.9. The value of 6.8, for the hydrated γ-Fe_2O_3, is in good agreement with the value of 6.7 obtained by Iwasaki et al.[2] for γ-Fe_2O_3, containing a small amount of lepidocrocite. The IEP value of 7.9 for hydrated α-Fe_2O_3 agrees well with the 8.0 value obtained by Johansen and Buchanan.[11]

The IEPs of γ- and α-Fe_2O_3 increased by 1.3 and 1.2 pH units respectively on hydration. Parks[3] calculated that there was an average of 2.1 pH units difference, between the IEPs of the hydrated and unhydrated oxides. Johansen and Buchanan[11] reported a decrease of 1.5 pH units in the IEP after dehydration.

The difference between the value of the IEPs of γ- and α-Fe_2O_3 was 1.2 pH units for the unhydrated samples and 1.1 pH units for the hydrated sample.

The reason why the IEPs of the oxides shift to the basic direction has been considered in terms of the formation of a hydrated layer[3] and the interacting forces between adjacent hydroxyl groups[13] at the particle surface. Ahmed and Maksimov[14,15] also reported the shift of PZC on hydration, and pointed out that the hydration is remarkable, when the amount of metal ions dissolved in the aqueous media, is of the order of the surface concentration of ions.

In this measurement, hydration caused a large increase in the IEP, whereas the PZC was nearly constant for at least a number of days. This discrepancy may be due to the fact that the concentration of the suspensions used in the microelectrophoretic method was smaller by a factor of 10^3 from the concentration used in the potentiometric titration method.

Effect of Crystal Structure. The difference in IEPs of the γ- and α-Fe_2O_3 samples can be considered to be due to the difference in their crystal structures, because the shapes of the particles, their specific surface areas and the cleaning and hydration operations applied to both of the samples were the same.

The crystal structures of γ- and α-Fe_2O_3 are the same as those of γ- and α-Al_2O_3, respectively. In both oxides, the γ-type has an inverse-spinel crystal structure, and the α-type has a corundum crystal structure.[16] Kozumina et al.[5] measured the IEP's of γ- and α-Al_2O_3, prepared by calcination of a gibbsite sample and obtained IEP values of 7.4 to 8.6 for the γ-Al_2O_3 and of 9.1 to 9.2 for the α-Al_2O_3 using the streaming potential method. The average difference in IEP between γ- and α-Al_2O_3, therefore, is 1.1 to 1.2 pH units, which is similar to the average difference in the IEP values between γ- and α-Fe_2O_3.

The unit lattice of γ-Fe_2O_3 is expressed by the following formula:

$$\underset{\text{Coordination Number}=4}{Fe^{3+}_8} \quad (\underset{\text{Coordination Number}=6}{Fe^{3+}_{40/3}} \ \square_{8/3}) \quad O^{2-}_{32}$$

In the above formula a vacant lattice point is indicated by □ at the position of the coordination number 6, i.e. 6 oxygen ions adjacent to the Fe^{3+} ion. Fe^{3+} ions having coordination numbers of 4 and 6 are present in the ratio of 3:5. On the other hand, α-Fe_2O_3 is a corundum-type oxide, in which all of the Fe^{3+} ions have a coordination number of 6.

The average IEP is more acidic by 2.6 pH units for four-coordinated ions than for six-coordinated metallic ions.[3] Thus, the difference in the IEPs between the γ-Fe_2O_3 and α-Fe_2O_3 is calculated to be 2.6×3/(3+5)=

1.0, assuming that the additivity rule holds.[17] Accordingly, the IEP of γ-Fe_2O_3 is about 1.0 pH units lower than that of α-Fe_2O_3. The lower IEP values of γ-Fe_2O_3 and the IEP differences of 1.2 and 1.1 for the hydrated and unhydrated samples respectively, coincide well with the above calculation.

Conclusion

1) The PZC and IEP of the unhydrated γ-Fe_2O_3 were 5.5 and the IEP of the hydrated γ-Fe_2O_3 was 6.8.

2) The PZC and IEP of γ-Fe_2O_3 were more acidic by 1.1 and 1.2 pH units than those of α-Fe_2O_3 for the hydrated and unhydrated stages respectively.

3) These differences were explained quantitatively in terms of the crystal structure.

The authors wish to thank Dr. S. Baker of Sony Corporation Research Center for reading the manuscript.

References

1) J. Seto, *J. Soc. Rheol. Jpn.*, **5**, 156 (1977).
2) I. Iwasaki, S. R. B. Cooke, and Y. S. Kim, *Trans AIME*, **223**, 113 (1962).
3) G. A. Parks, *Chem. Rev.*, **65**, 177 (1967).
4) T. W. Healy, A. P. Herring, and D. W. Fuerstenau, *J. Colloid Interface Sci.*, **21**, 435 (1966).
5) Z. P. Kozmina, M. P. Belova, and V. A. Sannikov, *Kolloidn. Zh.*, **25**, 169 (1963).
6) S. Kittaka, and T. Morimoto, *J. Colloid Interface Sci.*, **75**, 398 (1980).
7) S. Kachi, K. Moriyama, and S. Shimizu, *J. Phys. Soc. Jpn.*, **18**, 106 (1963).
8) G. A. Parks, and P. L. de Bruyn, *J. Phys. Chem.*, **66**, 967 (1962).
9) R. J. Hunter, "Zeta Potential in Colloid Science," Academic Press Inc., London (1981).
10) R. L. Parfitt, and R. S. C. Smart, *Soil Sci. Soc. Am. J.*, **42**, 48 (1978).
11) P. G. Johansen, and A. S. Buchanan, *Aust. J. Chem.*, **10**, 398 (1957).
12) I. Iwasaki, S. R. B. Cooke, and H. S. Choi, *Trans AIME*, **217**, 237 (1960).
13) T. Morimoto, and S. Kittaka, *Bull. Chem. Soc. Jpn.*, **46**, 3040 (1973).
14) S. M. Ahmed, and D. Maksimov, *Can J. Chem.*, **46**, 3841 (1968).
15) S. M. Ahmed, and D. Maksimov, *J. Colloid Interface Sci.*, **29**, 97 (1969).
16) R. W. G. Whyckoff, "Crystal Structure," 2nd ed., Interscience, New York (1963).
17) G. A. Parks, *Adv. Chem. Ser.*, **67**, 121 (1967).

Transport Properties of Cation-Exchange Membrane-Aqueous Electrolyte System

Yoshihiko NAGATA, Kazuyuki KOHARA, WongKang YANG, Akira YAMAUCHI, and Hideo KIMIZUKA*

Department of Chemistry, Faculty of Science, Kyushu University 33, Hakozaki, Higashi-ku, Fukuoka 812

(Received February 12, 1986)

Transport properties of a cation-exchange membrane-aqueous sodium chloride solution system have been studied. The membrane used was a sulfonated styrene-divinyl benzene copolymer, Neosepta C66-5T. The salt concentration was kept at 10^{-1} mol dm^{-3} on one side of the membrane and varied from 10^{-3} to 10^{-2} mol dm^{-3} on the other. The six elements of a conductance matrix have been experimentally determined according to the previous theory[1] and the membrane properties were discussed in terms of conductance elements. All the elements of the conductance matrix were positive within the concentration range studied. This would be characteristic of a cation-exchange membrane. The electrical ion conductance was greater than the diffusional ion conductance by a factor of 10 to 100. The ion-solvent coupling coefficient was much less than the interionic one, although the electroosmotic conductance was ten-times greater than the membrane conductance. The reflection coefficient was close to unity. The electroosmotic properties were also discussed in terms of the conductance matrix.

In the preceding papers,[1,2] six elements of a conductance matrix (phenomenological coefficients) were experimentally determined with the amphoteric ion-exchange membrane–aqueous electrolyte systems and the membrane properties were discussed in terms of the conductance matrix. All the transport properties in these systems could be explained in terms of the six elements. This indicates that six phenomenological coefficients are required for a characterization of a membrane–aqueous electrolyte system. It is, therefore, of interest to determine the phenomenological coefficients by using a variety of membranes and to understand how the coefficients reflect the membrane characters. Thus, a determination of the coefficients in the cation-exchange membrane-aqueous electrolyte system has been attempted. This paper describes the experimental results.

Experimental

Materials. The cation-exchange membrane used in the present study was a sulfonated styrene-divinyl benzene copolymer developed by Tokuyama Soda Co., Ltd. and coded as Neosepta C66-5T. The ion-exchange capacity was 2.45 meq. (g dry membrane)$^{-1}$, the water content 0.4 gH_2O (g dry membrane)$^{-1}$ and the thickness 0.15 mm. A pure specimen of sodium chloride as well as sucrose and twice-distilled water were used for preparing salt and sucrose solutions.

Procedures of Experiments. The experimental procedures were described elsewhere.[1] Regarding the aqueous phases separated by a membrane, the salt concentration of phase II was kept at 10^{-1} mol dm^{-3} and that of phase I was varied from 10^{-3} to 10^{-2} mol dm^{-3}. The sucrose concentration used for an osmotic flux measurement was 8.176×10^{-2} mol dm^{-3}. In the present study, current densities of 0.902×10^{-2}, 1.981×10^{-1}, and 2.971×10^{-1} mA cm^{-2} were passed through the paired Ag/AgCl electrodes of each system. The experiments were carried out at a regulated temperature of 25.0±0.1 °C.

Results and Discussion

The aim of the present work was to determine the phenomenological coefficients, g_{NaNa}—g_{ww}, in the phenomenological equation[1]

$$\begin{bmatrix} i_{Na} \\ i_{Cl} \\ Fj_w \end{bmatrix} = -\begin{bmatrix} g_{NaNa} & g_{NaCl} & g_{Naw} \\ g_{ClNa} & g_{ClCl} & g_{Clw} \\ g_{wNa} & g_{wCl} & g_{ww} \end{bmatrix} \begin{bmatrix} V-V_{Na} \\ V-V_{Cl} \\ -V_w \end{bmatrix}, \quad (1)$$

and to discuss the membrane properties in terms of the conductance matrix. In Eq. 1, the suffixes Na, Cl, and w refer to sodium and chloride ions and water, respectively. Also i denotes the ion current, j the flux, V the membrane potential, V_{Na} and V_{Cl} the pseudoequilibrium potential for sodium and chloride ions, respectively, and V_w the effective driving potential for water or the water potential. V_{Na}, V_{Cl}, and V_w are defined by

$$Z_\gamma FV_\gamma = RT \ln a_\gamma^{I}/a_\gamma^{II} - \bar{v}_\gamma \Delta P \quad (\gamma = \text{Na, Cl}) \quad (2)$$

and

$$FV_w = RT \ln a_w^{I}/a_w^{II} - \bar{v}_w \Delta P = \bar{v}_w(\Delta\pi - \Delta P), \quad (3)$$

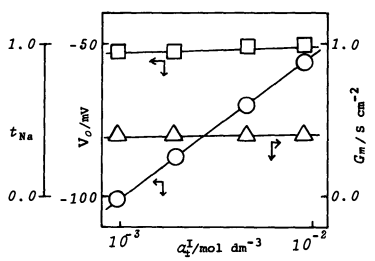

Fig. 1. Membrane potential at zero electric current, V_0, membrane conductance G_m and cationic transport number, t_{Na}, vs. mean electrolyte activity of phase I. ○: V_0, △: G_m, □: t_{Na}.

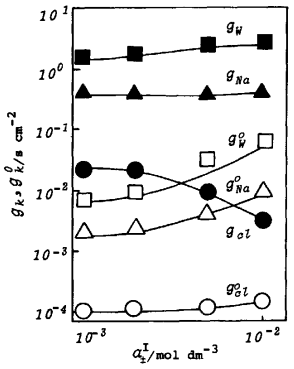

Fig. 2. Electrical ion and water conductances (g_{Na}, g_{Cl}, g_w) and diffusional ion and water conductances (g^0_{Na}, g^0_{Cl}, g^0_w) vs. mean electrolyte activity of phase I.
▲: g_{Na}, ●: g_{Cl}, ■: g_w, △: g^0_{Na}, ○: g^0_{Cl}, □: g^0_w.

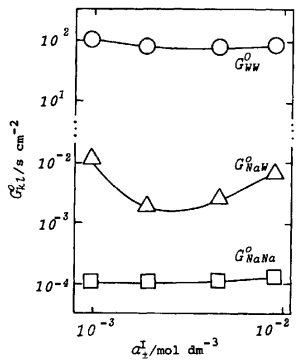

Fig. 3. G^0_{NaNa}, G^0_{Naw}, and G^0_{ww} as a function of mean electrolyte activity in phase I.
□: G^0_{NaNa}, △: G^0_{Naw}, ○: G^0_{ww}.

respectively, where the superscripts I and II refer to phases I and II, respectively. Here, F, R, and T denote the Faraday constant, the gas constant and the absolute temperature, respectively. Also, Z is the charge number, a the activity, $\bar{v}_\gamma$ (γ=Na, Cl, w) the partial molar volume of species γ (assumed to be constant for a given system), $\Delta\pi$ the osmotic pressure and ΔP ($=P^{II}-P^{I}$) the external pressure difference.

The equation for the membrane current, I, is obtained from Eq. 1 as follows[1]

$$I = i_{Na} + i_{Cl} = -G_m(V-V_0)$$
$$= -g_{Na}(V-V_{Na}) - g_{Cl}(V-V_{Cl}) + g_wV_w, \quad (4)$$

where g_{Na}, g_{Cl}, and g_w denote the electric conductances for the permeating species Na, Cl, and w, respectively,

$$g_k = g_{kNa} + g_{kCl} \quad (k=Na,\ Cl,\ w) \quad (5)$$

G_m, the membrane conductance is given by

$$G_m = g_{Na} + g_{Cl}. \quad (6)$$

V_0, the membrane potential at zero membrane current is

$$V_0 = t_{Na}V_{Na} + t_{Cl}V_{Cl} + t_wV_w, \quad (7)$$

and t_k, the transport number of a species k, is

$$t_k = g_k/G_m. \quad (8)$$

The transport numbers can be estimated from fluxes and the membrane currents according to the relations[1]

$$i_{Na} - i^0_{Na} = t_{Na}I$$

and

$$F(j_w - j^0_w) = t_wI, \quad (9)$$

where the superscript 0 refers to the fluxes at zero membrane current. The transport number of the cation t_{Na} is plotted in Fig. 1 together with the membrane potential V_0 and the membrane conductance G_m. This figure indicates that the membrane is selective to cations and that G_m is constant in the concentration range studied. The apparent transport number $(t_{Na})_{app.}$ estimated from the membrane potential vs. the logarithmic activity relation was close to t_{Na}.

The chloride ion conductance g_{Cl} was evaluated by subtracting g_{Na} ($=G_mt_{Na}$) from G_m. The conductances, g_{Na}, g_{Cl}, and g_w ($=G_mt_w$), are plotted against the salt activity as shown in Fig. 2. In the absence of a membrane current in the external solution, Eq. 1 is reduced to

$$\begin{bmatrix} i^0_{Na} \\ Fj^0_w \end{bmatrix} = -\begin{bmatrix} G^0_{NaNa} & G^0_{Naw} \\ G^0_{wNa} & G^0_{ww} \end{bmatrix} \begin{bmatrix} V_{Cl}-V_{Na} \\ -V_w \end{bmatrix}, \quad (10)$$

where

$$G^0_{NaNa} = g_{NaNa} - G_mt^2_{Na},$$
$$G^0_{Naw} = g_{Naw} - G_mt_{Na}t_w = G^0_{wNa},$$

and

$$G^0_{ww} = g_{ww} - G_mt^2_w. \quad (11)$$

A change in the water potential, ΔV_w, under constant values of V_{Na} and V_{Cl} gives rise to changes in the fluxes, Δi^0_{Na} and Δj^0_w, which are given as

$$\Delta j^0_{Na} = G^0_{Naw}\Delta V_w$$

and

$$F\Delta j^0_w = G^0_{ww}\Delta V_w, \quad (12)$$

provided that there is no appreciable change in the activity coefficients of ions as well as the phenomenological coefficients due to the addition of sucrose into one of the two aqueous phases. G^0_{NaNa} and G^0_{wNa} may be determined by using Eq. 10 provided G^0_{Naw} and G^0_{ww} are known. The result showed that G^0_{wNa} and G^0_{Naw} are close to each other, an indication of a reciprocal relation. Figure 3 shows G^0_{NaNa}, G^0_{Naw}, and G^0_{ww} as a function of the salt concentration in phase I. The diffusional conductances g^0_k (k=Na, Cl, w), calculated according to the relation

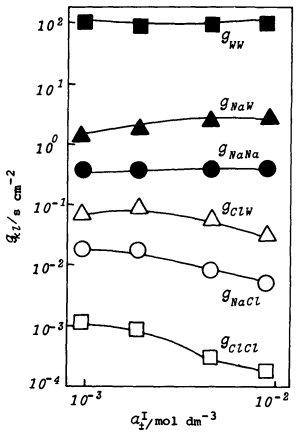

Fig. 4. Element of conductance matrix vs. mean electrolyte activity of phase I.
●: g_{NaNa}, □: g_{ClCl}, ○: g_{NaCl}, ▲: g_{Naw}, △: g_{Clw}, ■: g_{ww}.

$$g_k^0/g_k = (g_{NaNa}g_{ClCl} - g_{NaCl}^2)/g_{Na}g_{Cl} \quad (13a)$$
$$= G_{NaNa}^0/G_m t_{Na} t_{Cl}, \quad (13b)$$

are plotted in Fig. 2 together with the conductances g_k as functions of the electrolyte activity in the external solution. The value of g_k^0 can be estimated according to Eq. 13b, provided that g_k, G_m, and G_{NaNa}^0 are known.

Comparing Eqs. 11 and 5, we obtain a set of relations for estimating the elements of the conductance matrix as follows[2]

$$g_{NaNa} = G_m t_{Na}^2 + G_{NaNa}^0, \quad g_{Naw} = G_m t_{Na} t_w + G_{Naw}^0$$
$$g_{NaCl} = G_m t_{Na} t_{Cl} - G_{NaNa}^0, \quad g_{Clw} = G_m t_{Cl} t_w - G_{Naw}^0 \quad (14)$$
$$g_{ClCl} = G_m t_{Cl}^2 + G_{NaNa}^0, \quad g_{ww} = G_m t_w^2 + G_{ww}^0$$

Thus, the six elements of the conductance matrix can be estimated according to Eq. 14 after measurements of G_m, t_{Na}, t_w, G_{NaNa}^0, G_{Naw}^0, and G_{ww}^0. Figure 4 shows the six elements as functions of the mean electrolyte activity of phase I.

It can be seen in Fig. 4 that $g_{ww} > g_{Naw} > g_{NaNa} > g_{Clw} > g_{NaCl} > g_{ClCl}$ and that all the conductance elements are positive. This result is similar to that in the cation-exchange membrane-barium chloride system,[3] but differs from that in the amphoteric ion-exchange membrane-aqueous sodium chloride system,[1] $g_{ww} > g_{Naw} > |g_{Clw}| > g_{NaNa} \simeq g_{ClCl} > |g_{NaCl}|$, where g_{Clw} and g_{NaCl} are negative.

The lines in Fig. 2 indicate the values of g_k and g_k^0 calculated from g_{kl}'s (k,l=Na, Cl, w) in Fig. 4 according to Eqs. 5 and 13b, respectively. The calculated values are in good agreement with those obtained experimentally. This figure also indicates that the electrical ion conductance g_γ (γ=Na, Cl) is much greater than g_γ^0. This result agreed with that observed with the cation-exchange membrane-aqueous calcium chloride system[4] and can be ascribed to the small co-ion concentration in the membrane. In contrast, it was also reported that g_γ is much smaller than g_γ^0 in the amphoteric ion-exchange membrane-aqueous electrolyte system.[1,2] Rewriting Eq. 13a we have[1]

$$g_\gamma - g_\gamma^0 = g_{NaCl}/(1-t_\gamma). \quad (15)$$

Thus, it is seen that the positive value of g_{NaCl} in the cation-exchange membrane and the negative value of g_{NaCl} in the amphoteric ion-exchange membrane[2] are correlated to the difference between the conductive and diffusional ion conductances. Assuming the membrane controlling, we have from Eq. 15 an equation for the equivalent ion conductance[1]

$$\lambda_\gamma - \lambda_\gamma^0 = g_{NaCl}\delta/|Z_\gamma|\overline{C}_\gamma(1-t_\gamma), \quad (16)$$

where λ_γ denotes the equivalent ion conductance and λ_γ^0, that calculated from the diffution coefficient according to the Nernst-Einstein relation; δ the membrane thickness; and $\overline{C}_\gamma$, the concentration of γ ions within the membrane. Despić and Hills[5] ascribed the difference, $\lambda_\gamma - \lambda_\gamma^0$, to an electroosmotic effect. Since g_{NaCl} exhibits an interionic correlation, Despić and Hills' theory is not theoretically valid in view of nonequilibrium thermodynamics. Furthermore, the fact that the negative value of $(\lambda_\gamma - \lambda_\gamma^0)$ is observed in an amphoteric ion-exchange membrane can not be explained by Despić and Hills' theory, because the electroosmotic term is always positive.[5]

The reason why the positive and negative values of g_{NaCl} are observed in the cation-exchange membrane and the amphoteric ion-exchange membrane, respectively, has not yet been clear. However, it is of interest to point out that the negative value of g_{NaCl} in the amphotoric ion-exchange membrane is conformable with the positive cross term in phenomenological coefficients observed in an aqueous sodium chloride solution.[6]

The difference between the membrane conductance G_m and that without the electroosmotic effect, G_m' has been expressed as[1]

$$G_m - G_m' = g_v^2/g_p, \quad (17)$$

where g_v and g_p denote the electroosmotic volume-flow conductance and the hydrodynamic volume-flow conductance, respectively. Since the transport number of cations in the cation-exchange membrane is close to unity, Eq. 17 can be rewritten as

$$\lambda_{Na} - \lambda_{Na}' = \delta g_v^2/g_p \overline{C}_{Na}, \quad (18)$$

where δ is the membrane thickness and $\overline{C}_{Na}$, is the sodium ion concentration in the membrane. It has been shown in a preceding paper that under several assumptions Eq. 18 can be reduced to Despić and Hills' equation[1]

$$\lambda - \lambda' = (Fr)^2\overline{X}/8\eta, \tag{19}$$

where F denotes Faraday constant, r the capillary radius, $\overline{X}$ the counter-ion concentration in the membrane and η the solvent viscosity. It can be seen by comparing Eq. 16 with Eqs. 18 and 19 that the failure of Despic and Hills' theory lies in the replacement of λ_γ' by λ_γ^0. The electroosmotic contribution to the membrane conductance can be evaluated according to Eq. 17. The values of g_v and g_p can be estimated from g_{kl}'s given in Fig. 4 by using the relations given in the preceding paper.[1] The values of g_v and g_p were found to be almost the same as those of g_w and g_{ww}, respectively. The observed value of G_m was 0.39 S cm^{-2} in the range of concentration studied and the values of G_m' calculated according to Eq. 18 were 0.35—0.30 S cm^{-2}. On the other hand $g_\gamma(\lambda_\gamma)$ was greater than $g_\gamma^0(\lambda_\gamma^0)$ by a factor of 2 as shown in Fig. 2. These results indicate that the electroosmotic effect is not so appreciable as the diffusional effect.

The charge concentration per unit volume of the pore liquid X can be evaluated according to the relation[1]

$$X = g_v/g_p\bar{v}_w. \tag{20}$$

The value of X is given in Fig. 5. Equation 20 is equivalent to the effective charge density of a membrane proposed by Staverman.[7] The values of X were found to be 1—1.6 mol dm^{-3}, while the counter-ion concentration, $\overline{X}$, in the pore liquid evaluated from the exchange capacity and water content of the membrane was ca. 6 mole/KgH_2O. This might indicate that the counter-ions accompanying the electroosmotic flow are not all counter-ions within the membrane, as assumed in classical membrane theory.[8] The relation $X=\overline{X}$ was also assumed in Despić and Hills' theory.[5] It is interesting to note here that the ratio, $X/\overline{X}$, is near to the contribution of the electroosmotic effect in membrane conductance, $(G_m-G_m')/G_m$.

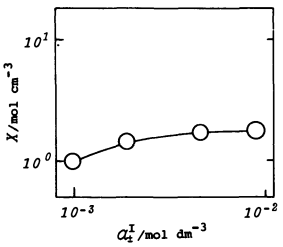

Fig. 5. Charge concentration per unit volume of the pore liquid vs. mean electrolyte activity of phase I.

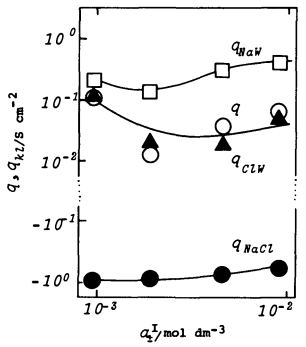

Fig. 6. Coupling coefficient vs. mean electrolyte activity of phase I.
○: q, ●: q_{NaCl}, □: q_{Naw}, ▲: q_{Clw}.

The present study deals with the three processes expressed by Eq. 1. The degree of coupling among these processes can be demonstrated by a coupling coefficient[1]

$$q_{kl} = -|g|_{kl}/(|g|_{kk}|g|_{ll})^{1/2}, \tag{21}$$

where $|g|_{kl}$ is the cofactor of an element g_{kl} in the conductance matrix. The coupling coefficients q_{NaCl}, q_{Naw}, and q_{Clw} calculated according to Eq. 21 is shown in Fig. 6. It is shown in this figure that q_{NaCl} is close to -1 while q_{Naw} and q_{Clw} are the order of 10^{-1} and 10^{-2}, respectively. This indicates that the ionic processes are more strongly coupled to each other than the coupling between ion and water transports. The remarkable difference between the diffusional and electric ion conductances reflects a strong interionic coupling. On the other hand, the ion-solvent interaction is weaker as shown in the electroosmotic effect, although it is appreciable. These facts indicate the importance of the cross coefficients in the membrane process. Thus, the cross coefficients in the phenomenological equation can not be ignored unless doing so is verified experimentally. The coupling coefficient q for the salt flow-volume flow coupling in the absence of an electric current is also shown in Fig. 6. The coefficient q is defined by

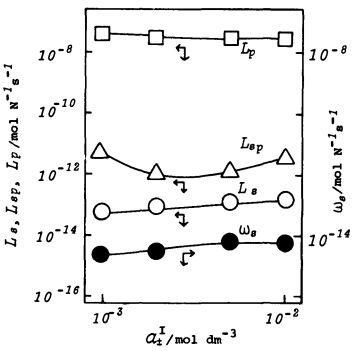

Fig. 7. Solute permeability(ω_s), thermodynamic permeability(L_s), mechanical filtration coefficient(L_{sp}) and hydrodynamic permeability(L_p) vs. mean electrolyte activity of phase I.
●: ω_s, ○: L_s, △: L_{sp}, □: L_p.

$$q = L_{sp}/(L_s L_p)^{1/2}, \tag{22}$$

where L_{sp} and L_s, and L_p are the phenomenological coefficients in the equation[1)]

$$\begin{bmatrix} \bar{v}_s J_s^0 \\ J_v^0 \end{bmatrix} = -\begin{bmatrix} L_s & L_{sp} \\ L_{sp} & L_p \end{bmatrix} \begin{bmatrix} \Delta\pi - \Delta\pi_s \\ \Delta p - \Delta\pi \end{bmatrix}. \tag{23}$$

This can be derived from Eq. 1 at a zero membrane current.[1)] In Eq. 23, the superscript 0 refers to a case where there is no membrane current; $\bar{v}_s$ denotes the partial molar volume of the salt; J_s^0 the salt flux; J_v^0 the volume flow; $\Delta\pi$ the osmotic pressure difference; Δp the external pressure difference; and $\Delta\pi_s$ the osmotic pressure difference of the salt. It is defind by[1)]

$$\bar{v}_s \Delta\pi_s = -2RT \ln a_{\pm}^{II}/a_{\pm}^{I}. \tag{24}$$

Here, $a_{\pm}$ denotes the mean activity of salt. It should be noted that the factors determining the correlation among the flow processes are not the relative magnitudes of the flows, but the coupling coefficients. For example, g_{ww} and g_w are greater than 100 and 10 times the membrane conductance, respectively, while the effects of the solvent flow on the interionic correlations are small as illustrated in the electro-osmotic effect on the membrane conductance. The ion fluxes can also be expressed by

$$\begin{bmatrix} i_{Na} \\ i_{Cl} \end{bmatrix} = -\begin{bmatrix} (g_{NaNa})_{app} & (g_{NaCl})_{app} \\ (g_{ClNa})_{app} & (g_{ClCl})_{app} \end{bmatrix} \begin{bmatrix} V - V_{Na} \\ V - V_{Cl} \end{bmatrix}, \tag{25}$$

where the subscript app refers to the apparent values, including the solvent effect.[1)] The deviation of $(g_{NaCl})_{app}$ from g_{NaCl} was comparable with that of G_m from G_m', although $(t_{Na})_{app}$ is close to t_{Na}.

Since the conductance matrix characterizes the system, all the transport properties of the membrane can be calculated from the elements of the conductance matrix. The thermodynamic solute permeability L_s, the mechanical filtration coefficient L_{sp}, the hydrodynamic permeability L_p and the solute permeability coefficient ω_s[1)] are related by

$$\omega_s = (L_s - L_{sp}^2/L_p)/\bar{v}_s. \tag{26}$$

These quantities were estimated for the present system as shown in Fig. 7. The reflection coefficient

$$\sigma = 1 - L_{sp}/L_p \tag{27}$$

was close to unity, 0.9998—0.9999, and is not plotted in this figure.

This work was supported by a Grant-in-Aid for Scientific Research No. 58470007 from the Ministry of Education, Science and Culture.

References

1) H. Kimizuka, Y. Nagata, and K. Kaibara, *Bull. Chem. Soc. Jpn.*, **56**, 2371 (1983).

2) H. Kimizuka, Y. Nagata, and W. Yang, "Membranes and Membrane Processes," ed by E. Drioli and M. Nakagaki, Plenum Press (1986), pp. 85—92.

3) E. Kumamoto and H. Kimizuka, *J. Phys. Chem.*, **85**, 635 (1981).

4) H. Kimizuka, K. Kaibara, E. Kumamoto, and M. Shirōzu, *J. Membrane Sci.*, **4**, 81 (1978).

5) A. Despić and G. J. Hills, *Diss. Faraday Soc.*, **21**, 150 (1956).

6) A. Katchalsky and P. F. Curran, "Nonequilibrium Thermodynamics in Biophysics," Harvard Univ. Press (1965).

7) A. J. Staverman, *Trans. Faraday Soc.*, **48**, 176 (1952).

8) N. Lakshminarayanaiah, "Transport Process in Membranes," Academic Press (1969).

 © 1986 The Chemical Society of Japan Bull. Chem. Soc. Jpn., 59, 2695—2698 (1986)

Effect of Pressure on the Adsorption and Micelle Formation of Aqueous Dodecyltrimethylammonium Chloride-Cyclohexane System

Michio YAMANAKA,*,† Makoto ARATONO, and Kinsi MOTOMURA
Department of Chemistry, Faculty of Science, Kyushu University 33, Fukuoka 812
(Received February 17, 1986)

The interfacial tension of aqueous dodecyltrimethylammonium chloride (DTAC) solution-cyclohexane system was measured as a function of pressure at concentrations around the critical micelle concentration (cmc). The derivative of interfacial tension with respect to pressure was observed to change abruptly at the cmc. The volume changes associated with the adsorption of DTAC from its monomeric and micellar states and the volume of micelle formation were calculated and compared with the corresponding ones of the aqueous DTAC solution-hexane system. It was found that the molar interfacial excess volume of the adsorbed film is slightly larger than the molar volume of micelle in the case of the cyclohexane system, while in the case of the hexane system the former is approximately equal to the latter. Further, it was concluded that the micellar particles solubilize molecules of the oil coexisting in equilibrium with the aqueous solution. It was also proved in the case of the present system that the micelle formation can be treated thermodynamically as the appearance of a macroscopic bulk phase in the solution.

In the preceding papers,[1,2] the interfacial tension of the aqueous solutions of dodecylammonium chloride (DAC) and dodecyltrimethylammonium chloride (DTAC) against hexane has been measured as a function of pressure. By applying the thermodynamic equations derived previously,[3] the volumes of adsorption of the surfactants from their monomeric and micellar states and the volume of micelle formation have been evaluated; the micelles of DAC and DTAC in equilibrium with hexane have been found to be similar in volumetric behavior to their adsorbed films at the solution/hexane interface. Further, our thermodynamic method has been proved to be useful.

On the other hand, organic liquids are known to have an influence on the critical micelle concentration and adsorption isotherm of surfactant.[4] Therefore, it is of interest to see if the above conclusions are drawn by using other organic liquid in place of hexane. Furthermore, it is important to investigate how the volumetric behavior of the micelle and adsorbed film of surfactant is affected by the organic liquid coexisting with its aqueous solution. In this work, we adopt cyclohexane as the organic liquid. The interfacial tension between aqueous DTAC solution and cyclohexane is measured as a function of pressure at various concentrations at a constant temperature.

Experimental

Dodecyltrimethylammonium chloride was prepared and purified as described in the previous papers.[2,5] Water was triply distilled from alkaline permanganate solution. Cyclohexane (Nakarai Chemicals, Ltd., UV spectrophotometric grade) was used after being distilled.

The equilibrium interfacial tension was measured by the pendant drop method[1,6] within an experimental error of 0.05 mN m^{-1}. The pendant drops were stood for 30 min to attain the thermodynamic equilibrium. The density of cyclohexane taken from the literature,[7] was used to calculate the interfacial tension at high pressures. The pressure range measured was from atmospheric pressure to the freezing pressure of cyclohexane (about 37 MPa). Temperature was kept constant at 298.15 K.

Results and Discussion

The interfacial tension γ between aqueous dodecyltrimethylammonium chloride (DTAC) solution and cyclohexane was measured as a function of pressure p at constant molality m_1 of DTAC and at 298.15 K. The γ vs. p curves at lower concentrations are shown in Fig. 1 and those at higher ones in Fig. 2. It is seen from Fig. 1 that the curves of the aqueous solutions of DTAC at concentrations below the critical micelle concentration (cmc; e.g., 21.89 mmol kg^{-1} at 0.1 MPa, see Fig. 5) are convex upward, while the curve of the pure water is linear. From Fig. 2, on the other hand, the curve at a concentration above the cmc is seen to be linear and have a very small slope compared to the curve of the pure water. At a concentration near the cmc, the curve has a linear portion, of which the upper limit is indicated by an arrow, at lower pressure.

The pressure effect on the adsorption can be visualized by plotting the slope of the γ vs. p curve, which is related directly to the volume change associated with the adsorption, against molality m_1 at several pressure values. Figure 3 shows the $\partial\gamma/\partial p$ vs. m_1 curves at 0.1, 15, and 30 MPa. It is seen that the $\partial\gamma/\partial p$ value varies with pressure in the concentration range below the cmc, while in the concentration range above the cmc it remains unvaried. Further, it is observed that the curve changes discontinuously at the cmc.

Next, let us consider the concentration dependence

† Present address: Laboratory of Chemistry, College of General Education, Kyushu University, Ropponmatsu, Fukuoka 810.

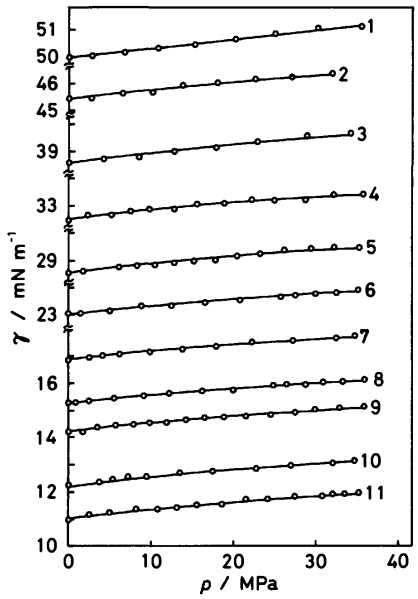

Fig. 1. Interfacial tension vs. pressure curves at constant total molality and at 298.15 K (lower concentration region). m_1=(1): 0 mmol kg^{-1}, (2): 0.20, (3): 1.03, (4): 2.61, (5): 4.02, (6): 6.94, (7): 12.04, (8): 14.00, (9): 14.97, (10): 17.71, (11): 19.56.

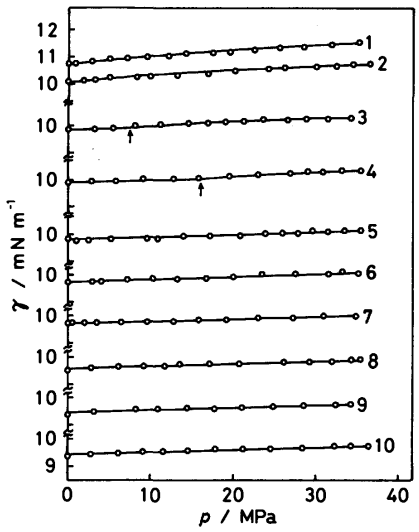

Fig. 2. Interfacial tension vs. pressure curves at constant total molality and at 298.15 K (higher concentration region). m_1=(1): 20.17 mmol kg^{-1}, (2): 21.49, (3): 22.22, (4): 22.54, (5): 23.32, (6): 25.02, (7): 27.10, (8): 30.60, (9): 35.03, (10): 40.19.

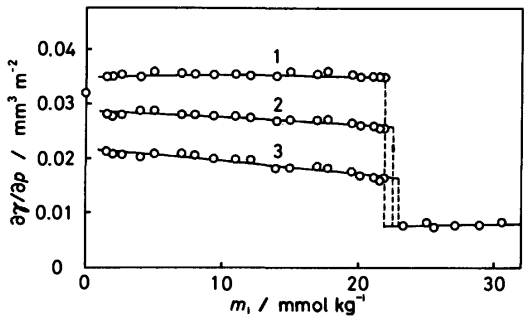

Fig. 3. Derivative of interfacial tension with respect to pressure vs. total molality curves at constant pressure and at 298.15 K. (1): 0.1 MPa, (2): 15 MPa, (3): 30 MPa.

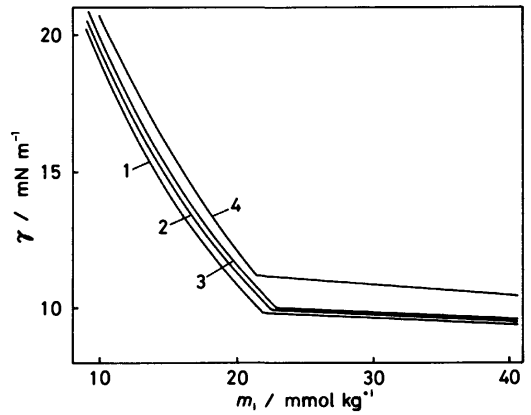

Fig. 4. Interfacial tension vs. total molality curves at constant pressure and at 298.15 K (around cmc). (1): 0.1 MPa, (2): 15 MPa, (3): 30 MPa, (4): aq DTAC/hexane, 0.1 MPa.

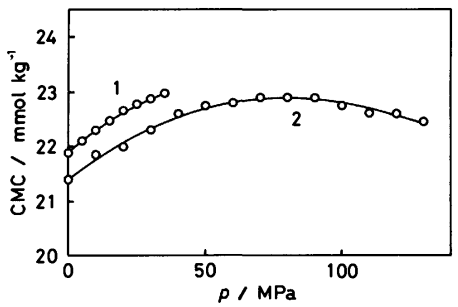

Fig. 5. Critical micelle concentration vs. pressure curves at 298.15 K. (1): aq DTAC/cyclohexane, (2): aq DTAC/hexane.

of the interfacial tension at constant pressure. In Fig. 4, the γ vs. m_1 curves, which are drawn by making use of the interpolated γ values taken from the γ vs. p curves in Figs. 1 and 2, are shown in the concentration range around the cmc. Included in this figure for comparison is the γ vs. m_1 curve of the system of aqueous DTAC solution and hexane at 0.1 MPa.[2] The γ vs. m_1 curve is observed to break at the cmc sharply enough to determine the precise value of the cmc. The dependence of the interfacial tension on pressure and concentration observed above is qualitatively similar to that made on the systems of the aqueous solutions of dodecylammonium chloride (DAC)[1] and DTAC[2] and hexane.

In Fig. 5, the cmc values obtained from the curves given in Fig. 4 and their analogs are shown as a

function of pressure and compared with those of the aqueous DTAC solution–hexane system.[2] The values of the cyclohexane system are found to be slightly different from those of the hexane system within the pressure range measured. Taking into account that the γ vs. m_1 curve of the cyclohexane system is shifted from that of the hexane system, such a difference suggests that the cyclohexane and hexane molecules take a place in the micelle formation of DTAC molecules in the aqueous solution.

According to the thermodynamic treatment developed previously,[1,3] the partial derivative of the interfacial tension with respect to pressure at constant temperature and molality shown in Fig. 3 provides the volume change per unit area associated with the adsorption of surfactant from its monomeric state, $\Delta v(1)$, at a concentration below the cmc and that from its micellar state, $\Delta v(\mathrm{M})$, at a concentration above the cmc; they are respectively defined by

$$\Delta v(1) = \Gamma_1^{\mathrm{H}}(v^{\mathrm{H}}/\Gamma_1^{\mathrm{H}} - v_1^{\mathrm{W}}) \tag{1}$$

and

$$\Delta v(\mathrm{M}) = \Gamma_1^{\mathrm{H}}(v^{\mathrm{H}}/\Gamma_1^{\mathrm{H}} - v^{\mathrm{M}}/N_1^{\mathrm{M}}), \tag{2}$$

where v^{H} is the interfacial excess volume per unit area, v^{M} the molar volume of micelle defined as the excess one with respect to the spherical dividing surface which makes the excess number of moles of water zero,[8] v_1^{W} the partial molar volume of monomeric surfactant, Γ_1^{H} the interfacial excess number of moles of surfactant per unit area, and N_1^{M} the number of surfactant ions in the micelle particle. Therefore, the curves in Fig. 3 turn out to be the $\Delta v(1)$ vs. m_1 and $\Delta v(\mathrm{M})$ vs. m_1 curves.

The values of $\Delta v(1)$ and $\Delta v(\mathrm{M})$ at the cmc, which are obtained by extrapolation, are plotted with those of the aqueous DTAC solution–hexane system[2] against pressure in Fig. 6. It is found again that the $\Delta v(\mathrm{M})$ value is independent of pressure and the $\Delta v(1)$ value depends on pressure. Further, the $\Delta v(1)$ and $\Delta v(\mathrm{M})$ values of the cyclohexane system are seen to be larger than those of hexane system. Therefore, it is possible to say that the molar interfacial excess volume of the adsorbed film at the cmc becomes slightly larger than the molar volume of micelle though their pressure dependence is similar to each other, when cyclohexane is used in place of hexane. This may be related closely to the experimental fact that the volume of interface formation of the pure water/cyclohexane interface has a larger value than that of the pure water/hexane interface.[9]

Let us now consider the volume of micelle formation $\Delta_{\mathrm{W}}^{\mathrm{M}}v$ defined by

$$\Delta_{\mathrm{W}}^{\mathrm{M}}v = v^{\mathrm{M}}/N_1^{\mathrm{M}} - v_1^{\mathrm{W}}. \tag{3}$$

The value of $\Delta_{\mathrm{W}}^{\mathrm{M}}v$ can be evaluated by use of the equation[8]

$$\Delta_{\mathrm{W}}^{\mathrm{M}}v = 2(RT/\mathrm{cmc})(\partial \mathrm{cmc}/\partial p)_T. \tag{4}$$

The $\Delta_{\mathrm{W}}^{\mathrm{M}}v$ vs. p curve obtained from the cmc vs. p curve in Fig. 5 is compared with that of the hexane system in Fig. 7. It is seen from this figure that the micelle formation in the cyclohexane system shows the volumetric behavior slightly different from that in the hexane system. Therefore, we may say that the micelle particles solubilize molecules of the oil coexisting in equilibrium with the aqueous solution.

Finally, let us examine whether the micelle particle behaves thermodynamically like a macroscopic bulk phase. Combining Eqs. 1, 2, and 3, the following equation is obtained:

$$\Delta v(1) - \Delta v(\mathrm{M}) = \Gamma_1^{\mathrm{H}}\Delta_{\mathrm{W}}^{\mathrm{M}}v. \tag{5}$$

The left side of Eq. 5 is the difference between the $\Delta v(1)$ and $\Delta v(\mathrm{M})$ values given in Fig. 6 and the right side the product of the Γ_1^{H} value, which is evaluated

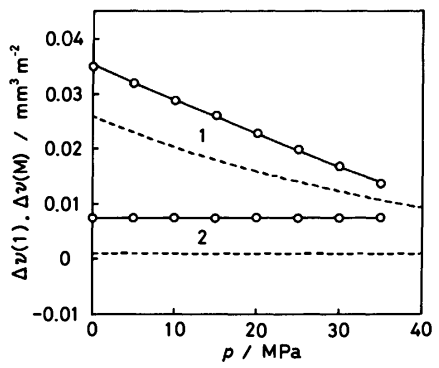

Fig. 6. Volume change associated with the adsorption from monomeric state ($\Delta v(1)$) vs. pressure and volume change associated with the adsorption from micellar state ($\Delta v(\mathrm{M})$) vs. pressure at cmc and at 298.15 K. (1): $\Delta v(1)$ vs. p, (2): $\Delta v(\mathrm{M})$ vs. p, (○): aq DTAC/cyclohexane, (— — —) aq DTAC/hexane.

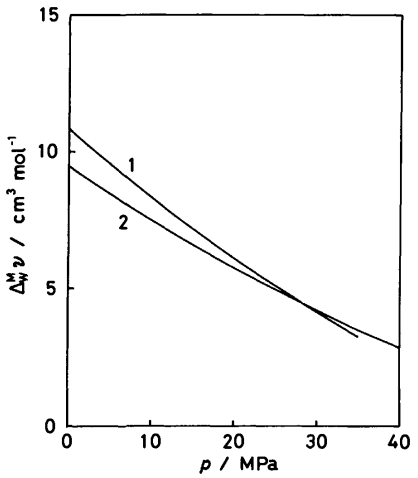

Fig. 7. Volume of micelle formation vs. pressure curves at 298.15 K. (1): aq DTAC/cyclohexane, (2): aq DTAC/hexane.

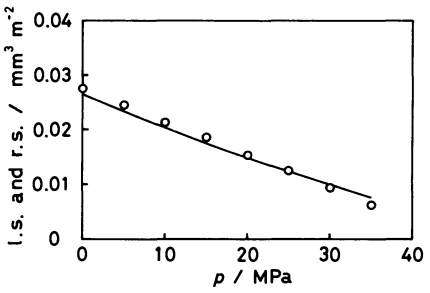

Fig. 8. Comparison between left side ($\Delta v(1)-\Delta v(M)$) and right side ($\Gamma_1^{II}\Delta_W^M v$) of Eq. 5. (○): left side, (——): right side.

from the γ vs. m_1 curve in Fig. 4, and the $\Delta_W^M v$ value given in Fig. 7; both the sides are compared in Fig. 8. They are in good agreement with each other over the entire pressure range measured. Therefore, we again arrive at the conclusion that irrespective of the phase coexisting in equilibrium with its aqueous solution, the micelle formation of surfactant can be treated thermodynamically as the appearance of a macroscopic bulk phase.[1-3,5]

References

1) M. Yamanaka, H. Iyota, M. Aratono, K. Motomura, and R. Matuura, *J. Colloid Interface Sci.*, **94**, 451 (1983).

2) M. Yamanaka, M. Aratono, K. Motomura, and R. Matuura, *Colloid Polymer Sci.*, **262**, 338 (1984).

3) K. Motomura, S. Iwanaga, M. Yamanaka, M. Aratono, and R. Matuura, *J. Colloid Interface Sci.*, **86**, 151 (1982).

4) S. J. Rehfeld, *J. Phys. Chem.*, **71**, 738 (1967).

5) M. Yamanaka, M. Aratono, H. Iyota, K. Motomura, and R. Matuura, *Bull. Chem. Soc. Jpn.*, **55**, 2744 (1982).

6) N. Matubayasi, K. Motomura, S. Kaneshina, M. Nakamura, and R. Matuura, *Bull. Chem. Soc. Jpn.*, **50**, 523 (1977).

7) H. Kashiwagi, T. Fukunaga, Y. Tanaka, H. Kubota, and T. Makita, *Rev. Phys. Chem. Jpn.*, **49**, 70 (1979).

8) K. Motomura, M. Yamanaka, and M. Aratono, *Colloid Polymer Sci.*, **262**, 948 (1984).

9) K. Motomura, H. Iyota, M. Aratono, M. Yamanaka, and R. Matuura, *J. Colloid Interface Sci.*, **93**, 264 (1983).

The Phase Transition of 1,4-Dialkyl-1,4-diazoniabicyclo[2.2.2]octane Dibromides, C_n-DABCO-C_{n+2}-Br

Kengo IMAMURA, Jun SHIMIZU, and Takashi NOGAMI*
Department of Applied Chemistry, Faculty of Engineering, Osaka University,
Yamada-oka, Suita, Osaka 565
(Received March 13, 1986)

The phase transition of 1,4-dialkyl-1,4-diazoniabicyclo[2.2.2]octane dibromide (diquaternary salt) in which the difference in the carbon numbers of the two alkyl groups is two, was studied by means of differential scanning calorimetry, infrared absorption spectroscopy, and a study of the bromide-anion conductivities. DSC measurements revealed the existence of the metastable phase. The conversion rate from the metastable phase to the stable phase was too slow to be followed. The phase transition could be explained by the free energy-temperature relation. The temperature-dependence of the infrared absorption spectra showed that the band progressions due to two different alkyl chains disappeared at the transition temperature. This shows that the *trans*-zigzag conformation in the low-temperature phase is destroyed by the conformational change of the alkyl chain at the transition temperature. The free energy-temperature relation was also confirmed by the IR spectra. Discontinuous increases in the bromide-anion conductivities were observed at the transition temperatures. The conductivity jump was explained by the voids caused by the conformational change in the alkyl chain.

There have been extensive studies of the solid–solid phase transitions of alkanes and their derivatives[1] and of alkylammonium salts.[2] Especially, IR, Raman, and wide-line NMR spectroscopy have revealed that the transition was caused by the rotation of the alkyl chain. Two types of "rotation" have been recognized: one is the rotation of the whole molecule without changing its conformation,[3] and the other, the rotation involving conformational change.[4] In the cases of alkanes and their derivatives, the rotation of a whole molecule in the solid has long been postulated for the phase transition.[5] However, nonplanar conformers have recently been found for alkanes longer than n-$C_{21}H_{44}$ by IR spectroscopy.[6] These phase transitions have attracted much attention, because they are the best models for such fundamental chemical phenomena as the melting of materials and the glass transition temperatures of polymers.

In connection with this, we have found that a series of symmetrical 1,4-dialkyl-1,4-diazoniabicyclo[2.2.2]-octane dibromides (diquaternary salts) exhibited first-order phase transitions, with a concomitant increase in the halide-anion conductivities by two to three orders of magnitude.[7,8] The temperature dependences of the IR spectra showed that the band progressions due to the *trans*-zigzag conformation of the long alkyl chains in the low-temperature phase disappeared completely at the transition temperature.[8] This shows that the conformational change in the alkyl chain occurs at every site of the methylene carbons of the alkyl chain, contrasting with the case of the phase transitions of alkanes; band progressions did not disappear even after the transition in the alkanes. Snyder et al. reported that the conformational change in n-$C_{21}H_{44}$ occurs mainly within four carbons from either end of the molecule; the *trans*-zigzag conformation is almost retained at the central part of the molecule.[9] Thus, the phase transition of the salts of 1,4-diazabicyclo[2.2.2]octane (DABCO) is peculiar case in that the *trans*-zigzag conformation is completely destroyed. Although the transition temperatures of alkanes are a few degrees below their melting points, those of the DABCO salts are more than one hundred degrees lower than the melting points or the decomposition points. Since the phase-transition temperatures and the transition enthalpies tend to increase with the increase in the alkyl-chain length in the symmetric diquaternary salts, it is noteworthy how these properties are modified in the case of the unsymmetric salts. All of the symmetric diquaternary salts exhibited one transition temperature.[7,8] Thus, it is especially interesting to determine whether or not the phase transition takes place at several temperatures, as a result of the difference in the alkyl chains in the unsymmetric diquaternary salts. The effect of the unsymmetric substitution on the halide-anion conductivities and the IR absorption spectra are also noteworthy. As an extension of the previous studies, we have investigated the phase transitions of the unsymmetric diquaternary salts of DABCO on the basis of their differential scanning calorimetry curves, bromide-anion conductivities, and

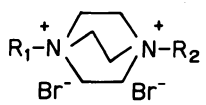

C_{10}-DABCO-C_{12}-Br :	R_1=$C_{10}H_{21}$,	R_2=$C_{12}H_{25}$
C_{11}-DABCO-C_{13}-Br :	$C_{11}H_{23}$,	$C_{13}H_{27}$
C_{12}-DABCO-C_{14}-Br :	$C_{12}H_{25}$,	$C_{14}H_{29}$
C_{13}-DABCO-C_{15}-Br :	$C_{13}H_{27}$,	$C_{15}H_{31}$
C_{14}-DABCO-C_{16}-Br :	$C_{14}H_{29}$,	$C_{16}H_{33}$
C_{15}-DABCO-C_{17}-Br :	$C_{15}H_{31}$,	$C_{17}H_{35}$
C_{16}-DABCO-C_{18}-Br :	$C_{16}H_{33}$,	$C_{18}H_{37}$

Fig. 1. 1,4-Dialkyl-1,4-diazoniabicyclo[2.2.2]octane dibromides.

infrared-absorption spectra. The materials studied possess two long alkyl chains; the difference in their carbon numbers was fixed at two. The materials studied are shown in Fig. 1. The names of the materials are abbreviated by the numbers of alkyl carbons. For example, 4-Decyl-1-aza-4-azoniabicyclo-[2.2.2]octane bromide and 1-decyl-4-dodecyl-1,4-diazoniabicyclo[2.2.2]octane dibromide are abbreviated as C_{10}-DABCO-Br and C_{10}-DABCO-C_{12}-Br respectively. Thus, the materials in Fig. 1 can be described generally as C_n-DABCO-C_{n+2}-Br.

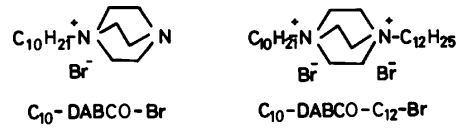

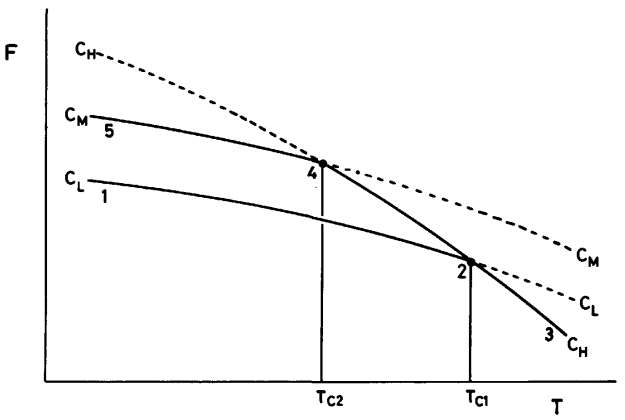

Fig. 2. Free energy (F)-temperature (T) relation of unsymmetric diquaternary salts of DABCO.

Experimental

Materials. The methyl alcohol and acetonitrile were purified as has been described before.[7,8] The ethyl acetate was washed with aqueous sodium hydrogencarbonate, and then aqueous sodium chloride, dried over magnesium sulfate, and distilled. The ethyl alcohol was distilled. The diethyl ether, DABCO, and all of the alkyl bromides were used without purification.

Syntheses of 4-Alkyl-1-aza-4-azoniabicyclo[2.2.2]octane Bromides. The synthesis of 4-alkyl-1-aza-4-azoniabicyclo-[2.2.2]octane bromide (monoquaternary salt) will be described for C_{10}-DABCO-Br as a typical example. To the acetonitrile solution (50 ml) of DABCO (5.6 g, 50 mmol) we stirred in, drop by drop, 11.05 g (50 mmol) of decyl bromide for a 30-min period, at room temperature. The solvent was then evaporated, and 500 ml of benzene was added to the residue to obtain a white precipitate. It was recrystallized from a mixed solvent of benzene (1 l) and acetonitrile (50 ml). The same procedures were adopted for the synthesis of C_{11}-DABCO-Br. In the case of C_n-DABCO-Br ($n \geqq 12$), the acetonitrile solution was directly poured into diethyl ether to obtain the crude product. It was recrystallized from ethyl acetate.

Syntheses of Unsymmetric Diquaternary Salts of DABCO. The synthesis of unsymmetric diquaternary salt of DABCO will be described for C_{10}-DABCO-C_{12}-Br as a typical example. A methanol (20 ml) solution of C_{10}-DABCO-Br (2 g, 6 mmol) and dodecyl bromide (1.49 g, 6 mmol) was refluxed for 48 h. After it had then been cooled to room temperature, it was poured into diethyl ether (500 ml) to obtain a white precipitate. The crude product was recrystallized five times from acetonitrile. Essentially the same reaction conditions were adopted for the other materials. The solvents of recrystallization were acetonitrile for C_n-DABCO-C_{n+2}-Br (n=10, 11, 12, 13, 14) and ethyl alcohol for C_n-DABCO-C_{n+2}-Br (n=15, 16).

Measurements. The measurements of the DSC, the IR absorption spectra, and the bromide-anion conductivities were made by the methods described previously.[7,8]

Results and Discussion

Syntheses of Unsymmetric Diquaternary Salts of DABCO. Unsymmetric diquaternary salts of DABCO were synthesized by two-step reactions, i.e., the synthesis of monoquaternary salt, followed by that of the diquaternary salt. In the first step, the reaction of equimolar amounts of DABCO and alkyl bromide readily gave the monoquaternary salt in 30 min at room temperature. Diquaternary salt was not obtained in this case, however, because the reaction rate from the monoquaternary salt to the diquaternary salt is much slower than that from DABCO to the monoquaternary salt. The diquaternary salt was obtained by the reaction with the monoquaternary salt with alkyl bromide under more vigorous reaction conditions in the second step. Since one nitrogen converts to N^+ in the monoquaternary salt, the lone-pair electron at the other nitrogen will be attracted by N^+ by means of Through-bond interaction.[10] This effect causes the lowering of the lone-pair MO level and the decrease in the lone-pair electron density, both of which consequently reduce the rate of the second step of the reaction. MINDO/2 calculation[11] revealed that the former effect is dominant over the latter.[12] In reality, the monoquaternary salt and alkyl bromide did not give the diquaternary salt under the same conditions as in the first step of the reaction. Only after the solution of the reactants had been refluxed for a prolonged period of time (48 h) could the diquaternary salt be obtained.

DSC Measurements. DSC measurements were made while changing the temperature by 5 °C/min. When the virgin samples were heated, single endothermic signals ($\Delta H_{en,1}$) were observed at T_{c1}. However, no reproducible T_{c1} values were obtained; they varied by several degrees in several runs. C_{12}-DABCO-C_{14}-Br and C_{16}-DABCO-C_{18}-Br exhibited three and two transitions respectively. When the samples were

Table 1. Unsymmetric Diquaternary Salts of DABCO, Transition Temperatures (T_{c1} and T_{c2}), Transition Enthalpies ($\Delta H_{en,2}$), Transition Entropies (ΔS), and Ratios of Bromide-anion Conductivities Before (σ_l) and After (σ_h) Transition

Materials	T_{c1}[a] / °C	T_{c2} / °C	$\Delta H_{en,2}$ / kJ mol^{-1}	ΔS / J mol^{-1} deg^{-1}	σ_h/σ_l
C_{10}-DABCO-C_{12}-Br	(92)	46	46.9	128	770
C_{11}-DABCO-C_{13}-Br	(95)	60	57.3	173	2170
C_{12}-DABCO-C_{14}-Br	(93, 95, 99)	64	56.8	169	700
C_{13}-DABCO-C_{15}-Br	(96)	74	69.0	199	2070
C_{14}-DABCO-C_{16}-Br	(101)	74	71.6	206	1290
C_{15}-DABCO-C_{17}-Br	(102)	79	86.7	246	3000
C_{16}-DABCO-C_{18}-Br	(90, 103)	84	88.8	249	3070

a) Since the values of T_{c1}'s are not strictly reproducible, they are shown in parentheses as only approximate values.

cooled after they had once been heated above T_{c1}, exothermic signals ($\Delta H_{exo,1}$) were observed at much lower temperatures (T_{c2}) than T_{c1}; $T_{c1}>T_{c2}$. Reproducible T_{c2}'s were obtained. The succeeding heating-cooling cycles showed reproducible endothermic ($\Delta H_{en,2}$) and exothermic ($\Delta H_{exo,1}$) signals at around T_{c2}, but did not show any signal at T_{c1}, even when DSC was measured after the samples had been kept at room temperature for weeks. The absolute values of $\Delta H_{en,1}$, $\Delta H_{en,2}$, and $\Delta H_{exo,1}$ were within the range of experimental error. The annealed sample which gives the phase transition at T_{c2} is designated as C_M; it is assumed to be a metastable phase[13] on the basis of our related studies of the phase transition of C_{10}-DABCO-C_n-Br ($13 \leqq n \leqq 22$).[14] For these systems, DSC measurements exhibited phenomena similar to those described above. However, C_M was found to be converted slowly to the stable phase (C_L) when the sample was kept at room temperature. The larger the difference in the carbon numbers of the two alkyl groups attached to DABCO nitrogens, the faster was the conversion rate from C_M to C_L. For example, the conversion rates of C_{10}-DABCO-C_{14}-Br and C_{10}-DABCO-C_{18}-Br were one week and one day respectively. Since the difference in the carbon numbers is only two in the present systems, the conversion rates are too slow to be followed. The above thermodynamic phenomena can be understood by the free energy (F)-temperature (T) relation shown in Fig. 2. In this figure, the virgin sample (C_L) follows the F-T curve from 1 to 2 when the sample is heated. Phase transition takes place at 2 (temperature: T_{c1}), and the sample follows the curve of the high-temperature phase (C_H) from 2 to 3. When the sample is then cooled, it follows the F-T curve of C_H from 3 through 2 to 4. Phase transition takes place at 4 (temperature: T_{c2}), and the sample follows the F-T curve of the metastable phase (C_M) from 4 to 5.

Part of Table 1 shows T_{c1}, T_{c2}, $\Delta H_{en,2}$, and ΔS ($=\Delta H_{en,2}/T_{c2}$). The values of T_{c1} are shown in parentheses, because they are not strictly reproducible.

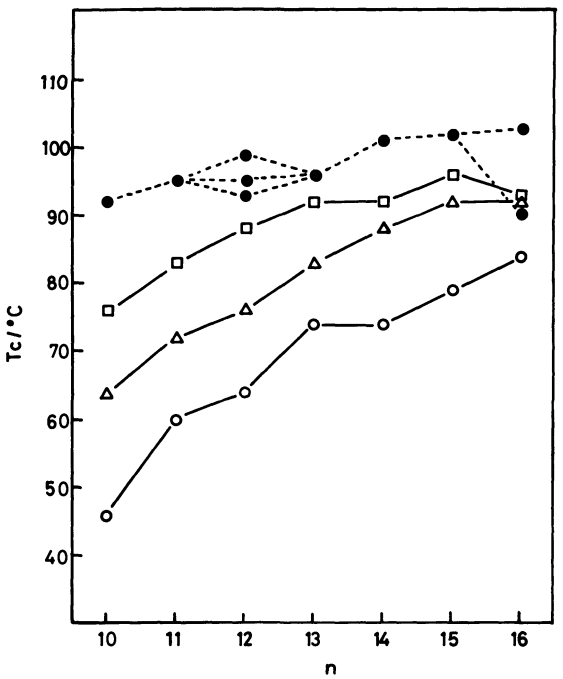

Fig. 3. The plot of the transition temperatures against the carbon numbers of alkyl groups attached to DABCO nitrogens.
○: T_{c2} for C_n-DABCO-C_{n+2}-Br, △: T_c for C_n-DABCO-C_n-Br, □: T_c for C_{n+2}-DABCO-C_{n+2}-Br, ●: T_{c1} for C_n-DABCO-C_{n+2}-Br. Since T_{c1} is not strictly reproducible, the black circles were connected with dotted lines.

They are shown only as approximate values. All of the transition temperatures were obtained from the onsets of the endothermic peaks. The characteristic points of the DSC measurements will be discussed below. Figure 3 plots the T_{c1} and T_{c2} values against the carbon numbers of the alkyl chains. This figure also shows the plots of the transition temperatures of the symmetric diquaternary salts of DABCO[8] for the sake of comparison. All of the transition temperatures tend to increase with the increase in the alkyl-chain lengths. The order of the transition temperature is as

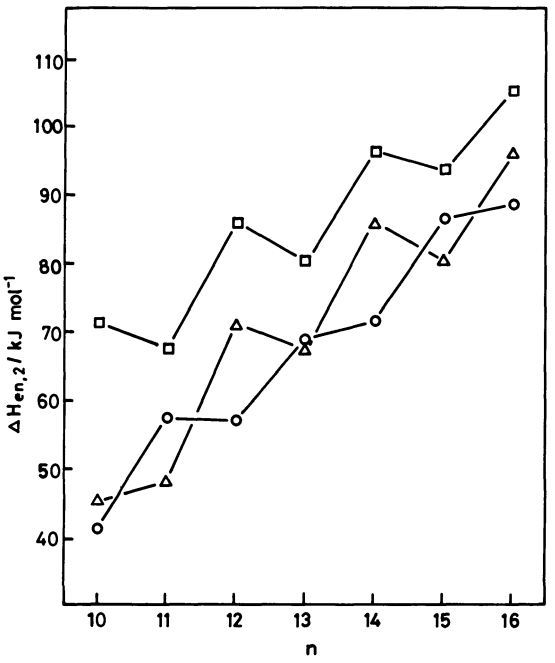

Fig. 4. The plot of the transition enthalpies ($\Delta H_{en,2}$) against the carbon numbers of alkyl groups attached to DABCO nitrogens.
○: C_n–DABCO–C_{n+2}–Br, △: C_n–DABCO–C_n–Br, □: C_{n+2}–DABCO–C_{n+2}–Br.

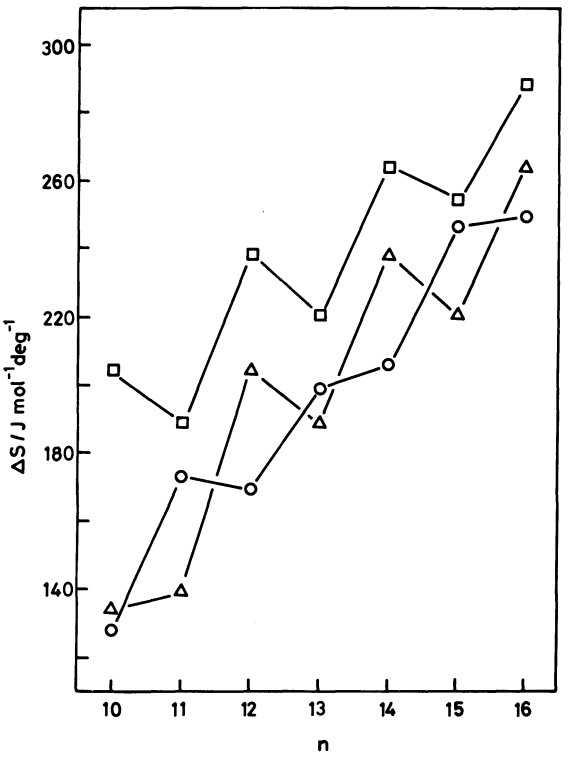

Fig. 5. The plot of the transition entropies ΔS (= $\Delta H_{en,2}/T_{c2}$) against the carbon numbers of alkyl groups attached to DABCO nitrogens.
○: C_n–DABCO–C_{n+2}–Br, △: C_n–DABCO–C_n–Br, □: C_{n+2}–DABCO–C_{n+2}–Br.

follows, if the carbon number of the alkyl group is fixed: $T_{c1}>T_c$ for C_{n+2}–DABCO–C_{n+2}–Br$>T_c$ for C_n–DABCO–C_n–Br$>T_{c2}$. An even-odd number effect of carbon was found for T_{c2}. The difference between T_{c1} and T_{c2} tends to decrease with the increase in the alkyl-chain length, but it is always in the range of 6—50 °C. Since the difference in the alkyl-chain length is only two, the general tendency of the transition temperature with the alkyl-chain length is similar to that of the symmetric diquaternary salts. The great difference in the unsymmetric salts from the symmetric salts is that the metastable phase can be found for the former salts. Figure 4 shows the plots of $\Delta H_{en,2}$ against the carbon numbers of the alkyl chains. This figure also shows the transition enthalpies of the symmetric salts[8] for the sake of comparison. An even-odd number effect of carbon was clearly observed in a reverse manner from the symmetric salts, i.e., up-down for the unsymmetric salts and down-up for the symmetric salts. $\Delta H_{en,2}$ tends to increase with the increase in the alkyl-chain length. The following order of the transition enthalpy is noteworthy, although the reason is as yet not clear; ΔH for C_{2n+2}–DABCO–C_{2n+2}–Br$>\Delta H$ for C_{2n}–DABCO–C_{2n}–Br$>\Delta H$ for C_{2n}–DABCO–C_{2n+2}–Br. ΔH for C_{2n+1}–DABCO–C_{2n+1}–Br$>\Delta H$ for C_{2n-1}–DABCO–C_{2n+1}–Br$>\Delta H$ for C_{2n-1}–DABCO–C_{2n-1}–Br. Figure 5 shows the plots of the transition entropies ($\Delta S=\Delta H_{en,2}/T_{c2}$) against the carbon numbers of the alkyl groups. This figure also shows the plot of the transition entropies of the symmetric salts for the sake of comparison.[15] The ΔS's also tend to increase with the increase in the alkyl-chain lengths. The even-odd number effect of carbon on ΔS was quite similar to that on the $\Delta H_{en,2}$ shown in Fig. 4. The transition entropies also exhibited order similar to that found for $\Delta H_{en,2}$; i.e., ΔS for C_{2n+2}–DABCO–C_{2n+2}–Br$>\Delta S$ for C_{2n}–DABCO–C_{2n}–Br$>\Delta S$ for C_{2n}–DABCO–C_{2n+2}–Br. ΔS for C_{2n+1}–DABCO–C_{2n+1}–Br$>\Delta S$ for C_{2n-1}–DABCO–C_{2n+1}–Br$>\Delta S$ for C_{2n-1}–DABCO–C_{2n-1}–Br. The numbers of sites (W) after phase transition were estimated from the $\Delta S=R\ln W$ relation, and the W's were in the range of 4.9×10^6—9.8×10^{12}.[16] Although T_{c1} could not be obtained correctly, the estimated transition entropies gave the values of W as 10^6—10^{12}. Thus, comparable structural changes seem to occur at T_{c1} and T_{c2}. The large values of W's will be discussed later, together with the IR absorption spectra.

Infrared Absorption Spectroscopy. The temperature dependence of the infrared absorption spectra was measured in order to obtain more information on the phase transition and on the metastable phase. Figure 6 shows the temperature dependence of the IR spectra of C_{14}–DABCO–C_{16}–Br for a KBr disk sample, as a typical example, when the sample is heated from room temperature to 103 °C and then cooled to room

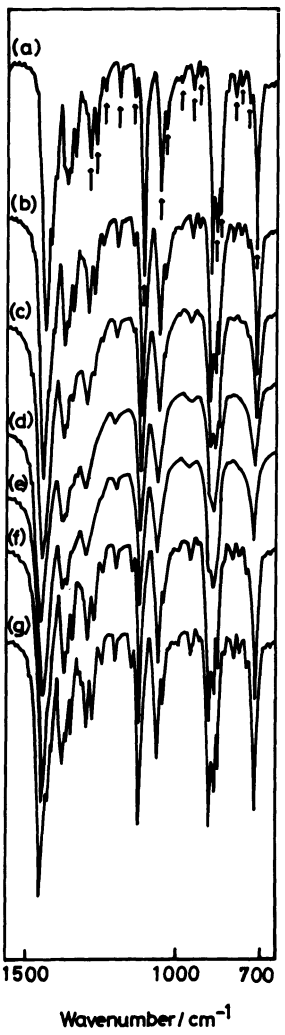

Fig. 6. Temperature dependence of the IR spectra of C_{14}–DABCO–C_{16}–Br for the KBr pellet sample.
(a): 29 °C, (b): 79 °C, (c): 98 °C, (d): 103 °C, (e): 80 °C, (f): 61 °C, (g): 33 °C. The virgin sample was heated from (a) to (d), and then cooled from (d) to (g).

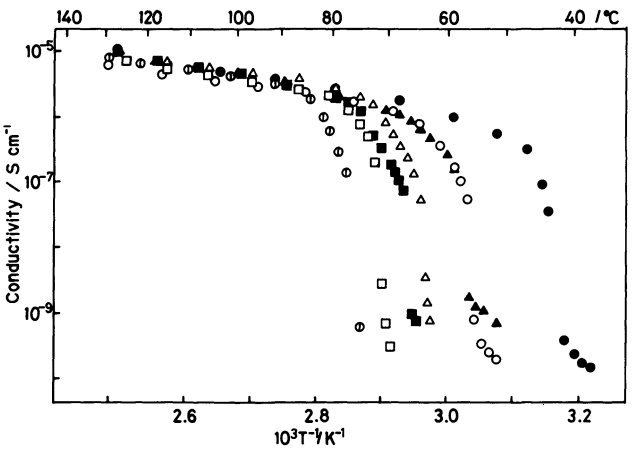

Fig. 7. Temperature dependence of the bromide-anion conductivities of C_n–DABCO–C_{n+2}–Br.
●: $n=10$, ○: $n=11$, ▲: $n=12$, △: $n=13$, ■: $n=14$, □: $n=15$, ⓓ: $n=16$.

temperature. The resulting IR spectra are shown sequentially from the top to the bottom in this figure. The IR spectra of the virgin sample (C_L) at 29 °C exhibited several structures, shown by the arrows. The absorption positions of these structures were compared with band progressions of n-$C_{15}H_{32}$ and n-$C_{17}H_{36}$,[17] which have the same numbers of CH_2 units as the alkyl groups of C_{14}–DABCO–C_{16}–Br. The good coincidence[18] leads to the conclusion that the structures in Fig. 6 can be assigned to the band progressions of the two alkyl groups.

The absorption spectra at 29 °C (a) and 79 °C (b) were not so different. When the temperature of the sample approached T_{c1} (101 °C), all of the absorptions were broadened (see Spectrum (c) at 98 °C), but the band progressions could still be seen. However, all of the band progressions disappeared at 103 °C (d). This shows that the *trans*-zigzag conformation of the alkyl groups of the low-temperature phase (C_L) is destroyed at T_{c1}. When the temperature of the sample was lowered after it had once been raised above T_{c1}, the band progression did not appear between T_{c1} and T_{c2}. For example, the absorption spectra (b) and (e) were measured at almost the same temperature, but they are quite different; the Spectrum (b) exhibited the band progressions, but (e) did not show them. This observation is consistent with the DSC result. Since the Spectrum (e) corresponds to the point between 2 and 4 on the F–T curve of the C_H phase in Fig. 2, the *trans*-zigzag conformation of the alkyl chain is still destroyed. Only after the temperature had been lowered below T_{c2} (74 °C) did the band progressions appear again (see Spectrum (f)) to convert to the C_M phase. Since no difference in the spectra was found between (a) and (g) in Fig. 6, the *trans*-zigzag conformation is assumed to be recovered in the C_M phase. However, judging from the broader powdered X-ray diffractions of the C_M phase than the C_L phase,[13] the crystallinity of the C_M phase can be said to be lower than the C_L phase. The high potential barrier between C_M and C_L prevents C_M from going back to C_L.

DSC measurements gave a large numbers of sites (W) above the transition temperature. This is consistent with the results of the IR absorption spectra. Since band progressions disappeared completely above T_{c1} or T_{c2}, the conformational change is assumed to occur at every site of the alkyl carbons. This gives rise to a large numbers of sites. Thus, the conformational changes in the present systems and previous systems[8] are quite different from those in *normal* alkanes,[9] because the *trans*-zigzag conformation still remains above the transition temperature for

the latter materials. Although the phase transitions of the diquaternary DABCO salts were ascribed to the conformational change in the alkyl groups, there is some possibility that the portion of DABCO may rotate around the N–N direction.[19] However, the present study could not confirm this possibility.

Bromide-anion Conductivities. All of the samples have already been confirmed as bromide-anion conductors.[7,8] The ionic conductivities were measured for the compressed pellet samples by an AC method. The impedance and a phase shift were measured, and the real and imaginary parts of the impedances were plotted for various frequencies (25 Hz—500 kHz). The resistance of the sample was obtained by a method described previously.[8] The temperature dependences of the bromide-anion conductivities were measured while raising the temperature of the sample slowly (about 0.5 °C min^{-1}) from room temperature; they are shown in Fig. 7. Conductivities less than 10^{-9} S cm^{-1} are below the limit of our measurements. Since the samples were dried overnight under a dynamic vacuum above T_{c1} before the measurements, they were converted to C_M phases. The proton conduction due to moisture was negligible. The following facts are noteworthy from this figure: (1) All of the samples show abrupt increases in the ionic conductivities by two to three orders of magnitude resulting from the phase transitions around T_{c2}. (2) The longer the alkyl chain, the higher the transition temperature. (3) The longer the alkyl chain, the lower the bromide-anion conductivities below T_{c2}. However, the bromide-anion conductivities were close to each other above T_{c2}, with their activation energies of about 30 kJ mol^{-1}.

The second and third characteristics above are also those of the halide-anion conductivities of the symmetric diquaternary salts of DABCO, and they may be explained as before.[8] Table 1 shows the materials and the ratios of the bromide-anion conductivities before (σ_l) and after (σ_h) the phase transition, i.e., σ_h/σ_l. The two steps of the conductivity changes were observed around T_{c2}; the first rapid increase, followed by the slower increase in the conductivities. The changes in the conductivities around T_{c2} were found to be in the range of 770—3070. However, the conductivity jumps in Fig. 7 are slightly broader than those of the symmetric diquaternary salts,[8] because the slower increases in the conductivities were not observed for the latter materials. The virgin samples (C_L) can also be expected to show an abrupt change in the ionic conductivities at T_{c1}. However, no measurement was made for this transition, because DSC measurements did not give reproducible results. Although abrupt increases in the bromide-anion conductivities were observed around T_{c2}, the transition temperatures obtained by DSC were higher than those obtained by the bromide-anion conductivities; the latter transition temperatures were defined as the middle points of the conductivity jumps. This shows that the conductivity jump starts before the considerable structural change sets in. Since ionic conductivities are sensitive to the structure, the conductivity jump takes place at the temperature region of the pre-transition where the local movement of the alkyl groups begins. Since the low-temperature phase possesses a close-packed crystal structure, the conduction pathway of the bromide anion is assumed to be narrow. However, the situation changes considerably at the transition temperature. The conductivity jump can be explained by the formation of voids caused by the onset of the movement of the alkyl chains.

Summary. The phase transitions of the unsymmetric diquaternary salts of DABCO, C_n–DABCO–C_{n+2}–Br ($10 \leqq n \leqq 16$), were studied by means of the DSC, the IR spectra, and the bromide-anion conductivities. The DSC measurements revealed the existence of the metastable phase. The temperature dependence of the IR spectra showed that, with a rise in the temperature, the band progressions in the low-temperature phase disappeared completely at T_{c1} and then appeared again at T_{c2} when the temperature was lowered after it had once been raised above T_{c1}. These results are consistent with the existence of the metastable phase. Abrupt increases in the bromide-anion conductivities by two to three orders of magnitude were found at the transition temperatures (T_{c2}). However, the conductivity jumps were slightly broader than those of the symmetric diquaternary salts. The conductivity jump at the transition temperature was explained by the formation of voids caused by the onset of the conformational change in the alkyl chains.

We are grateful to Professor Shigekazu Kusabayashi and Dr. Shunsuke Takenaka, Faculty of Engineering, Osaka University, for the use of the DSC apparatus. We are also grateful to Dr. Yasuhiko Kondo, Faculty of Engineering, Osaka University, for his suggestion that the rate difference in the quaternization reaction of DABCO may be explained by the Through-bond interaction.

References

1) M. G. Taylor, E. C. Kelusky, C. P. Smith, H. L. Casal, and D. G. Cameron, *J. Chem. Phys.*, **78**, 5108 (1983).
2) H. Ishida, R. Ikeda, and D. Nakamura, *Bull. Chem. Soc. Jpn.*, **59**, 915 (1986).
3) D. W. McClure, *J. Chem. Phys.*, **49**, 1830 (1968).
4) M. Maroncelli, S. P. Qi, H. L. Strauss, and R. G. Snyder, *J. Am. Chem. Soc.*, **104**, 6237 (1982).
5) T. Ishinabe, *J. Chem. Phys.*, **72**, 353 (1980).
6) R. G. Snyder, M. Maroncelli, S. P. Qi, and H. L. Strauss, *Science*, **214**, 188 (1981).
7) J. Shimizu, T. Nogami, and H. Mikawa, *Solid State Commun.*, **54**, 1009 (1985).
8) J. Shimizu, K. Imamura, T. Nogami, and H. Mikawa,

Bull. Chem. Soc. Jpn., **59**, 1443 (1986).

9) R. G. Snyder, M. Maroncelli, H. L. Strauss, C. A. Ellinger, D. G. Cameron, H. L. Casal, and H. H. Mantsch, *J. Am. Chem. Soc.*, **105**, 133 (1983).

10) R. Hoffmann, *Acc. Chem. Res.*, **4**, 1 (1971).

11) M. J. S. Dewar and E. Haselbach, *J. Am. Chem. Soc.*, **92**, 590 (1970); N. Bodor, M. J. S. Dewar, A. Harget, and E. Haselbach, *J. Am. Chem. Soc.*, **92**, 3854 (1970).

12) MINDO/2 calculation was done for DABCO and the 4-methyl-1-aza-4-azoniabicyclo[2.2.2]octane cation (CH_3-DABCO$^+$) in order to see the quaternization effect on the lone-pair electron density of nitrogen and the orbital energy of the HOMO level. The nitrogen lone-pair electron densities of DABCO and CH_3-DABCO$^+$ are calculated to be 1.75 and 1.72 respectively; those values are not very different. Since the contribution of the nitrogen lone-pair is the largest for HOMO, the large difference in the HOMO levels ($\varepsilon_{DABCO}=-7.76$ eV, $\varepsilon_{CH_3\text{-}DABCO^+}=-13.31$ eV) is assumed to cause the large difference in the activation energy of the quaternization reaction.

13) Powdered X-ray diffractions of the virgin samples (C_L) showed several sharp diffractions. On the other hand, the annealed sample (C_M) exhibited somewhat broader diffractions. This suggests that C_M is disordered, possibly by the *gauche* conformation of the alkyl groups. This fact also supports the assumption that C_M is in a metastable phase.

14) J. Shimizu, K. Imamura, T. Nogami, and H. Mikawa, *Bull. Chem. Soc. Jpn.*, in press.

15) From the transition enthalpies and the transition temperatures shown in Ref. 8, the transition entropies (J mol^{-1} deg^{-1}) of the symmetric salts (C_n-DABCO-C_n-Br) were obtained as follows: 134 for n=10, 139 for n=11, 204 for n=12, 189 for n=13, 237 for n=14, 220 for n=15, 263 for n=16, 254 for n=17, 288 for n=18, and 311 for n=22.

16) The numbers of sites of the symmetric diquaternary salts of DABCO were estimated from the transition entropies shown in Ref. 15; they are in the range of 1.0×10^7—1.9×10^{16}.

17) R. G. Snyder and J. H. Schachtschneider, *Spectrochim. Acta*, **19**, 85 (1963).

18) Since the difference between the carbon numbers of the two alkyl groups is only two, the band progressions of the two alkyl groups have almost the same absorption positions. Thus, we could not assign the band progressions separately to the individual alkyl group.

19) We are grateful to Professor Hiroshi Suga, Department of Chemistry, Faculty of Science, Osaka University, who suggested that the portion of DABCO may rotate above the transition temperature.

 © 1986 The Chemical Society of Japan Bull. Chem. Soc. Jpn., 59, 2707—2710 (1986)

The Crystal and Molecular Structure of Diphenyl-2-pyridylmethyl Methacrylate

Hiroyuki KAGEYAMA,†† Kunio MIKI, Nobutami KASAI,* Haruhiko MOHRI,†
Yoshio OKAMOTO,† and Koichi HATADA†
Department of Applied Chemistry, Faculty of Engineering, Osaka University,
Yamadaoka, Suita, Osaka 565
†Department of Chemistry, Faculty of Engineering Science, Osaka University,
Machikaneyama, Toyonaka, Osaka 560
(Received March 31, 1986)

The molecular structure of diphenyl-2-pyridylmethyl methacrylate has been determined by means of X-ray diffraction. Crystals are monoclinic, space group $P2_1/n$, a=10.334(2), b=22.093(3), c=8.415(1) Å, β=110.92(2)°, and Z=4. The structure was established by the direct method, and refined by the block-diagonal least-squares procedure to R=0.052 (R_w=0.064) for 1702 observed reflections. The molecule has an *antiperiplanar-synperiplanar* conformation. One of the two phenyl groups attached to the C(5) atom is *trans*, and the other phenyl and 2-pyridyl groups are *gauche* to the C(1).

Recently, in a series of studies on the molecular structures of methacrylates and their reactivties in the asymmetric selective polymerization with Grignard reagnt-(−)-sparteine derivatives, molecular structures of (*RS*)-1,2-diphenylethyl methacrylate (1,2-DPEMA),[1] (*RS*)-α-*t*-butylbenzyl methacrylate (*t*-BBMA),[1] (*RS*)-1,2,2,2-tetraphenylethyl methacrylate(TrBzMA),[2] and (1*S*,2*R*)-(+)-1-benzyl-3-dimethylamino-2-methyl-1-phenylpropyl methacrylate (ChMA)[2] have been determined by means of X-ray diffraction. In addition, in order to clarify the role of the α-substituents on the ester group in the sterospecific polymerization of diphenylmethyl methacrylate derivatives with *n*-BuLi, molecular structures of diphenylmethyl methacrylate (DPMMA),[3] 1,1-diphenylethyl methacrylate (1,1-DPEMA),[4] and triphenylmethyl methacrylate (TrMA)[4] have been determined. This paper describes the structural study on diphenyl-2-pyridylmethyl methacrylate (2-PyMA), a new diphenylmethyl methacrylate derivative, which gave a highly isotactic polymer not only by anionic polymerization but also by radical polymerization.[5]

Experimental

Colorless crystals of 2-PyMA were recrystallized from toluene. Unit-cell parameters and reflection intensities were measured on a Rigaku automated, four-circle diffractometer. Nickel-filterd Cu $K\alpha$ radiation was used.

Crystal Data. 2-PyMA, $C_{22}H_{19}O_2N$, M 329.4, monoclinic, space group $P2_1/n$, a=10.334(2), b=22.093(3), c=8.415(1) Å, β=110.92(2)° V=1794.6(4) Å^3, D_c=1.219 g cm^{-3} for Z=4, μ(Cu $K\alpha$)=6.27 cm^{-1}.

Integrated intensities were measured by the θ-2θ scan technique(2θ<110°). The 2θ scan rate and scan width were 4° min^{-1} and $\Delta 2\theta$=(2.0+0.3 tanθ)°, respectively. Backgrounds were counted for 7.5 s before and after each scan. Four standard reflections were measured after every 60 reflections, which showed no intensity decrease during the intensity measurement. The usual Lorentz and polarization corrections were applied but no correction for absorption and extinction was carried out. A total of 1702 reflections was collected($|F_o|>3\sigma(F_o)$).

Structure Solution and Refinement

The structure was solved by the direct method (*MULTAN* 78),[6] and refined by the block-diagonal least-squares procedure (*HBLS* V)[7] minimizing $\Sigma w(\Delta F)^2$. Anisotropic temperature factors were applied for nonhydrogen atoms and isotropic ones for hydrogen atoms. Atomic scattering factors were taken from

Table 1. Final Atomic Coordinates of Non-hydrogen Atoms and the Equivalent Isotropic Temperature Factors[9] with Estimated Standard Deviations in Parentheses

Atom	x	y	z	B_{eq}/Å^2
O (1)	0.2219 (3)	0.18044 (10)	−0.2049 (3)	4.08
O (2)	0.4432 (3)	0.15879 (12)	−0.1719 (4)	5.78
N	0.1749 (3)	0.01633 (12)	−0.2427 (4)	4.04
C (1)	0.3492 (4)	0.19408 (16)	−0.2043 (5)	4.29
C (2)	0.3569 (4)	0.25932 (16)	−0.2484 (5)	5.02
C (3)	0.2447 (5)	0.29643 (18)	−0.2813 (7)	7.07
C (4)	0.4873 (5)	0.2777 (3)	−0.2574 (7)	7.70
C (5)	0.1953 (4)	0.12056 (13)	−0.1496 (4)	3.42
C (6)	0.2993 (4)	0.10999 (15)	0.0320 (4)	3.80
C (7)	0.3089 (4)	0.15542 (18)	0.1511 (5)	5.29
C (8)	0.4030 (5)	0.1492 (3)	0.3178 (6)	6.83
C (9)	0.4841 (5)	0.0984 (3)	0.3646 (6)	7.43
C (10)	0.4732 (5)	0.0533 (3)	0.2489 (6)	6.58
C (11)	0.3826 (4)	0.05925 (18)	0.0823 (5)	4.95
C (12)	0.0473 (4)	0.12515 (14)	−0.1502 (4)	3.33
C (13)	−0.0472 (4)	0.16640 (15)	−0.2534 (5)	4.64
C (14)	−0.1824 (4)	0.16648 (16)	−0.2577 (6)	5.29
C (15)	−0.2269 (4)	0.12622 (17)	−0.1640 (5)	4.89
C (16)	−0.1339 (4)	0.08434 (16)	−0.0633 (5)	4.38
C (17)	0.0017 (4)	0.08428 (15)	−0.0564 (4)	3.84
C (18)	0.1945 (3)	0.07344 (14)	−0.2826 (4)	3.30
C (19)	0.2001 (4)	0.08826 (17)	−0.4399 (5)	4.58
C (20)	0.1897 (4)	0.0426 (2)	−0.5566 (5)	5.58
C (21)	0.1721 (4)	−0.01570 (18)	−0.5149 (5)	5.14
C (22)	0.1648 (4)	−0.02717 (15)	−0.3579 (5)	4.66

†† Present address: Government Industrial Research Institute, Osaka Agency of Indutrial Science and Technology, Midorigaoka, Ikeda, Osaka 563, Japan

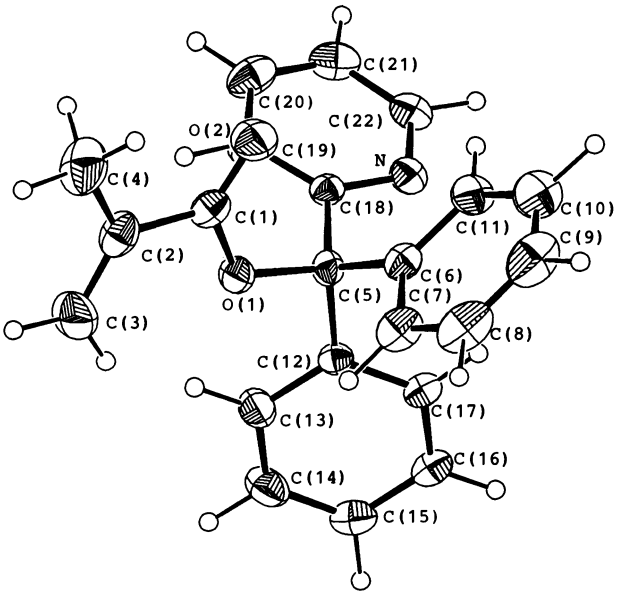

Fig. 1. A perspective view[10] of the 2-PyMA molecule with the atom labelling.
Non-hydrogen atoms are represented as thermal ellipsoids with 30% probability level, hydrogen atoms as spheres with $B=1.0$ Å^2.

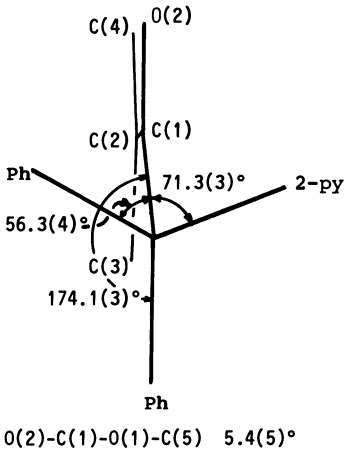

O(2)-C(1)-O(1)-C(5) 5.4(5)°

Fig. 2. Conformation about the C(5)–O(1) bond.

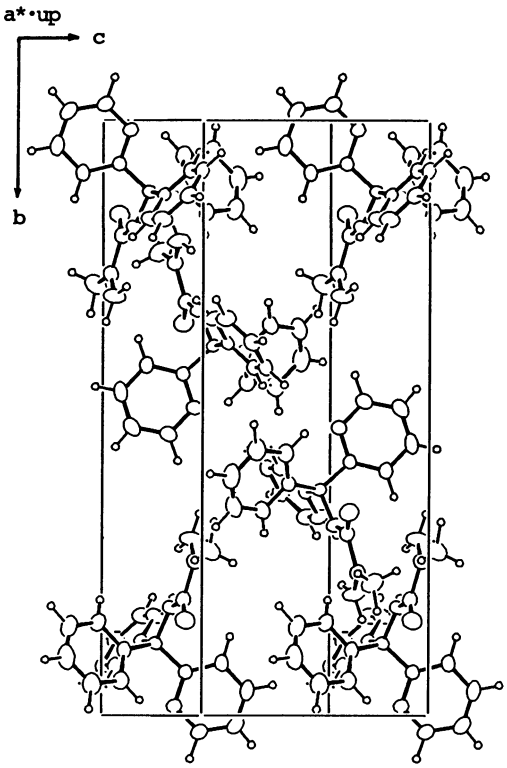

Fig. 3. Crystal structure projected along the a* axis.[10]

International Tables for X-Ray Crystallography.[8] Finally, the R value converged to 0.053 (R_w=0.064). The weighting scheme used at the final stage was $w=\{\sigma^2(F_o)-0.00438\,|F_o|+0.00170|F_o|^2\}^{-1}$ for $|F_o|>0$. σ is the standard deviation obtained by the counting statistics.

The final atomic parameters and equivalent temperature factors are given in Table 1.††† All computations were done on an ACOS 850 computer at the Crystallographic Research Center, Institute for Protein Research, Osaka University.

Results and Discussion

Molecular Structure. Figure 1 shows a perspective view[10] of 2-PyMA molecule with the atom labelling. Selected bond lengths and bond angles are given in Table 2, and some least-squares planes and dihedral angles in Table 3.

This molecule has an *antiperiplanar-synperiplanar (ap-sp)* structure: the conformation of the C(2)=C(3) [1.366(7) Å] and C(1)=O(2) [1.199(5) Å] double bonds about the C(1)-C(2) [1.498(5) Å] is *ap* and that of the C(1)=O(2) and the C(5)-O(1) ester bond [1.461(4) Å] about the C(1)-O(1) is *sp*, which is different from those of α-substituted diphenylmethyl methacrylates, 1,1-DPEMA and TrMA but similar to DPMMA. However, TrMA and 2-PyMA act similarly in the stereospecific polymerization; both monomers afford almost 100% isotactic polymers in the anionic polymerization, and even radical polymerization produce the isotactic polymers.[5,11] Therefore, the conformation of the C(2)=C(3) and C(1)=O(2) of the methacrylates in the solid state may not be important for the stereospecific polymerization. In solution both monomers likely take the same conformation considering from the results by ^{1}H NMR study with a shift reagent.[12]

The methacryloyl residue is planar within 0.04 Å (Plane 1), and the dihedral angle between the plane defined by the C(1), C(2), C(3), and C(4) atoms (Plane 2) and that made by the C(1), C(2), O(1), and O(2) (Plane 3) is only 1.7(2)°. Two benzene and a pyridine

††† Tables of anisotropic temperature factors, coordinates of hydrogen atoms, and the observed and calculated structure factors are kept at the Chemical Society of Japan, Document No. 8641.

Table 2. Selected Bond Lengths and Bond Angles with Estimated Standard Deviations in Parentheses

Bond lengths[l/Å]			
O (1) - C (1)	1.348 (4)	O (1) - C (5)	1.461 (4)
O (2) - C (1)	1.199 (5)	C (1) - C (2)	1.498 (5)
C (2) - C (3)	1.366 (7)	C (2) - C (4)	1.435 (7)
C (5) - C (6)	1.540 (5)	C (5) - C (12)	1.531 (4)
C (6) - C (7)	1.397 (5)	C (12) - C (13)	1.391 (5)
C (6) - C (11)	1.384 (5)	C (12) - C (17)	1.388 (5)
C (7) - C (8)	1.400 (6)	C (13) - C (14)	1.385 (6)
C (8) - C (9)	1.372 (7)	C (14) - C (15)	1.373 (6)
C (9) - C (10)	1.368 (7)	C (15) - C (16)	1.384 (6)
C (10) - C (11)	1.386 (6)	C (16) - C (17)	1.381 (5)
C (5) - C (18)	1.527 (4)	C (18) - C (19)	1.385 (5)
C (18) - N	1.339 (4)	C (19) - C (20)	1.385 (6)
C (22) - N	1.343 (5)	C (20) - C (21)	1.364 (6)
		C (21) - C (22)	1.373 (5)
Bond angles [ϕ/°]			
C (1) - O (1) - C (5)	119.7 (3)	O (1) - C (1) - O (2)	124.5 (4)
O (1) - C (1) - C (2)	110.7 (3)	O (2) - C (1) - C (2)	124.9 (4)
C (1) - C (2) - C (3)	120.8 (4)	C (1) - C (2) - C (4)	114.8 (4)
C (3) - C (2) - C (4)	124.4 (5)	O (1) - C (5) - C (6)	108.0 (3)
O (1) - C (5) - C (12)	103.9 (3)	O (1) - C (5) - C (18)	109.7 (3)
C (6) - C (5) - C (12)	110.9 (3)	C (6) - C (5) - C (18)	116.3 (3)
C (12) - C (5) - C (18)	107.4 (3)	C (5) - C (6) - C (7)	116.6 (3)
C (5) - C (6) - C (11)	124.3 (3)	C (7) - C (6) - C (11)	119.0 (4)
C (6) - C (7) - C (8)	119.7 (4)	C (7) - C (8) - C (9)	120.2 (5)
C (8) - C (9) - C (10)	120.3 (5)	C (9) - C (10) - C (11)	120.3 (5)
C (6) - C (11) - C (10)	120.5 (4)	C (5) - C (12) - C (13)	121.6 (3)
C (5) - C (12) - C (17)	119.8 (3)	C (13) - C (12) - C (17)	118.4 (4)
C (12) - C (13) - C (14)	119.6 (4)	C (13) - C (14) - C (15)	121.8 (4)
C (14) - C (15) - C (16)	118.9 (4)	C (15) - C (16) - C (17)	119.9 (4)
C (12) - C (17) - C (16)	121.4 (4)	C (5) - C (18) - C (19)	123.3 (3)
C (5) - C (18) - N	114.8 (3)	C (19) - C (18) - N	121.6 (3)
C (18) - C (19) - C (20)	119.1 (4)	C (19) - C (20) - C (21)	119.3 (4)
C (20) - C (21) - C (22)	118.7 (4)	C (21) - C (22) - N	123.1 (4)
C (18) - N - C (22)	118.2 (3)		

rings attached to the C(5) atom are all planar within 0.01 Å. Bond lengths [av. 1.385 and 1.384 Å] and bond angles [both 120.0°] in phenyl rings are normal. The nitrogen atoms of the 2-pyridyl group is located far from the methacryl residue. The N-C(18) [1.339(4) Å] and N-C(22) [1.343(5) Å] bond lengths are respectively equal to the corresponding lengths in the pyridine molecule at 153 K [1.336 Å].[13] The C(19)-C(20) bond length [1.385(6) Å] is slightly longer than the corresponding C-C length in pyridine [1.378 Å]. The C(18)-N-C(22) angle [118.2(3)°] is slightly larger and the N-C(18)-C(19) [121.6(3)°] smaller than the C-N-C [116.6°] and N-C-C [123.7°] angle in pyridine, respectively. Among the bond angles around the C(5) atom, the C(6)-C(5)-C(18) angle [116.3(3)°] is much larger, whereas the O(1)-C(5)-C(12) [103.9(3)°] is much smaller than the tetrahedral angle.

The molecular conformation about the O(5)-C(1) bond is shown in Fig. 2. Similar to 1,1-DPEMA,[4] one of the two phenyl groups attached to the C(5) atom is trans to the C(1), and the other and the 2-pyridyl group gauche. This conformation is also similar to those of TrMA[4] and ChMA,[2] each of which has no hydrogen atom on the C(5).

Crystal Structure. The packing mode of molecules in the crystal is shown in Fig. 3[10] Close intermolecular contacts between non-hydrogen atoms of pyridine rings in adjacent molecules are observed: C(21)(x, y, z)···C(22)($-x$, $-y$, $-1-z$)=3.392(6), N(x, y, z)···C(21)($-x$, $-y$, $-1-z$)=3.435(5), and C(20)(x, y, z)···C(22)($-x$, $-y$, $-1-x$)=3.489(6) Å. The C(15)(x, y, z)···O(2) ($-1+x$, y, z) distance is also short [3.461(5) Å].

References

1) H. Kageyama, K. Miki, N. Kasai, Y. Okamoto, E. Yashima, K. Hatada, H. Yuki, *Makromol. Chem.*, **185**, 913 (1984).

2) H. Kageyama, Y. Yanagisawa, N. Kasai, Y. Okamoto,

Table 3. Least-Squares Planes, Deviations of Atoms from the Planes [l/Å], Dihedral Angles between the Planes [ϕ/°], and Angles between the Vector and Plane [ϕ/°] (The planes are defined in terms of Cartesian coordinates by $AX+BY+CZ=D$, where the X and Y axes are parallel to the a and b axes, respectively, and the Z axis parallel to the c* axis.) Estimated Standard Deviations in Parentheses

Plane 1: O(1), O(2), C(1), C(2), C(3), and C(4)
A, B, C, and D in Å=0.0546, −0.2470, −0.9675, −0.7258

O(1)	O(2)	C(1)	C(2)	C(3)	C(4)
0.006(9)	−0.007(9)	−0.001(9)	−0.010(10)	−0.020(10)	0.034(10)

Plane 2: C(1), C(2), C(3), and C(4)
A, B, C, and D in Å=−0.0326, 0.2455, 0.9689, 0.6387

C(1)	C(2)	C(3)	C(4)
−0.002(19)	0.009(19)	−0.006(19)	−0.005(19)

Plane 3: O(1), O(2), C(1), and C(2)
A, B, C, and D in Å=0.0613, −0.2441, −0.9678, −0.7640

O(1)	O(2)	C(1)	C(2)
−0.000(12)	−0.001(12)	0.002(12)	−0.001(12)

Plane 4: O(1), O(2), and C(5)
A, B, C, and D in Å=0.0802, −0.3352, −0.9387, −0.4089

Plane 5: C(6), C(7), C(8), C(9), C(10), and C(11)
A, B, C, and D in Å=−0.8570, −0.4492, 0.2524, 3.5959

C(6)	C(7)	C(8)	C(9)	C(10)	C(11)
−0.001(5)	0.006(6)	−0.005(7)	−0.005(7)	−0.011(7)	−0.005(6)

Plane 6: C(12), C(13), C(14), C(15), C(16), and C(17)
A, B, C, and D in Å=−0.0246, 0.6470, 0.7621, −0.8115

C(12)	C(13)	C(14)	C(15)	C(16)	C(17)
0.004(6)	−0.008(7)	0.002(7)	0.006(7)	−0.006(6)	0.001(6)

Plane 7: C(18), C(19), C(20), C(21), C(22), and N
A, B, C, and D in Å=−0.9178, 0.1284, −0.3756, 1.5709

C(18)	C(19)	C(20)	C(21)	C(22)	N
−0.010(7)	0.010(8)	0.001(8)	−0.006(7)	0.000(7)	0.005(7)

Dihedral angles:
between planes 2 and 3: 178.4(2)
between planes 3 and 4: 5.6(3)
between planes 1 and 5: 100.4(2)
between planes 1 and 6: 154.0(2)
between planes 1 and 7: 73.6(2)

Angles between the vector and plane:
between the C(5)-O(1) vector and the plane 5: 47.8(2)
between the C(5)-O(1) vector and the plane 6: 20.6(2)
between the C(5)-O(1) vector and the plane 7: 2.8(2)

E. Yashima, T. Takeda, K. Hatada, *Makromol. Chem.*, **185**, 933 (1984).

3) H. Kageyama, K. Miki, N. Tanaka, N. Kasai, Y. Okamoto, K. Hatada, H. Yuki, *Makromol. Chem.*, **183**, 2863 (1982).

4) H. Kageyama, Y. Hayashi, S. Harada, Y. Kai N. Kasai, Y. Okamoto K. Hatada, *Makromol. Chem.* **186**, 203 (1985).

5) Y. Okamoto, M. Ishikawa, K. Hatada. H. Yuki, *Polym. J.*, **15**, 851 (1983)

6) P. Main, E. E. Hull, L. Lessinger, G. Germain, J.-P. Declercq, M. M. Woolfson, *MULTAN* 78, "A System of Computer Programs for the Automatic Solution of Crystal Structures from X-Ray Data", Univ. of York, England (1978).

7) T. Ashida, *HBLS* V, "The Univeral Crytallographic Computing System-Osaka," The Compuation Ceter, Osaka Univ., (1979), p. 53.

8) Internatioal Tables for X-Ray Crytallography, Kynoch Press, Birmingham, Vol. IV (1974), p. 71.

9) W. C. Hamilton, Acta Crystallogr., **12**, 609 (1959).

10) C. K. Johnson, *ORTEP* II, Report ORNL-5138, Oak Ridge National Laboratory, Tennessee (1976).

11) H. Yuki, K. Hatada, T. Niinomi, Y. Kikuchi, *Polym. J.*, **1** 36 (1970).

12) Y. Okamoto, E. Yashima, K. Hatada, H. Kageyama, N. Kasai, unpublished data

13) D. Moots, H.-G. Wussow, *J. Chem. Phys.*, **75**, 1517 (1981).

Proton Transfer Reactions in the Triplet State of Benzophenone Studied by Nanosecond Laser Flash Photolysis

Masahiko Hoshi and Haruo Shizuka*
Department of Chemistry, Gunma University,
Kiryu, Gunma 376
(Received April 1, 1986)

Proton-transfer reactions in the triplet state of benzophenone in H_2O–acetonitrile (4:1) at 20 °C have been studied by means of nanosecond nitrogen laser flash photolysis at 337 nm. The proton association (k_1) and dissociation (k_2) rates are determined to be 5.0 (±0.5)×10^9 mol^{-1} dm^3 s^{-1} and 3.3 (±0.3)×10^9 s^{-1} respectively by a transient kinetic treatment. These rates are large enough to make an acid-base equilibrium during the lifetime of the triplet state. The acidity constants (pK_a*) in the triplet state of benzophenone obtained by the transient kinetic treatment, the Ware plot, and the T_n←T_1 absorbance titration curve are the same [0.18 (±0.1)]. The pK_a* value determined by the titration method is appreciably dependent upon the delay time after the start of pulsing (the accurate value was obtained at the delay time 20 ns). There is no proton-induced quenching in the triplet state of benzophenone, since electrophilic protonation occurs at the oxygen atom in the carbonyl group. The reactive state for protonation in the triplet state is not $^3(n,\pi^*)$, but $^3(\pi,\pi^*)$, judging from the large k_1 value and the pK_a* value.

Proton-transfer reactions in the excited states of aromatic compounds are elementary processes in both chemistry and biochemistry. The acid-base properties in the excited state of aromatic compounds are closely related to electronic structure, which is considerably different from that in the ground state. A large number of studies on the acidity constants pK_a* in the excited state of aromatic compounds have been reported showing that the pK_a* values are significantly different from the acidity constants in the ground state.[1–9] It is known that the pK_a* values can be estimated by means of the Förster cycle,[1–3,10] the fluorescence titration curve,[2,3] and the triplet–triplet absorbance titration curve.[11] These methods involve the assumptions that proton transfer in the excited state is very fast and that the prototropic equilibrium may be accomplished during the lifetime in the excited state.

However, it has been shown recently that proton-induced quenching (^1k_q) is competitive with the proton-transfer reaction in the excited singlet state of naphthylamines (that is, simple acid-base equilibrium cannot be attained during the lifetime in the excited state of aromatic amines) and that a dynamic analysis containing the quenching process is, therefore, needed in order to obtain the accurate pK_a* values.[12] The dynamic analyses by means of nanosecond time-resolved spectroscopy with fluorimetry have been applied to 1-pyrenylamine,[13] 1-anthrylamine,[14] phenanthrylamines,[15] and naphthols.[16] The Stuttgart group[17] has supported our method to determine the pK_a* values of naphthylamines. Similar experimets for excited naphthols have been reported by Harris and Selinger.[18] For the proton-induced quenching mechanism, it has been demonstrated that the quenching proceeds via electrophilic protonation at one of carbon atoms of the aromatic ring in the excited singlet state, leading to proton exchange (or isotope exchange).[19] An intramolecular CT structure in the excited state is responsible for the quenching.[15,19,20] A linear relationship between the values of $\log {}^1k_q$ and the charge densities in the excited state of aromatic compounds has been shown.[20] Examples for no excited-state acid-base equilibria of aromatic compounds have been shown.[21–23] Establishment of prototropic equilibria at moderate acid concentrations have been reported for benzophenone[24,25] and phenyl ketones.[25] For the triplet state, its lifetime is relatively long enough to establish the prototropic equilibrium.[25] Very recently, it has been shown that the proton-induced quenching occurs scarcely in the triplet state of methoxynaphthalenes.[26] There has been considerable interest in photochemical and photophysical properties of aromatic compounds in the presence of protons.[27]

In the course of a study on the excited-state proton transfer reaction,[27] we became interested in the proton transfer reaction in the triplet state of benzophenone studied by nanosecond laser flash photolysis. This work was studied to answer the following questions: (1) How fast are the proton association and dissociation rates in the triplet state of benzophenone? (2) Is there really no proton-induced quenching in the triplet state? (3) How about pK_a* values in the triplet state of benzophenone determined by a transient kinetic treatment, the Ware plot, and the T_n←T_1 absorbance titration curve? (4) Which is the reactive state for protonation in the triplet state, $^3(n,\pi^*)$ or $^3(\pi,\pi^*)$?

Experimental

Materials. Benzophenone (a G. R. grade product from Tokyo Kasei) was purified by repeated recrystallizations from H_2O–EtOH mixtures. Sulfuric acid (97%, Wako) was used without further purification. Distilled water and acetonitrile (G. R. grade, Wako) were used as a H_2O–CH_3CN mixture (4:1 by volume). The concentration of benzophenone was 3.2×10^{-3} mol dm^{-3}. The pH values of samples were recorded with a pH meter (Corning M-125). The samples were thoroughly degassed by freeze-pump-

Table 1. Transient Absorbance (Ab^0) at 525 nm at 20 ns after the Start of Pulsing, Observed Decay Constant (τ_{obsd}^{-1}) and Lifetime (τ_{obsd}) of the 525 nm Transient at Different Acidities

pH or H_0	wt. % H_2SO_4 [a]	Ab^0	$\tau_{obsd}^{-1}/10^6\ s^{-1}$ [b]	τ_{obsd}/ns [b]
7.00		0.0506	0.74	1.35×10^3
2.33		0.0506	0.84	1.19×10^3
1.07		0.0466	9.62	104
0.64		0.0406	17.9	56
0.28		0.0281	30	33
−0.43[a]	11.4	0.0108	67	15
−1.67[a]	29.3	0.0021	77	13
−2.34[a]	38.9	0.0032	77	13

a) Data taken from M. J. Jorgenson, D. R. Hartter, *J. Am. Chem. Soc.*, **85**, 878 (1963). b) Errors within 5%.

thaw cycles on a high vacuum line. All experiments were carried out at 20 °C.

Nanosecond Laser Flash Experiments. Laser flash photolysis studies were carried out using a nanosecond N_2 laser system at 337 nm (Japan Dynamic JS-1000L; pulse width 5 ns, laser power 5 mJ). The monitoring system consisted of a pulsed UXL-150D xenon lamp. A MC-20N monochromator (Ritsu) and a HTV R928 photomultiplier tube were used for the detection part. The transient signal was recorded with a transient memory (Kawasaki Electronica, MR-50E) and a 100 MHz storage oscilloscope (Iwatsu TS-8123).

Results and Discussion

Nanosecond Laser Flash Photolysis of Benzophenone. It is well known that triplet formation through intersystem crossing is very rapid (<10 ps),[28] according to the El-Sayed's rule.[29] For benzophenone (BP), a strong absorption band with a maximum at 525 nm (ε=7800 $mol^{-1}\,dm^3\,cm^{-1}$)[30] was observed just after pulsing, which decayed by first-order kinetics with a decay rate of $(\tau_0)^{-1}=7.4\times10^5\ s^{-1}$. This band is ascribed to the $T_n\leftarrow T_1$ absorption.[31,32] The protonated benzophenone triplet, ^{3}BP+H*, has a very weak absorption band at 505 nm.[25] The ^{3}BP+H* species produced in a 4 mol dm^{-3} H_2SO_4 solution decayed with a lifetime of 13 ns. The observed decay rate of triplet benzophenone (^{3}BP*) monitored at 525 nm increased significantly with an increase of proton concentration. The experimental data of the 525 nm transient absorbance (Ab) at 20 ns after the start of pulsing and the observed decay rate constants (τ_{obsd}^{-1}) or the apparent lifetimes (τ_{obsd}) in various acid concentrations are summarized in Table I. Judging from the relatively low value of absorbance at 525 nm, there is no triplet-triplet annihilation of BP under the experimental conditions. There is little or no quenching of ^{3}BP* by the counter anion SO_4^{2-}.[33]

Dynamic Analyses by Means of a Transient Kinetic Treatment. The experimental results can be accounted for by Scheme 1.

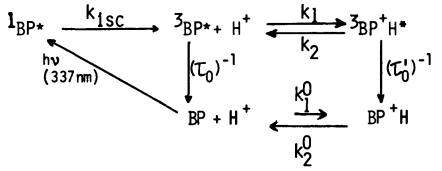

Scheme 1.

where BP and ^{3}BP* represent the ground and triplet states of benzophenone respectively, τ_0 and τ_0' the lifetimes of ^{3}BP* (in the absence of protons) and ^{3}BP+H* respectively, k_1 and k_2 the protonation and dissociation rate constants in the triplet state, respectively, and ^{3}BP+H* protonated benzophenone triplet. At the highest acidities used, the ground state of benzophenone is unprotonated,since the pK_a value in the ground state of BP is very low (−5.7).[34] when BP is excited by a laser pulse at 337 nm, ^{3}BP* is produced very quickly within 10 ps[28] via fast intersystem crossing[29] of the singlet state of benzophenone (^{1}BP*).

At first, a transient kinetic treatment for the acid-base reaction of benzophenone has been made. The decay function of $Ab(t)$ of the transient absorbance at 525 nm for ^{3}BP* can be expressed as[35]

$$Ab(t) = c(e^{-\lambda_1 t}+Ae^{-\lambda_2 t}) \quad (1)$$

where c denotes the constant and $A=(X-\lambda_1)(\lambda_2-X)^{-1}$. The decay parameters λ_1 and λ_2 are

$$\lambda_{1,2} = \frac{1}{2}[X+Y\mp\{(Y-X)^2+4k_1k_2[H^+]\}^{1/2}] \quad (2)$$

where $X=\tau_0^{-1}+k_1[H^+]$ and $Y=(\tau_0')^{-1}+k_2$. The observed decay function at 525 nm is approximately the same as the undistorted decay function of Eq. 1, since the pulse width is relatively small (5 ns). The experimental value of τ_0^{-1} ($7.4\times10^5\ s^{-1}$) was used. The values of k_1, k_2, and $(\tau_0')^{-1}$ were varied. With use of the values of λ_1 and λ_2 obtained from Eq. 2, fitting of the decay function of $Ab(t)$ was carried out. Figure 1a shows the observed and calculated results of the function $Ab(t)$ at 20 °C at the concentrations of protons (1) $8.5_2\times10^{-2}$, (2) 0.22_8, and (3) 0.52_1 mol dm^{-3}. The best fitted values of λ_1 and λ_2 as a function of $[H^+]$ are shown in Fig. 1b. The values of k_1, k_2, and $(\tau_0')^{-1}$ were determined to be 5.0 ($\pm$0.5)$\times10^9$ $mol^{-1}\,dm^3\,s^{-1}$, 3.3 ($\pm$0.3)$\times10^9\ s^{-1}$, and 7.9 ($\pm$0.7)$\times10^7\ s^{-1}$, respectively. The value of the protonation rate constant (k_1) is close to that of the diffusion rate. It is noteworthy that the value of $(\tau_0')^{-1}$ obtained is approximately the same as the decay rate constant ($7.7\times10^7\ s^{-1}$) of ^{3}BP+H* at higher acid concentrations (see Table 1). The values of k_1 and k_2 are very much greater than those of the competitive processes: i.e., $k_1\gg\tau_0^{-1}$; $k_2\gg(\tau_0')^{-1}$. That is, an acid-base equilibrium in Scheme 1 is established in the excited

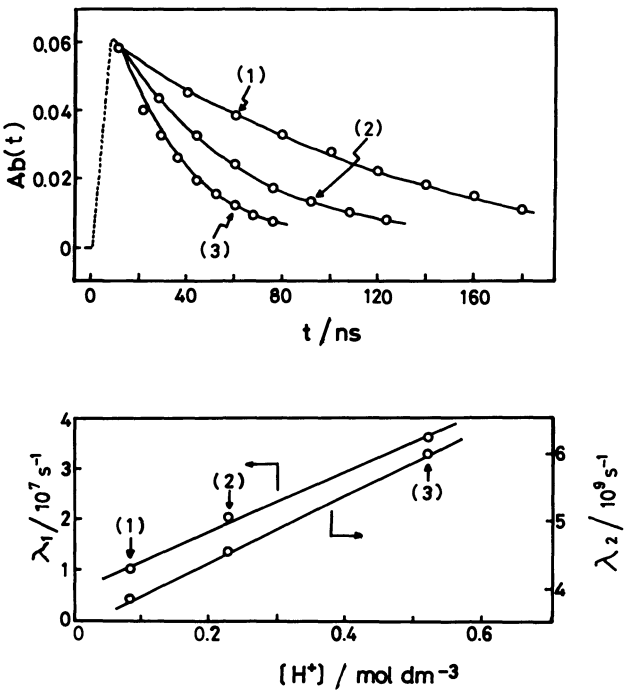

Fig. 1. (a) The decay function $Ab(t)$ of the 525 nm transient at the concentration of protons: (1) $8.5_2\times10^{-2}$, (2) 0.22_8, (3) 0.52_1 mol dm^{-3}. Circle: observed; solid curve; calculated. (b) The decay parameters λ_1 and λ_2 fitted to $Ab(t)$ as a function of $[H^+]$; e.g., (1)$\lambda_1=1.0\times10^7$s^{-1}, $\lambda_2=3.8\times10^9$s^{-1}; (2) $\lambda_1=2.0\times10^7$s^{-1} and $\lambda_2=4.5\times10^9$s^{-1}; and (3) $\lambda_1=3.5\times10^7$s^{-1} and $\lambda_2=5.9_5\times10^9$s^{-1}. For details see text.

state. The value of K_a^* ($=k_2/k_1$) was evaluated to be 0.66 mol dm^{-3}. The acidity constant of triplet benzophenone (pK_a^*) was determined to be 0.18 by means of the transient kinetic treatment. Very recently, a similar treatment has been employed in the hydrogen-atom transfer reaction from triplet naphthol to ground benzophenone.[30]

The Ware Plot. In the above section, it is shown that the prototropic equilibrium in the triplet state of BP is established within the triplet lifetime. Therefore, the Ware equation[36] can be applied to the present system. The Ware equation reads

$$\{\tau_{obsd}^{-1}-\tau_0^{-1}\}^{-1}=\{(\tau_0')^{-1}-\tau_0^{-1}\}^{-1}\left\{1+\frac{K_a^*}{[H^+]}\right\}. \quad (3)$$

The Ware plot of $(\tau_{obsd}^{-1}-\tau_0^{-1})^{-1}$ as a function of $[H^+]^{-1}$ is shown in Fig. 2. From the slope and intercept, the values of K_a^* and $(\tau_0')^{-1}$ are determined as 0.64 mol dm^{-3} and 7.5×10^7 s^{-1} respectively. The pK_a^* value is evaluated to be 0.19 from the Ware plot. As for $(\tau_0')^{-1}$ the values obtained by the decay rate constant of ^{3}BP$^+$H*, the transient kinetic treatment, and the Ware plot are approximately the same each other within experimental errors. The pK_a^* value (0.19) obtained is approximately the same as that (0.18) determined by the transient kinetic treatment.

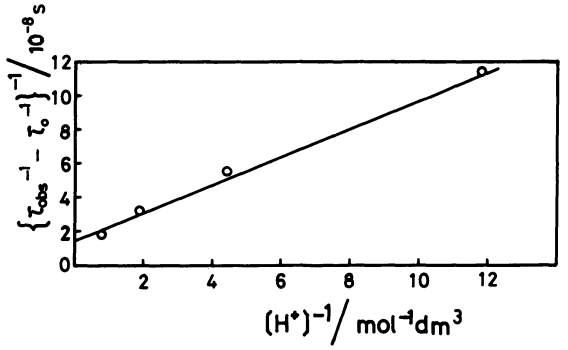

Fig. 2. The Ware plot of $[\tau_{obsd}^{-1}-\tau_0^{-1}]^{-1}$ vs. $[H^+]^{-1}$. See text.

Triplet-Triplet Absorbance Titration Curve. This method is the most popular one to estimate the pK_a^* value in the triplet state, when a prototropic equilibrium is established within the lifetime in the excited state.[11] Usually, the pK_a^* value can be estimated from the midpoint of the $T_n\leftarrow T_1$ absorbance titration curve obtained by nanosecond laser flash photolysis or microsecond flash photolysis just after pulsing. However, little attention has been paid to a relation between the pK_a^* value and the delay time to measure the titration curve. Here, it is demonstrated that there is a large dependence of the pK_a^* value upon the decay time. Figure 3 shows the dependence of the $T_n\leftarrow T_1$ absorbance titration curve on the delay time after the start of pulsing. The midpoint of the titration curve is shifted to higher pH values with an increase of the delay time. The pK_a^* value (0.18) obtained by the titration method at 20 ns after the start of pulsing is the best fit to that obtained by the transient kinetic analysis or the Ware plot. This value is positively deviated as the delay time increases, since the decay rate $[(\tau_0')^{-1}=7.7\ (\pm0.3)\times10^7\ s^{-1}]$ of ^{3}BP$^+$H* is extremely large compared to that $[\tau_0^{-1}=7.4\times10^5\ s^{-1}]$ of free ^{3}BP*. The short lifetime (13 ns) of ^{3}BP$^+$H*, the triplet benzophenone protonated at the oxygen atom of the carbonyl group, is not due to the proton-induced quenching, but the decay nature of ^{3}BP$^+$H* itself. In the triplet state of BP, electrophilic attack occurs on the oxygen atom of the carbonyl group of ^{3}BP* to produce ^{3}BP$^+$H*, since intramolecular charge migration from phenyl groups to the carbonyl group takes place appreciably in ^{3}BP* as discussed later. There is no electrophilic protonation (i.e., proton-induced quenching)[19] at one of carbon atoms of aromatic rings under the experimental conditions. The proton association and dissociation rates (k_1 and k_2) in the triplet state of BP are very fast enough to make an acid-base equilibrium within the lifetime in the excited state as stated above. Therefore, the delay time at 20 ns after the start of pulsing is a reasonable time to measure the titration curve in the present system.

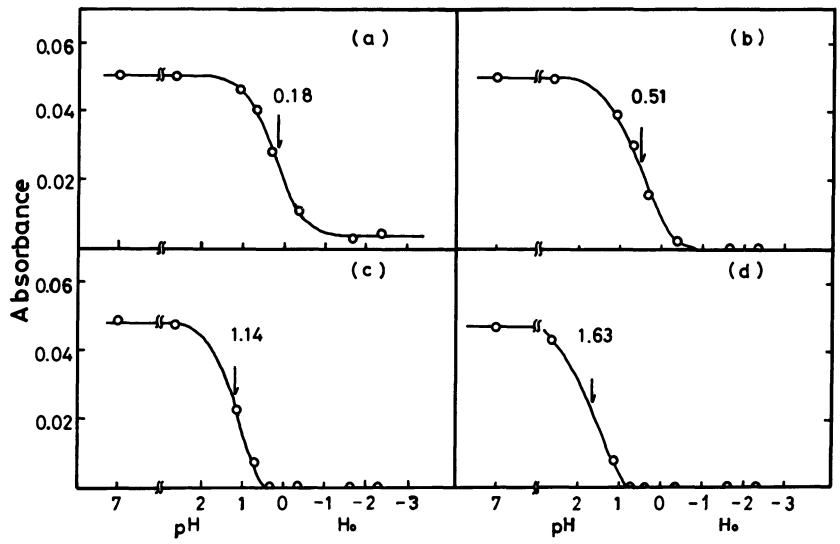

Fig. 3. The 525 nm transient absorbance curves observed at various delay times: (a) 20 ns, (b) 40 ns, (c) 100 ns, and (d) 200 ns after the start of pulsing.

Electronic Structure of Triplet Benzophenone. It is known that the lowest triplet state of BP is $^3(n,\pi^*)$ even in polar media.[37] There is a problem whether the reactive state of $^3BP^*$ for protonation is $^3(n,\pi^*)$ or $^3(\pi,\pi^*)$. In a previous paper,[25] the pK_a^* value for aromatic ketones is expressed as

$$pK_a^* = \rho^*\sigma^* + (pK_a^*)_0 \quad (4)$$

where ρ^* is equal to -1.33 and $(pK_a^*)_0$ denotes the pK_a^* value of acetophenone (0.60). The +I effect of a substituent of the carbonyl group increases the charge density (i.e., basicity) at the oxygen atom of the carbonyl group, resulting in an increase of the pK_a^* value. For BP, a positive deviation from the line according to Eq. 4 is observed.[25] The pK_a^* value of BP (0.18) has a greater value than that (-0.2) expected from its σ^* value ($+0.600$).[38] This fact cannot be explained by the difference in the lowest triplet character between $^3(n,\pi^*)$ (BP) and $^3(\pi,\pi^*)$ (phenyl alkyl ketones) in polar media. The charge density at the carbonyl group in the $^3(n,\pi^*)$ state should be smaller than that in the $^3(\pi,\pi^*)$ state, since the former state involves back charge transfer (from the carbonyl group to the phenyl ring). Both $^3(n,\pi^*)$ and $^3(\pi,\pi^*)$ states are perturbed by one another because the energy separation between them is very small in polar media, as has been discussed previously.[25,33b] The rapid rate of k_1 for protonation to $^3BP^*$ strongly supports that the reactive state of $^3BP^*$ is not $^3(n,\pi^*)$ but $^3(\pi,\pi^*)$. The $^3(\pi,\pi^*)$ state may have an intramolecular CT structure; charge migration from phenyl groups to the carbonyl group occurs in polar media, leading to a relatively high basicity in the triplet state. Thus, it can be understood that the pK_a^* value (0.18) in the triplet state of benzophenone increases drastically compared to that (-5.7)[34] in the ground state.

Concluding Remarks

The following remarks can be drawn from the results reported: (1) The protonation (k_1) and proton dissociation (k_2) rate constants in the triplet state of benzophenone in H_2O–CH_3CN (4:1) at 20 °C are determined to be $5.0\ (\pm0.5)\times10^9\ mol^{-1}\ dm^3\ s^{-1}$ and $3.3\ (\pm0.3)\times10^9\ s^{-1}$ respectively by means of a transient kinetic treatment. These rates are very much greater than those of their competitive decay processes, leading to produce an acid-base equilibrium in the excited state. (2) There is no proton-induced quenching in $^3BP^*$, because protons attack the oxygen atom of the carbonyl group. (3) The pK_a^* values for $^3BP^*$ obtained by means of the transient kinetic treatment, the Ware plot, and the $T_n \leftarrow T_1$ absorbance titration method are the same (0.18 ± 0.1) each other. The pK_a^* value determined by the titration curve depends upon the delay time to measure its curve; the accurate pK_a^* value is obtained at the delay time 20 ns after the start of pulsing. (4) The reactive state for protonation in the triplet state of benzophenone is not $^3(n,\pi^*)$ but $^3(\pi,\pi^*)$, considering the relatively large protonation rate k_1 and the pK_a^* value.

This work was supported by a Scientific Research Grant-in-Aid (No. 58470001) of the Ministry of Education.

References

1) The Förster, *Z. Elektrochem. Angew. Phys. Chem.*, **54**, 42, 531 (1950).

2) A. Weller, *Ber. Bunsenges. Phys. Chem.*, **56**, 662 (1952);

ibid., **66**, 1144 (1956).
3) A. Weller, *Prog. React. Kinet.*, **1**, 189 (1961).
4) H. Beens, K. H. Grellmann, M. Gurr, and A. Weller, *Discuss. Faraday Soc.*, **39**, 183 (1965).
5) E. V. Donckt, *Prog. React. Kinet.*, **5**, 273 (1970).
6) E. L. Wehry and L. B. Rogers, "Fluorescence and Phosphorescence Analyses," ed by D. M. Hercules, Wiley-Interscience, New York (1966), p. 125.
7) S. G. Shulman, "Modern Fluorescence Spectroscopy," ed by E. L. Wehry, Pleum, New York (1976), Vol. 2; S. G. Shulman, "Fluorescence and Phosphorescence Spectroscopy," Pergamon, Oxford (1977).
8) J. F. Ireland and P. A. H. Wyatt, *Adv. Phys. Org. Chem.*, **12**, 131 (1976) and references cited therein.
9) W. Klöpffer, *Adv. Photochem.*, **10**, 311 (1977).
10) Z. R. Grabowski and A. Grabowska, *Z. Phys. Chem. (Wiesbaden)*, **101**, 197 (1976); Z. R. Grabowski and W. Rubaszewska, *J. Chem. Soc., Faraday Trans. 1*, **73**, 11 (1977).
11) G. Jackson and G. Porter, *Proc. R. Soc. London, Ser. A*, **260**, 13 (1961).
12) K. Tsutsumi and H. Shizuka, *Chem. Phys. Lett.*, **52**, 485 (1977); *Z. Phys. Chem. (Wiesbaden)*, **111**, 129, (1978).
13) H. Shizuka, K. Tsutsumi, H. Takeuchi, and I. Tanaka, *Chem. Phys. Lett.*, **62**, 408 (1979); *Chem. Phys.*, **59**, 183, (1981).
14) H. Shizuka and K. Tsutsumi, *J. Photochem.*, **9**, 334 (1978).
15) K. Tsutsumi, S. Sekiguchi, and H. Shizuka, *J. Chem. Soc., Faraday Trans. 1*, **78**, 1087 (1982).
16) K. Tsutsumi and H. Shizuka, *Z. Phys. Chem. (Wiesbaden)*, **122**, 129 (1980).
17) F. Hafner, J. Wörner, U. Steiner, and M. Hauser, *Chem. Phys. Lett.*, **72**, 139 (1980).
18) C. M. Harris and B. K. Selinger, *J. Phys. Chem.*, **84**, 891, 1366 (1980).
19) H. Shizuka and S. Tobita, *J. Am. Chem. Soc.*, **104**, 6919 (1982); S. Tobita and H. Shizuka, *Chem. Phys. Lett.*, **75**, 140 (1980).
20) H. Shizuka and K. Tsutsumi, *Bull. Chem. Soc. Jpn.*, **56**, 629 (1983).
21) H. Shizuka, K. Kameta, and T. Shinozaki, *J. Am. Chem. Soc.*, **107**, 3956 (1985).
22) H. Shizuka, M. Nakamura, and T. Morita, *J. Phys. Chem.*, **83**, 2019 (1979).
23) H. Shizuka, T. Ogiwara, and E. Kimura, *J. Phys. Chem.*, **89**, 4302 (1985).
24) D. M. Rayner and P. A. H. Wyatt, *J. Chem. Soc., Faraday Trans. 2*, **70**, 945 (1974).
25) H. Shizuka and E. Kimura, *Can. J. Chem.*, **62**, 2041 (1984).
26) H. Shizuka, M. Fukushima, T. Fuju, T. Kobayashi, H. Ohtani, and M. Hoshino, *Bull. Chem. Soc. Jpn.*, **58**, 2107 (1985).
27) H. Shizuka, *Acc. Chem. Res.*, **18**, 141 (1985), and references cited therein.
28) R. W. Anderson, Jr., R. M. Hochstrasser, H. Lutz, and G. W. Scott, *J. Chem. Phys.*, **61**, 2500 (1974); *Chem. Phys. Lett.*, **28**, 153 (1978).
29) M. A. El-Sayed, *J. Chem. Phys.*, **36**, 573 (1962); *ibid.*, **38**, 2834 (1963); *ibid.*, **41**, 2462 (1964).
30) H. Shizuka, H. Hagiwara, and M. Fukushima, *J. Am. Chem. Soc.*, **107**, 7816 (1985).
31) M. B. Ledger and G. Porter, *J. Chem. Soc., Faraday Trans. 1*, **68**, 539 (1972).
32) E. J. Land, *Proc. R. Soc. London, Ser A*, **305**, 457 (1968).
33) a) H. Shizuka, M. Nakamura, and T. Mortia, *J. Phys. Chem.*, **84**, 989 (1980); b) H. Shizuka and H. Obuchi, *ibid.*, **86**, 1297 (1982).
34) T. G. Bonner and J. Phillips, *J. Chem. Soc., B*, 650, (1966).
35) J. B. Birks, "Photophysics of Aromatic Molecules," John Wiley & Sons, London (1970).
36) W. R. Ware, D. Watt, and D. Holmes, *J. Am. Chem Soc.* **96**, 7853 (1974).
37) A. A. Lamola, *J. Chem. Phys.*, **47**, 4810 (1967).
38) R. W. Taft, Jr., "Steric Effects in Organic Chemistry," ed by M. S. Newman, John Wiley & Sons, New York (1956), p. 619.

 © 1986 The Chemical Society of Japan Bull. Chem. Soc. Jpn., 59, 2717—2722 (1986)

Electrocatalytic Oxygen Reduction at (Tetrasulfonatophthalocyaninato)-cobalt Incorporated Polypyrrole Film Electrode

Tetsuya OSAKA,* Katsuhiko NAOI, Takayuki HIRABAYASHI, and Sadako NAKAMURA†
Department of Applied Chemistry, School of Science and Engineering, Waseda University, Shinjuku-ku, Tokyo 160
†Department of Chemistry, Japan Women's University, Mejirodai, Bunkyo-ku, Tokyo 112
(Received April 8, 1986)

Electrocatalytic activity of oxygen reduction was strikingly improved at a GC(glassy carbon)/PPy(polypyrrole)/CoTSP((tetrasulfonatophthalocyaninato)cobalt) electrode among the other CoTSP doped polymer electrodes. The GC/PPy/CoTSP electrode was formed by electro-oxidized polymerization of pyrrole on a glassy carbon(GC) electrode in methanol solution containing CoTSP. The catalytic oxygen reduction at the GC/PPy/CoTSP electrode was mainly analyzed with RRDE technique. Oxygen reduction reaction at the GC/PPy/CoTSP electrode in 0.05 mol dm^{-3} H_2SO_4 showed ca. 0.5 V more anodic onset potential than the value obtained with a GC electrode in 0.05 mol dm^{-3} H_2SO_4 containing 10^{-3} mol dm^{-3} CoTSP. Kouteckty-Levich plot, i.e., the relation between I_{lim}^{-1} and $\omega^{-1/2}$ for the GC/PPy/CoTSP electrode gave almost the same slope of theoretical four-electron reduction at the limiting current region. It was indicated that the apparent oxygen reduction is occurred through direct four-electron exchange process. On the other hand, the GC electrode in dissolved CoTSP gave almost the same slope as of theoretical two-electron reduction. A diagnostic criterion for oxygen reduction proposed by Wroblowa et al.[19] indicated that the parallel pathways of two- and four-electron reduction exist for the GC/PPy/CoTSP electrode.

Catalytic properties of macrocyclic transition metal complexes such as metal porphyrins and phtalocyanines for an electrochemical oxygen reduction have been recognized and examined extensively by many workers.[1,2] An active, inexpensive and also stable catalyst system, however, has not yet been discovered.[14-17] In this connection, special efforts have been made to enhance the activity of electrode catalysts such as graphite by modifying their surfaces with some active materials. Utilization of modified catalytic electrode at monolayer level has not been so successful in that they lack stability and conductivity in a doped state due to an unstable and insulating nature of adsorbed species on the substrate.[3-5] Recently, incorporation of electrocatalytic materials into polymer-coated electrode has been introduced as an easy and potential means for fixing a large metal complexes as active catalyst on a substrate.[6-9] Polymer films can be deposited on an electrode by electro-oxidized polymerization simultaneously with the incorporation of active materials from the supporting electrolyte.

In this paper, we mainly adopted polypyrrole for coating glassy carbon(GC) electrode by considering the following advantages. First, pyrrole can easily be polymerized and form a fairly stable film which adheres well to the substrate. Second, polypyrrole shows a good electronic conductivity, and can be an excellent current collector and an electron shuttle. Third, polymerized polypyrrole shows an easy incorporation of dopants during the film formation.

Bull et al.[6] reported that there was no remarkable change in catalytic activity by doping FeTSP in PPy film. However, a considerable improvement on catalytic activity of O_2 reduction was observed by doping [5,10,15,20-tetrakis(4-sulfonatophenyl)porphyrinato] metals such as CoTPPS, FeTPPS and MnTPPS in polypyrrole films.[7,8] In the previous communication,[9] we briefly surveyed some PPy modified metal porphyrins such as FeTPPS, CoTPPS, FeTSP, and CoTSP for the activity of O_2 reduction. Among these, we found that the GC/PPy/CoTSP electrode showed the highest activity with respect to an onset potential of O_2 reduction reaction. The main motivation of the paper is to throw a light on the interpretation of oxygen reduction mechanism for the GC/PPy/CoTSP electrode with RRDE (rotating ring-disk electrode) technique.

Experimental

CoTSP was synthesized and purified after an usual way,[10] and was then identified by an absorption spectrum using the same method in Refs.[11,12] Electrocatalytic activities for oxygen reduction reaction were mainly examined by rotating Pt ring-GC disk electrode (RRDE) at various rotating speeds. The ring and disk electrodes were pretreated by polishing with alumina grain (0.3 μmϕ) suspended in water. The ring-disk electrode was calibrated with the iron(II)/iron(III) couple. The value of collection efficiency, N, determined in this manner was 0.40 which was well consistent with the value of 0.40 obtained from the geometry of electrodes. An Ag/AgCl was used as a reference electrode and all the potentials for electrochemical measurements were referred to it. Pt wire was used as a counter electrode. Polymer coated CoTSP electrodes were deposited on GC by potentiostatic electropolymerization in methanol or aqueous solution containing CoTSP. The film thickness of polymer films was controlled by passing 90 mC cm^{-2}. GC/PPy/CoTSP and GC/PMP(poly(N-methylpyrrole))/CoTSP were formed at 1.2 V vs. Ag/Ag$^+$ in methanol solution containing 0.1 mol dm^{-3} monomer and 10^{-3} mol dm^{-3} CoTSP. GC/PPr(polypyrene)/CoTSP was formed at 1.2 V vs. Ag/Ag$^+$ in methanol containing

0.01 mol dm^{-3} monomer and 10^{-3} mol dm^{-3} CoTSP. GC/PAn(polyaniline)/CoTSP was formed at 0.8 V vs. Ag/AgCl in an aqueous solution containing 0.1 mol dm^{-3} monomer, 0.2 mol dm^{-3} H_2SO_4 and 10^{-3} mol dm^{-3} CoTSP. Solutions with various pH values were used as follows; 0.05 mol dm^{-3} H_2SO_4 (pH=1.2), 0.05 mol dm^{-3} KH_2PO_4+5.6×10^{-3} mol dm^{-3} NaOH (pH=6.0), and 0.025 mol dm^{-3} Na_2HPO_4+3.3×10^{-3} NaOH (pH=10.9). The intermediate hydrogen peroxide generated by two-electron reduction of O_2 was detected by ring electrode which was polarized at 1.10 V (pH=1.2), 0.82 V (pH=6.0), and 0.53 V (pH=10.9) while scanning the disk electrode potential at a scan rate of 10 mV s^{-1}.

Results and Discussion

Figure 1 shows typical O_2 reduction curves for GC/Polymer/CoTSP electrodes at 960 rpm where the background currents in N_2 atmosphere are already subtracted. GC/PPy/CoTSP, GC/PMP/CoTSP and GC/PAn/CoTSP electrodes have almost the same onset potentials at ca. 0.50 V which are the most favorable potential compared with the other two electrode systems, viz., GC/PPr/CoTSP and GC electrode in dissolved CoTSP. However, the ring current behavior of each electrode indicates that GC/PPy/CoTSP electrode is the most active oxygen reduction catalyst because of the occurrence of the four-electron transfer process to H_2O at the potential cathodic to 0.00 V. Therefore, the GC/PPy/CoTSP electrode was considered to be the most active oxygen reduction catalyst among the other polymer coated electrodes and worthwhile examining further.

Typical pH dependence of RRDE polarization curves for the GC/PPy/CoTSP is shown in Fig. 2. Oxygen reduction current at the GC/PPy/CoTSP disk electrode has onset potentials of ca. 0.50 V (pH=1.2), ca. 0.25 V (pH=6.0), and ca. 0.00 V

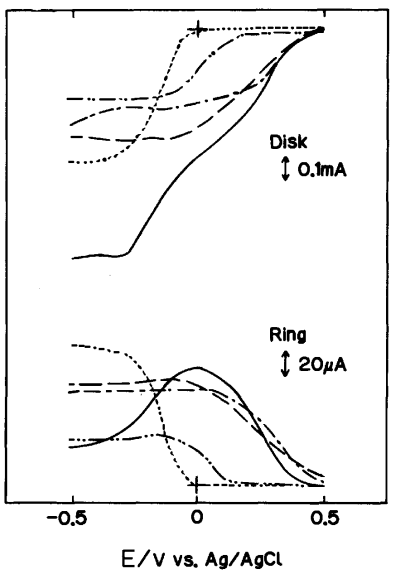

Fig. 1. Ring-disk current vs. potential curves for GC/CoTSP electrodes coated with various conductive polymers at 960 rpm in 0.05 mol dm^{-3} H_2SO_4. Film preparation conditions are indicated in the experimental section.
——: CoTSP/Polypyrrole, — — —: CoTSP/Poly(*N*-methylpyrrole) —·—: CoTSP/Polyaniline, —··—: CoTSP/Polypyrene, ------: GC electrode in 10^{-3} mol dm^{-3} CoTSP.

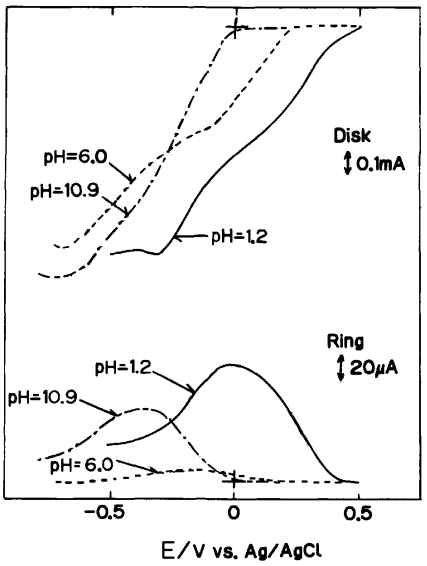

Fig. 2. pH dependence of RRDE curves for O_2 reduction at GC/PPy/CoTSP electrode at 960 rpm. pH=1.2 : 0.05 mol dm^{-3} H_2SO_4, pH=6.0 : 0.05 mol dm^{-3} KH_2PO_4+5.6×10^{-3} mol dm^{-3} NaOH, pH=10.9 : 0.025 mol dm^{-3} Na_2HPO_4+3.3×10^{-3} mol dm^{-3} NaOH.

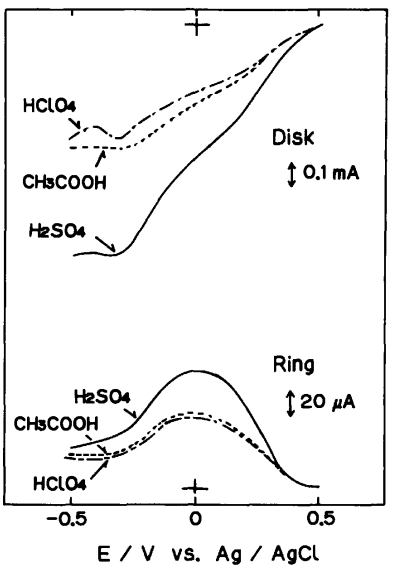

Fig. 3. Supporting electrolyte dependence of RRDE curves at GC/PPy/CoTSP electrode at 960 rpm. The pH values for all solutions were adjusted to 1.2.

(pH=10.9). As proton concentration increases, the onset potentials of O_2 reduction are observed to shift to the anodic side. In the solution of pH=1.2, the disk current shows the most anodic onset potential and a relatively clear limiting current is observed. The ring current shows a peak at ca. 0.00 V, and decreases until −0.32 V at which disk current exactly shows a maximum, and finally becomes constant current. At the potential more cathodic than 0.00 V, the four-electron process seems to occur. In the solution of pH=6.0, both disk and ring current curves have an onset potential at 0.25 V. Although disk current shows a substantial increase, the ring current shows almost zero change, indicating that the direct reduction from O_2 to H_2O is dominantly involved. In the solution of pH=10.9, the two- and the four-electron process seems to occur in parallel. The following study is focused on the behavior of GC/PPy/CoTSP electrode in the acidic solution of pH=1.2.

Figure 3 shows polarization curves for O_2 reduction reaction in three different supporting electrolytes, viz., H_2SO_4, CH_3COOH, and $HClO_4$ at pH=1.2. O_2 reduction current for H_2SO_4 electrolyte keeps the highest values than those in the other electrolyte. Polarization curves for O_2 reduction curves are observed to be very sensitive to the electrolyte anions used for the O_2 reduction measurements. The reason for that is still unclear at the present stage, but the behavior of polarization curves may have a close relationship with the mobility of anions in electrolyte solutions and the polymer film resistances with anion doped states.

Polarization curve of O_2 reduction at a GC/PPy electrode without CoTSP dopants and at the GC/PPy/CoTSP electrode are compared as shown in Fig. 4. As is evident from the disk currents, an onset potential for the GC/PPy electrode is 0.0 V, which is less anodic than that for the GC/PPy/CoTSP. Ring currents for the GC/PPy/CoTSP and the GC/PPy electrodes have onset potentials at 0.50 V and 0.00 V, respectively. For the GC/PPy/CoTSP electrode, two-electron reduction of O_2 is observed to occur at ca. 0.50 V, and has peak value at 0.00 V. At the potentials cathodic to 0.00 V, four-electron reduction gradually became to be involved. On the other hand, for the GC/PPy electrode, only two-electron O_2 reduction process occurs at the potential cathodic to 0.00 V. By incorporating CoTSP into PPy film, catalytic activity of O_2 reduction is found to be highly improved.

Oxygen Reduction Mechanism at GC/PPy/CoTSP Electrode. Figure 5 shows polarization curves for the GC/PPy/CoTSP electrode. Background currents for the GC/PPy/CoTSP electrode in N_2 atmosphere are almost the same for given range of rotation speeds. The background currents at given rotation speeds are already subtracted so that the polarization curves reflect only O_2 reduction reaction. At potentials from −0.2 V to −0.3 V, the polarization curves have the plateaus and can reasonably be understood as the limiting currents. Therefore, the Kouteckty-Levich plots can be applied to these curves. According to the

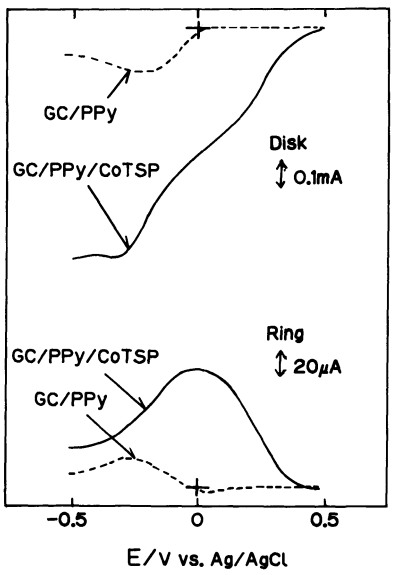

Fig. 4. Ring-disk current vs. potential curves for GC/PPy/CoTSP electrode (solid line) and GC/PPy (dashed line) formed at 1.2V vs. Ag/AgCl in 0.1 mol dm^{-3} Na_2SO_4+0.1 mol dm^{-3} pyrrole monomer at 960 rpm in 0.05 mol dm^{-3} H_2SO_4.

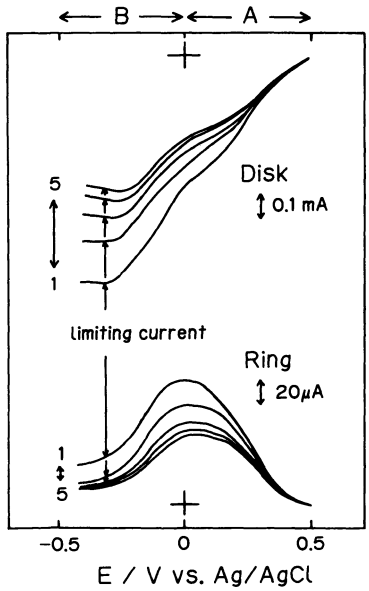

Fig. 5. Ring-disk current vs. potential curves for GC/PPy/CoTSP electrode at various rotation speeds in 0.05 mol dm^{-3} H_2SO_4 in O_2(solid lines) and N_2 (dashed line) atmosphere. The numbers 1, 2, 3, 4, and 5 correspond to 960, 610, 420, 310, and 240 rpm, respectively.

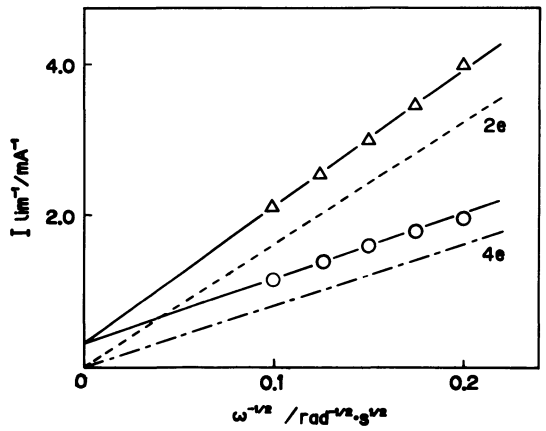

Fig. 6. Kouteckty-Levich plots for O_2 reduction reaction at GC/PPy/CoTSP electrode (—○—) and GC electrode in 10^{-3} mol dm^{-3} CoTSP (—△—) in 0.05 mol dm^{-3} H_2SO_4. Theoretical lines for two- and four-electron exchange reactions of O_2 reduction at bare electrode are indicated in the figure.

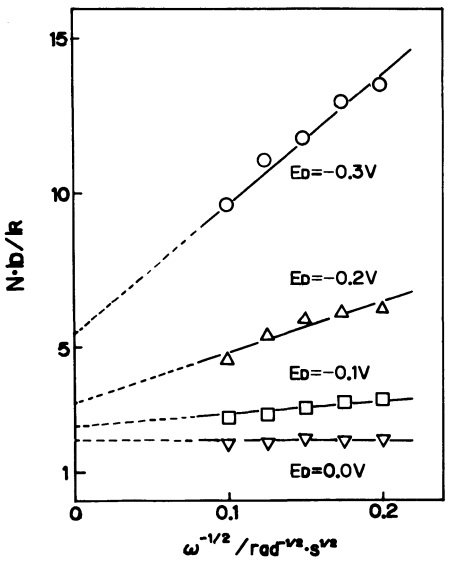

Fig. 7. NI_D/I_R vs. $\omega^{-1/2}$ plots for O_2 reduction reaction at GC/PPy/CoTSP electrode at various disk potentials in 0.05 mol dm^{-3} H_2SO_4. The disk potentials are indicated in the figure.

shape of ring currents, O_2 reduction mechanism can be discussed in two potential regions, viz., **A**: 0 V to 0.5 V, **B**: −0.50 V to 0 V. For the GC/PPy/CoTSP electrode in region **A**, O_2 reduction appears to occur from ca. 0.5 V, partly via H_2O_2, and the ring current steadily increases. In region **B**, the ring current of the GC/PPy/CoTSP electrode shows reverse behavior to that in region **A**, and the intermediate H_2O_2 gradually decreases for the GC/PPy/CoTSP electrode. It is assumed that O_2 reduction at the GC/PPy/CoTSP electrode partly became to involve four-electron transfer process at the transition potential region from **A** to **B**. Thus, for the GC/PPy/CoTSP electrode, the reaction path changed partly from two-electron process to four-electron process in this potential region.

Figure 6 shows the Kouteckty-Levich plots for the GC/PPy/CoTSP electrode and the GC electrode in dissolved CoTSP at the potential at which the limiting current was observed. The disk limiting current(I_{lim}) can generally be expressed as follows;[18]

$$1/I_{lim} = 1/I_k + 1/(I_d)_{lim} \quad (1)$$

$$(I_d)_{lim} = 0.62\,nFAD^{2/3}\nu^{-1/6}\omega^{1/2}Cb, \quad (2)$$

where $(I_d)_{lim}$, I_k, Cb, D, ν are the diffusion limiting current, the reaction controlled current, the dissolved O_2 concentration, the diffusion coefficient of O_2, the kinematic viscosity of the solution, respectively. Theoretical values for two- and four-electron reduction are calculated by using Eq.2 and the values of D and ν in Ref.[13] For both electrodes, the linear relationship between the reciprocal of limiting current and (rotation speed)$^{-1/2}$ are shown. The plot for the GC electrode in dissolved CoTSP is in good agreement with the theoretical two-electron reduction.

In contrast, for the GC/PPy/CoTSP electrode, the slope is almost the same as the theoretical four-electron reduction. The reaction controlled current is observed at the intercept with I_{lim} axis for the GC/PPy/CoTSP eletrode.

Figure 7 shows NI_D/I_R vs. $\omega^{-1/2}$ plots as a function of disk potentials. All plots yield straight lines with their intercepts above unity. The increase of the slope is observed with an increase of cathodic potential. Further information on an apparent electroreduction can be obtained from the diagnostic criterion suggested by Wroblowa et al.[19] By postulating a generalized scheme[19] for possible oxygen electroreduction at the GC/PPy/CoTSP, disk current(I_D) to ring current(I_R) ratio was derived as follows:

$$N(I_D/I_R) = 1 + 2k_1/k_2 + A + (k_{-5}/Z\omega^{1/2})A$$

where

$$A = (2k_1/k_2k_5)(k_{-2}+k_3+k_4) + (2k_3+k_4)/k_5 \quad (3)$$

$$Z = 0.62D^{2/3}\nu^{-1/6}$$

with N, D, ν, and ω are the collection efficiency, the diffusion coefficient of peroxide, the kinematic viscosity and the angular velocity of electrode. Equation 3 involves the two main reaction pathways, i.e., four-electron reduction to H_2O (k_1) and two-electron reduction to H_2O_2 (k_2). Adsorbed H_2O_2 proceeds to the following reactions; **1**. further two-electron reduction to H_2O(k_3), **2**. reoxidation to O_2(k_{-2}), **3**. catalytic decomposition of adsorbed H_2O_2 to O_2 and H_2O(k_4), **4**. desorption of adsorbed H_2O_2(k_5).

Equation 3 reduces to Eq. 4 with the intercept(J) and slope (s) of the NI_D/I_R vs. $\omega^{-1/2}$ plots.

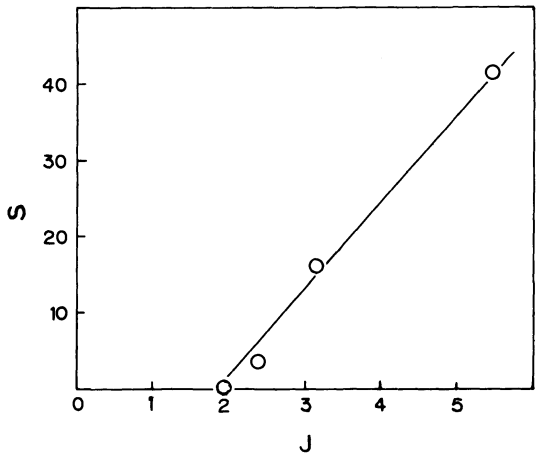

Fig. 8. Intercept(J) vs. slope (S) plot for O_2 reduction at GC/PPy/CoTSP electrode as a function of disk potentials.

$$J = 1 + 2k_1/k_2 + SZ/k_{-5} \quad (4)$$

Slope (S) was plotted against J at several disk potentials and indicated in Fig. 8. A straight line with the intercept $J'=2$ was yielded. When $k_1 \neq 0$, and k_1/k_2 is independent of potential, J vs. S plots should become linear with the intercept $J'>1$ as follows:

$$J' = 1 + 2k_1/k_2 \quad (5)$$

Hence, there is a parallel mechanism of four-electron direct reduction to H_2O and two-electron reduction to H_2O_2 process. The increase of S with an increase of cathodic potential is considered to be caused mainly by the occurrence of further oxidation from H_2O_2 to H_2O.

Cyclic Voltammograms for GC/PPy/CoTSP Electrode and GC Electrode in Dissolved CoTSP. One of the reasons of the high catalytic improvement for GC/PPy/CoTSP electrode would be deduced from the results in Fig. 9. In Fig. 9 a), a small redox peak was observed at around 0.3 V which may due to the redox reaction of CoTSP doped PPy film. The peaks are not so distinct because of the hindrance of PPy background, but they can be identified as ca. 0.31 V and ca. 0.22 V for anodic and cathodic peak potentials in N_2 atmosphere. The cathodic current peak at 0.22 V was increased when the solution was saturated with O_2. This catalytic reduction can be caused by the mediation effect of the redox couple at 0.30 V. As shown in Fig. 9b), O_2 reduction occurred at ca. 0.00 V which was far cathodic to the onset potential for the GC/PPy/CoTSP electrode. Therefore, the GC/PPy/CoTSP electrode has a favorable conditions with respect to the onset potential of O_2 reduction reaction. For the GC/PPy/CoTSP electrode, PPy matrix makes the redox potential more cathodic, which, as a result,

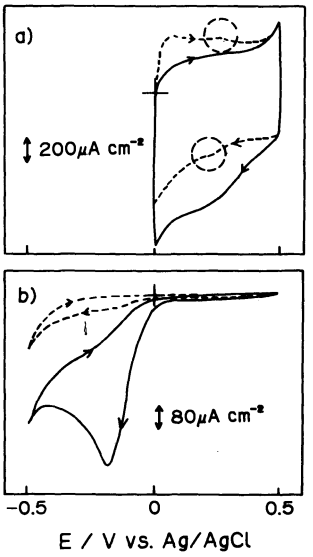

Fig. 9. Cyclic voltammograms for a) GC/PPy/CoTSP electrode and b) GC electrode in 10^{-3} mol dm^{-3} CoTSP at a scan rate of 50 mV s^{-1} in 0.05 mol dm^{-3} H_2SO_4 solution in O_2 (solid line) and N_2 (dashed line) atmosphere.

happen to form a favorable energy level of the CoTSP metal center for the formation of O_2 adduct with Co metal center of CoTSP.

The authors are indebted to Prof. Noboru Oyama and Dr. Takeo Ohsaka at Tokyo University of Agriculture and Technology for their valuable discussions and Mrs. Michiko Maeda at Japan Women's University for supplying CoTSP.

References

1) e.g., Proc. of Symp. on Electrocatalysis, ed by M. W. Breiter, Electrochem. Soc., 1974.

2) H. Behret, W. Clauberg, and G. Sandstede, *Z.Phys. Chem. NF*, **113**, 97 (1978).

3) A. Bettelheim, R. Parash, and D. Ozet, *J. Electrochem. Soc.*, **129**, 2247 (1982).

4) J. P. Collman, P. Denisevich, Y. Konai, M. Marroco, C. Koval, and F. C. Anson, *J. Am. Chem. Soc.*, **102**, 6027 (1980).

5) D. A. Butty and F. C. Anson, *J. Am. Chem. Soc.*, **106**, 59 (1984).

6) R. A. Bull, F. R. Fan, and A. T. Bard, *J. Electrochem. Soc.*, **131**, 687 (1983).

7) K. Okabayashi, O. Ikeda, and H. Tamura, *J. Chem. Soc., Chem. Commun.*, **1983**, 684.

8) O. Ikeda, K. Okabayashi, N. Yoshida, and H. Tamura, *J. Electroanal. Chem.*, **191**, 157 (1985).

9) T. Osaka, M. Nishikawa, and S. Nakamura, *Denki Kagaku*, **52**, 370 (1984).

10) J. H. Weber and D. H. Busch, *Inorg. Chem.*, **4**, 489 (1965).

11) L. D. Rollman and R. T. Iwamoto, *J. Am. Chem. Soc.*, **90**, 1455 (1968).

12) H. Kobayashi, Y. Torii, and N. Fukuda, *Nippon Kagaku Zasshi*, **81**, 694 (1960).
13) J. Zagal, P. K. Sen, and E. Yeager, *J. Electrochem. Soc.*, **87**, 207 (1977).
14) J. Zagal, P. Bindra, and E. Yeager, *J. Electrochem. Soc.*, **127**, 1506 (1980).
15) R. A. Bull, F. F. Fan, and A. J. Bard, *J. Electrochem. Soc.*, **129**, 1009 (1982).
16) A. Diaz, J. M. V. Vallejo, and A. M. Duran, *IBM J. Res. Develop.*, **25**, 42 (1981).
17) H. Behret, H. Binder, G. Sandante, and G. G. Scherer, *J. Electroanal. Chem.*, **117**, 29 (1981).
18) e.g., A. J. Bard and L. R. Faulkner, "Electrochemical Method, Fundametal and Application," Wiley, New York (1980).
19) H. S. Wroblowa, Y. CH. Pan, and G. Razumney, *J. Electroanal. Chem.*, **69**, 195 (1976).

 © 1986 The Chemical Society of Japan Bull. Chem. Soc. Jpn., 59, 2723—2728 (1986)

Photochemical Magnetic-Field Effects of Isoquinoline *N*-Oxide in Various Alcohols

Norisuke HATA
Department of Chemistry, College of Science and Engineering, Aoyama Gakuin University, Chitosedai, Setagaya-ku, Tokyo 157
(Received April 8, 1986)

A pronounced solvent dependence of the magnetic-field effect due to the HFI-J mechanism was found for the first time in the case of a photochemical isomerization of isoquinoline *N*-oxide into lactam (1-isoquinolone). The chemical yield of the lactam showed a minimum at a higher magnetic field as one changes the reaction medium from *t*-butyl alcohol to 2-propanol (or ethanol) and then to methanol, which was the same order as the pK_a value (*t*-butyl alcohol>2-propanol≈ethanol>methanol). Such a solvent dependence provides corroborating evidence that the photoisomerization proceeds via the S_1-born singlet radical-ion-pair intermediate, which is linked by a hydrogen bond between the N→O group in the cation radical of *N*-oxide and the OH group in the anion radical of alcohol. Another interesting finding was that, in the case of the photochemical isomerization in *t*-butyl alcohol, the chemical yield of the lactam showed distinct maxima at approximately 0.9T and 1.35T in addition to a minimum at about 0.72T. The anomalous magnetic-field effect in a high field region (>0.8T) could reasonably be explained in terms of an HFI-J mechanism by assuming the T_1-born triplet hydrogen-bonded radical-ion pair to have an electron-exchange interaction larger than that in the S_1-born singlet hydrogen-bonded radical-ion pair.

As has been described in a previous paper,[1] the photochemical isomerization of isoquinoline *N*-oxide in ethanol was found to show a new type of magnetic-field effect in 1976, the chemical yield of the product (1-isoquinolone) having a minimum at approximately 1T. This phenomenon was successfully interpreted in terms of a hyperfine-interaction mechanism including an electron-exchange interaction (HFI-J mechanism) in the S_1-born singlet hydrogen-bonded radical ion-pair, assumed to be a transient intermediate of this reaction. In 1979 the photochemical magnetic-field effect was found to depend greatly on the pK_a of the alcohol (methanol, ethanol, 2-propanol, or *t*-butyl alcohol) used as a reaction medium; further, in the case of a *t*-butyl alcoholic solution, an anomalous field dependence of the chemical yield was observed at a magnetic field higher than 0.8T.[2] These findings were partly reported in a preliminary form.[2] The present paper will present further details of these phenomena, together with an interpretation.

Experimental

The isoquinoline *N*-oxide **1** used as a sample was prepared and purified according to the method described in a previous paper;[1] mp 103—105 °C. The 1,3-cyclohexadiene used as a triplet quencher was a reagent-grade product of the Tokyo Kasei Kogyo Co., which was further purified by distillation; bp 80—81 °C. The methanol, 2-propanol, and *t*-butyl alcohol used as the photoreaction medium were reagent-grade products of Wako Pure Chemical Industries.

The experimental procedure was quite similar to that described proviously;[1] a 50-cm^3 portion of an alcoholic solution (methanol, 2-propanol or *t*-butyl alcohol) containing 35 mg of isoquinoline *N*-oxide in a quartz vessel (44×45×25 mm) was irradiated with a 500W Ushio super-high-pressure Mercury Lamp (USH-500D) equipped with a Toshiba filter UV-31 for 15 min in the cases of methanolic and 2-propanolic solutions (or 10 min in the case of a *t*-butyl alcoholic solution), while nitrogen was being bubbled in, in a magnetic field of 0—1.65T at room temperature. A similar experiment was also performed on a *t*-butyl alcoholic solution containing the *N*-oxide (35 mg) and 1,3-cyclohexadiene (4.80×10^{-1} mol dm^{-3}). In the case of a methanolic or 2-propanolic solution, unreacted *N*-oxide **1** and a photoproduct (lactam) **2** were separated by means of silica-gel TLC (Merck silica-gel plate $60F_{254}$; layer thickness, 2 mm; the eluent, benzene–ethanol–diethyl ether (5:1:2)). In the case of a *t*-butyl alcoholic solution, the irradiated solution was chromatographed on an alumina column (Wako activated aluminium oxide, about 300 mesh) by elution with chloroform–diethyl ether (1:3), chloroform–ethanol (40:1), and then chloroform–ethanol (20:1) to separate some decomposition products, unreacted *N*-oxide **1** and then lactam **2**. The amounts of the unreacted *N*-oxide **1** and the product **2** were determined spectrophotometrically. The UV absorption spectra were taken with a Shimadzu recording spectrophotometer, UV-220.

Results and Discussion

The irradiation of isoquinoline *N*-oxide **1** in hydroxylic solvent (ROH) leads to the isomerization into lactam **2** (1-isoquinolone) and 1,3-benzoxazepine **3** (Eq. 1), but the latter product **3** is quite unstable and can not be isolated.[1,3]

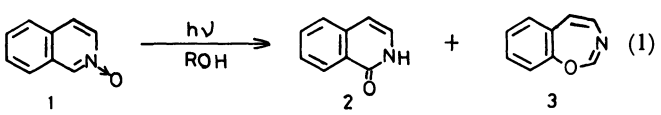

1 2 3 (1)

As has been reported previously,[1] when the photochemical isomerization of isoquinoline *N*-oxide **1** in ethanol was carried out in the presence of a magnetic field, the chemical yield of lactam **2** showed a minimum at approximately 1T (Fig. 2). In order to interpret this phenomenon, "the radical-ion-pair mechanism" (as shown in Scheme 1) has been proposed for the photoisomerization of isoquinoline

N-oxide **1** into lactam **2** in hydroxylic solvents (ROH).[1] In this scheme, the field-sensitive singlet radical-ion-pair intermediate **2a** responsible for the formation of lactam **2** was reasonably assumed to be formed by the transfer of an electron (πO:) from the excited singlet *N*-oxide (S_1) to the hydrogen-bonded alcohol (ROH). The exchange interaction between the unpaired electrons in the pair **2a** is thought to be larger than the electron-nuclear hyperfine interaction, for the radical centers are in close proximity as a result of hydrogen-bonding interaction between the radical ions. This means that, as is shown in Scheme 2, the singlet (S) and triplet ($T_{0,\pm}$) levels of the S_1-born radical-ion pair (**2a** and **2a'**) are nondegenerate, having an energy gap of $2|J|$, where J denotes the electron-exchange integral. Therefore, the hyperfine-induced intersystem crossing ($S \leftrightarrow T_{0,\pm}$) of the pair does not occur at the zero field. As can be seen from Scheme 2, however, the application of the magnetic field to this system causes a crossing of the levels of S and T_+ at a particular magnetic field, H_1. Consequently, the chemical yield of the lactam **2** as an S_1-born cage product comes to show a minimum at this field strength, H_1 (ca. 1T in Fig. 2), i.e., the magnetic-field dependence of the chemical yield of the S_1-born cage product due to the HFI-J mechanism.[4]

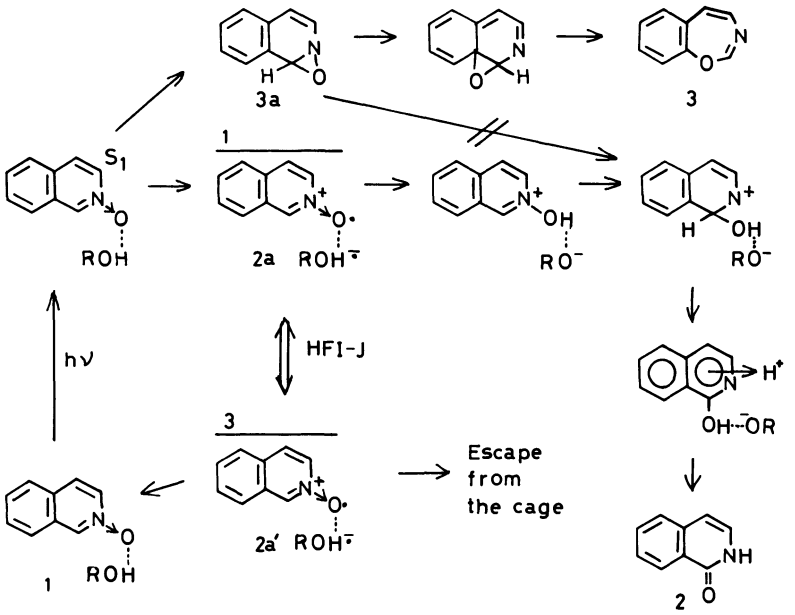

Scheme 1.

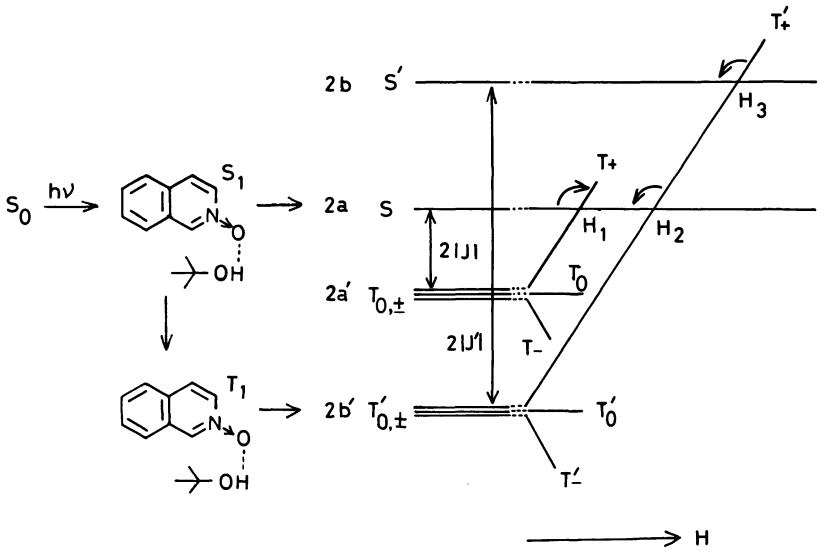

Scheme 2.

If this interpretation is valid, the magnetic field, H_1, should be progressively shifted to a higher field as the electron-exchange interaction in the radical-ion pair **2a** increases, because the electron-exchange interaction determines the singlet-triplet splitting ($2|J|$) of the pair.[6] The exchange integral, $J(r)$, depends exponentially on the interradical distance, r, according to:

$$J(r) = J_0\exp(-\alpha r) \quad (2)$$

where α is a parameter.[6a] In the photochemical system under consideration, the distance between the radical centers of the pair **2a** can be assumed to vary with the pK_a of the reaction medium (ROH) which is linked by hydrogen bond to the oxygen atom of the *N*-oxide. This, in turn, leads to the idea that the electron-exchange interaction is dependent on the pK_a of the alcohol used as a reaction medium. The values of pK_a of some conventional aliphatic alcohols are known to be in the following order:[7] *t*-butyl alcohol>2-propanol≈ethanol>methanol. Accordingly, the magnetic field, H_1, responsible for the minimal yield of lactam **2** can be expected to be shifted to a progressively higher field as the reaction medium is changed from *t*-butyl alcohol to 2-propanol (or ethanol) and then methanol. In order to determine whether or not this presumption is correct, therefore, the photochemical isomerizations of isoquinoline *N*-oxide in the various alcohols were examined in either the absence or presence of a magnetic field.

In the absence of a magnetic field, the chemical yield of lactam **2** was dependent on the nature of the alcohol used as a reaction medium, decreasing in this order: methanol (ca. 74%), ethanol (ca. 67%), 2-propanol (ca. 55%) and *t*-butyl alcohol (ca. 43%), where the values in parentheses are the chemical yields.

Figures 1 to 4 show the results when the chemical yield of lactam **2** in various alcohol is plotted as a function of the magnetic-field strength. In the case of a 2-propanolic solution (Fig. 3), the minimal yield (ca. 44%) was observed at approximately 1T, just as in the case of an ethanolic solution (Fig. 2) reported previously.[1] In the case of a methanolic solution (Fig. 1), the chemical yield of lactam **2** was ca. 74% at a magnetic field below 1.4T, but it decreased steeply with an increase in the field strength reaching ca. 68% at 1.62T. It may safely be concluded from this finding that a minimal yield would appear in the vicinity of

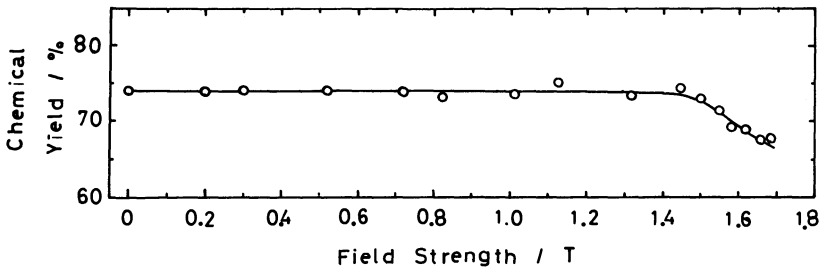

Fig. 1. Photochemical magnetic field effect of isoquinoline *N*-oxide **1** in methanol. Chemical yield of lactam **2** vs. magnetic field strength. [**1**]=4.81×10^{-3} mol dm^{-3}. Irradiation time: 15 min. Conversion: ca.18%.

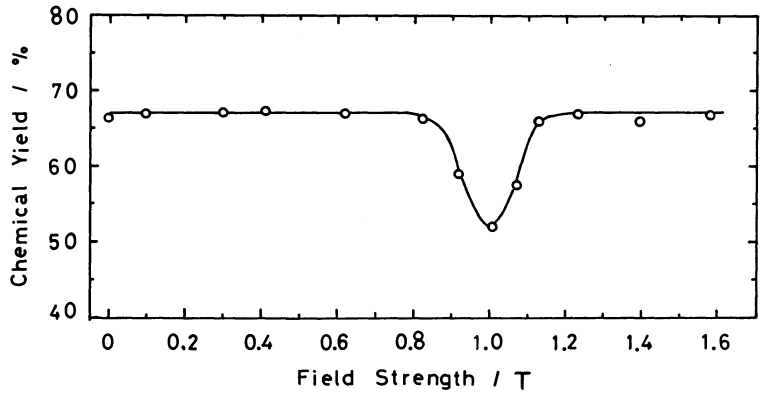

Fig. 2. Photochemical magnetic field effect of isoquinoline *N*-oxide **1** in ethanol. Chemical yield of lactam **2** vs. magnetic field strength.[1] [**1**]=4.82×10^{-3} mol dm^{-3}. Irradiation time: 10 min. Conversion: ca. 17%.

1.7T, although the measurement was not performed at a magnetic field above 1.65T because of the limited capability of the electromagnet employed in the experiment. In the case of a *t*-butyl alcoholic solution, unexpectedly, the complicating magnetic-field effect shown by Curve (a) in Fig. 4 was observed; the chemical yield of lactam **2** showed two maxima (ca. 50 and 55%), at approximately 0.9 and 1.35T, as well as a minimum (ca. 34%) at about 0.72T. The anomalous magnetic-field effect in the high-field region (>0.8T) disappeared completely upon the addition of 1,3-cyclohexadiene, C_6H_8, (triplet quencher)[8] to the reaction system, while a minimum of the chemical yield was still observed at approximately 0.75T (Curve (b) in Fig. 4). The results indicate clearly that the quencher-insensitive-field effect around 0.7T should be assigned to the HFI-J magnetic-field effect, which can itself be ascribed to the S_1-born singlet hydrogen-bonded radical-ion pair **2a**. The anomalous and quencher-sensitive magnetic-field effect will be discussed later.

The experimental results described above are, surprisingly, in fair agreement with the presumption that a minimum in the chemical yield of lactam **2** may appear at a higher magnetic field as one changes the reaction medium in the order: *t*-butyl alcohol, 2-propanol (or ethanol) and methanol. Hence, the observed solvent dependence can be taken as corroborating evidence that, as is shown in Scheme 1, the photochemical isomerization of isoquinoline *N*-oxide **1** into lactam **2** in hydroxylic solvents (ROH) occurs with the intervention of the S_1-born singlet hydrogen-bonded radical-ion pair **2a**, but it does not proceed via the S_1-born oxaziridine **3a** previously postulated as an intermediate of this reaction (cf. Ref. 1).

Next, let us discuss the anomalous field dependence of the chemical yield that is observed only in the case of *t*-butyl alcoholic solution in a magnetic field above 0.8T. As can be seen from Fig. 4, the chemical yield of lactam **2** showed distinct maxima at approximately 0.9 and 1.35T, but this effect disappeared upon the

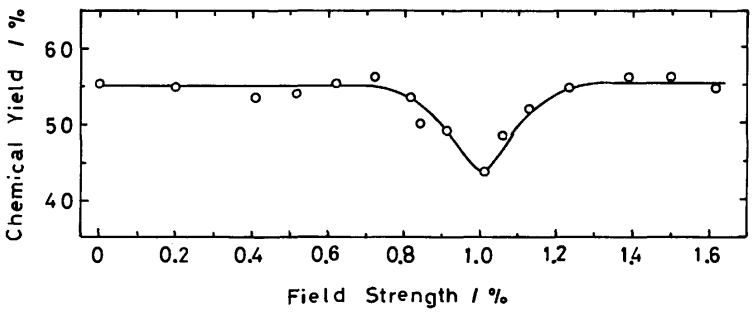

Fig. 3. Photochemical magnetic field effect of isoquinoline *N*-oxide **1** in 2-propanol. Chemical yield of lactam **2** vs. magnetic field strength. $[\mathbf{1}]=4.82\times10^{-3}$ mol dm^{-3}. Irradiation time: 15 min. Conversion: ca. 16%.

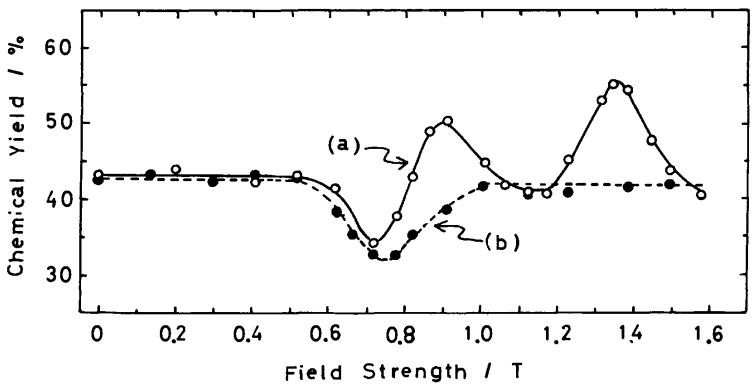

Fig. 4. Photochemical magnetic field effect of isoquinoline *N*-oxide **1** in *t*-butyl alcohol. Chemical yield of lactam **2** vs. magnetic field strnegth. $[\mathbf{1}]=4.81\times10^{-3}$ mol dm^{-3}.
(a) —○—: $[C_6H_8]=0$. Irradiation time: 10 min. Conversion: ca. 17%.
(b) --●--: $[C_6H_8]=4.80\times10^{-1}$ mol dm^{-3}. Irradiation time: 10 min. Conversion: ca. 12%.

addition of the triplet quencher. The quencher-sensitive magnetic-field effect showed, of course, the same pattern as that for the field dependence of the chemical yield of the T_1-born cage product due to the HFI-J mechanism (cf. Fig. 6 in Ref. 5).[4] This strongly suggests that the transfer of an electron (πO:) from the *N*-oxide to the hydrogen-bonded alcohol occurs not only in the S_1 state, but also in the T_1 state, to produce two kinds of field-sensitive radical-ion-pair intermediates (**2a** and **2b′**) quite similar to each other (Scheme 2). The only difference between the two pairs is the magnitude of the electron-exchange interaction. The exchange interaction in the T_1-born radical ion pair, **2b′**, should be much larger than that in the S_1-born radical ion pair, **2a**, since the maximal yields of the lactam **2** as a T_1-born cage product appear in a higher-field region compared to the minimal yield of the lactam **2** as an S_1-born cage product. For the formation of such radical-ion pairs, a hydrogen-bonding interaction between the oxygen atom of the *N*-oxide and the alcoholic solvent has to be much stronger in the T_1 state than in the S_1 state.

Kubota et al.[9] have demonstrated clearly, prior to 1972, from solvent-effect studies of the absorption (singlet–singlet and singlet–triplet) and fluorescence spectra of some heterocyclic *N*-oxides, that the hydrogen-bonding ability of the oxygen atom of the N→O group is much larger in the S_0 and T_1 states than in the S_1 state; this is in conformity with the result of molecular-orbital consideration that the charge transfer from the oxygen atom of the N→O group to the ring π-electron system is much larger in the S_1 state than in the S_0 and T_1 states. The results strongly support the idea that the T_1-born triplet hydrogen-bonded radical-ion pair **2b′** has an electron-exchange interaction (J') much larger than that (J) in the S_1-born singlet hydrogen-bonded radical-ion pair **2a**.

One may construct a schematic energy-level diagram (as is shown in Scheme 2) for the hydrogen-bonded radical-ion pairs produced from the S_1 and T_1 states, by considering that the singlet-triplet splitting ($2|J'|$) in the T_1-born radical-ion pair is greater than that ($2|J|$) in the S_1-born radical-ion pair. On the basis of this diagram, the observed photochemical magnetic-field effect of isoquinoline *N*-oxide in *t*-butyl alcohol can be reasonably interpreted in terms of an HFI-J mechanism as follows.

In the absence of an external magnetic field, the hyperfine-induced intersystem crossing ($S \rightarrow T_{0,\pm}$ or $T'_{0,\pm} \rightarrow S'$) from the S_1-born singlet or T_1-born triplet radical-ion pair (**2a** or **2b′**) does not occur at the zero field because of the large electron-exchange interaction. As a result, the S_1-born singlet hydrogen-bonded radical-ion pair **2a** mostly undergoes a geminate reaction within a solvent cage to give rise to lactam **2** as an S_1-born cage product, whereas the T_1-born triplet hydrogen-bonded radical-ion pair **2b′** undergoes a diffusive separation into the solvent bulk. However, the application of the magnetic field to this system resolves the triplet level $T_{0,\pm}$ (or $T'_{0,\pm}$) into three sublevels, T_0, T_+, and T_- (or T'_0, T'_+, and T'_-), and the T_+ (or T'_+) level approaches the S and S′ levels as the field strength increases. Consequently, a crossing of the levels of S and T_+ occurs first at the magnetic field of H_1 and the chemical yield of the lactam **2** as an S_1-born cage product becomes minimal, corresponding to a minimal yield around 0.7T (Fig. 4). A further increase in the field strength causes an intersystem crossing of $T'_+ \rightarrow S$ at the magnetic field H_2,[10] followed by a crossing from the T'_+ to S′ levels at the magnetic field H_3. As a result, the chemical yield of the lactam **2** as a T_1-born cage product comes to show maxima at the magnetic fields of H_2 and H_3, corresponding probably to maximal yields at approximately 0.9 and 1.35T (Curve (a) in Fig. 4).

In the case of a methanolic, ethanolic or 2-propanolic solution, no such anomalous field effect was observed at all at any magnetic field below 1.65T (Figs. 1 to 3). This is probably because a hyperfine-induced intersystem crossing between the T'_+ and S (or S′) levels can not occur in this field region because of a large electron-exchange interaction in the hydrogen-bonded radical-ion-pair intermediate.

Conclusion

Remarkable solvent dependences of the magnetic-field effect attributable to the HFI-J mechanism were found for the first time in the case of a photochemical isomerization of isoquinoline *N*-oxide **1** into lactam **2** in alcoholic solvents. First, the chemical yield of the lactam **2** as an S_1-born cage product showed a minimum at a particular magnetic field, which was progressively shifted to a higher field as the reaction medium (ROH) was changed from *t*-butyl alcohol to 2-propanol (or ethanol) and then methanol. Such a solvent dependence was attributable to the influence of an electron-exchange interaction on the hyperfine-induced intersystem crossing of the S_1-born singlet hydrogen-bonded radical-ion pair **2a**, assumed to be a transient intermediate of this reaction. Second, in the case of a *t*-butyl alcoholic solution, the chemical yield of lactam **2** showed two maxima in the field region of 0.8—1.4T, in addition to a minimum at ca. 0.7T. This phenomenon was also reasonably explained in terms of an HFI-J mechanism by assuming the formation of the triplet hydrogen-bonded radical-ion pair **2b′** from the T_1 state (Scheme 2). The present studies demonstrate definitely that the photochemical isomerization of isoquinoline *N*-oxide in hydroxylic solvent proceeds according to the mechanism shown in Scheme 1.

References

1) N. Hata, *Bull. Chem. Soc. Jpn.*, **58**, 1088 (1985); Preliminary reports, N. Hata, *Chem. Lett.*, **1976**, 547; **1978**, 1359.

2) N. Hata, Y. Ono, and F. Nakagawa, *Chem. Lett.*, **1979**, 603; N. Hata and A. Yagi, *Chem. Lett.*, **1983**, 309.

3) As to the photochemistry of aromatic amine *N*-oxides, see, for example, G. G. Spence, E. C. Taylor, and O. Buchardt, *Chem. Rev.*, **70**, 231 (1970); F. Bellamy and J. Streith, *Heterocycles*, **4**, 1391 (1976); A. Albini and M. Alpegiani, *Chem. Rev.*, **84**, 43 (1984).

4) The magnetic-field dependence of the chemical yield is currently classified into six patterns, depending on whether the product is a cage- or escape-product and an S_1-or T_1-born product, and also on whether the magnetic perturbation is due to the Δg, HFI, or HFI-J mechanism. See Appendix in Ref. 5.

5) N. Hata and N. Nishida, *Bull. Chem. Soc. Jpn.*, **58**, 3423 (1985).

6) The influence of an electron-exchange interaction on the magnetic-field effect has been reported recently for biradicals of polymethylene-linked compounds (A-$(CH_2)_n$-D)[a] or cyclohexanones.[b] a) A. Weller, H. Staerk, and R. Treichel, *Faraday Discuss. Chem. Soc.*, **78**, 271 (1984); b) M. B. Zimmt, C. Doubleday, Jr., and N. J. Turro, *J. Am. Chem. Soc.*, **107**, 6726 (1985).

7) W. K. McEwen, *J. Am. Chem. Soc.*, **58**, 1124 (1936).

8) The excitation energy of the T_1 state of isoquinoline *N*-oxide has been estimated from the phosphorescence maximum to be about 224.5 kJ mol^{-1}; I. Ono and N. Hata, *Bull. Chem. Soc. Jpn.*, **46**, 3658 (1973).

9) T. Kubota and H. Miyazaki, *Chem. Pharm. Bull.*, **9**, 948 (1961); N. Mataga and T. Kubota, "Molecular Interaction and Electronic Spectra," M. Dekker, New York (1970), Chap. 7; T. Kubota, M. Miyazaki, M. Yamakawa, and Y. Mizuno, *Bull. Chem. Soc. Jpn.*, **45**, 3282 (1972).

10) The fact that the chemical yield of lactam **2** shows a maximum at the magnetic field of H_2 (ca. 0.9T in Fig. 2) indicates explicitly that the intersystem crossing $T'_+ \rightarrow S$ occurs, while the $S \rightarrow T'_+$ does not. This is probably because a geminate reaction (**2a**→**2b**) of the singlet hydrogen-bonded radical-ion pair **2a** takes place much faster than the intersystem crossing $S \rightarrow T'_+$.

Basis Set Dependency of Molecular Electronic Structures

Hiroshi Ichikawa,* Keiichiro Sameshima, and Yukiko Ebisawa
Hoshi College of Pharmacy, Shinagawa-ku, Tokyo 142
(Received April 14, 1986)

The total atomic charges as well as the kinetic and potential energies calculated using 22 different basis sets were compared. It was shown that polarization functions must be added to atoms of the first row as well as the hydrogen atom in order to obtain well-balanced wave functions. The STO-*N*G (*N*=3, 4, 5, or 6) method, which is considered to give poor wave functions, is shown to give well-balanced wave functions.

It is unnecessary to say that ab initio molecular orbital (MO) theories have been frequently used in explaining various molecular properties in terms of electronic structures. Energy partitioning based on ab initio MO theories has been effectively applied in analyses of chemical bonds[1] and aromaticity.[2,3]

So far, quantum chemists have proposed various types of basis sets (i.e. MO theories). However, much effort in creating a new basis set has been devoted to the lowering of the total energy and to reproducing the observed geometries; the electron distribution has been treated less effectively. As a result, electron distributions can be greatly changed according to the type of basis set used. There have been method-to-method comparisons reported between different basis sets, mainly by the originaters of new basis sets. However, the number of such comparisons is too small for determining the general aspects of various MO theories. This paper is to show how the electronic structures and partitioned energies are dependent on the adopted basis set. For this purpose we have examined those quantities using 22 different basis sets in the GAUSSIAN-80 program.[4,5]

Partitioning of Molecular Energies

If wave functions are to provide an understanding of the behavior of electrons in a molecule, one must try to extract, in some way, information on the physically essential features of electronic energies. One of the trends along this line is energy partitioning.[6] Since in LCAO MO theory each MO is expanded by a linear combination of atomic orbitals (AO's), and since via the Fock matrix three- and four-center integrals out of the two-electron integrals can be reduced to two-center terms, the energy (E) based on either the restricted[7] or unrestricted Hartree-Fock equation[8] is *formally* expressed by the sum of monocentric (E_A) and bicentric (E_{AB}) terms,

$$E = \sum_{A} E_A + \sum_{A>B} E_{AB}. \quad (1)$$

These terms were further partitioned as

$$E_A = E_A^V + E_A^J + E_A^T \quad (2)$$

and

$$E_{AB} = E_{AB}^V + E_{AB}^J + E_{AB}^N + E_{AB}^T, \quad (3)$$

where E^V, E^J, and E^T are the one-electron potential, two-electron potential and kinetic energies of the electrons. E_{AB}^N is the nuclear-repulsion energy between atoms A and B and is, of course, one of the potential energies in the given system. A detailed calculation method has been given elsewhere.[3]

According to the method of Mulliken population analysis,[9] the kinetic and potential energies concerning electrons belonging to a specified atom, X, KE(X) and PE(X) are, respectively, defined as,

$$\mathrm{KE(X)} = E_X^T + 1/2 \sum_{A} E_{XA}^T \quad (4)$$

and

$$\mathrm{PE(X)} = E_X^V + E_X^J + 1/2 \sum_{A>B} (E_{XA}^V + E_{XA}^J + E_{XA}^N). \quad (5)$$

Since the kinetic and potential energies are considered to be basic quantities with apparent physical meanings, we examined them in addition to the total atomic charges of the Mulliken population analysis.

Results and Discussion

1. Total Atomic Charge. The Mulliken population analysis[9] is probably the most-widely applied method in the analyses of the electronic structures in the various fields of chemistry. It is important to note that the total atomic charge obtained in a Mulliken population analysis must be dependent on the basis set since any assignment of charges to atoms in a molecule is necessarily arbitrary. Therefore, the absolute charges calculated by a Mulliken population analysis also tend to be dependent on the basis set. First, we show how much they are dependent.

Figure 1 shows the total atomic charge of the hydrogen atoms of vinylamine by 22 different ab initio MO methods,[5] where a geometry optimization was carried out for each MO calculation. We also obtained results for the hydrogen of methane, which appears to be almost the same as those of H_a. It is clearly shown that the calculated total atomic charge varies significantly according to the calculation method. However, there seem to be some tendencies in the results. It can

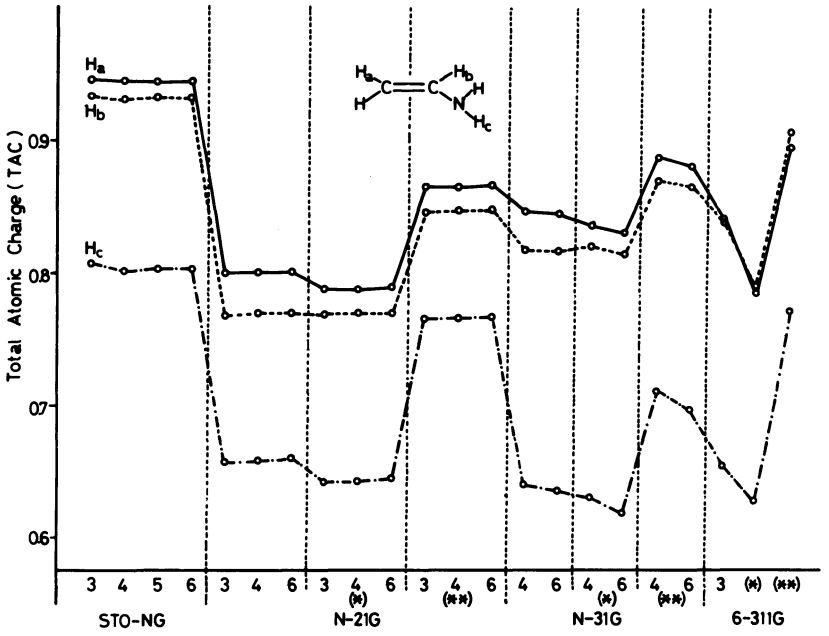

Fig. 1. Dependence of total atomic charge on basis set in hydrogen atoms of vinylamine.

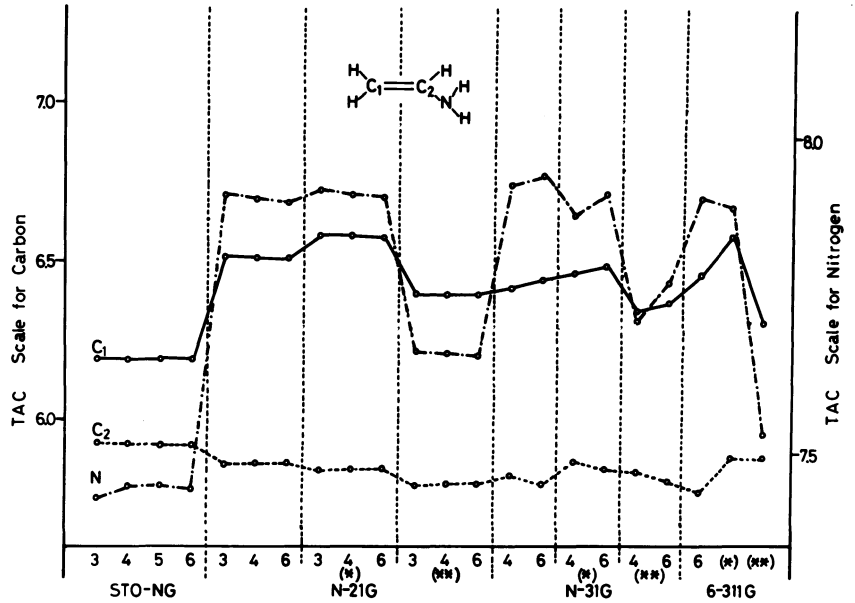

Fig. 2. Dependence of total atomic charge on basis set in carbon and nitrogen atoms of vinylamine.

be generally said that similar methods give similar electronic structures. The STO-*NG* series give almost the same total atomic charges, independently of the contraction number *N*.

In the split-valence methods, the number of the primitive gaussian functions for an inner-shell 1*s* AO has almost nothing to do with the total atomic charge of the hydrogen. "Single-star" methods generally give a total atomic charge for hydrogen that is too low, while "double-star" methods compensate such a loss of electrons on the hydrogen atoms. A good example is the difference of the results between the 6-311G* and 6-311G** methods, where the difference is most prominent.

Figure 2 shows the total atomic charges of C_1, C_2, and N for optimized structures of vinylamine. If we consider that the 6-311G** method gives the best-balanced wave function at present, any other split-

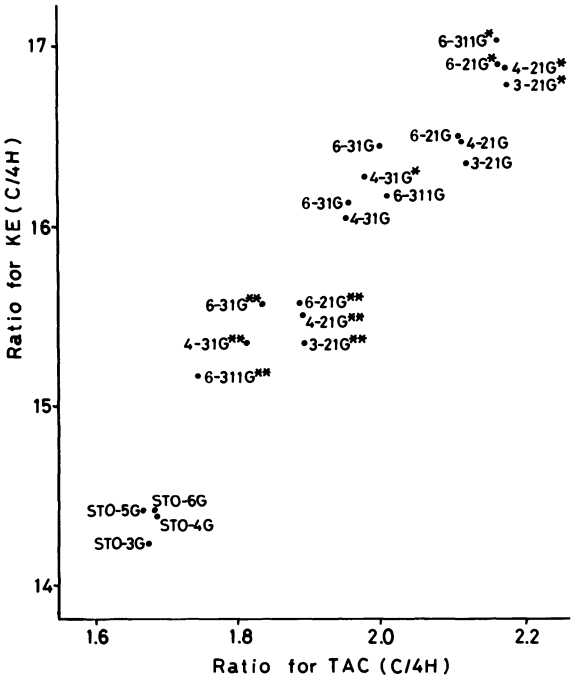

Fig. 3. Ratio of kinetic energies (C/4H) vs. ratio of total atomic charge (C/4H).

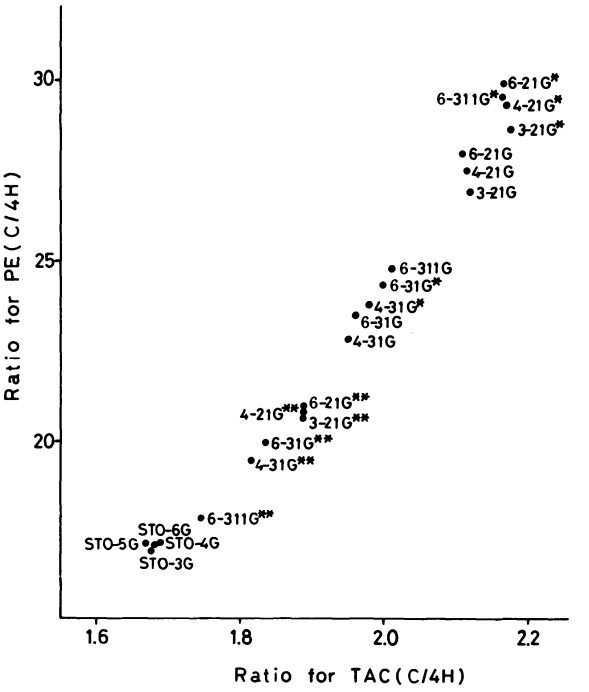

Fig. 4. Ratio of potential energies (C/4H) vs. ratio of total atomic charges (C/4H).

valence method without a "double-star" seems to produce off-balanced wave functions. Interestingly, the STO-*N*G method gives a very similar result to that of 6-311G**.

The above results suggest that the addition of polarization functions allows much freedom for electrons, resulting in a large electronic population on atoms with polarization functions. This indicates that polarization functions must be added to both the atoms of the first row and hydrogen atoms in order to obtain a well-balanced wave function. It should be stressed here that the total atomic charge obtained by STO-*N*G is very close to that obtained by 6-311G**, which is considered to be very close to the Hartree-Fock limit.

2. The Relationship between Total Atomic Charge and Partitioned Energies. Since the total energy is dependent on the basis set, a direct comparison of the partitioned energy with that of a different basis set is meaningless. As a matter of fact, we usually do not need the absolute energy, but only the relative energy or relative distribution of energy in a molecule with respect to the change of the molecular geometry. Accordingly, we examined the ratios of the total atomic charge and partitioned energies.

The horizontal axis of Figs. 3 or 4 represents the ratios of the total atomic charge of the carbon atom to the sum of those for four hydrogen atoms in methane. The ratios range from 1.685 to 2.174. It can again be said that a similar method gives similar results: a "single-star" series give results that are very different from that of 6-311G** because of an *unfair* addition of electronic freedom (only for carbon). The addition of a polarization function on hydrogen improves such a deformed wave function.

The vertical axes of Figs. 3 and 4 are for the ratios of the kinetic and potential energies, respectively. There is a close linear relationship between the ratios of the total atomic charge and that of the potential energy or the kinetic energy.

3. Basis Set Dependency of Partitioned Potential and Kinetic Energies. It was very fortunate to be able to obtain the result that STO-*N*G can reproduce a well-balanced wave function since STO-*N*G is a feasible method that can be applied to systems that are as large as those in which organic chemists show interest. We extended a similar examination in order to determine whether or not STO-*N*G gives a well-balanced wave function, regardless of the position of the bisection. Since it became clear that a similar method gives similar results, we only examined STO-3G, 3-21G, 4-31G, 6-31G*, and 6-311G**, and assumed that 6-311G** gives the best-balanced wave function out of all the methods.

Table 1 shows the results for carbon monoxide, formaldehyde, and ketene, where the ratios of the kinetic energies (KE(X)/KE(Y)) and the potential energies (PE(X)/PE(Y)) are also listed. We chose the oxygen-containing compounds as models, since such compounds are most liable to show a large depen-

Table 1. Ratios of the Potential and Kinetic Energies in Divided Systems

X†Y		STO-3G	3-21G	4-31G	6-31G*	6-311G**
C†O	KE[a]	0.5116	0.5003	0.5021	0.5060	0.5057
	PE[b]	0.4993	0.4835	0.4874	0.4958	0.4982
H_2†C=O	KE	0.0117	0.0108	0.0108	0.0107	0.0116
	PE	0.0100	0.0058	0.0066	0.0069	0.0102
H_2C†O	KE	0.5224	0.5185	0.5205	0.5214	0.5219
	PE	0.5166	0.5027	0.5049	0.5087	0.5124
H_2†C=C=O	KE	0.0082	0.0069	0.0071	0.0070	0.0077
	PE	0.0064	0.0012	0.0026	0.0023	0.0047
H_2C†C=O	KE	0.3483	0.3460	0.3462	0.3470	0.3461
	PE	0.3489	0.3450	0.3460	0.3501	0.3470
H_2C=C†O	KE	1.0338	1.0236	1.0265	1.0277	1.0284
	PE	1.0207	0.9918	0.9979	1.0019	1.0099

a) Ratio KE(X)/KE(Y). b) Ratio PE(X)/PE(Y).

Table 2. Ratios of the Potential and Kinetic Energies of Two Functional Groups

X†Y		STO-3G	3-21G	4-31G	6-31G*	6-311G**
CH_3†CH=CH_2	KE[a]	0.5105	0.5114	0.5115	0.5117	0.5109
	PE[b]	0.5111	0.5111	0.5116	0.5121	0.5074
CH_3†C≡CH	KE	0.5151	0.5178	0.5178	0.5192	0.5175
	PE	0.5162	0.5130	0.5114	0.5179	0.5122
CH_3†CN	KE	0.4267	0.4278	0.4282	0.4288	0.4276
	PE	0.4267	0.4246	0.4243	0.4271	0.4220
H†CN	KE	0.0057	0.0052	0.0053	0.0053	0.0063
	PE	0.0045	0.0006	0.0014	0.0016	0.0042
CH_3†NC	KE	0.4242	0.4254	0.4261	0.4276	0.4273
	PE	0.4212	0.4142	0.4135	0.4192	0.4196
H†NH_2	KE	0.0117	0.0101	0.0099	0.0097	0.0114
	PE	0.0082	0.0041	0.0034	0.0028	0.0079
CH_3†NH_2	KE	0.7121	0.7092	0.7096	0.7113	0.7106
	PE	0.7087	0.6985	0.6971	0.7014	0.7031
H†OH	KE	0.0089	0.0072	0.0072	0.0067	0.0089
	PE	0.0057	0.0013	0.0006	0.0004	0.0052
CH_3†OH	KE	0.5252	0.5223	0.5228	0.5237	0.5238
	PE	0.5225	0.5119	0.5119	0.5127	0.5159

a) Ratio KE(X)/KE(Y). b) Ratio PE(X)/PE(Y).

dence on the basis set. Comparing those ratios, we could again conclude that the STO-3G method reproduces the results of 6-311G** very well.

Next, we examined the partitioned energies bisected by a functional group. Table 2 shows the ratios of the kinetic and potential energies of the two functional groups. The ratios are similar, independent of the method unless one of the functional groups is hydrogen. As shown in the former section, the total atomic charge of hydrogen is most susceptible to a change in the basis set: the split-valence methods and the split-valence methods with polarization functions only for first row atoms ("single-star" series) are liable to cause a low electron distribution on hydrogen resulting in a large difference in the energy ratios from the STO-*N*G or 6-311G** methods. It was again ascertained that the STO-3G method gives the closest ratios to those by the 6-311G** method in all kinds of functional partitionings.

Thus, we have obtained very instructive results regarding the choice of the basis set in a MO calculation. It is well known that the larger is the adopted basis set, the better the molecular wave function. It can be obtained simply because of the lower total energy. However, this does not apply to the electron distribution in the system. The addition of polarization functions to only first row atoms gives the most deformed wave functions. Instead, the STO-*N*G method, which was considered to give a poor wave function, was found to produce a well-balanced wave function. Recently, contour maps have been widely used in an explanation of the molecular properties and the reaction processes in cases where the shape of molecular wave function is the decisive factor.

Finally, Fig. 5 shows a comparison of the computation time (cpu time) of 22 different basis sets for some small molecules. The computer used was a HITAC

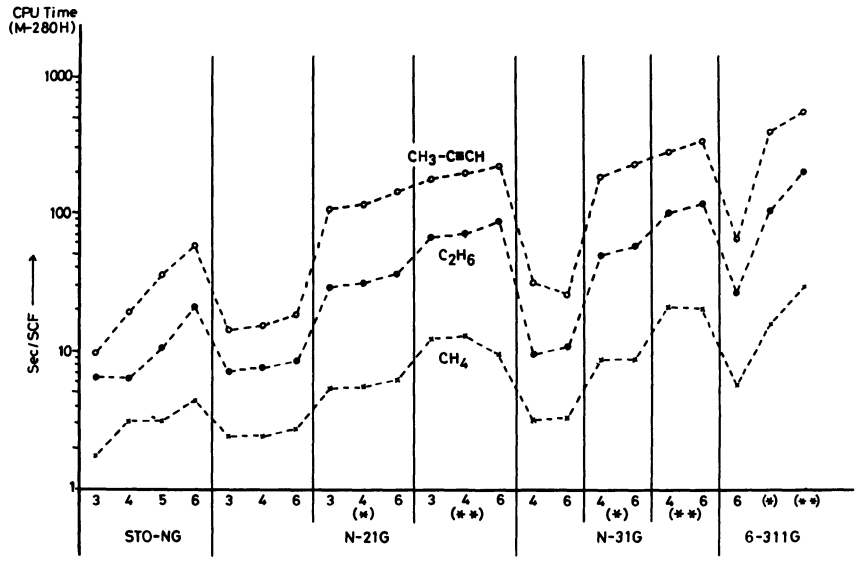

Fig. 5. Computer cpu time (HITAC M-280H) required for a single SCF calculation by 22 different MO methods.

M-280H system at the Computer Center of the University of Tokyo.

References

1) e.g. a) J. B. Moffat and H. E. Popkie, *Int. J. Quantum Chem.*, **2**, 565 (1968); b) F. Driessler and W. Kutzelnigg, *Theor. Chim. Acta (Berl.)*, **43**, 1 (1976); *ibid.*, **43**, 307 (1977); c) H. Kollmar, *ibid.*, **50**, 235 (1978).

2) H. Ichikawa, *J. Am. Chem. Soc.*, **105**, 7457 (1983); *ibid.*, **106**, 6249 (1984).

3) H. Ichikawa and Y. Ebisawa, *J. Am. Chem. Soc.*, **107**, 1161 (1985).

4) We have used GAUSSIAN 80H program (a Hitac version of GAUSSIAN 80 (QCPE No. 437, Indiana University, IN)) at the Computer Center of the University of Tokyo.

5) a) STO-3G basis set: J. B. Collins, P. v. R. Schleyer, J. S. Binkley, and J. A. Pople, *J. Chem. Phys.*, **64**, 5142 (1976); b) STO-4G basis set: W. J. Hehre, R. Ditchfield, R. F. Stewart, and J. A. Pople, *ibid.*, **51**, 2657 (1969); c) 3-21G and 6-21G basis sets: J. S. Binkley, J. A. Pople, and W. J. Hehre, *J. Am. Chem. Soc.*, **102**, 939 (1980); M. S. Gordon, J. S. Binkley, J. A. Pople, W. J. Pietro, and W. J. Hehre, *ibid.*, **104**, 2797 (1982); d) 4-21G basis set: P. Pulay, G. Fogarasi, F. Pang, and J. E. Boggs, *ibid.*, **101**, 2250 (1979); e) 3-21G* basis set: W. J. Pietro, M. M. Francl, W. J. Hehre, D. J. DeFrees, J. A. Pople, and J. S. Binkley, *J. Am. Chem. Soc.*, **104**, 5039 (1982); f) 4-31G basis set: R. Ditchfield, W. J. Hehre, and J. A. Pople, *J. Chem Phys.*, **54**, 724 (1971); W. J. Hehre and J. A. Pople, *ibid.*, **56**, 4233 (1972); J. D. Dill and J. A. Pople, *ibid.*, **62**, 2921 (1975); g) 6-31G basis set: W. J. Hehre, R. Ditchfield, and J. A. Pople, *ibid.*, **56**, 2257 (1972); J. S. Binkley and J. A. Pople, *ibid.*, **66**, 879 (1977); J. D. Dill and J. A. Pople, *ibid.*, **62**, 2921 (1975); h) 6-31G* and 6-31G** basis sets: P. C. Hariharan and J. A. Pople, *Theor. Chim. Acta*, **28**, 213 (1973); J. D. Dill and J. A. Pople, *J. Chem. Phys.*, **62**, 2921 (1975); i) 6-311G and 6-311G** basis sets: R. Krishnan, J. S. Binkley, R. Seeger, and J. A. Pople, *ibid.*, **72**, 650 (1980); The GAUSSIAN-80 program includes other basis sets, whose exponents and contraction coefficients are listed in "Handbook of Gaussian Basis Sets," ed by R. Poirier, R. Kari, and I. G. Csizmadia, Elsevier Pub. Co., Amsterdam (1985).

6) The method of energy partitioning was proposed and rigorously evaluated by Reudenberg (K. Reudenberg, *Rev. Mod. Phys.*, **34**, 326 (1962)). There are some problems in partitioning the total energy by an HF SCF method into mono- and bicentric terms since a Fock operator contains the potentials from three- and four-center interactions in an averaged form. However, since there are no other means to see inside of a large molecular system, this method has been frequently applied to the analysis of chemical bonds as shown in Ref. 1.

7) G. G. Hall, *Proc. R. Soc. London, Ser. A*, **205**, 541 (1951); C. C. J. Roothaan, *Rev. Mod. Phys.*, **23**, 69 (1951).

8) J. A. Pople and R. K. Nesbet, *J. Chem. Soc.*, **1964**, 571.

9) R. S. Mulliken, *J. Chem. Soc.*, **23**, 1822 (1955); *ibid.*, **23**, 1841 (1955); *ibid.*, **23**, 2338 (1955); *ibid.*, **23**, 2343 (1955).

Photochemical Reactions of Bromoanthraquinones in Ethanol at Room Temperature Studied by Steady-State Photolysis and Laser Photolysis

Kumao HAMANOUE,* Toshihiro NAKAYAMA, Kazuhide SAWADA, Yoshiaki YAMAMOTO, Susumu HIRASE, and Hiroshi TERANISHI
Department of Chemistry, Kyoto Institute of Technology, Matsugasaki, Sakyo-ku, Kyoto 606
(Received April 14, 1986)

Photolyses of α-bromoanthraquinones (1-bromo-, 1,5-dibromo-, and 1,8-dibromoanthraquinones) with 366-nm light in ethanol at room temperature gave rise to the formation of debrominated 9,10-anthracenediol as a final product. This was interpreted in terms of the sequence of the formation of α-bromo-9,10-anthracenediols followed by the photochemical dehydrobromination yielding the corresponding anthraquinones with one less bromine atom than original ones. Photolysis of 2-bromoanthraquinone gave rise to the formation of 2-bromo-9,10-anthracenediol, and no dehydrobromination was observed. Combined with the values of the quantum yields of photoreduction, the results of the laser photolyses revealed that the rate constant for the hydrogen-atom abstraction from ethanol decreased as an increase of the $\pi\pi^*$ character of the lowest triplet states of α-bromoanthraquinones.

The photochemistry of quinones has been extensively studied on account of its importance in the understanding of the degradative action of light upon biological materials, photophosphorylation and the initiation of biological electron transport via excited quinones.

In connection with our recent interest in photophysics and photochemistry of aromatic carbonyl compounds, we have investigated the phosphorescences and triplet–triplet ($T'\leftarrow T_1$) absorptions of a series of halogenoanthraquinones:[1,2] Our finding is that the lowest triplet states (T_1) of α-haloanthraquinones are of mixed $n\pi^*$–$\pi\pi^*$ or $\pi\pi^*$ character, while the $n\pi^*$ triplet states are the lowest ones for β-haloanthraquinones. The much shorter lifetimes of the T_1 states and small phosphorescence quantum yields of α-haloanthraquinones were indicative that the depopulation of the T_1 states was mainly due to a special rapid nonradiative process.

Although the reason for this was not clear, a possible conjecture was that the dehalogenation of α-haloanthraquinones affects the triplet lifetimes, because we observed the formation of anthraquinone during the steady-state photolysis of 1-chloroanthraquinone in ethanol with 366-nm light. However, this is ruled out by our findings that: (1) Steady-state photolysis of α-chloroanthraquinones (1-chloro-, 1,5-dichloro-, and 1,8-dichloroanthraquinones) with 366-nm light in ethanol gave rise to the sequence of the formation of α-chloro-9,10-anthracenediols followed by the photochemical dehydrochlorination yielding the corresponding anthraquinones with one less chlorine atom than original ones and the final photoproduct was 9,10-anthracenediol. No dechlorination was observed upon the 366-nm photolysis of 2-chloroanthraquinone.[3,4] (2) The hydrogen-atom abstraction of α-chloroanthraquinones from ethanol originated from the T_1 state in spite of its mixed $n\pi^*$–$\pi\pi^*$ or $\pi\pi^*$ character, though the reactivity for hydrogen-atom abstraction decreased as an increase of the $\pi\pi^*$ character in the T_1 state.[5,6]

This paper deals with the photochemical reactions of bromoanthraquinones. Since the lifetimes of the T_1 states of α-bromoanthraquinones (1-bromo-, 1,5-dibromo-, and 1,8-dibromoanthraquinones) are much shorter than those of α-chloroanthraquinons,[1,2] the purpose of our present study is to examine the photochemical reactivity of bromoanthraquinones in order to confirm whether our previous conclusion made for chloroanthraquinones[3–6] can generally be applicable or not.

Experimental

Chemicals. The details of the methods of preparation of 1-bromo-, 2-bromo-, 1,5-dibromo-, and 1,8-dibromoanthraquinones (1-BAQ, 2-BAQ, 1,5-DBAQ, 1,8-DBAQ) have been given in our previous paper.[1] Spectral-grade ethanol (Nakarai) was used as a solvent without further purification. The sample solutions were degassed by several freeze-pump-thaw-cycles.

Steady-State Photolysis. Irradiation of bromoanthraquinones was carried out using a USH-500D super-high pressure mercury lamp. Light of 366-nm monochromatic wavelength was selected by the combination of two Toshiba color glass filters (UV-35 and UV-D35) and a filter solution ($CuSO_4 \cdot 5H_2O$, 100 g dm^{-3}; path length, 3 cm), while 313-nm light was selected by the combination of two Toshiba color glass filters (UV-29 and UV-D33S) and a filter solution ($Ni_2SO_4 \cdot 6H_2O$, 50 g dm^{-3}; path length, 2 cm). Photolysis of α-bromo-9,10-anthracenediols was performed with lights of longer wavelengths than 450 nm which were selected by the combination of a USL-500D Xe lamp, two Toshiba color glass filters (UV-35 and VY-46) and a filter solution of $CuSO_4$ (loc. cit). Absorption and fluorescence spectra were recorded using a Hitachi 200-20 spectrophotometer and a Hitachi MPF-4 fluorescence spectrophotometer, respectively. Since we observed a relatively rapid dark reaction

immediately after the photolysis of 1,8-DBAQ, the time variation of the absorption spectrum was measured with a Unisoku rapid scan spectrophotometer (USP-450), where a Xe (at 330—450 nm) and a D_2 (at 290—390 nm) lamps were used as the monitoring-light sources. Unless otherwise stated, all experiments were carried out in ethanol at room temperature and the concentrations of sample solutions were $2—5\times10^{-4}$ M (1 M=1 mol dm^{-3}). The quantum yield of the photoreduction was determined by the Hatchard-Parker's potassium trisoxalatoferrate(III) actinometry method.[7] The yield of the photoproduct was determined by measuring its absorbance. To confirm the participation of the solvent in the dehydrobromination reaction, photolysis of 1-bromo-9,10-anthracenediol was carried out in benzene-d_6 (G.R.-grade, Wako) and anthraquinone produced was analyzed by using a Shimadzu QP-1000 GC-MS spectrometer with an OV-101 wall-coated capillary column (Ionization potential, 70 eV).

Laser Photolysis. The decays of the triplet-triplet ($T'\leftarrow T_1$) absorptions of bromoanthraquinones were measured at 380 nm in ethanol at room temperature. The third harmonic (355 nm) from a picosecond mode-locked Nd^{3+}:YAG laser was used for sample excitation, and the pulse width was 15 ps. Although the details of this laser photolysis system have been given elsewhere by Sumitani and Yoshihara,[8] a minor modification was performed: The monitoring light was generated by focusing the fundamental light onto the electrode of a Xe flash lamp (FX265 B203). The detection system for the absorption spectroscopy was composed of a monochromator (Shimadzu-Baush-Lomb, 1350 grooves/mm), a photomultiplier (HTV RI 294UZC3I8), an osciloscope (Tektronix 7104 with 7A29 and 7B10 plag-in units), a photo-oscillo unit (San-ei Instrument, 5R32) and a microcomputer (NEC PC9801m). The concentrations of the deaerated sample solutions in a cell of 10-mm path length were 3.5×10^{-4}, 1.8×10^{-4}, and 1.6×10^{-4} M for 1-BAQ, 1,5-DBAQ, and 1,8-DBAQ, respectively.

Results

Steady-State Photolysis. Photoreduction of 2-BAQ in ethanol was studied by the absorption spectral change upon photolysis. Figure 1 indicates the depletion of 2-BAQ and the buildup of a photoproduct during 366-nm photolysis. The existence of an isosbestic point at 353 nm supports quantitative conversion of 2-BAQ to the product. Exposure to oxygen caused quantitative oxidation of the product back to 2-BAQ. This reaction is very similar to those of anthraquinone (AQ)[3,4,9-11] and 2-chloroanthraquinone.[4] Moreover, absorption and fluorescence spectra of the photoproduct of 2-BAQ are similar to those of 9,10-anthracenediol (AQH_2) and 2-chloro-9,10-anthracenediol. Thus one can safely conclude that the new absorption in Fig. 1 is due to 2-bromo-9,10-anthracenediol.

Photoreactions of 1-BAQ upon 366-nm photolysis gave rise to rather complicated absorption spectral changes as shown in Fig. 2-a: No isosbestic point could be seen as observed for 2-BAQ, and the absorption bands of the reactant and the products shifted to the blue during photolysis. Spectrum F with λ_{max}=382 nm was assigned to AQH_2, because absorption and fluorescence spectra of the final product were identical with those of AQH_2. Moreover, exposure to oxygen caused quantitative oxidation of the final photoproduct to AQ with λ_{max}=325 nm. On the other hand, photolysis of 1-BAQ with 313-nm light caused a simple absorption spectral change similar to that in photoreduction of 2-BAQ, that is, the depletion of 1-BAQ and the buildup of a product with λ_{max}=387 nm were observed, accompanied by an isosbestic point at 359 nm (Fig. 2-b). No spectral shifts

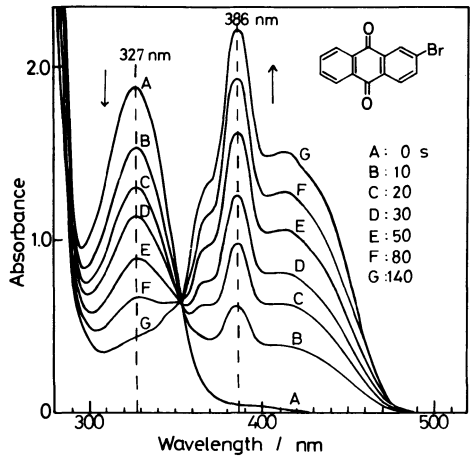

Fig. 1. Absorption spectral change of 2-BAQ in ethanol upon irradiation with 366-nm light at room temperature.

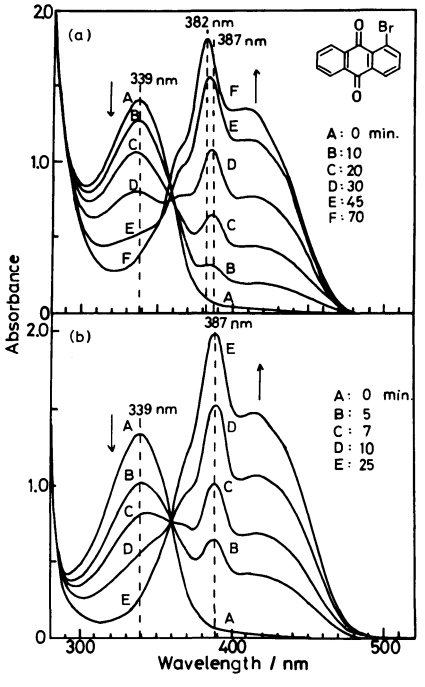

Fig. 2. Absorption spectral changes of 1-BAQ in ethanol upon irradiation with 366-nm (a) and 313-nm (b) lights at room temperature.

of the reactant and the product were observed during irradiation. (Extended photolysis gave rise to the decrease and the blue-shift in the absorption band at 387 nm). Spectrum E with λ_{max}=387 nm in Fig. 2-b is identical with Spectra B and C in Fig. 2-a, and the photoproduct can be identified as 1-bromo-9,10-anthracenediol (1-BAQH$_2$) by its reaction with oxygen on exposure to air, giving 1-BAQ.

Figure 3 shows the absorption spectral change of 1-BAQH$_2$ upon the photolysis with lights of longer wavelengths than 450 nm, indicating the formation of a product at the expense of 1-BAQH$_2$, accompanied by an isosbestic point at 348 nm. The photoproduct with λ_{max}=325 nm was identified as AQ by comparison of the absorption spectrum with that of the authentic sample of AQ. Further irradiation of this photoproduct with 366-nm light yielded AQH$_2$. The photolysis of 1-BAQH$_2$ was also performed in benzene-d_6, and the result of GC-MS analysis indicated that only AQ (not deuterated AQ) was produced.

In Fig. 4-a, we display much complicated photoreactions of 1,5-DBAQ upon 366-nm photolysis. Spectral shifts of the absorption bands of the reactant and the products can also be seen during photolysis, and the final photoproduct was AQH$_2$. (In Spectrum C, the absorption band with λ_{max}=387 nm is identical with that of 1-BAQH$_2$). However, photolysis of 1,5-DBAQ with 313-nm light gave rise to a simple reaction as shown in Fig. 4-b. The photoproduct has an absorption band with λ_{max}=393 nm which is identical with that of Spectrum B in Fig. 4-a, and the photoproduct was identified as 1,5-dibromo-9,10-anthracenediol (1,5-DBAQH$_2$), because it changed to 1,5-DBAQ on exposure to air. Further photolysis of 1,5-DBAQH$_2$ with lights of longer wavelengths than 450 nm gave a photoproduct with λ_{max}=339 nm which was identified as 1-BAQ by comparison of the absorption spectrum with that of the authentic sample (Fig. 5).

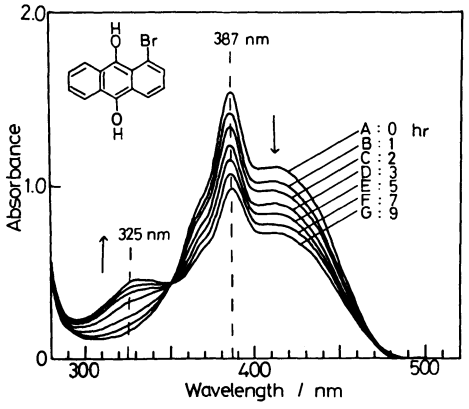

Fig. 3. Absorption spectral change of 1-BAQH$_2$ in ethanol upon irradiation with lights of longer wavelengths than 450 nm at room temperature.

The photochemical reactions of 1,8-DBAQ were not different from those of 1,5-DBAQ as shown in Figs. 6 and 7: The final photoproduct with λ_{max}=382 nm in Fig. 6-a was identified as AQH$_2$ and the absorption spectrum of the final photoproduct with λ_{max}=393 nm in Fig. 6-b was assigned to 1,8-dibromo-9,10-anthracenediol (1,8-DBAQH$_2$), because it changed to 1,8-DBAQ on exposure to air. By $\lambda \geq$450-nm excitation (Fig. 7), 1,8-DBAQH$_2$ was dehydrobrominated to 1-BAQ. By using a Unisoku rapid scan spectrophotometer, however, we observed that the absorption spectra taken immediately after the photolysis (7 or 10 min) of 1,8-DBAQ changed with time by a dark reaction (cf. Fig. 8); the absorption around 300 nm decreased and those of 1,8-DBAQ and 1,8-DBAQH$_2$ increased simultaneously, accompanied by an isosbestic point at 325 nm. (Such a spectral change was not observed for 1-BAQ, 2-BAQ, and 1,5-DBAQ.) For the sake of comparison, we also show the similar results for 1,8-

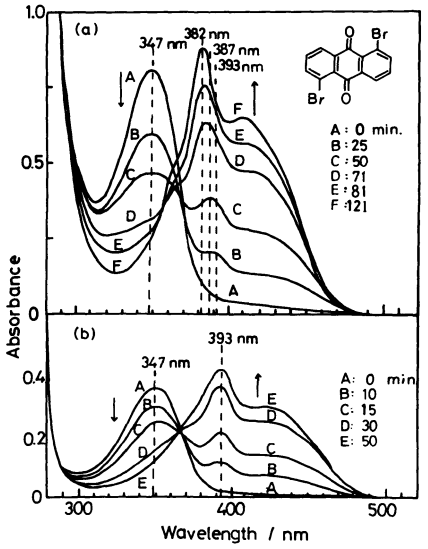

Fig. 4. Absorption spectral changes of 1,5-DBAQ in ethanol upon irradiation with 366-nm (a) and 313-nm (b) lights at room temperature.

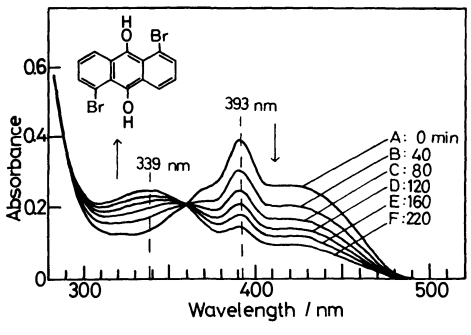

Fig. 5. Absorption spectral change of 1,5-DBAQH$_2$ in ethanol upon irradiation with lights of longer wavelengths than 450 nm at room temperature.

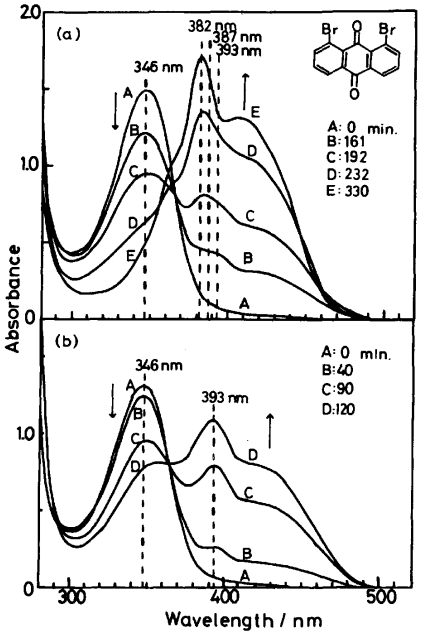

Fig. 6. Absorption spectral changes of 1,8-DBAQ in ethanol upon irradiation with 366-nm (a) and 313-nm (b) lights at room temperature.

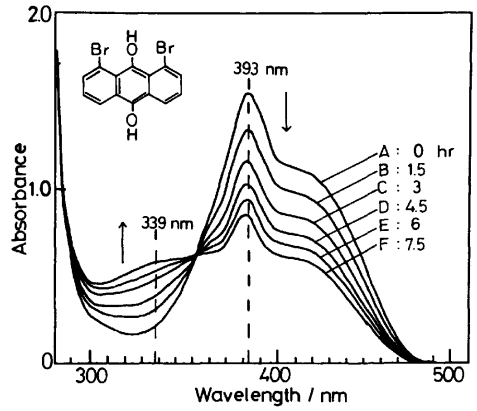

Fig. 7. Absorption spectral change of 1,8-DBAQH$_2$ in ethanol upon irradiation with lights of longer wavelengths than 450 nm at room temperature.

dichloroanthraquinone (1,8-DCAQ) in Fig. 9, where spectra were taken by a Hitachi 200-20 spectrophotometer (a)[3,4] and a Unisoku rapid scan spectrophotometer (USP-450) (b). Since the both results are identical with each other, the result for 1,8-DBAQ in Fig. 8 may be reliable.

In Table 1, we show the quantum yields of photoreduction of α-bromoanthraquinones upon the 313-nm photolysis. For the sake of comparison, we also show the results for α-chloroanthraquinones.[4]

Laser Photolysis. Since the T′←T$_1$ absorptions of α-bromoanthraquinones have the strong absorptions at ≈380 nm and weak one at ≈500 nm,[2] the decays of

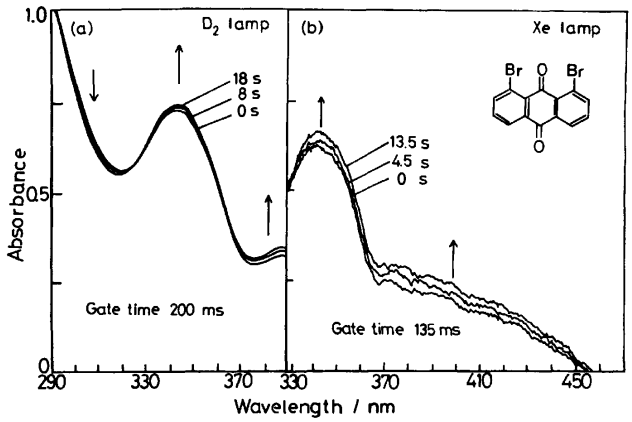

Fig. 8. Dark reactions of the complex of two 1,8-DBAQH· in ethanol at room temperature after irradiation of 1,8-DBAQ for 7 min (a) and 10 min (b), where spectra were taken by a Unisoku rapid scan spectrophotometer (USP-450) using a D_2 (a) and a Xe (b) lamps as the monitoring light sources.

the T$_1$ states were monitored at 380 nm. In Fig. 10, we display the time variation of the transient absorptions (full curves). According to the mechanism established by Wilkinson[9] and Tickle and Wilkinson,[10] the photoreduction of anthraquinone (AQ) in alcohol (R_2CHOH) is given by

$$AQ^*(T_1) \longrightarrow AQ, \quad (1)$$

$$AQ^*(T_1) + R_2CHOH \longrightarrow AQH\cdot + R_2\dot{C}OH, \quad (2)$$

$$R_2\dot{C}OH + AQ \longrightarrow AQH\cdot + R_2CO, \quad (3)$$

$$2AQH\cdot \longrightarrow AQ + AQH_2, \quad (4)$$

where AQ*(T$_1$) and AQH· are triplet anthraquinone and anthrasemiquinone radical, respectively. Since the transient absorptions decayed monotonously and the quantum yields of photoreduction were very small as shown in Table 1, the absorptions due to anthrasemiquinone radicals may be negligible. Thus, the triplet decay constant (k_T) of α-bromoanthraquinones were determined by analyzing the most probable smooth curves (broken lines) as a single exponential curve. (The first-order plots of the absorbances against time are inserted in Fig. 10 by open circles and dotted lines). The values of k_T thus obtained are also listed in Table 1, together with those for α-chloroanthraquinones.[5,6]

Discussion

The results of the steady-state photolysis indicate that only the photoreduction occurs upon the photolysis of 2-BAQ. For α-bromoanthraquinones, 313-nm photolysis yielded the corresponding bromo-9,10-anthracenediols, and no photochemical dehydrobromination was observed. However, the photolysis of α-bromo-9,10-anthracenedilols with lights of

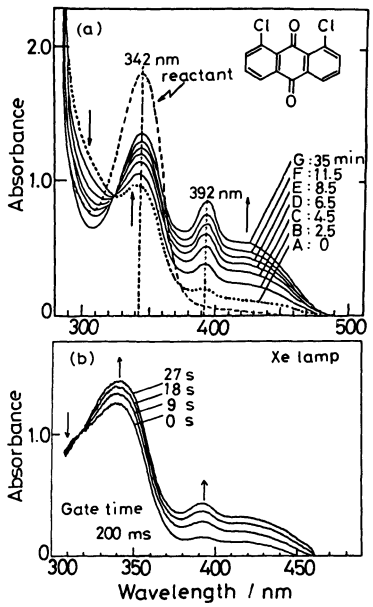

Fig. 9. Dark reactions of the complex of two 1,8-DCAQH· in ethanol at room temperature after irradiation of 1,8-DCAQ for 12 min (a) and 3 min (b), where spectra were taken by a Hitachi 200–20 spectrophotometer (a)[3,4] and a Unisoku rapid scan spectrophotometer (USP-450) (b). In the latter case, a Xe lamp was used as a monitoring light source.

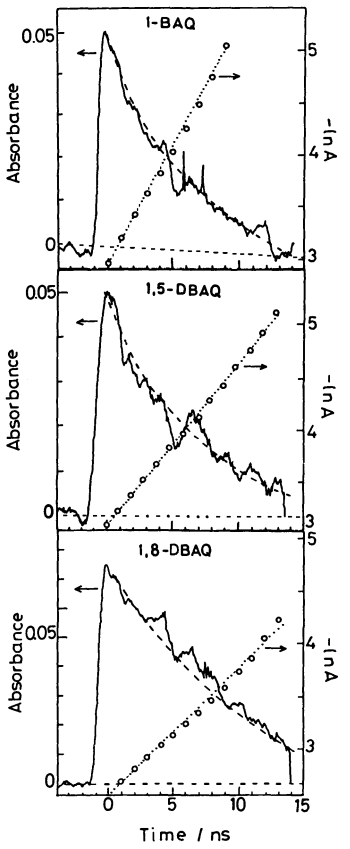

Fig. 10. Decay curves of the $T' \leftarrow T_1$ absorptions of 1-BAQ, 1,5-DBAQ, and 1,8-DBAQ (full curves), where the absorbances were monitored at 380 nm and the data represent the average of 20 shots of laser pulses. The broken lines are the most probable decay curves and their first-order plots are shown by the dotted lines.

longer wavelengths than 450 nm gave rise to the dehydrobromination yielding AQ (or 1-BAQ), accompanied by a clear isosbestic point. Since AQ and α-bromoanthraquinones (and their bromo-9,10-anthracenediols) have appreciable absorptions at 366-nm, the results of 366-nm photolyses are interpreted in terms of the following consecutive reactions, in accordance with the results for α-chloroanthraquinones:[3,4]

$$\text{1,5- or 1,8-DBAQ} \xrightarrow{h\nu} \text{1,5- or 1,8-DBAQH}_2 \xrightarrow{h\nu} \text{1-BAQ} \xrightarrow{h\nu} \text{1-BAQH}_2 \xrightarrow{h\nu} \text{AQ} \xrightarrow{h\nu} \text{AQH}_2.$$

Based on this conclusion, the decrease and the blue-shift in the absorption bands of the photoproducts upon the extended 313-nm photolyses of α-bromoanthraquinones may be due to the consecutive reactions mentioned above.

In Fig. 6-b, a clear isosbestic point can be seen. Such an isosbestic point was not observed for 1,8-DCAQ, where we observed the initial spectral increase around 300 nm instead of a small yield of 1,8-dichloro-9,10-anthracenediol (1,8-DCAQH$_2$):[3,4] By a dark reaction (cf. Fig. 9), the absorption around 300 nm decreased and those of 1,8-DCAQH$_2$ and 1,8-DCAQ increased simultaneously, accompanied by an isosbestic point at 322 nm. The decay constant of the 300-nm absorption was nearly equal to the rate constants for the formation of 1,8-DCAQH$_2$ and 1,8-DCAQ,[4] i.e., $\approx 5.8\times10^{-3}$ s^{-1}. Thus, we have assigned the 300-nm absorption to a complex of two 1,8-dichloroanthrasemiquinone radicals (1,8-DCAQH·). Actually, the rate constant for the buildup of the 300-nm absorption ($\approx 2\times10^{9}$ M^{-1} s^{-1})[4] was nearly equal to the decay constant of 1,8-DCAQH·, i.e., 5.8×10^{8}—2.2—4.1×10^{9}

Table 1. The Quantum Yields(Φ) of the Photoreduction of α-Bromoanthraquinones, Their Triplet Decay Constants (k_T) and the Rate Constants (k_r) for the Hydrogen-Atom Abstraction from Ethanol

	1-BAQ	1,5-DBAQ	1,8-DBAQ
Φ	0.04 (1.0)[a]	0.03 (0.9)[a]	0.003 (0.04)[a]
k_T/s^{-1}	2.3×10^{8} (2.3×10^{6})[b]	1.6×10^{8} (1.6×10^{6})[b]	1.2×10^{8} (4.0×10^{5})[b]
k_r/s^{-1}	9.3×10^{6} (2.3×10^{6})[b]	4.8×10^{6} (1.4×10^{6})[b]	3.6×10^{5} (1.6×10^{4})[b]

The values in parentheses are those for the corresponding α-chloroanthraquinones. a) Ref. 4. b) Refs. 5 and 6.

$M^{-1}s^{-1}$, though the value of the decay constant depends on the assumption of the extinction coefficient of 1,8-DCAQH·.[6]

Since we could not observe any absorption due to a complex of two 1,8-dibromoanthrasemiquinone radicals (1,8-DBAQH·) during the spectral measurements using a Hitachi 200-20 spectrophotometer, the complex of two 1,8-DBAQH· may be more unstable than that of 1,8-DCAQH·. This is consistent with our findings that: (1) The result in Fig. 8 clearly shows the existence of a relatively rapid dark reaction. (2) A clear isosbestic point was observed even for 1,8-DCAQ, when each spectrum was taken at the delay time of 20 min after the 313-nm photolysis (1 min) of 1,8-DCAQ.[4]

As reported in our previous paper,[4] the quantum yields of photoreduction were 1.0, 1.0, 0.9, and 0.04 for AQ, 1-chloro-, 1,5-dichloro-, and 1,8-dichloroanthraquinones, respectively. This decrease in the quantum yields as an increase of the $\pi\pi^*$ character in the T_1 states of α-chloroanthraquinones was also observed for α-bromoanthraquinones as shown in Table 1. (The value for 2-BAQ was 1.0). Thus one can safely conclude that much shorter lifetimes of the T_1 states and small phosphorescence quantum yields of α-haloanthraquinones are not due to the photoreactions but are due to the modification of the geometrical molecular structure by the interaction of the carbonyl group with halogen atom(s) at the α-positions, causing the T_1 states to be of $\pi\pi^*$ character with short lifetimes. Of course, the internal heavy-atom effect of halogen atoms may also affect the triplet lifetimes.[12]

As can be seen in Table 1, the decay constants (k_T) of the T_1 states of α-bromoanthraquinones are much greater than those of α-chloroanthraquinones.[5,6] Combined with the results of quantum yields of photoreduction, the rate constants (k_r) of hydrogen-atom abstraction from ethanol were estimated as shown in Table 1, indicating that the reactivity of triplet α-bromoanthraquinones decreases as an increase of the $\pi\pi^*$ character of the T_1 state, in accordance with our previous results for α-chloroanthraquinones.[5,6]

Since the result of GC-MS analysis indicated that only AQ (not deuterated AQ) was produced upon the photolysis of 1-BAQH$_2$ in benzene-d_6, a possible reaction mechanism may be given by Scheme 1: Namely, the homolysis of the C–Br bond may give rise to the formation of two caged radicals. If the electron transfer from the semiquinone radical to the bromine radical in the solvent cage is followed by the rapid deprotonation, it looks like that the solvent does not participate in the overall reaction. If this scheme is correct, however, the rate of dehydrochlorination of α-chloro-9,10-anthracenediols should be slower than that of dehydrobromination of α-bromo-9,10-anthracenediols, because the bond dissociation energy of C–Cl bond is expected to be larger than that of C–Br bond. This is inconsistent

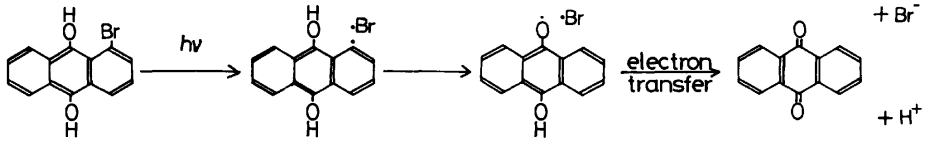

Scheme 1.

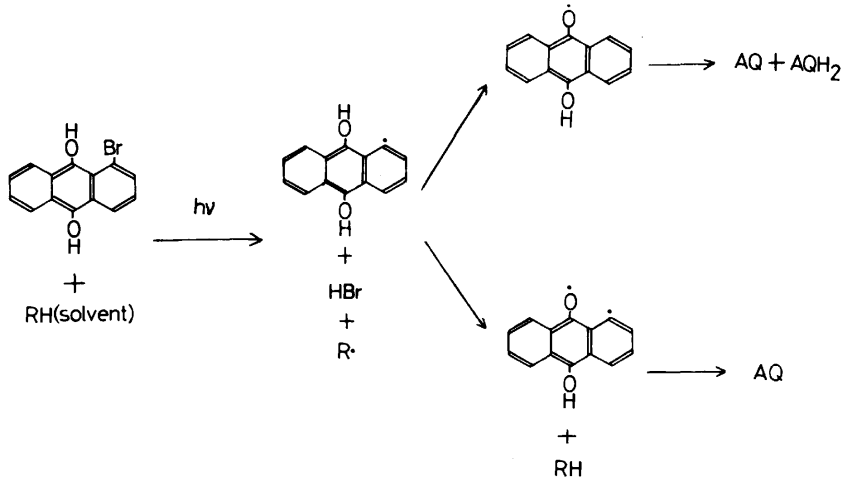

Scheme 2.

with our present finding that the rates of dehydrobromination are extremely slower than those of dehydrochlorination. (The possibility of Scheme 1 may be also excluded, based on the fact that photolysis of 2-BAQH$_2$ does not give rise to the formation of AQ.)

An alternative reaction mechanism may be given by Scheme 2. However, this is also ruled out based on the discussion in our previous paper,[4] where we proposed that the dehydrochlorination of α-chloro-9,10-anthracenediols occurs via the intramolecular elimination of hydrogen chloride. Since dehydrobromination is also observed only for α-bromo-9,10-anthracenediols, the dehydrohalogenation reaction may be affected by the proximity effect of halogen(s), that is, the structural proximity of the hydroxyl group to the halogen atom(s) may make it possible to cause intramolecular elimination of hydrogen halide. The faster rates of dehydrochlorination than those of dehydrobromination support our previous suggestion[4] that an intramolecular hydrogen bonding between the hydroxyl group and the halogen atom at the α-position enhances the rate of dehydrohalogenation. This is based on the fact that the electronegativity of chlorine atom is larger than that of bromine atom, indicating that the hydrogen-bonding character (or charge-transfer character) between the chlorine atom and the hydroxyl group is larger than that between the bromine atom and the hydroxyl group. For β-halo-9,10-anthracenediols (2-chloro- and 2-bromo-9,10-anthracenediols), therefore, it is expected that the hydroxyl group and the halogen atom are located too much separately to cause the intramolecular dehydrohalogenation.

In summary, one can say that our previous conclusion made for the photochemical reactions of chloroanthraquinones is generally applicable to those of bromoanthraquinones.

We wish to express our sincere thanks to Professor Keitaro Yoshihara and Dr. Minoru Sumitani of Institute for Molecular Science for the help in the measurements of the triplet decay constants using a Nd^{3+}:YAG laser. Thanks are also due to Mr. Toshihiko Nagamura of Unisoku Co. Ltd. for the help in the measurements of the dark reactions using a rapid scan spectrophotometer.

References

1) K. Hamanoue, Y. Kajiwara, T. Miyake, T. Nakayama, S. Hirase, and H. Teranishi, *Chem. Phys. Lett.*, **94**, 276 (1983).

2) Y. Kajiwara, Master Thesis of Faculty of Engineering and Design, Kyoto Institute of Technology (1982).

3) K. Hamanoue, K. Yokoyama, T. Miyake, T. Kasuya, T. Nakayama, and H. Teranishi, *Chem. Lett.*, **1982**, 1967.

4) K. Hamanoue, K. Sawada, K. Yokoyama, T. Nakayama, S. Hirase, and H. Teranishi, *J. Photochem.*, **33**, 99 (1986).

5) K. Hamanoue, K. Yokoyama, Y. Kajiwara, K. Nakajima, T. Nakayama, and H. Teranishi, *Chem. Phys. Lett.*, **110**, 25 (1984).

6) K. Hamanoue, T. Nakayama, A. Tanaka, Y. Kajiwara, and H. Teranishi, *J. Photochem.*, **34**, 73 (1986).

7) C. G. Hatchard and C. A. Parker, *Proc. R. Soc., London, Ser. A*, **235**, 518 (1956).

8) M. Sumitani and K. Yoshihara, *Bull. Chem. Soc. Jpn.*, **55**, 85 (1982).

9) F. Wilkinson, *J. Phys. Chem.*, **66**, 2569 (1962).

10) K. Tickle and F. Wilkinson, *Trans. Faraday Soc.*, **61**, 1981 (1965).

11) S. A. Carlson and D. M. Hercules, *Photochem. Photobiol.*, **17**, 123 (1973).

12) Inoue et al.[13] proposed that the photoreduction originated via direct electron transfer from ethanol to triplet $\pi\pi^*$ haloanthraquinones. If this were correct, the much shorter lifetimes of the T_1 states of α-haloanthraquinones studied by us might be attributed to the formation of an exciplex between ethanol and triplet $\pi\pi^*$ α-haloanthraquinones, because the rates of photoreduction of anthraquinones were enhanced by the addition of triethylamine (TEA) and it was confirmed that the photoreduction originated via the formation of the exciplexes between TEA and the lowest triplet anthraquinones.[14] In the absence of TEA, however, no evidence for electron transfer from ethanol to the triplet α-haloanthraquinones was obtained.[5,6]

13) H. Inoue, K. Ikeda, H. Mihara, M. Hida, N. Nakashima, and K. Yoshihara, *Chem. Phys. Lett.*, **95**, 60 (1983).

14) K. Hamanoue, K. Yokoyama, Y. Kajiwara, M. Kimoto, T. Nakayama, and H. Teranishi, *Chem. Phys. Lett.*, **113**, 207 (1985); K. Hamanoue, M. Kimoto, Y. Kajiwara, T. Nakayama, and H. Teranishi, *J. Photochem.*, **31**, 143 (1985).

 © 1986 The Chemical Society of Japan Bull. Chem. Soc. Jpn., 59, 2743—2750 (1986)

Nuclear Magnetic Resonance Studies of Copper(I) Complexes of Imidazoles. I. Their Preparation, Characterization, Equilibria, and Reaction with Carbon Monoxide

Susumu KITAGAWA* and Megumu MUNAKATA
Department of Chemistry, Faculty of Science and Technology, Kinki University, Kowakae, Higashi-Osaka 577
(Received December 12, 1985)

Various copper(I) complexes with monodentate imidazole(im) have been prepared from $[Cu(CH_3CN)_4]X$ ($X=ClO_4^-$ and PF_6^-) in acetone. Their characterization has principally been made by ^1H NMR spectroscopy. Binary copper(I) complexes are $[Cu(im)_2]^+$ (**2**) and $[Cu(im)_3]^+$ (**3**), while the monoimidazole complex is a ternary two- or four-coordinate complex (**1**). In contrast with **2** and **3**, quantitative formation of $[Cu(im)_4]^+$ (**4**) does not occur in acetone. Even at [im]/[Cu]<2, **2** forms more preferentially than **1**. This is due to the linear structure of **2**. **2** and **3** provide stable CO adducts, both of which display complete reversibility. The affinity for CO of **3** is much stronger than that of **2**. Pyrazole copper(I) complexes were also prepared and examined as a comparison with imidazole complexes. Monodentate pyrazole hardly gives two- and three-coordinate complexes. This is attributable to its low basicity in contrast with that of imidazole.

The presence of copper(I)–imidazole binding[1–3] in copper proteins has been demonstrated physicochemically. Keen interest in the relationship between their functions and the structure of a copper(I)–imidazole moiety has prompted the syntheses and characterizations of low-molecular weight copper(I) compounds including ligation from histidine, histamine, imidazole,[4–5] and their derivatives.[6–17] Binary copper(I) compounds having only imidazole are significant in connection with the environment of "type 3" copper moiety[1–3] in copper proteins. Two-coordinate copper(I) compounds of chelating benzimidazole-containing ligands have been isolated, where the copper atom is linearly coordinated by two nitrogen atoms.[9,14] Tetrakis(imidazole)copper(I)[4] has been isolated and the structure has been demonstrated to be tetrahedral. This geometric feature is not necessarily rare in copper(I) compounds[18–23] as well as in silver(I) and mercury(II) compounds.[24] On the other hand, no binary three-coordinate complex of imidazole has ben found. Regarding a structural model of deoxyhemocyanin,[3] the synthesis and characterization of three-coordinate imidazole complexes are of great importance; furthermore, a detailed knowledge of their behavior in solution, such as equilibria and reactivity, is valuable.

In this work, we try to challenge the preparation of various coordination copper(I) compounds of imidazole. Another purpose of this work is to explore the coordination chemistry of an imidazole–copper(I) system by inquiring into the chemical reactivity in a solution together with equilibrium. Finally, we aimed at the establishment of a methodology to investigate a copper(I)–imidazole system since ESR and the visible absorption spectroscopy are of very little use in these complexes. NMR spectroscopy is a very important tool for copper(I) complexes in solution, and helps to answer such questions as to what and how many donors are coordinated to copper(I).[25,26] Consequently, the characterizations of the imidazole–copper(I) compounds studied here are due to NMR spectroscopy.

Experimental

Materials. $[Cu(CH_3CN)_4]ClO_4$ and $[Cu(RCN)_4]ClO_4$ ($R=C_2H_5$ and C_6H_5) were synthesized from copper(I) oxide[27] and copper wire,[28] respectively. $[Cu(CH_3CN)_4]PF_6$ was also prepared by a method described in the literature.[29] The obtained compounds were all checked by elementary analysis and optical absorption method with the aid of the absorbance at 440 nm of a derived bis(2,2′-bipyridine)copper(I) in acetone (ε_{max}=4800 M^{-1} cm^{-1}(1 M=1 mol dm^{-3})).[30] Copper(I) oxide and copper wire were commercially available, refreshed with dilute HCl, washed with water and dried before use. Imidazole(im), pyrazole(pz), and 1-methylimidazole(1-meim) were commercially available. The first two were recrystallized several times from benzene and dried in vacuo, while the latter was dried over KOH and distilled at a reduced pressure.

Acetone-d_6 (Merck, 99.8%) was used as a solvent for ^1H and ^{31}P NMR measurements after drying with molecular sieves. High-purity nitrogen (99.9998%) and carbon monoxide (>99.95%) were utilized.

Preparation of Copper(I)-Imidazole Compounds. A solution of imidazole (2.0 mg, 2.9×10^{-5} mmol) and $[Cu(CH_3CN)_4]ClO_4$ (5.1 mg, 1.5×10^{-5} mmol) in 5 mL of acetone-d_6 was stirred under nitrogen for 5 min. In order to vary the ratio of [im] to [Cu], a stock solution of imidazole was added to a constant amount of copper(I). While maintaining a nitrogen atmosphere, the resultant solutions were transferred into an NMR sample tube and the NMR spectra were recorded.

Carbonylated compounds were prepared by passing carbon monoxide through a solution of imidazole copper(I) compounds. Low-pressure carbon monoxide was obtained[33] by mixing nitrogen with carbon monoxide and making adjustments with three Kusano KG-1 rotameters and three precise needle valves. The rotameters were individually calibrated throughout their ranges with nitrogen and carbon monoxide.

Physical Measurements. 200 MHz ^1H NMR spectra were obtained with a JEOL FX200 spectrometer. Between 200 and 1000 transients were accumulated using a 14-μs (90°) pulse;

8 K data points were collected over a band width of 2500 Hz. A probe temperature was set at −90 °C, being calibrated to an accuracy of ±1 °C using the temperature-dependent difference between the CH_3 and OH shifts of pure methanol. ^{31}P NMR spectra operating at 80.79 MHz were recorded: 500 transients were accumulated using an 18-μs (80°) pulse and 8 K data points were collected over a band width of 4000 Hz. The solution of copper(I) imidazole containing 50 mM copper(I) with a ratio [im]/[Cu]=2 and 3 was transferred under a nitrogen atmosphere into a sealed IR cell constructed with KBr plates having a 0.05 mm path length. The IR spectrum was recorded at 25 °C. The remaining solution was then exposed to carbon monoxide for 5 min; that solution was transferred to a sealed IR cell and the spectrum was again recorded. All the spectra were calibrated with the aid of polystyrene film.

Results and Discussion

^{1}H NMR Spectra of Imidazole Complexes of Copper(I). $[Cu(CH_3CN)_4]ClO_4$ reacts with imidazole under anaerobic conditions to give various copper(I) complexes whose formation depends upon the concentration of imidazole. All of the complexes are colorless and show no optical spectra. Thus, their formation and structural characterization were investigated by ^{1}H NMR spectroscopy.

Three metal-free imidazole signals with integrated intensities of 1:1:2 were assigned[31,32] from the downfield region to 1-H, 2-H, and 4,5-H, respectively. The coordinated imidazole generally gave four resolved signals,[6,32] with the downfield shift assigned from downfield to 1-H, 2-H, 5-H, and 4-H. Those imidazole copper(I) species in solution encounter a chemical-exchange effect at ambient temperature and exhibit four averaged broad ^{1}H NMR signals. This averaging of the signals is released when a solution is cooled to −90 °C.[30]

Formation of Binary Copper(I) Complexes. By ^{1}H NMR spectroscopy, we can distinguish the species in a solution. Figure 1 illustrates these features as a function of [im]. The metal-binding imdazole gives well resolved signals which are reproducible within, at most, ±0.02 ppm on repeated runs. Especially, imidazole C-H proton signals are good markers for a species in solution. Now we will focuss on imidazole C-H protons in the 6—9 ppm region. When a small amount of imidazole (r=[im]/[Cu]≤1) was added to $[Cu(CH_3CN)_4]ClO_4$, three signals ($A_{2,4,5}$) appeared. As [im] further increased, the new signals ($B_{2,4,5}$) increased with a decrease in the intensity of signals $A_{2,4,5}$ (Fig. 1(2)). Signals $A_{2,4,5}$ were located at the upfield region more than signals $B_{2,4,5}$. Signals $A_{2,4,5}$ are assigned to mono(imidazole)complex(**1**), while signals $B_{2,4,5}$ are attributable to bis(imidazole)complex(**2**). Complex **2** was predominantly formed by the addition of ca. two equivalent of imidazole. When more than two equivalent of imidazole was added to $[Cu(CH_3CN)_4]ClO_4$, a set of new signals($C_{2,4,5}$) appeared, located at higher field than signals for **1** and **2**. We successfully detected signals $C_{2,4,5}$ concurrently with those of **2** at [im]/[Cu]=2.5 (Fig. 1(4)). These signals $C_{2,4,5}$ were ascribed to tris(imidazole)copper(I) (**3**). Nearly equal intensities of signals B and C (Fig. 1(4)) support the quantitative formation of **2** and **3**. As [im] further increased [im]/[Cu]=3—4), signals $C_{2,4,5}$ apparently broadened, even at low temperatures, accompanying a slight upfield shift. Under these concentrations, the principal species was **3**. At an imidazole concentration greater than four equivalent, signals were further broadened, indicating a signal-averaging between the coordinated and metal-free imidazole. This broadening makes it difficult to detect tetrakis(imidazole)copper(I) (**4**). At r=4, **4** is a likely minor species. Interestingly, excess imidazole ([im]/[Cu]>4) turned a colorless solution blue at the ambient temperature. This reveals the occurrence of the oxidation of copper(I).[33] The observed ^{1}H NMR chemical shifts obtained here are listed in Table 1.

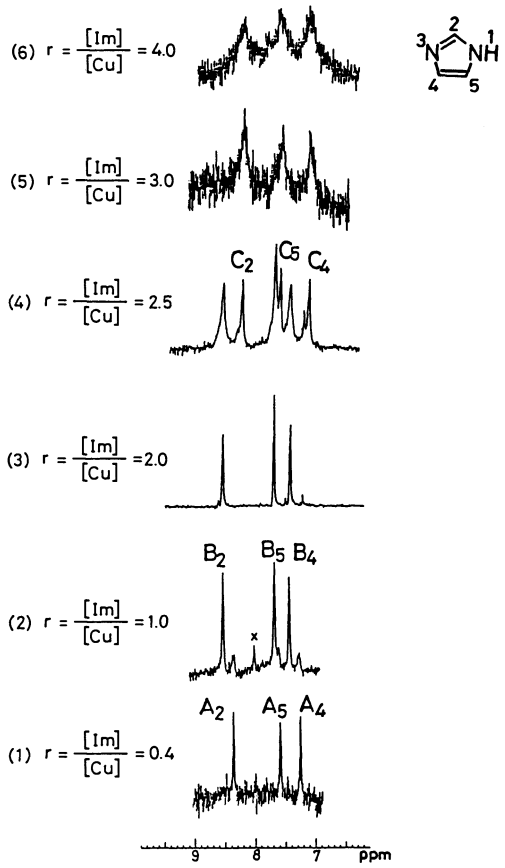

Fig. 1. ^{1}H NMR spectra at −90°C of acetone-d_6 solution of copper(I) complexes of imidazole. A, B, and C corresponds to signals of compound **1**, **2**, and **3**, respectively. Suffix denotes the assignement of proton signals of imidazole. x=impurity.

What structures have the solution species **1**—**4**? Among copper(I) complexes which have so far been

Table 1. Observed ^{1}H NMR Chemical Shifts[a] of Mononuclear Copper(I) Complexes,[b] $[CuL_nL'_m]ClO_4$

L(n)	L'(m)	1-H(Me)	2-H	4-H	5-H
Imidazole(metal-free)		13.06	7.97	7.25	7.25
(1)	CH_3CN[c]	12.49	8.38	7.28	7.61
(2)	—	12.61	8.53	7.42	7.68
(2)	CO (1)[d]	12.47	8.35	7.25	7.60
(3)	—	12.41	8.22	7.12	7.59
(3)	CO (1)	12.42	8.21	7.11	7.58
1-Methylimidazole (metal-free)		3.74	7.69	6.98	7.21
(2)	—	3.94	8.32	7.34	7.57

a) Shifts in ppm from $Si(CH_3)_4$. Error limit, ±0.02 ppm. Observed at −90 °C. b) $[Cu(CH_3CN)_4]ClO_4$ was used as a starting material. c) Number of coordinated molecules was not determined. d) The observed shifts at $P_{CO}=1$ atm. Under $P_{CO}=0.1$ atm, 12.48, 8.42, 7.32, and 7.63 ppm for 1-, 2-, 3-, and 5-H, respectively.

Table 2. Observed ^{1}H NMR Chemical Shifts[a] of Nitriles[b]

Solution[c]	CH_3CN	C_2H_5CN		C_6H_5CN		
		CH_3	CH_2	o-H	m-H	p-H
Metal-free	2.22	1.23	2.55	7.94	7.70	7.84
$[Cu(nitrile)_4]^+$	2.41	1.30	2.76	8.11	7.77	7.94
$[Cu(im)(nitrile)_m]^+$	2.32	1.28	2.71	7.98	7.73	7.90
$[Cu(im)_2]^+$	2.20	1.23	2.55	7.96	7.72	7.86
$[Cu(im)_2(CO)]^+$	2.22	1.23	2.56	7.96	7.71	7.86
$[Cu(im)_3]^+$	2.19	1.23	2.55	7.96	7.71	7.85
$[Cu(im)_3(CO)]^+$	2.20	1.23	2.55	7.96	7.71	7.85

a) Shifts in ppm from $Si(CH_3)_4$. Error limit ±0.02 ppm. Observed at −90 °C. b) $[Cu(nitrile)_4]ClO_4$ as a starting material was used in order to prepare copper(I)-imidazole complexes. c) The solution in which a principal copper(I)-imidazole complex forms. The predominant species are denoted in this column.

Table 3. Effect of Nitriles[a] on the Observed ^{1}H NMR Chemical Shifts[b] of Imidazole in Copper(I) Complexes

RCN[a]	Complexes	1-H	2-H	4-H	5-H
C_2H_5CN	$[Cu(im)(C_2H_5CN)_m]^+$	12.61	8.54	7.43	7.69
	$[Cu(im)_2]^+$	12.66	8.53	7.42	7.68
	$[Cu(im)_2(CO)]^+$	12.47	8.35	7.25	7.60
	$[Cu(im)_3]^+$	12.41	8.22	7.12	7.59
	$[Cu(im)_3(CO)]^+$	12.47	8.21	7.11	7.58
C_6H_5CN	$[Cu(im)(C_6H_5CN)_m]^+$	12.47	8.41	7.30	7.62
	$[Cu(im)_2]^+$	12.64	8.53	7.42	7.68
	$[Cu(im)_2(CO)]^+$	12.51	8.34	7.24	7.59
	$[Cu(im)_3]^+$	12.41	8.21	7.12	7.59
	$[Cu(im)_3(CO)]^+$	12.42	8.21	7.11	7.58

a) $[Cu(RCN)_4]ClO_4$ was used as a starting material. Solvent was acetone-d_6. b) Shifts in ppm from $Si(CH_3)_4$. Error limit, ±0.02 and ±0.04 ppm for 2,4,5-H, and 1-H, respectively. Observed nitrile shifts were catalogued in Table 2.

synthesized and characterized, four-coordinate tetrahedral species[23] are popular. Recently, various two-[7,9,14,18–22] and three-coordinate[13,34–46] copper(I) complexes have been synthesized; these types have become familiar. Two-coordinate complexes display a linear structure, while three-coordinate structures exhibit a triangular[34–43] or T-shape form,[15,44–46] the former being more preferable when the usual monodentate ligands coordinate. We have clarified the number of coordinating imidazole among **1**—**4**. Next, other ligands should be determined among solution species **1**—**3**. In our systems, potential donor ligands are ClO_4^-, CH_3CN, and acetone. The latter can be excluded from the donor groups due to its very poor coordinating ability against a soft metal ion.[47] Concerning (1) nitrile and (2) counter anion binding, we have used various starting materials of copper(I) such as $[Cu(RCN)_4]ClO_4$ (R=CH_3, C_2H_5, and C_6H_5). Also, we have demonstrated[25] that methyl proton signals of CH_3CN distinguish well between the coordinated and dissociated CH_3CN. Thus, signals of the nitriles for solutions of **2** and **3** have been examined. Table 2 shows the observed shifts of the nitriles. All of the ^{1}H signals locate at metal-free positions, indicating no coordination of acetonitrile. The imidazole signals of **2** and **3** have also been recorded as a function of R, and the obtained shifts are listed in Table 3. An inspection of Table 3 reveals that the imidazole signals of **2** and **3** show independence upon starting nitrile derivatives. Lastly, with the aid of ascorbic acid as a reducing agent, **2** was also synthesized from $Cu^{II}(ClO_4)_2$ and imidazole; such a system is free from nitrile. Both the ^{1}H NMR spectra with and without CH_3CN show that those imidazole signals[48] completely agree with each other.

Species **1** was checked, although it was the most difficult case to be characterized by NMR. **1** is formed only if $r<1$, wherein the principal species in solution are binary $[Cu(CH_3CN)_n]^+$ (n=2 or 3)[49,60] rather than **1**. Even at −90°, ^{1}H NMR spectroscopy failed to detect separated CH_3 signals of the CH_3CN ascribed to each species. This is because CH_3CN is chemically exchanged faster than the NMR time scale and its signal is averaged out. The chemical exchange is not depressed for nitrile. Table 2 reveals that only **1** gives nitrile signals different from a metal-free position. Imidazole proton signals of **1** show a nitrile-dependence as illustrated in Tables 1 and 3; these shift downfield by 0.08—0.16 ppm when a starting copper source $[Cu(CH_3CN)_4]$ is replaced by $[Cu(C_6H_5CN)_4]$. This nitrile-dependence is significantly associated with the coordination of CH_3CN in **1**. Consequently, it is concluded that the binding of nitrile occurs in **1** while not in **2** and **3**.

In order to clarify the coordination of a perchlorate ion, PF_6^- is used instead of ClO_4^-: The former possesses much less coordinating ability[24] than ClO_4^-. ^1H NMR signals of perchlorate salts of **1—3** are the same as those from their hexafluorophosphate salts. ^{31}P NMR spectra of the resultant species were measured as to whether or not the ^{31}P NMR signal shifts to the position denoting a strong association with copper(I). Both imidazole-free and imidazole-containing (two-equivalents) solutions of $[Cu(CH_3CN)_4]PF_6$ gave a single ^{31}P signal, appearing at −143.9 ppm from H_3PO_4, that are characteristic of a metal-free PF_6^-. Accordingly, the counter anion proves to be dissociated for all the species, **1—3.**

Now, we conclude that **2** and **3** are two- and three-coordinate copper(I) complexes, respectively, wherein neither nitrile nor an anion is bound to copper(I). The results regarding **2** are in good agreement with the accepted view that 1:2 complexes with monodentate ligands like NH_3[58] are truely two-coordinate in solution. **2** is possibly linear, as has been demonstrated by its X-ray structure,[7,9,14] while **3** is trigonal. This is reasonable since 1:3 complexes of copper(I) are easily formed with CN^-,[34,52] pyridine,[53,54,59] Cl^-, and CH_3CN.[55-57] **1** has at least one ligand other than imidazole. In referring to structures which have so far been demonstrated for copper(I) compounds, $[Cu(im)(CH_3CN)]^+$ or $[Cu(im)(CH_3CN)_3]^+$ is considered as a possible species. Mono-, bis-, and tris(imidazole)complexes are successfully prepared in an acetone solution; their formation and equilibria are summarized in Scheme 1. Throughout this investigation, $[Cu(CH_3CN)_4]ClO_4$ has been proven to be equivalent to $[Cu(CH_3CN)_4]PF_6$ concerning a reaction with imidazole.

It is noteworthy in Table 1 that the increase in the coordiation number from **2** to **3** causes imidazole signals to shift upfield. This is accounted for by the delocalization of a positive charge upon the imidazole ring.[6] The downfield shift upon coordination to copper(I) is attributable to a scattering of positive charge onto imidazole ring, and the increase in the number of coordinating imidazole dilutes the scattered positive charge on each imidazole ring. Chemical shifts for **1** are not directly compared with those for **2** and **3** because the former is a ternary compound.

Formation of Carbonylated Copper(I) Imidazole Complexes. When CO gas was passed into a solution of **1—3**, the resultant colorless solution gave new sharp ^1H NMR signals whose chemical shifts are different from those of the precursor (Fig. 2). The binding of CO causes an upfield shift of coordinating imidazole. The carbonylated complex (**3-a**) of **3** has been definitely determined to be $[Cu(im)_3(CO)]^+$ since dissociated imidazole signals were not observed.

We have determined the structure of a carbonylated species as well as the binary systems mentioned in the previous section. The coordinated imidazole signals of **2-a** and **3-a** showed no dependence upon the starting materials of $[Cu(RCN)_4]ClO_4$ (R=CH_3, C_2H_5, and C_6H_5), indicating no nitrile-binding in **2-a** and **3-a**. Also, no anion binding to copper(I) in **2-a** and **3-a** has demonstrated by ^1H and ^{31}P NMR for imidazole-$[Cu(CH_3CN)_4]PF_6$ systems. Consequently, these species are $[Cu(im)_2(CO)]^+$ and $[Cu(im)_3(CO)]^+$. Figure 2(3) reveals that the signal intensities of $[Cu(im)_2(CO)]^+$ and $[Cu(im)_3(CO)]^+$ are nearly equal, indicating the occurrence of only addition reaction of CO (Fig. 1(4)).

CO-bubbling into the solution of **1** gave imidazole ^1H shifts that just correspond to those of **2-a.** This is either because the carbonylated compound of **1** accidentally gives the same chemical shifts as **2-a**, or because carbon monoxide drives the equilibrium to the formation of **2-a** rather than the addition to **1.** To determine which is more probable is beyond the abilities of the present NMR method.

Decarbonylation was carried out by passing nitrogen into the solution. **3-a** is the most stable and, thus, prolonged nitrogen bubbling is required. This stability reminds us that $[Cu(dien)(CO)]^+$ [61] and $[Cu(HB(pz)_3)(CO)]^+$ [63] (dien=diethylenetriamine ;HB-$(pz)_3$=hydrotris(pyrazol-1-yl)borate). Neither compounds lose CO, even at high temperatures or in

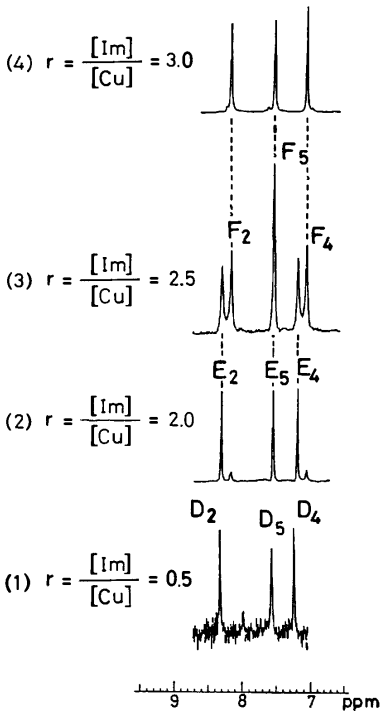

Fig. 2. ^1H NMR spectra at −90 °C of acetone-d_6 solution of copper(I) complexes of imidazole. All samples were prepared under CO atmosphere. D, E, and F correspond to signals of complexes **1-a**, **2-a**, and **3-a**, respectively. Suffix denotes the assignment of proton signals of imidazole.

vacuo in the solid state. These copper(I) complexes and **3-a** commonly have a tetrahedral structure with an N_3C donor set. The greater is the basicity of the N donor ligand, the more the electron density on copper increases.[62] Therefore, the rich electron density on copper enhance the π back-bonding and stabilize the Cu–CO bond. The basicity of dien is greater in five pK_a units[59] than that of imidazole. This gap in basicity is significantly associated with a reversible binding of CO. The carbonyl–decarbonyl cycle can be repeated many times for all a solutions of copper(I) imidazole compounds in this work, while dien system can not. The obtained reversible reactions are summarized in Scheme 1.

Sorrell et al.[7] have reported by use of IR spectra that bis(imidazole)copper(I) does not react with CO unless other bases are present in solution. On the basis of the inertness of bis(imidazole)copper(I) species, they suggest that the coordination sphere of each copper in hemocyanin is a two-coordinate; however, near one of the copper centers is an additional donor that can coordinate and promote CO binding to that copper. Indeed, three-coordinate copper(I) tends to readily provide a monocarbonyl complex, as has also been demonstrated here. However, the reactivity of bis(imidazole)copper(I) against CO appears opposite to our results. They have also illustrated that bis(pyrazole)copper(I) readily reacts with CO to produce its monocarbonyl adduct. Then, two questions arise: (1) Whether or not bis(imidazole)copper(I) reacts with CO? and (2) why there are marked difference in reactivity toward CO between copper(I) complexes of pyrazole and imidazole? In response to question (2), we point out that the difference in the ligand basicity, which contributes to the stability[7] of a precursor, is of significance. The answer to question (1) is that **2** does react with CO, contrary to Sorrell's conclusion. It should be noted that the NMR spectra were measured at different conditions from the IR spectra. The clearest difference is the temperature: −90 °C was established for the NMR measurement, while the ambient temperature was set for IR. Does this low temperature render an equilibrium shift to the formation of a carbonylated complex? For example, $[CuCl(bpy)]_2$ in acetone under a P_{co}=1 atm at 25 °C gives a monocarbonyl adduct[30] with ca. 57% yield to the precursor. This adduct was completely formed at −90 °C. Figure 2 ((2) and (3)) reveals the quantitative formation of **2-a** and **3-a**, amounts that clearly correspond to those of precursors, **2** and **3** (Fig. 1(4)), respectively. This fact was obtained at low temperature and does not exhibit any marked difference in the reactivity[7] of **2** and **3**.

In comparison with a low-temperature species, the species formed at ambient temperature were checked by the IR spectra. The stretching frequencies (ν_{co}) of the coordinated CO was measured for carbonyl complexes in an acetone solution. Fortunately, acetone gives no significant absorption bands at 2000—2200 cm^{-1}. Solutions prepared with a ratio of [im]/[Cu]=2 provided a single band at 2076 cm^{-1}, while a degassed solution gave no band in this region (Fig. 3). This band is attributable to ν_{co} of the coordinating CO. A band at 2069 cm^{-1} having the stronger intensity appeared at r=3. The band at r=2 is broader than that at r=3. The gap (7 cm^{-1}) between two bands is not large enough to be seen as two different bands, since the linewidth of those IR bands are broad. The ν_{co} band of $[CuL_3(CO)]^+$ appeared in the region lower than 2100 cm^{-1}, while that of

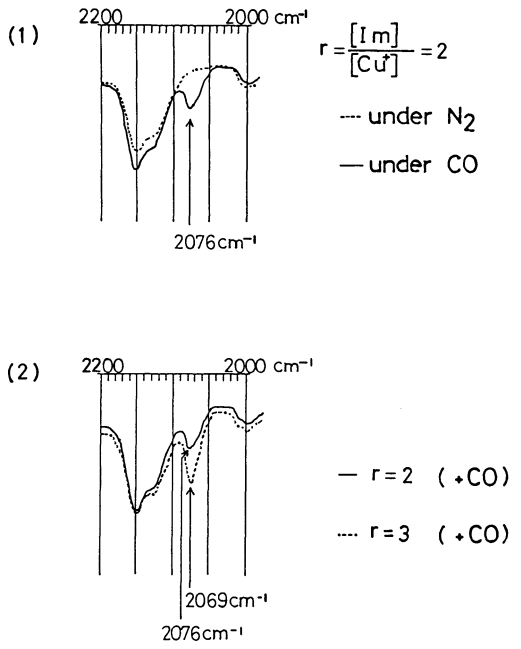

Fig. 3. Infrared spectra at 25 °C of carbonylated copper(I) complexes in acetone. The band ascribed to carbonyl stretching is indicated by an arrow together with its wave number.

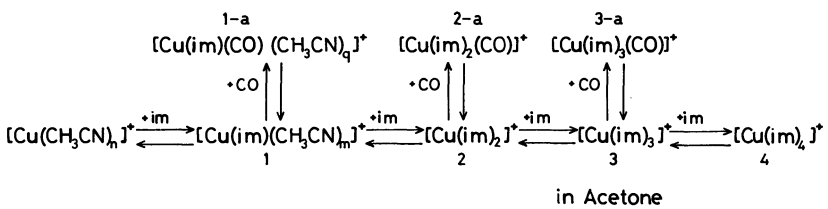

Scheme 1.

$[CuL_2(CO)]^+$ appeared in the region greater than 2100 cm^{-1} (L=pyrazole and its derivatives).[7] Accordingly to these facts, these bands were assigned to ν_{CO} of $[Cu(im)_3(CO)]^+$. Even at r=2, the detection of **3-a** indicates that **3-a**[64] forms more readily than **2-a**. The IR spectra of solution samples require a very high concentration of the coordinating CO. The concentration of 50—100 mM is 25—50 fold larger than in the case of ^1H NMR measurements. Therefore, the IR spectrum fails to detect its ν_{CO} signal when **2-a** is present as a minor species. The detection is dependent on the degree in the stability constants of the resultant CO adduct. In conclusion, **2** does react with CO, giving 100% **2-a** at −90 °C, and less **2-a** at ambient temperature.

Copper(I) Pyrazole Complexes. Similarly, copper(I) pyrazole (pz) compounds were also examined by ^1H NMR spectroscopy at −90 °C.[65] From the ^1H NMR spectra obtained at r=[pz]/[Cu]=0.5—4, various chemical exchange phenomena were found. At r=1—2, the 3-H signal was broadened accompanying with a slight shift, while 5-H and 4-H signals remain sharp. This broadening is not due to the paramagnetic copper(II) species generated by the oxidation of copper(I) species because of its selective broadening. This selective broadening is attributable to a chemical exchange[66] among $[Cu(pz)L_x]^+$ (L= another ligand, possibly CH_3CN), $[Cu(pz)_2]^+$, and L. Such a chemical exchange phenomena is in good contrast with the case of imidazole. At r=2—3, all the signals of pyrazole became broadened, indicating a chemical exchange[67] between a metal-free and coordinating ($[Cu(pz)_n]^+$; n=2 and 3) pyrazoles; thus, the presence of a considerable amount of metal-free pyrazole in solution. On the other hand, the chemical exchange rate in $[Cu(im)_n]^+$ (n=2 and 3) at r=2.5 was so slow that the ^1H NMR spectra were simultaneously observed (Fig. 1). Accordingly, the formation of $[Cu(pz)_3]^+$ is harder than that of $[Cu(im)_3]^+$. The difference between copper(I) complexes of pyrazole and imidazole is ascribed to the basicity of the ligand,[48,53] A chelating ligand of pyrazole is required if a stable and less labile copper(I)-pyrazole complexes is to be synthesized. Carbonylated copper(I) complexes of pyrazole are quantitatively formed and all their signals are sharp, revealing a slow chemical exchange.[69] Of course, the carbonyl-decarbonyl cycle is readily repeated. In summarizing these results, there was the remarkable difference in forming two-coordinate copper(I) complexes between pyrazole and imidazole. Also, no distinguishable difference between their carbonylated copper(I) complexes were detected by low temperature ^1H NMR spectroscopy.

A knowledge of the equilibria and reactivity and the accumulated ^1H NMR data on imidazole in various copper(I) complexes would contribute to an advancement in the copper(I) chemistry involving imidazole and its derivatives and an application to copper proteins.

We appreciate the assistance of Mr. Hirotoshi Konoike, Mr. Hiroki Nagai, and Mr. Norimitsu Izumi for the recording the NMR spectra. This work was supported in part by a Grant-in-Aid for Scientific Research No. 59740303 from the Ministry of Education, Science and Culture.

References

1) "Metal Ions in Biological Systems," ed by H. Sigel, Marcel Dekker, Inc, New York (1981), Vol. 13.

2) "Copper Coordination Chemistry. Biochemical and Inorganic Perspectives," ed by K. D. Karlin, J. Zubieta, Adenine Press, New York (1983).

3) W. P. J. Gaykema, W. G. J. Hol, J. M. Vereijken, N. M. Soeter, H. J. Bak, and J. J. Beintema, *Nature*, **309**, 23 (1984).

4) a)W. Clegg, S. R. Ascott, and C. D. Garner, *Acta Crystallogr., Sect. C*, **40**, 768 (1984); b) W. Clegg, S. R. Acott, and C. D. Garner, *J. Chem. Soc., Chem. Commun.*, **1984**, 2581.

5) H. A. Henricksson, B. Sjoeberg, and R. Oesterberg, *J. Chem. Soc., Chem. Commun.*, **1976**, 130.

6) P. A. Temussi and A. Vitagliano, *J. Am. Chem. Soc.*, **97**, 1572 (1975).

7) T. N. Sorrell and D. L. Jameson, *J. Am. Chem. Soc.*, **105**, 6013 (1983).

8) T. N. Sorrell and D. L. Jameson, *J. Am. Chem. Soc.*, **104**, 2053 (1982).

9) H. M. J. Hendriks, P. J. M. W. L. Birker, J. Rijn, G. C. Verschoor, and J. Reedijk, *J. Am. Chem. Soc.*, **104**, 3607 (1982).

10) P. J. M. W. L. Birker, E. F. Godefroi, J. Helder, J. Reedijk, *J. Am. Chem. Soc.*, **104**, 7556 (1982).

11) M. G. Simmons, C. L. Merrill, L. J. Wilson, L. A. Bottomley, and K. M. Kadish, *J. Chem. Soc., Dalton. Trans.*, **1980**, 1827.

12) J. V. Dagdigian and C. A. Reed, *Inorg. Chem.*, **18**, 2623 (1979).

13) T. N. Sorrell and M. R. Malachowski, *Inorg. Chem.*, **22**, 1883 (1983).

14) M. J. Schilsfra, P. J. M. W. L. Birker, G. C. Verschoor, and J. Reedijk, *Inorg. Chem.*, **21**, 2637 (1982).

15) J. V. Dagdigian, V. Mckee, and C. A. Reed, *Inorg. Chem.*, **21**, 1332 (1982).

16) M. Pasquali, G. Marini, C. Floriani, A. G. Manfredotti, and C. Guastini, *Inorg. Chem.*, **19**, 2525 (1980).

17) L. Casella, M. E. Silver, and J. A. Ibers, *Inorg. Chem.*, **23**, 1409 (1984).

18) H. Siebert and D. Gunamer, *Z. Anorg. Chem.*, **420**, 265 (1976).

19) D. N. Waters and B. Basak, *J. Chem. Soc., Dalton Trans.*, **1971**, 2734.

20) J. Kaiser, G. Brauer, F. A. Schroeder, I. F. Taylor, and S. E. Rasmussen, *J. Chem. Soc., Dalton Trans.*, **1974**, 1490.

21) G. A. Bowmaker and D. A. Rogers, *J. Chem. Soc., Dalton Trans.*, **1982**, 1873.

22) P. Leoni, M. Pasquali, and C. A. Ghilardi, *J. Chem. Soc., Chem. Commun.*, **1983**, 240.

23) F. H. Jardine, *Adv. Inorg. Chem. Radiochem.*, **17**, 115 (1975), and references cited therein.
24) F. A. Cotton and G. Wilkinson, "Advanced Inorganic Chemistry," 4th ed, Interscience, New York (1980).
25) S. Kitagawa, M. Munakata, and M. Miyaji, *Inorg. Chem.*, **21**, 3842 (1982).
26) S. Kitagawa and M. Munakata, *Inorg. Chem.*, **23**, 4388 (1984).
27) P. Hemmerich and C. Sigwart, *Experientia*, **19**, 488 (1963).
28) M. Kubota and D. J. Johnston, *J. Inorg. Nucl. Chem.*, **29**, 769 (1967).
29) D. F. Shriver, "Inorganic Syntheses," Wiley-Interscience, New York (1979), Vol. 19, p. 90.
30) S. Kitagawa and M. Munakata, *Inorg. Chem.*, **20**, 2261 (1981).
31) A. Mannschreck, W. Seitz, and H. A. Staab, *Chem. Ber.*, **67**, 1963 (1963).
32) N. S. Rowan, C. B. Storm, and R. Rowman, *Inorg. Biochem.*, **14**, 59 (1981).
33) This shows that copper(I) complexes are oxidized to copper(II) complexes. The blue color of the solution was also reproduced when the solution was exposed to air.
34) C. Kappenstein and R. P. Hugel, *Inorg. Chem.*, **17**, 1945 (1978).
35) M. S. Weininger, G. W. Hunt, and E. L. Amma, *J. Chem. Soc., Chem. Commun.*, **1972**, 1140.
36) D. Covcouvanis, C. N. Murphy, and S. K. Kanodia, *Inorg. Chem.*, **19**, 2993 (1980).
37) P. G. Eller and P. W. R. Corfield, *J. Chem. Soc., Chem. Commun.*, **1971**, 105.
38) P. G. Nicpon and D. W. Meek, *J. Am. Chem. Soc.*, **87**, 4951 (1965).
39) J. M. Bret, P. Castan, G. Jugie, and A. Dubourg, *J. Chem. Soc., Dalton Trans.*, **1983**, 301.
40) P. H. Davis, R. L. Belford, and I. C. Poul, *Inorg. Chem.*, **12**, 213 (1973).
41) M. Barrow, H. B. Burgi, D. K. Johnson, and L. M. Venanzi, *J. Am. Chem. Soc.*, **98**, 2536 (1976).
42) J. A. Tiethof, J. Stalik, and D. W. Meek, *Inorg. Chem.*, **12**, 1170 (1973).
43) L. G. Dance, L. J. Fizpatrick, and M. L. Scudder, *J. Chem. Soc., Chem. Commun.*, **1983**, 546.
44) R. G. Gagne, R. P. Kreh, and J. A. Dodge, *J. Am. Chem. Soc.*, **101**, 6917 (1979).
45) K. D. Karlin, Y. Gultneh, J. P. Hutchinson, and J. Zubieta, *J. Am. Chem. Soc.*, **104**, 5240 (1982).
46) T. N. Sorrell, M. R. Malachowski, and D. L. Jameson, *Inorg. Chem.*, **21**, 3250 (1982).
47) a) M. Munakata, S. Kitagawa, and M. Miyajima, *Inorg. Chem.*, **24**, 1638 (1985); b) We have obtained no direct evidence concerning the coordination of acetone molecules by NMR spectroscopy. Although acetone is a weak ligation molecule and there is no cases where acetone binds copper(I), we cannot exclude the possibility of the ligation of acetone because large excess of acetone is present.
48) The reduction was made by refluxing the solution. These copper(I) compounds reduced by ascorbic acid definitely gave the same ^{1}H NMR signals of coordinating imidazole as those obtained from copper(I) sources. Additional signals were also observed which are easily assigned to oxidized ascorbic acid.
49) ^{63}Cu NMR spectra are available for an investigation of tetrahedrally coordinated copper(I) compounds.[26] Due to the great quadrupolar interaction, other copper(I) compounds having the lower symmetry give hardly detected ^{63}Cu NMR signal as a consequence of the broadening. By use of ^{63}Cu NMR spectroscopy, it has been demonstrated that acetone solution of $[Cu(CH_3CN)_4]ClO_4$ provides no ^{63}Cu signal, indicative of significant decomposition[50,51] of $[Cu(CH_3CN)_4]^+$ into the lower coordination form. On the other hand, its acetonitrile solution clearly gave single signal ascribed to $[Cu(CH_3CN)_4]^+$.
50) S. Kitagawa and M. Munakata. Unpublished work.
51) U. Ochsenbein and C.W.Schlaepfer, *Helv. Chim. Acta*, **63**, 1926 (1980).
52) R. M. Izatt, H. D. Johnston, G. D. Watt, and J. J. Christensen, *Inorg. Chem.*, **6**, 132 (1967).
53) B. R. James and R. J. P. Williams, *J. Chem. Soc.*, **1961**, 2007.
54) A. D. Zuberbuehler, "Metal Ions in Biological Systems," ed by H. Sigel, Marcel Dekker Inc., New York (1976), Vol. 5, Chap. 7, p. 325.
55) A. Guenter and A. D. Zuberbuehler, *Chimia*, **24**, 340 (1970).
56) S. E. Manaham and R. T. Iwamoto, *J. Electroanal. Chem.*, **14**, 213 (1967).
57) T. Hurlen, *Acta Chem. Scand.*, **15**, 1231 (1961).
58) V. R. Nast and C. Schultze, *Z. Anorg. Chem.*, **307**, 15 (1960).
59) R. E. Smith and A. E. Martell, "Critical Stability Constants," Plenum Press, New York (1975), Vol. 2.
60) P. Hemmerich, "The Biochemistry of Copper," ed by J. Peisach, P. Aisen, W. E. Blumberg, Academic Press, New York (1966), p. 15.
61) M. Pasquali, F. Marchetti, and C. Floriani, *Inorg. Chem.*, **17**, 1684 (1978).
62) a) S. Kitagawa, M. Munakata, and N. Miyaji, *Bull. Chem. Soc. Jpn.*, **56**, 2258 (1983); b) D. T. Clark, A. Sgamelloti, and F. Tarantelli, *Inorg. Chem.*, **20**, 2602 (1981).
63) M. I. Bruce and A. P. P. Ostazewski, *J. Chem. Soc., Dalton Trans.*, **1973**, 2433.
64) Exact addition of two equivalent of imidazole at the concentration is very difficult problem. If a slight excess of imidazole is present in solution, **3-a** may readily form under CO atmosphere.
65) A metal-free pyrazole gave three ^{1}H NMR signals at 13.1 (1-H), 7.83 (3- and 5-H), and 6.42 ppm (4-H), with relative intensities of 1, 2, and 1, respectively. In copper(I)-pyrazole systems, well-separated four signals were obtained, and the coordination shift for all pyrazole protons was appreciated, ranging from 0.11—0.43 ppm. At $r<1$, except for 1-H (13.3 ppm) very sharp signals displaying multiplets were obtained, whose assignment is 5-H (8.26), 3-H (7.94), and 4-H (6.70). The chemical shift of 4-H and 5-H signals is insensitive to the structures such as $[Cu(pz)_n]^+$ and $[Cu(pz)_m(CO)_p]^+$. On the other hand, 3-H signal is sensitive, indicative of a good probe to inquire into the structure in solution.
66) At $1\leq r\leq 2$, several exchange processes are considered from ^{1}H NMR spectra, which show characteristic broadening of 3-H signal. Possible processes are considered as follows:

$$[Cu_A(pz)L_n]^+ + [Cu_B(pz)(pz)^*]^+ \rightleftharpoons [Cu_A(pz)(pz)^*]^+ + [Cu_B(pz)L_n]^+, \quad \text{(i)}$$

$$[Cu(pz)L_x]^+ + L \rightleftharpoons [Cu(pz)L_{x+1}]^+, \quad \text{(ii)}$$

wherein L is another ligand, possibly CH_3CN. This is characteristic of copper(I)-pyrazole system.

67) The linewidth of all the signals increases with increase in r. Hence, the line-broadening of signals is attributable to the following chemical exchange processes (iii) and/or (iv).

$$Cu(pz)_2 + pz^* \rightleftharpoons Cu(pz)(pz^*) + pz \quad \text{(iii)}$$

$$Cu(pz)_3 + pz^* \rightleftharpoons Cu(pz)_2(pz^*) + pz \quad \text{(iv)}$$

68) "Stability Constants of Metal-Ion Complexes," ed by D. D. Perrin, IUPAC Chemical Data Series No. 22, Pergamon, Oxford (1979).

69) At r=1—3, three different ^1H NMR spectra were obtained. They all displayed well-separated and sharp four signals. The tentative structure of these carbonylated complexes is determined in analogy with that of copper(I)-imidazole complexes. At r=1, $[Cu(pz)(CO)L_x]^+$ (L=another ligand; x=1 or 2) forms, whose signals are assigned to 1-H (13.4 ppm), 5-H (8.27), 3-H (7.89), and 4-H (6.70). At r=2, four signals at 13.2 (1-H), 8.25 (5-H), 7.74 (3-H), and 6.68 (4-H) are ascribed to $[Cu(pz)_2(CO)_y]^+$ (possibly y=2). Finally, at r=3, $[Cu(pz)_3(CO)]^+$ gives signals at 8.25 (5-H), 7.67 (3-H), and 6.67 (4-H).

Nuclear Magnetic Resonance Studies of Copper(I) Complexes of Imidazoles. II. Their Reaction with Ethylene, Phosphite, and Isocyanides

Susumu KITAGAWA* and Megumu MUNAKATA
Department of Chemistry, Faculty of Science and Technology, Kinki University, Kowakae, Higashi-Osaka 577
(Received December 12, 1985)

The reaction of binary copper(I) complexes of monodentate imidazole(im) with π acceptor ligands (ethylene, triethyl phosphite, *p*-tolyl isocyanide, and phenyl isocyanide) have been carried out in acetone. The resultant copper(I) complexes have been characterized by ^{1}H and ^{31}P NMR spectroscopy. Ethylene reacts with $[Cu(im)_2]^+$ (**2**) to give $[Cu(im)_2(C_2H_4)]^+$ (**2-b**), but does not react with $[Cu(im)_3]^+$ (**3**). This shows a clear difference in reactivity between **2** and **3**. Phosphite and isocyanides give rise to a substitution reaction for im in **2** and **3**, accompanying with addition reaction. Among the copper(I) compounds prepared here, two- and four-coordinate forms show sharp ^{1}H NMR signals of coordinated im, indicating that they are in the slow-exchange regime. This proved that ^{1}H NMR spectroscopy is a useful tool to characterize diamagnetic copper(I)-imidazole complexes in solution.

Part I of this study[1] has demonstrated that binary copper(I) complexes of monodentate imidazole (im) are produced quantitatively in acetone at low temperature. Bisimidazolecopper(I) perchlorate, $[Cu(im)_2]ClO_4$ (**2**), and trisimidazolecopper(I) perchlorate, $[Cu(im)_3]ClO_4$ (**3**), are quite interesting in relation to the active site of deoxyhemocyanin,[2,3] of which copper(I) reacts with π acceptor ligands such as carbon monoxide[4] and isocyanide.[5] Furthermore, certain copper(I) complexes provide an ethylene adduct,[6,7] indicative of a possible receptor[6-8] of ethylene, which is a plant hormone. From these points of view, knowledge of such coordination chemistry as the coordination number, geometry and reactivity for π acceptor ligands of copper(I)–imidazole systems is important for an intrinsic understanding of the copper(I) active site. This manuscript is concerned with a reaction of **2** and **3** with π acceptor ligands of ethylene, phosphites, and isocyanides and their equilibrium in solution.

Experimental

Materials. Triethyl phosphite was commercially available. Its purity was checked by ^{1}H and ^{31}P NMR spectroscopy and used without further purification. Phenyl and *p*-tolyl isocyanide were synthesized from corresponding amines.[9]

Acetone-d_6 (99.8%)(Merck) was utilized as a solvent for ^{1}H and ^{31}P NMR studies after drying with molecular sieves. High-purity nitrogen (99.9998%) and ethylene (99.9%) were utilized.

$[Cu(im)_2]ClO_4$ (**2**) and $[Cu(im)_3]ClO_4$ (**3**) were prepared according to the method of Part I.[1] A 2.9×10^{-3} M (1 M=1 mol dm^{-3}) acetone solution of **2** (or **3**) was prepared under nitrogen. While maintaining a nitrogen atmosphere, a stock solution of triethyl phosphite (L) was added to the copper(I) solution in order to vary the ratio of [L]/[Cu]. The mixed solution was stirred for 30 min and then transferred into an NMR sample tube and sealed therein. Ethylene compounds were prepared by passing C_2H_4 gas through a solution of **2** (or **3**).

200 MHz ^{1}H and 80.79 MHz ^{31}P NMR spectra were obtained as previously described.[1]

Results and Discussion

Phosphites and isocyanides are good π acceptor ligands.[10] **2** and **3** react with them to give ternary copper(I) complexes; these are thermally stable, but air-sensitive. Because ternary copper(I) complexes are generally substitution labile, we should find the optimum conditions under which the objective ternary copper(I) complexes predominantly form. Of most significance is the characterization of copper(I) species in solution for the isolation of a copper(I) complex. We have demonstrated[1] that the ^{1}H NMR spectra of imidazole give coordination shift that is sensitive to the structure of copper(I) complexes; this indicated that these signals are also applicable to the inquirement of ternary copper(I) complexes in solution.

Reaction with Ethylene. The ^{1}H NMR spectra at -90 °C of **2** and **3** under ethylene atmosphere were studied as to whether they react with C_2H_4 to give adducts or not. **2** affords an ^{1}H NMR spectrum, displaying the formation of an ethylene complex (**2-b**), whose chemical shifts are presented in Table 1. **2-b** is thermally stable to a loss of ethylene. Upon the binding of ethylene,[11] no dissociation of im occured, indicating an addition reaction of ethylene. Monoolefin copper(I) compounds have recently been synthesized: A four-coordinate compound is $[Cu(HB(3,5\text{-}Me_2pz)_3)(C_2H_4)]$,[6a] ($HB(3,5\text{-}Me_2pz)_3$=hydrotris(3,5-dimethyl-1-pyrazolyl)borate), while a three-coordinate is $[Cu(biL)(C_2H_4)]^+$ (biL=1,10-phenanthroline, 2,2′-bipyridine, etc.).[6b,7] In analogy with $[Cu(biL)(C_2H_4)]^+$, **2-b** is assigned to $[Cu(im)_2(C_2H_4)]^+$. The reaction of **3** with C_2H_4 is in good contrast with that of **2**. An ethylene atmosphere did not influence the ^{1}H NMR spectrum of **3** even at -90 °C; this reveals that no formation of $[Cu(im)_3(C_2H_4)]^+$ takes place. The solution of **3** turned blue when C_2H_4 was bubbled at ambient

Table 1. Observed ^{1}H NMR Shifts[a] of Coordinated Imidazoles of Mixed-Ligand Copper(I) Complexes, $[Cu(im)_nL_m]^+$

L	Coordination No.					
	n	*m*	1-H	2-H	4-H	5-H
Metal-free			13.06	7.97	7.25	7.25
—[b]	2	0	12.61	8.53	7.42	7.68
—[b]	3	0	12.41	8.22	7.12	7.59
C_2H_4	2[c]	1	12.54	8.35	7.28	7.64
$P(OC_2H_5)_3$	2	1	12.56	8.42	7.34	7.64
	2	2	12.46	8.17	7.16	7.56
	3	1	12.59	8.13	7.13	7.54
	1	3	12.48	8.23	7.22	7.59
$CH_3C_6H_4NC$	2	2		8.32	7.31	7.56
	1	3		8.45	7.45	7.63
C_6H_5NC	2	2		8.36	7.30	7.61
	1	3		8.48	7.47	7.65

a) Shift in ppm, from $Si(CH_3)_4$. Error limit, ± 0.02 ppm. b) Binary complexes in Ref. 1. c) $[Cu(im)_3]^+$ does not react with C_2H_4.

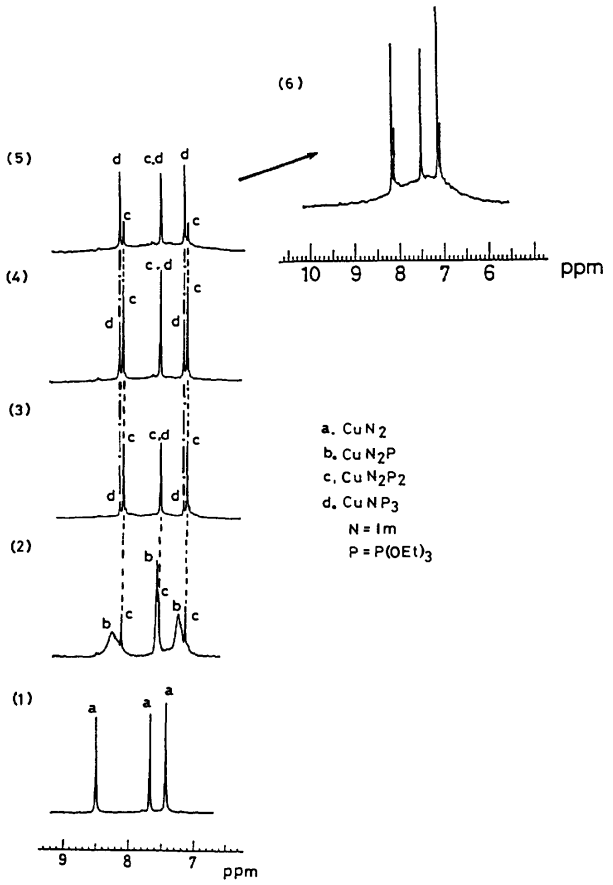

Fig. 1. ^{1}H NMR spectra at -90 °C of acetone-d_6 solution of mixed-ligand copper(I) complexes. Titration of $P(OC_2H_5)_3$ to the solution of **2**. $r=[P(OC_2H_5)_3]/[Cu^+]$: (1) 0; (2) 1.0; (3) 2.0; (4) 3.0; (5) and (6) 4.0. (6) was recorded at wider spectral width than other five spectra in order to examine the base line.

temperature for a long time. The resultant blue species were associated with copper(II) complexes. Hence, it is concluded that **3** does not react with C_2H_4.[12] In the case of a carbon monoxide atmosphere, thermally very stable $[Cu(im)_3(CO)]^+$ predominantly forms, and gives well resolved ^{1}H NMR signals.[1] The difference in the reactivity of C_2H_4 and CO against **3** is of much interest in probing the copper(I) active site in a protein.

A four-coordinate complex, $[Cu(HB(3,5\text{-}Me_2pz)_3)(C_2H_4)]$, is in good contrast with $[Cu(im)_3(C_2H_4)]^+$. This pyrazole derivative is stable even in olefin-free solvents, and the prolonged exposure of a solution to an inert atmosphere[6] is indispensable for removing the coordinated olefin. From this difference in reactivities between these two copper(I) precursors, two factors governing the affinity for C_2H_4 are considered. One is the bonding nature of N donor ligands such as imidazole and pyrazole. The basicity of imidazole is much greater than that of pyrazole. According to the Dewar-Chatt-Duncanson model,[13,14] the more basic ligand, when it binds copper(I), promotes the π back-bonding of copper(I) and results in stable bonding. Imidazole complexes are more stable than pyrazole complexes as was demonstrated regarding binary copper(I) complexes in Part I.[1] Such a stability of the binary copper(I) complex is associated with its reactivity with ethylene.

The geometry of a complex is another factor influencing the reactivity of copper(I). Tridentate chelating ligands, especially tripodal ligands, are structurally fixed, being correlated to (1) the hybridization of copper(I) orbitals to form the more stable bond with ethylene, and (2) the controlling the steric interaction between chelating groups and the fourth ligand. $[Cu(HB(3,5\text{-}Me_2pz)_3)]$ has, if present, a trigonal-pyramidal form with copper at an apex. This is indicative of the unusual structure in copper(I) chemistry. In fact, $[Cu(HB(3,5\text{-}Me_2pz)_3)]_2$ is easily dimerized to give $[Cu(HB(3,5\text{-}Me_2pz)_3)]_2$,[15] revealing that this monomer is very reactive and requires another ligand at the fourth position, giving a tetrahedral complex. In this case, the presence of ethylene as a donor is just appropriate to give a four-coordinate monomer. On the other hand, a structural change might be needed when C_2H_4 binds copper(I) of **3** to give a tetrahedral complex. A number of three-coordinate triangular copper(I) complexes have been found with monodentate ligands. Typical examples are $Na_2[Cu(CN)_3]$,[16] $[Cu(SPh)_3][BPh_4]_2$ (Ph=phenyl),[17] and $[Cu(2\text{-methylpyridine})_2]ClO_4$.[18] According to these facts, **3** at least, has a structure dissimilar to $[Cu(HB(3,5\text{-}Me_2pz)_3)]$, and is supposed to be nearly triangular. The energy barrier on the structural change from a triangular to a tetrahedral form can affect the reactivity of copper(I). It is interesting to

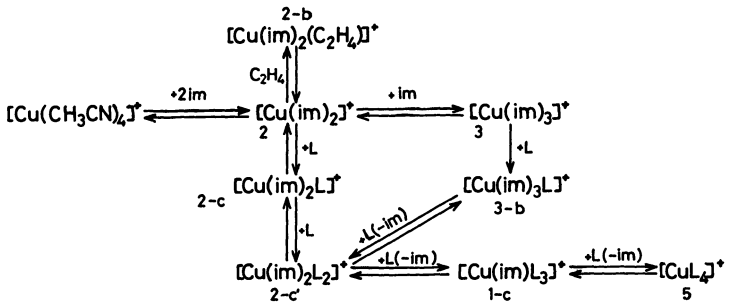

L=phosphite or isocyanide

Scheme 1.

consider the reaction of CO[1] in **3**, where CO readily provides its adduct. Structural factors concerning the affinity for C_2H_4 is significantly associated with the stable formation of four-coordinate ethylene adducts.[19] From this point of view, the systematic synthesis of copper(I) complexes of various tripodal imidazole- or pyrazole- containing chelates is most important in order to elucidate the relationship between the reactivity and structure of three-coordinate imidazole-copper(I) complexes.

Reaction of Phosphite and Isocyanides. We have also utilized triethyl phosphite, phenyl, and *p*-tolyl isocyanide. So long as a high pressure was not provided in the case of ethylene, the concentration was restricted to the solubility at 1 atm. On the contrary, phosphite and isocyanides are available for controlling their concentrations (from high to low) in solution. Typical example of their reaction with binary copper(I) imidazole complexes is presented in Fig. 1. Triethyl phosphite was successively added to a solution of **2** with varying r (=[$P(OC_2H_5)_3$]/[Cu]=0—4). With an increase in r ($0<r<1$), ternary compounds, $[Cu(im)_2(P(OC_2H_5)_3)_n]^+$ (n=1 and 2), successively appeared. Copper(I) complexes from two- to four-coordinate have so far been synthesized and characterized.[21] It is to be noted that copper(I) complexes of more than five-coordination hardly form. The further appearance of signals d in Fig. 1 (3)—(5) indicates the occurrence of a substitution reaction at $r>2$. Signals d are attributable to $[Cu(im)(P(OC_2H_5)_3)_3]^+$. $[Cu(im)_2(P(OC_2H_5)_3)_2]^+$ (**2-c'**) and $[Cu(im)(P(OC_2H_5)_3)_3]^+$ (**1-c**) gave sharp signals, indicating that these four-coordinate complexes undergo slow chemical exchanges, while the main signals at the condition r=1 are broad. This indicates a partial chemical exchange between **2** and **2-c**. These signals in Fig. 1 were completely assigned in analogy with those illustrated previously for binary and ternary copper(I) complexes.[1]

In order to inquire into the behavior[22] of $P(OC_2H_5)_3$, the ^{31}P NMR spectra of these solutions were measured. A single broad ^{31}P NMR signal at 120±0.5 ppm from $H_3{}^{31}PO_4$ as an external reference was observed at $r<2$ and no metal-free signal of $P(OC_2H_5)_3$ were detected in this region. This indicates that $P(OC_2H_5)_3$ is chemically exchanged among coordinated ones of copper(I) species, as confirmed by the ^1H NMR spectra (Fig. 1). On the other hand, at $r>2$ a quartet signal centered at 127 ppm appeared (J_{Cu-P}=1180 Hz), which could be easily assigned to $[Cu(P(OC_2H_5)_3)_4]^+$ (**5**).[23,24] With an increase in r, the ^{31}P signal for ternary copper(I) complexes decreases; it is then covered with the main signal of **5**, and finally disappears. Hence, it is concluded that **5** is a principal species at $r>3$ and that $P(OC_2H_5)_3$ has a high affinity for Cu(I).

At $r>3$, excess metal-free imidazole must be present in solution. However, Fig. 1 (4)—(6) apparently reveal no metal-free signals of imidazole. The wide ^1H NMR spectrum (6 kHz) exhibits a rising baseline at the region 7—9 ppm in Fig. 1 (6). This is averaged broad imidazole signals due to very rapid exchange between the bulk and the coordinated imidazole of binary copper(I) complexes.[25] Imidazoles of **2-c'** and **1-c** are free from this exchange mechanism because their sharp resonances can be simultaneously detected (Fig. 1 (5)). It is important to examine the reactions of **3** in comparison with **2**. The ^1H and ^{31}P NMR spectra were monitored when $P(OC_2H_5)_3$ was also successively added to **3**. As was expected, $[Cu(im)_3(P(OC_2H_5)_3]^+$ (**3-b**) firstly formed with a little broadening. Also, and with an increase in [$P(OC_2H_5)_3$], **2-c** and **2-c'** appeared, followed by **1-c** and **5**. These facts indicate that the reaction occurring here are all reversible. We can, thus, summarize these reactions in one part of Scheme 1.

In the case of isocyanides, the same trend in ^1H NMR signals as in Fig. 1 has been observed. $[Cu(im)_2L_2]^+$ and $[Cu(im)L_3]^+$ (L=phenyl and *p*-tolyl isocyanide) successively form with the isocyanide addition to **2**. ^1H NMR imidazole signals are sharp enough to resolve various species in solution, denoting the downfield shift more than those in the case of phosphite (Table 1). Phenyl-group signals of isocyanide accidentally collapse with each other; hence, their separations are difficult. Of course, their signal positions are shifted downfield more than those of metal-free species, indicating a coordination to

copper(I).

In conclusion, the generated species with C_2H_4 (and CO) are only adduct compounds, while in the case of phosphite and isocyanides, a substitution reaction principally occurs accompanied by a dissociation of imidazole to produce their mono-, bis-, tris-, and finally tetrakis-coordination compounds. The remarkable difference in the reactivity of **2** from **3** is also found in the case of ethylene. Concerning the ^1H NMR spectra, four-coordinate mixed-ligand complexes, such as $[Cu(im)_nL_m]^+$ (n=3 and m=1; n=2 and m=2; n=1 and m=3), are in the slow-exchange regime and are readily detected using low-temperature NMR. The lower coordination complexes encounter a chemical-exchange effect to give broad and averaged signals, indicating the labile nature of such complexes.

We appreciate the assistance of Mr. Hiroki Nagai and Mr. Katsumasa Kanai in recording of the NMR spectra. This work was supported in part by a Grant-in-Aid for Scientific Research No. 60307004 from the Ministry of Education, Science and Culture.

References

1) S. Kitagawa and M. Munakata, *Bull. Chem. Soc. Jpn.*, **59**, 2743 (1986) (Part I.).

2) W. P. J. Gaykema, W. G. J. Hol, J. M. Vereijken, N. M. Soeter, H. J. Bak, and J. J. Beintema, *Nature*, **309**, 23 (1984).

3) B. Linzen, N. M. Soeter, A. F. Riggs, H. J. Schneider, W. Schartau, M. D. Moore, E. Yokota, P. Q. Behrens, H. Nakashima, T. Takagi, T. Nemoto, J. M. Vereijken, H. J. Bak, J. J. Beintema, A. Volbeda, W. P. J. Gaykema, and W. G. J. Hol, *Science*, **229**, 519 (1985).

4) W. Vanneste and H. S. Mason, "The Biochemistry of Copper," ed by J. Peisach, P. Aisen, and W. E. Blumberg, Academic Press, N. Y. (1966), p. 465.

5) E. J. Wood and W. H. Bannister, *Nature*, **215**, 1091 (1967).

6) a) J. S. Thompson, R. L. Harlow, and J. F. Whitney, *J. Am. Chem. Soc.*, **105**, 3522 (1983); b) J. S. Thompson and J. F. Whitney, *Inorg. Chem.*, **23**, 2813 (1984).

7) M. Munakata, S. Kitagawa, S. Kosome, and A. Asahara, *Inorg. Chem.*, **25**, 2622 (1986).

8) R. Dagani, *Chem. Eng. News*, **1984**, 21.

9) W. P. Weber and G. W. Gokel, *Tetrahedron Lett.*, **1972**, 637.

10) F. A. Cotton and G. Wilkinson, "Advanced Inorganic Chemistry," 4th ed, Wiley-Interscience, New York (1980), Part I, p. 82.

11) Acetone solution under ethylene gives single ethylene ^1H NMR signal with the intensities much larger than imidazole signals. This reveals the great dissolution of ethylene in acetone. Hence, ethylene ^1H NMR signal is averaged due to chemical exchange phenomena, such as

$$Cu(im)_2(C_2H_4)^* + C_2H_4 \rightleftarrows Cu(im)_2(C_2H_4) + C_2H_4.^*$$

12) Prolonged passing of nitrogen into the solution of **3** changed the colorless solution into pale blue. This blue color solution gave broad ^1H NMR imidazole signals, whose intensity is considerably weakened. When the solution of **3** remains for a long time, **3** is oxidized by O_2 contained in nitrogen, or coming from air into synthetic apparatus. Thus, **3** is very sensitive to O_2. On the other hand, CO-passing causes no change in color of the solution even for a long time, indicative of a much better stability against O_2. Under ethylene-passing, a phenomenon similar to the case of nitrogen occurs.

13) M. J. S. Dewar, *Bull. Soc. Chim. Fr.*, **18**, C71(1979).

14) J. Chatt and L. A. Duncanson, *J. Chem. Soc.*, **1953**, 293.

15) C. Mealli, C. S. Arcus, J. W. L. Wilkinson, T. J. Marks, and J. A. Ibers, *J. Am. Chem. Soc.*, **98**, 71 (1976).

16) C. Kappenstein and R. P. Hugel, *Inorg. Chem.*, **17**, 1945 (1978).

17) D. Covcouvanis, C. N. Murphy, and S. K. Kanodia, **19**, 2993 (1980).

18) A. H. Lewin and R. J. Michl, *J. Chem. Soc., Chem. Commun.*, **1962**, 661.

19) Concerning a steric interaction, the orientation of a coordinated ligand is likely to be important. CO binds Cu(I) in end-on form,[20] while C_2H_4 does in side-on one.[6,7] The latter potentially encounters steric interaction with coordinated imidazole. From this point of view, a tripodal chelate is considered to be a ligand avoiding this type interaction. This can be proved by the use of chelating systems, including these types of stuctural factors.

20) M. Munakata, S. Kitagawa, and K. Goto, *J. Inorg. Biochem.*, **16**, 319 (1982).

21) See Part I and references threrein.

22) Triplet methyl and quartet methylene signals of coordinated $P(O(C_2H_5)_3)$ appear near 1 and 4 ppm, respectively. Methylene signals for **2-c**, **2-c'**, and **1-c** collapse with each other; thus, reading their shifts are difficult. Methyl signals of **2-c**, **2-c'**, and **1-c** are 1.24, 1.21, and 1.27, respectively.

23) S. I. Shupack and B. Wagner, *J. Chem. Soc., Chem. Commun.*, **1966**, 548.

24) R. W. King, T. J. Huttemann, and J. G. Verkade, *J. Chem. Soc., Chem. Commun.*, **1965**, 561.

25) The greater [L] becomes, the more **5** forms and metal-free imidazole increases. Under this condition, equilibria are very complicated. In addition to **2-c'** and **1-c**, binary complexes such as **3** also likely to form. Binary ones easily undergo a chemical exchange with metal-free imidazole as was demonstrated in Part I.[1]

 © 1986 The Chemical Society of Japan Bull. Chem. Soc. Jpn., 59, 2755—2760 (1986)

Azide-, Thiocyanate- or Cyanate-Bridged Di- and Trinuclear Copper(II) Complexes with *N,N,N',N'*-Tetramethylethylenediamine, *N,N*-Diethylethylenediamine, 2,2'-Bipyridyl or 1,10-Phenanthroline

Yasuo NAKAO,* Hideo NAKAMURA, Wasuke MORI,† Takeshi SAKURAI,†
Shinnichiro SUZUKI,† and Akitsugu NAKAHARA†
Chemical Laboratory, Faculty of Education, Okayama University, Okayama 700
†Institute of Chemistry, College of General Education, Osaka University, Toyonaka, Osaka 560
(Received December 26, 1985)

A series of di- and trinuclear copper(II) complexes containing *N,N,N',N'*-tetramethylethylenediamine (tmen), *N,N*-diethylethylenediamine(deen), 2,2'-bipyridyl(bpy) or 1,10-phenanthroline(phen) and azide, thiocyanate or cyanate ions have been prepared and characterized by their magnetic susceptibilities, infrared, electronic, and ESR spectra, and electric conductances. Magnetic susceptibility data for the dimeric complex $[Cu_2(tmen)_2(N_3)_2](ClO_4)_2$ shows the presence of a ferromagnetic interaction (Weiss constant θ=+30 K) above 150 K, whereas the two copper(II) ions are apparently non-coupled below 150 K. On the other hand, the dimeric complex $[Cu_2(bpy)_2(N_3)_2](ClO_4)_2$ shows the presence of a large antiferromagnetic exchange interaction (μ_{eff}<0.6 B.M. at room temperature). The complex $[Cu_3(tmen)_3(NCS)_3](ClO_4)_3\cdot 1.5H_2O$ is estimated to have the trimeric structure; the temperature-dependence of the magnetic susceptibility for this compound indicates the existence of an antiferromagnetic exchange interaction with a J value of $-175\ cm^{-1}$.

It is well-known that azide, thiocyanate, and cyanate ions act as a bridging ligand between metal atoms. The azide ligand can bridge two metal ions in an end-to-end fashion as in (1) or in an end-on fashion as in (2).[1-22] On the other hand,

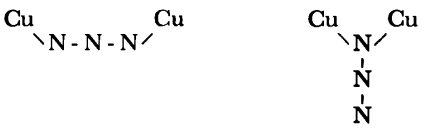

(1) (2)

three bridging modes are available for the thiocyanate and cyanate ions ((3)—(5)).[15,23-29] Some dimeric copper complexes

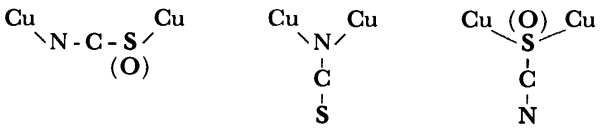

(3) (4) (5)

containing these bridging groups are of particular interest as synthetic models for the natural dinuclear copper proteins and their derivatives.[9,11,12,20]

In this paper we report the preparation and characterization of dimeric and trimeric copper(II) complexes containing *N,N,N',N'*-tetramethylethylenediamine(tmen), *N,N*-diethylethylenediamine (deen), 2,2'-bipyridyl(bpy) or 1,10-phenanthroline(phen) and azide, thiocyanate or cyanate anions.

Experimental

Preparation of Copper(II) Complexes. $Cu_2(tmen)_2X_4\cdot nH_2O$ (X=N_3, NCS, and NCO), 1, 4, and 6. To a mixture of $Cu(ClO_4)_2\cdot 6H_2O$ (1.85 g, 5 mmol) and 20 cm^3 of ethanol were added tmen(0.58 g, 5 mmol) and NaX(X=N_3, NCS, or NCO, 10 mmol). The reaction mixture was stirred at room temperature for 1 h, and then allowed to stand for several hours in a refrigerator. After it had been filtered off, the precipitate was recrystallized from ethanol.

$Cu_2(deen)_2X_4\cdot nH_2O$(X=$N_3$, NCS, and NCO), 7, 9, and 10. These complexes were also prepared in the same way as that for $Cu_2(tmen)_2X_4\cdot nH_2O$, and then recrystallized from ethanol.

$Cu_2(tmen)_2(N_3)_2(ClO_4)_2$, 2 and $Cu_3(tmen)_3(NCS)_3(ClO_4)_3\cdot 1.5H_2O$, 5. Except that 4 mmol of NaX(X=N_3 or NCS) was used, the same procedure as that for the preparation of $Cu_2(tmen)_2X_4\cdot nH_2O$ was adopted. The products obtained were washed by ethanol.

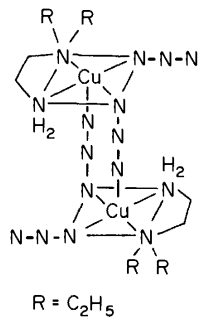

R = C_2H_5
I

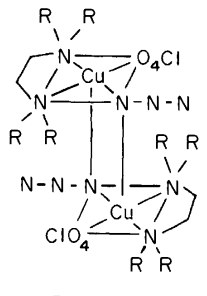

R = CH_3
II

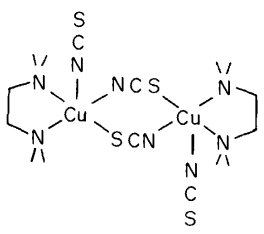

III

Table 1. Analytical Data for the Complexes

No.	Complex	H(%)		C(%)		N(%)	
		Found	Calcd	Found	Calcd	Found	Calcd
1	$Cu_2(tmen)_2(N_3)_4$	6.07	6.12	27.56	27.31	42.45	42.48
2	$Cu_2(tmen)_2(N_3)_2(ClO_4)_2$	5.15	5.03	22.70	22.43	21.95	21.80
3	$Cu_2(tmen)_2(N_3)_2(NO_3)_2 \cdot 2.5H_2O$	5.70	6.10	23.16	23.52	27.74	27.44
4	$Cu_2(tmen)_2(NCS)_4$	5.31	5.46	32.12	32.46	18.72	18.94
5	$Cu_3(tmen)_3(NCS)_3(ClO_4)_3 \cdot 1.5H_2O$	5.09	4.96	24.30	24.27	11.90	12.14
6	$Cu_2(tmen)_2(NCO)_4 \cdot 1.5H_2O$	6.03	6.37	35.08	34.64	19.81	20.21
7	$Cu_2(deen)_2(N_3)_4$	5.90	6.12	26.82	27.31	42.52	42.48
8	$Cu_2(deen)_2(N_3)_2(ClO_4)_2$	4.88	5.03	22.14	22.43	21.74	21.80
9	$Cu_2(deen)_2(NCS)_4 \cdot 0.5H_2O$	5.21	5.55	31.61	31.98	18.61	18.65
10	$Cu_2(deen)_2(NCO)_4$	6.10	6.13	36.26	36.42	20.95	21.24
11	$Cu_2(bpy)_2(N_3)_4$	2.68	2.66	39.54	39.53	36.61	36.89
12	$Cu_2(bpy)_2(N_3)_2(ClO_4)_2$	2.36	2.24	34.14	33.25	19.17	19.39
13	$Cu_2(bpy)_2(NCS)_4$	2.47	2.41	43.00	42.90	16.63	16.68
14	$Cu_2(bpy)_2(NCO)_4$	2.67	2.66	47.19	47.44	17.95	18.45
15	$Cu_2(phen)_2(N_3)_4$	2.51	2.46	44.03	43.96	33.71	34.19

The complex $Cu_2(tmen)_2(N_3)_2(NO_3)_2 \cdot 2.5H_2O$, **3** was isolated by the same way using $Cu(NO_3)_2 \cdot 3H_2O$.

$Cu_2(deen)_2(N_3)_2(ClO_4)_2$, 8. This was obtained by the same method as **2** by use of deen.

$Cu_2(bpy)_2X_4$(X=N_3, NCS, and NCO), and $Cu_2(phen)_2(N_3)_4$, 11, 13, 14, and 15. These were prepared by the same method as **1** using bpy or phen instead of tmen. Recrystallization was carried out using aqueous ethanol (1:1 by volume).

$Cu_2(bpy)_2(N_3)_2(ClO_4)_2$, 12. Except that 5 mmol of NaN_3 was used, the same method as that for the preparation of **11** was adopted. The purification was carried out by washing with ethanol.

The analytical data for the compounds described above are collected in Table 1.

Measurements. Infrared absorption spectra were measured with a JASCO A-102 infrared spectrophotometer with KBr disk. Visible absorption spectra of DMF solutions were recorded on a Hitachi 200-10 double beam spectrophotometer. Magnetic susceptibility at room temperature was determined by using a Gouy magnetic apparatus. The magnetic susceptibility measurements over the range of liquid helium temperature to room temperature were carried out by Faraday method. The instrument was calibrated with $CuSO_4 \cdot 5H_2O$. The X-band ESR spectra of powdered sample at 77 K were recorded at 9.3 GHz and 100 kHz modulation frequency with a JEOL JES-FE-1X. The g values were calibrated based on Li-TCNQ (g= 2.0025). The X-ray powder patterns were recorded by the use of a Rigaku RAD-1B diffractometer at room temperature, with the Cu-$K\alpha$ line filtered through nickel. The differential scanning calorimetry measurement was carried out by the use of Rigaku DSC 8230. A Toa Denpa Conduct Meter CM-7B was used for conductivity measurements.

Results and Discussion

Copper(II) Complexes with tmen and deen. The dimeric copper(II) complex **1** had already been prepared and characterized by Bkouche-Waksman et al.[13] The similar type of complexes (**1**—**10**) bridged by N_3^-, NCS^-, and NCO^- were newly prepared by the method described in the Experimental section. The color of crystals, magnetic moments at room temperature, IR spectral and electric conductance data are given in Table 2. The complex **1** has centrosymmetric dimeric units with two asymmetric end-to-end azide bridges.[13] However, it has been pointed out that the two copper(II) ions are magnetically non-coupled in the complex **1**.[13] The complex **7** shows the similar magnetic moment and λ_{max} due to d-d transition(Table 3) as those for **1**, hence this compound is estimated to have the dimeric structure I like the corresponding complex **1**. The magnetic moments of the complexes **2** and **8** at room temperature are higher than that of copper(II) complex having no interaction. In order to obtain detailed information on the structure of these complexes, the magnetic susceptibility of **2** was measured over the temperature range 4.2—300 K. Figure 1 shows the temperature-dependence of the magnetic susceptibility. The χ_A^{-1}—T profile in this Figure curves at about 150 K, indicating the possibility of phase transition. The differential scanning calorimetry(DSC) curve for **2** showed the existence of a single broad endotherm at ca. 138 K. These results for **2** suggest that there is a ferromagnetic exchange interaction(Weiss constant θ=+30 K) between the two copper(II) ions above ca. 150 K. However, the two copper(II) ions are essentially non-coupled below 150 K. The similar behavior was recently observed for complexes $[Cu_2(2\text{-Pca=Hist})_2(N_3)_2](ClO_4)_2$[31] and $[Cu_2(2\text{-Pca=}\beta\text{-Ala})_2(N_3)_2] \cdot 2H_2O$.[31] Thus, the complex **2** is considered to have the dimeric structure II like $[Cu_2(2\text{-Pca=Hist})_2(N_3)_2]$ $(ClO_4)_2$ with the end-on azide bridging. The splitting of ClO_4^- vibration(1090, 1115, and 1145 cm^{-1}) in IR spectrum supports the validity of this structure. The structure of **8** is

Table 2. Physical Properties of the Complexes

Complex No.	Color	μ_{eff}/BM(K)	IR	Λ
			$\nu_{asym}(N_3^-)$ or $\nu(C\equiv N)$/cm^{-1}	S cm^2 mol^{-1}
1	Dark green	1.85 (286)	2025 vs, 2080 vs, 2100 vw	14
2	Grey blue	2.02 (287)	2050 vs, 2080 vs	133
3	Dark green	1.92 (299)	2080 vs, 2100 vs	143
4	Dark green	1.90 (287)	2080 vs, 2110 vs	73
5	Dark green	1.34 (286)	2110 vs, 2140 vw	255
6	Blue violet	1.78 (285.5)	2190 vs, 2230 vs	35
7	Dark green	1.81 (288.5)	2015 vw, 2030 vs, 2050 vs, 2075 vw	9
8	Dark green	1.99 (287.5)	2070 vs, 2110 w	141
9	Green	1.87 (288)	2100 vs, 2125 vs	66
10	Violet blue	1.83 (288)	2190 vs, 2205 vw	10
11	Dark green	1.89 (293)	2020 s, 2070 vs	6
12	Brown green	<0.6 (288)	2070 vw, 2100 vs	136
13	Green	1.90 (293)	2100 vs, 2125 vs	61
14	Blue	1.86 (296)	2190 s, 2210 vs	13
15	Brown green	1.87 (289.5)	2030 vs, 2060 vs	6

Table 3. Electronic Spectral Data of the Complexes[a)]

Complex No.	λ_{max}/nm(log ε/mol^{-1} dm^3 cm^{-1})
1	615 (2.53), 450 sh (3.2)[b)] 390 (3.46)
2	656 (2.27), 394 (3.40)
3	656 (2.34), 394 (3.51)
4	656 (2.18), 374 (3.16)
5	664 (2.06), 372 (3.01)
6	641 (2.06), 330 sh (3.4)[b)]
7	608 (2.58), 384 (3.60)
8	672 (2.40), 386 (3.48)
9	673 (2.20), 363 (3.10)
10	654 (2.04), 315 sh (3.4)[b)]
11	628 (2.49), 448 sh (3.4)[b)] 393 (3.54)
12	678 (2.28), 398 (3.47)
13	680 (2.05), 388 (3.02)
14	655 (1.89), 335 sh (3.4)[b)] 318 (3.51)
15	636 (2.51), 450 (3.40) 395 (3.57)

a) Solvent: DMF. b) sh=shoulder.

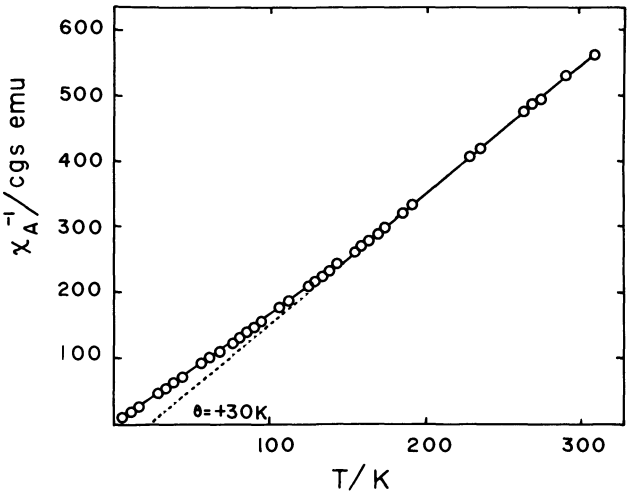

Fig. 1. Temperature-dependence of the magnetic susceptibility of **2**.

expected to be analogous to that of **2** because of its similar magnetic moment and the splitting mode of ClO_4^- (1090, 1120, and 1145 cm^{-1}) in IR spectrum. The above structures are also born out by the ESR parameters of both the complexes **2** ($g_{//}$=2.18 and $g_{\perp}$=2.07) and **8** ($g_{//}$=2.15 and $g_{\perp}$=2.05). Further, the signals due to triplet state were found at g=3.0 and g=1.2 for **8** (Fig. 2), which exhibits that the complex is a dinuclear copper(II) complex. The spectral lines in the ΔM_s=1 region of Fig. 2 are not easily interpreted. Because the sample **8** is a good crystalline solid, we consider that the amount of impurities (probably the copper(II) monomers of unknown composition) is very slight. However, the ΔM_s=1 signal in Fig. 2 may be attributed to some contaminants.

The room-temperature magnetic moments of the thiocyanate containing complexes **4** and **9** were close to the values for non-interacting or weakly interacting copper(II) complexes. The IR spectra of these complexes showed two C-N stretching vibrations of thiocyanato group in the region 2080—2125 cm^{-1} (Table 2). This suggests that there are two kinds of thiocyanato group of different bonding modes in each complex. It is pointed out that the complexes bridged by thiocyanate exhibit ν(CN) above 2100 cm^{-1}.[24)] In addition, the wavenumbers of the two ν(CN) vibrations for **4** and **9** are close to those for α- and β-$[Cu_2(NCS)_4(dmtp)_4]$[28)] which have the skeleton

, hence two Cu-NCS bonds. Thus the

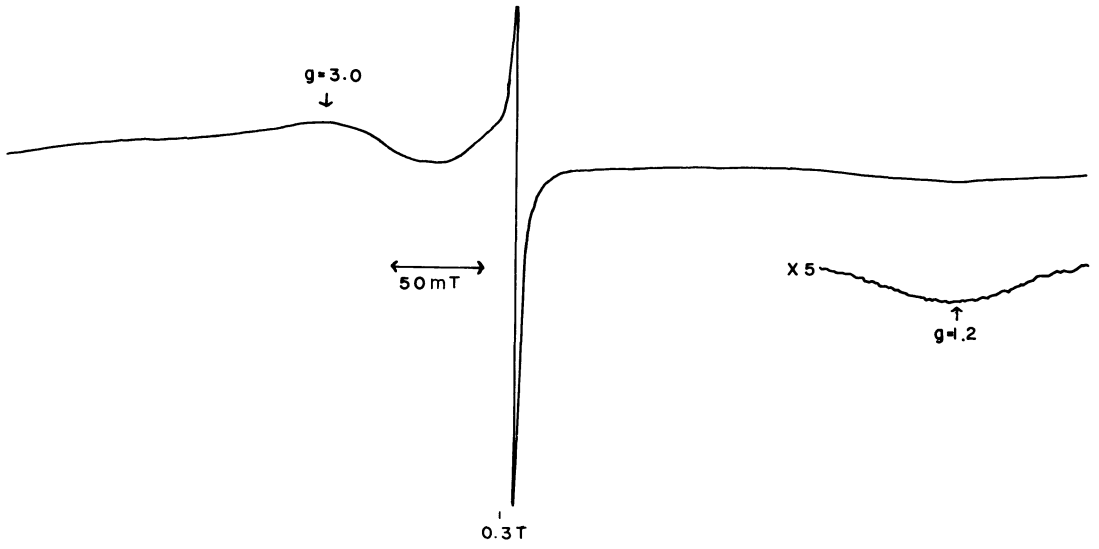

Fig. 2. ESR spectrum of **8** at 77 K.

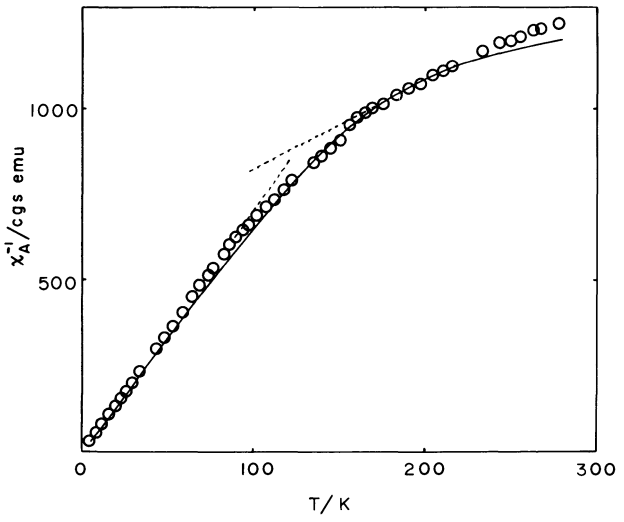

Fig. 3. Temperature-dependence of the magnetic susceptibility of **5**. The solid line shows theoretical susceptibility calculated by Eq. 1 with the parameters described in the text.

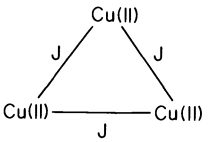

Fig. 4. Spin-spin interaction in triangular trinuclear copper(II) complexes.

complexes **4** and **9** may have the dimeric structure III. The complex **5** shows an effective magnetic moment smaller than the spin-only value at room temperature. The magnetic susceptibility was measured over the range from liquid helium temperature to room temperature. Figure 3 represents the temperature-dependence of the magnetic susceptibility. The observed susceptibility obeyed the Curie-Weiss law in the temperature range $T \gtrsim 160$ K and $T \lesssim 90$ K: the Curie and Weiss constants were determined as C_h=0.38 emu K mol^{-1} and θ_h=−210 K for the high temperature range, and C_l=0.143 emu K mol^{-1} and θ_l=0 K for the low temperature range. Furthermore, the ratio C_h/C_l is 2.7. This magnetic behavior indicates that the complex **5** is the compound containing three copper(II) ions magnetically interacted. The theoretical susceptibility, χ_A, for triangular trinuclear complex is given by a solid line in Fig. 3. The calculation of these χ_A values was carried out according to the Eq. 1[30]

$$\chi_A = \frac{Ng^2\mu_B^2}{12kT} \times \frac{1+10\exp(3J/kT)}{1+2\exp(3J/kT)} + N\alpha, \quad (1)$$

where J denotes the exchange integral between copper(II) ions as indicated in Fig. 4. Magnetic parameters were as follows: g=2.16, $N\alpha$=60×10^{-6} cgs emu mol^{-1}, J=−175 cm^{-1}. Thus the complex **5** is considered to have the triangular trimeric structure bridged by thiocyanate ions. This complex indicates the rhombic ESR spectrum with g_1=2.18, g_2=2.13, and g_3=2.07 in the ΔM_s=1 region.

The ΔM_s=2 transition in the X-band ESR spectra for cyanate containing complexes **6** and **10** was not observed at half-field. The same results were found for the thiocyanato complexes **4** and **9**. Although there are no other evidences for dimeric structure of **6** and **10**, these compounds are also supposed to have a dinuclear structure similar to III proposed for thiocyanato complexes.

The electric conductances (Table 2) of **1**, **7**, and **10** show that these complexes are non-electrolytes in DMF solutions. Accordingly, the structures in the solid state of **1**, **7**, and **10** are supposed to be

maintained in DMF. The molar conductances of **2**, **3**, and **8** are in the range found for 1:2 electrolytes, suggesting that these compounds undergo significant structural changes upon dissolution. Also, a partial dissociation of NCS^- for **4** and **9** takes place in DMF.

All of the azido complexes display an intense band at 380—390 nm(log ε, ca. 3.5) (Table 3). These bands are assigned to azide to copper CT transitions.[32,33] The CT bands are also observed for the thiocyanato complexes around 370 nm (Table 3).[33] The similar $N_3^- \rightarrow$ and $SCN^- \rightarrow$Cu CT bands are observed in metazido- and metthiocyanato-hemocyanin in which the peroxide of oxy-hemocyanin is displaced by N_3^- and NCS^-, respectively.[33]

Copper(II) Complexes with bpy and phen. The copper(II) complexes **11**—**15** were prepared by the same method as that for **1**—**10** by using 2,2′-bipyridyl or 1,10-phenanthroline. The complexes with same compositions with ours, $[Cu(bpy)(N_3)_2]$, $[Cu(bpy)(NCS)_2]$, and $[Cu(phen)(N_3)_2]$ were described by Dutta and De.[34] Bushnell and Kahn[6] reported the crystal and molecular structure of $[Cu(bpy)(N_3)_2]$,[34] which has the polymeric structure with asymmetric end-on azide bridges. No difference was observed in IR spectra of $[Cu(bpy)(N_3)_2]$ and **11**. However, the low-angle lines of X-ray powder diffraction patterns (Fig. 5) for both complexes are fairly different in location and relative intensity. This indicates a somewhat different

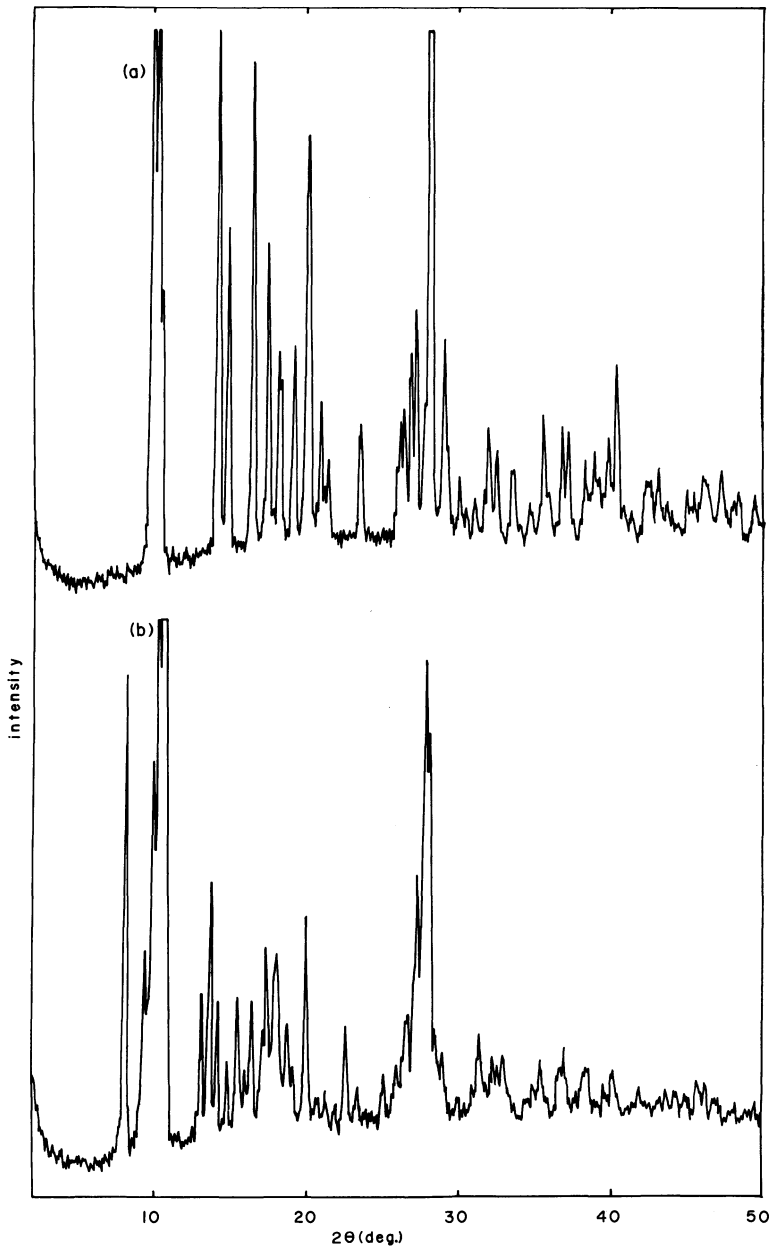

Fig. 5. Comparison of X-ray powder diffraction patterns for **11** (a) and $[Cu(bpy)(N_3)_2]$ (b).

packing arrangement in the unit cells of [Cu(bpy)$(N_3)_2$][6] and **11**. Although more precise measurements of magnetic susceptibilities and the determination of the crystal structure of **11** will be required for elucidating the difference between [Cu(bpy)$(N_3)_2$][6] and **11**, it may be suggested that **11** has a dimeric structure similar to **1**. The magnetic moment of **12** at room temperature shows 0.6 B.M. However, we consider that the compound **12** has a property near diamagnetism, since the presence of several % of paramagnetic impurities in the solid sample **12** is confirmed from the experiment on variable-temperature magnetic susceptibility. Antiferromagnetic interactions have been found in many copper(II) complexes containing end-to-end azide bridges.[8,9,11,13,22] The complex **12** is, therefore, considered to have the structure with end-to-end azide bridging. Also, we imagine that the two copper(II) coordination planes are nearly coplanar and the azide ions bridge the two copper(II) ions in the coordination planes, because the large spin-spin interaction usually operates only when the coplanality of the bridging group 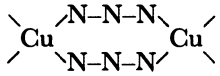 is attained.[8,9,11,13,22] Thus, we consider that the diamagnetic metazido-hemocyanins[35,36] derived from the hemocyanins of *Busycon canaliculatum* and *Limulus polyphemus* contain 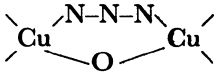 plane. These complexes **11**—**15** exhibit the similar behaviors as **1**—**10** in electronic spectra and electric conductances (Tables 2 and 3).

We thank Miss Sachiyo Nishi for her collaboration in the preparation of compounds. We also indebted to Dr. Isao Kusachi of Okayama University for obtaining the results of the X-ray diffraction and Mr. Sakira Kaneko of Rigaku Denki Co. for DSC measurement and his valuable disscussion. This work was supported in part by a Grant-in-Aid for Scientific Reserch (C) (No. 58540389) from the Ministry of Education, Science and Culture.

References

1) I. Agrell, *Acta Chem. Scand.*, **21**, 2647 (1967).
2) I. Agrell and S. Lamnevik, *Acta Chem. Scand.*, **22**, 2038 (1968).
3) J. Drummond and J. S. Wood, *J. Chem. Soc., Chem. Commun.*, **1969**, 1373.
4) D. M. Duggan and D. N. Hendrickson, *Inorg. Chem.*, **12**, 2422 (1973).
5) C. G. Barraclough, R. W. Brookes, and R. L. Martin, *Aust. J. Chem.*, **27**, 1843 (1974).
6) G. W. Bushnell and M. A. Kahn, *Can. J. Chem.*, **52**, 3125 (1974).
7) G. R. Hall, D. M. Duggan, and D. N. Hendrickson, *Inorg. Chem.*, **14**, 1956 (1975).
8) T. R. Felthouse and D. N. Hendrickson, *Inorg. Chem.*, **17**, 444 (1978).
9) Y. Agnus, R. Louis, and R. Weiss, *J. Am. Chem. Soc.*, **101**, 3381 (1979).
10) M. G. B. Drew, M. McCann, and S. M. Nelson, *J. Chem. Soc., Chem. Commun.*, **1979**, 481.
11) V. McKee, J. V. Dagdigian, R. Bau, and C. A. Reed, *J. Am. Chem. Soc.*, **103**, 7000 (1981).
12) J. Comarmond, P. Plumere, J.-M. Lehn, Y. Agnus, R. Louis, R. Weiss, O. Kahn, and I. Morgenstern-Badarau, *J. Am. Chem. Soc.*, **104**, 6330 (1982).
13) I. Bkouche-Waksman, S. Sikorav, and O. Kahn, *J. Cryst. Spect. Res.*, **13**, 303 (1983).
14) O. Kahn, S. Sikorav, J. Gouteron, S. Jeannin, and Y. Jeannin, *Inorg. Chem.*, **22**, 2877 (1983).
15) Y. Nakao, M. Yamazaki, S. Suzuki, W. Mori, A. Nakahara, K. Matsumoto, and S. Ooi, *Inorg. Chim. Acta*, **74**, 159 (1983).
16) S. Sikorav, I. Bkouche-Waksman, and O. Kahn, *Inorg. Chem.*, **23**, 490 (1984).
17) Y. Agnus, R. Louis, J.-P. Gisselbrecht, R. Weiss, *J. Am. Chem. Soc.*, **106**, 93 (1984).
18) M. A. S. Goher and T. C. W. Mak, *Inorg. Chim. Acta*, **85**, 117 (1984).
19) I. Bkouche-Waksman, M.-L. Boillot, O. Kahn, and S. Sikorav, *Inorg. Chem.*, **23**, 4454 (1984).
20) V. McKee, M. Zvagulis, J. V. Dagdigian, M. G. Patch, and C. A. Reed, *J. Am. Chem. Soc.*, **106**, 4765 (1984).
21) M.-L. Boillot, O. Kahn, C. J. O'Connor, J. Gouteron, S. Jeannin, and Y. Jeannin, *J. Chem. Soc., Chem. Commun.*, **1985**, 178.
22) K. Matsumoto, S. Ooi, K. Nakatsuka, W. Mori, S. Suzuki, A. Nakahara, and Y. Nakao, *J. Chem. Soc., Dalton Trans.*, **1985**, 2095.
23) E. J. Laskowski, D. M. Duggan, and D. N. Hendrickson, *Inorg. Chem.*, **14**, 2449 (1975).
24) K. Nakamoto, "Infrared and Raman Spectra of Inorganic and Coordination Compounds," Wiley, New York (1977), p. 270.
25) M. G. B. Drew, M. McCann, and S. M. Nelson, *J. Chem. Soc., Dalton Trans.*, **1981**, 1868.
26) S. M. Nelson and F. S. Esho, *J. Chem. Soc., Chem. Commun.*, **1981**, 388.
27) M. Nelson, F. S. Esho, and M. G. B. Drew, *J. Chem. Soc., Dalton Trans.*, **1982**, 407.
28) J. G. Haasnoot, W. L. Driessen, and J. Reedijk, *Inorg. Chem.*, **23**, 2803 (1984). The ligand, dmtp, represents 5,7-dimethyl[1,2,4]triazolo[1,5-*a*]pyrimidine.
29) M.-L. Boillot, O. Kahn, C. J. O'Connor, J. Gouteron, S. Jeannin, and Y. Jeannin, *J. Chem. Soc., Chem. Commun.*, **1985**, 178.
30) "Theory and Applications of Molecular Paramagnetism," ed by E. A. Boudreaux and L. M. Mulay, John Wiley, New York (1976).
31) These complexes are described in a previous paper.[22] The ligands, 2-Pca=Hist and 2-Pca=β-Ala, represent Schiff bases derived from 2-pyridinecarbaldehyde and histamine, and 2-pyridinecarbaldehyde and β-alanine, respectively.
32) S. Masatatsu, H. Kanatomi, Y. Demura, and I. Murase, *Bull. Chem. Soc. Jpn.*, **57**, 1003 (1984).
33) R. S. Himmelwright, N. C. Eickman, C. D. LuBien, and E. I. Solomon, *J. Am. Chem. Soc.*, **102**, 5378 (1980).
34) R. L. Dutta and D. De, *J. Indian Chem. Soc.*, **46**, 1 (1969).
35) G. L. Woolery, L. Powers, M. Winkler, E. I. Solomon, and T. G. Spiro, *J. Am. Chem. Soc.*, **106**, 86 (1984).
36) D. E. Wilcox, J. R. Long, and E. I. Solomon, *J. Am. Chem. Soc.*, **106**, 2186 (1984).

 © 1986 The Chemical Society of Japan Bull. Chem. Soc. Jpn., 59, 2761—2765 (1986)

Preparation of Cubic $HZr_2(PO_4)_3$ and Related Compounds

Akira ONO* and Yoshiyuki YAJIMA
National Institute for Research in Inorganic Materials, Namiki, Ibaraki 305
(Received January 11, 1986)

A single phase of cubic $NH_4Zr_2(PO_4)_3$ with a langbeinite-type structure was prepared at 235 °C by a hydrothermal method. A series of analogous compounds containing various monovalent cations or vacancies were made by starting with cubic $NH_4Zr_2(PO_4)_3$. They are polymorphs with respect to Nasicon-type compounds and have rigid skeleton structures with interstitial spaces partially occupied by monovalent ions and water molecules. Maximum water contents of the cubic compounds decrease with increasing sizes of the monovalent ions. Proton-bearing cubic compound exhibited ion exchange reactions with NaCl and LiCl solutions at 20 °C. This suggests the existence of bottlenecks large enough for permitting diffusion of Na^+ and Li^+ ions. Low thermal expansion of cubic $NaZr_2(PO_4)_3$ was studied by high-temperature X-ray diffraction.

Phosphate compounds with the formula $AM_2(PO_4)_3$ where A is an alkali metal atom, H_3O, H, or NH_4 and M is Zr or Ti have three dimensional skeleton structures. Most of the compounds have rhombohedral Nasicon-type structures, but cubic langbeinite-type compounds are also known.[1,2] Here, Nasicon is a solid solution series of the formula $Na_{1+x}Zr_2Si_xP_{3-x}O_{12}$ ($3>x>0$), and langbeinite is a mineral formulated as $K_2Mg_2(SO_4)_3$. Recently, we have prepared cubic $AZr_2(PO_4)_3$ (abbreviated as AZP) and $Zr_4P_6O_{23}$ (abbreviated as VZP, V stands for a vacancy) by a series of heat treatments of cubic NH_4ZP under dry and hydrothermal conditions and ion-exchange reactions between HZP and alkali chloride solutions.[3] The novel cubic compounds, however, were not investigated in detail because of the presence of a considerable amount of monoclinic ZrO_2. This paper describes the preparation and properties of a single phase of cubic NH_4ZP and its related compounds. The cubic phases obtained were characterized by X-ray powder diffraction, high temperature X-ray diffraction, thermal gravimetric analysis(TG), differential thermal analysis(DTA), infrared(IR) spectroscopy and scanning electron microscopy(SEM). An analysis of complex impedance data on cubic HZP[4] will be reported in the near future.

Both cubic and rhombohedral skeleton structures consist of corner-sharing ZrO_6 octahedra and PO_4 tetrahedra with interstitial spaces partially occupied by monovalent cations. Their structures have been explained by a cubic or hexagonal packing of rods[5] consisting of a repeating sequence $A,(A),O_3ZrO_3$, O_3ZrO_3 or A,O_3ZrO_3,O_3ZrO_3, respectively, where (A) is a vacancy. Rhombohedral AZP has one M_1 octahedral site occupied by an A^+ ion and three vacant M_2 sites per formula unit. The M_1 and M_2 sites constitute a three-dimensional network. Any M_1 site is surrounded by six M_2 sites. The spaces linking the M_1 and M_2 sites are considered to be ion-pathways.[6,7]

Cubic AZP has two kinds of cation sites occupied by A^+ ions, and half of the sites are vacant in a statistical sense. Figure 1 illustrates the schematic view parallel to [111] showing the two cation sites in a large ellipsoidal cage which is bounded by a network of six 6-membered and three 4-membered rings consisting of corner-sharing ZrO_6 octahedra and PO_4 tetrahedra. The monovalent ion is surrounded by nine oxygen atoms.[2] Judging from the rapid ion-exchange reaction between cubic HZP and a LiCl or NaCl solution,[3] diffusion of Na and Li ions took place rapidly through the windows of the 6-membered rings.

Experimental

Hydrothermal syntheses were carried out in a Teflon-lined bomb of 20 cm^3 capacity. The bomb was heated in an oven at a prescribed temperature. The pressure was believed

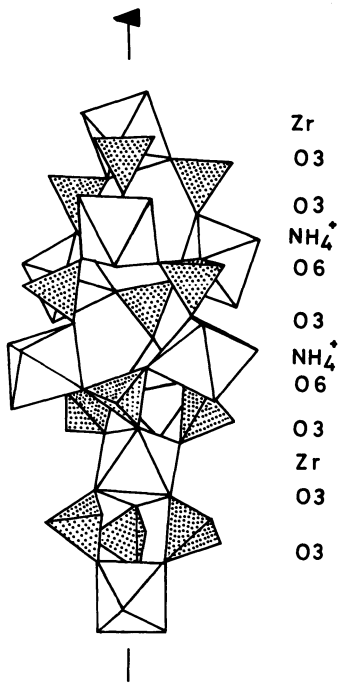

Fig. 1. The schematic view showing the framework of an ellipsoidal cage occupied by a monovalent ion. Two kinds of sites are available for an NH_4^+ ion.

to be about 0.1 to 0.2 GPa calculated from the per cent fill of the container. Two kinds of starting materials were used for the preparation of cubic NH_4ZP. The first one was obtained as follows: $ZrOCl_2 \cdot 8H_2O$, $(NH_4)_2HPO_4$, and $NH_4H_2PO_4$ were mixed in a Teflon container, and then water was added. NH_4F and NH_4NO_3 solutions of 1.5 mol dm^{-3} were also used in some experiments to promote crystallization reactions. The precipitate obtained was well homogenized by stirring with a rod made of bamboo. The Zr/P ratio of the precipitate was 2/3 judging from the mixing ratio of the starting materials. The pH values of the solutions were adjusted by changing the mixing ratio of $NH_4H_2PO_4$ and $(NH_4)_2HPO_4$, but in a few cases a dilute solution of HCl or aqueous ammonia was added to the starting materials. Experimental conditions are given in Table 1.

The other starting material was a gel obtained by mixing solutions of $NH_4H_2PO_4$ and $ZrOCl_2 \cdot 8H_2O$ under controlled pH values.[8] The gel was crystallized in a dilute HCl solution. A small amount of NH_4F or LiCl was added as a mineralizer in a few runs. Experimental conditions are summarized in Table 2.

The yields were filtered and washed with distilled water after the determination of the pH values of the solutions. The products were examined by X-ray methods, IR spectra, TG, DTA, and SEM. All the measurements were carried out on the same laboratory equipment and by the methods described previously.[3,8] Various cubic compounds were prepared from cubic NH_4ZP by the same procedure used before.[3] Chemical compositions of these cubic phases were determined by the combined data of lattice constants, IR spectra, and TG, assuming that the Zr/P ratio of all the cubic phases studied here was 2:3. To confirm the validity of this method, sodium in cubic NaZP was analyzed by the atomic absorption method. The sample was brought into solution in the mixed acid of HF and H_2SO_4.

The interplanar spacing d_{311} of cubic NaZP was measured up to 520 °C for the determination of the coefficient of linear thermal expansion. X-Ray diffraction patterns were recorded with a high-temperature X-ray powder diffractometer, JEOL, DX-COH-V2, using Ni-filtered Cu $K\alpha$ radiation with a scanning speed of 0.25° 2θ min^{-1}. The temperature was measured with a Pt-Pt13%Rh thermocouple in contact with a platinum sample holder which was also heater. Quartz was used as an internal standard. The spacing d_{310} of quartz at 520 °C was calculated by using the lattice constants given in the literature.[9] During the slow heating up to 520 °C, seven lattice constants were measured under constant temperatures, and two lattice constants during the cooling process.

Results and Discussion

Preparation of Cubic AZP. Table 1 shows the results of experiments which were carried out at 235 °C using the precipitates made in a Teflon-container. Cubic NH_4ZP was obtained as a main product under high pH values, but a minor rhombohedral phase was present when no mineralizer was used. A single phase of cubic NH_4ZP was prepared by the addition of a small amount of NH_4F. At low pH values both rhombohedral and cubic NH_4ZP were pepared, but a considerable amount of amorphous materials were obtained together with cubic and rhombohedral phases in a pH range 7—8.3.

Cubic NH_4ZP obtained in NH_4F solutions exhibited euhedral crystal forms with 0.5—1.2 μm in sizes under the SEM. At 925 °C for 25 min this compound loses NH_3 and H_2O to yield cubic VZP which has crystal forms retaining the morphology of the original cubic compound. We could not find any effects of degassing of volatile components on the crystal surfaces of VZP. This may be due to a small volume difference between NH_4ZP and VZP.

For the hydration of VZP at 340 °C and 0.1 GPa,[3] the duration was 5 h previously, but it was 9 h in the

Table 1. Hydrothermal Crystallization at 235 °C

Sample	Time / h	Zr^+ / g	pH	V / cm^3	Product : Remarks
8-45	96	5.22	8.68	9	R+C(0.06)
7-38	95	3.22		7	R+C(0.05)
7-44	72	3.22	8.82	12	R+C(0.16) : NH_4OH added
8-28	96	3.22	8.66	12	R+C+amp(0.12)
7-43	72	3.22	8.55	12	R+C(0.08)
8-27	73	3.22	8.09	12	R+C+amp(0.18)
7-45	27	3.22	7.95	12	R+C+amp(0.67)
8-39	115	3.22	7.05	13	R+C+amp(0.83)
7-42	72	3.22	1.75	12	R+C(0.9)
7-41	72	3.22	1.01	10	R+C(1.8)
7-69	72	3.22	0.35	12	R+C(0.86) : HCl added
9-05	86	3.22	8.58	12	C : 1.5 mol dm^{-3} NH_4F
9-09	87	3.22	8.70	12	C : 0.75 mol dm^{-3} NH_4F
9-12	78	3.22	8.32	12	C+amp : 0.5 mol dm^{-3} NH_4NO_3

R: rhombohedral phase, C: cubic phase, amp: amorphous phase, ( ): X-ray intensity ratio of rhombohedral 012 to cubic 111, Zr^+: weight of $ZrOCl_2 \cdot 8H_2O$, V: volume of solution added.

present study that was long enough for the formation of cubic H_3OZP. The weight loss of cubic H_3OZP took place in the two temperature ranges as shown in Fig. 2A. Cubic HZP was formed after the first water loss of 3.9 wt%, and cubic VZP after the second water loss of 1.85 wt%. The TG curve of cubic HZP showed a weight gain due to absorption of moisture in the temperature range 25 to 220 °C as shown in Fig. 2B. Actually, rehydration of cubic HZP, i.e. formation of H_3OZP, occurred rapidly at 25 °C by addition of a small amount of water. Hydrated VZP ($Zr_4P_6O_{23}\cdot 4H_2O$) was obtained by the hydration of cubic VZP at 100 °C for 24 h under one atmosphere.

Preparation of cubic H_3OZP was undertaken by the hydration of VZP at 245 °C for 48 h in the Teflon-lined bomb. The material obtained showed a water loss of 1.0 wt% in the temperature range 500—900 °C,

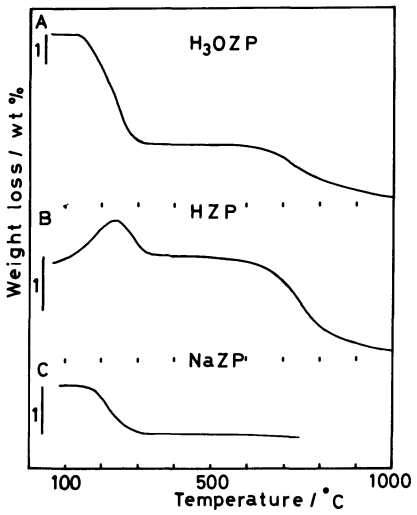

Fig. 2. TG curves of three cubic AZP.
A, C: Materials prepared hydrothermally, B: HZP heated at 500 °C and quenched to room temperature. Scale bar: 1 wt%. Heating rate: 10 °C min^{-1}.

which indicated that H_3O^+ ions occupy 60% of the available cation sites. The hydrated phase obtained was heated at 400 °C in air to prepare a proton-bearing compound which might exhibit an ion-exchange reaction with a NaCl solution at room temperature. The ion-exchange reaction, monitored by a pH meter, mainly took place within 0.5 min after the mixing of the solid and the liquid phases and was completed after 48 h. The final product did not show a weight loss above 500 °C, suggesting the complete exchange of protons by sodium ions. The sodium content of the final product is 2.7 wt% determined by the atomic absorption method. It is, therefore, concluded that sodium ions occupy 56% of the available cation sites that is in good agreement with the value obtained by the water loss datum.

Cubic LiZP was prepared at room temperature by the ion-exchange reaction between cubic HZP and a LiCl solution. In a dilute HCl solution cubic LiZP was changed to cubic H_3OZP after 80 h at 25 °C.

The results of experiments performed by using gels are summarized in Table 2. Cubic NH_4ZP was prepared together with the rhombohedral phase in most of the products. The amount of the cubic phase varied depending upon the different starting gels, and it did not show any systematic relationships to the pH values of the solutions. With respect to this problem, no rhombohedral phase was present when 1.5 mol dm^{-3} solution of NH_4F was added to the dilute HCl solution of 4 cm^3, although the pH value was below 2.0 (Table 2, 9—39). The fluorine ions in the solvent are the strong influencing factor for the formation of the cubic phase. On the other hand, the aging of a gel promoted the formation of the rhombohedral phase over the cubic phase. The result is presented in Table 2, 9—51 for the xerogel aged for 90 d at room temperature before heating.

Stability of Cubic AZP. The thermodynamical stabilities of cubic and rhombohedral AZP are

Table 2. Hydrothermal Crystallization at about 0.15 GPa

Sample	Gel / g	Vol / cm^3	Temp / °C	Time / h	Yield / g	pH	Additives	Products[a)]
9-32	4	12	255	67	3.1	0.79		R+amp
9-33	4	10.7	235	41				amp
9-36	4	9	245	92	1.35	0.45		R+C(6.6)
9-39	4	8	245	68	2.15	1.76	NH_4F	C
9-42	4	7	245	86	2.7	0.25		R+C(1.7)
9-43	2.4	7.8	245	72	1.7	0.34	LiCl	R+C(1.5)
9-44	3	7.9	255	67	1.9	0.61		R+C(0.8)
9-46	3.7	7	243	72	2.4	0.25		R+C(0.18)
9-48	3.2	7	243	72	2.4	0.25		R+C(1.0)
9-50	3.2	7.2	243	72	2.7	0.58		R+C(1.3)
9-51	2.0	6.7	240	64	1.4	0.50		R+C(9.6)

vol: volume of solution, a): see Table 1.

Table 3. X-Ray Data for Cubic AZP[a)]

	$NaZr_2(PO_4)_3 \cdot 0.3H_2O$		$Zr_4P_6O_{23}$	
hkl	d/Å	I_{obsd}	d/Å	I_{obsd}
111	5.89	70	5.86	51
210	4.564	100	4.537	100
211	4.166	47	4.142	35
221	3.401	34	3.382	30
310	3.227	80	3.208	56
311	3.077	37	3.059	27
320	2.830	28	2.814	10
321	2.727	92	2.711	67
400	2.551	9	2.536	4
410	2.475	14	2.461	9
331			2.327	5
422	2.083	12	2.071	9
430	2.041	11	2.029	7
510	2.001	11	1.990	8
511	1.964	15	1.952	11
520	1.895	37	1.884	26
521	1.863	17	1.852	11

a) Data obtained with Ni-filtered Cu $K\alpha$ radiation. Quartz used as an internal standard. Space group; $P2_13$.

problematic because formation of the phases depend on the nature of the starting materials, the pH value and the anion species in the solution equilibrated with the solid phase. According to the previous study,[3)] however, cubic NH_4ZP crystallized at 340 °C and 0.1 GPa at the initial stage of the reaction, and was then gradually changed to the rhombohedral phase by further heating. This result indicates the instability of cubic NH_4ZP above 340 °C under 0.1 GPa.

Here, we have carried out experiments to evaluate the stability of cubic H_3OZP under hydrothermal conditions. Cubic VZP sealed in a gold capsule together with water was heated in a cold sealed pressure vessel for various times. At 350 °C and 0.1 GPa cubic H_3OZP was formed after 9 h, but it was transformed completely to the rhombohedral phase after the subsequent hydrothermal heating for 6 h. It is evident that cubic H_3OZP is a metastable transient phase at 350 °C. At 410 °C and 0.1 GPa, rhombohedral H_3OZP crystallized together with the cubic phase after 1 h. However, on further heating both phases decomposed partially to give unknown oxide compounds. Thus, both cubic and rhombohedral H_3OZP are unstable at 410 °C under 0.1 GPa. The stability ranges of cubic NH_4ZP and H_3OZP, if present, are below 350 °C under 0.1 GPa according to the available data.

Properties of Cubic AZP. X-Ray powder data of cubic VZP and NaZP are listed in Table 3. Here, the intensity (I_{obsd}) was measured as the peak height above the background. The other compounds obtained here showed similar X-ray powder patterns to those listed in Table 3 or Table 1 of the literature.[3)] Chemical formulas and lattice constants of cubic AZP prepared in hydrous conditions are listed in Table 4 together with those of anhydrous cubic compounds which were obtained by heating the hydrous compounds at 500 °C in air. The amount of zeolitic water in the hydrous AZP was estimated by the weight loss taking place mainly in the temperature range 110—300 °C. An example of TG curves is given in Fig. 2 C.

Table 4. Lattice Constants of Cubic AZP

Crystalline material	Lattice constant/Å
$NH_4Zr_2(PO_4)_3$	10.192
$H_3OZr_2(PO_4)_3 \cdot 0.1H_2O$	10.190
Na $Zr_2(PO_4)_3 \cdot 0.3H_2O$	10.205
Li $Zr_2(PO_4)_3 \cdot 0.7H_2O$	10.200
$Zr_4P_6O_{23} \cdot 4H_2O$	10.218
Na $Zr_2(PO_4)_3$	10.173
Li $Zr_2(PO_4)_3$	10.168
H $Zr_2(PO_4)_3$	10.165
$Zr_4P_6O_{23}$	10.146

Lattice constants of hydrous AZP are similar and do not show any relationships to the size of the monovalent ions. The hydrous cubic phases appear to have similar dimensions and configurations of the rigid framework structures. The lattice constant of hydrous cubic AZP is larger than that of the anhydrous one, and hydrous VZP has the largest lattice constant as listed in Table 4. These facts suggest that the lattice constant of cubic AZP may increase by the incorporation of water molecules into the vacant sites located in the large ellipsoidal cages shown in Fig. 1. If the vacant sites were completely occupied by water molecules, the lattice constant of hydrous AZP would be larger than the value given in Table 4. Since such a hypothetical highly hydrous phase could not be prepared, hydrous cubic AZP must become unstable when its lattice constant exceeded a certain value by the increasing number of water molecules in the structure. This value may be in the narrow range 10.190 to 10.205 Å for various cubic AZP. If this is true, the amount of zeolitic water is highly dependent on the size of the monovalent ion, because effects of a water molecule on the expansion of the ellipsoidal cage may be more effective when a water molecule is incorporated into the sites located nearby the larger monovalent ions. Actually, the amount of the zeolitic water in the cubic phases decrease systematically with increasing sizes of the monovalent ions as shown in Table 4.

The lattice constants of the anhydrous cubic phases increase slightly with the increasing sizes of the monovalent ions. The difference in the molar

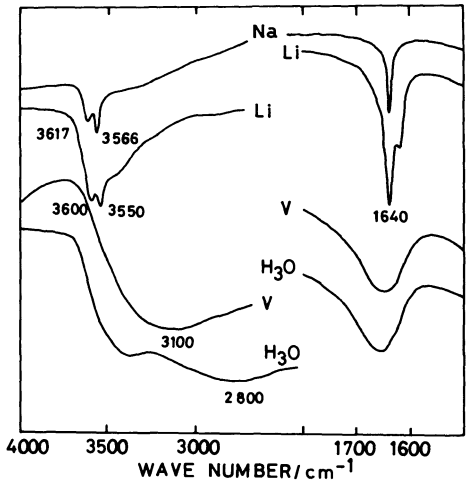

Fig. 3. IR spectra of hydrated cubic phases. Na, Li, V and H_3O are cations located in the interstitial sites of the framework. Here, V stands for a vacancy.

volumes of NH_4ZP and LiZP is 1.1 cm^3 for the cubic phases and 7.2 cm^3 for the rhombohedral phases.[8] The small difference in the cubic phases may be due to the presence of rigid and large ellipsoidal cages which various monovalent ions occupy without considerable changes in the configuration.

Hydrous LiZP and NaZP showed narrow absorption bands in the frequency range 1500 to 4000 cm^{-1} as illustrated in Fig. 3. The wave number of the sharp bands depends on the nature of the monovalent cation. These narrow bands are attributed to OH absorption bands of water molecules whose oxygen atoms interact with adjacent Li or Na ions (ion-dipole interaction). Similar narrow absorption bands of water are common for zeolites.[10]

Cubic H_3OZP showed a broad absorption band near 2800 cm^{-1} which was absent for hydrated VZP. The latter phase exhibited a broad band near 3100 cm^{-1} which could be attributed to a hydrogen-bonded OH stretching vibration.

The d_{310} values of cubic NaZP were approximately constant up to 520 °C. The lattice constant at 520 °C is 10.186 Å which is similar to the value (10.173 Å) at room temperature. The coefficient of linear thermal expansion is 1.6×10^{-6} K^{-1}.

The existence of large vacant sites in a skeleton structure is a necessary condition for the materials of low thermal expansion. Nasicon-type compounds fulfil this requirement and $Ca_{0.5}Zr_2(PO_4)_3$, $ZrNb(PO_4)_3$, and $KTi_2(PO_4)_3$ were demonstrated to be of low thermal expansion.[11–14] Structural analysis of a single crystal of Nasicon has revealed that configurations of polyhedra exhibited little temperature dependence.[6] Therefore, the thermal expansion of Nasicon was mainly caused by changes of bond angles between the adjacent polyhedra.

Cubic AZP has also a three dimensional skeleton structure. Moreover, half of the interstitial cation sites are vacant. These structural features satisfy the requirement for low thermal expansion. Therefore, cubic AZP may have low thermal expansion.

Lattice constants of cubic AZP do not increase considerably when the monovalent cations were completely replaced by the other larger ions as mentioned earlier. This suggests that an increase in size of a monovalent ion caused by a rise in temperature has little effect on the lattice constant of cubic AZP. In fact, cubic NaZP was proved to be of low thermal expansion by high temperature X-ray diffraction.

References

1) L. Hagman and P. Kierkegaard, *Acta Chem. Scand.*, **22**, 1822 (1968).
2) R. Masse, A. Durif, J-C. Guitel, and I. Tordjman, *Bull. Soc. Fr. Mineral. Cryistallogr.*, **95**, 47 (1972).
3) A. Ono, *J. Mater. Sci. Lett.*, **4**, 936 (1985).
4) M. Ohta, F. P. Okamura, and A. Ono, *Abst. Solid State Ionics (Jpn)*, **12**, 65 (1985).
5) M. O'Keefe and S. Andersson, *Acta Crystallogr., Sect. A*, **33**, 914 (1977).
6) D. Tranqui, J. J. Capponi, J. C. Jourbert, and R. D. Shannon, *J. Solid State Chem.*, **39**, 219 (1981).
7) H. Kohler, H. Schulz, and O. Melinikov, *Mater. Res. Bull.*, **18**, 1143 (1983).
8) A. Ono, *J. Mater. Sci.*, **19**, 2691 (1984).
9) D. Taylor, *Mineral. Mag.*, **38**, 593 (1972).
10) L. Bertsch and H. W. Habgood, *J. Phys. Chem.*, **67**, 1621 (1963).
11) R. Roy, D. K. Agrawal, J. Alamo, and R. A. Roy, *Mater. Res. Bull.*, **19**, 471 (1984).
12) D. K. Agrawal and V. S. Stubican, *Mater. Res. Bull.*, **20**, 99 (1985).
13) G. E. Lenain, H. A. McKinstry, S. Y. Limaye, and A. Woodward, *Mater. Res. Bull.*, **19**, 1451 (1984).
14) T. Oota and I. Yamai, *Ann. Rep. Ceram. Engin. Res. Lab. Nagoya Inst. Tech.*, **10**, 9 (1983).

Splitting Parameters in Ligand Field Absorption Bands of Cobalt(III) Ammine Complexes with Chloro or Aqua Ligands

Yoshihiro MITSUTSUKA,* Ichiji KONDO, and Masayoshi NAKAHARA†
Department of Chemistry, Faculty of Science and Engineering, Meisei University, Hodokubo, Hino 191
†Department of Chemistry, Faculty of Science, Rikkyo University, Nishiikebukuro, Toshima-ku, Tokyo 171
(Received January 28, 1986)

The splitting parameters of ligand field absorption bands for cobalt(III) ammine complexes containing aqua or chloro ligands were investigated by microspectrophotometry. The polarized absorption spectra were measured for these crystals. The spectra obtained were separated into Gaussian components according to a nonlinear least-squares method. The splitting parameters were determined from the locations of the components for the first absorption band.

The splitting pattern of the ligand field absorption band for cobalt(III) complexes with different ligands was predicted according to a semiempirical procedure proposed by Yamatera,[1] the so-called Yamatera's rule. Further, the rule was applied to the ligand field bands of cobalt(III) chelate complexes by Matsuoka et al.[2]; it is well-known that the rule does hold in the splitting pattern of the band.

The present work was carried out in order to establish the splitting parameters of some ligands in cobalt(III) complexes. In an aqueous solution it should be possible to determine the parameters of shifting and splitting in spectral patterns, but some complexes are more or less subject to hydrolysis in an aqueous solution and an exact spectrum cannot be obtained. Therefore, a spectral measurement in a crystalline solid is preferable.

In this study, polarized spectra were measured for a single crystal in order to intensify particular components of the absorption band of the complex and to increase the reliability of the spectral analyses. The microspectrophotometric technique was used for the spectral measurement since it is very difficult to grow a single crystal large enough to measure the absorption spectra by a common technique.

Experimental

Microspectrophotometer. The electronic spectra were recorded on a Shimadzu D40R-w spectrophotometer. A part of the optical construction in the microphotometer is illustrated in Fig. 1. Two photomultipliers (R928, Hamamatsu TV) were used for the measurement. Polarized light was obtained by using a Glan Thompson prism in front of a mirror chopper. A sample beam was focused on a crystal of the complex salt with a reflecting objective (MO30X, Olympus) and collected on a photomultiplier with another objective. Since the intensity of the sample beam decreased by approximately 60%, the reference beam was balanced by adjusting an attenuator. The size of the focused beam was 0.03 mm in width and 0.06 mm in length; the width could be reduced by narrowing the slit of the spectrophotometer.

Sample. A large single crystal of the complex salt was required for this experiment. Cobalt(III) ammine complexes, containing chloro and aqua as ligands, were used because these complexes form large single crystals. Since these ligands differ regarding ligand field strength from each other, the components of the absorption band could be distinctly observed. As a result it was easy to analyze the spectrum. The complexes prepared by conventional means were identified by chemical analyses as well as IR and UV spectrophotometry. When the absorbance of the crystal was too high, the crystal was sliced[3] in the desired direction and was then polished smooth and flat.

Measurement. To ensure the best alignment of the electric vector of the incident beam with the axis of maximum absorbance, a Glan Thompson prism was turned until the absorbance reached a maximum. The spectrum of a single crystal was then recorded. After the optical axis of the prism was rotated 90°, another polarized spectrum was also measured. After the crystal was removed from the light beam, a base line was recorded. A net spectrum was obtained by subtracting the base-line absorbance from the observed spectrum.

Curve Analysis. It was proposed by Mead[4] that the absorption curve of the complex was empirically represented by the sum of Gaussian error functions. The absorption

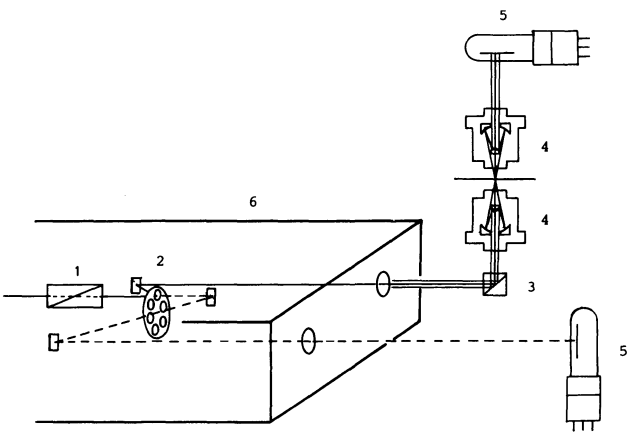

Fig. 1. Apparatus for microspectrophotometry.
1: Glan Thompson prism, 2: chopper, 3: total reflection prism, 4: reflecting objectives, 5: photomultipliers, 6: spectrophotometer.

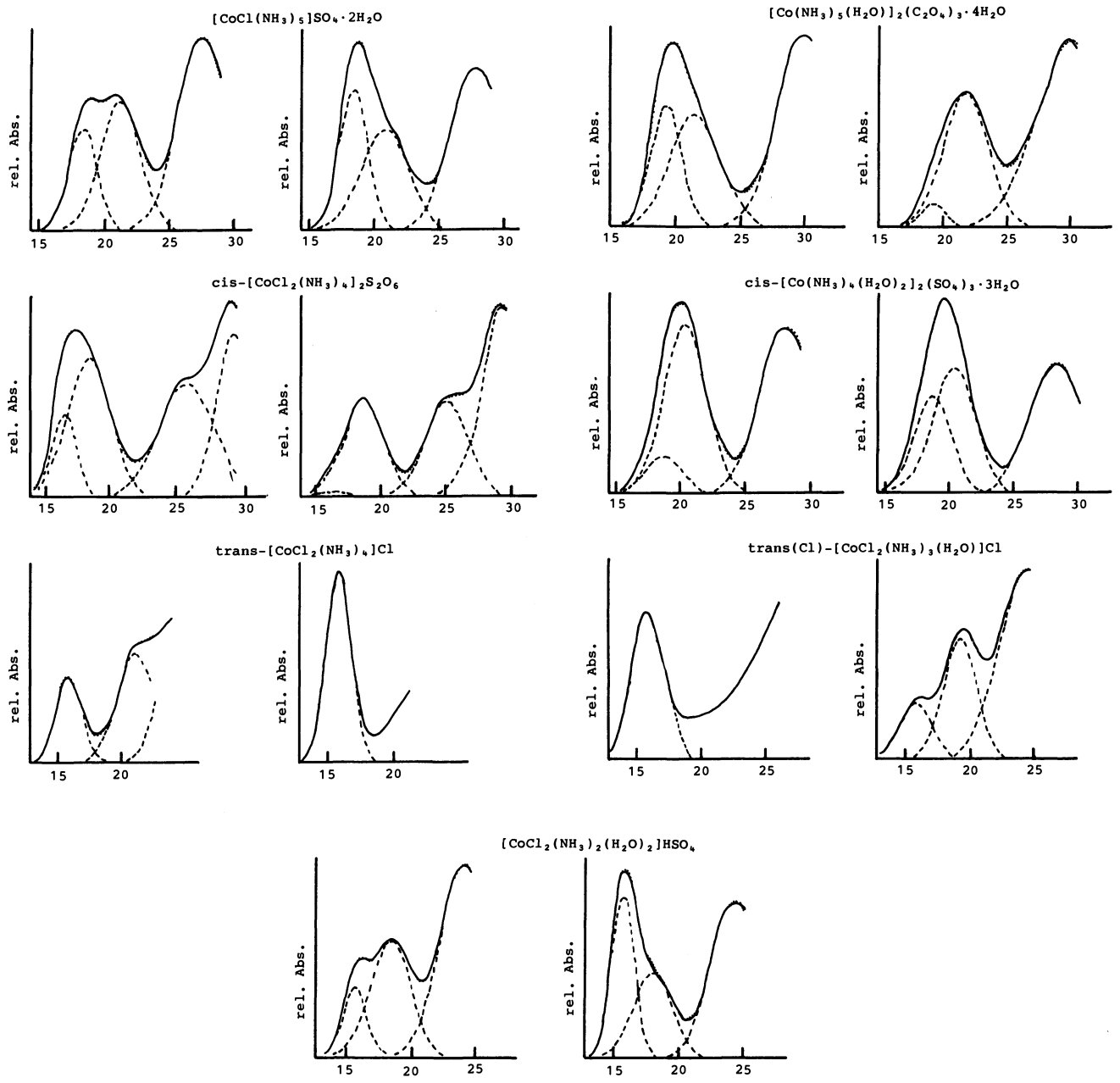

Fig. 2. Polarized crystal spectra of the complexes: solid line, observed spectra; dashed line, calculated Gaussian component; dotted line, sum of the Gaussian components. The numbers on the abscissa indicate wave number ($\times 10^3$ cm^{-1}).

curve obtained was statistically separated into its band components by using the nonlinear least-squares method (SSVM method[5]).

Results and Discussion

Figure 2 shows the electronic spectra of the complexes studied and the calculated curves. The peak positions of the calculated Gaussian components are summarized in Table 1. The splitting components can be clearly distinguished for the so-called first absorption band ($^1T_{1g} \leftarrow {}^1A_{1g}$ in O_h complexes and the corresponding transitions in the complexes of lower symmetries). In this case, no explicit splitting was observed in the so-called second absorption band, ($^1T_{2g} \leftarrow {}^1A_{1g}$ in O_h complexes and the corresponding transitions in the complexes of lower symmetries); the rule of average environment was followed. Furthermore, the second band in some cases somewhat overlapped the charge-transfer band. Thus, the average position of the band is listed in Table 1.

The splitting pattern of the absorption band for octahedral and pseudooctahedral complexes having various ligands has been qualitatively explained according to Yamatera's rule. The rule was applied to

Table 1. Positions of the Absorption Bands of Amminecobalt(III) Complexes

Complex	Analyzed component positions of the first absorption band/$\times 10^3$ cm^{-1}		Average value of the second absorption band/$\times 10^3$ cm^{-1}
$[CoCl(NH_3)_5]SO_4 \cdot 2H_2O$	18.28	21.27	27.55
cis-$[CoCl_2(NH_3)_4]_2S_2O_6$	16.41	18.66	25.53
trans-$[CoCl_2(NH_3)_4]Cl$	15.87	21.05	—
$[Co(NH_3)_5(H_2O)]_2(C_2O_4)_3 \cdot 4H_2O$	19.34	21.61	29.95
cis-$[Co(NH_3)_4(H_2O)_2]_2(SO_4)_3 \cdot 3H_2O$	18.69	20.32	28.34
trans(*Cl*)-$[CoCl_2(NH_3)_3(H_2O)]Cl$	15.75	19.21	24.15
$[CoCl_2(NH_3)_2(H_2O)_2]HSO_4$	15.63	18.48	24.10

Table 2. Band Positions and Expressions Corresponding to the Skeleton

Complex	Skeleton	Components of the first band	Observed position/$\times 10^3$ cm^{-1}
$[Co(NH_3)_6](ClO_4)_3$	$\begin{matrix} N \\ N+N \\ N \end{matrix}$	$\delta(NH_3)$	21.30
$[CoCl(NH_3)_5]SO_4 \cdot 2H_2O$	$\begin{matrix} Cl \\ N+N \\ N \end{matrix}$	$\frac{1}{4}\delta(Cl^-) + \frac{3}{4}\delta(NH_3)$	18.28
	$\begin{matrix} N \\ N+N \\ N \end{matrix}$	$\delta(NH_3)$	21.27
cis-$[CoCl_2(NH_3)_4]_2S_2O_6$	$\begin{matrix} Cl \\ N+Cl \\ N \end{matrix}$	$\frac{1}{2}\delta(Cl^-) + \frac{1}{2}\delta(NH_3)$	16.41
	$\begin{matrix} Cl \\ N+N \\ N \end{matrix}$	$\frac{1}{4}\delta(Cl^-) + \frac{3}{4}\delta(NH_3)$	18.66
trans-$[CoCl_2(NH_3)_4]Cl$	$\begin{matrix} Cl \\ N+N \\ Cl \end{matrix}$	$\frac{1}{2}\delta(Cl^-) + \frac{1}{2}\delta(NH_3)$	15.87
	$\begin{matrix} N \\ N+N \\ N \end{matrix}$	$\delta(NH_3)$	21.05
$[Co(NH_3)_5(H_2O)]_2(C_2O_4)_3 \cdot 4H_2O$	$\begin{matrix} O \\ N+N \\ N \end{matrix}$	$\frac{1}{4}\delta(H_2O) + \frac{3}{4}\delta(NH_3)$	19.34
	$\begin{matrix} N \\ N+N \\ N \end{matrix}$	$\delta(NH_3)$	21.61
cis-$[Co(NH_3)_4(H_2O)_2]_2(SO_4)_3 \cdot 3H_2O$	$\begin{matrix} O \\ N+O \\ N \end{matrix}$	$\frac{1}{2}\delta(H_2O) + \frac{1}{2}\delta(NH_3)$	18.69
	$\begin{matrix} O \\ N+N \\ N \end{matrix}$	$\frac{1}{4}\delta(H_2O) + \frac{3}{4}\delta(NH_3)$	20.32

the spectra of the complete series of $[Co(ox)_x(gly)_y(en)_z]$ chelate complexes as reported by Matsuoka et al.[2] They suggested that the rule describes the band location and shape for these chelate complexes. In the present work, complexes including only unidentate ligands were employed in order to eliminate the chelate effect.

According to Yamatera's rule, the first band of octahedral and pseudooctahedral complexes consists of three components corresponding to the transitions $d_{xy} \rightarrow d_{x^2-y^2}$, $d_{yz} \rightarrow d_{y^2-z^2}$, and $d_{zx} \rightarrow d_{z^2-x^2}$. When a complex has the same six ligands, the three transition energies should be the same; therefore, it appears that the first absorption band shows no splitting. However, the presence of two or more kinds of ligands in a complex gives rise to band splitting. In this study Yamatera's parameter was somewhat modified and used as follows. For example, when a $d_{xy} \rightarrow d_{x^2-y^2}$ transition takes place in a plane including the four ligands of L1, L2, L3, and L4 (located on the X and Y axes), the

Table 3. δ Values of Amminecobalt(III) Complexes

Complex	$\delta(NH_3)$ $\times 10^3$ cm^{-1}	δ(L) $\times 10^3$ cm^{-1}	
$[Co(NH_3)_6](ClO_4)_3$	21.30[6]	—	
$[CoCl(NH_3)_5]SO_4\cdot 2H_2O$	21.27	$\delta(Cl^-)$	9.30
cis-$[CoCl_2(NH_3)_4]_2S_2O_6$	20.91	$\delta(Cl^-)$	11.91
trans-$[CoCl_2(NH_3)_4]Cl$	21.05	$\delta(Cl^-)$	10.69
$[Co(NH_3)_5(H_2O)]_2(C_2O_4)_3\cdot 4H_2O$	21.61	$\delta(H_2O)$	12.53
cis-$[Co(NH_3)_4(H_2O)_2]_2(SO_4)_3\cdot 3H_2O$	21.95	$\delta(H_2O)$	15.43

energy of the transition can be represented by the sum of the $(1/4)\delta$(L) contributions to the ligand field strength from individual ligands:

$$\frac{1}{4}[\delta(L1)+\delta(L2)+\delta(L3)+\delta(L4)].$$

Expressions corresponding to the other transitions can be similarly represented. The skeletons and expressions of their band positions are shown in Table 2. The δ(L) for each ligand in an individual complex is readily calculated from their expressions in the respective complex. Yamatera's parameters δ(L), thus obtained, are also listed in Table 3.

It is known[6] that the positions of the absorption maxima of various complexes in a crystal vary with the kind of counter ion; for example, the maximal degree in band shifts due to counter ions is about 300 cm^{-1} in $[Co(NH_3)_6]X_3$ crystals, except for the occurrence of strong association absorption bands or charge-transfer bands. Therefore, the $\delta(NH_3)$ values of these complexes are in fair agreement with each other (Table 3). Then, it can be assumed that the usable value of $\delta(NH_3)$ is 21.3×10^3 cm^{-1}. However, the treatment of a δ(L) other than $\delta(NH_3)$ is not so simple. The order of δ(L) (L=H_2O, Cl^-) obtained from $[CoL(NH_3)_5]$ and also from *cis*-$[CoL_2(NH_3)_4]$ agrees with that of the spectrochemical series.[7,8] The values of $\delta(Cl^-)$ obtained from $[CoCl(NH_3)_5]$, *cis*-$[CoCl_2(NH_3)_4]$, and *trans*-$[CoCl_2(NH_3)_4]$ are 9.31, 11.91, and 10.69×10^3 cm^{-1}, respectively. These values differ from one another depending on their coordination states. The difference of (1/4) δ(L) values is considered here for the following skeletons:

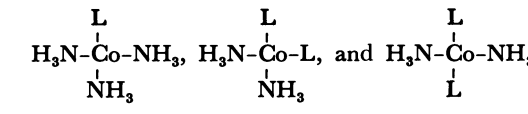

The δ value of ligand L is variable, depending on the other ligands at the cis or trans position. Therefore, particular consideration is necessary for these results. Since the ligand field splitting, 10 Dq, essentially corresponds to the energy difference between $e_g^*(\sigma)$ and $t_{2g}^*(\pi)$, or between σ and π antibonding levels, the difference stated above in the δ(L)'s in chloro and aquacomplexes also arises from the differences in their splitting effects. NH_3 is a fairly strong σ donor but a poor π donor. On the other hand, H_2O and Cl^- with one or two π donor electron pairs will have a much larger ligand-to-metal π interaction than that of NH_3. While the values of $\delta(NH_3)$, 21.30×10^3 cm^{-1}, are nearly the same for any complex, the values of $\delta(Cl^-)$ and $\delta(H_2O)$ vary according to their coordination structure, as described above. Thus δ(L) values of such ligands should be adopted according to the respective coordination structure.

Here, the δ values determined above are applied to a complex whose structure is known. The first absorption band in *trans*(Cl)-$[CoCl_2(NH_3)_3(H_2O)]Cl$, dichro salt,[10] should split into three components corresponding to the skeletons of

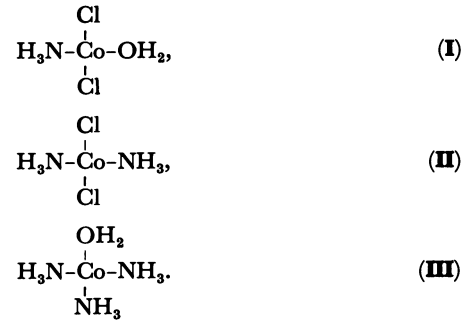

(I)

(II)

and

(III)

Since the $\delta(H_2O)$ for the skeleton (I) was not obtained, the δ value is taken to be the same as that for (III); then, the calculated positions corresponding to three skeletons are:

$$\frac{1}{2}\delta(Cl^-)+\frac{1}{4}\delta(H_2O)+\frac{1}{4}\delta(NH_3)=13.80, \quad (1)$$

$$\frac{1}{2}\delta(Cl^-)+\frac{1}{2}\delta(NH_3)=15.99, \quad (2)$$

$$\frac{1}{4}\delta(H_2O)+\frac{3}{4}\delta(NH_3)=19.11. \quad (3)$$

The values of (2) and (3) agree well with the observed band positions, 15.75 and 19.21×10^3 cm^{-1} (Table 1). In spite of careful experiments extending as far as ca. 1100 nm (9000 cm^{-1}), the band corresponding to (I) could not be found. The question arises as to why the band splits into only two components. A possible explanation is that the predicted $\delta(H_2O)$ value for (I) is different from that for (III). The presence of two Cl^- ligands at the cis positions for H_2O would increase the $\delta(H_2O)$ value for (I). To make this more clear, the spectra of $[CoCl_2(NH_3)_2(H_2O)_2]HSO_4$ were measured (Table 1). Although the crystal structure of this complex has not been clarified, Kyuno[11] has given a coordination structure which was presumed from its UV and IR spectra; two chloro ligands coordinate in the trans positions, as well as two ammine and two aqua ligands in the cis positions. Therefore, the first band should consist of two components corresponding to

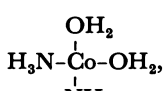

(IV)

and

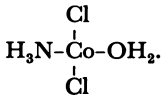

(V)

The position corresponding to skeleton (**IV**) can then be calculated from the values in Table 3:

$$\frac{1}{2}\delta(H_2O) + \frac{1}{2}\delta(NH_3) = 18.37 \quad (4)$$

The value is in good agreement with the observed value, 18.48×10^3 cm^{-1} (Table 1). Therefore, skeleton (**V**) should correspond to the value observed at 15.63×10^3 cm^{-1}; thus

$$\frac{1}{2}\delta(Cl^-) + \frac{1}{4}\delta(H_2O) + \frac{1}{4}\delta(NH_3) = 15.63. \quad (5)$$

From the resuls described above, the component corresponding to (1) should appear at about 15.63×10^3 cm^{-1}. Thus, it is considered that in a dichro salt, the band which could not been found overlaps with the component (2) in the band at 15.75×10^3 cm^{-1}.

It has been shown for a series of aqua and chloro amminecobalt(III) complexes that the positions of components of the first absorption band qualitatively follow Yamatera's rule and also that an excellent quantitative agreement between the rule and experiments can be obtained by using parameter values which are derived by taking into account the effect of coexisting ligands.

The authors are greatly indebted to Dr. Masahiro Morita of the Science University of Tokyo for making programming and computer time available for this study. They also thank Dr. Haruo Yamamoto of Meisei University for the technical service regarding the apparatus. One of authors (Y. M.) thanks Dr. Hisao Hidaka of Meisei University for his encouragement.

References

1) H. Yamatera, *Bull. Chem. Soc. Jpn.*, **31**, 95 (1958).
2) N. Matsuoka, J. Hidaka, and Y. Shimura, *Bull. Chem. Soc. Jpn.*, **40**, 1868 (1967).
3) Y. Mitsutsuka and I. Kondo, *Research Bulletin of Meisei Univ. (Phys. Sci. Engin.)*, **19**, 23 (1983).
4) A. Mead, *Trans. Faraday Soc.*, **30**, 1052 (1934).
5) E. G. Philip, M. Walter, and H. W. Margaret, "Practical Optimization," Academic Press, London (1981), p. 126.
6) Y. Kondo, *Science of Light*, **10**,156 (1961).
7) Y. Shimura and R. Tsuchida, *Bull. Chem. Soc. Jpn.*, **29**, 311 (1956).
8) The spectral data of pentaammine complexes, $[CoX(NH_3)_5]$, (X=F$^-$, and OH$^-$), were obtained by the same method as this experiment. The values of $\delta(F^-)$ and $\delta(OH^-)$ for them were also calculated by this procedure. However, the order in the two-dimensional spectrochemical series[9] should be considered for the complexes with F$^-$ and OH$^-$. A detail report of them will appear elsewhere.
9) J. Glerup, O. Monsted, and C. E. Schaffer, *Inorg. Chem.*, **15**, 1399 (1976).
10) Y. Tanito, Y. Saito, and H. Kuroya, *Bull. Chem. Soc. Jpn.*, **25**, 328 (1952).
11) E. Kyuno, *Nippon Kagaku Zasshi*, **80**, 36 (1959).

 © 1986 The Chemical Society of Japan Bull. Chem. Soc. Jpn., 59, 2773—2778 (1986)

Synthesis and Electrical Conductivity of a New Family of Pt Mixed Valence Complexes: $Pt_6(NH_3)_{14}Cl_{10}X_4$ (X=ClO_4, BF_4, and PF_6)

Masako TANAKA* and Ikuji TSUJIKAWA
Department of Chemistry, Faculty of Science, Kyoto University,
Kitashirakawaoiwake-cho, Sakyo-ku, Kyoto 606
(Received February 10, 1986)

A new family of Pt mixed valence complexes: $Pt_6(NH_3)_{14}Cl_{10}X_4$ (X=ClO_4, BF_4, and PF_6) was synthesized from the Magnus green salt (MGS) by the partial oxidation using an oxidant of H_2O_2 or by electrochemical method. On partial oxidation, the 1/6 of Cl^- ligands in MGS are randomly replaced by NH_3 ligands and simultaneously counter ions X are introduced. These complexes comprise of one-dimensional chains with direct contact between Pt atoms and consequently a quasi-one-dimensional band made up of $5d_{z^2}$ orbital of Pt is formed. The average valence of Pt is +2.33 and the distance between Pt atoms along a chain is shorter than or comparable to that of $K_2[Pt(CN)_4]Br_{0.3}\cdot xH_2O$ (KCP). The electrical conductivity σ of these complexes was measured from 80 K to r.t. The σ(r.t.) is rather high in spite of the measurement on the powder pressed pellets. This suggests that σ along a chain direction may be as high as that of KCP if single crystals can be obtained. The conductivity data were fitted using a gap energy with various temperature dependence. In the complex with X=PF_6, there may be a phase transition caused by ordering of PF_6^- ions at about 110 K.

In the last decade, many quasi-one-dimensional compounds have been synthesized and intensively studied.[1] They comprise both organic and inorganic substances. Among organic charge transfer complexes, tetrathiafulvalene-tetracyanoquinodimethane (TTF-TCNQ) was most intensively studied in 1970's. TTF-TCNQ shows very high and anisotropic conductivity and shows metallic behavior down to 57 K at which it shows sharp metal-insulator(MI) transition, that is, the three-dimensional Peierls transition.[2] Since then, many analogues of TTF-TCNQ have been synthesized to suppress the Peierls transition and to obtain metallic state or superconductivity at low temperature.[3] Consequently, the first organic superconductor $(TMTSF)_2PF_6$ (TMTSF: tetramethyltetraselenafulvalene) was obtained, which has T_c of about 1 K under a pressure of 1.2 GPa.[4] Subsequently, $(TMTSF)_2ClO_4$, a superconductor below 1.4 K at an ambient pressure, was synthesized.[5] Recently a new class of sulfur-based organic conductors $(BEDT\text{-}TTF)_2X$ (X=ReO_4, I_3, IBr_2)(BEDT-TTF: bis(ethylenedithio)tetrathiafulvalene) have been synthesized and studied intensively.[6] At present it arrives at the stage of seeking a superconductor with higher transition temperature in organic compounds. On the other hand, in transition metal mixed valence complexes, KCP, one of Krogmann salts,[7] was the most studied substance in 1970's.[2,8] It shows a high and anisotropic conductivity at room temperature and shows a giant Kohn anomaly characteristic of one-dimensional compounds. But it does not show distinct transition of three-dimensional ordering to the Peierls state, because of the randomness caused by Br^- which occupies 60% of the crystallographic sites and partially oxidizes Pt atoms. And it has been found that the metal dithiolates such as $Li_{0.8}[Pt(mnt)_2](H_3O)_{0.3}\cdot 1.7H_2O$[9] (mnt: maleonitriledithiolate) and the metallomacrocycle complexes such as Ni(Pc)I[10] (Pc: phthalocyanine) have rather high conductivity, though their conductivity is due to π electrons. Recently, the transition metal trichalcogenide MX_3 and the blue bronze attract much attention from the fact that the theoretically expected Peierls–Fröhlich state is realized in these compounds.[8] In any way, since 1980, none of transition metal complexes with conductivity due to d electrons has attracted interests. Only the third model of excitonic superconductor by KCP-like complex was proposed by W. A. Little.[11]

As mentioned above, though KCP is a good model as the quasi-one-dimensional conductor, which comprises the quasi-one-dimensional band made up of $5d_{z^2}$ orbital of transition metal, the elucidation of its physical properties has not yet been achieved. Therefore, it will be worthwhile that the transition metal complexes with more excellent properties than KCP will be found, that is, with higher conductivity, with free of randomness and with lower temperature of the Peierls transition.

We intended to elucidate the mechanism of the MI transition in the one-dimensional conductor with $5d_{z^2}$ band, so that we planned to synthesize new substances which are free from randomness and do not contain water of crystallization which drastically changes physical properties. For the preparation of such compounds, we choose the Magnus green salt $[Pt(NH_3)_4][PtCl_4]$ (abbreviated as MGS hereafter) as a starting material, which has the columnar structure and the filled band made up of $5d_{z^2}$ orbitals of Pt atoms. Then, MGS is partially oxidized by replacing a ligand NH_3 or Cl^- with another ligand with a different charge. Once Pt^{2+} is oxidized to Pt^{4+}, the position vertical to the coordination plane is labile and readily coordinated by donor ligands, such as Cl, Br, I, H_2O, etc. Therefore, the oxidation reaction must take place in a strong acid solution without any other ligands to coordinate in order to retain the one-dimensional chain structure.[12] Hence, the oxidation was proceeded in a $HClO_4$, HBF_4 or HPF_6 acid solution. As the result, we could obtain new mixed valence complexes of Pt; $Pt_6(NH_3)_{14}Cl_{10}X_4$ (X=ClO_4, BF_4, and PF_6)(hereafter abbreviated as POC, POB, and POP respectively). The synthesis, crystal structure

and electrical conductivity of the complexes are reported in this paper.

Experimental

Preparation. Powder of MGS is suspended in 10% $HClO_4$, HBF_4, or HPF_6 solution at room temperature and is oxidized for a few weeks by oxidant of H_2O_2 or by electrochemical method. Consequently, green MGS is changed to the partially oxidized salt POC, POB, or POP. They are brown with metallic luster. Partially oxidized salts thus obtained are in powder form, however, fibrous small needles crystallize from the filtrate. The acids, HPF_6, and HBF_4 are decomposed on heating so POB and POP cannot be recrystallized from these acids, while recrystallization of POC can be made from 2—40% $HClO_4$ solution. The crystals are dichroic with dark brown and colorless for polarized light parallel and perpendicular to the needle axis, respectively.

Structure. Though complete analysis of structure has not been achieved because of the smallness of single crystals of these three compounds, the lattice constants are determined from powder patterns of X-ray diffraction and from X-ray oscillation photographs about the needle axis as well for POC and POB. For POB, lattice constants could be determined on a four-circle diffractometer. IR spectra of POC are observed with KBr pellets.

Electrical Conductivity. The d.c. conductivities of pressed pellets of POC, POB, and POP prepared under pressure of 2.7—3.6×10⁸ Pa were measured between r.t. and 80 K by the two probe method using silver paste for electrodes' contact.

In addition, thermal properties were examined using a DSC between 100 K and r.t.

Results

Elemental analyses were carried out mainly for POC, because POC could be prepared with high purity by the recrystallization, as mentioned above. Found: H, 2.10; N, 8.77; Cl, 22.97; O, 12.06%. Calcd for $Pt_3N_7H_{21}Cl_7O_8$: H, 1.96; N, 9.07; Cl, 22.96; O, 11.84%. POC and POB were determined to be isomorphous from X-ray powder patterns. For POP, Found: H, 1.94; N, 8.41%. Calcd for $Pt_3N_7H_{21}Cl_{10}P_2F_{12}$: H, 1.81; N, 8.37%.

Table 1. Lattice Constants of POC, POB, and POP (Å)

	POC	POB	POP
a	15.07	14.917	6.93
c	5.62	5.696	5.78

POC, POB, and POP belong to tetragonal system and their lattice constants are listed in Table 1. There were no diffuse lines in oscillation photographs of POC and POB. IR spectra for POC which are consistent with the T_d symmetry of ClO_4 suggest that ClO_4 is introduced not as ligand but as a counter ion. The data are listed in Table 2 together with the data from literature.[13]

The experimental results of the electrical conductivity σ measured on heating from liquid N_2 temperature to room temperature are shown in Fig. 1. Conductivity maxima σ_{max} appear at about 287 K(T_{max}) and 273 K

Table 2. IR Spectra of POC with Respect to Molecular Vibrations of ClO_4^- (cm^{-1})

POC	$Cu(ClO_4)_2\cdot 6H_2O$	$Cu(ClO_4)_2\cdot 2H_2O$	$Cu(ClO_4)_2$
1140 s	1160	1158 vs	1270
	≀ sb		≀ sb
			1245
1104 s			1130 s
1090 s	1085		
		1030 vs	1030 w
920 vw	947 wsh	920 vs	948 s
			920 s
	800 vw		
626 m		660 w	665 m
		648 s	647 m
		626 s	624 m
		605 s	600 s

T_d: ClO_4^- C_{3v}: -O-ClO_3^- C_{2v}: $\begin{matrix}-O\\-O\end{matrix}\!\!>\!ClO_2^-$

s: strong, vs: very strong, sb: strong and broad, m: medium, w: weak, vw: very weak, wsh: weak shoulder.

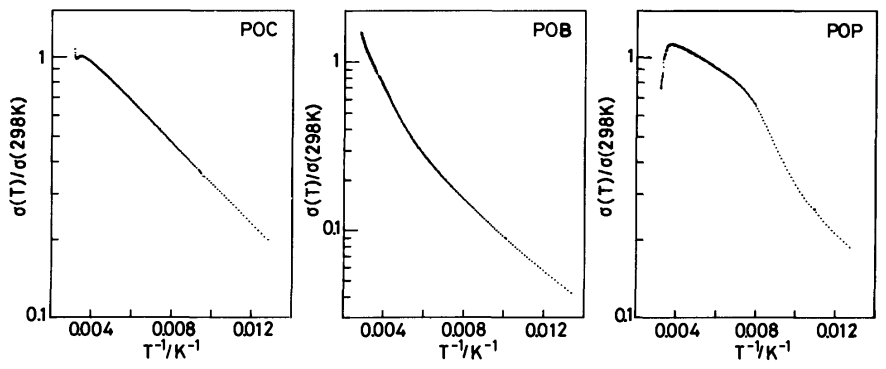

Fig. 1. Electrical conductivity of POC, POB, and POP. Conductivity normalized by the value at room temperature is plotted in a log scale against T^{-1}.

for POC and POP, respectively and below T_{max}, POC and POP are semiconductive. POB is semiconductive in all temperature region observed, though a slight shoulder is observed at 276 K. If σ in the semiconductive region is expressed as $\sigma=\sigma_0\exp(-E_a/k_BT)$, the activation energy E_a becomes considerably small. They are listed in Table 3 together with the values of the conductivity at room temperature. Above T_{max}, they are metallic in the sense of $d\sigma/dT<0$. The MI transition mentioned above takes place in temperature region rather broad as in KCP or NMP-TCNQ (NMP: *n*-methylphenazine). Above 313 K(T_{min}) for POC, σ is again semiconductive with a rather large E_a of an order of 1 eV. While, their starting material MGS is semiconductive over all temperature region with $E_a\simeq0.19$ eV.

No anomalies can be detected in thermal analyses by the DSC for MGS and its partially oxidized complexes unlike a ligand substituting mixed valence complex $Pt_6(NH_3)_{10}Cl_{10}(HSO_4)_4$ (POS) where a glass transition caused by freezing of internal rotation of substituted ligand of HSO_4^- and a structural transition were observed.[14]

Discussion

In MGS, the Pt atoms coordinated in plane by NH_3 and by Cl are stacked alternately and form one-dimensional chains with direct contact of Pt. In the present partially oxidized complexes, the repeating distance in the chain direction is twice of the distance between Pt atoms, retaining the periodicity of the starting material MGS. On the other hand, the averaged valence of Pt, +2.33 evaluated from the formula, suggests that the repeating distance in the chain direction is six times of the distance between Pt atoms. This implies that two of twelve Cl ligands of three molecules of MGS -[$Pt(NH_3)_4$]-[$PtCl_4$]-[$Pt(NH_3)_4$]-[$PtCl_4$]-[$Pt(NH_3)_4$]-[$PtCl_4$]- are randomly replaced by NH_3 ligands in such a way that NH_3 ligands locate in positions trans to Cl^- ligands, which results from a stronger trans-effect of Cl^- than that of NH_3. Then introduced counter ions are assumed to locate between the chains and to form the hydrogen bonding with NH_3. The ligand substitution and the introduction of counter ions result in the partial oxidation, as the result of which 1/6 of Pt atoms changes their valence from +2 to +4 to provide a mixed valence state. The averaged valence of Pt becomes +2.33. This value itself is commensurate with the lattice unlike in KCP. Because of this partial oxidation, the distances between Pt atoms along a chain become shorter from 3.25 Å for MGS[15] to 2.81, 2.85, and 2.89 Å for POC, POB, and POP, respectively. They are comparable to or shorter than that of KCP (2.89 Å)[8] and closer to the value for Pt metal of 2.77 Å. This shrinkage of the distance between Pt atoms comes from the smallness of the substituted ligand of NH_3, which excludes the steric hindrance, and reflects the bare effect of the partial oxidation.

Proposed structure viewed along the chains is given in Fig. 2. The lattice parameter a for POB is smaller than that of POC. This can be explained by the difference in the bond lengths in the counter anions of 1.43 Å[16] and 1.44 Å[16] for B-F (in BF_4^-) and Cl-O (in ClO_4^-), respectively. The parameter a is twice the distance between the nearest neighbour chains. This must come from the lack of the inversion center in a tetrahedral counter anion. The disorder in a chain could not bring about such doubled periodicity. A counter anion with a T_d symmetry can have two probable orientation. The difference in the orientation causes the doubled periodicity. On the other hand, for POP, in which there are octahedral PF_6^- ions, the lattice constant a is the distance between the nearest neighbour chains. The bond length of P-F (1.58 Å (in PF_6^-))[17] is longer than those of Cl-O and B-F, but the lattice constant a is shorter than a half of those of POC and POB. POP may have a different form of packing of counter anions from that in POC and POB.

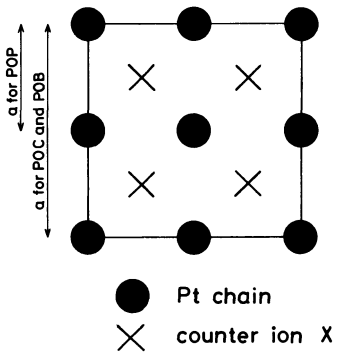

Fig. 2. Proposed structure perpendicular to the chain direction.

Table 3. Conductivity at Room Temperature and Activation Energy in Semiconductive Region for Compressed Pellets Together with the Distances between Pt Atoms

	POC	POB	POP	POS	KCP	Pt
$\sigma_{r.t.}$/S cm^{-1}	1.98×10^{-2}	2.20×10^{-2}	1.17×10^{-2}	2×10^{-4}	8×10^{-2} [23] 3×10^{-3} [24]	
E_a/m eV	16	28	10—30	20	72	—
d(Pt-Pt)/Å	2.81	2.85	2.89	3.25	2.89	2.775

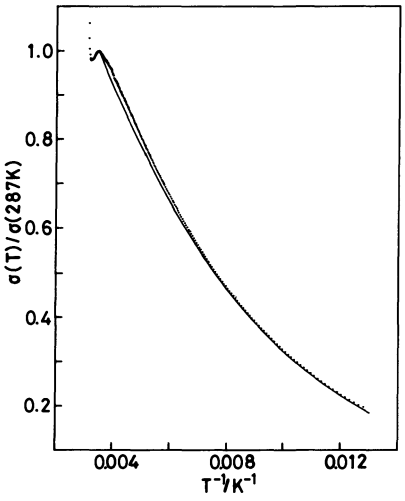

Fig. 3. Electrical conductivity of POC. Dots are the experimental data. Solid line is calculated using $\sigma=\sigma_0 \ln(1+\exp(-E_g/2k_BT))$ with $E_g=390$K (34 meV).

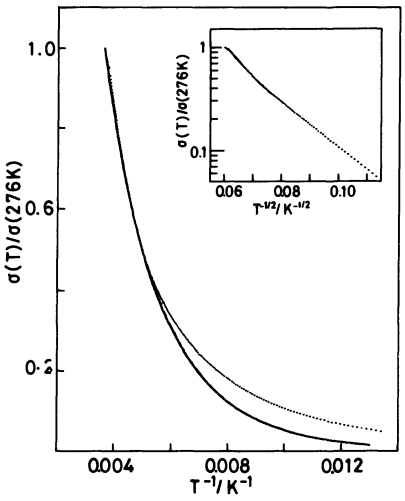

Fig. 4. Electrical conductivity of POB. Dots are the experimental data. Solid line is calculated using the gap energy with temperature dependence of $E_g(T)=E_g(0)(1-T^2/T_c^2)$, where $E_g(0)=760$K (65 meV) and $T_c=276$K. The plot of $\sigma(T)/\sigma(276\text{K})$ against $T^{-1/2}$ is shown in the inset.

Next, we will discuss the temperature dependence of the d.c. conductivity of these new mixed valence complexes of Pt. The conductivity values of the partially oxidized complexes are alike each other and rather high in spite of the measurements on the powder compressed pellets. It is surprising when we notice that the densities of electrons in conductivity of the present complexes comes from the fact that Pt atoms are partially oxidized and the distance between Pt atoms becomes shorter. The values of σ are almost the same as that of KCP. This suggests the conductivity along the chain axis will be as high as that of KCP ($\sigma_{//}=3.5\times10^2$ S cm^{-1} at r.t.),[18] if single crystals can be obtained. We obtained the conductivity only for compressed pellets as mentioned above, so we cannot analyse it quantitatively but may discuss its temperature dependence. The temperature dependence of these complexes differs each other. POC and POP show gradual MI transition at 287 and 273 K, respectively, and for POB at about 276 K a slight shoulder is observed in the conductivity. The MI transition mentioned above is probably the Peierls transition as in KCP. The transition temperature is higher and the activation energy is smaller than those of KCP. Though the temperature dependence of the conductivity above the transition temperature is also of interest in elucidating the nature of this transition, our data are not yet sufficient to make extensive analysis. Therefore, we will only discuss the temperature dependence below the transition temperature. Since the gap energy $E_g(=2E_a)$ is rather small and comparable to k_BT, we must use an explicit form of the Fermi distribution function $f(E)=1/(1+\exp(\beta(E-\zeta)))$ on calculating the number of electrons n in a conduction band, where ζ is the chemical potential and $\beta=1/k_BT$. As n is thought to be small, the temperature dependence in ζ is neglected. Assuming the energy independent constant density of state $N(0)$ at the conduction band, n is derived to be $n=N(0)k_BT\ln(1+e^{\beta\zeta})$. When the origin of energy is taken to the bottom of a conduction band, $\zeta=-E_g/2$, where E_g is the gap energy open up due to the Peierls transition. Since the conductivity σ is expressed using relaxation time τ and effective mass m^* as $\sigma=ne^2\tau/m^*$, $\sigma=\sigma_0\ln(1+\exp(-E_g/2k_BT))$ when we take $\tau\propto T^{-1}$ as in a metal. Even though there will remain the probability that random potential due to ligand substitution do randomly localize electrons in a chain. In this case $\zeta=-E_g$ is taken in the above formulation. The electrical conductivity data are usually fitted empirically using a gap energy with a various temperature dependence[14,19]; BCS-type $E_g(T)=E_g(0)(1-T/T_c)^{1/2}$, $E_g(T)=E_g(0)(1-T^2/T_c^2)$, and $E_g(T)=E_g(0)/(1+\exp(T-T_c)/T)$ and temperature dependent mobility[20] $\mu\propto T^{-\alpha}$. Then, the temperature dependent gap energy is taken as the order parameter. When there exists structural disorder in one-dimensional system, all electrons are localized at $T=0$K. Therefore, electrical conductivity can occur mainly by phonon assisted hopping. Then the conductivity can be expressed[21] as $\ln(\sigma/\sigma_0)=-(T_0/T)^{1/2}$.

For POC, $\sigma=\sigma_0\ln(1+\exp(-E_g/2k_BT))$ with temperature independent gap energy $E_g=390$ K(34 meV) gives a good agreement with experimental values as shown in Fig. 3. If the temperature dependence is introduced in the gap energy, the deviation becomes appreciable especially in higher temperature region. This temperature independence of the gap energy indicates

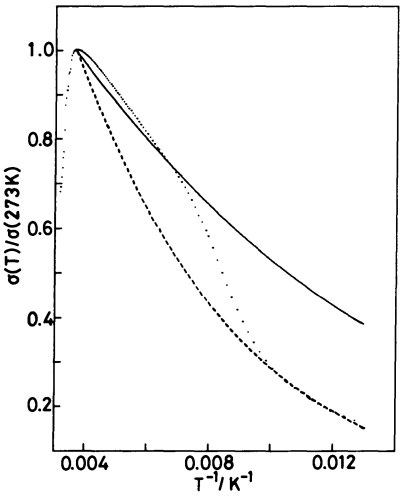

Fig. 5. Electrical conductivity of POP. Dots are the experimental data. Solid line and broken line are calculated using $\sigma=\sigma_0 \ln(1+\exp(-E_g/2k_BT))$ with E_g=240K (21 meV) and E_g=440K (38 meV) respectively.

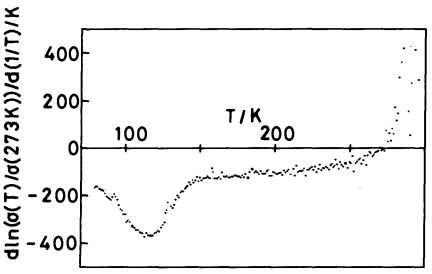

Fig. 6. Logarithmic derivation of the conductivity dln $(\sigma(T)/\sigma(273\text{K}))/\text{d}(1/T)$ plotted as a function of the temperature for POP.

that none of the previous forms of the gap function is applicable. Hence, the MI transition might be induced by structural phase transition, though anomaly cannot be detected in the DSC measurement. Conductivity of POB cannot be expressed in a single formula of σ. Above about 200 K, the gap energy with a temperature dependence of $E_g(T)=E_g(0)(1-T^2/T_c^2)$ gives best fit to the data, where $E_g(0)$=760 K(65 meV) and T_c=276 K. In the region from 77 K to 150 K, the plot of $\log\sigma$ against $T^{-1/2}$ gives linear relation as shown in Fig. 4. This suggests defects or imperfections in a chain and that conductivity due to hopping is dominant at lower temperature as observed in KCP. Conductivity of POP differs considerably from those of POC and POB. There is a change in the temperature dependence at about 110 K. The temperature independent gap energy about 240 K(21 meV) above 110 K and that about 440 K(38 meV) below 140 K give best fit to the experimental results as shown in Fig. 5. A plot of $\text{d}(\ln(\sigma/\sigma_{298\text{K}}))/\text{d}(1/T)$ against T shows minimum at about 110 K as shown in Fig. 6. There is a possibility that the structural phase transition takes place at 110 K. Above 110 K, counter ions PF_6^- freely rotate or librate between two statistically equivalent positions, and below 110 K PF_6^- ions takes a kind of ordering. Such behavior of octahedral anions is observed for $(TMTTF)_2SbF_6$ (TMTTF: tetramethyltetrathiafulvalene) at 154 K where MI transition takes place.[22]

We could synthesize a new family of transition metal complexes $Pt_6(NH_3)_{14}Cl_{10}X_4$. The conductivity is very high, though randomness cannot be excluded. Various kinds of temperature dependent conductivity are observed in these complexes. The behavior depends on the counter anions. Counter anions both tetrahedral and octahedral can be introduced by altering the acid on synthesis. The syntheses of complexes with other anions such as ReO_4^- and AsF_6^- are in progress. We are also trying to grow single crystals in order to make clear the crystal structure and physical properties. Furthermore, conductivity measurements with four-probe and under a high pressure are in progress in order to elucidate the gradual MI transition.

The authors wish to express their sincere thanks to Professor Tsuyoshi Murao and Dr. Yoshitami Ajiro of Kyoto University for their helpful discussions. We also would like to thank to Dr. Koshiro Toriumi of I.M.S. and Professor Tasuku Ito of Tohoku University for obtaining the lattice constants of POB on a four-circle diffractometer.

References

1) "Chemistry and Physics of One-Dimensional Metals," ed by H. J. Keller, Plenum Press, New York (1977).

2) "Quasi-One Dimensional Conductors I," ed by S. Barisic et al., Springer-Verlag, Berlin (1979); G. A. Toombs, *Phys. Rep.*, **C40**, 181 (1978).

3) D. Jerome, A. Mazaud, M. Ribault, and K. Bechgaard, *J. Phys. Lett. (Paris)*, **41**, L-95 (1980).

4) M. Ribault, G. Benedek, D. Jerome, and K. Bechgaard, *J. Phys. Lett. (Paris)*, **41**, L-397 (1980).

5) M. Ribault, J. P. Pouget, D. Jerome, and K. Bechgaard, *J. Phys. Lett. (Paris)*, **41**, L-607 (1980).

6) S. S. P. Parkin, E. M. Engler, R. R. Schumaker, R. Logier, V. Y. Lee, J. C. Scott, and R. L. Greene, *Phys. Rev. Lett.*, **50**, 270 (1983); E. B. Yabubskii, I. F. Shchegolev, V. N. Laukhin, P. A. Kononovich, M. V. Martsovnic, A. V. Zvarykina, and L. I. Buravov, *Pis'ma Zh. Eksp. Teor. Fiz.*, **39**, 12 (1984); J. M. Williams, T. J. Emge, H. H. Wang, M. A. Beno, P. T. Copps, L. N. Hall, K. D. Carlson, and G. W. Grabtree, *Inorg. Chem.*, **23**, 2558 (1984).

7) K. Krogmann and H. D. Hausen, *Z. Anorg. Allg. Chem.*, **358**, 67 (1968).

8) K. Carneiro, "Electronic Properties of Inorganic Quasi-One-Dimensional Compounds," ed by P. Monceau, D. Reidel (1985), Part II, p. 1.

9) M. M. Ahmad and A. E. Underhill, *J. Chem Soc., Dalton Trans.*, **1982**, 1065.

10) R. P. Scaringe, C. J. Schramm, D. R. Stojakovic, B. M. Hoffman, J. A. Ibers, and T. J. Marks, *J. Am. Chem. Soc.*, **102**, 6702 (1980).
11) W. A. Little, *Int. J. Quantum Chem.*, **15**, 545 (1981).
12) W. Gitzel, H. J. Keller, H. H. Rupp, and K. Seibold, *Z. Naturforsch., B*, **27**, 365 (1972).
13) B. J. Harthaway and A. E. Underhill, *J. Chem. Soc.*, **1961**, 3091.
14) R. Inoue, T. Enoki, and I. Tsujikawa, *J. Phys. Soc. Jpn.*, **51**, 3592 (1982).
15) M. Atoji, J. W. Richardson, and R. E. Rundle, *J. Am. Chem. Soc.*, **79**, 3017 (1957).
16) "International Table for X-Ray Crystallography," Kynoch Press, Birmingham (1974).
17) H. Bode and H. Clausen, *Z. Anorg. Chem.*, **265**, 229 (1951).
18) H. R. Zeller and A. Beck, *J. Phys. Chem. Solids*, **35**, 77 (1974).
19) J. F. Thomas, *Solid State Commun.*, **42**, 571 (1982).
20) A. J. Epstein, E. M. Conwell, and J. S. Miller, *Ann. N. Y. Acad. Sci.*, **313**, 183 (1978).
21) A. N. Bloch, R. B. Weisman, and C. M. Varma, *Phys. Rev. Lett.*, **28**, 753 (1972).
22) R. Laversanne, C. Coulon, B. Gallois, J. P. Pouget, and R. Moret, *J. Phys. Lett. (Paris)*, **45**, L303 (1985).
23) L. V. Interrante and F. P. Bundy, *Solid State Commun.*, **11**, 1641 (1972).
24) J. F. Thomas, *Solid State Commun.*, **42**, 571 (1982).

 © 1986 The Chemical Society of Japan Bull. Chem. Soc. Jpn., 59, 2779—2783 (1986)

The Solvent-Extraction Equilibrium of Vanadium(III, IV, V) with Acetylacetone in Nonpolar Solvents

Hisanori IMURA and Nobuo SUZUKI*
Department of Chemistry, Faculty of Science, Tohoku University, Sendai 980
(Received April 9, 1986)

The extraction of vanadium(III, IV, V) with 0.01—0.1 mol dm^{-3} acetylacetone in such nonpolar organic solvents as heptane, benzene, and chloroform has been investigated at pH 1—7 under a nitrogen atmosphere. The extraction constant, the partition coefficient, and the stability constant for the vanadium(III) and vanadium(IV) chelate were determined. Vanadium(V) was found to have been extracted as the vanadium(IV) chelate with reduction.

Vanadium is present in aqueous solutions in +2, +3, +4, and +5 oxidation states. In the presence of air, the quadrivalent and quinquevalent states are stable. Recently, the extraction equilibrium of vanadium has been investigated by using some chelating agents such as 8-quinolinol for vanadium(V)[1] and dithizone for vanadium(IV, V).[2] On the other hand, the spectrophotometric determination of vanadium using the extraction of vanadium(III) with 50% acetylacetone in chloroform has been previously reported.[3] However, little is known about the extraction equilibrium of vanadium in lower oxidation states, especially of vanadium(III).

In the present paper, the extraction chemistry of vanadium (III, IV, V), which are expected to occur in nature, is systematically studied in acetylacetone-nonpolar organic solvent systems.

Experimental

Reagents. A radioisotope, ^{48}V, was produced from high-purity titanium foils by a (p,n) reaction with 18 MeV protons using a cyclotron of Tohoku University. The titanium targets were dissolved in diluted sulfuric acid, and an excess amount of hydrogen peroxide was added to oxdize the titanium carrier to the quadrivalent state. After the excess of hydrogen peroxide has been removed by heating, carrier-free ^{48}V was extracted with 0.02 M(1 M=1 mol dm^{-3}) diethylammonium diethyldithiocarbamate in carbon tetrachloride at pH 4.5—5, washed with an aqueous solution at pH 4.5, and back-extracted with 10 M nitric acid. This solution was evaporated to dryness and dissolved in concentrated hydrochloric acid. Then the solution was fed into an anion-exchange column (Dowex 1X8, 0.8 cm inner diameter ×10 cm height) and eluted with concentrated hydrochloric acid. The ^{48}V fraction was collected and evaporated to dryness. To the residue, concentrated nitric acid was added, and the mixture was heated to completely decompose organic impurities and then evaporated to dryness. Finally, ^{48}V was dissolved in 0.01 M perchloric acid or sulfuric acid.

A carrier solution of vanadium(V) (ca. 0.02 M) was prepared by dissolving high-purity vanadium(V) oxide (Specpure; Johnson Matthey Chem., Ltd.) in perchloric acid or sulfuric acid. The radioactive vanadium(V) solution (10^{-4}—10^{-2} M) was prepared by mixing an appropriate amount of the vanadium(V) carrier and carrier-free ^{48}V, evaporating the mixture to dryness, dissolving it in 0.5 M perchloric acid, and heating it for about 1 h. To confirm the isotopic equilibrium of vanadium, the radioactive vanadium(V) in a 0.1 M sodium hydroxide solution was also prepared and used for the extraction of vanadium(V). The radioactive vanadium(IV) solution was prepared by reducing the vanadium(V) with sodium hydrogensulfite: to the radioactive vanadium(V) in a sulfuric acid solution, sodium hydrogensulfite (ca. 1 M) was added, and the excess of sulfite was removed by heating.

The 2,4-pentanedione(acetylacetone, Hacac) was washed with a diluted ammonia solution and water and then doubly-distilled through a fractionating column after drying. The tris(acetylacetonato)vanadium(III)[V(acac)$_3$] was prepared by the method of Dilli and Patsalides[4] and used to examine its stability in solutions for air oxidation. The oxobis(acetylacetonato)vanadium(IV)[VO(acac)$_2$] was obtained from Dojindo Laboratories. The chloroform was of a spectroscopic grade and was washed with redistilled water several times before use. The other organic solvents were purified by the usual methods. Unless otherwise stated, the reagents used were of a guaranteed reagent grade.

The ionic strength of an aqueous phase was kept at 0.10 M by the use of perchloric acid and sodium hydroxide. The pH of the aqueous phase was adjusted with 0.01—0.10 M perchloric acid, 0.01 M acetic acid, and 0.01 M sodium hydroxide. All the reagent solutions used for the extraction of vanadium(III) and vanadium(IV) were purged for 30 min with nitrogen which had been purified through a pyrogallol-potassium hydroxide solution just before use.

Apparatus. The γ-activity of ^{48}V was measured with an NaI(Tl) well-type scintillation counter. The electronic spectrum of the vanadium chelate was measured with a doublebeam spectrophotometer. The pH value of the equilibrated aqueous phase was measured with a glass electrode.

Extraction Procedure of Vanadium(III). When vanadium(III) was prepared by the reduction of vanadium(V), the purification of the vanadium(III) formed was found to be inevitable if reliable extraction data were to be obtained. Hence, an organic vanadium(III) solution was prepared and purified as follows, and the distribution ratio of vanadium(III) was determined by the back-extraction technique. A stream of purified nitrogen was passed through an 80-cm^3 extraction vessel with three necks in order to displace the air. An aqueous solution (pH 3—5) containing radioactive vanadium(V) (ca. 1×10^{-4} M) and an organic solvent containing 0.01—0.1 M Hacac were then placed in the vessel, and the mixture was stirred. A small amount of 2 M

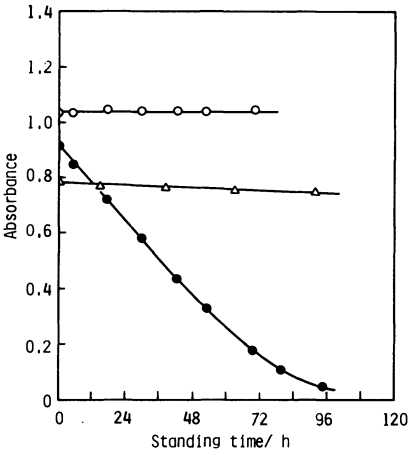

Fig. 1. Stability of $V(acac)_3$ in heptane solutions saturated with nitrogen or air.
○: 1.2×10^{-4} M $V(acac)_3$ at 348 nm under nitrogen atmosphere, ●: 1.1×10^{-4} M $V(acac)_3$ at 348 nm in air, △: 8.9×10^{-5} M $V(acac)_3$ –0.05 M Hacac at 355 nm in air.

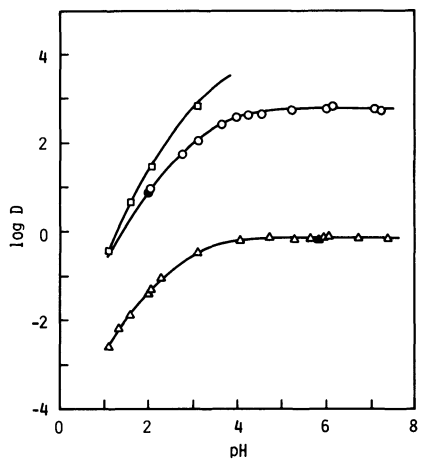

Fig. 2. Extraction of vanadium(III) with 0.10 M Hacac in various organic solvents. The solid lines indicate the computed values.
△: Heptane, ○: benzene, □: chloroform; ●▲: obtained from forward extraction.

sodium dithionite as a reducing agent was added to the contents to make up about a 0.05 M concentration of dithionite. Then the contents were vigorously stirred for 1—3 h. After the mixture had been left to stand, the organic phase was taken out and stirred again with a perchloric acid solution in an appropriate concentraion (0.01—0.1 M) to remove a small amount of the vanadium(IV) complexes from the organic phase. To the purified organic phase containing $V(acac)_3$ we then added an appropriate amount of Hacac, after which the solution was diluted with the organic solvent to adjust it to the desired concentrations of Hacac (0.01—0.1 M) and $V(acac)_3$ (10^{-6}—10^{-5} M). This organic solution (5 cm^3) was shaken with an aqueous solution (5 cm^3) for 1—24 h at pH 1—7 in a stoppered centrifuge tube in which the air had been displaced with nitrogen. After centrifugation, an aliquot was pipetted out from each phase, and the γ-activity was measured. The distribution ratio(D) of vanadium(III) was calculated by the counting rates. The equilibrium pH value was measured immediately after shaking. To confirm the extraction equilibrium, the forward extraction was also performed, and the distribution ratio was measured. Vanadium(III) was back-extracted with 1.0 M perchloric acid from the organic phase. A 0.5-cm^3 portion of the aqueous vanadium(III) solution was added to the centrifuge tube containing the organic (5 cm^3) and the aqueous phase (4.5 cm^3), and the contents were shaken. All the extraction procedures were performed under a nitrogen atmosphere at 25 °C.

Extraction Procedure of Vanadium(IV). An aqueous solution (5 cm^3) containing 1×10^{-5} M radioactive vanadium(IV) was shaken with an organic solution (5 cm^3) containing 0.1 M Hacac for 1—6 h in a centrifuge tube. After centrifugation, an aliquot was pipetted out from each phase, and the γ-activity was measured. In the back-extraction, the organic phase obtained by the forward-extraction was shaken with a fresh aqueous phase. All the extraction procedures were performed under a nitrogen atmosphere at 25 °C.

Extraction Procedure of Vanadium(V). An aqueous solution (5 cm^3) containing 10^{-6}—10^{-4} M radioactive vanadium(V) was shaken with an organic solution (5 cm^3) containing 0.01—0.1 M Hacac for 24 h at 25 °C. The distribution ratio was determined in the same manner as that in vanadium(III, IV). Only the back-extraction was performed under a nitrogen atmosphere.

Theoretical

The extraction equilibrium of a metal ion, M^{n+}, with a chelating agent, HA, can be expressed as follows:

$$M^{n+} + nHA_{org} \rightleftharpoons MA_{n,org} + n\,H^+ \quad (1)$$

$$K_{ex} = \frac{[MA_n]_{org}[H^+]^n}{[M^{n+}][HA]^n_{org}}, \quad (2)$$

where the subscript "org" denotes the organic phase, and K_{ex}, the extraction constant. The distribution ratio of the metal can be written as:

$$D = \frac{[MA_n]_{org}}{[M^{n+}] + \sum_{m=1}^{n} [MA_m{}^{(n-m)+}]}. \quad (3)$$

Equation 3 can be rewritten by using the partition coefficient of the neutral chelate(MA_n), P_M, and the overall stability constant of $MA_m{}^{(n-m)+}$ in the aqueous phase, β_m:

$$D = \frac{P_M\beta_n[A^-]^n}{1 + \sum_{m=1}^{n} \beta_m[A^-]^m} \quad (4)$$

$$= K_{ex}\left(\frac{P_{HA}}{K_{HA}}\right)^n \frac{[A^-]^n}{1 + \sum_{m=1}^{n} \beta_m[A^-]^m}, \quad (5)$$

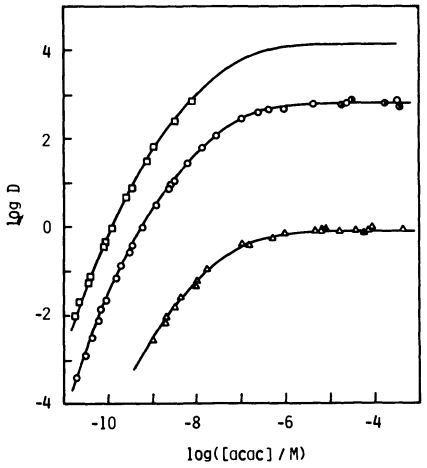

Fig. 3. Distribution ratio of vanadium(III) as a function of acac concentration in the aqueous phase. The solid lines indicate the computed values.
0.01—0.10 M Hacac, 7.5×10^{-7}—6.8×10^{-5} M V(III), pH 1.1—7.4.
△: Heptane, ○: benzene, □: chloroform, ◑▲: successively back-extracted.

where P_{HA} and K_{HA} denote the partition coefficient and the acid-dissociation constant of HA.

Results and Discussion

Extraction of Vanadium(III). Since vanadium(III) is unstable in the presence of oxygen, the stability of $V(acac)_3$ solutions was examined by using the chelate synthesized in an inert gas atmosphere. Figure 1 shows the absorbance of the chelate in heptane solutions as a function of the standing time. It gradually decomposes in a heptane solution saturated with air until it has completely decomposed after standing for four days. In that solution, the formation of $VO(acac)_2$ due to the oxidation of $V(acac)_3$ was observed from the absorption spectrum. However, the addition of Hacac significantly prevents the oxidation decomposition, even in the presence of air. In addition, the vanadium(III) chelate is quite stable in a heptane solution saturated with nitrogen.

Under a nitrogen atmosphere, the extraction of vanadium(III) with Hacac in an organic solvent was first attempted using an aqueous vanadium(V) solution and a strong reducing agent, such as sodium dithionite or sodium borohydride. However, it was found that the complete conversion of vanadium(V) to vanadium(III) was difficult. Hence, in order to obtain accurate distribution data on vanadium(III), we adopted the back-extraction technique described above. Figure 2 shows the extraction curves of vanadium(III) with 0.10 M Hacac in heptane, benzene, and chloroform. The distribution ratio obtained from the forward extraction is in good agreement with that obtained from the back extraction. This fact means that the extraction equilibrium was completely

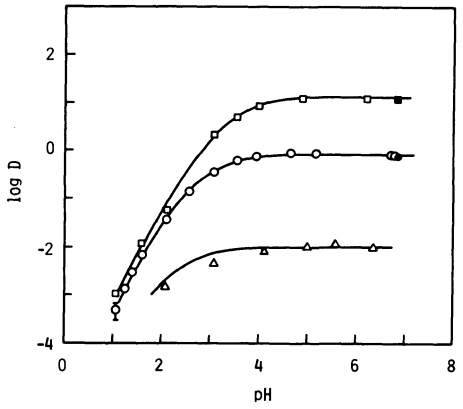

Fig. 4. Extraction of vanadium(IV) with 0.10 M Hacac in various organic solvents. The solid lines indicate the computed values.
△: Heptane, ○: benzene; □: chloroform, ●■: obtained from back extraction.

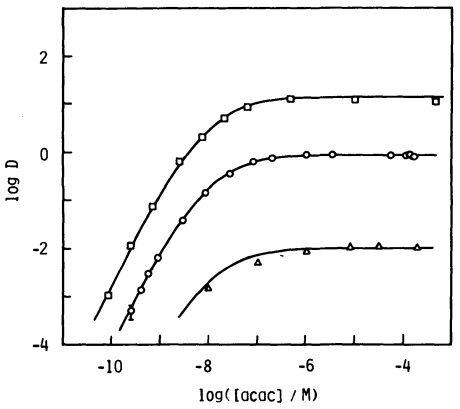

Fig. 5. Distribution ratio of vanadium(IV) as a function of acac concentration in the aqueous phase. The solid lines indicate the computed values.
0.08—0.10 M Hacac, 1.0×10^{-5} M V(IV), pH 1.1—6.9.
△: Heptane, ○: benzene, □: chloroform.

achieved within the agitation time given in each solvent system; 1—120 min for the heptane system, 2—6 h for the benzene system, and 18—24 h for the chloroform system, at pH 1—2. The solid lines indicate the values calculated using the equilibrium constants determined as below.

Moreover, the detailed extraction of vanadium(III) was performed with a different amount of Hacac in the organic solvent (0.01—0.10 M) at pH 1—7. Figure 3 shows the plots of log D against the logarithm of the equilibrium concentration of the acac anion in the aqueous phase. The equilibrium concentration of acac was calculated by using the following equation:

$$[A^-] = \frac{C_{HA}}{(P_{HA}+1)[H^+]/K_{HA}+1}, \quad (6)$$

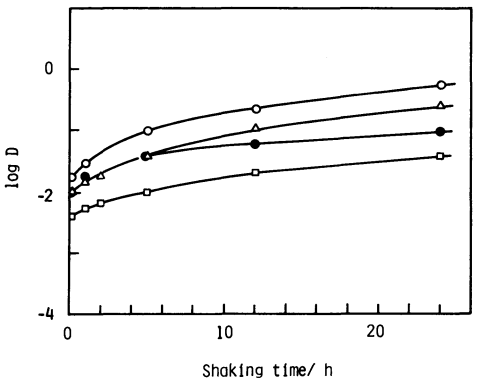

Fig. 6. Effect of shaking time on the extraction of vanadium(V).
1.0×10^{-5} M V(V).
□: 0.10 M Hacac-benzene at pH 2.61, △: 0.10 M Hacac-chloroform at pH 2.61, ○: 0.10 M Hacac-chloroform at pH 4.69, ●: 0.01 M Hacac-chloroform at pH 4.69.

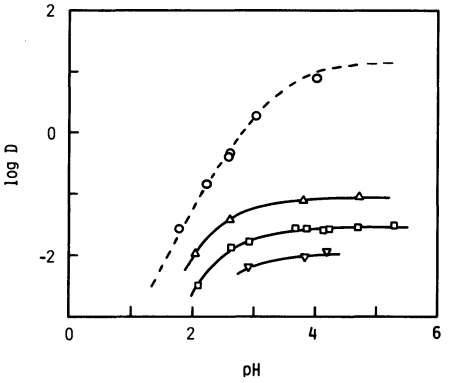

Fig. 7. Extraction and back extraction of vanadium (V) with 0.10 M Hacac in chloroform. The broken line shows the extraction curve of vanadium(IV).
1.0×10^{-5} M V(V).
▽,□,△: Forward extraction at shaking time 5 min, 1 h, 6 h respectively, ○: back extraction at shaking time 1 h.

where C_{HA} denotes the initial concentration of Hacac. The literature values of K_{HA} and P_{HA} were used; i.e., log K_{HA} was -8.82,[5] and log P_{HA} was -0.052 for heptane,[6] 0.736 for benzene,[7] and 1.367 for chloroform.[7] In the low-concentration region of acac, the slope for the plots of log D vs. log [acac] is 3, as is to be expected from the extraction of $V(acac)_3$. The equilibrium constants, P_M and β_m, can be determined according to Eq. 4: the P_M values in the heptane and benzene system were directly determined as the limiting value of the distribution ratio in the high-concentration region of acac. The stability constants, β_1, β_2, and β_3, were determined by the least-square fitting (SALS program, University of Tokyo) on the basis of Eq. 4, using the distribution data in the benzene system. The P_M value in the chloroform system was determined by the least-square fitting using the β_1, β_2, and β_3 values obtained above. The K_{ex} value was calculated as $K_{ex}=P_M\beta_3K_{HA}^3P_{HA}^{-3}$. The equilibrium constants are listed in Table 1. The solid lines in Fig. 3 indicate the values computed using these equilibrium constants, they are in good agreement with the experimental plots.

Extraction of Vanadium(IV). Figure 4 shows the extraction curves of vanadium(IV) with 0.10 M Hacac in heptane, benzene, and chloroform. The distribution ratio of vanadium(IV) did not vary at various agitation times from 1 to 6 h. The distribution ratio obtained from the back-extraction is in good agreement with that obtained from the forward extraction, and the extraction equilibrium is completely achieved. Figure 5 shows the plots of log D against log[acac]. In the low-concentration region of acac, the slope for the plots is 2, as is to be expected from the extraction of $VO(acac)_2$. The P_M value in each solvent system was directly determined as the limiting value of the distribution ratio in the high-concentration region of acac. The stability constants, β_1 and β_2, were determined by the least-square fitting on the basis of Eq. 4, using the distribution data in the benzene system. The K_{ex} value was calculated as $K_{ex}=P_M\beta_2K_{HA}^2P_{HA}^{-2}$. These values are listed in Table 1. The solid lines in Figs. 4 and 5 indicate the values computed using these equilibrium constants; they are in good agreement with the experimental plots.

Extraction of Vanadium(V). The extractability of vanadium(V) was much lower than those of vanadium(III) and vanadium(IV) and the extraction equilibrium could not be achieved. Figure 6 shows that the distribution ratio of vanadium(V) very gradually increases with an increase in the shaking time in both the benzene and chloroform systems. This phenomenon was also observed even at lower vanadium(V) concentrations such as 8.2×10^{-7} M. In such a low-concentration region, polynuclear species of vanadium(V), especially of metavanadates, which are relatively slow equilibrium species, are not formed.[8] Figure 7 shows the plots of log D against the pH at several shaking intervals. The gradual increase in log D is seen at pH 2—5 in the forward-extraction. On the other hand, the distribution ratios in the back-extraction are in agreement with those of vanadium(IV). This result was also obtained in the benzene system under similar extraction and back-extraction conditions. These facts suggest that vanadium(V) is reduced to vanadium(IV) and extracted as stable $VO(acac)_2$. This conclusion is consistent with the previous observation that the vanadium(V)-acetylacetone complex cannot be isolated because of its ready reduction to the quadrivalent state.[3]

Equilibrium Constants of Vanadium(III, IV). The equilibrium constants are summarized in Table 1. No data for vanadium(III) have been reported thus far. It was revealed that not only P_M, β_1, β_2, and β_3 for

Table 1. Equilibrium Constants in the Extraction of V(III) and V(IV) at 25 °C

Chelate	Solvent	$\log K_{ex}$	$\log P_M$	$\log \beta_1$	$\log \beta_2$	$\log \beta_3$
$V(acac)_3$	Heptane	−0.31	−0.112			
	Benzene	0.23	2.793	10.19	19.18	26.10
	Chloroform	−0.32	4.141			
$VO(acac)_2$	Heptane	−3.42	−1.979			
	Benzene	−3.08	−0.066	8.59	16.10	
	Chloroform	−3.12	1.157			

vanadium(III) are all almost the same as those for iron(III) in a series of first-transition metal(III)–acetylacetone chelates,[9] i.e., the equilibrium constants of iron(III) in the benzene system, log P_M=2.785, log β_1=10.63, log β_2=19.26, and log β_3=26.22. Such similarities are supported by the fact that the ionic radius of vanadium(III), 0.640×10^{-8} cm,[10] is quite close to that of iron(III), 0.645×10^{-8} cm[10]; additionally, the metal-oxygen-bond length in $V(acac)_3$ obtained by the X-ray crystallography, 1.982×10^{-8} cm,[11] is close to that in $Fe(acac)_3$, 1.992×10^{-8} cm.[11] These results suggest that the nature of the coordination bonds in the vanadium(III) chelate is hardly different from that in the iron(III) chelate. Consequently, the agreement of the partition coefficient between the vanadium(III) and the iron(III) chelate may be attributed to the similarity in the polarity of their bonds and in the solute-solvent interactions between the chelate and the organic solvent or water.

The equilibrium constants of $VO(acac)_2$ was compared with those of bis(acetylacetonato) chelates of the first-transition metals(II). It was found that the stability constant of the vanadium(IV) chelate is larger than that of the copper(II) chelate, *i.e.*, log β_1=7.93 and log β_2=14.56,[12] which are largest values among the first-transition metal(II) chelates. On the other hand, the partition coefficient of the vanadium(IV) chelate was considerably smaller than that of the copper(II) chelate; i.e., the log P_M in the benzene system is 0.897.[12] These facts may be attributed to the higher charge of the central metal as +4 as well as to the polarity of the oxo group in the vanadium(IV) chelate.

References

1) A. Yuchi, S. Yamada, and M. Tanaka, *Anal. Chim. Acta*, **115**, 301 (1980).

2) H. Akaiwa, H. Kawamoto, and E. Hiyamuta, *Bull. Chem. Soc. Jpn.*, **54**, 3409 (1981).

3) J. P. Mckaveney and H. Freiser, *Anal. Chem.*, **30**, 562 (1958).

4) S. Dilli and E. Patsalides, *Aust. J. Chem.*, **29**, 2389 (1976).

5) J. Rydberg, *Svensk Kem. Tidskr.*, **67**, 499 (1955).

6) H. Watarai and N. Suzuki, *Bull. Chem. Soc. Jpn.*, **52**, 2778 (1979).

7) T. Wakahayashi, S. Oki, T. Omori, and N. Suzuki, *J. Inorg. Nucl. Chem.*, **26**, 2255 (1964).

8) C. F. Baes, Jr. and R. E. Mesmer, "The Hydrolysis of Cations," John Wiley & Sons, New York (1976), p. 197.

9) H. Imura, J. Kodera, and N. Suzuki, 8th Symposium on Solution Chemistry, Kanazawa, 1985, Abstr., p. 72.

10) R. D. Shannon and C. T. Prewitt, *Acta Cryst.* **B25**, 925 (1969).

11) J. P. Fackler, Jr., and A. Avdeef, *Inorg. Chem.*, **13**, 1864 (1974).

12) H. Imura and N. Suzuki, *J. Radioanal. Nucl. Chem.*, **88**, 63 (1985).

 © 1986 The Chemical Society of Japan Bull. Chem. Soc. Jpn., 59, 2785—2788 (1986)

A Voltammetric Detection System for Measuring the Concentration of Chloride Ions in Fresh Concrete

Akifumi YAMADA,* Kazunori HODOUCHI, Koichi KATOH,† Nozomu OTSUGA,††
Choichi HASHIDA,††† and Tetsuo HONDA††††
Department of Materials Science and Technology, Technological University of Nagaoka, Nagaoka 940-21
†Department of Applied Chemistry, Faculty of Engineering, Niigata University, Ikarashi 2-No-Cho 8085, Niigata 950-21
††Department of Inorganic Materials, Tokyo Institute of Technology, Ookayama, Meguro-ku, Tokyo 152
†††Yoshikawa Sangyo Co., Kurosaki-machi, Niigata 950-11
††††Frontex Co., 1408 Ubagayama, Niigata 950
(Received April 25, 1986)

A voltammetric detection system for measuring the concentration of chloride ions in fresh concrete has been developed. A comparative determination using the Volhard titration method showed that the voltammetric system works as well in slushy concrete as in an aqueous chloride solution. No interference from the admixture was observed.

There is a growing trend to use sea sand instead of river sand for making concrete. However, sea sand is likely to contain a lot of chloride which can assist in the corrosion of reinforcing steel.[1,2] It is important, therefore, to determine the on-the-spot chloride content in fresh concrete in order to avoid exceeding the maximum limit. At present, various photoelectric, conductometric, and ion-selective detectors are available for measuring chloride ions in solution.[3] These detectors, however, present considerable technical difficulties when chloride-ion detection is attempted in fresh concrete.[3,4]

Preliminary studies[5,6] of a voltammetric method have shown that a voltammetric sensor has an excellent response to chloride in sea sand and fresh concrete samples. This paper reports the results of a study designed to develop a voltammetric system that seems to work as well in slushy concrete as in an aqueous solution.

Experimental

Instrumentation. A schematic diagram of the voltammetric detection system is shown in Fig. 1 together with the voltammetric sensor which consists of a small silver electrode (working electrode), a lead(II) sulfate/sodium sulfate electrode (reference electrode), and a stainless-steel electrode (counter electrode). Details regarding the voltammetric sensor have been previously described.[5]

The sensor was connected to a computer-controlled potentiostat consisting of an adder, a current-voltage converter(I/V), a sample-and-hold circuit(S/H), an analog-to-digital converter(A/D), display devices (LED, digital printer and x-y polotter), and a microcomputer. Bias and pulse voltages are applied to the adder through a summing resistor (omitted in Fig. 1), respectively. The pulse width of the pulse voltage is established by a pulse-time switch (digital). The start signal, initiated by depressing the start switch in the digital timing and control section, gates the pulse from the analog waveform generator to the potential

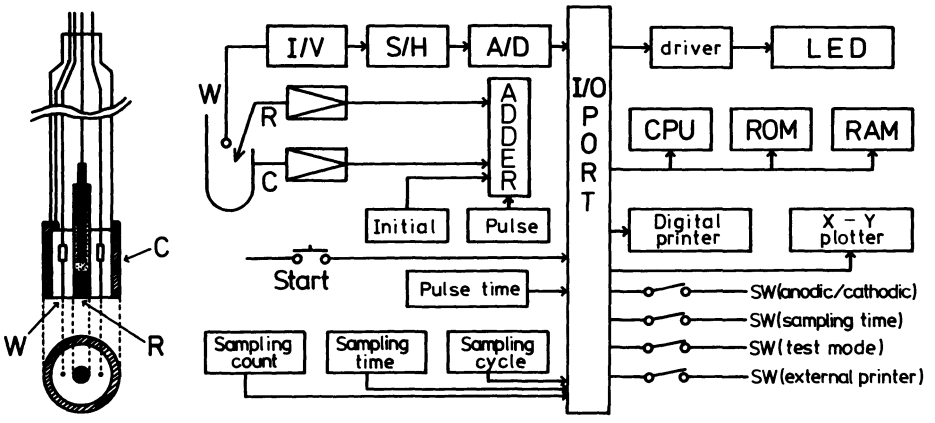

Fig. 1. Schematic diagram of the voltammetric sensor and the voltammetric detection system used for the determination of chloride ions in fresh concrete.
W: Working electrode, C: counter electrode, R: reference electrode, I/V: current-voltage converter, S/H: sample-and-hold, A/D: analog-to-digital converter, CPU: microcomputer, ROM: read-only memory, RAM: random-access memory.

control circuit and the cell. This also initiates a timing routine which controls the read signals to the analog-to-digital converter.

The current-monitoring sequence is accomplished by selecting three digital switches on a patchboard which controls the sampling count, sampling time and sampling cycle. The number of measurements and the interval of each run are controlled by a sampling-count switch and a sampling-cycle switch. A sample-and-hold circuit operates after the elapsed sampling time and the instantaneous current on chlonoamperogram is obtained. The analog-to-digital converter measures and converts the analog voltages from the current-measuring circuit. The digital information is stored in a random-access-memory unit. Upon completion of the measurements, the stored information can be recalled, then printed or plotted on an x-y plotter by operating a manual switch in the control section.

For a chloride determination, the electrolysis current is monitored only after the double-layer charging current has decayed. The working curve is stored in a read-only-memory unit and a fast determination of the chloride content is accomplished after comparing the current due to the chloride with a standard sample.

Procedure. During operation, the sensor is immersed in a concrete paste or paste filtrate with the working electrode held at 0.1 volt; at this potential silver chloride is reduced. Then, a 0.6-volt square-wave potential is applied to the working electrode and both the oxidation and reduction currents are monitored as a function of time. The electrode reaction is given by

$$Ag + Cl^- \longrightarrow AgCl + e \quad \text{(anodic)} \qquad (1)$$

and

$$AgCl + e \longrightarrow Ag + Cl^- \quad \text{(cathodic)}. \qquad (2)$$

The results of the oxidation currents are mainly described in this paper. Usually, the following values are used for measurements: 10—15 for sampling count, 30—50 ms for sampling time, and 1 s for a sampling cycle. The current data correspond to the sampling count; an average of these data are printed out by a digital printer. Current-time curves can be plotted on an x-y plotter if necessary.

Materials. Fresh concrete was prepared by mixing ordinary portland cement (Asano, Onoda, Denka, and Kaihatsu), mineral aggregate, and water. It also contained some air and sometime air-entraining agents (Pozzolith No. 70, obtained from Pozorisu Bussan Co.). Reagent-grade sodium chloride was added to the mixing water to make a solution of the desired chloride concentration.

Reagent-grade silver nitrate, ammonium thiocyanate, ammonium iron(III) sulfate and nitrobenzene were used in Mohr[7] or Volhard[8] titration.

Results and Discussion

When portland cement is mixed with water, the cement particles become dispersed in the water. This suspension changes from the liquid state (slurry) to a plastic or a stiff paste with time. At the same time, a series of reactions occur between the two materials. These reactions are aggregately called the hydration of the cement and are frequently discussed in the literature:[9,10]

$$2(3CaO\cdot SiO_2) + 6H_2O \longrightarrow 3CaO\cdot 2SiO_2\cdot 3H_2O + 3Ca(OH)_2 \qquad (3)$$

$$2(2CaO\cdot SiO_2) + 4H_2O \longrightarrow 3CaO\cdot 2SiO_2\cdot 3H_2O + Ca(OH)_2 \qquad (4)$$

$$3CaO\cdot Al_2O_3 + 6H_2O \longrightarrow 3CaO\cdot Al_2O_3\cdot 6H_2O \qquad (5)$$

$$4CaO\cdot Al_2O_3\cdot Fe_2O_3 + 2Ca(OH)_2 + 10H_2O \longrightarrow 3CaO\cdot Al_2O_3\cdot 6H_2O + 3CaO\cdot Fe_2O_3\cdot 6H_2O \qquad (6)$$

Rapid hydration occurs primarily between the tricalcium aluminate of the cement and water. Simultaneously, the water becomes saturated mainly with calcium hydroxide, calcium aluminate, and gypsum; slurry-cement solutions exhibit remarkably strong alkaline nature.

It has been known that a number of insoluble complex salts such as $3CaO\cdot Al_2O_3\cdot CaCl_2\cdot 10H_2O$ (Friedel salt), $3CaO\cdot Fe_2O_3\cdot CaCl_2\cdot 10H_2O$, and $3CaO\cdot Al_2O_3\cdot CaCl_2\cdot 32H_2O$ are formed with chloride ions if chloride is present in the solution.[11] In fresh concrete, however, a major portion of the chloride is present as free chloride ions. The chloride determination was tested under various analytical conditions.

Working Curve in Chloride Solutions. The current-concentration characteristics of the voltammetric sensor were tested in chloride solutions with varying sodium chloride concentrations. The anodic current was measured at 50 ms after the beginning of electrolysis. Typical examples of the results are plotted in Fig. 2; a well-defined working curve was obtained in the range 0—1% NaCl (by weight).

The analyst usually wishes to measure the concentration of the chloride ions rather than their currents; thus concentration standards are necessary. When a sodium chloride solution is used for calibrating the electrode, the linearity in the standard seems to be excellent (Fig. 2). Thus, the working curve in the computer's memory was standardized before use.

Working Curve of Chloride in Cement Paste. A working curve for a cement paste which was prepared from different (Onoda, Denka, and Kaihatsu) commercially available cements was tested. Also 50 g of

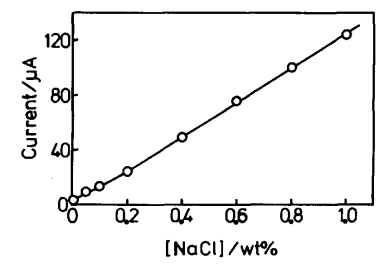

Fig. 2. Current-concentration characteristics of voltammetric sensor obtained in sodium chloride solutions (20 °C). sampling time=50 ms; sampling cycle=1 s.

portland cement was dissolved into 28 g of water containing various concentrations of sodium chloride. This cement paste was vigorously agitated in the thermostat(25 °C) for 20—30 min. Then, the sensor was immersed in a slushy paste and the current was measured fifteen times for a sampling time of 20 ms and a sampling cycle of 1 s. The average current for fifteen measurements was plotted against the chloride concentration after subtracting the background current.

The results are shown in Fig. 3. Although the background current due to the chloride-free-cement paste was somewhat different for each sample, a linear relation was found among those working curves: the slopes of the working curves were consistent with each other.

Reproducibility of Currents. The reproducibility of currents in a series of measurements was tested for a sodium chloride solution, a cement paste and fresh concrete. The composition of a cement paste is only cement and water, while fresh concrete contains water, cement, sand, gravel, and an air-entraining agent.

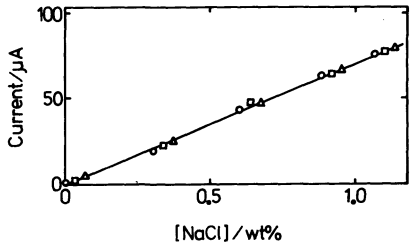

Fig. 3. Current-concentration characteristics of the voltammetric sensor obtained in cement pastes containing sodium chloride (25 °C).
Water/cement ratio=56%; sampling time=20 ms; sampling cycle=1 s.
○: Onoda cement, △: Denka cement, □: Kaihatsu cement.

The sensor was directly immerced in the solution, cement paste or mortar, and the current was measured every second with an appropriate sampling time (20—50 ms).

Examples of raw-current data for ten runs are given in Table 1. Though the voltammetric sensor used in these measurements was not the same, a good reproducibility was seen for different media. The precision between runs varied from 1.5 to 5% over a range of 0.05 to 0.5% chloride. The last two columns are the currents for ten determinations, which involve ten runs in each measurement.

In general, the currents obtained in fresh concrete and cement paste were found to be smaller than those of a sodium chloride solution; this might be caused by a higher viscosity of the cement and by a bleeding phenomenon. When a concrete, after consolidation but still plastic, is allowed to stand unagitated, water usually appears at the surface. This autogeneous flow of mixing water within (or its emergence from freshly placed concrete, mortar or paste) is called bleeding, or water gain.[12]

Determination of Chloride in Fresh Concrete. Many different concretes are now being produced under different technical and economical conditions for a wide variety of purposes. Selections of concrete ingredients should be based on the construction conditions, the type of concrete structure, and the price and properies of the ingredients. In experiments, two types of fresh concretes with different consistencies were prepared; one was the normal concrete (slump=12 cm) and the other was hard concrete (slump=3 cm).

Fresh-concrete types were produced, according to JIS A 1138,[13] by mixing ordinary portland cement, natural sand, crushed stone, an air-entraining agent, and water. A proper amount of sodium chloride was

Table 1. Reproducibility of the Current Data Obtained in Fresh Concretes, Cement Pastes, and Sodium Chloride Solutions (25 °C)[a]

0.1 wt% NaCl solutions current/μA		Cement paste[b] containing 0.1 wt% NaCl current/μA		Fresh concrete[c] containing 0.2 wt% NaCl and admixtures			
				current/μA		current[d]/μA	
43.2	42.0	12.8	13.0	44.7	44.3	44.6	45.8
42.8	42.0	12.6	13.0	44.8	44.2	44.4	47.3
42.8	41.6	12.8	13.0	44.6	44.1	46.0	46.9
42.4	41.6	12.8	13.0	44.6	44.0	42.3	44.2
42.4	41.6	12.8	13.0	44.2	44.2	46.9	45.0
avg=42.3		avg=12.9		avg=44.4		avg=45.3	
σ=1.2%		σ=1.0%		σ=0.59		σ=3.2%	
t=50 ms		t=20 ms		t=50 ms		t=50 ms	

a) The sensor used for each measurement is different. Figures in the left column correspond to runs 1 through 5, and those in right column, to runs 6 through 10. σ represents the relative standard deviation of a single determination, and t is the sampling time. Sampling cycle is 1 s. b) Water/cement ratio=56%. c) Water/cement ratio=61%, Sand/aggregate ratio=50%. d) Data for ten determinations. A single determination gives an average of 10 runs.

Table 2. Proportioning of Test Concrete

No.	Max. size[a] mm	Slump cm	Entrapped air %	Water-cement ratio %	Sand-aggregate ratio %	Component in 1 m³ of compacted concrete/kg					Chloride content[c] %
						Water	Cement	Fine[b] aggregate	Coarse aggregate	Admixture	
1											0
2	25	12	4.5	55.0	42.0	161	300	770 (757)	1069	0.750	0.02
3											0.05
4											0.10
5	25	2—3	4.5	47.7	43.6	140	300	825 (811)	1069	0.750	0.05

a) Maximum size of coase aggregate. b) The number in parentheses represents the weight of dry sand. c) Weight percent of NaCl for the weight of dry sand used.

Table 3. Determination of Chloride in Fresh-Concrete Samples

No.	Chloride content wt%	Slump cm	Entrapped air %	Chloride content found[a]/wt%		Difference[b] %
				Voltammetric method	Volhard method	
1	0	12.0	4.5	0.0075	0.0070	+7.1
2	0.02	11.0	4.5	0.0247	0.0236	+4.7
3	0.05	12.5	4.6	0.0538	0.0536	+0.4
4	0.10	12.0	4.6	0.103	0.104	−1.0
5	0.05	3.0	4.8	0.0532	0.0529	+0.6

a) Weight percent of NaCl for the weight of dry sand used. b) Difference between the voltammetric method and Volhard method.

added to the mixing water. The water/cement ratio was 48—55% and the sand/aggregate ratio was 42—44%. Table 2 summarizes the mix proportion used for the production of test concrete. The chloride concentration is usually expressed as the weight of sodium chloride divided by the weight of the small aggregate in a unit volume of concrete; this is the sodium chloride-sand ratio by weight.

The fresh-concrete types were filtered by an aspirator and the chloride content was measured by the voltammetric system. The chloride content was also determined by the Volhard method. Table 3 summarizes the results of the chloride content, slump and air content. The results show that the slump and air content agree with their target values; an adjustment of the batch weights for the test concrete was carried out satisfactory. Sample 1 (corresponding to no chloride content) showed a slight presence of chloride. This may have been caused by chloride contamination from the cement, air-entraining agent or water. However, it can be seen that the mutual relation between the voltammetric and Volhard methods was sufficiently estimated from the result of the measurements given in Table 3 (sample 1 through 4). The result of sample 5 shows that the voltammetric determination worked well for lower-water-content concrete; this method is applicable for concrete produced in general construction.

In conclusion, the convenience of this voltammetric system suggests that it could find on-the-spot applications in concrete manufacturing, in the construction industry, or for other consumers of concrete for a quality control of concrete.

The authors express their sincere thanks to Dr. Yoshikiyo Kato of Yamagata University for his continuous encouragements.

References

1) K. Kobayashi, T. Akaishi, K. Kishitani, M. Tokita, T. Fujii, Y. Kakegai, M. Kondou, Y. Nojiri, and H. Sawai, *Concrete Kougaku*, **22**, 2 (1984).

2) Proceedings of Japan National Council on Concrete, "Symposium on Effects of Chlorides in Reinforcing Concrete," Tokyo (1975).

3) A. Yamada and C. Hashida, *Denki Kagaku*, **52**, 728 (1984).

4) M. Tokita and H. Sakamoto, *Concrete J.*, **12**, 47 (1974).

5) A. Yamada and K. Hodouchi, *Denki Kagaku*, **52**, 633 (1984).

6) A. Yamada, K. Hodouchi, N. Otsuga, K. Ueda, and C. Hashida, *Chem. Lett.*, **1985**, 751.

7) "Shin-Jikken Kagaku Koza," ed by Chemical Society of Japan, Maruzen, Tokyo (1976), Vol. 9, p. 243.

8) Ref. 7, p. 244.

9) S. Popovics, "Concrete Making Materials," McGraw-Hill, New York (1979).

10) F. M. Lea, "The Chemistry of Cement and Concrete," 3rd ed, Chemical Publishing Company, New York (1971).

11) M. H. Roberts, *Mag. Concrete Res.*, **14**, 143 (1962).

12) S. Popovics, "Fundamentals of Portland Cement Concrete: A Quantitative Approach," John Wiley & Sons, New York (1982), Vol. 1.

13) Japanese Industrial Standard, "Method of Making Test Samples of Concrete in the Laboratory," Japanese Standards Association, Tokyo (1978).

Mössbauer and DTA Studies of K_2SO_4-$ZnSO_4$-$Fe_2(SO_4)_3$ Glasses

Tetsuaki NISHIDA* and Yoshimasa TAKASHIMA
Department of Chemistry, Faculty of Science, Kyushu University 33,
Hakozaki, Higashiku, Fukuoka 812
(Received April 30, 1986)

A structural study of ternary sulfate glasses has been performed to elucidate the nature of the chemical bond and the local structure of these glasses. Mössbauer parameters (isomer shift and quadrupole splitting) show drastic decrease with an increase in the K_2SO_4 content. This is ascribed to the gradual change in the coordination number of iron (Fe^{3+}) from six (Oh) to four (Td) when the K_2SO_4 content is higher than about 60 mol%. Lattice dynamic information obtained from low-temperature Mössbauer measurements suggests that the chemical bond between the iron and the neighboring oxygen is essentially ionic. All the Mössbauer results for the ternary sulfate glasses suggest that the Fe^{3+} ions are present at the vacant sites (voids) of the pseudospherical SO_4^{2-} ions which are considered to be randomly packed to constitute the ionic glasses. Glass transition temperature (T_g) of these sulfate glasses, obtained from DTA measurements, also shows a gradual decrease with increasing K_2SO_4 content. This result is very similar to the composition dependency of the Mössbauer parameters described above, and suggests that the ionic field strength of the sulfate glasses decreases with increasing K_2SO_4 content. These experimental results are ascribed to the increased intermolecular bond length between the pseudospherical SO_4^{2-} units.

Zinc sulfate-based glasses are considered to be constituted of randomly packed SO_4^{2-} ions which have essentially spherical geometry.[1-5] The feature of these glasses will lie in the essentially ionic nature of the chemical bond between the SO_4^{2-} ions and in the lack of so-called network structure. This is quite distinguishable from the case of ordinary oxide glasses such as silicate and borate glasses, in which each network-forming atom (Si and B) is covalently bonded with each other by oxygen atoms. As for the ionic salt glasses other than the $ZnSO_4$-based glasses, nitrate, nitrite, carbonate, formate, and acetate glasses are known to be present.[1] These ionic salt glasses seem to be very interesting and important materials from the scientific point of view, because their glass structure is quite different from the structure of ordinary oxide glasses, as described above. Coulombic interaction between cation (e.g., K^+ and Zn^{2+}) and anion (e.g., SO_4^{2-}) and a packing effect of them are therefore considered to be predominant factors for the preparation of the ionic salt glasses. Physical properties of some $ZnSO_4$-based glasses, such as density, refractive index, glass transition temperature, and heat capacity, have been studied by Rao et al.[2,3] They reported that the increase in the $ZnSO_4$ content results in gradual increases in density and refractive index of these glasses. A structural model for the K_2SO_4-$ZnSO_4$ glasses was proposed on the basis of the composition dependency of these physical properties.[2] A few structural studies of $ZnSO_4$-based glasses have been performed by means of X-ray diffraction[4] and ESR.[5,6] Coordination numbers of K^+, Na^+, and Zn^{2+} in the $ZnSO_4$-based glasses are known to be twelve, eight, and six, respectively.[2-4] An ESR study of binary K_2SO_4-$ZnSO_4$ glasses doped with Cu^{2+} or Mn^{2+} suggests that these transition metal ions occupy the octahedral sites, just as in the case of the Zn^{2+} ions surrounded by six oxygen atoms given by six SO_4^{2-} tetrahedra.[2]

The present Mössbauer and DTA (Differential Thermal Analysis) studies of the ternary K_2SO_4-$ZnSO_4$-$Fe_2(SO_4)_3$ glasses were carried out in order to obtain the structural information such as the coordination number and the symmetry of metal ions and the nature of the chemical bond between the metal ions and the SO_4^{2-} ions. Mössbauer spectroscopy is well utilized for the structural study of several inorganic glasses[7-18] by the authors. Mössbauer study of some halide glasses, i.e., KCl-$ZnCl_2$[17] and BaF_2-ZrF_4,[18] revealed that these glasses are constituted of three-dimensional network of $ZnCl_4$ tetrahedra and of the one- or two-dimensional chain-like polymer of ZrF_6 octahedra, respectively. DTA measurements also give us some useful information on the structure of glasses. In general, the increase in the coordination number of network-forming atom is known to result in a gradual increase in the glass transition temperature (T_g).[15,19-23] For example, step-by-step structural changes of network formers from BO_3 to BO_4 units and from GeO_4 to GeO_6 units are well reflected in T_g in borate and germanate glasses, respectively. This is probably due to the increased degree of bridging in the glass skeleton. On the other hand, a decreased degree of bridging in the glass skeleton, brought about by the formation of nonbridging oxygen atom, is observed as a gradual decrease in T_g.[15,22,23] As for the T_g of the $ZnSO_4$-based glasses, a composition dependency has so far been observed only in a ternary K_2SO_4-Na_2SO_4-$ZnSO_4$ glass system,[3] in which an increase in T_g is ascribed to the increased coordination number of alkali metal ion caused by the substitution of K_2SO_4 for Na_2SO_4.

Experimental

A series of K_2SO_4-$ZnSO_4$-$Fe_2(SO_4)_3$ glasses, in which $Fe_2(SO_4)_3$ content is lower than 12 mol%, were prepared by

fusing the individual mixtures (1 g) of K_2SO_4, $ZnSO_4 \cdot 7H_2O$, and $Fe_2(SO_4)_3$, of a guaranteed reagent grade, at 640—740 °C for 2—40 min using an electric muffle furnace. The anhydrous $Fe_2(SO_4)_3$ was prepared by heating the commercially available $Fe_2(SO_4)_3 \cdot nH_2O$ at 235 °C for 6 h, because the simultaneous DTA and TG (Thermal Gravity) measurements of the hydrous iron(III) sulfate proved to be almost completely dehydrated when heated at 235 °C. Each melt in a platinum crucible was quenched with ice-cold water after the fusion. All the glass samples prepared in this way show transparent and brown color. Mössbauer measurements were performed by a constant acceleration method at various temperatures with a proportional counter and a 1024 channel-multichannel scaler. Cobalt-57 (10 mCi) diffused into a palladium foil was used as the Mössbauer source. As for the reference material of isomer shift, a metallic iron foil enriched with iron-57 was used. Calibration of the Mössbauer spectrometer was also performed using the iron foil. Every Mössbauer spectrum obtained from room-temperature measurement was analyzed into a quadrupole doublet, having the same width and intensity with each other, due to Fe^{3+} ions. On the other hand, each Mössbauer spectrum obtained at temperatures lower than room temperature was analyzed into two kinds of quadrupole doublets due to Fe^{3+} and Fe^{2+} ions. Mössbauer measurements were performed in such a condition that the thickness of the glass sample should be as thin as possible. Simultaneous DTA and TG measurements were performed for each glass sample of 20 mg with a heating rate of 5 °C min^{-1}. The DTA and TG measurements were performed over the range from room temperature to 700 °C, using Al_2O_3 powder as a standard material for the DTA measurement.

Results and Discussion

The glass-forming region for the ternary K_2SO_4–$ZnSO_4$–$Fe_2(SO_4)_3$ glasses prepared in the present study is shown with a solid line in Fig. 1, in which open circles indicate the formation of glass samples. Closed and half-closed circles in Fig. 1 indicate the formations of ceramics (devitrified) and glass-ceramics (partially devitrified), respectively. It is seen from Fig. 1 that the glass-forming region for the binary K_2SO_4–$ZnSO_4$ system is in the range of 35—65 mol%, which is approximately consistent with the already published results.[2-4,24-26] At the early stage of the present study, ternary glass system K_2SO_4–$ZnSO_4$–$FeSO_4$ was also tried to prepare with $FeSO_4 \cdot 7H_2O$ or $FeSO_4 \cdot (NH_4)_2SO_4 \cdot 6H_2O$. As the result, the latter reagent proved to be useful for the preparation. The ternary $ZnSO_4$-based glasses prepared with $FeSO_4 \cdot (NH_4)_2SO_4 \cdot 6H_2O$, however, showed the absorption only due to Fe^{3+} ions in the Mössbauer spectra. This will be due to the oxidation reaction of Fe^{2+} to Fe^{3+} during the sample preparation, because all of the sample preparations was performed in the atmosphere. The glass-forming region for the ternary $ZnSO_4$-based glasses prepared with $FeSO_4 \cdot (NH_4)_2SO_4 \cdot 6H_2O$ is shown by a dotted line in Fig. 1. Sample preparation for the ternary K_2SO_4–$ZnSO_4$–Fe_2O_3 system was also attempted in the present study, but no vitreous sample could be obtained.

A typical Mössbauer spectrum of the ternary K_2SO_4–$ZnSO_4$–$Fe_2(SO_4)_3$ glass system is shown in Fig. 2a. The spectrum indicates that the iron is present as a paramagnetic Fe^{3+} ion in these glasses. It is speculated from Fig. 2a that only a small amount of Fe^{2+} ions is also present in these glasses. (Note that a weak peak around 2 mm s^{-1} is a part of the quadrupole doublet due to Fe^{2+} ions and that the relative absorption intensity of the Fe^{2+} peak is comparable to the amplitude of the scattering of the points around the base line.) Each Mössbauer spectrum measured at room temperature is therefore analyzed into a quadrupole doublet only due to Fe^{3+} ions, as is shown by a solid line in Fig. 2a.

Mössbauer parameters for the ternary $ZnSO_4$-based glasses are summarized in Table 1, in which the Mössbauer parameters for the anhydrous $Fe_2(SO_4)_3$ used for the preparation of the glass samples are also

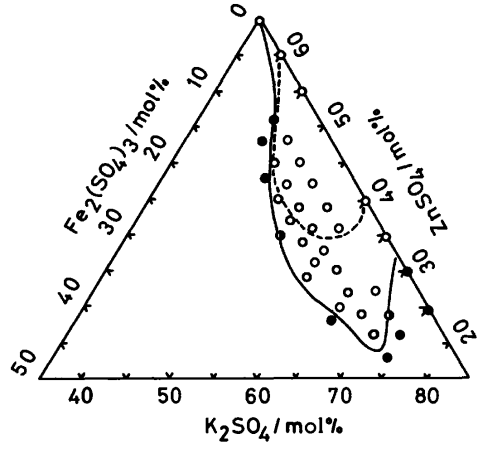

Fig. 1. Glass-forming region for the K_2SO_4–$ZnSO_4$–$Fe_2(SO_4)_3$ system.

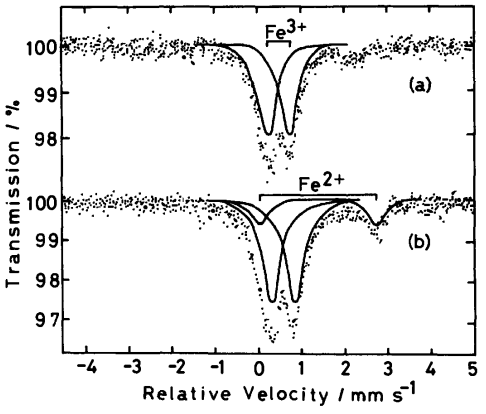

Fig. 2. Mössbauer spectra of $47K_2SO_4 \cdot 45ZnSO_4 \cdot 8Fe_2(SO_4)_3$ glass. (a): At room temperature (296 K), (b): at 78 K.

shown for comparison. Table 1 demonstrates that the isomer shift and the quadrupole splitting show drastic and gradual decreases when the K_2SO_4 content increases. On the other hand, linewidth shows a gradual increase with the increase in the K_2SO_4 content. The magnitude of the linewidth is larger than that of the ordinary crystalline compounds, which is usually smaller than ca. 0.4 mm s^{-1} in the case of ^{57}Fe-Mössbauer spectroscopy. (Compare to the linewidth of the anhydrous $Fe_2(SO_4)_3$ shown in Table 1.) The absorption peak with large linewidth is ascribed to the increased irregularities in the interatomic bond length and bond angle. Figure 3 shows the drastic decrease in the isomer shift with an increase in the K_2SO_4 content. The drastic change in the isomer shift corresponds to a gradual change in the coordination number of Fe^{3+} from six to four. The isomer shifts of Fe^{3+} with octahedral symmetry are known to be larger than ca. 0.4 mm s^{-1}.[7-14] On the other hand, the isomer shifts are usually smaller than ca. 0.4 mm s^{-1} in the case of tetrahedral Fe^{3+} ions.[7-14] In the several Mössbauer studies of oxide and halide glasses[7-18] performed until now by the authors, the coordination number of iron or tin has shown single values even if the composition changes. The change in the coordination number of iron from six to four shown in Fig. 3 is, therefore, considered to be a very rare case. It is speculated from Fig. 3 that the coordination number of iron is essentially six when the K_2SO_4 content is lower than about 60 mol% in the case of K_2SO_4–$ZnSO_4$–$Fe_2(SO_4)_3$ glasses containing 8 mol% $Fe_2(SO_4)_3$. In such glasses, Fe^{3+} ions are considered to be present at the substitutional sites of Zn^{2+} ions which are reported to be octahedrally surrounded by six oxygen atoms originating from six SO_4^{2-} tetrahedra.[2-6] On the other hand, the Fe^{3+} ions in the ternary K_2SO_4–$ZnSO_4$–$Fe_2(SO_4)_3$ glasses are speculated to occupy tetrahedral sites surrounded by four oxygen atoms when the K_2SO_4 content is higher than 60 mol%. The four oxygen atoms in these glasses will be provided by four SO_4^{2-} ions. Within the authors' knowledge, the four-fold coordinated metal ions are not observed in the $ZnSO_4$-based glasses until now, and most of the transition metal ions have been considered to occupy the octahedral sites at the substitutional sites of Zn^{2+} ions.[5,6] In the binary or ternary K_2SO_4–$ZnSO_4$ glasses, by the way, the increase in the K_2SO_4 content is known to result in decreases in density and ionic field strength of the glasses.[2-4] A decrease in the density seems to suggest the prolonged intermolecular distance between SO_4^{2-} ions. In such a condition, the interatomic distance between iron and the neighboring oxygen atom will also be prolonged, because every Fe^{3+} ion is considered to be present at the vacant sites (voids) surrounded by six or four SO_4^{2-} ions. The gradual increase in the interatomic distance between the iron and the oxygen will reduce the crystal field strength, and the coordination number of iron will gradually decrease from six to four with increasing K_2SO_4 content. The isomer shift of anhydrous $Fe_2(SO_4)_3$ used for the sample preparation (Table 1) is typical of the octahedral Fe^{3+} ion with high ionicity, and is in good agreement with the published data for the ionic crystals containing iron.[27,28]

The gradual change in the coordination number of iron from six to four seems to be correlated with the

Table 1. Mössbauer Parameters for K_2SO_4–$ZnSO_4$–$Fe_2(SO_4)_3$ Glasses Measured at 296 K

Composition	δ[a] / mm s^{-1}	Δ[b] / mm s^{-1}	Γ[c] / mm s^{-1}
$47K_2SO_4 \cdot 45ZnSO_4 \cdot 8Fe_2(SO_4)_3$	0.45	0.57	0.44
$50K_2SO_4 \cdot 42ZnSO_4 \cdot 8Fe_2(SO_4)_3$	0.42	0.54	0.48
$53K_2SO_4 \cdot 39ZnSO_4 \cdot 8Fe_2(SO_4)_3$	0.41	0.51	0.43
$56K_2SO_4 \cdot 36ZnSO_4 \cdot 8Fe_2(SO_4)_3$	0.43	0.56	0.48
$59K_2SO_4 \cdot 33ZnSO_4 \cdot 8Fe_2(SO_4)_3$	0.39	0.49	0.45
$62K_2SO_4 \cdot 30ZnSO_4 \cdot 8Fe_2(SO_4)_3$	0.29	0.45	0.51
$65K_2SO_4 \cdot 27ZnSO_4 \cdot 8Fe_2(SO_4)_3$	0.32	0.49	0.55
$68K_2SO_4 \cdot 24ZnSO_4 \cdot 8Fe_2(SO_4)_3$	0.27	0.30	0.56
$71K_2SO_4 \cdot 21ZnSO_4 \cdot 8Fe_2(SO_4)_3$	0.25	0.33	0.53
$Fe_2(SO_4)_3$	0.48	0.24	0.37

a) Isomer shift. b) Quadrupole splitting. c) Linewidth.

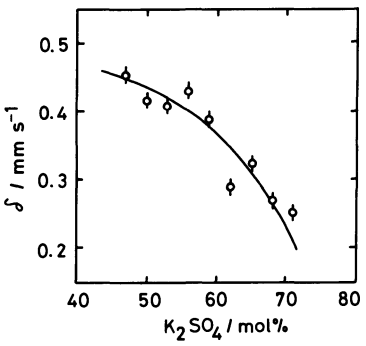

Fig. 3. Change in the isomer shift of Fe^{3+} with K_2SO_4 content of the K_2SO_4–$ZnSO_4$–$Fe_2(SO_4)_3$ glasses.

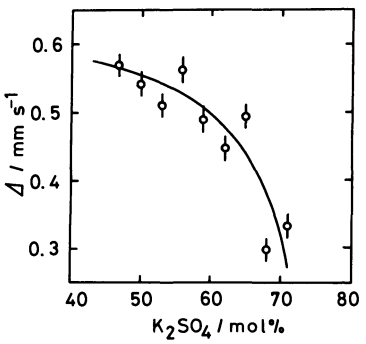

Fig. 4. Change in the quadrupole splitting of Fe^{3+} with K_2SO_4 content of the K_2SO_4–$ZnSO_4$–$Fe_2(SO_4)_3$ glasses.

composition dependency of the quadrupole splitting. This is shown in Fig. 4, from which it is seen that the quadrupole splitting decreases drastically with increasing K_2SO_4 content. Very small quadrupole splittings (0.30 and 0.33 mm s^{-1}) are observed when the K_2SO_4 content is close to 70 mol%; the quadrupole splittings are smaller than the linewidths of the corresponding absorptions, i.e., 0.56 and 0.53 mm s^{-1} in the cases of the glasses with the K_2SO_4 contents of 68 and 71 mol%, respectively. From the distinct decrease in the quadrupole splitting for the higher K_2SO_4-content glasses (Fig. 4), it is concluded that the symmetry around the Fe^{3+} ion increases with increasing K_2SO_4 content. (Each Fe^{3+} ion has a symmetric electron configuration of $3d^5$ in the outer-most orbital, and therefore only the electric field gradient caused by the neighboring atoms or ions, i.e., oxygen atoms in the present study, will be the primary origin of the quadrupole splitting.) The gradual decrease in the quadrupole splitting with increasing K_2SO_4 content therefore suggests that the symmetry around the Fe^{3+} ion is higher when surrounded by four SO_4^{2-} ions than when surrounded by six SO_4^{2-} ions. It is seen from Table 1 that the quadrupole splitting for the anhydrous $Fe_2(SO_4)_3$ is smaller than those for the ternary K_2SO_4–$ZnSO_4$–$Fe_2(SO_4)_3$ glasses. The very small quadrupole splitting for the Fe^{3+} ion is in agreement with the published data,[27,28] and reflects the nearly cubic symmetry. All the Mössbauer parameters for the anhydrous $Fe_2(SO_4)_3$ shown in Table 1 therefore suggest that the local environment of iron in the ternary K_2SO_4–$ZnSO_4$–$Fe_2(SO_4)_3$ glasses is quite different from that of iron in the anhydrous $Fe_2(SO_4)_3$ used for the preparation.

The composition dependency of the glass transition temperature (T_g), obtained from DTA measurements of the ternary K_2SO_4–$ZnSO_4$–$Fe_2(SO_4)_3$ glasses, is shown in Fig. 5. It is obvious from Fig. 5 that the T_g shows a distinct composition dependency similar to that of the isomer shift shown in Fig. 3. The gradual decrease in the T_g with an increase in the K_2SO_4 content suggests that the strength of the chemical bond between metal ions (K^+, Zn^{2+}, and Fe^{3+}) and

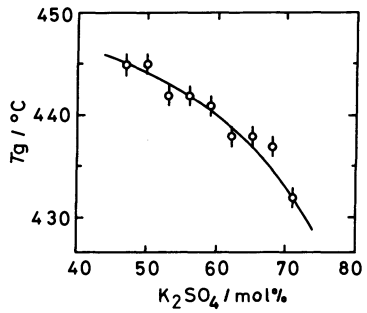

Fig. 5. Change in the glass transition temperature (T_g) with K_2SO_4 content of the K_2SO_4–$ZnSO_4$–$Fe_2(SO_4)_3$ glasses.

SO_4^{2-} ions becomes weakened when the fraction of the K_2SO_4 content increases. This is ascribed to the increased intermolecular distance between SO_4^{2-} ions and to the increased interatomic distance between the metal ions and the SO_4^{2-} ions, as described above. The increased intermolecular and interatomic distances are assumed from the decrease in the density observed in the binary K_2SO_4–$ZnSO_4$ or ternary K_2SO_4–Na_2SO_4–$ZnSO_4$ glasses when the K_2SO_4 content increases.[2-4] (The interatomic distance between the sulfur atom and the four oxygen atoms constituting a pseudospherical SO_4^{2-} ion is considered not to be changed even if the composition is changed.)

Mössbauer measurements of a ternary K_2SO_4–$ZnSO_4$–$Fe_2(SO_4)_3$ glass, at various temperatures lower than room temperature, were also performed to know the nature of the chemical bonds between metal ions and SO_4^{2-} ions and between two SO_4^{2-} ions. Measurements of Mössbauer spectra at low temperatures have already been performed on germanate[15,16] and BaF_2–ZrF_4–FeF_2[18] glasses, and some useful information on the intermolecular force constant has been obtained by the authors. The intermolecular force constant (θ^2M) is expressed by

$$\theta^2M = 3E^2/kc^2(-\mathrm{d}\ln f/\mathrm{d}T)^{-1}, \quad (1)$$

where E and f are transition energy (14.4 keV in the case of ^{57}Fe-Mössbauer spectroscopy) and recoil-free fraction in the Mössbauer spectrum, respectively. In the Eq. 1, k and c are Boltzmann constant and the velocity of light, respectively. It is easily understood from Eq. 1 that the value of θ^2M, in which θ is so-called Debye temperature and M is the mass of Mössbauer nucleus, can be obtained by dividing $3E^2/kc^2$, i.e., 7.76×10^3 in the present study, with the slope of the straight line obtained in the $\ln f$ vs. temperature (T) plot. In the present study, an absorption area (A) is plotted instead of the recoil-free fraction f, because $\mathrm{d}\ln f/\mathrm{d}T$ can be approximated by $\mathrm{d}\ln A/\mathrm{d}T$ when a very thin sample is used.

Mössbauer spectrum of $47K_2SO_4\cdot45ZnSO_4\cdot8Fe_2(SO_4)_3$ glass at lower temperatures consists of two quadrupole doublets, as is also shown in Fig. 2b, due to Fe^{3+} and Fe^{2+} ions. At lower temperatures, the relative absorption area of the Fe^{2+} peak proved to be somewhat higher than that at room temperature. For example, the absorption area amounts to 17.5% at 78 K (Fig. 2b), showing a gradual decrease with increasing temperature. The formation of Fe^{2+} species is probably due to an electron transfer from a part of SO_4^{2-} ions, which are considered to be thermally decomposed into SO_2 and O_2 during the fusion, to the Fe^{3+} ions. All the Mössbauer parameters for the $47K_2SO_4\cdot45ZnSO_4\cdot8Fe_2(SO_4)_3$ glass, obtained at lower temperatures, are summarized in Table 2. It is obvious from Table 2 that the isomer shift and the quadrupole splitting of the Fe^{3+} absorptions show

Table 2. Mössbauer Parameters of $47K_2SO_4 \cdot 45ZnSO_4 \cdot 8Fe_2(SO_4)_3$ Glass Measured at Lower Temperatures

Temperature / K	Fe^{3+}			Fe^{2+}		
	δ[a] / mm s^{-1}	Δ[b] / mm s^{-1}	Γ[c] / mm s^{-1}	δ[a] / mm s^{-1}	Δ[b] / mm s^{-1}	Γ[c] / mm s^{-1}
78	0.54	0.62	0.50	1.34	2.69	0.43
104	0.54	0.61	0.51	1.34	2.73	0.45
140	0.53	0.60	0.50	1.30	2.62	0.45
167	0.51	0.59	0.51	1.28	2.52	0.49
200	0.49	0.59	0.50	1.27	2.41	0.52
230	0.48	0.58	0.50	1.24	2.39	0.55
252	0.47	0.58	0.51	1.22	2.43	0.48
284	0.44	0.57	0.47	1.17	2.24	0.47

a) Isomer shift. b) Quadrupole splitting. c) Linewidth.

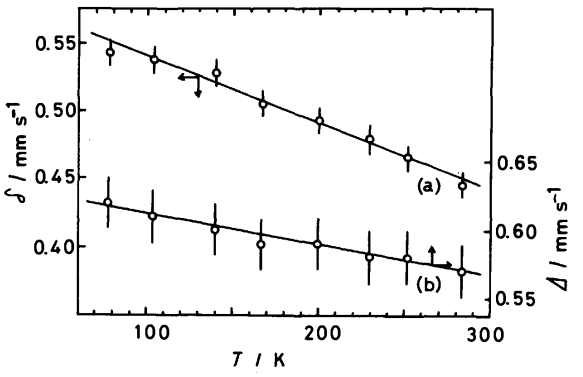

Fig. 6. Changes in the isomer shift(a) and quadrupole splitting(b) of Fe^{3+} in the $47K_2SO_4 \cdot 45ZnSO_4 \cdot 8Fe_2(SO_4)_3$ glass with temperature.

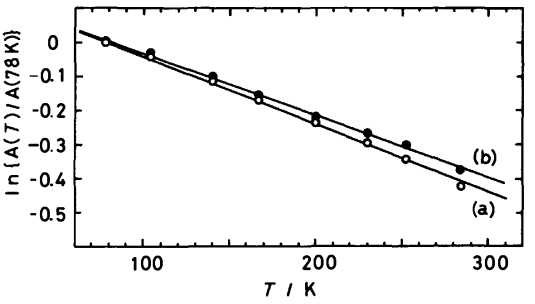

Fig. 7. Changes in the absorption area for the $47K_2SO_4 \cdot 45ZnSO_4 \cdot 8Fe_2(SO_4)_3$ glass with temperature. (a): Fe^{3+} plus Fe^{2+}, (b): only Fe^{3+}.

distinct decreases when the temperature increases. This is illustrated graphically in Fig. 6, from which it is seen that both Mössbauer parameters show linear relationships with temperature. These results indicate that no structural change, such as a phase transition observed in a BaF_2–ZrF_4–FeF_2 glass,[18] occurs in the ternary K_2SO_4–$ZnSO_4$–$Fe_2(SO_4)_3$ glass within the temperature region ranging from 78 to 284 K. In the case of the BaF_2–ZrF_4–FeF_2 glass,[18] the corresponding plots of isomer shift and quadrupole splitting vs. temperature were found to be individually composed of two straight lines crossed with each other at the phase transition temperature of 225 K. Changes in the isomer shift and the quadrupole splitting of the Fe^{2+} absorptions are not graphically shown in the present study because they have large experimental errors. However, they also have a tendency to decrease almost linearly with increasing temperature.

Change in the absorption area with temperature is shown in Fig. 7, where the absorption area of Fe^{3+} plus Fe^{2+} (Fig. 7a) and that of only Fe^{3+} (Fig. 7b) are plotted separately. It is obvious from Fig. 7a and b that the absorption area shows a linear relationship with temperature. The linear correlationship between $\ln A$ and T suggests that a Debye model can be applied to the so-called lattice dynamic study of the K_2SO_4–$ZnSO_4$–$Fe_2(SO_4)_3$ glass, and that no structural change occurs within the temperature range of 78 to 284 K. This is consistent with the results for the isomer shift and the quadrupole splitting described above. In Fig. 7, each absorption area is normalized by the absorption area at 78 K. From the slope of the straight line shown in Fig. 7a, θ^2M value proved to be 3.9×10^6. This is almost the same as the θ^2M value of 4.3×10^6 obtained from the corresponding plot of the absorption area of only Fe^{3+} ions (Fig. 7b). Anyhow, these values are larger than the representative values ($1-3\times10^6$) reported for the monomer or polymer compounds[29] of which chemical bond is known to be essentially covalent. The θ^2M value is known to reflect the degrees of bridging and packing as well as the nature of the chemical bonds of several crystalline and non-crystalline compounds.[15,16,18,29] Considering the experimental results together with the structural model proposed for binary K_2SO_4–$ZnSO_4$ or ternary K_2SO_4–Na_2SO_4–$ZnSO_4$ glasses, that the glasses consist of random close packing of pseudospherical SO_4^{2-} ions,[2-4] the θ^2M values obtained in the present study seem to reflect the essentially ionic nature of the chemical bonds between metal ions and SO_4^{2-} ions and between two SO_4^{2-} ions. It seems that the θ^2M values obtained for the $47K_2SO_4 \cdot 45ZnSO_4 \cdot 8Fe_2(SO_4)_3$ glass in the present study are a little smaller than those for the representative ionic compounds such as $BaSnO_3$ and SnO_2, of which θ^2M values are estimated to be 22.4×10^6 and 8.9×10^6, respectively.[15] This is probably due to the difference in the degree of packing effect. ($BaSnO_3$ and SnO_2 are known to be rigid ionic crystals of perovskite- and rutile-type structures, respectively.) Mössbauer studies of several germanate glasses[15,16] containing 2 mol% SnO_2 revealed that the θ^2M value has a close correlationship with the composition of glass, ranging from 6.2×10^6 to 8.7×10^6. In the germanate glasses,[15,16] tin (IV) proved to be ionically present at the interstitial sites of the three-dimensional network composed of GeO_4 and GeO_6 units. In the case of $25BaF_2 \cdot 65ZrF_4 \cdot 10FeF_2$ glass,[18] the θ^2M value showed a drastic change from

6.9×10^6 to 1.9×10^6 at the phase transition temperature described above. In the ZrF_4 -based glass,[18] iron(III) proved to be ionically present at the interstitial sites of one- or two-dimensional zigzag chains composed of ZrF_6 octahedra. Judging from all the experimental results discussed in the present paper, the chemical bonds between metal ions (K^+, Zn^{2+}, and Fe^{3+}) and SO_4^{2-} ions and between two SO_4^{2-} ions are concluded to be essentially ionic. The K_2SO_4–$ZnSO_4$–$Fe_2(SO_4)_3$ glasses are therefore concluded to be composed of random close packing of pseudospherical SO_4^{2-} ions. Potassium, zinc, and iron ions are considered to be ionically present at the vacant sites (voids) made by the pseudospherical SO_4^{2-} ions.

The authors are grateful to Misses Setsuko Saruwatari and Maori Horiuchi for their kind help in the experiments. One of the authors (TN) is grateful to the Itoh Science Foundation for the financial support.

References

1) N. J. Kreidl, "Inorganic Glass-Forming Systems," in "Glass: Science and Technology," ed by D. R. Uhlmann and N. J. Kreidl, Academic Press, New York and London (1983), Vol. 1, Chap. 3.
2) P. S. L. Narasimham and K. J. Rao, *J. Non-Cryst. Solids*, **27**, 225 (1978).
3) H. G. K. Sundar and K. J. Rao, *J. Chem. Soc., Faraday Trans. 1*, **76**, 1617 (1980).
4) H. G. K. Sundar, B. G. Rao, and K. J. Rao, *Phys. Chem. Glasses*, **23**, 90 (1982).
5) C. S. Sunandana and K. V. R. G. Sharma, *Proc. XIV Int. Congr. Glass, India*, **1986**, 170.
6) H. G. K. Sundar and K. J. Rao, *J. Non-Cryst. Solids*, **50**, 137 (1982).
7) T. Nishida and Y. Takashima, *J. Non-Cryst. Solids*, **37**, 37 (1980).
8) T. Nishida, T. Shiotsuki, and Y. Takashima, *J. Non-Cryst. Solids*, **41**, 161 (1980).
9) T. Nishida, T. Hirai, and Y. Takashima, *J. Non-Cryst. Solids*, **43**, 221 (1981).
10) T. Nishida, T. Hirai, and Y. Takashima, *Phys. Chem. Glasses*, **22**, 94 (1981).
11) T. Nishida, T. Hirai, and Y. Takashima, *Bull. Chem. Soc. Jpn.*, **54**, 3735 (1981).
12) T. Nishida, T. Shiotsuki, and Y. Takashima, *J. Non-Cryst. Solids*, **43**, 115 (1981).
13) T. Nishida, T. Shiotsuki, and Y. Takashima, *J. Non-Cryst. Solids*, **43**, 123 (1981).
14) T. Nishida, Y. Miyamoto, and Y. Takashima, *Bull. Chem. Soc. Jpn.*, **56**, 439 (1983).
15) T. Nishida, M. Katada, and Y. Takashima, *Bull. Chem. Soc. Jpn.*, **57**, 3566 (1984).
16) T. Nishida, M. Katada, and Y. Takashima, *Bull. Chem. Soc. Jpn.*, **58**, 1745 (1985).
17) T. Nishida, A. Nakamura, and Y. Takashima, *Chem. Lett.*, **1984**, 1683.
18) T. Nishida, T. Nonaka, and Y. Takashima, *Bull. Chem. Soc. Jpn.*, **58**, 2255 (1985).
19) R. M. Almeida and J. D. Mackenzie, *J. Chem. Phys.*, **74**, 5954 (1981).
20) E. N. Boulos and N. J. Kreidl, *J. Am. Ceram. Soc.*, **54**, 368 (1971).
21) J. L. Piguet and J. E. Shelby, *J. Am. Ceram. Soc.*, **68**, 450 (1985).
22) J. E. Shelby, *J. Am. Ceram. Soc.*, **57**, 436 (1974).
23) J. E. Shelby, *J. Appl. Phys.*, **46**, 193 (1975).
24) A. Ishii and K. Akawa, *Rep. Res. Lab. Asahi Glass Co.*, **15**, 1 (1965).
25) C. Angell, *J. Am. Ceram. Soc.*, **48**, 540 (1965).
26) V. Kolesova, *Fiz. Khim. Stekla*, **1**, 290 (1975).
27) Y. Haven and R. E. Noftle, *J. Chem. Phys.*, **67**, 2825 (1977).
28) G. J. Long, "A Mössbauer Effect and Magnetic Study of $Fe_2(SO_4)_3$ and $Fe_2(MoO_4)_3$, Two L-Type Ferrimagnets," in "Chemical Mössbauer Spectroscopy," ed by R. H. Herber, Plenum Press, New York and London (1984), Chap. IV.
29) S. Matsubara, M. Katada, K. Sato, I. Motoyama, and H. Sano, *J. Phys. (Paris), Colloq. C2*, **40**, 363 (1979).

 © 1986 The Chemical Society of Japan Bull. Chem. Soc. Jpn., 59, 2795—2799 (1986)

Binuclear Metal Complexes. 58.[1] Synthesis and Properties of Mixed-Valence Diiron(III,IV) Complexes of Salen Analogs with Pendant Thioether Group

Hisashi Ōkawa,* Kaoru Horiuchi, Wakako Kanda, Hiroki Oshio,† and Sigeo Kida†

Department of Chemistry, Faculty of Science, Kyushu University, Hakozaki, Higashiku, Fukuoka 812

(Received May 6, 1986)

Iron complexes of the composition $[Fe_2(L)_2O]PF_6$ have been obtained with *N,N'*-disalicylidene-2-methyl-4-(1-methylethylthio)-1,2-butanediamine (H_2L^1) and *N,N'*-disalicylidene-2-methyl-4-ethylthio-1,2-butanediamine (H_2L^2). They were characterized as mixed-valence diiron(III,IV) complexes composed of high-spin iron(III) and low-spin iron(IV). Cryomagnetic measurements demonstrated the operation of an antiferromangetic spin-exchange interaction ($J=-12.3--13.9\,cm^{-1}$) between the Fe^{III} and Fe^{IV} ions. ESR signals at liquid nitrogen temperature ($g=4.03$ and 2.00) were reasonably attributed to the ground spin state ($S_T=3/2$) in the spin-coupled dimer. In the Mössbauer spectra two quadrupole splitting doublets due to iron(III) and iron(IV) were observed. The complexes were discussed in comparison with mixed-valence complexes of *N,N'*-disalicylideneethylenediamine (H_2salen), $[Fe_2(salen)_2O]X$, composed of high-spin iron(III) and high-spin iron(IV).

It is worthwhile to design pentadentate ligands consisting of a planar unsaturated tetradentate system and an axial base, because such a pentacoordinate environment is often seen at the active site of metalloenzymes such as hemoglobin[2] and myoglobin.[3] For this purpose there have been synthesized some pentadentate salen analogs (H_2salen=*N,N'*-disalicylideneethylenediamine) possessing a pyridyl,[4] hydroxyphenyl,[5] methoxyphenyl,[5] or alkylthio group[6,7] as the pendant group. Salen analogs with thioether pendant group were recently synthesized in our laboratory.[6] These ligands formed pentacoordinate cobalt(II) complexes with the thioether sulfur at the axial site under nitrogen atmosphere while hexacoordinate O_2-adducts in the presence of molecular oxygen. In this study we have synthesized iron complexes of salen analogs, *N,N'*-disalicylidene-2-methyl-4-(1-methylethylthio)-1,2-butanediamine (H_2L^1) and *N,N'*-disalicylidene-2-methyl-4-ethylthio-1,2-butanediamine (H_2L^2) (see Fig. 1). The objects of this study are to characterize the complexes and to elucidate the sulfur coordination effect on the property of the complexes. A similar ligand, (*S*)-*N,N'*-disalicylidene-4-methylthio-1,2-butanediamine, was prepared by Amundsen et al.[7] However, they found no evidence of thioether coordination in its iron(III) complex.

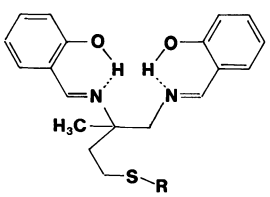

Fig. 1. Chemical structure of ligands: R=*i*-C_3H_7, H_2L^1; R=C_2H_5, H_2L^2.

Experimental

Preparation. The synthesis of H_2L^1 is described in the previous paper.[6] H_2L^2 was prepared in this study in nearly the same way as that of H_2L^1 except for the use of 4-ethylthio-2-butanone instead of 4-(1-methylethylthio)-2-butanone as the starting material.

Iron complexes were obtained as follows. Iron(II) sulfate heptahydrate (1×10^{-3} mole) and the ligand (1×10^{-3} mole) were dissolved in ethanol (50 cm^3), and the mixture was heated at 80 °C for 30 min. To this was added NH_4PF_6 (2×10^{-3} mole), and the mixture was heated for 3 h with stirring. Insoluble materials were separated by filtration, and the solvent was evaporated to dryness. The residue was dissolved in dichloromethane, and the solution was allowed to stand for one week. The crude product thus obtained was dissolved in dichloromethane and reprecipitated by adding ether to this solution. This operation was repeated five times to give brown microcrystals.

$[Fe_2(L^1)_2O]PF_6$, yield ca. 90 mg. Found: C, 50.81; H, 5.04; N, 5.40%. Calcd for $C_{44}F_6Fe_2H_{52}N_4O_5PS_2$; C, 50.92; H, 5.05; N, 5.40%.

$[Fe_2(L^2)_2O]PF_6$, yield ca. 70 mg. Found: C, 49.98; H, 4.91; N, 5.66%. Calcd for $C_{42}F_6Fe_2H_{48}N_4O_5PS_2$: C, 49.96; H, 4.79; N, 5.55%.

Physical Measurements. Infrared spectra were obtained on a Hitachi-Parkin-Elmer 225 grating IR spectrometer on KBr disks. Electronic spectra were recorded on a Shimadzu MPS-5000 spectrometer. Magnetic susceptibilities were measured by the Faraday method in the range 80—300 K. The apparatus was calibrated using $Hg[Co(NCS)_4]$.[8] Diamagnetic corrections were carried out using Pascal's constants.[9] Cyclic voltammograms and differential pulse polarograms were recorded on a Yanagimoto P-1000 voltammetric analyzer in freshly distilled dichloromethane. The measurements were carried out with a three-electrode

† Present address: Coordination Chemistry Laboratories, Institute for Molecular Science, Okazaki National Research Instiutes, Myodaiji, Okazaki 444.

cell equipped with a glassy-carbon working electrode, a platinum-coil auxiliary electrode, and a calomel electrode as the reference electrode. Tetrabutylammonium perchlorate (0.1 mol dm^{-3}) was added as the supporting electrolyte. All the potentials were normalized by the use of ferrocene as an internal standard.[10] ESR spectra (X-band) were recorded on a JEOL JES-FE-3X instrument on powder samples at room temperature and liquid nitrogen temperature. Mössbauer spectra were measured with a constant-acceleration spectrometer (Ausin Science Associates) using a cobalt 57 source diffused into palladium foil. All the spectra were fitted to the Lorentzian line shape using the least-squares method. The velocity scale was normalized with respect to the center of the spectrum of metallic iron at 297 K.

Results and Discussion

Analytical results satisfactorily coincided with the formula $[Fe_2(L)_2O]PF_6$, which suggested the formation of oxo-bridged mixed-valence diiron(III,IV) complexes.

The effective magnetic moments (μ_{eff} per metal ion) for the L^1- and L^2-complexes were 4.28 and 4.36 BM, respectively. As the temperature was lowered to the liquid nitrogen temperature, the moments decreased to 3.45 and 3.58 BM, respectively. The temperature-dependence of the magnetic moments is presumably due to an antiferromagnetic spin-exchange interaction through the oxo-bridge but not due to other effects such as spin-crossover phenomenon.

For analyzing the magnetism of the complexes, a spin Hamiltonian for an isotropic exchange interaction for a dimer ($\mathcal{H}=-2J\hat{S}_1\cdot\hat{S}_2$) was adopted, where J is the exchange integral and $\hat{S}_1$ and $\hat{S}_2$ are the spin operators for metals 1 and 2, respectively. Magnetic susceptibility equation for the case $Fe^{III}(S=5/2)$-$Fe^{IV}(S=2)$ have been derived by Wojciechowski as follows:[11]

$$\chi_M = \frac{Ng^2\beta^2}{4kT} \times \frac{165\exp(-24J/kT)+84\exp(-15J/kT)+35\exp(-8J/kT)+10\exp(-3J/kT)+1}{5\exp(-24J/kT)+4\exp(-15J/kT)+3\exp(-8J/kT)+2\exp(-3J/kT)+1} + N\alpha$$

With this equation Wollmann and Hendrickson well explained the magnetisms of their mixed-valence diiron(III,IV) complexes, $[Fe_2(salen)_2O]X$, which is structurally similar to the present complexes. When this equation was applied to the present complexes, however, very poor fits to the experimental data were obtained.

It is noted that the magnetic moments for the L^1- and L^2-complexes are considerably lower than that of $[Fe_2(salen)_2O]PF_6$ at room temperature (≈4.7 BM at 300 K), but are higher than that of $[Fe_2(salen)_2O]PF_6$ at liquid nitrogen temperature (≈3.0 BM at 78 K). This suggests that for the present complexes the highest total-spin quantum number is smaller than that ($S_T=9/2$) for $Fe^{III}(S=5/2)$-$Fe^{IV}(S=2)$ and the lowest total-spin quantum number is larger than that ($S_T=1/2$) for $Fe^{III}(S=5/2)$-$Fe^{IV}(S=2)$. Such a situation occurs only when either of the iron(III) or iron(IV) is in low-spin state. Therefore, magnetic simulations were attempted with the susceptibility equations for $Fe^{III}(S=5/2)$-$Fe^{IV}(S=1)$ and $Fe^{III}(S=1/2)$-$Fe^{IV}(S=2)$, together with those for $Fe^{III}(S=3/2)$-$Fe^{IV}(S=2)$, $Fe^{III}(S=3/2)$-$Fe^{IV}(S=1)$, $Fe^{III}(S=1/2)$-$Fe^{IV}(S=2)$, and $Fe^{III}(S=1/2)$-$Fe^{IV}(S=1)$. As the result, only the equation for the $Fe^{III}(S=5/2)$-$Fe^{IV}(S=1)$ case,

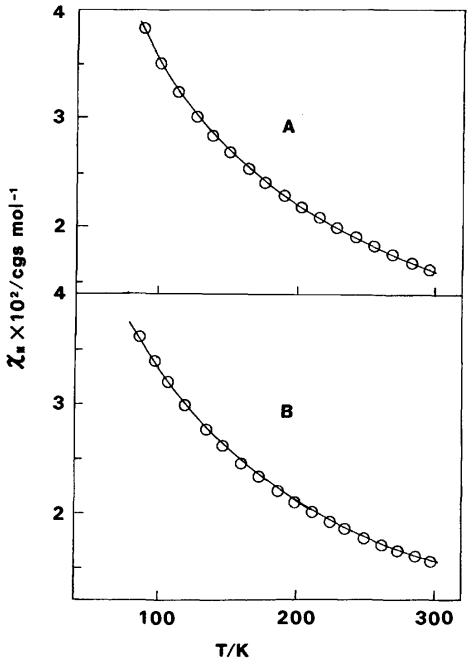

Fig. 2. Temperature-variations of magnetic susceptibility of $[Fe_2(L^1)_2O]PF_6$ (A) and $[Fe_2(L^2)_2O]PF_6$ (B). Solid curves are drawn based on the equation for the spin-coupled (S=5/2)-(S=1) system (see text), with the paramenters $J=-12.3$ cm^{-1} and $g=2.01$ for A and $J=-13.9$ cm^{-1} and $g=2.00$ for B.

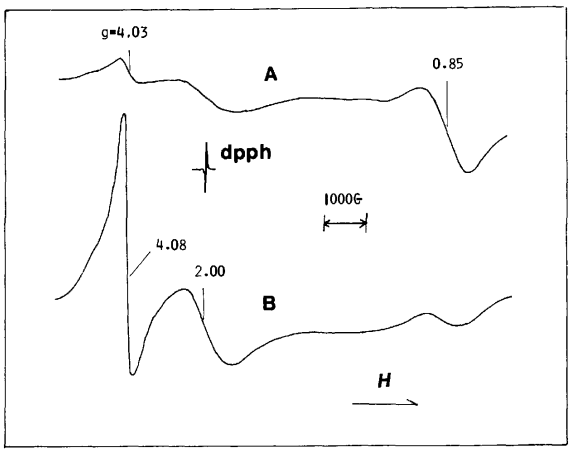

Fig. 3. X-band ESR spectra of $[Fe_2(L^1)_2O]PF_6$ at room temperature (trace A) and at liquid nitrogen temperature (trace B).

$$\chi_M = \frac{Ng^2\beta^2}{4kT} \times \frac{84\exp(-12J/kT)+35\exp(-5J/kT)+10}{4\exp(-12J/kT)+3\exp(-5J/kT)+2} + N\alpha,$$

could reasonably explain the temperature variation of magnetic susceptibilities for the L^1- and L^2-complexes as shown in Fig. 2. The magnetic parameters obtained by best-fit technique are $J=-12.3\,cm^{-1}$ and $g=2.01$ for the L^1-complex and $J=-13.9\,cm^{-1}$ and $g=2.00$ for the L^2-complex; the temperature-independent paramagnetism $N\alpha$ being assumed to be zero in this simulation.

Thus, magnetic investigations demonstrate the presence of low-spin iron(IV) in the present complexes. It must be emphasized that the complexes $[Fe_2(salen)_2O]X$ involve high-spin iron(IV).[12] The low-spin state of the iron(IV) in $[Fe_2(L)_2O]PF_6$ presumably results from the coordination of the pendant thioether sulfur to the metal ion. On the other hand, it is unclear at present whether the sulfur coordination to the iron(III) occurs or not in these complexes.

X-band ESR spectra of the L^1-complex were obtained on powder sample at room temperature and liquid nitrogen temperature (Fig. 3). The spectrum at room temperature (trace A) exhibits three signals at $g=4.03$, 2.00, and 0.85. At liquid nitrogen temperature (trace B) the $g=0.85$ signal practically disappeared, whereas the $g\approx4.0$ and 2.0 signals increased their intensities. It is likely that the $g=4.08$ and 2.00 signals in trace B are due to the ground spin state and the $g=0.85$ signal in trace A is due to one of the excited spin states of the mixed-valence diiron(III,IV) complex. The low temperature spectrum (trace B) can be reasonably interpreted in terms of the total-spin ground state ($S_T=3/2$) of the spin-coupled $Fe^{III}(S=5/2)$-$Fe^{IV}(S=1)$ dmer; the $g=2.00$ and 4.08 signals being attributed to the $g_{//}$ and $g_{\perp}$ components of the $(+1/2\leftrightarrow-1/2)$ transition, respectively. The signal due to the $(+3/2\leftrightarrow+1/2)$ and $(-1/2\leftrightarrow-3/2)$ transitions are not observed probably because of a large zero-field splitting owing to the low molecular symmetry and the spin-orbit coupling interaction. Therefore, the ESR spectral result also strongly supports the presence of low-spin iron(IV) in $[Fe_2(L)_2O]PF_6$. In contrast to this, for $[Fe_2(salen)_2O]X$ only a broad signal with a line width of $\approx$650 G has been observed near $g=2.0$.[12]

Cyclic voltammogram (CV) and differential pulse polarogram (DPP) for the L^1-complex are shown in Fig. 4. The CV and DPP both showed two reduction waves at -0.40 and -1.58 V. The L^2-complex also showed two reduction waves at -0.56 and -1.52 V. For analyzing the electrochemical behaviors of the present complexes, the electrochemical data for $[Fe(salen)]_2O$[13] seemed helpful. In our measurements, this complex showed one reduction wave at -1.55 V, attributable to the process $Fe^{III}Fe^{III}/Fe^{II}Fe^{III}$.[13] Notably this potential well corresponds to the second reduction potential for $[Fe_2(L)_2O]PF_6$. Thus, we may assign the second wave to the $Fe^{III}Fe^{III}/Fe^{II}Fe^{III}$ process and the first wave to the $Fe^{III}Fe^{IV}/Fe^{III}Fe^{III}$ process. Electrochemical results, therefore, support the fact that $[Fe_2(L)_2O]PF_6$ are mixed-valence diiron(III,IV) complexes.

The ^{57}Fe Mössbauer spectra of the L^1-complex were obtained at 296, 80, and 15 K. The spectra were practically independent of temperature. The spectrum at 80 K is shown in Fig. 5. The spectrum consists of two doublets of closely similar isomer shifts and quadrupole splittings, implying the presence of two kinds of iron, i.e., Fe^{III} and Fe^{IV}. The spectrum was analyzed by computer technique into four peaks with nearly equal intensity and half-band width (Fig. 5). We tentatively assigned the peaks 1 and 3 to the iron(IV) and the peaks 2 and 4 to the iron(III). Another pairing (1 and 4; 2 and 3) is also possible, but our assignment is based on the general concept that

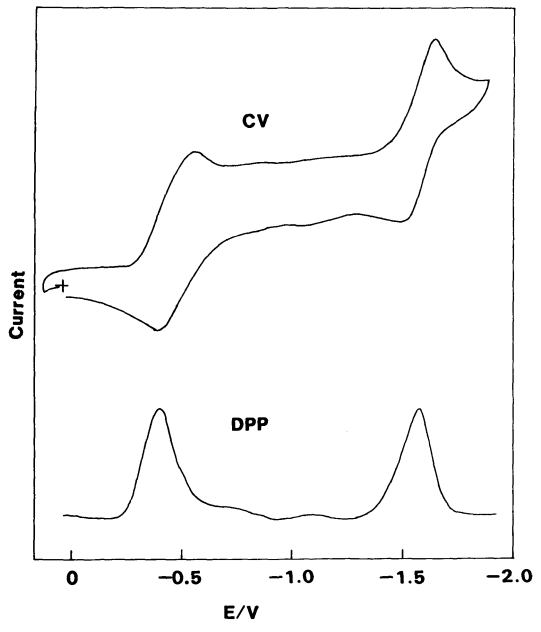

Fig. 4. Cyclic voltammogram and differential pulse polarogram of $[Fe_2(L^1)_2)]PF_6$: concd $=1.02\times10^{-3}$ M (1 mol dm^{-3}); scan rate $=0.01$ V s^{-1} for both CV and DPP; in CH_2Cl_2.

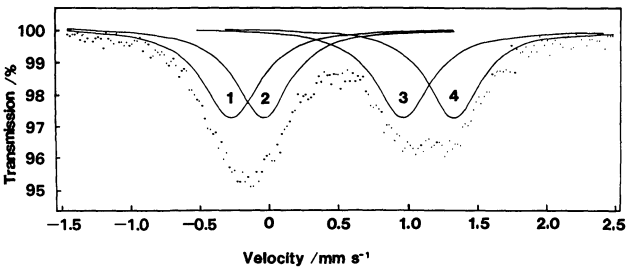

Fig. 5. Mössbauer spectrum of $[Fe_2(L^1)_2O]PF_6$ at 80K.

Table 1. Mössbauer Parameters for $[Fe_2(L^1)_2O]PF_6$

T/K	Fe^{III}		Fe^{IV}	
	δ	Δ	δ	Δ
295	0.463	1.478	0.310	1.054
80	0.647	1.399	0.343	1.256
15	0.673	1.368	0.344	1.296

δ, isomer shift/mm s^{-1}; Δ, quadrupole splitting/mm s^{-1}.

the isomer shift for iron(IV) is smaller than that for iron(III). The results are given in Table 1. The isomer shift and quadrupole splitting assigned to the high-spin iron(III) are quite reasonable. On the other hand, Mössbauer spectral data for low-spin iron(IV) are very limited.[14-16] Of these complexes, tris(disubstituted dithiocarbamato)iron(IV) tetrafluoroborates show isomer shift falling in the range 0.45—0.57 mm s^{-1} relative to sodium pentacyanonitrosylferrate(III).[16] Thus the isomer shift assigned to the iron(IV) of the L^1-complex does not seem unreasonable.

From the above results, it is concluded that the $[Fe_2(L)_2O]PF_6$ complexes are mixed-valence diiron(III,IV) complexes, probably bridged by oxo group. Oxo-bridged diiron(III,III) complexes have been characterized by an intense IR band in the 800—900 cm^{-1} region, which is assigned to the asymmetric Fe–O–Fe stretching mode.[17] The present complexes do not show such a band in the 800—900 cm^{-1} region. We also examined far IR spectra of the complexes, in comparison with the spectra of the nickel(II) complexes of H_2L^1 and H_2L^2. However, any characteristic IR band was seen for the diiron complexes. It should be noted that $[Fe_2(salen)_2O]X$[12] also showed no IR band attributable to the Fe–O–Fe stretch. As suggested by Wollmann and Hendrickson,[12] it is probable that the Fe–O–Fe band of $[Fe_2(L)_2O]PF_6$ is weakened in intensity, shifted in position, and obscured by ligand vibrations.

Mixed-valence complexes generally show intervalence transfer bands in visible or near IR region.[18-20] The electronic spectra of $[Fe_2(L)_2O]PF_6$ in dichloromethane showed absorption bands at 260, 320, 420, and 500 nm. The spectrum of the L^1-complex is given in Fig. 6. No absorption was found in the near IR region. Despite the different spin state of iron(IV), $[Fe_2(L)_2O]PF_6$ showed an absorption spectrum very similar to that of $[Fe_2(salen)_2O]PF_6$.[12] By the inspection of the spectra of $[Fe(salen)]_2O$ and $[Fe_2(salen)_2O]X$, Wollmann and Hendrickson tentatively assigned the ≈500 nm band of the latter complex to the intervalence transfer band.[12] According to Hush,[20] the energy of an intervalence transfer band should vary with $(1/n^2)$-$(1/D)$ of solvent, where n is the refractive index and D the dielectric constant of solvent. The electronic spectra of $[Fe_2(L)_2O]PF_6$ were

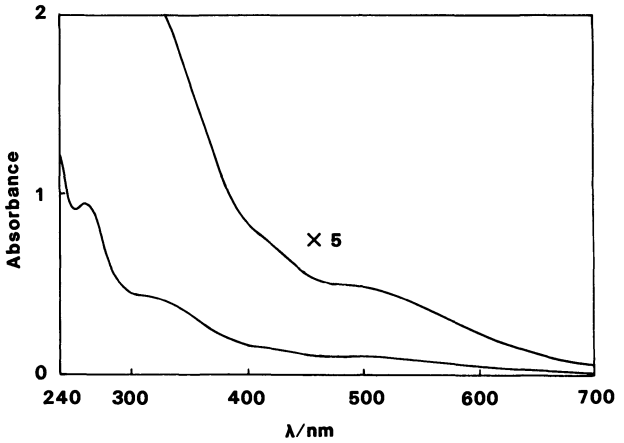

Fig. 6. Electronic spectra of $[Fe_2(L^1)_2O]PF_6$: concd= 2.377×10^{-5} M; in CH_2Cl_2.

measured in various solvents (CH_2Cl_2, $CHCl_3$, CH_3CN, CH_3OH, dioxane), and it was found that the frequency of the ≈500 nm band was practically independent of the solvents. Probably this band is not intervalence transfer band but a charge transfer band from the phenolic oxygen to the iron(III) or iron(IV). Since intramolecular electron transfer from high-spin iron(III) to low-spin iron(IV) should produce the mixed-valence state composed of intermediate-spin iron(III) and high-spin iron(IV), the intervalence transfer band for $[Fe_2(L)_2O]PF_6$ must be located at a higher energy region than 500 nm and concealed by more intense absorptions.

References

1) Part 57: M. Handa, Z. J. Zhong, M. Mikuriya, H. Ōkawa, and S. Kida, *J. Chem. Soc., Dalton Trans*, in press.
2) S. E. V. Phillips, *Nature (London)*, **273**, 247 (1978).
3) B. Shaanan, *Nature (London)*, **296**, 683 (1982).
4) J. P. Collman, H. Takaya, B. Winkler, L. Libit, S. S. Koon, G. A. Rodley, and W. T. Robinson, *J. Am. Chem. Soc.*, **95**, 1656 (1973).
5) W. Kanda, H. Ōkawa, and S. Kida, *Bull. Chem. Soc. Jpn.*, **56**, 3268 (1983).
6) K. Nakamoto, H. Oshio, H. Ōkawa, W. Kanda, K. Horiuchi, and S. Kida, *Inorg. Chim. Acta*, **108**, 231 (1985).
7) A. R. Amundsen, J. Whelan, and B. Bosnich, *Inorg. Chem.*, **18**, 206 (1979).
8) B. N. Figgis and R. S. Nyholm, *J. Chem. Soc.*, **1959**, 331.
9) F. E. Mabbs and D. J. Machin, "Magnetism and Transition Metal Complexes," Chapman and Hall, London (1973), p. 5.
10) R. R. Gagne, C. A. Koval, and G. C. Lisensky, *Inorg. Chem.*, **19**, 2854 (1980).
11) W. Wojciechowski, *Inorg. Chem. Acta*, **1**, 324 (1967).
12) R. G. Wollmann and D. N. Hendrickson, *Inorg. Chem.*, **16**, 723 (1977).
13) S. E. Wenk and F. A. Schultz, *J. Electroanal. Chem.*, **101**, 89 (1979).
14) G. Simonneaux, W. F. Scholz, C. A. Reed, and G.

Lang, *Biochim. Biophys. Acta*, **716**, 1 (1982).
15) J. T. Groves, R. Quinn, T. J. McMurry, M. Nakamura, G. Lang, and B. Boso, *J. Am. Chem. Soc.*, **107**, 354 (1985).
16) E. A. Pasek and D. K. Straub, *Inorg. Chem.*, **11**, 259 (1972).
17) K. S. Murray, *Coord. Chem. Rev.*, **12**, 1 (1974).
18) M. B. Robin and P. Day, *Adv Inorg. Chem. Radiochem.*, **10**, 247 (1967).
19) G. C. Allen and N. S. Hush, *Prog. Inorg. Chem.*, **8**, 357 (1967).
20) N. S. Hush, *Prog. Inorg. Chem.*, **8**, 391 (1967).

X-Ray and Neutron-Diffraction Study of a Stereoselectively Deuterated Benzyl *t*-Butyl Sulfoxide. A Revised Configuration Assignment for the Chiral Carbon Atom Due to Isotopic Substitution

Yoichi Iitaka,* Akiko Itai, Nobuo Tomioka, Yoshio Kodama,†
Kazuo Ichikawa,† Ken Nishihata,† Motohiro Nishio,†,*
Masashi Izumi,†† and Kenji Doi††
Faculty of Pharmaceutical Sciences, The University of Tokyo, Hongo, Bunkyo-ku, Tokyo 113
†Central Research Laboratories, Meiji Seika Kaisha Ltd., Morooka-cho, Kohoku-ku, Yokohama 222
††Division of Physics, Japan Atomic Energy Research Institute, Tokai, Ibaraki 319-11
(Received December 10, 1985)

X-Ray analysis of a stereoselectively monodeuterated benzyl *t*-butyl sulfoxide, PhCHDSO-tBu, revealed that the *t*-butyl and phenyl groups are oriented anti to each other in this molecule. Integrated intensities for ten reflections were measured on a two-circle neutron diffractometer and the relative intensity distribution was compared with the calculated neutron structure factors, assuming the atomic parameters obtained by the X-ray analysis. It is concluded that the benzylic hydrogen which is flanked by S-O and *t*-Bu was replaced by deuterium. The results require that the earlier assignment for the relative configuration of PhCHDSO-tBu, should be revised; an important conclusion in view of current discussions of sulfur stereochemistry.

It has been reported that the isotopic exchange and the alkylation of benzyl alkyl sulfoxides, $PhCH_2SO$-Me (**1**) and $PhCH_2SO$-tBu (**2**), proceed via different stereochemical pathways;[1] retention of the configuration for the H-D exchange, and inversion of the configuration for the methylation (Fig. 1). The configuration assignments of the partially deuterated sulfoxides, **1**-*d*[2] and **2**-*d*,[1b] were made by correlating them chemically to optically active benzyl-α-*d* alcohols, the configuration of which has been believed to be established; [(+)-(*S*) and (−)-(*R*)].[3]

The opposite stereochemical outcome for the H-D exchange and the methylation (Fig. 1) is unusual in the current understanding of carbanion chemistry, since electrophilic substitution reactions are more reasonably expected to occur with retention of the intermediate carbanion configuration. In order to examine this point, we prepared crystals of a stereoselectively deuterium-labelled benzyl *t*-butyl sulfoxide (**2**-*d*), and determined the relative disposition of the deuterium atom with respect to the S-O bond by X-ray and neutron diffraction study.

The problem is to know which hydrogen atom (H_{7A} or H_{7B} in Fig. 2) was exchanged by D; it is possible to distinguish the H and D atoms at the benzyl methylene by calculating the structure factors of neutron diffraction which is based on the result of X-ray analysis. Analyses of the crystallographic data revealed that the relative configuration of **2**-*d*, which has been believed to date,[1b,4] should be reversed. This is an important conclusion in view of current discussions of the stereochemistry of sulfoxides.[1,4,5]

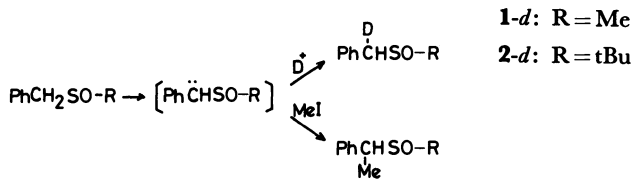

1-*d*: R=Me
2-*d*: R=tBu

Fig. 1.

Experimental

Materials. A solution of benzyl *t*-butyl sulfoxide (**2**, 10 mmol) in dry tetrahydrofuran (100 ml) was treated, under nitrogen at −70°, with a hexane solution of butyllithium (12 mmol). After standing for 5 min, the reaction mixture was treated with deuterium oxide (10 ml), and then diluted with water (50 ml). This was neutralized and extracted with ether (200 ml). The ether layer was washed 3 times with water, dried over $MgSO_4$, and then concentrated to give a crude solid of the monodeuterated product. The solid was crystallized from ligroin. This was again crystallized from ligroin solution by slow cooling. A large crystal of approximate dimensions 4×2.5×0.2 mm was chosen for

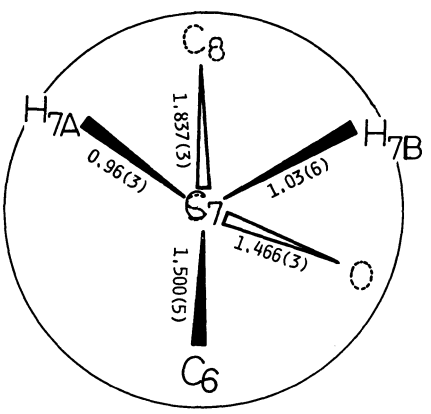

Fig. 2. Newman projection of the compound **2**, viewing along C_7–S axes.

neutron diffraction study. NMR (CCl_4, ppm): 3.64 (1H, s, CHD), 1.25 (9H, s, *t*-Bu), 7.26 (5H, s, Ar).

Crystal Data. Benzyl *t*-butyl sulfoxide, $C_{11}H_{16}OS$, M.W.= 196, Partially-deuterated compound, $C_{11}H_{15}DOS$. Monoclinic, Space group $P2_1/n$, Z=4. For full hydrogen compound, a=14.284(7), b=13.185(7), c=6.015(4) Å, β= 93.83(5)°, U=1130 Å^3, D_{calcd}=1.1508 g cm^{-3}, μ for Cu $K\alpha$ radiation 21.8 cm^{-1}.

X-Ray measurement was carried out using a small crystal of the deuterated compound of approximate dimensions 0.2×0.3×0.1 mm. Intensities were measured on a Philips PW1100 diffractometer using graphite monochromated Cu $K\alpha$ radiation. 2543 Reflections were measured within the 2θ range of 6° through 156°. 466 Reflections were below the 2σ(I) level and regarded as unobserved. A total of 2077 reflections were then used for the structure determination.

The structure was determined by the direct method using MULTAN[6] and refined by the block-diagonal least-squares method to an R value of 0.072. All the 16 hydrogen atoms were found on the difference electron-density map and they were included in the refinement process with isotropic temperature factors.

Results and Discussions

The final atomic parameters are listed in Table 1. The bond lengths and angles are listed in Tables 2 and 3.[7] The values observed in the present molecule are typical of the related compounds. Some relevant torsional angles are listed in Table 4.

Figure 2 illustrates the orientation of the phenyl group (represented by C_6) to the S–O bond and to the *t*-butyl group (represented by C_8). A stereoview of the molecule is shown in Fig. 3. It is clear that the *t*-butyl group is flanked by the two hydrogen atoms and that the *t*-butyl and the phenyl groups are oriented anti to each other.

It is interesting to compare this conformation with those found in the diastereoisomeric pair of 1-phenylethyl *t*-butyl sulfoxides, [(α *R*, *SS*/*SS*, *SR*)- and (α *R*, *SR*/α *S*, *SS*)-**3**], determined by X-ray methods[8] (Fig. 4). In both of these compounds, the *t*-butyl group has been shown to be gauche to the phenyl group and anti to the methyl group (Fig. 4d, e). The conformation of **3** has been shown to be maintained in solutions by NMR (LIS),[9] ORD[8b] and dipole moment measurements[10]; the conclusion was supported by molecular force-field calculations[11].

The conformation of **2** in solution was also studied by various methods. Although the force-field calculations[11] favored a gauche conformation of *t*-butyl and phenyl groups (Fig. 4c), the energy difference between the anti conformer (Fig. 4a) is small. A dipole moment[10] study favored the anti conformation. NMR

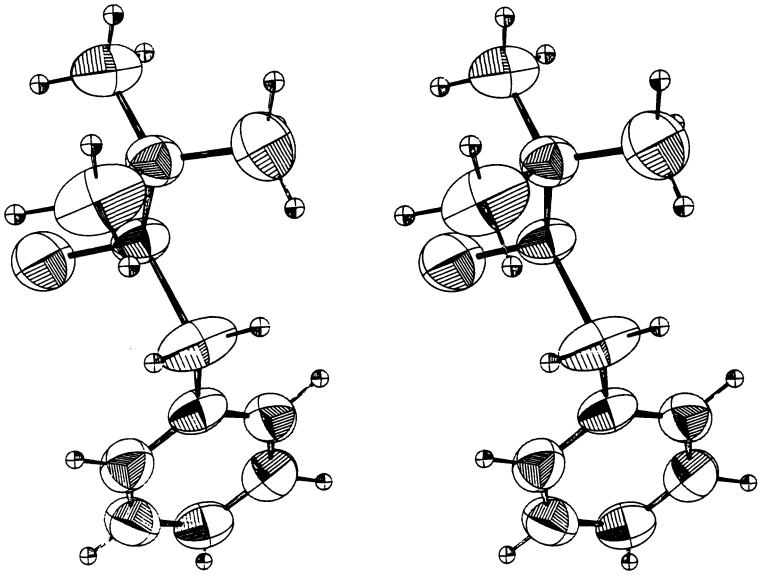

Fig. 3. Stereoview of the molecule **2** drawn by ORTEP.[13]

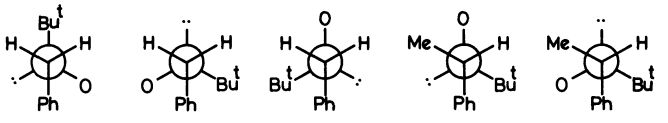

(a) (b) (c) (d) (e)

(αS, *SR*)-**3** (αS,*SS*)-**3**

Fig. 4. Conformations in solution of the compounds **2** and **3** (one of the enantiomers is illustrated).

Table 1. Final Coordinates of Compound **2** with e.s.d's in Parentheses

Equivalent positions

X	Y	Z
$1/2-X$	$1/2+Y$	$1/2-Z$

and their inverted coordinates

No.	Atom	X 10^5	Y 10^5	Z 10^5	B_{eq} A^2
1	S1	24300(4)	43270(5)	28960(11)	4.72(.01)
No.	Atom	X 10^4	Y 10^4	Z 10^4	B_{eq} A^2
2	O1	2208(2)	4173(2)	505(4)	7.85(.05)
3	C1	52(2)	3706(2)	2314(5)	5.76(.04)
4	C2	−629(2)	2964(3)	2403(5)	6.00(.05)
5	C3	−716(2)	2424(2)	4316(6)	5.78(.04)
6	C4	−115(2)	2602(2)	6125(5)	6.04(.05)
7	C5	575(2)	3338(2)	6061(5)	5.52(.04)
8	C6	658(2)	3900(2)	4144(5)	4.92(.04)
9	C7	1369(2)	4737(2)	4115(7)	7.02(.06)
10	C8	3147(2)	5480(2)	3247(4)	4.75(.04)
11	C9	2685(3)	6357(3)	1965(7)	7.99(.07)
12	C10	4060(2)	5217(3)	2234(6)	6.34(.05)
13	C11	3290(3)	5716(4)	5704(7)	8.93(.08)
No.	Atom	X 10^3	Y 10^3	Z 10^3	B_{eq} A^2
14	H1	14(2)	407(2)	104(4)	5.5(0.6)
15	H2	−102(2)	289(2)	121(5)	5.7(0.6)
16	H3	−118(2)	196(2)	433(5)	6.1(0.6)
17	H4	−22(2)	224(2)	767(5)	6.4(0.7)
18	H5	101(2)	346(2)	736(4)	5.6(0.6)
19	H7A	155(2)	501(2)	557(5)	6.9(0.7)
20	H7B	118(2)	532(2)	302(5)	7.0(0.7)
21	H9A	206(2)	655(2)	252(5)	6.7(0.7)
22	H9B	313(2)	692(2)	185(5)	7.7(0.8)
23	H9C	256(2)	612(3)	10(5)	8.4(0.8)
24	H10A	432(2)	473(2)	317(4)	5.8(0.6)
25	H10B	394(2)	504(2)	67(4)	5.0(0.5)
26	H10C	450(2)	580(2)	245(5)	5.9(0.6)
27	H11A	357(2)	511(2)	615(5)	6.5(0.6)
28	H11B	384(2)	622(2)	587(5)	6.8(0.7)
29	H11C	268(2)	602(2)	625(5)	6.3(0.6)

$T=\exp\{-2\pi^2(U_{11}h^2a^{*2}+U_{22}k^2b^{*2}+U_{33}l^2c^{*2}+2U_{12}hka^*b^*+2U_{13}hla^*c^*+2U_{23}klb^*c^*)\}$

U_{ij}'s are multiplied by 10^5

No.	Atom	U_{11}	U_{22}	U_{33}	U_{12}	U_{13}	U_{23}
1	S1	4993(33)	5291(34)	7758(43)	−29(22)	1307(30)	−1050(26)

U_{ij}'s are multiplied by 10^4

1	Atom	U_{11}	U_{22}	U_{33}	U_{12}	U_{13}	U_{23}
2	O1	854(16)	1251(20)	876(16)	−248(14)	56(12)	−413(14)
3	C1	751(17)	757(17)	692(15)	57(14)	126(13)	136(13)
4	C2	628(16)	846(19)	796(17)	19(14)	−48(13)	−92(15)
5	C3	607(15)	599(14)	1004(20)	−29(12)	156(14)	−44(14)
6	C4	803(19)	687(17)	819(18)	105(14)	156(15)	128(14)
7	C5	617(15)	775(17)	703(15)	86(13)	26(12)	−72(13)
8	C6	514(12)	528(12)	845(17)	38(10)	191(12)	−76(11)
9	C7	669(17)	608(16)	1438(30)	−105(14)	425(19)	−257(18)
10	C8	545(13)	590(13)	668(14)	−57(10)	35(10)	−84(11)
11	C9	916(24)	661(19)	1495(36)	133(16)	347(23)	265(20)
12	C10	556(15)	837(20)	1027(22)	−76(14)	126(14)	−52(17)
13	C11	998(29)	1533(39)	856(23)	−295(26)	22(20)	−437(23)

Table 1. Continued

No.	Atom	U_{11}
	U_{ij}'s are multiplied by 10^3	
14	H1	70(7)
15	H2	72(8)
16	H3	77(8)
17	H4	81(8)
18	H5	70(8)
19	H7A	87(8)
20	H7B	89(9)
21	H9A	85(8)
22	H9B	97(10)
23	H9C	106(10)
24	H10A	73(8)
25	H10B	63(7)
26	H10C	75(8)
27	H11A	82(8)
28	H11B	86(9)
29	H11C	79(8)

Table 2. Bond Lengths (l/Å)

S1	-O1	1.466(2)
S1	-C7	1.810(4)
S1	-C8	1.837(3)
C1	-C2	1.383(5)
C1	-C6	1.378(4)
C2	-C3	1.366(5)
C3	-C4	1.361(4)
C4	-C5	1.386(4)
C5	-C6	1.382(4)
C6	-C7	1.501(4)
C8	-C9	1.516(5)
C8	-C10	1.516(4)
C8	-C11	1.511(5)
C1	-H1	0.920(26)
C2	-H2	0.887(27)
C3	-H3	0.911(29)
C4	-H4	1.064(30)
C5	-H5	0.980(26)
C7	-H7A	0.964(29)
C7	-H7B	1.033(31)
C9	-H9A	1.002(32)
C9	-H9B	0.983(32)
C9	-H9C	1.166(31)
C10	-H10A	0.912(27)
C10	-H10B	0.973(23)
C10	-H10C	0.994(29)
C11	-H11A	0.923(31)
C11	-H11B	1.027(32)
C11	-H11C	1.035(31)

Table 3. Bond Angles (ϕ/°)

O1	-S1	-C7	107.9(2)
O1	-S1	-C8	108.0(1)
C7	-S1	-C8	100.5(1)
C2	-C1	-C6	120.4(3)
C3	-C2	-C1	120.3(3)
C4	-C3	-C2	119.7(3)
C5	-C4	-C3	120.7(3)
C6	-C5	-C4	120.0(3)
C7	-C6	-C1	121.1(3)
C7	-C6	-C5	120.0(3)
C1	-C6	-C5	118.8(3)
C9	-C8	-S1	110.6(2)
C9	-C8	-C10	109.1(3)
C9	-C8	-C11	111.5(3)
S1	-C8	-C10	104.6(2)
S1	-C8	-C11	108.7(2)
C10	-C8	-C11	112.1(3)
S1	-C7	-C6	111.8(2)

and mechanistic considerations[4b] suggested that this compound takes a folded conformation (Fig. 4b); this conclusion rests, however, on the configuration assignments of the monodeuterated benzyl *t*-butyl sulfoxides (αR, $SS/\alpha S$, SR)- and (αR, $SR/\alpha S$, SS)-**2**-*d*,[1b,4] which is correlated chemically to the optically active benzyl-α-*d* alcohol.[3]

To identify which benzyl hydrogen atom (H_{7A} or H_{7B}) is replaced by deuterium atom, two sets of neutron structure factors were calculated assuming the atomic parameters listed in Table 1; $F_A(hkl)$ based on the model A, in which only H_{7A} is exchanged by D, and $F_B(hkl)$ for model B in which only H_{7B} is exchanged by D. Since the crystal is flattened on (010) plane and it is easier to measure the $h0l$ reflection intensities, ten $h0l$ reflections were chosen having the largest $|F_A|$or$|F_B|$ and the largest $||F_A|-|F_B||$ values. The values are listed in Table 5. Neutron scattering lengths b were taken from the International Tables for X-ray Crystallography III.[12] They were S 0.310, C 0.661, N 0.935, O 0.578, H −0.378, D 0.650 (10^{-12} cm). Integrated intensities for the ten $h0l$ reflections were measured on a two-circle neutron diffractometer at the Japan Atomic Energy Research Institute in Tokai (JAERI). The primary beam was monochromated by a crystal monochromator giving radiation of wavelength 2.338 Å. The observed $|F(h0l)|$ values are normalized to $|F(101)|$ and are listed in Table 5. Inspection of the Table shows that the H–D exchange took place on H_{7B}; the hydrogen atom flanked by S–O and the *t*-butyl groups.

From the above results, we conclude that the configuration assignment of the stereoselectively deuterated sulfoxide (**2**-*d*), reported by Durst et al.,[1b] is in error.

In view of the revised assignment, the paradoxes in the sulfoxide stereochemistry may well be understood. Thus, as expected, the stereochemical pathways for the H–D exchange and the methylation of **2** are the same. A gauche conformation was suggested for **2** (Fig. 4b) by LIS measurements and mechanistic con-

Table 4. Dihedral Angles

	Atom 1=(D1)=Atom	2=(D2)=Atom	3=(D3)=Atom 4	Tau (STD)
O1	=1.466=S1	=1.810=C7	=1.501=C6	69.72(15)
O1	=1.466=S1	=1.837=C8	=1.516=C9	50.95(20)
O1	=1.466=S1	=1.837=C8	=1.516=C10	−66.38(17)
O1	=1.466=S1	=1.837=C8	=1.511=C11	173.62(18)
C7	=1.810=S1	=1.837=C8	=1.516=C9	−61.89(19)
C7	=1.810=S1	=1.837=C8	=1.516=C10	−179.28(15)
C7	=1.810=S1	=1.837=C8	=1.511=C11	60.83(21)
C2	=1.383=C1	=1.378=C6	=1.501=C7	−176.83(20)
C2	=1.383=C1	=1.378=C6	=1.382=C5	0.65(39)
C6	=1.501=C7	=1.810=S1	=1.837=C8	−177.31(21)
C3	=1.366=C2	=1.383=C1	=1.378=C6	1.03(40)
C4	=1.361=C3	=1.366=C2	=1.383=C1	−1.63(40)
C5	=1.386=C4	=1.361=C3	=1.366=C2	1.26(41)
C6	=1.382=C5	=1.386=C4	=1.361=C3	−0.59(38)
C7	=1.501=C6	=1.382=C5	=1.386=C4	176.47(16)
C1	=1.378=C6	=1.382=C5	=1.386=C4	−0.88(35)
S1	=1.810=C7	=1.501=C6	=1.378=C1	−84.78(23)
S1	=1.810=C7	=1.501=C6	=1.382=C5	98.10(20)

Table 5. The Calculated and Observed Values of Structure Factors in Neutron Diffraction, with e.s.d's in Parentheses

	Calculated		Observed
(*hkl*)	$\|F_A\|$	$\|F_B\|$	$\|F_o\|$
101	100	100	100(8.0)
$\bar{7}01$	61	52	54(7.2)
$\bar{8}02$	53	59	61(7.9)
$\bar{4}02$	40	4	9(3.2)
$\bar{3}01$	66	54	73(7.5)
$\bar{1}01$	39	5	7(2.4)
301	1	34	33(5.1)
501	45	62	60(7.3)
701	53	65	50(7.8)
$\bar{2}02$	28	4	0(2.4)

siderations.[4b] With the revised assignment, the solution conformation of **2** is concluded as *t*-Bu/Ph anti (Fig. 4a); this is the conformation found in crystals and is compatible with the results obtained by dipole moment measurements.[10] The alcoholic analogue of **2**, ($PhCH_2CHOH$-tBu),[14] has been shown to have the *t*-Bu/Ph anti conformation in solutions. This, again, is consistent with the above conclusion regarding the solution conformation of **2**.

A question remains, however, as to the origin of the erroneous configuration assignment of **2**-*d*. At present, we do not know whether this arose from the chemical correlation process,[1b] or originated from the absolute configuration assignment of optically active benzyl alcohol.[3]

We wish to thank Professors Shigeru Oae (Okayama College of Science), Atsuyoshi Ohno (Kyoto Univ.), and Ukon Nagai (Mitsubishi Institute of Life Sciences) for useful discussions.

References

1) a) K. Nishihata and M. Nishio, *Chem. Commun.*, **1971**, 958; b) T. Durst, R. Viau, and M. R. McClory, *J. Am. Chem. Soc.*, **93**, 3077 (1971); c) K. Nishihata and M. Nishio, *J. Chem. Soc., Perkin Trans. 2*, **1972**, 1730. In Ref. 1b, a wrong absolute configuration was quoted for optically active **2**-*d*.

2) J. E. Baldwin, R. E. Hackler, and R. M. Scott, *Chem. Commun.*, **1969**, 1415.

3) A. Streitwieser, Jr., J. R. Wolfe, Jr., and W. D. Schaeffer, *Tetrahedron*, **6**, 338 (1959); R. U. Lemieux and J. Howard, *Can. J. Chem.*, **41**, 303 (1963); V. E. Althouse, D. M. Feigl, W. A. Sanderson, and H. S. Mosher, *J. Am. Chem. Soc.*, **88**, 3595 (1966); D. Arigoni and E. L. Eliel, *Top. Stereochem.*, **4**, 127 (1967).

4) a) K. Nishihata and M. Nishio, *Tetrahedron Lett.*, **1972**, 4839; b) **1977**, 2105.

5) M. Nishio, *Chem. Pharm. Bull.*, **17**, 262, 274 (1969); *Chem. Commun.*, **1969**, 560; R. Viau and T. Durst, *J. Am. Chem. Soc.*, **95**, 1346 (1973); M. B. D'Amore and J. I. Brauman, *J. Chem. Soc., Chem. Commun.*, **1973**, 398; J. F. Biellmann and J. J. Vicens, *Tetrahedron Lett.*, **1974**, 2915; **1978**, 467; G. Chassaing, R. Lett, and A. Marquet, *ibid.*, **1978**, 471; S. Oae and N. Kunieda, "The Stereochemistry of Sulfur Compounds," Chap. 3 in "Chemistry of Sulfur Compounds-Reaction Mechanism," ed by S. Oae, Kagaku Dojin (1982); G. Solladie, *Synthesis*, **1980**, 185.

6) G. Germain, P. Main, and M. M. Woolfson, *Acta Crystallog., Sect. A*, **27**, 368 (1971).

7) The list of F_o and F_c may be obtained from one of the authors (Y. K.) upon request.

8) a) Y. Iitaka. Y. Kodama, K. Nishihata, and M. Nishio, *J. Chem. Soc., Chem. Commun.*, **1974**, 389; b) Y. Kodama, K. Nishihata, M. Nishio, and Y. Iitaka, *J. Chem. Soc., Perkin Trans. 2*, **1976**, 1490.

9) Y. Kodama, K. Nishihata, and M. Nishio, *J. Chem. Res.(S)*, **1977**, 102; Y. Kodama, S. Zushi, K. Nishihata, M. Nishio, and J. Uzawa, *J. Chem. Soc., Perkin Trans., 2*, **1980**, 1306.

10) M. Hirota, Y. Takahashi, M. Nishio, and K. Nishihata, *Bull. Chem. Soc. Jpn.*, **51**, 2358 (1978).

11) M. Hirota, T. Sekiya, K. Abe, H. Tashiro, M. Karatsu, M. Nishio, and E. Osawa, *Tetrahedron*, **39**, 3091 (1983).

12) "International Table for X-Ray Crystallography" Kynoch Press, Birmingham (1962) Vol. III, pp. 228—231.

13) C. K. Johnson, *ORTEP.*, Oak Ridge National Report ORNL-3794.

14) S. Zushi, Y. Kodama, Y. Fukuda, K. Nishihata, M. Nishio, M. Hirota, and J. Uzawa, *Bull. Chem. Soc. Jpn.*, **54**, 2113 (1981).

 © 1986 The Chemical Society of Japan Bull. Chem. Soc. Jpn., 59, 2807—2810 (1986)

Photochemical Reactions of Aryltriethylgermanes and Diethyldiphenylgermane

Michio KOBAYASHI* and Masanori KOBAYASHI
Department of Chemistry, Faculty of Science, Tokyo Metropolitan University, Setagaya-ku, Tokyo 158
(Received January 16, 1986)

Aryltriethylgermanes and diethyldiphenylgermane were found to split easily to generate germyl radicals by irradiation with a medium-pressure mercury lamp in hexane or cyclohexane. The germyl free radicals produced reacted with hydrocarbon radicals generated from the solvent by hydrogen abstraction either by recombination or by disproportionation.

There have been only a few studies[1] of the photochemical reaction of organogermanium compounds. We have investigated the photochemical behavior of several alkylarylgermanes and found that germanium–carbon bonds are cleaved readily by irradiation to generate germyl free radicals and the results will be described in this paper.

Results and Discussion

Photochemical reactions of three aryltriethylgermanes, Et_3GeAr (**1a**, Ar=Ph; **1b**, Ar=*p*-$CH_3C_6H_4$; **1c**, Ar=*p*-$NO_2C_6H_4$) and diethyldiphenylgermane Et_2GePh_2 (**1d**) were examined.

When a solution of **1a** (or **1b**) in hexane was irradiated under an argon atmosphere with a 450 W medium-pressure mercury lamp through a Vycor filter for 20—30 min, about 40% of the substrate was photolyzed. Hexyltriethylgermanes, Et_3GeR (**2a**, R=*n*-C_6H_{13}; **2b**, R=$CH(CH_3)C_4H_9$; **2c**, R=$CH(C_2H_5)$-C_3H_7(*n*-), hexaethyldigermane (**3**), benzene (or toluene in the case of **1b**) and dodecanes (**5**) were identified as products. Structure assignment was performed by GC–MS, IR, ^1H NMR, and ^{13}C NMR. The yields were estimated by GLC and HPLC. The results are summarized in Table 1.

$$\underset{\mathbf{1}}{Et_3GeAr} \xrightarrow[\text{hexane}]{250\text{ nm}} \underset{\mathbf{2}}{Et_3GeR} + \underset{\mathbf{3}}{(Et_3Ge)_2} + \underset{\mathbf{4}}{ArH} + \underset{\mathbf{5}}{C_{12}H_{26}}$$

a: Ar=Ph
b: Ar=*p*-Tol

In the case of **1a**, some polymers were also formed. The relative yields of **2b** and **2c** could not be determined, since these two products have almost the same GLC retention time.

Formation of hexaethyldigermane (**3**), hexyltriethylgermanes (**2a—c**) and large amounts of benzene (or toluene) indicates that the aryl–germanium bond, not the alkyl–germanium bond, splits in the photolysis as is shown in the following reaction sequences.

$$Et_3GeAr \longrightarrow Et_3Ge\cdot + Ar\cdot$$
$$RH + Ar\cdot \longrightarrow R\cdot + ArH$$
$$Et_3Ge\cdot + R\cdot \longrightarrow Et_3GeR$$
$$2Et_3Ge\cdot \longrightarrow (Et_3Ge)_2$$
RH=hexane

In the first step, the aryl–Ge bond is cleaved. Since the germyl free radical is known[1,2] to possess little ability to abstract hydrogen atom from alkanes, the aryl radical must play a major role to abstract a hydrogen atom from the solvent (hexane or cyclohexane). Hexyl radicals may recombine with a germyl radical to give triethylhexylgermanes or with other hexyl radicals to form a dodecane mixture. The germyl radical can also dimerize to hexaethyldigermane.

The ratio **2a**/(**2b**+**2c**) after statistical correction (10/18 with **1a**; 4/15 with **1b**) evaluates the relative reactivity for primary to secondary C–H toward hydrogen abstraction from a hexane by a phenyl radical. Relative selectivities of hydrogen abstraction from primary, secondary, and tertiary C–H by a phenyl radical generated thermally from phenylazotriphenylmethane was reported as 1 : 9.3 : 44 at 60 °C.[3] Compared with the latter figures, the selectivities of the aryl radical from **1a** or **1b** are about 1/2 to 1/4.

The reason for the preferential cleavage of the aryl–Ge bond instead of the alkyl–Ge bond may be explained as follows. The UV absorption maximum of aryltriethylgermane (**1a**, **1b**) lies near the 257 nm region, which corresponds to a ^1L_a transition of the

Table 1. Photolysis of Aryltriethylgermanes

Ar	Irr. time / min	Products (yield/%)[a]					Recovered **1**/%
		2a	**2b** **2c**	**3**	**4**	**5**	
Ph (**1a**)	20	5	6	13	78	Trace	49
p-$CH_3C_6H_4$ (**1b**)	30	12	30	57	97	Trace	65

a) Yields were based on the starting materials consumed.

benzene pi orbital. Since in the present photochemical experiments, a medium pressure mercury lamp was used as the light source, 253.7 nm radiation with highest intensity is considered to excite the aryl pi electron of the arylgermanes, accompanied by a weakening of the aryl–Ge bond, thus subsequently resulting in its splitting before the energy transfer to an ethyl–Ge bond occurred effectively.

The effects of the triplet sensitizer was examined using acetophenone. When **1b** was irradiated in hexane for 30 min in the presence of acetophenone (0.1 mol/mol of **1b**), the extent of the photolysis of **1b** was found to be about 7%, much lower than that in the absence of acetophenone. This finding suggests that the photolysis proceeds via a singlet excited state. The decrease of the extent of the photolysis may be attributed to the quenching effects of acetophenone.

The photochemical behavior of *p*-nitrophenyltriethylgermane (**1c**) was different from those of **1a** and **1b**. Irradiation of **1c** in cyclohexane for 15 min (or in benzene for 5 h) with a 450 W medium-pressure mercury lamp through a Vycor filter under an argon atmosphere resulted in the formation of a complex mixture. Small amounts of phenyltriethylgermane (**1a**) (3%), *p*-hydroxyphenyltriethylgermane (14%) and cyclohexanone (11%) were detected among the products. (the yields in parenthesis are conversion yields. 78% of **1c** was recovered). No cyclohexyltriethylgermane was detected. These findings suggest that the nitro group of **1c** suffers photolysis more readily than the carbon–germanium bond.

When diethyldiphenylgermane (**1d**) was irradiated in hexane for 30 min under argon with radiation of wavelength >250 nm, the main products were diethylphenylgermane (**6a**), diethylphenylgermylhexanes (**7a—c**), benzene, and dodecanes (**5**).

$$\underset{\textbf{1d}}{Et_2GePh_2} \xrightarrow[\text{hexane}]{} \underset{\textbf{6a}\ 23\%}{Et_2GeH(Ph)} + \underset{\textbf{7a};\ R=\text{hexyl}\ 12\%;\ \textbf{7b};\ R=\text{1-methylpentyl}\ 26\%;\ \textbf{7c};\ R=\text{1-ethylbutyl}\ 5\%}{Et_2GeR(Ph)} + \underset{133\%}{PhH}$$

$$+ \underset{\text{trace}}{C_{12}H_{26}} + \underset{77\%}{\text{recovered } \textbf{1d}}$$

(yields are conversion yields)

The remarkable difference of the photochemical behavior of **1d** from those of **1a** or **1b** is the production of hydrogermane (**6a**) and no formation of digermane $(Et_2GePh)_2$. In order to confirm that the hydrogen atom of hydrogermane **6a** originated from the solvent hexane, **1d** was irradiated in cyclohexane-d_{12}. Formation of deuteriogermane, Et_2GePhD (**6b**) was confirmed by GC-MS. As mentioned before, the germyl free radical is believed to lack ability to abstract a hydrogen atom from alkanes.[1,2] The only known examples of hydrogen abstraction by a germyl radical are the cases of the reaction in toluene or 2-propanol as solvent.[2] Formation of **6a** may be explained by a disproportionation reaction between a diethylphenylgermyl radical and hexyl radicals (hexyl, 1-methylpentyl and 1-ethylbutyl radical), as shown in the following equation:

$$Et_2\dot{G}ePh + \cdot C_6H_{13} \longrightarrow \underset{\textbf{6a}}{Et_2GeH(Ph)} + C_6H_{12}$$

Formation of a saturated and an unsaturated compound by a disproportionation reaction between two free radicals is well known among aliphatic hydrocarbon radicals. To confirm the formation of hexenes required in the disproportionation, bromine was added to the solvent recovered by distillation. After being kept for a few h in the dark, the mixture was concentrated and the residue subjected to GC–MS analysis. Formation of 6% of a dibromohexane mixture (1,2-, 2,3-, and 3,4-) was observed, thus verifying the formation of hexenes in the photoreaction of diethyldiphenylgermane in hexane. When the photolysis of **1d** was carried out in cyclohexane, formation of hydrogermane **6a** (23%) and cyclohexene (10% as dibromocyclohexane) was detected. The absence of digermane among the products in the photolysis of **1d** may be attributed to the steric hindrance toward recombination of the diethylphenylgermyl radical.

The possibility of the photochemical generation of germylene (**9**) from **1d** was also examined. If two geminal phenyl groups of **1d** split off from germanium atom simultaneously, diethylgermylene and biphenyl would be formed. When **1d** was photolyzed in the presence of 2,3-dimethyl-1,3-butadiene, (which is known as a good scavenger for germylene,[4]) in cyclohexane as solvent, only a trace of 1,1-diethyl-3,4-dimethyl-3-germacyclopentene and 0.5—1.0% of biphenyl were detected by GC–MS. This finding indicates that the Ph–Ge bond splitting occurs stepwise in the photolysis of **1d**.

$$Et_2GePh_2 \begin{cases} \longrightarrow Et_2\dot{G}ePh + Ph\cdot \\ \not\longrightarrow Et_2Ge: + Ph\text{-}Ph \end{cases}$$

9

In this reaction, no products which should arise from the addition of diethylphenylgermyl radical to diene were detected by GC-MS. The main products in this experiment were those from the recombination of a cyclohexyl radical and a germyl radical as in the absence of 2,3-dimethyl-1,3-butadiene.

Experimental

GLC and HPLC were performed on a Hitachi 163 Gas Chromatograph with SE-30 10% coated column (2 m) and a Hitachi 655 Liquid Chromatograph with Hitachi 638-

41 UV monitor. IR and UV spectra were recorded on a Hitachi 260-10 IR spectrophotometer and Hitachi 220 A UV spectrophotometer respectively. The proton NMR spectra were recorded at 60 MHz using a JNM-PMX-60 spectrometer with TMS as an internal standard in $CDCl_3$ or C_6D_6. Mass spectra were measured with a JMS-DX300 high resolution mass spectrometer.

Materials. *p*-Tolyltriethylgermane (**1b**),[5] *p*-nitrophenyltriethylgermane (**1c**),[6] diethyldiphenylgermane (**1d**)[7] and hexaethyldigermane (**3**)[8] were prepared according to the literature.

Phenyltriethylgermane (1a): Bromotriethylgermane (5.00 g; 20.9 mmol) in benzene (20 cm^3) was added to the phenylmagnesium bromide prepared from bromobenzene (4.00 g; 25.0 mmol) and magnesium (0.60 g ; 25.0 m gatom) in ether (30 cm^3). The mixture was refluxed for 3.5 h, then hydrolyzed with ice and dilute hydrochloric acid. After the usual work-up and purification by silica-gel column chromatography with hexane as an eluent and fractional distillation, **1a** was obtained in 94% yield. Bp 77—78 °C/1 mmHg (1 mmHg=133.322 Pa)(lit,[5] 117—118 °C/13.5 mmHg). UV; λ_{max}=257 nm, ε=230. ^{1}H NMR δ=0.97—1.03 (m, 15H), 7.34—7.37 (m, 5H). MS; *m/z* 238 (M^+).

Hexyltriethylgermane (2a): Bromotriethylgermane (2.00 g; 8.34 mmol) in tetrahydrofuran (50 cm^3) was added to hexylmagnesium bromide prepared from 1-bromohexane (2.75 g; 16.7 mmol) and magnesium (0.41 g; 16.7 m gatom) in THF (50 cm^3). The reaction mixture was refluxed for 17 h. After the usual work-up, the product was purified by silica-gel column chromatography and fractional distillation. Yield 97%. Bp 60 °C/0.7 mmHg (lit, [9] 117 °C/20 mmHg). ^{1}H NMR δ=0.45—1.53 (m, 28H). MS; *m/z* 246 (M^+).

1-Methylpentyltriethylgermane (2b): This compound was synthesized from bromotriethylgermane (4.00 g; 16.7 mmol) and 1-methylpentylmagnesium bromide, prepared from 2-bromohexane (5.15 g; 33.4 mmol), in a similar way as **2a**. Yield 43%. Bp 56—57 °C/0.5 mmHg. MS; *m/z* 246 (M^+): Exact MS; Found, 217.0995, Calcd for $C_{10}H_{23}Ge$ ($M^+-C_2H_5$) 217.1011. ^{1}H NMR; δ=0.40—1.67 (m, 28H).

1-Ethylbutyltriethylgermane (2c) was synthesized from bromotriethylgermane and 3-bromohexane in a similar way as **2b**. Yield 59%. Bp 62—64 °C/1.05 mmHg. MS; *m/z* 246 (M^+): Exact MS; Found, 217.1004, Calcd for $C_{10}H_{23}Ge$ ($M^+-C_2H_5$) 217.1011. ^{1}H NMR; δ=0.43—1.67 (m, 28H).

Bromodiethylphenylgermane (8): Bromine (5.61 g; 35.1 mmol) in 1,2-dibromoethane (10 cm^3) was added to diethyldiphenylgermane (10.0 g; 35.1 mmol) in 1,2-dibromoethane (100 cm^3) at 80—85 °C. The mixture was refluxed for 2 h, then the solvent was distilled off under reduced pressure. The residue was purified by fractional distillation. Yield 80%. Bp 110—112 °C/4 mmHg (lit,[10] 141 °C/18 mmHg). MS; *m/z* 288 (M^+). ^{1}H NMR; δ=0.85—1.90 (m, 10H), 7.17—7.70 (m, 5H).

Diethylphenylgermane (6a): **8** (2.00 g; 6.95 mmol) in dry ether (10 cm^3) was slowly added to lithium aluminum hydride (0.26 g; 6.95 mmol) in ether (20 cm^3) with stirring and refluxing. The reaction mixture was refluxed for 2 h. The reaction was quenched by slow addition of water with cooling and followed by 3 M sulfuric acid. The organic layer was separated within 10 min and dried over sodium sulfate. After expelling the solvent, the residue was purified by fractional distillation. Yield 83%. Bp 100—102 °C/21 mmHg. MS; *m/z* 210 (M^+). ^{1}H NMR; δ=0.75—1.28 (m, 10H), 4.40—4.63 (m, 1H), 7.03—7.60 (m, 5H). IR (neat); 2007 cm^{-1} (ν_{Ge-H}). Exact MS; *m/z* Found, 210.0548, Calcd for $C_{10}H_{16}{}^{74}Ge$ 210.0462.

1-(Diethylphenylgermyl)hexane (7a): **8** (3.01 g; 10.5 mmol) in THF (50 cm^3) was added to hexylmagnesium bromide prepared from 1-bromohexane (3.44 g; 20.9 mmol) and magnesium (0.51 g; 20.9 m gatom) in THF (100 cm^3). The reaction mixture was refluxed for one night and hydrolyzed with ice and water. The THF layer was separated and the aqueous layer extracted with ether. After the solvent was evaporated, the residue was purified by silica-gel column chromatography and fractional distillation. Yield 48%. Bp 100 °C/0.6 mmHg. MS; *m/z* 265 ($M^+-C_2H_5$): Exact MS; Found, 265.1043, Calcd for $C_{14}H_{23}Ge$ ($M^+-C_2H_5$) 265.1011. ^{1}H NMR; δ=0.63—1.70 (m, 23H), 7.07—7.57 (m, 5H).

2-(Diethylphenylgermyl)hexane (7b): This compound was synthesized from **8** (2.94 g; 10.2 mmol) and 1-methylpentylmagnesium bromide prepared from 2-bromohexane (3.44 g; 20.9 mmol) in a similar way to **7a**. Yield 45%. Bp 95—96 °C/0.55 mmHg. MS; *m/z* 294 (M^+): Exact MS; Found, 265.0978, Calcd for $C_{14}H_{23}Ge$ ($M^+-C_2H_5$) 265.1011. ^{1}H NMR δ=0.67—1.63 (m, 23H), 7.07—7.55 (m, 5H).

3-(Diethylphenylgermyl)hexane (7c) was prepared from **8** (1.60 g; 5.56 mmol) and 1-ethylbutylmagnesium bromide in a similar way to **7a**. Yield 43%. Bp 101 °C/0.85 mmHg. MS; *m/z* 294 (M^+): Exact MS; Found, 265.0964, Calcd for $C_{14}H_{23}Ge$ ($M^+-C_2H_5$), 265.1011. ^{1}H NMR; δ=0.60—1.77 (m, 23H), 7.07—7.57 (m, 5H).

Photolysis: A typical example of the photolysis is described in the case of **1a**. A solution containing 210.7 mg (0.89 mmol) of **1a** in 230 cm^3 hexane was irradiated under an argon atmosphere with a 450 W medium-pressure mercury lamp (Hanovia) through a Vycor filter for 20 min. After the removal of the solvent by distillation, the products were analyzed by GC-MS. Products **2**, **3**, and **5** were identified by comparison of their GLC retention time and mass fragment pattern with those of authentic samples.

Photolysis of 1d in cyclohexane-d_{12}: A solution containing 4.14 mg of **1d** in 0.7 cm^3 of cyclohexane-d_{12} was externally irradiated with a 450 W medium-pressure mercury lamp through a Vycor filter for 30 min. The photolysate was analyzed by GC-MS. Although a parent peak of deuterated germane (**6b**) was not observed, its fragment peaks, *m/z* 182 (**6b**$-C_2H_5$) and 153 (**6b**$-2C_2H_5$) (base peak) were observed with high intensity.

Thanks are due to The Asai Germanium Research Institute for donation of tetrachlorogermane.

References

1) H. Sakurai, "Free Radicals," ed by J. K. Kochi, Wiley-Interscience, New York (1973), Vol. 2, Chap. 25; P. Rivière, M. Rivière-Baudet, and J. Satgé, "Comprehensive Organometallic Chemistry," ed by G. Wilkinson, F. G. A. Stone, and E. W. Abel, Pergamon Press, Oxford (1982), Vol. 2, Chap. 10.

2) P. Rivière, A. Castel, and J. Satgé, *J. Organomet. Chem.*, **212**, 351 (1981).

3) R. F. Bridgan and G. A. Russell, *J. Am. Chem. Soc.*, **85**, 3744 (1963).
4) J. Satgé, M. Massol, and P. Rivière, *J. Organomet. Chem.*, **56**, 1 (1973); M. Schriewer and W. P. Neumann, *J. Am. Chem. Soc.*, **105**, 897 (1983).
5) C. Eaborn and K. C. Pande, *J. Chem. Soc.*, **1960**, 3200.
6) C. Eaborn, K. Leyshon, and K. C. Pande, *J. Chem. Soc.*, **1960**, 3423.
7) E. A. Flood, *J. Am. Chem. Soc.*, **54**, 1663 (1932).
8) E. J. Bulten and J. G. Noltes, *Tetrahedron Lett.*, **1966**, 4389; E. J. Bulten and J. G. Noltes, *J. Organomet. Chem.*, **29**, 397 (1971).
9) N. S. Vyazankin, G. A. Razuvaev, E. N. Gladyshev, and S. P. Korneva, *J. Organomet. Chem.*, **7**, 353 (1967).
10) M. Lesbre, P. Mazerolles, and J. Satgé, "The Organic Compounds of Germanium," Wiley-Interscience, New York (1971), Chap. 5.

 © 1986 The Chemical Society of Japan Bull. Chem. Soc. Jpn., 59, 2811—2818 (1986)

Synthesis and Photolysis of Tricyclo[5.3.1.$0^{2,6}$]undeca-3,9-dien-8-ones and -4,9-dien-8-ones. Formation of Novel Trishomocubanones[1)]

Toshio Ogino* and Kazuyuki Awano*,†
Department of Chemistry, Faculty of Education, Niigata University,
Ikarashi, Niigata 950-21
†Department of Industrial Chemistry, Nagaoka Technical College,
Nishikatagai, Nagaoka 940
(Received February 14, 1986)

A series of 10-substituted tricyclo[5.3.1.$0^{2,6}$]undeca-3,9-dien-8-ones (**6**) and the 4,9-dien-8-one isomers (**7**) were synthesized and photolyzed. Upon irradation, whereas most of the derivatives underwent [2+2] photocyclization to give the corresponding novel trishomocubanones, the methyl and phenyl derivatives of **7** afforded products attributable to intramolecular hydrogen abstraction by the β-carbon of the α,β-unsaturated ketone along with the photocyclization products.

Because of the efficient construction of strained polycyclic molecules and the storage of solar energy, intramolecular photochemical [2+2] cyclizations of bridged dienes or dienones have attracted considerable attention in recent years. In particular, the conversion of dicyclopentadienone (**I**) to bishomocubanone is the best known example of such a reaction.[2)] However, there have been no systematic studies on the photochemistry of the homologous dienones such as **II** or **III**, whose structural feature is very unique from the point of view that they have an allylic system facing to the conjugated enone moiety in the rigid molecule. These compounds are expected to undergo not only [2+2] photocyclization to give novel trishomocubane frameworks but also competitive intramolecular allylic hydrogen abstraction by the excited enones. Only a few examples are known for the photochemical reactions in which intramolecular hydrogen abstraction occurs competitively along with [2+2] photocyclization.[3,4)]

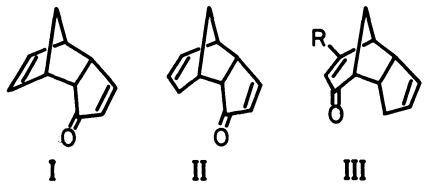

I II III

It seems to us of interest to synthesize the derivatives of **III** (**6a—d**) variously substituted at the β-carbon of the α,β-unsaturated enone and their isomers **7a—d** and to study their photochemical behavior. Details of such a study are reported herewith.

Results and Discussion

Syntheses of 10-Substituted Tricyclo[5.3.1.$0^{2,6}$]undecadienones. Scheme 1 shows the outline of the syntheses for **6a—d** and **7a—d**. The key compounds **6a** and **7a** were first synthesized starting from the diol **1**, which had been prepared by phase-transfer-assisted permanganate oxidation of *endo*-dicyclopentadiene in dichloromethane followed by treatment with an aqueous base.[5)] Since it was difficult to oxidize **1** directly into the α-diketone **5**, the conversion was accomplished in the following manner. The diol (**1**) was partially acetylated with acetic anhydride at room temperature to give an isomeric mixture of the monoacetates **2**. Chromium trioxide oxidation of **2** followed by alkaline hydrolysis of the resulting keto acetates **3** afforded the α-ketol **4** as an isomeric mixture in 60% overall yield from **1**. The conversion of **4** into **5** with conventional oxidizing agents ($FeCl_3$–HCl, $Cu(OAc)_2$–AcOH, and $CuSO_4$–pyridine) failed. However, treatment of **4** with DMSO at 80—90 °C in the presence of P_2O_5[6)] afforded **5** as a single product in 56% yield. The structure of **5** was supported by the spectral characteristics [IR 1770 and 1750 cm^{-1}; UV 475 nm (ε 24)], which are quite similar to those reported for camphorquinone.[7)]

Treatment of **5** with diazomethane in diethyl ether in the presence of a small amount of methanol[8)] gave an isomeric mixture of **6a** and **7a** in a 6 : 4 ratio via ring expansion and subsequent methylation of the resulting β-diketone. The mixture was separated by

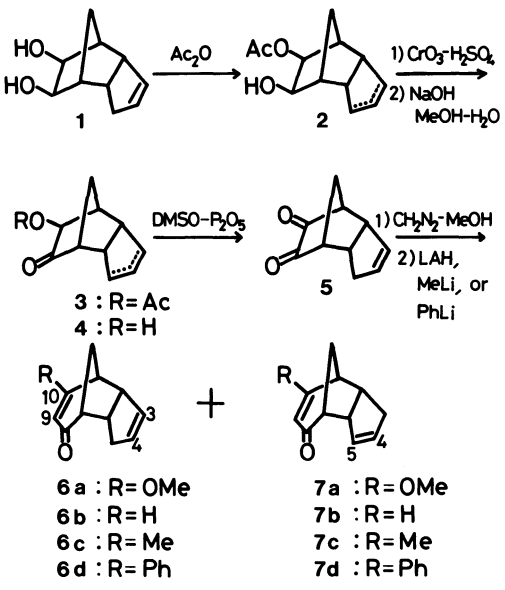

Scheme 1.

preparative GLC or column chromatography on silica gel-$AgNO_3$. The IR (1640 and 1600 cm^{-1} for both **6a** and **7a**) and UV spectra [254 nm (ε 9300) for **6a**; 254 nm (ε 12900) for **7a**] exhibited the characteristic absorptions of α,β-unsaturated β-methoxycyclohexenone.

The assignments of the double-bond position in the cyclopentene rings of **6a** and **7a** were established by NMR studies using $Eu(dpm)_3$ as the shift reagent. The induced shifts determined for the olefinic proton signals are summarized in Table 1. Since the extremely large shift ($\Delta\delta$=5.56 ppm) observed for an olefinic proton of **7a** could be attributed to proximity of this hydrogen to the carbonyl group, **7a** were assigned to the structure having the double bond at C_4–C_5, and hence **6a** to the one having the double bond at C_3–C_4. This was further supported by the structures of the photoproducts of these compounds (vide infra).

The compound **6a** was then converted to **7b** (R=H), **7c** (R=Me), and **7d** (R=Ph) by reactions with LAH, MeLi, and PhLi, respectively, followed by acid treatment. In a similar fashion, **7a** was converted to **6b** (R=H), **6c** (R=Me), and **6d** (R=Ph). The structures of all the new compounds were evidenced by spectroscopic data (see Experimental), and the assignments of the double bond position were also compatible with the results of photolysis as described below.

Photolyses of the Tricyclo[5.3.1.$0^{2,6}$]undecadienones (6a—d and 7a—d). Irradiation of a benzene solution of **6a** in a Pyrex tube gave the [2+2] photocycloaddition product **8a** exclusively. The structure of the product was supported by the IR absorption at 1700 cm^{-1}, which indicated the presence of a six-membered cyclic ketone as expected from the structure of **6a** (but not **7a**), and also by the ^1H NMR spectrum, which was devoid of signals attributable to olefinic protons downfield from the methoxyl signal at δ 3.20.

Table 1. Induced Shifts of the Vinyl Proton Signals by $Eu(dpm)_3$

Compound	Hydrogen	$\Delta\delta^{a)}$ ppm
6a	C_3-H	1.52
	C_4-H	1.52
7a	C_4-H	2.45
	C_5-H	5.56

a) Changes in chemical shift at the molar ratio $Eu(dpm)_3$/substrate = 1 extrapolated from the data observed at the ratio 0—0.18.

Treatment of **8a** with an acid in methanol gave **10**, a novel tetracyclic diketone, whose structure was deduced from the IR bands at 1765 (cyclobutanone) and 1700 cm^{-1} (cyclohexanone), and from the ^1H NMR spectrum (devoid of methoxyl signals).

In a similar fashion, irradiation of **7a** gave an unstable cylization product **9a**, which was more easily transformed into the tetracyclic diketone **11** upon treatment with an acid, or even on standing in a refrigerator overnight, possively due to acidic impurities on the glass wall or in the solvent. The structure of **11** was also deduced from the spectroscopic data [IR absorption at 1735 cm^{-1} (cyclopentanone) and NMR spectrum devoid of methoxyl signal].

The formation of **10** and **11** can be rationalized by the retro-aldol type β-scission of the photoproducts (de Mayo reaction)[9] induced by protonation of the carbonyl groups and subsequent hydrolysis of the oxonium ions (**14** and **15**) as depicted in Scheme 2.

Recently, Zwanenburg, and co-workers[10] have reported a similar acid-catalyzed ring opening of methoxy-substituted bishomocubanone **16**. In this case, however, the initial scission of the C_4–C_5 bond is followed by subsequent C_2–C_3 bond cleavage, thus giving the tricyclic enedione **18**. The absence of signals due to olefinic protons in the ^1H NMR spectra of **10** and **11** can exclude the analogous enedione structures (**19** and **20**) for the ring opening products from **8a** and **9a**.

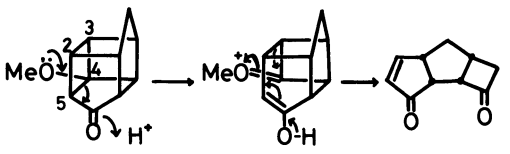

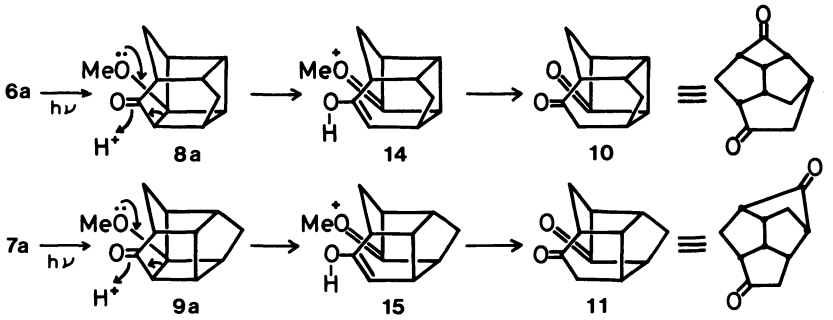

Scheme 2.

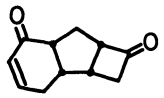

19

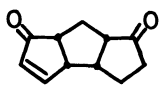

20

Irradiation of **6b—d** in benzene all resulted in the exclusive formation of trishomocubanones **8b—d** via [2+2] photocycloaddition (Scheme 3). The structures of the products were assigned by the IR absorptions (**8b**: 1695 cm^{-1}, **8c**: 1685 cm^{-1}, and **8d**: 1700 cm^{-1}) which are compatible with cyclohexanones in polycyclic rigid systems[11] and by the ^{13}C NMR spectra which displayed no resonances for sp^2-hybridized carbon other than those assigned to the carbonyl carbon and the aromatic ring. Further evidence was given by the mass spectra which are almost superimposable on those of the corresponding starting dienones.

Irradiation of **7b** gave **9b** exclusively, whereas irradiation of **7c** and **7d** produced not only the photocyclization products **9c** and **9d**, but also additional photoproducts **12c**[12] and **12d**, respectively. The product ratios estimated by ^1H NMR were 5 : 1 for **9c**/**12c**, and 4 : 1 for **9d**/**12d**. Since any attempts to separate the products by chromatography failed in both cases, **9c** and **9d** were converted to the tricyclic dienones **13c** and **13d** by treatment with acids,[13] and then regenerated by irradiation after the chromatographic separation from unchanged **12c** and **12d**, respectively (Scheme 4).

Again, the structures of **9b—d** were supported by the IR spectra (**9b**: 1720 cm^{-1}, **9c**: 1710 cm^{-1}, and **9d**: 1725 cm^{-1}), the ^1H NMR spectra (devoid of all low-field signals), and the ^{13}C NMR spectra (no resonances for sp^2-hybridized carbon other than those assigned to the carbonyl carbon and the aromatic ring). In addition, the mass-fragmentation patterns of this series of compounds (**9b—d**) were found to be quite similar to those of the dienones **13b—d**, respectively. The latter compounds have been obtained by acid or Rh(I)-catalyzed cycloreversion of **9b—d** and shown to reproduce the trishomocubanones (**9b—d**) upon irradiation (Scheme 4).[13,14] Recently, Mehta and coworkers have also established the similar interconversion between the pentacyclic diones **21** and the bis(enone)s **22**.[15]

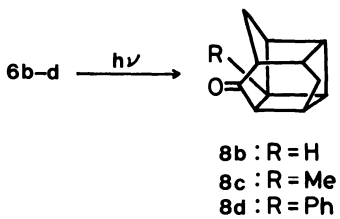

Scheme 3.

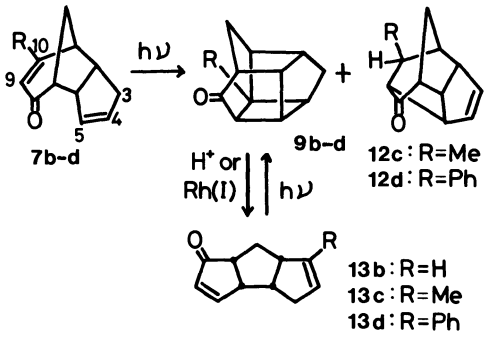

Scheme 4.

On the other hand, the ^1H NMR spectra of **12c** and **12d**, particularly the two olefinic proton signals at δ 5.79 (dd, J=6 and 3 Hz) and 6.10 (dd, J=6 and 3 Hz) for **12c**, and at δ 5.90 (dd, J=6 and 2.5 Hz) and 6.33 (dd, J=6 and 2.5 Hz) for **12d**, indicated that the double bond in the cyclopentene ring is retained in these compounds. This observation, coupled with the empirical formulae, $C_{12}H_{14}O$ for **12c** and $C_{17}H_{16}O$ for **12d**, determined by high-resolution mass spectra and elemental analysis suggested that these products have tetracyclic structures which are expected by intramolecular hydrogen abstraction. This was supported by the off-resonance ^1H decoupled ^{13}C NMR spectra. Namely, of the eleven skeletal carbons in each compound, one was accounted for by a signal for a carbonyl carbon [δ=219.2 (s) for **12c** and δ=218.5 (s) for **12d**], two were by signals for olefinic carbons [δ=133.6 (d) and 129.0 (d) for **12c**, and δ=134.8 (d) and 128.9 (d) for **12d**], seven were by signals for methine carbons [δ=54.5, 53.2, 52.7, 46.9, 45.8, 38.9, and 35.9 (all d) for **12c**, and δ=54.3, 52.9, 48.8, 46.5, 46.2, 45.8, and 40.6 (all d) for **12d**], and the remaining one was by a signal for a methylene carbon [δ=43.5 (t) for **12c**, and δ=42.4 (t) for **12d**]. These data, coupled with the appearance of the methyl signal as a doublet at δ 0.95 in ^1H NMR of **12c**, indicated that the hydrogen abstraction occurred at the β-carbon of the conjugated enone. Furthermore, of all the possible structures expected by hydrogen abstraction, only those depicted as **12c** and **12d** satisfied the IR spectra (1735 cm^{-1} for both **12c** and **12d**) which indicated the presence of the cyclopentanone rings.

Although a fair number of examples of the photoreactions which involve intramolecular allylic or benzylic hydrogen abstraction by the β-carbon of a conjugated enone have been reported,[16] a few examples of the reactions in which hydrogen abstrac-

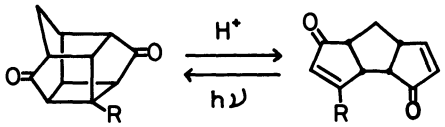

21 22

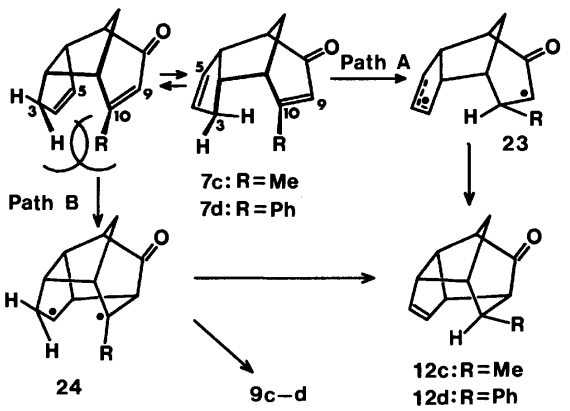

Scheme 5.

tion by the β-carbon occured along with intramolecular [2+2] photocyclization are known mainly with citral and related compounds.[4a] The mechanistic possibilities (which cannot presently be distinguished) include the following.

Initial abstraction of the C_3-hydrogen atom by the β-carbon of a triplet enone (possively common to [2+2] cyclization) gives biradical **23** (path A in Scheme 5), which in turn collapses to **12**. Dreiding model examination of **7c—d** indicated that the β-carbon-to-C_3-hydrogen distance is 1.9—2.5 Å, which is within the limit for the sum of the van der Waals radii of 2.90 Å suggested for hydrogen abstraction by carbon.[17] Furthermore, this inspection of the model disclosed that the substitution at C_{10} causes changes of the conformation so that the β-carbon-to-hydrogen distance becomes shorter and the hydrogen atom to be transferred becomes axial owing to the steric repulsion between the substituent and C_3-hydrogen. In this conformation, on the contrary, the spatial relationship of the two carbon-carbon double bonds comes to be unfavorable for the [2+2] cycloaddition reaction.

An alternative mechanism involves the initial bond formation between C_5 and C_9 to give the biradical **24** which may be a common intermediate for both **9c—d** and **12c—d** (path B in Scheme 5). A similar mechanism has been proposed for the photoreaction of citral (**25**) in which the biradical intermediate **26** derived from a triplet precursor led to both the [2+2] photocyclization product **27** and the hydrogen

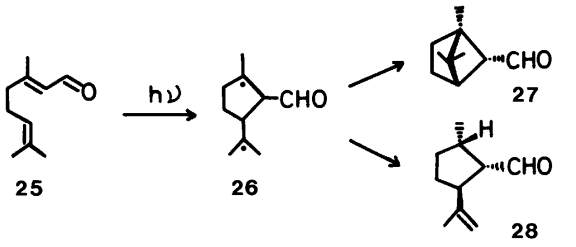

abstraction product **28**.[4a] In addition, a same mechanism has been also proposed for the intermolecular photoreaction between 2-cyclohexenone and 2-methylpropene on the basis of the formation of 2-(2-methylallyl)cyclohexanone together with the corresponding cycloaddition product.[18]

Although we prefer path A because this provides the explanation for the production of the hydrogen transfer products from the reaction of **7c** and **7d**, the present results do not define the detailed mechanism of the photoreaction.

Experimental

General. Melting points are uncorrected. IR spectra (in $CHCl_3$, unless otherwise noted) were recorded on JASCO A-102 and A-3 spectrometers. UV spectra were obtained on Hitachi 200-10 and JASCO UVIDEC-505 spectrometers. ^1H NMR spectra (in $CDCl_3$, unless otherwise noted) were determined on JEOL JNM-PMX 60 and Hitachi R-600 spectrometers with tetramethylsilane as the internal standard. ^{13}C NMR spectra (in $CDCl_3$) were obtained with a JEOL JNM-GX 270 spectrometer. GLC was performed on a Hitachi 063 gas chromatograph using PEG 20 M, DEGS, or Silicone SE-30. Mass spectra were taken on a Hitachi M-60 mass spectrometer at an ionization potential of 70 eV. High-resolution mass measurements were carried out on JEOL JMS-D-300 and Hitachi RMU-7MG mass spectrometers. Photochemical reactions were carried out in Pyrex tubes using 300 and 500 W high pressure mercury lamps, with running water cooling under a nitrogen atmosphere.

Preparation of Monoacetate 2. A solution of 3.05 g (18.3 mmol) of **1**[5] in 50 cm^3 of freshly distilled Ac_2O was stirred at 30 °C for 19 h. The mixture was then poured into water (170 cm^3), stirred at room temperature for 2.5 h, and extracted with four 40 cm^3 portions of $CHCl_3$. The extracts were combined, washed with saturated aqueous $NaHCO_3$ and saturated brine, and dried ($MgSO_4$). Removal of the solvent under reduced pressure gave an oily residue which was purified on a silica-gel column (benzene–Et_2O) to afford pure **2** (3.12 g, 85%) as colorless crystals: Mp 68—70 °C. ^1H NMR (CCl_4) δ=2.00 (3H, s), 3.79 (1H, br. t, J=4 Hz), 4.50 (1H, t, J=6 Hz), and 5.62 (2H, br. s). IR 3600, 1720, and 1090 cm^{-1}. Found: C, 69.23; H, 7.67%. Calcd for $C_{12}H_{16}O$: C, 69.21; H, 7.74%.

Jones' Oxidation of 2 to Keto Acetate 3. To a well stirred solution of **2** (3.01 g, 14.5 mmol) in acetone (60 cm^3) was added Jones' reagent (12 cm^3) dropwise over a period of 1.5 h at 0 °C. After continued stirring for 30 min, the mixture was treated with 25% aqueous $NaHSO_3$ (20 cm^3), and concentrated to one-third of its original volume. The residue was poured into water, and extracted with $CHCl_3$ (60 cm^3×5). The combined extracts were washed with saturated aqueous $NaHCO_3$ and saturated brine, and dried over $MgSO_4$. Evaporation of the solvent in vacuo gave **3** (2.32 g, 78%) as pale yellow crystals. An analytical sample was prepared by recrystallization from Et_2O–pet. ether: Mp 62—64 °C. ^1H NMR (CCl_4) δ=2.00 (3H, s), 4.59 (1H, dd, J=14 and 3 Hz), and 5.67 (2H, m). IR 1755 and 1735 cm^{-1}. Found: C, 69.29; H, 6.84%. Calcd for $C_{12}H_{14}O_3$: C, 69.05; H, 6.94%.

Hydrolysis of 3 to α-Ketol 4. To a stirred solution of **3** (2.20 g, 10.7 mmol) in methanol (30 cm^3) was added a methanolic solution (10 cm^3) of NaOH (0.6 g, 15.0 mmol) dropwise over a period of 10 min at room temperature under

a nitrogen atmosphere, and stirring was continued for 5 min. After evaporation of most part of the solvent, the residue was poured into water, and extracted with $CHCl_3$ (40 cm^3×5). The extracts were washed with saturated brine, dried over $MgSO_4$, and evaporated in vacuo to give **4** (1.59 g, 91%) as pale yellow crystals. An analytical sample was prepared by recrystallization from Et_2O–pet. ether: Mp 64—69 °C. ^1H NMR (CCl_4) δ=3.30 (1H, m), 3.54 (1H, m), and 5.60 (2H, br. s). IR 3600, 1750, and 1055 cm^{-1}. Found: C, 72.54; H, 7.80%. Calcd for $C_{10}H_{12}O_2$: C, 73.14; H, 7.37%.

DMSO Oxidation of 4 to α-Diketone (5). To a solution of **4** (6.18 g, 37.6 mmol) in dimethyl sulfoxide (110 cm^3) was added a solution of phosphorus pentoxide (16 g, 113 mmol) in DMSO (60 cm^3) at 90 °C over a period of 5 min. After standing for 30 min at 90 °C, the mixture was cooled, poured into water, and extracted with $CHCl_3$ (100 cm^3×5). The extracts were washed with water, saturated aqueous $NaHCO_3$, and saturated brine and dried over $MgSO_4$. After removal of the solvent at reduced pressure, the residue was purified on a silica-gel column (benzene–Et_2O) to afford 3.42 g (56%) of **5** as yellow crystals. An analytical sample was prepared by recrystallization from Et_2O–pet. ether: Mp 58—60 °C. ^1H NMR δ=1.85—3.85 (8H, m) and 5.53 (2H, br s). IR 1770 and 1750 cm^{-1}. UV (EtOH) 263 (ε 141) and 475 nm (ε 24). MS *m/z* 162 (M^+). Found: C, 73.17; H, 6.05%. Calcd for $C_{10}H_{10}O_2$: C, 74.06; H, 6.21%.

Preparation of 10-Methoxytricyclo[5.3.1.$0^{2,6}$]undeca-3,9-dien-8-one (6a) and 10-Methoxytricyclo[5.3.1.$0^{2,6}$]undeca-4,9-dien-8-one (7a) from 5. To a stirred solution of **5** (1.91 g, 11.8 mmol) in Et_2O (10 cm^3) were added an ethereal solution (100 cm^3) of diazomethane and MeOH (5 cm^3) in small portions at 0 °C, and the mixture was stirred overnight at room temperature. After evaporation of the solvent, separation of the residual oil (1.97 g) by preparative GLC (20% PEG 20 M on Chromosorb W-AW-DMCS, 230 °C) gave **6a** (0.89 g, 40%) as colorless crystals and **7a** (0.54 g, 24%) as a colorless oil. **6a**: Mp 67.5—69 °C. ^1H NMR δ=1.50—2.35 (4H, m), 2.50—3.50 (4H, m), 3.53 (3H, s), 4.93 (1H, s), and 5.50 (2H, m). IR 1640 and 1600 cm^{-1}. UV (EtOH) 254 nm (ε 9300). MS *m/z* (rel intensity) 190 (M^+, 100), 175 (4), 125 (89), 124 (98), 109 (29), 106 (15), 96 (9), 92 (10), 91 (9). Found: C, 75.73; H, 7.26%; *m/z* 190.0983. Calcd for $C_{12}H_{14}O_2$: C, 75.76; H, 7.42%; M, 190.0993. **7a**: ^1H NMR δ=1.50—2.35 (4H, m), 2.50—3.50 (4H, m), 3.64 (3H, s), 4.91 (1H, s), and 5.48 (2H, s, $W_{1/2}$=4 Hz). IR 1640 and 1600 cm^{-1}. UV (EtOH) 254 nm (ε 12900). MS *m/z* (rel intensity) 190 (M^+, 100), 175 (3), 162 (10), 147 (20), 130 (11), 129 (11), 125 (61), 124 (100), 109 (60), 106 (91), 98 (21). Found: C, 75.20; H, 7.67%; *m/z* 190.0997. Calcd for $C_{12}H_{14}O_2$: C, 75.76; H, 7.42%; M, 190.0993.

Preparation of Tricyclo[5.3.1.$0^{2,6}$]undeca-3,9-dien-8-one (6b) from 7a. To a refluxing mixture of $LiAlH_4$ (108 mg, 2.84 mmol) and dry Et_2O (20 cm^3) was added an anhydrous ethereal solution (5 cm^3) of **7a** (120 mg, 0.64 mmol). After refluxing for 2 h the mixture was cooled, treated with AcOEt (4 cm^3), and stirred with 25% H_2SO_4 (25 cm^3) at room temperature for 18 h. The organic solvent was evaporated in vacuo, and the aqueous solution was extracted with CH_2Cl_2 (15 cm^3×4). The extracts were washed with saturated aqueous $NaHCO_3$ and saturated brine, dried over $MgSO_4$, and evaporated in vacuo. Purification of the residue by silica-gel chromatography (benzene–Et_2O) gave pure **6b** (55 mg, 55%); Mp 49—53 °C. ^1H NMR δ=1.54—2.45 (4H, m), 2.65—3.30 (3H, m), 3.35—3.90 (1H, m), 5.56 (2H, br s, $W_{1/2}$=6 Hz), 5.90 (1H, d, *J*=10 Hz), and 6.93 (1H, dd, *J*=10 and 2 Hz). IR 1665 cm^{-1}. UV (EtOH) 230 nm (ε 4860). MS *m/z* (rel intensity) 160 (M^+, 26), 132 (5), 95 (100), 94 (30), 91 (13), 77 (25), 66 (38), 65 (13). Found: C, 81.99; H, 7.65%; *m/z* 160.0875. Calcd for $C_{11}H_{12}O$: C, 82.46; H, 7.55%; M, 160.0888.

Preparation of Tricyclo[5.3.1.$0^{2,6}$]undeca-4,9-dien-8-one (7b) from 6a. To a suspension of lithium aluminum hydride (120 mg, 3.1 mmol) in dry Et_2O (45 cm^3) was added a solution of **6a** (121 mg, 0.64 mmol) in dry Et_2O (5 cm^3) under reflux and the mixture was heated for 1.5 h. Working up and purification similar to those employed for the synthesis of **6b** gave pure **7b** (52 mg, 51%) as colorless crystals: Mp 40—45 °C. ^1H NMR δ=1.50—2.46 (4H, m), 2.53—3.25 (3H, m), 3.35—3.80 (1H, m), 5.55 (2H, s), 5.83 (1H, dd, *J*=10 and 2 Hz), and 7.10 (1H, br t, *J*=8 Hz). IR 1665 cm^{-1}. UV (EtOH) 236 nm (ε 5800). MS *m/z* (rel intensity) 160 (M^+, 41), 132 (53), 131 (20), 117 (86), 104 (27), 95 (37), 94 (18), 91 (57), 79 (32), 78 (61), 77 (45), 67 (29), 66 (100), 65 (36). Found: C, 82.16; H, 7.60%; *m/z* 160.0957. Calcd for $C_{11}H_{12}O$: C, 82.46; H, 7.55%; M, 160.0888.

Preparation of 10-Methyltricyclo[5.3.1.$0^{2,6}$]undeca-3,9-dien-8-one (6c) from 7a. To a stirred solution of **7a** (118 mg, 0.62 mmol) in dry Et_2O (20 cm^3) at room temperature under nitrogen atmosphere was added a solution of methyllithium in Et_2O (1.85 mol dm^{-3}, 2.7 cm^3) over a period of 45 min. The reaction mixture was refluxed for 2 h, cooled to 0 °C, and treated with H_2SO_4 (3 mol dm^{-3}, 15 cm^3) for 50 min with vigorous stirring. Most of the organic solvent was evaporated, and the aqueous solution was extracted with $CHCl_3$ (30 cm^3×3). The extracts were washed with saturated aqueous $NaHCO_3$, 3% aqueous Na_2SO_3 (20 cm^3) and saturated brine, dried ($MgSO_4$), and evaporated. Bulb-to-bulb (Kugelrohr) distillation of the residue [123—124 °C (1333 Pa)] gave pure **6c** (75 mg, 69%): Mp 42—45 °C. ^1H NMR δ=1.70—2.36 (4H, m), 1.83 (3H, s), 2.40—3.26 (3H, m), 3.40—3.83 (1H, m), 5.53 (2H, br s, $W_{1/2}$=3 Hz), and 5.66 (1H, br s, $W_{1/2}$=5 Hz). IR 1655 and 1620 cm^{-1}. UV (EtOH) 238 nm (ε 7950). MS *m/z* (rel intensity) 174 (M^+, 32), 159 (4), 109 (100), 108 (31), 91 (18), 79 (12), 77 (14), 66 (13), 65 (12). Found: C, 82.35; H,8.25%; *m/z* 174.1028. Calcd for $C_{12}H_{14}O$: C, 82.72; H, 8.10%; M, 174.1045.

Preparation of 10-Methyltricyclo[5.3.1.$0^{2,6}$]undeca-4,9-dien-8-one (7c) from 6a. To a stirred solution of **6a** (121 mg, 0.64 mmol) in dry Et_2O (20 cm^3) was added an ethereal solution of methyllithium (1.85 mol dm^{-3}, 2 cm^3) under nitrogen atmosphere at room temperature over a period of 50 min. The reaction mixture was worked up and purified by a method similar to that employed for the synthesis of **6c** to give **7c** (73 mg, 66%) as a colorless oil: ^1H NMR δ=1.70—2.43 (4H, m), 2.02 (3H, s), 2.60—3.30 (3H, m), 3.30—3.80 (1H, m), 5.55 (2H, br s, $W_{1/2}$=2 Hz), and 5.65 (1H, br s, $W_{1/2}$=5 Hz). IR 1655 and 1620 cm^{-1}. UV (EtOH) 237 nm (ε 7300). MS *m/z* (rel intensity) 174 (M^+, 68), 159 (4), 146 (50), 131 (100), 117 (27), 106 (40), 105 (27), 93 (33), 92 (96), 91 (51), 80 (48). Found: C, 82.52; H, 8.13%; *m/z* 174.1025. Calcd for $C_{12}H_{14}O$: C, 82.72; H, 8.10%; M, 174.1045.

Preparation of 10-Phenyltricyclo[5.3.1.$0^{2,6}$]undeca-3,9-dien-8-one (6d) from 7a. To a stirred solution of **7a**

(275 mg, 1.45 mmol) in dry Et_2O (30 cm^3) was added an ethereal solution of phenyllithium (1.66 mol dm^{-3}, 5.5 cm^3) at 0 °C over a period of 40 min under nitrogen atmosphere. The reaction mixture was refluxed for 3 h, poured into ice-cold 25% H_2SO_4 (20 cm^3), and stirred for 1 h. Most of the organic solvent was evaporatd, and the aqueous solution was extracted with $CHCl_3$ (50 cm^3×3). The extracts were washed with saturated aqueous $NaHCO_3$ and saturated brine, dried ($MgSO_4$), and evaporated. The residue was chromatographed on silica-gel (benzene–Et_2O) to give **6d** (214 mg, 62%) as colorless crystals: Mp 98—100 °C. ^1H NMR δ=1.70—2.43 (4H, m), 2.83—3.33 (2H, m), 3.35—3.93 (2H, m), 5.43 (2H, m), 6.22 (1H, s), and 7.42 (5H, br s). IR 1655 and 1600 cm^{-1}. UV (EtOH) 222 (ε 7530) and 290 nm (ε 13800). MS *m/z* (rel intensity) 236 (M^+, 57), 171 (100), 170 (71), 153 (56), 152 (22), 142 (20), 141 (21), 128 (21), 115 (36), 77 (23). Found: C, 86.28; H, 6.90%; *m/z* 236.1263. Calcd for $C_{17}H_{16}O$: C, 86.41; H, 6.82%; M, 236.1202.

Preparation of 10-Phenyltricyclo[5.3.1.$0^{2,6}$]undeca-4,9-dien-8-one (7d). To a stirred solution of **6a** (406 mg, 2.13 mmol) in dry Et_2O (45 cm^3) was added an ethereal solution of phenyllithium (1.66 mol dm^{-3}, 6.5 cm^3) at 0 °C under nitrogen atmosphere over a period of 1 h, and refluxed for another 40 min. The reaction mixture was poured into ice-cold 25% H_2SO_4 (40 cm^3), stirred vigorously for 100 min, and then worked up and purified by a method similar to that employed for the synthesis of **6d** to give **7d** (368 mg, 73%) as pale yellow crystals: Mp 68—71 °C. ^1H NMR δ=1.80—2.50 (4H, m), 3.00—3.36 (2H, m), 3.40—3.90 (2H, m), 5.57 (2H, br s), 6.20 (1H, s), and 7.43 (5H, br s). IR 1655 and 1600 cm^{-1}. UV (EtOH) 222 (ε 9540) and 290 nm (ε 15800). MS *m/z* (rel intensity) 236 (M^+, 77), 208 (34), 194 (29), 171 (56), 170 (57), 167 (31), 166 (29), 155 (100), 154 (43), 153 (21), 142 (93), 141 (54), 129 (26), 128 (38), 117 (24), 115 (72), 106 (99). Found: C, 86.15; H, 6.85%; *m/z* 236.1179. Calcd for $C_{17}H_{16}O$: C, 86.41; H, 6.82%; M, 236.1202.

Photochemical Transformation of 6a into 7-Methoxypentacyclo[5.4.0.$0^{2,6}$.$0^{3,10}$.$0^{5,8}$]undecan-9-one (8a). A solution of **6a** (10 mg) in benzene (3 cm^3) was irradiated for 6 h. Evaporation of the solvent in vacuo gave **8a** (10 mg) as a colorless oil, which was analyzed without purification because of its instability: ^1H NMR δ=1.50—1.83 (2H, m), 1.85—2.16 (2H, m), 2.50—3.83 (7H, m), and 3.20 (3H, s). IR 1700 cm^{-1}.

Acid Treatment of 8a. To a solution of **8a** (33 mg) in methanol (3 cm^3) was added ten drops of hydrochloric acid (1 mol dm^{-3}) at 50 °C. The mixture was stirred for 1.5 h, poured into saturated aqueous $NaHCO_3$ (10 cm^3), and extracted with $CHCl_3$ (10 cm^3×3). The extracts were washed with saturated brine, dried ($MgSO_4$), and evaporated to give the diketone **10** (25 mg, 82%) as colorless crystals: Mp 154—156 °C. IR 1765 and 1700 cm^{-1}. MS *m/z* (rel intensity) 176 (M^+ 4), 148 (72), 133 (14), 110 (18), 106 (11), 105 (34), 83 (12), 82 (100), 80 (12), 79 (34), 78 (29). Found: *m/z* 176.0838. Calcd for $C_{11}H_{12}O_2$: M, 176.0837.

Photochemical Transformation of 7a into 7-Methoxypentacyclo[5.4.0.$0^{2,6}$.$0^{3,10}$. $0^{4,8}$]undecan-11-one (9a). Irradiation of a solution of **7a** (10 mg) in benzene (3 cm^3) for 2.5 h and evaporation of the solvent gave **9a** (10 mg) as an unstable colorless oil. ^1H NMR δ=1.50—2.50 (6H, m), 2.50—3.30 (5H, m), 3.50 (3H, s). IR 1730—1700 cm^{-1}.

Acid Treatment of 9a. To a solution of **9a** (12 mg) in methanol (2 cm^3) was added five drops of hydrochloric acid (1 mol dm^{-3}) at 75 °C. The mixture was stirred for 2 h, and worked up by a method similar to that described in the reaction of **8a** to give **11** (7 mg, 63%) as colorless crystals: Mp 118—120 °C. ^1H NMR δ=1.20—3.40 (12H, m). IR 1735 cm^{-1}. MS *m/z* (rel intensity) 176 (M^+, 100), 147 (65), 133 (16), 131 (25), 130 (12), 106 (13), 94 (22). Found: *m/z* 176.0868. Calcd for $C_{11}H_{12}O_2$: M, 176.0837.

Photochemical Transformation of 6b into Pentacyclo[5.4.0.$0^{2,6}$.$0^{3,10}$.$0^{5,8}$]undecan-9-one (8b). Irradiation of a solution of **6b** (28 mg) in benzene (5 cm^3) for 2 h and purification of the product by column chromatography (benzene–Et_2O) gave **8b** (26 mg, 94 %) as a colorless oil. ^1H NMR δ=1.50—2.16 (4H, m) and 2.20—3.43 (8H, m). ^{13}C NMR δ=217.3 (s), 58.1 (d), 47.0 (d), 46.9 (d), 46.8 (d), 41.1 (d), 40.2 (d), 40.0 (d), 39.9 (t), 37.7 (d), and 34.6 (t). IR 1695 cm^{-1}. MS *m/z* (rel intensity) 160 (M^+, 31), 132 (15), 117 (27), 95 (100), 94 (35), 91 (27), 79 (15), 78 (21), and 77 (24). Found: C, 82.21; H, 7.60%; *m/z* 160.0876. Calcd for $C_{11}H_{12}O$: C, 82.46; H, 7.55%; M, 160.0888.

Photochemical Transformation of 6c into 7-Methylpentacyclo[5.4.0.$0^{2,6}$.$0^{3,10}$.$0^{5,8}$]undecan-9-one (8d). Irradiation of a solution of **6c** (87 mg) in benzene (7 cm^3) for 3 h and purification of the product by chromatography (benzene–Et_2O) gave **8c** (70 mg, 81%) as a colorless oil. ^1H NMR δ=1.17 (3H,s), 1.47—2.10 (4H, m), and 2.15-3.30 (7H, m). ^{13}C NMR δ=217.1 (s), 57.1 (d), 54.0 (d), 46.4 (d), 46.1 (d), 45.1 (s), 44.0 (d), 43.7 (d), 38.0 (d), 38.0 (t), 34.8 (t), and 23.4 (q). IR 1685 cm^{-1}. MS *m/z* (rel intensity) 174 (M^+, 24), 159 (3), 146 (9), 131 (17), 109 (100), 108 (40), 93 (10), 92 (17), and 91 (29). Found: C, 82.45; H, 8.15%; *m/z* 174.0994. Calcd for $C_{12}H_{14}O$: C, 82.72; H, 8.10%; M, 174.1045.

Photochemical Transformation of 6d into 7-Phenylpentacyclo[5.4.0.$0^{2,6}$.$0^{3,10}$.$0^{5,8}$]undecan-9-one (8d). Irradiation of a solution of **6d** (75 mg) in benzene (56 cm^3) for 10 h and purification of the product by chromatography (benzene–Et_2O) gave **8d** (30 mg, 40%): Mp 61—65.5 °C. ^1H NMR δ=1.60—1.90 (2H, m), 2.13 (2H, br s), 3.07 (5H, br s), 3.41 (2H, m), and 7.25 (5H, m). ^{13}C NMR δ=216.1 (s), 145.4 (s), 128.5 (d, 2C), 126.1 (d), 124.8 (d, 2C), 57.1 (d), 54.4 (d), 50.9 (s), 47.8 (d), 46.3 (d), 44.3 (d), 43.7 (d), 38.8 (t), 38.7 (d), and 34.82 (t). IR 1700 cm^{-1}. MS *m/z* (rel intensity) 236 (M^+, 25), 172 (11), 171 (100), 170 (61), 165 (15), 155 (16), 154 (16), 153 (40), 152 (20), 141 (21), 128 (16), 115 (34), and 102 (14). Found: C, 86.35; H, 6.85%; *m/z* 236.1206. Calcd for $C_{17}H_{16}O$: C, 86.41; H, 6.82%; M, 236.1202.

Photochemical Transformation of 7b into Pentacyclo[5.4.0.$0^{2,6}$.$0^{3,10}$.$0^{4,8}$]undecan-11-one (9b). Irradiation of a solution of **7b** (30 mg) in benzene (5 cm^3) for 2 h and purification by chromatography (benzene–Et_2O) gave **9b** (26 mg, 89%) as colorless crystals: Mp 116—118 °C. ^1H NMR δ=1.35—3.35 (12H, m). ^{13}C NMR δ=218.8 (s), 52.5 (d), 51.4 (d), 50.5 (d), 45.8 (d), 45.1 (d, 2C), 42.2 (t), 41.7 (d), 39.6 (d), and 35.6 (t). IR 1720 cm^{-1}. MS *m/z* (rel intensity) 160 (M^+, 43), 132 (56), 131 (25), 117 (100), 104 (30), 95 (28), 91 (60), 79 (64), 78 (81), 77 (38), 67 (23), and 66 (63). Found: C, 82.25; H, 7.62%; *m/z* 160.0909. Calcd for $C_{11}H_{12}O$: C, 82.46; H, 7.55%; M, 160.0888.

Photochemical Transformation of 7c into 7-Methylpentacyclo[5.4.0.$0^{2,6}$.$0^{3,10}$.$0^{4,8}$]undecan-11-one (9c) and 10-Methyltetracyclo[5.3.1.$0^{2,6}$.$0^{5,9}$]undec-3-en-8-one (12c). Irradiation of a solution of **7c** (92 mg) in benzene (7 cm^3) for 2 h gave an

inseparable mixture of **9c** and **12c** as a colorless solid. The ratio of **9c** to **12c** (5 : 1) was determined by the relative intensities of methyl proton signals in ^{1}H NMR. The mixture was treated with p-TsOH (50 mg) in benzene (10 cm^3) for 10 h at room temperature, washed with aqueous $NaHCO_3$ and brine, dried ($MgSO_4$). After evaporation of the solvent, the residue (79 mg) was chromatographed on silica gel to give **12c** (17 mg) and **13c**[13] (48 mg). **12c**: Mp 42—43 °C. ^{1}H NMR δ=0.95 (3H, d, J=7 Hz), 1.40—2.75 (7H, m), 2.80—3.40 (2H, m), 5.79 (1H, dd, J=6 and 3 Hz), and 6.10 (1H, dd, J=6 and 3 Hz). ^{13}C NMR δ=219.2 (s), 133.6 (d), 129.0 (d), 54.5 (d), 53.2 (d), 52.7 (d), 46.9 (d), 45.8 (d), 43.5 (t), 38.9 (d), 35.9 (d), and 16.5 (q). IR 1735 cm^{-1}. MS m/z (rel intensity) 174 (M$^+$, 56), 159 (14), 146 (54), 145 (31), 132 (26), 131 (82), 130 (24), 129 (31), 128 (29), 118 (37), 117 (69), 115 (51), 109 (72), 93 (76), 92 (87), and 91 (100). Found: C, 82.53; H, 8.12%; m/z 174.1017. Calcd for $C_{12}H_{14}O$: C, 82.72; H, 8.10%; M, 174.1044.

Regeneration of 9c from 13c: Irradiation of a solution of **13c** (37 mg) in benzene (5 cm^3) for 3 h and purification of the product by chromatography (benzene–Et_2O) gave **9c** (34 mg, 94%) as colorless crystals: Mp 82—84 °C. ^{1}H NMR δ=1.10 (3H, s), 1.45—2.05 (4H, m), and 2.10—3.10 (7H, m). ^{13}C NMR δ=218.5 (s), 57.4 (d), 53.6 (s), 52.7 (d), 52.6 (d), 50.6 (d), 46.7 (d), 44.4 (d), 40.4 (d), 36.2 (d), 34.3 (t), and 23.1 (q). IR 1710 cm^{-1}. MS m/z (rel intensity) 174 (M$^+$, 69), 159 (6), 146 (56), 131 (100), 117 (31), 115 (21), 109 (80), 108 (35), 106 (34), 105 (30), 93 (77), 92 (99), and 91 (72). Found: C, 82.62; H, 8.11%; m/z 174.1017. Calcd for $C_{12}H_{14}O$: C, 82.72; H, 8.10%; M, 174.1045.

Photochemical Transformation of 7d into 7-Phenylpentacyclo[5.4.0.0^{2,6}.0^{3,10}.0^{4,8}]undecan-11-one (9d) and 10-Phenyltetracyclo[5.3.1.0^{2,6}.0^{5,9}]undec-3-en-8-one (12d). Irradiation of a solution of **7d** (64 mg) in benzene (6 cm^3) for 1.5 h gave a mixture of **9d** and **12d**. The ratio of **9d** to **12d** (4 : 1) was determined by the relative intensities of phenyl proton signals of **9d** and olefinic proton signals of **12d** in the ^{1}H NMR. The mixture was stirred with **3** drops of BF_3 etherate in benzene (10 cm^3) for 40 min at room temperature, washed with aqueos $NaHCO_3$ and brine, dried ($MgSO_4$), and the solvent was evaporated. Chromatography of the products (55.3 mg) gave **12d** (16 mg) and **13d**[13] (35.2 mg). **12d**: Mp 102—104 °C. ^{1}H NMR δ=1.9—3.5 (9H, m), 5.90 (1H, dd, J=6 and 2.5 Hz), 6.33 (1H, dd, J=6 and 2.5 Hz), and 7.28 (5H, m). ^{13}H NMR δ=218.2 (s), 142.7 (s), 134.8 (d), 128.9 (d), 128.4 (d, 2C), 127.6 (d, 2C), 126.1 (d), 54.3 (d), 52.9 (d), 48.8 (d), 46.5 (d), 46.2 (d), 45.8 (d), 42.4 (t), and 40.6 (d). IR 1735 cm^{-1}. MS m/z (rel intensity) 236 (M$^+$, 42), 208 (13), 171 (16), 170 (27), 166 (24), 155 (48), 154 (28), 143 (20), 142 (100), 141 (21), 129 (34), 128 (40), 117 (53), 116 (28), 115 (83), and 106 (66). Found: C, 86.26; H, 6.98%; m/z 236.1201. Calcd for $C_{17}H_{16}O$: C, 86.41; H, 6.82%; M, 236.1202.

Regeneration of 9d from 13d: Irradiation of a solution of **13d** (38 mg) in benzene (7 cm^3) for 90 min and purification of the product by column chromatography gave **9d** (31 mg, 82%) as colorless crystals: Mp 36.5—38 °C. ^{1}H NMR δ=1.50—2.40 (5H, m), 2.45—3.25 (6H, m), and 6.90—7.50 (5H, m). ^{13}C NMR δ=218.5 (s), 146.0 (s), 128.5 (d, 2C), 126.16 (d), 124.9 (d, 2C), 60.1 (s), 56.0 (d), 55.9 (d), 52.3 (d), 50.9 (d), 47.6 (d), 44.8 (d), 40.9 (t), 36.5 (d), and 35.7 (t). IR 1725 cm^{-1}. MS m/z (rel intensity) 236 (M$^+$, 40), 208 (16), 171 (35), 170 (29), 165 (15), 156 (14), 155 (100), 154 (26), 153 (16), 142 (41), 141 (29), and 115 (40). Found: C, 86.05; H, 7.01%; m/z 236.1221. Calcd for $C_{17}H_{16}O$: C, 86.41; H, 6.82%; M, 236.1202.

The authors wish to thank to Professors Hajime Katayama and Akira Kato of Niigata College of Pharmacy for the measurements of high-resolution mass spectra, and Professor Teruo Fujimoto and Mr. Takeo Kazama of Technological University of Nagaoka for the NMR measurements at 270 MHz. We also wish to express our thanks to Professor Koji Isogai and Mr. Jun-ichi Sakai of Niigata University for the measurements of mass spectra and their helpful discussions. This work was partially supported by Grant-in-Aids for Scientific Research (No. 56540295 and No. 58740240) from the Ministry of Education, Science and Culture.

References

1) A part of this study has been previously reported: T. Ogino and K. Awano, *Chem. Lett.*, **1982**, 891.

2) R. C. Cookson, R. R. Hill, and J. Hudec, *Chem. Ind. (London)*, **1958**, 100; R. C. Cookson, J. Hudec, and R. O. Williams, *Tetrahedron Lett.*, **1960**, 29; G. Jones, II and B. R. Ramachandran, *J. Org. Chem.*, **41**, 798 (1976).

3) For examples of photoreactions which involve intramolecular hydrogen abstraction by the α-carbon of an α,β-unsaturated ketone system as well as intramolecular [2+2] cyclization, see T. W. Gibson and W. F. Erman, *J. Org. Chem.*, **37**, 1148 (1972); F. Nobs, U. Burger, and K. Schaffner, *Helv. Chim. Acta*, **60**, 1607 (1977); W. Oppolzer and T. G. C. Bird, *ibid.*, **62**, 1199 (1979); T. R. Hoye, S. J. Martin, and D. R. Peck, *J. Org. Chem.*, **47**, 331 (1982).

4) For examples of photoreactions which involve intramolecular hydrogen abstraction by the β-carbon of α,β-unsaturated ketone as well as intramolecular [2+2] cyclization, see a) R. C. Cookson, J. Hudec, S. A. Knight, and B. R. D. Whitear, *Tetrahedron*, **19**, 1995 (1963); G. Büchi and H. Wüest, *J. Am. Chem. Soc.*, **87**, 1589 (1965); F. Barany, S. Wolff, and W. C. Agosta, *ibid.*, **100**, 1946 (1978); **102**, 2378 (1980); b) M. Yoshioka, K. Ishii, and H. R. Wolf, *Helv. Chim. Acta*, **63**, 571 (1980); W. K. Appel, T. J. Greenhough, J. R. Scheffer, J. Trotter, and L. Walsh, *J. Am. Chem. Soc.*, **102**, 1160 (1980).

5) T. Ogino and K. Mochizuki, *Chem. Lett.*, **1979**, 443.

6) C. L. Stevens, *J. Org. Chem.*, **33**, 1586 (1968).

7) N. B. Haynes, D. Redmore, and C. J. Timmons, *J. Chem. Soc.*, **1963**, 2420.

8) von B. Eistert, D. Greiber, and I. Caspari, *Liebigs Ann. Chem.*, **654**, 64 (1962).

9) P. de Mayo and H. Takeshita, *Can. J. Chem.*, **41**, 440 (1963); B. D. Challand, H. Hikino, G. Kornis, G. Lange, and P. de Mayo, *J. Org. Chem.*, **34**, 794 (1964).

10) A. J. H. Klunder, G. J. A. Ariaans, and B. Zwanenburg, *Tetrahedron Lett.*, **25**, 5457 (1984).

11) K. Hirao, M. Taniguchi, O. Yonemitsu, J. L. Flippen, and B. Witkop, *J. Am. Chem. Soc.*, **101**, 408 (1979); K. Hirao, Y. Kajikawa, E. Abe, and O. Yonemitsu, *J. Chem. Soc., Perkin Trans. 1*, **1983**, 1791.

12) The compound **12c** was initially overlooked because it escaped detection even by GLC.[1]

13) T. Ogino, K. Awano, T. Ogihara, and K. Isogai, *Tetrahedron Lett.*, **24**, 2781 (1983).
14) T. Ogino, K. Awano, T. Ogihara, and K. Isogai, *Chem. Lett.*, **1984**, 2023.
15) G. Mehta and A. Srikrishna, *J. Chem. Soc., Chem. Commun.*, **1982**, 218.
16) For examples of the photoreactions which involve intramolecular allyic or benzylic hydrogen abstraction by the β-carbon of an α,β-unsaturated ketone system, see Y. Tamura, H. Ishibashi, and M. Ikeda, *J. Org. Chem.*, **41**, 1277 (1976); F. M. Schell and P. M. Cook, *ibid.*, **43**, 4420 (1978); S. Wolff, W. L. Schreiber, A. B. Smith, III, and W. C. Agosta, *J. Am. Chem. Soc.*, **94**, 7797 (1972); M. Tada, H. Saiki, H. Mizutani, and K. Miura, *Bull. Chem. Soc. Jpn.*, **51**, 343 (1978); M. Tada, T. Maeda, and H. Saiki, *ibid.*, **51**, 1516 (1978).
17) J. R. Scheffer and A. A. Dzakpasu, *J. Am. Chem. Soc.*, **100**, 2163 (1978).
18) E. J. Corey, J. D. Bass, R. LeMahieu, and R. B. Mitra, *J. Am. Chem. Soc.*, **86**, 5570 (1964).

 © 1986 The Chemical Society of Japan Bull. Chem. Soc. Jpn., 59, 2819—2825 (1986)

Reaction of Carbocations Derived from Alkanes with Carbon Monoxide in HF-SbF_5 Superacid

Norihiko YONEDA,* Yukio TAKAHASHI,† Tsuyoshi FUKUHARA, and Akira SUZUKI
Department of Applied Chemistry, Faculty of Engineering, Hokkaido University, Sapporo 060
(Received February 15, 1986)

Alkanes readily react with CO and H_2O in HF-SbF_5 at 30 °C under atmospheric pressure and give considerably different product distributions from those in the usual Koch-Haaf reaction. When using C_5- or C_6-alkanes with tertiary C-H bonds, a considerable amount of secondary carboxylic acids are produced by the reaction of CO with secondary alkyl cations. Such cations may appear as transient intermediates in the course of the carbon skeletal isomerization of initially formed tertiary cations. For the straight-chain alkanes, the protonolysis at C-C bonds initiated the reaction to give fragment alkyl cations. This resulted in the formation of carboxylic acids with a lower number of carbon atoms than the starting alkanes. Intermolecular hydride shift between the fragment cations and the starting alkanes occurred at the same time to form a large amount of carboxylic acids with the alkyl group of the same number of carbon atoms as the starting alkane. On the other hand, for alkanes with more than seven carbon atoms, β-scission occurs exclusively to produce C_4-, C_5-, and C_6-carboxylic acids.

Ionization of alkanes to the corresponding alkyl cations in superacid media such as FSO_3H-SbF_5 and HF-SbF_5 has been well investigated.[1] The reaction of alkyl cations thus obtained with nucleophiles such as benzene[2] and carbon monoxide[3] has also been described. Paatz and Weisgerber reported that the reactions of isopentane, methylcyclopentane or cyclohexane with carbon monoxide in the presence of HF-SbF_5 at room temperature under atmospheric pressure gave C_6- or C_7-acids along with some ketones.[4] The reaction is highly interesting, especially because of the mild reaction conditions.[5,6] However, no extensive studies of the reaction have been reported to date. We have therefore undertaken a detailed study, using alkanes with various skeletal structures in order to clarify the reaction of alkyl cations derived from the alkanes with carbon monoxide in superacidic media.[7]

In this report, we shall discuss the reaction, initiated by the ionization of σ-bonds in alkanes, followed by trapping with carbon monoxide and quenching with water to give carboxylic acids. Our discussion will be based on the detailed analysis of the composition and isomer distribution of the products.

Experimental

Materials. Pure alkanes and carbon monoxide were of commercially available and were used without further purification. SbF_5 and anhydrous hydrogen fluoride were distilled, twice and once, respectively.

General Procedure of Carboxylation. A solution of HF-SbF_5 (5:1 molar ratio, ca. 20 ml) was placed in a 100-ml Kel-F three-necked reaction vessel under vigorous stirring at an appropriate temperature. The substrate (5—20 mmol) was added dropwise during 15 min to the acid solution, while carbon monoxide was introduced at a constant flow rate of 20 ml min^{-1} at 30 °C. After the reaction was completed, the resulting solution was hydrolyzed with ice-water, and the product obtained after usual work-up[8] were identified by means of GLC, GC-mass, IR, NMR spectrometry, and by comparison with authentic samples.

Carboxylic Acids as Authentic Samples. Propanoic acid (**1**), 2-methylpropanoic acid (**2**), 2,2-dimethylpropanoic acid (**3**), 2-methylbutanoic acid (**4**) and 2,2-dimethylbutanoic acid (**8**) are commercially available. 2-Methylpentanoic acid (**5**),[21] 2-ethylbutanoic acid (**6**),[21] 2,3-dimethylbutanoic acid (**7**),[22] 2,2-dimetylbutanoic acid (**8**),[23] 2,2,3-trimethylbutanoic acid (**9**),[24] 2-ethyl-2-methylbutanoic acid (**10**),[15] 2,2-dimethylpentanoic acid (**11**),[15] 2-ethyl-3-methylbutanoic acid (**12**),[25] 2,3-dimethylpentanoic acid (**13**),[26] 2-methylhexanoic acid (**14**),[27] 2-ethylpentanoic acid (**15**),[28] 2,3,3-trimethylbutanoic acid (**16**),[29] 2,4-dimethylpentanoic acid (**17**)[30] and 2,2,3,3-tetramethylbutanoic acid (**18**),[31] were prepared according to Hussey's[9] or/and Creper's[10] methods and identified with the aid of IR, NMR, and MS. All products were liquid except for **18** (mp 198—199 °C, lit,[30] 198.5—199.5 °C) and exhibited reasonable spectra. These were esterified with diazomethane.[8] The retention times and volumes of GLC (Hitachi FID-063, Column: Silicon DC-550. 45 m, 150 °C) of these methyl esters were appropriate as a means of qualitative and quantitative identification for the products.

Results and Discussion

The results of the reaction of C_5- and C_6-alkanes with carbon monoxide are shown in Tables 1 and 2. Tables 1 and 2 indicate that the isomer distribution of the major products (C_6-acids and C_7-acids) are independent of the individual skeletal structures of the starting alkanes under the same conditions. A considerably high yield of secondary carboxylic acids are found in the products. In a marked contrast, it was reported that tertiary carboxylic acids were exclusively produced from nonbranched alkenes or alcohols in the Koch-Haaf carboxylation using usual strong acids such as H_2SO_4.[11] It is likely that the reaction of branched C_5- and C_6-alkanes is readily initiated by

† Present address: Department of Industrial Chemistry, Kitami Institute of Technology, Kitami 090.

Table 1. Carboxylation of C_5- and C_6-Alkanes

Alkane	Total yield %	Composition and distribution of carboxylic acids/%									
		C_3-Acid	C_4-Acid	C_5-Acids		C_6-Acids				C_7-Acids	C_8-Acids
		1	**2**	**3**	**4**	**5**	**6**	**7**	**8**		
Pentane	53	3	26	14		57				Some	—
				25	75	12	11	38	39		
2-Methylbutane	55	Some	Some	4		96				Some	—
				67	33	13	11	38	38		
Hexane	69	2	10	18		5				65	Some
				13	87	11	10	41	39		
2-Methylpentane	61	—	Some	3		3				94	—
				67	33	10	9	41	40		
3-Methylpentane	66	—	Some	4		3				93	—
				20	80	10	10	40	40		
2,3-Dimethylbutane	63	—	4	Some		5				91	—
						9	9	40	42		
2,2-Dimethylbutane	57	—	Some	10		15				75	—
				80	20	10	11	39	40		

Reaction conditions: Reaction time, 1 h; reaction temp, 30 °C; alkane, 20 mmol; SbF_5/alkane molar ratio, 2; HF/SbF_5 molar ratio, 5.

Table 2. Isomer Distribution of C_7-Acids in the Carboxylation of Hexanes[a)]

Substrate	React. time h	Isomer distribution of C_7-acids/%									Sec./tert. ratio
		Tert. acids			Sec. acids						
		9	**10**	**11**	**12**	**13**	**14**	**15**	**16**	**17**	
Hexane	1.0	12	9	12	15	11	4	7	25	5	67/33
2-Methylpentane	1.0	10	9	10	16	12	5	7	26	5	71/29
3-Methylpentane	1.0	10	9	11	16	13	5	7	24	5	70/30
2,3-Dimethylbutane	1.0	10	9	11	16	12	5	7	26	5	70/30
2,3-Dimethylbutane	1.0	11	9	12	16	12	4	7	25	4	68/32
Hexanes[b)]	0.2	15	20	20	10	7	3	3	19	3	45/55
Hexanes[b)]	0.5	13	16	15	14	10	3	5	22	3	56/44
Hexanes[b)]	1.0	10	9	11	16	13	5	7	24	5	70/30
Hexanes[b)]	3.0	7	8	8	17	13	5	8	28	7	75/25
Hexanes[b)]	5.0	6	8	8	18	12	6	9	28	7	78/22

a) Reaction conditions: See footnote in Table 1. b) 3-Methylpentane. 2-Methylpentane and 2,3-dimethylbutane gave almost the same results.

protonolysis[12)] at their tertiary C–H bonds to give the corresponding tertiary alkyl cations which in turn undergo skeletal isomerization via secondary alkyl cations.[13)] The alkyl cations under the present conditions seem more electrophilic[14)] than those expected in the reaction of alkenes, alcohols or alkyl halides under the Koch–Haaf conditions. The Koch–Haaf conditions usually require either high temperature and pressure or a high concentration of carbon monoxide achieved by use of copper(I) carbonyl catalyst under highly acidic conditions.[15,16)] These alkyl cations can react with carbon monoxide to form acyl cations which give the corresponding carboxylic acids by quenching with water as shown in Scheme 1. When the reaction time is longer, as is the case with the reaction of hexanes as shown in Table 2, the ratio of secondary carboxylic acids **12—17** to tertiary ones **9—11** is increased and the isomer distributions in the product seem to attain an equilibrated state after 3 h. Tertiary alkyl cations, **A–C** in Scheme 1, derived from starting alkanes (2-methylpentane, 3-methylpentane and 2,3-dimethylbutane) rearrange rapidly to reach an equilibrium with each other which can be observed by NMR as demonstrated by Brouwer.[13)] Secondary alkyl cations **D–I** may form as transient intermediates in the course of the re-

arrangement of initially formed tertiary alkyl cations to other tertiary skeletal ones. Although spectroscopic attempts to observe the formation of such secondary cations in superacids were unsuccessful.[17] These alkyl cations may be in a high concentration and/or have a sufficiently long life time in a HF-SbF_5 solution to bring about the reaction with carbon monoxide. Thus, isomer distributions of carboxylic acids found in the initial stage of reaction depend largely on the equilibrium mixtures of these isomeric alkyl cations

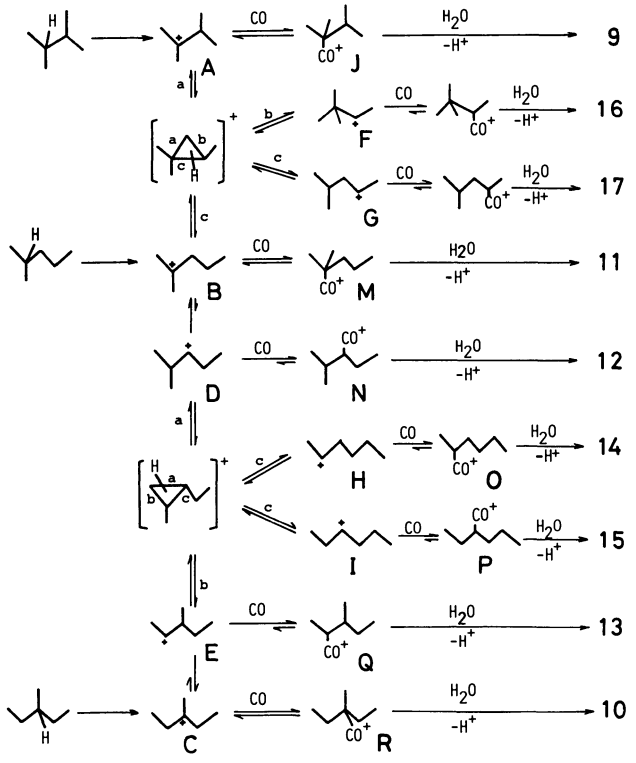

Scheme 1.

A–I including the secondary ones. On the other hand, when the reaction time is longer, an actual increase in the ratio of the secondary carboxylic acids **12—17** to tertiary ones **9—11** occurs. This seems unreasonable because of the rearrangement from more stable tertiary carbocations to less stable secondary ones is unlikely. This would probably result from the equilibration of alkanoyl cations **J–R**.[18,19]

For straight chain C_5- or C_6-alkanes, on the other hand, the protonolysis at carbon-carbon bonds takes place to give fragment alkyl cations **S–T** and C_1- — C_4-alkanes where the protonolysis at secondary C–H bonds in the substrate is preferred as shown in Scheme 2. The fragment alkyl cations **S–U** thus formed are responsible for the preferred formation of carboxylic acids **1—4** with the alkyl group of a lower number of carbon atoms than the starting alkanes (Eqs. 1—4). They are also responsible for the ionizaton of starting alkanes by the abstraction of hydride ion at secondary C–H bonds which in turn produced carboxylic acids with the alkyl group with the same number of carbon atoms as in the starting alkanes (Eq. 5). Thus, compared with the reaction of branched C_5- and C_6-alkanes, a considerably large amount of gaseous hydrocarbons, i.e., methane, ethane, propane and butanes were observed in these reactions.

The isomer distribution of C_6- and C_7-carboxylic acids are the same as that in the reaction of branched alkanes. As shown in Table 1, however, there is a distinction among the isomer distributions of C_5-carboxylic acids produced in the reactions of C_5- and C_6-alkanes. This can be explained by the slow occurrence of the skeletal isomerization of butyl cations arising from suitable protonolysis at carbon-carbon bonds in the substrates compared to those of pentyl, **Y** and **Z**, or higher alkyl cations as demonstrated by Brouwer.[13]

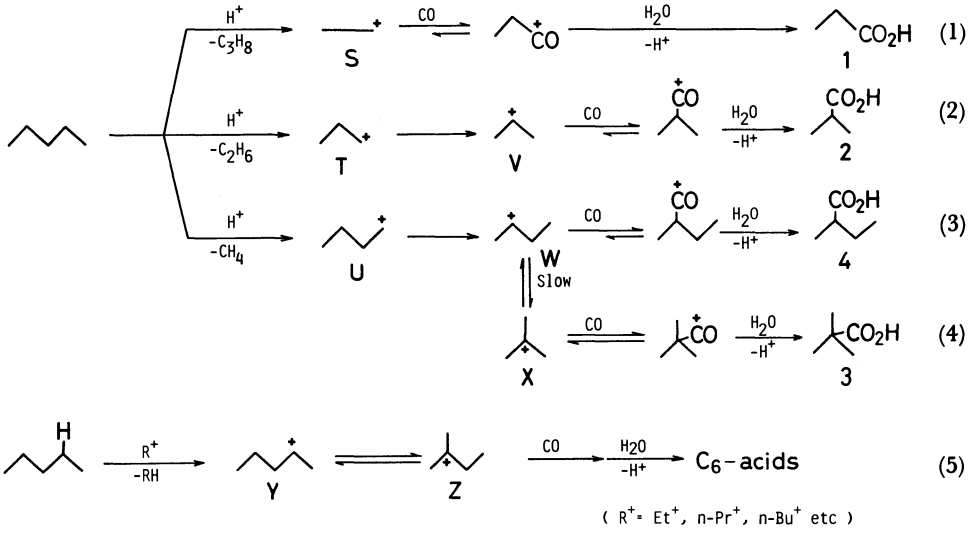

Scheme 2.

Table 3. Carboxylation of C_7-, C_8-, and C_9-Alkanes

Alkane	Total yield %	Composition and distribution of carboxylic acids/%									
		C_3-Acid	C_4-Acid	C_5-Acids		C_6-Acids				C_7-Acids	C_8-Acids
		1	2	3	4	5	6	7	8		
Heptane	80	Some	47	48		5				Some	Some
				90	10	17	10	35	38		
3-Methylhexane	98	—	4	92		4				Some	—
				96	4	12	10	36	42		
2,4-Dimethylpentane	92	—	79	21		Some				Some	Some
				98	2						
2,3-Dimethylpentane	94	—	70	28		2				Some	Some
				98	2	13	10	33	44		
2,3,4-Trimethylbutane	102	—	65	35		Some				Some	Some
				99	1						
Octane	90	Some	6	87		7				Some	Some
				90	10	15	10	37	38		
2,4,4-Trimethylpentane	102	—	—	100		—				—	—
				100	—						
Nonane	75	Some	34	31		33				2	—
				87	13	12	10	40	38		

Reaction conditions: See footnote in Table 1.

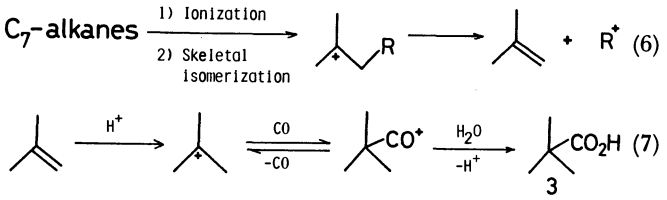

Scheme 3.

In contrast to C_5- or C_6-alkanes, the reactions of such substrates having seven or eight carbon atoms gave C_4- and/or C_5-carboxylic acids almost exclusively, as shown in Table 3. In other words, these alkanes can give a small amount of C_8-, C_9- or C_{10}-carboxylic acids with an alkyl group of the same number of carbon atoms of starting alkanes. From the product distribution, these alkanes, as shown in Eqs. 6 and 7 in Scheme 3, were ionized in the same fashion as those in the case of C_5- or C_6-alkanes. They gave alkyl cations which easily undergo exclusive β-scission and produce fragment alkyl cations R^+ and 2-methylpropene resulting from the preferential formation of **3** under the present reaction conditions. Interestingly, the product distribution obtained in the reaction of C_7-alkanes is quite different from those found in the reaction of alcohols or halides having the same carbon skeletal structure as alkanes under the same reaction conditions. 2,4-Dimethyl-2-pentanol, for example, reacted with carbon monoxide and water to give a considerable amount of C_6- and C_7-carboxylic acids together with C_4- and C_5-carboxylic acids. This is in contrast with the product distribution in the reaction of 2,4-dimethylpentane which yielded 79% of **2** and 21% of **3** without any other products under the same conditions as shown in Scheme 4. C_7-alkyl cations, which were formed in the reaction of the alcohols in a HF–SbF_5 solution, may be abundant and may give rise to oligocondensation to produce such alkyl cations which have fourteen or more carbon atoms. These oligocondensed alkyl cations undergo β-scission to give *t*-butyl cation and C_6-cations which in turn gave C_5- and C_7-carboxylic acids, respectively. C_6-acids may arise from C_5-alkyl cations derived from another β-scission process of these or other oligocondensed alkyl cations. 2,4-Dimethylpentane, on the other hand, may be ionized slowly to yield the alkyl cation, because mass transfer between acid and the hydrocarbon phase is a rate-determining step. Such an alkyl cation may take place in a limited oligocondensation with each other. Thus, β-scission of the alkyl cation may take place predominantly to produce 2-methylpropene and isopropyl cation which in turn gave C_4- and C_5-carboxylic acids.

Another characteristic feature in the reaction of C_7-alkanes is the product compositions which differ from each other as shown in Table 4. The exact reaction pathway giving these product distributions is not clear, but fragment alkyl cation R^+ (*t*-butyl or isopropyl cation), produced by β-scission of parent alkyl cations, may play an important role in the formation of C_5- and C_4-carboxylic acids and also in the ionization of the starting alkanes. This resulted in

Table 4. Products Found in Gaseous Phase in the Carboxylation of Tertiary C_7 Alkanes

Substrate	Products found in the gaseous phase/%				
	Isobutane	Butane	Propane	Ethane	Methane
3-Methylhexane	Some	1	90	8	Some
2,4-Dimethylpentane	82	Some	17	Some	—
2,3-Dimethylpentane	68	—	27	4	Some
2,2,3-Trimethylbutane	60	—	39	Some	Some

Reaction conditions: See footnote in Table 1.

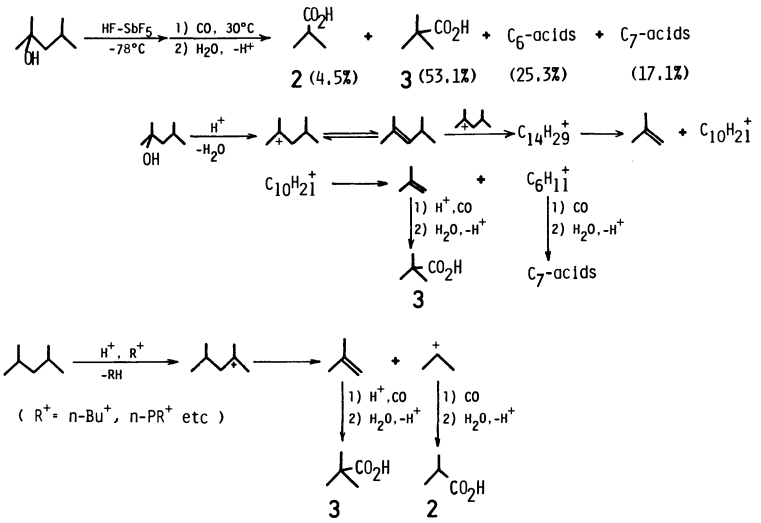

Scheme 4.

the formatiom of C_7-alkyl cations, and then propane and isobutane are produced by the intermolecular hydride ion transfer reaction as shown in Scheme 5. For C_7-alkanes, other than 2,4-dimethylpentane, initially formed C_7-alkyl cations must be rearranged in such an alkyl cation to give isopropyl and *t*-butyl cations by β-scission, since initially formed C_7-alkyl cations have unfavorable skeletal structures for β-scission reaction (Eqs. 8 and 10). The preferential formation of **2** prior to **3** and isobutane prior to propane in the reactions of 2,4-dimethylpentane, 2,3-dimethylpentane, and 2,2,3-trimethylbutane (Tables 3 and 4) are observed. *t*-Butyl cation, formed in Eq. 9, seems to play a much more important role to undergo intermolecular hydride abstraction from the starting C_7-alkanes in preference to that undergone by isopropyl cation in Eq. 9. Such a predominant occurrence of hydride abstraction with *t*-butyl cation may be attributed to the equilibrations in the reaction of these alkyl cations and carbon monoxide. Namely, the equilibrium of the reaction of isopropyl cation and carbon monoxide to produce isobutyryl cation leans far toward the isobutyryl cation compared to the reaction of *t*-butyl cation and carbon monoxide to produce pivaloyl cation[18] as seen in Eqs. 2 and 4 in Scheme 2. By these equilibrations, *t*-butyl cation may always exist in a higher concentration than isopropyl cation in the reaction mixture. The hydride abstraction of the substrate with the *t*-butyl cation (R^+) may proceed in Eqs. 8—10. On the other hand, in the case of C_7-alkanes, there is a much higher steric hindrance against the intermolecular hydride abstraction with *t*-butyl cation, than with the isopropyl cation. Such a steric hindrance may be expected in the following C_7-alkanes order.

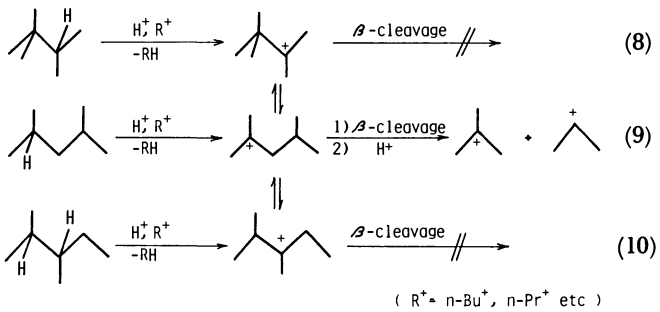

Scheme 5.

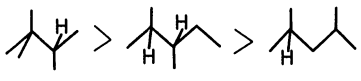

Thus, this steric factor renders the ratio of the products, i.e., between **2** and **3** or between isobutane and propane in these reactions variable as shown in

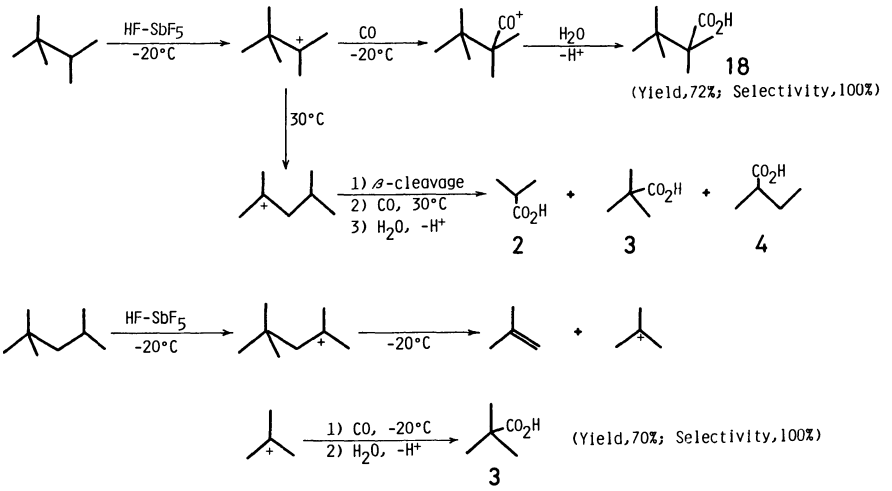

Scheme 6.

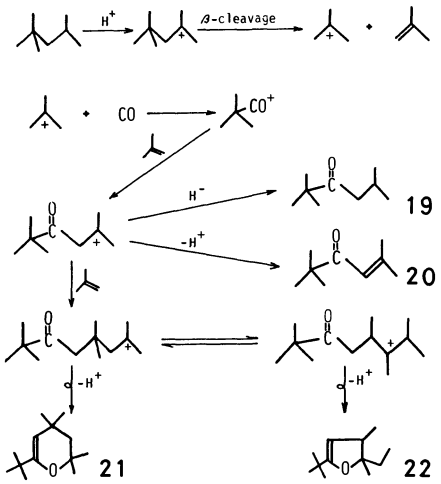

Scheme 7.

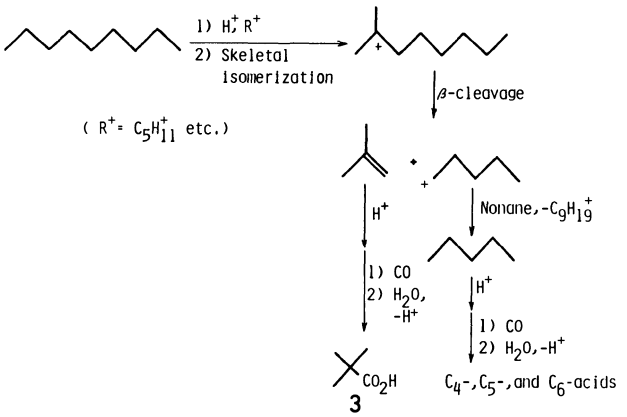

Scheme 8.

Tables 3 and 4. The preferred formation of **3** in the reaction of 2- or 3-methylhexane is still unclarified. However, judging from the preferred formation of propane in this case, it seems that the β-scission of the alkyl cations derived from these alkanes can afford *s*-propyl cation which is a highly reactive electrophile and can readily attack the tertiary C–H bond in the starting alkane.

In general, the lower the reaction temperature, the β-scission of alkyl cations is more difficult. The exclusive formation of **18** was observed in the reaction of 2,2,3-trimethylbutane in good yield at −20 °C as shown in Scheme 6. However, in the reaction of 2,2,4-trimethylpentane, initially formed 1,1,3,3-tetramethylbutyl cation undergoes the reaction involving the β-scission remarkably even at −20 °C to give *t*-butyl cation and 2-methylpropene which in turn reacts with carbon monoxide to yield **3** exclusively.

As shown in Scheme 7, when 2,2,3-trimethylpentane is in excess relative to SbF_5 (alkane/SbF_5 molar ratio 2, HF/SbF_5 molar ratio 10), ketones (**19**/(20%), **20**/(31%)) and cyclic ethers (**21**+**22**/29%) were produced together with **3** and 2-methylpropane.[20] A large amount of 2-methylpropene was formed from the β-scission of initially formed 1,1,3,3-tetramethylbutyl cation may react directly with pivaloyl cation resulting in the formation of these ketones and cyclic ethers.

In the reaction of nonane, a large amount of C_6-carboxylic acids together with C_4- and C_5-carboxylic acids were formed as shown in Table 3. The principal reaction path accompanied with β-scission of initially formed alkyl cation may be again well accounted for in the product composition as shown in Scheme 8. The intermolecular hydride ion shift between the substrate and primary pentyl cation produced by the β-scission of the initially formed alkyl cation will give rise to pentane and C_9-alkyl cations. Pentane, thus formed, could react with carbon monoxide and water to yield C_4-, C_5-, and

C_6-carboxylic acids. Hence, the product composition in the reaction of nonane exhibited an almost similar product composition that was observed in the reaction of pentane itself as shown in Table 1. The only difference in the composition is that it has a relatively high distribution of **3** which may have arisen mostly from the reaction of 2-methylpropene formed by the β-scission of C_9-alkyl cations.

References

1) G. A. Olah, Y. Halpern, J. Shen, and Y. K. Mo, *J. Am. Chem. Soc.*, **95**, 4960 (1973); G. A. Olah, G. K. S. Prakash, and J. Sommer, "Superacids," John Wiley & Sons, New York (1985).

2) R. Miethchen and K. Wald, *Z. Chem.*, **14**, 53, 240, 354 (1974); *ibid.*, **15**, 135 (1975); G. A. Olah, P. Schilling, Y. Halpern, and J. A. Olah, *J. Am. Chem. Soc.*, **97**, 6807 (1975); D. Farcasiu, M. Siskin, and R. P. Rhodes, *ibid.*, **101**, 7671 (1979).

3) H. Hogeveen, J. Lukas, and C. F. Roobeek, *J. Chem. Soc., D*, **1969**, 920.

4) R. Paatz and G. Weisgerber, *Chem. Ber.*, **100**, 984 (1967).

5) The reaction of 2-methylbutane with carbon monoxide in the presence of $AlCl_3$ under the pressure of 150 atm and at 60 °C for 36 h was reported to give some ketones and a trace of carboxylic acids together with some polymers.[6)]

6) A. T. Balaban and C. D. Nenitzescu, *Justus Liebigs Ann. Chem.*. **625**, 66 (1959); H. Pines, V. N. Ipatieff, *J. Am. Chem. Soc.*, **69**, 1337 (1947); H. Hoff, *Angew. Chem.*, **60**, 245 (1948).

7) N. Yoneda, Y. Takahashi, T. Fukuhara, and A. Suzuki, *Chem. Lett.*, **1983**, 17.

8) N. Yoneda, Y. Matsushima. M. Matsubara, and H. Ohtsuka, *Bull. Jpn. Petr. Inst.*, **14**, 178 (1972); M. Matsubara, Y. Matsushima, N. Yoneda, and H. Ohtsuka, *Kogyo Kagaku Zasshi*, **73**, 2147 (1970).

9) A. S. Hussey, *J. Am. Chem. Soc.*, **73**, 1364 (1951).

10) P. L. Creger, *J. Am. Chem. Soc.*, **92**, 1397 (1970).

11) H. Bahrmann, "New Syntheses with Carbon Monoxide," ed by J. Falbe, Springer-Verlag, N. Y. (1980), p. 372.

12) G. A. Olah, Y. Halpern, J. Shen, and Y. K. Mo, *J. Am. Chem. Soc.*, **93**, 1251 (1971).

13) D. M. Brouwer and J. M. Oelderik, *Recl. Trav. Chim. Pays-Bas*, **87**, 319 (1968).

14) N. Yoneda, T. Fukuhara, Y. Takahashi, and A. Suzuki, *Chem. Lett.*, **1979**, 1003.

15) H. Koch, *Brennstoff-Chemie*, **36**, 321 (1955); K. E. Moller, *ibid.*, **47**, 10 (1966); H. Koch and W. Haaf, *Justus Liebigs Ann. Chem.*, **618**, 251 (1958).

16) Y. Souma, H. Sano, and J. Iyoda, *J. Org. Chem.*, **38**, 2016 (1973); Y. Souma and H. Sano, *Bull. Chem. Soc. Jpn.*, **46**, 3237 (1973); N. Yoneda, T, Fukuhara, Y, Takahashi, and A. Suzuki, *Chem. Lett.*, **1974**, 607; N. Yoneda, T. Fukuhara, Y. Takahashi, and A. Suzuki, *Bull. Chem. Soc. Jpn.*, **51**, 2347 (1978).

17) G. A. Olah and J. A. Olah, "Alkylcarbonium Ions," in "Carbonium Ions," ed by G. A. Olah and P. von R. Schleyer, Wiley-Interscience, New york (1970), Vol. 3, Chap. 17, pp. 715—782.

18) G. A. Olah, E. B. Baker, W. S. Tolgyesi, J. S. McIntyre, and I. J. Bastier, *J. Am. Chem. Soc.*, **86**, 1360, (1964).

19) H. Hogeveen, *Adv. Phys. Org. Chem.*, **10**, 29 (1973).

20) Y. Takahashi, H. Fujimori, N. Yoneda, and A. Suzuki, *Nippon Kagaku Kaishi*, **1977**, 1861.

21) F. F. Bentley, M. T. Ryan, and J. E. Katon, *Spectrochim. Acta*, **20**, 685 (1964).

22) J. K. Stille, F. Huang, and M. T. Ryan, *J. Am. Chem. Soc.*, **96**, 1518 (1974).

23) W. L. Senn, Jr. and A. Pine, *Anal. Chim. Acta*, **31**, 441 (1964).

24) N. J. Turro, G. W. Byers, and P. A. Leemakers, *J. Am. Chem. Soc.*, **86**, 955 (1964).

25) G. Slomp, Jr. and J. L. Johnson, *J. Am. Chem. Soc.*, **80**, 915 (1958).

26) P. Pino, R. Rossi, and P. Bucci, *Tetrahedron Lett.*, **1966**, 3295.

27) D. L. Guertin, S. E. Wiberley, W. H. Bauer, and J. Goldson, *Anal. Chem.*, **28**, 1194 (1956).

28) R. M. Adams and C. A. Van der Werf, *J. Am. Chem. Soc.*, **72**, 4368 (1950).

29) R. S. Shell and R. H. Reihenbacher, *J. Am. Chem. Soc.*, **90**, 3436 (1968).

30) K. Alder and H. R. Brackel, *Justus Liebigs Ann. Chem.*, **651**, 141 (1962).

31) L. Tsai, T. Miwa, and N. S. Newman, *J. Am. Chem. Soc.*, **79**, 2530 (1957).

 © 1986 The Chemical Society of Japan Bull. Chem. Soc. Jpn., 59, 2827—2831 (1986)

A Convenient Preparative Method of Nitrile Oxides by the Dehydration of Primary Nitro Compounds with Ethyl Chloroformate or Benzenesulfonyl Chloride in the Presence of Triethylamine

Tomio SHIMIZU,* Yoshiyuki HAYASHI, Hiroshi SHIBAFUCHI, and Kazuhiro TERAMURA
Department of Color Chemistry and Technology, Faculty of Industrial Arts,
Kyoto Institute of Technology, Matsugasaki, Sakyo-ku, Kyoto 606
(Received February 17, 1986)

Three nitrile oxides (MeOCOC≡N→O, PhC≡N→O, and EtC≡N→O) were effectively generated in situ by dehydration of the corresponding primary nitro compounds (RCH_2NO_2) with $PhSO_2Cl$ or ClCOOEt in the presence of triethylamine. Various cycloadducts were prepared by the reaction of them with dipolarophiles. Some advantages of these methods are described in comparison with other known methods.

1,3-Dipolar cycloaddition reaction using nitrile oxides is one of the versatile methods for the preparation of five-membered heterocycles.[1] Preparation of nitrile oxides by the dehydration of primary nitro compounds has been known so far.[2-8] Following combinations of reagents have been known to be effective for the dehydration; (a) PhNCO and Et_3N,[3] (b) Ac_2O and AcONa,[4] (c) AcCl and MeONa,[5] (d) *p*-TsOH,[6] (e) $POCl_3$,[3d] (f) Diketene and Na,[7] and (g) H_2SO_4.[8] The most widely used one among these methods is (a). Though the method has been known to be sufficiently effective for the preparation of a variety of heterocycles, an equimolar amount of *N,N'*-diphenylurea is formed as a by-product during the reaction. In many cases, separation of the by-product from the reaction mixture can be accompilshed easily by filtration because diphenylurea shows very low solubilities towards many organic solvents. But, in some cases, the desired heterocyclic compounds also show solubilities similar to that of diphenylurea towards organic solvents, thus, the separation is often tedious. Recently, we reported the cycloaddition reactions of dipolarophiles with nitrile oxides prepared by the action of a catalytic amount of *p*-TsOH on primary nitro compounds [method (d)].[6a] Though this reaction gave no such by-products and the yields of the desired heterocycles are also comparable to those by the method (a), good results could not be attained in some cases where the primary nitro compounds bear thermally labile functional groups because of the necessity of the high reaction temperature (>140 °C).

Hydrolysis of ethyl chloroformate or benzenesulfonyl chloride gives water soluble products, (EtOH+HCl+CO_2) or ($PhSO_3H$+HCl). The use of these reagents for the dehydration of primary nitro compounds has the advantage that the by-products can be removed easily by washing the reaction mixture with water. We report here the usefulnes of the combination of reagents such as ClCOOEt/Et_3N and $PhSO_2Cl$/Et_3N for the dehydration of primary nitro compounds.

Results and Discussion

The reaction of methyl nitroacetate (**1**) with allyl *p*-nitrophenyl ether in the presence of various amounts of ClCOOEt and Et_3N in several kinds of solvents was examined in order to search the optimum reaction conditions. Table 1 summarizes the results along with yields of the cycloadduct, methyl 5-(*p*-nitrophenoxymethyl)-2-isoxazoline-3-carboxylate (**2f**). Table 1 suggests that the maximum yield of the cyclo-

Table 1. Reaction of Methyl Nitroacctate (**1**) with Allyl *p*-Nitrophenyl Ether under Various Conditions

Run	Molar ratio of **1** : CH_2=$CHCH_2OAr$: ClCOOEt : Et_3N				Solv.	Reaction time/h	Temp °C	Yield of **2f**/%
1	1	1	1	1	C_6H_6	20	80	30
2	1	1	2	2	C_6H_6	20	r.t.*	30
3	1	1	3	3	—	6	80	41
4	1	1	2	2	C_6H_6	6	80	43
5	1	1	2	2	$CHCl_3$	6	60	34
6	1	1	2	2	THF	6	67	34
7	1	1	2	2	CH_3CN	6	82	21
8	1	1	2	2	Et_2O	6	34	10
9	1	1	2	2	DMF	6	50	5
10	1	1	3	3	C_6H_6	6	80	34

* Room temperature.

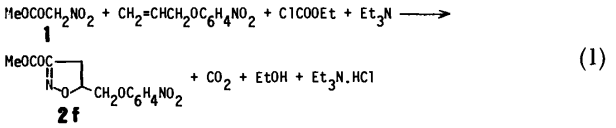

(1)

adduct was obtained by the treatment of the substrates with two molar amount of the dehydrating agents in benzene at the refluxing temperature (Method A). As expected, evolution of CO_2 gas and formation of ethanol were observed.

We also examined the reactions of (nitromethyl)benzene (**4**) with allyl *p*-nitrophenyl ether in the presence of benzenesulfonyl chloride (or methanesulfonyl chloride) and Et_3N under various conditions (Table 2). In

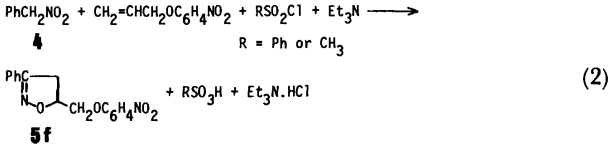

(2)

this case, the optimum conditions for the cycloadduct, 3-phenyl-5-(*p*-nitrophenoxymethyl)-2-isoxazoline (**5f**), were as follows; the use of two molar amounts of benzenesulfonyl chloride and Et_3N, and chloroform as a solvent at room temperature (Method B). Reactions of some primary nitro compounds (**1**, **4**, and **7**) with a number of dipolarophiles were carried out under these conditions (Method A and B). Table 3 summarized the results. The yields obtained in the reaction by use of another dehydrating agents are also shown for convenience of comparison.

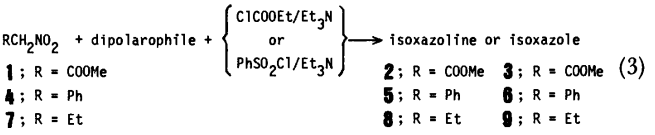

(3)

The structure of the cycloadducts, 2-isoxazolines (**2**, **5**, and **8**) and isoxazoles (**3**, **6**, and **9**), were established by the comparison of the spectral and physical proper-

Table 2. Reaction of (Nitromethyl)benzene (**4**) with Allyl *p*-Nitrophenyl Ether under Various Conditions

Run	4	CH_2=$CHCH_2OAr$	RSO_2Cl	Et_3N	Solv.	Reaction time/h	Temp °C	Yield of **5f**
1	1	1	1.2(R=CH_3)	1.2	C_6H_6	6	80	12%
2	1	1	1.2(R=CH_3)	1.2	CCl_4	6	77	16%
3	1	1	1.2(R=CH_3)	1.2	$CHCl_3$	6	60	10%
4	1	1	1.2(R=Ph)	1.2	C_6H_6	6	80	40%
5	1	1	1.2(R=Ph)	1.2	CCl_4	6	77	39%
6	1	1	1.2(R=Ph)	1.2	$CHCl_3$	6	60	48%
7	1	1	1.2(R=Ph)	1.2	C_6H_6	15	r.t.	41%
8	1	1	1.2(R=Ph)	1.2	$CHCl_3$	15	r.t.	47%
9	1	1	2 (R=Ph)	2	C_6H_6	15	r.t.	40%
10	1	1	2 (R=Ph)	2	$CHCl_3$	15	r.t.	73%
11	1	1	3 (R=Ph)	3	$CHCl_3$	15	r.t.	68%

Table 3. Yields of Cycloadducts[a] by Method A, B, and Other Known Methods

Dipolarophile		Method A	Method B	Other Method		Method A	Method B	Other Method		Method A	Method B	Other Method
Norbornene	**2a**	45%	50%		**5a**	83%	64%		**8a**	10%	72%	
CH_2=$CHOC_4H_9$-*n*	**2b**	74%	40%		**5b**	80%	45%		**8b**	6%	34%	62%[b]
CH_2=$CHOCOCH_3$	**2c**	27%			**5c**	20%	43%	84%[c]	**8c**		57%	89%[b]
CH_2=$CHC_{12}H_{25}$-*n*	**2d**	33%	2%	25%[d]	**5d**	31%	78%	45%[d]	**8d**		49%	
CH_2=$CHCH_2Ph$	**2e**	21%		15%[d]	**5e**	24%	60%	29%[d]	**8e**	17%	46%	
CH_2=$CHCH_2O$-$C_6H_4NO_2$-*p*	**2f**	43%	5%	22%[d]	**5f**	53%	73%	42%[d]	**8f**		42%	
CH_2=CHPh	**2g**	47%	19%		**5g**	22%	75%		**8g**	6%	58%	58%[b]
CH_2=CHCN	**2h**	40%			**5h**	30%	59%		**8h**	3%	30%	92%[b]
CH_2=$CHCOOCH_3$	**2i**	5%			**5i**	64%	50%		**8i**		45%	45%[e]
Methyl methacrylate	**2j**	6%			**5j**	49%	75%		**8j**	4%	65%	
Dimethyl fumarate	**2k**	24%	3%	36%[d]	**5k**	46%	83%	76%[f]	**8k**		37%	58%[d]
N-Phenylmaleimide	**2l**	6%		70%[d]	**5l**	57%	73%	54%[d]	**8l**		42%	58%[d]
Phenylacetylene	**3a**	26%			**6a**	25%	70%	47%[f]	**9a**	6%	31%	30%[g]
MeOCOC≡CCOOMe	**3b**	30%	32%	20%[f]	**6b**	35%	80%	82%[h]	**9b**	13%	29%	30%[h]

a) The cycloadduct obtained from monosubstituted olefins, methyl methacrylate, and phenylacetylene is found to be 5-substituted regioisomer. b) Lit, 3a. c) Lit, 3b. d) Lit, 6a. e) Lit, 3d. f) Lit, 5a. g) Lit, 3e. h) Lit, 4a.

ties of the cycloadducts with those of anthentic specimens (see Experimental Section).

Almost cycloadducts can be easily isolated from the reaction mixtures after washing the reaction mixtures with water followed by usual work-up. However, in some cases by Method A, formation of an unexpected product made the isolation of desired cycloadducts difficult. The structre of the unexpected product was found to be R-C(Cl)=NOCO$_2$Et (**10a**: R=COOMe, **10b**: R=Ph, **10c**: R=Et) on the basis of elemental and spectral analyses, In fact, a considerable amount of **10** was obtained along with furazan 2-oxide, dimer of the nitrile oxide, in the rections of primary nitro compounds with ClCOOEt/Et$_3$N in the absence of dipolarophile. The formation of methyl 2-chloro-2-(benzoyloxyimino)acetate (**11**), MeOCOC(Cl)=NOCOPh, which has a structure similar to **10a**, has been reported in the dehydration reaction of **1** with benzoyl chloride and MeONa, and explained on the basis of 1,3-addition of benzoyl chloride to nitrile

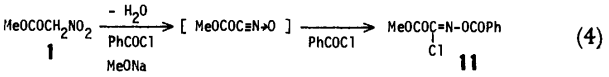

(4)

oxide.[5a] The formation of **10** in the present reaction may also be explained by a similar mechanism. The mechanism for the formation of nitrile oxide from primary nitro compounds by both Method A and B can be explained as shown in Scheme 1; i) abstraction of α-hydrogen of the primary nitro compounds by triethylamine gives its nitronate anion (**12**), ii) substitution reaction of ClCOOEt or PhSO$_2$Cl with the nitronate anion gives ethoxycarbonyl or benzenesulfonyl nitronate (**13** or **14**), respectively, and iii) elimination of EtOCO$_2$H or PhSO$_3$H from the nitronates via a cyclic transition state gives the nitrile oxides.

The present two methods for generation of nitrile oxides were found to be usefull ones for the preparation of 2-isoxazolines and isoxazoles because of the easiness of the operation and of the use of low-priced dehydrating agents.

Experimental

Measurements. All melting and boiling points are uncorrected. The ^{1}H NMR spectra were measured on a Varian T-60A instrument with Me$_4$Si as an internal standard; chemical shifts are given in δ units and coupling constants (J) are in herz units: s=singlet; d=doublet; t=triplet; q=quartet; m=multiplet br=broad singlet. The IR spectra were recorded on a Hitachi 215 Infrared Spectrophotometer. All new products gave satisfactory elemental analyses (±0.3% for C, H, and N).

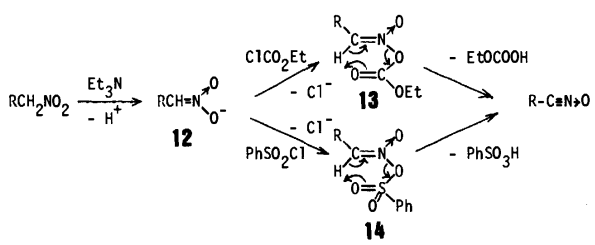

Scheme 1.

Materials. Methyl nitroacetate (**1**)[9] and (nitromethyl) benzene (**4**)[10] were prepared according to the method described in the literatures. Chloroform was used after passing through column chromatography on almina for the purpose of removal of contaminant ethanol which exists in the solvent as a stabilizer. The other chemicals were of commercial origin and were used without further purification.

Reation of Primary Nitro Compounds with Dipolarophiles in the Presence of Ethyl Chloroformate and Triethylamine (Method A). General Procedure. To a stirred benzene solution (50 ml) of primary nitro compound (0.01 mol), dipolarophile (0.01 mol), and ethyl chloroformate (2.17 g, 0.02 mol) was added a benzene solution (10 ml) of triethylamine (2.02 g, 0.02 mol) at room temperature. Gradual evolution of CO_2 (trapped as $CaCO_3$) and ethanol was observed in the course of the reaction. (Sometimes evolution of a small amount of ethyl chloride was also observed). After refluxing the benzene solution for 6 h, the reaction mixture was cooled and washed with water several times. The benzene solution was dried over sodium sulfate and evaporated in a rotary evaporator to give crude products. Crystalline crude products were recrystallized from the solvents and oily crude products were purified by the fractional distillation. In some cases, a small amount of R-C(Cl)=NOCOEt (R=CO$_2$Me, Ph, and Et) or Et$_2$NCO$_2$Et was also isolated by the fractional distillation. Yields of the cycloadducts are shown in Table 3. Similar yields of the cycloadducts were attained from the reaction using ClCOOMe instead of ClCOOEt.

Reaction of Primary Nitro Compounds with Dipolarophiles in the Presence of Benzenesulfonyl Chloride and Triethylamine (Method B). General Procedure. To a stirred chloroform solution (50 ml) of primary nitro compound (0.01 mol), dipolarophile (0.01 mol), and benzenesulfonyl chloride (3.53 g, 0.02 mol) was added triethylamine (2.02 g, 0.02 mol) below 10 °C. The mixture was stirred for 15 h at room temperature and then washed with water several times. The chloroform solution was dried over sodium sulfate and evaporated in a rotary evaporator. Distillation of PhSO$_2$Cl in vacuo from the residue gave crude products. Crystalline or oily products were purified according to the Method A. Complete elimination of PhSO$_2$Cl from the crude products can be easily attained by stirring them with aqueous 2-aminoethanol, though this operation can not be used for the compounds bearing ester functional group. Yields of the cycloadducts are shown in Table 3. Similar yields of the cycloadducts were obtained from the reaction using p-toluenesulfonyl chloride instead of PhSO$_2$Cl. Compounds (**2d—f**,[6a] **2g**,[12] **2l**,[6a] **3a**,[12] **3b**,[5a] **5a**,[11] **5c**,[3b] **5d—f**,[6a] **5g**,[13] **5h**,[14] **5i—j**,[15] **5k**,[5a] **5l**,[6a] **6a**,[5a] **6b**,[4a] **8b—c**,[3a] **8g—h**,[3a] **8i**,[3d] **8k—l**,[6a] **9a**,[3c] and **9b**[4a]) obtained by the Methods (A and/or B) were identified on the basis of the melting (or boilig) points and the spectral data. Melting (or boiling) points, NMR spectral data, and analytical data of the other cycloadducts were as follows; **2a**: Bp 115 °C/1.1 mmHg(1 mmHg=133.322 Pa); ^{1}H NMR (CDCl$_3$)

0.9—1.8 (m, 6H), 2.6 (br, 2H), 3.3 (d, 1H, J=8), 3.83 (s, 3H), 4.7 (d, 1H, J=8). Found: C, 61.49; H, 6.68; N 7.22%. Calcd for $C_{10}H_{13}NO_3$: C, 61.52; H, 6.71; N, 7.18%. **2b**: Bp 137 °C/5 mmHg; ^{1}H NMR ($CDCl_3$) δ=0.9 (t, 3H, J=7), 1.1—1.9 (m, 4H), 2.97 (dd, 1H, J=3 and 18), 3.33 (dd, 1H, J=6 and 18), 3.3—4.0 (m, 2H), 3.9 (s, 3H), 5.73 (dd, 1H, J= 3 and 6). Found: C, 53.85; H, 7.50; N, 7.02%. Calcd for $C_9H_{15}NO_4$: C, 53.72; H, 7.51; N, 6.96%. **2c**: Bp 115 °C/1 mmHg; ^{1}H NMR ($CDCl_3$) δ=2.1 (s, 3H), 3.13 (dd, 1H, J=3 and 19), 3.53 (dd, 1H, J=6 and 19), 3.93 (s, 3H), 6.8 (dd, 1H, J=3 and 6). Found: C, 44.90; H, 5.04; N, 7.44%. Calcd for $C_7H_9NO_5$: C, 44.92; H, 4.85; N, 7.48%. **2h**: Bp 116 °C/1 mmHg; ^{1}H NMR ($CDCl_3$) δ=3.6 (d, 2H, J=9), 3.93 (s, 3H), 5.47 (t, 1H, J=9). Found: C, 46.90; H, 3.95; N, 18.42%. Calcd for $C_6H_6N_2O_3$: C, 46.76; H, 3.92; N, 18.18%. **2i**: Bp 130 °C/4 mmHg; ^{1}H NMR ($CDCl_3$) δ=3.5 (d, 2H, J=9), 3.8 (s, 3H), 3.9 (s, 3H), 4.22 (dd, 1H, J=9 and 11). Found: C, 44.99; H, 4.73; N, 7.55%. Calcd for $C_7H_9NO_5$: C, 44.92; H, 4.85; N, 7.48%. **2j**: Bp 122 °C/1.7 mmHg; ^{1}H NMR ($CDCl_3$) δ=1.67 (s, 3H), 3.03 (d, 1H, J=18), 3.75 (d, 1H, J=18), 3.8 (s, 3H), 3.9 (s, 3H). Found: C, 47.75; H, 5.49; N, 7.00%. Calcd for $C_8H_{11}NO_5$: C, 47.76; H, 5.51; N, 6.96%. **5b**: Bp 141 °C/1 mmHg; ^{1}H NMR ($CDCl_3$) δ=0.9 (t, 3H, J=7), 1.1—1.9 (m, 4H), 3.1 (dd, 1H, J=3 and 18) 3.45 (dd, 1H, J=6 and 18), 3.4—4.0 (m, 2H), 5.67 (dd, 1H, J=3 and 6), 7.2—7.6 (m, 3H), 7.6—7.8 (m, 2H). Found: C, 71.07; H, 7.69; N, 6.54%. Calcd for $C_{13}H_{17}NO_2$: C, 71.20; 7.82; 6.39%. **8a**: Bp 88 °C/1 mmHg; ^{1}H NMR ($CDCl_3$) δ=0.9—1.8 (m, 9H), 2.0—2.6 (m, 4H), 3.0 (d, 1H, J=8), 4.4 (d, 1H, J=8). Found: C, 72.88; H, 9.01; N, 8.51%. Calcd for $C_{10}H_{15}NO$: C, 72.69; H, 9.15; N, 8.48%. **8d**: Mp 35—36 °C (from methanol), bp 163 °C/1 mmHg: ^{1}H NMR ($CDCl_3$) δ=0.7—1.7 (m, 28H), 2.35 (q, 2H, J=7), 2.5 (dd, 1H, J=9 and 18), 3.0 (dd, 1H, J=11 and 18), 4.3—4.8 (m, 1H). Found: C, 76.30; H, 12.44; N, 5.21%. Calcd for $C_{17}H_{33}NO$: C, 76.33; H, 12.44; N, 5.24%. **8e**: Bp 144 °C/3.4 mmHg; ^{1}H NMR ($CDCl_3$) δ=1.1 (t, 3H, J=7), 2.3 (q, 2H, J=7), 2.55—3.3 (m, 4H), 4.5—5.1 (m, 1H), 7.27 (s, 5H). Found: C, 76.34; H, 8.22; N, 7.45%. Calcd for $C_{12}H_{15}NO$: C, 76.15: H, 7.99; N, 7.40%. **8f**: Mp 83—85 °C (from ethanol); ^{1}H NMR ($CDCl_3$) δ=1.2 (t, 3H, J=7), 2.4 (q, 2H, J=7), 2.9—3.2 (m, 2H), 4.1 (d, 2H, J=6), 4.6—5.2 (m, 1H), 6.97 (d, 2H, J=8), 8.2 (d, 2H, J=8). Found: C, 57.61; H, 5.63; N, 11.10%. Calcd for $C_{12}H_{14}N_2O_4$: C, 57.59; H, 5.64; N, 11.20%. **8j**: Bp 83 °C/1.7 mmHg; ^{1}H NMR ($CDCl_3$) δ=1.15 (t, 3H, J=7), 1.6 (s, 3H), 2.35 (q, 2H, J=7), 2.77 (d, 1H, J=18), 3.47 (d, 1H, J=18), 3.75 (s, 3H). Found: C, 56.08; H, 7.66; N, 8.11%. Calcd for $C_8H_{13}NO_3$: C, 56.12; H, 7.65; N, 8.18%.

An Equimolar Reaction of Primary Nitro Compounds with ClCOOEt in the Presence of Triethylamine. An equimolar (0.02 mol) mixture of primary nitro compound (**1**, **4**, or **7**), ClCOOEt, and triethylamine in benzene (50 ml) was refluxed for 6 h. The reaction mixture was washed with water several times, and then evaporated in a rotary evaporator. In the case of $PhCH_2NO_2$ (**4**), residual crystals were recrystallized from ethanol to give pure 3,4-diphenylfurazan 2-oxide in 60% yield; mp 112—114 °C (lit,[16] 114 °C). In the case of $MeOCOCH_2NO_2$ (**1**), residual oil was distilled in vacuo to give pure dimethyl 3,4-furazan-dicarboxylate 2-oxide in 25% yield; bp 115 °C/2 mmHg (lit,[16] 151 °C/10 mmHg). In the case of 1-nitropropane, distillation of residual oil gave recovered nitropropane (30%) and ethyl diethylcarbamate (20%) [bp 73 °C/25 mmHg (lit,[17] bp 165 °C)].

Reaction of Primary Nitro Compounds with Double the Molar Quantity of ClCOOEt and Triethylamine. To a benzene solution (50 ml) of primary nitro compound (0.02 mol) and ClCOOEt (0.04 mol) was added triethylamine (0.04 mol) and then the mixture was refluxed for 6 h. After filtration of triethylamine hydrochloride the filtrate was evaporated to give oily residue, which was distilled in vacuo to give esters of chloroximes; **methyl 2-chloro-2-(ethoxycarbonyldioxyimino)acetate (10a)**: 25% Yield, bp 100 °C/1 mmHg; ^{1}H NMR (δ) in $CDCl_3$; 1.4 (t, 3H, J=7), 4.0 (s, 3H), and 4.2 (q, 2H, J=7). Found: C, 34.64; H, 3.96; N, 6.69; Cl, 16.72%. Calcd for $C_6H_8NO_3Cl$: C, 34.37; H, 3.82; N, 6.68; Cl, 16.95%.

α-Chloro-α-(ethoxycarbonyloxyimino)toluene (10b): 70% Yield, bp 110—115 °C/0.3 mmHg, mp 32—34 °C (from hexane), ^{1}H NMR (δ) in $CDCl_3$: 1.4 (t, 3H, J=7), 4.3 (q, 2H, J=7), 7.3—7.6 (m, 3H), and 7.8—8.1 (m, 2H). IR (nujol): 1780 cm^{-1} (-OCOO-). Found: C, 52.96; H, 4.38; N, 6.27; Cl, 15.50%. Calcd for $C_{10}H_{10}NO_3Cl$; C, 52.75; H, 4.40; N, 6.15; Cl, 15.57%.

1-Chloro-1-(ethoxycarbonyldioxyimino)propane (10c): 3% Yield, bp 70—74 °C/1.3 mmHg, ^{1}H NMR (δ) in $CDCl_3$: 1.25 (t, 3H, J=7), 1.37 (t, 3H, J=7), 2.7 (q, 2 H, J=7), and 4.33 (q, 2H, J=7).

References

1) For reviews, see a) C. Grundmann and P. Grünanger "The Nitrile Oxides," Springer-Verlag, New York (1971); b) P. Caramella and P. Grünanger, "1,3-Dipolar Cycloaddition Chemistry Vol. 1," ed by A. Padwa, John Wiley & Sons, New York (1984), Chap. 3, pp. 291—392.

2) See Ref. 1a pp. 31—61.

3) a) T. Mukaiyama and T. Hoshino, *J. Am. Chem. Soc.*, **82**, 5339 (1960); b) R. Paul and S. Tchelitcheff, *Bull. Soc. Chim. Fr.*, **1962**, 2215; c) *ibid.*, **1963**, 140; d) G. B. Bachmann and L. E. Strom, *J. Org. Chem.*, **28**, 1150 (1963); e) P. Vita Finzi and P. Grünanger, *Chim. Ind. (Milan)*, **47**, 516 (1965).

4) a) A. Mckillop and R. J. Kobylecki, *Tetrahedron*, **30**, 1365 (1974); b) A. Rahman, N. Razzaq, and A. Jabbar, *Pak. J. Sci. Ind. Res.*, **30**, 91 (1978); c) A. Rahman, M. Younas, and N. A. Khan, *J. Chem. Soc. Pak.*, **5**, 243 (1983).

5) a) K. Harada, E. Kaji, and S. Zen, *Chem. Pharm. Bull.*, **28**, 3296 (1980); b) *Idem. Nippon Kagaku Kaishi*, **1981**, 1195.

6) a) T. Shimizu, Y. Hayashi, and K. Teramura, *Bull. Chem. Soc. Jpn.*, **57**, 2531 (1984); b) R. G. Duranleau, J. M. Larkin, and S. R. Newman, U. S. Patent 4089867 (1978); *Chem. Abstr.*, **89**, 109515 (1978).

7) S. Tsushima, T. Tsujikawa, and O. Aki, Japan Patent 24902 (1968); *Chem. Abstr.*, **70**, 87344 (1969).

8) I. V. Vigalok, I. E. Moisak, and N. V. Svetlakov, *Khim. Geterotsikl. Soedin.*, 175 (1969); *Chem. Abstr.*, **71**, 3330 (1969).

9) S. Zen, M. Koyama, and S. Kato, *Org. Synth.*, **55**, 77 (1976).

10) A. P. Black and F. H. Barbers, *Org. Synth.*, Coll. Vol. **2**, 512 (1966).

11) W. Fliege and R. Huisgen, *Justus Liebigs Ann. Chem.*, 2038 (1973).

12) T. Shimizu, Y. Hayashi, and K. Teramura, *Bull.*

Chem. Soc. Jpn., **58**, 2519 (1985).
13) G. Stagno d'Alcontres and P. Grünanger, *Gazz. Chim. Ital.*, **80**, 831 (1950).
14) G. Stagno d'Alcontres and P. Grünanger, *Gazz, Chim. Ital.*, **80**, 741 (1950).
15) A. Quilico, G. Stagno d'Alcontres, and P. Grünanger, *Gazz. Chim. Ital.*, **80**, 479 (1950).
16) J. V. R. Kaufman, and J. P. Picard, *Chem. Rev.*, **59**, 429 (1959).
17) J. A. Campbell, *J. Org. Chem.*, **22**, 1259 (1957).

 © 1986 The Chemical Society of Japan Bull. Chem. Soc. Jpn., 59, 2833—2837 (1986)

Preparation and Thermal Ring Opening of 1-(Methylthio)cyclopropenes

Hiroshi YOSHIDA,* Hiroe SANO, Makoto KATO, Tsuyoshi OGATA, and Kiyoshi MATSUMOTO†
Department of Applied Chemistry, Faculty of Engineering, Shizuoka University, Hamamatsu 432
†College of Liberal Arts and Sciences, Kyoto University, Kyoto 606
(Received March 13, 1986)

The reaction of (methylthio)diphenyl- and methyl(methylthio)phenylcyclopropenium salts with Grignard reagents (methyl, 1-methylethyl, and phenyl) yielded 1-(methylthio)cyclopropenes as major products together with isomeric 3-methylthio-1-cyclopropenes in moderate total yields. Phenyllithium also reacted similarly with the salt to afford cyclopropenes in lower yields. Thermal ring opening of 1-(methylthio)cyclopropenes took place readily at room temperature or on heating at around 80 °C to give indene and/or butadiene derivatives in good yields. Product analysis of the reaction in methanol as well as kinetic studies of one of 1-(methylthio)cyclopropenes gave strong evidence for the intermediacy of vinylcarbene in the ring opening of cyclopropene.

Cyclopropenes have long intrigued chemists because of their strained structure. Indeed, extensive as well as intensive studies on preparation of new cyclopropenes,[2-5] photochemical and thermal ring opening,[6-14] and synthetic utilization of cyclopropenes[15-19] have been of continuing interest.

In continuation of our studies on the reactions of mono(alkylthio)cyclopropenium salts,[20] we found an easy route for the preparation and facile ring-opening reaction of 1-(alkylthio)cyclopropenes (**2**). In this paper we report full details of the results.

The reaction of tris(alkylthio)cyclopropenium salts with nucleophiles have been reported to yield substitution products (cyclopropenes or ring-opened products) proceeding through an addition-elimination mechanism.[19]

1-Sulfinyl- and 1-sulfonylcyclopropenes are obtained by the photolysis of the corresponding 3*H*-pyrazoles at −30 °C.[21,22] In contrast, there is no report describing any 1-alkylthiocyclopropene as a stable compound.[23,24]

Table 1. The Reaction of **1a** with PhMgBr or PhLi

Reactant /mol[a]	Reaction conditions[b]		Products(Yield/%)	
	Solvent	Additive[c]	**2a**	**3a**
PhMgBr (3)	Ether		64	23
(5)	Ether		72	5
(5)	Ether	c	69	4
(5)	THF		64	5
(5)	THF	c	55	14
PhLi (5)	Ether		39	15
(5)	Ether	c	26	11
(5)	THF		14	9
(5)	THF	c	17	0
(5)	THF[d]		0	0

a) Moles of the reactant to one mole of **1a**. b) Reaction at room temperature otherwise noted. c) *N,N,N',N'*-Tetramethylethylenediamine (TMED, 5 mol) was added. d) At −50°C.

To a suspension of 1-methylthio-2,3-diphenylcyclopropenium bromide (**1a**)[20] in dry benzene was added phenylmagnesium bromide (3 times excess) in one portion, and the mixture was stirred giving a clean solution. After 5 min the resulting solution was quenched with ice water and the organic layer was separated. ^{1}H NMR spectroscopic analyses revealed that the crude product was a mixture of two isomeric cyclopropenes **2a** and **3a**. The major component was separated by column chromatography and confirmed to be 1-methylthio-2,3,3-triphenylcyclopropene (**2a**) on the basis of IR, ^{1}H and ^{13}C NMR, and mass spectral data. The other isomer **3a** decomposed upon attempted chromatographic separation. All attempts to improve yields or to change product ratios of **2a** and **3a** were unsuccessful as shown in Table 1. The use of phenyllithium gave large amounts of unidentified by-products. The reaction of trisubstituted cyclopropenium salts with Grignard reagents provides a general route for the preparation of cyclopropenes.[6,9,12,14] This is indeed the case for **1a**. The reaction of **1a** with Grignard reagent in ether or THF produced 1-(alkylthio)cyclopropenes, though no change in product ratio was observed on addition of tetramethylethylenediamine (TMED).[25]

Similar treatment of **1a** and **1b** with other Grignard reagents, R'MgX, gave the corresponding cyclopropenes **2** in good yields together with isomeric cyclopropenes **3** (Table 2). Cyclopropene **3a**, which

Table 2. The Reaction of **1a** and **1b** with Grignard Reagents

1	Reactants R'MgX	Products(Yield/%)	
1a	PhMgBr	**2a**(64)	**3a**(23)
1a	*i*-PrMgBr	**2b**(90)	**3b**(0)
1a	MeMgI	**2c**(83)	**3c**(12)
1b	MeMgI	**2d**(96)	**3d**(0)
1b	PhMgBr	**2a**(82)	

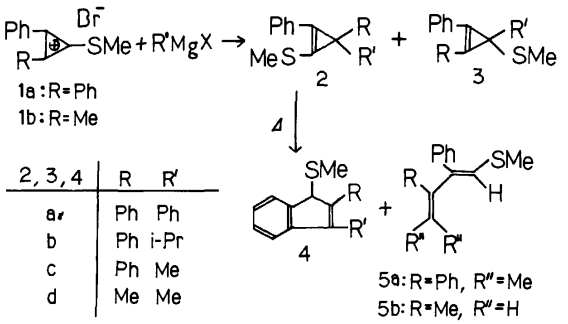

Scheme 1.

could not be purified by chromatography, was independently prepared from triphenylcyclopropenium perchlorate and methanethiol in the presence of triethylamine.

An examination of the distribution of the products **2** and **3** suggests that Grignard reagents preferentially attack the carbon atom unsubstituted by sulfur, this regioselectivity being attributed to the strong electron-releasing properties of methylthio group and steric repulsion between the substituents (MeS and/or Ph) of **1** and Grignard reagents.

Tetraphenylcyclopropene rearranges at temperatures as high as 235—240 °C to give triphenylindene,[26] whereas the ring opening reaction of 1-(methylthio)-cyclopropenes **2a—d** took place easily at room temperature or on heating at 80 °C, producing indene **4** and/or butadiene derivatives **5** in good yields as shown in Table 3, although 3-(methylthio)-1,2,3-triphenylcycloprop-1-ene (**3a**) was stable even at 200 °C. The structures of the products **4a—c** and **5a,b** was confirmed on the basis of their spectroscopic studies.

Theoretical calculations suggest that the ring opening of cyclopropene proceeds directly to a diradical planar intermediate.[27,28] To explain the photolysis products of cyclopropene, a diradical and/or vinylcarbene has been postulated.[6,9,10–14,29] Few studies have been performed as to the mechanistic aspects of thermal ring opening of cyclopropenes.[30]

The relatively stable cyclopropene **2b** was subjected to precise studies for the ring-opening reaction. Thermolysis of **2b** in benzene gave indene **4b** and butadiene **5a** in a 1:1 ratio (Table 3), whereas thermolysis of **2b** in boiling methanol afforded methyl ether **6E** and **6Z** in 51% yield along with **4b** and **5a** in 43% yield. Addition of triethylamine or sodium hydroxide to the methanol solution increased the total yield of **6E** and **6Z** to a maximum of 82%. The structure of **6E** and **6Z** was confirmed by ^{1}H NMR data as well as by conversion to aldehydes **7E** and **7Z** on treatment with mercury(II) acetate in acetic acid. The stereochemistry of **6** and **7** was assigned on the assumption that the protons of a group R cis to the phenyl are shielded and appear at higher field than

Table 3. Thermolysis of **2a—d** and **3a** in Benzene

Reactant	Reaction conditions		Product(Yield/%)
	Temp/°C	Time/h	
2a	25	3	**4a**(95)
2b	80	30	**4b**(46), **5a**(44)
2c	80	2	**4c**(87)
2d	80	4	**5b**(82)
3c	200	100	Recovery

Table 4. Rate Constants for the Thermolysis of **2b**

Solvent (ε)	Temp/°C	$10^5 k_1$ s^{-1}
PhCl (5.61)	65.3	3.45±0.15
Pyridine (12.3)	65.3	2.66±0.16
PhCN (25.2)	65.3	2.77±0.13
CD_3OD (32.6)	60.2	2.69±0.10
	65.3	4.57±0.19, 4.41±0.23[a] 4.60±0.25[b]
	69.8	7.37±0.43
	75.0	11.8 ±0.43
$PhNO_2$ (34.6)	65.3	2.67±0.17
$MeNO_2$ (38.6)	65.3	3.01±0.17

To a solution of **2b** (0.09—0.13 mol dm^{-3}) NaOD was added at a) 0.07 and b) 0.14 mol dm^{-3}.

those of the group R trans to the phenyl.[31] The ratios of **6E** and **6Z**, and **7E** and **7Z** were determined to be 7:3 and 2:1, respectively, by ^{1}H NMR analysis, though separation of mixtures of E and Z by chromatography was unsuccessful.

We have performed a kinetic experiment in order to help clarify a reasonable mechanism for the ring opening of **2**. The rate was followed at suitable time intervals by analyzing the ^{1}H NMR spectra of the methylthio group of **2b** by using methyl phenyl sulfide or dimethyl sulfone internal standard. The disappearance of **2b** gave a good first-order rate constant k_1. The change of the solvent from chlorobenzene to nitromethane (ε 5.6—38.6) did not affect significantly the reaction rate (Table 4).

With regard to formation of the methyl ether, the kinetic experiment ruled out a mechanism involving a nucleophilic attack of alkoxide onto the cyclopropene ring of **2b** to give **6E** and **6Z**, since addition of sodium hydroxide to the methanol solution had no effect on the rate constants.

Tetraphenylcyclopropene has been reported to rearrange to indene with the activation energy of 167 kJ mol^{-1},[26] while the rearrangement of **2b** requires 98.6 kJ mol^{-1}.

These results indicate a sequence involving ring opening of **2b** to give a more stable vinylcarbene, stabilized by the adjacent alkylthio group,[32] followed by intramolecular hydrogen abstraction to afford **4b**

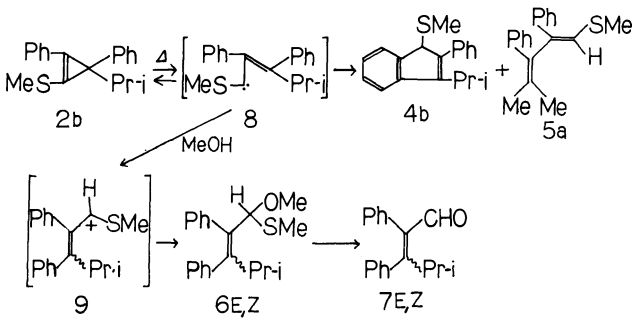

Scheme 2.

and/or **5a**. In contrast to tetraphenylcyclopropene[26] and **3a**, the introduction of alkylthio groups on carbon-1 of the cyclopropene ring made the ring opening easier. The fact that the addtion of a base to the methanolic solution of **2b** increased the yields of methyl ethers **6E** and **6Z** might be attributable to the high reactivity of methoxide with the protonated vinylcarbene (the alkylthiocarbonium ion **9**).

Laser flash photolysis technique has provided insight on the chemistry of the carbene intermediate.[33-35] Carbene reacts with alcohols to give either C–H or O–H insertion products depending on its multiplicity.[33-35] Singlet ground state carbenes yield ethers by the reaction with alcohols.[33,34a,b,36]

It has been clarified that protonation and ylide formation mechanisms are possible for the ether generation depending on the structure of carbene.[37]

Products analyses of photochemical ring opening of 5-(alkylthio)pyrazoline[23,24] and thermal ring opening of 1-sulfinyl- and 1-sulfonylcyclopropenes[21,22] have revealed the intermediacy of thio-, sulfinyl-, and sulfonylvinylcarbenes. Furthermore, an alkoxcarbene intermediate, e.g., an oxygen analogue of **8**, has been postulated and trapped by methanol or ethanol in the photochemical reaction of nortricyclanone and related compounds.[38]

Sulfur-substituted carbenes are known to serve either as a nucleophle or an electrophile, depending on the substituent and reaction conditions.[37] We feel, though not well-founded, that **8** is protonated prior to nucleophilic attack by methanol or methoxide ion since the electron-releasing property of the methylthio group would stabilize a carbonium ion intermediate **9** as revealed in the facile ring-opening reaction of **1a** with cyclic and acyclic 1,3-diketones.[20]

In summary, an appropriate substitution of cyclopropenes with an alkylthio group permits thermally facile ring opening leading to indene and/or butadiene derivatives in good yields.

Experimental

1) General. Melting points were uncorrected. The ^{13}C FT NMR spectra were recorded either on a JEOL JNM FX-60 spectrometer (15.04 MHz) or JEOL JNM FX-90Q (22.49 MHz) and ^1H NMR spectra on a Hitachi-Perkin Elmer R-24 (60 MHz). The IR spectra were recorded on a JASCO A-3 spectrometer.

2) Preparation of (Methylthio)cyclopropenium Salts. (Methylthio)cyclopropenium salts **1** and triphenylcyclopropenium salt were prepared as previously described.[20]

3) The Reaction of Cyclopropenium Salts 1 with Grignard Reagents to Give Cyclopropenes 2 and 3. General Procedure. To a cooled suspension of **1** (3 mmol) in benzene (20 ml) was added a Grignard reagent (9 mmol or 15 mmol in ether or in THF 15 ml prepared before hand and TMED was added in some runs) for 5 min with stirring. The mixture was stirred for additional 5 min to give a clean solution. Crushed ice (30 g) was added to the solution portionwise, and the organic layer was separated and dried over sodium carbonate. The ^1H NMR and IR spectroscopic studies indicated that the crude product was a mixture of two isomeric cyclopropenes. The yields of the respective products were estimated by ^1H NMR integration using dimethyl sulfone as an inner standard and the results are shown in Table 1.

The reaction of **1a** with phenylmagnesium bromide yielded a mixture of cyclopropenes. The major product was isolated by chromatography over silica gel and identified to be 1-methylthio-1,2,3-triphenyl-1-cyclopropene (**2a**). Oil; IR(neat) 1790 cm^{-1}; ^1H NMR($CDCl_3$) δ=2.44 (3H, s, MeS) and 6.9—7.6 (15H, m, 3 Ph). **2a** was thermally unstable even at room temperature to yield **4a** (see the next section). The minor product was not isolated, but its IR and ^1H NMR spectrum indicated the presence of 3-methylthio-1,2,3-triphenylcycloprop-1-ene (**3a**) in the crude reaction product.

Independent preparation of **3a** was undertaken. A suspension of triphenylcyclopropenium perchlorate (1 mmol)in a mixture of methanethiol (3 mmol), triethylamine (2 mmol) and dry benzene (20 ml) was stirred at room temperature for 3 h. After the separation of the precipitate, the benzene solution was condensed and the residue was crystallized from hexane to yield colorless crystals of **3a** in a 67% yield. **3a**: Mp 121.5—122.5 °C; IR (KBr) 1820 cm^{-1}; ^1H NMR ($CDCl_3$) δ=1.95 (3H, s, MeS) and 7.0—7.9 (15H, m, 3 Ph); MS (*m/z*) 314 (M^+). Found: C, 83.45; H, 5.77%. Calcd for $C_{22}H_{18}S$: 84.03; H, 5.77%.

The reaction of **1a** with 1-methylethylmagnesium bromide yielded 3-(1-methylethyl)-2-methylthio-1,3-diphenylcyclopropene (**2h**): Oil; IR (neat) 1780 cm^{-1}; ^1H NMR ($CDCl_3$) δ=0.89 and 0.92 (6H, d, *J*=7 Hz, 2Me), 2.48 (3H, s, MeS), 2.87 (1H, sept, *J*=7 Hz $Me_2C\underline{H}$), and 7.0—7.7 (10H, m, 2Ph); ^{13}C NMR ($CDCl_3$) δ=17.2 (q, MeS), 21.1 and 21.4 (q, $\underline{Me}_2CH$), 30.8 (d, $Me_2\underline{C}H$), 43.7 (s, C_3), 115.3 (s), 117.2 (s), 125.4 (d), 127.0 (d), 127.2 (d), 127.8 (d), 128.0 (d), 128.6 (d), 129.2 (s), and 145.8 (s); MS (*m/z*) 280 (M^+). Found: C, 80.54; H, 7.02%. Calcd for $C_{19}H_{20}S$: C, 81.38; H, 7.19%.

The reaction of **1a** with methylmagnesium iodide yielded two cyclopropenes. The major product was isolated over silica-gel chromatography and was found to be 3-methyl-2-methylthio-1,3-diphenylcyclopropene (**2c**): Oil; IR (neat) 1780 cm^{-1}; ^1H NMR ($CDCl_3$) δ=1.71 (3H, s, C_3-Me), 2.39 (3H, s, MeS), and 6.9—7.6 (10H, m, 2Ph); ^{13}C NMR ($CDCl_3$) δ=16.5 (q, C_3-$\underline{Me}$), 22.1 (q, MeS), 31.9 (s, C_3), 116.0 (s), 117.6 (s), 125.3 (d), 125.9 (s), 126.1 (d), 127.2 (d), 127.8 (d), 128.0 (d), and 146.8 (s); MS (*m/z*) 252 (M^+). Found: C, 80.62; H, 6.31%.

Calcd for $C_{17}H_{16}S$: C, 80.90; H, 6.38%.

The minor product was not isolated(decomposed during chromatography), but found to be 3-methyl-3-methylthio-1,2-diphenylcyclopropene (**3c**): IR (neat) 1810 cm^{-1}; ^1H NMR ($CDCl_3$) δ=1.42 (3H, s, Me), 2.07 (3H, s, MeS).

The reaction of 1-methyl-2-methylthio-3-phenylcyclopropenium bromide (**1b**) with methylmagnesium iodide yielded 3,3-dimethyl-1-methylthio-2-phenylcyclopropene (**2d**) as a major product. **2d**: Oil; IR (neat) 1760 cm^{-1}; ^1H NMR ($CDCl_3$) δ=1.39 (6H, s, 2Me), 2.54 (3H, s, MeS), and 7.1—7.5 (5H, m, Ph); MS (*m/z*) 190 (M^+). Found: C, 75.31; H, 7.42%. Calcd for $C_{12}H_{14}S$: C, 75.73; H, 7.41%.

4) Thermolysis of 2 and 3a. A solution of **2** or **3a** in benzene was heated at appropriate temperature. The reaction was checked by means of TLC (silica gel, $CHCl_3$–petroleum ether, 1:4) at suitable time intervals. After the reaction, the mixture was either chromatographed over silica gel or recrystallized from an appropriate solvent.

Upon heating at 80 °C or on standing at room temperature **2a** gave 1-methylthio-2,3-diphenylindede (**4a**): Mp 158 °C (2-propanol); ^1H NMR ($CDCl_3$) δ=1.41 (3H, s, MeS), 4.82 (1H, s, 1-CH), and 7.0—8.1 (14H, m, Arom); ^{13}C NMR ($CDCl_3$) δ=9.1 (q, MeS), 52.0 (d, C_1) , 120.3 (d), 124.1 (d), 126.0 (d), 127.2 (d), 127.5 (d), 127.6 (d), 127.9 (d), 128.6 (d), 129.4 (d), 134.6 (s), 134.9 (s), 140.7 (s), 142.0 (s), 144.1 (s), and 144.7 (s); MS (*m/z*) 314 (M^+). Found: C, 84.14; H, 5.84%. Calcd for $C_{22}H_{18}S$: C, 84.03; H, 5.77%.

Upon heating **2b** yielded 3-(1-methylethyl)-1-methylthio-2-phenylindede **4b** and 4-methyl-1-methylthio-2,3-diphenyl-1,3-pentadiene (**5a**). **4b**: Mp 108—109 °C (2-propanol); ^1H NMR ($CDCl_3$) δ=1.30 (3H, d, *J*=7 Hz, Me CH), 1.39 (3H, s, MeS), 1.46 (3H, d, *J*=7 Hz, MeCH), 3.32 (1H, m, Me_2CH), 4.69 (1H, s, C_1H), and 7.2—7.9 (10H, m, 2 Ph); MS (*m/z*) 280 (M^+). Found: C, 81.11; H, 7.16%. Calcd for $C_{19}H_{20}S$: C, 81.38; H, 7.19%.

5a: Mp 103—104 °C (2-propanol); ^1H NMR ($CDCl_3$) δ=1.71 (3H, s, CH_3), 1.84 (3H, s, CH_3), 2.25 (3H, s, MeS), 6.06 (1H, s, C_1–H), and 7.0—7.5 (10H, m, 2 Ph); MS (*m/z*) 280 (M^+). Found: C, 80.86; 7.09%. Calcd for $C_{19}H_{20}S$: C, 81.38; H, 7.19%.

Upon heating at 80 °C for 2 h **2c** yielded **4c** in 87% yield. 3-Methyl-1-methylthio-2-phenylindene (**4c**): Mp 89—91 °C (MeOH); ^1H NMR ($CDCl_3$) δ=1.30 (3H, s, MeS), 2.23 (3H, d, *J*=2 Hz. 3-Me), 4.72 (1H, q, *J*=2 Hz, 1-CH), and 6.9—7.8 (9H, m, Arom); ^{13}C NMR ($CDCl_3$) δ=9.2 (q, MeS), 11.8 (q, 3-Me), 52.0 (d, 1-CH), 119.0 (d), 123.7 (d), 125.8 (d), 127.1 (d), 127.5 (d), 128.2 (d), 129.1 (d), 135.5 (s), 135.9 (s), 141.4 (s), 143.9 (s), and 145.6 (s); MS (*m/z*) 252 (M^+). Found: C, 80.73; 6.43%. Calcd for $C_{17}H_{16}S$: C, 80.90; H, 6.38%.

On heating **2d** gave 3-methyl-1-methylthio-2-phenyl-1,3-butadiene (**5b**): Mp 41 °C (hexane); ^1H NMR ($CDCl_3$) δ=1.93 (3H, bs, CH_3), 2.16 (3H, s, MeS), 4.43 (1H, bs, CH), 4.80 (1H, bs, CH), 6.20 (1H, bs, CH), and 6.9—7.6 (5H, m, Ph); MS (*m/z*) 190 (M^+). Found: C, 75.51; H, 7.43%. Calcd for $C_{12}H_{14}S$: C, 75.73; H, 7.41%.

5) Thermolysis of 2b in Methanol. A solution of **2b** (200 mg) in methanol (10 ml) was heated at reflux and the reaction was monitored by means of TLC (silica gel, chloroform–petroleum ether, 1:4). After the reaction (24 h) the mixture was condensed and chromatographed over silica gel to give two mixtures. The former elution was a mixture of **4b** and **5a** in 43% yield, products from thermolysis of **2b**, and the latter was a mixture of (*E*)- and (*Z*)-1-methoxy-4-methyl-1-methylthio-2,3-diphenyl-2-pentenes (**6E**) and (**6Z**). Although the separation of the two methyl ethers by chromatography was unsuccessful, ^1H NMR spectra of the mixture showed two groups of signals corresponding to **6E** and **6Z** in a ratio of 3:7. **6E**: ^1H NMR ($CDCl_3$) δ=0.98 and 1.00 (6H, d, *J*=7 Hz, Me_2CH), 2.13 (3H, s, MeS), 2.5—3.2 (1H, m, Me_2CH), 3.46 (3H, s, MeO), 5.29 (1H, s, CH), and 6.6—7.6 (10H, m, 2Ph). **6Z**: δ=0.78 (6H, d, *J*=7 Hz, Me_2), 1.75 (3H, s, MeS), 2.5—3.2 (1H, m, Me_2CH), 3.16 (3H, s, MeO), 4.56 (1H, s, CH), and 6.6—7.6 (10H, m, 2 Ph). MS (*m/z*) 312 (M^+). Found: C, 76.75; H, 7.78%. Calcd for $C_{20}H_{24}OS$: C, 76.88; H, 7.74%.

Desulfurization of a mixture of **6E** and **6Z** with mercury(II) acetate in aqueous chloroform (bilayers reaction) gave a mixture of two aldehydes (*E*)- and (*Z*)-4-methyl-2,3-diphenyl-2-pentenal (**7E** and **7Z**) in a 58% yield. ^1H NMR spectrum of the mixture ($CDCl_3$) showed two sets of signals: δ=1.05 (6H, d, *J*=7 Hz, Me_2), 3.83 (1H, sept, *J*=7 Hz, Me_2CH), and 10.18 (1H, s, CHO), and 0.85 (6H, d, *J*=7 Hz, Me_2), 2.72 (1H, sept, *J*=7 Hz, Me_2CH), and 9.13 (1H, s, CHO) corresponding to **7E** and **7Z** (2:1) together with 6.4—7.5 (m, Ph); MS (*m/z*) 222 (M^+). Found: C, 86.94; H, 7.28%. Calcd for $C_{18}H_{18}O$: C, 86.36; H, 7.25.

Addition of triethylamine (1 ml) or sodium hydroxide (0.3 g) to a solution of **2b** (0.2 g) in methanol (10 ml) increased the yield of the methyl ether **6** to 82% and no **4b** and **5a** were isolated.

5) Kinetic Experiment of Thermolysis of 2b. A solution of **2b** (0.09—0.13 M (1 mol dm^{-3})) and methyl phenyl sulfide or dimethyl sulfone as an inner standard in an appropriate solvent was sealed in an NMR sample tube and was kept stand in a thermostated bath (±0.1 °C); the rate was followed at suitable time intervals (at least 10 times) by analyzing the ^1H NMR spectra of the methyl groups of **2b** and the internal standard by the peak-height method averaging 5 measurements. The results are summarized in Table 4.

References

1) A preliminary communication of this work appeared in *J. Org. Chem.*, **50**, 1145 (1985).

2) W. Ando, Y. Hanyu, T. Tanaka, and K. Ueno, *J. Am. Chem. Soc.*, **106**, 2216 (1984).

3) W. E. Billups, L.-J. Lin, and E. W. Casserly, *J. Am. Chem. Soc.*, **106**, 3698 (1984).

4) S. W. Staley and T. D. Norden, *J. Am. Chem. Soc.*, **106**, 3699 (1984).

5) B. A. Hess. Jr., D. Michalska, and L. J. Schaad, *J. Am. Chem. Soc.*, **107**, 1449 (1985).

6) A. Padwa, U. Chiacchio, A. Compagnini, A. Corsano, and G. Purrello, *J. Chem. Soc., Perkin Trans. 1*, **1984**, 2671.

7) T. Eicher, H. Pielartzik, and P. Zacheus, *Tetrahedron Lett.*, **25**, 4495 (1984).

8) A. Krebs, W. Cholcha, M. Müller, T. Eicher, H. Pielartzik, and H. Schnöckel, *Tetrahedron Lett.*, **25**, 5027 (1984).

9) A. Padwa, W. F. Rieker, and R. J. Rosenthal, *J. Am. Chem. Soc.*, **107**, 1710 (1985).

10) M. G. Steinmetz and R. T. Mayes, *J. Am. Chem. Soc.*, **107**, 2111 (1985).

11) C. J. Abelt and H. D. Roth, *J. Am. Chem. Soc.*, **107**,

3840 (1985).
12) M. W. Klett and R. P. Johnson, *J. Am. Chem. Soc.*, **107**, 3963 (1985).
13) T. J. Stierman and R. P. Johnson, *J. Am. Chem. Soc.*, **107**, 3971 (1985).
14) H. E. Zimmermann and S. A. Fleming, *J. Org. Chem.*, **50**, 2539 (1985).
15) P. Mueller and D. Rodriguez, *Helv. Chim. Acta*, **66**, 2540 (1983).
16) M. L. Deem, *Synthesis*, **1982**, 701.
17) D. L. Boger and C. E. Brotherton, *J. Am. Chem. Soc.*, **106**, 805 (1984).
18) W. E. Billups, B. E. Arney. Jr., and L.-J. Lin, *J. Org. Chem.*, **49**, 3436 (1984).
19) S. Inoue and T. Hori, *Bull. Chem. Soc. Jpn.*, **56**, 171 (1983) and references cited therein.
20) H. Yoshida, M. Nakajima, T. Ogata, K. Matsumoto, R. M. Acheson, and J. D. Wallis, *Chem. Lett.*, **1983**, 155; *Bull. Chem. Soc. Jpn.*, **56**, 3015 (1983); H. Yoshida, M. Nakajima, T. Ogata, and K. Matsumoto, *Bull. Chem. Soc. Jpn.*, **57**, 734 (1984); K. Masumoto and Y. Ikemi, *Heterocycles*, **14**, 1445 (1980). K. Matsumoto, T. Uchida, Y. Yagi and R. M. Acheson, *Heterocycles*, **23**, 2041 (1985).
21) M. Franck-Neumann and J. J. Lohmann, *Angew. Chem. Int. Ed. Engl.*, **16**, 323 (1977).
22) M. Franck-Neumann and J. J. Lohmann, *Tetrahedron Lett.*, **1979**, 2397. Authors express thanks to Prof. R. W. Hoffmann for calling our attention to these two references (21 and 22).
23) M. Franck-Neumann and J. J. Lohmann, *Tetrahedron Lett.*, **1978**, 3729.
24) M. Franck-Neumann and J. J. Lohmann, *Tetrahedron Lett.*, **1979**, 2075.
25) M. Braun, R. Veith, and G. Moll, *Chem. Ber.*, **118**, 1058 (1985).
26) M. A. Battiste, B. Halton, and R. H. Grubbs, *J. Chem. Soc., Chem. Commun.*, **1967**, 907.
27) J. H. Davis, W. A. Goddard III, and R. G. Bergman, *J. Am. Chem. Soc.*, **99**, 2427 (1977).
28) A. Savin and L. Arnaud-Danaon, *J. Org. Chem.*, **46**, 2346 (1981).
29) A. Padwa, *Acc. Chem. Res.*, **12**, 310 (1979).
30) E. J. York, J. D. Stevens, and R. G. Bergmann, *J. Am. Chem. Soc.*, **95**, 5680 (1973).
31) L. M. Jackman and S. Sternhell, "Application of Nuclear Magnetic Resonance Spectroscopy in Organic Chemistry" 2nd ed, Pergamon Press, Oxford (1969).
32) E. Block, "Reactions of Organosulfur Compounds," Academic Press, New York (1978), p. 221.
33) D. Griller, A. S. Nazran, and J. C. Scaiano, *Acc. Chem. Res.*, **17**, 283 (1984).
34) Recent works: a) C. Chuang, S. C. Lapin, A. K. Schrock, and G. B. Schuster, *J. Am. Chem. Soc.*, **107**, 4243 (1985); b) P. B. Grasse, J. J. Zupancic, S. C. Lapin, M. P. Hendrich, and G. B. Schuster, *J. Org. Chem.*, **50**, 2352 (1985); c) H. L. Casal, N. H. Weistiuk, and J. C. Scaiano, *J. Org. Chem.*, **49**, 5214 (1984); d) B. B. Wright and M. S. Platz, *J. Am. Chem. Soc.*, **106**, 4175 (1984).
35) S. Oikawa and M. Tsuda, *J. Am. Chem. Soc.*, **106**, 1940 (1985).
36) W. Kirmse, *Justus Liebigs Ann. Chem.*, **666**, 9 (1963); D. Bethell, G. Stevens, and P. Tickle, *J. Chem. Soc. D*, **1970**, 792; H. Tomioka, T. Miwa, S. Suzuki, and Y. Izawa, *Bull. Chem. Soc. Jpn.*, **53**, 753 (1980).
37) P. M. Warner and I.-S. Chu, *J. Am. Chem. Soc.*, **106**, 5366 (1984).
38) P. Yates, *Pure Appl. Chem.*, **16**, 93 (1968).

 © 1986 The Chemical Society of Japan Bull. Chem. Soc. Jpn., 59, 2839—2842 (1986)

Regioselectivity in the Catalytic Hydrogenolysis of 1-Amino-1-cyclopropanecarboxylic Acid and Its Methyl Ester

Koji ISOGAI,* Jun-ichi SAKAI, Keiji YAMAUCHI, and Katsuya WATANABE
Department of Applied Chemistry, Faculty of Engineering, Niigata University, Ikarashi, Niigata 950-21
(Received March 17, 1986)

The title compounds were hydrogenolyzed over Pd-C. The ring-bond cleavage in the hydrogenolysis of the acid in water or methanol occurred at both the C_1–C_2 bond and the C_2–C_3 bond in nearly equal proportion, whereas the C_1–C_2 bond was cleaved mainly in the presence of ammonia and the C_2–C_3 bond was cleaved mainly in acetic acid. Selective hydrogenolysis of the C_1–C_2 bond of ester occurred in hexane or methanol, whereas the C_2–C_3 bond was hydrogenolyzed mainly in acetic acid. The role of the amino group is discussed.

Although many studies on the regioselectivity in the catalytic hydrogenolysis of substituted cyclopropanes have been reported,[1] little attention has been given to the catalytic hydrogenolysis of aminocyclopropanes. Recently, Musso[2] reported that 1-amino-1-cyclopropanecarboxylic acid was hydrogenolyzed selectively at the opposite bond of the amino group in methanol in the absence or in the presence of ammonia by the use of a palladium catalyst. On the contrary, we found previously that *exo*-7-aminobicyclo[4.1.0]heptane and *exo*-6-aminobicyclo[3.1.0]hexane were hydrogenolyzed exclusively at the adjacent bond of the amino group in hexane using both palladium and nickel catalysts.[3] In order to make clear the role of the amino group which might cause these conflicting results, we have investigated the hydrogenolysis of methyl 1-amino-1-cyclopropanecarboxylate (**1**) and 1-amino-1-cyclopropanecarboxylic acid (**2**) in neutral, basic or acidic solution.

Table 1. Hydrogenolysis of Methyl 1-Amino-1-cyclopropanecarboxylate (**1**)

Run No.	Solvent	Conversion %	Composition of products/%		
			C_2–C_3 Fission		C_1–C_2 Fission
			3	**4**	**5**
1[a]	Hexane	0	—	—	—
2[b]	Hexane	64	—	2	98
3[a]	CH_3OH	0	—	—	—
4[b]	CH_3OH	28	17	—	83
5[a]	CH_3COOH	28	84	12	4

Substrate: 58 mg, 0.5 mmol. Catalyst: Pd-C, 50 mg. Reaction time: 24 h. a) Room temperature, atmospheric pressure. b) 80°C, 50 kg cm^{-2}.

The hydrogenolysis of **1** and **2** was carried out by the use of palladium-charcoal (Pd-C) catalyst and the results are shown in Tables 1 and 2.

The hydrogenolysis of **1** was made easy by increasing the reaction temperature and the hydrogen pressure. The hydrogenolysis of **1** in hexane gave selectively methyl 2-aminobutanoate (**5**) as the C_1–C_2 bond cleaved product, accompanied by a slight amount of methyl 2-amino-2-methylpropanoate (**4**) as the C_2–C_3 bond cleaved product. The hydrogenolysis of **1** in methanol also gave mainly **5**, accompanied by a small amount of methy 2-methylpropanoate (**3**) as the C_2–C_3 bond cleaved product. On the other hand, when acetic acid was used as a solvent, selective hydrogenolysis of the C_2–C_3 bond of **1** occurred at

Table 2. Hydrogenolysis of 1-Amino-1-cyclopropanecarboxylic Acid (**2**)

Run No.	Solvent	Conversion %	Composition of products/%[g]		
			C_2–C_3 Fission		C_1–C_2 Fission
			3	**4**	**5**
6[a]	H_2O	100	28	17	55
7[a]	H_2O-NH_3[c]	86	9	3	88
8[a]	H_2O-CH_3COOH[d]	93	88	4	8
9[a]	CH_3OH	100	49	3	48
10[a]	CH_3OH-NH_3[e]	93	9	—	91
11[b]	CH_3COOH[f]	18	14	78	8
12[b]	CH_3COOH	17	86	14	—

Substrate: 100 mg (1 mmol). Catalyst: Pd-C, 200 mg. Solvent: 10 ml. Reaction time: 24 h. a) 100 °C, 80 kg cm^{-2}. b) Room temperature, atmospheric pressure. c) NH_3 is contained in amounts eight times the molar quantity of **2**. d) CH_3COOH is contained in amounts ten times the molar quantity of **2**. e) NH_3 is contained in amounts five times the molar quantity of **2**. f) PtO_2 (50 mg) is used instead of Pd-C. g) Products were determined as methyl esters.

room temperature under atmospheric pressure to give **3** and **4**, accompanied by a slight amount of **5**.

The hydrogenolysis of **2** was carried out in water and the reaction products were converted into methyl esters to submit to vapor-phase chromatography (VPC). The ring-bond cleavage of **2** in water occurred at both the C_1–C_2 bond and the C_2–C_3 bond in nearly equal proportion, whereas the C_1–C_2 bond was cleaved mainly in the presence of aqueous ammonia and the C_2–C_3 bond was cleaved mainly in the presence of acetic acid. The results (Run No. 9, 10, and 11) obtained by the reinvestigation under the conditions reported by Musso[2] were analogous to that described above.

According to Musso's report,[2] the ratios of 2-amino-2-methylpropanoic acid and 2-aminobutanoic acid obtained in the hydrogenolysis of **2** using Pd–C in methanol, Pd–C in methanol–ammonia and Pt in acetic acid were reported, respectively, as follows: 90%, 10%; 98.5%, 1.5%; 23%, 77%. He explained the results on the basis of his proposal,[4] concerning the regioselective effect of substituents in the hydrogenolysis of cyclopropanes, in the following manner. The amino group plays as an electron-donating group in the neutral or the basic solvent and the hydrogenolysis occurs at the weakened C_2–C_3 bond preferentially, whereas the amino group plays as an electron withdrawing group in the acidic solvent and causes the C_1–C_2 bond cleavage mainly.

Contrary to his explanation, however, our finding suggests strongly that the amino group of **2** contributes mainly to the cleavage of the C_1–C_2 bond when the hydrogenolysis is carried out under the condition in which the amino group behaves as a free amine, whereas the C_2–C_3 bond cleavage is prefered under the condition in which the amino group forms an ammonium ion. Additionally, the C_2–C_3 bond cleavage was accompanied by the elimination of the amino group.

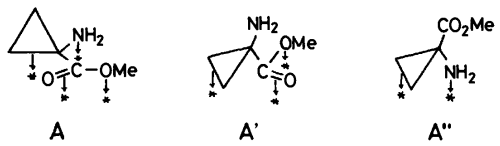

Fig. 1. Adsorbed states of **1** in neutral solvents.

The obtained results may be explained by considering the adsorbed states of **1** and **2** on the catalyst. The probable adsorbed states of **1** are shown in Fig. 1. The adsorbed state A which is adsorbed with the amino group, the methoxycarbonyl group and the C_1–C_2 bond of the cyclopropane ring seems to be preferable to A′ which is adsorbed with the methoxycarbonyl group and the C_2–C_3 bond or A″ which is adsorbed with the amino group and the C_2–C_3 bond. Therefore, it is expected that the predominant product is the C_1–C_2 bond cleaved product in the hydrogenolysis of **1** in the neutral solvent as shown in Path (1) in Scheme 1. The obtained results support this consideration.

A pathway of the formation of the minor products **3** and **4** is shown in Path (2) in Scheme 1. The C_2–C_3 bond cleavage of the adsorbed state A′ occurs more easily than that of the adsorbed state A″ because the unadsorbed amino group behaves as an electron-donating group and contributes to weakening the C_2–C_3 bond. The elimination of the amino group can be explained as an example of the elimination in the half-hydrogenated state.[5–8] In the half-hydrogenated state C′ formed from A′ via B′, the combination with the chemisorbed hydrogen competes with the elimination of the amino group caused by the donation of the electron of the carbon–metal bond to the C_1–C_2 bond. The tendency toward the elimination seems to be enhanced by the solvation of the leaving group with protic solvents such as methanol and water.

In the acidic solvent, the amino group of **1** is converted to ammonium ion and loses the ability of

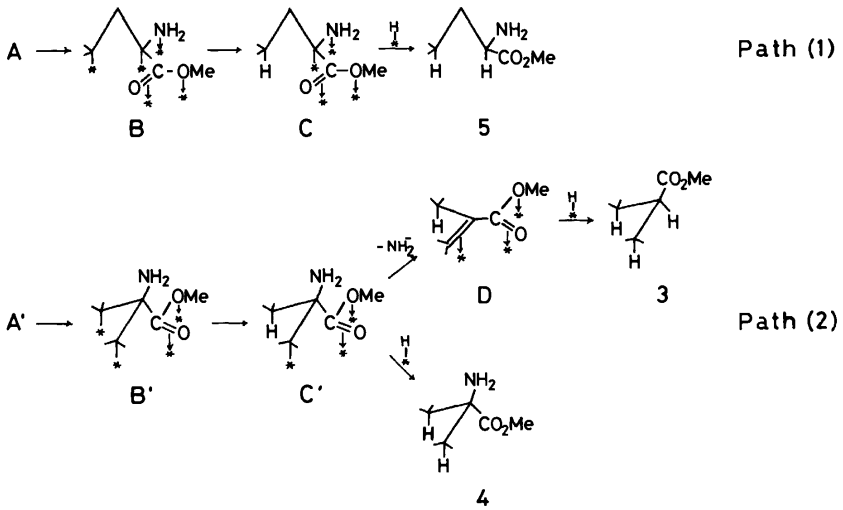

Scheme 1.

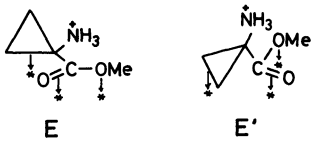

Fig. 2. Adsorbed states of **1** in acidic solvents.

adsorption to the catalyst. Therefore, two forms of the adsorbed states E and E′, adsorbing with the methoxycarbonyl group and the C_1–C_2 bond or the C_2–C_3 bond, can be considered as shown in Fig. 2.

Although the hydrogenolysis of methyl cyclopropanecarboxylate has not been reported, it is expected that the C_1–C_2 bond is cleaved selectively because cyclopropyl methyl ketone is hydrognolyzed at the C_1–C_2 bond selectively.[9] If the ammonio group in **1** behaves as an electron withdrawing group and contributes to cleaving the adjacent C_1–C_2 bond as mentioned in Musso's proposal, it is expected that the combined influences of the ammonio and the methoxycarbonyl groups would cause the exclusive C_1–C_2 bond cleavage of **1**. On the contrary, the selective cleavage of the opposite C_2–C_3 bond and the elimination of the ammonio group were observed in our experiment. These results suggest that **1** is adsorbed mainly in the adsorbed state E′ and the hydrogenolysis proceeds according to the similar pathway shown in Path (2) in Scheme 1.

However, the hydrogenolysis of **1** in acetic acid proceeded more easily than in hexane or methanol and was accompanied by considerable elimination of the ammonio group. Therefore, it seems to be necessary to consider the relationship between the accelaration of the C_2–C_3 bond cleavage and the easy elimination of the ammonio group.

It is well-known that the accelerating effect in the solvolysis of cyclopropyl tosylates[10] or halides[11] is explained by the concept of σ-participation. In the adsorbed state E′, π-adsorption of the C_2–C_3 bond to the catalyst surface and the C–NH_3^+ bond are opposite in direction. Because the relationship in direction is preferable stereoelectronically, the acceleration of the hydrogenolysis in acidic solvent may be explained somewhat more clearly by the concept of the σ-participation. An increase of the polarization in C–NH_3^+ bond caused by the solvation makes the C_2–C_3 bond cleavage easy and the elimination of the ammonio group proceeds predominantly, competing with the combination of chemisorbed hydrogen as shown in Scheme 2.

Since the details of experimental conditions were not described in Musso's report, it is difficult to point out the cauces of discrepancies observed in the hydrogenolysis of **2**. However, the obtained results can be explained reasonably in the following manner. In aqueous solution, equilibrium is established among the dipolar ion of **2** and the anion and the

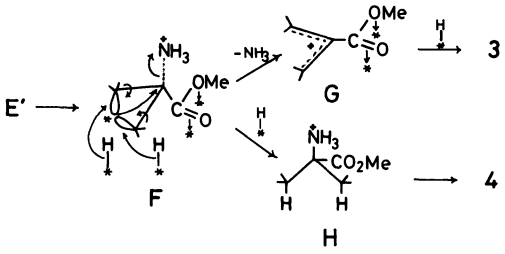

Scheme 2.

cation forms of **2**, whereas it is largely in the anion form in basic solution and largely in the cation form in acidic solution. Therefore, the composition of products in the hydrogenolysis of **2** in water is dependent on the equilibrium of the three forms of **2**. The anion form is adsorbed mainly with the C_1–C_2 bond, the amino group and the carboxyl group to give the C_1–C_2 bond cleaved product, whereas the dipolar ion and the cation form are adsorbed mainly with the C_2–C_3 bond and the carboxyl group to give the C_2–C_3 bond cleaved products being accompanied by the elimination of the ammonio group. The behavior of **2** in the hydrogenolysis in methanol, methanol–ammonia or acetic acid may be explained in a similar manner as above.

Experimental

Infrared spectra were recorded on a Hitachi 270-30 spetrometer. ^{1}H NMR spectra were recorded on a JEOL JNM-PMX 60 spectrometer. Chemical shifts (δ) are recorded in ppm downfield Me_4Si.

1-Amino-1-cyclopropanecarboxylic Acid (2). **2** was prepared according to the method described in the literature.[12] To a solution of 1-[(diphenylmethylene)amino]-1-cyclopropanecarbonitrile, mp 77—80 °C, lit,[12] mp 77—80 °C, (7.5 g, 30.5 mmol) in ether (75 ml) was added 1 mol dm^{-3} hydrochloric acid (150 ml) and the mixture was stirred for 12 h at room temperature. The layers were separated and the aqueous layer was refluxed with concentrated hydrochloric acid (150 ml) for 4 h. After removal of the water, the residue was taken up in a small volume of water and passed through a column packed with weakly basic anion-exchange resin Bio-Rad AG3-X4A) to give 2.8 g of **2**: Mp 229—231 °C, lit,[12] mp 229—231 °C; ^{1}H NMR (D_2O)[12] δ=1.5 (2H, m, C$\underline{H}_2$), 1.2 (2H, m, C$\underline{H}_2$); IR(KBr) 1626 (ν_{COO^-}), 1538 ($\delta_{NH_3^+}$); Found: C, 47.36; H, 6.79; N, 13.97%. Calcd for $C_4H_7NO_2$: C, 47.52; H, 6.98; N, 13.85%.

Methyl 1-Amino-1-cyclopropanecarboxylate (1). To a solution of **2** (2.5 g, 24.8 mmol) in methanol (10 ml) was passed dried hydrogen chloride and refluxed for 12 h. After removal of the methanol the residue was made basic with diluted sodium carbonate solution and extracted with chloroform. The fractional distillation gave 0.6 g of **1**: Bp 45—47 °C/27 mmHg (1 mmHg=133.322 Pa); ^{1}H NMR (CCl_4) δ=3.60 (3H, s, OC$\underline{H}_3$), 1.77 (2H, s, N$\underline{H}_2$), 1.15 (2H, m, C$\underline{H}_2$), 0.92 (2H, m, C$\underline{H}_2$); IR (CCl_4) 3396 (ν_{NH}), 1724 ($\nu_{C=O}$), 1622 (δ_{NH}), 1192 (ν_{CO}); Found: C, 52.08; H, 7.92; N, 12.21%. Calcd for $C_5H_9NO_2$: C, 52.16; H, 7.88; N, 12.16%.

Hydrogenolysis of 1. A solution of **1** (58 mg, 0.5 mmol) in hexane, methanol or acetic acid (5 ml) was stirred with Pd-C (50 mg, Kawaken Fine Chemical Co.: Pd-C(M)) at room temperature under hydrogen at atmospheric pressure or at 80 °C under hydrogen pressure of 50 kg cm^{-2} for 24 h. When hexane was used as a solvent, the reaction mixture was submitted directly to VPC to determine the composition of products. When methanol or acetic acid was used as a solvent, hexane (15 ml) was added to the reaction mixture and washed with water to remove the methanol or the acetic acid and submitted to VPC.

Hydrogenolysis of 2. A solution of **2** (100 mg, 1 mmol) in water (10 ml) in the absence or in the presence of aqueous ammonia (8 mmol) or acetic acid (10 mmol) was stirred with Pd-C (200 mg) at 100 °C under hydrogen pressure of 80 kg cm^{-2} for 24 h. After the catalyst and the water were removed from the reaction mixture, the residue was esterified with methanol in the presence of hydrogen chloride and submitted to VPC.

A solution of **2** (100 mg, 1 mmol) in methanol (10 ml) in the absence or in the presence of ammonia (5 mmol) was stirred with Pd-C (200 mg) at 100 °C under hydrogen pressure of 80 kg cm^{-2} for 24 h. The reaction mixture was esterified in a similar manner as above and submitted to VPC.

A solution of **2** (100 mg, 1 mmol) in acetic acid (10 ml) was stirred with Pd-C (200 mg) or PtO_2 (50 mg) at room temperature under hydrogen at atmospheric pressure for 24 h. The reaction mixture was esterified with methanol and submitted to VPC.

Identification of Products. The products were identified by comparison with ^{1}H NMR, IR spectra and the values of T_R in VPC of authentic samples prepared by the esterification of the corresponding carboxylic acids in the usual way.

Methyl 2-Methylpropanoate (3): Bp 92—93 °C, lit,[13] bp 91.5 °C/742 mmHg; ^{1}H NMR (CCl_4) δ=3.16 (3H, s, $OC\underline{H}_3$), 2.73—2.27 (1H, m, J=7.0 Hz, C$\underline{H}$), 1.14 (6H, d, J=7.0 Hz, $C\underline{H}_3$×2); IR (CCl_4) 1736 ($\nu_{C=O}$), 1200 (ν_{CO}), 1156 (ν_{CO}).

Methyl 2-Amino-2-methylpropanoate (4): Bp 132—134 °C, lit,[14] bp 133—134 °C; HCl salt: Mp 182—183 °C, lit,[14] mp 182—183 °C; ^{1}H NMR(CCl_4) δ=3.62 (3H, s, $OC\underline{H}_3$), 1.41 (2H, s, $N\underline{H}_2$), 1.25 (6H, s, $C\underline{H}_3$×2); IR (CCl_4) 3396 (ν_{NH}), 1730 ($\nu_{C=O}$), 1192 (ν_{CO}), 1142 (ν_{CO}).

Methyl 2-Aminobutanoate (5): Bp 68—70 °C; HCl salt: mp 149—150 °C, lit,[15] mp 150—151 °C; ^{1}H NMR (CCl_4) δ=3.60 (3H, s, $OC\underline{H}_3$), 3.23 (1H, t, J=7.0 Hz, C$\underline{H}$), 1.92—1.23 (2H, m, $C\underline{H}_2$), 1.30 (2H, s, $N\underline{H}_2$), 0.92 (3H, t, J=7.0 Hz, $C\underline{H}_3$); IR (CCl_4) 3404 (ν_{NH}), 1738 ($\nu_{C=O}$), 1174 (ν_{CO}), 1140 (ν_{CO}).

References

1) A. P. G. Kieboom and V. van Rantwijk, "Hydrogenation and Hydrogenolysis in Synthetic Organic Chemistry," Delft University Press, Delft (1977), p. 102.

2) H. Musso, "IUPAC Current Trends in Organic Synthesis," ed by H. Nozaki, Pergamon Press, Oxford and New York (1983), p. 371.

3) K. Isogai, J. Sakai, and K. Yamauchi, *Nippon Kagaku Kaishi*, **1986**, 214.

4) C. Groger, H. Musso, and I. Roβnagel, *Chem. Ber.*, **113**, 3261 (1980).

5) S. Mitsui, M. Fujimoto, Y. Nagahisa, and T. Sukegawa, *Chem. Ind. (London)*, **1969**, 241.

6) K. Isogai and K. Kitahara, *Nippon Kagaku Kaishi*, **1978**, 280.

7) K. Isogai and S. Hirabayashi, *Bull. Chem. Soc. Jpn.*, **52**, 3757 (1979).

8) K. Isogai, N. Nishizawa, T. Saito, and J. Sakai, *Bull. Chem. Soc. Jpn.*, **56**, 1555 (1983).

9) A. L. Schultz, *J. Org. Chem.*, **36**, 383 (1971).

10) C. H. DePuy, L. G. Schnack, and J. W. Hausser, *J. Am. Chem. Soc.* **88**, 3343 (1966).

11) S. J. Cristol, R. M. Seqeira, and C. H. DePuy, *J. Am. Chem. Soc.*, **87**, 4007 (1965).

12) M. J. O'Donnell. W. A. Bruder, T. M. Eckrich, D. F Shullenberger, and G, S. Staten, *Synthesis*, **1984**, 127.

13) D. Lim and O. Wichterle, *J. Polymer Sci.*, **29**, 579 (1958).

14) S.M. McElvain and E. H. Pryde, *J. Am. Chem. Soc.*, **71**, 326 (1949).

15) R. L. Smith and W. J. Polglase, *J. Biol. Chem.*, **180**, 1209 (1949).

 © 1986 The Chemical Society of Japan Bull. Chem. Soc. Jpn., 59, 2843—2849 (1986)

Retentive Solvolysis. 13.[1] The Number and the Stability of Carbocation Intermediate in the S_N1 Phenolysis. Salt Effect on Retentive Phenolyses of Optically Active 2,2-Dimethyl-1-(*p*-substituted phenyl)propyl *p*-Nitrobenzoates†

Tomomi KINOSHITA, Keizo IKAI, Tugunori KASHIMURA, Masataka FUJIWARA, and Kunio OKAMOTO*

Department of Hydrocarbon Chemistry, Faculty of Engineering, Kyoto University, Kyoto 606

(Received April 7, 1986)

The salt effect of $(n\text{-Bu})_4NClO_4$ and NaOPh on the polarimetric and titrimetric rate constants (k_p and k_t, respectively) has been examined for the S_N1 solvolyses of optically active 2,2-dimethyl-1-(*p*-methoxyphenyl)-propyl (**1**) and 2,2-dimethyl-1-phenylpropyl *p*-nitrobenzoates (**2**) in pure phenol solvent. Four patterns, A, B, C, and D of the k_p–k_t profile against the added salt concentration have been observed for the phenolyses of **1**, **2**, and 2,2-dimethyl-1-(*p*-nitrophenyl)propyl *p*-nitrobenzoate (**3**). The patterns can specify the number of the sequential ion-pair intermediates (i.e., one or two), the product-forming stage (i.e., the 1st or the 2nd intermediate), and the species of reactant at the product-forming step (i.e., solvent phenol molecule, the phenoxide, or the perchlorate). The feature of the pattern of the k_p–k_t profile is predominantly controlled by two factors, (i) the stability of the carbocation intermediate derived from the substrates **1**—**3** and (ii) the nucleophilicity of the added salt. The patterns of salt effect on the product distribution (% of ROPh, *o*- and *p*-RC_6H_4OH) are also compatible with such rationalization of the four patterns.

In view of the recent recognition of multiple intermediates in S_N1 solvolysis,[2] we need to know how many ion-pair intermediates exist in each solvolysis, before we consider about the structure of the ion pair as the intermediate. However, the example which actually presents experimental evidence for the presence of multiple intermediates has not so often been reported except by Winstein's[3,4] and our groups.[5–8]

As a result of such dearth of examples in the literature, there has been seen diversity of suggested structures on the ion-pair intermediates, especially for the second stage.[9] By the same token, there has been little direct proof[10] to a view that, as the reactivity of substrate is varied, the relative proportions of simultaneous nucleophilic attack at the different intermediate stages will change.[10,11]

It was previously reported that retentive phenolyses of optically active aralkyl systems can apparently be classified into two groups in which the products derived from either the first or the second ion-pair intermediate, on the basis of four patterns of the salt effect of sodium phenoxide on k_p (polarimetric rate constant) and k_t (titrimetric rate constant) profile.[5,6] However, the examples were so insufficient to correlate explicitly the ion-pair stage (the first or the second) of the product formation with the ion-pair stability (or the reactivity).

Recently, we have further investigated on the salt effect of two salts with different nucleophilicity (i.e., sodium phenoxide and tetrabutylammonium perchlorate) on the k_p and k_t and also on the product distribution (% of ROPh, *o*-, and *p*-RC_6H_4OH) for the phenolyses of 2,2-dimethyl-1-(*p*-methoxyphenyl)propyl (**1**) and 2,2-dimethyl-1-phenylpropyl *p*-nitrobenzoates (**2**). Thus, it has led us to recognize that products come from "the second ion-pair intermediate" alone in the phenolysis of **1**, whereas only "the first ion-pair intermediate" is the source of the products in that of **2**, reflecting the stability sequence of the carbocation intermediate derived from **1** and **2**.

In addition, it has been disclosed in the phenolysis of **2** that the added salts, i.e., sodium phenoxide and tetrabutylammonium perchlorate, can change the k_p–k_t pattern from the pattern B to the pattern C depending on their nucleophilicity, and hence the virtual reactant toward the ion-pair intermediate can be specified as the phenoxide in the presence of sodium phenoxide and as the phenol molecule in the presence of tetrabutylammonium perchlorate.

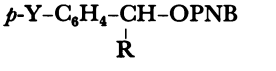

(1) R=*t*-Bu, Y=MeO
(2) R=*t*-Bu, Y=H
(3) R=*t*-Bu, Y=NO_2

Results and Discussion

Phenolysis Rates and Stability of the Ion-Pair Intermediates. The titrimetric rate constants for the phenolyses in phenol at 125 °C in the presence of sodium phenoxide (0.1 M (1 M=1 mol dm^{-3})) have previously been reported for **1**—**3**.[6] The $k_{t,rel.}$ and the k_p values, which were not cited in the previous paper,[6]

† Presented in part by K. O. at the 7th IUPAC Conference on Physical Organic Chemistry, in Auckland, New Zealand, August, 1984.

Table 1. Phenolysis Rates of *p*-Substituted 2,2-Dimethyl-1-phenylpropyl *p*-Nitrobenzoates **1**—**3** in the Presence of Sodium Phenoxide at 125 °C

Substrate[a]	$[NaOPh]_o$/M	k_t/s^{-1} [b,c]	$k_{t,rel.}$	k_p/s^{-1} [d]
1	0.111	4.13×10^{-3}	1.78×10^{5}	
	0.142			6.36×10^{-3}
2	0.104	1.50×10^{-6}	6.49×10	
	0.114			1.78×10^{-6}
3	0.117	2.31×10^{-8}	1.00	

a) $[Substrate]_o=0.10$—0.11 M. b) Cited from Ref. 6. c) Accurate to within ±1.0%. d) Accurate to within ±3.0%.

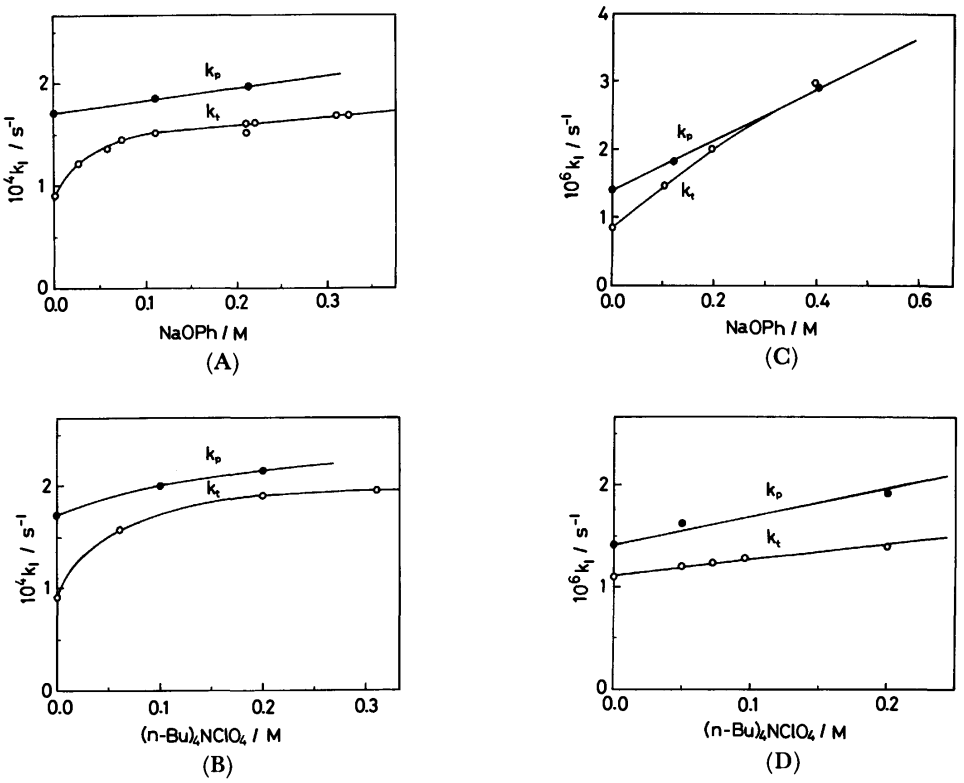

Fig. 1. Effect of added salt concentration on the first-order rate constants (k_p and k_t) in the phenolyses.
(A): (1) in the presence of NaOPh at 75 °C.
(B): (1) in the presence of $(n\text{-Bu})_4NClO_4$ at 75 °C.
(C): (2) in the presence of NaOPh at 125 °C.
(D): (2) in the presence of $(n\text{-Bu})_4NClO_4$ at 125 °C.

are shown along with the k_t values in Table 1.

The k_t decreases in the sequence **1**>**2**>**3** (relative rate; 178000:64.9:1.00). The k_p ($k_p/k_t<1.4$) decreases in the same sequence **1**>**2**. Thus, each of the phenolysis intermediate should become less stable in the order of rate sequence.

Salt Effect on Phenolysis Rates. The measurement of k_p and k_t values were carried out at variable concentrations of added sodium phenoxide or tetrabutylammonium perchlorate for the optically active substrates **1** at 75 °C and **2** at 125 °C. Subsequently, the k_p and k_t were plotted against the salt concentration (Fig. 1).

Such k_p-k_t diagrams can in general be classified into four patterns, A–D (Fig. 2), provided that there is no normal salt effect.[6]

A common feature of patterns A and B is seen in "the special salt effect" on k_t, which has first been recognized in acetolyses of many substrates by Winstein and his coworkers.[3,4,9,15] The special salt effect indicates that the added salt reacts with an ion-pair intermediate making the rate of ion-pair return negligibly low as compared with the rate of the product formation.

Table 2. Salt Effect on k_p-k_t for the Phenolyses of 2,2-Dimethyl-1-(*p*-substituted phenyl)propyl *p*-Nitrobenzoates **1**—**3** in Phenol

Substrate[a]	Salt	Temp °C	k_t° [b,c] s^{-1}	$k_{t,ext}^{\circ}/k_t^{\circ}$ [b]	$[Salt]_{1/2}$ [b] M	b_t [b]	k_p° [a,c] s^{-1}	b_p [b]	k_p-k_t pattern[d]
1	NaOPh	125[e]	2.93×10^{-3}	1.74	0.10	0.50	5.90×10^{-3}	0.52	A
		75	9.31×10^{-5}	1.58	0.025	0.40	1.71×10^{-4}	0.61	A
	TBAP[f]	75	9.31×10^{-5}	1.58	0.01	1.6	1.71×10^{-4}	1.7	A
2	NaOPh[e]	125	8.50×10^{-7}	1.67	0.041	2.54	1.42×10^{-6}	2.54	B
	TBAP[f,g]	125	8.50×10^{-7}	1.00	—	4.00	1.42×10^{-6}	2.32	C
3[e]	NaOPh	125	1.75×10^{-8}	1.00	—	2.71	—	—	D[h]

a) $[Substrate]_0=0.10$—0.12 M. b) See the text. c) Accurate to within ±2% for k_t° and within ±3% for k_p° unless otherwise noted. d) The pattern of salt effect on k_p-k_t (see Fig. 2). e) Cited from Ref. 6. f) Tetrabutylammonium perchlorate. g) In the presence of 2,6-di-*t*-butyl-4-methylpyridine (0.1 M). h) Concluded from the k_t diagram against the added NaOPh concentration and from no racemization of the reclaimed substrate at 50% conversion.

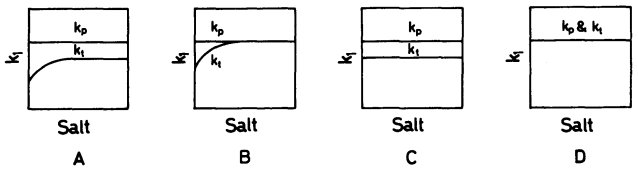

Fig. 2. Four patterns of salt effect on k_p and k_t in S_N1 solvolysis (in the absence of normal salt effect; cited from Ref. 6).

In pattern A, the k_p exceeds the k_t over the whole range of the added salt concentration and the k_p/k_t ratio is constant at higher concentrations of the salt. This indicates the existence of two kinetically-distinguishable intermediates in the solvolysis system as pointed out by Winstein and his coworkers.[3,4]

By contrast, in pattern B the discrepancy between k_p and k_t virtually disappears with increase in the salt concentration. The coincidence in the k_p and k_t values at higher salt concentrations suggests that the consumption rate of the ion-pair intermediate becomes far greater than the return rate and consequently that the solvolysis proceeds via a single ion-pair intermediate alone.

The k_t values in patterns C and D are invariant despite of increase in concentration of the added salt. Thus, the patterns C and D indicate that not the salt but a solvent molecule alone participates in the formation of the product. They clearly indicate that the intermediate is so reactive as to react with the solvent molecule before it does with the added salt. Consequently, we can see from the patterns C and D the existence of a single ion-pair intermediate alone in the reaction system.

In the pattern C, in addition, the intermediate partially returns to the substrate, partially reacts with the solvent molecule, and partially racemizes in itself. In the pattern D, however, all of the intermediate is scavenged by the solvent molecule alone.*

We can characterize such salt effect on k_p and k_t, using the parameters proposed by Winstein and his coworkers,[13] i.e., $k_{t,ext}^{\circ}/k_t^{\circ}$ ($k_{t,ext}^{\circ}$: k_t value extrapolated at [salt]=0 from its linear part at higher salt concentrations, k_t°: k_t value at [salt]=0) and $[salt]_{1/2}$ (salt concentration corresponding to $0.5(k_{t,ext}^{\circ}+k_t^{\circ})$) for special salt effect, and also using Winstein's equations[13] $k_p=k_p^{\circ}(1+b_p[salt])$ (k_p°: k_p value at [salt]=0) and $k_t=k_{t,ext}^{\circ}(1+k_t[salt])$ for normal salt effect on k_p and k_t, respectively. Such parameters for phenolyses of **1**—**3**, which include some previously-reported,[6] are tabulated in Table 2.

The phenolysis of **1** in the presence of NaOPh or $(n\text{-Bu})_4NClO_4$, follows pattern A (Fig. 1 and Table 2; $k_{t,ext}^{\circ}/k_t^{\circ}>1$, $[salt]_{1/2}>0$, and $k_p/k_t>1$) which suggests that both NaOPh and $(n\text{-Bu})_4NClO_4$ attack the second intermediate (I_2).

The other examples of pattern A have been observed in the phenolysis of 1-(*p*-methoxyphenyl)ethyl *p*-nitrobenzoate in the presence of NaOPh[5] and also in the acetolyses of *threo*-2-(*p*-methoxyphenyl)-1-methylpropyl brosylate and tosylate in the presence of $LiClO_4$.[3]

The k_p-k_t profile for **2** against the added NaOPh concentration, which belongs to pattern B (Fig. 1 and Table 2; $k_{t,ext}^{\circ}/k_t^{\circ}>1$, $[salt]_{1/2}>0$, and $k_p/k_t=1$), indicates that the phenoxide ion attacks the first ion-pair intermediate to result in neither ion-pair return nor racemization of the intermediate itself at higher NaOPh concentrations. The other examples of pattern B have been found in the phenolyses of 2,2-dimethyl-1-(*p*-methoxyphenyl)propyl trifluoroacetate,[6] 1-ethyl-1,5-dimethylhexyl chloride and *p*-nitrobenzoate,[7] and 1-methylheptyl tosylate,[7] the acetolysis of

* The intermediate may return without racemization and also without isotope scrambling of two oxygen atoms in the *p*-nitrobenzoyloxy group of leaving one.

2-(*p*-methoxyphenyl)propyl tosylate,[4] and the trifluoroacetolysis of 1-methylpropyl tosylate.[14]

In this context, it deserves to mention that Winstein and his coworkers measured the sum ("k_1"$=k_t+k_r$) of the k_t for 2-(*p*-methoxyphenyl)propyl tosylate and the rearrangement rate (k_r) to 1-(*p*-methoxyphenyl)-1-methylethyl tosylate as the ionization rate constant instead of the k_p and they regarded the "k_1"$-k_t$ (instead of k_p-k_t) profile for the acetolysis of 2-(*p*-methoxyphenyl)propyl tosylate as pattern A in the presence of $LiClO_4$.[4] However, the ratios of "k_1"$/k_t$ for this system are calculated to be 1.24, 1.14, and 1.03 at $LiClO_4$ concentrations 0.0300, 0.0600, and 0.100 M, respectively, by the use of their rate data.[4] Thus, it certainly decreases to 1.00 at higher $LiClO_4$ concentrations. In other words, the "k_1" and k_t lines must coincide with each other at the higher salt concentration than 0.1 M. Consequently, the profile should not belong to pattern A, but to pattern B, and hence the nucleophile should attack the first, not the second, ion-pair intermediate in the acetolysis.

The phenolysis of **2** in the presence of $(n\text{-Bu})_4NClO_4$† exhibits pattern C (Fig. 1 and Table 2; $k^\circ_{t,ext}/k^\circ_t=1$, $[salt]_{1/2}=0$, and $k_p/k_t>1$) instead of B. The added perchlorate is less nucleophilic than NaOPh and the intermediate is scavenged by the solvent phenol instead of the perchlorate. Thus, this is reflected in the changeover of the pattern from B to C (Table 2).

The same pattern C has been observed in the other phenolyses of 1-phenylethyl,[5] 1-phenylpropyl,[6] 2-methyl-1-phenylpropyl,[6] 1-methyl-1-phenylpropyl,[6] *p*-chlorobenzhydryl *p*-nitrobenzoates[6] in the presence of NaOPh), and 1-phenylethyl chloride (in the presence of $PhNH_2$††). The same pattern C has been also found in the acetolysis of *exo*-2-norbornyl brosylate in the presence of KOAc.†††,[16]

The *p*-nitrobenzoate (**3**) should give a relatively less stable and short-lived ion-pair intermediate, and the racemization was not observed in the reclaimed substrate at a half life. Hence, although the k_p was not measured for **3**, it is most probable that **3** follows pattern D (Table 2; $k^\circ_{t,ext}/k^\circ_t=1$, $[salt]_{1/2}=0$, and $k_p/k_t=1$). The phenolyses of 1-(*p*-nitrophenyl)ethyl *p*-nitrobenzoate[5] and 1-ethyl-1,5-dimethylhexyl trifluoroacetate in the presence of NaOPh[6] and the acetolysis of *endo*-2-norbornyl brosylate in the presence of KOAc†††,[16] offer the other examples of pattern D.

Among the phenolyses of the three substrates **1**—**3**, the reaction temperature (75 °C) for **1** in the presence of $(n\text{-Bu})_4NClO_4$ is lower than those for the others (see Table 2). However, the pattern A for **1** has been observed in the presence of NaOPh at both 125[6] and 75 °C (Table 2). Therefore, the k_p-k_t pattern for $(n\text{-Bu})_4NClO_4$ would most probably follow pattern A even at 125 °C.

Accordingly, under the exactly identical conditions the k_p-k_t profiles for phenolyses of **1**—**3** should exhibit pattern A for **1**, B in the presence of NaOPh for **2**, C in the presence of $(n\text{-Bu})_4NClO_4$ for **2**, and D for **3**.

The similar feature of the k_p-k_t profile has been observed for the phenolysis of 1-phenylethyl system, A for $p\text{-}CH_3O$, C for unsubstituted, and D for $p\text{-}NO_2$.[5]

These results, in turn, show that the k_p-k_t pattern should change in the order A→B→C→D as the stability of phenolysis intermediate decreases and also as the nucleophilicity of added salt decreases. For **1** which gives the most stable carbocation among the homologue, the second ion-pair intermediate (I_2) is attacked by both NaOPh and $(n\text{-Bu})_4NClO_4$. For **2** which generates relatively less stable carbocation, the phenoxide ion and a solvent molecule (in a solvation shell) attack the first ion-pair intermediate (I_1), but $(n\text{-Bu})_4NClO_4$ can not have the chance to react with I_1. For **3** which produces the most reactive carbocation among the homologue, I_1 reacts instantly with the solvent phenol molecule alone as it forms.

A similar tendency is seen in the comparison of acetolyses of *threo*-2-(*p*-methoxyphenyl)-1-methylpropyl and 2-(*p*-methoxyphenyl)propyl tosylates; their rates (k°_p) decrease in the sequence the former (2.70×10^{-5} s^{-1} at 25 °C[3]) > the latter (1.79×10^{-5} s^{-1} at 50 °C[4]) and follow the k_p-k_t patterns A and B, respectively (vide supra).

It has been claimed that in the S_N1 solvolysis the product may be produced via some or all of possible intermediates.[2] In addition, a view[10,11] has been presented that as the stability of the intermediates varies, the relative portions of nucleophilic attack stages will change. However, little direct evidence[10] has been given to the view. Our result shows that, conservatively speaking of the phenolysis, all of the products are substantially derived from a single ion-pair intermediate, either I_1 or I_2.

Thus, from the k_p-k_t patterns, we can determine the number of ion-pair intermediate, in the other words, the product-forming stage and the species of reactant (the solvent molecule or the added salt). Hence, the intermediate stage of nucleophilic attack is fundamen-

† 2,6-Di-*t*-butyl-4-methylpyridine was added to the phenolysis of **2** in the presence of $(n\text{-Bu})_4NClO_4$ in order to neutralize the liberated acid which might cause the rearrangement of the phenyl ether to the alkylphenols.[15]

†† Although the pattern A was previously reported for the phenolysis of 1-phenylethyl chloride in the presence of aniline,[8] reexamination of the salt effect for the system in our laboratory has now disclosed that it does not follow pattern A, but C.

††† For the acetolyses of *exo*-[16] and *endo*-2-norbornyl brosylates,[17] the rates were measured only at one or two concentrations of added KOAc. The k_p-k_t patterns, however, can be estimated to be C for the exo-isomer and D for the endo-isomer.

Table 3. Features of Four Patterns of the k_p-k_t Diagram against Concentration of Added salt in the Phenolyses of 2,2-Dimethyl-1-(*p*-substituted phenyl)propyl *p*-Nitrobenzoates **1**—**3**

X[a]	Pattern[b]	No. of intermediate	Added salt	Nucleophile[c]	Ion-pair return	Ion-pair intermediate		
						Life	Stability (Reactivity)	Racemization
CH_3O **1**	A	2	NaOPh TBAP[d]	NaOPh TBAP[d]	Exists	Longer	Higher (Lower)	More
H **2**	B	1	NaOPh	NaOPh	Exists[e]	Shorter	Lower (Higher)	Less[f]
H **2**	C	1	TBAP[d]	PhOH	Exists	Shorter	Lower (Higher)	Less
NO_2 **3**	D	1	NaOPh	PhOH	Not exist	Much shorter	Much lower (Much higher)	No

a) *p*-Substituent. b) See the text for each profile. c) Reacting with ion-pair intermediate. d) Tetrabutylammonium perchlorate. e) Not exist at higher salt concentration. f) No racemization at higher salt concentrations.

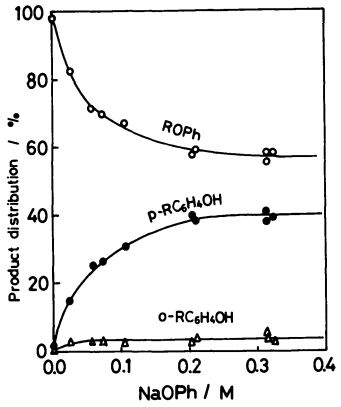

Fig. 3. Product distribution in the phenolysis of 2,2-dimethyl-1-(*p*-methoxyphenyl)propyl *p*-nirtobenzoate (**1**) in the presence of added sodium phenoxide in phenol at 75 °C.

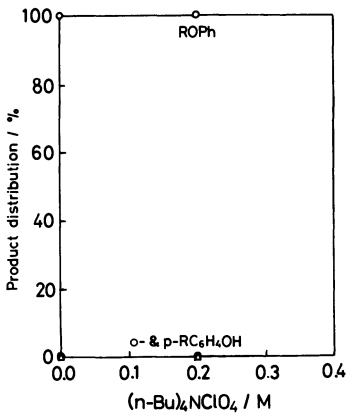

Fig. 4. Product distribution in the phenolysis of 2,2-dimethyl-1-(*p*-methoxyphenyl)propyl *p*-nitrobenzoate (**1**) in the presence of added tetrabutylammonium perchlorate in phenol at 75 °C (at 0% reaction extrapolated from product distributions at 5—70% reaction).

tally dependent on the stability (the reactivity or the life span) of S_N1 ion-pair intermediate and the nucleophilicity of the added salt or the solvent molecule. These are summarized in Table 3.

Salt Effect on Product Distribution. The product distribution (% of ROPh, *o*-, and *p*-RC_6H_4OH) was examined by the use of GLPC for the phenolyses of **1** with variable concentrations (0—0.3 M) of added NaOPh or $(n\text{-Bu})_4NClO_4$ at 75 °C under conditions identical with those employed in rate measurements. When the distribution was plotted against the concentration of added salt, patterns similar to the salt effect on k_t were observed in the diagrams; the results are shown in Figs. 3—5, along with that for **2** which was reported in the previous paper.

For **1** and **2** in the presence of NaOPh, the yield of *p*-alkylphenol increases and that of alkyl phenyl ether decreases in a pattern similar to the special salt effect on k_t (Figs. 2 and 4). The yield of *o*-alkylphenol is

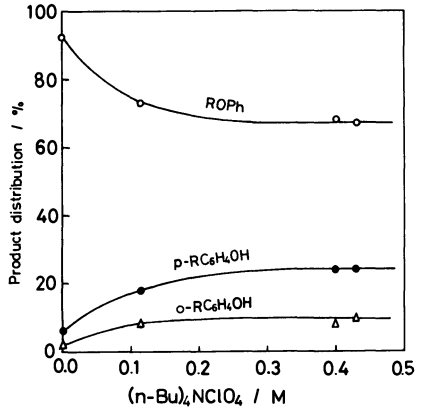

Fig. 5. Product distribution in the phenolysis of 2,2-dimethyl-1-phenylpropyl *p*-nitrobenzoate (**2**) in the presence of added sodium phenoxide in phenol at 125 °C (cited from Ref. 6).

almost invariable. From constancy of the product distribution at higher salt concentrations, it is concluded that almost all of the products at higher salt concentrations are derived from the reaction of the phenolysis intermediate with the added salt, not with the solvent phenol molecule.

For **1** in the presence of $(n\text{-Bu})_4NClO_4$, the product distribution is almost invariable inspite of increase in the added salt concentration and predominantly the phenyl ether alone (extrapolated at 0% reaction from product distribution curves at 5—70% reaction¶; Fig. 3).

Thus, the special salt effect by NaOPh appears on both the k_t value and the product distribution, whereas the special salt effect by $(n\text{-Bu})_4NClO_4$ does not appear on the product distribution but on the k_t value alone.

The perchlorate certainly reacts with the intermediate to give another intermediate, which is rapidly consumed by the solvent phenol molecule alone. On the role of $(n\text{-Bu})_4NClO_4$ at the product formation stage, further examination is in progress.

In conclusion, only after confirmation of the ion-pair stage of nucleophilic attack, we can deduce the detailed structure of the ion-pair intermediates from the stereochemical outcomes for both O- and C-alkylations in phenolyses. The ion-pair structure will be discussed in the following paper.

Experimental

^{13}C and ^1H NMR spectra were taken with a JEOL model JNM FX-100 25 MHz and a Hitachi model R-24 60 MHz instruments, respectively; IR spectra with a Hitachi model 215 spectrophotometer, and GLPC was performed with Hitachi model 163 and model 023-6003 instruments. Optical rotations were measured with a JASCO DIP-SL polarimeter.

Materials. Optically active **1** and **2** were synthesized in the previously-reported manner.[6] Sodium phenoxide was prepared by refluxing a toluene solution of phenol with sodium metal. Tetrabutylammonium perchlorate, an analytical reagent grade, was recrystallized from ethanol and dried in vacuo. 2,6-Di-*t*-butyl-4-methylpyridine was prepared by a known method.[18]

Titrimetric Rate Constants (k_t). The usual aliquot technique[5,6] was employed for measurement of k_t. The diminution in base concentration in the presence of NaOPh was followed by titration in acetone with standard hydrochloric acid; the increase in acid concentration in the presence of $(n\text{-Bu})_4NClO_4$ or in the absence of added salt was followed by titration with aqueous sodium hydroxide solution. Methyl Red was used as an indicator. The k_t values are tabulated in Table 2.

Polarimetric Rate Constants (k_p). The previously-reported procedure[5,6] was followed. The rate data against the added salt concentration are summarized in Table 2.

Product Distribution Analysis. Product distributions of phenolyses were analyzed by GLPC in a manner similar to that reported earlier.[19]

The authors thank the Ministry of Education, Science, and Culture for a Grant-in-Aid for Scientific Research.

¶ The extrapolation was carried out in order to eliminate the effect of the liberated acid which caused the rearrangement of the phenyl ether to the alkylphenols.[15]

References

1) Part 12, K. Okamoto, K. Takeuchi, and K. Inoue, *J. Chem. Soc., Perkin Trans. 2*, **1980**, 842.

2) For recent reviews, a) S. Winstein, B. Appel, R. Baker, and A. Diaz, *Chem. Soc., Spec. Pub.*, **19**, 109 (1965) and their many earlier papers cited therein; b) D. J. Raber, J. M. Harris, R. E. Hall, and P. v. R. Schleyer, *J. Am. Chem. Soc.*, **93**, 4821 (1971); c) V. J. Shiner, Jr., and R. D. Fisher, *ibid.*, **93**, 2553 (1971); d) H. L. Goering and H. Hopf, *ibid.*, **93**, 1224 (1971); e) C. D. Ritchie, *Acc. Chem. Res.*, **5**, 348 (1972); f) F. G. Bordwell, *ibid.*, **5**, 374 (1972); g) R. A. Sneen, *ibid.*, **6**, 46 (1973); h) D. J. Raber, J. M. Harris, and P. v. R. Schleyer in "Ions and Ion Pairs in Organic Reactions," ed by M. Szwarc, John Wiley & Sons, New York, N. Y. (1974), Chap. 3; i) J. M. Harris, *Progr. Phys. Org. Chem.*, Vol. **11**, pp. 88—174 (1974); j) T. W. Bentley and P. v. R. Schleyer, *Adv. Phys. Org. Chem.*, Vol. **14**, pp. 1—67 (1977); k) D. Bethell in "Reactive Intermediates," ed by M. Jones, Jr., and R. A. Moss, John Wiley & Sons, New York, N. Y. (1978), Vol. **1**, Chap. 4.

3) S. Winstein and G. C. Robinson, *J. Am. Chem. Soc.*, **80**, 169 (1958).

4) S. Winstein and A. H. Fainberg, *J. Am. Chem. Soc.*, **80**, 459 (1958).

5) K. Okamoto, T. Kinoshita, Y. Takemura, and H. Yoneda, *J. Chem. Soc., Perkin Trans. 2*, **1975**, 1426.

6) K. Okamoto, T. Kinoshita, T. Oshida, T. Yamamoto, Y. Ito, and M. Dohi, *J. Chem. Soc., Perkin Trans. 2*, **1976**, 1617.

7) K. Okamoto and T. Kinoshita, *Bull. Chem. Soc. Jpn.*, **45**, 2802 (1972).

8) K. Okamoto, K. Takeuchi, and H. Shingu, *Bull. Chem. Soc. Jpn.*, **35**, 525 (1962); detailed reexamination for the salt effect on k_p-k_t will be described in a following paper.

9) For solvent-saparated ion pair, Refs. 1, 2, and 3: For anion-cation-stabilized ion pair, L. S. Miller, D. Zazzaron, J. J. Dannenberg, R. Metras, and M. Gillard, *J. Org. Chem.*, **45**, 641 (1980): For quadruplet, A. D. Topsom in C. K. Ingold, "Structure and Mechanism in Organic Chemistry," 2nd Ed., Cornell Univ. Press, Ithaca, New York, N. Y. (1969), p. 500: For four-centre ion pair, a) K. Okamoto, H. Yamada, I. Nitta, and H. Shingu, *Bull. Chem. Soc. Jpn.*, **39**, 299 (1966); b) K. Okamoto, T. Kinoshita, and H. Shingu, *ibid.*, **43**, 1545 (1970): For rear-side shielded ion pair, K. Okamoto, T. Kinoshita, and Y. Osada, *J. Chem. Soc., Perkin Trans. 2*, **1975**, 253 and references therein: and so on.

10) C. D. Ritchie, *J. Am. Chem. Soc.*, **93**, 7324 (1971).

11) a) S. Winstein, E. Clippinger, A. H. Fainberg, R. Heck, and G. C. Robinson, *J. Am. Chem. Soc.*, **78**, 328 (1956); b) J. M. Harris, D. Clark, A. Becker, and J. F. Fagan, *ibid.*, **96**, 4478 (1974).

12) S. Winstein, E. Clippinger, A. H. Fainberg, and G. C. Robinson, *Chem. Ind. (London)*, **1954**, 664.
13) a) S. Winstein, E. Clippinger, A. H. Fainberg, and G. C. Robinson, *J. Am. Chem. Soc.*, **76**, 2597 (1954); b) A. H. Fainberg and S. Winstein, *ibid.*, **78**, 2763 and 2767 (1956); c) S. Winstein and E. Clippinger, *ibid.*, **78**, 2784 (1956); d) S. Winstein and J. Sonnenberg, *ibid.*, **83**, 3235 (1961).
14) A. D. Allen, I. C. Ambidge, and T. T. Tidwell, *J. Org. Chem.*, **48**, 4527 (1983).
15) K. Okamoto, T. Kinoshita, O. Makino, and H. Shingu, *Bull. Chem. Soc. Jpn.*, **47**, 1770 (1974).
16) S. Winstein and D. Trifan, *J. Am. Chem. Soc.*, **74**, 1154 (1952).
17) S. Winstein and D. Trifan, *J. Am. Chem. Soc.*, **74**, 1147 (1952).
18) A. G. Anderson and P. J. Stang, *J. Org. Chem.*, **41**, 3034 (1976).
19) K. Okamoto, K. Matsubara, T. Kinoshita, and H. Shingu, *Bull. Chem. Soc. Jpn.*, **45**, 1191 (1972).

Synthesis of Vinylcyclopropanes, Cyclopropyl Vinyl Ketones, and 3-Pyrazolyl Vinyl Ketones from 1-Diazo-3-trimethylsilylpropanone

Otohiko Tsuge,* Shuji Kanemasa, Toshiro Suzuki, and Koyo Matsuda
Research Institute of Industrial Science, and Department of Molecular Science and Technology, Interdisciplinary Graduate School of Engineering Sciences, Kyushu University, Kasugakoen, Kasuga 816
(Received April 12, 1986)

Reaction of 1-diazo-3-trimethylsilylpropanone with olefins in the presence of cupric acetylacetonate ($Cu(acac)_2$) affords cyclopropyl trimethylsilylmethyl ketones. One-flask procedure for the formation of these silylated ketones and subsequent treatment with organometallics or with lithium diisopropylamide (LDA) and then carbonyl compounds gives a variety of vinylcyclopropanes or cyclopropyl vinyl ketones in good yields, respectively. Cycloaddition of 1-diazo-3-trimethylsilylpropanone with acetylenes and similar carbon–carbon bond formation at the side chain of the cycloadducts lead to 3-pyrazolyl vinyl ketones.

Rapidly growing importance of organosilanes in recent organic synthesis owes to their wide utility in carbanion chemistry. Silicon–carbon bond can be smoothly desilylated by action with a silylophile leading to the regioselective formation of carbanion, and deprotonation can be performed by action with a base at the carbon substituted by the silyl moiety generating silyl-stabilized carbanion.[1] The resulting carbanionic species can be utilized for carbon–carbon bond-forming reactions. Accordingly, addition of a silyl moiety to functionalized molecule produces a new reagent of multi-functionalized type.[2]

Silicon–carbon bond is relatively inert under normal conditions so that the compounds bearing this bond may be often isolated and the silyl moiety may survive on a chemoselective reaction at the preexisting functionality. Use of the both functionalities in separate steps, one by one in two different orders, adds new synthetic potentials to the parent molecule providing a new reagent.

The present report describes the synthetic utility of 1-diazo-3-trimethylsilylpropanone (**1**) which bears a diazo ketone and a silyl functionalities. Though this diazo compound **1** has been known for these seven years, there is no report available on its utilization to organic synthesis.[3] Here, the diazo ketone functionality is to be first used for the cyclopropanation of olefins or the cycloaddition reaction with acetylenes, and the silyl functionality on the resulting cyclopropanes or cycloadducts is to be utilized for the subsequent carbon–carbon bond formation.

Results and Discussion

1-Diazo-3-trimethylsilylpropanone (**1**) was previously synthesized by the reaction of diazomethane with trimethylsilylacetyl chloride,[3] which is available from commercially available chloromethyltrimethylsilane via trimethylsilylacetic acid.[4] We first investigated to open a more convenient route to **1** starting from readily available materials. For this purpose, acetic acid was converted into its dianion by treatment with LDA and the anion was silylated with two equivalent amounts of chlorotrimethylsilane to give 70% of trimethylsilylacetic acid after hydrolysis (Scheme 1). The carboxylic acid was then transformed into trimethylsilylacetyl chloride or isopropyl trimethylsilylacetyl carbonate in 83 or 89% yield, respectively. The diazo compound **1** was obtained by the subsequent treatment of the silylacetyl chloride or the silylacetyl carbonate with diazomethane in ether. This method makes possible to prepare large quantities of **1** from less expensive acetic acid and chlorotrimethylsilane.

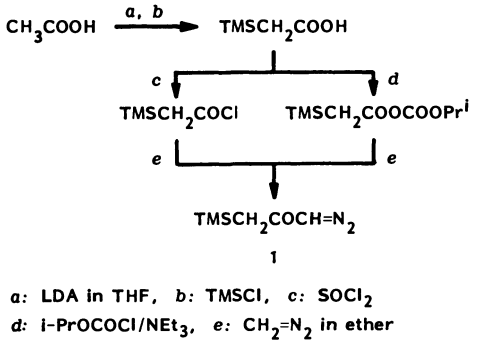

Scheme 1.

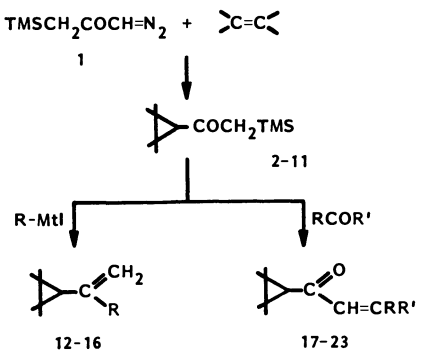

Scheme 2.

Table 1. Cyclopropanation of Olefins with 1-Diazo-3-trimethylsilylpropanone (**1**)[a]

Olefin	Solvent[b]	Product		Yield/%[c]
Styrene	A	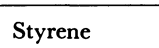	**2**	55
1-Octene	A	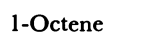	**3**	49 (72[d])
2-Methyl-1-pentene	A	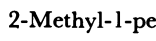	**4**	57 (68[d])
Cyclohexene	A		m=$(CH_2)_4$ **5**	65
Cycloheptene	A		m=$(CH_2)_5$ **6**	53 (62[d])
Cyclooctene	A		m=$(CH_2)_6$ **7**	50
Bicyclo[2.2.1]hept-2-ene	B	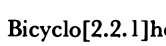	**8**	60
Acenaphthylene	B	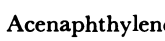	**9**	61[d]
Ethyl vinyl ether	A	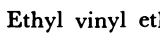	**10**	45
Vinyl acetate	A	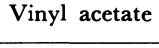	**11**	51

a) All reactions were carried out at 60 °C in the presence of 5 mol% of $Cu(acac)_2$. b) A: Olefin (0.5 ml for 1 mmol of **1**) was used as solvent. B: Benzene. c) Isolated yield by vacuum distillation. d) Determined by GLC.

Table 2. One-Pot Synthesis of Vinylcyclopropanes **12**—**16** from **1**[a]

Cyclopropyl silylmethyl ketone	Organometallics[b]	Conditions[c]	Product	R	Yield/%[d]
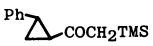	*n*-BuLi	A	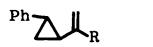	**12a** *n*-Bu	50
	n-HepMgBr	B		**12b** *n*-Hep	56
2	CH_2=CHLi	B	**12**	**12c** CH_2=CH[e]	50[f]
	PhLi	A		**13a** Ph	60
	PhMgBr	B	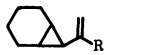	**13a** Ph	50
	n-BuLi	A		**13b** *n*-Bu	55
5	*n*-HepMgBr	B	**13**	**13c** *n*-Hep	57
	CH_2=CHLi	B		**13d** CH_2=CH[e]	51[f]
	PhLi	A		**14a** Ph	53
	PhMgBr	B		**14a** Ph	41
	n-BuLi	A		**14b** *n*-Bu	42
7	CH_2=CHLi	B	**14**	**14c** CH_2=CH[e]	53[f]
	PhLi	A		**15a** Ph	53
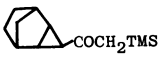	PhMgBr	B	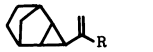	**15a** Ph	40
	n-BuLi	A		**15b** *n*-Bu	57
8	CH_2=CHLi	B	**15**	**15c** CH_2=CH[g]	49[h]
	PhLi	A		**16a** Ph	51
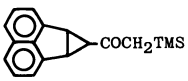	PhMgBr	B	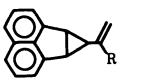	**16a** Ph	40
	n-BuLi	A		**16b** *n*-Bu	45
9	CH_2=CHLi	B	**16**	**16c** CH_2=CH[e]	44[f]

a) Cyclopropyl silylmethyl ketones are first prepared from **1** and olefins according to the procedure shown in Table 1. Dry THF and then organometallics are added by syringe. All reactions are carried out under dry nitrogen. b) PhLi: In cyclohexane-diethyl ether (7 : 3); PhMgBr: In THF; *n*-BuLi: In hexane; *n*-HepMgBr: In THF; CH_2=CHLi: Prepared in situ from tetravinyltin and butyllithium in THF. These organometallics are used in a slight excess (1.2—1.3 equivalent to **1**). c) A: 1 h at 0 °C; B: 1 h at −78 °C and then 30 min at room temperature. After the reaction is completed, the mixture is treated with aqueous acetic acid. d) Isolated yield based on **1**. e) Isolated as a cycloadduct with dimethyl fumarate. f) Yield of the fumarate cycloadduct. g) Isolated as a cycloadduct with *N*-methylmaleimide. h) Yield of the maleimide cycloadduct.

Reactions of **1** with a variety of olefins proceeded rapidly and cleanly at 60 °C in the presence of a catalytic amount of $Cu(acac)_2$ to give cyclopropyl trimethylsilylmethyl ketones **2—11** (Scheme 2 and Table 1). As the carbene generated from **1** by the elimination of nitrogen tends to undergo ready coupling dimerization reaction giving 3-hexene-2,5-dione after spontaneous desilylation, this reactive species has to be captured as soon as it is generated.[5] Therefore, olefins were used as solvents if they are liquid, and were used in large excess in dry benzene if solid. When the diazo compound **1** was slowly added by syringe to the mixture of olefin and catalyst preheated at 60 °C, formation of the coupling product became negligible. This addition took at least 30 min when 1 mmol of **1** was employed. Copper powder could be used instead of $Cu(acac)_2$, but yields of the cyclopropanes were found less satisfactory.

Although they are able to be isolated, the cyclopropyl trimethylsilylmethyl ketones **2—11** thus obtained are quite sensitive to moisture in the air suffering from ready protodesilylation. As the separation or purification procedure through column chromatography on silica gel met with awful loss of the silylated products, the crude reaction mixture was directly subjected to vacuum distillation to give pure **2—11** in fairly good yields (Table 1). The yields of some high-boiling products were determined on the basis of GLC analysis.

Nucleophilic addition of organometallics onto the carbonyl group of trimethylsilylacetyl substituent of **2**, **5**, and **7—9** gave vinylcyclopropanes **12—16** after elimination of trimethylsilanol (Scheme 2). One-flask procedure was most conveniently applied to the sequence of cyclopropanation and nucleophilic addition. Thus, the reaction of **1** with an olefin was first carried out under the conditions shown in Table 1. The reaction mixture was diluted with dry tetrahydrofuran (THF) and an organometallic reagent previously prepared was added. After the completion of nucleophilic addition, the mixture was treated with acetic acid to give vinylcyclopropanes **12—16** (Table 2).

Use of Grignard reagents as organometallics at the

Table 3. One-Pot Synthesis of Cyclopropyl Vinyl Ketones **17—23** from **1**[a]

Cyclopropyl silylmethyl ketone	Carbonyl compounds	Product		R	R′	Yield/%[b]
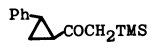 **2**	PhCHO	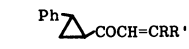 **17**	**17a**	H	Ph	60
	PhCH=CHCHO (t)		**17b**	H	PhCH=CH (t)	55
	EtCHO		**17c**	H	Et	50
	i-PrCHO		**17d**	H	*i*-Pr	52
	MeCOMe		**17e**	Me	Me	49
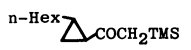 **3**	PhCHO	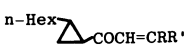 **18**	**18a**	H	Ph	58
	2-furyl-CHO		**18b**	H	2-furyl	50
	EtCHO		**18c**	H	Et	55
	i-PrCHO		**18d**	H	*i*-Pr	56
4	PhCHO	**19**	**19a**	H	Ph	59
	EtCHO		**19b**	H	Et	59
	i-PrCHO		**19c**	H	*i*-Pr	58
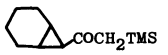 **5**	PhCHO	**20**	**20a**	H	Ph	69
	EtCHO		**20b**	H	Et	58
	i-PrCHO		**20c**	H	*i*-Pr	54
	MeCOMe		**20d**	Me	Me	52
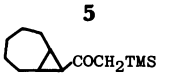 **6**	PhCHO	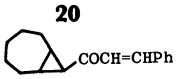 **21**				49
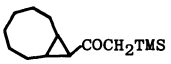 **7**	PhCHO	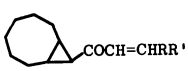 **22**	**22a**	H	Ph	59
	2-furyl-CHO		**22b**	H	2-furyl	55
	EtCHO		**22c**	H	Et	53
	i-PrCHO		**22d**	H	*i*-Pr	50
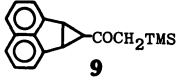 **9**	PhCHO	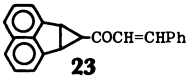 **23**				50

a) Cyclopropyl silylmethyl ketones are first prepared from **1** and olefins according to the procedure shown in Table 1 under argon. The resulting mixture is added slowly by syringe to a solution of LDA, previously prepared from butyllithium and diisopropylamine in THF, at −78 °C. After 45 min, carbonyl compounds are added and the mixture is allowed to stir at −78 °C for 1 h and then at room temperature for 1 h (under nitrogen). b) Isolated yield based on **1**.

second step in the above one-flask procedure resulted in extremely decreased yields of vinylcyclopropanes. Coupling reaction products of the Grignard reagents were far major products in these cases. When the Grignard reagents were slowly added at −78 °C, this undesired coupling reaction could be significantly suppressed. However, yields of the vinylcyclopropanes were not satisfactory yet. Employment of organolithiums instead of Grignard reagents afforded better yields of the vinylcyclopropanes **13**—**16** (Table 2).

The silyl-stabilized carbanions generated by the deprotonation of cyclopropyl silylmethyl ketones **2**—**7** and **9** with LDA smoothly reacted with a variety of carbonyl compounds to afford cyclopropyl vinyl ketones **17**—**23** (Scheme 2). One-flask procedure for the sequence of cyclopropanation, anion generation, carbonyl addition, and silanol elimination was again employed without any serious troubles (Table 3).

Thus, 1-diazo-3-trimethylsilylpropanone (**1**) was successfully utilized to the synthesis of a variety of vinylcyclopropanes **12**—**16** and cyclopropyl vinyl ketones **17**—**23** through a simple one-flask procedure.

We further continued to use **1** in the synthesis of heterocyclic compounds. Cycloaddition reaction of **1** with *N*-phenylmaleimide or dimethyl fumarate produced the corresponding cycloadducts **A**. However, these cycloadducts were found to undergo ready protodesilylation during their separation procedure through column chromatography over silica gel to give 3-acetyl-2-pyrazolines **24** and **25** (Scheme 3).

Similar reaction of **1** with an acetylenic dipolarophile such as dimethyl acetylenedicarboxylate or dibenzoylacetylene produced the corresponding cycloadduct **B**, which again suffered from ready desilylation to give 3-acetylpyrazole **26** or **27** in excellent yield. Treatment of the crude reaction mixture, which nearly consisted of silylated cycloadduct **B**, with more than two equivalents of LDA and the subsequent reaction with benzaldehyde gave 3-pyrazolyl vinyl ketone **28** or **29** (Scheme 4).

Although all the above one-flask reactions are successful examples of consecutive use of the diazo ketone functionality and then the silyl moiety of 1-diazo-3-trimethylsilylpropanone (**1**), use of these functional groups in the different order was found not fruitful. For example, **1** was treated with benzaldehyde in the presence of tetrabutylammonium fluoride (TBAF) to give 60% yield of 3-diazo-4-hydroxy-4-phenyl-2-butanone (**30**). This product was presumably formed by the initial generation of carbanion **C** through desilylation of **1**, a 1,3-proton migration leading to another carbanion **D**, and its addition with benzaldehyde (Scheme 5).

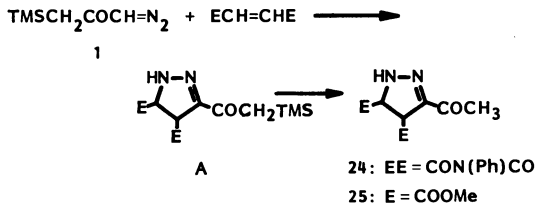

Scheme 3.

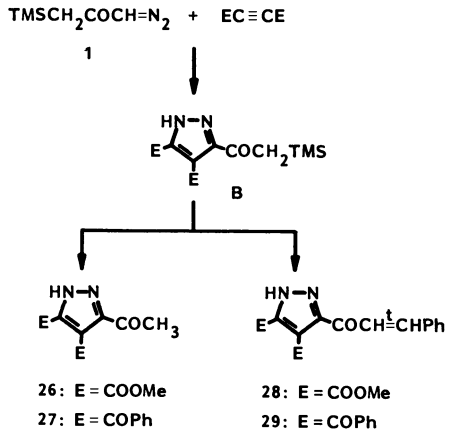

Scheme 4.

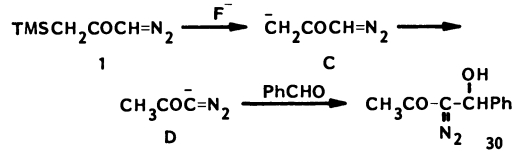

Scheme 5.

Experimental

General. Melting points were determined on a Yanagimoto micro melting point apparatus and are uncorrected. IR spectra were taken with a JASCO IRA-1 or a JASCO A-702 spectrometer. ^{1}H NMR spectra were recorded on a Hitachi R-40 (90 MHz) or a JEOL FX-100 instrument (100 MHz) and ^{13}C NMR spectra on a JEOL FX-100 spectrometer at 25.05 MHz. Chemical shifts are expressed in parts per million downfield from tetramethylsilane as internal standard. Mass spectra were measured with a JEOL JMS-01SG-2 spectrometer at 70 eV of ionization energy. Elemental analyses were performed on a Hitachi 026 CHN micro analyzer. Thin-layer chromatography (TLC) was accomplished on 0.2 mm precoated plates of silica gel 60 F-254 (Merck) or of aluminum oxide 60 F-254 type-E (Merck). Visualization was made with ultraviolet light (254 and 365 nm), iodine, molybdophosphoric acid (5% in ethanol), or *p*-anisaldehyde (5% in ethanol containing 5% of sulfuric acid). For preparative column chromatography, Wakogel C-200, C-300 (Wako), or Kieselgel 60 (Merck, 230—400 mesh) was used. Flash chromatography was carried out on an EYELA EF-10 apparatus using a column (20×180 mm) packed with Silicagel 60 (Merck, size: 0.04—0.063 mm). Gas liquid chromatography (GLC) was accomplished on a Yanaco G-2800 gas chromatography (Yanagimoto) with a flame ionization detector using a glass column (SE-30, 3×

2000 mm). Micro vacuum distillation was carried out with a Sibata GTO-250R Kugelrohr distilling apparatus. Solvents were evaporated with a Tokyo Rikakikai rotary evaporator type-V at about 50 °C unless otherwise stated.

Trimethylsilylacetic Acid. To a solution of diisopropylamine (3.0 g, 29.7 mmol) in dry THF (20 ml) was added dropwise butyllithium (18.7 ml, 29.7 mmol) at 0 °C under nitrogen. After 10 min, acetic acid (0.84 g, 14 mmol) in THF (1 ml) was added dropwise. After 1.5 h at 0 °C chlorotrimethylsilane (3.64 ml, 28 mmol) was added, the mixture was stirred for 2 h, poured into saturated sodium chloride solution, acidified to pH 3 with 1 M-HCl (1 M=1 mol dm^{-3}), and extracted with ether (20 ml). The ether was evaporated and the residue was treated with aqueous methanol overnight. This mixture was poured into ice water and extracted with ether (20 ml). The ether was dried and evaporated to give colorless solid of the acid (1.3 g, 70%): Mp 40 °C; ^{1}H NMR ($CDCl_3$) δ=0.23 (9H, s, TMS), 1.98 (2H, s, CH_2), and 10.20 (1H, br, OH).

This silylacetic acid was also obtained in 81% yield from chloromethyltrimethylsilane via its Grignard reagent according to the known method.[4]

Isopropyl Trimethylsilylacetyl Carbonate. To a mixture of trimethylsilylacetic acid (2.32 g, 17.6 mmol) and isopropyl chloroformate (2 ml, 17.6 mmol) in dry ether (20 ml) was added slowly triethylamine (2.44 ml, 17.6 mmol) at room temperature. The mixture was stirred for 12 h and colorless precipitate separated was removed by filteration. The filtrate was distilled under vacuum to give colorless liquid of the carbonate (3.4 g, 89%): Bp 101—103 °C/8398 Pa; IR (neat) 1790, 1250, and 850 cm^{-1}; ^{1}H NMR ($CDCl_3$) δ=0.18 (9H, s, TMS), 1.32 (6H, d, *i*-Pr), 2.00 (2H, s, CH_2), and 4.91 (1H, m, *i*-Pr); MS *m/z* (rel intensity, %) 117 (41), 75 (93), and 43 (base peak). Found: C, 49.65; H, 8.26%. Calcd for $C_9H_{18}O_4Si$: C, 49.52; H, 8.32%.

1-Diazo-3-trimethylsilylpropanone (1). To a solution of trimethylsilylacetic acid (5.2 g, 39 mmol) in dry petr. ether (10 ml) was added dropwise thionyl chloride (5.01 g, 42 mmol). The mixture was heated at 45—50 °C for 1 h and distilled under vacuum to give trimethylsilylacetyl chloride (bp 60—61 °C/4000 Pa, 4.88 g, 83%): IR (neat) 1805, 1715, 1250, 1095, and 845 cm^{-1}; ^{1}H NMR ($CDCl_3$) δ=0.22 (9H, s, TMS) and 2.51 (2H, s, CH_2).

The chloride (3 g, 19.9 mmol) was slowly added to the ether solution of diazomethane at 0 °C, which was previously prepared from *N*-methyl-*N*-nitroso-*p*-toluenesulfonamide (21.5 g, 100 mmol) and distilled with ether. The mixture was stirred at 0 °C for 30 min and then at room temperature for 12 h. The ether and unreacted diazomethane were removed under vacuum below room temperature. The residue was distilled under vacuum to give **1** (bp 46 °C/107 Pa, 2.24 g, 72%): IR (neat) 2110, 1620, 1330, and 840 cm^{-1}; ^{1}H NMR ($CDCl_3$) δ=0.14 (9H, s, TMS), 2.03 (2H, s, CH_2), and 5.04 (1H, s, CH=N_2); MS *m/z* (rel intensity, %) 156 (M^+, 10), 116 (22), 84 (65), 75 (31), and 73 (base peak).

When isopropyl trimethylsilylacetyl carbonate was employed instead of trimethylsilylacetyl chloride in the above procedure, 62% yield of **1** was obtained.

General Procedure for the Cyclopropanation of Olefins with 1. A mixture of olefins (0.5 ml) and $Cu(acac)_2$ (13 mg, 0.05 mmol) was heated at 60 °C under nitrogen. When olefins are solid, they were dissolved in dry benzene (4 mmol in 1 ml). To this mixture, **1** (1 mmol) was slowly added by syringe in a period of 30 min. After the addition was completed, the mixture was subjected to vacuum distillation on a Kugelrohr micro distilling apparatus to give pure cyclopropyl trimethylsilylacetyl ketones **2**—**11**, except for **9** which could not be distilled. Results are summarized in Table 1.

2: Colorless liquid; bp 135 °C/53 Pa; IR (neat) 1675, 1250, and 850 cm^{-1}; ^{1}H NMR ($CDCl_3$) δ=0.08 (9H, s, TMS), 1.1—2.2 (4H, m, *c*-Pr), 2.32 (2H, s, CH_2), and 6.9—7.4 (5H, m, Ph); ^{13}C NMR ($CDCl_3$) δ=−1.06 (q, TMS), 18.71 (t, CH_2 of *c*-Pr), 28.65, 33.47 (each d, CH of *c*-Pr), 39.83 (t, CH_2), 126.07, 126.48, 128.60 (each d), 140.72 (s), and 206.90 (s, CO); MS *m/z* (rel intensity, %) 232 (M^+, 24), 142 (23), 141 (35), 115 (35), 75 (24), and 73 (base peak). HRMS Found: *m/z* 232.1287. Calcd for $C_{14}H_{20}OSi$: M, 232.1284.

3: Colorless liquid; bp 145 °C/67 Pa; IR (neat) 1675, 1410, 1255, and 855 cm^{-1}; ^{1}H NMR ($CDCl_3$) δ=1.03 (9H, s, TMS), 0.6—2.0 (17H, m, *n*-Hex and *c*-Pr), and 2.30 (2H, s, CH_2); MS *m/z* (rel intensity, %) 240 (M^+, 6), 115 (38), 75 (46), and 73 (base peak). HRMS Found: *m/z* 240.1898. Calcd for $C_{14}H_{28}OSi$: M, 240.1908.

4 (Mixture of two stereoisomers): Colorless liquid; bp 80 °C/67 Pa; IR (neat) 1670, 1255, and 855 cm^{-1}; ^{1}H NMR ($CDCl_3$) δ=0.12 (9H, s, TMS), 0.7—1.8 (10H, m, *n*-Pr and *c*-Pr), 1.10, 1.13 (3H, each s, Me), 2.30, and 2.35 (2H, each s, CH_2, 3:1); ^{13}C NMR ($CDCl_3$) δ=−0.94 (q, TMS), 14.24, 15.41, 20.06, 20.59 (each q, Me), 22.59, 23.30, 24.65 (each t), 30.24, 30.71 (each s, q-C), 33.36 (t), 35.65, 36.24 (each d), 40.71, 40.94, 43.71 (each t), and 207.31 (s, CO); MS *m/z* (rel intensity, %) 212 (M^+, 11), 115 (37), 93 (27), 75 (44), and 73 (base peak). HRMS Found: *m/z* 212.1515. Calcd for $C_{12}H_{24}OSi$: M, 212.1595.

5: Colorless liquid; bp 100 °C/27 Pa; IR (neat) 1680, 1660, 1405, 1245, and 840 cm^{-1}; ^{1}H NMR ($CDCl_3$) δ=0.12 (9H, s, TMS), 1.1—1.9 (11H, m, CH_2 and CH), and 2.29 (2H, s, CH_2); ^{13}C NMR ($CDCl_3$) δ=−1.00 (q, TMS), 21.12, 23.12 (each t), 25.06, 35.65 (each d), 39.71 (t), and 208.60 (s, CO); MS *m/z* (rel intensity, %) 210 (M^+, 35), 75 (55), and 73 (base peak). HRMS Found: *m/z* 210.1436. Calcd for $C_{12}H_{22}OSi$: M, 210.1439.

6: Colorless liquid; bp 110 °C/20 Pa; IR (neat) 1660, 1420, 1240, and 840 cm^{-1}; ^{1}H NMR ($CDCl_3$) δ=0.11 (9H, s, TMS), 0.8—2.4 (13H, m, CH_2 and CH), and 2.28 (2H, s, CH_2); ^{13}C NMR ($CDCl_3$) δ=−1.06 (q, TMS), 28.77, 29.71 (each t), 30.53 (d), 32.47 (t), 37.59 (d), 39.65 (t), and 208.02 (s, CO); MS *m/z* (rel intensity, %) 224 (M^+, 4), 75 (32), and 73 (base peak). HRMS Found: *m/z* 224.1573. Calcd for $C_{13}H_{24}OSi$: M, 224.1594.

7: Colorless liquid; bp 140 °C/53 Pa; IR (neat) 1670, 1430, 1250, and 850 cm^{-1}; ^{1}H NMR ($CDCl_3$) δ=0.12 (9H, s, TMS), 1.1—2.2 (15H, m, CH_2 and CH), and 2.29 (2H, s, CH_2); MS *m/z* (rel intensity, %) 238 (M^+, 9), 115 (25), 75 (36), and 73 (base peak). HRMS Found: *m/z* 238.1774. Calcd for $C_{14}H_{26}OSi$: M, 238.1752.

8: Colorless liquid; bp 150 °C/200 Pa; IR (neat) 1670, 1245, and 840 cm^{-1}; ^{1}H NMR ($CDCl_3$) δ=0.12 (9H, s, TMS), 0.6—1.9 (11H, m, CH_2 and CH), and 2.24 (2H, s, CH_2); ^{13}C NMR ($CDCl_3$) δ=1.17 (q, TMS), 25.41 (d), 28.47 (t), 28.71 (d), 28.94 (t), 36.00 (d), 40.12 (t), and 208.54 (s, CO); MS *m/z* (rel intensity, %) 222 (M^+, 34), 75 (25), and 73 (base peak). HRMS Found: *m/z* 222.1438. Calcd for $C_{13}H_{22}OSi$: M,

222.1439.

9: Colorless liquid; ^{1}H NMR ($CDCl_3$) δ=0.12 (9H, s, TMS), 1.91 (1H, t, J=2.5 Hz, CH), 2.33 (2H, s, CH_2), 3.49 (2H, t, J=2.5 Hz, CH), and 7.3—7.6 (6H, m, Ar); ^{13}C NMR ($CDCl_3$) δ=0.99 (q, TMS), 30.65 (d), 39.98 (t), 49.50 (d), 120.41, 123.64, 127.46 (each d), 131.39, 142.90, 143.25 (each s), and 204.66 (s, CO). As pure **9** could not be obtained, its protodesilylated derivative was submitted for elemental analysis: Colorless prisms (hexane); mp 98—99 °C; IR (KBr) 1660 cm^{-1}; MS m/z (rel intensity, %) 208 (M^+, 10) and 165 (base peak). HRMS Found: m/z 208.0894. Calcd for $C_{15}H_{12}O$: M, 208.0888.

10: Colorless liquid; bp 90 °C/40 Pa; IR (neat) 1670, 1425, 1240, and 840 cm^{-1}; ^{1}H NMR ($CDCl_3$) δ=0.15 (9H, s, TMS), 1.0—1.3 (5H, m, Et and CH_2), 2.22 (2H, s, CH_2TMS), 2.2—2.4 (1H, m, CH), and 3.2—3.6 (3H, m, Et and CH); ^{13}C NMR ($CDCl_3$) δ=−1.06 (q, TMS), 15.00 (q), 17.71 (t), 30.18 (d), 39.53 (t), 62.77 (d), 66.65 (t), and 206.90 (s, CO); MS m/z (rel intensity, %) 200 (M^+, 3), 81 (42), 75 (28), and 73 (base peak). HRMS Found: m/z 200.1251. Calcd for $C_{10}H_{20}O_2Si$: M, 200.1231.

11: Colorless liquid; bp 95 °C/53 Pa; IR (neat) 1750, 1670, 1240, 1225, and 845 cm^{-1}; ^{1}H NMR ($CDCl_3$) δ=0.15 (9H, s, TMS), 1.1—1.5 (2H, m, c-Pr), 2.00 (3H, s, MeCO), 2.37 (2H, s, CH_2), and 4.25 (1H, m, c-Pr); ^{13}C NMR ($CDCl_3$) δ=−1.06 (q, TMS), 15.68 (t, CH_2), 20.72 (q, MeCO), 28.88 (d), 39.98 (t, CH_2TMS), 56.36 (d), 170.74 (s, COO), and 205.72 (s, CO); MS m/z (rel intensity, %) 154 (M^+−70, 16), 75 (40), 73 (93), 45 (23), and 43 (base peak). This compound showed no parent ion peak, the elemental analysis through HRMS being impossible.

General Procedure for the One-Pot Synthesis of Vinylcyclopropanes 12—16 from 1. Cyclopropyl silylmethyl ketones **2**, **5**, and **7—9** were prepared according to the method mentioned above. To the crude product was added dry THF (2 ml for 1 mmol of **1**), and then a solution of organometal previously prepared was added dropwise by syringe. When the reaction was over (the reaction conditions are shown in Table 2), aqueous acetic acid was added and the mixture was stirred at room temperature for 1 h. This acidic solution was neutralized with aqueous sodium hydrogencarbonate and extracted with diethyl ether (10 ml×2). The combined extracts were dried over magnesium sulfate and evaporated in vacuo. The residue was chromatographed over silica gel with hexane-ethyl acetate (15:1) to give vinylcyclopropanes **12—16**. The results are listed in Table 2.

12a: Colorless liquid; IR (neat) 1640 and 1605 cm^{-1}; ^{1}H NMR ($CDCl_3$) δ=0.87 (3H, t, Me of n-Bu), 0.7—2.2 (10H, m, CH_2 and CH), 4.60 (2H, s, =CH_2), and 6.9—7.3 (5H, m, Ph); ^{13}C NMR ($CDCl_3$) δ=13.94 (q, Me), 15.50, 22.42 (each t, CH_2), 25.49, 28.56 (each d, CH), 30.26, 36.11 (each t, CH_2), 106.28 (t, =CH_2), 125.43, 125.63, 128.20 (each d), 142.88 (s), and 149.90 (s); MS m/z (rel intensity, %) 200 (M^+, 7), 143 (base peak), 141 (33), 129 (69), 128 (65), 116 (22), 115 (81), 104 (23), 103 (21), 91 (95), 80 (44), 79 (23), 78 (27), and 77 (46). HRMS Found: m/z 200.1552. Calcd for $C_{15}H_{20}$: M, 200.1564.

12b: Colorless liquid; IR (neat) 1640 and 1605 cm^{-1}; ^{1}H NMR ($CDCl_3$) δ=0.91 (3H, m, Me of n-Hep), 1.0—2.2 (16H, m, CH_2 and CH), 4.65 (2H, s, =CH_2), and 6.9—7.3 (5H, m, Ph); ^{13}C NMR ($CDCl_3$) δ=14.08 (q, Me), 15.50, 22.66 (each t, CH_2), 25.53 (d, CH), 28.12 (t, CH_2), 28.60 (d, CH), 29.19, 29.34, 31.87, 36.45 (each t, CH_2), 106.28 (t, =CH_2), 125.43, 125.67, 128.20 (each d), 142.92 (s), and 149.99 (s); MS m/z (rel intensity, %) 242 (M^+, 8), 143 (base peak), 129 (35), 128 (26), 115 (25), 91 (48), and 80 (31). HRMS Found: m/z 242.2037. Calcd for $C_{18}H_{26}$: M, 242.2033.

Diels-Alder Cycloadduct of 12c with Dimethyl Fumarate (Mixture of two stereoisomers): Colorless liquid; IR (neat) 1740 and 1610 cm^{-1}; ^{1}H NMR ($CDCl_3$) δ=0.9—2.9 (10H, m, CH_2 and CH), 3.60 (6H, s, COOMe), 5.37 (1H, m, 2-H), and 6.8—7.3 (5H, m, Ph); ^{13}C NMR ($CDCl_3$) δ=14.00, 14.65 (each t, CH_2), 23.12, 23.71 (each d, CH), 28.00 (t, CH_2), 29.12 (d, CH), 29.88, 30.06 (each t, CH_2), 41.35, 41.65 (each d, CH), 51.89 (q, COOMe), 118.13 (d, 2-C), 125.77, 125.89, 128.48 (each d), 135.83 (s), 142.83 (s, 1-C), and 175.36 (s, COOMe); MS m/z (rel intensity, %) 314 (M^+, 15), 255 (22), 254 (base peak), 195 (52), 194 (33), 117 (64), 115 (27), and 91 (87). Found: C, 72.62; H, 7.09%. Calcd for $C_{19}H_{22}O_4$: C, 72.59; H, 7.06%.

13a: Colorless liquid; IR (neat) 1625 and 1450 cm^{-1}; ^{1}H NMR ($CDCl_3$) δ=1.1—2.2 (11H, m, CH_2 and CH), 4.73, 5.08 (each 1H, d, J=1.5 Hz, =CH_2), and 7.1—7.5 (5H, m, Ph); ^{13}C NMR ($CDCl_3$) δ=20.37 (d, CH), 22.13, 24.19 (each t, CH_2), 29.06 (d, CH), 108.20 (t, =CH_2), 126.70, 127.87, 128.75, 129.34 (each d), 142.72 (s), and 150.71 (s); MS m/z (rel intensity, %) 198 (M^+, 14), 155 (30), 142 (31), 141 (67), 129 (33), 128 (64), 115 (84), 103 (24), 102 (32), 91 (52), 89 (21), 79 (20), 78 (27), 77 (79), and 38 (base peak). HRMS Found: m/z 198.1390. Calcd for $C_{15}H_{18}$: M, 198.1408.

13b: Colorless liquid; IR (neat) 1640 cm^{-1}; ^{1}H NMR ($CDCl_3$) δ=0.8—2.1 (20H, m, Me, CH_2, and CH), 4.43, and 4.48 (each 1H, br s, =CH_2); ^{13}C NMR ($CDCl_3$) δ=14.03 (q, Me), 19.54 (d, CH), 21.49, 22.52, 23.59 (each t, CH_2), 29.04 (d, CH), 30.46, 36.60 (each t, CH_2), 103.84 (t, =CH_2), and 152.09 (s); MS m/z (rel intensity, %) 178 (M^+, 18), 136 (58), 135 (26), 121 (84), 107 (32), 95 (23), 94 (34), 93 (73), 81 (62), 80 (25), 79 (84), 77 (42), and 42 (base peak). HRMS Found: m/z 178.1697. Calcd for $C_{13}H_{22}$: M, 178.1698.

13c: Colorless liquid; IR (neat) 1640 cm^{-1}; ^{1}H NMR ($CDCl_3$) δ=0.87 (3H, m, Me of n-Hep), 1.1—2.1 (23H, m, CH_2 and CH), 4.39, and 4.43 (each 1H, br s, =CH_2); ^{13}C NMR ($CDCl_3$) δ=14.08 (q, Me), 19.49 (d, CH), 21.49, 22.71, 23.63 (each t, CH_2), 28.26 (d, CH), 29.04, 29.38, 29.73, 31.92, 36.94 (each t, CH_2), 103.89 (t, =CH_2), and 151.98 (s); MS m/z (rel intensity, %) 220 (M^+, 7), 136 (20), 121 (22), 93 (26), 91 (24), 81 (27), 79 (39), 77 (22), and 40 (base peak). HRMS Found: m/z 220.2203. Calcd for $C_{16}H_{28}$: M, 220.2190.

Diels-Alder Cycloadduct of 13d with Dimethyl Fumarate (Mixtures of two stereoisomers): Colorless liquid; IR (neat) 1730 cm^{-1}; ^{1}H NMR ($CDCl_3$) δ=0.7—2.9 (17H, m, CH_2 and CH), 3.65 (6H, s, COOMe), and 5.28 (1H, m, 2-H); ^{13}C NMR ($CDCl_3$) δ=16.94, 17.59 (each d, CH), 21.47, 23.53, 28.18 (each t, CH_2), 29.77 (d, CH), 30.18 (t, CH_2), 41.59, 41.89 (each d, CH), 51.83 (q, COOMe), 115.95 (d, 2-C), 137.43 (s, 1-C), 175.48, and 175.60 (each s, COOMe); MS m/z (rel intensity, %) 292 (M^+, 13), 232 (base peak), 173 (49), 172 (20), 105 (25), and 91 (66). Found: C, 69.88; H, 7.99%. Calcd for $C_{17}H_{24}O_4$: C, 69.84; H, 8.27%.

14a: Colorless liquid; IR (neat) 1620, 1485, 1460, and 1440 cm^{-1}; ^{1}H NMR ($CDCl_3$) δ=0.7—2.3 (15H, m, CH_2 and CH), 4.80, 5.10 (each 1H, d, J=1.5 Hz, =CH_2), and 7.0—7.6 (5H, m, Ph); ^{13}C NMR ($CDCl_3$) δ=25.47 (d, CH_2), 26.71, 26.88 (each t, CH_2), 28.77 (d, CH), 29.71 (t, CH_2), 108.13 (t,

=CH_2), 126.24, 127.42, 128.31 (each d), 142.25, and 149.89 (s); MS *m/z* (rel intensity, %) 226 (M^+, base peak), 169 (27), 156 (38), 155 (67), 143 (48), 142 (24), 141 (40), 130 (30), 129 (45), 128 (32), 115 (29), and 91 (36). HRMS Found: *m/z* 226.1717. Calcd for $C_{17}H_{22}$: M, 226.1720.

14b: Colorless liquid; IR (neat) 1630, 1460, and 1440 cm^{-1}; ^1H NMR ($CDCl_3$) δ=0.8—2.1 (24H, m, Me, CH_2, and CH), 4.39, and 4.44 (each 1H, br s, =CH_2); ^{13}C NMR ($CDCl_3$) δ=14.06 (q, Me), 22.53 (t, CH_2), 25.18 (d, CH), 26.71, 26.94 (each t, CH_2), 29.36 (d, CH), 29.71, 30.48, 36.71 (each t, CH_2), 104.54 (t, =CH_2), and 151.89 (s); MS *m/z* (rel intensity, %) 206 (M^+, 8), 149 (25), 107 (22), 95 (24), 93 (39), 91 (35), 81 (47), 79 (59), 77 (36), and 42 (base peak). HRMS Found: *m/z* 206.2039. Calcd for $C_{15}H_{26}$: M, 206.2033.

Diels-Alder Cycloadduct of 14c with Dimethyl Fumarate (Mixture of two stereoisomers): Colorless liquid; IR (neat) 1730, 1460, and 1430 cm^{-1}; ^1H NMR ($CDCl_3$) δ=0.6—2.9 (21H, m, CH_2 and CH), 3.60 (6H, s, COOMe), and 5.25 (1H, m, 2-H); ^{13}C NMR ($CDCl_3$) δ=22.77, 23.41, 26.64, 26.88, 28.18, 29.71, 30.06, 30.24, 41.59 (d), 41.89 (d), 51.89 (q, COOMe), 116.30 (d, 2-C), 137.13 (s, 1-C) and 175.66 (s, COOMe); MS *m/z* (rel intensity, %) 320 (M^+, 3), 91 (23), and 59 (base peak). Found: C, 70.75; H, 9.01%. Calcd for $C_{19}H_{28}O_4$: C, 71.22; H, 8.81%.

15a (Mixture of two stereoisomers): Colorless liquid; IR (neat) 1620 cm^{-1}; ^1H NMR ($CDCl_3$) δ=0.7—1.6 (10H, m, CH_2 and CH), 2.47 (1H, br s, CH), 4.78, 5.12 (each 1H br s, =CH_2), and 7.1—7.5 (5H, m, Ph); ^{13}C NMR ($CDCl_3$) δ=14.16, 18.36 (each d, CH), 22.75 (t, CH_2), 25.49 (d, CH), 28.95, 29.54, 31.69 (each t, CH_2), 36.23 (d, CH), 109.13 (t, =CH_2), 126.27, 127.54, 128.32 (each d), 142.48 (s), and 148.63 (s); MS *m/z* (rel intensity, %) 210 (M^+, 97), 195 (22), 182 (30), 181 (21), 168 (25), 167 (58), 165 (31), 156 (67), 155 (48), 154 (22), 153 (27), 152 (24), 143 (30), 142 (50), 141 (69), 130 (30), 129 (51), 128 (66), 115 (83), 103 (42), 91 (94), and 77 (base peak). HRMS Found: *m/z* 210.1411. Calcd for $C_{16}H_{18}$: M, 210.1408.

15b (Mixture of two stereoisomers): Colorless liquid; IR (neat) 1640 cm^{-1}; ^1H NMR ($CDCl_3$) δ=0.5—2.1 (19H, m, Me, CH_2, and CH), 2.23 (1H, br s, CH), 4.40, and 4.45 (each 1H, br s, =CH_2); ^{13}C NMR ($CDCl_3$) δ=14.11 (q, Me), 18.69 (d, CH), 22.66 (t, CH_2), 24.95, 28.90, 29.64 (each t, CH_2), 30.37, 30.66 (t, CH_2), 35.28, 36.72 (d, CH), 36.91, 37.21 (t, CH_2), 105.61 (t, =CH_2), and 150.59 (s); MS *m/z* (rel intensity, %) 190 (M^+, 24), 148 (36), 133 (41), 120 (25), 105 (24), 94 (37), 92 (21), 91 (57), 82 (24), 81 (88), 80 (base peak), 79 (26), and 78 (62). HRMS Found: *m/z* 190.1677. Calcd for $C_{14}H_{22}$: M, 190.1720.

Diels-Alder Cycloadduct of 15c with *N*-Methylmaleimide (Mixture of stereoisomers): Colorless liquid; IR (neat) 1775, 1710, and 1690 cm^{-1}; ^1H NMR ($CDCl_3$) δ=0.5—2.7 (16H, m, CH_2 and CH), 2.90 (3H, s, NMe), 3.00 (1H, m, CH), and 5.42 (1H, m, 6-H); ^{13}C NMR ($CDCl_3$) δ=19.30, 22.47, 22.83 (each d, CH), 24.24 (t, CH_2), 24.94 (d, CH), 25.83, 28.53, 29.47 (each t, CH_2), 35.88, 39.53, 39.77 (each d, CH), 118.42 (d, 6-C), 140.54 (s), 180.25, and 180.54 (each s, CON); MS *m/z* (rel intensity, %) 271 (M^+, 23), 216 (24), 192 (35), 129 (24), 128 (22), 117 (32), 116 (37), 93 (21), 92 (25), 91 (base peak), 80 (52), 79 (50), 78 (40), and 77 (57). Found: C, 75.01; H, 7.99; N, 5.11%. Calcd for $C_{17}H_{21}NO_2$: C, 75.25 H, 7.80; N, 5.16.

16a: Pale yellow liquid; IR (neat) 1610, 1605, and 1490 cm^{-1}; ^1H NMR ($CDCl_3$) δ=1.82 (1H, t, *J*=3.0 Hz, CH), 3.16 (2H, d, *J*=3.0 Hz, CH_2), 5.00, 5.27 (each 1H, s, =CH_2), and 7.1—7.5 (11H, m, Ar); ^{13}C NMR ($CDCl_3$) δ=33.24, 44.12 (each d, CH), 109.66 (t, =CH_2), 119.66, 123.19, 126.13, 127.66, 127.89, 128.13, 128.48, 128.90 (each d), 132.13, 137.60, 140.96, 145.42, and 147.42 (each s); MS *m/z* (rel intensity, %) 268 (M^+, 44) and 165 (base peak). HRMS Found: *m/z* 268.1248. Calcd for $C_{21}H_{16}$: M, 268.1251.

16b: Pale yellow liquid; IR (neat) 1625, 1605, and 1460 cm^{-1}; ^1H NMR ($CDCl_3$) δ=0.8—2.2 (9H, m, Me, CH_2, and CH), 2.90, 3.04, 3.32 (each 1H, m, CH), 4.65, 4.72 (each 1H, br s, =CH_2), and 6.8—7.7 (6H, m, Ar); MS *m/z* (rel intensity, %) 248 (M^+, 8), 166 (58), 165 (base peak), 153 (39), and 152 (29). HRMS Found: *m/z* 248.1563. Calcd for $C_{19}H_{20}$: M, 258.1564.

Diels-Alder Cycloadduct of 16c with Dimethyl Fumarate (Mixture of stereoisomers): Pale yellow liquid; IR (neat) 1738 and 1700 cm^{-1}; ^1H NMR ($CDCl_3$) δ=1.41 (1H, t, *J*=3.0 Hz, CH), 2.25 (4H, m, CH_2), 2.82 (2H, m, CH), 3.01 (2H, d, *J*=3.0 Hz, CH), 5.34 (1H, m, 2-H), and 7.1—7.5 (6H, (m, Ar); ^{13}C NMR ($CDCl_3$) δ=27.88, 29.41 (each t, CH_2), 30.36, 30.94, 41.24, 41.53, 45.65 (each d, CH), 51.95 (q, NMe), 118.95, 119.48, 122.95, 127.54, 128.48 (each d), 132.01, 135.01, 137.36, 145.48 (each s), 175.19, and 175.36 (each s, COOMe); MS *m/z* (rel intensity, %) 362 (M^+, 5), 165 (62), 152 (23), 91 (29), and 59 (base peak). HRMS Found: *m/z* 362.1627. Calcd for $C_{23}H_{22}O_4$: M, 362.1517.

General Procedure for the One-Pot Synthesis of Cyclopropyl Vinyl Ketones 17—23 from 1. Cyclopropyl silylmethyl ketones **2—7** and **9** were prepared under argon according to the procedure described above. The resulting mixture was slowly added at −78 °C by syringe to a solution of lithium diisopropylamide (1.1 equivalent) which had been previously prepared from butyllithium (in hexane) and diisopropylamine in THF at −78 °C. After 45 min, a carbonyl compound (1 equivalent) in dry THF (1 ml/1 mmol) was added, the mixture was stirred at −78 °C for 1 h, and then at room temperature for 1 h. All these procedures were carried out under nitrogen. The resulting mixture was poured into aqueous ammonium chloride, extracted with diethyl ether (20 ml×2), the combined extracts were dried over magnesium sulfate, and finally evaporated in vacuo. The residue was chromatographed over silica gel with hexane-ethyl acetate (20—50:1) to give cyclopropyl vinyl ketones **17—23**. The results are listed in Table 3.

17a: Colorless prisms (ethyl acetate-hexane); mp 80—81 °C; IR (KBr) 1655 and 1595 cm^{-1}; ^1H NMR ($CDCl_3$) δ=1.2—1.4, 1.6—1.8 (each 1H, m, CH_2 of *c*-Pr), 2.2—2.6 (2H, m, CH of *c*-Pr), 6.63, 7.38 (each 1H, d, *J*=16.5 Hz, -CH=CHPh), and 6.8—7.4 (10H, m, Ph); ^{13}C NMR ($CDCl_3$) δ=19.26 (t, CH_2 of *c*-Pr), 29.65, 31.70 (each d, CH of *c*-Pr), 126.05, 126.46, 128.28, 128.46, 128.87, 130.34 (each d), 134.50, 140.49 (each s), 142.31 (d, =CHPh), and 197.74 (s, CO); MS *m/z* (rel intensity, %) 248 (M^+, 24), 131 (59), 117 (21), 116 (48), 115 (94), 104 (30), 103 (83), 102 (33), 91 (54), 89 (22), 78 (26), and 77 (base peak). HRMS Found: *m/z* 248.1175. Calcd for $C_{18}H_{16}O$: M, 248.1200.

17b: Colorless prisms (ethyl acetate-hexane); mp 128.5—129.5 °C; IR (KBr) 1650 and 1575 cm^{-1}; ^1H NMR ($CDCl_3$) δ=1.2—1.5, 1.6—1.9 (each 1H, m, CH_2 of *c*-Pr), 2.2—2.7 (2H, m, CH of *c*-Pr), 6.23 (1H, d, *J*=15.0 Hz, -COCH=), and 6.6—7.4 (13H, m, Ph and =CHPh); ^{13}C NMR ($CDCl_3$) δ=19.18 (t, CH_2 of *c*-Pr), 29.47, 31.59 (each d, CH of *c*-Pr), 126.24, 126.60, 126.83, 127.36, 128.65, 128.95, 130.01 (each d), 136.18, 140.83 (each s), 141.66, 142.60 (each d, COCH=CHCH=

CHPh), and 198.01 (s, CO); MS *m/z* (rel intensity, %) 274 (M^+, base peak), 183 (39), 170 (28), 157 (67), 129 (37), 128 (71), 127 (30), 117 (31), 115 (38), 104 (21), and 91 (38). Found: C, 87.56; H, 6.61%. Calcd for $C_{20}H_{17}O$: C, 87.88; H, 6.66%.

17c: Colorless liquid; IR (neat) 1670, 1650, and 1615 cm^{-1}; ^1H NMR ($CDCl_3$) δ=1.05 (3H, t, Me of Et), 0.8—1.8 (3H, m, CH_2 and CH of *c*-Pr), 2.23 (2H, m, CH_2 of Et), 2.2—2.7 (1H, m, CH of *c*-Pr), 6.12 (1H, br d, *J*=15.5 Hz, -COCH=), 6.84 (1H, dt, *J*=15.5, 6.6, and 6.6 Hz, EtCH=), and 6.9—7.3 (5H, m, Ph); ^{13}C NMR ($CDCl_3$) δ=12.24 (q, Me of Et), 18.88 (t, CH_2 of *c*-Pr), 25.53 (t), 29.12, 30.59 (each d), 126.18, 126.54, 128.60, 129.83 (each d), 140.83 (s), 148.83 (d, =CHEt), and 198.25 (s, CO); MS *m/z* (rel intensity, %) 200 (M^+, 4), 117 (28), 116 (35), 115 (base peak), 91 (70), 89 (24), 83 (57), 78 (22), and 77 (25). HRMS Found: *m/z* 200.1198. Calcd for $C_{14}H_{16}O$: M, 200.1196.

17d: Colorless liquid; IR (neat) 1675, 1650, and 1620 cm^{-1}; ^1H NMR ($CDCl_3$) δ=1.02, 1.09 (each 3H, d, *J*=7.3 Hz, Me of *i*-Pr), 1.2—1.8 (3H, m, CH_2 and CH of *c*-Pr), 2.2—2.7 (2H, m, CH of *c*-Pr and CH of *i*-Pr), 6.04 (1H, br d, *J*=15.9 Hz, -COCH=), 6.78 (1H, dd, *J*=15.9 and 6.9 Hz, *i*-PrCH=), and 6.2—7.3 (5H, m, Ph); ^{13}C NMR ($CDCl_3$) δ=19.14 (t, CH_2 of *c*-Pr), 21.31 (q, Me of *i*-Pr), 29.24, 30.76, 31.18 (each d), 126.05, 126.35, 127.75, 128.40 (each d), 140.61 (s), 153.41 (d, *i*-PrCH=), and 198.32 (s, CO); MS *m/z* (rel intensity, %) 214 (M^+, 23), 171 (21), 117 (29), 116 (30), 115 (70), 97 (55), 91 (56), and 41 (base peak). HRMS Found: *m/z* 214.1355. Calcd for $C_{15}H_{18}O$: M, 214.1355.

17e: Colorless liquid; IR (neat) 1670 and 1620 cm^{-1}; ^1H NMR ($CDCl_3$) δ=1.2—1.8 (3H, CH_2 and CH of *c*-Pr), 1.85, 2.13 (each 3H, s, Me), 2.3—2.6 (1H, m, CH of *c*-Pr), 6.12 (1H, br s, -COCH=), and 6.9—7.3 (5H, m, Ph); ^{13}C NMR ($CDCl_3$) δ=18.88 (t, CH_2 of *c*-Pr), 20.82, 27.65 (each q, Me), 29.06, 34.24 (each d, CH of *c*-Pr), 124.72, 126.24, 126.48, 128.60 (each d), 141.13 (s), 155.13 (s, $=C(Me)_2$), and 198.60 (s, CO); MS *m/z* (rel intensity, %) 200 (M^+, 44), 115 (37), 91 (26), 83 (base peak), and 55 (53). HRMS Found: *m/z* 200.2794. Calcd for $C_{14}H_{16}O$: M, 200.2794.

18a: Colorless liquid; IR (neat) 1675, 1645, and 1605 cm^{-1}; ^1H NMR ($CDCl_3$) δ=0.86 (3H, m, Me of *n*-Hex), 1.1—2.1 (14H, CH_2 and CH), 6.72 (1H, d, *J*=16.5 Hz, -COCH=), 7.2—7.5 (5H, m, Ph), and 7.47 (1H, d, *J*=16.5 Hz, PhCH=); ^{13}C NMR ($CDCl_3$) δ=14.12 (q, Me of *n*-Hex), 18.71 (t, CH_2 of *c*-Pr), 22.71, 26.88, 27.94, 29.06, 29.24, 31.88, 33.53 (CH_2 and CH), 126.77, 128.88, 129.13, 130.42 (each d), 135.01 (s), 141.89 (d, =CHPh), and 199.78 (s, CO); MS *m/z* (rel intensity, %) 256 (M^+, 8), 147 (27), 131 (base peak), 103 (79), 91 (26), and 77 (50). HRMS Found: *m/z* 256.1826. Calcd for $C_{18}H_{24}O$: M, 256.1826.

18b: Pale yellow liquid; IR (neat) 1670, 1635, and 1605 cm^{-1}; ^1H NMR ($CDCl_3$) δ=0.87 (3H, t, Me of *n*-Hex), 1.1—1.5 (11H, m, CH_2 and CH), 1.90 (1H, m, CH of *c*-Pr), 6.46 (1H, dd, *J*=3.5 and 2.0 Hz, 4-H of furyl), 6.63 (1H, d, *J*=3.5 Hz, 3-H of furyl), 6.75 (1H, d, *J*=15.8 Hz, -COCH=), 7.34 (1H, d, *J*=15.8 Hz, furylCH=), and 7.46 (1H, d, *J*=2.0 Hz, 5-H of furyl); ^{13}C NMR ($CDCl_3$) δ=14.12 (q, Me of *n*-Hex), 18.59 (t, CH_2 of *c*-Pr), 22.71 (t), 26.83, 28.47 (each d, CH of *c*-Pr), 29.06, 29.30, 31.88, 33.54 (each t, CH_2), 112.65, 115.59 (each d, 3- and 4-C of furyl), 123.89 (d, -COCH=), 128.07 (d, furylCH=), 144.89 (d, 5-C of furyl), 151.66 (s, 2-C of furyl), and 199.31 (s, CO); MS *m/z* (rel intensity, %) 246 (M^+, 11), 121 (65), 65 (82), and 41 (base peak). HRMS Found: *m/z* 246.1628. Calcd for $C_{16}H_{22}O_2$: M, 246.1619.

18c (Mixture of two stereoisomers): Colorless liquid; IR (neat) 1680, 1660, and 1625 cm^{-1}; ^1H NMR ($CDCl_3$) δ=0.85, 1.06 (each 3H, t, Me of *n*-Hex and Et), 1.2—2.4 (16H, m, CH_2 and CH), 6.59 (1H, br d, *J*=16.0 Hz, -COCH=), and 6.81 (1H, dt, *J*=16.0, 5.7, and 5.7 Hz, *n*-HexCH=); ^{13}C NMR ($CDCl_3$) δ=12.41, 13.82, 14.11 (each q, Me of *n*-Hex and Et), 18.24 (CH_2 of *c*-Pr), 22.71, 24.47, 25.59, 26.35, 26.53, 26.93, 29.06, 29.30, 29.83, 31.88, 33.53 (CH_2 and CH), 129.95, 131.19 (each d, -COCH=), 147.54, 148.01 (each d, EtCH=), 198.72, and 200.07 (each s, CO); MS *m/z* (rel intensity, %) 208 (M^+, 9), 98 (28), 95 (21), 83 (base peak), and 55 (69). HRMS Found: *m/z* 208.1829. Calcd for $C_{14}H_{24}O$: M, 208.1821.

18d (Mixture of two stereoisomers): Colorless liquid; IR (neat) 1675, 1650, and 1620 cm^{-1}; ^1H NMR ($CDCl_3$) δ=0.89 (3H, m, Me of *n*-Hex), 1.09 (6H, d, Me of *i*-Pr), 1.2—2.7 (15H, CH_2 and CH), 6.12 (1H, br d, *J*=16.2 Hz, -COCH=), and 6.79 (1H, dd, *J*=16.2, 6.3, and 6.3 Hz, *i*-PrCH=); ^{13}C NMR ($CDCl_3$) δ=14.06 (q, Me of *n*-Hex), 18.24 (t, CH_2 of *c*-Pr), 21.43, 22.65, 24.47, 25.65, 26.35, 26.47, 26.94, 29.00, 29.24, 29.77, 31.18, 31.88, 33.43 (CH_2 and CH), 128.01, 129.24 (each d, -COCH=), 152.30, 152.72 (each d, *i*-PrCH=), 198.96, and 200.25 (each s, CO); MS *m/z* (rel intensity, %) 222 (M^+, 6), 97 (49), 69 (25), and 40 (base peak). HRMS Found: *m/z* 222.1978. Calcd for $C_{15}H_{26}O$: M, 222.1982.

19a (Mixture of two stereoisomers): Colorless liquid; IR (neat) 1675, 1650, and 1610 cm^{-1}; ^1H NMR ($CDCl_3$) δ=0.9—1.6 (9H, m, Me, CH_2, and CH), 1.20 (3H, s, Me), 2.24 (1H, m, CH of *c*-Pr), 6.97 (1H, br d, *J*=16.0 Hz, -COCH=), 7.4—7.7 (5H, m, Ph), and 7.68 (1H, d, *J*=16.0 Hz, PhCH=); ^{13}C NMR ($CDCl_3$) δ=14.24, 15.53 (each q, Me of *n*-Pr and Me), 20.12, 20.47, 22.18, 22.94, 24.41, 31.18, 31.77, 33.77, 34.12, 34.65, 43.47 (CH_2 and CH), 128.18, 128.36, 129.07, 130.30 (each d), 135.01 (s), 141.42 (d, PhCH=), and 198.01 (s, CO); MS *m/z* (rel intensity, %) 228 (M^+, 49), 146 (28), 131 (base peak), 129 (20), 128 (21), 115 (26), 103 (74), 102 (27), 91 (34), and 77 (68). HRMS Found: *m/z* 228.1504. Calcd for $C_{16}H_{20}O$: M, 228.1513.

19b (Mixture of two stereoisomers): Colorless liquid; IR (neat) 1680, 1655, and 1620 cm^{-1}; ^1H NMR ($CDCl_3$) δ=0.6—2.3 (18H, m, Me, CH_2, and CH), 6.00 (1H, br d, *J*=15.5 Hz, -COCH=), and 6.66 (1H, dt, *J*=15.5, 6.0, and 6.0 Hz, EtCH=); ^{13}C NMR ($CDCl_3$) δ=12.41, 14.24, 15.47 (each q, Me of *n*-Pr, Me of Et, and Me), 20.06, 20.41, 21,65, 22.34, 24.35, 25.47, 30.30, 30.88, 33.06, 33.59, 33.77, 43.53 (CH_2 and CH), 131.30 (d, -COCH=), 147.31, 147.42 (each d, EtCH=), and 198.13 (s, CO); MS *m/z* (rel intensity %) 180 (M^+, 16), 83 (76), 81 (21), 67 (22), and 55 (base peak). HRMS Found: *m/z* 180.1619. Calcd for $C_{12}H_{20}O$: M, 180.1513.

19c (Mixture of two stereoisomers): Colorless liquid; IR (neat) 1675, 1650, and 1610 cm^{-1}; ^1H NMR ($CDCl_3$) δ=0.7—2.6 (14H, Me, CH_2, and CH), 1.06 (6H, d, Me of *i*-Pr), 6.11 (1H, br d, *J*=16.5 Hz, *i*-PrCH=), and 6.73 (1H, dd, *J*=16.5 and 6.3 Hz, -COCH=); ^{13}C NMR ($CDCl_3$) δ=14.30, 15.47 (each q, Me of *n*-Pr and Me), 19.30, 20.06, 20.41, 21.53, 21.77, 22.47, 24.41, 30.36, 30.93, 31.12, 33.18, 33.77, 43.59 (Me, CH_2, and CH), 129.42 (d, -COCH=), 152.19, 152.30 (each d, *i*-PrCH=), and 198.48 (s, CO); MS *m/z* (rel intensity, %) 194 (M^+, 7), 97 (34), 69 (24), and 40 (base peak). HRMS Found: *m/z* 194.1670. Calcd for $C_{13}H_{22}O$: M, 194.1670.

20a: Colorless liquid; IR (neat) 1670, 1645, and 1605 cm^{-1}; ^1H NMR ($CDCl_3$) δ=0.7—2.0 (11H, m, CH_2 and CH), 6.64

(1H, d, J=16.2 Hz, -COCH=), 7.1—7.4 (5H, m, Ph), and 7.35 (1H, d, J=16.2 Hz, PhCH=); ^{13}C NMR ($CDCl_3$) δ=21.14 23.45 (each t, CH_2), 26.36, 34.30 (each d, CH), 126.70, 128.16, 128.81, 130.10 (each d), 134.86 (s), 141.08 (d, PhCH=), and 199.32 (s, CO); MS m/z (rel intensity, %) 226 (M^+, 82), 225 (23), 183 (base peak), 145 (37), 134 (21), 131 (28), 129 (35), 105 (22), 103 (56), 102 (34), 91 (49), and 75 (35). HRMS Found: m/z 226.1349. Calcd for $C_{16}H_{18}O$: M, 226.1357.

20b: Colorless liquid; IR (neat) 1680, 1655, and 1620 cm^{-1}; ^{1}H NMR ($CDCl_3$) δ=1.09 (3H, t, Et), 1.2—2.0 (11H, m, CH_2 and CH), 2.25 (2H, q, Et), 6.15 (1H, d, J=16.2 Hz, -COCH=), and 6.87 (1H, dt, J=16.2, 6.3, and 6.3 Hz, EtCH=); ^{13}C NMR ($CDCl_3$) δ=12.29 (q, Me of Et), 21.12, 23.18, 25.47 (each t, CH_2), 25.71, 33.12 (each d, CH), 129.95 (d, -COCH=), 147.36 (d, EtCH=), and 199.95 (s, CO); MS m/z (rel intensity, %) 178 (M^+, 12), 107 (28), 91 (21), 83 (37), 79 (32), 77 (30), 67 (31), and 40 (base peak). HRMS Found: m/z 178.1357. Calcd for $C_{12}H_{18}O$: M, 178.1357.

20c: Colorless liquid; IR (neat) 1675, 1655, and 1620 cm^{-1}; ^{1}H NMR ($CDCl_3$) δ=1.06 (6H, d, Me of i-Pr), 1.1—2.0 (10H, CH_2 and CH), 2.44 (1H, m, CH of i-Pr), 6.05 (1H, br d, J=16.0 Hz, -COCH=), and 6.70 (1H, dd, J=16.0 and 6.3 Hz, i-PrCH=); ^{13}C NMR ($CDCl_3$) δ=21.14, 21.43, 23.25, 25.95, 31.12, 33.35 (Me, CH_2, and CH), 127.87 (d, -COCH=), 152.00 (d, i-PrCH=), and 200.09 (s, CO); MS m/z (rel intensity, %) 192 (M^+, 14), 149 (39), 107 (43), 97 (25), 91 (26), 81 (24), 79 (35), 77 (33), 69 (23), and 41 (base peak). HRMS Found: m/z 192.1511. Calcd for $C_{13}H_{20}O$: M, 192.1513.

20d: Colorless liquid; IR (neat) 1660 and 1620 cm^{-1}; ^{1}H NMR ($CDCl_3$) δ=1.1—1.8 (11H, m, CH_2 and CH), 1,83, 2.10 (each 3H, br s, Me), and 6.16 (1H, br s, -COCH=); ^{13}C NMR ($CDCl_3$) δ=20.24 (q, Me), 20.65, 21.18 (each t, CH_2), 23.30 (d, CH), 25.53 (q, Me), 36.59 (d, CH), 125.07 (d, -COCH=), 153.13 (s, $(Me)_2C$=), and 200.72 (s, CO); MS m/z (rel intensity, %) 178 (M^+, 46), 163 (22), 135 (base peak), 122 (22), 121 (38), 109 (70), 96 (26), 83 (97), 79 (23), 67 (21), and 55 (75). HRMS Found: m/z 178.1331. Calcd for $C_{12}H_{18}O$: M, 178.1357.

21: Colorless needles (ethyl acetate–hexane); mp 85—86 °C; IR (KBr) 1655, 1640, and 1600 cm^{-1}; ^{1}H NMR ($CDCl_3$) δ=0.8—2.1 (13H, m, CH_2 and CH), 6.66 (1H, d, J=16.5 Hz, -COCH=), 7.1—7.5 (5H, m, Ph), and 7.41 (1H, d, J=16.5 Hz, PhCH=) ^{13}C NMR ($CDCl_3$) δ=28.71, 29.83 (each t, CH_2), 31.65 (d, CH), 32.41 (t, CH_2), 38.36 (d, CH), 126.78, 128.36, 129.01, 130.30, each d), 135.01 (s), 141.48 (d, PhCH=), and 198.90 (s, CO); MS m/z (rel intensity, %) 240 (M^+, base peak), 183 (91), 131 (46), 103 (40), 91 (25), and 77 (40). Found: C, 84.77; H, 8.37%. Calcd for $C_{17}H_{20}O$: C, 84.96; H, 8.39%.

22a: Colorless needles (ethyl acetate–hexane); mp 94—95 °C; IR (KBr) 1650, 1625, and 1600 cm^{-1}; ^{1}H NMR ($CDCl_3$) δ=0.8—2.2 (15H, m, CH_2 and CH), 6.70 (1H, d, J=16.5 Hz, -COCH=), 7.1—7.6 (5H, m, Ph), and 7.42 (1H, d, J=16.5 Hz, PhCH=); ^{13}C NMR ($CDCl_3$) δ=26.35, 29.24 (CH_2), 31.41, 34.41 (each d, CH), 127.07, 128.42, 129.07, 130.36 (each d), 135.13 (s), 141.54 (d, PhCH=), and 199.60 (s, CO); MS m/z (rel intensity, %) 254 (M^+, 15), 183 (53), 146 (45), 131 (97), 128 (20), 103 (base peak), 102 (23), 91 (33), and 77 (93). Found: C, 85.12; H, 8.85%. Calcd for $C_{22}H_{16}O$: C, 84.99; H, 8.72%.

22b: Colorless prisms (ethyl acetate–hexane); mp 74—75 °C; IR (KBr) 1650 and 1595 cm^{-1}; ^{1}H NMR ($CDCl_3$) δ= 1.1—2.2 Z(15H, m, CH_2 and CH), 6.36 (1H, dd, J=3.3 and 2.0 Hz, 4-H of furyl), 6.52 (1H, d, J=3.3 Hz, 3-H of furyl), 6.59 (1H, d, J=16.2 Hz, -COCH=), 7.20 (1H, d, J=16.2 Hz, furylCH=), and 7.37 (1H, d, J=2.0 Hz, 5-H of furyl); ^{13}C NMR ($CDCl_3$) δ=26.35, 26.47, 29.24 (each t, CH_2), 31.36, 34.93 (each d, CH), 112.60, 115.36, 124.18, 127.77 (each d), 144.77 (d, 5-C of furyl), 151.66 (s, 2-C of furyl), and 199.24 (s, CO); MS m/z (rel intensity, %) 244 (M^+, 12), 173 (20), 121 (80), 94 (22), 91 (23), 81 (28), 79 (24), 77 (22), and 65 (base peak). Found: C, 78.65; H, 8.25%. Calcd for $C_{16}H_{20}O_2$: C, 78.87; H, 8.33%.

22c: Colorless needles (ethyl acetate–hexane); mp 28—29 °C; IR (KBr) 1670, 1650, and 1620 cm^{-1}; ^{1}H NMR ($CDCl_3$) δ=1.06 (3H, t, Et), 1.2—2.1 (15H, m, CH_2 and CH), 2.19 (2H, m, Et), 6.12 (br d, J=15.9 Hz, -COCH=), and 6.83 (1H, dt, J=15.9, 6.0, and 6.0 Hz, EtCH=); ^{13}C NMR ($CDCl_3$) δ=12.35 (q, Me of Et), 25.51, 26.30, 26.47, 29.23 (each t, CH_2), 30.77, 33.30 (each d, CH), 130.07 (d, -COCH=), 147.60 (d, EtCH=), and 199.84 (s, CO); MS m/z (rel intensity, %) 206 (M^+, 1), 83 (49), 81 (21), 79 (30), 77 (23), 67 (27), and 56 (base peak). HRMS Found: m/z 206.1682. Calcd for $C_{14}H_{22}O$: M, 206.1670.

22d: Colorless plates (ethyl acetate–hexane); mp 52.5—54 °C; IR (KBr) 1650 and 1600 cm^{-1}; ^{1}H NMR ($CDCl_3$) δ=1.07 (6H, d, Me of i-Pr), 0.8—2.1 (15H, m, CH_2 and CH), 2.45 (1H, m, CH of i-Pr), 6.07 (1H, br d, J=15.6 Hz, -COCH=), and 6.73 (1H, dd, J=15.6 and 6.0 Hz, i-PrCH=); ^{13}C NMR ($CDCl_3$) δ=21.41 (q, Me), 26.30, 26.47, 29.18 (each t, CH_2), 30.94, 31.12, 33.47 (each d, CH), 128.13 (d, -COCH=), 152.42 (d, i-PrCH=), and 200.25 (s, CO); MS m/z (rel intensity, %) 220 (M^+, 4), 177 (20), 149 (23), 107 (28), 97 (base peak), 95 (26), 93 (28), 91 (38), 81 (55), 79 (58), 77 (31), and 69 (39). HRMS Found: m/z 220.1835. Calcd for $C_{15}H_{24}O$: M, 220.1826.

23: Colorless needles (ethyl acetate–hexane); mp 154.5—155.5 °C; IR (KBr) 1660 and 1605 cm^{-1}; ^{1}H NMR ($CDCl_3$) δ=2.30 (1H, t, J=2.8 Hz, CH of c-Pr), 3.59 (1H, d, J=2.8 Hz, CH of c-Pr), 6.64 (1H, d, J=15.5 Hz, -COCH=), 7.1—7.5 (11H, m, Ar), and 7.38 (1H, d, J=15.5 Hz, PhCH=); ^{13}C NMR ($CDCl_3$) δ=35.30, 46.53 (each d, CH), 120.95, 124.01, 126.36, 127.71, 128.48, 129.07, 130.65, 131.67, 134.66, 143.01 (d), 143.54 (s), and 195.89 (s, CO); MS m/z (rel intensity, %) 296 (M^+, 13), 165 (base peak), 164 (28), 163 (32), 131 (65), 103 (32), and 77 (27). Found: C, 89.24; H, 5.60%. Calcd for $C_{22}H_{16}O$: C, 89.16; H, 5.44%.

Reaction of 1 with *N*-Phenylmaleimide Leading to 24. A mixture of **1** (312 mg, 2 mmol) and *N*-phenylmaleimide (346 mg, 2 mmol) in dry benzene (5 ml) was stirred under nitrogen at room temperature for 10 h. The solvent was evaporated in vacuo and the residue was chromatographed over silica gel with hexane–ethyl acetate (1:1) to tive **24** (262 mg, 51%): Pale yellow prisms (ethyl acetate–hexane); mp 160.5—161.5 °C; IR (KBr) 3400, 1720, and 1670 cm^{-1}; ^{1}H NMR ($CDCl_3$) δ=2.41 (3H, s, COMe), 4.72, 5.06 (each 1H, d, J=10.5 Hz, 3a- and 6a-H), and 7.1—7.6 (6H, m, Ph and NH); ^{13}C NMR ($CDCl_3$) δ=25.92 (q, COMe), 50.34 (d, 3a-C), 64.42 (d, 6a-C), 126.21, 128.94, 129.13 (each d), 131.12 (s), 143.70 (s, 3-C), 170.85, 173.18 (each s, CON), and 192.09 (s, CO); MS m/z (rel intensity %) 257 (M^+, 75), 228 (46), 119 (base peak), 95 (78), 93 (29), 91 (20), and 55 (54). HRMS Found: m/z 257.0800. Calcd for $C_{13}H_{11}N_3O_3$: M, 257.0800.

Reaction of 1 with Dimethyl Fumarate Leading to 25. The reaction of **1** (156 mg, 1 mmol) with dimethyl fumarate (144 mg, 1 mmol) under the same conditions gave

25 (139 mg, 62%): Pale yellow liquid; IR (neat) 3350, 1740, and 1660 cm^{-1}; ^1H NMR ($CDCl_3$) δ=2.26 (3H, s, COMe), 3.60, 3.64 (each 3H, s, COOMe), 4.21, 4.60 (each 1H, d, J=5.4 Hz, 4- and 5-H), and 7.07 (1H, br, NH); ^{13}C NMR ($CDCl_3$) δ=25.58 (q, COMe), 50.92 (d, 4-C), 53.02, 53.16 (each q, COOMe), 66.42 (d, 5-C), 146.87 (s, 3-C), 169.87, 170.21 (each s, COOMe), and 192.87 (s, CO); MS m/z (rel intensity, %) 228 (M^+, 9), 195 (24), 169 (83), 137 (48), 125 (33), 95 (33), 93 (base peak), 83 (29), and 59 (32). HRMS Found: m/z 228.0745. Calcd for $C_9H_{12}N_2O_5$: M, 228.0756.

Reaction of 1 with Dimethyl Acetylenedicarboxylate Leading to 26. A mixture of **1** (312 mg, 2 mmol) and dimethyl acetylenedicarboxylate (284 mg, 2 mmol) in dry benzene (4 ml) was heated under reflux for 3.5 h under nitrogen. The solvent was evaporated in vacuo. ^1H NMR of the residue showed a quantitative formation of the cycloadduct **B** (E=COOMe). The residue was chromatographed over silica gel with hexane–ethyl acetate (3:1) to give **26** (431 mg, 95%): pale yellow plates (ethyl ether); mp 55—56 °C; IR (KBr) 3200, 1730, and 1680 cm^{-1}; ^1H NMR ($CDCl_3$) δ=2.58 (3H, s, COMe), 3.87, 3.95 (each 3H, s, COOMe), and 7.29 (1H, br, NH); ^{13}C NMR ($CDCl_3$) δ=26.77 (q, COMe), 52.90, 53.13 (each q, COOMe), 117.54, 135.03, 146.89 (each s), 158.99, 164.45 (each s, COOMe), and 191.98 (s, CO); MS m/z (rel intensity, %) 226 (M^+, 4), 195 (13), 93 (33), 79 (14), 67 (17), 66 (13), 65 (19), and 43 (base peak). HRMS Found: m/z 226.0591. Calcd for $C_9H_{10}N_2O_5$: M, 226.0589.

Reaction of 1 with Dibenzoylacetylene Leading to 27. The reaction of **1** (134 mg, 0.86 mmol) with dibenzoylacetylene (218 mg, 0.86 mmol) under reflux in dry THF (2 ml) for 3 h and the followed chromatographic separation gave **27** (198 mg, 73%): Colorless prisms; mp 154—155 °C; IR (KBr) 3220, 1660, and 1630 cm^{-1}; ^1H NMR ($CDCl_3$) δ=2.36 (3H, s, COMe), 7.1—8.0 (10H, m, Ph), and 11.70 (1H, br, NH); ^{13}C NMR ($CDCl_3$) δ=27.94 (q, COMe), 116.89, 125.42 (each s), 128.54, 128.89, 129.36, 130.30 (each d), 133.66, 134.07, 136.13, 137.42 (each s), 186.13, 190.01, and 191.84 (each s, CO); MS m/z (rel intensity, %) 318 (M^+, 44), 241 (45), 223 (22), 105 (66), and 77 (base peak). Found: C, 71.43; H, 4.39; N, 9.01%. Calcd for $C_{19}H_{14}N_2O_3$: C, 71.64; H, 4.43; N, 8.80%.

General Procedure for the One-Pot Synthesis of 3-Pyrazolyl Vinyl Ketones 28 and 20. 3-Silylacetylpyrazoles **B** (E=COOMe or COPh) were prepared in dry THF (1 mmol in 2 ml) according to the method shown above. This mixture was added to LDA (2 mmol in THF) at −78 °C. After 30 min at −78 °C, benzaldehyde (1 mmol) in THF (1 ml) was added dropwise, the mixture was stirred at 0 °C for 2 h, poured into aqueous ammonium chloride, and extracted with diethyl ether (20 ml). The ether was dried over magnesium sulfate and evaporated in vacuo. The residue was chromatographed over silica gel with chloroform-ethyl acetate (12:1) to give **28** or **29**.

28: Yield 53%; Colorless plates (ethyl ether); mp 145—146 °C; IR (KBr) 3200, 1720, 1650, and 1580 cm^{-1}; ^1H NMR ($CDCl_3$) δ=3.86, 3.92 (each 3H, s, COOMe), 7.2—7.5 (6H, m, Ph and NH), 7.51, and 7.81 (each 1H, d, J=15.6 Hz, CH=CH); ^{13}C NMR ($CDCl_3$) δ=53.12, 53.32 (each q, COOMe), 118.41 (s), 121.39, 129.05, 131.20 (each d), 134.62, 135.16 (each s), 146.04 (d), 148.09 (s), 159.37, 164.50 (each s, COOMe), and 182.56 (s, CO); MS m/z (rel intensity, %) 314 (M^+, 28), 283 (27), 282 (80), 224 (20), 131 (26), 103 (base peak), 102 (38), 93 (24), and 77 (65); Found: C, 61.34; H, 4.63; N, 8.96%. Calcd for $C_{16}H_{14}N_2O_5$: C, 61.14; H, 4.49; N, 8.91%.

29: Yield 41%; Pale yellow prisms (ethyl ether); mp 180—181 °C; IR (KBr) 3170, 1640, and 1580 cm^{-1}; ^1H NMR ($CDCl_3$) δ=6.9—7.6 (12H, m, Ar), 7.44, 7.77 (each 1H, d, J=15.8 Hz, CH=CH), and 7.7—8.0 (4H, m, Ar); MS m/z (rel intensity, %) 406 (M^+, 12), 105 (56), 103 (30), and 77 (base peak). Found: C, 76.71; H, 4.40; N, 6.95%. Calcd for $C_{26}H_{18}N_2O_3$: C, 76.83; H, 4.46; N, 6.89%.

Reaction of 1 with Benzaldehyde in the presence of TBAF Leading to 30. To a mixture of **1** (232 mg, 1.5 mmol) and benzaldehyde (160 mg 1.5 mmol) in dry THF (2 ml) was added TBAF (2.25 ml, 2.25 mmol) at room temperature. The mixture was stirred under nitrogen at room temperature for 30 min and poured into water (30 ml). Organic layer was extracted with dichloromethane (20 ml×2), the combined extracts were dried over magnesium sulfate and evaporated in vacuo. The residue was chromatographed over silica gel with hexane–ethyl acetate (1:1) to give **30** (170 mg, 60%): Colorless liquid; IR (neat) 3400, 2050, and 1625 cm^{-1}; ^1H NMR ($CDCl_3$) δ=2.22 (3H, s, COMe), 3.40 (1H, br s, OH), 5.94 (1H, s, CH), and 7.2—7.5 (5H, m, Ph); ^{13}C NMR ($CDCl_3$) δ=25.54 (q, COMe), 67.11 (d, CH), 125.41, 127.93, 128.52 (each d), 139.32 (s), and 190.80 (s, CO); MS m/z (rel intensity, %) 190 (M^+, 13), 162 (27), 161 (50), 148 (62), 143 (65), 119 (48), 107 (31), 105 (43), 102 (22), 91 (65), 80 (39), 78 (77), and 43 (base peak). Found: C, 61.30; H, 4.57; N, 8.65%. Calcd for $C_{16}H_{14}O_5$: C, 61.14; H, 4.49; N, 8.91%.

References

1) As reviews: D. J. Ager, *Synthesis*, **1984**, 384; W. P. Weber, "Silicon Reagents for Organic Synthesis," Springer-Verlag, Heidelberg (1983); E. W. Colvin, "Silicon in Organic Synthesis," Butterworth, London (1981); W. C. Groutas and D. Felker, *Synthesis*, **1980**, 861; I. Fleming, "Organic Silicon Chemistry," in "Comprehensive Organic Chemistry," ed by D. H. R. Barton and W. D. Ollis, Pergamon, Oxford (1979), Vol. 3, p. 539.

2) We have been studying on α-functionalized silanes such as silylmethyl azide (O. Tsuge, S. Kanemasa, and K. Matsuda, *Chem. Lett.*, **1983**, 1131; O. Tsuge, S. Kanemasa, H. Suga, and K. Matsuda, *Heterocycles*, **22**, 1955 (1984)), *N*-(silylmethyl)imines, and *N*-silylmethyl heterocumulenes (O. Tsuge, S. Kanemasa, A. Hatada, *Chem. Lett.*, **1984**, 801; O. Tsuge, S. Kanemasa, and K. Matsuda, *J. Org. Chem.*, **49**, 2688 (1984)).

3) A. S. Kostyuk, Zh. G, Boyadzhan, V. N. Zaitseva, V. N. Sergeev, N. I. Savel'eva, Yu. I. Baukov, and I. F. Lutsenko, *Zh. Obshch. Khim.*, **49**, 1543 (1979).

4) L. H. Sommer, J. R. Gold, G. M. Goldberg, and N. S. Marans, *J. Am. Chem. Soc.*, **71**, 1509 (1949).

5) 3-Hexene-2,5-dione is known to form in the thermal decomposition of 1-diazopropanone in the presence of copper catalyst (J. Quintana, M. Torres, and F. Serratosa, *Tetrahedron*, **29**, 2065 (1973) and references cited therein).

 © 1986 The Chemical Society of Japan Bull. Chem. Soc. Jpn., 59, 2861—2863 (1986)

Effect of the Structure of Insoluble Pyridinium-Type Polymer on Its Ability to Capture Bacteria in Water

Nariyoshi KAWABATA,* Takaya HAYASHI, and Masaru NISHIKAWA
Department of Chemistry, Faculty of Engineering and Design,
Kyoto Institute of Technology, Matsugasaki, Sakyo-ku, Kyoto 606
(Received April 14, 1986)

Effect of the structure of insoluble pyridinium-type polymer on its ability to capture bacteria in water was investigated. Strong ability of the polymer was further confirmed by an equilibrium capture experiment. The ability was quantitatively evaluated by the removal coefficient reported previously based on initial rate of decrease of viable cell counts caused by the presence of the polymer. The coefficient uniformly increased with the content of pyridinium group, and considerably increased when the content of divinylbenzene became smaller. The coefficient also increased with the content of 4-vinylpyridine in the polymer matrix. Based on these observations, presence of pyridinium group was concluded to be essentially important in the affinity of the polymer for bacterial cells. Hydrophilicity and high degree of swelling in water of the polymer matrix appeared to enhance the ability to capture bacteria.

A recent publication from this laboratory described a novel and remarkable ability of cross-linked poly(4-vinylpyridinium halide) to remove bacteria from water.[1] This insoluble pyridinium-type polymer captured many bacteria alive by contact with them. The polymer was found to capture virus in water strongly with keeping the viral activity.[2] This nature of the polymer appears to be of wide application in microbiology and biotechnology.

We are now attempting to immobilize microbial cells on this polymer in order to apply the new technology to the production of useful materials by biochemical reactions. Although various methods are known for the immobilization of enzymes and microbial cells, continuous efforts are being made to pursue new materials and techniques for the immobilization.[3] Immobilization of these biocatalysts to solid materials by chemical reaction is apt to result in damage to the enzyme activity. Entrapment of them in the gel of polymeric substances is apt to result in a decrease of the contact of substrates with enzymes and microbial cells. Adsorption onto ion-exchange resin is not strong and is reversible. However, immobilization on the insoluble pyridinium-type polymer can be realized without chemical reaction and entrapment. Surface-immobilized, live bacteria entities on this polymer are expected to show useful properties.

Prior to this research work, it is necessary to obtain information about basic properties of the insoluble pyridinium-type polymer. As was reported previously,[1] the capturing ability of the polymer is not limited to viable cells. The difference in the ability for viable and killed bacteria was insignificant, and physicochemical interaction appeared to be much more important than physiological action in the phenomenon. In this work, we have investigated effect of the structure of the polymer on its ability to capture bacteria.

Experimental

Materials. 4-Vinylpyridine provided by Koei Chemical Co. Ltd., Osaka, and commercial products of divinylbenzene,[5] styrene, ethanol and toluene were purified by distillation before polymerization. Commercial products of 2,2′-azobisisobutyronitrile, benzyl bromide, and other chemicals were used without further purification.

Insoluble Pyridinium-Type Polymer. Cross-linked poly(*N*-benzyl-4-vinylpyridinium bromide) was used as the insoluble pyridinium-type polymer. Procedure for the preparation of the polymer is given below. Polymerizations were carried out in a 2-l round-bottomed three-necked flask under a nitrogen atmosphere. Copolymerization of 4-vinylpyridine with divinylbenzene, and that of 4-vinylpyridine with styrene and divinylbenzene were carried out using 2,2′-azobisisobutyronitrile as initiator at 75 °C for 5 to 6 h according to the procedure of Katchalsky et al.[4] with minor modifications.[5]

The copolymer was converted to the insoluble pyridinium-type polymer as follows. The copolymer was added to methanol, and the mixture was kept at room temperature for about 20 h. Methanol was separated by filtration. The swollen copolymer was added to toluene in a three-necked flask connected with a mechanical stirrer and a reflux condenser. The mixture was stirred gently, and the prescribed amount of benzyl bromide was added: The solution was allowed to react at 60 to 80 °C for 3 h under stirring. After the reaction, the polymer was separated by filtration, and was washed by benzene, methanol and water followed by drying in vacuo to constant weight. In order to determine content of pyridinium group, the polymer in the bromide form was transferred into the polymer in the nitrate form by treatment with excess 1 M† potassium nitrate in a column method. Titration of the eluted solution with standard 0.1 M silver nitrate using eosin as indicator showed the content of pyridinium group in the polymer.

For comparison with the insoluble pyridinium-type polymer, four commercial resins were used in this work. Amberlite IRA-900 and IRA-400 supplied by Rohm & Haas Co., Philadelphia, Pa., were used as strong base anion-exchange resins, which had a styrene-divinylbenzene matrix with quaternary ammonium group. The resins were preconditioned according to a usual method,[5] and were

† 1M=1 mol dm^{-3}.

used in the chloride form. Amberlite IRA-45 supplied by Rohm & Haas Co. was used as a weak base anion-exchange resin, which had a styrene-divinylbenzene matrix with primary, secondary, and tertiary amino groups. The resin was preconditioned to the free base form in a similar manner. Amberlite XAD-4 supplied by Rohm & Haas Co. was used as porous styrene-divinylbenzene resin with no ion-exchange functional group. This nonionic resin was preconditioned by washing with methanol followed by washing with water.

Bacteria. *Escherichia coli* was incubated and treated as was reported previously.[1]

Procedure. All procedures of the removal experiments were carried out under aseptic conditions as was reported previously.[1]

Serial dilutions of cell suspensions were done of the medium prepared by dissolving KH_2PO_4 (4.5 g), Na_2HPO_4 (6.0 g), L-cystin·HCl (0.5 g), and tween 80 (0.5 g) in 1000 ml of water. The diluted cell suspensions were transferred to plates of Eosin-Methylene Blue-agar (BBL). The measurements of viable cell counts were done after incubation at 37 °C for 24 h.

Results and Discussion

Ability of the insoluble pyridinium-type polymer to capture bacteria was evaluated by the removal coefficient defined as:[1]

$$\text{Removal coefficient} = \frac{V}{Wt}\log\,[N(0)/N(t)]$$

Here, $N(0)$ is the initial viable cell count, $N(t)$ is the viable cell count at contact time t, V is the volume of viable cell suspension, W is the dry weight of the polymer, and t is the contact time. The coefficient was shown to be independent on initial cell count $N(0)$ and concentration of insoluble polymer W/V.[1] Although the difference in the content of pyridinium group should be taken into consideration, cross-linked poly(*N*-benzyl-4-vinylpyridinium bromide and chloride) were most effective among the polymers examined. Although commercial resins also showed the ability to some extent, that of the insoluble pyridinium-type polymer was outstanding.

The removal coefficient is a dynamic index of the ability of polymers to capture bacteria, and is based on initial rate of decrease of viable cell counts. On the other hand, equilibrium capture experiment would also be important for the evaluation of the basic and definitive ability of the polymer to capture bacteria.[6] Thus we have performed the equilibrium capture experiment at 37 °C. After the mixture of polymer and *E. coli* in sterilized physiological saline reached equilibrium, viable cell counts were determined. The experimental isotherm for *E. coli* on the insoluble pyridinium-type polymer is shown in Fig. 1 (graph A). The isotherm on cross-linked poly(4-vinylpyridine), i.e., the polymer without pyridinium group is shown in Fig. 1 (graph D). The isotherms on various other polymers are also shown in Fig. 1 (graphs B, C, and E). As can be seen in Fig. 1, the insoluble pyridinium-type polymer was confirmed to have a much stronger ability to capture bacteria when compared with that of other types of polymers examined.

The ability of the insoluble pyridinium-type polymer to capture bacteria appeared to depend on the content of pyridinium group.[1] We have examined the effect using cross-linked poly(*N*-benzyl-4-vinylpyridinium bromide) containing various amount of the pyridinium group. In Fig. 2 is shown the result. The coefficient uniformly increased with the content of pyridinium group. This result indicates the importance of the presence of pyridinium group in the ability of the polymer to capture bacteria on its surface. Electrostatic interaction between the positive charge on the surface of the polymer and the negative charge of the microbial cell surface appears to be

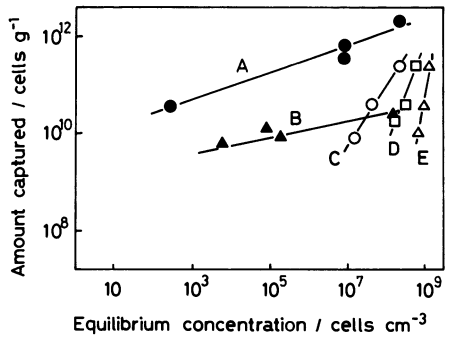

Fig. 1. Experimental isotherms of the capture of *E. coli* by insoluble polymers. (A): Cross-linked poly(N-benzyl-4-vinylpyridinium bromide) containing 72 mol% of 4-vinylpyridine and 2.9 mmol g^{-1} of the pyridinium group, (B): Amberlite IRA-45 in the free base form, (C): Amberlite XAD-4, (D): Cross-linked poly(4-vinylpyridine) containing 72 mol% 4-vinylpyridine, (E): Amberlite IRA-400 in the chloride from.

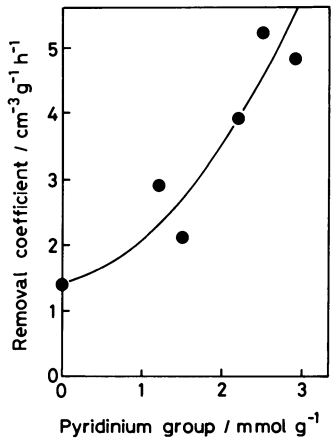

Fig. 2. Effect of the content of pyridinium group in the insoluble pyridinium-type polymer on the removal coefficient for *E. coli*. The polymer contained 72 mol% of 4-vinylpyridine.

Table 1. Effect of the Structure of Cross-Linked Poly(*N*-benzyl-4-vinylpyridinium Bromide) on the Removal Coefficient for *Escherichia Coli*

Run	Monomer content/mol%			Pyridinium group	$N(0)$	W[d]	Removal coefficient
	4-VP[a]	DVB[b]	ST[c]	mmol g^{-1}	cells cm^{-3}	dry g	$cm^3\ g^{-1}\ h^{-1}$
1	72	28	0	2.9	4.3×10^6	4.0	4.8
2	72	20	8	2.9	6.9×10^7	4.4	6.9
3	72	10	18	2.9	1.5×10^7	5.8	7.1
4	72	3	25	3.1	1.5×10^7	4.5	∞[e]
5	72	28	0	2.2	6.9×10^7	3.5	3.9
6	54	28	18	2.1	4.1×10^7	2.7	2.7
7	36	28	36	2.1	4.1×10^7	3.2	1.6

a) 4-Vinylpyridine. b) Divinylbenzene. c) Styrene. d) The volume of bacterial suspension, V, was 20 ml. e) Viable cells were not detected even at the contact time of 0.5 h.

important, although the strong effect of the benzyl group is not clear.

Cross-linked poly(*N*-benzyl-4-vinylpyridinium bromide) was prepared under various conditions in order to examine the effect of higher structure of the polymer upon its ability to capture bacteria. Results are given in Table 1.

Runs 1 to 4 were performed to examine the effect of the degree of cross-linking of the polymer. Here, content of 4-vinylpyridine and that of the pyridinium group were kept nearly constant, and part of divinylbenzene was replaced by styrene. As is obvious in Table 1, the removal coefficient increased with the decrease of the content of divinylbenzene. The result shows that decrease of the degree of cross-linking caused the increase of the ability of the polymer to capture bacteria. In this case, the polymer swells very well in water. The effective surface area in water is much larger, which enhances the ability of the polymer to capture bacterial cells.

Runs 5 to 7 were carried out to examine effect of composition of the matrix of the polymer. In these cases, content of pyridinium group was kept nearly constant at 2.1 mmol g^{-1}, and that of divinylbenzene was also fixed around 28%. As can be seen in Table 1, the removal coefficient increased with the content of 4-vinylpyridine. This result shows that hydrophilicity of the polymer matrix enhanced the affinity of the polymer for bacterial cells.

It would be noteworthy to remind that cross-linked poly(*N*-alkly-4-vinylpyridinium bromides) were much less effective than cross-linked poly(*N*-benzyl-4-vinylpyridinium bromide) for the capture of bacterial cells.[1] Hydrophobicity of the long alkyl group of the polymer did not strengthen the ability to capture bacteria. The *N*-dodecyl polymer and the *N*-hexadecyl polymer showed smaller values of the removal coefficient than that of the polymer with no pyridinium group, i.e., cross-linked poly(4-vinylpyridine). Hydrophobicity of the polymer seems to diminish its ability to capture bacteria.

The ability of the insoluble pyridinium-type polymer to capture bacteria is much higher than that of tetraalkylammonium-type anion-exchange resins. With respect to the strength of positive charge, tetraalkylammonium-type resin would not be inferior to the insolube pyridinium-type polymer. The difference between the two types of polymers in the ability to capture bacteria seems to be ascribable mainly to the difference in hydrophilicity. The pyridinium group is highly hydrophilic. For example, linear polymer of poly(*N*-benzyl-4-vinylpyridinium bromide) is hygroscopic.

References

1) N. Kawabata, T. Hayashi, and T. Matsumoto, *Appl. Environ. Microbiol.*, **46**, 203 (1983).

2) N. Kawabata, T. Hashizume, and T. Matsumoto, *Agric. Biol. Chem.*, **50**, 1551 (1986).

3) S. Fukui and A. Tanaka, *Ann. Rev. Microbiol.*, **36**, 145 (1982).

4) A. Katchalsky, K. Rosenheck, and A. Altman, *J. Polymer Sci.*, **23**, 955 (1957).

5) N. Kawabata and K. Ohira, *Environ. Sci. Technol.*, **13**, 1396 (1979).

6) K. DeNicola and D. J. Kirwan, *Biotechnol. Bioeng.*, **22**, 1283 (1980).

 © 1986 The Chemical Society of Japan Bull. Chem. Soc. Jpn., 59, 2865—2867 (1986)

The Stereochemistry of the Reduction of Carbon-Carbon Double Bond with the Cultured Cells of *Nicotiana tabacum*

Takayuki SUGA,* Toshifumi HIRATA, and Hiroki HAMADA†
Department of Chemistry, Faculty of Science, Hiroshima University,
Higashisenda-machi, Naka-ku, Hiroshima 730
(Received April 19, 1986)

The stereochemistry in the reduction of the C–C double bond adjacent to the carbonyl group with the cultured cells of *Nicotiana tabacum* was investigated by feeding (4*R*)-[6-^{2}H]-(−)-carvone to the cultured cells. It was found that the hydrogen attack to the C–C double bond takes place stereospecifically from the *si*-face at C-1 and the *re*-face at C-6, being trans-addition.

A general mechanism for the biological reduction of a C–C double bond is briefly reviewed.[1] On the other hand, the reduction of a C–C double bond in living cells has been described for the biotransformation of steroids with plant cultured cells,[2–4] but little is reported on the stereochemical aspect of the reduction in the plant tissue cultures. We recently found that the cultured cells of *Nicotiana tabacum* reduce the C–C double bond adjacent to the carbonyl group of carvone (**1**) and then the carbonyl group, whereas the cells do not attack the C–C double bond in the 1-methylethenyl group.[5] It was found that the hydrogen attack to the conjugated C–C double bond takes place stereospecifically from the *si*-face at C-1.[5] However, the stereochemistry of the hydrogen attack at C-6 of **1** has not been elucidated yet. To complete the stereochemical studies on the reduction of the conjugated C–C double bond with the cultured cells of *N. tabacum*, we have now investigated the stereochemistry of the hydrogen addition to the 6-position of carvone by examining the orientation of deuterium in a resultant product in the biotransformation of ^{2}H-labeled carvone with the cultured cells.

Results and Discussion

Incubation of (4*R*)-[6-^{2}H]-(−)-carvone (**2**) (deuterated by 97.6 atom %) with the cultured cells of *N. tabacum* was carried out in a manner similar to that described in our previous paper[5] to yield neodihydrocarveol (**3**) as a main product. The mass spectrum of **3** showed a molecular ion peak at *m/z* 155 and $[M-H_2O]^+$ ion peak at *m/z* 137. The relative intensities of the peaks indicated that 97% of the molecules of **3** were labeled with deuterium. The proton noise decoupled ^{13}C NMR spectrum of the product **3** closely resembled to the spectrum of the nonlabeled neodihydrocarveol (**4**), except that the C-6 signal of **3** at δ_c 27.8 was a somewhat weak triplet ($J_{^{13}C-^2H}$=20 Hz), whereas the corresponding signal of the nonlabeled compound **4** was a singlet. This indicates that one of the hydrogen atoms at C-6 is deuterated.

The orientation of deuterium in the product **3** was determined by comparison of its ^{1}H NMR spectrum with that of the nonlabeled compound **4**, as given in Fig. 1. Complete assignments of the ^{1}H NMR signals of **3** and **4** were made on a 500 MHz NMR spectrum and are shown in Table 1. The assignments were confirmed by a two-dimensional H/H shift correlation NMR spectrum of the nonlabeled compound **4**; all correlations expected were found in the spectrum. The disappearance of the 6α-H signal in the ^{1}H NMR spectrum of **3** indicates the 6α-atom to be deuterium. Thus, it was demonstrated that the *R* hydrogen atom at the 6-position of **3** was added when the carbocyclic double bond of carvone (**2**) was reduced in the cultured cells of *N. tabacum*.

As has been described in our previous paper,[5] the cultured cells of *N. tabacum* have the ability to reduce (4*R*)- and (4*S*)-carvones; (4*R*)-carvone was transformed to (1*R*,2*S*,4*R*)-neodihydrocarveol and (4*S*)-carvone to (1*R*,4*S*)-isodihydrocarvone and (1*R*,2*S*,4*S*)-neoisodihydrocarveol. The formation of these compounds indicates that carvone is stereospecifically reduced to the compound with the chirality of *R* at the C-1 and that of *S* at the C-2 in its biotransformation with the cultured cells. Putting the previous and present results together, thus, the mode of the hydrogen

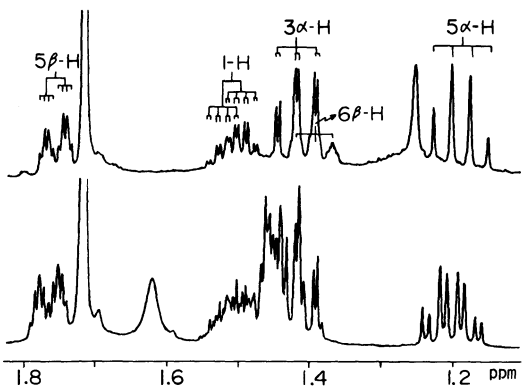

Fig. 1. Comparison of the ^{1}H NMR spectrum of ^{2}H-labeled product **3** (upper) with that of nonlabeled (+)-neodihyrocarveol (**4**) (lower).

† Present address: Department of Fundamental Natural Science, Okayama University of Science, Ridai-cho, Okayama 700.

Table 1. ^{1}H NMR Spectral Data[a] of ^{2}H-Labeled Product **3** and Nonlabeled (+)-Neodihydrocarveol (**4**)

Protons	**3**		**4**	
	δ	J/Hz	δ	J/Hz
1-H	1.52 dqd	12.7, 6.5, 2.4	1.53 dqt	12.6, 6.6, 2.5
2-H	3.89 dt	3.2, 2.4	3.89 dtd	3.2, 2.5, 0.3
3α-H	1.42 ddd	13.2, 12.4, 2.4	1.42 ddd	13.3, 12.4, 2.5
3β-H	1.92 dddd	13.2, 3.3, 3.2, 3.1	1.92 dddd	13.3, 3.3, 3.2, 3.1
4-H	2.28 tt	12.4, 3.3	2.28 tt	12.4, 3.3
5α-H	1.19 dt	12.5, 12.4	1.20 dtd	12.5, 12.4, 4.5
5β-H	1.76 dtd	12.5, 3.3, 3.2	1.77 ddtd	12.5, 3.5, 3.3, 3.2
6α-H	Not detected		1.44 ddddd	12.7, 4.5, 3.5, 2.5, 0.3
6β-H	1.40 br t	12.7	1.42 dddd	12.7, 12.6, 12.4, 3.3
9-H$_2$	4.69 q	1.1	4.69 q	1.0
1-Me	0.97 d	6.5	0.97 d	6.6
8-Me	1.72 t	1.1	1.72 t	1.0

a) Measured at 500 MHz in $CDCl_3$.

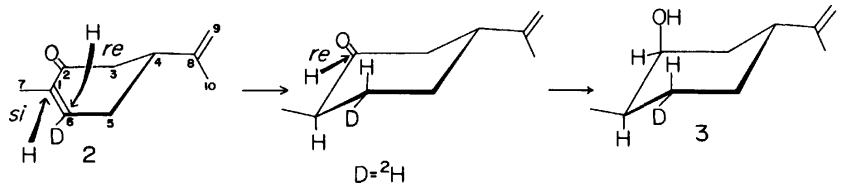

Fig. 2. Stereospecific hydrogen attack in the reduction of the C–C double bond and the carbonyl group of (−)-carvone (**2**) by the suspension cells of *N. tabacum*.

addition in the reduction of carvone with the cultured cells of *N. tabacum* was perfectly established as shown in Fig. 2; at first, the hydrogen attack to the carbocyclic double bond takes place stereospecifically from the *si*-face at C-1 and the *re*-face at C-6. Accordingly, the mode of the hydrogen addition to the C–C double bond conjugated with the carbonyl group is trans. After occurrence of this C–C double bond reduction, the hydrogen attack to the carbonyl group at the 2-position takes place stereospecifically from the *re*-face.

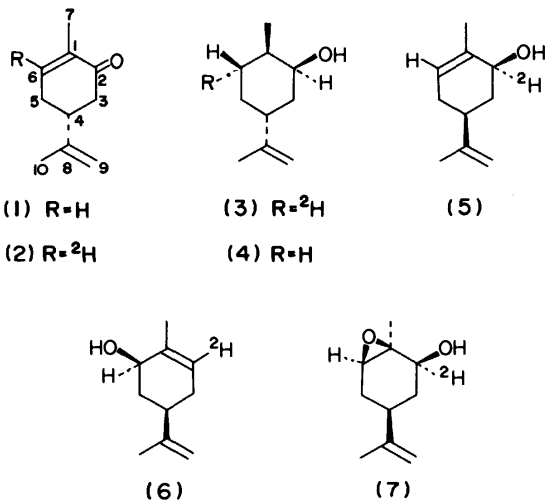

Experimental

Analytical and preparative TLC were carried out on 0.25-mm and 0.5-mm thick silica-gel plates (Merck silica gel 60, GF_{254}). GLC analyses were performed on an instrument equipped with FID and a glass column (3 mm×2 m) packed with 15% DEGS, 15% PEG-20M, and 2% OV-17 on Chromosorb W (AW-DMCS; 80—100 mesh) at 100, 120, and 90—200 °C (3 °C min^{-1}), respectively. ^{1}H NMR spectra were obtained at 90 and 500 MHz in $CDCl_3$ with TMS as an internal standard. GC–MS spectra were recorded on a mass spectrometer equipped with a gas chromatograph with 15% DEGS column (3 mm×2 m) by EI mode at 70 eV.

Substrate. (4*R*)-[6-^{2}H]-(−)-Carvone (**2**) was prepared by reduction of (+)-carvone with NaB^2H_4, isomerization of the resultant (+)-*cis*-carveol (**5**) to (−)-enantiomer **6**,[6] and then oxidation of the enantiomer **6**, as described below.

(i) (4*S*)-[2-^{2}H]-(+)-*cis*-Carveol (5). To a soln of (+)-carvone (3.8 g) ($[\alpha]_D^{25}$ +59.0° (neat); n_D^{25} 1.4990) in MeOH (20 cm^3), NaB^2H_4 (3.0 g) was added by portions at 0 °C. After standing for 30 min at room temp, the reaction mixture was extracted with ether and then subjected to preparative TLC with hexane-EtOAc (7:3, v/v) to give (4*S*)-[2-^{2}H]-(+)-*cis*-carveol (**5**) (3.0 g): *m/z* (rel intensity) 153 (M^+, 2), 135 (M^+-H_2O, 38), 120 (23), and 85 (100).

(ii) 1,3-Transposition of 5. According to the reported procedure,[6] the ^{2}H-labeled (+)-*cis*-carveol (**5**) (3.0 g) was oxidized with *t*-butyl hydroperoxide and oxobis(2,4-pentanedionato-*O*,*O*′)vanadium(IV) to give a ^{2}H-labeled epoxy-alcohol **7** (1.3 g). This epoxy-alcohol **7** was converted to the mesylate derivative (1.8 g) with mesyl chloride-triethylamine. Treatment of the mesylate (1.8 g) with a

sodium-naphthalene reagent[6] dissolved in THF afforded (4*R*)-[6-^{2}H]-(−)-*cis*-carveol (**6**) (0.48 g): ^{1}H NMR (90 MHz) δ=1.64 (s, 6H, 1- and 8-Me), 4.09 (m, 1H, 2-H), and 4.60 (m, 2H, 9-H_2); *m/z* (rel intensity) 153 (M^+, 1), 135 (M^+-H_2O, 35), 120 (23), and 85 (100).

(iii) Oxidation of 6. To a soln of the ^{2}H-labeled (−)-*cis*-carveol (**6**) (0.41 g) in CH_2Cl_2 (50 cm^3), pyridinium-chromium trioxide[7] (2.2 g) was added drop by drop at 5 °C. The mixture was stirred for 1 h at room temp. After filtration, the product was extracted with ether, dried (Na_2SO_4), and freed of the solvent. The residue was subjected to preparative TLC with hexane-EtOAc (95:5, v/v) to give (4*R*)-[6-^{2}H]-(−)-carvone (**2**) (0.28 g): $[\alpha]_D^{25}$ −59.3° (*c* 1.5, EtOH); n_D^{25} 1.4997 (lit,[5] $[\alpha]_D^{25}$ −60.4°, n_D^{25} 1.5000); >99% pure on GLC; *m/z* (rel intensity) 151 (M^+, 6), 136 (M^+-CH_3, 3), and 83 (100); ^{1}H NMR (90 MHz) δ=1.76 (bs, 6H, 1- and 8-Me) and 4.78 (bs, 2H, 9-H_2). The signal at δ 6.78 for C(6)-H, which is observed in the ^{1}H NMR spectrum of nonlabeled carvone, disappeared in the NMR spectrum of **2**. The relative intensities of the molecular ion peaks in the mass spectra of **2** and nonlabeled carvone indicated that 97.6% of the molecules of carvone were labeled with deuterium.

Incubation of (4*R*)-[6-^{2}H]-(−)-Carvone (2) with the Tobacco Suspension Cells. The suspension cells of *N. tabacum* "Bright Yellow" were prepared as described in Ref. 5; the cells were cultured in a 300-ml conical flask containing 100 ml of Murashige and Skoog's medium.[8] To the flask containing the suspension cells (about 50—70 g fresh wt/flask), the ^{2}H-labeled carvone (**2**) (10 mg/flask; total 500 mg) was administered, and then the cultures were incubated at 25 °C for 10 d on a rotary shaker (70 rpm) in the dark.

Isolation and Identification of the Product. The cultured mixture was worked up in a manner similar to that described in Ref. 5; a product was extracted with ether and subjected to preparative TLC on silica gel with hexane-EtOAc (1:4, v/v). The product was identified by direct comparison of TLC, GLC, and spectral data with those of an authentic sample. The physical constants and spectral data of the product were as shown below.

(1*R*,2*S*,4*R*)-[6-^{2}H]-(+)-neodihydrocarveol (3): $[\alpha]_D^{25}$ +30.0° (*c* 0.15, EtOH); IR ν_{max} (film) 3435 (OH) and 1645 (C=C) cm^{-1}; ^{1}H NMR (90 MHz) δ=0.98 (3H, d, *J*=6 Hz, 1-Me), 1.71 (3H, s, 8-Me), 3.88 (1H, bs, >CH-OH), 4.68 (2H, bs, >C=CH_2), (500 MHz) see Table 1; ^{13}C NMR (22.6 MHz, in $CDCl_3$) δ_c=150.2 (s, C-8), 108.7 (t, C-9), 71.0 (d, C-2), 38.8 (t, C-3), 37.8 (d, C-4), 36.1 (d, C-1), 31.4 (t, C-5), 27.8 (bm, C-6), 21.0 (q, C-7), 18.3 (q, C-10); *m/z* (rel intensity) 155 (M^+, 4), 137 (M^+-H_2O, 77), 122 (79), 108 (100), 94 (66), and 79 (62).

Preparation of Authentic Neodihydrocarveol (4). Following the procedure described in the Ref. 9, (+)-neodihydrocarveol (**4**) was prepared from (−)-carvone by the reduction with zinc powder: $[\alpha]_D^{25}$ +29.9° (*c* 0.30, EtOH) (lit,[5] $[\alpha]_D^{25}$ +29.1°), IR ν_{max} (film) 3442 (OH) and 1645 (C=C) cm^{-1}; ^{1}H NMR (90 MHz) δ=0.98 (3H, d, *J*=6 Hz, 1-Me), 1.70 (3H, s, 8-Me), 3.90 (1H, br, >CH-OH), 4.71 (2H, bs, >C=CH_2), (500 MHz) see Table 1; *m/z* (rel intensity) 154 (M^+, 5), 136 ($M-H_2O$, 55), 121 (67), 79 (57), and 41 (100).

The authors thank Takasago Perfumery Co. Ltd. for a gift of the sample of (−)-carvone, Drs. Akio Yasui and Shigetoshi Amiya of Central Research Laboratories of Kuraray Co. Ltd. for the measurement of the 500 MHz ^{1}H NMR, and the JEOL Co. Ltd. for the measurement of the two-dimensional H/H shift correlation NMR. The present work was in part supported by Grant-in-Aids for Developmental Scientific Research No. 57840030 (1982) and 59840013 (1984) from the Ministry of Education, Science and Culture.

References

1) M. Akhtar and C. Jones, *Tetrahedron*, **34**, 813 (1978).
2) T. Furuya, M. Hirotani, and K. Kawaguchi, *Phytochemistry*, **10**, 1013 (1971).
3) S. J. Stohs and M. M. El-Olemy, *Phytochemistry*, **11**, 1397 (1972).
4) M. Hirotani and T. Furuya, *Phytochemistry*, **13**, 2135 (1974).
5) T. Hirata, H. Hamada, T. Aoki, and T. Suga, *Phytochemistry*, **21**, 2209 (1982).
6) A. Yasuda, H. Yamamoto, and H. Nozaki, *Bull. Chem. Soc. Jpn.*, **52**, 1757 (1979).
7) E. J. Corey and G. Schmidt, *Tetrahedron Lett.*, **1979**, 399.
8) T. Murashige and F. Skoog, *Physiol. Plant.*, **15**, 473 (1962).
9) Y. Noma and C. Tatsumi, *Nippon Nogei Kagaku Kaishi*, **47**, 705 (1973).

 © 1986 The Chemical Society of Japan Bull. Chem. Soc. Jpn., 59, 2869—2871 (1986)

Phenolic Solvent-Assisted Hydrogenolysis of *trans*-Stilbene

Tatsuro MIZUKI, Shigeru FUTAMURA,* and Yoshio KAMIYA
Department of Reaction Chemistry, Faculty of Engineering, The University of Tokyo,
Hongo, Bunkyo-ku, Tokyo 113
(Received April 21, 1986)

Phenolic solvents such as phenol, 3,4-xylenol, 2-naphthol, and 5,6,7,8-tetrahydro-2-naphthol greatly promote toluene formation in the hydrogenolysis of *trans*-stilbene, compared with hydroaromatic hydrocarbon solvents. Toluene is afforded in the thermal decomposition of the phenolic solvent adduct to *trans*-stilbene, not via bibenzyl.

It is well-known that mixed solvents composed of phenols and tetralin greatly promote coal liquefaction.[1-7]

Considerable amounts of phenolic compounds are produced inherently in coal liquefaction[3] and their ambident character is quite interesting as acid catalyst[4] and polar media penetrating into the micropores of coal and dissolving polar and high molecular weight components of coal liquids formed during coal liquefaction.[3,6]

Mechanisms for the action of phenols have already been investigated by some groups, using model compounds such as di-2-naphthyl ether,[4] *p*-hydroxyphenyl phenyl ether,[8] benzyl phenyl ether, and dibenzylamines.[9] In these systems, however, unified interpretations have not been made on the source of donatable hydrogen and hydrogen transfer mechanism (homolytic[4,9] or heterolytic[8] cleavage of the O-H bond).

Quite recently, we have shown that phenolic solvents are greatly effective in the hydrogenolysis of *trans*-stilbene, compared with hydroaromatic hydrocarbon solvents.[10] Since olefinic structures can be formed transiently during coal liquefaction, it is significant to clarify the reactivity of phenols toward aromatic olefins in their hydrogenolysis and solvent addition.

In this paper, we present that phenolic solvents can act as hydrogen-donor solvent under coal liquefaction conditions and that they promote hydrogenolysis of aromatic olefins such as *trans*-stilbene via solvent addition.

Experimental

Materials. The following substrates and solvents were commercially purchased and further purified if needed by the conventional method: *trans*-stilbene, bibenzyl, phenol, 3,4-xylenol, 2-naphthol, 5,6,7,8-tetrahydro-2-naphthol(THN), tetralin, 9,10-dihydroanthracene(DHA), and naphthalene.

Instrumental. The GC analyses were carried out on a Shimadzu GC-9A-TCD apparatus equipped with a stainless steel column of 5% OV 17 on Chromosorb W(DMCS). The ^{1}H NMR spectra of the products were obtained on a Varian EM 360A NMR Spectrometer (60 MHz), using Me_4Si as an internal standard.

Batch Experiments. 10 mmol of *trans*-stilbene or bibenzyl and a 10-fold molar excess of a solvent were put into a 90 ml SUS 316 magnetically stirred autoclave. After being pressurized up to 2.0 MPa, the autoclave was heated up to the prescribed temperature within 30 min and maintained at the temperature for 30 min. After the reaction, the autoclave was cooled by an electric fan to room temperature. The products were recovered with tetrahydrofuran and subjected to GC analysis using chlorobenzene as an internal standard.

Product Analyses. The yields of toluene, bibenzyl, *o*- and *p*-benzylphenols were analyzed by GC. (1,2-Diphenylethyl)-phenols[11] were isolated by silica-gel column chromatography and identified by means of ^{1}H NMR and GC-MS. Their ^{1}H NMR and GC-MS data are as follows: δ=3.17 (d, 2H, J=7.2 Hz), 4.33 (t, 1H, J=7.2 Hz), 5.14 (s, 1H, exchangeable with D_2O), 6.62—7.06 (m, 14H). m/z=274 (2.5 (M^+)), 183 (100), 165 (46), 91 (17).

Results and Discussion

As Table 1 shows, phenolic solvents such as 3,4-xylenol, 2-naphthol, and THN show higher hydrogen-

Table 1. Solvent Effect on Hydrogenolysis of *trans*-Stilbene(t-ST)

Solvent	Conv. of t-ST/mol%	Yield of BB/mol%	Yield of TOL/mol%	Conv. of Solvent/mol%
DHA	100	97	6	
2-Naphthol	91	67	16	17
THN	84	59	25	12
3,4-Xylenol	91	54	26	22
Tetralin	33	27	1.1	5.4
Naphthalene	13	13	—	

t-ST 10 mmol; solvent 100 mmol; reaction temperature 400 °C; initial hydrogen pressure 2.0 MPa; reaction time 30 min. BB = Bibenzyl, TOL = toluene.

Table 2. Solvent Effect on Molar Ratio [Toluene(TOL)]/[Bibenzyl(BB)] in the Hydrogenolyses of *trans*-Stilbene(t-ST) and BB

Solvent	[TOL]/[BB] from t-ST=A	[TOL]/[BB] from BB=B	Ratio A/B
Phenol	1.38	0.04	34.5
2-Naphthol	0.24	0.008	30
THN	0.43	0.01	43
Tetralin	0.02	0.01	2.0

Substrate 10 mmol; solvent 100 mmol; reaction temperature 400 °C; initial hydrogen pressure 2.0 MPa; reaction time 30 min.

Table 3. Activation Energies(*Ea*) and Frequency Factors for the Hydrogenolysis of *trans*-Stilbene

Solvent	*Ea*/kcal mol^{-1} [a]	*A* factor/mol^{-1} s^{-1}
2-Naphthol	32.6	6×10^{7}
THN	31.1	9×10^{6}
Tetralin	29.4	8×10^{5}

a) 1 cal=4.184 J.

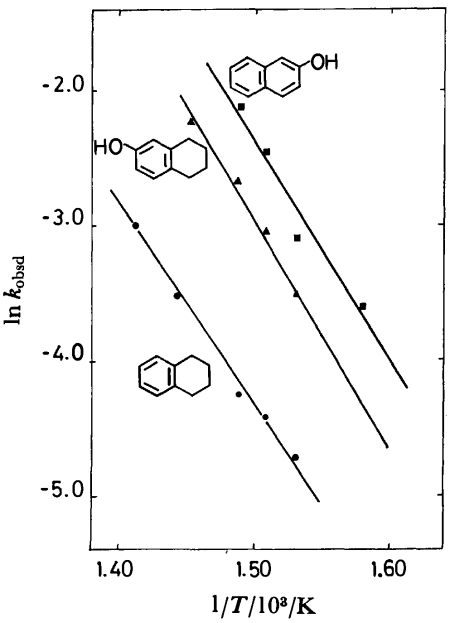

Fig. 1. The plot of ln k_{obsd} versus $1/T$ for *trans*-stilbene conversion.

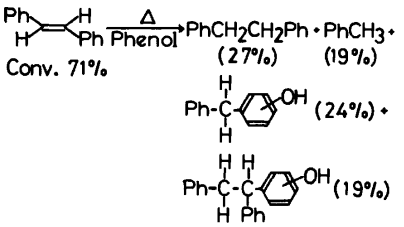

Fig. 2. Hydrogenolysis of *trans*-stilbene in phenol. Parentheses denote selectivities.

donatabilities than tetralin in the hydrogenolysis of *trans*-stilbene at 400 °C. It is noteworthy that toluene formation is greatly promoted by these solvents, contrasting with hydroaromatic hydrocarbon solvents.

Table 2 shows a solvent effect on molar ratio of toluene/bibenzyl in the hydrogenolyses of *trans*-stilbene and bibenzyl. If toluene is afforded exclusively via the thermal cracking of bibenzyl, ratio A/B in Table 2 is expected to fall around unity. In fact, this ratio is given as 2 for tetralin as solvent. On the other hand, 30- to 40-fold increase in ratio A/B is observed for the phenolic solvents. These facts suggest that in the phenolic solvents, toluene could be given in the common mechanism other than the thermal cracking of bibenzyl.

A good linearity was observed in the first-order plot for *trans*-stilbene conversion in the temperature range of 380—435 °C. Figure 1 shows the plot of ln k_{obsd} versus $1/T$ depicted on the basis of the above data. As Table 3 shows, almost no difference is observed in the activation energies for 2-naphthol, THN, and tetralin as solvent.

On the other hand, 10 to 100 times larger values of frequency factor are obtained for the phenolic solvents compared with tetralin. Such difference still has to be unravelled, but it may indicate that some ionic interaction between phenols as weak acids and *trans*-stilbene as π-base is effective in formation of the encounter complex.

Thus, hydrogenolysis of *trans*-stilbene in phenol was carried out in order to understand the reaction profile. As Fig. 2 shows, 71% of *trans*-stilbene was converted in this reaction, and bibenzyl, toluene, benzylphenol, and (1,2-diphenylethyl)phenol(DPEP) were afforded in 27, 19, 24, and 19% selectivities, respectively. Neither benzene nor ethylbenzene was obtained in this reaction. According to GC analysis, benzylphenol was a 2.7:1.0 mixture of *o*- and *p*-forms. Phenol adduct to *trans*-stilbene, DPEP is considered to be formed in the coupling of 1,2-diphenylethyl radical and phenoxyl radical or in the addition of 1,2-diphenylethyl radical to phenol followed by loss of a hydrogen atom. Since 1,2-diphenylethyl radical is detected by ESR[12] and is known to be produced in the pyrolysis of bibenzyl,[13] it can be also produced in the monohydrogen transfer from phenol to *trans*-stilbene.

1,2-Diphenyl-1-phenoxyethane(DPPE), one of the solvent adducts was not obtained in this reaction. Thermal instability of benzyl phenyl ether at 340 °C[14] suggests that all of DPPE decompose thermally at 400 °C.

The larger value for ratio toluene/bibenzyl from *trans*-stilbene in phenol (1.38) in Table 2 may reflect less steric hindrance of phenol or phenoxyl radical toward the approach of 1,2-diphenylethyl radical.

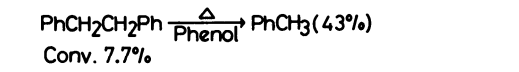

Fig. 3. Hydrogenolysis of bibenzyl in phenol. Parenthesis denotes selectivity.

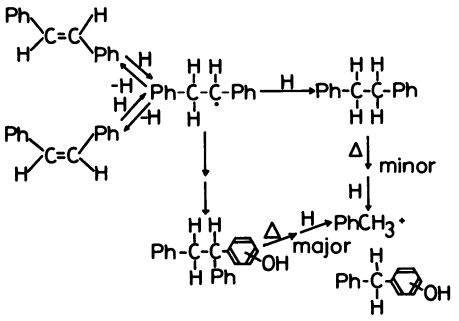

Fig. 4. Possible mechanism for the hydrogenolysis of *trans*-stilbene in phenol.

In these systems, isomerization of stilbene from trans to cis is observed during the course of the reaction. Although no *cis*-stilbene can be detected, using DHA as solvent, about 5% of stilbene is recovered as a cis-form in the phenolic solvents at 380 °C. This value is a little larger than that obtained in the isomerization of *trans*-stilbene to *cis*-stilbene in naphthalene. Such solvent effect on the distribution of the stilbene isomers also supports the homolytic monohydrogen transfer mechanism from phenolic solvents to *trans*-stilbene, and the concerted mechanism can be precluded.

Under these reaction conditions, only 7.7% of bibenzyl was converted to give toluene in 43% selectivity. No benzylphenol was detected by GC in this reaction(see Fig. 3). Therefore, it is unlikely that toluene and benzylphenol were derived from the benzyl radical produced in the thermal cracking of bibenzyl under the reaction conditions. 68% of DPEP decomposed to afford benzylphenol and toluene in 66 and 61% selectivities, respectively, under the same conditions. Since the carbon to carbon single bond in DPEP is more labile than that of bibenzyl, toluene and benzylphenol could be produced in the thermal cracking of DPEP as Fig. 4 shows.

Proton transfer from phenol to *trans*-stilbene is another possibility,[5] but bibenzyl formation from 1,2-diphenylethyl cation cannot be explained by this mechanism.

Here remains the question as to the transferable hydrogen in the phenolic solvents. Comparison of the hydrogen donatabilities of 2-naphthol and naphthalene in Table 1 suggests the involvement of phenolic hydrogens in the hydrogen-transfer process. Thus, hydrogenation of *trans*-stilbene was carried out using a 7:3 mixture of 2-NpOD and 2-NpOH. GC–MS analysis shows that deuterated bibenzyls are formed as

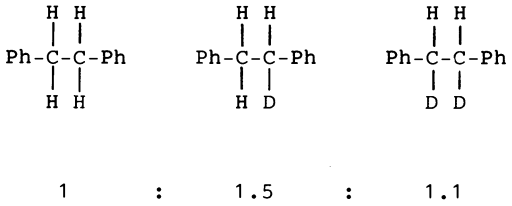

Fig. 5. Deuterium distribution in bibenzyl.

shown in Fig. 5. According to GC analysis, the conversion of 2-naphthol(2-NpOD+2-NpOH) was lower than that of 2-NpOH by 10%. ^{1}H NMR spectroscopy showed that scrambling between phenolic hydrogens and aromatic ring hydrogens was negligible under the reaction conditions. All these facts suggest that phenolic hydrogens are really used in the hydrogenolysis of *trans*-stilbene.

In conclusion, it has been shown that hydrogenolysis of *trans*-stilbene is promoted by the phenolic solvents such as phenol, 3,4-xylenol, 2-naphthol, and 5,6,7,8-tetrahydro-2-naphthol via the phenolic solvent adduct to *trans*-stilbene. Hydrogen-transfer from these phenolic solvents is considered to proceed by radical mechanism.

The authors are very grateful to Dr. Akio Nishijima and Mr. Hiromichi Shimada at the National Research Institute for Industry for the measurement of the GC–MS spectra.

References

1) A. Pott and H. Broche, *Fuel*, **13**, 125 (1934).
2) M. Orchin and H. H. Storch, *Ind. Eng. Chem.*, **40**, 1385 (1948).
3) D. D. Whitehurst, M. Farcasiu, and T. O. Mitchell, "The Nature and Origin of Asphaltenes in Processed Coals," EPRI Annual Report AF-252, Electric Power Research Institute, Palo Alto, 1976.
4) Y. Kamiya, H. Sato, and T. Yao, *Fuel*, **57**, 681 (1978).
5) J. A. Franz, *Fuel*, **58**, 405 (1979).
6) A. A. Awadalla and B. E. Smith, *Fuel*, **61**, 631 (1982).
7) E. J. Volker and B. C. Bockrath, *Fuel*, **63**, 285 (1984).
8) D. F. McMillen, W. C. Ogier, and D. S. Ross, *J. Org. Chem.*, **46**, 3322 (1981).
9) H.-H. King and L. M. Stock, *Fuel*, **61**, 1172 (1982).
10) Y. Kamiya, S. Futamura, T. Mizuki, M. Kajioka, and K. Koshi, *Fuel Proc. Tech.*, in press.
11) Isomer distribution of benzylphenol indicates that the hydroxyl group is attached at the 2- and 4-positions in a 2.7:1.0 ratio.
12) R. Livingston, H. Zeldes, and M. S. Conradi, *J. Am. Chem. Soc.*, **101**, 4312 (1979).
13) R. E. Miller and S. E. Stein, *J. Phys. Chem.*, **85**, 580 (1981).
14) 81% of benzyl phenyl ether decomposed in tetralin at 340 °C to afford toluene and phenol in ca. 50% selectivities. M. Kajioka, S. Futamura, and Y. Kamiya, unpublished results.

Esterification, Etherification, and Aldol Condensation Using Cathodically-Generated Organic Olate Anions

Toshio FUCHIGAMI,* Takeshi AWATA, Tsutomu NONAKA,* and Manuel M. BAIZER†
Department of Electronic Chemistry, Graduate School at Nagatsuta,
Tokyo Institute of Technology, Nagatsuta, Midori-ku, Yokohama 227
†Department of Chemistry, University of California, Santa Barbara,
California 93106, U.S.A.
(Received May 1, 1986)

Cathodic methods for the esterification of carboxylic acids and the etherification of phenol and benzenethiol under mild conditions were developed. The esterification was successfully carried out at room temperature by the reaction of alkylating reagents with cathodically-generated quaternary ammonium carboxylates. The etherification was similarly achieved using electrogenerated quaternary ammonium phenolate and halonitrobenzenes. A hindered phenolate anion cathodically-generated from 2,6-di-*t*-butyl-*p*-cresol remarkably promoted aldol condensation of aromatic ketones and aldehydes, and allowed subsequent Michael reaction to provide efficiently symmetrical 1,5-diketones.

Recently, there has been an increasing interest in the utilization of anionic species with onium counter cations in organic synthesis, since their reactivities are sometimes quite different from those of the anions with metal counter cations.[1] However, the preparation of the anionic species with onium counter cations from the corresponding ones with alkali metal cations is often troublesome and not practical since the use of expensive crown ethers and onium fluorides is required. Phase transfer catalysts (PTC's) enhance the nucleophilicity of anionic moieties, however, they are not always applicable owing to their instability under heating[2] and the impossibility of realizing completely dry reaction media.

Cathodic reduction of organic compounds generates anionic species with onium counter cations such as R_4N^+[3,4] and R_3S^+[4] when onium salts ($R_4N^+X^-$ and $R_3S^+X^-$) are used as supporting electrolytes. Therefore, cathodic reduction seems to be a convenient and versatile method for the generation of such active anionic species.

Therefore, as part of a broad program of the application of electrogenerated active species to organic synthesis,[3-6] cathodic esterification of carboxylic acids and etherification of phenols through S_NAr reaction were at first successfully achieved.[7]

Negatively charged species behave not only as nucleophiles but also as bases. Iversen and Lund[8] first demonstrated that an anionic species electrogenerated from azobenzene allows ylide formation from a phosphonium salt and the subsequent Wittig reaction. One (M.M.B.) of the authors named such anionic species and their precursors "electrogenerated bases (EGB's)" and "pro-bases (PB's)", respectively, and studied intensively and systematically synthetic utilization of some types of EGB's derived from azobenzene derivatives,[9,10] active olefins,[11] oxygen,[5,12-15] and carbon tetrachloride.[16] Most recently, we have found novel EGB-catalyzed polymerization of *N*-carboxy anhydrides of amino acids.[6]

Shono and Kashimura[17] have also explored the application of EGB's to organic synthesis and found that a base electrogenerated from 2-pyrrolidone possesses intriguing reactivity to promote various reactions with high selectivity. Although EGB's seem to be promising bases for organic synthesis, only a limited number of types of PB's have been reported so far.[8-17]

In a continuation of study on the utilization of EGB's, we have explored new ones and found that a certain type of phenolate anion also can be a useful base, that is, a hindered phenolate anion derived from 2,6-di-*t*-butyl-*p*-cresol remarkably promoted aldol condensation and allowed subsequent Michael reactions to provide efficiently symmetrical 1,5-diketones.

Results and Discussion

Cathodic Esterification of Carboxylic Acids. The esterification of carboxylic acids is an important and well-established reaction in organic synthesis. Reasonably, simple methods for the esterification under mild conditions should be required in many cases. One of the "simple methods" may be to react metal salts of carboxylic acids with alkylating reagents but this is generally "not mild" because of the high temperatures required.[18] In a previous paper,[19] one (M.M.B.) of the authors reported that quaternary ammonium salts of carboxylic acids reacted with alkyl halides to give the corresponding esters in high yields. In this method, the esterification reaction itself could proceed smoothly at room temperature, in other word, under "mild" conditions, but the preparation of either quaternary ammonium hydroxides or their carboxylates (**2**) was not very "simple". Afterword, some other methods which seemed to be mild were proposed but they were not simple because of the use of special and expensive reagents such as 1,8-diazabicyclo[5.4.0]-undec-7-ene,[20,21] 1-ethyl-2-fluoropyridinium tetrafluoroborate,[22] and alkyl chloroformates.[23]

With this in mind, a convenient method for

Table 1. Cathodic Esterification of Carboxylic Acids

RCOOH **1**	R'X	Method[a]	Charge passed /F mol^{-1}	Yield of ester **3**[b] /%
MeCOOH	*n*-BuCl	A	1.2	24
MeCOOH	*n*-BuBr	A	1.2	60
MeCOOH	*n*-BuI	A	1.2	25
MeCOOH	*n*-BuOTs	A	1.1	48
MeCOOH	*n*-BuCl	B	1.1	27
MeCOOH	*n*-BuBr	B	1.1	68
MeCOOH	*n*-BuI	B	1.1	96
n-PrCOOH	EtI	B	1.1	96
n-PrCOOH	EtOTs	A	1.1	70
PhCOOH	MeI	B	1.1	80
PhCOOH	EtI	B	1.1	83
PhCOOH	MeOTs	A	1.1	75
$HOOC(CH_2)_4COOH$	MeI	B	1.0	24[c]
$HOOC(CH_2)_4COOH$	MeI	B	2.2	80[c]
PhCHCOOH (OH)	EtI	B	1.1	90
$ClCH_2COOH$	MeI	B	1.1	42
MeCH=CHCOOH	MeI	B	1.0	77
HC≡CCOOH	MeI	B	1.0	58
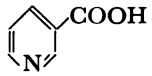	MeI	B	1.1	70

a) See text. b) Determined by gas chromatography. c) Dimethyl adipate.

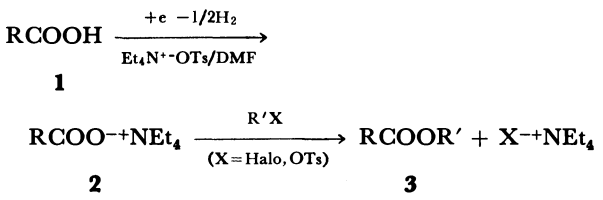

Scheme 1.

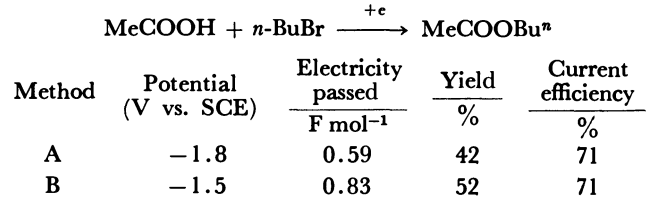

Method	Potential (V vs. SCE)	Electricity passed / F mol^{-1}	Yield / %	Current efficiency / %
A	−1.8	0.59	42	71
B	−1.5	0.83	52	71

Scheme 2.

preparing quaternary ammonium salts of carboxylic acids (**2**) by cathodic reaction and the successive one-pot esterification in a cathode chamber was developed as shown in Scheme 1.

Two procedures for the esterification were employed as follows: In the presence of alkylating reagents, electrolytic reduction of carboxylic acids was carried out in DMF containing Et_4NOTs (Method A). In other method (Method B), the alkylating reagents were added to the catholyte after the electrolysis.

At first, we examined the esterification of acetic acid with butyl bromide by controlled-potential electrolysis. As shown in Scheme 2, the esterification proceeded at room temperature in both procedures to give butyl acetate. Since the amounts of electricity passed were smaller than the theoretical amount for the formation of the acetate anion because of decrease of the current during electrolysis, the yields were low although the current efficiencies were satisfactory.

Constant current electrolysis was found to improve the yield remarkably regardless of the procedures as shown in Table 1.

The yield of butyl acetate formed in Method A was greatly affected by kind of butyl halides used as alkylating reagents. The less electrophilic chloride gave a lower yield than the bromide. Although the iodide should be more electrophilic than the bromide, the former gave a lower yield. This fact is rationalized as due to a less negative reduction potential of the iodide than the bromide: It was confirmed that considerable amounts of the iodide were simultaneously reduced to the corresponding hydrocarbon. Butyl tosylate was also used in the esterification, but it did not give a higher yield than the bromide.

In order to prevent the simultaneous reduction of alkylating reagents, they were added to the catholyte after completion of the electrolysis (Method B). In the esterification of acetic acid with butyl halides by this method, the most electrophilic iodide and the least electrophilic chloride gave the highest and lowest

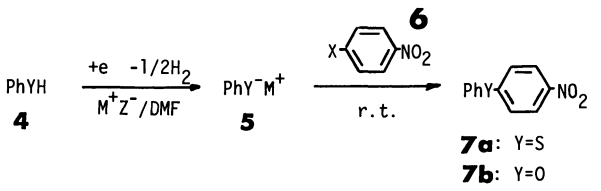

Scheme 3.

yields, respectively. Method B also resulted in high or reasonable yields in the esterification of other simple acids such as propionic and benzoic acids.

The esterification was successfully extended to somewhat complicated acids. It is noticeable that adipic acid gave the diester, though only 1.0 F mol^{-1} of charge was passed. When stoichiometric amounts of charge and methyl iodide for the formation of the diester were used, the yield of the diester reached to 80%. An α-hydroxy acid (mandelic acid) was also esterified in a high yield. Acids with electroreducible groups such as chloro, 1-propenyl, ethynyl, and 3-pyridyl groups could be esterified without the simultaneous reduction of their electroreducible groups.

Although Method A was inferior to Method B in yield, the former is much simpler than the latter and therefore the former may be more useful for esterification in some cases.

Shono and Kashimura have reported another excellent cathodic esterification using a base electrogenerated from 2-pyrrolidone.[17c] However, our method is simpler and does not require the use of any electrogenerated bases.

Cathodic Etherification. Preparation of Diarylethers Using Electrogenerated Phenolate Anions. Nucleophilic aromatic substitution with phenolate anions to give diaryl ethers is also one of important reactions in organic synthesis. Recently, diarylether derivatives have found to be effective as pesticides, particulary as herbicides and certain types of such ethers are now commercially produced.[24] However, substituents of the aromatic rings often eliminate and thus provide undesired by-products because of the high temperatures required in their synthesis. Because of this, most recently, many efforts have been made to solve such problems using PTC's.[25] However, there are limitations to their utilization because the usual type of PTC's are sometimes consumed due to their reaction with phenolate anions under heating; therefore special thermally-stable PTC's must be employed in these cases.[2]

These problems prompted us to attempt nucleophilic aromatic substitution using electrogenerated phenolate anion. At first, the reaction of benzenethiolate anion, an analogue of the phenolate, with halonitrobenzenes was examined. Benzenethiolate anion (**5a**) was cathodically generated from benzenethiol; subsequent reaction of the resulting **5a** with various *p*-halonitrobenzenes (**6**) was carried out in DMF at room temperature, as shown in Scheme 3.

Table 2. Preparation of Diaryl Ethers **7** from Halonitrobenzenes and Electrogenerated Benzenethiolate and Phenolate Anions

Run	4 Y	6 X	Supporting electrolyte[a]	Reaction time/h	Yield of 7[b] /%
1	S	F	A	0.5	96
2	S	Cl	A	0.5	95
3	S	Br	A	0.5	98
4	S	Br	B	0.5	97
5	S	I	A	0.5	96
6	O	F	A	0.5	95
7	O	Cl	A	3.0	62
8	O	Cl	A	Over night	82
9	O	Br	A	0.5	75
10	O	Br	B	0.5	Trace
11	O	I	A	Over night	72
12	O	*o*-Cl	A	5.0	31[c]

a) A=Et_4NOTs, B=$NaClO_4$. b) Isolated yield. c) *o*-Nitrophenyl phenyl ether (**7c**).

The results are summarized in Table 2.

The reaction proceeded almost quantitatively to give *p*-nitrophenyl phenyl sulfide (**7a**). This cathodic thioetherification was not affected by the kind of halogen atoms of **6** and the supporting electrolytes (M^+Z^-) probably because the benzenethiolate anion is inherently so reactive.

Next, the reaction was similarly carried out using phenol instead of benzenethiol to give *p*-nitrophenyl phenyl ether (**7b**) in good to excellent yields. In this case, the yield of **7b** depended on the kind of halogen atoms of **6**. *p*-Fluoronitrobenzene gave the best result since fluorine atom is known to be an excellent leaving group in such S_NAr reaction (Run 6). *p*-Iodonitrobenzene usually gives a poor yield in such a reaction; however, a satisfactory yield could be achieved by this cathodic method (Run 11).

Although *o*-chloronitrobenzene is sterically hindered to S_NAr reaction, the etherification proceeded to provide **7c**, though its yield was rather low (Run 12).

Furthermore, it is noticeable that the reaction was greatly affected by the cation of the supporting electrolyte as follows: The etherification did not proceed when sodium perchlorate was employed instead of Et_4NOTs as a supporting electrolyte (Run 10). This fact suggests that the nucleophilicity of quaternary ammonium salt of phenolate anion cathodically generated is much higher than that of the corresponding sodium salt.[26] In order to comfirm the effect of a counter cation, the reaction of *p*-bromonitrobenzene with sodium phenolate prepared by the treatment of phenol with sodium hydride was

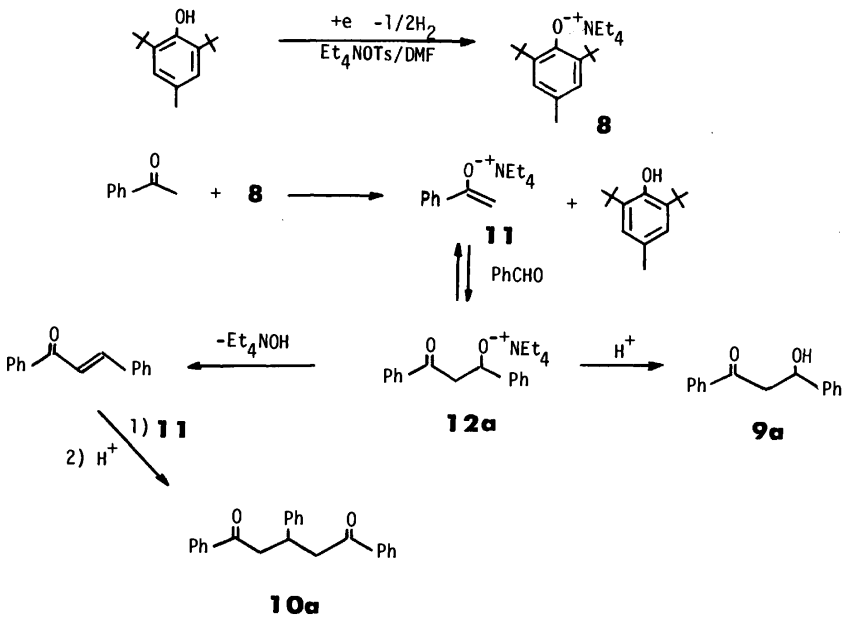

Scheme 4.

Table 3. Hindered Phenolate Anion-Promoted Aldol Condensation of Acetophenone with Benzaldehyde

Run	Reaction time/h	Reaction temp/°C	Counter cation of **8**	Yield[a]/%	
				9a	**10a**
1	1.5	−15	Et_4N^+	39	trace
2	0.5	0	Et_4N^+	20	0
3	3.0	0	Et_4N^+	0	83
4	1.0	r.t.	Et_4N^+	0	74
5	3.0	r.t.	Et_4N^+	0	85
6[b]	0.5	r.t.	Na^+	0	42[c]
7[d]	2.0	r.t.	Et_4N^+	12	16

a) Isolated yield. b) The sodium salt of **8** was prepared using sodium hydride. c) Large amounts of inseparable by-products were formed. d) A catalytic amount of **8** (0.05 equivalent) was used.

also examined under the same conditions as in the electrolysis. Expectedly, the reaction scarcely proceeded and provided only trace amounts of the desired product **7b**.

Thus, the cathodic method has an advantage as follows: The reactivity of anions can be controlled by the selection of supporting electrolytes, particularly their counter cations. It was demmonstrated here that quaternary ammonium phenolate cathodically prepared has a potential utility for the facile synthesis of *p*-nitrophenyl aryl ethers under mild conditions.

Aldol Condensation Promoted by Electrogenerated Hindered Phenolate Anion. Just like LDA, hindered phenolate anions seem to possess much lower nucleophilicity compared to ordinary phenolates. In fact, the reaction of *p*-bromonitrobenzene with the anion **8** cathodically derived from 2,6-di-*t*-butyl-*p*-cresol was found not to proceed at all. Therefore, this hindered phenolate anion seems to be one of promising candidates for EGB's.

Brown[27] and Corey[28] have successfully employed lithium and potassium salts of **8** for the generation of enolate anions from ketones and α-halo ketones; this allowed successive carboxylation and homologation, respectively.

These facts prompted us to investigate aldol condensations using hindered phenolate anion **8** since the reaction sought here is a typical base-promoted one.[29] Aldol condensation of acetophenone and benzaldehyde was at first attempted under various conditions as follows: 2,6-di-*t*-butyl-*p*-cresol was reduced cathodically in DMF containing Et_4NOTs and then the catholyte was added to a mixed solution of acetophenone and benzaldehyde.

The results are summarized in Table 3.

Aldol product **9a** was found to be formed only at temperatures below 0 °C (Runs 1 and 2). When the reaction time was longer even at 0 °C, 1,5-diketone **10a** was obtained solely in a high yield (Run 3). At ambient temperature, **10a** was obtained in good yields regardless of the reaction time (Runs 4 and 5). On the other hand, the sodium salt of the phenolate anion **8** gave large amounts of various by-products together with 1,5-diketone **10** (up to 42% yield), regardless of both the reaction temperature and reaction time (Run 6). The reaction giving **10a** seems to proceed stepwise as shown in Scheme 4.

Although the aldol condensation is an efficient method for forming new carbon–carbon bonds, the product selectivity is not always satisfactory under equilibrium conditions.[30] It is known that the intermediate keto alkoxide **12** is stabilized by six-

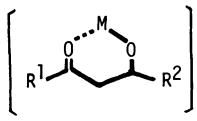

Fig. 1.

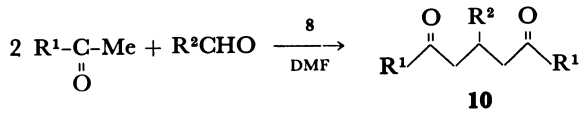

Scheme 5.

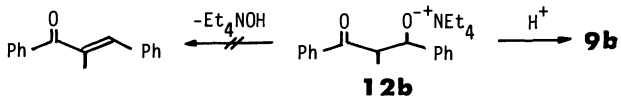

Scheme 6.

Table 4. Preparation of Symmetrical 1,5-Diketones (**10**) from acetophenones Using Electrogenerated Phenolate Anion **8**

Run	R^1	R^2	Reaction time/h	Yield of **10**[a] /%
1	Ph	Ph	3	85
2	Ph	*p*-$MeOC_6H_4$	Over night	59
3[b]	Ph	*p*-$MeOC_6H_4$	3	31[c]
4	Ph	*m*-$MeOC_6H_4$	3	60
5	Ph	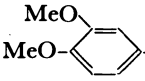	Over night	25
6	Ph	*p*-ClC_6H_4	1	89
7	Ph	*n*-Bu	Over night	0
8	Ph	allyl	Over night	0
9	*p*-ClC_6H_4	Ph	3	79
10	*p*-MeC_6H_4	Ph	3	41
11	*p*-$MeOC_6H_4$	Ph	3	41
12	Ph[d]	Ph	Over night	18[e]

a) Isolated yield. b) Reaction temp = 50 °C. c) Large amounts of various by-products were formed. d) Propiophenone was used. e) The product **9b** (: threo/erythro ≈ 1, ^{1}H NMR) was formed.

membered cyclic metal chelate formation (Fig. 1) in the presence of a divalent metal cation thus providing a single aldol product.[31] On the contrary, the intermediate **12** lacking such stabilization often leads to various side reactions such as retrograde aldol, poly-condensations, and enone formation followed by Michael addition; therefore inseparable mixtures of aldol products are obtained. Although a quaternary ammonium salt of the intermediate **12a** belongs to the latter case, the aldol condensation followed by dehydration and Michael addition proceeded highly selectively to provide 1,5-diketone in excellent yields in contrast to the case of the corresponding sodium salt (Run 6).

The same aldol condensation was examined by using quaternary ammonium phenolate (**5b**) instead of **8**, however the reaction became so complicated that no products could be separated probably because simultaneous nucleophilic attack of the phenolate anion to the starting compounds and/or products took place. It was also comfirmed that the reaction did not proceed smoothly with catalytic amount of **8** (Run 7).

Since the quaternary ammonium salt of hindered phenolate anion **8** was found to be an effective base for the formation of symmetrical 1,5-diketone **10**, this reaction was similarly carried out using various ketones and aldehydes (Scheme 5).

As shown in Table 4, 1,5-diketones **10** were prepared in moderate to good yields from aromatic ketones and aromatic aldehydes, whereas no products were obtained from aliphatic analogues (Runs 7 and 8). Moreover, the aldol product, keto alcohol **9b**, was obatined solely instead of 1,5-diketone from propiophenone and benzaldehyde although the yield was rather low (Run 12). This may be due to the difficulty of dehydrating the intermediate keto alkoxide **12b** (Scheme 6). It was also found that the yield of **10** was greatly affected by the substituents on the benzene rings of both ketones and aldehydes. Since the initial step of the aldol condensation reaction is abstraction of a proton from α-carbon of the ketones, the observed substituent effect was easily understood, as shown in Scheme 4.

Since the products thus obtained are known to be easily converted into pyrylium salts which possess wide utility for various organic synthesis,[32] this base-promoted reaction seems to be highly useful.

Experimental

^{1}H NMR spectra were recorded at 60 MHz on a Varian EM 360 NMR spectrometer using $CDCl_3$ and Me_4Si as solvent and internal standard, respectively. IR spectra were obtained with a Hitachi 295 infrared spectrometer. Mass spectra were obtained with a JEOL JMS-D100 mass spectrometer.

Electrolytic Procedure. An H-type electrolytic cell divided with a glass filter diaphragm was used. Platinum plates (2×3 cm) were used as cathode and anode. The catholyte was 40 cm^3 of 0.5 mol dm^{-3} Et_4NOTs or $NaClO_4$/

anhydrous DMF containing 6—10 mmol of substrates (**1**, **4**, **8**). Constant current (1.6A dm^{-2}) electrolysis was mainly carried out by passing 1.0—1.2F (1F=96480C) mol^{-1} of charge under a nitrogen atmosphere at room temperature.

Cathodic Esterification of Carboxylic Acids. Method A: Alkylating reagents (11 mmol of alkyl halides or tosylates) had been added to the catholyte containing carboxylic acids (10 mmol) before the current was turned on. After the electrolysis, the catholyte was allowed to stand for 1 h at room temperature.

Method B: Similar to Method A except that the alkylating reagents were added to the catholyte after the current had been turned off. In both methods, the catholyte was poured into water and then extracted with dichloromethane. The extract was analyzed by gas chromatography using a 2 m PEG 20M column at 100—200 °C.

Preparation of Diaryl Ethers (7) Using Electrogenerated Phenolate Anions. After the electrolysis of 6 mml of benzenethiol or phenol had been carried out by passing 1.0F mol^{-1}, the catholyte was added to a stirred solution of 5 mmol of *o*- or *p*-halonitrobenzene in 10 cm^3 of DMF. The reaction mixture was stirred at room temperature, and then the mixture was poured into water. After extraction with ether, the extracts were dried over anhydrous sodium sulfate. After removal of the solvent, the remaining residue was chromatographed on silica gel. Elution with a mixed solvent of hexane and ethyl acetate (50:1) provided pure products **7**. The products, *p*-nitrophenyl phenyl sulfide (**7a**)[33] and *p*-nitrophenyl phenyl ether (**7b**)[34] were identified by spectroscopic comparison with authentic samples.

***o*-Nitrophenyl Phenyl Ether (7c):** Yellow oil. IR (KBr): 1520 cm^{-1} (ν_{NO_2}). ^1H NMR δ=6.85—7.75 (m, 8H, Ar-H) and 7.80—8.05 (m, 1H, Ar-H). MS *m/z* 215 (M^+). Found: C, 66.71; H, 4.22; N, 6.18%. Calcd for $C_{12}H_9O_3N$: C, 66.97; H, 4.21; N, 6.51%.

Aldol Condensation Promoted by Electrogenerated Hindered Phenolate Anion (8). After the electrolysis had been carried out in 40 cm^3 of DMF containg 10 mmol of 2,6-di-*t*-butyl-*p*-cresol, 13.3 cm^3 of the catholyte was added to a stirred solution of 3 mmol of ketone and 3 mmol of aldehyde in 7 cm^3 of DMF under a nitrogen atmosphere. After stirring (TLC control), the reaction mixture was poured into an aqueous solution of NaCl and then extracted with ether. After drying and concentrating, the remaining residue was chromatographed on silica gel. Elution with a mixed solvent of hexane and diethyl ether (4:1) provided keto alcohol (**9**) or 1,5-pentanedione (**10**).

The products, 3-hydroxy-1,3-diphenyl-1-propanone (**9a**),[31] 1,3,5-triphenyl-1,5-pentanedione (**10a**),[31] 3-(4-methoxyphenyl)-1,5-diphenyl-1,5-pentanedione,[35] 3-(3,4-dimethoxyphenyl)-1,5-diphenyl-1,5-pentanedione,[35] 3-(4-chlorophenyl)-1,5-diphenyl-1,5-pentanedione,[35] 3-phenyl-1,5-di-*p*-tolyl-1,5-pentanedione,[36] 1,5-bis(4-methoxyphenyl)-3-phenyl-1,5-pentanedione[37] were identified by spectroscopic comparison with authentic samples.

3-(3-Methoxyphenyl)-1,5-diphenyl-1,5-pentanedione: Mp 88—90 °C. IR (KBr): 1680 cm^{-1} ($\nu_{C=O}$). ^1H NMR δ=3.15—3.50 (m, 2H, CH_2), 3.65—4.35 (s, 3H, CH_3O and m, 1H, CH), and 6.55—8.10 (m, 14H, Ar-H). MS *m/z* 358 (M^+). Found: C, 80.29; H, 5.97%. Calcd for $C_{24}H_{22}O_3$: C, 80.42; H, 6.19%.

1,5-Bis(4-chlorophenyl)-3-phenyl-1,5-pentanedione: Mp 125—127 °C. IR (KBr): 1690 cm^{-1} ($\nu_{C=O}$). ^1H NMR δ=3.30—3.65 (m, 4H, CH_2), 3.90—4.35 (m, 1H, CH), and 7.20—8.10 (m, 13H, Ar-H). MS *m/z* 400 (M^++4), 398 (M^++2), and 396 (M^+). Found: C, 69.83; H, 4.83; Cl, 18.17%. Calcd for $C_{23}H_{18}O_2Cl_2$: C, 69.53; H, 4.57; Cl, 17.85%.

3-Hydroxy-2-methyl-1,3-diphenyl-1-propanone (9b): Colorless oil. IR (liquid film): 3500 (ν_{OH}) and 1670 cm^{-1} ($\nu_{C=O}$). ^1H NMR δ=0.85—1.30 (d, 3H, CH_3), 3.20—3.90 (m, 2H, OH and MeCH), 4.77—5.13 (d, 1H, CHOH), and 7.05—8.10 (m, 10H, ArH). MS *m/z* 240 (M^+). Found: C, 79.67; H, 6.66%. Calcd for $C_{16}H_{16}O_2$: C, 79.97; H, 6.71%.

References

1) For examples: a) I. Kuwajima and E. Nakamura, *J. Am. Chem. Soc.*, **97**, 3257 (1975); b) R. Noyori, K. Yokoyama, J. Sakata, I. Kuwajima, E. Nakamura, and M. Shimizu, *J. Am. Chem. Soc.*, **99**, 1265 (1977); c) R. Noyori, I. Nishida, and J. Sakata, *J. Am. Chem. Soc.*, **105**, 1598 (1983).

2) D. J. Brunelle and D. A. Singleton, *Tetrahedron Lett.*, **1984**, 3383.

3) T. Awata, M. M. Baizer, T. Nonaka, and T. Fuchigami, *Chem. Lett.*, **1985**, 371.

4) M. Minato, T. Nonaka, and T. Fuchigami, *Chem. Lett.*, **1986**, 1071.

5) M. Sugawara and M. M. Baizer, *J. Org. Chem.*, **48**, 4931 (1983).

6) T. Komori, T. Nonaka, and T. Fuchigami, *Chem. Lett.*, **1986**, 11.

7) For a preliminary communication, see Ref. 3.

8) P. E. Iversen and H. Lund, *Tetrahedron Lett.*, **1969**, 3523.

9) T. Troll and M. M. Baizer, *Electrochim. Acta*, **20**, 33 (1975).

10) R. C. Hallcher and M. M. Baizer, *Justus Liebig Ann. Chem.*, **1977**, 737.

11) M. M. Baizer, J. L. Chruma, and D. A. White, *Tetrahedron Lett.*, **1973**, 5209.

12) P. M. Allen, C. S. Foote, and M. M. Baizer, *Synth. Commun.*, **12**, 123 (1982).

13) W. T. Monte, M. M. Baizer, and R. D. Little, *J. Org. Chem.*, **48**, 803 (1983).

14) M. Sugawara and M. M. Baizer, *Tetrahedron Lett.*, **24**, 2223 (1983).

15) M. Sugawara, M. M. Baizer, W. T. Monte, R. D. Little, and U. Hess, *Acta, Chem. Scand., Ser. B*, **37**, 509 (1983).

16) S. T. Nugent, M. M. Baizer, and R. D. Little, *Tetrahedron Lett.*, **23**, 1339 (1982).

17) a) T. Shono, S. Kashimura, K. Ishizaki, and O. Ishige, *Chem. Lett.*, **1983**, 1311; b) T. Shono, S. Kashimura, and H. Nogusa, *J. Org. Chem.*, **49**, 2043 (1984); c) T. Shono, O. Ishige, H. Uyama, and S. Kashimura, *J. Org. Chem.*, **51**, 546 (1986); d) T. Shono, S. Kashimura, and H. Nogusa, *Chem. Lett.*, **1986**, 425.

18) R. H. Mill, M. W. Farrar, and O. J. Weinkauff, *Chem. Ind. (London)*, **1962**, 2144.

19) J. H. Wagenknecht, M. M. Baizer, and J. L. Chruma, *Synth. Commun.*, **2**, 215 (1972).

20) N. Ono, T. Yamada, T. Sato, T. Tanaka, and A. Kaji, *Bull. Chem. Soc. Jpn.*, **51**, 2401 (1978).

21) C. G. Rao, *Org. Prep. Proc. Int.*, **12**, 225 (1980).

22) S. Shoda and T. Mukaiyama, *Chem. Lett.*, **1980**, 391.

23) S. Kim, Y. C. Kim, and J. I. Lee, *Tetrahedron Lett.*, **1983**, 3356.

24) H. Yoshioka, C. Takayama, and N. Matsuo, *Yuki*

Gosei Kagaku Kyokaishi., **42**, 809 (1984).
25) W. P. Weber and G. W. Gokel, "Phase Transfer Catalysis in Organic Synthesis," Spring-Verlag; W. Berlin (1977).
26) The high reactivity of ammonium phenolate has been reported, but its preparation is troublesome: J. Ugelstad, T. Ellingsen, and A. Berge, *Acta Chem. Scand.*, **20**, 1593 (1966).
27) H. C. Brown, H. Nambu, and M. M. Rogic, *J. Am. Chem. Soc.*, **91**, 6852 (1969).
28) a) E. J. Corey and R. H. K. Chen, *J. Org. Chem.*, **38**, 4086 (1973); b) E. J. Corey and R. H. K. Chen, *Tetrahedron Lett.*, **1973**, 3817.
29) EGB (aldehyde radical anion)-promoted aldol condensation of aldehydes has been reported: T. Shono, S. Kashimura, and K. Ishizaki, 47th National Meeting of the Chemical Society of Japan, April 1983, Kyoto, Abstr. No. 3E 28.
30) H. O. House, "Modern Synthetic Reactions," 2nd ed., W. A. Benjamin; Menlo Park, CA, 1972; Chap. 10.
31) H. O. House, D. S. Crumrine, A. Y. Teranishi, and H. D. Olmstead, *J. Am. Chem. Soc.*, **95**, 3310 (1973).
32) A. T. Balaban, A. Dinculescu, G. N. Dorofeenko, G. W. Fischer, A. V. Koblik, and V. V. Mezheritskill, "Pyrylium Salts: Syntheses, Reactions, and Physical Properties," ed by A. R. Katritzky, Academic Press, New York (1982).
33) H. Gilman and A. Broadbent, *J. Am. Chem. Soc.*, **69**, 2055 (1947).
34) C. M. Suter, *J. Am. Chem. Soc.*, **51**, 2581 (1929).
35) R. L. Frank and R. P. Seven, *J. Am. Chem. Soc.*, **71**, 2632 (1949).
36) W. Dilthey and S. Windmueller, *J. Prakt. Chem.*, **159**, 273 (1942).
37) W. Schneider, G. Gramms, and W. Riedel. *Chem. Ber.*, **69**, 2543 (1936).

 © 1986 The Chemical Society of Japan Bull. Chem. Soc. Jpn., 59, 2881—2884 (1986)

The Oxidation of Methylbenzenes and Naphthalenes to Quinones with H_2O_2 in the Presence of Palladium Catalyst

Satoru YAMAGUCHI, Masami INOUE,* and Saburo ENOMOTO
Faculty of Pharmaceutical Sciences, Toyama Medical and Pharmaceutical University,
2630 Sugitani, Toyama 930-01
(Received January 24, 1986)

Methylbenzenes and naphthalenes were oxidized to quinones with aqueous(60%) H_2O_2 in acetic acid in the presence of a 0.24 wt% Pd(II)-sulfonated polystyrene type resin. The selectivities to quinones were higher in naphthalenes than in methylbenzenes. Among the naphthalenes used, 2-methylnaphthalene, 2,3-dimethylnaphthalene, and 2,6-dimethylnaphthalene gave 1,4-quinones in good yields(50—64%). The increase in the reaction temperature increased the selectivity to quinones from 40% at 20 °C to 70% at 70 °C.

The oxidation of 2-methylnaphthalene with chromium trioxide to 2-methyl-1,4-naphthoquinone (vitamin K_3) is known to be a practical process.[1] Recently, various quinones have been prepared from aromatic hydrocarbons with chromium trioxide by the addition of 18-crown-6 ether.[2] However, catalytic oxidation is valuable since the use of a large amount of chromium trioxide gives rise to problems in the treatment of waste water. Along this line, the oxidation of aromatic hydrocarbons to quinones with H_2O_2 in the presence of acid catalysts has been claimed.[3] As for metal-ion catalysts, naphthalenes and anthracenes have been oxidized with ammonium peroxodisulfate under the coexistence of ammonium cerium(IV) sulfate and silver(I) nitrate[4] in an emulsified solution. From a practical standpoint, a solid catalyst is useful in the separation of the catalyst from the reaction products.

In the oxidation of 2-methylnaphthalene to 2-methyl-1,4-naphthoquinone, we have found a palladium catalyst supported on sulfonated polystyrene type resins.[5] In this work palladium catalysts were applied to the oxidation of methylbenzenes and naphthalenes since several quinone compounds showed antitumor or antibiotic activities.

The reaction rates and selectivities to the quinones differed widely with the substituents on methylbenzenes and naphthalenes.

Experimental

Reagents and Preparation of the Catalyst. Methyl benzenes, naphthalenes, 1,2-naphthoquinone, 1,4-naphthoquinone, 2-methyl-1-naphthol, 2,3,5-trimethylhydroquinone, 2-methyl-1,4-naphthoquinone, 2,5-dimethyl-p-benzoquinone, and 2,3,5,6-tetramethyl-*p*-benzoquinone, were purchased commercially. Aqueous (60%) H_2O_2 was obtained from Mitsubishi Gas Chemical Co. The conditioning of sulfonated polystyrene type(SP) resin (DOWEX 50w-x8, 200-400 mesh, H-form, 1 g, water content 50%) was carried out by allowing it to stand for 1 h in 30 ml of acetic acid. The solvent was removed and the SP resin was washed with acetic acid; then, a 0.24 wt% Pd(II)-SP resin catalyst was prepared from 5 mg of $Pd(AcO)_2$ and the SP resin (1 g) by stirring in 20 ml of acetic acid for 5 h at 50 °C. The catalyst was separated and washed three times with acetic acid. Melting points were determined with a Yanagimoto micro melting-point apparatus and were uncorrected.

2,3-Dimethyl-1,4-naphthoquinone. 2,3-Dimethyl-naphthalene (385 mg, 2.5 mmol) was oxidized with 60% H_2O_2 (0.7 ml, 15.6 mmol) at 50 °C for 8 h in 10 ml of acetic acid in the presence of the 0.24 wt% Pd(II)-SP resin catalyst (1 g). After the catalyst had been separated, the reaction mixture was diluted with water to 40 ml and poured into the separating funnel with hexane to extract the quinone from the reaction mixture. The hexane layer was washed with water, dried, and evaporated. The quinone was crystallized from methanol; mp 126—127 °C. Lit,[6] mp 127 °C. Found: C, 77.68; H, 5.46%. Calcd for $C_{12}H_{10}O_2$: C, 77.40; H, 5.41%.

2,6-Dimethyl-1,4-naphthoquinone. 2,6-Dimethylnaphthalene (768 mg, 5.0 mmol) was oxidized with 60% H_2O_2 (1.05 ml, 23.4 mmol) at 50 °C for 8 h in 20 ml of acetic acid in the presence of the 0.24 wt% Pd(II)-SP resin catalyst (2 g). The quinone was obtained from the reaction mixture in the same way as 2,3-dimethyl-1,4-naphthoquinone; mp 137—138 °C. Lit,[7] mp 136—137 °C. Found: C, 77.30; H, 5.41%. Calcd for $C_{12}H_{10}O_2$: C, 77.40; H, 5.41%.

2,3,5-Trimethyl-*p*-benzoquinone. 2,3,5-Trimethyl-*p*-benzoquinone was prepared from 2,3,5-trimethyl-*p*-hydroquinone with chromium trioxide in dichloromethane/diethyl ether according to a method described in the literature[2]; mp 30 °C. Lit,[2] mp 32 °C. Found: C, 71.41; H, 6.92%. Calcd for $C_9H_{10}O_2$: C, 71.98; H, 6.71%.

2-Methyl-1,4-naphthalenediol. 2-Methyl-1,4-naphthalenediol was prepared by reducing 2-methyl-1,4-naphthoquinone with sodium dithionite according to a method from the literature[1]. Mp 150—160 °C. Found: C, 75.94; H, 5.57%. Calcd for $C_{11}H_{10}O_2$: C, 75.84; H, 5.79%.

General Procedure for the Oxidation of Methylbenzenes and Naphthalenes. Naphthalenes (2.5 mmol), acetic acid (10 ml), and the 0.24 wt% Pd(II)-SP resin catalyst (1 g) were added to a 50 ml flask. Oxidation was initiated by the addition of 60% H_2O_2 (0.35 ml, 7.8 mmol) under magnetic stirring. After 4 h, an additional 0.35 ml of 60% H_2O_2 was added and the solution was heated until the oxidation was almost completed. The products were analyzed by high-performance liquid chromatography (HPLC) (M & S pack C-18, 4.6×150 mm column, Gilson Co. model 302) using MeOH–H_2O (100:15) as the eluent (flow rate, 0.5 ml min^{-1}; detector, UV at 285 nm). 2,6-Dimethylnaphthalene or 2-methylnaphthalene was used as an internal standard. Retention times were 1,2-naphthoquinone 3.9 min, 1,4-naphthoquinone 4.6 min, 2-methyl-1,4-naphthoquinone 5.5 min, 2,3-dimethyl-1,4-naphthoquinone 7.0 min, 2,6-dimethyl-1,4-naphthoquinone 6.6 min, 2,5-dimethyl-*p*-benzo-

quinone 4.4 min, 2,3,6-trimethyl-*p*-benzoquinone 5.2 min, 2,3,5,6-tetramethyl-*p*-benzoquinone 6.8 min, naphthalene 7.2 min, 2-methylnaphthalene 9.6 min, 2,3-dimethylnaphthalene 12.9 min, 2,6-dimethylnaphthalene 13.8 min, *p*-xylene 7.8 min, 1,2,4-trimethylbenzene 10.7 min, and 1,2,4,5-tetramethylbenzene 14.0 min, respectively.

Results and Discussion

Oxidation of Methylbenzenes and Naphthalenes. In the oxidation of 2-methylnaphthalene to 2-methyl-1,4-naphthoquinone, the composition of the catalysts and the reaction conditions such as metal ions, anions, the supports of palladium, and solvents have been studied previously.[5] The best catalyst was prepared from palladium salts and sulfonated polystyrene-type resins in acetic acid by an ion-exchanging procedure at 50 °C for a 5-h heating. When a 0.24 wt% palladium-sulfonated polystyrene type resin (SP resin) was used, the conversion of 97% and the selectivity of 55% were attained at 50 °C for 8 h. Though the SP resin itself catalyzed the oxidation, the activity was poor; a conversion of 54% and a selectivity of 37% were obtained under the same reaction conditions. Acetic acid was an effective solvent for the oxidation. In our oxidation system 2-methyl-1,4-naphthoquinone was sufficiently stable in separated experiments; a quinone of 9.9% was decomposed after 8 h at 50 °C.

In this report, the oxidation of methylbenzenes and naphthalenes was carried out with aqueous 60% H_2O_2 by using palladium catalysts. Results are shown in

Table 1. Oxidation of Methylbenzenes and Naphthalenes to Quinones

Substrate	Quinone	Temp °C	Time h	Conv %	Yield %
Naphthalene	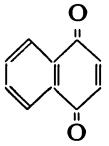	50	8	67.9	12.6
2-Methylnaphthalene	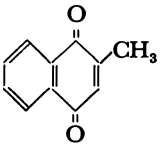	60	8	92.9	59.9
2,3-Dimethylnaphthalene	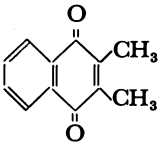	50	6	95.1	51.2
2,6-Dimethylnaphthalene	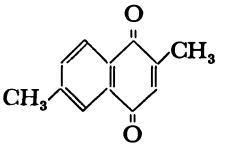	50	8	97.9	64.7
p-Xylene	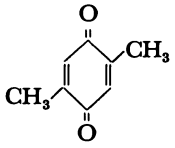	70	8	37.2	6.6
1,2,4-Trimethylbenzene	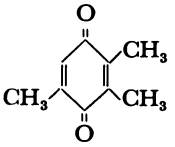	70	10[a]	77.6	3.3
1,2,4,5-Tetramethylbenzene	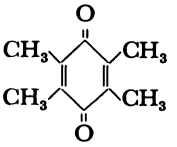	70	8	74.8	8.4

Substrate (2.5 mmol), 60% H_2O_2 (0.7 ml, 15.6 mmol), 0.24 wt% Pd(II)-SP resin (DOWEX 50 w-x8, 200—400 mesh) 1 g, and AcOH 10 ml were used. a) H_2O_2 of one equivalent to 1,2,4-trimethylbenzene was added each at 0 h, 4 h, and 7 h.

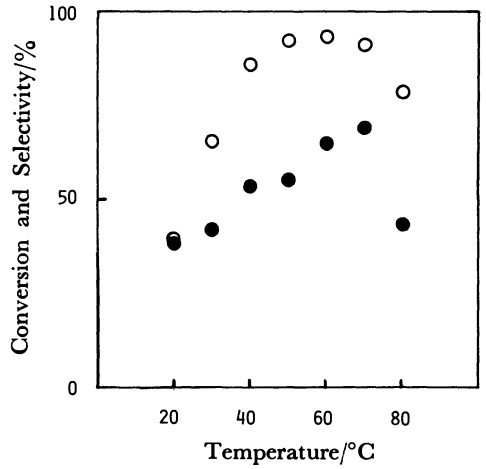

Fig. 1. Effect of the temperature on the conversion and the selectivity of the oxidation of 2-methylnaphthalene to 2-methyl-1,4-naphthoquinone with H_2O_2. 2-Methylnaphthalene 0.35 g(2.5 mmol), 60% H_2O_2 0.7 ml(15.6 mmol), 0.24 wt% Pd(II)-SP resin (DOWEX 50w-x8, 200—400 mesh) 1 g, and AcOH 10 ml were used. The oxidation was carried out for 8 h. ○: Conversion, ●: Selectivity.

Table 1. Methylbenzenes such as *p*-xylene, 1,2,4-trimethylbenzene, and 1,2,4,5-tetramethylbenzene were oxidized to give 2,5-dimethyl-*p*-benzoquinone, 2,3,5-trimethyl-*p*-benzoquinone, and 2,3,5,6-tetramethyl-*p*-benzoquinone, respectively, with poor yields of 3—8% at 70 °C. On the other hand, naphthalenes were oxidized easily to give methylnaphthoquinones; 2-methyl-, 2,3-dimethyl-, and 2,6-dimethylnaphthalene gave corresponding 1,4-quinones from naphthalenes with selectivities of 54, 53, and 66%, respectively. The only quinone from naphthalene was 1,4-naphthoquinone, since the decomposition of 1,2-naphthoquinone occurred vigorously.

Figure 1 shows the effect of the reaction temperature on the conversion and the selectivity in the oxidation of 2-methylnaphthalene. The conversion increased upon increasing the reaction temperature up to 50 °C and a constant value of around 90% was attained. However, a further increase in the reaction temperature (80 °C) collapsed the catalyst and the activity decreased drastically.

The selectivity also increased linearly upon increasing the reaction temperature to 70 °C. Therefore, we carried out the oxidation at temperatures between 50 and 70 °C. Usually, a higher selectivity is expected when mild reaction conditions are employed. Our results were contrary to the general tendency. For this complicated result, the presence of two different types of active species working under different temperature ranges are considered, i.e., hydroxyl cations[8] worked mainly at higher temperatures to give quinones and hydroxyl radicals at lower temperatures to afford polymerized compounds as by-products.[9]

Table 2. Oxidation Rates of 2-Methylnaphthalene, 2-Methyl-1-naphthol, and 2-Methyl-1,4-naphthalenediol

Substrate	Initial rate[a] $\times 10^{-4}$ mol dm^{-3} min^{-1}	Select.[b] %
2-Methylnaphthalene	5.9	55
2-Methyl-1-naphthol	72.2	61
2-Methyl-1,4-naphthalenediol	1500	100

Substrate (5.0 mmol), 60% H_2O_2 (one equivalent to the substrates), 0.24 wt% Pd(II)-SP resin (DOWEX 50w-x8, 200—400 mesh) 2 g, and AcOH 20 ml were used. The oxidation was carried out at 50 °C. a) The rate of formation of 2-Methyl-1,4-naphthoquinone. b) The selectivity to 2-methyl-1,4-naphthoquinone.

The Oxidation of Various Substituted Benzenes and Naphthalenes. The yields of quinones varied with the position and the number of the methyl groups attached to benzenes and naphthalenes (Table 1). As a tendency, electron-donating substituents, such as methyl and methoxyl groups at carbon-2, accelerated the oxidation. On the other hand, nitro groups greatly retarded the oxidation; the ratios for the initial oxidation rates were MeO:Me:H:Cl:NO_2=11.1:3.4:1.0:0.6:0.1. The large substituent effect and an ionic media of our reaction system suggested that an electrophilic attack of peroxigenated palladium at the 1-position of naphthalenes to give 1-naphthols is a key step for the quinone formation followed by the hydroxylation to carbon-4. 2-Methyl-1-naphthol and 2-methyl-1,4-naphthalenediol, the supposed intermediates, were easily oxidized to give quinones as shown in Table 2.

The nature of the palladium catalysts in the oxidation with peroxides is still ambiguous. Recently, a peroxidized palladium complex has been prepared from *t*-BuOOH and $Pd(AcO)_2$ and used for the oxidation of olefins to ketones.[10] In our catalyst, *t*-BuOOH was inactive to the oxidation of 2-methylnaphthalene.

The oxidations of methoxybenzenes with chromium trioxide have afforded benzoquinones selectively.[11] Also, 1,2,3-trimethoxybenzene has been oxidized to give dimethoxy-*p*-benzoquinones with H_2O_2 in acetic acid in the presence of hexacyanoferrate.[12] On the other hand, the palladium-SP resin catalyst easily oxidized *o*-, *m*-, and *p*-dimethoxybenzenes with H_2O_2 to give polymerized tars.

References

1) L. F. Fieser, *J. Biol. Chem.*, **133**, 391 (1940).
2) M. Juaristi, J. M. Aizpurua, B. Lecea, and C. Palomo, *Can. J. Chem.*, **62**, 2941 (1984).
3) J. Sugano, Y. Kuriyama, Y. Ishiuchi, and Y. Minamikawa, *Ger. Offen* DE 2341468 (1974); *Chem. Abstr.*,

81, 3694n (1974); R. Baba, E. Takanobu, Y. Saito, and K. Sakuma, Japan Patent, 7850147 (1978); *Chem. Abstr.*, **89**, 90142n (1978); E. Takanobu, R. Baba, Y. Saito, and Y. Yokoyama, Japan Patent 77108959 (1977); *Chem. Abstr.*, **88**, 37500 f (1978).

4) J. Skarżewski, *Tetrahedron*, **40**, 4997 (1984).

5) S. Yamaguchi, M. Inoue, and S. Enomoto, *Chem. Lett.*, **1985** 827; S. Yamaguchi, M. Inoue, and S. Enomoto, *Chem. Pharm. Bull.*, **34**, 445 (1986).

6) R. T. Arnold and R. Larson, *J. Org. Chem.*, **5**, 250 (1940); L. I. Smith and I. M. Webster, *J. Am. Chem. Soc.*, **59**, 662 (1937).

7) L. F. Fieser and A. M. Seligman, *J. Am. Chem. Soc.*, **56**, 2690 (1934).

8) D. F. Sangster, "The Chemistry of the Hydroxyl Group," ed by S. Patai, Interscience Publishers (1971), p. 172; R. A. Sheldon and J. K. Kochi, "Metal-Catalyzed Oxidations of Organic Compounds," Academic Press (1981), p. 381.

9) J. Sugita, *Nippon Kagaku Zasshi*, **87**,1082 (1966).

10) H. Mimoun, R. Charpentier, A. Mitschler, J. Fischer, and R. Weiss, *J. Am. Chem. Soc.*, **102**, 1047 (1980).

11) G. Cainelli and G. Cardillo, "Chromium Oxidations in Organic Chemistry," Springer-Verlag (1984), p. 101.

12) M. Matsumoto, H. Kobayashi, and Y. Hotta, *J. Org. Chem.*, **50**, 1766 (1985).

Effect of Pore-Size Distribution on the Catalytic Performance for Coal Liquefaction. II. Carbonaceous and Metallic Deposition on the Catalyst

Hiromichi SHIMADA,* Minoru KURITA, Toshio SATO, Yuji YOSHIMURA, Yoshinori KOBAYASHI, and Akio NISHIJIMA
National Chemical Laboratory for Industry, Yatabe, Ibaraki 305
(Received February 18, 1986)

The behavior of carbonaceous and metallic depositions on catalysts during hydroliquefaction of coal was investigated by using several kinds of catalyst supports with different pore-size distribution values in order to obtain the fundamental data for designing long-life catalysts. Higher concentration of carbonaceous deposition was observed on large-pore and bimodal catalysts than was observed on the comparative small-pore and unimodal catalysts, respectively. However, the carbonaceous deposit was distributed more evenly inside large pores than it was inside small pores. The micropores of the bimodal catalysts were more effectively used than were those of the unimodal catalysts. Thus, the unimodal catalysts with small pores suffered more severe pore-mouth poisoning than the bimodal or the large-pore catalysts. The penetration behavior of the metallic components was found to be different for each metal. Discrete minerals such as clay could not penetrate into the catalyst pores and were deposited on the external surface of the catalyst particle. While, the metallic components coordinated with organic compounds such as phenolates or chelates deposited inside the macro- and mesopores. Easy access of the large asphaltenic molecules to the active sites resulted in high coal-liquefaction activity for the catalyst. This was accompanied by large amounts of both carbonaceous and metallic depositions. It is concluded that large-pore or bimodal pore structure is required for both high liquefaction activity and suppression of pore-mouth poisoning.

In the previous paper,[1] the authors reported that the pore-size distribution of the catalyst support have a great effect on the catalytic activity and selectivity for direct liquefaction of coal. The results are summarized as follows;

1. Catalysts with large pores are more advantageous in the production of asphaltenes (toluene-solubles) from coal than those with small pores.
2. Small pores tend to produce light products such as oils (hexane-solubles).
3. Bimodal catalysts with macroporosity ($r>300$ nm) and microporosity ($r<10$ nm) performed excellently in terms of both total liquefaction and oil production.

Another important catalytic performance required for hydrotreating catalysts, besides activity and selectivity, is long life time, which depends strongly upon carbonaceous deposition and metallic foulants on the catalyst. The recent development of catalysts for hydrotreating petroleum fractions has shown that it is necessary to clarify the behavior of the poisoning materials on the catalyst in order to design a new type of catalyst with longer life.[2-7]

Several investigations have been undertaken on the effects of the pore structure of the catalyst support on its aging behavior during hydroliquefaction of coal[8,9] or hydrotreating of coal-derived liquids.[10,11] They have demonstrated the beneficial effects of increasing pore radius or bimodal pore-size distribution of the catalyst support. As for the behavior of the carbonaceous and metallic foulants on the catalyst, it was found that there was a higher rate of deposition of the foulants during coal liquefaction as compared with petroleum hydroprocessing.

Bertolacini et al.[8] reported that the slowest decline of activity for hydroliquefaction of coal was found for bimodal catalyst with large micropores ($r\approx10$ nm). They indicated that the surface area and pore volume decreased more rapidly for catalysts with small micropores than those with large pores. They also found that carbonaceous deposition caused a shift in micropore-size distribution with time on stream to lower pore diameter. Stiegel et al.[11] reported slower deactivation for catalysts with bimodal pore-size distribution than those with unimodal pores during hydrotreating of coal-derived liquids. They found that the former accumulates larger amounts of metallic foulants than the latter in spite of similar coke concentrations on all of the catalysts. Several researchers have applied electron microprobe (EPMA) analysis to the profiling of metallic components in catalyst particles and have reported different penetrations by the elements.[12-14]

In spite of these efforts, there still remain several questions unresolved concerning the aging behavior of catalysts because of the lack of information about the behavior of the poisoning materials on the catalyst. For example, it is still inclear why bimodal catalysts are much better than unimodal catalysts in terms of aging, although the superiority of the bimodal catalysts in the initial activity could be attributed to the high effective diffusivity.[1,15,16] It is not clear how each metallic foulant behaves on the catalyst and decreases the activity.

In the present paper, the authors aimed to clarify the behavior of foulants on catalysts in order to obtain the fundamental data needed for understanding the

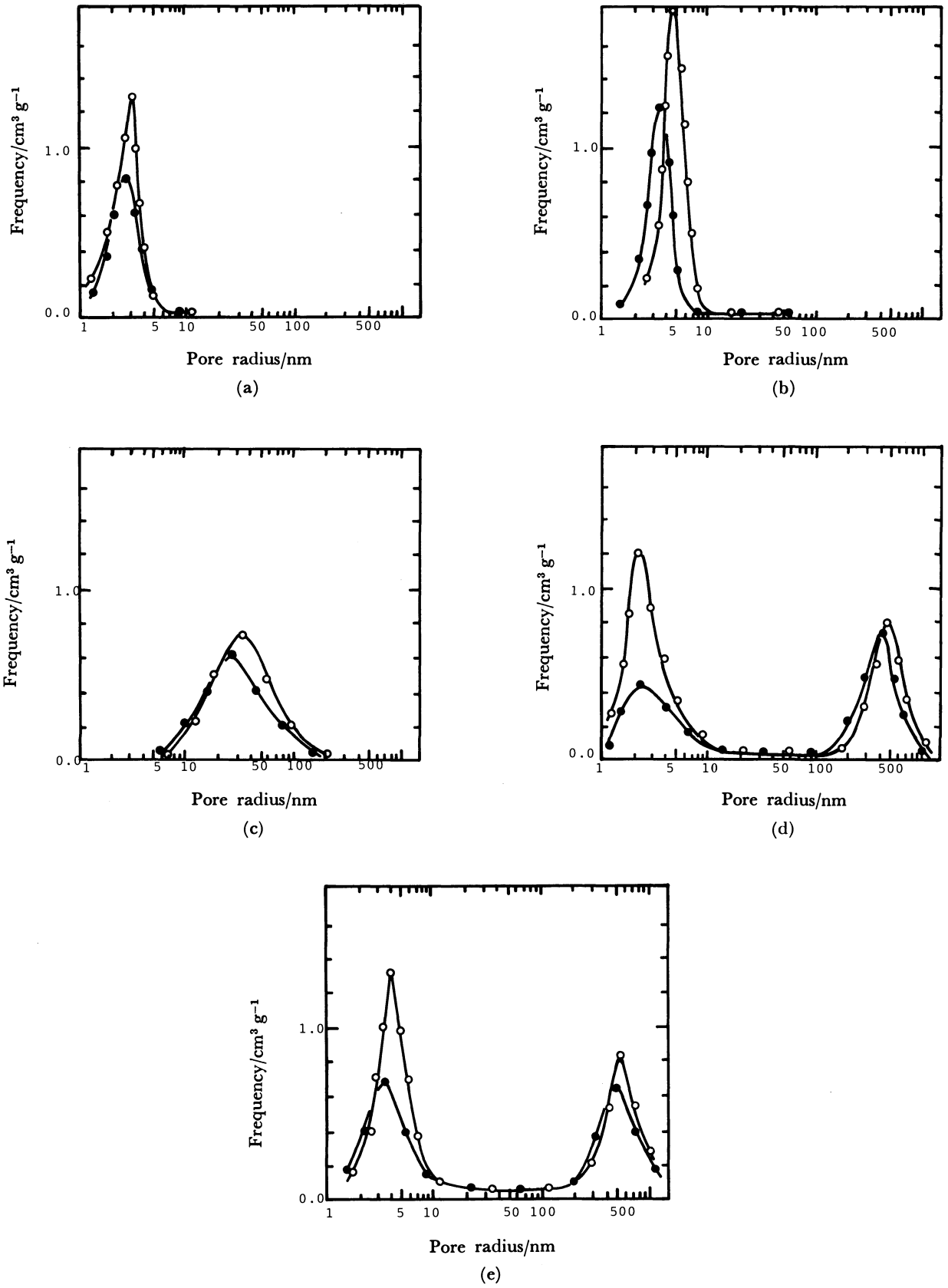

Fig. 1. Changes in pore-size distributions of the catalysts A (a), B (b), C (c), D (d), and E (e).
○: Fresh catalyst, ●: Used catalyst.

aging behavior of catalysts. Emphasis was placed on the effect of the pore structure on the deposition behavior. For this purpose, detailed analysis was carried out on five used catalysts with micro- ($r<10$ nm), meso- ($10<r<100$ nm) and macroporosity ($r>100$ nm) employing new surface analytical techniques such as X-ray photoelectron spectroscopy (XPS) and secondary ion mass spectrometry (SIMS) to investigate the metallic deposit.

Experimental

Catalysts. The molybdenum based catalysts were prepared by impregnation of Al_2O_3 supports (sphere with a diameter of 1.5 mm). The details of the procedures used are described in a previous paper.[3] The physical properties and chemical composition of the freshly prepared catalysts are summarized in Table 1. Pore-size distribution curves for the catalysts are shown in Fig. 1.

Reaction Procedure. The coal used was a subbituminous Taiheiyo coal containing 16.1% ash (dry base). All the reactions were carried out in a 500-cm^3 autoclave with a magnetically-driven stirrer. The reaction conditions are as follows: hydrogen initial pressure (at 27 °C), 9.8 MPa; temperature, 400 °C; time, 2 h. Other details for procedures used are described in the previous paper.[1]

Characterization of the Catalyst. The catalyst used was Soxhlet extracted with tetrahydrofuran for 16 h and dried in vacuo at 300 °C before analysis. Analytical techniques employed in this study of the fresh and used catalysts were as follows.

The carbonaceous deposit on the catalyst was determined by using a CHN analyzer (Yanagimoto, MT-3). A mercury porosimeter (AMINCO, 60000 psi) was used for the determination of the specific surface area, pore volume, and pore-size distribution of the catalyst. The amounts of Fe, Ca, and Ti deposited on the catalysts were measured by an X-ray fluorescence analyzer. An atomic absorption spectrometer was used in the determination of Na and Mg. An X-ray photoelectron spectrometer (XPS, Shimadzu ASIX-1000) with Mg anode (270 w) was used for evaluating the concentration of carbon and metallic elements on the surface of the catalyst particles.

A secondary ion mass spectrometer (SIMS, Hitachi IMA-2) was employed for the depth profiling of each metallic element around the external surface of the used catalyst. All the samples were bomberded by 10-keV O_2^+ ions at a current of about 2×10^{-6} A. A beam of electrons was applied to the sample's surface during analysis to prevent charge build-up.

Table 1. Properties of the Fresh and the Used Catalysts

Catalyst	A	B	C	D	E
Fresh catalyst					
Phase of Al_2O_3[a]	γ	γ	α	γ	γ
S.A.[b]/m^2 g^{-1}	276	211	39	316	261
P.V.[c]/cm^3 g^{-1}	0.37	0.48	0.55	0.76	0.84
MoO_3/wt%	3.4	3.2	2.8	3.5	2.9
Coal conversion activity					
TS[d] yields/%	89.9	93.2	94.4	94.7	95.7
Used catalyst					
Carbonaceous deposition					
Carbon/wt%[e]	6.9	6.7	2.0	10.7	10.1
Carbon/mg m^{-2} [f]	0.25	0.32	0.51	0.34	0.39
Physical properties					
S.A./m^2 g^{-1}	175	199	41	147	180
r(S.A.)[g]	0.63	0.94	1.0	0.47	0.69
P.V./cm^3 g^{-1}	0.26	0.35	0.49	0.55	0.61
r(P.V.)[h]	0.70	0.73	0.89	0.72	0.73

a) Decided by X-ray diffraction. b) Surface area. c) Pore volume. d) Asphaltene and oil (Toluene soluble). e) Calculated basing on the weight of fresh catalyst. f) Calculated basing on the surface area of the fresh catalyst. g) The ratio of the surface area for the used catalyst relative to that of the fresh one. h) The ratio of the pore volume for the used catalyst relative to that of the fresh one.

Results and Discussion

Carbonaceous Materials. Table 1 shows the amount of carbon contained in the carbonaceous materials deposited on the catalyst during coal liquefaction. For unimodal catalysts, the carbon concentration on the surface of the catalyst increased with the pore radius of the catalyst support. This is in agreement with the trend observed for the catalysts used in hydrotreating petroleum residue.[2,4] This trend is attributed to the severe pore-diffusion limitation of the large molecules which cause carbonaceous deposition. It is also shown in Table 1 that carbonaceous materials were deposited in higher concentration on the bimodal catalysts (catalysts D and E) than they were on the unimodal catalysts (catalysts A and B). On the contrary, Stiegel et al.[11] reported that similar concentrations of carbon were deposited on both unimodal and bimodal catalysts during hydrotreating of coal-derived liquids. This discrepancy may be attributed to the difference in pore diffusion between coal and coal-derived liquids.

The changes in physical properties of the catalyst after coal liquefaction are also shown in Table 1. The r(S.A.) values (the ratio of the surface area of the used catalyst to that of the fresh one) increased with the pore radius, showing that the loss in the surface area was greater for small-pore catalysts than for large-pore catalysts. The bimodal catalysts (catalysts D and E) gave smaller r(S.A.) values than did the unimodal catalysts (catalysts A and B), again contrary to the results by Stiegel et al.[11], who reported similar concentration of carbon on both the catalysts. This discrepancy can be partly attributed to the fact that they chose bimodal catalysts with large micropores and unimodal catalysts with small micropores.

Figure 1 clearly shows the changes in pore-size distribution. Small micropores (Fig. 1 (a) and (d))

suffered severe pore plugging, while meso- and macroporosity did not change appreciably. More accumulated carbonaceous deposit was observed on the micropores of the bimodal catalysts than on those of the unimodal catalysts, which is consistent with Table 1.

It is clear that carbonaceous deposition is caused by large asphaltenic molecules, especially those containing heteroatoms such as nitrogen or oxygen.[17] Due to diffusion limitation of the large molecules, an increase in the concentration of the deposit was observed with increasing pore size. On the contrary, the smaller decrease in surface area and pore volume for the former than the latter indicated that the deposits were evenly distributed on the inner surface of large pores, while they localized around the mouth of the small pores (Fig. 2).

In the case of bimodal catalysts, the macroporosity enhanced the diffusion of large molecules into the micropores which are the branches between the macropores. The small pores of unimodal catalysts are narrow and long, while those of bimodal catalysts are connected to macropores, and are shallower (Fig. 2). Thus, the macroporosity caused a higher concentration of carbonaceous deposition on the inner surface of the micropores for the bimodal catalysts.

It has already been shown that most of the carbonaceous deposition on catalysts during the initial stage of a run is by reversibly adsorbed molecules.[2,18] Therefore, high concentrations of reversibly adsorbed carbonaceous deposits on bimodal or large-pore catalysts during the initial stage of a run occurs on the inner surface of the catalyst and does not necessarily result in rapid deactivation of the catalyst. In fact, high total conversion was given over the large-pore catalyst, C, and the bimodal catalysts, D and E, (Table 1). It is apparent that the unimodal catalysts with microporosity suffered the most severe pore-mouth poisoning. It is important to prevent the production of inactive coke on the catalyst in order to reduce the deactivation rate of the catalyst. High pore diffusion may play an important role in the suppression of this production.

Metallic Foulants. Table 2 shows the amount of metallic foulants on the catalyst during coal liquefaction. In the table, the total amount deposited on each catalyst (5 g) is given. For each metallic component, the amount deposited increased with the pore radius of the catalyst support. The tendency was quite evident for Ca and Ti, but not as clear for Na.

Comparison of the amount of metal deposited on the catalyst with the total amount in coal showed that Ti and Mg were deposited on the large-pore catalysts preferentially. Little Si was deposited on the catalyst, although it was the most abundant metallic element in coal.

Table 3 shows the concentration, by XPS, of each metallic component on the external surface of the

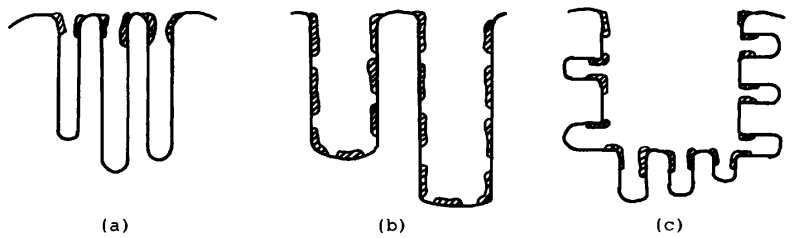

Fig. 2. Schematic diagram of pore structure of catalyst support and deposition behavior of carbonaceous materials (a): Small-pore catalyst (b): Large-pore catalyst (c): Bimodal catalyst ▨: Carbonaceous materials.

Table 2. Deposited Metals[a] on the Used Catalysts

Catalyst	A	B	C	D	E	Coal ash[b]
P.R.[c]/nm	2.5	4.5	30	2.5, 350	4.5, 450	
Na_2O/mg	12	11	14	18	23	155
MgO/mg	4	3	9	11	14	61
CaO/mg	3	4	15	13	16	540
TiO_2/mg	1	4	7	11	17	83
Fe_2O_3/mg	5	7	13	16	17	500

a) The total amount deposited on all the catalyst (5 g). b) The total amount contained in the coal (60 g). Other major components are SiO_2 (6300 mg), Al_2O_3 (2000 mg), and K_2O (61 mg). The amount of SiO_2 and Al_2O_3 on the used catalyst could not be determined because they are the components of the fresh catalysts. The amount of K_2O was too little to be determined. c) Most probable pore radius.

catalyst. For all of the catalysts the XPS analysis gave a much higher concentration for each of the metallic foulants than was obtained by chemical analysis. It should be emphasized that very high concentrations of Ca, Ti, and Si were observed on the external surface layer, even for the small-pore catalysts (catalysts A and B), in spite of there being relatively little deposition through the entire catalyst particle.

The authors utilized a secondary ion mass spectrometer (SIMS) to investigate the penetration behavior of metallic foulants into the inner part of catalyst particles.[19,20] SIMS analysis gave more detailed information on the profiling around the external surface of the particle as compared with EPMA. Figure 3 shows the depth-profile curves measured by SIMS. The ordinate, $I_{M\,cor}$ (corrected intensity for element M), is given by :

$$I_{M\,cor}(t) = \frac{I_M(t)/I_{Al}(t)}{I_M(0)/I_{Al}(0)},$$

Where $I_M(t)$ is the observed intensity for element M at sputtering time, t. The abscissa, sputtering time, is proportional to the depth from the external surface layer of the catalyst particle.

Figure 3 clearly displays the difference in the behavior between the metallic elements. In the case of the small-pore catalyst A, Na showed much greater penetration than other elements. On the other hand, in the catalyst E with micro- and macropores, Ca, Mg, Ti, and Fe penetrated more deeply into the inner part of the catalyst particle than Na. For both catalysts, the profiles of Si and K decreased rapidly. Na could even penetrate into the catalyst particles having no large pores, while Ca, Ti, Fe, and Mg could not enter small pores. Si and K could not intrude even into large pores.

Table 3. Deposited Metals on the External Surface of the Catalyst Sphere[a)]

Catalyst	A	B	C	D	E
Na_2O/wt%	3.7	3.0	3.9	3.0	3.9
CaO/wt%	1.8	1.7	1.9	1.4	1.9
TiO_2/wt%	3.6	4.3	4.0	5.4	4.9
Fe_2O_3/wt%	4.5	3.3	4.9	3.0	2.1
SiO_2/wt%	23.	39.	18.	15.	34.

a) The determination was carried out by using XPS. And calculated basing on the measured area of the spectra and cross section given by Scofield.[21]

The above data, Tables 2, 3, and Fig. 3, clearly indicated that the metallic deposition behavior is quite different for each metal. The behavior of each metallic component is dependent upon its coordination which affects its effective particle size and its interaction with the catalyst. The metallic components can be classified into two categories.[22] The first is as mineral matter present as discrete particles such as pyrite, quartz, and other clay minerals. The second is as organic matter which can be classified into two subcategories. One consists of inorganic salts of organic acids and the other as organic chelates.

The results indicate that most of the silicon in the coal occurs in the minerals, such as quartz, calcite, or kaolinite which could be observed as crystalline materials by X-ray diffraction. The particle size of the minerals is larger than the pore mouth of the macropores. High concentrations of Si on the external surface of the catalyst particles (Table 3) indicate the "filtration" of the minerals by the surface of the catalyst. It is inferred that most of the potassium occurs in the minerals also. This is in agreement with the results obtained by Gorin[22] which indicated that K is an exception among alkali and alkaline earth metals.

Other elements, at least in part, will be associated with the organic matter. The major portion of the

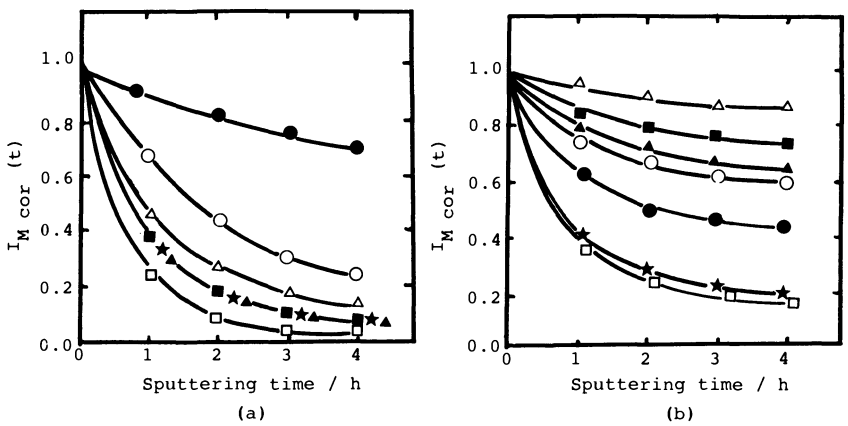

Fig. 3. Depth profiles of metal elements for the catalyst A (a) and the catalyst E (b).
●: Na, ○: Fe, △: Ca, ■: Mg, ★: Si, ▲: Ti, □: K.

alkali and alkaline earth metals in coal are present as inorganic salts of organic acids. The low pore-diffusion limitation seen for Na suggests that it is present as inorganic salts of low molecular weight organic acids such as phenols. Na from these phenolates was probably exchanged for protons from the acidic sites of the catalyst during deposition.

The next deepest penetration into the small-pore catalysts was observed for Fe (Fig. 3), which is consistent with the results in Table 2 that showed Fe was the second most abundant metallic foulant on small-pore catalysts. While, the ratio of the deposited amount to the total amount in coal was very low (Table 2). These results suggest that most of the iron is in the form of inorganic minerals, but that some of the iron is present in a small molecular weight component which can penetrate into catalyst pores. It cannot be excluded that a part of the iron is present as fine particles of minerals such as pyrite.

The low pore diffusion found for Mg and Ca indicated that these metals are present in large asphaltenic molecules, such as humates. Ca was deposited in a lower amount on the catalyst relative to the total amount in coal as compared with Mg (Table 2). This indicates that some of the Ca is present in minerals. The deposition behavior of Ti resembled that of Mg, indicating the presence of organotitanium chelate compounds.[22-24]

Inorganic minerals are deposited on the external surface of the catalyst, which causes pore-mouth poisoning. More rapid deactivation of small particle size catalysts[9] can be attributed to this poisoning. Macroporosity of bimodal catalysts enhances the diffusion of large asphaltenic molecules into micropores, while it prevents the access of the minerals to the inner surface of the catalyst particle. The deposition of metals coordinated with organic compounds was caused by the decomposition of the organic matter. In fact, higher rate of metal deposition in the large-pore (catalyst C) or the bimodal (catalysts D and E) catalysts was accompanied by high coal-liquefaction activity of the catalyst (Table 1). As a consequence, it may be impossible to suppress the deposition without decreasing coal liquefaction activity. Therefore, high resistance against metallic deposition is required for catalysts with high activity and long life time.

As has been described above, the pore-size distribution greatly affects the deposition behavior of carbonaceous and metallic materials. On the large-pore and the bimodal catalysts, higher rates of deposition were observed than that found for the small-pore and the unimodal catalysts, respectively. However, deposition (except that due to inorganic minerals) results from the effective use of the inner surface of the catalyst which leads to high coal liquefaction activity. It was also found that large-pore or bimodal catalysts are more advantageous than microporous unimodal catalysts from the view point of pore-mouth poisoning.

References

1) H. Shimada, M. Kurita, T. Sato, Y. Yoshimura, T. Kawakami, S. Yoshitomi, and A. Nishijima, *Bull. Chem. Soc. Jpn.*, **57**, 2000 (1984).

2) H. Beuther, O. A. Larson, and A. J. Perrotta, "The Mechanism of Coke Formation on Catalysts," in "Catalyst Deactivation," ed by B. Delmon and G. F. Froment, Elsevier, Amsterdam (1980), pp. 271—282.

3) S. T. Sie, "Catalyst Deactivation by Poisoning and Pore Plugging in Petroleum Processing," in "Catalyst Deactivation," ed by B. Delmon and G. F. Froment, Elsevier, Amsterdam (1980), pp. 545—569.

4) O. Togari, H. Takahashi, and M. Nakamura, *Sekiyu Gakkaishi*, **23**, 256 (1980).

5) M. Nakamura, O. Togari, and T. Ono, Proc. Pan-Pasific Synfuels Conference, Tokyo, (1982), E-9.

6) K. Nomura, Y. Sekido, and Y. Ohguchi, *Sekiyu Gakkai Shi.*, **23**, 321 (1980).

7) K. Nomura, Y. Sekido, and Y. Ohguchi, *Sekiyu Gakkai Shi* **24**, 253 (1981).

8) R. J. BertoLacini, L. C. Gutberlet, D. K. Kim, and K. K. Robinson, EPRI Report AF-1084 (1979).

9) L. M. Polinski, G. J. Stiegel, and R. E. Tischer, "1980 Status Review-Hydroliquefaction of Coal with Supported Catalysts," DOE/PETC/TR-81/2 (1981).

10) Y. Yoshimura, M. Kurita, T. Sato, H. Shimada, and A. Nishijima, *Kagaku Kogaku Ronbunshu*, **11**, 238 (1985).

11) G. J. Stiegel, R. E. Tiscer, and L. M. Polinski, *Ind. Eng. Chem., Prod. Res. Dev.*, **22**, 411 (1983).

12) J. J. Stanulonis, B. C. Gates, and J. H. Olson, *AIChE. J.*, **22**, 576 (1978).

13) T. L. Cable and F. E. Massoth, *Fuel Processing Technol.*, **4**, 265 (1981).

14) G. B. Freeman, B. D. Adkins, M. J. Moniz, and B. H. Davis, *Applied Catalysis*, **15**, 49 (1985).

15) L. M. Polinski, G. J. Stiegel, and L. Saroff, *Ind. Eng. Chem., Proc. Des. Dev.*, **21**, 477 (1982).

16) P. N. Ho and S. W. Weller, *Fuel Processing Technol.*, **4**, 21 (1981).

17) E. Furimsky, *Fuel Processing Technol.*, **6**, 1 (1982).

18) M. Ternan, E. Furimsky, and G. I. Parsons, *Fuel Processing Technol.*, **2**, 45 (1979).

19) H. Shimada, M. Kurita, T. Sato, Y. Kobayashi, Y. Yoshimura, and A. Nishijima, *Chem. Lett.*, **1983**, 181.

20) H. Shimada, Y. Kobayashi, M. Kurita, T. Sato, Y. Yoshimura, and A. Nishijima, Proc. 4th Int. Conf. on Secondary Ion Mass Spectrometry, Osaka (1983), p. 283.

21) J. H. Scofield, *J. Electron Spectrosc. Relat. Phenom.*, **8**, 129 (1976).

22) E. Gorin, "Fundamentals of Coal Liquefaction," in "Chemistry of Coal Utilization Second Supplementary Volume," ed by M. A. Elliot, John Wiley & Sons, New York (1981), p. 1904.

23) A. Robbat, Jr., D. H. Finseth, and R. G. Lett, *Fuel*, **63**, 1710 (1984).

24) R. Campo, H. J. Callot, P. Albrecht, and J. P. Kintzinger, *Tetrahedron Lett.*, **25**, 24 (1984).

A ^{14}N NMR Relaxation Study of Aqueous Alkyltrimethylammonium Salt Solutions

Yuhei Uzu,* Jiro Nakagawa, and Masatoki Yokoi
Department of Chemistry, Faculty of Science, Shinshu University,
Asahi, Matsumoto 390
(Received March 13, 1986)

Synopsis. ^{14}N spin-lattice and spin-spin relaxation times were measured in a series of alkyltrimethylammonium salts at higher concentrations above the critical micell concentration. Octyltrimethylammonium bromide and dodecyltrimethylammonium chloride form spherical micelles at all concentrations, while decyl- and dodecyltrimethylammonium bromides form larger and rodlike micelles such as the hexadecyltrimethylammonium bromide suggested previously.

The transition of the shape of micelles in aqueous solutions is known to occur for various surfactants. In connection with this phenomenon, a change from spherical to rodlike micelles at higher concentrations has, also, been observed by macroscopic techniques, such as light scattering, viscosity and electron microscopic observation etc.[1-3] The significance of the spectroscopic work is evident for the dynamical study of the micellar phenomenon at the molecular level. Here, nuclear magnetic resonance (NMR) is a very powerful tool; thus, that many ^{1}H, $^{2}H(D)$, and ^{13}C studies have been reported in this field.[4-6] It has been shown that the longitudinal relaxation time, T_1, and the transverse relaxation time, T_2, can give information about the intensity of molecular motions. The time scale of the molecular motions is usually characterized by the parameter τ_c, the rotational correlation time. Recently, a study of ^{14}N relaxation times, T_1 and T_2, of hexadecyltrimethylammonium bromide (CTAB) and chloride (CTAC) micellar solutions has been reported by Henriksson et al.,[7] suggesting a change from spherical to rodlike form for the CTAB micellar shape.

With the aim of further documenting changes in the micellar shape, we have undertaken a systematic study of a series of alkyltrimethylammonium systems using the applicability of ^{14}N NMH.

The surfactants used in this study were alkyltrimethylammonium bromides with 8, 10, and 12 carbon atoms in the aliphatic chain, and dodecyltrimethylammonium chloride (DTAC). Dodecyltrimethylammonium bromide (DTAB), decyltrimethylammonium bromide (DeTAB) and DTAC were supplied from Kanto Chemical Inc. and purified through several recrystallizations from an ethanol-ether mixture. Octyltrimethylammonium bromide (OTAB) was synthesized by reacting equimolar quantities of trimethylamine and octyl bromide in ethanol at −3 °C for 5 d. As a check of the purity of the surfactants, cmc determinations were performed by means of a surface-tension method; the cmc's agreed closely with those values from the literature.[8] Deuterium oxide was used without further purification. ^{14}N relaxation times were measured at 6.42 MHz by a JEOL-FX90QFT NMR. The experimental temperature was 27 °C. Its reliability was monitored by the alternative insertion of a thermister into the sample position; the temperature was found to be ±0.5 °C. Spectra were recorded in the FT mode and T_1 was obtained by the 180°—τ—90° pulse sequence. T_2 was calculated from the half-width of the absorption signal in the fourier transform spectrum using the relation $(\pi\ T_2)^{-1}=\Delta\nu-\Delta\nu_{inhom}$, where $\Delta\nu$ is the experimental line width and $\Delta\nu_{inhom}$ is the contribution to the line width from magnetic field inhomogeneities. $\Delta\nu_{inhom}$ was determined from the spectrum of an aqueous solution of ammonium nitrate, which has a negligible contribution to the line width from relaxation.

The observed ^{14}N relaxation times, T_1 and T_2, for several alkyltrimethylammonium bromides are plotted in Fig. 1 as functions of the surfactant concentration. For a comparison, the result at 28.5 °C for CTAB reported by Henriksson et al.[7] is also given in the Fig. 1. All measurements obtained here have been performed at concentrations well above the cmc. When the concentration is increased, there is a gradual decrease in the relaxation times, and both T_1 and T_2 values initially have the same values, as are those for normal micellar solutions which extreme narrowing condition is fulfilled. At higher concentrations, T_2 still continues to decrease with increasing concentration, while T_1 becomes rather larger compared with T_2; consequently, T_1 differs from T_2, except for OTAB. For DTAB, a broader minimum in T_1 was

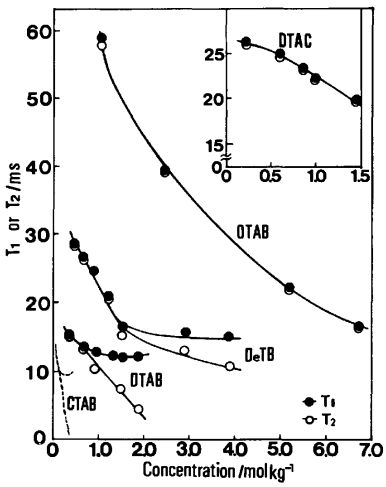

Fig. 1. ^{14}N relaxation times T_1 and T_2 vs. concentration at 27 °C for various surfactants. For comparison, the result for CTAB at 28.5 °C by Henriksson et al.[7] is included as the dashed curve.

also observed at $c \approx 1.5$ mol kg^{-1}, just as that for CTAB.[7] In such a case, it was suggested that the rotational motion about the principal axis of the electric field gradient at the nitrogen nucleus, the N-C$_\alpha$ bond, would not be described by a single correlation time based upon the rotational motion of isotropically reorienting molecule. Henriksson et al.[7] explained this observation by assuming that two kinds of molecular motions are effective for the relaxation. One is a local fast anisotropic motion of the molecule and the other is a slower motion over a distance of the order of micellar dimensions. For the fast motion which makes approximately constant contribution to the relaxation, the correlation time is $\tau_c^f = 4.5 \times 10^{-10}$ s at 27 °C in DTAB micelles.[9] On the other hand, the correlation time for the slow motion, τ_c^s, increases rapidly with the concentration.[7] This can be regarded as the slow motion that is tied to the distribution of aggregation numbers of the micelles, implying that the overall motion becomes more important for the relaxation. The calculation with τ_c^s value in DTAB micelles gives approximately 1.53×10^{-8} s[9] at $c = 1.5$ mol kg^{-1}, which is obviously much larger than τ_c^f. These values are of similar magnitude to those calculated for CTAB micelles by Henriksson et al., indicating that the same types of larger micelles are present in both systems. As the alkyl chain length is shortened, the discontinuous change tends to be shifted to the higher-concentration region and the relaxation times become larger. At the same time, it is suggested that T_1 gradually approaches T_2.

On the other hand, the relaxation behavior for OTAB seems to be different from the other surfactants and $T_1 = T_2$ holds throughout the concentration range examined. The differences in micellar size and shape would bring about a different relaxation behavior. This result is certainly expected since the concentrated solution of OTAB consists of spherical micelles.[2] Also, the behavior in aqueous solutions of DTAB and DTAC in Fig. 1 is found to be quite different and the relaxation times are about twice as long for the DTAC as for the DTAB solutions. The most likely explanation is that bromide ions can lower the electrostatic repulsion between the cationic head groups in the DTAB micelles and make a closer packing and tighter binding of the surfactant molecules on the micellar surface.[7] This seems to be caused by a phase change in the molecular packing accompanied by a phenomenon similar to that of the transition from spherical to rod-shaped micelles at high concentrations. In analogy with the above discussion, no change in the micellar shape occurs with DTAC and the micelles tend to remain spherical over all the concentration range, as already noted by Ozeki and Ikeda.[11] Accordingly, these results can be best explained by the occurrence of both rodlike (in which $T_2 < T_1$) and spherical (in which $T_1 = T_2$) micelles.

References

1) S. Ozeki and S. Ikeda, *J. Colloid Interface Sci.*, **87**, 424 (1982).
2) P. Ekwall, L. Mandell, and P. Solyom, *J. Colloid Interface Sci.*, **35**, 519 (1971).
3) T. Imae, R. Kamiya, and S. Ikeda, *J. Colloid Interface Sci.*, **108**, 215 (1985).
4) J. Clifford, *Trans. Faraday Soc.*, **61**, 1276 (1965).
5) E. Williams, B. Sears, A. Allerhand, and E. H. Cordes, *J. Am. Chem. Soc.*, **95**, 4871 (1973).
6) J. Ulimius, B. Lindman, G. Lindblom, and T. Drakenberg, *J. Colloid Interface Sci.*, **65**, 88 (1978).
7) U. Henriksson, L. Odberg, J. C. Eriksson, and L. Westman, *J. Phys. Chem.*, **81**, 76 (1977).
8) P. Mukerjee, K. J. Mysels, "Critical Micelle Concentration of Aqueous Surfactant Systems," Nat. Stand. Ref. Data Series, Nat. Bur. Stand. (U.S) Feb., 1961.
9) Following Henriksson et al.,[7] τ_c^f and τ_c^s were calculated from the modified relations, $1/T_1$ and $1/T_2$, for the nuclear quadrupole relaxation.[10]
10) A. Abragam, "The Principles of Nuclear Magnetism," Oxford University Press, Oxford (1961).
11) S. Ozeki and S. Ikeda, *Bull. Chem. Soc. Jpn.*, **54** 552 (1981).

The Magnetic Properties of the Copper(II) Compounds with 3- and 4-Piperidinecarboxylic Acids

Shuji EMORI,* Nobuhide MORISHITA, and Yoneichiro MUTO
Department of Chemistry, Faculty of Science and Engineering, Saga University, Honjo-machi, Saga 840
(Received March 20, 1986)

Synopsis. Compounds of formula $[CuX_2(C_5H_{11}NCOO)_2]\cdot 3H_2O$ (X=NO_3, Cl, Br), $[Cu(NO_3)_2(C_5H_{11}NCOO)_2]\cdot 2(NH_2)_2CO$, and $Cu[(CH_3)_2CHCOO]_2\cdot(NH_2)_2$ CO have been prepared. The correlation of their magnetic properties with the pK_a values of their parent carboxylic acids is discussed.

A recent X-ray study[1] of a compound formed by the reaction of copper(II) nitrate with β-alanine has shown that four 3-ammoniopropionates bridge two copper(II) ions, forming a dimeric structure similar to that of copper(II) acetate monohydrate.[2,3] Previously, we also found that dinuclear copper(II) ω-ammonio carboxylates were obtained during a treatment of ω-amino carboxylic acids with copper(II) halides.[4] Since there still remain unclear points about the influence of a carboxylato substituent on the magnetic properties of dinuclear copper(II) carboxylates,[5] these ammonio carboxylates seem to be appropriate for studying the substitution effects. Then, as a continuation of our studies, we have prepared several new copper(II) compounds with 3- and 4-piperidinecarboxylic acids (nipecotic and isonipecotic acids) and examined the relation between their magnetic properties and the pK_a values of their parent acids. For the sake of discussion, the urea adduct of copper(II) isobutyrate was also prepared.

Compounds with a stoichiometry of $[CuX_2(C_5H_{11}NCOO)_2]\cdot 3H_2O$ (X=NO_3, Cl, Br) were prepared by a previously described method for copper(II) ω-amino carboxylates.[4] The urea adducts, $[Cu(NO_3)_2(C_5H_{11}NCOO)_2]\cdot 2(NH_2)_2CO$ and $Cu[(CH_3)_2CHCOO]_2\cdot(NH_2)_2CO$, were prepared according to the reported general procedure.[6]

The IR spectra of the copper(II) piperidinecarboxylate show bands near 1585—1593 cm^{-1} connected with NH_2^+ deformations[7] in addition to the characteristic bands in the ranges of 1430—1450 and 1600—1660 cm^{-1} connected with symmetric and unsymmetric COO stretching vibrations of the carboxyl groups.[8]

The effective magnetic moments (Table 1) were evaluated from the room-temperature magnetic susceptibilities, which were corrected for the diamagnetic contribution of constituent atoms using Pascal constants[9] and $N\alpha=60\times10^{-6}$ emu mol^{-1} (1 emu=$4\pi\times10^{-6}$ m^3). The temperature dependence of the magnetic susceptibilities (80—300 K) of $[Cu(NO_3)_2(3\text{-}C_5H_{11}NCOO)_2]\cdot 3H_2O$, $[Cu(NO_3)_2(4\text{-}C_5H_{11}NCOO)_2]\cdot 3H_2O$, and $Cu[(CH_3)_2CHCOO]_2\cdot(NH_2)_2CO$ were measured. The results agreed well with the Bleaney-Bowers equation,[10] using the following parameters: $g=2.13$ and $2J=-314$ cm^{-1}, $g=2.14$ and $2J=-330$ cm^{-1}, and $g=2.18$ and $2J=-342$ cm^{-1} for the compounds with 3- and 4-piperidinecarboxylic acids and isobutyric acid, respectively, indicating the presence of a dinuclear unit, which contains four zwitterionic (piperidinio)formate ($C_5H_9NH_2^+$–COO^-) bridges between the copper(II) ions similarly to copper(II) acetate monohydrate.

For dimers with this type of structure, it has been pointed out that the magnitude of a superexchange interaction through carboxylato bridging groups is inversely related to the basicity of the bridging group, as measured by the pK_a value of its parent acid.[11] In a previous study of copper(II) (substituted propionate)s, we found that this trend was maintained for a series of copper(II) ω-ammonio carboxylates.[4] In the present study, the bridging groups were substituted isobutyrate ligands and the pK_a values of the parent acids

Table 1. Analytical Data and Effective Magnetic Moments at 20 °C

Compound	Found(Calcd)/%					μ_{eff}/BM
	Cu	X	H	C	N	
$[Cu(NO_3)_2(3\text{-}C_5H_{11}NCOO)_2]\cdot 3H_2O$	12.78		5.63	29.06	11.29	1.37
	(12.71)		(5.65)	(28.83)	(11.21)	
$[CuCl_2(3\text{-}C_5H_{11}NCOO)_2]\cdot 3H_2O$	14.15	16.18	5.97	32.47	6.25	1.32
	(14.22)	(15.87)	(6.32)	(32.26)	(6.27)	
$[Cu(NO_3)_2(4\text{-}C_5H_{11}NCOO)_2]\cdot 3H_2O$	12.82		5.59	28.94	11.24	1.34
	(12.71)		(5.65)	(28.83)	(11.21)	
$[Cu(NO_3)_2(4\text{-}C_5H_{11}NCOO)_2]\cdot 2(NH_2)_2CO$	11.31		5.36	29.61	19.66	1.37
	(11.23)		(5.34)	(29.71)	(19.80)	
$[CuBr_2(4\text{-}C_5H_{11}NCOO)_2]\cdot 3H_2O$	11.82	29.51	5.12	26.90	5.19	1.31
	(11.86)	(29.83)	(5.27)	(26.90)	(5.23)	
$Cu[(CH_3)_2CHCOO]_2\cdot(NH_2)_2CO$	21.11		6.08	35.77	10.22	1.33
	(21.34)		(6.09)	(36.30)	(9.41)	

varied from 3.53 and 4.03 (estimated from the Branch–Calvin equation[12]) for 3- and 4-piperidinecarboxylic acids to 4.63 for isobutyric acid. The singlet-triplet separation value ($-2J$) of $[Cu(NO_3)_2(4\text{-}C_5H_{11}NCOO)_2]\cdot 3H_2O$ ($330cm^{-1}$) is larger than that of $[Cu(NO_3)_2(3\text{-}C_5H_{11}NCOO)_2]\cdot 3H_2O$ ($314\,cm^{-1}$), and also the magnetic moment of $[Cu(NO_3)_2(4\text{-}C_5H_{11}NCOO)_2]\cdot 2(NH_2)_2CO$ (1.37 BM) is larger than that of $Cu[(CH_3)_2CHCOO]_2\cdot(NH_2)_2CO$ (1.33 BM). Therefore, the order for the extent of an antiferromagnetic interaction between the two copper(II) ions is isobutyrate>4-piperidinecarboxylate>3-piperidinecarboxylate, indicating that the magnetic interaction in the series of copper(II) dialkylacetates also tends to decrease as the acid strength of the parent acid becomes stronger.

References

1) M. E. Kamwaya, E. Papavinasam, and S. G. Jeoh, *Acta Crystallogr.*, **C40**, 2043 (1984).
2) J. N. van Niekerk and F. R. L. Schoening. *Acta Crystallogr.*, **6**, 227 (1953).
3) G. M. Brown and R. Chidambaram, *Acta Crystallogr. Sect. B*, **29**, 2393 (1973).
4) S. Emori, T. Noguchi, and Y. Muto, *Bull. Chem. Soc. Jpn.*, **58**, 2733 (1985).
5) Y. Muto, A. Sasaki, T. Tokii, and M. Nakashima, *Bull. Chem. Soc. Jpn.*, **58**, 2572 (1985).
6) M. Kishita, M. Inoue, and M. Kubo, *Inorg. Chem.*, **3**, 237 (1964).
7) L. J. Bellamy, "The Infrared Spectra of Complex Molecules," 3rd ed., Chapman and Hall (1975).
8) S. Yamada, H. R. Nakamura, and R. Tsuchida, *Bull. Chem. Soc. Jpn.*, **31**, 303 (1958).
9) G. Foex, "Constants Sélectionées, Diamagnétisme et Paramagnétisme," Masson, Paris (1957).
10) J. Lewis, Y. C. Lin, L. K. Royston, and R. C. Thomson, *J. Chem. Soc.*, **1965**, 1171.
11) R. W. Jotham, S. F. A. Kettle, and J. A. Marks, *J. Chem. Soc., Dalton Trans.*, **1972**, 428.
12) G. E. K. Branch and M. Calvin, "The Theory of Organic Chemistry," Prentice-Hall, Inc., New York (1941).

Activation Analysis of Oxygen in SnO_2 and Zn_2SnO_4 Crystals

Ryoichi YOSHIDA, Yoshihisa HASEGAWA, Iwao YAMAI,† Kohei KODAIRA,*,†† and Toru MATSUSHITA††
Government Industrial Development Laboratory, Hokkaido, Sapporo 061-01
†Ceramic Engineering Research Laboratory, Nagoya Institute of Technology, Tajimi 507
††Department of Applied Chemistry, Faculty of Engineering, Hokkaido University, Sapporo 060
(Received March 26, 1986)

Synopsis. Oxygen content of SnO_2 and Zn_2SnO_4 crystals grown by the vapor phase method was determined by 14 MeV neutron activation analysis. The oxygen contents in the crystals were a little smaller than the theoretical values. The oxygen deficiency in the crystals was found to be related to their inherent semiconductive properties and density.

Many oxides show a semiconductive property originating in the deviation of oxygen from stoichiometry. The authors have already reported on the growth of SnO_2,[1-3] ZnO,[4] and Zn_2SnO_4[5] crystals by the vapor phase method. There is a possible of oxygen deficiency in these crystals because they grew with high growth rate. Therefore, informations on the deviation of oxygen from stoichiometry is important to understand their properties.

Activation analysis has been applied to the determination of the oxygen contents in many organic or inorganic compounds.[6-10] However, its application of oxygen analysis to oxide single crystals is quite a few.

In the present paper, the determination of oxygen contents in SnO_2 and Zn_2SnO_4 crystals was carried out by activation analysis.

Experimental

Samples used in this study were SnO_2 (with/without additives), and Zn_2SnO_4 crystals grown at 1300 °C for 2 hours in porcelain crucible by the vapor phase method. The SnO_2 crystals were obtained from the mixture of SnO_2 and Sn powders, and the Zn_2SnO_4 were also from ZnO and Sn powders. SnO_2 powder (chemical reagent) and ZnO_2 powder (special reagent) were used as reference sample. Sample (ca. 0.1 g) and graphite powder (reagent for spectroscopy, ca. 2.7 g) were mixed sufficiently. The pellets (1.25 cm×1 cm) of the mixed sample were sealed in cylindrical polyethylene containers of 1.5 cm×2 cm. The containers containing samples were transferred from the position of the sample charger to the target area with a pneumatic tube. Samples in the containers were bombarded with 14 MeV neutron with 5×10^9 n s^{-1} of neutron intensity for 30 second at target area. After being bombarded, the containers were transferred to a 4.44 cm×5 cm sodium iodide well-type detector with a pneumatic tube to measure the 6.13 MeV γ-ray from 7.35 sec-halflife ^{16}N produced by the reaction of $^{16}O(n,p)^{16}N$. A neutron generator (by Toshiba Co. Ltd) accelerates deuterium ion to generate 14 MeV neutron by the $^3T(d,n)^4He$ reaction: $^3_1T+^2_1d\rightarrow^4_2He+^1_0n+17.59$ (MeV). As a standard sample for calibration, sucrose (guaranteed reagent) was used. The calibration curve on the basis of sucrose-graphite standard sample shows a good linearity in the range of 0 mg to 26.0 mg of oxygen.

Results and Discussion

Table 1 shows the average values on measurements of 3 to 4 times. The values of SnO_2 powder and ZrO_2 powder as reference samples show close agreement with their theoretical values. The values of undoped, antimony-doped and chromium-doped SnO_2 crystals were of the same value, 20.9%. There are no significant differences between the theoretical and the measured values within experimental errors. The oxygen contents is nearly theoretical value. On the other hand, that of vanadium-doped SnO_2 crystals showed clearly a smaller value, 19.9%, than the three others. The density of V-doped crystals was between 5.4 and 5.8. The values were smaller than 6.15 for undoped SnO_2 crystals and 6.12—6.29 for Sb-doped crystals grown at the same vapor phase method. The electrical resistivitiy of the crystals along the growth direction of an a-axis showed semiconductivity at temperatures from 150° to 400 °C. Accordingly, the semiconductive property of V-doped SnO_2 crystals will be due to oxygen defect.[2]

In regards to Zn_2SnO_4 crystals grown under the same conditions, dendrite crystals grown in the initial stage of reaction contain somewhat lower oxygen (19.3%) than that (19.6%) of needle crystals grown in the latter stage of reaction. Both Zn_2SnO_4 crystals showed a lower oxygen content than the theoretical value (20.4%). The electrical resistivity of the needle crystals along growth direction was about 10^3—10^4 ohm cm at room temperature.

On a survey of analytical results, the values of oxygen contents in the vanadium-doped SnO_2 and Zn_2SnO_4 crystals were somewhat smaller than the theoretical values, though antimony-doped and

Table 1. Oxygen Content in SnO_2 and Zn_2SnO_4 Crystals by 14 MeV Newtron Activation Analysis

Crystals	Radiated sample Irradiated /mg	Oxygen content %	Theoretical value/%
SnO_2 powder	80.7	21.0	21.2
ZrO_2 powder	82.6	26.1	26.0
SnO_2	83.7	20.9	21.2
Sb-doped SnO_2	93.9	20.9	21.2
V-doped SnO_2	95.7	19.9	21.2
Cr-doped SnO_2	87.4	20.9	21.2
Zn_2SnO_4(needle)	87.1	19.6	20.4
Zn_2SnO_4(dendrite)	89.8	19.3	20.4

chromium-doped ones had nearly theoretical value. Accordingly, the crystals with low oxygen contents used in the present experiments will have an oxygen deficiency leading to semiconductivity.

References

1) T. Matsushita and I. Yamai, *Nippon Kagaku Kaishi*, **1974**, 1893.
2) R. Yoshida, Y. Yoshida, J. Saito, Y. Yamada, K. Kodaira, T. Matsushita, and I. Yamai, *J. Mater. Sci. Lett.*, **2**, 741 (1983).
3) T. Matsushita, Y. Yamai, K. Kodaira, J. Saito, and R. Yoshida, "Bull. Facul. Eng., Hokkaido University," No. 122, 41 (1984).
4) K. Kodaira, T. Matsushita, J. Saito, and R. Yoshida, *Chem. Lett.*, **1975**, 589.
5) R. Yoshida, Y. Yoshida, I. Yamai, K. Kodaira, and T. Matsushita, *J. Cryst. Growth*, **36**, 181 (1976).
6) I. Fujii, H. Muto, K. Ogawa, and T. Tani, *J. Atom. Energ. Soc, Jpn*, **5**, 455 (1963).
7) K. Yabe, S. Ueda, Y. Hasegawa, and T. Sato, *Radioisotopes*, **21**, 80 (1972).
8) M. Chiba and T. Ando, *Bunseki Kagaku*, **31**, 294 (1982).
9) T. Nagashima, M. Kamo, H. Tanaka, and Y. Inomata, *Yogyo Kyokai Shi*, **88**, 511 (1980).
10) H. Ishikawa, M. Nakane, and Y. Miyake, *Nippon Kagaku Kaishi*, **1973**, 56.

Tautomeric Equilibrium of Salicylidene Schiff Base. UV-Visible Absorption and Raman Spectroscopic Studies

Ho-hi LEE and Teizo KITAGAWA*
Institute for Molecular Science, Okazaki National Research Institutes, Okazaki 444
(Received February 24, 1986)

Synopsis. The solvent effect and temperature dependence on the Raman and absorption spectra demonstrated the existence of a tautomeric equilibrium for the title compound between the enol form and the protonated Schiff base form in methanol; the latter form is more stable by ca. 850 cal mol^{-1}(1 cal=4.184 J) than the former. Characteristic Raman bands for the two tautomers have been identified.

An intramolecular proton transfer has been considered to be a major factor for controlling the activity of some biological molecules.[1] Aspartate aminotransferase, having a pyridoxal Schiff base as a cofactor, is an example for which the enzymic activity has been associated with the protonation state of the cofactor,[2] although the detailed mechanism has not yet been established. Salicylidene Schiff bases are expected to serve as a good model for the active site of the pyridoxal enzyme. Previous IR and UV-visible absorption studies[3-5] suggested that the Schiff base exists as a tautomeric mixture in a polar solvent; however there has been no firm spectroscopic evidence for this idea. Accordingly, in this study, the UV-visible and Raman spectra were investigated for the simplest Schiff base of this class, namely, *N*-salicylidene methylamine (SAL-MA) and *N*-(*o*-methoxybenzylidene)methylamine (ANIS-MA) (Fig. 1), in which the vibrational contribution from the amine moiety is minimized. SAL-MA has a proton that can be transferred whereas ANIS-MA does not. Thus, ANIS-MA can serve as a model of tautomer **1** in Fig. 1.

Experimental

SAL-MA and ANIS-MA were synthesized by a direct condensation of salicylaldehyde or *o*-anisaldehyde with methylamine in alkaline methanol (MeOH), respectively. The absorption spectra were recorded on a Hitachi 220S spectrometer. For Raman measurements, the off-resonance condition was chosen so that Raman signals from both tautomers could be observed simultaneously. The 514.5 nm line of an Ar^+ ion laser (NEC GLG3200) was used for the excitation. Excitation at shorter wavelengths brought about an intense fluorescence which hindered us from measuring the resonance Raman spectrum of each tautomer. Raman spectra were recorded on a JEOL-400D Raman spectrometer equipped with a cooled RCA-31034a photomultiplier. Low-temperature measurements for absorption and Raman spectra were carried out in a specially designed glass Dewar. A quartz cell with a 1-mm path length was placed inside the Dewar and cooled with cold ethanol. The temperature of the sample was monitored by a thermocouple attached to the sample cell.

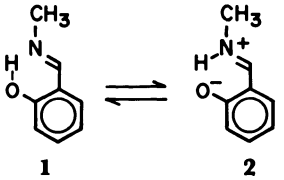

1 2

Fig. 1. Tautomeric structures of SAL-MA. For ANIS-MA the OH group is replaced by the OCH_3 group in **1**.

Results and Discussion

The UV-visible absorption spectrum of SAL-MA in pure MeOH is shown in the inset of Fig. 2. Two bands were observed around 300 and 400 nm. For convenience, the bands at 300 and 400 nm are designated as Band A and B, respectively. When the solvent was changed from pure MeOH to pure $CHCl_3$, the 400-nm band disappeared and in a mixed solvent of MeOH/$CHCl_3$ SAL-MA gave an intermediate spectrum (not shown). On the other hand, ANIS-MA gave a single peak near 300 nm both in MeOH and $CHCl_3$. As the temperature was lowered, the relative intensity of Band B to Band A for SAL-MA increased. Isosbestic points were obtained at 283, 338, and 435 nm. The solvent effect and the temperature dependence suggest that there are two species in a MeOH solution of SAL-MA; one absorbs light at 300 nm and the other at 400 nm. The latter species should have a more polar structure than the former. In Fig. 2 the logarithm of the ratio of the peak intensities are plotted against the reciprocal absolute temperature. A fairly good straight line was obtained; its slope indicates that the species giving rise to Band B is more stable than the other by ca. 850 cal mol^{-1}. This is comparable to the value for *N*-(2-hydroxy-1-naphthylmethylene) aniline reported by Dudek.[6]

Figure 3 shows the temperature dependence and solvent effect on the Raman spectra of SAL-MA,

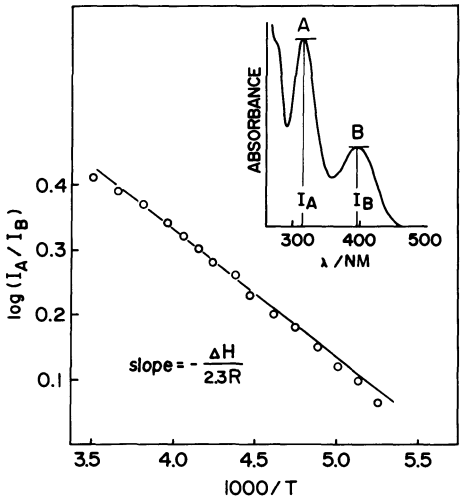

Fig. 2. Plot of the logarithm of the ratio of peak intensities versus the reciprocal absolute temperature. The inset is UV-visible absorption spectrum of SAL-MA in MeOH at 295 K.

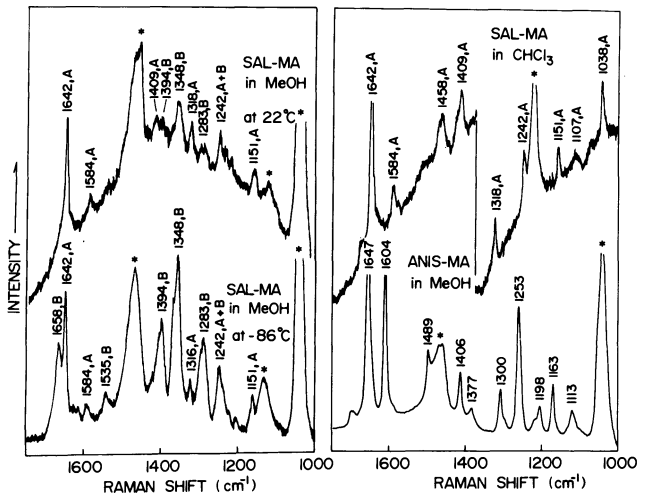

Fig. 3. Raman spectra of SAL-MA and ANIS-MA. left panel; Raman spectra of SAL-MA in MeOH at 22 °C (top) and at −86 °C (bottom), right panel; Raman spectra of SAL-MA in $CHCl_3$ (top) and ANIS-MA in MeOH (bottom) at room temperature. Excitation 514.5 nm, 150 mW, spectral slit-width 5 cm^{-1}. Solvent peaks are denoted by asterisks.

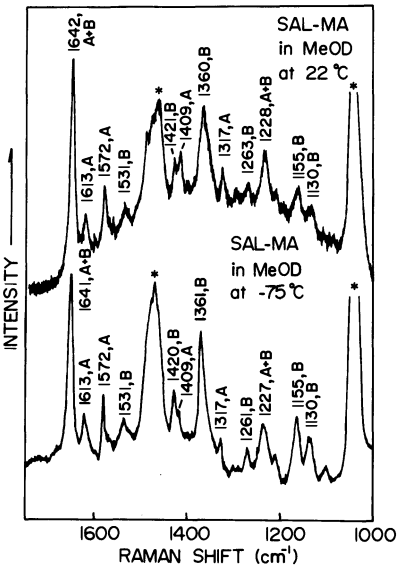

Fig. 4. Temperature dependence of Raman spectra of SAL-MA in MeOD. Excitation 514.5 nm, 100 mW, spectral slit-width 5 cm^{-1}.
Solvent peaks are denoted by asterisks.
The 1228 cm^{-1} and 1155 cm^{-1} bands contain marginal intensity contributions from the solvent.

together with the spectrum of ANIS-MA in MeOH. As the temperature of the MeOH solution of SAL-MA is lowered, the intensities of the Raman bands marked by B increase at the expense of intensities of the Raman bands marked by A. Most noticeable are the doublet features around 1650 cm^{-1} which fall in the C=N stretching region. This temperature dependence for Raman bands A and B is comparable with that observed for Bands A and B in the UV-visible absorption spectrum. In $CHCl_3$ SAL-MA shows only Raman bands marked by A. Consequently, it follows that the species yielding Bands A and B in the UV-visible spectra give rise to Raman bands A and B, respectively. It is noteworthy that the Raman spectrum of ANIS-MA is much closer to the Raman spectrum of A than to that of B.

The A bands of SAL-MA at 1642 and 1242 cm^{-1} correspond to the bands of ANIS-MA at 1647 and 1253 cm^{-1}, respectively. In MeOD the 1642 cm^{-1} band remained unshifted but the 1242 cm^{-1} band was shifted to lower frequency by 14 cm^{-1} (as shown in Fig. 4). The spectrum of O-deuterated SAL-MA in $CHCl_3$, which gives exclusively A peaks, showed the unshifted 1642 cm^{-1} band but lacked the 1242 cm^{-1} band, although the lower-frequency side of the 1242 cm^{-1} band was masked by the solvent band. The C-OH stretching mode of phenol shifts from 1252 to 1241 cm^{-1} upon O-deuteration.[7] Therefore, the 1642 and the 1242 cm^{-1} bands can be assigned to the -C=N- and C-OH stretching modes, respectively. The bands of SAL-MA at 1584, 1151, and 1038 cm^{-1} are assigned to the benzene ring modes (ν_{8a}, ν_{9a}, and ν_{18a}, respectively). These results suggest that species A corresponds to the enol form (**1** in Fig. 1). With regard to the Raman spectrum of species B, on the other hand, a comparison of Fig. 3 with Fig. 4 suggests that the 1658 cm^{-1} band undergoes a low-frequency shift by 15 cm^{-1} and the 1283 cm^{-1} band seems to disappear when the solvent is changed from MeOH to MeOD. The former can be assigned to the -C=NH^+-stretching mode because the higher frequency for the -C=NH^+- stretch compared to the -C=N- stretch and the proximity of the -C=ND^+- stretching frequency to the -C=N- one are consistent with the results for retinal Schiff base derivatives.[8] The latter is a candidate for the NH bending mode of the -C=NH^+- group, although the frequency seems to be too low for this mode. The effects of *N*-deuteration on the other B peaks are rather complicated; this prevents us from giving consistent band assignments. However, the data shown here strongly suggest that the B species takes a protonated Schiff base, structure **2**.

In conclusion, clear evidence for the tautomerism of a salicylidene Schiff base between **1** and **2** in Fig. 1 was obtained for the first time from the Raman spectrum; this will help in an interpretation of the resonance Raman spectrum of the pyridoxal enzyme.

The authors are grateful to Mr. Shinji Hashimoto for help with the low-temperature experimental arrangement.

References

1) D. E. Metzler, *Adv. Enzymol.*, **50**, 1 (1979).
2) A. E. Braunstein, *Enzymes*, **IX B**, 379 (1973).
3) D. Heinert and A. E. Martell, *J. Am. Chem. Soc.*, **84**, 3257 (1962).
4) J. W. Ledbetter Jr., *J. Phys. Chem.*, **81**, 54 (1977).
5) J. W. Lewis and C. Sandorfy, *Can. J. Chem.*, **60**, 1727 (1982).
6) G. O. Dudek and E. P. Dudek, *J. Am. Chem. Soc.*, **88**, 2407 (1966).
7) J. C. Evans, *Spectrochim. Acta*, **16**, 1382 (1960).
8) S. O. Smith, J. Lugtenburg, and R. A. Mathies, *J. Membr. Biol.*, **85**, 95 (1985), and the references therein.

Optical Spectra of Tocopheroxyl Model Radicals

Kazuo MUKAI,* Yoshiko WATANABE, and Kazuhiko ISHIZU
Department of Chemistry, Faculty of Science, Ehime University, Matsuyama 790
(Received March 17, 1986)

Synopsis. Tocopheroxyl model radicals have been prepared by the reaction between tocopherol models and stable phenoxyl radical in ethanol under nitrogen atmosphere. Optical spectra were recorded, and wavelength of absorption peaks (λ_{max}) and molar extinction coefficients (ε) were correctly determined.

The role of vitamin E (α-, β-, γ-, and δ-tocopherols) as an important biological antioxidant has been well recognized in recent years.[1] The antioxidant properties of the tocopherols have been ascribed to the initial oxidation of the phenolic hydroxyl group, producing tocopheroxyl radicals. Therefore, recently, several investigators including present authors have studied the ESR spectra of tocopheroxyl radicals, and determined the proton hyperfine splittings exactly.[2-4] By using pulse radiolysis technique, Packer et al. reported direct evidence for a free radical interaction between vitamin E (α-tocopherol) and vitamin C in vitro.[5] In the work, they observed the transient absorption spectrum of α-tocopheroxyl radical, showing an absorption peak (λ_{max}) at 425 nm. However, the value of molar extinction coefficient (ε) has not been reported, because of a rapid decrease in absorption at 425 nm.

Structure

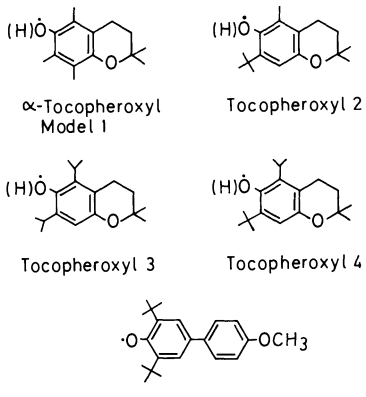

Recently, we have prepared the tocopherol model compounds **1**, **2**, **3**, and **4** having large alkyl substituents at both ortho positions (C-5 and C-7).[6] The tocopheroxyl radicals produced by the oxidation of the above tocopherols are fairly stable. Therefore, in the present work, we have succeeded in measuring the absorption spectra of the tocopheroxyls **2**, **3**, and **4**, and determined the values of λ_{max} and ε for these tocopheroxyls. However, in the case of α-tocopheroxyl model **1**, the radical is unstable, and thus we could only determine the wavelengths of absorption peaks.

Experimental

The preparation of tocopherol model compounds was reported in a previous paper.[6]

The 2,6-di-*t*-butyl-4-(4-methoxyphenyl)phenoxyl (abbreviated to phenoxyl **5** hereafter) was prepared according to the method of Müller et al.[7] Radical concentration of **5** was obtained from the results of the paramagnetic susceptibility measurements at 20 °C, after correcting for the diamagnetic contribution ($\chi_{dia}=-0.220\times10^{-3}$ emu mol^{-1}) calculated by the Pascal's method. The value was 100% for **5** assuming the Curie law.

Tocopheroxyl radicals **1**, **2**, **3**, and **4** have been prepared by the reaction between stable phenoxyl radical **5** and corresponding tocopherols in ethanol at 23 °C under nitrogen atmosphere.

The visible spectra were recorded with a Hitachi EPS-3T spectrophotometer.

Results and Discussion

The phenoxyl radical **5** is very stable in the absence of tocopherol, and shows absorption peaks at λ_{max}=376 nm (ε=17600) and 580 nm (ε=4280). Phenol precursor of **5** and tocopherol model **4** show absorption peaks at λ_{max}=267 nm (ε=19500) and λ_{max}=295 nm (ε=3610), respectively, in ethanol: no absorptions were observed in the visible absorption region. By adding the ethanol solution of tocopherol **4** (6.0×10^{-4} M) to the solution of phenoxyl **5** (4.0×10^{-4}M)(1:1 in volume) at 23 °C, the absorption spectrum of phenoxyl **5** immediately changed to that of tocopheroxyl **4** (see Fig. 1). Here, new absorptions at visible region (λ_{max}=341, 400, and 419 nm) are due to tocopheroxyl **4**, and the weak absorption at 580 nm is due to remaining phenoxyl **5** (5.0%). The tocopheroxyl **4** is considerably stable at 23 °C, and the absorption intensity only gradually decreases with time. There-

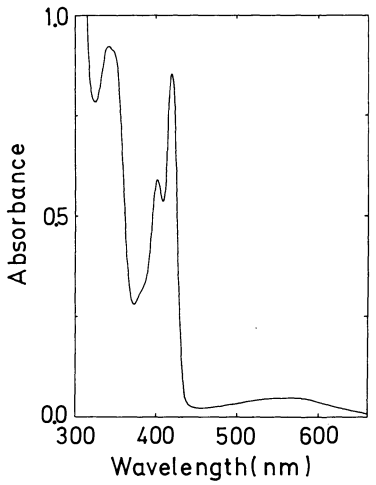

Fig. 1. Absorption spectrum of tocopheroxyl **4** in ethanol.
The weak absorption at 580 nm and the shoulder at 376 nm are due to remaining phenoxyl **5** (5.0%).

Table 1. Absorption Peaks (λ_{max}) and Molar Extinction Coefficients (ε) of Tocopheroxyl Radicals **1**, **2**, **3**, and **4** in Ethanol

1	λ_{max} (nm)	340	405	427
	ε (M^{-1} cm^{-1})	—	—	—
2	λ_{max}	338	398	419
	ε	3720	2390	3910
3	λ_{max}	338	401	420
	ε	4100	2490	4010
4	λ_{max}	341	400	419
	ε	3990	2510	3990

fore, the molar extinction coefficients are calculated to be ε=3990 M^{-1} cm^{-1} at 341 nm, ε=2510 M^{-1} cm^{-1} at 400 nm, and ε=3990 M^{-1} cm^{-1} at 419 nm for tocopheroxyl **4**, after correcting for the remaining phenoxyl **5** (5.0%). Similarly, tocopherols **1**, **2**, and **3** were reacted with phenoxyl **5**, and the optical spectra of tocopheroxyls **1**, **2**, and **3** were observed. The remaining phenoxyl radical **5** was 4.4% for **1**, 9.5% for **2**, and 11.9% for 3. The values of λ_{max} and ε obtained are listed in Table 1. However, in the case of α-tocopherol model **1**, the tocopheroxyl radical **1** produced is unstable, and absorption decreases rapidly with time.[6] Therefore, the value of ε cannot be determined.

As it is clear from the results listed in Table 1, the values of λ_{max} in tocopheroxyls **1**, **2**, **3**, and **4** are similar to each other as expected. Further, the values of ε obtained for tocopheroxyls **2**, **3**, and **4** are very similar to each other at three absorption peaks, where the difference in the ε value is 9% at most. The result suggests that the ε value of α-tocopheroxyl model is also similar to those of tocopheroxyls **2**, **3**, and **4**. As described in a previous section, Packer et al. have observed the absorption peak at 425 nm in water-2-propanol-acetone mixtures. In the present work, we have observed three absorption peaks (340, 405, and 427 nm) at visible region for α-tocopherol model **1**. The value of λ_{max} at the longest wavelength (427 nm) in α-tocopheroxyl model shows good accordance with that (425 nm) of α-tocopheroxyl reported by Packer et al.

We are very grateful to Miss Kimiko Takamatsu, Miss Ayako Ono, and Mr. Yuichi Uemoto for their help in the preparation of tocopherols.

References

1) M. L. Scott, "The Fat-Soluble Vitamins" ed by H. F. Deluca, Plenum Press, New York (1978), pp. 133—210.
2) K. Mukai, N. Tsuzuki, S. Ouchi, and K. Fukuzawa, *Chem. Phys. Lipids*, **30**, 337 (1982), and references cited therein.
3) M. Matsuo and S. Matsumoto, *Lipids*, **18**, 81 (1983).
4) J. Tsuchiya, E. Niki, and Y. Kamiya, *Bull. Chem. Soc. Jpn.*, **56**, 229 (1983).
5) J. E. Packer, T. F. Slater, and R. L. Willson, *Nature*, **278**, 737 (1979).
6) K. Mukai, K. Takamatsu, and K. Ishizu, *Bull. Chem. Soc. Jpn.*, **57**, 3507 (1984).
7) E. Müller, A. Schick, and K. Scheffler, *Chem. Ber.*, **92**, 474 (1959).

Selective Allylation of Sodium Naphtholate

Shigetoshi YAMADA,* Toru TAKESHITA,† and Juntaro TANAKA
Department of Industrial Chemistry, Junior College of Technology, Shizuoka University, Hamamatsu 432
†Teijin Institute for Biomedical Reserch, Hino, Tokyo 191
(Received March 19, 1986)

Synopsis. The reaction of 1- or 2-naphthol with allylic halides (1-chloro-3-methyl-2-butene, 1-chloro-3,7-dimethyl-2,6-octadiene, *trans*-1-chloro-2-butene and *trans*-1-chloro-2-hexene) in the presence of metallic sodium gave naphthols having the corresponding allylic group selectively.

1,4-Naphthoquinones and 1,4-naphthalenediols which have polyprenyl units as side chains are widely distributed from bacteria to higher plants and animals, and many of these compounds are known as biological active compounds.[1]

In previous papers,[2-4] we described that the reaction of phenols with allylic halides in the presence of alkali metals gave ortho-allylated phenols in high yields. This procedure was considered to be applicable to the synthesis of the naturally occurring compounds. Therefore, we now wish to report the allylation of 1- or 2-naphtholate which gives 2- or 1-allylic naphthol selectively.

Table 1. The Effects of Alkali Metals

Metals	Convn. %	Product/%			Unknown
		3	**5**	**6**	
Li	73	63	12	4	21
Na	96	82	3	2	13
K	88	77	6	4	13

In regard to C-allylation of naphthols, Sharma et al.[5] have reported that the naphthols were treated with isoprene and iodotrimethylsilane in acetonitrile to give C-allylated naphthols. Whiting et al.[6] also have reported that 1-(3-methyl-2-butenyl)-2-naphthol was prepared from the (phenylthio)naphtho[2,1-*b*]pyran derivative. However, the yields of allylic naphthols in each cases were quite poor.

By contrast, when this reaction actually was attempted with our method, C-allylated compounds were obtained in good yields. In the reaction of 1-(**1**) or 2-naphthol (**2**) with 1-chloro-3-methyl-2-butene in the presence of metallic sodium, 2-(3-methyl-2-butenyl)-1-naphthol (**3**) or 1-(3-methyl-2-butenyl)-2-naphthol (**4**) was obtained in a yield of 82% or 86%, respectively. As the minor products, 1-naphthyl 3-methyl-2-butenyl ether (**5**), 2,2-dimethyl-3,4-dihydro-2*H*-naphtho[1,2-*b*]pyran (**6**), 2-naphthyl 3-methyl-2-butenyl ether (**7**) and 3,3-dimethyl-1,2-dihydro-3*H*-naphtho[2,1-*b*]pyran (**8**) were found in very poor yields, respectively.

The effect of the alkali metals in this reaction is shown in Table 1.[7] From this result, it was found that the metallic sodium was useful for obtaining selectively naphthols having 3-methyl-2-butenyl group.

In a same manner as above, the reaction of

Table 2. Spectral and Analytical Data for Compounds

Compd	IR (cm^{-1})	^1H NMR (δ, CCl_4)	Formula	Found (%) (Required) C	H
3	3450, 1210, 845, 810, 750	1.70(s, 6), 3.30(d, 2), 5.15(s, 1), 5.18 (t, 1), 6.85—8.10(m, 6)	$C_{15}H_{16}O$	85.08 (84.87)	6.46 (6.71)
4	3450, 1200, 810, 795, 750	1.53(s, 3), 1.68(s, 3), 3.53(d, 2), 6.05 (t, 1), 5.55(s, 1), 6.65—7.80(m, 6)	$C_{15}H_{16}O$	84.62 (84.87)	6.91 (6.71)
9	3470, 1660, 1200, 870, 810, 745	1.32(s, 3), 1.42(s, 3), 1.48(s, 3), 1.65 —1.95(m, 4), 3.09(d, 2), 4.68(s, 1), 4.98(t, 2), 6.65—7.70(m, 6)	$C_{20}H_{24}O$	85.48 (85.66)	8.85 (8.63)
10	3450, 1660, 1200, 860, 810, 745	1.42(s, 6), 1.55(s, 3), 1.80—2.05(m, 4), 3.55(d, 2), 4.80(s, 1), 5.05(t, 2), 655—765(m, 6)	$C_{20}H_{24}O$	85.89 (85.66)	8.35 (8.63)
11	3500, 1660, 1210, 980, 810, 750	1.62(d, 3), 3.30—3.50(m, 2), 4.10(s, 1), 5.25—5.65(m, 2), 6.90—8.20(m, 6)	$C_{14}H_{14}O$	84.59 (84.81)	7.43 (7.12)
12	3300, 1660, 1220, 975, 815, 750	1.50(d, 3), 3.55—3.80(m, 2), 4.10(s, 1), 5.35—5.55(m, 2), 6.70—7.65(m, 6)	$C_{14}H_{14}O$	85.02 (84.81)	7.05 (7.12)
13	3500, 1680, 1210, 980, 810, 750	0.88(t, 3), 1.33(sext, 2), 1.96(q, 2), 3.28—3.50(m, 2), 5.40—5.80(m, 3), 6.90—8.20(m, 6)	$C_{16}H_{18}O$	84.87 (84.91)	8.45 (8.02)
14	3300, 1660, 1205, 975, 810, 745	0.80(t, 3), 1.25(sext, 2), 1.85(q, 2), 3.50—3.80(m, 2), 6.75—7.90(m, 6)	$C_{16}H_{18}O$	84.96 (84.91)	8.25 (8.02)

naphthols (**1**, **2**) with 1-chloro-3,7-dimethyl-2,6-octadiene, *trans*-1-chloro-2-butene and *trans*-1-chloro-2-hexene gave good yields of (3,7-dimethyl-2,6-octadienyl)naphthols (**9**, **10**), (*trans*-2-butenyl)naphthols (**11**, **12**) and (*trans*-2-hexenyl)naphthols (**13**, **14**), respectively.[8]

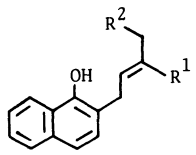

			Yield/%	(convn. %)
3	$R^1=CH_3$,	$R^2=H$	82	(96)
9	$R^1=CH_3$,	$R^2=C_5H_9$	80	(91)
11	$R^1=R^2=H$		75	(90)
13	$R^1=H$,	$R^2=C_2H_5$	73	(84)

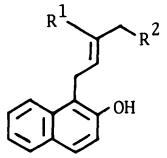

			Yield/%	(convn. %)
4	$R^1=CH_3$,	$R^2=H$	86	(95)
10	$R^1=CH_3$,	$R^2=C_5H_9$	82	(90)
12	$R^1=R^2=H$		80	(88)
14	$R^1=H$,	$R^2=C_2H_5$	79	(78)

Experimental

The following procedure is the typical experimental conditions used in the reaction of naphthols with allylic halides in the presence of metallic sodium.

The reaction of 1-naphthol with 1-chloro-3-methyl-2-butene. To an ethereal solution (15 ml) of 1-naphthol (2.88 g, 0.02 mol), metallic sodium (0.46 g, 0.02 g atom) was added. After the mixture was stirred for 1 h, 1-chloro-3-methyl-2-butene (2.09 g, 0.02 mol) was added slowly and the mixture was refluxed for 30 min. Then, the solution was acidified with 0.1 mol dm^{-3} aq HCl and extracted with ether. The ethereal solution was treated with 10% aq NaOH to remove the unreacted naphthol, and washed with Claisen's alkali. The Claisen's alkali phase was acidified with 1 mol dm^{-3} aq HCl and extracted with ether, and the ether layer was washed with water and dried over anhydrous sodium sulfate. After the removal of the solvent by distillation under reduced pressure, 2-(3-methyl-2-butenyl)-1-naphthol (**3**) was obtained in the yield of 82%. In order to identify the minor products, the ether layer, which was washed with Claisen's alkali as described above, was chromatographed over alumina. The alumina column was eluted with hexane and 1-naphthyl 3-methyl-2-butenyl ether (**5**) and 2,2-dimethyl-3,4-dihydro-2*H*-naphtho[1,2-*b*]pyran (**6**) were obtained in 3 and 2% yields, respectively. The structures of these products were identified by means of the IR, ^1H NMR and elemental analysis (Table 2).

References

1) G. D. Manners and L. Jurd, *J. Chem. Soc., Perkin Trans. 1*, **1977**, 405.; T. Kusumi, M. Ishitsuka, T. Kinoshita, and H. Kakisawa, *Chem. Lett.*, **1979**, 277; M. Ochi, H. Kotsuki, and A. Inoue, *ibid.*, **1979**, 831; B. H. Howard, K. Clarkson, and R. L. Berstein, *Tetrahedron Lett.*, **1979**, 4449.

2) S. Yamada, F. Ono, T. Katagiri, and J. Tanaka, *Synth. Commun.*, **5**, 181 (1975).

3) S. Yamada, F. Ono, T. Katagiri, and J. Tanaka, *Nippon Kagaku Kaishi*, **1980**, 733.

4) S. Yamada, F. Ono, T. Katagiri, and J. Tanaka, *Nippon Kagaku Kaishi*, **1981**, 1192.

5) P. Barua, N. C. Barua, and R. P. Sharma, *Tetrahedron Lett.*, **24**, 5801 (1983).

6) S. E. N. Mohamed, P. Thomas, and D. A. Whiting, *J. Chem. Soc., Chem. Commun.*, **1983**, 738.

7) The reaction was carried out under conditions described below: (**1**) (0.02 mol), 1-chloro-3-methyl-2-butene (0.02 mol), alkali metal (0.02 g atom), ether (15 ml), reflux, reaction time 30 min.

8) It was found that these compounds (**9**—**13**) are composed of approximately 90—93% of E-type configuration by means of HPLC. HPLC was performed with a JASCO BIP-I instrument equipped with a UV detector (250 nm) using a Finepak SIL reversed-phase column (4.6 mm×25 cm) and methanol/H_2O (17/4) as an eluent at a flow speed of 1.0 ml min^{-1}.

Thermal Isomerization Equilibrium between 2′-Hydroxychalcones and Flavanones

Yukio HOSHINO* and Noboru TAKENO†
Department of Natural Science, Muroran Institute of Technology, Mizumoto-cho, Muroran 050
†Department of Industrial Chemistry, Muroran Institute of Technology, Mizumoto-cho, Muroran 050
(Received March 19, 1986)

Synopsis. Nine substituted 2′-hydroxychalcones and the corresponding flavanones were heated separately at 230±0.2 °C in nitrogen atmosphere. Both materials were mutually isomerized under these reaction conditions and the equilibrium constants of this isomerization were measured by means of HPLC analyses. The substituent effect on the equilibrium is discussed and thermodynamic functions (ΔG, ΔH, and ΔS) are calculated.

2′-Hydroxychalcones (**1**) and flavanones (**2**) constitute an important class of naturally occuring pharmacological compounds[1] and are intermediates in the biosynthesis of flavonoids.[2] Both materials are the structual isomers of each other; the isomerization of 2′-hydroxychalcones results in the corresponding flavanones and is usually effected under the influence of mineral acids and enzymes.[3] Kinetic studies on the isomerization equilibrium between **1** and **2** in an aqueous alkali and in an alkaline methanolic medium have also been reported.[4]

In the related work on flavonoids, we discovered the fact that **1** and **2** are mutually isomerized (partially) in a column (TENAX-GC) of gas chromatography at 285 °C. We now report on experimental results concerning the thermal isomerization equilibrium between **1** and **2** in a none-solvent environment at temperatures above those melting points.

Table 1. Equilibrium Constants of the Thermal Isomerization between 2′-Hydroxychalcones and Flavanones

Compd 1, 2	K[a]	Temp °C
a	1.41	200
	1.38	210
	1.33	220
	1.29	230
	1.18	240
	1.16	250
b	0.626	230
c	0.886	
d	0.943	
e	1.05	
f	1.47	
g	1.40	
h	1.55	
i	1.69	

a) $K=C_f/C_c$, where C_c and C_f are the concentrations of 2′-hydroxychalcones and flavanones, respectively.

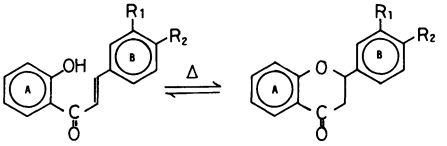

a $R_1=R_2=H$ **b** $R_1=H$, $R_2=OCH_3$ **c** $R_1=H$, $R_2=CH_3$ **d** $R_1=H$, $R_2=CH(CH_3)_2$ **e** $R_1=CH_3$, $R_2=H$ **f** $R_1=H$, $R_2=Cl$ **g** $R_1=H$, $R_2=Br$ **h** $R_1=Cl$, $R_2=H$ **i** $R_1=Br$, $R_2=H$

When 2′-hydroxychalcone (**1a**) and flavanone (**2a**) were heated separately at 230±0.2 °C, both materials mutually isomerized. These equilibria were attained in about 5 h. The equilibrium constants were measured as the concentration ratio of **2a** to **1a** by means of an HPLC analysis using the calibration method of the peak area ratio vs. the concentration ratio. The attainment of equilibrium was confirmed by an agreement of both equilibrium constants within the experimental error.

Under the same reaction conditions and using the same analytical procedures, 3 or 4-substituted chalcones (**1b—i**) and the corresponding flavanones (**2b—i**) were examined. The results are summarized in Table 1. In all cases, no material was detected outside of the chalcones and the flavanones. Nitro derivatives of **1** and **2** could not be correctly examined because of considerable resinification or the carbonization.

Although extreme equilibrium shifts due to the introduction of substituents were not observed, Table 1 shows that the equilibrium constant decreased due to the electron-donating group on the B-ring; this increased as a result of the electron-withdrawing group. These results gave an excellent Hammett-type linear free energy relationship using Brawn-

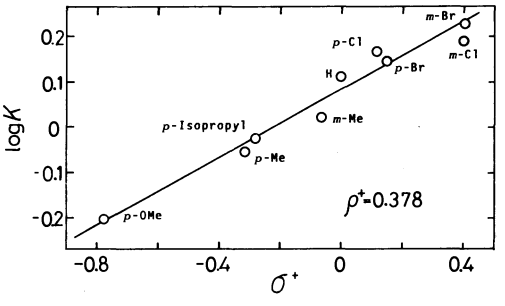

Fig. 1. Hammett plots for the thermal isomerization equilibrium between 2′-hydroxychalcones and flavanones.

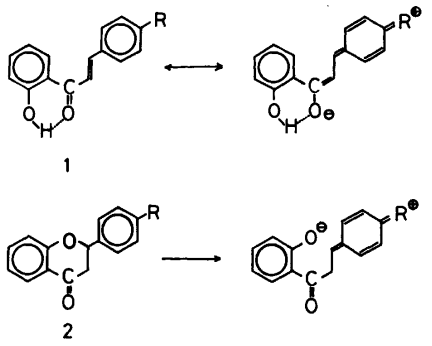

Scheme 1.

Okamoto's σ^+ constant (r=0.996, Fig. 1). In the liquid state, **1** seem to have a strong intramolecular hydrogen bond and the electron-donating groups on the para-position in the B-ring tend to strengthen it further by resonance (Scheme 1). Thus those groups can prevent the cyclization of **1** into **2**; this can result in a decrease in the equilibrium constant, i.e., the advantage of **1**. On the other hand, the above-mentioned substituents can facilitate a bond cleavage between the oxygen atom of heterocycle and C_2-carbon atom in the case of the conversion of **2** into **1** as shown in Scheme 1, and also bring about a similar effect regarding equilibrium.

In order to obtain the thermodynamic parameters, the equilibrium constants at several temperatures were measured regarding the interconversion of **1a** and **2a**. The obtained results are also shown in Table 1. These results show that the equilibrium shifts to **1a** as the temperature rises. **1a** might be more stable than **2a** at high temperatures. According to Eq. 1, the thermodynamic parameters (ΔG, ΔH, and ΔS) for this equilibrium condition were calculated on the basis of a plot

$$RT \ln K = -\Delta G = -\Delta H + T\Delta S \quad (1)$$

of $\ln K$ vs. $1/T$ (Fig. 2). The following values were obtained: $\Delta G^{503}=-1.07$ (kJ mol^{-1}), $\Delta H=-8.78$ (kJ mol^{-1}) and $\Delta S=-15.5\pm0.2$ (J mol^{-1} K^{-1}). The negative value of ΔS might be due to a decrease in the degree of freedom owing to cyclization. From the value of ΔH, it is clear that the conversion of **1a** into **2a** is an exothermic reaction.

Experimental

Materials. Chalcones and flavanones were prepared according to the known procedures;[5] related physical data have already been reported,[6] except for the following derivatives. Melting points are uncorrected.

4-Methyl-2′-hydroxychalcone (1c): Mp 120.0—121.5 °C; ^{1}H NMR (CCl_4) δ=2.36 (3H, s, 4-CH_3), 6.70—7.88 (10H, m, Olefin and Aromatic), 12.66 (1H, s, 2′-OH). Found: C, 80.73; H, 5.75%. Calcd for $C_{16}H_{14}O_2$: C, 80.65; H, 5.92%.

4-Isopropyl-2′-hydroxychalcone (1d): Mp 74—75 °C; ^{1}H NMR (CCl_4) δ=1.26 (6H, d, $CH(\underline{CH_3})_2$, J=6.5 Hz), 2.91 (1H, septet, $\underline{CH}(CH_3)_2$, J=6.5 Hz), 6.72—7.92 (10H, m, Olefin and Aromatic), 12.65 (1H, s, 2′-OH). Found: C, 81.11; H, 6.71%. Calcd for $C_{18}H_{18}O_2$: C, 81.17; H, 6.81%.

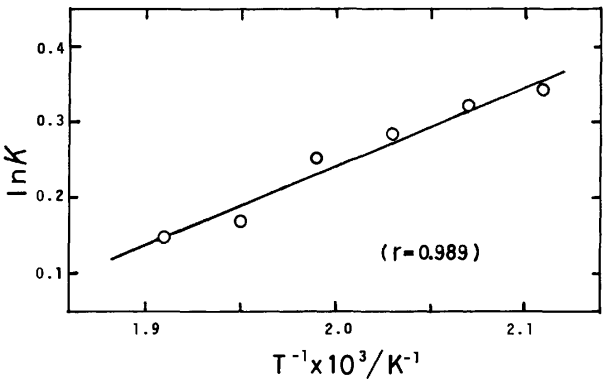

Fig. 2. Temperature dependence of the equilibrium constants of the thermal isomerization.

4-Bromo-2′-hydroxychalcone (1g): Mp 146—147 °C; ^{1}H NMR ($CDCl_3$) δ=6.82—7.92 (10H, m, Olefin and Aromatic), 12.68, (1H, s, 2′-OH). Found: C, 59.42, H, 3.64, Br, 26.30%. Calcd for $C_{15}H_{11}O_2Br$: C, 59.43, H, 3.66, Br, 26.36%.

3-Chloro-2′-hydroxychalcone (1h): Mp 104—105 °C; ^{1}H NMR (CCl_4) δ=6.75—7.86 (10H, m, Olefin and Aromatic), 12.49 (1H, s, 2′-OH). Found: C, 69.46, H, 4.15, Cl, 13.65%. Calcd for $C_{15}H_{11}O_2Cl$: C, 69.64, H, 4.29, Cl, 13.70%.

3-Bromo-2′-hydroxychalcone (1i): Mp 104—106 °C; ^{1}H NMR (CCl_4) δ=6.73—7.86 (10H, m, Olefin and Aromatic), 12.46 (1H, s, 2′-OH). Found: C, 59.20, H, 3.59, Br, 26.25%. Calcd for $C_{15}H_{11}O_2Br$: C, 59.43, H, 3.66, Br, 26.36%.

4′-Isopropylflavanone (2d): Mp 76—77 °C; ^{1}H NMR (CCl_4) δ=1.27 (6H, d, $CH(\underline{CH_3})_2$, J=9.0 Hz), 2.64—3.14 (3H, m, $\underline{CH}(CH_3)_2$ and C_3-H_{ax}, H_{eq}), 5.37 (1H, d·d, C_2-H_{ax}, $J_{ax\cdot ax}$=12.5 Hz, $J_{ax\cdot eq}$=5.0 Hz), 6.88—7.49 (7H, m, Aromatic), 7.85 (1H, d·d, C_5-H, J_{ortho}=8.5 Hz, J_{meta}=2.0 Hz). Found: C, 81.10, H, 6.70%. Calcd for $C_{18}H_{18}O_2$: C, 81.17, H, 6.81%.

General Procedure. In two test tubes (15 mmϕ×105 mm), ca. 0.1 g of **1a** and **2a** were placed separately, and the air in the tubes was displaced with nitrogen to avoid any resinification or carbonization. Then, these tubes were tightly sealded with Uni-stoppers and were dipped in a silicone oil bath adjusted to 230±0.2 °C. After about 5 h, the reaction mixtures were rapidly cooled at room temperature and solved in chloroform (50 ml). Then, the equilibrium constants were determined by an HPLC analysis using instruments by Yanagimoto High Speed Liquid Chromatograph L-2000.

References

1) K. Formanek and H. J. A. Hoeller, *Pharm. Sci.*, **29**, 217 (1961).

2) M. Flammang, C. G. Wermuth, and H. Delassue, *Chim. Ther.*, **5**, 431 (1970).

3) W. Barz and R. Wiemann, "Flavonoids and Bioflavonoids, 1981," ed by L. Farkas, M. Gábor, F. Kállay, and H. Wagner, Elsevier, Amsterdam-Oxford-New York (1982), p. 185.

4) J. J. P. Furlong and N. S. Nudelman, *J. Chem. Soc., Perkin Trans. 2*, **1985**, 633.

5) a) N. S. Poonia, K. Chhabra, C. Kumer, and V. W. Bhagwat, *J. Org. Chem.*, **42**, 3311 (1977). b) T. A. Geissman and R. O. Clinton, *J. Am. Chem. Soc.*, **68**, 697 (1946).

6) a) Y. Hoshino, T. Oohinata, and N. Takeno, *Nippon Kagaku Kaishi*, **1985**, 2104; b) Y. Hoshino and N. Takeno, *Nippon Kagaku Kaishi.*, **1986**, 157; c) Y. Hoshino and N. Takeno, *Bull. Chem. Soc. Jpn.*, **59**, 2351 (1986).

NAD(P)$^+$-NAD(P)H Models. 59. 1,2- Versus 1,4-Reduction of β,γ-Unsaturated α-Keto Ester

Atsuyoshi OHNO,* Tsuneo YASUMA, Kaoru NAKAMURA, and Shinzaburo OKA
Institute for Chemical Research, Kyoto University, Uji, Kyoto 611
(Received March 29, 1986)

Synopsis. Depending on the reactivity of the reducing agent, β,γ-unsaturated α-keto ester is reduced into either β,γ-unsaturated α-hydroxy ester or saturated α-keto ester as the result of 1,2- or 1,4-reduction.

It has been reported that the asymmetric reduction by a chiral NAD(P)H model, *N*-(α-methylbenzyl)-1-propyl-2,4-dimethyl-1,4-dihydronicotinamide (Me_2-PNPH), is a useful tool in obtaining a chiral alcohol as a building block of natural products and many other bio-active compounds.[1] Namely, the reduction of α-keto esters results in excellent enantio-specificity. In order to extend the scope of this interesting asymmetric reduction, we further studied the reduction of α-keto esters that have various functional groups.

Table 1. Reduction of β,γ-Unsaturated and Other α-Keto Esters with 4*R*, 9*R*-Me_2PNPH

Substrate	Product	Conv. %[a]	Chem. Yield/%	e.e. %[b]
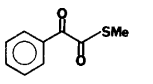	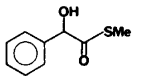	—[c]	71[d]	86.6
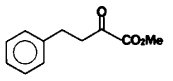	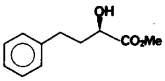 [9]	91	80[e]	63.1
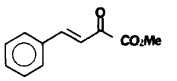	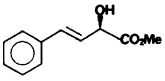 [10]	100	89[d]	95.2
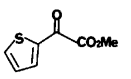	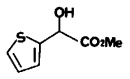	100	—[c]	93.5
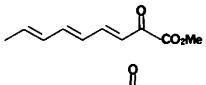	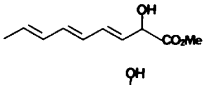	97	—[c]	76.9
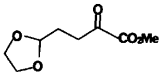	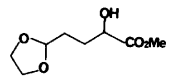	95	—[c]	75.4
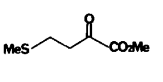	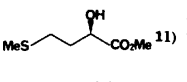 [11]	100	65[e]	95.4
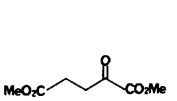	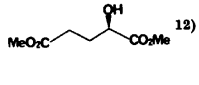 [12]	—[c]	60[e]	62.5
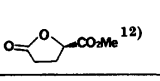 [12]		—[c]	30[e]	62.5

a) Amount of substrate consumed. b) Determined by 400 MHz ^{1}H NMR spectroscopy and/or on VPC of the *R*-(+)-α-methoxy-α-(trifluoromethyl)phenylacetates (MTPA esters). When the absolute configurations of the products are known, they are indicated on the structures. c) Not observed. d) Isolation yield. e) Yield measured on VPC.

Results and Discussion

The results are summarized in Table 1, which apparently shows that the presence of various functional groups in the substrate does not interfere the reduction both in chemical yield and in enantio-specificity.

Among these, the reduction of methyl (*E*)-2-oxo-4-phenyl-3-butenoate (**1**) is especially interesting. The reduction of this keto ester with 1-propyl-1,4-dihydronicotinamide (PNAH) or with the Hantzsch ester (HEH) was recently studied by Meijer and Pandit[2] and it was reported that the sole product was the corresponding saturated α-keto ester (**2**) as a result of the 1,4-reduction. Since Me_2PNPH is more reactive reducing agent than PNAH due to electron-releasing substituents, two methyl groups on the 1,4-dihydropyridine ring and an α-methylbenzyl group on the amide nitrogen, the difference in the product seems to stem from the difference in reactivity of these reagents. Therefore, we also studied the reduction with *N*-(α-methylbenzyl)-1-propyl-1,4-dihydronicotinamide (PNPH), which is expected to have medium reactivity and found that the reaction affords **2**, methyl (*E*)-2-hydroxy-4-phenyl-3-butenoate (**3**) and methyl 2-

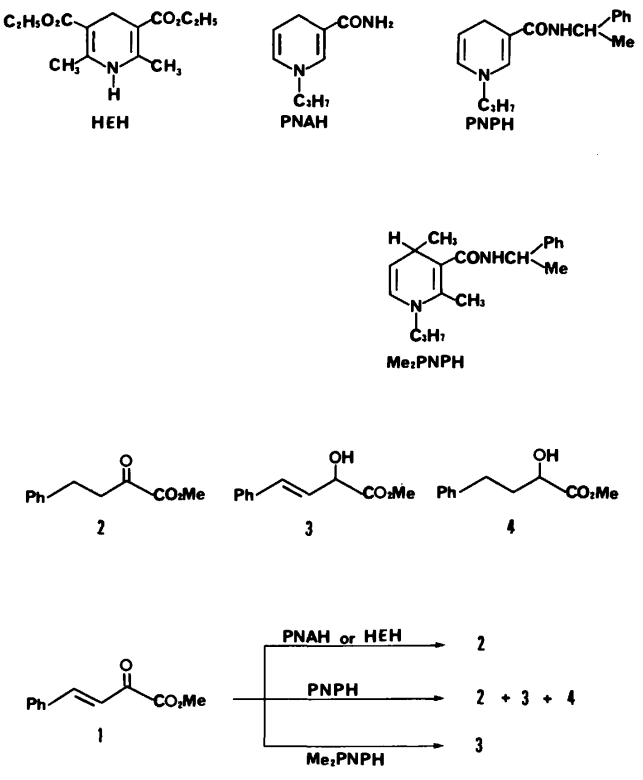

Scheme 1.

hydroxy-4-phenylbutanoate (**4**) in 14, 14, and 7% yields, respectively (Scheme 1). Since it is known that PNPH has no ability to reduce an α-hydroxy olefin, there remains no doubt that **4** is the reduction product from **2**.

The origin of the reactivity-selectivity relationship is not known at present. However, the present result seems to support our prvious proposal that the reduction is composed of succesive transfers of an electron, a proton, and an electron: The reactivity of the reducing agent is defined by its ability for the initial electron transfer. When the activation energy for this process becomes small, the activation energy for the proton-transfer process overwhelms the former and the reaction becomes to appear as if it proceeded with the transfer of a hydrogen atom or a hydride.[3,4] Since the transfer of an electron is the orbital-controlled process, the reaction takes place at the soft reaction center, the olefinic carbon, to result in the 1,4-reduction, whereas the hydride-like species prefers to attack harder reaction center, the carbonyl-carbon, through the charge-density-controlled reaction to result in the 1,2-reduction.

Experimental

Materials. General procedures for the preparation of the 1,4-dihydronicotinamide derivatives were described in the previous papers.[1,3]

Methyl 2-oxo-4-phenyl-3-butenoate[2,5] and methyl 2-oxo-3,5,7-nonatrienoate[6] were respectively prepared according to the literature procedures. Methyl 2-oxo-4-phenylbutanoate, methyl 2-oxo-2-(2-thienyl)acetate, and methyl 2-oxo-4-(1,3-dioxolan-2-yl)butanoate were synthesized by the reaction of the corresponding Grignard reagents and dimethyl oxalate in tetrahydrofuran according to the general procedure.[7]

Methyl 2-oxo-4-(methylthio)butanoate was obtained by methylation of 2-oxo-4-(methylthio)butanoic acid, which was prepared from D,L-methionine by oxidation with D-amino acid oxidase.[8] Dimethyl 2-oxoglutalate was obtained by methylation of 2-oxoglutalic acid. *S*-Methyl 2-oxo-2-phenylethane-thioate is a kind gift from Prof. K. Ogura of Chiba University.

Procedure. The reaction was run with 1.1 equivalent amount of PNAH, PNPH, or Me_2PNPH in the presence of 1 equivalent amount of magnesium perchlorate in acetonitrile for appropriate period (about a day) under an argon atmosphere in the dark at room temperature.

Isolation of the reaction products and the method to determine the enantiomer excess by ^{1}H NMR spectroscopy and on VPC were described in the previous papers.[1,3]

References

1) A. Ohno, M. Ikeguchi, T. Kimura, and S. Oka, *J. Am. Chem. Soc.*, **101**, 7036 (1979).
2) L. H. P. Meijer and U. K. Pandit, *Tetrahedron*, **41**, 467 (1985).
3) A. Ohno, H. Yamamoto, and S. Oka, *J. Am. Chem. Soc.*, **103**, 2041 (1981).
4) S. Yasui and A. Ohno, *Bioorg. Chem.*, in press.
5) H. D. Stecher and H. F. Ryder, *J. Am. Chem. Soc.*, **74**, 4392 (1952).
6) F. G. Fischer and O. Wiedemann, *Justus Liebigs Ann. Chem.*, **513**, 251 (1934).
7) A. Ohno, T. Kimura, S. G. Kim, H. Yamamoto, S. Oka, and Y. Ohnishi, *Bioorg. Chem.*, **6**, 21 (1977).
8) A. Meister, *J. Biol. Chem.*, **197**, 309 (1952).
9) V. Prelog and M. Wilhelm, *Helv. Chim. Acta*, **37**, 1634 (1954).
10) The configuration was determined after hydrogenation on Pd/C.
11) M. Winitz, L. Bloch-Frankenthal, N. Izumiya, S. M. Birnbaum, C. G. Baker, and J. P. Greenstein, *J. Am. Chem. Soc.*, **78**, 2423 (1956).
12) L. Garanti, L. M. Pagnoni, and F. Bellesia, *Ann. Chim. (Rome)*, **63**, 759 (1973).

Insertion of Benzyne and Substituted Benzynes into the S-S Bond of Diphenyl and Di-*p*-tolyl Disulfides Yielding the Corresponding *o*-Bis(arylthio)benzenes

Juzo NAKAYAMA,* Takayuki TAJIRI, and Masamatsu HOSHINO
Department of Chemistry, Faculty of Science, Saitama University,
Urawa, Saitama 338
(Received April 10, 1986)

Synopsis. Benzyne and substituted benzynes undergo insertion into the S-S bond of diphenyl and di-*p*-tolyl disulfides to afford the corresponding *o*-bis(arylthio)benzenes in low but reproducible yields.

Petragnani and Toscano reported that benzyne, generated by thermolysis of diphenyliodonium-2-carboxylate monohydrate,[1] inserts into the Se–Se and Te–Te bonds of diphenyl diselenide and bis(*p*-ethoxyphenyl) ditelluride to afford *o*-bis(phenylseleno)- and *o*-bis(*p*-ethoxyphenyltelluro)benzenes, respectively, but it fails to insert into the S–S bond of diphenyl disulfide, the latter being recovered quantitatively.[2] In connection with our continuing study on reactions of benzyne with sulfur compounds, we reexamined the reaction of benzyne with diphenyl disulfide and found that benzyne reacts with diphenyl disulfide to give *o*-bis(phenylthio)benzene in a low but reproducible yield. Herein we report the insertion of benzyne and substituted benzynes into the S–S bond of diphenyl and di-*p*-tolyl disulfides yielding the corresponding *o*-bis(arylthio)benzenes.

First the reaction of benzyne with diphenyl disulfide was reinvestigated under the conditions that were reported by Petragnani and Toscano.[2] Thus 2 equivalents of diphenyliodonium-2-carboxylate monohydrate was heated with diphenyl disulfide in boiling *o*-dichlorobenzene for 0.5 h. The resulting brown mixture was evaporated and the residue was chromatographed on a column of silica gel. Elution with hexane afforded *o*-bis(phenylthio)benzene (**1**) in 8% yield with quantitative recovery of the unreacted diphenyl disulfide. The structure of **1** was established by comparison with the authentic sample prepared by an alternative systhesis.[3]

Next benzyne, generated by aprotic diazotization of anthranilic acid,[4] was allowed to react with diphenyl disulfide. Thus a solution of anthranilic acid in dioxane was added to a gently refluxing solution of isopentyl nitrite and diphenyl disulfide in 1,2-dichloroethane (anthranilic acid:isopentyl nitrite:diphenyl disulfide=2:2.1:1). Workup of the mixture with silica-gel column chromatography afforded the sulfide **1** in 14% yield with quantitative recovery of the unreacted disulfide.

Thus it is clear that, contrary to the previous report,[2] benzyne is able to insert into the S–S bond of diphenyl disulfde. The reaction probably proceeds via the intitial formation of the betaine intermediate (**2**) as depicted below. The initial formation of betaine intermediates by reaction of benzyne with organic sulfides is well-documented.[5]

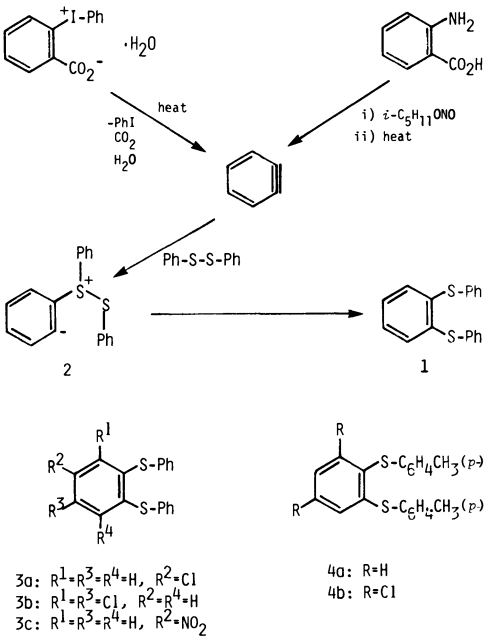

In order to know more about the generality and chracteristics of the present reaction, reactivities of substituted benzynes toward diphenyl and di-*p*-tolyl disulfides were examined. 4-Chloro-, 3,5-dichloro, and 4-nitrobenzynes were generated by aprotic diazotization of 4-chloro-, 3,5-dichloro-, and 4-nitroanthranilic acids, respectively. These benzynes, produced from 2 equivalents of anthranilic acids, reacted with diphenyl disulfide to afford the sulfides **3a**, **3b**, and **3c** in 25, 19, and 30% yields, respectively. Benzyne and 3,5-dichlorobenzyne reacted with di-*p*-tolyl disulfide to give the sulfides **4a** and **4b** in 17 and 14% yields, respectively.

The present reaction involves the initial electrophilic attack of benzynes on the sulfur atom of the disulfides, and therefore more electrophilic benzynes would be expected to give higher yields of the insertion products. However, the above results do not show such a tendency markedly. This is due to the fact that a competitive side reaction, addition of isopentyl alcohol (produced from isopentyl nitrite) to benzynes yielding isopentyl aryl ethers, occurs to consume benzynes, especially when benzynes are strongly eletrophilic.

In conclusion insertion of benzyne and substituted benzynes into diaryl disulfides generally occurs to yield *o*-bis(arylthio)benzenes in low but reproducible yields.[6]

Experimental

Diphenyliodonium-2-carboxylate monohydrate was purchased from Lancaster Synthesis Ltd. Anthranilic acid and 4-chloro- and 3,5-dichloroanthranilic acids were obtained from Tokyo Kasei Kogyo and 4-nitroanthranilic acid from Aldrich. Column chromatography was carried out on 70—230 mesh Merck silica gel. Isopentyl nitrite was prepared by the literature method.[7]

Reaction of Diphenyl Disulfide with Benzyne Generated from Diphenyliodonium-2-carboxylate Monohydrate. A mixture of 549 mg (2.5 mmol) of diphenyl disulfide and 1.717 g (5 mmol) of diphenyliodonium-2-carboxylate monohydrate in 10 ml of *o*-dichlorobenzene was refluxed for 0.5 h. The resulting brown mixture was evaporated under reduced pressure and the residue was chromatographed on a column of silica gel. Elution with hexane afforded 505 mg (92%) of diphenyl disulfide and then 56 mg (8%) of *o*-bis(phenylthio)benzene (**1**). ^{1}H NMR and IR spectra of **1** agreed with those of the authentic sample prepared by an alternative synthesis.[3]

Reaction of Diphenyl Disulfide with Benzyne Generated by Aprotic Diazotization of Anthranilic Acid. To a gently refluxing mixture of 2.18 g (10 mmol) of diphenyl disulfide and 2.46 g (21 mmol) of isopentyl nitrite in 100 ml of 1,2-dichloroethane was added dropwise a solution of 2.74 g (20 mmol) of anthranilic acid in 10 ml of dioxane over a period of 0.5 h. After the completion of the addition, the mixture was refluxed for 0.5 h and evaporated. The resulting residue was chromatographed on a column of silica gel. Elution with hexane gave 1.86 g (86%) of diphenyl disulfide and then 0.42 g (14%) of *o*-bis(phenylthio)benzene (**1**).

Reaction of Diphenyl Disulfide with 4-Chloro-, 3,5-Dichloro-, and 4-Nitrobenzynes. 4-Chloro-, 3,5-dichloro-, and 4-nitrobenzynes were generated by aprotic diazotization of two equivalents of 4-chloro-, 3,5-dichloro-, and 4-nitroanthranilic acids, respectively, and allowed to react with an equivalent of diphenyl disulfide in a similar manner described above. Chromatographic purification afforded the following new *o*-bis(phenylthio)benzenes.

1,2-Bis(phenylthio)-4-chlorobenzene (3a): Yield, 25%; viscous oil; ^{1}H NMR (CCl_4) δ=6.8—7.0 (3H, m), 7.23 (5H, s), and 7.30 (5H, s). Found: C, 65.73; H, 3.94; Cl, 10.80; S, 19.28%. Calcd for $C_{18}H_{13}ClS_2$: C, 65.74; H, 3.98; Cl, 10.78; S, 19.50%.

1,2-Bis(phenylthio)-3,5-dichlorobenzene (3b): Yield, 19%; mp 87—88 °C; ^{1}H NMR (CCl_4) δ=6.43 (1H, d, J=1.6 Hz), 6.9—7.3 (6H, m), and 7.36 (5H, s). Found: C, 59.37; H, 3.29; Cl, 19.72; S, 17.50%. Calcd for $C_{18}H_{12}Cl_2S_2$: C, 59.51; H, 3.33; Cl, 19.52; S, 17,65%.

1,2-Bis(phenylthio)-4-nitrobenzene (3c): Yield, 30%; yellow viscous oil; ^{1}H NMR (CCl_4) δ=6.70 (1H, d, J=9.0 Hz), 7.23 (5H, s), 7.30 (5H, s), and 7.6—7.9 (2H, m). Found: C, 63.56; H, 3.86; N, 4.22; S, 18.53%. Calcd for $C_{18}H_{13}NO_2S_2$: C, 63.69; H, 3.86; N, 4.13; S, 18.89%.

Reaction of Di-*p*-tolyl Disulfide with Benzyne and 3,5-Dichlorobenzyne. Di-*p*-tolyl disulfide was allowed to react with benzyne and 3,5-dichlorobenzyne generated from 2 equivalents of the corresponding anthranilic acids in a manner described above to give *o*-bis(*p*-tolylthio)benzene (**4a**) and 1,2-bis(*p*-tolylthio)-3,5-dichlorobenzene (**4b**).

4a: Yield, 17%; mp 75.5 °C; ^{1}H NMR (CCl_4) δ=2.32 (6H, s), 6.97 (4H, s), and 7.0—7.5 (8H, m). Found: C, 74.52; H, 5.63; S, 19.88%. Calcd for $C_{20}H_{18}S_2$: C, 74.49; H, 5.63; S, 19.88%.

4b: Yield, 14%; mp 70—72 °C; ^{1}H NMR (CCl_4) δ=2.23 (3H, s), 2.37 (3H, s), 6.43 (1H, d, J=2.0 Hz), and 6.8—7.5 (9H, m). Found: C, 61.42; H, 4.09; Cl, 18.25; S, 16.40%. Calcd for $C_{20}H_{16}Cl_2S_2$: C, 61.38; H, 4.12 Cl, 18.12; S, 16.38%.

References

1) E. Le Goff, *J. Am. Chem. Soc.*, **84**, 3786 (1962).
2) N. Petragnani and V. G. Toscano, *Chem. Ber.*, **103**, 1652 (1970).
3) J. Nakayama, T. Fujita, and M. Hoshino, *Chem. Lett.*, **1983**, 249.
4) L. Friedman and F. M. Logullo, *J. Org. Chem.*, **34**, 3089 (1969)
5) R. W. Hoffmann, "Dehydrobenzene and Cycloalkynes," Academic Press, New York (1967), p. 164.
6) We are currently investigating the reaction of dialkyl disulfides with benzyne. The raction does not afford the products resulting from the insertion of benzyne to the S–S bond. For example, the reaction of dimethyl disulfide with benzyne affords thioanisole and diphenyl sulfide as the major products.
7) W. A. Noyes, *Org. Synth.*, Coll. Vol. 2, 108, (1966).

Preparation of Some 1,3-Selenazin-4-ones

Masataka YOKOYAMA,* Katsushi KUMATA, Hidekatsu HATANAKA, and Tadashi SHIRAISHI
Department of Chemistry, Faculty of Science, Chiba University,
Yayoi-cho, Chiba 260
(Received April 12, 1986)

Synopsis. 2-Cyano-3-hydroseleno-3-(methylthio)acrylamide reacts with carbonyl compounds in the presence of sulfuric acid and aroyl chlorides in the presence of pyridine to give the corresponding 2,3-dihydro-4*H*-1,3-selenazin-4-ones and 4*H*-1,3-selenazin-4-ones in moderate yields, respectively.

In the chemistry of heterocycles containing selenium and nitrogen atoms, many literatures concerning 1,3-selenazoles have appeared and their features have been well documented.[1] However, only some reports have been published on the synthesis of 4*H*-1,3-selenazines perhaps because of the synthetic difficulty.[2] During the course of studies on heteroatom rearrangements[3] we have fond a convenient preparative procedure for *S*,*S*-dimethyl dithioselenocarbonate (**1**).[4] As is synthetic application it was found that

Table Compounds **3** and **4** Prepared

Product	Yield %	Mp θ_m/°C	Molecular Formula[a]	IR cm^{-1}	^{1}H NMR(solv./TMS) δ(ppm)	MS[b] m/z(M$^+$)
3a	53	189—190	$C_8H_{10}N_2OSSe$	3120, 3020 (NH); 2200 (CN); 1640 (CO)	($CDCl_3$) 1.89(s, 6H, CH_3); 2.65(s, 3H, SCH_3); 6.73 (br, 1H, NH)	262
3b	90	204—205	$C_{11}H_{14}N_2OSSe$	3120, 3020 (NH); 2200 (CN); 1640 (CO)	($CDCl_3$) ca. 1.3(m, 6H, CH_2); ca. 2.0(m, 4H, CH_2); 2.7(s, 3H, SCH_3); 8.1(br, 1H, NH)	302
3c	41	162—163	$C_9H_{12}N_2OSSe$	3120, 3020 (NH); 2200 (CN); 1640 (CO)	($CDCl_3$) ca. 1.0(m, 3H, CH_3); ca. 1.5(m, 2H, CH_2); ca. 2.0 (m, 2H, CH_2); 2.7(s, 3H, SCH_3); 5.16(d, 1H, CH, J=4 Hz); 6.14(br, 1H, NH)	276
3d	51	214—215	$C_{12}H_{10}N_2OSSe$	3120, 3020 (NH); 2200 (CN); 1640 (CO)	(Py-D_5) 2.7(s, 3H, SCH_3); 6.5 (br, 1H, CH); ca. 7.5(m, 5H, C_6H_5); 10.5(br, 1H, NH)	310
3e	72	195—196	$C_{10}H_8N_2O_2SSe$	3250(NH); 2200(CN); 1650(CO)	($CDCl_3$) 2.7(s, 3H, SCH_3); 6.2 (br, 1H, CH); 6.26, 6.45, 6.53 (m, 3H, C_4H_3O); 7.5(br, 1H, NH)	300
4a	59	188—189	$C_{12}H_8N_2OSSe$	2220(CN); 1640(CO)	($CDCl_3$) 2.8(s, 3H, SCH_3); 7.5, 7.7(m, 3H, C_6H_5); 8.0(m, 2H, C_6H_5)	308
4b	70	235—236	$C_{16}H_{10}N_2OSSe$	2220(CN); 1640(CO)	($CDCl_3$-DMSO) 2.8(s, 3H, SCH_3); 7.4—8.0(m, 6H, $C_{10}H_7$); 8.4(s, 1H, $C_{10}H_7$)	358
4c	48	137—138	$C_{13}H_{10}N_2O_2SSe$	2210(CN); 1630(CO)	($CDCl_3$-DMSO) 2.4(s, 3H, CH_3); 2.7(s, 3H, SCH_3); 5.8 (d, d, 2H, C_6H_4, J=8 Hz); 6.8(d, d, 2H, C_6H_4, J=8 Hz)	338
4d	66	228—229	$C_{12}H_7N_2OSSeCl$	2210(CN); 1640(CO)	($CDCl_3$-DMSO) 2.8(s, 3H, SCH_3); 7.4(d, d, 2H, C_6H_4, J=8 Hz); 7.8(d, d, 2H, C_6H_4, J=8 Hz)	342
4e	62	186—187	$C_{11}H_7N_3OSSe$	2210(CN); 1640(CO)	(DMSO-D_6) 2.8(s, 3H, SCH_3); 7.4, 8.1, 8.6, 8.9(m, 4H, C_5H_4N)	309

a) Satisfactory microanalyses obtained: C±0.30, H±0.22, N±0.28. b) M$^+$ based on ^{80}Se isotope peak.

Scheme

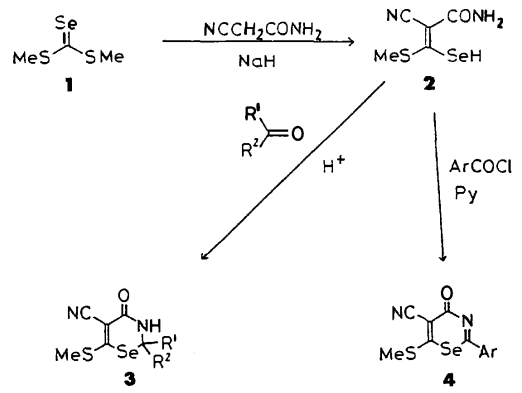

3a $R^1=R^2=CH_3$ **4a** Ar=Phenyl
3b $R^1,R^2=-(CH_2)_5-$ **4b** Ar=2-Naphthyl
3c $R^1=n\text{-}C_3H_7$, $R^2=H$ **4c** Ar=*p*-Methoxyphenyl
3d $R^1=C_6H_5$, $R^2=H$ **4d** Ar=*p*-Chlorophenyl
3e $R^1=$Furyl, $R^2=H$ **4e** Ar=3-Pyridyl

several 4*H*-1,3-selenazin-4-ones could be easily synthesized starting from **1**. Herein we wish to report their preparations.

Compound **1** reacted with cyanoacetamide in the presence of sodium hydride under the oxygen-free conditions to give 2-cyano-3-hydroseleno-3-(methylthio)-acrylamide (**2**) (77% yield), which could be kept for two or three weeks in a refrigerator without decomposition. Compound **2** was allowed to react with various carbonyl compounds in the presence of sufuric acid and some aroyl chlorides in the presence of pyridine to afford the corresponding 2,3-dihydro-4*H*-1,3-selenazin-4-ones (**3**) and 4*H*-1,3-selenazin-4-ones (**4**) in moderate yields, respectively (see Table). In this reaction the use of acetophenone, benzophenone, and acyl chlorides did not give a satisfactory result.

Experimental

Microanalyses were performed with a Perkin-Elmer 240 elemental analyser at the Analytical Center of Chiba University. IR spectra were recorded on a Hitachi 215 spectrometer. ^1H NMR spectra were determined with Japan Electron Optics Lab. (JEOL) JNM-FX-270 and MH-100. The chemical shifts are given in ppm with $(CH_3)_4Si$ as an internal standard. Mass spectra were measured on a Hitachi M-60 spectrometer at an ionizing energy at 70 eV. Chloroform and pyridine were purified by standard procedure, and tetrahydrofuran (THF) was distilled from benzophenone ketyl.

2-Cyano-3-hydroxyseleno-3-(methylthio)acrylamide (2): A 100 ml two-necked round flask equipped with a reflux condenser and a Teflon-coated magnetic bar, is dried in vacuo and then flushed with argon. In this flask are placed sodium hydride (60% dispersion, 1.6 g, 40 mmol) and THF (40 ml). To the resulting slurry solution is added cyanoacetamide (0.84 g, 10 mmol). After stirring at room temperature for 20 min, *S,S*-dimethyl dithioselenocarbonate (2.2 g, 12 mmol) solution in THF (10 ml) is added and the mixture is refluxed with stirring for 2.5 h until orange coloration is produced. The reaction is quenched with dropping of a degassed water under ice cooling, and a mixture of benzene (40 ml) and degassed water (40 ml) is added to the resulting solution. After shaking in a separatory funnel flushed with argon, an aqueous layer is transfered to a 100 ml Erlenmeyer flask containing hexane (20 ml). The aqueous solution is acidified with 6M-HCl (1 M=1 mol dm^{-3}) under ice cooling. The obtained material is collected, washed with degassed water (20 ml×2), and dried in a vacuum desiccator; yellow powder of mp 102—104 °C; 1.7 g, yield 77% ; IR (KBr) 3380, 3280, 3200 (s), 2200 (vs), and 1650 cm^{-1} (vs); ^1H NMR ($CDCl_3$) 2.72 (s, 3H, SCH_3), 7.26 (br, 2H, NH_2), and 16.38 (s, 1H, SeH).

Compound **2** thus obtained is used for the following procedures without purification because **2** decomposes to some extent on recrystallization.

5-Cyano-6-methylthio-2-propyl-2,3-dihydro-4*H*-1,3-selenazin-4-one (3c). Typical Procedure: A mixture of **2** (0.44 g, 2 mmol), *n*-butyraldehyde (0.2 g, 3 mmol)[3], 6M-H_2SO_4 (2 ml), and methanol (8 ml) is stirred for 4 h at room temperature. The reaction is quenched with water, thus obtained crystals are collected, and recrystallized from isopropyl alcohol to give **3c** as pale yellow needles; 0.22 g, yield 41%.

5-Cyano-2-(*p*-chlorophenyl)-6-methylthio-4*H*-1,3-selenazin-4-one (4d). Typical Procedure: A mixture of **2** (0.66 g, 3 mmol, *p*-chlorobenzoyl chloride (1.2 g, 7.6 mmol), pyridine (1.6 ml), and chloroform (10 ml) is shaken for 3 h at room temperature. The reaction is quenched with water and then ethanol, the obtained material is collected, dried in a vacuum desiccator; cream-colored powder (recry. from chloroform–hexane); 0.66 g, yield 66%.

Nicotinoyl chloride is prepared according to the literature.[5] The others are prepared from the reaction of the corresponding carboxylic acids with thionyl chloride in the usual way.

References

1) E. Bulka, "Advances in Heterocyclic Chemistry," ed by A. R. Katritzky, Academic Press, (1963), Vol 2, p. 344.

2) M. Takahashi, S. Watanabe, and T. Kasai, *Heterocycles*, **14**, 1921 (1980); K. T. Potts, F. Huang, and R. K. Khattak, *J. Org. Chem.*, **42**, 1644 (1977); G. Simchen and G. Entenmann, *Justus Liebigs Ann. Chem.*, **8**, 1249 (1977); M. Dzurilla and P. Kristian, *Chem. Zvesti.*, **33**, 792 (1979); F. I. Luknitskii, D. O. Taube, and B. A. Vovsi, *Zh. Org. Khim.*, **5**, 1844 (1969); A. Shafiee, F. Assadi, and V. I. Cohen, *J. Heterocycl. Chem.*, **15**, 39 (1978); M. Dzurilla and P. Kristian, *Collect. Czech. Chem. Commun.*, **41**, 1388 (1976).

3) M. Yokoyama, T. Shiraishi, H. Hatanaka, and K. Ogata, *J. Chem. Soc., Chem. Commun.*, **1985**, 1704 and related references therein.

4) M. Yokoyama and H. Hatanaka, *Synthesis*, **9**, 891 (1985).

5) A. M. Grigorovskii and Z. M. Kimen *J. Gen. Chem.*, **18**, 171 (1948).

The Microwave Spectrum of (*Z*)-(Propionaldehyde Oxime)

Makoto KATAYAMA, Takeshi SAKAIZUMI, Ichiro YAMAGUCHI, and Osamu OHASHI*
Department of Chemistry, Faculty of Science and Technology, Sophia University, Chiyoda-ku, Tokyo 102
(Received March 28, 1986)

Synopsis. The microwave spectrum of (*Z*)-(propionaldehyde oxime) was observed in the frequency region of 10 to 30 GHz. The rotational constants (MHz) for the ground vibrational state were determined to be A=15453.95±0.20, B=2733.60±0.03, and C=2394.85±0.02. The conformation has been plausibly deduced to be the *ap*, *Z*-form from the rotational constants. The dipole moments were determined by the Stark effect: μ_a=0.889±0.010 and μ_b=0.364±0.025 *D*.

From its rotational spectrum propionic acid has been shown to exist predominantly in *sp*-conformation in which the methyl group eclipses the carbonyl bond and the hydroxyl hydrogen is located between the two oxygen atoms.[1] Nuclear magnetic resonance spectroscopic study[2] of propionaldehyde oxime has suggested that this molecule exists in two stereoisomeric forms, termed *E* and *Z* forms with respect to the C=N bond. Each of the conformers has four possible rotational conformations with respect to the C_2–C_3 single bond if the OH bond is assumed to be at the trans position to the C=N bond just as in acetaldehyde oxime[3,4] and acrylaldehyde oxime,[5,6] as shown in Fig. 1. The microwave spectroscopic study[7] has revealed that (*E*)-(propionaldehyde oxime) exists in an *ac*, *E*-conformation (See Fig. 1).

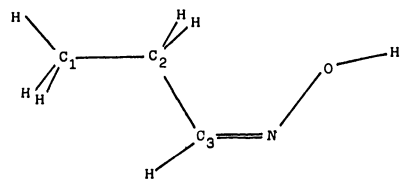

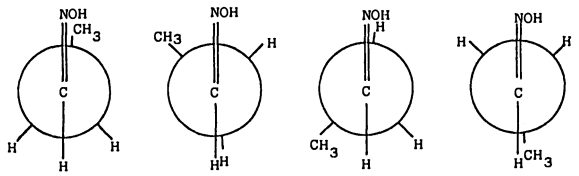

	sp	sc	ac	ap
A/MHz	7954.8	8514.4	11838	15658
B/MHz	5618.3	4321.4	3062.7	2773.5
C/MHz	3434.9	3264.4	2740.3	2418.1
ΔI/amu·Å^2	-6.35	-21.5	-23.3	-6.35

Fig. 1. Four possible rotatonal conformers, their calculated rotational constants, and the numbering of carbon atoms of an *ap*, (*Z*) -(propionaldehyde oxime)

Experimental

Propionaldehyde oxime was prepared by the method described elsewhere.[7]

The microwave spectrometer employed was the same one as described elsewhere.[7] The spectrum was observed at room temperature.

Results and Discussion

A survey of the spectrum was made in the frequency region of 19 to 22 GHz in which the J=4—3 transition lines were expected to be observed from the molecular model calculation of the rotational constants.

The six absorption line frequencies of the J=4—3 transtions led to the preliminary rotational constants which were employed to predict the other transition lines. The assignments of the transition lines were made on the basis of their characteristic Stark effects. The frequencies of the transitions assigned to the

Table 1. Rotational Transition Frequencies (MHz) of (*Z*)-(Propionaldehyde Oxime) in the Ground Vibrational State

Transition	Obsd	$\Delta\nu$[a]	Transition	Obsd	$\Delta\nu$[a]
	a-Type R-branch		5_{15}—4_{14}	24766.63	−0.32
2_{12}—1_{11}	9918.21	0.03	5_{05}—4_{04}	25509.59	0.20
2_{02}—1_{01}	10250.25	0.02	5_{24}—4_{23}	25627.49	−0.01
2_{11}—1_{10}	10596.01	0.34	5_{23}—4_{22}	25760.37	0.13
3_{13}—2_{12}	14873.01	−0.10	5_{14}—4_{13}	26458.98	0.01
3_{03}—2_{02}	15358.64	−0.01		b-Type Q-branch	
3_{22}—2_{21}	15385.27	−0.19	4_{13}—4_{04}	14665.65	−0.07
3_{21}—2_{20}	15412.11	−0.04	5_{14}—5_{05}	15615.12	−0.18
3_{12}—2_{11}	15889.19	−0.09	6_{15}—6_{06}	16806.89	0.18
4_{14}—3_{13}	19823.05	−0.13	7_{16}—7_{07}	18265.27	0.13
4_{04}—3_{03}	20447.18	0.03	8_{17}—8_{08}	20016.18	0.18
4_{23}—3_{22}	20508.82	0.10	9_{18}—9_{09}	22084.18	−0.18
4_{22}—3_{21}	20575.41	0.08	10_{19}—10_{010}	24488.40	−0.07
4_{13}—3_{12}	21177.73	0.04			

a) $\Delta\nu = \nu_{obsd} - \nu_{calcd}$

Table 2. Rotational Transitions of (*Z*)-(Propionaldehyde Oxime) in the Excited States (MHz)

Transition	$v=1$		$v=2$	
	Obsd	$\Delta\nu$[a)]	Obsd	$\Delta\nu$[a)]
$2_{02}-1_{01}$	10311.97	0.26	10376.34	−0.34
$2_{12}-1_{11}$	9998.82	0.27	10075.82	0.49
$2_{11}-1_{10}$	10637.27	−0.13	10689.33	−0.09
$3_{03}-2_{02}$	15452.25	0.05	15549.95	−0.08
$3_{13}-2_{12}$	14994.03	0.02	15209.26	−0.03
$3_{12}-2_{11}$	15952.36	0.15	16030.50	0.13
$3_{22}-2_{21}$	15477.40	−0.03	15572.07	−0.07
$3_{21}-2_{20}$	15501.39	−0.64		
$4_{04}-3_{03}$	20574.31	−0.02	20705.56	0.07
$4_{14}-3_{13}$	19984.75	−0.25	20138.83	−0.11
$4_{13}-3_{12}$	21262.11	−0.14	21366.74	0.06
$4_{23}-3_{22}$	20632.08	0.30		
$4_{22}-3_{21}$	20693.43	0.26		

a) $\Delta\nu=\nu_{obsd}-\nu_{calcd}$

Table 3. Rotational Constants of (*Z*)-(Propionaldehyde Oxime)

	Ground state	Excited state	
	$v=0$	$v=1$	$v=2$
A/MHz	15453.95 (20)	15014 (155)	14354 (180)
B/MHz	2733.60 (3)	2739.18 (14)	2749.19 (12)
C/MHz	2394.85 (2)	2419.76 (14)	2442.15 (11)
κ	−0.948120 (37)	−0.949 (24)	−0.948 (29)
ΔI/amu·Å^2	−6.552 (4)	−9.3 (4)	−12.1 (5)

$\Delta I=I_c-I_a-I_b$

Table 4. Structural Parameters Assumed for (*Z*)-(Propionaldehyde Oxime)

Bond length	*r*/Å	Bond angle	θ/°
C_1-C_2	1.525	HC_1H	109.5
C_2-C_3	1.510	HC_2H	109.5
C_1-H	1.087	HC_1C_2	109.5
C_2-H	1.087	HC_2C_3	109.5
C_3-H	1.086[a)]	$C_1C_2C_3$	109.5
C_3=N	1.276[a)]	HC_3=N	122.0[a)]
N-O	1.408[a)]	C_2C_3=N	126.0[a)]
O-H	0.956[a)]	C_3=NO	110.2[a)]
		NOH	102.7[a)]

Structural parameters of ethyl group were estimated from mono-substituted ethyl derivatives.
a) See Ref. 7: K. Yoshida et al., *Bull. Chem. Soc. Jpn.*, **59**, 1620 (1986).

Table 5. Stark Coefficients (Hz/(V/cm)^2) and Dipole Moments (D) of (*Z*)-(Propionaldehyde Oxime)

Transition	|M|	Obsd	Calcd
$3_{13}-2_{12}$	1	5.493	5.499
	2	21.50	21.81
$3_{12}-2_{11}$	1	−4.665	−4.716
	2	−17.59	−17.12
	$\mu_a=0.889\pm0.010$		
	$\mu_b=0.364\pm0.025$		
	$\mu_c=0$(assumed)		
	$\mu_t=0.961\pm0.019$		

ground vibrational state of (*Z*)-(propionaldehyde oxime) are listed in Table 1.

From comparison between the observed and calculated rotational constants and values of $\Delta I(=I_c-I_a-I_b)$ listed in Table 3 and Fig. 1, it has been reasonably concluded that the conformation of (*Z*)-(propionaldehyde oxime) with respect to the C_2–C_3 bond is an *ap* form in contrast to the *ac* form for (*E*)-(propionaldehyde oxime).[7] Table 4 shows the structural parameters of this molecule used for a model calculation of the rotational constants.

Two satellite lines which could be attributable to vibrationally excited states were observed in the vicinity of the ground state lines. The results of the least squares analysis of data are given in Tables 2 and 3. From the trends of changes in the rotational constants and values of ΔI given in Table 3, these two satellites should be ascribed to one vibrational mode that may be the torsional motion around the C_2–C_3 bond.

The dipole moments were determined by the measurements of the Stark effects of the 3_{13}—2_{12} and 3_{12}—2_{11} transition lines. The electric field in the absorption cell was calibrated with OCS[8] as a standard. The observed and calculated Stark coefficients are given in Table 5 together with the dipole moments experimentally determined.

Table 5 shows that the observed Stark coefficients are in good agreement with the ones calculated from the dipole moments determined by the least squares analysis assuming $\mu_c=0$. The above fact is consistent with that the conformation of (*Z*)-(propionaldehyde oxime) is an *ap*, *Z*-form.

References

1) Otto L. Stiefvaster, *J. Chem. Phys.*, **62**, 233 (1975).
2) W. D. Phillips, *Ann. N.Y. Acad. Sci.*, **70**, 817 (1958).
3) O. Ohashi, R. Ishihara, T. Sakaizumi, M. Onda, and I. Yamaguchi, *Bull. Chem. Soc. Jpn.*, **49**, 891 (1976).
4) O. Ohashi, H. Hara, K. Noji, T. Sakaizumi, M. Onda, and I. Yamaguchi, *Bull. Chem. Soc. Jpn.*, **50**, 834 (1977).
5) M. Niwase, K. Kubota, K. Yoshida, T. Sakaizumi, M. Onda, O. Ohashi, and I. Yamaguchi, *Bull. Chem. Soc. Jpn.*, **57**, 2408 (1984).
6) M. Terashima and O. Ohashi, *Bull. Chem. Soc. Jpn.*, **58**, 3647 (1985).
7) K. Yoshida, T. Sakaizumi, O. Ohashi, and I. Yamaguchi, *Bull. Chem. Soc. Jpn.*, **59**, 1620 (1986).
8) D. Muenter, *J. Chem. Phys.*, **48**, 4544 (1968).

Tris(tellurato)cobaltate(III) and Tris(ethylenediamine)tris(tellurato)-tetracobaltate(III) Complexes[1)]

Yoichi SHIMURA* and Yutaka HOSOKAWA
Department of Chemistry, Faculty of Science, Osaka University,
Toyonaka, Osaka 560
(Received April 24, 1986)

Synopsis. Alkali metal salts of two new telluratocobaltate(III) complexes, $[Co(TeO_6H_4)_3]^{3-}$ and $[Co_4Te_3O_{18}(en)_3]^{6-}$, have been prepared. The latter heteropoly type complex and the related periodate analogue $[Co_4I_3O_{18}(en)_3]^{3-}$ have been optically resolved.

Only a limited number of telluratocobalt(III) complexes have been known such as $[Co(TeO_6H_4)(en)_2]Cl\cdot 3H_2O$[2)] and $K_3[Co(TeO_6H_4)_2(OH)_2]$.[3,4)] We report here two new entries, $K_3[Co(TeO_6H_4)_3]\cdot 2H_2O$ and $Na_3H_3[Co_4Te_3O_{18}(en)_3]\cdot 6H_2O$, of which the former belongs to a trischelate type and the latter to a hexol-like heteropoly type[5)] as seen in Fig. 1.

Experimental

$K_3[Co(TeO_6H_4)_3]\cdot 4H_2O$. To a solution of 0.84 g (3.1 mmol) of *cis*-$K[Co(CO_3)_2(NH_3)_2]\cdot H_2O$[6)] in 20 cm³ of water was added a solution of 2.5 g (11 mmol) of $Te(OH)_6$ in 20 cm³ of water with mechanical stirring. After the evolution of carbon dioxide ceased, a solution of 1.12 g (20 mmol) of potassium hydroxide in 20 cm³ of water was added gradually, and the mixture was stirred for a few hours at about 75 °C. The resulting solution was kept in a refrigerator overnight and filtered to remove a pale green precipitate of unknown nature. The filtrate was kept in a refrigerator for week. Then the dark green product was washed with methanol, ethanol, and acetone, and dried in a desiccator over silica gel. Found: H, 1.80; Co, 6.0; K, 12.4; Te, 40.8%. Calcd for $H_{20}O_{22}CoK_3Te_3$: H, 2.16; Co, 6.3; K, 12.6; Te, 41.1%.

$Na_3H_3[Co_4Te_3O_{18}(en)_3]\cdot 6H_2O$. A solution of 2.3 g (10 mmol) of $Te(OH)_6$ in 15 cm³ of water was added to a mixed solution of 2.6 g (9.4 mmol) of *trans*-$[CoCl_2(NH_3)_2(en)]Cl\cdot H_2O$[7)] and 1.0 g (3.0 mmol) of *cis*-$[Co(NH_3)_4(H_2O)_2](SO_4)_{1.5}\cdot 1.5H_2O$ in 30 cm³ of water. A solution of 2.4 g (60 mmol) of sodium hydroxide in 20 cm³ of water was added gradually to the mixture with mechanical stirring, and the stirring was continued at about 60 °C until the evolution of ammonia ceased. After cooling to room temperature an appropriate amount of ethanol was added gradually and the resulting solution was kept in a refrigerator overnight. The greenish brown product deposited was separated by a centrifuge, recrystallized twice from a 0.001 mol dm⁻³ sodium hydroxide solution by adding a small amount of ethanol, and washed with methanol and acetone several times. Found: C, 5.76; H, 3.54; N, 6.60; Co, 17.6; Te, 29.0%. Calcd for $C_6H_{39}N_6O_{24}Co_4Na_3Te_3$: C, 5.69; H, 3.10; N, 6.63; Co, 18.6; Te, 30.2%.

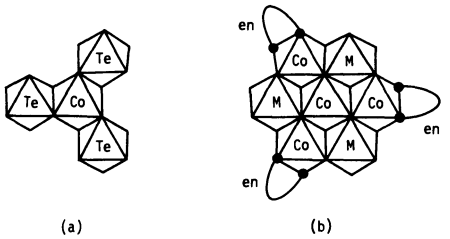

Fig. 1. Schematic structure of (a) Δ-$[Co(TeO_6H_4)_3]^{3-}$ and (b) $\Delta\Lambda'(\Lambda'')_3$-$[Co_4M^{(x)}{}_3O_{18}(en)_3]^{(24-3x)-}$ ($M^{(x)}$= Te^{VI} or I^{VII}). For the notation of absolute configuration, see the text.

$Na_3[Co_4I_3O_{18}(en)_3]\cdot 11H_2O$. This periodate complex was prepared in the same way as for the corresponding tellurate one by using H_5IO_6 instead of $Te(OH)_6$ at 80 °C. Found: C, 5.11; H, 3.26; N, 6.27%. Calcd for $C_6H_{46}N_6O_{29}Co_4I_3Na_3$: C, 5.33; H, 3.43; N, 6.22%. The visible-UV absorption spectrum was identical to that of the known free acid $H_3[Co_4I_3O_{18}(en)_3]\cdot 5H_2O$[8)] which was prepared from $H_3[Co_4I_3O_{18}(H_2O)_6]\cdot 8H_2O$.[8,9)]

Optical Resolution of $[Co_4M^{(x)}{}_3O_{18}(en)_3]^{(24-3x)-}$ ($M^{(x)}$=Te^{VI} and I^{VII}). A solution of 0.02 g of the resolving agent Λ-$(+)_{589}$-$[Co(en)_3]Br_3\cdot H_2O$ in 30 cm³ of water was added by portions with vigorous stirring to a solution of 0.1 g of $Na_3H_3[Co_4Te_3O_{18}(en)_3]\cdot 6H_2O$ dissolved in 100 cm³ of a 0.001 mol dm⁻³ sodium hydroxide solution. The mixture was concentrated to about 40 cm³ at 5—15 °C in air. The greenish brown less-soluble diastereomer deposited was separated by a centrifuge and washed with water–methanol (1:3). The diastereomer was stirred in a 0.001 mol dm⁻³ sodium hydroxide solution with a cation exchanger SP-Sephadex C-25 (Na^+ form) while being cooled in an ice-bath. The solution was filtered to remove the Sephadex, and CD (circular dichroism) of the filtrate was measured. $\Delta\varepsilon_{589}$=+0.31 cm⁻¹ mol⁻¹ dm³.

The corresponding periodate complex was resolved similarly using a solution of 0.12 g of $H_3[Co_4I_3O_{18}(en)_3]\cdot 5H_2O$ in 150 cm³ of a sodium hydroxide solution (pH 12) and a solution of 0.012 g of Λ-$(+)_{589}$-$[Co(en)_3]Br_3\cdot H_2O$ in 25 cm³ of water. The enantiomer obtained from the less-soluble diastereomer has $\Delta\varepsilon_{589}$=−0.68 cm⁻¹ mol⁻¹ dm³. An attempt was made to resolve the $[Co(TeO_6H_4)_3]^{3-}$ complex by a similar way, but only slight CD intensity was observed in the visible region.

Measurements. A Shimadzu UV-200 spectrophotometer and a JASCO MOE-1 spectropolarimeter were used for the absorption and CD measurements, respectively, of aqueous solutions at room temperature.

Results and Discussion

The absorption spectrum of $[Co(TeO_6H_4)_3]^{3-}$ ion was measured in a cooled 0.1 mol dm⁻³ potassium hydroxide solution (Fig. 2). The first spin-allowed d-d absorption band is located at 16500 cm⁻¹ and the position of tellurate ligand $TeO_6H_4^{2-}$ is determined in the spectrochemical series of oxygen chelate ligands: acetylacetonate(1−) 16900>oxalate(2−) 16570>tellurate(2−) 16500>malonate(2−) 16460>nitrate(1−) 16400>carbonate(2−) 15500 (values in the series mean the wavenumbers of the first d-d absorption bands of trischelate complexes). The strong absorption band at 27500 cm⁻¹ [log (ε/cm⁻¹ mol⁻¹ dm³)=3.18] is assigned to a ligand-to-metal charge transfer transition

Table 1. CD and Absorption Data[a] in the First d-d Transition Region

Complex	$\sigma_{ext}(\Delta\varepsilon)$	$\sigma_{max}(\log\varepsilon)$	Chromophore
$[Co(TeO_6H_4)_3]^{3-}$		16.5(1.82)	CoO_6
$(+)^{CD}_{589}$-$[Co_4Te_3O_{18}(en)_3]^{6-}$	15.0(−0.65)		CoO_6
	17.0(+3.01)	17.7(2.47)	CoO_4N_2
	19.7(−0.24)		CoO_4N_2
$(-)^{CD}_{589}$-$[Co_4I_3O_{18}(en)_3]^{3-}$	15.9(+0.37)		CoO_6
	17.8(−1.12)	18.2(2.61)	CoO_4N_2

a) Energies of CD extrema, σ_{ext}, and absorption maxima, σ_{max}, are given in 10^3 cm^{-1}, and the intensities $\Delta\varepsilon$ and ε in cm^{-1} mol^{-1} dm^3.

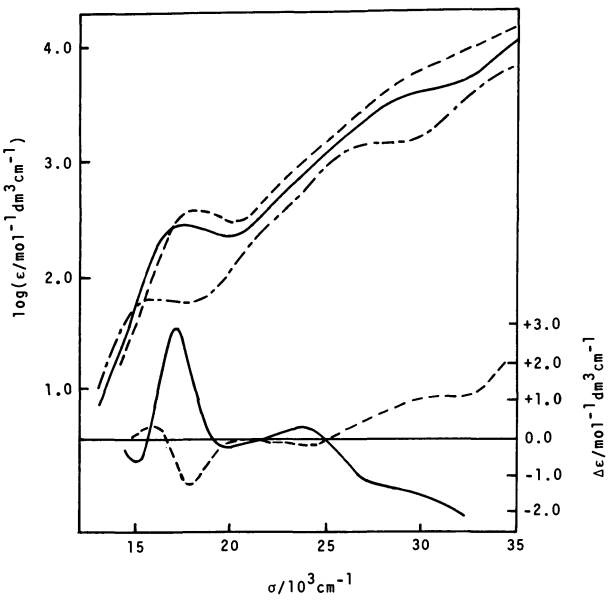

Fig. 2. Absorption and CD spectra of $(+)^{CD}_{589}$-$[Co_4Te_3O_{18}(en)_3]^{6-}$ (——) and $(-)^{CD}_{589}$-$[Co_4I_3O_{18}(en)_3]^{3-}$ (----), absorption spectrum of $[Co(TeO_6H_4)_3]^{3-}$ being also shown (——).

$e_g(Co)\leftarrow p_\pi(O)$ concerning the bridging oxo ligands.[10]

The tris(ethylenediamine)tris(tellurato)tetracobaltate(III) complex has a composition quite similar to that of the known periodate complex[8] $[Co_4I_3O_{18}(en)_3]^{3-}$. The parent aqua ion $[Co_4I_3O_{18}(H_2O)_6]^{3-}$ had been established in full detail from X-ray crystallography by two independent groups of workers.[11,12] A less characterized aqua derivative of the tellurato heteropoly compound had also been reported briefly.[3,4] For the present preparation of the heteropoly type tris(ethylenediamine) complexes, it was essential to use a mixed solution of two kinds of cobalt(III) complexes, one containing ethylenediamine and the other not.

$$3[CoCl_2(NH_3)_2(en)]Cl + [Co(NH_3)_4(H_2O)_2](SO_4)_{1.5} + 3Te(OH)_6 + 15NaOH \longrightarrow Na_3H_3[Co_4Te_3O_{18}(en)_3] + 9NaCl + 1.5Na_2SO_4 + 10NH_3 + 17H_2O$$

When only one kind of complex $[CoCl_2(NH_3)_2(en)]Cl$ was used, the main products containing tellurate ligands were a brown hexanuclear and a blue pentanuclear condensate of chain structure.[10] On the other hand, by using another kind of cobalt(III) complex $[Co(NH_3)_4(H_2O)_2](SO_4)_{1.5}$, the tris(tellurato)-cobalt(III) complex was obtained.

The $(+)^{CD}_{589}$-tellurato and $(-)^{CD}_{589}$-periodato heteropoly complexes show the similar CD patterns, the signs of the corresponding CD bands being opposite (Fig. 2 and Table 1). The enantiomer shown in Fig. 1 has the absolute configuration Δ concerning the $Co(MO_6)_3$ moiety, while Λ' the $Co(CoO_4en)_3$ moiety. In addition, the same enantiomer has three Λ'' peripheral chromophores $Co(en)(MO_6)_2$ (M=Te or I). Thus the total absolute configuration of this isomer should be represented by $\Delta\Lambda'(\Lambda'')_3$. From the well-known criterion that the Λ isomer of a trischelate cobalt(III) complex has a sign (+) for the main CD band in the first d-d absorption region,[13] the $(+)^{CD}_{589}$-$[Co_4Te_3O_{18}(en)_3]^{6-}$ isomer with a main positive CD band in the CoO_4N_2 chromophore region (Table 1) is assigned to be $\Delta\Lambda'(\Lambda'')_3$ configuration and the $(-)^{CD}_{589}$-$[Co_4I_3O_{18}(en)_3]^{3-}$ isomer to the $\Lambda\Delta'(\Lambda'')_3$ configuration. Unfortunately, the optical resolution of trischelate type complex $[Co(TeO_6H_4)_3]^{3-}$ was achieved only partially, and the quantitative CD curve was not obtained.

References

1) Partly presented at the 37th National Meeting of the Chemical Society of Japan, Yokohama, April 1978, Abstr., No. 3J37.
2) Y. Hosokawa and Y. Shimura, *Bull. Chem. Soc. Jpn.*, **52**, 1051 (1978).
3) M. W. Lister and Y. Yoshino, *Can. J. Chem.*, **40**, 1490 (1962).
4) Y. Yoshino, T. Takeuchi, and H. Kinoshita, *Nippon Kagaku Zasshi*, **86**, 978 (1965).
5) Y. Shimura, *Rev. Inorg. Chem.*, **6**, 149 (1984).
6) M. Shibata, *Nippon Kagaku Zasshi*, **87**, 771 (1966).
7) C. J. Hawkins, J. A. Stark, and C. L. Wong, *Aust. J. Chem.*, **25**, 273 (1972).
8) T. Ama, J. Hidaka, and Y. Shimura, *Bull. Chem. Soc. Jpn.*, **46**, 2145 (1973).
9) J. M. Williams and C. J. Nyman, *Inorg. Synth.*, **9**, 142 (1967).
10) Y. Hosokawa and Y. Shimura, *Bull. Chem. Soc. Jpn.*, **53**, 3202 (1980).
11) L. C. W. Baker, L. Lebioda, J. Grochowski, and H. G. Mukherjee, *J. Am. Chem. Soc.*, **102**, 3274 (1980); L. Lebioda, M. Ciechanowicz-Rutkowska, L. C. W. Baker, and J. Grochowski, *Acta Crystallogr., Sect. B*, **36**, 2530 (1980).
12) H. Kondo, A. Kobayashi, and Y. Sasaki, *Bull. Chem. Soc. Jpn.*, **55**, 2113 (1982).
13) A. J. McCaffery, S. F. Mason, and R. E. Ballard, *J. Chem. Soc.*, **1965**, 2883.

Optical Resolution of *erythro*-2-Amino-1,2-diphenylethanol by Reciprocal Crystallization of the Diastereomeric Salts with (−)-Mandelic Acid on Alternate Seeding

Kazuhiko SAIGO,* Izuru SUGIURA, Ikuko SHIDA, Kouzou TACHIBANA, and Masaki HASEGAWA
Department of Synthetic Chemistry, Faculty of Engineering, The University of Tokyo, Hongo, Bunkyo-ku, Tokyo 113
(Received April 10, 1986)

Synopsis. *erythro*-2-Amino-1,2-diphenylethanol was efficiently resolved into a pair of enantiomers by reciprocal crystallization of the diastereomeric salts with (−)-mandelic acid on alternate seeding.

Racemic *erythro*-2-amino-1,2-diphenylethanol (**1**), which can be easily prepared from commercially available benzoin oxime, has a similar fundamental structure to ephedrine. Therefore, optically active **1** is considered to be useful as an artificial chiral source. From this viewpoint optically active **1** has been applied in our laboratory as a chiral auxiliary in optical resolutions[1] and asymmetric syntheses.[1,2] Optically active **1** can be obtained by the fractional crystallization of the diastereomeric salts of racemic **1** with D-glutamic acid[3] or with (+)-10-camphorsulfonic acid,[4] by the preferential crystallization of the enantiomeric salts of racemic **1** with cinnamic acid,[1] and by chromatographic separation of diastereomeric 2-oxazolidinone derivative of racemic **1**.[5] The fractional crystallization, however, requires several recrystallization to get (+)- and (−)-**1** in high optical purities. The resolution efficiency of the preferential crystallization is not so high as observed in usual one although (+)- and (−)-**1** are obtained in high optical purities by simple operation. Moreover, the chromatographic separation includes multiple step and has a limitation in a quantity per one operation. We therefore examined another method to prepare optically active **1** more efficiently and easily.

Treatment of (+)- and (−)-**1**, which was prepared by preferential crystallization,[1] with an equimolar amount of (−)-mandelic acid (**2**) gave a pair of diastereomeric salts. Between the solubilities of these two salts in methanol and ethanol, there was little difference, meaning that it is impossible to resolve simply these diastereomeric salts by fractional crystallization. Actually a mixture of both diastereomeric salts with ethanol of crystallization deposited on cooling a hot clear ethanol solution of the mixture. By contrast, (+)-**1**·(−)-**2**·EtOH salt deposited preferentially when the supersaturated solution was cooled to about 40 °C by standing at room temperature and seeded with a small amount of diastereomerically pure (+)-**1**·(−)-**2**·EtOH salt. Moreover, seeding of (−)-**1**·(−)-**2**·EtOH salt to the filtrate gave (−)-**1**·(−)-**2**·EtOH salt preferentially. On the basis of specific rotations, these salts were found to be highly diastereomerically pure. This result means that racemic **1** can be resolved by "reciprocal crystallization of diastereomeric salts on alternate seeding," which is very rare in the optical resolution of diastereomers.

By repeating alternate seeding of (+)-**1**·(−)-**2**·EtOH and (−)-**1**·(−)-**2**·EtOH salts in this order to the mother liquor, which was supersaturated in a similar magnitude on addition of (±)-**1**·(−)-**2**·salt, both diastereomeric salts were reciprocally obtained in high diastereomeric purities. The result is shown in the Table. This procedure could be carried out in 0.10—0.05 mol scale to give both of diastereomeric salts in large quantities with high diastereomeric purities.

The recrystallized diastereomeric salts were dissolved in hot water and treated with aqueous ammonia to give white precipitates, respectively. Recrystallization of them from ethanol gave optically pure (+)- and (−)-**1**.

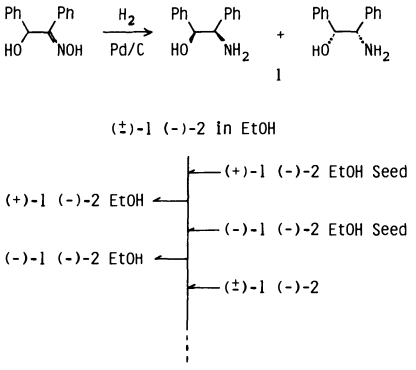

Experimental

All melting points were measured by a Laboratory Devices MEL-TEMP apparatus and are uncorrected. Optical rotations were recorded on a JASCO DIP-360 Digital Polarimeter.

Table 1. Reciprocal Crystallization of (±)-**1**·(−)-**2** Salt on Alternate Seeding

Run[a]	(±)-**1**·(−)-**2** Salt Supplied (g)	Signs of Seed **1**·**2**·EtOH	Yield g	Diastereomeric Purity/%
1	—	(+) (−)	1.37	94
	—	(−) (−)	1.37	99
2	2.32	(+) (−)	1.33	96
	—	(−) (−)	0.99	97
3	2.13	(+) (−)	1.09	96
	—	(−) (−)	1.37	99

a) The initial composition of the mother liquor: (±)-**1**·(−)-**2** salt (3.65 g) in ethanol (60 ml).

(±)-*erythro*-2-Amino-1,2-diphenylethanol (**1**) was synthesized by hydrogenation of commercially available benzoin oxime.[1,3] A pair of optically active **1** was prepared by the preferential crystallization of enantiomeric salts of racemic **1** with cinnamic acid salt.[1] (−)-Mandelic acid (**2**) is of commercial origin and was used without any purification.

Preparation of (+)-1·(−)-2·EtOH and (−)-1·(−)-2·EtOH Salts for Seeds. The reaction of (+)- or (−)-**1** with (−)-**2** in ethanol, followed by recrystallization from ethanol, gave the corresponding diastereomeric salts in pure state, respectively. The salts, dried at room temperature for 12 h over P_2O_5 in vacuo, contained an equimolar amount of ethanol of crystallization. They were used as seeds for the reciprocal crystallization of diastereomeric salts on alternate seeding.

(+)-**1**·(−)-**2**·EtOH salt: Mp 167—168.5 °; $[\alpha]_{435}^{17}$ +93.9° (*c* 1.00, MeOH). (−)-**1**·(−)-**2**·EtOH salt: Mp 162—163.5 °; $[\alpha]_{435}^{15}$ −259.7° (*c* 1.00, MeOH).

Drying at 80 °C for 24 h over P_2O_5 in vacuo gave the dastereomeric salts without ethanol of crystallization.

(+)-**1**·(−)-**2** salt: Mp 165—167 °C; $[\alpha]_{435}^{17}$ +105.7 ° $[\alpha]_{D}^{17}$ +49.0° (*c* 1.00, MeOH).

Found: C, 72.49; H, 6.08; N, 3.96%. Calcd for $C_{22}H_{23}NO_4$: C, 72.31 H, 6.34; N, 3.83%.

(−)-**1**·(−)-**2** salt: Mp 156—158 °C; $[\alpha]_{435}^{15}$ −292.5°, $[\alpha]_{D}^{15}$ −134.4° (*c* 1.00, MeOH).

Found: C, 72.39; H, 6.20; N, 3.62%. Calcd for $C_{22}H_{23}NO_4$: C, 72.31; H, 6.34; N, 3.83%.

The diastereomeric purities of the deposited precipitates by reciprocal crystallization on alternate seeding and the recrystallized diastereomeric salts were calculated on the basis of the specific rotations of the salts with or without ethanol of crystallization, respectively.

Optical Resolution by Reciprocal Crystallization of Diastereomeric Salts on Alternate Seeding. A solution of (±)-**1** (2.13 g, 10 mmol) and (−)-**2** (1.52 g. 10 mmol) in 99% ethanol (60 ml) was refluxed until the solution became clear. The solution was cooled to about 40 °C by standing at room temperature and then seeded with (+)-**1**·(−)-**2**·EtOH salt (10 mg), followed by standing overnight at room temperature. The white precipitate deposited was collected by filtration and dried over P_2O_5 at room temperature in vacuo to give (+)-**1**·(−)-**2**·EtOH salt (1.37 g, 67%): $[\alpha]_{435}^{13}$ +83.8° (*c* 1.00, MeOH); 94% diastereomeric purity.

The filtrate was again refluxed, cooled, and seeded with (−)-**1**·(−)-**2**·EtOH salt. On standing the solution overnight at room temperature, white precipitate deposited. The precipitate was collected by filtration and dried at room temperature for 12 h in vacuo to give (−)-**1**·(−)-**2**·EtOH salt (1.37 g, 67%): $[\alpha]_{435}^{16}$ −257.9° (*c* 1.00, MeOH); 99% diastereomeric purity.

To the mother liquor was added (±)-**1**·(−)-**2** salt (2.32 g) and the solution was similarly refluxed, cooled, and seeded with (+)-**1**·(−)-**2**·EtOH and (−)-**1**·(−)-**2**·EtOH salts, successively. The process was repeated in a similar manner supplying 2.1—2.3 g of (±)-**1**·(−)-**2** salt in each run to give (+)-**1**·(−)-**2**·EtOH and (−)-**1**·(−)-**2**·EtOH salts in high diastereomeric purities. The initial three runs are shown in the Table.

The crystals of the same diastereomer were combined, recrystallized from ethanol, and dried at about 80 °C for 24 h in vacuo to give optically pure (+)-**1**·(−)-**2** and (−)-**1**·(−)-**2** salts.

(+)-**1**·(−)-**2** salt: 84% recrystallization yield; mp 165—167 °C; $[\alpha]_{435}^{15}$ +105.6 ° (*c* 1.00, MeOH); 100% diastereomeric purity.

(−)-**1**·(−)-**2** salt: 84% recrystallization yield; mp 156—157 °C; $[\alpha]_{435}^{15}$ −292.5 °C (*c* 1.00, MeOH); 100% diastereomeric purity.

Decomposition of the Diastereomeric Salts. In 530 ml of water (+)-**1**·(−)-**2** salt (28.61 g) was dissolved at 70 °C and then treated with aqueous ammonia (28 ml). Recrystallization of the resulting precipitate from ethanol gave (+)-**1** (11.57 g, 86%): Mp 142.5—144 °C; $[\alpha]_{D}^{19}$ +7.7° (*c* 0.60, EtOH); 100% optical purity (lit,[1] mp 143—144 °; $[\alpha]_{D}^{24}$ +7.7° (*c* 0.63, EtOH)).

Similar treatment of (−)-**1**·(−)-**2** salt (22.40 g), followed by recrystallization, gave (−)-1 (10.16 g, 80%): Mp 143—144.5 °C; $[\alpha]_{D}^{16}$ −7.5° (*c* 0.60, EtOH); over 99% optical purity (lit,[1] mp 143—144 °C; $[\alpha]_{D}^{32}$ −7.6° (*c* 0.60, EtOH).

References

1) K. Saigo, S. Ogawa, S. Kikuchi, A. Kasahara, and H. Nohira, *Bull. Chem. Soc. Jpn.*, **55**, 1568 (1982).

2) K. Saigo, A. Kasahara, and H. Nohira, *Tetrahedron Lett*, **24**, 511 (1983).

3) J. Weijland, K. Pfister 3rd, E. F. Swanezy, C. A. Robinson, and M. Tishler, *J. Am. Chem. Soc.*, **73**, 1216 (1951).

4) I. G. Vasi and R. K. Desai, *Indian J. Chem., Sect. B*, **14B**, 625 (1976).

5) W. H. Pirkle and K. A. Simmons, *J. Org. Chem.*, **48**, 2520 (1983).

Photoreaction of *N*-Alkylamides Containing Iron(III) Chloride by Monochromatic Light

Yasushi YOKOYAMA, Takahiro SUZUKI, and Yukio KURITA*
Department of Materials Chemistry, Faculty of Engineering, Yokohama National University, Tokiwadai, Hodogaya-ku, Yokohama 240
(Received January 8, 1986)

Synopsis. The photolysis of *N*-alkylamides containing $FeCl_3$ using monochromatic light corresponding to the absorption maxima were examined by ESR. Irradiation by 313-nm light resulted mainly in a hydrogen abstraction from the aliphatic carbon adjacent to either CO or NH, whereas 366-nm light produced an acyl radical in larger amounts.

The photoreduction of coordinated metal ions, accompanied by an oxidation of their ligands, is an interesting problem.[1] Recently, we have reported on an ESR study of the photolysis of some *N*-alkylamides containing $FeCl_3$ by UV light irradiation (300—400 nm).[2] We showed that: 1) Some amides gave a mixture of radicals consisting of **a** and **b** or **c** at liquid-nitrogen temperature and 2) amide–$FeCl_3$ complexes gave two absorption maxima in a $CHCl_3$ solution at 312 and 350 nm. Here, we report that the irradiation of amide–$FeCl_3$ complexes with 313-nm light, corresponding to one of the absorption maxima, gave mainly a hydrogen-abstracted radical (**b** or **c**). However, irradiation with 366-nm light, corresponding to another absorption maxima, gave an increased relative molar ratio of the acyl radical **a**.

$RCH_2\dot{C}O$ $RCH_2CONH\dot{C}HR'$ $R\dot{C}HCONHCH_2R'$
a **b** **c**

Photoreaction experiments were carried out on eight amides. Here, a typical example is given. The irradiation of the *N*-ethyl-acetamide (**2**)–$FeCl_3$ mixture at 77 K by 313-nm light for 20 min gave the ESR spectrum shown in Fig. 1a. It was analyzed and shown to be a 72/28 mixture of a 1:4:6:4:1 quintet

Table 1. Radicals Generated from Photoirradiated Amide–$FeCl_3$ Mixture and Their Relative Molar Ratio Observed by ESR at 77 K

Amides	313 nm[a] *g*-Value, A_H/mT	(**b** or **c**)/**a**	366 nm[b] *g*-Value, W_{msl}/mT	(**b** or **c**)/**a**
$CH_3CONHCH_3$	CO-side[c]	31/69	Acetyl	42/58
1	2.002, 2.20		2.001, 1.5	
$CH_3CONHCH_2CH_3$	NH-side[d]	72/28	Acetyl[d]	48/52
2	2.002, 2.05		2.001, 1.5	
$CH_3CH_2CONHCH_3$	CO-side[e]	69/31	Propanoyl[e]	50/50
3	2.002, 2.44		2.001, 1.3	
$CH_3CH_2CONHCH_2CH_3$	f)	59/41	Propanoyl	56/44
4	2.003, 2.05		2.001, 1.3	
$CH_3CH_2CONH(CH_2)_2CH_3$	CO-side[d,g]	82/18	Propanoyl[d]	71/29
5	2.002, 2.42		2.001, 1.25	
$CH_3CH_2CONH(CH_2)_5CH_3$	CO-side[d,g,h]	83/17	Propanoyl[d]	80/20
6	2.002, 2.42		2.001, 1.2	
$CH_3(CH_2)_2CONHCH_2CH_3$	NH-side[g]	69/31	Butanoyl	39/61
7	2.002, 2.21		2.001, 1.5	
$CH_3CH_2CONHCH(CH_3)_2$	CO-side	95/5	Propanoyl	82/18
8	2.002, 2.40		2.001, 1.5	

a) Irradiation by 313 nm light always generated a small to medium amount of acyl radical together with hydrogen-abstracted radical. Values at the right side of this column are the relative molar ratio of hydrogen-abstracted radical/acyl radical. In the cases of **2**, **5**, and **6**, the numerators contain the contribution from the alkyl radical generated from the acyl radical. "NH-side" refers to the radical -CONHĊH-(**b**), and "CO-side" refers to the radical -ĊHCONH-(**c**). Because A_H^{α} is indistinguishable from A_H^{β} in every case, both of them are represented by A_H. b) Irradiation by 366 nm light always generated a hydrogen-abstracted radical and an acyl radical. Values at the right side of this column are the relative molar ratios of the hydrogen-abstracted radical/acyl radical. c) Yield of the radicals was very low. d) Also containing the alkyl radical decarbonylated from the acyl radical **a**. e) Also containing $\cdot N{=}CH_2$ (g=2.002, A_H=8.9 mT) generated from $HN{=}CH_2$.[2,10] f) Undetermined.[11] g) On irradiation by 313 nm light, amides **5**, **6**, and **7** produced the 1 : 4 : 6 : 4 : 1 radicals which we assigned to $-X\dot{C}HCH_3$, not $-X\dot{C}HCH_2-$ (X=NH or CO) which occasionally shows a 1 : 2 : 2 : 2 : 1 quintet,[12] because **5**-d_2 ($CH_3CH_2CONHCD_2CH_2CH_3$) gave a quintet (g=2.002, A_H=2.43 mT) similar to that of **5**. h) Small amount of $-CH_2\dot{C}HCH_2-$ type radical was also existing.[9]

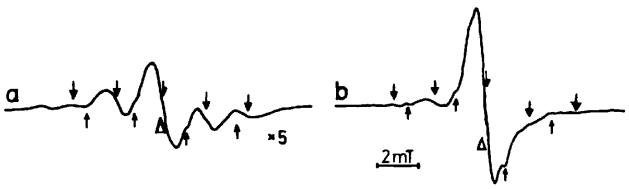

Fig. 1. (a) ESR spectrum of 313nm-irradiated **2**-$FeCl_3$ mixture. (b) ESR spectrum of 366nm-irradiated **2**-$FeCl_3$ mixture. Methyl radical is denoted by an upward arrow, **2a** by a delta, and **2b** by a downward arrow.

(g=2.002, A_H=2.1 mT, **2b**[3]) and a singlet (g=2.001, W_{msl}=1.5 mT, **2a**[5]),[6] together with a small amount of the methyl radical generated by decarbonylation from the acetyl radical.[2]

When the amide (**2**)-$FeCl_3$ mixture was irradiated by 366-nm light, the spectrum shown in Fig. 1b was obtained. This time, it was analyzed and shown to be a 48/52 mixture of **2b** and **2a**, along with (again) a small amount of the methyl radical.

The results obtained in a similar manner are summarized in Table 1.

In all cases, 313-nm light gave rise to the predominant formation of the hydrogen-abstracted radical **b** or **c**, except the amide **1** which produced a little amount of the radical; 366-nm light gave rise to the formation of a larger relative amount of the acyl radical **a** in most cases. This shows a difference in the natures of the two absorption bands in the UV spectra.[7]

The hydrogen-abstracted radicals generated by 313-nm light were classified into two groups. Group-one amides (**2** and **7**) generated a radical having an unpaired electron on the carbon atom adjacent to the NH group (**b**), whereas for group-two (**1**, **3**, **5**, **6**, and **8**), the electron appeared on the carbon atom adjacent to the CO group (**c**).[8]

In the case of amide **6**, a small amount of $-CH_2\dot{C}HCH_2-$ radical[9] was also observed upon irradiation with 313-nm light. Because amide **6** has an ethyl group on the carbonyl and the main hydrogen abstraction occurred on this side, the inner radical must be on the hexyl moiety on the NH group. This was confirmed by a GC–MS measurement (see below). From this experiment, the formation of three reaction products (*N*-(3-hexenyl)propanamide (**9**), *N*-hexyl-2-chloropropanamide (**10**), and *N*-(4-chlorohexyl)propanamide (**11**) was confirmed. Chloride **10** corresponds to a product from **6a**, and **9** and **11** are from the inner radical.

In some cases, the ESR spectrum after 313 or 365 nm irradiation showed the presence of alkyl radicals generated by a decarbonylation of the corresponding mother acyl radicals (**2**, **5**, and **6**).[2]

Experimental

Amides used in this study were prepared by a condensation of the corresponding monoalkylamine and acid chloride in benzene in the presence of pyridine, and purified by several distillations under a reduced pressure. Their purities were examined by gas chromatography (column SP-1000, 100—220 °C).

ESR Measurement. A sample for ESR measurement was prepared by dissolving $FeCl_3$ (Wako Pure Chem., chemical grade) in amide ($3—5\times10^{-3}$ mol dm^{-3}) under a nitrogen atmosphere and then degassed by a freeze-pump-thaw technique (three times) in a quartz sample tube.

Photoirradiation was carried out using a USH-500D 500W ultra-high-pressure mercury lamp (Ushio Co.).

Filters for 313-nm light irradiation[13] (9% transmittance at 313 nm) were water (cell length 50 mm), aqueous potassium hydrogen phthalate (5 g dm^{-3}, cell length 10 mm), potassium chromate in 0.1% aqueous sodium hydroxide (0.2 g dm^{-3}, cell length 10 mm), aqueous nickel(II) sulfate hexahydrate (100 g dm^{-3}, cell length 50 mm), and UV-D35 glass filter (Toshiba Glass Co., 3 mm thick). Filters for 366 nm light[13] (25% transmittance at 366 nm) were water (cell length 50 mm), Pyrex glass (2.5 mm thick), UV-35 and UV-D36A glass filters (both Toshiba Glass Co., 3 mm thick).

ESR spectra were recorded by a JEOL JES-ME-3X ESR spectrometer at liquid-nitrogen temperature immediately after irradiation for an adequate period (ca. 1—20 min) at that temperature.

GC-MS Measurement of Photoirradiation Product of 6-$FeCl_3$. Amide **6** containing $FeCl_3$ was irradiated by >300-nm light for about 6 h under a nitrogen atmosphere at room temperature. The resulting mixture was extracted with hexane, followed by an examination with GC–MS (JEOL D-300 Mass Spectrometer, column PG-20E, 80—160 °C. The oven temperature was increased at a rate of 8 °C per minute). **9**: Retention time 4′35″; m/z 155 (M^+; 15), 98 ($(M-CH_3CH_2CO)^+$; 29), 70 (29), 69 ($(CH_3CH_2CH{=}CHCH_2)^+$, allylic cleavage; 100), and 57 ($CH_3CH_2CO^+$; 35). **10**: Retention time 6′25″; m/z 191 (M^+; 7), 156 ($(M-Cl)^+$; 28), 128 ($M-CH_3CHCl)^+$; 64), 123 (7), 122 (8), 121 (24), 120 (23), 85 ($(M-CH_3CHClCONH)^+$; 100), 65 (CH_3CHCl^+; 7), and 63 (CH_3CHCl^+; 20). **11**: Retention time 8′05″; m/z 193 (M^+; 3), 191 (M^+; 10), 156 ($(M-Cl)^+$; 39), 155 ($(M-HCl)^+$; 20), 114 ($(M-CH_3CH_2CHCl)^+$; 55), 100 ($(M-CH_3CH_2CHClCH_2)^+$; 25), 87 (63), 86 ($CH_3CH_2CONHCH_2^+$; 89), 74 (35), 73 ($CH_3CH_2CONH^+$; 80), 58 (64), and 57 ($CH_3CH_2CO^+$; 100).

References

1) T. Imamura, T. Jin, T. Suzuki, and M. Fujimoto, *Chem. Lett.*, **1985**, 847, and references cited therein.

2) Y. Kurita, Y. Yokoyama, J. Shirokaze, and Y. Fujii, *Nippon Kagaku Kaishi*, **1982**, 1111.

3) We assigned the quintet to **2b** because **2c** is expected to give a broad triplet. The observed coupling constant of 2.1 mT is comparable to that of a radical $H_2NCONH\dot{C}HCH_3$ (A_{CH}=1.83 mT, A_{Me}=2.3 mT).[4]

4) T. S. Jaseja and R. S. Anderson, *J. Chem. Phys.*, **35**, 2192 (1961).

5) S. Noda, K. Fueki, and Z. Kuri, *J. Chem. Phys.*, **49**, 3287 (1968).

6) Relative molar ratio of the radicals was determined by simulation.

7) It seems to be quite reasonable to assign the 312-nm absorption band as the CT band from Cl^- to Fe(III) and the 350-nm band as the CT band from amide to Fe(III). The former caused the generation of Cl, which might abstract hydrogen from an amide molecule. The latter generated an amide cation radical which decomposed into an acyl radical, an imine, and a proton[2] when irradiated on the absorption maxima.

8) We could not clarify what nature of amides would determine the course of the hydrogen abstraction. However,

there is an apparent tendency that an $-X\dot{C}HCH_3$ type radical (X=NH or CO) is apt to be generated.

9) g-Value=2.001, $A_H^{\alpha}=A_H^{\beta}=3.23$ mT. see; A. Lund, *J. Phys. Chem.*, **76**, 1411 (1972).

10) D. Banks and W. Gordy, *Mol. Phys.*, **26**, 1555 (1973).

11) Because both NH- and CO- side radicals generated from **4** would give a quintet having a similar g-value and A_H, we could not assign the observed radical. However, we think that it would be an NH-side radical, judging from the fact that the A_H value is closer to that of **2b** than to that of **3c**.

12) Yu. A. Kruglyak and V. S. Kuts, *Zh. Strukt. Khim.*, **9**, 33 (1968).

13) J. G. Calvert, J. N. Pitts, Jr., "Photochemistry," John Wiley and Sons, Inc., New York(1966), p. 728.

Structure Model for Liquid Neopentane

Keiko NISHIKAWA
Department of Chemistry, Faculty of Science, Gakushuin University,
Mejiro, Toshima-ku, Tokyo 171
(Received October 21, 1985)

Synopsis. Structure simulation studies for liquid neopentane have been carried out by the use of real space expansion and reciprocal space expansion based on the local lattice structure model. A body centered cubic (bcc) model has reproduced Narten's experimental data very well.

X-Ray diffraction studies for liquid neopentane were carried out by Narten.[1] He measured the diffraction intensities from the liquid at eight different temperatures under high pressure from −17° (melting point) to 150 °C (cf. the critical point, 161 °C and 32 bar). He also attempted structure analysis, constructing an intermolecular correlation function from Percus-Yevick theory using the analytical solution for hard spheres. He reported that the calculated correlation function was in very good agreement with the experimental curves for values of $s \leq 1.5$ Å^{-1} but the deviation from the experimental intensity became large with increase of s ($s=4\pi\sin\theta/\lambda$).

In order to understand orientational correlation of molecular liquids, it is useful to construct a model in which we visualize a structure model which is to be tested against the experimental intensity. Such modeling for liquid structure, such as the "local lattice structure model" is usually formulated in the form of "real space expansion."[2-4] Recently a new method named "reciprocal space expansion" has been introduced by the present author and her coworker.[5,6] The real space expansion and reciprocal space expansion are complementary to each other; with good convergence in larger s-values for the former and the good convergence in the smaller s-region for the latter. The two methods were successfully applied to liquid carbon tetrachloride[4-6] based on the local lattice model of a bcc arrangement with head-tail head-tail packing.

In the present work the two methods have been applied to the structure simulation for liquid neopentane using the same bcc model. The diffraction intensities of liquid neopentane observed by Narten[1] are used.

First, the real space expansion was tried, and the weighted structure function $si(s)$ was used for the comparison of the simulated scattering intensities with the experimental ones. The least-squares refinement was carried out with four parameters; the lattice constant of the bcc cell a, the Prins parameter D,[7] the radius of the discrete structure region R_c and its temperature factor l_c. Because of the large values of l_{ij}, the more rigorous expression $\sin s(r_{ij}-l_{ij}^2/r_{ij})$[8] was used in the calculation instead of $\sin sr_{ij}$ of Eq. 4 in Ref. 4. For the values of the intramolecular distances r_{C-Me} and r_{Me-Me} and their root mean-square amplitudes l_{C-Me} and l_{Me-Me}, those obtained by the gas electron diffraction[9] were used. The group scattering factor for CH_3 group introduced by Narten[1] was used.

The number of molecules first contained in the discrete structure region was nine (a central molecule and the first nearest neighbors) at the initial trial, which was increased during the least-square refinements up to 51. That is the number of molecules included in the fourth nearest neighbors around the central molecule. Further increase of the number of molecules in the structure region no longer changed the feature of the calculated $si(s)$ curve. Scattering intensities ranging from 1 to 6 Å^{-1} have been used, because for the s-region smaller than 1 Å^{-1} spurious peaks inevitably appear whereas for the s-region larger than 6 Å^{-1} the calculated $si(s)$ is approximately equal to that of a free neopentane molecule and is considered hardly affected by the intermolecular interference. The results of the least-squares refinements for the

Table 1. The Refined Parameters of the bcc Model for Liquid Neopentane[a]

t/°C	a/Å	d/Å	D/Å	R_c/Å	l_c/Å	R factor[b]
−17	7.09(9)	6.14	0.057(16)	13.0(4)	1.8(8)	0.14
0	7.21(10)	6.24	0.058(16)	13.2(4)	1.9(10)	0.14
25	7.31(10)	6.33	0.069(17)	13.3(4)	2.1(10)	0.11
50	7.33(11)	6.38	0.074(18)	13.3(3)	2.2(9)	0.10
75	7.52(12)	6.51	0.091(25)	13.3(3)	2.5(9)	0.09
100	7.71(15)	6.68	0.113(35)	13.9(4)	2.1(10)	0.08
125	7.82(18)	6.77	0.128(48)	14.1(4)	2.3(12)	0.07
150	7.97(22)	6.90	0.151(51)	14.3(5)	2.6(16)	0.07

a) a: the lattice constant of the bcc lattice, d: the nearest neighbor distance calculated from a, D: the Prins parameter, R_c: the radius of the structure region, l_c: temperature factor for R_c. The values in parentheses are the standard deviations in the last significant digit. b) The reliability factor R is defined by

$$R = \left[\frac{\sum \{si(s)_{exp} - si(s)_{calc}\}^2}{\sum (si(s)_{exp})^2} \right]^{1/2}$$

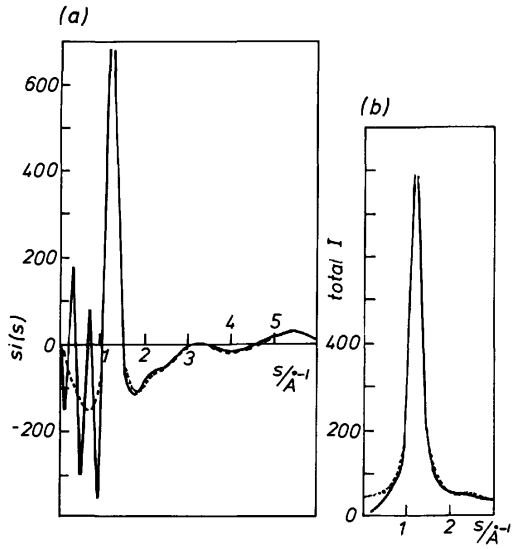

Fig. 1. The scattering intensities of liquid neopentane at −17 °C. The solid curves are the calculated intensities and the broken curves are Narten's experimental values. (a) Reduced intensity $si(s)$. The calculated one is obtained by the real space expansion based on the bcc model. (b) Total coherent intensity $I(s)$. The calculated one is obtained by the reciprocal space expansion.

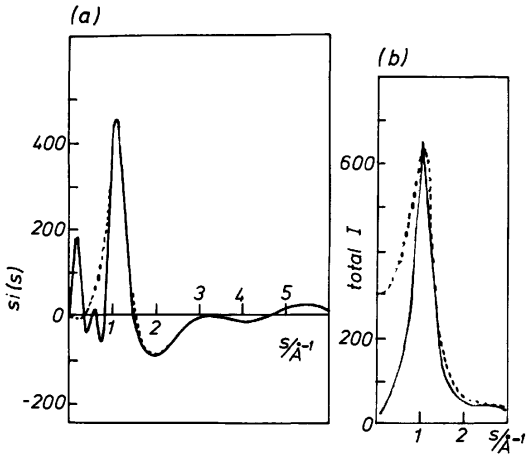

Fig. 2. The scattering intensities of liquid neopentane at 150 °C. See the caption of Fig. 1 for other details.

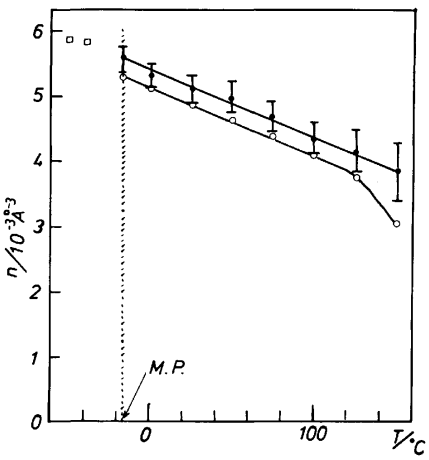

Fig. 3. Number densities n of neopentane. Dots show the values obtained by the bcc model, open circles those from Refs. 11 and 12 cited in Ref. 1 and squares for the plastic crystal phase.[13,14]

eight temperatures are shown in Table 1. The values of the nearest neighbor distance d are also given. The calculated $si(s)$ curves at −17° and 150 °C are respectively compared in Figs. 1(a) and 2(a) with Narten's experimental data.

Next, the reciprocal space expansion was carried out using the same a and D parameters. In this calculation reciprocal lattice points up to 600 are included. For the 600 the magnitude of the reciprocal lattice point vector is 5.32 Å^{-1} in the case of the data at −17 °C. The total coherent intensity is adopted, because it distinguishes the discrepancy between the experimental and simulated intensities in the small s-region. The results at −17° and 150 °C are shown in Figs. 1(b) and 2(b).

As seen in Figs. 1 and 2, X-ray scattering intensities from liquid neopentane could be well simulated by the bcc model, in the range of $s \geq 1$ Å^{-1} by the use of the real space expansion and in the range of $0.5 \leq s \leq 3$ Å^{-1} by the use of the reciprocal space expansion. Two peaks on the calculated curves at an s-region smaller than 1 Å^{-1} in Figs. 1(a) and 2(a) are all spurious due to the sudden onset of the continuum region to the discrete region, which do not appear in the total coherent intensity curves calculated by the reciprocal space expansion. A difference between the experimental and calculated intensities by the use of the reciprocal spece expansion is seen in the region of $s \leq 0.5$ Å^{-1}. The experimental scattering intensity near $s \approx 0$ Å^{-1} has a finite value because of the density fluctuation of the liquids.[10] With increase of temperature the density fluctuation increased and especially near the critical point this became significantly large. The density fluctuation was not included in the present formulation by the local lattice structure model.

From the variation of the lattice constants a's determined for the bcc model at different temperatures, the number densities of the liquid were calculated, these are shown in Fig. 3. The number densities decreased almost linearly with the increase of temperature. For comparison, the values tabulated in Narten's paper[1] are also given in Fig. 3. He obtained them by interpolating the values from the measurements of Gonzales and Lee[11] and from the values listed in the book by Timmermans.[12] The number density obtained from the present bcc model is approximately 5% larger than these values. The difference of these number densities may be explained by the possibility that the volatile neopentane contains many voids in its structure. The number densities for the plastic crystal at −40° and −50 °C calculated from values of the mass density determined by means of powder diffraction[13,14] are also shown in Fig. 3.

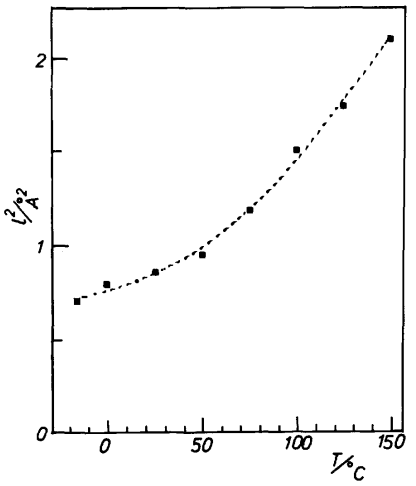

Fig. 4. Temperature dependence of the mean square deviation, l^2, of the neighboring neopentane molecules.

The mean square deviations of liquids increased as the distance between the central molecule and surrounding ones increased, and the deviations in the case of liquid neopentane were described well by the Prins relation $l_{ij}^2=2Dr_{ij}$.[7]

For harmonic oscillators at high temperature or low frequencies the mean square deviation of l^2 becomes[15]

$$l^2 = \frac{kT}{4\pi^2\mu\nu^2},$$

where ν is the frequency of the ocillator, T absolute temperature, and μ the reduced mass. Then l^2 is proportional to T. For several acceptable potentials with anharmonicity, the mean square deviation l^2 was calculated and found to be approximately proportional to T in this temperature range.[16] The observed l^2 was therefore expected to be nearly proportional to T. This however was not true in the present case, as is shown in Fig. 4. It exhibits a nearly parabolic increase with increase of temperature. This temperature dependence of the mean square deviations can be considered as the direct reflection of the effective potential that a molecule in the liquid feels. More detailed investigation on the mean square deviations will give information concerning the dynamical properties of the liquid but this is left for future studies.

The author wishes to express her thanks to Professor Takao Iijima, Gakushuin University, for his helpful suggestions and discussion.

References

1) A. H. Narten, *J. Chem. Phys.*, **70**, 299 (1979).
2) A. H. Narten, M. D. Danford, and H. A. Levy, *Discuss. Faraday Soc.*, **43**, 97 (1967).
3) A. H. Narten and H. A. Levy, *Science*, **165**, 447 (1969).
4) K. Nishikawa and T. Iijima, *Bull. Chem. Soc. Jpn.*, **58**, 1215 (1985).
5) T. Iijima and K. Nishikawa, *Chem. Phys. Lett.*, **115**, 522 (1985).
6) K. Nishikawa and T. Iijim, *Bull. Chem. Soc. Jpn.*, **59**, 117 (1986).
7) J. Frenkel, "Kinetic Theory of Liquids," Dover Publications, New York (1955).
8) Y. Morino, Y. Nakamura, and T. Iijima, *J. Chem. Phys.*, **32**, 643 (1960).
9) L. S. Bartell and W. Bradford, *J. Mol., Struct.*, **37**, 113 (1977).
10) C. Croxton, "Introduction to Liquid State Physics," John Wiley & Sons, London (1975).
11) M. H. Gonzales and A. L. Lee, *J. Chem. Eng. Data*, **13**, 68 (1968).
12) J. Timmermans, "Physico-chemical Constants of Pure Organic Compounds," Elsevier, New York (1965).
13) A. Mones and B. Post, *J. Chem. Phys.*, **20**, 755 (1952).
14) R. Rudman and B. Post, *Mol. Cryst.*, **5**, 95 (1968).
15) Y. Morino, K. Kuchitsu, A. Takahashi, and K. Maeda, *J. Chem. Phys.*, **21**, 1927 (1953).
16) K. Nishikawa and T. Iijima, to be published.

Mössbauer Spectroscopic Study on the Mixed-Valence States of 1′,1‴-Bis(*o*-methylbenzyl)-, 1′,1‴-Bis(*m*-methylbenzyl)-, and 1′,1‴-Bis(*p*-methylbenzyl)biferrocenium Triiodide

Satoru NAKASHIMA, Motomi KATADA, Izumi MOTOYAMA, and Hirotoshi SANO*
Department of Chemistry, Faculty of Science, Tokyo Metropolitan University, Fukasawa, Setagaya-ku, Tokyo 158
(Received April 19, 1986)

Synopsis. 1′,1‴-Bis(*o*-methylbenzyl)-, 1′,1‴-bis(*m*-methylbenzyl)-, and 1′,1‴-bis(*p*-methylbenzyl)biferrocene were synthesized and Mössbauer spectroscopic measurements of their monocation salts were carried out at various temperatures in order to study the effect of the substituents on the mixed-valence states.

Biferrocene derivatives are easily monooxidized to give the corresponding monocations, which show a mixed-valence state. It is known that those compounds can be classified into two types of valence states of iron atoms, a trapped-valence type and an averaged-valence type, by means of Mössbauer spectroscopy.[1] The former type has different states of iron atoms corresponding to ferrocene-like bivalent and ferricenium-like tervalent iron atoms, while the latter has an equivalent state averaged over ferrocene-like bivalent and ferricenium-like tervalent iron atoms.

It has been reported that the triiodide salt of biferrocene itself is of the trapped-valence type from a low temperature to room temperature.[2] However, Iijima et al. observed the interesting temperature-dependence of the mixed-valence states for 1′,1‴-diethyl- and 1′,1‴-dipropylbiferrocenium triiodide which show an averaged-valence type near room temperature but a trapped-valence type at low temperatures.[3]

Recently, it was reported that the triiodide salts of monocationic 1′,1‴-di-*n*-butyl- and 1′,1‴-dibenzylbiferrocenium show a temperature-dependence similar to those observed in 1′,1‴-diethyl- and 1′,1‴-dipropylbiferrocenium triiodide, suggesting that the environment surrounding each cation in the solids should determine whether or not an intramolecular electron transfer occurs.[4]

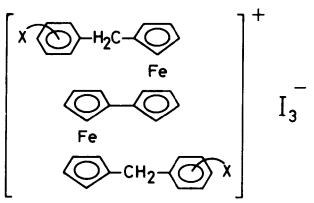

Fig. 1. Compounds.
(1) 1′,1‴-Bis(*o*-methylbenzyl)biferrocenium triiodide (X=*o*-CH_3)
(2) 1′,1‴-Bis(*m*-methylbenzyl)biferrocenium triiodide (X=*m*-CH_3)
(3) 1′,1‴-Bis(*p*-methylbenzyl)biferrocenium triiodide (X=*p*-CH_3)

The introduction of a methyl group to the benzyl substituent in 1′,1‴-dibenzylbiferrocene is expected to influence the packing of those cations in the solids. In the present paper, the triiodide salts of 1′,1‴-bis(*o*-methylbenzyl)-, 1′,1‴-bis(*m*-methylbenzyl)-, and 1′,1‴-bis(*p*-methylbenzyl)biferrocene (Fig. 1) were synthesized and investigated by means of Mössbauer spectroscopy in order to study the effects of the substituents on the valence states of iron atoms.

Experimental

Materials. 1′,1‴-Bis(*o*-, *m*-, and *p*-methylbenzyl)biferrocene were prepared by Ullmann coupling at 100—110 °C for 18 h of 1-bromo-1′-(*o*-, *m*-, and *p*-methylbenzyl)ferrocene, respectively. The products were checked by using ^{1}H NMR and elemental analysis. The data of elemental analysis for 1′,1‴-bis(*o*-, *m*-, and *p*-methylbenzyl)biferrocene are shown below, respectively: Found: C, 74.51; H, 4.64%, Found: C, 73.24; H, 6.57%, and Found: C, 75.18; H, 6.74%. Calcd for $C_{36}H_{34}Fe_2$: C, 74.76; H, 5.93%

The triiodide salts were prepared by partial oxidation of the corresponding 1′,1‴-bis(*o*-, *m*-, and *p*-methylbenzyl)-biferrocene in benzene with a stoichiometric amount of I_2. All the analytical data of 1′,1‴-bis(*o*-, *m*-, and *p*-methylbenzyl)biferrocenium triiodide salt are shown below, respectively: Found: C, 45.01; H, 4.17%, Found: C, 44.61; H, 4.19%, and Found: C, 42.99; H, 3.98%. Calcd for $C_{36}H_{34}Fe_2I_3$: C, 45.08; H, 3.57%.

Mössbauer Spectroscopic Measurements. ^{57}Co(Rh) moving in a constant-acceleration mode was used as the radioactive source for Mössbauer spectroscopic measurements. Mössbauer spectra were obtained by using an Austin Science Associates Mössbauer spectrometer and a proportional counter. The isomer shifts were referred to a metallic iron foil. The Mössbauer parameters were obtained by least-squares fitting to Lorentzian peaks.

Results and Discussion

Mössbauer spectroscopic measurements of 1′,1‴-bis(methylbenzyl)biferrocenes were carried out at 78 and 298 K. The Mössbauer spectroscopic data are shown in Table 1 together with those of 1′,1‴-dibenzylbiferrocene. It can be seen from Table 1 that all the spectral data show ferrocene-type bivalent iron, although the value of quadrupole splitting (ΔE_q) for 1′,1‴-bis(*o*-methylbenzyl)biferrocene is a little smaller than those of 1′,1‴-bis(*m*-methylbenzyl)- and 1′,1‴-bis(*p*-methylbenzyl)biferrocene.

Mössbauer spectroscopic measurements of 1′,1‴-bis(methylbenzyl)biferrocenium triiodides were carried out at 78 and 298 K. The Mössbauer spectra of 1′,1‴-bis(*o*-methylbenzyl)-, 1′,1‴-bis(*m*-methylbenzyl)-, and 1′,1‴-bis(*p*-methylbenzyl)biferrocenium tri-

iodide are shown in Figs. 2, 3, and 4, respectively. These Mössbauer spectroscopic data are summarized in Table 2 together with those of 1′,1‴-dibenzylbiferrocenium triiodide.

Table 1. Mössbauer Parameters

Compound	Temperature /K	δ[a]/mm s^{-1}	ΔE_q/mm s^{-1}
1′,1‴-Dibenzyl-	298	0.45	2.31
biferrocene	78	0.53	2.32
1′,1‴-Bis(*o*-methyl	298	0.44	2.28
benzyl)biferrocene	78	0.52	2.29
1′,1‴-Bis(*m*-methyl-	298	0.45	2.31
benzyl)biferrocene	78	0.53	2.32
1′,1‴-Bis(*p*-methyl-	298	0.44	2.30
benzyl)biferrocene	78	0.53	2.32

a) Isomer-shift data are reported with respect to metallic iron foil.

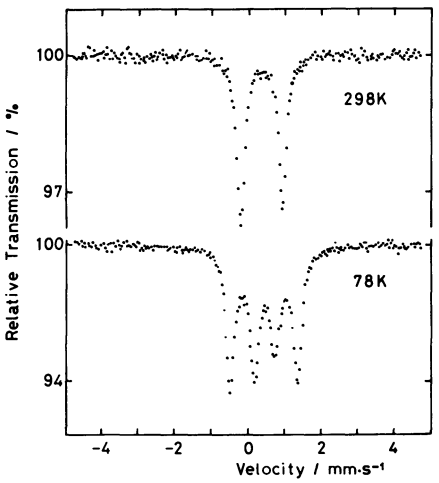

Fig. 2. Mössbauer spectra of 1′,1‴-bis (*o*-methylbenzyl) biferrocenium triiodide at 78 and 298K.

1′,1‴-Dibenzylbiferrocenium triiodide shows the remarkable temperature-dependence in its Mössbauer spectra; i.e., the spectra are of the trapped-valence type at low temperatures and of the averaged-valence type at high temperatures near room temperature.

Mixed-valence states observed in the present study depend on the position of methyl group in the benzyl

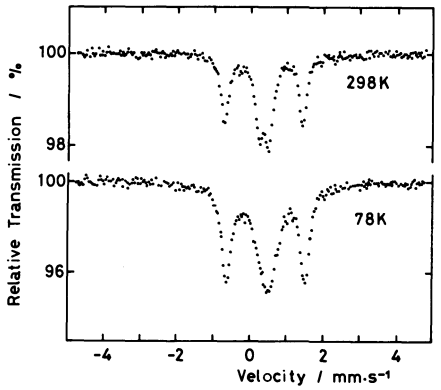

Fig. 3. Mössbauer spectra of 1′,1‴-bis (*m*-methylbenzyl) biferrocenium triiodide at 78 and 298K.

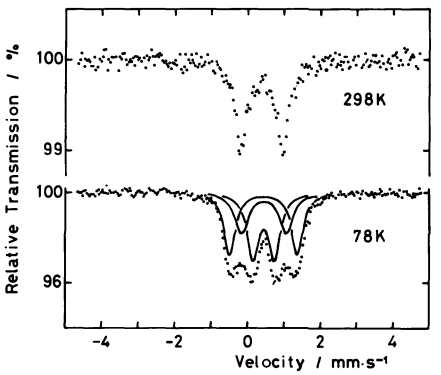

Fig. 4. Mössbauer spectra of 1′,1‴-bis(*p*-methylbenzyl) biferrocenium triiodide at 78 and 298K.

Table 2. Mössbauer Parameters

Compound	Temperature/K	δ[a]/mm s^{-1}	ΔE_q/mm s^{-1}	Area/%
1′,1‴-Dibenzylbiferrocenium$^+$ I_3^-	298	0.44	1.11	100
	78	0.53	2.00	43
		0.51	1.21	14
		0.53	0.44	43
1′,1‴-Bis(*o*-methylbenzyl)-	298	0.44	1.14	100
biferrocenium$^+$ I_3^-	78	0.53	1.85	50
		0.54	0.57	50
1′,1‴-Bis(*m*-methylbenzyl)-	298	0.44	2.14	45
biferrocenium$^+$ I_3^-		0.45	0.26	55
	78	0.53	2.15	42
		0.58	ca. 0	58
1′,1‴-Bis(*p*-methylbenzyl)-	298	0.46	1.13	100
biferrocenium$^+$ I_3^-	78	0.53	1.87	35
		0.54	1.24	28
		0.54	0.59	37

a) Isomer-shift data are reported with respect to metallic iron foil.

substituent. In 1′,1‴-bis(*o*-methylbenzyl)biferrocenium triiodide, the spectrum at 78 K consists of an inner and an outer doublet with nearly 1:1 ratio in areal intensity, which are ascribable to ferricenium-like tervalent and ferrocene-like bivalent iron, respectively, while the spectrum consists of only one doublet at room temperature. The Mössbauer spectroscopic data for the doublet at 298 K show a close resemblance to those for 1′,1‴-dibenzylbiferrocenium triiodide at 298 K.

On the other hand, the Mössbauer spectra obtained in 1′,1‴-bis(*m*-methylbenzyl)biferrocenium triiodide show a trapped-valence state both at 78 and 298 K. Although the Mössbauer spectrum of 1′,1‴-bis(*p*-methylbenzyl)biferrocenium triiodide at 298 K shows an averaged-valence state as in the case of 1′,1‴-bis(*o*-methylbenzyl)biferrocenium triiodide at 298 K, the spectrum at 78 K seems to have both a trapped-valence state and an averaged-valence state.

The values of ΔE_q of outer ferrocene-like doublet found in *o*- and *p*-methylbenzyl derivatives at 78 K are a little smaller than that found in *m*-methylbenzyl derivative at 78 K, while the values of ΔE_q of inner ferricenium-like doublet found in *o*- and *p*-methylbenzyl derivatives at 78 K are a little larger than that found in *m*-methylbenzyl derivative at 78 K. This suggests that the interaction between Fe(II) and Fe(III) in *o*- and *p*-methylbenzyl derivatives is stronger than that in *m*-methylbenzyl derivative even at 78 K.

These results suggest that the position of methyl group in the benzyl substituent has important effects on the mixed-valence states of 1′,1‴-bis(methylbenzyl)-biferrocenium triiodides. In 1′,1‴-bis(*m*-methylbenzyl)biferrocenium triiodide, one of the terminal iodine atoms of the I_3^- anion is supposed to be situated closer to the Fe(III) atom of a cation(both at 78 and at 298 K) based on the assumption made on the studies of 1′,1‴-di-*n*-butyl- and 1′,1‴-dibenzylbiferrocenium triiodide[4] and the ^{129}I-Mössbauer spectroscopic studies of ferricenium, biferrocenium and 1′,1‴-dihalobiferrocenium iodide salts,[5] although further structual information on the compounds used is needed to verify the assumption.

References

1) "Mixed-Valence Compounds," ed by D. B. Brown, D. Reidel Publishing Company, Dordrecht (1980).

2) W. H. Morrison, Jr. and D. N. Hendrickson, *J. Chem. Phys.*, **59**, 380 (1973).

3) S. Iijima, R. Saida, I. Motoyama, and H. Sano, *Bull. Chem. Soc. Jpn.*, **54**, 1375 (1981).

4) T.-Y. Dong, D. N. Hendrickson, K. Iwai, M. J. Cohn, S. J. Geib, A. L. Rheingold, H. Sano, I. Motoyama, and S. Nakashima, *J. Am. Chem. Soc.*, **107**, 7996 (1985).

5) M. Katada, S. Nakashima, Y. Uchida, I. Motoyama, H. Sano, H. Sakai, and Y. Maeda, *J. Radioanal. Nucl. Chem., Lett.*, in press.

Study of Packing State in Lipid Bilayers with the Aid of Ultraviolet Spectroscopy

Yoshio INOUE,* Yuji SEIYA, Minoru SAKURAI, and Riichiro CHÛJÔ
Department of Polymer Chemistry, Tokyo Institute of Technology,
O-okayama 2, Meguro-ku, Tokyo 152
(Received April 3, 1986)

Synopsis. The packing states of lipid bilayers of three phosphocholines were investigated based on the density dependent UV shifts of probes incorporated into bilayers. As UV probes, two retinal Schiff bases were used. It was confirmed that the packing state of the fatty acyl chain region is well probed by UV spectroscopy.

Lipids are prerequisite for an activation of membrane enzymes.[1] Lipid bilayers would contribute the stabilization of enzyme conformation required for an activation. In many cases, fluidity of lipid is also necessary for the enzyme activity.[2-4] For these reasons, many spectroscopic methods have been applied, for example, NMR,[5-11] ESR,[12-15] fluorescence,[16-19] IR,[20-22] etc. Up to now, an investigation of the state of lipid bilayers using an UV spectroscopy notwithstanding its high sensitivity has not been reported. In this note, we will show that the UV shifts could provide the information on packing states of lipid bilayers.

Experimental

Three types of phosphocholine(PC) were used; egg yolk phosphocholine(EPC), 1,2-dimyristoyl-*sn*-glycero-3-phosphocholine(DMPC), and 1,2-dipalmitoyl-*sn*-glycero-3-phosphocholine(DPPC). As UV probes, retinal Schiff bases, i.e., *N*-retinylidene-butylamine(NRB) and α-(*t*-Butyloxycarbonyl)-ε-*N*-retinylidene-L-lysyl-L-phenylalanyl-L-tyrosine methyl ester(PEP) were used (Fig. 1). Methods of syntheses and characterization of these compounds were described elsewhere.[23,24] The molar ratio of probe to lipid was almost 1/10. Homogeneous vesicle dispersion in distilled water containing 100 mM NaCl (1 M=1 mol dm^{-3}) is prepared by sonication with TOMY model UR-200P sonicator at frequency 20 kHz and output power 200 W under cooling by ice/water until translucence (about 20 min). It has confirmed that the incorporation of retinal less than 20 mol% causes the slight expansion of EPC vesicle size but dose not induce the obvious disruption.[25] UV spectra were observed on a Beckman model 25 spectrometer with a probe concentration of ca. 5×10^{-2} mol dm^{-3}.

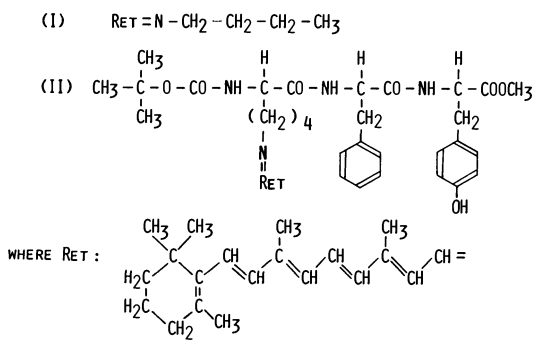

Fig. 1. Chemical structure of UV probes. (I) NRB and (II) PEP(peptide probe).

Results and Discussion

Retinal moiety of the peptide probe PEP is located in the region of fatty acyl chains in the bilayers.[24] NRB is also seemed to locate in the same region, but not near the polar head group, because of its higher hydrophobicity. PEP in EPC vesicle shows UV absorption maximum λ_{max} of retinal moiety at 380 nm, which is more bathochromic than in EPC inverted micell (in hexane, λ_{max}=360 nm).[24] This shift is mainly due to the van der Waals effect which depends on the density of medium. Similar shift has been observed in normal hydrocarbons as solvents, where the λ_{max} value of retinal Schiff base shifts to more bathochromic as the density of the solvent becomes larger.[26] Fatty acyl chains of EPC in inverted micell are not so densely packed compared with those in EPC bilayer vesicle. The λ_{max} value in vesicle is, therefore, in longer wavelength region than that in inverted micell. It suggests that by using the λ_{max} shift we can study the packing state of fatty acyl chain region of lipid bilayers.

Figure 2 shows the temperature dependence of the λ_{max} values of two probes in three different PC vesicles. At 5—10 °C, the λ_{max} values of probes in DPPC are larger than those in DMPC and EPC. This result suggests that DPPC bilayers are more densely packed than the other two PC bilayers. The bilayers of pure DPPC, DMPC, and EPC show phase transition at

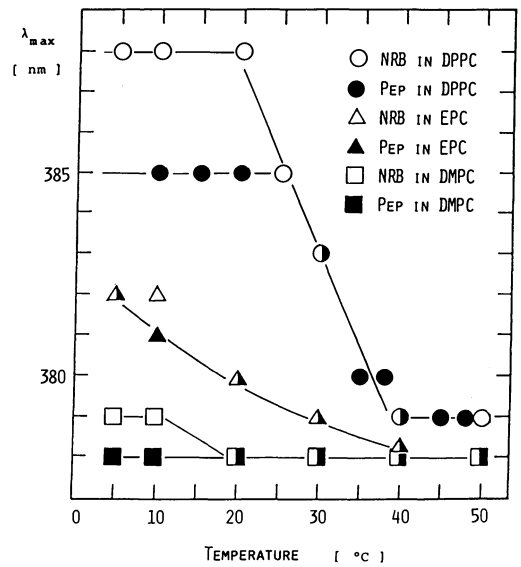

Fig. 2. Temperature dependence of λ_{max} values of UV probes in phosphocholine(PC) bilayers. Errors in temperature and λ_{max} are ±2.0 °C and ±1 nm, respectively.

temperatures (T_c) of 41.3,[27] 23.8, and −15.0 °C,[28] respectively. At the temperature range 5—10 °C, DMPC and DPPC would be in the gel state, while EPC in the fluid state. When the fatty acyl chains consist of saturated carbon-carbon bonds and the bilayers are in the gel state, the packing effect depends on the length of the acyl chains. Raman studies in the gel state showed that DMPC is more perturbed and its fatty acyl chains are more rich in gauche conformers than the case of DPPC.[27,29,30] The packing strength is influenced by the perturbation which becomes larger with a decreasing of the chain length.[30] Our UV result in the gel state parallel that from Raman study. Almost all acyl chains of EPC are longer than those of DPPC, but they contain a lot of unsaturated bonds,[28] loosening the packing of the bilayers. In DPPC bilayers, the λ_{max} value of NRB is larger than that of peptide probe PEP, indicating that the packing of DPPC acyl chains is affected by the nature of the probes. The smaller perturbation of NRB compared with PEP reflects the better compatibility of the former with the lipid bilayers.

On the other hand, the differences between the λ_{max} values of NRB and PEP are very small in DMPC and EPC bilayers. The packing of these bilayers may be not so dense by nature to be affected significantly by NRB and PEP.

At 40—50 °C, the bilayers of three PC types containing the UV probes would have almost the same packing density, since the λ_{max} values are almost the same and constant. The probes in EPC bilayers show small blue shift with an increase of temperature. EPC bilayers are in the fluid state in this temperature range and their packing becomes looser as temperature rises.

The λ_{max} values of both UV probes in the DPPC bilayers show large blue shifts with an increase in temperature from about 25 to 35 °C, indicating a large change in the packing state of bilayers. IR studies have showed that the acyl chain packing of DPPC changes from an orthorhombic to a hexagonal subcell between 36—38 °C (pretransition), which is lower than a main phase transition temperature T_c.[31,32] The UV λ_{max} shifts may correspond to this change in packing state. Thus this change would accompany the density change. For PC with saturated acyl chains, more gauche isomers exist in the fluid state than in the gel state.[30,31] The structural disorder of the fatty acyl chains would cause the loosening of the packing.

On the other hand, λ_{max} value in DMPC bilayers is almost constant both below and above T_c. For DMPC, consisting of shorter acyl chains, the alignment of acyl chains in the gel state are originally much disturbed[30] and the density would not change so much with phase transition. In this case, the packing would not be so strong even in the gel state.

From these UV results, it is confirmed that the packing strength of acyl chain region of bilayers is affected mainly by the length and the chemical structure of the fatty acyl chains when the polar head group is identical, and it also depends on the order or fluidity of bilayers. Further it is confirmed that UV spectroscopy is one of the best methods for the study of the packing state of lipid bilayers. Although the probe is used in this work at a relatively high concentration, it is easy to lower its concentration because of its high UV sensitivity. By using an UV probe bound to a protein, such as retinal which can bind to a protein through a lysine side chain by forming a Schiff base linkage as found in rhodopsin[33] and bacteriorhodopsin,[34] it would be possible to obtain the information on the state of lipid surrounding the protein and on the lipid-protein interaction.

References

1) H. Sandermann, Jr., *Biochim. Biophys. Acta*, **515**, 209 (1978).
2) H. K. Kimelberg and D. Papahadjopoulos, *Biochim. Biophys. Acta*, **282**, 277 (1972).
3) H. K. Kimelberg and D. Papahadjopoulos, *J. Biol. Chem.*, **249**, 1071 (1974).
4) D. F. O'Brien, L. F. Costa, and R. A. Ott, *Biochemistry*, **16**, 1295 (1977).
5) L. K. Tamm and J. Seelig, *Biochemistry*, **22**, 1474 (1983).
6) A. Bienvenue, M. Bloom, J. D. Davis, and P. F. Devaux, *J. Biol. Chem.*, **257**, 3032 (1982).
7) R. J. Wittebort, A. Blume, T. H. Huang, S. K. Das Gupta, and R. G. Griffin, *Biochemistry*, **21**, 3487 (1982).
8) M. Engelsberg, S. R. Dowd, V. Simplaceanu, B. W. Cook, and C. Ho, *Biochemistry*, **21**, 6985 (1982).
9) J. L. Browning, *Biochemistry*, **20**, 7123 (1981).
10) S. Rajan, S. Y. Kang, H. S. Gutowsky, and E. Oldfield, *J. Biol. Chem.*, **256**, 1160 (1981).
11) R. E. Stark, J. L. Manstein, W. Curatolo, and B. Sears, *Biochemistry*, **22**, 1474 (1983).
12) M. G. McNamee, J. F. Ellena, and A. W. Daziel, *Biophys. J.*, **37**, 103 (1982).
13) A. Watts, I. D. Volotovski, R. Pates, and D. Marsh, *Biophys. J.*, **37**, 94 (1982).
14) A. Kusumi, M. Tsuda, T. Akino, S. Ohnishi, and Y. Terayama, *Biochemistry*, **22**, 1165 (1983).
15) A. Kusumi and J. S. Hyde, *Biochemistry*, **21**, 5978 (1982).
16) F. Jähnig, H. Vogel, and L. Best, *Biochemistry*, **21**, 6790 (1982).
17) M. P. Heyn, R. J. Cherry, and N. A. Dencher, *Biochemistry*, **20**, 840 (1981).
18) A. Ikegami, *Biophysics(Seibutsu-butsuri)*, **23**, 1 (1983).
19) M. R. Alecio, D. E. Golan, W. R. Veatch, and R. R. Rando, *Proc. Natl. Acad. Sci. U. S. A.*, **79**, 5171 (1982).
20) R. Mendelsohn, R. A. Dluhy, D. G. Cameron, and H. H. Mantsch, *Biophys. J.*, **37**, 83 (1982).
21) M. Cortijo, A. Alonso, J. G. Gomez-Fernandez, and D. Chapman, *J. Mol. Biol.*, **157**, 597 (1982).
22) R. A. Dluhy, R. Mendelsohn, H. L. Casal, and H. H. Mantsch, *Biochemistry*, **22**, 1170 (1983).
23) Y. Inoue, Y. Tokitô, R. Chûjô, and Y. Miyoshi, *J. Am. Chem. Soc.*, **99**, 5592 (1977).
24) Y. Seiya, S. Tomomasa, M. Sakurai, Y. Inoue, and R. Chûjô, *Rep. Prog. Polym. Phys. Jpn.*, **25**, 769 (1982).
25) Y. Inoue, Y. Hanafusa, M. Toda, and R. Chûjô, *Bull. Chem. Soc. Jpn.*, **55**, 540 (1982).
26) R. S. Becker, G. Hug, P. K. Das, A. M. Schaffer, T. Takemura, N. Yamamoto, and W. Waddell, *J. Phys. Chem.*, **80**, 2265 (1976).
27) C. Huang, J. R. Lapides, and I. W. Levin, *J. Am. Chem. Soc.*, **104**, 5926 (1982).

28) S. Hidaka and F. Toda, *Yuki Gosei Kagaku Kyokai Shi,* **40**, 377 (1982).
29) J. F. Mason and C. Huang, *Lipid,* **16**, 604 (1981).
30) C. Huang and I. W. Levin, *J. Phys. Chem.,* **87**, 1509 (1983).
31) D. G. Cameron, H. L. Casal, E. F. Gudgin, and H. H. Mantsch, *Biochim. Biophys. Acta,* **596**, 463 (1980).
32) D. G. Cameron, H. L. Casal, and H. H. Mantsch, *Biochemistry,* **19**, 3665 (1980).
33) D. Bownds, *Nature,* **216**, 1178 (1967).
34) D. Oesterhelt and W. Stoeckenius, *Nature, New Biol.,* **233**, 149 (1971).

Resonance Raman Spectra of Red-Shifted Retinal Schiff's Base

Toshiharu SUGIHARA and Teizo KITAGAWA*,†
Department of Home Economics, Gifu University, Yanagido, Gifu 501-11
†Institute for Molecular Science, Okazaki National Research Institutes, Myodaiji, Okazaki 444
(Received January 7, 1986)

Synopsis. We have found that the visible absorption maximum (λ_{max}) of retinal Schiff's base in fluoro alcohols is considerably red-shifted. The C=N stretching Raman line exhibits a frequency shift in deuterated fluoro alcohols, indicating that the Schiff's base is protonated. Frequencies of the in-phase C=C stretching Raman lines ($\nu_{C=C}$) changed linearly with λ_{max}, and the $\nu_{C=C}$ vs. λ_{max} correlation coincides with that observed for retinoid proteins.

In attempts to elucidate the structure-function relationship of retinoid proteins, resonance Raman (RR) spectroscopy has been extensively used to explore the molecular events which befall the chromophore of visual pigments[1-7] and bacteriorhodopsin[8-13] upon light irradiation. One of the remaining problems to be clarified is the origin of the opsin shift, that is, the large red shift of the absorption maximum of a retinal Schiff's base (RSB) in proteins compared with that in organic solvents. Recently we found that RSB in fluoro alcohols such as 1,1,1,3,3,3-hexafluoro-2-propanol (HFIP) and 2,2,2-trifluoroethanol (TFE) (Abbreviations for the chemical substances are summarized in the footnote of Table 1) gives an absorption band which is strongly red-shifted at the expense of the ordinary band in the blue region.[14] The amount of the red shift is larger than that usually observed for protonation of a Schiff's base by a strong acid, and the relative intensity of the red-shifted band to the ordinary band depends on the solvent composition and temperature; dilution of the fluoro alcohol solution with an inert solvent such as chloroform or rise of temperature decreases the relative intensity of the red-shifted band to the blue band. We are curious to know what occurs on the chromophore which exhibits such a large red shift of λ_{max}. In this note we report on RR spectra of all-*trans*-RSB of Ile-Ala-Phe-OBzl (RetIAF) and of butylamine (RetBu) in the fluoro alcohols, pointing out that the interaction between the Schiff's base nitrogen and alcoholic hydroxyl group alters the π delocalization of retinal and changes $\nu_{C=C}$ in linear correlation with λ_{max}.

Experimental

RetIAF was synthesized by mixing all-*trans*-retinal with Ile-Ala-Phe-OBzl[15] in ethyl acetate. 40 mg of HCl Ile-Ala-Phe-OBzl was dissolved in 5 ml of water and the solution was adjusted to pH 9 by 5% $NaHCO_3$. The solution became a gel. After extraction with 15 ml of ethyl acetate the organic layer was dried over Na_2SO_4 and filtered. Molecular sieve (3A) was added to the filtrate and then 100 mg of all-*trans*-retinal was incorporated into the solution, which was left to stand at 0 °C for 24 h. After removal of the molecular sieve, the solution was evaporated to give a yellow oil. The slightly yellow precipitate, which was formed on addition of hexane, was collected, washed with hexane, and dried in vacuum; the yield was 24 mg. The purity of the compound was confirmed by ^1H and ^{13}C NMR. RetBu was prepared according to the literature.[16] Deuterated HFIP or TFE was obtained by distillation of a mixture of D_2O and the fluoro alcohol (4:1). Other solvents were distilled immediately before use. The Schiff's base solution at a concentration of ca. 0.1 mM (1 M=1 mol dm^{-3}) was used for the Raman measurements. Raman spectra were measured with a JEOL-400D Raman spectrometer and an Ar laser (Spectra Physics, model 164) or a He/Cd laser (Kinmon Electrics, CDR80SG). The laser power at the sample point was 2—24 mW. About 50 µl of the sample solution in a cylindrical cell kept at 4 °C was used for the measurement.

Results and Discussion

The RR spectra of RetIAF and RetBu in the 1400—1700 cm^{-1} region are shown in Figs. 1(A) and (B), respectively. It is seen that the frequencies of the Raman lines are sensitive to the solvent and this solvent effect is most pronounced for the C=C and C=N stretching modes. The in-phase C=C stretching modes ($\nu_{C=C}$) of RetIAF and RetBu appear at 1576 and

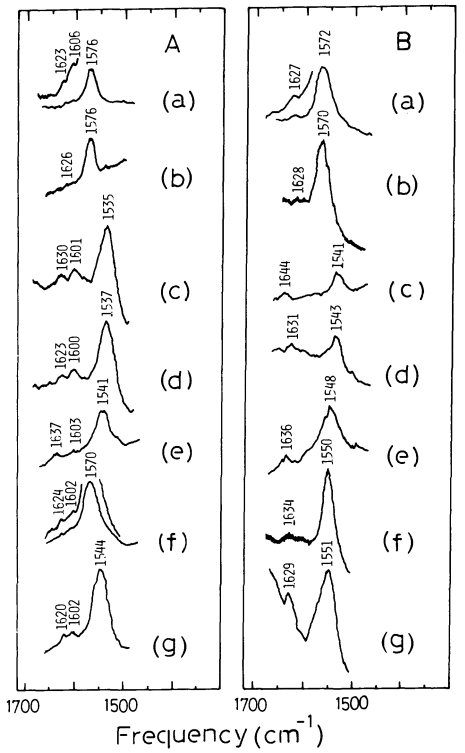

Fig. 1. The resonance Raman spectra of RetIAF (A) and RetBu (B) in the 1400—1700 cm^{-1} region. Excitation wavelengths and solvents are as follows: a): 441.6 nm, chloroform, b): 514.5 nm, chloroform, c): 514.5 nm, HFIP, d): 514.5 nm, HFIP (deuterated), e): 514.5 nm, TFE, f): 441.6 nm, TFE, g): 514.5 nm, TFE (deuterated).

1572 cm^{-1}, respectively, in chloroform (a) but they are shifted to 1535 and 1541 cm^{-1} in HFIP (c) and to 1541 and 1548 cm^{-1} in TFE (e). The Schiff's base C=N stretching modes ($\nu_{C=N}$) of RetIAF and RetBu appear at 1623 and 1627 cm^{-1}, respectively, in chloroform (a) but they are shifted to 1630 and 1644 cm^{-1} in HFIP (c) and to 1637 and 1636 cm^{-1} in TFE (e). Thus, the C=C and C=N stretching modes shift in opposite directions and their magnitudes are not correlated.

The visible absorption spectrum of RetIAF in TFE exhibits two absorption maxima at 368 and 494 nm, and the RR spectrum excited at 441.6 nm (f) is distinctly different from that excited at 514.5 nm (e). Therefore, it is deduced that there exist two molecular species in equilibrium in the TFE solution, each giving rise to an absorption band at either 368 or 494 nm. These are tentatively called the U and P species, respectively, in this paper. The bands in the 514.5 nm- and 441.6 nm-excited RR spectra are considered to arise predominantly from the P and U species, respectively. The U species gives the $\nu_{C=C}$ and $\nu_{C=N}$ lines at 1570 and 1624 cm^{-1} (f), respectively, while the P species gives the lines at 1541 and 1637 cm^{-1} (e). The RR spectrum of the TFE solution excited at 441.6 nm (f) is very close to that of the chloroform solution (a). The $\nu_{C=N}$ line of the P species exhibits frequency shift in deuterated fluoro alcohols [(d) and (g) in Figs. 1A and B], but that of the U species does not. Therefore, the P and U species are inferred to have protonated and unprotonated Schiff's bases, respectively.

On the other hand, protonation of RetIAF and RetBu in chloroform by a strong acid such as CF_3COOH caused frequency shifts of the $\nu_{C=C}$ mode by -32 and -15 cm^{-1}, respectively, and the $\nu_{C=N}$ mode by $+17$ and $+23$ cm^{-1}, respectively. The magnitude of the shift is smaller than the frequency difference between the chloroform and fluoro alcohol solutions for $\nu_{C=C}$, but it is larger for $\nu_{C=N}$. Table 1 summarizes the values of λ_{max}, $\nu_{C=C}$, and $\nu_{C=N}$ of RetIAF and RetBu in various solvents. When the values of λ_{max} are plotted against the values of $\nu_{C=C}$, it gives a straight line as displayed in Fig. 2. The linear correlation between λ_{max} and $\nu_{C=C}$ was previously reported for retinoid proteins,[5,9] but it is noteworthy here that the values of λ_{max} and $\nu_{C=C}$ of the present compounds in various solvents fall on the identical line with that of the retinoid proteins. This means that the solvent effect on the chromophore found in the present study is qualitatively the same as the role of surrounding proteins regarding the spectral property. Since the strength of the C=C bond in the conjugated linear molecules generally becomes weaker and thus the $\nu_{C=C}$ frequency becomes lower as delocalization of π electrons increases, the linear correlation between λ_{max} and $\nu_{C=C}$ suggests that the red-shift of λ_{max} of RetIAF and RetBu in fluoro alcohols as well as of retinylidene chromophore in proteins can be attributed to increas-

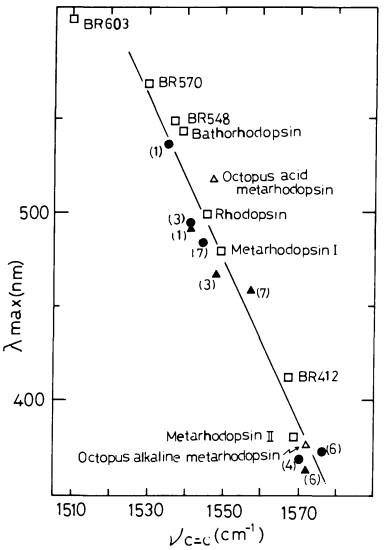

Fig. 2. Correlation between λ_{max} and $\nu_{C=C}$ for the present compounds and retinoid proteins. Data are obtained from rhodopsin,[3] bathorhodopsin,[1] metarhodopsin I and II,[5] bacteriorhodopsin,[12] octopus metarhodopsin,[7] and Table 1 (●: RetIAF and ▲: RetBu). Numbers besides the points represent the compounds specified in Table 1.

Table 1. Raman Frequencies and Absorption Maxima of RetIAF and RetBu in Various Solvents

	Solvent	Ret IAF[a]			Ret Bu[a]		
		$\nu_{C=N}$ / cm^{-1}	$\nu_{C=C}$ / cm^{-1}	λ_{max} / nm	$\nu_{C=N}$ / cm^{-1}	$\nu_{C=C}$ / cm^{-1}	λ_{max} / nm
(1)	HFIP[b]	1630	1535	536	1644	1541	494
(2)	HFIP[b] (deuterated)	1623	1537		1631	1543	
(3)	TFE[b]	1637	1541	494	1636	1548	467
(4)	TFE[c]	1624	1570	368			
(5)	TFE[b] (deuterated)	1620	1544		1629	1551	
(6)	Chloroform[c]	1623	1576	372	1627	1572	363
(7)	Chloroform + TFA[b]	1640	1544	484	1650	1557	458

a) Abbreviations used are; RSB, retinal Schiff's base; RetIAF, RSB with Ile-Ala-Phe-OBzl; RetBu, RSB with butylamine; HFIP, 1,1,1,3,3,3-hexafluoro-2-propanol; TFE, 2,2,2-trifluoroethanol. b) Raman frequencies are obtained from the spectrum excited at 514.5 nm. c) Raman frequencies are obtained from the spectrum excited at 441.6 nm.

ed π delocalization. It is important to note that such π delocalization is controlled by the interaction at the Schiff's base.

An interesting feature of this study is that the $\nu_{C=N}$ modes of the red-shifted RetIAF and RetBu shift to lower frequencies in deuterated fluoro alcohols. Upon deuteration of HFIP, the $\nu_{C=N}$ modes of RetIAF (1630 cm^{-1}) and RetBu (1644 cm^{-1}) exhibit the frequency shift of −7 and −13 cm^{-1}, respectively, while the deuteration of TFE gives corresponding shifts of −17 and −7 cm^{-1}, respectively. This type of frequency shift is usually seen upon deuteration of proteins having protonated RSB.[3] Accordingly, it is likely that the alcoholic hydroxyl group acts as a Lewis acid and a proton is shared between the Schiff's base nitrogen and the alcoholic oxygen. If this were simply a hydrogen-bonding interaction in which the Schiff base nitrogen serves as a proton acceptor, the $\nu_{C=N}$ line would not exhibit such a large frequency shift upon deuteration of the alcohols. Therefore, the interaction between the N and H atoms is rather of a weak covalent type but it would not be categorized as a hydrogen bond. Thus, RetIAF and RetBu in fluoro alcohols behave as if they were protonated RSB. The solvent-dependent difference in frequency shifts upon deuteration reflects that the degree of coupling between the C=N stretching and the N–H in-plane bending modes varies depending on the strength of the quasi-covalent N–H bond. It is due to this vibrational coupling that the frequency of $\nu_{C=N}$ is not correlated with the frequency of $\nu_{C=C}$ or the values of λ_{max} despite the fact that the C=N bond is also affected by the π delocalization. We would stress finally that fluoro alcohol is more effective than a strong acid in shifting λ_{max} to red and on lowering $\nu_{C=C}$.

We wish to thank Prof. E. R. Blout of Harvard Medical School for his valuable suggestions and discussions.

References

1) A. R. Oseroff and R. H. Callender, *Biochemistry*, **13**, 4243 (1984).
2) R. H. Callender, A. Doukas, R. Crouch, and K. Nakanishi, *Biochemistry*, **15**, 1621 (1976).
3) R. H. Callender and B. Honig, *Ann. Rev. Biophys. Bioeng.*, **6**, 33 (1977).
4) R. Mathies, T. B. Freeman, and L. Stryer, *J. Mol. Biol.*, **109**, 367 (1977).
5) A. Doukas, B. Aton, R. H. Callender, and T. G. Ebrey, *Biochemistry*, **17**, 2430 (1978).
6) G. Eyring, B. Curry, R. Mathies, R. Fransen, I. Palings, and J. Lutenburg, *Biochemistry*, **19**, 2410 (1980).
7) T. Kitagawa and M. Tsuda, *Biochim. Biophys. Acta*, **624**, 211 (1980).
8) R. H. Lozier and W. Stockenius, *Proc. Natl. Acad. Sci. U.S.A.*, **71**, 4462 (1974).
9) B. Aton, A. Doukas, R. H. Callender, B. Becher, and T. G, Ebrey, *Biochemistry*, **16**, 2955 (1977).
10) M. A. Marcus and A. Lewis, *Biochemistry*, **17**, 4772 (1978).
11) J. Terner, C. Hsieh, A. R. Burns, and M. A. El-Sayed, *Biochemistry*, **18**, 3629 (1979).
12) M. Stockburger, W. Klusmann, H. Gattermann, G. Massig, and R. Peters, *Biochemistry*, **18**, 4886 (1979).
13) M. Braiman and R. Mathies, *Biochemistry*, **19**, 5421 (1980).
14) T. Sugihara, and E. R. Blout, in preparation.
15) T. Sugihara, E. R. Blout, and B. A. Wallace, *Biochemistry*, **21**, 3444 (1982).
16) P. E. Blatz, R. H. Johnson, J. H. Mohler, S. K. Al-Dilaimi, S. H. Dewhurst, and J. O. Erickson, *Photochem. Photobiol.*, **13**, 237 (1971).

Cubic Relation between Thermodynamic Functions and Natural Variables for Chemical Thermodynamic Systems

Makoto ISIHARA
Department of General Education, Shotoku-Gakuen Women's Junior College,
Nakauzura 1-38, Gifu 500
(Received January 16, 1986)

Synopsis. The relation between thermodynamic functions and natural variables for chemical thermodynamic systems is represented in terms of the geometry of a cube. Besides being helpful in understanding the abstractive nature of thermodynamic relation, this leads to a useful mnemonic as well.

It is well known that thermodynamic functions are characterized by natural variables and that they are related to one another through the Legendre transformation.[1] What we intend to show in this note is that the relation between thermodynamic functions and natural variables for chemical thermodynamic systems can be represented in terms of the geometry of a cube. Being simple, this does not seem to be trifling. Although it is quite probable that someone has noticed the fact already, no description of it can be seen in thermodynamic and chemical thermodynamic literature, as far as the author knows.[2] Only two kinds of thermodynamic squares,[3-5] which are mnemonic diagrams, have some relation with it, as mentioned later. The author is very afraid that his finding might be really a small rediscovery, but yet he believes that the fact is worth communicating here. It gives both conceptual and practical profits to workers studying and making use of chemical thermodynamics.

In general the thermodynamic function has the Pfaffian form consisting of several constituents, each of which is specified by the conjugate pair of extensive and intensive quantities. Let us denote the extensive and the intensive quantities for the i-th constituent, respectively, by $[1]_i$ and $[-1]_i$, which are rewritten as $[\sigma_i]_i$ with the parameter σ_i taking 1 or -1. We write $-\sigma_i$ as $\bar{\sigma}_i$ and -1 as $\bar{1}$ in the following. Denoting the thermodynamic function of natural variables $[\sigma_1]_1, \cdots, [\sigma_m]_m$ by $[\sigma_1 \cdots \sigma_m]$, we can put its Pfaffian form as

$$\mathrm{d}[\sigma_1 \cdots \sigma_m] = \sum_{i=1}^{m} \sigma_i [\bar{\sigma}_i]_i \mathrm{d}[\sigma_i]_i, \tag{1}$$

from which it follows immediately that

$$\left(\frac{\partial[\sigma_1 \cdots \sigma_m]}{\partial[\sigma_k]_k}\right)_{[\sigma_i]_i (i \neq k)} = \sigma_k [\bar{\sigma}_k]_k. \tag{2}$$

For the Legendre transformation changing one of natural variables from $[\sigma_k]_k$ into $[\bar{\sigma}_k]_k$ it is relevant to define the operator L_k as

$$L_k[\cdots \sigma_k \cdots] = [\cdots \sigma_k \cdots] - \sigma_k [\bar{\sigma}_k]_k [\sigma_k]_k. \tag{3}$$

This definition naturally gives

$$\mathrm{d}L_k[\cdots \sigma_k \cdots] = \mathrm{d}[\cdots \bar{\sigma}_k \cdots], \tag{4}$$

which allows us to put

$$L_k[\cdots \sigma_k \cdots] = [\cdots \bar{\sigma}_k \cdots]. \tag{5}$$

Substituting Eqs. 2 and 5 into Eq. 3, replacing σ_k with $\bar{\sigma}_k$, we have a generalized expression for the Gibbs–Helmholtz type equations

$$[\cdots \sigma_k \cdots] = [\cdots \bar{\sigma}_k \cdots] - [\bar{\sigma}_k]_k \left(\frac{\partial[\cdots \bar{\sigma}_k \cdots]}{\partial[\bar{\sigma}_k]_k}\right)_{[\sigma_i]_i (i \neq k)}. \tag{6}$$

On the other hand, From Eq. 2 the Maxwell relations are summarized in the form

$$\sigma_j \left(\frac{\partial[\bar{\sigma}_j]_j}{\partial[\sigma_k]_k}\right)_{[\sigma_j]_j} = \sigma_k \left(\frac{\partial[\bar{\sigma}_k]_k}{\partial[\sigma_j]_j}\right)_{[\sigma_k]_k} \quad (j \neq k), \tag{7}$$

the fixed variables other than $[\sigma_j]_j$ and $[\sigma_k]_k$ being suppressed for brevity. The abstractive nature of thermodynamic relation is succinctly expressed with the above notation.[6]

Now we confine ourselves to the three-constituent case. Surely this is a restriction, but it yields no serious loss of applicability. Putting $m=3$, we immediately see that our notation is ready to fit the geometry of a cube: Assign $[1]_i$'s and $[\bar{1}]_i$'s to six faces, $[\bar{1}]_i$ being opposite to $[1]_i$, assign $[\sigma_1\sigma_2\sigma_3]$ to the vertex formed by the three faces $[\sigma_1]_1$, $[\sigma_2]_2$, and $[\sigma_3]_3$, and assign L_i to the four edges connecting the vertices around $[1]_i$ with the vertices around $[\bar{1}]_i$. The scheme of the assignment is illustrated in Fig. 1 with a cubist-like manner. It is easy to find the geometrical counterparts of the equations mentioned in the preceding paragraph (vide infra). The cube tells us concisely the cyclic character of thermodynamic relation. Such geometrical emblematization seems to be impossible for general multi-constituent cases within usual "visible" polyhedrons.

The Pfaffian form of the internal energy U of the ν-component chemical thermodynamic system is written as

$$\mathrm{d}U = T\mathrm{d}S - p\mathrm{d}V + \sum_{\kappa=1}^{\nu} \mu_\kappa \mathrm{d}n_\kappa, \tag{8}$$

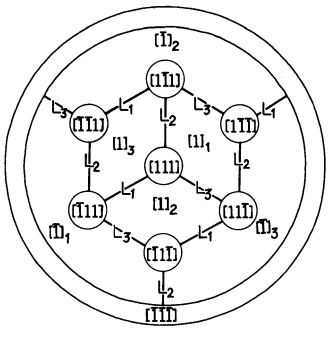

Fig. 1. Cubic relation.
The surrounding double circle stands for a vertex as well as small circles.

where T, S, p, V, μ_κ, and n_κ are the temperature of the system, the entropy, the pressure, the volume, the chemical potential and the amount of substance for the κ-th component, respectively. We have to treat more than three constituents except for the single-component case. It is never unpractical, however, to exclude the thermodynamic function of which natural variables are the chemical potential for some component(s) and the amount of substance for the other component(s). Using μ and n as representatives of μ_κ's and n_κ's, we can work actually within three constituents for chemical thermodynamic systems.[7] Thus the most typical and important choice is: $[1]_1=S$, $[\bar{1}]_1=T$, $[1]_2=-V$, $[\bar{1}]_2=p$, $[1]_3=n$, $[\bar{1}]_3=\mu$, and $[111]=U$. We have $[\bar{1}11]$ as the Helmholtz function A, $[1\bar{1}1]$ as the enthalpy H, and $[\bar{1}\bar{1}1]$ as the Gibbs function G. The grand (canonical) function, well-known in statistical mechanics and often denoted by Ω, corresponds to $[\bar{1}1\bar{1}]$. The others, $[11\bar{1}]$, $[1\bar{1}\bar{1}]$, and $[\bar{1}\bar{1}\bar{1}]$ have neither prevalent symbols nor names. We refer to this cube as U-cube.

Another choice to be mentioned comes from a famous rearrangement in Eq. 8

$$dS = \frac{1}{T}dU + \frac{p}{T}dV - \sum_{\kappa=1}^{\nu}\frac{\mu_\kappa}{T}dn_\kappa. \tag{9}$$

We set: $[1]_1=U$, $[\bar{1}]_1=1/T$, $[1]_2=V$, $[\bar{1}]_2=p/T$, $[1]_3=n$, $[\bar{1}]_3=-\mu/T$, and $[111]=S$. The three generalized Massieu functions[8] correspond to $[\bar{1}11]$, $[1\bar{1}1]$, and $[\bar{1}\bar{1}1]$; the first one and the third are the Massieu function J and the Planck function Y, respectively. We have $[\bar{1}1\bar{1}]$ as the Kramers function.[9] The others are nameless. This is S-cube. We can obtain various "thermodynamic cubes" likewise.

Next we show that thermodynamic cubes are useful and powerful as a mnemonic tool for thermodynamic relation. For this purpose it is appropriate to exemplify how to have the information from thermodynamic cubes. Let us take U-cube as an example. The view around the vertex G is shown in Fig. 2. We see that G has T, p, and n as natural variables, or reversely, that the thermodynamic function having T, p, and n as natural variables is G. We have the Pfaffian form

$$dG = -SdT + Vdp + \mu dn, \tag{10}$$

noting the faces behind and an extra negative sign for an intensive natural variable. A few views around edges are presented in Figs. 3 and 4 with some pliancy. In Fig. 3 we see that G is related to A through the Legendre transformation

$$G = A + pV \tag{11}$$

and that T and n are common natural variables in G and A. Figure 4 illustrates the way of obtaining the Gibbs–Helmholtz equations;

$$U = A - T\left(\frac{\partial A}{\partial T}\right)_{Vn}, \tag{12}$$

$$H = G - T\left(\frac{\partial G}{\partial T}\right)_{pn}. \tag{13}$$

The view around the face n is shown in Fig. 5. This indicates the four thermodynamic functions of which natural variables include n. Their partial derivatives with respect to n are μ (behind). This view is also adaptable for the two-constituent case of no chemical variable. Figure 6 concerns the following two Maxwell relations.

$$\left(\frac{\partial S}{\partial p}\right)_{Tn} = -\left(\frac{\partial V}{\partial T}\right)_{pn}, \tag{14}$$

$$\left(\frac{\partial p}{\partial T}\right)_{Vn} = \left(\frac{\partial S}{\partial V}\right)_{Tn}. \tag{15}$$

Note that an extra negative sign is supposed for every differentiation with respect to an intensive variable. The way of obtaining the Maxwell relations is completely analogous with that of thermodynamic squares. It should be emphasized that thermodynamic cubes have the neat sign convention throughout.

For mnemonics in thermodynamics,[10] we already have two kinds of thermodynamic squares, the Born

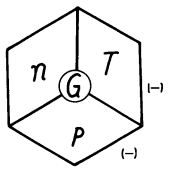

Fig. 2. Natural variables.

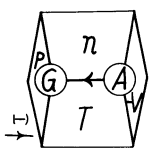

Fig. 3. The Legendre transformation.

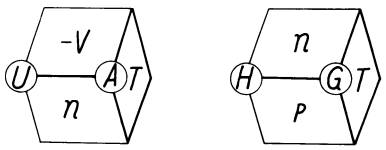

Fig. 4. The Gibbs–Helmholtz equations.

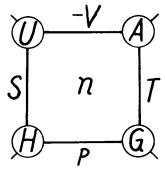

Fig. 5. Thermodynamic functions of a common natural variable.

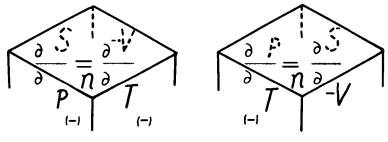

Fig. 6. The Maxwell relations.

diagram[3,4,11] and the Christie diagram,[5,12] which are suited to the Maxwell relations. Sign convention aside, a square in a thermodynamic cube gives the Christie diagram, which corresponds essentially to the Born diagram. The latter has thermodynamic functions and natural variables at sides and vertices, respectively, contrarily to the former. They work equivalently, as far as one square is concerned. Anyhow, no mnemonic is seriously necessary in the case of the two constituents (S,T) and (p,V). It is other cases that need a mnemonic tool.[13] It is undoubtful that a thermodynamic cube is far more excellent and general, even as a mnemonic, than a set of several thermodynamic squares with individual assignment of thermodynamic functions and natural variables.[3]

References

1) For example, H. B. Callen, "Thermodynamics," John Wiley & Sons, New York (1960), Chap. 5.

2) The author has checked a lot of descriptions related to the subject. There exist, however, so many books and articles on thermodynamics and chemical thermodynamics that he remains far away from the exhaustive inquiry.

3) H. B. Callen, "Thermodynamics," John Wiley & Sons, New York (1960), Section 7.2.

4) E. O. Koenig, *J. Chem. Phys.*, **3**, 29 (1935).

5) D. E. Christie, *Am. J. Phys.*, **25**, 486 (1957).

6) Thermodynamics itself is abstractive in the sense that it concerns no concrete form of thermodynamic functions.

7) As the case may be, we have additional terms $Xdx+\cdots$, say, due to an external field in Eq. 8. Even in such cases, if we choose three constituents relevantly with the rest of the Pfaffian form fixed, the cubic relation is valid within a defined family of thermodynamic functions. The relevant choice will be almost exclusively the original three.

8) H. B. Callen, "Thermodynamics," John Wiley & Sons, New York (1960), Section 5.4.

9) No symbol seems to prevail for this function.

10) As tabulation of its own value, we should cite Shaw's Jacobian table as well as Bridgman's table, which are more than mnemonics: A. N. Shaw, *Phil. Trans. Roy. Soc. London A*, **234**, 299 (1935); P. W. Bridgman, "Condensed Collection of Thermodynamic Formulas," Harvard University Press, Cambridge, Massachusetts (1926); J. C. Slater, "Introduction to Chemical Physics," McGraw-Hill, New York (1939), p. 27.

11) Not a few books contain description of such a thermodynamic square as quoted in Callen's book (Ref. 3). This kind of thermodynamic squares was initiated by M. Born in his lecture in 1929 according to L. Tisza, who named it the Born diagram: L. Tisza, "Generalized Thermodynamics," MIT Press, Cambridge, Massachusetts (1966), p. 64.

12) The Christie diagram originates from a mnemonic of natural variables for the $(S,T)-(p,V)$ case; see the references cited in Christie's note (Ref. 5). U-cube may be regarded as an improved generalization of the Christie diagram.

13) As a "real" mnemonic tool we recommend a truncated cube with symbols of thermodynamic functions on triangular faces, the edges around which are, of course, spurious.

Diode Laser Spectrum of the ν_8 Band of CH_3SH

Kuniaki NAKAGAWA,* Takeshi KOJIMA, and Eizi HIROTA†
Department of Physics, Faculty of Science, Toyama University, Gofuku, Toyama 930
†Institute for Molecular Science, Okazaki 444
(Received March 14, 1986)

Synopsis. The Stark effect was used to assign four series of the transitions in the heavily perturbed spectrum of methanethiol in the 14 μm region: K=0 and two K=1 series of A torsional symmetry and K=0 series of E symmetry. Effective parameters were determined for each series. The K=0 levels of A symmetry in the ν_8 state were found to be perturbed by a Fermi-type resonance.

Studies on the torsion-rotation energy levels in the excited states of the vibrations other than the torsion provide detailed information on hindered internal rotation. Most of the studies reported so far[1-4] are on methanol in the 9—10 μm region. In the present work, the torsion-rotation levels in the first excited ν_8 state of methanethiol (C-S stretching, 710 cm^{-1})[5] are studied.

The diode laser spectrometer described previously[6] was used in the present work. The frequency-modulated laser beam was passed through a cell of 55 cm in length equipped with parallel Stark plates separated by about 3 mm. A commercially available sample of methanethiol was used without further purification. The sample pressure was in the region of 0.3—2 Torr (1 Torr=133.322 Pa). About one thousand absorption lines were observed with four laser diodes in the range of 703.3—718.2 cm^{-1}. The absorption line frequencies were measured by interpolating the CO_2 ν_2 band lines[7,8] using etalon fringes. The absolute accuracy in the frequencies is estimated to be better than 0.003 cm^{-1} for unoverlapped lines.

At a medium resolution, the ν_8 band looked like a parallel band of a symmetric top, but once the P- and R-branches were resolved at a high resolution, their structures were much more complicated than those expected for a parallel band. Several series of lines were found in the complicated structures with the help of a Loomis-Wood diagram. Each of the series is composed of transitions with different J, the total angular momentum quantum number, and with the same quantum numbers, n, σ, and K,[9] where n is the torsional quantum number, σ specifies the torsional symmetry (σ=0 for A- and 1 for E-species), and K is the quantum number of the component of the total angular momentum along the internal rotation axis.[10] It was found, however, impossible to explain the spectrum on the basis of the conventional internal axis method (IAM)[10,11] by choosing appropriate torsional and rotational parameters for the excited vibrational state, because the ν_8 state was seriously perturbed by the torsionally excited states in the ground vibrational state. Accordingly, no assignment could readily be made for any of the series without further information, except that a pair of the $A(\sigma=0)$, K=1 series were identified unambiguously by their characteristic K-doubling pattern. The pair series are listed in the latter half of Table 1.

The Stark effect of the spectral lines provided another clue. The observed Stark-modulated spectrum was congested with Stark components and was very complicated. In contrast, a source-modulated spectrum with a DC field was found to be much simpler and readily gave a rough estimate of the magnitude of the Stark effect of each line. As the DC field was increased, most of the absorption lines were broadened and their peak intensities were decreased. Only the lines with a small Stark effect were left relatively unaffected in the spectrum even by a field as strong as 670 V/cm. An example is shown in Fig. 1. Since the transitions involving the K=0 levels do not show the first-order effect, they must be assigned to

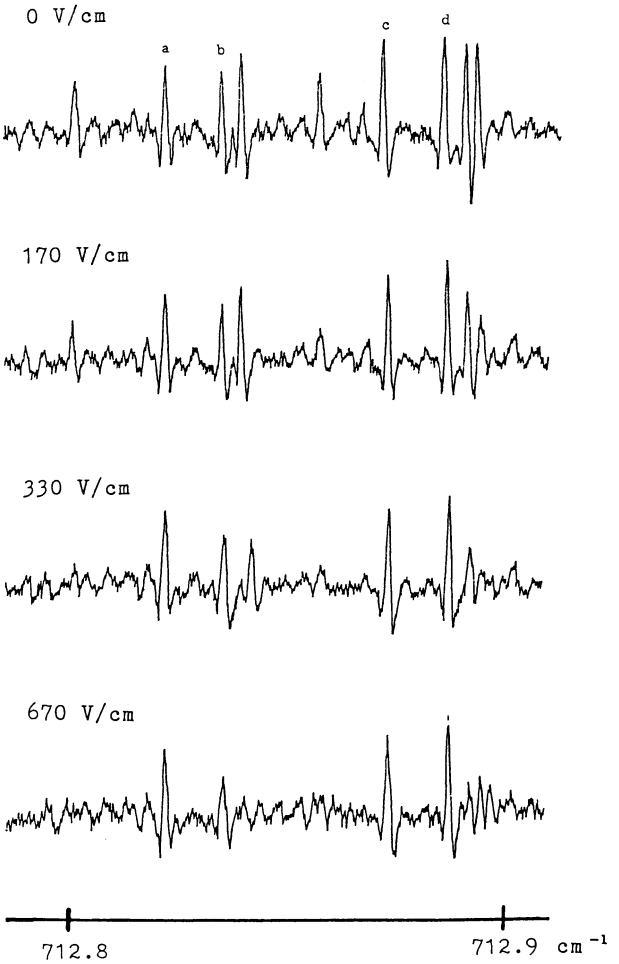

Fig. 1. Source modulated spectra of the CH_3SH ν_8 R(2) transitions with various DC Stark fields applied. At the Stark field of 670 V/cm, four lines, a—d, with relatively small Stark effect remain. a) 712.821, A, K=1, b) 712.835, unassigned, c) 712.874, A, K=1, d) 712.887 cm^{-1}, E, K=0.

Table 1. Assigned ν_8 Band Transitions and Fitting of the ν_8 Energy Levels of CH_3SH[a)]

Transition		Energy level[c)]			
	Obsd[b)]		Obsd[b,d)]	Calcd[e)]	(O-C)×10[3]
$A(\sigma=0)$, $K=0$ Series					
P (8)	703.957 (1)	7_{07}	734.309 (2) *	734.310	−1
P (7)	704.843 (3)	6_{06}	728.454 (3) *	728.454	0
P (6)	705.724 (3)	5_{05}	723.434 (3) *	723.435	−1
P (5)	706.600 (2)	4_{04}	719.251 (2)	719.251	0
P (4)	707.469 (3)	3_{03}	715.904 (3)	715.903	1
P (3)	708.331 (2)	2_{02}	713.392 (2)	713.392	0
R (3)	714.187 (5)	4_{04}	719.248 (5)	719.251	−3
R (4)	715.001 (3)	5_{05}	723.436 (3)	723.435	1
R (6)	716.602 (4)	7_{07}	734.312 (4) *	734.310	2
Obtained parameters[f)]					
$w_{A0}=710.8809(12)$, $b_{A0}=0.41857(10)$, $d_{A0}=3.5(15)\times10^{-6}$					
$E(\sigma=1)$, $K=0$ Series					
P (8)	703.476 (3)	7_0	733.828 (3)	733.825	3
P (7)	704.358 (2)	6_0	727.968 (2)	727.970	−2
P (6)	705.239 (2)	5_0	722.949 (2)	722.950	−1
P (5)	706.114 (2)	4_0	718.765 (2)	718.765	0
P (4)	706.981 (3)	3_0	715.416 (3)	715.417	−1
P (3)	707.846 (4)	2_0	712.907 (4)	712.906	1
P (2)	708.702 (5)	1_0	711.233 (5)	711.232	1
R (2)	712.887 (3)	3_0	715.418 (3)	715.417	1
R (3)	713.705 (3)	4_0	718.766 (3)	718.765	1
R (4)	714.518 (5)	5_0	722.953 (5)	722.950	3
R (5)	715.320 (3)	6_0	727.971 (3)	727.970	1
R (6)	716.117 (3)	7_0	733.827 (3)	733.825	2
R (7)	716.905 (3)	8_0	740.515 (3)	740.515	0
R (8)	717.687 (2)	9_0	748.039 (2)	748.039	0
Obtained parameters[f)]					
$w_{E0}=710.3943(12)$, $b_{E0}=0.41863(6)$, $d_{E0}=4.0(6)\times10^{-6}$					
$A(\sigma=0)$, $K=1$ Series					
P (8)	703.500 (1)	7_{17}	737.076 (3) *	737.078	−2
P (7)	704.377 (2)	6_{16}	731.277 (3) *	731.280	−3
P (6)	705.250 (2)	5_{15}	726.308 (2) *	726.310	−2
P (5)	706.117 (3)	4_{14}	722.166 (3) *	722.167	−1
P (4)	706.978 (2)	3_{13}	718.854 (2)	718.854	0
P (3)	707.831 (3)	2_{12}	716.367 (3)	716.368	−1
P (2)	708.680 (4)	1_{11}	714.712 (4)	714.711	1
R (2)	712.821 (2)	3_{13}	718.853 (2)	718.854	−1
R (3)	713.632 (1)	4_{14}	722.168 (1)	722.167	1
R (4)	714.435 (2)	5_{15}	726.311 (2)	726.310	1
R (5)	715.231 (2)	6_{16}	731.280 (2) *	731.280	0
R (6)	716.022 (3)	7_{17}	737.080 (3) *	737.078	2
R (7)	716.804 (3)	8_{18}	743.704 (3) *	743.704	0
Obtained parameters[f)]					
$w_{A1}=713.8828(13)$, $b_{A1L}=0.41426(8)$, $d_{A1L}=1.1(11)\times10^{-6}$					
$A(\sigma=0)$, $K=1$ Series					
P (8)	703.358 (1)	7_{16}	737.562 (2) *	737.562	0
P (7)	704.254 (1)	6_{15}	731.642 (1) *	731.642	0
P (5)	706.029 (2)	4_{13}	722.340 (2) *	722.340	0
P (4)	706.907 (2)	3_{12}	718.957 (2)	718.957	0
P (3)	707.778 (3)	2_{11}	716.419 (3)	716.420	−1
P (2)	708.644 (4)	1_{10}	714.728 (4)	714.728	0
R (2)	712.874 (3)	3_{12}	718.958 (3)	718.957	1
R (3)	713.700 (3)	4_{13}	722.341 (3)	722.340	1
R (4)	714.518 (5)	5_{14}	726.568 (5)	726.569	−1

Table 1. (Continued)

Transition		Energy level[c]			
	Obsd[b]		Obsd[b,d]	Calcd[e]	(O-C)×10³
R (5)	715.333 (4)	6_{15}	731.644 (4) *	731.642	2
R (6)	716.140 (4)	7_{16}	737.564 (4) *	737.562	2
R (7)	716.938 (5)	8_{17}	744.326 (5) *	744.326	0
R (8)	717.730 (2)	9_{18}	751.934 (3) *	751.934	0
Obtained parameters[f]					
$w_{A1}=713.8822\,(6)$, $b_{A1U}=0.42292\,(3)$, $d_{A1U}=1.3\,(4)\times10^{-6}$					

a) All values in cm^{-1}. b) Values in parentheses are estimated errors in units of 10^{-3} cm^{-1}. c) Energy level notation for A species follows that for asymmetric rotors, $J_{Ka,\,Kc}$. d) Energy is given relative to the $J=K=0$ level of each species in the ground state. The energies without an asterisk are obtained from the observed infrared frequencies in the left column and the observed microwave frequencies.[12,13] For the asterisked levels, the ground state energy levels were calculated from the constants[12] and their estimated errors include the uncertainties in the calculation. e) Calculated by Eq. 1 from the parameters given below. f) Parameters in Eq. 1 determined by weighted least-squares. The numbers in parentheses are standard errors in units of the last digit of the parameter.

some of these lines least affected by Stark effects. Two series involving the $K=0$ levels were thus identified. The one at higher-frequency was assigned to the A-species and the other one at lower frequency to the E-species, as shown in the former half of Table 1, on the basis of the following consideration. In the Loomis-Wood diagram, the lower series is in a cluster of several series, whereas the higher one is separated from the cluster by about 0.5 cm^{-1}. The shift can be explained by a resonance of the $n=0$, A, $K=0$ stack of the ν_8 state with the $n=4$, A, $K=0$ stack in the ground vibrational state, which is located at about 40 cm^{-1} below the former stack. On the other hand, there are no nearby perturbing levels around the ν_8, $n=0$, E, $K=0$ stack.

The assigned transitions are combined with the ground state torsion-rotation energy levels[12,13] to give the vibration-torsion-rotation levels in the ν_8 state. The levels in the ν_8 state are fitted to

$$E(\sigma,\ J,\ K) = w_{\sigma K} + b_{\sigma K}J(J+1) - d_{\sigma K}\{J(J+1)\}^2, \quad (1)$$

by the weighted least-squares method; the results are shwon in Table 1. The fact that the values of b_{A0} and d_{A0} are close to those of b_{E0} and d_{E0} suggests that the resonance is of the Fermi type. The further analysis requires information on the perturbing $n=3$ and 4 levels in the ground vibrational state.

One of the authors, Kuniaki Nakagawa, would like to thank the late Professor Tsunetake Fujiyama for his encouragement in the early stage of the work. He is also grateful to Dr. Chikashi Yamada for his technical assistance. The authors are indebted to Professors Kozo Kuchitsu and Kojiro Takagi for critical reading of the manuscript. The medium resolution spectrum which served as a guide to the present measurement was kindly provided by Professor Fujiyama and Dr. Shi-aki Hyodo. This work was partly supported by the Joint Studies Program (1981—82 and 84—85) of the Institute for Molecular Science and by a Grant-in-Aid for Scientific Research No. 60740256 from the Ministry of Education, Science and Culture.

References

1) J. P. Sattler, T. L. Worchesky, and W. A. Riessler, *Infrared Phys.*, **19**, 217 (1979); **18**, 521 (1978).
2) J. O. Henningsen, *J. Mol. Spectrosc.*, **85**, 282 (1981); **102**, 399 (1983).
3) W. H. Weber, D. H. Leslie, and C. W. Peters, *J. Mol. Spectrosc.*, **89**, 214 (1981).
4) W. H. Weber and P. D. Maker, *J. Mol. Spectrosc.*, **93**, 131 (1982).
5) I. W. May and E. L. Pace, *Spectrochim. Acta, Part A*, **24**, 1605 (1968).
6) C. Yamada, K. Nagai, and E. Hirota, *J. Mol. Spectrosc.*, **85**, 416 (1981).
7) R. Paso, J. Kauppinen, and R. Anttila, *J. Mol. Spectrosc.*, **79**, 236 (1980).
8) K. Jolma, *J. Mol. Spectrosc.*, **111**, 211 (1985).
9) As long as the levels with $n=0$ are discussed, the quantum number n is often dropped in the present note. Only the $\Delta K=0$ selection rule is considered because methanethiol is a near-symmetric top molecule and the ν_8 band is nearly a parallel band. The quantum number σ is the same as μ in Ref. 10.
10) T. Itoh, *J. Phys. Soc. Jpn.*, **11**, 264 (1956).
11) C. C. Lin and J. D. Swalen, *Rev. Mod. Phys.*, **31**, 841 (1959).
12) T. Kojima, *J. Phys. Soc. Jpn.*, **49**, 1197 (1980).
13) R. M. Lees and M. A. Mohammadi, *Can. J. Phys.*, **58**, 1640 (1980).

A Consideration on the Mechanism of the Wacker Reaction from the Viewpoint of the Trans Influence of Ligands ($OH^->Cl^->H_2O$)

Sumio SHINODA, Yasuyuki KOIE, and Yasukazu SAITO*
Institute of Industrial Science, The University of Tokyo,
22-1, Roppongi 7 Chome, Minato-ku, Tokyo 106
(Received February 22, 1986)

Synopsis. The trans influence of three ligands (OH^-, Cl^-, and H_2O) was compared for the first time according to the same experimental standard ($^1J(PtP_{trans})$). Based on the extremely high trans influence of the OH^- ligand, a mechanism was proposed for the palladium(II) oxidation of ethylene, which includes the rate-determining external attack of H_2O on a possible intermediate, *trans*-$[PdCl_2(OH)(C_2H_4)]^-$.

Although the palladium(II) oxidation of ethylene (the Wacker reaction) has been studied extensively, its mechanistic details (the stereochemistry of the hydroxypalladation and the nature of the rate-determining step) are still the subject of some debate.[1,2] While the mechanism proposed by Henry (rate-determining *syn*-hydroxypalladation) is consistent with the kinetics,[1] Bäckvall et al.[3] proposed a mechanism of the Wacker reaction which reconciles the anti stereochemistry of the hydroxpalladation step with the kinetics. The important point is that the hydroxylation occurs in a *reversible* reaction by the external attack of water on $[PdCl_2(OH_2)(C_2H_4)]$ (Eq. 1), followed by a rate-determining step in which the loss of chloride ion from $[HOCH_2CH_2PdCl_2(OH_2)]^-$ (Eq. 2) takes place.

$$[PdCl_2(OH_2)(C_2H_4)] + H_2O \rightleftharpoons [HOCH_2CH_2PdCl_2(OH_2)]^- + H^+ \quad (1)$$

$$[HOCH_2CH_2PdCl_2(OH_2)]^- \rightleftharpoons [HOCH_2CH_2PdCl(OH_2)] + Cl^- \quad (2)$$

However, the reversibility of Eq. 1 was seriously questioned on the basis of the deuterium isotope effect for ethylene-1,1-d_2,[4] and later on the basis of the relative rate of isomerization vs. oxidation with allyl-1,1-d_2 alcohol adopted as a substrate (very slow isomerization via hydroxypalladation-deoxypalladation processes, despite the rate expression for oxidation being the same as that for ethylene oxidation).[5,6] Thus, if anti stereochemistry is assumed for the hydroxypalladation step, the most likely mechanism which is consistent with the kinetics would be a rate-determining attack of H_2O on a $[PdCl_2(OH)(C_2H_4)]^-$ species.[7] In the present paper, we would like to discuss the possibility of this mechanism from the points of view of (i) the activation of coordinated ethylene toward the external attack of an H_2O molecule, (ii) the nature of the ethylene–palladium(II) bond, and (iii) the trans influence of the OH^- ligand. Some of the experimental data are our own and are presented here for the first time.

In a previous paper,[4] we suggested that the displacement of the coordinated ethylene to an unsymmetrical position was important in the Wacker reaction; its transition-state structure contrasts with that of ethylene methoxy-mercuration, which is accompanied by considerable C–O bond formation.[10] Actually, Eisenstein and Hoffmann[11] showed that a symmetrically η^2-coordinated olefin was deactivated toward attack by an external nucleophile, and that olefin slipping, a deformation to η^1 coordinantion, played a crucial role in activating the olefin, with an increase in the overlap population between the π^* orbital of the olefin and the electron pair of the nucleophiles. This idea was supported by recent experimental findings.[12]

The bonding nature of metal-ethylene π-complexes $[MCl_3(C_2H_4)]^-$ (M=Pd, Pt) was investigated by means of ab initio calculations on an extended basis,[13] where the creditability of the calculations was ensured by the agreement between the calculated and observed values for both the geometry and the barrier to rotaion in $[PtCl_3(C_2H_4)]^-$. For this complex, the amounts of σ-donation and π-back-donation were evaluated as 0.24 and 0.22 electrons respectively. As for $[PdCl_3(C_2H_4)]^-$ the corresponding values are 0.12 (σ-donation) and 0.07 (π-back-donation) electrons, indicating the weakness of the Pd-ethylene bond relative to the Pt-ethylene bond. By comparing these two values (0.12>0.07), it was also concluded that σ-donation is more important than π-back-donation in the case of $[PdCl_3(C_2H_4)]^-$. In fact, many kinds of experiments support these trends.[14–16]

Previously, an unexpectedly high trans influence of the OH^- ligand in comparison with the Cl^- ligand was pointed out[4] on the ground of the $^1J_{PtP}$ values for the Pt(II) complexes $[PtX(CH_3)(Ph_2PCH_2CH_2PPh_2)]$.[17] We determined here the corresponding value for the aqua complex, together with the acetone complex (Table 1), to complete the comparison of the trans influence among OH^-, Cl^-, and H_2O ligands. Table 1 unequivocally confirms that the trans influence of

Table 1. ^{195}Pt-^{31}P Nuclear Spin Coupling Constants of $[PtX(CH_3)(dppe)]$ Complexes ($dppe=Ph_2PCH_2CH_2PPh_2$)[a]

Complex	J_{PtP} (trans to X) / Hz	J_{PtP} (trans to CH_3) / Hz
$[Pt(H_2O)(CH_3)(dppe)]BF_4$[b]	4722	1821
$[Pt(Me_2CO)(CH_3)(dppe)]BF_4$[b]	4619	1821
$[Pt(Cl)(CH_3)(dppe)]$	4255 (4224)	1729 (1737)
$[Pt(OH)(CH_3)(dppe)]$	3474 (3546)	1829 (1804)

a) Measured at 30 °C in CH_2Cl_2 (0.3 mol dm^{-3}; JEOL FX-60Q, 24.20 MHz). Data in parentheses are from Ref. 17. b) Prepared according to the literature methods.[17,28]

Table 2. Some Characteristics of OH^-, Cl^-, and H_2O Ligands

Ligand	$P_L/V^{a)}$	*trans*-[ML(CO)$(PPh_3)_2$] (M=Rh, Ir)				E_{homo}/a.u.[d]
		ν_{CO}/cm^{-1} [b]		$E_{1/2}^{ox}/V$[c]		
		Rh	Ir	Rh	Ir	
OH^-	−1.55	1961	1949	−2.45	−2.68	−0.0941
Cl^-	−1.19	1980	1965	−2.05	−2.22	
H_2O						−0.7121

a) $P_L=E_{1/2}^{ox}[Cr(CO)_5L]-E_{1/2}^{ox}[Cr(CO)_6]$. From Ref. 29. b) From Ref. 30. c) Standard: Ag/Ag^+ 0.1 mol dm^{-3} CH_3CN solution. From Ref. 31. d) From Ref. 20.

OH^- is far stronger than not only Cl^- but also H_2O. Since the $^1J_{PtP}$ value reflects well the σ-bond strength between the platinum and phosphorus atoms, [18] it can be said that the Pt–P(trans) σ bond is most weakened in the case of the hydroxo complex because of the strongest σ bonding between the platinum(II) and the OH^- ligand.[19]

As far as we know, there are no other data available for comparing these three ligands on the same experimental standard. However, some relevant data are collected in Table 2. It is obvious from Table 2 that OH^- is the most electron-donating among the three. With respect to theoretical studies, the CNDO/2 calculations of pentaammine complexes $[M(NH_3)_5X]$ ($M=Co^{2+}$, Co^{3+}, Fe^{2+}, and Fe^{3+}; X=FH, OH_2, CO, NH_3, pyridine, OH^-, F^-, and CN^-) showed that the M-NH_3 bond was weakened when the trans ligand was changed from H_2O to OH^-.[20] Recently, on the basis of the equilibrium geometry obtained by ab initio calculations with energy-gradient methods, the trans influene order of $OH^->Cl^->NH_3>H_2O$ was concluded.[21]

According to the analysis of the palladium(II)–ethylene bond (vide supra), σ-donation (from the ethylene π orbital to the Pd d_σ orbital) is important. Taking into consideration the strong trans influence of the OH^- ligand (relative to Cl^- and H_2O), it is quite conceivable that the η^2-coordinated ethylene slips most easily when its trans position is occupied by this ligand.[22] If this process occurs exclusively for the hydroxo complex, the observed kinetics is compatible with the anti stereochemistry of hydroxy-palladation.

References

1) P. M. Henry, "Palladium Catalyzed Oxidation of Hydrocarbons," Reidel, New York (1980), Chap. 2.

2) H. E. Bryndza, *Organometallics*, **4**. 406 (1985), and the references cited therein.

3) J. E. Bäckvall, B. Åkermark, and S. O. Ljunggren, *J. Am. Chem. Soc.*, **101**, 2411 (1979).

4) Y. Saito and S. Shinoda, *J. Mol. Catal.*, **9**, 461 (1980); M. Kosaki, M. Isemura, Y. Kitaura, S. Shinoda, and Y. Saito, *J. Mol. Catal.*, **2**, 351 (1977).

5) W. K. Wan, K. Zaw, and P. M. Henry, *J. Mol. Catal.*, **16**, 81 (1982).

6) N. Gregor, K. Zaw, and P. M. Henry, *Organometallics,*, **3**, 1251 (1984).

7) Bäckvall et al.[3] and Henry et al.[5] noted that the nucleophilic attack on a negatively charged π-olefin-metal complex is unlikely. However, even if this reaction is supposed to be driven by a cationic charge on the coordinating carbon atom, its charge density would not necessarily be determined by the formal charge of the complexed ion as a whole. Rather, the trans influence of ligands,[8] either ionic or neutral, seems more important. For instance, the ^1H chemilcal shifts and ν(Ir-H) of a series of hydridoiridium(III) complexes *trans*-[H(L)Ir(CO)(Cl)$(PPh_3)_2$] were shown to be understandable in terms of the σ-donor strength of the trans ligand L,[9] quite independent of the formal charge of the complex.

8) T. G. Appleton, H. C. Clark, and L. E. Manzer, *Coord. Chem. Rev.*, **10**, 335 (1973).

9) B. Olgemöller and W. Beck, *Inorg. Chem.*, **22**, 997 (1983).

10) S. Shinoda, M. Isemura, and Y. Saito, *Bull. Chem. Soc. Jpn.*, **52**, 1855 (1979).

11) O. Eisenstein and R. Hoffmann, *J. Am. Chem. Soc.*, **103**, 4308 (1981); **102**, 6148 (1980).

12) L. Maresca and G. Natile, *J. Chem. Soc., Chem. Commun.*, **1983**, 40.

13) P. J. Hay, *J. Am. Chem. Soc.*, **103**, 1390 (1981).

14) D. W. Wertz and M. A. Moseley, *Inorg. Chem.*, **19**, 705 (1981); *Spectrochim. Acta A*, **36A**, 467 (1980).

15) H. Kurosawa, T. Majima, and N. Asada, *J. Am. Chem. Soc.*, **102**, 6996 (1980).

16) W. Partenheimer, *J. Am. Chem. Sco.*, **98**, 2779 (1976).

17) T. G. Appleton and M. A. Bennett, *Inorg. Chem.*, **17**, 738 (1978).

18) Y. Koie, S. Shinoda, and Y. Saito, *Inorg. Chem.*, **20**, 4408 (1981).

19) E. J. Shustrovich, *J. Am. Chem. Soc.*, **100**, 7513 (1978).

20) E. Kai, T. Misawa, and K. Nishimoto, *Bull. Chem. Soc. Jpn.*, **53**, 2481 (1980).

21) H. Basch, M. Krauss, W. J. Stevens, and D. Cohen, *Inorg. Chem.*, **24**, 3313 (1985).

22) Due to the strong trans influence of ethylene, the formation of *trans*-$[PdCl_2(H_2O)(C_2H_4)]$ is substantial.[1] It is well known that the proton-dissociating ability of H_2O is enhanced by coordination with metal ions.[23] Further, this effect is emphasized when there is an olefin ligand at its trans position.[24] Leden and Chatt estimated the acid-dissociation constant of $[PtCl_2(H_2O)(C_2H_4)]$ to be of the order 10^{-5},[25] while Henry assumed 10^{-6} as the corresponding value of $[PdCl_2(H_2O)(C_2H_4)]$.[26] Although he claimed the presence of kinetically significant amounts of the intermediate *cis*-$[PdCl_2(OH)(C_2H_4)]^-$ on this standard (also assuming about 10% *cis*-form in the total), the acid-dissociation constant may be much higher in view of the extremely high affinity of Pd(II) to OH^- in comparison with Pt(II) (Eqs. 3 and 4).[27]

$$[PdCl_4]^{2-} + OH^- \rightleftharpoons [PdCl_3(OH)]^{2-} + Cl^-, \quad \log_{10} K = 5.7 \ (\mu = 1.0,\ 19\text{—}50\ ^\circ C) \tag{3}$$

$$[PtCl_3(OH)]^{2-} + Cl^- \rightleftharpoons [PtCl_4]^{2-} + OH^-, \quad \log_{10} K = 8.66 \ (\mu = 1.0,\ 25\ ^\circ C) \tag{4}$$

23) F. Basolo and R. G. Pearson, *Progr. Inorg. Chem.*, **4**, 381 (1962); M. I. Gel'fman, *Koord. Khim.*, **2**, 1369 (1976).
24) Yu. N. Kukushkin, K. M. Trusova, V. F. Budanova, and G. N. Sedova, *Koord. Khim.*, **4**, 436 (1978).
25) I. Leden and J. Chatt, *J. Chem. Soc.*, **1955**, 2936.
26) P. M. Henry, *J. Am. Chem. Soc.*, **86**, 3246 (1964).
27) F. R. Hartley, "The Chemistry of Platinum and Palladium," Applied Science Publishers, London (1973), pp. 237—238.
28) D. P. Arnold and M. A. Bennett, *J. Organomet. Chem.*, **199**, 119 (1980).
29) J. Chatt, C. T. Kan, G. J. Leigh, C. J. Pickett, and D. R. Stanley, *J. Chem. Soc., Dalton Trans.*, **1980**, 2032.
30) L. Vaska and J. Peone, Jr., *Chem. Commun.*, **1971**, 418.
31) G. Schiavon, S. Zecchin, and G. Pilloni, *J. Inorg. Nucl. Chem.*, **39**, 115 (1977).

Crystal and Molecular Structure of a Binuclear Copper(II) Complex with 1,2,3,4-Tetrakis(salicylideneamino)-2,3-dimethylbutane[1)]

Masahiro MIKURIYA,*,† Tatsuo IZUMITANI, Hisashi ŌKAWA, and Sigeo KIDA*,†
Department of Chemistry, Faculty of Science, Kyushu University 33,
Hakozaki, Higashi-ku, Fukuoka 812
(Received April 23, 1986)

Synopsis. The crystal structure of a binuclear copper(II) complex with 1,2,3,4-tetrakis(salicylideneamino)-2,3-dimethylbutane (abbreviated as H_4sata), Cu_2(sata), was determined by the single-crystal X-ray diffraction method. The complex molecule has two coordination units formed by a planar 6-5-6 fused chelate ring and takes a nonstacked form.

In recent years there has been a considerable interest in binuclear metal complexes because of their unique properties arising from the two metal ions in close proximity. As a face-to-face binucleating ligand, Ōkawa et al. have prepared 1,2,3,4-tetrakis(salicylideneamino)-2,3-dimethylbutane (abbreviated as H_4sata) which contains two "salpn" moieties (H_2salpn=*N,N'*-disalicylidene-1,2-propanediamine) combined at the 2-carbon atom of the diamine chain (Fig. 1).[2)] This ligand forms binuclear complexes M_2(sata) (M=Cu, Ni, Fe, Mn) which take two possible configurations, (i.e., stacking and nonstacking), caused by the rotation about the bridging C–C bond. The electronic and ESR spectra and electrochemical data suggested that the two MN_2O_2 planes are stacked in a face-to-face manner and interact with each other in solution.[3)] The structures of these complexes have not yet been confirmed by X-ray analysis, since we have obtained no crystal suitable for the analysis. In this study, however, another batch of crystals have proved to have better quality, thus we have carried out the X-ray structure analysis of Cu_2(sata).

Experimental

The Cu_2(sata) complex was prepared by the method previously reported.[2)] Crystals suitable for X-ray study were obtained as dark brown plates by crystallization from a dilute ethanol solution after standing one year. Anal. Found: C, 56.03; H, 4.83; N, 7.21%. Calcd for $C_{36}H_{40}Cu_2N_4O_7$=Cu_2(sata)·C_2H_5OH·$2H_2O$: C, 56.31; H, 5.25; N, 7.30%. A crystal with dimensions of 0.11×0.36×0.40 mm^3 was used for the X-ray analysis. The unit-cell parameters and intensities were measured on a Rigaku AFC-5 automated four-circle diffractometer with graphite-monochromated Mo Kα radiation (λ=0.71073 Å) at 24±1 °C.

Crystal Data: $C_{36}H_{40}Cu_2N_4O_7$, F.W.=767.83; triclinic; $P\bar{1}$; a=16.691(1), b=17.106(1), c=15.641(1) Å; α=117.25(1), β=117.95(1), γ=88.83(1)°; D_m=1.50; D_c=1.50 g cm^{-3}; Z=4.

The intensity data were collected by the 2θ-ω scan technique with a scan rate of 3° min^{-1} in ω. A total of 8144 reflections with 2θ<43° were collected. The intensity data were corrected for the Lorentz and the polarization effects, but not for absorption. 4829 Independent reflections with $|F_o|>3\sigma(|F_o|)$ were considered as "observed" and were used for the structure analysis. The structure was solved by the direct method and refined by the block-diagonal least-squares method. The ethyl groups of ethanol molecules could not be located probably due to the disorder in the solvent molecules. Hydrogen atoms are not included in the calculation. In the least-squares refinement a weighting scheme, $w=(6.81+|F_o|+0.005|F_o|^2)^{-1}$ was employed. The final discrepancy factors were $R_1=\sum||F_o|-|F_c||/\sum|F_o|=0.080$ and $R_2=[\sum w(|F_o|-|F_c|)^2/\sum w|F_o|^2]^{1/2}=0.119$.

The atomic scattering factors and the anomalous dispersion corrections were taken from International Tables for X-Ray Crystallography.[4)] All the calculations were carried out on the FACOM M-200 computer in the Computer Center of Kyushu University by the use of a local version of the UNICS-III programs.[5)] The final positional and thermal parameters are given in Table 1. The anisotropic thermal parameters and the F_o—F_c tables have been deposited as a Document No. 8643 at the Office of the Editor.

Results and Discussion

The crystal contains two crystallographically independent binuclear molecules; they are represented as A and B. There are no significant differences in bond lengths and angles between A and B. The molecular structure of A is shown in Fig. 2, the "en-chelated structure" (Fig. 1) which was supposed from the electronic spectrum[2)] has been confirmed. The molecule consists of two "Cu(salpn)" moieties linked by the C(8)–C(8)′ bond. All the coordination geometries are nearly square planar, four donor atoms around a copper atom being coplanar with the deviations within ±0.14 Å. Each "Cu(salpn)" moiety does not form a rigorous plane, and may be described as "umbrella-shape."[6)] The five-membered chelate rings (Cu–N(1)–C(8)–C(9)–N(2), Cu′–N(1)′–C(8)′–C(9)′–N(2)′) assume a gauche conformation similar to that observed in the Cu(salpn)[7)] and Cu(salen)[8)] complexes (H_2salen=*N,N'*-disalicylidene-1,2-ethanediamine). Bond lengths and angles of the "Cu(salpn)"

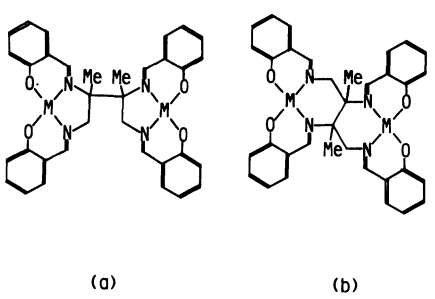

Fig. 1. Possible structures of Cu_2(sata): (a) en-chelated and (b) tn-chelated structures.

† Present address: Coordination Chemistry Laboratories, Institute for Molecular Science, Okazaki National Research Institutes, Okazaki 444.

Table 1. Fractional Positional Parameters ($\times 10^4$) and Thermal parameters of Non-Hydrogen Atoms with Their Estimated Standard Deviations in Parentheses

Atom	x	y	z	B_{eq}/Å^2	Atom	x	y	z	B_{eq}/Å^2
Cu(A)	432(1)	561(1)	−528(1)	5.3	C(11A)′	5212(10)	−1221(9)	748(13)	5.3
Cu(A)′	3610(1)	−863(1)	−1187(1)	4.9	C(12A)′	5928(11)	−1327(12)	1629(15)	6.9
Cu(B)	1391(1)	5863(1)	1064(1)	5.0	C(13A)′	6369(13)	−2027(13)	1418(17)	8.2
Cu(B)′	4566(1)	4436(1)	3475(1)	5.2	C(14A)′	6062(13)	−2668(12)	267(19)	8.5
O(1A)	−566(8)	225(9)	−1972(10)	8.5	C(15A)′	5360(12)	−2587(11)	−624(16)	7.2
O(2A)	−37(7)	1566(7)	23(10)	6.9	C(16A)′	4943(10)	−1826(10)	−376(13)	5.9
O(1A)′	3152(8)	−1324(8)	−2726(8)	8.0	C(17A)′	2629(10)	1350(8)	318(11)	5.1
O(2A)′	4314(7)	−1744(7)	−1248(8)	6.3	C(1B)	2448(11)	6057(10)	160(14)	6.6
O(1B)	1851(9)	6331(8)	461(11)	8.2	C(2B)	2745(14)	6519(14)	−268(18)	8.8
O(2B)	680(7)	6728(6)	1184(9)	6.3	C(3B)	3374(15)	6308(14)	−551(18)	9.0
O(1B)′	5565(7)	4784(9)	3364(10)	8.3	C(4B)	3852(14)	5636(14)	−437(18)	9.0
O(2B)′	5041(7)	3438(7)	3498(9)	7.1	C(5B)	3615(13)	5220(13)	6(16)	8.2
N(1A)	1062(8)	−328(7)	−1051(9)	5.5	C(6B)	2933(10)	5408(9)	305(12)	5.5
N(2A)	1371(7)	793(7)	950(9)	4.5	C(7B)	2779(9)	4933(9)	791(10)	5.3
N(1A)′	2764(7)	−81(7)	−1109(9)	4.5	C(8B)	2206(9)	4607(8)	1791(9)	4.2
N(2A)′	4153(7)	−282(7)	410(8)	4.6	C(9B)	1227(9)	4521(9)	1615(11)	5.0
N(1B)	2238(7)	5079(7)	1213(8)	4.7	C(10B)	196(9)	5493(9)	1786(10)	4.9
N(2B)	829(7)	5260(7)	1521(9)	5.1	C(11B)	−217(10)	6215(9)	1761(11)	5.6
N(1B)′	3922(7)	5338(7)	3215(8)	5.1	C(12B)	−930(12)	6346(13)	2029(13)	7.4
N(2B)′	3623(7)	4211(8)	3785(8)	5.1	C(13B)	−1347(13)	7068(15)	2093(15)	9.0
C(1A)	−687(14)	−434(13)	−2891(16)	9.2	C(14B)	−1034(14)	7691(13)	1870(13)	8.8
C(2A)	−1568(18)	−596(19)	−3898(17)	14.0	C(15B)	−374(12)	7576(12)	1577(13)	7.5
C(3A)	−1701(22)	−1261(24)	−4922(21)	19.7	C(16B)	67(10)	6855(10)	1526(11)	6.1
C(4A)	−1136(26)	−1857(22)	−5035(20)	19.7	C(17B)	2383(10)	3654(8)	1340(10)	5.2
C(5A)	−272(20)	−1822(18)	−4104(17)	14.5	C(1B)′	5714(13)	5458(14)	3238(15)	9.7
C(6A)	−98(14)	−1017(14)	−3005(14)	9.5	C(2B)′	6559(18)	5593(19)	3260(21)	14.4
C(7A)	760(12)	−971(11)	−2054(13)	7.8	C(3B)′	6696(21)	6318(21)	3109(24)	16.2
C(8A)	2022(10)	−257(9)	−112(12)	5.6	C(4B)′	6114(22)	6879(21)	2897(25)	16.1
C(9A)	1946(11)	146(10)	945(13)	6.1	C(5B)′	5264(19)	6807(15)	2977(18)	12.3
C(10A)	1468(10)	1396(10)	1885(13)	5.9	C(6B)′	5073(14)	6061(12)	3125(14)	8.6
C(11A)	924(11)	2084(10)	1973(13)	6.4	C(7B)′	4232(11)	5986(11)	3168(12)	7.7
C(12A)	1161(13)	2750(13)	3105(18)	9.2	C(8B)′	2967(10)	5274(9)	3111(11)	5.1
C(13A)	644(19)	3389(14)	3251(22)	12.2	C(9B)′	3059(10)	4866(10)	3855(12)	5.9
C(14A)	−24(17)	3443(11)	2332(24)	11.9	C(10B)′	3532(10)	3586(11)	3998(11)	5.9
C(15A)	−245(12)	2837(10)	1275(18)	8.2	C(11B)′	4071(11)	2910(11)	3975(13)	6.7
C(16A)	211(11)	2150(10)	1067(15)	6.5	C(12B)′	3822(13)	2275(13)	4213(14)	9.0
C(17A)	2240(11)	−1201(10)	−357(15)	7.0	C(13B)′	4320(19)	1591(16)	4190(19)	12.6
C(1A)′	2537(11)	−1053(10)	−3357(12)	6.4	C(14B)′	4986(18)	1542(13)	3905(15)	12.3
C(2A)′	2316(14)	−1515(13)	−4497(13)	8.8	C(15B)′	5258(14)	2165(12)	3662(13)	9.4
C(3A)′	1614(17)	−1307(14)	−5241(16)	10.1	C(16B)′	4766(11)	2859(9)	3693(10)	6.1
C(4A)′	1197(14)	−621(13)	−4900(15)	8.7	C(17B)′	2764(11)	6188(9)	3614(13)	6.9
C(5A)′	1402(11)	−192(11)	−3800(12)	6.9	O(SA1)	1911(13)	−1435(16)	2013(20)	17.1
C(6A)′	2063(11)	−408(9)	−3030(12)	5.6	O(SA2)	1574(19)	−3222(23)	−3148(29)	23.7
C(7A)′	2231(10)	65(9)	−1912(12)	5.5	O(SA3)	1141(23)	−3806(19)	−5258(21)	23.1
C(8A)′	2784(9)	393(8)	−25(10)	4.3	O(SB1)	6897(12)	3571(14)	3464(16)	15.8
C(9A)′	3786(9)	497(9)	884(11)	5.2	O(SB2)	3452(20)	−1682(26)	3533(22)	26.1
C(10A)′	4805(10)	−477(9)	1108(13)	5.3	O(SB3)	3879(22)	−1160(18)	2446(25)	22.3

moieties fall in the range of the values reported for a series of Cu(salen)-type complexes.[6–8]

It was pointed out that the ligand was diastereomeric (dl and meso) with respect to the 2- and 3-carbon atoms of the 2,3-dimethyl-1,2,3,4-butanetetramine moiety, and its configuration was inferred as the dl-form from the configurational study for the related complexes.[9] The present structural data have confirmed that the configuration of the tetramine moiety is the dl-form.

The Cu_2(sata) molecule in the crystal takes a nonstacked form though the discussions based on the

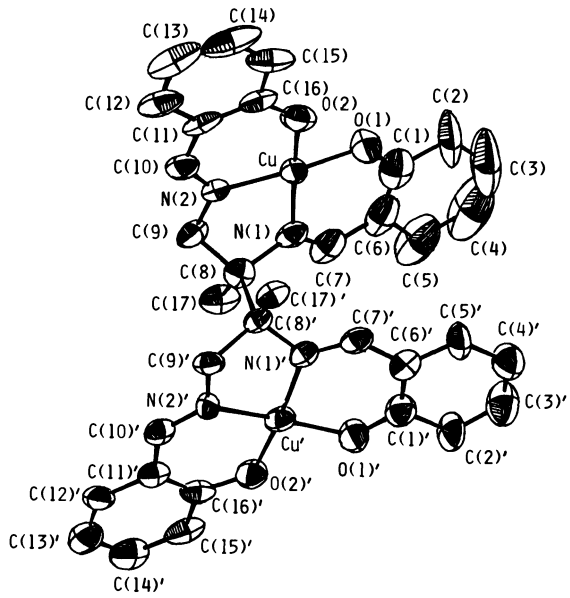

Fig. 2. Molecular structure of the Cu_2(sata) complex with thermal ellipsoids (35% probability level). Distances (l/Å): Cu–O(1) 1.879(12), 1.876(20); Cu–O(2) 1.879(12), 1.876(11); Cu–N(1) 1.921(13), 1.936(12); Cu–N(2) 1.936(11), 1.949(17); Cu′–O(1)′ 1.887(12), 1.888(16); Cu′–O(2)′ 1.888(12), 1.875(13); Cu′–N(1)′ 1.932(12), 1.950(13); Cu′–N(2)′ 1.921(11), 1.944(15). Angles (ϕ/°): O(1)–Cu–O(2) 87.2(5), 88.7(7); O(1)–Cu–N(1) 94.8(5), 95.2(6); N(1)–Cu–N(2) 84.9(5), 84.0(6); O(2)–Cu–N(2) 94.2(5), 93.1(6); O(1)′–Cu′–O(2)′ 88.1(6), 87.7(7); O(1)′–Cu′–N(1)′ 94.7(6), 94.7(6); N(1)′–Cu′–N(2)′ 84.3(5), 84.1(6); O(2)′–Cu′–N(2)′ 93.8(5), 94.6(6). Dihedral angles (τ/°) between the coordination planes, O(1)–N(1)–N(2)–O(2) and O(1)′–N(1)′–N(2)′–O(2)′: 11.2, 10.4 for molecules A and B, respectively.

electronic and ESR spectra and electrochemical properties in solution all pointed a stacked form. The intramolecular copper-copper distance is 6.118(3) Å. There is neither axial coordination nor intermolecular association, the closest atom, N(2), of neighboring molecule being separated from the copper atom by 3.447(14) Å. The present results do not contradict the conclusions derived from the solution studies, since the rotation about the C(8)–C(8)′ bond is feasible in solution so that the two coordination planes stack.

References

1) Binuclear Metal Complexes Part 60 (Part 59: D. Liao, J.-Z. Zhuang, H. Ōkawa, and S. Kida, submitted to *Inorg. Chim. Acta*, for publication.

2) T. Izumitani, H. Ōkawa, and S. Kida, *Chem. Lett.*, **1981**, 483; T. Izumitani, M. Nakamura, H. Ōkawa, and S. Kida, *Bull. Chem. Soc. Jpn.*, **55**, 2122 (1982).

3) H. Ōkawa, M. Kakimoto, T. Izumitani, M. Nakamura, and S. Kida, *Bull. Chem. Soc. Jpn.*, **56**, 149 (1983); M. Nakamura, H. Ōkawa, and S. Kida, *Inorg. Chim. Acta*, **75**, 9 (1983); M. Nakamura, *Bull. Chem. Soc. Jpn.*, **56**, 2529 (1983); H. Ōkawa, A. Honda, M. Nakamura, and S. Kida, *J. Chem. Soc., Dalton Trans.*, **1985**, 59.

4) "International Tables for X-Ray Crystallography", Kynoch Press, Birmingham (1974), Vol. IV.

5) S. Kawano, *Rep. Comp. Cent. Kyushu Univ.*, **16**, 113 (1983); T. Sakurai and K. Kobayashi, *Rep. Inst. Phys. Chem. Res.*, **55**, 69 (1979); C. K. Johnson, Report No. 3794, Oak Ridge National Laboratory, Oak Ridge, Tennessee (1965).

6) M. Calligaris, G. Nardin, and L. Randccio, *Coord. Chem. Rev.*, **7**, 385 (1972).

7) F. J. Llewellyn and T. N. Waters, *J. Chem Soc.*, **1960**, 2639.

8) D. Hall and T. N. Waters, *J. Chem. Soc.*, **1960**, 2644.

9) H. Ōkawa, M. Kakimoto, T. Izumitani, and S. Kida, *Bull. Chem. Soc. Jpn.*, **55**, 2671 (1982).

Tetraoxotetraazaparacyclophanes with Various Alkyl Chains as Hosts for Hydrophobic Compounds

Masato KODAKA* and Toshio FUKAYA
National Chemical Laboratory for Industry, Tsukuba, Ibaraki 305
(Received March 29, 1986)

Synopsis. Tetraoxotetraazaparacyclophanes with short or long alkyl chains and tertiary amino groups were synthesized. It was shown that *NN'N''N'''*-tetrakis-(3-dimethylaminopropyl)-3,10,21,28-tetraoxo-2,11,20,29-tetraaza[3.3.3.3]paracyclophane and *NN'N''N'''*-tetrakis-(5-dimethylaminopentyl)-3,10,21,28-tetraoxo-2,11,20,29-tetra-aza-[3.3.3.3]paracyclophane as well as *NN'N''N'''*-tetrakis-(10-dimethylaminodecyl)-3,10,21,28-tetraoxo-2,11,20,29-tetra-aza-[3.3.3.3]paracyclophane could undergo a complex formation with picrate and 8-anilino-1-naphthalenesulfonic acid, while the dissociation constants for the former cyclophanes were larger than those for the latter cyclophane. The hydrolysis of *p*-nitrophenyl hexanoate was also studied in the presence of the cyclophanes and azide ion (N_3^-), but the reaction was not significantly activated.

Chemical reactions in vivo are catalyzed by enzymes, where host-guest complexes are formed between substrates and enzymes before reactions take place. Another typical example of host-guest complexes can be seen in antigen-antibody reactions. Murakami et al. designed several tetraoxotetraazaparacyclophanes possessing four or eight long alkyl chains (octopus azaparacyclophanes) and characterized the complex formation with hydrophobic compounds.[1-3] Other types of water-soluble cyclophanes were synthesized by Tabushi et al.[4,5] and Odashima et al.,[6] which could undergo complex formations with some hydrophobic anionic compounds.

In the present work, we have studied the former type of cyclophanes, which have shorter alkyl chains than those characterized by Murakami et al.[1-3] and have tertiary amino groups. The substrate-binding ability of such tetraoxotetraazaparacyclophanes with shorter alkyl chains has not been studied so far.

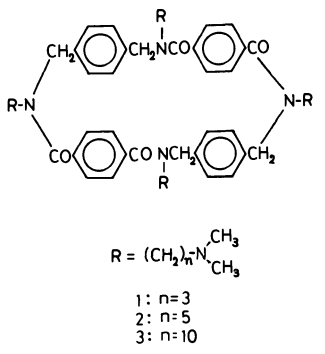

Experimental

Tetraoxotetraazaparacyclophanes (**1**, **2**, **3**) were synthesized in a similar manner as reported.[1,2] Potassium picrate (Kanto Chemical Co.), 8-anilino-1-naphthalenesulfonic acid magnesium salt (ANS) (Nakarai Chemicals) and *p*-nitrophenyl hexanoate (*p*-NPH) (Tokyo Kasei Kogyo Co.) were used as supplied. Other reagents used were of the purest grade available.

Electronic absorption and fluorescence spectra were taken on a Beckman Model 34 spectrophotometer and a JASCO FP-4 fluorescence spectrophotometer, respectively, at pH 6.3 (0.1 mol dm^{-3} Na_2HPO_4–0.1 mol dm^{-3} NaH_2PO_4 buffer) and 25 °C. The hydrolysis of *p*-NPH was investigated under the conditions: pH 8.1 (0.05 mol dm^{-3} NaH_2PO_4–0.025 mol dm^{-3} $Na_2B_4O_7$ buffer), μ=0.1 (KCl) and 32 °C. The reaction rate was determined by measuring the absorbance at 400 nm, originating from the liberated *p*-nitrophenol, with a Beckman Model 34 spectrophotometer.

Results and Discussion

The absorption spectrum of potassium picrate changed upon the addition of **1**, **2**, or **3**. Typical spectral changes caused by **3** are shown in Fig. 1. By assuming the formation of a 1:1 complex between picrate and the cyclophane, the dissociation constants (K_d) were evaluated by the Benesi-Hildebrand plot[1] and are summarized in Table 1. In Fig. 2 is shown a typical plot for **1**. It should be noted that **1** and **2** form relatively stable complexes with picrate but their dissociation constants are larger than that with **3**.

It is generally known that the fluorescence intensity of ANS is significantly increased when it is situated in hydrophobic environments.[7] Thus, the dissociation constants for the complexes formed with ANS and the cyclophanes were obtained from the fluorescence measurements. Figure 3 shows the typical Benesi-

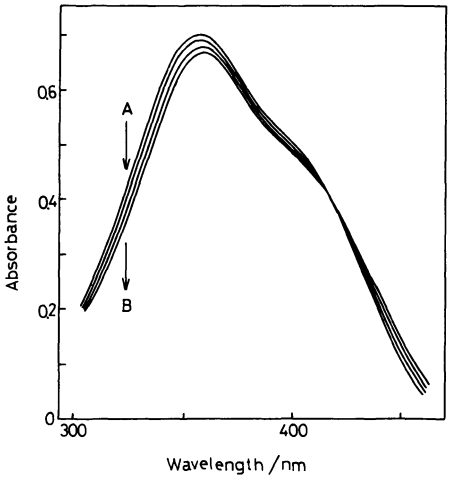

Fig. 1. Absorption spectra of potassium picrate at various concentrations of **3**: pH 6.3(0.1 mol dm^{-3} Na_2HPO_4–0.1 mol dm^{-3} NaH_2PO_4 buffer); 25 °C. The concentrations(mol dm^{-3}) of **3** are 0, 5×10^{-6}, 5×10^{-5} and 1×10^{-4}; read from A to B. The concentration of potassium picrate is 5×10^{-5} mol dm^{-3}.

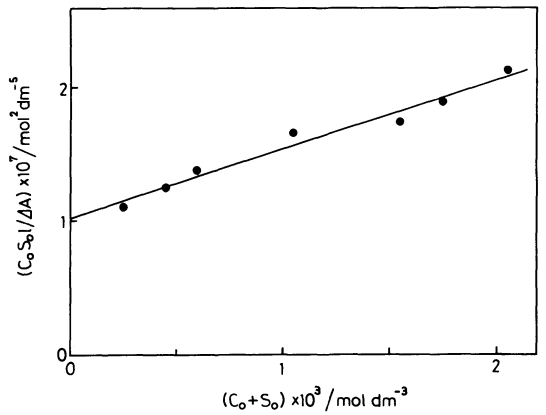

Fig. 2. Benesi–Hildebrand plot for the complex formation between potassium picrate and **1**: pH 6.3(0.1 mol dm^{-3} Na_2HPO_4–0.1 mol dm^{-3} NaH_2PO_4 buffer); 25 °C.
C_0: Concentration of **1**.
S_0: Concentration of picrate (5×10^{-5} mol dm^{-3}).
1: Cell length(0.1 dm).
ΔA: Change of absorbance at 340 nm.

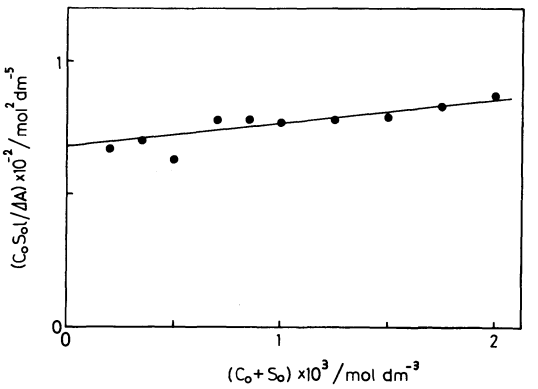

Fig. 3. Benesi–Hildebrand plot for the complex formation between ANS and **1**: pH 6.3(0.1 mol dm^{-3} $NaHPO_4$–0.1 mol dm^{-3} NaH_2PO_4 buffer); 25 °C. The concentration of ANS is 1×10^{-6} mol dm^{-3}. The excitation wavelength is 365 nm and the emission wavelength is 480 nm.
C_0: Concentration of **1**.
S_0: Concentration of ANS(1×10^{-6} mol dm^{-3}).
1: Cell length(0.1 dm).
ΔA: Change of relative fluorescence intensity.

Table 1. Dissociation Constants of Complexes between Cyclophanes(**1**, **2**, **3**) and Substrates[a]

Cyclophane	Dissociation constant(10^3K_d) / mol dm^{-3}	
	Picrate	ANS
1	2.0	8.0
2	1.0	5.7
3	0.25	0.31

a) pH 6.3 (0.1 mol dm^{-3} Na_2HPO_4 - 0.1 mol dm^{-3} NaH_2PO_4 buffer), 25 °C.

Table 2. Pseudo-First-Order Rate Constant (k) for the Hydrolysis of *p*-NPH[a]

Cyclophane	$[N_3^-]\times10^2$ / mol dm^{-3}	$k\times10^2$ / min^{-1}	$(\Delta k/C)\times10^{-2}$[b] / min^{-1} mol^{-1} dm^3
None	0	0.13	
None	1	1.6	
1(1×10^{-3} mol dm^{-3})	1	1.7	1
2(1×10^{-3} mol dm^{-3})	1	1.7	1
3(5×10^{-5} mol dm^{-3})	1	1.8	40
3(1×10^{-4} mol dm^{-3})	1	2.1	50

a) pH 8.1 (0.05 mol dm^{-3} NaH_2PO_4–0.025 mol dm^{-3} $Na_2B_4O_7$ buffer), μ=0.1(KCl), 32 °C. b) Increase in the k value per mol dm^{-3} cyclophane.

Hildebrand plot for **1**. The determined K_d values are summarized in Table 1. Here, as in the case of picrate, **1** and **2** form relatively stable complexes with ANS, although **3** forms a much more stable complex with ANS than **1** and **2**. The relative deficiency of the stability for the complexes with **1** and **2** seems to be ascribed to the inefficient hydrophobicity provided by the shorter alkyl chains. The hydrophobicity of the cyclophane-skeleton seems to give an important effect on the complex formation in the case of **1** and **2** in comparison with the case of **3**.

The hydrolyses of active esters have been widely studied as catalyzed by enzyme-mimetic compounds or systems. Various cyclophanes have been used as enzyme models in the hydrolyses of active esters.[1,2,5,8] In the present study, the hydrolysis of *p*-nitrophenyl hexanoate (*p*-NPH) in the presence of the cyclophanes (**1**, **2**, and **3**) and azide ion(N_3^-) was investigated. Under the present experimental conditions, the cyclophanes may attract *p*-NPH by a hydrophobic interaction and N_3^- by an electrostatic force. The reaction followed the pseudo-first-order kinetics until the conversion of ca. 70%, although the rate enhancement was not so large. The pseudo-first-order rate constants (k) are shown in Table 2. In the presence of N_3^- (1×10^{-2} mol dm^{-3}) and **1** or **2** (1×10^{-3} mol dm^{-3}), k was increased by ca. 6% as compared with that in the presence of only N_3^-. In the case of **3**, the increase in the k value per mol dm^{-3} cyclophane ($\Delta k/C$) was much larger than in the cases of **1** and **2**. The strong binding ability of **3** toward *p*-NPH may be responsible for the larger rate acceleration. The enhancement was, however, not so significant as a whole, probably owing to the poor ability of **3** to bind N_3^-.

In the present study, tetraoxotetraazaparacyclophanes with shorter alkyl chains (**1** and **2**) and the one with relatively long alkyl chains (**3**) have been characterized. As a result, **1** and **2** have been found to include the hydrophobic anionic compounds (picrate and ANS), whereas the binding ability of **1** and **2** is not so large as that of **3**. These cyclophanes enhanced the hydrolysis of *p*-NPH to a minor extent.

References

1) Y. Murakami, A. Nakano, R. Miyata, and Y. Matsuda, *J. Chem. Soc., Perkin Trans. 1*, **1979**, 1669.
2) Y. Murakami, A. Nakano, K. Akiyoshi, and K. Fukuya, *J. Chem. Soc., Perkin Trans. 1*, **1981**, 2800.
3) Y. Murakami, J. Kikuchi, M. Suzuki, and T. Takaki, *Chem. Lett.*, **1984**, 2139.
4) I. Tabushi, H. Sasaki, and Y. Kuroda, *J. Am. Chem. Soc.*, **98**, 5727 (1976).
5) I. Tabushi, Y. Kimura, and K. Yamamura, *J. Am. Chem. Soc.*, **100**, 1304 (1978).
6) K. Odashima, T. Soga, and K. Koga, *Tetrahedron Lett.*, **22**, 5311 (1981).
7) F. Cramer, W. Saenger, and H. Ch. Spatz, *J. Am. Chem. Soc.*, **89**, 14 (1967).
8) I. Tabushi, Y. Kimura, and K. Yamamura, *J. Am. Chem. Soc.*, **103**, 6486 (1981).

Selective 2′-*O*-Methylation of Pyrimidine-Ribonucleosides by Trimethylsulfonium Hydroxide in the Presence of Mg^{2+} and Ca^{2+} Ions[1)]

Kiyoshi YAMAUCHI,* Toru NAKAGIMA, and Masayoshi KINOSHITA
Department of Applied Chemistry, Osaka City University, Sumiyoshi-ku, Osaka 558
(Received March 31, 1986)

Synopsis. Reactions of various ribonucleosides with trimethylsulfonium hydroxide were investigated in the presence of Mg^{2+} and Ca^{2+} ions. The 2′-OH groups of pyrimidine-ribonucleosides were methylated selectively.

The 2′-OH group of a ribonucleoside is assumed to be similar in reactivity toward various acylating and alkylating reagents to the 2′-OH groups of other ribonucleosides.[2)] In this paper we wish to report that (a) the 2′-OH groups of pyrimidine-ribonucleosides were methylated selectively by trimethylsulfonium hydroxide [$(CH_3)_3S^+$ OH^-, abbreviated as Me_3SOH hereafter] in the presence of Mg^{2+} and Ca^{2+} ions and (b) the selectivity was much higher than that observed in purine-ribonucleosides.

Methylation reactions were carried out by stirring a mixture of ribonucleosides and 1.5—2 equivalents of Me_3SOH in the presence and absence of 0.25—1 equivalent of $Mg(acac)_2$ or $Ca(acac)_2$ (acac=acetylacetonato) in DMF at 70 °C for 1 h. The metal salts were soluble in the solvent and allowed the reactions to occur in homogeneous solutions. Me_3SOH is a SN2-type reagent which reacts with nucleophiles according to the general scheme of Eq. 1.[3)] Methylation of the acetylacetone ligand by Me_3SOH was negligible under the conditions used. Typical results are listed in Table 1. One may draw the following conclusions.

(i) In the absence of $Mg(acac)_2$ and $Ca(acac)_2$, methylation occurred rather randomly on the ribose and the purine or pyrimidine moieties of the starting nucleosides (Entries 1, 4, 6, and 8).

(ii) In the presence of $Mg(acac)_2$ and $Ca(acac)_2$, Ado gave chiefly a mixture of 2′-MeAdo and 3′-MeAdo in a ratio of ca. 2.5:1 (entries 2 and 3).[1)] The combined extents of 2′-*O*-methylation and 3′-*O*-methylation[4)], however, showed only slight increases to 39 and 19% from 31 and 11%, respectively, which were observed in the absence of the metal salts. The use of the metal salts did not offer any merits of 2′-*O*- and 3′-*O*-methylations of other purine-ribonucleosides such as Guo, N^6-MeAdo and 1-MeGuo, either (the results are omitted in the Table).

(iii) By contrast, $Mg(acac)_2$ and $Ca(acac)_2$ allowed Me_3SOH to attack selectively and efficiently the 2′-OH groups of the pyrimidine-ribonucleosides such as Cyd, 3-MeUrd and 3-BenzylUrd (Entries 5 and 9—11). The yields of the 2′-*O*-methyl derivatives were better than those of the previous procedures.[5-8)] Urd gave 3,2′-Me_2Urd in a modest yield perhaps through 2′-*O*-methylation of the primary product, 3-MeUrd (Entry 7). The ratio of the 2′-*O*-methylation to the 3′-*O*-methylations were more than 10.

Many transition metal ions including Sn^{2+} and Cu^{2+} ions have been known to promote 2′-*O*- and 3′-*O*-methylations of both purine- and pyrimidine-nucleosides, affording the corresponding 2′-*O*-methyl and 3′-*O*-methyl derivatives with ratios of 2—5:1,[5-8)] and the effects have been attributed to the increased nucleophilicity of the 2′(3′)-*O*-atom upon their chelation with the metal ions.[9,10)] The same concept

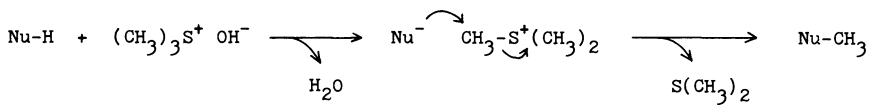

(1)

may be applied to an efficient 2′-*O*- and 3′-*O*-methylations of 2′,3′-*O*-(dibutylstannylene)uridine with methyl iodide.[11)] Although it has been unsettled why a combination of Me_3SOH and $Mg(acac)_2$ or $Ca(acac)_2$ permitted the pyrimidine-nucleosides to undergo selective 2′-*O*-methylation, yet the results would be ascribed most likely to the chelating property of the metal ions (to the nucleosides) which might be different from the transition metal ions. The mechanism of the 2′-*O*-methylation is now under investigation.

Experimental

Ado, Cyd, and Urd were the highest purities obtainable commercially. 3-MeUrd and authentic samples (2′-MeAdo, 3′-MeAdo, N^6,2′-Me_2Ado, N^6,3′-Me_2Ado, 2′-MeCyd, 3′-MeCyd, N^4-MeCyd, 2′-MeUrd, 3,2′-Me_2Urd, and 3-MeUrd) were prepared previously.[8,13)] 3-BenzylUrd was synthesized by treating Urd (2.0 g, 8.2 mmol) in DMF (10 ml) with sodium hydride (60% in oil, 0.33 g, 8.2 mmol) followed by addition of benzyl bromide (1.7 g, 10 mmol) and refluxing the turbid mixture for 3 h. The reaction mixture was concentrated and applied to a silica-gel column. Elution with a mixture of chloroform and methanol (10–1 v/v) afforded 3-BenzylUrd, which was recrystallized from water; 2.4 g (88%), mp 179—181 °C, UV λ_{max} (H_2O) 261 nm (ε 7500) at pH 1 and 6, 261 nm (ε 7500) at pH 11.

Similarly, 2′-MeUrd was benzylated a the *N*-3 position to give 3-Benzyl, 2′-MeUrd in a 75% yield: Mp 156—158 °C; UV λ_{max} (H_2O) 260.5 nm (ε 10700) at pH 1 and 6, 262 nm (ε 10400) at pH 11; NMR ($CDCl_3$–CD_3OD, 2–1 v/v) δ=7.95 (d, 1, $J_{5,6}$=8.2 Hz), 7.35 (m, 5, C_6H_5), 5.88 (d, 2, $J_{1',2'}$=3.0 Hz), 5.77 (d, 2, $J_{5,6}$=8.2 Hz), 5.11 (s, 2, $CH_2C_6H_5$), 3.8—4.3 (m, 5, $C_{2'}H$, $C_{4'}H$, and $C_{5'}2H$), and 3.56 (s, 3, CH_3). Found: C,

Table 1. Methylation of Various Ribonucleosides with Me_3SOH in the Presence and Absence of $Mg(acac)_2$ and $Ca(acac)_2$[a]

Entry	Nucleoside	Metal ion	Products				
			TLC-UV Yields/% [Yields of Isolated Products][b]				
			2′-MeAdo	3′-MeAdo	N^6-MeAdo	N^6,2′-Me_2Ado	N^6,3′-Me_2Ado
1		none	19	7	18	12	4
2	Ado	Mg^{2+}	30[21]	13[3]	7	9	5
3		Ca^{2+}	28	12	8	10	3
			2′-MeCyd	3′-MeCyd	N^3-MeCyd		
4	Cyd	none	27	8	10		
5		Mg^{2+}	66[43]	5[2]	7		
			3,2′-Me_2Urd	3,3′-Me_2Urd	3-MeUrd		
6	Urd	none	45	12	23		
7		Mg^{2+}	35[21]	trace	40		
			3,2′-Me_2Urd	3,3′-Me_2Urd	3,2′,3′-Me_3Urd		
8		none	31	8	6		
9	3-MeUrd	Mg^{2+}	82[65]	trace	9		
10		Ca^{2+}	71	trace	8		
			3-Benzyl,2′-MeUrd				
11	3-BenzylUrd	Mg^{2+}	83[62]	c)			

a) Reaction conditions: nucleoside-Me_3SOH-$Mg(acac)_2$ or $Ca(acac)_2$-DMF=2 mmol-3.4 mmol-1 mmol-8 ml; reaction temperature and time: 70 °C and 1 h, respectively. b) The TLC-UV yields of the products in the reaction mixtures were determined in a manner similar to that mentioned previously (Ref. 13). The major products were isolated in the yields shown in the brackets. The isolated compounds had the following physical constants. 2′-MeAdo, mp 202—203 °C (from ethanol)(lit,[7] 202—203.5 °C); UV λ_{max} (H_2O) 259 nm (ε 14000) at pH 6. 3′-MeAdo, mp 176—177 °C (from ethanol)(lit,[7] 174—176 °C); UV λ_{max} (H_2O) 259 nm (ε 24500) at pH 6. N^6,2′-Me_2Ado, mp 104—105 °C (from acetone-hexane)(lit,[8] 103—105 °C); UV λ_{max} (H_2O) 265 nm (ε 14200) at pH 6. N^6,3′-Me_2Urd, mp 189—190 °C (from acetone-hexane)(lit,[8] 189—191 °C); UV λ_{max} (H_2O) 265 nm (ε 16500) at pH 6. 2′-MeCyd, mp 252—254 °C (from ethanol)(lit,[7] 251—254 °C); UV λ_{max} (H_2O) 271 nm (ε 8900) at pH 6. 3′-MeCyd, mp 209—210 °C (from ethanol)(lit,[7] 210—211 °C); UV λ_{max} (H_2O) 271 nm (ε 9000) at pH 6. 3,2′-MeUrd, mp 138—140 °C (from hexane)(lit,[14] 140—141 °C); UV λ_{max} (H_2O) 261 nm (ε 9800) at pH 6. 3-Benzyl,2′-MeUrd, mp as well as UV and NMR spectra were identical with those of the authentic sample (see the experimental section). c) The reaction of the Entry 11 gave 3-Benzyl,2′-MeUrd exclusively.

58.40; H, 6.05; N, 7.84%. Calcd for $C_{17}H_{20}N_2O_6$: C, 58.61; H, 5.78; N, 8.04%.

General Mathylation Procedure. A mixture of nucleoside (2.0 mmol) and 1.7 equivalents of a 0.7 M methanol solution (1 M=1 mol dm^{-3}) of Me_3SOH[3] was concentrated in the absence and presence of one equivalent of $Mg(acac)_2$ or $Ca(acac)_2$ below 20 °C. DMF (8 ml) was added to the resulting residue, and the mixture was stirred magnetically at 70 °C for 0.5—1 h. A product-distribution in the methylation reaction using authentic samples and isolation of major products were conducted in a manner similar to that mentioned previously.[8,13] A ratio, 2′-*O*-methyl nucleoside/3′-*O*-methyl isomer, was determined from the area ratio of the corresponding methoxyl groups in the NMR spectrum of the mixture which was separated from the reaction mixture by silica gel chromatography.

Optimal amounts of Me_3SOH and the $M(acac)_2$s were about 1.5—2 equivalents and 0.5 equivalent, respectively, to the starting nucleosides. The use of the excess $M(acac)_2$s did not improve overall yields of methylation. The optimal reaction temperature was 60—80 °C. At higher temperature, Me_3SOH underwent significantly decomposition to methanol and dimethyl sulfide.

References

1) Abbreviations used are: adenosine, Ado; cytidine, Cyd; guanosine, Guo; uridine, Urd; 3-benzyluridine, 3-BenzylUrd; N^6-methyladenosine, N^6-MeAdo; 2′-*O*-methyladenosine, 2′-MeAdo; 3′-*O*-methyladenosine, 3′-MeAdo; 1-methylguanosine, 1-MeGuo; 3-methyluridine, 3-MeUrd; 3,2′,-*O*-dimethyluridine, 3,2′-Me_2Urd; 3-benzyl-2′-*O*-methyluridine, 3-Benzyl-2′-MeUrd; Similar abbreviations for other methyl nucleosides.

2) N. K. Kochetkov and E. I. Budovskii, "Organic Chemistry of Nucleic Acids," Plenum, London (1971), Part B, p. 449.

3) K. Yamauchi, T. Tanabe, and M. Kinoshita, *J. Org. Chem.*, **44**, 638 (1979); K. Yamauchi, Y. Hisanaga, and M. Kinoshita, *J. Am. Chem. Soc.*, **105**, 538 (1983).

4) A combined extent of 2′(3′)-*O*-methylation=summation of TLC yields of 2′(3′)-*O*-methyl nucleosides.

5) M. J. Robins, M. MacCoss, and A. S. K. Lee, *Biochem. Biophys. Res. Commun.*, **12**, 194 (1973); **70**, 356 (1976).

6) M. J. Robins, A. S. K. Lee, and F. A. Norris, *Carbohydrate Res.*, **41**, 304 (1975).

7) M. J. Robins, S. R. Naik, and A. S. K. Lee, *J. Org. Chem.*, **39**, 1891 (1974).

8) K. Yamauchi, T. Nakagima, and M. Kinoshita, *J. Org. Chem.*, **45**, 3865 (1980).

9) Y. H. Chao and D. R. Kearns, *J. Am. Chem. Soc.*, **99**, 6245 (1977); G. L. Eichhorn, "Inorganic Biochemistry," ed by G. L. Eichhorn, Elsevier, Amsterdam (1973), Vol. 2, p. 1210.

10) Cu^{2+} and other transition metal ions were less selective than Mg^{2+} and Ca^{2+} ions in methylating the 2′-OH

groups of ribonucleosides. For instance, when Ado and Cyd were subjected to methylation reactions using 0.5 equivalent of $Cu(acac)_2$ under the conditions similar to those of Entry 2 and 5 of Table 1, the former provided 2′-MeAdo and 3′-MeAdo in 41 and 37%, respectively, and the latter furnished 2′-MeCyd and 3′-MeCyd in 60 and 22%, respectively.[8] A combination of diazomethane and tin(II) chloride converted Ado into 2′-MeAdo and 3′-MeAdo in 44 and 56%, respectively.[6,7] No detectable methylation of Ado was observed with the systems of diazomethane and Mg^{2+} and Ca^{2+} ions.[6]

11) D. Wagner, J. P. H. Verheyden, and J. G. Moffatt, *J. Org. Chem.*, **39**, 24 (1974).

12) UV spectra were measured with a Hitachi 3T spectrometer. NMR spectra were recored on a Jeol PS-100 using dilute solution in $CDCl_3$ or a mixture of $CDCl_3$–CD_3OD (2–1 v/v) with tetramethylsilane as an internal standard.

13) K. Yamauchi, T. Nakagima, and M. Kinoshita, *J. Chem. Soc., Perkin Trans. 1*, **1980**, 2787.

14) Y. Furukawa, K. Kobayashi, Y. Kanai, and M. Honjo, *Chem. Pharm. Bull. (Tokyo)*, **13**, 1273 (1965).

Synthesis of 2,3-Dihydro-2-alkyl-3-(substituted amino)-1*H*-isoindol-1-ones. 2-Alkylation of 2,3-Dihydro-3-(substituted amino)-1*H*-isoindol-1-ones in a Phase-Transfer Catalyst System

Ryu SATO,* Toshihide SENZAKI, Takehiko GOTO, and Minoru SAITO
Department of Resource Chemistry, Faculty of Engineering, Iwate University, Morioka 020
(Received April 17, 1986)

Synopsis. A variety of 2,3-dihydro-2-alkyl-3-(substituted amino)-1*H*-isoindol-1-ones were conveniently synthesized by selective 2-alkylation of 2,3-dihydro-3-(substituted amino)-1*H*-isoindol-1-ones, which were derived from 2-cyanobenzaldehyde, with some alkyl halides in a phase-transfer catalyst system.

We recently reported the formation of γ-lactams, 2,3-dihydro-3-(substituted amino)-1*H*-isoindol-1-ones, from the reaction of 2-cyanobenzaldehyde with primary and secondary alkylamines at room temperature in excellent yields, and also revealed that the amines used were introduced regioselectively into the 3-position, not into the 2-position, of the 2,3-dihydro-3-(substituted amino)-1*H*-isoindol-1-ones.[1] Since 2-alkylated isoindol-1-ones could not be obtained directly by the method, our interests focused on the selective alkylation at the 2-position of 2,3-dihydro-3-(substituted amino)-1*H*-isoindol-1-ones. Although, to our knowledge, there have been no reports on the direct 2-alkylation of the isoindol-1-ones, the selective *N*-alkylation of amides in the presence of a phase-transfer catalyst have recently appeared.[2] We also reported the one-pot synthesis of alkyl aryl trithiocarbonates from benzenethiols and carbon disulfide with alkyl halides in the presence of a phase-transfer catalyst in good yields.[3] Thus, because of the experimetal simplicity, superior regioselectivity and high yields of the products, the phase-transfer catalyst(PTC) has been used widely for alkylations of some nitrogen or sulfur organic compounds which are difficult to be alkylated regioselectively.[4] This elegant technique encouraged us to explore the regioselective 2-alkylation of 2,3-dihydro-3-(substituted amino)-1*H*-isoindol-1-ones with alkyl halides. In this paper, we wish to report a first example for the 2-alkylation of 2,3-dihydro-3-(substituted amino)-1*H*-isoindol-1-ones(**2**), which are derived from 2-cyanobenzaldehyde(**1**),[1] in the phase-transfer catalyst(PTC) system to give 2,3-dihydro-2-alkyl-3-(substituted amino)-1*H*-isoindol-1-ones(**3**) in high yields (Scheme 1).

Table 1. 2-Alkylations of 2,3-Dihydro-3-(substituted amino)-1*H*-isoindol-1-ones (**3**) with Alkyl halides in a Phase-Transfer Catalyst System

Run[a]	Substrate		Halide		React		Yield of **3**		Mp
	R^1	R^2		R^3X	Temp/°C	Time/min	% [b]		θ_m/°C
1	H	H	**2a**	$4\text{-}CH_3C_6H_4CH_2Br$	20	10	75	**3aa**	106
2			**2a**	$BrCH_2COOC_2H_5$	20	20	90	**3ab**	77
3	H	CH_3	**2b**	$2\text{-}ClC_6H_4CH_2Cl$	20	3(h)	83	**3bc**	107
4			**2b**	$3,4\text{-}Cl_2C_6H_3CH_2Cl$	20	3(h)	66	**3bd**	108
5	H	$C(CH_3)_3$	**2c**	CH_3I	20	5(h)	83	**3ce**	171
6			**2c**	$C_6H_5CH{=}CHCH_2Br$	20	60	90	**3cf**	137
7			**2c**	$2,4\text{-}Cl_2C_6H_3CH_2Cl$	20	2(h)	63	**3cg**	157
8	C_2H_5	C_2H_5	**2d**	CH_3I	20	24(h)	94	**3de**	53
9			**2d**	$ClCH_2CN$	20	30	95	**3dh**	69
10			**2d**	$C_6H_5CH_2Br$	20	10	94	**3di**	79
11			**2d**	$4\text{-}CH_3C_6H_4CH_2Br$	20	10	97	**3da**	64
12			**2d**	$2\text{-}CH_3C_6H_4CH_2Br$	60	10	96	**3dj**	87
13			**2d**	$4\text{-}ClC_6H_4CH_2Cl$	60	90	95	**3dk**	69
14			**2d**	$2\text{-}ClC_6H_4CH_2Cl$	60	40	94	**3dc**	88
15			**2d**	$2,4\text{-}Cl_2C_6H_3CH_2Cl$	60	30	91	**3dg**	126
16			**2d**	$3,4\text{-}Cl_2C_6H_3CH_2Cl$	60	15	92	**3dd**	74
17			**2d**	$CH{\equiv}CCH_2Br$	60	4(h)	90	**3dl**	62
18	$-CH_2CH_2OCH_2CH_2-$		**2e**[6]	CH_3I	20	4(h)	92	**3ee**	115
19			**2e**	$CH_2{=}CHCH_2Br$	20	4(h)	97	**3em**	64
20			**2e**	$2\text{-}CH_3C_6H_4CH_2Br$	20	10	97	**3ej**	114
21	$-CH_2(CH_2)_3CH_2-$		**2f**[6]	$ClCH_2CN$	20	40	54	**3fh**	98
22			**2f**	$4\text{-}ClC_6H_4CH_2Cl$	20	2(h)	91	**3fk**	121

a) Tetrabutylammonium iodide was used as phase-transfer catalyst. b) Isolated yields based on the substrates.

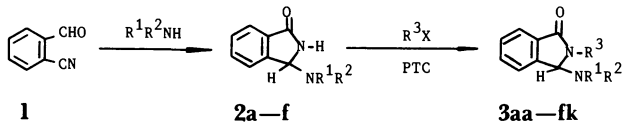

1 2a—f 3aa—fk

Scheme 1.

Many 2,3-dihydro-2-alkyl-3-(substituted amino)-1*H*-isoindol-1-ones(**3**) were obatained in high yields as shown in Table 1. It should be noted that the synthesis of many functionalized isoindol-1-ones(**3**) containing cyano, chloro and unsaturated alkyl groups in the molecules as shown in the table was carried out successfully, of which antiflammatory activity has been observed.[5] In the absence of the phase-transfer catalyst, the substrate, isoindol-1-one(**2**), was not alkylated at all. Various quarternary ammonium salts, for example, methyltrioctylammonium chloride(TOMAC) and tetrabutylammonium bromide and iodide could be used, and little difference by the catalyst was observed in the present reaction. On the other hand, a considerable increase of the yield of 2-alkylated isoindol-1-ones(**3**) could be confirmed when the concentration of sodium hydroxide aqueous solution was changed to 50% from 20%. It is noteworthy that a high selectivity was observed in this reaction. Thus, 2-alkylated isoindol-1-ones(**3aa-cg**) were obtained by treating 3-amino(**2a**), 3-methylamino(**2b**), and 3-(*t*-butylamino)-2,3-dihydro-1*H*-isoindol-1-one(**2c**) with alkyl halide in the presence of tetrabutylammonium iodide in high yields without any 3-(alkylated amino)-2,3-dihydro-1*H*-isoindol-1-one (Runs 1—7). These reactions proceeded smoothly at 20 °C to 60 °C.

Consequently, a novel route to 2-alkyl-3-(substituted amino)-2,3-dihydro-1*H*-isoindol-1-ones(**3**) from 2-cyanobenzaldehyde(**1**) was confirmed.

Experimental

Measurements. All the melting points were uncorrected. NMR, IR and Mass spectra were recorded with a HITACHI R-22, HITACHI 295 and HITACHI RMU-6M, respectively. Elemental analysis were determined with YANAGIMOTO MT-3.

Materials. 2,3-Dihydro-3-(substituted amino)-1*H*-isoindol-1-ones(**2**) were obtained from reactions of 2-cyanobenzaldehyde(**1**) with the corresponding amines.[1]

General Procedure for the Preparation of 2,3-Dihydro-2-alkyl-3-(substituted amino)-1*H*-isoindol-1-ones(3) from 2,3-Dihydro-3-(substituted amino)-1*H*-isoindol-1-ones(2). An alkyl halide (1.1 mmol) was added dropwise to a mixture of 1.0 mmol of 2,3-dihydro-3-(substituted amino)-1*H*-isoindol-1-ones(**2**), 0.2 mmol of tetrabutylammonium iodide, 5 ml of benzene and 5 ml of 50% aqueous sodium hydroxide. The order of addition of the materials did not affect the results. After the completion of the addition, stirring was continued at 20 °C until the substrate disappeared (monitoring by TLC). Water (5 ml) was added to the reaction mixture and then the benzene layer was separated. The aqueous layer was extracted with benzene three times (5 ml each), and the organic layers were combined. Evaporation of the solvent from the combined benzene solution after drying with magnesium sulfate gives a yellow oil. Desired 2,3-dihydro-2-alkyl-3-(substituted amino)-1*H*-isoindol-1-ones(**3**) were obtained as clear colorless crystals by column chromatgraphy of the oil on silica gel (Wako gel C-300) using chloroform as eluent, followed by repeated recrytallization from chloroform-hexane. All products were new compounds, being assigned by physical, spectral and analytical data as follows.

3aa. Colorless crystals, mp 106 °C; IR (KBr) 3370, 3000, 2900, and 1685 cm^{-1}; ^1H NMR ($CDCl_3$) δ=1.80 (s, 2H, NH_2), 2.31 (s, 3H, CH_3), 4.37 and 5.10 (d, 2H, J=15.0 Hz, CH_2), 5.90 (s, 1H, CH) and 7.00—7.90 (m, 8H, arom); MS (70 eV) *m/z* 252 (M^+); Found: C, 76.14; H, 6.39; N, 11.10%. Calcd for $C_{16}H_{16}N_2O$: C, 76.16; H, 6.39; N, 11.10%.

3ab. Colorless crystals, mp 77 °C; IR (KBr) 3390, 3300, 2960, 1760, and 1690 cm^{-1}; ^1H NMR ($CDCl_3$) δ=1.27 (t, 3H, 6.5 Hz, CH_3), 1.84 (s, 2H, NH_2), 4.14 and 4.52 (d, 2H, 17.0 Hz, CH_2), 4.18 (d, 2H, 6.5 Hz, CH_2), 5.42 (s, 1H, CH) and 7.45—7.85 (m, 4H, arom); MS (70 eV) *m/z* 234 (M^+); Found: C, 61.32; H, 6.02; N, 11.67%. Calcd for $C_{12}H_{14}N_2O_3$; C, 61.53; H, 6.02; N, 11.96%.

3bc. Colorless crystals, mp 107 °C; IR (KBr) 3340, 2925, and 1690 cm^{-1}; ^1H NMR ($CDCl_3$) δ=1.94 (s, 3H, CH_3), 2.08 (bs, 1H, NH), 4.50 and 5.16 (d, 2H, 15.0 Hz, CH_2), 5.27 (s, 1H, CH) and 7.10—7.90 (m, 8H, arom); MS (70 eV) *m/z* 287 (M^+); Found: C, 66.88; H, 5.18; N, 9.76%. Calcd for $C_{16}H_{15}N_2OCl$: C, 67.02; H, 5.27; N, 9.77%.

3bd. Colorless crystals, mp 108 °C; IR (KBr) 3320, 2900, and 1690 cm^{-1}; ^1H NMR ($CDCl_3$) δ=2.00 (s, 3H, CH_3), 4.28 and 5.09 (d, 2H, 15.0 Hz, CH_2), 5.22 (s, 1H, CH), 7.08—7.92 (m, 7H, arom); MS (70 eV) *m/z* 321 (M^+); Found: C, 59.65; H, 4.32; N, 8.72%. Calcd for $C_{16}H_{14}N_2OCl_2$: C, 59.83; H, 4.39; N, 8.72%.

3ce. Colorless crystals, mp 171 °C; IR (KBr) 3325, 2955, and 1670 cm^{-1}; ^1H NMR ($CDCl_3$) δ=1.33 (s, 9H, CH_3), 3.07 (s, 3H, CH_3), 5.20 (s, 1H, CH) and 7.35—7.83 (m, 4H, arom); MS (70 eV) *m/z* 218 (M^+); Found: C, 71.12; H, 8.43; N, 12.87%. Calcd for $C_{13}H_{18}N_2O$: C, 71.53; H, 8.31; N, 12.83%.

3cf. Colorless crystals, mp 137 °C; IR (KBr) 3320, 2960, 2900, and 1690 cm^{-1}; ^1H NMR ($CDCl_3$) δ=1.30 (s, 9H, CH_3), 1.40 (b, 1H, NH), 4.07 (dd, 1H, 16.0,6.5 Hz, CH_2), 4.64 (dd, 1H, 16.0, 3.5 Hz, CH_2), 5.35 (s, 1H, CH), 6.00—6.60 (m, 2H, CH=CH) and 7.10—7.88 (m, 9H, arom); MS (70 eV) *m/z* 320 (M^+); Found: C, 78.67; H, 7.64; N, 8.84%. Calcd for $C_{21}H_{24}N_2O$: C, 78.71; H, 7.55; N, 8.74%.

3cg. Colorless crystals, mp 157 °C; IR (KBr) 3350, 2970, and 1700 cm^{-1}; ^1H NMR ($CDCl_3$) δ=1.16 (s, 9H, CH_3), 1,47 (b, 1H, NH), 4.85 (d, 2H, 6.0 Hz, CH_2), 5.28 (s, 1H, CH) and 6.89—7.90 (m, 7H, arom); MS (70 eV) *m/z* 363 (M^+); Found: C, 62.76; H, 5.49; N, 7.69%. Calcd for $C_{19}H_{20}N_2OCl_2$: C, 62.82; H, 5.55; N, 7.71%.

3de. Colorless crystals, mp 53 °C; IR (KBr) 2960, 2825, and 1700 cm^{-1}; ^1H NMR ($CDCl_3$) δ=1.06 (t, 6H, 7.5 Hz, CH_3), 2.62 (q, 4H, 7.5 Hz, CH_2), 3.08 (s, 3H, CH_3), 5.22 (s, 1H, CH) and 7.30—7.86 (m, 4H, arom); MS (70 eV) *m/z* 218 (M^+); Found: C, 71.29; H, 8.23; N, 12.60%. Calcd for $C_{13}H_{18}N_2O$: C, 71.53; H, 8.31; N, 12.83%.

3dh. Colorless crystals, mp 69 °C; IR (KBr) 2975, 2840, 2250, and 1710 cm^{-1}; ^1H NMR ($CDCl_3$) δ=1.13 (t, 6H, 7.5 Hz, CH_3), 2.64 (q, 4H, 7.5 Hz, CH_2), 4.22 and 4.75 (d, 2H, 17.5 Hz, CH_2), 5.48 (s, 1H, CH) and 7.35—7.93 (m, 4H, arom); MS (70 eV) *m/z* 243 (M^+); Found: C, 69.00; H, 7.09; N, 16.98%. Calcd for $C_{14}H_{17}N_3O$: C, 69.11; H, 7.04; N, 17.27%.

3di. Colorless crystals, mp 79 °C; IR (KBr) 2950, 2820, and 1680 cm^{-1}; ^1H NMR ($CDCl_3$) δ=0.98 (t, 6H, 7.3 Hz, CH_3), 2.54 (q, 4H, 7.3 Hz, CH_2), 4.24 and 5.23 (d, 2H, 15.0 Hz, CH_2), 5.15 (s, 1H, CH) and 7.20—7.95 (m, 9H, arom); MS (70 eV) *m/z* 294 (M^+); Found: C, 77.22; H, 7.54; N, 9.31%. Calcd for $C_{19}H_{22}N_2O$: C, 77.52; H, 7.53; N, 9.52%.

3da. Colorless crystals, mp 64 °C; IR (KBr) 2960, 2825, and 1690 cm^{-1}; ^1H NMR ($CDCl_3$) δ=1.00 (t, 6H, 7.5 Hz, CH_3), 2.30 (s, 3H, CH_3), 2.54 (q, 4H, 7.5 Hz, CH_2), 4.19 and 5.20 (d, 2H, 15.0 Hz, CH_2), 5.14 (s, 1H, CH) and 6.98—7.88 (m, 8H, arom); MS (70 eV) *m/z* 308 (M^+); Found: C, 77.78; H, 7.97; N, 8.93%. Calcd for $C_{20}H_{24}N_2O$: C, 77.89; H, 7.84; N, 9.08%.

3dj. Colorless crystals, mp 87 °C; IR (KBr) 2960, 2840, and 1690 cm^{-1}; ^1H NMR ($CDCl_3$) δ=0.98 (t, 6H, 7.3 Hz, CH_3), 2.37 (s, 3H, CH_3), 2.53 (q, 4H, 7.3 Hz, CH_2), 4.30 and 5.20 (d, 2H, 15.0 Hz, CH_2), 5.10 (s, 1H, CH) and 7.08-7.95 (m, 8H, arom); MS (70 eV) *m/z* 308 (M^+); Found: C, 77.85; H, 7.93; N, 9.00%. Calcd for $C_{20}H_{24}N_2O$: C, 77.89; H, 7.84; N, 9.08%.

3dk. Colorless crystals, mp 69 °C; IR (KBr) 2950, 2820, and 1680 cm^{-1}; ^1H NMR ($CDCl_3$) δ=1.00 (t, 6H, 7.5 Hz, CH_3), 2.54 (q, 4H, 7.5 Hz, CH_2), 4.26 and 5.13 (d, 2H, 15.0 Hz, CH_2), 5.14 (s, 1H, CH), 7.25 (s, 4H, arom) and 7.35—7.93 (m, 4H, arom); MS (70 eV) *m/z* 329 (M^+); Found: C, 69.01; H, 6.39; N, 8.54%. Calcd for $C_{19}H_{21}N_2OCl$: C, 69.40; H, 6.44; N, 8.51%.

3dc. Colorless crystals, mp 88 °C; IR (KBr) 2960, 2830, and 1690 cm^{-1}; ^1H NMR ($CDCl_3$) δ=0.97 (t, 6H, 7.5 Hz, CH_3), 2.53 (q, 4H, 7,5 Hz, CH_2), 4.63 and 5.13 (d, 2H, 15.5 Hz, CH_2), 5.24 (s, 1H, CH) and 7.10—7.96 (m, 8H, arom); MS (70 eV) *m/z* 329 (M^+); Found: C, 69.17; H, 6.44; N, 8.47%. Calcd for $C_{19}H_{21}N_2OCl$: C, 69.40; H, 6.44; N, 8.51%.

3dg. Colorless crystals, mp 126 °C; IR (KBr) 2960, 2825, and 1700 cm^{-1}; ^1H NMR ($CDCl_3$) δ=0.97 (t, 6H, 7.4 Hz, CH_3), 2.52 (q, 4H, 7.4 Hz, CH_2), 4.60 and 5.04 (d, 2H, 15.5 Hz, CH_2), 5.20 (s, 1H, CH) and 7.10—7.93 (m, 7H, arom); MS (70 eV) *m/z* 363 (M^+); Found: C, 62.58; H, 5.41; N, 7.64%. Calcd for $C_{19}H_{20}N_2OCl_2$: C, 62.82; H, 5.55; N, 7.71%.

3dd. Colorless crystals, mp 74 °C; IR (KBr) 2960, 2825, and 1690 cm^{-1}: ^1H NMR ($CDCl_3$) δ=1.00 (t, 6H, 7.4 Hz, CH_3), 2.53 (q, 4H, 7.4Hz, CH_2), 4.24 and 5.07 (d, 2H, 15.0 Hz, CH_2), 5.13 (s, 1H, CH) and 7.05—7.94 (m, 7H, arom); MS (70 eV) *m/z* 363 (M^+); Found: C, 62.20; H, 5.57; N, 7.62%. Calcd for $C_{19}H_{20}N_2OCl_2$: C, 62.82; H, 5.55; N, 7.71%.

3dl. Colorless crystals, mp 62 °C; IR (KBr) 3230, 2960, 2800, and 1700 cm^{-1}; ^1H NMR ($CDCl_3$) δ=1.07 (t, 6H, 7.5 Hz, CH_3), 2.18—2.27 (m, 1H, -C≡CH), 2.62 (q, 4H, 7.5 Hz, CH_2), 3.94, and 4.74 (dd, 2H, 17.0, 2.8 Hz, CH_2), 5.51 (s, 1H, CH) and 7.25—7.87 (m, 4H, arom); MS (70 eV) *m/z* 242 (M^+); Found: C, 74.14; H, 7.44; N, 11.44%. Calcd for $C_{15}H_{18}N_2O$: C, 74.35; H, 7.49; N, 11.56%.

3ee. Colorless crystals, mp 115°C; IR (KBr) 2870, 2820, and 1700 cm^{-1}; ^1H NMR ($CDCl_3$) δ=2.40—2.80 (m, 4H, CH_2), 3.14 (s, 3H, CH_3), 3.67 (t, 4H, 4.8 Hz, CH_2), 5.04 (s, 1H, CH) and 7.36—7.88 (m, 4H, arom); MS (70 eV) *m/z* 232 (M^+); Found: C, 67.20; H, 7.01; N, 11.76%. Calcd for $C_{13}H_{16}N_2O_2$: C, 67.22; H, 6.94; N, 12.06%.

3em. Colorless crystals, mp 64 °C; IR (KBr) 2945, 2840, and 1700 cm^{-1}; ^1H NMR ($CDCl_3$) δ=2.35—2.83 (m, 4H, CH_2), 3.65 (t, 4H, 4.8 Hz, CH_2), 3.87 (dd, 1H, 15.0, 7.3 Hz, CH_2), 4.53 (dd, 1H, 15.0, 5.0 Hz, CH_2), 5.10—5.33 (m, 2H, -C=CH_2), 5.14 (s, 1H, CH), 5.63—6.06 (m, 1H, -CH=C) and 7.30—7.90 (m, 4H, arom); MS (70 eV) *m/z* 258 (M^+); Found: C, 69.68; H, 7.11; N, 11.79%. Calcd for $C_{15}H_{18}N_2O_2$: C, 69. 74; H, 7.02; N, 10.84%.

3ej. Colorless crystals, mp 114 °C; IR (KBr) 2940, 2840, and 1700 cm^{-1}; ^1H NMR ($CDCl_3$) δ=2.24—2.84 (m, 4H, CH_2), 2.39 (s, 3H, CH_3), 3.68 (t, 4H, 4.8 Hz, CH_2), 4.34 and 5.23 (d, 2H, 14.5 Hz, CH_2), 4.86 (s, 1H, CH) and 7.10—7.98 (m, 8H, arom); MS (70 eV) *m/z* 322 (M^+); Found: C, 74.53; H, 6.94; N, 8.54%. Calcd for $C_{20}H_{22}N_2O_2$: C, 74.51; H, 6.88; N, 8.69%.

3fh. Colorless crystals, mp 98 °C; IR (KBr) 2940, 2800, and 1705 cm^{-1}; ^1H NMR ($CDCl_3$) δ=1.30—1.75 (b, 6H, CH_2), 2.30—2.75 (b, 4H, CH_2), 4.27 and 4.68 (d, 2H, 17.0 Hz, CH_2), 5.25 (s, 1H, CH) and 7.35—7.90 (m, 4H, arom); MS (70 eV) *m/z* 255 (M^+); Found: C, 70.33; H, 6.69; N, 16.51%. Calcd for $C_{15}H_{17}N_3O$: C, 70.56; H, 6.71; N, 16.46%.

3fk. Colorless crystals, mp 121 °C; IR (KBr) 2930, 2800, and 1700 cm^{-2}; ^1H NMR ($CDCl_3$) δ=1.35—1.70 (b, 6H, CH_2), 2.20—2.70 (b, 4H, CH_2), 4.28 and 5.09 (d, 2H, 14.0 Hz, CH_2), 4.89 (s, 1H, CH), 7.24 (s, 4H, arom) and 7.35—7.90 (m, 4H, arom); MS (70 eV) *m/z* 341 (M^+); Found: C, 70.42; H, 6.24; N, 8.40%. Calcd for $C_{20}H_{21}N_2OCl$: C, 70.48; H, 6.21; N, 8.22%.

References

1) R. Sato, T. Senzaki, T. Goto, and M. Saito, *Chem. Lett.*, **1984**, 1599.

2) a) T. Gaida and A. Zwierzak, *Synthesis*, **1981**, 1005; b) E. V. Dehnlow, *Chimica*, **34**, 19 (1980).

3) A.Sugawara, M. Shirahata, S. Sato, and R. Sato, *Bull. Chem. Soc. Jpn.*, **57**, 3353 (1984).

4) a) J. Dockx, *Synthesis*, **1973**, 441; b) M. Makosza, *Pure Appl. Chem.*, **43**, 439 (1975); c) E. V. Dehnlow, *Angew. Chem., Int. Ed. Engl.*, **16**, 493 (1977); d) G. W. Gokel and W. P. Weber, *J. Chem. Educ.*, **55**, 350 (1978); e) J. M. Lehn, *Acc. Chem. Res.*, **11**, 49 (1980); f) G. Mouzin, H. Cousse, and J. M. Autin, *Synthesis*, **1981**, 448; g) D. Nasipuri, S. Banerjee, B. V. Alaka, and N. P. Daw, *Synthesis*, **1982**, 1073; h) P. Cocagne, J. Elguero, and R. Gallo, *Heterocycles*, **20**, 1379 (1983); i) D. J. Brunello, *J. Org. Chem.*, **49**, 1309 (1984).

5) a)S. Ogata, Japan Patent, 80127389; *Chem, Abstr*, **95**, 25058z (1981); b) M. H. Sherlock, U. S. Patent, 3296276 (1967); *Chem. Abstr.*, **67**, 73519u (1967).

6) R. R. Schmidt and E. Schlipf, *Chem. Ber.*, **103**, 3783 (1970).

The Absolute Configuration of Isoprelaurefucin[1)]

Minoru SUZUKI,* Kazuya KURATA,† Teruaki SUZUKI, and Etsuro KUROSAWA*
Department of Chemistry, Faculty of Science, Hokkaido University, Sapporo 060
†Department of Industrial Chemistry, Hakodate Technical College, Hakodate 042
(Received April 2, 1986)

Synopsis. (3*Z*)-Isoprelaurefucin has been isolated as a major metabolite from the red alga *Laurencia nipponica* Yamada, and its structure was confirmed by chemical correlation with isoprelaurefucin. Furthermore, the absolute configuration of isoprelaurefucin was established on the basis of chemical evidence.

During our continuing studies on the constituents of the red marine alga *Laurencia nipponica* Yamada, one of the Japanese species of the genus *Laurencia* (Rhodomelaceae; Rhodophyta), we have newly collected at Asari and Hariusu, near Otaru, Hokkaido, and isolated (3*Z*)-isoprelaurefucin (**1**) in 20 and 23% yields of the extracts, respectively. (3*Z*)-Isoprelaurefucin has previously been obtained as the minor metabolite from *L. subopposita*[2)] and *L. nipponica*.[3)] In this note we describe the structural confirmation of (3*Z*)-isoprelaurefucin (**1**) and the absolute configuration of isoprelaurefucin (**2**).[4)]

(3*Z*)-Isoprelaurefucin (**1**), $C_{15}H_{20}O_2Br_2$ (*m/z* 394, 392, and 390; M^+), colorless oil, $[\alpha]_D^{21}$ −75.5° (*c* 1.41; $CHCl_3$), indicated in its IR, UV, ^1H NMR, and MS spectra the presence of a *cis*-2-penten-4-ynyl grouping [ν_{max} 3300, 2120, and 760 cm^{-1}; λ_{max} 222 nm (ε 14600); δ=3.11 (1H, d, *J*=2 Hz), 5.59 (1H, br d, *J*=11 Hz), and 6.08 (1H, ddd, *J*=11, 7, 7 Hz); *m/z* 329, 327, and 325; $M^+-C_5H_5$]. The spectral data of **1** were very similar to those of isoprelaurefucin (**2**),[4)] which has previously been isolated as a minor component from *L. nipponica* collected at Moheji, near Hakodate, Hokkaido, suggesting that **1** is the geometric isomer of the double bond at C-3 of **2**. Hydrogenation of **1** over PtO_2 in ethanol gave the hexahydro derivative, $C_{15}H_{26}O_2Br_2$, which was identical with the hydrogenated product **3**[4)] of isoprelaurefucin (**2**) in all respects.

Of the six chiral centers at C-6, C-7, C-9, C-10, C-12, and C-13 in isoprelaurefucin (**2**), the absolute configurations at C-6, C-7, and C-9 were unambiguously established as 6*R*, 7*R*, and 9*R*, respectively,[4)] on the basis of the chemical correlation with the known compound, hexahydrolaurefucin (**4**).[5)] The remaining configurations at C-10, C-12, and C-13, however, were inferred from the biogenetical viewpoint and the chemical observation that the elimination reaction of the hexahydro derivative (**3**) with zinc and acetic acid generated 9-*cis*-12-*trans*-pentadeca-9,12-diene-6,7-diol.[4)] Therefore, in order to confirm the absolute stereochemistries at C-10, C-12, and C-13, we carried out the following chemical correlation with the known compounds.

Treatment of hexahydroisoprelaurefucin (**3**) with zinc and acetic acid in methanol yielded two unsaturated alcohols, **5** and **6**, which have the same molecular formula $C_{15}H_{27}O_2Br$. One of the unsaturated alcohols, compound **6** was hydrogenated in ethanol over PtO_2 to give a saturated compound which was identical with compound **7**,[6)] which has been derived from compound **8**,[6,7)] kumausallene,[6)] and kumausynes.[8)] Hence the absolute configuration at C-10 in **1** was established as *R*.

Another unsaturated alcohol, compound **5** showed in its mass spectrum the relatively intense fragments at *m/z* 219 and 217 ($M^+-C_6H_{13}O$) and 197 ($M^+-C_3H_6Br$), thus indicating that compound **5** was generated from **3** by the oxolane ring cleavage to contain an oxepane ring with 1-bromopropyl and 1-hydroxyhexyl side chains. Furthermore, compound **5** was brominated with carbon tetrabromide and triphenylphosphine[9)] in benzene to give a dibromo ether **9**, $C_{15}H_{26}OBr_2$, whose IR spectrum indicated no hydroxyl absorption. Compound **9**, on treatment with zinc and acetic acid in methanol, afforded two unsaturated bromohydrins **10** and **11**, $C_{15}H_{27}OBr$. Hydrogenation of **10** over PtO_2 in ethyl acetate yielded the saturated bromohydrin **12**, $C_{15}H_{31}OBr$, $[\alpha]_D^{18}$ −3.14°. The fragment ions at *m/z* 185 ($M^+-C_3H_6Br$) and 153 and 151 ($M^+-C_{11}H_{23}$) in the mass spectrum of **12** showed that the bromohydrin **12** is 3-bromo-4-pentadecanol.

On the other hand, treatment of hexahydrolaureatin (**13**)[10)] with zinc and acetic acid in methanol resulted in the cleavage of oxetane ring in **13** to give an unsaturated alcohol **14**, $C_{15}H_{27}O_2Br$, which was further brominated with carbon tetrabromide and triphenylphosphine to yield a dibromo ether **15**, $C_{15}H_{26}OBr_2$, with the concomitant formation of a dehydrobromination product **16**, $C_{15}H_{25}OBr$. Moreover, treatment of **15** with zinc and acetic acid in methanol yielded two unsaturated bromohydrins **17** and **18**, $C_{15}H_{27}OBr$. One of the bromohydrins, compound **17** showed almost identical spectral data with those of **10** derived from isoprelaurefucin. In the ^1H NMR spectra of **10** and **17**, the shape of the signals of the C_8–H_2, flanked by two double bonds, at δ 2.7—2.9 and the olefinic protons at δ 5.1—5.8 is slightly different, indicating that the double bond at C-6 in **10** and **17** cosisted of a mixture of *cis* and *trans* double bonds whose ratio were different. Hydrogenation of **17** over PtO_2 in ethyl acetate gave the saturated bromohydrin, (3*S*,4*R*)-3-bromo-4-pentadecanol (**12**), $[\alpha]_D^{17}$ −2.88°, which was completely identical with the bromohydrin **12** derived from isoprelaurefucin. Thus, the absolute configurations of the remaining chiral centers at C-12 and C-13 were established as *R* and *S*, respectively. Consequently, the structures, including the absolute configuration, of (3*Z*)-isoprelaurefucin and isoprelaurefucin are represented by formulae **1** and **2**, respectively.

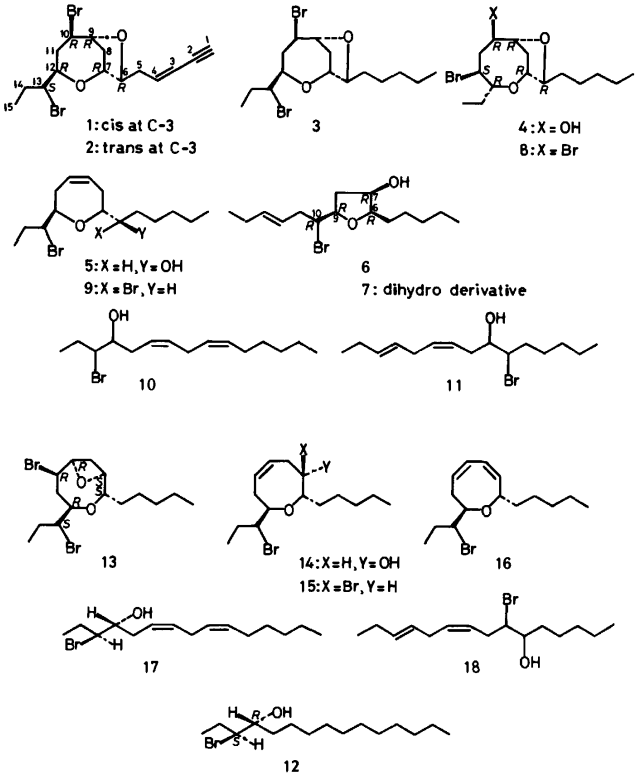

Experimental

The IR spectra were measured on a Hitachi EPI-G2 or a JASCO A-102 spectrophotometers. The UV spectra were obtained on a Shimadzu UV-240 spectrophotomer. The ^1H and ^{13}C NMR spectra were recorded on a JEOL JNM-FX 100 or a JEOL JNM-FX 270 spectrometers, using tetramethylsilane as an internal reference in $CDCl_3$. The low and high resolution mass spectra were taken with a JEOL JMS-D300 or a JEOL JMS-DX300 spectrometers. Optical rotations were determined on a JASCO DIP-140 or a Atago Polax polarimeters in $CHCl_3$. Silica gel (Merck, Kieselgel 60, 70—230 mesh) was used for column chromatography. High-performance liquid chromatography was performed on a JASCO TRI ROTAR-III with a Megapak SIL CN column.

Collection. Algae were collected at Asari and Hariusu, near Otaru, Hokkaido, in June 18, 1982.

Isolation of (3Z)-Isoprelaurefucin (1). Half-dried alga (60 g), collected at Asari, was extracted with MeOH, and the resulting MeOH extract was treated with 0.5 mol dm^{-3} aqueous KOH in the usual manner to give a neutral oil (0.77 g) which was chromatographed on a silica-gel column. The earlier benzene fraction was further subjected to repeated silica-gel column chromatography to yield pure (3Z)-isoprelaurefucin (**1**) (150 mg); oil; $[\alpha]_D^{21}$ −75.5° (*c* 1.41); UV (EtOH), λ_{max} 222 (ε 14600) and λ_{inf} 214 (ε 12800) and 231 (ε 10900) nm; IR (film), ν_{max} 3300, 2120, 1293, 1245, 1200, 1140, 1105, 1088, 1075, 1055, 1020, 975, 863, and 760 cm^{-1}; ^1H NMR and ^{13}C NMR, Table 1; MS (70 eV), *m/z* (rel intensity) 394, 392, 390 (0.3:0.6:0.3; M^+), 329, 327, 325 (5:11:6; $M^+-C_5H_5$), 313, 311 (12:11; M^+—Br), 271, 269 (7:4; $M^+-C_3H_6Br$), 231 (22; M^+—Br-HBr), 137 (24), 123 (26), 121 (54), 119 (21), 109 (45), 107 (27), 95 (59), 93 (66), 91 (23), 81 (43), 79 (38), 71 (35), and 69 (31). Found: *m/z* 311.0648. Calcd for $C_{15}H_{20}O_2$ ^{79}Br: M–Br, 311.0647.

Hydrogenation of (3Z)-Isoprelaurefucin (1). (3Z)-Isoprelaurefucin (**1**) (296 mg) was hydrogenated in EtOH over PtO_2-catalyst. After removal of the catalyst and the solvent, the residual oil was chromatographed on silica-gel column to yield **3** (287 mg); oil; $[\alpha]_D^{22}$ −48.6° (*c* 1.20); IR (film), ν_{max} 1197, 1180, 1140, 1108, 870, 835, 792, 759, and 691 cm^{-1}; ^1H NMR, δ=0.89 (3H, br t, *J*=6 Hz), 1.06 (3H, dd, *J*=7, 7 Hz), 3.6—3.9 (2H, m), 4.1—4.4 (3H, m), and 4.61 (1H, br d, *J*=7 Hz); MS (75 eV), *m/z* 319, 317 (12:12; M^+—Br), 318, 316 (20:19; M^+—HBr), 277, 275 (2:2; $M^+-C_3H_6Br$), 238 (14; M^+—Br-Br), 237 (74; M^+—Br-HBr), 167 (12), 137 (39), 123 (100), 122 (57), 109 (34), 99 (35), 95 (26), 93 (50), 71 (28), 67 (43), 55 (32), 43 (26), and 41 (34). These spectral data were consistent with those of hexahydroisoprelaurefucin (**3**).[4]

Table 1. ^{13}C and ^1H NMR Data for (3Z)-Isoprelaurefucin (**1**)

Carbon	$^{13}C^{a)}/\delta$	$^1H^{b)}/\delta$	Multiplicity (*J* in Hz)
1	82.3 (d)	3.11	d, *J*=2
2	79.9 (s)		
3	110.5 (d)	5.59	br d, *J*=11
4	140.5 (d)	6.08	ddd, *J*=11, 7, 7
5	33.3 (t)	2.88	br ddd, *J*=14.5, 8, 7
		2.66	br ddd, *J*=14.5, 7, 7
6	81.7 (d)	3.89	ddd, *J*=8, 7, 2
7	76.0 (d)[c)]	4.31	dd, *J*=4, 2
8	40.5 (t)	2.44	br d, *J*=14
		2.19	br ddd, *J*=14, 8.5, 4
9	82.9 (d)	4.63	br d, *J*=8.5
10	50.2 (d)	4.16	br dd, *J*=11, 6
11	29.4 (t)	2.56	br dd, *J*=15, 6
		2.29	ddd, *J*=15, 11, 9
12	75.6 (d)[c)]	4.29	dd, *J*=9, 4
13	62.0 (d)	3.89	ddd, *J*=10, 4, 4
14	27.5 (t)	1.93	ddddd, *J*=14, 7, 7, 7, 4
		1.79	ddddd, *J*=14, 7, 7, 7, 10
15	12.8 (q)	1.07	dd, *J*=7, 7

a) Spectrum was measured at 25.0 MHz in $CDCl_3$ (TMS as int. standard). b) Spectrum was recorded at 270 MHz in $CDCl_3$ (TMS as int. standard). Assignments were made with the aid of 2D-COSY and spin decoupling (in part) experiments. c) Assignments may be reversed.

Treatment of 3 with Zn-AcOH. To a solution of **3** (230 mg) in MeOH (5 ml) was added zinc dust (500 mg) and acetic acid (0.25 ml). The mixture was stirred for 15 h at room temperature and then filtered to remove the zinc dust. The filtrate was extracted with ether. The ethereal solution was successively washed with water, 5% aqueous $NaHCO_3$, and water, dried over Na_2SO_4, and then evaporated to leave a residual oil, which was chromatographed on silica-gel column to give **5** (97 mg) and **6** (15 mg): **5**; oil; $[\alpha]_D^{22}$ −5.23° (*c* 2.86); IR (film), ν_{max} 3440, 3020, 1657, 1218, 1195, 1132, 1100, 1020, 1000, 929, 905, and 795 cm^{-1}; ^1H NMR, δ=0.89 (3H, br t, *J*=6 Hz), 1.08 (3H, dd, *J*=7, 7 Hz), 3.48 (1H, m), 3.9—4.4 (3H, m), and 5.70 (2H, m); MS (75 eV), *m/z* 320, 318 (1:1; M^+), 302, 300 (0.6:0.6; M^+-H_2O), 239 (9; M^+—Br), 238 (15; M^+—HBr), 219, 217 (47:43; $M^+-C_6H_{13}O$), 197 (61; $M^+-C_3H_6Br$), 139 (33), 137 (100), 121 (53), 119 (24), 114 (24), 109 (98), 99 (52), 97 (33), 95 (49), 93 (73), 83 (40), 81 (31), 79 (43), 71 (33), 67 (82), 55 (51), and 41 (44).

Hydrogenation of 6. Compound **6** (12 mg) was hydrogenated in EtOH over PtO_2-catalyst in the usual manner to give **7** (12 mg); oil; $[\alpha]_D^{22}$ +3.46° (*c* 0.867); whose spectral

properties were compatible with those of compound **7**,[6] which was derived from compound 8,[7] kumausallene,[6] and kumausynes.[8]

Conversion of 5 into 9. A solution of **5** (54 mg) in dry benzene (3.5 ml) was refluxed with triphenylphosphine (110 mg) and carbon tetrabromide (140 mg) for 1 h in N_2 atmosphere. The subsequent removal of the solvent gave a residual substance, which was purified by silica-gel column chromatography to afford **9** (64 mg); oil; $[\alpha]_D^{22}$ −5.36° (*c* 0.933); IR (film), ν_{max} 3010, 1217, 1168, 1092, 1022, 799, and 670 cm^{-1}; ^1H NMR, δ=0.90 (3H, br t, *J*=6 Hz), 1.07 (3H, dd, *J*=7 Hz), 3.9—4.3 (4H, m), and 5.70 (2H, m); MS (75 eV), *m/z* 384, 382, 380 (0.9:1.7:1.1; M^+), 261, 259 (41:40; $M^+-C_3H_6Br$), 232, 230 (10:10; $M^+-Br-C_5H_{11}$), 219, 217 (60:61; $M^+-C_6H_{12}Br$), 151 (38), 137 (40), 109 (100), 95 (39), 93 (30), 81 (30), 79 (40), 67 (69), 55 (28), and 41 (39).

Treatment of 9 with Zn-AcOH. To a solution of **9** (60 mg) in MeOH (1.2 ml) was added zinc dust (150 mg) and acetic acid (0.06 ml). The mixture was stirred for 22 h at room temperature and then worked up in a manner similar to the case of **3**. The resulting oily substance was subjected to HPLC eluted with hexane-isopropyl alcohol (100:0.25) to yield **10** (13 mg) and **11** (8 mg): **10**; oil; $[\alpha]_D^{17}$ +5.21° (*c* 1.30); IR (film), ν_{max} 3420, 3020, 1285, 1050, 1037, 1027, 970, and 803 cm^{-1}; ^1H NMR, δ=0.88 (3H, br t, *J*=6 Hz), 1.08 (3H, dd, *J*=7, 7 Hz), 2.41 (2H, t, *J*=5.5 Hz), 2.7—2.9 (2H, m), 3.76 (1H, br ddd, *J*=5.5, 5.5, 5.5 Hz), 4.07 (1H, ddd, *J*=8, 5.5, 5 Hz), and 5.1—5.8 (4H, m); MS (70 eV), *m/z* 223 (11; M^+-Br), 205 (20; M^+-Br-H_2O), 95 (44), 93 (30), 81 (58), 79 (53), 71 (100), 69 (58), 67 (81), 55 (66), 43 (92), and 41 (73); **11**; oil; ^1H NMR, δ=0.90 (3H, br t, *J*=6 Hz), 0.97 (3H, dd, *J*=7, 7 Hz), 2.40 (2H, t, *J*=6 Hz), 2.7—2.9 (2H, m), 3.74 (1H, m), 4.19 (1H, m), and 5.1—5.8 (4H, m).

Hydrogenation of 10. Compound **10** (13 mg) was hydrogenated in EtOAc over PtO_2-catalyst in the usual manner to yield **12** (12 mg); oil; $[\alpha]_D^{18}$ −3.14° (*c* 1.21); IR (film), ν_{max} 3400, 1285, 1125, 1075, 1055, 1040, 1020, 920, and 803 cm^{-1}; ^1H NMR, δ=0.88 (3H, br t, *J*=6 Hz), 1.08 (H, dd, *J*=7, 7 Hz), 3.69 (1H, m), and 4.09 (1H, ddd, *J*=7.5, 6, 3.5 Hz); MS (70 eV), *m/z* 291, 289 (0.3:0.3; M^+-H_2O+H), 227 (2; M^+-Br), 185 (85; $M^+-C_3H_6Br$), 153, 151 (4:4; $M^+-C_{11}H_{23}$), 111 (69), 97 (97), 83 (94), 69 (100), 57 (59), 55 (89), 43 (89), and 41 (92).

Treatment of Hexahydrolaureatin (13) with Zn-AcOH. To a solution of hexahydrolaureatin (**13**)[10] (500 mg) in MeOH (12.5 ml) was added zinc dust (1.25 g) and acetic acid (0.63 ml). The mixture was stirred for 110 min at room temperature and then worked up in a manner similar to the case of **3**. The resulting oil was chromatographed on silica-gel column to give **14** (183 mg); oil; $[\alpha]_D^{22}$ +93.7° (*c* 1.33); IR (film), ν_{max} 3450, 3010, 1655, 1280, 1195, 1120, 1060, 1045, 797, and 692 cm^{-1}; ^1H NMR, δ=0.89 (3H, br t, *J*=6 Hz), 1.09 (3H, dd, *J*=7, 7 Hz), 3.5—4.1 (4H, m), and 5.6—6.0 (2H, m); MS (70 eV), *m/z* 320, 318 (0.5:0.5; M^+), 239 (5; M^+-Br), 220, 218 (6:6; $M^+-C_5H_{11}-C_2H_5$), 197 (28; $M^+-C_3H_6Br$), 121 (37), 114 (79), 113 (83), 109 (67), 95 (75), 67 (100), 55 (97), 43 (77), and 41 (69).

Bromination of 14. A solution of **14** (150 mg) in dry benzene (6 ml) was refluxed with triphenylphosphine (280 mg) and carbon tetrabromide (350 mg) for 70 min in N_2 atmosphere. After removal of the solvent, the residual oil was chromatographed over silica-gel column to yield **15** (23 mg) and **16** (30 mg): **15**; oil; $[\alpha]_D^{22}$ −34.1° (*c* 1.40); IR (film), ν_{max} 3020, 1660, 1285, 1219, 1198, 1070, 1089, 1071, 1050, and 695 cm^{-1}; ^1H NMR, δ=0.90 (3H, br t, *J*=6 Hz), 1.07 (3H, dd, *J*=7, 7 Hz), 3.8—4.2 (4H, m), and 5.5—5.9 (2H, m); MS (70 eV), *m/z* 384, 382, 380 (0.3:0.6:0.3; M^+), 303, 301 (25:25; M^+-Br), 261, 259 (30:32; $M^+-C_3H_6Br$), 220, 218 (44:45), 203, 201 (99:100; $M^+-C_5H_{11}-C_2H_5$), 192, 190 (45:45), 179 (39), 151 (35), 95 (40), 79 (39), 67 (55), 55 (37), 43 (28), and 41 (35); **16**; oil; $[\alpha]_D^{17}$ +151° (*c* 1.40); UV (EtOH), λ_{max} 225 nm (ε 4930); IR (film), ν_{max} 3010, 1080, 1060, 1020, 805, and 792 cm^{-1}; ^1H NMR, δ=0.88 (3H, br t, *J*=6 Hz), 1.06 (3H, dd, *J*=7, 7 Hz), 3.5—4.3 (3H, m), 5.27 (1H, dd, *J*=10.5, 8 Hz), and 5.2—6.2 (3H, m); MS (75 eV), *m/z* 302, 300 (4:4; M^+), 231, 229 (4:4; $M^+-C_5H_{11}$), 221 (68; M^+-Br), and 79 (100).

Treatment of 15 with Zn-AcOH. To a solution of **15** (23 mg) in MeOH (0.5 ml) was added zinc dust (50 mg) and acetic acid (0.03 ml). The mixture was stirred for 3 h at room temperature and then worked up in a manner similar to the case of **3**. The resulting oil was subjected to HPLC eluted with hexane-isopropyl alcohol (100:0.20) to give **17** (12 mg) and **18** (5 mg): **17**; oil; $[\alpha]_D^{18}$ +6.33° (*c* 1.29); whose spectral data were almost identical with those of **10** derived from isoprelaurefucin; **18**; oil; ^1H NMR, δ=0.90 (3H, br t, *J*=6 Hz), 0.97 (3H, dd, *J*=7, 7 Hz), 2.5—2.9 (4H, m), 4.16 (1H, m), and 5.3—5.7 (4H, m).

Hydrogenation of 17. Compound **17** (12 mg) was hydrogenated in EtOAc over PtO_2-catalyst in the usual manner to give **12** (10 mg); oil; $[\alpha]_D^{17}$ −2.88° (*c* 1.14); whose spectral properties were identical with those of **12** derived from isoprelaurefucin.

References

1) Part 65 of "Constituents of Marine Plants," Part 64; H. Kikuchi, T. Suzuki, M. Suzuki, and E. Kurosawa, *Bull. Chem. Soc. Jpn.*, **58**, 2437 (1985).

2) S. J. Wratten and D. J. Faulkner, *J. Org. Chem.*, **42**, 3343 (1977).

3) H. Kikuchi, T. Suzuki, M. Suzuki, and E. Kurosawa, *Bull. Chem. Soc. Jpn.*, **58**, 2437 (1985).

4) E. Kurosawa, A. Fukuzawa, and T. Irie, *Tetrahedron Lett.*, **1973**, 4135.

5) A. Fukuzawa, E. Kurosawa, and T. Irie, *Tetrahedron Lett.*, **1972**, 3; A. Furusaki, E. Kurosawa, A. Fukuzawa, and T. Irie, *ibid.*, **1973**, 4579.

6) T. Suzuki, K. Koizumi, M. Suzuki, and E. Kurosawa, *Chem. Lett.*, **1983**, 1639.

7) A. Furusaki, T. Matsumoto, H. Kikuchi, T. Suzuki, M. Suzuki, and E. Kurosawa, *Bull. Chem. Soc. Jpn.*, **56**, 2523 (1983).

8) T. Suzuki, K. Koizumi, M. Suzuki, and E. Kurosawa, *Chem. Lett.*, **1983**, 1643.

9) This bromination usually proceeds in S_N2 mechanism with inversion of configuration. J. G. Calzada and J. Hooz, *Org. Synth.*, **54**, 63 (1974).

10) T. Irie, M. Izawa, and E. Kurosawa, *Tetrahedron Lett.*, **1968**, 2091; T. Irie, M. Izawa, and E. Kurosawa, *Tetrahedron*, **26**, 851 (1970); E. Kurosawa, A. Furusaki, M. Izawa, A. Fukuzawa, and T. Irie, *Tetrahedron Lett.*, **1973**, 3857.

Pseudo-Sugars. XVI. Facile Synthesis of Pseudo-α-D and L-Glucopyranoses[1]

Seiichiro OGAWA,* Kazufumi NAKAMURA, and Tohei TAKAGAKI
Department of Applied Chemistry, Faculty of Science and Technology, Keio University, Hiyoshi, Yokohama 223
(Received March 19, 1986)

Synopsis. Optically active pseudo-α-glucopyranoses have been synthesized from enantiomeric (1,3,5/2,4)-2,3-diacetoxy-4,5-dibromo-1-cyclohexanecarboxylic acids, obtained by optical resolution of the racemic modification using (+)- and (−)-α-methylbenzylamines.

Recently, pseudo-α-DL-glucopyranose[2] has been shown to inhibit glucokinase activity and glucose-stimulated insulin release.[3] Accordingly, it has become necessary to provide quantities of the pseudo-sugars, as optically active forms, for a further biological and biochemical studies. We now describe a facile synthesis of pseudo-α-D and L-glucopyranoses, starting from (−) and (+)-enantiomers of (1,3,5/2,4)-2,3-diacetoxy-4,5-dibromo-1-cyclohexanecarboxylic acid (**2**), respectively, obtained by an optical resolution[4] of the racemic modification.[5]

Pseudo-α-D-glucopyranose has already been synthesized from D-glucose by two research groups.[6,7] The sequence of the present synthesis could readily be conducted with a high selectivity and a high overall yield, and has an advantage to furnish both D- and L-enantiomers with ease.

The racemic acid (±)-**2** was successfully resolved by use of commercially available (+)- and (−)-α-methylbenzylamines. Thus, a mixture of (*R*)-(+)-amine salts of (−)-**2** and (+)-**2** was fractionally crystallized from ethanol to give, in 54% yield, the pure (*R*)-(+)-amine salt of (−)-**2**, from which the free acid (−)-**2** ($[\alpha]_D$ −5.1°) was obtained by treatment with sodium carbonate followed by hydrochloric acid. Similarly, the acid (+)-**2** ($[\alpha]_D$ +5.2°) was obtained by use of the (*S*)-(−)-amine. The absolute configuration of (−)-**2** could be estabilised as shown in Scheme by identification with the authetic sample derived from (3*S*)-(+)-2-*exo*-bromo-4,8-dioxatricyclo[4.2.1.0^{3,7}]nonan-5-one[8] (**1**) by treatment with hydrogen bromide in acetic acid.

The present synthesis of **9** was carried out in the following sequence,[5] previously used for the preparation of the racemic modification.

Treatment of the acid (−)-**2** with methanol and acetyl chloride gave the methyl ester (−)-**3** in 91% yield. Compound (−)-**2** was debrominated with zinc dust in acetic acid to give 96% yield of the olefin (−)-**4**. Similarly, (−)-**3** was converted into the olefin (−)-**5** in 92% yield. Oxidation of (−)-**5** with osmium tetraoxide and hydrogen peroxide in *t*-butyl alcohol, followed by acetylation, afforded selectively the tetraacetate (+)-**6** in 85% yield.[9] *O*-Deacetylation of (+)-**6** with methanolic sodium methoxide gave the methyl ester (+)-**7** ($[\alpha]_D$ +48°) quantitatively. Reduction of (+)-**6** with lithium aluminum hydride in tetrahydrofuran, followed by acetylation, gave the pentaacetate (+)-**8** ($[\alpha]_D$ +57°) in 98% yield. *O*-Deacetylation of (+)-**8** gave pseudo-α-D-glucopyranose (+)-**9** ($[\alpha]_D$ +67°)[10] quantitatively. The overall yield of (+)-**9** from (−)-**2** was about 70%.

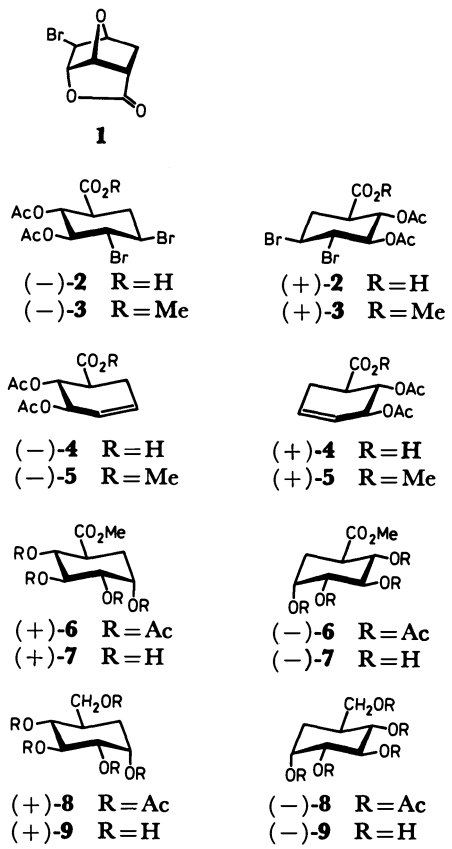

Likewise, pseudo-α-L-glucopyranose (−)-**9** ($[\alpha]_D$ −67°) was obtained from (+)-**2**.

The structures of **8** and **9** were established on the basis of the ^{1}H NMR spectra.[2,11]

Experimental

Melting points were determined on a MEL-TEMP capillary melting-point apparatus and are uncorrected. Optical rotations were measured on a Jasco DIP-4 polarimeter. The ^{1}H NMR spectra were recorded on a Varian EM-390 (90 MHz) spectrometer for solution of chloroform-*d* or deuterium oxide. The silica gel used for column chromatography was Wakogel C-300 (Wako Co., Osaka). The structures of the optically active compounds synthesized were confirmed by comparison of the ^{1}H NMR spectra with those of the corresponding racemic modifications.[2,5,11]

Optical Resolution of DL-(1,3,5/2,4)-2,3-Diacetoxy-4,5-dibromo-1-cyclohexanecarboxylic Acid[2] [(±)-2]. To a solution of the acid (±)-**2** (20 g, 50 mmol) in ethanol (200 ml) was

added (*R*)-(+)-α-methylbenzylamine[12] (7.7 ml, 60 mmol), and the mixture was kept in a refrigerator (0—5 °C) overnight. The precipitates, a mixture of the salts, were collected by filtration and washed with 2-propanol. The salts were fractionally crystallized from ethanol to give the pure (*R*)-(+)-amine salt of (−)-**2** (6.8 g, 52%) as white needles: Mp 187—190 °C; $[\alpha]_D^{20}$ +8.7° (*c* 1.0, MeOH).

Found: C, 43.68; H, 4.74; N, 2.67%. Calcd for $C_{19}H_{25}Br_2NO_6$: C, 43.62; H, 4.82; N, 2.67%.

Similarly, by use of (*S*)-(−)-α-methylbenzylamine, the (*S*)-(−)-amine salt of (+)-**2** was obtained in 47% yield, needles (from EtOH): Mp 187—190 °C; $[\alpha]_D^{21}$ −8.6° (*c* 0.90, MeOH).

Found: C, 43.58; H, 4.75; N, 2.55%.

A portion (1.46 g, 3.13 mmol) of (*R*)-(+)-amine salt of (−)-**2** was treated with 2 M aqueous sodium carbonate (40 ml) (1 M=1 mmol dm^{-3}) at room temperature for 2 h, and then the solution was extracted with ether (20 ml×3). The solvent was removed to leave recovered (*R*)-(+)-amine (0.36 g 92%). The aqueous layer was acidified with 1 M hydrochloric acid and extracted with ether (100 ml×3). The extracts were dried over anhydrous sodium sulfate and concentrated to give a crystalline residue. Recrystallization from 2-propanol gave the acid (−)-**2** (1.19 g, 95%) as prisms: Mp 180—181 °C; $[\alpha]_D^{19}$ −5.1° (*c* 0.90, EtOH).

Found: C, 33.10; H, 3.69; Br, 39.45%. Calcd for $C_{11}H_{14}Br_2O_6$: C, 32.86; H, 3.51; Br, 39.75%.

From (*S*)-(−)-amine salt of (+)-**2**, the acid (+)-**2** was obtained in 93% yield, prisms (from *i*-PrOH): Mp 180—181 °C; $[\alpha]_D^{21}$ +5.2° (*c* 1.8, EtOH).

Found: C, 31.99; H, 3.21%. Calcd for $C_{11}H_{14}Br_2O_6 \cdot 0.5\,H_2O$: C, 32.14: H, 3.68%.

Preparation of (−)-2 from (3*S*)-(+)-2-*exo*-Bromo-4,8-dioxatricyclo[4.2.1.0^{3,7}]nonan-5-one[7] (1). The bromolactone **1** (1.0 g, 4.6 mmol) was heated with 20% hydrogen bromide–acetic acid (6 ml) in a sealed tube at 85 °C for 42 h. The reaction mixture was poured into ice–water (70 ml) containing sodium hydrogencarbonate (2 g) and the precipitates, after standing overnight in a refrigerator, were collected by filtration. Recrystallization from ethanol gave (−)-**2** (0.86 g, 44%) as prisms: Mp 182—183 °C; $[\alpha]_D^{23}$ −4.7° (*c* 0.72, EtOH).

Methyl (1*S*)-(−) [(−)-3] and (1*R*)-(+)-(1,3,5/2,4)-2,3-Diacetoxy-4,5-dibromo-1-cyclohexanecarboxylate [(+)-3]. A mixture of (−)-**2** (0.91 g, 2.3 mmol), acetyl chloride (0.1 ml), and methanol (10 ml) was heated at reflux for 2 h, and then neutralized with sodium hydrogencarbonate. The reaction mixture was concentrated and the residue was acetylated with acetic anhydride (5 ml) and pyridine (5 ml) overnight at room temperature. The mixture was concentrated, the residue was taken up in ethyl acetate (30 ml), and the solution was washed with 1 M hydrochloric acid, saturated aqueous sodium hydrogencarbonate, and water, dried, and concentrated. Recrystallization of the residue from ethanol gave (−)-**3** (0.85 g, 91%) as needles: Mp 140—141 °C; $[\alpha]_D^{20}$ −15.5° (*c* 1.4, $CHCl_3$).

Found: C, 34.48; H, 3.88; Br, 38.53%. Calcd for $C_{12}H_{16}Br_2O_6$: C, 34.64; H, 3.88; Br, 38.41%.

Similarly, (+)-**2** was converted into the ester (+)-**3**; needles (from EtOH): Mp 140—141 °C; $[\alpha]_D^{20}$ +15.4° (*c* 0.85, $CHCl_3$).

Found: C, 34.97; H, 3.89%.

(1*S*)-(−) [(−)-4] and (1*R*)-(+)-(1,3/2)-2,3-Diacetoxy-4-cyclohexene-1-carboxylic Acid [(+)-4]. To a solution of (−)-**2** (0.93 g, 2.3 mmol) in acetic acid (20 ml) was added zinc dust (1.5 g, 23 matom) in portions at 70 °C for 0.5 h. The insoluble material was filtered and the filtrate was concentrated. The residue was taken up in ethyl acetate (20 ml) and the solution was washed with saturated aqueous sodium hydrogencarbonate and water, dried, and concentrated. Recrystallization of the residue from carbon tetrachloride gave (−)-**4** (0.54 g, 96%) as prisms: Mp 113—115 °C; $[\alpha]_D^{17}$ −2.5° (*c* 1.9, EtOH).

Found: C, 54.32; H, 5.70%. Calcd for $C_{11}H_{14}O_6$: C, 54.54; H, 5.83%.

Similarly, (+)-**4** was obtained from (+)-**2**; prisms (from CCl_4): Mp 113—115 °C; $[\alpha]_D^{17}$ +2.7° (*c* 2.7, EtOH).

Found: C, 54.38; H, 5.73%.

Methyl (1*S*)-(−) [(−)-5] and (1*R*)-(+)-(1,3/2)-2,3-Diacetoxy-4-cyclohexene-1-carboxylate [(+)-5]. The ester (−)-**3** (0.50 g, 1.2 mmol) was treated with zinc dust in acetic acid as described for the preparation of (−)-**4** to give (−)-**5** (0.28 g, 92%) as needles (from ether): Mp 45—47 °C; $[\alpha]_D^{18}$ −22° (*c* 1.6, $CHCl_3$).

Found: C, 55.87; H, 5.96%. Calcd for $C_{12}H_{16}O_6$: C, 56.25; H, 6.29%.

Similarly, the ester (+)-**3** was converted into (+)-**5**; needles (from ether): Mp 45—47 °C; $[\alpha]_D^{17}$ +21° (*c* 0.96, $CHCl_3$).

Found: C, 55.98; H, 6.07%.

Methyl (1*S*)-(+) [(+)-6] and (1*R*)-(−)-(1,3/2,4,5)-2,3,4,5-Tetraacetoxy-1-cyclohexanecarboxylate [(−)-6]. A mixture of (−)-**5** (0.51 g, 2.0 mmol), *t*-butyl alcohol (11 ml) containing 30% hydrogen peroxide (2 ml), and *t*-butyl alcohol (3.8 ml) containing osmium tetraoxide (19 mg) was stirred at room temperature for 24 h. Excess peroxide was decomposed by addition of sodium sulfite and the mixture was concentrated. The residue was acetylated in a usual way and the product was eluted from a column of silica gel (30 g) with 2-butanone–toluene (1:8) to give (+)-**6** (0.63 g, 85%) as prisms (from EtOH): Mp 79—80 °C; $[\alpha]_D^{23}$ +56° (*c* 1.1, $CHCl_3$).

Found: C, 51.30; H, 5.87%. Calcd for $C_{16}H_{22}O_{10}$: C, 51.34; H, 5.92%.

Similarly, (−)-**6** was obtained from (+)-**5**; prisms (from EtOH): Mp 79—80 °C; $[\alpha]_D^{22}$ −58° (*c* 1.1, $CHCl_3$).

Found: C, 51.08; H, 5.77%.

Methyl (1*S*)-(+) [(+)-7] and (1*R*)-(−)-(1,3/2,4,5)-2,3,4,5-Tetrahydroxy-1-cyclohexanecarboxylate [(−)-7]. Compound (+)-**6** (45 mg, 0.12 mmol) was treated with 0.1 M methanolic sodium methoxide (2 ml) at room temperature for 2 h, and then the mixture was neutralized by passage through a short column of Amberlite IR 120B (H^+) resin. The eluate was concentrated to give (+)-**7** (25 mg, 100%) as a syrup: $[\alpha]_D^{20}$ +48° (*c* 0.71, MeOH).

Found: C, 45.59; H, 6.66%. Calcd for $C_8H_{14}O_6 \cdot 0.25H_2O$: C, 45.60; H, 6.94%.

Similarly, (−)-**7** was obtained from (−)-**6**; syrup: $[\alpha]_D^{20}$ −48° (*c* 0.98, MeOH).

Found; C, 46.61; H, 6.58%. Calcd for $C_8H_{14}O_6$: C, 46.60; H, 6.84%.

(1*S*)-(+) [(+)-8] and (1*R*)-(−)-(1,3/2,4,5)-2,3,4,5-Tetraacetoxycyclohexanmethanol [(−)-8]. The ester (+)-**6** (100 mg, 0.27 mmol)was treated with lithium aluminum hydride (55 mg, 1.4 mmol) in tetrahydrofuran (2 ml) at room temperature for 8 h. The mixture was processed in a usual way to give a hydroxy compound, which was acetylated with acetic anhydride in pyridine. The product was purified by passage through a short column of alumina with chloroform to give (+)-**8** (103 mg, 98%) as a syrup: $[\alpha]_D^{21}$ +57° (*c* 0.90, $CHCl_3$) [lit,[6] $[\alpha]_D^{22}$ +37° ($CHCl_3$)] (Found: C, 52.44; H, 6.01%).

Similarly, (−)-**8** was obtained from (−)-**6**; syrup: $[\alpha]_D^{20}$ −56° (*c* 1.1, $CHCl_3$).

(1*S*)-(+) [(+)-9] and (1*R*)-(−)-(1,3/2,4,5)-2,3,4,5-Tetrahydroxycyclohexanemethanol [(−)-9]. Compound (+)-**8** (56 mg, 0.14 mmol) was treated with 0.1 M methanolic sodium methoxide (2 ml) at room temperature for 3 h. The mixture was neutralized with Amberlite IR 120B (H^+) resin to give (+)-**9** (27 mg, 100%) as a syrup: $[\alpha]_D^{21}$ +67° (*c* 0.50, MeOH) [lit,[6] $[\alpha]_D^{25}$ +30° (MeOH)].

Similarly, the pentol (−)-**9** was obtained from (−)-**8**:

syrup: $[\alpha]_D^{21}$ −67° (*c* 1.5, MeOH).

Found: C, 47.32; H, 7.66%. Calcd for $C_7H_{14}O_5$: C, 47.18; H, 7.92%.

The authors are grateful to Prof. Tetsuo Suami for a kind advice, and to Mr. Saburo Nakada and Mr. Akio Takahashi for elementary analyses. The present work was partially supported by a grand of the Asahi Glass Foundation for the contribution to industrial technology.

References

1) Part XV, see T. Suami, S. Ogawa, Y. Uematsu, and A. Suga, *Bull. Chem. Soc. Jpn.*, **59**, 1261 (1986).

2) S. Ogawa, Y. Tsukiboshi, Y. Iwasawa, and T. Suami, *Carbohydr. Res.*, **136**, 77 (1985).

3) I. Miwa, H. Hara, J. Okuda, T. Suami, and S. Ogawa, *Biochem Int.*, **11**, 809 (1985).

4) Since the yield of the reaction producing **2** was rather low, an optical resolution of (±)-**2** seemed to be more effective for the present synthesis.

5) S. Ogawa, Y. Yato, K. Nakamura, M. Takata, and T. Takagaki, *Carbohydr. Res.*, **148**, 249 (1986).

6) T. Suami, K. Tadano, Y. Kameda, and Y. Iimura, *Chem. Lett.*, **1984**, 1919.

7) J. Cleophax, S. D. Gero, P. Krausz, A. S. Machado, M. Philippe, B. Sire, C. Tachdjian, and G. Vass, 3rd European Symposium on Carbohydrates, Grenoble-France, September 1985, Abstr., No. B.2-5.

8) S. Ogawa, Y. Iwasawa, T. Nose, T. Suami, S. Ohba, M. Ito, and Y. Saito, *J. Chem. Soc., Perkin Trans. 1*, **1985**, 903.

9) The oxidation of **5** has been found to be more selective reaction than that of the correspondind bromomethyl compound, giving a pseudo-sugar derivative with the α-gluco configuration, see Ref. 11.

10) The remarkable discrepancy between the values of optical rotation of (+)-**9** and that of an authentic sample[6] might be explained by their homogeneity rather than by optical purity. The present results seem to be convincing, because optical rotations of both enantiomers synthesized are equal and opposite.

11) S. Ogawa, T. Toyokuni, T.Kondoh, Y. Hattori, S. Iwasaki, M. Suetsugu, and T. Suami, *Bull. Chem. Soc. Jpn.*, **54**, 2739 (1981).

12) (*R*)-(+) and (*S*)-(−)-α-methylbenzylamine were perchased from Tokyo Kasei Kogyo Co. Ltd. and showed specific rotations of +38.4 and −38.4° (neat), respectively, corresponding to ca. 96% optical purity.

The Addition of Alcohol to 1,2-Naphthoquinone Promoted by Metal Ions. A Facile Synthesis of 4-Alkoxy-1,2-naphthoquinones

Akio TAKUWA,* Osamu SOGA, Hidetoshi IWAMOTO, and Kazuhiro MARUYAMA†
Department of Chemistry, Faculty of Science, Shimane University,
Nishikawatsu-cho, Matsue 690
†Department of Chemistry, Faculty of Science, Kyoto University,
Sakyo-ku, Kyoto 606
(Received February 20, 1986)

Synopsis. In the presence of some metal ions and sodium iodate, 1,2-naphthoquinone (**1**) readily reacted with methanol to give 4-methoxy-1,2-naphthoquinone (**2a**). The activity of the metal ions increased in the following order: Co(II)<Ni(II) ≪ Cu(II)<La(III) ≪ Ce(III). The reaction was remarkably affected by the reaction temperature, reaction time, and molar ratio of the chelating agent. By the use of 1 equivalent of cerium salt to **1**, the yield of **2a** increased to 81% at 20 °C for 30 min. In higher alcohols, the addition reaction proceeded under similar conditions to give 4-alkoxy-1,2-naphthoquinones (**2b**—f) in 46—75% yields.

The quinone moiety plays an extremely important role in biological systems. A large number of methods have been applied for preparations of *o*- and *p*-quinones.[1] In these methods, two main approaches have been frequently used to synthesize 1,2-naphthoquinones, either by the oxidation of 1-amino-2-naphthols or a suitably substituted naphthol, or by the Michael addition of a nucleophile to the parent quinone.[1] In the addition reaction of a nucleophile, alcohols do not normally add to the quinones and, therefore, methyl or ethyl alcohol has been used as a recrystallizing solvent for some 1,2-naphthoquinone derivatives.[2]

Recently, M. Matsuoka et al.[3] and M. Hida et al.[4] independently reported an excellent direct amination of aminoanthraquinone or anthraquinone in the presence of metal salts or a metal complex. Moreover, hypervalent iodine oxides have been found to oxidize various dihydroxy aromatics to the corresponding quinones in high yields under very mild conditions.[5]

In this paper, we wish to report a novel and simple method for the preparation of 4-alkoxy-1,2-naphthoquinones (**2**) from the addition reaction of 1,2-naphthoquinone (**1**) with aliphatic alcohols in the presence of metal halides and sodium iodate as the oxidizing agent. The quinones, except for 4-methoxy-1,2-naphthoquinone, are unknown.

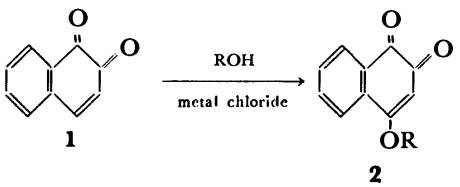

1 **2**

a: R=CH_3, **b**: R=C_2H_5, **c**: R=n-C_3H_7, **d**: R=i-C_3H_7, **e**: R=n-C_4H_9, **f**: R=$CH_2CH{=}CH_2$

Results and Discussion

No reaction of **1** with methanol occurred in the absence of metal chlorides; however, in the presence of metal chlorides, methanol was added to **1** at room temperature to afford **2a**. The activities of metal chlorides in this methoxylation are shown in Table 1. Metal chlorides were arranged in the order of reactivities as follows: Ce(III) ≫ La(III)>Cu(II) ≫ Ni(II)> Co(II). The activity of the cerium(III) ion was particularly superior to those of other metal ions examined in this work. The water of crystallization was slightly effective regarding the activities of cobalt(II) and copper(II) salts (Runs 3 and 6).[6]

The effect of the reaction time and temperature on the reaction of **1** with methanol in the presence of cerium(III) chloride heptahydrate is shown in Table 2. The yield of **2a** increased up to 30 min at 20 °C and gradually decreased with a prolonged reaction time. Suprisingly, an unexpected product, i.e., 2-methoxy-1,4-naphthoquinone (**3**), began to be produced after 1 h; it became the exclusive product after 10 h (Runs 11—13). The reaction was also considerably affected by the reaction temperature. Within 30 min, only **2a** was obtained at temperatures below 20 °C; at higher temperatures, the yield of **3** increased and it was the sole product under reflux for 30 min (Run 18). These results indicate that **2a** is converted into **3** under these conditions.[7]

Next, we examined the effect of the molar ratio of

Table 1. Effect of Metal Chloride on the Reaction of **1** with Methanol[a]

Run	Metal chloride	Yield[b,c]/% **2a**
1	None	0
2	$CoCl_2$	3
3	$CoCl_2 \cdot 6H_2O$	10
4	$NiCl_2 \cdot 6H_2O$	15
5	$CuCl_2$	40
6	$CuCl_2 \cdot 2H_2O$	51
7	$LaCl_3 \cdot 7H_2O$	66
8	$CeCl_3 \cdot 7H_2O$	79

a) A methanol solution of **1**(0.4 mmol) was stirred for 30 min in the presence of a metal salt(0.4 mmol) and sodium iodate(0.4 mmol) at room temperature. b) Yields were based on the quinone used. c) Determined by ^1H NMR spectra.

Table 2. Effect of the Reaction Temperature and Time on the Methoxylation of **1** in the Presence of $CeCl_3 \cdot 7H_2O$[a]

Run	Time / min	Temperature / °C	Yield[b),c)] / % **2a**	**3**
9	15	20	60	0
10	30	20	81	0
11	60	20	51	8
12	120	20	39	17
13	600	20	0	63
14	30	4	36	0
15	30	20	81	0
16	30	30	72	trace
17	30	50	25	35
18	30	Reflux	0	60

a) Reactions of **1** in methanol were carried out in the presence of cerium salt(1 equiv) and sodium iodate(1 equiv). b), c) See footnote in Table 1.

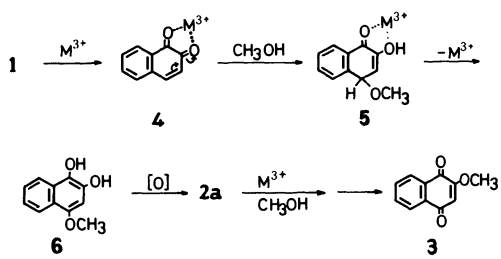

Scheme 1.

Table 3. Effect of the Molar Ratio of $CeCl_3 \cdot 7H_2O$ in the Reaction of **1** with Methanol at 20 °C for 30 min[a]

Run	Metal/**1**	Yield[b),c)] / % **2a**
19	0.1	15
20	0.5	68
21	1.0	81
22	2.0	70
23	3.0	70
24	5.0	70

a) Reactions were carried out in the presence of 1 equivalent of sodium iodate. b), c) See footnote in Table 1.

Table 4. Reactions of **1** with Various Alcohols[a]

Run	Alcohol	Time / h	Yield[b)] / % **2**
25	Methanol	0.5	**2a** (72)
26	Ethanol	0.5	**2b** (70)
27	Propanol[c)]	0.6	**2c** (75)
28	2-Propanol[c),d)]	4.0	**2d** (46)
29	Butanol[c),d)]	1.2	**2e** (75)
30	Allyl alcohol[c),d)]	2.0	**2f** (52)

a) The reactant, **1**(0.8 mmol) was stirred in alcohol with $CeCl_3 \cdot 7H_2O$(0.8 mmol) and sodium iodate(0.8 mmol). b) Isolated yield. c) Cerium salt was dissolved in 0.4 ml of water. d) The quinone was dissolved in acetonitrile(3 ml).

cerium salt to **1** on the yield of **2a**; the results are shown in Table 3. The yield of **2a** increased with an increase in the molar ratio of cerium salt up to 1.0. The additional amounts of the cerium ion slightly depressed the yield to 70% (Runs 22—24). Therefore, the optimum reaction conditions for the preparation of **2a** were as follows: 20 °C for the temperature, 30 min for the reaction time, and one equivalent mol of cerium(III) chloride heptahydrate to 1.

On the bases of our experimental results, a tentative reaction mechanism is proposed as shown in Scheme 1. The formation of a chelate complex (**4**), in which 1- and 2-carbonyl oxygens of **1** are coordinated to the metal ion,[8] enhances the electrophilic character of the C_4-carbon in **1**, and facilitates a nucleophilic attack of methanol on that carbon. A similar role of the cerium ion has been observed during the addition of aromatic amines to 5,8-quinolinedione.[9] The 2,5-cyclohexadienone intermediate (**5**) may be enolized to afford 4-methoxy-1,2-naphthalenediol (**6**), and **6** is oxidized into **2a**. For a prolonged reaction time, the metal ion presumably recoodinates to **2a** and the methanol adds to the chelated quinone to give a hemiacetal. It finally results in the formation of **3**.[7] The details of the reaction mechanism for each step are still not clear, however, and are under investigation.

Other aliphatic alcohols also reacted with **1** in the presence of $CeCl_3 \cdot 7H_2O$ under similar conditions to afford **2b—f** in good yields (Table 4). Since cerium salt and **1** were slightly soluble in higher alcohols, a minimum amount of water and acetonitrile were necessarily added to dissolve both components (Runs 27—30). In addition, a prolonged reaction time was required for some alcohols in order to improve the yields of **2d—f**. Thus, the direct alkoxylation of 1,2-naphthoquinone in the presence of $CeCl_3 \cdot 7H_2O$ is synthetically useful method for the preparation of 4-alkoxy-1,2-naphthoquinones.

Experimental

1,2-Naphthoquinone was prepared according to a method described in the literature.[10] All metal chlorides and sodium iodate were reagent-grade and were used without further purification. Alcohols were purified by distillation. Column chromatography was performed on silica gel (Merck Kisel gel 60, Art. 7734), using chloroform as an eluent. Authentic samples of **2a**[11] and **3**[12] were prepared by the methods described in the literatures. All the yields were based on **1** that was used.

General Procedure. (a) A mixture of **1**, metal salt, sodium iodate, and methanol was stirred in a flask (see Tables 1, 2, and 3). The mixture was then poured into a 10%

aqueous solution of ammonium chloride, and extracted with chloroform. The organic layer was thoroughly washed with water, dried (Na_2SO_4), and concentrated in vacuo. The yields of **2a** and **3** were determined by ^1H NMR integrations of methoxyl and quinonoid protons. The products were isolated by TLC (ether:hexane=4:1) (R_f 0.28 for **2a**; 0.43 for **3**). The physical properties of **2a** and **3** were identical with those of authentic samples. The reaction with ethanol was carried out by the same procedure, and **2b** was separated by column chromatography. (Table 4).

(b) As cerium salt and **1** were slightly soluble in higher alcohols, the reactions were modified as follows: An alcohol (11 ml) was added to acetonitrile (3 ml) solution of **1** (0.8 mmol), and then cerium salt dissolved in 0.4 ml of water and sodium iodate (0.8 mmol) were added to the solution. The mixture was stirred for the time indicated in Table 4 at 20 °C. After a workup as described above, the product was separated by column chromatography. The yields of the products are summarized in Table 4.

Identification of the Products. 4-Ethoxy-1,2-naphthoquinone (2b): Orange needles (benzene-hexane); mp 121—123 °C; IR (KBr) 1705 (m) and 1657 (s) cm^{-1} (C=O); ^1H NMR ($CDCl_3$) δ=1.55 (t, 3H, J=7.0 Hz), 4.23 (q, 2H, J=7.0 Hz), 5.90 (s, 1H), and 7.52—8.11 (m, 4H). Found: C, 71.01; H, 4.82%. Calcd for $C_{12}H_{10}O_3$: C, 71.28; H, 4.98%.

4-Propoxy-1,2-naphthoquinone (2c): Yellow needles (benzene-hexane); mp 115.5—116.5 °C; IR (KBr) 1700 (m) and 1650 (s) cm^{-1} (C=O); ^1H NMR ($CDCl_3$) δ=1.11, (t, 3H, J=7.0 Hz), 1.95 (sex, 2H, J=7.0 Hz), 4.12 (t, 2H, J=7.0 Hz), 5.95 (s, 1H), and 7.52—8.18 (m, 4H). Found: 72.49; H, 5.49%. Calcd for $C_{13}H_{12}O_3$: C, 72.21; H, 5.59%.

4-Isopropoxy-1,2-naphthoquinone (2d): Orange yellow needles (benzene-hexane); mp 124—125 °C; IR (KBr) 1700 (m) and 1645 (s) cm^{-1} (C=O); ^1H NMR ($CDCl_3$) δ=1.48 (d, 6H, J=7.0 Hz), 4.72 (sev, 1H, J=7.0 Hz), 5.90 (s, 1H), and 7.50—8.10 (m, 4H). Found: C, 71.19; H, 5.67%. Calcd for $C_{13}H_{12}O_3$: C, 72.21; H, 5.59%.

4-Butoxy-1,2-naphthoquinone (2e): Yellow needles (benzene-hexane); mp 95.5—96.5 °C; IR (KBr) 1690 (m) and 1640 (s) cm^{-1} (C=O); ^1H NMR ($CDCl_3$) δ=1.02 (t, 3H, J=7.0 Hz), 1.36—1.72 (m, 2H), 1.90 (quint, 2H, J=7.0 Hz), 4.13 (t, 2H, J=7.0 Hz), 5.91 (s, 1H), and 7.48—8.12 (m, 4H). Found: C, 78.55; H, 6.77%. Calcd for $C_{14}H_{14}O_3$: C, 78.48; H, 6.59%.

4-Allyloxy-1,2-naphthoquinone (2f): Yellowish brown needles (benzene-hexane); mp 121.5—123.5 °C; IR (KBr) 1700 (m) and 1650 (s) cm^{-1} (C=O); ^1H NMR ($CDCl_3$) δ=4.65 (m, 2H, OCH_2), 5.35—5.57 (m, 2H, $C=CH_2$), 5.91 (s, 1H), 5.96—6.44 (m, 1H, CH=C), and 7.49—8.11 (m, 4H). Found: C, 72.61; H, 4.55%. Calcd for $C_{13}H_{10}O_3$: C, 72.89; H, 4.71%.

The authors wish to thank Mr. Kazutoshi Yamasaki and Miss. Keiko Kurahashi for their assistance in carring out some of the experiments.

References

1) W. M. Horspool, *Quart. Rev.* (London), **23**, 204 (1969); R. H. Thomson, "Synthesis," and K. T. Finley, "The Addition and Substitution Chemistry of Quinones," in "The Chemistry of the Quinonoid Compounds," ed by S. Patai, John Wiley (1974), Part 1, pp. 116—161 and Part 2, pp. 878—1126.

2) R. W. A. Oliver, R. M. Rashman, and A. W. Somerville, *Tetrahedron*, **24**, 4067 (1968).

3) M. Matsuoka, *Yuki Gosei Kagaku Kyokai Shi*, **40**, 114 (1982) and references cited therein.

4) K. Mita, T. Yamagishi, and M. Hida, *Nippon Kagaku Kaishi*, **1980**, 1855.

5) T. Tanaka, R. Tajima, and W. Ando, *J. Org. Chem.*, **48**, 4764 (1983).

6) The catalytic effect of water was observed in the nucleophilic addition of amines to esters. E. M. Arnett, J. G. Miller, and A. R. Day, *J. Am. Chem. Soc.*, **72**, 5635 (1950).

7) Actually, the reaction of 4-methoxy-1,2-naphthoquinone (**2a**) (0.4 mmol) with methanol (7 ml) in the presence of $CeCl_3 \cdot 7H_2O$ (0.4 mmol) and $NaIO_3$ (0.4 mmol) at room temperature for 15 h afforded 2-methoxy-1,4-naphthoquinone (**3**) in 70% yield.

8) P. J. Crowley reported that 9,10-phenanthrenequinone formed complexes with a range of transition metals. P. J. Crowley and H. M. Haender, *Inorg. Chem.*, **1**, 904 (1962).

9) Y. T. Pratt, *J. Org. Chem.*, **27**, 3905 (1962).

10) A. H. Blatt, *Org. Synth.*, Coll. Vol. II, 430 (1948).

11) H-J. Teuber and N. Gotz, *Chem. Ber.*, **87**, 1236 (1954).

12) L. F. Fieser and R. H. Brown, *J. Am. Chem. Soc.*, **71**, 3609 (1949).

 © 1986 The Chemical Society of Japan Bull. Chem. Soc. Jpn., 59, 2963—2968 (1986)

Studies on Special Type Surfactants. XVI. Preparation of Telomer-Type Surfactants Containing 4-Vinylpyridine and Oxidative Polymerization of 2,6-Xylenol Using Their Copper Complexes

Yoshifumi KOIDE,* Yasuyuki EDA, and Kimiho YAMADA
Department of Synthetic Chemistry, Faculty of Engineering, Kumamoto University, Kurokami, Kumamoto 860
(Received January 13, 1986)

The polymerization of 2,6-xylenol (XOH) was catalyzed by using a copper complex of a telomer-type surfactant containing 4-vinylpyridine, 1-benzyl-4-vinylpyridinium chloride, and methyl acrylate or styrene (L-VP-Q, L-VP-Q-MA, L-VP-St, and L-VP-Q-St). A copper complex of L2.5VP3.9Q2.2MA catalyzed an emulsion polymerization of XOH more than that of L-VP-Q, 4-vinylpyridine polymer (VP-Q), or pyridine. Furthermore, the oxidative polymerization of XOH in several organic solvents was more effective than emulsion polymerization. The copper complexes formed reversed-micelles in water (3—10 vol%)-DMSO, and the catalytic actions were in the following order: L-VP-Q>VP-Q>pyridine. The acceleration by the L-VP-Q complex was considered to be due to the adsorption of XOH on reversed micelles.

Telomer-type surfactants have been characterized by the terminal alkyl group and polyfunctional groups.[1] Telomer-type surfactants bearing 4-vinylpyridine and 1-benzyl-4-vinylpyridinium chloride (L-VP-Q), oriented at the interface of water and an immisible organic solution, emulsify these solutions.[2] The emulsion polymerization of XOH using the L-VP-Q–copper complex was more catalytically active than that using the corresponding polymer (VP-Q) complex or a pyridine(py) complex in a water–benzene solvent.[2]

The oxidative polymerization of XOH was studied in detail by Tsuchida et al. using a VP-Q polymer complex and several solvents.[3,4] The catalytic activity was accelerated by a nonpolar field in the polymer ligand[3] and the nonpolar solvent.[4] Therefore, a telomer-type surfactant is expected to be an excellent catalyst since the surfactant forms a nonpolar field consisting dodecyl groups; a highly condensed catalytic active site consists of pyridyl groups above the critical micelle concentration (cmc). However, the oxidative polymerization of XOH using a catalyst of a surfactant-copper complex has not yet been seen. In this study, cotelomer-type surfactants bearing 4-vinylpyridine, 1-benzyl-4-vinylpyridinium chloride, and methyl acrylate or styrene were prepared and the oxidative polymerization of XOH using their copper complexes were examined in comparison with the VP-Q polymer or the py ligand for obtaining information regarding the catalytic character of a telomer-type surfacant.

Experimental

Syntheses of Cotelomer-Type Surfactants. The L-VP-Q telomer-type surfactants and the VP-Q polymer were obtained as described in a previous paper.[2] The cotelomer-type surfactants bearing 4-vinylpyridine, 1-benzyl-4-vinylpyridinium chloride, and methyl acrylate (L-VP-Q-MA) or styrene (L-VP-Q-St) were derived from the corresponding 4-vinylpyridine cotelomers (L-VP-MA, L-VP-St).

The preparation of L-VP-Q-MA was as follows: 4-Vinylpyridine (26.3—27.3 g), methyl acrylate (15.5—54.2 g), and 0.5 wt% of 2,2′-azobisisobutyronitrile (per weight of the mixed monomers) were added to 1-dodecanethiol (30.3—44.4 g); then, the reaction mixture was stirred at 70 °C for 6 h. After cooling to room temperature, the light-brown L-VP-MA was precipitated by adding hexane to the solution mixture. The crude L-VP-MA was reprecipitated twice with hexane after dissolving in chloroform. Then, benzyl chloride (1.0—1.2 g) was added dropwise to 100 cm^3 of a 2% L-VP-MA methanolic solution and the mixture was refluxed for 24 h. After cooling to room temperature, the reaction mixture was poured into 200 cm^3 of ether. The resulting precipitate, L-VP-Q-MA, was filtered and rinsed with ether. The cotelomer-type surfactant-bearing 4-vinylpyridine, 1-benzyl-4-vinylpyridinium chloride, and styrene, L-VP-Q-St, was obtained with styrene instead of methyl acrylate by the same procedure as the preparation of L-VP-Q-MA.

The compositions of the cotelomers (L-VP-MA, L-VP-Q-MA, L-VP-St, and L-VP-Q-St) were determined by means of molecular-weight (Corona 114 vapor-pressure osmometer) and the analytical data of nitrogen from elementary analyses. Detailed descriptions for preparing L-VP-MA and L-VP-St were reported in a preceding paper.[5] Then, the L-VP-Q-MA and L-VP-Q-St that quaternized with benzyl chloride were confirmed by the pyridinium absorption at 1640 cm^{-1} in the IR spectrum and the benzyl peak of 7.2 ppm in the NMR spectrum. The quaternized percent was calculated from the absorption ratio of the IR spectrum[2] or the integrated values of the NMR spectrum. The benzyl chloride reacted with the pyridyl groups of L-VP-MA in 90—95% yields. The chemical formulas and the elementary analyses of the cotelomers are shown in Table 1. The calculated values of C, H, and N based on the chemical formulas agreed with the analytical data.

Polymerization of XOH. The polymerization rate was measured in terms of the oxygen consumption.[2] The polymerization of XOH in an organic solution was as follows: The copper ($CuCl_2$ or CuCl) complex of telomer-type surfactant and the equimolar sodium hydroxide dissolved in a 10 cm^3 of organic solution was added to a 10 cm^3 of organic solution containing the known amount of XOH in a 100 cm^3 flask. The mixed solution was thermostated at 30 °C and shaken until a termination of oxygen absorption. Then, the solution was first added to 450 cm^3 of methanol and the resulting diphenoquinone (DQ) was filtered out. Then, 50 cm^3 of 35%-hydrochloric acid was added to the methanol. The resulting polyphenylene oxide (PPO) was

Table 1. Elementary Analyses of Cotelomers

Cotelomer	Composition[a]	Calcd[b] (Found) (%)			Molecular weight (Found)
		C	H	N	
L4.0VP1.6MA	L-$VP_{4.0}$-$MA_{1.6}$	73.46 (73.63)	8.45 (8.60)	7.39 (7.25)	760 (749)
L6.4VP2.2MA	L-$VP_{6.4}$-$MA_{2.2}$-$H_2O_{0.2}$	73.89 (73.63)	7.98 (8.20)	8.41 (8.41)	1067 (1059)
L7.7VP9.4MA	L-$VP_{7.7}$-$MA_{9.4}$-$H_2O_{1.3}$	67.47 (67.90)	7.60 (7.72)	5.85 (5.85)	1842 (1820)
L6.8VP2.5St	L-$VP_{6.8}$-$St_{2.5}$-$H_2O_{2.0}$	78.90 (78.61)	8.12 (8.31)	7.86 (7.84)	1212 (1206)
L0.8VP3.2Q1.6MA	L-$VP_{0.8}$-$Q_{3.2}$-$MA_{1.6}$-$H_2O_{1.9}$	68.98 (68.08)	7.56 (7.42)	4.68 (4.60)	1198 (—[c])
L2.5VP3.9Q2.2MA	L-$VP_{2.5}$-$Q_{3.9}$-$MA_{2.2}$-$H_2O_{3.2}$	69.13 (68.55)	7.35 (7.12)	5.55 (5.19)	1614 (—[c])
L1.5VP6.2Q9.4MA	L-$VP_{1.5}$-$Q_{6.2}$-$MA_{9.4}$-$H_2O_{8.2}$	64.12 (63.28)	7.18 (7.13)	3.92 (4.55)	2750 (—[c])
L3.1VP3.7Q2.5St	L-$VP_{3.1}$-$Q_{3.7}$-$St_{2.5}$-$H_2H_{10.6}$	69.05 (68.81)	7.73 (7.18)	5.19 (5.18)	1835 (—[c])

a) L: $C_{12}H_{25}S$-; VP: -(CH_2CH)-; Q: -(CH_2CH)-; MA: -(CH_2CH)-; St: -(CH_2CH)-. b) Calculated values based on the composition. c) The molecular weight could not be measured because of the chloroform-insoluble compound.

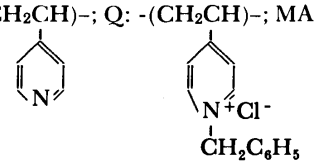

centrifuged, reprecipitated twice with a 35%-hydrochloric acid (10 vol%)-methanol (90) mixture after dissolving in chloroform, and dried.

Results and Discussion

Emulsion Polymerization of XOH. It is known that a plot of the volume of oxygen consumption against the amount of resulting PPO gives a straight line for a large excess of XOH.[6] Therefore, the polymerization rate can be determined by a measurement of the oxygen-consumption rate, with an error of about 2 $mm^3 min^{-1}$.

The emulsion polymerization of XOH using the L-VP-Q-copper complex was more catalytically active than that using the VP-Q polymer complex in a water–benzene solvent.[2] Moreover, the polymerization rate (66 $mm^3 min^{-1}$) using a L2.5VP3.9Q2.2MA complex which contains methoxycarbonyl groups was 1.4-times faster than that (47 $mm^3 min^{-1}$) using the L3.0VP5.0Q complex at pH 7.5. The acceleration was considered to be due to a slight increase in the nonpolarity formed by the methoxycarbonyl groups[3] in addition to the emulsification.[2] However, the resulting PPO were 3100—5100 of molecular weight and the by-product, DQ, yielded more than 10%. Consequently, the following polymerizations were carried out in a DMSO or a methanol–*o*-dichlorobenzene (DCB) mixture.

Oxidative Polymerization in DMSO. The high molecular weight of PPO and a small amount of DQ were obtained for the above-mentioned solvents by Tsuchida et al. using a VP-Q polymer complex.[7] The polymerization rate was accelerated under alkaline

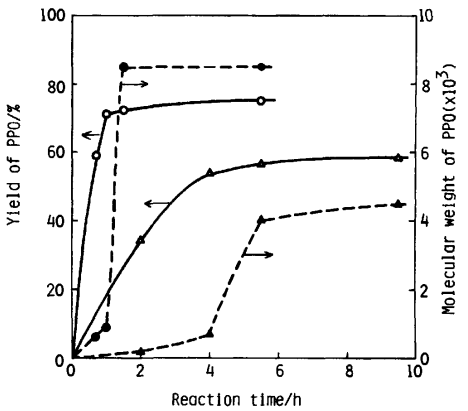

Fig. 1. Effect of reaction time.
XOH: 0.5 mol dm^{-3}; $CuCl_2$: 0.01 mol dm^{-3}; [VP unit]/[Cu]=2; [py]/[Cu]=20. Solvent: 20 cm^3 of water(10 vol%)-DMSO(90) mixture; Temp: 30°C; Oxidation: under aerobic conditions.
○,● L5.1VP8.7Q, △,▲ Pyridine.

conditions because of the low oxidation potential of XOH; however, a higher pH made the copper complex hydrolysis.[6] Therefore, equimolar sodium hydroxide was added to a copper complex.

The polymerization of XOH in a water (10 vol%)–DMSO(90) mixture was examined using the L5.1VP8.7Q or pyridine complex. The effects of the reaction time are indicated in Fig. 1. The yield of PPO increased with the passage of time, while the molecular weight of PPO increased steeply near the conclusion of the reaction (the oxygen consumption ceased). Therefore, the reaction was allowed to continue twice as long as

Table 2. Polymerizations in Water-DMSO Mixture

	Water	Polymerization rate	PPO Yield	PPO Molecular weight
	vol%	$mm^3 min^{-1}$	wt%	
L0.8VP3.2Q1.6MA	3	25.5	70	8000
L0.8VP3.2Q1.6MA	10	8.0	64	10700
L0.8VP3.2Q1.6MA	50	4.5	77	8000
L1.5VP6.2Q9.4MA	3	14.2	84	10300
L5.1VP8.7Q	10	18.8	65	14800
L5.1VP8.7Q	50	6.5	45	7700
62VP26Q	3	9.0	0[a)]	—[a)]
62VP26Q	10	6.8	0[a)]	—[a)]
62VP26Q	50	6.6	7	2000

a) XOH: 0.5 mol dm^{-3}; $CuCl_2$: 0.01 mol dm^{-3}; [VP unit]/[Cu]=1.5. Solvent: 20 cm^3 of water-DMSO mixture; pH: 13.5; Temp: 30 °C; Oxidation: under aerobic conditions. a) PPO did not precipitate from methanol, which molecular weight seemed low.

the time necessary for a consumption of oxygen (the polymerization rate reduced nearly to zero). PPO was yielded in 75% with the L5.1VP8.7Q complex and 58% with the pyridine complex, and DQ yielded in 6% with the L5.1VP8.7Q complex and 8% with the pyridine complex.

Then, the effect of the water content in a DMSO solution was examined (Table 2). On the whole, the polymerization rates were not so fast at pH 13.5 when the VP-unit ratio to copper was 1.5 (the Cu complex is not hydrolyzed). However, the polymerization rate using the surfactant-copper complex was highly affected by the water content: L0.8VP3.2Q1.6MA 25.5 mm^3 min^{-1} at 3 vol% water in DMSO, 26.0 $mm^3 min^{-1}$ at 5 vol%, 22.0 $mm^3 min^{-1}$ at 7 vol%, 8.0 $mm^3 min^{-1}$ at 10 vol%, and 4.5 mm^3 min^{-1} at 50 vol%. On the other hand, the polymerization rates using the 62VP26Q polymer complex were nearly constant in 3—50 vol% of water contents (9.0 $mm^3 min^{-1}$ at 3 vol%, 7.5 mm^3 min^{-1} at 5 vol%, 7.0 $mm^3 min^{-1}$ at 7 vol%, 6.8 mm^3 min^{-1} at 10 vol%, and 6.6 $mm^3 min^{-1}$ at 50 vol%). Similar results had been obtained by Tsuchida et al.[7] Usually, a surfactant in a nonaqueous solution tends to aggregate or to form reversed micelles, and the structure varies with the water content.[8] The cmc of L5.1VP8.7Q-copper complex was actually confirmed in a water (5vol%)-DMSO(95) mixture by conductometric titration (cmc 4.8×10^{-4} mol dm^{-3}); however, that of the L5.1VP8.7Q complex in a water (50 vol%)-DMSO (50) mixture and those of 34VP51Q complex in a water (5 vol%)-DMSO(95) and a water (50 vol%)-DMSO(50) mixture were not found. The XOH anion would adsorb on the cationic reversed micelles or the cationic aggregated-surfactants in 3—10 vol% of water contents. The K_1 (the reciprocal of the Michaelis constant K_m) calculated from the Lineweaver-Burk plots were py-Cu 22 $dm^3 mol^{-1}$,[7] VP-Q-Cu 190,[7] and L-VP-Q-Cu 800—900, which means the affinity of the catalyst for the substrate.[9] Therefore, the rate using the telomer-type surfactants would become fast in the 3—10 vol% of water contents because the XOH was more condensed to the reversed micelles (about 40-times that of py) in addition to the nonpolar effect of the dodecyl group. The catalytic action of L5.1VP6.2Q9.4MA was more active than that of L0.8VP3.2Q1.6MA in the water (3 vol%)-DMSO(97) mixture. This difference is probably due to the extent of nonpolarity based on the methoxycarbonyl groups.

Then, the repeated use of telomer-type surfactants was examined. L0.8VP3.2Q1.6MA, the less active catalyst, was used repeatedly for the oxidative polymerization of XOH in a half scale of the abovementioned concentration (Table 2). Then, 60 cm^3 of 0.25 M (M=mol dm^{-3}) XOH in water (3 vol%)-DMSO (97) mixture was polymerized by 5×10^{-3} M $CuCl_2$ and 6.3×10^{-2} M L0.8VP3.2Q1.6MA at 30 °C under aerobic conditions. After the oxidative polymerization, the reaction mixture was divided in two parts; 10-cm^3 of the reaction mixture was used for a determination of PPO and 50 cm^3 of the remainder was subjected for further polymerization: 10 cm^3 of 0.5-M XOH in water (3 vol%)-DMSO mixture was added to 50 cm^3 of the reaction mixture. The resulting PPO were first 4800 of molecular weight in 64% yield, second 4800 in 69%, and third 4200 in 62%. In spite of the half-scale concentration, and the L0.8VP3.2Q1.6MA-copper solution was then diluted in series, the three findings were similar. Furthermore, the other telomer-type surfactants were confirmed their repeating use in similar reactivities.

Solvent Effects. The catalytic action of the VP-Q polymer complex was much affected by the solvent polarity.[4] Therefore, the effects of solvent polarity were examined on the assumption that the dielectric constant of mixed solvent D is equal to the sum of the individual products of the dielectric constant of the mixing species and its volume ratio.[10] The polarity was expressed as a dielectric parameter E; $E=(D-1)(2D+1)^{-1}$,[11] The E values for the 3—50 vol% water in DMSO were 0.485—0.488 (Table 2). The tendency that the catalytic action increased with a decrease in the solvent polarity could be recognized, but the

Table 3. Effects of Solvents and Ligands on Polymerizations of XOH

Ligand	Polymerization rate	PPO Yield	PPO Reduced viscosity	DQ Yield
	$mm^3 min^{-1}$	wt%	($\eta_{sp}C^{-1}$)	wt%
Water (10 vol%)-DMSO(90) E=0.486				
L5.1VP8.7Q	70	75	0.24	10
L0.8VP3.2Q1.6MA	26	66	0.12	6
L-VP-Q-St	29	54	0.13	6
34VP51Q	25	0[a]	—[a]	0
py	20	58	0.15	8
MeOH(10 vol%)-DCB(90) E=0.441				
L5.1VP8.7Q	85	74	0.33	9
L-VP-Q-St	200	65	0.25	10
34VP51Q	70	62	0.16	6
py	60	62	0.78	4
MeOH(10 vol%)-DMSO(90) E=0.484				
L5.1VP8.7Q	23	45	0.05	9
MeOH(10 vol%)-Bz(90) E=0.371				
L5.1VP8.7Q	100	63	0.31	8

XOH: 0.5 mol dm^{-3}; $CuCl_2$: 0.01 mol dm^{-3}; [VP unit]/[Cu]=2. Volume: 20 cm^3; Temp: 30°C: Oxidation: under aerobic conditions. a) PPO did not precipitate from methanol.

Table 4. Polymerizations of XOH by Cu(II) Complexes in MeOH-DCB-py Mixture

Ligand	Solvent Composition vol%			Dielectric parameter (E)	Polymerization rate	PPO Yield	PPO Reduced viscosity	DQ Yield
					$mm^3 min^{-1}$	wt%	($\eta_{sp}C^{-1}$)	wt%
	(MeOH-DCB-py)							
L5.1VP8.7Q	10	90	0	0.441	85	74	0.33	8
L5.1VP8.7Q	10	87	3	0.441	100	80	0.74	4
L5.1VP8.7Q	10	10	80	0.449	64	59	0.43	2
None	10	87	3	0.441	0[a]	—[a]	—[a]	0
None	10	10	80	0.449	106	58	0.11	0.4

XOH: 0.5 mol dm^{-3}; $CuCl_2$: 0.01 mol dm^{-3}; [VP unit]/[Cu]=2. Volume: 20 cm^3; Dielectric parameter $E\{=(D-1)(2D+1)^{-1}\}$: 0.441, 0.449; Temp: 30°C; Oxidation: under aerobic conditions. a) PPO did not precipitate from methanol.

range of the E values was too narrow to discuss. The polymerization using the L-VP-St complex was examined in a py(20 vol%)-organic solvent (80) mixture; E value: py-benzene (Bz) 0.342, py-chlorobenzene (CB) 0.399, py-DCB 0.431, and py-nitrobenzene (NB) 0.476. The polymerization rate decreased with an increase in the solvent polarity, while the reduced viscosity of PPO was independent of the solvent polarity in the E range 0.342—0.476.

Then, the catalytic actions in a water (10 vol%)-DMSO (90) mixture (E 0.486) and in a MeOH (10 vol%)-DCB (90) mixture (E 0.441) were examined (Table 3). The polymerization rates of XOH in an MeOH-DCB mixture were higher than that in a water-DMSO mixture. Moreover, the catalytic actions in an MeOH (10 vol%)-DMSO (90) mixture (E 0.484) and in an MeOH (10 vol%)-Bz (90) mixture (E 0.371) were evaluated by using the L5.1VP8.7Q complex. The polymerization rates were as follows: In MeOH-Bz > MeOH-DCB > water-DMSO > MeOH-DMSO. The order of these rates was according to the order of solvent polarities, except for the water-DMSO mixture. It was proven by Tsuchida et al. that the rate-determining step for the oxidative polymerization of XOH using the VP-Q polymer complex was the reoxidation step in a polar solvent and was the electron-transfer step in a nonpolar solvent. Also, the total polymerization rate was fast in a nonpolar solvent.[4] However, the rate using the L5.1VP8.7Q complex in a polar water-DMSO mixture was higher than that in a less polar MeOH-DMSO mixture. The cmc of L5.1VP8.2Q complex in 3—10 vol% water in DMSO was found but that in an MeOH-DMSO mixture was not. Therefore, the higher rate in the water-DMSO mixture was presumably due to the concentration of XOH to the reversed-micelles. In these solvents the polymerization rate using the L5.1VP8.7Q, L0.8VP3.2Q1.6MA or L-VP-Q-St complex was faster than that using the 34VP51Q or pyridine complex because of the large aggregation.

Effect of Pyridine. The oxidative polymerization of XOH was considerably affected by adding pyridine.[4] The catalytic actions in MeOH-DCB-py solutions are shown in Table 4. Although the E values of these solutions are nearly equal to 0.44 (0.441—0.449), the polymerization rate and the reduced viscosity of PPO

Table 5. Polymerizations of XOH by Cu(I) Complexes in MeOH-DCB-py Mixture

Ligand	Solvent vol%			Polymerization Rate	Time	PPO Yield	PPO Reduced viscosity	DQ Yield
				$mm^3 min^{-1}$	h	wt%	($\eta_{sp}C^{-1}$)	wt%
	(MeOH-DCB-py)							
L5.1VP8.7Q	20	70	10	70	2	75	0.74	4
L5.1VP8.7Q	50	40	10	80	2	72	0.51	7
L5.1VP8.7Q	80	10	10	76	2	68	0.38	8
34VP51Q	20	70	10	120	1	73	0.69	4
34VP51Q	50	40	10	99	1	61	0.48	7
34VP51Q	80	10	10	66	2	47	0.20	9
None	20	70	10	255	0.7	77	0.57	4
None	50	40	10	160	1	60	0.49	7
None	20	60	20	70	3	63	0.55	4
None	20	50	30	10	10	82	0.69	5
	(MeOH-CB-py)							
L5.1VP8.7Q	20	70	10	146	1.3	77	0.75	3
None	20	70	10	430	0.5	79	0.62	4
	(MeOH-Bz-py)							
L5.1VP8.7Q	20	70	10	205	1	78	0.79	3
None	20	70	10	520	0.3	79	0.66	3

XOH: 0.2 mol dm^{-3}; CuCl: 5×10^{-3} mol dm^{-3}; [VP unit]/[Cu]=2. Volume: 40 cm^3; Temp: 30 °C; Oxidation: under oxygen atmosphere.

using the L5.1VP8.7Q complex increased at 3 vol% of the pyridine content. A similar result was also obtained upon using the L-VP-St complex. On the other hand, the catalytic actions without the telomer-type surfactants were, on the whole, less. Catalysts for the oxidative polymerization of XOH are known to possess the following structures:[4,12]

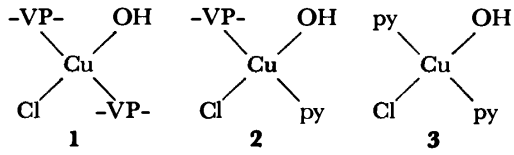

Presumably, the **2** that formed upon adding pyridine (3 vol%) was easier to use for forming complexes with XOH than **1** with a rigid structure; also, oxygen was more easy of access to the resulting **2**-XOH complex because of less steric hindrance.[12] Consequently, the addition of pyridine would accelerate the polymerization rate. However, in a large excess of the pyridine content (80 vol%) the polymerization rate using the L5.1VP8.7Q complex was slow and the reduced viscosity of PPO was low. By a further addition of pyridine, the structure of **2** could be converted to the inactive structure VP-$CuCl(py)_2$ etc. Similarly, the polymerization rate became slow when the VP-unit ratio in the L0.8VP3.2Q1.6MA to the copper was increased, i.e., 31.9 $mm^3 min^{-1}$ at ratio 5, 4.6 mm^3 min^{-1} at ratio 7, and 1.8 $mm^3 min^{-1}$ at ratio 10. On the other hand, the rate without the L5.1VP8.7Q in the 3 vol% of pyridine content was very slow and the rate in the 80 vol% of pyridine content was fast but the reduced viscosity was very low. The structures would be CuCl(OH)py and **3** or $CuCl(py)_3$.

Polymerization under Oxygen Atmospere. The polymerization of XOH was examined by using a Cu(I) complex under an oxygen atmosphere instead of the Cu(II) complex under aerobic conditions (Table 5). The polymerization rates using the 34VP51Q polymer and the pyridine monomer complexes were very fast in comparison with that using the L5.1VP8.7Q telomer complexes. Their catalytic actions in MeOH-DCB-py solutions became more active at a lower MeOH content and the order of the catalytic actions was in MeOH-Bz-py>MeOH-CB-py>MeOH-DCB-py. The polymerization-rate ratio (using L5.1VP8.7Q to the rate using the pyridine complex in the MeOH-DCB-py (10 vol%) mixture) was larger than the ratio in the MeOH-CB-py or the ratio in the MeOH-Bz-py mixture. The Cu(I) complex of a telomer-type surfactant would aggregate or form reversed-micelles in these solutions. The approach of oxygen to the surfactant complex would be more difficult than the pyridine complex because of a steric hindrance, even if the oxygen pressure increased. Then, the rate-determining step in a polar solvent was the reoxidation step and that in a nonpolar solvent was the electron-transfer step.[4] Therefore, the dependence of the polymerization rate on the catalyst in the more polar solvent (MeOH-DCB-py) would be larger than that in the more nonpolar solvent (MeOH-Bz-py). Nevertheless, the reduced viscosity of PPO using the L5.1VP8.7Q complex was the highest in the MeOH-DCB-py mixture. Furthermore, the increase of pyridine made the polymerization rate slow, but made the reduced viscosity high. The structure of the complex would become **3**. Naturally, the polymerization rate

Table 6. Effects of Hexadecyltrimethylammonium Bromide

Ligand	HTAB	Polymerization rate	PPO Yield	PPO Reduced viscosity	DQ Yield
	mol dm^{-3}	mm^3 min^{-1}	wt%	($\eta_{sp}C^{-1}$)	wt%
L5.1VP8.7Q	0	70	75	0.74	4
L5.1VP8.7Q	0.025	26	76	0.86	5
34VP51Q	0	120	73	0.69	4
34VP51Q	0.025	28	69	0.85	3
None	0	255	77	0.57	4
None	0.025	32	78	0.67	4

XOH: 0.2 mol dm^{-3}; CuCl: 5×10^{-3} mol dm^{-3}; [VP unit]/[Cu]=2. HTAB: hexadecyltrimethylammonium bromide; Solvent: 40 cm^3 of MeOH(20 vol%)-DCB(70)-py(10) mixture; E: 0.451; Temp: 30°C; Oxidation: under oxygen atmosphere.

increased under an oxygen atmosphere, and the rate when using the telomer-type surfactant was relatively disadvantageous in comparison with the rate when using pyridine. However, the characters of the telomer-type surfactants for the polymerization of XOH were substantially similar to that under aerobic conditions.

Then, the effects of hexadecyltrimethylammonium bromide (HTAB) on the oxidation polymerization of XOH were examined (Table 6). By the addition of HTAB, the reduced viscosity of PPO became high. However, the yields of PPO and DQ were nearly constant, and all the polymerization rates became slow (about 30 mm^3 min^{-1} while the reaction time became long). These results suggested that the HTAB interfered with the formation of catalyst–XOH complex because the HTAB attracted the XOH anions, and that the HTAB kept the growing PPO highly dispersed.

References

1) K. Yamada and Y. Koide, *Yukagaku*, **30**, 2 (1981).

2) K. Yamada, Y. Koide, M. Kinno, and H. Shosenji, *Nippon Kagaku Kaishi*, **1980**, 1875.

3) E. Tsuchida, H. Nishikawa, and E. Terada, *J. Polym. Sci., Polym. Chem. Ed.*, **14**, 825 (1976).

4) H. Nishide, H. Nishikawa, and E. Tsuchida, *Nippon Kagaku Kaishi*, **1974**, 771; H. Nishide, H. Nishikawa, and E. Tsuchida, *ibid.*, **1974**, 809.

5) K. Yamada, Y. Koide, M. Sakiyama, and I. Sakuma, *Yukagaku*, **34**, 1021 (1985).

6) M. Kaneko, H. Nishide, E. Tsuchida, *Kogyo Kagaku Zasshi*, **74**, 1194 (1971).

7) E. Tsuchida, H. Nishide, and T. Nishiyama, *Nippon Kagaku Kaishi*, **1974**, 784.

8) A. Kitahara, *Yukagaku*, **9**, 169 (1960); **11**, 613 (1962); **17**, 140 (1968).

9) E. Tsuchida, M. Kaneko, and H. Nishide, *Makromol. Chem.*, **151**, 221 (1971).

10) N. Tokura, *Yuuki Gosei Kagaku Kyokai Shi*, **21**, 598 (1963).

11) R. W. Alder, R. Baker, J. M. Brown, "Mechanism in Organic Chemistry," John Wiley & Sons., (1971), p. 44.

12) E. Tsuchida, M. Kaneko, H. Nishide, and S. Nishi, *Kogyo Kagaku Zasshi*, **74**, 2370 (1971).

 © 1986 The Chemical Society of Japan Bull. Chem. Soc. Jpn., 59, 2969—2971 (1986)

The Enantioselective Hydrogenation of Methyl Levulinate on the Interactive and Noninteractive Sites of Nickel Surfaces with Preadsorbed Asymmetric Compounds

Michio Yokozeki, Kazuo Shimokoshi, and Eizo Miyazaki*
Department of Chemistry, Tokyo Institute of Technology, 2-12-1, Ohokayama, Meguro-ku, Tokyo 152
(Received February 2, 1986)

The gaseous hydrogenation of methyl levulinate on the Ni surface modified with the optically active tartaric, malic and lactic acids was studied. It was found that γ-valerolactone is formed on an unmodified surface, while optically active methyl 4-hydroxypentanoate [MHP] and γ-valelolactone [VL] are formed consecutively on modified surfaces. Using these results and the temperature dependency of the reaction rates, along with previous theoretical results [*J. Phys. Chem.*, **89**, 2397 (1985)], it was concluded that, on an Ni surface modified with preadsorbed optically active acids, there are two different and independently operative sites, i.e., noninteractive (nonselective) and interactive (selective) sites which give the enantioselectivity. Further, the fractions of the noninteractive sites in the total amount of active sites were estimated to be about 18 and 13% for TA- and MA-modified surfaces respectively. A similar character of the active sites was found for the enantioselective hydrogenation of methyl acetoacetate [MAA] to methyl 3-hydroxybutyrate [MHB] on TA-modified Ni, where the fraction of noninteractive sites was evaluated to be about 15%.

It is known that such transition metal catalysts as Ni, when an optically active molecule such as tartaric acid is preadsorbed on their catalyst surfaces, become enantioselective for the hydrogenation of methyl acetoacetate.[1-3] Two different mechanisms for this selectivite reaction have been proposed as important processes on the surface:[3,5,6] (1) The complex formation with the substrate and modifiers,[4,5] and (2) the control of the orientations of the reactants by rather strong interaction between reactants and modifiers. In the previous theoretical studies based on the molecular orbital calculations with the MNDO method,[7] it was predicted that the hydrogen-bond-like interactions between reactants and preadsorbed hydroxy acids can control the form of the reactants on the surface.

On the other hand, as has been reported by Harada et al. in their study of liquid phase reactions,[8] the enantioselectivity of these systems is dependent upon the nature of the surface sites on which the reaction occurs; i.e., the high enantioselectivity is expected only from the reactions on the appropriately modified surface sites. In fact, the low-pressure gaseous hydrogenation of methyl acetoacetate (MAA) on the modified Ni surface provided an optical yield of, at most about 50%.[3] Therefore, in order to clarify the enantio-face-differentiating activity of the catalysts, it is desirable to obtain detailed knowledge of the processes occurring on both modified and unmodified surface-active sites. Harada et al. have clarified, using KBr as the site selective preadsorber in the modifier solution, that the Raney-Ni surface has two kinds of sites, i.e., effective and noneffective sites for the enantioselectivity.[8]

In the present work we investigated the hydrogenation of methyl levulinate (ML) on a nickel catalyst with and without the modification of optically active hydroxy acids, and found that the products formed on modified surfaces were different from those on an unmodified nickel surface. Using this reactant, we could obtain an insight into the processes on the modified surface. Further, this information on the surface sites of the modified Ni could be made use of in giving reasonable interpretations to the enantioselective hydrogenation of MAA in the gas phase, because the hydrogenation of MAA produced only methyl 3-hydroxybutylate (MHB) on both surfaces of Ni.

In the present paper, first we will describe the results of the enantioselective hydrogenation of methyl levulinate on nickel surfaces modified with various optically active hydroxy acids, and then the results obtained by applying a similar method to the analyses of the enantioselective hydrogenation of MAA to MHB.

Experimental

The apparatus used for the preparation of the catalysts and the reaction was the same as that reported previously.[3a] The modifiers used were (*R,R*)-tartaric acid (TA), (*S*)-malic acid (MA), (*S*)-3-hydroxybutyric acid (HBA), and (*S*)-lactic acid (LA). The modification was made by introducing 0.1 mol l^{-1} solutions of hydroxy acids at room temperature into a reaction cell which contained the nickel previously reduced by hydrogen. The pH of the modifier solutions was controlled at 5.0 by the use of sodium hydroxide. After 1.5 h of contact, the catalyst was washed by deaired methanol in a storage area attached to the cell. These processes were performed in the vacuum system.

Hydrogen of 2.66×10^4 Pa was circulated through the liquid ML (or MAA) storage, and a gaseous mixture of H_2 and the reactants was introduced into the reaction cell. The partial pressure of the ML vapour was 90 Pa. The reaction rates of hydrogenation were monitored by the change in the total pressure. The products were collected by means of liquid-nitrogen trap and analyzed by the use of a gas chromatograph (Yanagimoto G2800-F) using a 200 cm glass column packed with polyethylene glycol 20M (20%) on Celite 545 at 110 C. The optical rotation of the products was measured by means of a Yanagimoto OR-50 polarimeter.

Two different products, methyl 4-hydroxypentanoate (MHP) and γ-valerolactone (VL), were obtained by the hydrogenation of ML on TA-modified Ni. The optical yield

Table 1. Rates of the Product Formation, Ratioes of MHP in the Products and the Relative Rates [$\%r=(100-\%\mathrm{MHP})R_1/R_2$] of Nonselective Sites on Unmodified, TA-, and MA-modified Ni

Reaction temperature	Unmodified Ni		TA-modified Ni			MA-modified Ni		
	Rate(R_1)	MHP	Rate(R_2)	MHP	r[a)]	Rate(R_2)	MHP	r[a)]
K	$\times10^{-11}$	%	$\times10^{-11}$	%	%	$\times10^{-11}$	%	%
323	4.8	<0.5	2.8	68	18.6	1.7	64	12.7
333	6.6	<0.5	3.6	67	18.0	2.4	63	13.4
343	9.9	<0.5	4.7	62	18.0	3.3	61	13.0
353	13.0	<0.5	6.0	58	18.9	4.2	57	13.5

a) % fraction of nonselective sites [$=(100-\%\mathrm{MHP})R_1/R_2$].

Table 2. Optical Rotation of the Products Befoere and After Conversion and the Enantioselectivities [ES (%e.e.)]

Reaction temperature	Before conversion			After conversion		
	[α][a)]	MHP	VL	[α][a)]	VL	ES[b)]
K		%	%		%	%
322	−0.16	14.0	4.0	+0.22	12.3	5.1
343	−0.24	18.3	7.5	+0.36	21.8	4.7

a) Optical rotation. b) Enantioselectivity (% enantio excess).

of the products was calculated based on the value of $[\alpha]_D^{22}=-35.1$ (neat) for (*S*)-γ-valerolactone.[9] In the present experiments, in order to obtain the optical rotation accurately, the mixture was heated with Amberlyt 15 to convert all the MHP to VL. The enantioselectivities, ES, were defined as the percentage of enantiomer excess in the products.

Results and Discussion

In the hydrogenation of ML on TA-modified Ni catalysts at 323 to 353 K, two kinds of products, methyl 4-hydroxypentanoate (MHP) and γ-valerolactone (VL), were obtained, whereas on an unmodified Ni surface nearly 100% of the ML was converted to VL. The following consecutive mechanism, consisting of two steps, I and II, has been reported for this reaction on the surface.[10]

$$\underset{\text{ML}}{CH_3\overset{\overset{O}{\|}}{C}CH_2CH_2COOCH_3} + H_2 \xrightarrow{\text{I}}$$

$$\underset{\text{MHP}}{CH_3\underset{\underset{OH}{|}}{CH}CH_2CH_2COOCH_3} \xrightarrow{\text{II}} \underset{\text{VL}}{CH_3\overset{\overset{O}{\diagup\diagdown}}{CH}\underset{\underset{CH_2-CH_2}{|\quad|}}{CO}} + CH_3OH$$

The ratio of MHP to the total products (VL+MHP) was about 60—70% in the former case, it decreased gradually with the increase in the reaction temperature. The hydrogenation character on Ni modified with other hydroxy acids, such as MA, LA, and HBA, was similar to that on TA-modified Ni; the ratios of MHP at 323 K were 69 (TA), 64 (ML), 62 (LA), and 60% (HBA). However, the enantioselectivity observed on ML modified Ni was less than that on TA-modified Ni, and on LA- and HBA-modified Ni the enantioselectivities were too low to be detected. The observed reaction rates at various temperatures on the unmodified (R_1) and modified (R_2) catalysts and also the % MHP in the products on Ni modified with TA and MA are compared in Table 1.

Unfortunately, the quantity of MHP in the gas-phase-reaction products was not large enough to measure the rotation of MHP and VL separately, and the optical rotation of MHP has not been reported. The optical rotations of the products were, therefore, measured before and after all the MHP, obtained initially, had been converted thermally into VL. Table 2 lists the optical rotations, the proportions, and the optical yield of the products. As may be seen in the table, the optical rotation was opposite in direction for the samples before and after the conversion. Since the rotating directions of VL and MHP in the same configuration are opposite to the reported value, $[\alpha]_D^{24}=+10.5$, for the related acid [(*S*)-4-pentanoxiacid] of MHP, the observed change indicates that (*R*)-MHP was formed on the modified surface and converted to (*R*)-VL by thermal treatment. The effect of the preadsorbed optically active hydroxy acids on the enantioselectivity is, therefore, apparent, even though their optical yields are not very high.

Figure 1 shows the variations in the rates of the product formation on the unmodified and TA- or MA-modified Ni surfaces with the reaction temperature. It may be seen that the apparent activation energy (33 kcal†mol^{-1}) obtained for VL formation on the unmodified Ni was very close to those on the TA- and MA-modified Ni, i.e., 33 and 31 kcal mol^{-1} respectively, while the energies for MHP on the two

† 1 cal=4.184 J.

Table 3. Rates, Enantioselectivities and r Values for MAA Hydrogenation to MHB on TA-modified Ni

Reaction temperature	Unmodified Ni Rate	TA-modified Ni Rate	ES	r
K	$\times 10^{-11}$	$\times 10^{-11}$	%	%
323	23.5	6.6	45.0	15
333	38.0	10.1	43.2	15
343	60.0	14.4	39.1	15
353	90.0	19.0	38.0	13

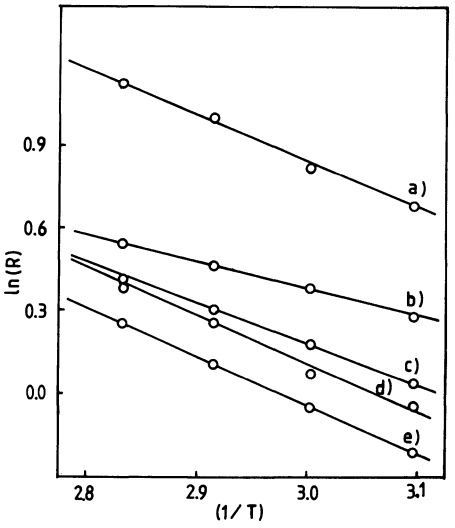

Fig. 1. The variation of the rate of the product formation as a function of reciprocal reaction temperature.
R: The rate of the formation ($\times 10^{-11}$ molecules $s^{-1} cm^{-2}$).
a) VL formation on unmodified Ni, b) MHP on TA-modified Ni, c) MHP on TA-modified Ni, d) VL on TA-modified Ni, and e) VL on MA-modified Ni.

surfaces modified with TA (18 kcal mol^{-1}) and MA (28 kcal mol^{-1}) were quite different. These results, therefore, strongly suggest that the nature of the reaction for the formation of VL is similar on both unmodified and modified surfaces. Further, in order to estimate the fraction of the surface sites for VL formation in the total amount of active sites for the hydrogenation, the value $\%r=(100-\%MHP)R_1/R_2$ was calculated at each temperature. The values, shown in Table 1, were found to be independent of the reaction temperature, but dependent on the modifiers used, i.e., about 18 and 13% for TA- and MA-modified surfaces respectively.

These results suggest that MHP and VL are formed on different surface sites. On the nickel surfaces modified with the preadsorbed hydroxy acids, there might be two different and independently operative sites, (a) the "interactive" (selective) and (b) "noninteractive" (nonselective) sites. In the hydrogenation of ML on the interactive sites, the reaction may cease at Step I to form MHP, while the reaction proceeds further to Step II on such noninteractive sites as the bare nickel surfaces.

On the other hand, Table 3 summarizes the rates and enantioselectivities obtained for the hydrogenation of methyl acetoacetate (MAA) to methyl 3-hydroxybutyrate (MHB) on TA-modified Ni. It can reasonably be assumed that, in the enantioselective hydrogenation of MAA on modified nickel surfaces, the reaction proceeds on the interactive sites, where the reactants are controlled by neighboring preadsorbed hydroxy acid molecules to form an optically active product preferentially.[7] Therefore, the fraction of the noninteractive sites of a modified surface can be estimated in a manner similar to that described above; i.e., by dividing the rate of the nonstereospecific reaction on TA-modified catalyst by that on the corresponding unmodified catalyst at each temperature. The calculated results are listed in Table 3. The values ($\%r$), as expected, were found to hold almost constant (15%) throughout the reaction temperatures.

In conclusion, Ni surfaces modified with optically active acids are divided into interactive and noninteractive parts. The fraction of the noninteractive sites in the total amount of active sites is in the range of 10 to 20%, depending on the modifiers used. These sites seem to exist independently; thereby, it may be suggested that one can suppress the reaction rate on noninteractive sites using some appropriate reagents which cover the noninteractive sites preferentially.

References

1) Y. Izumi, *Angew. Chem. Int. Ed.*, **10**, 871 (1971).
2) Y. Izumi, *Adv. in Catal.* **32**, 250 (1983).
3) a) I. Yasumori, M. Yokozeki, and Y. Inoue, *Faraday Discus. Chem. Soc.*, **72**, 385 (1981); b) Y. Nitta, T. Imanaka, and S. Teranishi, *J. Catal.*, **80**, 31 (1983).
4) E. I. Klabunovskii, A. A. Vadenyapin, E. I. Karpeiskaya, V. A. Pavlov, and N. D. Zelinskii, *Proc. Int. Congr. Catal.*, **7**, 1980, 390.
5) A. Hoek and W. M. H. Sachtler, *J. Catal.*, **58**, 2376 (1979).
6) A. Tai, T. Harada, Y. Hiraki, and S. Murakami, *Bull. Chem. Soc. Jpn.*, **56**, 1414 (1983).
7) M. Yokozeki, K. Shimokoshi, and E. Miyazaki, *J. Phys. Chem.*, **89**, 2397 (1985).
8) T. Harada, M. Yamamoto, S. Onaka, M. Imaida, H. Ozaki, A. Tai, and Y. Izumi, *Bull. Chem. Soc. Jpn.*, **54**, 2232 (1981).
9) H. Minato, *Chem. Pharm. Bull.*, **9**, 625 (1961).
10) R. W. Thomas, H. A. Schuette, and M. A. Cowley, *J. Am. Chem. Soc.*, **53**, 3861 (1931).

 © 1986 The Chemical Society of Japan Bull. Chem. Soc. Jpn., 59, 2973—2978 (1986)

Solubilities and Free Energies of Transfer for Lanthanoid Iodates in Dimethyl Sulfoxide-Water Mixtures

Hiroshi Miyamoto,* Hiroko Iijima, and Masako Sugawara
Department of Chemistry, Faculty of Education, Niigata University, Ikarashi-2, Niigata 950-21
(Received February 14, 1986)

The solubilities of lanthanoid iodates in dimethyl sulfoxide (DMSO)-water mixtures at 25 °C were measured. Thirteen lanthanoid iodate dihydrates $Ln(IO_3)_3 \cdot 2H_2O$ (Ln=Ce, Pr, Nd, Sm, Eu, Gd, Tb, Dy, Ho, Er, Tm, Yb, and Lu) were used. From the measured solubilities, the Gibbs free energies of the transfer of the iodates from water into aqueous DMSO solutions were calculated. The tetrad effect behavior reported by Peppard et al. was observed in both the variation with the lanthanoid atomic number of the solubility data and that with the atomic number of the free energies of transfer. The tetrad effect behavior seems to depend on a change in the solvation of the lanthanoid ions in variation with the crystal radii of the trivalent lanthanoid ions. In each system the logarithm of the solubility of the iodates decreases almost linearly with the reciprocal of the dielectric constant of the mixtures, as is expected from the Born equation or its modification when dealing with mixtures with narrow dielectric constant, ranging between 78.5 and 78.0.

As is well-known, variations in the thermodynamic data regarding lanthanoid(III) ions in aqueous solutions show no simple correlation with the crystal radii of the trivalent cations. A plot of the thermodynamic data as a function of the radius often exhibits a break somewhere in the middle of the lanthanoid series. For example, a plot of the stability constants of many lanthanoid complex systems against the lanthanoid atomic number shows a gadolinium break.[1,2] Peppard et al.[3] have reported that in certain liquid-liquid extraction systems the behavior of lanthanoid(III) ions has been interpreted in terms of four tetrads, rather than in terms of two octads. The tetrad effect proposed by Peppard et al. has been theoretically studied by Nugent.[4] He stated that the effect originates mainly from the quantum mechanical interelectronic repulsion energy of the q electrons in a $4f^q$ electron configuration.

Siekierski and Salomon[5,6] have studied the thermodynamic behavior of the solubility phenomena using recently published critically evaluated solubility and activity data of lanthanoid nitrates. They stated that the variations of the thermodynamic and congruent melting points as a function of atomic number can be interpreted mainly in terms of changes in the inner-sphere coordination number for both solid hexahydrates and aquo ions. Bertha and Choppin[7] have measured the heats of solution and the solubilities of the lanthanoid iodates in water at 25 °C and from these data the thermodynamic parameters of hydration were calculated. They proposed that the variations of the entropies of hydration across the lanthanoid series support the suggestion of a change in the hydration number of the lanthanoid ions somewhere in the middle of the series.

The lanthanoid iodates were chosen for this study of the solubility phenomena for several reasons. For all of the lanthanoid iodates except lanthanum and promethium salts their dihydrates could be prepared. Their relative insolubility allowed an easy determination of the solubility product values. They exhibited desirable precipitation characteristics with no evidence of colloidal suspension.

The solubility data of lanthanoid iodates in water at 25 °C except those of cerium, promethium and lutetium iodates have been reported by Firsching and Paul.[8] Bertha and Choppin[7] have also measured the solubilities of the iodates in water at 25 °C except that of promethium iodate. However, the solubilities of lanthanoid iodates in a variety of binary solvent mixtures have not yet been studied systematically. Monk[9,10] measured the solubilities of lanthanum iodate only in various solvent mixtures, and discussed the relation between the solubility of the iodates and the dielectric constant of aqueous solvent mixtures. Miyamoto, Shimura, and Sasaki[11] have reported the solubilities of lanthanoid iodates except lanthanum and promethium iodates in aqueous methanol media and in aqueous ethanol media. They also pointed out that the neodymium and erbium breaks appeared in addition to the gadolinium break in these systems.

In this study, the solubilities of thirteen iodates of the lanthanoid series in dimethyl sulfoxide (DMSO)-water mixed solvents were measured. From the solubility data, the Gibbs free energies of transfer from water into aqueous DMSO solutions were calculated. The dependence of the solubility of the lanthanoid iodates in aqueous aprotic solvent mixtures on the crystal radii of trivalent lanthanoid ions and on the lanthanoid atomic number was studied, and the dependence of the free energies of transfer on those was also considered.

Experimental

Preparation of Lanthanoid Iodates. The lanthanoid iodates were prepared by a dropwise addition of both the acidic solutions of lanthanoid nitrates and the aqueous potassium iodate solution. The agreement between the chemically found and the theoretically calculated values for dihydrate salts was within ±0.5 %. The results of chemical analyses of the prepared iodates were supported by thermal analyses.

Preparation details and analytical methods of the iodates

Table 1. Solubility of Lanthanoid Iodates in Dimethyl Sulfoxide-Water Mixtures at 25 °C

DMSO mass%	DMSO mol%	Dielectric constant	Solubility 10^3 mol dm^{-3}			
			$Ce(IO_3)_3$	$Pr(IO_3)_3$	$Nd(IO_3)_3$	$Sm(IO_3)_3$
0(This work)		78.54[a]	1.963±0.001	1.098±0.001	1.044±0.001	0.771±0.002
0(Ref. 11)		78.40[b]	1.96	1.12	1.03	0.82
5.03	1.21	78.31[a]	1.495±0.003	0.881±0.006	0.855±0.001	0.631±0.001
10.03	2.51	78.07[a]	1.261±0.002	0.733±0.003	0.693±0.001	0.518±0.001
20.09	5.48	77.42[a]	0.905±0.001	0.493±0.001	0.476±0.001	0.359±0.001
40.03	13.34	76.01[a]	0.428±0.001	0.226±0.008	0.209±0.001	$0.164\pm0.000_3$
			$Eu(IO_3)_3$	$Gd(IO_3)_3$	$Tb(IO_3)_3$	
0(This work)		78.54[a]	0.782±0.003	0.893±0.002	0.933±0.001	
0(Ref. 11)		78.40[b]	0.79	0.88	0.93	
5.03	1.21	78.31[a]	0.647±0.003	0.747±0.002	0.776±0.001	
10.03	2.51	78.07[a]	$0.534\pm0.000_2$	$0.614\pm0.000_4$	0.627±0.001	
20.09	5.48	77.42[a]	$0.369\pm0.000_2$	$0.422\pm0.000_4$	0.427±0.001	
40.03	13.34	76.01[a]	0.166±0.001	$0.185\pm0.000_3$	0.177±0.001	
			$Dy(IO_3)_3$	$Ho(IO_3)_3$	$Er(IO_3)_3$	
0(This work)		78.54[a]	1.010±0.001	1.162±0.001	$1.379\pm0.000_1$	
0(Ref. 11)		78.40[b]	1.02	1.16	1.36	
5.03	1.21	78.31[a]	0.836±0.004	0.965±0.003	1.120±0.001	
10.03	2.51	78.07[a]	0.687±0.001	0.786±0.001	0.904±0.001	
20.09	5.48	77.42[a]	0.453±0.001	$0.505\pm0.000_3$	$0.573\pm0.000_2$	
40.03	13.34	76.01[a]	$0.181\pm0.000_3$	$0.193\pm0.000_0$	0.208±0.002	
			$Tm(IO_3)_3$	$Yb(IO_3)_3$	$Lu(IO_3)_3$	
0(This work)		78.54[a]	1.467±0.001	1.620±0.003	2.036±0.005	
0(Ref. 11)		78.40[b]	1.47	1.63	2.04	
5.03	1.21	78.31[a]	$1.217\pm0.000_2$	1.343±0.001	1.629±0.001	
10.03	2.51	78.07[a]	$0.978\pm0.000_2$	1.085±0.001	1.304±0.004	
20.09	5.48	77.42[a]	$0.616\pm0.000_1$	0.662±0.001	$0.794\pm0.000_3$	
40.03	13.34	76.01[a]	$0.214\pm0.000_1$	0.227±0.001	$0.258\pm0.000_1$	

a) Data for pure water and for DMSO-water mixture from Ref. 12. b) Data for pure water from Ref. 13.

were previously reported.[11]

Preparation of Binary Aqueous Solvent Mixtures. Guaranteed grade DMSO was purchased from Wako Chemicals Co., and was distilled under reduced pressure three times. Redistilled water with a specific conductivity of 0.98±0.05 μS cm^{-1} was used. The binary solvent mixtures by weight were made from the purified DMSO and the redistilled water.

Solubility Measurements. The supersaturation method was used. The purified lanthanoid iodates and DMSO-water mixtures were placed into glass-stoppered bottles, which were slowly rotated in a thermostat at 27 °C for about 12 h. The temperature was lowered to 25.00±0.05 °C and the bottles were continuously rotated for 48 h, after which no further change was observed within the relative average deviation of 0.3%. The solubilities of the iodates were determined in water and in 40 mass percent DMSO solvent mixtures.

After settling in a thermostat at 25 °C for about one hour, the solutions were filtered through a vaccum-jacketed sintered-glass filter. The filtrates were kept in the thermostat at 25 °C for about one hour. Aliquots were diluted with redistilled water for adjusting to a suitable concentration for titration. Aqueous potassium iodide and hydrochloric acid were added and the liberated iodine was titrated with a sodium thiosulfate solution that had been standardized with potassium iodate using a starch indicator. In cases where the solubility was small, aliquots of the saturated solution were added to a known amount of potassium iodate and the mixtures were back-titrated with a standardized thiosulfate solution. All solubility measurements were performed in duplicate.

Results and Discussion

Solubilities of Lanthanoid Iodates in DMSO–Water Solvent Mixtures. The observed solubilities of lanthanoid iodate dihydrates $Ln(IO_3)_3 \cdot 2H_2O$ (Ln=Ce, Pr, Nd, Sm, Eu, Gd, Tb, Dy, Ho, Er, Tm, Yb, and Lu) in DMSO-water mixtures at 25 °C are given in Table 1 along with the standard deviations of each solubility determination. The dielectric constants of DMSO-water mixtures[12] and of water[13] are also listed in Table 1.

The solubility determination of lanthanum iodate in the mixtures was not performed since the iodate dihydrate crystals could not be prepared. The solubility of promethium iodate is also missing from the table since a starting material such as promethium oxide or nitrate for the preparation of promethium iodate could not be purchased.

The solubilities of lanthanoid iodates in water at 25 °C have been reported by Firsching and Paul,[8] and Bertha and Choppin.[7] Miyamoto, Shimura, and Sasaki[11] measured the solubilities of the iodates in water at 25 °C and have reported the recommended values of the iodate solubilities in water at 25 °C by applying the evaluation guidelines[14] of the IUPAC Solubility Data Project. Our results regarding the solubility determination of the iodates are in good agreement with the recommended values.

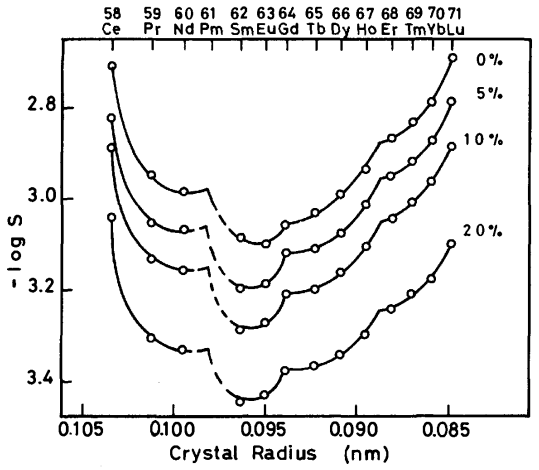

Fig. 1. Dependence of the logarithm of the solubility on the crystal radii (nm) of lanthanoid ions(III).

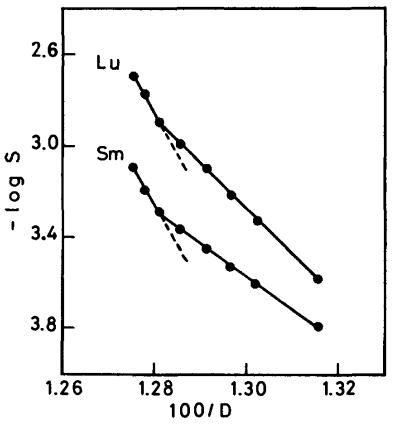

Fig. 2. Dependence of the logarithm of the solubility of samarium and lutetium iodates on the reciprocal of the dielectric constant of DMSO-water mixtures.

In this study, the DMSO concentrations of the solvent mixtures were in the range from 0 to 40 mass percent. At concentrations above 40 mass percent, the solubility could not be determined by an iodometric titration because the end point of the titration was not clear.

The relation between the logarithm of the solubility of lanthanoid iodates in DMSO-water mixtures and the lanthanoid atomic number is shown in Fig. 1., which also shows the dependence of the solubility of the iodates on the crystal radii of the trivalent lanthanoid ions. Recently, the ionic radii of many cations in aqueous solutions containing trivalent lanthanoid ions were theoretically determined by Marcus,[15] but the data of some cations in a series of trivalent lanthanoid ions are lacking. Therefore, the crystal radii of trivalent lanthanoid ions reported by Templeton and Dauben[16] were adopted.

In Fig. 1, although the points corresponding to lanthanum and promethium are lacking, it can be seen that the solubility curves pass through a minimum at atomic number 62 (samarium). By analyzing the solubility curves in further detail, the points on a plot of the logarithm of the solubility of lanthanoid iodates in DMSO-water mixtures vs. atomic number may be grouped, through the use of four smooth curves without inflections, into four tetrads with the gadolinium point being common to the second and third tetrads and the extended smooth curves intersecting, additionally, in the 60—61 and 67—68 atomic number regions.

As is well known, a plot of the stability constants of many lanthanoid complex systems[1,2] against the lanthanoid atomic number shows a gadolinium break. Peppard et al.[3] have reported that in certain liquid-liquid extraction systems the behavior of trivalent lanthanoid ions can be interpreted in terms of four tetrads, rather than in terms of two octads. The present solubility study also reveals the three break points, and the tetrad effect reported Peppard et al.[3] was observed.

The solubility of sparingly soluble salts as a function of the static dielectric constant of mixtures has been related to the Born equation[17] or its modification.[18-20] An example of the relation between the logarithm of the solubility and the reciprocal of the dielectric constant of the mixtures is shown in Fig. 2 for samarium iodate-DMSO-water and lutetium iodate-DMSO-water systems. In addition to the solvent mixtures having DMSO concentrations of 5, 10, 20, and 40 mass percent, solvents of DMSO with concentrations of 15, 25, and 30 mass percent were also used to determine the solubilities of the two systems. The circles indicate the observed solubilities of the iodates and dash lines are from a modified Born equation.

In each system the logarithm of the solubility of the iodates decreases almost linearly with the reciprocal of the dielectric constant of the mixtures, as is expected from the Born equation[17] or its modification[18-20] when dealing with mixtures of the narrow dielectric constant range of 78.5—78.0, but when dealing with mixtures of the dielectric constant range of 78.0—76.0 deviation from the Born equation was found. The dielectric constant range of 78.5—78.0 where a plot of the logarithm of the solubility vs. the reciprocal of the dielectric constant of the binary aqueous solvent mixtures follows the modified Born equation is narrower than that of methanol-water[11] and ethanol-water[11] systems.

For example, the relation between the logarithm of the solubility of the sparingly soluble salts and the reciprocal of the dielectric constant of mixed solvents is given by Davis, Ricci and Sauter[18] as

$$\ln (S_w/S_x) = (Z_+Z_-e^2/2rkT)/(1/D_x - 1/D_w), \quad (1)$$

where S and D represent the solubility of the iodates based on the molar scale and the dielectric constant of the mixtures, respectively, and the subscripts w and x

Table 2. The $2r$ Values of Lanthanoid Iodates Systems Calculated from Eq. 1 (10^9 units)

Index	Ce	Pr	Nd	Sm	Eu	Gd	Tb	Dy	Ho	Er	Tm	Yb	Lu
S_wS_5	2.3	2.9	3.2	3.2	3.3	3.5	3.5	3.3	3.4	3.0	3.4	3.4	2.8
S_wS_{10}	2.9	3.2	3.1	3.2	3.4	3.4	3.2	3.3	3.3	3.1	3.2	3.2	2.9
S_wS_{20}	4.0	3.9	3.9	4.1	4.1	4.1	4.0	3.9	3.7	3.6	3.6	3.5	3.3
S_wS_{40}	4.7	4.5	4.6	4.6	4.5	4.5	4.2	3.8	3.7	3.7	3.7	3.6	3.5
$S_{10}S_{20}$	5.5	4.6	4.8	4.9	4.9	4.8	4.7	4.3	4.1	4.0	3.9	3.7	3.7
$S_{10}S_{40}$	5.4	5.0	4.9	5.1	5.0	4.9	4.6	4.4	4.2	4.0	3.8	3.7	3.5

refer to the water system and the mixed solvent systems, respectively. Equation 1 corresponds to the first term of Koizumi's equation,[20] and the r value (solvation radius) was defined as Eq. 2:

$$1/r = (1/2)(1/r_+ + 1/r_-) \quad (2)$$

The $2r$ values calculated from Eq. 1 are given in Table 2. In "Index" column of Table 2, S_w and S_x (x=5, 10, 20, and 40) represent the solubility of iodates in water and that in the mixed solvent of the DMSO concentration x based on the mass percent scale, respectively, which were used to calculated the $2r$ values.

The physical properties of a DMSO–water system have been extensively studied.[13,21,22] These data point to strong interactions between water and DMSO in mixtures, which may be attributed to hydrogen bonding. Fox and Whittingham[21] have reported that the maximum interaction occurs in the region of about 0.3 mole fraction, enhancement of water structure expects perhaps at very low concentration (<0.01 mole fraction). The extensive literature[23] dealing with the DMSO–water interaction indicates that the solution properties of aqueous DMSO are dominated by 2:1 H_2O–DMSO complex, and only one result reported by Glasel[24] has been given 3:1 H_2O:DMSO complex.

When the electrolytes were added to DMSO–water solvent mixtures, the maximum interaction of DMSO and water changed distinctly. Indeed, Mastroianni, Pikal and Lindenbaum[25] have reported that the heats of dilution for lithium bromide in aqueous DMSO solutions exhibit a maximum around 20 mol% DMSO.

In a solubility study involving silver halides in DMSO–water mixtures,[26] the variation in the solubility data shows no simple correlation with the DMSO concentration in the mixtures. The solubility of silver chloride increases with an increase in the DMSO concentration, but those of silver bromide and iodide are reversed. From these results, the solubility phenomena of electrolytes in DMSO–water mixtures are no simple behavior.

In this study, as are given in Table 2 and shown in Fig. 2, the $2r$ values are classified into two categories. In each iodate system, one group consists of the $2r$ values for the lower DMSO concentration range (<2.5 mol%), and the other is those for the DMSO concentration of 20 and 40 mass percent (>5.0 mol%). The change of the slope depends on that of the solvation of lanthanoid ions, and it may also reflect the change of the DMSO–water interaction effected by lanthanoid ions.

Gibbs Free Energies of Transfer of Lanthanoid Iodates from Water into Aqueous DMSO Media. The aim of this section is to explore the dependence of the free energy of transfer for lanthanoid iodates from water into aqueous DMSO solutions on the lanthanoid atomic number.

The free energy of transfer of lanthanoid iodates from water into binary aqueous solvent mixtures is given by

$$\Delta G_t^\circ[\mathrm{Ln(IO_3)_3}] = RT \ln [K_{sp}(w)/K_{sp}(x)], \quad (3)$$

and the solubility product K_{sp} can be calculated from

$$K_{sp} = 27S^4\gamma_\pm^4. \quad (4)$$

Here, S and $\gamma_\pm$ represent the solubility of the iodates based on the molar scale and the molar activity coefficient of the iodates, respectively.

The solubilities of the iodates in water S_w and in DMSO–water mixtures S_x are related to the free energy of transfer from water into binary aqueous solvent mixtures:

$$\Delta G_t^\circ[\mathrm{Ln(IO_3)_3}] = 4RT \ln [S_w\gamma_\pm(w)/S_x\gamma_\pm(x)]. \quad (5)$$

From the solubility data, Blandamer, Burgess, and Duffield[27] have calculated the free energies of transfer of potassium cyanide from water into binary aqueous solvent mixtures. In the study, three methods were adopted to calculate the free energy of transfer. One approach was by an estimation of molar mean activity coefficients using the Debye–Hückel limiting law;[28] the other was also by an estimation of activity coefficients using the Güntelberg equation;[28] the rest was by the calculation of the quantity ΔG_t° on the molar scale from the observed solubility assuming $\gamma_\pm(w)/\gamma_\pm(x) \simeq 1$ in Eq. 5. For example, in pure DMSO the free energies calculated by using the Debye–Hückel equation and that calculated by using the Güntelberg equation were 21.8 and 21.9 kJmol^{-1}, respectively, and that calculated from the solubility assuming $\gamma_\pm(w)/\gamma_\pm(x) \simeq 1$ was 23.2 kJmol^{-1}. The relative average deviation is 2.7%. A comparison of the three results of the free energy of transfer to a series of pure solvent has been shown that the assumption $\gamma_\pm(w)/\gamma_\pm(x) \simeq 1$ was reasonable.

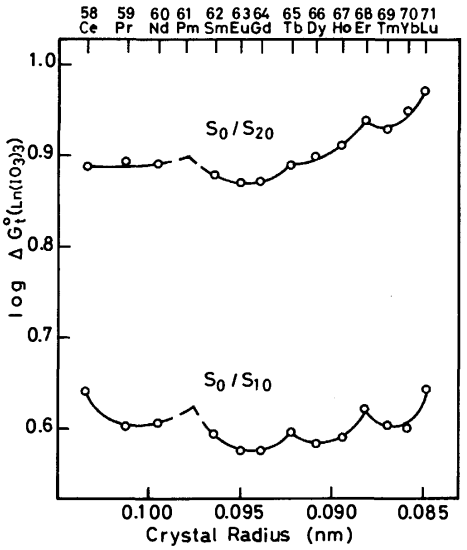

Fig. 3. Dependence of the logarithm of the free energy of transfer on the crystal radii (nm) of lanthanoid ions(III).

In this study, an estimation of molar activity coefficients used the Güntelberg equation[28] and the Davies equation.[28] Also, the free energies of transfer of the lanthanoid iodates from water into aqueous DMSO solutions were calculated from the observed solubility using Eq. 5. Further, Eq. 5 assuming $\gamma_{\pm}(w)/\gamma_{\pm}(x)\simeq 1$ was also used to calculate the free energies of transfer. From the results for samarium and lutetium iodate systems, the relative average deviation of the free energy of transfer calculated using the three methods was the range of 1.0—2.0%. The results are better than that of potassium cyanide in pure DMSO. Therefore, the free-energy values of the iodates calculated from the assumption $\gamma_{\pm}(w)/\gamma_{\pm}(x)\simeq 1$ were used in Fig. 3.

The dependence of free energy of transfer for lanthanoid iodates from water into aqueous DMSO solutions on the lanthanoid atomic number is shown in Fig. 3. The ratios S_0/S_{10} and S_0/S_{20} (Fig. 3) refer to the solubility ratio given explicitly in Eq. 5 and subscripts 0, 10, and 20 refer to the organic co-solvent concentrations of the mixtures. In Fig. 3, the points on a plot of the free energy of transfer against the lanthanoid atomic number can be divided into four curves with break points at atomic number 68 (erbium) and 65 (terbium) and in the 61—62 region. The behavior of trivalent lanthanoid ions is interpreted in terms of four tetrads, rather than in terms of two octads. Although the break points obtained in this free-energy study differ slightly from the behavior of the normal tetrad effect reported by Peppard et al.,[3] it can be seen that a tetrad-effect-like behavior is also observed in this free-energy study. However, Fujisawa and Suzuki[29] have reported that from a stability constant study the three break points were placed at 60 (neodymium), 64 (gadolinium) and 68 (erbium). Nugent[4] has stated that the variation in the interelectronic-repulsion-stabilization energy for the lanthanoid aqueous ions results in a tetrad effect at the 1/4, 1/2, and 3/4 filled shells of a 4f electronic configuration. However, a more detailed theoretical treatment as well as additional experimentation are necessary.

The figures referring to solubility ratios S_0/S_5 and S_0/S_{40} are not shown here, but the behavior of the curves is almost similar to that of S_0/S_{10} and S_0/S_{20}.

References

1) T. Moeller, "The Lanthanides, in Comprehensive Inorganic Compounds," ed by A. F. Trotman-Dickenson, Pergamon Press, London (1973), Vol. 4, p. 1.
2) S. Misumi, *Nippon Kagaku Zasshi*, **89**, 723 (1968).
3) D. F. Peppard, C. A. A. Bloomquist, E. P. Horwitz, S. Lewey, and G. W. Mason, *J. Inorg. Nucl. Chem.*, **32**, 339 (1970).
4) L. J. Nugent, *J. Inorg. Nucl. Chem.*, **32**, 3485 (1970).
5) S. Siekierski and M. Salomon, *J. Solution Chem.*, **14**, 473 (1985).
6) S. Siekierski, T. Mioduski, and M. Salomon, "Scandium, Yttrium, Lanthanum and Lanthanide Nitrates (IUPAC Solubility Data Series, Vol. 13)," Pergamon Press, London (1983).
7) S. L. Bertha and G. R. Choppin, *Inorg. Chem.*, **8**, 613 (1969).
8) F. H. Firsching and T. R. Paul, *J. Inorg. Nucl. Chem.*, **28**, 2414 (1966).
9) C. B. Monk, *J. Chem. Soc.*, **1951**, 2723.
10) C. B. Monk, *Trans. Faraday Soc.*, **47**, 1233 (1951).
11) H. Miyamoto, H. Shimura, and K. Sasaki, *J. Solution Chem.*, **14**, 485 (1985).
12) E. Tommila and A. Pajunen, *Soum. Kemistil. B*, **41**, 172 (1968).
13) R. L. Kay, G. A. Vidulich, and K. S. Pribadi, *J. Phys. Chem.*, **73**, 445 (1969).
14) IUPAC Commission on Solubility Data, "Solubility Data Series Guidelines for Compilers, Evaluators and Editors," ed by A. F. M. Barton, Pergamon Press, London, (1984).
15) Y. Marcus, *J. Solution Chem.*, **12**, 271 (1983).
16) D. H. Templeton and C. H. Dauben, *J. Am. Chem. Soc.*, **76**, 5237 (1954).
17) M. Born, *Z. Phys.*, **1**, 45 (1920).
18) T. W. Davis, J. E. Ricci, and C. G. Sauter, *J. Am. Chem. Soc.*, **61**, 3274 (1939).
19) P. B. Davies and C. B. Monk, *J. Chem. Soc.*, **1951**, 2718.
20) E. Koizumi, *Nippon Kagaku Kaishi*, **68**, 19 (1947).
21) M. F. Fox and K. P. Whittingham, *J. Chem. Soc., Faraday Trans. 1*, **71**, 1407 (1975).
22) For example: (Density and Viscosity) S. A. Schichman and R. L. Amey, *J. Phys. Chem.*, **75**, 98 (1971); (Heat of Mixing) H. L. Clever and S. P. Pigott, *J. Chem. Thermodyn.*, **3**, 221 (1971); (Vapor Pressure) S. Y. Lam and R. L. Benoit, *Can. J. Chem.*, **52**, 718 (1974); (Molal Volume and Heat Capacity) O. Kiyohara, G. Perron, and J. E. Desnoyers, *Can. J. Chem.*, **53**, 3263 (1975).
23) For example: E. M. Arnett and D. R. McKelvey, *J. Am. Chem. Soc.*, **88**, 2598 (1966); G. Yagil, *J. Phys. Chem.*, **73**, 1610 (1969); S. A. Schichman and R. L. Amey, *J. Phys. Chem.*, **75**, 98 (1971).
24) J. A. Glasel, *J. Am. Chem. Soc.*, **92**, 372 (1970).

25) M. J. Mastroianni, M. J. Pikal, and S. Lindenbaum, *J. Phys. Chem.*, **76**, 3050 (1972).
26) B. G. Cox and R. Natarajan, *J. Chem. Soc., Faraday Trans. 1*, **75**, 1780 (1979).
27) M. J. Blandamer, J. Burgess, and A. J. Duffield, *J. Chem. Soc., Dalton Trans.*, **1980**, 1.
28) See, for example, R. A. Robinson and R. H. Stokes, "Electrolyte Solutions," 2nd edn., Butterworths, London, (1959), Chap. 9.
29) M. Fujisawa and Y. Suzuki, 30th Conference on Coordination Chemistry, Tokyo, Japan, (1980), p. 296.

 © 1986 The Chemical Society of Japan Bull. Chem. Soc. Jpn., 59, 2979—2982 (1986)

Effects of Cyclodextrins on the Fluorescence of Diphenyl Phosphate in Aqueous Solution

Sanyo HAMAI
Department of Physics, Miyazaki Medical College, Kiyotake, Miyazaki 889-16
(Received February 14, 1986)

The effects of α-, β-, and γ-cyclodextrin (CD) on intramolecular excimer formation between the two phenyl groups of diphenyl phosphate (DP) in aqueous solution were investigated by means of absorption and fluorescence spectra. It was found that DP forms 1 : 1 inclusion compounds with α-, β-, and γ-CDs. In the inclusion compound with α- or β-CD, only one phenyl group of a DP molecule is incorporated in the cavity of a CD molecule. In the case of γ-CD, however, the cavity can accommodate either one or two phenyl groups of a DP molecule. The pH dependence of the equilibrium constant for the formation of the inclusion compound between DP and β-CD has also been examined. Over the pH range from 3.46 to ≈10 the equilibrium constant does not change, whereas for pH values above ≈11 it decreases drastically.

Cyclodextrins (CDs) are cyclic oligosacharides consisting of more than five glucopyranose units. CDs containing 6, 7, and 8 glucose units are specified as α-CD, β-CD, and γ-CD, respectively. The effects of these CDs on the fluorescence properties of various aromatic compounds have been studied extensively.[1-8] The fluorescence intensity of a guest molecule is usually enhanced by the formation of an inclusion compound with CD.[1-5,7,8]

There have been several studies on the inclusion compounds of CDs with 1,3-bichromophoric substances which form an intramolecular excimer between two biphenyl groups or two naphthyl groups.[9-12] Bis(4-biphenylylmethyl)ammonium chloride (BBA) exhibits both a monomer and an excimer fluorescence in aqueous solution. The effects of CDs on the two emission bands have been reported by Emert et al.[9] The addition of α-CD to a BBA aqueous solution results in the reduction of the excimer fluorescence. No excimer peak is observed when β-CD is added. In contrast, excimer fluorescence is enhanced by the addition of γ-CD. The authors have suggested that the smaller cavity of α- and β-CDs which can accommodate only one aryl residue inhibits excimer formation, whereas the larger cavity of γ-CD, which can host two aryl moieties, enhances excimer formation considerably. For 1,3-bichromophoric substances possessing two naphthyl groups, it has also been shown that two naphthyl groups in the same molecule can be located inside the γ-CD cavity.[9-12]

Among the 1,3-bichromophoric compounds investigated up to now, dibenzylammonium chloride (DA) is the only compound that possesses two phenyl groups.[9] The addition of α-, β-, and γ-CDs have no effects on both the monomer and the excimer fluorescence of DA. This result has been explained as due to the prevention of a deep penetration of DA by both the second benzene moiety and the positively charged nitrogen.

Although the formation of an inclusion compound with CD is affected by other factors than the cavity size of CD and the molecular size and shape of a guest molecule, it appears that two phenyl groups, which are less bulky than two naphthyl groups, can be incorporated in the same γ-CD cavity. Thus, as a 1,3-bichromophoric compound having two phenyl groups, we selected diphenyl phosphate which was found to show both monomer and excimer fluorescence in aqueous solutions, and investigated the formation of inclusion compounds of diphenyl phosphate with α-, β-, and γ-CDs by means of absorption and fluorescence spectra.

Experimental

Diphenyl phosphate, purchased from Nakarai, was recrystallized twice from cyclohexane. β-Cyclodextrin (β-CD) from Nakarai was recrystallized three times from water. α- and γ-CDs obtained from Nakarai and Tokyo Kasei, res ectively, were used without further purification.

The absorption spectra were measured with a Shimadzu 260 spectrophotometer, and the fluorescence spectra were recorded on a Shimadzu RF-501 spectrofluorometer equipped with a cooled EMI 9789QA photomultiplier. Fluorescence was viewed at right angles to the direction of excitation, and the spectra were corrected for the spectral response of the detection system as previously described.[5] The absorption and fluorescence spectra were measured at 25±0.1 °C unless otherwise stated. Aerated sample solutions were used throughout this work.

Results and Discussion

Complex Formation of Diphenyl Phosphate (DP) with α- and β-Cyclodextrins (CDs). Since DP is a monoprotic acid, DP can take both anionic and neutral forms. By using a conventional titration method, the pK_a of DP was determined to be 2.4. At the DP concentration (5×10^{-4} mol dm^{-3}) used for this work, the pH of an aqueous DP solution was 3.46. Therefore, the DP at 5×10^{-4} mol dm^{-3} is predominantly in its anionic form in aqueous solution.

Figure 1 shows the absorption spectra of 5×10^{-4} mol dm^{-3} DP in aqueous solutions containing varying concentrations of β-CD. The absorption band of DP is red-shifted with isosbestic points at 228 and 254 nm as the concentration of β-CD is increased. This finding indicates a simple equilibrium involving a 1:1

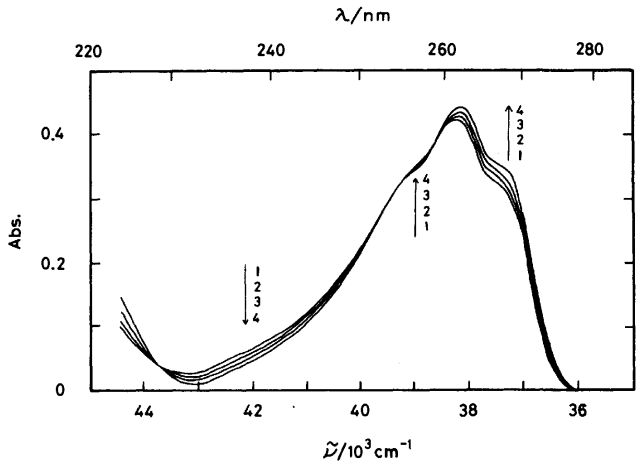

Fig. 1. Absorption spectra of DP (5×10^{-4} mol dm^{-3}) in aqueous solution in the presence of β-CD. Concentration of β-CD: (1) 0 mol dm^{-3}; (2) 10^{-3} mol dm^{-3}; (3) 2×10^{-3} mol dm^{-3}; (4) 5×10^{-3} mol dm^{-3}; (5) 10^{-2} mol dm^{-3}.

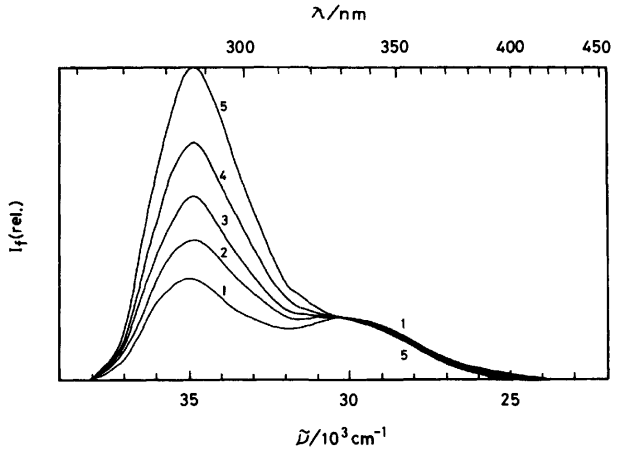

Fig. 2. Fluorescence spectra of DP (5×10^{-4} mol dm^{-3}) in aqueous solution in the presence of β-CD. Concentration of β-CD: (1) 0 mol dm^{-3}; (2) 10^{-3} mol dm^{-3}; (3) 2×10^{-3} mol dm^{-3}; (4) 4×10^{-3} mol dm^{-3}; (5) 10^{-2} mol dm^{-3}.

inclusion compound of DP formed with β-CD. The equilibrium between DP and a 1:1 inclusion compound of DP with β-CD can be represented by the following scheme:

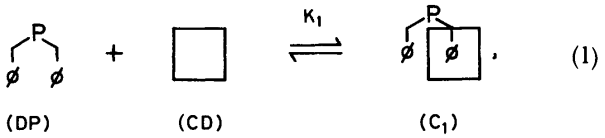

(1)

where C_1 is a 1:1 inclusion compound of DP with CD in which only one phenyl group of a DP molecule is incorporated in the cavity of a CD molecule, and K_1 is an equilibrium constant for the formation of C_1. Because of a very small variation in the absorbance, we could not reliably determine the value of the equilibrium constant from the absorption data.

Figure 2 illustrates the fluorescence spectra of DP (5×10^{-4} mol dm^{-3}) in aqueous solutions with varying concentrations of β-CD. The fluorescence spectrum of DP alone exhibits two bands whose maxima are at 286 and 330 nm, respectively. The 286-nm band can be assigned to a monomer fluorescence since phenyl dihydrogenphosphate shows only one fluorescence band with a maximum at 288 nm in aqueous solution. The 330-nm band can be assigned to the intramolecular excimer fluorescence of DP from the following. (1) Even at a DP concentration as low as 5×10^{-5} mol dm^{-3}, the fluorescence spectrum was identical to that for a 5×10^{-4} mol dm^{-3} DP solution. (2) The excitation spectrum for the 330-nm band was the same as that for the 286-nm band. (3) The maxima of the excimer emissions of benzene and 1,3-diphenylpropane are reported to be 320 and 333 nm, respectively.[13,14] Corresponding to the C–C–C carbon-atom skeleton in the cases of 1,3-bichromophoric propanes, the three-atom molecular chain, O–P–O, in a DP molecule is responsible for the formation of the intramolecular excimer.

The addition of β-CD results in a remarkable enhancement of the DP monomer band without a shift in the maximum position of the monomer band. In contrast to the dibenzylammonium chloride studied by Emert et al., the effect of β-CD on the DP fluorescence is evident. To evaluate the intensity of excimer emission, the fluorescence spectrum of phenyl dihydrogenphosphate was assumed to be the same as that of the DP monomer, and the tail of its emission, which extends to ≈380 nm, was subtracted from the excimer portion of the spectrum. The true intensity of the excimer band decreased upon increasing the β-CD concentration.

In the cases of benzene and naphthalene derivatives, the equilibrium constants for the formation of inclusion compounds, obtained from the absorption and fluorescence spectrophotometric methods, almost coincide with each other.[5,16] The rate constants of the association and dissociation reactions for the systems of a naphthalene derivative and β-CD are of the order of 10^7 mol^{-1} s^{-1} and 10^4 s^{-1}, respectively.[15] Although the corresponding rate constants for DP are not available, the above values are small compared with the expected decay rate constant (the order of 10^8 s^{-1}) of the singlet excited state of DP. Therefore, it is likely that an equilibrium between excited DP and β-CD cannot be established within the lifetime of excited DP. Thus, K_1 was evaluated to be 200 mol^{-1} dm^3 from the intensity change in the monomer fluorescence of DP, according to the method previously described.[5] This value is in good agreement with the equilibrium constants reported for the 1:1 inclusion compound formed between benzene and β-CD (196±10 (28 °C) and 169±1 (25 °C) mol^{-1} dm^3).[16,17]

When α-CD was added to a DP aqueous solution, similar changes were observed both in the absorption

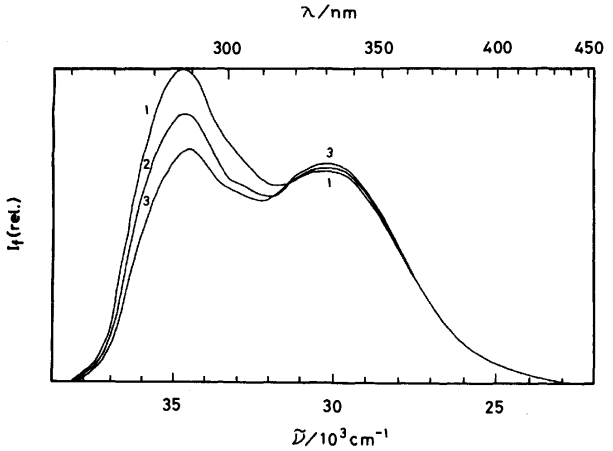

Fig. 3. Fluorescence spectra of an aqueous DP (5×10^{-4} mol dm^{-3}) solution in the presence of γ-CD at 43°C. Concentration of γ-CD: (1) 0 mol dm^{-3}; (2) 10^{-2} mol dm^{-3}; (3) 2×10^{-2} mol dm^{-3}.

and fluorescence of DP except that these changes were much smaller than those for β-CD, indicating the formation of the C_1 inclusion compound between DP and α-CD to a smaller extent. For α-CD, K_1 was determined to be 0.85 mol^{-1} dm^3 from measurements of the DP monomer fluorescence. The equilibrium constant for the formation of the 1:1 inclusion compound between benzene and α-CD has been reported to be 31.6±0.1 mol^{-1} dm^3 at 25°C.[17] A marked disparity between the equilibrium constant of α-CD with DP and that with benzene suggests a strong obstruction against complex formation by the substituent group (-O-P(-O$^-$)(=O)-O-Ph) in the DP molecule.

Complex Formation of DP with γ-CD. Below a γ-CD concentration of $\approx3\times10^{-2}$ mol dm^{-3}, the spectral change in the DP absorption was similar to that for β-CD. However, above a γ-CD concentration of $\approx3\times10^{-2}$ mol dm^{-3}, no isosbestic points were observed in the absorption spectra. This finding indicates the coexistence of at least two different equilibria between DP and γ-CD at a high γ-CD concentration. In this work, therefore, we restricted the γ-CD concentration up to 3×10^{-2} mol dm^{-3}. We found that a spectral change of the DP fluorescence caused by the addition of γ-CD varied significantly with temperature. In the lower-temperature range (below ≈10°C), the DP monomer fluorescence was enhanced with a decrease in the excimer fluorescence by the addition of γ-CD. As in the cases of α- and β-CDs, the enhancement of the monomer fluorescence is due to the formation of the 1:1 inclusion compound, C_1, of DP with γ-CD. From the fluorescence measurements, K_1 was evaluated to be 1.5 mol^{-1} dm^3 at 3°C. Figure 3 shows the DP fluorescence spectra at 43°C in the absence and presence of γ-CD. A decrease in the DP monomer fluorescence was observed in the higher-temperature range (above ≈25°C), accompanied by an enhancement of the DP excimer

Table 1. ΔH and ΔS for the Formation of the 1:1 Inclusion Compounds (C_1) of DP with α- and β-CDs

	DP		Benzene[a]	
	α-CD	β-CD	α-CD	β-CD
ΔH/kJ mol^{-1}	−37	−8.0	−13.1	−1.9
ΔS/J K^{-1} mol^{-1}	130	15	−15.5[b]	36.1[b]

a) From Ref. 17. b) Calculated from the equilibrium constant and the corresponding enthalpy change shown in Table 1 of Ref. 17.

fluorescence. The result in the higher-temperature range is similar to that for 1,3-bichromophoric compounds possessing two naphthyl or two biphenyl groups, indicating that two phenyl groups in a DP molecule are inserted into the same cavity of a γ-CD molecule.[9-12] The change in the DP fluorescence spectra in the higher-temperature range can be interpreted by the following equilibrium:

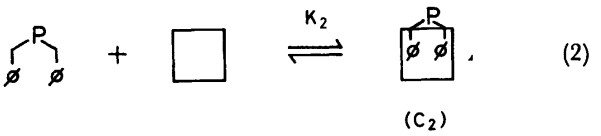

(2)

where C_2 is an inclusion compound in which two phenyl groups in a DP molecule are incorporated in the same cavity and K_2 is an equilibrium constant for the formation of C_2. In the case of C_2, it is likely that excited DP changes its geometrical conformation inside the γ-CD cavity within its lifetime and emits both a monomer and an excimer fluorescence. Even at a high temperature, C_1 in Eq. 1 can exist in a DP solution containing γ-CD. Since C_1, if it exists, contributes to both an increase in the monomer band and a decrease in the excimer band, the reverse intensity changes, a decrease in the monomer band and an increase in the excimer band (Fig. 3), is due mainly to the existence of C_2. By assuming that the presence of C_1 was negligible, K_2 at 43°C was determined to be 30 mol^{-1} dm^3 from the intensity change in the monomer fluorescence. At such a high temperature as 43°C, the increase in the DP excimer fluorescence at the expense of the DP monomer fluorescence may suggest that the enthalpy change (ΔH) for the C_2 formation is close to zero and, on the other hand, the entropy change (ΔS) for that is a positive value. Unfortunately, the thermodynamic parameters for K_1 and K_2 in the DP-γ-CD system could not be estimated because neither C_1 nor C_2 could be ignored over the fairly wide temperature range examined.

Temperature Dependence of K_1 for α- and β-CDs. From the temperature dependence of K_1 for α- and β-CDs, ΔH, and ΔS for the formation of C_1 could be obtained. The results are listed in Table 1 together with the data of benzene reported by Tucker and Christian.[16] For the inclusion compound of β-CD, positive values of

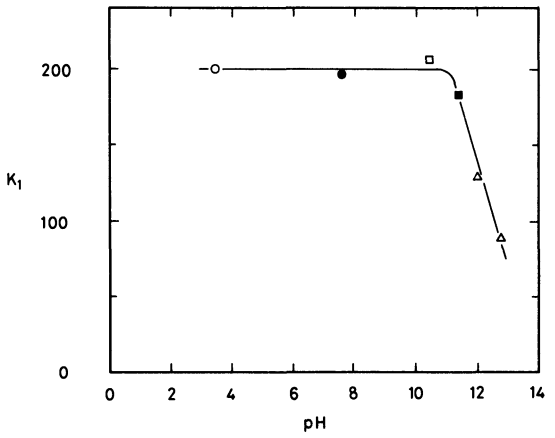

Fig. 4. pH dependence of K_1 for β-CD: (○) without buffer; (●) KH_2PO_4–NaOH buffer; (□) $NaHCO_3$–NaOH buffer; (■) Na_2HPO_4–NaOH buffer; (△) KCl–NaOH buffer.

ΔS were obtained for both DP and benzene. The larger $-\Delta H$ value for DP than that for benzene suggests that the substituted benzene ring fits more tightly the size of the β-CD cavity than the unsubstituted benzene nucleus. In the case of α-CD, ΔS for benzene is negative, whereas that for DP is positive. This result may show that a benzene molecule is more rigidly incorporated in the α-CD cavity than a DP molecule is. The larger $-\Delta H$ of α-CD both for DP and benzene than those of β-CD reveal that the cavity size of α-CD is more appropriate to the complexation with the benzene ring than that of β-CD.

pH Dependence of K_1 for β-CD. In order to further study the inclusion processes of DP, we examined the pH dependence of K_1 for β-CD. In Fig. 4, the values of K_1 are plotted as a function of pH. K_1 is constant at pH values between 3.46 and ≈10. However, K_1 abruptly decreases as the pH is increased above ≈11. The pK_a value for α-CD is known to be 11.8.[18] Since both α- and β-CDs are constituted from the identical glucopyranose units, nealy the same value of pK_a is expected for β-CD. As already mentioned, DP exists as an anionic form over the whole pH range studied. Therefore, the sharp drop of K_1 in Fig. 4 indicates an electrostatic repulsion between an anionic DP and an anionic β-CD molecule. In addition, if the deprotonation of β-CD at pH≈11 causes a conformation change in β-CD, this change can play an important role in the reduction of K_1.

The author wishes to thank Professor Fumio Hirayama for his valuable discussion.

References

1) C. J. Seliskar and L. Brand, *Science*, **171**, 799 (1971).
2) H. Kondo, H. Nakatani, and K. Hiromi, *J. Biochem.*, **79**, 393 (1976).
3) H. E. Edwards and J. K. Thomas, *Carbohydrate Res.*, **65**, 173 (1978).
4) A. Ueno, K. Takahashi, and T. Osa, *J. Chem. Soc., Chem. Commun.*, **1980**, 921.
5) S. Hamai, *Bull. Chem. Soc. Jpn.*, **55**, 2721 (1982).
6) K. Kano, I. Takenoshita, and T. Ogawa, *J. Phys. Chem.*, **86**, 1833 (1982).
7) A. Nakajima, *Spectrochim. Acta*, **39A**, 913 (1983).
8) S. Scypinski and J. M. Drake, *J. Phys. Chem.*, **89**, 2432 (1985).
9) J. Emert, D. Kodali, and R. Catena, *J. Chem. Soc., Chem. Commum.*, **1981**, 758.
10) N. J. Turro, T. Okubo, and G. C. Weed, *Photochem. Photobiol.*, **35**, 325 (1982).
11) R. Arad-Yellin and D. F. Eaton, *J. Phys. Chem.*, **87**, 5051 (1983).
12) M. Itoh and Y. Fujiwara, *Bull. Chem. Soc. Jpn.*, **57**, 2261 (1984).
13) J. B. Birks, C. L. Braga, and M. D. Lumb, *Proc. Roy. Soc. London, Ser. A*, **283**, 83 (1964).
14) F. Hirayama, *J. Chem. Phys.*, **42**, 3163 (1965).
15) N. J. Turro, T. Okubo, and Chao-Jen Chung, *J. Am. Chem. Soc.*, **104**, 1789 (1982).
16) M. Hoshino, M. Imamura, K. Ikehara, and Y. Hama, *J. Phys. Chem.*, **85**, 1820 (1981).
17) E. E. Tucker and S. D. Christian, *J. Am. Chem. Soc.*, **106**, 1942 (1984).
18) R. L. VanEtten, G. A. Clowes, J. F. Sebastian, and M. L. Bender, *J. Am. Chem. Soc.*, **89**, 3253 (1967).

 © 1986 The Chemical Society of Japan Bull. Chem. Soc. Jpn., 59, 2983—2989 (1986)

Heterogeneous Hydration of Acrylonitrile over the Metal Oxide Catalysts in Liquid Phase

Kazuo SUGIYAMA,* Hiroshi MIURA, Yasushi NAKANO, Hideyuki SEKIWA, and Tsuneo MATSUDA
Department of Applied Chemistry, Faculty of Engineering, Saitama University, Shimo-okubo, Urawa 338
(Received February 15, 1986)

The liquid-phase hydration of acrylonitrile has been examined over various single metal oxide catalysts at 65 °C. Numerous metal oxides have proved to be active for hydration and have been used to produce three products: acrylamide, ethylene cyanohydrin, and bis(2-cyanoethyl) ether. These oxide catalysts could be divided into two groups with respect to the acrylamide selectivity with 100% or not. A good relationship between the catalytic abilities (activity and selectivity) and the solid acid-base properties of each metal oxide group examined in benzene or in water was observed. Differences in the hydration selectivity to either a C≡N or a C=C bond of acrylonitrile over the catalysts could be explained on the basis of the IR spectra of two adsorbed states of acrylonitrile on the metal oxide surface. It was proved that the liquid-phase hydration of acrylonitrile over the insoluble metal oxide catalysts was an acid-base-catalyzed reaction proceeding on the acidic or basic surface hydroxyl groups.

Acrylonitrile (AN) is a reactive organic molecule owing to two kinds of reactive unsaturated bonds: a C≡N triple bond and a C=C double bond. Many derivatives were produced by an addition reaction to the AN.[1] For example, a water molecule could easily be added to the two functional groups in either acidic or basic media.[2,3] Using sulfuric acid, the acrylamide sulfate was produced during the initial stage of a stoichiometoric reaction as follows:

$$\underset{\text{acrylonitrile (AN)}}{CH_2{=}CH{-}C{\equiv}N} + H_2SO_4 + H_2O \longrightarrow CH_2{=}CHCONH_2{-}H_2SO_4 \quad (1)$$

Acrylamide (AA) could be obtained by the neutralization of the sulfate with an alkali solution such as aqueous ammonia.

$$CH_2{=}CHCONH_2{-}H_2SO_4 + 2NH_3 \longrightarrow \underset{\text{acrylamide (AA)}}{CH_2{=}CHCONH_2} + (NH_4)_2SO_4 \quad (2)$$

On the other hand, in a basic medium using an aqueous sodium hydroxide,[4] the hydration of AN catalytically proceeded to produce ethylene cyanohydrin (ECH), bis(2-cyanoethyl) ether (BCE), and AA as follows:

$$CH_2{=}CH{-}C{\equiv}N + H_2O \longrightarrow \underset{\text{ethylene cyanohydrin (ECH)}}{HOCH_2CH_2C{\equiv}N} \quad (3)$$

$$CH_2{=}CH{-}C{\equiv}N + HOCH_2CH_2C{\equiv}N \longrightarrow \underset{\text{bis(2-cyanoethyl) ether (BCE)}}{O(CH_2CH_2C{\equiv}N)_2} \quad (4)$$

$$CH_2{=}CH{-}C{\equiv}N + H_2O \longrightarrow CH_2{=}CHCONH_2 \quad (5)$$

In the case of metal oxides, the heterogeneous catalytic hydration of AN could also be observed,[5-10] and produced the same products as those in the case of the homogeneous hydration. The product distributions on the catalysts were similar to those in homogeneous acid-bese hydration of AN. Consequently, it is considered that the catalytic abilities (hydration activity and selectivity) are correlated with the solid acid-base properties of the metal oxide catalysts.

In this study the relationship between the catalytic behaviors of various metal oxides and their solid acid-base properties was examined in order to confirm whether the mechanism in the liquid-phase hydration of AN could be applied to a heterogeneous acid-base catalytic reaction.

Experimental

Catalyst Preparation: Metal oxides as catalyst were generally prepared by the decomposition of the hydroxides or carbonates of metals-to-metal oxides at 110 °C for 12 h or at >200 °C for 3 h. The surface areas of the catalysts were determined by the B.E.T. method. The catalysts used in this study are listed in Table 1. The detailed preparation methods are as follows;

(1) MnO_2: Commercially available electrolytic manganese dioxide (type FM-H, Toyo Soda Manuf. Co.) was used without further purification.

Samples 2 to 5 were chemically prepared in accordance with a method described by Kanungo[11] as below:

(2) α-MnO_2: $MnSO_4$ was dissolved in 0.5-M (1 M=1 mol dm^{-3}) hot sulfuric acid at 80 °C, precipitated with ammonium peroxodisulfate until the pink color of the solution disappeared. The precipitate was thoroughly washed with deionized water and then dried.

(3) β-MnO_2: $Mn(NO_3)_2$ was thermally decomposed in a stream of air.

(4) γ-MnO_2: An aqueous $Mn(NO_3)_2$ was oxidized with a dilute $KMnO_4$ solution.

(5) δ-MnO_2: An aqueous (0.38 M) $KMnO_4$ was reduced with 6-M aqueous HCl at 80 °C.

Other samples were prepared as follows;

(6) Co_3O_4: Cobalt hydroxide was precipitated from an aqueous $Co(NO_3)_2$ with aqueous NaOH, followed by a thorough washing of the precipitate and drying.

(7) Co_3O_4: Cobalt carbonate was thermally decomposed in a stream of air.

(8) Co_3O_4: Cobalt hydroxide was precipitated from a

$Co(NO_3)_2$ solution with aqueous ammonia.

(9) Co_3O_4: Cobalt hydroxide was precipitated from a $CoCl_2$ solution with aqueous NaOH.

(10) NiO(A): Nickel hydroxide was precipitated from a $Ni(NO_3)_2$ solution with aqueous NaOH, as reported in a previous paper.[10]

(11) CuO(A): Copper hydroxide was precipitated from a $Cu(NO_3)_2$ solution with aqueous NaOH.

(12) Fe_2O_3: Iron hydroxide was precipitated from an $Fe(NO_3)_3$ solution with aqueous ammonia.

(13) PbO_2: Lead nitrate was thermally decomposed in a stream of air.

(14) WO_3: Ammonium parawolframate was thermally decomposed in a stream of air.

(15) SiO_2: Commercially available silica sol (Catalloid H-20, Catalysts & Chemicals Ind. Co.) was dried in air and then calcined.

(16) TiO_2: Titanium hydroxide was precipitated from a $Ti(SO_4)_2$ solution with aqueous ammonia.

(17) Al_2O_3(A): Commercially available alumina (Neobead GB, Mizusawa Chem. Co.) was used.

(18) MnO: Manganese carbonate was thermally decomposed in a stream of nitrogen.

(19) MgO: Basic magnesium carbonate was thermally decomposed in air.

(20) ZnO: Zinc carbonate was thermally decomposed in air.

(21) Cu_2O: Copper(II) oxide was partially reduced in a stream of 2 vol% of propylene diluted by nitrogen, in accordance with the manner described by Mikhal'chenko et al.[12]

(22) NiO(B): Basic nickel carbonate was thermally decomposed in a stream of air, as reported in the previous paper.[10]

(23) CuO(B): Basic copper carbonate was thermally decomposed in a stream of air.

(24) Ag_2O: The precipitate was obtained from an $AgNO_3$ solution with aqueous NaOH.

(25) La_2O_3: Lanthanum hydroxide was precipitated from a $La(NO_3)_3$ solution with aqueous ammonia.

(26) Al_2O_3(B): Aluminum tri-isopropoxide was hydrolyzed, followed by washing of the precipitate and then dried.

(27) PbO: Lead hydroxide was precipitated from a $Pb(NO_3)_2$ solution with aqueous KOH.

Activity Measurement: The hydration of AN was carried out by the use of a four-necked flask equipped with a mechanical stirrer, a reflux condenser, a thermometer and a screw cap for sampling. Pure water (100 ml) and AN (8.5 ml) purified by distillation were introduced into the reactor and kept at 65 °C. The catalyst (2.5±0.1 g) was transferred from the calcination glass-tube to the reactor, followed by stirring. The rotation speed was 2000 rpm. The reaction products were analyzed by an FID gas chromatograph. Column packing used were both a Porapak QS (4 mmϕ×1 m, 170 °C) for analysis of AN, AA, and ECH and a PS 400 on Chromosorb W (4 mmϕ×2 m, 170 °C) for BCE.

Acid-Base Strength Distribution of Dark-Colored Solid Oxides: As the active catalysts for the hydration of AN to AA were dark-colored metal oxides, the acid-base strength distribution on these colored samples was determined by the modified indicator method that we developed. A characteristics of this method is that a commercially available separate ground-glass Gooch crucible for measuring the acidic or basic properties of the samples can be used, and the dark-colored sample and a white standard probe with a known acidity or basicity is situated in the upper and lower parts separated by a glass filter with a pore size of 20—30 μ. The detailed procedure was described in a previous paper.[13]

Equi-Acid-Base Point (EABP) of Metal Oxides: The value of EABP of metal oxide represents the acid-base properties of the solid catalysts dispersed in water.[14,15] The EABP of metal oxide catalysts was determined by a pH shift method in accordance with the manner described by Tari et al.[16] The metal oxide sample (2.5±0.1 g) and pure water (100 ml) were introduced into an Erlenmeyer flask equipped with a glass stopper in a decarbonated nitrogen atmosphere and then permitted to stand for one week. The pH value of the supernatant solution in the flask was measured with a pH meter.

IR Measurements: Infrared spectroscopic measurements of the AN adsorbed on both SiO_2 and MgO catalysts were made using a JEOL JIR-100 FTIR spectrometer. Sample treatment and adsorption of AN gas were carried out with a glass gas-handling system capable of achieving a 10^{-6} Torr vacuum. The quartz IR cell used was a conventional T-shaped cell with separate zones for heating and for taking spectra. CaF_2 windows were used. Spectra were collected by co-adding 100 scans at a resolution of 4 cm^{-1}. SiO_2 or MgO sample wafers were prepared by pressing 20 mg of a sample under a pressure of 200 kg cm^{-2} to form a disk about 20 mm in diameter. After SiO_2 and MgO wafers were, respectively, heated at 500 °C for 2 h in a cell, AN vapor (45 Torr (1 Torr=133.322 Pa)) was adsorbed to the sample at room temperature for 15 min and then evacuated for 3 min. All spectra were recorded at room temperature.

Amount of AN Adsorbed: Preheated MnO_2 (at 110 °C) or MgO (at 700 °C) sample (2.5 g) was, respectively, put into an Erlenmeyer flask with glass stopper, and then 100 ml of a 2.5 wt% AN aqueous solution was poured into the flask. After stirring for 6 h, the sample was allowed to stand for 40 h at room temperature and then kept at 40 °C for 4 h. The amount of adsorbed AN was determined from the difference of the concentration of AN before and after adsorption. The concentration of AN was measured by gas chromatographically.

Results and Discussion

Catalytic Activity and Selectivity: The catalytic activity (conversion of AN) and selectivity of the liquid-phase hydration of AN over various insoluble metal oxides were examined at 65 °C for 6 h in a batch reactor. The reaction results are summarized in Table 1. Many metal oxides had shown the catalytic activity of the AN hydration, and gave three products: AA, ECH, and BCE. The catalysts used in the AN hydration could be classified into two groups with respect to AA selectivity. One group, defined as "Group A," represents the metal oxides with a 100% AA selectivity and another, defined as "Group B," represents other metal oxides with a low AA selectivity.

The order of the catalytic activity of the oxides in Group A resulted as follows:

$MnO_2 > Co_3O_4 > NiO(A) > CuO(A) > Fe_2O_3 > PbO_2$, $WO_3 > SiO_2$, TiO_2, Al_2O_3(A).

Table 1. Catalytic Activity and Selectivity on Various Single Metal Oxides

Catalyst	Raw materials	Calcination temp/°C	Surface area/$m^2 g^{-1}$	Conversion of AN/%	Selectivity/%		
					AA	ECH	BCE
Group A							
1 MnO_2	electrolytic MnO_2	110	33.2	13.3	100	0	0
		200	28.5	10.9	100	0	0
		300	16.3	7.3	100	0	0
2 α-MnO_2	$MnSO_4+(NH_4)_2S_2O_4$	110	20.5	8.2	100	0	0
3 β-MnO_2	$Mn(NO_3)_2$	200	3.9	0.7	100	0	0
4 γ-MnO_2	$Mn(NO_3)_2+KMnO_4$	110	22.4	5.7	100	0	0
5 δ-MnO_2	$KMnO_4+HCl$	110	140	12.7	100	0	0
6 Co_3O_4	$NaOH+Co(NO_3)_2$	250	38.1	7.8	100	0	0
		400	28.2	6.4	100	0	0
		500	25.9	3.7	100	0	0
7 Co_3O_4	$2CoCO_3 \cdot 3Co(OH)_2$	400	47.8	6.9	100	0	0
8 Co_3O_4	$Co(NO_3)_2+NH_3$ aq.	300	17.8	3.4	100	0	0
9 Co_3O_4	$CoCl_2+NaOH$	250	—	2.3	100	0	0
10 NiO(A)	$Ni(NO_3)_2+NaOH$	300	60.9	4.6	100	0	0
11 CuO(A)	$Cu(NO_3)_2+NaOH$	250	32.5	3.6	100	0	0
12 Fe_2O_3	$Fe(NO_3)_3+NH_3$ aq.	400	68.6	1.2	100	0	0
13 PbO_2	$Pb(NO_3)_2$	350	1.4	0.7	100	0	0
14 WO_3	$(NH_4)_{10}W_{12}O_{41}$	500	<1	0.5	100	0	0
15 SiO_2*	colloidal silica	500	482	1.0	100	0	0
16 TiO_2*	$Ti(SO_4)_2+NH_3$ aq.	500	75.5	0.9	100	0	0
17 Al_2O_3(A)*	MIZUSAWA Chem.	500	271	0.9	100	0	0
Group B							
18 MnO	$MnCO_3$ in N_2	500	14.2	64.8	15.4	28.7	55.9
19 MgO	$4MgCO_3 \cdot Mg(OH)_2$	700	65.0	57.2	3.4	12.6	84.0
20 ZnO	$5ZnO \cdot 2ZnCO_3$	500	20.7	35.1	20.8	31.7	47.5
21 Cu_2O	CuO in $C_3^{\prime}$	250	—	20.8	24.8	9.1	66.1
22 NiO(B)	$NiCO_3 \cdot 2Ni(OH)_2$	300	16.7	15.6	22.4	34.5	43.1
23 CuO(B)	$CuCO_3 \cdot Cu(OH)_2$	400	20.7	10.6	41.9	27.4	30.7
24 Ag_2O	$AgNO_3+NaOH$	110	1.6	5.0	28.4	27.3	44.3
25 La_2O_3	$La(NO_3)_3+NH_3$ aq.	500	13.8	2.3	37.8	23.0	39.2
26 Al_2O_3(B)	$Al[OCH(CH_3)_2]_3+H_2O$	400	—	0.8	62.6	14.1	23.3
27 PbO	$Pb(NO_3)_2+KOH$	250	<1	0.6	64.9	8.3	26.8

Reaction temperature: 65°C (*120°C in autoclave): Reaction time; 6 h: 6.4 wt% AN solution; 108.5 ml: Catalyst weight; 2.5±0.1 g.

Especially, MnO_2, Co_3O_4, NiO(A), and CuO(A) were effective catalysts for AA formation with 100% selectivity. The catalytic activity of both MnO_2 and Co_3O_4 strongly depended on both the catalytic preparation method and the pretreatment temperature.

The order of the catalytic activity of the oxides in Group B was as follows:

$$MnO > MgO > ZnO > Cu_2O > NiO(B) > CuO(B) > Ag_2O > La_2O_3 > Al_2O_3(B), PbO.$$

MnO was the most active catalyst for AN hydration in all the metal oxide catalysts examined. The more active catalysts in Group B showed the lower selectivity to AA.

It should be noted that the NiO, CuO, and Al_2O_3 prepared with two kinds of methods had different AA selectivities, regardless of their same crystal structure, which was determined by an X-ray diffraction method. Also, both carbonates and hydroxides of the manganese, cobalt, nickel and copper were inactive for liquid-phase AN hydration. When their salts were decomposed to the corresponding oxides, a hydration activity just appeared.

From the results of solid acid-base properties summarized by Tanabe[17] it could be proved that almost all the catalysts of Group A possessed a solid acidity, while the catalysts of Group B were rich in basic properties. It seems that the solid acid-base properties of the metal oxide catalysts are closely related to the catalytic activity and selectivity of AN hydration. This correlation is clarified in the next section.

Electronegativity of the Metal Ion and Selectivity to AA: A qualitative acid-base property of metal oxides can be explained by the electronegativity of the metal ion of an oxide.[18] The relationship between the selectivity to AA and the electronegativity of the metal ion of metal oxide catalysts is illustrated in Fig. 1. A good relation was obtained. The value of the electronegativity of Co_3O_4 could be expressed using the value of arithmetic mean of Co^{2+} and Co^{3+} ion. All the metal oxides for which the electronegativity was 11 or greater showed 100% selectivity to AA. The selectivity to AA of the catalysts decreased with decreasing electronegativity of the metal ion. Differences of the selectivity to AA on the NiO, CuO, and Al_2O_3 catalysts could not be

Table 2. The Acidity and Basicity of the Active Catalysts on the Liquid-Phase Hydration of Acrylonitrile

Catalyst	Selectivity to AA/%	Basicity/mmol g^{-1} $H_-\geqq+9.3$	Acidity/mmol g^{-1} $H_0\leqq+6.8$	$H_0\leqq+4.8$	$H_0\leqq+3.3$
Group A					
1 MnO_2	100	0	0.101	0.078	0.006
6 Co_3O_4	100	0	0.029	0.022	0.003
10 NiO(A)	100	0	0.088	0.037	0
11 CuO(A)	100	0	0.028	0.022	0
12 Fe_2O_3	100	0	0.049	0.018	0.012
Group B					
18 MnO	15.4	0.297	0	—	—
19 MgO	3.4	0.239	0	—	—
20 ZnO	20.8	0.070	0	—	—
22 NiO(B)	22.4	0.023	0.014	0	—
23 CuO(B)	41.9	0.099	0.027	0.013	0

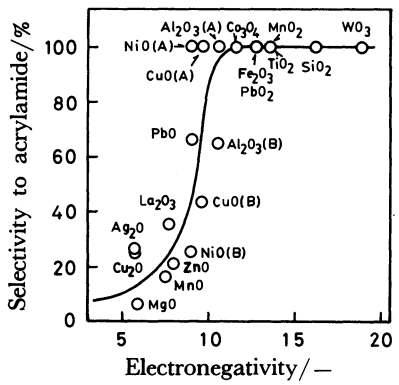

Fig. 1. Relationship between the selectivity to acrylamide and electronegativity of metal cation of metal oxide catalysts.

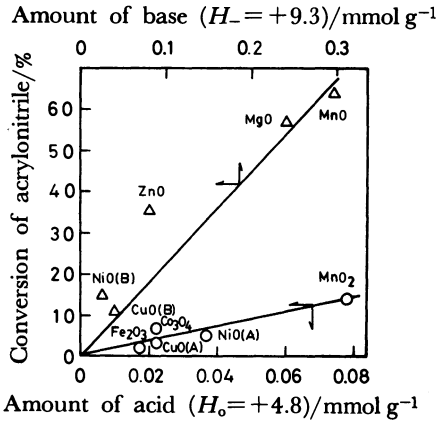

Fig. 2. Relationship between the conversion of acrylonitrile and the amount of acid-base of metal oxide catalysts.

explained from the electronegativity since it is a qualitative measure of the solid acidity or basicity of metal oxide catalysts.

Acid-Base Property on the Metal Oxides: A quantitative measurements of the acidity and basicity on the metal oxide catalysts can be generally made using the indicator titration method. However, the properties of dark-colored solid samples are difficult to measure by this method. Accordingly, our modified titration method[13] was adapted during the course of this. The acid-base properties of some metal oxide catalysts for AN hydration in Group A or B were obtained as shown in Table 2, although not all the catalysts shown in Table 1 were examined.

The Group A catalysts with 100% AA selectivity showed acidic strength between pK_a 3.3 and 6.8; that is, a rather weak acidic site is related to AA formation. On the other hand, Group B catalysts with a low AA selectivity exhibited a pK_a value of 9.3 or greater. The acidic and basic sites on the NiO(B) and CuO(B) catalyst surfaces showed a pK_a of 4.8 or less and a pK_a of 15.0 or greater, respectively. Consequently, the acidic sites on the metal oxide surface participate with the hydration of the C≡N bond in an AN molecule and the basic sites do the same with C=C bond.

As shown in Fig. 2, a good relationship between the catalytic activity of the metal oxides and the amount of acid at p$K_a\leqq+4.8$ or of base at p$K_a\geqq+9.3$ was obtained. Thus, rather weak acid-base properties on metal oxides are closely related to AN hydration. The pK_a value of the oxonium (H_3O^+) or hydroxide (OH^-) ion was −1.7 or +15.7, respectively.[19] Consequently, it is considered that the acidic or basic site of metal oxides ranging in a pK_a range between −1.7 and +15.7 effectively act for AN hydration. One can conclude that a metal oxide catalysts having moderate acid-base properties is suitable for the liquid-phase hydration of AN.

Equi-Acid-Base Point (EABP) of the Metal Oxides: The acid-base property of an insoluble metal oxide dispersed in water can be represented by the EABP; the pH value is used as a measure of acidity or basicity on the oxides.[15] The EABP values of the metal oxide catalysts used were obtained in the pH range of 3.6—11.2; in this pH range a homogeneous AN hydration in acidic or basic liquid phase did not progress.[20] The EABP value of the metal oxides in Group A was below 7, i.e., rather acidic, while that of the oxides in the Group B was above 7, i.e., rather basic. These results

indicate that each of the metal oxides in Group A or B has both acidic or basic properties, even in water. A typical solid acid catalyst, SiO_2–Al_2O_3 showed an EABP value of 7, showing that it is inactive for AN hydration.

Figure 3 illustrates the relationship between the AA selectivity and the EABP value of the catalysts. The metal oxide catalysts which have an acidic property in water showed 100% selectivity to AA. While in the case of the metal oxides which had basic properties in water, the AA selectivity of the catalysts decreased upon increasing their basicity. Figure 4 shows the logarithm of the catalytic activity against the EABP values of the metal oxides, indicating the pattern of a character of

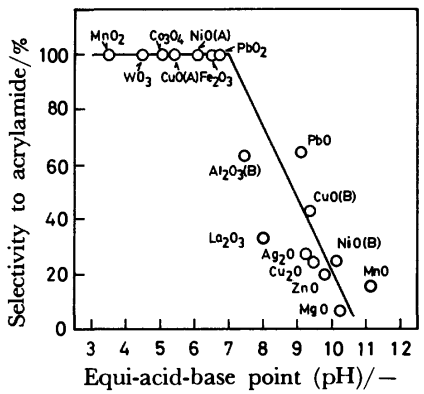

Fig. 3. Relationship between the selectivity to acrylamide and the value of equi-acid-base point of metal oxide catalysts.

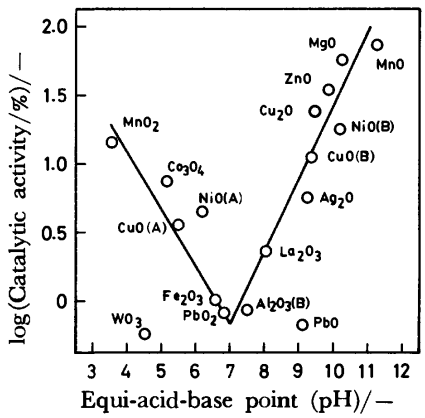

Fig. 4. Relationship between the catalytic activity and the value of equi-acid-base point of metal oxide catalysts.

"V." The EABP value of the bottom of the "V" was just 7. These results suggested that the hydration activity of the metal oxides are proportional to the amount of acidic or basic sites on the oxide surface.

Effect of Poisoning: As shown in Table 3, the catalytic activity of MnO_2 was depressed by the addition of such basic materials as sodium hydroxide, whereas the activity of an MgO catalyst was inhibited by the addition of such acidic materials as phosphoric acid. Furthermore, by the addition of a buffer solution of pH=7 (such as a tetrachlorozincate anion complex ($ZnCl_4^{2-}$)[20]) the catalytic activity of both MnO_2 and MgO was entirely lost. These results also indicate that the acidic site on MnO_2 and the basic site on MgO act as the active sites of the catalysts for AN hydration.

Effectiveness of the Metal Oxide Surface: The effectiveness of the metal oxide surface on the active sites for the heterogeneous liquid-phase hydration of AN was determined by a comparison of the homogeneous AN hydration in an aqueous acidic or basic solution. As shown in Table 4, heterogeneous AN hydration did not progress in an aqueous H_2SO_4 solution adjusted to pH 3.6, which was the same pH value of EABP of MnO_2 catalyst. AA was not observed until the pH value in the solution became to 2.1. In the case of a basic AN solution, a small amount of products was formed in an aqueous NaOH solution adjusted to pH 10.3. Only when the supernatant solution of MgO catalyst was used, a slight conversion of AN was observed. In conclusion, the AN conversion of homogeneous catalysts was extremely small compared with that of metal oxide catalysts with the same pH value.

In addition, the lower apparent activation energy of MnO_2 and MgO catalysts than that of H_2SO_4 and NaOH could be calculated, and the AN adsorption to

Table 3. Poisoning Effect of the Additives to MnO_2 and MgO Catalyst on the Hydration of Acrylonitrile

Additive	Catalyst	
	MnO_2	MgO
NaOH (0.1 mol)	○	×
H_3PO_4 (0.1 mol)	×	○
Buffer solution of pH=7.0	○	○

○: Detected. ×: Not detected. Reaction conditions are the same as those in Table 1.

Table 4. Hydration of Acrylonitrile in Hetero- and Homogeneous Liquid Phase

Catalyst	Phase	pH[a]	AN conv.[b]	AA sel.[b]	ΔE	Adsorbed AN
			%	%	kcal mol^{-1}	(×10^{-4} mol/g-cat)
MnO_2	heterogeneous	(3.6)	13.3	100	15	5.3
H_2SO_4	homogeneous	3.6	0	—	36[c]	—
MgO	heterogeneous	(10.3)	57.2	3.4	16	0.4
$Mg(OH)_2$	homogeneous	10.3	2.9	15.5	—	—
NaOH	homogeneous	10.3	8.8	27.2	19[d]	—

a) EABP value of the oxide catalyst was shown in parentheses. b) Reaction conditions are the same as those in Table 1. c) Ref. 27. d) The value calculated in the previous paper: Ref. 4.

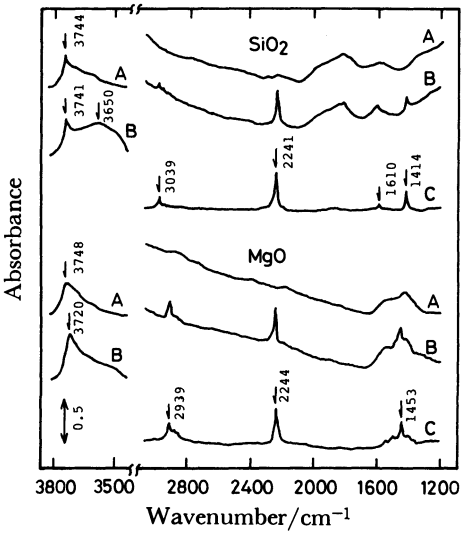

Fig. 5. IR spectra of acrylonitrile adsorbed on SiO_2 and MgO catalysts: (A): Background, (B): after adsorption of acrylonitrile, (C): subtracted spectrum.

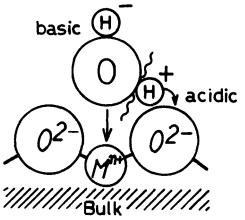

Fig. 6. Hydrated surface model of metal oxide.

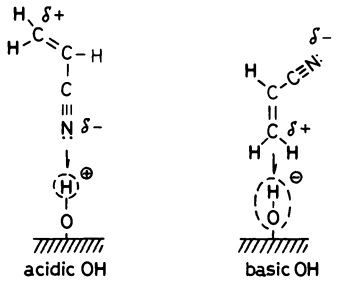

Fig. 7. Adsorbed model of acrylonitrile on surface OH group of metal oxide.

the MnO_2 and MgO surface was actually observed in the liquid phase. Consequently, it can be concluded that the acidic or basic site on metal oxide surface acts as the active site for the liquid-phase hydration of AN.

IR Spectra of Adsorbed AN: The IR spectra of the AN adsorbed on the metal oxides were examined in order to obtain more detailed information with respect to the hydration selectivity to either a C≡N triple bond or a C=C double bond in an AN molecule. The IR spectra of AN adsorbed on SiO_2 and MgO are shown in Fig. 5. The IR spectrum of liquid-state AN shows three characteristic absorption bands; C≡N stretching vibration at 2230 cm^{-1}. C=C stretching vibration at 1609 cm^{-1} and CH_2 deformation vibration at 1415 cm^{-1}, respectively.[21,22] When AN was adsorbed on the SiO_2 C≡N band shifted to higher band (2241 cm^{-1}) and a new broad absorption band of surface OH group at ca. 3650 cm^{-1} appeared. This result suggests that the covalent coordination through an N(2s) lone pair of electrons of the AN[23] takes place on the surface OH group of a SiO_2 catalyst. On the other hand, when AN was adsorbed on the MgO surface, two new bands appeared at 1453 and 2939 cm^{-1} and the C≡N band shifted to a higher frequency. These new absorption bands (1453, 2939 cm^{-1}) instead of indicating the disappearance of the vinyl-group absorption bands could be, respectively, assigned to the C–H bending and stretching vibrations of a chain $-CH_2-$ in the ECH molecule. The broad absorption band of the OH stretching vibration from 3400 to 3700 cm^{-1} appears to indicate the formation of an alcoholic bond between the surface OH group and the terminal carbon atom in the AN molecule. These results suggest that σ- or π-component coordination through the C=C double bond of the AN[24] arises on the surface OH groups of an MgO catalyst.

It is known that an acidic or a basic OH group is formed on a metal oxide surface when a water molecule adsorbs to the surface as shown in Fig. 6.[25,26] The EABP value of the metal oxide mentioned before is the difference of the surface concentration between acidic and basic OH groups.[14] The difference of selectivity to the hydration products of the metal oxide catalysts could be explained according to the EABP values of the catalysts. Therefore, the adsorbed state of AN on the acidic or basic OH groups on the metal oxide surface can be schematically depicted as shown in Fig. 7, based on the IR data. It is considered that the selectivity of AN hydration is controlled by acidic or basic OH groups on the metal oxide surface, and that the catalytic activity is also proportional to the amount of surface OH groups on the catalyst.

Conclusions

On the basis of the results described above, we conclude that the liquid-phase hydration of AN on a metal oxide is an acid-base-catalyzed reaction and that the active sites are probably the acidic or basic OH groups on the metal oxide surface.

1) The metal oxide catalysts on liquid-phase hydration of AN could divided into two groups with respect to AA selectivity. Group A is the oxide which gives the AA selectivity with 100% and Group B is the oxide which forms three kinds of products, ECH, BCE, and AA.

2) A good relationship between the hydration abilities (activity and selectivity) of AN on a metal oxide catalysts and the acid-base properties on metal oxides determined by the indicator titration method was observed. The catalytic activity of catalysts of Group A or B is proportional to the number of acid sites at $pK_a \leqq +4.8$ or basic sites at $pK_a \geqq +9.3$, respectively. A

moderate strength of an acid or base ($3.3<pK_a\leqq9.3$) is effective for the liquid-phase hydration of AN.

3) The equi-acid-base point (EABP) values of the metal oxide catalysts of Group A were below 7, and the catalytic conversion increased upon decreasing the EABP value. The EABP value of Group B metal oxides was above 7, and the catalytic activity increased with increasing the EABP value.

4) Two types of the adsorption states assigned to either cyano or vinyl group of AN were observed on the metal oxides.

References

1) A. Kanbara, "Acrylonitrile-Chemistry and Industry," Gihodo, Tokyo (1959), p. 46, 57.

2) Z. Rappoport, "The Chemistry of the Cyano Group," Interscience Publishers, London (1979), p. 256.

3) E. N. Zil'berman, *Russian Chemical Reviews*, **53**, 900 (1984).

4) K. Sugiyama, H. Miura, Y. Nakano, A. Matsukawa, and T. Matsuda, *Nippon Kagaku Kaishi*, **1986**, 19.

5) L. R. Haeffele and H. J. Young, *Ind. Eng. Chem., Prod. Res. Dev.*, **11**, 364 (1972).

6) H. C. Misra, S. K. Roy, P. K. Roy, S. K. Roy, and S. C. Roy, *J. Indian Chem. Soc.*, **56**, 208 (1979).

7) S. K. Roy, S. C. Roy, and P. K. Roy, *J. Indian Chem. Soc.*, **57**, 195 (1980).

8) H. Miura, K. Sugiyama, S. Kawakami, T. Aoyama, and T. Matsuda, *Chem. Lett.*, **1982**, 183.

9) F. Nozaki, T. Sodesawa, T. Yamamoto, *J. Catal.*, **58**, 419 (1983).

10) K. Sugiyama, H. Miura, A. Matsukawa, and T. Matsuda, *Nippon Kagaku Kaishi*, **1986**, 208.

11) S. B. Kanungo, *J. Catal.*, **58**, 419 (1979).

12) V. G. Mikhal'chenko, V. D. Sokolovskii, and G. K. Boreskov, *Kinetika i Kataliz*, **14**, 698 (1973).

13) K. Sugiyama, Y. Nakano, H. Miura, and T. Matsuda, *Bull. Chem. Soc. Jpn.*, **58**, 1825 (1985).

14) T. Hirai, I. Tari, "Surface Electrochemistry," ed by T. Takamura, A. Kozawa, Japan Scientific Societies Press, Tokyo (1978), p. 124.

15) K. Mushiake and N. Masuko, *Seisan Kenkyu*, **29**, 2 (1977).

16) I. Tari, K. Fujii, and T. Hirai, *Denki Kagaku*, **49**, 517 (1981).

17) K. Tanabe, "CATALYSIS-Science and Technology," ed by J. R. Anderson, M. Boudart, Springer-Verlag, Berlin (1981), p. 2.

18) K. Tanaka and A. Ozaki, *J. Catal.*, **8**, 1 (1967).

19) K. Tanabe, "GENDAI KAGAKU," ed by M. Oki, M. Tanaka, Iwanami, Tokyo (1979), Vol. 9, p. 73.

20) A. Kozawa, *J. Electrochem. Soc.*, **106**, 553 (1959).

21) F. Halverson, F. R. Stamm, and J. J. Whalen, *J. Chem. Phys.*, **16**, 808 (1948).

22) R. E. Kitson and N. E. Griffith, *Anal. Chem.*, **24**, 334 (1952).

23) P. J. Chong and G. Curthoys, *J. Chem. Soc., Faraday Trans. 1*, **77**, 1639 (1981).

24) P. J. Chong and G. Curthoys, *J. Chem. Soc., Faraday Trans. 1*, **77**, 1649 (1981).

25) H. P. Boehm, *Angew. Chem.*, **78**, 617 (1966).

26) H. P. Boehm, *Discuss. Faraday Soc.*, **52**, 264 (1972).

27) E. P. Grigorian, G. F. Vytonv, and R. N. Rodyukova, *Zh. Prikl. Khim.*, **49**, 2043 (1976).

 © 1986 The Chemical Society of Japan Bull. Chem. Soc. Jpn., 59, 2991—2996 (1986)

ESR Study of Glass-Like Carbons

Kazuro KAWAMURA* and Shiushichi KIMURA†
Department of Chemistry, National Defense Academy, 1-10-20, Hashirimizu, Yokosuka 239
†Research Laboratory of Engineering Materials, Tokyo Institute of Technology,
Nagatsuta, Midori-ku, Yokohama 227
(Received March 26, 1986)

ESR studies were carried out on a variety of glass-like carbons made from different precursors heat-treated in the range 300—2500 °C. It was found that the behaviors of unpaired electrons were nearly identical. The temperature dependence of ESR spectrum showed that the behavior of localized unpaired electrons in the glass-like carbons changed to that of delocalized ones at HTT about 2500 °C. The ESR spectrum of the glass-like carbons heat-treated at 800 °C consisted of a single line under a pressure of above 10^{-4} Torr but split into two components when air was admitted. This strong interaction with unpaired electrons and air (oxygen molecules) is caused by the active structure related to micropores in the glass-like carbons. We suppose that the polyene type radicals are the most suitable as the active structure to interpret the behavior of unpaired electrons in glass-like carbons heat-treated at 800 °C. As another major point in this study, it was found that there is a correlation between unpaired electron concentration and the g value.

In general carbonized organic materials contain high concentrations of unpaired electrons produced by bond breaking during the pyrolysis. The unpaired electrons are usually stable at room temperature or below, and their behavior is easily observed by ESR absorption measurements. There are many reports of ESR studies on carbonized materials and excellent reviews have been made by Singer,[1] Mizushima,[2] and Mrozowski.[3] ESR studies of glass-like carbons made from cure resins have also been reported.[4–6] There have been few studies on ESR absorption measurements for glass-like carbons made from different precursors which have been heat-treated in a temperature range as wide as 300—2500 °C. Heat treatments in this temperature range cover the process of carbon precursor formation and those of carbonization and graphitization, and are required for ESR study of glass-like carbon to get informations on the behavior of the localized and delocalized unpaired electrons through the microstructural change in the course of heat treatment.

In the present paper, ESR absorption measurements are reported for glass-like carbons prepared from three kinds of cure resins heat-treated between 300 and 2500 °C. The effect of adsorbed air on the ESR absorption spectrum is investigated for glass-like carbons obtained at 800 °C in the temperature range −170—200 °C.

Experimental

Three kinds of cure resins, epoxy resin cured with 2,4,6-trinitrophenol (Epikote 828/TNP =90/10), furfuryl alcohol resin and phenol-formaldehyde resin were heat-treated at temperatures between 300 and 2500 °C under the same conditions as those described previously.[7] ESR absorption spectra were measured for the samples by a JEOL X-band spectrometer, model JES-PE-lX, using 100 KHz magnetic field modulation with the microwave power of 8 mW and crystal current of 0.2 mA. No saturation on the spectrum could be seen under this condition. Temperature was measured by a standard copper-constantan thermocouple put close to the sample in the microwave cavity. The temperature in the cavity was controlled within ±1 °C in the temperature range −170—200 °C by flowing cold gas from liquid nitrogen or hot air through the inside of the cavity by a JES-VT-3A variable temperature controller. Samples were powdered and contained in quartz tubes of 6 mm o.d. To study the effect on adsorbed air for the samples, two vacuum conditions were employed: (1) a low vacuum, the sample was sealed in the quartz tube with a pressure of about 10^{-2} Torr (1 Torr=133.322 Pa), (2) a high vacuum, the sample was sealed in the quartz tube after evacuating to a pressure of above 10^{-4} Torr with heating at 150 °C for 1 h.

The g values of the samples were determined by comparison with that of Mn^{2+} in MgO placed in the cavity close to the sample. The g value for Mn^{2+} was predetermined by comparison with that of DPPH (g=2.0036).[8] The g value of the sample was calculated by the equation $g=g_s H/(H-\Delta H_{diff})$, where g_s and H are the g value and the field at resonance of the standard samples, and ΔH_{diff} is the difference between the field at resonance for the test sample and that for the standard sample. The accuracy of the measurement of the g value was ± 0.0002. The line shapes of the ESR spectra for all samples investigated were almost Lorentzian shape. The area S, which is proportional to the absorption intensity was estimated by the equation, $S=(\pi/3)(\Delta H)^2 \cdot h$,[9] where ΔH is the line width of the first derivative spectrum and h is the peak-to-peak height. The unpaired electron concentration was determined by comparing the area on the spectrum of the sample with that of DPPH.

Results

1. Examination in High Vacuum. The ESR absorption spectra of glass-like carbons made from the three kinds of resins heat-treated at the temperatures in the range 300—2500 °C were nearly identical. Figure 1 shows an example of the typical change of the ESR absorption spectrum of glass-like carbons with heat treatment temperature (HTT). The results in Fig. 1 were measured for the glass-like carbon from epoxy resin cured with TNP. The spectra for HTT up to 2000 °C consist of a narrow single line, while the spectrum for HTT of 2500 °C contains two com-

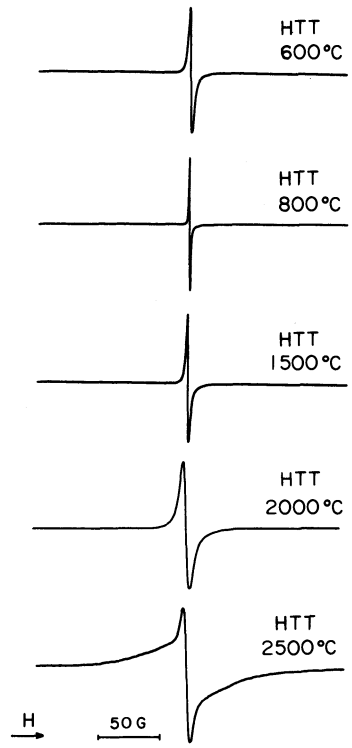

Fig. 1. Change of ESR absorption spectrum of glass-like carbon made from epoxy resin cured with 10 wt% of TNP at different HTT in a high vacuum.

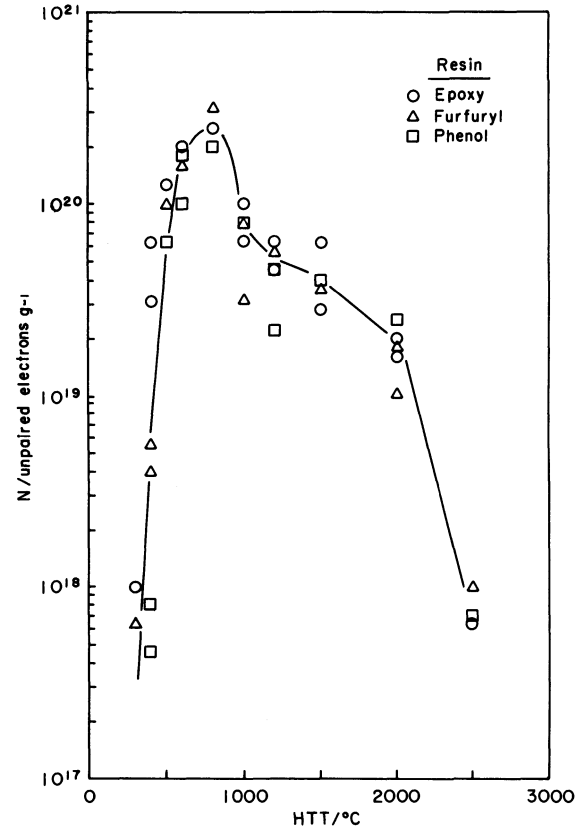

Fig. 2. Changes of unpaired electron concentrations (N) in glass-like carbons with HTT in a high vacuum.

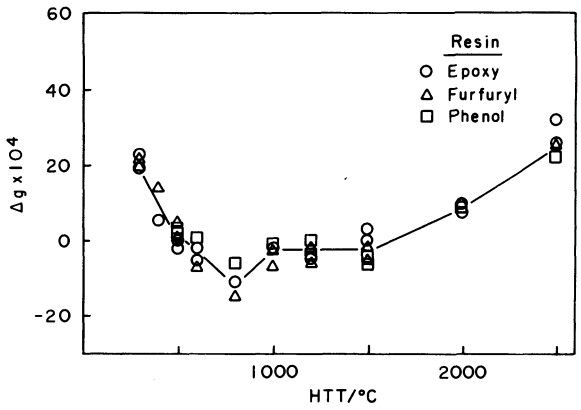

Fig. 3. Changes of Δg on ESR absorption spectra of glass-like carbons with HTT in a high vacuum.

ponents, narrow- and broad-line components. The line widths for narrow-line components are 5—9 G and that for broad one is about 30 G. Broad-line component is not clear to detect quantitatively.

The unpaired electron concentration (N) and the g value of the three kinds of glass-like carbons are shown in Figs. 2 and 3 plotted as a function of HTT. It should be noted that a maximum occurs in N vs. HTT curve at HTT of about 800 °C and a shoulder in the HTT range 1200—1500 °C as shown in Fig. 2. Similar data have been reported by Mrozowski[10] and Toyoda et al.[5] The g values of the glass-like carbons are very close to that of the free spin, g=2.0023, but small change in g with HTT can be seen. As shown in Fig. 3, as with increasing HTT the g shift Δg(Δg= g_s−2.0023, g_s: g value of each sample), decreases steeply to a minimum at HTT of 800 °C at first, increases a little bit to a value at 1000 °C, keeps the value up to HTT of 1500 °C, and then increases gradually. If we combine the results in Figs. 2 and 3, it is seen that an inverse relation exists between N and Δg.

Figure 4 shows the typical temperature dependence of the line width, ΔH, and the peak-to-peak height, h of the spectra at HTT's 800 and 2500 °C. At HTT of 800 °C ΔH decreases gradually and h increases monotonically, as the temperature is decreased. This behavior is similar to that of DPPH, which is characteristic of localized unpaired electrons.[11] At HTT of 2500 °C, little change in ΔH or h against temperature is observed.

In Fig. 5 the S_t/S_{20} is plotted as a function of inverse temperature for glass-like carbons heat-treated at various temperatures, where S_t and S_{20} are the areas of ESR absorption spectra of t °C and 20 °C, respectively. A good linear relationship is resulted at each HTT. The slopes of the straight lines are positive for HTT lower than 2000 °C, and that is slightly negative at HTT of 2500 °C.

2. Examination in Low Vacuum. Figure 6 shows the temperature dependence of the ESR absorption spectrum of glass-like carbon made from epoxy resin

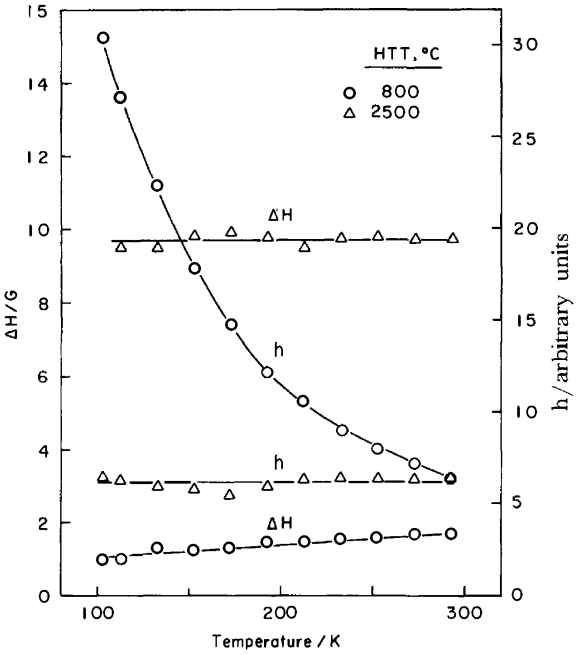

Fig. 4. Temperature dependence of line width (ΔH) and intensity of peak-to-peak height (h) of ESR absorption spectrum of glass-like carbon made from epoxy resin cured with 10 wt% of TNP in a high vacuum.

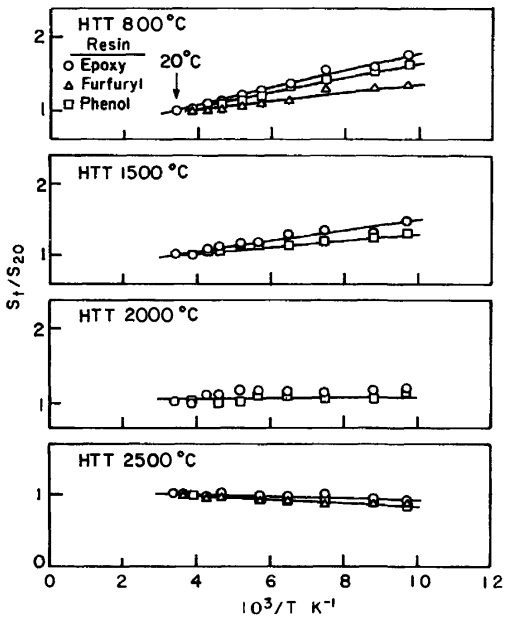

Fig. 5. Relation between relative absorption intensity (S_t/S_{20}) and $1/T$ of glass-like carbons in a high vacuum.

cured with TNP heat-treated at 800°C. In contrast with the spectrum in high vacuum the ESR absorption spectra measured for HTT of 800°C in a low vacuum at room temperature consist of two components, narrow- and broad-line components. The spectrum is common for all three cure resins heat-treated at

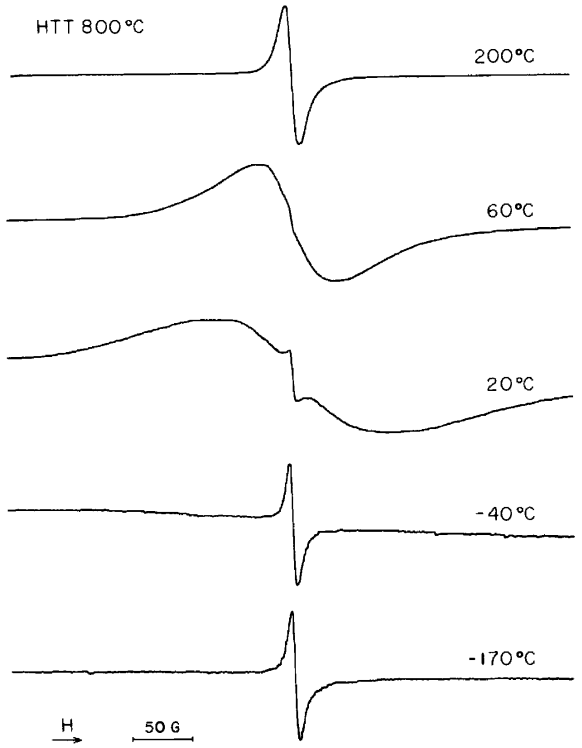

Fig. 6. Change in ESR absorption spectrum of glass-like carbon made from epoxy resin cured with 10 wt% of TNP in a low vacuum.

800°C. The line width of the broad-line component ranges 100 to 500 G and the width of the narrow one 2 to 5 G. The vacuum condition and the measurement temperature affect the line width and the intensity of the broad-line component strongly. The broad-line spectrum observed under a low vacuum changed back to the narrow-line spectrum in high vacuum as shown in Fig. 1 (HTT 800°C), and the line broadening appears immediately when air is admitted. The line-broadening seen in the glass-like carbons heat-treated at 800°C was also observed in the glass-like carbon made from furfuryl alcohol resin heat-treated at 1000°C, but not observed in glass-like carbons prepared at other HTT in the range 300—2500°C.

The broad-line component in the spectrum observed at 20°C shown in Fig. 6 becomes broader and weaker as the temperature is decreased, and the line width increases to the width broaden than 1000 G at −60°C. At a temperature below −70°C the broad-line component is too wide to be detected. When the temperature is increased above room temperature, the broad-line component is narrowed, and the narrow-line component can be seen as a slight shoulder on the broad-line component at 60°C as shown in Fig. 6. The narrow-line component is imperceptible on the broad one at 70°C by narrowing of the broad-line component, and the line width of the broad one at 200°C ranges 10—20 G. Therefore, the line width of the broad-line component increases, and the intensity

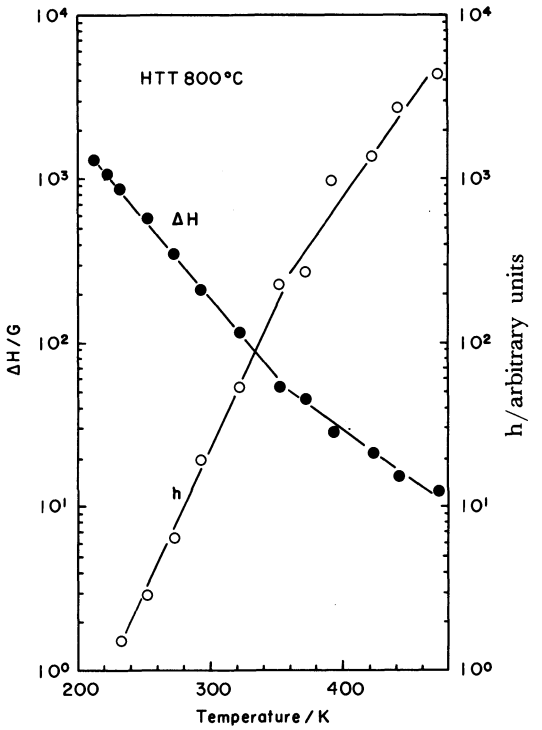

Fig. 7. Temperature dependence of line width (ΔH) and intensity of peak-to-peak height (h) of broad-line component of ESR spectrum of glass-like carbon made from epoxy resin cured with 10 wt% of TNP in a low vacuum.

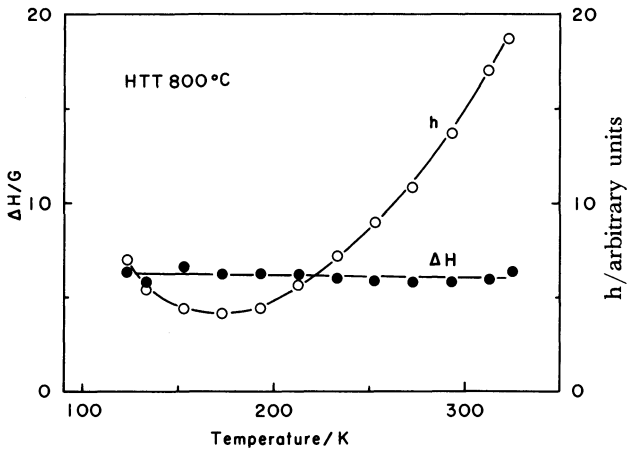

Fig. 8. Temperature dependence of line width (ΔH) and intensity of peak-to-peak height (h) of narrow-line component of ESR spectrum of glass-like carbon made from epoxy resin cured with 10 wt% of TNP in a low vacuum.

decreases markedly, as the temperature is decreased. The trend is shown in Fig. 7. On the other hand, as shown in Fig. 8, the line width of the narrow-line component is almost constant, and with decreasing temperature the peak-to-peak height decreases to a minimum at around 173 K (−100°C) and then increases. The ratio S_t/S_{20} is plotted as a function of inverse temperature for narrow- and broad-line components for HTT of 800°C in Fig. 9. A minimum

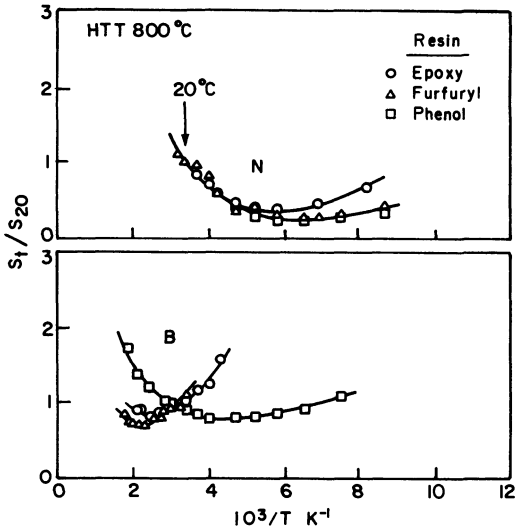

Fig. 9. Relation between relative absorption intensity (S_t/S_{20}) and $1/T$ of glass-like carbons in a low vacuum, N for narrow-line component and B for broad-line component.

of the narrow-line component appeares in the range 153—183 K. On the other hand, a minimum is also observed for broad-line component, but the minimum appears at higher temperature than that for the narrow-line component.

Discussion

1. Examination in High Vacuum. The unpaired electrons at HTT 800°C are mainly localized because of the positive slope of the S_t/S_{20} vs. $1/T$ plots (Fig. 5). The decrease of the slope with increasing HTT indicates that there is a gradual decrease in the localized spin centers and increase in the delocalized spin centers, and the decrease is probably due to the growth of the carbon layer planes. The behavior of the localized unpaired electrons observed in these carbonized resins changes to delocalized one at HTT around 2500°C, because of the slight negative slope as shown in Fig. 5.[12]

The change of g value with HTT is very small in each sample in the HTT range 300—2500°C, but this change is strongly correlated to the unpaired electron concentration as mentioned in Results (Figs. 2 and 3). Logarithm of the value of the unpaired electron concentration shows a good linear relationship against Δg as shown in Fig. 10. The relationship can be fitted to $\log N = A + B \cdot \Delta g \times 10^4$, by a linear least-squares analysis, where $A = 19.7 \pm 0.4$, $B = -0.068 \pm 0.025$. The interaction of unpaired electrons becomes stronger as the unpaired electron concentration is increased, and the strong interaction makes the g value to decrease.

2. Examination in Low Vacuum. Singer et al. studied the effect of paramagnetic gases on the ESR absorption of carbon material[13] and found that O_2 and NO affects strongly on broadening the ESR ab-

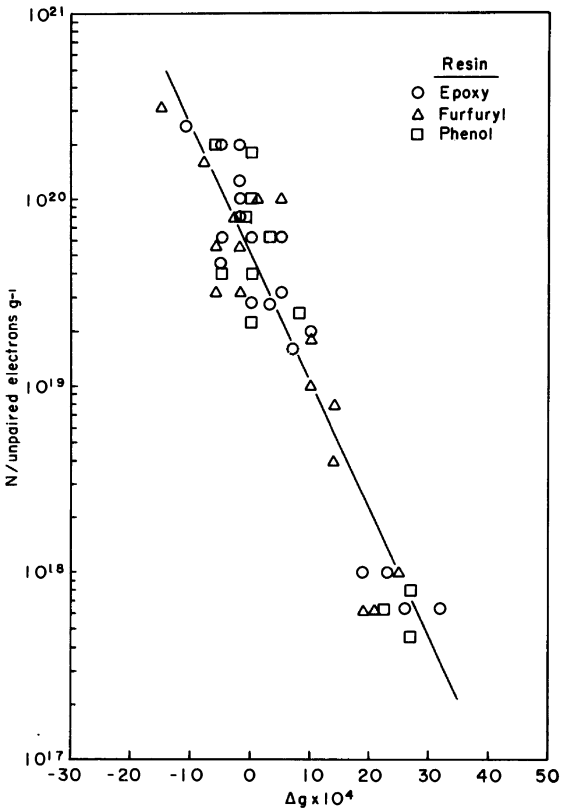

Fig. 10. Unpaired electron concentration as a function of Δg for glass-like carbons made from cure resins.

sorption spectrum, while N_2 no influence. Therefore, line broadening seen in the spectrum for HTT of 800°C is caused by the strong interaction between unpaired electrons in glass-like carbons and adsorbed oxygen molecules. The broadening phenomenon was also observed by Fielder et al. in the ESR study of pyrolysis of acrylonitrile homopolymer fibers (PAN).[14] They found that the ESR spectrum of char made from PAN pyrolysis at 700—850°C showed a single narrow line in vacuum. When the sample was exposed to air, the spectrum separated into two components with a narrow line of about 2 G width and a broad line of about 40 G width, and only a broad line was observed after a long exposure to air. Analysis of the volatile products produced from PAN during pyrolysis at 800°C showed that the major constituent was HCN, and most likely nitrogen came from heteroaromatics, thus leaving highly reactive fragments. They assumed that this effect of air on the spectrum is the formation of the highly reactive fragments produced by the rupture of heteroaromatics. Our finding of the broadening of the ESR absorption spectrum of glass-like carbons in low vacuum at HTT 800°C is basically the same phenomenon. In addition, we believe that the strong physical adsorption of air on the surface of glass-like carbons at HTT 800°C is caused by micro-pores developed during pyrolysis. Noda et al.[15] and Fitzer et al.[16] reported that the surface area attained in the glass-like carbons showed a maximum at HTT near 800°C, indicating development of an open micropores. As shown in Fig. 9, changes in narrow-line components of three glass-like carbons are almost the same as those in broad-line components except a little difference in temperature for the minimum point. These trends indicate that the narrow-line component is also influenced by the adsorption of air indirectly. Since for localized unpaired electrons S_t/S_{20} increases with increasing inverse temperature and for delocalized unpaired electrons S_t/S_{20} decreases, the variations in Fig. 9 are due to a mixed behavior for the localized and the delocalized unpaired electrons. Unpaired electrons in glass-like carbon heat-treated at 800°C are very much influenced by oxygen molecules adsorbed on the surface.

The formation of unpaired electrons through the pyrolysis of cure resins can be explained as follows;

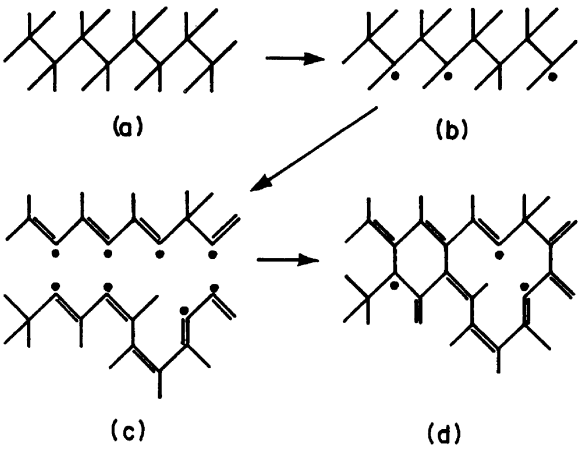

Here, the Structure (a) indicates the hydrocarbon chain in the original cure resin. The unpaired electrons appear by the dehydrogenation reaction and chain breaking during pyrolysis as shown in Structure (b). The unpaired electrons in radical structures increase at near HTT of 800°C as shown in Structure (c) and decrease gradually by the recombination of unpaired electrons as shown in Structure (d) as HTT is increased. A strong interaction of unpaired electrons caused by the exchange of the position is expected in the polyene type radicals (Structure (c)). And also the behavior of this type of radicals can be easily affected by oxygen molecules adsorbed on the active surface on which micropores are developed well. A strong exchange interaction between unpaired electrons of glass-like carbons and oxygen molecules makes the spin-spin relaxation time T_2 shorter, T_2 is given by $T_2=\hbar/\sqrt{3}g\beta\Delta H$, where $\hbar$ is the Plank constant devided by 2π and β is the Bohr magneton,[17] and as the result broadening of the ESR absorption spectrum is observed.

Summary

ESR studies were carried out for glass-like carbons

prepared from the cure resins (epoxy resin, phenol-formaldehyde resin and furfuryl alcohol resin) in the HTT range 300—2500°C. The measurements were made at temperatures in the range −170—200°C under conditions of a high and a low vacuum. The ESR absorption spectra of the glass-like carbons obtained from these resins were almost identical. The unpaired electron concentration shows a maximum at HTT near 800°C. When air is admitted to the glass-like carbons obtained at HTT 800°C, the ESR absorption spectra split into two components. This splitting is caused by the exchange interaction of unpaired electrons in the glass-like carbons and oxygen molecules absorbed on the surface. From the ESR data in a high vacuum, for the glass-like carbons made from the cure resins heat-treated at the temperature around 2500°C unpaired electrons are delocalized ones. The value of the unpaired electron concentration (N) and the g-shift, $\Delta g(\Delta g=g_s-2.0023)$ can be fitted to $\log N = A+B\cdot\Delta g$, independent of the particular carbon.

References

1) L. S. Singer, *Proc. Fifth Conf. Carbon*, **2**, 37 (1962).
2) S. Mizushima, TANSO, No. 47, 30 (1966), No. 50. 20 (1967).
3) S. Mrozowski, *J. Low Temp. Phys.*, **35**, 231 (1979).
4) C. Jackson and W. F. K. Wynne-Jones, *Carbon*, **2**, 227 (1964).
5) S. Toyoda, S. Sugawara, and T. Furuta, *Carbon*, **8**, 473 (1970).
6) S. Orzesko and K. T. Yang, *Carbon*, **12**, 493 (1974).
7) K. Kawamura and S. Kimura, *Bull. Chem. Soc. Jpn.*, **56**, 2499 (1983).
8) J. E. Wertz, *Chem. Rev.*, **55**, 919 (1955).
9) M. Kinoshita, "Yuki Handotai," Jikken Kagaku Koza, Zoku 13, Maruzen (1967), pp. 235—244.
10) S. Mrozowski, *Carbon*, **9**, 97 (1971).
11) S. Toyoda, T. Yamakawa, Y. Yamada, and K. Kobayashi, TANSO, No. 72, 8 (1973).
12) K. Kamiya, S. Yugo, M. Inagaki, H. Saito, and T. Tsuzuku, *Bull. Chem. Soc. Jpn.*, **41**, 2782 (1968).
13) L. S. Singer and W. J. Spry, *Bull. Am. Phys. Soc., Series II*, **1**, 214 (1956).
14) A. K. Fielder, E. Fitzer, and F. Rozpłoch, *Carbon*, **11**, 426 (1973).
15) T. Noda, M. Inagaki, and S. Yamada, *J. Non-Cryst. Solids*, **1**, 285 (1969).
16) E. Fitzer, W. Schäfer, and S. Yamada, *Carbon*, **7**, 643 (1969).
17) R. S. Alger, "Electron Paramagnetic Resonance: Techniques and Applications," John Wiley and Sons, New York (1968).

 © 1986 The Chemical Society of Japan Bull. Chem. Soc. Jpn., 59, 2997—3001 (1986)

Polarized Raman and Infrared Spectra of [$^1H_4$]- and [$^2H_4$]Pyridazines

Yoshimi Ozono, Yoshinori Nibu,† Hiroko Shimada,* and Ryoichi Shimada†
Department of Chemistry, Faculty of Science, Fukuoka University, Nanakuma, Jonan-ku, Fukuoka 814-01
†Department of Chemistry, Faculty of Science, Kyushu University 33, Hakozaki, Higashi-ku, Fukuoka 812
(Received March 28, 1986)

The polarized Raman and infrared spectra of [$^1H_4$]- and [$^2H_4$]pyridazines were studied. Assignments of the normal vibrations made by previous workers were reexamined on the basis of polarization behavior of the Raman and infrared bands and also through the normal coordinate calculation, and reasonable assignments are presented.

Although the vibrational spectra of aromatic azines such as pyridine, pyrimidine, and pyrazine have been studied by many workers, few informations are available for the normal vibrations of pyridazine. Vibrational analyses of the Raman and infrared spectra of pyridazine were made by Ito et al.[1] and Lord et al.[2] on the basis of intercomparison with the normal vibrations of benzene, pyridine, and diazines, and by Stidham and Tucci[3] on the basis of the isotopic effect on the vibrational frequencies. Their vibrational assignments, however, are not consistent with each other. Especially for the assignments of the non-totally symmetric vibrations, there are many discrepancies in the vibrational modes and frequencies. Therefore, definite experimental evidences are needed for the reasonable assignments of the normal vibrations.

In this work, vibrational assignments for [$^1H_4$]- and [$^2H_4$]pyridazines are reexamined through measurements of the polarization behavior of the Raman and infrared spectra and also through the normal coordinate calculation and reliable assignments of the normal vibrations are given.

Experimental

Material. [$^2H_4$]Pyridazine was synthesized by the exchange reaction of [$^1H_4$]pyridazine, which was obtained from Aldrich Chemical Company, with D_2O and NaOD. Isotopic purity of the product was determined by the nuclear magnetic resonance measurement. The samples used for the experiment were purified by repeated distillation under reduced pressure.

Optical Measurements. Polarization measurement of the Raman spectrum was made in liquid and single crystal phases with a JEOL 400 T Laser Raman Spectrophotometer. The sample was excited with the 514.5 nm line from an Ar^+ ion laser. [$^1H_4$]- and [$^2H_4$]Pyridazines crystalize at −8 °C. Although single crystals of the sample could be easily obtained by the Bridgman method, samples with rectangular shape needed for the quantitative observation of the polarized Raman spectrum could not be prepared because pyridazine is quite volatile and hygroscopic and the crystal surface became opaque and deliquesced immediately after the crystal was cut off with a razor blade. Thus the polarized Raman spectrum was observed in the following way. Single crystals were grown in capillary glass tubes of 3 mm in diameter having a sharp conical end by the Bridgman method and a well grown single crystal was selected. The extinction directions of the crystal were determined under the polarized light. The direction of crystal growth which was along the capillary tube was found to be one of the extinction directions. Determination of another extinction direction was made by rotating the capillary tube, which was supported horizontally, around the crystal growth direction under the light polarized perpendicular to the capillary tube. The extinction direction thus detected was more clearly confirmed by tilting the capillary tube from the horizontal orientation. These two extinction directions will be referred to as u and v axes, respectively. The w axis is taken to be perpendicular to both the u and v axes. These procedures were carried out in a box where the temperature was kept at −12 °C. The crystal specimen was held in a Raman sample cell kept at −12 °C in such a way that the u axis of the crystal was directed parallel to the polarization direction of the excitation laser beam and the Raman scattering was observed at right angles with the laser beam. The observation was made with two crystal orientations. In the first orientation the v axis and in the second the w axis were directed parallel to the propagation direction of the laser beam, respectively. Thus the uu, uv, and uw polarized Raman spectra were obtained, where the first letter refers to the direction of polarization of the excitation laser beam and the latter to that of the scattering light.

The infrared spectrum was observed in vapor and single crystal phases with a Hitachi Infrared Spectrophotometer Model 345. Preparation of the single crystal sample and the method of measurement of the polarized infrared spectrum are exactly the same as those described previously.[4]

Normal Coordinate Calculation

The normal coordinate calculations for [$^1H_4$]- and [$^2H_4$]pyridazines were performed through the standard GF matrix method with a FACOM M-200 computer at the Computer Center of Fukuoka University. The molecular structure of [$^1H_4$]pyridazine was taken from the data determined by Almenningen et al.[5] The F matrix elements for the in-plane and out-of-plane vibrations were evaluated with the potential fields of an improved modification of the Urey–Bradley and valence force fields, respectively, as described previously.[4,6,7] Values of the force constants for the in-plane and out-of-plane vibrations are given in Tables 1 and 2, respectively. The notations of the force constants are the same as those described previously.[4,6,7] Calculated vibrational frequencies and modes are listed in Tables 3 and 4, respectively.

Table 1. Force Constants for In-Plane Vibrations

$K_{N\text{-}N}$	5.5	$F_{N\cdots C}$	0.6
$K_{N\text{-}C}$	5.3	$F_{C\cdots C}$	0.8
$K_{C\text{-}C}$	4.5	$F_{N\cdots H}$	0.55
$K_{C\text{-}H}$	4.6	$F_{C\cdots H}$	0.45
H_{CNN}	0.5	k_{rr}^{o}	0.05
H_{NCC}	0.35	k_{rr}^{m}	−0.05
H_{CCC}	0.4	k_{RR}^{m}	−0.1
H_{NCH}	0.2	$f_{\beta\beta}^{o}$	0.12
H_{CCH}	0.27	ρ	0.37

Force consatants denoted by K, H, F, ρ, and k are given in hN m^{-1} (=mdyn/Å) and f in aNmrad^{-2} (=mdynÅ/rad^2) units. R refers to the N-N, C-N and C-C bonds, r to the C-H bond and β to the ∠NCH and ∠CCH. Superscripts o and m refer to ortho and meta, respectively.

Table 2. Force Constants for Out-of-Plane Vibrations

$Q_{N\text{-}N}$	0.17	q^{m}	0.01
$Q_{N\text{-}C}$	0.19	p^{o}	0.06
$Q_{C\text{-}C}$	0.21	p^{m}	−0.06
P_{H}	0.33	t_{N}^{o} [a]	−0.03
q_{N}^{o} [a]	−0.04	t_{C}^{o} [a]	−0.02
q_{C}^{o} [a]	−0.03	t^{m}	−0.01

Force constants are given in aNmrad^{-2} (=mdynÅ/rad^2) units. a) Subscript N indicates that the force constants are concerned with the torsional coordinates involving the C-N and N-N bonds and subscript C the C-C bond. Superscripts o and m refer to ortho and meta, respectively.

Results and Discussion

The relative intensities of the Raman bands in the polarized Raman spectrum are governed by the orientation of the molecules in crystal, that is, the relative intensities depend on the direction cosines between the molecular and crystal axes in the oriented gas model approximation. Therefore, the molecular vibrations belonging to the same symmetry species should show the same polarization behavior in the polarized Raman spectrum observed with a certain crystal orientation with respect to the polarization directions of the excitation and scattering lights. If the crystal structure is known, the relative intensities of the bands can be calculated from the direction cosines between the crystal and molecular axes and thus, the observed polarization behavior of the Raman bands gives a quantitative justification for the assignments of the normal vibrations. Even if the crystal structure is unknown, the polarized Raman spectrum can be observed along the extinction directions. The extinction axes of the crystal coincide with the crystal axes in general and thus the observed polarization behavior of the Raman bands gives a qualitative information for the classification of the observed Raman bands into a certain symmetry species. We applied this experimental procedure for the assignments of the normal vibrations of halosubstituted pyrimidines[8] and pyridine[9] and obtained satisfactory results.

The polarized Raman and infrared spectra of [$^1H_4$]-

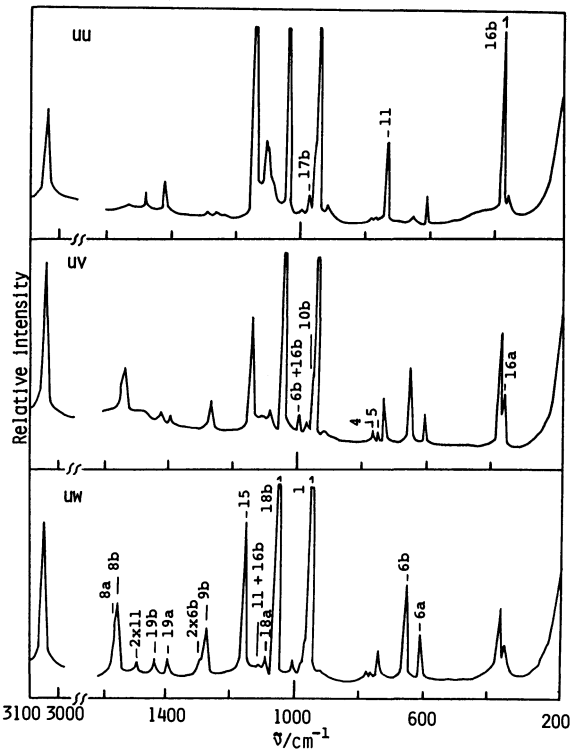

Fig. 1. Polarized Raman spectrum of [$^1H_4$]pyridazine single crystal.

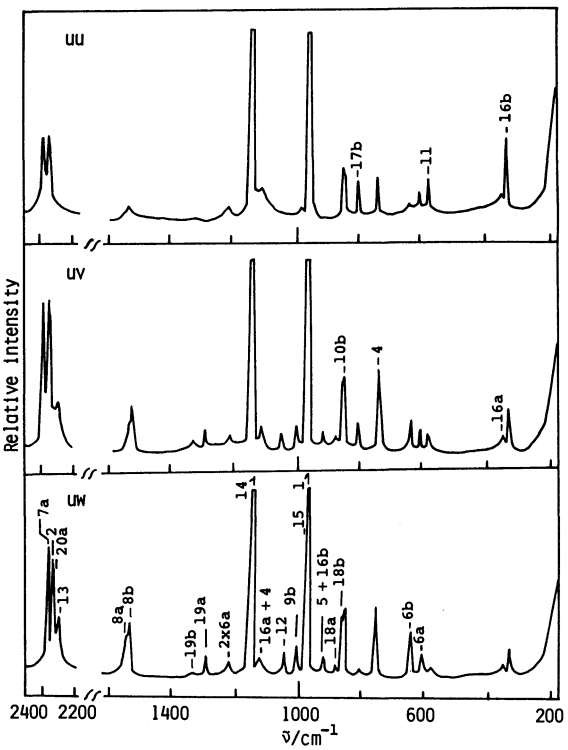

Fig. 2. Polarized Raman spectrum of [$^2H_4$]pyridazine single crystal.

and [$^2H_4$]pyridazines observed in single crystals are shown in Figs. 1, 2, 3, and 4, respectively. The nontotally symmetric vibrational bands in the polarized Raman spectrum of a single crystal can be classified

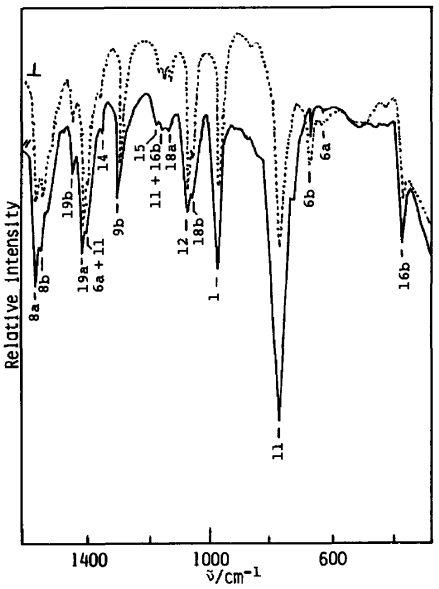

Fig. 3. Polarized infrared spectrum of [$^1H_4$]pyridazine single crystal.

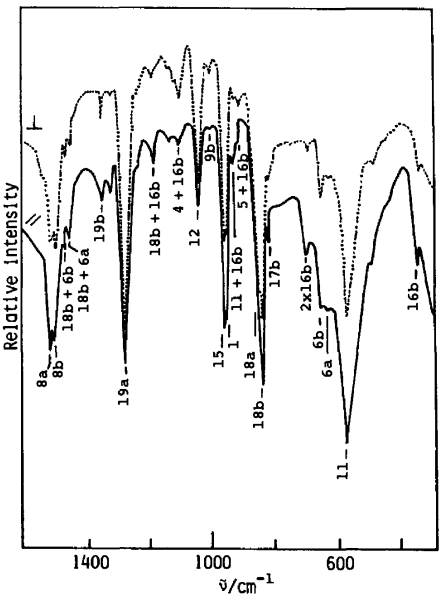

Fig. 4. Polarized infrared spectrum of [$^2H_4$]pyridazine single crystal.

into three types of polarization behavior as can be seen in Figs. 1 and 2. The intensity relationship of the polarized Raman bands belonging to the first type is $I_{uw} > I_{uv} \gg I_{uu}$, the second type $I_{uu} > I_{uv} > I_{uw}$ and the third type $I_{uv} > I_{uw} > I_{uu}$. These three types of polarization behavior are referred to as types α, β, and γ, respectively. The polarized infrared spectra measured with the incident lights polarized parallel and perpendicular to the crystal growth direction are referred to as // and $\perp$ spectra and drawn with the solid and dotted lines, respectively. The infrared bands in crystal can be classified into three types I, II, and III based on their polarization behavior. The intensity relationship of the bands belonging to the first type is $I_{//} \simeq I_{\perp}$, the second and third types $I_{//} > I_{\perp}$ and $I_{//} < I_{\perp}$, respectively.

The moments of inertia calculated from the molecular structure suggest that the infrared bands belonging to a_1, b_2, and b_1 symmetry species show A, B, and C band contour in [$^1H_4$]pyridazine and B, A, and C contour in [$^2H_4$]pyridazine, respectively. Therefore, each Raman and infrared bands can be experimentally classified into a certain symmetric species based on the polarization behavior observed in crystal phase together with the band contour in vapor phase. The determination of the vibrational modes can be made based on the normal coordinate calculation.

[$^1H_4$]Pyridazine. a_1 Species: Strongly polarized Raman bands observed at 3070, 3053, 1441, 1352, 1150, 1063, and 963 cm^{-1} in liquid phase can be straightforwardly assigned to the totally symmetric ν_{7a}, ν_2, ν_{19b}, ν_{14}, ν_{15}, ν_{18b}, and ν_1 vibrations, respectively, by referring the normal coordinate calculation. The infrared band corresponding to the ν_1 vibration shows A band contour in vapor and the type I polarization in crystal. Infrared bands at 1555 and 632 cm^{-1} show the type I polarization in crystal and therefore these bands were assigned to the ν_{8a} and ν_{6a} vibrations, respectively, although the corresponding Raman band at 1570 cm^{-1} seems to be depolarized in liquid due to overlapping of a band assigned to the ν_{8b} vibration and the corresponding Raman band at 622 cm^{-1} is very slightly polarized in liquid.

b_2 Species: Infrared bands observed at 1408, 1283, 1058, and 663 cm^{-1} show B band contour in vapor and therefore can be assigned to the b_2 vibrations. Thus these bands were assigned to the ν_{19a}, ν_{9b}, ν_{12}, and ν_{6b} vibrations, respectively. The corresponding infrared and Raman bands observed in crystal show the type III and type α polarization, respectively. Raman bands at 3080, 3041, 1564, and 1113 cm^{-1} show also the type α polarization in crystal and the corresponding infrared bands show the type III polarization in crystal. Therefore, these bands were assigned to the ν_{20a}, ν_{13}, ν_{8b}, and ν_{18a} vibrations, respectively.

b_1 Species: Infrared bands at 760 and 372 cm^{-1} show C band contour in vapor and hence these bands were assigned to the ν_{11} and ν_{16b} vibrations of b_1 species, respectively. The corresponding infrared and Raman bands observed in crystal show the type II and type β polarization, respectively. A Raman band at 986 cm^{-1} shows the type β polarization in crystal and thus this band was assigned to the ν_{17b} vibration.

a_2 Species: Depolarized Raman bands at 786, 775, and 363 cm^{-1} in liquid show the type γ polarization in crystal and therefore these bands were assigned to the ν_4, ν_5, and ν_{16a} vibrations of a_2 species, respectively, because the Raman bands showing the types α and β polarization in crystal were already assigned to the bands belonging to the b_2 and b_1 vibrations, respectively. A Raman band at 970 cm^{-1} which was not clearly

Table 3. Normal Vibrations of [$^1H_4$]Pyridazine

Sym spec	Mode	Stidham[a]	This work						
			Raman			Infrared			Calcd
		$\tilde{\nu}$/cm^{-1}	$\tilde{\nu}$/cm^{-1}	Pol		$\tilde{\nu}$/cm^{-1}	Pol		$\tilde{\nu}$/cm^{-1}
				liq	cry		vap	cry	
a_1	ν_{7a}	3064	3070	p					3083
	ν_2	3052	3053	p					3077
	ν_{8a}	1572	1570	dp?		1555		I	1573
	ν_{19b}	1417	1441	p		1440		I	1453
	ν_{14}	1347	1352	p		1340		I	1355
	ν_{15}	1063	1150	p		1153		I	1122
	ν_{18b}	1150	1063	p		1055		I	1058
	ν_1	964	963	p		960	A	I	973
	ν_{6a}	630	622	dp?		632		I	631
b_2	ν_{20a}	3056	3080	dp	α				3097
	ν_{13}	3085	3041	dp	α				3040
	ν_{8b}	1556	1564	dp	α	1540		III	1587
	ν_{19a}	1450	1401	dp	α	1408	B	III	1424
	ν_{9b}	1283	1287	dp	α	1283	B	III	1286
	ν_{18a}	1129	1113	dp	α	1112		III	1110
	ν_{12}	1032	1052	dp	α	1058	B	III	1049
	ν_{6b}	667	660	dp	α	663	B	III	656
b_1	ν_{17b}	842	986	dp	β				982
	ν_{11}	760	755	dp	β	760	C	II	777
	ν_{16b}	370	370	dp	β	372	C	II	374
a_2	ν_{10b}	861	970		γ				958
	ν_4	753	786	dp	γ				788
	ν_5	938	775	dp	γ				774
	ν_{16a}	410	363	dp	γ				371

a) H. D. Stidham and J. V. Tucci, *Spectrochim. Acta*, **23A**, 2233 (1967).

resolved in liquid shows the type γ polarization in crystal and thus this band was assigned to the ν_{10b} vibration.

The normal vibrations thus assigned are summarized in Table 3 together with those given by Stidham and Tucci.[3] Stidham and Tucci assigned the infrared band observed at 1417 cm^{-1} to the a_1 vibration but this band shows B band contour in vapor and the type III polarization in crystal. Thus this band should be assigned to the b_2 vibration. They also assigned the Raman bands observed at 1450, 1129, and 1032 cm^{-1} to the b_2 vibrations but the first two bands are polarized in liquid and the last shows a_2 polarization behavior in crystal. Therefore, the bands observed at 1417, 1450, 1129, and 1032 cm^{-1} by them were assigned to the ν_{19a}, ν_{19b}, $\nu_{11}+\nu_{16b}$, and $\nu_{6b}+\nu_{16b}$ vibrations, respectively. They observed a weak Raman band at 938 cm^{-1} and assigned to the a_2 vibration. This band, however, shows neither b_2, b_1, nor a_2 polarization behavior in crystal and thus we assigned it to the $\nu_{8a}-\nu_{6a}$ vibration. Stidham and Tucci observed very weak Raman bands at 753, 861, 842, and 410 cm^{-1} and assigned those to the out-of-plane vibrations but these bands could not be clearly observed in this work.

[$^2H_4$]Pyridazine. a_1 Species: Strongly polarized Raman bands observed at 2295, 2276, 1318, 1130, 965, 946, 835, and 600 cm^{-1} can be assigned to the ν_{7a}, ν_2, ν_{19b}, ν_{14}, ν_{15}, ν_1, ν_{18b}, and ν_{6a} vibrations, respectively. The corresponding infrared bands show the type I polarization in crystal. An infrared band at 1515 cm^{-1} shows the type I polarization in crystal and hence this band was assigned to the ν_{8a} vibration, although the corresponding Raman band at 1532 cm^{-1} seems to be depolarized in liquid due to overlapping of a band assigned to the ν_{8b} vibration.

b_2 Species: Infrared bands observed at 1268 and 1035 cm^{-1} show A band contour in vapor and the type III polarization in crystal, and the corresponding Raman bands show the type α polarization in crystal. Therefore, these bands were assigned to the ν_{19a} and ν_{12} vibrations, respectively. Raman bands observed at 2272, 2247, 1525, 980, 865, and 639 cm^{-1} show the type α polarization in crystal and the corresponding infrared bands show the type III polarization in crystal. Therefore these bands were assigned to the ν_{20a}, ν_{13}, ν_{8b}, ν_{9b}, ν_{18a}, and ν_{6b} vibrations, respectively.

b_1 Species: Infrared bands observed at 562 and 321 cm^{-1} show C band contour in vapor and the type II polarization in crystal. The corresponding Raman bands show the type β polarization in crystal. Hence these bands were assigned to the ν_{11} and ν_{16b} vibrations, respectively. A Raman band observed at 802 cm^{-1} shows the type β polarization in crystal and the corresponding infrared band shows the type II polarization

Table 4. Normal Vibrations of [$^2H_4$]Pyridazine

Sym spec	Mode	Stidham[a]	This work						
			Raman			Infrared			Calcd
		$\tilde{\nu}$/cm^{-1}	$\tilde{\nu}$/cm^{-1}	Pol		$\tilde{\nu}$/cm^{-1}	Pol		$\tilde{\nu}$/cm^{-1}
				liq	cry		vap	cry	
a_1	ν_{7a}	2303	2295	p					2267
	ν_2	2277	2276	p					2262
	ν_{8a}	1545	1532	dp?		1515		I	1505
	ν_{19b}	1270	1318	p		1307		I	1308
	ν_{14}	1203	1130	p					1158
	ν_{15}	835	965	p		950		I	966
	ν_1	950	946	p		945		I	956
	ν_{18b}	894	835	p		833		I	827
	ν_{6a}	608	600	p		610		I	615
b_2	ν_{20a}	2259	2272	dp	α				2274
	ν_{13}	2303	2247	dp	α				2245
	ν_{8b}	1528	1525	dp	α	1505		III	1535
	ν_{19a}	1318	1272	dp	α	1268	A	III	1281
	ν_{12}	973	1032	dp	α	1035	A	III	1023
	ν_{9b}	1038	980	dp	α	983		III	969
	ν_{18a}	853	865	dp	α	860		III	894
	ν_{6b}	642	639	dp	α	633		III	647
b_1	ν_{17b}	710	802	dp	β	800		II	808
	ν_{11}	563	578	dp	β	562	C	II	588
	ν_{16b}	327	330	dp	β	321	C	II	324
a_2	ν_{10b}	727	820	dp	γ				823
	ν_4	686	738	dp	γ				723
	ν_5	766							592
	ν_{16a}	351	347	dp	γ				335

a) H. D. Stidham and J. V. Tucci, *Spectrochim. Acta*, **23A**, 2233 (1967).

in crystal. Therefore this band was assigned to the ν_{17b} vibration.

a_2 Species: Depolarized Raman bands at 820, 738, and 347 cm^{-1} show the type γ polarization in crystal and therefore these bands were assigned to ν_{10b}, ν_4, and ν_{16a} vibrations, respectively. The ν_5 vibrational band could not be resolved in the polarized Raman spectrum.

The normal vibrations of [$^2H_4$]pyridazine thus assigned are summarized in Table 4 together with those given by Stidham and Tucci.[3] Stidham and Tucci assigned the Raman bands at 1270 and 1318 cm^{-1} to the a_1 and b_2 vibrations, respectively. However the former shows b_2 and the latter a_1 polarization behavior, and thus we assigned these bands to the ν_{19a} and ν_{19b} vibrations, respectively. A polarized Raman band at 1203 cm^{-1} in liquid was assigned the $2\nu_{6a}$ vibration although Stidham and Tucci assigned it to the ν_{14} vibration. A strong and polarized Raman band at 1130 cm^{-1}, which was assigned to the $2\nu_{11}$ vibration by them, was assigned to the ν_{14} vibration in this work. Stidham and Tucci assigned a very weak Raman band at 710 cm^{-1} to the b_1 vibration, but this band shows neither b_2, b_1, nor a_2 polarization behavior in single crystal, and therefore, this band was assigned to the $\nu_{19b}-\nu_{6a}$ vibration. They also assigned very weak Raman bands at 686 and 766 cm^{-1} to the a_2 vibrations, but these bands could not be observed in this work.

Agreements between observed and calculated vibrational frequencies for both [$^1H_4$]- and [$^2H_4$]pyridazines are satisfactory. We believe that the polarization behavior of the Raman and infrared bands gives clear and definite experimental justification for the assignments, and the normal vibrations determined in this work are quite reliable.

References

1) M. Ito, R. Shimada, T. Kuraishi, and W. Mizushima, *J. Chem. Phys.*, **25**, 597 (1956).

2) R. C. Lord, A. L. Marston, and F. A. Miller, *Spectrochim. Acta*, **9**, 113 (1957).

3) H. D. Stidham and J. V. Tucci, *Spectrochim. Acta*, **23A**, 2233 (1967).

4) S. Kizuki, Y. Ishibashi, H. Shimada, and R. Shimada, *Mem. Fac. Sci. Kyushu Univ., Ser. C*, **13**, 7 (1981).

5) A. Almenningen, G. Bjørnsen, T. Ottersen, R. Seip, and T. G. Strand, *Acta Chem. Scand., Ser A*, **31**, 63 (1977).

6) Y. Ishibashi, R. Shimada, and H. Shimada, *Bull. Chem. Soc. Jpn.*, **55**, 2765 (1982).

7) Y. Ishibashi, F. Arakawa, H. Shimada, and R. Shimada, *Bull. Chem. Soc. Jpn.*, **56**, 1327 (1983).

8) S. Nakama, H. Shimada, and R. Shimada, *Bull. Chem. Soc. Jpn.*, **57**, 2584 (1984).

9) Y. Ozono, M. Maehara, Y. Nibu, H. Shimada, and R. Shimada, *Bull. Chem. Soc. Jpn.*, **59**, 1617 (1986).

 © 1986 The Chemical Society of Japan Bull. Chem. Soc. Jpn., 59, 3003—3006 (1986)

Synergistic Extraction of Copper(II) and Zinc(II) with Tributyl Phosphate and Crown Ether

Yuko HASEGAWA,* Hirofumi MIYATA, and Satoshi YOSHIDA
Department of Chemistry, Science University of Tokyo, Kagurazaka, Shinjuku-ku, Tokyo 162
(Received March 29, 1986)

The solvent extraction of copper(II) and zinc(II) with 12-crown-4 (12C4) or 15-crown-5 (15C5) as picrates into chloroform containing tributyl phosphate (TBP) has been studied. The following conclusions have been reached. i) Even in the presence of TBP which is more basic than crown ether, either copper(II) or zinc(II) is extracted in association with 2 moles of 12C4 or 15C5. ii) The crown ether complex of either copper(II) or zinc(II) forms 1 : 1 : 1 (metal(II) : crown ether : TBP) stoichiometric adducts in chloroform. iii) The 12C4 complex of either copper(II) or zinc(II) forms more stable adducts with TBP than the 15C5 complex. iv) The extraction of the metal (II) with 15C5 and TBP is better than that of 12C4 and TBP. v) The copper(II) complex with 12C4 or 15C5 forms more stable TBP adducts than those from zinc(II) complex.

It has been previously reported[1] that the extraction of zinc(II) with crown ether and picrate ion is not very different from that of copper(II), while the extraction of zinc(II) with β-diketones such as acetylacetone is remarkably poorer than that of copper(II).[2] The different behavior of the ion pair extraction of zinc(II) from the chelate extraction has been explained in terms of the difference in coordination structure of the extracted metal(II) species. This leads to the idea that the adduct formation or the solvation of zinc(II) complexes in organic phase may be different between the ion pair and the chelate.

In the present work, the adduct formation constants between the crown ether–picrate ion pair of zinc(II) or copper(II) and tributylphosphate (TBP) in chloroform have been determined by the solvent extraction method to compare with those of the chelates.

Experimental

All reagents employed were of analytical grade. Tributylphosphate ex. Tokyo Kasei Inc. was purified by washing with water, 0.1 M (M=mol dm^{-3}) sodium hydroxide solution, and 0.1 M perchloric acid.

Copper(II) or zinc(II) nitrate (2.5×10^{-2}M), lithium picrate, and a crown ether were agitated in a stoppered glass tube by a mechanical shaker for an hour with same volume of chloroform containing TBP of various concentrations. The metal(II) in organic phase was then back-extracted with 0.1 M perchloric acid and its concentration was measured by means of atomic absorption spectrometer. Detailed procedures have been described previously.[1]

The distribution ratio D was defined as

$$D=\frac{[M(II)]_{o,total}}{[M(II)]_{a,total}},$$

where the subscripts "o" and "a" denote the organic and aqueous phases, respectively.

Results and Discussion

When zinc(II) and copper(II) were extracted from lithium picrate solution containing a given amount of 12C4 or 15C5 into chloroform in the presence of 0.1 M TBP, the distribution ratio increased in proportion to the square of the anion concentration. This result indicates that one mole of the metal ions are extracted with two moles of picrate ions, in the similar manner to the extraction of the metal(II)–crown ether–picrate into chloroform reported earlier.[1]

The distribution ratio of the metal(II) between lithium picrate solution and TBP–chloroform is plotted against the concentration of TBP in Fig. 1 (symbols are triangles). The log–log plots give straight lines with inclination of 2, although the plots deviate from the straight line in a higher concentration region. It indicates that the ion pair between the metal(II) and picrate ion is accompanied by 2 moles of TBP. From the slope analysis, the extraction constants ($Kex_{02}=D[A^-]_a^{-2}[TBP]_o^{-2}$) of copper(II) and zinc(II) from lithium picrate solution into TBP–chloroform were determined to be 1.3 and 0.4 as log Kex_{02}, respectively.

In the higher concentration region these metal ions seem to be extracted with more than 2 moles of TBP. Hence, the data obtained in the TBP region lower than 0.3M were employed to the data analysis in the present study.

It has been reported[1] that the ion pair between the metal(II) and picrate ion is accompanied by 1 or 2 moles of crown ethers when extracted. Therefore, when the ion pair including a crown ether forms adducts with TBP, the distribution ratio can be represented as

$$D=\frac{\sum[ME_lA_2]_o+[MT_2A_2]_o+\sum[ME_mT_nA_2]_o}{[M^{2+}]_a}, \quad (1)$$

where M, E, A, and T denote the metal(II), crown ether, picrate ion, and TBP, successively, l, m, and n being the integer 1 or 2.

Equation 1 can be rewritten by introducing the extraction constants as follows:

$$D=\{(Kex_{10}[E]_a+Kex_{20}[E]_a^2)+Kex_{02}[T]_o^2+\sum Kex_{mn}[E]_a^m[T]_o^n\}[A^-]_a^2 \quad (2)$$

Figure 1 also shows the relationship between distribution ratio and TBP concentration in the case of metal(II) extraction from an aqueous solution contain-

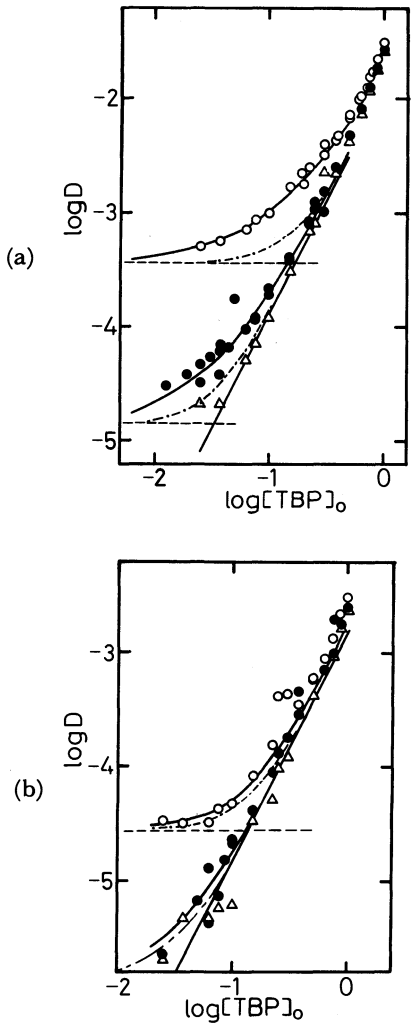

Fig. 1 Extraction of Cu(II)(a) and Zn(II)(b) from 2.5×10^{-2} M lithium picrate solution containing 2.5×10^{-2} M 15C5(○), 12C4(●) or no crown ether(△) into TBP-chloroform.
Solid lines are calculated by the following equation using the constants listed in Table 1.

$$D=\left(\frac{K_{ex10}}{1+K_D}E_T+\frac{K_{ex20}}{(1+K_D)^2}E_T^2+K_{ex02}[T]_o^2+\frac{K_{ex11}}{1+K_D}E_T[T]_o\right)[A^-]^2$$

Chain lines are calculated using only the first three terms in the equation, i.e. ignoring adduct formation.

ing lithium picrate and crown ether into TBP–chloroform. The chain curves in Fig. 1 are obtained by combining the extraction with crown ether $\{(K_{ex10}[E]_a+K_{ex20}[E]_a^2)[A^-]^2\}$ with the extraction with TBP $(K_{ex02}[T]_o^2[A^-]^2)$. The observed distribution ratio is higher than the calculated value given by the chain line. The difference will be ascribed to the adduct formation represented by the third term of the numerator in Eq. 1. Then the extraction constants of the mixed complex or the complex solvated with TBP can be determined as

Table 1. Summary of Equilibrium Constants When the Metal(II) is Extracted as Picrates with Crown Ethers and/or TBP into Chloroform

	Cu(II)		Zn(II)	
	12C4	15C5	12C4	15C5
$\log K_{ex10}$[1)]	0.64	2.09	−0.15	1.01
$\log K_{ex20}$[1)]	3.07	4.44	1.80	3.28
$\log K_{ex11}$	2.54	3.49	1.25	1.69
$\log K_{ex02}$	1.30		0.36	
$\log\bar{\beta}_{11}$	1.90	1.40	1.40	0.68

$$K_{ex_{mn}}=\frac{[ME_mT_nA_2]_o}{[M^{2+}]_a[E]_a^m[T]_o^n[A^-]_a^2}$$

m and n = 0, 1, or 2

$$\bar{\beta}_{11}=\frac{[MEA_2T]_o}{[MEA_2]_o[T]_o}$$

$$D/[A^-]_a^2-K_{ex02}[T]_o^2=K_{ex10}[E]_a+K_{ex20}[E]_a^2+(K_{ex11}[E]_a+K_{ex21}[E]_a^2)[T]_o+(K_{ex12}[E]_a+K_{ex22}[E]_a^2)[T]_o^2+\cdots \quad (3)$$

When the left side of Eq. 3 was plotted against $[T]_o$, straight lines were obtained for the data in Fig. 1. It indicates that the dominant species extracted is accompanied by one mole of TBP in these systems. The slope is $(K_{ex11}[E]_a+K_{ex21}[E]_a^2)$. Since the data in Fig. 1 were obtained at a constant crown ether concentration, $K_{ex11}[E]_a$ and $K_{ex21}[E]_a^2$ can not be calculated separately. As the first approximation, K_{ex21} was ignored and only K_{ex11} was determined. The constants obtained are listed in Table 1.

To check the validity of K_{ex11}, the distribution ratio of the metal(II) between an aqueous solution containing crown ether and lithium picrate (2.5×10^{-2} M) and 0.1 M TBP–chloroform has been measured. Figure 2 shows the plot of the distribution ratio against the total concentration of crown ether. The chain curves were obtained by combining the metal(II) extraction from an aqueous solution containing lithium picrate of constant concentration without crown ether into chloroform containing 0.1 M TBP (flat lines given by broken lines in Fig. 2) with the extraction from lithium picrate solution with crown ethers into chloroform containing no TBP (another broken line in Fig. 2). The observed distribution ratio is higher than the calculated one due to the adduct formation. The situation is thus similar to that in Fig. 1.

The solid curves in Figs. 1 and 2 calculated using the constants fit well with the observed distribution ratios.

The validity of K_{ex11} was also confirmed by measuring the distribution ratio at a higher concentration, 0.1 M, of crown ether, because the relationship between the distribution ratio and concentrations of crown ether and TBP in Eq. 3 applies to all concentrations. Figure 3 gives the plot of the distribution ratio against TBP concentration in the logarithmic units.

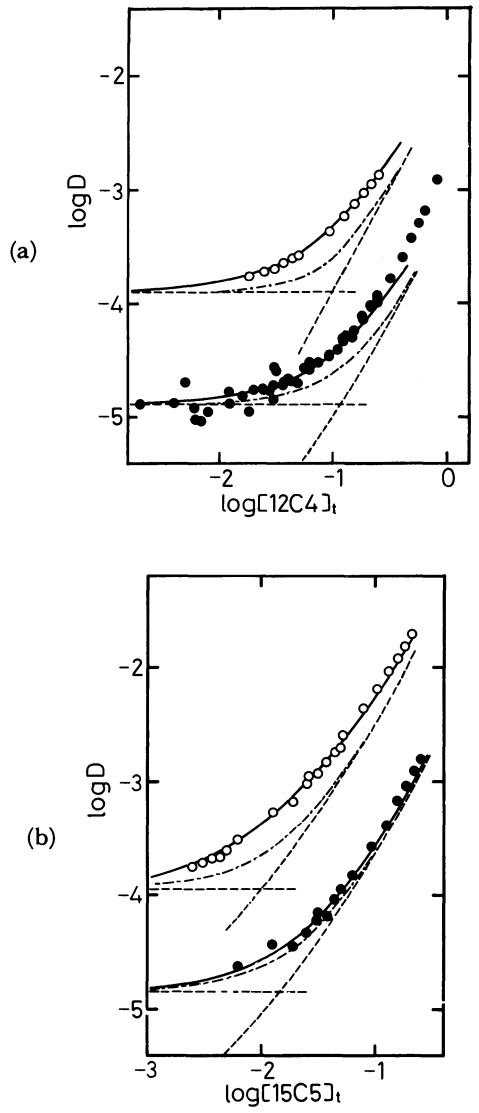

Fig. 2. Distribution ratio of Cu(II)(O) and Zn(II)(●) between 2.5×10^{-2} M lithium picrate solution contaning 12C4(a) and 15C5(b) and 0.1M TBP chloroform as a function of crown ether concentration.
Broken lines shows the extraction with TBP (flat lines) or a crown ether as picrates. Chain lines are obtained by combining the two lines above mentioned.
Solid lines are calculated by the equations denoted in Fig. 1 using the constants in Table 1.

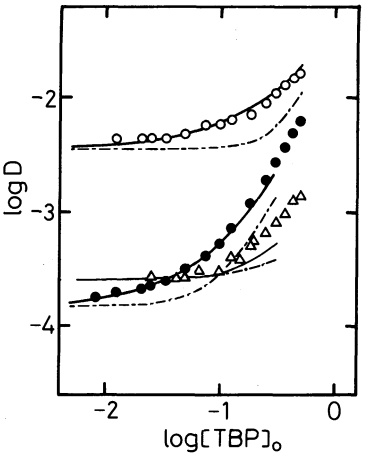

Fig. 3. Extraction of copper(II) with 0.1M 15C5(O) and 12C4(●) or of zinc(II) with 15C5(△) from 2.5×10^{-2} M lithium picrate solution into TBP-chloroform.
Solid lines are calculated by the equation in Fig. 1 using the constants in Table 1.
Chain lines are calculated on assuming no adduct formation.

The calculated values by using the constants in Table 1 are shown by solid line in Fig. 3. The calculated values fit well the experimental data for copper(II). However, the fitness does not appear for zinc(II) in the higher TBP concentration range, although the constants explain well the data in Figs. 1 and 2. The result may suggest that in the extraction with such a high concentration of crown ether, TBP could form adducts with bis-crown ether complex, ZnE_2A_2 as well as the mono-complex, $ZnEA_2$.

The present study reveals that the crown ether complex of either copper(II) or zinc(II) forms 1:1:1 (metal(II): crown ether: TBP) stoichiometric adducts similar to those formed between neutral ligands and metal(I)-crown ether complexes.[3,4] Since TBP seems to be more basic than crown ether, crown ether in the complexes could be replaced by TBP, although the metal(II) can be extracted in association with two moles of crown ether in the absence of TBP. However, Fig. 2 shows that the limiting slope of the plot between crown ether concentration and the distribution ratio is two, indicating that the complex with 2 moles of crown ether may be extracted even in the presence of TBP.

The formation constant of the adducts can be represented as

$$MEA_{2(o)} + T_{(o)} \rightleftharpoons MEA_2T_{(o)}$$

$$\bar{\beta}_{11} = \frac{[MEA_2T]_o}{[MEA_2]_o[T]_o} \quad (4)$$

and $\bar{\beta}_{11}$ can be obtained from the relation

$$\bar{\beta}_{11} = Kex_{11}/Kex_{10}. \quad (5)$$

The formation constants of the adducts are listed in Table 1. As seen in Table 1, the complex of either copper(II) or zinc(II) with 12C4 will form more stable adducts with TBP than the metal complex with 15C5, of which cavity size being larger than 12C4. However, the increase of the extraction with the adduct formation is more remarkable in 15C5 complexes than in 12C4 complexes as seen in Fig. 1. The larger enhancement in the extraction with 15C5 in spite of smaller formation constant of the adduct can be explained as follows: the extractability of the adduct (Kex_{11}) depends on the extractability of the parent crown ether complex as

well as on the property of adduct formed in the organic solvent ($\bar{\beta}_{11}$), i.e., the 12C4 complex forms more stable adducts than the 15C5 complex, while the 15C5 complex as picrate is extracted better than the 12C4 complex. Consequently, the enhancement in the extraction is more remarkable with 15C5–TBP than with 12C4–TBP.

Table 1 also shows that the adducts from copper(II) complexes with crown ether are more stable than those from zinc(II) complexes. The tendency seems to be opposite to the chelate extraction system. For example, Sekine and Ihara reported[2] that the first formation constant of the adduct between TBP and (trifluoroacetylacetonato)copper(II) is 2.16 in logarithmic unit, whereas that of the zinc(II) chelates is 4.29, that is, zinc(II) chelate forms more stable adduct with TBP than copper(II) chelate. They further suggested,[2] as a general tendency of adduct formation of metal chelates, that the chelate easily extractable forms less stable adducts. For example, the extraction of tfa–zinc(II) (tfa means trifluoroacetylacetonato) was much poorer than that of tfa–copper(II) under the same conditions. They explained the difference between the extractability of copper(II) and zinc(II) with chelating agents and the difference of adduct stability between copper(II) and zinc(II) in terms of the different coordination structures; when zinc(II) is extracted with β-diketones, zinc(II) takes the coordination number of 6, so that the zinc(II) chelate with β-diketone may hydrate with water molecules. Therefore, the extraction of (β-diketonato)zinc(II) is poorer than that of (β-diketonato)copper(II). Furthermore, since the hydrated water molecules may be replaced with neutral ligands such as TBP, the adduct from zinc(II) chelate is more stable than that from copper(II) chelate. On the other hand, since zinc(II) takes the coordination number of four when the metal(II) is extracted as the ion pair,[1,5] zinc(II) does hardly have a room to accept extra ligand. The different electronic structure of zinc(II) and copper(II) will be one of the reasons why the adduct formation is different between their chelates and their ion pairs.

When the adduct formation of the crown ether complex in the present study is compared with the adduct formation in chelates, the behavior of adduct formation of ion pair or cationic complex in organic phase seems to be very different from that of metal chelates.

References

1) Y. Hasegawa, H. Tanabe, and S. Yoshida, *Bull. Chem. Soc. Jpn.*, **58**, 3649 (1985).
2) T. Sekine and N. Ihara, *Bull. Chem. Soc. Jpn.*, **44**, 2942 (1971).
3) Y. Hasegawa, K. Suzuki, and T. Sekine, *Chem. Lett.*, **1981**, 1075.
4) Y. Takeda, *Bull. Chem. Soc. Jpn.*, **54**, 526 (1981).
5) H. Moriya and T. Sekine, *Bull. Chem. Soc. Jpn.*, **45**, 1626 (1972).

Effects of EDTA Derivatives on the Photoreduction of Methyl Viologen by a Thiacarbocyanine Sensitizer in a Micellar Solution

Masayuki NAKAGAKI, Hiroaki KOMATSU,* Hiromi TANAKA, and Tetsurou HANDA†
Faculty of Pharmaceutical Sciences, Kyoto University, Yoshida-shimoadachi-cho, Sakyo-ku, Kyoto 606
†Gifu Pharmaceutical University, Mitahorahigashi, Gifu 502
(Received April 1, 1986)

The photoinduced reduction of Methyl Viologen (MV^{2+}) by ethylenediaminetetraacetate (EDTA), 1,2-propanediamine-*N,N,N′,N′*-tetraacetate (MeEDTA), and *trans*-1,2-cyclohexanediamine-*N,N,N′,N′*-tetraacetate (CyDTA) was investigated by using 3,3′-dioctadecylthiacarbocyanine (C^{+}_{18-18}) as a sensitizer in a micellar solution of a nonionic surfactant, heptaethylene glycol monododecyl ether. The production rate of reduced Methyl Viologen ($MV^{+\cdot}$) decreased with the light-irradiation time, while the deceleration increased in the order of: CyDTA<MeEDTA<EDTA. The concentration of the EDTA derivatives at the micellar surface was estimated to be in the order of EDTA<MeEDTA<CyDTA, this difference in the concentration being attributed to such hydrophobic groups as methyl group and cyclohexane ring in the EDTA-derivative molecules. The high concentration of the EDTA derivatives at the surface accelerated the reaction of the sensitizer divalent cation radical ($C^{2+\cdot}_{18-18}$) with the EDTA derivatives, prevented the consumption of $MV^{+\cdot}$ through the back reaction of $C^{2+\cdot}_{18-18}$ with $MV^{+\cdot}$, and facilitated the efficient photoproduction of $MV^{+\cdot}$. It was demonstrated that the hydrophobic interaction between the EDTA-derivative molecules and the micellar surface is an important factor in determining the efficiency of the photoinduced $MV^{+\cdot}$ production.

The phtotoreduction of an electron acceptor (A) by a photoexcited sensitizer (S*) has received much attention in recent years (Reaction 1).[1-4] One common feauture of such a reaction is the high efficiency of the dark reaction of recombination (Reaction 2), which is facilitated by the energetics and the initial proximity of the reactants:

$$S^* + A \longrightarrow S^+ + A^- \quad (1)$$

$$S^+ + A^- \longrightarrow S + A \quad (2)$$

It is often desirable to maximize the yield of photoreduction, and techniques to minimize the recombination have been much studied. Such techniques have generally involved physically separating the products of the photoreaction and then removing one of them by means of an added substance. In order to separate the products, charged micellar,[5] charged vesicular[6] or colloidal SiO_2 surfaces[7] and vesicular bilayers[8,9] have been used. The additives used to remove S^+ from the systems are generally good reducing agents or electron donors (D).[10] Thus,

$$D + S^+ \longrightarrow D^+ + S. \quad (3)$$

The overall reaction in such a three-component system is given as follows:

$$D + S^* + A \longrightarrow D^+ + S + A^-. \quad (4)$$

In the system involving S in the micellar phase and D and A in the bulk aqueous phase, the high concentration of D at the micellar surface prevents the recombination (Reaction 2) and leads to the high efficiency of the photoreduction. Accordingly, the efficient photoreduction can be expected to be realized by the use of a substance as D, which can be strongly bound to the micellar surface. To demonstrate the above concept, we investigated the photoinduced reduction of Methyl Viologen by means of three kinds of ethylenediaminetetraacetate derivatives as a reducing agent in an aqueous phase sensitized by 3,3′-dioctadecylthiacarbocyanine incorporated in a nonionic micelle, composed of heptaethylene glycol monododecyl ether. The difference in the reaction rate between the ethylenediaminetetraacetate derivatives is examined. The results obtained are discussed in terms of the binding between the ethylenediaminetetraacetate derivatives and the micellar surface.

Experimental

The 3,3′-dioctadecyl-2,2′-thiacarbocyanine (C^{+}_{18-18}) bromide (the structure is shown in Fig. 1a) and 3,3′-diethyl-2,2′-thiacarbocyanine (C^{+}_{2-2}) bromide were purchased from the Japan Research Institute for Photosensitizing Dye Co., Ltd., and were used without further purification. The disodium ethylenediaminetetraacetate (EDTA), 1,2-propanediamine-*N,N,N′,N′*-tetraacetate (MeEDTA), and *trans*-1,2-cyclohexanediamine-*N,N,N′,N′*-tetraacetate (CyDTA) (the structures of these EDTA derivatives are shown in Fig. 1) were obtained from Dojindo Laboratories. The Methyl Viologen (1,1′-dimethyl-4,4′-bipyridinium, MV^{2+}) dichloride was received from the Sigma Chemical Company. The nonionic surfactant, heptaethylene glycol monododecyl ether (HED), was obtained from the Nikko Chemicals Co., Ltd.; the reported value of the critical micelle concentration is 8×10^{-5} M (1 M=1 mol dm^{-3}).[11] The monoethylene glycol monohexyl ether (MEH) was purchased from the Tokyo Chemical Industry Co., Ltd. The water was doubly distilled from a quartz still.

The preparation of HED micellar solutions containing a sensitizer has been described elsewhere.[12] C^{+}_{18-18} is insoluble in water[13] and may be considered to be incorporated in the micellar phase. The sample solution (5×10^{-7} M C^{+}_{18-18}, 2×10^{-3} M MV^{2+}, 2×10^{-2} M HED in a buffered solution with 2×10^{-3} M EDTA derivatives and 2×10^{-3} M tris(hydroxymethyl)aminomethane, Tris, at pH 7.0) was placed in a quartz cell

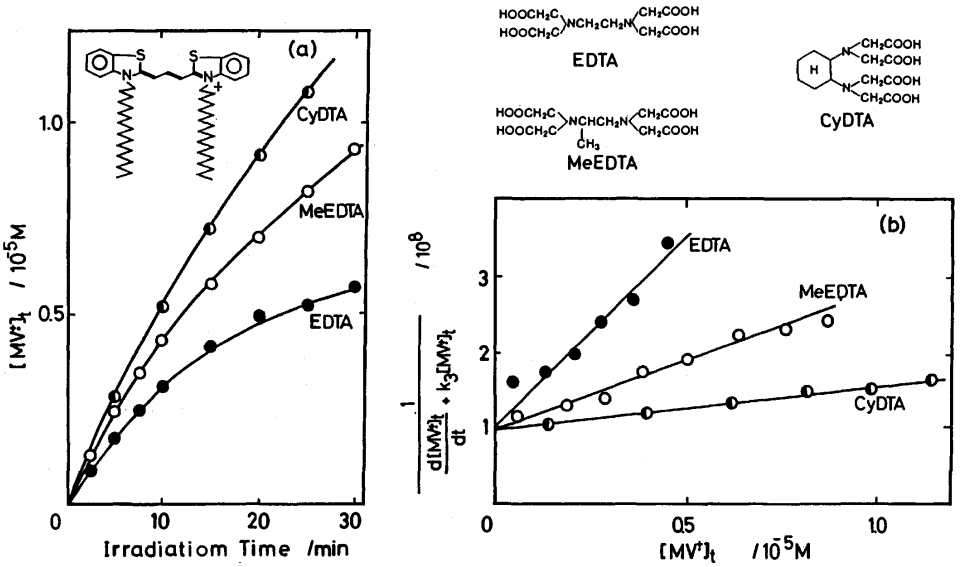

Fig. 1. (a) Built-up of $MV^{+\cdot}$ as a function of irradiation time at 25 °C. 5×10^{-7} M of C^{+}_{18-18} is solubilized in 2×10^{-2} M HED micellar solution (2×10^{-3} M EDTA derivatives, 2×10^{-3} M MV^{2+} and 2×10^{-3} M Tris at pH 7.0). Chemical structure of a sensitizer (C^{+}_{18-18}) is shown in the margin. (b) Variation of $1/(d[MV^{+\cdot}]_t/dt+k_3[MV^{+\cdot}]_t)$ as a function of $[MV^{+\cdot}]_t$ according to Eq. 8, and chemical structures of EDTA derivatives.

(1×1×4 cm) fitted with a stopcock was freed of oxygen by bubbling a nitrogen gas for 15 min, and was then degassed by aspiration at 2700 Pa (20 mmHg) prior to irradiation.

Irradiations were carried out using a Kondo-Sylvania 1 kW tungsten halogen lamp. A Toshiba KL-56 interference filter was used to obtain monochromic light, λ=560±5 nm (the absorption maximum of C^{+}_{18-18} in the HED micellar phase was about 560 nm). The intensity of light incident upon the cell was 3.26×10^{15} quanta s^{-1} as determined by trisoxalateferrate(III) actinometry.[14]

The production of reduced Methyl Viologen ($MV^{+\cdot}$) after intervals of irradiation was monitored by means of the absorption spectra on a Shimadzu UV-180 spectrophotometer. The concentration of $MV^{+\cdot}$ was calculated from the absorbance of the solution at 395 nm by taking $\varepsilon_{395nm}=3.8\times10^{4}$ M^{-1} cm.[15]

The measurements of the partition coefficient of EDTA derivatives from aqueous to water-saturated MEH phases were performed by the following procedure. The mixture of MEH solution, previously saturated with water, and a 2×10^{-3} M EDTA-derivative buffer solution was stirred well. After the centrifugation of the mixture, the aqueous phase was collected. Then, the decrease in the concentration of the EDTA derivatives in the aqueous phase was measured by chelatometry using magnesium chloride.

All the measurements were carried out at 25 °C.

Results

Photoreduction of MV^{2+}. A deoxygenated solution containing C^{+}_{18-18} in the HED micellar phase and MV^{2+} in the aqueous phase was irradiated with green light. As a result, the solution turned dark blue; a development of absorption maxima at about 395- and 603-nm was observed in the presence of EDTA derivatives. The development of the absorption maxima is characteristic of the formation of $MV^{+\cdot}$.[15] The subsequent introduction of air into the cuvette resulted in the prompt reoxidation of $MV^{+\cdot}$ to MV^{2+}, as manifested by decolorization.[16] In the dark or in the absence of the EDTA derivatives, no $MV^{+\cdot}$ was produced.

In Fig. 1a, the concentrations of $MV^{+\cdot}$ formed by irradiation with light are plotted against the irradiation time. In all the EDTA derivatives, the production rate of $MV^{+\cdot}$ decreased with the increase in the irradiation time. The degree of the deceleration increased in this order: CyDTA<MeEDTA<EDTA.

After the removal of the light, the concentration of $MV^{+\cdot}$ gradually decreased with the increase in the time as a result of the reoxidation of $MV^{+\cdot}$ to MV^{2+} by the small amount of oxygen dissolved in the solution.[17] In a previous study,[12] it was found that this reoxidation in the dark followed pseudo first-order kinetics and that the rate constant (k_3) was 5.4×10^{-5} s^{-1} under our conditions. Such a reoxidation of $MV^{+\cdot}$ to MV^{2+} may be considered to proceed not only after the removal of light, but also during irradiation with light.

The mechanism of the reaction which was proposed in a previous report[12] is depicted in Fig. 2. Assuming that the concentration of the sensitizer cation radical ($C^{2+\cdot}_{18-18}$) is constant in a stationary state and that the moles of MV^{2+}, $MV^{+\cdot}$, and EDTA derivatives in the HED micellar phase are much smaller than the total moles of the respective components in the solution, the measureable production rate of $MV^{+\cdot}$ during irradiation with light may be described by:

$$\frac{d[MV^{+\cdot}]_t}{dt}=\frac{k_1k_2[{}^3C^{+*}_{18-18}]_m[MV^{2+}]_m[EDTAd^{3-}]_m^{1/2}}{k_{-1}(P_{MV^+}[MV^{+\cdot}]_t)+k_2[EDTAd^{3-}]_m^{1/2}}-(k_3'P_{MV^+}[O_2]_m+k_3''[O_2]_a)[MV^{+\cdot}]_t, \quad (5)$$

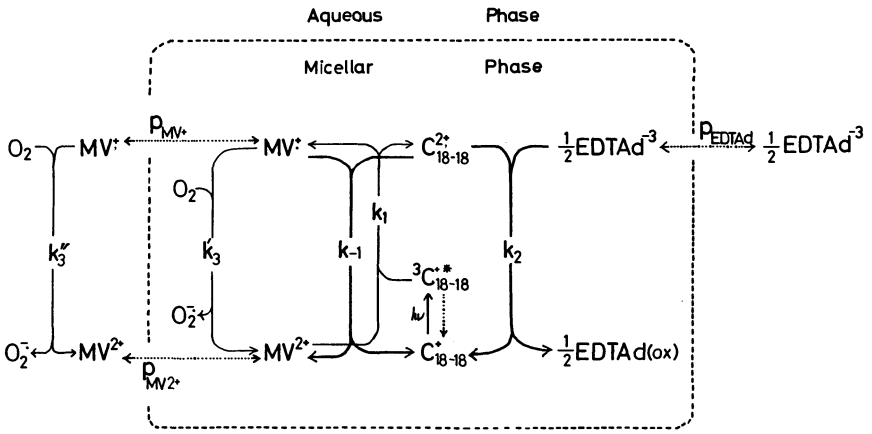

Fig. 2. The proposed mechanism of the photoreduction of MV^{2+} by EDTA derivatives. C^{+}_{18-18} and $^3C^{+*}_{18-18}$, sensitizers in the ground and the triplet excited states in the micellar phase; $C^{2+\cdot}_{18-18}$, sensitizer cation radical; EDTAd and EDTAd(ox), EDTA derivatives and the oxidated form of EDTAd; P_{MV2+}, P_{MV+}, and P_{EDTAd}, partition coefficients of MV^{2+}, $MV^{+\cdot}$, and $EDTAd^{3-}$ from the aqueous phase to the micellar pseudophase; k_1, k_{-1}, k_2, k_3' and k_3'', the rate constants of each reaction.

where $^3C^{+*}_{18-18}$ and $EDTAd^{3-}$ represent the sensitizer in the triplet excited state and the EDTA derivatives respectively. P_{MV+} stands for the partition coefficient of $MV^{+\cdot}$ from the bulk aqueous phase to the micellar pseudophase, defined as $P_{MV+}=[MV^{+\cdot}]_m/[MV^{+\cdot}]_a$. The subscripts a and m denote the concentration at the aqueous phase and at the micellar pseudophase, while the subscript t denotes the total concentration in the micellar solution. The initial rate of $MV^{+\cdot}$ production (V_{init}), which can be obtained from Eq. 5 at $[MV^{+\cdot}]_t \to 0$, is given as follows:

$$V_{init} = k_1[^3C^{+*}_{18-18}]_m[MV^{2+}]^0_m. \tag{6}$$

Here, $[MV^{2+}]^0_m$ is the initial value of $[MV^{2+}]_m$. Since, in this experiment, $[MV^{2+}]_t \gg [MV^{+\cdot}]_t$, and $[MV^{2+}]_m$ in Eq. 5 is nearly equal to $[MV^{2+}]^0_m$ and is a constant, Eq. 5 becomes:

$$\frac{d[MV^{+\cdot}]_t}{dt} = \frac{V_{init}k_2[EDTAd^{3-}]_m^{1/2}}{k_{-1}(P_{MV+}[MV^{+\cdot}]_t) + k_2[EDTAd^{3-}]_m^{1/2}} - k_3[MV^{+\cdot}]_t, \tag{7}$$

where $k_3=k_3'P_{MV+}[O_2]_m+k_3''[O_2]_a$. The second term on the right-hand side of Eq. 7 corresponds to the reoxidation rate of $MV^{+\cdot}$ to MV^{2+} in the dark after the removal of the light. Equation 7 indicates that the deceleration in the production rate of $MV^{+\cdot}$ with the increase in the time arises from the decrease in the first and the second terms on the right-hand side of the equation with the increase in $[MV^{+\cdot}]_t$.

Equation 7 may be transformed to:

$$\frac{1}{\frac{d[MV^{+\cdot}]_t}{dt} + k_3[MV^{+\cdot}]_t} = \frac{k_{-1}P_{MV+}}{V_{init}k_2[EDTAd^{3-}]_m^{1/2}}[MV^{+\cdot}]_t + \frac{1}{V_{init}}. \tag{8}$$

Plots of $1/(d[MV^{+\cdot}]_t/dt+k_3[MV^{+\cdot}]_t)$ vs. $[MV^{+\cdot}]_t$ according to Eq. 8 are shown in Fig. 1b. Here, the observed values evaluated from Eqs. 9 and 10 were substituted for the values of $d[MV^{+\cdot}]_t/dt$ and $[MV^{+\cdot}]_t$ respectively:

$$\frac{d[MV^{+\cdot}]_t}{dt} = \frac{[MV^{+\cdot}]_{t(n+1)} - [MV^{+\cdot}]_{t(n)}}{t(n+1) - t(n)} \tag{9}$$

and

$$[MV^{+\cdot}]_t = \frac{[MV^{+\cdot}]_{t(n+1)} + [MV^{+\cdot}]_{t(n)}}{2}. \tag{10}$$

Here, $[MV^{+\cdot}]_{t(n)}$ and $[MV^{+\cdot}]_{t(n+1)}$ are $[MV^{+\cdot}]_t$ at the measuring time $t=t(n)$ and at $t=t(n+1)$ respectively. These plots give straight lines, and the slope and the intercept lead to values for V_{init} and $(k_2[EDTAd^{3-}]_m^{1/2})/(k_{-1}P_{MV+})$ respectively, as is shown in Table 1.

The values of V_{init} in all the EDTA derivatives are the same, but the values of $(k_2[EDTAd^{3-}]_m^{1/2})/(k_{-1}P_{MV+})$ increase in this order; EDTA<MeEDTA<CyDTA. In the case of EDTA, the value of V_{init} with monochromic light (λ=560±5 nm, percent transmission of the filter at 560 nm, T_{560nm}=25%) is smaller than that with visible light (λ>460 nm, using Y-46 cut-off filter, T_{560nm}=90%). The values of $(k_2[EDTAd^{3-}]_m^{1/2})/(k_{-1}P_{MV+})$ are, however, the same in both irradiation intensities. These results correspond to the expectation that V_{init} is dependent on the intensity of the incident light, which is propotional to $[^3C^{+*}_{18-18}]$, but is independent of the kind of EDTA derivatives, as may be seen from Eq. 6, and that $(k_2[EDTAd^{3-}]_m^{1/2})/(k_{-1}P_{MV+})$ is affected by the kind of EDTA derivatives, but not by the light intensity.

Absorption Maxima of Sensitizer Dye in Various Solvents. Previously,[18] it was demonstrated that C^{+}_{2-2} and C^{+}_{18-18} showed considerably large shifts in their absorption maxima in various aliphatic alcohols used as solvents; the wave numbers at their absorption

Table 1. Experimental Values on Photoreduction of MV^{2+}

EDTAd	V_{init} / $M\,s^{-1}$	$\frac{k_2[EDTAd^{3-}]_m^{1/2}}{k_{-1}P_{MV+}}$ / $M^{1/2}$	P^*_{EDTAd}	Irradiation light
EDTA	1.00×10^{-8}	0.20×10^{-5}	1.2×10^{-2}	Monochromic[a]
	12.71×10^{-8}	0.19×10^{-5}		Visible[b]
MeEDTA	1.02×10^{-8}	0.56×10^{-5}	2.4×10^{-2}	Monochromic[a]
CyDTA	1.02×10^{-8}	1.45×10^{-5}	3.0×10^{-2}	Monochromic[a]

a) Monochromic, monochromic light (λ=560 nm, percent transmission at 560 nm, $T_{560\,nm}$=25%); b) visible, visible light (λ>460 nm, $T_{560\,nm}$=90%).

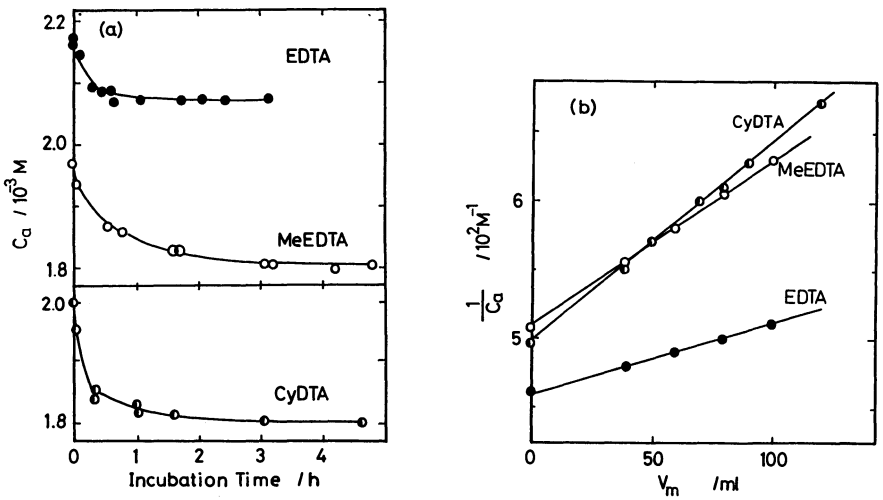

Fig. 3. (a) Time course of partition of $EDTAd^{3-}$ from aqueous to water-saturated MEH phase in the case of V_a=10 ml and V_m=40 ml at 25 °C. (b) Plots of $1/C_a$ versus V_m according to Eq. 12 in the case of V_a=10 ml. C_a, the concentration of $EDTAd^{3-}$ in the aqueous pase; V_a and V_m, the volumes of the aqueous and the water-saturated MEH phases.

maxima ($\tilde{\nu}_{max}$) increase with the dielectric constant (D) of alcohols. The value of D in the vicinity of the chromophore of C^+_{18-18} in the HED micellar phase, which has been defined as the effective dielectric constant (D_{eff}), was estimated as D_{eff}=20.0 using the values of $\tilde{\nu}_{max}$ and D for alcohols.[18] Similar procedures led to the D_{eff} value of 19.4 for C^+_{2-2} in a water-saturated MEH solution. These D_{eff} values correspond to the polarity of 1-propanol or 1-butanol, and indicate that the chromophore of C^+_{2-2} in the water-saturated MEH solution is dissolved in an environment with a micropolarity similar to that of C^+_{18-18} in the HED micellar phase.

Partition of EDTA Derivatives from Aqueous to Water-Saturated MEH Phases. The time course of the partition of EDTA derivatives between aqueous and water-saturated MEH phases was investigated; the results are shown in Fig. 3a. The partition equilibrium was established after about 3 h under our conditions. The partition coefficient of the EDTA derivatives from the aqueous to the water-saturated MEH phases (P^*_{EDTAd}) is given by:

$$P^*_{EDTAd} = \frac{C_m}{C_a} = \frac{V_a}{V_m}\left(\frac{C^0_a}{C_a} - 1\right), \qquad (11)$$

where C_a, C_m, and C^0_a are the concentration of the EDTA derivatives in the aqueous and water-saturated MEH phases, and the initial concentration of the EDTA derivatives in the aqueous phase respectively. Here, V_a and V_m are the volumes of the aqueous and water-saturated MEH phases respectively. Equation 11 may be rewritten as:

$$\frac{1}{C_a} = \frac{P^*_{EDTAd}}{C^0_a V_a} V_m + \frac{1}{C^0_a}. \qquad (12)$$

Plots of $1/C_a$ versus V_m according to Eq. 12 are shown in Fig. 3b in the case of V_a=10 ml. These plots give straight lines, and their slopes and intercept lead to the values for P^*_{EDTAd} shown in Table 1. These results indicate that the concentrations of the EDTA derivatives in the water-saturated MEH phase increase in the order of EDTA<MeEDTA<CyDTA at the partition equilibrium.

Discussion

The photoinduced reduction of MV^{2+} by EDTA has been carried out with various sensitizer dyes such as tris(2,2'-bipyridine)ruthenium,[1-6,8] porphyrins,[1-7,9,10,19]

and phatalocyanines[20] by numerous workers, and every effort has been made to maximize the efficiency of the photoinduced production of $MV^{+\cdot}$, for $MV^{+\cdot}$ is capable of generating hydrogen from water when platinum dioxide is used as a catalyst.[21] In our studies, 3,3'-dioctadecylthiacarbocyanine in a nonionic micelle has been adopted as a sensitizer.[12,13] This dye has been known as a probe for investigating the membrane potentials of erythrocyte membranes[22] and cell membranes of bacteria[23] and as a strong inhibitor of the endogeneous respiration of Ehrlich ascites tumor cells.[24]

In this study, in order to minimize the recombination of photoproducts (Eq. 13, corresponding to Eq. 2), EDTA derivatives are used as reducing agents, resulting in the removal of $C_{18\text{-}18}^{2+\cdot}$ from the system (Eq. 14, corresponding to Eq. 3) and in the prevention of the recombination of $C_{18\text{-}18}^{2+\cdot}$ with $MV^{+\cdot}$ (Eq. 9):

$$(C_{18\cdot18}^{2+\cdot})_m + (MV^{+\cdot})_m \xrightarrow{k_{-1}} (C_{18\text{-}18}^{+})_m + (MV^{2+})_m, \quad (13)$$

$$(C_{18\text{-}18}^{2+\cdot})_m + (EDTAd^{3-})_m \xrightarrow{k_2} (C_{18\cdot18}^{+})_m + (EDTAd(ox))_m. \quad (14)$$

It can be expected that the faster the process shown as Eq. 14 is, that is, the higher $[EDTAd^{3-}]_m$ and/or the rate constant (k_2) of this process is, the larger is the efficiency of the $MV^{+\cdot}$ production. As may be seen from Fig. 1, the production rates of $MV^{+\cdot}$ decrease with the increase in the time, and the deceleration is the smallest in CyDTA and the largest in EDTA. Equation 7, showing the production rate of $MV^{+\cdot}$, indicates that the deceleration of the $MV^{+\cdot}$ production arises from the decrease in the first and second terms on the right-hand side of Eq. 7 with the increase in $[MV^{+\cdot}]_t$. Furthermore, since V_{init}, k_3, k_{-1}, and P_{MV+} are independent of the kind of the EDTA derivatives and constant, Eq. 3 indicates that the larger $[EDTAd^{3-}]_m$ and/or k_2 is, the smaller is the deceleration of the $MV^{+\cdot}$ production.

As may be seen from the proposed mechanism, $MV^{+\cdot}$ is produced through the following process:

$$(^3C_{18\cdot18}^{+*})_m + (MV^{2+})_m \xrightarrow{k_1} (C_{18\text{-}18}^{2+\cdot})_m + (MV^{+\cdot})_m. \quad (15)$$

On the other hand, $MV^{+\cdot}$ disappears through the processes shown by Eqs. 13, 16, and 17:

$$(MV^{+\cdot})_m + (O_2)_m \xrightarrow{k_3'} (MV^{2+})_m + (O_2^{-\cdot})_m \quad (16)$$

$$(MV^{+\cdot})_a + (O_2)_a \xrightarrow{k_3''} (MV^{2+})_a + (O_2^{-\cdot})_a \quad (17)$$

Therefore, by using the reaction rate of these processes, the efficiency of $MV^{+\cdot}$ production (E) is introduced as follows:

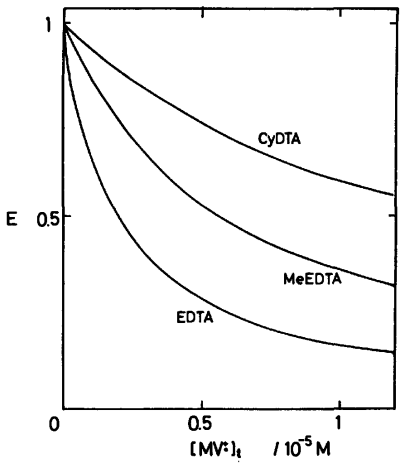

Fig. 4. Comparison of the efficiency of $MV^{+\cdot}$ production (E) between the three $EDTAd^{3-}$ as a function of $[MV^{+\cdot}]_t$. The values of E were evaluated using Eq. 19 and the values in Table 1.

$$E = \frac{k_1[^3C_{18\cdot18}^{+*}]_m[MV^{2+}]_m - k_{-1}[C_{18\text{-}18}^{2+\cdot}]_m[MV^{+\cdot}]_m - k_3[MV^{+\cdot}]_t}{k_1[^3C_{18\cdot18}^{+*}]_m[MV^{2+}]_m}$$

$$= 1 - \frac{k_3}{V_{Init}}[MV^{+\cdot}]_t - \frac{1}{1+\left(\frac{k_2[EDTAd^{3-}]_m^{1/2}}{k_{-1}P_{MV+}}\right)\frac{1}{[MV^{+\cdot}]_t}} \quad (18)$$

Here, $[C_{18\text{-}18}^{2+\cdot}]_m$ is constant and is equal to $V_{init}/(k_{-1}P_{MV+}[MV^{+\cdot}]_t + k_2[EDTAd^{3-}]_m^{1/2})$ in a stationary state (see Fig. 2). Since the value of k_3 is 10^{-5}-order and since the values of V_{init} are 10^{-8}-order, it may be considered that $k_3[MV^{+\cdot}]_t/V_{init} \ll 1$ at $[MV^{+\cdot}]_t$ below about 1×10^{-5} M. Therefore, Eq. 18 may reduce to:

$$E = \frac{1}{1+[MV^{+\cdot}]_t/\left(\frac{k_2[EDTAd^{3-}]_m^{1/2}}{k_{-1}P_{MV+}}\right)}. \quad (19)$$

Figure 4 compares the E values between the three EDTA derivatives as a function of $[MV^{+\cdot}]_t$. The values of E were calculated using the values of $(k_2[EDTAd^{3-}]_m^{1/2})/(k_{-1}P_{MV+})$ in Table 1. As may be seen from Fig. 4, the value of E for CyDTA decreases gradually with the increase in $[MV^{+\cdot}]_t$. On the other hand, the value of E for EDTA decreases rapidly in the region of small values of $[MV^{+\cdot}]_t$. Equation 19 indicates that the slower decrease of E for CyDTA with the increase in the $[MV^{+\cdot}]_t$ may be ascribed to the relatively high value of $[EDTAd^{3-}]_m$, i.e. $[CyDTA^{3-}]_m$ and/or k_2.

The binding between the EDTA derivatives and the HED micelle (P_{EDTAd}) was measured with the ultrafiltration method. However, the binding was slight and was not clearly detected. As has been mentioned before, the D_{eff} for $C_{18\text{-}18}^{+}$ in the HED micellar phase is 20.0 and corresponds to the polarity of 1-propanol or 1-butanol. This indicates that the chromophore of $C_{18\text{-}18}^{+}$ accommodated in the HED micellar phase is pro-

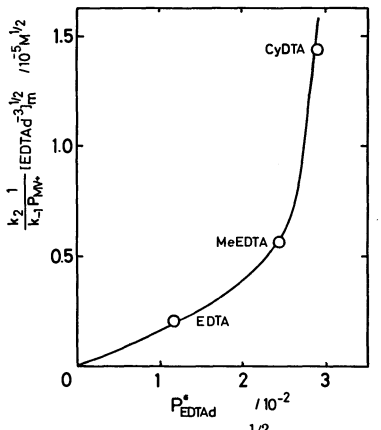

Fig. 5. Plots of $(k_2[EDTAd^{3-}]_m^{1/2})/(k_{-1}P_{MV+})$ versus P^*_{EDTAd}.

vided with a remarkably less polar environment than that in the aqueous phase, but it seems to be in a more polar environment than in a liquid hydrocarbon. These results indicate that the chromophore is located in the surface region of the HED micelle,[12] probably in its ethylene glycol mantle. The D_{eff} value for C^+_{2-2}, which has the same chromophore as C^+_{18-18}, in a water-saturated MEH solution is 19.4; this indicates that C^+_{2-2} is dissolved in a micropolarity similar to that of C^+_{18-18} in the HED micellar phase. Therefore, the concentration of the EDTA derivatives at the HED micellar surface (the binding between the EDTA derivatives and the HED micelle) was estimated from the partition coefficient (P^*_{EDTAd}) of the EDTA derivatives from the aqueous to the water-saturated MEH phases. As a result, the concentration of CyDTA in the water-saturated MEH phase is the highest,while that of EDTA is the lowest, in the three EDTA derivatives. These differences in the concentration of the EDTA derivatives in the water-saturated MEH phase may be attributed to the hydrophobic groups, such as the methyl group and cyclohexane ring in the EDTA-derivative molecules. The order of the concentration of EDTA derivatives in the water-saturated MEH phase coincides with that of the efficiency of $MV^{+\cdot}$ production (E), indicating that the local concentration of the EDTA derivatives at the HED micellar surface ($[EDTAd^{3-}]_m$) is an important factor in determining E.

Figure 5 shows the plots of the values of $(k_2[EDTAd^{3-}]_m^{1/2})/(k_{-1}P_{MV+})$ versus P^*_{EDTAd}. These plots suggest the close correlation between E and P^*_{EDTAd}. The difference in the value of k_2 in the three EDTA derivatives is probably a result of difference in the oxidation potential of the EDTA derivatives, their proximity to $C^{2+\cdot}_{18-18}$ in the micellar surface, which are also associated with their partition coefficient (P_{EDTAd}). Thus, though the k_2 values are somewhat different in the three EDTA derivatives, the agreement in the order in the EDTA derivatives between the ease of the partition to the MEH phase and the efficiency of $MV^{+\cdot}$ production indicates that the local concentration of the EDTA derivatives at the HED micellar surface is an important factor in determining the efficiency of $MV^{+\cdot}$ production.

In conclusion, it seems that the high concentration of EDTA derivatives at the micellar surface is essential for the efficient photoproduction of $MV^{+\cdot}$. It is also suggested that not only the electrostatic interaction, demonstrated by many workers, but also the hydrophobic interaction between EDTA derivatives and the micellar surface is important for the achievement of a high concentration of EDTA derivatives at the micellar surface and for the effective production of $MV^{+\cdot}$.

References

1) M. Calvin, *Acc. Chem. Res.*, **11**, 4701 (1978).
2) J. H. Fendler, *Acc. Chem. Res.*, **13**, 7 (1980).
3) M. Grätzel, *Acc. Chem. Res.*, **14**, 376 (1981).
4) "Photochemical Conversion and Storage of Solor Energy," ed by J. S. Connolly, Academic Press, New York (1981).
5) P. P. Infelta, M. Grätzel, and J. H. Fendler, *J. Am. Chem. Soc.*, **102**, 1479 (1980).
6) T. Nagamura, K. Takuma, Y. Tsutsui, and T. Matsuo, *Chem. Lett.*, **1980**, 503.
7) I. Willner, J. W. Otvos, and M. Calvin, *J. Am. Chem. Soc.*, **103**, 3203 (1981).
8) W. E. Ford, J. W. Otvos, and M. Calvin, *Nature*, **274**, 508 (1978).
9) H. Komatsu, K. Togawa, K. Watanabe, T. Katsu, and Y. Fujita, *Nippon Kagaku Kaishi*, **1984**, 345.
10) G. O. Pradevan and M. P. Pileni, *J. Chim. Phys.*, **78**, 203 (1981).
11) H. Lange, *Proc. Inter. Cong. Surface Activity*, **3**, 279 (1960).
12) M. Nakagaki, H. Komatsu, and T. Handa, *Bull. Chem. Soc. Jpn.*, **58**, 3197 (1985).
13) T. Handa, H. Komatsu, and M. Nakagaki, *Progr. Colloid, Polymer Sci.*, **68**, 33 (1983).
14) J. G. Calvert and J. N. Pitts, "Photochemistry," Wiley, New York (1967), p. 784.
15) M. S. Tunuli and J. H. Fendler, *J. Am. Chem. Soc.*, **103**, 2507 (1981).
16) E. M. Kosower and J. L. Cotter, *J. Am. Chem. Soc.*, **86**, 5524 (1964).
17) F. M. Hawkridge and T. Kumana, *Anal. Chem.*, **45**, 1021 (1973).
18) T. Handa, H. Komatsu, K. Matsuzaki, and M. Nakagaki, *Nippon Kagaku Kaishi*, **1984**, 8.
19) S. Aono, I. Okura, and A. Yamada, *J. Phys. Chem.*, **89**, 1593 (1985).
20) T. Tanno, B. Wohrle, M. Kaneko, and A. Yamada, *Ber. Bunsenges. Phys. Chem.*, **84**, 1032 (1980).
21) J. Kiwi ahd M. Grätzel, *J. Am. Chem. Soc.*, **101**, 7214 (1979).
22) P. J. Sims, A. S. Wagguner, C. Wang, and J. H. Hoffman, *Biochemistry*, **13**, 3315 (1974).
23) P. C. Laris and H. A. Pershadsingh, *Biochem. Biophys. Res. Commun.*, **57**, 620 (1974).
24) E. Okimasu, J. Akiyama, N. Shiraishi, and K. Utsumi, *Physiol. Phys.*, **11**, 425 (1979).

 © 1986 The Chemical Society of Japan Bull. Chem. Soc. Jpn., 59, 3013—3018 (1986)

o-Quinodimethane Generation from α,α′-Dihalo-o-xylenes by Use of Sodium Benzenetellurolate

Nobuaki KAMBE, Takashi TSUKAMOTO, Noritaka MIYOSHI, Shinji MURAI, and Noboru SONODA*
Department of Applied Chemistry, Faculty of Engineering, Osaka University, Suita, Osaka 565
(Received April 2, 1986)

Treatment of α,α′-dihalo-o-xylenes with sodium benzenetellurolate gave o-quinodimethane which readily reacted with dienophiles leading to Diels–Alder adducts. The best yields were obtained when the reaction was carried out in refluxing ethanol using two molar equivalents of the benzenetellurolate to α,α′-dihalo-o-xylenes. This reaction competes with substitution of the halogen atoms with the benzenetellurolate anion to afford α,α′-bis(phenyltelluro)-o-xylene, which did not give o-quinodimethane under identical conditions. It is likely that the reaction proceeds through nucleophilic attack of benzenetellurolate anion at the tellurium atom of α-halo-α′-phenyltelluro-o-xylene which is formed in situ by the substitution of one of the halogen atoms of the starting α,α′-dihalo-o-xylene with the benzenetellurolate anion. When sodium benzeneselenolate was employed, no evidence of o-quinodimethane formation was observed under similar conditions.

Since Cava and his co-worker first recognized the intermediacy of α,α′-dibromo-o-quinodimethane in the reaction of α,α,α′,α′-tetrabromo-o-xylene with sodium iodide,[1] a variety of methods for the generation of o-quinodimethane intermediates have been developed and used for organic synthesis.[2–10] Recent advances in this methodology have enabled the facile generation of o-quinodimethanes under mild conditions[4m–r] with stereocontrol of the subsequent Diels–Alder reaction with a dienophile (intermolecularly or intramolecularly), leading to the successful preparation of polycyclic compounds such as steroids, alkaloids, terpenoids and some antibiotics.

For the syntheses of relatively simple compounds via Diels–Alder reaction of the unsubstituted o-quinodimethane, α,α′-dihalo-o-xylenes may be the first choice because of their ready availability as starting materials. The heterogeneous 1,4-dehalogenation of α,α′-dihalo-o-xylenes proceeds through reductions with Zn,[4d,e] Fe,[4f] or Cu[4g] metals. Only one homogeneous reduction[9] was reported using iodide anion.[4a–c] Dehalogenation of vic-dihalides[11] or α-halo carbonyls[12] with iodide ion is a well-known and versatile reaction, but dehalogenation of α,α′-dihalo-o-xylenes to o-quinodimethanes with iodide anion was restricted to activated systems having alkoxyl substituents on the aryl rings[4b,c] or halogens in the benzylic positions.[4a]

In this paper we report a new o-quinodimethane generation from nonactivated α,α′-dihalo-o-xylenes (**1**) promoted by sodium benzenetellurolate giving rise to Diels–Alder adducts in the presence of dienophiles (Scheme 1).

Dehalogenation with tellurolate anions has been successfully achieved in the cases of α-halo carbonyls,[13] vic-dihalides,[14] 1,4-dibromo-2-enes,[15] and 3,7-dibromo-5-cyclooctadiene,[16] but no precedence has been reported for the generation of o-quinodimethanes from α,α′-dihalo-o-xylenes.

Results and Discussion

Dehalogenation of *vic*-dihalides[14] was reported using sodium hydrogen telluride (NaTeH), prepared from tellurium and sodium borohydride.[17] These successful results prompted us to investigate the dehalogenation of α,α′-dihalo-o-xylenes with NaTeH to generate o-quinodimethanes. The reaction in refluxing ethanol for 5 h in the presence of excess diethyl maleate gave diethyl 2,3-tetralindicarboxylate in 24% yield. In the cases of ethyl acrylate and other dienophiles, reduction of the C–C double bond of the dienophiles with NaTeH predominated, resulting in very poor yields of the desired adducts. In order to preclude this side reaction, we investigated the use of sodium benzenetellurolate (PhTeNa), as the nucleophile.

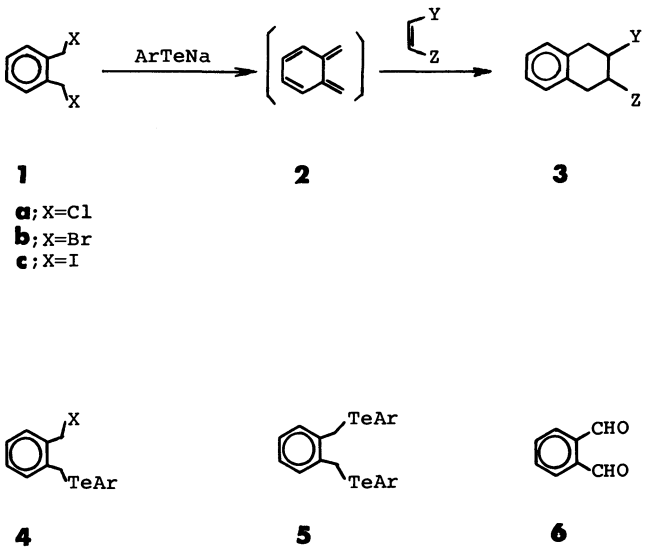

Scheme 1.

The reaction of α,α′-dihalo-o-xylenes with PhTeNa prepared from diphenyl ditelluride and sodium borohydride[18] was carried out in refluxing ethanol in the presence of an excess of a dienophile. Several dienophiles were examined using different arenetellurolate anions. The results are summarized in Table 1. Ethyl acrylate, methyl vinyl ketone, and acrylonitrile gave the corresponding Diels–Alder adducts in moderate yields. It should be noted that a similar reaction using sodium

Table 1. Generation of Quinodimethane[a)]

Haloxylene	Ar_2Te_2	Dienophile	Product	Yield/%
	Ph_2Te_2		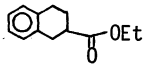	45
	Ph_2Te_2		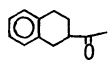	36
	Ph_2Te_2		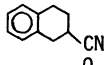	30
	Ph_2Te_2		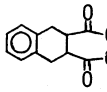	35
	$(p\text{-Me-}C_6H_4)_2Te_2$		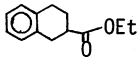	31[b)]
	$(m\text{-Cl-}C_6H_4)_2Te_2$		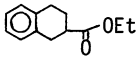	20[b)]
	$(p\text{-MeO-}C_6H_4)_2Te_2$		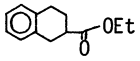	31[b)]
	Ph_2Te_2		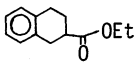	53[b)]
	Ph_2Te_2		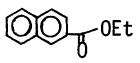	<10

a) Reaction conditions: Ar_2Te_2 (5 mmol), α,α'-dihalo-*o*-xylene (5 mmol), dienophile (50 mmol), $NaBH_4$ (10.5 mmol, 400 mg), EtOH (30 mL), reflux, 2 h. b) GLC yield.

benzeneselenolate, PhSeNa, gave α,α'-bis(phenylseleno)-*o*-xylene in 75% yield together with the Michael adduct of benzeneselenolate to ethyl acrylate instead of the desired Diels–Alder adduct (see Experimental section).

When the reaction was carried out at room temperature, no apparent change was observed and no adduct was detected. After reaching reflux, the reaction mixture turned red, which may be due to the color of diaryl ditelluride, suggesting that reduction with arenetellurolate had occurred. Monitoring of the reaction by GLC showed that the reaction was complete within 1 h. When $\alpha,\alpha,\alpha',\alpha'$-tetrabromo-*o*-xylene was employed, the expected adduct,[19] ethyl 2-naphthoate, was formed in very poor yield. This is in marked contrast[20] to the iodide ion induced quinodimethane formation in which the corresponding adduct was formed in 65% yield from $\alpha,\alpha,\alpha',\alpha'$-tetrabromo-*o*-xylene by the treatment with sodium iodide in the presence of *N*-phenylmaleimide.[4a)]

In all reactions in Table 1, the dialdehyde **6** was obtained as a by-product in about 30% yield based on the dihalide used. It is known that benzyl tellurolate is oxidized in air at room temperature to give benzaldehyde.[21] So the aldehyde is assumed to be formed by the oxidation of α,α'-bis(phenyltelluro)-*o*-xylene. In order to ensure this hypothesis, a control experiment was carried out. When a ethanol solution of PhTeNa and α,α'-dibromo-*o*-xylene was refluxed for 2 h, a new NMR singlet at δ 4.17 appeared, which was assigned to the methylene protons of α,α'-bis(phenyltelluro)-*o*-xylene (**5**). The mixture was then exposed to air and stirred at r.t. overnight, and the dialdehyde **6** was isolated in 60% yield. In a similar manner, α,α'-bis(phenyltelluro)-*o*-xylene (**5**) was isolated and conversion of **5** to **6** was monitored by NMR (see Experimental section).

The reaction of the α,α'-dibromo-*o*-xylene with sodium benzenetellurolate at room temperature or below resulted in substitution of bromide with $PhTe^-$ and no Diels–Alder adduct was detected by GLC. The reaction proceeds only when refluxed.

Another important factor was the molar ratio of PhTeNa to α,α'-dihalo-*o*-xylene. The yields of the desired adduct and the dialdehyde were plotted against the molar ratio of PhTeNa to α,α'-dibromo-*o*-xylene as shown in Fig. 1. The best yield of the adduct was obtained when the ratio was 2.0. As the ratio was increased the substitution predominated resulting in an increase of dialdehyde formation. An explanation for these results is that the excess of $PhTe^-$ displaces both halogen atoms of the dihalides before the reaction mixture reached reflux, and gave α,α'-bis(phenyltelluro)-*o*-xylene (**5**) which is not converted to the quinodimethane under these reaction conditions.

α,α'-Dichloro-*o*-xylene did not give the corresponding Diels–Alder adduct. When NaI was added to the reaction mixture of the α,α'-dichloro-*o*-xylene, the Diels–Alder adduct was obtained in a moderate yield,

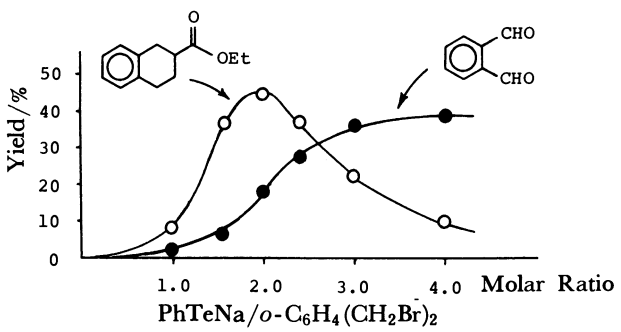

Fig. 1. Yields of the adducts at the different ratios of PhTeNa/*o*-$C_6H_4(CH_2Br)_2$.

probably due to the substitution of the chlorine atom with the iodine atom.

In order to elucidate the reaction path, some NMR studies were performed. When α,α'-dibromo-*o*-xylene was treated with two equivalents of PhTeNa in the presence of methyl acrylate at −20 °C in a mixed solvent of $CDCl_3$ and CD_3OD, the NMR indicated a mixture of the starting dibromide (benzylic protons of **1** at δ 4.64), α-bromo-α'-phenyltelluro-*o*-xylene (those of **4** at δ 4.43 and at δ 4.37), and α,α'-bis(phenyltelluro)-*o*-xylene (those of **5** at δ 4.17). Heating the mixtute to 60 °C, the first two compounds disappeared and the Diels–Alder adduct had formed. While the peak for **5** remained unchanged. This result indicated that substitution of one of the bromine atoms on the benzylic positions of **1b** with benzenetellurolate anion is a fast reaction even at low temperatures, and that substitution of the second bromine atom with $PhTe^-$ may compete with the quinodimethane formation giving rise to **5** which is not a precursor to **2** but to **6**. This conclusion is also supported by the evidence that when excess benzenetellurolate anion was used, formation of the dialdehyde **6** predominated and quinodimethane formation was suppressed as shown in Fig. 1. The fact that the yield of the Diels–Alder adduct was very low when a stoichiometric amount of benzenetellurolate anion was used may indicate that Path A in which quinodimethane was formed by direct attack of $PhTe^-$ at one of the bromine atoms of **1** can be ruled out, or if any, can not be the main path. So the next question is which does $PhTe^-$ attack the halogen atom or the tellurium atom of **4** in the subsequent step of the reaction.

There are some precedents on the reaction of alkyl halides with chalcogenolate anions. The direct attack at halogen atoms by tellurolate anions was suggested in the dehalogenation of *vic*-dihalides supported by the stereochemistry of the olefinic products formed from stereochemically pure *vic*-dihalides, i.e., anti elimination.[14c] In similar reactions using PhSeNa,[22] *vic*-dibromide, 2-iodoalkyl chloride, and 2-(phenylseleno)alkyl chloride undergo anti elimination by the direct attack of $PhSe^-$ at bromine, iodine, and selenium atoms, respectively. On the other hand the elimination of *vic*-dichloride proceeds in net syn fashion, indicating that the displacement of one of the chlorine atoms with $PhSe^-$ preceded the subsequent anti elimination which is caused by the nucleophilic attack of $PhSe^-$ on selenium of the in situ formed 2-(phenylseleno)alkyl chloride.

In the dehalogenation of α-halo ketones or α-halo amides to the parent ketones or amides by tellurolate anions, it has been proposed that the reduction is initiated by the displacement of the halide with $ArTe^-$ followed by the nucleophilic attack of a second molecule of tellurolate anion at the tellurium of the substituted intermediate.[13b] It has been previously reported that reactions of α-halo ketones[23] and benzyl halides[24] with thiolate and selenolate anions often give mixtures of reduction and substitution products depending on both the nature of the substrates and that of the reagents used as well as the reaction conditions. In the reaction with 3,7-dibromo-1,5-cyclooctadiene, thiolate and selenolate anions displaced bromide but tellurolate anion preferred the nucleophilic attack at one of the bromine atoms leading to the formation of a bicyclic compound.[16]

As described above, both examples of the nucleophilic attack of tellurolate anion at the halogen atoms and that at the chalcogen atoms are known, and both Path B and Path C seem probable. But we would like to propose that $PhTe^-$ attacks the tellurium atom of **4** than the halogen atom, since it is likely that bromide and iodide anions are expected to be better leaving groups than the benzenetellurolate anion from our knowledge obtained in the study about the tellurium chemistry in out laboratory. Contribution of iodide anion as the nucleophile to attack the tellurium or the iodine atoms of **4** or **5** can be ruled out by the fact that the presence of large excess of NaI in the reaction of **1c** with PhTeNa did not affect the yield of the adduct. The fact that **5** did not give the quinodimethane in the reaction with PhTeNa in the presence of NaI may also indicated that iodide anion does not substitute for the $PhTe^-$ group in the benzylic positions under these reaction conditions. So Path B seems to be the most probable, but the alternative pathways such as electron transfer[13c] in some stage of the reaction could not be ruled out.

In conclusion a new and facile homogeneous reaction for the generation of *o*-quinodimethane by use of benzenetellurolate anion has been discovered. The key step of this reaction is proposed to be the nucleophilic attack of benzenetellurolate anion at tellurium of intermediate **4**.

Experimental

General. Instruments used were as follows: melting points, Yanagimoto Micro Melting Point Apparatus; ^1H NMR, Hitachi R-24B or Japan Electron Optics JNM-PS-100; IR, Shimadzu IR-400; MS, Hitachi RMU-6A. Chemical shifts are expressed in parts per million using tetramethyl-

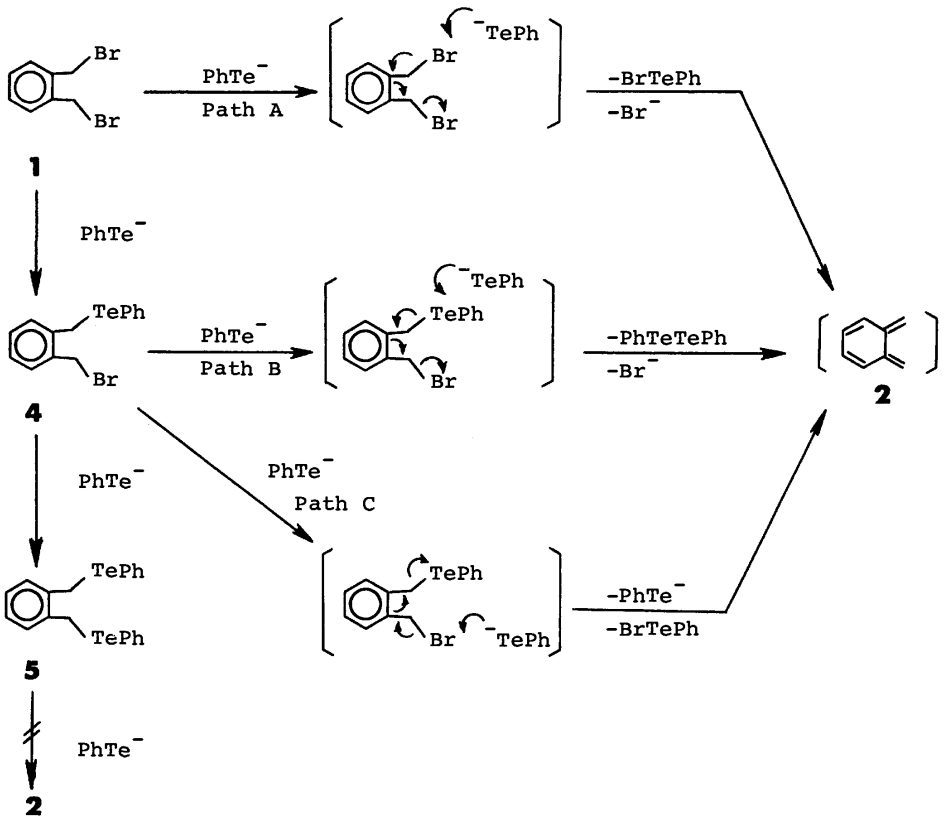

Scheme 2.

silane (TMS) as the internal standard.

Diaryl ditellurides and diphenyl diselenide were prepared as discribed in the literature[23b,25] or by similar procedures. α,α'-Dihalo-*o*-xylenes, dienophiles, solvent (tetrahydrofuran: THF), and other materials used were all purchased from commercial sources and used after purification by distillation or recrystallization.

Reaction of α,α'-Dibromo-*o*-xylene with NaTeH. Following the reported procedure,[17] NaTeH was prepared from Te (5 mmol, 650 mg) and $NaBH_4$ (19.8 mmol, 750 mg, added in three portions) in EtOH (20 ml) at the reflux, and to this solution was added diethyl maleate (10 mmol, 1.6 ml) under N_2. Deposition of tellerium was observed at this stage. α,α'-Dibromo-*o*-xylene (5 mmol, 1.32 g) was then added and the mixture was heated at reflux for 5 h. After the precipitates were filtered, the product was extracted into ether and dried over $MgSO_4$. The solvent and remaining diethyl maleate were removed in vacuo and the residue was chromatographed on silica gel (benzene/ether=9/1) to give 24% of diethyl 2,3-tetralindicarboxylate.[4n,8]

General Reaction, Reaction of α,α'-Dibromo-*o*-xylene with PhTeNa. To a solution of PhTeNa generated from Ph_2Te_2 (5 mmol, 2.05 g) and $NaBH_4$ (10.5 mmol, 400 mg) in EtOH (30 ml) at 25 °C, was added a THF (15 ml) solution of ethyl acrylate(50 mmol) and α,α'-dibromo-*o*-xylene (5 mmol, 1.32 g). The mixture was refluxed for 2 h with stirring. The resulting red solution was then stirred in contact with the air overnight at 25 °C. The red color faded and a white precipitate was formed. The precipitate was filtered, and the product was extracted into ether and dried over $MgSO_4$. The solvent was evaporated and the residue chromatographed on silica gel (benzene) to give a 45% yield of ethyl 2-tetralincarboxylate.[4n,9]

Reaction of α,α'-Dibromo-*o*-xylene with Sodium Benzeneselenolate. A THF solution (5 ml) of α,α'-dibromo-*o*-xylene (1 mmol, 264 mg) was added at 25 °C to an ethanol solution (10 ml) of ethyl acrylate (5 mmol, 0.53 ml) and PhSeNa (2 mmol) generated from diphenyl diselenide (1 mmol, 313 mg) and $NaBH_4$ (2.1 mmol, 80 mg). The reaction was continued at reflux for 2 h. The solution turned slightly yellow and white precipitates were observed. GLC analysis showed no formation of the Diels-Alder adduct. After the reaction was complete, 20 ml of benzene was added to the mixture. The precipitates were filtered and the solvent evaporated. The residue was chromatographed on silica gel (pentane/ether=95/5) to give 316 mg of α,α'-bis(phenylseleno)-*o*-xylene[26] (0.75 mmol, 75% based on α,α'-dibromo-*o*-xylene used) and 150 mg (0.58 mmol) of ethyl 3-(phenylseleno)propionate: IR (neat) 2980, 1732, 1583, 1220, 1025, 739, 694 cm^{-1}; ^1H NMR(TMS, CCl_4) δ=1.22 (t, 3H, J=7.2 Hz), 4.07 (q, 2H, J=7.2 Hz), 7.10—7.55 (m, 5H) and essentially two triplets (2H, each) centered at δ=2.60 and δ=3.03, each line shows further fine splitting due to partial conformational freezing; MS (m/z, ^{80}Se) 258 (M^+); Found: C, 51.12; H, 5.51%. Calcd for $C_{11}H_{14}O_2Se$: C, 51.37; H, 5.49%.

Formation of Phthalaldehyde 6 from 1b. To an ethanol solution of PhTeNa (10 mmol in 30 ml) formed as described above was added α,α'-dibromo-*o*-xylene (5 mmol, 1.32 g) in THF (15 ml) and the reaction was refluxed for 2 h. The resulting mixture was exposed to the air at 25 °C and stirred overnight. The product was extracted into ether and dried. Evaporation followed by column chromatography on silica gel (benzene) gave **6**[27] in 60% yield.

Intermediacy of 5 in the Formation of Phthalaldehyde 6. To an ethanol solution (20 ml) of PhTeNa formed from Ph_2Te_2 (4.5 mmol, 1.85 g) and $NaBH_4$ (9.5 mmol, 360 mg)

was added a THF (20 ml) solution of **1b** (4.5 mmol, 1.19 g). The solution turned yellow and a white precipitate formed immediately. The mixture was stirred at 25 °C for 2 h. The solvent was removed in vacuo and benzene (50 ml) was added to the residue. The precipitate was filtered under N_2 and the filtrate was evaporated to give 1.91 g of a red solid. The NMR spectrum showed two singlets at δ 4.17 and δ 6.87 with 1:1 ratio which was assigned to the methylene and the aromatic protons of **5**, respectively, together with the aromatic protons of the PhTe groups of **5** and Ph_2Te_2 as the impurity (δ=7.20—7.50, m and δ=7.70—8.00, m). By subtracting the integral due to Ph_2Te_2 in the ^1H NMR spectrum, the yield of **5** was estimated to be 66%. In the MASS spectrum of the mixture, a peak appeared at 311 (**5**, *m/z*, M^+—PhTe) together with the parent peak of Ph_2Te_2 (*m/z*=414), but the parent peak of **5** was not observed. Allowing the NMR sample to stand at r.t., the peaks at δ 4.17 and δ 6.87 gradually decreased and a new peak appeared at δ 10.45 which was assigned to aldehyde protons of **6**. An attempt for isolation and purification of **5** failed due to its instability toward oxygen and/or light.

References

1) M. P. Cava and D. R. Napier, *J. Am. Chem. Soc.*, **79**, 1701 (1957).

2) Generation of quinodimethane can be classified into Ref. 3—8 according to the types of the reactions and those of precursors.

3) From benzocyclobutenes by thermolysis: a) F. R. Jensen and W. E. Coleman, *J. Am. Chem. Soc.*, **80**, 6149 (1958); b) T. Kametani, H. Nemoto, H. Ishikawa, K. Shiroyama, H. Matsumoto, and K. Fukumoto, *J. Am. Chem. Soc.*, **99**, 3461 (1977); c) B. D. Gowland and T. Durst, *Can. J. Chem.*, **57**, 1462(1979); d) R. W. Franck, T. V. John, and K. Olejniczak, *J. Am. Chem. Soc.*, **104**, 1106 (1982); e) A. Z. Bimanand, Y. N. Gupta, M. J. Doa, T. A. Eaton, K. N. Houk, and F. R. Fronczek, *J. Org. Chem.*, **48**, 403 (1983); f) P. Schiess, M. H.-Francotte, and C. Vogel., *Tetrahedron Lett.*, **26**, 3959 (1985); g) W. S. Trahanovsky and B. W. Surber, *J. Am. Chem. Soc.*, **107**, 4995 (1985).

4) From α,α'-substituted *o*-xylenes by 1,4-elimination: reduction of α,α'-dihalo-*o*-xylenes, a) M. P. Cava, A. A. Deana, and K. Muth, *J. Am. Chem. Soc.*, **81**, 6458 (1959); b) J. F. W. McOmie and D. H. Perry, *Synthesis*, **1973**, 416; c) F. A. J. Kerdesky, R. J. Ardecky, M. V. Lakshmikantham, and M. P. Cava, *J. Am. Chem. Soc.*, **103**, 1992 (1981); d) K. Alder and M. Fremery, *Tetrahedron*, **14**, 190 (1961); e) G. M. Rubottom and J. E. Wey, *Synthetic Commun.*, **14**, 507 (1984); f) H. Nozaki and R. Noyori, *Tetrahedron*, **22**, 2163 (1966); g) Y. Ito, K. Yonezawa, and T. Saegusa, *J. Org. Chem.*, **39**, 2769 (1974); Hofman Elimination, h) L. A. Errede, *J. Am. Chem. Soc.*, **83**, 949 (1961); 1,4-elimination of hydrogen halide, i) H. Hart, J. A. Hartlage, R. W. Fish, and R. R. Rafos, *J. Org. Chem.*, **31**, 2244 (1966); j) P. Schiess and M. Heitzmann, *Angew. Chem. Int. Ed. Engl.*, **16**, 469 (1977); k) S. K. Pollack, B. C. Raine, and W. J. Hehre, *J. Am. Chem. Soc.*, **103**, 6308 (1981); 1,4-elimination of methanol, l) R. J. Moss, R. O. White, and B. Rickborn, *J. Org. Chem.*, **50**, 5132 (1985); F^- induced 1,4-elimination, m) Y. Ito, M. Nakatsuka, and T. Saegusa, *J. Am. Chem. Soc.*, **102**, 863 (1980); n) *idem*, *ibid.*, **104**, 7609 (1982); o) S. Djuric, T. Sarkar, and P. Magnus, *ibid.*, **102**, 6885 (1980); p) J. L. Charlton, *Tetrahedron Lett.*, **26**, 3413 (1985); q) Y. Ito, E. Nakajo, K. Sho, and T. Saegusa, *Synthesis*, **1985**, 698; r) S. V. Kessar, P. Singh, and D. Venugopal, *Chem. Commun.*, **1985**, 1258.

5) From benzo-fused cyclic compounds by reverse Diels-Alder or cheletropic elimination of Z: Z=SO_2, a) M. P. Cava and A. A. Deana, *J. Am. Chem. Soc.*, **81**, 4266 (1959); b) E. K. Chess, P.-H. Lin, and M. L. Gross, *J. Org. Chem.*, **48**, 1522 (1983); c) L. A. Levy, *Synthetic Commun.*, **13**, 639 (1983); d) T. Durst, E. C. Kozma, and J. L. Charlton, *J. Org. Chem.*, **50**, 4829 (1985); Z=N_2, e) L. A. Carpino, *J. Org. Chem.*, **34**, 461 (1969); f) C. R. Flynn and J. Michl, *J. Am. Chem. Soc.*, **96**, 3280 (1974); Z=CO, g) G. Quinkert, J. Palmowski, H.-P. Lorenz, W.-W. Wiersdorff, and M. Finke, *Angew. Chem. Int. Ed. Engl.*, **10**, 198 (1971); Z=CO_2, h) R. J. Spangler, B. G. Beckmann, and J. H. Kim, *J. Org. Chem.*, **42**, 2989 (1977); Z=Te, i) E. Cuthbertson and D. D. MacNicol, *Tetrahedron Lett.*, **1975**, 1893.

6) From dimetallacyclohexenes: W. H. Hersh and R. G. Bergman, *J. Am. Chem. Soc.*, **103**, 6992 (1981).

7) From *o*-methylbenzaldehydes or *o*-methylstyrenes by photolysis: a) P. G. Sammes, *Tetrahedron* **32**, 405 (1976); b) J. M. Hornbach and R. D. Barrows, *J. Org. Chem.*, **47**, 4285 (1982).

8) From 5,6-dimethylenebicyclo[2.2.0]hex-2-ene by thermolysis: N. L. Bauld, F. R. Farr, and C.-S. Chang., *Tetrahedron Lett.*, **1972**, 2443.

9) Recently homogeneous reduction of α,α'-dibromo-*o*-xylenes with $CrCl_2$ in a mixed solvent of THF and HMPT was reported; D. Stephan, A. Gogues, and A. L. Coq, *Tetrahedron Lett.*, **25**, 5649 (1984).

10) Reviews in *o*-quinodimethane chemistry: a) W. Oppolzer, *Angew. Chem. Int. Ed. Engl.*, **16**, 10 (1977); b) *idem*, *Synthesis*, **1978**, 793; c) T. Kametani and H. Nemoto, *Tetrahedron*, **37**, 3 (1981); d) Y. Ito, *Yuki Gosei Kagaku Kyokai Shi*, **40**, 559 (1982).

11) a) W. M. Schubert, H. Steadly, and B. S. Rabinovitch, *J. Chem. Soc.*, **1955**, 5755; b) P. E. Sonnet and J. E. Oliver, *J. Org. Chem.*, **41**, 3284 (1976).

12) a) G. A. Olah, Y. D. Vankar, and A. P. Fung, *Synthesis*, **1979**, 59; b) G. A. Olah, M. Arvanaghi, and Y. D. Vankar, *J. Org. Chem.*, **45**, 3531 (1980); c) A. L. Gemal and J. L. Luche, *Tetrahedron Lett.*, **21**, 3195 (1980).

13) a) D. L. J. Clive and P. L. Beaulieu, *J. Org. Chem.*, **47**, 1124 (1982); b) L. Engman and M. P. Cava, *ibid.*, **47**, 3946 (1982); c) A. Osuka and H. Suzuki, *Chem. Lett.*, **1983**, 119.

14) a) K. Ramasamy, S. K. Kalyanasundaram, and P. Shanmugam, *Synthesis*, **1978**, 311; b) *idem*, *ibid.*, **1978**, 545; c) L. Engman, *Tetrahedron Lett.*, **23**, 3601 (1982).

15) L. Engman and S. E. Byström, *J. Org. Chem.*, **50**, 3170 (1985).

16) E. Cuthbertson and D. D. MacNicol, *Chem. Commun.*, **1974**, 498.

17) D. H. R. Barton and S. W. McCombie, *J. Chem. Soc., Perkin Trans. 1*, **1975**, 1574.

18) D. L. J. Clive, G. J. Chittattu, V. Farina, W. A. Kiel, S. M. Menchen, C. G. Russell, A. Singh, C. K. Wong, and N. J. Curtis, *J. Am. Chem. Soc.*, **102**, 4438 (1980).

19) Another expected product, ethyl 2,3-dibromo-2-tetralincarboxylate, was not obtained.

20) In the iodide induced reaction simple α,α'-dihalo-*o*-xylenes could not be dehalogenated(see Ref. 4a—c).

21) a) H. K. Spencer and M. P. Cava, *J. Org. Chem.*, **42**,

2937 (1977); b) H. K. Spencer, M. V. Lakshmikantham, and M. P. Cava, *J. Am. Chem. Soc.*, **99**, 1470 (1977).
22) M. Sevrin, J. N. Denis, and A. Krief, *Tetrahedron Lett.*, **21**, 1877 (1980).
23) a) M. Oki, W. Funakoshi, and A. Nakamura, *Bull. Chem. Soc. Jpn.*, **44**, 828 (1971); b) H. J. Reich, J. M. Renga, and I. L. Reich, *J. Am. Chem. Soc.*, **97**, 5434 (1975); c) R. Seshadri, W. J. Pegg, and M. Israel, *J. Org. Chem.*, **46**, 2596 (1981).
24) L. Hevesi, *Tetrahedron Lett.*, **1979**, 3025.
25) a) W. S. Haller and K. J. Irgolic, *J. Organomet. Chem.*, **38**, 97 (1972); b) M. R. Detty, B. J. Murray, D. L. Smith, and N. Zumbulyadis, *J. Am. Chem. Soc.*, **105**, 875 (1983).
26) H. Higuchi, T. Otsubo, F. Ogura, H. Yamaguchi, Y. Sakata, and S. Misumi, *Bull. Chem. Soc. Jpn.*, **55**, 182 (1982).
27) T. C. Chaudhuri, *J. Am. Chem. Soc.*, **64**, 315 (1942).

Polymerization of Styrene Adsolubilized in Surfactant Adsorbed Bilayer on Pigments

Kenjiro MEGURO, Toshikazu YABE, Sayuri ISHIOKA, Kazufumi KATO, and Kunio ESUMI*
Department of Applied Chemistry and Institute of Colloid and Interface Science,
Science University of Tokyo, Kagurazaka, Shinjuku-ku, Tokyo 162
(Received April 7, 1986)

The polymerization of styrene adsolubilized in a surfactant-adsorbed bilayer formed on the surface of inorganic pigments (iron oxide, titanium dioxide) was attempted in order to modify their surface properties. After the polymerization, the amount of polystyrene formed on the pigments gradually increased with an increase in the amount of styrene adsolubilized. Further, the molecular weight of the polystyrene formed changed with an increase in the amount of styrene. The surface properties of pigments after the polymerization were characterized by FTIR-PAS, turbidity, and zeta potential measurements.

Recently, seeded polymerization has been employed to modify the surface properties of particles. Cho et al.[1] have studied the mechanism with respect to the emulsion polymerization of PMMA-seeded styrene. Similar research has been achieved by Okubo,[2,3] Whang,[4] Hawkett,[5] Morgan,[6] and Hergeth.[7] From their studies, it has been confirmed that the polymerization of organic polymers on the surfaces of organic substances occurs easily. However, when the polymerization of organic monomers is performed in the presence of inorganic particles, it is known that seed nucleation and the growth of organic monomers progress independently of the inorganic particles due to a deficiency of the affinity between monomers and inorganic particles.[8]

On the other hand, it has been reported that inorganic particles can be encapsulated by organic polymers due to an enhancement of the interfacial affinity by a treatment of water-soluble polymers[8,9] or monomers of the hydrophilic acrylic series.[10] It is also well-known[11] that ionic surfactants form adsorbed bilayers on particle surfaces. By using such adsorbed bilayers, there is a great possibility that hydrophobic monomers can be adsolubilized into the surfactant adsorbed bilayers which exhibit hydrophobic properties and can then be polymerized.

In this work, styrene was adsolubilized into surfactant bilayers on the surface of a pigment and the polymerization of styrene adsolubilized was examined.

Experimental

Materials. Iron oxide (α-Fe_2O_3) and titanium dioxide (anatase) used were supplied by Titan Kogyo Co. Ltd. The surface area of the former was 3.4 $m^2 g^{-1}$, and 40.7 $m^2 g^{-1}$ for the latter. Sodium dodecyl sulfate (SDS) was supplied by Wako Pure Chemical Industries, Ltd., which was purified twice by recrystallization from ethanol. Styrene obtained from Wako Pure Chemical Industries, Ltd., was distilled under reduced pressure. Other chemicals were of all analytical grade.

Procedure. All the polymerization was performed in a 1-liter separable flask under nitrogen gas purging. The polymerization temperature was controlled at 70 °C by a thermostatic water bath. Before polymerization, 1 g of the pigment and 100 ml of aqueous electrolyte solution ($FeCl_3$ for iron oxide, $AlCl_3$ for titanium dioxide) were mixed in order to obtain a pigment with a high positive zeta potential.[11] Then, in order to form adsorbed bilayers of surfactant on the pigment, 100 ml of a 15 mM SDS solution was added, whereas the zeta potential of the adsorbed bilayer on pigment surface was negative. Styrene (as a monomer) was adsolubilized into the adsorbed bilayers of the surfactant on the pigment under 400 rpm of agitation speed for 2 h and then potassium peroxodisulfate (as an initiator) was added into the solution. The weight ratio of potassium peroxodisulfate to styrene was 1:100. The obtained products were washed several times with ethanol.

The amount of ethylbenzene adsolubilized was determined by using the same solution mentioned above; the concentration of ethylbenzene was obtained by measuring the absorbance at 260 nm.

Measurements. The coated amount of polystyrene on the pigments was determined gravimetrically: The total amounts of polystyrene on the pigments were obtained from the difference of weight before and after the calcination of the samples at 500 °C. The THF-unextractive coated amount of polystyrene was also determined gravimetrically.

The zeta potential of uncoated and polystyrene-coated pigments was measured with an Electrophoresis apparatus (Laser Zee 500, Pen Kem, Inc.) in ethanol. The zeta potential of styrene latex prepared by using SDS alone was also measured for a comparison.

The turbidity of pigments in water or hexane was measured as follows: A known weight of sample was put into a sedimentation tube in which deionized water or hexane was contained and then the obtained suspension was treated by sonication for ten minutes. After one hour standing, the absorbance of the suspension was measured at 500 nm with a spectrophotometer (Hitachi, Ltd., 220A).

The weight-average molecular weight of polystyrene which had been extracted from the coated pigments with THF was determined by gel permeation chromatography (Japan Spectroscopic Co. Ltd.).

The surfaces of the coated pigments were measured using a FTIR-PAS (FPA-84, Japan Spectroscopic Co., Ltd.).

Results and Discussion

It is known[11] that positively charged particles can be flocculated and redispersed by the addition of anionic surfactants, resulting in the formation of an adsorbed

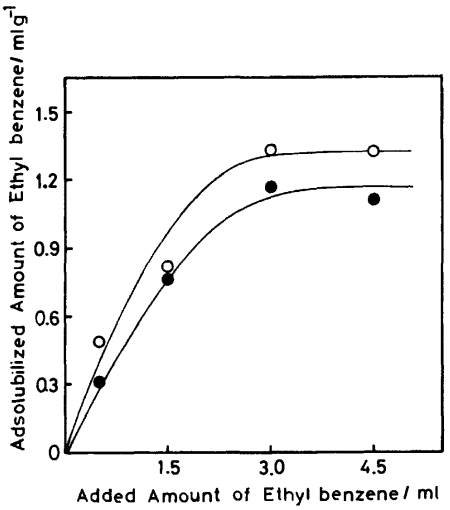

Fig. 1. The change in the amount of ethylbenzene adsolubilized into SDS-double layer on the pigment as a function of added amount of ethylbenzene at 25°C; (○) iron oxide, (●) titanium dioxide.

bilayer of surfactant on the particles. This adsorbed bilayer is expected to provide a field of polymerization of hydrophobic monomers since it exhibits hydrophobic property.

Figure 1 shows the amount of ethylbenzene adsolubilized into an SDS-adsorbed bilayer on the pigments as a function of the added amount of ethylbenzene at 25°C. Here, it is postulated that the amount of ethylbenzene adsolubilized is similar to that of styrene. In both pigments, the amount of ethylbenzene adsolubilized gradually increased and attained a constant value.

Then, the polymerization of adsolubilized styrene was carried out at 60°C using potassium peroxodisulfate as an initiator for 3 h. From a measurement of FTIR-PAS for the samples after polymerization, the absorption bands attributable to polystyrene (3200—2900 cm^{-1}, 1480—1360 cm^{-1}, 1130—1100 cm^{-1}) and SDS (1220 cm^{-1}, 1040 cm^{-1}) were observed, indicating that the surface of pigments are covered with a polystyrene layer.

Figure 2 shows the total amount of polystyrene and the THF-unextractive amount of polystyrene on pigments as a function of added amount of styrene. In the case of iron oxide, it is apparent that the THF-unextractive amount is approximately constant in spite of various added amounts. On the other hand, for titanium dioxide, the THF-unextractive amount was very small, but the THF-extractive amount increased with the added amount of styrene. The change in the weight-average molecular weight of the THF-extractive polystyrene as a function of the added amount of styrene is shown in Fig. 3. In the case of iron oxide, the weight-average molecular weight of the THF-extractive polystyrene decreased with an increase of the added amount of styrene. This result can be explained

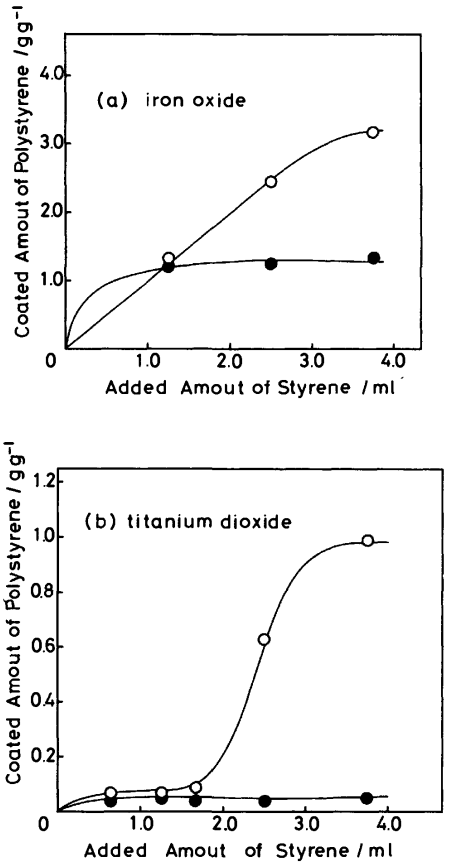

Fig. 2. The change in the coated amount of polystyrene on pigments as a function of added amount of styrene; (●) amount of unextractive polystyrene after THF extraction, (○) total coated amount of polystyrene.

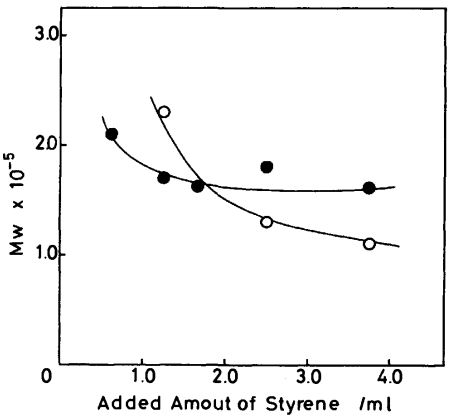

Fig. 3. The change in the weight-average molecular weight of THF-extractive polystyrene on pigment as a function of added amount of styrene; (○) iron oxide, (●) titanium dioxide.

as follows: The adsolubilized amount of styrene gradually increases with the added amount of styrene, while the amount of the initiator becomes in excess against the adsolubilized amount of styrene, resulting in a decrease in the molecular weight. Similarly, in the case of titanium dioxide, the weight-average molecular

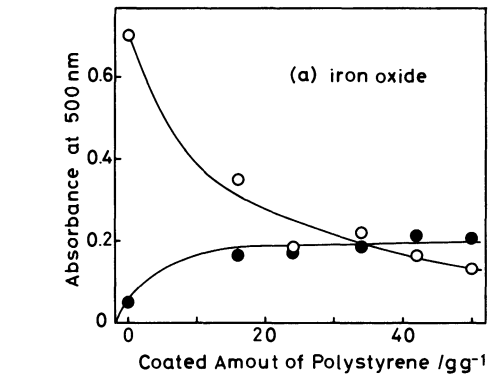

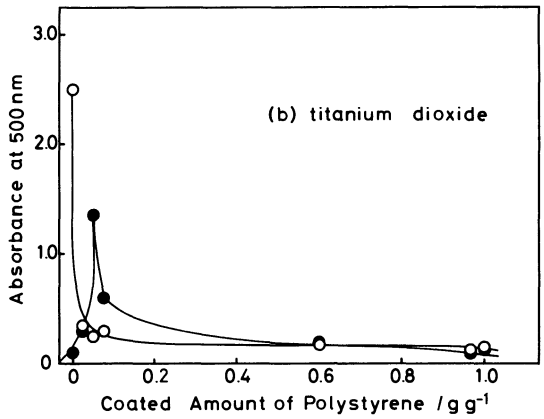

Fig. 4. The change in the absorbance at 500 nm as a function of coated amount of polystyrene on pigment; (○) in water, (●) in hexane.

weight decreases slightly. The zeta potential of the pigments after the polymerization was measured: the zeta potential was almost zero in ethanol compared with both the untreated sample and the latex prepared by using SDS alone having a large zeta potential, suggesting that the pigment surface is reasonably coated by polystyrene for both pigments.

Figure 4 shows the change in the absorbance of pigments after polymerization, in water and hexane, respectively. Here, a high absorbance value indicates a high stability. In water, the absorbance of both pigments decreased upon increasing the coated amount of polystyrene; however, in hexane an opposite change was observed for iron oxide, indicating that the surface of pigment becomes hydrophobic after polymerization. On the other hand, the absorbance of titanium dioxide in hexane showed a maximum value at some coated amount of polystyrene.

Schematics of the adsorbed bilayer of a surfactant adsolubilized with styrene and of pigment particles

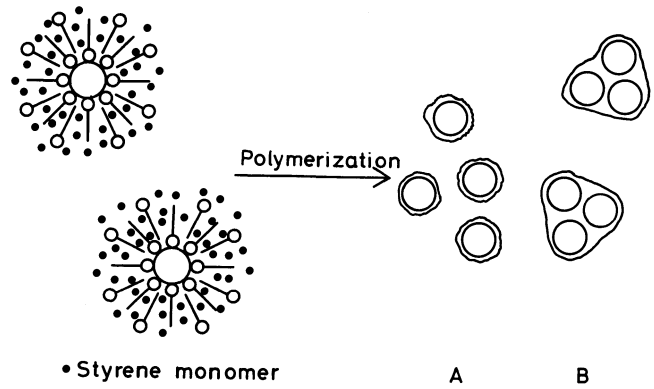

Fig. 5. Models of coated pigments by polystyrene.

after polymerization are presented in Fig. 5. For both iron oxide and titanium dioxide, there is a possibility that the coated pigments belong to model A or B since the coated amount of polystyrene and the molecular weight changed gradually with an increase in the added amount of styrene. Thus, it is concluded that this method of using a surfactant adsorbed bilayer is a useful encapsulation technique for the modification of a particle surface.

The authors are indebted to Japan Spectroscopic Co. Ltd., for measurement of FTIR-PAS.

References

1) I. Cho and K. W. Lee, *J. Appl. Polym. Sci.*, **30**, 1903 (1985).

2) M. Okubo, S. Yamaguchi, and T. Matsumoto, *Kobunshi Ronbunshu*, **42**, 17 (1985).

3) M. Okubo, Y. Katsuta, and T. Matsumoto, *J. Polym. Sci., Polym. Lett. Ed.*, **18**, 481 (1980).

4) B. C. Y. Whang, D. H. Napper, M. J. Ballard, and R. G. Gilbert, *J. Chem. Soc., Faraday Trans. 1*, **78**, 1117 (1982).

5) B. S. Hawkett, D. H. Napper, and R. G. Gilbert, *J. Chem. Soc., Faraday Trans. 1*, **76**, 1323 (1980).

6) L. W. Morgan, *J. Appl. Polym. Sci.*, **27**, 2033 (1982).

7) W. D. Hergeth and K. Schmutzler, *Acta Polymerica*, **36**, 472 (1985).

8) K. Furusawa, Y. Kimura, and T. Tagawa, *Kobunshi Ronbunshu*, **40**, 697 (1983).

9) K. Furusawa, Y. Kimura, and T. Tagawa, *J. Colloid Interface Sci.*, **109**, 69 (1986).

10) K. Kakutani, J. Kuze, S. Wataya, and T. Matsumoto, Japan Patent, 15281 (1980).

11) K. Meguro, S. Tomioka, N. Kawashima, and K.Esumi, *Progr. Colloid. Polym. Sci.*, **68**, 97 (1983).

 © 1986 The Chemical Society of Japan Bull. Chem. Soc. Jpn., 59, 3023—3028 (1986)

State of Polarization of Light Scattered by Colored Spheroids

Yoh SANO* and Masayuki NAKAGAKI†
National Institute of Agrobiological Resources, Tsukuba Science City, Yatabe, Ibaraki 305
†Faculty of Pharmaceutical Science, Kyoto University, Sakyo-ku, Kyoto 606
(Received April 9, 1986)

Using the light-scattering theory of Rayleigh–Gans for spheroids, theoretical expressions were derived for the polarization state of light scattered by randomly oriented small and colored spheroidal particles in the case of linearly polarized incident light with an angle of inclination of ψ to the scattering plane. The azimuth angle ζ of the ellipse of the scattered light did not depend on the axial ratio p and the relative complex refractive index m ($=m_0-ik_0$), but was a function of only the scattering angle θ and ψ; also, the ellipticity of the ellipse of the scattered light was always equal to 0 and the scattered light was partially linearly polarized for linearly polarized incident light. The degree of polarization of the scattered light for spheroidal particles, P, defined as the ratio of the polarized component to the intensity of the scattered light, depended strongly on p, m_0, k_0, and θ together with the angle ψ. This P was found to be smaller than 1. In the case of spherical particles, P was always equal to 1 at any θ; this means that the scattered light was perfectly polarized. It has been concluded that a determination of P as a function of ψ and θ gives good information regarding the shape and the optical constants (m_0 and k_0) of the colored spheroidal particles.

The light-scattering of colorless systems has been studied quite extensively by many investigators.[1,2] However, some biocolloids such as cytochrome C, hemoglobin, ferritin et al., dyes, membrane fragments or metal colloids are colored. These colored biocolloids or colloids often exhibit absorption maxima in the visible region. Under usual experimental conditions, incident light over a visible region is used. Therefore, the light-scattering phenomena are very complicated since we must take into consideration the effects of the absorption together with light scattering. In the case of colored spherical particles, the extinction, scattering and absorption of light have been theoretically studied by means of the Mie theory.[3,4] For absorbing spheroidal particles, the electrodichroic ratio has also been calculated as well as the effect of a complex refractive index and of the axial ratio of the spheroids upon the electrodichroic ratio.[5] However, to the author's knowledge no theory exists for taking into consideration the anisometry effect on the scattering and absorption of light by colored nonspherical particles.

Even if we use completely polarized incident light, the scattered light by anisotropic scatterers will generally be partially polarized and will contain an unpolarized component, since the direction of the induced dipole in an anisotropic particle is different from the direction of the electric vector of incident light. To give a complete description of a partially elliptically polarized beam of scattered light, we must state the intensity associated with both the polarized and unpolarized components, and also give the full specification of the polarized ellipse.

Three parameters must be used to completely define the elliptical polarization of the scattered light: that is, the ratio of the minor and the major axes of the ellipse, η (called the ellipticity), the inclination ζ of the major semi-axes of the ellipse with respect to the scattering plane (called the azimuth), and the direction of the motion of the end point of the electric vector of the light (similarly defined as for circular polarization). Ellipticity can vary between zero and unity, and the azimuth angle varies between 0 and $\pm 90°$. Linear and circular forms of polarization can be defined as special cases of elliptical polarization, that is, the ellipticity is 0 or 1, respectively.

The purpose of this work was to study the light scattering of a colored system having a complex index of refraction due to absorption in the above-mentioned visible region. For this purpose, the state of polarization of light scattered by randomly oriented, identical colored spheroidal particles was calculated on the basis of Rayleigh[6] and Gans[7] theorem. This will always be refered to as the Rayleigh–Gans theory of spheroids (RGS theory) in order to avoid any confusion with the well-known Rayleigh–Gans (RG) scattering theory involving the restrictive assumption that the refractive index of a particle is close to that of the surrounding medium.

Theory

General Consideration. Let us consider a system of colored and relatively small spheroidal particles dispersed in a colorless medium, where the dispersed phase (consisting of the particles) is optically isotropic and has neither intrinsic birefringence nor intrinsic dichroism. When linearly polarized incident light with its electric vector oriented obliquely to the scattering plane (observation plane) reaches the scattering volume element, the scatterer changes the state of light polarization and the scattered light generally becomes elliptically polarized, but contains unpolarized component as well.

All the possible states of the scattered light can be most easily analyzed by making use of Stokes parameters, and a Mueller or scattering matrix which depends only on the characteristics of the scattering medium.[8] The Stokes parameters (I, Q, U, and V), which completely characterize the intensity and the polarization properties of a beam of light, including

partially polarized and unpolarized light, is defined in terms of time averages of the electric-field components of an electromagnetic wave.

$$\begin{aligned} I &= \langle E_\pi E_\pi^* + E_\sigma E_\sigma^* \rangle, \\ Q &= \langle E_\pi E_\pi^* - E_\sigma E_\sigma^* \rangle, \\ U &= \langle E_\pi E_\sigma^* + E_\sigma E_\pi^* \rangle, \\ V &= \mathrm{i}\langle E_\pi E_\sigma^* - E_\sigma E_\pi^* \rangle. \end{aligned} \tag{1}$$

The subscripts π and σ refer to components of the electric field parallel and perpendicular, respectively, to the scattering plane, the brackets denote time averages, and an asterisk denotes a conjugate complex value. The four elements of the Stokes vector can be thought of as describing the total intensity (I), the excess π-polarization over the σ-polarization intensity (Q), the excess intensity of +45° linear polarization over −45° linear polarization (U), and the excess of right (as opposed to left) circular polarization intensity (V).

The Stokes vectors describing incident, $\boldsymbol{S}_0$, and scattered, $\boldsymbol{S}$, light are connected by a 4×4 matrix called Mueller's matrix or scattering matrix, $\boldsymbol{M}$,

$$\boldsymbol{S} = \boldsymbol{M}\boldsymbol{S}_0, \tag{2}$$

where $\boldsymbol{S}=[I, Q, U, V]$ and $\boldsymbol{S}_0=[I_0, Q_0, U_0, V_0]$ are the Stokes vectors of the incident and scattered light.

Scattering Matrix. The matrix elements are functions of Euler's angles, the scattering angle θ and the optical constants of the particle. If a particle is sufficiently small compared to the wavelength of light, it can be assumed that one dipole is introduced in the particle and that the oscillation of the dipole radiates scattered light according to a theorem proposed by Rayleigh[6] and Gans[7] (RGS theory). The scattering matrix $\boldsymbol{M}$ for randomly oriented spheroids in suspension is given by the following form (discussed by Van de Hulst[9]):

$$\boldsymbol{M} = \begin{pmatrix} S_{11} & S_{12} & 0 & 0 \\ S_{12} & S_{22} & 0 & 0 \\ 0 & 0 & S_{33} & 0 \\ 0 & 0 & 0 & S_{44} \end{pmatrix}, \tag{3}$$

where the matrix elements S_{11}, S_{12}, S_{22}, S_{33}, and S_{44} depend upon the shape of the particle and its complex refractive index. Averaging over Euler's angles for a completely random orientation of particles gives[10]

$$\begin{aligned} S_{11} &= F_1(1+\cos^2\theta) + 2|B|^2/15, \\ S_{12} &= F_1(\cos^2\theta - 1), \\ S_{22} &= F_1(\cos^2\theta + 1), \\ S_{33} &= 2F_1\cos\theta, \text{ and} \\ S_{44} &= (2F_1 - 2|B|^2/15)\cos\theta, \end{aligned} \tag{4}$$

where

$$F_1 = \{|A|^2 + 2[\mathrm{Re}A\cdot\mathrm{Re}B + \mathrm{Im}A\cdot\mathrm{Im}B]/3 + 2|B|^2/15\}/2. \tag{5}$$

ReA and ImA are the real and imaginary parts of A, respectively. In the case of a spheroidal particle, A and B are calculated as:

$$\begin{aligned} A &= \alpha^3(m^2-1)/\{3p^2[1+(m^2-1)L_b]\}, \text{ and} \\ B &= \alpha^3(m^2-1)/\{3p^2[1+(m^2-1)L_a]\} - A, \end{aligned} \tag{6}$$

where the parameter α is the relative particle radius defined by

$$\alpha = 2\pi a/\lambda. \tag{7}$$

Here, a is the length of semiaxis symmetry for the spheroid, and λ is the wavelength of light in the medium. The shape parameters L_i in the i-direction (i=a or b) are functions of the axial ratio p (=a/b) for a prolate ($p>1$) and an oblate ($p<1$) spheroid[11]

$$\begin{aligned} L_b(p>1) &= (1/2)[p^2/(p^2-1)][1-(1/\{p(p^2-1)^{1/2}\})\times \\ &\qquad \ln\{p+(p^2-1)^{1/2}\}], \\ L_b(p<1) &= (1/2)[p^2/(1-p^2)][(1/\{p(1-p^2)^{1/2}\})\arccos p - 1], \end{aligned} \tag{8}$$

and

$$L_a + 2L_b = 1. \tag{9}$$

The refractive index, n_2, of a colored particle is complex and can be written[9] as

$$n_2 = n_{20}(1-\mathrm{i}k). \tag{10}$$

Then, the relative complex refractive index, m, is

$$m = n_2/n_0 = m_0 - \mathrm{i}k_0, \tag{11}$$

where n_0 is the refractive index of the colorless medium; also,

$$m_0 = n_{20}/n_0 \text{ and } k_0 = m_0 k. \tag{12}$$

If the particle is colorless, k and k_0 are both zero.

State of Polarization of the Scattered Light. The scattered light is, in general, partially polarized. The partially polarized light behaves as an incoherent sum of the totally polarized, I_p (subscript "p" signify the polarized component), and the unpolarized, I_u (subscript "u" signify unpolarized), components. Both components are related to the Stokes parameters of the scattered light (I, Q, U, V) as follows:

$$\begin{aligned} I_p &= (Q^2+U^2+V^2)^{1/2}, \text{ and} \\ I_u &= I - I_p. \end{aligned} \tag{13}$$

In general, the polarized component is elliptically polarized, i.e., the end point of the electric vector moves periodically along an ellipse, which may, of course, reduce in special cases to a circle or a straight line. It is often convenient and sufficient for many experiments to give what is known as the degree of polarization of the light, together with a description of the shape,

azimuth and handedness of the ellipse of the polarized component of the scattered light. The degree of polarization, P, is defined as the ratio of the intensity of the polarized portion to the total intensity[12]

$$P = I_p/I. \tag{14}$$

It is generally known that the description of the polarization ellipse of the scattered light is also related to the Stokes parameters of the scattered light as follows:[12]

(1) The azimuth angle of the ellipse of the polarized component is

$$\zeta = (1/2) \arctan (U/Q), \text{ and} \tag{15}$$

(2) the ellipticity, η, of the ellipse is deduced from

$$2\eta/(1+\eta^2) = V/(Q^2+U^2)^{1/2}. \tag{16}$$

The linear polarization corresponds to $\eta=0$.

If we consider linearly polarized incident light with an electric vector that subtends an angle ψ with the scattering plane, the normalized Stokes parameters of the incident light beam are

$$I_0 = 1, Q_0 = \cos 2\psi, U_0 = \sin 2\psi, \text{and } V_0 = 0. \tag{17}$$

By substituting S_0 in Eq. 2, we can obtain the Stokes parameters of scattered light, and we can calculate the characteristics of each parameter of a partially polarized scattered light as follows:

$$\begin{aligned} &I_p = I_p^\circ(1-\sin^2\theta\cos^2\psi),\\ &I = I_p^\circ(1-\sin^2\theta\cos^2\psi) + I_u,\\ &I_u = 2|B|^2/15, I_p^\circ = 2F_1,\\ &\tan\zeta = \tan\psi/\cos\theta, \text{and}\\ &\eta = 0. \end{aligned} \tag{18}$$

According to the RGS theory for an electric dipole, the I_u term is only a function of B; this indicates an optical anisotropy. The term I_p is linearly polarized when the incident light is linearly polarized. This is because the direction of the induced dipole is different from the direction of the incident electric vector due to the anisometry of the particle.

The total intensity I during RGS scattering can be divided into two parts: one is the polarized component I_p which depends on the scattering angle θ together with ψ, m_0, k_0, and p, and the other is the unpolarized component I_u which is independent of the scattering angle and the angle of inclination of the incident light ψ.

According to Eqs. 6, 11, and 18, the intensities I and I_p are zero if k_0 is zero and m_0 is unity. That is, scattering does not occur in a colorless system if the refractive index of particles and the medium are equal. In the case of a colored system, however, scattering occurs even when m_0 is equal to unity. Generally, there exists no value of m_0 which can make the intensities I and/or I_p equal to zero when k_0 is not zero.

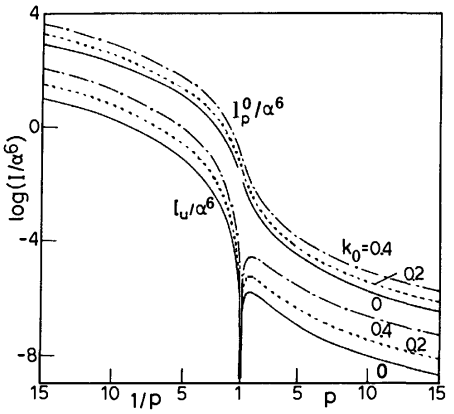

Fig. 1. Variation of $\log(I_u/\alpha^6)$ and $\log(I_p^\circ/\alpha^6)$ with the axial ratios p for spheroids of $m_0=1.20$ and various k_0 values; $k_0=0$ (——), $k_0=0.2$ (----), and $k_0=0.4$ (—·—). For the oblate ($p<1$) spheroids, $1/p$ (instead of p) is plotted on the abscissa to the left direction.

For an isotropic, spherical, colloidal particle, that is for Rayleigh scattering, the degree of polarization is always equal to 1 over the entire range of θ since $B=0$. In the case of spheroids, the degree of polarization is smaller than 1 and depends on m_0, k_0, and p, but it is independent of α in the RGS approximation.

In the case of linearly polarized incident light, the ellipticity, η, of the polarized component of the scattered light is equal to 0; this means that the component is linearly polarized. The azimuth angle of the polarized component, ζ, for the spheroids as well as for the spherical particles is equal to 90° in the case of $\theta=90°$ (according to Eq. 18) for both colored and colorless systems. The ζ is equal to ψ when $\theta=0°$; this means that the direction of the electric field of the forward-scattered light is equal to that of the incident light for both Rayleigh scattering as well as the RGS approximation (if the orientation of particles is completely random).

Numerical Results and Discussion

Variation of the Intensity of the Scattered Light. Numerical calculations were made with an ACOS 850/20 computer at the Computer Center of the Ministry of Agriculture and Forestry. Figure 1 shows the variation of the intensities of the scattered light for the unpolarized component I_u and the maximum of the polarized component I_p° for prolate and oblate spheroids in the case $k=k_0/m_0<1$ (that is $k_0<m_0$) as a function of the axial ratio p and of a given m_0 value (the case $m_0=1.20$ is given as an example). We call the quantity I (as well as I_p and I_u) the "intensity" of the scattered light; however, it is actually a dimensionless quantity which is equal to the Rayleigh ratio multiplied by $(2\pi/\lambda)^2$ per particle. The scattered intensities, I_u and I_p°, for a colored system become greater with increasing k_0 since they include absorp-

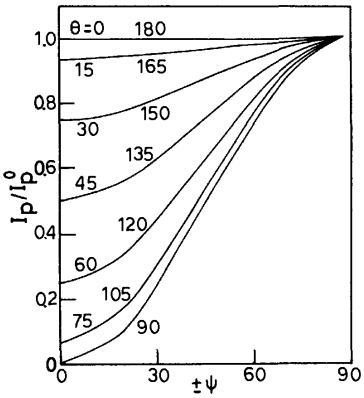

Fig. 2. Variation of I_p/I_p° with $\pm\psi$ (degree) for various values of θ. Dependences on m_0, k_0, α, and p are cancelled by taking the ratio of I_p to I_p°, in the RGS approximation.

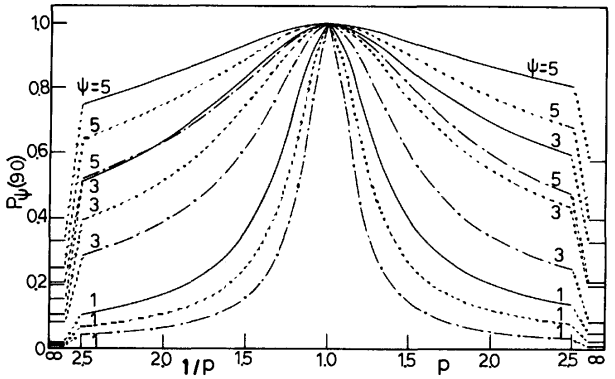

Fig. 3. Variation of the degree of polarization at $\theta=90°$, $P_\psi(90)$, with axial ratio of the prolate spheroid (p) or of the oblate spheroid ($1/p$) at $m_0=1.20$ and various k_0 values; $k_0=0$ (——), $k_0=0.2$ (– – –), and $k_0=0.4$ (—·—). Horizontal lines on both sides indicate the limiting values at $p\to\infty$ (infinitesimally thin rod) and $p\to0$ (infinitesimally thin disk), respectively.

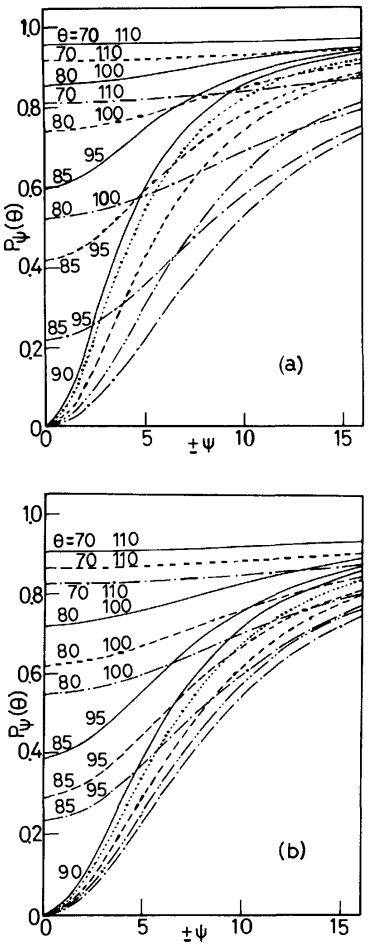

Fig. 4. Variation of the degree of polarization, $P_\psi(\theta)$ with ψ (degree) for (a) the prolate spheroid at $p=15$ and (b) the oblate spheroid at $p=1/15$ and $m_0=1.20$. Parameters are scattering angle θ (degree). The $P_\psi(\theta)$ for various k_0 values at $\theta=90°$ indicates $k_0=0$ (——), $k_0=0.1$ (------), $k_0=0.2$ (------), $k_0=0.3$ (—··—), and $k_0=0.4$ (—·—).

tion contributions to the scattering.

Figure 2 shows the variation of the polarized component I_p with the azimuth angle of the linearly polarized incident light ψ. By taking the ratio I_p/I_p°, all dependencies on m_0, k_0, α, and p can be cancelled just as in an RGS approximation. As shown in Eq. 18, the intensities I_p and I are functions of $\cos^2\theta$; therefore, they are symmetric around the $\theta=90°$ axis.

Variation of the Degree of Polarization. The degree of polarization P defined by Eq. 14 is, together with Eq. 18,

$$P_\psi(\theta) = (1-\sin^2\theta\cos^2\psi)/[(1-\sin^2\theta\cos^2\psi) + I_u/I_p^\circ]. \tag{19}$$

Thus, when $\theta=90°$,

$$P_\psi(90) = \sin^2\psi/(\sin^2\psi + I_u/I_p^\circ). \tag{20}$$

Figure 3 shows the variation of P_ψ (90) with the axial ratio p of the spheroids for various k_0 and ψ at $m_0=1.20$. The P_ψ (90) depends strongly on p and ψ, especially for a ψ value smaller than 5°. The P_ψ (90) is nearly equal to 1.0 if ψ is larger than 45° since I_u is about 1/100 of I_p° (Fig. 1). If $p=1$, P_ψ (90) is equal to 1.0 irrespective of the value of ψ and k_0 since I_u is equal to zero. The dependence of P_ψ (90) on p becomes greater as k_0 increases. Also, P_ψ (90) decreases monotonously upon increasing of p or $1/p$.

The horizontal lines in Fig. 3 are the limiting values for $p\to\infty$ ($L_a=0$ and $L_b=1/2$) on the right side and for $p\to0$ ($L_a=1$ and $L_b=0$) on the left side. The P_ψ (90) for an infinitesimally thin disk is much smaller than that for the rodlike particle.

Figure 4 shows the variation of the degree of polarization, $P_\psi(\theta)$, in Eq. 19 with $\pm\psi$ at various scattering angles θ. The cases of a prolate spheroid at $p=15$ and of an oblate spheroid at $p=1/15$ are shown here as examples. The intensities, I and I_p, are functions of $\sin^2\theta$; therefore, the degree of polarization is also symmetric around $\theta=90°$. At $\theta=90°$, $P_\psi(\theta)$ increases monotonously from 0 to almost 1 with an

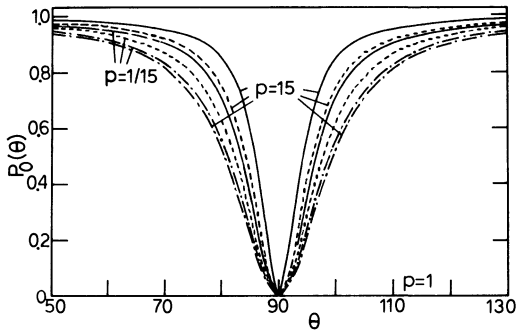

Fig. 5. Variation of the degree of polarization, at $\psi=0$, $P_0(\theta)$, for the prolate spheroid at $p=15$, the oblate spheroid at $p=1/15$, the spherical particle ($p=1$) of $m_0=1.20$ and various k_0 values; $k_0=0$ (——), $k_0=0.2$ (----), and $k_0=0.4$ (—·—).

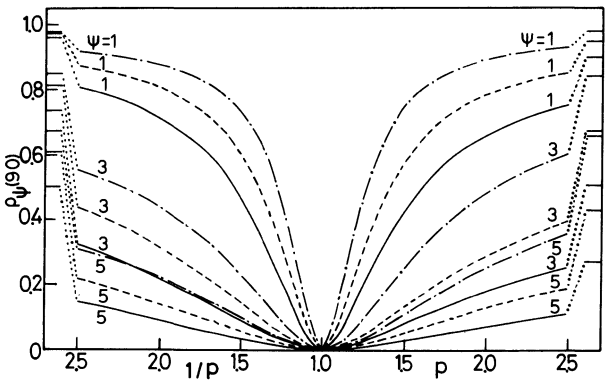

Fig. 6. Variation of the degree of depolarization at $\theta=90°$, $\rho_\psi(90)$, with axial ratio p or $1/p$ for $m_0=1.20$ and various k_0 values; $k_0=0$ (——), $k_0=0.2$ (----), and $k_0=0.4$ (—·—).
Horizontal lines on both sides indicate the limiting values at $p\to\infty$ (infinitesimally thin rod) and $p\to0$ (infinitesimally thin disk), respectively.

increase in $\pm\psi$; its value at a given ψ decreases with increasing k_0. The $P_\psi(\theta)$ at constant θ increases monotonously with an increasing $\pm\psi$. The dependence of $P_\psi(\theta)$ on $\pm\psi$ becomes smaller as the deviation of θ from 90° becomes larger and is larger as k_0 becomes larger. The variation of $P_\psi(\theta)$ for an oblate spheroid is shown in Fig. 4(b). The value of the degree of polarization $P_\psi(\theta)$ for an oblate spheroid at $p=1/15$ is a little smaller than that for a prolate spheroid at $p=15$ since an oblate spheroid has two major axes (b) which are responsible for producing an unpolarized component of scattered light while the prolate spheroid has only one major axis (a).

For $\psi=0°$, Eq. 19 can be rewritten as:

$$P_0(\theta) = \cos^2\theta/[\cos^2\theta + I_u/I_p^\circ] \tag{21}$$

Figure 5 shows the variation of $P_0(\theta)$; its value is symmetric around $\theta=90°$ and increase from 0 to almost 1. The $P_0(\theta)$ at $\theta=85°$ (or 95°) for a colorless system ($k_0=0$) is about 0.6, since $\cos^2 85°=0.0076$ (which is of the order of magnitude of $I_u/I_p°$). For a colored system $P_0(85)$ is about 2/3 of that for a colorless system at $k_0=0.2$ and about 1/3 at $k_0=0.4$.

Variation of the Degree of Depolarization. It has been said that the various kinds of degrees of depolarization to be defined can be given as combinations of two fundamental degrees of depolarization, ρ_π and ρ_σ:

$$\begin{aligned}\rho_\pi(\theta) &= I_{\pi\pi}(\theta)/I_{\pi\sigma}(\theta), \text{ and}\\ \rho_\sigma(\theta) &= I_{\sigma\pi}(\theta)/I_{\sigma\sigma}(\theta),\end{aligned} \tag{22}$$

where π and σ indicate the parallel and perpendicular directions, respectively, of the electric vector of light to the scattering plane. The first and the second subscripts are for incident and scattered light, respectively.[13] For example, the degree of depolarization for unpolarized incident light, ρ_u, is given by ρ_π and ρ_σ as

$$\rho_u = \frac{I_{u\pi}}{I_{u\sigma}} = \frac{I_{\pi\pi}+I_{\sigma\pi}}{I_{\pi\sigma}+I_{\sigma\sigma}} = \rho_\sigma\frac{1+\rho_\pi}{1+\rho_\sigma} \tag{23}$$

if the particles are either spherical or spheroids oriented completely randomly so that the following Krishnan reciprocity theorem holds.

$$I_{\pi\sigma} = I_{\sigma\pi}. \tag{24}$$

In the RGS approximation for completely random orientation,[14]

$$\begin{aligned}I_{\pi\pi}(\theta) &= I_p^\circ\cos^2\theta + (1/2)I_u,\\ I_{\pi\sigma}(\theta) &= I_{\sigma\pi}(\theta) = (1/2)I_u, \text{ and}\\ I_{\sigma\sigma}(\theta) &= I_p^\circ + (1/2)I_u.\end{aligned} \tag{25}$$

Therefore, for unpolarized incident light

$$\rho_u(\theta) = [\cos^2\theta + I_u/I_p^\circ]/[1+I_u/I_p^\circ]. \tag{26}$$

This is equal to $\cos^2\theta$ and is not equal to zero, even if the unpolarized component I_u is zero (if the angle θ is other than 90°). For $\theta=90°$,

$$\rho_u(90) = I_u/[I_p^\circ+I_u] = 1 - P_{90}(90), \tag{27}$$

where $P_{90}(90)$ is the degree of polarization for $\psi=90°$ and $\theta=90°$.

Instead of unpolarized light, if linearly polarized light with the azimuth angle of ψ is used as the incident light, the degree of depolarization is

$$\rho_\psi(\theta) = \frac{I_{\psi\pi}(\theta)}{I_{\psi\sigma}(\theta)} = \frac{I_{\pi\pi}(\theta)\cos^2\theta + I_{\sigma\pi}(\theta)\sin^2\theta}{I_{\pi\sigma}(\theta)\cos^2\theta + I_{\sigma\sigma}(\theta)\sin^2\theta} \tag{28}$$

In the RGS approximation,

$$\rho_\psi(\theta) = [2\cos^2\psi\cos^2\theta + I_u/I_p^\circ]/[2\sin^2\psi + I_u/I_p^\circ], \tag{29}$$

and, for $\theta=90°$

$$\rho_\psi(90) = I_u/[2I_p^\circ\sin^2\psi + I_u]. \tag{30}$$

These equations show that for $\psi=0°$, $\rho_0(90)=\rho_\pi(90)=1$; for $\psi=90°$, $\rho_{90}(\theta)=\rho_\sigma(\theta)=I_u/[2I_p°+I_u]$ which is independent of θ and is very small because $I_u/I_p°$ is the order of 10^{-2} as was shown in Fig. 1; for $\psi=45°$, $\rho_{45}(\theta)=\rho_u(\theta)$ is approximately equal to $\cos^2\theta$ if θ is different

from 90°, but at $\theta=90°$, $\rho_u(90)$ is nearly equal to $2\rho_\sigma$ and is very small at the order of 10^{-2}.

In the RGS approximation, the variation of $\rho_\psi(90)$ for various ψ values as a function of the axial ratio p of the particle for $m_0=1.20$ is shown in Fig. 6. It seems to be very similar to Fig. 3 if the direction of the ordinate is inverted.

For the Determination of Parameter Values. As is shown in Figs. 3—6, the degree of polarization or degree of depolarization strongly depends on the axial ratio p, m_0, and k_0 of the spheroids, and is independent of α. If we measure $P_\psi(\theta)$, $P_\psi(90)$, or $P_\psi(90)$, the axial ratio for a colorless system is determined directly if the value of m_0 is known. For a colored system, if we measure $P_\psi(\theta)$ at several values of ψ and θ, it is possible to determine both k_0 and p from the curve-fitting method to the theoretical values and to determine whether the particle is prolate or oblate. On the contrary, if the value of the axial ratio p of the colored spheroid is known from the other physicochemical techniques, it is also possible to determine both m_0 and k_0 values of the colored spheroid. In conjunction with the knowledge of the axial ratio, the value of α is also obtained from the values of the intensities (I, I_p, and I_u), which are obtained simultaneously. Knowledge about α and p immediately gives information regarding the molecular weight M of the spheroid (for both colored and colorless systems) if the partial specific volume is known separately.

The value of k_0 can be large if the particles are colored. It can even be infinitely larger if the particles are made of a good conductor; however, the extinction of the dispersed system as a whole can be made as small as possible in experiments by diluting the dispersed system. Therefore, extremely small k_0 values are experimentally interesting. In particular, the value of the refractive index of a colored system is not practically equal to that of a colorless system if the value of k_0 is larger than 10^{-4}.[3]

Measurement of Degree of Polarization with the Analyzer. The intensity of the irradiance transmitted through the analyzer with a transmission axis inclined by χ to the scattering plane, $I_{\psi\chi}(\theta)$, is calculated by using the Mueller matrix for an ideal linear analyzer as follows:[8]

$$I_{\psi\chi}(\theta) = (I_u/2) + I_p\{1+\cos 2(\chi-\zeta)\}/2 = I\frac{1+P_\psi(\theta)\cos 2(\chi-\zeta)}{2}, \quad (31)$$

where ζ is the azimuth angle of the scattered polarized component. In the case of the degree of depolarization the two special cases of $\chi=0°$ (parallel) and $\chi=90°$ (perpendicular to the scattering plane) is generally discussed.

The variation of $I_{\psi\chi}(\theta)$ is shown in Fig. 7. When χ is changed by rotating the analyzer, the intensity of the transmittance $I_{\psi\chi}(\theta)$ has maximum, $I_{max}(\theta)$, and minimum, $I_{min}(\theta)$, values at $\chi=\zeta$ and $\chi=\zeta+\pi/2$, respectively

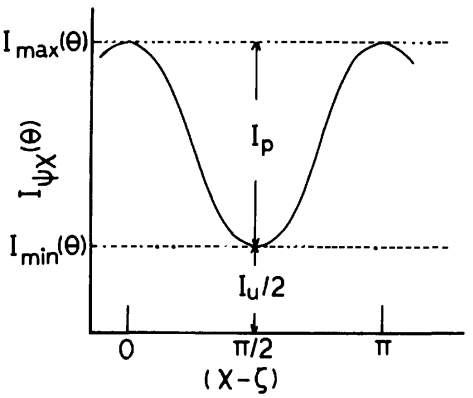

Fig. 7. Variation of transmitted intensity of the partially polarized light with analyzer orientation.

(Fig. 7). The degree of polarization can, therefore, be experimentally measured by rotating the analyzer by using

$$P_\psi(\theta) = [I_{max}(\theta)-I_{min}(\theta)]/[I_{max}(\theta)+I_{min}(\theta)]. \quad (32)$$

This is equivalent to thinking of the beam as being made up of two linearly polarized orthogonal incoherent beams with intensities $I_{max}(\theta)$ and $I_{min}(\theta)$.

As mentioned in the INTRODUCTION, it is important to determine the size and shape of the colored biocolloids such as cytochrome C, hemoglobin, ferritin et al., dyes, membrane fragments prepared from the plant plasma membrane, and/or the various kinds of metal colloids. It is also important to determine the k_0 values in order to determine the physico-chemical properties of these colored molecules. For this purpose, the theory presented in this paper can be efficiently applied to these colored systems.

References

1) M. Kerker, The Scattering of Light and Other Electromagnetic Radiation, Academic Press, New York (1969).
2) M. B. Huglin, Light Scattering from Polymer Solutions, Academic Press, New York (1972).
3) M. Nakagaki, *Bull. Chem. Soc. Jpn.*, **31**, 980 (1958); **38**, 2130 (1965).
4) F. C. Chromey, *J. Opt. Soc. Amer.*, **50**, 730 (1960).
5) M. Kerker and D. D. Cooke, *App. Opt.*, **10**, 2670 (1971).
6) L. Rayleigh, *Phil. Mag.*, **44**, 28 (1897).
7) R. Gans, *Ann. Phys.*, **62**, 331 (1920).
8) W. A. Shurcliff, Polarized Light, Harvard University Press, Massachusetts (1962).
9) H. C. Van de Hulst, Light Scattering by Small Particles, Wiley, New York (1957).
10) Y. Sano and M. Nakagaki, *J. Colloid Interface Sci.*, **105**, 348 (1985).
11) Y. Sano and M. Nakagaki, *J. Phys. Chem.*, **88**, 95 (1984).
12) M. Born and E. Wolf, Principles of Optics, Pergamon Press, New York (1965).
13) W. Heller and M. Nakagaki, *J. Chem. Phys.*, **61**, 3619 (1974).
14) M. Nakagaki, *Bull. Chem. Soc. Jpn.*, **34**, 834 (1961).

 © 1986 The Chemical Society of Japan Bull. Chem. Soc. Jpn., 59, 3029—3032 (1986)

Studies of Spin-Labeled Sodium Dodecyl Sulfate. II. Effect of Sodium Chloride on ESR Line Width

Takeo YAMAGUCHI,* Akira YAMAUCHI,† Eiji KIMOTO, and Hideo KIMIZUKA†
Department of Chemistry, Faculty of Science, Fukuoka University, Jonan-ku, Fukuoka 814-01
†Department of Chemistry, Faculty of Science, Kyushu University 33, Hakozaki, Higashi-ku, Fukuoka 812
(Received April 11, 1986)

The ESR spectra of spin-labeled sodium dodecyl sulfate were examined by changing the concentration, temperature, and ionic strength. The broadening of ESR lines due to a monomer surfactant could be explained in terms of an electron-spin exchange and a monomer-micelle exchange. The spin-exchange rate increased with increasing temperature and decreased with increasing ionic strength, i.e., the spin-exchange frequency was closely related to the viscosity of the medium. On the basis of an analysis of the line width above the critical micelle concentration, it was found that the aggregation number of the micelle of this compound and the monomer-micelle exchange frequency were dependent on the ionic strength.

Recent investigations on the micelle have stressed its dynamic properties. The diffusion coefficients of the micelles have been obtained by means of quasi-elastic light-scattering spectroscopy.[1,2] Kinetic studies of micellar systems by pressure-jump, temperature-jump, and ultrasonic absorption have shown that there are two relaxation processes for micelle formation.[3] The slow process, which is characterized by a relaxation time of the order of 10^{-3} s, represents the fluctuation of the total number of the micelles. On the other hand, the fast relaxation process of the order of 10^{-6} s corresponds to the association/dissociation equilibrium of monomeric ion to/from micelles. The NMR and ESR spectra also give useful information regarding the monomer-micelle exchange frequency. NMR data showed that its exchange frequency was below 10^{-5} s.[4] Nakagawa and Jizomoto[5] demonstrated that the lifetime of the spin probe molecules solubilized into micelle was 10^{-6} s. However, there are only a few reports on the dynamic properties of micelles composed of spin-labeled surfactants. Of these, Fox[6] studied the monomer-micelle exchange using cationic surfactant spin-labeled at polar head group and reported that the line broadening due to the monomer-micelle exchange was not observed. On the other hand, Schmidt et al.[7] have investigated the kinetics on micellization of spin-labeled lecithin and correlated the line broadening above the critical micelle concentration (cmc) to the monomer-micelle exchange reaction.

Here, it would be important to confirm the existence of the monomer-micelle exchange by the ESR spectra and, furthermore, to obtain information regarding the dynamic behavior of surfactant molecules in micellar solutions. From such a standpoint, we synthesized the spin-labeled sodium dodecyl sulfate (SL-SDS) labeled with a nitroxide radical.[8,9] Using this spin-labeled surfactant, we studied the properties of an aqueous SL-SDS solution in the absence of salt on the basis of its ESR spectra and conductivity data.[9] In the present work, the effect of added salt on the spin-exchange interaction and the micelle formation of SL-SDS is described.

Experimental

Materials. SL-SDS, sodium salt of 2-ethyl-2-[9-(hydroxysulfonyloxy)nonyl]-4,4-dimethyl-3-oxazolidinyloxyl, was synthesized by the procedure previously described.[8,9]

Viscosity. The viscosity of the medium containing NaCl was calculated according to the Othmer rule.[10,11]

Measurement of ESR. The samples were carefully deoxygenated by the repetitive freeze-thaw technique and then substituted by a dry nitrogen gas. ESR measurements were carried out with a JEOL FE-1X spectrometer equipped with a variable temperature accessory. The temperature control was checked with a copper-constantan thermocouple and was found to be stable within ±0.5°C. The usual spectrometer settings were 100 KHz modulation amplitude, 0.5 G; microwave power, 1 mW; scan range, 200 G; scan speed, 8 min.

Results and Discussion

As we have already noted regarding the properties of an aqueous SL-SDS solution without added salt, the three sharp ESR lines due to nitroxide radicals become broad and eventually coalesce into a single broad line with increasing radical concentration. Such spectral changes have been interpreted in terms of an electron-spin exchange.[9,12] On the basis of the conductivity data, it has been determined that the cmc of SL-SDS is 21.6 mmol kg^{-1} at 25°C and its aggregation number is about 6.[9] Because of a small aggregation number and its high cmc, such superimposed ESR signals due to monomer and micellar surfactants as seen above cmc in other spin-labeled surfactants[6,7] were not observed. Figure 1 shows the ESR spectra of 50 mmol kg^{-1} SL-SDS solutions containing various concentrations of NaCl (0.1—1.0 mol kg^{-1}). The ESR signal in the absence of NaCl was considerably distorted with an increased number of collisions between surfactant molecules. With an increasing NaCl concentration, however, the triplet lines due to monomer surfactant became sharp and a single broad line ascribed to the micelles gradually appeared at the central field. This suggests that, with increasing the amount of added salt, the aggregation number of the micelles increases and the monomer concentration decreases.

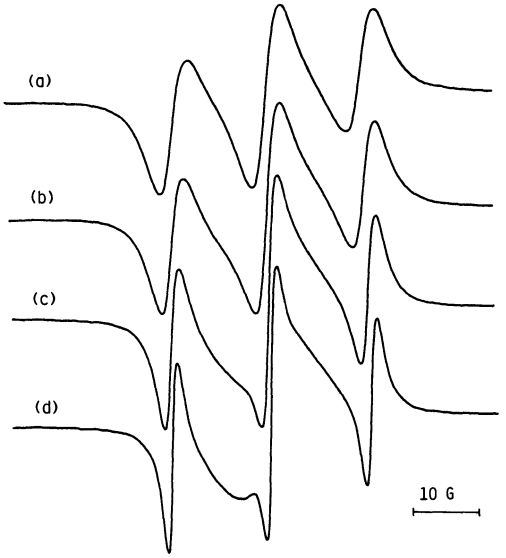

Fig. 1. ESR spectra of 50 mmol kg^{-1} SL-SDS solution containing a) 0, b) 0.1, c) 0.5, and d) 1.0 mol kg^{-1} NaCl, respectively, at 19°C.

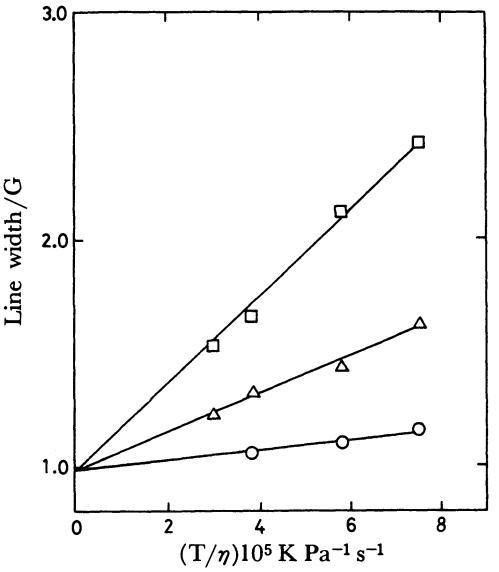

Fig. 3. Width of the $M=+1$ line vs. T/η for SL-SDS solution containing 1 mol kg^{-1} NaCl in 1 (○), 4 (△), and 8 mmol kg^{-1} (□), respectively.

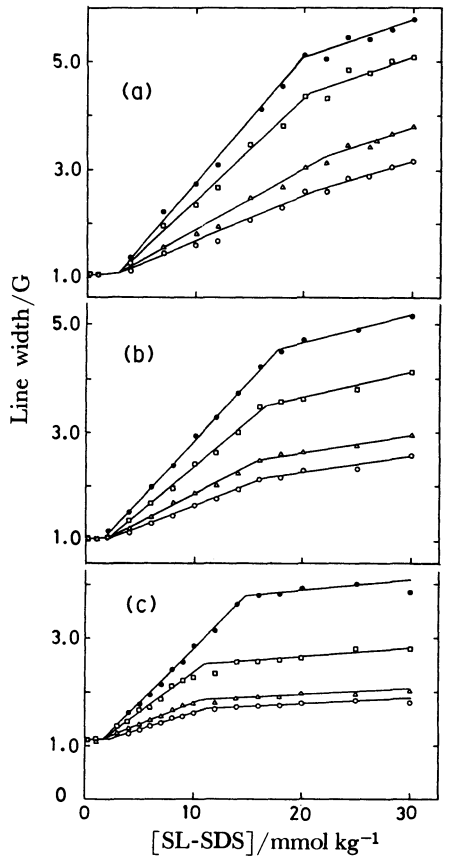

Fig. 2. Width of the $M=+1$ line vs. concentration of SL-SDS at 25 (○), 35 (△), 55 (□), and 70°C (●) in the presence of 0.1 (a), 0.5 (b), and 1.0 mol kg^{-1} NaCl (c).

As shown in Fig. 2, the relationship between the line width of the signal ($M=+1$ line, where M is the nuclear spin quantum number) at low field and SL-SDS concentration was examined at various temperatures (25, 35, 55, and 70°C) and NaCl concentrations (0.1, 0.5, and 1.0 mol kg^{-1}). The plots of the line width vs. the SL-SDS concentration show two inflection points. At low concentrations of SL-SDS (0.5 and 1.0 mmol kg^{-1}), the line widths were almost independent of both the temperature and the ionic strength. This indicates that the contribution of spin rotational relaxation[12] to the line width is negligibly small, regardless of the added salt. At a constant temperature and NaCl concentration, the line width became broader with increasing radical concentration. Generally, in free nitroxide radical molecules, the line broadening observed with increasing radical concentration can be attributed to either an electron-spin exchange or an electron spin-electron spin dipole interaction. The relaxation process due to the spin-exchange interaction is dependent on T/η, while that due to dipole-dipole interaction depends on η/T, where η is the viscosity of the medium and T is the absolute temperature.[13] Therefore, the relation of the line width vs. T/η was examined at various concentrations of SL-SDS in the presence of 1 mol kg^{-1} NaCl. As shown in Fig. 3, the line width varied linearly as a function of T/η. This indicates that spin exchange is predominant relaxation process in the range of this concentration. Thus, the line broadening observed between the two inflection points is attributed to the spin-exchange interaction. In the absence of NaCl, the plots of the line width vs. the SL-SDS concentration deviate from a straight line above about 20 mmol kg^{-1}.[9] However, this inflection point shifted to a lower concentration of SL-SDS with increasing NaCl concentration, i.e., it changed from 20 to 11 mmol kg^{-1} by an addition of 1 mol kg^{-1} NaCl. The linewidth variation with the SL-SDS concentration above the higher inflection point is small compared with

Table 1. Effects of Temperature and Ionic Strength on Second-Order Rate Constant [a)]

Temp/°C	$k_2 \times 10^{-9}$/kg mol^{-1} s^{-1}			
	Added NaCl/mol kg^{-1}			
	0[b)]	0.1	0.5	1.0
25	2.2 (3.6)	1.9 (3.6)	1.8 (3.5)	1.4 (3.3)
35	2.7 (4.7)	2.4 (4.6)	2.3 (4.5)	1.8 (4.2)
55	4.0 (7.2)	4.0 (7.1)	3.9 (6.7)	3.1 (6.4)
70	5.0 (9.3)	5.1 (9.2)	5.0 (8.8)	4.4 (8.3)

a) Calculated k_2' values are shown in parentheses. b) Data from Ref. 9.

that below its inflection point. For micellar solutions, it is well known that the cmc decreases upon adding salts and the monomer concentration remains constant above cmc.[14] Taking these facts into account, it is considered that the inflection point at higher concentrations corresponds to the cmc of the surfactant molecules.

The spin exchange between SL-SDS molecules is regarded as a second-order reaction.[13] The second-order rate constants (k_2) are obtained from the slope of the line width vs. the radical concentration by

$$k_2 = \frac{3\sqrt{3}}{4}|\gamma_e|h, \tag{1}$$

where γ_e is a magnetogyric ratio of a free electron, and h is the slope of the line width-surfactant concentration plots. The obtained values of k_2 are given in Table 1. The values of k_2 decreased upon adding salts at each temperature. The values of k_2 in all cases were of the order 10^9 kg mol^{-1} s^{-1}, indicating that the spin exchange of SL-SDS is a diffusion-controlled process.[12,13] For such a reaction, the reaction rate is greatly influenced by the viscosity of the solvent. Using the theory of Smoluchowski,[15] we could obtain the rate constant (k_2') for the bimolecular encounters:

$$k_2' = \frac{N_A}{1000\,\rho}\frac{4kT}{3\eta}, \tag{2}$$

where N_A is Avogadro's number and ρ, the density of the solution. The values of k_2' are also given in Table 1. The values of k_2' are in agreement with those of $2k_2$. Similar results, i.e., $2k_2$, is equal to k_2', have also been reported by other workers.[12,16-18] The frequency of the spin exchange is markedly dependent on the charge and size of the radical. For example, the spin-exchange rate of anion radicals with a large repulsive charge increases due to the offset of a coulombic repulsion between these radicals with increasing ionic strength.[19] Eastman et al.[19] demonstrated that the spin-exchange rate of the di-*t*-butyl nitroxide radical decreased markedly with increasing ionic strength. In order to explain such a phenomenon, they have proposed that aggregates of the radicals are caused by the hydrophobicity of the *t*-butyl groups. In the present work, the spin-exchange rates of SL-SDS obtained in the presence and absence of NaCl were closely dependent on the viscosity of the medium, suggesting that neither the polar head group nor the hydrocarbon chain of SL-SDS molecule play any significant role in the spin-exchange interaction.

In spin-labeled surfactants, monomer amphiphilic molecules incorporated into micelles undergo a fast spin exchange, causing a line broadening. Therefore, the increase in line width above cmc (Fig. 2) can be ascribed to the monomer-micelle exchange and was examined according to the treatment of Schmidt et al.[7] On the basis of Aniansson's kinetic theory on the micellization, they have given the following kinetic expression on the monomer-micelle exchange in order to explain the ESR line broadening of the monomer surfactant above cmc.

$$\Delta W = \frac{k^+}{\bar{n}}(C - C_m), \tag{3}$$

where ΔW is the line-width variation in frequency unit, k^+ is the rate constant for the association of monomer to micelle, $\bar{n}$ is the aggregation number of the micelle, C_m is the critical micelle concentration, and C is the total concentration of the surfactant. According to Eq. 3, the slope of plots of the line width vs. the surfactant concentration equals to $k^+/\bar{n}$. As the aggregation number of SL-SDS without NaCl is about 6 at 25 °C,[9] 1.3×10^9 kg mol^{-1} s^{-1} is obtained as the value of k^+. This is in rough agreement with the value of 1.8×10^9 kg mol^{-1} s^{-1} obtained using Eq. 1 from the relation between the line width and the SL-SDS concentration above cmc. This suggests that the monomer surfactant becomes associated with the micelles as if a bimolecular reaction occurs. The values of the association constant k^+ reported for various surfactants are between 10^8 and 10^9 dm^3 mol^{-1} s^{-1}, which exist in the expected range for a diffusion-controlled reaction.[3,15] Therefore, it is considered that the values of k^+ characterized with the diffusion-controlled reaction should be approximately independent of ionic strength and hydrocarbon chain length of surfactants.[3,7] On the other hand, the rate constant (k^-) for the dissociation of one amphiphilic ion from the micelles is strongly dependent on the alkyl chain length of the surfactant and ionic strength.[3,7] The rate constant k^- is obtained from the following relation developed by Aniansson et al.,[3]

$$k^- = k^+ \cdot \text{cmc}. \tag{4}$$

The calculated value of k^- for SL-SDS is 2.8×10^7 s^{-1}. The values of k^+ and k^- obtained from the ESR line width for SL-SDS in this study are compared with those, i.e., $k^+=1.2\times10^9$ dm^3 mol^{-1} s^{-1} and $k^-=1.0\times10^7$ s^{-1}, from chemical relaxations for SDS by Aniansson et al.[3] It seems that the agreement is well satisfied. The temperature and ionic strength dependences of $k^+/\bar{n}$ are given in Table 2. At any temper-

Table 2. Effects of Temperature and Ionic Strength on Association Constant ($k^+/\bar{n}$)

Temp/°C	$k^+/\bar{n}\times10^{-8}$/kg mol^{-1} s^{-1}			
	Added NaCl/mol kg^{-1}			
	0[a)]	0.1	0.5	1.0
25	2.2	1.7	0.70	0.27
35	2.3	1.9	0.86	0.32
55	2.4	1.9	1.3	0.45
70	2.5	2.0	1.6	0.72

a) Data from Ref. 9.

ature, the values of $k^+/\bar{n}$ decrease greatly with increasing ionic strength. As mentioned above, the changes in k^+ values for the ionic strength are small. On the other hand, the aggregation number of SL-SDS micelles increases drastically with increasing ionic strength (Fig. 1). Therefore, the decreases in $k^+/\bar{n}$ upon adding salt are mainly attributed to an increase in the aggregation number, whereas the change in $k^+/\bar{n}$ with temperature is small compared with that for the ionic strength. With increasing ionic strength, the temperature dependence of $k^+/\bar{n}$ becomes large. This can be interpreted in terms of both the increase in k^+ and the decrease in $\bar{n}$ with increasing temperature. In order to obtain detailed information concerning the effect of NaCl on the micellar kinetics of SL-SDS, it is necessary to examine the aggregation number of SL-SDS micelles in the presence of any added salt.

The authors wish to thank Mr. Toshihiko Kiyohara for his technical assistance.

References

1) D. F. Evans, S. Mukherjee, D. J. Mitchell, and B. W. Ninham, *J. Colloid Interface Sci.*, **93**, 184 (1983).
2) G. D. J. Phillies, *J. Colloid Interface Sci.*, **86**, 226 (1982).
3) E. A. G. Aniansson, S. N. Wall, M. Almgren, H. Hoffmann, I. Kielmann, W. Ulbricht, R. Zana, J. Lang, and C. Tondre, *J. Phys. Chem.*, **80**, 905 (1976).
4) T. Nakagawa and K. Tori, *Kolloid Z. Z. Polym.*, **194**, 143 (1964).
5) T. Nakagawa and H. Jizomoto, *Kolloid Z. Z. Polym.*, **250**, 594 (1972).
6) K. K. Fox, *J. Chem. Soc., Faraday Trans. 1*, **74**, 220 (1978).
7) D. Schmidt, CH. Gähwiller, and C. Von Planta, *J. Colloid Interface Sci.*, **83**, 191 (1981).
8) T. Yamaguchi, A. Yamauchi, and H. Kimizuka, *Chem. Lett.*, **1978**, 941.
9) T. Yamaguchi, A. Yamauchi, E. Kimoto, and H. Kimizuka, *Bull. Chem. Soc. Jpn.*, **53**, 372 (1980).
10) A. Korosi and B. M. Fabuss, *J. Chem. Eng. Data*, **13**, 548 (1968).
11) D. F. Othmer and E. S. Yu, *Ind. Eng. Chem.*, **60**, 22 (1968).
12) J. E. Wertz and J. R. Bolton, "Electron Spin Resonance: Elementary Theory and Practical Applications," McGraw-Hill, New York (1972), p. 201.
13) M. P. Eastman, R. G. Kooser, M. R. Das, and J. H. Freed, *J. Chem. Phys.*, **51**, 2690 (1969).
14) K. Shinoda, T. Nakagawa, B. Tamamushi, and T. Isemura, "Colloidal Surfactants," Academic Press, New York (1963), Chap. 1.
15) E. A. Moelwyn-Hughes, "The Chemical Statics and Kinetics of Solutions," Academic Press, New York and London (1971), Chap. 5.
16) G. Martini and M. Bindi, *J. Colloid Interface Sci.*, **108**, 133 (1985).
17) T. A. Miller and R. N. Adams, *J. Am. Chem. Soc.*, **88**, 5713 (1966).
18) M. T. Jones, *J. Chem. Phys.*, **38**, 2892 (1963).
19) M. P. Eastman, G. V. Bruno, and J. H. Freed, *J. Chem. Phys.*, **52**, 2511 (1970).

On the Relationship Between the Chemical Structure and the Carcinogenicity of Polycyclic and Chlorinated Monocyclic Aromatic Compounds as Studied by Means of ^{13}C NMR

Yohko SAKAMOTO* and Shosuke WATANABE†
School of Pharmaceutical Science, Toho University, 2-2-1 Miyama, Funabashi, Chiba 274
†Nihon Junior College of Economics, 5-24-10 Sakai, Musashino, Tokyo 180
(Received April 12, 1986)

The relationship between chemical structure and carcinogenicity was investigated in thirty-eight polycyclic aromatic compounds and forty-four chlorinated aromatic hydrocarbons by means of ^{13}C NMR. As an "index" serving as a measure of the electronic structure of aromatic compounds, which is closely related to the carcinogenicity, the averaged ^{13}C NMR chemical shift over all the aromatic carbons in the molecule was used. In polycyclic aromatic compounds, the averaged chemical shifts of the carcinogenic compounds are within the range from 127.11 to 127.87 ppm, but those of the noncarcinogenic compounds are not within this range. In chlorinated monocyclic aromatic compounds, the carcinogenic compounds was within the range from 127.76 to 132.64 ppm. Thus, we proposed that the "index" is very useful for the discernment of the carcinogenicity of polycyclic and chlorinated monocyclic aromatic compounds.

It is known that aromatic compounds sometimes have carcinogenicity.[1-3] In order to obtain useful information about the detailed mechanism of their carcinogenicity, several approaches have been employed. One of them is the quantum-chemical approach,[4-10] which has provided insight into the close relationship between the carcinogenicity and the electronic structure and has also made possible an interesting prediction as to the carcinogenicity of aromatic compounds. Nevertheless, this approach is not practical for the discrimination of the carcinogenicity. Another approach is to relate the carcinogenicity to a physical quantity such as the ionization potential.[11-15]

It has been reported that aromatic hydrocarbons with an ionization potential within any specified range show carcinogenic activity and that the carcinogenicity increases with a decrease in the potential energy.

It is known that ^{13}C NMR chemical shifts of the aromatic compounds considered here are closely related to the electronic environments of the individual carbon and to the ionization potential.[16,17] This means that the ^{13}C NMR chemical shift of aromatic compounds provides a measure of whether or not the molecules have carcinogenic activity.

The purpose of this paper is to study the relationship between the carcinogenicity and the averaged ^{13}C chemical shifts over all the carbons in the ring structure of aromatic compounds, and to clarify whether or not the averaged ^{13}C chemical shift is useful for the discernment of the carcinogenicity.

The averaged chemical shifts employed in this work reflect the electronic structure and electronic state of the molecules as follows. The dominant factor governing the ^{13}C chemical shift of a nucleus i is the paramagnetic contribution as given by Eq. 1, with an average excitation energy approximation.

$$\delta_i \propto \frac{1}{\Delta E} \cdot Q_i, \tag{1}$$

where ΔE is the averaged excitation energy of a molecule and Q is a factor containing electron density and bond order. Thus, the averaged chemical shift defined above is expressed by Eq. 2:

$$\begin{aligned} \bar{\delta} &\propto \frac{1}{N} \sum_i^N \frac{1}{\Delta E} \cdot Q_i \\ &= \frac{1}{\Delta E} \cdot \frac{1}{N} \sum_i^N \cdot Q_i \\ &= \frac{1}{\Delta E} \cdot \bar{Q} \end{aligned} \tag{2}$$

$$\text{in which } \bar{Q} = \frac{1}{N} \sum_i^N Q_i,$$

where N is the number of carbon atoms considered here. As may be seen from this equation, the averaged chemical shift involves information on the averaged excitation energy and the averaged value of Q. Thus, we can indirectly get information on the electronic structure and electronic state of the aromatic compounds through the observation of the averaged chemical shift for all the carbons in the ring structure of the molecule.

Experimental

Twelve compounds (**1**)—(**12**) (see Table 1) and forty-four compounds (**1**)—(**44**) (see Table 2) were obtained from the Tokyo Kasei Co. and were used without further purification.

The ^{13}C NMR spectra were recorded with Fourier Transform spectrometers, Hitachi R-900 FT and JEOL GX-400 FT, operating at 22.6 MHz and 100.4 MHz respectively, at 35 °C and at 27 °C, using an external lock system and a deuterated lock system. Deuteriochloroform was used as the solvent. The concentration of the sample solution was 25—62%(w/v). The chemical shift was significantly independent of the concentration of the sample within this concentration range.

The chemical shifts were expressed in ppm relative to tetramethylsilane.

The number of accumulations is about 400—14000: data points, 16K or 32K: spectral width, 1800 Hz: flip angle, 25°,

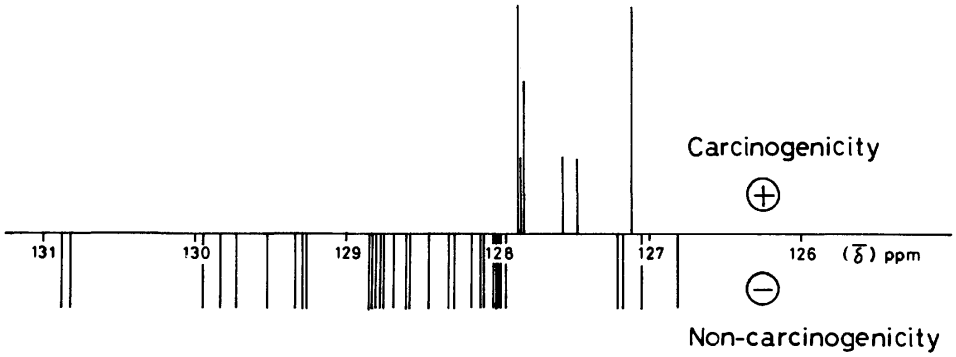

Fig. 1. The relationship between the averaged ^{13}C NMR chemical shifts (δav) of individual polycyclic aromatic compound and their carcinogenicity.

and interval of pulse to pulse, 3 s. (The detailed assignment of the ^{13}C NMR spectra for some samples is carried out by means of T_1 measurement,[18] selective decoupling[19a,b] and an isotope-label shift.[20])

Results and Discussion

Polycyclic Aromatic Hydrocarbons. The averaged ^{13}C NMR chemical shifts (δ av) over all the ring carbons in polycyclic aromatic compounds and their subsituted compounds, together with the ionization potential and the known carcinogenicity, are shown in Table 1, while the relationship between the averaged ^{13}C NMR chemical shifts (δ av) of the individual compounds and their carcinogenicities is shown in Fig. 1.

The averaged ^{13}C NMR chemical shift values for the compounds have already been estimated from the reported data.[23a,b] On the other hand, some compounds (**1**)—(**12**) with carcinogenicity have already been investigated.[4,5,17b,21,22,23b,25] Hawever, in many compounds the carcinogenicity is unknown. Thus, the compounds listed in Table 1 are divided into three groups: carcinogenic, noncarcinogenic, and undetermined groups. It has been reported that benz[*a*]anthracene (**4**), dibenz[*a*,*h*]anthracene (**8**), benzo[*a*]pyrene (**9**), 7-methylbenz[*a*]anthracene (**11**), and 7,12-dimethylbenz[*a*]anthracene (**12**) are carcinogenic.[4,22,23,25] The values of δ av for the corresponding compounds are within the range from 127.11 to 127.87 ppm. On the other hand, it is found that the averaged ^{13}C chemical shift values for naphthalene (**1**) and anthracene (**2**) are larger than 127.87 ppm, while those for 9,10-dimethylanthracene (**10**) and triphenylene (**6**) are smaller than 127.11 ppm. These compounds are not carcinogenic.[4,17,22,23b] These findings suggest that there is a correlation between the averaged chemical shifts and the carcinogenicity, and that the chemical shift range from 127.11 to 127.87 ppm, the "index range," can be used to discern whether or not compounds being considered are carcinogenic. For phenanthrene (**3**), contrary results on its carcinogenicity have been reported.[4,5] The averaged chemical shift was 128.68 ppm. Thus, according to the above "index" range, phenanthrene (**3**) can be expected to be noncarcinogenic. Next, let us consider pyrene (**5**) and dibenz[*a*,*c*]anthracene (**7**), which have been reoported to be noncarcinogenic.[4,5,17b,22]

The values of these compounds are slightly higher than that of 7,12-dimethylbenz[*a*]anthracene (**12**), which is carcinogenic: they are the lowest values in the "carcinogenic index." This means that it is not easy to determine clearly, by the use of the carcinogenic index, whether compounds which are near the lower limit of the carcinogenic index are carcinogenic or noncarcinogenic. When methyl groups were substituted into polycyclic aromatic hydrocarbons, the increase in carcinogenicity or the appearance of the carcinogenic activity were recognized in some compounds.[17a] For methyl-substituted benz[*a*]anthracene (**4**), the increase in the carcinogenicity has been well-confirmed in 7-methylbenz[*a*]anthracene (**11**) and 7,12-dimethylbenz[*a*]anthracene (**12**). However, methyl-substituted naphthalene and anthracene are known to be noncarcinogenic. Such experimental findings will be studied through the averaged ^{13}C chemical shifts of methyl-substituted aromatic hydrocarbons.

We predicted the carcinogenicity of the methyl-substituted compounds to be as is shown in Table 1; we did so on the basis of the averaged chemical shifts. The values of δ av for all methyl-substituted compounds, (**14**)—(**16**) and (**19**)—(**28**), appear at a field lower by from 0.17 to 2.54 ppm than that of naphthalene. This suggests that these compounds are noncarcinogenic. Also, the values of the δ av for 1-methylnaphthalene (**13**), 1,4-dimethylnaphthalene (**17**), and 1,5-dimethylnaphthalene (**18**) appear at a field higher than that of naphthalene by ca. from 0.05 to 0.09 ppm; these values are not in the range from 127.11 to 127.87 ppm. Therefore, it may be suggested that these compounds are noncarcinogenic. The values of δ av for di-, tri-, and tetramethyl-substituted anthracene, (**32**)—(**38**), showed a variety of shifts ranging from ca. 0.16 to 1.66 ppm.

None of them is carcinogenic, since all of them showed a field shift lower than the "index." 1-Methylanthracene (**29**) and 2-methylanthracene (**30**) also seem to be noncarcinogenic, judging from their low

Table 1. The Averaged ^{13}C NMR Chemical Shifts over All the Ring Carbons of Polycyclic Aromatic Hydrocarbons, Ionization Potentials, and Their Carcinogenicities

Compound	Averaged Chemical Shift/ppm	Ionization Potential IP/eV	1/IP	Predicted Carcinogenicity[a]	Carcinogenicity[b] Literature
Naphthalene (**1**)	128.28	8.13	0.1230		− (4, 22)
Anthracene (**2**)	128.17	7.43	0.1346		− (4, 22)
Phenanthrene (**3**)	128.68	8.19	0.1221	−	± (4, 5, 21)
Benz[*a*]anthracene (**4**)	127.86	7.54	0.1326		+ (4, 22, 25)
Pyrene (**5**)	127.16	7.50	0.1333		− (4, 5, 17b))
Triphenylene (**6**)	126.82	8.15	0.1227		− (4, 22)
Dibenz[*a*,*c*]anthracene (**7**)	127.21				− (4, 5, 22)
Dibenz[*a*,*h*]anthracene (**8**)	127.83	7.58	0.1319		++ (4, 22)
Benzo[*a*]pyrene (**9**)	127.11	7.23	0.1383		+++ (4, 22, 25)
9,10-Dimethylanthracene (**10**)	127.06	7.14	0.1401		− (17a), 23b))
7-Methylbenz[*a*]anthracene (**11**)	127.47	7.37	0.1357		+ (4, 23b))
7,12-Dimethylbenz[*a*]anthracene (**12**)	127.87	7.22	0.1385		+++ (4, 23b))
1-Methylnaphthalene (**13**)	128.08[c]			−	
2-Methylnaphthalene (**14**)	128.75[c]			−	
1,2-Dimethylnaphthalene (**15**)	128.45[c]			−	
1,3-Dimethylnaphthalene (**16**)	128.82[c]			−	
1,4-Dimethylnaphthalene (**17**)	128.02[c]			−	
1,5-Dimethylnaphthalene (**18**)	128.10[c]			−	
1,6-Dimethylnaphthalene (**19**)	128.76[c]			−	
1,7-Dimmethylnaphthalene (**20**)	128.83[c]			−	
1,8-Dimethylnaphthalene (**21**)	130.87[c]			−	
2,3-Dimethylnaphthalene (**22**)	129.26[c]			−	
2,6-Dimethylnaphthalene (**23**)	129.52[c]			−	
2,7-Dimethylnaphthalene (**24**)	129.73[c]			−	
2,3,5-Trimethylnaphthalene (**25**)	129.32[c]			−	
2,3,6-Trimethylnaphthalene (**26**)	129.96[c]			−	
1,6,7-Trimethylnaphthalene (**27**)	129.26[c]			−	
1,5,8-Trimethylnaphthalene (**28**)	130.82[c]			−	
1-Methylanthracene (**29**)	127.96[d]			−	
2-Methylanthracene (**30**)	128.61[d]			−	
9-Methylanthracene (**31**)	127.57[d]			+	
1,4-Dimethylanthracene (**32**)	127.97[d]			−	
1,8-Dimethylanthracene (**33**)	127.99[d]			−	
1,4,9-Trimethylanthracene (**34**)	128.59[d]			−	
2,7,9-Trimethylanthracene (**35**)	128.33[d]			−	
1,4,5,9-Tetramethylanthracene (**36**)	128.84[d]			−	
1,4,5,8-Tetramethylanthracene (**37**)	127.94[d]			−	
1,4,5,8,9-Pentamethylanthracene (**38**)	129.83[d]			−	

a) − For noncarcinogenic and + for carcinogenic. b) Carcinogenicity reported by reference. This may be due to biochemical evidence or molecular orbital calculation. −: For noncarcinogenic, +: for carcinogenic, ±: for noncarcinogenic or carcinogenic, ++, +++: for strongly carcinogenic. c) From Ref. 23a). d) From Ref. 23b).

chemical shifts. However, 9-methylanthracene (**31**) falls in the range of the "index." The carcinogenicity in the compound has not yet been determined, but the observed value of δ av suggests that the compound is carcinogenic. Most polycyclic aromatic compounds form charge-transfer complexes which consist of an electron-donor part and an acceptor part.

It has been proposed that any specified value of the ionization potential formation for charge-transfer complexes is associated strongly with the ionization potential. This causes steric hindrance effects to the DNA conformation, and so such compounds are carcinogenic. The relationship among the ionization potential, the averaged ^{13}C NMR chemical shift, and the carcinogenicity is shown in Table 1. The ionization potentials and their reciprocals in some compounds are shown in Table 1. It is known that carcinogenic compounds have ionization potentials of from 7.22 to 7.58 eV and that naphthalene (**1**), phenanthrene (**3**), and triphenylene (**6**), with higher ionization potentials than this range, are not carcinogenic. In the carcinogenic compounds, those with lower ionization potentials showed stronger carcinogenicities. However, 9,10-dimethylanthracene (**10**), which has the lowest ionization potential, anthracene (**2**) and pyrene (**5**), all within the range from 7.22 to 7.58 eV, are not carcinogenic. In these cases, the local electronic state in the molecules should be determined in addition to the ionization potential in order to estimate their carcinogenicity.

Chlorinated Aromatic Hydrocarbons. The relationship between the averaged ^{13}C NMR chemical shift

Table 2. The Averaged ^{13}C NMR Chemical Shifts over All the Ring Carbons of Chlorinated Aromatic Hydrocarbons, Ionization Potentials, and Their Carcinogenicities

Compound	Averaged Chemical Shift/ppm	Ionization Potential IP/eV	1/IP	Predicted carcinogenicity	Carcinogenicity[b] Literature
Chlorobenzene (**1**)	129.77[c]	9.42	0.1062		+ (26)
o-Dichlorobenzene (**2**)	131.48[c]	9.06	0.1104		+ (26)
m-Dichlorobenzene (**3**)	130.65	9.80	0.1020		+ (26)
p-Dichlorobenzene (**4**)	131.21	9.67	0.1078		+ (26)
1,2,4-Trichlorobenzene (**5**)	130.24				+ (26)
3,4,5,6-Tetrachlorobenzene (**6**)	131.49				+ (26)
1,2,4,5-Tetrachlorobenzene (**7**)	131.52				+ (26)
1,2,3,4,5-Pentachlorobenzene (**8**)	131.90				+ (26)
p-Chlorobenzyl chloride (**9**)	132.23[c]			+	
Benzyl chloride (**10**)	130.75[c]				+ (27a), b))
Benzylidene dichloride (**11**)	131.23				+ (27a), b))
Benzylidyne trichloride (**12**)	131.80				+ (27a))
Benzoyl chloride (**13**)	132.30				+ (28a), b))
o-Chloroacetophenone (**14**)	129.43			+	
m-Chloroacetophenone (**15**)	131.30			+	
p-Chloroacetophenone (**16**)	131.23			+	
2,6-Dichloroacetophenone (**17**)	131.38			+	
1-Chloro-2,4-dinitrobenzene (**18**)	131.82			+	
2,4-Dichloroacetophenone (**19**)	129.85			+	
2,3-Dimethyl-6-chlorobenzene (**20**)	131.63[c]			+	
o-Chloronitrobenzene (**21**)	129.70			+	
2-Chloro-6-nitrotoluene (**22**)	132.82			−	
4-Chloro-2-nitroanisole (**23**)	131.92			+	
p-Chlorofluorobenzene (**24**)	134.68[d]			−	
p-Chlorobenzonitrile (**25**)	137.10[e]			−	
2,6-Dichlorobenzonitrile (**26**)	133.55				− (29a), b), c))
2,3,4,5,6-Pentachloro-1-nitrobenzene (**27**)	131.72			+	
Ethyl α-(*p*-Chlorophenoxy)isobutyrate (**28**)	132.80				− (29a), b), c)) (30a), b), c))
o-Chlorophenol (**29**)	127.76	9.28	0.1078		+ (29a), b), c)) (31a)—h))
m-Chlorophenol (**30**)	128.82	8.98	0.1114		+ (29a), b), c)) (31a)—h))
p-Chlorophenol (**31**)	131.51	9.07	0.1103		+ (29a), b), c)) (31a)—h))
2,4,5-Trichlorophenol (**32**)	128.94				+ (29a), b), c)) (31a)—h))
2,4,6-Trichlorophenol (**33**)	130.57				+ (29a), b), c)) (31a)—h))
Pentachlorophenol (**34**)	132.64				+ (29a), b), c))
4-Chloro-*m*-cresol (**35**)	129.89			+	
2,4-Dichlorophenoxyacetic acid (**36**)	130.03				+ (29a), b), c))
o-Chloroaniline (**37**)	125.70	8.30	0.1205	−	
m-Chloroaniline (**38**)	126.56	8.60	0.1163	−	
p-Chloroaniline (**39**)	128.41	8.18	0.1223	+	
p-Chloro-*o*-anisidine (**40**)	120.26			−	
1-Chloro-4-nitroaniline (**41**)	128.29			+	
4-Chloro-1,2-phenylenediamine (**42**)	124.60			−	
3,4-Dichloroaniline (**43**)	126.97			−	
(4-Chloro-*N*-methylanilino)cyanide (**44**)	129.25[f]			+	

a) − For noncarcinogenic and + for carcinogenic. b) Carcinogenicity reported by reference. +: For carcinogenic, −: For noncarcinogenic. c) From Ref. 32). d) From Ref. 33). e) From Ref. 34). f) From Ref. 35).

and the carcinogenicity of chlorinated monocyclic aromatic compounds is shown in Table 2 and Fig. 2. These compounds also were divided into three groups: the carcinogenic, noncarcinogenic, and undetermined groups. Chlorobenzene (**1**) and di-, tri-, tetrachlorobenzene (**2**)—(**8**), benzyl chloride and its derivatives (**10**)—(**13**), di-, tri-, and pentachlorophenol (**29**)—(**34**), and 2,4-dichlorophenoxyacetic acid (**36**) have all been reported to be carcinogenic. The averaged chemical shifts in these carcinogenic compounds were within the range from 127.76 to 132.64 ppm. The averaged chemical shift of two non-carcinogenic compounds, 2,6-dichlorobenzonitrile (**26**) and ethyl α-(*p*-chlorophenoxy)isobutyrate (**28**), were larger than those of the carcinogenic compounds. From these "index" values, we predicted the carcinogenicity of the *p*-chlorobenzyl chloride (**9**), (**14**)—(**25**), (**27**), whose carcinogenicities have not yet been studied. *p*-Chlorobenzyl chloride (**9**), chloroacetophenones (**14**)—(**17**), (**19**) chlorobenzene derivatives (**18**), (**20**), (**21**), (**27**), and 4-chloro-2-nitroanisole (**23**) would seem to be carcinogenic, since the averaged chemical shifts of these compounds are within the range of 127.76—132.64 ppm, the index of carcinogenic chlorinated

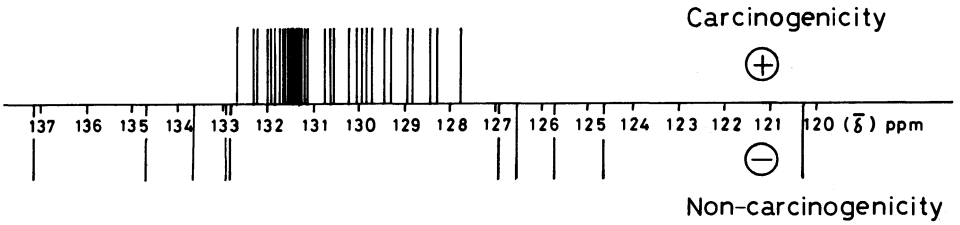

Fig. 2. The relationship between the averaged ^{13}C NMR chemical shifts (δav) of individual chlorinated-monocyclic aromatic compound and their carcinogenicity.

compounds. The averaged chemical shifts of 2-chloro-6-nitrotoluene (**22**), *p*-chlorofluorobenzene (**24**), and *p*-chlorobenzonitrile (**25**) were larger than the "index value" and similar to that of the noncarcinogenic compounds, (**26**) and (**28**). Therefore, we predicted that these compounds would be noncarcinogenic.

In 2-chloro-6-nitrotoluene (**22**), electrons in the ring are attracted by the high electronegativity of the Cl and NO_2 groups, and so the number of electrons in the ring decreased. This moved the averaged chemical shifts downfield. In compound (**24**), the electrons in the ring are attracted to subsituted halogen; this moves its averaged chemical shifts downfield. In *p*-chlorobenzonitrile (**25**) and 2,6-dichlorobenzonitrile (**26**), the electronegativity of the cyano group is so large that the electrons in the ring are attracted by the δ-I effect; therefore, the averaged chemical shifts move downfield as a whole. The larger the δ-I effect, the less the electron density in para positions within the benzene ring.

Next, let us consider the monocyclic chlorine-substituted compounds (**29**)—(**36**). In this table, all of the compounds except 4-chloro-*m*-cresol (**35**) have been reported to be carcinogenic.[29,30,31]

Compound (**35**) also would be carcinogenic judging from the "carcinogenic index" for chlorine-substituted aromatic compounds. The averaged chemical shift value of (4-chloro-*N*-methylanilino)cyanide (**44**) was 129.25 ppm; therefore, the compound seems to have carcinogenicity. The downfield shift may be due to the fact that electrons in the ring are attracted to the Cl group by its large electronegativity, and so the number of electrons in the ring is decreased. In the case of the alkaline compounds, it seems that the downfield shift occurs by means of the solvation in solution. The chlorine atom in the para position may decrease the electrons in the benzene ring rather than that in the meta position, and it seems to cause the averaged chemical shifts downfield as a whole. In general, acid and neutral monocyclic chlorine compounds seem to be carcinogenic, whereas alkaline ones are usually of no carcinogenicity.

As in the case of polycyclic aromatic hydrocarbons, there seems to be a correlation between the carcinogenicity and the ionization potential of the chlorinated aromatic hydrocarbons.

As is shown in Table 2, the ionization potentials of the carcinogenic compounds are within the range from 8.98 to 9.80 eV. We can see the correlation of the averaged ^{13}C NMR chemical shift, the ionization potential, and the carcinogenicity.

Our idea of using the averaged value of the ^{13}C NMR chemical shifts which link the electronic structure and the electronic state was carried out; we found that we could predict the carcinogenicity in aromatic compounds from the chemical-shift value.

The averaged chemical shifts of the known carcinogenic polycyclic aromatics are within the range from 127.11 to 127.87 ppm, while those of the known chlorinated aromatics are within the range from 127.76 to 132.64 ppm: the difference might reflect the slight difference in the mechanism of carcinogenicity between the two types of compounds. There are a few noncarcinogenic compounds that have averaged chemical shifts values within the "carcinogenic index". Therefore, there would be a secondary criterion to judge their carcinogenicity, such as a local electronic state, even though the averaged chemical shift remains the more primary, simple, and useful criterion for carcinogen. Furthermore, a close investigation of carcinogenic compounds and noncarcinogenic compounds with only slightly different chemical-shift values should give insight into the mechanism of carcinogenicity.

The authors are indebted to Dr. Isao Ando of the Tokyo Institute of Technology for his useful discussions and advice and are grateful to Professor Sinzo Tamura and Yasuoki Murakami of Toho University for their kind support and encouragement.

References

1) M. A. Mainster and J. D. Memory, *Biochim. Biophys. Acta.*, **148**, 605 (1967).
2) O. Schmidt, *Naturwissenschaften.*, **29**, 146 (1941).
3) V. Sjentpaly and Laszlo, *J. Am. Chem. Soc.*, **106**, 6021 (1984).
4) A. Pullman and B. Pullman, *Advan. Cancer Res.*, **3**, 117 (1955).
5) I. A. Smith, G. D. Berger, P. G. Seybold, and M. P. Serve, *Cancer Research*, **38**, 2968 (1978).
6) M. S. Noor, Indian. *J. Biochem. Biophys.*, **22**, 0301 (1985).
7) L. Ciquan, S. Ziutan, W. Ying, and D. Shusan, *Fenzi Kexue Xuebao.*, **1**, 19 (1981).
8) Link and Ewa, *Pr. Biol. Mol.*, **8**, 253 (1981).
9) H. Darong, *Huanjing Huaxue.*, **1**, 35 (1982).

10) J. C. Acros and M. F. Argus, *Advan. Cancer Res.*, **11**, 305 (1968).
11) W. R. Woolfenden and D. M. Grant, *J. Am. Chem. Soc.*, **88**, 1496 (1966).
12) G. C. Nelson, G. C. Levy, and J. D. Cargioli, *J. Am. Chem. Soc.*, **94**, 3089 (1972).
13) T. D. Algh, D. M. Grant, and E. G. Paul, *J. Am. Chem. Soc.*, **88**, 5397 (1966).
14) B. Norden, U. Edlund, D. Johnels, and S. Wold, *Pharmacol. Chem. Biol.*, **2**, 73 (1983).
15) P. Lazzeretti and F. Taddei, *Org. Magn. Reson.*, **3**, 283 (1971).
16 E. L. Cavalieri, E. G. Rogan, R. W. Roth, R. K. Saugier, and A. Hakam, *Chem-biol. Interactions.*, **47**, 87 (1983).
17) a) R. S. Ozubko, G. W. Buchanan, and I. C. P. Smith, *Can. J. Chem.*, **52**, 2493 (1974); b) G. W. Buchanan and R. S. Ozubko, *Can. J. Chem.*, **53**, 1829 (1975).
18) T. Yoshida, Y. Maekawa, H. Uchino, and S. Yokokawa, *Bull. Chem. Soc. Jpn.*, **52**, 3676 (1979).
19 a) E. Carvalieri and M. Calvin, *Proc. Nat. Acad. Sci. U.S.A.*, **68**, 1251 (1971); b) B. Birdsall, *J. Chem. Soc. Chem. Commun.*, **1972**, 316.
20) R. H. Martin, J. Moriau, and N. Defay, *Tetrahedron.*, **30**, 179 (1974).
21) S. Berger and K. P. Zeller, *Org. Magn. Reson.*, **11**, 303 (1978).
22) A. C. Allison and T. Nash, *Nature*, **197**, 758 (1963).
23) a) D. Dalling, K. H. Ladner, D. M. Grant, and W. R. Woolfenden, *J. Am. Chem. Soc.*, **99**, 7142 (1977); b) M. Y. Ronl, J. B. Stothers, and N. K. Wilson, *Can. J. Chem.*, **53**, 1958 (1975).
24) "The Bay-Region Theory A. Quantum Mechanical Approach to Aromatic Hydrocarbon-induced Carcinogenicity," ed by D. M. Jerina and R. E. Lehr, in "Microsomes and Drug Oxidations," ed by V. Ullrich, I. Roots, A. G. Hildelrant, R. W. Estabroak, and A. H. Conney Pergamon Press, Oxford (1977), pp. 709—720.
25) "Bay Region Epoxides of Dihydrodiols. A. Concept Explaining the Mutagenic and Carcinogenic Activity of Benzo(a)pyrene and Benzo(a)anthracene," ed by D. M. Jerina, R. E. Lehr, R. M. Schaefer, H. Yagi, J. M. Karle, D. R. Thakker, A. H. Wood, and A. H. Conney, in "Origins of Human Cancer," ed by H. Hiatt, J. D. Watson, and I. Winstin Cold Spring Harbor, New York (1977), pp. 639—638.
26) *IARC Monographs*, **7**, 231 (1974).
27) a) K. Fukuda, H. Matsushita, H. Sakabe, and K. Takemoto, *Gann.*, **72**, 655 (1981); b) K. Fukuda, H. Matsushita, and K. Takemoto, Proceedings of the Japanese Cancer Association, The 38th Annual Meeting, September, 1979 (Tokyo). c) *IARC Monographs*, **11**, 217 (1976).
28) a) H. Sakabe, H. Matsushita, and S. Koshi, *Ann. N. Y. Acad. Sci.*, **271**, 67 (1976); b) H. Sakabe and K. Fukuda, *Ind. Health*, **15**, 173 (1977).
29) a) R. K. Boutwell and D. K. Bosch, *Cancer Research*, **19**, 413 (1959); b) *IARC Monographs*, **20**, 303 (1979); c) "Outline of Pepticides" ed by S. Mutoh (1970).
30) a) R. I. Levy, *Ann. Intern. Med.*, **77**, 267 (1972); b) J. M. Falko, *Amer. J. Med.*, **66**, 303 (1979).
31) a) K. Fukuda, *Mutation Research*, **4**, 36 (1981); b) Y. Yamanzoe and T. Kamataki, *Mutation Research*, **4**, 72 (1981); c) R. Kato, *Mutation Research*, **4**, 14 (1981); d) M. Uchiyama, *Mutation Research*, **4** 47 (1981); e) R. Kato and Y. Yamazoe, *Research*, **1979**, 71; f) J. C. Loper, *Mutation Research*, **76**, 241 (1980); g) T. H. Maugh, *Science.*, **211**, 694 (1981); h) *IARC Monographs* Supplement 1, **1979**, 33.
32) "American Petroleum Institute research Project 44," ^{13}C NMR Spectral Data (Texas A and M University) (1975).
33) G. Miyajima, S. Akiyama, and K. Nishimoto, *Org. Magn. Reson.*, **4**, 811 (1972).
34) R. W. Stephany, M. J. A. De Bie Mjadebie, and W. D. Rent, *Org. Magn. Reson.*, **6**, 45 (1974).
35) R. W. Storek, G. E. Hard, and F. Ritsch, *Org. Magn. Reson.*, **5**, 419 (1973).

 © 1986 The Chemical Society of Japan Bull. Chem. Soc. Jpn., 59, 3039—3041 (1986)

Magnetic Field Effects on the Primary Photoprocess of Anthrone in Micellar Solution by Laser Flash Photolysis and Two-Step Laser Excitation Fluorescence

Yoshifumi TANIMOTO,* Etsuko SHIMADA, and Michiya ITOH
Faculty of Pharmaceutical Sciences, Kanazawa University, Takara-machi, Kanazawa 920
(Received April 16, 1986)

The magnetic field effects on hydrogen abstraction reaction of anthrone have been studied in micellar solution by laser flash photolysis and two-step laser excitation (TSLE) fluorescence. The decaytime of the anthrone ketyl radical determined by laser flash photolysis increases from 370 ns at zero field to 890 ns at 80 mT. The results are in accordance with the magnetic field effects on the risetime of the cage product by the TSLE fluorescence. All of the results are discussed in terms of the radical pair model.

Particular interest has recently been taken in the effects of magnetic field on chemical reactions.[1] This is caused by versatile applicability such as the enrichment of nuclear magnetic isotopes. Mangetic field effects on photochemical reactions in condensed phase are interpreted mainly in terms of the radical pair model, where the lifetime of radical pair determines significance of the effects. In homogeneous solution, diffusion of radicals is so fast that the lifetime of the pair is as short as 10^{-8}—10^{-9} s, and usually no significant effects are expected for the chemical reaction. In this context, aqueous micellar solution will provide an excellent environment for enhancement of chemical reaction by magnetic field. Since organic compounds are solubilized in the micellar phase of normal micelle system due to hydrophobic interaction, the radical pair generated is confined in micellar cages; this results in long lifetime of 10^{-6} s or so. Based on this reason, we have studied the effects of magnetic field on photochemical reactions in micellar solution.[2-5]

In the present paper, we report results of the effect of magnetic field on the hydrogen abstraction reaction of anthrone in micellar solution by laser flash photolysis and two-step laser excitation (TSLE) fluorescence technique. Transient absorption of the anthrone ketyl radical and the TSLE fluorescence of cage product are strongly influenced by the magnetic field ($\leqslant$ 80 mT). All of the results are discussed in terms of the radical pair model.

Experimental

Anthrone (Tokyo Kasei Co.) and sodium dodecyl sulfate (Nakarai Co., for biological use, denoted as SDS hereafter) were used as received. Distilled water was further deionized. All solutions were deaerated by flowing nitrogen for 10 min.

In the laser flash photolysis, an N_2 laser (Molectron UV-12, 337 nm) and a xenon arc lamp were used as excitation and probe light sources, respectively. Two-step laser excitation (TSLE) fluorescence was measured by means of an excimer laser (Lambda Physik EMG-50E, 308 nm) and an N_2 laser pumped dye laser (Molectron UV-12 and DL-14, 406 nm), as the first and the second laser, respectively. Timing of each laser was adjusted with a home-made delay circuit. Magnetic field was applied with a home-made Helmholtz coil ($\leqslant$ 80 mT). Details of the systems were similar to those described elsewhere.[3,6] All measurements were carried out at room temperature.

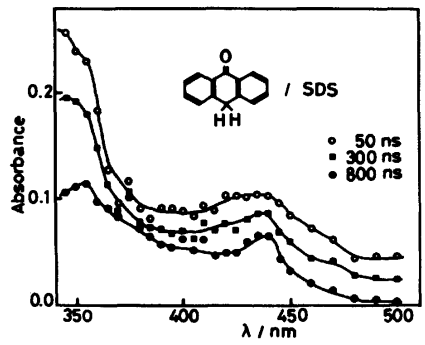

Fig. 1. Transient absorption spectra of anthrone (2×10^{-3} mol dm^{-3}) in SDS (0.4 mol dm^{-3}) micellar solution.

Results and Discussion

Transient Absorption and Mechanism. Figure 1 shows transient absorption spectra of anthrone in SDS micellar solution. The absorption band around 350 nm is assigned to the anthrone ketyl radical with reference to the literature,[7] though the spectrum at 50 ns delay is slightly shifted to shorter wavelength, because of the overlap with the short-lived triplet–triplet absorption band of anthrone. The risetime of the ketyl radical was estimated to be 40 ns. We have reported several hydrogen abstraction reactions of aromatic carbonyls in the triplet states,[2-4] whose reaction mechanism is shown in Scheme 1. By analogy with

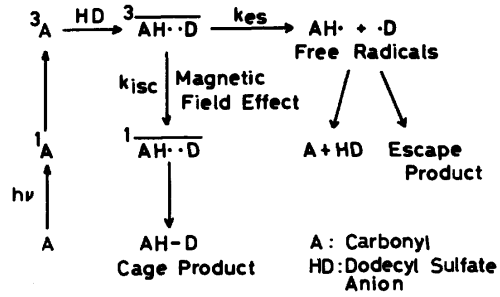

Scheme 1. Photoreaction pathways of aromatic carbonyls in SDS micellar solution.

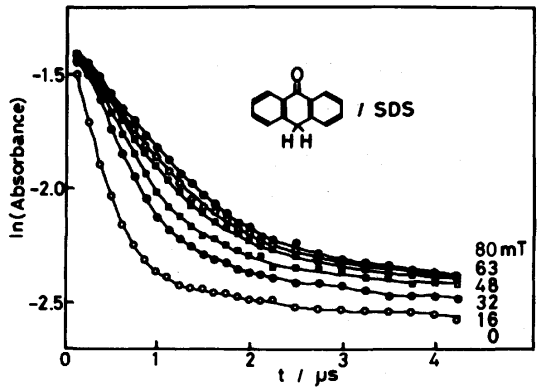

Fig. 2. Magnetic field effects on the decay of the anthrone ketyl radical at 355 nm.

the photoreactions of these carbonyls reported, the excited triplet anthrone may abstract a hydrogen atom from an SDS surfactant to yield a triplet pair between anthrone ketyl radical and dodecyl sulfate anion radical. The triplet pair disappears via two competing processes, i.e., the intersystem crossing to singlet pair followed by geminate cage reaction, and the dissociation of triplet pair into the component free radicals (escape products). The adduct of the ketyl radical with the surfactant seems responsible to the geminate cage reaction,[10] while 9-anthrol to the escape product. In a radical pair, the triplet-singlet intersystem crossing as well as relaxation within the triplet manifold occurs via electron-nuclear hyperfine interaction and these rates are decreased by applying a magnetic field because of the Zeeman splitting of the triplet sublevels.[1] Therefore, in a magnetic field, the decay rate of the triplet radical pair and also the formation rate of the cage product are expected to be reduced.

Figure 2 shows the effects of magnetic fields on the decay of ketyl radical observed at 355 nm. Without applying field, the decay of the radical appears to consist of fast and slow processes, though the decay does not proceed exponentially. In the presence of magnetic field, the decay rate of the fast process becomes slow and the apparent intensity at 4 μs delay increases. When the generation of the triplet pair and the geminate cage reaction are very fast and the decay of the ketyl radical escaped from the pair is slow enough within the time scale of microsecond, as shown in the Scheme, the absorption intensity of the ketyl radical, $I(t)$, can be expressed as follows:[2]

$$I(t) \propto I_f \exp(-k_f t) + I_s, \quad (1)$$

where $k_f = k_{isc} + k_{es}$, $I_f = k_{isc}/(k_{isc}+k_{es})$, and $I_s = k_{es}/(k_{isc}+k_{es})$. The first and the second terms in the right side of Eq. 1 represent the concentrations of the ketyl radical in the triplet pair and in the escaped free radical, respectively. Thus, Fig. 2 indicates that the external magnetic field reduces the decay rate of the triplet pair and enhances the yield of the escaped free radical. Decay curves in Fig. 2 were analysed by Eq. 1 in order to estimate k_f (Table 1).[11] In the presence of a magnetic field (80 mT), the decay rate of triplet pair is reduced by ≈60%, as expected from the Scheme.

Table 1. Magnetic Field Effects on k_f and k_r ($10^6\,s^{-1}$)

	H/mT					
	0	16	32	48	63	80
k_f	2.7	1.8	1.6	1.3	1.2	1.1
k_r	2.6					1.4

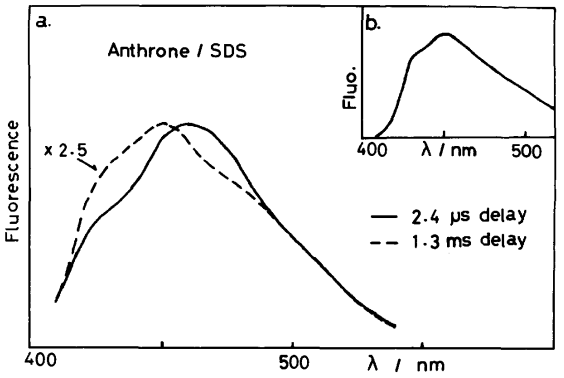

Fig. 3. (a) The TSLE fluorescence spectra of anthrone (3×10^{-4} mol dm^{-3}) in SDS (0.4 mol dm^{-3}) micellar solution. (b) Fluorescence spectrum of 9-anthrol in SDS micellar solution.

Two-Step Laser Excitation (TSLE) Fluorescence. In order to analyse the magnetic field effects on photoadduct formation, we examined the TSLE fluorescence of anthrone in SDS micellar solution; two steps consist of the initial laser excitation as the reaction light source and the following probe laser excitation. Figure 3a shows the TSLE fluorescence spectra of anthrone in the solution. The spectrum at 2.4 μs delay after the first laser excitation has a peak around 460 nm, and the peak shifts to the shorter wavelength by ≈10 nm at 1.3 ms delay. The lifetime of TSLE fluorescence seems to be composed of two decay components (3—4 and 12 ns). On the other hand, 9-anthrol, synthesized by reduction of anthrone, has a fluorescence band maximum around 450 nm (lifetime 12 ns) (Fig. 3b). Thus the TSLE fluorescence band around 450 nm, which appears at 1.3 ms delay after the first laser excitation, is attributable mainly to 9-anthrol. The TSLE fluorescence around 460 nm at 2.4 μs delay is likely to be due to the photoadduct of the anthrone ketyl radical with the SDS surfactant (a product of the geminate cage reaction). Figure 4 demonstrates the magnetic field effects on the time evolution of the TSLE fluorescence at 460 nm. The risetime $1/k_r$ was estimated to be 380 ns at zero field and 710 ns at 80 mT, k_r being the formation rate of the photoadduct. The TSLE fluorescence intensity at 6.4 μs delay decreases by ≈10% in the magnetic field (80 mT). These results imply that the rate of formation and the yield of cage product, the photoadduct, is reduced

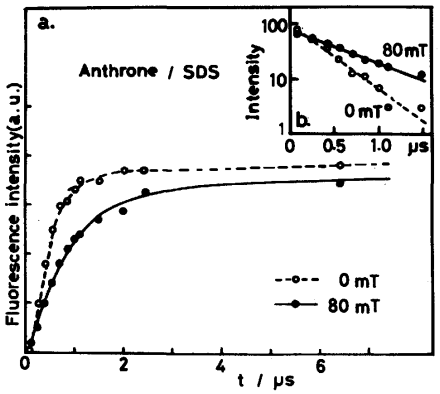

Fig. 4. (a) Magnetic field effects on the time evolution of the TSLE fluorescence at 460 nm. (b) Semilogarithmic plots of the intensities of (a), $I_\infty - I(t)$, the intensity at 5 μs delay, where it reaches plateau, being used as I_∞.

in the magnetic field.

Furthermore, the risetimes $1/k_r$ of the adduct with and without magnetic field (80 mT) determined by the TSLE fluorescence agree with the corresponding decaytimes $1/k_f$ of the anthrone ketyl radical by laser flash photolysis within experimental error (Table 1). This coincidence implies that the fast deactivation process of the triplet radical pair, composed of anthrone ketyl radical and dodecyl sulfate anion radical, is attributable to the intersystem crossing to the singlet pair followed by the fast geminate cage reaction as shown in Scheme 1. The decrease in the yield of cage product, determined by TSLE fluorescence, with concomitant increase in the escaped radical yield, determined by laser flash photolysis, in a magnetic field also supports the mechanism proposed (Scheme 1), in which both processes compete to each other.

In the previous papers,[3] we studied the transient absorption and the TSLE fluorescence of anthraquinone in SDS micellar solution in magnetic field. The decays and yields of anthrasemiquinone radical as well as those of photoadduct of semiquinone with surfactant are influenced by the external magnetic field. Present results agree well with those in the studies mentioned above.

In conclusion, by combining results by laser flash photolysis with those by TSLE fluorescence, it is unequivocally demonstrated that radical pair intervenes as a short-lived intermediate in the reaction and that intersystem crossing as well as relaxation of the radical pair is reduced by external magnetic field.

We wish to acknowledge the financial support from the Takeda Science Foundation for this research.

References

1) See, for instance: "Spin Polarization and Magnetic Effects in Radical Reactions," ed by Yu. N. Molin, Elsevier, Amsterdam (1984).

2) Y. Tanimoto and M. Itoh, *Chem. Phys. Lett.*, **83**, 626 (1981); Y. Tanimoto, H. Udagawa, Y. Katsuda, and M. Itoh, *J. Phys. Chem.*, **87**, 3976 (1983).

3) Y. Tanimoto, H. Udagawa, and M. Itoh, *J. Phys. Chem.*, **87**, 724 (1983); Y. Tanimoto, K. Shimizu, and M. Itoh, *Photochem. Photobiol.*, **39**, 511 (1984); *J. Am. Chem. Soc.*, **106**, 7257 (1984); *Chem. Phys. Lett.*, **112**, 217 (1984).

4) Y. Tanimoto, M. Takashima, and M. Itoh, *Chem. Phys. Lett.*, **100**, 442 (1983); *Nippon Kagaku Kaishi*, **1984**, 1747; *J. Phys. Chem.*, **88**, 6053 (1984); *Chem. Lett.*, **1984**, 1981.

5) Y. Tanimoto, K. Shimizu, H. Udagawa, and M. Itoh, *Chem. Lett.*, **1983**, 353; Y. Tanimoto, M. Takayama, M. Itoh, R. Nakagaki, and S. Nagakura, *Chem. Phys. Lett.*, in press.

6) M. Itoh, T. Adachi, and K. Tokumura, *J. Am. Chem. Soc.*, **106**, 850 (1984).

7) N. Kanamaru and S. Nagakura, *J. Am. Chem. Soc.*, **90**, 6905 (1968).

8) J. C. Scaiano, E. B. Abuin, and L. C. Stewart, *J. Am. Chem. Soc.*, **104**, 5673 (1982).

9) Y. Sakaguchi, H. Hayashi, and S. Nagakura, *J. Phys. Chem.*, **86**, 3177 (1982).

10) The photoadduct may have the following structure by analogy with the photoproduct of benzophenone in SDS micellar solution,[8,9] though we failed in its chemical identification because of instability to air.

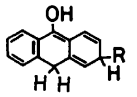

, R = Dodecyl Sulfate Anion

11) The absorption due to the photoadduct may also appear at 355 nm. However, we can estimate the k_f values, since the risetime of the adduct is the same as the decaytime of the triplet pair.

 © 1986 The Chemical Society of Japan Bull. Chem. Soc. Jpn., 59, 3043—3046 (1986)

A Molecular Orbital Study of Conformational Behavior of 9,9′-Bifluorenylidene

Osamu KIKUCHI,* Ken-ichi MATSUSHITA, Kenji MORIHASHI, and Mitsunobu NAKAYAMA
Department of Chemistry, The University of Tsukuba, Sakura, Ibaraki 305
(Received April 28, 1986)

The conformation of 9,9′-bifluorenylidene and the $E \rightarrow Z$ isomerization of its derivatives were examined by a two-configuration SCF calculation with the MINDO/3 approximation. The twisted conformation was calculated to be more stable than the folded one. The E-Z isomerization occurs between two twisted conformers and the 90°-twisted structure is the transition state. The structural dependence of the rotational barrier of the isomerization is discussed.

Bifluorenylidene, **1**, is a highly overcrowded ethylene[1] and is expected to exist in one of the two possible conformations, the twisted or folded conformation, in order to avoid large repulsive interactions around the central C_9–$C_{9'}$ double bond. In the twisted form,

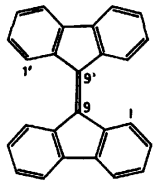

1

the two 9-fluorenylidene fragments make a large twist angle but maintain planarity. In the folded form, the fragments are folded away from each other without rotation about the C_9–$C_{9'}$ bond. The Newman projections of these two structures are shown in Fig. 1.

Gault et al.[2] assumed in their NMR study of substituted 9,9′-bifluorenylidenes in solution that the compounds existed in folded forms. In the solid state, an X-ray analysis showed that **1** has the twisted conformation with approximately planar 9-fluorenylidene fragments.[3] The substituted 9,9′-bifluorenylidenes have a barrier of 80—100 kJ mol^{-1} for a rotation about the C_9–$C_{9'}$ double bond in the E-Z isomerization.[4,5] These values are remarkably low in comparison with the rotational barrier of ethylene, 273 kJ mol^{-1}.[6]

Conformations and the E-Z isomerization of 9,9′-bifluorenylidenes have been studied by molecular

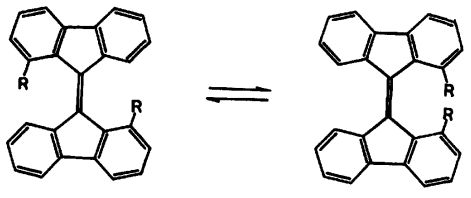

E **Z**

mechanics calculations.[7,8] As a molecular orbital calculation on 9,9′-bifluorenylidene, Meyer and Yinnon employed the π-electron calculation method to estimate the twist angle of 40°.[9] The present study examined the conformation of **1** on the basis of all-valence-electron MO calculations and analyze the E-Z isomerization process of substituted 9,9′-bifluorenylidenes.

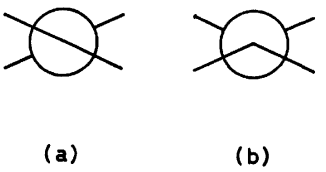

(a) (b)

Fig. 1. Newman projections of 9,9′-bifluorenylidene. (a) Twisted form and (b) folded form.

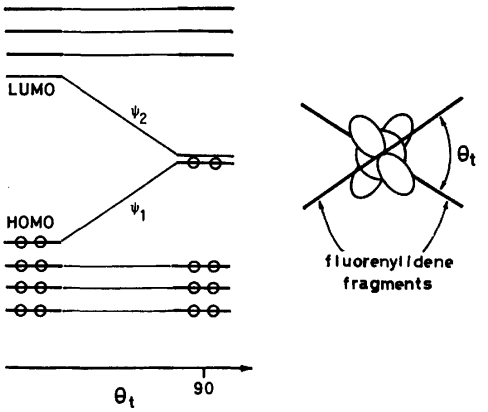

Fig. 2. Qualitative variation of orbital energies of 9,9′-bifluorenylidene with the twist angle about the central C–C double bond. The ψ_1 and ψ_2 orbitals are the bonding and anti-bonding π-orbitals of the ethylenic double bond, respectively.

Method

The electronic structure of the 90°-twisted 9,9′-bifluorenylidene can not appropriately be calculated by the closed-shell SCF method. It can be treated by the method applied to 10,10′-bianthrone.[10] As the twist angle about the 9–9′ double bond of 9,9′-bifluorenylidene increases, the energy separation between the bonding (ψ_1) and antibonding (ψ_2) π-orbitals associated with the C_9–$C_{9'}$ double bond decreases (Fig. 2). In the 90°-twisted 9,9′-bifluorenylidene, the ψ_1 and ψ_2 orbitals are degenerate, and the two closed-shell configurations, Φ_1 and Φ_2, contribute equally to the lowest singlet state.

$$\Phi_1 = |\cdots\psi_1\bar{\psi}_1|$$

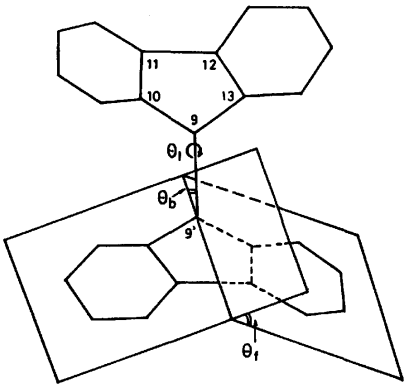

Fig. 3. Molecular parameters which represent the 9,9′-bifluorenylidene structure. For the six-membered ring, C-C=1.418 Å, C-H=1.084 Å, and all the valence angles=120° were fixed in the calculation.

and

$$\Phi_2 = |\cdots\psi_2\overline{\psi}_2|.$$

Thus, 9,9′-bifluorenylidene with a large twist angle should be calculated by two-configuration SCF (TCSCF) wave function,

$$\Phi_G = C_1|\cdots\psi_1\overline{\psi}_1| + C_2|\cdots\psi_2\overline{\psi}_2|. \quad (1)$$

9,9′-Bifluorenylidene is too large in size for ab initio calculations and the MINDO/3 approximation[11] was used. A small model compound cannot be used for the present purpose, since the conformational behavior of 9,9′-bifluorenylidene is essentially controlled by steric interactions. Only a part of molecular structure was optimized. The parameters are shown in Fig. 3. These parameters were determined by using a closed-shell SCF calculation. The TCSCF method was used for the energy calculation when the twist angle was changed from 0 to 90° and the other parameters were fixed at the optimized values.

In order to understand the energy change associated with the conformational change, the total energy of the TCSCF wave function was divided into three parts,

$$E_{total} = E_1 + E_2 + E_{1-2},$$

where E_1 and E_2 are the energies of two 9-fluorenylidene fragments and E_{1-2} is the inter-fragment energy between the two fragments.

Results and Discussion

The molecular structures are listed in Table 1. The calculated values of the twisted form agree well with experimental values.[3] The variations in the energy vs. the twist angle are shown in Fig. 4. The most stable conformation of 9,9′-bifluorenylidene was a twist form with θ_t=45°. This agrees with the structures in solid state[3] and of molecular mechanics calculations.[8] The lowest folded form has θ_t=0° and lies 27 kJ mol^{-1} above the twisted conformation. Table 2 shows the energy components in the twisted and folded forms. The energy of each 9-fluorenylidene fragment is lower in the twisted form by 58 kJ mol^{-1} due to the planarity of the fragments maintained in the twisted form. On the other hand, the interaction energy between two fragments, E_{1-2}, is lower in the folded form by 89 kJ mol^{-1}. This comes from the favorable resonance interaction between the C_9 and $C_{9'}$ atoms in the folded form; this stronger interaction can be seen in the shorter C_9–$C_{9'}$ bond in the folded form.

Table 1. Structure Parameters of Folded and Twisted Forms of 9,9′-Bifluorenylidene in Their Lowest Energy Conformations[a]

Parameter[b]	Folded	Twisted	Exp. (twisted)[c]
$R_{9-9'}$	1.381	1.392	1.377
R_{9-10}	1.538	1.529	1.48 — 1.49
α	53.1	51.9	52.5 — 53.4
β	108.4	109.4	106.7—109.5
θ_t	0	45.0	43
θ_f	27.7	0	0
θ_b	14.8	0	0

a) Bond lengths are in Å and bond angles are in degrees. b) α is the half of the C_{10}–C_9–C_{13} angle and β is the C_{11}-C_{10}–C_9 angle which are measured before folding the 9-fluorenylidene fragment. c) Ref. 3.

Table 2. Energy Components in the Folded and Twisted Structures

	Twisted(θ_t=45°)	Folded(θ_t=0°)	ΔE/kJ mol^{-1}
E_1	−1754.218 eV	−1753.619 eV	58
E_2	−1754.218	−1753.619	58
E_{1-2}	−17.990	−18.914	−89

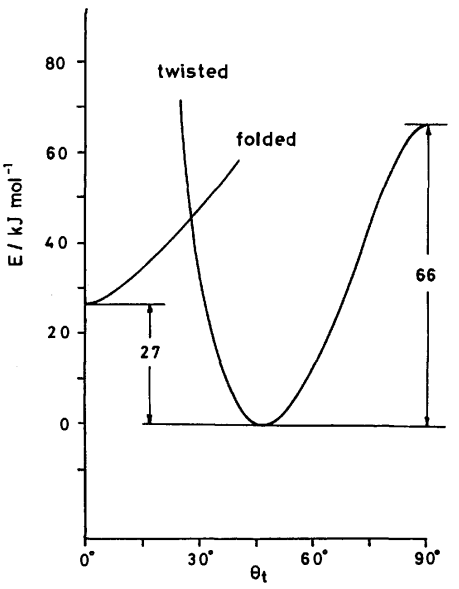

Fig. 4. Potential energy curves of 9,9′-bifluorenylidene with the twist angle θ_t. The energy is relative one with respect to the lowest twisted structure.

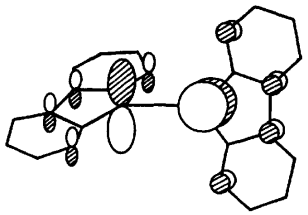

π_1 π_2

Fig. 5. Two π-orbitals of 9-fluorenylidene fragments. The ψ_1 and ψ_2 orbitals for $\theta_t=90°$ in Fig. 2 are expressed by linear combination of these two π-orbitals.

The contribution of the second configuration in Eq. 1 to the Φ_G wave function was 4—6% when $\theta_t \leqq 50°$. It increased when $\theta_t \geqq 60°$ and reached 50% at $\theta_t=90°$. The wave function of the 90°-twisted structure was, thus,

$$\Phi_G = \frac{1}{\sqrt{2}}|\cdots\psi_1\bar{\psi}_1| - \frac{1}{\sqrt{2}}|\cdots\psi_2\bar{\psi}_2|, \quad (2)$$

where the ψ_1 and ψ_2 orbitals were expressed by π_1 and π_2 orbitals each of which belongs to one of

$$\psi_1 = \frac{1}{\sqrt{2}}(\pi_1+\pi_2)$$
$$\psi_2 = \frac{1}{\sqrt{2}}(\pi_1-\pi_2) \quad (3)$$

the orthogonal 9-fluorenylidene fragment (Fig. 5). By using Eq. 3, Eq. 2 can be expressed in terms of the π_1 and π_2 orbitals by

$$\Phi_G = \frac{1}{\sqrt{2}}\{|\cdots\pi_1\bar{\pi}_2| + |\cdots\pi_2\bar{\pi}_1|\},$$

indicating that the lowest singlet state of the 90°-twisted 9,9′-bifluorenylidene is a diradical in which the two orthogonal π_1 and π_2 orbitals are occupied by unpaired electrons.

The present calculations show that *E*–*Z* isomerization is an interconversion between two twisted forms via the transition state of the 90°-twisted conformation. This is an interesting contrast with the *E*–*Z* isomerization of 10,10′-bianthrone where the 90°-twisted structure is not the transition state.[10,12] The barrier to the isomerization of 9,9′-bifluorenylidene was shown to be 66 kJ mol^{-1}, which is somewhat smaller than the value estimated from experiments, 108 kJ mol^{-1}.[13] Two factors need to be considered in an elucidation of structural effects on the low barrier for *E*–*Z* isomerization. First is the ground-state destabilization due to the steric repulsion around the 9–9′ bond, and the second is the stabilization of the diradical transition state by a large conjugated system. These two factors were examined by using the 1,1′-dichloro derivative, **2**, and the benzo-annelated compound, **3**. Table 3 shows the calculated energies of *E*-twisted, *Z*-twisted, and 90°-twisted structures of **2** and **3**. In the compound **2**, the *E*-form is more stable than the *Z*-form by 7 kJ mol^{-1}. This agrees with the experimental facts that in the 1,1′-disubstituted 9,9′-bifluorenylidenes, the *E*-form is more stable than the *Z*-form by 2—4 kJ mol^{-1}.[4,5] The activation energy calculated for the *E*→*Z* isomerization of **3**, 65 kJ mol^{-1}, is larger than that of **2**, 43 kJ mol^{-1}: this is parallel to the experimental findings.[4,5] The lowering of the rotational barrier by the introduction of chlorine atoms at the 1,1′-positions is attributed to the higher repulsion between fragments. This was reflected in the large twist angle, 53°, and was confirmed by the energy components analysis.

Table 3. Relative Energies of Conformers and the 90°-Twisted Structure of 9,9′-Bifluorenylidenes

Compound	Conformation	θ_t	Energy/kJ mol^{-1}
1	Twisted	45°	0
	90°-twisted	90°	66
2	*E*	53°	0
	Z	58°	7
	90°-twisted	90°	43
3	*E*	45°	0
	Z	45°	0
	90°-twisted	90°	65

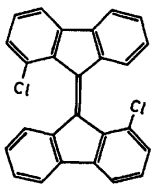

2

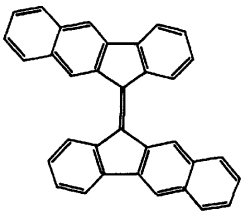

3

The extension of the conjugated system is considered to stabilize the transition-state diradical and lower the barrier for the *E*–*Z* isomerization.[5] However, the lowering of the activation energy calculated for **3** was very small, 1 kJ mol^{-1}. The ground state is also expected to be stabilized by extension of the conjugated system, and the benzo-annelation stabilizes both the ground state and the transition state in the same extent.

References

1) J. H. Day, *Chem. Rev.*, **63**, 65 (1963).
2) I. R. Gault, W. D. Ollis, and I. O. Sutherland, *Chem. Commun.*, **1970**, 269.
3) N. A. Bailey and S. E. Hull, *Acta Crystallog., Sect. B*, **34**, 3289 (1978).
4) I. Agranat, M. Rabinovitz, A. Weitzen-Dagan, and I. Gosnay, *Chem. Commun.*, **1972**, 732.
5) M. Rabinovitz, I. Agranat, and A. Weitzen-Dagan, *Tetrahedron Lett.*, 1241 (**1974**).
6) M. C. Lin and K. J. Laider, *Can. J. Chem.*, **46**, 973 (1968).

7) D. Lenoir and P. Lemmen, *Chem. Ber.*, **113**, 3112 (1980).
8) G. Favini, M. Simmonetta, M. Sottocornola, and R. Todeschini, *J. Comput. Chem.*, **3**, 178 (1982).
9) A. Y. Meyer and H. Yinnon, *Tetrahedron*, **28**, 3915 (1972).
10) O. Kikuchi and Y. Kawakami, *J. Mol. Struct.*, **137**, 365 (1986).
11) R. C. Bingham, M. J. S. Dewar, and D. H. Lo, *J. Am. Chem. Soc.*, **97**, 1285 (1975).
12) I. Agranat and Y. Tapuhi, *J. Org. Chem.*, **44**, 1941 (1979).
13) W. J. Leigh and D. R. Arnold., *Can. J. Chem.*, **59**, 609 (1981).

Reaction of Hydroxide Ion with Electron Acceptors in Dimethyl Sulfoxide

Kisaburo UMEMOTO* and Nobuyuki OKAMURA
Department of Pure and Applied Sciences, College of Arts and Sciences, The University of Tokyo, Komaba, Meguro-ku, Tokyo 153
(Received October 24, 1985)

In dimethyl sulfoxide, the reaction of hydroxide ion with several electron acceptors—iodine, tetracyanoquinodimethan, Nitro Blue Tetrazolium chloride, 2,3,5-triphenyltetrazolium chloride, anthraquinone, and benzophenone—gave reaction products identical to those obtained by the reaction of these electron acceptors with electron donors. The reaction pathways of these electron acceptors were found to be composed of successive one-electron reactions similar to the electrochemical reduction of these electron acceptors. These results indicate that hydroxide ion acts as a reductant in dimethyl sulfoxide.

Hydroxide ion is known to be oxidized at +0.75 V vs. SCE in dimethyl sulfoxide,[1] but the reducing property of hydroxide ion is so weak in aqueous solution that hydroxide ion has been paid little attention as a reductant. Recently, 1-oxo-2,2,6,6-tetramethylpiperidinium salt,[2] anthraquinone,[3] and several electron acceptors[4] were found to be reduced by hydroxide ion in dichloromethane,[2] dimethyl sulfoxide,[3] and acetonitrile.[4] These observations are suggestive of the enhanced reducing power of hydroxide ion in nonaqueous aprotic solvents.

In the present paper, the reaction of hydroxide ion with several electron acceptors of various reduction potentials were studied in order to exemplify the reducing property of hydroxide ion. Dimethyl sulfoxide was used as the solvent, since this solvent is widely used as a useful nonaqueous solvent, while little has been known[3] about the reducing property of hydroxide ion in this solvent.

Experimental

As the sources of hydroxide ion, tetrabutylammonium hydroxide (0.38 M aqueous TBAOH), tetraethylammonium hydroxide (0.69 M aqueous TEAOH), and potassium hydroxide (1M aqueous KOH) were used (1 M=1 mol dm^{-3}). Potassium *t*-butoxide (tBOK, dissolved in ethanol in 0.03 M) and potassium hyperoxide (KO_2, dissolved in DMSO with 18-crown-6-ether in 0.002 M) were used as the electron donors. Iodine, tetracyanoquinodimethan (TCNQ), Nitro Blue Tetrazolium chloride (NBT), 2,3,5-triphenyltetrazolium chloride (TTC), anthraquinone (AQ), and benzophenone (BP) were used as the electron acceptors. Dimethyl sulfoxide (DMSO) was purified as described previously.[5]

The reaction of the hydroxides with the electron acceptors were carried out in a spectrophotometric cell equipped with an airtight sealing cap: a 3 ml of the DMSO solution containing (0.5—10)×10^{-5} M of an electron acceptor was taken in the cell, deaerated with nitrogen gas, and followed by the addition of the aqueous solution of 0.2—10 μl of hydroxide with a microsyringe. The concentration of the electron acceptor and the amount of the added hydroxide were chosen depending on the efficiency of each reaction. The ESR measurements were carried out by taking out an aliquot of the solution under nitrogen. The stopped-flow experiments carried out for observing the kinetic traces of the absorption spectra of the reaction intermediates were performed by using a Furue Science JP-V microfieder. The electrochemical studies were performed as described previously.[5] For the measurement of absorption spectra of electrochemically generated unstable species, the electrolysis was carried out by using an H-type cell as shown in Fig. 1, the cathode compartment of which was composed of a spectrophotometric cell. The cathode was a Pt gauze (0.5×2.0 cm) and the anode was a Pt wire. The salt bridge connected to the SCE was put in the anode compartment. Nitrogen gas was bubbled through both compartments in order to agitate the solution for an efficient electrolysis, to deaerate, and to secure the homogeneity of the solution.

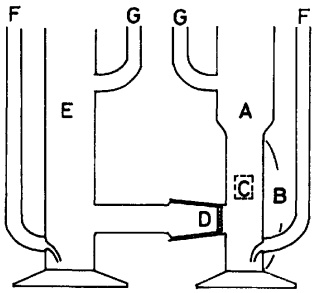

Fig. 1. Electrolysis cell. A: Cathode compartment, B: made of a spectrophotometric cell (1.0 cm×1.0 cm×5.0 cm), C: path of light beam, D: sintered glass filter, E: anode compartment, F: nitrogen inlet, G: nitrogen outlet.

Results and Discussion

Hydroxide ion is known to be gradually decomposed in DMSO, but 0.069 M TEAOH and 0.038 M TBAOH in DMSO were found to remain the same titers after 30 min of standing, indicating that hydroxide ion is stable in DMSO for the time period of ca. 30 min required for the measurement of each spectrum.

The identification of the reaction products and the reaction intermediates generated from the electron acceptors was performed by electrochemical, spectrophotometric, and ESR measurements as summarized as follows.

Iodine. Iodine reacts with the hydroxides and the electron donors very fast and the color of iodine disappeared instantaneously on addition of an excess amount of the hydroxides and the electron donors examined. The generation of iodate in the reactions

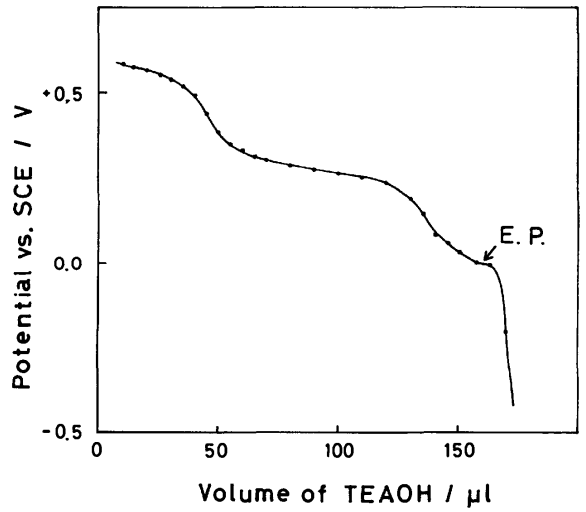

Fig. 2. Titration of iodine with TEAOH in DMSO. Iodine: 20 ml of 5.36 mM (as I) in DMSO. TEAOH: 0.69 M aqueous solution. End point (E.P.): 160 μl of TEAOH. Indicator electrode: Pt.

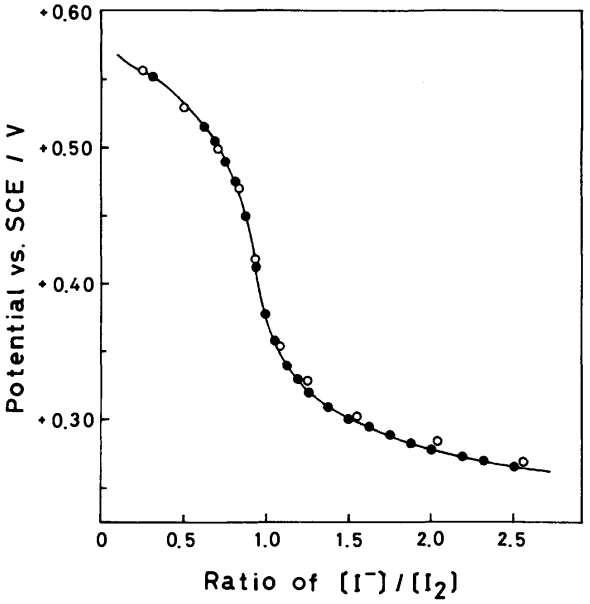

Fig. 3. The equiliblium potential change of I_2/I_3^- system in DMSO.
●: Titration of 20 ml of 3.6 mM iodine (as I_2) with 43.7 mM potassium iodide in DMSO.
○: Titration of iodine with TEAOH. The ratio of $[I^-]/[I_2]$ was calculated from the first inflection point of the titration curve shown in Fig. 2. Indicator electrode: Pt.

was ruled out since iodate is sparingly soluble in DMSO, while no precipitate was found in the solutions. The reaction of iodine with the hydroxides gave a redox titration curve as shown in Fig. 2. The potential change at the first inflection point agreed well with that obtained for the titration of iodine with KI as shown in Fig. 3, indicating iodine being reduced to iodide ion on reaction with hydroxide ion. By taking one-electron reaction, the clear-cut disappearance of

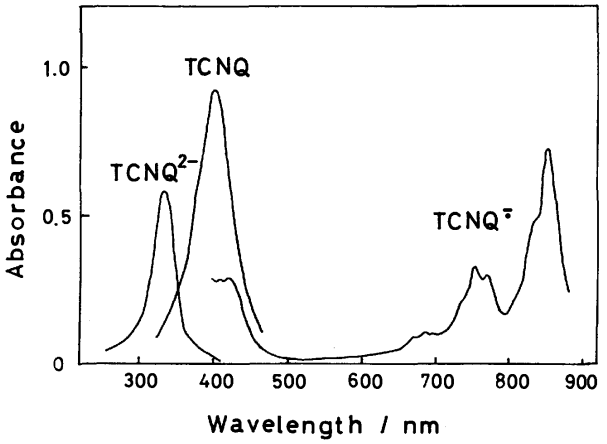

Fig. 4. Absorption spectra of reduction products of TCNQ obtained from 3.7×10^{-5} M of TCNQ in DMSO.

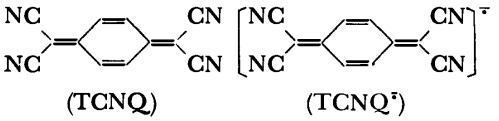

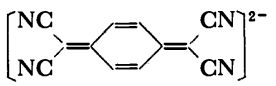

(TCNQ²⁻)

the color of iodine was found to occur at the stoichiometrically equivalent end point of the titration; a ratio of $[I]/[OH^-]=1:1.03$ was found experimentally.

TCNQ. The cyclic voltammogram of TCNQ showed two reversible one-electron redox waves with reduction potential of +0.25 and −0.30 V vs. SCE, respectively. By the controlled potential electrolysis at the first reduction wave, an ESR active green colored solution of $TCNQ^-$ was obtained. By the constant potential electrolysis at the second reduction wave, $TCNQ^-$ was reduced to the colorless $TCNQ^{2-}$. Upon addition of TCNQ to the solution containing $TCNQ^{2-}$ alone, $TCNQ^-$ was found to be generated. By taking these results, the redox reaction scheme of TCNQ is given as follows.

$$TCNQ \overset{e}{\rightleftharpoons} TCNQ^- \overset{e}{\rightleftharpoons} TCNQ^{2-} \quad (1)$$

$$TCNQ^{2-} + TCNQ \longrightarrow 2\,TCNQ^- \quad (2)$$

The absorption spectra of these reduction products are given in Fig. 4.

On reaction with the hydroxides and the electron donors examined, TCNQ gave $TCNQ^-$ when the concentration of the hydroxides or the electron donors is less than the equivalent amount of TCNQ and with the addition of an excess amount of the hydroxides or the electron donors, $TCNQ^-$ was reduced to $TCNQ^{2-}$. The rate of reaction of TCNQ with the hydroxides and the electron donors was so fast that the color change of the solution occurred instantaneously upon mixing the reactants. From the observations of the stepped

generation of $TCNQ^{\cdot-}$ and $TCNQ^{2-}$ from TCNQ, TCNQ is considered to be reduced by hydroxide ion by successive one-electron reactions as shown as follows.

$$TCNQ + OH^- \longrightarrow TCNQ^{\cdot-} + OH \quad (3)$$

$$TCNQ^{\cdot-} + OH^- \longrightarrow TCNQ^{2-} + OH \quad (4)$$

The hydroxy radical is known to be unstable to give oxygen and water[1] or hydrogen peroxide[2] according to the following reactions.

$$2\,OH \longrightarrow H_2O_2 \quad (5)$$

$$H_2O_2 \longrightarrow H_2O + \frac{1}{2}O_2 \quad (6)$$

The consumption of hydroxide ion in the reaction was detected by using a pH meter. As the response of the glass electrode in pure DMSO is not specified, the measurement was carried out after dissolving 10 ml of DMSO into 30 ml of water. In this solvent mixture, the 0.69 M TEAOH showed the same titer as in aqueous solution. The indicator of the pH meter was calibrated by adding a known amount of hydroxide in 10 ml of DMSO before mixing with 30 ml of water. When no hydroxide was added, the meter indicated at pH 5.0 (880 mV), and when 15 μl of 0.69 M TEAOH was added in 10 ml of DMSO (1.0×10^{-3} M), the meter indicated at pH 10.8 (530 mV). When 15 μl of 0.69 M TEAOH was added into 10 ml of DMSO containing 1.37×10^{-3} M TCNQ, the pH meter showed pH 5.3 (860 mV), indicating almost no hydroxide ion being left in the solution after the reaction with TCNQ proceeded. No oxygen was detected as the reaction product as evidenced by the observation of no oxygen wave at −0.8 V vs. SCE on the cyclic voltammogram taken after the reaction of hydroxide ion with TCNQ completed. The detection of hydrogen peroxide was unsuccessful because of the reactivity of DMSO on the permanganate method and of the color interference of TCNQ on the titanium chloride method. The hydroxy radical is known to react with some solvents,[6] but the reaction product of OH and DMSO was not confirmed or excluded in the present work.

NBT. On the cyclic voltammogram of NBT^{2+}, three predominant reduction waves were observed at −0.28, −1.28, and −1.66 V vs. SCE. The first wave which has a slight shoulder was attributed to the reduction of the tetrazolium ring as shown below. The second and the third waves are considered to correspond to the reduction of the nitro group of NBT^{2+}, since these potentials are close to those of para-substituted nitrobenzene derivatives. At the early stage of the constant potential electrolysis at −0.55 V vs. SCE, corresponding to the first reduction wave, a blue colored solution of monoformazan (MF, λ_{max}=680 nm) was obtained. The solution also gave an ESR spectrum identified to that of bitetrazole cation radical ($NBT^{\cdot+}$). The monoformazan thus generated turned to

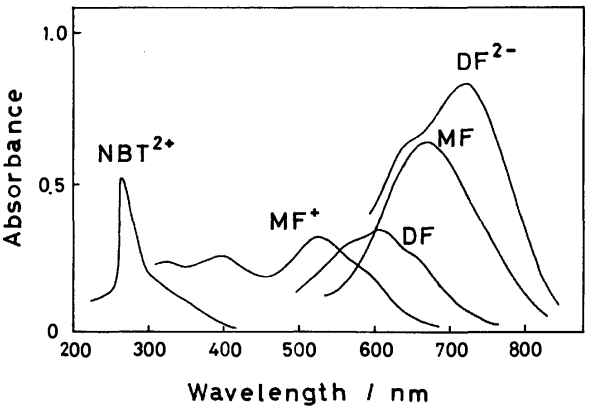

Fig. 5. Absorption spectra of reduction products of NBT obtained from 8.2×10^{-6} M of NBT in DMSO.

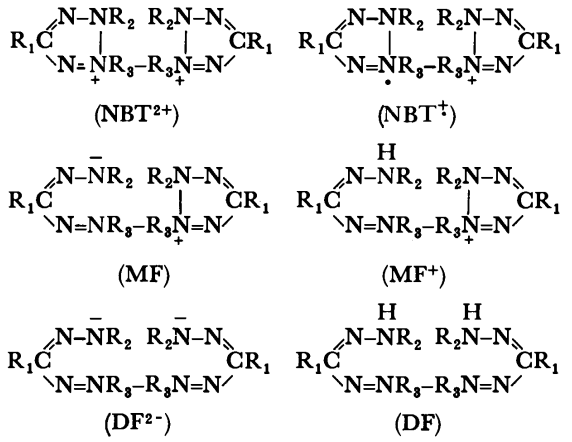

$R_1 = C_6H_5$, $R_2 = p\text{-}NO_2C_6H_4$, $R_3 = m\text{-}CH_3OC_6H_3$

the monoformazan ion (MF^+, λ_{max}=530 nm) on addition of acids. Upon completion of the controlled potential electrolysis at −0.55 V vs. SCE, a sky blue solution of biformazan dianion (DF^{2-}, λ_{max}=724 nm) was obtained with the consumption of overall four electrons for each molecule of NBT^{2+}. The biformazan dianion was turned to biformazan (DF) on addition of acids. The reaction scheme of NBT^{2+} was given as follows.[7]

$$NBT^{2+} \xrightarrow{e} NBT^{\cdot+} \xrightarrow{e} MF \xrightarrow{H^+} MF^+ \quad (7)$$

$$MF \xrightarrow{2e} DF^{2-} \xrightarrow{2H^+} DF \quad (8)$$

The characteristic absorption bands of these species are given in Fig. 5. The formation of MF according to the following disproportionation reaction of $NBT^{\cdot+}$ is also probable,[7]

$$2\,NBT^{\cdot+} \rightleftharpoons NBT^{2+} + MF \quad (9)$$

but it was not confirmed whether MF is formed by the electronation or the disproportionation of $NBT^{\cdot+}$. It is most reasonable to consider that both reactions are operative in the reduction process of NBT^{2+}.

On reaction with the hydroxides, NBT^{2+} immediately gave a blue-colored solution of MF. The solution

also gave an ESR spectrum identified to $NBT^{\ddagger}$. The MF and $NBT^{\ddagger}$ thus generated were converted to MF^+ on addition of acids. The reaction scheme of NBT^{2+} with hydroxide ion is considered to be as follows.

$$NBT^{2+} + OH^- \longrightarrow NBT^{\ddagger} + OH \quad (10)$$

$$NBT^{\ddagger} + OH^- \longrightarrow MF + OH \quad (11)$$

and/or

$$2\,NBT^{\ddagger} \rightleftharpoons NBT^{2+} + MF \quad (9)$$

The consumption of hydroxide ion in this reaction was confirmed by using a pH meter as in the case of TCNQ. The reaction of the hydroxides with NBT^{2+} was fast but not so effective as in the reactions of iodine and TCNQ. For example, by the reaction of 8.2×10^{-6} M NBT^{2+} with 1.64×10^{-5} M TEAOH required from the stoichiometry of the reactions shown by Eqs. 10, 11, or 9, only half amount of NBT^{2+} was reduced. As the reduction potential of NBT^{2+} is more negative than those of iodine and TCNQ, the electron donating property of hydroxide ion is considered to be less effective for NBT^{2+} than for iodine and TCNQ.

TTC. The electrochemical study of TTC showed that 2,3,5-triphenyltetrazolium ion (TT^+) is reduced to a tetrazolyl radical ($TT^{\cdot}$) and to 1,3,5-triphenylformazan anion (TF^-, λ_{max}=536 nm) at −0.49 and −0.74 V vs. SCE, respectively. TF^- was also generated by the disproportionation reaction of $TT^{\cdot}$ generated by the constant potential electrolysis at −0.55 V vs. SCE.[5] The reaction scheme of TT^+ is given as follows.[5]

$$TT^+ \xrightarrow{e} TT^{\cdot} \xrightarrow{e} TF^- \xrightarrow{H^+} TF \quad (12)$$

$$2\,TT^{\cdot} \rightleftharpoons TT^+ + TF^- \quad (13)$$

The characteristic absorption bands of these species are given in Fig. 6.

Upon reaction with the hydroxides, TT^+ gave a highly red colored solution of TF^-. The solution also gave an ESR spectrum identified to $TT^{\cdot}$. On addition of acids, the ESR spectrum disappeared and the solution gave an absorption spectrum characteristic to 1,3,5-triphenylformazan (TF, λ_{max}=485 nm). The reaction of TTC with hydroxide ion is given as follows.

$$TT^+ + OH^- \longrightarrow TT^{\cdot} + OH \quad (14)$$

$$TT^{\cdot} + OH^- \longrightarrow TF^- + OH \quad (15)$$

and/or

$$2\,TT^{\cdot} \rightleftharpoons TT^+ + TF^- \quad (13)$$

The reaction of TTC with hydroxide ion was less effective than the reactions of iodine, TCNQ, and NBT^{2+} as predicted from the reduction potential of TTC which is more negative than the reduction potentials of iodine, TCNQ, and NBT^{2+}. For example,

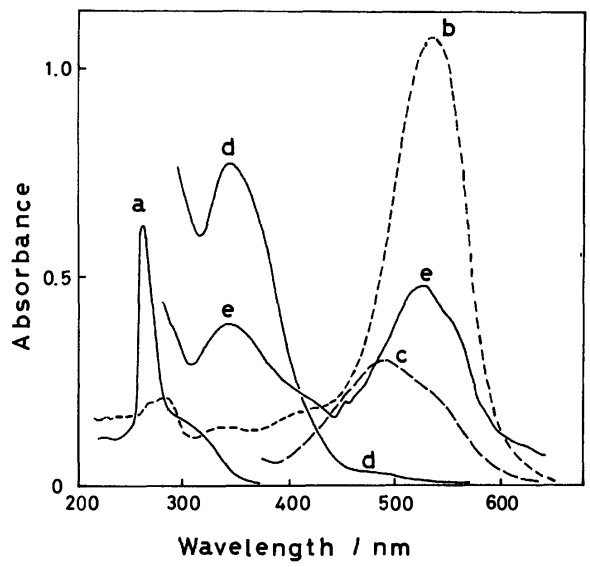

Fig. 6. Absorption spectra of (a): 3.5×10^{-5} M TTC, (b): TF^- generated from (a) by the reaction with TBAOH, (c): TF generated from (b) with the addition of benzoic acid, (d): $TT^{\cdot}$ generated by the reaction of TF^- with TT^+ in DMSO–benzene mixture (DMSO:benzene=20:80 in volume), (e): $TT^{\cdot}$ and TF^- obtained 2 s after mixing of 1.0×10^{-4} M TTC and 1.0×10^{-2} M TBAOH by flowing the solutions.

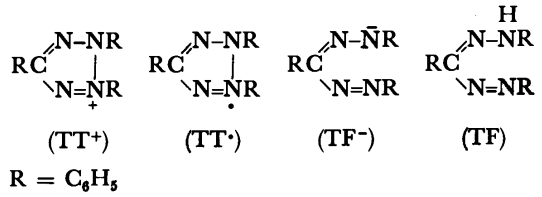

when 3.5×10^{-5} M TTC was reacted with 7.0×10^{-5} M TEAOH, only one third of the amount of TTC was reduced.

Although $TT^{\cdot}$ was detected by the ESR method in the reaction of TTC with an equimolar amount of hydroxide, any absorption band attributable to $TT^{\cdot}$ was not observed in pure DMSO. However, when benzene was added into the solution of TF^- with an excess amount of TTC, the color of the solution turned from red to yellow and a new absorption band appeared at 345 nm with the consumption of the absorption band of TF^- as shown in Fig. 6d. In a typical experiment, 1 ml of DMSO solution of TF^- generated by the reaction of 3.5×10^{-5} M TTC with 5×10^{-4} M TBAOH was added into 8 ml of pure benzene. The solution showed an absorption spectrum of TF^- alone. To this solution 1 ml of DMSO solution containing 3×10^{-3} M TTC was added. The color of the solution turned from red to yellow. The yellow colored solution gave an intense ESR spectrum identical to that of $TT^{\cdot}$ as shown in Fig. 7. Thus, the absorption band at 345 nm was identified to that of $TT^{\cdot}$. This band was gradually substituted by that of TF^- with the successive increase of the content of DMSO in the DMSO–benzene mixture. These observa-

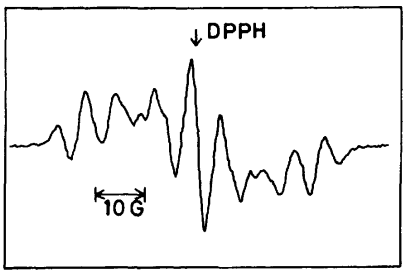

Fig. 7. ESR spectrum of TT·, generated by the reaction of TTC with TBAOH in DMSO.

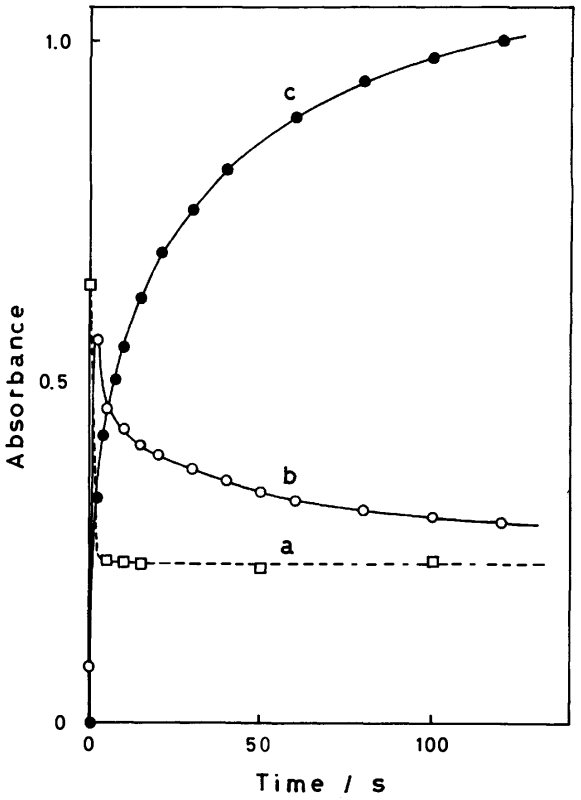

Fig. 8. Stopped-flow kinetic traces of absorption bands observed in the reaction of 7.0×10^{-5} M TTC with 7.6×10^{-3} M TBAOH in DMSO.
(a): TT^+ at 258 nm, (b) TT· at 345 nm (the range of absorbance: ×2), and (c): TF^- at 536 nm.

tions indicate that in pure DMSO the equilibrium constant of the disproportionation reaction (Eq. 13) is so large that the concentration of TT· is kept too low to be detected by the spectrophotometric method at the equilibrium state. However, if the reaction of TTC with hydroxide ion is induced by the electron transfer from hydroxide ion to TT^+, the transient accumulation of TT· should be observed at the early stage of the reaction. In order to verify the probable accumulation of TT·, the reaction was studied by a flow method. The reactants were introduced into a spectrophotometric flow-cell by using a double-channeled microfeeder. On the absorption spectrum taken immediately after mixing the reactants, absorption bands of both TT· and TF^- were observed as shown

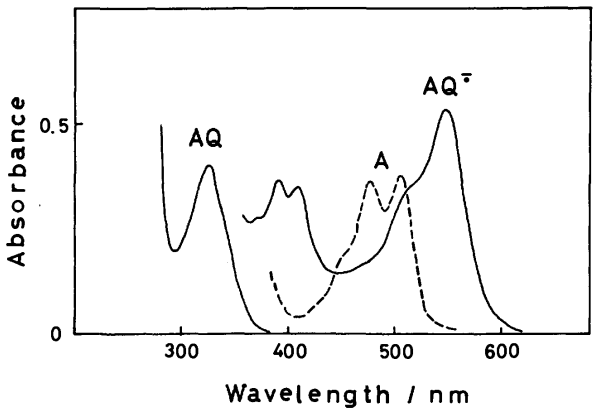

Fig. 9. Absorption spectra of reaction products of anthraquinone (AQ) in DMSO.
AQ: 8.0×10^{-5} M. AQ^- and A: generated from 2.3×10^{-3} M of AQ by the reaction with TEAOH.

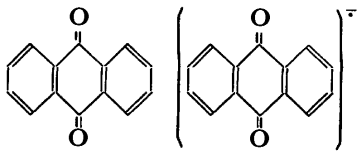

in Fig. 6e. The stopped-flow kinetic traces of absorption bands of TT^+, TT·, and TF^- are given in Fig. 8. Although the time courses of these kinetic traces are not so simple as to allow a rigorous kinetic analysis; the rate of increase of TF^- is seen to be well intercorrelated with the rate of decrease of TT·, indicating that TT· is working as a precursor of TF^- in the reaction sequence.

Anthraquinone. The cyclic voltammetry of AQ showed that AQ is reversibly reduced to AQ^- and AQ^{2-} at −0.83 and −1.53 V vs. SCE, respectively. The constant potential electrolysis at the first reduction wave gave a red colored solution of AQ^- (λ_{max}=550 nm) as shown in Fig. 9.

On reaction with the hydroxides, AQ gave a red-colored solution of AQ^-. The solution showed an ESR signal. The reaction of AQ with the hydroxides was not so effective as in the reactions of iodine, TCNQ, NBT, and TTC as predicted from the reduction potential of AQ which is the most negative among these electron acceptors. In order to obtain an absorption spectrum of AQ^-, higher concentration of AQ was required as compared with the other electron acceptors examined. AQ^- turned gradually to a yellow colored species (shown by A in Fig. 9) on standing, which did not give any ESR signal and has not been identified yet.

Benzophenone. The electrochemical study of BP showed that BP is reduced to blue colored BP^- at −1.77 V vs. SCE. However, BP did not react with the hydroxides and the electron donors examined. The reduction potential of BP is too negative to be reduced by the hydroxides and the electron donors examined.

Conclusion. The reaction products and intermediates identified in the reactions of the electron

Table 1. Reaction Products Identified in the Reaction of Electron Acceptors with Hydroxides and Electron Donors in DMSO

Electron acceptor	Hydroxides			Electron donors			Reduction potential vs. SCE/V
	TBAOH	TEAOH	KOH	tBOK	KO_2	Electrochemical reduction	
I_2	I^-	I^-	I^-	I^-	I^-	I^-	+0.53 (I_2/I_3^-) +0.28 (I_3^-/I^-)
TCNQ	$TCNQ^{\cdot-}$ $TCNQ^{2-}$	$TCNQ^{\cdot-}$ $TCNQ^{2-}$	$TCNQ^{\cdot-}$ $TCNQ^{2-}$	$TCNQ^{\cdot-}$ $TCNQ^{2-}$	$TCNQ^{\cdot-}$ $TCNQ^{2-}$	$TCNQ^{\cdot-}$ $TCNQ^{2-}$	+0.25 −0.30
NBT	NBT^{+}, MF	NBT^{+}, MF	NBT^{+}, MF	NBT^{+}, MF, DF^{2-}	NBT^{+}, DF^{2-}	NBT^{+}, MF, DF^{2-}	−0.28
TTC	$TT^{\cdot}$, TF^-	$TT^{\cdot}$, TF^-	$TT^{\cdot}$, TF^-	$TT^{\cdot}$, TF^-	$TT^{\cdot}$, TF^-	$TT^{\cdot}$, TF^-	−0.49
AQ	$AQ^{\cdot-}$	$AQ^{\cdot-}$	$AQ^{\cdot-}$	$AQ^{\cdot-}$	$AQ^{\cdot-}$	$AQ^{\cdot-}$, AQ^{2-}	−0.83
BP	—	—	—	—	—	$BP^{\cdot-}$	−1.77

acceptors with the hydroxides and the electron donors in DMSO are summarized in Table 1. As shown in Table 1, the reaction of the electron acceptors with the hydroxides gave reaction products or intermediates identical to those obtained by the reaction of these electron acceptors with the electron donors. The efficiency of the reactions was shown to have a qualitative correlation with the reduction potentials of the electron acceptors: the less negative the reduction potential, the more efficiently the reaction proceeded. These observations would lead us to suppose that hydroxide ion acts as an electron donor in the reactions examined.

The reducing property of hydroxide ion is of interest, since this property may possibly play an essential role in some, not all, of the so-called base-catalyzed reactions. Further studies to clarify the role of hydroxide ion are also required in analytical chemistry, since the reducing property of hydroxide ion has been paid little attention in the acid-base reactions in nonaqueous solvents.

The authors thank Dr. Ryo Hirasawa and Master Kazuo Sakamoto for their kind permission and outstanding assistances in using their ESR spectrometer.

References

1) A. D. Goolsby and D. T. Sawyer, *Anal. Chem.*, **40**, 83 (1968).
2) T. Endo, T. Miyazawa, S. Shiihashi, and M. Okawara, *J. Am. Chem. Soc.*, **106**, 3877 (1984).
3) S. Arai, S. Kato, and M. Hida, *Bull. Chem. Soc. Jpn.*, **58**, 1458 (1985).
4) K. Umemoto, *Chem. Lett.*, **1985**, 1415.
5) K. Umemoto, *Bull. Chem. Soc. Jpn.*, **58**, 2051 (1985).
6) J. L. Roberts, M. M. Morrison, and D. T. Sawyer, *J. Am. Chem. Soc.*, **100**, 329 (1978).
7) B. H. J. Bielski, G. G. Shiue, and S. Bajuk, *J. Phys. Chem.*, **84**, 830 (1980).

Ylide-Metal Complexes. XI.[1] The Preparation and Properties of VIA Group Metal (Te) Complexes of Alkylidenetriphenylphosphoranes and the Corresponding Selenium Compounds

Yoshihisa YAMAMOTO
Faculty of Pharmaceutical Sciences, Higashi Nippon Gakuen University, Ishikari-Tobetsu, Hokkaido 061-02
(Received March 12, 1986)

Reactions of $(C_6H_5)_3P{=}CH_2$ (**L**) with $TeCl_4$ of mole ratios 2 : 1 and 3 : 1 yield new compounds: dichlorobis(methylenetriphenylphosphorane)tellurium dichloride, $[L_2TeCl_2]Cl_2$ (**1**), and chlorotris(methylenetriphenylphosphorane)tellurium trichloride, $[L_3TeCl]Cl_3$ (**2**), respectively. The reaction of ylide **L** with compound **1** yields a new compound: tetrakis(methylenetriphenylphosphorane)tellurium tetrachloride, $[L_4Te]Cl_4$ (**3**). The structure of compounds **1**—**3** is a distorted tetrahedron. The color of **1**—**3** is yellow. The electronic absorption spectra of compounds **2** and **3** show six absorption bands in the region 200—500 nm in dry dichloromethane. The reactions of ylide **L** with $(C_6H_5)_2SeCl_2$ of mole ratios 1 : 1 and 2 : 1 yield new compounds: chloro(methylenetriphenylphosphorane)diphenylselenium chloride, $[LSe(Cl)(C_6H_5)_2]Cl$ (**9**), and bis(methylenetriphenylphosphorane)diphenylselenium dichloride, $[L_2Se(C_6H_5)_2]Cl_2$ (**11**), respectively. The color of the selenium compounds is white. The tellurium and selenium compounds are thermally stable in the solid state.

A previous paper[2] of this series was concerned with a study of methylenetriphenylphosphorane, bis(methylenetriphenylphosphorane)gold(I) chloride and the corresponding copper(I) chloride by X-ray photoelectron spectroscopy. Also, we have been concerned with the preparation, properties and structures of ylide-metal complexes for I—IV group metals with unstable phosphoranes.[3-6] In the VIA group, the preparation of several selenium compounds with phosphoranes, $(C_6H_5)_3P{=}CHR$ (R: H, CH_3, SC_6H_5), has been reported.[7-10] However, the preparation of a tellurium compound with phosphorane has not been reported except for a tellurium compound with stable (ethoxycarbonylmethylene)triphenylphosphorane,[11,12] $(C_6H_5)_3P{=}CHCOOC_2H_5$. Very little is known of the preparation, properties and structures of selenium and tellurium compounds with phosphoranes[3,13-15] and arsoranes.[16,17] Thus, the present paper deals with the preparation and properties of dichlorobis(methylenetriphenylphosphorane)tellurium dichloride, $[\{(C_6H_5)_3PCH_2\}_2TeCl_2]Cl_2$, chlorotris(methylenetriphenylphosphorane)tellurium trichloride, $[\{(C_6H_5)_3PCH_2\}_3TeCl]Cl_3$, and tetrakis(methylenetriphenylphosphorane)tellurium tetrachloride, $[\{(C_6H_5)_3PCH_2\}_4Te]Cl_4$, and deals with the preparation of chloro(methylenetriphenylphosphorane)diphenylselenium chloride, $[(C_6H_5)_3PCH_2Se(Cl)(C_6H_5)_2]Cl$, and bis(methylenetriphenylphosphorane)diphenylselenium dichloride, $[\{(C_6H_5)_3PCH_2\}_2Se(C_6H_5)_2]Cl_2$.

Experimental

Measurements. The NMR spectra were measured with an R-40 (Hitachi) spectrometer, XL-200 (Varian) spectrometer for ^1H NMR, and with an FX-60 spectrometer (JEOL) for ^{13}C NMR. The electric conductivities of the solutions were determined by the use of a conductometric meter, CM-30 (Shimadzu) in dry methanol and dry dichloromethane. The electronic absorption spectra were recorded with a Shimadzu UV-210 recording spectrophotometer.

Starting Material. The methylene-[18] and ethylidene[19] triphenylphosphorane were prepared from the corresponding phosphonium bromide by the sodium amide method.

Preparation of Ylide–Metal Complexes. Dichlorobis(methylenetriphenylphosphorane)tellurium Dichloride (1): The methylene ylide (0.43 g, 1.56 mmol) was dissolved in dry THF (20 cm^3) at 0 °C under nitrogen. The THF solution was added to powder $TeCl_4$ (0.2 g, 0.74 mmol) at 0 °C. The mixture was stirred for 10 min at 0 °C. The precipitated light yellow complex was filtered and dried under vacuum. Yield: 0.50 g (82%). Decomp: 124 °C. Found: C, 56.00; H, 4.35%. Calcd for $C_{38}H_{34}P_2TeCl_4$ (MW 822.04) C, 55.52; H, 4.17%.

Chlorotris(methylenetriphenylphosphorane)tellurium Trichloride (2): The dry THF (20 cm^3) solution of methylene ylide (0.47 g, 1.70 mmol) was added to powder $TeCl_4$ (0.15 g, 0.56 mmol) under nitrogen. The mixture was stirred at room temperature for 1 d. The precipitated yellow complex was filtered, washed with pentane and dried under vacuum. Yield: 0.52 g (85%). Decomp: 106 °C. Found: C, 62.24; H, 5.01%. Calcd for $C_{57}H_{51}P_3TeCl_4$ (MW 1098.36) C, 62.33; H, 4.68%. Electronic absorption spectrum: 240 nm (ε=13100), 260 (9200), 267 (10100), 274 (8530), 350 (730), and 435 (1630) in dry dichloromethane. Λ=193 S cm^2 mol^{-1} in dry methanol solution at 19 °C; a 29.4 mg sample was dissolved 27-cm^3 of dry methanol. Complex **2** was also prepared from the reaction mixture of ylide and $TeCl_4$ in a mole ratio of 4:1 in THF.

Tetrakis(methylenetriphenylphosphorane)tellurium Tetrachloride (3): The dry THF (20 cm^3) solution of methylene ylide (0.31 g, 1.12 mmol) was added to powder $TeCl_4$ (0.15 g, 0.56 mmol) at 0 °C. The mixture was stirred for 10 min at 0 °C. Then, the THF solution (10 cm^3) of methylene ylide (0.34 g, 1.23 mmol) was added to the reaction mixture at 0 °C under nitrogen. The mixture was stirred for 150 min at room temperature. A deep-yellow complex was filtered, washed with pentane and dried. Yield: 0.63 g (82%). Decomp: 116 °C. Found: C, 66.15; H, 5.20%. Calcd for $C_{76}H_{68}P_4TeCl_4$ (MW 1374.67) C, 66.40; H, 4.99%. Electronic absorption spectrum: 238 nm (ε=18300), 262 (13000), 267 (14200), 275 (11700), 360 (900), and 447 (2030) in dry dichloromethane. Λ=328 S cm^2 mol^{-1} in dry methanol solution at 19 °C; a 34.9 mg sample was dissolved 25-cm^3 of dry methanol. Λ=75 S cm^2 mol^{-1} in dry dichloromethane solution at 21 °C; a 49.6 mg sample was dissolved in dry dichloromethane 36 cm^3.

Chloro(methylenetriphenylphosphorane)diphenylselenium Chloride (9): Diphenylselenium dichloride (0.19 g, 0.62

Table 1. ^1H and ^{13}C NMR Data of Complexes and Ylide

^1H	CH_2P		C_6H_5	Solvents
	δ/ppm	$^2J_{HCP}$/Hz	δ/ppm	
1	3.15 d (2H)	13.7	7.4—8.1 m (15H)	CD_2Cl_2
2	3.20 d (2H)	13.7	7.4—7.9 m (15H)	CD_2Cl_2
	2.94 d (2H)	14.0	7.5—8.0 m (15H)	CD_3OD
3	3.30 d (2H)	13.7	7.3—8.0 m (15H)	CD_2Cl_2
	2.93 d (2H)	14.0	7.5—8.0 m (15H)	CD_3OD
L[a]	−0.13 d (2H)	7.5	6.2—7.2 m (15H)	C_6D_6[b]

^{13}C	CH_2P		C_6H_5 δ/ppm (J_{CP}/Hz)			
	δ/ppm	J_{CP}/Hz	c-1	*o*	*m*	*p*
1	10.56 d	55.7	119.4 (87.9)	133.5 (10.7)	130.5 (13.7)	135.2 (2.9)
2	10.36 d	57.6	119.6 (87.9)	133.6 (10.7)	130.4 (12.7)	135.2 (3.9)
3	10.30 d	55.7	119.6 (87.9)	133.5 (9.8)	130.4 (11.8)	135.1 (2.9)
L[c]	−4.3 d	98.6				

Standard: ^1H NMR; internal TMS (δ=0), ^{13}C NMR; CD_2Cl_2 (δ=53.6 ppm). Solvent: CD_2Cl_2. a): Ref. 27; b): external TMS (δ=0); c): Ref. 6.

mmol) was added to a dry THF solution (8 cm^3) of methylene ylide (0.17 g, 0.62 mmol) under nitrogen. The mixture was stirred for 20 h. Then, the precipitated compound was filtered, washed with ether and dried. Yield: 0.19 g (52%). Decomp: 162 °C. Found: C, 64.48; H, 4.93%. Calcd for $C_{31}H_{27}PSeCl_2$ (MW 580.39) C, 64.15; H, 4.69%.

Chloro(ethylidenetriphenylphosphorane)diphenylselenium Chloride (10): Diphenylselenium dichloride (0.23 g, 0.76 mmol) was added to a dry THF solution (8 cm^3) of ethylidene ylide (0.25 g, 0.86 mmol) under nitrogen. The mixture was stirred for 18 h at room temperature. The precipitated white compound was filtered, washed with ether and dried. Yield: 0.28 g (62%). Decomp: 160 °C. Found: C, 64.35; H, 4.79%. Calcd for $C_{32}H_{29}PSeCl_2$ (MW 594.42) C, 64.66; H, 4.92%.

Bis(methylenetriphenylphosphorane)diphenylselenium Dichloride (11): Diphenylselenium dichloride (0.19 g, 0.62 mmol) was added to a dry THF solution (8 cm^3) of methylene ylide (0.37 g, 1.34 mmol) under nitrogen. The mixture was stirred for 1 d. The precipitated compound was filtered, washed with ether and dried. Yield: 0.28 g (52%). Decomp: 203 °C. Found: C, 70.35; H, 5.34%. Calcd for $C_{50}H_{44}P_2SeCl_2$ (MW 856.71) C, 70.10; H, 5.18%.

Bis(ethylidenetriphenylphosphorane)diphenylselenium Dichloride (12): Diphenylselenium dichloride (0.19 g, 0.62 mmol) was added to a dry THF solution (10 cm^3) of ethylidene ylide (0.40 g, 1.38 mmol) under nitrogen. The mixture was stirred for 20 h. The precipitated compound was filtered, washed with ether and dried. Yield: 0.30 g (54%). Decomp: 193 °C. Found: C, 70.43; H, 5.54%. Calcd for $C_{52}H_{48}P_2SeCl_2$ (MW 884.76) C, 70.59; H, 5.47%.

Results and Discussion

Dichlorobis(methylenetriphenylphosphorane)tellurium dichloride, $[\{(C_6H_5)_3PCH_2\}_2TeCl_2]Cl_2$ (**1**), and chlorotris(methylenetriphenylphosphorane)tellurium trichloride, $[\{(C_6H_5)_3PCH_2\}_3TeCl]Cl_3$ (**2**), were isolated from the reaction mixtures of methylenetriphenylphosphorane, $(C_6H_5)_3P{=}CH_2$ (**L**), and $TeCl_4$ in mole ratios of 2:1 and 3:1, respectively. Tetrakis(methylenetriphenylphosphorane)tellurium tetrachloride, $[\{(C_6H_5)_3PCH_2\}_4Te]Cl_4$ (**3**), was isolated from a reaction mixture of **L** and complex **1** in a mole ratio of 2:1. Complexes **1**—**3** are soluble in chloroform, dichloromethane, DMF, DMSO and water, but are insoluble in benzene, tetrahydrofuran (THF), pentane and ether. Complexes **1**—**3** in water give phosphonium chloride, $[(C_6H_5)_3PCH_3]Cl$ (**4**). Complexes **2** and **3** are stable in alcohols, though complex **1** is unstable. Their color is yellow, and they are thermally stable in the solid state.

The ^1H NMR spectra of **1**—**3** showed a doublet signal for methylene group at 2.9—3.3 ppm and a multiplet signal for phenyl groups at 7.4—8.1 ppm in a ratio of 2:15 at room temperature in dichloromethane-d_2. The coupling constant ($^2J_{HCP}$) of the methylene group is larger than that of **L**, and the chemical shift is at a lower field than that of **L** as is shown in Table 1. In the ^{13}C NMR spectra in dichloromethane-d_2, the chemical shift for methylene group is at a lower field than that of **L**, and the coupling constant (J_{CP}) for methylene group is smaller than that of **L** as is shown in Table 1. These spectral properties were similar to those of bis(methylenetriphenylphosphorane)-metal chloride, $[(C_6H_5)_3PCH_2\text{-}M\text{-}CH_2P(C_6H_5)_3]Cl_2$ (**5**) (M: IIB group metals),[5] and the corresponding ylide-metal complexes such as $[(C_6H_5)_3PCH_2\text{-}M\langle^{Cl}_{Cl}\rangle M\text{-}CH_2P(C_6H_5)_3]Cl_2$ (**6**) (M: IIA group metals)[3] and $[(C_6H_5)_3PCH_2\text{-}M(C_6H_5)_3]Cl$ (**7**) (M: IVA group metals).[4] Thus, the ylide in complexes **1**—**3** is bonded to the metal atom through the carbanionic donor atom.[19]

Complex **1** is not polymeric[20] since it is soluble in dichloromethane. The elemental analysis of **1** agreed with that of L_2TeCl_4. The structures of $TeCl_4$[21,22] and $(C_6H_5)_2TeBr_2$[23,24] (**8**) were found to be monomeric

distorted tetrahedrons by X-ray diffraction, i.e., the observed bond angles were 178.0±0.2° for Br–Te–Br and 96.3±1.2° for C–Te–C. Two bromine atoms in **8** are bonded to the axial positions and are at a position cis for the lone pair. Thus, we suggest that the structure of **1** is a distorted tetrahedron as is shown in Scheme 1.

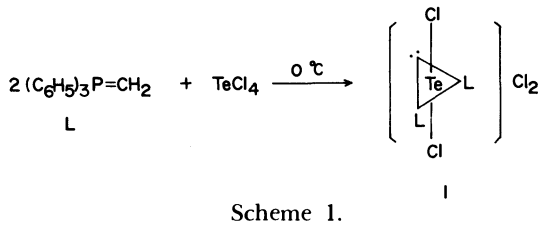

I

Scheme 1.

Complex **2** is not polymeric[20] since it is soluble in dichloromethane and alcohols. The elemental analysis of **2** agreed with that of L_3TeCl_4. Complex **2** has free anion, judging from the molar conductance (cf. Experimental section). Thus, the structure of **2** is either **2a** or **2b** (distorted tetrahedron) as is shown in Scheme 2. We believe that the structure of **2** is **2a**:

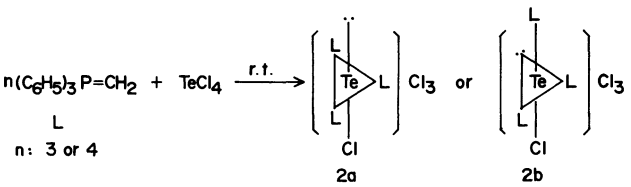

Scheme 2.

The chlorine atoms in complex **1** are substituted with ylides, and complex **1** changes to complex **3** (described below) which is not obtained from the reaction mixture of ylide and $TeCl_4$ in the mole ratio 4:1. This difference is due to the configuration (cis or trans) between the chlorine atom and lone pair in the complex. Thus, the chlorine atom in the position cis for the lone pair can be substituted with ylide. This was confirmed in the preparation of complexes **9**—**11** (described below), which were obtained from the mixture of ylide and diphenylselenium dichloride since the chlorine atoms in diphenylselenium dichloride are in a position cis for the lone pair according to X-ray diffraction.[24,25] Thus, the chlorine atom in **2** might be in a position trans to a lone pair such as **2a**.

Complex **3** is not polymeric[20] since it is soluble in dichloromethane and alcohols. The elemental analysis of **3** agreed with that of L_4TeCl_4. Complex **3** has free anion, judging from the molar conductance. Complex **3** has been isolated only from a reaction mixture of **L** and complex **1** in the mole ratio 2:1. Thus, we suggest that the structure of **3** is a distorted tetrahedron as is shown in Scheme 3.

The electronic absorption spectra of the ylide metal complexes were observed. The spectra of **2** and **3** showed six absorption bands in dry dichloromethane as

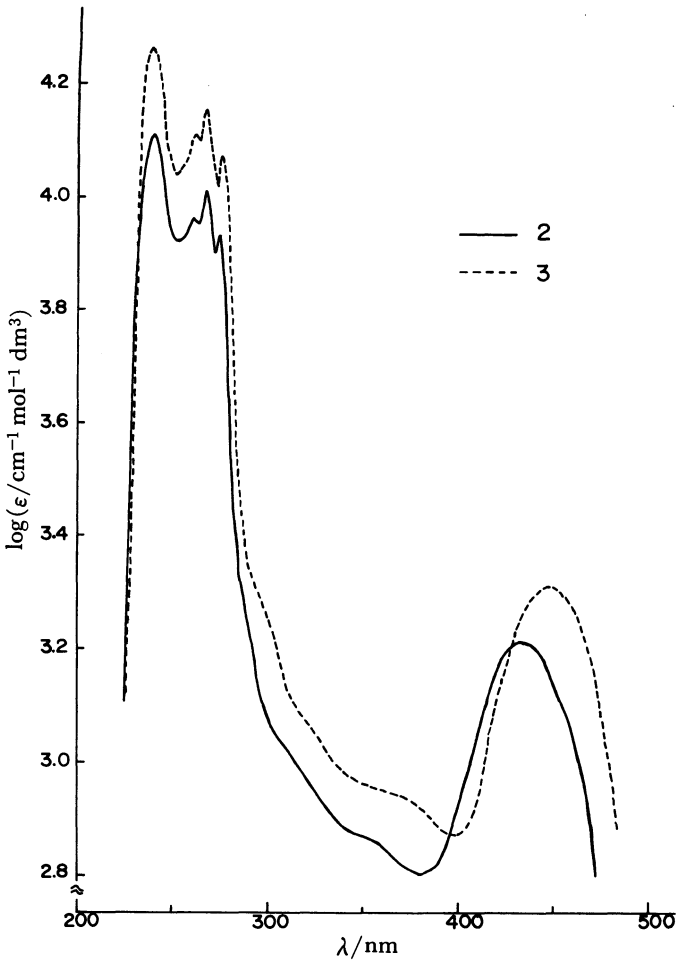

Fig. 1. The electronic absorption spectra of **2** and **3** complexes in dichloromethane.
2: $[\{(C_6H_5)_3PCH_2\}_3TeCl]Cl_3$. **3**: $[\{(C_6H_5)_3PCH_2\}_4Te]$-$Cl_4$.

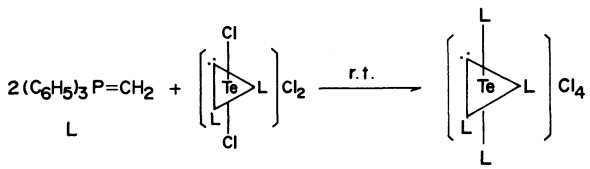

3

Scheme 3.

is shown in Fig. 1 and Experimental section. The absorption band at 435 nm or 447 nm can be assigned to the charge-transfer band. The absorption spectra[26] for phosphoranes did not show in the 400—500 nm region.

Chloro(methylene(or ethylidene-)triphenylphosphorane)diphenylselenium chloride (**9**, **10**) and bis(methylene(or ethylidene-)triphenylphosphorane)diphenylselenium dichloride (**11**, **12**) have been isolated from the reaction mixtures of diphenylselenium dichloride and methylene ylide (**L**) or ethylidenetriphenylphosphorane, $(C_6H_5)_3P=CH(CH_3)$ (**L'**), in the mole ratio 1:1 or 1:2.

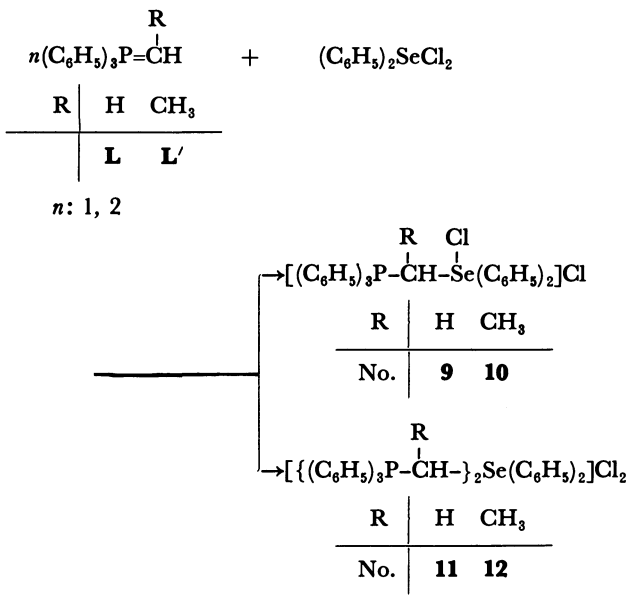

They are soluble in alcohols, dichloromethane, chloroform, water, DMSO and DMF, but insoluble in benzene and acetone. The ^{1}H NMR spectra of **9—12** could not be observed since compounds **9—12** are unstable in alcohols, dichloromethane and chloroform at −80 °C and give the corresponding phosphonium salt (**4**). However, their decomposition temperatures differ from the melting points of the ylides **L** and **L'** and salt **4**. Their color is white, and they are thermally stable in the solid state. The elemental analyses of **9—10** and **11—12** agreed with those of [(**L** or **L'**)Se(Cl)(C_6H_5)$_2$]Cl, and [(**L** or **L'**)$_2$Se(C_6H_5)$_2$]Cl_2, respectively. Thus, the ylides are bonded to the Se atom in the solid state such as complexes **6** and **7**.[3,4] The structures of diphenylselenium dibromide, (C_6H_5)$_2$$SeBr_2$[24] (**13**), and di(*p*-tolyl)selenium dibromide, (*p*-$CH_3C_6H_4$)$_2$-$SeBr_2$[24,25] (**14**), and the corresponding dichloride[24,25] have been found to be monomeric distorted tetrahedron by X-ray diffraction. The observed C–Se–C bond angles were ca. 110° and the observed X–Se–X bond angles were ca. 180°; therefore two halogen atoms are in the position *cis* for the lone pair. Thus, the chlorine atoms in diphenylselenium dichloride are substituted with ylides, and complexes **9—12** are formed. From the above, we suggest that the structure of **9—12** is a distorted tetrahedron as is shown in Scheme 4.

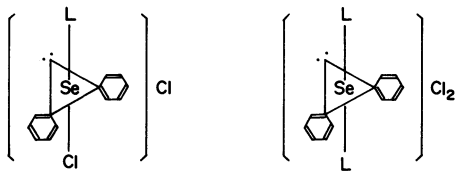

9 11

Scheme 4.

The different characteristics between tellurium complexes **1—3** and selenium compounds **9—12** are their colors and stabilities in solution. The color of tellurium complexes is yellow, but that of the selenium compounds is white. The tellurium complexes are stable in methanol and dichloromethane at room temperature, but the selenium compounds are unstable in alcohols and dichloromethane at −80 °C.

References

1) Part X: Ref. 2.
2) Y. Yamamoto and H. Konno, *Bull. Chem. Soc. Jpn.*, **59**, 1327 (1986).
3) Y. Yamamoto, *Bull. Chem. Soc. Jpn.*, **56**, 1772 (1983).
4) Y. Yamamoto, *Bull. Chem. Soc. Jpn.*, **55**, 3025 (1982).
5) Y. Yamamoto and H. Sugimoto, *Bull. Chem. Soc. Jpn.*, **53**, 3176 (1980).
6) Y. Yamamoto and Z. Kanda, *Bull. Chem. Soc. Jpn.*, **52**, 2560 (1979).
7) H. Schmidbaur, C. Zybill, C. Krüger, and H.-J. Kraus, *Chem. Ber.*, **116**, 1955 (1983).
8) N. Petragnani, J. V. Comasseto, R. Rodrigues, and T. J. Brocksom, *J. Organomet. Chem.*, **124**, 1 (1977).
9) N. Petragnani, R. Rodrigues, and J. V. Comasseto, *J. Organomet. Chem.*, **114**, 281 (1976).
10) T. Mukaiyama, S. Fukuyama, and T. Kumamoto, *Tetrahedron Lett.*, **1968**, 3787.
11) D. Seyferth and G. Singh, *J. Am. Chem. Soc.*, **87**, 4156 (1965).
12) N. Petragnani and M. de Moura Campos, *Chem. Ind. (London)*, **1964**, 1461.
13) Y. Yamamoto, *Bull. Chem. Soc. Jpn.*, **57**, 43 (1984).
14) Y. Yamamoto, *Chem. Lett.*, **1980**, 311.
15) H. Schmidbaur, *Acc. Chem. Res.*, **8**, 62 (1975).
16) Y. Yamamoto, *Bull. Chem. Soc. Jpn.*, **57**, 2835 (1984).
17) W. Richter, Y. Yamamoto, and H. Schmidbaur, *Chem. Ber.*, **110**, 1312 (1977).
18) R. Koster, D. Simic, and M. A. Grassberger, *Justus Liebigs Ann. Chem.*, **739**, 211 (1970).
19) Y. Yamamoto and H. Schmidbaur, *J. Organomet. Chem.*, **96**, 133 (1975).
20) Y. Yamamoto and H. Schmidbaur, *J. Organomet. Chem.*, **97**, 479 (1975).
21) A. W. Searcy, *J. Chem. Phys.*, **31**, 1 (1959).
22) D. P. Stevenson and V. Schomaker, *J. Am. Chem. Soc.*, **62**, 1267 (1940).
23) G. D. Christofferson and J. D. McCullough, *Acta Crystallogr.*, **11**, 249 (1958).
24) R. J. Gillespie, *Can. J. Chem.*, **39**, 318 (1961).
25) J. D. McCullough and R. E. Marsh, *Acta Crystallogr.*, **3**, 41 (1950).
26) L. Horner and H. Oediger, *Chem. Ber.*, **91**, 437 (1958).
27) H. Schmidbaur, H. Stühler, and W. Vornberger, *Chem. Ber.*, **105**, 1084 (1972).

 © 1986 The Chemical Society of Japan Bull. Chem. Soc. Jpn., 59, 3057—3061 (1986)

Spectrophotometric Determination of Micro Amounts of Pentathionate via Permanganate Reaction

Yasuyuki MIURA* and Tomozo KOH
Department of Chemistry, Faculty of Science, Tokai University, 1117, Kitakaname, Hiratsuka, Kanagawa 259-12
(Received March 20, 1986)

A method has been developed for the determination of micro amounts of pentathionate. It is based on the reaction of pentathionate with a given amount of permanganate in a dilute sulfuric acid medium and on the spectrophotometric measurement of iodine as triiodide, which is formed by the oxidation of iodide with an excess of permanganate. The analytical conditions were established by varying the temperature, reaction time, and amounts of sulfuric acid and permanganate. The present method can be successfully applied to a determination of pentathionate in the range 2×10^{-7} to 1.4×10^{-5} mol dm^{-3} (0.5—35.9 μg $S_5O_6^{2-}$ in 10 cm^3) and gives a higher sensitivity than any previous method without solvent extraction. In eleven determinations for 10 cm^3 sample solutions containing 0.080 μmol of pentathionate, the present method gave a mean value of 0.080 μmol, with a standard deviation of 0.0006 μmol and a relative standard deviation of 0.75%.

A simple, accurate and sensitive determination of polythionates (tri-, tetra-, penta-, and hexathionate) is increasingly desirable from the viewpoint of sulfur chemistry. When polythionates react with cyanide, sulfite, hydroxide or mercury(II) thiocyanate, thiocyanate or thiosulfate (or both species equivalent to each of polythionates) is formed. Thiocyanate and thiosulfate can easily be measured spectrophotometrically with iron(III) and iodine, respectively. Therefore, various investigations have been made concerning the cyanolysis,[1-7] the sulfitolysis,[8-11] the alkaline decomposition[12,13] and the mercury(II) thiocyanate reaction[14] of polythionates and have led to the development of spectrophotometric methods for the determination of polythionates at concentrations as low as the 10^{-4} mol dm^{-3} level. Moreover, a sensitive method has been proposed for the determination of tetra-, penta-, and hexathionate, based on the solvent extraction of thiocyanate formed by their cyanolysis as an ion pair with Methylene Blue.[15] The cyanolysis and sulfitolysis of polythionates have also played a critical role in the development of methods for the analysis of mixtures of polythionates[16-20] as well as mixtures of sulfite, thiosulfate and each of the polythionates.[8-11] High-performance liquid chromatography (HPLC)[21-25] has been used for the separation of mixtures of polythionates. Takano et al.[24] sulfitolyzed polythionates prior to HPLC separation and determined even tri- and tetrathionate in mixtures with the other polythionates (which can not be separated chromatographically).

In a previous paper,[26] the present authors devised a sensitive method for the determination of thiocyanate up to 4×10^{-5} mol dm^{-3}; it was based on the consumption of permanganate by its reaction with thiocyanate in an acid medium. It has been found that pentathionate is also oxidized by permanganate. No consideration was given to the spectrophotometric determination of polythionates by means of their reactions with permanganate. In the present study, the optimal conditions under which pentathionate can be oxidized quantitatively by permanganate were established. The proposed method is based on the reaction of pentathionate with a given amount of permanganate in dilute sulfuric acid and on the spectrophotometric measurement of any formed iodine (as triiodide) after a reaction of excess permanganate with iodide to form iodine.

Experimental

Apparatus. All spectrophotometric measurements were made at 350 nm using a Shimadzu Model UV-240 recording spectrophotometer with 10-mm quartz cells. Desired temperatures were controlled by a Taiyo Coolnit Model CL-15 thermoregulator. In all the experiments, redistilled water was used, which was freed from any permanganate-consuming impurities with a Nippon Millipore, Ltd., Model Milli-QII apparatus.

Reagents. All chemicals were of analytical grade and were used without further purification.

Potassium pentathionate. Potassium pentathionate was prepared as described by Goehring and Feldmann.[27] The obtained pentathionate ($K_2S_5O_6\cdot1.5H_2O$) was recrystallized twice in an acid medium of 0.5 mol dm^{-3} hydrochloric acid, and then dried at room temperature before storage at -10 ± 2°C. The pentathionate was confirmed to be sufficiently pure for the present purpose; its purity was estimated by the sulfitolysis method[10] to be 92.5% as $K_2S_5O_6$.

Standard Pentathionate Solution. A 1×10^{-3} mol dm^{-3} pentathionate solution was prepared by dissolving 180.8 mg of potassium pentathionate in water and diluting to 500 cm^3. The stock solution of 1×10^{-3} mol dm^{-3} standard pentathionate could be used for at least four months without any measurable changes as long as it was stored at 5 ± 2°C. The working solution was prepared by suitable dilution.

Standard Permanganate Solution.[28] A 0.02 mol dm^{-3} permanganate solution was prepared by heating a potassium permanganate solution to boiling, keeping it at a temperature slightly below the boiling point for 1 h, and then allowing it to stand for 3 d at room temperature. After manganese dioxide had been filtered off by suction with a sintered glass filter (3SG4), the filtrate was standardized by titration with standard sodium oxalate. The stock solution of 0.02 mol dm^{-3} standard permanganate proved to be stable; even after six months, no measurable change was found by the present method when it was stored at room temperature in the dark. A working solution of 2×10^{-4} mol dm^{-3} permanganate

could be used for 2 d.

Standard Thiosulfate Solution. A 0.1 mol dm^{-3} thiosulfate solution was prepared by dissolving sodium thiosulfate pentahydrate in freshly boiled and cooled water containing a small amount of sodium carbonate as a stabilizer. The thiosulfate solution was standardized by iodimetry a week after preparation. A 5×10^{-4} mol dm^{-3} thiosulfate solution was obtained by diluting the standardized thiosulfate solution.

Iodide Solution. A 0.5 mol dm^{-3} iodide solution was prepared by dissolving 41.7 g of potassium iodide in water containing 200 mg of sodium carbonate as a stabilizer and by then diluting it to 500 cm^3.

Recommended Procedure. A mixture of 1.5 cm^3 of 1 mol dm^{-3} sulfuric acid and 4 cm^3 of 2×10^{-4} mol dm^{-3} standard potassium permanganate solution was placed in a 25 cm^3 volumetric flask. To this mixture, 10 cm^3 of a sample solution containing pentathionate up to 0.140 μmol was added. The mixture was then allowed to stand for 20 min at temperatures ranging from 5 to 40 °C to complete the oxidation of pentathionate. Then, 1 cm^3 of 0.5 mol dm^{-3} potassium iodide was added to form iodine equivalent to excess permanganate, and 3 cm^3 of 5×10^{-4} mol dm^{-3} sodium thiosulfate was added to decrease the absorbance of the iodine as triiodide to an appropriate value, otherwise the absorbance for the reagent blank becomes so high as much as 1.94. The flask was filled to the mark with water. The absorbance of a solution of the triiodide complex, thus formed, was measured against water at 350 nm about 5 min after the dilution.

A permanganate-free reagent blank was prepared by adding 1.5 cm^3 of 1 mol dm^{-3} sulfuric acid, 14 cm^3 of water in place of both 4 cm^3 of 2×10^{-4} mol dm^{-3} permanganate and 10-cm^3 of a sample solution containing pentathionate, and 1 cm^3 of 0.5 mol dm^{-3} iodide in a 25-cm^3 volumetric flask. After the flask had been filled to the mark with water, the absorbance was measured against water at 350 nm after about 5 min. This absorbance value was subtracted from each of the absorbances for pentathionate and the reagent blank, for iodide is susceptible to air-oxidation in an acid medium.

Results and Discussion

Reaction of Pentathionate with Permanganate. In order to determine the stoichiometric relationship between pentathionate and permanganate in an acid medium, the reaction was investigated by the molar-ratio method. For the application of this method, 4 cm^3 of permanganate with various molar concentrations and 10-cm^3 of each of 0.3×10^{-5}, 0.6×10^{-5}, 1×10^{-5} and 1.4×10^{-5} mol dm^{-3} pentathionate solutions were used with varying the molar ratio of permanganate to pentathionate. Pentathionate was allowed to react with permanganate for 20 min, where sodium thiosulfate was not added. The results are shown in Fig. 1. When straight portions of each graph were extrapolated, each line (dotted lines) intersected the abscissa at a point of 3.5. This fact proves that 2 mol of pentathionate reacted exactly with 7 mol of permanganate under the conditions of the recommended procedure.

Calibration Plots. Figure 2 shows the calibration graphs obtained by treating a series of standard solutions of pentathionate according to the recommended procedure, and the plots obtained by treating a series of standard permanganate solutions according to the recommended procedure except that 4 cm^3 of redistilled water was used instead of 4 cm^3 of 2×10^{-4} mol dm^{-3} permanganate. The graph for permanganate was prepared to confirm the stoichiometry and the completion

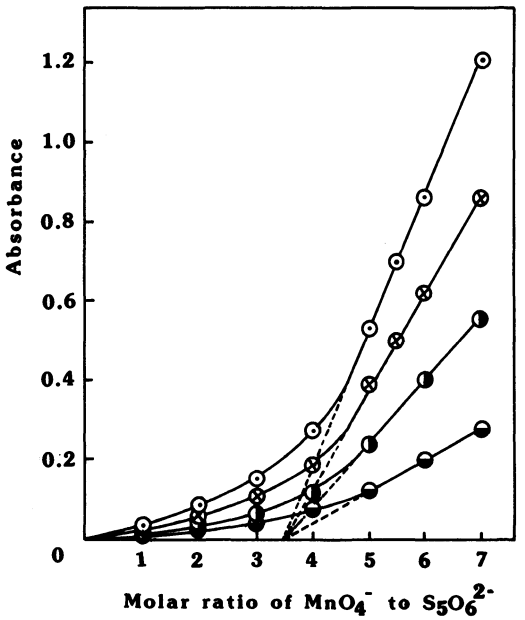

Fig. 1. Molar ratio plots for the reaction of pentathionate with permanganate.
⊙: 1.4×10^{-5} mol dm^{-3} $S_5O_6^{2-}$, ⊗: 1×10^{-5} mol dm^{-3} $S_5O_6^{2-}$, ◑: 0.6×10^{-5} mol dm^{-3} $S_5O_6^{2-}$, ◒: 0.3×10^{-5} mol dm^{-3} $S_5O_6^{2-}$.

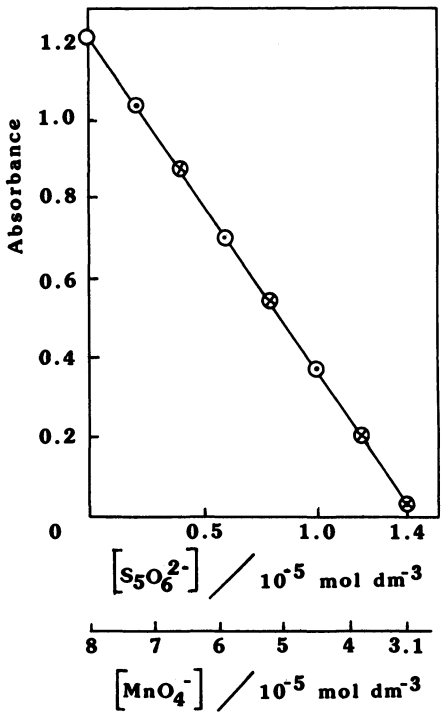

Fig. 2. Calibration plots.
○: Reagent blank, ⊙: $S_5O_6^{2-}$, ⊗: MnO_4^- (expected value).

of the reaction of pentathionate with permanganate. As described above, if 2 mol of pentathionate reacts with 7 mol of permanganate stoichiometrically, the graph for pentathionate should coincide with that for permanganate (the expected graph). Figure 2 proves that the reaction proceeded to stoichiometric completion under the conditions of the recommended procedure.

The precision was estimated from eleven results for 10-cm^3 aliquots of a solution containing 0.080 μmol of pentathionate. The present method gave a mean value of 0.080 μmol, with a standard deviation of 0.0006 μmol and a relative standard deviation of 0.75%. This method gives a higher sensitivity than previous methods without any need for solvent extractions.

Rate of Reaction of Pentathionate with Permanganate. The reaction rate was investigated at temperatures ranging from 5 to 40°C. The amounts of the reagents and the addition order were the same as in the above procedure. The results are given in Table 1. The reaction was gradually accelerated by an increase in the temperature. The absorbances for 1.2×10^{-5} mol dm^{-3} pentathionate reached those for 3.8×10^{-5} mol dm^{-3} permanganate, which are the expected values, in 20 min at 5°C, in 10 min at 10 and 20°C, in 5 min at 30°C and in 3 min at 40°C, and then kept constant until 60 min had passed. These facts confirm that the reaction proceeds to completion as long as the reaction is carried out for 20 min at temperatures of 5 to 40°C. On the other hand, when pentathionate was allowed to react with permanganate in a low-acidity solution using 1.5 cm^3 of 0.6 mol dm^{-3} sulfuric acid, the reaction did not proceed to completion. Therefore, the effect of acidity was investigated at 20°C. The results are shown in Table 2.

Table 1. Reaction Rate of Pentathionate with Permanganate at Various Temperatures

t / min	Absorbance of I_3^- (350 nm)				
	1.2×10^{-5} mol dm^{-3} $S_5O_6^{2-}$				
	5°C	10°C	20°C	30°C	40°C
	0.206[a]	0.205[a]	0.205[a]	0.206[a]	0.204[a]
1	0.249	0.243	0.242	0.231	0.229
3	0.237	0.235	0.236	0.221	0.203
5	0.226	0.225	0.222	0.211	0.205
10	0.218	0.210	0.206	0.206	0.203
20	0.208	0.205	0.205	0.208	0.204
30	0.203	0.203	0.204	0.205	0.203
45	0.203	0.204	0.205	0.203	0.205
60	0.204	0.205	0.203	0.205	0.204

a) Absorbances for 3.8×10^{-5} mol dm^{-3} permanganate which are expected values.

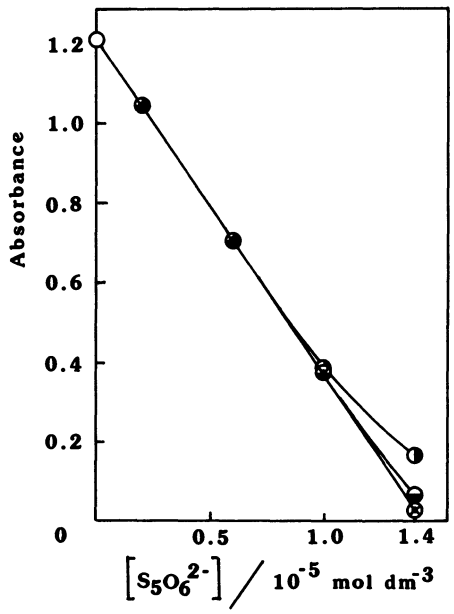

Fig. 3. Effect of amounts of permanganate on the reaction with pentathionate.
○: Reagent blank, ◑: $S_5O_6^{2-}$ with 2.5 cm^3 of 2×10^{-4} mol dm^{-3} MnO_4^-, ◒: $S_5O_6^{2-}$ with 3.0 cm^3 of 2×10^{-4} mol dm^{-3} MnO_4^-, ⊗: $S_5O_6^{2-}$ with 3.5, 4.0, or 4.5 cm^3 of 2×10^{-4} mol dm^{-3} MnO_4^-, ⊙: $S_5O_6^{2-}$ obtained under the conditions of the recommended procedure.

Table 2. Effect of Various Amounts of Sulfuric Acid on the Reaction of Pentathionate with Permanganate at 20°C

t / min	Absorbance of I_3^- (350 nm)			
	1.2×10^{-5} mol dm^{-3} $S_5O_6^{2-}$			
	0.6 mol dm^{-3} H_2SO_4	0.8 mol dm^{-3} H_2SO_4	1 mol dm^{-3} H_2SO_4	2 mol dm^{-3} H_2SO_4
	0.207[a]	0.205[a]	0.207[a]	0.204[a]
1	0.261	0.250	0.242	0.248
3	0.243	0.240	0.236	0.238
5	0.229	0.227	0.222	0.223
10	0.224	0.208	0.206	0.209
20	0.222	0.203	0.205	0.208
30	0.220	0.204	0.204	0.209
45	0.220	0.205	0.205	0.207
60	0.218	0.207	0.203	0.205

a) Absorbances for 3.8×10^{-5} mol dm^{-3} permanganate which are expected values. The volume of sulfuric acid used was 1.5 cm^3.

Table 3. Effect of Diverse Ions

Foreign ion	Added as	Amount μg	Amount of $S_5O_6^{2-}$ found μg	Error %	Foreign ion	Added as	Amount μg	Amount of $S_5O_6^{2-}$ found μg	Error %
None			20.5		Cr^{3+}	$Cr(NO_3)_3 \cdot 9H_2O$	500	20.4	−0.5
Na^+	Na_2SO_4	10000	20.6	0.5	F^-	NaF	30000	20.5	0
K^+	K_2SO_4	10000	20.6	0.5	Cl^-	NaCl	10000	20.5	0
NH_4^+	$(NH_4)_2SO_4$	10000	20.5	0	Br^-	KBr	500	20.6	0.5
Mg^{2+}	$Mg(NO_3)_2 \cdot 6H_2O$	10000	20.5	0	I^-	KI	100	20.5	0
Ca^{2+}	$Ca(NO_3)_2 \cdot 4H_2O$	10000	20.5	0	NO_3^-	KNO_3	10000	20.6	0.5
Zn^{2+}	$ZnSO_4 \cdot 7H_2O$	10000	20.5	0	NO_2^-	KNO_2	1	20.7	1.0
Cd^{2+}	$Cd(OAc)_2 \cdot 2H_2O$	10000	20.6	0.5			1000[b]	20.2	−1.5
Mn^{2+}	$MnSO_4 \cdot 5H_2O$	50	20.5	0	CO_3^{2-}	Na_2CO_3	10000	20.5	0
Co^{2+}	$CoSO_4 \cdot 7H_2O$	10000	20.5	0	S^{2-}	$Na_2S \cdot 9H_2O$	0.1	20.6	0.5
Ni^{2+}	$NiSO_4 \cdot 6H_2O$	10000	20.5	0	HSO_3^-	$NaHSO_3$	1	20.7	1.0
Cu^{2+}	$CuSO_4 \cdot 5H_2O$	1000	20.1	−2.0	$S_2O_3^{2-}$	$Na_2S_2O_3 \cdot 5H_2O$	0.1	20.6	0.5
Pb^{2+}	$Pb(NO_3)_2$	1000	20.1	−2.0	$H_2PO_4^-$	$NaH_2PO_4 \cdot 2H_2O$	10000	20.5	0
Fe^{2+}	$FeSO_4 \cdot 7H_2O$	1	20.8	1.5	Borate ion	H_3BO_3	10000	20.6	0.5
Fe^{3+}	$Fe(NO_3)_3 \cdot 9H_2O$	1	20.5	0	Silicate ion	(as SiO_2)	10000	20.5	0
		1000[a]	20.2	−1.5	OAc^-	$NaOAc \cdot 3H_2O$	10000	20.6	0.5
Al^{3+}	$Al(NO_3)_3 \cdot 9H_2O$	10000	20.5	0	$H_2NSO_3^-$	$HOSO_2NH_2$	5000	20.5	0

a) Three cm^3 of 0.5 mol dm^{-3} NaF was added. b) One cm^3 of 0.05 mol dm^{-3} sulfamic acid was added.

The absorbances for 1.2×10^{-5} mol dm^{-3} pentathionate coincided with the expected value in 10 min with respect to 1.5 cm^3 of each of 0.8, 1, and 2 mol dm^{-3} sulfuric acid, and then remained constant. Consequently, 1.5 cm^3 of 1 mol dm^{-3} sulfuric acid was employed in this experiment.

Effect of Amounts of Permanganate. For measuring the effect of amounts of permanganate, pentathionate was allowed to react with various amounts of potassium permanganate for 20 min at 20 °C. In this experiment, thiosulfate, which is used in order to reduce the absorbance in the recommended procedure, was not added. The absorbance, therefore, increased with increasing amounts of permanganate employed. The resulting graphs given in Fig. 3 were normalized in such way that each calibration graph for pentathionate with various amounts of permanganate was permitted to shift in parallel fashion to cause each reagent blank to accord with that obtained under the conditions of the recommended procedure. When 2.5 and 3 cm^3 of 2×10^{-4} mol dm^{-3} permanganate were used, the reaction did not go to completion because the amounts of permanganate were insufficient; even in this case, the reagent blank gave high absorbances of 1.215 and 1.453, respectively. When 3.5, 4.0, or 4.5 cm^3 of the permanganate solution were used, the graphs for pentathionate yielded a straight line and coincided exactly with that obtained under the conditions of the recommended procedure. Consequently, 4 cm^3 of 2×10^{-4} mol dm^{-3} permanganate was employed, and 3 cm^3 of 5×10^{-4} mol dm^{-3} thiosulfate was added to decrease the reagent blank to an appropriate value by reducing the iodine formed.

Effect of Diverse Ions. A 10-cm^3 portion of a solution containing 20.5 μg of pentathionate and various amounts of diverse ions was treated exactly as in the recommended procedure. For the determination of pentathionate with an error of below 2% by the present method, foreign ions can be tolerated at the levels given in Table 3. Iron(II), nitrite, thiosulfate, sulfide, and sulfite gave positive errors, even when present in trace amounts, because they reduce permanganate. However, the interference of nitrite could be eliminated by decomposing it with sulfamic acid. Iron(III) gave a negative interference in amounts of 10 μg because it oxidizes iodide to form iodine, but its interference was removed by masking with fluoride. Trithionate gave a very weak interference, but tetrathionate and hexathionate gave strong interferences with the determination of pentathionate because they also were oxidized by permanganate.

References

1) P. J. Urban, *Z. Anal. Chem.*, **179**, 422 (1961).
2) T. Koh, A. Wagai, and Y. Miura, *Anal. Chim. Acta*, **71**, 367 (1974).
3) O. A. Nietzel and M. A. DeSesa, *Anal. Chem.*, **27**, 1839 (1955).
4) P. J. Urban, *Z. Anal. Chem.*, **180**, 110 (1961).
5) T. Koh and I. Iwasaki, *Bull. Chem. Soc. Jpn.*, **39**, 352 (1966).
6) T. Koh, *Bull. Chem. Soc. Jpn.*, **38**, 1510 (1965).
7) T. Koh and I. Iwasaki, *Bull. Chem. Soc. Jpn.*, **38**, 2135 (1965).
8) I. Iwasaki and S. Suzuki, *Bull. Chem. Soc. Jpn.*, **39**, 576 (1966).
9) T. Koh, K. Taniguchi, Y. Miura, and I. Iwasaki, *Nippon Kagaku Kaishi*, **1979**, 348.
10) T. Koh, K. Taniguchi, and I. Iwasaki, *Bull. Chem. Soc. Jpn.*, **51**, 164 (1978).
11) T. Koh and K. Taniguchi, *Anal. Chem.*, **46**, 1679 (1974).
12) Y. Miura and T. Koh, *Nippon Kagaku Kaishi*, **1983**,

1597.
13) Y. Miura, *Bunseki Kagaku*, **33**, 537 (1984).
14) Y. Miura and T. Koh, *Anal. Chem.*, **52**, 1855 (1980).
15) T. Koh, N. Saito, and I. Iwasaki, *Anal. Chim. Acta*, **61**, 449 (1972).
16) T. Koh and I. Iwasaki, *Bull. Chem. Soc. Jpn.*, **39**, 703 (1966).
17) T. Koh and K. Taniguchi, *Anal. Chem.*, **45**, 2018 (1973).
18) D. P. Kelly, L. A. Chambers, and P. A. Trudinger, *Anal. Chem.*, **41**, 898 (1969).
19) T. Mizoguchi and T. Okabe, *Bull. Chem. Soc. Jpn.*, **48**, 1799 (1975).
20) T. Koh, Y. Aoki, and I. Iwasaki, *Analyst*, **104**, 41 (1979).
21) J. N. Chapman and H. R. Beard, *Anal. Chem.*, **45**, 2268 (1973).
22) A. W. Wolkoff and R. H. Larose, *Anal. Chem.*, **47**, 1003 (1975).
23) R. N. Reeve, *J. Chromatogr.*, **177**, 393 (1979).
24) B. Takano, M. A. McKibben, and H. L. Barnes, *Anal. Chem.*, **56**, 1594 (1984).
25) S. B. Rabin and D. M. Stanbury, *Anal. Chem.*, **57**, 1130 (1985).
26) Y. Miura and T. Koh, *Bull. Chem. Soc. Jpn.*, **59**, 741 (1986).
27) M. Goehring and U. Feldmann, *Z. Anorg. Chem.*, **257**, 223 (1948).
28) I. M. Kolthoff, E. B. Sandell, E. J. Meehan, and S. Bruckenstein, "Quantitative Chemical Analysis," 4th ed., Macmillan Company, London (1969), p. 825.

 © 1986 The Chemical Society of Japan Bull. Chem. Soc. Jpn., 59, 3063—3066 (1986)

Trachit Change of the $ZrSiO_4$ Single Crystal During Crystal Growth Studied by the $Na_2O \cdot 3V_2O_5$ Flux Method

Masumi USHIO* and Yoshihiro SUMIYOSHI
Department of Applied Chemistry, Faculty of Engineering, Gunma University, Tenjin-cho, Kiryu 376
(Received April 3, 1986)

The appearance and disappearance of the crystal faces of the $ZrSiO_4$ single crystal during crystal growth under the conditions of a growth temperature of 900 °C and a Δt value (temperature difference) of 1 °C have been studied by means of the $Na_2O \cdot 3V_2O_5$ flux method. A spherical seed prepared from a natural zircon single crystal was used. The c{001}, a{100}, and m{110} appeared at the earliest stage, and next appeared r{115}, u{015}, p{111}, e{011}, and q{021} after 20 h of growth time. However, the u-face, r-face, and q-face disappeared after 400 h, and the c-face and a-face began to disappear after 500 h. The final morphology after 1400 h was a first-order prism and a pyramid consisting of only the m-face and the p-face. It was found that the m-face and the p-face were dominant on a flux-grown $ZrSiO_4$ single crystal, and that this tendency was unchangeable after 2500 h.

$ZrSiO_4$ (zircon) is a widely distributed accessory mineral in ogneous rocks. Ushio et al.[1] have reported the growth of the $ZrSiO_4$ single crystal by means of the $Na_2O \cdot 3V_2O_5$ flux method, using a natural zircon seed, the growth rate with the time; the normal growth rates of the c-face, the a-face, the p-face, and the m-face; the growth patterns on the p-face and the m-face; the step-advanced rates of the growth layers on the p-face and the m-face, etc. In this crystal-growth procedure, when a spherical seed was used, the trachit change in the crystal face was observed according to the increase in the growth time. An attempt to reproduce this interesting phenomenon is elucidated in detail.

The trachit change in a crystal may be caused by the different rates of growth of the various faces. A large number of factors can affect the trachit change of a crystal, e.g., the type of solvent, the pH of the solution, the degree of supersaturation or supercooling, the temperature of the crystal growth, the presence of impurities, the rate of cooling, the degree of agitation, the presence of a surface-active agent (surfactant), the flow of solution, the presence of defects (dislocation, twinning, and so on.), the growth time, and frequency and intensity of applied ultrasonic waves.[2]

In this paper, the purpose is to investigate, in detail, the trachit change in the crystal face of a zircon crystal in the initial, intermediate, and final stages, when the zircon crystals are grown slowly by means of the $Na_2O \cdot 3V_2O_5$ flux method using of natural spherical seeds.

Experimental

The experimental apparatus and the configurations of the crucible were previously reported.[1] The inner volume of the platinum crucible was ca. 400 ml, and natural zircon single crystals from Viet Nam and Brazil were used as seeds. There was no difference between the two crystals except for the number of cracks and their colors. The natural zircon single crystals were cut and their surfaces polished to a spherical form close to a true sphere about 5 mm in diameter.

The starting materials of oxides (V_2O_5, ZrO_2, and SiO_2) and a carbonate (Na_2CO_3), used as flux and nutrient, were used as the first-class reagents.

Runs were carried out under the conditions of 900 and 1000 °C for growth temperature (near the upper part of the nutrient) and 0.5 to 5 °C for Δt, which signifies the temperature difference between the seed and the upper part of the nutrient. The growth temperature, the supersaturation, and, especially, the growth time may have a influence on the trachit change in the crystal surface. For this reason, these factors have been controlled electrically as much as possible.

A 800 g portion of the flux and 120 g of the nutrient were charged into the platinum crucible. After confirming the saturation by the nutrient dissolved into the flux melt, a spherical seed tied up with a platinum wire was inserted into the flux melt. The growing seed was pulled up from the flux melt after having soaked for the fixed growth time, and then washed a hot alkaline solution and acid to dissolve the flux solid adhering to the seed surface. After observing the crystal surface of the growing seed with microscopes, this seed was again soaked in the melt. This procedure of inserting the seed into the flux melt and then pulling it, was repeated 30 times.

To identify the grown crystal faces of the zircon seed, an inclination-angle microscope and a scanning electron microscope were used. The former was used mainly to measure the angle between the two grown crystal faces of zircon seed, but also to confirm the existence and shape of the grown crystal faces.

Results

A run carried out under the conditions of a growth temperature of 900 °C and a temperature difference of 1 °C will now be described.

After 20 h of growth time, c{001} appeared in the neighborhood of poles, and a{100} and m{110} in the equator, but at this early stage, all the faces developed as flats and did not yet come into contact with one another. Small pyramid faces of r{115}, u{015}, e{011}, and then q{021} appeared between the c-face and the m- or a-faces.

After 50 h, pairs of faces, namely, the c-face and the r-face, the c-face and the u-face, the p-face and the w-face, the e-face and the q-face, the w-face and the m-face, and the q-face and the a-face, came into contact with each other, and then, appearance marked each step. At the growth time between 120 and 250 h, two groups of steps consisting of c-u-e-faces and c-r-p-faces were observed. However, the u-face and the r-face, the e-face

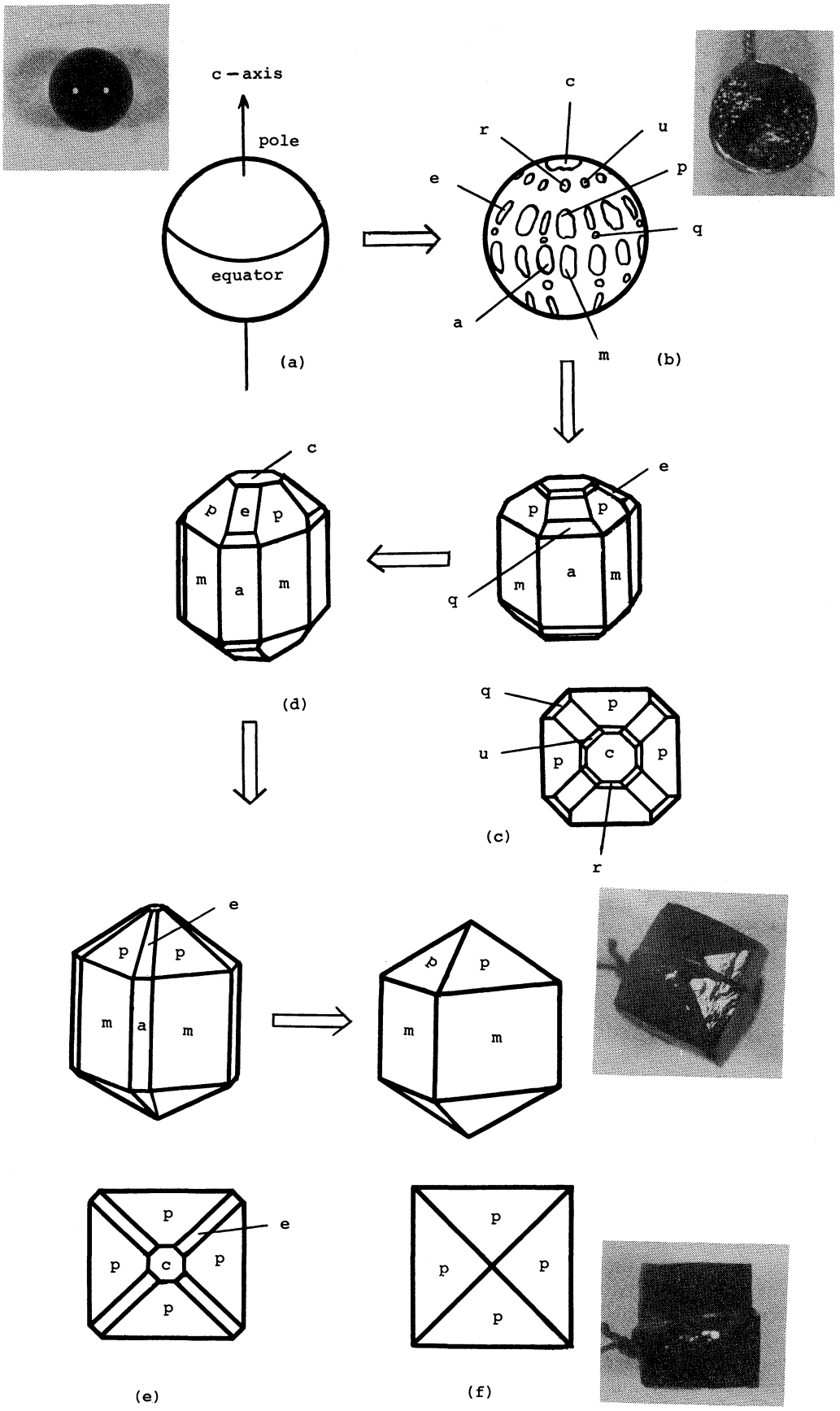

Fig. 1. Schematic drawing of appearance and disappearance of crystal faces during growth.
(a): Spherical seed. (b): after growth time between 20 and 100 h. (c): after 300 to 400 h. (d): 500 to 700 h. (e): after 900 to 1200 h. (f): after above 1400 h.

Table 1. Experimental Results of Interfacial Angle of Grown Zircon Xrystal

Angle between two faces	$Angle_{obsd}$
r{115}∧m{110}	79±0.5°
p{111}∧m{110}	45±0.5°
w{221}∧m{110}	29±0.5°
u{015}∧ a{100}	82±0.5°
e{011}∧ a{100}	57±0.5°
q{201}∧ a{100}	38±0.5°
e{011}∧e'{011}	46±0.5°
p{111}∧p'{111}	57±0.5°

and the p-face, and the m-face and the a-face did not make contact with each other.

After 300 h, the crystal domain of both c-u-e-faces and c-r-p-faces got much bigger, and the lateral faces of the a-face and the m-face came into contact with each other. The u-face, the r-face, the q-face, and the w-face disappeared after 400 h, while the c-face, the e-face, and the p-face grew further.

After 500 h, the p-face and the e-face were observed as pyramid faces, but the crystal-surface domain of the p-face was better developed than that of the e-face. After 700 h, the c-face and the a-face began to disappear. The e-face was also found to disappear.

After 900 h, only the p-face as a pyramid face and m-face as a lateral face grew much larger. The very small c-face, the e-face, and the a-face still remained, but these faces disappeared as growth went on.

The morphology after 1400 h was a first-order prism and a pyramid consisting of only the m-face and the p-face. The grown seed was elongated only in the direction of the *c*-axis after 2000 h and was bounded with the same faces. It was found that the m-face, and the p-face were dominant on the flux-grown $ZrSiO_4$ single crystal, and that this tendency was unchangeable after 2500 h.

A schematic drawing of the trachit changes during the growth of the $ZrSiO_4$ single crystal is shown in Fig. 1, while experimental results of the interfacial-angle measurements given in Table 1.

In the case a growth temperature of 1000°C, each face appeared and disappeared much faster than was the case at 900°C, while in the case of the same growth temperature, e.g., at 900°C, the increasing temperature difference had a tendency to promote the growth rate of each face.

Discussion

As has been mentioned above, the habit and trachit changes of a crystal are influenced by various factors.

The crystal faces most frequently observed in the natural zircon single crystal were c{001} as a basal face, m{110} and a{100} as prisms, and p{111}, u{331}, x{311} and e{011} as pyramids.[3]

By using a spherical and natural zircon single crystal as a seed, a basal c-face and prisms of the a-face and the m-face near the equator appeared mainly in the earliest stage, and then c-r-p-m-faces and c-u-q-a-faces appeared between the pole and the equator of a spherical seed. These faces made several flights of steps. Among these faces, the growth rate increase of the u-face, the r-face, and the q-face was much faster, and these faces also disappeared much faster. Judging from the experimental results on the order of disappearance, the u-face and the r-face disappeared almost simultaneously, and after a while the q-face disappeared. Then surface of the c-face became apparantly rough, and finally disappeared. The final crystal form was bounded by the p-face as a pyramid and the m-face as a prism in this experimental range. These faces were a prism and a pyramid of the first order. An a-face, etc., forming a prism and the pyramid faces of the second order disappeared. No w-face formed between the p-face and the m-face was observed because of the very high growth rate. A w-face belongs to the pyramid of the first order. Pyramid faces of the second order, e.g., the e-face, the u-face, and the q-face, remained from 900 to 1200 h.

From a stereographic projection for a crystal of zircon, a continuous series of steps of the c-u-e-q-a-faces would be observed in the direction of the *a*-axis if each face appeared, and we could expect a continuous series of steps of the c-r-p-w-m-faces to appear in the direction inclined at 30°C from the *a*-axis. No x-face was observed because of the higher growth rate.

Hartman[4] reported the morphology of zircon by applying the periodic-bond-chain theory, and calculated the lattice energy and the attachment energies of several faces. He concluded that, if it was assumed that the displacement velocities of the F-faces were proportional to the attachment energies, a "theoretical habit" of zircon crystals was bounded by two forms only: a{100} and e{011}.

These faces produced an "equilibrium form" and were a second-order prism and a pyramid. However, as has been stated previously, the "growth form" of the zircon single crystal prepared in this experiment was bounded by the first-order prism and pyramid faces, i.e, m{110} and p{111}. In comparison with the Kombinationspersistenz (*P*-value) and the Fundortspersistenz (*F*-value),[4,5] it was found that these values of crystal faces producing both forms, e.g., the equlibrium and growth forms, were relatively closer than those of the other faces. For this reason, it may be assumed that the ease of formation of both forms is influenced by the environmental conditions surrounding a zircon crystal, e.g., the kinds of the solute and the solvent and growth temperature.

From Hartman's result from the calculation of the attachment energies of the crystal faces of zircon by using the electrostatic energy, the order of attachment energy was found to be follows:

$$a\{100\} < m\{110\} < e\{011\} < p\{111\} < c\{001\}$$

The attachment energy of a {100} was the smallest one, m{110} ranked second, and so on. The F-face (flat face) is a{100}, m{110}, e{011}, if we considers the P.B.C vector numbers. It is possible that a F-face has a higher attachment energy than a S-face (stepped face) has. The c-face, the u-face, the r-face, the p-face, the m-face, and the a-face were observed in the initial stage of crystal growth, but trachit change was observed with the crystal growth proceeding and only the p-face and m-face were finally observed. In this experimental result, the growth form of zircon single crystal was a tetragonal prism with a bipyramid, bounded by the p-face and the m-face only. From these experimental findings concerning the appearance and disappearance of each face from the observed normal growth rates, the order of the normal growth rate for each face of zircon single crystal was determine to be as follows:

$$a\{100\} > c\{001\} > p\{111\} > m\{110\}$$

The observed value of the normal growth rate of the a-face was $5.0—7.0\times10^{-4}$ mm h^{-1}; the c-face, $2.0—3.5\times10^{-4}$ mm h^{-1}; the p-face, $1.2—2.0\times10^{-4}$ mm h^{-1}, and the m-face, $0.9—1.0\times10^{-4}$ mm h^{-1}.[1] From this fact, when a spherical crystal was used as a seed, the pyramid face appeared mainly in the initial stage, but almost disappeared in the intermediate stage because of the higher growth rates. A c-face as a basal face appeared mainly in the initial stage and remained until the final stage, but soon disappeared. Therefore, a normal growth rate for each face can be presumed to be one in which the trachit of growth in the zircon single crystal changes.

A small zircon single crystal grown by spontaneous nucleation formation at the bottom or on the wall of the crucible was bounded by the m-face and the p-face, which grew progressively greater, and by very small faces, e.g., the a-face, the q-face, and the c-face. At the bottom of the crucible, the growth rate of the zircon single crystal was usually slower in order to have a small temperature difference and a small convection velocity of the flux melt. Therefore, it was expected that a zircon single crystal was grown by a phenomenon close to the diffusion process. Small crystal faces of the a-face, the q-face, the c-face, etc. may remain without disappearing.

A process in which the solute molecule is carried to a seed by heat convection and incorporated in a seed surface may occur, but the process in which the solute is carried by a phenomenon close to heat convection, and therefore a seed grows, may more probably be expected.

References

1) M. Ushio and Y. Nishitani, *Nippon Kagaku Kaishi*, **1982**, 756.

2) D. Elwell and H. J. Schell,"Crystal Growth from High Temperature Solutions," Academic Press., New York (1975), p. 202.

3) E. S. Dana and W. E. Ford, "A Textbook of Mineralogy," John Wiley and Sons, New York (1967), p. 610.

4) P. Hartman, *Acta Crystallogr.*, **11**, 721 (1956); *ibid*, **12**, 429 (1959).

5) P. Niggli, *Z. Kristallogr.*, **58**, 490 (1923).

 © 1986 The Chemical Society of Japan Bull. Chem. Soc. Jpn., 59, 3067—3072 (1986)

Studies on Dissolved Metalloenzymes in Lake Water. II. Seasonal Variations in Phosphatase Activity in Lake Kasumigaura

Kensei KOBAYASHI,[a] Shinya HASHIMOTO, Koichi IWASE,[b] Akira OTSUKI,† Kitao FUJIWARA, Keiichiro FUWA, and Hiroki HARAGUCHI*

Department of Chemistry, Faculty of Science, The University of Tokyo, 7-3-1, Hongo, Bunkyo-ku, Tokyo 113
†National Institute for Environmental Studies, 16-2, Onogawa, Yatabe-machi, Ibaraki 305

(Received April 18, 1986)

Alkaline phosphatase activity in Lake Kasumigaura was determined periodically and characterized by high-performance liquid chromatography and isoelectric focusing electrophoresis. There are two peaks in dissolved alkaline phosphatase activity; the bigger one in summer and the smaller one in winter. Molecular weight of ca. 89000 and isoelectric points 5—6 were found for most phosphatases in samples collected during the summer. A considerable part of the winter alkaline phosphatases, however, have much higher molecular weights, and major isoelectric points for these were ca. 4. These alkaline phosphatases were metalloenzymes activated by zinc. The observations above suggest that there are seasonal changes in the dominant microbial species producing dissolved alkaline phosphatase; i.e., blue-green algae, a procaryote, in summer and diatoms and flagellates, eucaryotes, in winter. The peak of alkaline phosphatase activity in lake water was predictive of a following increase in algal species therein.

Phosphorus is recognized as a key to fertilization in natural waters, i.e., orthophosphate is one essential nutrient for microorganisms such as algae and bacteria. When studying the cycle of phosphorus and the regulation of microorganisms, alkaline phosphatase activity should be considered in both its intracellular and extracellular (dissolved) forms.

Alkaline phosphatase (orthophosphoric monoester phosphohydrolyase with activity optimum in alkaline pH) is a typical metalloenzyme, containing several zinc ions at its active sites, and these zinc ions are essentially related to the appearance of phosphatase activity.[1] In most organisms, from primitive procarytes such as bacteria to eucaryotes such as mammals, alkaline phosphatase is found mostly in their periplasmic spaces.[2,3]

Alkaline phosphatase activity in lake waters[4] and seawater[5–7] has been reported by several researchers: Reichardt et al. first determined phosphatase activity not only in unfiltered freshwater but also in water which had been filtered through a 0.6 μm membrane. This suggested the existence of extracellular (dissolved) phosphatase in lake waters.[8] Since then, several researchers have found activity attributed to dissolved phosphatase in lake waters[9–11] and seawaters,[12] and have considered its role in the phosphorus cycle in natural waters.[13,14] In the previous paper,[15] it was confirmed that dissolved phosphatase activity in natural waters was due to the metalloenzymes (zinc-containing alkaline phosphatase).

In the present paper, seasonal variations in alkaline phosphatase in Lake Kasumigaura are examined by high performance liquid chromatography and isoelectric focusing electrophoresis.

a) Present address: Laboratory of Chemical Evolution, Department of Chemistry, University of Maryland, College Park, Maryland 20742, U.S.A.

b) Present address: Agency of Science and Technology, 1-1-1, Kasumigaseki, Chiyoda-ku, Tokyo 100.

Field Description[16]

Lake Kasumigaura, the second largest lake in Japan, is situated in the eastern part of the Kanto Plain, about 50 km north-east of Tokyo. The lake basin is smooth and shallow, with a surface area of 171 km^2, a mean depth of 4 m, and a maximum depth of 7.4 m near the mouth of Takahamairi Bay. Due to the shallowness of the water and its constant agitation by wind, distinct thermal stratifications do not develop even in summer, except for a few calm days. Heavy blooms of blue-green algae are to be seen over the whole lake in summer. The bloom usually starts at the innermost parts of both Takahamairi and Tsuchiurairi Bays, which receive nutrient-rich inflowing waters, and gradually spreads to the center of the lake. By August, the bloom covers the whole lake.

Experimental

Chemicals. *E. coli* alkaline phosphatase purchased from Boehringer-Mannheim Co. (No. 15429) was used as a standard; its specific activity is 20 U mg^{-1} and molecular weight (M. W.) 89000.[12] In addition to *E. coli* alkaline phosphatase, the following enzymes purchased from Boehringer-Mannheim Co. were used as molecular weight standards for high performance liquid chromatography (HPLC): Urease (Jack bean; M. W. 480000); ferritin (indicator protein; M. W. 450000); Bovine carbonic anhydrase (M. W. 31000); and cytochrome c (indicator protein; M. W. 12500). To determine alkaline phosphatase activity, 1 mM (M=mol dm^{-3}) *p*-nitrophenyl dihydrogen phosphate (*p*-NPP) dissolved in 0.6 M tris(hydroxymethyl)methanamine (Tris) hydrochloride buffer (pH 8.0) was used as a substrate. LBK Ampholine Carrier Ampholite (pH 3.5—10) was used as an isoelectric focusing solution.

Instruments. A Shimadzu UV-210A spectrophotometer with a SFU-6 semiauto flow cell unit (optical path of absorption cell: 10mm) was used to determine enzymatic activity. A Shimadzu LC-3A high performance liquid chromatograph was used for HPLC separation, using Shimadzu aqueous

gel column Type W-71; detection was accomplished by using an SPD-2A spectrophotometric detector. An LBK Ampholine 8100-1 Electrofocusing Equipment (column volume: 110 mL) with a power supply (Atto Co., V-C Stabilizer SJ-1061; maximum voltage: 1000 V) was used for isoelectric focusing. Ultrafiltration was performed with an Amicon Diaflo Cell Type 202. A Thermostatic Bath Circulator (Thomas Scientific Co., Model TRL-111SP), a fraction collector (Toyo Kagaku Sangyo Co., Signal Fracon SF-60L), and a peristaltic pump (Toyo Kagaku Sangyo Co., Signal Pump TMP-6L) were also used in HPLC and electrophoresis fractionation.

Pretreatment of Lake Water Samples. Lake water was sampled at 10 points in Lake Kasumigaura (Ibaraki Prefecture), once a month as from April 1980 through March 1982 (see Fig. 1). The collected water was filtered with glass fiber membrane filters (pore size: 1.0 μm), and then filtered with Toyo Kagaku UK-2 membrane filters (pore size: 0.45 μm) or UK-4 (pore size: 0.2 μm) to exclude bioorganisms. All the filtrations were performed immediately after sampling, and the samples were then stored in a cold room (4 C).

An unfiltered sample, to which 2 v/v% of chloroform was added, was also kept in a cold room to determine total phosphatase activity.

Before separation by HPLC or electrophoresis, the 0.45 μm-filtered sample was concentrated ca. 1000 times by ultrafiltration, using a Toyo Kagaku UK-10 type ultrafilter, with which only molecules larger than M. W. 10000 can be concentrated. Samples were kept under constant temperature at 4 C throughout ultrafiltration and storage. Experimental vessels and containers were cleaned and sterilized by heating to 110 C, by soaking in 40% ethanol aqueous solution and/or by soaking in 7 M nitric acid.

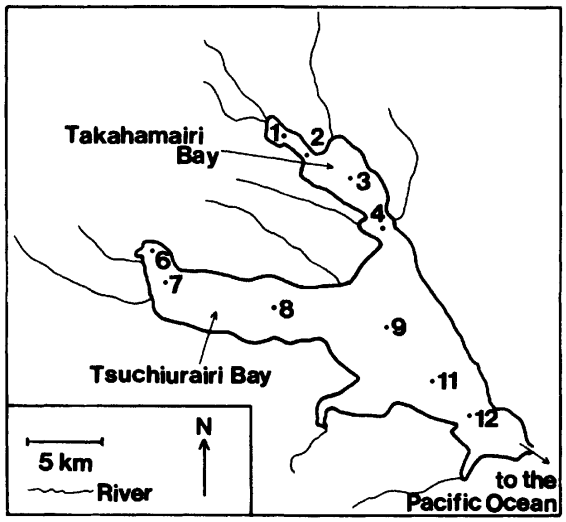

Fig. 1. Sampling stations in Lake Kasumigaura.

Determination of Phosphatase Activity. Alkaline phosphatase catalyzes the hydrolysis of *p*-NPP to *p*-nitrophenol:

$$O_2N\text{-}C_6H_4\text{-}OPO_3H_2 + H_2O \rightarrow O_2N\text{-}C_6H_4\text{-}OH + H_3PO_4 \quad (1)$$

The rate of production of the *p*-nitrophenol is followed spectrophotometrically and provides a measure of the concentration of the catalyst. Dissolved alkaline phosphatase activity was determined by using 0.2 μm-filtered lake water as a sample, as described in our previous paper.[15] Total alkaline phosphatase activity was determined in the same way as dissolved alkaline phosphatase activity, using an unfiltered sample; the *p*-NPP substrate was saturated with chloroform for its bacteriostatic effect.[17]

HPLC Chromatograms. For HPLC separation, two aqueous porous gel columns (both Type W-71) were available, one column 7.9 mm i.d.×30 cm and the other 7.9 mm i.d.×50 cm. Either column was used or both were joined to make an 80-cm length. Instead of the phosphate buffer, which is generally used as a carrier for the W-71 column, 0.1 M Tris-HCl buffer (pH 8.0) was used for determining the phosphatase activity of the untreated effluent, because phosphate ion inhibits phosphatase activity. The effluent was fractionated every 0.5—1.0 min (0.5—1.0 cm^3) with a fraction collector, and the phosphatase activity of the thirty or so individual fractions was then measured.

Isoelectric Focusing Chromatograms. Isoelectric focusing was carried out in accordance with the instruction manual of LKB Ampholine 8100 electrofocusing equipment. The solutions used in the present experiment are shown in Table 1. The system was thermostated, and electrofocusing was carried out at 4 C for 48 h. After the electrode solutions had been removed from the column, the electrofocused solution was fractionated every 2.5 cm^3 with a peristaltic pump and a fraction collector. The phosphatase activities of the individual fractions were determined by the method described earlier.

Results

Distribution of Phosphatase Activity in Lake Kasumigaura. Total phosphatase activity (TPA) and dissolved phosphatase activity (DPA) in Lake Kasumigaura from April, 1981 to March, 1982

Table 1. Solutions Used for Isoelectric Focusing

Solution	Content		Total Volume
Dense gradient solution	Sucrose	27 g	54 cm^3
	Ampholine	2 cm^3	
	concd. sample plus water	35 cm^3	
Light gradient solution	Sucrose	2.7 g	54 cm^3
	Ampholine	0.7 cm^3	
	concd. sample plus water	50.3 cm^3	
Cathode solution	0.25 M NaOH	10 cm^3	10 cm^3
Anode solution	Sucrose	15 g	25 cm^3
	0.25 M H_2SO_4	16 cm^3	

Table 2. Phosphatase Activities in Lake Kasumigaura from April, 1981 to March, 1982 (activity: nmol dm^{-3} min^{-1})

Sta.		Apr	May	Jun	Jul	Aug	Sep	Oct	Nov	Dec	Jan	Feb	Mar
1	DPA[a]	5.1	2.0	3.1	1.3	0.9	0.8	1.0	0.6	0.8	1.2	1.2	1.5
	TPA[b]	27.1	18.0	20.7	14.2	18.9	16.0	17.5	11.5	14.6	26.0	18.9	19.6
2	DPA	1.5	3.2	3.4	4.3	1.0	1.7	0.4	2.3	1.0	1.3	1.0	2.2
	TPA	14.7	41.2	56.2	17.6	12.8	18.5	10.5	26.5	37.3	24.5	24.3	21.4
3	DPA	1.7	2.3	0.9	3.7	2.1	0.4	<0.4	1.1	0.9	1.6	1.4	5.1
	TPA	19.8	29.2	14.5	12.4	11.0	7.0	9.7	18.9	34.4	17.3	32.1	23.0
4	DPA	3.1	4.8	0.4	1.0	1.0	0.4	0.4	<0.4	1.0	1.2	1.4	3.1
	TPA	20.3	40.0	12.7	11.3	10.3	10.4	11.8	12.6	37.5	12.7	19.3	14.3
6	DPA	1.7	1.9	1.3	0.7	0.9	0.5	0.4	0.6	0.9	1.2	0.5	1.4
	TPA	9.1	23.2	23.0	12.1	19.6	13.7	5.5	3.7	14.6	8.7	6.9	5.6
7	DPA	2.9	4.1	0.7	1.9	1.0	<0.4	0.4	0.9	1.9	1.1	0.6	1.2
	TPA	13.1	82.2	18.3	16.6	15.3	13.7	8.9	14.2	35.4	11.4	15.0	8.4
8	DPA	1.9	5.4	0.7	1.1	1.5	0.5	0.6	1.0	1.4	1.5	0.9	1.7
	TPA	18.3	61.2	18.6	9.1	11.5	9.6	11.8	20.2	37.5	13.0	18.5	10.8
9	DPA	2.4	3.2	1.7	1.2	0.9	<0.4	<0.4	0.5	1.5	1.2	0.8	1.7
	TPA	18.4	42.8	45.9	4.6	6.9	12.0	9.7	11.0	42.9	17.8	22.4	14.5
11	DPA	—	4.3	1.2	2.7	<0.4	<0.4	<0.4	<0.4	1.5	0.9	1.1	1.6
	TPA	—	38.2	33.0	6.8	5.0	6.5	8.7	13.9	37.1	11.9	17.0	10.8
12	DPA	—	3.6	1.3	1.1	0.8	<0.4	<0.4	1.4	1.5	0.9	0.5	1.8
	TPA	—	32.0	32.7	10.5	5.0	7.2	10.1	19.7	52.0	15.1	17.5	15.3

a) DPA=Dissolved phosphatase activity. b) TPA=Total phosphatase activity.

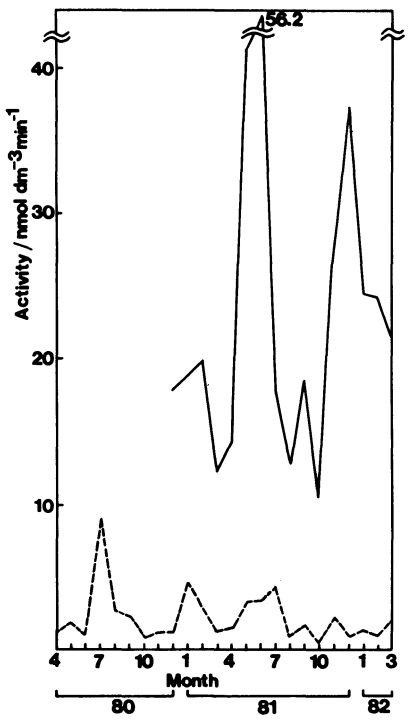

Fig. 2. Seasonal variations in total and dissolved phosphatase activities at Sta. 2 in Lake Kasumigaura. ——: Total alkaline phosphatase activity; -----: dissolved alkaline phosphatase activity.

are shown in Table 2. Average DPA levels in Lake Kasumigaura were ca. 1 nmol dm^{-3} min^{-1}, about the same as those determined in the Shinobazu pond[15] and in Lake Kinneret.[6] At each location, average TPA was about ten times higher than DPA, but phosphatase activity near the edge of the lake ((e.g., Stations (Stas.) 1, 2, 6, and 7)) was greater than in the center of the lake (e.g., Sta. 9). This trend was more obvious in the summer than in spring.

Seasonal Variations in Phosphatase Activity. Seasonal variations in DPA and TPA at Sta. 2 in Lake Kasumigaura are shown in Fig. 2. Very distinct peaks were observed in summer, and other smaller peaks were observed in winter. The patterns of the two curves are almost the same.

Alkaline phosphatase activity in lake water in all seasons was diminished when samples were treated with chelating agents, such as 2,6-pyridinedicarboxylic acid; the activity was restored on addition of zinc ion (see Table 3.)

HPLC Chromatograms. HPLC chromatograms of concentrated lake water sample in August and December, 1980, are shown in Figs. 3 and 4. In summer (Fig. 3), a very distinct single peak was seen at the elution time of *E. coli* alkaline phosphatase. The chromatograms for winter (Fig. 4) through spring had more complicated features, showing the presence

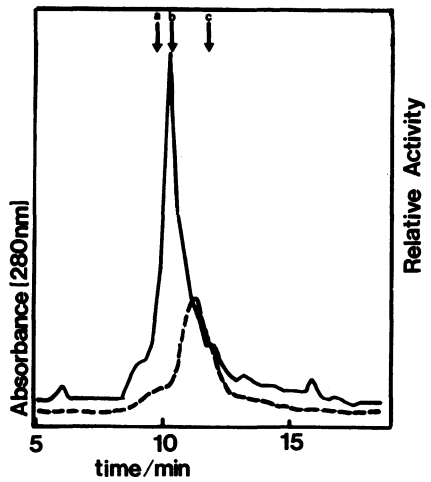

Fig. 3. HPLC chromatograms of concentrated lake water collected in August, 1980.
Sample: concentrated (×2300) water sample collected in Lake Kasumigaura (Sta. 2) on August 16, 1980; sample volume: 100 mm^3; column: Shimadzu aqueous porous gel column W-71 (7.9 mm i.d.×50 cm); carrier: 0.01 M Tris-HCl buffer (pH 8.0); flow rate: 1.0 $cm^3 min^{-1}$.
——: Phosphatase activity; -----: UV absorbance at 280 nm. Elution time of standard proteins are as follows:
a: Urease (M.W.: 480000); b: *E. coli* alkaline phosphatase (M.W.: 89000); c: Bovine carbonic anhydrase (M.W.: 31000).

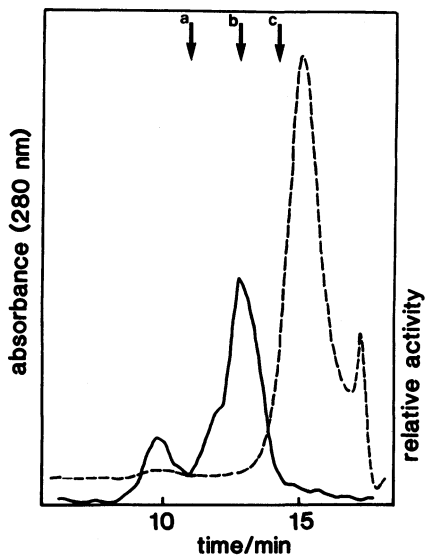

Fig. 4. HPLC chromatograms of concentrated lake water collected in December, 1980.
Sample: concentrated (×1400) water sample collected in Lake Kasumigaura (Sta. 2) on December 22, 1980; sample volume: 200 mm^3, column: Shimadzu W-71 (7.9 mm×50 cm); carrier: 0.1 M Tris-HCl buffer (pH 8.0); flow rate: 1.0 $cm^3 min^{-1}$.
——: Phosphatase activity; -----: absorbance at 280 nm. a: Ferritin (M.W.: 450000); b: *E. coli* alkaline phosphatase (M.W.: 89000); c: Bovine carbonic anhydrase (M.W.: 31000).

Table 3. Recovery Ratios of Phosphatase Activity when Various Metal Ions Added to Lake Water Treated with Chelating Agent

Metal ion	Relative activity	
	August, 1980[a)]	May, 1981[b)]
None	0%	0%
Manganese(II)	41	25
Cobalt(II)	32	27
Nickel(II)	4	18
Copper(II)	9	0
Zinc(II)	100	100
Cadmium(II)	4	0

a) Cited from Ref. 15. b) A mixture of 33 mm^3 of concentrated (×440) lake water (Sta. 2) and 17 mm^3 of 10 mM 2,6-pyridinedicarboxylic acid (pH 7.0) was used as an "apo-sample." Fifty μg of each metal ion(II) was added to the apo-sample.

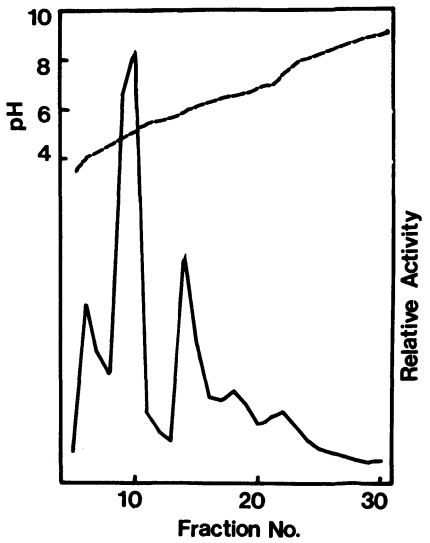

Fig. 5. Isoelectric focusing chromatogram of concentrated lake water for October, 1980.
Sample: concentrated water sample collected in Lake Kasumigaura (Sta. 2) on October 22, 1980.

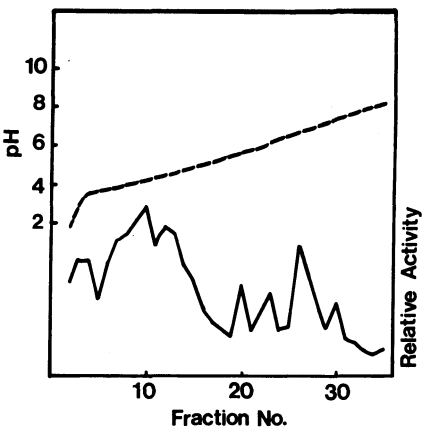

Fig. 6. Isoelectric focusing chromatogram of concentrated lake water for April, 1981.
Sample: concentrated water sample collected in Lake Kasumigaura (Sta. 2) on April 21, 1981.

of alkaline phosphatase with a greater molecular weight than those of *E. coli*.

Isoelectric Focusing Chromatograms. Figures 5 and 6 show the isoelectric focusing (IEF) chromatograms of concentrated lake water in October, 1980 and April, 1981, individually. All the chromatograms had several peaks of phosphatase activity, but the isoelectric points (pI) of the peaks showing high phosphatase activity were not the same. In summer and fall (Fig. 5), the peaks of phosphatase activity at pI 5—6 were significant, but those at ca. pI 4 were dominant in other seasons (Fig. 6). These results show seasonal changes in the composition of the isozymes of alkaline phosphatase in Lake Kasumigaura.

Discussion

Horizontal and Vertical Distribution of Phosphatase Activity. Lake Kasumigaura is notable as one of the most fertilized lake in Japan. This can be attributed mainly to its shallowness and the large inflow of nutrient-rich waters. The shallowness of the lake and the constant agitation of the water by the wind mean that there is little vertical variation of phosphatase activity in the water. Thus vertical variations of phosphatase activity can be ignored.[15]

As shown in Table 2, phosphatase activity varied appreciably with sampling location. Coastal waters in Takahamairi Bay (Stas. 1 and 2) or Tsuchiurairi Bay (Sta. 6) generally gave high TPA and DPA values that seemed to relate to the degree of fertilization or the biomass of microorganisms.

Seasonal Changes in Phosphatase Activity. In Lake Kasumigaura, heavy blooms of *Microcystis aeruginosa*, a species of blue-green algae, are to be seen covering the whole lake in summer. Other algae such as diatoms and flagellates can not breed during this period. When the blue-green algae decrease in autumn, other algae can increase.[18] The correlation between the peaks of DPA and of the biomass can be seen; the peak of DPA in summer corresponded to that of blue-green algae; the smaller peaks of DPA in winter and spring might correspond to those of diatoms and flagellates. The peaks of DPA (or TPA) slightly preceded the bloom of algae. This suggests that algae produce more alkaline phosphatase before multiplying.

Bacteria may also put alkaline phosphatase into the lake water, although the biomass of bacteria is much less than that of algae.[19] Thus, while most of the DPA originated from algae, DPA originating from bacteria could not be ignored.

HPLC and IEF Chromatograms. The seasonal variations described above are also shown as the HPLC and IEF chromatograms. Figures 3—6 show that various isozymes of alkaline phosphatase were present as dissolved enzymes in the lake water. The very distinct single peak in the HPLC chromatograms for summer (Fig. 3) is believed to be *Microcystis aeruginosa* alkaline phosphatase, whose molecular weight is close to that of *E. coli* alkaline phosphatase (89000). Alkaline phosphatases of higher molecular weight (eluted earlier than *E. coli* alkaline phosphatase) are seen in Fig. 4. These appear to be alkaline phosphatase originating from eucaryotes such as diatoms and flagellates. The eucaryotic alkaline phosphatase, unlike *E. coli* alkaline phosphatase, are glycoproteins, whose amino acid compositions, however, are strikingly similar to that of *E. coli* alkaline phosphatase.[20] Consequently eucaryotic alkaline phosphatase seems to elute rather sooner than might be estimated from the calibration curve for simple proteins.

There were several peaks in each IEF chromatogram, but the dominant peaks differed according to the sample. Unlike the HPLC chromatogram, which gave only a single dominant peak, a number of major peaks appeared in the IEF chromatogram for summer and fall (Fig. 5). This suggests that the procaryotic alkaline phosphatases, which could not be separated using a method based on molecular weight, can be separated using electrophoresis. The positions of the dominant IEF peaks (ca. pI 4) for winter and spring were markedly different from those for summer and fall (pI 5—6), and this also reflected the seasonal changes in the algae in Lake Kasumigaura.

Conclusion

Phosphatase activity in Lake Kasumigaura varied seasonally. The peak of phosphatase activity seemed to predict the increase in a certain species of algae. In addition to the change in total activity, a change in isozymes was observed in the HPLC and IEF chromatograms. This was interpreted as being caused by seasonal changes in phosphatase in natural water in Lake Kasumigaura; i.e., procaryotes (blue-green algae) in summer and eucaryotes (such as diatoms and flagellate) in winter and spring.

The various alkaline phosphatases found in the different seasons were all zinc-containing metalloenzymes, and are therefore also of interest as a significant source of zinc in natural water.[15,21] This suggests that other heavy metals may similarly be found in biochemical substances in natural water.

The amount of phosphatase in natural water is influenced not only by the biomass of microorganisms producing enzymes, but also by orthophosphate.[22] The nature of the relationship between alkaline phosphatase activity and concentration of various phosphorus compounds and the role of alkaline phosphatase in phosphorus cycles in lake water will be considered in the following paper.

The present authors thank Dr. Lawrence J. Sacks, Laboratory of Chemical Evolution, Department of Chemistry, University of Maryland, for his kind help in preparation of the manuscript.

This research has been supported by the Grant-in-

Aid for Environmental Science from the Ministry of Education, Science and Culture.

References

1) J. E. Coleman, "Inorganic Biochemistry," ed by G. L. Eichhorn, Elsevier, Amsterdam (1973), Vol. 1, Chap. 17.
2) J. E. Coleman and J. F. Chlebowski, "Advances in Inorganic Biochemistry," ed by G. L. Eichhorn and L. G. Marzilli, Elsevier, New York (1979), Vol. 1, Chap. 1.
3) J. F. Chlevowski and J. E. Coleman, "Metal Ions in Biological Systems," ed by H. Sigel, Marcel Dekker, New York (1976), Vol. 6, Chap. 1.
4) M. Steiner, *Naturwissenschaften*, **26**, 723 (1938).
5) R. Y. Morita and R. A. Howe, *Deep-Sea Research*, **4**, 254 (1957).
6) H. Goldschmiedt, *Chem. Ztg.*, **83**, 442 (1959).
7) M. J. Perry, *Mar. Biol.*, **15**, 113 (1972).
8) W. Reichardt, J. Overbeck, and L. Steubing, *Nature*, **216**, 1345 (1967).
9) T. Berman, *Nature*, **224**, 1231 (1969).
10) J. Olah and E. O. Toth, *Aquaculture Hungarica (Szarvas)*, **1**, 15 (1978).
11) M. Jansson, *Science*, **194**, 320 (1976).
12) N. Taga and H. Kobori, *Mar. Biol.*, **49**, 223 (1978).
13) R. J. Stevens and M. P. Parr, *Freshwater Biol.*, **7**, 351 (1977).
14) H. Kobori and N. Taga, *J. Exp. Mar. Biol. Ecol.*, **36**, 23 (1979).
15) K. Kobayashi, K. Iwase, M. Matsui, M. Watanabe, H. Ueda, K. Fujiwara, H. Haraguchi, and K. Fuwa, *Bull. Chem. Soc. Jpn.*, **55**, 3459 (1982).
16) A. Otsuki, S. Kasuga, and T. Kawai, *Verh. Internat. Verein. Limnol.*, **21**, 602 (1981).
17) T. Berman, *Limnol, Oceanogr.*, **15**, 663 (1970).
18) M. Imamura and M. Yasuno, *Res. Rep. Natl. Inst. Environ. Stud.*, **22**, 123 (1981).
19) M. Aizaki and T. Nakajima, *Res. Rep. Natl. Inst. Environ. Stud.*, **22**, 63 (1981).
20) F. N. Fernley, "The Enzymes," ed by P. D. Boyer, 3rd Ed., Academic Press, New York (1971), Vol. 4, Chap. 18.
21) K. Kobayashi, M. Matsui, H. Haraguchi, and K. Fuwa, *J. Inorg. Biochem.*, **18**, 41 (1983).
22) K. Kobayashi, S. Hashimoto, K. Fujiwara, H. Haraguchi, K. Fuwa, and A. Otsuki, *Chem. Lett.*, **1984**, 565.

Metallation of Aliphatic Carbon Atoms. IV. Syntheses and Characterization of the Cyclopalladated Complexes of 2-*t*-Butylbenzothiazole

Katsuma HIRAKI,* Yoshio FUCHITA, Motoharu NAKASHIMA, and Hirofumi HIRAKI
Department of Industrial Chemistry, Faculty of Engineering, Nagasaki University, Bunkyo-machi, Nagasaki 852
(Received April 23, 1986)

2-*t*-Butylbenzothiazole reacts with palladium(II) acetate in acetic acid to produce the cyclopalladated dimer [{Pd(CH_2CMe_2-C_7H_4NS)(μ-$MeCO_2$)}$_2$] (**2**) (C_7H_4NS=2-benzothiazolyl). Complex **2** shows temperature-dependent ^{1}H NMR spectra, which have been interpreted on the basis of the inversion motion of the acetato bridges. Metatheses of **2** with lithium chloride and sodium iodide result in the formation of the chloro- and iodo-bridged analogues, [{Pd(CH_2CMe_2-C_7H_4NS)(μ-Cl)}$_2$] (**3**) and [{Pd(CH_2CMe_2-C_7H_4NS)(μ-I)}$_2$] (**4**), respectively, each of which is found to be composed of cis and trans isomers. The ^{1}H NMR spectra of **3** and **4** depend on temperature and are ascribed to rapid exchange between the two isomers. Equimolar amounts of **3** and **4** afford a μ-chloro-μ-iodo binuclear complex, [(C_7H_4NS-CMe_2CH_2)Pd(μ-Cl)(μ-I)Pd(CH_2CMe_2-C_7H_4NS)]. The reaction of **3** with thallium(I) acetylacetonate [Tl(acac)] produces a mononuclear cyclopalladated complex [Pd(CH_2CMe_2-C_7H_4NS)(acac)]. Complexes **2** and **3** react with CO in methanol to give $MeO_2CCH_2CMe_2$-C_7H_4NS, the formation of which comfirms also the cyclopalladated structure of 2-*t*-butylbenzothiazole in **2** and **3**.

It has been demonstrated that the activation of C–H bonds in saturated organic compounds is one of the most intriguing goals of organometallic chemistry.[1,2] We have been challenging this theme through cyclometallation reactions. Up to date we have achieved the cyclopalladations of alkyl groups in 2-neopentylpyridine,[3] *N*,*N*-dimethylneopentylamine,[4] 1,3-di(2-pyridyl)propane,[5] and 2-(trimethylsilyl)pyridine[6] by using palladium(II) acetate as a metallating reagent. In this paper we wish to report the new C–H bond activation of *t*-butyl group in 2-*t*-butylbenzothiazole by palladium(II) acetate and the dynamic behavior of the resulting binuclear cyclopalladated complexes.

Results and Discussion

Synthesis of the Cyclopalladated Complexes. 2-*t*-Butylbenzothiazole reacted with an equimolar amount of sodium tetrachloropalladate(II) in the presence of sodium acetate at 80—85 °C to afford a crystalline complex **1**. The ^{1}H NMR spectrum of **1** was not clear owing to its low solubility. On the basis of the elemental analysis and the similarity of the IR spectrum of **1** to that of 2-*t*-butylbenzothiazole, **1** was assigned to a dinuclear addition complex [{(Pd(μ-Cl)Cl(CMe_3-C_7H_4NS)}$_2$] (C_7H_4NS=2-benzothiazolyl group).

2-*t*-Butylbenzothiazole and palladium(II) acetate reacted in acetic acid at 80—85 °C to give yellow crystals, [{Pd(CH_2CMe_2-C_7H_4NS)(μ-CH_3CO_2)}$_2$] (**2**). Its IR spectrum showed characteristic bridged acetato bands at 1415 and 1580 cm^{-1}.[7] The ^{1}H NMR spectrum of **2** at −22 °C showed an AB type quartet at δ 2.20 (2H, $\Delta\delta$=0.26, $^2J_{HH}$=8 Hz) and a singlet at δ 2.49 (2H), ascribable to methylene group, which was formed by the cyclopalladation of one methyl group

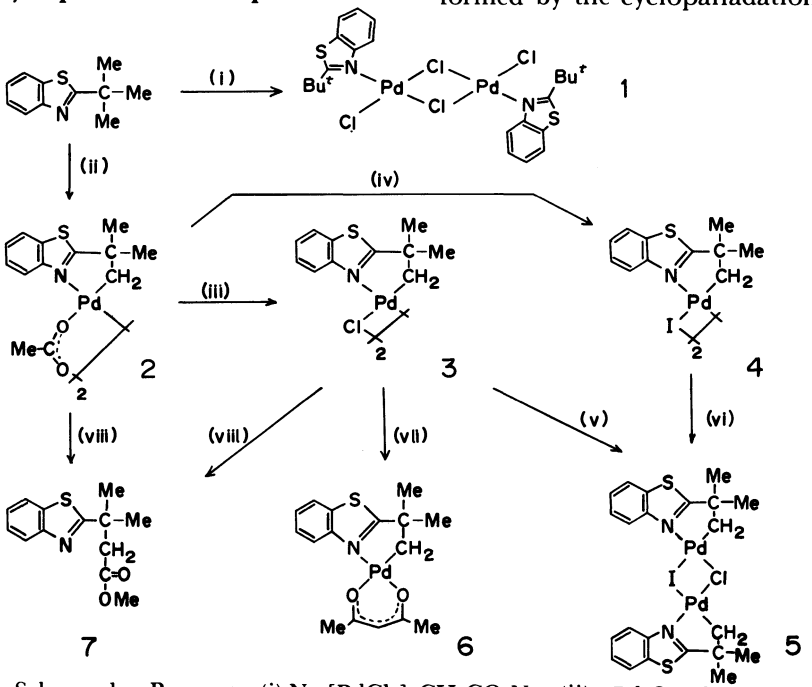

Scheme 1. Reagents: (i) $Na_2[PdCl_4]$-CH_3CO_2Na. (ii) $Pd(CH_3CO_2)_2$. (iii) LiCl. (iv) NaI. (v) **4**. (vi) **3**. (vii) Tl(acac). (viii) CO at 50 atm.

in 2-*t*-butylbenzothiazole. In addition, the spectrum exhibited three singlets due to the methyl protons of the bridging acetato ligands at δ 2.09 (1.5H), 2.15 (3.0H), and 2.21 (1.5H). The central singlet at δ 2.15 is assignable to a trans isomer with a C_2 symmetry, whereas the other two singlets at δ 2.09 and 2.21 are ascribable to a cis isomer with a C_s symmetry. On the basis of these results and the elemental analysis together with the characterization of derivatives from **2**, **2** was assigned to a 1:1 mixture of trans and cis isomers of novel binuclear cyclopalladated complex, di-μ-acetato-bis[2-(2-benzothiazolyl)-2-methylpropyl-C^1, N]dipalladium(II) [{Pd(CH_2CMe_2-C_7H_4NS)(μ-CH_3CO_2)}$_2$]. The trans isomer was palladated at *a*- and *h*-positions (**2-*ah***), as shown in Fig. 1, whereas the cis isomer was done at *a*- and *g*-positions (**2-*ag***). The formation of the two kinds of isomers has been observed in other several acetato-bridged cyclopalladated complexes.[3,4,6,8]

The acetato-bridged complex **2** was converted into the corresponding chloro-bridged analogue [{Pd(CH_2-CMe_2-C_7H_4NS)(μ-Cl)}$_2$] (**3**) and iodo-bridged one [{Pd(CH_2CMe_2-C_7H_4NS)(μ-I)}$_2$] (**4**) by the metathetical reactions of **2** with lithium chloride and sodium iodide, respectively, in THF. The equimolar mixture of these two complexes afforded an interesting mixed halogeno-bridged binuclear complex, [(C_7H_4NS-CMe_2-CH_2)Pd(μ-Cl)(μ-I)Pd(CH_2CMe_2-C_7H_4NS)] (**5**) in a high yield. Furthermore, mononuclear cyclopalladated complex **6**, [Pd(CH_2CMe_2-C_7H_4NS)(acac)] (acac=acetylacetonato) was obtained by treating **3** with Tl(acac) in dichloromethane. Characteristic *O*,*O*′-chelating acac bands were observed at 1510 and 1580 cm^{-1} in the IR spectrum of **6**.

All the complexes (**2**—**6**) synthesized in this study are fairly stable in air. Their elemental analyses, yields, and ^{1}H NMR data are summarized in Tables 1 and 2.

Dynamic Behavior of the Acetato-Bridged Dimer 2. Complex **2** showed temperature-dependent ^{1}H NMR spectra (Fig. 2). At −22 °C, the methylene protons of **2-*ah*** showed the AB type quartet and the protons of the two remaining methyl groups were nonequivalent, resonating as two singlets at δ 0.70 and 1.14. The methyl protons of **2-*ag*** appeared also as two singlets at δ 1.45 and 1.54. These facts indicate unambiguously that the both isomers of **2** have a folded structure,

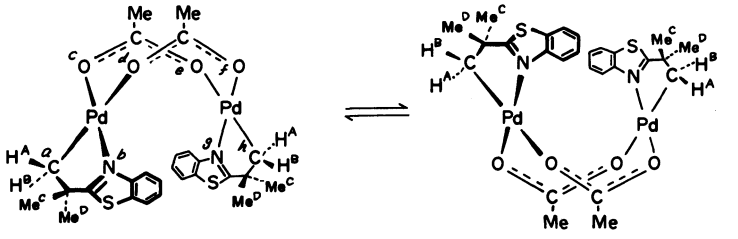

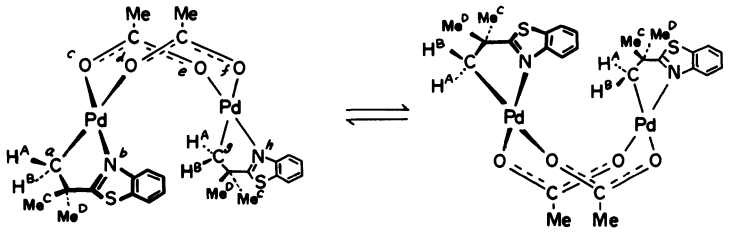

Fig. 1. Inversion motions of the isomers of **2**.

Table 1. Yield and Elemental Analyses

Compound	Yield	Mp[a]	Found (Calcd) (%)		
	%	θ_m/°C	C	H	N
1	45	185—190	36.02(35.84)	3.69(3.55)	3.53(3.80)
2	51	199—202	43.75(43.89)	4.21(4.25)	4.00(3.94)
3	88	250—252	38.91(39.78)	3.66(3.64)	4.12(4.22)
4	61	225—227	30.82(31.19)	2.99(2.86)	3.17(3.31)
5	72	205—207	35.22(34.96)	3.23(3.20)	3.60(3.71)
6	75	116—118	48.09(48.55)	4.99(4.84)	3.57(3.54)
7	96[b]	—[c]	62.51(62.63)	6.12(6.06)	5.57(5.62)

a) With decomposition. b) From 3. c) Oil.

Table 2. ^{1}H NMR Data[a)]

Compd	Temp[b)] °C	CH_2	CH_3	2-Benzothiazolyl group[c)] 4-H	5- and 6-H's		7-H	Others[d)]
2-*ah*	−22	2.20q[e)]	0.70s 1.14s	8.15d	7.15t	7.42t	7.86d	2.15s(CH_3CO_2)
2-*ag*	−22	2.49s	1.45s 1.54s	7.75d	6.62t	7.38t	7.60d	2.09s(CH_3CO_2) 2.21s(CH_3CO_2)
2-*ah*	43	2.21s	1.05brs	8.33d	7.17t	7.43t	8.01d	2.10s(CH_3CO_2)
2-*ag*	43	2.51s	1.36brs	7.76d	6.72t	7.41t	7.60d	2.04s(CH_3CO_2) 2.16s(CH_3CO_2)
3	−32	2.50s 2.59s[f)]	1.63s	8.60d 8.85d[f)]	7.46t	7.61t	7.89d	—
	54	2.56s	1.60s	8.80d	7.44t	7.60t	7.86d	—
4	−35	2.42s 2.54s	1.66s	8.63d 8.87d	7.46t	7.54t	7.83d	—
	50	2.48s	1.66s	8.85d	7.45t	7.52t	7.81d	—
3+4[g)]	50	2.45s	1.59s	8.84brd	7.45t	7.52t	7.79d	—
5	−35	2.33s	1.62s	8.77d	7.39t	7.54t	7.82d	—
	50	2.40s	1.60s	8.87d	7.38t	7.52t	7.79d	—
6	24	2.38s	1.58s	8.93d	7.38t	7.52t	7.78d	1.96s, 2.06s(acac-CH_3) 5.33s(acac-CH)
7	24	2.84s	1.58s	7.86d	7.21t	7.35t	7.77d	3.54s(CH_3O)

a) δ Value from TMS. Recorded in $CDCl_3$ on a JEOL JNM-MH 100 spectrometer. b) Measured temperature. c) Coupling constants between the adjacent protons in this ring ($^3J_{HH}$) are ca. 7 Hz. d) Assignment is given in the parentheses. e) $\Delta\delta$=0.26, $^2J_{HH}$=8 Hz. f) Corresponding to the major isomer. g) **3**+**4** in a 2:1 molar ratio. See the text.

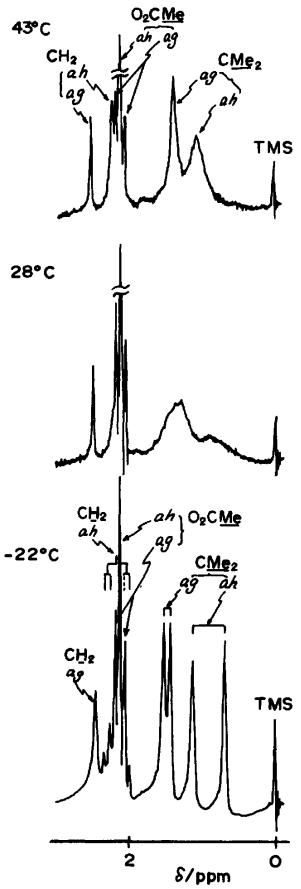

Fig. 2. The temperature-dependent ^{1}H NMR spectra of **2**.

as other acetato-bridged binuclear palladium(II) complexes have.[9-11] As for **2-*ah***, the protons of the both methyl groups resonated at higher fields in comparison with the corresponding methyl protons in **2-*ag***. This seems to be associated with the anisotropic shielding by the facing benzothiazolyl group.[10] Furthermore, the anisotropic shielding acts on one of the methylene protons situated at the innerside of the folded structure in **2-*ah***, shifting the resonance to the higher field (at δ 2.07). However, the methylene protons of **2-*ag*** do not undergo such anisotropic shielding owing to the mirror image relationship of the structure, resonating at δ 2.49 as a singlet.

On raising the measured temperature, the two methyl resonances in each of **2-*ah*** and **2-*ag*** coalesced at 28 °C, and then became broad singlets at δ 1.05 and 1.36, respectively, at 43 °C. However, these two singlets did not coalesce at 60 °C, indicating that the exchange between **2-*ah*** and **2-*ag*** did not occur even at this temperature. The temperature-dependency of the ^{1}H NMR spectra of **2** is attributable to such the typical inversion motion of the acetato bridges (Fig. 1) as the other acetato-bridged complexes exhibit.[4,6,10,11]

Dynamic Behavior of the Halogeno-Bridged Binuclear Complexes. The chloro-bridged dimer **3** also exhibited the temperature-dependent ^{1}H NMR spectra. At −32 °C palladium-bonded methylene protons resonated as two singlets at δ 2.50 (1.4H) and 2.59 (2.6H), whereas 4-H of the 2-benzothiazolyl moiety appeared as two doublets at δ 8.60 (0.7H) and 8.85 (1.3H). These data indicate that **3** consists of two isomers, trans type with (*a*-C, *b*-N; *e*-N, *f*-C) chelations and cis one with (*a*-C, *b*-N; *e*-C, *f*-N) chelations as seen in Fig. 3.

The former two singlets at δ 2.50 and 2.59 coalesced at 3 °C and changed to one sharp singlet at

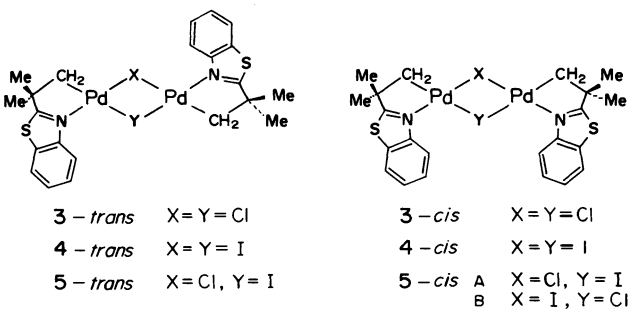

Fig. 3. Isomers of the halogeno-bridged binuclear complexes.

δ 2.56 at 54°C. Similarly, the latter two doublets at δ 8.60 and 8.85 were turned into one doublet at δ 8.80 at the same temperature. This temperature-dependent ^{1}H NMR spectra did not change at all by adding 10-fold excess of acetone or water to the NMR sample solution of **3** in $CDCl_3$. Such temperature dependence is attributed to an exchange between the cis and trans isomers rather than that between **3** and a mononuclear species [Pd(CH_2CMe_2–C_7H_4NS)ClL] (L=Me_2CO or H_2O). This is also supported by easy formation and isolation of the chloro-iodo-mixed bridged binuclear complex as stated later. The iodo-bridged dimer **4** also exhibited similar temperature-dependent ^{1}H NMR spectra in the range of −35—+50 °C (Table 2), indicating that **4** consisted of cis and trans isomers (Fig. 3) and a rapid exchange between the two isomers took place above −10°C. Galli et al.[12] reported recently the analogous exchange between the cis-trans isomers of halogeno-bridged cyclopalladated dimers of *t*-butyl methyl ketone *N*-methyl-*N*-phenylhydrazone [{Pd[CH_2CMe_2C(=N-NMePh)Me]-X}$_2$] (X=Cl, Br, and I).

When the ^{1}H NMR spectra of the equimolar mixture of **3** and **4** were measured in $CDCl_3$, only one set of signals, corresponding neither to **3** nor **4**, was obtained. Moreover, this species also showed temperature-dependent ^{1}H NMR spectra. At 50°C, the palladium-bonded methylene protons and 4-H of the 2-benzothiazolyl moiety resonated as one singlet at δ 2.40 and one doublet at δ 8.87, respectively. On lowering the temperature, these signals broadened at 18°C, and then changed again to one sharp singlet at δ 2.33 and one resolved doublet at δ 8.77 at −35°C. This species could be isolated as a chloro-iodo-bridged binuclear complex [(C_7H_4NS-CMe_2CH_2)-Pd(μ-Cl)(μ-I)Pd(CH_2CMe_2-C_7H_4NS)] (**5**). Of course, **5** showed the same temperature-depending ^{1}H NNR spectra as the above-mentioned mixture of **3** and **4**. It is interesting that **5** showed only one set of ^{1}H NMR signals, though there are three possible isomers, trans, cis-A, and cis-B, as shown in Fig. 3.

When the mixture of **3** and **4** in a molar ratio of 2:1 was run in a ^{1}H NMR tube, there appeared three sets of signals; one corresponded to **5** and the other two did to two sets observed for **3** at −35°C. On increasing the temperature all the three sets coalesced at 25°C, and then appeared as one single set of signals at 60°C. These results clearly indicate that the chloro-bridged dimer **3** as well as the iodo-bridged dimer **4** experiences exchange between cis- and trans-isomers. In other words at high temperature (ca. 50°C) the exchange between the two species is rapid, giving averaged single set of signals, and at low temperature (ca. −35°C) the exchange is actually quenched to result in affording two sets of signals corresponding to cis and trans isomers.

Carbonylation of the Cyclopalladated Complexes, 2 and 3. The acetato-bridged dimer **2** as well as the chloro-bridged one **3** reacted with carbon monoxide in methanol in an autoclave to give methyl 3-(2-benzothiazolyl)-3-methylbutyrate (**7**) in almost quantitative yields. This fact unambiguously indicates that metallation occurs on the methyl carbon of the 2-*t*-butylbenzothiazole, and that methoxycarbonyl group can be introduced quantitatively and regiospecifically onto one of the methyl groups via cyclopalladated complex.

Experimental

2-*t*-Butylbenzothiazole[13] and thallium(I) acetylacetonate[14] were synthesized as published. General procedures were as described previously.[8]

Reaction of 2-*t*-Butylbenzothiazole with $Na_2[PdCl_4]$. 2-*t*-Butylbenzothiazole (215 mg), sodium acetate (92 mg), and $Na_2[PdCl_4]$ (300 mg) were mixed in 20 cm^3 of acetic acid, and then the mixture was heated at 80—85°C for 6 h. The resulting precipitates were collected, and washed with water and diethyl ether. Recrystallization from benzene and hexane gave 170 mg of [{Pd(μ-Cl)Cl(CMe_3-C_7H_4NS)}$_2$] (**1**) as beige crystals.

Reaction of 2-*t*-Butylbenzothiazole with $Pd(CH_3CO_2)_2$. The mixture of 2-*t*-butylbenzothiazole (940 mg) and Pd-$(CH_3CO_2)_2$ (1000 mg) in 15 cm^3 of acetic acid was heated at 80—85°C for 2.5 h. The solvent was evaporated and the residue was chromatographed on a silica-gel column (200 mesh, 1.2×12 cm). A pale yellow-brown fraction eluted by THF/CH_2Cl_2 (1/1) was collected and evaporated to dryness. Recrystallization from dichloromethane and hexane afforded 800 mg of [{Pd(CH_2CMe_2-C_7H_4NS)(μ-CH_3CO_2)}$_2$] (**2**) as yellow crystals.

Metathesis of 2 with Lithium Chloride. Lithium chloride (107 mg) was added to a THF suspension (10 cm^3) of **2** (360 mg). The suspension became clear and was stirred for 1 d at room temperature. The solvent was removed and the residue was dissolved in 10 cm^3 of benzene. Pale beige crystals were precipitated after a few minutes, and were collected and washed with water, methanol, and then diethyl ether to give 295 mg of [{Pd(CH_2CMe_2-C_7H_4NS)(μ-Cl)}$_2$] (**3**).

Metathesis of 2 with Sodium Iodide. A clear THF solution (20 cm^3) of sodium iodide (421 mg) and **2** (400 mg) was left overnight and evaporated to dryness. The residue was extracted with dichloromethane. Hexane was added to the extract and 290 mg of [{Pd(CH_2CMe_2-C_7H_4NS)(μ-I)}$_2$] (**4**) was obtained as brown crystals.

Reaction of 3 with 4. Complex **3** (55 mg) was added to a dichloromethane solution (15 cm^3) of **4** (70 mg), and the

resulting mixture was stirred at room temperature for 12 h. After the mixture was evaporated to dryness, the residue was recrystallized from benzene and hexane to give 100 mg of [(C_7H_4NS-CMe_2CH_2)Pd(μ-Cl)(μ-I)Pd(CH_2CMe_2-C_7H_4NS)] (**5**) as yellow crystals.

Reaction of 3 with Thallium(I) Acetylacetonate. Thallium(I) acetylacetonate (286 mg) was added to a stirred solution of **3** (204 mg) in 10 cm^3 of dichloromethane. After 17 h, the resulting milk-white suspension was centrifugalized. The supernatant solution was purified through a short silica-gel column and evaporated at reduced pressure to 4 cm^3. Addition of hexane afforded 181 mg of [Pd(CH_2-CMe_2-C_7H_4NS)(acac)] (**6**) as pale yellow crystals.

Reaction of 2 or 3 with CO in MeOH. In 20 cm^3 of methanol, **2** (500 mg) was carbonylated at 80 °C under a carbon monoxide pressure of 50 atm for 20 h under stirring. The mixture was filtered to remove palladium black, and then evaporated to dryness. The product, methyl 3-(2-benzothiazolyl)-3-methylbutyrate (**7**), was isolated by extracting the resulting oil with pentane and evaporating and drying up in vacuo. Yield 268 mg (83%), colorless oil.

The compound **7** was also obtained from **3** by the similar way as described above. Yield, 200 mg (96%) from 300 mg of **3**.

Analytical and ^1H NMR data of **7** are also given in Tables 1 and 2, respectively.

We wish to thank Mr. Eiji Ueda of Shikamachi Technical High School for preparing the complex **1**. The present work was partially suported by a Grant-in-Aid for Scientific Research No. 58550572 from the Ministry of Education, Science and Culture.

References

1) D. E. Webster, *Adv. Organomet. Chem.*, **15**, 147 (1977).
2) A. H. Janowicz and R. G. Bergman, *J. Am. Chem. Soc.*, **105**, 3929 (1983).
3) Y. Fuchita, K. Hiraki, and T. Uchiyama, *J. Chem. Soc., Dalton Trans.*, **1983**, 897.
4) Y. Fuchita, K. Hiraki, and Y. Matsumoto, *J. Organomet. Chem.*, **280**, C51 (1985).
5) K. Hiraki, Y. Fuchita, and Y. Matsumoto, *Chem. Lett.*, **1984**, 1947.
6) Y. Fuchita, M. Nakashima, and K. Hiraki, 7th International Symposium on Organosilicon Chemistry, Kyoto, September 1984, Abstr., No. PM16.
7) H. Onoue and I. Moritani, *J. Organomet. Chem.*, **43**, 431 (1972).
8) K. Hiraki, Y. Fuchita, H. Nakaya, and S. Takakura, *Bull. Chem. Soc. Jpn.*, **52**, 2531 (1979).
9) M. R. Churchill, H. J. Wasserman, and G. J. Young, *Inorg. Chem.*, **19**, 762 (1980).
10) A. J. Deeming and I. P. Rothwell, *J. Organomet. Chem.*, **205**, 117 (1981).
11) J. Powell, *J. Am. Chem. Soc.*, **91**, 4311 (1969).
12) B. Galli, F. Gasparrini, B. E. Mann, L. Maresca, G. Natile, A. M. Manotti-Lanfredi, and A. Tiripicchio, *J. Chem. Soc., Dalton Trans.*, **1985**, 1155.
13) J. Metzger and H. Plank, *Bull. Soc. Chim. Fr.*, **1956**, 1692.
14) W. H. Nelson, W. J. Randall, and D. F. Martin, *Inorg. Syn.*, **9**, 53 (1971).

^{17}O NMR Studies on a Series of Manganese Carbonyl Derivatives with Sn-Mn Bond(s)[1)]

Satoru ONAKA,*,† Tadashi SUGAWARA, Yuzo KAWADA,†† Yukihiro YOKOYAMA,††† and Hiizu IWAMURA*
†Department of Chemistry, Nagoya Institute of Technology, Gokiso-cho, Showa-ku, Nagoya 466
Division of Applied Molecular Science, Institute for Molecular Science, Myodaiji, Okazaki 444
(Received April 24, 1986)

^{17}O NMR spectra were measured for a series of manganese carbonyl derivatives, $(CH_3)_xCl_{3-x}Sn$-$Mn(CO)_{5-y}L_y$ and $(CH_3)_{3-x}Sn[Mn(CO)_{5-y}L_y]_{x+1}$(L=$P(OPh)_3$). ^{17}O chemical shifts were correlated with carbonyl stretching frequencies, ^{119}Sn-Mössbauer isomer shifts, and ^{55}Mn NMR chemical shifts. From these correlations, ^{17}O chemical shifts were interpreted in terms of σ- and π-electron acceptance of the tin moieties. It was also clarified that ^{17}O NMR spectroscopy is a direct method to study electronic nature around the oxygen atoms in metal cluster compounds such as $Me_2Sn[Mn(CO)_5]_2$ and $MeSn[Mn(CO)_5]_3$. ^{55}Mn NMR spectra were also measured for some of these compounds to corroborate the ^{17}O NMR results.

The tin atom forms a variety of compounds with transition metals.[2)] Their chemistry has been developed actively by Gorsich, Graham, Clark, Nesmeyanov, and others from the interests to extend the knowledge of "metal-metal bonds," and to look for potential models which emulate metal alloys of relevant metal stoms and/or to find effective new catalysts.[3)] Some series of these compounds have been also the targets of many kinds of spectroscopic studies such as IR, Raman, Mössbauer, NMR, and NQR to elucidate the bonding nature between the tin and transition metal atoms and/or to explore the influence of ligands which are coordinated to the tin and transition metal atoms on the tin-transition metal bonds.[4-7)] We reported similar spectroscpic studies on a series of $R_xX_{3-x}Sn$-$Mn(CO)_{5-y}L_y$-type compounds.[8)] In these studies, our attention was mainly focused on the change of the Sn-Mn, Sn-X, and Sn-R bondings as functions of R, X, and L. Variation of electron distribution around the oxygen and carbon atoms is usually investigated by normal coordinate analyses. Although we can get an insight into the bonding nature of the carbonyl groups in terms of C-O and Mn-C stretching force constants from normal coordinate analyses, the information obtained therefrom on the electronic nature of CO groups is somewhat indirect and obscured by introduction of several stretch-stretch interaction force constants to attain better agreement between the observed and calculated frequencies. However, recent technical improvement of NMR spectroscopy, that is, the pulsed FT-NMR technique, has made it possible to obtain ^{17}O NMR spectra of the metal carbonyl derivatives at the naturally abundant ^{17}O-level[9,10)] together with ^{13}C NMR spectra. Direct information on the electron distribution at the oxygen and carbon atoms is available from ^{17}O and ^{13}C NMR data. We have adopted a series of tin-manganese bonded compounds, $R_xCl_{3-x}Sn$-$Mn(CO)_{5-y}L_y$ and $R_{3-x}Sn[Mn(CO)_{5-y}L_y]_{x+1}$ for ^{17}O and ^{13}C NMR studies from our renewed interest in these types of compounds and to deepen our understanding on ^{17}O and ^{13}C NMR data by correlating these with other spectroscopic results obtained in the series of previous studies.[8)] During the course of this study, we have found that ^{13}C NMR spectra of CO groups are broad and unresolved for axial and equatorial carbonyls because of the nuclear quadrupole moment of ^{55}Mn, but the ^{17}O NMR spectra are reasonably sharp and clearly resolved for axial and equatorial carbonyls in these compounds. This observation promises that ^{17}O NMR which has recently been expeditiously employed as a structural and bonding prove for metal carbonyl derivatives,[9-11)] is an eligible alternative to ^{13}C NMR for investigating the bonding nature of CO groups and/or structures of these compounds. Kump and Todd reported similar observation during the course of this study.[10f)] We now report ^{17}O NMR spectra of some tin-manganese bonded compounds together with ^{55}Mn NMR data to supplement our previous spectroscopic studies on these compounds and to demonstrate how ^{17}O NMR is instrumental for disclosing the bonding of CO groups in metal carbonyl derivatives in which the nuclear quadrupole moment of the metal atom is greater than 1/2.

Experimental

Materials. All the syntheses were made under a purified nitrogen atmosphere. The series of $(CH_3)_xCl_{3-x}Sn$-$Mn(CO)_5$ compounds, that is Cl_3Sn-$Mn(CO)_5$ (**1**), $Cl_2(CH_3)Sn$-$Mn(CO)_5$ (**2**), $Cl(CH_3)_2Sn$-$Mn(CO)_5$ (**3**), and $(CH_3)_3Sn$-$Mn(CO)_5$ (**4**) were prepared according to the previous paper.[8b)] Literature methods were employed to obtain $(CH_3)_2Sn[Mn(CO)_5]_2$ (**5**)[12a)] and $CH_3Sn[Mn(CO)_5]_3$ (**6**).[12b)] The syntheses of $(CH_3)_3Sn$-$Mn(CO)_4L$ (**7**),[13)] $(CH_3)_2Sn[Mn(CO)_4L]_2$ (**8**),[13)] and $(CH_3)_3Sn$-$Mn(CO)_3L_2$ (**9**)[8m)] are described elsewhere.

NMR Measurements. ^{17}O and ^{55}Mn NMR spectra were measured for ca. 1 mol dm^{-3} toluene solutions at ca. 80 °C (**5** and **6**), benzene-d_6 solutions (**4**, **7**, **8**, and **9**) and chloroform-d solutions at 30 °C (**1**, **2**, and **3**) on a Varian FT-80A spectrometer operated at 10.782 and 19.708 MHz respectively with Fourier transform mode for naturally abundant levels (0.037 and 100% for ^{17}O and ^{55}Mn nuclei, respectively). The spectra were recorded using a 10 mm o.d. sample tube.

††Present address: Department of Chemistry, Ibaraki University, 2-1-1 Bunkyo, Mito 310.
†††Present address: Department of Synthetic Cheimistry, Nagoya Institute of Technology, Gokiso-cho, Showa-ku, Nagoya 466.

Table 1. ^{17}O and ^{55}Mn NMR Chemical Shifts and Relevant Carbonyl Stretching Frequencies

Compound[a]	$\delta(^{17}O)$/ppm[b] equatorial	axial	$\delta(^{55}Mn)$/ppm[c]	$\nu(CO)/cm^{-1}$
Cl_3Sn-$Mn(CO)_5$ (**1**)	390	383	−2024[d]	2126(A_1^2) 2046(E) 2040(A_1^1)[d]
$Cl_2(CH_3)Sn$-$Mn(CO)_5$ (**2**)	386	380	−2312[d]	2114(A_1^2) 2032(E) 2020(A_1^1)[d]
$Cl(CH_3)_2Sn$-$Mn(CO)_5$ (**3**)	384	373	−2520[d]	2102(A_1^2) 2008(E) 2016(A_1^1)[d]
$(CH_3)_3Sn$-$Mn(CO)_5$ (**4**)	382	369	−2660[d]	2090(A_1^2) 1994(E) 2002(A_1^1)[d]
$(CH_3)_2Sn[Mn(CO)_5]_2$ (**5**)	387	372	−2559	2102(w) 2089(w) 2077(s) 2005(vs) 1980(s, sh)[e]
$CH_3Sn[Mn(CO)_5]_3$ (**6**)	391	376	−2558	2109(w) 2075(s) 2012(s) 1995(vs)[e]
$(CH_3)_3Sn$-$Mn(CO)_4L$ (**7**)	377		−2869[g]	2050(A_1^2) 1956(E)[f]
$(CH_3)_2Sn[Mn(CO)_4L]_2$ (**8**)	380		not observed	2065(vw) 2039(w) 1995(sh) 1075(vs) 1995(sh)[f]
$(CH_3)_3Sn$-$Mn(CO)_3L_2$ (**9**)	367	372	−3458	2019(A_1^2) 1952(E, A_1^1)[f]

a) L denotes triphenyl phosphite, $P(OC_6H_5)_3$. b) Chemical shifts from $H_2{}^{17}O$. c) Chemical shifts from $K^{55}MnO_4$. d) Data from Ref. 8b. e) Data from Ref. 8o. f) C_6H_6 solution; g: doublet with the spacing of 782.2 Hz.

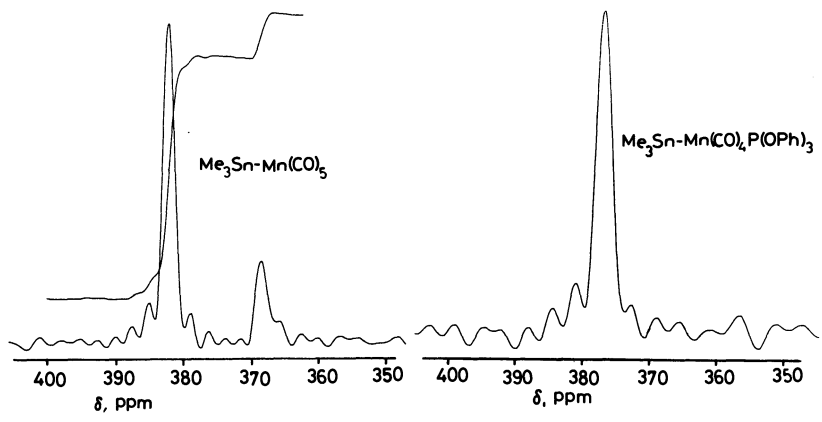

^{17}O NMR Spectra

Fig. 1. ^{17}O NMR spectra of $(CH_3)_3Sn$-$Mn(CO)_5$ in $CDCl_3$ and $(CH_3)_3Sn$-$Mn(CO)_4P(OPh)_3$ in C_6D_6.

Accumulated transients were ca. 5×10^5 (0.02 s acquisition time) for ^{17}O and ca. 10^6 (0.05 s) for ^{55}Mn with 90° pulses. The spectral widths were 8000 Hz both for ^{17}O and ^{55}Mn nuclei and available data points were 323 and 807 for ^{17}O and ^{55}Mn in the time-domain spectra by keeping the Fourier number at 16384. Chemical shifts were measured in parts per million as frequency shifts from synthesizer frequencies, 8.532 and 17.385 MHz respectively for ^{17}O and ^{55}Mn and they were recalculated in the sense that a positive chemical shift designates a resonance to a lower field than that of water oxygen (10.78317 MHz) for ^{17}O, while a positive chemical shift for ^{55}Mn designates a resonance to a higher field than that of potassium permanganate (19.70807 MHz). The ^{17}O NMR spectra of these compounds were reasonably sharp (half band widths of 20—30 Hz). The ^{55}Mn NMR spectra were also sharp for a series of $(CH_3)_xCl_{3-x}Sn$-$Mn(CO)_5$, $(CH_3)_2Sn[Mn(CO)_5]_2$, and $CH_3Sn[Mn(CO)_5]_3$, but the spectra were broad for **7** and **9**. The NMR data are collated in Table 1 together with $\nu(CO)$ frequencies.

Spectral Results, Assignment, and Trends

^{17}O NMR Spectra. The compounds **1—4** which possess four equatorial and one axial carbonyls show two peaks with relative intensity of 4:1, whereas the compounds **7** and **8** which contain only equatorial carbonyls display one peak (Fig. 1). The stronger peaks of **1—4** are assigned to the equatorial carbonyls and the weaker peaks to axial carbonyls. For **5** and **6** which

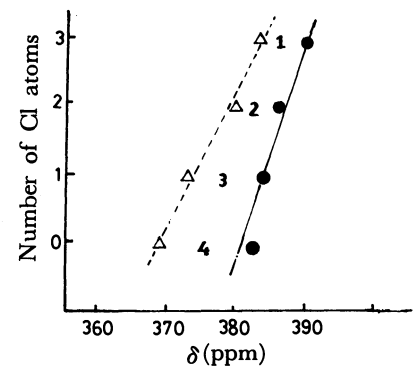

Fig. 2. Plots of ^{17}O chemical shifts vs. the number of the chlorine atoms for $(CH_3)_xCl_{3-x}Sn$-$Mn(CO)_5$.

possess two kinds of carbonyl groups, that is, four cis carbonyls and one trans carbonyl for each $Mn(CO)_5$ group with respect to each Sn-Mn bond, we observe two peaks with relative intensity of 4:1; a similar assignment as above is applicable. All the ^{17}O NMR

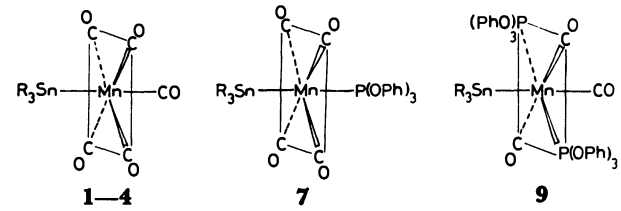

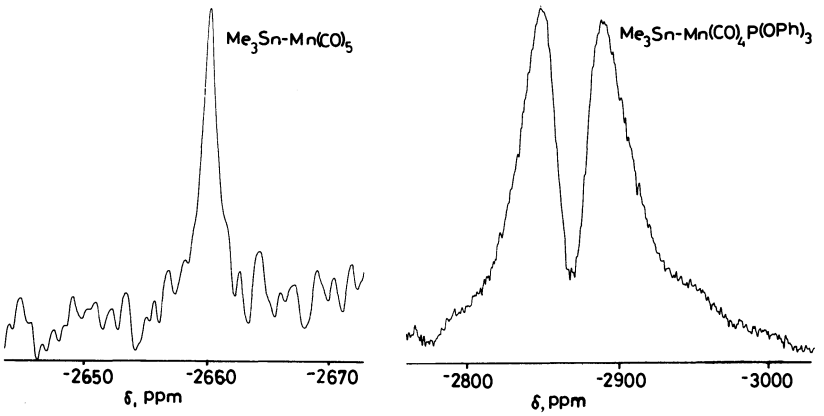

^{55}Mn NMR Spectra

Fig. 3. ^{55}Mn NMR spectra of $(CH_3)_3Sn$-$Mn(CO)_{5-x}L_x$ in toluene.

signals are reasonably sharp (half-band width=20—40 Hz under these conditions). The spectrum of compound **9** which has two peaks with a relative intensity of 2:1 are overlapped and broad (half-band width=120 Hz), suggesting the presence of a number of conformers and the exchange process thereof. The spectral results is a good example to demonstrate that ^{17}O NMR is superior to IR spectroscopy for polynuclear metal carbonyl derivatives such as **5** and **6** to assess the electron distribution and/or bond order of CO groups; in IR spectra of **5** and **6**, several CO stretching peaks are observed. We are forced to carry out rather a laborious normal coordinate analysis in order to cull information on the electronic nature of CO groups. Attempts were also made to get ^{13}C NMR spectra of CO groups for the present compounds. However, unresolved broad peaks were observed for some of these compounds. For series of $(CH_3)_xCl_{3-x}Sn$-$Mn(CO)_5$ compounds, the resonances due to axial carbonyl oxygen show monotonous up-field shifts as large as 14 ppm, whereas those of equatorial carbonyls shift 8 ppm to up-field as we replace a chlorine atom with a methyl group (Fig. 2). The observation indicates that the axial carbonyl is more strongly influenced than equatorial carbonyls by this substitution. For a series of $(CH_3)_{3-x}Sn[Mn(CO)_5]_{x+1}$ compounds, **4**, **5**, and **6**, the resonances of the equatorial carbonyl oxygen shifts to downfield quite similarly to those of axial carbonyls with the increase of the number of the manganese carbonyl moiety. For the substitution of carbonyls with triphenyl phosphite(s), the equatorial carbonyls resonate at a higher field with the increase of the triphenyl phosphite ligand(s), while the axial carbonyls are less influenced by this substitution.

^{55}Mn NMR Spectra. In a series of $(CH_3)_{3-x}Sn[Mn(CO)_5]_{x+1}$ compounds, ^{55}Mn chemical shift moves only slightly to lower field and the line width remains almost constant at 27 Hz with the increase of x from 0 to 2. The one-bond Sn-Mn coupling cannot be observed. In contrast, ^{55}Mn NMR spectra exhibit a drastic change as we replace CO with triphenyl phosphite in $(CH_3)_3Sn$-$Mn(CO)_{5-y}L_y$; (**7**) shows a doublet signal with the separation of 782.2 Hz and the center of this split peaks is at ca. 210 ppm up-field compared with the resonance position of **4** (Fig. 3). For x=2, the signal is very broad ($\Delta\nu_{1/2}$=1340 Hz) and the center is further in the up-field. The observed splitting and broadening are probably due to spin-spin coupling with the phosphorus nucleus, although the ^{31}P NMR of **9** shows a slightly broadened singlet ($\Delta\nu_{1/2}$=31 Hz). It is very often the case that the nucleus with I=1/2 may not show splitting due to coupling but just broadening when coupled with a quadrupolar nucleus which relaxes with fast to intermediate rates.[14] An alternative possibility that this splitting could be derived from the presence of a stereoisomer of **7** where the triphenyl phosphite group occupies a cis position with respecpt to the Sn-Mn bond is rather unlikely, since ^{17}O NMR spectrum of **7** exhibits only one peak. The ^{55}Mn NMR spectra of a series of $(CH_3)_xCl_{3-x}Sn$-$Mn(CO)_5$ are reported in the previous paper.[8b]

Discussion

Correlation of ^{17}O NMR Chemical Shifts with Other Spectroscopic Data. A first attempt was made to correlate the ^{17}O NMR chemical shift values with previously obtained spectral data for **1**—**4**, **7**, and **9**. In Fig. 4 is given the relationship between ^{17}O chemical shifts of axial and equatorial carbonyls and CO stretching frequencies of the carbonyl groups, where A_1^2 mode denotes the symmetric stretching essentially due to equatorial carbonyls and A_1^1 mode denotes the symmetric stretching essentially due to axial carbonyl. It is generally understood that the electron taken up in the part of CO is situated in the antibonding orbital and therefore leads to lowering of the stretching frequencies. Good linear relationship holds for ^{17}O chemical shifts and CO stretching frequencies of A_1^2 mode. For axial carbonyl, however, the plot for **9** deviates conspicuously from the line. Figure 5 shows relationships between ^{17}O chemical shifts and ^{55}Mn chemical shifts for a series of $(CH_3)_xCl_{3-x}Sn$-

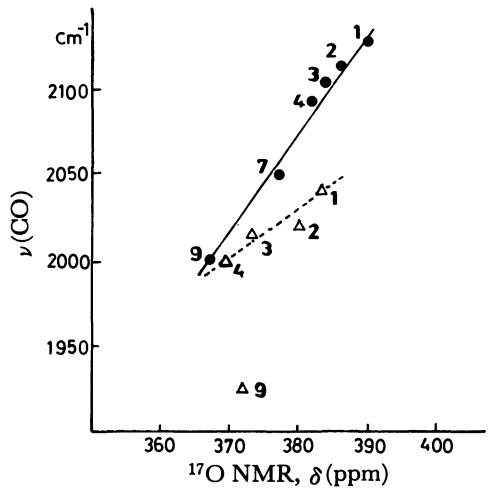

Fig. 4. Correlations of ^{17}O chemical shifts with carbonyl stretching frequencies for $(CH_3)_xCl_{3-x}Sn-Mn(CO)_{5-y}L_y$; ● denotes A_1^2 mode and △ denotes A_1^1 mode.

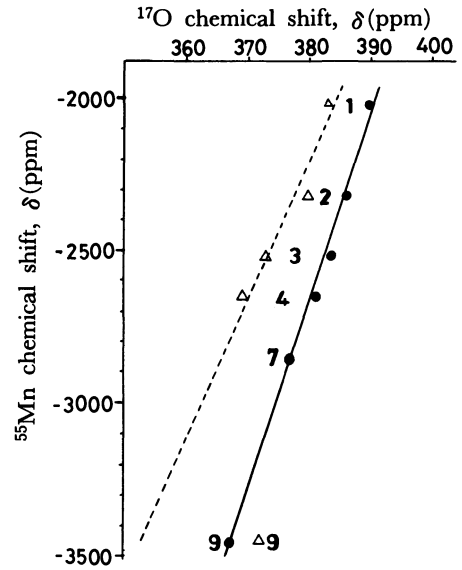

Fig. 5. Relationships between ^{17}O and ^{55}Mn NMR chemical shifts for $(CH_3)_xCl_{3-x}Sn-Mn(CO)_{5-y}L_y$; ● and △ represent chemical shifts for the equatorial and axial carbonyls, respectively.

$Mn(CO)_{5-y}L_y$ compound. Good linear relationship is observed for equatorial carbonyls, but the plot for axial carbonyl of **9** is far from the line drawn for plots of **1**—**4**. Significant deviation of ^{17}O chemical shift for axial carbonyl of **9** against ν(CO) and ^{55}Mn NMR chemical shift observed in Figs. 4 and 5 leads us to assume that a certain factor other than electronic origin might provoke anomaly of ^{17}O chemical shift of the axial carbonyl in **9**. In Fig. 6, correlation between ^{17}O chemical shifts and ^{119}Sn-Mössbauer isomer shifts is examined for a series of $(CH_3)_xCl_{3-x}Sn-Mn(CO)_5$ and a series of $(CH_3)_{3-x}Sn[Mn(CO)_5]_{x+1}$. ^{17}O chemical shifts move to lower field with the increase of ^{119}Sn isomer shift. Since the increase of ^{119}Sn-Mössbauer isomer shift means s-electron deposit on the tin nucleus,[8a]

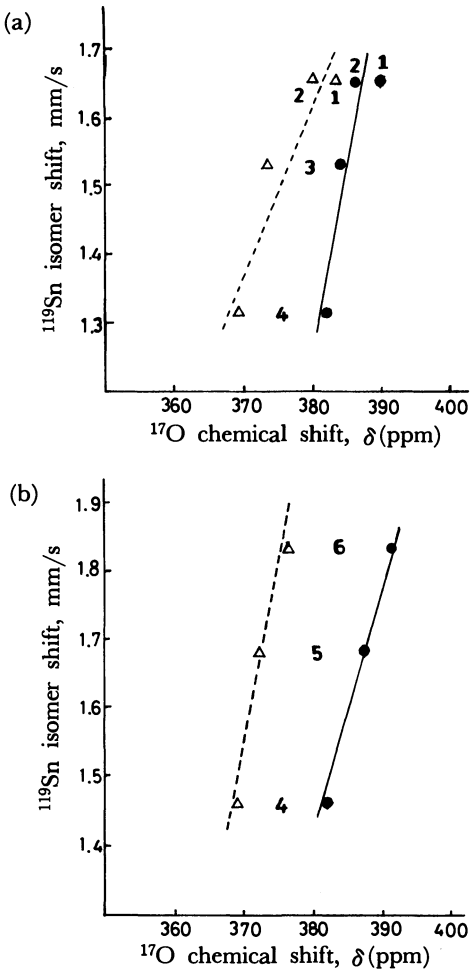

Fig. 6(a): Relationships between ^{17}O NMR chemical shifts and ^{119}Sn-Mössbauer isomer shifts for $(CH_3)_xCl_{3-x}Sn-Mn(CO)_5$. (b): Relationships between ^{17}O NMR chemical shifts and ^{119}Sn-Mössbauer isomer shifts for $(CH_3)_{3-x}Sn[Mn(CO)_5]_{x+1}$; ● represents data for equatorial carbonyls and △ for axial carbonyls.

the correlation indicates sσ-electron transfer from the manganese carbonyl moiety to the tin atom.

Interpretation of ^{17}O Chemical Shifts. The chemical shifts of ^{17}O NMR are dominantly determined by the local paramagnetic contribution to the total screening constant σ.[15,16] The paramagnetic screening σ_p is expressed by Pople in the form

$$\sigma_p = -\text{const} \langle \Delta E \rangle^{-1} \{ \langle r_p^{-3} \rangle (Q_{aa} + Q_{ab})_p \} \quad (1)$$

where ΔE is a mean excitation energy, $\langle r_p^{-3} \rangle$ is the mean inverse cube radius of the valence p-electron, and $(Q_{aa}+Q_{ab})_p$ terms are dependent on the charge imbalance in the ground state valence p-orbitals of the atom **a** and the bond order between the atom **a** and the adjacent atom **b**, respectively. In the previous report from this laboratory,[9b] it was demonstrated that ^{17}O chemical shift is dominantly determined by the change of electron density through σ-donating and π-accepting ability of the group R for $RMn(CO)_5$-type compounds, that is, Q_{aa} term is operative for

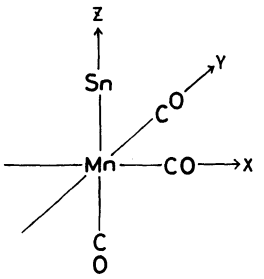

Fig. 7. Coordinate axes for $(CH_3)_xCl_{3-x}Sn-Mn(CO)_{5-y}L_y$.

paramagnetic shift of ^{17}O resonance. The series of $(CH_3)_xCl_{3-x}Sn-Mn(CO)_5$ type compounds, **1**—**4**, are appropriate to see the electronic effect of the tin moiety on the ^{17}O chemical shift. As is shown in Figs. 2 and 6(a), ^{17}O resonances of carbonyl groups are shifted to a lower field by replacing the methyl group with more electronegative chlorine atom and the trend of the shift is more pronounced for axial carbonyl than for equatorial carbonyls. If we choose coordinate axes as is shown in Fig. 7, the axial carbonyl can exploit two π-orbitals (d_{xz} and d_{yz}) which interact with the π-orbitals of the tin atom, whereas the equatorial carbonyl can utilize one π-orbital (d_{xz} or d_{yz}) for π bondings between carbonyls and manganese atom. From this symmetry consideration, we find that the increase of π-electron withdrawal by the more electronegative tin moiety reduces π-interactions between manganese and equatorial and axial carbonyls and the reduction of this π-interaction should be enhanced for axial carbonyl and σ-electron-withdrawing by the tin moiety reduces electron density of only axial carbonyl. Thus, the change of σ- and π-electron-withdrawing ability of the tin moiety should be more strongly reflected on the change of charge density around the oxygen atom of axial carbonyl than that of equatorial carbonyls. The observed trend of enhanced deshielding of ^{17}O nuclei for axial carbonyl than that for equatorial carbonyls is interpreted in terms of increased σ- and π-electron acceptance of the tin moiety with the increase of the number of chlorine atoms. Similar conclusion was obtained in the previous spectroscopic studies for this series of compounds,[8a–c] but the effect of the substitution is more adequately reflected on the ^{17}O chemical shift than, for instance, on a set of force constants of carbonyl groups; in the previous normal coordinate analyses, the effect of this substitution was enhanced for equatorial carbonyls than for axial carbonyls when the Mn–C and C–O stretching force constants of equatorial and axial carbonyls were compared for **1** and **4**.[8c]

The substitution of CO group(s) with triphenyl phosphite(s) which is a weaker π-accepting ligand than CO affects π-interactions between the tin and manganese atoms and between the remaining CO groups and the manganese atom in a similar manner. When the axial carbonyl is replaced with triphenyl phosphite, the π-interaction between the tin and manganese atoms and between the manganese atom and equatorial carbonyls should be enhanced. When equatorial carbonyls are replaced with triphenyl phosphites, the π-interactions between the manganese atom and axial carbonyl and between the manganese atom and the remaining equatorial carbonyls are increased. However, the π bond order between carbon and oxygen atoms is decreased by synergetic effect for both types of substitution. The change of the π-interaction between the tin and manganese atoms was already discussed in the previous ^{119}Sn-Mössbauer study[8d,81] and the attention is now focused on the ^{17}O chemical shift. By replacing axial and/or equatorial carbonyls with triphenyl phosphite as in the case of **7** and **9**, ^{17}O resonance of equatorial carbonyl shifts to a higher field. This observation is in agreement with our expectation that the π bond order between the carbon and oxygen atoms of the remaining carbonyls is reduced by this substitution and reduction of π bond order should lead to a higher field shift of ^{17}O resonance of equatorial carbonyls in **8** by substituting the triphenyl phosphite for axial carbonyl in **7**. However, ^{17}O chemical shift of the axial carbonyl in **9** shifts slightly to a lower field by this substitution. A plausible explanation of this anomaly is that deshielding effect due to diamagnetic phenyl groups which are arranged just in the position to deshield the axial carbonyl might contribute to a lower field shift to some extent, although exact discussion must wait for further study on ^{17}O chemical shift of similar metal carbonyl derivatives.

For a series of $Me_{3-x}Sn[Mn(CO)_5]_{x+1}$ compounds, ^{17}O resonances of both equatorial and axial carbonyls shift monotonously to a lower field with the increase of manganese carbonyl moiety. A heuristic treatment of ^{17}O chemical shifts is shown in Fig. 6(b), that is, a plot of ^{17}O chemical shifts versus ^{119}Sn-Mössbauer isomer shifts shows that ^{17}O chemical shift moves to a lower field with the number of the $Mn(CO)_5$ group and/or with the increase of ^{119}Sn-Mössbauer isomer shift. The result indicates that the more electronegnative tin atom accepts more sσ-electron from the manganese carbonyl moieties with the increase of $Mn(CO)_5$ groups[17] and σ-electron term in Eq. 1 is operative for ^{17}O chemical shift for this series of compounds.

The crux of the matter clarified in this study is that ^{17}O NMR spectroscopy is very convenient and useful technique to investigate the change of electron distribution of the carbonyl groups in metal cluster compounds such as **5** and **6**, and ^{17}O chemical shifts reflect σ- and π-electron acceptance of the tin moiety.

References

1) This work was presented at the 29-th Symposium for Coordination Chemistry held by Chem. Soc. Jpn. on October, 1979 in Hamamatsu.

2) N. S. Vyazankin, G. A. Razuvaev, and O. A. Kruglaya,

Organometal. Chem. Rev. (A)., **3**, 323 (1968) and references therein.

3) H. C. Clark and J. H. Tsai, *Inorg. Chem.*, **5**, 1407 (1966).

4) K. L. Watters and W. M. Risen, Jr., *Inorg. Chim. Acta Rev.*, **1969**, 129 and references therein.

5) D. D. Spencer, J. L. Kirsh, and T. L. Brown, *Inorg. Chem.*, **9**, 235 (1970) and references therein.

6) G. M. Bancroft, K. D. Butler, A. T. Rake, and B. Dale, *J. Chem. Soc., Dalton Trans.*, **1972**, 2025 and references therein.

7) D. H. Harris, M. F. Lappert, J. S. Poland, and W. McFarlane, *J. Chem. Soc., Dalton Trans.*, **1975**, 311.

8) a) S. Onaka, Y. Sasaki, and H. Sano, *Bull. Chem. Soc. Jpn.*, **44**, 726 (1971); b) S. Onaka, T. Miyamoto, and Y. Sasaki, *ibid.*, **44**, 1851 (1971); c) S. Onaka, *ibid.*, **44**, 2135 (1971); d) S. Onaka and H. Sano, *ibid.*, **45**, 1271 (1972); e) S. Onaka, *Nippon Kagaku Kaishi*, **1972**, 1978; f) Y. Kume, D. Nakamura, M. Kubo, and S. Onaka, *J. Magn. Reson.*, **10**, 58 (1973); g) S. Onaka, *Bull. Chem. Soc. Jpn.*, **46**, 2444 (1973); h) S. Onaka, *Bull. Nagoya Inst. Tech.*, **1973**, 133; i) S. Onaka, *Nippon Kagaku Kaishi*, **1974**, 255; j) S. Onaka, *J. Inorg. Nucl. Chem.*, **36**, 1721 (1974); k) S. Onaka, *Bull. Chem. Soc. Jpn.*, **48**, 319 (1975); l) S. Onaka and H. Sano, *ibid.*, **48**, 258 (1975); m) S. Onaka, Y. Yoshikawa, and H. Yamatera, *J. Organomet. Chem.*, **157**, 187 (1978); n) S. Onaka, *Chem. Lett.*, **1978**, 1163; o) S. Onaka and N. Furuichi, *J. Organomet. Chem.*, **173**, 77 (1979).

9) a) Y. Kawada, T. Sugawara, and H. Iwamura, *J. Chem. Soc., Chem. Commun.*, **1979**, 291; b) S. Onaka, T. Sugawara, Y. Kawada, and H. Iwamura, *J. Chem. Soc., Dalton Trans.*, **1982**, 257.

10) a) J. P. Hickey, J. R. Wilkinson, and L. J. Todd, *J. Organomet. Chem.*, **179**, 159 (1979); b) J. P. Hickey, I. M. Baibich, I. S. Butler, and L. J. Todd., *Spectrosc. Lett.*, **11**, 671 (1978); c) D. Cozak, I. S. Butler, J. P. Hickey, and L. J. Todd, *J. Magn. Reson.*, **33**, 149 (1979); d) S. Aimer, L. Milone, D. Osella, G. E. Hawkes, and E. W. Randall, *J. Organomet. Chem.*, **178**, 171 (1979); e) R. L. Kump and L. J. Todd, *J. Chem. Soc., Chem. Commun.*, **1980**, 292; f) R. L. Kump and L. J. Todd, *J. Organomet. Chem.*, **194**, C43 (1980).

11) S. Aime, D. Osella, L. Milone, G. E. Hawkes, and E. W. Randall, *J. Am. Chem. Soc.*, **103**, 5920 (1981).

12) a) W. Jetz, P. B. Simons, J. A. J. Thompson, and W. A. G. Graham, *Inorg. Chem.*, **5**, 2218 (1966); b) A. J. Thompson and W. A. G. Graham, *ibid.*, **6**, 1365 (1967).

13) S. Onaka, Y. Kondo, N. Furuichi, K. Toriumi, and T. Ito, *Bull. Chem. Soc. Jpn.*, **56**, 87 (1983).

14) a) L. J. Todd and J. R. Wilkinson, *J. Organomet. Chem.*, **80**, C31 (1974); b) S. Aime, G. Gervasic, L. Milone, and E. Rosenberg, *Transition Metal Chem.*, **1**, 177 (1976).

15) L. O. Anderson and J. Mason, *J. Chem. Soc., Dalton Trans.*, **1974**, 202.

16) K. A. K. Ebraheem and G. A. Webb, *J. Magn. Reson.*, **25**, 399 (1974).

17) C. Whynter and L. Chandler, *Bull. Chem. Soc. Jpn.*, **43**, 2115 (1970).

^{121}Sb Mössbauer and ^{1}H and ^{13}C NMR Spectroscopic Studies of a Series of Organoantimony(V) Compounds, R_3SbX_2

Makoto YANAGA,* Taichi MIURA, Kazutoyo ENDO, Hiromichi NAKAHARA, and Masuo TAKEDA†
Department of Chemistry, Faculty of Science, Tokyo Metropolitan University, Fukasawa, Setagaya, Tokyo 158
†Department of Chemistry, Faculty of Science, Toho University, Miyama, Funabashi, Chiba 274
(Received April 26, 1986)

The ^{121}Sb Mössbauer spectroscopic and the ^{1}H and ^{13}C NMR nuclear magnetic resonance studies have been performed for a series of organoantimony(V) compounds: R_3SbX_2 (R=CH_3, C_6H_5, p-$CH_3C_6H_4$; X=F, Cl, Br, I). For the trimethylantimony dihalides, the isomer shifts and quadrupole coupling constants of the ^{121}Sb Mössbauer spectra indicated that the withdrawal of the bonding electrons from the antimony atom along Sb–X increased, as the electronegativity of the halogen increased. The chemical shifts of the ^{1}H and ^{13}C NMR spectra showed that the electron population around the methyl group increased with increasing electronegativity of halogen. For phenyl and p-tolyl derivatives, both ^{121}Sb Mössbauer and ^{13}C NMR data showed a trend similar to the methyl compounds. The results suggest that the electron cloud around the antimony atom spreads, with an increase in the electronegativity of the halogen, not only toward the halogen atoms but also toward the plane perpendicular to the bonding direction with the halogen atoms.

Mössbauer spectroscopy is a sensitive tool for studying the effect of the chemical environment on the electron density at and around a Mössbauer atom. Antimony contains 57.25% of the naturally occuring isotope ^{121}Sb. The nuclear radius factor, $\Delta R/R$, of ^{121}Sb is considerably large (about -1×10^{-3}).[1] Hence, a large change in the isomer shift can be expected for varieties of antimony compounds, although a large natural line width of 2.11 mm s^{-1} will result in an inaccuracy in the evaluation of the data.

If Mössbauer spectroscopy is used in combination with other spectroscopies, it is possible to elucidate how an electron is redistributed throughout a molecule when some ligands are varied.[2-5] For example, the effect of various ligands on the electron distribution, especially around tin atoms in the molecules of $R_{3-x}X_xSn$–$Mn(CO)_5$ (R=CH_3, C_6H_5; X=Cl, Br), was successfully studied by combining ^{119}Sn Mössbauer spectroscopy and ^{1}H and ^{55}Mn NMR.[3]

For trimethyl- and triphenylantimony dihalides, several structural studies by the X-ray diffraction method[6,7] and infrared and Raman spectroscopy[8-12] have been reported. ^{121}Sb Mössbauer spectra have also been reported for some of trimethyl- and triphenylantimony dihalides.[13-15]

In the present work, we have examined the correlation between the electronic state at antimony atoms, deduced from the isomer shifts and the nuclear quadrupole coupling constants of ^{121}Sb Mössbauer spectra, and the electron distributions of the ligands, revealed by their chemical shifts in ^{1}H and ^{13}C NMR spectra for a series of organoantimony(V) compounds, trimethylantimony dihalides $(CH_3)_3SbX_2$ (X=F, Cl, Br, I), triphenylantimony dihalides $(C_6H_5)_3SbX_2$ (X=Cl, Br, I), and tri-p-tolylantimony dihalides $(p$-$CH_3C_6H_4)_3SbX_2$ (X=Cl, Br, I). Mössbauer spectra were measured at 20 K and analyzed by using the transmission integral in order to take into account the effect of the thickness of the absorber on the spectra.

Experimental

Preparation of Compounds. All the compounds were prepared by methods described in the literature[8,16,17] or analogous methods. For example, tri-p-tolylantimony dichloride was synthesized by the following method. Antimony trichloride (25 g) dissolved in 250 ml of dry benzene was added slowly to the Grignard reagent prepared from 9.5 g magnesium and 72 g p-bromotoluene dissolved in 250 ml of absolute ether, and the mixture was boiled for thirty hours. The filtrate was distilled under reduced pressure, and the soluble residue was removed by extraction with small quantities of ethanol. The tri-p-tolylstibine was further purified by crystallization from carbon tetrachloride (yield; 20.5 g, 47.3%). Tri-p-tolylstibine (5 g), dissolved in 30 ml of carbon tetrachloride, was treated with chlorine until the solution became yellow. Most of the solvent and the excess chlorine were then removed using a steam bath. The tri-p-tolylantimony dichloride was separated from the cold concentrated solution, and recrystallized from carbon tetrachloride (yield; 3.2 g, 54.2%).

The purity of the compounds studied in the present work was checked by elemental analyses of carbon and hydrogen, and by IR and/or NMR.

Mössbauer Spectra. The ^{121}Sb Mössbauer absorption spectra were obtained using $\simeq$440 μCi $Ca^{121m}SnO_3$ source moving in a constant acceleration mode. The source and the absorber containing 13—25 mg cm^{-2} of Sb were both kept at 20 K in a cryostat[18] and the 37.14 keV resonance γ-rays were detected by counting the escape peak in a Xe–CO_2 proportional counter. Generally, the measurement was continued until $1-3\times10^4$ counts/channel was achieved. The velocity scale was calibrated by using a laser interferometer.

The spectra were analyzed by the program of least-squares fitting of transmission integrals,[19-22] edited by L. H. Bowen.[23] The value of 1.34 was used as a fixed parameter for $Q(7/2)/Q(5/2)$ in analyses.[24]

^{1}H and ^{13}C NMR Spectra. The ^{1}H and ^{13}C NMR spectra were observed at room temperature for the chloroform-d solution containing 1% tetramethylsilane (TMS) as the internal standard. A PMX 60SI spectrometer and a JNM-FX60, Fourier transform spectrometer were used for the measurement of ^{1}H and ^{13}C NMR, respectively.

Results and Discussion

The observed ^{121}Sb Mössbauer spectra for the trimethylantimony dihalides are shown in Fig. 1. The Mössbauer parameters obtained in the present work for a series of compounds are summarized in Table 1. The absolute value of the isomer shift (IS) decreases and that of the quadrupole coupling constant (e^2q_zQ) increases as the electronegativity of the halogen increases for all the trimethyl, triphenyl, and tri-*p*-tolyl compounds.

On the assumption that the contribution of the core electrons to the electron density at the nucleus of antimony is, as a first approximation, the same for all the compounds studied and that the shielding effect on the 5s electrons by 5d electrons is considerably smaller than that by the 5p electrons, 5s and 5p electrons can be considered mainly responsible for the observed Mössbauer parameters. As the absolute value of the IS is proportional to the electron density at the antimony nucleus, the trend of the IS shows that the s electron density decreases as the electronegativity of the ligand halogen atom increases. This fact implies the withdrawal of s electrons from the antimony atom along Sb–X.

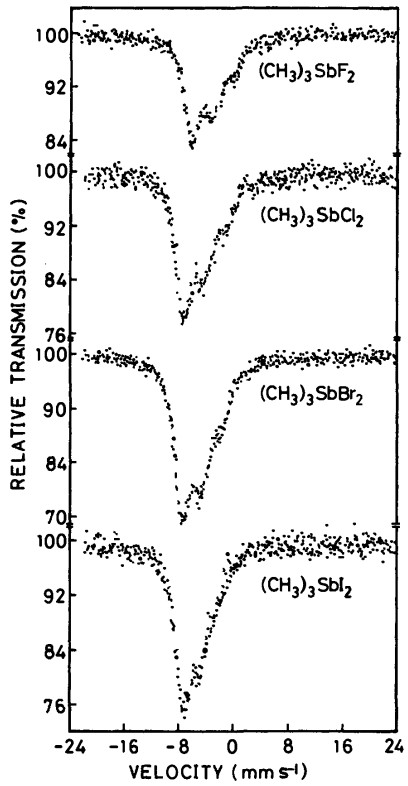

Fig. 1. ^{121}Sb Mössbauer spectra of $(CH_3)_3SbX_2$ (X=F, Cl, Br, I) against a $Ca^{121m}SnO_3$ source at 20 K.

All the compounds investigated are found to have large negative e^2q_zQ, indicating the main component of the electric field gradient, eq_z, is positive since the quadrupole moment, eQ, of the ^{121}Sb nucleus is negative.

X-Ray structural studies for R_3SbX_2 (R=CH_3, C_6H_5; X=Cl, Br, I) revealed that the trigonal bipyramidally coordinated antimony atom has two halogen atoms occupying the apical positions along the *z*-axis and three organic ligands situating in the *x*–*y* plane,[6,7] and the sp^3d hybrid is expected.[15] Neglecting 5d orbital contributions, the electric field gradient, eq_z, due to the asymmetric p electrons and the asymmetric factor, η, can be written in general as

$$eq_z = C\{-N_{Pz}+1/2(N_{Px}+N_{Py})\}$$

and

$$\eta = 3(N_{Px}-N_{Py})/\{-2N_{Pz}+(N_{Px}+N_{Py})\},$$

where N_{Pi} with $i=x, y, z$ represents the orbital population along the three directions and C is a constant with the positive sign. This axial symmetry allows us to put $N_{Px}=N_{Py}$ and $\eta=0$. The observed positive eq_z means that the p electron density along the *x* and *y* directions is greater than that along the *z*-axis. The trend that the electric field gradient at the antimony nuclear site increases as the electronegativity of the halogen atoms increases suggests that the electrons in the p_z orbital is withdrawn toward the halogen atom along Sb–X.

Two ^{121}Sb Mössbauer parameters, IS and e^2q_zQ, both show that the electron attraction by the halogen

Table 1. ^{121}Sb Mössbauer Parameters for R_3SbX_2 Compounds

Compound	IS/mm s^{-1} [a]	e^2q_zQ/mm s^{-1} [b]	Γ_{exp}/mm s^{-1}
$(CH_3)_3SbF_2$	−4.90±0.03	−24.1±0.3	2.53±0.04
$(CH_3)_3SbCl_2$	−6.01±0.04	−23.1±0.3	2.49±0.05
$(CH_3)_3SbBr_2$	−6.23±0.02	−21.6±0.1	2.29±0.04
$(CH_3)_3SbI_2$	−6.44±0.03	−18.3±0.3	2.42±0.01
$(C_6H_5)_3SbCl_2$	−6.00±0.02	−21.1±0.2	2.29±0.04
$(C_6H_5)_3SbBr_2$	−6.22±0.02	−19.4±0.2	2.32±0.01
$(C_6H_5)_3SbI_2$	−6.42±0.03	−17.2±0.3	2.26±0.03
$(p\text{-}CH_3C_6H_4)_3SbCl_2$	−5.84±0.05	−20.9±0.5	2.16±0.07
$(p\text{-}CH_3C_6H_4)_3SbBr_2$	−6.07±0.03	−19.7±0.3	2.27±0.07
$(p\text{-}CH_3C_6H_4)_3SbI_2$	−6.14±0.07	−17.2±0.7	2.68±0.02

a) Relative to a $Ca^{121m}SnO_3$ source. b) $Q(7/2)/Q(5/2)=1.34$ was used as a fixed parameter and the listed values were estimated for the $Q(5/2)$ value.

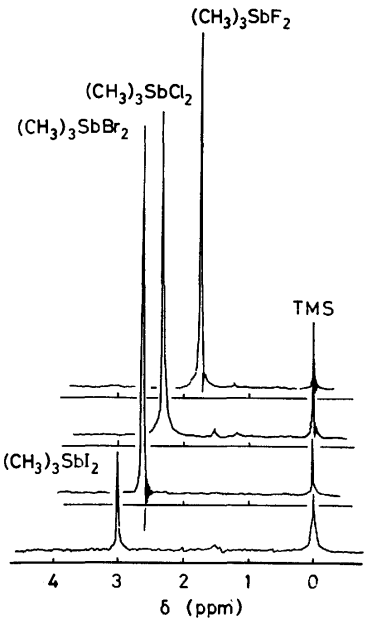

Fig. 2. ^{1}H NMR spectra of $(CH_3)_3SbX_2$ (X=F, Cl, Br, I) in $CDCl_3$ at room temperature. Tetramethylsilane (TMS) was used as the internal standard.

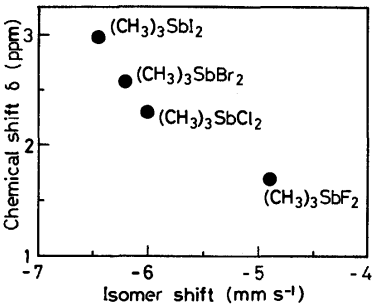

Fig. 3. Relationship between ^{121}Sb Mössbauer isomer shift (relative to a $Ca^{121m}SnO_3$ source) and ^{1}H NMR chemical shift (with respect to TMS).

Table 2. ^{1}H and ^{13}C NMR Parameters for $(CH_3)_3SbX_2$ Compounds

Compound	^{1}H chemical shift	^{13}C chemical shift
	ppm[a)]	ppm[a)]
$(CH_3)_3SbF_2$	1.70	9.3
$(CH_3)_3SbCl_2$	2.30	22.9
$(CH_3)_3SbBr_2$	2.57	26.5
$(CH_3)_3SbI_2$	2.98	31.9

a) Relative to $(CH_3)_4Si$ (TMS).

increases, as the electronegativity difference between the halogen and antimony increases.

It is further noted that the absolute values of the IS decrease slightly for the same halogen atom in the order of $(CH_3)_3SbX_2$, $(C_6H_5)_3SbX_2$, and $(p\text{-}CH_3C_6H_4)_3SbX_2$ as shown in Table 1, when we compare the effects of ligands in the x-y plane. The electron releasing ability of these substituents is known to be in the order of methyl>p-tolyl>phenyl group. In fact, for the p-tolyl and phenyl derivatives, the electron density of the carbon bonded to the antimony atom was found to increase with this sequence, which will be shown later (^{13}C NMR data in Table 3). In the foregoing discussion, the shielding effects of the 5s electrons by 5d electrons were ignored in comparison to those due to the 5p electrons. However, as a minor effect, the s electron density at the ^{121}Sb nuclear site will slightly decrease with an increase of the density on the 5d orbitals. In the case of $(p\text{-}CH_3C_6H_4)_3SbX_2$, the electron-donating methyl group bonded to the phenyl ring may cause the π-electron density of the carbon bonded to the antimony higher. Although the X-ray diffraction data have not yet been available for the p-tolyl derivative, the π-orbital may interact with the vacant $5d_{xz}$ and $5d_{yz}$ orbitals of antimony. This interaction may enhance the shielding effects, resulting in the decrease of 5s electron density at the ^{121}Sb nuclear site. This will be one of the possible reasons for the observed Mössbauer parameters.

In order to examine in more detail the electron distribution around antimony, we compared the ^{1}H and ^{13}C NMR data with the ^{121}Sb Mössbauer data. The ^{1}H NMR spectra of trimethylantimony dihalides are shown in Fig. 2. In Fig. 3 is illustrated the relationship between the ^{121}Sb Mössbauer isomer shift and ^{1}H NMR chemical shift; ^{1}H chemical shift smoothly decreases as the absolute value of the isomer shift decreases. The values of the chemical shift, δ, of ^{1}H and ^{13}C NMR for trimethylantimony dihalides are listed in Table 2. Both ^{1}H and ^{13}C NMR chemical shifts are observed at higher fields as the electronegativity of the halogen coordinated to the antimony increases. This implies that the electron population becomes larger around the methyl group when the more electronegative halogen is attached to the antimony atom. The s electron density at the antimony itself decreases as shown by the Mössbauer isomer shift. The present NMR data are consistent with those on the streching force constant (k) of antimony-carbon atoms obtained for $(CH_3)_3SbX_2$ (X=F, Cl, Br) by far-infrared spectroscopy (k decreases in the order of X=F, Cl, Br).[11] The present observation is, however, contrary to the one reported on methyl halides CH_3X, where the chemical shifts of ^{1}H NMR are observed at lower fields as the electronegativity of the halogen increases.[25]

The values for ^{13}C chemical shift of the triphenyl and tri-p-tolylantimony dihalides are summarized in Table 3. In the case of triphenyl and tri-p-tolylantimony dihalides, the δ value for the carbon atom coordinated to the antimony atom shifts toward a higher field as the electronegativity of the halogen increases, indicating that the electron population increases at the carbon atom coordinated to the antimony atom. This trend agrees with the case of trimethylantimony dihalides. However, Table 3 also shows that the δ values of the o- and p-carbon atoms shift toward lower fields although

Table 3. ^{13}C NMR Parameters for $(C_6H_5)_3SbX_2$ and $(p\text{-}CH_3C_6H_4)_3SbX_2$ Compounds

Compound	Chemical shift/ppm[a]				
	C-1	C-2	C-3	C-4	C-5
$(C_6H_5)_3SbCl_2$	140.0	134.2	129.6	131.8	—
$(C_6H_5)_3SbBr_2$	141.0	133.6	129.5	131.6	—
$(C_6H_5)_3SbI_2$	141.3	133.2	129.5	131.4	—
$(p\text{-}CH_3C_6H_4)_3SbCl_2$	136.6	133.9	130.1	142.1	21.4
$(p\text{-}CH_3C_6H_4)_3SbBr_2$	137.7	133.5	130.1	142.0	21.4
$(p\text{-}CH_3C_6H_4)_3SbI_2$	138.0	133.1	130.1	141.8	21.5

a) Relative to $(CH_3)_4Si$ (TMS).

the δ values for the *m*-carbon stays constant. This implies that the π-electron density is withdrawn from the phenyl or *p*-tolyl group to the antimony, indicating the electrophilic nature of the antimony atom.

These results may imply that the electron cloud around the antimony atom spreads in the x–y plane as well as in the z direction with an increase in the electronegativity of the halogen atom. Therefore, the electron density on the carbon coordinated to the antimony might be increased.

Conclusion

In a series of organoantimony(V) compounds R_3SbX_2 (R=CH_3, C_6H_5, *p*-$CH_3C_6H_5$; X=F, Cl, Br, I), the ^{121}Sb Mössbauer spectra and ^1H and ^{13}C NMR spectra were measured. Interesting information concerning the electron distribution around the antimony atom was obtained.

As the electronegativity of the halogen occupying the apical position along the z-axis in the trigonal bipyramidal structure increases, (1) the ^{121}Sb Mössbauer data show an increasing withdrawal of the electron density from the antimony atom to the halogen atom, and (2) the ^1H and ^{13}C NMR chemical shifts show the increase of the electron population at the methyl group in trimethylantimony dihalides and on the carbon coordinated to the antimony of the aromatic group in the triphenyl and tri-*p*-tolylantimony dihalides. These facts suggest that the cloud of the electrons around the antimony atom spread along the x and y directions with an increasing tendency for the withdrawal of the electron density from the antimony along the z-axis.

The authors gratefully acknowledge the cooperation of Drs. Yasuyuki Miyazawa, Haruo Matsuyama, and Masato Yoshida, and Prof. Dr. Michio Kobayashi of Tokyo Metropolitan University in the measurements of the ^1H and ^{13}C NMR spectra. We would also like to thank Dr. Masashi Takahashi of Toho University for measurements of the ^{121}Sb Mössbauer spectra. The authors are also indebted to Prof. Dr. Lawrence H. Bowen at North Carolina State University for a least-squares fitting program of transmission integrals.

References

1) D. E. Fenton and J. J. Zuckermann, *J. Am. Chem. Soc.*, **90**, 6226 (1968).
2) S. Onaka, Y. Sasaki, and H. Sano, *Bull. Chem. Soc. Jpn.*, **44**, 726 (1971).
3) A. K. H. Al-Sa'ady, C. A. McAuliffe, K. Moss, R. V. Parish, and R. Fields, *J. Chem. Soc., Dalton Trans.*, **1984**, 491.
4) S. W. Hedges and L. H. Bowen, *Inorg. Chem.*, **23**, 1458 (1984).
5) L. H. Bowen, "^{121}Sb Mössbauer Spectroscopy," in "Mössbauer Effect Data Index 1972," ed by J. G. Stevens and V. E. Stevens, IFI/Plenum, New York, N. Y. (1973), p. 71.
6) A. F. Wells, *Z. Kristallogr., Kristallgeom., Kristallphys., Kristallchem.*, **99**, 367 (1938).
7) T. N. Polynova and M. A. Porai-Koshits, *J. Struct. Chem.*, 7, 691 (1966).
8) G. G. Long, G. O. Doak, and L. D. Freedman, *J. Am. Chem. Soc.*, **86**, 209 (1964).
9) G. O. Doak, G. G. Long, and L. D. Freedman, *J. Organomet. Chem.*, **4**, 82 (1965).
10) R. G. Goel, E. Maslowsky, Jr., and C. V. Senoff, *Inorg. Nucl. Chem. Lett.*, **6**, 833 (1970).
11) R. G. Goel, E. Maslowsky, Jr., and C. V. Senoff, *Inorg. Chem.*, **10**, 2572 (1971).
12) C. Woods and G. G. Long, *J. Mol. Spectrosc.*, **38**, 387 (1971).
13) G. G. Long, J. G. Stevens, R. J. Tullbane, and L. H. Bowen, *J. Am. Chem. Soc.*, **92**, 4230 (1970).
14) K. Dehnicke, K. Fleck, K. Schmidt, and J. Pebler, *Z. Anorg. Allg. Chem.*, **451**, 109 (1979).
15) L. H. Bowen and G. G. Long, *Inorg. Chem.*, **15**, 1039 (1976).
16) G. T. Morgan and G. R. Davies, *Proc. Roy. Soc. (London)*, **A110**, 523 (1926).
17) H. H. Willard, L. R. Perkins, and F. F. Blicke, *J. Am. Chem. Soc.*, **70**, 737 (1948).
18) T. Takano, Y. Ito, and M. Takeda, *Radioisotopes*, **29**, 341 (1980).
19) S. Margulies and J. R. Ehrman, *Nucl. Instrum. Methods*, **12**, 131 (1961).
20) G. K. Shenoy and J. M. Friedt, *Phys. Rev. Lett.*, **31**, 419 (1970).
21) G. K. Shenoy and J. M. Friedt, *Nucl. Instrum. Method*, **116**, 573 (1974).
22) G. K. Shenoy, J. M. Friedt, H. Maletta, and S. L. Ruby, "Curve Fitting and the Transmission Integral: Warnings and Suggestions," in "Mössbauer Effect Methodology,"

ed by I. J. Gruverman, C. W. Seidel, and K. Dieterly; Plenum Press, New York, N. Y. (1974), Vol. 9, pp. 277—305.
23) L. H. Bowen (private communication, 1984).
24) J. G. Stevens and S. L. Ruby, *Phys. Lett.*, **A322**, 91 (1970).
25) R. L. Pecsok, L. D. Shields, T. Cairns, and I. G. McWilliam, "Modern Methods of Chemical Analysis," 2nd ed, John Wiley & Sons, New York, N. Y. (1976), Chap. 15.

 © 1986 The Chemical Society of Japan Bull. Chem. Soc. Jpn., 59, 3091—3095 (1986)

The Reaction of *cyclo*-Triphosphate with Ethanolamines

Mitsutomo Tsuhako,* Chiyoko Sueyoshi, Tohru Miyajima,† Shigeru Ohashi,†
Hiroyuki Nariai,†† and Itaru Motooka††

Kobe Women's College of Pharmacy, Kitamachi, Motoyama, Higashinada-ku, Kobe 658
†Department of Chemistry, Faculty of Science, Kyushu University 33, Hakozaki, Higashi-ku, Fukuoka 812
††Department of Chemistry, Faculty of General Education, Kobe University, Tsurukabuto, Nada-ku, Kobe 657
(Received April 30, 1986)

The reaction of *cyclo*-triphosphate(P_{3m}) with mono-(MEA), di-(DEA), or triethanolamine(TEA) in an aqueous solution was investigated under various conditions (mixing ratio of MEA, DEA, or TEA to P_{3m}, pH, temperature, and reaction time). 1) In the pH region of 7—12, P_{3m} reacted with MEA or DEA to yield tri-, di-, and monophosphate derivatives of MEA or DEA. The phosphoric acid ester of MEA or DEA was not formed at all. 2) The reactivities of MEA and DEA to P_{3m} were in the order of MEA > DEA, and TEA did not react with P_{3m}. 3) The reactivity of P_{3m} with MEA or DEA decreased with the decrease in the pH, and no reaction took place under acidic conditions. 4) The maximum yields of triphosphate derivatives of MEA, *N*-(2-hydroxyethyl)-triphosphoramidate(P_3-(N)MEA) and of DEA, *N*-bis(2-hydroxyethyl)triphosphoramidate (P_3-(N)DEA), were about 75 and 60% respectively at a molar ratio of 1 : 1, at pH 12, and at room temperature. 5) P_3-(N)MEA and P_3-(N)DEA easily recyclized to the raw material, P_{3m}, under acidic conditions. 6) The mechanism of the reaction between P_{3m} and MEA or DEA was investigated.

Inorganic condensed phosphates can be roughly classified into the following three types: 1) linear polyphosphates, 2) cyclic phosphates, and 3) ultraphosphates (network-like phosphates).[1] Among them, linear poly- and ultraphosphates are widely used for drugs, food additives, fertilizers, detergents, water treating agents, and industrial chemicals.[2-4] However, as to cyclic phosphates, few practical applications[5-7] have been known, and few reports[8,9] have been presented on fundamental investigations of them. Since Feldmann reported, in 1965—1969, that P_{3m} reacts with alkylamines,[10] phenols,[11] and amino acids,[12] P_{3m} has been attracting much attention as a phosphorylating agent for organic compounds. Rabinowitz[13,14] reported the reaction of P_{3m} with amino acids (glycine and alanine); Saffhill,[15] the phosphorylation of nucleosides with P_{3m}, and Dombrovskii and Dorosh,[16] the reaction of P_{3m} with 1,6-hexanediamine. However, in these studies paper chromatography has been principally used to analyze the reaction products; it provides only a semiquantitative discussion. In the present study, the reaction of P_{3m} with mono- (MEA), di- (DEA), or triethanolamine (TEA) has been examined in order to develop studies of the application of P_{3m} as a phosphorylating agent. Both ^{31}P-NMR and anion-exchange chromatography have been used to determine the structure and the amounts of the reaction products. The reaction mechanism is also discussed.

Experimental

Chemicals. Sodium *cyclo*-triphosphate hexahydrate, $Na_3P_3O_9 \cdot 6H_2O$, was obtained by recrystallizing it three times from an aqueous solution of industrial-grade anhydrous sodium *cyclo*-triphosphate (98%) from Rasa Kogyo, Ltd. Unless otherwise stated, guaranteed grade mono-, di-, and triethanolamine were used without further purification.

Reaction between *cyclo*-Triphosphate and Ethanolamine. In the reaction of P_{3m} with MEA, DEA, or TEA, 50 cm^3 of a 0.5 mol dm^{-3} aqueous sodium *cyclo*-triphosphate (P_{3m}) solution and 50 cm^3 of a 0.5—5 mol dm^{-3} aqueous mono-, di-, or triethanolamine solution were mixed. The pH values of the mixed solution were about 12.0—12.5 in MEA, 11.6—11.9 in DEA, and 10.5—10.7 in TEA. These mixed solutions were then adjusted to the prescribed pH value (pH 12, 10, 7, or 4) by the use of a 6 mol dm^{-3} sodium hydroxide aqueous solution and hydrochloric acid, and the reaction was allowed to proceed at room temperature or 50 °C. Since the pH of the mixed solution gradually fell with the progress of the reaction, a sodium hydroxide solution was added to it to maintain the prescribed pH value.

Anion-exchange chromatography and the measurement of ^{31}P-NMR were carried out by the methods described in a previous paper.[17]

Results and Discussion

Reaction of P_{3m} with MEA. Aqueous solutions of P_{3m} and MEA were mixed in a molar ratio of 1 : 1. The pH of the mixed solution was adjusted to 12 with a sodium hydroxide solution, and the reaction was allowed to proceed at room temperature. With the progress of the reaction, the pH of the mixed solution gradually decreased to about 9.3 after 1 d. This fact indicates that P_{3m} reacts with water or MEA to produce linear phosphates or their derivatives. In order to examine this, the present authors investigated the reaction products and their amounts by the use of anion-exchange chromatography and ^{31}P-NMR.

As an example, two representative anion-exchange chromatograms of the reaction products are shown in Fig. 1. Immediately after the reaction, a large peak due to an unknown compound appeared at about 880 cm^3 of the effluent (designated as Compound C). The peak of the pyrophosphate (P_2) was also observed, though its amount was slight. The amount of Compound C increased with the passage of the reaction time, but in a reaction over a long period its amount gradually decreased due to hydrolysis. As can be seen from Fig. 1, when the reaction was allowed to proceed for 44 d, in addition to Compound C four peaks due to un-

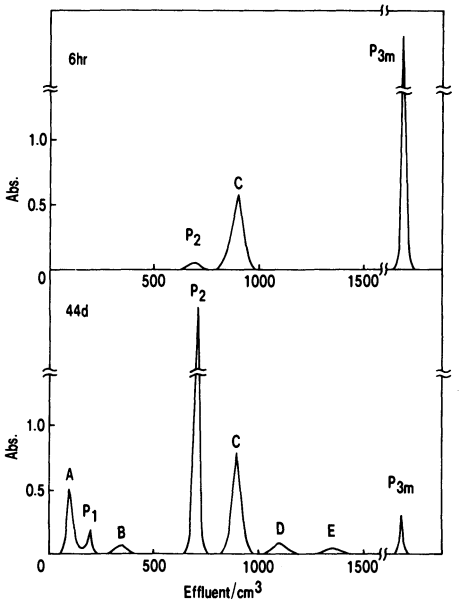

Fig. 1. Elution patterns of the reaction products of P_{3m} with MEA at pH 12.
P_{3m}: MEA = 0.5 mol dm^{-3}: 0.5 mol dm^{-3}.

known compounds (Compounds A, B, D, and E) were found at about 100, 350, 1150, and 1360 cm^3 of the effluent. Moreover, almost no production of triphosphate (P_3) was found in this reaction.

Figure 2 shows the ^{31}P-NMR spectra of the reaction products of P_{3m} and MEA at a molar ratio of 1 : 10 and pH 12. It can be seen that the main product, Compound C, is a triphosphate derivative of MEA, *N*-(2-hydroxyethyl)triphosphoramidate(P_3-(N)MEA). In the ^{1}H-decoupling spectrum of Fig. 2, the doublets at δ −0.5 and −4.3 ppm were assigned to the end phosphorus atoms of P_3-(N)MEA, P_α and P_γ, respectively, while the triplet at −20.3 ppm corresponded to the middle phosphorus atom, P_β. In the ^{1}H-coupling spectrum, each of the doublets of P_α ought to split into triplets because of the two hydrogen atoms of the methylene (-NHCH$_2$-) group, but actually a quintet was observed as a result of overlapping.

The ^{31}P-NMR spectra do not always indicate that Compound C is P_3-(N)MEA, with a P-N bond in the molecule. There is another possibility that Compound C is a triphosphoric acid ester of MEA, 2-aminoethyl triphosphate, with a P-O-C bond in the molecule. In order to check this possibility, an aqueous solution of Compound C was made acidic (pH 3). Since Compound C easily recyclized to P_{3m}, it was concluded that Compound C is a triphosphate derivative of MEA, P_3-(N)MEA, with a P-N bond in the molecule.[18,19] The singlet at δ 4.7 ppm in Fig. 2 is attributed to the phosphorus atom of a monophosphate derivative of MEA,

N-(2-hydroxyethyl)phosphoramidate$^-$O-P(=O)(O$^-$)-NHCH$_2$CH$_2$OH (P_1-(N)MEA).

This phosphorus atom splits into a triplet in the ^{1}H-coupling due to the influence of two hydrogen atoms of the methylene group. Compound A, whose amount is next to P_3-(N)MEA, was estimated to be a monophosphate derivative of MEA, P_1-(N)MEA, with a P-N bond in the molecule. Singlets at δ 4.0 and −5.1 ppm were attributed to PO_4^{3-} and $P_2O_7^{4-}$ ions.[20]

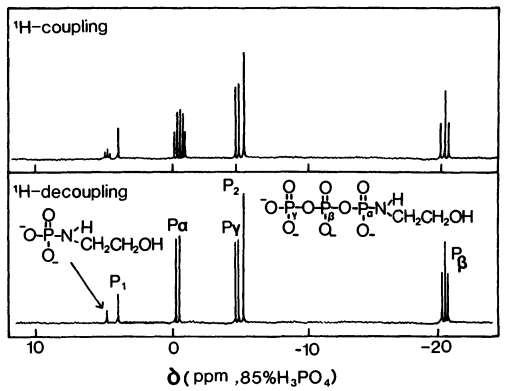

Fig. 2. ^{31}P-NMR spectra of the reaction products in the P_{3m}-MEA series.

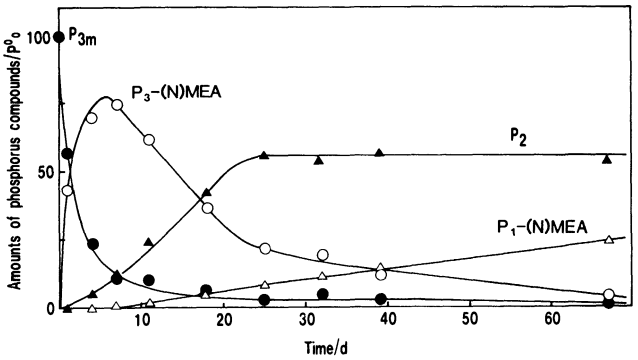

Fig. 3. Changes of the amounts of phosphorus compounds in the reaction of P_{3m} with MEA at pH 12.
P_{3m}: MEA = 0.5 mol dm^{-3}: 0.5 mol dm^{-3}.

The structures of Compounds B, D, and E have not yet been characterized because they were formed in only minute amounts and could not be isolated in a pure form. However, based upon the fact that, when a solution containing much of Compound B was made acidic (pH=3), it was hydrolyzed to produce P_2, Compound B was estimated to be *N*-(2-hydroxyethyl)diphosphoramidate(P_2-(N)MEA). On the other hand, the orthophosphoric acid ester of MEA, 2-aminoethyl dihydrogenphosphate, was not produced in the reaction of P_{3m} with MEA. Thus, it was found that the phosphorylation of MEA with P_{3m} takes place at the position of the NH_2 group in MEA.

Amounts of P_3-(N)MEA, P_2-(N)MEA, and P_1-(N)MEA. Figure 3 shows the changes in the amounts of the various phosphates formed by the reaction of P_{3m} with MEA at a molar ratio of 1 : 1, pH 12, and room temperature. P_3-(N)MEA began to be produced immediately after the start of the reaction; the yield reached

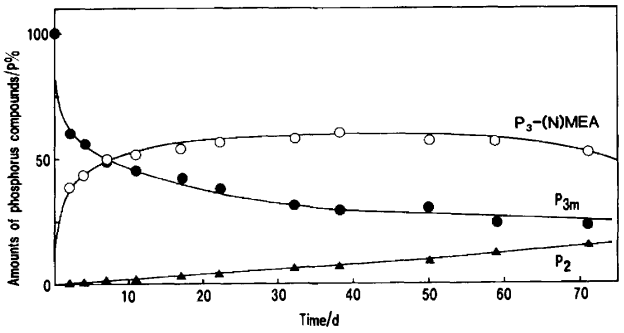

Fig. 4. Changes of the amounts of phosphorus compounds in the reaction of P_{3m} with MEA at pH 10.
P_{3m}: MEA = 0.5 mol dm^{-3}: 0.5 mol dm^{-3}.

about 75% after 7 d. After that, however, it gradually decreased as the reaction progressed. On the other hand, P_1-(N)MEA increased with the reaction time, attaining about 24% after 67 d. Also, the amount of P_2 increased with the progress of the reaction, and the crystals of tetrasodium pyrophosphate decahydrate, $Na_4P_2O_7 \cdot 10H_2O$, began to precipitate after 25 d. However, the amount of $Na_4P_2O_7 \cdot 10H_2O$ precipitated was not taken into consideration in Fig. 3. The amounts of P_1, P_2-(N)MEA, and Compounds D and E were so small (P_1, 4.4; P_2-(N)MEA, 4.7; Compound D, 6.6, and E, 11.5%) that they were omitted in Fig. 3.

Figure 4 shows the changes in the amounts of phosphorus compounds formed by the reaction between P_{3m} and MEA (P_{3m} : MEA = 1 : 1) at pH 10 and room temperature. The raw material, P_{3m}, gradually decreased with the progress of the reaction, showing that the reaction of P_{3m} with MEA at pH 10 was slower than that at pH 12. The main product, P_3-(N)MEA, attained to about 50% after 7 d. After that, the amount was constant (about 55—60%) until 60 d after the reaction. P_1, P_1-(N)MEA, P_2-(N)MEA, and Compounds D and E were not formed until 20 d after the reaction. No precipitate of $Na_4P_2O_7 \cdot 10H_2O$ was observed under these conditions.

In the reaction of P_{3m} with MEA at a molar ratio of 1 : 1, pH 7, and room temperature, the amount of P_3-(N)MEA was very small amounting only to about 2.3% even after 60 d. At pH 4, the phosphorylation of MEA with P_{3m} was not observed at all. Instead, the hydrolysis products of P_{3m}, i.e., P_3, P_2, and P_1 were obtained. From the above experimental results (pH 12, 10, 7, and 4), it can be concluded that P_{3m} and MEA react well in highly alkaline regions, that the reactivity decreases with the decrease in the pH, and that no reaction takes place under acidic conditions. This is ascribable to the formation of inactive $H_3{}^+NCH_2CH_2OH$ under acidic conditions.

Figure 5 shows the changes in the amounts of phosphorus compounds when the reaction was allowed to proceed at a molar ratio of 1 : 10, pH 12, and room temperature. P_{3m} rapidly decreased after the start of the reaction, and it became almost zero after several hours. On the contrary, P_3-(N)MEA began to be produced

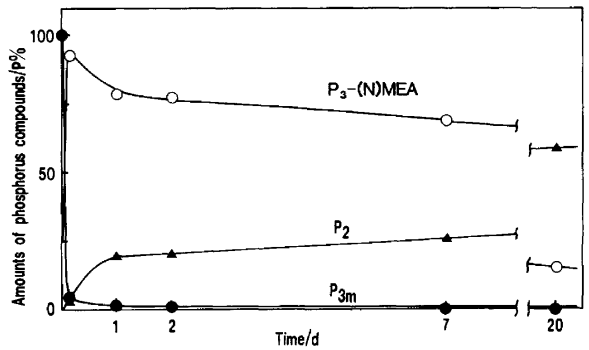

Fig. 5. Changes of the amounts of phosphorus compounds in the reaction of P_{3m} with MEA at pH 12.
P_{3m}: MEA = 0.5 mol dm^{-3}: 5 mol dm^{-3}.

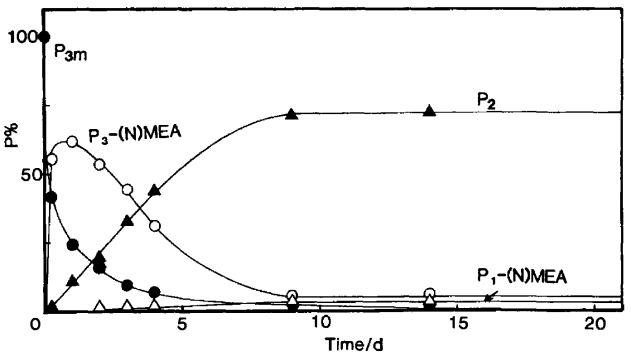

Fig. 6. Changes of the amounts of phosphorus compounds in the reaction of P_{3m} with MEA at 50 °C.
P_{3m}: MEA = 0.5 mol dm^{-3}: 0.5 mol dm^{-3}, pH 12.

rapidly, and it was produced about 92% within 3.5 h. The amount of P_3-(N)MEA gradually decreased after that with the lapse of the reaction time. The production rate of P_3-(N)MEA was faster, and its amount was larger at a molar ratio of 1 : 10 than that at 1 : 1 (Fig. 3). Since the amounts of P_1, P_1-(N)MEA, and P_2-(N)MEA were small (about 7.1, 8.0, and 2.7% respectively), they are not shown in Fig. 5. No Compound D or E was produced under these experimental conditions.

In Fig. 6, the amounts of P_3-(N)MEA, P_1-(N)MEA, and P_2 formed by the reaction of P_{3m} with MEA (molar ratio = 1 : 1) at pH 12 and 50 °C are plotted against the time. The reaction proceeded faster than that at room temperature (Fig. 3). The pattern of the formation of P_3-(N)MEA, P_1-(N)MEA, and P_2 was, however, similar to that at room temperature. The amount of P_3-(N)MEA increased to the maximum value of about 61% after 1 d, thereafter, it gradually decreased.

Reaction of P_{3m} with DEA. A representative anion-exchange chromatogram for the products resulting from the reaction of P_{3m} and DEA at a molar ratio of 1 : 1, pH 12, and room temperature is shown in Fig. 7. Other than the peaks of P_1, P_2, and P_3, three peaks due to unknown compounds were found at about 100, 440, and 815 cm^3 of the effluent (designated as Compounds I, II, and III). In the reaction of P_{3m} with DEA, the production of P_3 was remarkable. This may be due to the lower reactivity of

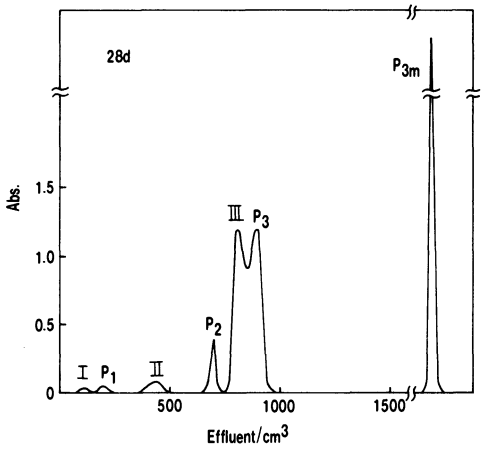

Fig. 7. Elution pattern of the reaction products of P_{3m} with DEA at pH 12.
P_{3m}: DEA = 0.5 mol dm^{-3}: 0.5 mol dm^{-3}.

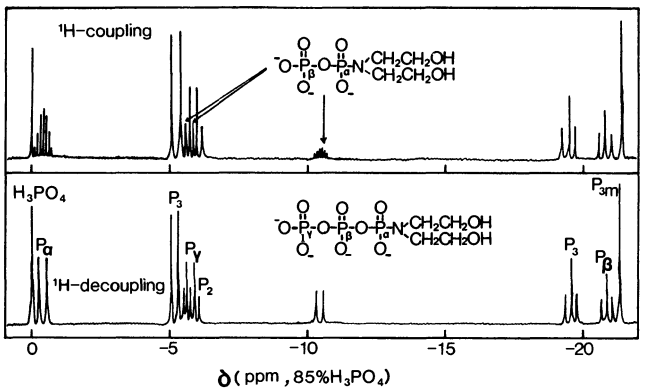

Fig. 8. ^{31}P-NMR spectra of the reaction products in the P_{3m}-DEA series.

P_{3m} with DEA compared with that with MEA. The hydrolysis of P_{3m} in such an alkaline solution can not be neglected in this case. In order to clarify the structures of Compounds I, II, and III, ^{31}P-NMR of the reaction products of P_{3m} and DEA was measured (Fig. 8). At δ −0.3, −5.4, and −20.8 ppm in the ^{1}H-decoupling spectrum, peaks due to P_α (doublet), P_γ (doublet), and P_β (triplet) of a triphosphate derivative of DEA, *N*-bis(2-hydroxyethyl)-triphosphoramidate (P_3-(N)DEA) are found. In the ^{1}H-coupling, the P_α of P_3-(N)DEA was split into seven peaks due to the four hydrogen atoms of two methylene groups,

$$\left(\text{P-N}\begin{matrix}\text{CH}_2\text{-}\\ \text{CH}_2\text{-}\end{matrix}\right).$$

Since P_β and P_γ are not influenced by these hydrogen atoms, no coupling due to a proton is recognized. It is interesting that, at δ −5.3 and −10.3 ppm, two doublets due to the P_β and P_γ of a diphosphate derivative of DEA, *N*-bis(2-hydroxyethyl)diphosphoramidate (P_2-(N)DEA), were found. One doublet (δ −5.1 ppm) and one triplet (δ −19.7 ppm) are due to phosphorus atoms of the end PO_4 and to the middle PO_3 of P_3[20] respectively. From the peak heights (amounts) of Compounds II and III on an anion-exchange chromatogram (Fig. 7), it was deduced that Compound II is a diphosphate derivative of DEA, P_2-(N)DEA, while III is a triphosphate derivative of DEA, P_3-(N)DEA. Another proof that Compound III is a triphosphate derivative of DEA with a P-N bond in the molecule is the fact that Compound III was easily recyclized to P_{3m} when the solution of Compound III was made acidic (pH 3).

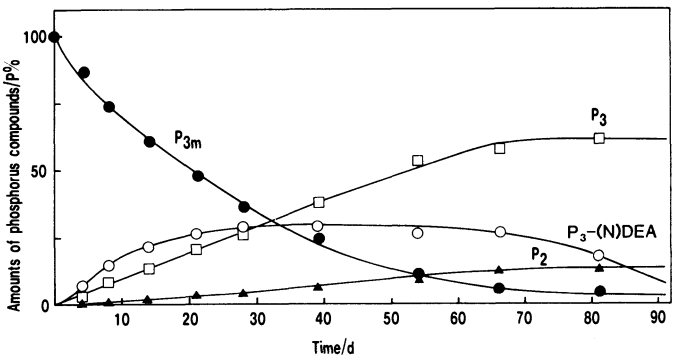

Fig. 9. Changes of the amounts of phosphorus compounds in the reaction of P_{3m} with DEA at pH 12.
P_{3m}: DEA = 0.5 mol dm^{-3}: 0.5 mol dm^{-3}.

From the fact that P_2-(N)DEA was not produced at the initial stage of the reaction, but was produced with the progress of the reaction, it can be considered that P_2-(N)DEA is produced by the hydrolysis of P_3-(N)DEA. That is, the P_3-(N)DEA formed at the initial stage of the reaction is gradually hydrolyzed to yield P_2-(N)DEA and P_1.

It was impossible to determine the structure of Compound I because of its small yield. However, it can be anticipated that Compound I is a monophosphate derivative of DEA, *N*-bis(2-hydroxyethyl)phosphoramidate (P_1-(N)DEA), because P_1 was produced when an aqueous solution of Compound I was made acidic (pH 3).

Amounts of P_3-(N)DEA, P_2-(N)DEA, and P_1-(N)-DEA. Figure 9 shows the changes in the amounts of phosphates formed by the reaction of P_{3m} and DEA at a molar ratio of 1 : 1, pH 12, and room temperature. Compared with the reaction of MEA, the production of P_3-(N)DEA was very slow; after 28 d it attained a maximum level of about 30%, smaller than that observed in the reaction of MEA. After that, it was gradually hydrolyzed. On the other hand, the amount of P_3 increased linearly up to 70 d, and it showed a constant value of about 60%. Since the amounts of P_1-(N)DEA, P_2-(N)DEA, and P_1 were very small (P_1-(N)DEA, 0.8; P_2-(N)DEA, 2.0; P_1, 0.5%), they are omitted in Fig. 9. A characteristic phenomenon is that the production of P_3 was dominant in the P_{3m}-DEA series, although the production of P_2 was remarkable in the P_{3m}-MEA series. Therefore, it is considered that, in the P_{3m}-MEA series, P_3-(N)MEA is produced at the first stage of the reaction and that this is hydrolyzed principally to P_1-(N)MEA and P_2. On the contrary, in the P_{3m}-DEA series, the

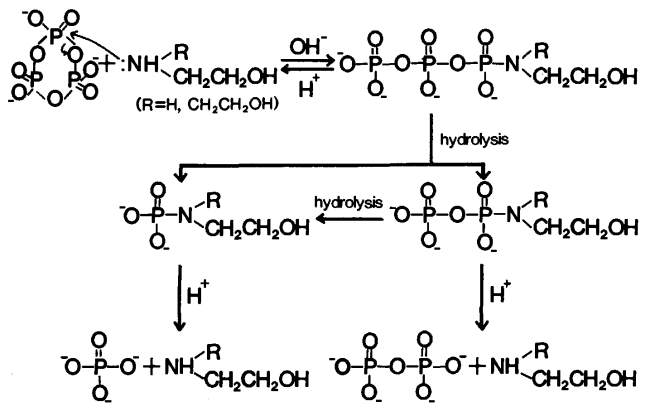

Fig. 10. The reaction mechanism of P_{3m} with MEA or DEA.

hydrolysis of P_{3m} to P_3 proceeded at the same time as the phosphorylation of DEA. With the lapse of the reaction time, P_3-(N)DEA was gradually hydrolyzed to P_2-(N)DEA and P_1.

The reaction of P_{3m} with TEA was allowed to proceed under the same conditions as those in the P_{3m}-MEA and P_{3m}-DEA series. However, no reaction took place in the P_{3m}-TEA series. This is due to the absence of a hydrogen atom directly bonded to the nitrogen atom in the TEA molecule. That is, no ring cleavage of P_{3m} takes place because of the absence of a dissociable hydrogen atom in TEA when the lone-pair of the nitrogen atom of TEA nucleophilically attacks the phosphorus atom of P_{3m}. On the other hand, Feldmann[10] reported that P_{3m} easily reacts with methylamine and dimethylamine to yield triphosphate derivatives of them, but not with trimethylamine. That is, P_{3m} easily reacts with primary and secondary amines in alkaline regions, but does not react with tertiary amines. This fact agrees well with our experimental results.

Mechanism of the Reaction of P_{3m} with MEA or DEA. The mechanism of the reaction of P_{3m} with MEA or DEA in alkaline solutions is shown in Fig. 10. The lone-pair of the nitrogen atom of MEA or DEA nucleophilically attacks the phosphorus atom of P_{3m}, causing a ring cleavage of P_{3m} to produce a triphosphate derivative of MEA or DEA, P_3-(N)MEA or P_3-(N)DEA, with a P-N bond in the molecule. These compounds are gradually hydrolyzed in the reaction solution to form di- and monophosphate derivatives of MEA or DEA. When P_3-(N)MEA and P_3-(N)DEA were made acidic (pH 3), they were easily recyclized to P_{3m}. From this fact, it is clear that the reaction of P_{3m} with MEA or DEA proceeds reversibly, depending upon the pH. When di- and monophosphate derivatives of MEA or DEA are made acidic, they are easily hydrolyzed to yield P_2 and P_1 respectively. Based upon the fact that the phosphoric acid ester of MEA or DEA was not formed in this reaction, it can be estimated that the reactivity of the NH_2 group to P_{3m} is higher than that of the OH group in ethanolamines. When the reaction of P_{3m} with MEA, DEA, or TEA was compared, the reactivity was in the order of MEA>DEA, and TEA did not react with P_{3m}.

References

1) J. Van Wazer, "Phosphorus and Its Compounds," Interscience Publishers, New York (1958), Vol. 1, p. 601.
2) J. Van Wazer, "Phosphorus and Its Compounds," Interscience Publishers, New York (1961), Vol. 2, p. 1462.
3) E. Kobayashi, "Chemistry and Application of Phosphates," ed by S. Hori Kagaku Kogyosha (1969), p. 115.
4) K. Hirata, "New Food Industry," Shokuhin Shizai Kenkyukai (1973), p. 34.
5) Stevens, Langner, Parry, and Rollinson, British Patent, 770565 (1957).
6) K. Kainuma, T. Oda, and S. Suzuki, *Denpun Kogyo Gatsukaishi*, **14**, 24 (1967).
7) R. C. Ropp, N. Caldwell, and H. D. Layman, U. S. Patent, 3318818 (1967).
8) S. Y. Kalliney, "Topics in Phosphorus Chemistry," ed by M. Grayson and E. J. Griffith John Wiley and Sons, New York (1972), Vol. 7, p. 255.
9) G. Kura, T. Nakashima, and F. Oshima, *J. Chromatogr.*, **219**, 385 (1981).
10) W. Feldmann, *Z. Chem.*, **1**, 26 (1965).
11) W. Feldmann, *Chem. Ber.*, **99**, 3251 (1966).
12) W. Feldmann, *Z. Chem.*, **4**, 154 (1969).
13) J. Rabinowitz, *Helv. Chim. Acta*, **52**, 2663 (1969); **53**, 1350 (1970); **54**, 1483 (1971).
14) J. Rabinowitz, *Nature*, **224**, 795 (1969).
15) R. Saffhill, *J. Org. Chem.*, **35**, 2881 (1970).
16) N. M. Dombrovskii and A. I. Dorosh, *Russ. J. Inorg. Chem.*, **17**, 981 (1972).
17) M. Tsuhako, A. Nakajima, T. Miyajima, S. Ohashi, H. Nariai, and I. Motooka, *Bull. Chem. Soc. Jpn.*, **58**, 3092 (1985).
18) O. T. Quimby, A. Narath, and F. H. Lohman, *J. Am. Chem. Soc.*, **82**, 1099 (1960).
19) W. Feldmann and E. Thilo, *Z. Anorg. Allg. Chem.*, **328**, 113 (1964).
20) V. Mark, C. Dungan, M. Crutchfield, and J. Van Wazer, "Topics in Phosphorus Chemistry, ^{31}P Nuclear Magnetic Resonance," ed by M. Grayson and E. J. Griffith John Wiley and Sons, New York (1967), Vol. 5, p. 319.

 © 1986 The Chemical Society of Japan Bull. Chem. Soc. Jpn., 59, 3097—3101 (1986)

Ring-Opening Reactions of Thiophene Derivatives by the Use of the Birch Reduction

Takanobu KUMAMOTO,* Kumiko HOSOYA, Satoshi KANZAKI, Kazuhiro MASUKO, Mikio WATANABE, and Kozo SHIRAI
Department of Chemistry, Faculty of Science, Tokai University, Kitakaname, Hiratsuka, Kanagawa 259-12
(Received December 14, 1985)

It was found that the Birch reduction of 2-(2-thienyl)alkanoic acid and subsequent alkylation with benzyl bromide resulted in the formation of 2-alkyl-3-benzylthio-3-hexenoic acid selectively. Further, the Birch reduction of a 2,3-dialkylthiophene and subsequent alkylation with benzyl bromide gave a tetrasubstituted olefin which was formed by a selective C–S bond fission between the 1 and 5 positions of the thiophene nuclei. In contrast to these results, the Birch reduction of 3-thiophenecarboxylic acid derivatives and subsequent benzylation gave 2-alkyl-4-benzylthio-3-butenoic acid which was formed by a C–S bond fission between the 1 and 2 positions of the thiophene nuclei.

It is well-known that a Birch reduction of thiophene gives a mixture of dihydrothiophenes and ring-opening products, 2- and 3-butene-1-thiols.[1] In recent few years, several reports showed the formation of regioselective-ring-opening compounds by a Birch reduction of the thiophene derivatives. For example, Joullié et al. reported that the Birch reduction of 2-thiophenecarboxylic acid (**1**) gave (*Z*)-5-mercapto-3-pentenoic acid (**2**) which was formed by a reductive cleavage of the bond between the sulfur atom and C-2 of the thiophene nuclei.[2] However, we have reported that the product which was formed by the C–S bond fission between the 1 and 5 positions of the thiophene nuclei, 4-benzylthio-3-ethyl-3-alkenoic acid (**4**) or (*Z*)-3-benzylthio-3-hexenoic acid (**6**), was obtained by the Birch reduction of 2-(3-thienyl)alkanoic acid (**3**) or 2-thienylacetic acid (**5**) and subsequent alkylation with benzyl bromide.[3]

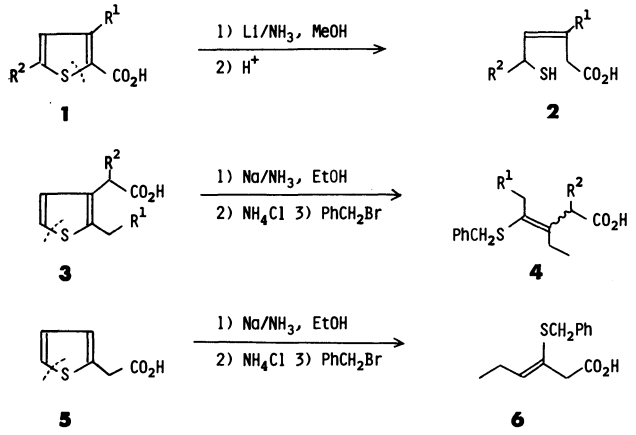

1 **2** **3** **4** **5** **6**

These results show that the regioselectivity of the C–S bond fission and the position of the double bond in the products are largely affected by the substituents of the thiophene derivatives. From this point of view, we investigated Birch reductions of several types of thiophenes in order to clarify the effects of the substituents on the regioselectivity of the ring-opening reactions.

Results and Discussion

Preparations of Thiophenes. The preparations of 2-(2-thienyl)alkanoic acids (**9a—c**) were carried out as follows: The reaction of lithium enolate of ethyl 2-thienylacetate (**7**), prepared from **7** with lithium diisopropylamide (LDA) in THF, with alkyl halides gave ethyl 2-(2-thienyl)alkanoate (**8**) in good yields. Further, **9** was obtained by the hydrolysis of **8**.

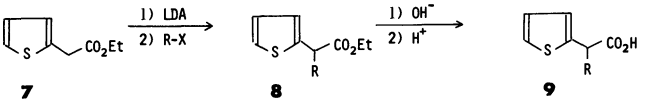

7 **8** **9**

a: R = CH_3-, **b**: R = $CH_3(CH_2)_3$-, **c**: R = CH_2=CH-CH_2-

2-Thienylacetone (**11**) was prepared by the Jones oxidation of 1-(2-thienyl)-2-propanol (**10**) which was obtained by successive treatments of thiophene at −30 °C with butyllithium and propylene oxide.

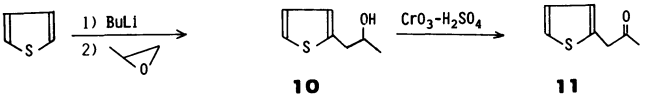

10 **11**

2,3-Dialkylthiophenes (**15a—c**) were prepared by the following two methods. Commercially available 3-methylthiophene (**12**) was used as the starting material for the preparation of 2-alkyl-3-methylthiophenes (**15a, b**). 2-Bromo-3-methylthiophene (**13**) was prepared from **12** and *N*-bromosuccinimide (NBS) by the procedure of Kellogg et al.[4] The resulting **13** was converted to the Grignard reagent **14** in ether and **14** was allowed to react with two equivalents of an alkyl *p*-toluenesulfonate[5] to give **15a, b** in good yields (Scheme 1).

3-Ethyl-2-propylthiophene (**15c**) was prepared by modifing the method reported by Meltz et al.[6] as shown in Scheme 2.

The Birch Reductions of Thiophenes. The Birch reduction of 2-(2-thienyl)propanoic acid (**9a**) with 5 equivalents of sodium in liquid ammonia in the presence of ethanol and a subsequent treatment with ammonium chloride and benzyl bromide resulted in

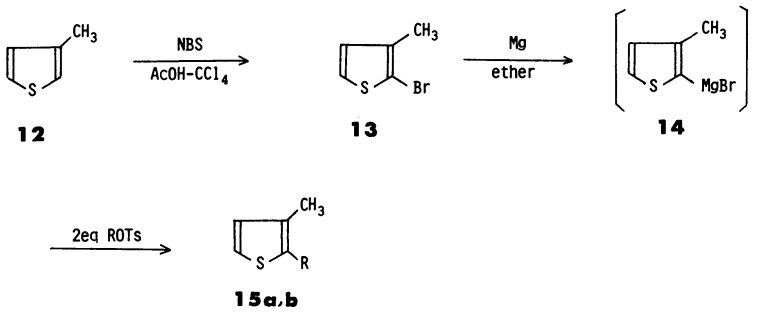

Scheme 1.

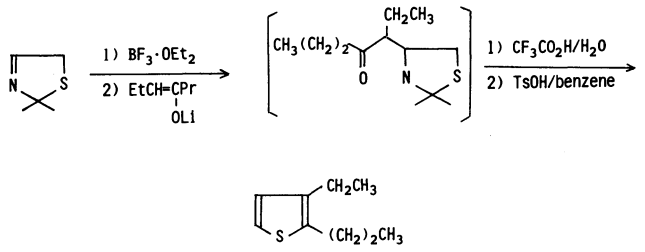

Scheme 2.

the formation of (*Z*)-3-benzylthio-2-methyl-3-hexenoic acid (**16a**) in 63% yield. The Birch reductions of 2-(2-thienyl)hexanoic acid (**9b**) and 2-(2-thienyl)-4-pentenoic acid (**9c**) under similar reaction conditions also gave (*Z*)-3-benzylthio-2-butyl-3-hexenoic acid (**16b**) and (*Z*)-2-allyl-3-benzylthio-3-hexenoic acid (**16c**) in 77 and 76% yields, respectively. These products were formed by the cleavage of the bond between the sulfur atom and C-5 of the thiophene nuclei.

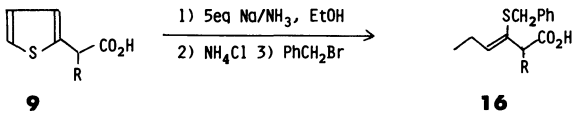

However, the Birch reduction of 2-thienylacetone (**11**) (which contains a carbonyl group at the same position as **9**) did not give ring-opening products. When **11** was treated with 4 equivalents of sodium and benzyl bromide, a dialkylated compound **17** was obtained without the formation of ring-opening products. This result shows that the formation of a carbanion at the α-carbon of the carbonyl group of **11** is faster than the reduction of the thiophene nuclei.

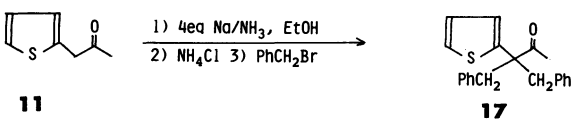

In a previous report,[3] we found that the Birch reduction of 2-propylthiophene under similar reaction conditions gave (*Z*)-4-benzylthio-3-heptene. In the present report, the Birch reduction and alkylation of 3-methylthiophene (**12**) was examined. The reduction of **12** with 4 equivalents of sodium under reaction conditions similar to those reported before gave a mixture of many products. A careful separation of the products by silica-gel column chromatography and an NMR study clarified that 1-benzylthio-2-methyl-2-butene (**18**), 1-benzylthio-3-methyl-2-butene (**19**), 1-benzylthio-2-methyl-1-butene (**20**), and 1-benzylthio-3-methyl-1-butene (**21**) were formed in the ratio of 10:4:4:1.

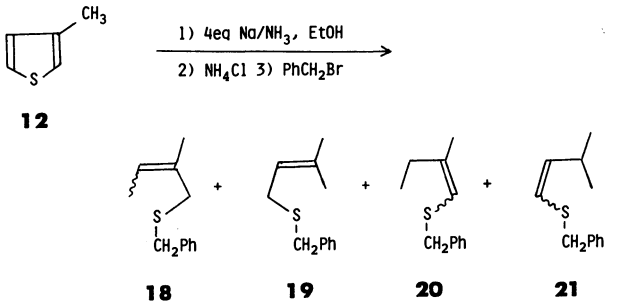

The ratio of the trisubstituted and disubstituted olefins in the above products was 18:1. This result indicates that the product distribution is dependent on the thermodynamic stability of the olefins. Therfore, Birch reductions of 2,3-dialkylthiophene (**15**) were examined with an expectation that tetrasubstituted olefins would be formed.

When 2-butyl-3-methylthiophene (**15a**) was allowed to react with 4 equivalents of sodium by the procedure reported previously, 4-benzylthio-3-methyl-3-octene (**22a**) was obtained in 60% yield as expected. Similarly, a Birch reduction of 3-methyl-2-octylthiophene (**15b**) and 3-ethyl-2-propylthiophene (**15c**) also gave tetrasubstituted olefins **22b** and **22c** in 37 and 52% yields, respectively. These results show that the reductive

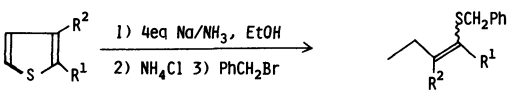

a: R^1= $CH_3(CH_2)_3$- R^2= CH_3-
b: R^1= $CH_3(CH_2)_7$- R^2= CH_3-
c: R^1= $CH_3(CH_2)_2$- R^2= CH_3CH_2-

cleavage of the bond between the sulfur atom and C-5 of the thiophene nuclei gave thermodynamically stable tetrasubstituted olefins.

Next, it was found that the regioselectivity of the ring-opening reactions of 3-thiophenecarboxylic acid (**23a**) and its derivatives was different from that of the above-mentioned reactions. When **23a** was allowed to react with 5 equivalents of sodium and benzyl bromide, (*Z*)-4-benzylthio-2-methyl-3-butenoic acid (**24a**) was obtained in 51% yield. Similarly, the Birch reduction and alkylation of 2-methyl-3-thiophenecarboxylic acid (**23b**) gave (*Z*)-4-benzylthio-2-ethyl-3-butenoic acid (**24b**) in 69% yield. In these reactions, a reductive cleavage of the thiophene ring occurred between the sulfur atom and C-2 of the thiophene nuclei and the resulting products were disubstituted olefins rather than trisubstituted olefins. Further, the Birch reduction and alkylation of 2-(α-hydroxybenzyl)-3-thiophenecarboxylic acid (**25**) resulted in the formation of an over-reduced product, (*Z*)-4-benzylthio-2-(2-phenylethyl)-3-butenoic acid (**26**) in 48% yield.

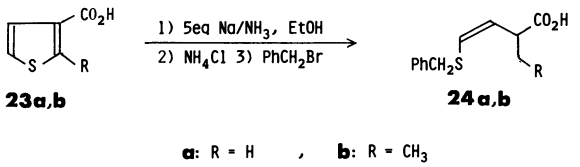

23a,b **24a,b**

a: R = H , **b**: R = CH_3

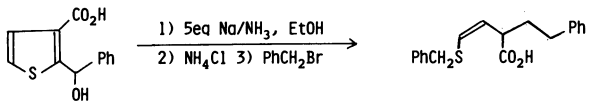

25 **26**

In conclusion, the ring-opening reactions of thiophene derivatives are classified into three types. (A) The ring-opening reaction occurs between the sulfur atom and C-5 of the thiophene nuclei and the double bond remains at the 2 position. Birch reductions of **3**, **5**, **9**, and **15** belong to type-A. (B) The ring-opening reaction occurs between the sulfur atom and C-2 of thiophene and the double bond remains at the 3 position. A Birch reduction of **1** belongs to type-B. (C) The position of a C-S bond fission is the same as type-B, but the double bond remains at the 4 position. Birch reductions of **23** and **25** belong to type-C.

These selectivities of the ring-opening reaction can be reasonably explained by the two mechanisms shown in Shemes 3 and 4.

In these mechanisms, the reduction and the protonation of the thiophene derivatives of type-A forms thermodynamically stable dihydrothiophene (**I**) as the intermediate (Scheme 3). The formation of 2,3-dihydrothiophene (**III**) as the intermediate in Scheme 4 by the reduction and the protonation of radical anion **II**, which is produced by the reduction of the thiophene derivatives of the type-C, can be affected by the

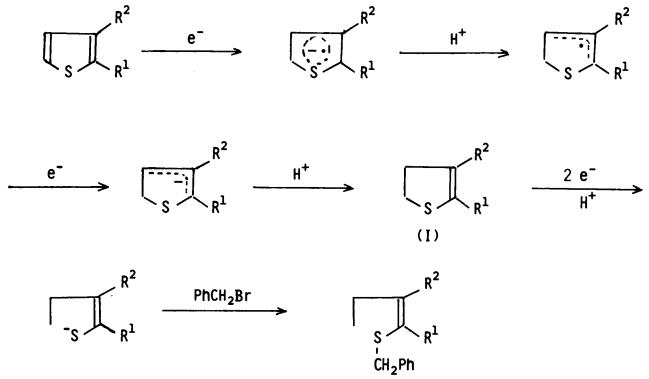

Scheme 3.

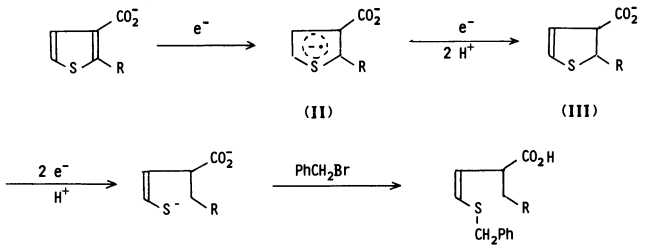

Scheme 4.

position of the carboxyl group. However, the reason of the formation of **III** is not clear.

Experimental

The Preparation of 2-(2-Thienyl)propanoic Acid (9a). A solution of ethyl 2-thienylacetate (**7**) (1.72g, 10 mmol) in 10 ml of THF was added into a solution of lithium diisopropylamide which was prepared from diisopropylamine (1.11 g, 11 mmol) and butyllithium (11 mmol) in 15 ml of THF at −30 °C under argon. After the addition of **7**, a white precipitate was observed in the reaction mixture. The reaction mixture was stirred for 0.5 h and was added to methyl iodide (2.13 g, 15 mmol) in 10 ml of THF at −30 °C. Additional stirring was continued for 1 h and the reaction mixture was quenched with 10% hydrochloric acid. The mixture was extracted with ether and the ether layer was dried over magnesium sulfate. After removing the solvent, the residue was chromatographed on silica gel using benzene as the solvent to give ethyl 2-(2-thienyl)propanoate (**8a**) [1.72 g (94%)]. IR (NaCl) 1730 cm^{-1} (C=O); NMR ($CDCl_3$) δ=1.27 (3H, t), 1.63 (3H, d), 4.03 (1H, q), 4.20 (2H, q), 6.90—7.47 (3H, m); MS *m/z* 184 (M^+).

Thus prepared, **8a** (1.66 g, 9 mmol) was stirred with 50 ml of 5% sodium hydroxide solution at room temperature for 2h. The reaction mixture was acidified with 10% hydrochloric acid and extracted with ether. The ether layer was washed with a saturated sodium chloride solution and dried over magnesium sulfate. After removing the solvent, the residue was chromatographed on silica gel using benzene–ether (2:1) as the solvent to give 2-(2-thienyl)propanoic acid (**9a**) [1.35 g (96%)]. Further purification of **9a** was performed by distillation, bp 138—140 °C (11 mmHg, 1 mmHg=133.32 Pa). IR (NaCl) 3600—2300 cm^{-1} (CO_2H), 1700 cm^{-1} (C=O); NMR ($CDCl_3$) δ=1.63 (3H, d), 4.07 (1H, q), 6.87—7.43 (3H, m), 11.30 (1H, brs); MS *m/z* 156 (M^+).

Similarly, ethyl 2-(2-thienyl)hexanoate (**8b**), 2-(2-thienyl)-hexanoic acid (**9b**), ethyl 2-(2-thienyl)-4-pentenoate (**8c**), and 2-(2-thienyl)-4-pentenoic acid (**9c**) were prepared by the reactions of **7** with corresponding alkyl halides. The yields and spectral data are as follows.

8b: Yield 71%; IR (NaCl) 1720 cm^{-1} (C=O); NMR ($CDCl_3$) δ=0.75—1.62 (10H, m), 2.01 (2H, m), 3.92 (1H, t), 4.52 (2H, q), 6.92—7.53 (3H, m); MS m/z 226 (M^+).

9b: Yield 86%; IR (NaCl) 3600—2400 cm^{-1} (CO_2H), 1700 cm^{-1} (C=O); NMR ($CDCl_3$) δ=0.72—2.22 (9H, m), 3.78 (1H, t), 6.72—7.18 (3H, m), 11.32 (1H, s); MS m/z 198 (M^+).

8c: Yield 87%; IR (NaCl) 1720 cm^{-1} (C=O), 1640 cm^{-1} (CH=CH_2); NMR ($CDCl_3$) δ=1.22 (3H, t), 2.17—3.04 (2H, m), 3.86 (1H, t), 4.05 (2H, q), 4.78—5.17 (2H, m), 5.35—6.03 (1H, m), 6.63—7.20 (3H, m); MS m/z 210 (M^+).

9c: Yield 99%; IR (NaCl) 3600—2300 cm^{-1} (CO_2H), 1710 cm^{-1} (C=O), 1650 cm^{-1} (CH=CH_2); NMR ($CDCl_3$) δ=2.23—3.08 (2H, m), 3.85 (1H, t), 4.76—5.19 (2H, m), 5.31—6.01 (1H, m), 6.67—7.19 (3H, m), 11.34 (1H, s); MS m/z 182 (M^+). Found: C, 54.17; H, 5.36%. Calcd for $C_9H_{10}O_2S$: C, 54.29; H, 5.54%.

The Preparation of 2-Thienylacetone (11). To a solution of thiophene (1.72 g, 20 mmol) in 20 ml of THF, a solution of butyllithium in hexane (22 mmol) was added at −30 °C with stirring under an argon atmosphere. After stirring for one hour at −30 °C, the reaction mixture was cooled to −70 °C. Into the reaction mixture, a solution of propylene oxide (1.22 g, 22 mmol) in 20 ml of THF was added at −70 °C. The reaction temperature was maintained at −70 °C for 0.5 h and then slowly raised to room temperature. Further, the reaction mixture was refluxed for 3 h. The mixture was acidified with 10% hydrochloric acid and extracted with ether. After the ether layer was washed with saturated sodium chloride solution, it was dried over magnesium sulfate. The solvent was removed under a reduced pressure and the residue was chromatographed on silica gel using benzene–ether (1 : 1) as the solvent to give 1-(2-thienyl)-2-propanol (**10**) [1.77 g (63%)]. IR (NaCl) 3500 cm^{-1} (OH); NMR ($CDCl_3$) δ=1.19 (3H, d), 2.31—2.62 (1H, brs), 3.89 (2H, d), 3.95 (1H, sex), 6.73—7.27 (3H, m); MS m/z 142 (M^+).

Into a solution of **10** (2.84 g, 20 mmol) in 50 ml of acetone, a mixture of chromium trioxide (2.60 g, 26 mmol), concd sulfuric acid (23 ml), and water (5 ml) was added at −20 °C over a period of 1 h. Further, additional stirring was continued for 1 h at −20 °C and the mixture was poured into 2-propanol (20 ml) and sodium hydrogencarbonate solution. After the precipitate was filtered, the filtrate was extracted with ether. The ether layer was washed with a saturated sodium chloride solution and was dried over magnesium sulfate. After removing the solvent, the residue was chromatographed on silica gel using benzene–petroleum ether (4 : 1) as the solvent to give 2-thienylacetone (**11**) [1.16 g (41%)]. IR (NaCl) 1700 cm^{-1} (C=O); NMR ($CDCl_3$) δ=2.22 (3H, s), 3.93 (2H, s), 6.92—7.48 (3H, m); MS m/z 140 (M^+).

Preparation of 2-Butyl-3-methylthiophene (15a). The preparation of 2-bromo-3-methylthiophene (**13**) was performed by the procedure of Kellog et al.[4] from 3-methylthiophene (**12**) and *N*-bromosuccinimide.

A solution of **13** (5.31 g, 30 mmol) in 25 ml of ether was added to magnesium (0.74 g, 31 mmol) with stirring at room temperature under nitrogen. The reaction mixture was stirred for 2.5 h at room temperature and was refluxed for 15 min. Into the reaction mixture, a solution of butyl *p*-toluenesulfonate (13.08 g, 60 mmol) in 25 ml of ether was added at reflux temperature. After refluxing was continued for 7.5 h, the solution was acidified with 10% hydrochloric acid. The resulting mixture was extracted with ether and the ether layer was washed with saturated sodium chloride solution. The layer was dried over magnesium sulfate. After removing the ether, the residue was chromatographed on silica gel and 2-butyl-3-methylthiophene (**15a**) was obtained by the elution with petroleum ether [2.27 g (49%)]. Thus prepared **15a** was further purified by distillation, bp 78—82 °C (18 mmHg). IR (NaCl) 700 cm^{-1} (thiophene); NMR ($CDCl_3$) δ=0.70—1.90 (7H, m), 2.09 (3H, s), 2.65 (2H, t), 6.83 (1H, d), 6.87 (1H, d); MS m/z 154 (M^+).

In a similar procedure, 3-methyl-2-octylthiophene (**15b**) was prepared. The spectral data and boiling point of **15b** are as follows: yield 60%, bp 140—142 °C (14 mmHg). IR (NaCl) 700 cm^{-1} (thiophene); NMR ($CDCl_3$) δ=0.63—1.81 (15H, m), 2.09 (3H, s), 2.65 (2H, t), 6.59 (1H, d), 6.81 (1H, d); MS m/z 210 (M^+).

The Preparation of 3-Ethyl-2-propylthiophene (15c). The preparation of 3-ethyl-2-propylthiophene (**15c**) was performed by the modified procedure of Meltz et al.[6] The adduct, prepared from 4-heptanone (3.42 g, 30 mmol) and 2,2-dimethyl-3-thiazoline (3.45 g, 30 mmol) by the reported method, was hydrolyzed with trifluoroacetic acid (3.5 ml) in ethanol (15 ml) and water (5 ml) under stirring for 1 h. After removing the solvent, the residue was refluxed in benzene (100 ml) for 10 h with catalytic amounts of *p*-toluenesulfonic acid using a water-separating apparatus. The reaction mixture was washed with 10% sodium hydrogencarbonate solution and a saturated sodium chloride solution. The benzene layer was dried over magnesium sulfate. After removing the solvent, the residue was chromatographed on silica gel and **15c** was obtained by the elution with petroleum ether [0.95 g (21%)]. IR (NaCl) 700 cm^{-1} (thiophene); NMR ($CDCl_3$) δ=0.98 (3H, t), 1.18 (3H, t), 1.45—2.12 (2H, m), 2.32—2.90 (4H, m), 6.77 (1H, d), 6.98 (1H, d); MS m/z 154 (M^+).

General Procedure for the Birch Reduction and Benzylation of Thiophene Derivatives. To a mixture of thiophene derivatives (10 mmol), absolute ethanol (4 ml) and liquid ammonia (50 ml), small pieces of sodium (4.4 or 5.5 equivalents) were added over a period of 1 h under reflux. After the mixture then had been stirred for 1 h in refluxing ammonia, solid ammonium chloride (3 equivalents) was added and the mixture was stirred for 0.5 h. Next, benzyl bromide (2.0 ml) was added to the mixture, and the mixture was stirred for 0.5 h. Further, additional benzyl bromide (1.0 ml) was added into the mixture and the mixture was stirred for 1 h with refluxing. The ammonia was then evaporated and the residue was added 20 ml of 10% hydrochloric acid and 20 ml of ether. The mixture was stirred for 1 h and then the ether layer was separated. The ether layer was washed with saturated sodium chloride solution and dried over magnesium sulfate. After removing the solvent, the residue was chromatographed on silica gel. The yield, the solvent of chromatography, spectral data, and analytical data of the products are as follows.

(*Z*)-3-Benzylthio-2-methyl-3-hexenoic acid (**16a**); yield 63% [elution with benzene–ether (5 : 1)]; an oily product; IR (NaCl) 3250—2950 cm^{-1} (CO_2H), 1700 cm^{-1} (C=O); NMR ($CDCl_3$) δ=0.90 (3H, t), 1.34 (3H, d), 2.25 (2H, qu), 3.42 (1H, q), 3.87 (2H, s), 6.01 (1H, t, J=8.4 Hz), 7.35 (5H, s), 12.31 (1H, brs); MS m/z 206 (M^+). Found: C, 67.06; H, 7.72%. Calcd for

$C_{14}H_{18}O_2S$: C, 67.17; H, 7.26%.

(*Z*)-3-Benzylthio-2-butyl-3-hexenoic acid (**16b**); yield 77% [elution with benzene–ether (5:1)]; an oily product; IR (NaCl) 3700—2300 cm^{-1} (CO_2H), 1700 cm^{-1} (C=O); NMR ($CDCl_3$) δ=0.70—1.97 (12H, m), 2.20 (2H, qu), 3.21 (1H, t), 3.81 (2H, s), 5.92 (1H, t, J=7.0 Hz), 7.19 (5H, s), 10.54 (1H, brs); MS m/z 248 (M^+). Found: C, 69.77; H, 8.46%. Calcd for $C_{17}H_{24}O_2S$: C, 69.82; H, 8.29%.

(*Z*)-2-Allyl-3-benzylthio-3-hexenoic acid (**16c**); yield 76% [elution with benzene–ether (4:1)]; an oily product; IR (NaCl) 3550—2200 cm^{-1} (CO_2H), 1700 cm^{-1} (C=O), 1640 cm^{-1} (CH=CH_2); NMR ($CDCl_3$) δ=0.86 (3H, t), 1.92—2.66 (4H, m), 3.32 (1H, t), 3.82 (2H, s), 4.85—5.83 (3H, m), 5.96 (lH, t, J=7.0 Hz), 7.22 (5H, s), 11.40 (lH, brs); MS m/z 214 (M^+). Found: C, 69.64; H, 7.53%. Calcd for $C_{16}H_{20}O_2S$: C, 69.50; H, 7.31%.

4-Benzylthio-3-methyl-3-octene (**22a**); yield 60% (elution with petroleum ether); an oily product; IR (NaCl) 2950 cm^{-1} (CH_2), 2920 cm^{-1} (CH_2), 700 cm^{-1} (C_6H_5); NMR ($CDCl_3$) δ=0.63—1.62 (10H, m), 1.67 (3H, s), 1.97—2.42 (4H, m), 3.62 (2H, s), 7.02 (5H, s); MS m/z 248 (M^+). Found: C, 77.54; H, 9.63%. Calcd for $C_{16}H_{24}S$: C, 77.37; H, 9.74%.

4-Benzylthio-3-methyl-3-dodecene (**22b**); yield 37% (elution with petroleum ether); an oily product; IR (NaCl) 2920 cm^{-1} (CH_2), 2850 cm^{-1} (CH_2), 700 cm^{-1} (C_6H_5); NMR ($CDCl_3$) δ=0.61—1.64 (18H, m), 1.67 (3H, s), 1.97—2.46 (4H, m), 3.69 (2H, s), 7.27 (5H, s); MS m/z 304 (M^+). Found: C, 78.92; H, 10.72%. Calcd for $C_{20}H_{32}S$: C, 78.89; H, 10.59%.

4-Benzylthio-3-ethyl-3-heptene (**22c**); yield 52% (elution with petroleum ether); an oily product; IR (NaCl) 2950 cm^{-1} (CH_2), 2870 cm^{-1} (CH_2), 690 cm^{-1} (C_6H_5); NMR ($CDCl_3$) δ=0.64—1.12 (9H, m), 1.22—1.78 (2H, m), 1.80—2.50 (6H, m), 3.72 (2H, s), 7.21 (5H, s); MS m/z 248 (M^+). Found: C, 77.38; H, 10.20%. Calcd for $C_{16}H_{24}S$: C, 77.37; H, 9.74%.

(*Z*)-4-Benzylthio-2-methyl-3-butenoic acid (**24a**); yield 51% (elution with benzene); an oily product; IR (NaCl) 3400—2300 cm^{-1} (CO_2H), 1700 cm^{-1} (C=O); NMR ($CDCl_3$) δ=1.26 (3H, d), 3.29—3.86 (1H, m), 3.92 (2H, s), 5.72 (1H, t), 6.20 (1H, d, J=10 Hz), 7.33—7.65 (5H, m), 11.29 (1H, s); MS m/z 222 (M^+). Found: C, 64.75; H, 6.60%. Calcd for $C_{12}H_{14}O_2S$: C, 64.85; H, 6.35%.

(*Z*)-4-Benzylthio-2-ethyl-3-butenoic acid (**24b**); yield 69% [elution with petroleum ether–ethyl acetate (1:1)]; an oily product; IR (NaCl) 3300—2200 cm^{-1} (CO_2H), 1690 cm^{-1} (C=O); NMR ($CDCl_3$) δ=0.98 (3H, t), 1.05—1.51 (2H, m), 1.51—2.13 (1H, m), 3.97 (2H, s), 5.79 (1H, t), 6.40 (1H, d, J=8 Hz), 7.56 (5H, s), 11.54 (1H, brs); MS m/z 236 (M^+). Found: C, 66.36; H, 7.01%. Calcd for $C_{13}H_{16}O_2S$: C, 66.08; H, 6.83%.

(*Z*)-4-Benzylthio-2-(2-phenylethyl)-3-butenoic acid (**26**); yield 48% [elution with petroleum ether–ethyl acetate (1:1)]; mp 104—105 °C (recrystallization from petroleum ether–benzene); IR (KBr) 3400—2300 cm^{-1} (CO_2H), 1700 cm^{-1} (C=O); NMR ($CDCl_3$) δ=2.00 (2H, q), 2.60 (2H, t), 3.50 (1H, q), 3.88 (2H, s), 5.65 (1H, t), 6.24 (1H, d, J=10 Hz), 7.05—7.52 (10H, m), 11.59 (1H, s); MS m/z 312 (M^+). Found: C, 73.64; H, 6.54%. Calcd for $C_{19}H_{20}O_2S$: C, 73.06; H, 6.45%.

References

1) S. F. Birch and D. T. McAllan, *J. Chem. Soc.*, **1951**, 2565; **1951**, 3411.

2) W. G. Blenderman, M. M. Joullie, and G. Preti, *J. Org. Chem.*, **48**, 3206 (1983).

3) M. Sado, H. Abe, N. Inuzuka, K. Shirai, and T. Kumamoto, *Bull. Chem. Soc. Jpn.*, **56**, 1665 (1983).

4) R. M. Kellog, A. P. Schaap, E. T. Hanper, and H. Wynberg, *J. Org. Chem.*, **33**, 2902 (1968).

5) F. F. Blicke and F. Leonard, *J. Am. Chem. Soc.*, **68**, 1934 (1946).

6) C. N. Meltz and R. A. Volkman, *Tetrahedron Lett.*, **24**, 4503 (1983).

 © 1986 The Chemical Society of Japan Bull. Chem. Soc. Jpn., 59, 3103—3108 (1986)

The Total Synthesis of (±)-Pisiferin

Takashi MATSUMOTO,* Sachihiko IMAI, Takashi YOSHINARI, and Shigeo MATSUNO
Department of Chemistry, Faculty of Science, Hiroshima University, Higashisenda-machi, Naka-ku, Hiroshima 730
(Received March 14, 1986)

The conversion of racemic α-cyclocitral into 3-(3-isopropyl-4-methoxyphenethyl)-4,4-dimethyl-2-methylenecyclohexanone (**2**) was carried out in five steps via 3-(3-isopropyl-4-methoxyphenethyl)-2,4,4-trimethyl-1-cyclohexene. An intramolecular cyclization of **2** with polyphosphoric acid produced the corresponding two tricyclic ketones possessing *cis*- and *trans*-A/B ring junctions. Each of these ketones was further converted into 12-mesyloxy-9(10→20)-*abeo*-abieta-1(10),8,11,13-tetraene in four steps. The mesylate was reduced with lithium aluminium hydride to give (±)-pisiferin.

Pisiferin (**1**), a rare tricyclic diterpene phenol possessing a rearranged abietane skeleton, has been isolated from the leaves[1] and seeds[2] of *Chamaecyparis pisifera* (Cupressaceae). As a part of our synthetic studies in the naturally-occurring diterpenes, we have attempted a synthesis of pisiferin.[3] The synthetic strategy was developed from a retrosynthetic analysis of the natural product **1**, which involved the disconnection illustrated in Scheme 1. That is, two C_{10} units, including A and C rings of the natural compound, were first condensed to give a C_{20} unit which was converted into an α,β-unsaturated ketone (**2**). An intramolecular cyclization of **2** with acid led to the corresponding tricyclic ketone; this was then transformed into the natural compound.

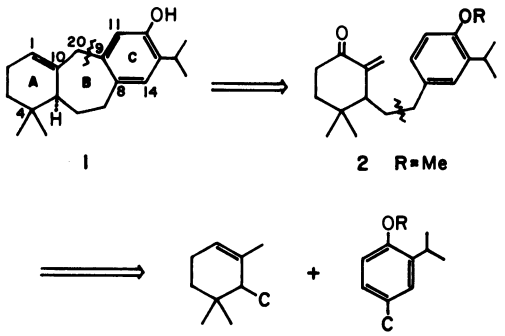

Scheme 1.

The Wittig reaction[4] of racemic α-cyclocitral (**3**) with (3-isopropyl-4-methoxybenzyl)triphenylphosphonium chloride (**4**) in benzene in the presence of butyllithium gave 3-(3-isopropyl-4-methoxystyryl)-2,4,4-trimethyl-1-cyclohexene (**5**) in 75.3% yield. This was submitted to a partial catalytic hydrogenation to give the corresponding phenethyl derivative (**6**) in 86.3% yield. The oxidation of **6** with *m*-chloroperbenzoic acid in dichloromethane at room temperature afforded an epoxide which, without purification, was treated with lithium diethylamide[5,6] in refluxing hexane to give an alcohol (**7**) in 60.5% yield from **6**. The oxidation of **7** with pyridinium chlorochromate in dichloromethane at room temperature afforded the corresponding α,β-unsaturated ketone (**2**) in 89.1% yield. The IR spectrum of **2** showed a conjugated carbonyl band at 1693 cm^{-1} and its ^1H NMR spectrum showed two doublet signals at δ 4.91 (1H, J=2.5 Hz) and 5.69 (1H, J=2.5 Hz) due to an *exo*-methylene group. Intramolecular cyclization of **2** with polyphosphoric acid at 80—85 °C afforded two stereoisomers, **8** and **9**, in 73.2 and 17.4% yields, respectively. In order to determine the stereochemistry of the A/B ring junction in these tricyclic ketones, the following conversion was carried out. A reduction of the minor ketone **9** in ether with lithium aluminium hydride, followed by acetylation with acetic anhydride in pyridine, yielded a mixture of the C-1 epimeric acetates (**10a** and **10b**) in a ratio of ca. 7 : 3. The ^1H NMR spectrum of the mixture showed broad signals due to C-1 protons at δ 4.2—4.75 ($W_{1/2}$=19 Hz) for **10a** and at δ 5.10 ($W_{1/2}$=9 Hz) for **10b**, suggesting the presence of axial and equatorial C-1 protons, respectively. The crude mixture (**10a** and **10b**) in acetic acid was oxidized with chromium trioxide at room temperature to give a ketone (**11**) in 22.9% yield from **9**. The ^1H NMR spectrum of **11** showed a singlet signal due to a C-1 acetoxyl group at δ 2.18, a multiplet due to a C-1 proton at δ 4.35—4.75, and two singlets due to C-11 and C-14 aromatic protons at δ 6.46 and 7.60. The appearance of the C-14 proton signal in very low field (δ 7.60) suggested the presence of a carbonyl group at the C-7 position. The 7-oxo compound **11** was reduced with sodium borohydride in methanol to give a mixture of the C-7 epimeric alcohols (**12**), which was immediately dehydrated by refluxing with *p*-toluenesulfonic acid in benzene to give a tetraene derivative (**13**) in 97.8% yield from **11**. The ^1H NMR spectrum of **13** showed two double doublet signals due to the C-6 and C-7 olefinic protons at δ 5.78 (J=4 and 13 Hz) and 6.47 (J=2 and 13 Hz). When both olefinic proton signals at δ 5.78 and 6.47 were irradiated, the C-5 proton appeared at δ 1.88 as a doublet with a coupling constant of 12 Hz. The large coupling constant ($J_{5,10}$=12 Hz) indicated an axial-axial coupling and suggested that the relative configuration of the C-5 and C-10 protons in **13** is trans. Thus, the stereochemistries of the A/B ring junction in **8** and **9** were assigned to be cis and trans, respectively. A reduction of the major ketone **8** with lithium aluminium hydride afforded the C-1 epimeric alcohols, **14a** (82.2%) and **14b** (17.0%), which were converted into the corresponding acetates, **15a** and **15b**.

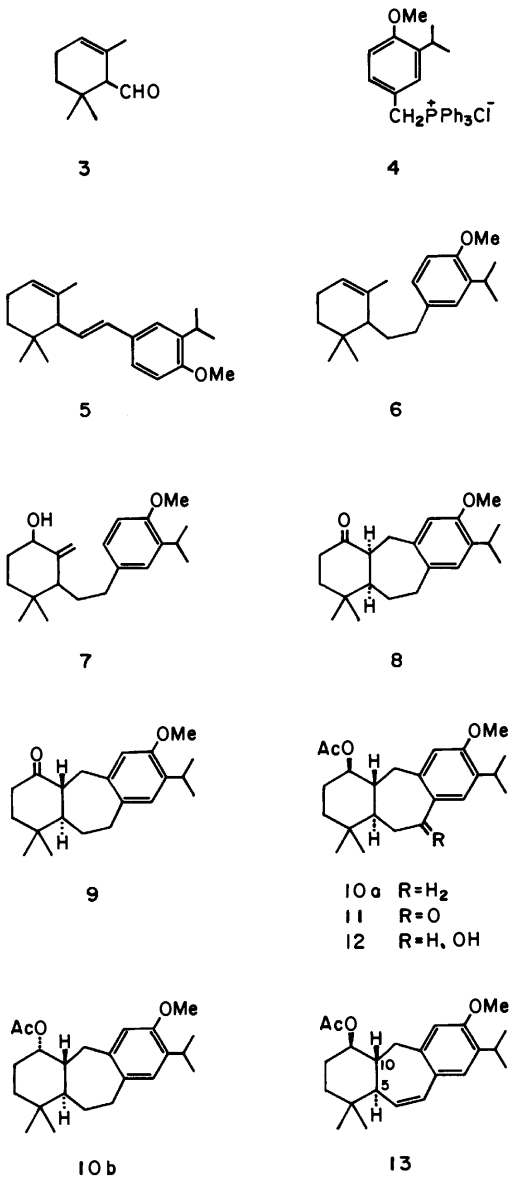

The stereochemistries of the acetoxyl groups in **15a** and **15b** were assigned, respectively, to be equatorial and axial conformations from their ^{1}H NMR spectra which showed signals due to the C-1 protons at δ 4.1—4.7 ($W_{1/2}$=19 Hz) and 5.09 ($W_{1/2}$=6 Hz). Thus, the conformations of the hydroxyl groups in **14a** and **14b** were also determined to be equatorial and axial, respectively. The *cis*-A/B-ring compound can exist in two A-ring chair conformations as shown in I and II. Of these two conformers, I is more stable than II because a 1,3-diaxial strain between the C-1 substituent (R=H, R'=OH or OAc) and the C-6 methylene group in I is fairly smaller than that between the C-4 methyl and the C-20 methylene groups in II. The other strains in the A-ring of both conformers are expected to be nearly equal. Thus, the *cis*-A/B-ring compound must exist in a preferred conformation I. From these considerations, the configurations of the hydroxyl groups in the C-1 epimeric alcohols were assigned to be an α disposition for **14a** and β for **14b**.

Mesylation of a mixture of **14a** and **14b** with mesyl chloride in pyridine at room temperature, followed by refluxing of the resulting mesylates (**16**) with 2,4-lutidine under a stream of nitrogen, produced a separable mixture of the disubstituted (**17**) and trisubstituted (**18**) olefins in 68.7% yield (ca. 2:9 ratio). A mixture of **17** and **18** was also obtained from a mixture of **14a** and **14b** by heating with hexamethylphosphoric triamide at 195—205 °C under a stream of nitrogen in 80.2% yield (ca. 5:8 ratio). Demethylation of **18** with anhydrous aluminium chloride and ethanethiol[7] in dichloromethane at room temperature provided only a dienone compound in 68.4% yield, but the desired pisiferin (**1**) could not be isolated. The dienone had the molecular formula $C_{20}H_{28}O$ based on the mass spectrum (M^+, m/z 284) and an elementary analysis. The IR spectrum indicated a conjugated carbonyl band at 1655 cm^{-1} but no hydroxyl band. The ^{1}H NMR spectrum showed signals at δ 0.95 (3H, singlet) and 1.03 (3H, singlet) due to a *gem*-dimethyl, at δ 1.06 (6H, doublet) and 2.98 (1H, multiplet) due to an isopropyl, and at δ 6.20 (1H, singlet) and 6.38 (1H, singlet) due to two olefinic protons. The ^{13}C NMR spectrum showed three singlet signals at δ 186.7, 176.1, 143.5, and two doublet signals at δ 147.2, 122.8 in the sp^2 carbon region, indicating the presence of a dienone moiety. The remaining fifteen carbons appeared in a δ 17—41 region as three singlets, two doublets, six triplets, and four quartets. From these spectral data the structure **19** was tentatively assigned to the dienone. Since the conversion of **18** into pisiferin (**1**) was unsuccessful, another synthetic route was examined. The alcohol **14a** was demethylated with anhydrous aluminium chloride and ethanethiol in dichloromethane to give a diol (**20a**) in 94.6% yield. On the other hand, a similar demethylation of **14b** gave only the dienone **19** in 90.3% yield. The expected diol **20b** corresponding to **20a** could not be isolated. These different results from demethylations of **14a** and **14b** can be explained as follows. The alcohol **14a** possessing an equatorial hydroxyl group was normally demethylated to give the expected diol **20a**, while under the same reaction conditions the epimer **14b** possessing an axial hydroxyl group was easily dehydrated by antiperiplanar elimination to give the trisubstituted olefin **18**. This was then demethylated and the resulting pisiferin (**1**) was further isomerized to the dienone **19**. Isomerization of **1** into **19** is described later. The diol **20a** was mesylated and the resulting dimesylate (**21**) was refluxed with 2,4-lutidine to give a mixture of the corresponding disubstituted (**22**) and trisubstituted (**23**) olefins in 87.1% yield (ca. 2:9 ratio), from which pure crystalline **23** was obtained by repeated column chromatography on silica gel and recrystallization. Treatment of **23** with lithium aluminium hydride in refluxing tetrahydrofuran afforded a phenolic compound (**1**) (98.4% yield) which gave an acetate (**24**). The ^{1}H NMR spectrum of the synthetic **1** was identical with that of natu-

ral pisiferin. The synthetic **1** was further isomerized to the dienone **19** by a treatment with anhydrous aluminium chloride and ethanethiol at room temperature in 93.0% yield. Similarly, the *trans*-ketone **9** was also converted into a mixture of the corresponding mesylates, **25** and **23** in 40.7% yield (ca. 1 : 4 ratio) from **9**.

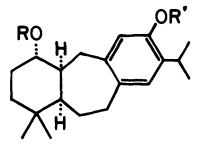

14a R=H, R'=Me
15a R=Ac, R'=Me
20a R=R'=H
21 R=R'=Ms

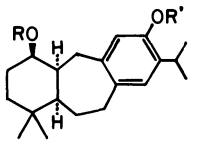

14b R=H, R'=Me
15b R=Ac, R'=Me
20b R=R'=H

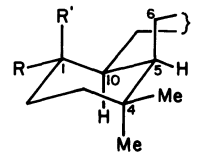

I

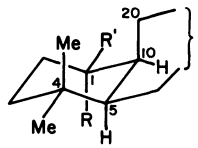

II

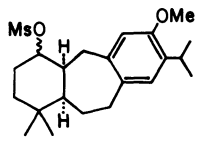

16

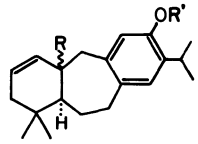

17 R=αH, R'=Me
22 R=αH, R'=Ms
25 R=βH, R'=Ms

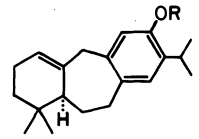

18 R=Me
23 R=Ms
24 R=Ac

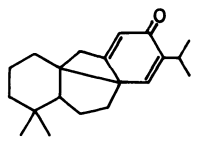

19

Experimental

All melting points are uncorrected. The IR spectra were measured in chloroform and the ^{1}H NMR spectra in deuteriochloroform at 60 MHz, with tetramethylsilane as an internal standard, unless otherwise stated; s: singlet, bs: broad singlet, d: doublet, bd: broad doublet, dd: double doublet, t: triplet, q: quartet, m: multiplet. The column chromatography was performed using Merck silica gel (0.063 mm).

3-(3-Isopropyl-4-methoxyphenethyl)-2,4,4-trimethyl-1-cyclohexene (6). A solution of butyllithium in hexane (15%: 7.9 ml) was added at 7—9 °C to a suspension of (3-isopropyl-4-methoxybenzyl)triphenylphosphonium chloride (**4**) (5.816 g) in dry benzene (60 ml) under a stream of nitrogen. The mixture was stirred at 7—9 °C for 30 min and a solution of racemic α-cyclocitral[8] (**3**) (1.200 g) in dry benzene (2.0 ml) was added at 7—9 °C. After stirring at this temperature for 1 h and then at room temperature for 3 h, the mixture was poured into ice-dilute hydrochloric acid and extracted with ether. The ether extract was washed with brine, dried over sodium sulfate, and evaporated in vacuo. The residue was triturated with hexane (100 ml) and the precipitated triphenylphosphine oxide was removed by filtration. The filtrate was evaporated and the residue was chromatographed on silica gel (40 g), using hexane as the eluent, to give 3-(3-isopropyl-4-methoxystyryl)-2,4,4-trimethyl-1-cyclohexene (**5**) as an oil (1.772 g: 75.3%).

A suspension of **5** (5.124 g) and 10% Pd-C (1.30 g) in ethanol (55 ml) was stirred at room temperature in an atmosphere of hydrogen. After one equivalent of hydrogen had been absorbed, the mixture was filtered. The filtrate was evaporated and the residue was purified by column chromatography on silica gel (70 g), using hexane as the eluent, to give **6** as an oil (4.450 g: 86.3%). The IR and ^{1}H NMR spectra of **6** were identical with those of an authentic optically-active sample.[3]

3-(3-Isopropyl-4-methoxyphenethyl)-4,4-dimethyl-2-methylenecyclohexanol (7). A solution of **6** (4.111 g) and 80% *m*-chloroperbenzoic acid (2.951 g) in dichloromethane (105 ml) was stirred at room temperature for 1.5 h and then diluted with ether. The solution was washed successively with 10% aqueous potassium iodide, aqueous sodium thiosulfate, aqueous sodium hydrogencarbonate, and brine. The dried solution was evaporated in vacuo to give a crude epoxide as an oil (4.530 g). ^{1}H NMR (CCl_4) δ=0.83 (3H, s) and 0.88 (3H, s) (-C(CH$_3$)$_2$), 1.21 (6H, d, J=7 Hz, -CH(CH$_3$)$_2$), 1.29 (3H, s, -O-CCH$_3$), 3.23 (1H, m, -CH(CH$_3$)$_2$), 3.78 (3H, s, -OCH$_3$).

A solution of the crude epoxide (4.530 g) in dry hexane (38 ml) was added at −50—−60 °C for 15 min to a stirred solution of lithium diethylamide which was prepared from butyllithium in hexane (15%: 42.8 ml) and diethylamine (7.1 ml) in dry hexane (40 ml) at −45—−60 °C for 30 min under a stream of nitrogen. The mixture was stirred at room temperature for 30 min, refluxed for 5 h, cooled, and then poured into aqueous ammonium chloride. The mixture was extracted with ether. The ether extract was washed with brine, dried over sodium sulfate, and evaporated in vacuo. The crude product was chromatographed on silica gel (220 g), using ether-benzene (1 : 99) as the eluent, to give **7** as an oil (2.621 g: 60.5%); IR 3600, 3435, 1645 cm^{-1}; ^{1}H NMR (CCl_4) δ=0.71 (3H, s) and 0.90 (3H, s) -C(CH$_3$)$_2$), 1.18 (6H, d, J= 7 Hz, -CH(CH$_3$)$_2$), 3.21 (1H, m, -CH(CH$_3$)$_2$), ca. 3.65—4.1 (1H, m, overlap, -CH(OH)-), 3.77 (3H, s, -OCH$_3$), 4.74 (1H, bs) and 5.17 (1H, bs) (-C=CH$_2$), 6.46—6.9 (3H, m, aromatic protons). Found: C, 79.98; H, 10.39%. Calcd for $C_{21}H_{32}O_2$: C, 79.70; H, 10.19%.

3-(3-Isopropyl-4-methoxyphenethyl)-4,4-dimethyl-2-methylenecyclohexanone (2). A solution of **7** (1.736 g) in dichloromethane (9.5 ml) was added to a stirred suspension of pyridinium chlorochromate (2.010 g) in dichloromethane (19.0 ml) at room temperature for 15 min. After stirring for 3 h, the mixture was poured into aqueous sodium carbonate (10%: 30 ml) and extracted with ether. The ether extract was washed with brine, dried over sodium sulfate, and evaporated in vacuo. The residue was chromatographed on silica gel (60 g), using ether-benzene (1 : 99) as the eluent, to give **2** as an oil (1.537 g: 89.1%); IR 1693 cm^{-1}, ^{1}H NMR (CCl_4) δ=0.99 (3H, s) and 1.05 (3H, s) (-C(CH$_3$)$_2$), 1.18 (6H, d, J= 7 Hz, -CH(CH$_3$)$_2$), 3.22 (1H, m, -CH(CH$_3$)$_2$), 3.77 (3H, s,

$-OCH_3$), 4.91 (1H, d, J=2.5 Hz) and 5.69 (1H, d, J=2.5 Hz) ($-\underline{C}=CH_2$), 6.48—6.9 (3H, m, aromatic protons). Found: C, 80.28; H, 9.86%. Calcd for $C_{21}H_{30}O_2$: C, 80.21; H, 9.62%.

Intramolecular Cyclization of 2. Polyphosphoric acid was prepared from 85% phosphoric acid (25 ml) and phosphorus pentaoxide (25 g) by heating at 100 °C for 2 h.

A stirred mixture of **2** (2.172 g) and polyphosphoric acid (32.6 ml) was heated at 80—85 °C for 1 h. After cooling, the mixture was diluted with water and extracted with ether. The ether extract was washed with brine, dried over sodium sulfate, and evaporated in vacuo. The residue was recrystallized from hexane to give 12-methoxy-9(10→20)-10α*H*-*abeo*-abieta-8,11,13-trien-1-one (**8**) (1.280 g: 58.9%), mp 155—156 °C; IR 1703 cm^{-1}, ^1H NMR (90 MHz, CCl_4) δ=0.98 (3H, s) and 1.01 (3H, s) ($-\underline{C}(CH_3)_2$), 1.15 (6H, d, J=7 Hz, $-CH(C\underline{H}_3)_2$), 3.19 (1H, m, $-C\underline{H}(CH_3)_2$), 3.75 (3H, s, $-OCH_3$), 6.43 (1H, s, C_{11}-H), 6.84 (1H, s, C_{14}-H). Found: C, 80.41; H, 9.64%. Calcd for $C_{21}H_{30}O_2$: C, 80.21; H, 9.62%.

The mother liquor of recrystallization was evaporated in vacuo and the residue was chromatographed on silica gel (40 g), using benzene as the eluent, to give an additional **8** (0.310 g: 14.3%) and 12-methoxy-9(10→20)-*abeo*-abieta-8,11,13-trien-1-one (**9**) as an oil (0.378 g: 17.4%); IR 1702 cm^{-1}, ^1H NMR (CCl_4) δ=1.00 (3H, s) and 1.02 (3H, s) ($-\underline{C}(CH_3)_2$), 1.14 (d, J=7 Hz) and 1.16 (d, J=7 Hz) (6H, $-CH(C\underline{H}_3)_2$), 3.75 (3H, s, $-OCH_3$), 6.54 (1H, s, C_{11}-H), 6.75 (1H, s, C_{14}-H).

1β-Acetoxy-12-methoxy-9(10→20)-*abeo*-abieta-8,11,13-trien-7-one (11). Lithium aluminium hydride (13 mg) was added to a stirred solution of **9** (70 mg) in dry ether (2.0 ml) with cooling in an ice-water bath. The mixture was stirred at room temperature for 1 h, poured into dilute hydrochloric acid, and extracted with ether. The ether extract was washed with brine, dried over sodium sulfate, and evaporated in vacuo. The residue was acetylated with acetic anhydride (0.5 ml) in pyridine (0.5 ml) at 75—80 °C for 2 h to give an oily mixture of the C-1 epimeric acetates (**10a** and **10b**) in a ratio of ca. 7:3. ^1H NMR of **10a** δ=0.76 (3H, s) and 0.94 (3H, s) ($-\underline{C}(CH_3)_2$), 1.18 (d, J=7 Hz) and 1.20 (d, J=7 Hz) (6H, $-CH(C\underline{H}_3)_2$), 2.15 (3H, s, $-OCOCH_3$), 3.79 (3H, s, $-OCH_3$), 4.2—4.75 (1H, m, $W_{1/2}$=19 Hz, C_1-H), 6.52 (1H, s, C_{11}-H), 6.86 (1H, s, C_{14}-H). ^1H NMR of **10b** δ=0.76 (3H, s) and 0.98 (3H, s) ($-\underline{C}(CH_3)_2$), 1.18 (d, J=7 Hz) and 1.20 (d, J=7 Hz), (6H, $-CH(C\underline{H}_3)_2$), 2.10 (3H, s, $-OCOCH_3$), 3.75 (3H, s, $-OCH_3$), 5.10 (1H, bs, $W_{1/2}$=9 Hz, C_1-H), 6.57 (1H, s, C_{11}-H), 6.86 (1H, s, C_{14}-H).

A stirred mixture of the C-1 epimeric acetates (**10a** and **10b**) was oxidized with chromium trioxide (43 mg) in acetic acid (2.0 ml) at room temperature for 5 h. The mixture was diluted with water and extracted with ether. The ether extract was washed successively with water, aqueous sodium hydrogencarbonate, and water. The dried solution was evaporated in vacuo. The residue was chromatographed on silica gel (10 g), using ether-benzene (2:98) as the eluent, to give **11** as an oil (19 mg: 22.9% from **9**); IR 1720, 1655 cm^{-1}; ^1H NMR, δ=0.92 (6H, s, $-\underline{C}(CH_3)_2$), 1.21 (6H, bd, J=7 Hz, $-CH(C\underline{H}_3)_2$), 2.18 (3H, s, $-OCOCH_3$), 3.86 (3H, s, $-OCH_3$), 4.35—4.75 (1H, m, C_1-H), 6.46 (1H, s, C_{11}-H), 7.60 (1H, s, C_{14}-H).

1β-Acetoxy-12-methoxy-9(10→20)-*abeo*-abieta-6,8,11,13-tetraene (13). Sodium borohydride (10 mg) was added to a stirred solution of **11** (19.0 mg) in methanol (2.0 ml) with cooling in a water bath. The solution was stirred at room temperature for 1 h, diluted with ether, poured into dilute hydrochloric acid, and extracted with ether. The ether extract was washed with brine, dried over sodium sulfate, and evaporated in vacuo to give an oily mixture of the C-7 epimeric alcohols (**12**); IR 3600, 3410, 1720 cm^{-1}.

A mixture of the above crude **12** and *p*-toluenesulfonic acid (10 mg) in dry benzene (2.0 ml) was refluxed for 1 h. After cooling, the mixture was diluted with ether and the solution was washed with brine. The dried solution was evaporated in vacuo and the residue was chromatographed on silica gel (5.0 g), using benzene as the eluent, to give **13** as an oil (17.8 mg: 97.8% from **11**); IR 1720 cm^{-1}, ^1H NMR (90 MHz) δ=0.88 (3H, s) and 0.96 (3H, s) ($-\underline{C}(CH_3)_2$), 1.18 (6H, d, J=7 Hz, $-CH(C\underline{H}_3)_2$), 2.10 (3H, s, $-OCOCH_3$), 3.25 (1H, m, $-C\underline{H}(CH_3)_2$), 3.80 (3H, s, $-OCH_3$), 4.45—4.8 (1H, m, C_1-H), 5.78 (1H, dd, J=13 and 4 Hz, C_6-H), 6.47 (1H, dd, J=13 and 2 Hz, C_7-H), 6.52 (1H, s, C_{11}-H), 6.92 (1H, s, C_{14}-H).

12-Methoxy-9(10→20)-10α*H*-*abeo*-abieta-8,11,13-trien-1α-ol (14a) and Its C-1 Epimer (14b). Lithium aluminium hydride (69.4 mg) was added to a stirred solution of **8** (1.150 g) in dry ether (50 ml) with cooling in an ice-water bath. The mixture was stirred at room temperature for 1 h, poured into ice-dilute hydrochloric acid, and extracted with ether. The ether extract was washed with water, dried over sodium sulfate, and evaporated in vacuo. The residue was recrystallized from acetone-hexane to give **14a** (813 mg: 70.3%), mp 151—151.5 °C; IR 3600, 3430 cm^{-1}; ^1H NMR δ=0.75 (3H, s) and 0.94 (3H, s) ($-\underline{C}(CH_3)_2$), 1.18 (d, J=7 Hz) and 1.20 (d, J=7 Hz) (6H, $-CH(C\underline{H}_3)_2$), 3.78 (3H, s, $-OCH_3$), 6.58 (1H, s, C_{11}-H), 6.99 (1H, s, C_{14}-H). Found: C, 79.59; H, 10.41%. Calcd for $C_{21}H_{32}O_2$: C, 79.70; H, 10.19%.

The mother liquor of recrystallization was evaporated in vacuo and the residue was repeatedly chromatographed on silica gel, using benzene as the eluent, to give an additional **14a** (138 mg: 11.9%) and **14b** as an oil (196 mg: 17.0%); IR 3620, 3440 cm^{-1}; ^1H NMR δ=0.72 (3H, s) and 0.98 (3H, s) ($-\underline{C}(CH_3)_2$), 1.17 (d, J=7 Hz) and 1.20 (d, J=7 Hz) (6H, $-CH(C\underline{H}_3)_2$), 3.78 (3H, s, $-OCH_3$), 3.91 (1H, br, $W_{1/2}$=9 Hz, C_1-H), 6.54 (1H, s, C_{11}-H), 6.89 (1H, s, C_{14}-H).

Acetylation of 14a and 14b. a): The alcohol **14a** (100 mg) was acetylated with acetic anhydride (1.0 ml) in pyridine (1.0 ml) at 75—80 °C for 2 h to give a crude acetate (**15a**); IR 1718 cm^{-1}, ^1H NMR δ=0.77 (3H, s) and 0.96 (3H, s) ($-\underline{C}(CH_3)_2$), 1.19 (d, J=7 Hz) and 1.21 (d, J=7 Hz) (6H, $-CH(C\underline{H}_3)_2$), 2.18 (3H, s, $-OCOCH_3$), 3.23 (1H, m, $-C\underline{H}(CH_3)_2$), 3.80 (3H, s, $-OCH_3$), 4.1—4.7 (1H, m, $W_{1/2}$=19 Hz, C_1-H), 6.58 (1H, s, C_{11}-H), 6.84 (1H, s, C_{14}-H).

b): The alcohol **14b** was acetylated with acetic anhydride in pyridine to give a crude acetate (**15b**); IR 1718 cm^{-1}, ^1H NMR δ=0.73 (3H, s) and 1.00 (3H, s) ($-\underline{C}(CH_3)_2$), 1.15 (d, J=7 Hz) and 1.18 (d, J=7 Hz) (6H, $-CH(C\underline{H}_3)_2$), 2.11 (3H, s, $-OCOCH_3$), 3.78 (3H, s, $-OCH_3$), 5.09 (1H, bs, $W_{1/2}$=6 Hz, C_1-H), 6.52 (1H, s, C_{11}-H), 6.85 (1H, s, C_{14}-H).

12-Methoxy-9(10→20)-10α*H*-*abeo*-abieta-1,8,11,13-tetraene (17) and 12-Methoxy-9(10→20)-*abeo*-abieta-1(10),8,11,13-tetraene (Pisiferin Methyl Ether) (18). a): A mixture of **14a** and **14b** (100.7 mg) was mesylated with mesyl chloride (0.10 ml) in pyridine (0.7 ml) at room temperature for 3.5 h. The mixture was poured into dilute hydrochloric acid and extracted with ether. The ether extract was washed with brine, dried over sodium sulfate, and evaporated in vacuo to give a crude mesylate (**16**) (129 mg).

The crude **16** (129 mg) in 2,4-lutidine (0.7 ml) was refluxed for 2.5 h under a stream of nitrogen. The mixture was cooled, poured into dilute hydrochloric acid, and extracted with ether. The ether extract was washed successively with dilute hydrochloric acid, aqueous sodium hydrogencarbonate, and brine. The dried solution was evaporated in vacuo and the residue was repeatedly chromatographed on silica gel, using hexane as the eluent, to give two oily products, **17** (12.0 mg: 12.6%) and **18** (53.2 mg: 56.1%). ^{1}H NMR (90 MHz) of **17** δ=0.73 (3H, s) and 0.94 (3H, s) (-C(CH$_3$)$_2$), 1.18 (d, J=7 Hz) and 1.20 (d, J=7 Hz) (6H, -CH(CH$_3$)$_2$), 3.28 (1H, m, -CH(CH$_3$)$_2$), 3.79 (3H, s, -OCH$_3$), 5.4—5.7 (2H, m, C$_1$-H and C$_2$-H), 6.61 (1H, s, C$_{11}$-H), 6.96 (1H, s, C$_{14}$-H). ^{1}H NMR (90 MHz) of **18** δ=0.88 (3H, s) and 0.92 (3H, s) (-C(CH$_3$)$_2$), 1.18 (d, J=7 Hz) and 1.20 (d, J=7 Hz)(6H, -CH(CH$_3$)$_2$), 3.23 (1H, m, -CH(CH$_3$)$_2$), 3.30 (2H, s, C$_{20}$-H$_2$), 5.43 (1H, t, J=4 Hz, C$_1$-H), 6.60 (1H, s, C$_{11}$-H), 6.90 (1H, s, C$_{14}$-H).

b): A mixture of **14a** and **14b** (400 mg) was heated with hexamethylphosphoric triamide (4.0 ml) at 195—205 °C for 1 h under a stream of nitrogen. The solution was cooled, poured into dilute hydrochloric acid, and extracted with ether. The ether extract was washed with brine, dried over sodium sulfate, and evaporated in vacuo. The crude product was purified by column chromatography on silica gel (100 g), using hexane as the eluent, to give an oily mixture of **17** and **18** (302 mg: 80.2%) in a ratio of ca. 5:8.

Demethylation of 18. Anhydrous aluminium chloride (13.3 mg) was added to a stirred solution of **18** (10.0 mg) and ethanethiol (0.015 ml) in dichloromethane (0.5 ml) with cooling in an ice-water bath. The mixture was stirred at room temperature for 4 h, poured into ice-dilute hydrochloric acid, and extracted with ether. The ether extract was washed with brine, dried over sodium sulfate, and evaporated in vacuo. The residue was chromatographed on silica gel (10 g), using ether-benzene (1:99) as the eluent, to give a dienone (**19**) (6.5 mg: 68.4%) as a solid, whose IR and ^{1}H NMR spectra were identical with those of the authentic sample (vide infra).

Demethylation of 14a and 14b. a): A solution of **14a** (597.0 mg) in dichloromethane (8.0 ml) was demethylated with anhydrous aluminium chloride (754.6 mg) and ethanethiol (0.85 ml) at room temperature for 4 h. After the work-up as described above, the crude product was recrystallized from acetone-hexane to give a diol (**20a**) (510.0 mg: 89.4%), mp 183.5—184.5 °C; IR 3600, 3360 cm^{-1}; ^{1}H NMR δ=0.75 3H, s) and 0.93 (3H, s) (-C(CH$_3$)$_2$), 1.24 (6H, d, J=7 Hz, -CH(CH$_3$)$_2$), 4.89 (1H, bs, -OH), 6.50 (1H, s, C$_{11}$-H), 7.00 (1H, s, C$_{14}$-H). Found: C, 79.48; H, 10.30%. Calcd for C$_{20}$H$_{30}$O$_2$: C, 79.42; H, 10.00%. The mother liquor of recrystallization was evaporated in vacuo and the residue was chromatographed on silica gel (20 g), using ether-benzene (5:95) as the eluent, to give an additional **20a** (27.9 mg: 5.2%).

b): A solution of **14b** (111.0 mg) in dichloromethane (2.1 ml) was demethylated with anhydrous aluminium chloride (139.8 mg) and ethanethiol (0.15 ml) at room temperature for 4 h. After the work-up as described above, the crude product was chromatographed on silica gel (10 g), using ether-benzene (5:95) as the eluent, to give a dienone (**19**) (90.1 mg: 90.3%), which was recrystallized from hexane, mp 107—109 °C; IR 1655 cm^{-1}, UV λ_{max}^{EtOH}: 255 nm (ε 15300). ^{1}H NMR (90 MHz) δ=0.95 (3H, s) and 1.03 (3H, s) (-C(CH$_3$)$_2$), 1.06 (6H, d, J=7 Hz, -CH(CH$_3$)$_2$), 2.98 (1H, m, -CH(CH$_3$)$_2$), 6.20 (1H, s, C$_{11}$-H), 6.38 (1H, bs, C$_{14}$-H). ^{13}C NMR ($CDCl_3$) δ=17.6 (t), 20.0 (q), 21.9 (q), 21.9 (q), 24.1 (q), 25.9 (d), 27.7 (t), 30.5 (t), 31.0 (t), 34.7 (s), 35.8 (t), 35.8 (t), 37.2 (d), 39.7 (s), 40.4 (s), 122.8 (d), 143.5 (s), 147.2 (d), 176.1 (s), 186.7 (s); MS m/z 284 (M$^+$). Found: C, 84.39; H, 10.04%. Calcd for C$_{20}$H$_{28}$O: C, 84.45; H, 9.92%.

12-Mesyloxy-9(10→20)-10α*H*-*abeo*-abieta-1,8,11,13-tetraene (22) and 12-Mesyloxy-9(10→20)-*abeo*-abieta-1(10),8,11,13-tetraene (23). a): A mixture of **20a** (102.0 mg) and mesyl chloride (0.08 ml) in pyridine (1.0 ml) was allowed to stand at room temperature for 16.5 h and then diluted with ether. The ether solution was washed successively with dilute hydrochloric acid and brine. The dried solution was evaporated in vacuo to give a crude dimesylate (**21**) (130 mg) which was used, without purification, in the next reaction. ^{1}H NMR δ=0.79 (3H, s) and 0.96 (3H, s) (-C(CH$_3$)$_2$), 1.23 (d, J=7 Hz) and 1.25 (d, J=7 Hz) (6H, -CH(CH$_3$)$_2$), 3.12 (3H, s) and 3.19 (3H, s) (2-OSO$_2$CH$_3$), 4.1—4.6 (1H, m, C$_1$-H), 7.03 (1H, s) and 7.10 (1H, s) (C$_{11}$-H and C$_{14}$-H).

b): A solution of the crude **21** (130 mg) in 2,4-lutidine (1.5 ml) was refluxed for 2.5 h under a stream of nitrogen. The solution was cooled, diluted with ether, and washed successively with dilute hydrochloric acid and brine. The dried solution was evaporated in vacuo and the residue was purified by repeated column chromatography on silica gel and recrystallization from methanol to give **22** (18.6 mg: 15.2%) as an oil and **23** (87.9 mg: 71.9%) as a crystalline, mp 138—140 °C. ^{1}H NMR (90 MHz) of **22** δ=0.73 (3H, s) and 0.95 (3H, s) (-C(CH$_3$)$_2$), 1.21 (d, J=7 Hz) and 1.23 (d, J=7 Hz) (6H, -CH(CH$_3$)$_2$), 3.16 (3H, s, -OSO$_2$CH$_3$), 5.5—5.7 (2H, m, C$_1$-H and C$_2$-H), 7.02 (1H, s) and 7.08 (1H, s) (C$_{11}$-H and C$_{14}$-H). ^{1}H NMR (90 MHz) of **23** δ=0.88 (3H, s) and 0.92 (3H, s) (-C(CH$_3$)$_2$), 1.21 (d, J=7 Hz) and 1.23 (d, J=7 Hz) (6H, -CH(CH$_3$)$_2$), 2.7—2.9 (2H, m, C$_7$-H$_2$), 3.16 (3H, s, -OSO$_2$CH$_3$), 3.25 (1H, m, -CH(CH$_3$)$_2$), 3.31 (2H, s, C$_{20}$-H$_2$), 5.43 (1H, t, J=4 Hz, C$_1$-H), 7.00 (1H, s) and 7.02 (1H, s) (C$_{11}$-H and C$_{14}$-H). Found: C, 69.61; H, 8.21%. Calcd for C$_{21}$H$_{30}$O$_3$S: C, 69.57; H, 8.34%.

(±)-Pisiferin (1). A solution of **23** (23.4 mg) in dry tetrahydrofuran (2.0 ml) was reduced with lithium aluminium hydride (9.8 mg) by refluxing for 1.5 h. The mixture was poured into dilute hydrochloric acid and extracted with ether. The ether extract was washed with brine, dried over sodium sulfate, and evaporated in vacuo. The crude product was chromatographed on silica gel (5.0 g), using benzene as the eluent, to give **1** as an oil (18.1 mg: 98.4%); IR 3600, 3350 cm^{-1}; ^{1}H NMR (90 MHz) δ=0.88 (3H, s) and 0.91 (3H, s) (-C(CH$_3$)$_2$), 1.22 (d, J=7 Hz) and 1.24 (d, J=7 Hz) (6H, -CH(CH$_3$)$_2$), 2.74 (2H, m, C$_7$-H$_2$), 3.12 (1H, m, -CH(CH$_3$)$_2$), 3.27 (2H, s, C$_{20}$-H$_2$), 4.46 (1H, s, -OH), 5.41 (1H, t, J=4 Hz, C$_1$-H), 6.48 (1H, s, C$_{11}$-H), 6.88 (1H, s, C$_{14}$-H). The ^{1}H NMR spectrum of **1** was identical with that of natural pisiferin. MS m/z 284 (M$^+$).

Acetylation of 1. A solution of **1** (11.8 mg) and acetic anhydride (0.5 ml) in pyridine (0.5 ml) was heated at 75—80 °C for 2 h. After the usual work-up, the crude product was chromatographed on silica gel (5.0 g), using benzene as the eluent, to give an acetate (**24**) as an oil (12.2 mg: 90.4%), IR 1753 cm^{-1}, MS m/z 326 (M$^+$), ^{1}H NMR (90 MHz) δ=0.87 (3H, s) and 0.91 (3H, s) (-C(CH$_3$)$_2$), 1.18 (d, J=7 Hz) and 1.20 (d, J=7 Hz) (6H, -CH(CH$_3$)$_2$), 2.27 (3H, s, -OCOCH$_3$), 3.30 (2H, s, C$_{20}$-H$_2$), 5.42 (1H, t, J=4 Hz, C$_1$-H), 6.70 (1H, s, C$_{11}$-H), 6.98 (1H, s, C$_{14}$-H).

Conversion of 1 into 19. A solution of **1** (43.0 mg) and ethanethiol (0.07 ml) in dichloromethane (2.8 ml) was treated with anhydrous aluminium chloride (60.4 mg) at room temperature for 4 h. After the work-up as described above, the crude product was chromatographed on silica gel (10 g), using ether–benzene (5 : 95) as the eluent, to give **19** (40.0 mg: 93.0%), whose IR and ^{1}H NMR spectra were identical with those of the authentic sample.

Conversion of 9 into 23 and 12-Mesyloxy-9(10→20)-*abeo*-abieta-1,8,11,13-tetraene (25). The ketone **9** (261.1 mg) in dry ether (5.0 ml) was reduced with lithium aluminium hydride (15.8 mg) at room temperature for 1 h to give a mixture of the C-1 epimeric alcohols (240 mg).

A solution of the above crude alcohols (240 mg) and ethanethiol (0.37 ml) in dichloromethane (4.0 ml) was treated with anhydrous aluminium chloride (332.1 mg) at room temperature for 4 h. The crude product (235 mg) was immediately mesylated with mesyl chloride (0.2 ml) in pyridine (1.0 ml) at room temperature for 16 h and the resulting crude mesylate was refluxed with 2,4-lutidine (2.0 ml) for 2.5 h under a stream of nitrogen. After the work-up as described above, the crude product was chromatographed on silica gel (20 g), using hexane–benzene (1 : 1) as the eluent, to give a mixture of **23** and **25** (122.4 mg: 40.7% from **9**) in a ratio of ca. 4 : 1.

The authors are grateful to Professor Yoshiyuki Hirose, Science University of Tokyo, for kindly supplying the spectra of natural pisiferin and to Dr. Yasuto Uchio of this department for measurement of ^{13}C NMR spectrum.

References

1) M. Yatagai and T. Takahashi, *Phytochemistry*, **19**, 1149 (1980).

2) S. Hasegawa, Y. Hirose, M. Yatagai, and T. Takahashi, *Chem. Lett.*, **1984**, 1837.

3) Although the formulas represent only one enantiomer, they should be taken to indicate racemates.

4) T. Matsumoto and S. Usui, *Bull. Chem. Soc. Jpn.*, **52**, 212 (1979).

5) J. K. Crandall and L. C. Lin, *J. Org. Chem.*, **33**, 2375 (1968).

6) T. Matsumoto and S. Usui, *Bull. Chem. Soc. Jpn.*, **56**, 491 (1983).

7) M. Node, K. Nishide, M. Sai, K. Ichikawa, K. Fuji, and E. Fujita, *Chem. Lett.*, **1979**, 97.

8) W. M. B. Könst, L. M. van der Linde, and H. Boelens, *Tetrahedron Lett.*, **1974**, 3175; R. N. Gedye, P. C. Arora, and K. Deck, *Can. J. Chem.*, **49**, 1764 (1971).

 © 1986 The Chemical Society of Japan Bull. Chem. Soc. Jpn., 59, 3109—3112 (1986)

Spacer-Assisted Catalytic Action of Imidazole-Appended γ-Cyclodextrin

Akihiko Ueno,* Fumio Moriwaki, Tetsuo Osa,* Tsukasa Ikeda,† Fujio Toda,† and Kenjiro Hattori††
Pharmaceutical Institute, Tohoku University, Aobayama, Sendai 980
†Department of Chemical Engineering, Faculty of Engineering, Tokyo Institute of Technology, O-okayama, Meguro-ku, Tokyo 152
††Department of Industrial Chemistry, Faculty of Engineering, Tokyo Institute of Polytechnics, Atsugi, Kanagawa 244-02
(Received March 20, 1986)

Catalytic activity of γ-cyclodextrin bearing an imidazole moiety (**1**) was compared with that of the corresponding β-cyclodextrin derivative (**2**) in the hydrolysis of *p*-nitrophenyl acetate. The catalysts **1** and **2** hydrolyzed the ester 80 and 172 times, respectively, as fast in the complexes as the buffer without any catalyst. The binding of **1** for the ester was 40% weaker than that of **2**. When sodium 1-naphthaleneacetate was present in the catalytic systems, the hydrolysis rate was enhanced for **1**, but depressed for **2**. This rate enhancement of **1** suggests that sodium 1-naphthaleneacetate acts as a spacer which facilitates **1** to bind the substrate by narrowing the large γ-cyclodextrin cavity. The time dependency of *p*-nitrophenol formation under the conditions of large excess of *p*-nitrophenyl acetate to **1** or **2** exhibited that the inhibitory effect of the product was remarkable for **2**, but negligible for **1**.

Cyclodextrins (CDs) are a series of cyclic oligomers consisting of six or more α-1,4-linked D-glucopyranose units. The number of glucopyranose unit is designated by a Greek letter: α for six, β for seven, γ for eight, so on. They have a hydrophobic cavity in which various hydrophobic guests can be included.[1] Because of their remarkable ability to form inclusion complexes, CDs, particularly α- and β-CDs, have been used as enzyme models.[1,2] Ester hydrolysis accelerated by CDs has been extensively studied as a serine protease model in which an alkoxide anion of secondary hydroxyls of CDs attacks the carbonyl of bound substrates.[3-5] Since pK_a of the hydroxyls is 12.1,[4] the acceleration by CDs occurs only at high pHs, in contrast to chymotrypsin which exhibits maximal rate at pH 8. Another fault of native CDs as enzyme models is that they are not real catalyst because acylated CDs thus produced are stable. There have been many attempts to convert CDs to better enzyme models by attaching appropriate functional groups.[1] Imidazole is one of those functional groups, which itself works as a catalyst at around pH 8, and actually plays an important role in catalytic action of chymotrypsin. From this viewpoint, imidazole-modified α- and β-CDs have been studied as effective catalysts which have both binding site (CD unit) and functional group (imidazole).[6-8]

The use of γ-CD as a binding site of such enzyme models has not yet been attempted so far mainly due to its large cavity size. However, in recent years, γ-CD has excited much attention because it was shown that γ-CD can include two guest molecules in its large cavity.[9] It was also shown that good-sized molecules or attached moieties can act as spacers which enable γ-CD to include a variety of guests by narrowing the large cavity.[10-12] In connection with this unique property of γ-CD, we have prepared imidazole-appended γ-CD (**1**) in the present work to examine its catalytic activity, turnover ability and effects of additives by using the corresponding β-CD derivative (**2**) as a reference catalyst.

Table 1. Pseudo-First-Order Rate Constants for Ester Hydrolysis[a]

Catalyst	$10^5 k_{obsd}/s^{-1}$
None	4.83±0.27
β-CD	10.6±0.04
γ-CD	8.49±0.20
1	63.4±1.4
2	182±7
3	29.7±0.05

a) 25 °C in pH 8.16 (I=0.200 (KCl)) 0.05 mol dm^{-3} Tris-HCl buffer with 0.40% (v/v) acetonitrile added; [Catalyst]=2.5×10^{-3} mol dm^{-3}; [*p*-Nitrophenyl acetate]=2.5×10^{-5} mol dm^{-3}.

Results and Discussion

Table 1 shows the pseudo-first-order rate constants obtained at 25 °C in pH 8.16 buffer solution by using *p*-nitrophenyl acetate as a substrate. Even under these mild conditions, the ester decomposes spontaneously. β- and γ-CDs enhance the hydrolysis rate slightly, showing 2.2 and 1.8-fold larger values, respectively, than the simple buffer solution. The data suggest stronger binding ability of β-CD than that of γ-CD.[12] The imidazole-appended β-CD **2** revealed 38-fold increase in the rate constant, while the rate increase of the corresponding γ-CD derivative **1** was 13-fold. The inferior activity of **1** is probably due to the large cavity size of its γ-CD unit. It is obvious that the CD parts of **1** and **2** contribute remarkably as binding sites to the acceleration of the reaction, as shown by two and six times larger rate constants for **1** and **2**, respectively, than that of the reference imidazole compound **3**. The reaction, therefore, proceeds according to the Scheme 1,

$$\mathrm{ImCD} + \mathrm{S} \underset{k_{-1}}{\overset{k_1}{\rightleftharpoons}} \mathrm{ImCD \cdot S} \xrightarrow{k_2} \mathrm{ImCD \cdot S'} \xrightarrow{k_3} \mathrm{ImCD} + \mathrm{P_2}$$
$$\mathrm{ImCD \cdot S'} + \mathrm{P_1}$$

Scheme 1.

Table 2. Kinetic Parameters for Ester Hydrolysis by **1** and **2**[a)]

Catalyst	$10^3k_2/s^{-1}$[b)]	K_m/mmol dm^{-3}[c)]	$10(k_2/K_m)$/dm^3 mol^{-1} s^{-1}
1	3.86±0.42	14.9±2.0	2.60±0.07
2	8.33±0.28	8.90±0.08	9.35±0.23

a) Hydrolysis of *p*-nitrophenyl acetate at 25 °C in pH 8.16 (I=0.200 (KCl)) 0.05 mol dm^{-3} Tris-HCl buffer with 0.40% (v/v) acetonitrile added. b) Rate constant of intracomplex hydrolysis. c) Dissociation constant of the substrate-catalyst complexes.

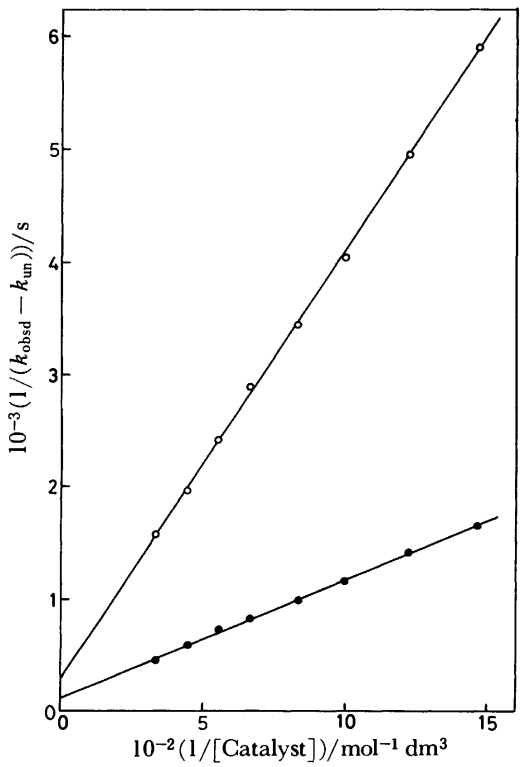

Fig. 1. Lineweaver-Burk plots for hydrolysis of *p*-nitrophenyl acetate with **1** (○) and **2** (●) (25 °C in pH 8.16 Tris-HCl buffer).

where ImCD is **1** or **2**, S is *p*-nitrophenyl acetate, P_1 is *p*-nitrophenol and P_2 is acetic acid.

The rate constants for the intracomplex reaction k_2 and the dissociation constants (Michaelis constants) K_m were evaluated by the Lineweaver-Burk plots[13)] of Eq. 1 (Fig. 1) as shown in Table 2,

$$\frac{1}{k_{obsd}-k_{un}} = \frac{K_m}{(k_2-k_{un})[Catalyst]} + \frac{1}{(k_2-k_{un})}, \quad (1)$$

where k_{obsd} and k_{un} denote the rate constants in the presence and absence of catalyst, respectively. The catalysts **1** and **2** hydrolyze the ester 80 and 172 times, respectively, as fast in the complexes as the buffer without any catalyst. The catalyst **2** has a dissociation constant that is 40% smaller than that of **1**. These data demonstrate that size-fitting between CD cavity and guest and positions of imidazole and ester carbonyl in the complex are better for **2**, resulting in 3.6-fold larger overall reaction rate k_2/K_m than that of **1**.

It seems interesting to examine the effect of additives

Table 3. Spacer Effect of Sodium 1-Naphthaleneacetate on Ester Hydrolysis Catalyzed by **1** and **2**[a)]

Catalyst	Spacer[b)]/mol dm^{-3}	$10^5k_{obsd}/s^{-1}$
1	0	63.4±1.4
1	0.005	74.9±0.3
1	0.01	78.7±0.04
2	0	182±7
2	0.005	162±0.3
2	0.01	150±4
3	0	29.7±0.05
3	0.005	29.7±0.06
3	0.01	29.9±0.04

a) 25 °C in pH 8.16 (I=0.200 (KCl)) 0.05 mol dm^{-3} Tris-HCl buffer with 0.40% (v/v) acetonitrile added; [Catalyst]=2.5×10^{-3} mol dm^{-3}; [*p*-Nitrophenyl acetate]=2.5×10^{-5} mol dm^{-3}. b) Sodium 1-naphthaleneacetate.

in the catalytic system of **1** since the additives might operate as spacers which enable the substrate to be included more strongly by narrowing the large γ-CD cavity. Table 3 shows the variation of the pseudo-first-order rate constant observed when sodium 1-naphthaleneacetate (**4**) was added as a spacer. The rate value for **2** diminished with increasing concentration of **4**, while **1** showed 24% increase in the value at [**4**]=0.01 mol dm^{-3}. The results imply that **4** acts as an inhibitor for **2** but as an effector for **1**. This effector behavior of **4** should be due to the spacer effect of **4** as shown in Fig. 3. This spacer effect was also confirmed by the fact that the catalyst **3**, which has no cavity, afforded the same rate value independently of the concentration of **4**. Since similar rate enhancement was

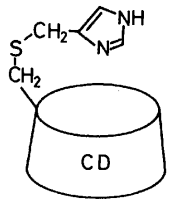

1 CD = γ-CD

2 CD = β-CD

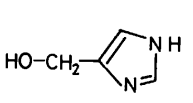

3

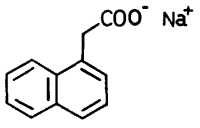

4

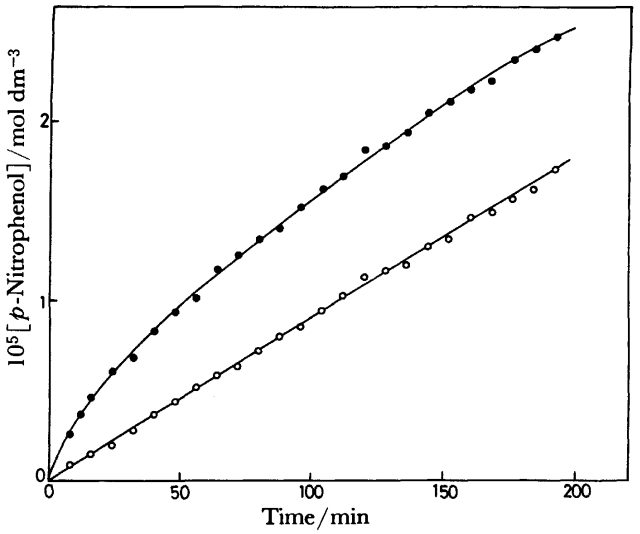

Fig. 2. Concentration of *p*-nitrophenol produced by hydrolysis of *p*-nitrophenyl acetate as a function of time under the conditions of large excess of substrate to **1** (○) or **2** (●) (25 °C in pH 7.02 (I=0.200 (KCl)) phosphate buffer). [*p*-Nitrophenyl acetate]=1.00×10^{-3} mol dm^{-3}. [**1**] or [**2**]=1.00×10^{-5} mol dm^{-3}.

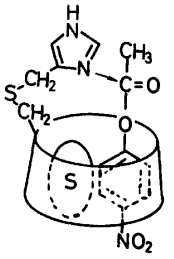

Fig. 3. Schematic representation of spacer(S)-assisted hydrolysis of *p*-nitrophenyl acetate in **1**.

observed when cyclohexanone and (−)-borneol were used in place of **4**,[14] this spacer effect is considered to occur widely in γ-CD systems.

The turnover abilities of **1** and **2** were examined under the conditions of large excess (100-fold) of *p*-nitrophenyl acetate. Figure 2 shows the time dependency of the amount of *p*-nitrophenol. The amounts of hydrolyzed *p*-nitrophenyl acetate are 1.7-fold and 2.5-fold larger for **1** and **2**, respectively, than the quantity of the catalysts at 200 min of the reaction time. This confirms that the deacylation step in Scheme 1 proceeds, regenerating the catalysts which can hydrolyze other substrate molecules again. The plots of *p*-nitrophenol vs. time exhibit different features for **1** and **2**, being curved for **2** and linear for **1**. The depressed rate observed for **2** in the period after the initial stage may be explained in terms of the inhibitory effect of produced *p*-nitrophenol. It means that the product competes with the substrate for complexing with **2**. In contrast to the remarkable binding ability of **2** to *p*-nitrophenol, the catalyst **1**, which has a large γ-CD cavity, seems hard to form 1:1 complex with *p*-nitrophenol. In other words, **1** is likely to be good host for the substrate and poor host for the product. Although the present study gave no data indicative of the formation of the ternary complex of **1**, substrate and *p*-nitrophenol, it is noted that *p*-nitrophenol may act as a spacer in the catalytic system of **1** as **4** does if its concentration is appropriate. The spacer-assisted or product-assisted binding of substrate cannot be expected to occur in α- and β-CD systems.

The present γ-CD system **1** was not a better catalyst than the β-CD system **2** even in the presence of spacers, but the results obtained here present guideline for designing effective catalytic systems of γ-CD. As an extension of this study, construction of some γ-CD systems having both spacer and catalytic moiety are now under way.

Experimental

Materials. β-CD (Tokyo Kasei) was recrystallized from water and dried in vacuo. γ-CD was kindly gifted from Nihon Shokuhin Kako Ltd., and was used without further purification. *p*-Nitrophenyl acetate (Tokyo Kasei) was recrystallized from ethanol. 4-(Hydroxymethyl)imidazole (Aldrich) and sodium 1-naphthaleneacetate (Tokyo Kasei) were used without further purification. Aqueous buffers were prepared with deionized water.

Tosyl-β-CD was prepared in pyridine, so that one of primary hydroxyls of β-CD was sulfonated.[15,16] The crude product was purified by repeated recrystallization from the mixed solvent of 1-butanol, ethanol, and water (5:4:3 by volume). The TLC of the obtained crystals showed a single spot on the plate (Merck, Kieselgel 60 F_{254}) when the plate was treated with *p*-anisaldehyde solution and then heated: R_f 0.49 (1-butanol: ethanol: water=5:4:3).

6-*O*-(2-naphthylsulfonyl)-γ-CD was prepared from 2-naphthalenesulfonyl chloride and γ-CD by the method previously reported.[17]

Measurements. The kinetic runs were performed with a Shimadzu UV-360 spectrophotometer. Reaction temperature was kept at 25±0.1 °C by using a Haake water circulation instrument. A kinetic run was initiated by injecting a solution of substrate in acetonitrile into the catalyst solution. The absorbance at 400 nm of *p*-nitrophenol was monitored as a function of time. The data were fitted to a simple exponential curve for a first-order reaction. The pseudo-first-order rate constants in Tables 1 and 3 were averages of at least two runs. The kinetic parameters shown in Table 2 represent the averages of three runs of Lineweaver-Burk plots. Figure 1 shows the results of one run of the plots for **1** and **2**.

6-Deoxy-6-(4-imidazolylmethylthio)-γ-cyclodextrin (1). 4-(Mercaptomethyl)imidazole hydrochloride (430 mg) and 6-*O*-(2-naphthylsulfonyl)-γ-CD (1 g) were dissolved in 200 ml of 30% aqueous ethanol solution. After adding sodium carbonate to adjust pH of the solution at 10.0, the solution was stirred 4 d under nitrogen. The reaction mixture was neutralized with 1M HCl (1M=1 mol dm^{-3}) and concentrated to 15 ml. Purification was performed by desalting with Bio-Bead ™SM-4 and SP-Sephadex C-25 resins, followed by column chromatography with Sephadex G-15 (yield 0.25 g (25%)). R_f=0.21 (28% aqueous NH_3: H_2O: AcOEt: 2-PrOH= 1:4:3:5); ^{1}H NMR (DMSO-d_6, 20 °C) δ=3.09—3.94 (br,

50H, CH_2 protons of mercaptomethyl-4-imidazole and CD protons other than C_1H and OH), 4.54 (7H, O_6H), 4.88 (8H, C_1H), 5.79 (16H, O_2H and O_3H), 6.63—7.17 (1H, aromatic), 7.52 (1H, aromatic), 11.90 (1H, NH); Found: C, 41.51; H, 6.51; N, 1.93; S, 2.19%. Calcd for $C_{52}H_{84}N_2O_{39}S \cdot 6H_2O$: C, 41.60; H, 6.45; N, 1.87; S, 2.14%.

6-Deoxy-6-(4-imidazolylmethylthio)-β-cyclodextrin (2). This compound was prepared previously.[18] In the present work, **2** was prepared according to the procedure described in the synthesis of **1** (yield 27%): R_f=0.28 (28% aqueous NH_3 : H_2O : AcOEt : 2-PrOH=1 : 4 : 3 : 5). Found: C, 43.56; H, 6.31; N, 1.95; S, 2.80. Calcd for $C_{46}H_{74}N_2O_{34}S \cdot 2H_2O$: C, 43.60; H, 6.20; N, 2.21; S, 2.53%.

We thank Nihon Shokuhin Kako Co Ltd. for providing γ-CD. Support of this work by a Grant-in-Aid (No. 60104003) for Special Project Research from the Ministry of Education, Science and Culture is gratefully acknowledged.

References

1) M. L. Bender and M. Komiyama, "Cyclodextrin Chemistry," Springer-Verlag (1978).
2) I. Tabushi, *Acc. Chem. Res.*, **15**, 66 (1982).
3) N. Heinrich and F. Cramer, *J. Am. Chem. Soc.*, **87**, 1121 (1965).
4) R. L. VanEtten, J. F. Sebastian, G. A. Clowes, and M. L. Bender, *J. Am. Chem. Soc.*, **89**, 3242, 3253 (1967).
5) R. Breslow, M. F. Czarniecki, J. Emert, H. Hamaguchi, *J. Am. Chem. Soc.*, **102**, 762 (1980); R. Breslow and G. Trainor, *J. Am. Chem. Soc.*, **103**, 154 (1981); R. Breslow, G. Trainor, and A. Ueno, *J. Am. Chem. Soc.*, **105**, 2739 (1983).
6) F. Cramer and G. Mackensen, *Angew. Chem.*, **78**, 641 (1966).
7) Y. Iwakura, K. Uno, F. Toda, S. Onozuka, K. Hattori, and M. L. Bender, *J. Am. Chem. Soc.*, **97**, 4432 (1975).
8) T. Ikeda, R. Kojin, C. -J. Yoon, H. Ikeda, M. Iijima, K. Hattori, and F. Toda, *J. Incl. Phenom.*, **2**, 669 (1984).
9) A. Ueno, K. Takahashi, and T. Osa, *J. Chem. Soc., Chem. Commun.*, **1980**, 921; A. Ueno, F. Moriwaki, T. Osa, F. Hamada, and K. Murai, *Bull. Chem. Soc. Jpn.*, **59**, 465 (1986) and references therein.
10) A. Ueno, K. Takahashi, Y. Hino, and T. Osa, *J. Chem. Soc., Chem. Commun.*, **1981**, 194.
11) A. Ueno, Y. Tomita, and T. Osa, *J. Chem. Soc., Chem. Commun.*, **1983**, 976.
12) A. Ueno, F. Moriwaki, Y. Hino, and T. Osa, *J. Chem. Soc., Perkin Trans. 2*, **1985**, 921.
13) H. Lineweaver and D. Burk, *J. Am. Chem. Soc.*, **56**, 658 (1934).
14) Unpublished data.
15) A. Ueno and R. Breslow, *Tetrahedron Lett.*, **23**, 3451 (1982).
16) K. Takahashi, K. Hattori, and F. Toda, *Tetrahedron Lett.*, **25**, 3331 (1984).
17) A. Ueno, Y. Tomita, and T. Osa, *Chem. Lett.*, **1983**, 1635.
18) R. Breslow, P. Bovy, and C. L. Hersh, *J. Am. Chem. Soc.*, **102**, 2115 (1980).

 © 1986 The Chemical Society of Japan Bull. Chem. Soc. Jpn., 59, 3113—3116 (1986)

Stopped-Flow Investigation of Antioxidant Activity of Tocopherols

Kazuo MUKAI,* Yoshiko WATANABE, Yuichi UEMOTO, and Kazuhiko ISHIZU
Department of Chemistry, Faculty of Science, Ehime University, Matsuyama 790
(Received March 22, 1986)

It was observed by ESR measurement that the oxidation of α-, β-, γ-, and δ-tocopherols (vitamin E) with a stable phenoxyl radical in benzene immediately gives corresponding tocopheroxyl radicals. The rates of reaction of α-, β-, γ-, and δ-tocopherols with the stable phenoxyl radical in ethanol solution have been determined spectrophotometrically using stopped-flow technique, as a model reaction of tocopherols with unstable free radicals (ROO·, RO·, and HO·) in biological systems. The second-order rate constants obtained are $(5.12\pm0.36)\times10^3$ (α-Toc), $(2.24\pm0.04)\times10^3$ (β-Toc), $(2.42\pm0.16)\times10^3$ (γ-Toc), and $(0.51\pm0.01)\times10^3$ (δ-Toc), $M^{-1}s^{-1}$ in ethanol at 25.0 °C. The relative rates agree well with those obtained from studies of the reactivities of tocopherols toward poly(styrylperoxyl) and galvinoxyl radicals by O_2 consumption and by ESR method, respectively. The results suggest that the relative reactivities, that is, relative antioxidant activities of tocopherols do not depend on the kinds of unstable free radicals reacted.

Vitamin E (α, β-, γ-, and δ-tocopherols) is known to scavenge peroxyl, alkoxyl, and hydroxyl radicals.[1,2] The above free radical scavenging actions by vitamin E have been ascribed to the initial reaction of the phenolic hydroxyl group with the production of a tocopheroxyl* radical.[3,4] Therefore, several investigators have measured the oxidation rates k_1 of α-tocopherol by peroxyl radicals (ROO·), using different experimental methods such as chemiluminescence, pulse radiolysis, and O_2 consumption.[5–10]

$$ROO\cdot + Toc \longrightarrow ROOH + Toc\cdot \qquad (1)$$

However, considerable variations in the values of k_1 have been observed when different experimental methods were used, because the techniques employed to measure k_1 for α-tocopherol are indirect.[11]

Recently, Burton et al. have measured rate constants for reactions of the α-, β-, γ-, and δ-tocopherols with poly(styrylperoxyl) radicals, using O_2 consumption method.[11,12] They suggested that the reactivity of the tocopherols towards peroxyl radicals parallels their biological activity (α>β>γ>δ-tocopherol). Further, Niki et al. have measured the rate constants for reactions between galvinoxyl radical incorporated into dimyristoyl phosphatidylcholine (abbreviated to PC) liposomes and α-, β-, γ-, and δ-tocopherols incorporated into different dimyristoyl PC liposomes by ESR technique.[13] The observed pseudo-first-order rate constants of tocopherols decreased in the order of α>β≅γ>δ-tocopherol.

In this study we have used a stopped-flow technique to examine the reaction of tocopherols with a stable phenoxyl radical, i. e., 2,6-di-*t*-butyl-4-(4-methoxyphenyl)-phenoxyl (PhO·) (see Fig. 1), as a model reaction of tocopherols with unstable free radicals (ROO·, RO·, and HO·) in biological systems. The reactions were performed in the presence of excess tocopherol in ethanol, giving the pseudo-first-order rate constants, k_{obsd}. The second-order rate constants, k_s, may be immediately calculated from the k_{obsd} values, using the relation, $k_{obsd}=k_s[Toc]$. That is, the k_s value can be directly obtained from the above stopped-flow experiments. Therefore, this method will give more reliable values of rate constants than the other methods. By comparing the relative reactivities of α-, β-, γ-, and δ-tocopherols found by different experimental methods, we discussed the antioxidant activity of tocopherols.

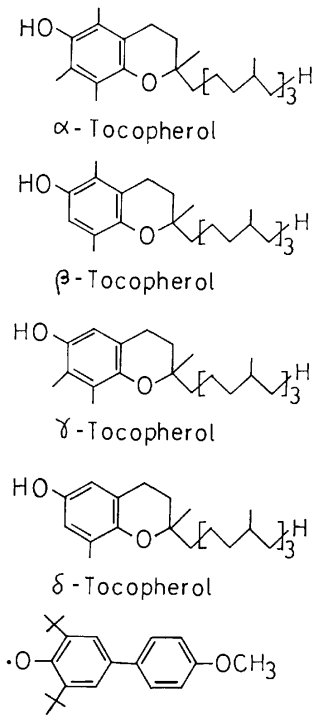

Fig. 1. Molecular structures of α-, β-, γ-, and δ-tocopherols and phenoxyl radical (PhO·).

Experimental

d-α-, d-β-, d-γ-, and d-δ-tocopherols were kindly supplied from Eisai Co., Ltd.

The 2,6-di-*t*-butyl-4-(4-methoxyphenyl)phenoxyl (PhO·)

* The phenoxyl radicals generated from tocopherols are named in this paper as widely used tocopheroxyl radicals for convenience rather than tocopheryloxyl radicals that conform to rules of nomenclature.

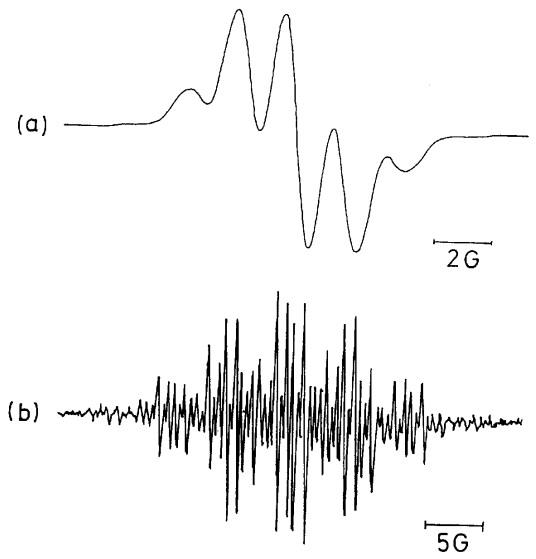

Fig. 2. ESR spectra of (a) phenoxyl radical and (b) α-tocopheroxyl radical at 25°C in benzene under vacuum.

(abbreviated to "phenoxyl" hereafter) was prepared according to the method of Müller et al.[14] Radical concentration of the phenoxyl radical was obtained from the results of the paramagnetic susceptibility measurements at 20°C, after correcting for the diamagnetic contribution ($\chi_{dia} = -0.220 \times 10^{-3}$ emu mol^{-1}) calculated by the Pascal's method. The value was 100% for phenoxyl, assuming the Curie law.

The ESR measurements were carried out using a JES-FE-2XG spectrometer with 100 KHz magnetic field modulation. UV. visible spectra were recorded on a JASCO UVIDEC-1 spectrophotometer. The stopped-flow data were obtained on a UNISOKU stopped-flow spectrophotometer Model RS-450 by mixing equal volumes of ethanol solutions of phenoxyl and tocopherol. The oxidation reactions were studied under pseudo-first-order conditions, and the observed rate constants, k_{obsd}, were calculated in the usual way using a standard least-squares analysis. All measurements were performed at 25.0 ± 0.5 °C.

Results and Discussion

ESR Studies of the Oxidation of Tocopherols with Phenoxyl Radical. Figure 2(a) shows an ESR spectrum of the phenoxyl radical in benzene at 25°C under vacuum.[15] When two benzene solutions containing 2.50 mM phenoxyl and 5.00 mM α-tocopherol (1 : 1 in volume), respectively, were mixed at 25°C under vacuum, phenoxyl disappeared instantaneously, and a new spectrum due to α-tocopheroxyl radical appeared (Fig. 2(b)). The above reaction can be represented by the following equation.

$$\text{PhO}\cdot + \text{Toc} \xrightarrow{k_s} \text{PhOH} + \text{Toc}\cdot \qquad (2)$$

Similarly, β-, γ-, and δ-tocopherols were reacted with the phenoxyl, and the ESR spectra due to β- and γ-tocopheroxyl radicals were observed. However, in the case of δ-tocopherol, the radical is very unstable, and the clear ESR spectrum cannot be observed. The observed hyperfine splittings are listed in Table 1. There have been many ESR studies of tocopheroxyl radicals published.[16] However, the spectrum is fairly complex and has only recently been completely resolved, first by Mukai (one of the present authors) et al.,[3,17] and, then, by Matsuo et al.[18] and Tsuchiya et al.[19] The hyperfine splittings in Table 1 show good accordance with those reported previously.[3,17]

Table 1. Hyperfine Couplings (a_i^H) of Tocopheroxyl Radicals in Benzene at 25°C

	a_5^H	a_7^H	a_4^H	a_8^H
α-Toc	6.04G	4.52G	1.48G	0.93G
β-Toc	6.39	4.63	1.76	0.81
γ-Toc	5.97	4.80	1.17	1.17
δ-Toc	—	—	1.52	1.04

Stopped-Flow Studies of the Reaction Rates of Tocopherols with Phenoxyl. The phenoxyl radical is stable in the absence of tocopherol, and shows absorption peaks at $\lambda_{max} = 376$ nm ($\varepsilon = 17600$ M^{-1} cm^{-1}) and 580 nm ($\varepsilon = 4280$ M^{-1} cm^{-1}) in ethanol. The phenol precursor of the phenoxyl and α-tocopherol show absorption peaks at $\lambda_{max} = 267$ nm ($\varepsilon = 19500$ M^{-1} cm^{-1}) and $\lambda_{max} = 295$ nm ($\varepsilon = 3610$ M^{-1} cm^{-1}), respectively, in ethanol; no absorptions were observed in the visible region.

By adding an ethanol solution of α-tocopherol (5.00 mM) to an ethanol solution of phenoxyl (0.10 mM) (1 : 1 in volume) at 25.0°C, the absorption spectrum of the phenoxyl immediately changed to that of α-tocopheroxyl. The absorption spectrum of α-tocopheroxyl shows weak absorption peaks at 425 and 405 nm.[20] However, the α-tocopheroxyl is unstable, and the absorption peaks rapidly disappeared. Similarly, the phenoxyl radical has been reacted with excess β-, γ-, and δ-tocopherols, showing rapid decrease of the absorption spectrum, respectively. On the other hand, the absorption spectra of the corresponding tocopheroxyls were not observed in these cases, because these tocopheroxyls are more unstable than α-tocopheroxyl.

Therefore, the oxidation rates of tocopherols by phenoxyl were studied spectrophotometrically using stopped-flow technique in the presence of excess tocopherol in ethanol. The rate was measured by following the decrease in absorbance at 376 and 580 nm of phenoxyl radical. The time dependence of the decrease in absorbance at 376 nm observed when 0.10 mM ethanol solution of phenoxyl is mixed with 5.00 mM ethanol solution of α-thcopherol (1 : 1 in volume; final concentration of phenoxyl is 0.05 mM) is shown in Fig. 3. A typical Guggenheim plot versus time was linear to >90% completion, as shown in Fig. 4. The pseudo-first-order rate constants, k_{obsd}, obtained by varying the concentration of phenoxyl and α-tocopherol are presented in Table 2. The stopped-flow reactions were performed at 25.0 ± 0.5 °C.

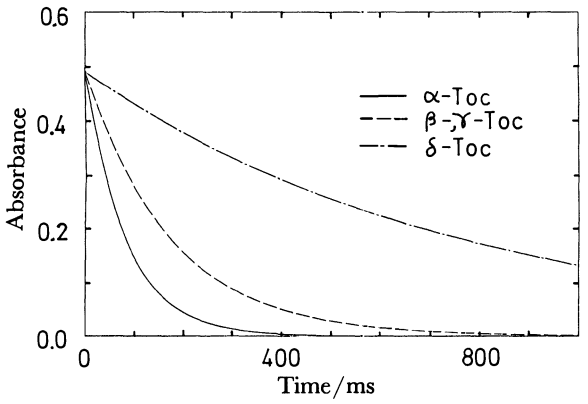

Fig. 3. The decay of phenoxyl radicals for the reaction of phenoxyls with α-, β-, γ-, and δ-tocopherols in ethanol at 25.0 °C.
$[PhO\cdot]_{t=0}$ 0.05 mM and $[Toc]_{t=0}$ 2.50 mM. At 376 nm.

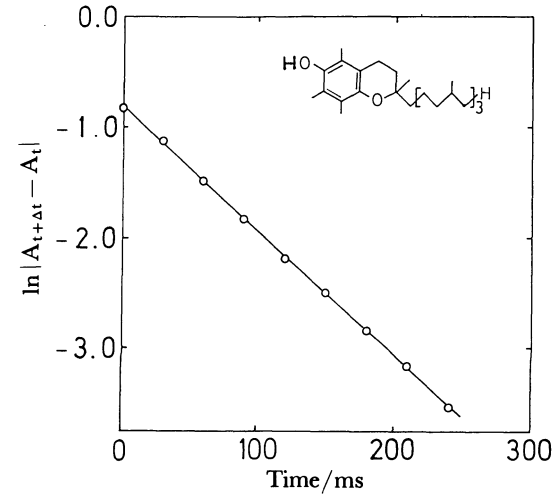

Fig. 4. First-order Guggenheim plot of the data of α-tocopherol in Fig. 3; $k_{obsd}=12.0\,s^{-1}$.

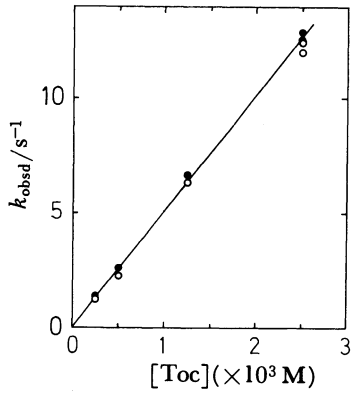

Fig. 5. The dependence of the pseudo-first-order rate constant, k_{obsd}, on [α-Toc] in ethanol. (○): observed at 376 nm. (●): observed at 580 nm.

The pseudo-first-order rate constants, k_{obsd}, observed at 376 and at 580 nm were linearly dependent on the concentration of tocopherol as shown in Fig. 5. Therefore, the rate law is expressed as

Table 2. Pseudo-First-Order (k_{obsd}) and Second-Order (k_s) Rate Constants for Oxidation of α-Tocopherol by the Phenoxyl Radical in Ethanol at 25.0 °C

λ_{max}	Ratio [PhO·]:[Toc]	k_{obsd} / s^{-1}	$10^{-3}k_s$ / $M^{-1}s^{-1}$
376 nm	2 :50	12.5	4.98
	1.5:50	12.4	4.94
	1[a]:50	12.0	4.76
	1 :25	6.34	5.15
	1 :10	2.62	5.31
	1 : 5	1.29	5.22
580 nm	2 :50	12.5	4.98
	1.5:50	12.5	4.98
	1 :50	12.9	5.10
	1 :25	6.65	5.41
	1 :10	2.61	5.29
	1 : 5	1.32	5.34

a) $[PhO\cdot]_{t=0}=0.05$ mM. For PhO·, see text and Fig. 1.

$$-d[PhO\cdot]/dt = k_{obsd}[PhO\cdot] = k_s[Toc][PhO\cdot], \quad (3)$$

where k_s is the second-order rate constant for oxidation of tocopherol by phenoxyl radical. The k_s values were calculated from k_{obsd} values in 12 independent experiments (0.25—2.50 mM tocopherol), respectively, and listed in Table 2. The average value for k_s was $(5.12\pm0.36)\times10^3\ M^{-1}\ s^{-1}$ in ethanol at 25.0 °C. Similarly, the second-order rate constants, k_s, were obtained for β-, γ-, and δ-tocopherols. For each tocopherol, k_s was measured in 4—12 independent experiments. The experimental error in k_s values was $<\pm7\%$ in every case. The values of the k_s observed are listed in Table 3. The results listed in Table 3 demonstrate that α-tocopherol is about two times as reactive as β-tocopherol, whereas β-tocopherol is, within our limits of error, as reactive as γ-tocopherol. However, δ-tocopherol is only ca. 10% as reactive as α-tocopherol.

Century and Horwitt reported that biological activities of tocopherols decrease in the order of $\alpha>\beta>\gamma>\delta$, and that in vivo and in vitro tests of their relative biological activities change depending on the kinds of test (see Table 2 in Ref. 21).[21] As described in a previous section, Burton et al. have reported absolute second-order rate constants, k_s', for the reaction of α-, β-, γ-, and δ-tocopherols with poly(styrylperoxyl) radicals, using the O_2 consumption method (see Table 3).[11,12] The suggested that the relative magnitude of the second-order rate constant, k_s', of α-, β-, γ-, and δ-, tocopherols is in agreement with in vivo and in vitro tests of their relative biological activities which yield: $\alpha>\beta>\gamma>\delta$-tocopherol.[21] Niki et al. have measured the pseudo-first-order rate constants (k_f) (see Table 3) for the reaction between galvinoxyl radical incorporated into dimyristoyl PC liposomes and α-, β-, γ-, and δ-tocopherols incorporated into different dimyristoyl PC liposomes, by ESR technique.[13] By comparing the k_f value for α-tocopherol with those found for β-, γ-, and δ-tocopherol, they suggested that the reactivities of

Table 3. Second-Order Rate Constants (K_s) and Relative Rate Constants (k_s/k_s (α-Toc)) for Oxidation of Tocopherols by Phenoxyl Radical in Ethanol at 25.0 °C

	Present Work $10^{-3}\,k_s$ ($M^{-1}s^{-1}$)	k_s/k_s (α-Toc)	Ingold et al.[a] $10^{-6}\,k'_s$ ($M^{-1}s^{-1}$)	k'_s/k'_s (α-Toc)	Niki et al.[b] $10^4\,k_f$ (s^{-1})	k_f/k_f (α-Toc)
α-Toc	5.12±0.36	(1.00)	3.24±0.15	(1.00)	10.1[c]	(1.00)
β-Toc	2.24±0.04	(0.44)	1.66±0.33	(0.51)	5.44	(0.54)
γ-Toc	2.42±0.16	(0.47)	1.59±0.42	(0.49)	5.00	(0.50)
δ-Toc	0.51±0.01	(0.10)	0.65±0.13	(0.20)	4.76	(0.47)
Technique	Stopped-flow Spectrophotometer		O_2 Consumption		ESR	
Radical	Phenoxyl[d]		Poly(styrylperoxyl)		Galvinoxyl	
T/°C	25		30		30	

a) See Ref. 11 and 12. b) See Ref. 13. c) Experimental errors are not indicated. d) The structure is shown in Fig. 1.

tocopherols toward galvinoxyl radical decrease in the order of $\alpha > \beta \cong \gamma > \delta$.

In the present work, we have measured the rate constants k_s for the reaction of α-, β-, γ-, and δ-tocopherols with the stable phenoxyl radical in ethanol, using a stopped-flow spectrophotometer. As listed in Table 3, the relative k_s values ($\alpha:\beta:\gamma:\delta = 1.00:0.44:0.47:0.10$) obtained by the stopped-flow technique are in good agreement with the values (1.00:0.51:0.49:0.20) obtained by the O_2 consumption method, except for δ-tocopherol, although the absolute k_s values are about 600 times smaller than those for the reaction of tocopherols with poly(styrylperoxyl) radical in chlorobenzene.[11,12] Further, the above relative magnitude of the second-order rate constants, k_s, of α-, β-, γ-, and δ-tocopherols is also in satisfactory agreement with that (1.00:0.54:0.50:0.47) of the pseudo-first-order rate constant, k_f, obtained by ESR technique, except for δ-tocopherol.[13] The results suggest that the relative reactivities, that is, relative antioxidant activities obtained by the three different experimental methods agree well with each other. In addition, the above results indicate that the relative antioxidant activities do not depend on the kinds of radicals (phenoxyl, poly (styrylperoxyl), and galvinoxyl radical) used, while the absolute rates are considerably different from each other. As described above, biological activities of tocopherols decrease in the order of $\alpha > \beta > \gamma > \delta$, and in vivo and in vitro tests of their relative biological activities change depending on the kinds of test.[21] For instance, the relative biopotencies of α-, β-, γ-, and δ-tocopherols have been reported as 100, 25, 18, and 0.3 in an erythrocyte hemolysis test and as 100, 55, 5, and 4 in respiratory decline test, respectively.[21] The result shows that the relative biological activity and antioxidant activity of tocopherols do not always agree with each other, suggesting that the function of tocopherols in biological system is not simple, but manifold.

We are very grateful to Prof. Yoichi Kitamura for use of stopped-flow spectrophotometer and his helpful discussions.

References

1) P. Schudel, H. Mayer, and O. Isler, "The Vitamins," 2nd ed, ed by W. H. Sebrell, Jr. and R. S. Harris, Academic Press, New York (1972), Vol. 5, pp. 168—218.
2) M. L. Scott, "The Fat-Soluble Vitamins," ed by H. F. Deluca, Plenum Press, New York (1978), pp. 133—210.
3) K. Mukai, N. Tsuzuki, S. Ouchi, and K. Fukuzawa, *Chem. Phys. Lipids*, **30**, 337 (1982).
4) M. T. Craw and M. C. Depew, *Rev. Chem. Intermediates*, **6**, 1 (1985).
5) A. A. Kharitonova, Z. G. Kozlova, V. F. Tsepalov, and G. P. Gladyshev, *Kinet. Katal.*, **20**, 593 (1979).
6) J. E. Packer, T. F. Slater, and R. L. Willson, *Nature (London)*, **278**, 737 (1979).
7) Ye. B. Burlakova, Ye. N. Kukhtina, I. P. Ol'khovskaya, I. K. Sarycheva, Ye. B. Sinkina, and N. G. Khrapova, *Biophysics*, **24**, 989 (1980).
8) G. W. Burton, Y. Le. Page, E. J. Gabe, and K. U. Ingold, *J. Am. Chem. Soc.*, **102**, 7791 (1980).
9) M. G. Simic, *J. Chem. Educ.*, **58**, 125 (1981).
10) E. Niki, R. Tanimura, and Y. Kamiya, *Bull. Chem. Soc. Jpn.*, **55**, 1551 (1982).
11) G. W. Burton and K. U. Ingold, *J. Am. Chem. Soc.*, **103**, 6472 (1981).
12) G. W. Burton, L. Hughes, and K. U. Ingold, *J. Am. Chem. Soc.*, **105**, 5950 (1983).
13) E. Niki, J. Tsuchiya, Y. Yoshikawa, Y. Yamamoto, and Y. Kamiya, *Bull. Chem. Soc. Jpn.*, **59**, 497 (1986).
14) E. Müller, A. Schick, and K. Scheffler, *Chem. Ber.*, **92**, 474 (1959).
15) A. Rieker and K. Scheffler, *Liebigs Ann. Chem.*, **689**, 78 (1965).
16) T. Ozawa, A. Hanaki, S. Matsumoto, and M. Matsuo, *Biochim. Biophys. Acta*, **531**, 72 (1978), and references cited therein.
17) K. Mukai, N. Tsuzuki, K. Ishizu, S. Ouchi, and K. Fukuzawa, *Chem. Phys. Lipids*, **29**, 129 (1981).
18) M. Matsuo and S. Matsumoto, *Lipids*, **18**, 81 (1983).
19) J. Tsuchiya, E. Niki, and Y. Kamiya, *Bull. Chem. Soc. Jpn.*, **56**, 229 (1983).
20) W. Boguth and H. Niemann, *Internat. Z. Vit. Forschung*, **39**, 429 (1969).
21) B. Century and M. K. Horwitt, *Fed. Proc. Am. Soc. Exp. Biol.*, **24**, 906 (1965).

Mechanism of Carboxylic Acid-Catalyzed Reduction of Substituted Nitrosobenzenes by 1-Benzyl-3,5-bis(1-pyrrolidinylcarbonyl)-1,4-dihydropyridine in Acetonitrile

Hiroshi AWANO and Waichiro TAGAKI*
Department of Applied Chemistry, Faculty of Engineering, Osaka City University, Sugimoto 3, Sumiyoshi-ku, Osaka 558
(Received March 20, 1986)

Mechanism of carboxylic acid-catalyzed reduction of substituted nitrosobenzenes by 1-benzyl-3,5-bis(1-pyrrolidinylcarbonyl)-1,4-dihydropyridine has been studied in acetonitrile at 25 °C. The major product was hydroxylamine when the dihydropyridine was used in excess over nitrosobenzene, while that was azoxybenzene in the reverse case. The observed second-order rate constant k_2^R are dependent on acid concentration in a first-order manner with the acid-catalyzed third-order rate constant k_H^R. The Hammett relationship for k_H^R for substituted nitrosobenzenes gave a ρ=−0.93. The Brönsted plot of log k_H^R vs. pK_a of acids gave a straight line with a slope of −0.34. The deuterium isotope effect for the catalysis by dichloroacetic acid was found to be k_H^R/k_D^R=2.80. These results indicate that a general acid catalysis by carboxylic acids plays an important role in the reduction of nitrosobenzene by dihydropyridine in acetonitrile.

Acid catalysis has been an interesting subject for the model studies of NAD(P)H coenzyme, since in certain dehydrogenases a protonated histidine residue is presumed to be involved as the general acid to activate substrate carbonyl group for hydride transfer from the coenzyme.[1,2] For the model studies of such acid catalysis, a problem is instability of conventional NADH analogs such as 1-benzyl-3-carbamoyl-1,4-dihydropyridine (**1**) toward acids.[3-6] This problem was solved by Shinkai et al. by the design of 1-benzyl-3-carbamoyl-1,4-dihydroquinoline (**2**) which is stable even in a strong aqueous acid solution.[7] Later, as reported previously,[8] we found that 1-benzyl-3,5-bis(1-pyrrolidinylcarbonyl)-1,4-dihydropyridine (**3**) is much more active reducing agent than **2** and more acid stable than **1** in the acid ($CHCl_2COOH$)-catalyzed reduction of substituted nitrosobenzenes in acetonitrile. In this paper, we wish to report the full accounts of the previous results[8] together with a more detailed study on the mechanism of this acid catalysis. Incidentally, it may be of interest to study the mechanisms of reduction of nitrosobenzene by NADH analogs in connection with the carcinogenesis in biological systems.[9-12]

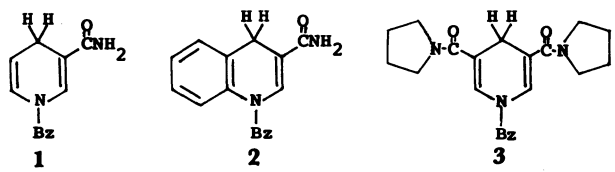

Experimental

All melting points were uncorrected. Spectra were recorded by using the following instruments: IR, Hitachi 215; UV-visible, Hitachi 220 and 220A; NMR, JEOL JMM-PS-100 (100 MHz) and Hitachi R-20 (60 MHz). HPLC was performed by using JASCO UNIDEC-100-II, UNIFLOW-211 and Shimadzu C-R1B.

Materials. Anhydrous acetonitrile was obtained by distilling over phosphorus pentaoxide. The carboxylic acids as catalysts were commercial samples of special grade and purified by recrystallization or distillation if necessary. Substituted nitrosobenzenes were prepared by the reduction of the corresponding commercially available nitrobenzenes with zinc powder in aqueous solution containing ammonium chloride according to the literature methods and purified by recrystallization from ethanol-water: *p*-CH_3, mp 48 °C (lit,[13] 48.5°); *m*-CH_3, mp 53 °C (lit,[13] 53°); *p*-Cl, mp 97 °C (lit,[14] 90°); *p*-CF_3, mp 56—57 °C (lit,[15] 51—53°); H, commercial sample, mp 68 °C. The IR and UV spectra of these nitrosobenzenes were in accord with reported ones.[16,17]

1-Benzyl-3,5-bis(1-pyrrolidinylcarbonyl)-1,4-dihydropyridine (3) was prepared as usual by treating 3,5-pyridinedicarbonyl dichloride with an excess of pyrrolidine in chloroform. The diamide was reacted with benzyl chloride in acetonitrile under reflux to give the pyridinium chloride. The salt was then reduced by sodium dithionite in water. The reaction mixture was extracted with dichloromethane, and the usual work-up of the extract, purification by cellulose-column chromatography and recrystallization from ethanol-water gave **3**, mp 46 °C: overall yield, 65%; UV (CH_3CN), λ_{max}=355 nm (ε=6072 $M^{-1}cm^{-1}$); ^1H NMR (ppm (δ) in $CDCl_3$/TMS), 1.67—1.95 (8H, m, pyrrolidine ring CH_2), 3.25—3.65 (10H, m, dihydropyridine ring 4-CH_2 plus pyrrolidine ring NCH_2), 4.41 (2H, s, CH_2Ph), 6.55 (2H s, dihydropyridine ring 2-CH and 6-CH), 7.45 (5H, s, benzyl aromatic). Found: C, 71.51; H, 7.48; N, 11.42%. Calcd for $C_{22}H_{27}N_3O_2$: C, 72.30; H, 7.45; N, 11.50%.

1-Benzyl-3-carbamoyl-1,4-dihydropyridine (1) and 1-benzyl-3-carbamoyl-1,4-dihydroquinoline (2) were prepared according to the literature methods, mp 118 °C (decomp) (lit,[18] 120—122°) and mp 155 °C (lit,[19] 158—160°), respectively.

Dichloroacetic acid-d was prepared by the hydrolysis of dichloroacetic anhydride in D_2O. The deuterium incorporation was 82% measured by NMR method.

Product analysis was performed for unsubstituted nitrosobenzene (X=H) by HPLC method using JASCO Finepak SIL C18-column and acetonitrile/water (2:1) solvent. Examples of retention times (min) for the reaction components were: phenylhydroxylamine (**5**) (2.3), benzaldehyde (internal standard) (2.9), nitrosobenzene (**4**, X=H) (3.4), azoxybenzene (**6**) (6.6), 1-benzyl-3,5-bis(1-pyrrolidinylcarbonyl)-1,4-dihydropyridine (**3**) (8.3). The major product was **5** when **3** was used in excess over **4**, while that was **6** in

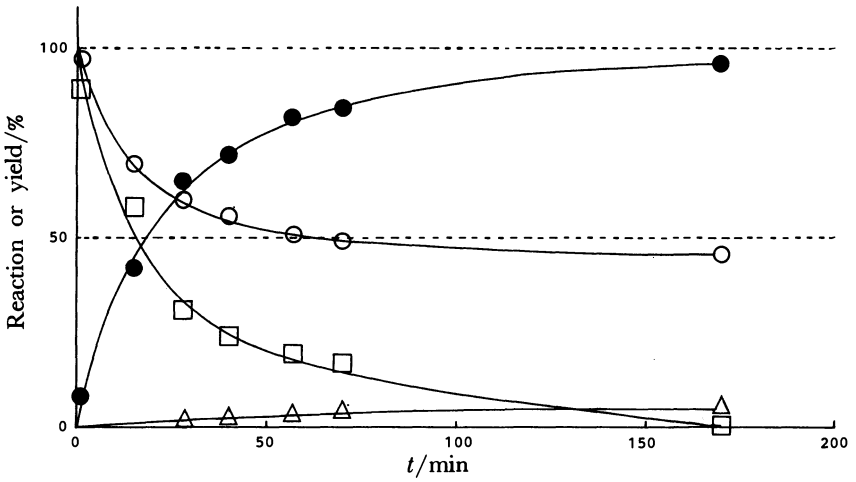

Fig. 1. Time dependent % reaction or yield: [**3**]=1.0×10^{-3} mol dm^{-3}, [**4**]=0.5×10^{-3} mol dm^{-3}, [$CHCl_2COOH$]=10.0×10^{-3} mol dm^{-3}, in acetonitrile, 25 °C. (**3**) (○), (**4**) (□), (**5**) (●), and (**6**) (△).

the reverse case. An example of the time course of a reaction mixture is shown in Fig. 1.

Kinetics. In a 1 cm quartz UV cell stoppered with a rubber septum cover was placed a 3 ml acetonitrile solution of a dihydropyridine and the solution was well bubbled with acetonitrile saturated pure nitrogen gas through inserted needles. Stock solutions of a carboxylic acid and nitrosobenzene were treated in the same way. Then the quartz cell was mounted on a water-jacketed UV cell holder and the acid and nitrosobenzene stock solutions in water bath were kept at 25 °C for 15 min. The reaction was started by adding acid and nitrosobenzene stock solutions to the quartz cell by a Hamilton microsyringe. The rates of reduction were followed by monitoring the decrease in absorbance of either dihydropyridine at 350 nm for **1** and **2**, and at 370 nm or 400 nm for **3** or nitrosobenzene near 307 nm. In most cases, the reaction was carried out under pseudo-first-order conditions with 20 molar excess of nitrosobenzene over a dihydropyridine.

Results

Products and Kinetics. The reduction reaction was carried out in anhydrous acetonitrile under the nitrogen atmosphere. The reaction was slow in the absence of an acid. The time-dependent composition of the reaction mixture could be successfully analyzed by HPLC. The results indicated the reaction to be quantitatively described by Eq. 1. As shown in Fig. 1, nitro-

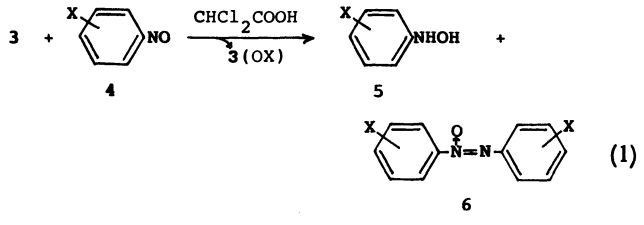

(1)

sobenzene (**4**, X=H) was quantitatively reduced to phenylhydroxylamine (**5**, X=H) when reacted with two molar excess of **3** in the presence of dichloroacetic acid, accompanied by the formation of a small amount of azoxybenzene (**6**). Figure 1 also shows that the disappearance of **3** and **4**, and the appearance of **5** occurred in almost the same rate and much faster than the formation of **6**. Furthermore, the curve for **3** indicates that after completion of reduction the remaining excess **3** was fairly stable without undergoing appraciable decomposition promoted by an acid. Under reversed conditions of excess **4** over **3** the major product was **6** which appeared to be formed by the acid-catalyzed condensation reaction between **5** and remaining **4**. Azoxybenzene **6** was stable without undergoing further redution by **3** under the present reaction conditions. The reduction occurred similarly in the case of

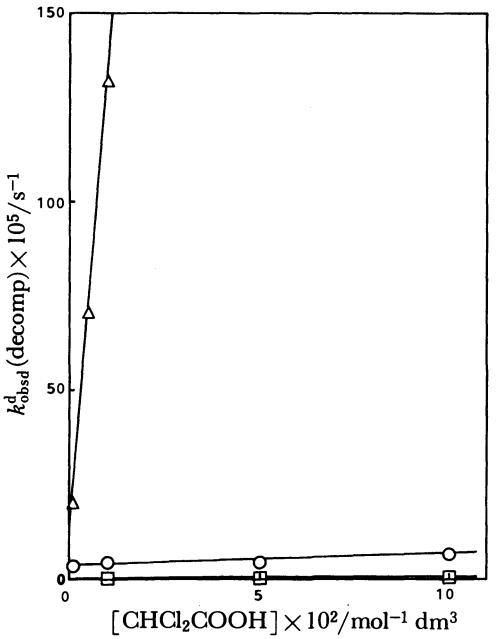

Fig. 2. Pseudo-first-order rate constants for the decomposition of (**1**) (△), (**2**) (□), and (**3**) (○) plotted as a function of the concentration of $CHCl_2COOH$ in acetonitrile at 25 °C.

Table 1. Rate Constants of the Acid-Catalyzed Decomposition of Dihydropyridines and of the Acid-Catalyzed Reduction of Nitrosobenzene by Dihydropyridines in Acetonitrile (25 °C)[a)]

Dihydropyridine	k_{un}^{d}	k_{H}^{d}	k_{un}^{R}	k_{H}^{R}
	s^{-1}	$mol^{-1}\,dm^3\,s^{-1}$	$mol^{-1}\,dm^3\,s^{-1}$	$mol^{-2}\,(dm^3)^2\,s^{-1}$
1	1.50×10^{-4}	1.09×10^{-1}	2.66	—
2	1.23×10^{-6}	7.50×10^{-6}	0.09	2.10
3	2.72×10^{-5}	3.72×10^{-4}	1.29	667

a) [**1**]=[**2**]=[**3**]=1.0×10^{-4} mol dm^{-3}, [**4**, X=H]=2.0×10^{-3} mol dm^{-3}.

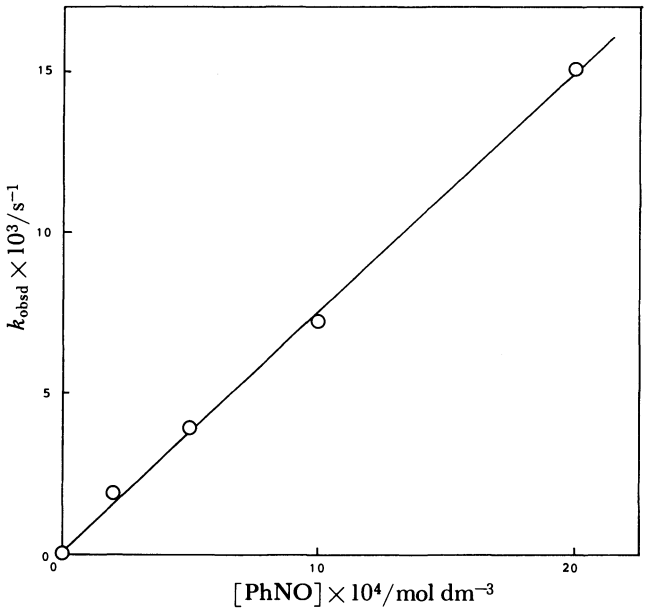

Fig. 3. A linear relationship between the observed pseudo-first-order rate constant and the concentration of nitrosobenzene in acetonitrile at 25 °C: [**3**]=1.0×10^{-4} mol dm^{-3}, [$CHCl_2COOH$]=1.0×10^{-2} mol dm^{-3}.

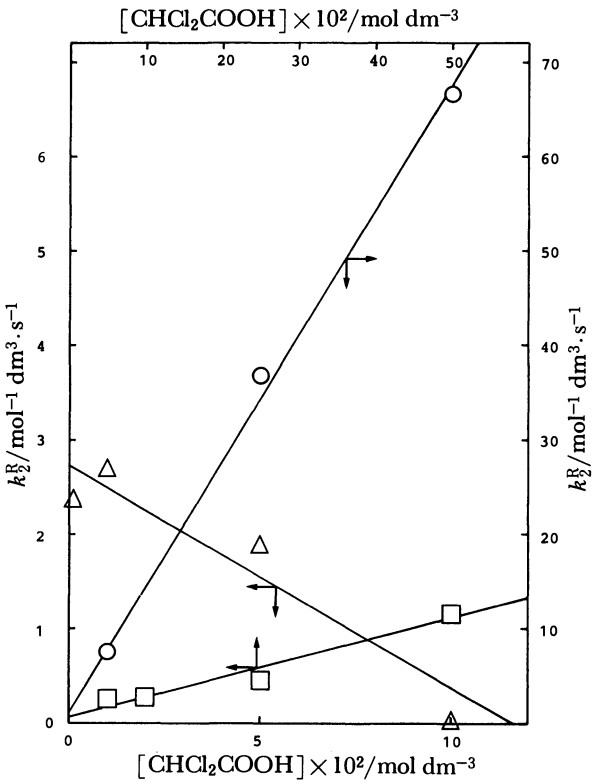

Fig. 4. Second-order rate constants for the reduction of nitrosobenzene by (**1**) (△), (**2**) (□), and (**3**) (○) plotted as a function of the concentration of $CHCl_2COOH$ in acetonitrile at 25 °C.

2, although the rate was much slower than in the case of **3**. The reduction was also observed with **1**, but the competing acid decomposition of **1** made the results complex. The decomposition of dihydropyridines by an acid were examined spectrophotometrically by measuring the rates of disappearance of dihydropyridine absorption (350 or 370 nm) in the absence of nitrosobenzene. As shown in Fig. 2, the pseudo-first-order rate constants for the decomposition (k_{obsd}^{d}) increase linearly with increasing concentration of dichloroacetic acid (AH) for all three dihydropyridines. Therefore the rate of decomposition can be represented by Eqs. 2 and 3.

$$\text{Rate(decomp)} = k_{obsd}^{d}[\text{dihydropyridine}] \quad (2)$$

$$k_{obsd}^{d} = k_{un}^{d} + k_{H}^{d}[AH] \quad (3)$$

The rate constants k_{un}^{d} obtained as the intercepts presumably arose from the air oxidation due to incomplete air extrusion from the reaction solutions. The rate constants k_{H}^{d} obtained as the slopes were those for the acid-catalyzed decomposition. These values are listed in Table 1. The Table indicates that the k_{H}^{d} value for **1** is far much larger than those for the other two. It is considered that **1** undergoes a ready acid promoted decomposition through an electrophilic addition of an acid on the enamine 5,6-double bond of dihydropyridine ring.[3-6)] Such an electrophilic addition seems to be much difficult to occur in the cases of **2** and **3** as discussed later.

The rates of reduction of nitrosobenzene were obtained similarly as the rates of disappearance of a dihydropyridine in the presence of nitrosobenzene (X=H). As shown in Fig. 3, the pseudo-first-order rate constants (k_{obsd}) were observed to increase linearly with increasing concentration of nitrosobenzene. Thus, combined with Eq. 2, the k_{obsd} value can be represented by Eq. 4 which allows to obtain a second-order rate constant for the reduction k_2^R as the slope of a straight line. Furthermore, as shown in Fig. 4, this k_2^R was observed to be linearly dependent on the acid con-

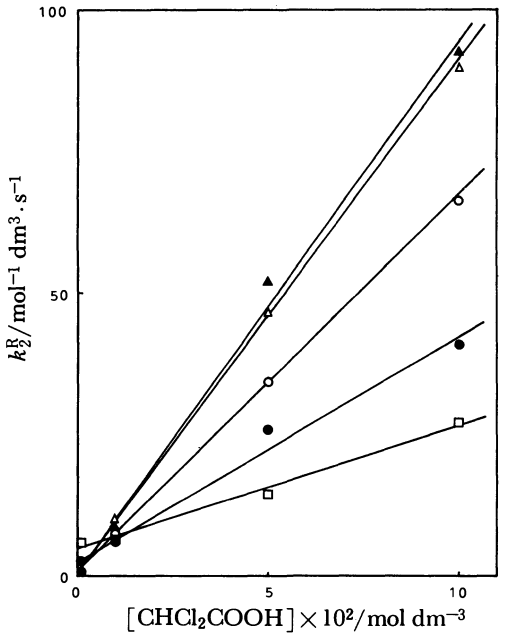

Fig. 5. Second-order rate constants for the reduction of substituted nitrosobenzenes by (**3**) as a function of the concentration of $CHCl_2COOH$ in acetonitrile at 25 °C: *p*-Me (△), *m*-Me (▲), H (○), *p*-Cl (●), and *p*-CF_3 (□).

centration and obeyed Eq. 5. Therefore, as summarized in Eq. 6, the k_{obsd} value is composed of four kinetic terms of decomposition and reduction. The corresponding four rate constants k_{un}^d, k_H^d, k_{un}^R, and k_H^R are shown in Table 1 for three dihydropyridines. As for the former two, it was described already.

$$k_{obsd} = k_{obsd}^d + k_2^R\,[\text{nitrosobenzene}] \quad (4)$$

$$k_2^R = k_{un}^R + k_H^R\,[AH] \quad (5)$$

$$k_{obsd} = k_{un}^d + k_H^d\,[AH] + k_{un}^R\,[\text{nitrosobenzene}] + k_H^R\,[AH][\text{nitrosobenzene}] \quad (6)$$

Of the two reduction rate constants, the uncatalyzed second-order one k_{un}^R indicates that a conventional dihydropyridine (**1**) is much more active than the other two (**2** and **3**) in the absence of an acid. However, Fig. 4 shows that the k_2^R for **1** decreases with increasing acid concentration with a line of negative slope, in contrast to the lines of positive slopes in the cases of **2** and **3**. The reason for such an inhibitory effect of an acid for **1** is not clear at present.[20] As discussed later, it may be conceivable that for more basic **1** than the other two, protonation of dihydropyridine moiety lowers its reducing activity together with the acid decomposition. On the other hand, the acid-catalyzed third-order rate constants k_H^R could be successfully obtained for **2** and **3**. As for the reactivities of **2** and **3**, the latter is much more active than the former in both uncatalyzed and catalyzed reaction: $k_{un}^R(\mathbf{3})/k_{un}^R(\mathbf{2})=15$ and $k_H^R(\mathbf{3})/k_H^R(\mathbf{2})=318$.

Hammett Substituent Effect. The present reduction is a hydride transfer from a dihydropyridine ring to the nitroso group.[21] Consequently, it is conceivable that the uncatalyzed (k_{un}^R) process is favored by an electron-withdrawing substituent of nitrosobenzene. On the other hand, if the above acid catalysis (k_H^R) is due to the activation of a nitroso group by protonation or hydrogen bonding, such process seems to be favored by an electron-donating substituent. What actually observed is shown in Fig. 5 which indicates that the plots of k_2^R vs. concentration of dichloroacetic acid give straight lines as seen for unsubstituted nitrosobenzene in Fig. 4. It is clear that the slopes of those straight lines (i.e. k_H^R) are larger for more electron-donating substituents. On the other hand, the intercepts (k_{un}^R) are larger for more electron-withdrawing substituent. These opposing substituent effects can be seen more clearly in the Hammett plots of Fig. 6, giving a positive $\rho=1.35$ for k_{un}^R and a negative $\rho=-0.93$ for k_H^R plot. As expected, the latter negative ρ value for k_H^R process suggests the activation of a substrate nitroso group by an acid, although its detailed mechanism, protonation or hydrogen bonding, is difficult to determine at this stage.

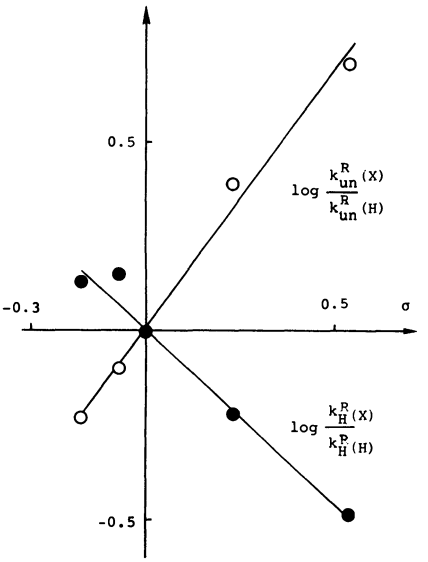

Fig. 6. Hammett plots of k_{un}^R(○) and k_H^R (●).

Brönsted Plots. The above k_H^R values for unsubstituted nitrosobenzene (X=H) were determined for eight carboxylic acids as shown in Table 2. The Table also lists the literature values of pK_a for the used carboxylic acids in water[22] and acetonitrile.[23] These values give two straight lines of Brönsted plots as shown in Fig. 7 and Eqs. 7 and 8. The α values are both negative,

$$\log k_H^R = -0.34\,pK_a(AN) + 6.88 \quad (7)$$

$$\log k_H^R = -1.17\,pK_a(\text{water}) + 4.77 \quad (8)$$

indicating a stronger acid being a more active catalyst.

Deuterium isotope effect was examined to get more insight into the mechanism of the above acid catalysis

Table 2. Acid-Catalyzed Rate Constants k_H^R with Eight Carboxylic Acids for the Reduction of Nitrosobenzene by (**3**) in Acetonitrile (25°C)[a)]

	Carboxylic acid	$(pK_a)_{AN}$[b)]	$(pK_a)_w$[c)]	k_H^d	k_H^R
				$mol^{-1}\,dm^3\,s^{-1}$	$mol^{-2}(dm^3)^2\,s^{-1}$
1	CF_3COOH		0.25	6.06×10^{-2}	2.95×10^{4}
2	CCl_3COOH		0.64	6.98×10^{-2}	1.76×10^{4}
3	$CHCl_2COOH$		1.30	3.72×10^{-4}	6.67×10^{2}
4	$CH_2ClCOOH$		2.86	1.03×10^{-4}	45.9
5	o-HOC_6H_4COOH	16.7	2.98	9.80×10^{-5}	22.8
6	3,5-$(NO_2)_2C_6H_3COOH$	16.9	2.82	3.13×10^{-5}	6.90
7	m-BrC_6H_4COOH	19.5	3.81	2.92×10^{-5}	1.20
8	CH_3COOH	22.3	4.76	6.31×10^{-6}	0.21

a) $[\mathbf{3}]=1.0\times10^{-4}$ mol dm^{-3}, [**4**, X=H]$=2.0\times10^{-3}$ mol dm^{-3}. The concentration of acids were varied from 2.0×10^{-4} mol dm^{-3} for CF_3COOH up to 2.0 mol dm^{-3} for CH_3COOH. b) pK_a values in acetonitrile.[22)] c) pK_a values in water.[21)]

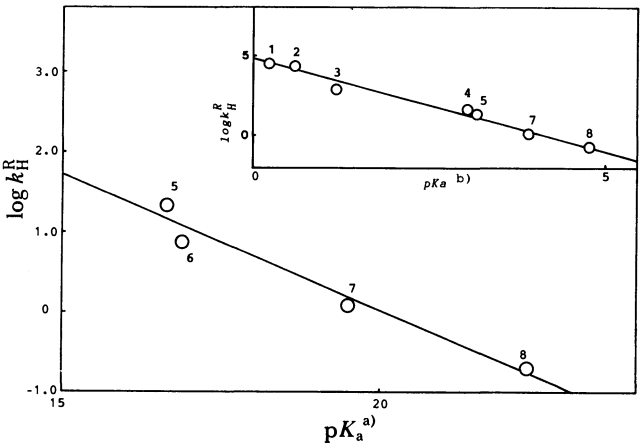

Fig. 7. Brönsted plots of the data in Table 2. Numbers in the figure correspond to the carboxylic acids in Table 2.
a) pK_a values in acetonitrile,[22)] b) pK_a values in water.[21)]

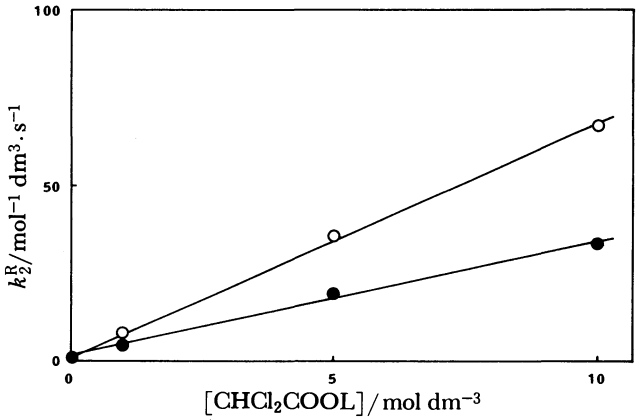

Fig. 8. Second-order rate constants for the reduction plotted as a function of the concentration of $CHCl_2COOH$ (○) and $CHCl_2COOD$ (●) in acetonitrile at 25°C. $[\mathbf{3}]=1.0\times10^{-4}$ mol dm^{-3}.

by using dichloroacetic acid-*d* (82% atom D-content), unsubstituted nitrosobenzene, and (**3**). The results are shown in Fig. 8. The slopes of the two straight lines are $k_D'(R)=315$ and $k_H^R=618$ in the unit of $mol^{-2}(dm^3)^2\cdot s^{-1}$ to give an isotope effect of $k_H^R/k_D'(R)=2.1$. This value can be corrected for the true isotope effect (k_H^R/k_D^R) based on Eqs. 9 and 10,

$$k'_D(R)([AD]+[AH]) = k_D^R[AD] + k_H^R[AH] \quad (9)$$

$$\frac{k_H^R}{k_D^R} = \frac{\gamma\cdot(k_H^R/k'_D(R))}{(1+\gamma)-(k_H^R/k'_D(R))} = 2.80 \quad (10)$$

where [AD] and [AH] are the concentrations of deuterium-labelled and unlabelled dichloroacetic acids, respectively, and $\gamma=[AD]/[AH]=82/18=4.56$ is used based on the above isotope content (82% D). In the same procedure, an isotope effect of $k_H^R/k_D^R=1.73$ was obtained for the reduction of *m*-nitrosotoluene.

Discussion

In the catalysis of lactate dehydrogenase and of related enzymes, the substrate carbonyl group is presumed to be activated by an acidic group toward the hydride transfer from NAD(P)H coenzyme.[1,2)] There have been known some model studies which support such acid catalysis. Salicylaldehyde[24)] or 3-hydroxy-4-pyridinecarbaldehyde[25)] undergoes a ready reduction by NADH analogs, in which the *o*-hydroxyl group is presumed to act as the acid to activate the neighboring carbonyl group through a hydrogen bonding. Intermolecular general acid catalysis was examined by using protonated amines as the acids.[26)] However, since protonated amines are usually very weak acids, they can only activate already activated substrates like hexachloroacetone[26a)] or Schiff base.[26b)] In order to examine the acid catalysis of stronger acids, one must make some device, such as to avoid a direct contact of a dihydropyridine moiety with an acid or to design a specially acid-stable NADH analog, since a conventional NADH analog like **1** is acid-unstable.[3-6)] Indeed Shinkai et al. was able to study the acid catalysis of a strong acid by using a specially designed acid-stable **2**[7)] Meanwhile we reported in the previous communications[8,27,28)] that **3** is also an acid-stable NADH analog having comparable reducing activity with that of **1**. A

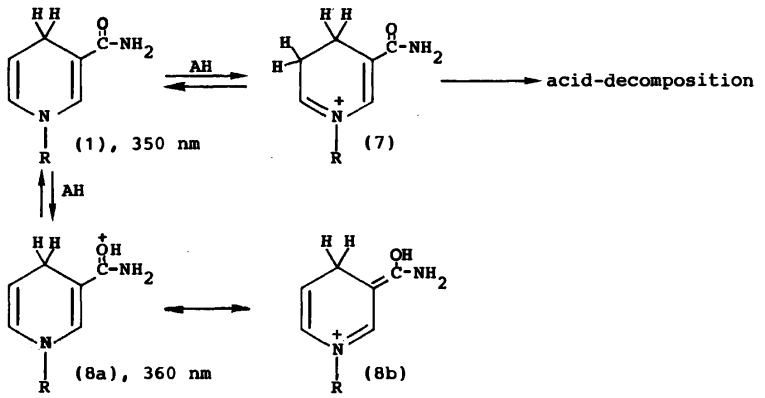

Scheme 1. Acid-promoted protonation and decomposition of (1).

more detailed features of acid catalysis of **3** are now reported for the reduction of nitrosobenzenes. Interests in the reduction of this substrate come from the following two reasons. One is from the mechanistic interests in that nitrosobenzene is much more reactive than carbonyl compounds and hence its reduction would allow to see more detailed features of acid catalysis by using acids of wide range of activity. The other is from the biochemical interests in the carcinogenesis promoted by the nitrosobenzene metabolism.[9-12]

As for the acid-stability, the data in Fig. 2 and Table 1 (k_H^d) indicate **1** to be the most acid-unstable among the three dihydropyridines examined. According to the literatures,[3-6] **1** undergoes a ready protonation to the 5,6-enamine double bond (Scheme 1, **7**). Such an electrophilic addition must be more difficult to occur in the cases of **2** and **3** because the 5,6-double bond is a part of aromatic ring in **2** and in conjugation with the carbonyl group at the 5-position in **3**. It is shown in Table 2 that the rates of decomposition (k_H^d) increase with increasing acidity (pK_a) of the acids. In a parallel way, the acid-catalyzed rates of reduction (k_H^R) also increase with increasing acid-acidity. However, it should be noticed that the rate of decomposition of **3** is negligibly small as compared to that of reduction, i.e. the oxidation of **3** by nitrosobenzene. For example, it can be calculated by using the rate data in Table 1 that the k_{obsd}^d of **3** is $6.44\times10^{-5}\,s^{-1}$ in the presence of 0.1 mol dm^{-3} dichloroacetic acid, while the corresponding k_{obsd} for reduction is $1.40\times10^{-1}\,s^{-1}$ in the presence of 2.0×10^{-3} mol dm^{-3} nitrosobenzene.

As for the reduction, the results in Fig. 4 may be the first to be discussed. The redution is inhibited by adding an acid in the case of **1** in contrast to the acceleration in the other two cases. In the case of **1**, concomitantly to the inhibition, a red-shift of dihydropyridine absorption occurs, even in a mixture of low concentration of [**1**]=[dichloroacetic acid]$=1.0\times10^{-4}$ mol dm^{-3}. Similar red shift is also observed for **3** (355 to 370 nm), but in the presence of a much higher acid concentration. In the case of **2**, the red shift is small or negligible. These red shifts are likely due to the protonation at the 3-carbamoyl group (Scheme 1, **8**).[3]

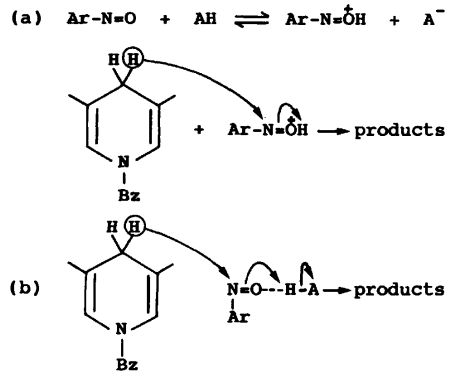

Scheme 2. Two possible mechanisms of acid catalysis.

Another protonation site is the 5-position **7**. Both of these protonation may deactivate the dihydropyridine ring as a hydride donor. Thus deactivation overcomes the catalysis in the case of **1**. On the other hand, since the protonation at 5-position is negligible in **2** or small in **3**, the total balance is over the catalysis rather than inhibition in these two cases.

The next to be discussed is the data in Figs. 6, 7, and 8, which were obtained by using **3**. In Fig. 6 are shown the two opposing Hammett plots. A positive $\rho=1.35$ for the uncatalyzed k_{un}^R indicates that, in the absence of an acid, an electron-withdrawing substituent helps the substrate to accept the hydride. On the other hand, a negative $\rho=-0.93$ for the acid-catalyzed k_H^R suggests that an electron-donating substituent helps the nitroso group to accept a proton from an acid and to become a better electrophile toward a hydride. Two mechanisms of acid catalysis are conceivable (Scheme 2): (a) Preequilibrium formation of protonated nitrosobenzene followed by a rate-limiting hydride transfer, and (b) a one-step concerted hydride transfer assisted by general acid-catalyzed proton transfer. These two mechanisms may be discernible by examining a Brönsted relationship and the H-D isotope effect. The Brönsted plots in Fig. 7 show a negative slope of $\alpha=-0.34$, based on the data in Table 2 and the pK_a of an acid in acetonitrile.[23] This result strongly suggests a mechanism of general acid catalysis,[29-31] i.e. the second mechanism (b) in Scheme 2. Namely the value 0.34 is

much smaller than 1.0, but rather close to 0.5, suggesting that the proton transfer is not complete, rather in a halfway at the transition state. The deuterium isotope effect shown in Fig. 8 also supports this general acid mechanism. A corrected value of $k_H^R/k_D^R=2.80$ is well in a range of primary isotope effect for general acid catalysis.[29-32]

The above general acid mechanism is of minor importance in aqueous buffer solutions, according to our previous observation.[27] The major mechanism observed at low pH is the hydronium ion (H_3O^+) catalysis, presumably similar to the first mechanism (a) in Scheme 2. Near neutral pH, the rates are independent of pH in aqueous media. These results indicate that the proton transfer is not important at the transition state in aqueous media. It seems to be reasonable that a general acid mechanism becomes important on changing the solvent from more polar water to less polar acetonitrile.

References

1) a) J. J. Holbrook, A. Liljas, S. J. Steindel, and M. G. Rossman, "The Enzymes," ed by P. D. Boyer, Academic Press, New York (1975), Vol. 11, pp. 19—293; b) J. I. Harris and M. Waters, *ibid.*, Vol. 13, pp. 1—49.

2) D. Moras, K. W. Olsen, M. N. Sabesan, M. Buchna, G. C. Ford, and M. G. Rossman, *J. Biol. Chem.*, **250**, 9137 (1975).

3) T. C. Bruice and S. J. Benkovic, "Bioorganic Mechanisms," Benjamin, New York (1966), Vol. 2, Chap. 9, pp. 301—349.

4) C. C. Johnston, J. L. Gardner, C. H. Suelter, and D. E. Metzler, *Biochemistry*, **2**, 689 (1963).

5) C. S. Y. Kim and S. Chaykin, *Biochemistry*, **7**, 2339 (1968).

6) a) S. Shinkai, R. Ando, and T. Kunitake, *Bull. Chem. Soc. Jpn.*, **48**, 1914 (1975); b) S. Shinkai, R. Ando, and T. Kunitake, *Bull. Chem. Soc. Jpn.*, **49**, 3652 (1976).

7) a) S. Shinkai, H. Hamada, T. Ide, and O. Manabe, *Chem. Lett.*, **1978**, 685; b) S. Shinkai, T. Nakano, H. Hamada, K. Kusano, and O. Manabe, *Chem. Lett.*, **1979**, 229; c) S. Shinkai, H. Hamada, and O. Manabe, *Tetrahedron Lett.*, **1979**, 1397.

8) H. Awano, T. Hirabayashi, and W. Tagaki, *Tetrahedron Lett.*, **25**, 2005, (1984).

9) D. C. Dittmer and J. M. Kolyer, *J. Org. Chem.*, **27**, 56 (1962).

10) E. N. Sol'nicova and A. S. Astakh'ova, *J. Gen. Chem. USSR* (Engl. Transl.), **37**, 1416 (1967).

11) M. L. C. Berheim, *Biochem. Biophys. Res. Comm.*, **46**, 1598 (1972).

12) A. R. Becker and L. A. Sternson, *Bioorg. Chem.*, **9**, 305 (1980).

13) E. V. Brown and W. H. Kipp, *J. Org. Chem.*, **36**, 170 (1971).

14) R. E. Lutz and M. R. Lytton, *J. Org. Chem.*, **2**, 68 (1937).

15) R. A. Abramovitch, S. R. Challand, and E. F. V. Scriven, *J. Org. Chem.*, **37**, 2705 (1972).

16) C. N. R. Rao and K. R. Bhaskar, "The Chemistry of Functional Groups-The chemistry of the nitro and nitroso groups," ed by H. Feuer, Interscience Publishers, New York, 1970, Chap. 3, pp. 137—163.

17) K. Tabei and S. Nagakura, *Bull. Chem. Soc. Jpn.*, **38**, 965 (1965).

18) D. Mauzerall and F. H. Westheimer, *J. Am. Chem. Soc.*, **77**, 2261 (1955).

19) S. Shinkai, H. Hamada, Y. Kusano, and O. Manabe, *J. Chem. Soc., Perkin Trans. 2*, **1979**, 699.

20) In the reduction of a certain quinone, it was demonstrated that the protonation of dihydropyridine ring inhibits the reduction: S. Fukuzumi, M. Ishikawa, and T. Tanaka, *J. Chem. Soc., Chem. Commun.*, **1985**, 1069; S. Fukuzumi, M. Ishikawa, and T. Tanaka, *Tetrahedron*, **42**, 1021 (1986).

21) Hydride is used here in formal sense without discriminating controversial one-step or multistep mechanism.

22) J. A. Dean (Ed.), "Lange's Handbook of Chemistry," 13th ed., McGraw-Hill, New York (1985).

23) a) J. F. Coetzee, *Progr. Phys. Org. Chem.*, **4**, 45 (1967); b) "Kagaku Binran," 3rd., ed., ed by Chem. Soc. Jpn., Maruzen, Tokyo (1984).

24) V. K. Pandit and F. R. Mass Cabre, *J. Chem. Soc., Chem. Commun.*, **1971**, 552.

25) a) S. Shinkai and T. C. Bruice, *J. Am. Chem. Soc.*, **94**, 8258 (1972); b) S. Shinkai and T. C. Bruice, *Biochemistry*, **12**, 1750 (1973).

26) a) S. Shinkai and T. Kunitake, *Chem. Lett.*, **1977**, 297; b) S. Shinkai and T. Kunitake, *Bull. Chem. Soc. Jpn.*, **49**, 3656 (1976).

27) H. Awano and W. Tagaki, *Chem. Lett.*, **1985**, 669.

28) H. Awano and W. Tagaki, *J. Chem. Soc., Chem. Commun.*, **1985**, 994.

29) Ref. 3, Vol. 1, Chap. 1.

30) W. P. Jencks, "Catalysis in Chemistry and Enzymology," McGraw-Hill, New York (1969).

31) A. Williams, "Isotopes in the diagnosis of mechanism," in "The Chemistry of Enzyme Action," ed by M. I. Page, Elsevier, Amsterdam (1984), Chap. 6.

32) F. H. Westheimer, *Chem. Rev.*, **61**, 265 (1961).

 © 1986 The Chemical Society of Japan Bull. Chem. Soc. Jpn., 59, 3125—3130 (1986)

Conformational Study of Acyclic Alcohols by NMR Spectroscopic Analysis, Molecular Force Field and Ab Initio Calculations

Kazuhisa ABE,* Kohichi ITO, Hiroko SUEZAWA, Minoru HIROTA, and Motohiro NISHIO†
Department of Synthetic Chemistry, Division of Materials Science and Chemical Engineering, Faculty of Engineering, Yokohama National University, 156 Tokiwadai, Hodogaya-ku, Yokohama 240
†Central Research Laboratotries, Meiji Seika Kaisha, Ltd. Morooka, Kohoku-ku, Yokohama 222
(Received April 3, 1986)

Conformations of a series of acyclic alcohols ($CH_3CH(R)CH(OH)CH_3$, $CH_3CH(R)CH(OH)CH(R')CH_3$, and $CH_3CH(R)CH(OH)Bu^t$) were studied (1) by measuring vicinal H-H coupling constants ($^3J_{H\text{-}H}$), (2) by lanthanoid-induced shift (LIS) analysis, (3) by molecular mechanics calculations (MM2), and (4) by ab initio (STO-3G, 4-31G geometry optimization) calculations. In the case of conformationally flexible alcohol as exemplified by 2-butanol and 3-pentanol, population of conformers determined by the LIS method do not agree with those determined by the $^3J_{H\text{-}H}$, MM2, and ab initio methods. The discrepancy comes from the fact that the LIS measurement gives the most stable conformation of the alcohol in the LSR-alcohol complex and not of the free alcohol. In some flexible molecules, the most stable conformer in the complex can be different from that of the free molecule. In general, the conformational equilibrium is shifted by coordination of the shift reagent to the conformer whose alkyl chain stretches opposite to the direction of the coordination site of the shift reagent.

Lanthanoid-induced shift (LIS) analysis[1,2] by NMR is a convenient method to investigate the conformation of organic compounds. The authors have reported the usefulness of the LIS simulation to the conformational studies of rather rigid molecules.[3-6] But a question about the effectiveness of LIS analysis arises when it is applied to conformationally flexible molecules because the shift reagent is bulky and the enthalpies (ΔH) of the complex formation between shift reagents and some substrates are fairly large (8—10 kcal mol^{-1} (1 cal=4.184 J)).[7,8] The conformational equilibria for the flexible molecules can be shifted significantly by the coordination of the shift reagent to the substrates because the free energy differences among the conformers of flexible molecules are considerably less than the ΔH of the complex formation. Conformational changes by the coordination of the lanthanoid shift reagents (LSR) were evidenced by the LIS measurement on dioxaphosphorinane derivatives[9] and *t*-butoxycarbonyl α-amino acids esters.[10] Therefore, conformations of flexible secondary alcohols were studied both experimentally [(1) the $^3J_{H\text{-}H}$ method and (2) the LIS analysis] and theoretically [(3) MM2 and (4) ab initio calculations]. Populations of the stable conformers obtained by these methods were compared with each other, and the reliability and the limitation of each method was discussed.

Experimental

Methods for Conformational Analyses. Conformations of acyclic secondary alcohols were determined by the following four methods. ^{1}H NMR spectra at an ambient temperature were recorded on a JEOL FX-90Q or a GX-400 spectrometer.

(1) $^3J_{H\text{-}H}$ Method: $^3J_{H\text{-}H}$ was measured with a GX-400 spectrometer on a homo decoupling mode. As the observed $^3J_{H\text{-}H}$ values reflect the populations of stable conformers, they were determined from the observed $^3J_{H\text{-}H}$ by assuming that the observed coupling constant ($^3J_{obsd}$) is the averaged value of ^3J_g and ^3J_t in proportion to their populations and in reference to the reported vicinal H-H coupling constants[11] for which conformation of vicinal protons are gauche (J_g=1.9 Hz) and trans (J_t=11.1 Hz).

(2) LIS Analysis: Yb(fod)$_3$ was used as an LSR in $CDCl_3$ because the contribution of the contact shift to LIS is negligibly small.[12] LIS_i^{obsd} of a nucleus i was determined experimentally from the induced chemical shift vs. [LSR]/[substrate] plots in the range of [LSR]/[substrate] to be 0—0.3. LIS_i^{calcd} was calculated from the sterical factor ($3\cos^2\theta-1/r^3$) of the McConnel-Robertson equation.[13,14] From these LIS data (LIS_i^{obsd} and LIS_i^{calcd}), the agreement factor (R)[15] was calculated by Eq. 1 and the geometry in which R showed minimal value was assigned to the most stable conformation.

$$R = [\sum_i (LIS_i^{obsd} - LIS_i^{calcd})^2 / \sum_i (LIS_i^{obsd})^2]^{1/2} \quad (1)$$

In non-rigid molecules, effective chemical shifts are evaluated by averaging the intrinsic chemical shift weighted by the populations of each conformer. Therefore, we had better take into account the differences of coordination ability of LSR towards each stable conformer and the relative accessibility of LSR to each coordination site of conformers (vide infra). By this LIS simulation we can correctly evaluate the LIS_i^{calcd} and R in Eq. 1.

The coordination ability[16] of each conformer was estimated by the competitive LIS experiment between conformationally rigid model compounds in which Yb(fod)$_3$ competitively coordinated to two model compounds. The coordination ability index of conformer **A** and **B** (C_A and C_B) was defined by Eq. 2.

$$C_A/C_B = [S_A^m/S_A^s(1-S_B^m/S_B^s)]/[S_B^m/S_B^s(1-S_A^m/S_A^s)] \quad (2)$$

S_A^m or S_B^m: LIS value induced by the competitive coordination of Yb(fod)$_3$ towards conformer **A** and **B**.

S_A^s or S_B^s are LIS values of conformer **A** and **B** induced by Yb(fod)$_3$.

The relative accessibility of Yb(fod)$_3$ to each coordination site of conformers is not thought to be equally favorable.

At the coordination sites 1, 2, and 3 of conformer k of the secondary alcohol illustrated below, the calculated LIS of nucleus i for conformer k is given by Eq. 3.

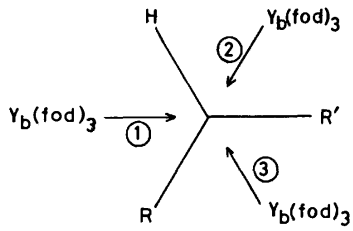

$$S_{k,i} = A_1S_{k,i}(1) + A_2S_{k,i}(2) + A_3S_{k,i}(3) \quad (3)$$

Here, A_1, A_2, and A_3 are relative accessibility of LSR at the coordination sites 1, 2, and 3, respectively.

$S_{k,i}(1)$, $S_{k,i}(2)$, and $S_{k,i}(3)$ are the calculated LIS's for nucleus i of conformer k in case LSR coordinated to the coordination site 1, 2, and 3, respectively.

By use of coordination ability index, C, and $S_{k,i}$ determined by Eqs. 2 and 3, the calculated LIS corresponding to the observed LIS for nucleus i on NMR spectra is derived by Eq. 4, if a secondary alcohol molecule is assumed to have three stable conformers **I**, **II**, and **III**.

$$S_i^{calcd} = C_IX_IS_{I,i} + C_{II}X_{II}S_{II,i} + C_{III}X_{III}S_{III,i} \quad (4)$$

Where X_I, X_{II}, X_{III} are population of the stable conformer **I**, **II**, **III**, respectively.

(3) MM2 Calculation:[17] The calculations were performed on a HITAC M-280H using the MM2 program modified by E. Osawa[18]. The geometry optimization was carried out for the expected stable conformers and the steric energy was calculated. From the relative steric energies of stable conformers, the population of each conformer was calculated tentatively by applying Boltzmann's theorem.

(4) Ab Initio Calculation: The ab initio calculations were performed on a HITAC M-200H by use of the Gaussian 80 (QCPE 13) program at the Computer Center of the Institute for Molecular Science. This program allows 127 Contracted Gaussian Type Orbitals (CGTO) for the purpose of the Hartree-Fock SCF calculation. However, geometry optimization can be carried out on the molecules with CGTO≦70. Geometries of conformers were optimized with the Hartree-Fock methods with the STO-3G or 4-31G basis set within the limit for the number of CGTO's. As the optimized geometries and relative energies between stable conformers obtained by MM2 geometry optimization calculations were nearly identical with those obtained by ab initio geometry optimization calculations with the STO-3G or 4-31G basis set (CGTO<70), optimized geometries obtained by MM2 were used as the input geometries for ab initio calculations and the energies were calculated with the STO-3G basis set in the case when the optimization by ab initio calculation is limited (CGTO>70).

Preparation of Materials. Commercially available secondary alcohols were purified by distillation. As commercially available 2,6-dimethylcyclohexanol is a mixture of three stereoisomers, each isomer was separated by column chromatography on silica gel (eluant; benzene-ether (v/v 6:1)) and by gas chromatography (column; SE-30, column Temp; 90 °C).

$Yb(fod)_3$ was prepared by reacting 1,1,1,2,2,3,3-heptafluoro-2,2-dimethyl-3,5-octanedione ($H(fod)_3$) with ytterbium nitrate in aqueous methanol solution at pH 4—6[19-21] and purified by sublimation in vacuo.

Results and Discussion

Coordination Ability of $Yb(fod)_3$ to the Conformers. Coordination ability of $Yb(fod)_3$ to each stable conformer of a secondary alcohol was estimated from the LIS for conformationally rigid model compounds. *t*-2-Methyl-*t*-6-methyl-*r*-1-cyclohexanol (a), *trans*-2-methylcyclohexanol (b), cyclohexanol (c), and *t*(or *c*)-2-methyl-*c*(or *t*)-6-methyl-*r*-1-cyclohexanol (d) were chosen as rigid model compounds. From the LIS by sole (S^s) or competitive (S^m) coordination of $Yb(fod)_3$ to the model compounds, coordination ability index (C) in reference to cyclohexanol of each model compound was evaluated (Table 1) by using Eq. 2.

Relative Accessibility of $Yb(fod)_3$. Relative accessibility (A) of $Yb(fod)_3$ at each coordination site of some secondary alcohols was estimated from the competitive experiment where the LIS's for two different alcohols were induced by competitive coordination of $Yb(fod)_3$. In the case of isopropyl alcohol R, R'=CH_3, for example, relative accessibilities A_1, A_2 (A_1=A_2), and A_3 were estimated from the competitive LIS experiment using a mixture (1 : 1 mol/mol) of isopropyl alcohol and *t*-butyl alcohol. From the LIS of each alcohol we can determine the ratio of coordination ability indexes of isopropyl alcohol (C_{iso}) and *t*-butyl alcohol (C_{tert}) by Eq. 2.

$$S_{Iso}/C_{tert} = 0.70 \times (1-0.25)/0.25 \times (1-0.70) = 7$$
$$(S_{Iso}^m/S_{Iso}^s = 0.70 \quad S_{tert}^m/S_{tert}^s = 0.25)$$
$$C_{Iso} : C_{tert} = 0.88 : 0.12$$

Table 1. Coordination Ability Indexes of $Yb(fod)_3$ to the Model Compounds for LIS Simulation of Acyclic Secondary Alcohols

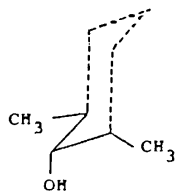	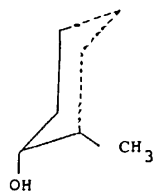		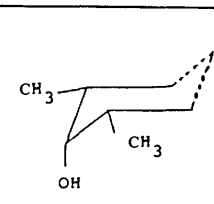
(a) *t*-2-Methyl-t-6-methyl-*r*-1-cyclohexanol	(b) *trans*-2-Methyl-cyclohexanol	(c) Cyclohexanol	(d) *t*(or *c*)-2-Methyl-*c*(or *t*)-6-methyl-*r*-1-cyclohexanol
0.18	0.57	1.0	0.22

From this ratio, the relative accessibility for each coordination site of isopropyl and *t*-butyl alcohols can be estimated as shown below by assuming that the coordination is solely dependent on the steric effect and that the coordination from the direction between the two methyl groups is equally favored in isopropyl and *t*-butyl alcohols.

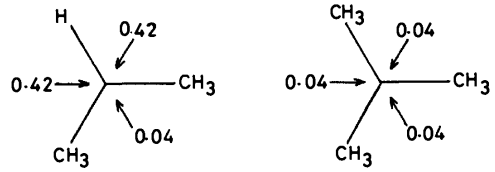

The relative accessibility at each coordination site of several secondary alcohols was determined in the same

Table 2. Relative Accessibility of Yb(fod)$_3$ to Each Coordination Site of RR'CHOH-Type Alcohols

R	R'	P_1	P_2	P_3
CH_3	CH_3	0.42	0.42	0.04
C_2H_5	CH_3	0.29	0.66	0.05
C_2H_5	t-C_4H_9	0.66	0.34	0.0
i-C_3H_7	CH_3	0.13	0.79	0.08
i-C_3H_7	C_2H_5	0.31	0.69	0.0
i-C_3H_7	t-C_4H_9	0.46	0.54	0.0

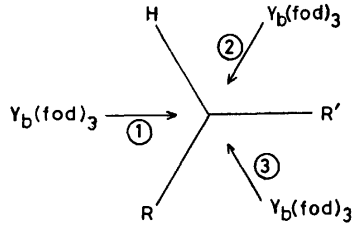

Table 3. Lanthanoid-Induced Shift (LIS) for $CH_3CH(R)CH(OH)CH_3$-, $CH_3CH(R)CH(OH)CH(R')CH_3$-, and $CH_3CH(R)CH(OH)C(CH_3)_3$- Type Acyclic Secondary Alcohols

	Proton (^{1}H)								Carbon (^{13}C)							
	1-H[a)]	2-H	3-H	4-H	5-H	2-CH_3	3-CH_3	4-CH_3	1	2	3	4	5	2-CH_3	3-CH_3	4-CH_3
(**1**) R=H	0.36	0.64	0.35 0.38	0.21	—	—	—	—	0.49	1.0	0.48	0.25	—	—	—	—
(**2**) R=CH_3	0.36	0.65	0.38	0.22	—	—	0.22	—	0.49	1.0	0.47	0.26	—	—	0.27	—
(**3**) R=H	0.21	0.34 0.39	0.64	0.34 0.39	0.21	—	—	—	0.26	0.48	1.0	0.48	0.26	—	—	—
(**4**) R=H, R'=CH_3	0.21	0.32	0.67	0.37 0.39	0.23	0.22	—	—	0.27	0.48	1.0	0.49	0.27	0.29	—	—
(**5**) R=R'=CH_3	0.20	0.36	0.67	0.36	0.20	0.25	—	0.25	0.26	0.50	1.0	0.50	0.26	0.31	—	0.31
(**6**) R=CH_3	0.22	—	0.67	0.30	0.21	0.22	—	0.30	0.27	0.48	1.0	0.49	0.25	0.27	—	0.35
(**7**) R=H	0.23	—	0.65	0.28 0.42	0.19	0.23	—	—	0.35	0.49	1.0	0.44	0.26	0.35	—	—

$CH_3CH(R)CH(OH)CH_3$: **1**—**2**, $CH_3CH(R)CH(OH)CH(R')CH_3$: **3**—**5**, $CH_3CH(R)CH(OH)C(CH_3)_3$: **6**—**7**.

a) The figures indicate the positional number of carbon atoms in IUPAC nomenclature. LIS values of ^{1}H and ^{13}C nuclei are normalized to the maximum LIS value in each compound.

Table 4. Population of Stable Conformers for $CH_3CH(R)CH(OH)CH_3$

	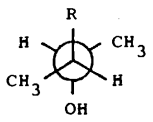	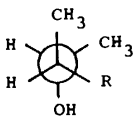	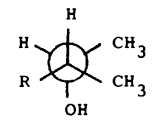
		2-Butanol (**1**) (R=H)	
	(I)	(II)	(III)
ab initio			
STO-3G	0.667	0.181	0.152
(ΔE)	(0.0)	(+0.782)	(+0.886)
4-31G	0.674	0.187	0.139
(ΔE)	(0.0)	(+0.769)	(+0.947)
MM2	0.597	0.250	0.153
(ΔE)	(0.0)	(+0.524)	(+0.821)
$^3J_{H-H}$	0.51	0.43	0.06
LIS	0.4	0.5	0.1
		3-Methyl-2-butanol (**2**) (R=CH_3)	
	(I)	(II)	(III)
MM2	0.428	0.186	0.386
(ΔE)	(0.0)	(+0.502)	(+0.062)
$^3J_{H-H}$	0.46	0.54	
LIS	0.6	0.3	0.1

(ΔE): Relative energy (kcal mol^{-1}).

Table 5. Population of Stable Conformers for $CH_3CH(R)CH(OH)CH(R)CH_3$

	3-Pentanol (**3**) (R=H, R'=H)								
	(I)	(II)	(III)	(IV)	(V)	(VI)	(VII)	(VIII)	(IX)
ab initio									
4-31G	0.235	0.182	0.191	0.182	0.01	—	0.191	—	—
(ΔE)	(0.0)	(+0.258)	(+0.208)	(+0.258)	(+2.490)	—	(+0.208)	—	—
MM2	0.373	0.135	0.106	0.155	0.006	0.062	0.104	0.057	0.002
(ΔE)	(0.0)	(+0.610)	(+0.759)	(+0.530)	(+2.500)	(+1.087)	(+0.766)	(+1.144)	(+3.291)
$^3J_{H-H}$		0.58			0.30			0.12	
LIS	0.0	0.4	0.1	0.4	0.0	0.0	0.1	0.0	0.0
	2-Methyl-3-pentanol (**4**) (R=H, R'=CH_3)								
	(I)	(IV)	(VII)	(II)	(V)	(VIII)	(III)	(VI)	(IX)
MM2	0.230	0.137	0.319	0.011	0.004	0.165	0.128	0.002	0.004
(ΔE)	(+0.199)	(+0.508)	(0.0)	(+2.209)	(+2.723)	(+0.399)	(+0.550)	(+2.954)	(+2.624)
$^3J_{H-H}$		0.71			0.22			0.07	
LIS	0.0	0.3	0.0	0.0	0.0	0.4	0.3	0.0	0.0
	2,4-Dimethyl-3-pentyanol (**5**) (R=CH_3, R'=CH_3)								
	(I)	(II)	(III)	(IV)	(V)	(VI)	(VII)	(VIII)	(IX)
MM2	0.007	0.003	0.490	0.011	0.0	0.013	0.446	0.007	0.022
(ΔE)	(+2.518)	(+3.012)	(0.0)	(+2.285)	(+4.272)	(+2.174)	(+0.056)	(+2.573)	(+1.865)
$^3J_{H-H}$		0.46			0.02			0.52	
LIS	0.0	0.3	0.0	0.3	0.0	0.2	0.0	0.2	0.0

(ΔE): Relative energy (kcal mol^{-1}).

Table 6. Population of Stable Conformers for $CH_3CH(R)CH(OH)C(CH_3)_3$

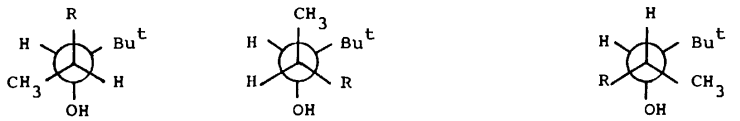

	2,2,4-Trimethyl-3-pentanol (**6**) (R=CH_3)		
	(I)	(II)	(III)
ab initio			
STO-3G	0.034	0.0	0.966
(ΔE)	(+2.412)	(+5.138)	(0.0)
MM2	0.121	0.007	0.872
(ΔE)	(+1.147)	(+2.914)	(0.0)
$^3J_{H-H}$	0.02	0.98	
LIS	0.2	0.0	0.8
	2,2-Dimethyl-3-pentanol (**7**) (R=H)		
	(I)	(II)	(III)
MM2	0.975	0.013	0.012
(ΔE)	(0.0)	(+2.599)	(+2.640)
$^3J_{H-H}$	0.93	0.01	0.06
LIS	1.0	0.0	0.0

(ΔE): Relative energy (kcal mol^{-1}).

way (Table 2).

Conformational Equilibrium of Acyclic Secondary Alcohols. The LIS's for the proton and carbon resonances of acyclic secondary alcohols **1**—**7** are listed in Table 3.

Populations of stable conformers for various types of alcohols (**1**—**7**) were estimated both experimentally and theoretically and given in Tables 4, 5, and 6.

Conformational Equilibrium Determined by the LIS Analysis: The conformational distribution derived from the LIS analysis is different from those of ab initio, MM2, and $^3J_{H-H}$ in the cases of conformationally flexible alcohols shown in Tables 4 and 5. In the case of 2-butanol, ab initio, MM2, and $^3J_{H-H}$ methods lead to the same conclusion on the conformer distribution. The most stable conformer **I** has a stretched alkyl chain, and the population decreases in the order **I**, **II**, and **III**. On the contrary, the LIS method concludes that conformer **II** is the most stable. This can be explained that conformational equilibrium is shifted by the complexation to Yb(fod)$_3$ on 2-butanol. Conformational preferences of alcohol molecules in the

LSR-alcohol complexes can be quite different from those of uncomplexed alcohols since the complexes are apt to lessen the steric strain around the metal ion by the conformational change of the flexible alcohol component. In this aspect, we considered the sterical crowdedness at the coordination sites of 2-butanol. It is unlikely that the conformational equilibrium will be shifted by coordination of $Yb(fod)_3$ at site 2 (the relative accessibility is the highest: 0.66) because the sterical crowdedness is not large. However, the change of the conformational equilibrium by coordination of $Yb(fod)_3$ at site 1 (relative accessibility is 0.29) is probable because the sterical congestion after complexation is estimated to be very large and the ethyl group is flexible. Therefore, a part of conformer **I** is expected to isomerize to conformer **II** by the coordination of $Yb(fod)_3$ at site 1 to avert the sterical congestion.

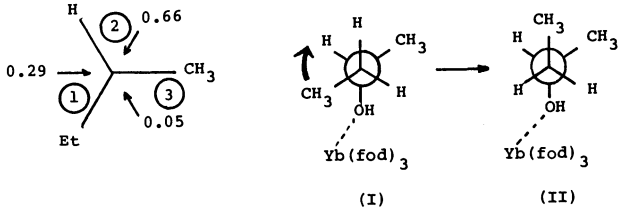

In the case of 3-methyl-2-butanol (**2**), we also find that the LIS method again predicts a conformational distribution different from those obtained by the three other methods, i.e., the LIS method leads to a larger population of conformer **I** and a less population of conformer **III** than the populations of the corresponding conformers estimated from the $^3J_{H\text{-}H}$ method and MM2. This shift in conformational equlibrium is thought to come from the conformation change from **III** to **I** by the coordination of $Yb(fod)_3$. As the sterical congestion around OH group is large in conformer **III**, it is easily converted to conformer **I** to relax the crowdedness.

Table 5 shows the populations of conformers for $CH_3CH(R)CH(OH)CH(R')CH_3$ (**3**, **4**, and **5**). Alcohols of this type have 9 stable conformations (Fig. 1) arising from the internal rotations about C_2-C_3 and C_4-C_3 bonds. In the case of 3-pentanol (**3**) both ab initio and MM2 calculations predict that conformer **I** is the most stable and the predicted conformational distribution from these calculations is similar. But LIS method predicts that **II** and **IV** are the most stable conformers which are favorable for complex formation with $Yb(fod)_3$. The LIS data suggest that a part of the most stable conformer **I** is converted to conformer **II** or **IV** by the coordination of $Yb(fod)_3$ and the conformational equilibrium is shifted. The same trends are also noticed in the cases of 2-methyl-3-pentanol (**4**) and 2,4-dimethyl-3-pentanol (**5**), where the LIS methods again resulted in the dominating conformers with favorable coordination site (s). From the results discussed above, it is certain that the conformational equilibria of flexible acyclic alcohols are shifted by the coordination of the shift reagent towards the conformer whose alkyl chains stretch opposite to the direction of the coordination site of the shift reagent.

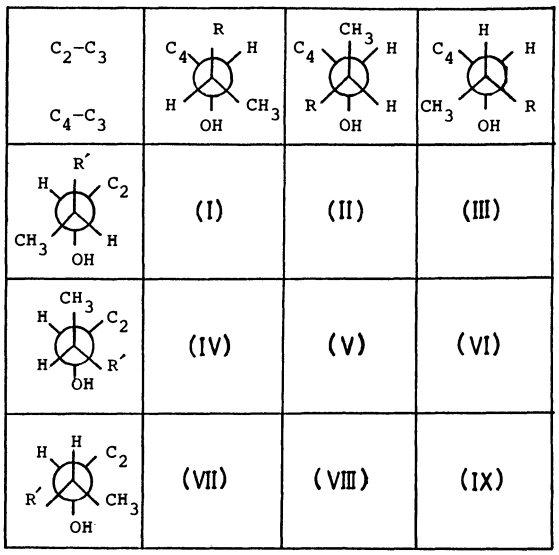

Fig. 1. Stable conformations for $CH_3CH(R)CH(OH)$-$CH(R')CH^3$-type alcohols.

On the contrary, the LIS method correctly predicts the conformational distribution of sterically congested $CH_3CH(R)CH(OH)Bu^t$-type secondary alcohols as shown in Table 6. In both cases (**6** and **7**) the conformational populations from the LIS method agreed with those from ab initio, MM2, and $^3J_{H\text{-}H}$ methods nearly quantitatively. All methods predict that the most stable conformer is **III** for **6** and **I** for **7**. Sterical congestion is so large in these alcohols that the conformational change during the complex formation with shift reagent becomes very difficult.[22]

Conformational Equlibrium Determined by MM2 and Ab Initio Calculations: In general, MM2 and ab initio calculations predict the conformational distribution correctly. From the geometry optimization study by MM2 and ab initio calculation on the every conformer of 2-butanol (**1**) (Table 3), it was shown that the populations and optimized geometries determined by the both calculations were almost the same. As proved by the several comparative studies shown above, the geometries and populations of the conformers can be predicted with enough accuracy by MM2. When we consider about the economical and technical restriction for ab initio calculation (CPU time, the number of CGTO), it is practical to use MM2 calculation for a conformational study of alcohols.

From the MM2 and ab initio studies, we considered the conformational equilibrium from a viewpoint of relative energy (ΔE) of each conformer. As shown in Table 4 and 5, ΔE's between the most stable and next stable conformers of **1**—**5** are very small (less than 1 kcal mol^{-1}). Therefore, we should recognize that the most stable conformers are convertible by the coordination of shift reagents in the cases of these conforma-

tionally flexible alcohols. The sequence of stability of the conformers can be perturbed by the complexation with shift reagents.

On the other hand, ΔE's between the most and the next stable conformers are pretty large in the cases of sterically congested alcohols. As shown in Table 6, ΔE's for **6** and **7** are larger (more than 2 kcal mol^{-1}) than those ΔE's for **1**—**5**. Sterical congestion in **6** and **7** is reflected on their optimized geometries determined by MM2. In the case of 2,2,4-trimethyl-3-pentanol (**6**), for example, widening of bond angles and deviation of dihedral angles from the normal values for both trans and gauche conformers were rationalized by the calculations. This fact, as well as their considerably large steric energies, suggests the presence of sterical congestion in these molecules. To avert the steric repulsion between gauche-positioned Bu^t, OH and CH_3 groups in the most stable conformer **III**, the dihedral angles between these groups Bu^t-C-C-CH_3, and HO-C-C-CH_3) are deviated from the normal value of 60° to ca. 90°.

Conformational Equilibrium Determined from the $^3J_{H\text{-}H}$: Application of the Karplus type equation on the observed $^3J_{H\text{-}H}$ predicts reasonable conformational distributions which agree with those obtained by MM2 and ab initio calculations. Though the $^3J_{H\text{-}H}$ method can not predict individual population of each conformer in the cases of **3**—**5** (Table 5), the summed-up populations ($X_1+X_2+X_3 : X_4+X_5+X_6 : X_7+X_8+X_9$) show fairly good agreement with those from the ab initio and MM2 calculations. The populations from the $^3J_{H\text{-}H}$ agreed even in the case of sterically congested alcohols (**6** and **7**). However, there remains a question whether $^3J_{H\text{-}H}$ method is applicable properly to the conformational equilibria of such distorted molecules.

In conclusion, the conformational equilibria for flexible alcohols can often be perturbed significantly by the complexation with LSR. Thus attention must be paid when the conclusions from the LIS analysis are compared with those from other theoretical and experimental methods. MM2 predicts the nearly identical populations of conformers and geometries with those derived from ab initio calculations and is proved to be a powerful tool in this field.

The authors are very grateful to Prof. Keiji Morokuma, the Institute for Molecular Science, for his kind permission to use a HITAC M-200H computer and the Gaussian 80 program and also for his valuable advice.

References

1) A. F. Cockerill, G. L. O. Davies, R. C. Harden, and D. M. Reckham, *Chem. Rev.*, **73**, 553 (1973).
2) R. E. Sievers, "NMR Shift Reagent," Academic Press, New York (1973).
3) J. Uzawa, S. Zushi, Y. Kodama, Y. Fukuda, K. Nishihata, K. Umemura, M. Nishio, and M. Hirota, *Bull. Chem. Soc. Jpn.*, **53**, 3623 (1980).
4) S. Zushi, Y. Kodama, K. Nishihata, J. Uzawa, and M. Hirota, *Bull. Chem. Soc. Jpn.*, **53**, 3631 (1980).
5) S. Zushi, Y. Kodama, Y. Fukuda, K. Nishihata, M. Nishio, M. Hirota, and J. Uzawa, *Bull. Chem. Soc. Jpn.*, **54**, 2113 (1981).
6) N. Kunieda, H. Endo, M. Hirota, Y. Kodama, and M. Nishio, *Bull. Chem. Soc. Jpn.*, **56**, 3110 (1983).
7) M. Hirota and S. Otsuka, *Chem. Lett.*, **1975**, 667.
8) H. Kojima, H. Nonaka, and M. Hirota, *Bull. Chem. Soc. Jpn.*, **55**, 2988 (1982).
9) W. G. Bentrude, H. W. Tan, and K. C. Yee, *J. Am. Chem. Soc.*, **94**, 3264 (1972).
10) H. Kessler and M. Molter, *J. Am. Chem. Soc.*, **98**, 5969 (1976).
11) L. M. Jackman and D. P. Kelly, *J. Chem. Soc. B*, **1970**, 102.
12) J. W. Apsimon, H. Beierkck, and J. K. Saunders, *Can. J. Chem.*, **51**, 3874 (1973).
13) H. M. McConnell and R. E. Robertson, *J. Chem. Phys.*, **28**, 749 (1958).
14) G. N. La Mair, W. D. Horrocks, Jr., and L. C. Allen, *J. Chem. Phys.*, **41**, 2126 (1964).
15) M. R. Wilcott, III, R. E. Lenkinski, and R. E. Davis, *J. Am. Chem. Soc.*, **94**, 1742 (1972).
16) Y. Nagawa, M. Ono, M. Hirota, Y. Hamada, and I. Takeuchi, *Bull. Chem. Soc. Jpn.*, **49**, 1322 (1976).
17) N. L. Allinger, *J. Am. Chem. Soc.*, **99**, 8127 (1977); N. L. Allinger and Y. H. Yuh, *QCPE*, No. 395.
18) Refined and new force field parameters for alcohols, amines, carboxylic acids, and alkyl halides that Allinger has set after the original MM2 version was issued in 1977 are supplemented in this program. Another point different from the original MM2 is that the modified MM2 takes into account the four-fold torsional potential terms (V_4) for the calculation of steric energies. This revised MM2 program is registered as a library program (Y4MM2) at the Computer Center of the University of Tokyo.
19) C. C. Hinckley, *J. Org. Chem.*, **35**, 2834 (1970).
20) K. J. Eisentraut and R. E. Sievers, *J. Am. Chem. Soc.*, **87**, 5254 (1965).
21) C. S. Springer, Jr., D. W. Meek, and R. E. Sievers, *Inorg. Chem.*, **6**, 1105 (1967).
22) Alternative explanation that the steric hindrance prevents these alcohols from forming a strong LSR-alcohol complex seems possible. However, the magnitude of their induced shifts are comparable to those of less hindered alcohols, and the contribution of weaker coordinate bond should be at most subsidiary.

 © 1986 The Chemical Society of Japan Bull. Chem. Soc. Jpn., 59, 3131—3136 (1986)

Preparation of 2-Azido-2-deoxypentose Derivatives

Hironobu HASHIMOTO,* Koichi ARAKI, Yoshihiro SAITO, Manabu KAWA, and Juji YOSHIMURA
Laboratory of Chemistry for Natural Products, Faculty of Science, Tokyo Institute of Technology, Nagatsuta, Midori-ku, Yokohama 227
(Received April 8, 1986)

2-Azido-2-deoxypentose derivatives having D-*xylo* and L-*arabino* configurations were prepared via azidonitration of 1,5-anhydro-2-deoxypent-1-enitols, that is, xylal and arabinal derivatives, respectively. The L-*ribo* isomer was prepared by substitution of 2-trifluoromethylsulfonyloxy and 2-(1-imidazolylsulfonyloxy) group with azide. The D-*xylo* isomer was converted into the corresponding D-*ribo* and D-*lyxo* isomers.

Recently 2-amino-2-deoxypentoses were reported as components of antibiotics such as glycocinnamoylspermidines (cinodine)[1] as well as adenine nucleosides[2] isolated from bacterial metabolites. On the other hand, 2-azido sugars have been used by preference on the occasion of synthesis of biologically important oligosaccharides[3] as a precursor of 2-amino sugars which are bonded through 1,2-cis glycosidic linkage. We have studied preparation of 2-azido-2-deoxypentoses as a part of total synthesis of cinodine which had an α-ureylene linkage through 2-amino-2-deoxy-D-xylose, while very recently this linkage was revised to be β in the course of structure elucidation of a closely related antibiotic, glycocinnasperimicin D.[4]

For the introduction of azido group the ring-opening reaction of epoxy derivatives and the substitution reaction have been used as the conventional methods. In the case of 2-azido-2-deoxypentopyranoside, however, both methods encounter synthetic difficulties. In the former, the conformational flexibility of pentopyransosides leads to lose the stereoelectronic control of the ring-opening reaction, that is, the reaction does not obey the Fürst-Plattner rule any more,[5] while in the latter the substitution at C-2 carbon are retarded by the neighboring anomeric center which has two polar carbon-oxygen bonds.[6] In this paper 2-azido-2-deoxypentopyranosides having D-*xylo* (and D-*lyxo* as minor component) and L-*arabino* configurations were prepared by the azidonitration method[7] and L-*ribo* isomer by substitution reaction of the reactive 2-*O*-sulfonyl derivatives with azide. Furthermore, D-*ribo* and L-*lyxo* isomers were derived from the D-*xylo* isomer by inversion of hydroxyl groups via the corresponding 3-ulose and 3,4-anhydro derivative, respectively.

Results and Discussion

Although the azidonitration of 3,4-di-*O*-acetyl-1,5-anhydro-2-deoxy-D-*threo*-pent-1-enitol (D-xylal diacetate, **1**) was first reported by Lemieux and Ratcliffe,[7] they reported only the ratio of D-*xylo* and D-*lyxo* isomers as 2:1. In this paper the isomer ratio was roughly estimated from the isolated yields after conversion into 1-acetates or methyl glycosides. For the former conversion once isolated and crude mixture of azidonitrates was acetylated with acetic anhydride and sodium acetate at 70 °C. For the latter methanol was added directly to the reaction solution of azidonitration. Methyl glycosides were obtained in higher yields than 1-acetates as shown in Table. In the case of **1**, it seems that the reaction temperature is one of the important factors controlling the ratio of two isomers (**3**/**6** or **4**/**7**) as reported for the azidonitration of D-glucal triacetate.[8] While at −10—−15 °C the ratio was about 2—3, at the lower temperature, albeit with higher molar ratios of cerium(IV) ammonium nitrate and sodium azide, the ratio increased to 12. However, more detailed experiments should be necessary for definitive explanation of the stereoselectivity. Thus,

Table 1. Azidonitration of 3,4-Di-*O*-acetyl-2-deoxy-D-*threo*-pent-1-enitol (**1**) and Its L-*Erythro* Isomer (**2**)

Glycal	Molar ratio[a]		Atmosphere	Temperature	Product	Ratio
	CAN[b]	NaN_3		°C	Yield/%	(eq-N_3/ax-N_3)[c]
1	2.0	1.1	N_2	−10	**3**(43), **6**(13)	3.3
1	2.0	1.5	N_2	−12	**3**(38), **6**(16)	2.4
1	2.0	5.2	N_2	−12	**3**(23), **6**(16)	1.4
1	3.0	1.1	N_2	−12	**3**(43), **6**(13)	3.3
1	3.0	1.5	N_2	−10	**3**(47), **6**(14)	3.4
1	2.0	1.5	air	−15	**3**(27), **6**(8)	3.3
1	4.3	2.3	air	−20	**3**(58), **6**(5)	12
1	4.0	2.0	air	−20	**4**(84), **7**[d]	>15
2	3.0	1.5	air	−10	**8**(55, α/β=1.8)	e)

a) Glycal=1.0. b) Cerium(IV) ammonium nitrate. c) eq=equatorial; ax=axial. d) Less than 5%. e) The product with ax-N_3 group colud not be isolated.

the reaction could be carried out even under aerobic conditions at −20 °C, for instance, to give **4** almost selectively in 84% yield, where the *lyxo* isomer (**7**) was obtained in trace amount.

On the other hand, the azidonitration of 3,4-di-*O*-acetyl-1,5-anhydro-2-deoxy-L-*erythro*-pent-1-enitol (L-arabinal diacetate, **2**), proceeded stereoselectively even at −10 °C to give D-*arabino* isomer (**9** or **10**) in a similar manner as D-galactal triacetate.[7] In this case the β-anomer of azidonitrate **8** could be isolated as crystals in 52% yield. The stereoselectivity can be explained by the steric hindrance of axially oriented 4-acetoxyl group in the half-chair conformation to favor the attack of azide radical from its opposite site.

The corresponding benzyl glycosides (**5** and **11**) were prepared by treatment of the azido nitrates with benzyl alcohol. The yield of **5** was 55% including the azidonitration step, while that of **11** from the nitrate **8** was 90%. Thus *xylo* and *arabino* isomers of 2-azido-2-deoxypentopyranose derivatives could be prepared by azidonitration method, and the remaining *ribo* and *lyxo* isomers was planned to be derived by different methods.

Preparation of 2-azido-2-deoxyribopyranosides was achieved by two methods. In the first method benzyl 3,4-*O*-isopropylidene-β-L-arabinopyranoside (**12**) was used as an easily-available starting compound and converted into the 2-triflate (**13**) and 2-(1-imidazole-sulfonate) (**14**), which are the derivatives of choice often used for the retarded substitution reaction.[9] Treatment of **13** and **14** with sodium azide gave the corresponding 2-azido derivative (**15**) in 27% (2 steps) and 80% yields, respectively. In the second method the configuration on C-3 of D-*xylo* isomer was inverted by oxidation and successive reduction. The deacetylated derivative (**16**) of **4** was benzoylated with benzoyl chloride and triethylamine in acetone at room temperature to give 3-benzoate (**17**), 4-benzoate (**19**), and 3,4-dibenzoate (**20**) in 5, 65, and 29% yields, respectively. Oxidation of **19** with dimethyl sulfoxide and trifluoroacetic anhydride followed by reduction of the resulting 3-ulose (**23**) with sodium borohydride afforded in 75% yield an another *ribo* isomer (**24**), which was further characterized as the 3-acetate (**25**). The corresponding benzyl glycoside derivatives (**26**—**28**) were prepared in a similar manner as described for the methyl glycosides (**16**, **19**, and **20**).

The remaining isomer of 2-azido-2-deoxypentose, that is, *lyxo* isomer could be also derived from the *xylo* isomer. The 3-mesylate (**21**) of **19** was treated with potassium hydroxide in methanol gave the 3,4-anhydro derivative (**31**) in 76% yield. Treatment of **31** with sodium acetate and acetic acid in *N*,*N*-dimethylformamide at 100 °C, followed by acetylation, gave the desired L-*lyxo* isomer (**32**) predominantly in 54% yield together with the D-*xylo* isomer **4** in 25% yield. Thus facile preparative methods of all stereoisomers of 2-azido-2-deoxypentose could be established.

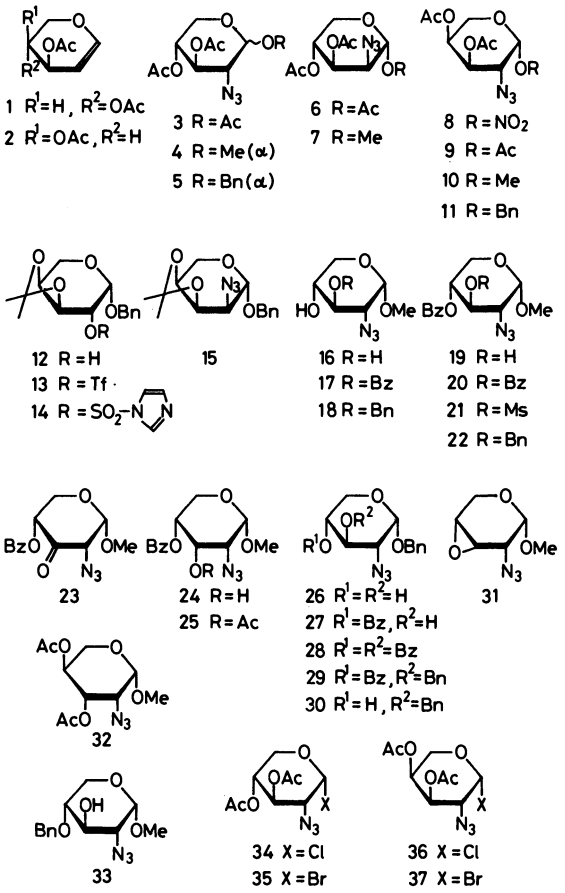

Furthermore, some *O*-benzyl derivatives and glycosyl halides were also prepared. Methyl 2-azido-3-*O*-benzyl-2-deoxy-D-xylopyranoside (**18**) were easily derived via **22** in 74% yield, by treatment of **19** with benzyl bromide and silver oxide followed by debenzoylation. The corresponding benzyl glycoside (**30**) of **18** was also prepared similarly via **29** from **27**. On the other hand, treatment of 3,4-*O*-dibutylstannylene derivative of **16** with benzyl bromide and tetraethylammonium bromide[10] gave the 4-*O*-benzyl derivative (**33**) predominantly in 70% yield together with **18** in 13% yield. This regioselectivity between two equatorial hydroxyl groups may be noteworthy. Acetohalogeno sugars of D-*xylo* and L-*arabino* configurations were derived from the corresponding acetate (**3**) and nitrate (**8**), respectively. Treatment of **3** with titanium tetrachloride and tetrabromide gave α-chloride (**34**) and α-bromide (**35**) in 77 and 63%, respectively. For the latter, bromination with hydrogen bromide in acetic acid gave a better yield. On the other hand, substitution of **8** with halide ions using tetraethylammonium halides gave β-chloride (**36**) and β-bromide (**37**) in 80 and 55%, respectively. These derivatives should be useful as synthetic intermediates for 2-amino-2-deoxypentose-containing antibiotics such as cinodine.

Experimental

Melting points were determined with a Mel-Temp appara-

tus and are not corrected. Optical rotations were measured using a 0.5-dm tube and a Carl Zeiss LEP-Al or JASCO DIP-4 polarimeter. IR spectra were recorded with a Hitachi EPI-G2 grating spectrometer. ^{1}H NMR spectra were recorded at 100 MHz with a JEOL PS-100 spectrometer in $CDCl_3$ with tetramethylsilane as the internal standard, unless stated otherwise. Column chromatography and preparative TLC were performed on Wakogel C-200 (Wako Pure Chemical Industries, Ltd.) and Kieselgel 60 HF_{254} (Merck), respectively. Evaporations were conducted under diminished pressure at 50 °.

Azidonitration of Glycals. To a solution of a glycal acetate (2.0 g, 10 mmol) in acetonitrile (70 ml) was added sodium azide (1.6—4.4 g, 11—30 mmol) and cerium(IV) ammonium nitrate (CAN, 10.9—23.5 g, 20—43 mmol) with stirring and cooling between −10 and −20 °C under nitrogen (occasionally under air). The solution was kept at the same temperature with stirring for 5—6 h, and mixed with ether and water. The ether layer was washed with water, dried and evaporated to give a crude syrupy mixture of 2-azido-1-nitrate derivatives.

1,3,4-Tri-*O*-acetyl-2-azido-2-deoxy-D-xylopyranose (3) and Its α-D-*Lyxo* Isomer (6). A crude mixture of azidonitrates obtained from **1** (17.0 g, 85 mmol), sodium azide (13 g, 200 mmol), and CAN (200 g, 365 mmol) at −20 °C under air as described above, was dissolved in acetic acid (100 ml) and heated at 70 °C for 2 h with stirring in the presence of sodium acetate (10 g). The reaction solution was evaporated and the residue was mixed thoroughly with chloroform and water. The organic layer was separated, dried and evaporated to give a syrup, which was fractionated on a silica-gel column with benzene-acetone (30 : 1) or toluene-ethyl acetate (19 : 1) to give **3** and **6** in 58 and 5% yields, respectively. Compound **3** was proved to be a mixture of α- and β-anomers with an approximate ratio of **10** by ^{1}H NMR.

3: Syrup, IR (NaCl) 2105 (azido) and 1750 (ester) cm^{-1}; ^{1}H NMR α-anomer δ=6.20 (d, $J_{1,2}$=3.9 Hz, H-1), 3.55 (dd, $J_{2,3}$=10.5 Hz, H-2), 5.44 (t, $J_{3,4}$=10.5 Hz, H-3), 4.99 (dt, $J_{4,5}$=10.5 Hz, $J_{4,5'}$=6.0 Hz, H-4), 3.67 (t, $J_{5,5'}$=10.5 Hz, H-5), 3.91 (dd, H-5′), 2.04, 2.12, and 2.18 (each s, OAc), β-anomer δ=5.50 (d, $J_{1,2}$=8.3 Hz, H-1), 3.60 (dd, $J_{2,3}$=9.0 Hz, H-2), 5.10 (t, $J_{3,4}$=9.0 Hz, H-3), 5.0 (H-4), 3.45 (dd, $J_{4,5}$=9.0 Hz, $J_{5,5'}$=11.8 Hz, H-5), 4.10 (dd, $J_{4,5'}$=4.9 Hz, H-5′), 2.04, 2.12, and 2.17 (each s, OAc).

Found: C, 43.89; H, 4.95; N, 13.95%. Calcd for $C_{11}H_{15}N_3O_7$: C, 43.86, H, 5.02; N, 13.95%.

6: Syrup, $[\alpha]_D$ +1.5° (*c* 1.0, $CHCl_3$). ^{1}H NMR δ=5.94 (d, $J_{1,2}$=5.1 Hz, H-1), 3.96 (dd, $J_{2,3}$=3.6 Hz, H-2), 5.36 (dd, $J_{3,4}$=7.1 Hz, H-3), 5.06 (m, H-4), 3.76 (dd, $J_{4,5}$=6.0 Hz, $J_{5,5'}$=12.0 Hz, H-5), 3.98 (dd, $J_{4,5'}$=3.8 Hz, H-5′) and 2.06—2.10 (OAc).

Found: C, 43.32; H, 5.07; N, 13.73%. Calcd for $C_{11}H_{15}N_3O_7$: C, 43.86; H, 5.02; N, 13.95%.

Methyl 3,4-Di-*O*-acetyl-2-azido-2-deoxy-α-D-xylopyranoside (4) and Its α-D-*Lyxo* Isomer (7). To a solution of the azidonitration reaction (**1** 2.4 g, NaN_3 1.57 g, CAN 26.6 g in CH_3CN 85 ml) carried out for 5.5 h in the same manner as described for **3** was added methanol (80 ml) together with chloroform (40 ml) and anhydrous magnesium sulfate. The mixture was stirred at room temperature for 16 h. Insoluble materials were filtered off and washed with chloroform. The filtrate was washed with water, dried and evaporated to give a syrup, which was fractionated on a silica-gel column with hexane-ethyl acetate (4 : 1) to give **4** in 84% yield and **7** in a trace amount. **4**: Syrup, $[\alpha]_D$ +128.5° (*c* 1.0, $CHCl_3$); IR (NaCl) 2103 (azido) and 1750 (ester) cm^{-1}; ^{1}H NMR δ=4.80 (d, $J_{1,2}$=3.3 Hz, H-1), 3.27 (dd, $J_{2,3}$=10.5 Hz, H-2), 5.46 (dd, $J_{3,4}$=9.6 Hz, H-3), 4.94 (dt, $J_{4,5}$=9.6 Hz, $J_{4,5'}$=6.0 Hz, H-4), 3.80 (dd, $J_{5,5'}$=10.8 Hz, H-5), 3.5 (H-5′), 2.04 and 2.11 (each s, OAc), and 3.46 (s, OMe).

Found: C, 44.39; H, 5.55; N, 15.11%. Calcd for $C_{10}H_{15}N_3O_6$: C, 43.96; H, 5.53; N, 15.38%.

7: Syrup, $[\alpha]_D$ −145.0° (*c* 1.0, $CHCl_3$). ^{1}H NMR δ=4.65 (d, $J_{1,2}$=2.7 Hz, H-1), 3.73 (dd, $J_{2,3}$=3.6 Hz, H-2), 5.10 (dd, $J_{3,4}$=6.3 Hz, H-3), 4.94 (dt, $J_{4,5}$=5.3 Hz, $J_{4,5'}$=3.8 Hz, H-4), 3.41 (dd, $J_{5,5'}$=12.2 Hz, H-5), 4.09 (dd, H-5′), 3.52 (s, OMe), 2.07 and 2.13 (each s, OAc).

Found: C, 43.73; H, 5.35; N, 15.14%. Calcd for $C_{10}H_{15}N_3O_6$: C, 43.96; H, 5.53; N, 15.38%.

Benzyl 3,4-Di-*O*-acetyl-2-azido-2-deoxy-α-D-xylopyranoside (5). A crude mixture of azidonitrates obtained from **1** (3.2 g, 16 mmol) in the same manner as described for **3**, was mixed with benzyl alcohol (7.8 ml, 69 mmol) in chloroform (30 ml). The solution was kept at room temperature for 24 h, washed with water, dried and evaporated to give a syrup, which was purified on a silica-gel column with benzene-acetone (30 : 1) to give **5** in 55% yield, $[\alpha]_D$ +104.7° (*c* 1.0, $CHCl_3$); ^{1}H NMR δ=4.98 (d, $J_{1,2}$=3.3 Hz, H-1), 3.22 (dd, $J_{2,3}$=10.4 Hz, H-2), 5.49 (dd, $J_{3,4}$=9.2 Hz, H-3), 2.04 and 2.10 (each s, OAc), 4.56 and 4.76 (ABq, J=12.8 Hz, CH_2 in Bn) and 7.36 (s, Ph).

Found: C, 54.83; H, 5.20; N, 11.65%. Calcd for $C_{16}H_{19}N_3O_6$: C, 55.01; H, 5.48; N, 12.03%.

3,4-Di-*O*-acetyl-2-azido-2-deoxy-1-*O*-nitro-β-L-arabinopyranose (8). Azidonitration of **2** (10 mmol) with sodium azide (15 mmol) and CAN (30 mmol) was carried out at −10 °C in the same manner as described for **3**. A crude azido nitrate was purified on silica-gel column to give a syrupy mixture of α- and β-nitrate (55%, α : β = 1.8 : 1) and only the β-anomer (**8**) was obtained as crystal from ether-hexane in 20% yield, mp 107—108.5 °C, $[\alpha]_D$ +18.4° (*c* 1.0, $CHCl_3$); ^{1}H NMR δ=5.57 (d, $J_{1,2}$=8.0 Hz, H-1), 3.86 (dd, $J_{2,3}$=9.7 Hz, H-2), 4.98 (dd, $J_{3,4}$=3.5 Hz, H-3), 5.26 (m, H-4), 4.10 (dd, $J_{4,5}$=2.6 Hz, $J_{5,5'}$=12.6 Hz, H-5), 3.78 (dd, $J_{4,5'}$=1.5 Hz, H-5′), 2.10 and 2.16 (each s, OAc).

Found: C, 35.85; H, 4.04; N, 18.05%. Calcd for $C_9H_{12}N_4O_8$: C, 35.53; H, 3.98; N, 18.42%.

1,3,4-Tri-*O*-acetyl-2-azido-2-deoxy-β-L-arabinopyranose (9). The glycosyl nitrate **8** (1.8 g, 5.6 mmol) was acetolyzed with acetic acid (10 ml) and anhydrous sodium acetate (0.8 g, 9.8 mmol) at 100 °C for 50 min. The residue obtained by direct evaporation of the reaction mixture was dissolved in chloroform. The solution was washed with water, dried and evaporated to give a syrup, which was purified on a silica-gel column with hexane-ethyl acetate (4 : 1) to afford **9** as crystal in 86% yield, mp 97—98 °C, $[\alpha]_D$ +128.2° (*c* 1.0, $CHCl_3$); ^{1}H NMR δ=6.28 (d, $J_{1,2}$=3.3 Hz, H-1), 3.96 (dd, $J_{2,3}$=10.5 Hz, H-2), 5.31 (dd, $J_{3,4}$=3.0 Hz, H-3), 5.31 (broad s, H-4), 3.80 (dd, $J_{4,5}$=1.8 Hz, $J_{5,5'}$=13.0 Hz, H-5), 4.04 (dd, $J_{4,5'}$=1.4 Hz, H-5′), 2.10 and 2.17 (each s, OAc).

Found: C, 44.12; H, 4.94; N, 13.75%. Calcd for $C_{11}H_{15}N_3O_7$: C, 43.86; H, 5.02; N, 13.95%.

Methyl 3,4-Di-*O*-acetyl-2-azido-2-deoxy-β-L-arabinopyranoside (10). The nitrate **8** (400 mg, 1.3 mmol) was dissolved in absolute methanol (10 ml) and the solution was kept at room temperature overnight with stirring in the

presence of molecular sieve 3 A. After removal of molecular sieve by filtration the filtrate was evaporated and the resulting syrupy residue was purified on preparative TLC on silica gel with benzene–acetone (40:3) to give **10** in 64% yield, $[\alpha]_D$ +218° (*c* 1.0, $CHCl_3$); ^1H NMR δ=4.89 (d, $J_{1,2}$= 3.4 Hz, H-1), 3.74 (m, H-2), 5.32 (dd, $J_{2,3}$=10.5 Hz, $J_{3,4}$=3.0 Hz, H-3), 5.29 (m, H-4), 3.70 (dd, $J_{4,5}$=1.8 Hz, $J_{5,5'}$=13.0 Hz, H-5), 3.96 (dd, $J_{4,5'}$=1.5 Hz, H-5'), 2.10 and 2.18 (each s, OAc), and 3.50 (s, OMe).

Found: C, 44.12; H, 5.27; N, 15.07%. Calcd for $C_{10}H_{15}N_3O_6$: C, 43.96; H, 5.53; N, 15.38%.

Benzyl 3,4-Di-*O*-acetyl-2-azido-2-deoxy-β-L-arabinopyranoside (11). The nitrate **8** (305 mg, 1.09 mmol) was stirred with benzyl alcohol (7 ml) and molecular sieve 3 A overnight at room temperature. The same work-up as described for **10** afforded **11** as a syrup in 90% yield, $[\alpha]_D$ +192° (*c* 1.0, $CHCl_3$); ^1H NMR δ=5.03 (d, $J_{1,2}$=3.3 Hz, H-1), 3.70 (dd, $J_{2,3}$=10.7 Hz, H-2), 5.36 (dd, $J_{3,4}$=3.3 Hz, H-3), 5.33 (broad s, H-4), 3.66 (dd, $J_{4,5}$=1.5 Hz, $J_{5,5'}$=12.5 Hz, H-5), 3.98 (dd, $J_{4,5'}$=1.3 Hz, H-5'), 2.07 and 2.14 (each s, OAc), 4.56 and 4.74 (ABq, J=12.8 Hz, CH_2 in Bn), and 7.34 (s, Ph).

Found: C, 54.82; H, 5.21; N, 12.41%. Calcd for $C_{16}H_{19}N_3O_6$: C, 55.01; H, 5.48; N, 12.03%.

Benzyl 2-*O*-(1-Imidazolylsulfonyl)-3,4-*O*-isopropylidene-β-L-arabinopyranoside (14). To a solution of **12** (1.6 g, 5.7 mmol) in pyridine (6 ml) was added imidazole (2.0 g, 30 mmol) and sulfuryl chloride (1.2 ml, 15 mmol) in two portions with stirring and cooling (ice-water). After being kept overnight at room temperature the mixture was poured into ice-water and extracted twice with chloroform. The extract was washed with water, dried and evaporated to give **14** (1.6 g) as a solid residue, which was characterized only by ^1H NMR δ=4.92 (d, $J_{1,2}$=2.7, H-1), 4.45 (H-2), 4.34 (dd, H-3), 4.20 (bd, H-4), 3.95 (bs, 2 H, H-5 and H-5'), 1.30 and 1.34 (each s, CMe_2), 4.45 and 4.69 (ABq, J=11.6 Hz, CH_2 in Bn), 7.03 (d), 7.87 (d), and 7.23 (dd) (Imidazyl), and 7.31 (s, Ph).

Benzyl 2-Azido-2-deoxy-3,4-*O*-isopropylidene-β-L-ribopyranoside (15). A. From 12 via Its 3-Triflate (13): To a solution of trifluoromethanesulfonic anhydride (1 ml, 7.1 mmol) in dichloromethane (20 ml) was added dropwise at −5—−10 °C a solution of pyridine (1 ml, 12 mmol) in dichloromethane (10 ml) and then a solution of **12** (1 g, 3.6 mmol) in dichloromethane (10 ml). The mixture was kept at the temperature for 0.5 h and then poured into ice-water containing sodium hydrogencarbonate. The dichloromethane layer was separated, washed with dilute hydrochloric acid, water, and sodium chloride solution, dried, and evaporated to give crude **13** as syrup, which was characterized only by ^1H NMR δ=5.09 (d, $J_{1,2}$=3.5 Hz, H-1), 5.37 (dd, $J_{2,3}$=6.9 Hz, H-2), 4.68 (d, H-3), 4.15 (H-4), 4.07 (bs, 2H, H-5 and H-5'), 1.40 and 1.56 (each s, CMe_2), 4.71 and 4.80 (ABq, J=10.0 Hz, CH_2 in Bn), and 7.36 (s, Ph).

A mixture of crude **13** and sodium azide (0.6 g, 9.2 mmol) in *N*,*N*-dimethylformamide (5 ml) was heated at 65—70 °C for 1 h, and then poured into ice-water, dried and evaporated to give a syrupy residue, from which was obtained the compound **15** by column chromatography on silica gel. Syrup, $[\alpha]_D$ +66.8° (*c* 1.1, $CHCl_3$); ^1H NMR δ=4.60 (d, $J_{1,2}$=3.6 Hz, H-1), 4.44 (dd, $J_{2,3}$=8.7 Hz, H-2), 4.7 (H-3), 4.18 (H-4), 4.0 (2 H, H-5 and H-5'), 1.34 and 1.50 (each s, CMe_2), 4.77 (s, CH_2 in Bn), and 7.33 (s, Ph).

Found: C, 58.76; H, 6.14; N, 13.42%. Calcd for $C_{15}H_{19}N_3O_4$: C, 59.01; H, 6.27; N, 13.76%.

B. From 14: A mixture of **14** (410 mg, 1.0 mmol), sodium azide (210 mg, 3.2 mmol), and tetrabutylammonium chloride (340 mg, 3.2 mmol) in toluene (5 ml) was heated under gentle reflux for 6 h. After addition of water the mixture was washed with water three times, dried and evaporated to give **14** (245 mg, 80%), which was identical with the 2-azido sugar described above.

Methyl 2-Azido-2-deoxy-α-D-xylopyranoside (16). Compound **4** (440 mg, 2.3 mmol) was dissolved in methanol containing catalytic amount of sodium. After standing at room temperature for 1 h and neutralization with acetic acid, the solution was evaporated and the residue was purified on a silica-gel column with ethyl acetate and hexane (3:2) to give **16** as a syrup in 82% yield, $[\alpha]_D$ +139.9° (*c* 1.0, methanol).

Found: C, 38.22; H, 5.84; N, 22.70%. Calcd for $C_6H_{11}N_3O_4$: C, 38.09; H, 5.86; N, 22.21%.

Benzoylation of 16. To a solution of **16** (6.11 g, 32.3 mmol) in acetone (70 ml) was added with stirring triethylamine (8.8 ml, 63.2 mmol) and benzoyl chloride (7.6 ml, 65.3 mmol), and the mixture was kept at room temperature for 36 h. After addition of water and further stirring for 2 h, the mixture was extracted with chloroform. The extract was washed with water, dried and evaporated to give a syrupy mixture of benzoates, which was fractionated on a silica-gel column with benzene–acetone (30:1) to give 3,4-dibenzoate (**20**), 4-benzoate (**19**) and 3-benzoate (**17**) in 29, 65, and 5%, respectively.

17: Syrup, $[\alpha]_D$ +134.9° (*c* 1.0, $CHCl_3$); ^1H NMR δ=4.82 (d, $J_{1,2}$=3.8 Hz, H-1), 3.40 (dd, $J_{2,3}$=10.5 Hz, H-2), 5.43 (dd, $J_{3,4}$=8.3 Hz, H-3), 3.6—4.1 (m, 3H, H-4, H-5, and H-5'), 3.46 (s, OMe), 7.2—7.6 and 8.0—8.1 (m, Ph).

Found: C, 53.34; H, 5.24; N, 13.96%. Calcd for $C_{13}H_{15}N_3O_5$: C, 53.24; H, 5.16; N, 14.33%.

19: Mp 85—89 °C, $[\alpha]_D$ +46.0° (*c* 1.0, $CHCl_3$); ^1H NMR δ=4.75 (d, $J_{1,2}$=3.6 Hz, H-1), 3.32 (dd, $J_{2,3}$=9.3 Hz, H-2), 4.23 (t, $J_{3,4}$=9.3 Hz, H-3), 5.05 (ddd, $J_{4,5}$=10.3 Hz, $J_{4,5'}$= 5.9 Hz, H-4), 3.63, (t, $J_{5,5'}$=10.6 Hz, H-5), 3.89 (dd, H-5'), 3.43 (s, OMe), 7.2—7.6 and 7.9—8.1 (m, Ph).

Found: C, 53.29; H, 5.03; N, 13.85%. Calcd for $C_{13}H_{15}N_3O_5$: C 53.24; H, 5.16; N, 14.33%.

20: Syrup, $[\alpha]_D$ +25.5° (*c* 1.0, $CHCl_3$); ^1H NMR δ=4.92 (d, $J_{1,2}$=3.8 Hz, H-1), 3.47 (dd, $J_{2,3}$=9.6 Hz, H-2), 5.95 (t, $J_{3,4}$=9.3 Hz, H-3), 5.31 (ddd, $J_{4,5}$=10.5 Hz, $J_{4,5'}$=6.0 Hz, H-4), 3.78 (t, $J_{5,5'}$=10.5 Hz, H-5), 4.04 (dd, H-5'), 3.52 (s, OMe), 7.3—7.6 and 7.9—8.2 (m, Ph).

Found: C, 59.82; H, 4.73; N, 10.80%. Calcd for $C_{20}H_{19}N_3O_6$: C, 60.45; H, 4.82; N, 10.58%.

Methyl 2-Azido-3-*O*-benzyl-2-deoxy-α-D-xylopyranoside (18). Compound **22** was debenzoylated with sodium methoxide in methanol in a conventional manner to give **18** in a quantitative yield, $[\alpha]_D$ +33.8°; ^1H NMR δ=4.66 (d, $J_{1,2}$=3.3 Hz, H-1), 3.2—3.8 (m, H-2—5), 3.47 (s, OMe), 4.68 and 4.88 (ABq, J=10.5 Hz, CH_2 in Bn), and 7.40 (s, Ph).

Found: C, 55.54; H, 6.09; N, 14.89%. Calcd for $C_{13}H_{17}N_3O_4$: C, 55.90; H, 6.14; N, 15.05%.

Methyl 2-Azido-4-*O*-benzoyl-2-deoxy-3-*O*-methylsulfonyl-α-D-xylopyranoside (21). Compound **19** was mesylated with methanesulfonyl chloride in pyridine in a conventional manner to give **21** in 85% yield, mp 53—54 °C, $[\alpha]_D$ −79.1° (*c* 1.0, $CHCl_3$); ^1H NMR δ=4.90 (d, $J_{1,2}$=3.5 Hz, H-1), 3.41 (dd, $J_{2,3}$=9.6 Hz, H-2), 5.08—5.36 (m, 3H, H-3, H-4, and H-5), 4.01 (dd, $J_{4,5'}$=5.4 Hz, $J_{5,5'}$=11.3 Hz), 3.47 (s, OMe), 3.04 (s, Ms) and 7.3—7.6 and 8.0—8.15 (m, Ph).

Found: C, 45.33: H, 4.51: N, 11.16; S, 8.85%. Calcd for $C_{14}H_{17}N_3O_7S$: C, 45.28; H, 4.61; N, 11.32; S, 8.63%.

Methyl 2-Azido-4-*O*-benzoyl-3-*O*-benzyl-2-deoxy-α-D-xylopyranoside (22). To a solution of **19** (527 mg, 1.8 mmol) in dry benzene (5 ml) was added benzyl bromide (0.85 ml, 7.1 mmol) and silver oxide (830 mg, 3.6 mmol) and the mixture was stirred under exclusion of light for 40 h. The undissolved material was filtered off and a residue obtained by evaporation of the filtrate was purified on a silica-gel column with hexane-ethyl acetate (7:1) to give **22** in 74% yield, syrup, $[\alpha]_D$ −52.2° (*c* 1.0, $CHCl_3$); IR (NaCl) 2100 (azido) and 1725 (ester) cm^{-1}; ^1H NMR δ=4.78 (d, $J_{1,2}$=1.2 Hz, H-1), 3.5 (H-2), 4.09 (t, $J_{2,3}=J_{3,4}$=9.5 Hz, H-3), 5.18 (ddd, $J_{4,5}$=10.5 Hz, $J_{4,5'}$=5.9 Hz, H-4), 3.60 (dd, $J_{5,5'}$=11.0 Hz, H-5), 3.90 (dd, H-5'), 3.46 (s, OMe), 4.72 and 4.80 (ABq, *J*= 11.4 Hz, CH_2 in Bn), 7.19 (s, Ph), 7.2—7.6 and 7.9—8.0 (m, Ph).

Found: C, 62.95; H, 5.60; N, 10.69%. Calcd for $C_{20}H_{21}N_3O_5$: C, 62.65; H, 5.52; N, 10.96%.

Methyl 2-Azido-4-*O*-benzoyl-2-deoxy-α-D-ribopyranoside (24). To a solution of **19** (1.7 g, 5.8 mmol) and dimethyl sulfoxide (2.3 g, 29.5 mmol) in dry dichloromethane (10 ml) was added with stirring at −78 °C a solution of trifluoroacetic anhydride (3.5 g, 1.8 mmol) in dry dichloromethane (5 ml), and then after 30 min, a solution of triethylamine (4.3 g, 43 mmol) in dichloromethane (5 ml). The temperature was kept for further 30 min and raised up to room temperature. Then, to the reaction solution was added with stirring methanol (20 ml) and sodium borohydride (0.43 g, 12 mmol) and the stirring was continued for 30 min. After addition of chloroform the reaction solution was washed with water, dried and evaporated to give a syrupy residue, which was purified on a silica-gel column with hexane-ethyl acetate (5:1) to afford **24** in 75% yield, $[\alpha]_D$ +110.3° (*c* 1.0, $CHCl_3$); ^1H NMR δ=4.78 (d, $J_{1,2}$=3.0 Hz, H-1), 3.43 (t, $J_{2,3}$=3.0 Hz, H-2), 4.43 (dt, $J_{3,4}$=3.0 Hz, $J_{3,OH}$=9.6 Hz, H-3), 5.07 (ddd, $J_{4,5}$=9.8 Hz, $J_{4,5'}$=5.1 Hz, H-4), 4.04 (dd, $J_{5,5'}$=11.4 Hz, H-5), 3.76 (dd, H-5'), 3.36 (d, OH), 3.56 (s, OMe), 7.3—7.6 and 8.0—8.2 (m, Ph).

Found: C, 53.83; H, 5.15; N, 14.03%. Calcd for $C_{13}H_{15}N_3O_5$: C, 53.24; H, 5.16; N, 14.33%.

Methyl 3-*O*-Acetyl-2-azido-4-*O*-benzoyl-2-deoxy-α-D-ribopyranoside (25). Acetylation of **24** in a usual manner gave **25** in 88% yield, syrup, $[\alpha]_D$ +60.2° (*c* 1.0, $CHCl_3$); ^1H NMR δ=4.66 (d, $J_{1,2}$=3.0 Hz, H-1), 3.5 (H-2), 5.54 (t, $J_{2,3}$=3.3 Hz, H-3), 5.21 (dt, $J_{3,4}$=3.3 Hz, H-4), 4.12 (dd, $J_{4,5}$=7.4 Hz, $J_{5,5'}$=11.6 Hz, H-5), 3.70 (dd, $J_{4,5'}$=3.9 Hz, H-5'), 2.13 (s, OAc), 3.55 (s, OMe), 7.3—7.6 and 7.9—8.1 (m, Ph).

Found: C, 53.41; H, 5.03; N, 12.20%. Calcd for $C_{15}H_{17}N_3O_6$: C, 53.73; H, 5.11; N, 12.53%.

Benzyl 2-Azido-2-deoxy-α-D-xylopyranoside (26). Compound **5** was deacetylated in the same manner as described for **16** and crude **26** was purified on a silica-gel column with hexane-ethyl acetate (2:1). Syrup, $[\alpha]_D$ +88.7° (*c* 1.0, methanol); ^1H NMR δ=4.91 (d, $J_{1,2}$=3.5 Hz, H-1), 3.15 (dd, $J_{2,3}$=9.5 Hz, H-2), 3.40—4.10 (m, other ring protons), 4.52 and 4.75 (ABq, *J*=12.0 Hz, CH_2 in Bn), and 7.35 (s, Ph).

Found: C, 54.10; H, 5.64; N, 15.81%. Calcd for $C_{12}H_{15}N_3O_4$: C, 54.33; H, 5.70; N, 15.84%.

Benzyl 2-Azido-4-*O*-benzoyl-2-deoxy-α-D-xylopyranoside (27) and Benzyl 2-Azido-3,4-di-*O*-benzoyl-2-deoxy-α-D-xylopyranoside (28). To a solution of **26** (2.42 g, 9.1 mmol) in acetone (30 ml) was added under cooling with ice-water triethylamine (2.5 ml, 18 mmol) and benzoyl chloride (1.6 ml, 14 mmol), and the mixture was stirred at room temperature for 16 h. A syrupy mixture of benzoates obtained by usual work-up was fractionated on a silica-gel column with benzene-acetone (100:1) to give 3,4-dibenzoate (**28**) and 4-benzoate (**27**) in 15 and 66% yields, respectively.

27: Mp 94—95 °C, $[\alpha]_D$ +64.5° (*c* 1.2, $CHCl_3$); ^1H NMR δ=5.04 (d, $J_{1,2}$=3.6 Hz, H-1), 3.37 (dd, $J_{2,3}$=10.5 Hz, H-2), 4.37 (t, $J_{3,4}$=9.3 Hz, H-3), 5.16 (m, H-4), 3.77 (t, $J_{4,5}=J_{5,5'}$=10.5 Hz, H-5), 3.99 (dd, $J_{4,5'}$=6.3 Hz, H-5'), 4.63 and 4.94 (ABq, *J*=11.4 Hz, CH_2 in Bn), 7.46 (s, Ph), 7.4—7.7 and 8.0—8.2 (m, Ph).

Found: C, 62.46; H, 5.18; N, 11.25%. Calcd for $C_{19}H_{19}N_3O_5$: C, 61.78; H, 5.19; N, 11.38%.

28: Syrup, $[\alpha]_D$ +37.9° (*c* 1.3, $CHCl_3$); ^1H NMR δ=5.17 (d, $J_{1,2}$=3.3 Hz, H-1), 3.49 (dd, $J_{2,3}$=10.2 Hz, H-2), 6.08 (dd, $J_{3,4}$=9.9 Hz, H-3), 5.40 (dt, $J_{4,5}$=9.9 Hz, $J_{4,5'}$=6.0 Hz, H-4), 3.90 (t, H-5), 4.14 (dd, $J_{5,5'}$=11.0 Hz, H-5'), 4.68 and 4.90 (ABq, *J*=11.6 Hz, CH_2 in Bn), 7.46 (s, Ph), 7.3—7.7 and 8.0—8.3 (m, Ph).

Found: C, 65.73; H, 4.87; N, 8.95%. Calcd for $C_{26}H_{23}N_3O_6$: C, 65.95; H, 4.90; N, 8.88%.

Benzyl 2-Azido-4-*O*-benzoyl-3-*O*-benzyl-2-deoxy-α-D-xylopyranoside (29). Compound **27** was benzylated in the same manner as described for **22** and the product was purified on a silica-gel column with hexane-ethyl acetate (1:0—4:1) to give **29** in 86% yield, syrup, $[\alpha]_D$ −6.2° (*c* 1.1, $CHCl_3$); ^1H NMR δ=5.04 (d, $J_{1,2}$=3.6 Hz, H-1), 3.50 (dd, $J_{2,3}$=10.1 Hz, H-2), 4.24 (t, H-3), 5.29 (ddd, $J_{3,4}$=9.6 Hz, $J_{4,5}$=10.2 Hz, $J_{4,5'}$=6.0 Hz, H-4), 3.74 (t, H-5), 4.01 (dd, $J_{5,5'}$=10.7 Hz, H-5'), 4.64 and 4.84 (ABq, *J*=12.0 Hz, CH_2 in Bn), 4.82 and 4.88 (ABq, *J*=11.3 Hz, CH_2 in Bn), 7.30 and 7.45 (each s, Ph), 7.3—7.7 and 8.0—8.3 (m, Ph).

Found: C, 67.92; H, 5.50; N, 8.86%. Calcd for $C_{26}H_{25}N_3O_5$: C, 67.96; H, 5.48; N, 9.15%.

Benzyl 2-Azido-3-*O*-benzyl-2-deoxy-α-D-xylopyranoside (30). Compound **29** was debenzoylated in the same manner as described for **18** to give **30** in a quantitative yield, mp 88—91 °C, $[\alpha]_D$ +50.9° (*c* 0.9, $CHCl_3$); ^1H NMR δ=4.97 (d, $J_{1,2}$=3.0 Hz, H-1), 3.33 (dd, $J_{2,3}$=9.0 Hz, H-2), 3.6—4.0 (m, 4H, H-3, H-4, H-5, and H-5'), 4.61 and 4.83 (ABq, *J*=12.0 Hz, CH_2 in Bn), 4.79 and 4.97 (ABq, *J*=11.3 Hz, CH_2 in Bn), and 7.44 (bs, Ph).

Found: C, 64.52; H, 5.94; N, 11.41%. Calcd for $C_{19}H_{21}N_3O_4$: C, 64.21; H, 5.96, N, 11.82%.

Methyl 3,4-Anhydro-2-azido-2-deoxy-α-D-ribopyranoside (31). Compound **21** (6.74 g, 18.1 mmol) was dissolved in 1.4 M (1M=1 mol dm^{-3}) methanolic potassium hydroxide (140 ml) and the solution was refluxed for 5 min. After addition of water the reaction mixture was extracted with chloroform. The extract was washed with water, dried and evaporated to give a syrupy residue, which was purified on a silica-gel column with benzene-ethanol (80:1). Yield 76%, mp 64—65 °C, $[\alpha]_D$ −16.8° (*c* 1.0, $CHCl_3$); ^1H NMR δ=4.60 (d, $J_{1,2}$=4.2 Hz, H-1), 3.2—3.6 (m, 3H, H-2, H-3, and H-4), 4.15 (bd, $J_{4,5}$=0.5 Hz, $J_{5,5'}$=13.7 Hz, H-5), 4.91 (dd, $J_{4,5'}$=3.0 Hz, H-5') and 3.50 (s, OMe).

Found: C, 44.05; H, 5.84; N, 20.49%. Calcd for $C_{10}H_{16}N_4O_5$: C, 44.11; H, 5.92; N, 20.58%.

Methyl 3,4-Di-*O*-acetyl-2-azido-2-deoxy-β-L-lyxopyranoside (32). To a solution of **31** (222 mg, 1.30 mmol) in dry *N*,*N*-dimethylformamide (10 ml) was added acetic acid (1 ml) and anhydrous sodium acetate (1 g), and the mixture was

heated with stirring at 100 °C for 16 h. After addition of acetic anhydride (3 ml) and pyridine (5 ml) the mixture was heated further at 100 °C for 1 h and then kept at room temperature for 4 h. The mixture was poured into ice-water and extracted five times with toluene. The extract was washed successively with water, 1 M hydrochloric acid, saturated sodium hydrogencarbonate, and water, and dried and evaporated to give a syrupy mixture. The mixture was fractionated on a silica-gel column with hexane–ethyl acetate (4 : 1) to give **32** (193 mg, 54%) and **4** (87 mg, 25%). **32**: Mp 79 °C (from ether), $[\alpha]_D$ +146.5° (*c* 1.8, $CHCl_3$), ^1H NMR δ=4.69 (d, $J_{1,2}$=3.0 Hz, H-1), 3.77 (t, $J_{2,3}$=3.5 Hz, H-2), 5.14 (dd, $J_{3,4}$=6.5 Hz, H-3), 4.97 (ddd, $J_{4,5}$=5.5 Hz, $J_{4,5'}$=3.5 Hz, H-4), 3.43 (dd, $J_{5,5'}$=12.5 Hz, H-5), 4.12 (dd, H-5′), 2.06 and 2.12 (each s, OAc), and 3.51 (s, OMe).

Found: C, 43.30; H, 5.48; N, 14.93%. Calcd for $C_{10}H_{15}N_3O_6$: C, 43.96; H, 5.53; N, 15.38%.

Methyl 2-Azido-4-*O*-benzyl-2-deoxy-α-D-xylopyranoside (33). A mixture of **16** (7.1 g, 38 mmol) and dibutyltin oxide (9.5 g, 38 mmol) in dry benzene (300 ml) was heated under reflux for 1 h. To this mixture was added benzyl bromide (9.1 ml, 77 mmol) and tetraethylammonium bromide (12.9 g, 61 mmol). Being heated under reflux for 17 h, the mixture was evaporated and the residue was fractionated on a silica-gel column with hexane–ethyl acetate (5 : 1) to give **33** and **18** in 70 and 13% yields, respectively. **33**: Syrup, $[\alpha]_D$ +94.5° (*c* 0.9, $CHCl_3$); IR (NaCl) 3450 (OH), and 2110 (azido) cm^{-1}. ^1H NMR δ=4.68 (d, $J_{1,2}$=3.9 Hz, H-1), 3.18 (dd, $J_{2,3}$=10.4 Hz, H-2), 3.38 (s, OMe), 4.64 (s, CH_2Ph), and 7.32 (s, Ph).

Found: C, 55.91; H, 5.81; N, 14.65%. Calcd for $C_{13}H_{17}N_3O_4$: C, 55.90; H, 6.14; N, 15.05%.

3,4-Di-*O*-acetyl-2-azido-2-deoxy-α-D-xylopyranosyl Chloride (34). To a solution of **3** (810 mg, 2.69 mmol) in dry dichloromethane (20 ml) was added titanium tetrachloride (1.0 g, 5.3 mmol). The solution was kept overnight at 25—30 °C diluted with chloroform, washed successively with ice-water, saturated aqueous sodium hydrogencarbonate, water, dried and evaporated to give crude **34** (660 mg, 88%), which was purified on a silica-gel column with hexane–ethyl acetate (4 : 1). Yield, 77%, mp 71—72 °C, $[\alpha]_D$ +149.4° (*c* 1.0, $CHCl_3$); ^1H NMR δ=6.10 (d, $J_{1,2}$=3.3 Hz, H-1), 3.78 (dd, $J_{2,3}$=9.8 Hz, H-2), 5.54 (t, $J_{3,4}$=9.8 Hz, H-3), 5.03 (dt, $J_{4,5}$=9.8 Hz, $J_{4,5'}$=6.9 Hz, H-4), 3.9—4.1 (m, H-5,5′), 2.07 and 2.10 (each s, OAc).

Found: C, 39.40; H, 4.37; N, 15.07%. Calcd for $C_9H_{12}N_3O_5Cl$: C, 38.93; H, 4.36; N, 15.13%.

3,4-Di-*O*-acetyl-2-azido-2-deoxy-α-D-xylopyranosyl Bromide (35). (a) With Titanium Tetrabromide: To a solution of **3** (430 mg, 1.43 mmol) in a mixture of dichloromethane (30 ml) and ethyl acetate (3 ml) was added titanium tetrabromide (2.10 g, 5.71 mmol). The mixture was kept at 25—30 °C for 36 h, poured into ice-water, and extracted with chloroform. A similar work-up of the extract as described for **34** gave a crude crystal (440 mg, 63%), mp 95—97 °C (dry ether), $[\alpha]_D$ +189.0° (*c* 1.5, $CHCl_3$); ^1H NMR δ=6.34 (d, $J_{1,2}$=4.0 Hz, H-1), 3.69 (dd, $J_{2,3}$=9.8 Hz, H-2), 5.47 (t, $J_{3,4}$=9.8 Hz, H-3), 5.00 (m, H-4), 3.88 (t, $J_{4,5}$=$J_{5,5'}$=10.5 Hz, H-5), 4.02 (dd, $J_{4,5'}$=6.3 Hz, H-5′), 2.06 and 2.12 (each s, OAc).

Found: C, 33.33; H, 3.63; N, 12.78%. Calcd for $C_9H_{12}N_3O_5Br$: C, 33.56; H, 3.76; N, 13.05%.

(b) With Hydrogen Bromide. To a solution of **3** (500 mg, 1.66 mmol) in dichloromethane (2 ml) was added dropwise a solution of 30% hydrogen bromide in acetic acid (0.6 ml) at 0 °C with stirring. The mixture was kept at the same temperature for 3 h and worked up in the same manner as described above to give **35** in 88% yield.

3,4-Di-*O*-acetyl-2-azido-2-deoxy-β-L-arabinopyranosyl Chloride (36). To a solution of **8** (3.5 g, 11 mmol) in acetonitrile (10 ml) was added tetraethylammonium chloride (7.0 g, 42 mmol). The mixture was stirred at room temperature for 16 h, diluted with chloroform, washed with water, dried and evaporated to give crude **36**, which was purified with hexane–ethyl acetate (4 : 1). Yield, 80%, mp 80—82 °C, $[\alpha]_D$ +185.7° (*c* 1.0, $CHCl_3$); ^1H NMR δ=6.16 (d, $J_{1,2}$=3.3 Hz, H-1), 4.12 (m, H-2), 5.34 (dd, $J_{2,3}$=10.5 Hz, $J_{3,4}$=3.0 Hz, H-3), 5.39 (dt, H-4), 3.89 (dd, $J_{4,5}$=1.8 Hz, $J_{5,5'}$=13.8 Hz, H-5), 4.26 (dd, $J_{4,5'}$=1.4 Hz, H-5′), 2.09 and 2.16 (each s, OAc).

Found: C, 38.65; H, 4.52; N, 14.86%. Calcd for $C_9H_{12}N_3O_5Cl$: C, 38.93; H, 4.36; N, 15.13%.

3,4-Di-*O*-acetyl-2-azido-2-deoxy-β-L-arabinopyranosyl Bromide (37). To a solution of **8** (1.0 g, 3.1 mmol) in acetonitrile (10 ml) was added lithium bromide (1.2 g, 14 mmol) and the mixture was kept at room temperature for 3 h. The same work-up as described for **36** gave **37** in 55% yield. ^1H NMR δ=6.47 (d, $J_{1,2}$=4.0 Hz, H-1), 4.03 (H-2), 5.32 (dd, $J_{2,3}$=9.5 Hz, $J_{3,4}$=3.6 Hz, H-3), 5.37 (broad s, H-4), 3.92 (dd, $J_{4,5}$=1.5 Hz, $J_{5,5'}$=13.8 Hz, H-5), 4.22 (dd, $J_{4,5'}$=0.9 Hz, H-5′), 2.07 and 2.15 (each s, OAc).

Found: C, 33.58; H, 3.91; N, 12.73%. Calcd for $C_9H_{12}N_3O_5Br$: C, 33.56; H, 3.76; N, 13.00%.

References

1) G. A. Ellestad, D. B. Cosulich, R. W. Broschard, J. H. Martin, M. P. Kunstmann, G. O. Morton, J. E. Lancaster, W. Fulmor, and F. M. Lovell, *J. Am. Chem. Soc.*, **100**, 2515 (1978).

2) T. Nakanishi, T. Iida, F. Tomita, and A. Furuya, *Chem. Pharm. Bull.*, **24**, 2955 (1976); Y. Iwai, A. Nakagawa, A. Nagai, K. Matsuyama, Y. Takahashi, M. Yamashita, A. Hirano, and S. Omura, *J. Antibiot.*, **32**, 1367 (1979).

3) H. Paulsen, *Angew Chem.*, **94**, 184 (1982); *Chem. Soc. Rev.*, **13**, 15 (1984).

4) K. Dobashi, K. Nagaoka, Y. Watanabe, M. Nishida, M. Hamada, H. Naganawa, T. Takita, T. Takeuchi, and H. Umezawa, *J. Antibiot.*, **38**, 1166 (1975).

5) N. R. Williams, *Adv. Carbohydr. Chem. Biochem.*, **25**, 109 (1970); H. Hashimoto, K. Araki, and J. Yoshimura, *Bull. Chem. Soc. Jpn.*, **54**, 3015 (1981).

6) For example: M. Miljković, M. Gligorijević, and D. Glišin, *J. Org. Chem.*, **39**, 3223 (1974).

7) R. U. Lemieux and R. M. Ratcliffe, *Can. J. Chem.*, **57**, 1244 (1979); J. Lehmann, W. Reuter, and D. Schoning, *Chem. Ber.*, **112**, 1470 (1979).

8) H. Paulsen, J. P. Lorentzen, and W. Kutschker, *Carbohydr. Res.*, **136**, 153 (1985).

9) Y. Ishido and N. Sakairi, *Carbohydr. Res.*, **97**, 151 (1981); S. Hanessian and J.-M. Vatele, *Tetrahedron Lett.*, **22**, 3579 (1981).

10) S. David, A. Thieffry, and A. Veyrieres, *J. Chem. Soc., Perkin Trans. 1*, **1981**, 1796.

 © 1986 The Chemical Society of Japan Bull. Chem. Soc. Jpn., 59, 3137—3143 (1986)

Synthetic Studies on Glycocinnamoylspermidine. II.[1] Synthesis of 4-*O*-(2-Azido-2-deoxy-D-xylopyranosyl)-2-azido-2-deoxy-D-xylopyranose Derivatives

Koichi ARAKI, Manabu KAWA, Yoshihiro SAITO, Hironobu HASHIMOTO,* and Juji YOSHIMURA
Laboratory of Chemistry for Natural Products, Faculty of Science, Tokyo Institute of Technology, Nagatsuta, Midori-ku, Yokohama 227
(Received April 8, 1986)

Synthetic intermediates for the aminopentose disaccharide moiety of glycocinnamoylspermidine were synthesized from D-xylose.

2-Amino-2-deoxy-D-xylose and 2,3-diamino-2,3-dideoxy-D-xylose, which are rare components in the field of carbohydrate antibiotics, constitute the disaccharide moiety of glycocinnamoylspermidine (cinodine)[2] in which the disaccharide is linked through a unique ureylene linkage with *p*-(bacillosaminyloxy)cinnamoylspermidine. In this paper we should like to report a detail of the previous comminucation[3] on the synthesis of the disaccharide. The synthesis of the *p*-(bacillosaminyloxy)cinnamate moiety was previously reported.[1]

First of all the synthesis of 2-azido-2-deoxy-D-xylopyranose disaccharide having $\beta(1\rightarrow4)$ glycosidic linkage was examined. In order to reduce the kinds of necessary protecting groups for amino function, the 2-azido group, albeit having no anchimeric assistance for the formation of the interglycosidic β-linkage, seems to be convenient. This substituent have also been considered as favorable for the formation of α-ureylene linkage at the reducing end, which was, however, recently revised to be β.[4] Moreover, the authors showed easy availability of 2-azido-2-deoxypentose derivatives in the preceding paper.[5] Three disaccharides (**14**, **15**, and **34**) were chosen as feasible starting compounds for the construction of the aminopentose disaccharide moiety.

The Koenigs-Knorr method[6,7] and trimethylsilyl triflate (TMSOTf) method[8] were examined using 3,4-di-*O*-acetyl-2-azido-2-deoxy-α-D-xylopyranosyl halides (**1** and **2**) or 1,3,4-tri-*O*-acetyl-2-azido-2-deoxy-D-xylopyranose (**6**) as glycosyl donor, and methyl 2-azido-3-*O*-benzyl-2-deoxy-α-D-xylopyranoside (**8**) or the corresponding 3-*O*-tetrahydropyranyl (THP) derivative (**9**) as glycosyl acceptor. The latter acceptor was prepared by treatment of methyl 2-azido-4-*O*-benzoyl-2-deoxy-α-D-xylopyranoside with 3,4-dihydropyran and pyridinium *p*-toluenesulfonate, followed by debenzoylation. In the Koenigs-Knorr

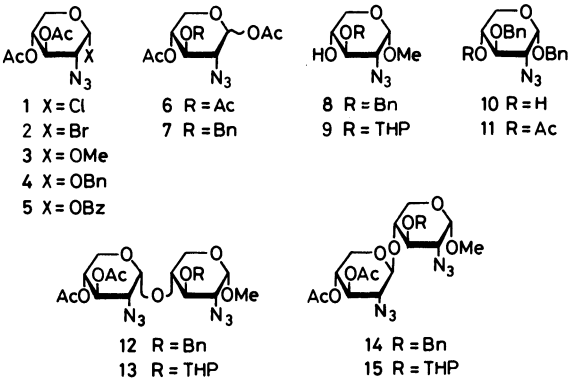

reaction of glycosyl halide having no participating group at C-2, β-glycoside formation are favored generally by the use of insoluble silver salts such as silver carbonate and silver silicate, or mercury(II) salts such as mercuric cyanide and mercury(II) bromide, which have weak affinity for halogens to promote the S_N2 type substitution of α-halide. Both types of promoters, however, proved to be not effective for **1** and **2** as shown in Table 1. In the coupling of α-chloride (**1**) with **8** a mixture of α-linked (**12**) and β-linked disaccharide (**14**) was obtained only using mercury(II) cyanide in a polar solvent in a very low yield. Even in the

Table 1. Disaccharide Formation

Donor	Acceptor	Reaction condition			Product and Yield/%	
		Promoter	Solvent	Temp/°C	α	β
1	**8**	$AgClO_4$, TMP	CH_3NO_2	−10	**12** 33	**14** 40
1	**8**	$Hg(CN)_2$	CH_3NO_2	60	**12** 5.3	**14** 4.7
1	**9**	$AgClO_4$, TMP	CH_3NO_2	−10	**13** 41	**15** 6
2	**9**	Ag_2CO_3	CH_2Cl_2	RT	**13** 16	
2	**9**	Ag_2O, I_2	CH_2Cl_2	RT	**13** 10	
2	**9**	HgO, $HgBr_2$	CH_2Cl_2	RT	**13** 11	
6	**8**	TMSOTf	$ClCH_2CH_2Cl$	0	**12** 16	**14** 36
1	**10**	$AgClO_4$, TMP	CH_3NO_2	RT	**33** 29	**35** 46

TMP: 2,4,6-Trimethylpyridine.

coupling of the more reactive α-bromide (**2**) with **9** only the α-linked disaccharide (**13**) was obtained in low yield with assistance of silver carbonate, silver oxide or mercury(II) bromide. Thus, 2-azido-2-deoxypentopyranosyl residue seems to be less reactive than the corresponding hexopyranosyl one. Therefore, glycosylation with silver perchlorate in nitromethane was examined in the presence of 2,4,6-trimethylpyridine. This method was proved to be suitable for β-glycoside formation in the cases of 3,4,6-triacetate of 2-*O*-benzyl- and 2-chloro-2-deoxy-α-D-glucopyranosyl chlorides.[9] The coupling of **1** and **8** gave **12** and **14** with predominance of the latter (4:5) in 73% yield, while the coupling of **1** with the benzyl glycoside (**10**) under the same conditions showed a slightly better selectivity to give a mixture of **32** and **34**, which were separated as *O*-deacetylated derivatives **33** and **35** in 29 and 46% yields, respectively. On the other hand, coupling of **1** with 3-*O*-THP derivative **9** exhibited a reverse selectivity to give α-linked (**13**) and β-linked disaccharide (**15**) in 41 and 6% yields, respectively. The result may be attributed to the lower reactivity of the 4-hydroxyl group in **9** due to the steric hindrance of bulky 3-*O*-THP moiety. Furthermore, coupling of 1-acetate (**6**) and **8** in the presence of TMSOTf gave **12** and **14** also with predominance of the latter (4:9) in 52% yield, respectively, to indicate a better selectivity for the formation of β-glycosidic linkage, albeit slightly in a lower yield. Considering that **6** consisted of almost α-anomer, S_N2 type substitution may predominate in this glycosylation.

Then, a precursor (**19**) of 2,3-diamino-2,3-dideoxy-D-xylose was derived via a 2,3-epimino derivative (**18**). 3-Mesylate (**16**) of methyl 2-azido-4-*O*-benzoyl-2-deoxy-α-D-xylopyranoside was hydrogenolyzed in the presence of platinum oxide to give 2-amino derivative (**17**) quantitatively, which was further converted into **18** in 73% yield, by treatment with sodium acetate in *N*,*N*-dimethylformamide at 80 °C. Azidolysis of **18** with sodium azide in the presence of tetraethylammonium chloride in 2-methoxyethanol-water at 95°C for 18 h afforded 3-azido derivative (**19**) preferentially in 85% yield. The structure of **19** was easily determined by ^{1}H NMR spectra, where $J_{2,3}$ and $J_{3,4}$ show 10.2 and 10.4 Hz, respectively, indicating *xylo* configuration.

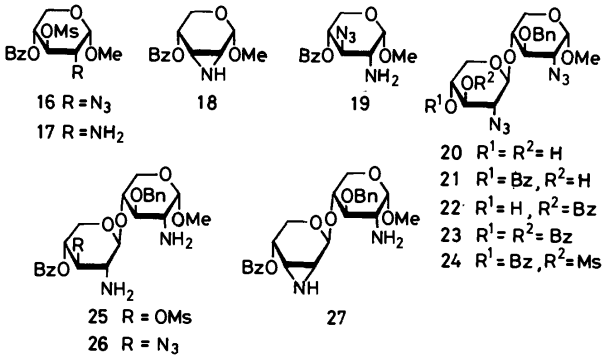

The same conversion was also substantiated in the case of disaccharide. The deacetylated derivative (**20**) of **14** was partially benzoylated with 2 molar equivalents of benzoyl chloride and triethylamine in acetone to give 4′-benzoate (**21**) in 61% yield together with 3′-benzoate (**22**) and 3′,4′-dibenzoate (**23**). The 3′-mesylate (**24**) obtained in 97% by a usual mesylation of **21** was successively hydrogenolyzed and treated with sodium acetate in the same manner as described above without any purification of the intermediate diamine (**25**) to give 2′,3′-epimino derivative (**27**) in a quantitative yield. Azidolysis of **27** with the same reagent as described above at 110 °C for 4 h give a desired isomer **26** in 63% yield. For the total synthesis of cinodine this method may assure an easy conversion of 2-azido-2-deoxy-D-xylopyranose moiety at the nonreducing end of the pseudo trisaccharide having interglycosidic ureylene linkage into 2,3-diamino-2,3-dideoxy-D-xylose moiety.

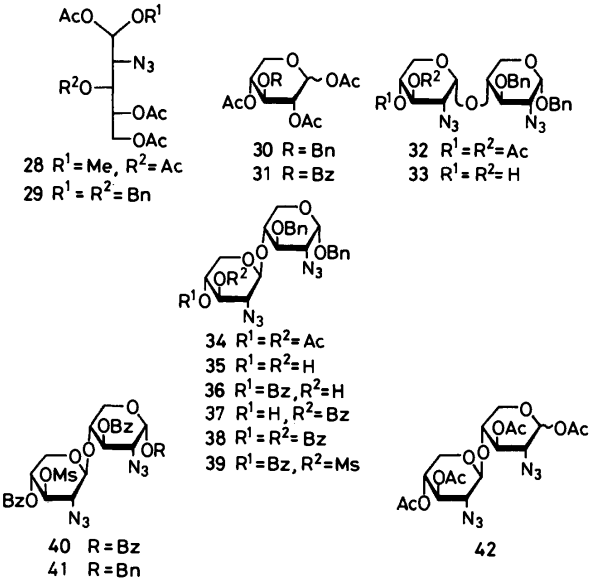

Finally deprotection of glycoside was examined, because it is necessary for formation of the ureylene linkage. Acetolysis of the glycosides, one of the most frequently used methods, proved to be unsuccesful. Treatment of 2-azido-2-deoxy-D-xylopyranoside derivative such as methyl 3,4-di-*O*-acetyl-2-azido-2-deoxy-α-D-xylopyranoside (**3**) and a benzyl glycoside (**10**) with acetic anhydride in the presence of acid gave acyclic products **28** and **29**, respectively, as shown in Table 2. These results may be attributed to the retarding effect of C_2-N_3 dipole against the cleavage of C_1-OMe bond to facilitate consequently cleavage of the bond between C_1 and ring oxygen. Presence of benzyl or glycosyl substituents on the glycosyl moiety seems to have no effect on this situation. It was noteworthy that acetolysis of **3** and **10** in the presence of perchloric and trifluoroacetic acid, respectively, gave acyclic products **28** and **29** in a quantitative and 81% yields, respectively, which were obviously higher than those obtained in

Table 2. Acetolysis and Hydrolysis[a] of 2-Azido-2-deoxy-α-D-xylopyranoside Derivatives

Substrate	Acid	Concd	Solvent	Temperature °C	Time h	Product and Yield/%
3	$HClO_4$	0.18%	Ac_2O	RT	1	**28** quantitative
10	H_2SO_4	0.02%	Ac_2O/AcOH (7:3)	RT	79	**29** 34, **11** 38
10	H_2SO_4	0.05%	Ac_2O/AcOH (6:5)	RT	99	**29** 41, **11** 60
10	CF_3CO_2H	5%	Ac_2O	RT	73	**29** 81, **11** 12
8	H_2SO_4	0.5 M	70% AcOH	100	7	**7** 29, **6** 13
10	H_2SO_4	0.5 M	70% AcOH	100	4	**7** 60, **11** 35
10	H_2SO_4	0.6 M	70% AcOH	100	6	**7** 27, **6** 26, **11** 20
10	H_2SO_4	1.0 M	70% AcOH	100	2.5	**7** 53, **11** 35

a) Products were isolated after acetylation. b) 1 M=1 mol dm^{-3}.

the presence of sulfuric acid (Table 2). In the latter case, the ratio of two isomers was 3:2. Furthermore, hydrolytic deprotection of the benzyl glycoside was attempted. Benzyl glycoside (**10**) could be hydrolyzed selectively in 70% aqueous acetic acid containing 0.5—1 M (1M=1 mol dm^{-3}) sulfuric acid at 100 °C to give **7** after acetylation in good yields (Table 2). These conditions, however, proved to be not effective for selective hydrolysis of benzyl glycoside in the presence of interglycosidic linkage. For instance, the latter linkage was hydrolyzed preferentially in the case of **35**.

Finally the glycosidic linkage at the reducing end could be selectively deprotected using the benzyl glycoside as substrates by two methods. One is oxidative conversion of benzyl into benzoyl group with chromium trioxide in acetic acid.[10] This method proved to function nicely for both benzyloxy groups at C-1 and C-3 in the case of benzyl 3,4-di-*O*-acetyl-2-azido-2-deoxy-α-D-xylopyranoside (**4**) and 1,2,4-tri-*O*-acetyl-3-*O*-benzyl-α-D-xylopyranose (**30**),[11] respectively. Oxidation of **4** and **30** with chromium trioxide in acetic acid at room temperature gave the corresponding *O*-benzoyl derivatives **5** and **31** in 58 and 28% yields respectively. In the presence of sulfuric acid the yield for the latter increased up to 90%. The suitable disaccharide intermediate (**39**), which was derived from **35** via **36** in the same manner as described for the corresponding methyl glycoside, was oxidized by this method to give 1,3,4′-tri-*O*-benzoylated disaccharide (**40**) in 50% yield, together with small amount of selectively oxidized product (**41**). On the other hand, the second *O*-debenzylation method consists of bromination with *N*-bromosuccinimide and bromine in carbon tetrachloride followed by hydrolysis. The disaccharide **34** was converted by this method into **42** after acetylation in 56% yield. This reaction seems to be useful in a wide range of synthetic purpose and the further aspects will be published elsewhere.[12]

Experimental

General Methods. All melting points are uncorrected. The solutions were concentrated under diminished pressure at 50 °C (bath). Optical rotations were measured with a Carl Zeiss LEP-Al polarimeter. IR spectra were recorded with a Hitachi EPI-G2 grating spectrometer. ^{1}H NMR spectra were recorded with a JEOL PS-100 or a GX-400 spectrometer for solutions in $CDCl_3$ (internal Me_4Si) unless otherwise stated. ^{13}C NMR spectra were recorded with a JEOL FX-90 spectrometer for solutions in $CDCl_3$ unless otherwise stated. Chromatography was performed on Wakogel C-200, flash Chromatography on Wakogel C-300, and preparative TLC (PTLC) on silica gel 60 (Merck).

3,4-Di-*O*-acetyl-2-azido-1-*O*-benzoyl-2-deoxy-α-D-xylopyranose (5). To a solution of **4**[5] (114 mg, 0.33 mmol) in acetic acid (2.5 ml) was added chromium trioxide (200 mg, 2.0 mmol), and the mixture was stirred for 1 h at room temperature. The same work-up as described for **31** gave **5** in 58% yield; ^{1}H NMR δ=6.33 (d, $J_{1,2}$=3.9 Hz, H-1), 3.26 (dd, $J_{2,3}$=10.5 Hz, H-2), 5.47 (t, $J_{3,4}$=10.5 Hz, H-3), 4.96 (dt, $J_{4,5a}$=10.5 Hz, $J_{4,5b}$=6.0 Hz, H-4), 3.65 (t, $J_{5a,5b}$=10.5 Hz, H-5a), 3.90 (dd, H-5b), 1.98 and 2.08 (each s, Ac), and 7.32—8.06 (m, Ph).

1,4-Di-*O*-acetyl-2-azido-3-*O*-benzyl-2-deoxyl-D-xylopyranose (7). To a solution of **10**[5] (300 mg, 0.85 mmol) in acetic acid (72 ml) was added 0.62 M aqueous sulfuric acid (29 ml), and the solution was heated at 100 °C for 1 h. After addition of 0.93 M sulfuric acid (4.2 ml) the temperature was kept further 3 h. To the cooled solution was added sodium hydrogencarbonate (5 g), and the product was extracted 8 times with chloroform (total 80 ml). The residue obtained by evaporation of the dried extract was acetylated in a usual manner, and the product was purified on a silica-gel column with hexane–ethyl acetate (7:3) to give **7** as an anomeric mixture (α:β=9:11) and **11** in 60 and 35% yields, respectively. Compound **7**: ^{1}H NMR δ=6.16 (d, $J_{1,2}$=3.0 Hz, H-1α), 3.60 (dd, H-2α), 3.94 (t, $J_{2,3}$=$J_{3,4}$=9.0 Hz, H-3α), 4.10 (dd, $J_{4,5a}$=5.3 Hz, $J_{5a,5b}$=12.0 Hz, H-5aα), 3.56 (dd, H-5bα); 5.44 (d, $J_{1,2}$=8.0 Hz, H-1β), 3.62 (t, H-2β), 3.66 (t, $J_{2,3}$=$J_{3,4}$=9.0 Hz, H-3β), 3.93 (dd, $J_{4,5a}$=6.0 Hz, $J_{5a,5b}$=11.7 Hz, H-5aβ), 3.33 (dd, $J_{4,5b}$=9.6 Hz, H-5bβ); 2.01 and 2.18 (each s, Ac), 4.72 and 4.88 (ABq, J=11.7 Hz, CH_2 in Bn), 4.73 and 4.86 (ABq, J=11.6 Hz, CH_2 in Bn), and 7.34 (s, Ph).

Found: C, 54.85; H, 5.51; N, 12.13%. Calcd for $C_{16}H_{19}N_3O_6$: C, 55.01; H, 5.48; N, 12.03%.

11: Mp 35—37 °C, $[\alpha]_D$ +85.7° (*c* 1.1, CH_2Cl_2), ^{1}H NMR δ=4.96 (d, $J_{1,2}$=3.0 Hz, H-1), 3.39 (dd, $J_{2,3}$=10.0 Hz, H-2), 4.04 (t, $J_{3,4}$=9.5 Hz, H-3), 5.0 (m, H-4), 3.84 (dd, $J_{4,5a}$=6.0 Hz, $J_{5a,5b}$=10.5 Hz, H-5a), 3.57 (t, $J_{4,5b}$=10.5 Hz, H-5b), 1.98 (s, Ac), 4.56 and 4.79 (ABq, J=12.0 Hz, CH_2 in Bn), 4.70 and 4.87 (ABq, J=11.5 Hz, CH_2 in Bn), 7.34 and 7.39 (each s, Ph).

Found: C, 63.70; H, 5.87; N, 10.48%. Calcd for $C_{21}H_{23}N_3O_5$: C, 63.46; H, 5.83; N, 10.58%.

Methyl 2-Azido-2-deoxy-3-*O*-tetrahydropyranyl-α-D-xylo-

pyranoside (9). To a solution of methyl 2-azido-4-*O*-benzoyl-2-deoxy-α-D-xylopyranoside[5] (1.5 g, 5.1 mmol) in dry dichloromethane (40 ml) was added 3,4-dihydropyran (0.65 g, 7.7 mmol) and a solution of pyridinium *p*-toluenesulfonate (125 mg, 0.5 mmol) in dichloromethane (15 ml). The mixture was kept at room temperature for 40 h, washed with aqueous sodium chloride, dried and evaporated to give 3-*O*-tetrahydropyranyl derivative as syrup quantitatively; IR (NaCl) 2100 (azido) and 1723 cm^{-1} (ester); ^1H NMR δ=4.84 (d, $J_{1,2}$=3.0 Hz, H-1), 3.26 (dd, $J_{2,3}$=10.0 Hz, H-2), 4.21 and 4.37 (each t, $J_{3,4}$=10.0 Hz, H-3), 5.14 (m, H-4), 3.63 (t, $J_{4,5a}$=$J_{5a,5b}$=10.0 Hz, H-5a), 3.89 (dd, $J_{4,5b}$=6.0 Hz, H-5b), 3.49 (s, OMe), 4.85 (dd, H-2 in THP), 1.2—2.0 (m, CH_2 in THP), 7.3—7.7 and 8.0—8.2 (m, Ph).

The 3-*O*-tetrahydropyranyl derivative was debenzoylated with sodium methoxide in methanol in a conventional manner to give **9** as syrup in 80% yield; IR (NaCl) 2095 cm^{-1} (azido); ^1H NMR δ=4.70 (d, $J_{1,2}$=3.3 Hz, H-1), 4.62 (m, H-2 in THP), 3.41 (s, OMe) and 1.35—2.1 (m, CH_2 in THP).

Found: C, 47.95; H, 7.36; N, 15.03%. Calcd for $C_{11}H_{19}N_3O_5$: C, 48.34; H, 7.01; N, 15.38%.

Methyl 4-*O*-(3,4-Di-*O*-acetyl-2-azido-2-deoxy-α-D-xylopyranosyl)-2-azido-3-*O*-benzyl-2-deoxy-α-D-xylopyranoside (12) and Its β-(1→4) Linked Isomer (14). A. Silver Perchlorate as a Promoter: To a solution of **8** (1.5 mmol) in nitromethane (2 ml) was added silver perchlorate (0.6 mmol), 2,4,6-trimethylpyridine (0.6 mmol) and Drierite (0.9 g), and the suspension was stirred with shielding from light at −10 °C for 1 h. To this suspension was added a solution of **1**[5] (0.5 mmol) in nitromethane (2 ml) and the temperature was kept for 60 h. Undissolved materials were filtered off and washed with chloroform. The filtrate was washed with water, dried and evaporated to give a syrupy residue, which was fractionated on a silica-gel column with benzene–acetone (6 : 1) to give **12** and **14** in 33 and 40% yields, respectively.

12: Syrup, $[\alpha]_D$ +41.3° (*c* 1.0, $CHCl_3$); IR (NaCl) 2100 (azido) and 1750 (ester) cm^{-1}; ^1H NMR δ=4.70 (d, $J_{1,2}$=3.6 Hz, H-1), 5.17 (d, $J_{1',2'}$=3.6 Hz, H-1'), 5.40 (dd, $J_{2',3'}$=9.3 Hz, $J_{3',4'}$=10.4 Hz, H-3'), 4.60—4.85 (m, H-4'), 3.2—4.1 (m, other ring protons), 2.04 and 2.10 (each s, Ac), 3.44 (s, OMe), 4.82 and 4.96 (ABq, J=9.8 Hz, CH_2 in Bn), and 7.32 (s, Ph).

Found: C, 51.20, H, 5.58; N, 15.82%. Calcd for $C_{22}H_{28}N_6O_9$: C, 50.77; H, 5.42; N, 16.15%.

14: Syrup, $[\alpha]_D$ +10.2° (*c* 1.0, $CHCl_3$); IR (NaCl) 2100 (azido) and 1750 (ester) cm^{-1}; ^1H NMR δ=4.67 (d, $J_{1,2}$=3.0 Hz, H-1), 4.35 (d, $J_{1',2'}$=8.1 Hz, H-1'), 4.76—5.10 (m, H-3' and H-4'), 3.1—4.1 (m, other ring protons), 2.03 and 2.11 (each s, Ac), 3.23 (s, OMe), 4.72 and 4.94 (ABq, J=10.2 Hz, CH_2 in Bn), and 7.34 (broad s, Ph).

Found: C, 50.65: H, 5.54; N, 16.46%. Calcd for $C_{22}H_{28}N_6O_9$: C, 50.77; H, 5.42; N, 16.15%.

B. Mercury(II) Cyanide as Promoter: To a solution of **1** (108 mg, 0.39 mmol) and **8**[5] (311 mg, 1.2 mmol) in dry benzene (2 ml) and nitromethane (2 ml) was added mercury(II) cyanide (240 mg, 0.88 mmol) and Drierite (0.3 g), and the mixture was stirred at 60 °C for 26 h. A similar work-up as described above and separation by preparative TLC gave **12** and **14** in 5.3 and 4.7% yields, respectively.

C. TMSOTf as a Catalyst: To a solution of **6** (104 mg, 0.38 mmol) and **8** (111 mg, 0.40 mmol) in dry 1,2-dichloroethane (2 ml) was added molecular sieve 4A (0.5 g) and TMSOTf (85 mg, 0.39 mmol) at 0 °C. The mixture was stirred at the same temperature for 24 h. Undissolved materials were filtered off and washed with chloroform. The filtrate was washed with saturated aqueous sodium hydrogencarbonate and water, dried and evaporated to give a syrupy residue, which was fractionated on PTLC to give **12** and **14** in 16 and 36% yields, respectively.

Methyl 4-*O*-(3,4-Di-*O*-acetyl-2-azido-2-deoxy-α-D-xylopyranosyl)-2-azido-2-deoxy-3-*O*-tetrahydropyranyl-α-D-xylopyranoside (13) and Its β-(1→4) Linked Isomer (15). A Silver Perchlorate as a Promoter: Compound **1** and **9** were coupled in the same manner as describe above to give **13** and **15** in 41 and 6% yields, respectively.

13: Syrup, $[\alpha]_D$ +94.0° (*c* 1.0, $CHCl_3$); IR (NaCl) 2940 (THP), 2100 (azido) and 1750 (ester) cm^{-1}; ^1H NMR δ=4.66 (d, $J_{1,2}$=3.2 Hz, H-1), 3.18 (d, $J_{2,3}$=9.5 Hz, H-2), 5.43 (d, $J_{1',2'}$=3.3 Hz, H-1'), 5.38 (t, $J_{2',3'}$=$J_{3',4'}$=9.0 Hz, H-3'), 4.81 (m, H-4'), 3.3—4.2 (m, other ring protons), 1.3—2.0 (m, CH_2 in THP), 2.04 and 2.09 (each s, Ac), and 3.39 (s, OMe).

Found: C, 46.47; H, 6.05; N, 16.02%. Calcd for $C_{20}H_{30}N_6O_{10}$: C, 46.69; H, 5.88; N, 16.34%.

15: Syrup, $[\alpha]_D$ −8.1° (*c* 1.0, $CHCl_3$); IR (NaCl) 2930 (THP), 2105 (azido) and 1750 (ester) cm^{-1}; ^1H NMR δ=4.74 (d, $J_{1,2}$=3.0 Hz, H-1), 3.28 (dd, $J_{2,3}$=9.5 Hz, H-2), 4.42 (d, $J_{1',2'}$=7.8 Hz, H-1'), 3.84—5.16 (m, H-3' and H-4'), 3.4—4.3 (m, other ring protons), 1.3—2.0 (m, CH_2 in THP), 2.04 and 2.12 (each s, Ac), and 3.44 (s, OMe).

Found: C, 47.02; H, 5.78; N, 15.98%. Calcd for $C_{20}H_{30}N_6O_{10}$: C, 46.69; H, 5.88; N, 16.34%.

B. Silver Carbonate as a Promoter: To a solution of **9** (270 mg, 1 mmol) in dry dichloromethane (6 ml) was added silver carbonate (550 mg, 2.2 mmol), molecular sieve 4A (1 g) and **2** (480 mg, 1.5 mmol). The mixture was stirred with shielding from light for 48 h at room temperature to give only **13** in 16% yield.

C. Silver Oxide-Iodine as Promoters: To a solution of **9** (137 mg, 0.5 mmol) in dry dichloromethane (3 ml) was added silver oxide (130 mg, 0.55 mmol) and molecular sieve 4A (0.6 g). After stirring under exclusion of light for 1 h iodine (30 mg) and a solution of **2** (161 mg, 0.5 mmol) in dry dichloromethane (2 ml) were added to the mixture. After 48 h at room temperature only **13** was obtained in 10% yield.

D. Mercury(II) Oxide-Mercury(II) Bromide as Promoters: To a solution of **9** (137 mg, 0.50 mmol) in dry dichloromethane (4 ml) was added mercury(II) oxide (119 mg, 0.55 mmol) and mercury(II) bromide (6 mg, 0.02 mmol). The mixture was stirred at room temperature with shielding from light for 30 min, and solution of **2** (161 mg, 0.50 mmol) was added. After 48 h at room temperature only **13** was obtained in 11% yields.

Methyl 2-Azido-4-*O*-benzoyl-2-deoxy-3-*O*-methylsulfonyl-α-D-xylopyranoside (16). Methyl 2-azido-4-*O*-benzoyl-2-deoxy-α-D-xylopyranoside[5] was treated with methanesulfonyl chloride in pyridine in a usual manner to give **16** in 85% yield, mp 53—54 °C, $[\alpha]_D$ −79.1° (*c* 1.0, $CHCl_3$); ^1H NMR δ=4.90 (d, $J_{1,2}$=3.5 Hz, H-1), 3.41 (dd, $J_{2,3}$=9.6 Hz, H-2), 5.08—5.36 (m, H-3 and H-4), 4.01 (dd, $J_{4,5a}$=5.2 Hz, $J_{5a,5b}$=10.6 Hz, H-5a), 3.66 (dd, $J_{4,5b}$=9.3 Hz, H-5b), 3.04 (s, Ms), 3.47 (s, OMe), and 7.26—7.63 and 8.00—8.16 (m, Ph).

Found: C, 45.33; H, 4.51; N, 11.16; S, 8.85%. Calcd for $C_{14}H_{17}N_3O_7S$: C, 45.28; H, 4.61; N, 11.32; S, 8.63%.

Methyl 2-Amino-3-azido-4-*O*-benzoyl-2,3-dideoxy-α-D-xylopyranoside (19). To a solution of **16** (0.2 mmol) in methanol (10 ml) was added platinum oxide (11 mg) and then introduced hydrogen until compound **16** disappeared

on TLC. The catalyst was filtered off and the filtrate was evaporated to give **17** quantitatively. To a solution of **17** in *N,N*-dimethylformamide–water (5 : 1, 2ml) was added sodium acetate trihydrate (122 mg). The solution was heated at 80 °C for 3 h, and evaporated to give a residue. Acetone was added to the residue and undissolved materials were filtered off. The filtrate was evaporated to give a syrup, which was purified on PTLC to give **18** in 73% yield; ^{1}H NMR δ=4.82 (d, $J_{1,2}$=3.4 Hz, H-1), 2.63 (dd, $J_{2,3}$=5.9 Hz, H-2), 2.79 (dd, $J_{3,4}$=3.9 Hz, H-3), 5.26 (ddd, $J_{4,5a}$=5.5 Hz, $J_{4,5b}$=7.3 Hz, H-4), 3.58 (dd, $J_{5a,5b}$=11.7 Hz, H-5a), 3.80 (dd, H-5b), 1.94 (NH), 3.45 (s, OMe), 7.20—7.60 and 7.95—8.10 (m, Ph).

To a solution of the epimino sugar **18** (0.5 mmol) in 2-methoxyethanol–water (14 : 1, 5 ml) was added sodium azide (2.5 mmol) and ammonium chloride (2.5 mmol). The mixture was heated at 95 °C for 18 h, and evaporated to give a residue. Acetone was added to the residue and undissolved materials were filtered off. The filtrate was evaporated to give a syrup, which was purified on PTLC to give **19** in 85% yield. This compound was characterized only by the following ^{1}H NMR data: δ=4.67 (d, $J_{1,2}$=3.3 Hz, H-1), 2.74 (dd, $J_{2,3}$=10.2 Hz, H-2), 3.59 (t, $J_{3,4}$=10.4 Hz, H-3), 5.00 (dt, $J_{4,5a}$=10.4 Hz, $J_{4,5b}$=5.4 Hz, H-4), 3.66 (t, $J_{5a,5b}$=10.4 Hz, H-5a), 3.94 (dd, H-5b), 2.02 (NH), 3.42 (s, OMe), 7.30—7.65 and 7.95—8.12 (m, Ph).

Methyl 2-Azido-4-*O*-(2-azido-2-deoxy-β-D-xylopyranosyl)-3-*O*-benzyl-2-deoxy-α-D-xylopyranoside (20). Deacetylation of **14** with sodium methoxide in methanol in a usual manner gave **20** quantitatively, $[\alpha]_D$ +41.3° (*c* 1.0, $CHCl_3$); ^{1}H NMR δ=4.76 (d, $J_{1,2}$=3.3 Hz, H-1), 4.36 (d, $J_{1',2'}$=7.5 Hz, H-1'), 3.1—4.1 (m, other ring protons) 3.48 (s, OMe), 4.80 and 5.03 (ABq, J=10.2 Hz, CH_2 in Bn), and 7.35—7.60 (m, Ph).

Found: C, 49.54; H, 5.56; N, 19.24%. Calcd for $C_{18}H_{24}N_6O_7$: C, 49.53; H, 5.54; N, 19.26%.

Partial Benzoylation of 20. To a solution of **20** (860 mg, 2.00 mmol) in acetone (8 ml) was added at 0 °C triethylamine (0.8 ml, 5.8 mmol) and benzoyl chloride (0.46 ml, 3.5 mmol), and the mixture was kept at room temperature for 18 h. After addition of water (2 ml) the mixture was stirred for 2 h, diluted with chloroform (30 ml), washed with water, dried and evaporated to give a mixture of three components, which was fractionated on a silica-gel column with benzene–acetone (30 : 1) to give **21**, **22**, and **23** in 61, 5, and 32% yields, respectively.

21: MP 118—122 °C, $[\alpha]_D$ −80° (*c* 1.0, $CHCl_3$); ^{1}H NMR δ=4.68 (d, $J_{1,2}$=3.6 Hz, H-1), 4.36 (d, $J_{1',2'}$=7.4 Hz, H-1'), 5.05 (dt, $J_{3',4'}$=$J_{4',5'a}$=9.0 Hz, $J_{4',5'b}$=5.5 Hz, H-4'), 4.14 (dd, $J_{5'a,5'b}$=11.6 Hz, H-5'b), 3.18—4.00 (m, other ring protons), 3.43 (s, OMe), 4.76 and 4.96 (ABq, J=10.2 Hz, CH_2 in Bn), 7.35 (s, Ph in Bn), and 7.24—7.66 and 7.93—8.08 (m, Ph in Bz).

Found: C, 56.01; H, 5.31; N, 15.79%. Calcd for $C_{25}H_{28}N_6O_8$: C, 55.55; H, 5.22; N, 15.55%.

22: Syrup, $[\alpha]_D$ +19.7° (*c* 1.0, $CHCl_3$); ^{1}H NMR δ=4.69 (d, $J_{1,2}$=3.2 Hz, H-1), 4.43 (d, $J_{1',2'}$=7.5 Hz, H-1'), 4.87 (dd, H-3'), 3.2—4.1 (m, other ring protons), 3.43 (s, OMe), 4.75 and 4.98 (ABq, J=11.7 Hz, CH_2 in Bn), 7.25—7.45 and 8.00—8.10 (m, Ph).

Found: C, 55.61; H, 5.29; N, 15.73%. Calcd for $C_{25}H_{28}N_6O_8$: C, 55.55; H, 5.22; N, 15.55%.

23: Syrup, $[\alpha]_D$ −61.2° (*c* 1.0, $CHCl_3$); ^{1}H NMR δ=4.72 (s, $J_{1,2}$=4.5 Hz, H-1), 4.59 (d, $J_{1',2'}$=7.5 Hz, H-1'), 5.49 (t, $J_{2',3'}$=$J_{3',4'}$=8.4 Hz, H-3'), 5.14 (dt, $J_{4',5'a}$=8.4 Hz, $J_{4',5'b}$=5.4 Hz, H-4'), 4.28 (dd, $J_{5'a,5'b}$=11.4 Hz, H-5'b), 3.18—4.04 (m, other ring protons), 3.47 (s, OMe), 4.80 and 5.02 (ABq, J=9.6 Hz, CH_2 in Bn), and 7.24—7.60 and 7.94—8.06 (m, Ph).

Found: C, 59.14; H, 5.00; N, 13.28%. Calcd for $C_{32}H_{32}N_6O_9$: C, 59.62; H, 5.00; N, 13.04%.

Methyl 2-Azido-4-*O*-(2-azido-4-*O*-benzoyl-2-deoxy-3-*O*-methylsulfonyl-β-D-xylopyranosyl)-3-*O*-benzoyl-2-deoxy-α-D-xylopyranoside (24). Treatment of **21** with methanesulfonyl chloride in pyridine in a usual manner gave **24** in 97% yield, mp 128—130 °C, $[\alpha]_D$ −32.3° (*c* 1.0, $CHCl_3$); ^{1}H NMR δ=4.53 (d, $J_{1,2}$=1.5 Hz, H-1), 4.45 (d, $J_{1',2'}$=7.7 Hz, H-1'), 4.53 (dd, $J_{2',3'}$=9.8 Hz, $J_{3',4'}$=9.0 Hz, H-3'), 5.10 (dt, $J_{4',5'a}$=9.0 Hz, $J_{4',5'b}$=5.1 Hz, H-4'), 4.26 (dd, $J_{5'a,5'b}$=12.0 Hz, H-5'b), 3.16—4.02 (m, other ring protons), 3.08 (s, Ms), 4.80 and 4.95 (ABq, J=10.2 Hz, CH_2 in Bn), and 7.28—7.64 and 7.98—8.16 (m, Ph).

Found: C, 50.42; H, 4.81; N, 13.55; S, 5.21%. Calcd for $C_{26}H_{30}N_6O_{10}S$: C, 50.48; H, 4.89; N, 13.59; S, 5.18%.

Methyl 2-Amino-4-*O*-(2-amino-3-azido-4-*O*-benzoyl-2,3-dideoxy-β-D-xylopyranosyl)-3-*O*-benzyl-2-deoxy-α-D-xylopyranoside (26). Azidolysis of **27** was carried out in the same manner as described for **19** to give **26** as a syrup in 63% yield, $[\alpha]_D$ −7.7° (*c* 1.0, $CHCl_3$); IR (NaCl) 3370 and 3300 (NH_2), 2100 (azido), and 1725 (ester) cm^{-1}; ^{1}H NMR δ=4.65 (d, $J_{1,2}$=1.5 Hz, H-1), 4.31 (d, $J_{1',2'}$=7.5 Hz, H-1'), 2.75 (dd, $J_{2',3'}$=10.2 Hz, H-2'), 5.10 (m, H-4'), 3.39 (s, OMe), and 7.28—8.16 (m, Ph).

Found: C, 57.93; H, 6.09; N, 13.29%. Calcd for $C_{25}H_{31}N_5O_7$: C, 58.47; H, 6.08; N, 13.64%.

Methyl 2-Amino-4-*O*-(4-*O*-benzoyl-2,3-dideoxy-2,3-epimino-β-D-ribopyranosyl)-3-*O*-benzyl-α-D-xylopyranoside (27). Hydrogenolysis of **24** in dichloromethane in the presence of platinum oxide in the same manner as described for **19** gave **25** quantitatively; ^{1}H NMR δ=4.66 (d, $J_{1,2}$=3.2 Hz, H-1), 2.80 (dd, $J_{2,3}$=9.2 Hz, H-2), 4.34 (d, $J_{1',2'}$=7.5 Hz, H-1'), 3.01 (dd, $J_{2',3'}$=9.3 Hz, H-2'), 3.80 (t, $J_{3',4'}$=9.3 Hz, H-3'), 5.22 (dt, $J_{4',5'a}$=9.3 Hz, $J_{4',5'b}$=6.0 Hz, H-4'), 4.27 (dd, $J_{5'a,5'b}$=12.0 Hz, H-5'b), 3.11—3.96 (m, other ring protons), 2.10 (NH), 3.01 (s, Ms), 3.40 (s, OMe), 4.62 and 5.00 (ABq, J=11.3 Hz, CH_2 in Bn), and 7.28—7.64 and 8.00—8.16 (m, Ph).

Treatment of **25** with sodium acetate in the same manner as described for **19** gave **27** as a syrup in 90% yield, $[\alpha]_D$ +47.9° (*c* 1.0, $CHCl_3$); IR (NaCl) 3360 and 3275 (OH and NH_2), and 1708 (ester) cm^{-1}; ^{1}H NMR (after D_2O exchange) δ=4.66 (d, $J_{1,2}$=3.0 Hz, H-1), 5.07 (s, H-1'), 2.30 (d, $J_{2',3'}$=5.0 Hz, H-2'), 2.8 (m, H-2 and H-3'), 4.96—5.14 (m, H-4'), 3.44—4.20 (m, other ring protons), 3.43 (s, OMe), 4.72 and 4.89 (ABq, J=11.4 Hz, CH_2 in Bn), 7.34 (s, Ph in Bn), and 7.26—7.62 and 7.96—8.14 (m, Bz).

Found: C, 63.53; H, 6.51; N, 5.66%. Calcd for $C_{25}H_{30}N_2O_7$: C, 63.82; H, 6.43; N, 5.95%.

1,3,4,5-Tetra-*O*-acetyl-2-azido-2-deoxy-D-xylose Methyl Hemiacetal (28). To a solution of **3**[5] (167 mg, 0.61 mmol) in acetic anhydride (1 ml) was added acetic anhydride (2 ml) containing one drop of 60% perchloric acid.

The mixture was kept at room temperature for 1 h, poured into saturated aqueous sodium hydrogencarbonate, and extracted with chloroform. The extract was washed with water, dried and evaporated to give **28** as a syrup quantitatively, $[\alpha]_D$ +21.2° (*c* 1.0, $CHCl_3$); ^{1}H NMR δ=5.74 (d, $J_{1,2}$=5.9 Hz, H-1), 3.67 (dd, $J_{2,3}$=3.0 Hz, H-2), 5.12—5.48 (m, H-3 and H-4), 3.98—4.44 (m, H-5a and H-5b), 3.51 (s, OMe) and 2.12 and 2.14 (Ac).

Found: C, 44.73; H, 5.57; N, 11.00%. Calcd for $C_{14}H_{21}N_3O_9$: C, 44.80; H, 5.64; N, 11.20%.

1,4,5-Tri-*O*-acetyl-2-azido-3-*O*-benzyl-2-deoxy-D-xylose Benzyl Hemiacetal (29). To a chilled solution of **10**[5] (58 mg, 0.16 mmol) in acetic anhydride (6 ml) was added trifluoroacetic acid (0.3 ml). The solution was kept at room temperature for 73 h and poured into saturated aqueous sodium hydrogencarbonate. Chloroform extract was washed with water, dried and evaporated to give a syrupy residue, which was purified on a silica-gel column with hexane-ethyl acetate (4:1) to give **29** in 81% yield. In its ^{1}H NMR spectrum signals due to two epimers were observed with a ratio of 3:2. ^{1}H NMR (400 MHz) major component δ=6.13 (d, $J_{1,2}$=6.8 Hz, H-1), 3.53 (dd, $J_{2,3}$=3.2 Hz, H-2), 3.98 (dd, $J_{3,4}$=6.2 Hz, H-3), 5.37 (dq, $J_{4,5a}$=7.0 Hz, $J_{4,5b}$=3.2 Hz, H-4), 4.20 (t, $J_{5a,5b}$=8.0 Hz, H-5a), 4.39 (dd, H-5b); Minor component δ=6.07 (d, $J_{1,2}$=5.4 Hz, H-1), 3.79 (t, $J_{2,3}$=4.2 Hz, H-2), 3.86 (t, $J_{3,4}$=4.4 Hz, H-3), 5.28 (dq, $J_{4,5a}$=7.0 Hz, $J_{4,5b}$=5.0 Hz, H-4), 4.17 (t, $J_{5a,5b}$=7.6 Hz, H-5a), 4.36 (dd, H-5b); 1.90—2.07 (m, Ac), 4.36—4.79 (m, CH_2 in Bn), and 7.20—7.40 (m, Ph).

Found: C, 59.79; H, 5.80; N, 8.19%. Calcd for $C_{25}H_{29}N_3O_8$: C, 60.11; H, 5.85; N, 8.41%.

1,2,4-Tri-*O*-acetyl-3-*O*-benzoyl-α-D-xylopyranose (31). To a mixture of acetic acid (2.5 ml) and acetic anhydride (0.2 ml) was added one drop of concd sulfuric acid, chromium trioxide (276 mg, 2.8 mmol) and **30**[10] (186 mg, 0.51 mmol). The mixture was kept at room temperature for 1 h, diluted with chloroform, and washed successively with water, aqueous sodium hydrogencarbonate, and water. The solution was dried and evaporated to give a syrup residue, which was purified on PTLC with hexane-ethyl acetate (7:3) to give **31** in 90% yield, $[\alpha]_D$ +48.8° (*c* 1.0, $CHCl_3$); ^{1}H NMR δ=6.29 (d, $J_{1,2}$=3.3 Hz, H-1),5.21 (dd, $J_{2,3}$= 9.8 Hz, H-2), 5.74 (t, $J_{3,4}$=9.8 Hz, H-3), 5.2 (m, H-4), 3.79 (t, $J_{4,5a}$=$J_{5a,5b}$=10.8 Hz, H-5a), 4.00 (dd, $J_{4,5b}$=6.0 Hz, H-5b), 1.93, 1.97 and 2.21 (each s, Ac), and 7.32—7.66 and 7.92—8.06 (m, Ph).

Found: C, 56.23; H, 5.08%. Calcd for $C_{18}H_{20}O_9$: C, 56.84; H, 5.30%.

Benzyl 2-Azido-4-*O*-(2-azido-2-deoxy-α-D-xylopyranosyl)-3-*O*-benzyl-2-deoxy-α-D-xylopyranoside (33) and Its β-Linked Isomer (35). Compounds **1** (1.51 g, 5.44 mmol) and **10** (3.80 g, 10.4 mmol) were coupled in the same manner as described for the preparation of **12** and **14** (Method A) to give a mixture of **32** and **34**, which was separated, after deacetylation with sodium methoxide in methanol, on a silica-gel column with benzene-acetone (6:1) to give **33** and **35** in 29 and 46% yields, respectively.

33: Syrup, $[\alpha]_D$ +88.2° (*c* 1.0, $CHCl_3$); ^{1}H NMR δ=4.92 (d, $J_{1,2}$=3.6 Hz, H-1), 3.36 (dd, $J_{2,3}$=9.8 Hz, H-2), 5.18 (d, $J_{1',2'}$=4.0 Hz, H-1'), 3.25 (dd, $J_{2',3'}$=10.2 Hz, H-2'), 3.48—4.10 (m, other ring protons), 4.32 (s, OH×2), 4.60 and 4.82 (ABq, J=11.7 Hz, CH_2 in Bn), 4.88 and 5.10 (ABq, J=9.9 Hz, CH_2 in Bn), and 7.48 (broad s, Ph).

Found: C, 56.43; H, 5.59; N, 16.27%. Calcd for $C_{24}H_{28}N_6O_7$: C, 56.24; H, 5.51; N, 16.40%.

^{1}H NMR data of 3',4'-diacetate (**32**): δ=4.93 (d, $J_{1,2}$=2.5 Hz, H-1), 4.38 (d, $J_{1',2'}$=8.0 Hz, H-1'), 4.53 and 4.75 (ABq, J=12.5 Hz, CH_2 in Bn), 4.85 and 4.97 (ABq, J=10.0 Hz, CH_2 in Bn), 2.03 and 2.11 (each s, Ac), and 7.35 (s, Ph).

35: Syrup, $[\alpha]_D$ +68.9° (*c* 1.0, $CHCl_3$); ^{1}H NMR δ=4.94 (d, $J_{1,2}$=3.6 Hz, H-1), 3.17 (dd, $J_{2,3}$=10.5 Hz, H-2), 4.34 (d, H-1').

Found: C, 55.88; H, 5.59; N, 15.99%. Calcd for $C_{24}H_{28}N_6O_7$: C, 56.24; H, 5.51; N, 16.40%.

^{1}H NMR data of 3',4'-diacetate (**34**): δ=4.90 (d, $J_{1,2}$=4.0 Hz, H-1), 3.35 (dd, $J_{2,3}$=10.5 Hz, H-2), 5.18 (d, $J_{1',2'}$=3.5 Hz, H-1'), 3.27 (dd, $J_{2',3'}$=10.0 Hz, H-2'), 5.46 (t, $J_{3',4'}$=8.5 Hz, H-3'), 4.51 and 4.77 (ABq, J=12.5 Hz, CH_2 in Bn), 4.87 and 5.03 (ABq, J=10.0 Hz, CH_2 in Bn), 2.00 and 2.07 (each s, Ac), and 7.38 (s, Ph).

Partial Benzoylation of 35. Treatment of **35** (1.80 g, 3.5 mmol) with benzoyl chloride (0.69 ml, 6.0 mmol) and triethylamine (1.4 ml, 10 mmol) in acetone (20 ml) in the same manner as described in the partial benzoylation of **21** gave, by separation on a silica-gel column with benzene-acetone (40:1), 4'-benzoate (**36**), 3'-benzoate (**37**), and 3'4'-dibenzoate (**38**) in 67, 13, and 17% yields, respectively.

36: Syrup, $[\alpha]_D$ +8.8° (*c* 1.0, $CHCl_3$); ^{1}H NMR δ=4.96 (d, $J_{1,2}$=3.3 Hz, H-1), 4.45 (d, $J_{1',2'}$=7.6 Hz, H-1'), 5.15 (dt, $J_{3',4'}$=$J_{4',5a'}$=9.8 Hz, $J_{4',5b'}$=5.3 Hz, H-4'), 4.22 (dd, $J_{5a,5b}$= 12.0 Hz, H-5'b), 3.24—4.10 (m, other ring protons), 4.61 and 4.83 (ABq, J=12.3 Hz, CH_2 in Bn), 4.85 and 5.06 (ABq, J=10.5 Hz, CH_2 in Bn), 7.46 (s, Ph in Bn), and 7.34—7.74 and 8.04—8.20 (m, Bz).

Found: C, 60.56; H, 5.16; N, 13.41%. Calcd for $C_{31}H_{32}N_6O_8$: C, 60.38; H, 5.23; N, 13.63%.

37: Syrup, $[\alpha]_D$ +30.1° (*c* 1.0, $CHCl_3$); ^{1}H NMR δ=4.95 (d, $J_{1,2}$=3.4 Hz, H-1), 4.50 (d, $J_{1',2'}$=8.1 Hz, H-1'), 3.56 (dd, $J_{2',3'}$=9.9 Hz, H-2'), 5.03 (t, H-3'), 3.17—3.45 (m, H-2 and H-4'), 3.75—4.20 (m, other ring protons), 4.60 and 4.82 (ABq, J=12.0 Hz, CH_2 in Bn), 4.86 and 5.08 (ABq, J=10.5 Hz, CH_2 in Bn), 7.45 (s, Ph in Bn), and 7.35—7.80 and 8.13—8.27 (m, Bz).

Found: C, 60.07; H, 5.35; N, 13.41%. Calcd for $C_{31}H_{32}N_6O_8$: C, 60.38; H, 5.23; N, 13.63%.

38: Syrup, $[\alpha]_D$ −28.1° (*c* 1.0, $CHCl_3$); ^{1}H NMR δ=4.97 (d, $J_{1,2}$=3.8Hz, H-1), 4.60(d, $J_{1',2'}$=7.7 Hz, H-1'), 5.55 (t, $J_{2',3'}$=$J_{3',4'}$=9.0 Hz, H-3'), 5.36 (dt, $J_{4',5'a}$=9.0 Hz, $J_{4',5'b}$=5.7 Hz, H-4'), 4.35 (dd, $J_{5'a,5'b}$=12.0 Hz, H-5'b), 3.32—4.16 (m, other ring protons), 4.62 and 4.82 (ABq, J=13.0 Hz, CH_2 in Bn), 4.86 and 5.09 (ABq, J=10.5 Hz, CH_2 in Bn), 7.45 (s, Ph in Bn), 7.35—7.70 and 7.96—8.20 (m, Bz).

Found: C, 63.21; H, 5.01; N, 11.93%. Calcd for $C_{38}H_{36}N_6O_9$: C, 63.33; H, 5.04; N, 11.66%.

Benzyl 2-Azido-4-*O*-(2-azido-4-*O*-benzyl-2-deoxy-3-*O*-methylsulfonyl-β-D-xylopyranosyl)-3-*O*-benzyl-2-deoxy-α-D-xylopyranoside (39). Methylsulfonylation of **36** in a usual manner gave **39** as a syrup quantitatively, $[\alpha]_D$ −10.3° (*c* 1.0, $CHCl_3$); ^{1}H NMR δ=4.96 (d, $J_{1,2}$=3.3 Hz, H-1), 3.25 (H-2), 4.50 (d, $J_{1',2'}$=8.3 Hz, H-1'), 3.56 (dd, $J_{2',3'}$=10.2 Hz, H-2'), 4.78 (t, $J_{3',4'}$=9.8 Hz, H-3'), 5.25 (dt, $J_{4',5'a}$=9.8 Hz, $J_{4,5'b}$=5.7 Hz, H-4'), 3.29 (dd, $J_{5'a,5'b}$=12.0 Hz, H-5'a), 4.29 (dd, H-5'b), 3.7—4.1 (m, other ring protons), 3.03 (s, Ms), 4.62 and 4.82 (ABq, J=12.0 Hz, CH_2 in Bn), 4.84 and 5.01 (ABq, J=10.8 Hz, CH_2 in Bn), 7.43 (s, Ph in Bn), and 7.32—7.66 and 8.0—8.22 (m, Bz).

Found: C, 55.27; H, 4.90; N, 11.81; S, 4.63%. Calcd for $C_{32}H_{34}N_6O_{10}S$: C, 55.32; H, 4.93; N, 12.10; S, 4.63%.

2-Azido-4-*O*-(2-azido-4-*O*-benzyl-2-deoxy-3-*O*-methylsulfonyl-β-D-xylopyranosyl)-1,3-di-*O*-benzoyl-2-deoxy-α-D-xylopyranose (40). Compound **39** was oxidized in the same manner as described for **32** to give **40** in 50% yield, $[\alpha]_D$ +24.3° (*c* 1.0, $CHCl_3$); ^{1}H NMR δ=6.57 (d, $J_{1,2}$=3.6 Hz, H-1), 3.81 (dd, $J_{2,3}$=10.5 Hz, H-2), 5.94 (dd, $J_{3,4}$=8.3 Hz, H-3), 4.49 (d, $J_{1',2'}$=7.5 Hz, H-1'), 3.56 (dd, $J_{2',3'}$=10.2 Hz, H-2'), 4.69 (dd,

$J_{3',4'}$=9.8 Hz, H-3'), 5.04 (dt, $J_{4',5'a}$=9.8 Hz, $J_{4',5'b}$=5.3 Hz, H-4'), 3.5—4.3 (m, other ring protons), 3.05 (s, Ms), and 7.37—7.80 and 8.04—8.32 (m, Bz).

Found: C, 53.30; H, 4.30; N, 11.43; S, 4.71%. Calcd for $C_{32}H_{30}N_6O_{12}S$: C, 53.18; H, 4.18; N, 11.63; S, 4.44%.

A partially oxidized product **41** was also obtained in 7% yield, mp 172—8 °C (decomp), $[\alpha]_D$ +11.3° (*c* 1.0 $CHCl_3$); ^1H NMR δ=5.10 (d, $J_{1,2}$=3.6 Hz, H-1), 3.32 (dd, $J_{2,3}$=10.5 Hz, H-2), 5.84 (dd, $J_{3,4}$=8.5 Hz, H-3), 4.45 (d, $J_{1',2'}$=7.5 Hz, H-1'), 3.53 (dd, $J_{2',3'}$=9.9 Hz, H-2'), 4.67 (t, $J_{3',4'}$=9.9 Hz, H-3'), 4.98 (m, H-4'), 3.63—4.20 (m, other ring protons), 3.05 (s, Ms), 4.69 and 4.89 (ABq, J=12.3 Hz, CH_2 in Bn), 7.48 (broad s, Ph in Bn), and 7.36—7.70 and 8.04—8.26 (m, Bz).

Found: C, 54.63; H, 4.60; N, 11.76; S, 4.48%. Calcd for $C_{32}H_{32}N_6O_{11}S$: C, 54.23; H, 4.55; N, 11.86; S, 4.52%.

1,3-Di-*O*-acetyl-4-*O*-(3,4-di-*O*-acetyl-2-azido-2-deoxy-β-D-xylopyranosyl)-2-azido-2-deoxy-D-xylopyranose (42). To a solution of **34** (50 mg, 0.084 mmol) in carbon tetrachloride (4.2 ml) was added with stirring *N*-bromosuccinimide (33 mg, 0.19 mmol) and a catalytic amount of bromine, and the mixture was kept at room temperature for 24 h. After a developed red color faded, undissolved materials were filtered off and washed with chloroform (5 ml). The filtrate was mixed with a solution of sodium hydrogencarbonate (0.05 g) in water (1 ml), stirred at room temperature for 2 h, and evaporated. The residue was acetylated in a conventional manner and fractionated on a silica-gel column with hexane–ethyl acetate (7 : 3) to give **42** (23 mg, 56%) as an anomeric mixture (α : β=2 : 3); ^1H NMR δ=6.15 (d, $J_{1,2}$=3.5 Hz, H-1α), 5.46 (d, $J_{1,2}$=8.0 Hz, H-1β), 4.30 (d, $J_{1',2'}$=7.5 Hz, H-1'), and 2.02—2.18 (many s, 12 H, Ac).

Found: C, 43.55; H, 4.93; N, 16.55%. Calcd for $C_{18}H_{24}N_6O_{11}$: C, 43.20; H, 4.83; N, 16.80%.

References

1) Part I: K. Araki, H. Hashimoto, and J. Yoshimura, *Carbohydr. Res.*, **109**, 143 (1982).

2) G. A. Ellestad, D. B. Cosulich, R. W. Broschard, J. H. Martin, M. P. Kunstman, G. O. Morton, J. E. Lancaster, W. Fulmor, and R. M. Lovell, *J. Am. Chem. Soc.*, **100**, 2515 (1978).

3) K. Araki, K. Miyazawa, H. Hashimoto, and J. Yoshimura, *Tetrahedron Lett.*, **23**, 1705 (1982).

4) K. Dobashi, K. Nagaoka, Y. Watanabe, M. Nishida, M. Hamada, H. Naganawa, T. Takita, T. Takeuchi, and H. Umezawa, *J. Antibiot.*, **38**, 1166 (1985).

5) H. Hashimoto, K. Araki, Y. Saito, M. Kawa, and J. Yoshimura, *Bull. Chem. Soc. Jpn.*, **59**, 3131 (1986).

6) K. Igarashi, *Adv. Carbohydr. Chem. Biochem.*, **34**, 243 (1977).

7) A. F. Bochkov and G. E. Zaikov, "Chemistry of the *O*-Glycosidic Bond," Pergamon Press, Oxford (1979), p. 16.

8) T. Ogawa, K. Beppu, and S. Nakabayashi, *Carbohydr. Res.*, **93**, C6 (1981).

9) K. Igarashi, J. Irisawa, and T. Honma, *Carbohydr. Res.*, **39**, 213 (1975).

10) S. J. Angyal and K. James, *J. Chem. Soc., Chem. Commun.*, **1969**, 617.

11) P. Kovać and J. Alfoldi, *Chem. Zvesti*, **33**, 785 (1979).

12) H. Hashimoto, M. Kawa, Y. Saito, T. Date, S. Horito, and J. Yoshimura, (submitted to *Tetrahedron Lett.*)

 © 1986 The Chemical Society of Japan Bull. Chem. Soc. Jpn., 59, 3145—3151 (1986)

Fusogenic Behavior of Single-Walled Vesicles Composed of Synthetic Peptide Lipids†

Yukito MURAKAMI,* Jun-ichi KIKUCHI, and Toshihiko TAKAKI
Department of Organic Synthesis, Faculty of Engineering, Kyushu University, Hakozaki, Higashi-ku, Fukuoka 812
(Received April 9, 1986)

Fusogenic behavior of the single-walled vesicles formed with mixed or individual synthetic peptide lipids, $N^+C_5Ala2C_n$ and $(SO_3^-)C_5Ala2C_n$ (n=14, 16), was investigated in the presence of various water-soluble polymers or a nonbilayer-forming lipid by means of electron microscopy, differential scanning calorimetry, and turbidity measurements. The following ionic polymers having opposite charges to the net surface charges of the vesicles immediately induced fusion via vesicle aggregation; heparin, chondroitin sulfate C, chondroitin, and potassium salt of poly(vinyl sulfate) for the cationic vesicles, and polybrene for the anionic ones. On the other hand, ionic polymers having electrostatic charges identical with the vesicular surface charges and nonionic ones, such as amylose, poly(vinyl alcohol), polyethylene glycol 20000, and polyethylene glycol 6000, induced neither fusion nor aggregation. A nonbilayer-forming lipid, QC_5Ala2C_{14}, incorporated into the $N^+C_5Ala2C_n$ vesicles induced fusion at kinetic rates much slower than those triggered by the ionic polymers. The observations were discussed with attention to the dehydration effect and the participation of nonbilayer structures in the fusion process.

In the field of membrane mimetic chemistry,[1] synthetic lipid membranes have been widely used in place of liposomes formed with natural phospholipids, because the former aggregates attain greater morphological stability relative to the latter and provide specified functions through chemical modifications. In the light of the Brockerhoff's concept[2] which claims that the intramembrane hydrogen-belt domain is much important for morphological stabilization of biomembranes, we have prepared various peptide lipids; each composed of a polar head moiety, a hydrophobic double-chain segment, and an amino acid residue interposed between them as a hydrogen-bonding component.[3-5] We have previously clarified the characteristic morphological features of aggregates composed of the peptide lipids. In general, ionic peptide lipids form multiwalled bilayer membranes in the aqueous dispersion state and the corresponding single-walled vesicles are formed upon sonication of the aqueous dispersions,[3-5] in analogy with morphological behavior observed for liposomal membranes. Physicochemical stability of the single-walled vesicles formed with the cationic lipids, $N^+C_5Ala2C_n$, is much larger than that of the liposomal membrane formed with dimyristoylphosphatidylcholine under comparable conditions.[5] Meanwhile, nonbilayer structures such as inverted hexagonal (H_{II}) and inverted cubic (C_{II}) phases can be created with the peptide lipids by controlling intramembrane interaction among polar head moieties of the lipids.[6-10] Such nonbilayer structures have been often observed in biological systems and claimed to play crucial roles in the membrane fusion process as key intermediates.[11] Thus, the peptide lipid system can be utilized as a suitable model for investigation of the plausible mechanism of nonbilayer-mediated fusion. In the present work, we studied on morphological changes of the single-walled vesicles as induced by fusogens such as water-soluble polymers and nonbilayer-forming lipids.

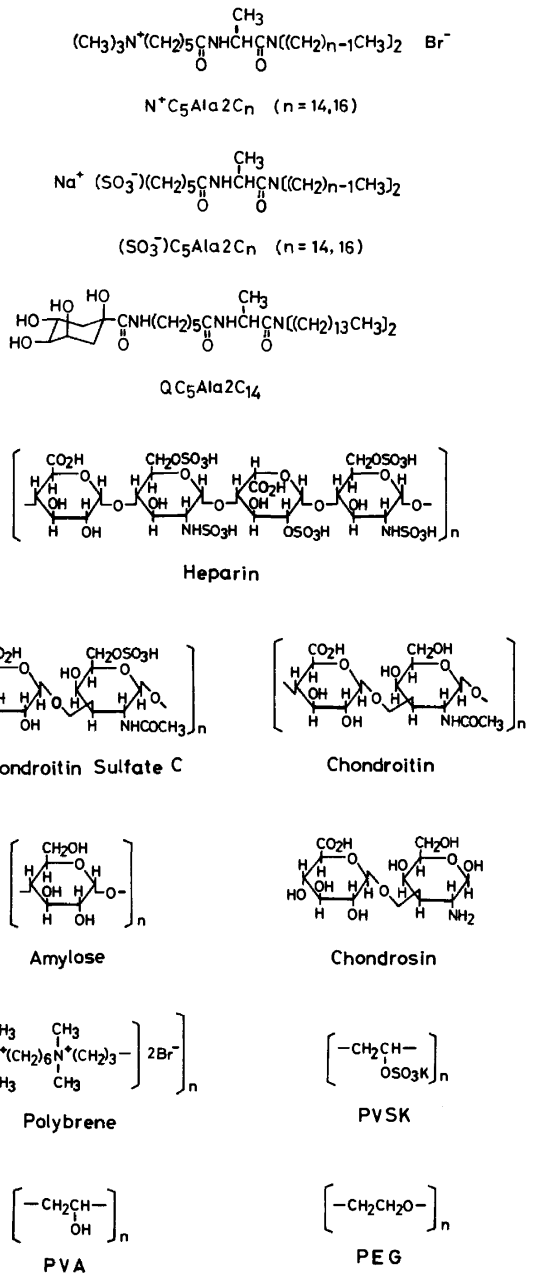

†Contribution No. 831 from this Department.

Experimental

Materials. The following compounds were obtained from commercial sources as the purest grade available and used without further purification: heparin, chondroitin 6-(sodium sulfate) (chondroitin sulfate C), amylose (molecular weight, ca. 2900), potassium salt of poly(vinyl sulfate) (PVSK: degree of polymerization (DP), 162.2; degree of esterification, 94.5%) (all four species from Nakarai Chemicals, Kyoto); 2,6-pyridinedicarboxylic acid, poly(vinyl alcohol) (PVA; DP, 1500—1800), polyethylene glycol 6000 (PEG 6000; DP, ca. 7500), polyethylene glycol 20000 (PEG 20000; DP, 20000 ±5000) (all four compounds from Wako Pure Chemical Industries, Osaka); chondroitin, 2-amino-2-deoxy-3-*O*-(β-D-glucopyranuronosyl)-α-D-galactopyranose (chondrosin) (both from Seikagaku Kogyo Co., Tokyo); poly[(dimethyliminio)-1,3-propanediyl(dimethyliminio)-1,6-hexanediyl dibromide] (polybrene; from Sigma Chemical Co., Missouri, U.S.A.). Preparation of the following lipids has been reported previously: *N,N*-ditetradecyl-N^{α}-[6-(trimethylammonio)hexanoyl]-L-alaninamide bromide ($N^+C_5Ala2C_{14}$),[5] *N,N*-dihexadecyl-N^{α}-[6-(trimethylammonio)hexanoyl]-L-alaninamide bromide ($N^+C_5Ala2C_{16}$),[5] sodium *N,N*-ditetradecyl-N^{α}-(6-sulfonatohexanoyl)-L-alaninamide [(SO_3^-)-C_5Ala2C_{14}],[7] sodium *N,N*-dihexadecyl-N^{α}-(6-sulfonatohexanoyl)-L-alaninamide [(SO_3^-)C_5Ala2C_{16}],[7] and *N,N*-ditetradecyl-N^{α}-[6-(quinoylamino)hexanoyl]-L-alaninamide (QC_5Ala2C_{14}); quinoyl being the conventional name for 1,3,4,5-tetrahydroxy-[1*R*-(1α,3α,4α,5β)]cyclohexylcarbonyl.[6]

Measurements. Aqueous dispersions of lipids were prepared according to the previous method.[7] Whenever necessary, a dispersion sample was subsequently sonicated with a Heat Systems-Ultrasonics W-220F probe-type sonicator and allowed to stand for 20 min at room temperature. The sonicated solution was adjusted to an appropriate pH with aqueous hydrochloric acid or aqueous potassium hydroxide. A Beckman Φ71 pH meter equipped with a Beckman 39505 combined electrode was used for the pH measurements after calibration with a combination of appropriate standard aqueous buffers. Turbidity measurements were run at 400 nm on a Union Giken SM-401 high sensitivity spectrophotometer equipped with a cell of 10.0- or 1.0-mm path length. A Daini Seikosha SSC-560U calorimeter was used for differential scanning calorimetry (DSC). The phase transition parameters (T_m, temperature at a peak maximum of the DSC thermogram; ΔH, enthalpy change for phase transition) were determined in a manner similar to that reported previously.[7] Electron micrographs were taken on a JEOL JEM-2000FX electron microscope installed at the Research Laboratory for High Voltage Electron Microscopy of Kyushu University. Negatively stained samples for the measurements were prepared in a manner as described previously.[7]

Results

First, we examined aggregation behavior of the single-walled vesicles by means of turbidity measurements as typically shown in Fig. 1. Addition of anionic polymers immediately caused aggregation of the cationic single-walled vesicles composed of $N^+C_5Ala2C_{16}$ with the diameter range 250—800 Å. When heparin or PVSK was added to the vesicular solution,

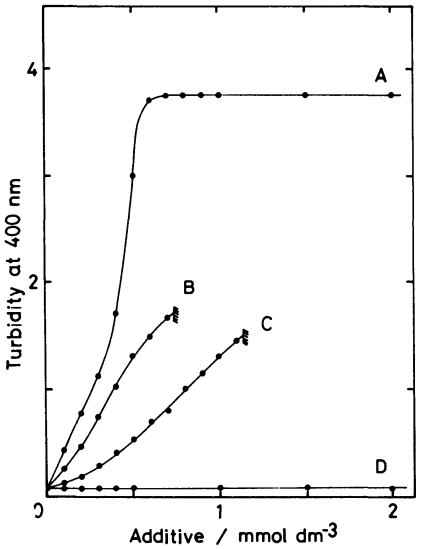

Fig. 1. Effects of additive-concentrations (in monosaccharide or monomer unit) on turbidity of the single-walled vesicles formed with $N^+C_5Ala2C_{16}$ (1.0 mmol dm^{-3}) at pH 7 and 40 °C.
A, heparin; B, chondroitin sulfate C; C, chondroitin; D, polybrene, PVA, PEG 20000, PEG 6000, amylose, or chondrosin.

turbidity increased and reached a maximum level under conditions that the whole cationic charges on the vesicular surfaces were completely neutralized with anionic charges involved in the polymer species at the 1 : 1 ratio of positive to negative charge, and further addition of the polymer gave no additional turbidity change (Fig. 1, line A). Addition of chondroitin sulfate C or chondroitin also resulted in an turbidity increase. However, precipitates were formed before neutralization of the cationic charges of the lipid vesicles with these anionic polymers (Fig. 1, lines B and C). On the other hand, a cationic polymer, polybrene, and nonionic ones, amylose, PVA, PEG 20000, and PEG 6000, did not trigger aggregation of the cationic vesicles (Fig. 1, line D) under the conditions employed here: [$N^+C_5Ala2C_{16}$], 1.0 mmol dm^{-3}; [polymer], 0—5 mmol dm^{-3} in a monosaccharide or a monomer unit. Anionic compounds with low molecular weights, chondrosin (measured at pH 5—11) and 2,6-pyridinedicarboxylic acid (measured at pH 6), also exhibited no capacity to induce aggregation of the $N^+C_5Ala2C_{16}$ vesicle.

The growth of single-walled vesicles to multiwalled lamellae was observed by negative staining electron microscopy (NSEM) for the $N^+C_5Ala2C_{16}$ membrane upon addition of one of the following anionic polymers; heparin (Fig. 2A), chondroitin sulfate C, chondroitin, and PVSK (Fig. 2B). On the other hand, the single-walled $N^+C_5Ala2C_{16}$ vesicle remained morphologically unchanged in the presence of any one of the following additives; polybrene (Fig. 2C), amylose, PVA, PEG 20000 (Fig. 2D), PEG 6000, chondrosin, and 2,6-pyridinedicarboxylic acid.

The vesicle growth observed by NSEM was also

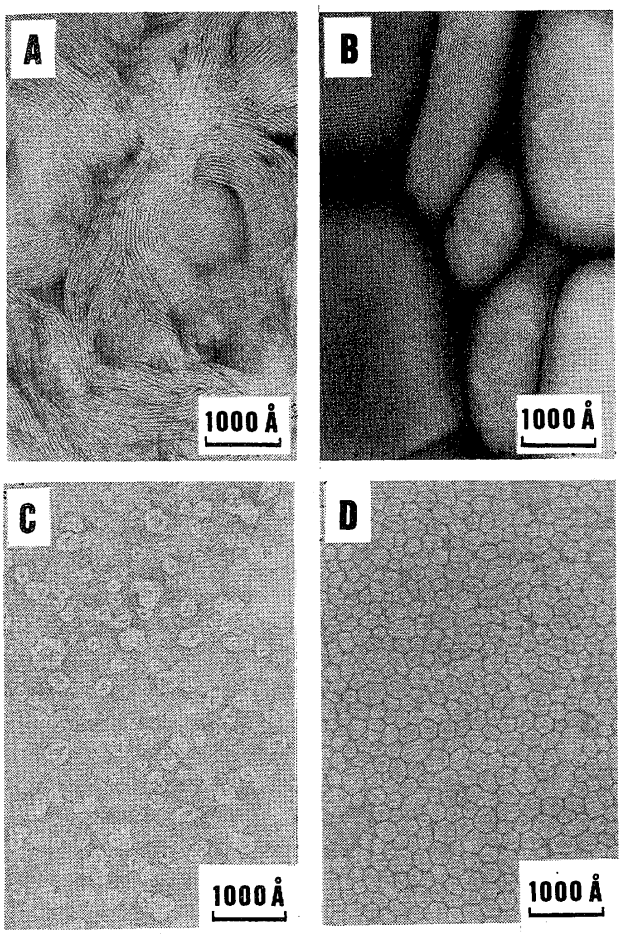

Fig. 2. Electron micrographs negatively stained with uranyl acetate.
Each specimen was prepared immediately after addition of the following additives to the single-walled vesicles formed with $N^+C_5Ala2C_{16}$ at pH 7 and 40 °C: A, heparin (2.5 mmol dm^{-3} in the anion unit); B, PVSK (0.8 mmol dm^{-3} in the monomer unit); C, polybrene (1.0 mmol dm^{-3} in the cation unit); D, PEG 20000 (5.0 mmol dm^{-3} in the monomer unit). Lipid concentrations: 5.0 mmol dm^{-3} for A and D; 1.0 mmol dm^{-3} for B and C.

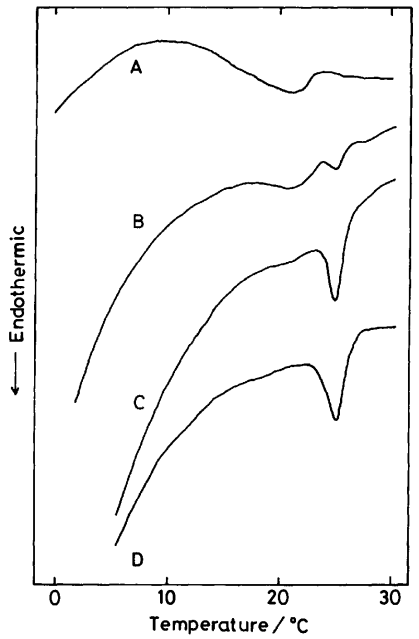

Fig. 3. Effect of added polymer on DSC behavior of the $N^+C_5Ala2C_{16}$ (5.0 mmol dm^{-3}) vesicle at pH 7.
A, aqueous solution sonicated for 3 min at 40 W without additives and incubated for 2 months at 20 °C; immediately after addition of heparin (B, 0.25 mmol dm^{-3}; C, 1.25 mmol dm^{-3}; D, 2.5 mmol dm^{-3}) at 20 °C to the aqueous solution sonicated for 3 min at 40 W. Concentrations of heparin are given in the anion unit.

confirmed by differential scanning calorimetry (DSC). The single-walled $N^+C_5Ala2C_{16}$ vesicle showed a broad phase transition at 20±5 °C (Fig. 3, curve A). The DSC thermogram remained unchanged after incubation without additives for 60 d at 20 °C or with PEG 20000 for 6 d at 20 °C. On the other hand, a phase transition peak, reflecting formation of the multi-walled bilayer membrane,[5] appeared immediately at 25.0 °C upon incubation of the vesicular solution in the presence of heparin. This DSC peak was intensified along with an increase in an amount of heparin added, and the peak originated from the single-walled vesicles nearly disappeared when a half portion of the positive charges of the lipid aggregates was neutralized with the negative ones of heparin (Fig. 3, curves B, C, and D). The results obtained from DSC measurements for the $N^+C_5Ala2C_{16}$ vesicle containing other additives, chondroitin sulfate C, chondroitin, PVSK, amylose, PVA, PEG 6000, chondrosin, and 2,6-pyridinedicarboxylic acid, were consistent with those from NSEM. Similar morphological behavior induced by anionic polymers was observed for the single-walled $N^+C_5Ala2C_{14}$ vesicle.

The aggregation-mediated vesicle growth was observed for the anionic vesicles formed with (SO_3^-)-C_5Ala2C_{16} upon addition of a cationic polymer, polybrene, as confirmed by NSEM and turbidity measurements. On the other hand, addition of heparin to the $(SO_3^-)C_5Ala2C_{16}$ vesicle did not cause any morphological changes.

In the mixed system composed of cationic and anionic peptide lipids, bilayer aggregates are formed under conditions that the total electrostatic charge on the membrane surface is not completely neutralized.[9] Multiwalled bilayers were observed in an aqueous dispersion of $N^+C_5Ala2C_{16}$ and $(SO_3^-)C_5Ala2C_{14}$ mixed at the 3:1 molar ratio (Fig. 4A), showing a relatively sharp phase transition peak (T_m) at 17.8 °C with a transition enthaply change (ΔH) of 24 kJ mol^{-1} (Fig. 5, curve A). Even though these individual lipids show phase transitions at 25.5 and 2.1 °C for $N^+C_5Ala2C_{16}$ and $(SO_3^-)C_5Ala2C_{14}$, respectively, in the aqueous dispersion state,[5,7] any phase separation between the cationic and anionic lipids was not detected by DSC when they were mixed. Upon sonication of the dispersion of the mixed lipid system for 2 min at 40 W, the

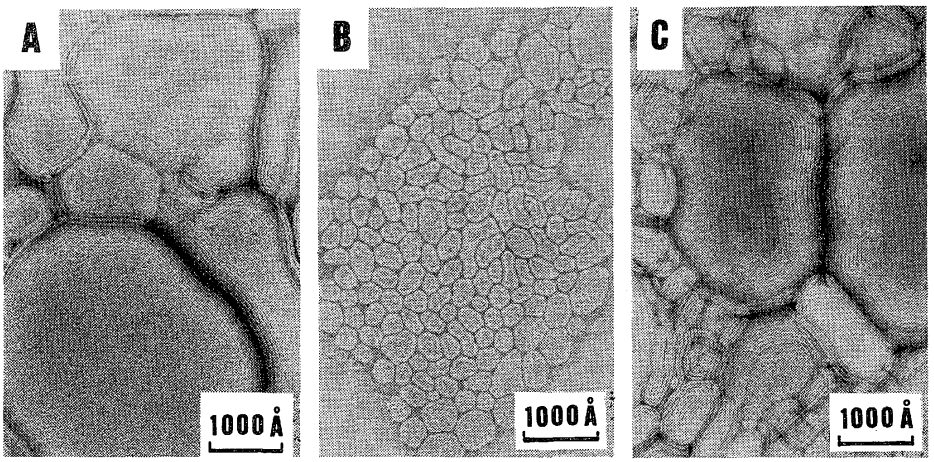

Fig. 4. Electron micrographs for a mixture of $N^+C_5Ala2C_{16}$ (1.88 mmol dm^{-3}) and $(SO_3^-)C_5Ala2C_{14}$ (0.63 mmol dm^{-3}), as negatively stained with uranyl acetate.
A, aqueous dispersion; B, aqueous solution sonicated for 3 min at 40 W; C, immediately after addition of heparin (2.0 mmol dm^{-3} in the anion unit) to B at pH 7 and 20 °C.

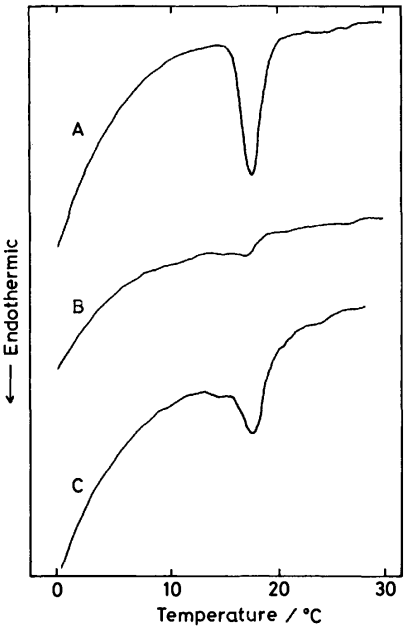

Fig. 5. DSC thermograms for a mixture of $N^+C_5Ala2C_{16}$ (1.88 mmol dm^{-3}) and $(SO_3^-)C_5Ala2C_{14}$ (0.63 mmol dm^{-3}).
Refer to the respective symbols (A, B, and C) in Fig. 4 for preparative conditions of samples.

aggregates were converted into the single-walled vesicles in the diameter range 250—800 Å (Fig. 4B), and a broad phase transition peak was observed at 17±5 °C (Fig. 5, curve B). Addition of heparin to the single-walled vesicles resulted in both aggregation and vesicle growth (Fig. 4C). The DSC thermogram showed a recovery of the sharp phase transition peak at 17.6 °C, without indicating any phase separation after such morphological changes (Fig. 5, curve C).

A mixed lipid system composed of the cationic $N^+C_5Ala2C_n$ and the nonionic QC_5Ala2C_{14} showed a unique vesicle-growing behavior in the absence of additives. The single-walled vesicles with the diameter range 200—500 Å were formed upon sonication of a homogeneous aqueous dispersion of $N^+C_5Ala2C_{14}$ and QC_5Ala2C_{14} at the 3:1 molar ratio (Fig. 6A). Although the vesicle aggregation was not detected by turbidity measurements, gradual growth of the aggregates was observed by NSEM. As shown in Fig. 6B, formation of elongated vesicles was observed in the specimen prepared after incubation for 0.5 h in addition to the original small single-walled vesicles. These aggregates were converted into larger vesicles with the diameter range 1000—4000 Å after incubation for 2 h (Fig. 6C). Such morphological changes were further examined with a combination of the cationic and nonionic lipids having different double-chain lengths. A homogeneous dispersion of $N^+C_5Ala2C_{16}$ and QC_5Ala2C_{14} at the 3:1 molar ratio showed a phase transition as detected by DSC: T_m, 19.9 °C; ΔH, 27 kJ mol^{-1}. A half-width of the endothermic peak is 3 °C and larger than that (2 °C) observed for the mixed lipid system composed of $N^+C_5Ala2C_{16}$ and (SO_3^-)-C_5Ala2C_{14} at the 3:1 molar ratio. This seems to indicate that the intramembrane domains formed by microscopic phase separation between the cationic and nonionic lipids are relatively larger than those in the cationic-anionic lipid system, although the nonlamellar phase formed with QC_5Ala2C_{14} alone was not detected by NSEM (Fig. 7A). Upon sonication of the dispersion, the multiwalled vesicles were converted into the single-walled ones with the diameter range 200—800 Å along with appearance of a broadened phase transition peak (T_m, 16±5 °C). The aggregate structure did not undergo an immediate change after sonication was performed (Fig. 7B). After the sonicated solution was allowed to stand for 3—6 d at 20 °C, very large vesicles in a diameter range of 1000—4000 Å were observed by NSEM (Fig. 7C). On the other hand,

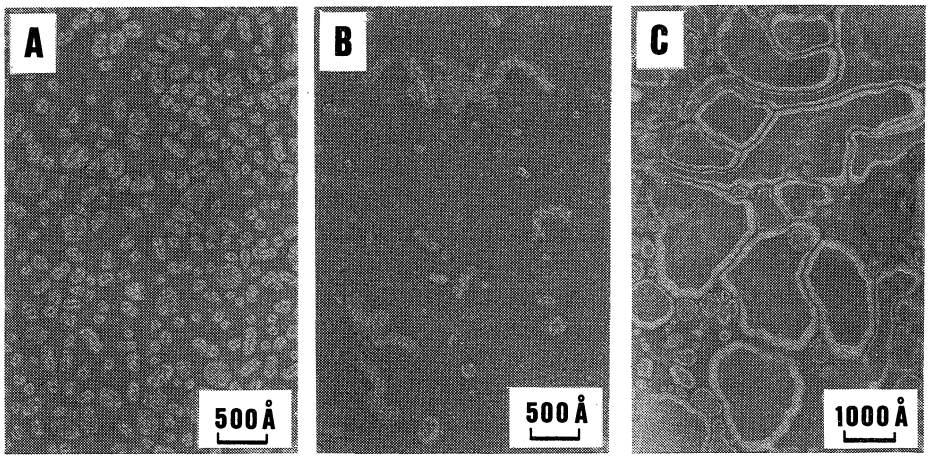

Fig. 6. Electron micrographs for a mixture of $N^+C_5Ala2C_{14}$ (3.75 mmol dm^{-3}) and QC_5Ala2C_{14} (1.25 mmol dm^{-3}), as negatively stained with uranyl acetate.
The aqueous solution sonicated for 3 min at 40 W was incubated at pH 7 and 20°C: A, immediately after sonication; B, for 0.5 h; C, for 2 h.

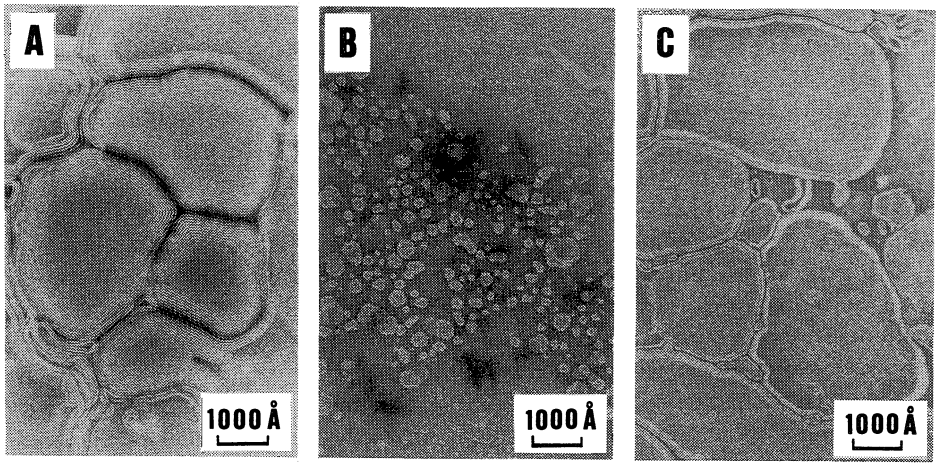

Fig. 7. Electron micrographs for a mixture of $N^+C_5Ala2C_{16}$ (3.75 mmol dm^{-3}) and QC_5Ala2C_{14} (1.25 mmol dm^{-3}), as negatively stained with uranyl acetate.
A, aqueous dispersion at pH 7 and 20°C; B, A being sonicated at pH 7 and 20°C for 3 min (40 W); C, B being left at 20°C for 6 d.

the DSC thermogram characteristic of single-walled vesicles remained practically unchanged even after incubation for 6 d.

Discussion

The membrane fusion is one of the most important phenomena for a wide variety of cellular activities, and molecular mechanisms involved in the fusion process have been extensively studied with the use of liposomal membranes.[12] The fusion of bilayer membranes is generally considered to proceed through the following sequential steps; (i) aggregation of vesicles, (ii) contact of two lipid bilayers at a limited area (adhesion), (iii) intermixing of lipid molecules by transient destabilization of bilayers at the contact point (joining), and (iv) restabilization of the bilayer structure by intermixing of separated aqueous compartments of vesicles (fission).[11a,13] Medium conditions such as temperature[13a,14] and pH,[14a,15] and many effectors such as divalent cations,[12b,16] polymers,[15,17] and lipophilic agents[18] have been reported to induce the fusion of liposomal membranes. Importance of local dehydration triggered by these fusogens has been emphasized for the adhesion step.[11b,19] Furthermore, deformation of the bilayer structure must take place in the joining step, and formation of nonbilayer structures (inverted micelles or small inverted hexagonal tubes) in the bilayer-connecting domain has been suggested.[11] In this article, we are to discuss the fusion behavior of the peptide lipid vesicles with attention to the dehydration effect and the participation of nonbilayer structures.

We have previously clarified fusogenic tendencies of the single-walled vesicles of $N^+C_5Ala2C_n$ by means of NMR, ESR, DSC, NSEM, and turbidity measurements.[3,5] The single-walled vesicles prepared upon sonication are so stable as to inhibit fusion of them under ordinary conditions and stay in solution over at

least a month without meaningful morphological change. Such structural stability of the peptide lipid vesicles is superior to that of liposomes and seems to originate partly from the formation of effective hydrogen-belt domains through intravesicular hydrogen-bonding interaction among the amino acid residues. On the other hand, nonlamellar assemblies composed of three-dimensional network of globular aggregates with small internal aqueous compartments (C_{II} phase) are formed with $N^+C_5Ala2C_n$ and $(SO_3^-)C_5Ala2C_n$ mixed at the 1 : 1 molar ratio in the aqueous dispersion state.[8,9] Since these cationic and anionic lipids form bilayer membranes individually, the polar head moieties of these lipids must be considerably dehydrated through an effective electrostatic interaction to afford such a nonlamellar phase.

It has been pointed out that the interbilayer hydration force is predominant at bilayer separations less than 20 to 30 Å and that the interaction between bilayers is dominated by electrostatic and van der Waals forces beyond about 30 Å separation.[11b,19] Thus, an essential part of fusion event must arise from the ability of membrane surfaces to overcome or circumvent the hydration barrier in order that bilayer surfaces get into contact with each other.[19] In our preliminary communication,[20] we have shown that fusion of the single-walled vesicles formed with peptide lipids takes place via formation of the intermediate nonlamellar phase as triggered by medium conditions, pH and/or temperature. Apparently, repulsion between the hydrated vesicular surfaces is circumvented by formation of the nonbilayer structure in which the lipid molecules are largely dehydrated due to an electrostatic intramembrane attraction. Dehydration of the peptide lipid bilayer may also be achieved through an electrostatic interaction on the membrane surface between lipid and additive molecules having opposite charges to each other. Indeed, fusion of the single-walled vesicles took place upon addition of polymers having the opposite charges (Figs. 2 and 3) via aggregation of the vesicles (Fig. 1). Thus, the electrostatic interaction between the vesicle and the polymer to give charge neutralization on the membrane surface becomes a potent driving force which allows not only the vesicles to aggregate but also the two membrane surfaces to come into contact. An amount of heparin, which neutralizes a half portion of the whole cationic charges of the lipid molecules present, is required for complete transformation of the cationic single-walled vesicle into the multiwalled bilayer, as confirmed by DSC (Fig. 3). This implies that the electrostatic interaction between the cationic vesicular surface and the anionic polymer is so large as to inhibit migration of the polymer molecule to the other vesicles. Since neither aggregation nor fusion was observed for the cationic vesicles in the presence of chondrosin or 2,6-pyridinedicarboxylic acid, the extended charge neutralization on the vesicular surface with polymer species seems to be essential to induction of the fusion. Accordingly, deformation of the bilayer structure can be achieved through strong electrostatic interactions between lipid and polymer molecules on the membrane surface and among charged head moieties of cationic and anionic peptide lipids.[8,9] Such changes in the packing mode of lipid molecules are accompanied undoubtedly with dehydration of lipid molecules so as to reduce the hydration barrier.

As for the mixed lipid systems composed of cationic and anionic peptide lipids, another characteristic feature was found to be present in the polymer-lipid interaction. The single-walled vesicles formed with $N^+C_5Ala2C_{16}$ and $(SO_3^-)C_5Ala2C_{14}$ at the 3 : 1 molar ratio underwent the heparin-induced fusion (Figs. 4 and 5), although the apparent surface charge density of the mixed-lipid vesicle is a half of that provided with the $N^+C_5Ala2C_{16}$ vesicle. Since homogeneous mixing of these ionic lipids was retained even after completion of the fusion as confirmed by DSC, a polymer-triggered phase separation does not seem to occur during the fusion. Thus, deformation of the bilayer structure, which results in the fusion, presumably comes from the cooperative assistance of polymer-lipid and lipid-lipid electrostatic interactions in the system.

QC_5Ala2C_{14} forms the inverted cubic phase through strong hydrogen-bonding interaction among the polar head moieties in the aqueous dispersion state.[6] Addition of this nonbilayer-forming lipid to the cationic peptide lipid, $N^+C_5Ala2C_n$, resulted in slow vesicle growth relative to the vesicle growth induced by ionic polymers (Figs. 6 and 7). In spite of such a disadvantage in the fusion rate, the membrane adhesion followed by deformation of the bilayer structure occurred in this system, QC_5Ala2C_{14} undoubtedly acting as a fusogen toward the vesicles. Formation of the elongated vesicles observed for the $N^+C_5Ala2C_{14}$-QC_5Ala2C_{14} (3 : 1) system (Fig. 6B) at the initial stage of morphological changes needs to be subjected to mechanistic consideration. Such vesicle growth to the transverse direction must be originated from a preferential fusogenic tendency of the vesicles at the surface domain having larger curvature. In fact, smaller liposomes formed with phosphatidylserine or phosphatidylcholine have an intrinsically greater capacity to fuse than larger vesicles.[14d,21] Relaxation of the packing strain imposed on the highly curved portion of the bilayers becomes a trigger of such vesicle growth. In the QC_5Ala2C_{14}-rich domains formed by microscopic phase separation as detected by DSC, such a strain effect must be much enhanced.

In conclusion, the fusion of single-walled vesicles formed with the ionic peptide lipids proceeds under the following conditions: (i) as for the vesicular systems of $N^+C_5Ala2C_n$ and $(SO_3^-)C_5Ala2C_n$ individually or mixed together to an extent that the surface charges are not completely neutralized, ionic polymers having the opposite charges to the net vesicular surface

charges are added; (ii) as for the $N^+C_5Ala2C_n$ vesicular system containing QC_5Ala2C_{14}, the latter lipid acts as a fusogen without polymer additives. Since vesicle aggregation is not always followed by fusion of bilayers,[21b,22] the present ionic polymers induce aggregation of the vesicles prior to the membrane adhesion and subsequently give out perturbation on the vesicular surface so that the bilayer structure is effectively deformed. Even in the absence of fusion-inducing polymers, incorporation of a nonbilayer-forming lipid into the vesicular system results in induction of the fusion process. Although the nonbilayer structure was not detected during the membrane fusion process under the present conditions, formation of such an intermediate phase in a microscopic portion of the bilayer-joining domain is much plausible as a consequence of dehydration of the polar head moieties of lipids.

References

1) J. H. Fendler, "Membrane Mimetic Chemistry," John Wiley, New York (1982), Chap. 6.

2) H. Brockerhoff, "Bioorganic Chemistry," ed by E. E. van Tamelen, Academic Press, New York (1977), Vol. 3, Chap. 1.

3) Y. Murakami, A. Nakano, and K. Fukuya, *J. Am. Chem. Soc.*, **102**, 4253 (1980).

4) Y. Murakami, A. Nakano, and H. Ikeda, *J. Org. Chem.*, **47**, 2137 (1982).

5) Y. Murakami, A. Nakano, A. Yoshimatsu, K. Uchitomi, and Y. Matsuda, *J. Am. Chem. Soc.*, **106**, 3613 (1984).

6) Y. Murakami, A. Nakano, J. Kikuchi, T. Takaki, and K. Uchimura, *Chem. Lett.*, **1983**, 1891.

7) Y. Murakami, J. Kikuchi, T. Takaki, K. Uchimura, and A. Nakano, *J. Am. Chem. Soc.*, **107**, 2161 (1985).

8) Y. Murakami, J. Kikuchi, T. Takaki, and K. Uchimura, *J. Am. Chem. Soc.*, **107**, 3373 (1985).

9) Y. Murakami, J. Kikuchi, T. Takaki, and K. Uchimura, *Bull. Chem. Soc. Jpn.*, **59**, 515 (1986).

10) Y. Murakami, J. Kikuchi, T. Takaki, and K. Uchimura, *Chem. Lett.*, **1986**, 325.

11) a) A. J. Verkleij, *Biochim. Biophys. Acta*, **779**, 43 (1984); b) R. P. Rand, *Ann. Rev. Biophys. Bioeng.*, **10**, 277 (1981); c) A. J. Verkleij, J. Leunissen-Bijvelt, B. De Kruijff, M. Hope, and P. R. Cullis, "Cell Fusion," Ciba Foundation Symposium 103, Pitman Books, London (1984), pp. 45—59.

12) a) M. Gratzel, C. Schudt, R. Ekerdt, and G. Dahl, "Membrane Structure and Function," ed by E. E. Bittar, John Wiley, New York (1980), Vol. 3, pp. 59—92; b) D. Papahadjopoulos, G. Poste, and W. J. Vail, *Methods Membr. Biol.*, **10**, 1 (1979).

13) a) S. W. Hui, T. P. Stewart, L. T. Boni, and P. L. Yeagle, *Science*, **212**, 921 (1981); b) P. R. Cullis and M. J. Hope, *Nature (London)*, **271**, 672 (1978).

14) a) A. M. Haywood and B. P. Boyer, *Biochemistry*, **21**, 6041 (1982); b) M. Wong, F. H. Anthony, T. W. Tillack, and T. E. Thompson, *ibid.*, **21**, 4126 (1982).

15) P. S. Uster and D. W. Deamer, *Biochemistry*, **24**, 1 (1985).

16) a) D. Papahadjopoulos, G. Poste, B. E. Schaefer, and W. J. Vail, *Biochim. Biophys. Acta*, **352**, 10 (1974); b) S. Nir, J. Bentz, J. Wilschut, and N. Düzgünes, *Prog. Surf. Sci.*, **13**, 1 (1983).

17) C.-Y. Wang and L. Huang, *Biochemistry*, **23**, 4409 (1984); A. E. Gad, B. L. Silver, and G. D. Eytan, *Biochim. Biophys. Acta*, **690**, 124 (1982); R. I. MacDonald, *Biochemistry*, **24**, 4058 (1985).

18) D. Papahadjopoulos, S. Hui, W. J. Vail, and G. Poste, *Biochim. Biophys. Acta*, **448**, 245 (1976); J. Sunamoto, T. Hamada, and H. Murase, *Bull. Chem. Soc. Jpn.*, **53**, 2773 (1980).

19) V. A. Parsegian, R. P. Rand, and D. Gingell, "Cell Fusion," Ciba Foundation Symposium 103, Pitman Books, London (1984), pp. 9—27.

20) Y. Murakami, J. Kikuchi, and T. Takaki, *Chem. Lett.*, **1985**, 1899.

21) a) J. Wilschut, N. Düzgünes, R. Fraley, and D. Papahadjopoulos, *Biochemistry*, **19**, 6011 (1980); b) J. Wilschut, N. Düzgünes, and D. Papahadjopoulos, *ibid.*, **20**, 3126 (1981); c) S. Nir, J. Wilschut, and J. Bentz, *Biochim. Biophys. Acta*, **688**, 275 (1982); d) J. Bentz and N. Düzgünes, *Biochemistry*, **24**, 5436 (1985); e) D. Lichtenberg, E. Freire, C. F. Schmidt, Y. Barenholz, P. L. Felgner, and T. E. Thompson, *ibid.*, **20**, 3462 (1981).

22) F. Schuber, K. Hong, N. Düzgünes, and D. Papahadjopoulos, *Biochemistry*, **22**, 6134 (1983); A. E. Gad, M. Bental, G. Elyashiv, and H. Weinberg, *ibid.*, **24**, 6277 (1985); L. A. M. Rupert, D. Hoekstra, and J. B. F. N. Engberts, *J. Am. Chem. Soc.*, **107**, 2628 (1985).

 © 1986 The Chemical Society of Japan Bull. Chem. Soc. Jpn., 59, 3153—3159 (1986)

Reaction of α,β-Unsaturated Carboxylic Acids with Manganese(III) Acetate in the Presence of Chloride Ion

Hiroshi YONEMURA, Hiroshi NISHINO, and Kazu KUROSAWA*
Department of Chemistry, Faculty of Science, Kumamoto University, Kurokami 2-39-1, Kumamoto 860
(Received April 12, 1986)

The reaction of 3-phenylpropenoic acids with manganese(III) acetate-Cl^- complex yielded 1,2,2-trichloro-1-phenylethanes, 1-acetoxy-2,2-dichloro-1-phenylethanes, and 2,2-dichloro-1-phenylethanols. (*E*)-2,3-Diphenylpropenoic acids gave 2,2-dichloro-1,2-diphenylethanones and 2-acetoxy-1,2-diphenylethanones. 3,3-Diphenylpropenoic acids yielded 2,2-dichloro-1,1-diphenylethenes, 1-acetoxy-2,2-dichloro-1,1-diphenylethanes, 2,2-dichloro-1,1-diphenyl-1-ethanols, and 2-hydroxy-2,2-diphenylethanal. Fluorenylideneacetic acid gave 9-chloro-9-(dichloromethyl)fluorene, 9-acetoxy-9-(dichloromethyl)fluorene, and 9-fluorenone. 1-Cyclohexenecarboxylic acid yielded 1,2-dichlorocyclohexanecarboxylic acid and 1-acetoxy-2-chlorocyclohexanecarboxylic acid. The reaction can be explained in terms of a free-radical mechanism involving manganese(III) acetate-Cl^- complexation, addition of $Cl^\cdot$ radical, decarboxylation, and the oxidation of chloroethenes which are the reaction intermediates.

Although there are many investigations into the reaction of manganese(III) acetate,[1] the reaction of manganese(III) acetate in the presence of Cl^- ion which forms a complex[2] has not been fully examined. The reaction of aromatic compounds with this complex gave chlorine-substituted products,[3] while olefins yielded mainly addition products.[2,3] In a previous paper[4] we have reported that the reaction of aryl ketones with manganese(III) acetate-LiCl gave α-chlorinated ketones in good yield. We have examined the reactions of α,β-unsaturated carboxylic acids, such as 3-phenylpropenoic acids, (*E*)-2,3-diphenylpropenoic acids, 3,3-diphenylpropenoic acids, fluorenylideneacetic acid, and 1-cyclohexenecarboxylic acid with the complex. These acids were chosen for the reason that they may provide a variety of products which reflect the nature of the reaction and that the products will be easily characterized by spectrometry. The reactions of these acids yielded chlorine addition and substitution products accompanied by decarboxylation. We will describe these reactions and the possible mechanisms in this paper.

Results and Discussion

3-Phenylpropenoic Acids (1a—g). When a mixture of (*E*)-3-phenylpropenoic aicd (**1a**), manganese(III) acetate[5,6] and LiCl in a molar ratio of 1 : 10 : 20 in AcOH was heated under reflux, it gave 1,2,2-trichloro-1-phenylethane (**2a**) and 1-acetoxy-2,2-dichloro-1-phenylethane (**3a**). The reaction was conducted at various molar ratios of manganese(III) acetate and LiCl, and the yields changed with changing the amounts of manganese(III) acetate and LiCl (Table 1,

Table 1. The Oxidations of 3-Phenylpropenoic Acids (**1a—g**) and 1-Chloro-2-phenylethene (**26a**) with Manganese(III) Acetate in the Presence of Chloride Ion at the Reflux Temperature

Entry	Substrate	Molar ratio[a]	Salt	Reaction time/min	Product (yield/%)[b]
1	**1a**	1 : 5 : 10	LiCl	170	**2a**(28)
2	**1a**	1 : 8 : 10	LiCl	310	**2a**(48)
3	**1a**	1 : 10 : 10	LiCl	300	**2a**(40)
4	**1a**	1 : 10 : 15	LiCl	350	**2a**(51)
5	**1a**	1 : 10 : 20	LiCl	410	**2a**(45) **3a**(6)
6	**1a**	1 : 10 : 20[c]	LiCl	310	**2a**(49) **3a**(3)
7	**1a**	1 : 10 : 30	LiCl	340	**2a**(36) **3a**(5)
8	**1a**	1 : 10 : 7.5	$CaCl_2$	570	**2a**(54) **3a**(4)
9	**1a**	1 : 10 : 15	NH_4Cl	660	**2a**(27)
10	**1a**	1 : 10 : 5	$AlCl_3$	30	**2a**(15) **3a**(6)
11	**1a**	1 : 10 : 15	NaCl	300	**2a**(10) **5** (6)
12	**1a**	1 : 10 : 15	HCl	510	**2a**(7) **5** (16)
13	**1a**	1 : 8 : 10	KCl	210	**2a**(15) **5** (6)
14	**1b**	1 : 8 : 16	LiCl	340	**3b**(54) **4b**(17)
15	**1c**	1 : 8 : 16	LiCl	150	**2c**(11) **3c**(52)
16	**1d**	1 : 8 : 16	LiCl	240	**2c**(8) **3c**(42) **6** (30)
17	**1e**	1 : 8 : 16	LiCl	410	**2e**(58)[d]
18	**1f**	1 : 8 : 16	LiCl	400	**2f**(51) **3f**(19) **4f**(4)[e]
19	**1g**	1 : 10 : 15	LiCl	340	**2g**(35) **7** (7)[f]
20	**26a**	1 : 4 : 12	LiCl	250	**2a**(51) **3a**(6)

a) Substrate:Manganese(III) acetate:Salt. b) Isolated yields based on the substrate added. c) Ac_2O (20 equivalents) was added. d) **1e** was recovered (5%). e) 4-Methylbenzoic acid was obtained (13%). f) **1g** was recovered (40%).

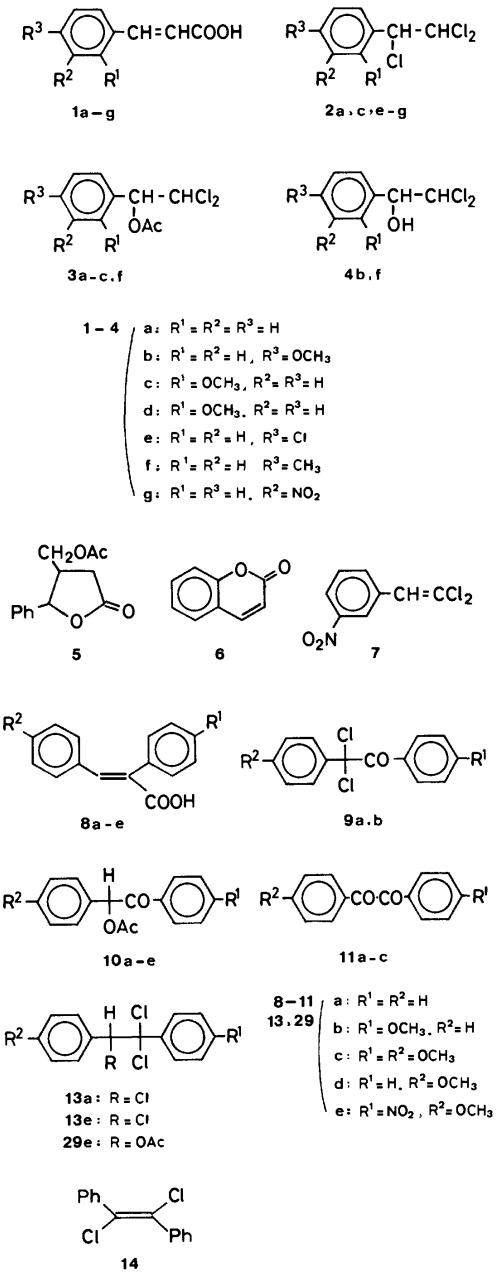

Entries 1—5, 7). Addition of Ac_2O to the reaction mixture caused no appreciable change in the yield, but shortened the reaction time considerably (Entry 6). It was observed that changing the Cl^- ion source affected the yield and $CaCl_2$ was as good as LiCl, but it took a longer reaction time. In the reactions using NaCl, HCl, or KCl, 4-acetoxymethyl-5-phenyl-4-butanolide (**5**) was isolated. Hereafter we employed LiCl as the Cl^- ion source. Then the reactions of (*E*)-3-(**4**-methoxyphenyl)- (**1b**), (*E*)-3-(2-methoxyphenyl)- (**1c**), (*Z*)-3-(2-methoxyphenyl)- (**1d**), (*E*)-3-(4-chlorophenyl)- (**1e**), (*E*)-3-(4-methylphenyl)- (**1f**), and (*E*)-3-(3-nitrophenyl)propenoic acid (**1g**) were examined. The structures of the products were determined by studying their ^1H NMR, IR, mass spectra and elemental analyses. A summary of the reaction conditions and the yields of the products are presented in Table 1.

(*E*)-2,3-Diphenylpropenoic Acids (8a—d). The reaction of (*E*)-2,3-diphenylpropenoic acid (**8a**) with manganese(III) acetate–Cl^- complex gave 2,2-dichloro-1,2-diphenylethanone (**9a**), 2-acetoxy-1,2-diphenylethanone (**10a**), 1,2-diphenylethanedione (**11a**), benzoic acid (**12**), 1,1,2-trichloro-1,2-diphenylethane (**13a**) and (*E*)-1,2-dichloro-1,2-diphenylethene (**14**). The reaction of (*E*)-2-(4-methoxyphenyl)-3-phenylpropenoic acid (**8b**) yielded the corresponding ethanones (**9b** and **10b**) and an ethanedione (**11b**). The reactions of (*E*)-2,3-bis(4-methoxyphenyl)propenoic acid (**8c**) and (*E*)-3-(4-methoxyphenyl)-2-phenylpropenoic acid (**8d**) yielded no chlorinated compounds, but gave 2-acetoxy-1,2-diphenylethanones (**10c** and **10d**) and 1,2-diphenylethanediones (**11b** and **11c**) (Table 2). It should be pointed out that the carbonyl carbon in the ethanones is assigned by ^1H NMR to the carbon on which the carboxyl group of the acid had been located and that the acetoxyl group is introduced more readily to the carbon attached to a methoxyphenyl group than to a phenyl group.

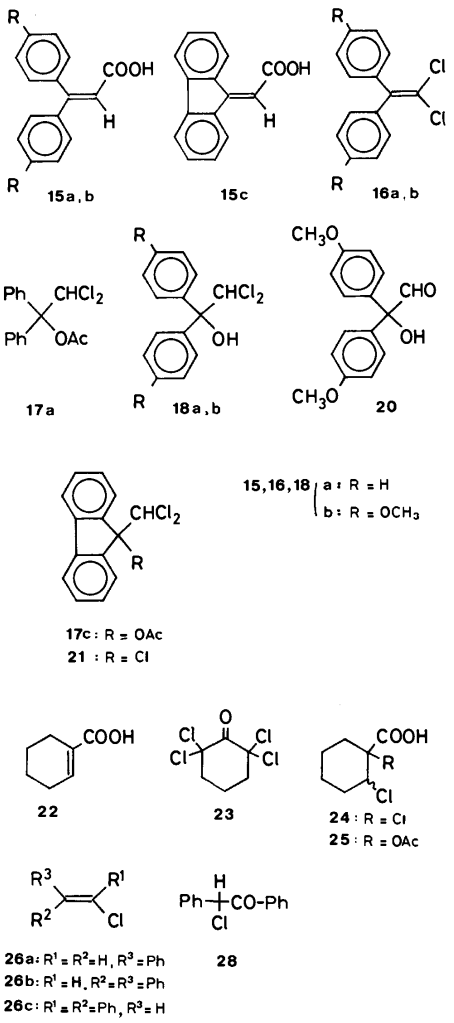

Fig. 1.

3,3-Diphenylpropenoic Acids (15a,b) and Fluorenylideneacetic Acid (15c). When 3,3-diphenylpropenoic

Table 2. The Oxidations of (*E*)-2,3-Diphenylpropenoic Acids (**8a—d**) and 1-Chloro-1,2-diphenylethene (**26c**) with Manganese(III) Acetate in the Presence of LiCl at the Reflux Temperature

Substrate	Molar ratio[a]	Reaction time/min	Product (yield/%)[b]				
8a	1 : 6 : 12	40	**9a**(50)	**10a**(6)	**11a**(13)	**13a**(5)	**14**(5)[c]
8b	1 : 6 : 12	116	**9b**(32)	**10b**(22)	**11b**(28)		
8c	1 : 6 : 12	160		**10c**(78)	**11c**(19)		
8d	1 : 6 : 12	120		**10d**(73)	**11b**(18)		
26c	1 : 4 : 12	80	**9a**(25)		**11a**(6)	**13a**(14)	**14**(17)

a) Substrate:Manganese(III) acetate:LiCl. b) Isolated yields based on the substrate added. c) Benzoic acid was obtained (9%).

Table 3. The Oxidation of 3,3-Diphenylpropenoic Acids (**15a, b**), Fluorenylideneacetic Acid (**15c**) and 2-Chloro-1,1-diphenylethene (**26b**) with Manganese(III) Acetate in the Presence of LiCl at the Reflux Temperature

Substrate	Molar ratio[a]	Reaction time/min	Product (yield/%)[b]			
15a	1 : 10 : 15	480	**16a**(9)	**17a**(42)	**18a**(40)	**19a**(4)
15a	1 : 10 : 15[c]	420	**16a**(10)	**17a**(72)		
15b	1 : 4 : 8	1	**16b**(46)		**18b**(3)	**20** (8)
15c	1 : 6 : 18	230		**17c**(37)	**19c**(12)	**21** (49)
26b	1 : 4 : 12	330	**16a**(20)	**17a**(41)	**18a**(35)	

a) Substrate:Manganese(III) acetate:LiCl. b) Isolated yields based on the substrate added. c) Ac_2O (15 equivalents) was added.

acid (**15a**) was oxidized with manganese(III) acetate–Cl^- complex in AcOH, 2,2-dichloro-1,1-diphenylethene (**16a**) and 1-acetoxy-2,2-dichloro-1,1-diphenylethane (**17a**), 2,2-dichloro-1,1-diphenylethanol (**18a**) and benzophenone (**19a**) were obtained. A remarkable change has been observed when Ac_2O was added to the reaction mixture, i.e. **17a** became the major product (Table 3). The reaction of 3,3-bis(4-methoxyphenyl)-propenoic acid (**15b**) with the complex in a molar ratio of 1 : 4 : 8 ended in extremely short reaction time, giving 2,2-dichloro-1,1-bis(4-methoxyphenyl)ethene (**16b**), 2,2-dichloro-1,1-bis(4-methoxyphenyl)ethanol (**18b**), and 2-hydroxy-2,2-bis(4-methoxyphenyl)ethanal (**20**). The reaction of fluorenylideneacetic acid (**15c**) yielded 9-acetoxy-9-(dichloromethyl)fluorene (**17c**), 9-fluorenone (**19c**), and 9-chloro-9-(dichloromethyl)fluorene (**21**).

1-Cyclohexenecarboxylic Acid (22). The reaction of **22** gave 2,2,6,6-tetrachlorocyclohexanone (**23**) (7%), 1,2-dichlorocyclohexanecarboxylic acid (**24**) (17%), and 1-acetoxy-2-chlorocyclohexanecarboxylic acid (**25**) (24%). These acids were separated and identified after methylation with diazomethane. The configuration of these acids could not be determined.

The reactions of 3-phenyl- and 3,3-diphenylpropenoic acids with manganese(III) acetate-Cl^- complex yielded chlorine-substituted ethenes and ethanes. By contrast, 2,3-diphenylpropenoic acids yielded 2,2-dichloro-1,2-diphenylethanones and 2-acetoxy-1,2-diphenylethanones. Addition of an acetoxyl group in place of a chlorine atom is often observed in these reactions. As postulated in the reaction of olefins with manganese(III) acetate in the presence of Cl^- ion,[2] the first step in the reaction of the acids must be the formation of a manganese(III) acetate-Cl^- complex which produces a Cl· radical. The Cl· radical adds to the C-2 of the substituted propenoic acid, producing a secondary or tertiary carbon radical A which is then oxidized to the corresponding carbonium ion B (Scheme 1). It seems also possible that the acid coordinates to the manganese(III) acetate–Cl^- complex and a chlorine atom is then transferred from the complex to the C-2 of the propenoic acid, forming the radical A. When the carboxyl group is eliminated from B as CO_2, then a chloroethene (**26a,b**) is formed which may react further with manganese(III) acetate-Cl^- complex to give another carbonium ion C. It was confirmed that 2,3-dichloro-3-phenylpropanoic acid (**27**) which could be formed by the addition of chlorine to the C=C bond in **1a**, was only partially decarboxylated and chlorinated under the reaction conditions to give 1,1,2-trichloro-2-phenylethane (**2a**) (17%), suggesting that this route makes only a small contribution for the formation of **2a**. The carbonium ion C gives dichloroethenes, 1,2,2-trichloroethanes, and 1-acetoxy-2,2-dichloroethanes depending on either losing a proton on the adjacent carbon or taking up a Cl^- ion and an acetate ion. If H_2O which may be contained in the reaction mixture attacks C, then alcohols are formed. The fact that the formation of **18a** was suppressed when the reaction of **15a** was conducted under anhydrous conditions (Table 3) confirms this view. In the reactions of **1b—d** and **15a**, an acetoxyl group was preferentially introduced onto the carbon bearing two phenyl groups or a methoxyphenyl group. The chlorine atom at the benzylic position could be readily replaced by an acetate

ion,[4] and **2c** was transformed into **3c** by heating in AcOH containing manganese(II) acetate. The formation of **10a** and **10b** in the reactions of **8a** and **8b** showed that the nucleophilic attack with acetate ion also takes place at the carbon attached to the phenyl group to a limited extent.

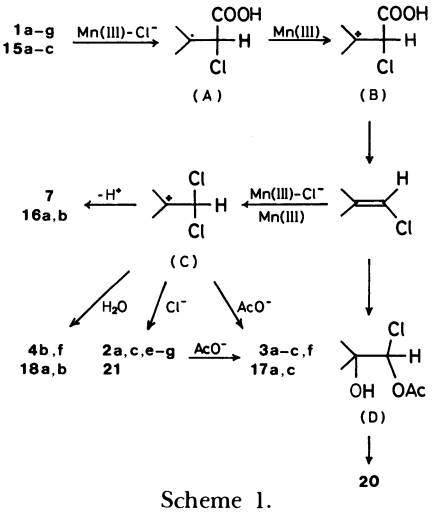

Scheme 1.

Chloroethenes as the postulated intermediates have not been found in the products, probably because they react faster than the original acid with manganese(III) acetate-Cl^- complex. In order to prove the involvement of chloroethenes as the reaction intermediate, 1-chloro-2-phenylethene (**26a**), which was prepared by an alternative method, was oxidized with the complex in AcOH and it did give the identical products with those from **1a** in a similar ratio (Table 1, Entry 20). Similarly, 2-chloro-1,1-diphenylethene (**26b**) was prepared and oxidized with the complex to yield **16a**, **17a**, and **18a** in a ratio similar to that from **15a** (Table 3). The formation of **20** in the reaction of **15b** deserves comment. It seems that because of the electron-donating effect of the two 4-methoxyphenyl groups in **15b**, the corresponding substituted 2-chloroethene, the intermediate, reacts with the complex via an electron-transfer mechanism[7] to give an α-glycol monoacetate (D) which can be hydrolyzed to **20**.

It has been mentioned already that the carbonyl carbon in 1,2-diphenylethanones (**9b** and **10b,d**) was assigned at the carbon on which the carboxyl group had been located. This was indicated by the presence of the characteristic lower field aromatic protons ortho to the carbonyl group of ethanones in their ^1H NMR spectra. This leads to a suggestion that the intermediate, 1-chloro-1,2-diphenylethene (**26c**), is converted into a 1,2-dichloro-1,2-diphenyl cation E which is in equilibrium with 1,1,2-trichloro-1,2-diphenylethane (**13a**) and eventually gives rise to 2-chloro-1,2-diphenylethanone (**28**) as shown in Scheme 2. In fact, the reaction of 1-chloro-1,2-diphenylethene (**26c**) gave **9a**, **11a**, **13a**, and **14** (Table 2) and the treatment of **13a** with manganese(II) acetate in AcOH yielded **28** in a

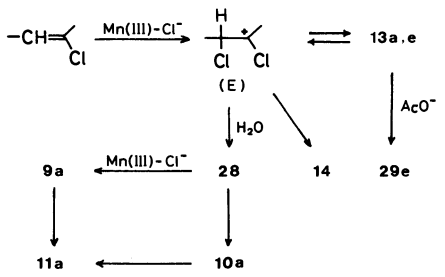

Scheme 2.

80% yield. For further confirmation of the mechanism for the formation of 2,2-dichloro-1,2-diphenylethanones and 2-acetoxy-1,2-diphenylethanones, the reaction of (*E*)-3-(4-methoxyphenyl)-2-(4-nitrophenyl)-propenoic acid (**8e**) with manganese(III) acetate-Cl^- complex was carried out. The corresponding 1,2-dichloro-1,2-diphenylethyl cation E from **8e** may be destabilized by the electron-withdrawing effect of the *p*-nitro group so that the equilibrium lies toward the right in favor of the formation of 1,1,2-trichloro (**13e**) and hence 2-acetoxy-1,1-dichloro derivative (**29e**). Accordingly, the cation E has less chance to form a 2-chloro-1,2-diphenylethanone (**28**). The reaction indeed yielded 2-acetoxy-1,1-dichloro-2-(4-methoxyphenyl)-1-(4-nitrophenyl)ethane (**29e**) as the major product (36%), accompanied with 2-acetoxy-2-(4-methoxyphenyl)-1-(4-nitrophenyl)ethanone (**10e**) (24%), and 1,1,2-trichloro-2-(4-methoxyphenyl)-1-(4-nitrophenyl)ethane (**13e**) (4%). The compound **28** can be either chlorinated to give **9a** or converted to **10a**,[4] and the routes to **11a** from **9a** and **10a** have been established.[8]

In the reaction of 1-cyclohexenecarboxylic acid (**22**) the yield of the decarboxylated product, 2,2,6,6-tetrachlorocyclohexanone (**23**), was poor, probably because the corresponding cation B is less stabilized and quickly takes up a chloride ion to form 1,2-dichlorocyclohexanecarboxylic acid (**24**). The compound **25** can be obtained from **24** on treatment with manganese(II) acetate in boiling AcOH.

It is thus concluded that the reaction of aryl-substituted propenoic acids with manganese(III)-Cl^- complex proceeds via chloro-substituted ethenes formed by chlorination and decarboxylation of the acids. Although there are several decarboxylation reactions to form alkyl or aryl halides[9,10] and our reaction is limited only to aryl-substituted propenoic acids, the use of manganese(III) acetate-Cl^- complex as a decarboxylating reagent is a method of choice when chloro-substituted phenylethanes and phenylethenes are needed.

Experimental

Measurements. The IR spectra were measured in chloroform solution on a JASCO A-102 infrared spectrometer. The ^1H NMR spectra were recorded on a Hitachi Perkin-Elmer R-24 spectrometer (60 MHz) with tetramethylsilane as an

internal standard; the chemical shifts are reported in δ values. The mass spectra were obtained with a JEOL JMS-DX300 and a JEOL JMS-DX303 mass spectrometer. The melting points were determined on a Yanagimoto micro-melting point apparatus and were not corrected.

Materials. (*E*)-3-(4-Methoxyphenyl)propenoic acid (**1b**),[11] (*E*)-3-(2-methoxyphenyl)propenoic acid (**1c**),[12] (*Z*)-3-(2-methoxyphenyl)propenoic acid (**1d**),[13] (*E*)-3-(4-methylphenyl)propenoic acid (**1f**),[14] fluorenylideneacetic acid (**15c**),[15] and 1-cyclohexenecarboxylic acid (**22**)[16] were prepared by the method described in the literature. (*E*)-2,3-Diphenylpropenoic acid (**8a**), (*E*)-2-(4-methoxyphenyl)-3-phenylpropenonic acid (**8b**), (*E*)-2,3-bis(4-methoxyphenyl)-propenoic acid (**8c**), (*E*)-3-(4-methoxyphenyl)-2-phenylpropenoic acid (**8d**), and (*E*)-3-(4-methoxyphenyl)-2-(4-nitrophenyl)propenoic acid (**8e**) were prepared from the corresponding arylacetic acid and benzaldehyde by Perkin condensation.[11]

(*E*)-2,3-Bis(4-methoxyphenyl)propenoic Acid (8c): Colorless needles; mp 212 °C (subl.); ^{1}H NMR (DMSO-d_6) δ=3.71 (3H, s, OCH_3), 3.79 (3H, s, OCH_3), 6.6—7.3 (8H, m, ar.H), 7.70 (1H, s, =CH-), and 12.3 (1H, br., COOH). Anal. ($C_{17}H_{16}O_4$) C, H.

3,3-Diphenylpropenoic acid (**15a**) and 3,3-bis(4-methoxyphenyl)propenoic acid (**15b**) were prepared from the corresponding benzophenone and ethyl bromoacetate by Reformatsky reaction.[17] (*E*)-3-Phenylpropenoic acid (**1a**), (*E*)-3-(4-chlorophenyl)propenoic acid (**1e**), and (*E*)-3-(3-nitrophenyl)-propenoic acid (**1g**) were purchased from Aldrich Chemical Company, Inc. and Wako Pure Chemical Industries, Ltd.

Oxidations of α,β-Unsaturated Carboxylic Acids with Manganese(III) Acetate-Cl^-. The general procedure for the oxidation of α,β-unsaturated carboxylic acids with manganese(III) acetate-Cl^- was as follows. To a heated solution of manganese(III) acetate[5] (4—10 mmol) and chloride anion (see Table 1) in AcOH (30 cm^3), a carboxylic acid (1 mmol) was added. The mixture was then heated under reflux until the brown color of the solution had become transparent. After removal of the solvent, 2 M (1 M=1 mol dm^{-3}) hydrochloric acid (40 cm^3) was added to the mixture, which was then extracted with benzene or chloroform (3×30 cm^3). The benzene (or chloroform) solution was washed with aqueous sodium hydrogencarbonate solution and evaporated in vacuo. The products were separated on preparative TLC (Kieselgel 60G or Wakogel B-10), with chloroform or benzene as the developing solvent. The aqueous sodium hydrogencarbonate solution was acidified with concd hydrochloric acid and extracted with either chloroform or ethyl acetate, which gave acidic products. The yields are summarized in Tables 1—3.

Oxidation Products of (*E*)-3-Phenylpropenoic Acid (1a). 1,2,2-Trichloro-1-phenylethane (2a): Bp 190 °C/2400 Pa (bath temperature); the ^{1}H NMR data agreed with those reported.[18]

1-Acetoxy-2,2-dichloro-1-phenylethane (3a): The ^{1}H NMR data agreed with those reported.[19]

4-Acetoxymethyl-5-phenyl-4-butanolide (5): Colorless liquid; bp 175 °C/1.3 Pa (bath temperature); IR 1780 (-COO-), 1755 cm^{-1} (OAc); ^{1}H NMR (CCl_4) δ=2.00 (3H, s, OAc), 2.0—3.0 (3H, m, >$CHCH_2$-), 4.17 (2H, d, J=5.4 Hz, -CH_2OAc), 5.21 (1H, d, J=6.0 Hz, >CH-O-), 7.32 (5H, m, ar.H). Anal. ($C_{13}H_{14}O_4$) C, H.

Oxidation Products of (*E*)-3-(4-Methoxyphenyl)propenoic Acid (1b). 1-Acetoxy-2,2-dichloro-1-(4-methoxyphenyl)-ethane (3b): Colorless liquid; IR 1747 cm^{-1} (OAc); ^{1}H NMR (CCl_4) δ=2.04 (3H, s, OAc), 3.66 (3H, s, OCH_3), 5.77 (1H, d, J=5.4 Hz, -$CHCl_2$), 5.93 (1H, d, J=5.4 Hz, >CHOAc), 6.76 (2H, m, H-3 and H-5), and 7.24 (2H, m, H-2 and H-6). Found: m/z 262.0154. Calcd for $C_{11}H_{12}{}^{35}Cl_2O_3$: M, 262.0164.

2,2-Dichloro-1-(4-methoxyphenyl)ethanol (4b): Colorless liquid; the ^{1}H NMR and IR spectra were identical with those reported.[20]

Oxidation Products of (*E*)-3-(2-Methoxyphenyl)propenoic Acid (1c) and (*Z*)-3-(2-Methoxyphenyl)propenoic Acid (1d). 1,2,2-Trichloro-1-(2-methoxyphenyl)ethane (2c): Colorless liquid; ^{1}H NMR (CCl_4) δ=3.84 (3H, s, OCH_3), 5.60 (1H, d, J=6.0 Hz, -$CHCl_2$), 6.06 (1H, d, J=6.0 Hz, -CHCl-), and 6.8—7.6 (4H, m, ar.H). Found: m/z 237.9735. Calcd for $C_9H_9{}^{35}Cl_3O$: M, 237.9719.

1-Acetoxy-2,2-dichloro-1-(2-methoxyphenyl)ethane (3c): Colorless needles; mp 108—109 °C (from ethanol); IR 1750 cm^{-1} (OAc); ^{1}H NMR ($CDCl_3$) δ=2.16 (3H, s, OAc), 3.78 (3H, s, OCH_3), 6.12 (1H, d, J=4.0 Hz, -$CHCl_2$), 6.57 (1H, d, J=4.0 Hz, >CHOAc), and 6.7—7.5 (4H, m, ar.H); MS m/z (rel intensity) 262, 264, 266 (M^+, 17), 179 (35), 137 (100), and 107 (45). Anal. ($C_{11}H_{12}Cl_2O_3$) C, H.

2*H*-1-Benzopyran-2-one (6): Mp 65—66 °C.

Oxidation Product of (*E*)-3-(4-Chlorophenyl)propenoic Acid (1e). 1,2,2-Trichloro-1-(4-chlorophenyl)ethane (2e): Colorless liquid.[21]

Oxidation Products of (*E*)-3-(4-Methylphenyl)propenoic Acid (1f). 1,2,2-Trichloro-1-(4-methylphenyl)ethane (2f): The ^{1}H NMR data agreed with those reported.[18]

1-Acetoxy-2,2-dichloro-1-(4-methylphenyl)ethane (3f): Colorless liquid.[22] **2,2-Dichloro-1-(4-methylphenyl)-ethanol (4f):** Colorless liquid.[23] **4-Methylbenzoic acid:** Mp 180 °C.

Oxidation Products of (*E*)-3-(3-Nitrophenyl)propenoic Acid (1g). 1,2,2-Trichloro-1-(3-nitrophenyl)ethane (2g): Colorless cubes; mp 59.8—60.7 °C (from methanol); IR 1534 and 1354 cm^{-1} (NO_2); ^{1}H NMR (CCl_4) δ=5.32 (1H, d, J=5.4 Hz, >CHCl), 6.05 (1H, d, J=5.4 Hz, -$CHCl_2$), 7.4—8.0 (2H, m, H-5 and H-6), and 8.1—8.4 (2H, m, H-2 and H-4). Anal. ($C_8H_6Cl_3NO_2$) C, H, N.

β,β-Dichloro-3-nitrostyrene (7): Colorless silky needles; mp 54.9—55.4 °C (from hexane); IR 1610 (C=C), 1531 and 1354 cm^{-1} (NO_2); ^{1}H NMR (CCl_4) δ=6.90 (1H, s, =CH-), 7.4—8.0 (2H, m, H-5 and H-6), and 8.0—8.5 (2H, m, H-2 and H-4). Anal. ($C_8H_5Cl_2NO_2$) C, H, N.

Oxidation Products of (*E*)-2,3-Diphenylpropenoic Acid (8a). 2,2-Dichloro-1,2-diphenylethanone (9a): Mp 62—63 °C (lit,[24] mp 61—62 °C). **2-Acetoxy-1,2-diphenylethanone (10a):** Mp 81—82 °C (lit,[25] mp 80—82 °C). **1,2-Diphenylethanedione (11a):** Mp 95 °C. **Benzoic acid (12):** Mp 122 °C. **1,2,2-Trichloro-1,2-diphenylethane (13a):** Mp 101—102 °C (lit,[26] mp 102—103 °C). **(*E*)-1,2-Dichloro-1,2-diphenylethene (14):** Mp 140.3—140.5 °C (lit,[27] mp 139 °C).

Oxidation Products of (*E*)-2-(4-Methoxyphenyl)-3-phenylpropenoic Acid (8b). 2,2-Dichloro-1-(4-methoxyphenyl)-2-phenylethanone (9b): Colorless needles; mp 57—58 °C (from ethanol); IR 1689 cm^{-1} (C=O); ^{1}H NMR ($CDCl_3$) δ=3.70 (3H, s, OCH_3), 6.71 (2H, m, H-3 and H-5), 7.1—7.8 (5H, m, Ph), and 7.76 (2H, m, H-2 and H-6). Anal. ($C_{15}H_{12}Cl_2O_2$) C, H.

2-Acetoxy-1-(4-methoxyphenyl)-2-phenylethanone (10b):

Mp 79.2—79.9 °C (lit,[28] mp 78—79 °C). **1-(4-Methoxyphenyl)-2-phenylethanedione (11b):** Mp 63 °C (lit,[29] mp 62—63 °C).

Oxidation Products of (*E*)-2,3-Bis(4-methoxyphenyl)propenoic Acid (8c). 2-Acetoxy-1,2-bis(4-methoxyphenyl)ethanone (10c): Mp 93.8—94.8 °C (lit,[30] mp 93.5 °C). **1,2-Bis(4-methoxyphenyl)ethanedione (11c):** Mp 132.7—133.3 °C (lit,[31] mp 133 °C).

Oxidation Products of (*E*)-3-(4-methoxyphenyl)-2-phenylpropenoic Acid (8d). 2-Acetoxy-2-(4-methoxyphenyl)-1-phenylethanone (10d): Colorless liquid.[32] **1-(4-Methoxyphenyl)-2-phenylethanedione (11b).**

Oxidation Products of 3,3-Diphenylpropenoic Acid (15a). 2,2-Dichloro-1,1-diphenylethene (16a): Mp 78.7—79.9 °C (lit,[33] mp 80 °C). **1-Acetoxy-2,2-dichloro-1,1-diphenylethane (17a):** Mp 98.7—99.2 °C (lit,[34] 102.4—104 °C). **2,2-Dichloro-1,1-diphenylethanol (18a):** Mp 95.7—96.7 °C (lit,[35] mp 94—97 °C). **Benzophenone (19a):** Mp 48 °C.

Oxidation Products of 3,3-Bis(4-methoxyphenyl)propenoic Acid (15b). 2,2-Dichloro-1,1-bis(4-methoxyphenyl)ethene (16b): Mp 110.3—110.6 °C (lit,[36] mp 109 °C).

2,2-Dichloro-1,1-bis(4-methoxyphenyl)ethanol (18b): Colorless cubes; mp 103.5—104.5 °C (from ethanol): IR 3568 cm^{-1} (OH): ^1H NMR ($CDCl_3$) δ=3.31 (1H, br s, OH), 3.65 (6H, s, 2×OCH_3), 6.47 (1H, s, -$CHCl_2$), 6.78 (4H, m, H-3′, H-3″, H-5′, and H-5″), and 7.37 (4H, m, H-2′, H-2″, H-6′, and H-6″). Found: *m/z* 326.0453. Calcd for $C_{16}H_{16}{}^{35}Cl_2O_3$: M, 326.0477.

2-Hydroxy-2,2-bis(4-methoxyphenyl)ethanal (20): Colorless liquid: IR 3488 (OH) and 1720 cm^{-1} (CHO); ^1H NMR ($CDCl_3$) δ=3.78 (6H, s, 2×OCH_3), 4.30 (1H, br s, OH), 6.84 (4H, m, H-3′, H-3″, H-5′, and H-5″), 7.24 (4H, m, H-2′, H-2″, H-6′, and H-6″), and 9.84 (1H, s, CHO). Found: *m/z* 272.1040. Calcd for $C_{16}H_{16}O_4$: M, 272.1049.

Oxidation Products of Fluorenylideneacetic Acid (15c). 9-Acetoxy-9-(dichloromethyl)fluorene (17c): Colorless cubes; mp 83.6—84.6 °C (from ethanol); IR 1745 cm^{-1} (OAc); ^1H NMR (CCl_4) δ=1.94 (3H, s, OAc), 6.79 (1H, s, -$CHCl_2$), and 7.1—7.8 (8H, m, ar.H). Anal. ($C_{16}H_{12}Cl_2O_2$) C, H.

9-Chloro-9-(dichloromethyl)fluorene (21): Colorless cubes; mp 88.0—88.6 °C (from ethanol); ^1H NMR (CCl_4) δ=6.14 (1H, s, -$CHCl_2$), and 7.0—7.7 (8H, m, ar.H). Anal. ($C_{14}H_9Cl_3$) C, H.

9-Fluorenone (19c): Mp 83 °C.

Oxidation Products of 1-Cyclohexenecarboxylic Acid (22). 2,2,6,6-Tetrachlorocyclohexanone (23): Mp 83.1—83.8 °C (lit,[37] mp 83 °C).

The acidic products of the oxidation of **22** were separated and identified after methylation with diazomethane.

Methyl 1,2-Dichlorocyclohexanecarboxylate (Methyl Ester of 24): Colorless liquid; IR 1740 cm^{-1} (-COO-); ^1H NMR (CCl_4) δ=1.0—2.7 (8H, m, -CH_2-), 3.73 (3H, s, OCH_3), and 4.52 (1H, br, -CHCl-); MS (for the acid **24**) *m/z* (rel intensity) 197, 199, 201 (100, $(M+1)^+$), 161, 163 (28), 133, 135 (51), and 127 (72).

Methyl 1-Acetoxy-2-chlorocyclohexanecarboxylate (Methyl Ester of 25): Colorless liquid; IR 1735 cm^{-1} (OAc and -COO-); ^1H NMR (CCl_4) δ=0.7—2.5 (8H, m, -CH_2-); 2.04 (3H, s, OAc), 3.70 (3H, s, OCH_3), and 4.19 (1H, br, -CHCl-); MS *m/z* (rel intensity) 235, 237 (100, $(M+1)^+$). Found: *m/z* 235.0729. Calcd for $C_{10}H_{16}{}^{35}ClO_4$: M, 235.0737.

Reaction of 2,3-Dichloro-3-phenylpropanoic Acid (27). A mixture of **27** (203 mg), manganese(III) acetate (497 mg), and lithium chloride (236 mg) in AcOH (25 cm^3) was heated under reflux for 110 min. The reaction mixture was diluted with water and extracted with benzene. After removal of the solvent in vacuo, the resulting substance was separated on TLC with chloroform as the developing solvent to give **2a** (33 mg, 17%) and **27** recovered (120 mg, 59%).

Conversion of 2c to 3c. A mixture of **2c** (86 mg), manganese(II) acetate tetrahydrate (704 mg), and acetic anhydride (1 cm^3) in AcOH (20 cm^3) was heated under reflux for 3 h. The reaction mixture was diluted with water and extracted with benzene. The solvent was evaporated in vacuo and the resulting substance was separated on TLC with benzene as the developing solvent to give **3c** (24 mg, 27%) and **2c** recovered (42 mg, 52%).

Oxidation of 1-Chloro-2-phenylethene (26a). The reaction of 1-chloro-2-phenylethene (**26a**)[38] under the reaction conditions similar to those for **1a** gave 1,2,2-trichloroethane (**2a**) and 1-acetoxy-2,2-dichloro-1-phenylethane (**3a**) (Table 1).

Oxidation of 2-Chloro-1,1-diphenylethene (26b). A similar reaction of 2-chloro-1,1-diphenylethene (**26b**) gave 2,2-dichloro-1,1-diphenylethene (**16a**), 1-acetoxy-2,2-dichloro-1,1-diphenylethane (**17a**), and 2,2-dichloro-1,1-diphenylethanol (**18a**) (Table 3).

Oxidation of 1-Chloro-1,2-diphenylethene (26c). The reaction of 1-chloro-1,2-diphenylethene (**26c**)[27] gave 2,2-dichloro-1,2-diphenylethanone (**9a**), 1,2-diphenylethanedione (**11a**), 1,1,2-trichloro-1,2-diphenylethane (**13a**), and (*E*)-1,2-dichloro-1,2-diphenylethene (**14**) (Table 2).

Conversion of 1,1,2-Trichloro-1,2-diphenylethane (13a) to 2-Chloro-1,2-diphenylethanone (28). A mixture of 1,1,2-trichloro-1,2-diphenylethane (**13a**, 260 mg), manganese(II) acetate tetrahydrate (1.79 g), and acetic anhydride (2.8 cm^3) in AcOH (25 cm^3) was heated under reflux for 3 h. After removal of the solvent in vacuo, the resulting substance was separated on TLC with chloroform as the developing solvent to give 2-chloro-1,2-diphenylethanone (**28**) (143 mg) and **13a** (39 mg) (80% conversion).

Oxidation of (*E*)-3-(4-Methoxyphenyl)-2-(4-nitrophenyl)propenoic Acid (8e). (*E*)-3-(4-Methoxyphenyl)-2-(4-nitrophenyl)propenoic acid (**8e**) gave 1,1,2-trichloro-2-(4-methoxyphenyl)-1-(4-nitrophenyl)ethane (**13e**), 2-acetoxy-1,1-dichloro-2-(4-methoxyphenyl)-1-(4-nitrophenyl)ethane (**29e**), 2-acetoxy-2-(4-methoxyphenyl)-1-(4-nitrophenyl)ethanone (**10e**), *p*-anisic acid, and *p*-nitrobenzoic acid.

1,1,2-Trichloro-2-(4-methoxyphenyl)-1-(4-nitrophenyl)ethane (13e): Colorless cubes; mp 127.3—127.8 °C (from ethanol); IR 1599 and 1350 cm^{-1} (NO_2); ^1H NMR ($CDCl_3$) δ= 3.78 (3H, s, OCH_3), 5.47 (1H, s, -CHCl-), 6.74 (2H, m, H-3″ and H-5″), 7.16 (2H, m, H-2″ and H-6″), 7.79 (2H, m, H-2′ and H-6′), and 8.18 (2H, m, H-3′ and H-5′); MS *m/z* (rel intensity) 359, 361, 363, 365 (M^+, 2), 289, 291 (11), 165 (18), and 154, 156 (100). Anal. ($C_{15}H_{12}Cl_3NO_3$) C, H, N.

2-Acetoxy-1,1-dichloro-2-(4-methoxyphenyl)-1-(4-nitrophenyl)ethane (29e): Colorless plates; mp 136.5—137.5 °C (from methanol); IR 1752 (OAc), 1529 and 1352 cm^{-1} (NO_2); ^1H NMR ($CDCl_3$) δ=2.10 (3H, s, OAc), 3.74 (3H, s, OCH_3), 6.31 (1H, s, CHOAc), 6.68 (2H, m, H-3″ and H-5″), 7.03 (2H, m, H-2″ and H-6″), 7.76 (2H, m, H-2′ and H-6′), and 8.15 (2H, m, H-3′ and H-5′). Anal. ($C_{17}H_{15}Cl_2NO_5$) C, H, N.

2-Acetoxy-2-(4-methoxyphenyl)-1-(4-nitrophenyl)ethanone (10e): Colorless liquid; IR 1740 (OAc), 1704 (C=O), 1530 and 1347 cm^{-1} (NO_2); ^1H NMR ($CDCl_3$) δ=2.19 (3H, s, OAc),

3.78 (3H, s, OCH_3), 6.79 (1H, s, $\geq$CHOAc), 6.90 (2H, m, H-3'' and H-5''), 7.40 (2H, m, H-2'' and H-6''), 8.00 (2H, m, H-2' and H-6'), and 8.23 (2H, m, H-3' and H-5'). Found: *m/z* 329.0860. Calcd for $C_{17}H_{15}NO_6$: M, 329.0899.

***p*-Anisic Acid:** Mp 183.5—184.0°C. ***p*-Nitrobenzoic Acid:** Mp 240°C (subl.).

Conversion of 2,2-Dichloro-1,2-diphenylethanone (9a) to 1,2-Diphenylethanedione (11a). A mixture of **9a** (80 mg), manganese(II) acetate tetrahydrate (450 mg), and acetic anhydride (0.7 cm^3) was heated under reflux for 1h. The reaction mixture was diluted with water and extracted with benzene. The solvent was evaporated in vacuo and the resulting substance was separated on TLC with benzene as the developing solvent to give **11a** (7 mg, 12%) and **9a** recovered (63 mg, 79%).

Conversion of 1,2-Dichlorocyclohexanecarboxylic Acid (24) to 1-Acetoxy-2-chlorocyclohexanecarboxylic Acid (25). A mixture of **24** (71 mg), manganese(II) acetate tetrahydrate (528 mg), and acetic anhydride (0.8 cm^3) in AcOH (20 cm^3) was heated under reflux for 3h. The reaction mixture was diluted with water and then extracted with benzene. After removal of the solvent in vacuo, a mixture of **24** and **25** was obtained in the molar ratio of **24**:**25**=3:2 (identified by ^1H NMR spectrum).

We wish to thank Professor Hitoshi Takeshita and Associate Professor Akira Mori of the Research Institute of Industrial Science, Kyushu University, for their measurements of the high-resolution mass spectra.

References

1) R. A. Sheldon and J. K. Kochi, "Metal-catalyzed Oxidation of Organic Compounds," Academic Press (1981).
2) K. D. Donnelly, W. E. Fristad, B. J. Gellerman, J. R. Peterson, and B. J. Selle, *Tetrahedron Lett.*, **25**, 607 (1984).
3) M. Okano, T. Kinoshita, Y. Muramoto, and T. Aratani, *Nippon Kagaku Kaishi*, **1978**, 578.
4) T. Tsuruta, T. Harada, H. Nishino, and K. Kurosawa, *Bull. Chem. Soc. Jpn.*, **58**, 142 (1985).
5) Although an oxo-centered trinuclear structure was proposed for manganese(III) acetate in solid state (Ref. 6), we have calculated the molar equivalent for the acetate as $Mn(OAc)_3 \cdot 2H_2O$ according to Dewar et al. (P. J. Andrulis, Jr., M. J. S. Dewar, R. Dietz, and R. L. Hunt, *J. Am. Chem. Soc.*, **88**, 5473 (1966)).
6) W. E. Fristad and J. R. Peterson, *J. Org. Chem.*, **50**, 10 (1985).
7) J. A. Norman, C. B. Thomas, and M. J. Burrow, *J. Chem. Soc., Perkin Trans. 1*, **1985**, 1087.
8) K. Oishi and K. Kurosawa, *Bull. Chem. Soc. Jpn.*, **53**, 179 (1980).
9) C. V. Wilson, *Org. React.*, **9**, 332 (1957).
10) J. K. Kochi, *J. Org. Chem.*, **30**, 3265 (1965).
11) J. R. Johnson, *Org. React.*, **1**, 211 (1942).
12) B. Jones and J. G. Watkin, *J. Chem. Soc.*, **1958**, 4064.
13) C. Stormer and R. Friemel, *Ber.*, **44**, 1843 (1911).
14) I. S. Dutt, *J. Indian Chem. Soc.*, **1**, 297 (1925).
15) E. D. Bergmann, H. Weiler-Feilchenfeld, and N. Mandel, *Vietnamica Chim. Acta*, **1966**, 129.
16) K. v. Auwers and F. Krollpfeiffer, *Ber.*, **48**, 1389 (1915).
17) R. L. Shriner, *Org. React.*, **1**, 1 (1942).
18) W. F. Reynolds and D. J. Wood, *Can. J. Chem.*, **49**, 1209 (1971).
19) M. C. Cabaleiro and M. D. Johnson, *J. Chem. Soc., (B)*, **1968**, 1022.
20) Y. Shimizu and R. Y. Hsu, *Chem. Pharm. Bull.*, **23**, 2179 (1975).
21) D. Woodcock, *J. Chem. Soc.*, **1949**, 203.
22) Y. G. Balon and M. D. Shulman, *Zh. Org. Khim.*, **12**, 1973 (1976); *Chem. Abstr.*, **86**, 55099v (1977).
23) I. I. Lapkin and E. V. Dormidontova, *Uch. Zap., Perm. Gos. Univ.*, **159**, 276 (1966); *Chem. Abstr.*, **68**, 114672e (1968).
24) B. Lachowicz, *Ber.*, **17**, 1161 (1884).
25) B. B. Corson and N. A. Saliani, *Org. Synth.* Coll. Vol. II, 69 (1943).
26) J. J. Sudborough, *J. Chem. Soc.*, **71**, 221 (1888).
27) R. E. Buckles, W. E. Steinmetz, and N. G. Wheeler, *J. Am. Chem. Soc.*, **72**, 2496 (1950).
28) P. D. Gardner, *J. Am. Chem. Soc.*, **78**, 3421 (1956).
29) A. McKenzie, E. M. Luis, M. Tiffeneau, and P. Weill, *Bull. Soc. Chim. Fr.*, **45**, 414 (1929).
30) R. P. Barnes and W. M. Lucas, *J. Am. Chem. Soc.*, **64**, 2258 (1942).
31) M. Bösler, *Ber.*, **14**, 323 (1881).
32) J. C. Sheehan, R. M. Willson, and A. W. Oxford, *J. Am. Chem. Soc.*, **93**, 7222 (1971).
33) A. Baeyer, *Ber.*, **6**, 220 (1873).
34) W. E. Craig, E. Y. Shropshire, and H. F. Wilson, U. S. Patent 2776988, (1957); *Chem. Abstr.*, **51**, 12144a (1957).
35) G. Koebrich, H. Trapp, K. Flory, and W. Drischel, *Chem. Ber.*, **99**, 689 (1966).
36) E. E. Harris and G. B. Frankforter, *J. Am. Chem. Soc.*, **48**, 3144 (1926).
37) R. Riemschneider and H. Rübner, *Z. Naturforsh.*, **8b**, 161 (1953).
38) F. Bergmann, A. Kalmus, and E. Breuer, *J. Am. Chem. Soc.*, **80**, 4540 (1958).

 © 1986 The Chemical Society of Japan Bull. Chem. Soc. Jpn., 59, 3161—3168 (1986)

Reaction of Olefins with Malonic Acid Derivatives in the Presence of Manganese(III) Acetate

Noriyuki FUJIMOTO, Hiroshi NISHINO, and Kazu KUROSAWA*
Department of Chemistry, Faculty of Science, Kumamoto University, Kurokami 2-39-1, Kumamoto 860
(Received April 15, 1986)

The reaction of methylmalonic acid with mono- and disubstituted olefins in the presence of manganese(III) acetate yielded 2-carboxy-2-methyl-4-butanolides in moderate to good yields. The reactions of bromomalonic acid and chloromalonic acid with a variety of olefins gave 2-halo-4-butanolides and/or 2-buten-4-olides. The reaction of ethyl hydrogen malonate with olefins in the presence of manganese(III) acetate yielded 2-ethoxycarbonyl-2-buten-4-olides, 2-ethoxycarbonyl-2-ethenyl-4-butanolide, 2,7-dioxaspiro[4.4]nonane-1,6-diones, 2-ethoxycarbonyl-4-butanolide, and ethyl 3-butenoate. These reactions can be accounted for in terms of a free-radical mechanism involving substituted dicarboxymethyl radicals.

The formation of γ-lactones is the most characteristic feature in the reaction of manganese(III) acetate with olefins.[1] In previous publications[2,3] it was described how the reaction of olefins with malonic acid in the presence of manganese(III) acetate yielded mainly 2,7-dioxaspiro[4.4]nonane-1,6-diones. We have continued the investigation into the reaction of olefins with malonic acid derivatives in order to obtain mono-γ-lactones rather than spirodi-γ-lactones because the former are encountered more frequently in synthetic organic chemistry. Therefore the reactions of methylmalonic acid, bromomalonic acid, chloromalonic acid, and ethyl hydrogen malonate with a variety of olefins in the presence of manganese(III) acetate were examined and the results are described in this paper.

Results and Discussion

Methylmalonic Acid. When a mixture of 1,1-diphenylethene (**1a**), methylmalonic acid, and manganese(III) acetate[4,5] in a molar ratio of 1 : 1 : 2 in AcOH was heated at 100 °C, 2-carboxy-2-methyl-4,4-diphenyl-4-butanolide (**2a**) was obtained as a sole product. The maximum yield was attained when the molar ratio was 1 : 1.2 : 2.4, but in this case a small amount of decarboxylated compound (**3a**) was also obtained. The reaction at 70 °C gave **3a** and 4,4-diphenyl-4-butanolide (**4**) in prolonged reaction time. Hereafter, we conducted all the reactions at 100 °C. The effects of additives such as Ac_2O and KOAc were next examined but neither showed any appreciable influence on the yield. The reaction was also carried out under an atmosphere of nitrogen, but it did not show any significant change either in the products or in the yield. The reactions of 1,1-bis(4-methoxyphenyl)ethene (**1b**), 1,1-bis(4-methylphenyl)ethene (**1c**), 2-phenylpropene (**1e**), acenaphthylene (**1f**), styrene (**1g**), methylenecyclohexane (**1h**), and 1-octene (**1i**) gave the corresponding 2-carboxy-2-methyl-4-butanolides (**2b**, **c**, **e**—**i**) in moderate to good yields under similar reaction conditions. In the case of **1f**, an acetoxy acid (**5**) was obtained together with **2f** and **3f**. The **2f** and **5** were isolated as their methyl esters. The reactions of 1,1,2-triphenylethene, phenanthrene, chalcone, and (*Z*)-α-acetoxystilbene did not

Table 1. The Reaction of Olefins (**1a**—**c**, **e**—**i**) with Methylmalonic Acid in the Presence of Manganese(III) Acetate in a Molar Ratio of 1:1.2:2.4 in AcOH at 100 °C

Entry	Olefin	Time / min	Recovery / %	Product (yield/%)[a]		Stereoisomer ratio	
1[b]	**1a**	2.5	9	**2a**(62)			
2	**1a**	4		**2a**(78)	**3a**(3)		
3[c]	**1a**	14 days			**3a**(81) **4**(5)		
4[d]	**1a**	3.5	4	**2a**(72)			
5[e]	**1a**	3.5	4	**2a**(74)	**3a**(3)		
6[f]	**1a**	4.5		**2a**(76)			
7	**1b**	3.5		**2b**(70)			
8	**1c**	3		**2c**(88)			
9	**1e**	3.5		**2e**(68)[g]		58 : 42	
10	**1f**	3	2	**2f**(13)[g]	**3f**(21) **5**(11)	100 : 0	for **2f**
						86 : 14	for **3f**
11	**1g**	2.5		**2g**(48)[g]		54 : 46	
12	**1h**	10		**2h**(56)			
13	**1i**	2.5		**2i**(30)[g]		63 : 37	
14[h]	**1i**	6		**2i**(42)[g,i]		55 : 45	

a) Isolated yields based on olefin added. b) A molar ratio of olefin: methylmalonic acid: Mn(III) was 1:1:2. c) At 70 °C. d) Ac_2O (4.8 molar equivalents) was added. e) KOAc (2.4 molar equivalents) was added. f) Under N_2 atmosphere. g) Isolated as a methyl ester. h) **1i**: methylmalonic acid: Mn(III) was 10:1:2. i) Yield based on Mn(III) added.

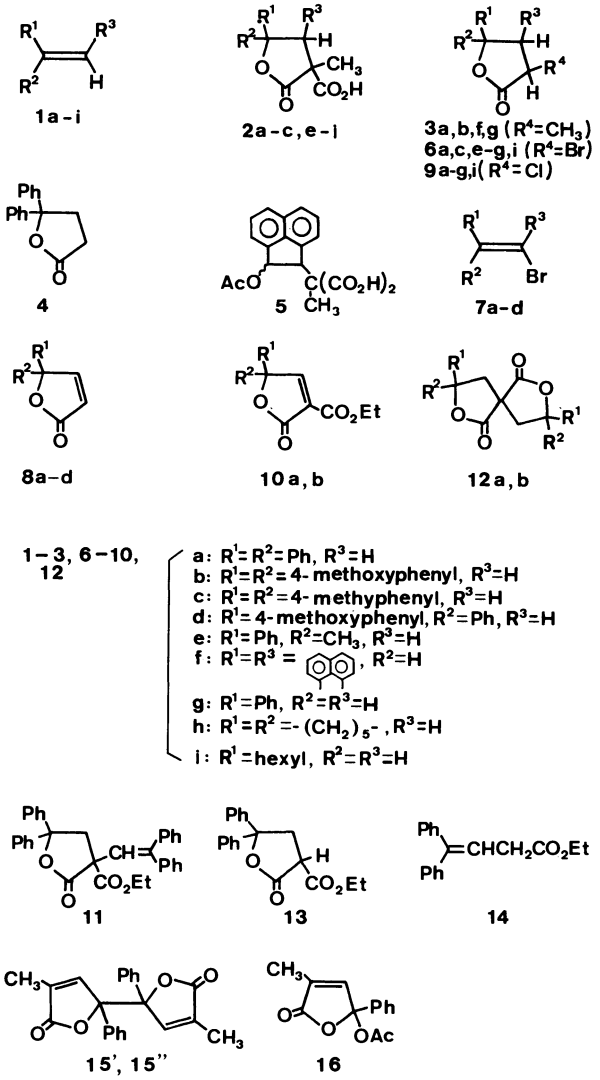

Fig. 1.

take place and the starting olefins were recovered. The 2-carboxy-2-methyl-4-butanolides obtained from **1e, g, i** were found to be a mixture of two diastereoisomers, their ratio being estimated by the ^{1}H NMR spectra or isolated yields. The stereochemistry of these lactones, however, could not be determined.

Bromomalonic Acid. When a mixture of **1a**, bromomalonic acid, and manganese(III) acetate in a molar ratio of 1:1.5:3 was heated at 100 °C, 2-bromo-4,4-diphenyl-4-butanolide (**6a**) was obtained together with 2-bromo-1,1-diphenylethene (**7a**). Similarly, **1e**, **1f**, and **1g** gave the corresponding 4-butanolides (**6e—g**). The olefin **1b** and 1-(4-methoxyphenyl)-1-phenylethene (**1d**), on the other hand, yielded 4,4-bis(4-methoxyphenyl)-2-buten-4-olides (**8b**) and 4-(4-methoxyphenyl)-4-phenyl-2-buten-4-olide (**8d**), respectively. The reaction of **1c** with bromomalonic acid-manganese(III) acetate gave 4,4-bis(4-methylphenyl)-2-buten-4-olide (**8c**) together with a small amount of 2-bromo-4,4-bis(4-methylphenyl)-4-butanolide (**6c**). These 2-bromo-4-butanolides (**6e—g**) consisted of two diastereoisomers which could be separated on TLC. The stereochemistry of each pair, however, could not be determined.

Chloromalonic Acid. The reaction of the olefins with chloromalonic acid-manganese(III) acetate gave results similar to those of bromomalonic acid except for the fact that the 2-chloro-4-butanolides (**9a—g, i**) are fairly stable.

Ethyl Hydrogen Malonate. When **1a** was oxidized with a mixture of ethyl hydrogen malonate and manganese(III) acetate in AcOH, it gave five products, i.e. 2-ethoxycarbonyl-4,4-diphenyl-2-buten-4-olide (**10a**), 2-ethoxycarbonyl-2-(2,2-diphenylethenyl)-4,4-diphenyl-4-butanolide (**11**), 3,3,8,8-tetraphenyl-2,7-dioxaspiro[4.4]-nonane-1,6-dione (**12a**), 2-ethoxycarbonyl-4,4-diphenyl-4-butanolide (**13**), and ethyl 4,4-diphenyl-3-butenoate

Table 2. Reaction of Olefins (**1a—g, i**) with Bromomalonic Acid and Chloromalonic Acid in the Presence of Manganese(III) Acetate in a Molar Ratio of 1:1.5:3 in AcOH at 100 °C

Entry	Olefin	Malonic acid	Time / min	Product (yield/%)[a]			Stereoisomer ratio
1	**1a**	Br	3	**6a**(68)	**7a**(3)		
2	**1a**	Cl	3	**9a**(82)			
3	**1b**	Br	4		**7b**(6)	**8b**(82)	
4	**1b**	Cl	3	**9b**(19)		**8b**(63)	
5	**1c**	Br	3.5	**6c**(4)	**7c**(5)	**8c**(69)	
6	**1c**	Cl	4	**9c**(74)			
7	**1d**	Br	3.5		**7d**(3)	**8d**(67)	
8	**1d**	Cl	3.5	**9d**(36)		**8d**(30)	Not determined
9	**1e**	Br	4	**6e**(54)			59 : 41
10	**1e**	Cl	4	**9e**(46)			54 : 46
11	**1f**	Br	4.5	**6f**(40)			68 : 32
12	**1f**	Cl	3	**9f**(32)			78 : 22
13	**1g**	Br	4	**6g**(28)			68 : 32
14	**1g**	Cl	4	**9g**(28)			75 : 25
15	**1i**	Cl	5.5	**9i**(6)			67 : 33

a) Isolated yields based on olefin added.

Table 3. Reaction of **1a** with Ethyl Hydrogen Malonate in the Presence of Manganese(III) Acetate in Boiling AcOH

Entry	Molar ratio[a]	Time	Recovery	Product (yield/%)[b]				
		min	%	**10a**	**11**	**12a**	**13**	**14**
1	2 : 1 : 4	15	9		57	8		17
2	2 : 1.2 : 4.8	300		3	69	4		12
3	1 : 1 : 2	3	3		17	6	12	12
4	1 : 1 : 3	6		3	45	17		7
5	1 : 1 : 4	110		4	32	22		
6	1 : 1 : 5	390		8	24	8		
7	1 : 2 : 5	80		20	27	8		
8	1 : 3 : 5	35		15	21	8		
9	1 : 4 : 5	20		13	16	6		
10	1 : 5 : 6	22		28	12	6		
11	1 : 6 : 7	21		29	9	7		
12[c]	1 : 6 : 7	22		25	12	11		
13	1 : 6 : 10	24		23	8	6		
14	1 : 6 : 12	32		24	3	3		
15	1 : 8 : 9	17		25	9	6		
16	1 : 10 : 11	13		23	2	7		

a) **1a**: ethyl hydrogen malonate: Mn(III). b) Isolated yields based on **1a** added. c) Ac_2O (16 molar equivalents) was added.

(**14**). The yield of **10a** was slightly improved with the increase of the amounts of ethyl hydrogen malonate and manganese(III) acetate at the expense of the yields of **11** and **12a**. In the reaction at a molar ratio of 1:1:2, the compounds **13** and **14** were formed in minor quantity along with **11** and **12a**. When the molar ratio was 2:1.2:4.8, **11** became the major product (Table 3, Entry 2). Addition of Ac_2O to the reaction mixture showed little effect on the product distribution. Similarly **1b** yielded **10b** (31%) and **12b** (8%).

The reaction of olefins with malonic acid derivatives-manganese(III) acetate proceeded smoothly at 100 °C in a few minutes to give substituted 4-butanolides and 2-buten-4-olides. As already described for the reactions of malonic acid[2] and malonamide[6] with olefin in the presence of manganese(III) acetate, the first step in the reaction of substituted malonic acid must be the formation of substituted malonic acid radical A as the result of the interaction between the malonic acid and manganese(III) acetate. The radical A reacts with an olefin to form a secondary or tertiary carbon radical B which is oxidized to the corresponding carbonium ion C. Upon cyclization followed by deprotonation, the carbonium ion C gives a 2-carboxy-4-butanolide which can be decarboxylated, while some 2-halo-4-butanolides are dehydrohalogenated to give 2-buten-4-olides. In fact, when 2-carboxy-2-methyl-4-butanolides (**2a, b, g**) were heated in AcOH, they gave the decarboxylated products (**3a, b, g**) in excellent yields. These are shown in Scheme 1. It should be pointed out that the substituted dicarboxymethyl radicals regiospecifically add to the less hindered site on the C=C bond. It should be noted also that the reactions of 4-methoxyphenyl (**1b** and **1d**) and 4-methylphenyl-substituted olefin (**1c**) with halomalonic acid tend to give 2-buten-4-olides rather than 2-halo-4-butanolides,

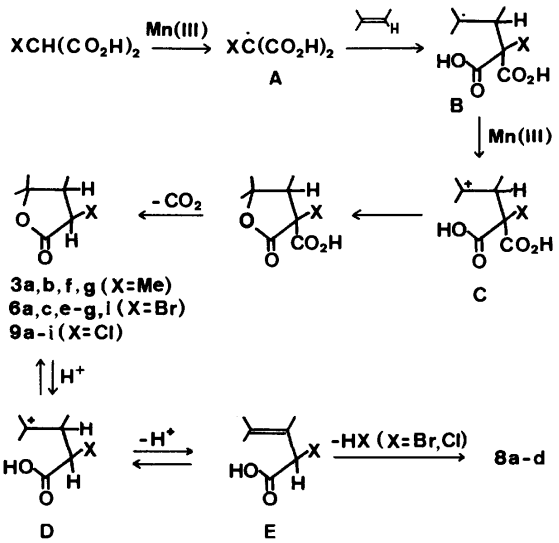

Scheme 1. Possible mechanisms for the formation of γ-lactones.

and some 2-bromo-4-butanolides having a 4-methoxyphenyl group also tend to give 2-buten-4-olides on spontaneous dehydrobromination. An attempt to dehydrohalogenate 4-phenyl-substituted 2-halo-4-butanolides with base failed to yield the corresponding 2-buten-4-olides. These facts may suggest that the carbonium ion D which is in equilibrium with 2-halo-4-butanolides suffered from deprotonation at the adjacent carbon to give 4,4-diaryl-2-halo-3-butenoic acid (E). The latter lactonized to give 2-buten-4-olides. In fact, **6a** was converted to **8a** in a 95% yield on heating in AcOH for 1 h. The formation of bromoethenes (**7a—d**) indicates that Br^- ion or $Br\cdot$ radical was produced in the reaction of bromomalonic acid with manganese(III) acetate.

The reactions of ethyl hydrogen malonate with olefins

in the presence of manganese(III) acetate are different from those of methyl-, bromo-, and chloromalonic acid. The reaction was previously reported by Fristad[3] and Corey[7] who both obtained 2-ethoxycarbonyl-4-butanoldie alone. When we repeated the reaction of **1a** with ethyl hydrogen malonate-manganese(III) acetate, it was found that several other products were also formed and the product distribution depended largely on the molar ratio of olefin and ethyl hydrogen malonate as shown in Table 3. The reaction of **13** with manganese(III) acetate gave **10a** (24%), and the reaction of **13** with a mixture of **1a** and manganese(III) acetate yielded **11** (79%) and **12a** (5%). Thus the pathway for the formation of **10a**, **11**, **12a**, and **14** can be depicted as shown in Scheme 2. Our results indicate that the reaction proved to be useful not only for the preparation of 2-ethoxycarbonyl-4-butanolides but also for the preparations of 2-ethoxycarbonyl-2-buten-4-olides and 2-vinyl-4-butanolides.

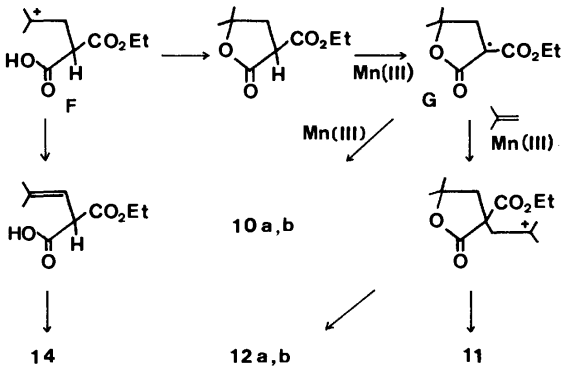

Scheme 2. Pathways for the reaction of olefins with ethyl hydrogen malonate in the presence of manganese(III) acetate.

The formation of 2-carboxy-2-methyl-4-butanolides (**2a—c**, **e—i**) by the reaction of an olefin with methylmalonic acid-manganese(III) acetate led us to investigate the reaction of acetylene with these reagents, since it might give rise to 2-methyl-2-buten-4-olides. The reaction of phenylacetylene with methylmalonic acid-manganese(III) acetate, however, yielded a mixture of isomeric 2,2′-dimethyl-4,4′-diphenyl-4,4′-bis(2-buten-4-olide) (**15′** and **15″**) (25%), and 4-acetoxy-2-methyl-4-phenyl-2-buten-4-olide (**16**) (7%). It was also observed that one of the isomers (**15″**) was converted to the other (**15′**) during recrystallization.

2-Methyl-4-butanolides and 2-chloro-4-butanolides were previously obtained by the reaction of an olefin with manganese(III) acetate in propionic acid[8] and in chloroacetic acid,[9] respectively, but in poor yields. The reaction of olefins with methylmalonic acid in the presence of manganese(III) acetate is a much better method for the preparation of 2-alkyl-4-butanolides, but for the preparation of 2-chloro-4-butanolides it was reported that the ruthenium(II)-catalyzed reaction of olefins with trimethylsilyl α-polychlorinated carboxylates gave γ-lactones in fairly good yields.[10] 2-Bromo-4-butanolides (**5a—c**, **e—i**) have not been synthesized before, therefore our reaction can be useful for the preparation of these compounds.

Experimental

Measurements. All the ^{1}H NMR spectra were recorded with a Hitachi Perkin-Elmer R-24 spectrometer (60 MHz) with tetramethylsilane as the internal reference. The IR spectra were measured in chloroform solution on a JASCO A-102 infrared spectrometer. The mass spectra were obtained with a Hitachi M-80B, a JEOL JMS-DX 300, and a JEOL JMS-OISG mass spectrometer. The melting points were determined with a Yanagimoto micromelting point apparatus and were not corrected.

Materials. The olefins (**1a—e**, h),[2] 1,1-bis(4-methylphenyl)-ethene (**1c**),[11] 1-(4-methoxyphenyl)-1-phenylethene (**1d**),[12] manganese(III) acetate,[4] bromomalonic acid,[13] and chloromalonic acid[13] were prepared by the method described in the literature. Acenaphthylene (**1f**), styrene (**1g**), and 1-octene (**1i**) were purchased from Wako Pure Chemical Industries, Ltd. Methylmalonic acid was commercially available from Aldrich Chemical Co.

Reaction of Olefins with Methylmalonic Acid in the Presence of Manganese(III) Acetate. To a heated solution of olefin (1 mmol) and methylmalonic acid (1.2 mmol) in AcOH (30 cm^3), manganese(III) acetate (2.4 mmol) was added. The solution was heated at 100 °C for the period of time shown in Table 1. After adding water (100 cm^3), the mixture was extracted with benzene. The solvent was removed under reduced pressure. When the resulting crude product was crystalline, the product was recrystallized from benzene and the filtrate was separated on TLC with benzene or chloroform as the developing solvent. In other cases, the product was separated on TLC with chloroform as developing solvent. In the cases of **2e**, g, i, the stereoisomers were further separated on TLC with 20—30% ether/light petroleum as the developing solvent after methylation with diazomethane.

Reaction Products of 1,1-Diphenylethene (1a) with Methylmalonic Acid-Mn(III). 2-Carboxy-2-methyl-4,4-diphenyl-4-butanolide (2a): Colorless plates (from benzene); mp 161.2—162.1 °C; IR 3600—2400 (COOH), 1777 (-COO-), and 1714 cm^{-1} (COOH); ^{1}H NMR (DMSO-d_6) δ=1.25 (3H, s, CH_3), 3.06 (1H, d, J=1.6 Hz, H-3), 3.55 (1H, d, J=12.6 Hz, H-3), 7.0 (1H, br. s, COOH), and 7.1—7.6 (10H, m, ar. H). Found: C, 72.75; H, 5.36%. Calcd for $C_{18}H_{16}O_4$: C, 72.96; H, 5.44%.

2-Methyl-4,4-diphenyl-4-butanolide (3a): Colorless plates (from methanol); mp 120.2—120.7 °C; IR 1770 cm^{-1} (-COO-); ^{1}H NMR ($CDCl_3$) δ=1.14 (3H, d, J=6.6 Hz, CH_3), 2.1—3.4 (3H, m, H-2 and 2×H-3), and 7.1—7.6 (10H, m, ar. H). Found: C, 80.90; H, 6.42%. Calcd for $C_{17}H_{16}O_2$: C, 80.93; H, 6.39%.

4,4-Diphenyl-4-butanolide (4): Colorless microcrystals (from ethanol); mp 89.9—91.1 °C (lit,[14] mp 87—90 °C).

Reaction Product of 1,1-Bis(4-methoxyphenyl)ethene (1b) with Methylmalonic Acid-Mn(III). 2-Carboxy-4,4-bis(4-methoxyphenyl)-2-methyl-4-butanolide (2b): Colorless needles (from benzene); mp 140.0—140.7 °C; IR 3600—2400 (COOH), 1773 (-COO-), and 1715 cm^{-1} (COOH); ^{1}H NMR ($CDCl_3$) δ=1.40 (3H, s, CH_3), 2.83 (1H, d, J=13.2 Hz, H-3), 3.53 (1H, d, J=13.2 Hz, H-3), 3.71 (3H, s, OCH_3), 3.75 (3H, s,

OCH_3), 6.6—7.5 (8H, m, ar. H), and 10.14 (1H, br. s, COOH). Found: C, 67.51; H, 5.37%. Calcd for $C_{20}H_{20}O_6$: C, 67.40; H, 5.66%.

Reaction Product of 1,1-Bis(4-methylphenyl)ethene (1c) with Methylmalonic Acid-Mn(III). 2-Carboxy-2-methyl-4,4-bis(4-methylphenyl)-4-butanolide (2c): Colorless needles (from benzene); mp 148.3—149.2 °C; IR 3600—2400 (COOH), 1775 (-COO-), and 1717 cm^{-1} (COOH); ^1H NMR ($CDCl_3$) δ=1.34 (3H, s, CH_3), 2.27 (3H, s, CH_3), 2.30 (3H, s, CH_3), 2.87 (1H, d, J=13.2 Hz, H-3), 3.51 (1H, d, J=13.2 Hz, H-3), 6.9—7.5 (8H, m, ar. H), and 10.53 (1H, br. s, COOH). Found: C, 74.10; H, 6.30%. Calcd for $C_{20}H_{20}O_4$: C, 74.06: H, 6.21%.

Reaction Product of 2-Phenylpropene (1e) with Methylmalonic Acid-Mn(III). Methyl Ester of 2-Carboxy-2-methyl-4-phenyl-4-pentanolide (2e'): From the upper fraction on TLC (developing solvent: 30% ether/light petroleum); liquid; IR 1771 (-COO-) and 1735 cm^{-1} ($COOCH_3$); ^1H NMR ($CDCl_3$) δ=1.35 (3H, s, CH_3), 1.74 (3H, s, CH_3), 2.47 (1H, d, J=13.2 Hz, H-3), 3.09 (1H, d, J=13.2 Hz, H-3), 3.80 (3H, s, $COOCH_3$), 7.31 (5H, s, Ph). Found: m/z 248.1065. Calcd for $C_{14}H_{16}O_4$: M, 248.1049.

Stereoisomeric Methyl Ester of 2-Carboxy-2-methyl-4-phenyl-4-pentanolide (2e''): From the lower fraction of TLC (developing solvent: 30% ether/light petroleum); colorless plates (from methanol); mp 91.7—92.2 °C; IR 1776 (-COO-) and 1736 cm^{-1} ($COOCH_3$); ^1H NMR ($CDCl_3$) δ= 1.57 (3H, s, CH_3), 1.72 (3H, s, CH_3), 2.31 (1H, d, J=13.2 Hz, H-3), 3.21 (3H, s, $COOCH_3$), 3.23 (1H, d, J=13.2 Hz, H-3), and 7.28 (5H, s, Ph). Found: C, 67.52; H, 6.40%. Calcd for $C_{14}H_{16}O_4$: C, 67.73; H, 6.50%.

Reaction Products of Acenaphthylene (1f) with Methylmalonic Acid-Mn(III). Methyl Ester of 9-Carboxy-9-methyl-*cis*-6b,9a-dihydroacenaphtho[1,2-*b*]furan-8(9*H*)-one (2f): Colorless needles (from benzene/hexane); mp 115.2—115.7 °C; IR 1773 (-COO-) and 1743 cm^{-1} ($COOCH_3$); ^1H NMR ($CDCl_3$) δ=1.80 (3H, s, CH_3), 2.88 (3H, s, $COOCH_3$), 4.25 (1H, d, J=7.8 Hz, H-6b), 6.23 (1H, d, J=7.8 Hz, H-9a), and 7.0—8.0 (6H, m, ar. H). Found: C, 72.36; H, 4.94%. Calcd for $C_{17}H_{14}O_4$: C, 72.33; H, 5.00%.

9-Methyl-*cis*-6b,9a-dihydroacenaphtho[1,2-*b*]furan-8(9*H*)-one (3f'): From the upper fraction on TLC (developing solvent: chloroform); liquid; IR 1766 cm^{-1} (-COO-); ^1H NMR (CCl_4) δ=1.48 (3H, d, J=7.8 Hz, CH_3), 2.2—2.8 (1H, m, H-7), 3.88 (1H, t, J=6.6 Hz, H-6b), 6.02 (1H, d, J=6.6 Hz, H-9a), and 7.0—8.0 (6H, m, ar. H). Found: m/z 224.0863. Calcd for $C_{15}H_{12}O_3$: M, 224.0837.

Stereoisomeric 9-Methyl-*cis*-6b,9a-dihydroacenaphtho-[1,2-*b*]furan-8(9*H*)-one (3f''): From the lower fraction on TLC (developing solvent: chloroform); colorless plates (from benzene/hexane); mp 123.9—124.2 °C; IR 1763 cm^{-1} (-COO-); ^1H NMR ($CDCl_3$) δ=1.29 (3H, d, J=7.8 Hz, CH_3), 3.20 (1H, dq, J=7.8 and 10.8 Hz, H-7), 4.50 (1H, dd, J=6.6 and 10.8 Hz, H-6b), 6.16 (1H, d, J=6.6 Hz, H-9a), and 7.1—8.0 (6H, m, ar. H). Found: C, 80.31; H, 5.43%. Calcd for $C_{15}H_{12}O_2$: C, 80.34; H, 5.39%.

1-Acetoxy-2-[1,1-bis(methoxycarbonyl)ethyl]acenaphthene (Dimethyl Ester of 5): Liquid; IR 1731 cm^{-1}; ^1H NMR ($CDCl_3$) δ=1.23 (3H, s, CH_3), 2.07 (3H, s, OAc), 3.66 (3H, s, $COOCH_3$), 3.80 (3H, s, $COOCH_3$), 4.57 (1H, d, J=1.8 Hz, H-2), 6.65 (1H, d, J=1.8 Hz, H-1), and 7.1—7.9 (6H, m, ar. H). Found: m/z 356.1279. Calcd for $C_{20}H_{20}O_6$: M, 356.1260.

Reaction Products of Styrene (1g) with Methylmalonic Acid-Mn(III). Methyl Ester of 2-Carboxy-2-methyl-4-phenyl-4-butanolide (2g'): From the upper fraction on TLC (developing solvent: 30% ether/light petroleum); colorless plates (from benzene/hexane); mp 81.2—81.6 °C; IR 1778 (-COO-) and 1736 cm^{-1} ($COOCH_3$); ^1H NMR (CCl_4) δ=1.49 (3H, s, CH_3), 1.99 (1H, dd, J=10.2 and 13.8 Hz, H-3), 3.04 (1H, dd, J=6.0 and 13.8 Hz, H-3), 3.78 (3H, s, $COOCH_3$), 5.40 (1H, dd, J=6.0 and 10.2 Hz, H-4), and 7.33 (5H, s, ar. H). Found: C, 66.69; H, 5.97%. Calcd for $C_{13}H_{14}O_4$: C, 66.66; H, 6.02%.

Stereoisomeric Methyl Ester of 2-Carboxy-2-methyl-4-phenyl-4-butanolide (2g''): From the lower fraction on TLC (developing solvent: 30% ether/light petroleum); liquid; IR 1778 (-COO-) and 1741 cm^{-1} ($COOCH_3$); ^1H NMR (CCl_4) δ=1.50 (3H, s, CH_3), 2.45 (1H, dd, J=7.2 and 12.6 Hz, H-3), 2.67 (1H, dd, J=8.4 and 12.6 Hz, H-3), 3.62 (3H, s, $COOCH_3$), 5.38 (1H, dd, J=7.2 and 8.4 Hz, H-4), and 7.25 (5H, s, ar. H). Found: m/z 234.0876; Calcd for $C_{13}H_{14}O_4$: M, 234.0892.

Reaction Product of Methylenecyclohexane (1h) with Methylmalonic Acid-Mn(III). 3-Carboxy-3-methyl-1-oxaspiro[4.5]decan-2-one (2h): Colorless microcrystals (from benzene); mp 147.8—148.3 °C; IR 3600—2400 (COOH), 1762 (-COO-), and 1714 cm^{-1} (COOH); ^1H NMR ($CDCl_3$) δ=1.0—3.0 (10H, m, 5×CH_2), 1.59 (3H, s, CH_3), 1.99 (1H, d, J=13.2 Hz, H-4), 2.72 (1H, d, J=13.2 Hz, H-4), and 11.52 (1H, s, COOH). Found: C, 62.14; H, 7.34%. Calcd for $C_{11}H_{16}O_4$: C, 62.25; H, 7.60%.

Reaction Products of 1-Octene (1i) with Methylmalonic Acid-Mn(III). Methyl Ester of 2-Carboxy-2-methyl-4-decanolide (2i'): From the upper fraction on TLC (developing solvent: 20% ether/light petroleum); liquid; bp 110—115 °C (bath temp)/0.002 mmHg (1 mmHg=133.322 Pa); IR 1771 (-COO-) and 1735 cm^{-1} ($COOCH_3$); ^1H NMR (CCl_4) δ=0.6—2.0 (13H, m, C_6H_{13}-), 1.42 (3H, s, CH_3), 1.70 (1H, dd, J=6.6 and 12.6 Hz, H-3), 2.65 (1H, dd, J=5.4 and 12.6 Hz, H-3), 3.72 (3H, s, $COOCH_3$), and 4.1—4.7 (1H, m, H-4). Found for the stereoisomeric mixture: C, 64.31; H, 9.06%. Calcd for $C_{13}H_{22}O_4$: C, 64.44; H, 9.15%.

Stereoisomeric Methyl Ester of 2-Carboxy-2-methyl-4-decanolide (2i''): From the lower fraction on TLC (developing solvent: 20% ether/light petroleum); liquid; bp 110—115 °C/0.002 mmHg; IR 1771 (-COO-) and 1740 cm^{-1} ($COOCH_3$); ^1H NMR (CCl_4) δ=0.6—2.0 (13H, m, C_6H_{13}-), 1.41 (3H, s, CH_3), 2.18 (1H, dd, J=7.2 and 13.2 Hz, H-3), 2.38 (1H, dd, J=8.4 and 13.2 Hz, H-3), 3.71 (3H, s, CH_3), and 4.1—4.6 (1H, m, H-4). Found for stereoisomeric mixture: C, 64.31; H, 9.06%. Calcd for $C_{13}H_{22}O_4$: C, 64.44; H, 9.15%.

Reaction of Olefins with Bromomalonic Acid and Chloromalonic Acid in the Presence of Manganese(III) Acetate. To a heated solution of the olefin (1 or 2 mmol) and halomalonic acid (1.5 or 3 mmol) in AcOH (30 cm^3), manganese(III) acetate (3 or 6 mmol) was added. The solution was heated at 100 °C for the period of time shown in Table 2. After removal of the solvent under reduced pressure, 2M hydrochloric acid (50 cm^3) was added and the mixture was extracted with chloroform. The solvent was removed under reduced pressure and the resulting crude product was separated on TLC with benzene or chloroform as the developing solvent.

Reaction Products of 1a with Bromomalonic Acid-Mn(III). 2-Bromo-4,4-diphenyl-4-butanolide (6a): Liquid; IR 1788 cm^{-1} (-COO-); ^1H NMR (CCl_4) δ=3.06 (1H, dd, J=10.2 and 13.8 Hz, H-3), 3.51 (1H, dd, J=7.8 and 13.8

Hz, H-3), 4.35 (1H, dd, J=7.8 and 10.2 Hz, H-2), 7.0—7.5 (10H, m, ar. H). Found: m/z 316.0090, 318.0072. Calcd for $C_{16}H_{13}{}^{79}BrO_2$: M, 316.0099; $C_{16}H_{13}{}^{81}BrO_2$: M, 318.0079.

2-Bromo-1,1-diphenylethene (7a): Liquid (lit,[15] mp 42 °C).

Reaction Product of 1a with Chloromalonic Acid-Mn(III). 2-Chloro-4,4-diphenyl-4-butanolide (9a): Colorless microcrystals (from ethanol); mp 90.0—91.4 °C; IR 1789 cm^{-1} (-COO-); ^1H NMR ($CDCl_3$) δ=2.95 (1H, dd, J=10.2 and 12.6 Hz, H-3), 3.51 (1H, dd, J=6.6 and 12.6 Hz, H-3), 4.44 (1H, dd, J=6.6 and 10.2 Hz, H-2), and 7.1—7.2 (10H, m, ar. H). Found: C, 70.35; H, 4.84%. Calcd for $C_{16}H_{13}ClO_2$: C, 70.46; H, 4.80%.

Reaction Products of 1b with Bromomalonic Acid-Mn(III). 2-Bromo-1,1-bis(4-methoxyphenyl)ethene (7b): Liquid (lit,[15] mp 80—82 °C). **4,4-Bis(4-methoxyphenyl)-2-buten-4-olide (8b):** Pale yellow needles (from ethanol); mp 133.2—134.2 °C; IR 1764 cm^{-1} (-COO-); ^1H NMR ($CDCl_3$) δ=3.74 (6H, s, 2×OCH_3), 6.08 (1H, d, J=6.0 Hz, H-2), 6.7—7.3 (8H, m, ar. H), and 7.81 (1H, d, J=6.0 Hz, H-3). Found: C, 72.80; H, 5.47%. Calcd for $C_{18}H_{16}O_4$: C, 72.96; H, 5.44%.

Reaction Products of 1b with Chloromalonic Acid-Mn(III). 4,4-Bis(4-methoxyphenyl)-2-buten-4-olide (8b). 2-Chloro-4,4-bis(4-methoxyphenyl)-4-butanolide (9b): Liquid; IR 1788 cm^{-1} (-COO-); ^1H NMR (CCl_4) δ=2.88 (1H, dd, J=10.8 and 13.2 Hz, H-3), 3.44 (1H, dd, J=7.8 and 13.2 Hz, H-3), 3.75 (6H, s, 2×OCH_3), 4.27 (1H, dd, J=7.8 and 10.8 Hz, H-2), 6.6—7.4 (8H, m, ar. H). Found: m/z 332.0824, 334.0829. Calcd for $C_{18}H_{17}{}^{35}ClO_4$: M, 332.0815; $C_{18}H_{17}{}^{37}ClO_4$: M, 334.0786.

Reaction Products of 1c with Bromomalonic Acid-Mn(III). 2-Bromo-4,4-bis(4-methylphenyl)-4-butanolide (6c): Liquid; IR 1788 cm^{-1} (-COO-); ^1H NMR ($CDCl_3$) δ=2.29 (6H, s, 2×CH_3), 2.99 (1H, dd, J=10.2 and 13.8 Hz, H-3), 3.45 (1H, dd, 7.8 and 13.8 Hz, H-3), 4.35 (1H, dd, J=7.8 and 10.2 Hz, H-2), 6.9—7.4 (8H, m, ar. H). Found: m/z 344.0336, 346.0412. Calcd for $C_{18}H_{17}{}^{79}BrO_2$: M, 344.0412; $C_{18}H_{17}{}^{81}BrO_2$: M, 346.0392.

2-Bromo-1,1-bis(4-methylphenyl)ethene (7c): Liquid (lit,[15] mp 55—57 °C). **4,4-Bis(4-methylphenyl)-2-buten-4-olide (8c):** Colorless needles (from methanol); mp 102.8—103.3 °C; IR 1763 cm^{-1} (-COO-); ^1H NMR ($CDCl_3$) δ=2.32 (6H, s, 2×CH_3), 6.11 (1H, d, J=6.0 Hz, H-2), 7.31 (8H, s, ar. H), and 7.84 (1H, d, J=6.0 Hz, H-3). Found: C, 81.56; H, 6.09%. Calcd for $C_{18}H_{16}O_2$: C, 81.79; H, 6.10%.

Reaction Products of 1d with Bromomalonic Acid-Mn(III). 2-Bromo-1-(4-methoxyphenyl)-1-phenylethene (7d): Liquid (a mixture of (*E*)- and (*Z*)-isomers); ^1H NMR (CCl_4) δ=3.69 and 3.75 (3H, s, s, CH_3), 6.5—7.4 (10H, m, =CH- and ar. H); MS m/z 288, 290. **4-(4-Methoxyphenyl)-4-phenyl-2-buten-4-olide (8d):** Colorless needles (from ethanol); mp 118.6—119.6 °C; IR 1763 cm^{-1} (-COO-); ^1H NMR ($CDCl_3$) δ=3.71 (3H, s, OCH_3), 6.06 (1H, d, J=5.4 Hz, H-2), 6.7—7.4 (9H, m, ar. H), 7.87 (1H, d, J=5.4 Hz, H-3). Found: C, 76.73; H, 5.33%. Calcd for $C_{17}H_{14}O_3$: C, 76.68; H, 5.30%.

Reaction Products of 1d with Chloromalonic Acid-Mn(III). 4-(4-Methoxyphenyl)-4-phenyl-2-buten-4-olide (8d). 2-Chloro-4-(4-methoxyphenyl)-4-phenyl-4-butanolide (9d): Liquid (a mixture of stereoisomers); IR 1790 cm^{-1} (-COO-); ^1H NMR (CCl_4) δ=2.5—3.1 (1H, m, H-3), 3.2—3.7 (1H, m, H-3), 3.69 (3H, s, OCH_3), 4.1—4.6 (1H, m, H-2), and 6.6—7.5 (9H, m, ar. H). Found: m/z 302.0667, 304.0692. Calcd for $C_{17}H_{15}{}^{35}ClO_3$: M, 302.0710; $C_{17}H_{15}{}^{37}ClO_3$: 304.0680.

Reaction Products of 1e with Bromomalonic Acid-Mn(III). 2-Bromo-4-phenyl-4-pentanolide (6e'): From the upper fraction on TLC (developing solvent: benzene); liquid; IR 1783 cm^{-1} (-COO-); ^1H NMR ($CDCl_3$) δ=1.83 (3H, s, CH_3), 2.72 (1H, dd, J=8.4 and 13.2 Hz, H-3), 3.11 (1H, dd, J=8.4 and 13.2 Hz, H-3), 4.44 (1H, t, J=8.4 Hz, H-2), and 7.32 (5H, s, ar. H). Found: m/z 253.9951, 255.9910. Calcd for $C_{11}H_{11}{}^{79}BrO_2$: M, 253.9943; $C_{11}H_{11}{}^{81}BrO_2$: 255.9922.

Stereoisomeric 2-Bromo-4-phenyl-4-pentanolide (6e''): From the lower fraction on TLC (developing solvent: benzene); liquid; IR 1776 cm^{-1} (-COO-); ^1H NMR ($CDCl_3$) δ=1.69 (3H, s, CH_3), 2.81 (1H, dd, J=7.2 and 13.8 Hz, H-3), 3.04 (1H, dd, J=7.2 and 13.8 Hz, H-3), 4.66 (1H, t, J=7.2 Hz, H-2), and 7.32 (5H, s, ar. H). Found: m/z 253.9949, 255.9954. Calcd for $C_{11}H_{11}{}^{79}BrO_2$: M, 253.9943; $C_{11}H_{11}{}^{81}BrO_2$: M, 255.9922.

Reaction Products of 1e with Chloromalonic Acid-Mn(III). 2-Chloro-4-phenyl-4-pentanolide (9e'): From the upper fraction on TLC (developing solvent: chloroform); liquid.[10]

Stereoisomeric 2-Chloro-4-phenyl-4-pentanolide (9e''): From the lower fraction on TLC (developing solvent: chloroform); liquid.[10]

Reaction Products of 1f with Bromomalonic Acid-Mn(III). 9-Bromo-*cis*-6b,9a-dihydroacenaphtho[1,2-*b*]furan-8(9*H*)-one (6f'): From the upper fraction on TLC (developing solvent: chloroform); pale yellow needles (from methanol); mp 127.6—128.5 °C; IR 1777 cm^{-1} (-COO-); ^1H NMR ($CDCl_3$) δ=4.4—4.7 (2H, m, H-6b and H-7), 6.30 (1H, d, J=5.4 Hz, H-9a), and 7.0—8.0 (6H, m, ar. H). Found: C, 58.14; H, 3.13%. Calcd for $C_{14}H_9BrO_2$: C, 58.16; H, 3.14%.

Stereoisomeric 9-Bromo-*cis*-6b,9a-dihydroacenaphtho[1,2-*b*]furan-8(9*H*)-one (6f''): From the lower fraction on TLC (developing solvent: chloroform); colorless needles (from methanol); mp 172.6—173.1 °C; IR 1785 cm^{-1} (-COO-); ^1H NMR ($CDCl_3$) δ=4.62 (1H, dd, J=6.0 and 10.2 Hz, H-6b), 5.10 (1H, d, J=10.2 Hz, H-7), 6.26 (1H, d, J=6.0 Hz, H-9a), and 7.3—8.0 (6H, m, ar. H). Found: C, 58.40; H, 3.14%. Calcd for $C_{14}H_9BrO_2$: C, 58.16; H, 3.14%.

Reaction Products of 1f with Chloromalonic Acid-Mn(III). 9-Chloro-*cis*-6b,9a-dihydroacenaphtho[1,2-*b*]furan-8(9*H*)-one (9f'): From the upper fraction on TLC (developing solvent: chloroform); pale yellow microcrystals (from benzene/hexane); mp 115.2—116.2 °C; IR 1782 cm^{-1} (-COO-); ^1H NMR ($CDCl_3$) δ=4.4—4.8 (2H, m, H-6b and H-7), 6.38 (1H, d, J=6.0 Hz, H-9a), and 7.2—8.0 (6H, m, ar. H). Found: m/z 244.0254, 246.0278. Calcd for $C_{14}H_9{}^{35}ClO_2$: M, 244.0291; $C_{14}H_9{}^{37}ClO_2$: M, 246.0262.

Stereoisomeric 9-Chloro-*cis*-6b,9a-dihydroacenaphtho-[1,2-*b*]furan-8(9*H*)-one (9f''): From the lower fraction on TLC (developing solvent: chloroform); colorless plates (from benzene); mp 192.5—193.5 °C; IR 1787 cm^{-1} (-COO-); ^1H NMR ($CDCl_3$) δ=4.68 (1H, dd, J=6.0 and 10.2 Hz, H-6b), 5.10 (1H, d, J=10.2 Hz, H-7), 6.22 (1H, d, J=6.0 Hz, H-9a), 7.2—8.0 (6H, m, ar. H). Found: m/z 244.0293, 246.0253. Calcd for $C_{14}H_9{}^{35}ClO_2$: M, 244.0291; $C_{14}H_9{}^{37}ClO_2$: M, 246.0262.

Reaction Products of 1g with Bromomalonic Acid-Mn(III). 2-Bromo-4-phenyl-4-butanolide (6g'): From the upper fraction on TLC (developing solvent: benzene); liquid; IR 1788 cm^{-1} (-COO-); ^1H NMR (CCl_4) δ=2.5—2.8 (2H, m, 2×H-3), 4.43 (1H, dd, J=3.0 and 5.4 Hz, H-2), 5.55 (1H, dd, J=6.6 and 7.8 Hz, H-4), and 7.26 (5H, s, Ph). Found: m/z 239.9777, 241.9780: Calcd for $C_{10}H_9{}^{79}BrO_2$: M, 239.9786;

$C_{10}H_9{}^{81}BrO_2$: M, 241.9766.

Stereoisomeric 2-Bromo-4-phenyl-4-butanolide (6g''): From the lower fraction on TLC (developing solvent: benzene); liquid; IR 1788 cm^{-1} (-COO-); ^1H NMR (CCl_4) δ=2.1—2.7 (1H, m, H-3), 2.9—3.5 (1H, m, H-3), 4.62 (1H, dd, J=8.4 and 9.6 Hz, H-2), 5.37 (1H, dd, J=6.6 and 9.6 Hz, H-4), and 7.23 (5H, s, Ph). Found: m/z 239.9801, 241.9808. Calcd for $C_{10}H_9{}^{79}BrO_2$: M, 239.9786; $C_{10}H_9{}^{81}BrO_2$: M, 241.9766.

Reaction Products of 1g with Chloromalonic Acid-Mn(III). 2-Chloro-4-phenyl-4-butanolide (9g'): From the upper fraction on TLC (developing solvent: chloroform); liquid.[10]

Stereoisomeric 2-Chloro-4-phenyl-4-butanolide (9g''): From the lower fraction on TLC (developing solvent: chloroform); liquid.[10]

Reaction Products of 1i with Chloromalonic Acid-Mn(III). 2-Chloro-4-decanolide (9i'): From the upper fraction on TLC (developing solvent: benzene); liquid.[16]

Stereoisomeric 2-Chloro-4-decanolide (9i''): From the lower fraction on TLC (developing solvent: benzene); liquid.[16]

Reaction of Olefins with Ethyl Hydrogen Malonate in the Presence of Manganese(III) Acetate. To a heated solution of olefin (1 or 2 mmol) and ethyl hydrogen malonate in AcOH (30 cm^3), manganese(III) acetate was added. The solution was heated under reflux for the period of time shown in Table 3. After adding water (100 cm^3), the mixture was extracted with benzene, and the solvent was removed under reduced pressure. The resulting crude product was separated on TLC with chloroform as the developing solvent.

Reaction Products of 1a with Ethyl Hydrogen Malonate-Mn(III). 2-Ethoxycarbonyl-4,4-diphenyl-2-buten-4-olide (10a): Colorless plates (from methanol); mp 107.9—109.4 °C; IR 1782 (-COO-), 1719 (-COOEt), and 1642 cm^{-1} (C=C); ^1H NMR ($CDCl_3$) δ=1.31 (3H, t, J=7.2 Hz, CH_3), 4.31 (2H, q, J=7.2 Hz, -CH_2-), 7.28 (10H, s, 2×Ph), and 8.57 (1H, s, =CH-). Found: C, 73.87; H, 5.21%. Calcd for $C_{19}H_{16}O_4$: C, 74.01; H, 5.23%.

2-Ethoxycarbonyl-4,4-diphenyl-2-(2,2-diphenylethenyl)-4-butanolide (11): Colorless needles (from benzene); mp 279.8—281.5 °C; IR 1776 (-COO-) and 1734 cm^{-1} (COOEt); ^1H NMR ($CDCl_3$) δ=0.94 (3H, t, J=7.2 Hz, CH_3), 2.72 (1H, d, J=12.6 Hz, H-3), 3.28 (1H, d, J=12.6 Hz, H-3), 3.62 (2H, q, J=7.2 Hz, -OCH_2-), 6.32 (1H, s, =CH-), and 6.9—7.6 (20H, m, 4×Ph). Found: C, 80.93; H, 5.58%. Calcd for $C_{33}H_{28}O_4$: C, 81.12; H, 5.78%.

3,3,8,8-Tetraphenyl-2,7-dioxaspiro[4.4]nonane-1,6-dione (12a): Colorless needles (from benzene); mp 284.5—285.0 °C (lit,[2] mp 284.5—285.0 °C).

2-Ethoxycarbonyl-4,4-diphenyl-4-butanolide (13): Colorless prisms (from benzene/hexane); mp 67.4—68.5 °C; IR 1782 (-COO-) and 1735 cm^{-1} (COOEt); ^1H NMR ($CDCl_3$) δ=1.17 (3H, t, J=7.2 Hz, CH_3), 3.0—3.8 (3H, m, -CH_2- and >CH-), 4.13 (2H, q, J=7.2 Hz, OCH_2-), and 7.1—7.5 (10H, m, 2×Ph). Found: m/z 310.1187. Calcd for $C_{19}H_{18}O_4$: M, 310.1205.

Ethyl 4,4-diphenyl-3-butenoate (14): Liquid.[17]

Reaction Products of 1b with Ethyl Hydrogen Malonate-Mn(III). 2-Ethoxycarbonyl-4,4-bis(4-methoxyphenyl)-2-buten-4-olide (10b): Liquid; IR 1781 (-COO-), 1717 (COOEt), and 1640 cm^{-1} (C=C); ^1H NMR (CCl_4) δ=1.26 (3H, t, J=7.2 Hz, CH_3), 3.66 (6H, s, 2×OCH_3), 4.16 (2H, q, J=7.2 Hz, OCH_2-), 6.5—7.3 (8H, m, ar. H), and 8.46 (1H, s, =CH-). Found: m/z 368.1258. Calcd for $C_{21}H_{20}O_6$: M, 368.1260.

3,3,8,8-Tetrakis(4-methoxyphenyl)-2,7-dioxaspiro[4.4]-nonane-1,6-dione (12b): Amorphous solid.[2]

Decarboxylation of 2a, b, g. 2-Carboxy-2-methyl-4-butanolide (**2a, b,** g) (1 mmol) was heated in AcOH (30 cm^3) under reflux. After adding water (100 cm^3), the mixture was extracted with benzene and the solvent was evaporated in vacuo. The resulting crude product was purified on TLC with chloroform as the developing solvent, and in the case of **3g** further purification was made by TLC with ether/light petroleum 30 : 70 as the developing solvent.

2-Methyl-4,4-diphenyl-4-butanolide (3a): Heated for 9 h; 90% yield.

2-Methyl-4,4-bis(4-methoxyphenyl)-4-butanolide (3b): Heated for 6 h; 54% yield: Colorless prisms (from benzene/hexane); mp 100.1—100.4 °C; IR 1765 cm^{-1} (-COO-); ^1H NMR ($CDCl_3$) δ=1.23 (3H, d, J=6.0 Hz, CH_3), 2.1—3.3 (3H, m, H-2 and 2×H-3), 3.74 (6H, s, 2×OCH_3), and 6.6—7.5 (8H, m, ar. H). Found: C, 73.16; H, 6.47%. Calcd for $C_{19}H_{20}O_4$: C, 73.06; H, 6.45%.

2-Methyl-4-phenyl-4-butanolide (3g) (a mixture of two diasteroisomers, **3g'** and **3g''**): Heated for 5.5 h; 71% yield. **3g'**: From the upper fraction on TLC; liquid.[18] **3g''**: From the lower fraction on TLC; liquid.[18]

Dehydrobromination of 6a in AcOH. The **6a** (53.2 mg) was heated in AcOH (5 cm^3) at 100 °C for 1 h. The solvent was removed in vacuo and the resulting crude product was purified on TLC with chloroform as the developing solvent, giving 4,4-diphenyl-2-buten-4-olide (**8a**) (37.9 mg, 95%), mp 131.7—132.7 °C (lit,[19] mp 131—131.5 °C).

Reaction of 13 with 1a in the Presence of Manganese(III) Acetate. To a heated solution of **1a** (211.5 mg) and **13** (128 mg) in AcOH (20 cm^3), manganese(III) acetate (347.2 mg) was added. The solution was heated under reflux for 55 min. After adding water (100 cm^3), the mixture was extracted with benzene. After removal of the solvent in vacuo the resulting crude product was separated on TLC with benzene as the developing solvent, giving **11** (79%) and **12a** (5%).

Reaction of 13 with Manganese(III) Acetate. To a heated solution of **13** (204.5 mg) in AcOH (20 cm^3), manganese(III) acetate (353.4 mg) was added. The solution was heated under reflux for 90 min. After adding water (100 cm^3), the mixture was extracted with benzene and purified on TLC with benzene as the developing solvent, giving **10a** (24%) and **4** (6%).

Reaction of Phenylacetylene with Methylmalonic Acid in the Presence of Manganese(III) Acetate. To a heated solution of phenylacetylene (204.6 mg) and methylmalonic acid (284.1 mg) in AcOH (30 cm^3), manganese(III) acetate (1.289 g) was added. The solution was heated at 100 °C for 2 min. After adding water (100 cm^3), the mixture was extracted with benzene. The solvent was removed in vacuo and then the resulting crude product was purified on TLC with benzene as the developing solvent, giving **15'**, **15''**, and **16**.

2,2'-Dimethyl-4,4'-diphenyl-4,4'-bi(2-buten-4-olide) (15'): 18% yield: Colorless needles (from benzene); mp 229.7—230.5 °C; IR 1762 (-COO-) and 1659 cm^{-1} (C=C); ^1H NMR ($CDCl_3$) δ=1.59 (6H, d, J=1.3 Hz, 2×CH_3), 7.31 (10H, s, 2×Ph), and 7.41 (2H, q, J=1.3 Hz, H-3 and H-3'). Found: C, 76.27; H, 5.23%. Calcd for $C_{22}H_{18}O_4$: C, 76.29; H, 5.24%.

Stereoisomeric 2,2'-Dimethoxy-4,4'-diphenyl-4,4'-bi(2-buten-4-olide) (15''): 7% yield: Colorless microcrystals (**15''** has changed to **15'** during recrystallization from benzene); IR

1763 (-COO-) and 1658 cm^{-1} (C=C); ^1H NMR ($CDCl_3$) δ=1.91 (6H, d, J=1.3 Hz, 2×CH_3), 7.15 (10H, s, 2×Ph), 7.33 (2H, q, J=1.3 Hz, H-3 and H-3′).

4-Acetoxy-2-methyl-4-phenyl-2-buten-4-olide (16): Liquid; IR 1783 (-COO-), 1748 (OAc), and 1664 cm^{-1} (C=C); ^1H NMR ($CDCl_3$) δ=1.95 (3H, d, J=1.3 Hz, CH_3), 2.04 (3H, s, OAc), 7.1—7.6 (5H, m, Ph), and 7.30 (1H, q, J=1.3 Hz, =CH-). Found: m/z 232.0731. Calcd for $C_{13}H_{12}O_4$: M, 232.0736.

We wish to thank Professor Hitoshi Takeshita and Associate Professor Akira Mori of the Research Institute of Industrial Science, Kyushu University, and Dr. Shinzaburo Hishida of Hitachi Ltd., for their measurements of the mass spectra.

References

1) J. B. Bush, Jr. and H. L. Finkbeiner, *J. Am. Chem. Soc.*, **90**, 5903 (1968); E. I. Heiba, R. M. Dessau, and W. J. Koehl, Jr., *ibid.*, **90**, 5905 (1968).

2) N. Ito, H. Nishino, and K. Kurosawa, *Bull. Chem. Soc. Jpn.*, **56**, 3527 (1983).

3) W. E. Fristad and S. S. Hershberger, *J. Org. Chem.*, **50**, 1026 (1985).

4) Although an oxo-centered trinuclear structure for manganese(III) acetate in solid state was proposed (Ref. 5), we have calculated the molar equivalent for the acetate as $Mn(OAc)_3 \cdot 2H_2O$ according to Dewar et al. (P. J. Andrulis, Jr., M. J. S. Dewar, R. Dietz, and R. L. Hunt, *J. Am. Chem. Soc.*, **88**, 5473 (1966)).

5) W. E. Fristad and J. R. Peterson, *J. Org. Chem.*, **50**, 10 (1985).

6) H. Nishino, *Bull. Chem. Soc. Jpn.*, **58**, 217 (1985).

7) E. J. Corey and A. W. Gross, *Tetrahedron Lett.*, **26**, 4291 (1985).

8) M. Okano, *Chem. Lett.*, **1973**, 165.

9) W. E. Fristad, J. R. Peterson, and A. B. Ernst, *J. Org. Chem.*, **50**, 3143 (1985).

10) T. Nakano, K. Ohkawa, S. Ikemori, H. Matsumoto, and Y. Nagai, *Nippon Kagaku Kaishi*, **1983**, 1778.

11) R. Anshütz and A. Hilbert, *Ber.*, **57**, 1697 (1924).

12) C. D. Hurd and C. N. Webb, *J. Am. Chem. Soc.*, **49**, 546 (1927).

13) M. Conrad and H. Reibach, *Ber.*, **35**, 1813 (1902).

14) W. S. Johnson, J. W. Petersen, and W. P. Schneider, *J. Am. Chem. Soc.*, **69**, 74 (1947).

15) D. F. Bender, T. Thippeswamy, and W. L. Rellahan, *J. Org. Chem.*, **35**, 939 (1970).

16) T. Nakano, K. Ohkawa, S. Ikemori, R. Hasegawa, Y. Sako, H. Matsumoto, and Y. Nagai, *Nippon Kagaku Kaishi*, **1983**, 1770.

17) V. K. Kasal and A. P. Bhaduri, *Z. Naturforsh.*, **34B**, 1567 (1979); *Chem. Abstr*, **92**, 110502x (1980).

18) A. P. Kozikowski and Y.-Y. Chen, *J. Org. Chem.*, **45**, 2236 (1980).

19) P. M. M. van Haard, L. Thijs, and B. Zwanenburg, *Tetrahedron Lett.*, **1975**, 803.

 © 1986 The Chemical Society of Japan Bull. Chem. Soc. Jpn., 59, 3169—3173 (1986)

Photochemical Addition of Benzyltriethylgermane and Dibenzyldiethylgermane to Olefins

Masanori KOBAYASHI, Masato YOSHIDA, and Michio KOBAYASHI*
Department of Chemistry, Faculty of Science, Tokyo Metropolitan University, Fukazawa, Setagaya-ku, Tokyo 158
(Received April 4, 1986)

A novel photochemical addition of a germyl radical to the olefinic double bond was discovered when benzyltriethylgermane or dibenzyldiethylgermane was irradiated with a medium-pressure mercury lamp in the presence of olefins.

There have been only scattered reports on the photochemical behavior of organogermanium compounds.[1] We have reported previously that the photolysis of aryltrialkylgermanes and diaryldialkyl-germanes generated germyl and aryl free radicals.[2] In order to widen the scope of this photochemical reaction, the photolysis of benzyltrialkylgermane and dibenzyldialkylgermane were investigated. Contrary to the arylalkylgermanes, which show no tendency to add to the olefinic double bond but to abstract a hydrogen atom from solvent hydrocarbon upon irradiation, the photolysis of benzylsubstituted germanes in the presence of olefins were found to readily form 1,2-adducts. Even in the absence of olefins, the photolysis of the Ge–benzyl bond of these benzylgermanes proceeded rapidly. The high photoreactivity of alkylbenzylgermanes makes a good contrast to the very low rate of conversion of analogous trimethylbenzylsilanes that have recently been reported.[3]

Results and Discussion

Photolysis of Benzyltriethylgermane and Diethyldibenzylgermane. The photolysis of benzyltriethylgermane (**1**) in hexane with a medium-pressure mercury lamp through a Vycor filter for 10 min resulted in the facile decomposition of **1** to give hexaethyldigermane (**2**)[5] and bibenzyl (**3**) as shown below:

$$\underset{\textbf{1}}{Et_3GeCH_2Ph} \xrightarrow[\text{hexane}]{h\nu,\ 10\text{min}} \underset{\textbf{2}\ 75\%}{(Et_3Ge)_2} + \underset{\textbf{3}\ 86\%}{(PhCH_2)_2} + \underset{\text{(recovered)}\ 9\%}{\textbf{1}}$$

The formation of the above two products can be explained by assuming the photochemical dissociation of the benzyl–germanium bond (Eq. 1) and a subsequent dimerization of triethylgermyl and benzyl radicals. Both the germyl radical (**4**) and the benzyl radical are known to be relatively inactive and to possess little ability to abstract hydrogen atoms from saturated aliphatic hydrocarbons such as hexane.[1]

$$Et_3GeCH_2Ph \xrightarrow{h\nu} \underset{\textbf{4}}{Et_3Ge\cdot} + PhCH_2\cdot \qquad (1)$$

When **1** was irradiated in benzene under similar conditions, a small amount of triethyl-*p*-tolylgermane (**5**) was detected among the products in addition to bibenzyl and digermane (**2**). The formation of **5** suggests an intramolecular rearrangement of the triethylgermyl group from the benzyl carbon to the benzene ring by recombination in a solvent cage of the benzyl radical and the triethylgermyl radical pair once generated by the homolysis of Ge–benzyl bond. A similar rearrangement was observed in the photolysis of trimethylbenzylsilane.[3] An intramolecular photorearrangement of the germyl group has also been observed in cinnamylgermanes.[4]

When dibenzyldiethylgermane (**6**) was irradiated in hexane under similar conditions for 3 min, about 40% of **6** was photolyzed to form bibenzyl (**3**) and 1,2-dibenzyl-1,1,2,2-tetraethyldigermane (**7**) as major products. However, in this case, small amounts of germane (**8**), toluene and heptylbenzene (**9**) were also detected.

$$\underset{\textbf{6}}{Et_2Ge(CH_2Ph)_2} \xrightarrow[\text{hexane}]{h\nu,\ 3\text{ min}} \underset{\textbf{7}\ 49\%}{(Et_2GeCH_2Ph)_2} + \underset{\textbf{3}\ 98\%}{(PhCH_2)_2} + PhCH_3 + \underset{\textbf{8}\ 12\%}{Et_2GeCH_2Ph} + \underset{\textbf{9}}{PhCH_2C_6H_{13}} \qquad (2)$$

The formation of bibenzyl and digermane (**7**) suggests the splitting of the Ge–benzyl bond under irradiation to give a diethylbenzylgermyl radical (**10**) and a benzyl radical, and a subsequent dimerization of each radical.

$$\textbf{6} \longrightarrow \underset{\textbf{10}}{Et_2\dot{G}eCH_2Ph} + PhCH_2\cdot \qquad (3)$$

$$\textbf{10} + \textbf{10} \longrightarrow (Et_2GeCH_2Ph)_2 \qquad (4)$$

$$2\,PhCH_2\cdot \longrightarrow (PhCH_2)_2 \qquad (5)$$

Since neither the germyl radical nor the benzyl radical can abstract hydrogen atom from a saturated hydrocarbon (as stated before), it is unreasonable to explain the formation of germane (**8**), toluene and **9** by the simple hydrogen abstraction of a germyl radical from hexane and a subsequent recombination of the hexyl and benzyl radicals. The formation of these products can be tentatively explained by the following reaction sequence:

$$\underset{\text{CH}_2\text{Ph}}{Et_2Ge\cdot} + PhCH_2\cdot \longrightarrow \underset{\textbf{8}}{Et_2GeHCH_2Ph} + \underset{\textbf{11}}{PhCH{:}} \qquad (6)$$

Table 1. Photochemical Addition of **1** to 1-Hexene

Product		Yield/%[a]
$Et_3GeCH_2\underset{\underset{CH_2Ph}{|}}{C}H(CH_2)_3CH_3$	(**12**)	50
$Et_3Ge(CH_2)_5CH_3$	(**13**)	35
$Et_3GeCH{=}CH(CH_2)_3CH_3$	(**14**)	
$Et_3GeCH_2CH{=}CH(CH_2)_2CH_3$	(**15**)	
$Et_3GeCH_2\underset{\underset{C_6H_{13}}{|}}{C}H(CH_2)_3CH_3$	(**17**)	15
$(PhCH_2)_2$	(**3**)	35

a) Yields were determined by GLC.

and

$$PhCH{:} + C_6H_{14} \longrightarrow \underset{\mathbf{9}}{PhCH_2C_6H_{13}} \qquad (7)$$

By a metathesis between **10** and benzyl radical or by a direct alpha elimination from **6**, phenylcarbene (**11**) which undergoes insertion into the C–H bond of the solvent (hexane) to give heptylbenzene (**9**).

Photolysis in the Presence of Olefins. When benzyltriethylgermane **1** was irradiated with a medium-pressure mercury lamp in the presence of 1-hexene for 1.5 h, **1** was completely consumed to give the following products (yields are shown in Table 1):

$$Et_3GeCH_2Ph + CH_3(CH_2)_3CH{=}CH_2 \xrightarrow{h\nu}$$
$$\underset{\mathbf{12}}{CH_3(CH_2)_3CH(CH_2Ph)CH_2GeEt_3} + \underset{\mathbf{13}}{CH_3(CH_2)_5GeEt_3} +$$
$$\underset{\mathbf{14}}{CH_3(CH_2)_3CH{=}CHGeEt_3} + \underset{\mathbf{15}}{CH_3(CH_2)_2CH{=}CHCH_2GeEt_3}$$
$$+ \mathbf{3} + C_{12}H_{26} \qquad (8)$$

This reaction can also be understood by assuming a splitting of the Ge–benzyl bond to give a triethylgermyl radical (**4**) and a benzyl radical (Eq. 1). **4** would add (Eq. 9) to 1-hexene to give a 1-(triethylgermylmethyl)-pentyl radical (**16**), which may recombine (Eq. 10) with a benzyl radical to form 1,2-adduct (**12**) or may disproportionate[2,5] (Eq. 11) to give 1-triethylgermylhexane (**13**) and 1-triethylgermyl-1-hexene (**14**) or 1-triethylgermyl-2-hexene (**15**), accompanying the dimerization of excess benzyl radicals to bibenzyl.

$$\underset{\mathbf{4}}{Et_3Ge\cdot} + C_4H_9CH{=}CH_2 \longrightarrow \underset{\mathbf{16}}{Et_3GeCH_2\dot{C}HC_4H_9} \qquad (9)$$

$$\mathbf{16} + PhCH_2\cdot \longrightarrow \mathbf{12} \qquad (10)$$

$$\mathbf{16} + \mathbf{16} \longrightarrow \mathbf{13} + \mathbf{14} + \mathbf{15} \qquad (11)$$

The formation of adduct **12** indicates the attack of a germyl radical to a terminal carbon atom of the olefinic double bond during the first step of the addition (Eq. 9), thus showing the higher addition ability of a germyl radical than that of a benzyl radical.

When **1** was photolyzed in the presence of cyclohexene under similar conditions for 1 h, the starting germane **1** was completely consumed. Products are summarized in Table 2.

Table 2. Photochemical Addition of **1** to Cyclohexene

Product		Yield/%[a]
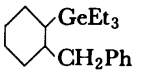	(**19**)	35 (cis:trans=1:4.4)
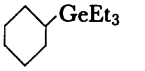	(**20**)	22
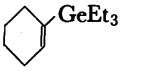	(**21**)	
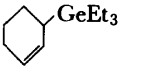	(**22**)	
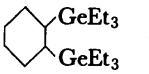	(**23**)	21 (cis and trans)
$(Et_3Ge)_2$	(**2**)	21
$(PhCH_2)_2$	(**3**)	45

a) Yields were determined by GLC.

The first step in this reaction was the cleavage of the Ge–benzyl bond (Eq. 1). The triethylgermyl radical (**4**) added to cyclohexene to form a 2-(triethylgermyl)cyclohexyl radical (**18**), which reacted either by recombination with a benzyl radical resulting in the formation of the 1,2-adduct (**19**), or by disproportionation to give triethylgermylcyclohexane (**20**), 1-(triethylgermyl)cyclohexene (**21**) and 3-(triethylgermyl)cyclohexene (**22**). Part of the triethylgermyl radical combined with **18** to form 1,2-bis(triethylgermy)cyclohexane (**23**) or dimerized to hexaethyldigermane (**2**).[5] About half of the benzyl radical dimerized to bibenzyl. The formation of digermane **2** and 1,2-digermyl compound **23** suggest that the triethylgermyl radical is rather stable and can diffuse out of the solvent cage to seek combinations with other free radicals.

1,2-Adduct **19** is a mixture of cis and trans isomers. The ratio of cis:trans is 1:4.4, indicating that the addition is mainly trans, but not strictly stereospecific. The formation of both cis and trans isomers indicates that addition is not concerted but proceeds by a two-step mechanism.

In order to survey the effects of substituents, the photolysis of **1** in the presence of di-, tri-, and tetrasubstituted olefins were also investigated.

Products of the photolysis of **1** in the presence of 2-hexene are shown in Table 3. Starting germane **1** was completely consumed in 1.5 h. Three types of 1,2-adducts (**24A**, **24B**, **24C**) were detected with GLC and GC-Mass but could not be separated from each other. Most probably, they are the 2- and 3-germyl isomers and their threo–erythro isomers.

Results of the photolysis of **1** in 2-methyl-2-pentene

Table 3. Photochemical Addition of **1** to 2-Hexene

Product[a]	Yield/%[b]
1,2-Adducts of **1** with 2-hexene (**24A**, **24B**, **24C**)	22
$(Et_3Ge)_2$ (**2**)	Trace
$(PhCH_2)_2$ (**3**)	40
$(Et_3Ge)_2O$	21

a) Germylhexanes, germylhexenes (total yield 21%), and germyldodecane (3%) were also detected by GC-MS. b) Yields were determined by GLC.

Table 4. Photochemical Addition of **1** to 2-Methyl-2-pentene

Product		Yield/%[a]
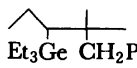	(**25**)	5
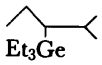	(**27**)	22
	(**28**)	
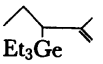	(**29**)	
$(Et_3Ge)_2$	(**2**)	Trace
$(Et_3Ge)_2O$		17
$(PhCH_2)_2$	(**3**)	40

a) Yields were determined by GLC.

Table 5. Photochemical Addition of **1** to 2,3-Dimethyl-2-butene

Product		Yield/%[a]
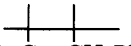	(**30**)	3
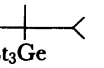	(**31**)	7
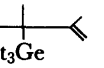	(**32**)	
$(Et_3Ge)_2$	(**2**)	45
$(Et_3Ge)_2O$		4
$(PhCH_2)_2$	(**3**)	71

a) Yields were determined by GLC.

Table 6. Photochemical Addition of **1** to 2,3-Dimethyl-1,3-butadiene

Product		Yield/%[a]
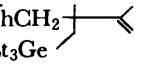	(**34**)	22
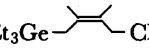	(**35**)	29
$(PhCH_2)_2$	(**3**)	17

a) Yields were determined by GLC based on the consumed **1**. 5% of **1** was recovered.

are summarized in Table 4. The structure of 1,2-adduct **25** indicates that the attack of triethylgermyl radical (**4**) occurred at a less-hindered olefinic carbon to give a more stable tertiary carbon radical **26**. The low yield of the 1,2-adduct **25** suggests a steric inhibition toward the recombination between **26** and the benzyl radical. A larger part of radical **26** disproportionated to afford germylhexane (**27**) and germylhexenes (**28** and **29**).

In the case of the photolysis of **1** in the presence of 2,3-dimethyl-2-butene, the yield of 1,2-adduct, 2-benzyl-2,3-dimethyl-3-(triethylgermyl)butane (**30**) was only 3%. The major products were hexaethyldigermane (**2**) and bibenzyl. Small amounts of 2,3-dimethyl-2-(triethylgermyl)butane (**31**) and 2,3-dimethyl-3-(triethylgermyl)-1-butene (**32**) were also detected. The formation of these germylbutane and germylbutene derivatives can be explained by a disproportionation of the adduct radical **33**.

In the reaction of **1** with a series of the substituted olefins, the yields of the 1,2-adduct greatly decreased with an increase in the number of the substituents on the olefinic carbon; this indicates the important role played by steric hindrance.

Photolysis in the Presence of 1,3-Dienes. The reaction of benzylgermane **1** with 1,3-diene is also interesting. When **1** was photolyzed in the presence of 2,3-dimethyl-1,3-butadiene, 1,2-adduct (**34**) and 1,4-adduct (**35**), both having triethylgermyl group on terminal carbon atom, were obtained in a 2:3 molar ratio (see Table 6). The orientation of the germyl group in the adducts again indicated a more preferential addition of the germyl free radical to diene than benzyl radical to.

Photochemical Reaction of Diethyldibenzylgermane with 1,3-Dienes. When diethyldibenzylgermane **6** was irradiated in the presence of 2,3-dimethyl-1,3-butadiene for 2 h under similar conditions as in the case of **1**, the major products were 1,2-adduct (**36**) and 1,4-adduct (**37**) in almost the same molar ratio (Table 7). However, in this reaction (although in low yield), the formation of 1,1-diethyl-3,4-dimethylgerma-3-cyclopentene (**38**)[7] was confirmed by GC-MS. The formation of **38** clearly indicated the generation of diethylgermylene (**39**) by the photolysis of **6**. Dimethylgermylene, thermally generated from 7-dimethylgerma-2,5-norbornadiene, is known to add to styrenes or dienes to give germacyclohexane or germacyclopentene derivatives respectively.[8]

The formation of 1,2- and 1,4-dibenzyl adducts (**40** and **41**) shows that benzyl radical can add to 1,3-diene, which was not observed in the reaction with simple olefins.

Table 7. Photochemical Addition of **6** to 2,3-Dimethyl-1,3-butadiene

Product		Yield/%[a]
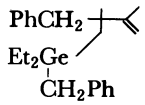	(**36**)	29
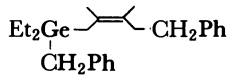	(**37**)	30
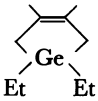	(**38**)	2
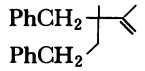	(**40**)	11
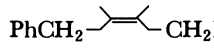	(**41**)	
$(PhCH_2)_2$	(**3**)	17

a) Yields were determined by GLC based on the consumed **6**. 3% of **6** was recovered.

Experimental

IR and UV spectra were recorded on a Hitachi 260-10 IR spectrometer and Hitachi 220A UV spectrometer, respectively. The proton and ^{13}C NMR spectra were recorded with TMS as an internal standard in $CDCl_3$ or benzene-d_6 at 60 MHz by JNM-PMX-60 and Jeol FX-60, respectively. Mass spectra were measured with a Jeol-DX300 high-resolution mass spectrometer with a JMA-5000 Mass Data System. GLC and HPLC were performed on a Hitachi 163 Gas Chromatograph with SE-30 10% coated column (2 m) and a Hitachi 655 Liquid Chromatograph with a Hitachi 638-41 UV monitor.

Materials. Benzyltriethylgermane (1): Bromotriethylgermane (5.00 g; 20.9 mmol) in ether (50 cm^3) was added to benzylmagnesium bromide prepared from 5.35 g (31.3 mmol) of benzyl bromide and magnesium (0.76 g; 31.3 mg atm) in ether (100 cm^3). The reaction mixture was refluxed for one night, then hydrolyzed with ice and dilute hydrochloric acid. After the usual work-up and purification by silica-gel column chromatography with hexane as an eluant and fractional distillation, **1** was obtained in 97% yield. Bp 71—73 °C/0.45 mmHg (1 mmHg=133.322 Pa). UV; 270 nm (ε 420). ^1H NMR ($CDCl_3$) δ=0.43—1.43 (m, 15H), 2.17 (s, 2H), 6.76—7.33 (m, 5H). ^{13}C NMR ($CDCl_3$) δ=3.9, 8.8, 21.1, 123.6, 127.7, 128.1, 141.7. MS *m/z* 252 (M^+). Exact MS; Found: *m/z* 252.0872. Calcd for $C_{13}H_{22}{}^{74}Ge$: 252.0933.

Dibenzyldiethylgermane (6): Dibromodiethylgermane[9] (11.03 g; 0.038 mol) in ether (30 cm^3) was added to benzylmagnesium bromide prepared from benzyl bromide (19.5 g; 0.114 mol) and magnesium (2.77 g; 0.114 g atom) in ether (90 cm^3). The reaction mixture was refluxed for one night and hydrolyzed with ice water. The product was purified by silica-gel column chromatography with hexane–ether (50:1 mixture) as an eluant and fractional distillation. Yield 96%. Bp 120—122 °C/0.12 mmHg. ^1H NMR ($CDCl_3$) δ=0.37—1.40 (m, 10H), 2.19 (s, 4H), 6.76—7.47 (m, 10H). ^{13}C NMR ($CDCl_3$) δ=4.2, 8.6, 21.2, 123.8, 127.9, 128.2, 141.0. MS *m/z* 314 (M^+). Exact MS; Found: *m/z* 314.1032. Calcd for $C_{18}H_{24}{}^{74}Ge$: 314.1089. UV; 267 nm (ε 840).

Photolysis. A solution of 0.93 mmol of **6** in 230 cm^3 of hexane was irradiated with a medium-pressure mercury lamp through a Vycor filter for 3 min under an argon atmosphere. The products were separated by preparative GLC and identified by GC-Mass, ^1H NMR, ^{13}C NMR and IR spectroscopy. Yields were determined by GLC.

Photochemical Addition. General procedure is shown in the case of benzyltriethylgermane in the presence of 1-hexene.

A solution of 2.4 mmol of **1** and 14.3 mmol of 1-hexene in 140 cm^3 of hexane was irradiated with a medium-pressure mercury lamp through a Vycor filter for 1.5 h under an argon atmosphere. The starting material was completely disappeared at this point. Products were isolated by GPC, preparative GLC and silica-gel column chromatography, and identified by ^1H NMR, ^{13}C NMR, IR, and GC-MS. Yields were determined by GLC using nonane, dodecane or tetradecane as an internal standard.

Physical Properties of the Product. 1,2-Dibenzyl-1,1,2,2-tetraethyldigermane (7): Colorless liquid; ^1H NMR ($CDCl_3$) δ=0.67—1.47 (m, 20H), 2.27 (s, 4H), 6.77—7.37 (m, 10H). ^{13}C NMR ($CDCl_3$) δ=6.7, 10.3, 22.8, 124.3, 128.2, 128.6, 142.3. MS *m/z* 355 (M^+-PhCH_2). Ex MS Found: *m/z* 353.0583. Calcd for $C_{15}H_{27}{}^{74}Ge^{72}Ge$: 353.0546.

1-Triethylgermyl-2-benzylhexane (12): Colorless liquid; ^1H NMR ($CDCl_3$) δ=0.43—1.13 (m, 18H), 1.13—2.17 (m, 9H), 2.52 (d, J=7.2 Hz, 2H), 6.97—7.43 (m, 5H). ^{13}C NMR ($CDCl_3$) δ=4.7, 8.9, 14.2, 17.1, 23.0, 28.8, 35.8, 37.1, 43.5, 125.5, 128.0, 129.2, 141.8. MS *m/z* 307 ($M^+-C_2H_5$). EX MS Found: *m/z* 307.1435. Calcd for $C_{17}H_{29}{}^{74}Ge$: 307.1481.

Diethylbenzylgermane (8): Colorless liquid; ^1H NMR (benzene-d_6) δ=0.72—1.17 (m, 10H), 2.20 (d, J=3 Hz, 2H), 3.90—4.20 (m, 1H), 6.87—7.14 (m, 5H). IR (neat) 2001 cm^{-1} (ν_{Ge-H}). MS *m/z* 224 (M^+). EX MS Found: *m/z* 224.0679. Calcd for $C_{11}H_{18}{}^{74}Ge$: 224.0620.

1-(Triethylgermyl)-2-benzylcyclohexane (19) (cis: trans= 1:4 mixture): Colorless liquid; ^1H NMR ($CDCl_3$) δ=0.57—2.03 (m, 25H), 2.49 (m, 2H), 6.92—7.48 (m, 5H). ^{13}C NMR ($CDCl_3$) δ=4.6, 9.4, 22.0, 25.6, 26.4, 28.3, 29.1, 29.8, 32.1, 33.4, 37.4, 39.0, 42.0, 43.6, 125.7, 128.2, 129.2, 141.7. MS *m/z* 305 ($M^+-C_2H_5$). EX MS Found: *m/z* 305.1284. Calcd for $C_{17}H_{27}{}^{74}Ge$: 305.1325.

1,2-Bis(triethylgermyl)cyclohexane (23) (cis-trans mixture): Colorless liquid; ^1H NMR ($CDCl_3$) δ=0.50—1.33 (m, 32H), 1.33—1.87 (m, 8H). ^{13}C NMR ($CDCl_3$) δ=5.1, 9.2, 25.3, 26.5, 27.2, 27.6, 30.1, 30.5. MS *m/z* 404 (M^+). EX MS; Found: *m/z* 243.1125. Calcd for $C_{12}H_{25}{}^{74}Ge$ (M^+-Et_3Ge): 243.1082.

1,2-Adduct of 1 with 2-Hexene (24A, 24B, 24C) (mixture of **3** isomer): Colorless liquid; ^1H NMR ($CDCl_3$) δ= 0.50—1.77 (m, 27H), 2.30—2.93 (m, 2H), 6.80—7.30 (m, 5H). MS *m/z* 307 ($M^+-C_2H_5$). EX MS: Found Isomer **A**; *m/z* 307.1443. Isomer **B**; *m/z* 307.1504. Isomer **C**, *m/z* 307.1418. Calcd for $C_{17}H_{29}{}^{74}Ge$; ($M^+-C_2H_5$): 307.1481.

2-Methyl-2-benzyl-3-trimethylgermylhexane (25): Colorless liquid; ^1H NMR ($CDCl_3$) δ=0.65—1.14 (m, 27H), 2.54 (s, 2H), 6.97—7.30 (m, 5H). ^{13}C NMR ($CDCl_3$) δ=6.1, 8.9, 14.7, 17.4, 26.0, 27.5, 37.4, 44.2, 49.0, 125.6, 127.5, 130.7, 139.7. MS *m/z* 307 ($M^+-C_2H_5$). EX MS Found *m/z* 307.1394. Calcd for $C_{17}H_{29}{}^{74}Ge$ ($M^+-C_2H_5$): 307.1481.

2,3,3-Trimethyl-4-phenyl-2-(triethylgermyl)butane (30): Colorless liquid; ^1H NMR ($CDCl_3$) δ=0.76—1.23 (m, 27H),

2.58 (s, 2H), 7.07—7.28 (m, 5H). MS *m/z* 307 ($M^+-C_2H_5$). EX MS Found: *m/z* 307.1481. Calcd for $C_{17}H_{29}{}^{74}Ge$ ($M^+-C_2H_5$); 307.1481.

2,3-Dimethyl-3-benzyl-4-triethylgermyl-1-butene (34): Colorless liquid; ^1H NMR ($CDCl_3$) δ=0.52—1.32 (m, 20H), 1.83 (s, 3H), 2.54, 2.78 (AB q, J=13.8 Hz, 2H), 4.51 (s, 1H), 4.73 (m, 1H), 6.93—7.37 (m, 5H). ^{13}C NMR ($CDCl_3$) δ=5.7, 9.0, 20.4, 25.6, 26.1, 42.9, 50.1, 111.4, 125.8, 127.4, 130.5, 139.2, 150.8. MS *m/z* 334 (M^+). EX MS Found: *m/z* 334.1699. Calcd for $C_{19}H_{32}{}^{74}Ge$: 334.1716.

2,3-Dimethyl-5-phenyl-1-triethylgermyl-2-pentene (35): Colorless liquid; ^1H NMR ($CDCl_3$) δ=0.43—1.30 (m, 17H), 1.65 (s, 6H), 2.47 (m, 4H), 6.93—7.47 (m, 5H). ^{13}C NMR ($CDCl_3$) δ=5.0, 8.9, 18.8, 20.3, 20.6, 34.9, 37.0, 123.9, 125.6, 127.5, 128.2, 128.4, 142.9. MS *m/z* 334 (M^+). EX MS Found: *m/z* 334.1781. Calcd for $C_{19}H_{32}{}^{74}Ge$: 334.1716.

2,3-Dimethyl-3-benzyl-4-diethylbenzylgermyl-1-butene (36): Colorless liquid; ^1H NMR ($CDCl_3$) δ=0.43—1.24 (m, 12H), 1.57 (s, 3H), 1.66 (s, 3H), 2.20 (s, 2H), 2.33, 2.51 (AB q, J=9 Hz, 2H), 4.48 (s, 1H), 4.72 (m, 1H), 6.77—7.43 (m, 10H). MS *m/z* 396 (M^+). EX MS Found: *m/z* 396.1837. Calcd for $C_{24}H_{34}{}^{74}Ge$: 396.1872.

2,3-Dimethyl-5-phenyl-1-diethylbenzylgermyl-2-pentene (37): Colorless liquid; ^1H NMR ($CDCl_3$) δ=0.38—1.33 (m, 12H), 1.56 (s, 6H), 2.33 (s, 2H), 2.49 (m, 4H), 6.96—7.32 (m, 10H). MS *m/z* 396 (M^+). EX MS Found: *m/z* 396.1846. Calcd for $C_{24}H_{34}{}^{74}Ge$: 396.1872.

5-(Triethylgermylmethyl)undecane (17): Colorless liquid; ^1H NMR ($CDCl_3$) δ=0.43—1.80 (m, 40H), ^{13}C NMR ($CDCl_3$) δ=4.8, 9.0, 11.7, 14.0, 14.2, 23.2, 23.3, 30.2, 30.5, 32.7, 33.8, 36.9, 38.5. MS *m/z* 301 ($M^+-C_2H_5$). EX MS Found: *m/z* 245.1331. Calcd for $C_{12}H_{27}{}^{74}Ge$ ($M^+-C_6H_{13}$): 245.1324.

1,1-Diethylgermacyclo-3,4-dimethyl-3-pentene (38): Due to the low yield this product could not be isolated in pure state in the photoreaction of diethyldibenzylgermane and 3,4-dimethyl-1,3-butadiene. Its mass fragmentation pattern [*m/z* 214 (M^+), 185 ($M^+-C_2H_5$, base peak), 157 ($M^+-2\,C_2H_5$), 132 (Et_2Ge), 115, and 103 (EtGe)] is identical with that of the authentic sample prepared as described below.

Synthesis of 38: To a solution of trichlorogermane (0.025 mol) in ether (20 ml) was added 2,3-dimethyl-1,3-butadiene (0.027 mol) in ether (10 ml) with stirring at room temperature. Stirring was continued for 1 h, and a precipitated white solid was filtered off. A filtrate containing 1,1-dichloro-3,4-dimethyl-1-germacyclo-3-pentene was added dropwise to a solution of ethylmagnesium bromide, prepared from ethyl bromide (0.25 mol) and magnesium (0.25 mol) in ether (200 ml), under reflux. After refluxing for 3 h, excess Grignard reagent was hydrolyzed with a saturated ammonium chloride solution. The solvent was expelled at room temperature and the residue was purified by silica-gel chromatography (eluant: hexane) and GPC to give **38**. Yield 22%. Bp 60 °C/7 mmHg (lit,[7] 102 °C/26 mmHg (1 mm Hg=133.322 Pa)). ^1H NMR δ=0.54—1.30 (m, 10H, C_2H_5), 1.47 (s, 4H, CH_2), 1.68 (s, 6H, CH_3). ^{13}C NMR δ=5.8, 9.2, 19.5, 22.9, 131.0. Mass: *m/z* 214 (M^+), 185, 157, 132 (Et_2Ge), 115, 103, 83, 75.

Thanks are due to ASAI Germanium Research Institute for donating the germanium tetrachloride.

References

1) H. Sakurai, "Free Radicals," ed by J. K. Kochi, Wiley-Interscience, New York (1973), Vol. 2, Chap. 25; P. Rivière, M. Rivière-Baudet, and J. Satgé, "Comprehensive Organometallic Chemistry," ed by G. Wilkinson, J. G. A. Stone, and E. W. Abel, Pergamon press, Oxford (1982), Vol. 2, Chap. 10.

2) M. Kobayashi and M. Kobayashi, *Bull. Chem. Soc. Jpn.*, **59**, 2807 (1986).

3) M. Kira, H. Yoshida, and H. Sakurai, *J. Am. Chem. Soc.*, **107**, 7767 (1985).

4) M. Kobayashi and M. Kobayashi, *Chem. Lett.*, **1986**, 385.

5) E. J. Bulten and J. G. Noltes, *Tetrahedron Lett.*, **1966**, 4389; E. J. Bulten and J. G. Noltes, *J. Organomet. Chem.*, **29**, 397 (1971).

6) N. S. Vyazankin, G. A. Razvaev, E. N. Gladyshev, and S. P. Korneva, *J. Organomet. Chem.*, **7**, 353 (1967).

7) P. Mazarolles and G. Manuel, *Bull. Soc. Chim. Fr.*, **1966**, 327.

8) J. Satgé, M. Massol, P. Rivière, *J. Organomet. Chem.*, **56**, 1 (1973); M. Schriever and W. P. Neumann, *J. Am. Chem. Soc.*, **105**, 897 (1983); J. Kocher and W. P. Neumann, *Organometallics*, **4**, 400 (1985).

9) M. Lesbre, P. Mazerolles, and J. Satgé, "The Organic Compounds of Germanium," Wiley-Interscience, New York (1971), Chap. 5.

Optically Active Cyclic Dipeptide Carrying 9-Anthryl Groups

Syun EGUSA, Masahiko SISIDO,†,* and Yukio IMANISHI
Department of Polymer Chemistry, Kyoto University, Yoshida, Sakyo-ku, Kyoto 606
†Research Center for Medical Polymers and Biomaterials, Kyoto University, Shogoin, Sakyo-ku, Kyoto 606
(Received April 15, 1986)

Optically active 3-(9-anthryl)alanine was synthesized for the first time and its cyclic dipeptide, cyclo(D-9-anthrylalanine)$_2$, was prepared. Conformation of the cyclic dipeptide in solution was investigated by means of ^{1}H NMR, absorption, circular dichroism (CD), and fluorescence spectroscopy. The coupling parameter $J_{NH\text{-}C^{\alpha}H}$, observed in the NMR spectra indicated a planar configuration for the 2,5-piperazinedione ring of the dipeptide. The cyclic dipeptide showed a moderately large exciton couplet in CD spectrum and a small splitting in the ^1B_b absorption band, but no excimer emission in fluorescence spectrum. These spectroscopic data suggest an unfolded-unfolded conformation for the side chains of the cyclic dipeptide.

Bichromophoric compounds in which two aromatic groups are linked to a ring system have been investigated.[1-3] Study on electronic interactions between two rigidly-fixed chromophores may provide basic information on photochemical processes in chromophoric assemblies, such as polymers, bilayers, and monolayers. In the previous paper, syntheses and conformational analyses of two cyclic dipeptides carrying 1- and 2-naphthyl groups, cyclo(L-1- and 2-naphthylalanine)$_2$ [c(1- and 2-napAla)$_2$] have been described.[4] The 2,5-piperazinedione ring of the two cyclic dipeptides was found to be nearly planar and the folded-unfolded asymmetric side-chain conformation was most populated. In this article, the same line of study was extended to a cyclic dipeptide carrying 9-anthryl group, cyclo(D-9-anthrylalanine)$_2$ [c(D-antAla)$_2$]. Its conformation in solution was studied by means of ^{1}H NMR, absorption, circular dichroism (CD), and fluorescence spectroscopy. The optically active 9-anthrylalanine was synthesized for the first time in this study. The determination of the absolute configuration of the amino acid has been described elsewhere.[5]

Experimental

Materials. D-3-(9-Anthryl)alanine and Cyclo(D-9-anthrylalanine)$_2$: Optically active 9-anthrylalanine was synthesized for the first time in this study. The cyclic dipeptide was prepared by a similar mannar as in the case of c(1- and 2-napAla)$_2$. The elimination of *N*-benzyloxycarbonyl group from a linear dipeptide was conducted by a catalytic hydrogenation using ammonium formate as a hydrogen donor.[6]

Ac-DL-9-antAla-OH[7]: Sodium (2.5 g) was dissolved in dry ethanol (200 ml) and diethyl acetamidomalonate (23.23 g) was added to the solution. 9-(Chloromethyl)anthracene (20 g) was then added and the mixture was refluxed for 4 h. After cooling to room temperature, sodium chloride was filtered off and the filtrate was evaporated. Diisopropyl ether (100 ml) was added to the residue and the mixture was cooled with ice to precipitate crude crystals of diethyl α-(9-anthrylmethyl)acetamidomalonate (25 g). The latter were dissolved in ethanol (200 ml) and 2M NaOH (100 ml, 1M=1 mmol dm^{-3}) was added. The mixture was heated to ca. 60 °C for 30 min and neutralized with concd HCl to pH= 3. Ethanol was evaporated and water was added to precipitate Ac-DL-antAla-OH. The curde material was redissolved in ethanol (100 ml) under heating and 2M NaOH (50 ml) was added. Crystalline precipitate was collected and treated with 1M HCl to obtain a free acid form of Ac-DL-antAla-OH, yield 15.9 g. Mp 265—267 °C. Found: C, 74.34; H, 5.28; N, 4.35%. Calcd for $C_{19}H_{17}NO_3$: C, 74.25; H, 5.57; N, 4.56%.

Resolution of Ac-DL-antAla-OH: The racemic acetylamino acid (14.8 g) was dissolved in ethanol (200 ml) under heating and *l*-ephedrine (9.5 g) was added. After standing overnight at room temperature the mixture was cooled with ice to precipitate Ac-D-antAla-OH *l*-ephedrine complex (the absolute configuration has been determined as described below). The complex was recrystallized twice from ethanol and redissolved in ethanol under heating. Concd HCl (10 ml) and water (300 ml) were added to the ethanol solution and the mixture was cooled with ice to precipitate Ac-D-antAla-OH, yield 3.3 g. Mp 269—270 °C. (Found: C, 74.04; H, 5.57; N, 4.47%). CD: $[\theta]_{258(max)}=1.12\times10^5$ (ethanol, $c=1.95\times10^{-4}$ M). Evaporation of the filtrate gave an L-rich Ac-antAla-OH *l*-ephedrine complex, from which the acetylamino acid containing more L-enantiomer was recovered.

Ac-D-antAla-OMe: Ac-D-antAla-OH was dissolved in methanol saturated with HCl and the solution was kept stirring at room temperature for 3 h. Evaporation gave crystals which was recrystallized from methanol/diisopropyl ether mixture. Mp 208—209 °C. Found: C, 74.53; H, 5.94; N, 4.41%. Calcd for $C_{20}H_{19}NO_3$: C, 74.75; H, 5.96; N, 4.36%.

D-antAla-OH·HCl: Ac-D-antAla-OH (3.3 g) was suspended in concd HCl (150 ml)/acetic acid (50 ml) mixture and refluxed for 4 h. After a further addition of water, the mixture was cooled with ice to precipitate crystalline D-antAla HCl, 2.84 g. Mp 244 °C. $[\alpha]_D=-43°$ (ethanol, $c=0.058$ g dl^{-1}, 21 °C).

D-antAla-OMe: D-AntAla·HCl (150 mg) was suspended in 1M HCl/methanol mixture and the suspension was refluxed for 1 h. The solvent was evaporated and the residual crystal was recrystallized from methanol/ether mixture to give D-antAla-OMe·HCl, yield 157 mg. Mp 229C°. The hydrochloride (50 mg) was treated with 3% $NaHCO_3$ and the free methyl ester was extracted with ethyl acetate, yield 30 mg. Mp 76 °C.

Absolute Configuration and Optical Purity of the 9-Anthryl-alanine Resolved by Using *l*-Ephedrine: The absolute configuration of the optically active amino acid was determined on the basis of the "Dnp-aromatic rule".[8] The *N*-dinitrobenzoyl derivative of the optically active antAla

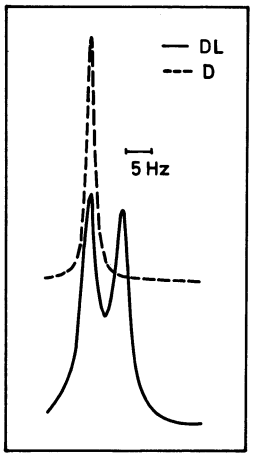

Fig. 1. Proton NMR spectra of D- and DL-antAla-OMe in the presence of 0.6 molar tris[3-(trifluoromethylhydroxymethylene)-*d*-camphorato]europium-(III) in deuteriochloroform. (——): DL-isomer, (-----): D-isomer.

showed a positive Cotton effect around 400 nm, which is indicative of D-configuration. The detail has been reported elsewhere.[5]

^{1}H NMR spectra of D- and DL-antAla-OMe were measured in $CDCl_3$ in the presence of 0.6 equivalent molar tris[3-(trifluoromethylhydroxymethylene)-*d*-camphorato]europium(III). Figure 1 shows the NMR spectra in the O-CH_3 proton region. The racemic compound showed two peaks whereas the D-isomer showed only one peak under the same conditions. The optical purity of the D-isomer is better than ca. 99%. It is interesting to note that the O-CH_3 signal of D-isomers of 1- and 2-naphthylalanine and 1-pyrenylalanine has been observed at lower field than that of the corresponding L-isomers. The present result in Fig. 1 conforms to this rule.

Z-D-antAla-OH: D-AntAla-OH·HCl (2.62 g) was dissolved in 1M NaOH (18 ml), and benzyloxycarbonyl chloride (2.0 ml) and 1M NaOH (9 ml) were added dropwise simultaneously at O°C under vigorous stirring. Precipitate appeared after one day. The mixture was acidified with HCl to pH=3 and the crystal precipitated was collected, washed with water and hexane, and dried. The curde crystal was recrystallized from ethyl acetate, yield 2.91 g. Mp 215—218°C.

Z-(D-antAla)$_2$-OMe: Z-D-antAla-OH (50 mg), D-antAla-OMe·HCl (39.5 mg), and triethylamine (17.4 l) were dissolved in DMF (2 ml), and water-soluble carbodiimide (26.4 mg) and 1-hydroxybenzotriazole hydrate (18.6 mg) were added under cooling with ice. The mixture was stirred under cooling for 4 h and at room temperature for 2 d. Precipitate, which appeared by the addition of 1M HCl (50 ml), was collected and washed with water, 3% $NaHCO_3$, and water. The crude solid was recrystallized from tetrahydrofuran/ethyl acetate mixture, yield 50 mg. Mp 238—240°C. Found: C, 78.02; H, 5.43; N, 4.53%. Calcd for $C_{43}H_{36}N_2O_5$: C, 78.16; H, 5.49; N, 4.24%.

Cyclo(D-antAla)$_2$: Z-(D-antAla)$_2$-OMe (40 mg) was dissolved in DMF (30 ml) and 10% palladium/activated carbon (100 mg) was added. Ammonium formate (40 mg) dissolved in methanol (5 ml) was added to the mixture under stirring at room temperature. The progress of the reaction was followed by TLC [Z-(D-antAla)$_2$-OMe, R_f=0.85, c(D-antAla)$_2$, R_f=0.4; ethyl acetate]. After 3 d, the catalyst was removed by filtration and the solvent was evaporated. The residual solid was reprecipitated from tetrahydrofuran (solvent)/methanol (nonsolvent), yield 10 mg, mp>300°C. TLC showed a single spot (chloroform, ethyl acetate). No impurity was found in IR, ^{1}H NMR (Fig. 2), UV (Fig. 3), and fluorescence (Fig. 5) spectra. IR (KBr disc): 1668 (amide C=O), 1438 (amide C-N) cm^{-1}.

Measurements. 90 MHz ^{1}H NMR spectra were recorded on a JEOL FX90Q instrument in DMF-d_7. Since the NH signal overlapped with the aromatic signals, the coupling parameter $J_{NH-C^\alpha H}$, was determined from the $C^\alpha H$ signals under irradiating $C^\beta H$ protons.

Circular dichroism was measured on a JASCO J-20 spectropolarimeter with quartz cells of 0.05 and 1.0 cm path lengths at the dipeptide concentration of 1.0×10^{-4} mol dm^{-3}. Fluorescence spectra were measured on a Hitachi MPF-4 instrument in a cuvette equipped with a stopcock. The sample solution was purged with nitrogen gas before each measurement.

Results and Discussion

Synthesis of Optically Active 9-Anthrylalanine. Synthesis of racemic 9-anthrylalanine has been reported[7] but its optical resolution has never been reported so far. Since optically active aromatic amino acids carrying large aromatic ring are important intermediate to prepare novel aromatic polypeptides in which aromatic groups are arranged regularly along a helical main chain, i.e., one-dimensional aromatic crystals, their preparation deserves special attention.

Optical resolution of antAla was attempted by a stereoselective deacylation of Ac-antAla with acylase at first, but the enzymic reaction did not occur at all. This contrasts the cases of 1- and 2-naphthylalanine, the acetyl derivatives of which were deacylated stereoselectively with acylase.[9,10] Enzymic deacylation of Ac-DL-pyrAla was also possible, although the yield was very low. The bulkiness of the 9-anthryl group may be the reason for the failure of the enzymic reaction.

Optical resolution by diastereomeric complex formation of Ac-DL-antAla-OH with 18 different chiral amino compounds was attempted. Only three of them, i.e., *l*-ephedrine, quinine, and *l*-cinchonidine formed ethanol-insoluble diastereomeric complex. These amines complexed preferentially with the D-enantiomer of Ac-antAla-OH. Among the three, the complex with *l*-ephedrine was most easily purified by recrystallization. The absolute configuration of antAla which forms insoluble complex with *l*-ephedrine was found to be a D-isomer according to the "Dnp-aromatic rule" as described above.[5]

Conformation of Cyclo(D-9-anthrylalanine)$_2$. ^{1}H NMR Spectra: Proton NMR spectrum of c(D-antAla)$_2$ in DMF-d_7 is shown in Fig. 2. The coupling parameter $J_{NH-C^\alpha H}$ was measured under irradiating $C^\beta H$ was protons and is shown in Table 1. The coupling parameter is related to the dihedral angle $\theta_{NH-C^\alpha H}$, which is approximately equal to ϕ+60° (for D-iso-

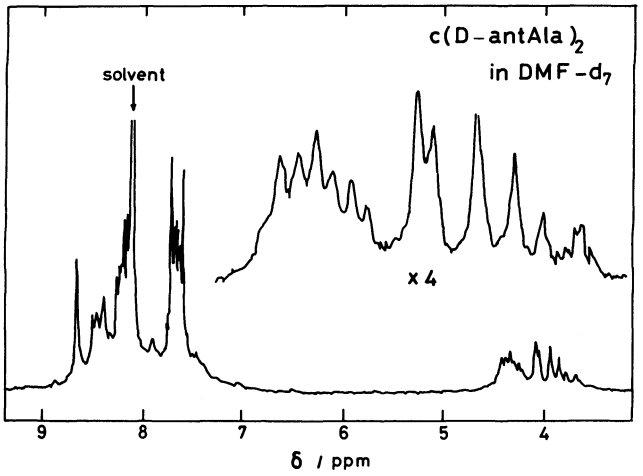

Fig. 2. Proton NMR spectrum of c(D-antAla)$_2$ in *N,N*-dimethylformamide-d_7. Concentration=4 mg/0.4 ml.

Table 1. The Coupling Parameter $J_{NH-C^{\alpha}H}$, and the Dihedral Angles $\theta_{NH-C^{\alpha}H}$, ϕ, and β for Cyclo(D-9-anthhrylalanine)$_2$ in *N,N*-Dimethylformamide-d_7

$J_{NH-C^{\alpha}H}$ (Hz)[a]	$\theta_{NH-C^{\alpha}H}$[b]	ϕ[c]	β[d]
2.6±0.2	±115°, ±57° (+57°)	−3°	3°

a) Estimated from the peak separation of $C^{\alpha}H$ signals under irradiating the $C^{\beta}H$ protons. b) θ was calculated according to the Bystrov equation: $J_{NH-C^{\alpha}H}=9.4\cos^2\theta-1.1\cos\theta+0.4$. c) $\phi=\theta-60°$. d) A supplement of the dihedral angle between two amide planes calculated assuming standard structural parameters for peptide bonds.

mer) where ϕ is the rotational angle of N-C^{α} bond defined according to the IUPAC-IUB nomenclature committee.[11] The dihedral angle and the rotational angle calculated according to the Bystrov equation[12] are also listed in Table 1. The Bystrov equation afforded four solutions for θ, but only one of the four, which is given in the parenthesis, corresponds to a reasonable skeletal conformation of the 2,5-piperazinedione ring. That is, the 2,5-piperazinedione ring is usually assumed to involve two planar amide bonds, and the dihedral angle between the two amide planes (β) may vary between ±45°. The θ value in the parenthesis corresponds to $\beta=3°$, whereas the other three solutions of the Bystrov equation gave β values outside the possible range. The determined β value indicates a planar conformation of the 2,5-piperazinedione ring of c(D-antAla)$_2$.

Circular Dichroism: CD and absorption spectra of c(D-antAla)$_2$ and Ac-D-antAla-OMe are shown in Fig. 3. The CD spectrum of the cyclic dipeptide shows a distinct exciton couplet at the ^1B_b absorption band. The molar ellipticities for one molar cyclic dipeptide are: $[\theta]_{248.5}=-3.1\times10^5$, $[\theta]_{262.5}=-5.3\times10^5$ deg cm^2 dmol^{-1}. According to the exciton coupling rule,[13]

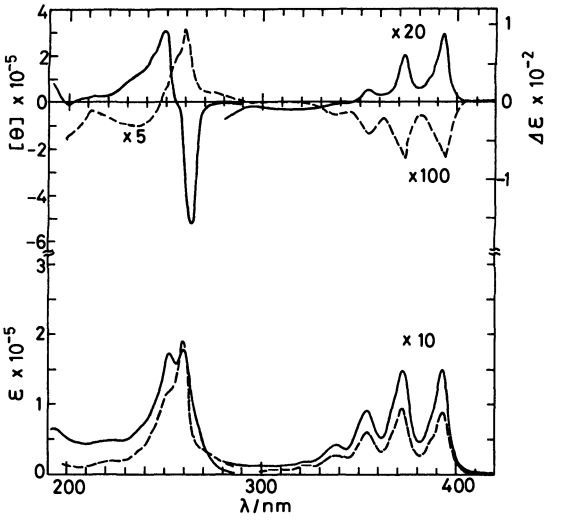

Fig. 3. Circular dichroism and absorption spectra of c(D-antAla)$_2$ (——) and Ac-D-antAla-OMe (----) in trimethyl phosphate. [antAla]=1.0×10^{-4} mol dm^{-3} for c(D-antAla)$_2$ and 1.9×10^{-4} mol dm^{-3} for Ac-D-antAla-OMe, room temperature. [θ] and ε are calculated with respect to two anthryl groups for c(D-antAla)$_2$ and one anthryl group for Ac-D-antAla-OMe.

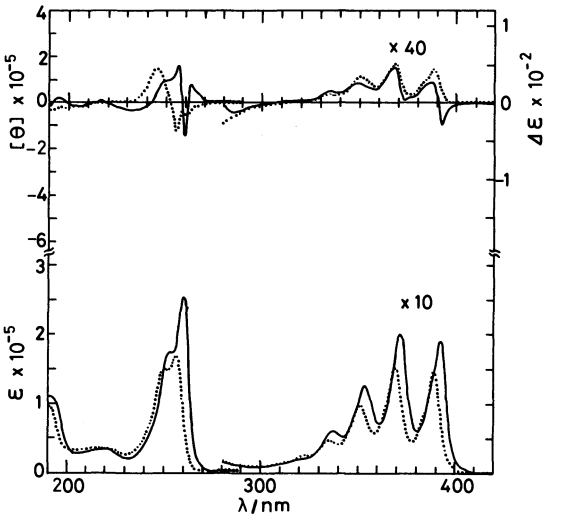

Fig. 4. Circular dichroism of Z-(D-antAla)$_2$ in trimethyl phosphate (—) and in 2,2,2-trifluoroethanol (·····). [antAla]=1.0×10^{-4} mol dm^{-3}, room temperature. [θ] and ε are calculated with respect to two anthryl groups.

the sign of the exciton couplet indicates that the transition dipole moments of the ^1B_b absorption which are parallel to the long axis of the anthryl group, are in a left-handed helical arrangement in c(D-antAla)$_2$.

Circular dichroic and absorption spectra of a linear dipeptide, Z-(D-antAla)$_2$-OMe in trimethyl phosphate (TMP) and in 2,2,2-trifluoroethanol (TFE) are shown in Fig. 4. A small and complex CD pattern is observed in TMP, whereas a small exction couplet at ^1B_b band in TFE. Two anthryl groups of the linear dipeptide may take a variety of orientations and the CD spectrum

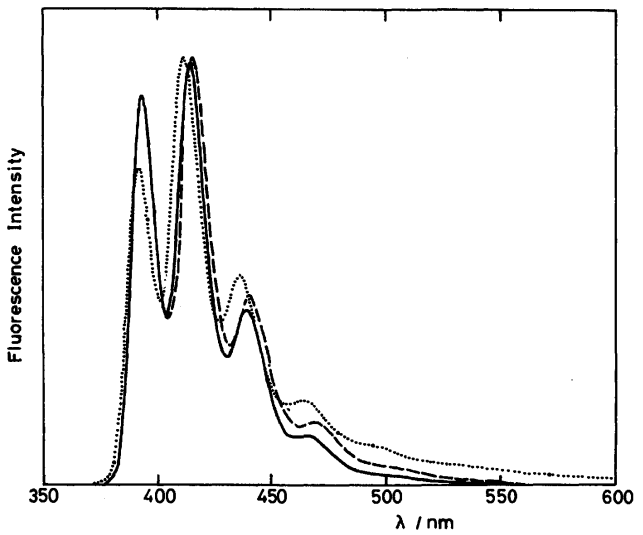

Fig. 5. Fluorescence spectra of c(D-antAla)$_2$ in trimethyl phosphate (—), and Z-(D-antAla)$_2$-OMe in trimethyl phosphate (-----) and in 2,2,2-trifluoroethanol (·····). [antAla]=1.0×10^{-5} mol dm^{-3}, room temperature.

should represent an average of these conformations. Rizzo and Jäckle[14] reported that linear dipeptides of aromatic amino acids (phenylalanine, histidine, tyrosine, and tryptophan) take extended conformations in aprotic solvents and folded conformations in protic solvents. This rule was also applicable to linear dipeptides of 1- and 2-naphthylalanines.[4] Hence the difference in CD spectrum in TMP (aprotic solvent) and TFE (protic solvent) may be interpreted by the different average conformations of Z-(D-antAla)$_2$-OMe in the two solvents.

Fluorescence Spectra: Figure 5 shows fluorescence spectra of c(D-antAla)$_2$ in TMP, and Z-(D-antAla)$_2$-OMe in TMP and in TFE. The cyclic dipeptide exhibits no excimer emission, indicating that the two anthryl groups are separated from each other by more than ca. 4 Å. The linear dipeptide shows no excimer in TMP but shows a small amount of excimer emission in TFE. The difference is consistent with the different conformations of the linear dipeptide in protic (TFE) and aprotic (TMP) solvent as described above. In the protic solvent the linear dipeptide takes folded compact conformations which favors excimer formation, whereas in the aprotic solvent the dipeptide takes extended conformations in which two anthryl groups are well separated from each other.

Conclusion on the Conformation of c(D-9-antAla)$_2$. Cyclo(D-antAla)$_2$ has a planar 2,5-piperazinedione ring in solution. It shows a moderately large exciton couplet in CD and a small exciton splitting in absorption spectrum, but no excimer emission in fluorescence spectrum. These spectroscopic properties suggest either folded-unfolded or unfolded-unfolded conformation of side chains. However, a CPK model analysis and a preliminary result of empirical conformational energy calculation[15] suggest that the folded (g$^+$) conformation is not allowed for the side chain of c(D-antAla)$_2$ due to a steric repulsion between the anthryl group and the 2,5-piperazinedione ring. Hence the side-chain conformation of c(D-antAla)$_2$ is concluded as unfolded-unfolded conformation. This conclusion is in contrast with the case of c(1- and 2-napAla)s, where folded-unfolded asymmetrical conformation was proposed.[4] In the latter two cases, the interaction between the 2,5-piperazinedione ring and the aromatic ring may not be so severe as to eliminate the folded conformation. In the unfolded-unfolded conformation of c(D-antAla)$_2$, the two anthryl groups are separated by about 10 Å. This interchromophore distance is evidently too far to form excimer in the excited state, but may be close enough to induce an exciton couplet in CD spectrum at the ^1B_b absorption band, which has very strong transition dipole moment.

The authors thank Mr. H. Sasaki for his assistance in preparing optically active anthrylalanine.

References

1) S. Ito, M. Yamamoto, and Y. Nishijima, *Bull. Chem. Soc. Jpn.*, **57**, 3295 (1984).
2) H. Masuhara, H. Shioyama, N. Mataga, T. Inoue, N. Kitamura, T. Tanabe, and S. Tazuke, *Macromolecules*, **14**, 1738 (1981).
3) P. Tundo and J. H. Fendler, *J. Am. Chem. Soc.*, **102**, 1760 (1980).
4) S. Egusa, J. Takagi, M. Sisido, and Y. Imanishi, *Bull. Chem. Soc. Jpn.*, **59**, 2195 (1986).
5) M. Kawai, T. Matsura, Y. Butsugan, S. Egusa, M. Sisido, and Y. Imanishi, *Bull. Chem. Soc. Jpn.*, **58**, 3047 (1985).
6) M. K. Anwer and A. F. Spatola, *Synthesis*, **1980**, 929.
7) W. Schreiber and W. Lautsch, *Z. Physiol. Chem.*, **340**, 95 (1965).
8) M. Kawai, U. Nagai, M. Katsumi, and A. Tanaka, *Tetrahedron*, **34**, 3435 (1978).
9) M. Sisido, S. Egusa, and Y. Imanishi, *J. Am. Chem. Soc.*, **105**, 1041 (1983).
10) M. Sisido, S. Egusa, and Y. Imanishi, *J. Am. Chem. Soc.*, **105**, 4077 (1983).
11) IUPAC-IUB Nomenclature Committee, *Biochemistry*, **9**, 3471 (1970).
12) V. F. Bystrov, V. T. Ivanov, S.L. Portonava, T.A. Balashova, and T. A. Ovchinnikov, *Tetrahedron*, **29**, 873 (1973).
13) N. Harada and K. Nakanishi, "Circular Dichroic Spectroscopy Exciton Coupling in Organic Stereochemistry," Univ. Sci. Books, N. Y. and Tokyo Kagaku Dojin, Tokyo (1982).
14) V. Rizzo and H. Jäckle, *J. Am. Chem. Soc.*, **105**, 4195 (1983).
15) M. Sisido and Y. Imanishi, in preparation.

 © 1986 The Chemical Society of Japan Bull. Chem. Soc. Jpn., 59, 3179—3183 (1986)

Oxidation of Lipids. XIV. Inhibition of Oxidation of Methyl Linoleate by Fatty Acid Esters of L-Ascorbic Acid

Mareyuki TAKAHASHI, Etsuo NIKI,* Akira KAWAKAMI, Akira KUMASAKA, Yorihiro YAMAMOTO, Yoshio KAMIYA, and Kunihiko TANAKA†

Department of Reaction Chemistry, Faculty of Engineering, The University of Tokyo, Hongo, Tokyo 113
†Sumitomo Chemical Co., Ltd., 3-1-98 Kasugade-naka, Konohana-ku, Osaka 554

(Received April 16, 1986)

Various kinds of fatty acid esters of L-ascorbic acid were synthesized and their role as chain-breaking antioxidant was studied in the oxidation of methyl linoleate in homogeneous solution. Fatty acid esters of ascorbic acid at either 6- or both 5- and 6-positions were effective as antioxidant and suppressed the oxidation of methyl linoleate, whereas those having ester group at 2-position did not act as antioxidant. 5,6-Erythorbyl dipalmitate was also effective as an antioxidant. Ascorbic acid esters inhibited the oxidation cooperatively with α- and δ-tocopherols as observed for free ascorbic acid. The antioxidant activity was correlated with the reactivity toward galvinoxyl radical.

The oxidations of lipids by molecular oxygen in biological systems and foods have received much attention recently in connection with their pathological, toxicological, and nutritional effects.[1-12] Tocopherols **1** (vitamin E)[13-16] and L-ascorbic acid **2** (vitamin C)[17-27] have been known to function as oil-soluble and water-soluble antioxidants, respectively,both in vivo and in vitro. In spite of much work on ascorbic acid and also the commercial production in large quantities, the chemistry of ascorbic acid has not been established in a manner that is scientifically satisfactory. The chemistry of ascorbic acid is in fact complicated partly because ascorbic acid can function as a radical scavenger, but it may also act as a prooxidant in combination with metal ions such as iron and copper.[28]

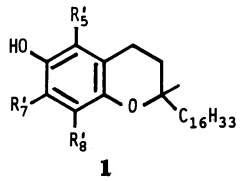

α-Tocopherol: $R_5'=R_7'=R_8'=CH_3$

δ-Tocopherol: $R_5'=R_7'=H$, $R_8'=CH_3$

1

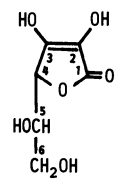

2

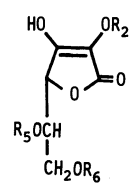

3

We have extended our study on the oxidation of lipids and its inhibition to study the role of ascorbic acid esters as chain breaking antioxidant in the oxidation of methyl linoleate in homogeneous solution. Various fatty acid esters of L-ascorbic acid **3** with different carbon numbers and positions have been prepared and examined. Erythorbic acid (D-isoascorbic acid) ester was also prepared and studied. Methyl linoleate was chosen as a substrate, since its oxidation has been shown to give four conjugated diene hydroperoxides quantitatively by a straight-forward mechanism.[29-31]

Table 1. Ascorbic Acid Esters **3** Used in This Study

Abbreviation	R_2	R_5	R_6
AsA	H	H	H
5,6-C_3-AsA	H	COC_2H_5	COC_2H_5
5,6-C_8-AsA	H	COC_7H_{15}	COC_7H_{15}
2,5,6-C_8-AsA	COC_7H_{15}	COC_7H_{15}	COC_7H_{15}
5,6-C_{14}-AsA	H	$COC_{13}H_{27}$	$COC_{13}H_{27}$
6-C_{16}-AsA	H	H	$COC_{15}H_{31}$
2,6-C_{16}-AsA	$COC_{15}H_{31}$	H	$COC_{15}H_{31}$
5,6-C_{16}-AsA	H	$COC_{15}H_{31}$	$COC_{15}H_{31}$
2,5,6-C_{16}-AsA	$COC_{15}H_{31}$	$COC_{15}H_{31}$	$COC_{15}H_{31}$
6-C_{18}-AsA	H	H	$COC_{17}H_{35}$
5,6-C_{18}-AsA	H	$COC_{17}H_{35}$	$COC_{17}H_{35}$
5,6-C_{22}-AsA	H	$COC_{21}H_{43}$	$COC_{21}H_{43}$
5,6-C_{16}-EA[a]	H	$COC_{15}H_{31}$	$COC_{15}H_{31}$

a) 5,6-Erythorbyl dipalmitate.

Experimental

Commercial methyl linoleate was purified by silica-gel column before use. Natural d-α-tocopherol and d-δ-tocopherol were provided by Eisai Co., Ltd. Various kinds of fatty acid esters of L-ascorbic acid were synthesized by the esterification of ascorbic acid at 2-, 5-, and 6-positions with corresponding fatty acids, followed by deacylation at 2-position in alcohol. Table 1 shows the ascorbic acid esters used in this study. 5,6-Erythorbyl dipalmitate was also synthesized similarly and studied. 2,2′-Azobis(2,4-dimethylvaleronitrile) (AMVN) was used as a radical initiator in order to generate initiating free radicals at a constant and known rate. Commercial galvinoxyl was used as received.

The oxidation was carried out at 37 °C under air in a glass ampoule immersed in a water bath. The rate of oxidation was measured in an automatic recording gas absorption apparatus by following the rate of oxygen uptake using a pressure transducer. The rate of free radical generation, that is, the rate of chain initiation was measured by conventional method from the induction period observed by the addition of a chain breaking antioxidant.[16] 2,6-Di-*t*-butyl-4-methylphenol (BMP) or α-tocopherol was used as the antioxidant. Commercial BMP was recrystallized from methanol before use. The rate of consumption of tocopherols was followed at 294 nm with a high-performance liquid chromatography (HPLC) by directly injecting 50 μl aliquots of the reaction mixture. The analytical system consisted of

JASCO liquid chromatograph equipped with a Finepak SIL-CN, 4.6×250 mm column, and samples were eluted with hexane–isopropyl alcohol–acetic acid (1000:15:1, v/v/v) at a flow rate of 1 ml min^{-1}. The rate of disappearance of ascorbic acid ersters was also measured with HPLC at 245 nm using 4.6×250 mm Finepak SIL-C_{18-5} column and metanol–water (85/15, v/v) containing 0.05% formic acid as an eluent (1 ml min^{-1}). The electron spin resonance (ESR) spectrum was recorded on X-band JEOL FE1X spectrometer.

Results and Discussion

Inhibition of Oxidation of Methyl Linoleate by Ascorbic Acid Esters. The rate of spontaneous autoxidation of methyl linoleate at ambient temperature is quite small, but it is oxidized at a constant rate without induction period in the presence of radical initiator AMVN. As shown in Fig. 1, when the fatty acid ester of ascorbic acid at either 6- or both 5-and 6-positions is added to the solution, the rate of oxidation was markedly suppressed and produced a clear induction period. During this induction period, the ascorbic acid ester was consumed linearly with time as shown in Fig. 2 and when it was depleted, the rate of oxidation increased to the same level as that without ascorbic acid ester. This is quite similar to the oxidation in the presence of α-tocoperhol and it clearly shows that ascorbic acid ester functions as a chain breaking antioxidant.

On the other hand, the ascorbic acid esters having ester group at 2-position did not show any antioxidant activity. 5,6-Erythorbyl dipalmitate was also effective in suppressing the oxidation.

Inhibition of Oxidation of Methyl Linoleate in Solution by the Combination of Ascorbic Acid Ester and Tocopherol. The pertinent results of the oxidations of methyl linoleate in chloroform initiated with AMVN and inhibited by both α-tocopherol and ascorbic acid ester are shown in Table 2. From the result of oxidation inhibited by α-tocopherol alone the constant ek_d was calculated as 2.87×10^{-6} s^{-1},

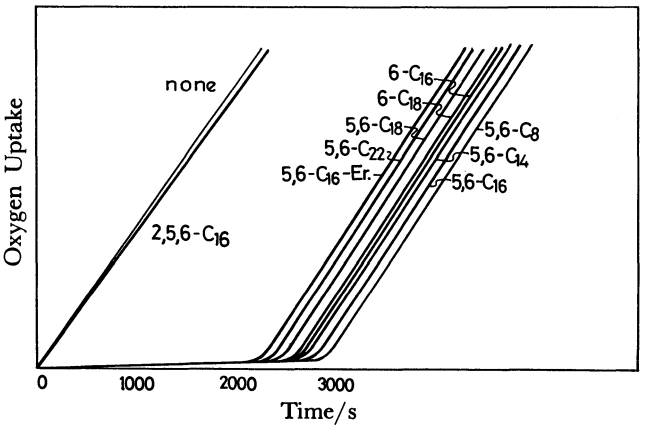

Fig. 1. Inhibition of oxidation of 145 mM methyl linoleate in solution by fatty acid esters of ascorbic acid at 37°C under air initiated with AMVN.

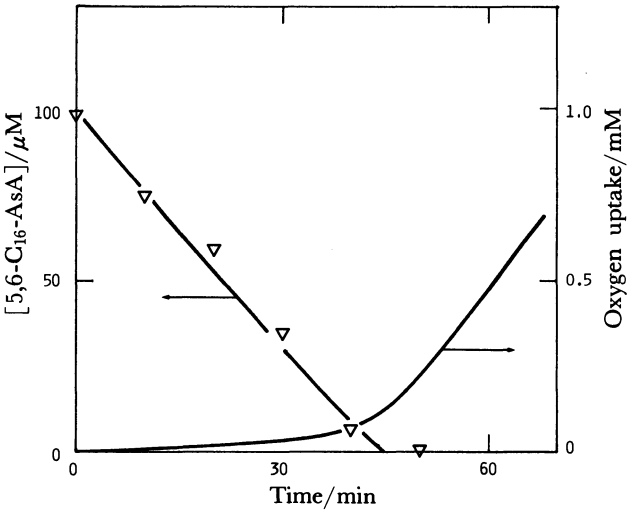

Fig. 2. Rates of oxygen uptake and consumption of 5,6-ascorbyl distearate in the oxidation of 159 mM methyl linoleate in benzene initiated with 10.1 mM AMVN at 37°C under air.

Table 2. Oxidation of Methyl Linoleate (LH) in Chloroform at 37°C Inhibited by α-Tocopherol and Ascorbic Acid Esters

LH	AMVN	α-Toc	AsAR		10^6R_i[a]	t_{inh}	n[b]	10^6R_p[c]	kcl[d]	$k_p/(2k_t)^{1/2}$[e]
mM	mM	μM	mM		M/s	s		M/s		$(Ms)^{-1/2}$
144	19.4	0			0.111	0		1.02	9.0	0.020
141	19.5	76.5			0.112	1365	2.0[f]	0.92	8.2	0.019
119	16.1	64.4	2,5,6-C_8	0.290	0.0924	1500	2.15	0.74	8.0	0.020
119	15.8	64.4	2,5,6-C_8	0.301	0.0907	1275	1.80	0.66	7.3	0.018
119	15.9	64.4	2,6-C_{16}	0.259	0.0913	1425	2.02	0.71	7.8	0.020
119	16.0	64.4	2,5,6-C_{16}	0.179	0.0918	1470	2.10	0.76	8.3	0.021
119	16.3	64.4	2,5,6-C_{16}	0.181	0.0936	1485	2.16	0.70	7.5	0.019
119	16.0	64.4	5,6-C_3	0.574	0.0918	>8500		n.d.[g]		
119	16.1	64.4	5,6-C_{16}	0.244	0.0924	5100	7.32	0.71	7.7	0.020
119	15.9	64.4	6-C_{18}	0.363	0.0913	7515	10.7	0.69	7.6	0.019

a) Rate of chain initiation calculated from Eq. 2. b) Apparent stoichiometric number for α-tocopherol calculated from Eq. 5. c) Rate of oxygen uptake after the induction period. d) Kinetic chain length, R_p/R_i. e) Oxidizability calculated from Eq. 7. f) Assumed. g) Not determined.

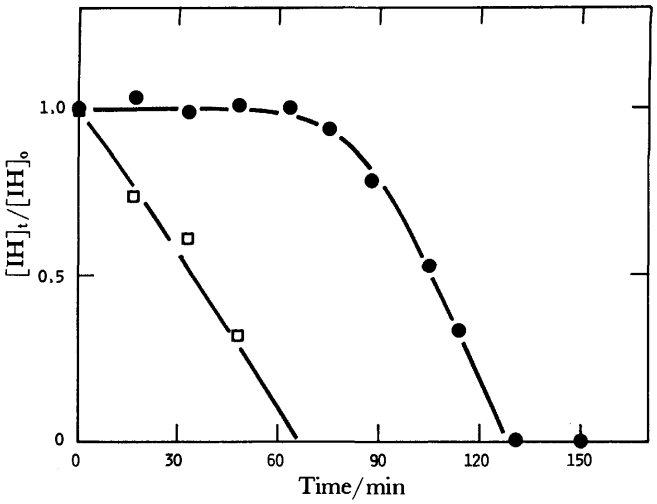

Fig. 3. Rate of consumption of antioxidant (IH) during the oxidation of 135 mM methyl linolate at 37°C. [AMVN]=18.1 mM, [α-tocoherol (●)]=50 mM, [5,6-C_{18}-AsA (□)]=500 mM.

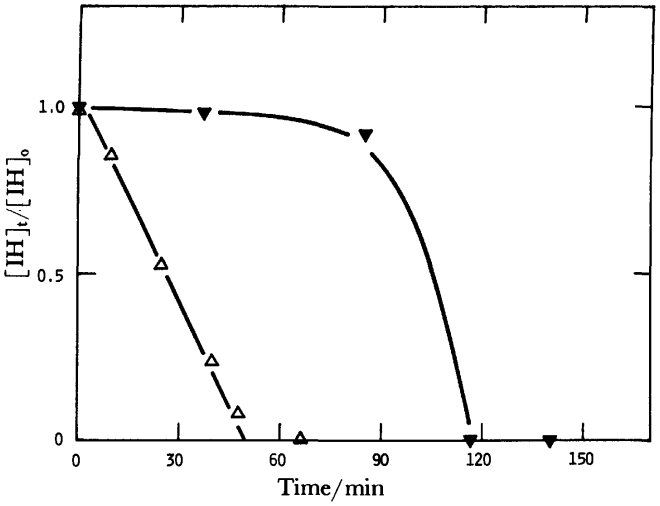

Fig. 4. Rate of consumption of antioxidant (IH) during the oxidation of 146 mM methyl linoleate under air at 37°C. [AMVN]=19.5 mM, [δ-tocopherol (▼)]=50 mM, [6-C_{18}-AsA (△)]=500 mM.

where A is $(CH_3)_2CHCH_2C(CH_3)CN-$ and e and k_d are the efficiency of free radical production and first-order rate constant for the decomposition of AMVN, respectively. The rate of chain initiation in other runs was calculated from Eq. 2 (M=mol dm^{-3}).

$$A\text{–}N{=}N\text{–}A \longrightarrow [A\cdot\ N_2\cdot\ A] \begin{cases} \nearrow 2eA\cdot & (1) \\ \searrow (1-e)A-A & (1') \end{cases}$$

$$R_i = 2ek_d[AMVN] = 5.74 \times 10^{-6}[AMVN]\ M\ s^{-1} \quad (2)$$

Both tocopherol and ascorbic acid esters (IH) scavenge peroxyl radicals by donating hydrogen atom (Eq. 3). The resulting radical, I·, may further trap peroxyl radicals (Eq. 4). The stoichiometric number of peroxyl radicals trapped by each antioxidant, n, is calculated from Eq. 5.

$$LO_2\cdot + IH \longrightarrow LOOH + I\cdot \quad (3)$$

$$(n-1)LO_2\cdot + I\cdot \longrightarrow \text{stable products} \quad (4)$$

$$n = R_i\cdot t_{inh}/[IH] \quad (5)$$

As Table 2 shows, the value of n in the absence of ascorbic acid is close to 2.0. That the apparent n values calculated from Eq. 5 are close to 2 in the presence of ascorbic acid esters which have ester group at 2-position suggests that these ascorbic acid esters do not function as radical scavenger. On the other hand, the apparent n values in the presence of 5,6-ascorbyl dipropionate, 5,6-ascorbyl dipalmitate, and 6-ascorbyl stearate are much higher than 2, suggesting that these ascorbic acid esters also function as hydrogen donor.

Figures 3 and 4 show that rate of consumption of tocopherol and ascorbic acid ester during the oxidation. Figure 3 shows that 5,6-ascorbyl distearate disappeared first linearly whereas α-tocopherol remained almost constant and it began to decrease after ascorbic acid ester was depleted. Similarly, as shown in Fig. 4, ascorbic acid ester was consumed first and δ-tocopherol was consumed after the ascorbic acid ester was depleted in the combination of δ-tocopherol and 6-ascorbyl stearate. Tocopherol (TH) must scavenge peroxyl radicals more rapidly than ascorbic acid ester (AH),[26] but the tocopheryl radical (T·) formed must react with ascorbic acid ester rapidly to regenerate tocopherol as observed in the combination of tocopherol and free ascorbic acid.[26,33,34]

$$LO_2\cdot \begin{cases} \overset{TH}{\nearrow} LOOH + T\cdot & (6) \\ \underset{AH}{\searrow} LOOH + A\cdot & (7) \end{cases}$$

$$T^{\cdot} + AH \longrightarrow TH + A\cdot \quad (8)$$

The ESR study supports the above conclusion. Galvinoxyl **4** is a stable phenoxyl radical, but it reacts with active hydrogens. For example, galvinoxyl reacts with good hydrogen donors such as tocopherols, ascorbic acid, cysteine, and glutathione.[35] As Fig. 5 shows, the ESR spectrum of galvinoxyl changed instantaneously to that of α-tocopheryloxyl radical when α-tocopherol was added to the benzene solution of galvinoxyl at 25°C. When 5,6-ascorbyl dipalmitate was added to the above solution, the ESR spectrum of α-tocopheryloxyl radical (Fig. 5, B) disappeared rapidly. On the other hand, when 2,5,6-ascorbyl tripalmitate was added instead of 5,6-ascorbyl dipalmitate, no change was observed for the ESR spectrum of α-tocopheryloxyl radical.

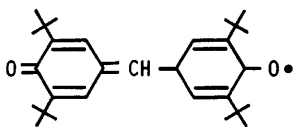

4

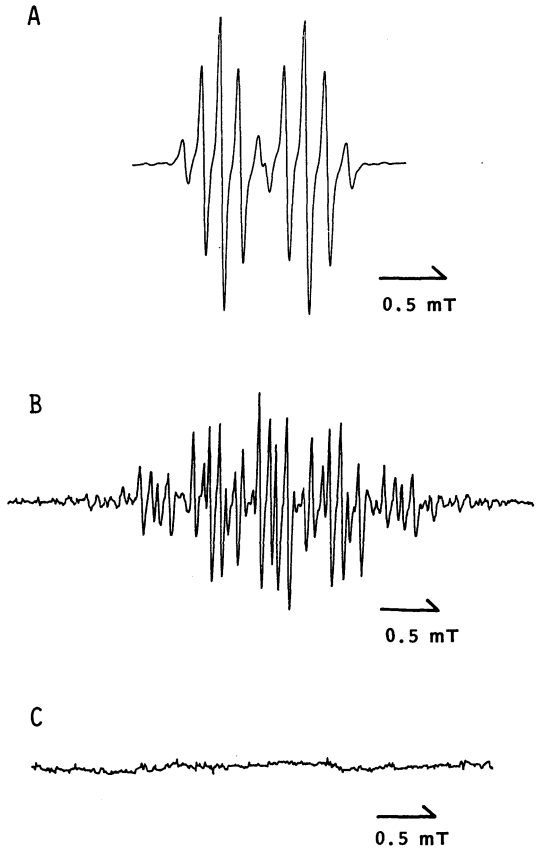

Fig. 5. Interaction of α-tocopheryloxyl radical with 5,6-ascorbyl dipalmitate in benzene at 25 °C under vacuum.
A: ESR spectrum of galvinoxyl radical in benzene. B: ESR spectrum observed when α-tocopherol was added to solution A. C: ESR spectrum observed when 5,6-ascorbyl dipalmitate was added to the solution B.

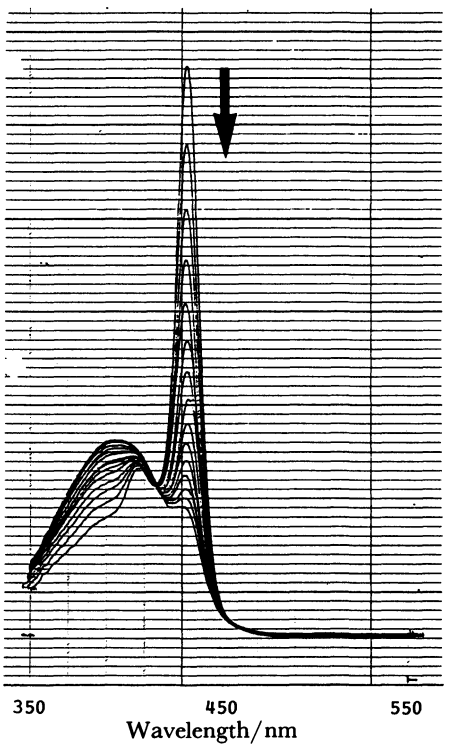

Fig. 6. Interaction of 20.8μM galvinoxyl with 28.9μM 5,6-ascorbyl dipropionate in chloroform at room temperature. The spectra were recorded every 2 min since 1 min after the mixing of galvinoxyl and 5,6-ascorbyl dipropionate.

When both tocopherol and ascorbic acid ester were depleted, the induction period was over and the rapid oxidation took place. Table 2 also shows the rate of oxygen uptake after the induction period. Under these conditions, the kinetic chain length is not very long, but nevertheless it is much larger than 1, suggesting that methyl linoleate is oxidized by a free radical chain mechanism. The oxidizability, $k_p/(2k_t)^{1/2}$, calculated from Eq. 9 is 0.020, where k_p and k_t are the rate constants for chain propagation and termination, respectively.

$$R_p = \frac{k_p}{(2k_t)^{1/2}}[LH]R_i^{1/2} \quad (9)$$

Interactions of Ascorbic Acid Esters with Galvinoxyl. The reactivity of hydrogen donor toward galvinoxyl gives the relative activity as a chain breaking antioxidant. Figure 6 shows the example of the result of interaction between galvinoxyl and ascorbic acid esters. It was found that all the ascorbic acid esters at either 6- or both 5- and 6-positions shown in Table 1 reacted with galvinoxyl at similar rate, whereas those substituted at 2-position did not interact with galvinoxyl.

The above results show that fatty acid esters of ascorbic acid and erythorbic acid at either 6- or both 5-and 6-positions act as chain-breaking antioxidant but that they are no more active as oxygen radical scavenger when ascorbic acid is esterified at 2-position. In other words, ascorbic acid esters function as antioxidant by donating the hydrogen atom at 2-position to oxygen radicals and interrupting free radical chain reaction. It may be worth noting, however, that even the ascorbic acid esters at 2-position may be effective as antioxidant in vivo when they are hydrolyzed by esterase.

Ascorbic acid derivatives have been previously prepared by several groups,[17,21,35] but many of the esters listed in Table 1 are novel compounds. Commercially available esters of ascorbic acid such as 6-ascorbyl palmitate and 6-ascorbyl stearate have solubility problem, but the fatty acid esters at both 5- and 6-positions of ascorbic acid improve the solubilities.

References

1) "Free Radicals in Biology," ed by W. A. Pryor, Academic Press, New York (1976—1984), Vol. I—VI.
2) "Tocopherol, Oxygen, and Biomembranes," ed by C. de Duve and O. Hayaishi, Elsevier, Amsterdam (1978).
3) "Oxygen Free Radicals and Tissue Damage," (Ciba Foundation Symp. 65), Excerpta Medica, Amsterdam (1979).
4) "Autoxidation in Food and Biological Systems," ed by

M. G. Simic and M. Karel, Plenum Press, New York (1980).
5) "Age Pigments," ed by R. S. Sohal, Elsevier/North Holland Biomedical Press, Amsterdam (1981).
6) "Free Radicals, Lipid Peroxidation and Cancer," ed by D. C. H. McBrien and T. F. Slater, Academic Press, London (1982).
7) "Lipid Peroxides in Biology and Medicine," ed by K. Yagi, Academic Press, New York (1982).
8) "Oxy Radicals and Their Scavenger Systems," ed by G. Cohen and R. A. Greenwald, Elsevier Biomedical, New York (1983).
9) "Oxygen Radicals in Chemistry and Biology," ed by W. Bors, M. Saran, and D. Tait, Walter de Gruyter, Berlin (1984).
10) W. A. Pryor, *Ann. New York Acad. Sci.*, **393**, 1 (1982).
11) B. Halliwell and J. M. C. Gutteridge, *Biomedical J.*, **219**, 1 (1984).
12) "Vitamin E," ed by L. J. Machlin, Marcel Dekker, New York (1980).
13) "Biology of Vitamin E," (Ciba Foundation Symp. 101), Pitman, London (1983).
14) G. W. Burton, T. Doba, E. J. Gabe, L. Hughes, F. L. Lee, L. Prasad, and K. U. Ingold, *J. Am. Chem. Soc.*, **107**, 7053 (1985).
15) E. Niki, J. Tsuchiya, Y. Yoshikawa, Y. Yamamoto, and Y. Kamiya, *Bull. Chem. Soc. Jpn.*, **59**, 497 (1986), and references cited therein.
16) W. M. Cort, *J. Am. Oil Chem. Soc.*, **51**, 321 (1974); *Adv. Chem. Ser.*, **200**, 533 (1982).
17) B. H. J. Bielski, H. W. Richter, and P. C. Chan, *Ann. New York Acad. Sci.*, **258**, 231 (1975).
18) A. D. Nadezhdin and H. B. Dunford, *Can J. Chem.*, **57**, 3017 (1979).
19) D. E. Cabelli and B. H. J. Bielski, *J. Phys. Chem.*, **87**, 1809 (1983).
20) W. A. Pryor, M. J. Kaufman, and D. F. Church, *J. Org. Chem.*, **50**, 281 (1985).
21) Y.-Y. Gwo, G. J. Flick, Jr., H. P. Dupuy, R. L. Ory, and W. L. Baran, *J. Am. Oil Chem. Soc.*, **62**, 1666 (1985).
22) E. Niki, T. Saito, and Y. Kamiya, *Chem. Lett.*, **1983**, 631.
23) L. R. C. Barclay, S. J. Locke, and J. M. MacNeil, *Can. J. Chem.*, **61**, 1288 (1983).
24) Y. Yamamoto, S. Haga, E. Niki, and Y. Kamiya, *Bull. Chem. Soc. Jpn.*, **57**, 1260 (1984).
25) E. Niki, T. Saito, A. Kawakami, and Y. Kamiya, *J. Biol. Chem.*, **259**, 4177 (1984).
26) E. Niki, A. Kawakami, Y. Yamamoto, and Y. Kamiya, *Bull.Chem. Soc. Jpn.*, **58**, 1971 (1985).
27) E. D. Wills, *Biochim. Biophys. Acta*, **98**, 238 (1965); A. W. Girotti, J. P. Thomas, and J. E. Jordan, *Photochem. Photobiol.*, **41**, 267 (1985).
28) H. W.-S. Chan and G. Levett, *Lipids*, **12**, 99 (1977).
29) N. A. Porter and D. G. Wujek, *J. Am. Chem. Soc.*, **106**, 2626 (1984), and preceding papers from this group.
30) Y. Yamamoto, E. Niki, and Y. kamiya, *Lipids*, **17**, 870 (1982).
31) E. N. Frankel, *J. Am. Oil Chem. Soc.*, **61**, 1908 (1984).
32) J. E. Packer, T. F. Slater, and R. L. Willson, *Nature*, **278**, 737 (1979).
33) E. Niki, J. Tsuchiya, R. Tanimura, and Y. Kamiya, *Chem. Lett.*, **1982**, 789.
34) J. Tsuchiya, T. Yamada, E. Niki, and Y. Kamiya, *Bull. Chem. Soc. Jpn.*, **58**, 326 (1985).
35) H. Tanaka and R. Yamamoto, *Yakugaku Zasshi*, **86**, 376 (1966).

Highly Enantioselective Reduction of Ethyl 2-Acyloxy-3-oxobutanoate with Immobilized Baker's Yeast

Takashi SAKAI, Toshiki NAKAMURA, Katsuyoshi FUKUDA, Eiichiro AMANO, Masanori UTAKA, and Akira TAKEDA*

Department of Synthetic Chemistry, School of Engineering, Okayama University, Tsushima, Okayama 700

(Received April 21, 1986)

Reduction of ethyl 2-acetoxy-3-oxobutanoate (**4a**) with immobilized baker's yeast in calcium alginate gel gave a 18:19:63 mixture of ethyl (2*R*,3*S*)- and (2*S*,3*S*)-2-acetoxy-3-hydroxybutanoates and ethyl (2*S*,3*S*)-2,3-dihydroxybutanoate each with >95% e.e. in 58% yield. A similar treatment of a 2-benzoyloxy analog of **4a** afforded a 6:94 mixture of ethyl (2*R*,3*S*)- and (2*S*,3*S*)-2-benzoyloxy-3-hydroxybutanoates (>95% e.e.) in 70% yield. Their absolute configurations were determined by comparison with authentic (2*R*,3*S*)- and (2*S*,3*S*)-2,3-dihydroxybutanoic acids. Effects of the immobilization and the pH of culture solution on the product ratio are also discussed.

Chiral (2*S*,3*S*)- and (2*R*,3*S*)-2,3-dihydroxybutanoic acids and their derivatives have been proved to be versatile key intermediates in a variety of natural poroduct syntheses[1–5] and hence convenient synthetic procedure for these compounds is desirable. In the reported method for the preparation of methyl (4*R*,5*S*)-2,2,5-trimethyl-1,3-dioxolane-4-carboxylate (**1**)[1] and its aldehyde analog (**2**),[2] their chiralities are derived from (2*R*,3*R*)-tartaric acid. (4*S*,5*S*)-2,2,5-Trimethyl-1,3-dioxolane-4-carbaldehyde (**3**)[3] has been elaborated from (4*S*,5*R*)-2,2,4-trimethyl-5-(2-phenylethenyl)-1,3-dioxolane which is obtainable from the baker's yeast promoted reaction of cinnamaldehyde with acetaldehyde.[4] Recently, aldehyde **3** has also been prepared efficiently via diastereo- and enantioselective reduction of 2-(1,2-dioxoalkyl)-1,3-dithian with baker's yeast.[5] As shown in these examples, the use of baker's yeast has been growing as one of the powerful synthetic methods for chiral alcohols, because of its high enantioselectivity by a simple procedure.

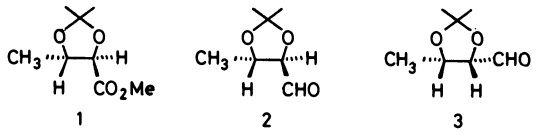

1 2 3

We describe here a novel, highly enantioselective synthetic method for (2*R*,3*S*)- and (2*S*,3*S*)-2,3-dihydroxybutanoic acid derivatives by the reduction of ethyl 2-acyloxy-3-oxobutanoates (**4a** and **4b**) with baker's yeast which is used by itself (method A) or as an immobilized one in calcium alginate gel[6] (method B) (Table 1). The immobilization of baker's yeast in an appropriate matrix has been realized not only to attain obvious advantages in the isolation and purification procedures,[6] but also to cause a definite change in an optical yield and/or a direction of rotation.[7] These advantages have encouraged us to use immobilized yeast. It enhanced erythro stereoselectivity in the reduction of **4a,b** and optical yields were more than 95% both in methods A and B.

Results and Discussion

The baker's yeast reduction of ethyl 2-acetoxy-3-oxobutanoate (**4a**)[8] gave ethyl (2*R*,3*S*)- and (2*S*,3*S*)-2-acetoxy-3-hydroxybutanoates (**5a** and **6a**) and ethyl (2*S*,3*S*)-2,3-dihydroxybutanoate (**7**)[9] as a major product (Scheme 1 and Table 1). The relative stereochemistry of **5** (threo) and **6** (erythro) were determined on the basis of ^{1}H NMR analysis which showed $J_{2,3}$=2.3—2.5 Hz for **5** and $J_{2,3}$=4 Hz for **6**.[10] Compound **7** was assigned to erythro after conversion to its acetonide as discussed below. The use of immobilized yeast improved the erythro-selectivity as well as the total yield of the reduction products. Prolonged reaction increased the ratio of **7** up to 63%, and decreased that of **6a**. Threo-(2*R*,3*S*) isomer of **7**, which is expected to be derived

Table 1. Reduction of Ethyl 2-Acyloxy-3-oxobutanoates (**4a, b**) with Fermenting Baker's Yeast

Ester	Method	Reaction Time/h	Product Yield/%[a]	Product Ratio/%[b]		
				5[c]	6[c]	7[c]
4a	A[d]	48	45	28	18	54
4a	B[e]	12	37	19	58	23
4a	B[e]	43	49	18	26	56
4a	B[e]	53	58	18	19	63
4b	A[d]	23	61	14	86	0
4b	B[e]	21	70	6	94	0
4b	B[f]	21	62	51	49	0

a) Isolated yield. b) Determined after separation by column chromatography. c) Optical purity is more than 95% e.e. d) A: Free baker's yeast was used. e) B: Immobilized baker's yeast was used. f) The pH of the calture solution was controlled at near 7 by addition of aqueous $NaHCO_3$.

from **5a**, was not detected in all cases. These facts suggest that only **6a** was hydrolyzed to **7** under the fermenting conditions. In a similar reduction of ethyl 2-benzoyloxy-3-oxobutanoate (**4b**), erythro-selectivity was further improved up to 94%. It is worth while to note here that the diastereoselection was not observed when the reaction was carried out under neutral conditions.

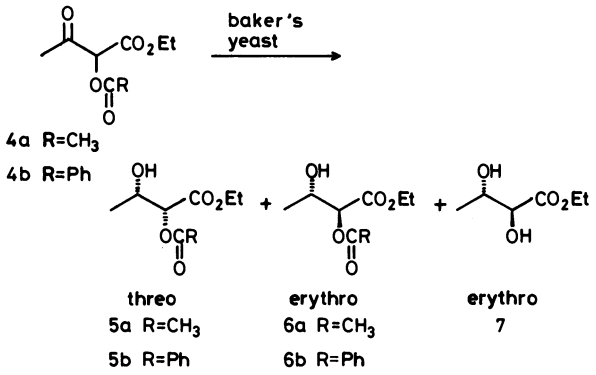

Scheme 1.

The absolute configurations of new chiral centers of these products were confirmed to be (3*S*) by comparison with authentic (2*R*,3*S*)- and (2*S*,3*S*)-2,3-dihydroxybutanoic acids (**8a** and **8b**) (Scheme 2). Thus the hydrolysis of threo esters **5a,b** and erythro ester **7** with 1 mol dm^{-3} methanolic $Ba(OH)_2$ gave the corresponding acids **8a** and **8b**, respectively. Interestingly, a similar treatment of erythro esters **6a,b** also afforded **8a** as a result of epimerization of C-2 position. The relative stereochemistry of **8a** and **8b** is distinguishable by means of ^{13}C NMR spectra (C-4 of **8a**: δ=19.3; that of **8b**[11]: 16.8). The stereochemical assignments are also acceptable in view of the Prelog rule.[12]

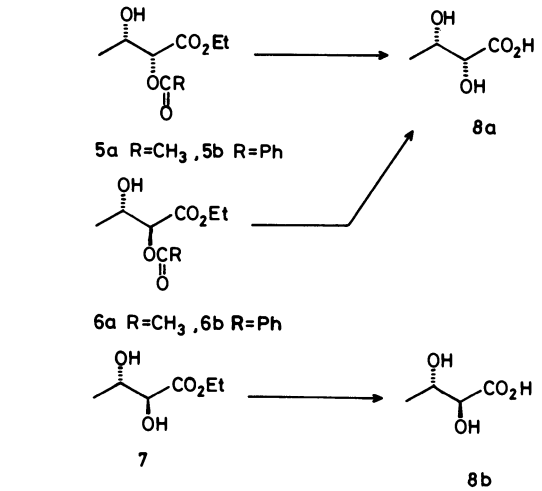

Scheme 2.

Optical purities of **5a**, **6a**, and **7** were estimated to be more than 95% e.e. based on the ^1H NMR spectral analysis with chiral shift reagent [Eu(hfc)$_3$] after conversion to acetonides **9a** and **9b** (Scheme 3). Namely, compounds **5a** and **7** could be converted to **9a** (trans) and **9b** (cis) with retention of the stereochemistry in a usual way by using 2,2-dimethoxypropane and *p*-toluensulfonic acid. However, erythro ester **6a** was transformed into **9a** with epimerization at C-2, as observed in the alkaline hydrolysis of **6a** to **8a**. The Eu(hfc)$_3$ induced ^1H NMR signal due to methyl group at C-5 in **9a** and **9b** thus obtained exhibited a doublet only, while that of the racemic ones, prepared from $NaBH_4$ reduction of **4a**, showed a couple of doublets with an equal intensity. The optical purities of **5b** and **6b** were also determined as >95% e.e. by comparing the ^1H NMR signal for C-4 proton in the presence of Eu(hfc)$_3$ with those for the $NaBH_4$ reduction products.

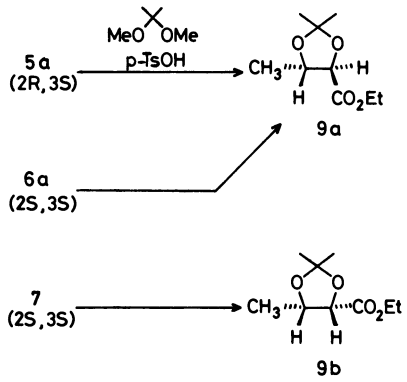

Scheme 3.

Experimental

Evaporative bulb-to-bulb distillation was done using a Büchi Kügelrohrofen. IR spectra were taken on a JASCO Model A-102 spectrometer. ^1H NMR spectra (60 MHz) were measured with a JEOL Model JNM-60 SI spectrometer and ^{13}C NMR spectra (25 MHz) were taken on a JEOL Model FX-100 spectrometer using Me_4Si as an internal standard. Preparative isolation by GLPC was done with Yanagimoto Model G-80 gas chromatograph (Apiezone Grease L on 10% Chromosorb, He 50 ml min^{-1}, oven temperature 140 °C). The preparative TLC was carried out on silica gel (Kieselgel 60 PF_{254}, Merck A. G. Darmstadt). Column chromatography was performed with silica gel (Silica Gel 60, 70—230 mesh, Katayama Chemical Co. Ltd., Tokyo). Elemental analysis was performed by E. A. Compound **4a** was prepared by the procedure of Henecka.[8]

Ethyl 2-Benzoyloxy-3-oxobutanoate (4b). A mixture of ethyl 2-chloro-3-oxobutanoate[8] (16.6 g, 0.101 mol), potassium benzoate·3H_2O (21.5 g, 0.10 mol), tetrabutylammonium bromide (1.51 g, 4.68 mmol) in benzene (150 ml) was heated under reflux for 3 h. The mixture was cooled, washed with aqueous $NaHCO_3$ and then with water, dried over $MgSO_4$, and concentrated. The residue was distilled under vacuum to give **4b** (16.2 g, 65% yield): Bp 115—122 °C (0.2 mmHg) (1 mmHg=133.322 Pa); IR (neat) 1760, 1730 cm^{-1}: ^1H NMR (CCl_4) δ=1.31 (3H, t, *J*=7 Hz), 2.31 (3H, s), 4.23 (2H, q, *J*=7 Hz), 5.53 (1H, s), 7.49 (3H, m), 8.09 (2H, m). Found: C, 62.62; H, 5.78. Calcd for $C_{13}H_{14}O_5$: C, 62.39; H, 5.64.

Preparation of Immobilized Baker's Yeast in Calcium Alginate Gel. The following preparation was done by the modification of the reported procedure.[6] Sodium alginate (14 g) was suspended in water (750 ml) by vigorous stirring at 50 °C for 1 h. To this was added dry baker's yeast

(14 g) (Oriental Yeast Co., Ltd., Tokyo; 98.5% yeast and 1.5% sorbitan fatty acid ester) and the mixture was stirred for additional 2 h untill it became as homogeneous as possible. The resulting suspension was added dropwise from a dropping funnel with a glass tube of 6 mm diameter into a 10% aqueous solution (750 ml) of $CaCl_2 \cdot 2H_2O$ with stirring to form small pieces of spherical calcium alginate gel with ca. 4 mm diameter immediately. Washing with water gave ca. 600 ml of immobilized baker's yeast gel which can be stored in a refrigerator for several weeks.

Typical Procedure for Baker's Yeast Reduction of Ethyl 2-Acyloxy-3-oxobutanoate. Reduction of Ethyl 2-Acetoxy-3-oxobutanoate (4a) with Immobilized Baker's Yeast. A culture solution involving $CaCO_3$ (2.5 g), $NH_4H_2PO_4$ (1 g), KH_2PO_4 (1 g), $MgSO_4$ (0.5 g, glucose (70 g) and boiled water (500 ml) was generally used. To this was added 350 ml of immobilized baker's yeast (8.2 g of baker's yeast) and stirred magnetically for 30 min at 35 °C. When brisk fermentation was confirmed by observing gel pieces to rise up to the surface of the mixture, compound **4a** (9.2 g, 48.9 mmol) was added and the stirring was continued for 20 h at 35 °C. Another batch of glucose (70 g) was added to the solution and the fermentation was continued for additional 23 h. The degree of its consumption was monitored by using glucose-test paper (Diasticks II, Mils-Sankyo Co. Ltd., Tokyo) in the course of the reaction and at the end of the reaction. The gel pieces and the aqueous layer were extracted with ethyl acetate separately. Combined organic layer was dried over $MgSO_4$ filtered and then concentrated. The residual oil was fractionated by column chromatography (140 g of silica gel; hexane-ethyl acetate-ether-acetic acid,30:10:10:0.5) to give **5a** (0.823 g, 9% yield), **6a** (1.19 g, 13% yield), and **7** (2.02 g, 28% yield). **5a**: $[\alpha]_D^{27}$ −30.0° (*c* 1.61, CH_2Cl_2); IR (neat) 3500, 1745 cm^{-1}: ^1H NMR (CCl_4) δ=1.27 (3H, t, *J*=7 Hz), 1.30 (3H, d, *J*=7 Hz), 1.96 (3H, s), 3.34 (1H, br s), 4.00 (1H, d, *J*=2.4 Hz), 4.18 (2H, q, *J*=7 Hz), 5.13 (1H, dq, *J*=2.4 Hz and 7 Hz); ^{13}C NMR ($CDCl_3$) δ=14.1 (q), 19.1 (q), 20.5 (q), 62.0 (t), 67.0 (d), 76.4 (d), 168.7 (s), 170.7 (s). Found: C, 50.59; H, 7.40. Calcd for $C_8H_{14}O_5$: C, 50.50; H, 7.42. **6a**: $[\alpha]_D^{27}$ +31.9° (*c* 1.71, CH_2Cl_2); IR (neat) 3490, 1742 cm^{-1}: ^1H NMR (CCl_4) δ=1.20 (3H, d, *J*=7 Hz), 1.27 (3H, t), 2.12 (3H, s), 3.19 (1H, br s), 3.8—4.30 (1H, m), 4.17 (2H, q, *J*=7 Hz), 4.76 (1H, d, *J*=4 Hz); ^{13}C NMR ($CDCl_3$) δ=14.2 (q), 16.1 (q), 20.9 (q), 62.0 (t), 71.1 (d), 73.0 (d), 170.2 (s), 172.3 (s). Found: C, 50.51; H, 7.69. Calcd for $C_8H_{14}O_5$: C, 50.50; H, 7.42. **7**: $[\alpha]_D^{27}$ +9.3° (*c* 1.69, CH_2Cl_2); IR (neat) 3440, 1730 cm^{-1}: ^1H NMR (CCl_4) δ=1.13 (3H, d, *J*=7 Hz) 1.30 (3H, t, *J*=7 Hz), 3.75—4.15 (2H, m), 4.20 (2H, q, *J*=7 Hz); ^{13}C NMR ($CDCl_3$) δ=14.2 (q), 17.3 (q), 61.6 (t), 69.2 (d), 74.8 (d), 172.7 (s). Found: C, 48.42; H, 8.15. Calcd for $C_6H_{12}O_4$; C, 48.64; H, 8.16.

Reduction of 4a with Free Baker's Yeast. To the culture solution (300 ml) prepared as before mentioned, was added dry baker's yeast (12 g) and stirred at 35 °C for 30 min. Compound **4a** (4.7 g, 25 mmol) was added and stirring was continued for 18 h at 35 °C. After addition of glucose (25 g) again, the mixture was stirred for additional 20 h. Celite was added to the mixture and filtered with suction. The organic layer was extracted with ethyl acetate and treated in a manner similar to that described above to give **5a** (607 mg, 13% yield), **6a** (390 mg, 8% yield), and **7** (898 mg, 25% yield).

Reduction of Ethyl 2-Benzoyloxy-3-oxobutanoate (4b) with Immobilized Baker's Yeast. A mixture of immobilized baker's yeast (50 ml) and **4b** (0.494 g, 1.97 mmol) in the culture solution (70 ml) was stirred at 35 °C for 20 h and worked up in a similar way. Crude products were fractionated by preparative TLC (hexane-ethyl acetate-ether, 1:1:1) to give ethyl (2*S*,3*S*)-2-benzoyloxy-3-hydroxybutanoate (**6b**) (R_f 0.47—0.70, 323 mg, 65.8% yield) and its (2*R*,3*S*)-isomer (**5b**) (R_f 0.70—0.75, 22 mg, 4.2% yield). **6b**: $[\alpha]_D^{21}$ +9.80° (*c* 1.96, CH_2Cl_2); IR (neat) 3500, 1730, 1600 cm^{-1}; ^1H NMR (CCl_4) δ=1.26 (3H, t, *J*=7 Hz), 1.27 (3H, d, *J*=7 Hz), 3.03 (1H, br s), 4.22 (2H, q, *J*=7 Hz), 4.00—4.30 (1H, m), 5.07 (1H, d, *J*=4 Hz, 2-H); ^{13}C NMR ($CDCl_3$) δ=14.0 (q), 19.2 (q), 61.7 (t), 67.3 (d), 76.6 (d), 128.5 (d), 129.2 (s), 129.9 (d), 133.4 (d), 166.0 (s), 168.6 (s).Found: C, 61.78; H, 6.40. Calcd for $C_{13}H_{16}O_5$: C, 61.90; H, 6.39. **5b**: $[\alpha]_D^{21}$ +21.4° (*c* 1.91, CH_2Cl_2); IR (neat) 3500, 1730, 1600 cm^{-1}; ^1H NMR (CCl_4) δ=1.16 (3H, t, *J*=7 Hz), 1.43 (3H, d, *J*=7 Hz), 2.96 (1H, s), 4.09 (2H, q, *J*=7 Hz), 4.00—4.35 (1H, m), 5.36 (1H, dq, *J*=2.5 Hz and 7 Hz), 7.40 (3H, m), 7.92 (2H, m); ^{13}C NMR ($CDCl_3$) δ=14.0 (q), 16.1 (q), 62.1 (t), 71.7 (d), 73.1 (d), 128.4 (d), 129.6 (d), 129.9 (s), 133.1 (d), 165.6 (s), 172.5 (s). Found: C, 61.96; H, 6.49. Calcd for $C_{13}H_{16}O_5$: C, 61.90; H, 6.39.

(2*R*,3*S*)-2,3-Dihydroxybutanoic Acid (8a). A mixture of ethyl (2*R*,3*S*)-2-acetoxy-3-hydroxybutanoate (**5a**) (300 mg, 1.6 mmol) in 5 ml of 1 mol dm^{-3} methanolic $Ba(OH)_2$ was stirred at room temperature for 10 h. After being acidified with 10% HCl and washed well with ether, the solvent was removed under reduced pressure. From the residue, organic material was extracted with several portions of methanol, bubled with carbon dioxide and filtered. Concentration of the filtrate gave an oil together with remaining inorganic materials. To this was added methanol and decanted. The procedure was repeated. Finaly, evaporation of the solvent gave spectroscopically pure **8a** (161 mg, 75% yield): $[\alpha]_D^{16}$ +8.8°[13] (*c* 1.0, H_2O) (lit,[11] $[\alpha]_D^{16}$ −13.51° (*c* 6.0, H_2O) for (2*S*,3*R*)-enantiomer); IR (neat) 3700—2300, 1735, 1310, 1238, 1146, 1083, 1070 cm^{-1}: ^1H NMR (CD_3OD) δ=1.22 (1H, d, *J*=6 Hz), 3.73—4.40 (2H, m),5.13 (3H, br s); ^{13}C NMR (CD_3OD) δ=19.6 (q), 69.7 (d), 75.7 (d), 176.2 (s).

A similar treatment of **5b**, **6a**, and **6b** also gave **8a**. The specific rotation[13] and yield in each experiment are as follows: $[\alpha]_D^{21}$ +13.1° (*c* 1.90, H_2O), 81% yield; $[\alpha]_D^{28}$ +9.1° (*c* 10.6, H_2O), 84% yield; $[\alpha]_D^{24}$ +8.4° (*c* 1.50, H_2O), 76% yield.

(2*S*,3*S*)-2,3-Dihydroxybutanoic Acid (8b).[11] Ester **7** was treated in a way similar to that described above to give **8b** (60% yield) as a viscous oil: $[\alpha]_D^{16}$ +8.8° (*c* 1.0, H_2O) [lit,[11] $[\alpha]_D^{20}$ +9.3° (*c* 0.5, H_2O)]; IR (neat) 3700—2300, 1735, 1260, 1220, 1190, 1082, 1060 cm^{-1}: ^1H NMR (CD_3OD) δ=1.19 (3H, d, *J*=6 Hz), 3.73—4.40 (2H, m), 5.13 (3H, br s); ^{13}C NMR (CD_3OD) δ=17.7 (q), 69.9 (d), 76.0 (d), 175.9 (s).

Ethyl (4*R*,5*S*)-2,2,5-Trimethyl-1,3-dioxolane-4-carboxylate (9a). A mixture of ester **5a** (130 mg, 0.68 mmol), 2,2-dimethoxypropane (140 mg, 1.34 mmol), and *p*-toluenesulfonic acid (1 mg, 0.006 mmol) in dichloromethane (0.75 ml) was heated under reflux for 45 h. The mixture was washed with aqueous $NaHCO_3$, dried over $MgSO_4$, and concentrated under reduced pressure. The residual oil was distilled to give **9a** (82 mg, 64% yield): Bp 60—65 °C (3 mmHg) (1 mmHg=133.322 Pa); $[\alpha]_D^{23}$ +15.2° (*c* 1.2, $CHCl_3$); IR (neat) 1760, 1730 cm^{-1}; ^1H NMR (CCl_4) δ=1.10—1.55 (12H, m), 3.65-4.20 (2H, m), 4.13 (2H, q); ^{13}C NMR ($CDCl_3$) δ=14.2 (q), 18.5 (q), 25.7 (q), 27.2 (q), 61.2 (t), 75.2 (d), 80.5 (d), 110.5 (s), 170.5 (s).

A similar treatment of compound **6a** also gave **9a** (73% yield): Bp 60—65 °C (3 mmHg).

Ethyl (4*S*,5*S*)-2,2,5-Trimethyl-1,3-dioxolane-4-carboxylate

(9b). Yield 72%; bp 60—65 °C (3 mmHg) (1 mmHg= 133.322Pa); $[\alpha]_D^{16}$ +24.7° (*c* 2.4, $CHCl_3$); IR (neat) 1760, 1730 cm^{-1}; ^1H NMR (CCl_4) δ=1.05—1.50 (12H, m), 4.07 (2H, q, *J*=7 Hz), 3.9—4.4 (2H, m); ^{13}C NMR ($CDCl_3$) δ=14.7 (q), 15.6 (q), 25.6 (q), 27.0 (q), 60.9 (t), 73.6 (d), 77.8 (d), 110.3 (s), 170.2 (s). Found: C, 57.74, H, 8.63. Calcd for $C_9H_{16}O_4$: C, 57.43; H, 8.57.

Ethyl (4*RS*,5*SR*)- and (4*RS*,5*RS*)-2,2,5-Trimethyl-1,3-dioxolane-4-carboxylates [(±)-9a and (±)-9b]. To a solution of ester **4a** (1.0 g, 5.26 mmol) in ethanol (5 ml), was added $NaBH_4$ (70 mg, 1.85 mmol). After being stirred at 4 °C for 10 min, the mixture was acidified with 10% HCl and ethanol was removed under reduced pressure. The residual oil[14] (762 mg) was added to a mixture of 2,2-dimethoxypropane (1.25 g, 12 mmol) and *p*-toluenesulfonic acid (5 mg, 0.03 mmol) in dichloromethane (3 ml). It was stirred under reflux for 12 h, cooled, washed with aqueous $NaHCO_3$, dried over $MgSO_4$, and then concentrated. The residue was purified by preparative TLC (hexane–ethyl acetate, 3:1; R_f 0.40—0.85) to give 228 mg (23% yield) of a mixture of (±)-**9a** and (±)-**9b**, which were separated by preparative GLPC [(±)-**9a**: retention time 7.3 min; (±)-**9b**: 9.3 min)].

Ethyl (2*RS*,3*SR*)- and (2*RS*,3*RS*)-2-Benzoyloxy-3-hydroxybutanoates [(±)-5b and (±)-6b]. Ester **4b** (504 mg, 3.02 mmol) was allowed to react with $NaBH_4$ (24.6 mg, 0.677 mmol) in ethanol (3 ml) at 0 °C for 5 min and worked up in a similar way. Crude products were fractionated by preparative TLC (hexane–ethyl acetate–ether, 1:1:1) to give (±)-**5b** (R_f 0.69—0.79, 165 mg, 33% yield) and (±)-**6b** (R_f 0.57—0.69, 49 mg, 10% yield).[15]

The present work was partly supported by a Grant-in-Aid for Special Project Research (No. 60119001) from Ministry of Education, Science and Culture.

References

1) A. Tanaka and K. Yamashita, *Chem. Lett.*, **1981**, 319.
2) G. Fronza, C. Fuganti, P. Grasselli, and G. Marinoni, *Tetrahedron Lett.*, **1979**, 3883.
3) G. Fronza, C, Fuganti, P. Grasselli, G. Pedrocchi-Fantoni, and C. Zirotti, *Tetrahedron Lett.*, **23**, 4143 (1982); S. Servi, *Tetrahedron Lett.*, **24**, 2023 (1983); C. Fuganti, S. Servi, and C. Zirotti, *Tetrahedron Lett.*, **24**, 5285 (1983).
4) C. Fuganti and P. Grasselli, *Chem. Ind.*, **17**, 983 (1977); G. Fronza, C. Fuganti, and P. Graselli, *J. Chem. Soc., Chem. Commun.*, **1980**, 442.
5) T. Fujisawa, E. Kojima, T. Itoh, and T. Sato, *Tetrahedron Lett.*, **26**, 6089 (1985).
6) M. Kierstan and C. Bucke, *Biotechnol. Bioeng.*, **19**, 387 (1977).
7) K. Nakamura, M. Higaki, K. Ushio, S. Oka, and A. Ohno, *Tetrahedron Lett.*, **26**, 4213 (1985).
8) H. Henecka, *Chem. Ber.*, **81**, 179 (1948).
9) Racemic compound: A Holy, *Collect. Czech. Chem. Commun.*, **47**, 173 (1982).
10) ^1H NMR spectral data of *threo*- and *erythro*-2,3-dihydroxypentanoic acid: N. Mori, S. Omura, and Y. Tsuzuki, *Bull. Chem. Soc. Jpn.*, **38**, 2199 (1965).
11) The spectral data were identical with those of the racemic sample prepared by the reported procedure: F. W. Bachelor and G. A. Miana, *Can. J. Chem.*, **47**, 4089 (1969).
12) V. Prelog, *Pure Appl. Chem.*, **9**, 119 (1964).
13) The specific rotation was not maximized because of difficulty in further purification of the compound but satisfactory to comfirm its direction.
14) Attempts for purification of the crude products were not successful. The products seem to involve racemic **5a** and **6a** together with their 3-acetoxy-2-hydroxy derivatives and so on.
15) Although HPLC analysis of **5b** and **6b** obtained showed a single peak (column SI-60, 8 mmϕ×250 mm; hexane–ethyl acetate–ethanol–ether, 20:10:9:1; 1.0 ml min^{-1}; (±)-**5b**: retention time 10.2 min; (±)-**6b**: 10.6 min), ^1H and ^{13}C NMR spectra of each compound indicate the presence of a small amount of impurities, probably due to 2-hydroxy-3-benzoyloxy analogs.

The Preparation of Polythia[n](1,1′)ruthenocenophanes. Their Platinum Group Metals Complexes and Their X-Ray Crystal Structures

Sadatoshi Akabori,* Sadao Sato,*,† Takehiko Tokuda, Yoichi Habata, Kayoko Kawazoe,† Chihiro Tamura,† and Masaru Sato††

Department of Chemistry, Faculty of Science, Toho University, Funabashi, Chiba 274
†Analytical and Metabolic Research Laboratories, Sankyo Co., Ltd., 1-2-58 Hiromachi, Shinagawa-ku, Tokyo 140
††Chemical Analysis Center, Saitama University, Urawa, Saitama 338

(Received April 23, 1986)

Polythia[n](1,1′)ruthenocenophanes were prepared by reaction of 1,1′-bis(2-chloroethylthio)ruthenocene with disodium alkanedithiolates in tetrahydrofuran/ethanol. The ruthenocenophanes efficiently formed 1 : 1 complexes with platinum and palladium dichlorides. X-Ray crystallography of complexes of the 1,4,7,10-tetrathia[n](1,1′)ruthenocenophane with $PtCl_2$ and $PdCl_2$ revealed that the Pt (or Pd) atom bonded selectively to the two sulfur atoms at the 4,7-positions among the four sulfur atoms in the bridge of the ligand with a slightly distorted cis square-planar configuration. The conformation of the organic moiety in the 1 : 1 complex is greatly changed from that of the metal-free ligand. Also, the 1 : 1 palladium complex is isomorphous with the 1 : 1 platinum complex.

Although a number of macrocyclic polyethers and their alkali and alkaline earth-metal complexes have already been reported,[1] few complexes of polythia-crown ethers with a platinum group metal are known.[2] We recently suggested[3,4] that the ruthenium atom of the complexes of polyoxa- and dioxapolythia[n](1,1′)-ruthenocenophanes (**1** and **2**) with soft cations such as mercury(II) and silver(I) ions interacted with the incorporated metal ions. Therefore, a similar interaction can be expected between the ruthenium atoms of ruthenocenocrown ethers and palladium(II) or platinum(II) ions which are soft cations. In a previous paper,[5] we reported an X-ray analysis of the Pt-complex with 4,7-dithia-1,10-dioxa[10]ruthenocenophane. In this complex, the platinum atom which has a slightly distorted square-planar configuration was selectively coordinated with two sulfur atoms at the 4,7-positions in the bridge. Therefore, the distance between the ruthenium and palladium atoms was too long to allow interaction. Furthermore, we have reported[6] on the syntheses of the polythia[n](1,1′)ruthenocenophanes (**6**, **7**, **8**, and **9**) by reactions of 1,1′-bis(2-chloroethylthio)ruthenocene with disodium 1,2-ethanedithiolate. Therefore, we have been interested in the stereochemistry of the complexes formed from polythia-[n](1,1′)ruthenocenophanes and *trans*-$[PdCl_2(CH_3CN)_2]$ (**11a**) or *cis*-$[PtCl_2(CH_3CN)_2]$ (**11b**). Here we report on the syntheses of complexes of polythia[n](1,1′)ruthenocenophanes with platinum group metals and their structural studies by spectral and X-ray crystallographic methods.

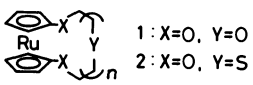

Syntheses of Polythia[n](1,1′)ruthenocenophanes. In order to obtain the starting material of polythia-[n](1,1′)ruthenocenophanes (**6**—**10**), ruthenocene-1,1′-dithiol (**3**),[6] which was prepared by the reduction of trithia[3](1,1′)ruthenocene, was reacted with 1-bromo-2-chloroethane in the presence of sodium hydroxide to give 1,1′-bis(2-chloroethylthio)ruthenocene (**5**) in 67% yield. A new series of polythia[n](1,1′)ruthenocenophanes were synthesized by the reaction of an equimolar amount of **5** with the disodium salt of 1,2-ethanedithiol and/or its homologs in several solvents. The best results were achieved when highly diluted conditions were realized by the combination of a slow addition and a high reaction temperature and when tetrahydrofuran (THF)–aqueous ethanol was used as the solvent. For example, the reaction of **5** with disodium 1,2-ethanedithiolate gave 1,4,7,10-tetrathia[10](1,1′)-ruthenocenophane (**6**) in 9.8% yield together with trace amounts of the unexpected 1,4-dithia[4](1,1′)ruthenocenophane (**7**), 1,4,7-trithia[7](1,1′)ruthenocenophane (**8**), and 1,4,7,10,13-pentathia[13](1,1′)ruthenocenophane (**9**).

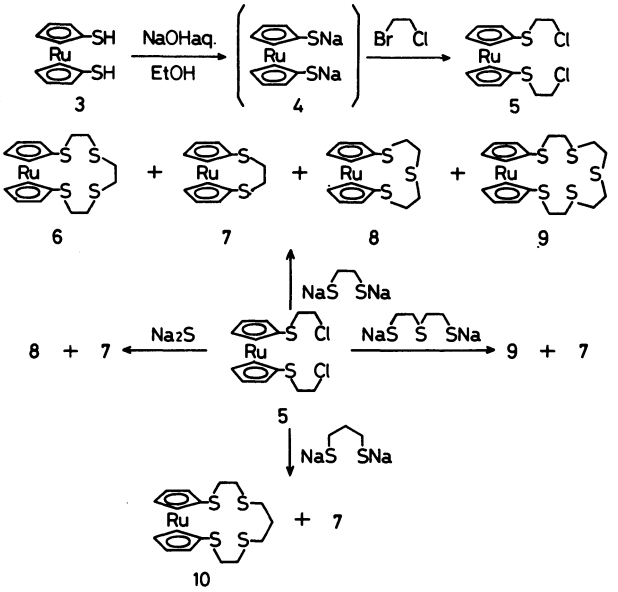

Similarly, **5** reacted with disodium 1,3-propanedithiolate, the disodium salt of bis(2-mercaptoethyl) sulfide, and sodium sulfide to give 1,4,8,11-tetrathia[11](1,1′)ruthenocenophane (**10**) (15%), **9** (23%), and **8** (15%) as the main products, respectively. Furthermore, in addition to the normal products, an unexpected product **7**

Table 1. ^{1}H NMR Spectral Data of **6**, **9**, and Their Palladium(II) and Platinum(II) Complexes (DMSO-d_6)

Compd	α-Protons	β-Protons	Methylene protons
6	4.64 (t, J=1.8 Hz, 4H)	4.81 (t, J=1.8 Hz, 4H)	3.10—2.79 (m, 12H)
12a	4.95 (s, 2H), 4.88 (s, 2H)	4.71 (t, J=1.8 Hz, 4H)	3.48—2.91 (m, 12H)
12b	5.02—4.85 (m, 4H)	4.71 (t, J=1.8 Hz, 4H)	3.44—2.91 (m, 12H)
9	4.65 (t, J=1.8 Hz, 4H)	4.79 (t, J=1.8 Hz, 4H)	3.03—2.74 (m, 16H)
13a	5.20—4.78 (m, 4H)	4.68 (broad-s, 4H),	3.48—2.84 (m, 16H)
13b	5.27—4.46 (m, 4H)	4.65 (broad-s, 4H)	3.75—2.59 (m, 16H)

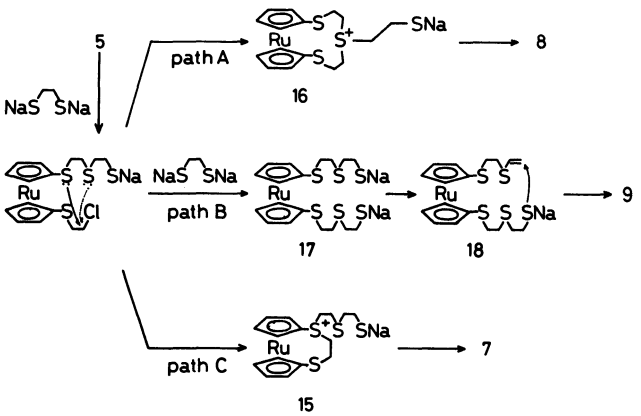

Scheme 1.

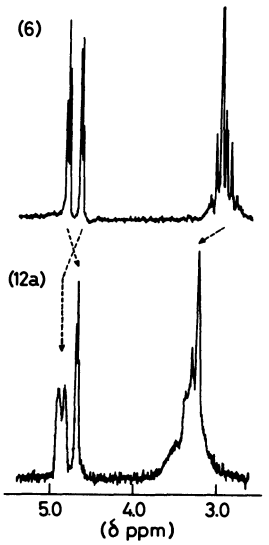

Fig. 1. ^{1}H NMR spectra of **6** and **12a**.

was also isolated in all cases. The structures of these products were established by their ^{1}H NMR and mass spectroscopic data and elemental analyses. A possible mechanism for the unexpected formation of **7**, **8**, and **9** in the reaction of **5** with disodium 1,2-ethanedithioate is proposed in Scheme 1. The formation of **7** can be rationalized in terms of the formation of the intermediate sulfonium ion **15** (path C) followed by dealkylation. The formation mechanisms of **8** and **9** can be interpreted similarly as follows (paths A and B): Dealkylation of **16** gives **8**, and elimination of SH^- from **17** gives the vinyl sulfide intermediate (**18**) followed by cyclization to give **9**. Also, a similar propagation reaction mechanism has been observed in the reaction of bis(2-chloroethyl) ether with sodium sulfide,[7] and the reaction of disodium 1,2-ethanedithiolate with 1,1′-bis(2-chloroethoxy)ferrocene[8] and 1,1′-bis(2-chloroethylthio)ferrocene.[9]

Palladium(II) and Platinum(II) Chloride Complexes of 6, 9, and 10. A solution of the ruthenocenothiacrown ether (**6**, **9**, and **10**) in acetonitrile was reacted with an equimolar amount of $MCl_2(CH_3CN)_2$ (**11a**: M=Pd or **11b**: M=Pt) in acetonitrile to give 1:1 complexes in 47—89% yields. The melting and decomposition points of these palladium and platinum complexes were higher than those of the corresponding metal-free ligands. As shown in Table 1 and Fig. 1, all of the α-protons of the ruthenocene nucleus and the methylene protons of complexes **12** and **13** were shifted downfield, and the signal shape of the α-protons became extremely complex. For example, the α- and the methylene protons of **12a**, compared with metal-free ligand **6**, shifted downfield by ca. +0.31—+0.24 and +0.38—+0.12 ppm, respectively, and the signal shape of the α-protons varied to two singlets from a triplet (J= 1.8 Hz). However, the β-protons of **12a** shifted upfield only a little (by −0.10 ppm). From the ^{1}H NMR spectral data, it is suggested that the palladium (or platinum) ion was coordinated with sulfur atoms outside of the polythia macrocyclic plane, so the structures of complexes **12** and **13** may be unsymmetrical. The far-IR spectra of **6** and **9** and their palladium and platinum complexes (**12** and **13**) were recorded using a CsI disk. These results are listed in Table 2. In complexes **12** and **13**, the Cp–Ru–Cp ring tilting and Cp–Ru stretching bands were slightly shifted to a lower frequency by ca. 10—20 cm^{-1}, respectively. In addition, new absorptions appeared at 2960 cm^{-1}, and 325 and 310 cm^{-1}, which were assigned to the C–H stretching vibrations of the Cp rings and *cis*-MCl_2 (M=Pd or Pt) stretching vibrations, respectively. The absorption bands at 325 and 310 cm^{-1} are in good agreement with the range reported for *cis*-MCl_2 (M=Pd or Pt) vibrations. These results suggest that the reaction of the ruthenocenocrown ethers with *trans*-$[PdCl_2(CH_3CN)_2]$ (**11a**) and *cis*-$[PtCl_2(CH_3CN)_2]$ (**11b**) gives only a cis-isomer.

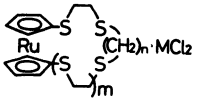

12a: m=1, n=2, M=Pd
12b: m=1, n=2, M=Pt
13a: m=2, n=2, M=Pd
13b: m=2, n=2, M=Pt
14a: m=1, n=3 M=Pd
14b: m=1 n=3 M=Pt

Table 2. IR Spectral Data[a] of **6**, **9**, and Their Palladium(II) and Platinum(II) Complexes (cm^{-1})

Compd	ν(C-H)		ν(C-C)			δ(C-H)	π(C-H)	Ring tilt	ν(Ru-Cp)	ν(M-Cl)	
6	3080		2910	1410		1025	808	450	382		
12a	3080	2960	2920	1410	1400(sh)[b]	1020	805	430	370	325(sh)	313
12b	3080	2960	2920	1420	1400(sh)	1020	805	432	370	325(sh)	312
9	3080		2920	1415		1025	817	450	395		
13a	3080	2960	2910	1410		1020	810	435	385	325(sh)	310
13b	3080	2950(sh)	2910	1410		1020	810	435(sh)	385	320(vw)[c]	610(vw)

a) CsI disk. b) Shoulder. c) Very weak.

Table 3. Fractional Atomic Coordinates (×10⁴) and Thermal Parameters (Å²)

	Atom	x	y	z	B_{eq}[a]
Molecule **6**	Ru	1685.7(3)	4150.9(3)	4087.7(6)	1.96
	C(1)	1151(3)	2261(4)	3590(8)	2.2
	C(2)	381(3)	2697(4)	1935(8)	2.5
	C(3)	10(3)	3447(4)	3437(9)	2.9
	C(4)	546(4)	3490(4)	6019(9)	3.0
	C(5)	1253(3)	2758(4)	6121(8)	2.7
	S(6)	1852(1)	1334(1)	2585(2)	3.0
	C(7)	1125(4)	−89(4)	2863(10)	2.9
	C(8)	1280(4)	−322(4)	5530(11)	3.9
	S(9)	2227(1)	−1129(1)	6682(3)	4.6
	C(10)	3428(4)	−264(5)	6404(11)	4.1
	C(11)	3890(5)	817(5)	8394(10)	4.2
	S(12)	5170(1)	1611(1)	8355(3)	5.1
	C(13)	4856(4)	2239(5)	5522(11)	3.8
	C(14)	4353(4)	3228(4)	5824(9)	3.4
	S(15)	3973(1)	3737(1)	2836(2)	3.0
	C(16)	3224(3)	4662(3)	3564(8)	2.2
	C(17)	2496(3)	5054(4)	1706(8)	2.5
	C(18)	2098(4)	5862(4)	3012(9)	2.8
	C(19)	2562(4)	5964(4)	5629(9)	3.0
	C(20)	3256(3)	5222(4)	5994(8)	2.5
Molecule **12b**	Pt	5884.3(8)	3119.2(3)	6547.9(11)	2.22
	Cl(1)	4197(6)	3026(2)	3235(8)	4.3
	Cl(2)	7180(6)	3590(2)	8796(8)	4.1
	Ru	2305(2)	4493.4(6)	1903(2)	2.6
	C(1)	942(20)	3941(7)	2608(29)	2.8
	C(2)	139(18)	4285(8)	1419(31)	3.9
	C(3)	348(23)	4746(8)	2392(33)	4.0
	C(4)	1209(27)	4680(8)	4051(31)	4.6
	C(5)	1647(23)	4190(9)	4249(27)	3.7
	S(6)	697(6)	3341(2)	2077(9)	3.6
	C(7)	2107(19)	3055(8)	3637(27)	3.1
	C(8)	3386(18)	3036(8)	2876(27)	2.8
	S(9)	4657(5)	2653(2)	4369(7)	2.6
	C(10)	5853(20)	2545(7)	2908(26)	2.7
	C(11)	6744(20)	2968(7)	2734(26)	2.9
	S(12)	7584(5)	3150(2)	5005(7)	2.7
	C(13)	8083(19)	3770(8)	4705(28)	3.3
	C(14)	7115(18)	4095(7)	3403(28)	2.5
	S(15)	5451(6)	4119(2)	4079(8)	3.2
	C(16)	4533(20)	4435(8)	2140(30)	3.6
	C(17)	3838(21)	4221(8)	458(28)	3.2
	C(18)	3084(22)	4615(9)	−560(30)	4.4
	C(19)	3275(21)	5021(8)	459(32)	3.8
	C(20)	4138(22)	4923(7)	2121(30)	3.3

a) W. C. Hamilton, *Acta Crystallogr.*, **12**, 609 (1959).

The metal free ligand **6** and its Pt complex **12b** were further characterized by X-ray crystallographic studies. The final atomic parameters are listed in Table 3, and bond lengths as well as bond and torsion angles are given in Tables 4 and 5 for **6** and **12b**, respectively. Perspective views of **6** and **12b** are shown in Fig 2.

For **6** the C–C bond lengths and C–C–C bond angles of the two Cp rings are in the range of 1.413(7)—

Table 4. Bond Lengths (l/Å), and Bond and Torsion Angles (ϕ/°) for **6**

1	2	3	4	1-2	1-2-3	1-2-3-4
Tetrathia-crown moiety						
S(6)	C(1)	C(2)	C(3)	1.750(5)	128.4(4)	175.4(3)
S(6)	C(1)	C(5)	C(4)		123.7(4)	−175.6(2)
C(2)	C(1)	S(6)	C(7)			22.5(5)
C(5)	C(1)	S(6)	C(7)			−162.0(4)
C(1)	S(6)	C(7)	C(8)		99.9(2)	169.8(4)
S(6)	C(7)	C(8)	S(9)	1.813(5)	109.7(4)	−175.7(1)
C(7)	C(8)	S(9)	C(10)	1.504(8)	112.4(4)	72.7(5)
C(8)	S(9)	C(10)	C(11)	1.808(6)	101.8(3)	72.0(5)
S(9)	C(10)	C(11)	S(12)	1.827(6)	113.3(4)	173.6(1)
C(10)	C(11)	S(12)	C(13)	1.510(9)	112.8(4)	74.6(5)
C(11)	S(12)	C(13)	C(14)	1.812(6)	104.6(3)	58.6(5)
S(12)	C(13)	C(14)	S(15)	1.806(6)	117.0(4)	−96.3(4)
C(13)	C(14)	S(15)	C(16)	1.511(8)	114.8(4)	−74.3(5)
C(14)	S(15)	C(16)	C(17)	1.822(6)	101.7(2)	84.7(5)
C(14)	S(15)	C(16)	C(20)			−98.0(4)
S(15)	C(16)	C(17)	C(18)	1.755(5)	127.9(4)	177.9(2)
S(15)	C(16)	C(20)	C(19)		124.6(4)	−178.1(2)
Cyclopentadienyl ring						
C(1)	C(2)	C(3)	C(4)	1.435(6)	108.1(4)	0.4(6)
C(2)	C(3)	C(4)	C(5)	1.425(7)	108.1(4)	0.1(6)
C(3)	C(4)	C(5)	C(1)	1.413(7)	108.7(4)	−0.5(6)
C(4)	C(5)	C(1)	C(2)	1.433(7)	107.4(4)	0.7(6)
C(5)	C(1)	C(2)	C(3)	1.432(7)	107.7(4)	−0.7(6)
C(16)	C(17)	C(18)	C(19)	1.434(7)	108.1(4)	0.0(6)
C(17)	C(18)	C(19)	C(20)	1.434(7)	108.0(4)	−0.2(6)
C(18)	C(19)	C(20)	C(16)	1.426(7)	108.2(4)	0.4(6)
C(19)	C(20)	C(16)	C(17)	1.425(7)	108.3(4)	−0.4(6)
C(20)	C(16)	C(17)	C(18)	1.435(6)	107.5(4)	0.3(5)

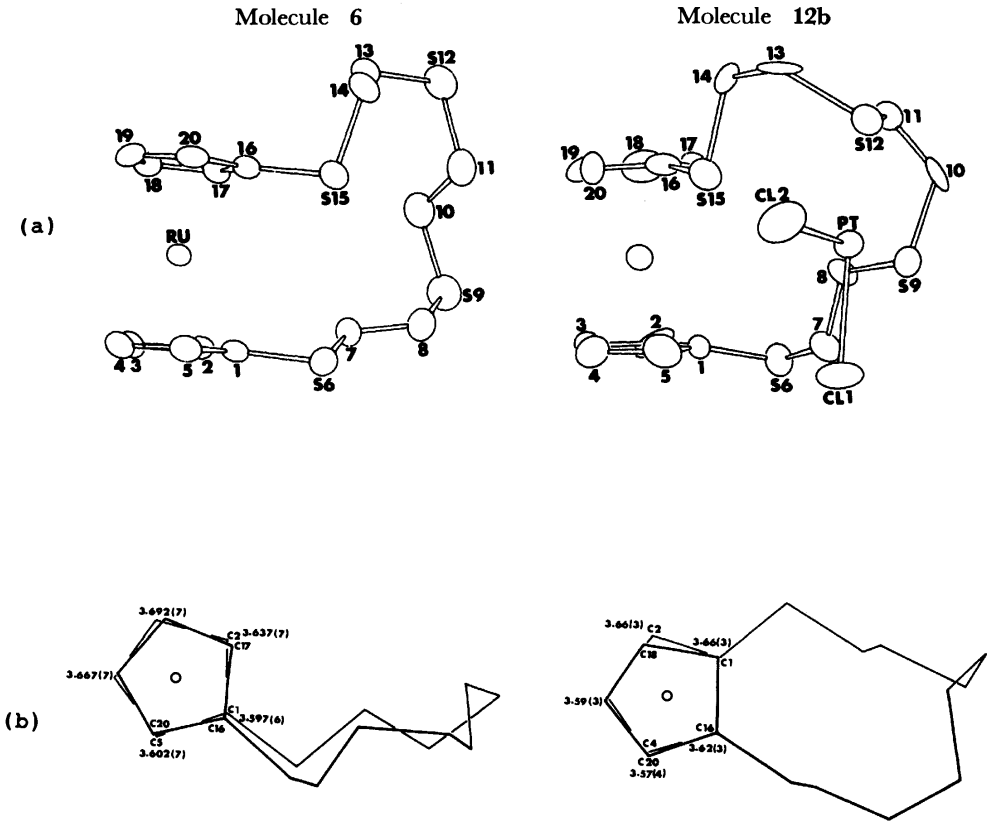

Fig. 2. (a) ORTEP (Johnson, 1965) drawings of molecules with atom numbering scheme. (b) Projections of the organic ligand moieties on the Cp ring containing the C(1) atom are also given with the C···C distance (A) between the rings. An open circle denotes Ru atom.

Table 5. Bond Lengths (l/Å) and Bond and Torsion Angles (ϕ/°) for **12b**

1	2	3	4	1-2	1-2-3	1-2-3-4
Tetrathia-crown moiety						
S(6)	C(1)	C(2)	C(3)	1.74(2)	118.5(17)	168.6(10)
S(6)	C(1)	C(5)	C(4)		132.6(17)	−165.5(15)
C(2)	C(1)	S(6)	C(7)			169.6(18)
C(5)	C(1)	S(6)	C(7)			−24.0(3)
C(1)	S(6)	C(7)	C(8)		103.3(11)	−86.8(18)
S(6)	C(7)	C(8)	S(9)	1.81(2)	111.5(16)	−170.6(3)
C(7)	C(8)	S(9)	C(10)	1.50(3)	108.1(15)	164.5(15)
C(8)	S(9)	C(10)	C(11)	1.85(2)	100.2(10)	74.2(17)
S(9)	C(10)	C(11)	S(12)	1.80(2)	113.2(14)	54.2(19)
C(10)	C(11)	S(12)	C(13)	1.50(3)	107.7(14)	−159.4(14)
C(11)	S(12)	C(13)	C14)	1.81(2)	103.6(10)	39(2)
S(12)	C(13)	C(14)	S(15)	1.84(2)	119.9(16)	57(2)
C(13)	C(14)	S(15)	C(16)	1.52(3)	109.0(15)	−171.3(16)
C(14)	S(15)	C(16)	C(17)	1.83(2)	97.2(10)	87(2)
C(14)	S(15)	C(16)	C(20)			−106(2)
S(15)	C(16)	C(17)	C(18)	1.79(2)	125.4(17)	171.6(13)
S(15)	C(16)	C(20)	C(19)		125.3(17)	−171.4(11)
Cyclopentadienyl ring						
C(1)	C(2)	C(3)	C(4)	1.44(3)	106(2)	−1(3)
C(2)	C(3)	C(4)	C(5)	1.48(3)	109(2)	2(3)
C(3)	C(4)	C(5)	C(1)	1.37(4)	110(2)	−3(3)
C(4)	C(5)	C(1)	C(2)	1.44(4)	107(2)	2(3)
C(5)	C(1)	C(2)	C(3)	1.46(3)	108(2)	−1(3)
C(16)	C(17)	C(18)	C(19)	1.44(3)	104(2)	−2(3)
C(17)	C(18)	C(19)	C(20)	1.46(3)	110(2)	1(3)
C(18)	C(19)	C(20)	C(16)	1.36(4)	109(2)	1(3)
C(19)	C(20)	C(16)	C(17)	1.39(3)	108(2)	−3(2)
C(20)	C(16)	C(17)	C(18)	1.43(3)	108(2)	3(2)
Pt coordination						
Cl(1)	Pt		Cl(2)	2.316(7)	91.0(2)	
Cl(2)	Pt		S(9)	2.315(7)	179.0(2)	
S(9)	Pt		Cl(1)	2.249(5)	89.5(2)	
S(12)	Pt		Cl(1)	2.239(6)	175.2(2)	
S(9)	Pt		S(12)		89.7(2)	
S(12)	Pt		Cl(2)		89.7(2)	

1.435(6) Å and 107.4(4)—108.7(4)° with average values of 1.429 Å and 108.0°, respectively. These average bond lengths and angles are in good agreement with those of ruthenocene.[11] In macrocyclic units, each average bond length of S-Csp^2, S-Csp^3, Csp^3-Csp^3 was 1.753, 1.816, and 1.508 Å; this is in agreement with each expected value. In the Cp moiety for **12b**, the bond lengths are in the range of 1.36(4)—1.48(3) Å with an average of 1.43 Å. Although the average value of the bond lengths is in good agreement with that of the metal-free ligand **6**, the bond lengths of C(3)-C(4), C(18)-C(19), and C(19)-C(20) are slightly shorter and C(2)-C(3), C(5)-C(1), and C(17)-C(18) are slightly longer than those found in the metal-free ligand **6**. The bond angles in the Cp rings are ranged over 104(2)—110(2)° with an average value of 108°. The difference (6°) of the bond angle is much larger than that (1.3°) in the free ligand **6**. The above results suggest a deformation of the Cp ring in the complex due to complexation. The Pt atom, which is complexed by the two S atoms of the tetradentate macrocyclic moiety, has a slightly distorted cis square-planar environment; the two S atoms at the 9- and 12-positions of the ligand occupy the other two cis positions. These results are consistent with those obtained from the IR spectral data. The Pt-S bond lengths are 2.249(5) and 2.239(7) Å. The bond lengths are slightly shorter than the sum of the covalent radii (2.32 Å)[12] and suggest that there is little π-bonding in the Pt-S bond. The Pt-Cl bond lengths have an average value of 2.315 Å, almost equal to the sum of the covalent radii, 2.28 Å. The interestingly selective coordination of the Pt atom to the S(9) and S(12) atoms is attributable to a steric hindrance of the two Cp rings to the S(6) and S(15) atoms. Moreover, the conformations of the organic ligand moiety differ greatly between ligand **6** and complex **12b**. The two Cp rings for both compounds take an eclipsed conformation and the dihedral angles between them are 2.5(2) and 2.4(10)° for **6** and **12b**, respectively. However, as shown in Fig. 1, the torsion angle (68°) between the C(1)-S(6) and S(15)-C(16) bonds around the z-axis of the ruthenocene nucleus in the complex **12b** is much larger than the corresponding one (5.3°) in the free ligand **6**. These results are quite similar to those obtained in 1,10-dioxa-4,7-dithia[10](1,1')ruthenocenophane.[5] Furthermore, X-ray crystal data, which are presented in the experi-

mental section, showed the two compounds (**12a** and **12b**) to be isostructural.

Experimental

The melting and decomposition points have not been corrected. The ^{1}H NMR spectra were obtained on a JEOL FX-90Q spectrometer with TMS as an internal standard. The mass spectra were measured on a Hitachi M80 mass spectrometer. The electronic spectra were recorded on a Hitachi 330 spectrometer. The IR spectra were taken by using a JASCO DS-701G Diffraction Grating Infrared Spectrometer in CsI pellets.

Materials. Ruthenocene,[13] 1-bromo-2-chloroethane,[14] dichlorobis(acetonitrile) complexes of palladium(II) and platinum(II)[10] were prepared according to previously reported methods. The synthesis of ruthenocene-1,1′-dithiol (**3**) was carried out as described previously.[4] All other solvents and reagents used were reagent grade.

1,1′-Bis(2-chloroethylthio)ruthenocene (5). 1-Bromo-2-chloroethane (25 g, 176 mmol) was added to a mixture of **3** (2.3 g, 7.0 mmol) and sodium hydroxide (0.70 g, 18 mmol) in ethanol (170 cm^3) containing water (5 cm^3). After the mixture was stirred for 4 h at room temperature, the reaction mixture was concentrated in vacuo and the residual solid was chromatographed on activated alumina (dichloromethane as eluent). The yellow fraction was collected and concentrated in vacuo. Recrystallization of the residual solid from benzene gave **5** as pale-yellow powder in 67% yield. Mp 92.5—93 °C. Found: C, 40.30; H, 3.80%. Calcd for $C_{14}H_{16}Cl_2S_2Ru$: C, 40.00; H, 3.84%. ^{1}H NMR ($CDCl_3$) δ=4.75 (t, J=1.8 Hz, 4H), 4.65 (t, J=1.8 Hz, 4H), 3.66 (t, J=6.1 Hz, 4H), 2.90 (t, J=6.1 Hz, 4H). MS (60 eV) m/z 421 (M^+).

1,4,7-Trithia[7](1,1′)ruthenocenophane (8). A mixture of **5** (0.31 g, 0.74 mmol) and sodium sulfide (0.22 g, 0.92 mmol) in THF–ethanol (1:4) (158 cm^3) was refluxed under nitrogen for 10 h. The reaction mixture was cooled, evaporated in vacuo and the residual solid was dissolved in dichloromethane (100 cm^3). After the insoluble material was filtered off, the filtrate was evaporated and then the residual solid was chromatographed on silica-gel TLC (benzene as eluent). The fourth (main) fraction was collected and evaporated. Recrystallization of the residual solid from hexane gave **8** as pale-yellow needles in 15% yield. Mp 154.0—154.6 °C. Found: C, 44.10; H, 4.20%. Calcd for $C_{14}H_{16}S_3Ru$: C, 44.07; H, 4.24%. ^{1}H NMR ($CDCl_3$) δ=4.83 (t, J=1.8 Hz, 4H), 4.61 (t, J=1.8 Hz, 4H), 3.22—2.88 (m, 8H). MS (60 eV) m/z 382 (M^+). From the third fraction, **7** was obtained in 9.8% yield. Mp 225.6—226.5 °C. Found: C, 44.56; H, 3.76%. Calcd for $C_{12}H_{12}S_2Ru$: C, 44.84; H, 3.77%. ^{1}H NMR ($CDCl_3$) δ= 5.06 (t, J=1.8 Hz, 4H), 4.57 (t, J=1.8 Hz, 4H), 3.14 (s, 4H). MS (60 eV) m/z 322 (M^+).

1,4,7,10-Tetrathia[10](1,1′)ruthenocenophane (6). **5** (0.58 g, 1.4 mmol) in THF (100 cm^3) and a mixture of sodium hydroxide (0.50 g, 13.0 mmol) and 1,2-ethanedithiol (0.50 g, 5.3 mmol) in 98% ethanol (100 cm^3) were added dropwise to the refluxing mixture of THF (200 cm^3) and ethanol (200 cm^3) in the same rate for a period of 3 h, and further refluxed for 14 h. The reaction mixture was cooled and evaporated, and the residue was extracted with three 50 cm^3 portions of chloroform. After the extracts were combined, the resulting solution was washed with water, dried and evaporated in vacuo. The residual oil was chromatographed on activated alumina (benzene as eluent). The third (main) fraction was collected and evaporated. Recrystallization of the residual solid from benzene gave **6** as pale-yellow needles in 9.8% yield. Similarly, trace amounts of **7**, **8**, and **9** were obtained from the first, second and fourth fractions, respectively. **6**: Mp 138.6—139.0 °C. Found: C, 44.48; H, 4.60%. Calcd for $C_{16}H_{20}S_4Ru$: C, 43.50; H, 4.57%. ^{1}H NMR ($CDCl_3$) δ=4.62 (t, J=1.8 Hz, 4H), 4.77 (t, J=1.8 Hz, 4H), 3.10 (s, 4H), 3.21—2.75 (m, 8H). MS (60 eV) m/z 441 (M^+). **9**: Mp 93.5—94.0 °C. Found: C, 42.82; H, 4.74%. Calcd for $C_{18}H_{24}S_5Ru$: C, 43.08; H, 4.83%. ^{1}H NMR ($CDCl_3$) δ=4.75 (t, J=1.8 Hz, 4H), 4.61 (t, J=1.8 Hz, 4H), 3.15—2.71 (m, 16H). MS (60 eV) m/z 501 (M^+). The structures of **7** and **8** were confirmed by comparison with the melting points, R_f values of TLC and the spectral data of the authentic samples.

1,4,7,10,13-Pentathia[13](1,1′)ruthenocenophane (9). Bis-(2-mercaptoethyl) sulfide (1.5 cm^3, 11 mmol) was reacted with **5** (0.80 g, 1.9 mmol) in the presence of sodium hydroxide (0.80 g, 20 mmol) under the same conditions described above. The reaction mixture was worked up according to the previously described procedure and chromatographed on activated alumina (benzene as eluent). The second (main) fraction was collected and evaporated. Recrystallization of the residual solid from hexane gave **9** as white needles in 27% yield. Also, **7** was obtained from the first fraction. The structures of these compounds were confirmed by comparison with the melting points, R_f values of TLC and the spectral data of the authentic samples.

1,4,8,11-Tetrathia[11](1,1′)ruthenocenophane (10). A mixture of 1,3-propanedithiol (0.55 g, 5.1 mmol) and **5** (0.50 g, 1.2 mmol) in THF (30 cm^3) was added to absolute ethanol (170 cm^3) containing sodium hydroxide (0.51 g, 13 mmol) at a refluxing temperature. After refluxing for 2 h, the reaction mixture was cooled, evaporated in vacuo and extracted with three 50 cm^3 portions of chloroform. The extracts were combined, washed with 10% of aq sodium hydroxide solution and concentrated, and then the residual solid was chromatographed on activated alumina (benzene as eluent). From the second (main) fraction, **10** was obtained in 15% yield. Mp 121.6—122.2 °C. Found: C, 45.03; H, 4.95%. Calcd for $C_{17}H_{22}S_4Ru$: C, 44.80; H, 4.88%. ^{1}H NMR ($CDCl_3$) δ=4.79 (t, J=1.8 Hz, 4H), 4.63 (t, J=1.8 Hz, 4H), 3.20—2.62 (m, 12H), and 2.08 (q, J=7.6 Hz, 2H). MS (60 eV) m/z 455 (M^+). Also, a trace amount of **7** was isolated from the first fraction.

Palladium(II) and Platinum(II) Complexes (12, 13, and 14) of Polythia[n](1,1′)ruthenocenophanes: General Procedure. Dichloro(1,4,7,10-tetrathia[10](1,1′)ruthenocenophane)platinum(II) (12b). **11** (35.6 mg, 0.102 mmol) in acetonitrile (5 cm^3) was slowly added to gently refluxing acetonitrile solution (10 cm^3) containing **6** (44.9 mg, 0.102 mmol). The resulting crystals were collected by filtration and washed with small amounts of acetonitrile to give **12b** in 51% yield as pale-yellow needles. Mp 257 °C (decomp). Found: C, 27.16; H, 2.85%. Calcd for $C_{16}H_{20}Cl_2S_4RuPt$: C, 27.19; H, 2.70%.

Dichloro(1,4,7,10-tetrathia[10](1,1′)ruthenocenophane)palladium(II) (12a). Yield (89%). Mp 248 °C (decomp). Found: C, 31.05; H, 3.26%. Calcd for $C_{16}H_{20}Cl_2S_4RuPd$: C, 30.98; H, 2.99%.

Dichloro(1,4,7,10,13-pentathia[13](1,1′)ruthenocenophane)palladium(II) (13a). Yield (79%). Mp 211—212 °C. Found: C, 31.39; H, 3.62%. Calcd for $C_{18}H_{24}Cl_2S_5RuPd$: C, 31.83; H, 3.56%.

Dichloro(1,4,7,10,13-pentathia[13](1,1′)ruthenocenophane)-

platinum(II) (13b). Yield (49%). Mp 218—218.5 °C. Found: C, 28.16; H, 3.15%. Calcd for $C_{18}H_{24}Cl_2S_5RuPt$: C, 28.06; H, 2.95%.

Dichloro(1,4,8,11-tetrathia[11](1,1')ruthenocenophane)palladium(II) (14a). Yield (73%). Mp 207—209 °C. Found: C, 32.26; H, 3.50%. Calcd for $C_{17}H_{22}Cl_2S_4RuPd$: C, 32.29; H, 3.47%.

Dichloro(1,4,8,11-tetrathia[11](1,1')ruthenocenophane)platinum(II) (14b). Yield (47%). Mp 212—213 °C. Found: C, 28.29; H, 3.07%. Calcd for $C_{17}H_{22}Cl_2S_4RuPt$: C, 28.15; H, 2.83%.

X-Ray Crystallography. Crystals of dimensions 0.4×0.15×0.1 mm for the metal-free ligand (**6**), 0.3×0.2×0.1 mm for the Pd-complex **12a**, and 0.4×0.1×0.05 mm for the Pt-complex **12b** were used for the X-ray crystallography. Crystal data are as follows: **6**, $C_{16}H_{20}S_4Ru$, MW=441.7. Triclinic, $P\bar{1}$, a=13.828 (2), b=11.890 (2), c=5.587 (2) Å, α=95.53 (2), β=105.39 (2), γ=102.22 (1)°, U=853.1 Å^3, Z=2, Dx=1.72 g·cm^{-3}, μ(Mo $K\alpha$)=1.4 mm^{-1}. **12a**, $C_{16}H_{20}Cl_2S_4RuPd$, MW=619.0, monoclinic, $P2_1/n$, a=9.925(4), b=28.148 (8), c=7.489 (3) Å, β=102.20 (3)°, U=2044.5 Å^3, Z=4, Dx=2.01 g·cm^{-3}, μ(Mo $K\alpha$)=2.3 mm^{-1}. **12b**, $C_{16}H_{20}Cl_2S_4RuPt$, MW=707.7, monoclinic, $P2_1/n$, a=9.912 (6), b=28.142 (9), c=7.521 (3) Å, β=102.08 (4)°, U=2053.3 Å^3, Z=4, Dx=2.29 g·cm^{-3}, μ(Mo $K\alpha$)=8.3 mm^{-1}.

An X-ray structural analysis was carried out on compounds **6** and **12b**, because **12a** was isostructural with **12b** as can be seen from each crystal data. Intensity data for 2θ=50° were recorded on a Rigaku AFC-5R with graphite-monochromatized Mo $K\alpha$ radiation. A Total of 3017 (**6**) and 3606 (**12b**) independent reflections were corrected for Lorentz and polarization factors but not for absorption. Both structures **6** and **12b** were solved by a combination of the heavy-atom technique and direct methods using MULTAN,[15] and refined by block diagonal least-squares methods. The positions of the hydrogen atoms were estimated using standard geometry. The final refinements with anisotropic temperature factors for the non-hydrogen atoms and isotropic temperature factors for the hydrogen atoms were lowered R values 0.031 (R_w=0.034, w=1.0, 2646 observed reflections with $F_o \geq 2\sigma(F_o)$) and 0.070 (R_w=0.055, $w=1/\sigma(F_o)$, 2528 observed reflections with $F_o \geq 2\sigma(F_o)$) for **6** and **12b**, respectively. Anomalous dispersion corrections were applied to the scattering factors of Pt, Ru, Cl, and S.[16]

Parameters for hydrogen atoms and the thermal parameters for non-hydrogen atoms (observed and calculated) as well as structure factors are kept at the Chemical Society of Japan (Document No. 8642).

References

1) R. E. Izatt and J. J. Christensen, "Synthetic Multidentate Macrocyclic Compounds," Academic Press, New York (1977).

2) B. Metz, D. Moras, and R. Weiss, *J. Inorg. Chem.*, **36**, 785 (1974); H. M. Colquhoun, *J. Chem. Soc., Chem. Commun.*, **1981**, 851.

3) Y. Habata, S. Akabori, and M. Sato, *Bull. Chem. Soc. Jpn.*, **58**, 3540 (1985).

4) S. Akabori, H. Munegumi, Y. Habata, S. Sato, K. Kawazoe, C. Tamura, and M. Sato, *Bull. Chem. Soc. Jpn.*, **58**, 2185 (1985).

5) S. Akabori, Y. Habata, S. Sato, K. Kawazoe, C. Tamura, and M. Sato, *Acta Crystallogr.*, **C42**, 682 (1986).

6) Preliminary reports: S. Akabori, H. Munegumi, S. Saito, and M. Sato, *J. Organomet. Chem.*, **272**, C54 (1984); S. Akabori, S. Sato, T. Tokuda, Y. Habata, K. Kawazoe, C. Tamura, and M. Sato, *Chem. Lett.*, **1986**, 121.

7) L. Mortillaro, M. Russo, J. Credali, and C. De. Checchi, *J. Chem. Soc. (C)*, **1966**, 428.

8) S. Akabori, S. Shibahara, Y. Habata, and M. Sato, *Bull. Chem. Soc. Jpn.*, **57**, 63 (1984).

9) M. Sato, S. Tanaka, S. Ebine, and S. Akabori, *Bull. Chem. Soc. Jpn.*, **57**, 1929 (1984).

10) a) F. R. Hartley, S. G. Murray, W. Levason, H. E. Soutter, and C. A. McAuliffe, *Inorg. Chim. Acta*, **35**, 265 (1979); b) R. A. Walton, *Spectrochimica Acta*, **21**, 1795 (1965).

11) G. L. Hardgrove and D. H. Templeton, *Acta Crystallogr.*, **12**, 28 (1959).

12) L. Pauling, "The Nature of the Chemical Bond," 3rd., ed by Cornell Unversity Press, Ithaca, New York (1969).

13) G. Wilkinson, *J. Am. Chem. Soc.*, **74**, 6146 (1952).

14) J. B. Cloke, R. T. Anderson, J. Lachmann, and G. E. Smith, *J. Am. Chem. Soc.*, **53**, 2791 (1931).

15) P. Main, L. Lessinger, M. M. Woolfson, G. Germain, and T. P. Declercq, "MULTAN 74: A System of Computer programs for the Atomic Solution of Crystal Structures from X-ray Diffraction Data," Universities of York, England, and Louvain, Belgium (1974).

16) "International Tables for X-ray Crystallography," Vol IV, Kynoch Press, Birmingham (1974), pp. 72—98 and pp. 149—150.

 © 1986 The Chemical Society of Japan Bull. Chem. Soc. Jpn., 59, 3197—3200 (1986)

The High Pressure Diels-Alder Reactions of 5-Methoxy-2-methyl-4-(*p*-nitrophenyl)oxazole with Ethylenic Dienophiles

Toshikazu IBATA,* Hiroyuki NAKAWA, Yasushi ISOGAMI, and Kiyoshi MATSUMOTO†
Institute of Chemistry, College of General Education, Osaka University, Toyonaka, Osaka 560
†College of Liberal Arts and Sciences, Kyoto University, Kyoto 606
(Received May 6, 1986)

The high pressure Diels-Alder reactions of 5-methoxy-2-methyl-4-(*p*-nitrophenyl)oxazole with ethylenic dienophiles such as *N*-methylmaleimide, *N*-phenylmaleimide, dimethyl maleate and dimethyl fumarate gave the corresponding adducts in good to excellent yields. The effects of pressure, temperature, solvents on the yields were investigated. The high pressure also increased the formation of 3-hydroxypyridine derivatives via the elimination of methanol from the adducts. The stereospecificity of the reaction was confirmed for the reactions with maleate and fumarate.

The Diels–Alder reactions of oxazoles have been studied extensively in connection with the synthesis of vitamin B_6.[1] The reasonable Diels–Alder reactivity of oxazoles opened their widespread use in organic synthesis.[2] The authors have reported the reactions with reactive dienophiles such as alkyl-substituted maleimides, diethyl azodicarboxylate, 4-phenyl-3*H*-1,2,4-triazole-3,5(4*H*)-dione, and dimethyl acetylenedicarboxylate.[3] However, some dienophiles were found to give adducts in very low yields or sometimes to give no adduct in the reactions under atmospheric pressure. As the acceleration of the cycloaddition reaction under high pressure is well documented,[4] the high pressure Diels–Alder reactions of 5-methoxy-2-methyl-4-(*p*-nitrophenyl)oxazole (**1**) with some typical ethylenic dienophiles were studied.

Results and Discussion

The Diels–Alder Reaction of 1 with *N*-Substituted Maleimides. *N*-Phenylmaleimide (**2a**) was reported to give Diels–Alder adducts with **1** in low yields under atmospheric pressure owing to the ready retro-Diels–Alder reaction.[3] In the reaction of **1** and **2a** at 40°C, the equilibrium lay to the side of the adducts but the rate was so slow that long time is required to reach the equilibrium. On the other hand, at 80°C the rate was fast enough but the equilibrium was on the side of the starting materials and the yields of the adducts became low. Therefore, the reaction was investigated under high pressure of 10 kbar. The reaction in benzene at 25°C and 10 kbar (Table 1, Run 4) gave the *endo* **3a** and the *exo*-adduct **4a** in 64.5 and 35.4% yields, without accompanying 3-hydroxypyridine derivative **5a**. Product ratios depend upon the reaction temperature and time (Table 1, Run 4—5), and the yield of the *exo*-adduct increased with the increase in reaction time.

This is ascribed to the fast retro-Diels–Alder reaction of the *endo*-adduct **3a** in comparison to that of the *exo*-adduct **4a**. That is to say, the **3a** produced preferentially at the initial stage of the reaction is decomposed by the retro-Diels–Alder reaction to give the starting **1** and **2a**, which affords **3a** and **4a** in the forward Diels–Alder reaction. In this manner, the yield of **4a** increased with the increase in the reaction time at the expense of the yield of **3a**. The retro-Diels–Alder reaction was not observed when the reaction was carried out for 2 h or less, showing constant product ratios within the experimental error (Table 2 (B)). When the reaction was continued more than 5 h, the retro-Diels–Alder reaction of **3a** apparently increased the composition of **4a** (Table 2(B)). The accelerating effect of the pressure was not enough under 1 kbar. However,

Table 1. Product Composition of the Diels–Alder Reaction of **1** and Maleimides

Run	R	Pressure/kbar	Solvent	Temp	Time	Product yield/%[a]			Total yield
				°C	h	**3**	**4**	**5**	%
1	C_6H_5	a.p.[b]	C_6H_6	40	240	43	17	—	60
2	C_6H_5	a.p.[b]	C_6H_6	60	25	41	18	—	59
3	C_6H_5	a.p.[b]	C_6H_6	80	50	13	21	—	34
4	C_6H_5	10	C_6H_6	60	25	64.5	35.4	—	99.9
5	C_6H_5	10	C_6H_6	60	100	45.1	54.0	—	89.1
6	C_6H_5	10	CH_2Cl_2	60	50	24.2	55.5	18.5	98.2
7	C_6H_5	10	CH_2Cl_2	60	100	0.2	0.5	97.8	98.5
8	C_6H_5	10	CH_3CN	60	100	4.7	—	85.8	90.5
9	CH_3	a.p.[b]	C_6H_6	60	25	52	14	—	66
10	CH_3	10	C_6H_6	60	50	55.2	30.8	12.2	98.2
11	CH_3	10	C_6H_6	60	100	47.0	9.9	43.0	99.9
12	CH_3	10	CH_2Cl_2	60	100	—	—	99.8	99.8

a) Isolated yields (%) using silica-gel column chromatography. b) Atomospheric pressure.

Table 2. Effect of Pressure, Time, and Solvent on the Product Composition[a] of the Diels–Alder Reaction of **1** and **2a**[b]

Solvent	Pressure	Time	Products/%			Recovered oxazole/%
	kbar	h	**3a**	**4a**	**5a**	
(A) Effect of Pressure						
C_6H_6	1	25	30	18	—	52
C_6H_6	3	25	68	32	—	—
C_6H_6	5	25	63	37	—	—
C_6H_6	10	25	65	35	—	—
(B) Effect of Reaction Time						
C_6H_6	10	1/6	80	20	—	—
C_6H_6	10	1/2	78	22	—	—
C_6H_6	10	1	80	20	—	—
C_6H_6	10	2	78	22	—	—
C_6H_6	10	5	74	26	—	—
C_6H_6	10	25	65	35	—	—
(C) Effect of Solvent						
C_6H_6	10	25	65	35	—	—
$CH_3COOC_2H_5$	10	25	65	35	—	—
$C_2H_5OC_2H_5$	10	25	63	19	18	—
CH_3CN	10	25	17	—	73	—
CH_3OH	10	25	—	—	100	—

a) Compositions of the products were calculated on the basis of the NMR intensities of OCH_3 and CH_3 groups of the products and unreacted **1**. b) The reactions were carried out at 60°C using an equimolar amount (0.2 mmol) of **1** and **2a**.

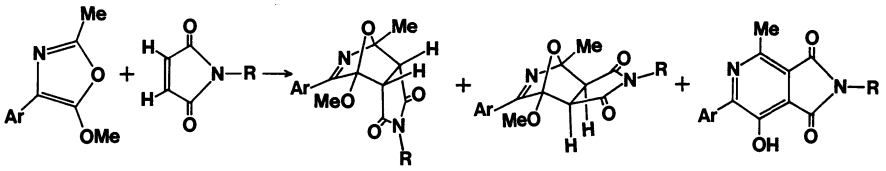

3 kbar was found enough for acceleration of this reaction (Table 2(A)).

When the reaction of **1** and **2a** was carried out in dichloromethane or acetonitrile, the elimination of methanol from **3a** and **4a** occured, and *N*-phenyl-5-hydroxy-2-methyl-6-(*p*-nitrophenyl)-3,4-pyridinedicarboxyimide (**5a**) was obtained along with the adducts **3a** and **4a**. This may be brought out by the catalytic action of protic species such as water contained in the solvents. The fact that the reaction in methanol gave **5a** as the sole product (Table 2) also supported the above explanation. Similar result was obtained in the reaction of **1** with *N*-methylmaleimide (**2b**). In this system, the reaction in benzene at 10 kbar also gave **5b** in a high yield which was different from the reaction in atmospheric pressure. The difference in the yields of **5a** and **5b** (Table 1, Run 5 and 11) indicates that the high pressure acceleration of methanol elimination from adducts is faster for the adducts of **2b** than for those of **2a**.

In order to compare the ability of methanol elimination, the equimolar amount (100 mg) of **3a** and **4a** dissolved in wet benzene[5] was treated at 60°C under 10 kbar for 50 h. The NMR measurement of the reaction mixture revealed that the *endo*-adduct **3a** was present unchanged completely. On the other hand, survived **4a** was 82% and the corresponding amount (18%) of **5a** was present. This means that the elimination of methanol occurs to the *exo*-adduct more easily.

The Diels–Alder Reaction of 1 with Dimethyl Maleate and Dimethyl Fumarate. The reaction of **1** with dimethyl maleate at 60°C under 10 kbar gave two adducts **6a** (mp 129.0°C) and **6b** (mp 159.0°C) together with a methanol elimination product **7**. The large coupling constants (J=10.3 and 9.1 Hz) of methine protons of both adducts indicate that the methine protons of each adducts locate in *cis* configuration. The stereochemistry of the dienophile is retained in the adducts. The possible structures of the adducts are **5**-*endo*-**6**-*endo* (**6a**) or **5**-*exo*-**6**-*exo* (**6b**). The assignment of the structures of **6a** and **6b** was based on the chemical shift of the methine protons. The adduct having signals of the methine protons at lower fields (δ 3.56 and 3.68) was assigned to **6a**, and the adduct with the methine proton signals at higher fields (δ 3.01 and 3.18) to **6b**, on the analogy of the adducts of *N*-substituted maleimide with **1**.[3] A larger coupling

Table 3. The Yields and NMR Chemical Shifts of the High-Pressure Diels-Alder Reaction Products of **1** with Dimethyl Maleate and Dimethyl Fumarate

Dienophile	Solvent	Temp	Time	Product yield/%				
		°C	h	**6a**	**6b**	**6c**	**6d**	**7**
(A) Yields								
Dimethyl maleate	C_6H_6	50	50	11.9	1.6	—	—	—[a]
	C_6H_6	60	100	7.4	0.6	—	—	70.5
	CH_2Cl_2	50	50	41.1	2.4	—	—	21.9
Dimethyl fumarate	C_6H_6	50	50	—	—	0.6	0.5	—[b]
	CH_2Cl_2	50	150	—	—	2.6	2.5	6.7[c]
	CH_2Cl_2	60	115	—	—	11.2	8.8	6.1[c]
(B) ^{1}H NMR Chemicals Shifts (/ppm) and Coupling Constants								
C-CH_3				2.00	2.15	1.83	2.12	2.55
O-CH_3				3.50	3.50	3.45	3.48	—[e]
O-CH_3				3.59	3.69	3.72	3.66	3.98
O-CH_3				3.65	3.77	3.84	3.84	4.02
Methine-H[d]				3.56	3.01	3.19	3.24	—
Methine-H[d]				3.67	3.18	3.82	3.47	—
J/Hz				10.3	9.1	5.7	5.4	—

a) 76% of **1** was recovered. b) 89% of **1** was recovered. c) A considerable amount of oxazole was recovered. d) Doublet signals were observed. e) A broad singlet signal of hydroxyl group was observed at δ 11.02.

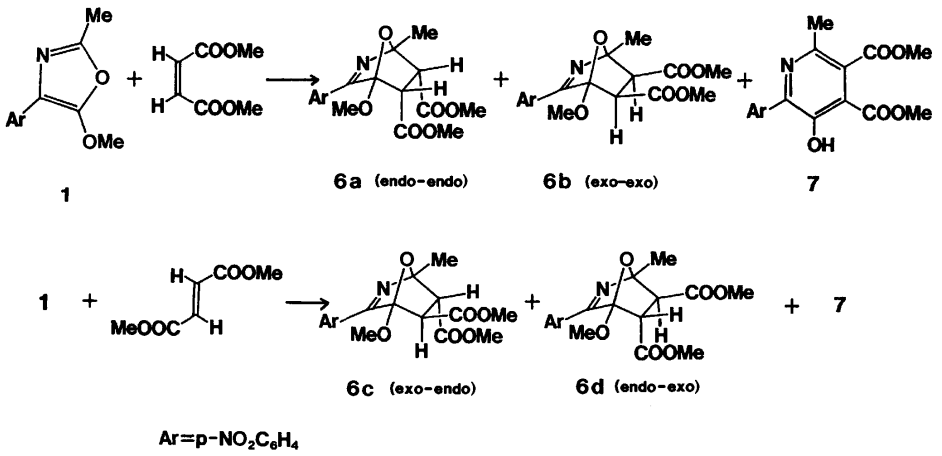

constant (J=10.3 Hz) of the *endo-endo*-adduct **6a** than the *exo-exo*-adduct **6b** (J=9.1 Hz)[6] supports the above assignment. In this case, the 5-*endo*-6-*endo*-adduct **6a** showed a C-CH_3 signal at a higher field (δ 2.00) than that of the 5-*exo*-6-*exo*-adduct **6b** (δ 2.15). This is probably caused by an anisotropic effect of closely located C=O of the ester group on C_6. The NMR spectrum of the third product shows two OCH_3 signals of ester groups (δ 3.98 and 4.02), a C-CH_3 (δ 2.55), an AB quartet of aromatic protons, and broad OH signal (δ 11.02). The absence of signals of third OCH_3 group and methine protons characterized the structure **7**, which was also supported by its IR spectrum and analytical data.

The reaction of dimethyl fumarate and **1** also gave two adducts and **7**. Although the adducts were difficult to isolate each other by silica gel column chromatography, NMR spectrum indicates that they are a mixture of two adducts which are different from **6a** and **6b**. Their smaller coupling constants (J=5.7 and 5.4 Hz) of methine protons indicate that the methine protons locate in *trans* configuration. The possible structures of the adducts having *trans* configuration are 5-*exo*-6-*endo* **6c** or 5-*endo*-6-*exo* **6d**, and the assignment was achieved by comparing of the chemical shift of the C-CH_3 group. The adduct having a C-CH_3 singlet at a higher field (δ 1.83) was assigned to 5-*exo*-6-*endo*-adduct **6c** by taking account of NMR feature of dimethyl maleate adducts described above. The reaction of dimethyl maleate was found to be faster than that of dimethyl fumarate in contrast to the usual Diels-Alder reaction.[7]

Experimental

The IR spectra were recorded on Perkin-Elmer model 983 and the ^{1}H NMR spectra were recorded in $CDCl_3$ solutions at 90 MHz on a Varian Spectrometer model EM390 using TMS as an internal standard.

Materials. 5-Methoxy-2-methyl-4-(*p*-nitrophenyl)oxazole (**1**) was prepared as described in the previous paper.[3] Solvents were dried in appropriate methods and stored over molecular sieves type 4A after distillation.

General Procedure of the High Pressure Diels-Alder Reaction of 1 with Maleimides. A solution of **1** (1.0 mmol) and maleimide (2.0 mmol) dissolved in 5 ml of a solvent was treated under the reaction conditions listed in the Table 1, using a Hikari Kouatsu high pressure reaction apparatus.[8] The reaction mixture was separated by silica gel column chromatography, and the isolated products were identified by comparison of its IR and NMR spectra with those of the samples obtained before.[3]

The Reaction of 1 with Dimethyl Maleate. A benzene solution of **1** (2.0 mmol) and dimethyl maleate (4.0 mmol) was treated under 10 kbar at 50°C for 25 h. After removal of solvent, the reaction mixture was separated by silica gel column chromatography to give three products.

First Product 6a: Pale yellow crystals; mp 128.0—129.0°C. Found: C, 54.17; H, 4.79; N, 7.38%. Calcd for $C_{17}H_{18}N_2O_8$: C, 53.97; H, 4.80; N, 7.41%.

Second Product 6b: Colorless crystals; mp 158.0—159.0°C. Found: C, 54.04; H, 4.75; N, 7.42%. Calcd for $C_{17}H_{18}N_2O_8$: C, 53.97; H, 4.80; N, 7.41%.

Third Product 7: Pale yellow needles; mp 198.0—200.0°C. Found: C, 55.38; H, 4.06; N, 8.04%. Calcd for $C_{16}H_{14}N_2O_7$: C, 55.49; H, 4.08; N, 8.09%.

The Reaction of 1 with Dimethyl Fumarate. The reaction was carried out in the same procedure as the reaction of dimethyl maleate. Column chromatography (silica gel/benzene–hexane) isolated **7** and a mixture of two adducts. However, the separation of the two adducts (**6c** and **6d**) was unsuccessful.

References

1) E. E. Harris, R. A. Firestone, K. Pfister III, R. R. Boetter, F. J. Cross, R. B. Currie, M. Monaco, E. R. Peterson, and W. Reuter, *J. Org. Chem.*, **27**, 2705 (1962).

2) A. R. Katritzky and A. Roulton, *J. Adv. Heterocycl. Chem.*, **17**, 99 (1974); and references cited therein.

3) T. Ibata, S. Nakano, H. Nakawa, J. Toyoda, and Y. Isogami, *Bull. Chem. Soc. Jpn.*, **59**, 433 (1986).

4) J. R. McCabe and C. A. Eckert, *Acc. Chem. Res.*, **7**, 251 (1974).

5) Distilled benzene was shaken with water in a separatory funnel and separated benzene layer was used without further treatment.

6) For example the *endo*- and *exo*-adducts of *N*-methylmaleimide with **1** show methine coupling constants, J= 7.5 and J=6.5 Hz, respectively.

7) R. Huisgen, R. Grashey, and J. Sauer, "The Chemistry of Alkene," Vol 1, p. 920; Interscience Publishers: New York (1964).

8) K. Matsumoto, A. Sera, and T. Uchida, *Synthesis*, **1985**, 1.

Selective Linear Codimerization of Terminal Acetylenes and 1,3-Butadienes Catalyzed by (η^4-1,5-Cyclooctadiene)(η^6-1,3,5-cyclooctatriene)ruthenium(0)-Trialkylphosphine

Take-aki MITSUDO,* Yoji HORI, and Yoshihisa WATANABE*
Department of Hydrocarbon Chemistry, Faculty of Engineering, Kyoto University, Kyoto 606
(Received May 8, 1986)

The reaction of terminal acetylenes with 1,3-butadienes catalyzed by (η^4-1,5-cyclooctadiene)(η^6-1,3,5-cyclooctatriene)ruthenium [Ru^0(COD)(COT)]-PR_3 (R=ethyl, butyl, octyl) in various solvents at 80 °C afforded linear codimers in good to excellent yield with high chemo-, regio-, and stereoselectivities. Reactions of deuterated acetylenes were also examined.

Recently, much attention has been focused on finding novel organic reactions catalyzed by ruthenium complexes.[1-18] With regard to carbon–carbon bond formation, however, characteristic organic syntheses with ruthenium catalysts are still limited.[1-9] In the course of our study on organic syntheses catalyzed by low-valent ruthenium complexes,[1,2] the first example of the selective linear codimerization of terminal aliphatic acetylenes and 1,3-butadienes catalyzed by dihydridotetrakis(trialkylphosphine)ruthenium [$RuH_2(PR_3)_4$, R= ethyl or butyl] has been found.[2] We now report a novel and versatile catalytic system, (η^4-1,5-cyclooctadiene)(η^6-1,3,5-cyclooctatriene)ruthenium [Ru(COD)(COT)]-PR_3 system, for this linear codimerization. The optimum reaction conditions, the effects of various phosphine ligands and solvents, and the reaction path of the codimerization are investigated.

Results and Discussion

1-Hexyne and 3,3-dimethyl-1-butyne readily reacted with 1,3-butadiene in the presence of a catalytic amount of Ru(COD)(COT)-PBu^n_3 in benzene at 80 °C for 4 h to give (*E*)-3-decen-5-yne (**1**) and (*E*)-7,7-dimethyl-3-octen-5-yne (**2**), respectively (Table 1, Runs 1 and 2). The reaction of ethyl 2-ethoxycarbonyl-4-pentynoate with 1,3-butadiene gave ethyl (*E*)-2-ethoxycarbonyl-6-nonen-4-ynoate (**3**) in 80% yield (Run 3). On the other hand, the reaction of 1-hexyne

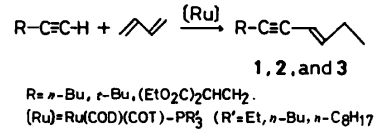

(1)

with methyl (*E*)-2,4-pentadienoate gave two isomers of the codimer, **4** and **5**, respectively (Run 4, Eq. 2).

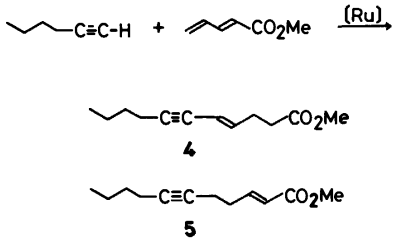

(2)

Table 1. Linear Codimerization of Acetylenes with 1,3-Dienes Catalyzed by Ru(COD)(COT)-PBu^n_3[a]

Run	Acetylene	1,3-Diene	Product	Yield/%[b]
1	C≡C-H		C≡C	**1** 94
2	C≡C-H		C≡C	**2** 96
3[c]	$(EtO_2C)_2CHCH_2C{\equiv}C$-H		$(EtO_2C)_2CHCH_2C{\equiv}C$	**3** 80(57)
4[d]	C≡C-H	CO_2Me	C≡C CO_2Me	**4** (32)
			C≡C CO_2Me	**5** **4**/**5**=64/36
5[e]	C≡C-H	CO_2Me	C≡C CO_2Me	**6** (45)

a) Acetylene, 10 mmol; Diene, 20 mmol; Ru(COD)(COT), 0.1 mmol; PBu^n_3, 0.2 mmol; Solvent, Benzene 5.0 cm^3; 80 °C; 4 h. b) Determined by GLC based on the amount of acetylene. Isolated yields were given in the parentheses. c) Ru(COD)(COT), 0.2 mmol; PBu^n_3, 0.4 mmol; 80 °C; 20 h. d) Acetylene, 10 mmol; Diene, 15 mmol; 80 °C, 8 h. e) 80 °C; 8 h.

Table 2. The Ru-Catalyzed Linear Codimerization of 1-Hexyne and 1,3-Butadiene[a] — Effects of Reaction Conditions

Run	Catalyst[b]	PBu^n_3	Reaction temp	Reaction time	Yield of (*E*)-3-decen-5-yne[c]
	mmol	mmol	°C	h	%
6	0.025	0.05	80	8	78
7	0.05	—	80	8	1
8	0.05	0.05	80	8	76
9	0.05	0.1	80	8	94
10	0.05	0.2	80	8	94
11	0.05	1.0	80	8	59
12	0.05	0.1	40	8	25
13	0.05	0.1	60	8	93
14	0.05	0.1	100	8	79
15	0.05	0.1	80	1	51
16	0.05	0.1	80	2	78
17	0.05	0.1	80	4	95
18	0.1	0.2	80	8	94
19	0.2	0.4	80	8	89(73)

a) 1-Hexyne, 10 mmol; 1,3-Butadiene, 20 mmol; Benzene, 5.0 cm^3. b) Catalyst=Ru(COD)(COT) (COD=cyclooctadiene, COT=cyclooctatriene). c) Determined by GLC based on the amount of 1-hexyne. Isolated yield was given in the parentheses.

The reaction of 1-hexyne with methyl (*E,E*)-2,4-hexadienoate gave methyl (*E*)-5-methyl-2-undecen-6-ynoate (**6**) in 45% yield (Run 5, Eq. 3). The optimum

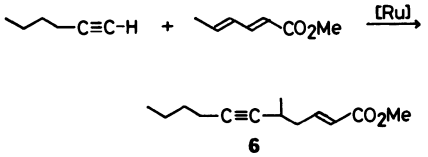

6 (3)

mole ratio of 1,3-diene/acetylene was 2 to perform the codimerization suppressing the homooligomerization of the acetylene. The high chemo-, regio-, and stereoselectivities observed are almost the same as those found in the reactions catalyzed by $RuH_2(PBu^n_3)_4$.[2] Since the preparation of Ru(COD)(COT) is much easier than that of $RuH_2(PBu^n_3)_4$ and the present catalyst system is easily modified by adding an appropriate phosphine, the present catalyst system is regarded to be an improved one. The effects of the amount of catalyst, the ratio of PBu^n_3/Ru, the reaction temperature and the reaction time in the reaction of 1-hexyne with 1,3-butadiene were examined and the results are summarized in Table 2. In the absence of PBu^n_3 under the reaction conditions shown in Run 7 of the Table 2, the yield of the codimer **1** was 1%. When a catalytic amount of PBu^n_3 was added, the yield of the codimer **1** increased dramatically (94%) (Run 9). The effect of the amount of the catalyst is shown in Fig. 1. The maximum yield of the codimer **1** was obtained by using 0.5 mol% of Ru(COD)(COT) and 1.0 mol% of PBu^n_3 at 80 °C for 4—8 h (yield 95%). The effect of the mole ratio PBu^n_3/Ru(COD)(COT) is shown in Fig. 2. When the ratio was 2—4, the codimer **1** was obtained in 94% yield. When the ratio was 20, the yield of the codimer decreased to 59%.

The effect of various phosphine ligands on the codimerization of 1-hexyne and 1,3-butadiene is summarized in Table 3. When triethylphosphine, tributylphosphine, or trioctylphosphine was added, the reac-

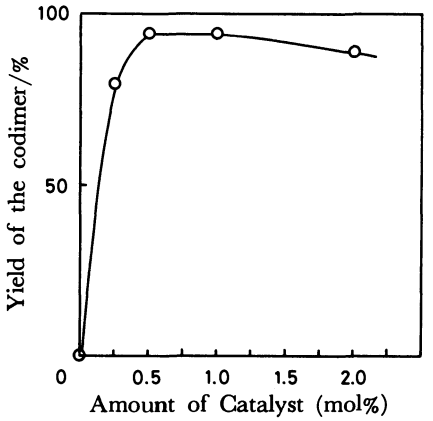

Fig. 1. The effect of the amount of catalyst. 1-Hexyne, 10 mmol; 1,3-Butadiene, 20 mmol; 80 °C; 8 h; PBu^n_3/Ru(COD)(COT)=2.

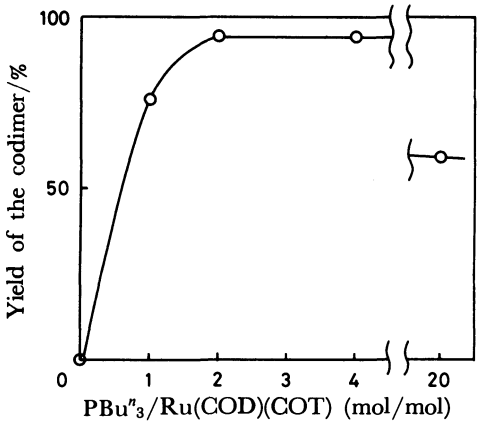

Fig. 2. The effect of the mole ratio PBu^n_3/Ru(COD)(COT). 1-Hexyne, 10 mmol; 1,3-Butadiene 20 mmol; Ru(COD)(COT) 0.5 mol%; 80 °C; 8 h.

tion proceeded rapidly and afforded the (*E*)-3-decen-5-yne (**1**) in the yields of 87, 95, and 90%, respectively (Runs 20—22). Trimethylphosphine, triisopropylphosphine, and tricyclohexylphosphine were not effective. When PEt_3, PBu^n_3, $P(C_8H_{17}{}^n)_3$, PMe_3, PPr^i_3, and $P(c\text{-}C_6H_{11})_3$ were compared, alkylphosphines with 130° of cone angle were effective. Neither phosphine ligands with an aryl group nor triisopropylphosphite with 130° of cone angle was effective.

The effects of various solvents on the codimerization of acetylenes and 1,3-butadiene are summarized in Table 4. The polarity of the solvents (benzene, THF, toluene, CH_3CN, CH_2Cl_2, DMF, or acetone) does not appreciably affect the yield of the codimers; the corresponding codimers were obtained in excellent yields (Runs 1, 2, 23—28). In pyridine, no reaction occurred (Run 29).

No codimer was obtained in the reactions of 1,3-butadiene with 3-hexyne, 2-propyn-1-ol, 2-methyl-3-butyn-2-ol, 2-propynyl acetate, ethyl 2-propynyl carbonate, 1-methoxy-2-propyne, or methyl propiolate.

Table 3. The Ru-Catalyzed Linear Codimerization of 1-Hexyne and 1,3-Butadiene with Phosphine Ligands[a,b]

Run	Ligand (cone angle°)		Yield of (*E*)-3-decen-5-yne[c] / %
20	PEt_3	(132)	87
21	PBu^n_3	(130)	95
22	$P(C_8H_{17}{}^n)_3$	(—)	90

a) 1-Hexyne, 10 mmol; 1,3-butadiene, 20 mmol; Ru(COD)(COT), 0.05 mmol; Ligand, 0.1 mmol; Benzene, 5.0 cm^3; 80°C; 4 h. b) PMe_3(118°), PPr^i_3(160°), $P(c\text{-}C_6H_{11})_3$(170°), PMe_2Ph(122°), $PMePh_2$(136°), PPh_3(145°), $P(o\text{-Tol})_3$(194°), 1,2-Bis(diphenylphosphio)ethane, 1,2-Bis(diethylphosphino)ethane, and $P(OPr^i)_3$(130°) were not effective. c) Determined by GLC based on the amount of 1-hexyne.

To obtain information on the reaction mechanism, the reactions of 1-pentyne-1-*d* or 3,3-dimethyl-1-butyne-1-*d* with 1,3-butadiene, methyl (*E,E*)-2,4-hexadienoate, or methyl (*E*)-2,4-pentadienoate were carried out. In the reaction of 3,3-dimethyl-1-butyne-1-*d* with methyl (*E,E*)-2,4-hexadienoate, erythro methyl (*E*)-5,8,8-trimethyl-2-nonen-6-ynoate-4-*d* (**7**) was obtained as a sole product (Eq. 4). The deuterium is introduced selectively at the 4 position of the codimer in a cis addition pathway.[2b] The reaction of 1-pentyne-1-*d* with methyl (*E*)-2,4-pentadienoate gave four isomers of the codimer, **8**—**11**. The ratio (**8**+**9**)/(**10**+**11**) was 6/4 and both ratios, **8**/**9** and **10**/**11** were 1/1 (Eq. 5). The reaction of 3,3-dimethyl-1-butyne-1-*d* with methyl (*E*)-2,4-pentadienoate also gave a result similar to that described above. It should be noted that no deuterium was introduced into the olefinic groups of the products. The reaction of 1-pentyne-1-*d* with 1,3-butadiene gave, to our surprise, (*E*)-3-

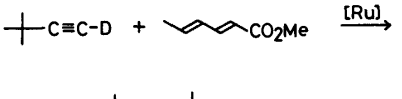

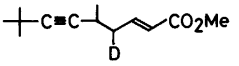

erythro **7** (4)

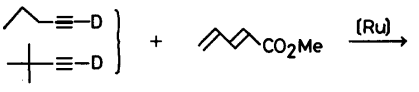

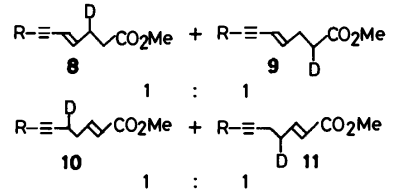

(5)

Table 4. The Ru-Catalyzed Linear Codimerization of Terminal Acetylenes with 1,3-Butadiene—Solvent Effects[a]

Run	Acetylene	Solvent	Product	Yield/%[b]
1	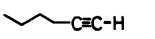	Benzene	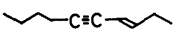	**1** 94
2	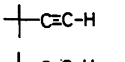	Benzene	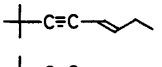	**2** 96
23	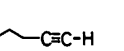	THF	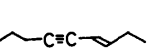	**2** 96(91)
24	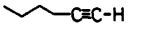	Toluene	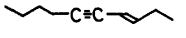	**1** 88
25	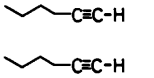	CH_3CN	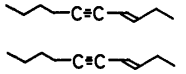	**1** 91(82)
26	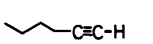	CH_2Cl_2	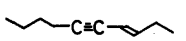	**1** 85
27	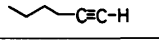	DMF	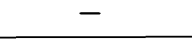	**1** 97
28	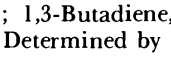	Acetone	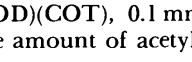	**1** 88
29		Pyridine	—	0

a) Acetylene, 10 mmol; 1,3-Butadiene, 20 mmol; Ru(COD)(COT), 0.1 mmol; PBu^n_3, 0.2 mmol; Solvent, 5.0 cm^3; 80°C; 4 h. b) Determined by GLC based on the amount of acetylene. Isolated yields were given in the parentheses.

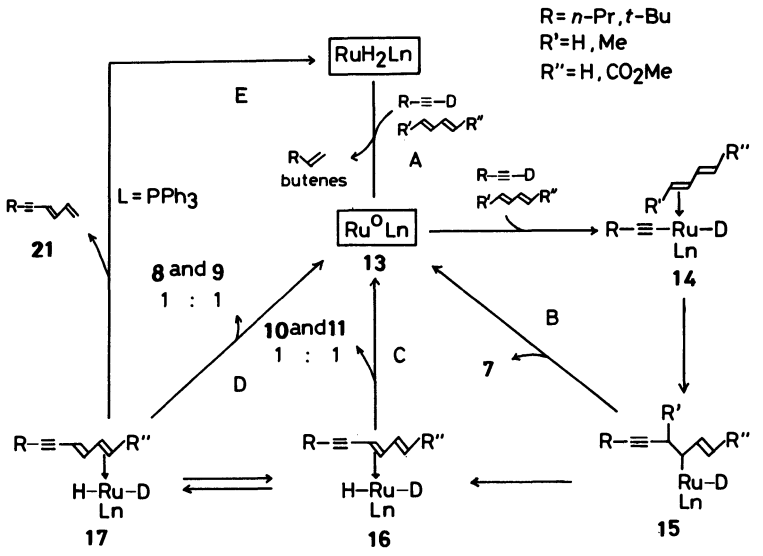

Scheme 1.

nonen-5-yne-2-*d* (**12**) as the sole product. Deuterium was introduced selectively at the 2 position of the codimer (Eq. 6). The reaction catalyzed by $RuH_2(PBu^n_3)_4$ also gave the same result.

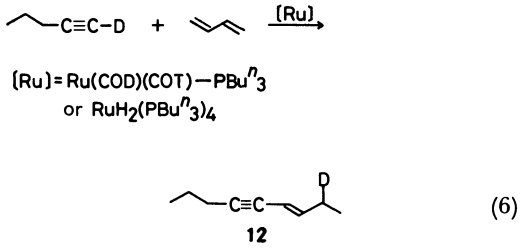

12 (6)

No clear-cut mechanism which explains these complicated results can be offered at the present time. Obviously, the mechanism of the formation of **7** is different from that of **12** because the position of the deuterium introduced is essentially different. The reaction path of the formation of the linear codimers **7** and **8—11** can be explained as follows (Scheme 1). Taking into account that both Ru(COD)(COT)-PBu^n_3 and $RuH_2(PBu^n_3)_4$ show almost the same catalytic activities and the identical distributions of the deuterium introduced in the reaction of deuterated acetylene (Eqs. 5 and 6), the reaction mechanism should be the same for both catalysts. The first step of the catalytic cycle would be the oxidative addition of acetylene to a zerovalent ruthenium complex **13** such as $Ru(PR_3)_n$ derived by the reaction of Ru(COD)-(COT) with trialkylphosphines or by the reaction of $RuH_2(PBu^n_3)_4$ with the dienes or acetylenes. It has been reported that the reaction of $RuH_2(PPh_3)_4$ with olefins such as ethylene or styrene gives zerovalent ruthenium complexes $Ru(olefin)(PPh_3)_3$[20] at the early step of the reaction.[21] The formation of a zerovalent ruthenium complex was also reasonably assumed in the [2+2] cross addition of norbornenes with acetylenes catalyzed by $RuH_2(PPh_3)_4$.[1] Then the η^2-coordination of the diene to the complex gives **14**. Insertion of the diene into the Ru-alkynyl bond would give **15**. If acetylene, instead of the diene, coordinates and inserts into the Ru-alkynyl bond, homooligomerization of acetylene proceeds. To prevent the insertion of acetylene, the mole ratio 2 of 1,3-diene/acetylene was required. When R′ and R″ in **15** are Me and CO_2Me, respectively, i.e. in the reaction of methyl (*E,E*)-2,4-hexadienoate, the reductive elimination of the ligands would give **7** selectively. Considering the high chemo- and regioselectivity of the reaction and the fact that deuterium is not introduced into the olefinic groups of **8—11**, the formation of an intermediate **18** with a branched skeletone or **19** derived by the insertion of the diene into the Ru-D bond is ruled out. Complex **18** will not give a linear codimer. Once **19** is formed, the formation of **8—11** having no deuterium at the olefinic group and the distributions of the deuterium can not be explained (vide infra).

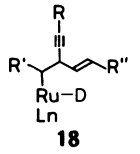

18

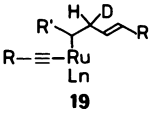

19

The possibility of the isomerization of **5** to **4** was investigated. The reaction of 1-hexyne with methyl (*E,E*)-2,4-hexadienoate was carried out in the presence of **5**; product **6** was obtained and **5** was recovered without the formation of **4** (Eq. 7). This fact and that

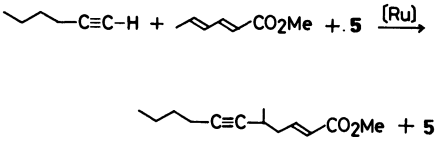

(7)

the deuterium is not introduced into the olefinic groups in **8—11** strongly suggest that when R′ is a hydrogen, i.e. in the reaction of methyl (*E*)-2,4-pentadienoate, β-elimination of **15** easily occurs giving the

equilibrium mixture of a deuteridohydrido(η^2-dienyne)-ruthenium complex **16** and its isomer **17**. The hydrogenation of the coordinated dienyne in **16** or **17** gives two pairs of olefins (**10** and **11**), and (**8** and **9**), in both pairs the equivalent amount of deuterium is introduced in the methylene groups and no deuterium is introduced into the olefinic groups. In these steps the zerovalent ruthenium complex **13** is reproduced (path C and D). It is unlikely that a π-allyl complex such as **20** plays the role of the key intermediate

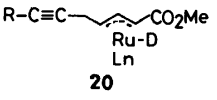

20

because the formation of **8**—**11** can not be explained. As has been reported in the previous paper,[2b] when the ligand L is triphenylphosphine and R″ is hydrogen in **16** or **17**, i.e. in the reaction of 1,3-butadiene, the dissociation of the dienyne easily occurs giving **21** (path E, Eq. 8). The main reason of the dissociation

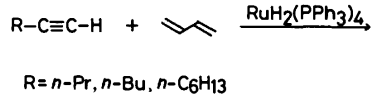

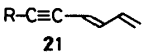

21 (8)

of **21** would be a larger cone angle of triphenylphosphine (145°) than that of tributylphosphine (130°).[22]

The explanation of the reaction path of the codimerization of 1-pentyne-1-*d* with 1,3-butadiene is confusing. The reaction path shown in the Scheme 1 should give **23** or the mixture of **12** and **22**; however, the result shows that the deuterium is selectively introduced into the 2 position of **12**. It is unlikely that the isomerization of **23** gives **12**, because in this case **24** should be detected in the products.

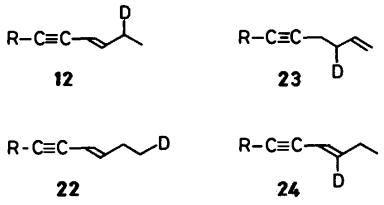

A speculated reaction path explaining these unusual results is shown in Scheme 2. If a monohydridoruthenium species **25** is present, a catalytic cycle via a π-allyl ruthenium complex could give **12** selectively. The first step of the reaction is a formation of a π-allyl ruthenium complex **26** by the coordination of 1,3-butadiene to hydridoruthenium species followed by the insertion of 1,3-butadiene to the hydrido-ruthenium bond. Oxidative addition of the 1-pentyne-1-*d* affords a π-allylalkynyldeuteridoruthenium complex **27**. Reductive elimination of the η^3-allyl group and the deuteride gives the alkynyl(π-olefin) complex **28**; insertion of the olefin into the alkynyl-Ru bond and β-elimination would give **12** selectively and the hydridoruthenium species again. As for the monohydridoruthenium species, it should be pointed out that complex **29** would be formed by the intramolecular oxidative addition of β-hydrogen of the tributylphosphine ligand (Eq. 9). Quite recently, similar intramolecular oxidative addition of an alkyl group of an alkylphosphine ligand has been reported.[19]

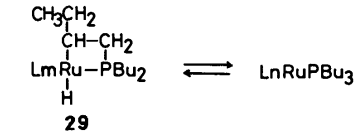

29 (9)

In conclusion, a versatile catalytic system for the selective linear codimerization of terminal acetylenes with 1,3-dienes was found providing a novel convenient tool for the construction of carbon skeletones with acetylenic and olefinic groups.

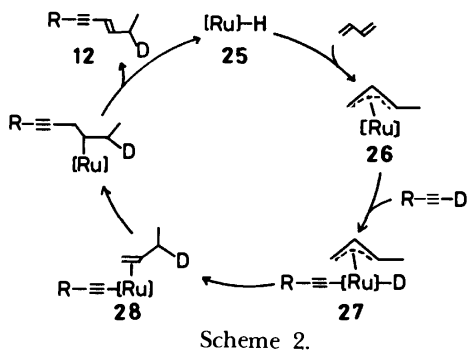

Scheme 2.

Experimental

All boiling points were uncorrected. Infrared spectra were recorded on a Hitachi Model 215 spectrometer and NICOLET 5-MX spectrometer as films. Proton nuclear magnetic resonance spectra were obtained on a JNM-FX-100 or NICOLET NT-300NB spectrometer as 20% solutions with tetramethylsilane as an internal reference. Carbon-13 nuclear magnetic resonance spectra were obtained on a JNM-FX-100 spectrometer as 30% solutions with tetramethylsilane as an internal reference. Mass spectra were taken on a JMS-01SG mass spectrometer. Microanalyses were performed by the Laboratory for Organic Elemental Microanalysis at the Faculty of Pharmaceutical Science at Kyoto University. Gas chromatographic analysis (GLC) were carried out on a 1.5 m×3 mm diameter column with OV 17. 1-Hexyne, 1,3-butadiene, methyl (*E*,*E*)-2,4-hexadienoate, and solvents were commercial samples and were purified by distillation under an atmosphere of argon before use. 3,3-Dimethyl-1-butyne,[23] 3,3-dimethyl-1-butyne-1-*d*,[24] and 1-pentyne-1-*d*[24] were prepared by the methods described in the literature. The complex Ru(COD)(COT) were prepared by the reported method.[25] All the catalytic reactions were carried out under an atmosphere of argon.

General Reaction Procedure. The reaction of 1-hexyne with 1,3-butadiene is representative. A mixture of 1-hexyne (0.82 g, 10 mmol), 1,3-butadiene (20 mmol), Ru(COD)(COT) (0.063 g, 0.2 mmol), PBu^n_3 (0.08 g, 0.4 mmol), and benzene (5.0 cm^3) was heated in a heavy-walled sealed tube at 80°C for 8 h. Careful vacuum distillation of the reaction mixture afforded 0.99 g (yield 73%) of (*E*)-3-decen-5-yne (**1**).

Other reactions were carried out in a similar manner. Codimers (**1**, **2**, **4**—**11**) were identified to be the products reported in the previous paper.[2b]

Ethyl (*E*)-2-Ethoxycarbonyl-6-nonen-4-ynoate (3). Colorless liquid, bp 108 °C (25 mmHg) (1 mmHg=133.322 Pa); IR (neat) 1745 cm^{-1}; ^1H NMR ($CDCl_3$) δ=6.08 (1H, dt, J=15.9 and 6.6 Hz), 5.39 (1H, dt, J=15.9 and 1.8 Hz), 4.22 (4H, q, J=7.1 Hz), 3.54 (1H, t, J=7.8 Hz), 2.86 (2H, dd, J=7.8 and 1.8 Hz), 2.09 (2H, qd, J=7.4 and 6.6 Hz), 1.28 (6H, t, J=7.1 Hz), and 0.98 (3H, t, J=7.4 Hz); ^{13}C NMR ($CDCl_3$) δ=167.9 (s), 145.5 (d), 108.7 (d), 83.8 (s), 81.1 (s), 61.5 (t), 51.6 (d), 26.1 (t), 19.4 (t), 14.1 (q), and 13.0 (q). MS m/z: 252. Found: C, 66.65; H, 8.15%. Calcd for $C_{14}H_{20}O_4$: C, 66.65; H, 7.99%.

(*E*)-3-Nonen-5-yne-2-*d* (12). Colorless liquid, bp 80 °C (85 mmHg); IR (neat) 2217 and 955 cm^{-1}; ^1H NMR ($CDCl_3$) δ=6.08 (1H, dd, J=15.6 and 6.3 Hz), 5.45 (1H, dm, J=15.6 Hz), 2.26 (2H, td, J=7.2 and 1.8 Hz), 2.09 (1H, m), 1.54 (2H, qt, J=7.2 and 7.2 Hz), 0.99 (3H, dm, J=7.5 Hz), 0.99 (3H, t, J=7.2 Hz); ^{13}C NMR ($CDCl_3$) δ=144.2 (d), 109.6 (d), 88.4 (s), 79.5 (s), 25.9 (t, J_{C-D}=19.5 Hz), 22.6 (t), 21.6 (t), 13.6 (q), and 13.2 (q).

The reaction of 1-Hexyne with Methyl (*E,E*)-2,4-Hexadienoate in the presence of 5. A mixture of 1-hexyne (8.2 mg, 0.1 mmol), methyl (*E,E*)-2,4-hexadienoate (12.7 mg, 0.1 mmol), methyl (*E*)-2-undecen-6-ynoate (**5**) (20 mg, 0.1 mmol), Ru(COD)(COT) (0.32 mg, 1 mol%), PBu^n_3 (0.40 mg, 2 mol%), and benzene (0.05 cm^3) was heated at 60 °C for 4 h. The GLC analysis showed the formation of the codimer **6** (yield 30%) and that **5** was completely recovered without the formation of **4**.

This work was partly supported by the Ministry of Education, Science and Culture (No. 60119001 and 61225012). We thank Dr. Richard M. Lain for helpful discussions.

References

1) T. Mitsudo, K. Kokuryo, T. Shinsugi, Y. Nakagawa, Y. Watanabe, and Y. Takegami, *J. Org. Chem.*, **44**, 4492 (1979).
2) a) T. Mitsudo, Y. Nakagawa, H. Watanabe, K. Watanabe, and Y. Watanabe, *J. Chem. Soc., Chem. Commun.*, **1981**, 496; b) T. Mitsudo, Y. Nakagawa, K. Watanabe, Y. Hori, H. Misawa, H. Watanabe, and Y. Watanabe, *J. Org. Chem.*, **50**, 565 (1985).
3) J. F. Knifton, *J. Am. Chem. Soc.*, **103**, 3959 (1981).
4) B. D. Dombeck, *J. Organomet. Chem.*, **250**, 467 (1983).
5) T. Nakano, K. Ohkawa, S. Ikemori, R. Hasegawa, R. Sako, H. Matsumoto, and Y. Nagai, *Nippon Kagaku Kaishi*, **1983**, 1770.
6) T. Nakano, K. Ohkawa, S. Ikemori, H. Matsumoto, and Y. Nagai, *Nippon Kagaku Kaishi*, **1983**, 1778.
7) N. Kamigata, J.-I. Ozaki, and M. Kobayashi, *J. Org. Chem.*, **50**, 5045 (1985).
8) H. Nagashima, K.-I. Ara, H. Wakamatsu, and K. Itoh, *J. Chem. Soc., Chem. Commun.*, **1985**, 518.
9) Y. Tsuji, H. Nishimura, K.-T. Huh, and Y. Watanabe, *J. Organomet. Chem.*, **286**, C44 (1985).
10) S.-I. Murahashi, K.-I. Ito, T. Naota, and Y. Maeda, *Tetrahedron Lett.*, **22**, 5327 (1981).
11) S.-I. Murahashi, K. Kondo, and T. Hakata, *Tetrahedron Lett.*, **23**, 229 (1982).
12) S. Cenini, M. Pizzotti, C. Crotti, F. Porta, and G. L. Monica, *J. Chem. Soc., Chem. Commun.*, **1984**, 1286.
13) M. Rotem and Y. Shvo, *Organometallics*, **2**, 1689 (1983).
14) Y. Blum and Y. Shvo, *J. Organomet. Chem.*, **282**, C7 (1985).
15) T. A. Smith, R. P. Aplin, and P. M. Maitlis, *J. Organomet. Chem.*, **291**, C13 (1985).
16) Y. Watanabe, Y. Tsuji, H. Ige, Y. Ohsugi, and T. Ohta, *J. Org. Chem.*, **49**, 3359 (1984).
17) Y. Tsuji, K.-T. Huh, Y. Ohsugi, and Y. Watanabe, *J. Org. Chem.*, **50**, 1365 (1985).
18) T. Mitsudo, Y. Hori, and Y. Watanabe, *J. Org. Chem.*, **50**, 1566 (1985).
19) B. Chaudret and R. Poilblanc, *Organometallics*, **4**, 1722 (1985).
20) S. Komiya, A. Yamamoto, and S. Ikeda, *J. Organomet. Chem.*, **42**, C65 (1972); *Bull. Chem. Soc. Jpn.*, **49**, 2552 (1976).
21) D. J. Cale-Hamilton and G. Wilkinson, *J. Chem. Soc., Chem. Commun.*, **1977**, 59.
22) C. A. Tolman, *Chem. Rev.*, **77**, 313 (1975).
23) W. L. Collier and R. S. Macomber, *J. Org. Chem.*, **38**, 1367 (1973).
24) A. F. Thomas, "Deuterium Labeling in Organic Chemistry," Appleton-Century-Croft, New York (1971), p. 57.
25) K. Itoh, H. Nagashima, T. Ohshima, N. Ohshima, and H. Nishiyama, *J. Organomet. Chem.*, **272**, 179 (1984).

 © 1986 The Chemical Society of Japan Bull. Chem. Soc. Jpn., 59, 3207—3212 (1986)

Synthesis and Antitumor Activity of *N*-Acetylmuramyl-L-alanyl-D-isoglutamine 6-Phosphate and Its Lipophilic Derivatives

Masahiro IMOTO, Shigeki KAGEYAMA, Shoichi KUSUMOTO, Morihiro KOHNO,† Kensuke MATSUMOTO,† Shinjiro HASHIMOTO,† Akiko TOHGO,† and Tetsuo SHIBA*

Department of Chemistry, Faculty of Science, Osaka University, Toyonaka, Osaka 560

†Research Institute, Daiichi Seiyaku Co., Ltd., Kitakasai 1-16-13, Edogawa-ku, Tokyo 134

(Received May 12, 1986)

6-Phosphate of *N*-acetylmuramyl-L-alanyl-D-isoglutamine and its lipophilic derivatives, i.e., 6-(octadecyl hydrogenphosphate) and 6-(2-docosyltetracosyl hydrogenphosphate) were synthesized after the structural feature of mycobacterial cell walls for the purpose to modify and possibly to enhance the immunostimulating activity of the muramyl dipeptide which is the minimum requisite for the activity. As expected, the latter more lipophilic phosphate showed a high activity in a tumor regression test.

As already described,[1,2] *N*-acetylmuramyl-L-alanyl-D-isoglutamine (**1**) is the minimum partial structure of bacterial peptidoglycan required for the expression of the immunostimulating activity. Our successive study demonstrated that lipophilic 6-*O*-acyl derivatives of the muramyl dipeptide which were synthesized in imitation of the structural feature of mycobacterial cell walls exhibit an antitumor activity characteristic of these natural cell walls.[3,4] However, the potency of the synthetic derivatives to inhibit the growth of tumor was still much less significant than the natural cell walls. In this respect, we continue synthetic studies towards derivatives of the muramyl dipeptide with more potent activities. One direction is syntheses of compounds with longer glycan structures.[5–7] As the second approach for the same purpose, we describe in this paper synthesis and antitumor activities of 6-*O*-phosphorylated derivatives of the muramyl dipeptide **1**.[8]

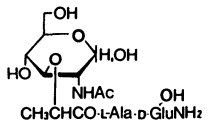

1

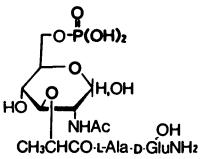

2

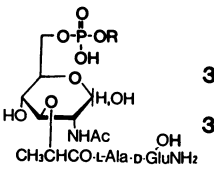

3a R = $(CH_2)_{17}CH_3$

3b R = $CH_2CH\langle^{(CH_2)_{21}CH_3}_{(CH_2)_{21}CH_3}$

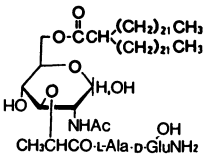

4

In cell walls of mycobacteria and related species, the 6-hydroxyl groups of muramic acid residues are bound through phosphodiester structures to arabinogalactan. It is further linked to mycolic acid, which is α-branched β-hydroxylated fatty acid with more than forty carbon atoms and thus render the cell wall highly lipophilic.[9] Since the 6-*O*-acylmuramyl dipeptides described above correspond to an oversimplified model of cell wall, both the phosphate and the polysaccharide parts being omitted and natural mycolic acid or analogous synthetic fatty acids being directly bound to the muramic acid residue, we were interested in testing the effect of the phosphate moiety on the biological activity of the molecule of the muramyl dipeptide. Especially, we anticipated that the simultaneous presence of the polar phosphate and the lipophilic part in the same molecule might have a significant effect. This consideration prompted us to synthesize *N*-acetylmuramyl-L-alanyl-D-isoglutamine 6-phosphate (**2**) and its lipophilic derivatives, i.e., the octadecyl derivative **3a** and the 2-docosyltetracosyl derivative **3b**. In the structures of **3a** and **3b**, the polysaccharide part is still lacking but the phosphodiester function is retained, the fatty acids present in the cell walls being replaced with long chain alcohols which are directly bound to the phosphate group.[10] In order to test the effect of different lipophilicity, two alcohols, i.e., 1-octadecanol and 2-docosyl-1-tetracosanol, were used. These two particular alcohols were chosen by taking into account the fact that 6-*O*-acylmuramyl dipeptides containing the fatty acids with the corresponding carbon chains showed characteristic activities. Namely, 6-*O*-stearoylmuramyl dipeptide showed the highest adjuvant activity among the acyl derivatives prepared,[11] and 6-*O*-(2-docosyltetracosanoyl)muramyl dipeptide **4** had a strong tumor suppressive activity.[4]

For the synthesis of 6-phosphate **2**, a known 4,6-*O*-benzylidene derivative of *N*-acetylmuramic acid α-benzyl glycoside (**5**) was prepared by slight modification of the reported conditions.[12] An improved yield was obtained at the formation of 2-carboxyethyl ether by reducing the amount of sodium hydride and by employing a lower reaction temperature. Benzyl esterification of **5** with phenyldiazomethane followed by acidic hydrolysis of the benzylidene group afforded **7** which is feasible for 6-*O*-phosphorylation.

When **7** was treated with diphenyl hydrogenphosphate[13] and 2,4,6-triisopropylbenzenesulfonyl chloride (TPS chloride) in pyridine, the desired 6-(diphenyl phosphate) **8** was obtained as a single product. The position of the phosphate moiety was confirmed by ^{13}C NMR, where a signal of methylene carbon (C-6) was observed which couples with ^{31}P of the phosphate group. After selective hydrogenolysis of the benzyl ester of **8**, the product was coupled with L-alanyl-D-isoglutamine benzyl ester to give the protected *N*-acetylmuramyl dipeptide 6-phosphate **9**, which was identified with the compound obtained via an alternative route described below. Deprotection of **9** was effected by catalytic hydrogenolysis in two steps, first with palladium black then with platinum oxide. Lyophilization from water gave the product **2** as colorless powder which gave a satisfactory result in elemental analysis. On treatment with diazomethane, **2** gave a trimethyl ester. Two of the methyl groups are bound to the phosphate residue as judged from the observation of through-three-bond H–P coupling in the ^1H NMR spectrum. Therefore, the presence of phosphomonoester structure in **2** was unequivocally assured, a possibility of the presence of a cyclic phosphodiester at 4 and 6 positions being thus excluded. The third methyl group was introduced at the carboxyl group of the isoglutamine residue.

Alternatively, the 6-phosphate **2** could be also prepared by phosphorylation after the dipeptide had been coupled with muramic acid. A partially protected derivative of muramyl dipeptide **10** prepared as an intermediate in our previous synthesis of 6-*O*-acyl muramyl dipeptide[14] was phosphorylated with the same reagents as above to give the 6-(diphenyl phosphate) which was identical with **9** obtained above. However, the yield of **9** was low (52%) because the undesired competitive dehydration occurred at the amide function of the isoglutamine residue to form a nitrile **11**. Consequently, the route described first was more favorable.

For the synthesis of lipophilic derivatives, **3a** and **3b**, the corresponding alkyl phenyl hydrogenphosphates were first prepared. Condensation of phenyl dihydrogenphosphate with 1-octadecanol or 2-docosyl-1-tetracosanol which had been prepared from methyl 2-docosyltetracosanoate by lithium aluminum hydride reduction was effected with dicyclohexylcarbodiimide (DCC) in pyridine. In case of the former alcohol, the reaction proceeded readily to give octadecyl phenyl hydrogenphosphate (**12a**) in a good yield. In contrast, the formation of the alkyl phenyl hydrogenphosphate was slow in case of the latter branched higher alcohol and more than 50% of the starting alcohol was recovered even after 70 h.

Octadecyl phenyl hydrogenphosphate was then treated with TPS chloride and muramic acid benzyl ester **7** in the same way as described for the synthesis of **2** to give a syrupy product **13a**, which was characterized by means of ^1H NMR and FD-MS. Hydrogenolysis of the benzyl ester of **13a** followed by condensation with the dipeptide benzyl ester afforded the protected muramyl dipeptide 6-(docosyl phenyl phosphate) **14a** as a solid after chromatographic purification. Hydrogenolysis in two steps followed by purification with a column of Bio-gel P-2 gave the muramyl dipeptide **3a** having octadecyl hydrogenphosphate at 6-position. Since the product gave a poorly resolved ^1H NMR spectrum due to aggregation, the structure was further characterized as its dibenzyl ester.

The 6-(2-docosyltetracosyl hydrogenphosphate) **3b** was also prepared in the same way. Like as the formation of the alkyl phenyl hydrogenphosphate **12b** described above, the yields of its condensation with muramic acid and the successive reaction with dipep-

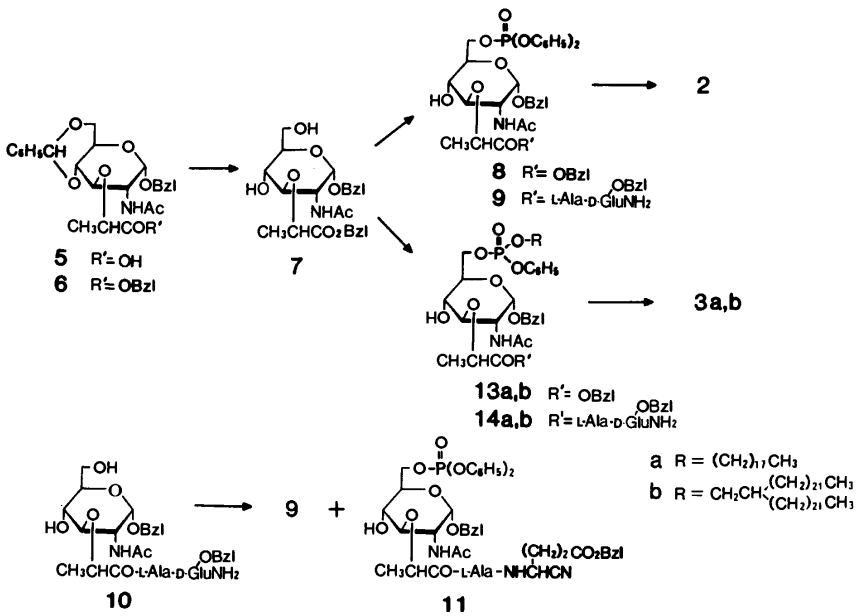

Table 1. Autitumor Effect of Synthetic Muramyl Dipeptide Derivatives on Meth-A Fibrosarcoma

Compound		Suppression Test[a]				Regression test[a]		
		Dose	Viability[b]	Suppression[c]	T/C[d]	Dose	Regression[c]	T/C[d]
		μg/mouse	%		%	μg/mouse		%
6-Phosphate	(**2**)	100	80	0/9	91.4			
6-(Octadecyl hydrogenphosphate)	(**3a**)	6.25	67	2/10	30.9			
6-(2-Docosyltetracosyl hydrogenphosphate)	(**3b**)	100	73	1/10	30.9	100	0/10	67.4
6-*O*-(2-Docosyl-tetracosanoate)	(**4**)	100	71	1/9	42.0	100	0/10	100.1
Nocardia CWS		100	96	2/9	32.1	100	0/8	59.2
Conrol		—	93	0/10	100	—	0/14	100

a) See the experimental part. b) The value represents the proportion of living/total cells before inoculation. c) Number of cured mice/number of treated mice. d) See Ref. 16 in the text.

tide were low presumably owing to a steric hindrance of the bulky alkyl group. The final product was also characterized after having been converted into the corresponding dibenzyl ester with phenyldiazomethane.

The antitumor activity of the synthetic compounds were first examined in the suppression test in which one can evaluate the ability of each compound to suppress the growth of tumor when tumor cells and the compound to be tested were simultaneously applied to animals.[15] Mice were inoculated intradermally with a mixture of the specified amount of the tumor cells and test materials given in Table 1. The weight of tumor was measured and compared with that of the control group where mice were given the tumor cells alone. The compound which gives smaller T/C value[16] is assumed to have higher suppression activity. The results are summarized in Table 1. While the hydrophilic 6-phosphate **2** showed no effect, both of the lipophilic derivatives, **3a** and **3b**, exhibited supression comparable to that obtained with *Nocardia* cell wall skeleton (CWS) which is known to have a potent antitumor activity.[17] 6-*O*-(2-Docosyltetracosanoyl)-muramyl dipeptide **4** of 6-*O*-acyl type prepared previously[4] also showed a similar activity in this test system. It should be noted here that the octadecyl derivative **3a** could not be used in higher doses because this compound kills the tumor cells by direct action probably due to its detergent-like character as shown by the decrease of viable tumor cells (Table 1). Tumor regression activity[18] of muramyl dipeptide 6-(2-docosyltetracosyl hydrogenphosphate) **3b** was then tested in comparison with *Nocardia* CWS and 6-*O*-(2-docosyltetracosanoyl)muramyl dipeptide **4**. In this test, growth inhibition with the compound is evaluated on the tumor which was previously inoculated and already grown up in mice. Therefore this system enables more strict estimation of the antitumor activity under conditions similar to actual immunotherapy. The result shown in Table 1 clearly indicate that compound **3b** prepared in this study shows high activity comparable to the natural cell wall preparation. On the contrary, 6-*O*-acyl type derivative **4** showed no effect in this regression test. Since **4** contains a carbon chain with the same length as that of **3b**, the difference in the biological activities could be attributed to the presence of the phosphate function in **3b**. As mentioned in the introduction of this paper, it could be speculated that simultaneous existence of both the phosphate moiety and the long alkyl chain would give a character like a phospholipid to the molecule and enhance the interaction with the membrane of host animals cells, resulting in expression of high biological activity.

Experimental

All melting points are uncorrected. Unless otherwise stated, ^{1}H and ^{13}CNMR spectra were measured at 100 and 22.5 MHz, respectively, for $CDCl_3$ solutions. FD mass spectra were obtained with a JEOL JMS-01SG mass spectrometer equipped with silicon emitter. Optical rotations were measured with a Perkin-Elmer 141 polarimeter. Column chromatography were carried out with Kieselgel 60 (0.063—0.2 mm), E. Merck.

Benzyl 2-Acetamido-4,6-*O*-benzylidene-3-*O*-[(*R*)-1-carboxyethyl]-2-deoxy-α-D-glucopyranoside (5). Sodium hydride (60% oil dispersion, 3.0 g, 75 mmol) was added to a solution of benzyl 2-acetamido-4,6-*O*-benzylidene-2-deoxy-α-D-glucopyranoside[19] (15.0 g, 37.6 mmol) in dry dioxane (750 ml). The mixture was kept at 60°C with stirring. (*S*)-2-Chloropropionic acid (16.4 g, 151 mmol) was added to the mixture and stirring was continued at 60°C. Soon after addition of the acid, a large amount of small crystals separated out which made efficient stirring difficult. Stirring again became possible within 10 min. Then NaH (7.5 g, 188 mmol) was again added. Stirring was continued at the same temperature for further 40 min. After addition of water (800 ml), the mixture was washed with hexane and then acidified with 6M[††] HCl. The separated crystals were collected by filtration, washed thoroughly with water, and dried. Recrystallization was effected from $CHCl_3$; Yield 14.8 g (84%); mp 230—234°C decomp.

Benzyl 2-Acetamido-4,6-*O*-benzylidene-3-*O*-[(*R*)-1-(benzyloxycarbonyl)ethyl]-2-deoxy-α-D-glucopyranoside (6). To a solution of **5** (4.70 g, 10.0 mmol) in $CHCl_3$ (470 ml) was added a solution of phenyldiazomethane in hexane. After

[††] 1 M=1 mol dm^{-3}.

usual work-up, the product was recrystallized from acetone; yield 5.51 g (98%); mp 178—181 °C. Found: C, 68.31; H, 6.22; N, 2.57%. Calcd for $C_{32}H_{35}NO_8$: C, 68.44; H, 6.28; N, 2.49%.

Benzyl 2-Acetamido-3-*O*-[(*R*)-1-(benzyloxycarbonyl)ethyl]-2-deoxy-α-D-glucopyranoside (7). A suspension of **6** (5.00 g, 8.90 mmol) in 60% AcOH (250 ml) was heated in a boiling water bath with shaking for 20 min. After usual work-up, the product was recrystallized from $CHCl_3$–ether–hexane; yield 3.75 g (89%); mp 120—123 °C (with sintering at 115 °C). Found: C, 63.10; H, 6.58; N, 3.02%. Calcd for $C_{25}H_{31}NO_8$: C, 63.41; H, 6.60; N, 2.96%.

Benzyl 2-Acetamido-3-*O*-[(*R*)-1-(benzyloxycarbonyl)ethyl]-2-deoxy-α-D-glucopyranoside 6-(Diphenyl Phosphate) (8). A mixture of **7** (500 mg, 1.05 mmol), diphenyl hydrogenphosphate (528 mg, 2.11 mmol), and TPS chloride (639 mg, 2.11 mmol) in dry pyridine (5 ml) was stirred at room temperature for 13 h. Diphenyl hydrogenphosphate (264 mg, 1.05 mmol) and TPS chloride (320 mg, 1.05 mmol) was added, and the mixture was stirred at room temperature for additional 19 h. After addition of water, the solvent was evaporated in vacuo. The residue was dissolved in $CHCl_3$, washed with water, and dried ($MgSO_4$). The product was isolated by column chromatography on silica gel (50 g, $CHCl_3$–MeOH 50:1) as colorless syrup; yield 674 mg (91%); ^{1}H NMR δ=7.1—7.5 (21H, aromatic H and NH); ^{13}C NMR δ=67.75 ($J_{P\text{-}O\text{-}C}$=6.1 Hz, C-6).

Benzyl L-Alanyl-D-isoglutaminate *N*-Acylated with Benzyl 2-Acetamido-2-deoxy-3-*O*-[(*R*)-1-carboxyethyl]-α-D-glucopyranoside 6-(Diphenyl Phosphate) (9). a) From **8**. Compound **8** (280 mg, 0.40 mmol) was dissolved in THF (8 ml) and hydrogenolyzed at room temperature in the presence of Pd-black for 2 h. The catalyst was filtered off and the solvent was evaporated in vacuo. The residue was again dissolved in THF (3 ml). L-Alanyl-D-isoglutamine benzyl ester trifluoroacetate (200 mg, 0.47 mmol), *N*-hydroxysuccinimide (HONSu) (55 mg, 0.48 mmol), triethylamine (65 μl, 0.47 mmol) and DCC (98 mg, 0.48 mmol) were added to the solution at 0 °C with stirring. The mixture was stirred overnight, being allowed to warm up to room temperature during this period. After usual work-up, the syrupy product obtained was subjected to column chromatography on silica gel (45 g, $CHCl_3$–MeOH 20:1) and recrystallized from $CHCl_3$–ether–hexane; yield 256 mg (71%); mp 106—108 °C. It was identical with the product obtained by the following method b).

b) From **10**. To a suspension of benzyl L-alanyl-D-isoglutaminate *N*-acylated with benzyl 2-acetamido-2-deoxy-3-*O*-[(*R*)-1-carboxyethyl]-α-D-glucopyranoside (**10**)[14] (336 mg, 0.50 mmol) in pyridine (3 ml) were added diphenyl hydrogenphosphate (250 mg, 1.0 mmol) and TPS chloride (302 mg, 1.0 mmol). The mixture had been stirred at room temperature for 3 h and worked up as usual. The crude product was subjected to silica-gel column chromatography (48 g). Elution with a mixture of $CHCl_3$–MeOH (10:1) first gave the nitrile derivative **11**, which was recrystallized from $CHCl_3$–ether; yield 100 mg (23%); mp 75—77 °C; IR (KBr) 2250 cm^{-1} (CN). Found: C, 60.67; H, 5.92; N, 6.16%. Calcd for $C_{45}H_{51}N_4O_{13}P$: C, 60.94; H, 5.80; N, 6.32%.

Further elution with the same solvent afforded **9** which was recrystallized from $CHCl_3$–ether: yield 235 mg (52%); mp 107—110 °C; $[\alpha]_D^{22}$ +57.2° (*c* 0.50, $CHCl_3$). Found; C, 59.29; H, 5.99; N, 6.03%. Calcd for $C_{45}H_{53}N_4O_{14}P\cdot 0.5H_2O$: C, 59.14; H, 5.96; N, 6.13%.

L-Alanyl-D-isoglutamine *N*-Acylated with 2-Acetamido-2-deoxy-3-*O*-[(*R*)-1-carboxyethyl]-D-glucose 6-Phosphate (2). Compound **9** (90 mg, 0.10 mmol) was dissolved in AcOH (5 ml) and stirred under atmospheric pressure of H_2 in the presence of Pd-black for 7 h. After catalyst had been filtered off, PtO_2 was added to the filtrate. The mixture was stirred under H_2 (5 kg cm^{-2}) at room temperature for 14 h. The catalyst was removed by filtration and the solvent was removed in vacuo. The residue was again dissolved in water. The solution was filtered through a Milipore filter (pore size 0.45 μm) and subjected to lyophilization to give colorless powder: yield 60 mg (quantitative); $[\alpha]_D^{22}$ +45.9° (*c* 0.51, MeOH). Found: C, 36.91; H, 6.04; N, 9.07; P, 4.73%. Calcd for $C_{19}H_{33}N_4O_{14}P\cdot 2.5H_2O$: C, 36.96; H, 6.20; N, 9.07; P, 5.02%.

The compound was dissolved in MeOH and treated with an ethereal solution of CH_2N_2. After evaporation of the solvent, the product was directly subjected to ^{1}H NMR measurement: (in $CDCl_3$–CD_3OD) δ=3.81 (6H, d, $J_{P\text{-}O\text{-}C\text{-}H}$= 11 Hz, $PO(OCH_3)_2$), 3.60 (3H, s, $COOCH_3$).

Octadecyl Phenyl Hydrogenphosphate (12a). A solution of 1-octadecanol (3.00 g, 11.1 mmol), phenyl dihydrogenphosphate (2.32 g, 13.3 mmol) and DCC (2.75 g, 13.3 mmol) in pyridine (30 ml) was stirred at room temperature for 13 h. Phenyl dihydrogenphosphate (0.97 g, 5.5 mmol) and DCC (1.14 g, 5.5 mmol) were added and the mixture was stirred for further 37 h. After usual work-up, the product was recrystallized from MeOH; yield 3.80 g (80%); mp 56—58 °C. Found: C, 67.71; H, 10.14%. Calcd for $C_{24}H_{43}O_4P$: C, 67.58; H, 10.16%.

Benzyl 2-Acetamido-3-*O*-[(*R*)-1-(benzyloxycarbonyl)ethyl]-2-deoxy-α-D-glucopyranoside 6-(Octadecyl Phenyl Phosphate) (13a). TPS chloride (1.28 g, 4.22 mmol) was added to a solution of the muramic acid benzyl ester **7** (1.00 g, 2.11 mmol) and octadecyl phenyl hydrogenphosphate (**12a**) (1.80 g, 4.22 mmol) in pyridine (20 ml). After the mixture had been stirred at room temperature for 23 h, the solvent was evaporated in vacuo and the residue subjected to silica-gel column chromatography (90 g, $CHCl_3$–MeOH 50:1) to give a syrupy product: yield 1.33 g (72%); FD-MS: *m/z* 882 $(M+H)^+$.

Benzyl L-Alanyl-D-isoglutaminate *N*-Acylated with Benzyl 2-Acetamido-2-deoxy-3-*O*-[(*R*)-1-carboxyethyl]-α-D-glucopyranoside 6-(Octadecyl Phenyl Phosphate) (14a). Compound **13a** (500 mg, 0.567 mmol) was dissolved in THF (15 ml) and hydrogenolyzed in the presence of Pd-black catalyst at room temperature for 45 min. After the catalyst had been filtered off, the solvent was once evaporated in vacuo and the residue was again dissolved in THF (5 ml). L-Alanyl-D-isoglutamine benzyl ester trifluoroacetate (300 mg, 0.711 mmol), HONSu (82 mg, 0.712 mmol), triethylamine (96 μl, 0.69 mmol), and DCC (140 mg, 0.679 mmol) were added to the solution cooled to 0 °C. The mixture was stirred overnight and worked up as usual. The product was purified by column chromatography on silica gel (50 g, $CHCl_3$–MeOH 10:1) and lyophilized from dioxane: yield 235 mg (38%); ^{1}H NMR δ=7.1—7.5 (15H, aromatic H), 5.09 (4H, s, $C_6H_5C\underline{H}_2$–), 1.90 (3H, s, CH_3CO), 1.2—1.5 (32H, broad, $-CH_2$).

L-Alanyl-D-isoglutamine *N*-Acylated with 2-Acetamido-2-deoxy-3-*O*-[(*R*)-1-carboxyethyl]-D-glucose 6-(Octadecyl Hydrogenphosphate) (3a) and Its Dibenzyl Ester. Compound **14a** (50 mg, 4.6 μmol) was dissolved in MeOH (5 ml). After a few drops of AcOH and Pd-black catalyst had been added, the

mixture was stirred under H_2 atmosphere (5 kg cm^{-2}) at room temperature for 48 h. The catalyst was filtered off, and the solvent was evaporated in vacuo. The residue was again dissolved in MeOH (5 ml) and the solution stirred under H_2 (5 kg cm^{-2}) for 3 h after addition of PtO_2. The product was dissolved in water and purified by a column of Bio-gel P-2 (100—200 mesh, 17 ml). Lyophilization from AcOH afforded colorless powder; yield 27 mg (71%); $[\alpha]_D^{22}$ +25.1° (*c* 1.00, $CHCl_3$–MeOH 5:1). Found: C, 51.83; H,8.26; N, 6.79%. Calcd for $C_{37}H_{69}N_4O_{14}P \cdot 2H_2O$: C, 51.62; H, 8.55; N, 6.51%.

Compound **3a** obtained from **14a** (0.10 mmol) was dissolved in $CHCl_3$, washed once with 1M HCl and then treated with phenyldiazomethane. The product was purified by preparative TLC on silica gel and lyophilized from benzene to give the dibenzyl ester; yield 35 mg; ^{1}H NMR; δ=7.2—7.4 (10H, aromatic H), 5.08 (4H, $C_6H_5C\underline{H}_2$). Found: C, 58.74; H, 7.98; N, 5.42; P, 2.52%. Calcd for $C_{51}H_{81}N_4O_{14}P \cdot 2H_2O$: C, 58.83; H, 8.23; N, 5.38; P, 2.97%.

2-Docosyl-1-tetracosanol. A mixture of 2-docosyltetracosanoic acid (5.00 g, 7.38 mmol) and concd H_2SO_4 (0.5 ml) in MeOH (50 ml) and CH_2ClCH_2Cl (50 ml) was heated under reflux for 5 h. After usual work-up, recrystallization from acetone afforded methyl 2-docosyltetracosanoate; yield 4.94 g (97%); mp 68—70°C.

To a suspension of this methyl ester (4.94 g, 7.15 mmol) in anhyd ether (200 ml) and anhyd THF (100 ml), a suspension of $LiAlH_4$ (271 mg, 7.15 mmol) in anhyd ether (75 ml) was added dropwise with stirring during 30 min. The mixture was heated under reflux for 3 h, $LiAlH_4$ (540 mg, 14.3 mmol) being added after 1.5 h. After usual work-up, the product was recrystallized from acetone; yield 4.46 g (94%); mp 65—67°C.

2-Docosyltetracosyl Phenyl Hydrogenphosphate (12b). DCC (1.66 g, 8.04 mmol) was added to a mixture of 2-docosyl-1-tetracosanol (4.46 g, 6.72 mmol) and phenyl dihydrogenphosphate (1.40 g, 8.04 mmol) in pyridine (50 ml). The mixture was stirred at room temperature for 55 h. Phenyl dihydrogenphosphate (1.17 g, 6.72 mmol) and DCC (1.38 g, 6.72 mmol) were added to the mixture and stirring was continued for further 16 h. After the mixture had been worked up as described for **12a**, the product and the unchanged 2-docosyl-1-tetracosanol were separated by means of silica-gel column chromatography (225 g, $CHCl_3$–MeOH 20:1 to 10:1).

2-Docosyl-1-tetracosanol recovered was recrystallized from acetone; 2.47 g (recovery 55%).

The product eluted from the column was dissolved in $CHCl_3$ and washed with 1M HCl and water. The residue obtained by evaporation of the solvent was recrystallized from acetone; yield 2.05 g (37%); mp 57—60°C. Found: C, 75.94; H, 12.06%. Calcd for $C_{52}H_{99}O_4P$: C, 76.23; H, 12.18%.

Benzyl 2-Acetamido-3-*O*-[(*R*)-1-(benzyloxycarbonyl)ethyl]-2-deoxy-α-D-glucopyranoside 6-(2-Docosyltetracosyl Phenyl Phosphate) (13b). TPS chloride (640 mg, 2.11 mmol) was added to a solution of muramic acid benzyl ester (**7**) (500 mg, 1.05 mmol) and **12b** (1.73 g, 2.11 mmol) in anhyd pyridine (15 ml). The mixture was stirred at room temperature for 48 h and worked up as described for **13a**. The product was isolated by column chromatography on silica gel (50 g, $CHCl_3$–MeOH 50:1) as colorless syrup; yield 550 mg (41%); FD-MS *m/z* 1175 $(M+H)^+$.

Benzyl L-Alanyl-D-isoglutaminate *N*-Acylated with Benzyl 2-Acetamido-3-*O*-[(*R*)-1-carboxyethyl]-α-D-glucopyranoside 6-(2-Docosyltetracosyl Phenyl Phosphate) (14b). Compound **13b** (545 mg, 0.427 mmol) was dissolved in THF (20 ml) and hydrogenolyzed in the presence of Pd-black catalyst for 1 h. The product was dissolved without purification in THF (7 ml). L-Alanyl-D-isoglutamine benzyl ester trifluoroacetate (270 mg, 0.641 mmol), HONSu (74 mg, 0.64 mmol), triethylamine (90 μl, 0.65 mmol) and DCC (106 mg, 0.514 mmol) were added to the solution. The mixture was stirred at room temperature for 17 h, worked up as described for **14a**. Silica-gel column chromatography (50 g, $CHCl_3$–MeOH 20:1) followed by lyophilization from dioxane afforded colorless powder; yield 233 mg (37%); $[\alpha]_D^{22}$ +34.0° (*c* 0.51, $CHCl_3$). Found: C, 67.92; H, 9.47; N, 3.88%. Calcd for $C_{85}H_{141}N_4O_{14}P$: C, 68.01; H, 9.67; N, 3.73%.

L-Alanyl-D-isoglutamine *N*-Acylated with 2-Acetamido-2-deoxy-3-*O*-[(*R*)-1-carboxyethyl]-D-glucose 6-(2-Docosyltetracosyl Hydrogenphosphate) (3b) and Its Dibenzyl Ester. Compound **14b** (60 mg, 41 μmol) was dissolved in a mixture of THF (20 ml)–MeOH (10 ml)–AcOH (1 ml) and hydrogenolyzed in the presence of Pd-black under H_2 (7 kg cm^{-2}) for 48 h. After removal of the catalyst, PtO_2 was added to the filtrate and again hydrogenolyzed at 7 kg cm^{-2} for 12 h. The solvent was evaporated in vacuo, the residue was dissolved in $CHCl_3$–MeOH (10:1) and filtered through a Fluoropore filter disk (pore size 0.45 μm) to remove small particles of insoluble materials. After evaporation of the solvent in vacuo, the residue was lyophilized from a mixture of benzene–AcOH to give **3b** as colorless powder; yield 48 mg (quantitative); $[\alpha]_D^{21}$ +18° (*c* 0.12, $CHCl_3$–MeOH 5:1).

The product (27 mg) was dissolved in $CHCl_3$ (10:1, 30 ml), washed with 1M HCl and treated with phenyldiazomethane. Purification by preparative TLC on silica gel followed by lyophilization from dioxane afforded the dibenzyl ester as colorless powder; yield 12.2 mg. Found: C, 67.29; H, 10.03; N, 4.06; P, 1.92%. Calcd for $C_{79}H_{137}N_4O_{14}P \cdot 0.5H_2O$: C, 67.45; H, 9.89; N, 3.98; P, 2.20%.

Tumor Suppression and Regression Tests. Antitumor effects of the muramyl dipeptide derivatives against Meth-A fibrosarcoma were evaluated by two distinct test systems using syngeneic BALB/c male mice (5 week-old, purchased from Shizuoka Laboratory Animal Center, Shizuoka, Japan). The suppression test was conducted according to the method of Yamamura et al.[15]: Briefly, a mixture of 2×10^5 tumor cells and a test compound in phosphate-buffered saline was inoculated intradermally into the right flank of mice. In the regression test,[18] mice were injected the same number of the tumor cells as above on day 0 and then given intratumor injection of a test compound seven times every other days from day 7. In both tests, mice were sacrificed three weeks after tumor cell inoculation and tumor growth inhibition was measured.[16]

References

1) F. Ellouz, A. Adam, R. Ciorbaru, and E. Lederer, *Biochem. Biophys. Res. Commun.*, **59**, 1317 (1974).

2) a) S. Kotani, Y. Watanabe, F. Kinoshita, T. Shimono, I. Morisaki, T. Shiba, S. Kusumoto, Y. Tarumi, and K. Ikenaka, *Biken J.*, **18**, 105 (1975); b) S. Kusumoto, Y. Tarumi, K. Ikenaka, and T. Shiba, *Bull. Chem. Soc. Jpn.*, **49**, 533 (1976).

3) I. Azuma, K. Sugimura, M. Yamawaki, M. Uemiya, S. Kusumoto, S. Okada, T. Shiba, and Y. Yamamura, *Infect. Immun.*, **20**, 600 (1978).

4) S. Kusumoto, M. Inage, T. Shiba, I. Azuma, and Y. Yamamura, *Tetrahedron Lett.*, **1978**, 4899.

5) S. Kusumoto, K. Yamamoto, and T. Shiba,

Tetrahedron Lett., **1978**, 4407.

6) S. Kusumoto, K. Yamamoto, M. Imoto, M. Inage, M. Tsujimoto, S. Kotani, and T. Shiba, *Bull. Chem. Soc. Jpn.*, **59**, 1411 (1986).

7) S. Kusumoto, M. Imoto, T. Ogiku, and T. Shiba, *Bull. Chem. Soc. Jpn.*, **59**, 1419 (1986).

8) A part of this work was presented at an International Symposium on "Immunomodulation by Microbial Product and Related Synthetic Compound" held at Osaka, July 27—29, 1981. See the book on the same title in "International Congress Series 563," ed by Y. Yamamura, S. Kotani, I. Azuma, A. Koda, and T. Shiba, Excerpta Medica, Amsterdam (1982), pp. 151—154.

9) I. Azuma, E. Ribi, T. Meyer, and B. Zbar, *J. Natl. Cancer Inst.*, **52**, 95 (1974).

10) We first attempted to use 2-aminoethanol as a linkage between a long chain carboxylic acid and the phosphate moiety (see Ref. 8 above). However, when a 2-(acylamino)-ethyl phenyl hydrogenphosphate was subjected to coupling with the 6-hydroxyl group of muramic acid, the desired product could not be isolated in a pure state. It decomposed spontaneously losing the acyl moiety. Therefore we connected long-chain alcohols directly to the phosphate moiety in the present study.

11) S. Kotani, F. Kinoshita, I. Morisaki, T. Shimono, T. Okunaga, H. Takada, M. Tsujimoto, Y. Watanabe, K. Kato, T. Shiba, S. Kusumoto, and S. Okada, *Biken J.*, **20**, 95 (1977).

12) H. M. Flowers and R. W. Jeanloz, *J. Org. Chem.*, **28**, 2983 (1963).

13) When dibenzyl hydrogenphosphate was used in place of diphenyl hydrogenphosphate, the desired 6-(dibenzyl phosphate) could not be isolated. TLC analysis of the reaction mixture indicated the disappearance of the starting material **7** and the presence of a polar product which was assumed to have a phosphate function because of the positive reaction against Dittmer-Lester reagent. This result could be explained by assuming that the desired product was once formed but decomposed because of the instability of the benzyl ester function in the phosphotriester.

14) S. Kusumoto, S. Okada, K. Yamamoto, and T. Shiba, *Bull. Chem. Soc. Jpn.*, **51**, 2122 (1978).

15) Y. Yamamura, I. Azuma, T. Taniyama, E. Ribi, and B. Zbar, *Gann*, **65**, 179 (1974).

16) T/C stands for the ratio of the mean tumor weight of a test group to that of the control group.

17) R. Tokuzen, M. Okabe, W. Nakahara, I. Azuma, and Y. Yamamura, *Gann*, **69**, 19 (1978).

18) M. Kohno, S. Abe, M. Yamazaki, and D. Mizuno, *Gann*, **73**, 484 (1982).

19) R. Kuhn, H. H. Bauer, and A. Seeliger, *Ann.*, **611**, 236 (1958).

 © 1986 The Chemical Society of Japan Bull. Chem. Soc. Jpn., 59, 3213—3216 (1986)

Dual-Mode Transport of Molecular Oxygen through the Membrane of the Poly(octyl methacrylate-co-4-vinylpyridine)(*N,N'*-disalicylideneethylenediaimine)cobalt(II) Complex

Hiroyuki NISHIDE, Manshi OHYANAGI, Hiroyoshi KAWAKAMI, and Eishun TSUCHIDA*
Department of Polymer Chemistry, Waseda University, Tokyo 160
(Received May 7, 1986)

Molecular oxygen transport through a polymeric membrane was enhanced in the membrane of poly(octyl methacrylate-co-4-vinylpyridine), complexed with (*N,N'*-disalicylideneethylenediamine)cobalt(II), which forms an oxygen adduct rapidly and reversibly. The cobalt complex in the membrane effectively acted as a fixed carrier on oxygen permeation. The oxygen-binding parameters determined spectroscopically were adequate to analyze the dual-mode transport model.

Recently there has been considerable interest in the production of oxygen-enriched air by the use of permselective membranes.[1] Metal complexes, such as iron porphyrin derivatives and cobalt Schiff base complexes, form oxygen adducts reversibly and have been successfully used for an oxygen-transporting fluid[2] and to an oxygen-separating liquid membrane.[3] However, an oxygen permselective membrane prepared from a polymer complexed with the metal complex acting as a fixed carrier on oxygen permeation has yet been reported. Recently the present authors preliminarily reported the preparation of polymer membranes containing the cobalt complexes as fixed carriers of oxygen which sorb and transport oxygen selectively by means of the Langmuir mode.[4,5] Drago and Balkus also recently reported that the cobalt-*N,N*-bis[3-(salicylideneamino)propyl]methylamine complex bound to a polystyrene membrane enhances the selectivity for oxygen permeation through a polystyrene membrane at low pressures.[6]

The present paper will describe the selective and dual-mode transport of molecular oxygen in a polymer complexed with a cobalt-Schiff base as a fixed carrier (Scheme 1). The polymer membrane was prepared by homogeneously complexing (*N,N'*-disalicylideneethylenediamine)cobalt(II) (CoS) to poly(octyl methacrylate-co-4-vinylpyridine)(POMP), whose sixth coordination site is vacant even in the solid state, to bind oxygen reversibly. Rapid and reversible oxygen binding to the polymer-bound complex (the fixed carrier) in the membrane was characterized in situ by means of spectroscopic methods. Oxygen permeation was measured in connection with the upstream oxygen pressure. The oxygen-permeation behavior through the membrane will be discussed in terms of the combination of the dual-mode transport theory and the spectroscopic data.

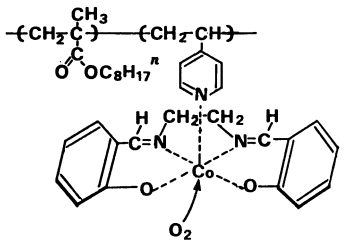

Scheme 1.

Experimental

Materials. (*N,N'*-disalicylideneethylenediamine)cobalt(II) (CoS) was synthesized as in the literature.[7] Poly(octyl methacrylate-co-4-vinylpyridine) (POMP) was obtained by the radical copolymerization of octyl methacrylate and 4-vinylpyridine, with azobisisobutyronitrile as an initiator. The vinylpyridine content and the molecular weight of POMP were determined to be 15 mol% and 150000 by elemental analysis and gel-permeation chromatography (with tetrahydrofuran as the solvent and polystyrene as the standard.), respectively. The toluene solution of POMP and CoS was carefully cast on a Teflon plate under an atmosphere without oxygen, followed by drying in vacuo, to yield a transparent and flexible membrane with thickness of 60 μm and containing 2.5 wt% CoS.

Spectroscopic Measurements. Reversible oxygen binding to the POMP–CoS complex in the membrane was observed with a spectral change in the visible absorption (using a highly sensitive spectrophotometer, Shimazu UV-2000). Rapid and reversible oxygen binding to the POMP–CoS complex in the membrane was also confirmed by means of flash photolysis (using a pulse and laser flash spectrophotometer equipped with a kinetic data processor; UNISOK FR-2000). The membrane was set at 45° to the laser-flash irradiation, and perpendicularily the rapid absorption change was recorded with a contact-type photomultiplier in order to cancel the noise signals caused by the scattering light.

Permeation Measurements. Oxygen and nitrogen permeation coefficients for various upstream gas pressures were measured with a low-vacuum permeation apparatus in the chamber for stable thermostating (Rika Seiki K-315 N-03).

Results and Discussion

Oxygen Binding to the Complex in the Membrane. The visible absorption spectrum of the transparent membrane is shown in Fig. 1. The color of the membrane was changed reversibly from brown to deep violet on exposure to oxygen and nitrogen. The spectral change in the membrane agreed with that of the polymer–CoS complex previously reported[2a]: UV and visible absorption maxima λ_{max}=555 nm (oxy: Co/O_2= 1/1 adduct), λ_{max}=345, 410 nm (deoxy: five-coordina-

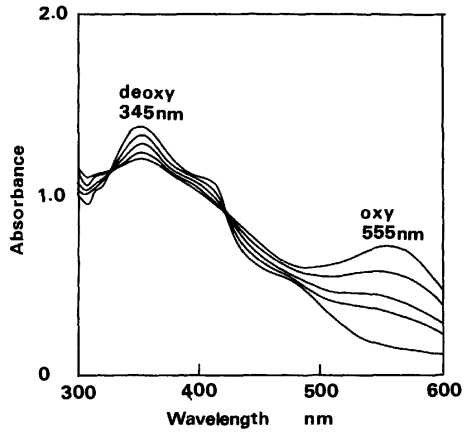

Fig. 1. UV and visible absorption spectral change in the oxygen binding to the POMP-CoS membrane at 30°C, [CoS]=2.5 wt%.

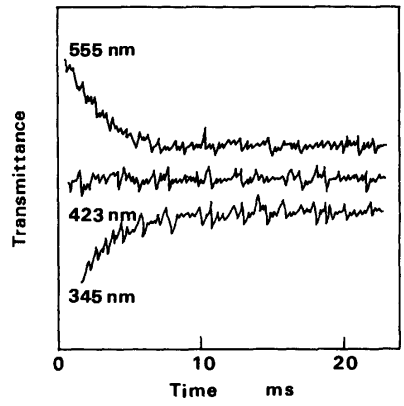

Fig. 2. Flash photolysis of the bound oxygen to the POMP-CoS membrane under exposing to air at 30°C, [CoS]=2.5 wt%.

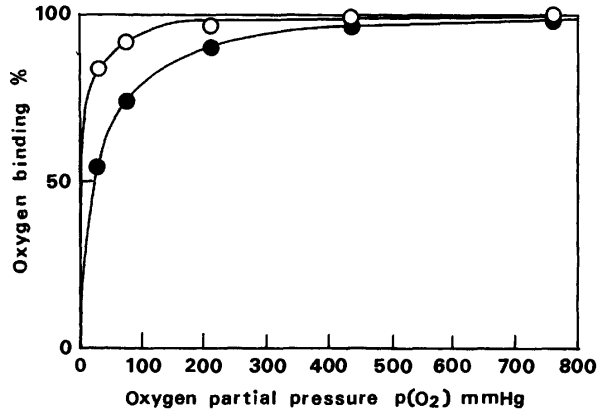

Fig. 3. Oxygen-binding equilibrium curve for the POMP-CoS membrane at O: 25°C, ●: 35°C, [CoS]=2.5 wt%.

tion), isosbestic points at 335, 423 nm.

The reversible oxy-deoxy spectral change occurred rapidly; e.g., for a 60 μm-thick membrane containing 2.5 wt% CoS, the oxygen-binding equilibrium was established within several minutes after the exposure to oxygen or in vacuo at 25°C. Although there have been several reports on the oxygen binding to a cobalt Schiff base complex or an iron porphyrin complex dispersed or bonded to the polymers in the solid state, oxygen adsorption and desorption to them occurred very slowly, even in a fine powder state with a large surface area.[8] It is important for a fixed carrier of oxygen that oxygen should be sorbed and desorbed rapidly in response to a partial oxygen pressure, even after fixation in a feasible membrane.

$$\text{POMP-CoS-O}_2 \xrightarrow{h\nu} \text{POMP-CoS} + \text{O}_2$$
$$\xrightarrow{k_{app}} \text{POMP-CoS-O}_2 \qquad (1)$$

$$\text{POMP-CoS} + \text{O}_2 \underset{k_{off}}{\overset{k_{on}}{\rightleftharpoons}} \text{POMP-CoS-O}_2 \qquad (2)$$

The photodissociation and recombination of the bound oxygen from and to the POMP-CoS complex in the membrane (Eq. 1) was successfully observed by means of pulse and laser flash spectroscopy. The oxygen-binding and -dissociation rate constants (k_{on} and k_{off} in Eq. 2) of the CoS complexed to the POMP membrane could be determined in situ as follows. By the changing in the monitoring wavelength from 300 to 600 nm, a differential spectrum before and after the flash photolysis was measured. The positive and negative extremes in the differential spectrum, 345 and 555 nm, were selected as the monitoring wavelengths for subsequent use (Fig. 2). These wavelengths agreed with the absorption maxima of the oxygen adduct and the deoxy complex in Fig. 1. The validity of these measurements is supported further by the following results: (i) The absorbance of 423 nm is kept constant before and after flash photolysis (Fig. 2); this wavelength agrees with the isosbestic point of the oxygen adduct and the deoxy complex as it shown in Fig. 1, and (ii) the absorbance changes followed at 345 and 555 nm are symmetric (Fig. 2).

The k_{on} and k_{off} values were estimated by means of pseudo-first-order kinetics and as given in Table 1. The k_{on} and k_{off} values of the CoS complexed to the POMP membrane were similar to those of the POMP-CoS complex in a toluene solution. This means that the CoS complex is active for the oxygen binding even, in the membrane, and that it acts as an effective fixed carrier of oxygen.

The oxygen-binding equilibrium constant ($K=k_{on}/k_{off}$) was determined by conducting oxygen-binding and -dissociation equilibrium measurements using Drago's equation.[9] The oxygen binding curves and the K values are given in Fig. 3 and Table 1. The K values of the complex in the membrane were much larger than those in the toluene solution. This result may be explained as follows: While the axial pyridyl group-ligation is in equilibrium in the solution system, the POMP-CoS complexation is completed and/or the pyridyl ligand in POMP is immobilized to

Table 1. Oxygen-Binding Rate.[a] Equilibrium Constant,[a] and Its Thermodynamic Parameters[b] for the POMP-CoS Membrane

Physical state	$10^{-5}k_{on}$	$10^{-2}k_{off}$	K	ΔH	ΔS
	$L\,mol^{-1}\,s^{-1}$	s^{-1}	$cmHg^{-1}$	$kcal\,mol^{-1}$	e.u.
Toluene soln.	1.8	2.7	1.1×10^{-3}	−30	−104
Membrane	4.8	0.44	4.3×10^{-1}	−16	−45

a) Data at 30°C. b) Data for van't Hoff plots ($\ln K$ in atm^{-1}).

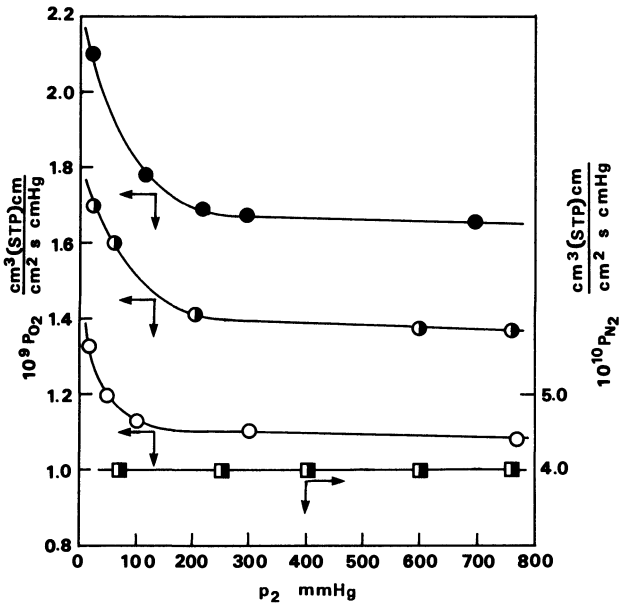

Fig. 4. Effect of upstream gas pressure on permeation coefficient for the POMP-CoS membrane. Oxygen: at O: 25°C, ◑: 30°C, ●: 35°C, Nitrogen: at ◧: 30°C.

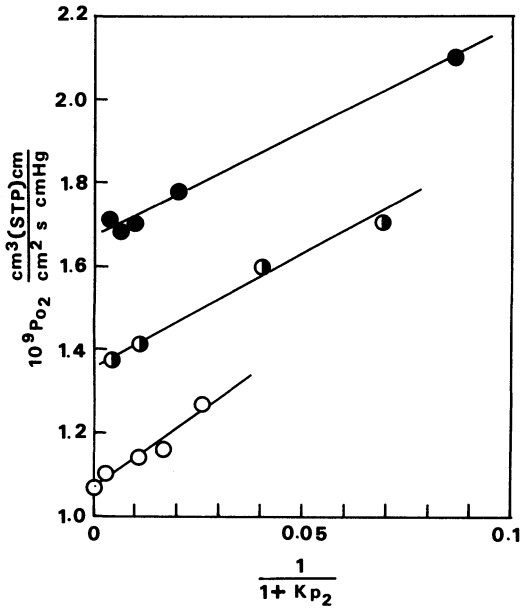

Fig. 5. Oxygen permeability in the POMP-CoS membrane plotted according to Eq. 3 at O: 25°C, ◑: 30°C, ●: 35°C.

CoS, which bring about a relatively stable oxygen adduct formation for the complex in the membrane. The thermodynamic parameters for the oxygen binding, as estimated from the temperature dependence of K, are also given in Table 1.

At any rate, the advantages of the membrane complexed with CoS are that the fixed carrier maintains its rapid and reversible binding capability of the penetrant even after fixation in the membrane and that the adsorption and desorption rates and the equilibrium constants of the penetrant to the carrier site can be evaluated in situ.

Oxygen Permeability in the Fixed Carrier Membrane. Figure 4 shows the effect of the upstream gas pressure (p_2) on the permeability coefficients (P_{O_2} and P_{N_2}) in a membrane containing 2.5 wt% CoS. Although the dependence of P on p_2 has been often reported for glassy polymers,[10] the glass-transition temperature was −8.0°C for the membrane containing CoS and the membrane was in a rubber state during permeability measurements. In fact, P_{N_2} was independent of $p_2(N_2)$, for the fixed carrier does not interact with nitrogen. P_{O_2} increases with a decrease in $p_2(O_2)$, which suggests that oxygen transport occurs by means of dual-mode transport[10] (Henry mode and additive Langmuir mode). That is, P is equal to the sum of a first term, representing the Henry mode, and the second term, for representing the Langmuir mode, which is a function of p_2:

$$P = k_D D_D[1+FR/(1+Kp_2)] \quad (3)$$

$$F = D_C/D_D,\ R = C_C'K/k_D$$

Here, P is the permeability coefficient, k_D is the solubility coefficient for Henry's law, D_D and D_C are the diffusion coefficients for Henry-type and Langmuir-type diffusions, C_C' is the saturated amount of oxygen reversibly bound to the binding site or the fixed carrier, K is the oxygen-binding and -dissociation equilibrium constant, and p_2 is the upstream gas pressure.

The effect of $p_2(O_2)$ on P_{O_2} was analyzed by using Eq. 3; that is, P_{O_2} was plotted against $1/(1+Kp_2)$ (Fig. 5). The plots show a linear relationship. The oxygen permeability in the membrane containing the complex as a fixed carrier can be explained in terms of the sum of the Henry mode attributed to the matrix and the Langmuir mode attributed to the fixed carrier, that is, the dual-mode theory.

The time lag (θ) for the oxygen permeation also depended on $p_2(O_2)$, as it shown in Fig. 6, in the same manner as the permeation coefficient. This behavior indicates that oxygen clearly interacts with the CoS complexed to the POMP membrane. This is further

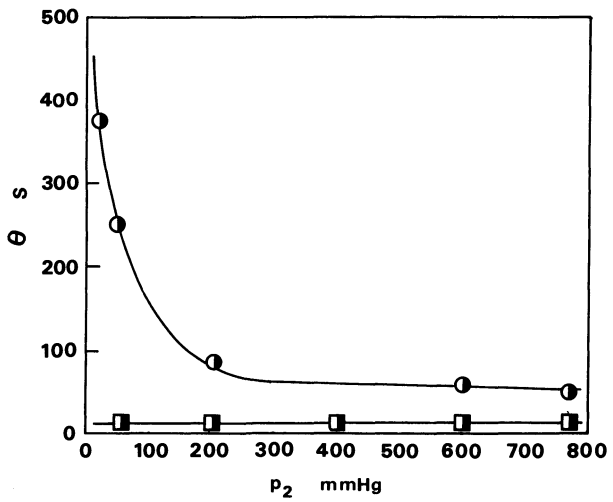

Fig. 6. Effect of upstream gas pressure on time lag for the POMP-CoS membrane. Oxygen: at ◑: 30°C, Nitrogen: at ◨: 30°C.

supported by the result that the value for the nitrogen permeation in the membrane containing the carrier is indepedent of the upstream gas pressures.

Although dual mode transport due to partial immobilization[10] has been reported for carbon-dioxide permeation in glassy polymers, the present authors have here verified the dual-mode transport by using a much simpler system.

This work was partially supported by a Grant-in-Aid from the Ministry of Education, Science and Culture.

References

1) a) W. Pusch and A. Walch, *Angew. Chem., Int. Ed. Engl.*, **10**, 81 (1982); b) W. J. Schell, *J. Membr. Sci.*, **22**, 217 (1985).

2) a) E. Tsuchida, *J. Macromol. Sci., Chem.*, **A13**, 545 (1979); b) E. Tsuchida, H. Nishide, M. Yuasa, E. Hasegawa, Y. Matsushita, and K. Eshima, *J. Chem. Soc., Dalton Trans.*, **1985**, 275; c) E. Tsuchida, *Ann. N.Y. Acad. Sci.*, **446**, 429 (1985); d) E. Tsuchida, *Chem. Eng. News, 14*, **1985**, 42.

3) I. C. Roman and I. W. Baker, Eur. Patent 0098731 (1983).

4) H. Nishide, M. Kuwahara, M. Ohyanagi, Y. Funada, H. Kawakami, and E. Tsuchida, *Chem. Lett.*, **1986**, 43.

5) H. Nishide, M. Ohyanagi, O. Okada, and E. Tsuchida, *Macromolecules*, **19**, 494 (1986).

6) R. S. Drago and K. J. Balkus, Jr., *Inorg. Chem.*, **25**, 716 (1986).

7) R. H. Bailes and M. Calvin, *J. Am. Chem. Soc.*, **69**, 1886 (1947).

8) a) D. Wohrle, H. Bohlen, and C. Aringer, *Makromol. Chem.*, **185**, 669 (1984); b) E. Tsuchida, K. Honda, and S. Hata, *Bull. Chem. Soc., Jpn*, **49**, 868 (1976).

9) T. Beugelsdijk and R. S. Drago, *J. Am. Chem. Soc.*, **97**, 6466 (1975).

10) a) D. R. Paul and W. J. Koros, *J. Polym. Sci., Phys. Ed.*, **14**, 675 (1976); b) D. R. Paul, *Ber. Bunsenges. Phys. Chem.*, **83**, 294 (1979).

Kinetics and Mechanism of Acid-Catalyzed Oxidation of Substituted Toluenes by Pyridinium Fluorochromate

Bharati BHATTACHARJEE, Manabendra Nath BHATTACHARJEE,* Mitra BHATTACHARJEE, and Apurba Krishna BHATTACHARJEE*,†
Department of Chemistry, North-Eastern Hill University, Shillong 793 003, India
†Department of Chemistry, Lady Keane Girls' College, Shillong 793 001, India
(Received November 25, 1985)

The kinetics of oxidation of substituted toluenes by pyridinium fluorochromate(VI) (PFC), $C_5H_5N\overset{+}{H}CrO_3F^-$, in aqueous acetic acid, in the presence of perchloric acid, have been studied. The main products are the corresponding aldehydes. While each of the oxidation is first order with respect to the oxidant, the rate is almost independent of the substrate concentration. The reactions depend on the first power of the concentration of acid. A kinetic isotope effect, $k_H/k_D=5.4$ at 30 °C, was observed. Electron-releasing groups were found to moderately facilitate the reaction, whereas the electron-withdrawing groups were found to have a retardation effect. Correlation with σ value yielded a ρ value of -2.0. The reaction does not induce polymerization of acrylonitrile. The effects of temperature and solvent compositions were studied and activation parameters evaluated. These and related data suggest that the initial reaction involves hydrogen abstraction forming an intermediate which subsequently produces the corresponding aldehyde.

Though the kinetics and mechanism of oxidation reactions using chromium(VI) oxidants are fairly well studied,[1–5] yet these reagents do not prove to be very satisfactory especially when some specific oxidations like oxidation of hydrocarbons, alcohols, thioethers etc. are desired. In recent years significant improvements were achieved by the use of pyridinium chlorochromate(VI) (PCC).[6–18] Of late, another effective chromium(VI) oxidant, pyridinium fluorochromate(VI) (PFC), $C_5H_5\overset{+}{N}HCrO_3F^-$, has been reported[19] which has several additional advantages over PCC, e.g., less acidity, selective oxidations under mild conditions, better solubility in nonaqueous solvents etc.

The oxidation of hydrocarbons is considerably less well understood and always present a mechanistic puzzle. In continuation with our interest in this subject,[20,21] we report in this investigation a detailed study of the kinetics and mechanism of the oxidation of side chains of mononuclear aromatic hydrocarbons such as toluene and substituted toluenes to their corresponding aldehydes. The common oxidizing agents (a) completely destroy the compound, (b) attack the nucleus, or (c) effect electrophilic substitution. The objective of the present investigation is not only to develop methods for oxidation of alkylarenes to the important aldehydes but also to get an insight to the reaction pathway.

Experimental

Materials. All the substrates were E. Merck grade and were purified by chromatography over alumina followed by distilation or recrystallization. Acetic acid (E. Merck) was distilled before use (bp 116 °C). Perchloric acid was a 'Baker analyzed' sample. $ArCD_3$ were prepared by the lithium aluminum deuteride reduction of their trichloromethyl derivative using the procedure reported earlier.[22] The materials used in the kinetic runs were repurified by chromatography and was shown to contain an insignificant amount of unlabeled, monodeuterio-, or dideuteriotoluenes, by the NMR spectra. Pyridinium fluorochromate (PFC) was synthesized by the method described in the literature.[19] The purity was checked by IR and UV analyses. The ionic strength of the medium was maintained constant by using sodium perchlorate, a Fluka purum product.

Kinetic Measurements. Both the substrate and oxidant solutions were thermostated and 30 °C for 3 h under nitrogen, and then mixed in equal volumes. The reaction mixture was homogeneous throughout the duration of the reaction. The reactions were followed by monitoring the absorption band at 444 nm, using a UV-VIS Beckmann spectrophotometer. This wavelength is the maximum absorption due to PFC, the absorption due to other reaction species being negligible. The reactions were performed under pseudo-first-order conditions by maintaining a large excess (10 times or greater) of the toluenes over PFC. Computations of the rate constants were made from the plot of log [PFC] against time. All infrared measurements were recorded on a Perkin-Elmer model 297 spectrophotometer and all NMR spectra were recorded on an EM-390 (Varian) 90-MHz spectrometer.

Product Analysis. The reactions were carried out in a manner similar to the kinetic experiments (using an excess of the substrate) and were allowed to proceed to completion in an atmosphere of nitrogen. The reaction mixture was diluted with ice-water saturated with sodium chloride, and was extracted several times with ether. The ether extract was washed with water, dried over anhydrous $MgSO_4$, and evaporated under reduced pressure. The material thus obtained was chromatographed over alumina, the toluene and xylenes being eluted with petroleum ether, and the corresponding aldehydes being eluted with 1:3 ether–petroleum ether. In each case, only toluene, xylenes, and the corresponding aldehydes were isolated. The aldehydes were characterized as the 2,4-dinitrophenylhydrazones, further characterized by using a standard method,[23] and confirmed by IR analyses.

Results and Discussion

Stoichiometry. Reaction mixtures containing an

Table 1. Rate Data for Oxidation of Toluene and Xylenes at 30±0.1 °C[a]

[Substrate]	[PFC]	[$HClO_4$]	$10^4 \times k_1/s^{-1}$			
M†$\times 10^{-3}$	M$\times 10^{-4}$	M	*p*-Xylene	*o*-Xylene	*m*-Xylene	Toluene
1.0	1.0	0.15	5.03	3.16	2.38	1.45
5.0	1.0	0.15	5.70	3.83	2.91	1.87
10.0	1.0	0.15	6.06	4.11	3.27	2.29
50.0	1.0	0.15	6.78	4.74	3.85	2.80
100.0	1.0	0.15	7.43	5.23	4.36	3.33
10.0	2.0	0.15	6.14	4.24	3.17	2.51
10.0	3.0	0.15	6.31	4.38	3.48	2.34
10.0	4.0	0.15	6.40	4.19	3.26	2.27
10.0	5.0	0.15	6.15	4.23	3.14	2.16
10.0	1.0	0.10	4.10	2.70	2.15	1.53
10.0	1.0	0.20	8.18	5.60	4.25	3.10
10.0	1.0	0.25	10.20	7.10	5.31	3.85
10.0	1.0	0.30	12.02	8.25	6.60	4.55
10.0	1.0	0.15	5.38[b]	3.43[b]	2.60[b]	1.63[b]
10.0	1.0	0.15	6.75[c]	4.80[c]	4.01[c]	2.98[c]
10.0	1.0	0.15	7.45[d]	5.50[d]	4.65[d]	3.67[d]

a) [$NaClO_4$]=0.155 M; HOAc: H_2O=95: 5 (v/v). b) 25 °C; c) 35 °C; d) 40 °C; (error limit: ±0.1 °C). †1 M=1 mol dm^{-3}.

excess of the oxidant (PFC) were allowed to react to completion under a nitrogen atomosphere at 30 °C and then analyzed spectrophotometrically for unchanged PFC and also by iodometric determination of the unreacted chromium(VI). The results gave a ratio of substrate and oxidant as 1:2, according to the equation:

$$XC_6H_4CH_3 + 2Cr^{6+} + H_2O \longrightarrow XC_6H_4CHO + 2Cr^{4+} + 4H^+ \quad (X=CH_3, OCH_3, Cl, Br). \quad (1)$$

This equation corroborates to a two-electron transfer and is in agreement with the proposal of Brown et al.,[24] who recently reported that the exact nature of the reaction product of PFC is not known. The idea is also supported from a recent report.[25] About 75—80% of the hydrocarbons were oxidized and about 80—85%, based on the hydrocarbons consumed, of the corresponding aldehydes were obtained.

Kinetic Results. The reactions were found to be first order with respect to the oxidant and near zero order in substrate (Table 1). The observed small but steady increase in the rate constant values for the hydrocarbons with increasing concentrations of the substrate and a plot of log k_1 against substrate concentrations show that the rates increase in very small fractions with the sequential increase in substrate concentration. This implies a probable complex formation between the substrate and the oxidant.

The order with respect to perchloric acid was determined in the same way (Table 1). A plot of log k_1 against log [H^+] gave a linear relationship with a slope of nearly unity. An attempt was made to correlate the rate data with the Hammett acidity function (H_o). Using H_o values from Wiberg's data,[5] plots of log k_1 against H_o gave slopes far different from unity. Thus under the present experimental conditions, it seemed appropriate to correlate the rates of these reactions with [H^+] rather than with H_o.

Table 2. Effect of Solvent Compositions at 30.0±0.1 °C[a]

HOAc : H_2O	$10^4 \times k_1/s^{-1}$		
%; v/v	*p*-Xylene	*o*-Xylene	*m*-Xylene
80 : 20	1.01	0.98	0.82
85 : 15	1.62	1.22	1.06
90 : 10	3.18	2.30	2.01
95 : 5	6.06	4.11	3.27

a) [Xylenes]=10$\times 10^{-3}$ M; [$HClO_4$]=0.15 M; [PFC]=1$\times 10^{-4}$ M; [$NaClO_4$]=0.155 M.

Table 3. Kinetic Isotope Effect at 30.0±0.1 °C[a]

Substrate	$10^5 \times k_1/s^{-1}$		
	$ArCH_3$ (k_H)	$ArCD_3$ (k_D)	k_H/k_D
p-$CH_3C_6H_4$-	60.6	11.0	5.4
o-$CH_3C_6H_4$-	41.1	8.0	5.1
m-$CH_3C_6H_4$-	32.7	6.0	5.4

a) [Substrates]=10$\times 10^{-3}$ M; [PFC]=1$\times 10^{-4}$ M; [$HClO_4$]=0.15 M; [$NaClO_4$]=0.155 M; HOAc : H_2O=95 : 5 (v/v).

The rates of the reactions were found to be unaffected by changes in the ionic strength of the medium. Similar observations were also reported earlier.[26-28] The oxidation processes were also studied in solutions containing varying proportions of acetic acid and water (Table 2). The reaction rate decreases with increase in dielectric constant of the medium suggesting that more polar solvents may require longer reaction time for the oxidation.[15] A plot of log k_1 against the inverse of dielectric constants of the media is a straight line with positive slope and implies the occurrence of an interaction between a dipole and a positive ion.[29]

A kinetic isotope effect, k_H/k_D=5.4, was observed (Table 3), indicating that the rate-determining step

Table 4. Effect of Substituents at 30.0±0.1 °C

[Substrate] 0.01 M	Substituted toluene $10^4 \times k_1/s^{-1}$	k/k_H
p-Methoxy	19.70	8.60
p-Methyl	6.06	2.64
m-Methyl	3.27	1.43
H	2.29	1.00
p-Chloro	0.81	0.35
p-Bromo	0.74	0.32
m-Chloro	0.38	0.16

[PFC]=1×10^{-4} M; [$HClO_4$]=0.15 M; [$NaClO_4$]=0.155 M; HOAc : H_2O=95 : 5 (v/v).

Table 5. Activation Parameters for the Oxidation Reactions

Substrate	ΔH^* kJ mol^{-1}	$-\Delta S^*$ J mol^{-1} K^{-1}	ΔG^* kJ mol^{-1}
Toluene	39.6	184.0	95.3
p-xylene	14.9	257.5	92.9
o-xylene	19.9	244.3	93.9
m-xylene	14.9	245.0	94.2

Error limit for ΔH^*, ΔS^*, and ΔG^* (at 303 K) are ±2.5 kJ mol^{-1}, ±4.0 J mol^{-1} K^{-1}, and ±3.0 kJ mol^{-1} respectively.

involved the cleavage of the carbon-hydrogen bond of the methyl group attached to the arene ring.

The oxidation was studied at different temperatures (vide Table 1) and the activation parameters have been evaluated (Table 5).

The effect of substituents was also determined (Table 4). A plot of the logarithm of the relative rates of reaction against the Hammett σ values gave a fair fit to a straight line with a slope of approximately −2.0 (Fig. 1).

The oxidation reaction, in an atmosphere of nitrogen, failed to induce polymerization of acrylonitrile. Further, no signal of radicals could be detected in the ESR spectra of each of the reactions carried out in a flow system (recorded on an E-4, Varian, EPR spectrometer). In control experiment without hydrocarbon, the concentration of PFC did not change.

The observed acid dependence of the reaction suggests that the reaction may be one between the alkylarenes and a protonated species of chromium(VI). This view is further supported[27] by the observance of linear plot of log k_1 against inverse of dielectric constant, and is in accord with the involvement of such species well established in chromium trioxide oxidation.[5,30] Again the observed ρ value (−2.0) does neither conclusively opt for a radical nor an ionic pathway. However, it implies that transfer of hydrogen nucleus is the essence of the mechanism of such reactions. The near constancy of the free energy of activation shows that the same mechanism is operative in all these oxidation processes.

Moreover, the order with respect to the substrate

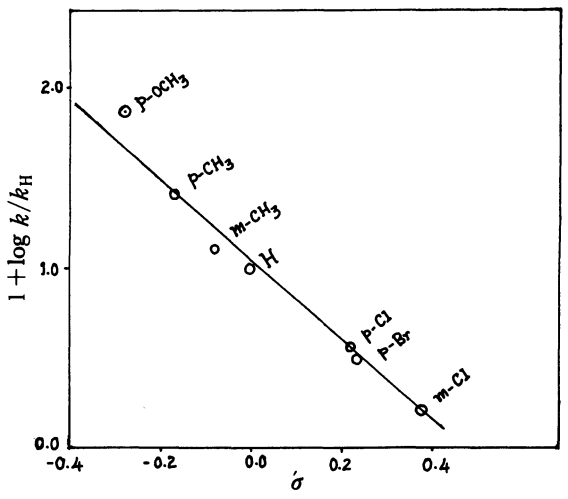

Fig. 1. Plot of log k/k_H against σ values for the oxidation of substituted toluenes at 30 °C (Hammett Plot).

(Table 1) is almost but not quite zero, suggesting a multistep reaction sequence via the formation of an intermediate complex between the substrate and PFC.

Though the reaction failed to give any significant ESR signal and to induce polymerization of acrylonitrile, the hydrogen abstraction mechanism cannot be ruled out as the initially-formed radical would be expected to react instantaneously with the Cr^{5+} species formed in the initial step. This observation is known to occur in the oxidation of saturated hydrocarbons by Cr(VI) compounds.[5,30] Again the large negative reaction constants (also ρ value) together with the substantial deuterium isotope effect indicate a considerable carbonium ion character in the transition state.

Thus the oxidation of the aromatic nuclei would appear to involve hydrogen transfer through an intermediate complex based on the following two mechanism:

(i) The intermediate complex consisting of a radical and a Cr^{5+} species or a carbonium ion and a Cr^{4+} species (Sceheme 1). The ambiguity regarding the intermediate could be overcome by considering the complex as a resonance hybrid in which the carbon atom has both radical and carbonium ion characters. This type of intermediate has also been reported earlier.[21,31-34]

(ii) Alternatively, it could be via the formation of an Etard type[35] complex as the intermediate (Scheme 2). Though no precipitate of the complex was observed yet it may be argued that owing to immediate hydrolysis no isolation of the intermediate was possible. Similar observation has been reported earlier in the chromium trioxide oxidation in aqueous acetic acid solution.[36]

However, as the intermediate complex could not be isolated, neither magnetic susceptibility study nor ESR study of the complex could be performed.

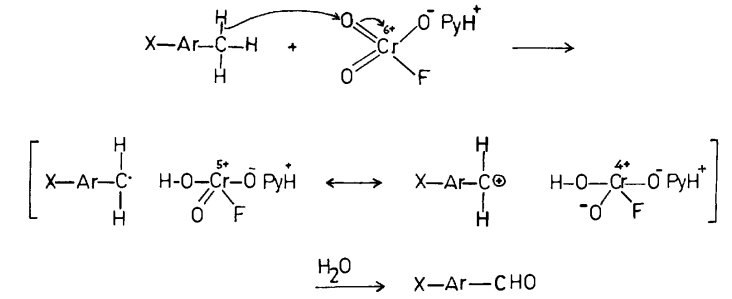

Scheme 1.

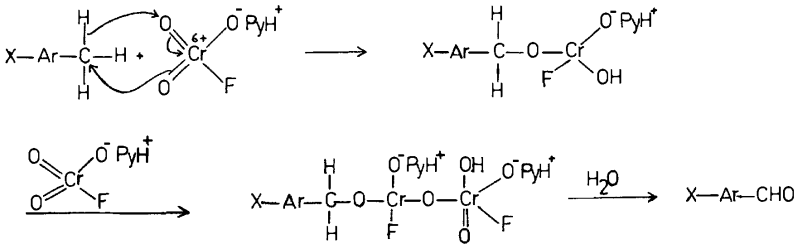

Scheme 2.

Moreover, the formation of Etard complex is not very much favorable in acetic acid medium.[35] Thus it seems reasonable to believe that the oxidation mechanism shown in Scheme 1 is the likely one involved in the present cases. Since the hybrid would have a lower energy than either of the two pairs, the stability of the intermediate could be expected. A large negative entropy of activation obtained in the present study may also support the view.

So the overall oxidation of the substituted toluenes would appear to involve initial electron transfer from the substituent group of the side chain hydrocarbon to the oxidant and the subsequent reaction of the resulting intermediate with the nucleophiles in the reaction solution to the formation of the products.

The authors wish to thank the Instrumentation Centre of the Central Research School for Chemistry of the Hungarian Academy of Sciences, Budapest, for recording the ESR spectra. One of us (A.K.B.) expresses his gratitude to Miss A. M. Marbaniang, Principal, Lady Keane Girls' College, Shillong for granting permission to carry out the work.

References

1) F. H. Westheimer, *Chem. Rev.*, **45**, 419 (1949).
2) G. T. E. Graham and F. H. Westheimer, *J. Am. Chem. Soc.*, **80**, 3030 (1958).
3) J. O. Edwards, *Chem. Rev.*, **50**, 455 (1952).
4) K. B. Wiberg and T. Mill, *J. Am. Chem. Soc.*, **80**, 3032 (1958).
5) K. B. Wiberg, "Oxidation in Organic Chemistry," Part A, Academic Press, New York (1965), pp. 71, 98—105.
6) E. J. Corey and G. W. J. Fleet, *Tetrahedron Lett.*, **1973**, 4499.
7) J. R. Holum, *J. Org. Chem.*, **26**, 4814 (1961).
8) A. Bowers, T. G. Hatshall, E. R. H. Jones, and A. J. Lemin, *J. Chem. Soc.*, **1953**, 2555.
9) J. C. Collins, W. W. Hess, and F. J. Frank, *Tetrahedron Lett.*, **1968**, 3363.
10) H. H. Sisler, W. C. L. Ming, E. Metter, and F. R. Hurley, *J. Am. Chem. Soc.*, **75**, 446 (1953).
11) F. S. Guziec, Jr. and F. A. Luzzio, *Synthesis*, **1980**, 691.
12) J. C. Collins and W. W. Hess, *Org. Synth.*, **52**, 5 (1972).
13) E. J. Corey and G. Schmidt, *Tetrahedron Lett.*, **1979**, 399.
14) G. I. Poos, G. E. Aoth, R. E. Beyber, and L. H. Sarett, *J. Am. Chem. Soc.*, **75**, 425 (1953).
15) E. J. Corey and J. W. Suggs, *Tetrahedron Lett.*, **1975**, 2647.
16) E. J. Corey and D. L. Boger, *Tetrahedron Lett.*, **1978**, 2461.
17) W. G. Dauben and D. M. Michno, *J. Org. Chem.*, **42**, 682 (1972).
18) G. Piancatelli, A. Scettri, and M. D'Auria, *Tetrahedron Lett.*, **1977**, 2199.
19) M. N. Bhattacharjee, M. K. Chaudhuri, H. S. Dasgupta, N. Roy, and D. T. Khathing, *Synthesis*, **1982**, 588.
20) A. K. Bhattacharjee and M. K. Mahanti, *Int. J. Chem. Kinet.*, **14**, 1113 (1982); *Indian. J. Chem.*, **22B**, 74 (1983); *React. Kinet. and Cat. Lett.*, **22**, 227 (1983); *Bull. Korean Chem. Soc.*, **4**, 102 (1983); *Gazz. Chim. Ital.*, **1983**, 113; *Bull. Soc. Chim. Fr.*, **1983**, I-270.
21) B. Bhattacharjee, M. N. Bhattacharjee, M. Bhattacharjee, and A. K. Bhattacharjee, *Int. J. Chem. Kinet.*, **17**, 629 (1985).
22) R. F. Nystrom and C. R. A. Berger, *J. Am. Chem. Soc.*, **80**, 2896 (1958).
23) A. I. Vogel, "A Text Book of Practical Organic Chemistry," ELBS & Longman, London (1958), p. 758.
24) H. C. Brown, C. Gundu Rao, and S. U. Kulkarni, *J. Org. Chem.*, **44**, 2809 (1979).
25) K. Rajasekharan, T. Baskran, and C. Gnanasekaran, *J. Chem. Soc., Perkin Trans. 2*, **1984**, 1183.
26) G. V. Bakore, K. K. Banerjee, and R. Shankar, *Z. Phys. Chem. (Frankfurt)*, **45**, 129 (1965).
27) K. K. Banerjee, *J. Chem. Soc., Perkin Trans. 2*, **1978**,

639; *Bull. Chem. Soc. Jpn.*, **51**, 2732 (1978).
28) M. N. Bhattacharjee, M. K. Chaudhuri, and H. S. Dasgupta, *Bull. Chem. Soc. Jpn.*, **57**, 258 (1984).
29) E. S. Amiss, "Solvent Effects on Reaction Rates and Mechanism," Academic Press, New York (1967), p. 42.
30) K. B. Wiberg and G. Fester, *J. Am. Chem. Soc.*, **83**, 423 (1961).
31) J. Roček, *Tetrahedron Lett.*, **1962**, 135.
32) N. L. Weinberg and H. R. Weinberg, *Chem. Rev.*, **68**, 449 (1968).
33) O. C. Musgrave, *Chem. Rev.*, **69**, 499 (1969).
34) R. N. Adams, *Acc. Chem. Res.*, **2**, 175 (1967).
35) W. H. Hartford and M. Darrin, *Chem. Rev.*, **58**, 1 (1958).
36) R. Slack and W. A. Waters, *J. Chem. Soc.*, **1949**, 599.

 © 1986 The Chemical Society of Japan Bull. Chem. Soc. Jpn., 59, 3223—3228 (1986)

Vibrational Spectrum of 2-Aminopyrazine

Arun Kumar KALKAR* and Comakshi C. ARS
Department of Chemical Technology, University of Bombay, Bombay 400 019, India
(Received January 16, 1986)

Infrared and polarized laser Raman spectra in the solid phase and in the solution phase in different solvents have been obtained within the spectral region between 4000 and 200 cm^{-1} and analyzed for the purpose of vibrational assignments. The impact of intermolecular hydrogen bonding on amino group frequencies has been discussed in length. The fundamentals arising out of aromatic nucleus in particular various assignments are consistent with predicted spectral changes due to the presence of strong electron-activating amino group resulting in considerable perturbation of the vibrational levels of "parent" molecule pyrazine.

Out of three diazabenzenes the optical spectroscopy of pyrazine has received considerable attention over the years. The pioneering work on vapor-phase ultraviolet spectrum by Innes et al.[1] is now well-known for the assignments of different transitions in n-π^* electronic transition. Nearly an ambiguous vibrational analysis of pyrazine has been also proposed by Innes et al.[2] and others.[3–13] Normal coordinate analysis of pyrazine has been carried out by many authors.[6,14,15] A complete and coherent vibrational spectral studies has been reported by Zarembowitch et al.[16] for pyrazine which supercedes all the previous reported work. By contrast, the spectroscopic studies of substituted pyrazines have received much less attention except the work on chloro-[17,18] and methylpyrazines.[18]

The present investigation is a part of the extensive program of work being undertaken on spectroscopic studies of various mono- and di-substituted pyrazines. Here the basic purpose of such studies is to study the effects of various electronic resonance interactions induced by different electron-activating and -deactivating substituent groups on electronic and vibrational transitions in pyrazine.

This paper is an endeavor to make precise assignments of the fundamental vibrational modes of 2-aminopyrazine, first time, based on our observations of the infrared and polarized Raman spectra of the solid and solution phases.

An introduction of an electron-activating group NH_2, at ortho position in pyrazine is expected to enhance the various electronic resonances by delocalizing and to some extent by relocalizing the (σ, π, n) electrons between parent molecule and substituent, resulting in the energy redistribution in various vibrational transitions. In the light of these electronic resonance interactions the assignments of different fundamentals have been made. Along with the infrared study of its isotopic modification containing ND_2 group, spectra with state of depolarization of Raman lines have been used in support of the assignments. In addition to these, the data from various papers and in particular by Innes et al.[2] and Zarembowitch et al.[16] on pyrazine,[4,8,11] and by Evans[19] and Tsuboi[20] on aniline have been extensively used.

Experimental

Chemically pure sample of 2-aminopyrazine obtained from M/s. Fluka AG was used without further purification. The solvents CCl_4, CS_2, and $CHCl_3$ used in recording infrared spectra, were of spectroscopic grade.

The infrared spectra of the sample in the solid state using KBr matrix and nujol mull were recorded. Various spectra were recorded carefully by changing the sample, and KBr powder mixture ratio and pressure used to prepare the KBr disc. The average peak values of different scan are used which were definitely differing by 2 to 3 cm^{-1}. Spectra were also recorded of polycrystalline form, formed on sodium chloride disc by using solvent evaporation method. The solution spectra in CCl_4, CS_2, and $CHCl_3$ were recorded at various concentrations using 0.1 mm path length solvent compensated liquid cells.

The isotopic exchange at amino group was obtained by various repeated exchange drying cycles, in a moisture-free nitrogen atmosphere by using 99.4% deuterated water (supplied by Bhabha Atomic Research Centre, Bombay), to obtain for the more complete deuteration. Absolute care was taken during deuterated sample mull preparation and spectra scan to avoid the rehydrogenation.

The maximum isotopic conversion, about 80%, was obtained by monitoring the relative intensity ratio of ND_2 bending mode to NH_2 bending mode.

All infrared measurements were carried out on a polystyrene film run calibrated Perkin-Elmer 397 spectrophotometer in the region 4000—400 cm^{-1}. A nicolet NIC-170SX (Model NIC-170SX) Fourier Transform interferometer was employed to scan the far infrared spectra in the region 400—200 cm^{-1}.

The Raman spectra were recorded on a Jobin Yvon Raman spectrophotometer equipped with double monochromator system consisting of concave halographic gratings with 2000 grooves per mm and one meter focal length. Spectra Physics Model 164 Ar^+ laser excitation at 488.0 nm was used as a excitation source. Calibration was done with the plasma lines from the laser.[21] Spectral widths of 3—5 cm^{-1} were used in recording the Raman spectra. The uncertainty of determination of wavenumber of around ±3 cm^{-1} in, infrared as well as in Raman spectra.

The samples were in the form of solid, sealed in glass capillaries. Polarization measurements were made by rotating the half-wave plate in two different, mutually perpendicular orientation.

Relatively low solubility, less than 25%, of 2-aminopyrazine in usual Raman solvents posed a major problem

Table 1. Correlation Diagram

Modes	Pyrazine D_{2h}	C_{2v}	2-Aminopyrazine C_s
1, 2, 6a, 8a, 9a	A_g (Raman)	A_1[IR, Raman (P)]	A′[IR, Raman(P)]
12, 13, 18a, 19a	B_{1u} (IR)		
3, 6b, 7b, 8b	B_{2g} (Raman)	B_1[IR, Raman(dp)]	
14, 15, 19b, 20b	B_{3u}(IR)		
10a	B_{1g} (Raman)	A_2[Raman (dp)]	A″[IR, Raman(dp)]
16a, 17a	A_u(Inactive)		
4, 5	B_{3g} (Raman)	B_2[IR, Raman(dp)]	
11, 16b	B_{2u} (IR)		

The authors assign the modes, 3, 10a, 13 to (C–X) vibrations in 2-aminopyrazine.

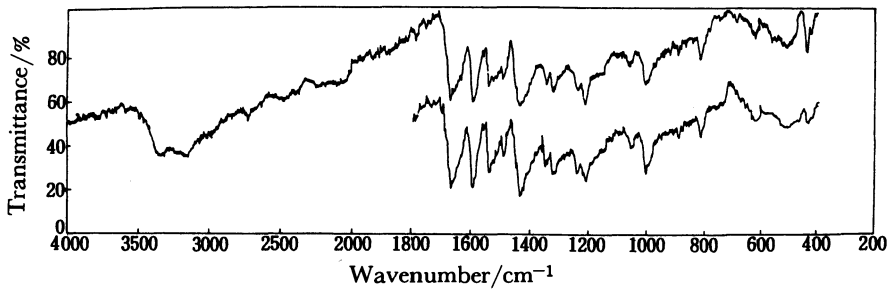

Fig. 1. Infrared spectrum of 2-aminopyrazine in KBr matrix.

to record solution phase Raman spectra. Finally, water was found to be the best Raman solvent in present case. Thus, essentially to ascertain the polarization character of fundamental vibrations obtained in solid phase, the solution phase polarized Raman spectra were recorded in aqueous solution.† Although the degree of polarization is high in aqueous phase rather than the solid phase, the polarizability confirmation in aqueous solution is the same as in the solid state. The uncertainty of measurement in depolarization ratio is of the order of ±0.02 in both the cases.

Results and Discussion

Molecular point group of 2-aminopyrazine has been reduced to C_s, due to inclusion of the nonplanar amino group, from its parent molecule which has D_{2h} point group and the vibrational fundamental modes become active as shown by diagram of correlation of point groups D_{2h}, C_{2v}, and C_s (Table 1).

The total thirty normal vibrations which are active both in the infrared and Raman spectra are divided into two categories:

i. 6 Vibrations of the NH_2 group

ii. 24 Vibrations of the aromatic nucleus

which reduces to 3a′+3a″ and 17a′+7a″ respectively. The Wilson[22] notation is used to label the various

†Few solution phase Raman spectra scans, were obtained on Spex Ramalog 1401 spectrometer from Spectroscopic Division, BARC, Bombay.

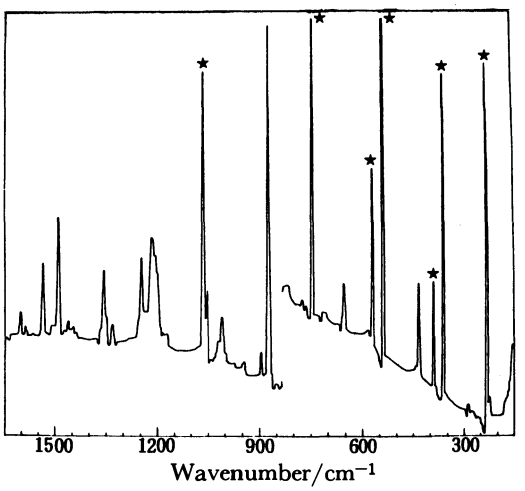

Fig. 2(a): Raman Spectrum of 2-aminopyrazine. Powder in capillary tube. Argon ion 480 nm excitation at 50 mW. Spectral slit width 5 cm⁻¹. ★ Plasma lines. (b): Raman spectrum of 2-aminopyrazine. Recorded on similar conditions as in Fig. 2a.

modes. As per symmetry selection rules, while the species a′ should give rise to polarized Raman lines, the species a″ will have depolarized Raman lines. However, exclusively on the basis of our depolarization measurement, it is interesting to note that some modes obey C_{2v} symmetry selection rules.

To facilitate the proper comparison in this paper, we follow the same set of molecular axis used by Innes et al.[2] for pyrazine, i.e. *Y* axis is taken perpendicular to the molecular plane and the *Z* axis through the two isoelectronic nitrogen atoms.

The infrared spectra recorded in KBr matrix and Raman spectra are reproduced in Figs. 1, 2(a), 2(b), and 3. The experimental observations and assignments are listed in Tables 2 and 3. Predominantly, the various band shapes have been used to relate the corresponding bands recorded in different phases to each other and listed in Table.[††] In following details, the different band values are from spectra recorded in KBr matrix.

Vibrations of the Amino Group: The spectra recorded at different concentrations clearly show that 2-aminopyrazine exhibits the dimer formation (Fig. 4) owing to intermolecular hydrogen bonding similar to 2-aminopyridine.

In general, it has been well established that vibrational spectra are significantly influenced by hydrogen-bond formation. This is particularly noticeable for stretching modes which are displaced to lower frequency upon association. This lowering of frequencies may be attributed to a decrease in force constant arising out of expected increased bond lengths upon association.[24]

All of the six normal fundamental vibrational modes arising out of the $-NH_2$ group and its isotopic modification containing the $-ND_2$ group motions have been assigned and listed in Table 2 along with aniline and 2-aminopyridine for comparison.

The 3500—3400 and 3250—3150 cm^{-1} regions shown two discrete sets of broad band profiles. Clearly, the bands at 3410 and 3510 cm^{-1} are due to symmetric (ν_s) and antisymmetric (ν_{as}), N-H stretches. It is reasonable to assume that the other two bands at 3165 and 3340 cm^{-1} are principally due to similar modes of

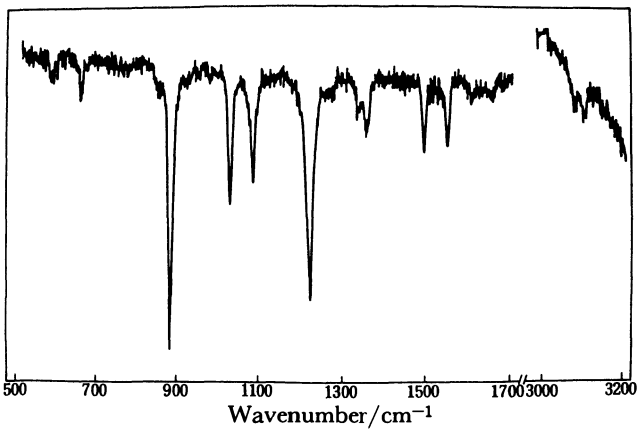

Fig. 3. Solution phase (in H_2O) Raman spectrum of 2-aminopyrazine.

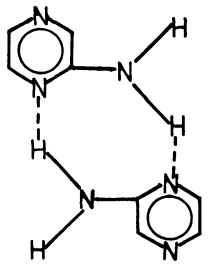

Fig. 4. 2-Aminopyrazine dimer.

Table 2. Internal Vibrational Frequencies (cm^{-1}) of NH_2 Group in 2-Aminopyrazine

Mode	Aniline Ref. 19	Aniline Ref. 20	2-Aminopyridine Ref. 25, 26	2-Aminopyrazine CS_2	CCl_4	$CHCl_3$	Nujol	KBr	Raman	ND_2AP in nujol
NH_2-Asymm.	3485	3481	3510(M)	3516	3516	3510	—	3510(M)	—	2520(M)
stretch	3440(NHD)	—	3335(D)	—	3347	3342	3330	3340(D)	3327(D)	2438(D)
	2592(ND_2)	—								
NH_2-Symm.	3401	3395	3420(M)	3415	3410	3402	—	3410(M)	—	2485(M)
stretch	2535(NHD)	—	3180(D)	—	3150	3165	3147	3165(D)	3165(D)	2400(D)
	2485(ND_2)	—								
NH_2 scissoring	1618	1619	1634(D)	—	—	1662(D)	—	1662(D)	—	1168(ND_2)
	1441(NHD)	—	1621(M)	—	—	1652(Sh)	—	1652(M)	1650R(L)	1335(NHD)
	1152(ND_2)	1150(ND_2)	—			(M)				
NH_2 twisting	1054	1115	1118	—	—	1200	—	1210	1213	1070(ND_2)
	—	797(ND_2)							1200(Sh)	
									1215R(L)	
NH_2 wagging	670	700	667	—	—	696	—	685	—	482(ND_2)
	420(ND_2)	600(ND_2)								
NH_2 torsion	440/2	—	435/2	—	—	430/2	224	218	218	—
	216.5†								212R(L)	

M=Monomer; D=Dimer; Sh=Shoulder; R(L)=Raman liquid phase in H_2O.
†Ref. 32.

††Detail table is available on request.

vibration in associated molecules. The corresponding bands in $-ND_2$ species are at 2485 and 2520 cm^{-1}, and 2400 and 2438 cm^{-1} for monomer and dimer respectively. In comparison to 2-aminopyridine[25,26] the large shift in bonded symmetric stretching frequency in present case may be due to the increased $=NH_2^+$ electronic nature[27] of the molecule resulting in increased strength of hydrogen bonding.[24] An advanced anharmonicity of 103 cm^{-1} is observed and calculated[28] bonded symmetric stretching viration resulting in extensive ∠HNH angle (143°)[29] opening very well reflects the stronger intermolecular hydrogen bond in present case.

Obviously, the effects of this strong intermolecular bond formation will be most pronounced on the various valence angle deformation modes rather than the resulting electronic activity out of animo group. Although, the enhanced electron attracting character of aromatic nucleus also contributes in raising the frequency and intensity markedly. The established range for NH (δ) scissoring mode is 1650—1590 cm^{-1} and in aniline[19,20] and 2-aminopyridine[25,26] this mode has been assigned to a band at 1620 cm^{-1}. One of the strongest band in present spectrum at 1662 cm^{-1}, with a shoulder at 1650 cm^{-1} has been assigned to this mode. The corresponding ND_2 species mode is found at 1168 cm^{-1}.

Under the same considerations, given for the scissoring mode, the other low frequency modes of the amino group, NH_2 twisting and wagging modes are assigned to the bands at 1210 and 685 cm^{-1} which shift to 1070 and 480 cm^{-1} respectively in the deuterated analog. The corresponding Raman band for twisting mode is at 1213 cm^{-1} and is polarized and weak in intensity.

The band at 218 cm^{-1} with a corresponding weak depolarized Raman band at 218 cm^{-1} is assigned to the low energy torsional motion around the C–N bond with its first overtone located at 431 cm^{-1}. The present torsional frequency agreement, with the value for 2-aminopyridine,[26,30] aniline,[31,32] and *m*-halo-substituted anilines[33] is excellent, and virtually localize the vibrational mode around 200—220 cm^{-1} in these molecules.

A particular aspect concerning the effect of the general anharmonicity induced by torsional motion of the amino group in present case has been visualized in enhanced intensity of combination bands with different amino internal deformation modes which even may contribute to frequency shifts to these characteristic group fundamentals.

Aromatic Nucleus Vibrations: Taking into account the effect of amino group substitution in present case, the phenyl nucleus vibrations are well identified and assigned by reference to instructive comprehensive analysis of the corresponding spectra of pyrazine[2,16] and the present work on 2-amino-d_2-pyrazine. The details are listed in Table 3 which is self explanatory. Only following few comments on spectral characteristic observations specially regarding

Table 3. Fundamental Vibrational Frequencies (in cm^{-1}) of 2-Aminopyrazine (Aromatic Nucleus Part)

Symmetry			Mode No. (22)	Assignment	Pyrazine										2-Aminopyrazine			
					L.M.M. (4)		C.A.S. (8)		S.I.B. (2)		S.S.R. (11)		Z.B.S (16)					
D_{2h}	C_{2v}	C_s			IR	R	IR	R	IR	R	IR	R	IR	R	IR	R(S)	R(L)	(σ_L)
Ag	A_1	A′	6a	βC-C	—	609	609	—	596.1	598	602	600	600	602P	590	582P	585P	0.59
			1	νC-C	—	1015P	1015	—	1015	1016	1016	1011	1016	1016P	862	870P	867P	0.62
			9a	βC-H	—	1232	1232	—	1230	1234	1246	1231	1233	1233P	1240	1245P	—	0.52
			8a	νC-C	—	1584P	1584	—	1578	1578	1581	1574	1580	1580P	1595	1600P	1595P	0.55
			2	νC-H	—	3051P	3060	—	3054	3054	3054	3052	3054	3054	3055	3055P		
A	A_2	A″	16a	γC-C	340	—	400	—	340 (estd)	—	423	—	350	—	355	—	—	
			17a	γC-H	950	—	950	—	950 (estd)	958	997	—	960	—	955	—	—	
B_{1u}	A_1	A′	13	$\nu C\text{-}NH_2$	3065	3069	3090	—	3066	—	3082	—	3012	—	1325	1325P	1320P	—
			19a	νC-C	1490	—	1490	—	1484	—	1491	—	1483	—	1490	1490P	1490P	0.63
			18a	βC-H	1067	—	1135	—	1144	—	1126	—	1130	—	1150	1175P	—	0.43
			12	βC-C	1022	—	1021	—	1110	—	1022	—	1018	—	1009	1009P	1012P	0.58
B_{3u}	B_1	A′	20b	νC-H	3066	—	3070	—	3066	—	3011	—	3063	—	3065	3074	3070P	—
			19b	νC-C	1418	—	1413	—	1418	—	1414	—	1411	—	1438	1445P	1447P	0
			14	νC-C	1342	—	1346	—	1067	—	1149	—	1149	—	1350	1355dp	1360dp	0.85
			15	βC-H	1148	—	1063	—	1022	—	1068	—	1063	—	1060	1050dp	1070dp	0.86
B_{2u}	B_2	A″	16b	γC-C	417	—	417	—	416	—	412	—	418	—	421	433	—	0.54
			11	γC-H	804	—	786	—	804	—	796	—	785	—	818	819dp	—	0.78
B_{1g}	A_2	A″	10a	$\gamma C\text{-}NH_2$	752	753	925	—	757	757	930	919	927	927dp	201	—	—	—
B_{3g}	B_2	A″	4	γC-C	—	641	703	—	703	703	765	—	756	756	745	755p	—	—
			5	γC-H	700	703dp	753	—	981.6	922dp	974	—	983	983	895	895p	—	0.63
B_{2g}	B_1	A′	6b	βC-C	—	516	641	—	516	—	699	701	704	704dp	630	651p	654p	0.30
			3	$\beta C\text{-}NH_2$	—	1118	1350	—	1118	—	1353	1343	1346	1345dp	408	—	—	—
			8b	νC-C	—	1523	1523	—	1524	1524	1522	1524	1525	1525dp	1540	1535dp	1535dp	0.76
			7b	νC-H	—	3038	—	—	3041	3041	3034	3040	3040	3040	3040	3045dp	3048dp	0.77

R(S)-Raman solid phase; R(L)-Raman liquid phase in H_2O; P-Polarized; dp-depolarized; ν-Stretching; β-in-plane deformation; γ-out-of-plane deformation; σ_L-Depolarization ratio liquid phase.

the various corresponding infrared inactive vibrations belonging to Au, B_{2g}, and B_{3g} symmetry species in pyrazine are worth mentioning.

The two infrared inactive Au species fundamentals are little effected in intensity gain due to reduction in symmetry in present case and are identified with weak bands at 355 cm^{-1} (ν_{16a}) and 955 (ν_{17a}) without corresponding Raman lines. Regarding the assignments of the B_{2g} species, planar Raman active fundamentals, our observation of the polarized 651 cm^{-1} Raman line strongly supports the 630 cm^{-1} weak band in infrared for ν_{6b} fundamental. The other two fundamentals ν_{8b} and ν_{7b} in this class show appreciable gain in intensity thus, it seems are sensitive to lowering of the symmetry. The strong infrared bands at 1540 and 3040 cm^{-1} with corresponding 1535 and 3045 cm^{-1} analogous Raman lines have been assigned to these fundamentals. Both the Raman lines are depolarized in character.

The remaining two Raman active nonplanar B_{3g} fundamentals have been identified with the weak infrared bands at 745 (ν_4) and 895 cm^{-1} (ν_5). The choice of these two infrared bands is based on the corresponding Raman lines at 755 and 895 cm^{-1} and their intensities in expected region. Here, the Raman lines are polarized in character.

Although our assignments for aromatic nucleus part are generally compatible with recent publications[11,16] there are some notable differences particularly in case of vibration ν_{14}. We prefer to localize this fundamental vibration at 1350 cm^{-1} with corresponding depolarised Raman line at 1355 cm^{-1} rather than 1149 cm^{-1} as proposed for pyrazine by Sbrane et al.[11] and Zarembowitch et al.,[16] spectrum does not show any strong band in the proposed region of 1150 cm^{-1}.

It is, however, important to note that the state of polarization of some of the Raman lines do not behave as per present C_s symmetry rules. Although, the symmetry of the molecule is C_s, an analogous assignments, considering higher C_{2v} symmetry, have been proposed in few cases. Assigning the vibrations in this way will give rise to an occasional depolarized B_1 Raman lines. Some of the vibrations belongs to B_{3u} and B_{2g} species fall under such characteristic class. This induced non-behaviorable character of these vibrations may be attributed to the coupling between the various NH_2 deformation modes, which ultimately results in various combination bands, particularly in the 3000—1700 cm^{-1} spectral region.

As mentioned earlier, 2-aminopyrazine form a dimer due to intermolecular hydrogen bonding. Various spectra recorded at low and higher concentrations, show that this bonding does not make a pronounced effect on the vibrational frequencies arising out of aromatic nucleus. In general the steady shift towards higher frequency side of these various fundamental modes in comparison to 2-aminopyridine clearly indicates that the heterocyclic aromatic nucleus here is more strong electron-accepting in nature and thus conjugate more with the amino nitrogen. However, the similarity of infrared spectrum with 2-aminopyridine is instructive.

In case of ring vibrations the behavior analogy with monosubstituted benzenes is remarkable. The symmetric hexagonal breathing mode ν_1 and trigonal breathing mode ν_{12} are closely coupled with the vibrational modes of the substituent groups in substituted benzens and has been discussed in detail.[34-36] Considering amino group as a light substituent,[34] one expect vibration ν_1 to show large decrement while ν_{12} remains relatively unchanged as is actually observed in present case.

Similar is the case with the degenerate ν_6 ring distortion vibration, of which the totally symmetric component decreases while the asymmetric component is somewhat localized.

Remaining other ring vibrations which get coupled predominantly with C-H in-plane deformation rather than other C-X vibrations and so are little effected on substitution.

We acknowledge the financial support made available under 19th Departmental Research Grant 1983—84, Department of Chemical Technology, University of Bombay, for this research project.

We are also thankful to Dr. V. B. Kartha, Spectroscopy Division, B. A. R. C., Bombay for providing necessary facilities for solution phase Raman Spectra.

References

1) K. K. Innes, J. Simmons, and S. Tilford, *J. Mol. Spectrosc.*, **11**, 257 (1963); K. K. Innes, J. P. Byrne, and I. G. Ross, *ibid.*, **22**, 125 (1967).

2) J. D. Simmons, K. K. Innes, and G. M. Begun, *J. Mol. Spectrosc.*, **14**, 190 (1964).

3) M. Ito, R. Shimada, T. Kuraishi, and W. Mizushima, *J. Chem. Phys.*, **25**, 597 (1956).

4) R. C. Lord, A. L. Marston, and F. A. Miller, *Spectrochim. Acta*, **9**, 113 (1957).

5) H. Shindo, *Chem. Pharm. Bull.*, **8**, 33 (1960).

6) D. B. Scully, *Spectrochim. Acta*, **17**, 233 (1961).

7) H. H. Perkampus and E. Baumgarten, *Spectrochim. Acta*, **19**, 1473 (1963).

8) S. Califano, C. Adembri, and G. Sbrana, *Spectrochim. Acta*, **20**, 385 (1964).

9) H. Takashashi, K. Mamola, and E. K. Plyler, *J. Mol. Spectrosc.*, **21**, 217 (1966).

10) V. Schettino, G. Sbrana, and R. Righini, *Chem. Phys. Lett.*, **13**, 284 (1972).

11) G. Sbrana, V. Schettino, and R. Righini, *J. Chem. Phys.*, **59**, 2441 (1973).

12) M. Ito and I. Suzuka, *Chem. Phys. Lett.*, **31**, 467 (1975).

13) N. Nishi, M. Kinoshita, T. Nakashima, R. Shimada, and Y. Kanda, *Mol. Phys.*, **33**, 31 (1977).

14) M. Scrocco, C. diLauro, and S. Califano, *Spectrochim. Acta*, **21**, 571 (1965).

15) V. I. Berezin and E. P. Krainov, *Opt. Spectrosk.*, **17**, 517 (1964).
16) J. Zarembowitch and L. Borobza-Sebagh, *Spectrochim. Acta, Part A*, **32**, 605 (1976).
17) R. C. Hirt, *Spectrochim. Acta*, **12**, 114 (1958).
18) S. B. Kartha, *Can. J. Spectroscopy*, **27**, 1 (1982).
19) J. C. Evans, *Spectrochim. Acta*, **16**, 428 (1960).
20) M. Tsuboi, *Spectrochim. Acta*, **16**, 505 (1960).
21) C. Norlen, *Phys. Scr.*, **8**, 249 (1973).
22) E. B. Wilson, *Phys. Rev.*, **45**, 706 (1934).
23) K. Venkata Ramiah and P. G. Puranik, *J. Mol. Spectrosc.*, **7**, 89 (1961).
24) G. C. Piemental and A. L. McClellan, "Hydrogen Bond," W. H. Freeman and Co., San Francisco (1960).
25) E. Spinner, *J. Chem. Soc.*, **1963**, 3860.
26) V. V. Bhujle, Ph. D. Thesis, University of Bombay (1969).
27) R. Flett, *Trans. Faraday Soc.*, **44**, 767 (1948).
28) L. J. Bellamy and R. L. Williams, *Spectrochim. Acta*, **9**, 341 (1957).
29) J. W. Linnett, *Trans. Faraday Soc.*, **41**, 223 (1945).
30) R. A. Kydd, *Spectrochim. Acta*, **35**, 409 (1979).
31) N. W. Larsen, E. L. Hansen, and F. M. Nicolsisen, *Chem. Phys. Lett.*, **43**, 584 (1976).
32) R. A. Kydd and P. J. Krueger, *Chem. Phys. Lett.*, **49**, 539 (1977).
33) R. A. Kydd and P. J. Krueger, *J. Chem. Phys.*, **69**, 827 (1978).
34) G. Vavsanyi, "Vibrational Spectra of Benzene Derivatives," Academic Press, New York (1969).
35) J. R. Scherer, *Spectrochim. Acta*, **21**, 321 (1965).
36) N. D. Patel, V. B. Kartha, and N. A. Narsimhan, *J. Mol. Spectrosc.*, **48**, 185 (1973).

 © 1986 The Chemical Society of Japan Bull. Chem. Soc. Jpn., 59, 3229—3232 (1986)

Solvent Extraction Separation of Germanium with Aliquat 336S from Citric Acid Solutions

Chandrashekhar P. VIBHUTE and Shripad M. KHOPKAR*
Department of Chemistry, Indian Institute of Technology, Bombay 400 076, India
(Received April 22, 1985)

Germanium was quantitatively extracted with 0.1 mol dm^{-3} Aliquat 336S in xylene from 1×10^{-3} mol dm^{-3} citric acid solution adjusted to pH 3.5. It was stripped with 0.5 mol dm^{-3} hydrochloric acid and determined spectrophotometrically at 530 nm as the complex with phenylfluorone. It was effectively separated from binary as well as ternary mixtures by taking advantage of the difference in the stability of the citrate complexes with metal ions in mineral acids. The method was applied to the determination of germanium in coal fly ash.

Germanium was extracted with carbon tetrachloride.[1] Tributyl phosphate in toluene could extract germanium in the presence of salting out agent.[2] The extraction was not quantitative with diisopropyl ether.[1] Trioctylamine in butanol[3] or with oxine[4] in chloroform was also used for extraction of germanium. Germanium was separated from tin and lead with Amberlite LA-1 in xylene.[5] Trioctylamine in kerosene was used for the extraction of germanium from oxalic acid,[6,7] however germanium was not separated from associated elements.

This paper describes, therefore, a systematic investigation on the solvent extraction of germanium with Aliquat 336S from citric acid solutions. Novel methods are developed for the separation of commonly interfering ions. The method is applied to the determination of germanium in a standard coal fly-ash sample.

Experimental

Apparatus and Reagents. Spectrophotometer GS866C (ECIL, India) with matched Corex glass cells, Orion Research Microprocessor ion analyzer/901 (Orion Ltd., USA), with glass and calomel electrodes and Wrist action flask shaker (Toshniwal, India) were used.

A stock solution of germanium was prepared as follows: About 0.32 g of germanium dioxide was fused with equal amount of sodium hydroxide in a platinum crucible. The cooled mass was extracted with water and the solution was neutralized with hydrochloric acid. It was then made up to 100 cm^3 with water and standardized gravimetrically.[8] It contained 2.2 mg cm^{-3} of germanium. The working solution containing 22 μg cm^{-3} of germanium was prepared by exact dilution with water. Phenylfluorone (BDH, AnalR) (0.05% ethanolic solution), Gelatin (1% aqueous solution), Amberlite LA-1, Amberlite LA-2 (Rohm and Hass, Co. USA), Aliquat 336S (General Mills Ltd., England) and TOA (Riedel-Haen, Germany) were used without further purification. The extractant was converted into the citrate form as described earlier.[9]

General Procedure. To an aliquot of solution containing 22 μg of germanium, 5 cm^3 of 0.01 mol dm^{-3} citric acid was added. The pH of the solution was adjusted to 3.5 with 0.01 mol dm^{-3} sodium hydroxide or citric acid. The total volume of the aqueous phase was made up to 10 cm^3 and the solution was transferred to a separatory funnel. It was equilibrated with 10 cm^3 of 0.1 mol dm^{-3} Aliquat 336S in xylene for 5 min on wrist action flask shaker. After allowing the phases to settle and separate the aqueous phase was discarded and the organic phase was shaken with 10 cm^3 of 0.5 mol dm^{-3} hydrochloric acid to strip germanium. To the solution thus obtained 1 cm^3 of 1% gelatin and 2 cm^3 of 0.05% phenylfluorone in ethanol were added and the volume was made up to 25 cm^3 with distilled water. The absorbance of the yellow orange colored complex was measured at 530 nm against the reagent blank. The concentration of germanium was obtained from a calibration curve.[10]

Results and Discussion

Effect of pH. The pH for the quantitative extraction was ascertained by carrying out extractions between pH 1.0 and 8.0 with various liquid anion exchangers (Fig. 1). The extraction of germanium

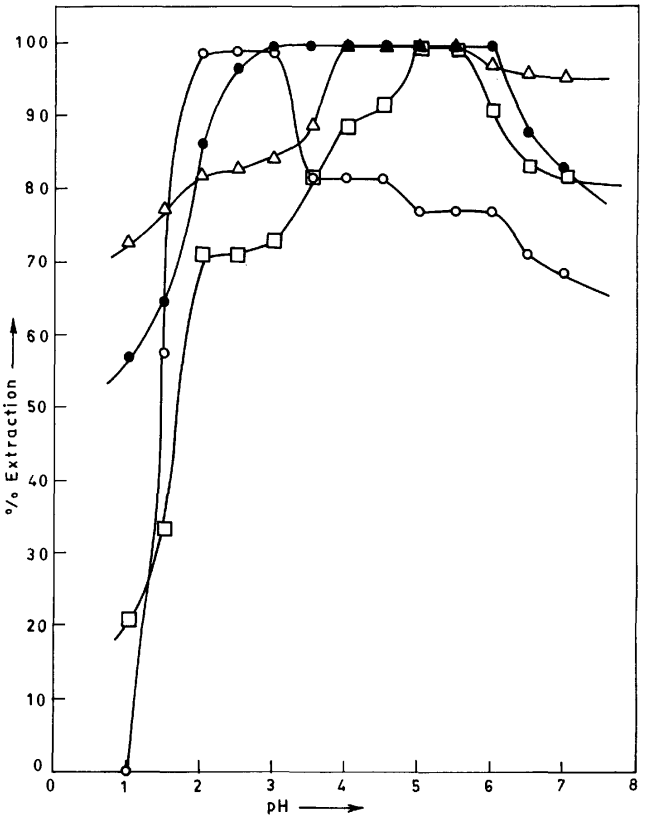

Fig. 1. Extraction of germanium with liquid anion exchangers.
●: Aliquat 336S (0.1M), ○: Amberlite LA-2 (0.08M), □: Amberlite LA-1 (0.1M), △: TOA (0.1M).

Table 1. Effect of Aliquat 336S Concentration
Ge=22 μg; pH=3.5

Concentration of Aliquat 336S 10^{-2} mol dm^{-3}	Extraction/%	Distribution ratio
1.00	59.3	1.5
1.25	64.3	1.8
2.50	86.0	6.1
3.75	88.9	8.0
5.00	93.1	13.5
6.25	96.6	29.5
7.50	99.9	999.0
8.75—10.0	99.9	999.0

Table 2. Effect of Citric Acid Concentration
Ge=22 μg; pH=3.5

Concentration of citric acid 10^{-4} mol dm^{-3}	Extraction/%	Distribution ratio
1	56.0	1.3
2	74.5	2.9
3	79.6	4.9
4	85.8	6.0
5	91.0	10.1
6	98.1	51.6
7	99.3	141.9
8-10	99.9	999.0

into xylene commenced below pH 1.0 for all the extractants except Amberlite LA-2. The extraction was quantitative from pH 3.0 to 6.0 with Aliquat 336S, pH 2.0 to 3.0 with Amberlite LA-2, pH 5.0 to 5.5 with Amberlite LA-1, and pH 4.0 to 4.5 with TOA in xylene. As the optimum pH range for the extraction was fairly broad. Aliquat 336S was used in further investigation. On the contrary the pH was quite broad (pH 3.0—6.0) with Aliquat 336S. Therefore Aliquat 336S was selected for further work.

Effect of Aliquat 336S Concentration. Germanium was extracted with varying concentrations of Aliquat 336S (1×10^{-2}—10^{-1} mol dm^{-3}) in xylene, while other factors were held at constant (Table 1). The extraction was almost quantitative when more than 7.5×10^{-2} mol dm^{-3} Aliquat 336S was used. Therefore 1×10^{-1} mol dm^{-3} Aliquat 336S was preferred throughout this investigation.

Effect of Citric Acid Concentration. The optimum concentration for the complete extraction was ascertained by extracting germanium from aqueous solution containing 1×10^{-4} to 10×10^{-3} mol dm^{-3} citrate. The extraction was incomplete below 5×10^{-4} mol dm^{-3} but quantitative above 7×10^{-4} mol dm^{-3} citrate (Table 2).

Effect of Various Diluents. A solution of 0.1 mol dm^{-3} Aliquat 336S was used in various diluents, such as, benzene, toluene, xylene, *n*-hexane, cyclohexane, carbon tetrachloride, chloroform, or nitrobenzene. The organic to aqueous phase volume ratio was maintained at 1:1. As shown in Table 3 chloroform and nitrobenzene are not effective as diluents perhaps due to their high polarities. The extraction was almost quantitative when xylene, *n*-hexane, cyclohexane, and carbon tetrachloride were used as diluents.

Effect of Stripping Agents. Germanium was stripped, after extraction, with 10 cm^3 of various concentrations of mineral acids and alkalis. Hydrochloric acid (0.5—4.0 mol dm^{-3}) and nitric, sulfuric, and hydrobromic acids (0.5—8 mol dm^{-3}) were capable of stripping germanium quantitatively. Similarly sodium hydroxide (0.1—2.0 mol dm^{-3}) or sodium carbonate (0.5—2.01 mol dm^{-3}) was also effective stripping agents. Hydrochloric acid was selected as a stripping agent considering its use in the separation and determination of germanium (Table 4).

Table 3. Effect of Various Diluents
Ge=22 μg, Citrate concentration=0.001 mol dm^{-3}, pH=3.5

Diluent	Dielectric constant	Extraction %	Distribution ratio
Benzene	2.28	94.0	15.6
Toluene	2.38	95.6	21.7
Xylene	2.30	99.9	999.0
Hexane	1.89	99.0	99.0
Cyclohexane	2.05	99.3	141.8
Carbon tetrachloride	2.24	98.3	57.8
Chloroform	4.8	45.6	0.6
Nitrobenzene	35.5	88.1	7.4

Nature of Extracted Species. The composition of the extracted species was investigated by plotting the logarithm of the distribution ratio of germanium against the logarithm of the concentration of Aliquat 336S at a constant citric acid concentration and the logarithm of the distribution ratio against the logarithm of the citric acid concentration at a constant concentration of Aliquat 336S. Linear relationship were obtained with slopes of 1.32 and 1.27, respectively. It is probable that the extracted species is $[R_4N^+\{Ge(OH)_2(Cit)^-\}]$. This postulation is supported by the observation of Pozhariskii et al.[12] who used trioctylamine in the extraction of germanium from citric and tartaric acid media.

Separation of Germanium from Foreign Metal Ions. Methods for the separation of germanium from foreign metal ions were investigated in the light of the difference in their complex forming abilities with citrate. Metal ions forming no complex or very weak complexes with citrate were not extracted and readily separated from germanium. A few metal ions forming weak complexes with citrate were readily removed from the organic extractant by washing with distilled water before stripping of germanium. Some metal ions forming stable complexes with citrate were strongly retained in the organic phase but these were effectively separated from germanium by using suitable stripping agents. Examples of the separation of germanium

Table 4. Effect of Different Stripping Agents Ge=22 μg

Stripping agents /mol dm^{-3}	Back stripping/%								
	0.1	0.25	0.5	1.0	2.5	4.0	5.0	6.0	8.0
HCl	0.0	94.0	99.9	99.9	99.8	99.7	10.5	0.0	0.0
HNO_3	67.8	99.9	99.9	100.0	99.9	99.1	100.0	99.8	99.8
H_2SO_4	20.3	99.0	99.9	99.1	100.1	100.0	99.8	99.9	99.8
HBr	0.0	99.7	99.9	99.9	99.9	99.9	100.0	99.0	0.0
Aqueous NH_3	50.0	62.7	69.5	70.0	—	—	—	—	—
NaOH	99.3	99.4	99.9	99.9	—	—	—	—	—
Na_2CO_3	76.3	99.3	99.8	99.5	—	—	—	—	—

Table 5. Separation from Binary Mixtures

Foreign ion	Added as	Tolerance limit/μg	Stripping agent†	Foreign ion	Added as	Tolerance limit/μg	Stripping agent†
Li^+	$Li_2SO_4 \cdot H_2O$	4500	Not extracted	Pb^{2+}	$Pb(NO_3)_2$	1850	H_2O
Na^+	NaCl	4400	Not extracted	Tl^+	Tl_2SO_4	1850	H_2O
K^+	KCl	4500	Not extracted	Ga	$GaCl_3$	275	0.5M HCL[b]
Rb^+	RbCl	4500	Not extracted	In	$InCl_3$	350	0.5M HCl[b]
Be^{2+}	$Be(NO_3)_2$	400	Not extracted	Tl^{3+}	$TlCl_3$	520	0.5M $HClO_4$[b]
Mg^{2+}	$MgSO_4 \cdot 7H_2O$	3200	Not extracted	Sn^{4+}	$SnCl_2$	325	0.5M H_2SO_4[b]
Ca^{2+}	$CaCl_2 \cdot 6H_2O$	3200	Not extracted	Sb^{3+}	$Sb(NO_3)_3$	410	0.5M H_2SO_4[b]
Sr^{2+}	$Sr(NO_3)_2 \cdot 2H_2O$	3200	Not extracted	Bi^{3+}	$Bi(NO_3)_3 \cdot 5H_2O$	130	0.5M H_2SO_4[b]
Ba^{2+}	$Ba(NO_3)_2 \cdot 4H_2O$	3000	Not extracted	Hg^{2+}	$HgCl_2$	240	0.1M NaOH[b]
Mn^{2+}	$MnSO_4 \cdot 7H_2O$	1000	H_2O	Sc^{3+}	$Sc(NO_3)_3$	200	5M HCl[a]
Fe^{2+}	$FeSO_4 \cdot 7H_2O$	1700	H_2O	Ti^{4+}	$Ti(SO_4)_2$	234	5M HCl[a]
Co^{2+}	$Co(NO_3)_2 \cdot 6H_2O$	970	H_2O	Zr^{4+}	$Zr(NO_3)_4 \cdot 4H_2O$	290	5M HCl[a]
Ni^{2+}	$Ni(NO_3)_2 \cdot 6H_2O$	1050	H_2O	Hf^{4+}	$Hf(SO_4)_2$	210	5M HCl[a]
Cu^{2+}	$CuSO_4 \cdot 5H_2O$	890	H_2O	V^{4+}	NH_4VO_3	320	5M HCl[a]
Zn^{2+}	$ZnSO_4 \cdot 7H_2O$	950	H_2O	U^{6+}	$UO_2(NO_3)_2 \cdot 6H_2O$	275	0.5M HCl[b]
Ag^+	$AgNO_3$	1650	H_2O	Th^{4+}	$Th(NO_3)_4 \cdot 4H_2O$	150	5M HCl[a]
Cd^{2+}	$3Cd(NO_3)_2 \cdot 8H_2O$	990	H_2O	Au^{3+}	$AuCl_3$	225	0.5M NaOH[b]
As^{3+}	$AsCl_3$	980	H_2O	pt^{4+}	$PtCl_4$	265	0.5M NaOH[b]
Al^{3+}	$Al(NO_3)_3$	1100	H_2O	Pd^{2+}	$PdCl_2$	435	5M HCl[a]

†1M=1 mol dm^{-3}.
a) Before stripping of germanium. b) After stripping of germanium.

from synthetic binary and ternary mixtures are given in Tables 5 and 6.

Application for the Determination of Germanium in Coal Fly Ash. About 0.5 g of a standard coal fly ash sample was dissolved in a mixture (10 ml cm^{-3}) of aqua regia and hydrofluoric acid (1:1) in a Teflon beaker. After removal of the excessive acids the content was dissolved in dilute hydrochloric acid and the solution was made up to 50 cm^3 [11] with distilled water. An aliquot of this solution was equilibrated with 10 cm^3 of 0.1 mol dm^{-3} Aliquat 336S in xylene as described above. Copper, cadmium, zinc, and cobalt were also extracted but these metals were readily removed by washing the extract with distilled water; thorium was then stripped with 6 mol dm^{-3} hydrochloric acid and finally germanium with 3 mol dm^{-3} hydrochloric acid. With duplicate determinations, the amount of germanium found was 18.7 and 18.5 ppm against the standard value of 19.0 ppm.

The separation of germanium from copper, zinc, lead, and antimony is interesting, as these elements are usually associated with each other in minerals. Similarly the separation of germanium from gallium, indium, and thallium is important because of their

Table 6. Separation of Germanium from Ternary Mixtures

S. No.	Mixture	Taken μg	Found μg	Recovery %	Stripping agents†
1	As(III)	210.5	210.4	99.9	H_2O
	Ge	22.4	22.3	99.5	4M HCl
	Hg	100.1	100.0	99.9	0.5M NaOH
2	Pb	314.2	314.0	99.9	H_2O
	Ge	22.4	22.4	100.0	3M HCl
	Sn	78.7	78.6	99.8	0.5M H_2SO_4
3	Al	278.0	277.5	99.6	H_2O
	Ge	22.4	22.2	99.1	3M HCl
	Bi	101.3	101.3	100.0	1M H_2SO_4
	Tl(III)	59.4	59.4	100.0	1M $HClO_4$
4	Ag/Zn	579.4	579.2	99.9	H_2O
	Ge	22.4	22.3	99.5	3M HCl
	Au	100.4	100.3	99.3	1M NaOH
5	Ge	22.4	22.3	99.5	4M HCl
	Sb	135.4	135.2	99.6	5M HNO_3
	In	100.0	99.8	99.8	0.5M HCl
6	Ge	22.4	22.2	99.1	3M HCl
	Bi	220.0	219.9	99.5	6M HCl
	Ga	125.0	124.8	99.8	0.5M HCl

† 1 M=1 mol dm^{-3}.

significant use in semiconductors. The proposed method is simple, rapid, and reproducible. The time required for complete separation and determination is 2 h. The standard deviation was 1.1% for 22 μg of germanium.

References

1) H. F. Turkalov, C. V. Zakolodyazhna, and I. V. Stasenko, *Zh. Khim.*, 19GDE 24 (1965); Abstr. No. 246128, *Anal. Abstr.*, **13**, 6800 (1966).

2) S. Kalyanaraman and S. M. Khopkar, *Indian J. Chem.*, **A 15**, 1031 (1977).

3) A. M. Andrianov and V. P. Koryukova, *Zh. Anal. Khim.*, **24**, 1117 (1969).

4) A. M. Andrianov and L. M. Avalasovich, *Zh. Prikl. Khim. (Leningrad)*, **41**, 2313 (1968); *Anal. Abstr.*, **18**, 1572 (1970).

5) G. Nakagawa, *Nippon Kagaku Zasshi*, **81**, 1255 (1960).

6) I. P. Aleksandrov, A. I. Perfil'ev, L. M. Avdasovich, and A. I. Sharkov, *Ukr. Khim. Zh.*, **40**, 980 (1974); *Anal. Abstr.*, **28**, 4B83 (1975).

7) K. Yakabe and S. Minaui, *Nippon Kagaku Kaishi*, **1981**, 969; *Chem. Abstr.*, **95**, 173159y (1981).

8) A. I. Vogel, "A Text Book of Quantitative Inorganic Analysis," Longman, Green, London (1964), p. 653.

9) C. P. Vibhute and S. M. Khopkar, *Anal. Lett.*, **16**, 1037 (1983).

10) A. I. Busev, V. G. Tiptsova, and V. M. Ivanov, "Analytical Chemistry of Rare Elements," Mir Publishers, Moscow (1981), p. 334.

11) R. A. Nadkarni, *Anal. Chem.*, **52**, 929 (1980).

12) A. F. Pozharitskii, N. M. Bobrovskaya, and Belousova, et al. *Zh. Neorg. Khim.*, **18**, 2482 (1973).

 © 1986 The Chemical Society of Japan Bull. Chem. Soc. Jpn., 59, 3233—3237 (1986)

Kinetics and Mechanism of Anation of Pentaammineaquarhodium(III) Ion by Malonate in Weakly Acidic Media[1)]

Chinmay CHATTERJEE* and Aya Singh BALI
Department of Chemistry, Indian Institute of Technology, Powai, Bombay 400 076, India
(Received August 5, 1985)

Anation of pentaammineaquarhodium(III) ion by malonic acid, hydrogenmalonate, and malonate ions to form the hitherto unknown pentaamminemalonatorhodium(III) complex has been studied as a function of $[H^+]$ for the acidity range $1.4 \leq pH \leq 5.0$, [total malonate], 0.3 mol dm^{-3} in the temperature range of 60 to 80 °C and at ionic strength 1.0 mol dm^{-3} adjusted with sodium perchlorate. Ion pairing is not significant between the complex and malonic acid but kinetically identifiable with hydrogenmalonate and malonate ions. Ion pair association constants for the hydrogenmalonate (Q_1) and malonate ion (Q_2) at 60 °C are 1.8 and 7.5 $mol^{-1}dm^3$ respectively. The values of the rate constants at 60 °C for anation by malonic acid, hydrogenmalonate, and malonate ions are $k_0=3.04\pm0.2\times10^{-5}$ $mol^{-1}dm^3s^{-1}$, $k_1=1.73\pm0.2\times10^{-4}$ s^{-1}, and $k_2=3.46\pm0.4\times10^{-4}$ s^{-1}. The activation parameters, ΔH^* and ΔS^* corresponding to anation rate constants, k_0, k_1, and k_2 are reported and the results discussed with reference to analogous reactions of Rh(III) and Co(III).

The kinetics and mechanism of replacement of the aqua ligand in pentaammineaquacobalt(III) ion by various anionic ligands have been the subject of several investigations. In contrast, limited data exist for the analogous reactions of corresponding rhodium(III) substrate and receiving attention in recent years, as these provide important mechanistic information for a comparative analysis of the reactivity of related octahedral and isoelectronic systems. Though the anation reactions of analogous complexes of Co(III) and Rh(III) often exhibit similar rate law, they actually proceed by different mechanism due to bond formation by the entering group being more significant in the case of rhodium than in cobalt as evident from water exchange and anation reactions of the complexes of the type $[M(NH_3)_5(OH_2)]^{3+}$, where M=Co(III)[2-10] and Rh(III).[11-17] The general applicability of the pronounced nucleophilic participation of the anating ligand in the transition state can be tested by extending the study to the anation reaction of $[Rh(NH_3)_5(OH_2)]^{3+}$ by carboxylate ligands which, so far, have been only sparingly studied.[18-20] In the present work, anation of pentaammineaquarhodium(III) ion by malonate has been presented. The reaction has been studied in aqueous malonate buffer of varying pH in order to assess the anation rate profile of malonic acid, hydrogenmalonate, and malonate ions. The results presented here show indeed a difference in mechanistic behavior between Co(III) and Rh(III).

Experimental

Materials and Reagents. Pentaammineaquarhodium(III) perchlorate was prepared according to standard procedures[21)] and purified by recrystallization. Chemical analysis confirmed the purity, as did a comparison with published UV-visible spectral data.[22)]

Pentaamminemalonatorhodium(III) perchlorate was prepared for the first time by digesting an aqueous solution of pentaammineaquarhodium(III) perchlorate with slight excess of malonic acid at 80 °C for 3 h followed by slow evaporation of the reaction mixture to one third of its original volume. Aqueous perchloric acid (30%) was added to the ice-cold reaction mixture to obtain the desired product as perchlorate salt. The white crystals that separated were filtered, washed successively with cold dilute perchloric acid, ethanol, and ether. The product was finally dried in air. The purity of the complex was ascertained by elemental analysis. Found: C, 7.30; H, 3.62; N, 14.20%. Calcd for $[Rh(O_2CCH_2CO_2H)(NH_3)_5](ClO_4)_2$: C, 7.35; H, 3.67; N, 14.29%.

The positions and intensities of the d-d bands of the complex (λ_{max} 322 nm, ε 165 $dm^3mol^{-1}cm^{-1}$, λ_{max} 265 nm, ε 130 $dm^3mol^{-1}cm^{-1}$) corresponding to $^1A_{1g}\rightarrow{}^1T_{1g}$ and $^1A_{1g}\rightarrow{}^1T_{2g}$ transitions respectively match well with those of the pentaamminecarboxylatorhodium(III) (N_5O type) complexes. Infrared spectrum of Nujol mull of hydrogenmalonato complex reveals two strong bands at 1630 and 1725 cm^{-1} assignable to carbonyl asymmetric stretching frequencies of coordinated and free carboxyl groups in the complex. Presence of one equivalent of titrable proton unambigously confirms the mode of bonding of coordinated malonate ligand in the molecule. Other chemicals used were of reagent grade quality or prepared in the pure state by suitable methods.

Rate Measurements. The kinetic measurements were performed employing a Varian Superscan-3UV-visible spectrophotometer. The acidities of the experimental solutions were attained by the addition of sodium hydroxide and perchloric acid as the case may be and measured by means of a PHM 64 (Radiometer Copenhagen) research pH meter. The course of the anation reaction of pentaammineaquarhodium(III) ion with malonate over the acidity range $1.4\leq pH\leq5.0$, for total malonate concentration up to 0.3 mol dm^{-3} in the temperature range of 60 to 80 °C was followed by measuring the increase in absorbance at 322 nm, where extinction coefficients of $[Rh(O_2CCH_2CO_2H)(NH_3)_5]^{2+}$ and $[Rh(NH_3)_5(OH_2)]^{3+}$ ions were 165 and 102 $dm^3mol^{-1}cm^{-1}$ respectively. The rate studies were made at ionic strength 1.0 mol dm^{-3} ($NaClO_4$) by a batch sampling technique,[20)] with the thermostat controlled to ±0.1 °C. The composition of the experimental solutions was such that the pseudo-first-order rate law was applicable and the pseudo-first-order rate constants, k_{obsd}, were computed from the gradients of the linear plots of $\log(A_\infty-A_t)$ vs. t by means of a least-squares program. Reported k_{obsd} values represent the average of at least duplicate runs which agreed within ±3%.

Table 1. Observed Rate Constants (k_{obsd}) as a Function of [Malonate]$_T$ and pH at Various Temperatures

Temp / °C	pH	Total malonate/mol dm^{-3}																
		0.02	0.03	0.04	0.05	0.06	0.08	0.10	0.12	0.125	0.15	0.16	0.175	0.18	0.20	0.225	0.25	0.30
		$k_{obsd}/10^{-5}$ s^{-1}																
60.0	1.4						0.3	0.4	0.5		0.6			0.7	0.8		0.9	1.1
	1.7							0.5			0.7				1.0		1.2	1.4
	2.0							0.7			1.0				1.3			2.0
	2.5				0.5			1.1			1.6				2.2			
	2.9			0.7	0.8		1.3	1.6	1.9		2.4			2.6	2.9		3.1	
	3.4				1.1			2.2			3.3				3.8		4.3	
	3.8				1.4		2.1	2.6	3.0		3.6			4.1	4.4			
	4.5				3.1		4.7	5.3	6.4		7.1				7.9			
	4.8				4.1		6.2		8.8		10.2			11.3	11.8			
	5.0				5.1		6.8	8.3	9.5		11.5			12.9	13.2			
70.0	1.4						0.7		1.0		1.2			1.4	1.5		2.1	2.5
	1.7				0.7						2.5				3.0		4.3	4.9
	2.0							1.9			2.7				3.7			5.7
	2.5				1.9			3.5			5.7				7.3			8.8
	2.9				3.1			5.7			8.7		9.5		10.3	10.9	11.5	
	3.4				4.0			7.9			11.5				14.0		16.0	18.0
	3.8				5.0			9.5			14.5		15.4		17.0	18.0	19.1	
	4.5			7.5	8.8		14.4		20.5		23.5							
	4.8		8.1		12.0		18.4	21.5	24.6		28.1			30.0				
	5.0			12.1	14.5		22.0	26.1	28.8		32.0			34.0				
80.0	1.4				1.2			1.9							4.0		4.8	6.4
	1.7				2.0			4.0			5.8				7.2			11.8
	2.0							6.4			8.9						14.1	16.9
	2.5	2.4			5.4			11.3			16.0				20.8			
	2.9				8.6		13.2	17.5	20.5		24.6		28.7			33.3	36.3	
	3.4			9.6			19.0		27.7			32.5			37.8			
	3.8				14.9		24.5	29.6		36.1	45.0		51.9		55.6	57.6		
	4.8	14.8	22.0	28.1	34.2	38.7	48.2	56.2										
	5.0	16.9		31.8		46.1	58.0	67.5	75.2									

Results and Discussion

Pentaammineaquarhodium(III) ion reacts with malonic acid, hydrogenmalonate ion, and malonate ion to form either $[Rh(O_2CCH_2CO_2H)(NH_3)_5]^{2+}$ or $[Rh(O_2CCH_2CO_2)(NH_3)_5]^{+}$ complex depending on the pH of the solution. The interpretation of the rate data, however, was not complicated by the presence of $[Rh(O_2CCH_2CO_2)(NH_3)_5]^{+}$ species at high pH, as it showed absorbance identical to that of protonated one at the experimental wavelength. In order to assess the anation rate profiles of malonic acid, hydrogenmalonate, and malonate ions, the reaction has been studied over a wide enough pH range to encompass all possible acidic and basic forms of anating species. The participation of $[Rh(NH_3)_5(OH)]^{2+}$ species is essentially eliminated by fixing the upper pH limit at 5.0 (pK_a of $[Rh(NH_3)_5(OH_2)]^{3+}$ at μ, 1.0 mol dm^{-3}=6.94[23]). Acid dissociation constant of $[Rh(O_2CCH_2CO_2H)(NH_3)_5]^{2+}$ at 25 °C and ionic strength 1.0 mol dm^{-3} was determined from conventional pH titrations employing a PHM 64 research pH meter. The pK_a value was estimated as 3.8±0.05, which is significantly lower than that of $CH_2C_2O_4H^-$ ion. This is ascribed to an increase in acidity of the ligand when coordinated to a metal ion. Values of the pseudo-first-order rate constant (k_{obsd}) under different sets of experimental conditions are summarized in Table 1. Representative plots of k_{obsd} versus malonate concentration for varying pH at 60 °C are illustrated in Fig. 1. The plots are noted to be linear at low pH, while curvature becomes apparent at pH≥2.5. Deviation from linearity at pH 2.5 and above suggests that the reactant association is not significant between aqua complex and malonic acid but kinetically identifiable with hydrogen malonate and malonate ions respectively, as the concentration of the latter species increases with increase in pH of the solution. Similar trends in k_{obsd} have also been noted at other experimental temperatures. The linearity of the plot at low pH suggests simple second-order kinetics for anation by malonic acid, as also reported for cobalt(III) analog.[10] The anation by basic forms of the anating ligand is thus proposed to involve the formation of ion pairs in a preequilibrium step followed by the rate determining interchange of coordinated aqua ligand by carboxylate ion. Consistent with the experimental results the anation scheme may be depicted as follows:

$$[Rh(NH_3)_5(OH_2)]^{3+} + CH_2C_2O_4H_2 \xrightarrow{k_0} [Rh(O_2CCH_2CO_2H)(NH_3)_5]^{2+} + H_3O^+$$

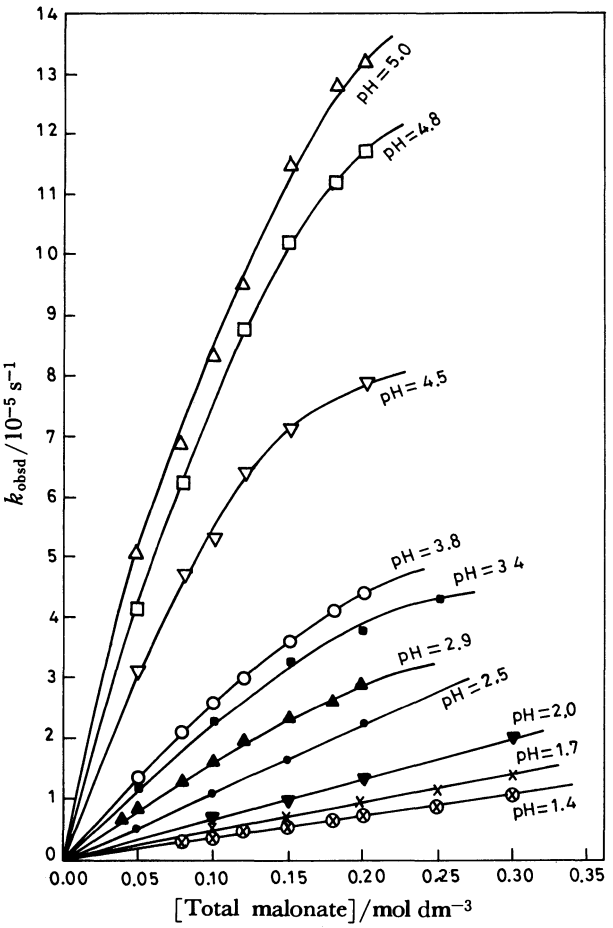

Fig. 1. k_{obsd} vs. [Total malonate] for various pH at 60.0±0.1 °C.
[Complex]; 0.002 mol dm^{-3}, μ; 1.0 mol dm^{-3}.

$$[Rh(NH_3)_5(OH_2)]^{3+} + CH_2C_2O_4H^- \overset{Q_1}{\rightleftharpoons} [Rh(NH_3)_5OH_2^{3+}\cdot CH_2C_2O_4H^-]$$

$$[Rh(NH_3)_5OH_2^{3+}\cdot CH_2C_2O_4H^-] \xrightarrow{k_1} [Rh(O_2CCH_2CO_2H)(NH_3)_5]^{2+} + H_2O$$

$$[Rh(NH_3)_5(OH_2)]^{3+} + CH_2C_2O_4^{2-} \overset{Q_2}{\rightleftharpoons} [Rh(NH_3)_5OH_2^{3+}\cdot CH_2C_2O_4^{2-}]$$

$$[Rh(NH_3)_5OH_2^{3+}\cdot CH_2C_2O_4^{2-}] \xrightarrow{k_2} [Rh(O_2CCH_2CO_2)(NH_3)_5]^{+} + H_2O,$$

where k_o signifies second order rate constant for anation of $[Rh(NH_3)_5(OH_2)]^{3+}$ by malonic acid, k_1, Q_1, and k_2, Q_2 are the rate and association constants of the hydrogenmalonate and malonate ion pair respectively. The theoretical rate law in accordance with the suggested scheme fits the equation

$$k_{obsd} = -\,d\ln[Rh(III)]_T/dt = \frac{k_0[CH_2C_2O_4H_2]+k_1Q_1[CH_2C_2O_4H^-]+k_2Q_2[CH_2C_2O_4^{2-}]}{1+Q_1[CH_2C_2O_4H^-]+Q_2[CH_2C_2O_4^{2-}]}. \quad (1)$$

At pH<3.5, the contribution of terms involving $CH_2C_2O_4^{2-}$ is too small to have any meaningful significance, and hence Eq. 1 reduces to

$$k_{obsd} = \frac{k_0[CH_2C_2O_4H_2]+k_1Q_1[CH_2C_2O_4H^-]}{1+Q_1[CH_2C_2O_4H^-]}. \quad (2)$$

At low pH, where mainly $CH_2C_2O_4H_2$ is present, the anation reaction follows simple second-order kinetics. Under these conditions, Eq. 2 can be simplified to

$$k_{obsd} = k_0[CH_2C_2O_4H_2]+k_1Q_1[CH_2C_2O_4H^-], \quad (3)$$

as $1+Q_1[CH_2C_2O_4H^-]\simeq 1$. The observed rate data under these conditions followed second-order kinetics such that

$$k_{obsd} = k_{an}[\text{total malonate}], \quad (4)$$

where k_{an} is the second-order rate constant. The Eqs. 3 and 4 on rearrangement leads to

$$k_{an} = k_0 + (k_1Q_1-k_0)\frac{[CH_2C_2O_4H^-]}{[\text{total malonate}]}. \quad (5)$$

The values of k_o at each experimental temperature were obtained from the intercept of k_{an} versus $[CH_2C_2O_4H^-]/[\text{total malonate}]$ plot. The Eq. 3 on rearrangement can be written as

$$\frac{k_{obsd}-k_0[CH_2C_2O_4H_2]}{[CH_2C_2O_4H^-]} = k_1Q_1-Q_1k_{obsd}. \quad (6)$$

The interchange rate constant (k_1) and association constant (Q_1) at each experimental temperature were evaluated from the slope and intercept of $\{k_{obsd}-k_0[CH_2C_2O_4H_2]\}/[CH_2C_2O_4H^-]$ versus k_{obsd} (Fig. 2) plot under the acidity range of pH≃pK_1 of malonic acid where the contribution of $CH_2C_2O_4H^-$ to the rate of reaction becomes significant. At pH≥4.0, the contribution of $k_0[CH_2C_2O_4H_2]$ to k_{obsd} is negligibly small and Eq. 1 reduces to

$$k_{obsd} = \frac{k_1Q_1[CH_2C_2O_4H^-]+k_2Q_2[CH_2C_2O_4^{2-}]}{1+Q_1[CH_2C_2O_4H^-]+Q_2[CH_2C_2O_4^{2-}]}. \quad (7)$$

The values of k_2 and Q_2 at each experimental temperature were estimated from the slope and intercept of the straight line plot of $\{k_{obsd}+(k_{obsd}-k_1)Q_1[CH_2C_2O_4H^-]\}/[CH_2C_2O_4^{2-}]$ versus k_{obsd} (Fig. 3). Activation parameters, ΔH^* and ΔS^* corresponding to anation rate constants were calculated using Eyring equation. Values of the anation rate constants and corresponding activation parameters together with their standard deviations as deduced by least-squares analysis are presented in Table 2. A comparison of the anating reactivity of malonic acid and its conjugate bases derived from second-order rate constants, k_o, k_1Q_1, and k_2Q_2 follow the sequence: $CH_2C_2O_4H_2 < CH_2C_2O_4H^- < CH_2C_2O_4^{2-}$. This can be explained satisfactorily considering higher reactivity of the deprotonated

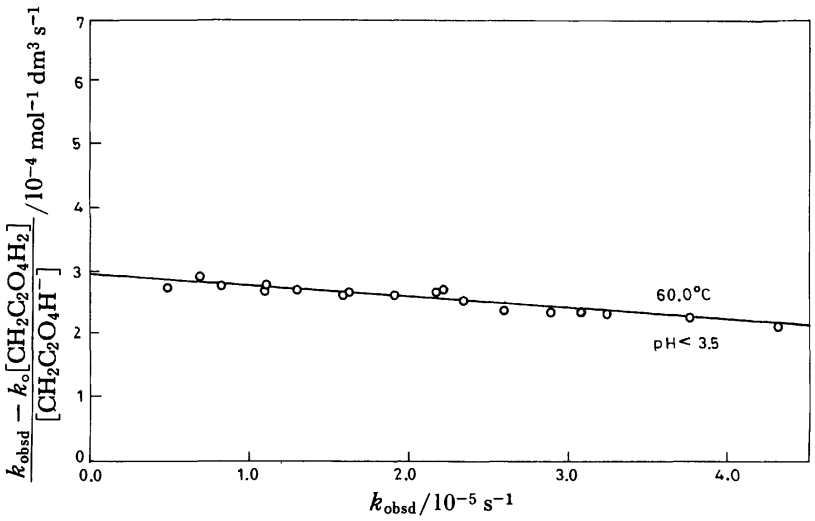

Fig. 2. $\frac{k_{obsd}-k_o[CH_2C_2O_4H_2]}{[CH_2C_2O_4H^-]}$ vs. k_{obsd} at 60.0±0.1℃.

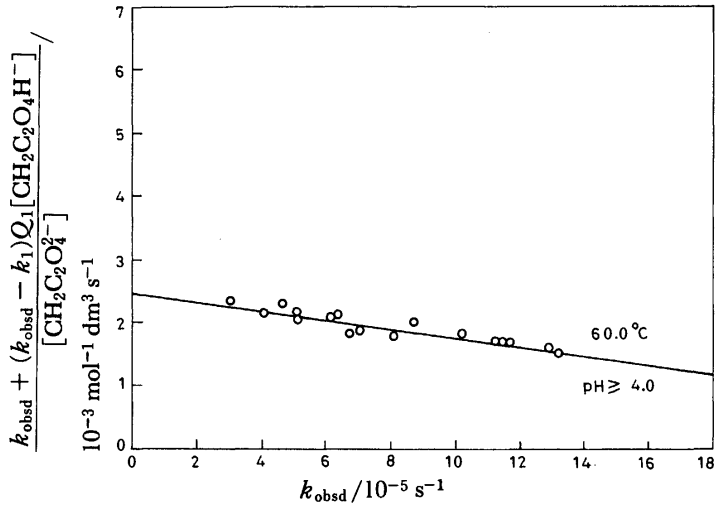

Fig. 3. $\frac{k_{obsd}+(k_{obsd}-k_1)Q_1[CH_2C_2O_4H^-]}{[CH_2C_2O_4^{2-}]}$ vs. k_{obsd} at 60.0±0.1℃.

Table 2. Rate and Activation Parameters for the Anation of $[Rh(NH_3)_5(OH_2)]^{3+}$ by Malonic Acid/Malonate Ions (μ=1.0 mol dm^{-3})

Rate parameter	Temperature/°C			Activation parameters	
	60.0±0.1	70.0±0.1	80.0±0.1	ΔH^*/kJ mol^{-1}	ΔS^*/J K^{-1} mol^{-1}
k_0/10^{-5} mol^{-1} dm^3 s^{-1}	3.04±0.2	7.22±0.2	15.44±0.3	79.0±2.9	−97.0±12.0
Q_1/mol^{-1} dm^3	1.7±0.1	1.8±0.3	1.9±0.2		
k_1/10^{-4} s^{-1}	1.73±0.2	5.96±0.5	16.93±0.7	104.0±5.6	−4.0±1.7
Q_2/mol^{-1} dm^3	7.1±0.3	7.8±0.3	7.6±0.4		
k_2/10^{-4} s^{-1}	3.46±0.4	9.1±0.7	24.24±1.0	96.5±6.0	−20.9±9.2

forms of the acid. Anation of pentaammineaquarhodium(III) ion by oxalic,[18] malonic, and propionic acid[20] studied so far offers a meaningful relation between k_o and pK values of the carboxylic acids. The value of k_o is found to decrease with an increase in pK value, i.e. with increasing basicity and O-H bond strength, of the acid, making the reaction more difficult to occur. This effect is accompanied by the increase in activation parameter as is expected for a less reactive species. The k_o value for the present system is comparable with the analogous reaction for cobalt(III) analog. In both cases no evidence for an ion pair is kinetically observed and the anation proceeded via a second-order kinetics, suggesting a simi-

larity in mechanism for both the systems. The observed rate constant for anation of $[Co(NH_3)_5(OH_2)]^{3+}$ ion by malonic acid at pH=1.5 is reported to decrease by a factor of 1.4 when D_2O instead of H_2O is used as solvent.[10] Based on the results of isotope effect and the relation between k_o and pK values of the carboxylic acid, the O-H bond fission on the -COOH group of the carboxylic acid has been suggested of significant importance in the rate-determining step of the anation mechanism.[10] Low ΔH^* and ΔS^* values corresponding to k_o for the complex under present investigation also corroborate the possibility of associative activation in the transition state. The value of essentially temperature-independent ion pair association constant (Q) is observed to be greater for malonate than for hydrogen malonate ion as expected on the basis of higher charge on the former, but are considerably higher than that for strong acid anions of the same charge viz., Cl^-, Br^-, SO_4^{2-}.[13] This may be attributed to the less extensive solvation of the carboxylates in comparison to that of strong acid anions.

According to Swaddle,[24] the magnitude of enthalpy of activation for anation rate constant offers better criteria to distinguish between the associative and dissociative character of interchange reactions. Similarity in ΔH^* and ΔS^* values corresponding to interchange rate constants, k_1 and k_2 for the present system seem to suggest near identity of the respective transition states. Moreover, both sets of activation parameters are observed to be fairly close to that of water exchange[11] of $[Rh(NH_3)_5(OH_2)]^{3+}$ ion as well as the substitution reaction involving replacement of coordinated aquo ligand by Cl^-, Br^-, I^-,[12,13] N_3^-, CH_3COO^-,[14] and $CH_3CH_2COO^-$[20] ions. The anation and water exchange reactions of $[Rh(NH_3)_5(OH_2)]^{3+}$ ion have been suggested to proceed by an interchange associative (I_a) mechanism. The negative volume of activations for the aquo exchange in $[Rh(NH_3)_5(OH_2)]^{3+}$ (ΔV^*, -4.1 ± 0.4 cm^3 mol^{-1})[16] and solvent exchange in $[Rh(NH_3)_5(dmf)]^{3+}$ (ΔV^*, -1.4 cm^3 mol^{-1}),[17] lend additional support to the associative character for rhodium(III) substrate. The ΔH^* values for the anation of $[Rh(NH_3)_5(OH_2)]^{3+}$ by hydrogenmalonate and malonate ions are observed to be 12—21 kJ mol^{-1} lower than for analogous reactions of cobalt(III) substrate. On the basis of the activation parameters, the anation of $[Co(NH_3)_5(OH_2)]^{3+}$ with hydrogenmalonate and malonate ions have proposed to take place by interchange dissociative (I_d) mechanism.[10] If the same type of mechanism is thought to be operative for the interchange reactions for the present system, owing to the greater loss of ligand field energy one would expect a higher enthalpy of activation for the Rh(III) complex compared to isostructural and isoelectronic (d^6) Co(III) substrate. The reverse trend in magnitude of ΔH^* cannot be explained by above mechanism but suggests significant bond formation by the entering group in the transition state in course of transformation of ion pair into the product complex. Moreover, a decrease in ΔS^* towards a more negative value, going from Co(III) to Rh(III) substrate, is also in conformity with a mechanism involving a more pronounced participation of the incoming nucleophile in the transition state for the latter.

References

1) C. Chatterjee and A. S. Bali, Proc. XXIIIrd International Coordination Chemistry Conference, Colorado, U. S. A. (1984), p. 24.

2) H. R. Hunt and H. Taube, *J. Am. Chem. Soc.*, **80**, 2642 (1958).

3) R. Van Aldik and G. M. Harris, *Inorg. Chem.*, **14**, 10 (1975).

4) P. R. Joubert and R. Van Eldik, *Inorg. Chim. Acta*, **12**, 205 (1975).

5) D. Banerjea and J. Roy, *Z. Anorg. Allg. Chem.*, **400**, 89 (1973).

6) P. R. Joubert and R. Van Aldik, *Inorg. Chim. Acta*, **14**, 259 (1975).

7) R. Van Eldik and P. R. Joubert, *J. Inorg. Nucl. Chem.*, **37**, 1887 (1975).

8) A. C. Dash and M. S. Dash, *J. Coord. Chem.*, **6**, 1 (1976).

9) R. Van Eldik, *J. Inorg. Nucl. Chem.*, **38**, 88 (1976).

10) P. R. Joubert and R. Van Eldik, *Int. J. Chem. Kinet.*, **8**, 411 (1976).

11) F. Monacelli and E. Veil, *Inorg. Chim. Acta*, **1**, 467 (1967).

12) H. L. Bott, A. J. Poe, and K. Shaw, *J. Chem. Soc. A*, **1970**, 1745.

13) F. Monacelli, *Inorg. Chim. Acta*, **2**, 263 (1968).

14) C. Chatterjee and P. Chaudhuri, *Indian J. Chem.*, **11**, 777 (1973).

15) A. J. Poe, K. Shaw, and M. J. Wendt, *Inorg. Chim. Acta*, **1**, 371 (1967).

16) T. W. Swaddle and D. R. Stranks, *J. Am. Chem. Soc.*, **94**, 8357 (1972).

17) S. T. D. Lo, M. J. Sisley, and T. W. Swaddle, *Can. J. Chem.*, **56**, 2609 (1978).

18) R. Van Eldik, *Z. Anorg. Allg. Chem.*, **416**, 888 (1975).

19) C. Chatterjee and A. K. Basak, *Bull. Chem. Soc. Jpn.*, **52**, 2710 (1979).

20) C. Chatterjee and A. S. Bali, *J. Coord. Chem.*, **11**, 179 (1981).

21) G. W. Bushnell, G. C. Lalor, and E. A. Moelwyn-Hughes, *J. Chem. Soc. A*, **1966**, 719.

22) H. H. Schmidtke, *Z. Phys. Chem. (Frankfurt am Main)*, **45**, 307 (1965).

23) L. H. Skibsted and P. C. Ford, *Acta Chem. Scand., Ser. A*, **34**, 109 (1980).

24) S. T. D. Lo, E. M. Ondeman, J. C. Hansen, and T. W. Swaddle, *Can. J. Chem.*, **54**, 3685 (1976).

Interaction of Dithiophosphinates of Cobalt and Nickel with Pyridine-Type Donors

Rabindra Nath MUKHERJEE,* Sanganabatla SHANKAR, and Denis Louis MASCARENHAS
Department of Chemistry, Indian Institute of Technology, Bombay 400 076, India
(Received September 17, 1985)

The relative isotropic ^{1}H NMR shifts of several pyridine-type base adducts of M(2,4-Me$_2$dtpi)$_2$ [where M=Co, Ni and 2,4-Me$_2$dtpi=bis(2,4-dimethylphenyl)dithiophosphinate] were measured. The opposite signs of ring and methyl proton resonance shifts in α- and γ-picoline complexes of nickel indicate that both σ- and π-mechanisms are operative. In the cobalt cases all proton resonances are shifted down-field suggesting a negative dipolar contribution in addition to contact interaction. The magnetic and electronic spectral studies on these compounds are consistent with either MS_4N or MS_4N_2 chromophores.

The proton isotropic shifts of pyridine-type donors in cobalt and nickel acetylacetonates[1] and β-keto esterates[2,3] have been reported. ^{1}H NMR studies on similar adducts of chelates of these metals with sulfur ligands have received much less attention.[4,5] Dithiophosphinates of transition metals were reported from our laboratory.[6,7] In the present article, complexes of bis(2,4-dimethylphenyl)dithiophosphinates of cobalt and nickel, M(2,4-Me$_2$dtpi)$_2$, with a series of pyridine-type donors have been subjected to magnetic, electronic, IR, and ^{1}H NMR investigations.

Experimental

All the chemicals used were either of analytical or chemically pure grade. Bis(2,4-dimethylphenyl)dithiophosphinic acid was synthesized by the procedure reported in literature.[8]

Preparation of Complexes. Co(2,4-Me$_2$dtpi)$_2$(L) (L= pyridine, α-picoline, β-picoline, γ-picoline, 2,6-lutidine, and 3,5-lutidine): The base (3 ml) was added to a methanolic solution (40 ml) of $CoCl_2 \cdot 6H_2O$ (1.1 g). Addition of methanolic solution (25 ml) of Na(2,4-Me$_2$dtpi) (3.1 g) afforded blue/greenish blue solid which was washed with methanol and dried.

Co(2,4-Me$_2$dtpi)$_2$(4-phenylpyridine): To a chloroform (25 ml) solution of Co(2,4-Me$_2$dtpi)$_2$ (1.5 g) methanolic solution (25 ml) of 4-phenylpyridine (0.4 g) was added. On slow addition of methanol (40 ml) bright green product precipitated out. This was washed with methanol and recrystallized from chloroform–methanol.

Co(2,4-Me$_2$dtpi)$_2$(L)$_2$ (L=pyridine and γ-picoline): A mixture of cobalt(II) chloride hexahydrate (1.3 g) and the base (10 ml) in methanol (40 ml) was treated with methanolic solution (30 ml) of sodium salt (3.7 g) of the ligand. The resulting pink crystalline solid was collected, washed with methanol containing a small amount of the base.

Ni(2,4-Me$_2$dtpi)$_2$(α-picoline): A chloroform solution (30 ml) of Ni(2,4-Me$_2$dtpi)$_2$ (1.5 g) was mixed with 3 ml of α-picoline. The resulting solution, on slow evaporation gave the brown adduct, which was washed with methanol and dried.

Ni(2,4-Me$_2$dtpi)$_2$(L) (L=β-picoline and γ-picoline): Nickel(II) chloride hexahydrate (1.1 g) in methanol (40 ml) was treated with 3 ml of base. Na(2,4-Me$_2$dtpi) (3.1 g) in methanol (25 ml) was added dropwise to this solution with stirring. The brown solid, which precipitated was isolated by filtration, washed with methanol and dried.

Ni(2,4-Me$_2$dtpi)$_2$(3,5-lutidine): A solution of Ni(2,4-Me$_2$dtpi)$_2$ (2.2 g) in chloroform (30 ml) was mixed with 3,5-lutidine (4 ml). The brown solid was forced from the resulting solution with methanol, filtered and then recrystallized from chloroform–methanol mixture in presence of small quantity of the base.

Ni(2,4-Me$_2$dtpi)$_2$(L)$_2$ (L=pyridine, β-picoline, and γ-picoline): The light green adduct was obtained by the interaction of a solution of Ni(2,4-Me$_2$dtpi)$_2$ (2.0 g) in chloroform (30 ml) with the base (6 ml) and on slow evaporation of the solvent. It was then recrystallized from chloroform–methanol in presence of base.

Ni(2,4-Me$_2$dtpi)$_2$(4-phenylpyridine)$_2$: A solution of 4-phenylpyridine (1.0 g) in chloroform (30 ml) was added slowly to a chloroform solution (30 ml) of Ni(2,4-Me$_2$dtpi)$_2$ (2.1 g). This solution on slow evaporation gave the green complex and was recrystallized from chloroform–methanol in presence of base.

Physical Measurements: A Pye-Unicam SP-2000 infrared spectrophotometer was used for recording IR spectra of the samples in KBr. The room-temperature magnetic measurements were carried out on a Gouy balance using Hg[Co(SCN)$_4$] as the standard. The electronic spectra were observed on a Varian Super Scan 3 UV-visible spectrophotometer. ^{1}H NMR spectra of the adducts in deuteriochloroform were recorded on a Varian XL-100 high resolution NMR spectrometer using tetramethylsilane as the internal calibrant.

Results and Discussion

The color, magnetic moment, analytical and thermal data of the complexes are given in Table 1.

The monoadducts of the composition Co(2,4-Me$_2$dtpi)$_2$(L) were obtained with pyridine, α-picoline, β-picoline, γ-picoline, 3,5-lutidine, 2,6-lutidine, and 4-phenylpyridine whereas the diadducts of the composition Co(2,4-Me$_2$dtpi)$_2$(L)$_2$ could be isolated only with pyridine and γ-picoline. Ni(2,4-Me$_2$dtpi)$_2$ forms 1:1 adducts with α-picoline and 3,5-lutidine whereas both 1:1 and 1:2 adducts have been obtained with β-picoline and γ-picoline. Electronic spectral studies show that a 1:2 adduct is also formed with 3,5-lutidine in solution. With pyridine and 4-phenylpyridine only 1:2 adducts could be isolated. Similar adducts with piperidine could not be isolated. However, the change in color of M(2,4-Me$_2$dtpi)$_2$ solution upon the addition of piperidine; electronic and

Table 1. Color, Magnetic Moment, Analytical, and Thermal Data of the Complexes

Complex[a]	Color	Magnetic moment	Found (Calcd)/%			Temp[e]
		BM	M[b]	S[c]	Loss of base[d]	°C
$Co(X)_2(py)$	Blue	4.64	7.95 (7.87)	17.27 (17.13)	10.48 (10.56)	140
$Co(X)_2(\alpha\text{-pic})$	Blue	4.63	7.61 (7.73)	16.67 (16.81)	12.08 (12.21)	155
$Co(X)_2(\beta\text{-pic})$	Blue	4.69	7.59 (7.73)	16.62 (16.81)	12.12 (12.21)	165
$Co(X)_2(\gamma\text{-pic})$	Blue	4.69	7.79 (7.73)	16.65 (16.81)	12.23 (12.21)	170
$Co(X)_2$(2,6-lut)	Greenish blue	4.66	7.42 (7.59)	16.37 (16.51)	13.56 (13.79)	140
$Co(X)_2$(3,5-lut)	Greenish blue	4.65	7.45 (7.59)	16.39 (16.51)	13.63 (13.79)	170
$Co(X)_2$(4-phpy)	Bright green	4.70	6.96 (7.14)	15.29 (15.55)	18.62 (18.81)	175
$Co(X)_2(py)_2$	Pink	5.09	7.06 (7.12)	15.28 (15.49)	19.02 (19.12)	140
$Co(X)_2(\gamma\text{-pic})_2$	Pink	4.89	6.78 (6.89)	14.72 (14.98)	21.59 (21.76)	170
$Ni(X)_2(\alpha\text{-pic})$	Brown	3.12	7.42 (7.70)	16.57 (16.82)	12.20 (12.21)	125
$Ni(X)_2(\beta\text{-pic})$	Brown	3.23	7.59 (7.70)	16.54 (16.82)	12.13 (12.21)	115
$Ni(X)_2(\gamma\text{-pic})$	Brown	3.14	7.47 (7.70)	16.69 (16.82)	12.24 (12.21)	135
$Ni(X)_2$(3,5-lut)	Brown	3.20	7.45 (7.56)	16.54 (16.51)	13.82 (13.80)	160
$Ni(X)_2(py)_2$	Light green	3.09	6.98 (7.09)	15.32 (15.49)	18.95 (19.10)	130
$Ni(X)_2(\beta\text{-pic})_2$	Light green	3.15	6.72 (6.86)	14.73 (14.99)	21.53 (21.76)	115
$Ni(X)_2(\gamma\text{-pic})_2$	Light green	3.22	6.83 (6.86)	14.57 (14.99)	21.49 (21.76)	135
$Ni(X)_2$(4-phpy)$_2$	Light green	3.25	5.83 (5.99)	12.89 (13.09)	31.43 (31.67)	170

a) X=2,4-Me_2dtpi. b) M=Metal (Co or Ni). c) S=Sulfur. d) Loss of the pyridine-type donor on heating. e) Temperature at which the complex was heated to estimate the loss of base.

^{1}H NMR spectral studies on the resulting solution confirm the formation of adducts in solution.

The IR spectra of these complexes show ν_{as}P-S and ν_sP-S around 650 and 585 cm^{-1} respectively.[9] The bands around 1470 and 1610 cm^{-1} are assigned to both C=C and C=N stretching vibrations.

The magnetic moments for the monoadducts of cobalt and nickel fall in the range 4.63—4.70 and 3.12—3.23 BM respectively consistent with the penta-coordinate geometry.[10,11] For the diadducts these values are around 5.0 and 3.2 BM respectively as expected for hexa-coordinate cobalt(II) and nickel(II) complexes.

The reflectance and solution spectra of Co(2,4-Me_2dtpi)$_2$(L) are similar and the observed d-d bands around 14800, 15600, and 17250 cm^{-1} are in agreement with those reported for other penta-coordinate compounds.[12] Since the overall pattern of the absorption bands for both trigonal bipyramidal as well as square pyramidal cobalt complexes is the same, the choice between the geometries based upon the spectral data is not categorically possible. The reflectance spectra of the pink diadducts exhibit a multicomponent band in the region 14800—21700 cm^{-1} which is assigned to $^4T_{1g}\rightarrow{}^4T_{1g}(P)$ transition in an octahedral stereochemistry.[13] The very weak two electron $^4T_{1g}\rightarrow{}^4A_{2g}$ transition expected in this region is obscured by the stronger $^4T_{1g}\rightarrow{}^4T_{1g}(P)$ transition. Thermogravimetric analysis of these compounds show two distinct dissociation steps (115 and 140 °C for pyridine and 125 and 170 °C for γ-picoline adducts respectively) indicating the presence of two base molecules in the adducts. The complexes decompose on prolonged exposure to air and are soluble in nonpolar solvents producing blue-colored solutions, indicating dissociation to penta-coordinate species.

The reflectance spectra of the monoadducts of Ni(2,4-Me_2dtpi)$_2$ show two ligand field bands around 13000 and 21000 cm^{-1} with a shoulder in the intermediate region (18000 cm^{-1}) and are consistent with a square pyramidal penta-coordinate stereochemistry.[14,15] The solid-state spectra of the diadducts exhibit ligand field bands around 13900 and 21600 cm^{-1} and are assigned to $^3A_{2g}\rightarrow{}^3T_{1g}$ and $^3A_{2g}\rightarrow{}^3T_{1g}(P)$ transitions in a trans octahedral symmetry of the NiS_4N_2 chromophore. Dis-

Table 2. Relative Isotropic Shifts for Ligands Coordinated with Metal Complexes

Ligand	Proton	Isotropic shifts in Ni(2,4-Me_2dtpi)$_2$ adducts	Isotropic shifts in Co(2,4-Me_2dtpi)$_2$ adducts
Piperidine	α-CH_2	−10.00	−10.00
	β-CH_2	−4.95	−4.02
	γ-CH_2	−2.81	−0.70
Pyridine	α-CH	−10.00	−10.00
	β-CH	−3.53	−3.92
	γ-CH	−0.93	−0.87
α-Picoline	α-CH	−10.00	−10.00
	β-CH	−3.42	−3.00
	γ-CH	−1.81	−0.93
	α-CH_3	+0.74	−0.18
β-Picoline	α-CH	−10.00	−10.00
	β-CH	−3.45	−3.50
	γ-CH	−0.56	−0.21
	β-CH_3	−0.51	−0.42
γ-Picoline	α-CH	−10.00	−10.00
	β-CH	−3.40	−3.87
	γ-CH_3	+1.10	−0.87
3,5-Lutidine	α-CH	−10.00	−10.00
	γ-CH	−0.62	−0.37
	β-CH_3	−0.56	−0.49
4-Phenylpyridine	α-CH	−10.00	−10.00
	β-CH	−3.17	−3.76
	α'-CH	−0.12	−0.55
	β'-CH	+0.11	−0.12
	γ'-CH	+0.11	−0.12

sociation of these complexes in chloroform solution could be prevented by addition of the base.

^{1}H NMR has been used to determine the distribution of unpaired spin density in the ligands of paramagnetic complexes in which the effective electron spin relaxation time is short. The existence of an isotropic hyperfine contact interaction between unpaired electrons and magnetic nuclei leads to large shifts in the nuclear resonance frequencies. Such a shift may be of contact or dipolar origin or a combination of both.[16] The isotropic shifts found for nickel chelates are assumed to arise solely from a contact interaction[17] while for cobalt compounds both contact and dipolar interactions[18] contribute for these shifts.

The observed shifts for dithiophosphinate moiety are very small hence our discussion is confined only to the base proton shifts. As the actual shifts depend upon the solution composition only relative shifts have been discussed. Absorption peaks were assigned to particular ligand protons by observing the approach to the known diamagnetic spectra upon the addition of more and more ligand. The observed shifts have been normalized to give a value of −10.00 for the α-proton shifts. Negative shifts are shifts to lower applied fields and positive shifts to higher applied fields.

The relative isotropic shifts for the protons of different bases complexed with nickel and cobalt dithiophosphinates are included in Table 2. In the nickel adduct with piperidine all the base proton resonances are shifted down-field and attenuate with the increasing number of intervening bonds between the metal ion and relevant proton. This pattern is characteristic of σ-delocalization and is observed in a number of complexes.[19,20] Similar observation was made for pyridine adduct in which all the proton shifts are down-field and the order is $\alpha > \beta > \gamma$. In contrast, the methyl protons of both α- and γ-picoline compounds are shifted up-field indicating the presence of unpaired π-electron density in addition to σ-spin density.

The observed isotropic shifts in cobalt complexes are compared with the corresponding nickel adducts and that of cobalt(II) acetylacetonates to get information about the nature of dipolar shifts. For piperidine adduct of Co(2,4-Me_2dtpi)$_2$ all the observed shifts are down-field in contrast to the up-field shifts reported for corresponding cobalt acetylacetonate derivative. Since piperidine has no π-orbitals, π-delocalization of magnetic t_{2g} electrons is not possible. The observed shift pattern can be explained by considering a negative dipolar contribution in addition to contact interaction while positive dipolar contribution has been reported for Co(acac)$_2$. This is supported by the down-field shift of the methyl protons of α- and γ-picolines in Co(2,4-Me_2dtpi)$_2$. If the spin-transfer mechanisms for nickel

and cobalt adducts are assumed to be the same, which of course have been shown to be true,[1,21] the methyl protons would have shifted up-field in the presence of small positive dipolar shifts. The observation of negative shifts for these protons rules out the possibility of positive dipolar contribution in these cobalt adducts. This is further supported by the down-field shift for β' and γ' protons in 4-phenylpyridine adduct, the corresponding protons in the cobalt acetylacetonate show up-field shifts. In the nickel complex the β' and γ' proton resonances are shifted up-field similar to that in the $Ni(acac)_2$ compound.

Isotropic shifts for all β-picoline protons of nickel adduct were observed down-field and the signs of shifts for β-CH and β-CH_3 protons are identical. The observation is similar to that reported for the corresponding acetylacetonate adduct. This behavior is in contrast to the results obtained for the α- and γ-picoline adducts which were explained on the basis of $(\sigma-\pi)$ configuration interaction. Similar observation was made for 3,5-lutidine adduct of $Ni(2,4\text{-}Me_2dtpi)_2$ in which α-CH, γ-CH, and β-CH_3 protons are shifted down-field. However, for the corresponding cobalt complexes the observation is similar to those of α- and γ-picoline adducts.

In $Co(2,4\text{-}Me_2dtpi)_2$(2,6-lutidine) the observed shifts have been normalized to give -10.00 for β-protons and the values obtained for γ-CH and α-CH_3 are -4.12 and -0.11 respectively. The signs of the shifts are identical to those for other bases. The corresponding nickel adduct could not be isolated and ^1H NMR spectrum did not provide evidence for complex formation in solution.

References

1) J. A. Happe and R. L. Ward, *J. Chem. Phys.*, **39**, 1211 (1963).
2) T. Maitani, M. Chikuma, and H. Tanaka, *J. Inorg. Nucl. Chem.*, **42**, 1689 (1980).
3) T. Maitani, M. Chikuma, and H. Tanaka, *J. Inorg. Nucl. Chem.*, **41**, 1115 (1979).
4) M. M. Dhingra, G. Govil, and C. R. Kanekar, *Chem. Phys. Lett.*, **10**, 86 (1971).
5) T. Maitani, M. Chikuma, and H. Tanaka, *J. Inorg. Nucl. Chem.*, **41**, 1121 (1979).
6) R. N. Mukherjee and M. D. Zingde, *J. Inorg. Nucl. Chem.*, **35**, 696 (1973).
7) R. N. Mukherjee, V. S. Vijaya, and P. K. Gogoi, *Indian J. Chem.*, **22A**, 564 (1983).
8) W. A. Higgins, P. W. Vogel, and W. G. Craig, *J. Am. Chem. Soc.*, **77**, 1864 (1955).
9) G. P. McQuillan and I. A. Oxton, *Inorg. Chim. Acta*, **29**, 69 (1978).
10) A. C. Villa, C. Gaustini, P. Porta, and A. A. G. Tomlinson, *J. Chem. Soc., Dalton Trans.*, **1978**, 956.
11) E. K. Barefield, D. H. Busch, and S. M. Nelson, *Quart. Rev.*, **22**, 457 (1968).
12) R. T. Boere, W. M. Brown, D. W. Stephan, and C. J. Willis, *Inorg. Chem.*, **24**, 593 (1985).
13) M. Shimoi, A. Ouchi, T. Uehiro, Y. Yoshino, S. Sato, and Y. Saito, *Bull. Chem. Soc. Jpn.*, **55**, 2371 (1982).
14) A. Sgamellotti, C. Furlani, and F. Magrini, *J. Inorg. Nucl. Chem.*, **30**, 2655 (1968).
15) J. R. Angus, G. M. Woltermann, and J. R. Wasson, *J. Inorg. Nucl. Chem.*, **33**, 3967 (1971).
16) R. W. Kluiber and W. D. Horrocks, Jr., *J. Am. Chem. Soc.*, **87**, 5350 (1965).
17) R. J. Fitzgerald and R. S. Drago, *Inorg. Chem.*, **8**, 2254 (1969).
18) I. Bertini, G. Canti, C. Luchinat, and F. Mani, *J. Am. Chem. Soc.*, **103**, 7784 (1981).
19) R. J. Fitzgerald and R. S. Drago, *J. Am. Chem. Soc.*, **90**, 2523 (1968).
20) A. Boyer and G. V. Fazakerley, *J. Inorg. Nucl. Chem.*, **43**, 1955 (1981).
21) W. D. Horrocks, Jr., R. C. Taylor, and G. N. LaMar, *J. Am. Chem. Soc.*, **86**, 3031 (1964).

Kinetics of the Iron(II) Reduction of Glycinatobis(malonato)-, *trans*-Bis(malonato)bis(pyridine)-, Nitrilotriacetato(malonato)-, and Nitrilotriacetato(oxalato)cobaltates(III)

Ramakrishnan VISWANATHAN and Venkatapuram Ramanujam VIJAYARAGHAVAN*
Department of Physical Chemistry, University of Madras, Guindy Campus, Madras 600 025, India
(Received September 17, 1985)

The kinetics of the iron(II) reduction of glycinatobis(malonato)-, *trans*-bis(malonato)bis(pyridine), nitrilotriacetato(malonato)-, and nitrilotriacetato(oxalato)cobaltates(III) have been studied in aqueous perchlorate medium at I=1.0 mol dm^{-3} ($LiClO_4$) and 30 °C in the [H^+] range 0.01—0.90 mol dm^{-3}. The reductions are found to be second order. The reduction of $[Co(gly)(mal)_2]^{2-}$ and $[Co(py)_2(mal)_2]^-$ is accelerated by H^+, while the reduction of $[Co(nta)(mal)]^{2-}$ and $[Co(nta)(ox)]^{2-}$ is independent of [H^+] in the range 0.1<[H^+]<0.9 mol dm^{-3}. The reduction of $[Co(nta)(mal)]^{2-}$ is, however, faster at [H^+]<0.1 mol dm^{-3}. The activation parameters for the reduction of $[Co(gly)(mal)_2]^{2-}$, $[Co(py)_2(mal)_2]^-$, $[Co(nta)(mal)]^{2-}$, and $[Co(nta)(ox)]^{2-}$ are respectively as follows:

$\Delta H^{\neq}$=49.8±4.8, 51.2±2.6, 41.1±3.2, and 41.4+3.6 kJ mol^{-1}

$\Delta S^{\neq}$=−98.3±8.3, −93.7±7.2, −119.2±9.7, and −114.6+9.6 J K^{-1} mol^{-1}.

The proposed mechanism invokes $[Co(L)(H_2O)(mal)(malH)]$ (L-py_2 or gly) formed in a H^+-assisted step as the reactive species for the bis(malonato) complexes. $[Co(nta)(mal)]^{2-}$ is proposed to be present as $[Co(nta)(malH)(H_2O)]^-$ while $[Co(nta)(ox)]^{2-}$ remains unaffected by H^+.

Extensive reports are available in literature on the inner-sphere reduction of cobalt(III) complexes, e.g. by Fe(II) and Cr(II). These studies indicate a variety of possibilities for the dependence of rate on [H^+].[1-5] The reduction rates of $[Co(en)(C_2O_4)_2]^-$,[1,2] $[Co(NH_3)_4(C_2O_4)]^+$,[3] and $[Co(en)_2(NH_2CH_2COO)]^{2+}$ [4] are independent of [H^+]. Rates showing an inverse dependence on [H^+] are observed in the reduction of $[Co(NH_3)_5(C_2O_4)]^+$ and $[Co(NH_3)_5(C_3H_2O_4)]^+$ $C_3H_2O_4^{2-}$= malonate ion (mal)[4] while the reduction of $[Co(C_3H_2O_4)_3]^{3-}$ [5] and $[Co(en)(C_3H_2O_4)_2]^-$ [2] is accelerated by H^+. Small increases in rates with increase in [H^+] have been attributed to medium effects, mainly when $NaClO_4$ is used as the ionic medium.[6] Extensive studies have been carried out in this laboratory to analyse the [H^+]-depencence of rates of reduction and the present report is in continuation of such studies.[2,7,8]

Experimental

Barium glycinatobis(malonato)cobaltate(III) sesqui-hydrate,[9] $Ba[Co(gly)(mal)_2]\cdot 1.5H_2O$, sodium *trans*-bis(pyridine)bis(malonato)cobaltate(III) dihydrate,[10] $Na[Co(py)_2(mal)_2]\cdot 2H_2O$, and disodium nitrilotriacetato(oxalato)cobaltate(III) monohydrate,[11] $Na_2[Co(nta)ox]\cdot H_2O$, were prepared and purified by literature methods. Disodium nitrilotriacetato(malonato)cobaltate(III) monohydrate $Na_2[Co(nta)(mal)]\cdot H_2O$ was prepared by a procedure similar to that for $Na_2[Co(nta)(ox)]$. The purities of the complexes were checked by UV-vis, IR, conductivity, and elemental analysis. Solutions of $Fe(ClO_4)_2$ were prepared by dissolving pure iron powder (Sarabhai M Chemicals) in ca. 2 M $HClO_4$ (1 M=1 mol dm^{-3}) in the presence of nitrogen and stored under nitrogen . [Fe(II)] and free [H^+] in the Fe(II) solution were determined by known methods.[12] Lithium perchlorate was prepared by neutralizing anhydrous Li_2CO_3 with $HClO_4$ and recrystallizing till free from Cl^- and SO_4^{2-} ions.[13] Perchloric acid (E Merck, reagent grade) was used as such. Doubly distilled water was used throughout the kinetic study.

Kinetics: Second order conditions were maintained in all kinetic runs, using equimolar concentrations of reactants. Solutions of the complexes and Fe(II) were thermostated separately and mixed at the time of reaction. Reactions were followed spectrophotometrically at 575 nm for $[Co(gly)(mal)_2]^{2-}$, 555 nm for $[Co(py)_2(mal)_2]^-$, 570 nm for $[Co(nta)(ox)]^{2-}$, and 563 nm for $[Co(nta)(mal)]^{2-}$ in a Carl Zeiss UV-vis recording spectrophotometer by measuring the absorbance at intervals of 30 seconds for 3 half lives. The reactions were studied in nitrogen atmosphere using serum caps to seal the cells. $HClO_4$ was used as the source of H^+. Studies at [H^+]-0.01 mol dm^{-3} were, however, in the presence of a glycine buffer. The ionic strength of the solutions was adjusted to 1 mol dm^{-3} with $LiClO_4$. Figure 1 shows the change in spectrum with time for the complex $[Co(py)_2(mal)_2]^-$ as an example. Rate constants were calculated from the slopes of $(A_o-A_t)(A_t-A_\infty)^{-1}$ versus time plots, where A_o is the initial absorbance, A_t- the absorbance at time t, and A_∞- the absorbance at the completion of the reaction. These plots were linear for three half-lives. Activation parameters were determined by carrying out the reactions at different temperatures ranging from 20 to 55 °C. The temperature dependence studies were made in the [H^+]-range in which the rates were [H^+]-independent.

The stoichiometry of the reactions was determined by measuring the Fe(III) and Co(II) produced from equimolar mixtures of the complex and Fe(II) after completion of reaction. Co(II) was determined as $CoCl_4^{2-}$ and Fe(III) as $Fe(NCS)_6^{3-}$ spectrophotometrically. The ratio of Fe(III) to Co(II) was found to be 1:1.

Results

Table 1 presents the second order rate constants k for the Fe(II) reduction of $[Co(gly)(mal)_2]^{2-}$ and $[Co(py)_2(mal)_2]^-$ in the range 0.01<[H^+]<0.7 mol dm^{-3}. Rate constants in the temperature range 30—55 °C are also given. The rate increases with [H^+] for both complexes, the increase being three to five-fold

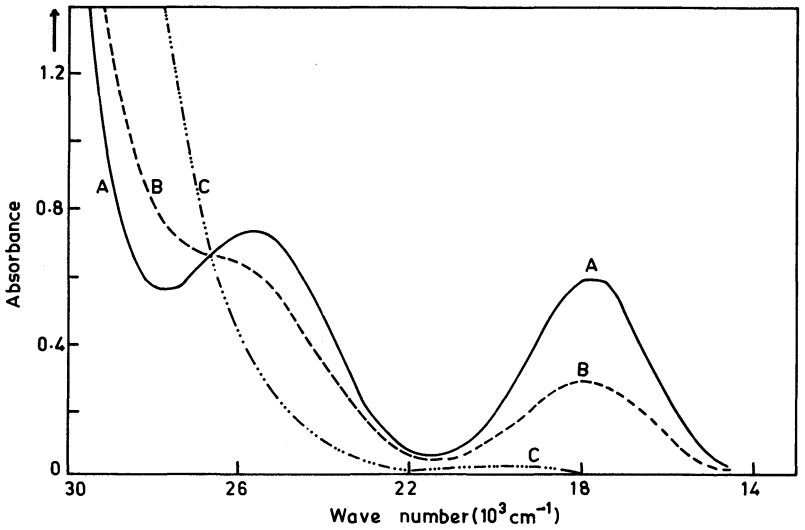

Fig. 1. Change in the visible spectrum during the Fe(II) reduction of *trans*-$[Co(py)_2(mal)_2]^-$.

$[Co(py)_2(mal)_2]^-=[Fe(II)]=8\times10^{-3}$ mol dm^{-3}

$[H^+]=0.2$ mol dm^{-3}.

$I=1.0$ mol dm^{-3} ($LiClO_4$).

Temp=30 °C.

A: Initial spectrum, B: After 10 min.,
C: After 60 min.

Table 1. Rate Constants[a] for the Iron(II) Reduction of $[Co(gly)(mal)_2]^{2-}$ and *trans*-$[Co(py)_2(mal)_2]^-$

Temp	$[H^+]$	k / dm^3 mol^{-1} s^{-1}	
°C	mol dm^{-3}	$[Co(gly)(mal)_2]^{2-}$	$[Co(py)_2(mal)_2]^-$
30	0.01	0.12	0.11
	0.025	0.14	—
	0.03	—	0.12
	0.05	0.15	0.14
	0.10	0.20	0.19
	0.20	—	0.28
	0.30	0.44	0.36
	0.40	0.53	0.40
	0.50	0.71	0.49
	0.60	—	0.54
	0.70	0.78	0.68
	0.80	—	0.83
	0.90	—	0.89
35	0.01	0.17	0.20
40	0.01	0.23	0.28
45	0.01	0.32	0.39
50	0.01	0.44	0.53
55	0.01	0.59	0.72

a) [Complex]=[Fe(II)]=0.01 mol dm^{-3}. $I=1.0$ mol dm^{-3} ($LiClO_4$).

Table 2. Rate Constants[a] for the Iron(II) Reduction of $[Co(nta)(mal)]^{2-}$ and $[Co(nta)(ox)]^{2-}$

Temp	$[H^+]$	k / dm^3 mol^{-1} s^{-1}	
°C	mol dm^{-3}	$[Co(nta)(mal)]^{2-}$	$[Co(nta)(ox)]^{2-}$
30	0.01	0.51	0.43
	0.025	0.45	—
	0.03	—	0.45
	0.05	0.41	—
	0.10	0.35	0.44
	0.20	0.34	0.45
	0.30	—	0.42
	0.40	0.31	0.46
	0.50	0.31	0.47
	0.60	—	0.45
	0.70	0.34	0.46
	0.80	0.32	0.52
	0.90	0.34	—
20	0.40	0.17	0.25
25	0.40	0.23	0.34
35	0.40	0.41	0.61
40	0.40	0.53	0.80
45	0.40	—	1.03

a) [Complex]=[Fe(II)]=0.01 mol dm^{-3}. $I=1.0$ mol dm^{-3} ($LiClO_4$).

over a ten-fold increase of $[H^+]$. Activation parameters were determined at $[H^+]=0.01$ mol dm^{-3}, the complexes being in the unprotonated form under these conditions. The values in the temperature range 30—55 °C are $\Delta H^{\neq}=49.8\pm4.8$ kJ mol^{-1}, $\Delta S^{\neq}=-98.3\pm8.3$ J K^{-1} mol^{-1} for $[Co(gly)(mal)_2]^{2-}$ and $\Delta H^{\neq}=51.2\pm2.6$ kJ mol^{-1}, $\Delta S^{\neq}=-93.7\pm7.2$ J K^{-1} mol^{-1} for $[Co(py)_2(mal)_2]^-$.

Table 2 presents the second order rate constants k for the Fe(II) reduction of $[Co(nta)(mal)]^{2-}$ and $[Co(nta)(ox)]^{2-}$. The rate constant decreases from

0.51 to 0.35 $dm^3 mol^{-1} s^{-1}$ in the range $0.01<[H^+]<0.1$ mol dm^{-3} and remains constant at ca 0.33 $dm^3 mol^{-1} s^{-1}$ at higher $[H^+]$ for $[Co(nta)(mal)]^{2-}$, while the value of k is 0.45 $dm^3 mol^{-1} s^{-1}$ in the range $0.01<[H^+]<0.8$ mol dm^{-3} for $[Co(nta)(ox)]^{2-}$. The activation parameters have been determined in the temperature range 20—45 °C and at $[H^+]=0.4$ mol dm^{-3}, the values being $\Delta H^{\neq}=41.1\pm3.2$ kJ mol^{-1}, $\Delta S^{\neq}=-119.2\pm9.7$ J $K^{-1} mol^{-1}$ for $[Co(nta)(mal)]^{2-}$ and $\Delta H^{\neq}=41.4\pm3.6$ kJ mol^{-1}, $\Delta S^{\neq}=-114.6\pm9.6$ J $K^{-1} mol^{-1}$ for $[Co(nta)(ox)]^{2-}$.

Discussion

Fe(II) reduction of $[Co(gly)(mal)_2]^{2-}$ and $[Co(py)_2(mal)_2]^-$: The dependence of the rate constants on $[H^+]$ (Table 1) may be expressed in the form

$$k = k_1 + k_2[H^+], \quad (1)$$

k_1 being the rate constant due to the unprotonated species present at pH 2. H^+ accelerations similar to that observed here have been observed in the Fe(II) reduction of $[Co(edta)]^-$[14] $[Co(mal)_3]^{3-}$[5] and $[Co(en)(mal)_2]^-$,[2] explained in terms of the involvement of an aqua complex generated by the H^+-assisted dechelation of the complexes. One should thus expect the reaction to proceed through the following steps:

$$[Co(gly)(mal)_2]^{2-} + H^+ + H_2O \overset{K_1}{\rightleftharpoons} [Co(gly)(mal)(OCOCH_2COOH)(H_2O)]^-, \quad (2)$$

$$[Co(gly)(mal)(OCOCH_2COOH)(H_2O)]^- + Fe^{2+} \overset{K_2}{\rightleftharpoons} \mathbf{1}, \quad (3)$$

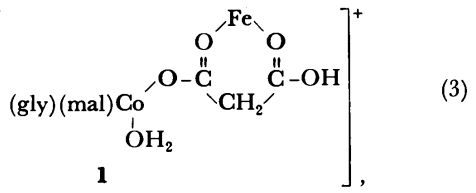

$$\mathbf{1} \xrightarrow[\text{slow}]{k_3} Co^{2+} + H_2mal + Fe^{3+} + gly, \quad (4)$$

k_2 being equal to $k_3K_1K_2$. K_1 and K_2 are too small in magnitude to permit observation of any limiting behavior. The values of k_2 for $[Co(gly)(mal)_2]^{2-}$ and $[Co(py)_2(mal)_2]^-$ are found to be 1.1—1.2 and 0.9 $dm^6 mol^{-2} s^{-1}$ respectively. These values suggest a significant kinetic advantage for the former due to $[H^+]$ acceleration. The values of k_1 for the two complexes are, however, similar, the values being 0.11 $dm^3 mol^{-1} s^{-1}$ for $[Co(gly)(mal)_2]^{2-}$ and 0.10 $dm^3 mol^{-1} s^{-1}$ for $[Co(py)_2(mal)_2]^-$.

Iron(II) reduction of $[Co(nta)(mal)]^{2-}$ and $[Co(nta)(ox)]^{2-}$: The rate constant (Table 2) for the reduction of $[Co(nta)(mal)]^{2-}$ decreases from 0.51 to 0.35 $dm^3 mol^{-1} s^{-1}$ as $[H^+]$ is increased from 0.01 to 0.1 mol dm^{-3} and reaches a limiting value of ca. 0.33 $dm^3 mol^{-1} s^{-1}$ in the range $0.1<[H^+]<0.9$ mol dm^{-3}. This is in contrast to the bis(malonato) complexes, where a $[H^+]$-assisted acceleration of reaction was observed. The observed $[H^+]$-dependence of rate for $[Co(nta)(mal)]^{2-}$ suggests the possibility of the presence of the species $[Co(nta)(H_2O)(OCOCH_2COO)]^{2-}$ and its protonated form in equilibrium. A similar inverse $[H^+]$-dependence has been observed in the Fe(II) reduction of $[Co(NH_3)_5(mal)]^+$ and $[Co(NH_3)_5(ox)]^+$.[4] The possibility of the presence of the species $[Co(nta)(H_2O)(OCOCH_2COO)]^{2-}$ was also verified by pH-titration of the complex with NaOH. The complex exhibited acid function as indicated by a buffer region in the pH range 4—6. No buffer region was observed for a similar titration with $[Co(nta)(ox)]^{2-}$. The possibility of the formation of the species $[Co(Hnta)(H_2O)(mal)]^-$, $[Co(Hnta)(H_2O)(ox)]^-$, $Co(Hnta)(H_2O)_2(Hmal)$, and $[Co(Hnta)(H_2O)(Hox)]$ may also be considered at high $[H^+]$. The formation of such species would be indicated by a $[H^+]$-dependent acceleration of rate, as observed for $[Co(gly)(mal)_2]^{2-}$, and *trans*-$[Co(py)_2(mal)_2]^-$. The absence of any acceleration of rate by H^+ for the Co(III)-nta complexes is an evidence against the possibility of $[Co(Hnta)(H_2O)_2(Hmal)]$ and the corresponding oxalato species.

Comparison of the rate constants for the Fe(II) reduction of $[Co(nta)(ox)]^{2-}$ with $[Co(nta)(mal)]^{2-}$ indicates an unusual trend. Generally the rates of reduction of oxalato complexes are higher by one or two orders of magnitude than the rates for the corresponding malonato complexes. For example, at $[H^+]$-0.4 mol dm^{-3} and at 30 °C the k values are 4.5×10^{-3} and 1.7×10^{-4} $mol^{-1} dm^3 s^{-1}$ for the Fe(II) reduction of $[Co(en)(ox)_2]^-$ and $[Co(en)(mal)_2]^-$ respectively[2] and 4.3×10^{-1} and 1.3×10^{-3} $mol^{-1} dm^3 s^{-1}$ for $[Co(NH_3)_5(ox)]^+$ and $[Co(NH_3)(mal)]^+$ respectively, at 25 °C.[4] However, the near similarity in rates viz. 0.46 and 0.32 $mol^{-1} dm^3 s^{-1}$ for $[Co(nta)(ox)]^{2-}$ and $[Co(nta)(mal)]^{2-}$ respectively in the $[H^+]$ range 0.4—0.8 mol dm^{-3} suggests a difference in the nature of the reactive species for the two complexes, viz. a chelated oxalate and a monodentate malonate. The reactivity of the latter is possibly due to precursor stabilization by chelation with Fe^{2+}.

References

1) B. Grossman and A. Haim, *J. Am. Chem. Soc.*, **93**, 6990 (1971).
2) R. Viswanathan and V. R. Vijayaraghavan, *Indian J. Chem.*, **23**, 1001 (1984).
3) C. Hwang and A. Haim, *Inorg. Chem.*, **9**, 500 (1970).
4) K. Ohashi, *Bull. Chem. Soc. Jpn.*, **49**, 1006 (1976).
5) Y. Sulfab and M. S. Al Obadie, *Polyhedron*, **1**, 149 (1982).
6) C. Lavalle and E. Deutsch, *Inorg. Chem.*, **11**, 3133 (1972).
7) P. N. Balasubramanian and V. R. Vijayaraghavan, *Inorg. Chim. Acta*, **38**, 49 (1980).
8) P. N. Balasubramanian and V. R. Vijayaraghavan,

Inorg. Chim. Acta, **53**, L209 (1981).
9) K. Yamasaki, J. Hidaka, and Y. Shimura, *Bull. Chem. Soc. Jpn.*, **42**, 119 (1969).
10) Y. Ida, S. Fujinami, and M. Shibata, *Bull. Chem. Soc. Jpn.*, **50**, 2665 (1977).
11) M. Mori, M. Shibata, E. Kyuno, and Y. Okubo, *Bull. Chem. Soc. Jpn.*, **31**, 940 (1985).
12) Y. Kurimura, K. Ohashi, T. Ohtsuki, and K. Yamamoto, *Bull. Chem. Soc. Jpn.*, **44**, 1293 (1971).
13) J. R. Ward and A. Haim, *J. Am. Chem. Soc.*, **92**, 475 (1970).
14) P. B. Wood and W. C. E. Higginson, *J. Chem. Soc.*, **1965**, 2116.

Synthesis, Dehydration Studies, and Cation-Exchange Behavior of a New Phase of Niobium(V) Phosphate

Mohsin QURESHI,* Anees AHMAD, Naseem Ahmad SHAKEEL, and Anek Pal GUPTA†
Chemical Laboratories, Z. H. College of Engg. and Tech., Aligarh Muslim University, Aligarh 202 001, India
(Received October 11, 1985)

Twenty-three samples of niobium(V) phosphate have been synthesized under different conditions using niobium sulfate and phosphoric acid solutions. The amorphous sample having the ion-exchange capacity of 1.06 mEq g^{-1} and niobium to phosphorus mole ratio of 0.670 was studied in detail for its cation-exchange behavior. Molar distribution coefficients for 25 cations have been studied on this gel at pH 1,2,3, and 5.5. Four quantitative separations of Mg^{2+}-Ca^{2+}, Mg^{2+}-Ba^{2+}, Zn^{2+}-Cd^{2+}, and Bi^{3+}-Zn^{2+} have successfully been achieved on it. The properties of this sample have been compared with those of niobium arsenate, niobium antimonate, and niobium molybdate. A tentative structural formula is proposed for this sample of niobium phosphate on the basis of chemical composition, cation-exchange capacity, pH-titration, IR spectra, T.G.A., water absorption, and heat treatment data.

Synthetic inorganic ion exchangers have been systematically studied during the last ten years owing to their resistance to heat and radiation. However, their analytical applications to the recovery of precious metals from radioactive wastes and to other chromatographic separations are of current interest. The inorganic ion exchangers based on zirconium have been most thoroughly studied followed by those based on tin, titanium and thorium. Very few studies have been reported on niobium(V) based inorganic ion exchanger.

Sukharev et al.[1-5] synthesized niobium phosphate and observed the effect of the presence of trivalent cation (Ce^{3+}, Fe^{3+}, or Cr^{3+}) upon its composition and sorptional behavior. The distribution coefficients were found higher for the precipitate prepared in the presence of trivalent ions. The phase synthesized at pH≤4 showed higher exchange capacity, improved kinetic parameters and ionic diffusion coefficients close to those in organic resin ($\simeq 10^{-8}$ cm s^{-1}). They also found that the amorphous niobium phosphate phases show a preferential uptake for $H_2[Fe(PO_4)_2]^-$ and $H_5[Fe(PO_4)_3]^-$. Shtin et al.[6,7] investigated the complexation of Nb(V) with phosphoric acid and the solubility of complexes of niobium phosphates $[Nb(OH)_3H_{4+z}(PO_4)_3$ where $z=2—5]$ as a function of H_3PO_4 concentrations within the ionic strength 2—20. They also studied the proton exchange in the coordination sphere of $Nb^{IV}(O_2^-)(OH^-)$ radical complexes. Posplev et al.[8,9] observed the effect of concentration of H_3PO_4 acid during synthesis on the properties of granular niobium phosphate $[NbO(OH)_3]_k[NbO(OH)_2]_l[HPO_4]_n[H_2O]_x$ and the effect of synthesis conditions on the composition and its properties. Chernokov et al.[10] prepared crystalline niobium phosphate having formula $NbO(PO_4)\cdot 2H_3PO_4\cdot 5H_2O$.

It is clear from what has been said above that considerable work has been done on the different phases of niobium(V) phosphate but no single phase has yet been exhaustively studied for its ion exchange behavior. Some aspects of these materials need elucidation and therefore we reinvestigated niobium phosphate in continuation of our systematic studies on niobium compounds such as niobium arsenate,[11-13] niobium antimonate,[14,15] and niobium molybdate.[16] The present manuscript describes our findings on a new phase of niobium phosphate.

Experimental

Reagents. Niobium pentaoxide was obtained from BDH (Poole, England). All other reagents of analytical reagent grade were used.

13.291 g Nb_2O_5 was heated with 400 ml of concd. H_2SO_4 containing 135 g $(NH_4)_2SO_4$ until a clear solution was obtained. After cooling the solution, 200 ml concd. H_2SO_4 was added to it and the whole mass was diluted to 1 liter with demineralized water (DMW) to give a 0.1 M solution (1 mol dm^{-3}) in niobium.

Apparatus. The following instruments were used. Elico pH-meter, Bausch and Lomb spectronic-710 colorimeter, DR-EL/4 (HATCH) spectrophotometer, IR Perkin Elmer Unit and Rich Seifort Iso Debyeflex 2002 X-ray diffractometer.

Synthesis. Numerous samples of niobium phosphate were synthesized by mixing acidic solution of 0.1 M niobium (sulfate) with phosphoric acid (Table 1). The concentration of H_3PO_4, mixing ratio, pH of precipitation, total refluxing time and the medium of reflux were the varying parameters. The precipitate so obtained was kept for 24 h with mother liquor to attain equilibrium. In each case the precipitate was separated from the mother liquor by decantation and washed with DMW until the wash solution had a pH of 6 and free from sulfate ions. The precipitate was dried at 40 °C and sieved to get the granules of 50—100 mesh size. The ion-exchange capacities were also determined by the column process for Na^+ ion. Sample 21 (NbP3) having the ion-exchange capacity (I.E.C.) of 1.06 mEq g^{-1} was chosen for detailed study.

Composition. 0.2 g NbP3 was dissolved in an acidic solution which was 10% in H_2SO_4 and 5% in HF. Niobium was determined as Nb_2O_5. It was precipitated with a 10% solution of cupferron[17] as niobium cupferronate. The white precipitate of niobium cupferronate was collected on ashless filter paper with repeated washings with 1% solution of cupferron. The precipitate with filter paper was first dried in

†Present address: Chemistry Department, Delhi College of Engg. Kashmere Gate, Delhi-110006, India.

Table 1. Synthesis and Ion Exchange Capacities of Niobium Phosphate Samples

S.No.	Sample No.	Refluxing		Time/h	Color of final precipitates	I.E.C./mEq g^{-1}
		State of precipitate	Medium			
1	NbP1	Solid	Nil	Nil	Shiny granules	0.94
2	NbP2	Wet	1M H_3PO_4	10	White	1.74
3	NbP3	Solid	1M H_3PO_4	10	Shiny granules	1.06
4	NbP4	Solid	1M H_3PO_4	24	White	1.20
5	NbP5	Solid	1M H_3PO_4	48	White	0.74

Note: Samples were prepared by mixing 0.1M solutions of niobium (sulphate) and phosphoric acid in the ratio of 1:4. The pH was adjusted to 1.1 by liquid ammonia.

Table 2. Solubility of Niobium(V) Phosphate in Different Solvents and Its Comparison to That of Arsenate, Antimonate, and Molybdate of Niobium

S.No.	Solvent	Niobium phosphate (NbP3)		Niobium arsenate[a] (Sample 2)		Niobium antimonate[b] (Sample AT 3)		Niobium molybdate[c]	
		Nb(mg L^{-1})	P(mg L^{-1})	Nb(mg L^{-1})	As(mg L^{-1})	Nb(mg L^{-1})	Sb(mg L^{-1})	Nb(mg L^{-1})	Mo(mg L^{-1})
1	4M H_2SO_4	1051.5	26.2	120.0	156.2	0.0	2.0	—	—
2	4M HNO_3	0.0	1.2	1.5	47.5	0.0	0.0	132.0	418.0
3	4M HCl	0.0	1.8	2.5	81.2	2.0	255.0	321.0	510.0[d]
4	1M Tartaric Acid	343.7	1.8	475.0	7.5	—	—	—	—
5	1M Acetic Acid	0.0	65.0	1.0	31.2	—	—	—	—
6	4M Ammonia	180.0	91.7	880.0	647.5[e]	352.0	659.0[e]	—	—
7	0.1M KOH	2000.0	675.0	—	—	460.0	560.0	Dissolved completely	
8	1M NaCl	0.0	62.5	—	—	—	—	—	—
9	1M NH_4NO_3	0.0	43.7	0.0	5.5	0.0	49.5	2.8	23.5
10	DMW[f]	0.0	10.4	0.0	11.5	0.0	4.2	3.6	20.1

a) From Ref. 12. b) From Ref. 14. c) From Ref. 16. d) In 2M HCl. e) In 1M Ammonia. f) Demineralized water.

Table 3. Ion-Exchange Capacities of NbP3 and NbP5 for Various Cations

S.No.	Cation	Salt used	pH of the eluent	Concn of salt	I.E.C./mEq g^{-1} (column process)	
					NbP3	NbP5
1	Li^+	LiCl	5.4	0.5 M	0.70	0.46
2	Na^+	NaCl	5.2	1.0 M	1.06	0.74
3	K^+	KCl	5.5	1.0 M	1.18	—
4	Mg^{2+}	$Mg(NO_3)_2$	5.7	0.5 M	0.96	—
5	Sr^{2+}	$SrCl_2$	5.8	0.5 M	1.00	—
6	Ba^{2+}	$BaCl_2$	5.5	0.5 M	1.56	1.34

the IR radiations and then heated in a silica crucible up to 1000 °C to convert it into Nb_2O_5. Phosphorus was obtained as ammonium magnesium phosphate by double precipitation from the former filtrate. The precipitate was heated up to 1000 °C in a silica crucible and determined as magnesium pyrophosphate[18] gravimetrically.

Chemical Stability. 0.2 g of NbP3 sample was shaken by batch process with different solvents for 24 h. The undissolved material was filtered off. The solutions were then analysed spectrophotometrically for the presence of niobium and phosphorus. Niobium was determined with KSCN[19] and phosphorus with ammonium molybdate-tin(II) chloride reagent.[20] The results are given in Table 2.

Ion Exchange Capacity. The I.E.C's of the samples of niobium phosphate were determined by column operation[21] using a column of 0.5 cm. (i.d.). The H^+ ions were eluted by percolating the required cationic solution through the column of the exchanger. The feed was passed until its pH became equal to that of the effluent collected. The hydrogen ions so eluted were titrated against standardized 0.1 M NaOH (Tables 1 and 3).

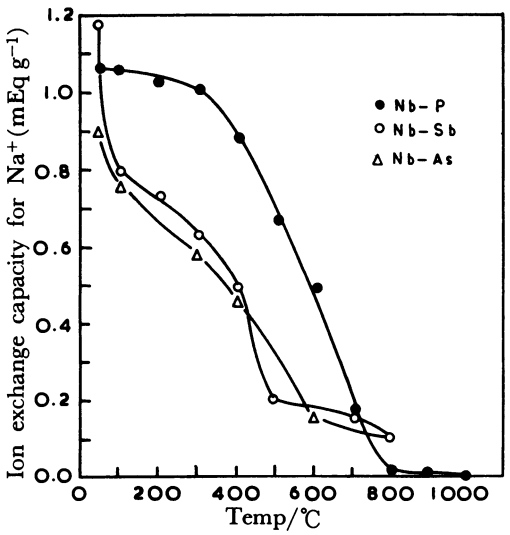

Fig. 1. Effect of temperature on ion-exchange capacities of various inorganic ion-exchangers.

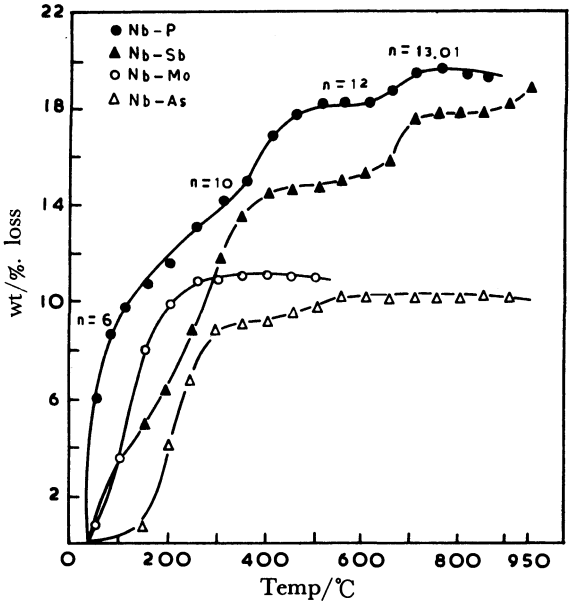

Fig. 2. T.G.A. curves of various inorganic ion-exchangers.

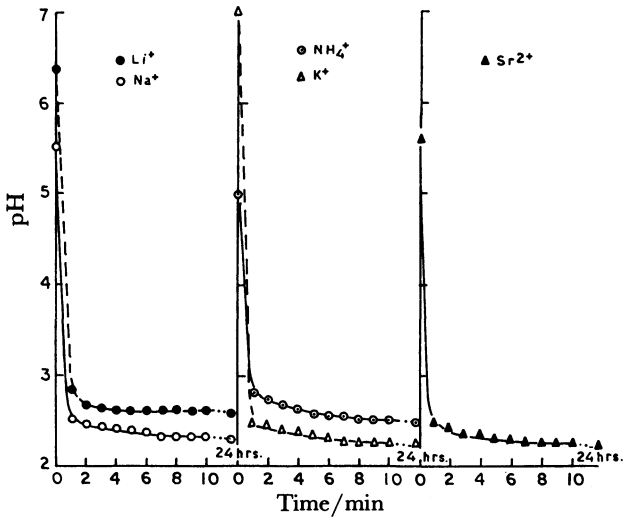

Fig. 3. Plots of pH as a function of time.

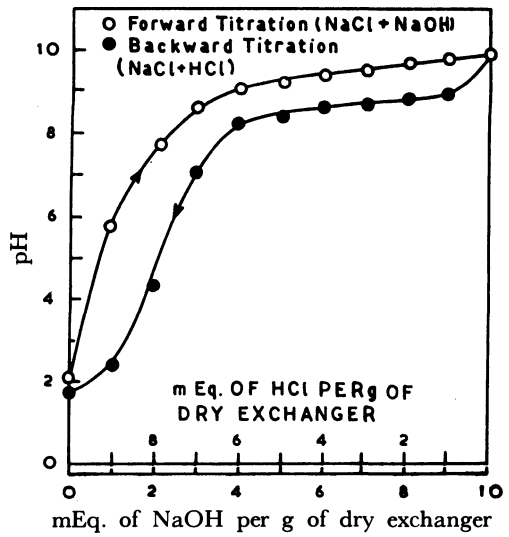

Fig. 4. pH titration curves for Na^+ on NbP_3.

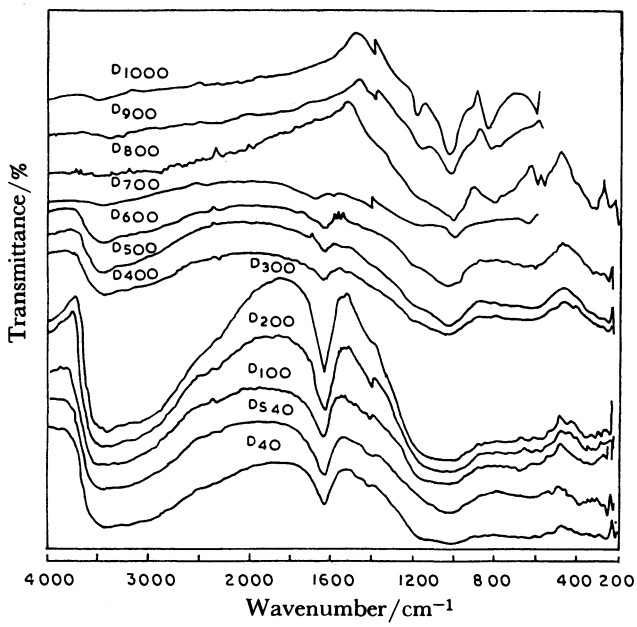

Fig. 5. IR spectra of niobium phosphate heated at various temperatures.
Abbreviations: D-sample 21 in H^+ form.
D_S-sample 21 in Na^+ form.
Subscripts 40—1000: Temperatures in °C.

Concentration Effect. 0.5 g samples of NbP3 in the H^+ form were equilibrated with 50 ml NaCl solution of different concentrations with intermittent shaking for 24 h in the stoppered conical flasks. The solid material was separated by decantation with repeated washings. The released hydrogen ions were titrated with standard NaOH solution.

Heat Treatment. To check the effect of temperature on the I.E.C. about 2 g of exchanger in the H^+ form was taken in different silica crucibles and each was heated in an automatic temperature controlled muffle furnace at different temperatures until the equilibrium reached. The I.E.C.'s of heated samples were determined with 1M NaCl without reconverting them to the H^+ form and plotted as a function of temperature in Fig. 1.

Thermogravimetric Analysis (T.G.A.). The thermogravimetric analysis was done by taking 0.5 g of the material in the H^+ form. It was heated at a rate of 10°C min^{-1} from 40 to 1000°C (accuracy ±5%) in an atmosphere of air and the weight loss as a function of temperature was recorded and shown in Fig. 2.

Water Absorption. 0.5 g of the sample in the H^+ form was heated at 100 and 200°C. The same sample in the Na^+ form was heated at 220°C for 1 h. The heated samples were stored in an air tight desiccator over a saturated solution of ammonium nitrate. The absorption of water was recorded at different time intervals.

Rate of Ion Exchange. The rate of ion exchange was measured by taking 50 ml of 1 M solution of the cation. The pH of the solution was measured and then 0.5 g of the exchanger in the H^+ form was added. The solution was shaken at short intervals and pH was recorded. The pH vs. time (in minutes) was plotted and shown in Fig. 3.

pH-Titration. The pH-titrations were performed by

the method of Topp and Pepper.[22] 0.1 g samples of dry exchanger in the H^+ form were shaken with 10 ml portions of 0.1 M (NaCl+NaOH) cationic solution in different conical flasks at 25±0.5°C. The ratio of NaCl/NaOH was varied from 0.1 M/0.01 M to 0.01 M/0.1 M in the equilibrating solution of the flasks. After 24 h the pH of the supernatant solution of each flask was recorded and plotted against the mEq of OH^- added per g of dry exchanger. For reverse titration, the Na^+ form of the exchanger was treated in a similar fashion with 0.1 M (NaCl+HCl) solution (Fig. 4).

X-Ray Diffractogram. Powder X-ray diffraction technique was used to take the diffractogram of the powdered sample using nickel filtered Cu $K\alpha$-radiation (λ=1.5404 Å).

IR Study. IR spectra of the material heated at various temperatures (i.e., from 40 to 1000°C) were recorded with the standard KBr disc technique. The spectrum of the material in the Na^+ form dried at 40°C was also recorded. The spectra are shown in Fig. 5.

Distribution Coefficients (K_d Values). K_d values of 25 cations on the exchanger sample were determined in DMW, 0.001, 0.01, and 0.1 M HNO_3 solutions (Tables 4a, 4b, 4c). The cations present in the solution were titrated with 10^{-3} M EDTA solution using the specific metal indicator. The distribution coefficient (K_d) was calculated as:

$$K_d(\text{ml g}^{-1}) = \frac{\text{Moles of metal ion per g of solid}}{\text{Moles of metal ion per ml of solution}}.$$

Separation Studies. The mixture of the metal ions were loaded on the exchanger and then the ions were eluted by suitable eluents. The flow rate of the effluent was maintained at 0.5 ml min^{-1} throughout the process. The released cations were estimated with standard 0.001 M EDTA solution (Table 5).

Results and Discussion

During these studies more than 20 samples of niobium phosphate have been synthesized under various conditions (results omitted to save space). Most of the samples were suitable for column operations and showed ion-exchange capacities varying from 0.16 to 1.2 mEq g^{-1} for the Na^+ ion. Only five of the samples (Table 1) were synthesized thrice, their ion-exchange capacities and chemical compositions were determined and found reproducible. They are designated as NbP1, NbP2,···, NbP5 respectively. The amorphous sample, NbP3 having Nb/P mole ratio of 0.67 and I.E.C. of 1.06 mEq g^{-1} was chosen first for detailed studies (reported in this manuscript). The studies on the rest of the samples is in progress and a part of it is reported elsewhere.[23]

Table 3 shows the ion-exchange capacities of samples 3 and 5 for various cations obtained by column process. The capacity increases as the hydrated radii of the cations decrease. The ion-exchange capacity of NbP3 increases from 0.86 to 1.06 mEq g^{-1} as the concentration of the eluent (NaCl) changes from 0.2 to 1 M and then becomes constant.

It is clear from Fig. 3 that the exchange is initially fast and then it slows down after one minute. Li^+, NH_4^+, and Sr^{2+} do not exchange as efficiently as Na^+ and K^+ ions.

The pH-titration of the material with NaOH in the presence of the added salt reveals its monofunctional behavior as it shows only one inflection point. The

Table 4a. K_d Values in DMW upon Phosphate, Arsenate, Molybdate, and Antimonate of Niobium

S.No.	Cation	Niobium phosphate	Niobium arsenate[a]	Niobium molybdate[b]	Niobium antimonate[c] (approximate)
1	Mg^{2+}	1028	171	26	20
2	Ca^{2+}	1078	298	30	398
3	Ba^{2+}	331	2980	20	398
4	Sr^{2+}	70	553	43	398
5	Fe^{3+}	45	115	—	1585
6	Ni^{2+}	71	1005	—	100
7	Co^{2+}	6437	387	—	—
8	Mn^{2+}	4500	1930	60	—
9	Cd^{2+}	5375	950	44	631
10	Cu^{2+}	4687	1600	>3500	399
11	Zn^{2+}	182	1100	27	100
12	Hg^{2+}	1875	31	0	398
13	Pb^{2+}	121	1850	—	2512
14	Zr^{4+}	2812	109	—	—
15	V^{5+}	295	540	—	340
16	Y^{3+}	734	9460	—	631
17	La^{3+}	1375	—	>3500	631
18	Ce^{3+}	375	—	—	795
19	Pr^{3+}	3312	9460	>3000	—
20	Sm^{3+}	112	9260	—	—
21	Eu^{3+}	75	2110	—	—
22	Gd^{3+}	316	2312	—	200
23	Al^{3+}	500	1930	17	251
24	Th^{4+}	110	—	400	631
25	Bi^{3+}	2575	—	1300	—

a) From Ref. 11. b) From Ref. 16. c) From Ref. 14.

Table 4b. K_d Values in 0.1M HNO_3 upon Phosphate Arsenate, Antimonate, and Hydrated Oxide of Niobium

S.No.	Cation	Niobium phosphate	Niobium arsenate[a)]	Niobium antimonate[b)]	Niobium hydrated oxide[c)]
1	Mg^{2+}	0	7	3	0
2	Ca^{2+}	99	22	18	0
3	Sr^{2+}	6	55	23	5
4	Ba^{2+}	120	85	280	62
5	Fe^{3+}	688	72	286	22
6	Ni^{2+}	4	13	27	12
7	Co^{2+}	3156	15	—	—
8	Mn^{2+}	70	11	—	—
9	Cd^{2+}	166	110	39	0
10	Cu^{2+}	115	65	26	3
11	Zn^{2+}	0	71	38	3
12	Hg^{2+}	366	12	410	370
13	Pb^{2+}	128	557	1066	425
14	Zr^{4+}	2813	193	—	—
15	V^{5+}	184	469	260	—
16	Y^{3+}	—	14	30	11
17	La^{3+}	1150	—	50	2
18	Ce^{3+}	675	—	20	0
19	Pr^{3+}	0	47	—	—
20	Sm^{3+}	11	20	—	—
21	Eu^{3+}	0	79	—	—
22	Gd^{3+}	20	10	34	0
23	Al^{3+}	963	133	160	0
24	Th^{4+}	110	—	95	50
25	Bi^{3+}	2575	—	—	—

a) From Ref. 11. b) From Ref. 14. c) From Ref. 14.

Table 4c. K_d Values upon Niobium Phosphate in HNO_3 at pH 2 and 3

S.No.	Cation	0.01M HNO_3	0.001M HNO_3	S.No.	Cation	0.01M HNO_3	0.001M HNO_3
1	Mg^{2+}	531	739	14	Bi^{3+}	2575	2575
2	Ca^{2+}	469	2281	15	Zr^{4+}	2813	2813
3	Sr^{2+}	77	118	16	V^{5+}	609	—
4	Ba^{2+}	281	156	17	Y^{3+}	174	268
5	Fe^{3+}	24	40	18	La^{3+}	1150	1375
6	Ni^{2+}	29	578	19	Ce^{3+}	675	675
7	Co^{2+}	6438	6437	20	Pr^{3+}	625	639
8	Mn^{2+}	4500	4500	21	Sm^{3+}	134	160
9	Cd^{2+}	5375	5375	22	Eu^{3+}	59	60
10	Cu^{2+}	68	4688	23	Gd^{3+}	25	—
11	Zn^{2+}	182	182	24	Al^{3+}	963	604
12	Hg^{2+}	328	—	25	Th^{4+}	110	110
13	Pb^{2+}	640	121				

Table 5. Separations Achieved on Niobium Phosphate Column

S.No.	Mixture loaded	Cation eluted	Eluent	Total volume of effluent collected	Amount loaded	Amount found	Error
				ml	μg	μg	%
1	Mg^{2+}-Ca^{2+}	Mg^{2+}	0.2M HNO_3	100	216	205	−5.09
		Ca^{2+}	0.2% $H_2C_2O_4$	25	160	168	+5.00
2	Mg^{2+}-Ba^{2+}	Mg^{2+}	0.2M HNO_3	110	216	216	0.00
		Ba^{2+}	0.2% $H_2C_2O_4$	25	448	450	+0.45
3	Zn^{2+}-Cd^{2+}	Zn^{2+}	0.2M HNO_3+0.25% NH_4NO_3	60	293	299	+2.05
		Cd^{2+}	1.0M HNO_3+0.5% NH_4NO_3	60	244	250	+2.46
4	Bi^{3+}-Zn^{2+}	Bi^{3+}	2% Na_2CO_3	30	214	219	+2.34
		Zn^{2+}	0.2M HNO_3+0.25% NH_4NO_3	70	290	294	+1.38

Table 6. Comparison of Theoretical and Observed Structural Data of Niobium Phosphate i.e., NbP3

S.No.	Properties	Observed	Theoretical	Remark
1	Behavior	Monofunctional	Monofunctional	$\overset{*}{H}PO_4^-$ — are exchange sites
2	Useful I.E.C. at 40°C	1.06 mEq g^{-1}	—	
3	I.E.C. by pH-titration	1.68 mEq g^{-1}	1.68 mEq g^{-1}	
4	Total I.E.C.	—	4.96 mEq g^{-1}	
5	Empirical formula	$2Nb_2O_5 \cdot 3P_2O_5(H_2O)_{2.96}10.05H_2O$	$2Nb_2O_5 \cdot 3P_2O_5(H_2O)_310H_2O$	
6	Mol. Wt.	1192.18	1192.00	
7	Nb/P ratio	0.67	0.67	

behavior appears to be reversible at lower pH values, i.e., pH 1—2. A hysteresis loop occurs at higher pH values. This may be due to the hydrolysis of niobium and phosphate groups at higher pH values which results in a totally different phase formation. This is in accordance with the chemical stability data that the material gets hydrolyzed in alkaline solution. It gave an ion-exchange capacity of 1.68 mEq g^{-1} for Na^+ ion.

The chemical dissolution data (Table 2) show that NbP3 is highly stable in 4 M HNO_3 and 4M HCl. It dissolves frequently in 4 M H_2SO_4, 1 M tartaric acid, 4 M ammonia and in 0.1 M KOH solutions probably due to complex formation. Its stability in 4 M HCl is remarkable as most exchangers which are stable in 4 M HNO_3 are unstable in 4M HCl. The comparison of NbP3 with the arsenate, antimonate, and molybdate of niobium shows that in most solutions NbP3 in only next to niobium antimonate in chemical stability.

In order to obtain some informations regarding the empirical formula and theoretical ion-exchange capacity of NbP3, thermoanalytical investigations were carried out. It is clear from Fig. 1 that the ion-exchange capacity of the various ion exchangers decreases with increase in temperature. It also shows that NbP3 is more thermally stable than niobium arsenate and antimonate as far as its ion-exchange behavior is concerned.

X-Ray diffraction studies of the material dried at 40°C revealed its amorphous behavior while the material heated above 400°C showed some signs of crystallinity. Only two weak lines viz. at d=8.01 and d=3.22 Å appeared in these samples. The intensities of these lines increased with increase in temperature.

The comparison of T.G.A. curves of various exchangers in the H^+ form (Fig. 2) shows that the curves of niobium molybdate and niobium arsenate are simple and similar up to 500°C. However, the T.G.A. of NbP3 is more complicated than that of the former compounds. It resembles more the curve for niobium antimonate. The most remarkable aspect of this curve is the highest weight loss than for any of the four compounds. Another interesting feature is the three-step weight loss which shows that there are at least three types of dehydrations occurring in this compound. This unusual behavior is probably due to the great affinity of the phosphate groups for water molecules and also due to large content of hydroxo-phosphate anionic part.

For niobium phosphate the weight loss is maximum (19.65%) up to 700°C. Assuming that at this temperature the composition of the sample is $2Nb_2O_5 \cdot 3P_2O_5$ (Nb:P=2:3, by chemical analysis) the number of moles of water lost per formula weight of the exchanger corresponding to the weight loss at different temperatures was calculated by the method of Alberti, et al.[24] and shown in Table 6.

If n is the number of moles of water per mole of "mixed oxide," then

$$\% \text{ weight loss} = \frac{1800\,n}{958+18\,n}, \tag{1}$$

(where mol. wt. of "mixed oxide" = 958).

From this equation the empirical formula can be obtained as follows:

Suppose

W_H = % weight loss in H^+-form of exchager up to 800 °C,

W_{Na} = % weight loss in Na^+-form of exchanger up to 800 °C,

n_H = number of moles of water corresponding to W_H,

n_{Na} = number of moles of water corresponding to W_{Na},

n_{ex} = number of moles of water from –OH groups responsible for exchange,

n_{ab} = number of moles of water absorbed or the water of crystallization,

then

$$n_{ex} = n_H - n_{Na}, \tag{2}$$

$$n_{ab} = n_H - n_{ex}. \tag{3}$$

Treatment of the experimental data according to Eqs. 1, 2, and 3 gives

$$n_{ex} = 2.96,$$

$$n_{ab} = 10.05.$$

Hence we can assign the following formula to NbP3 sample:

$$2Nb_2O_5 \cdot 3P_2O_5(H_2O)_{2.96}10.05\ H_2O.$$

Hence,

$$\text{the theoretical I.E.C.} = \frac{2.96 \times 2 \times 1000}{1192.18}$$

$$= 4.96\ \text{mEq g}^{-1}.$$

The sodium ions are exchanged only up to 1.63 mEq g^{-1} in alkaline medium. It is very low as compared to the theoretical exchange capacity (4.96 mEq g^{-1}) and corresponds to two protons per formula weight of the exchanger. It seems that under our experimental conditions only the surface protons take part in the exchange reaction as the ingoing cations are not able to reach all the exchange sites (six protons) in amorphous niobium(V) phosphate. Hence only a part (two protons) of the H^+ present are exchangeable.[25-31]

The exchanger in the H^+ form when heated to 100 and 200 °C shows a weight loss of 10.2% (n=6.04) and 11.8% (n=7.12), respectively. Upon storing these dried samples in air-tight desiccator over a saturated solution of NH_4NO_3 solution, the former reabsorbs 100% water within 20 h while the latter could absorb only 86.06% water (n=6.01) after 100 h. This shows that the loss of water at 100 °C is completely reversible while at 200 °C only 86% reversibility is obtained. When the same sample in the Na^+ form was heated to 200 °C and stored over a saturated solution of NH_4NO_3, it regained the lost water molecules at a slightly higher rate than that of the H^+ form. It recovered approximately all the weight loss within 100 h. This reveals that the hydrated Na^+ ion lies within the cavity and keeps it slightly expanded thus facilitating the reabsorption of the water molecules into the cavity.

The IR spectra of NbP3 heated at various temperatures are given in Fig. 5. All the spectra refer to the niobium phosphate in the H^+ form. Only D_{s40} refers to that of Na^+ form dried at 40 °C. A comparison of D_{40} and D_{s40} spectra is very interesting. Since the band between 3000 and 3600 cm^{-1} refer to strong hydrogen bonds between-OH groups of water molecules and hydrogen-bearing oxygen of phosphate groups, therefore this band may be attributed to the long hydrogen bond P-O-H····O-H and P-O-H····$O\langle^{H}_{H}$.[32] When the hydrogen ion of the P-OH group is replaced by Na^+, the hydrogen bonding is diminished and the band becomes narrower. A similar effect is observed for the band between 940 and 1180 cm^{-1}. This band can be assigned to the symmetric and antisymmetric vibrations for the phosphate groups.[32] When the hydrogen ion of P-OH is replaced by Na^+, which is more strongly ionized we obtain a much narrower peak in D_{s40} spectra in this region at 1020 cm^{-1}. The effect of heating on the band between 3000 and 3600 cm^{-1} and the peak at 1630 cm^{-1} can be interpreted as follows:

Since the band is due to P-O-H····$O\langle^{H}_{H}$ and the peak due to deformation vibration of H_2O and -OH groups it is possible that in the beginning, i.e., from 40 to 300 °C, the absorbed water molecules are lost and therefore the band and the peak become narrower as one goes from 40 to 300 °C. However, at 400 °C the P-OH groups of the phosphates begin to condense and this condensation is complete up to 800 °C. Therefore, at 800 °C (D_{800}) the band and the peak completely disappear. The effect of heat on the band between 940 and 1180 cm^{-1} is quite different. Since this band is due to P-O vibrations[32] it remains unaffected up to 300 °C with the loss of water molecules. Above 300 °C the band becomes narrower due to condensation of P-OH groups and the increase in the concentration of P-O-P groups. At 800 °C all the P-OH groups condense and hence a very sharp peak is obtained owing to the presence of P-O-P groups at 1020 cm^{-1}. This phase also shows some more peaks at 850, 620, 580, 350, and at 250 cm^{-1} corresponding O-P-O and O-Nb-O interatomic stretching vibrations.[32] In this way we can say that D_{800} is completely a new phase having no hydroxyl group or water of free ionic sites responsible for ion exchange.

Theoretical Interpretation of the Heating Effect. The schematic diagram and Fig. 1 show the amount and the type of water molecules lost with temperature. At 100 °C six water molecules attached to $\overset{*}{H}PO_4$ groups are lost. Up to 200 °C, 1.12 more water molecules are irreversibly removed from the cavity resulting in the cavity shrinkage and a negligible effect on the I.E.C. Up to 350 °C all the rest absorbed (probably coordinated to niobium) water molecules are lost. The condensation of phosphate groups starts above 400 °C and up to 550 °C two water molecules are lost as a result of intermolecular condensation of four phosphate groups.

$$(\overset{*}{H}PO_4^{2-})_2(HPO_4^{2-})_4 \xrightarrow[\approx 550°C]{-2H_2O} (\overset{*}{H}PO_4^{2-})_2(P_2O_7^{4-})_2$$

Intermolecular Condensation of Monomers

At 650 °C the dimer formation starts due to intramolecular condensation of the monomers and 0.5 water molecule per formula weight is lost from one of the $\overset{*}{H}PO_4^{2-}$ group and thus the I.E.C. is reduced to half.

$$2[(\overset{*}{H}PO_4^{2-})_2(P_2O_7^{4-})_2] \xrightarrow[\sim 650°C]{-H_2O} (\overset{*}{H}PO_4^{2-})_2(P_2O_7^{4-})_5$$

Monomers Dimer

Intramolecular Condensation

Above 700 °C two dimers combine together to give a tetramer. The condensation is complete up to 800 °C and at this stage all the exchange sites are exhausted.

$$2[(\overset{*}{H}PO_4^{2-})_2(P_2O_7^{4-})_5] \xrightarrow[>700°C]{-2H_2O} (P_2O_7^{4-})_{12}$$

Dimers Tetramer

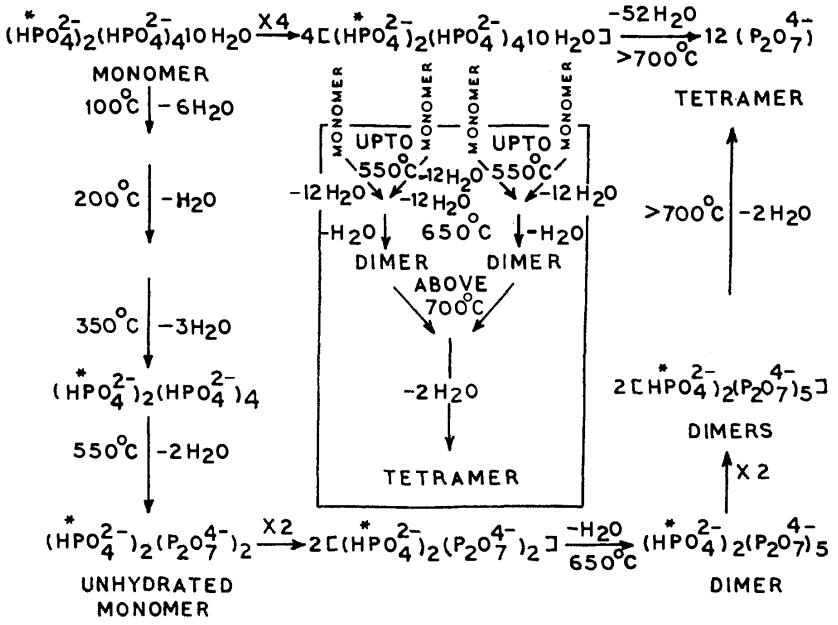

Schematic Representation of Heating Effect on Niobium Phosphate

The condensation process in this way agrees with IR, X-ray, T.G.A., and I.E.C. data and the niobium to phosphorus mole ratio remains constant at all the temperatures studied.

The K_d values of 25 metal ions on niobium phosphate (NbP3), niobium arsenate (Nb-As), niobium molybdate (Nb-Mo), and niobium antimonate (Nb-Sb) in DMW are given in Table 4a. All these materials show a high uptake for Cu^{2+}, Bi^{3+}, La^{3+}, Pr^{3+}, Y^{3+}, Sm^{3+}, and Gd^{3+}. Table 4b lists the K_d values on NbP3, Nb-As, Nb-Sb, and Nb_2O_5 which reflects that these exchangers show no absorption of Mg^{2+}, high or preferential uptake of Hg^{2+}, Pb^{2+}, Zr^{4+}, and V^{5+} and moderate preference towards lanthanides in 10^{-1} M HNO_3. Distribution coefficients on NbP3 in 10^{-2} M and 10^{-3} M HNO_3 decrease upon increasing the acid concentration as is evident from Table 4c.

The study of distribution coefficients in nitric acid solutions reveals the appreciable differences among the K_d values of a number of metal ions. The exchanger appears to be selective for Co^{2+} and Zr^{4+} in all the media. It seems that it can be used for the separation and purification of rare earth from various metal contaminants. These studies will require a careful examination of the problem. At present no attempt has been made in this direction, or rather, four quantitative separations of common cations namely, Mg^{2+}-Ca^{2+}, Mg^{2+}-Ba^{2+}, Zn^{2+}-Cd^{2+}, and Bi^{3+}-Zn^{2+} have been tried and successfully achieved on amorphous niobium(V) phosphate column. The results are presented in Table 5 which show that the recoveries of the metal ions lie within the limit of experimental errors.

The CSIR (India) is gratefully acknowledged for providing financial assistance under the Special Research Programme (Emeritus Scientist Scheme).

References

1) Yu. V. Egorov, Yu. I. Sukharev, and N. N. Pustovalov, *Tovarnyl, Znaki*, **46**, 22 (1969).

2) Yu. I. Sukharev, Yu. V. Egorov, and N. N. Pustovalov, *Zh. Neorg. Khim.*, **16**, 1026 (1971).

3) N. V. Dranitsina, Yu. V. Egorov, N. N. Kalugina, N. N. Pustovalov, and Yu. I. Sukharev, *Neorg. Ionooben. Mater.*, **1**, 97 (1974).

4) Yu. I. Sakharov, O. R. Glukhova, and Yu. V. Egorov, *Tr. Ural'sk Politekhn.*, **226**, 72 (1975).

5) R. M. Belkina, Yu. I. Sukharev, and Yu. V. Egorov, *Zh. Neorg. Khim.*, **21**, 1758 (1976).

6) A. M. Gorelov and A. P. Shtin, Deposited Publication VINITI **22**, 6694 (1973).

7) A. P. Shtin, V. L. Mamoshin, and A. D. Galaktinov, *Kimiya Tvenol. Tela (Sverdlovsk)*, **2**, 41 (1978).

8) A. A. Pospelov, V. N. Krylov, G. I. Deulin, L. M. Slobod-Chikova, and R. B. Dushin, *Iezisy. Dokl. Vses. Nauchno. Tekh. Knof. Tekhol Neorg. Veshchestu Miner Idobr.*, **1**, 141 (1974).

9) G. I. Deulin, N. V. Egorova, V. N. Krylov, V. G. Pitalve, A. A. Pospelov, and L. M. Slobodchikova, *Zh. Prikl. Khim.*, **54**, 1226 (1981).

10) N. G. Chernokov, M. P. Egorov, and V. F. Kutsepin, *Zh. Neorg. Khim.*, **24**, 1782 (1979).

11) M. Qureshi, J. P. Rawat, and A. P. Gupta, *J. Chromatogr.*, **118**, 167 (1976).

12) M. Qureshi, J. P. Rawat, and A. P. Gupta, *Chromatographia*, **11**, 202 (1978).

13) M. Qureshi, J. P. Rawat, and A. P. Gupta, *J. Indian Chem. Soc.*, **LVIII**, 855 (1981).

14) M. Qureshi, A. P. Gupta, T. Khan, and J. P. Gupta, *Chromatogr.*, **144**, 231 (1977).

15) M. Qureshi, A. P. Gupta, D. V. Nowell, and J. P. Gupta, *J. Inorg. Nucl. Chem.*, **40**, 545 (1978).

16) M. Qureshi, A. P. Gupta, J. S. Thakur, and V. P. Singh, *Sepn. Sci. Tech.*, **15**, 1255 (1980).

17) G. E. F. Lundell and J. I. Hoffman, "Outlines of Methods of Chemical Analysis," Wiley, New York (1958), p.

117.
18) N. H. Furman, "Standard Methods of Chemical Analysis," 6th ed, Van Nostrand, New York (1971), p. 812.
19) Alan D. Westland and Jerome Benzaire, *Anal. Chim. Acta*, **66**, 187 (1973).
20) APHA-AWWA-WPCF, "Standard Methods for the Examination of Water and Waste Water," 14th ed, (1975), p. 479.
21) O. Samuelson, Dissertation, Tek. Hogskelan, Stockholm, 1944.
22) N. E. Topp and K. W. Pepper, *J. Chem. Soc.*, **1949**, 3299.
23) Anees Ahmad, "Synthetic Inorganic Ion Exchangers," A Thesis submitted to A. M. U. Aligarh for the degree of Doctor of Philosophy in Chemistry, Aug, 1985.
24) G. Alberti, E. Torracà, and A. Conte, *J. Inorg. Nucl. Chem.*, **28**, 607 (1966).
25) J. S. Gill and S. N. Tandon, *J. Inorg. Nucl. Chem.*, **30**, 3885 (1972).
26) J. S. Gill and S. N. Tandon, *J. Radioanal. Chem.*, **13**, 391 (1973).
27) J. S. Gill and S. N. Tandon, *Talanta*, **19**, 1355 (1972).
28) J. S. Gill and S. N. Tandon, *J. Radioanal. Chem.*, **20**, 5 (1974).
29) J. S. Gill and S. N. Tandon, *Talanta*, **20**, 585 (1973).
30) J. S. Gill and S. N. Tandon, *J. Radioanal. Chem.*, **36**, 345 (1977).
31) J. S. Gill and S. N. Tandon, *J. Radioanal. Chem.*, **49**, 55 (1979).
32) J. A. Marinsky and Y. Marcus, "Ion Exchange and Solvent Extraction Series," Marcel Dekker, Inc., New York (1973), Vol. 5, p. 19.

 © 1986 The Chemical Society of Japan Bull. Chem. Soc. Jpn., 59, 3257—3262 (1986)

Photochemical Cis-Trans Isomerization of 5-Styryl-1,3-dimethyluracil

Eun Ju SHIN, Beom Shu AN, and Sang Chul SHIM*
Department of Chemistry, Korea Advanced Institute of Science and Technology, P. O. Box 150
Cheongyangni, Seoul 131, Korea
(Received July 15, 1985)

The cis-trans photoisomerization of 5-styryl-1,3-dimethyluracil is investigated. The fluorescence and photoisomerization quantum yields in various solvents of different viscosity and polarity, the effect of salt, pH, and heavy atom on the fluorescence and photoisomerization, the triplet sensitization of the photoisomerization, and the azulene quenching of the direct and sensitized isomerization indicate the singlet mechanism for the direct photoisomerization of the compound. The laser flash photolysis at room temperature showed a weak triplet-triplet absorption indicating some intersystem crossing from the excited singlet state to the triplet state.

The photochemical cis-trans isomerization of olefinic compounds has been extensively studied and is one of the best-known photoreactions.[1-4] Nonetheless, its mechanistic details have been the subject of much controversy.

From the theoretical calculations and spectroscopic observations for stilbene, it was proposed that the activated internal rotation about the central double bond in the excited ^1S state should be followed by internal conversion of ^1S to ^2S with a minimum energy for the twisted geometry leading to $^2S \rightarrow {}^0S$ internal conversion thereby isomerizing.[5-7]

The photochemical and photophysical properties of heteroaromatic compounds has been given much attention because the (n,π^*) states introduced by the heteroatom affect the photochemical behavior. The proximity of (n,π^*) states to the lowest (π,π^*) states increases radiationless transitions to deactivate the excited molecules. Azastilbenes, typical examples of olefins with heteroaromatic moiety, have attracted some interests.[8-11] With photoisomerization, a variety of reactions including photochemical addition, reduction, substitution, and elimination processes have been observed which evidently originate via hydrogen atom abstraction by an electron-deficient nitrogen.[12,13] The styrylpyridines (StP's) and 1,2-dipyridylethylenes (DPE's) have very low fluorescence and photoisomerization quantum yields when the heteroatom is in the ortho or para position[9,10] due to the fast deactivation of the excited singlet state through efficient internal conversion. The singlet mechanism has been proposed for the direct photoisomerization of StP's and DPE's.[9,10]

Pyrimidine nucleosides substituted at the C-5 position constitute a class of biologically significant molecules[14,15] and it is interesting to study the photochemical behavior of these molecules. We report here the cis-trans photoisomerization of (*E*)-5-styryl-1,3-dimethyluracil (5(*E*)-SDU) as a model for C-5 modified pyrimidine bases.

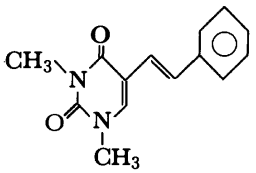

5(E)-SDU

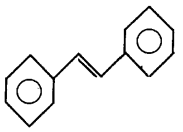

STILBENE

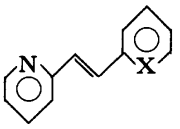

X = C, 2-StP
X = N, 2,2'-DPE

Experimental

Materials. (*E*)-5-Styryl-1,3-dimethyluracil (5(*E*)-SDU) was prepared by palladium-catalyzed reaction[16,17] of styrene and 1,3-dimethyluracil.[18] The reaction mixture was resolved on a silica-gel column using ethyl acetate-cyclohexane-chloroform (1/1/2, v/v) as the eluent, and recrystallized from 1-octanol: Mp 145.5—147.5 °C; Mass spectrum *m/z* 242 (molecular ion) 157 ($M^+-C_3ON_2H_5$) 115 ($M^+-C_5O_2N_2H_7$); UV ($CHCl_3$) λ_{max} 316 nm (ε 24500); ^1H NMR ($CDCl_3$) δ=7.25 (m, 5H, aromatic), 7.4 (d, 1H, phCH=), 6.8 (d, 1H, U-CH=), 3.53, 3.5 (s, 3H, N-CH_3). 5(*E*)-SDU in acetonitrile was irradiated with benzophenone as a sensitizer at 350 nm in a Rayonet photochemical reactor for 2 h after the solution was degassed by bubbling with N_2 gas for 1 h. 5(*Z*)-SDU was separated by column chromatography over silica gel and recrystallized from ethanol: UV ($CHCl_3$) λ_{max} 255, 305 nm (ε 5000); ^1H NMR ($CDCl_3$) δ=7.25 (m, 5H, aromatic), 7.3 (d, 1H, phCH=), 6.5 (d, 1H, U-CH=), 3.4, 3.2 (s, 3H, N-CH_3).

Benzophenone (Sigma) was recrystallized from cyclohexane. Azulene (Aldrich) was purified by vacuum sublimination. Commercially available styrene, uracil, mercury(II) acetate, trimethyl phosphate (Aldrich), and palladium chloride (Inuisho) were used without further purification. Extra pure solvents were used as received or after purification by distillation or standard methods.[19,20]

Spectra. NMR spectra were measured on a Varian T-60A spectrometer. Mass spectra were determined with a Hewlett Packard 5985 A GC/MS system by electron impact method. UV spectra were recorded on a Cary 17 spectrophotometer. Fluorescence spectra were recorded on an Aminco Bowman spectrofluorometer. Fluorescence quantum yields were determined using quinine hydrogen sulfate (Φ_f=0.546) as a reference. The fluorescence lifetime was measured at room temperature with SLM Model 480 phase modulation spectro-

Table 1. Phtoisomerization and Fluorescence Quantum Yields, Fluorescence Lifetimes, and Rotation Barriers of 5(*E*)-SDU and Other Stilbene Derivatives[9,10,24]

Compound	Φ_f	$\Phi_{t\to c}$	τ_f/ns	ΔE_f/kcal mol^{-1}
5(*E*)-SDU	0.023[a]	0.048[b]	0.042	3.0[c]
Stilbene	0.036	0.41	0.09	3.2
2-Stp	0.0008	0.25	0.007	2.0
3-StP	0.075	0.56	0.19	3.3
4-StP	0.0016	0.37	0.008	0.8
2,2′-DPE	0.005	0.01		
3,3′-DPE	0.13	0.08		
4,4′-DPE	0.0004	0.003		

a) In ethanol. b) In benzene. c) In methylcyclohexane-isopentane (1:1, v/v).

photofluorometer.

Quantum Yields of Isomerization. Three ml samples in Pyrex ampoules were degassed by freeze-pump-thaw method and then sealed. These samples were irradiated in a merry-go-round apparatus with Hanovia 450 W medium-pressure mercury arc lamp (Type 697A36). Corning glass filters CS 0-52 and 7-37 were used to isolate 366 nm UV light. Light intensities were measured by trioxalatoferrate(III) actinometry.[21] Samples were analyzed by HPLC on a Waters Associates Model 244 liquid chromatograph. Reactions were carried out to less than 5% conversion to avoid competition with the back reaction.

Laser Flash Photolysis. The nanosecond laser photolysis apparatus has been described elsewhere.[22] A XeF (351 nm) and a KrF (248 nm) excimer laser (Lambda Physik EMG101E) were used as excitation light sources. The concentrations (1.5×10^{-5}—5.9×10^{-5} M[†]) of 5(*E*)- and 5(*Z*)-SDU were adjusted such that suitable amount of the laser light was absorbed. The lifetime for decay of the transient of 5(*E*)-SDU was obtained from oscillograms.

Results and Discussion

Fluorescence Studies. The fluorescence quantum yield and lifetime of 5(*E*)-SDU are lower and shorter than those of stilbene and meta-isomers of StP's and DPE's, but higher and longer than those of ortho- and para-isomers of StP's and DPE's (Table 1). The lone-pair electrons of N-atoms are conjugated with olefinic π-electrons more easily in ortho- and para-positions than in meta-position, so that the $^1(n,\pi^*)$ electronic configuration, inducing the nonradiative process, is involved to more extent in the former positions than in the latter one. The results suggest that the lone-pair electrons of N-atoms in 5(*E*)-SDU is not sufficiently delocalized as in 3-StP[10,23] and 3,3′-DPE and give less contribution to radiationless transition than in 2- and 4-StP's and 2,2′- and 4,4′-DPE's. The fluorescence quantum yield is strongly enhanced at liquid nitrogen temperature and the laser flash photolysis experiments show low Φ_{isc} for 5(*E*)-SDU at room temperature. Therefore, the deactivation of 5(*E*)-SDU at room temperature is mainly attributable to internal conversion rather than to intersystem crossing.

† 1 M=1 mol dm^{-3}.

Table 2. Quantum Yields of Fluorescence and Direct Photoisomerization of 5-SDU in Various Solvents[a]

Solvent	η^b/cp	Φ_f[c]	$\Phi_{t\to c}$	$\Phi_{c\to t}$
Methylcyclohexane	0.69	0.013		
Ethanol	1.2	0.023	0.039	
Glycerol	7.0×10^2	0.048		
Acetonitrile-water[d]			0.048	
Benzene	0.625		0.048	
Chloroform	0.58		0.049	0.029
Acetonitrile	0.345		0.059	

a) 0.001 M 5-SDU at 366 nm. b) At 20 °C from Ref. 25. c) λ_{ex}=318 nm. d) 70: 30 by volume.

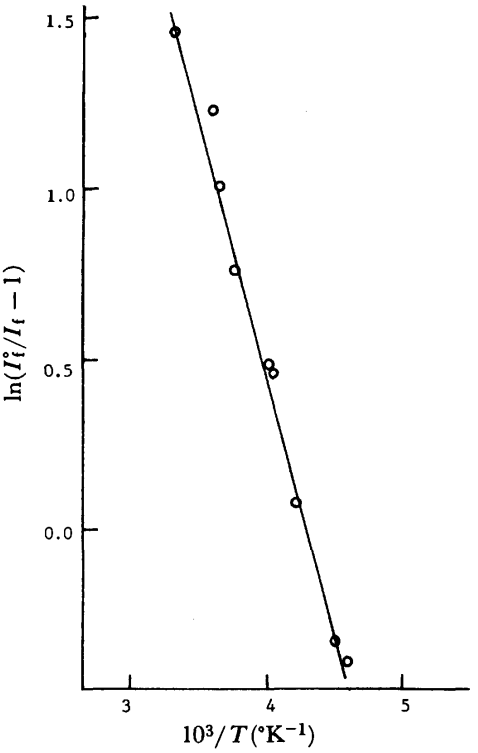

Fig. 1. Arrhenius plot for the temperature dependence of fluorescence intensity of (*E*)-5-styryl-1,3-dimethyluracil in methylcyclohexane-isopentane (1:1, v/v).

The fluorescence quantum yield depends on solvent viscosity (Table 2) and temperature (Fig. 1). If twisting in the first excited singlet state is postulated to be the activated process competing with fluorescence, the suggested mechanism for decay of 5(*E*)-SDU singlet state follows the scheme shown below.

$$t \xrightarrow{h\nu} {}^1t \quad (1)$$

$${}^1t \xrightarrow{k_f} t + h\nu \quad (2)$$

$${}^1t \xrightarrow{k_{ic}} t \quad (3)$$

$${}^1t \xrightarrow{k_{isc}} {}^3t \quad (4)$$

$${}^1t \xrightarrow{k_p} {}^1p \quad (5)$$

$${}^1p \xrightarrow{k_d} \alpha t + (1-\alpha)c \quad (6)$$

Here, t, c, and p represent trans, cis, and twisted geometry of 5-SDU, while k_f, k_{ic}, k_{isc}, k_p, and k_d are the rate constants for fluorescence, internal conversion, intersystem crossing, twisting, and decay, respectively. The fluorescence quantum yield is given by Eq. 7.

$$\Phi_f = k_f/(k_f + k_{ic} + k_{isc} + k_p) \quad (7)$$

Since step 5 is temperature dependent, k_p may be described by the Arrhenius equation (Eq. 8),

$$k_p = Ae^{-E_a/RT}. \quad (8)$$

The limiting fluorescence quantum yield at low temperature where the rate of twisting is too slow to compete with the other decay processes is

$$\Phi_f^0 = k_f/(k_f+k_{ic}+k_{isc}). \quad (9)$$

Therefore,

$$\frac{\Phi_f^0}{\Phi_f} = \frac{k_f+k_{ic}+k_{isc}+Ae^{-E_a/RT}}{k_f+k_{ic}+k_{isc}}$$

$$\ln(\Phi_f^0/\Phi_f-1) = \ln(I_f^0/I_f-1)$$
$$= \ln(A/(k_f+k_{ic}+k_{isc})) - E_a/RT.$$

If steps (2), (3), and (4) vs. step (5) is relatively independent of the temperature, plots of $\ln(I_f^0/I_f-1)$ vs. $1/T$ will be linear with a slope of $-E_a/R$. Values for I_f were estimated by modifying the method of Kirby and Steiner[40] and the best straight line relationship was obtained for $I_f^0=79$. An activation energy of 3.0 kcal mol^{-1} (1 cal=4.184 J) for the excited 5(*E*)-SDU is obtained from the slope.

In the fluorescence excitation polarization with λ_{em} 410 nm in ethanol, the 320 nm band is highly positive polarized ($P_{320\,nm}$=0.42) and flat in the longer wavelength, while the shoulder of 270 nm is relatively little positive polarized ($P_{270\,nm}$=0.21). The fluorescence polarization of 5(*E*)-SDU with excitation of 320 nm in ethanol is also highly positive polarized. This results imply that the lowest excited singlet state has (π,π^*) configuration in ethanol. 5(*Z*)-SDU has very weak fluorescence at room temperature, probably due to the fast internal conversion.

5(*E*)-SDU has very weak phosphorescence with the maxima of 580 and 620 nm in ethanol and isopentane–ethyl ether (1:1, v/v) at 77 K. The phosphorescence polarization of 5(*E*)-SDU with the excitation of 320 nm in ethanol is highly negative polarized. Accordingly, the lowest triplet state is thought to be $^3(\pi,\pi^*)$ state. Phosphorescence lifetime is shorter in ethanol (τ_{ph}=0.38 s) than in isopentane–ethyl ether (1:1, v/v) (τ_{ph}=0.41 s) and 5(*Z*)-SDU has no phosphorescence even at 77 K in ethanol.

Direct Photoisomerization. Direct photoisomerization quantum yields of 5-SDU in various solvents are reported in Table 2. The previous papers reported that the photoisomerization and fluorescence of stilbene depends on solvent viscosity[26] and couple with varying temperature in a highly viscous media.[27,28] This was explained by assigning the thermally activated process which competes with fluorescence and leads to isomerization to the twisted form from the fluorescing transoid form.[29] In solvents of low viscosity, there is an inherent thermal barrier to twisting about the central double bond. In certain viscosity regions the solvent imposes an additional barrier which must also be overcome before twisting about take place. Therefore, quantum yield of fluorescence increases and that of trans–cis photoisomerization decreases as solvent viscosity increases.

Both fluorescence and photoisomerization quantum yields of 5(*E*)-SDU are very low compared to stilbene, probably due to the presence of (n,π^*) state which can lead to very rapid radiationless decay. The photoisomerization quantum yield of 5(*E*)-SDU is similarly influenced by solvent viscosity (Table 2) as that of fluorescence while it is little affected by the solvent polarity. The energy levels of (π,π^*) and (n,π^*) states in 5-SDU are not close enough to affect the radiationless processes by solvent polarity in contrast to those of StP's.[11b,30] Effect of solvent viscosity suggest the presence of small energy barrier for the internal rotation around the central double bond as calculated in the fluorescence studies.

The quantum yield of cis→trans photoisomerization, $\Phi_{c\to t}$ of 5(*Z*)-SDU, is smaller than that of trans→cis photoisomerization, $\Phi_{t\to c}$ (Table 2) probably due to the shorter lifetime of the excited 5(*Z*)-SDU compared to 5(*E*)-SDU and/or to the fast competing reaction, photocyclization. Study of the direct cis–trans photoisomerization is complicated because of the facile photocyclization.[31]

Sensitized Photoisomerization. The quantum yields of benzophenone sensitized photoisomerization for 5-SDU in various solvents are given in Table 3. While the direct photoisomerization is very inefficient, 5-SDU undergoes fairly efficient photoisomerization when sensitized by benzophenone, indicating that the intersystem crossing in 5-SDU does not occur with measurable efficiencies and that the direct and sensitized isomerization pathways probably do not involve a common excited state. The azulene quenching studies lend further support to this contention. As the concentration of benzophenone increases, the photoisomerization quantum yield increases upto certain concentration of benzophenone and then decrease. When the concentration of benzophenone is low, benzophenone molecules do not absorb all the exciting radiation and the yield of the olefin triplet is low while self-quenching and triplet–triplet annihilation of benzophenone[32] becomes significant decreasing the energy transfer to 5-SDU at high benzophenone concentration. As Table 3 shows, the sensitized photoisomerization is strongly affected by the sol-

Table 3. Quantum Yields of Benzophenone-Sensitized Photoisomerization of 5-SDU in Various Solvents[a)]

Solvent	η^{b}/cp	Concentration of benzophenone/M	$\Phi_{t\to c}$	$\Phi_{c\to t}$	A/A^{0}[d)]
Ethanol	1.2	0.05	0.119		0.55
Acetonitrile-Water[c)]		0.05	0.289		0.55
Acetonitrile	0.345	0.05	0.377		0.55
Chloroform	0.58	0	0.049	0.029	1.00
		0.03	0.382		0.67
		0.05	0.393	0.103	0.55
		0.10	0.372		0.38
		0.30	0.230		0.17
Benzene	0.625	0.05	0.403		0.55

a) 0.001 M 5-SDU at 366 nm. b) At 20 °C from Ref. 25. c) 70:30 by volume. d) A/A^{0} is the fractions of photons absorbed by 5(*E*)-SDU in these conditions.

vent polarity in contrast to the direct photoisomerization which is affected by the solvent viscosity only. The sensitized photoisomerization quantum yield decreases with increasing the solvent polarity.

This result agrees with the observation that the lifetime of phosphorescence is shorter in the polar solvent than in the nonpolar solvent.

Salt, pH, and Heavy Atom Effect. The photoisomerization and fluorescence of 5(*E*)-SDU are little influenced by proton or salts supporting the results of solvent polarity effect. These results are in contrast with 2- and 4-StP.[30,36-38] The proton and alkali metal cation are expected to raise the energy level of $^{1}(n,\pi^{*})$ state in the similar manner like the polar solvents. The small Φ_{f} and short τ_{f} of 5(*E*)-SDU imply significant contribution of $^{1}(n,\pi^{*})$ state to the lowest excited singlet state and this leads to the reduction of isomerization efficiency occurring in the twisted $^{1}(\pi,\pi^{*})$ state. However, the results of pH and salt effects suggest that the $^{1}(n,\pi^{*})$ level is not close enough to $^{1}(\pi,\pi^{*})$ level and that even though the energy level of $^{1}(n,\pi^{*})$ state is raised by acids and salts, the fluorescent and isomerizable $^{1}(\pi,\pi^{*})$ state is little affected.

Fluorescence of 5(*E*)-SDU is quenched by ethyl iodide and photoisomerization increases with potassium iodide as shown in Table 4 suggesting that the triplet excited state increases due to the enhanced intersystem crossing induced by heavy atoms. The isomerization in the triplet state is more efficient than the direct isomerization as shown in the benzophenone sensitized photoisomerization. The results indicate that direct irradiation does not populate the triplet state significantly and radiative or radiationless deactivation processes from the singlet states determine the photoreactivity of 5-SDU.

Azulene Effect. Azulene quenches only the transoid singlet and triplet states of stilbene on direct and sensitized excitation,[26,39] but short lived cisoid excited state was not quenched. The following Stern-Volmer equation is derived assuming the selective quenching of transoid excited state by azulene and using the steady state approximation on excited species.

Table 4. Heavy Atom Effect on the Fluorescence and Direct trans→cis Photoisomerization of 5(*E*)-SDU in Methanol and Acetonitrile-Water (70:30, v/v), respectively[a)]

Concentration of ethyl iodide/M	I_{f}^{0}/I_{f}[b)]	Concentration of KI/M	$\Phi_{t\to c}$
0	1.00	0	0.043
0.07	1.14	1×10^{-3}	0.041
0.41	1.38	5×10^{-3}	0.040
0.22	1.68	1×10^{-2}	0.048
0.29	1.87	5×10^{-2}	0.052
0.38	2.61	1×10^{-1}	0.103

a) 0.001 M 5(*E*)-SDU. b) I_{f}^{0}; the fluorescence intensity in the absence of ethyl iodide. $\lambda_{ex}=318$ nm.

Table 5. Azulene Effect on the Direct and Sensitized Photoisomerization of 5(*E*)-SDU, Stilbene, StP, and BPE[a)]

Compound	Direct $k_{q}\tau/M^{-1}$	Sensitized[c)] $k_{q}\tau/M^{-1}$
5(*E*)-SDU[b)]	270	1120
Stilbene	16.1	79
4-Stp	18	130
3,3′-BPE	90	250
4,4′-BPE	70	280

a) Data from Ref. 11b in *t*-butyl alcohol. b) 0.001 M 5(*E*)-SDU in chloroform at 366 nm. c) 0.1 M Benzophenone sensitizer.

$$\Phi_{t\to c}^{0}/\Phi_{t\to c} = 1 + k_{q}\tau[Az],$$

where, k_{q} is the diffusion controlled quenching constant, τ is the lifetime of quenched species, and $\Phi_{t\to c}^{0}$ and $\Phi_{t\to c}$ are trans→cis photoisomerization quantum yields in the absence and presence of azulene, respectively.

Azulene effect on the direct and sensitized photoisomerization of 5(*E*)-SDU is summarized in Table 5. The results show much smaller slope for the direct isomerization compared to that for the benzophenone sensitized isomerization. The same phenomena were observed in the case of stilbene,[26] StP's, and DPE's.[11b]

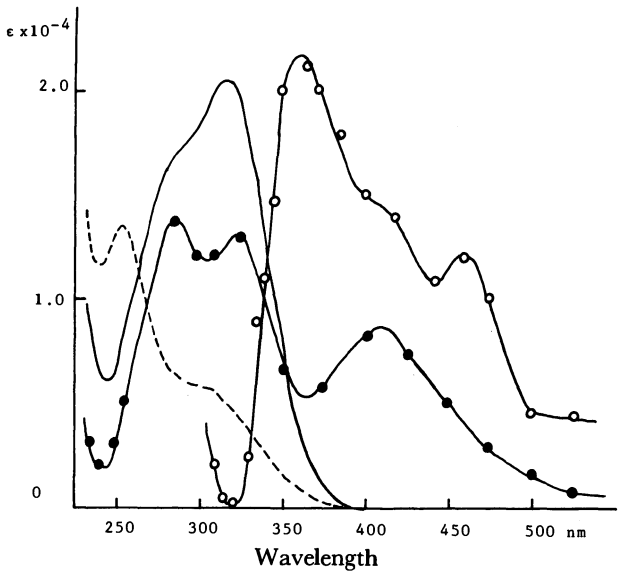

Fig. 2. UV absorption (——; 5(*E*)-SDU, -----; 5-(*Z*)-SDU) and triplet-triplet absorption spectrum (-O-O-O-: 5(*E*)-SDU, -●-●-●-: 5(*Z*)-SDU) of 5-SDU in ethanol.

This is consistent with a singlet mechanism for the direct isomerization.

Laser Flash Photolysis. Nanosecond time-resolved absorption spectra of 5-SDU in ethanol are shown in Fig. 2. In order to determine the molar absorption coefficient for triplet-triplet absorption, benz[*a*]anthracene which has molar absorption coefficient of 2.0×10^4 $M^{-1}cm^{-1}$ † at 455 nm is used as a reference compound. The intersystem crossing quantum yield, Φ_{isc}, of ca. 0.052 was obtained indicating that intersystem crossing of 5(*E*)-SDU is small but detectable and that the possibility of the involvement of triplet mechanism for direct photoisomerization is very small but cannot be excluded.

Irradiation of *cis*-stilbene in benzene gave only a long-lived absorption centered around 450 nm[34] which was attributed to 9,10-dihydrophenanthrene. Only long-lived transient of 5(*Z*)-SDU is observed at room temperature probably due to the formation of 9,10-dihydrophenanthrene derivative just like in the case of *cis*-stilbene.

The triplet energy of 5(*E*)-SDU was determined by the energy transfer method. Addition of *trans*-stilbene (E_T=50 kcal mol^{-1}) does not affect the transient absorption at 375 nm. With 9,10-diphenylanthracene (E_T= 41.8 kcal mol^{-1}), strong triplet-triplet absorption of 9,10-diphenylanthracene at 425 and 480 nm was observed. As benz[*a*]anthracene (E_T=47.2 kcal mol^{-1}) is added, strong triplet-triplet absorption of benz[*a*]-anthracene at 475 nm is detected with and without 5(*E*)-SDU. *trans*-1,3,5-Hexatriene gave no effect on the transient absorption curve of 5(*E*)-SDU. From these results, the triplet energy of 5(*E*)-SDU is estimated to lie between 41.8 and 47 kcal mol^{-1}. The plot of log A (absorbance) vs. time (ns) showed the straight line following first-order kinetics. From the decay curve of triplet-triplet absorption, the lifetime of triplet state for 5(*E*)-SDU was determined to be ca. 93 ns. This value is consistent with the triplet lifetime calculated by azulene quenching studies (Table 5) for the sensitized isomerization, assuming the diffusion controlled quenching ($k_q=1.2\times10^{10}$ $dm^3\,mol^{-1}\,s^{-1}$ at 20 °C in chloroform).

Conclusion

Fluorescence quantum yield of 5-SDU depends on the temperature and solvent viscosity increasing markedly at low temperature and high viscosity. The proton and salts have no effect on the fluorescence and photoisomerization. Addition of heavy atom affects the intensity of fluorescence and the quantum yield of direct photoisomerization strongly. The large difference is observed in the azulene quenching of the direct and sensitized photoisomerization. These observations strongly indicate the singlet mechanism for the direct photoisomerization and the intersystem crossing is not an important decay path at room temperature even though the laser flash photolysis shows detectable intersystem crossing at room temperature.

This investigation was supported by the Korea Science and Engineering Foundation. Authors thank Drs. K. Yoshihara and N. Nakashima of the Institute for Molecular Science, Okazaki, Japan and Dr. K. H. Chae of Chon Nam National University, Korea for the laser flash photolysis data.

References

1) a) J. Saltiel, J. T. D'Agostino, E. D. Megarity, L. Metts, K. R. Neuberger, M. Wrighton, and T. C. Zafiriou, *Org. Photochem.*, **3**, 1 (1973); b) J. Saltiel and J. L. Charlton, "Rearrangements in Ground and Excited States," ed by P. de Mayo, Academic Press, New York (1980), Vol. 3, p. 25.

2) U. Mazzucato, *Pure Appl. Chem.*, **54**, 1705 (1982).

3) G. G. Aloisi, U. Mazzucato, A. Spalletti, and G. Galiazzo, *Z. Phys. Chem. (Frankfurt am Main)*, **133**, 107 (1982).

4) a) J. Saltiel, G. R. Marchand, E. K. Kaminska, W. K. Smothers, W. B. Mueller, and J. L. Charlton, *J. Am. Chem. Soc.*, **106**, 3144 (1984); b) J. Saltiel, A. D. Rousseau, and B. Thomas, *ibid.*, **105**, 7631 (1983).

5) a) G. Orlandi and G. Marconi, *Nuovo Cimento*, **63B**, 332 (1981); b) G. Orlandi, P. Palmieri, and G. Poggi, *J. Am. Chem. Soc.*, **101**, 3492 (1979); c) G. Orlandi and W. Siebrand, *Chem. Phys. Lett.*, **30**, 352 (1975).

6) a) P. Tavan and K. Schulten, *Chem. Phys. Lett.*, **56**, 200 (1978); b) O. Teschke, E. P. Ippen, and G. R. Holton, *ibid.*, **52**, 233 (1977); c) E. Heumann, W. Triebel, R. Uhlmann, and B. Wilhelmi, *ibid.*, **45**, 425 (1977).

7) a) D. J. S. Birch and J. B. Birks, *Chem. Phys. Lett.*, **38**, 432 (1976); b) J. B. Birks, *ibid.*, **38**, 437 (1976).

8) H. Görner and D. Schulte-Frohlinde, *Chem. Phys. Lett.*, **101**, 79 (1983).
9) G. Bartocci, U. Mazzucato, and F. Masetti, *J. Phys. Chem.*, **84**, 847 (1980).
10) G. Orlandi, G. Poggi, and G. Marconi, *J. Chem. Soc., Farady Trans. 2*, **76**, 598 (1980).
11) a) A. R. Gutierrez and D. G. Whitten, *J. Am. Chem. Soc.*, **98**, 6233 (1976); b) D. G. Whitten and Y. J. Lee, *ibid.*, **94**, 9142 (1972).
12) D. G. Whitten and Y. J. Lee, *J. Am. Chem. Soc.*, **92**, 415 (1970).
13) F. R. Stermitz, C. C. Wei, and C. M. O'Donnell, *J. Am. Chem. Soc.*, **92**, 2745 (1970).
14) A. Kampf, R. L. Barfknecht, P. J. Shaffer, S. Osaki, and M. P. Mertes, *J. Med. Chem.*, **19**, 903 (1976).
15) a) Y. C. Cheng, B. A. Domin, R. A. Sharma, and M. Bobek, *Antimicrob. Agents Chemother.*, **10**, 119 (1976); b) L. S. Lee and Y. C. Cheng, *Biochemistry*, **15**, 3686 (1976).
16) a) C. F. Bigge, P. Kalaritis, and M. P. Mertes, *Tetrahedron Lett.*, **1979**, 1653; b) C. F. Bigge, P. Kalaritis, J. R. Deck, and M. P. Mertes, *J. Am. Chem. Soc.*, **102**, 2033 (1980).
17) D. E. Bergstrom and M. K. Ogawa, *J. Am. Chem. Soc.*, **100**, 8106 (1978).
18) K. Yamauchi and M. Kinoshita, *J. Chem. Soc., Perkin Trans 1*, **1973**, 391.
19) L. F. Fieser, "Experiments in Organic Chemistry" 3rd ed, D. C. Heath and Company, Boston, D. C. Heath and Co., Lexington, Massachusetts, p. 282.
20) J. F. O'Donnel, J. T. Ayres, and C. K. Mann, *Anal. Chem.*, **37**, 1161 (1965).
21) C. G. Hatchard and C. A. Parker, *Proc. Roy. Soc. (London)*, **A235**, 518 (1956).
22) N. Nakashima and K. Yoshihara, *J. Chem. Phys.*, **77**, 6040 (1982).
23) A. R. Gregory, W. Siebrand, and D. F. Williams, *J. Am. Chem. Soc.*, **101**, 1903 (1979).
24) D. G. Whitten and M. T. McCall, *J. Am. Chem. Soc.*, **91**, 5097 (1969).
25) J. A. Riddick and W. B. Bunger, "Techniques of Chemistry Vol. 2, Organic Solvents," 3rd ed., John Wiley & Sons, Inc., New York (1970).
26) J. Saltiel and E. D. Megarity, *J. Am. Chem. Soc.*, **94**, 2742 (1972).
27) S. Malkin and E. Fisher, *J. Phys. Chem.*, **68**, 1153 (1964).
28) J. Saltiel and J. T. D'Agostino, *J. Am. Chem. Soc.*, **94**, 6445 (1972).
29) J. Saltiel, O. C. Zafiriou, and E. D. Megarity, *J. Am. Chem. Soc.*, **90**, 4759 (1968).
30) G. Bartocci, P. Bortolus, and U. Mazzucato, *J. Phys. Chem.*, **77**, 605 (1973).
31) K. A. Muszkat and E. Fischer, *J. Chem. Soc., B*, **1967**, 662.
32) N. J. Turro, "Modern Molecular Photochemistry," Benjamin/Cummings Publicing Co. (1978), p. 146.
33) D. Schulte-Frohlinde and D. V. Bent, *Mol. Photochem.*, **6**, 315 (1974).
34) D. V. Bent and D. Schulte-Frohlinde, *J. Phys. Chem.*, **78**, 446 (1974).
35) a) D. V. Bent and D. Schulte-Frohlinde, *J. Phys. Chem.*, **78**, 451 (1974); b) H. Görner and D. Schulte-Frohlinde, *ibid.*, **82**, 2653 (1978).
36) P. Bortolus, G. Bartocci, and U. Mazzucato, *J. Phys. Chem.*, **79**, 21 (1975).
37) G. Favaro, U. Mazzucato, and F. Masetti, *J. Phys. Chem.*, **77**, 601 (1973).
38) G. Favaro, F. Masetti, and U. Mazzucato, *J. Phys. Chem.*, **79**, 2785 (1975).
39) a) J. Saltiel and E. D. Megarity, *J. Am. Chem. Soc.*, **91**, 1265 (1969); b) J. Saltiel, E. D. Megarity, and K. G. Kneipp, *ibid.*, **88**, 2336 (1966).
40) E. P. Kirby and R. F. Steiner, *J. Phys. Chem.*, **74**, 4480 (1970).

 © 1986 The Chemical Society of Japan Bull. Chem. Soc. Jpn., 59, 3263—3265 (1986)

A ^{15}N NMR Study of the Tautomeric Equilibria of Some 5-Substituted Tetrazoles

Elzbieta BOJARSKA-OLEJNIK, Lech STEFANIAK,* Michał WITANOWSKI, and Graham A. WEBB*,†
Institute of Organic Chemistry, Polish Academy of Sciences, 01-224 Warsaw, Kasprzaka 44/52, Poland
†Department of Chemistry, University of Surrey, Guildford, Surrey, U. K.
(Received December 28, 1985)

^{15}N NMR shielding data are presented for some 5-tetrazolones and some 5-tetrazolethiones. CNDO/S-SOS nitrogen shielding calculations are also performed for these compounds. The results obtained show that the compounds studied exist almost entirely in the oxo and thioxo forms, rather than the hydroxy or mercapto forms respectively, in DMSO solution.

We have previously reported some ^{15}N NMR data for both unsubstituted tetrazole[1] and some 5-mercapto-substituted[2] tetrazoles. In the case of some 5-hydroxy-tetrazoles electronic spectral data have been reported. Prototropic tautomerism is of some considerable interest in the field of azole chemistry.[4] The results reported indicate that the tetrazoles studied exist almost entirely in the thioxo and oxo forms rather than the mercapto and hydroxy forms respectively.

Our earlier studies have revealed that prototropic tautomerism of both unsubstituted and 5-(methylthio)-tetrazoles give rise to a predominance of the structure with a proton attached to N-1. In both cases this structure is reported to be present to the extent of about 85%.[1,2]

We now propose to investigate the possibility of prototropic tautomerism in 5-mercaptotetrazole and 1-methyl-5-hydroxytetrazole.

Results and Discussion

The results of a ^{15}N NMR investigation of 5-tetrazolone, 5-tetrazolethione and some related compounds are given in Table 1 together with the results of some CNDO/S-SOS nitrogen shielding calculations. The latter are reported on the absolute scale, whereas the experimental ^{15}N shieldings are given with respect to that of nitromethane. Consequently a one-to-one correspondence between these two sets of shielding data is not to be anticipated. However, for a given compound the calculated relative order of nitrogen shielding data is sufficiently reliable to permit their use for signal assignment purposes.[1]

In addition to the CNDO/S-SOS shielding results the nitrogen shielding assignments presented in Table 1 are obtained from a knowledge that pyrrole-type nitrogen atoms are highly shielded[5] with respect to pyridine-type nitrogen atoms. Bonding to another nitrogen atom produces a deshielding of the first nitrogen and bonding to two other nitrogens gives rise to a further nitrogen deshielding.[5]

Compounds **2** and **3** are studied as models for compound **1** which, in principle may exist as a tautomeric mixture of structures A, B, C, and D in DMSO. The structures of compounds **2** and **3** are known from literature data,[2] preparation and the assignments given in Table 1 of their ^{15}N NMR spectra are consistent with this.

The experimental data given in Table 1 for compound **1** is very similar to that of compound **3** which, of neccesity, exists as structure A. Therefore structure A is clearly the predominant one for compound **1**. However, we had initially anticipated that compound **1** would have existed mainly, if not entirely, in form B. Our reason for supposing this is by comparison with compound **2** which is demonstrated to consist of form B.[1] A possible explanation of our observation of form A for compound **1** is that solvent interactions lead to a preference of form A over form B.

Turning now to a consideration of the nitrogen shielding data for compounds **4** and **5**. In principle compound **4** may exist as a mixture of tautomers. In order to investigate this possibility compound **5** has been studied as a model compound.

The nature of the tautomeric equilibria in which compound **4** may be involved is as follows:

From a comparison of the results given in Table 1 for compounds **4** and **5** it is apparent that compound **4** exists in DMSO predominantly as form E. Any amount

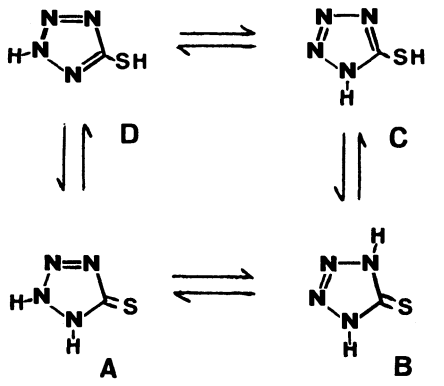

Fig. 1.

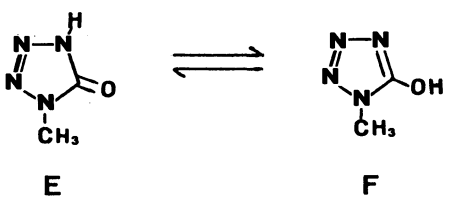

Fig. 2.

Table 1. ^{15}N NMR Shielding Data[a] for Some 5-Tetrazolones and Some 5-Tetrazolethiones Obtained by Experiment and Calculation by the CNDO/S-SOS Procedure

Number	Compound[a]	Nitrogen atom	Experimental results in DMSO	Theoretical results[b,c]
1	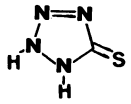	N-1	82.2	38.2
		N-2	70.4	35.1
		N-3	−3.9	−52.1
		N-4	50.4	−38.5
2	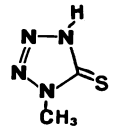	N-1	151.9	70.1
		N-2	25.4	−32.4
		N-3	17.4	−33.1
		N-4	145.7	64.2
3	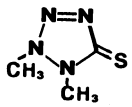	N-1	97.3	61.4
		N-2	70.9	45.2
		N-3	−4.5	−56.1
		N-4	47.7	−39.7
4	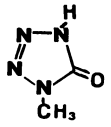	N-1	193.1	68.2
		N-2	43.2	−33.7
		N-3	33.6	−34.6
		N-4	187.7	62.4
5	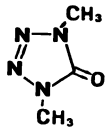	N-1	193.2	70.7
		N-4		
		N-2	39.1	−41.0
		N-3		
6	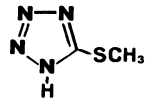	N-1	100.5	55.3
		N-4		−10.2
		N-2	4.5	−26.1
		N-3		−36.3
7	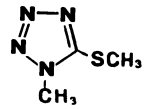	N-1	158.1	70.1
		N-2	7.1	−27.1
		N-3	−11.1	−36.9
		N-4	55.6	−9.8
8	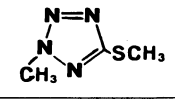	N-1	81.6	−27.6
		N-2	101.4	42.4
		N-3	−2.3	−50.9
		N-4	53.4	−35.3

a) All shielding data are reported in ppm. The experimental results relate to external nitromethane as standard; a possible increment corresponds to a shielding increase. b) The structures given are predominant in DMSO solutions and the theoretical shielding results relate to these structures. c) The theoretical results relate to absolute shieldings.

of form F present is predicted to be less than 5%. In the case of compound **4** the assignment of the N-2 and N-3 signals is consistent both with the deshielding influence of a β-effect and with the predictions of the CNDO/S-SOS shielding data. The relative assignments of the N-1 and N-4 signals are based on a comparison of the assignment of compound **2**, the shielding results observed for compound **5** and those calculated by the CNDO/S-SOS procedure for compound **4**.

In conclusion we observe that ^{15}N NMR spectroscopy is a very satisfactory procedure for investigating tautomeric equilibria of some 5-substituted tetrazoles. Additionaly, we note that CNDO/S-SOS parametrized shielding calculations are suitable for estimating the relative shieldings of the nitrogen atoms in the tetrazole ring.

Experimental

Compounds **1**,[6], **4**,[7] and **5**[7] were prepared by previously published procedures, while compound **2** was obtained commercially. Compound **3** was prepared by methylating the sodium salt of 2-methyl-5-mercaptotetrazole with dimethyl sulfate in equimolar amounts in methanol as solvent according to procedure published elsewhere.[1] The purity of all compounds employed was varified by means of ^{1}H and ^{13}C NMR measurements.

The ^{15}N NMR spectra were obtained on a Bruker WH 400 spectrometer using 10 mm sample tubes for 0.5 M (1 M=1 mol dm^{-3}) solutions at ambient temperatures. Nitromethane was used as an external standard. Typical operating conditions employed a delay of about 2s between pulses, a pulse angle of about 70° and an aquisition time of 0.5s. Gated

decoupling was used to suppress possible NOE effects.

The CNDO/S-SOS shielding calculations were performed on the CDC 7600 system of the University of London using a modified version of QCPE 174. The details of the calculations are presented elsewhere.[8] Standards geometries were used in the calculations.[9]

We are grateful for SERC enabling us to gain access to the regional NMR facility at the University of Warwick and to Drs. O. W. Howarth and E. Curzon for recording the spectra.

References

1) E. Bojarska-Olejnik, L. Stefaniak, M. Witanowski, B. T. Hamdi, and G. A. Webb, *Magn. Reson. Chem.*, **23**, 166 (1985).

2) E. Bojarska-Olejnik, L. Stefaniak, M. Witanowski, and G, A. Webb, *Bull. Pol. Acad. Chem.*, **33**, No 9-10 (1985).

3) J. P. Horwitz, B. E. Tisler, and A. J. Tomasewski, *J. Am. Chem. Soc.*, **81**, 3076 (1959).

4) A. R. Katritzky and C. W. Rees, "Comprehensive Hetrocyclic Chemistry," ed by O. Meth-Cohn, Pergamon Press (1984), Vol. 1, pp. 143—182.

5) L. Stefaniak, J. D. Roberts, M. Witanowski, and G. A. Webb, *Org. Magn. Reson.*, **22**, 215 (1984).

6) M. Freund and Th. Paradies, *Ber.*, **34**, 3110 (1901).

7) K. Hattori, E. Lieber, and J. P. Horwitz, *J. Am. Chem. Soc.*, **78**, 411 (1956).

8) I. Ando and G. A. Webb, "Theory of NMR Parameters," Academic Press, London (1983).

9) J. A. Pople and M. S. Gordon, *J. Am. Chem. Soc.*, **89**, 4253 (1967).

XPS Study of Silica-Supported Copper Catalyst Derived from Binuclear Copper(II) Acetate Monohydrate or Mononuclear Tetraammine Copper(II) Complex

Noriyoshi KAKUTA, Akio KAZUSAKA,* and Koshiro MIYAHARA
Research Institute for Catalysis, Hokkaido University, Sapporo 060
(Received February 28, 1986)

Synopsis. The surface copper(II) species on a CuO/SiO_2 catalyst derived from binuclear copper(II) acetate monohydrate has been studied using XPS in comparison with that from the mononuclear tetraammine copper(II) complex. From the binding energy of Cu $2p_{3/2}$ peak and the peak ratio of Cu $2p_{3/2}$ and Si 2p together with the results by EXAFS, it was deduced that the highly dispersed one or two dimensional copper oxide cluster, which is interacted more weakly with SiO_2, is developed on the copper(II) acetate monohydrate derived catalyst.

An active site on heterogeneous catalysts has become of interest in the recent year. We have examined to prepare a supported binuclear copper oxide catalyst from typical binuclear copper(II) acetate monohydrate [$Cu_2(CH_3COO)_4 \cdot 2H_2O$], and have compared it with a conventional catalyst from a mononuclear tetraammine copper(II) complex.[1-6] The recent EXAFS study, however, suggested that the one or two dimensional copper oxide cluster was developed on SiO_2 instead of the binuclear copper oxide.[6] Also, the copper(II) species derived from copper(II) acetate monohydrate has been found to show following properties: 1) It reacts easily with acetic acid to give the binuclear structure of copper(II) ions, which was identified by ESR[1,2] or IR,[2] 2) it shows a tremendous high catalytic activity for CO oxidation with N_2O, CO isotope equilibriation reaction,[1,2] or oxygen isotope-exchange reaction between CO and CO_2,[5] 3) it is reduced easily to metallic copper with CO under mild conditions.[3,6]

To obtain a further detailed information about it, we have applied a X-ray photoelectron spectroscopy (XPS) technique to above two kinds of silica-supported copper catalyst, finding that the acetate derived catalyst retains a highly dispersed copper oxide cluster.

Experimental

Two kinds of silica-supported copper catalyst were prepared from copper(II) acetate monohydrate (denoted Ac-Cu/SiO_2) and a copper(II) tetraammine complex (denoted Am-Cu/SiO_2), as described in earlier papers.[1,2] Each sample was found to contain copper of 3.7 or 3.4 wt%, respectively. A Vacuum Generators ESCA 3 system was used with Mg $K\alpha$ radiation (1253.6 eV) for XPS measurements. The samples pressed into disk were pretreated by the way similar to that in the previous paper[1,2] with an IR lamp in the preparation chamber of ESCA instrument. CuO was also used for reference measurements. The binding energies (BEs) were referenced to the Si 2p peak at 103.4 eV, or the C 1s peak at 285.0 eV. The binding energies reported here are in accuracy with ±0.2 eV.

Results and Discussion

Figure 1a shows the XPS spectrum in the Cu $2p_{3/2}$ region, which was obtained on the Ac—Cu/SiO_2 catalyst activated under vacuum from room temperature to 300°C and calcined with 100 Torr (1Torr=133.322Pa) of oxygen at 300°C; the binding energy of Cu $2p_{3/2}$ is evaluated at 933.8 eV. The identical value was obtained on the reference sample of CuO. The satelite peak usually observed for typical Cu(II) compounds was unable to detect clearly on this sample. It might be due to the low loading of copper on it. We have used the Ac-Cu/SiO_2 catalysts containing rather a small amount of copper, because the specific features described previously were found to be lost by increaseing it above ca.7 wt%. An effort to detect the satelite peak due to the Cu(II) species was made at liquid nitrogen temperature, but only the spectrum similar to that of Fig. 1a was observed on it. This result indicates that the Cu(II) species was not reduced during the XPS measurement, as pointed out by Kevan et al.[7]

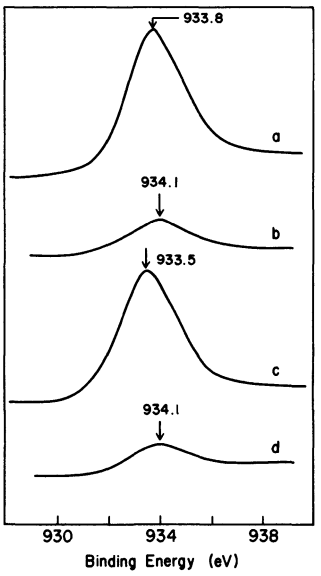

Fig. 1. Cu $2p_{3/2}$ XPS spectra of calcined Ac-Cu/SiO_2 (a), calcined Am-Cu/SiO_2 (b), reduced Ac-Cu/SiO_2 (c) or reduced Am-Cu/SiO_2 (d). All spectra were measured at room temperature.

Figure 1b shows the spectrum observed on the Am-Cu/SiO_2 catalyst, which was activated under vacuum at 300°C for 1 h and followed by calcining with 100 Torr of oxygen at 300°C for 1 h. This was also unable to identify the satelite peak in the Cu $2p_{3/2}$ region. The BE is evaluated at 934.1 eV. This value is higher than that of the Ac-Cu/SiO_2 catalyst or CuO.

In general, it is known that the BEs for metal oxides on supported catalysts tend to be higher than those of metal oxide themselves.[8,9] The authors have ascribed it to a coordination effects of supports or

Table 1. Surface Composition of Cu and Si on Ac-Cu/SiO_2 or Am-Cu/SiO_2

Treatment	$Cu(2p_{3/2})/Si(2p)$[a]	
	Ac-Cu/SiO_2	Am-Cu/SiO_2
Calcined	1.36	0.23
CO reduction	0.95	0.20

a) Estimated uncertainty is within ±5%.

the formation of the new compounds like MAl_2O_4, $MSiO_3$ etc. (M: metal cations). In this point of view, the copper(II) ions on the Ac-Cu/SiO_2 catalyst interacts more weakly with SiO_2 than those on the Am-Cu/SiO_2 catalyst.

The surface composition of Cu and Si can be evaluated from the peak intensities of their spectra. The ratios of Cu and Si are summarized in Table 1. Although both catalysts contain almost the same amount of copper as described previously, the Ac-Cu/SiO_2 catalyst has ca. 6 times higher concentration of the surface copper species than the Am-Cu/SiO_2 catalyst on their calcined states. These results are in agreement with those by EXAFS study[6]; it was found that one or two dimensional copper oxide cluster was loaded on the Ac-Cu/SiO_2 catalyst, while three dimensional one on the Am-Cu/SiO_2 catalyst.

When the calcined Ac-Cu/SiO_2 catalyst was reduced with 100 Torr of CO at 300°C for 1 h, followed by outgassing it at 300°C for 1 h, the spectrum was changed as shown in Fig.1c, giving the peak at 933.5 eV for Cu $2p_{3/2}$. It is somewhat higher than Cu_2O or metallic copper in literature.[10] The EXAFS study, however, showed that metallic copper was developed on the reduced Ac-Cu/SiO_2 catalyst.[6] The BE shift by the CO reduction therefore should be reflected by the presence of metallic copper.

On reducing the calcined Am-Cu/SiO_2 catalyst with 100 Torr of CO at 300°C, a little change was observed in the spectrum (Fig.1d). However, it seems to be broadened, suggesting that a small part of the copper(II) species was reduced by CO at 300°C. The Cu(I) species was detected by EXAFS experiment on it. The surface compositions of Cu and Si on the reduced samples are listed in Table 1.

In conclusion, the Ac-Cu/SiO_2 catalyst retains the highly dispersed low dimensional copper oxide cluster on silica, which is interacted weakly with the silica support. We believe that these features must give several particular catalytic properties different from the Am-Cu/SiO_2 catalyst.

We thank Prof. Nobutsune Takezawa of Hokkaido University for the valuable discussion.

References

1) N. Kakuta, A. Kazusaka, and K. Miyahara, *Chem. Lett.*, **1982**, 913.
2) N. Kakuta, A. Kazusaka, A. Yamazaki, and K. Miyahara, *J. Chem. Soc., Faraday Trans. 1*, **80**, 3245 (1984).
3) M. Nomura, A. Kazusaka, N. Kakuta, Y. Ukisu and K. Miyahara, *Chem. Phys. Lett.*, **122**, 538 (1985).
4) A. Kazusaka, A. Yamazaki, N. Kakuta, *J. Chem. Soc., Faraday Trans. 1*, **82**, 1553 (1986).
5) A. Kazusaka, A. Yamazaki, and N. Kakuta, to be published.
6) M. Nomura, A. Kazusaka, N. Kakuta, Y. Ukisu, and K. Miyahara, *J. Chem. Soc., Faraday Trans. 1*, in press.
7) S. Contarini and L. Kevan, *J. Phys. Chem.*, **90**, 1630 (1986).
8) R. B. Freidman, J. J. Freeman, and F. W. Lytle, *J. Catal.*, **55**, 10 (1978).
9) R. B. Shalvoy, P. J. Reucroft, and B. H. Davis, *J. Catal.*, **56**, 336 (1979).
10) S. Evans, *J. Chem. Soc., Faraday Trans. 2*, **71**, 1044 (1975).

A Time-Resolved ESR Study on the Photochemical Reduction of Nitrobenzene Derivatives in Alcoholic Solution

Kimio Akiyama, Yusaku Ikegami,* Tsuneo Ikenoue, and Shozo Tero-Kubota
Chemical Research Institute of Non-Aqueous Solutions, Tohoku University, Katahira 2-1-1, Sendai 980
(Received May 6, 1986)

Synopsis. Time-resolved ESR experiments have been carried out to elucidate the initial process in the photochemical reduction of aromatic nitro compounds. The first observation of CIDEP due to nitrobenzene anion radicals in the presence of an electron donor proved that radical generation takes place through a triplet mechanism.

A number of organic and physicochemical studies on the photoreduction and photosubstitution reactions of aromatic nitro compounds have been reported and various intermediates in these reactions have been detected. Among these, ESR studies revealed several types of intermediates in photochemical reactions involving nitrobenzenes. In the presence of electron donors, the observed ESR spectra could be interpreted as the photoreductive generation of anion radicals of the parent compounds. On the other hand, neutral radicals are generated from excited triplet states of aromatic nitro compounds by hydrogen abstraction and a successive reaction in the presence of hydrogen donors.[1] It is thought that the operative excited state in these reactions is the $n\pi^*$ triplet state by an analogy with the $n\pi^*$ excitation of aromatic carbonyl compounds, regardless of the low quantum yield of the excitation compared with that of the latter.

The present paper reports the initial process of the photoreduction of nitrobenzene derivatives contains the anisotropic intersystem crossing from the $n\pi^*$ singlet state to the triplet state. The study was carried out by means of time-resolved ESR spectroscopy for the photoreduction systems of unsubstituted (**1**), 4-methoxy- (**2**), and 4-chloro-nitrobenzenes (**3**).

Experimental

A transient ESR signal from the preamplifier output of a Varian E-109E EPR spectrometer was taken without any field modulation at arbitrary times after a laser pulse into a two-channel boxcar integrator. A nitrogen laser (5 mJ per pulse, 10-Hz repetition rate) was used as the source of the light pulse.[2] The sample solution was flowed in the ESR cavity in order to prevent any secondary reaction of the photochemical products formed from the nitrobenzene. All sample solutions were deoxygenated by bubbling of pure nitrogen gas before measurements.

Results and Discussion

Figure 1 shows the transient ESR spectra observed during the photoreduction of **1**—**3** in the presence of triethylamine (TEA) in 2-propanol. These spectra were confirmed to be due to the anion radicals of the corresponding nitro compounds by comparing them with the steady-state spectra measured under the same condition with continuous light irradiation.[1] The totally emissive CIDEP (chemically induced dynamic electron spin polarization) pattern of the spectra indicated that an electron transfer occurred between the excited triplet state of a nitro compound and the added electron donor. Obeying the interpretation of the CIDEP phenomena,[3] the emissive (E) polarization arises from an anisotropic intersystem crossing of the $n\pi^*$ excited singlet state to the triplet state in which the spin is most populated at the P_+ level; the electron transfer would proceed rapidly prior to a relaxation of the polarization in the excited triplet state.

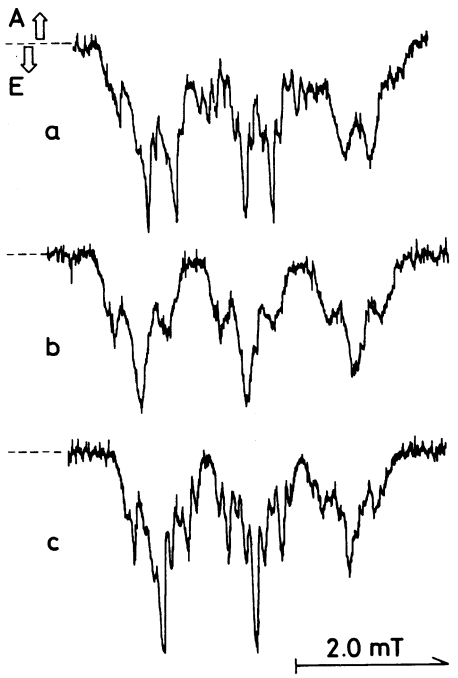

Fig. 1. Transient polarized ESR spectra of the anion radicals generated by photoreduction of unsubstituted (a), 4-methoxy- (b), and 4-chloronitrobenzenes (c) at room temperature. The spectra were taken at 1.0 μs after the laser pulse.

The same E polarization was observed for the CIDEP spectra of the anion radicals of **1**—**3** in the presence of dimethylamine (DMA) instead of TEA. According to Barltrop and Bunce,[4] the photoreduction products of nitrobenzenes varied depending on the reaction condition; also, the relative ratio of the produced aniline and azobenzene became reversed in the presence of TEA and DMA. However, the time-resolved ESR experiments showed the same CIDEP patterns in the presence of these two amines and gave no signal due to the hydrogen abstraction products. This suggests that the major photoreduction process is initiated by an electron transfer. Hydrogen abstraction from the α position of TEA is relatively slow and the polarization conserved in the hydrogen adduct may be very weak or completely diminished by the fast relaxation

of polarization within the excited triplet state of the aromatic nitro compound. Thus, the present behavior obviously differs from the CIDEP observations for the photolysis of aromatic carbonyl compounds in the presence of TEA in an alcoholic solution, which showed the spin polarization in the hydrogen-abstraction products.[5] A relatively lowered reduction potential of the aromatic nitro compounds may cause an efficient electron transfer from TEA to form anion radicals.

Since the ESR spectra of the hydrogen-abstraction products of nitrobenzene derivatives have been observed in photolysis under continuous light irradiation, it is expected that the polarized spectra of the hydrogen adducts can be observed. An examination to observe the polarized spectra of $ArNO_2H^{\cdot}$, however, has been unsuccessful, even for the active 4-chloronitrobenzene, by the use of good hydrogen donors: 2,6-di-*t*-butylphenol, benzhydrol, and cumene. Presumably, the hydrogen-abstraction rate of the triplet state of nitrobenzenes is slower than the rate of spin relaxation within the excited triplet state, even in the presence of reactive hydrogen donors.

The coexistence of hydrogen and electron donors in the above photoreduction systems also resulted in the same CIDEP spectra as that from the anion radicals. If equilibrium between the anion and its conjugated acid ($ArNO_2^{-}+H^{+}\rightleftharpoons ArNO_2H^{\cdot}$) is accompanied by a fast exchange, the appearance of another polarized signal is expected. Referring to the suggestion by Cu and Testa,[6] that the conversion rate between these two radical species should be the order of 10^8 s^{-1} in an acidic solution, the present result suggests that the spin polarization relaxed rapidly before conversion in the present neutral solution.

References

1) For example, see: a) R. L. Ward, *J. Chem. Phys.*, **38**, 2588 (1963); b) J. K. Brown and W. G. Williams, *J. Chem. Soc., Chem. Commun.*, **1966**, 495; c) D. J. Cowley and L. H. Sutcliffe, *J. Chem. Soc., Chem. Commun.*, **1968**, 201; d) C. Chachaty and F. Forchioni, *Tetrahedron Lett.*, **1968**, 307; e) E. G. Janzen and J. L. Gerlock, *J. Am. Chem. Soc.*, **91**, 3108 (1973); f) S. K. Wong and J. K. S. Wan, *Can. J. Chem.*, **51**, 753 (1973).

2) K. Akiyama, S. Tero-Kubota, Y. Ikegami, and T. Ikenoue, *J. Phys. Chem.*, **89**, 339 (1985).

3) F. J. Adrian, *Rev. Chem. Intermed.*, **3**, 3 (1979).

4) J. A. Barltrop and N. J. Bunce, *J. Chem. Soc. (C)*, **1968**, 1467.

5) K. Miyagawa, H. Murai, and Y. T. I'haya, *Chem. Phys. Lett.*, **118**, 140 (1985).

6) A. Cu and A. C. Testa, *J. Am. Chem. Soc.*, **96**, 1963 (1974).

EXAFS Study on One-Dimensional Halogen-Bridged Mixed-Metal (Pd, Pt) Mixed-Valence Complexes

Isao IKEMOTO,* Koichi KIKUCHI, Kumiko IWAI, Masahiro YAMASHITA,† Masaharu NOMURA,†† Kiyotaka ASAKURA,††† Nobuhiro KOSUGI,††† Kyuya YAKUSHI,††† and Haruo KURODA†††

Department of Chemistry, Faculty of Science, Tokyo Metropolitan University, Fukazawa, Setagaya-ku, Tokyo 158
†Laboratory of Chemistry, College of General Education, Kyushu University, Ropponmatsu, Chuo-ku, Fukuoka 810
††Photon Factory, National Laboratory for High Energy Physics, Ohmachi, Tukuba-gun, Ibaraki 305
†††Department of Chemistry, Faculty of Science, The University of Tokyo, Hongo, Bunkyo-ku, Tokyo 113

(Received May 19, 1986)

Synopsis. The EXAFS spectra of $[Pd(en)_2X_2Pt(en)_2](ClO_4)_4$ (en=ethylenediamine, X=Cl, Br, and I) were measured for Pd K and Pt L_{III} edges. The Fourier transforms of the Pd K- and Pt L_{III}- edge EXAFS show clearly that the halogen atoms are forming a chemical bond only to Pt(IV) and Pt-Cl, Pt-Br, and Pt-I bond lengths are 2.34, 2.47, and 2.83Å respectively.

Recently halogen-bridged one-dimensional mixed-valence complexes of Pt, Pd, and Ni have attracted much attention from the viewpoint of chemistry and physics of low-dimensional compounds.[1-4]

The compounds with the general formula of $[M(II)(AA)_2][M(IV)X_2(AA)_2]Y_4$ (M=Pt, Pd, and Ni; X=Cl, Br, and I; $(AA)_2$=(diamines)$_2$, linear tetramines, and tetraaza macrocycles; Y=ClO_4, BF_4 etc.) show various interesting phenomena such as strong inter-valence charge transfer, progressive resonance Raman spectra, and luminescence with a large Stokes shift. The effects of the metals, bridging halogens, counter anions, and in-plane ligands on the electronic structures of the complexes have been investigated by use of various different kinds of experimental methods.[5-12]

In the crystal structures, the four-coordinated M(II) and six-coordinated M(IV) units are stacked alternately, with bridging halogen atoms, constructing an infinite linear chain. The bridging halogen atom is located not at the middle point between M(II) and M(IV) atoms, but at the point closer to M(IV). In the compound of this type, the ratio of M(IV)-X and M(II)···X distances depends on metals, bridging halogens, counter anions, and in-plane ligands.

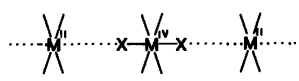

Toriumi and Yamashita[13] recently performed preliminary single-crystal X-ray structure analysis on the compounds where M(II)=Pd, M(IV)=Pt, AA= ethylenediamine, Y=ClO_4, and X=Cl, Br, or I, and showed that there is a disorder with regard to the position of bridging halogen atom. The halogen atom occupies two positions equidistant from the midpoint between the two metal atoms, Pt and Pd, with a half occupancy factor. Because of this disorder, it is hard to distinguish Pt and Pd sites, so that the metal sites are represented as(1/2)(Pt+Pd). Thus the state of halogen-metal bonding is not clear in the results of single-crystal X-ray structure analyses of those compounds. In order to establish the bonding of halogens to metals, we studied Pd K- and Pt L_{III}-edge EXAFS of the above-mentioned compounds. The measurements were carried out by use of the EXAFS facility at BL 10B[14] in

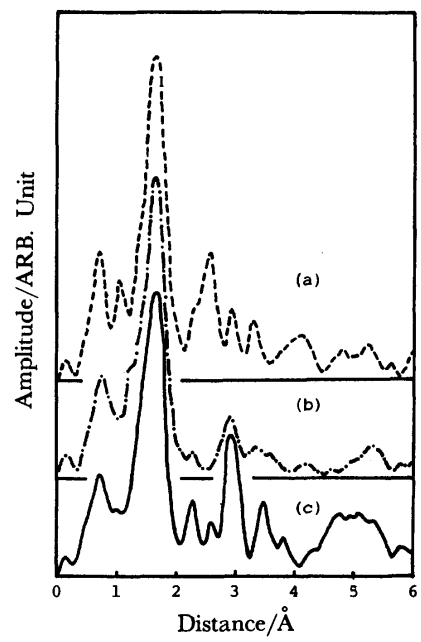

Fig. 1. The Fourier transforms for Pd K edge of (a) X=Cl, (b) X=Br, and (c) X=I.

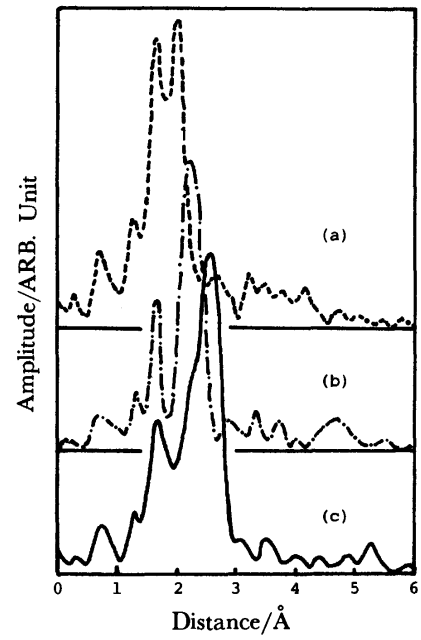

Fig. 2. The Fourier transforms for Pt L_{III} edge of (a) X=Cl, (b) X=Br, and (c) X=I.

Table 1. Bond Lengths/Å Obtained from the Analysis of EXAFS Data

	Pt-X	Pt-N	Pd-N
X=Cl	2.34	1.99	2.05
X=Br	2.47	2.05	2.06
X=I	2.83	2.08	2.05

the Photon Factory, National Laboratory for High Energy Physics (KEK-PF) utilizing a silicon (311) channel-cut monochromator.

The Fourier transform for Pd K edge EXAFS shows only one prominent peak (see Fig. 1). The position of this peak is the same for all the three compounds, therefore, the observed peak is attributable to Pd–N (in-plane ligand). We could not find a peak attributable to Pd-halogen. The Fourier transform for Pt L_{III} edge EXAFS (see Fig. 2) show two prominent peaks. The position of the peak at shorter distance remains the same for the three compounds, whereas the position of other peak shifts to longer distance as the halogen is changed from Cl to Br and to I. Thus we can attribute the former peak to Pt–N (in-plane ligand) and the latter to Pt–X. The results mentioned here clearly indicate that the bridging halogen atoms in the chain are at the position close to Pt(IV), possibly forming a chemical bond with Pt atom. Therefore, these results with XPS results[6] together indicate that these compounds are formulated as $[Pd(II)(en)_2][Pt(IV)X_2(en)_2](ClO_4)_4$.

Performing the inverse Fourier transformation over the region of the prominent peak of each Fourier transform, we carried out a further analysis for the obtained EXAFS oscillation by means of the nonlinear least square curve fitting method. The results are shown in Table 1. Previously it was reported that M(IV)-X distance is almost independent on the kinds of metals, in-plane ligands, and counter anions, although it is dependent on the kind of halogens. The results obtained in this study are quite consistent with those so far reportd.[4]

The data analyses were carried out on the HITAC M-280H computer system at the Computer Center of the University of Tokyo using the program, EXAFS1.[15]

Part of the present work was partially supported by a Grant-in-Aid for Scientific Research No.5947007 from the Ministry of Education, Science and Culture.

References

1) J. S. Miller and A. J. Epstein, *Prog. Inorg. Chem.*, **20**, 1 (1976).
2) I. F. Shchegolev, *Phys. Status Solidi A*, **12**, 9 (1972).
3) R. J. H. Clark, "Mixed-Valence Compounds," ed by D. B. Brown, Reidel, Dordrecht (1982), p. 271.
4) H. J. Keller, "Extended Linear Chain Compounds," ed by J. S. Miller, Plenum Press, New York (1982), Vol. 1.
5) Y. Wada, T. Mitani, M. Yamashita, and T. Koda, *J. Phys. Soc. Jpn.*, **54**, 3143 (1985).
6) M. Yamashita, I. Murase, T. Ito, Y. Wada, T. Mitani, and I. Ikemoto, *Bull. Chem. Soc. Jpn.*, **58**, 2336 (1985).
7) R. Aoki, Y. Hamaue, S. Kida, M. Yamashita, T. Takemura, Y. Furuta, and A. Kawamori, *Mol. Cryst. Liq. Cryst.*, **81**, 301 (1982).
8) H. Tanino and K. Kobayashi, *J. Phys. Soc. Jpn.*, **52**, 1446 (1983).
9) G. C. Papavassiliou and A. D. Zdetsis, *J. Chem. Soc., Faraday Trans. 2*, **76**, 104 (1980).
10) A. Kawamori, R. Aoki, and M. Yamashita, *J. Phys. C*, **18**, 5487 (1985).
11) R. J. H. Clark, M. L. Franks, and W. R. Trumble, *Chem. Phys. Lett.*, **41**, 287 (1976).
12) H. Tanino, N. Koshizuka, K. Kobayashi, M. Yamashita, and K. Hoh, *J. Phys. Soc. Jpn.*, **54**, 483 (1985).
13) K. Toriumi and M. Yamashita, to be published.
14) H. Oyanagi, T. Matsushita, M. Ito, and H. Kuroda, *KEK Report* 83-30 (1984).
15) N. Kosugi and H. Kuroda, Program EXAFS1, Research Center for Spectrochemistry, The University of Tokyo (1985).

The Preconcentration and Separation of a Trace Amount of Copper(II) in Water as Its Silica-Immobilized Salicylaldimine Chelate by Means of Column Chromatography

Takaharu HONJO* and Tetsuji MAKINO
Department of Chemistry, Faculty of Science, Kanazawa University, Marunouchi, Kanazawa 920
(Received March 31, 1986)

Synopsis. The behavior of a trace amount of copper(II) in solid-liquid extraction and back extraction has been examined with silica-immobilized salicylaldimine; the results have also been applied to the preconcentration and separation of a trace amount of copper(II) in water as its silica-immobilized salicylaldimine chelate by means of column chromatography.

Extraction chromatography has been applied to the concentration and separation of a trace amount of cobalt(II) in sea water as its 1-nitroso-2-naphtholate.[1] However, this technique has a weak point—the loss of 1-nitroso-2-naphthol from the stationary phase during the chromatographic process; this may decrease the usefulness of the column for the preconcentration of a trace amount of cobalt(II) in sea water. It has been generally known that salicylaldimine specifically reacts with copper(II) among transition metals to form a green chelate. After preliminary experiments on the solid-liquid extraction behavior of metals like copper(II), iron(III), nickel(II), palladium(II), cobalt(II), manganese(II), and zinc(II) with silica-immobilized salicylaldimine, it was found that copper(II) and iron(III) especially have high reactivities in a weakly acidic solution.

In this investigation, the behavior of a trace amount of copper(II) in solid-liquid extraction and back extraction with silica-immobilized salicylaldimine of a bidentate Schiff base has been examined in detail; the results have also been applied to the preconcentration and separation of a trace amount of copper(II) in water as its silica-immobilized salicylaldimine chelate by means of column chromatography. Some silica-immobilized salicylaldimines have already been prepared by the reaction of salicylaldehyde on silylated silica gel, and microgram amounts of iron(III), cobalt(II), nickel(II), copper(II), lead(II), vanadium(V), chromium(VI), and zinc(II) have also been collected with silica-immobilized salicylaldimine from weakly acidic and neutral solutions by means of solid-liquid extraction for subsequent X-ray fluorescence analysis.[2]

Experimental

The "aminopropyl silica gel" was prepared by a slight modification of the method of Aue and Hastings.[3] Silica-immobilized salicylaldimine was prepared as follows: A 50 g portion of aminopropyl silica gel was added to 100 cm³ of 5% salicylaldehyde in acetone, after which the mixture was stirred in a sealed flask for 2 h at about 50 °C. The product thus obtained was washed with acetone and dried under a vacuum at room temperature. The color of the product was brown. The solid-liquid extraction of copper(II) in water was carried out with silica-immobilized salicylaldimine as follows: A 0.1—2 g portion of the silica-immobilized salicylaldimine and 10 cm³ of a 1—1000 ppm copper(II) solution adjusted to pH 1—7 with 0.1M HCl (1M=1 mol dm^{-3}), 0.1M CH_3COOH 0.1M CH_3COONa, and 0.1M NaOH were

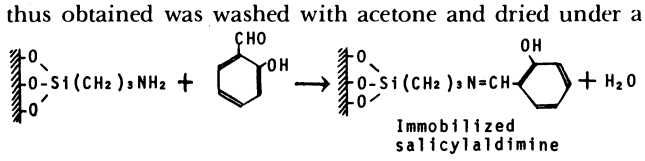

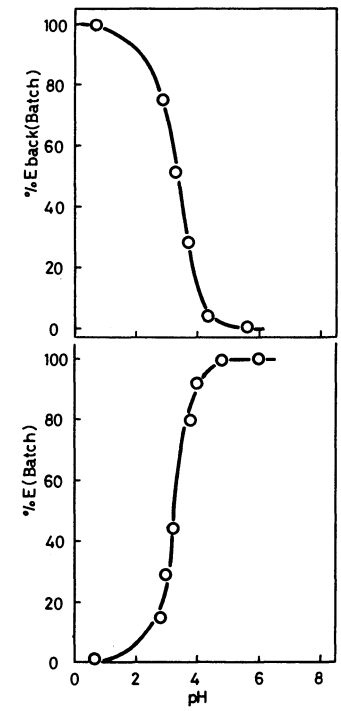

Fig. 1. Effect of pH on the extraction and the back extraction of copper(II) with silica-immobilized salicylaldimine.
Silica-immobilized salicylaldimine: 1.0 g, Cu(II): 100 μg, Aqueous solution: 10 cm³, Shaking time: 30 min.

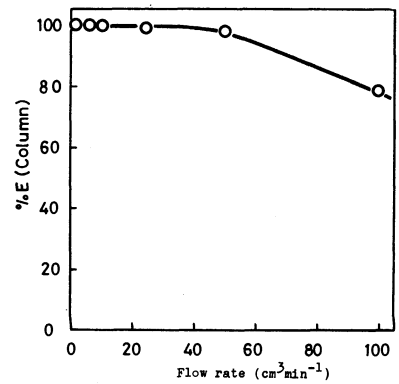

Fig. 2. Effect of flow rate on the preconcentration of copper(II) with silica-immobilized salicylaldimine column.
Silica-immobilized salicylaldimine: 1.0 g, Cu(II): 100 μg, pH 5.0.

Table 1. Recovery of Copper(II) in an Aqueous Solution of pH 5.0 with a Silica-Immobilized Salicylaldimine Column

Cu(II) spike/μg	Solution volume/cm³	Silica-immobilized salicylaldimine/g	Cu(II) recovery/%
100	10	1.0	100±2
100	100	1.0	97±2
10	500	1.0	100±2
10	1000	1.0	62±2
10	1000	2.0	100±2

Table 2. Content of Copper(II) in Distilled Water and Tap Water of Kanazawa University

Sample	Solution volume/cm³	Cu(II) collected/μg	Cu(II) collected/ppb
Distilled water	500	12.0, 13.5, 12.5	25.3±2.2
	1000	23.2, 23.7, 27.0, 24.0	24.5±1.5
	2000	46.6, 52.8	24.9
Tap water	2000	1.0, 1.4, 1.2	0.6±1

placed into a 30-cm³ centrifuged tube, and the mixtures were shaken for 1—30 min. The capacity of the silica-immobilized salicylaldimine was determined by adding 0.1 g silica-immobilized salicylaldimine to 10 cm³ of a 100 ppm copper(II) solution adjusted to pH 5.2, after which the mixtures were shaken for 30 min. The concentration of copper(II) in water was determined by the atomic-absorption method. The chromatographic column was prepared as follows: A 1.0—2.0 g portion of silica-immobilized salicylaldimine was added to a 0.1M acetate buffer solution of pH 5.0—6.0, and the mixtures were poured into a chromatographic glass tube (1 cm in inner diameter and 30 cm in length) with a fritted glass filter. The top of the column was covered with a small amount of glass fiber.

Results and Discussion

Silica-immobilized salicylaldimine was stable in the region of pH 3.5—7.0, and it reacted rapidly with copper(II) in water to form a green chelate.

When the behavior of a trace amount of copper(II) in solid-liquid extraction and back extraction has been studied with 1.0 g of silica-immobilized salicylaldimine, the quantitative extraction of 100 μg copper (II) is attained at pH 5.0—7.0 in about 1 min shaking (Fig. 1). Copper extracted as the silica-immobilized salicylaldimine chelate was easily back-extracted with an aqueous solution of 0.1—1M hydrochloric acid. On the basis of the experimental results described above, the chromatographic behavior of a trace amount of copper(II) in water was studied by means of 1.0 g of silica-immobilized salicylaldimine in a glass column at the flow rate of 0.8—200 $cm^3 min^{-1}$ under suction. The column capacity of silica-immobilized salicylaldimine with copper(II) was 0.10 $mmol g^{-1}$ at pH 5.2. A 10—1000 cm³ portion of 10—100 μg copper-(II) in water adjusted at pH 5.0—6.0 was passed through the column. It was found that the quantitative preconcentration of 0.01—10 ppm copper(II) was accomplished at the flow rate of 0.8—24 $cm^3 min^{-1}$ (Fig. 2). The results of the recovery (Table 1) of copper(II) in water adjusted at pH 5 with silica-immobilized salicylaldimine indicated that the preconcentration of trace amounts of copper(II) in water was quantitatively accomplished by using 1—2 g of silica-immobilized salicylaldimine. Foreign ions added, up to 100 μg of nickel(II), cobalt(II), manganese(II) and zinc(II) each, and 1000 μg of iron(III), did not interfere with the preconcentration of 10 μg copper in a 500 cm³ solution. Copper(II), probably held on silica-immobilized salicylaldimine by the 1:1 metal-chelate formation, as is seen in the case of metal-ion chelation chromatography on silica-immobilized 8-quinolinol,[4] was easily eluted with 10 cm³ of 1.0M hydrochloric acid within 1 min under increased pressure with air in order to prevent both the tailing of copper(II) and the hydrolysis of the silica-immobilized salicylaldimine during the process. About 70% of the collection ability of copper(II) with this reagent was lost when it was placed in contact with 1.0M hydrochloric acid for 30 min; however, there is no problem in concentrating traces of copper(II) for at least a few times by the procedure described above. The copper(II) was determined by the atomic-absorption method. The content of copper(II) in distilled water and tap water at Kanazawa University was determined by the preconcentration method described above. The results (Table 2) revealed that the concentration of copper(II) in distilled water prepared by means of an electric distillation apparatus constructed with copper plate (YAMATO WS-5) was about 25 ppb, while that of copper(II) in tap water was 0.6±1 ppb, which is compatible with the value of 0.5 ppb obtained with the column of 2-mercaptobenzothiazole supported on silica gel.[5]

The authors wish to thank the Ministry of Education for its Scientific Research Grant (No 56540340).

Thanks are also due to Prof. Kikuo Terada of Kanazawa University for his valuable advice.

References

1) T. Honjo, S. Abe, and T. Kiba, *Bull. Chem. Soc. Jpn.*, **51**, 1239 (1978).

2) K. Hirayama and N. Unohara, *Bunseki Kagaku*, **29**, 452 (1980).

3) W. A. Aue and C. R. Hastings, *J. Chromatogr.*, **42**, 319 (1969).

4) J. R. Jezorek and H. Freiser, *Anal Chem.*, **51**, 366 (1979).

5) K. Terada, A. Inoue, J. Inamura, and T. Kiba, *Bull. Chem. Soc Jpn.*, **50**, 1060 (1977).

Reaction of Bis(4-methyl-8-quinolinolato)nitrosylpyridinecobalt(II) with Nitrogen Monoxide in Dichloromethane

Eiichi MIKI,* Mikio TANAKA,† Kunihiko MIZUMACHI, and Tatsujiro ISHIMORI
Department of Chemistry, College of Science, Rikkyo University, Nishi-Ikebukuro, Toshima-ku, Tokyo 171
†Laboratory of Chemistry, Nippon Medical School, Kosugi, Nakahara-ku, Kawasaki 211
(Received April 16, 1986)

Synopsis. [Co(4mqn)$_2$(NO)(py)] (4mqn=4-methyl-8-quinolinolate ion, $C_{10}H_8NO^-$; py=pyridine) reacted with nitrogen monoxide in dichloromethane to produce a new compound, [NO][Co(4mqn)$_2$(NO$_3$)(py)], with liberation of dinitrogen oxide. The solid product was characterized by IR (including the ^{15}N-isotopic shifts), magnetic, and MS measurements.

It is well-known that transition-metal complexes react with nitrogen monoxide, NO, to make the NO disproportionation and transition-metal nitrosyls with NO^- group also react with NO to cause electrophilic attack by NO on the nitrosyl group.[1,2]

We have reported the reaction of NO with [$Co^{II}L_2$] (L=8-quinolinolate ion or its derivatives) or [$Co^{III}L_2$(NO)] with NO^- group in organic solvents.[3–6] In CH_2Cl_2 inhering poor coordinating ability to metal ion, [CoL_2] is nitrosylated or the nitrosyl group in the resulting nitrosyl complex reacts further with NO to give NO_3^-, NO_2^-, NO^+ (nitrosyl cation), and N_2O.[3,4] On the other hand, on the reaction of [CoL_2] with NO in pyridine having strong coordinating ability, [CoL_2] is nitrosylated followed by electrophilic attack of NO on the nitrosyl group to give NO_3^- or NO_2^-, and N_2O.[5,6]

In this paper, we report the reaction of [Co(4mqn)$_2$(NO)(py)] (4mqn=4-methyl-8-quinolinolate ion, py=pyridine) with NO in CH_2Cl_2. The solid product was [NO][Co(4mqn)$_2$(NO$_3$)(py)], the gaseous one being N_2O. The reaction is shown as follows;

$$Co^{3+} + NO^-(\text{coord}) + 5NO \longrightarrow Co^{2+} + NO^+ + NO_3^-(\text{coord}) + 2N_2O \quad (\text{coord} = \text{coordinating}).$$

Experimental

Dichloromethane was dried over Zeorum A-4, distilled and stored under argon. Nitrogen[^{15}N] monoxide was derived from $K^{15}NO_3$ (^{15}N atom%=99). The reactants, [Co(4mqn)$_2$(NO)(py)] with NO^- group and its ^{15}NO-labeled compound (^{15}N atom%=99), were prepared according to the literature.[6] Anal. ($CoC_{25}H_{21}O_3N_4$) Co, C, H, N.

The reactions were carried out using a vacuum line. Dichloromethane was degassed by three cycles of freeze-pump-thaw before use. The degassed CH_2Cl_2 (10 cm^3) was transferred to the reaction vessel containing the nitrosyl complex (0.3 mmol) and NO (5 mmol) which had been kept at the temperature of liquid nitrogen. The contents were stirred for ca. 50 h at room temperature after having been thawed under running water. The original yellowish khaki complex reacted rapidly with NO to give dark brown solution and gradually precipitate a khaki product in process of the reaction. The product was collected by filtration, washed with diethyl ether, and dried under vacuum. Yield: 60% (ca. 100 mg). Found: Co, 11.1; C, 54.6; H, 3.9; N, 12.8%. Calcd for [NO][Co($C_{10}H_8NO$)$_2$(NO$_3$)(C_5H_5N)] ($CoC_{25}H_{21}O_6N_5$): Co, 10.8; C, 55.0; H, 4.0; N, 12.8%.

The magnetic susceptibility of the solid product was measured by the Gouy method. The IR spectra of the solid products were measured as Nujol and poly(chlorotrifluoroethylene) oil mulls in the 200—4000 cm^{-1} region. The gaseous products were identified by a Hitachi M-80 double-focusing mass spectrometer equipped with a Hitachi M-003 data processor and by the IR bands (including ^{15}N-isotopic shifts) in the 1000—4000 cm^{-1} region.[6] The negative SIMS (secondary ion mass spectrometry) spectrum of the solid product was measured by the mass spectrometer with a SIMS unit and a negative ion measurement unit. The product was dissolved or suspended in a glycerol/3-mercapto-1,2-propanediol, glycerol/sulfolane, or diethanolamine/3-mercapto-1,2-propanediol matrix, and placed on a silver plate probe tip. Xenon was used to produce the primary ion.[7]

Results and Discussion

The khaki product in the solid state is stable in air but is decomposed in polar organic solvents such as DMF and DMSO.

The IR spectrum of the solid product showed some absorption bands characteristic of nitrosyl cation and

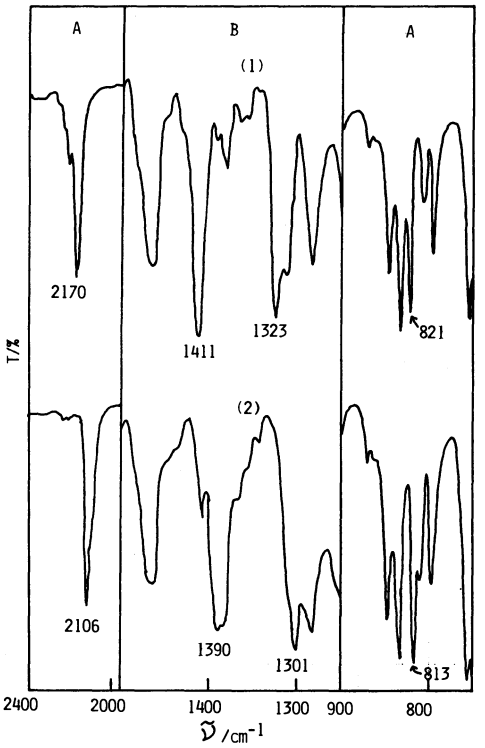

Fig. 1. IR spectra of [NO][Co(4mqn)$_2$(NO$_3$)(py)] (4mqn=4-methyl-8-quinolinolate ion, py=pyridine). (1): ^{14}N-complex, (2): ^{15}N-complex (^{15}N atom%=99). A region: Nujol mull, B region: poly(chlorotrifluoroethylene) oil mull.

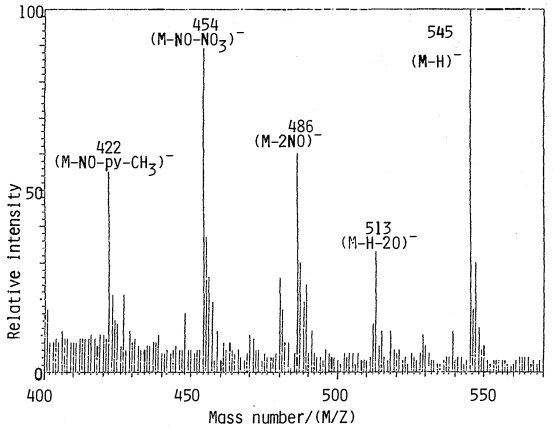

Fig. 2. Negative SIMS spectrum of [NO][Co(4mqn)$_2$-(NO_3)(py)] (4mqn=4-methyl-8-quinolinolate ion, py=pyridine) in the matrix, diethanolamine/3-mercapto-1,2-propanediol.

unidentate nitrate ion. These bands shifted downwards upon ^{15}N-substitution as shown in Fig. 1; the strong band at 2170 cm^{-1} shifted to 2106 cm^{-1}, and was assigned to the stretching vibration of nitrosyl cation.[3,4] The strong bands at 1411, 1323, and 821 cm^{-1} shifted to 1390, 1301, and 813 cm^{-1}, respectively, which were assigned to the NO_2 antisymmetric stretching, the symmetric stretching, and the out-of-plane bending vibrations of the NO_3^-, respectively.[3-6] The strong band at 327 cm^{-1} was assigned to the Co–N(pyridine) stretching vibration.[6]

The negative SIMS spectrum in diethanolamine/3-mercapto-1,2-propanediol showed the peaks at m/z= 545, 513, 486, 454, and 422. These ions correspond to $(M-H)^-$, $(M-H-2O)^-$, $(M-NO-NO)^-$, $(M-NO-NO_3)^-$, and $(M-NO-py-CH_3)^-$ where M is the molecular ion with m/z=546, respectively (see Fig. 2). These peaks were also observed in glycerol/3-mercapto-1,2-propanediol and glycerol/sulfolane matrices.

The elemental, IR, and MS analyses indicate that the solid compound is [NO][Co(4mqn)$_2$(NO_3)(py)] containing cobalt(II). The effective magnetic moment was 1.66 BM at 295 K, supporting low-spin d^7 configuration of the cobalt ion.

The IR and MS measurements clearly showed that the gaseous product was only dinitrogen oxide.

For tracing the nitrogen atoms in the reaction of the nitrosyl group with NO, the following isotopic combinations were used and the residual NO and the liberated N_2O were analysed by the mass spectrometer; A (the reaction of the ^{14}NO-complex with ^{15}NO gas) and B (the reaction of the ^{15}NO-complex with ^{14}NO gas). The molar ratio of ^{14}NO to ^{15}NO observed after the reaction was equal to that calculated from the amounts of the reactants before the reaction; the calculated and observed ratios in the case of A were 0.045 and 0.050±0.001, respectively, and those in the case of B, 19 and 20±3, respectively. This shows that the ^{14}N–^{15}N scrambling between the nitrosyl group and the NO gas occurred. Such a phenomenon has been observed for the reaction of [CoL_2(NO)] (L=8-quinolinolate ion or its derivatives) with NO in solvents having coordinating ability to metal ion.[5,6,8] The reproducibility of the same measurements for the liberated N_2O as the NO was poor, but the ^{14}N–^{15}N scrambling was also observed for N_2O. These scrambling phenomena suggest that the nitrosyl complex liberates NO in dissolution and the liberated NO together with original reactant, NO, reacts with the resulting cobalt(II) complex to attain the following equilibrium; Co^{II}+ $NO \rightleftarrows Co^{III}$–$NO^-$.[5,6] Thus, the reaction mechanism could not be elucidated.

In CH_2Cl_2, [Co(4mqn)$_2$(NO)] did not react with NO. The N–O stretching bands of [Co(4mqn)$_2$(NO)] and [Co(4mqn)$_2$(NO)(py)] are observed at 1658 and 1616 cm^{-1}, respectively, suggesting that electrophilicity of the nitrosyl group in the latter is stronger than that in the former due to coordination of pyridine. Thus, even in solvent having poor coordinating ability, the electrophilic attack of NO on the nitrosyl group would proceed to produce NO_3^-, NO^+ (nitrosyl cation), and N_2O as observed for the reaction of [Co(qn)$_2$(NO)] (qn=8-quinolinolate ion) with NO in CH_2Cl_2.[3]

There is a possibility that [Co(4mqn)$_2$L(py)] (L= NO_3^- or NO_2^-) is formed as a minor product in the present reaction considering our last paper.[6] However, the negative SIMS spectra showed no peaks corresponding to their molecular ion regions.

The present overall reaction can be represented as

$$Co^{3+} + NO^-(\text{coord}) + 5NO \longrightarrow Co^{2+} + NO^+ + NO_3^-(\text{coord}) + 2N_2O(\text{coord} = \text{coordinating}).$$

References

1) J. A. McCleverty, *Chem. Rev.*, **79**, 53 (1979).
2) K. K. Pandey, *Coord. Chem. Rev.*, **51**, 69 (1983).
3) E. Miki, *Chem. Lett.*, **1980**, 835.
4) E. Miki, K. Saito, K. Mizumachi, and T. Ishimori, *Bull. Chem. Soc. Jpn.*, **56**, 3515 (1983).
5) E. Miki, K. Ishimaru, K. Mizumachi, T. Ishimori, and M. Tanaka, *Bull. Chem. Soc. Jpn.*, **58**, 962 (1985).
6) E. Miki, M. Tanaka, K. Saito, T. Maejima, K. Mizumachi, and T. Ishimori, *Bull. Chem. Soc. Jpn.*, **58**, 1642 (1985).
7) The ionization method: electron impact; the primary ion accelerating potential: 8 kV.
8) T. Maejima, the master's thesis at Rikkyo University in 1985; to be published.

The Structure of Bis(μ-thiocyanato)-bis[tris(benzylamine)(thiocyanato)nickel(II)], $[Ni(SCN)_2(C_6H_5CH_2NH_2)_3]_2$

Masahiro TANIGUCHI* and Akira OUCHI
Department of Chemistry, College of Arts and Sciences, The University of Tokyo, Komaba, Meguro-ku, Tokyo 153
(Received May 9, 1986)

Synopsis. The crystal and molecular structure of the title complex was determined by means of a single-crystal X-ray diffraction method. A crystal of $Ni_2C_{46}H_{54}N_{10}S_4$, F. W. 992.67, is triclinic with a space group $P\bar{1}$, a=13.259(4), b=15.627(5), c=6.5150(16) Å, α=90.60(3), β=93.64(2), γ=112.601(19)°, U=1242.9(6) Å^3, Z=1, D_m=1.32(3), D_x=1.33 Mg m^{-3}, and μ(Mo $K\alpha$)=9.60 cm^{-1}. The central metal atom is hexa-coordinated, being ligated with three benzylamine and two thiocyanato (SCN) nitrogen atoms as well as one SCN sulfur atom. Two metal atoms are bridged by two SCN ions; however, the Ni-S bond length is 2.639(3) Å, which is a little longer than the sum of the Shannon's ionic radii. The distance Ni···Ni is 5.717(3) Å and the dimeric complexes are discrete in a crystal.

It has already been found that in Lewis-base adducts of thiocyanate (SCN) complexes, where the central metal is relatively soft (such as mercury, cadmium, or silver), the SCN ion bridges the metal atoms forming linear, planar, or three-dimensional networks.[1-7] On the other hand, in cases of the adducts of nickel(II) thiocyanate, many of them are monomeric and the metal atom is in an octahedral geometry.[8-10] However, Lipkowski has reported that in the case of 4-methylpyridine (pic) adduct, $[Ni(SCN)_2(pic)_3]_2$ (**2**), the adduct takes a dimer structure where two metal atoms are bridged by two SCN ions.[11] Since such types of nickel(II) complexes which include SCN bridges are not common, we started to find another example and obtained the title complex. Its structure was determined by an X-ray diffraction method using its single crystal.

Experimental

Synthesis of Bis(μ-thiocyanato)-bis[tris(benzylamine)(thiocyanato)nickel(II)] (1). Anhydrous nickel(II) thiocyanate (0.87 g, 5.0 mmol) and benzylamine (bza) (1.59 g, 15 mmol) are dissolved into warm methanol (20 cm^3), and the solution was left standing at ambient temperature. Pale-blue needle-like crystals were deposited, filtered off, washed with methanol and dried over a silica-gel desiccator. Yield: 1.9 g, 75%. Anal. ($Ni_2C_{46}H_{54}N_{10}S_4$), Ni, C, H, N.

Single-Crystal X-Ray Analysis. The crystal used for the structure determination was about 0.3×0.25×0.2 mm^3 in size, and was used without shaping. The reflections in the range of $3°<2\theta<60°$ were collected on a Rigaku AFC-6A automated 4-circle X-ray diffractometer with graphite-monochromated Mo $K\alpha$ radiation, by means of ω—2θ scan technique (scan speed, 4°min^{-1}: scan width 1.40+0.5 tanθ°(θ)). The intensities were corrected for Lorentz and polarization factors, but no correction was made for absorption and extinction. Of 7285 independent reflections collected, 3110 reflections with $|F_o|>3\sigma(|F_o|)$ were used for the structure determination. All the calculations were carried out on a HITAC M-280H computer at the Computer Center of the University of Tokyo, using the local version of UNICS.[12] The scattering factors were taken from Reference 13.

The structure was solved by the heavy-atom method. The positional parameters of all the non-hydrogen atoms converged, but as the equivalent isotropic temperature factors of C(35), C(36), and C(37) were found to be large, at the final refinement process, the positions of these three atoms were fixed at respective positions assuming their B_{iso} to be 15.0. Applying the anisotropic temperature factors for the other atoms, the final R value,[14] thus obtained, was 0.086.

Results and Discussion

The selected bond lengths and bond angles are shown in Table 1.[15] A projection of the complex together with the numbering scheme of the atoms is shown in Fig. 1, and the crystal packing diagram in Fig. 2.

The metal atom is hexa-coordinated and is in an octahedral geometry. Two nickel atoms are bridged by two SCN ions, where each nickel atom is ligated by the nitrogen atom of one ligand and the sulfur atom of the other. The eight-membered ring, which consists of

Table 1. Selected Bond Lengths and Bond Angles with Estimated Standard Deviations in Parentheses

Bond length (l/Å)					
Ni-S(1)	2.639(3)	Ni-N(1^i)	2.050(6)	Ni-N(2)	2.048(6)
Ni-N(11)	2.101(7)	Ni-N(21)	2.127(6)	Ni-N(31)	2.126(9)
S(1)-C(1)	1.638(7)	C(1)-N(1)	1.139(8)	S(2)-C(2)	1.623(7)
C(2)-N(2)	1.140(10)	N(11)-C(11)	1.499(10)	C(11)-C(12)	1.512(14)
N(21)-C(21)	1.471(9)	C(21)-C(22)	1.532(13)	N(31)-C(31)	1.35(2)
C(31)-C(32)	1.52(2)	Ni···Ni^i	5.717(3)	Ni···Ni^{ii}	6.515(3)
Bond angle (ϕ/°)					
S(1)-Ni-N(1^i)	92.05(17)	S(1)-Ni-N(2)	86.19(19)	S(1)-Ni-N(11)	84.4(2)
S(1)-Ni-N(31)	86.1(3)	N(1^i)-Ni-N(2)	177.9(3)	N(1^i)-Ni-N(11)	94.7(3)
N(1^i)-Ni-N(21)	86.6(2)	N(1^i)-Ni-N(31)	90.9(3)	N(2)-Ni-N(11)	86.3(3)
N(2)-Ni-N(21)	95.2(2)	N(2)-Ni-N(31)	87.8(3)	N(11)-Ni-N(21)	93.5(3)
N(21)-Ni-N(31)	96.1(3)	Ni-S(1)-C(1)	102.2(3)	Ni-N(1^i)-C(1^i)	164.9(6)
Ni-N(2)-C(2)	179.0(6)	S(1)-C(1)-N(1)	179.0(6)	S(2)-C(2)-N(2)	179.9(7)

Key to the symmetric operations: i, 1−x, 1−y, 1−z, ii, x, y, 1+z.

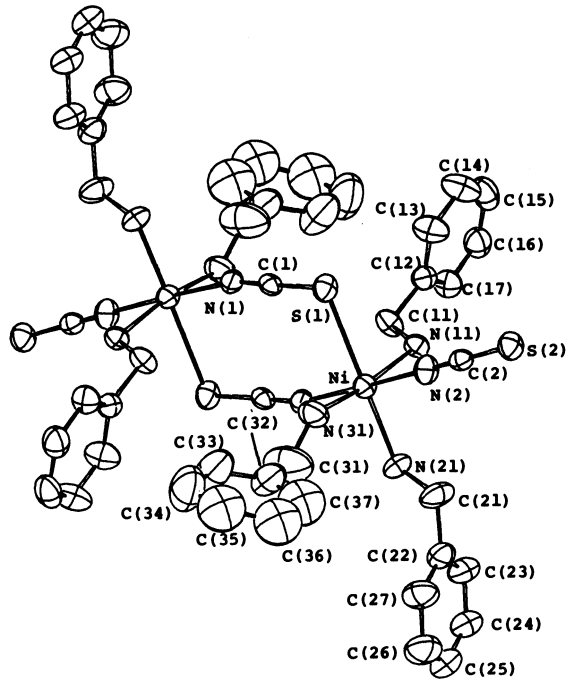

Fig. 1. A projection of the dimeric complex with the numbering scheme.

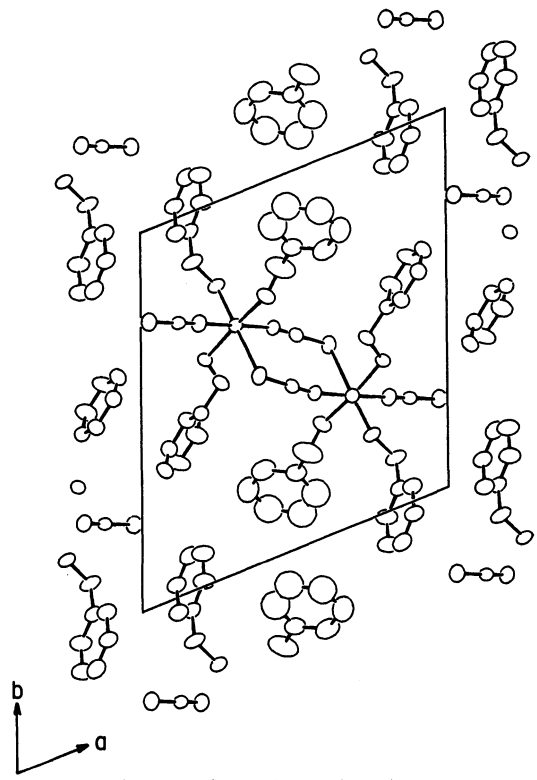

Fig. 2. Crystal packing diagram.

two nickel atoms and two bridging SCN ions, is about on a plane (average deviations of the atomic positions is 0.008 Å). A nitrogen atom of another SCN ion, as well as three bza nitrogen atoms, are coordinated to each metal atom. Each dimer complex is discrete in the crystal; neither ligand bridgings nor hydrogen bondings are found between them. Two SCN nitrogen atoms take trans configuration, and the sulfur atom of SCN ion is in the cis orientation from both of these nitrogen atoms; the other three positions are occupied by the bza nitrogen atoms. The bond length Ni–S(1) is 2.639(3) Å, which is a little longer than the sum of the Shannon's ionic radii, 2.53 Å (r_{Ni}=0.690 and r_S=1.84 Å).[16] The bond length Ni–N(bza) is 2.118 Å on the average, a little longer than that for Ni–N(SCN), 2.049 Å on the average. The latter value is a little shorter than the sum of the Shannon's ionic radii, 2.15 Å (where r_N=1.46 Å), probably due to the delocalization of the charge on the nitrogen atoms of the SCN ions.

Although the properties of bza and pic are quite different and their adducts of the metal complexes are expected to take different structures from each other, the structure of **1** is essentially similar to that of **2**: the orientation of the ligated atoms around the metal atom is the same in **1** and **2**.

However, in **2**, the Ni–S bond length (2.583 Å), as well as the Ni–N(pic) ones (2.085 Å on the average), are much shorter than the corresponding bond lengths of **1**, while those of Ni–N(SCN) are about the same.[11] Therefore, in **1** the Ni–S and Ni–N(Lewis base) bonds are thought to be weaker than the corresponding bonds of **2**. This fact may be, at least partially, due to the bulkiness of the bza ligand, which has a methylene group between the ligand nitrogen atom and the phenyl group; the ligand is not planar and it is hardly packed into a crystalline space, while the pic molecule is planar except for the methyl hydrogen atoms. Therefore, in the crystal packing, the steric hindrance of the Lewis base ligands makes the approach of the ligated atoms to the metal atoms in **1** more difficult than in **2**.

References

1) A. F. Wells, "Structural Inorganic Chemistry," 5th ed, Clarendon, Oxford, U. K. (1984), pp. 126, 935, 1159.
2) H. Kinoshita, M. Shimoi, A. Ouchi, and S. Sato, *Bull. Chem. Soc. Jpn.*, **58**, 2782 (1985).
3) H. Kinoshita, M. Shimoi, and A. Ouchi, *Bull. Chem. Soc. Jpn.*, **58**, 1304 (1985).
4) M. Taniguchi, M. Shimoi, and A. Ouchi, *Bull. Chem. Soc. Jpn.*, **59**, 2299 (1986).
5) P. C. Gagnon and A.L.Beauchamp, *Acta Crystallogr., Sect. B*, **35**, 166 (1979).
6) M. Cannas, G. Carta, A. Cristini, and G. Marongiu, *Inorg. Chem.*, **16**, 228 (1977).
7) N. K. Mills and A. H. White, *J. Chem. Soc., Dalton Trans.*, **1984**, 229.
8) A. R. Davis, F. W. B. Einstein, and A. C. Willis, *Acta Crystallogr., Sect. B*, **38**, 437 (1982).
9) L. M. Amzel, S. Baggio, and L. N. Becka, *J. Chem. Soc., A*, **1969**, 2066.
10) J. Garaj, M. Dunaj-Jurco, *J. Chem. Soc., Chem. Commun.*, **1968**, 518.
11) J. Lipkowski, *Transition Metal Chem.*, **3**, 117 (1978).
12) "The Universal Crystallographic Computation Program System (UNICS)," ed by T. Sakurai, Crystallographic Society of Jpn., Tokyo (1967).
13) "International Tables for X-Ray Crystallography," Kynoch Press, Birmingham (1974), Vol. IV, pp. 72, 149.
14) $R=\sum||F_o|-|F_c||/\sum|F_o|$.
15) The final atomic and thermal parameters, the final F_o-F_c table, and some additional data about the bond lengths and bond angles are deposited as Document No. 8644 at the Office of the Bull. Chem. Soc. Jpn.
16) R. D. Shannon, *Acta Crystallogr., Sect. A*, **32**, 751 (1976).

Reactions of α,β-Unsaturated Thiones with Diphenylcyclopropenone and Diphenylcyclopropenethione

Takayuki KARAKASA,† Satoshi TAKEDA, Takao SAITO, and Shinichi MOTOKI*
Department of Chemistry, Faculty of Science, Science University of Tokyo, Kagurazaka, Shinjuku-ku, Tokyo 162
†Nippon Dental University, Fujimi, Chiyoda-ku, Tokyo 102
(Received April 1, 1986)

Synopsis. 2-(Arylmethylene)tetralin-1-thione and 1-aryl-3-phenyl-2-propene-1-thione (thiochalcone) reacted with diphenylcyclopropenone across the =C–CO bond giving a thiophene derivative and a polysubstituted phenol with the arylketene/sulfur elimination, whereas the reaction with diphenylcyclopropenethione took place at the C=S bond affording a spiro compound.

Cyclopropenones and cyclopropenethiones have been known to be highly reactive compounds. Especially, many informations on the chemistry of cyclopropenones have accumulated in numerous papers and their cycloadditions were found to occur across the C=O, C=C, or the C–CO bond of the ring.[1,2] Previously, we reported that the α,β-unsaturated thiones such as 2-(arylmethylene)tetralin-1-thiones (**2**) and thiochalcones (**4**), which were generated by thermolysis of their dimers **1** and **3**, underwent cycloaddition reactions with various dienophiles to give 1:1-adducts.[3] As a continuation of the work, reactions of these thiones with diphenylcyclopropenone (**5**) and diphenylcyclopropenethione (**6**) have been investigated in the present study.

A mixture of 2-(phenylmethylene)tetralin-1-thione dimer, **1a**, and **5** in dry benzene was refluxed for 2.5 h. After the reaction was completed, the mixture was chromatographed to give 4,5-dihydro-2,3-diphenylnaphtho[1,2-*b*]thiophene (**7**) in a yield of 57%. Evidently, the product showed no band for a carbonyl group in the IR spectrum, and the ^{1}H NMR spectrum exhibited only signals of ethylene protons (4H) and aromatic protons (14H). In the mass spectrum, a molecular ion peak was observed at *m/z* 338 (100% intensity) which corresponded to that of *m/z* 456 (1:1-adduct) −118 (C_8H_6O). Since it is obvious from these spectral data that not less than one phenyl moiety was eliminated from a 1:1-adduct, reactions of 2-(*p*-methoxybenzylidene)tetralin-1-thione dimer (**1b**) and 2-(*p*-chlorobenzylidene)tetralin-1-thione dimer (**1c**) with **5** were examined. The product obtained in each case was the same compound **7** in which no *p*-methoxy- or *p*-chlorophenyl moiety was contained. The reaction of thiochalcone dimer, **3a**, with **5** afforded 2,3,5-triphenylthiophene (**8**) and 2,3,4,6-tetraphenylphenol (**9**) (Table 1). These interesting results are rationalized in terms of the [4+3]cycloaddition of the α,β-unsaturated thiones (**2**, **4**) and **5** with fission of the =C–CO bond of **5** and the subsequent elimination of the arylketene/sulfur atom from the intermediary 1:1-adducts (**10**, **11**). However, attempt to trap the ketene by methanol was unsuccessful. On the other hand, treatment of **1a** with **6** in refluxing benzene for 1 h gave a 1:1-adduct in a yield of 56%. The ^{1}H and ^{13}C NMR spectra of the adduct indicated the presence of a ethylene group, a methine group, and a quarternary carbon atom of the cyclopropene ring in addition to the olefinic and the aromatic moieties. The results suggest that both regioisomeric structures, **12** and **13**, are plausible for the adduct. We prefer the 1,3-dithiin structure because their mass fragmentation pattern[4] showed extrusion of a thiobenzaldehyde molecule from **12**, not from **13**. Similarly, the reactions of **1b**, **c** and **3a—c** with **6** gave the 1,3-dithiins **12b**, **c** and **14a—c**, respectively (Table 1).

Marked contrast between the reactions of the α,β-unsaturated thiones (**2**, **4**) with **5** and **6** can be recognized by the fact that thiocarbonyl group is usually more susceptible than carbonyl group to various addition reactions.[5] Actually, **2** and **4** react readily with ordinary thioketones such as thiobenzophenone to give the similar 1,3-dithiin adducts, whereas no reaction takes

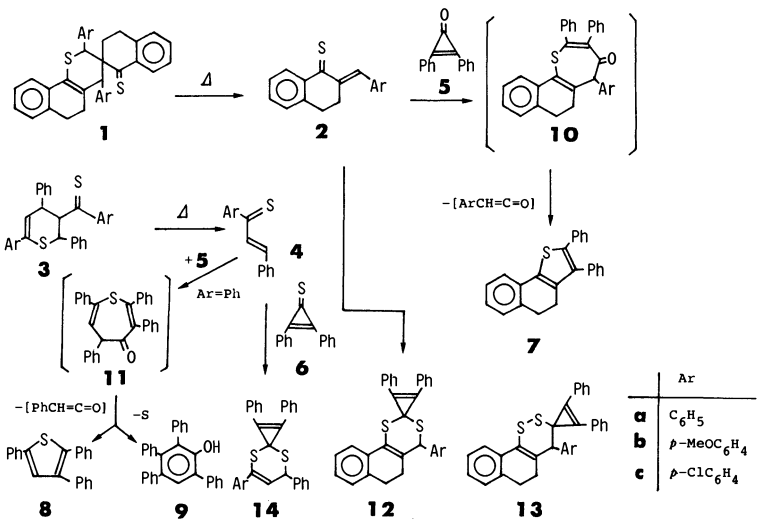

Table 1. Reaction of the Thione Dimers (**1**, **3**) with Diphenylcyclopropenone (**5**) and Diphenylcyclopropenethione (**6**)

Thione dimer	Dienophile	Reaction time/h	Product	Mp, θ_m/°C	Yield/%
1a	5	2.5	**7**		57
1b	5	1.5	**7**	166—168	52
1c	5	3.0	**7**		59
3a	5	8.0	**8**	132—134[a]	37
			9	96—97	19
1a	6	1.5	**12a**	200—202	56
1b	6	1.5	**12b**	204—206	63
1c	6	0.5	**12c**	203—205	59
3a	6	1.0	**14a**	146—147	62
3b	6	0.5	**14b**	176—178	88
3c	6	0.5	**14c**	160—163	62

a) Lit 9; mp 127°C, lit 10; mp 157°C.

place with ketones or aldehydes under the same reaction conditions.[6]

Experimental

All melting points are uncorrected. IR spectra were measured on a Hitachi Model 260-10 spectrometer. ^{1}H and ^{13}C NMR spectra were recorded on a JEOL JNM-FX 100 spectrometer and/or a JEOL PMX-60SI spectrometer in a $CDCl_3$ solution using tetramethylsilane as an internal standard. Mass spectra were recorded on a Hitachi double focusing mass spectrometer RMU-7M and/or M-80 with a data processing system M-003, operating at an ionizing potential of 100 or 70 eV. Elemental analyses were performed using a Yanagimoto Model MT-3 CHN corder.

2-(Arylmethylene)tetraline-1-thione dimers (**1a—c**) and thiochalcone dimers (**3a—c**) were prepared according to the method described previously.[3] Diphenylcyclopropenone (**5**)[7] and diphenylcyclopropenethione (**6**)[8] were prepared by the method given in the literature.

General Procedure for Reaction of the Thione Dimers (1, 3) with Diphenylcyclopropenone (5) or Diphenylcyclopropenethione (6). A mixture of **1** or **3** (4 mmol as a monomer) and **5** or **6** (4 mmol) in dry benzene (6 ml) was refluxed for a required period under a nitrogen atmosphere. After the reaction was completed, the solvent was removed and the residue was chromatographed on silica gel (Wakogel C-200) with benzene–hexane as an eluent. The crude product was recrystallized from an appropriate solvent.

4,5-Dihydro-2,3-diphenylnaphtho[1,2-*b*]thiophene (7). ^{1}H NMR δ=2.52—2.96 (m, 4H, CH_2CH_2), 7.04—7.40 (m, 14H, Ar-H); MS *m/z* 338 (100, M$^+$), 304 (5, M$^+$—H_2S), 261 (8, M$^+$—Ph); Found: M$^+$ 338.1131; Found: C, 85.03; H, 5.37%. Calcd for $C_{24}H_{18}S$: C, 85.17; H, 5.36%; M, 338.1129.

2,3,5-Triphenylthiophene (8). Colorless fluffy needles; IR (KBr) 1605, 765, and 705 cm^{-1}; ^{1}H NMR δ=7.0—7.7 (m, =CH, Ar-H); MS *m/z* 312 (100, M$^+$), 278 (14, PhCCPh$^+$), 191 (6, M$^+$—PhCS), 121 (13, PhCS$^+$).

2,3,4,6-Tetraphenylphenol (9). Yellow crystals; IR (KBr) 3440 cm^{-1}; ^{1}H NMR δ=6.73 (s, 1H, OH), 6.9—7.8 (m, 21H, Ar-H); MS *m/z* 398 (100, M$^+$), 321 (39, M$^+$—Ph), 293 (55, M$^+$—Ph-CO), 215 (32, M$^+$—2Ph—COH), 105 (72, PhCO$^+$).

5′,6′-Dihydro-2,3,4′-triphenylspiro[2-cyclopropene-1,2′-[4*H*]-naphtho[1,2-*d*][1,3]dithiin] (12a). ^{1}H NMR δ=2.82 (m, 4H, CH_2CH_2), 5.51 (s, 1H, CH-Ph), 7.0—7.7 (m, 19H, Ar-H); ^{13}C NMR δ=26.3 (t, CH_2CH_2), 28.5 (t, CH_2CH_2), 56.0 (d, C(1)), 70.2 (s, spiro-C(3)); MS *m/z* 472 (77, M$^+$), 440 (11, M$^+$—S), 350 (100, M$^+$—PhCS); Found: M$^+$ 472.1315. Found: C, 81.61; H, 5.19%. Calcd for $C_{32}H_{24}S_2$: C, 81.32; H, 5.12%; M, 472.1318.

5′,6′-Dihydro-4′-(*p*-methoxyphenyl)-2,3-diphenylspiro[2-cyclopropene-1,2′-[4*H*]naphtho[1,2-*d*][1,3]dithiin] (12b). ^{1}H NMR δ=2.82 (m, 4H, CH_2CH_2), 3.64 (s, 3H, OCH_3), 5.48 (s, 1H, CH-Ar), 6.5—7.7 (m, 18H, Ar-H); ^{13}C NMR δ=26.2 (t, CH_2CH_2), 28.6 (t, CH_2CH_2), 55.1 (d, C(1)), 55.8 (q, OCH_3), 70.5 (s, spiro-C(3)); MS *m/z* 502 (65, M$^+$), 470 (16, M$^+$—S), 350 (100, M$^+$—ArCHS). Found: C, 78.74; H, 5.01%. Calcd for $C_{33}H_{26}S_2$; C, 78.85; H, 5.21%.

5′,6′-Dihydro-4′-(*p*-chlorophenyl)-2,3-diphenylspiro[2-cyclopropene-1,2′-[4*H*]naphtho[1,2-*d*][1,3]dithiin] (12c). ^{1}H NMR δ=2.78 (m, 4H, CH_2CH_2), 5.40 (s, 1H, CH-Ar), 7.0—7.7 (m, 18H, Ar-H); ^{13}C NMR δ=26.3 (t, CH_2CH_2), 28.5 (t, CH_2CH_2), 55.1 (d, C(1)), 75.7 (s, spiro-C(3); MS *m/z* 507 (21, M$^+$), 475 (10, M$^+$—S), 350 (100, M$^+$—ArCHS). Found: C, 75.46; H, 4.46%. Calcd for $C_{32}H_{23}S_2Cl$: C, 75.79; H, 4.57%.

2,3,4′,6′-Tetraphenylspiro[2-cyclopropene-1,2′-[4*H*][1,3]dithiin] (14a). ^{1}H NMR δ=5.38 (s, 1H, H(4)), 6.41 (s, 1H, H(5)), 6.9—7.7 (m, 20H, Ar-H); ^{13}C NMR δ=59.74 (d, C(4)), 68.17 (s, C(2)); MS *m/z* 446 (60, M$^+$), 414 (41, M$^+$—S), 412 (92, M$^+$—H_2S), 325 (100, M$^+$—PhCS), 324 (70, M$^+$—PhCHS); Found: C, 80.53; H, 4.99%. Calcd for $C_{30}H_{22}S_2$: C, 80.71; H, 4.93%.

6′-(*p*-Methoxyphenyl)-2,3,4′-triphenylspiro[2-cyclopropene-1,2′-[4*H*][1,3]dithiin] (14b). ^{1}H NMR δ=3.77 (s, 3H, OCH_3), 5.40 (s, 1H, H(4)), 6.32 (s, 1H, H(5)), 6.7—7.7 (m, 19H, Ar-H); ^{13}C NMR δ=55.31 (q, OCH_3), 59.74 (d, C(4)), 68.22 (s, C(2)); MS *m/z* 476 (66, M$^+$), 444 (25, M$^+$—S), 354 (100, M$^+$—PhCHS); Found: C, 78.02; H, 5.11%. Calcd for $C_{31}H_{24}OS_2$: C, 78.15; H, 5.04%.

6′-(*p*-Chlorophenyl)-2,3,4′-triphenylspiro[2-cyclopropene-1,2′-[4*H*][1,3]dithiin] (14c). ^{1}H NMR δ=5.38 (s, 1H, H(4)), 6.38 (s, 1H, H(5)), 6.8—7.7 (m, 19H, Ar-H); ^{13}C NMR δ=59.64 (d, C(4)), 68.13 (s, C(2)); MS *m/z* 480 (51, M$^+$), 448 (21, M$^+$—S), 358 (100, M$^+$—PhCHS); Found: C, 74.76; H, 4.21%. Calcd for $C_{30}H_{21}S_2Cl$: C, 74.92; H, 4.37%.

References

1) K. T. Potts and J. S. Baum, *Chem. Rev.*, **74**, 189 (1974).

2) J. Cialattoni and G. A. Barchtold, *J. Am. Chem. Soc.*, **87**, 1404 (1965); R. Breslow and J. Pecoraro, *Tetrahedron Lett.*, **1972**, 4415.

3) T. Karakasa and S. Motoki, *J. Org. Chem.*, **43**, 4147 (1978); **44**, 4151 (1979); T. Karakasa, H. Yamaguchi, and S. Motoki, *ibid.*, **45**, 927 (1980); T. Karakasa and S. Motoki, *Chem. Lett.*, **1980**, 879.

4) U. Eisner and T. Krishnamurthy, *Tetrahedron*, **27**, 5753 (1971); P. Beslin, *J. Heterocyclic Chem.*, **20**, 1753 (1983).

5) E. Campaigne, "The Chemistry of the Carbonyl Group," in "The Chemistry of Functional Groups," ed by S. Patai, John Wiley & Sons, New York (1966), p. 938; S. M. Weinreb and R. R. Staib, *Tetrahedron*, **38**, 3087 (1982), and references cited therein.

6) S. Motoki et al., unpublished results.

7) R. Breslow and J. Posner, *Org. Synth.*, Coll. Vol. 5, 514 (1973).

8) Y. Kitahara and M. Funamizu, *Bull. Chem. Soc. Jpn.*, **37**, 1897 (1964).

9) A. Smith, *J. Chem. Soc.*, **57**, 647 (1890).

10) S. K. Mitra, *J. Indian Chem. Soc.*, **15**, 59 (1938); *Chem. Abstr.*, **32**, 4982 (1938).

Surface Analysis of MF-Aluminas and Related Supported Reagents by Scanning Electron Microscopy

Takashi ANDO,* James H. CLARK,† David G. CORK, and Takahide KIMURA
Department of Chemistry, Shiga University of Medical Science, Otsu, Shiga 520-21
†Department of Chemistry, University of York, Heslington, York YO1 5DD, U.K.
(Received April 11, 1986)

Synopsis. SEM of MF-aluminas (M=Na, K, and Cs, loaded at 2 mmol g^{-1} and dried at 90 °C/2.7 kPa), showed similar salt dispersions and surface morphologies, with salt clusters of ca. 1 μm diameter evident on the external surfaces. Less reactive, highly dried or highly loaded, reagents showed extensive surface crystallization. KCl- and KOH-aluminas showed the effect of anion basicity, giving greater clustering and surface destruction respectively.

Although supported inorganic salts have been employed in a wide variety of organic reaction types,[1,2] only in a few recent cases has the full potential of improved reagent selectivity, reactivity and stereospecificity begun to be realized, by careful study and optimization of predispersed reagent preparations.[3,4]

KF–Alumina is a most noteworthy supported reagent which acts as an efficient and convenient heterogeneous base.[5–7] We have previously shown that different loading and drying conditions can produce quite large changes in chemical reactivity, notably for noncatalytic base promoted reactions,[7] and that supported alkali metal fluoride reagents show the same cation effect on activity as do the unsupported salts ($NaF \ll KF < CsF$).[5] The reasons for the dramatic increase in MF basicity, when impregnated on Al_2O_3, and the subsequent reactivity variations have remained somewhat obscure despite IR, solids NMR, thermal, titrimetric and surface area analyses being performed.[7] The active basic species may involve a coordinatively unsaturated fluoride ion center, exhibiting basicity through its strong H-bonding capacity, but the basicity of species formed by reaction of F^- with Al_2O_3 cannot be discounted. In order to directly observe the effects of MF salt impregnation on the Al_2O_3 surface morphology and allow comparison with some related salts, we have now used scanning electron microscopy (SEM).

For the neutral chromatographic grade γ-alumina used, a 2 mmol g^{-1} loading of salt is calculated to give an approximate theoretical "monolayer" of ion pairs over the hydroxylated surface.[8] Although KF–alumina "monolayer" loadings and lower gave highly efficient basic catalysis, the optimum reagent preparation for a noncatalytic *O*-methylation of phenol involved a significantly higher loading (5 mmol g^{-1}, dried at 90 °C/2.7 kPa),[7] suggesting that surface coverage of salt, and active basic sites, are not maximized at the 2 mmol g^{-1} loading. Whereas X-ray powder diffraction of the reagents reveals little at these loadings (only at ca. 10 mmol g^{-1} does it give clear evidence for KF clustering and fluoroaluminate formation by chemisorption[7]), SEM directly shows the extent of salt clustering and surface deterioration.

A sample of deactivated alumina (aqueous washed, dried at 90 °C/2.7 kPa) shows that most of the particles have generally smooth surfaces (Fig. 1a) at

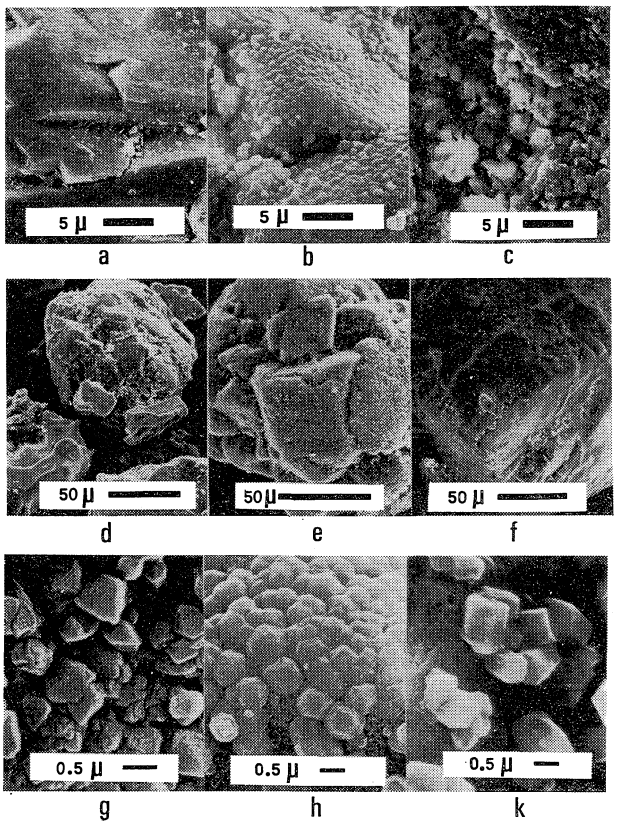

Fig. 1. Scanning electron microscopy of: (a) alumina, water washed and dried at 90 °C/2.7 kPa; (b), (e), and (h) KF-alumina 2 mmol g^{-1}, dried at 90 °C/2.7 kPa; (c) KF-alumina 2 mmol g^{-1}, dried at 600 °C; (d) KCl-alumina 2 mmol g^{-1}, dried at 90 °C/2.7 kPa; (f) KOH-alumina 2 mmol g^{-1}, dried at 90 °C/2.7 kPa; (g) NaF-alumina 2 mmol g^{-1}, dried at 90 °C/2.7 kPa; (k) CsF-alumina 2 mmol g^{-1}, dried at 90 °C/2.7 kPa.

magnification which cannot reveal their porous structure. Comparison with KF–alumina (Fig. 1b) at the 2 mmol g^{-1} loading, clearly shows the salt, in microcrystalline clusters of 0.5—1 μm diameter, well dispersed over the external surface. Microclusters of this size must contain in the order of 10^{10} KF ion pairs suggesting that a large amount of the 2 mmol of KF loaded is accommodated on the external surface in such clusters. It thus seems evident that "monolayer coverage" is not being obtained at this level of loading, and the 5 mmol g^{-1} KF–alumina may owe its optimum activity to the greater amount of KF available; a) to achieve greater coverage of the internal surface and b) to further cover the external alumina surface with salt microclusters. For reactions such as phenol alkylation, strong surface adsorption of reactants may well

hinder reaction if it takes place at unactive sites. Thus elimination of these sites, by more complete KF coverage, will be important for obtaining optimum reagent reactivity.[7]

Drying KF–alumina at up to 200 °C/13 Pa produced only limited local crystallization of the salt clusters, however 600 °C calcination produced a drastic change in the surface morphology (Fig. 1c) as chemisorption of KF is promoted. The surface crystallization is accompanied by a large drop in surface area (from 96 to 18 $m^2 g^{-1}$ Al_2O_3), a loss of noncatalytic activity, and also is associated with the detection of K_3AlF_6 by X-ray powder diffraction.[7]

Comparison of the alumina-supported potassium salts, KCl, KF, and KOH at 2 mmol g^{-1} loading (Fig. 1d, e, and f) shows the effect of salt basicity and surface affinity on the salt loading. The weakly basic chloride has little affinity for the alumina surface and the majority of the salt is deposited in large crystalline clusters of irregular size and shape, up to ca. 10—50 μm dimension. In contrast the highly basic hydroxide is deposited on the alumina surface in a fairly regular manner which produces some severe erosion of the surface, presumably by aluminate formation. The KF–alumina appears intermediate in terms of both the clustering of external salt, and the degree of surface damage caused by chemisorption reaction. Adsorption of KF causes little apparent surface erosion for the reagents dried at 90 °C.

The sequence of alumina-supported alkali metal fluorides, NaF, KF, and CsF at 2 mmol g^{-1} loading (Fig. 1g, h, and k) show that in all cases the external surface is covered with well dispersed microcrystalline clusters, of approximately 1 μm dimension. Although there is a large variation in the aqueous solubilities of these fluorides, increasing ca. 100 times in the above order, the similar appearance of the reagents suggests that the rate of salt precipitation onto the surface, during preparation by aqueous evaporation, does not greatly influence the cluster size and distribution. Rather, the high surface affinity of fluoride seems determinant. The clusters on all of these reagents must contain much of the salt loaded, but they do represent much smaller particles than could be obtained by conventional grinding procedures, consequently the reagents have a high salt surface area. The cation effect on the reactivity of the reagents is also in agreement with small salt clusters, rather than highly dispersed ion pairs, being responsible for the basicity.

Samples of KF- and KCl–alumina loaded at 10 mmol g^{-1} showed distinctly different external surface morphology, the fluoride having multilayers of clustered salt particles (2—3 μm size), whilst the chloride had relatively few crystal growths, covering large areas (typically 100—1000 μm^2). The greater interaction of KF, than KCl, with the alumina is also apparent in the measured BET surface areas of the two reagents.[7] KF–Aluminas continue to lose surface area with loading (38 $m^2 g^{-1}$ Al_2O_3 at 10 mmol g^{-1}) whereas the KCl–aluminas only lose surface area due to blockage of small pores, thus loadings at 2 and 10 mmol g^{-1} have quite similar surface areas, 104 and 93 $m^2 g^{-1}$ Al_2O_3 respectively.

In summary, SEM analysis has directly shown that MF–Al_2O_3 reagents possess most of their salt in microcrystalline clusters, which nevertheless are far smaller particles than would otherwise be obtainable. The KF salt dispersion and the KF–Al_2O_3 surface deterioration are intermediate between those of KCl– and KOH–Al_2O_3's further supporting the idea, from the reactivity order dependence on the MF cation ($Na \ll K < Cs$), that the supported reagent basicity largely originates from a great increase in salt surface area. Thus the enhanced basicity of MF–Al_2O_3 reagents would seem to be more a result of improved fluoride ion strong H-bonding ability than of F^-–Al_2O_3 reaction generating an alternative strong base.

Experimental

Preparation of Samples. The supported reagents were prepared by adding 5 g of alumina (Merck 90, neutral for chromatography) to the calculated weight of salt dissolved in ca. 30 ml of water, followed by rotary evaporation at ca. 50 °C and subsequent drying under the stated conditions (Fig. 1). Samples were mounted with double-sided sticky tape and coated with 10—15 nm of gold[9] in an evaporative ion coater. Observation by SEM was accomplished with a Hitachi S-500AS microscope operating at 15—25 kV accelerating voltage.

We thank the Japan Society for the Promotion of Science and the Royal Society (for a Fellowship to DGC) and Morita Kagaku Kogyo Co., Ltd for chemicals. We also thank Mr. Shinobu Nishitani for helpful discussions and assistance.

References

1) A. McKillop and D. W. Young, *Synthesis*, **1979**, 401, 481.

2) G. H. Posner, *Angew. Chem. Int. Ed. Engl.*, **17**, 487 (1978).

3) A. AlJazzaa, J. H. Clark, and M. Robertson, *Chem. Lett.*, **1982**, 405.

4) J. H. Clark and C. V. A. Duke, *J. Org. Chem.*, **50**, 1330 (1985); and unpublished results.

5) T. Ando, J. Yamawaki, T. Kawate, S. Sumi, and T. Hanafusa, *Bull. Chem. Soc. Jpn.*, **55**, 2504 (1982); J. Yamawaki, T. Kawate, T. Ando, and T. Hanafusa, *Bull. Chem. Soc. Jpn.*, **56**, 1885 (1983).

6) J. H. Clark, D. G. Cork, and M. S. Robertson, *Chem. Lett.*, **1983**, 1145.

7) T. Ando, S. J. Brown, J. H. Clark, D. G. Cork, T. Hanafusa, J. Ichihara, J. M. Miller, and M. S. Robertson, *J. Chem. Soc., Perkin Trans. 2*, **1986**, 1133.

8) Alumina BET surface area is 125 $m^2 g^{-1}$ Al_2O_3 and the estimated density of surface hydroxyl groups is 8—10 nm^{-2}.

9) Samples prepared for observation in "aquadag" carbon paste, without gold coverage, showed similar results but images generally suffered from charging effects.

The Reaction of 1,2-Epoxyalkylsilanes with Azidotrimethylsilane. A Novel Stereoselective Synthesis of (Z)-1-Alkenyl Azides

Shuji TOMODA,* Yuzo MATSUMOTO, Yoshito TAKEUCHI, and Yujiro NOMURA
Department of Chemistry, College of Arts and Sciences, The University of Tokyo, Komaba, Meguro-ku, Tokyo 153
(Received April 25, 1986)

Synopsis. The reaction of *trans*-1,2-epoxyalkylsilanes with azidotrimethylsilane in the presence of boron trifluoride-diethyl ether complex afforded regio- and stereoselectively (*Z*)-1-alkenyl azides.

1-Alkenyl azides, or more commonly vinyl azides, constitute an intriguing class of compounds because of their versatile utility in organic synthesis[1] as well as theoretical interests.[2] Methods available for the synthesis of these are rather limited, among which Hassner's procedure involving 2-iodoalkyl azides, prepared by addition of iodine azide to alkenes, has been most frequently employed.[3] Since this method fails to provide 2-substituted vinyl azides (**1**) except 3,3-dimethyl-1-butenyl azide, several attempts at synthesizing **1** have been made including azidoselenenylation[4] and azidosulfenylation[5] of alkenes.

In a synthetic project, we required stereochemically defined 2-substituted vinyl azides. With regard to the well-known stereoselective alkene synthesis originally reported by Peterson,[6] we thought that the reaction of 1,2-epoxyalkylsilanes (**2**)[7] with azide ion might ultimately afford the desired vinyl azides (**1**) stereoselectively. Herein we wish to report the novel reaction.

The azide ion source we have employed was azidotrimethylsilane (**3**).[8] Initial attempts at the reaction between **2** and **3** were uniformly unsuccessful in the absence of catalysts. After thorough screening of catalysts, it was found that boron trifluoride-diethyl ether is most effective for this reaction. Thus a 1:2 mixture of **2** and **3** was allowed to react at 0 °C to room temperature for 0.5 h in the presence of excess boron trifluoride-diethyl ether. The usual ethereal workup followed by chromatography provided **1** in the yields and stereoselectivities shown in Table 1. Five *trans*-1,2-epoxyalkylsilanes (**2a—e**) were employed. It should be noted that controlled experiments in NMR tube showed essentially quantitative conversion in all cases except **2e**, which gave mainly polymeric materials.

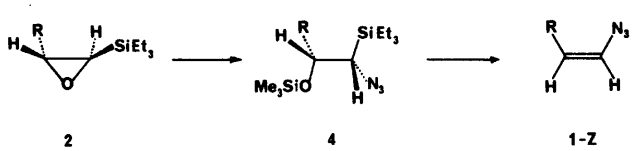

2 4 1-Z

As shown in Table 1, the stereoselectivity of the reaction is greater than 93%. ^{1}H NMR spectral analysis has shown that the olefinic proton resonances at C-2 of (*Z*)-isomers (δ=4.81—4.82) occur at higher field than those of (*E*)-isomers (δ=5.29—5.32) and that the coupling constants between the vinylic protons for (*Z*)-isomers (J=7.5—7.8 Hz) are less than those for (*E*)-isomers (J=13.5—14 Hz), thus confirming the stereochemical assignments discussed above. Virtually exclusive formation of (*Z*)-isomers is entirely consistent with the results of related reactions of **2** previously reported by Hudrlik et al.[9] As shown in Eq. 1, selective nucleophilic displacement by azide ion at the C-1 of **2** would produce intermediate **4**, which would then undergo *trans*-elimination to afford **1-Z**.

Table 1. Synthesis of 2-Substituted Vinyl Azide (**1**) from *trans*-1,2-Epoxyalkylsilanes (**2**)[a]

	2 R	**1** Isolated Yield/%	$Z:E$[b]
a	n-C_8H_{17}	91	93:7
b	n-C_6H_{13}	95	93:7
c	$Me_2CH(CH_2)_2$	88	95:5
d	$Ph(CH_2)_2$	93	95:5
e	Ph	8	100:0

a) Reactions were performed as described in Experimental Section. b) Determined by ^{1}H NMR.

It should be mentioned that the present method cannot be applied to *cis*-1,2-epoxyalkylsilanes, which generally undergo rapid polymerization in the presence of Lewis acids. For example, the cis isomer of **2a** was much less reactive toward **3** under the above conditions to provide a 2:3 mixture of **1-Z** and **1-E** in 12% isolated yield in addition to untractable white solids.

In summary, we have shown that (*Z*)-1-alkenyl azides (**1**) can be easily and stereoselectively obtained by a one-pot reaction from *trans*-1,2-epoxyalkylsilanes (**2**) in good yields. Although the reaction is not very successful for the case of **2e** (R=Ph), it clearly compensates the existing method.[3]

Experimental

Measurements and Materials. All reactions were performed under dry inert conditions. Solvents used were purified by distillation over appropriate drying agent under argon atmosphere. 1,2-epoxyalkylsilanes (**2**) were prepared from the corresponding alkenylsilanes according to the method of Stork.[7,10] Azidotrimethylsilane (**3**) was purchased from Chisso Chem. Co. and was distilled once under argon before use. Infrared spectra were measured on a JASCO DS403G spectrometer. ^{1}H NMR spectra were obtained as $CDCl_3$ solutions with a Varian EM-390 spectrometer at 90 MHz. ^{13}C NMR spectra were recorded in $CDCl_3$ on a JEOL FX90-Q spectrometer operated at 22.5 MHz. All chemical shifts were reported in relative to internal tetramethylsilane.

General Procedure to Prepare 1-Alkenyl Azides (1). To a mixture of **2** and **3** (2 molar equivalent) was added boron trifluoride-etherate (2 molar equivalent) at 0 °C and the mixture was stirred for 0.5 h at room temperature. It was then diluted with ether. The usual aqueous workup with saturated sodium hydrogencarbonate solution and anhydrous magnesium sulfate provided an oil after evaporation of the

solvent, which was purified by column chromatography on silica gel (Kieselgel 60, eluent hexane).

The yields of 1-alkenyl azides (**1**) are shown in Table 1. Analytical and spectroscopic data of the products **1** follow.

(Z)-1-Decenyl Azide (1a). Bp 43 °C/67 Pa. IR (liquid film) 2100 (s, $-N_3$), 1645 (m, C=C), and 725 (m, *cis*-CH=CH-) cm^{-1}. ^1H NMR ($CDCl_3$) δ=0.9 (m, 3H), 1.3 (br. s, 12H), 2.0 (m, 2H), 4.82 (d of t, J=7.5 and 7.5Hz, 1H) and 6.05 (d, J=7.5Hz, 1H). ^{13}C NMR ($CDCl_3$) δ= 14.1 (q), 22.7 (t), 25.8 (t), 29.2 (t), 29.3 (t), 29.4 (t), 31.9 (t), 121.2 (d), and 125.2 (d).

Found: C, 66.43; H, 10.39; N, 23.22%. Calcd for $C_{10}H_{19}N_3$: C, 66.26; H, 10.56; N, 23.18%.

(Z)-1-Octenyl Azide (1b). Bp 34 °C/52 Pa. IR (liquid film) 2100 (s, -N3), 1642 (m, C=C) and 727 (m, *cis*-CH=CH-) cm^{-1}. ^1H NMR ($CDCl_3$) δ=0.9 (m, 3H), 1.3 (br. s, 8H), 2.0 (m, 2H), 4.82 (d of t, J=7.5 and 7.5Hz, 1H) and 6.05 (d, J=7.5Hz, 1H). ^{13}C NMR ($CDCl_3$) δ=14.1 (q), 22.7 (t), 25.8 (t), 28.9 (t), 29.2 (t), 31.7 (t), 121.1 (d) and 125.3 (d).

Found: C, 62.76; H, 10.12; N, 27.51%. Calcd for $C_8H_{15}N_3$: C, 62.71; H, 9.87; N, 27.42%.

(Z)-5-Methyl-1-hexenyl Azide (1c). IR (liquid film) 2110 (s, $-N_3$), 1645 (m, C=C) and 728 (m, *cis*-CH=CH-) cm^{-1}. ^1H NMR ($CDCl_3$) δ=0.9 (m,6H), 1.3 (m,2H), 1.6 (m,1H), 2.1 (m, 2H), 4.81 (d of t, J=7.5 and 7.5 Hz, 1H) and 6.03 (d, J=7.5 Hz, 1H). ^{13}C NMR ($CDCl_3$) δ=22.4 (q), 23.7 (t), 27.6 (d), 38.3 (t), 121.1 (d), and 125.1 (d).

Found: C, 60.29; H, 9.58; N, 29.91%. Calcd for $C_7H_{13}N_3$: C, 60.40; H, 9.41; N, 30.19%.

(Z)-4-Phenyl-1-butenyl Azide (1d). Bp 70 °C/0.4 Torr (1 Torr=133.322 Pa). IR (liquid film) 2110 (s, $-N_3$), 1645 (m, C=C), 1605 (m, Ph), 1502 (m, Ph), 750 (m, Ph), 728 (m, *cis*-CH=CH-) and 700 (m, Ph) cm^{-1}. ^1H NMR ($CDCl_3$) δ=2.4 (m, 2H), 2.6 (m, 2H), 4.81 (d of t, J=7.5 and 7.0 Hz, 1H), 6.02 (d, 1H, J=7.5) and 7.4 (m, 5H). ^{13}C NMR($CDCl_3$) δ=27.4 (t), 35.4 (t), 119.8 (d), 125.9 (d), 126.0 (d), 128.5 (d), and 141.6 (s).

Found: C, 69.43; H, 6.14; N, 24.35%. Calcd for $C_{10}H_{11}N_3$: C, 69.34; H, 6.40; N, 24.26%.

(Z)-2-Phenylethenyl Azide (1e). IR (liquid film) 2120 (s, N_3), 1644 (s, C=C), 1602 (m, Ph), 1500 (m, Ph), 750 (m, Ph), 735 (m, *cis*-CH=CH-) and 695 (m, Ph). ^1H NMR ($CDCl_3$) δ=5.22 (d, J=6.7 Hz, 6.22 (d, J=6.7 Hz, 1H), 7.21 (m, 3H), and 7.60 (m, 2H).

Found: C, 66.31; H, 4.98; N, 28.64%. Calcd for $C_8H_7N_3$: C, 66.19; H, 4.86; N, 28.95%.

We wish to thank the Ministry of Education, Science and Culture for partial financial support of this work through Grant-in-Aid for Scientific Research No. 58540303.

References

1) Reviews: a) A. Hassner, *Acc. Chem. Res.*, **4**, 9 (1971); b) G. L'abbe, *Angew. Chem., Intern. Ed. Engl.*, **14**, 775 (1975). Recent examples: c) A. Hassner and B. A. Belinka, Jr., *J. Org. Chem.*, **102**, 6185 (1980); d) Y. Nomura, Y. Takeuchi, S. Tomoda, and M. M. Ito, *Bull. Chem. Soc. Jpn*, **54**, 261 (1981).

2) H. Bock, R. Dammel, and S. Aygen, *J. Am. Chem. Soc.*, **105**, 7681 (1983).

3) A. Hassner and F. W. Fowler, *J. Org. Chem.*, **33**, 2686 (1968).

4) J. N. Denis, J. Vicens, and A. Krief, *Tetrahedron Lett.*, **1979**, 2697.

5) B. M. Trost and T. Shibata, *J. Am. Chem. Soc.*, **104**, 3225 (1982).

6) Recent review: D. J. Ager, *Synthesis*, **1984**, 384.

7) E. W. Colvin, "Silicon in Organic Synthesis", Butterworths, London (1981), p. 83.

8) L. Birkofer and W. Kaiser, *Justus Liebigs Ann. Chem.*, **1975**, 266.

9) a) P. F. Hudrlik, A. M. Hudrlik, R. J. Rona, R. N. Misra, and G. P. Withers, *J. Am. Chem. Soc.*, **99**, 1993 (1977); b) A. P. Davis, G. J. Hughes, P. R. Lowndes, C. M. Robbins, E. J. Thomas, and G. H. Whitham, *J. Chem. Soc., Perkin Trans. 1*, **1981**, 1934.

10) G. Stork and E. W. Colvin, *J. Am. Chem. Soc.*, **93**, 2080 (1971).

Selective Oxidation of 2-Bromo-*m*-xylene to 2-Bromo-3-methylbenzoic Acid or 2-Bromoisophthalic Acid

Sotaro MIYANO,* Hiroshi FUKUSHIMA, Hideho INAGAWA, and Harukichi HASHIMOTO
Department of Applied Chemistry, Faculty of Engineering, Tohoku University, Aramaki-Aoba, Sendai 980
(Received May 1, 1986)

Synopsis. Aqueous sodium dichromate oxidation of 2-bromo-*m*-xylene (**1**) under a carbon dioxide pressure gave 2-bromoisophthalic acid (58%), while NBS-bromination of **1** followed by Sommelet oxidation to aldehyde and then potassium permanganate oxidation enabled the isolation of 2-bromo-3-methylbenzoic acid in 42% yield.

Herein, we wish to report that 2-bromo-*m*-xylene (**1**) serves as readily available starting material for the synthesis of 2-bromo-3-methylbenzoic acid (**2**) and 2-bromoisophthalic acid (**3**) (Scheme 1), both

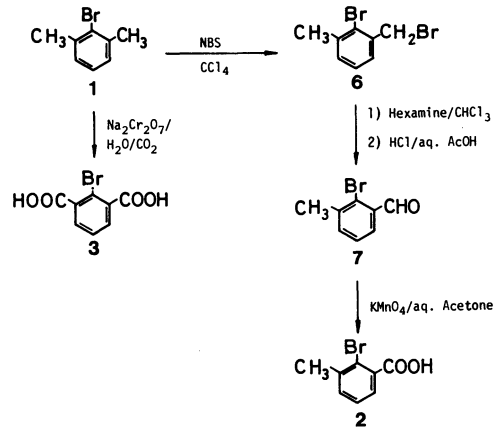

Scheme 1.

of which have been obtained with difficulty by the literature procedure. In the course of our study on the construction of axially chiral biaryl skeletons,[1] we needed **2** as a coupling component in the Ullmann biaryl synthesis. Unexpectedly, a search of the literature revealed only one precedent synthesis of **2** by Bunnett and Rauhut which involes bromination of *p*-nitrotoluene and then treatment of the resulting 2-bromo-4-nitrotoluene with KCN in water (the von Richter reaction).[2,3] The process was not appealing to us for large scale synthesis because of the low overall yield of **2** (7—8% based on *p*-nitrotoluene) and the tedious handling of massive quantities of toxic cyanide.

We have recently reported an improved oxidation of 1-bromo-2-methylnaphthalene (**4**) to 1-bromo-2-naphthoic acid (**5**) by an aqueous sodium dichromate under a carbon dioxide atmosphere according to the method of Yamashita et al.[4,5] The simplicity of the procedure, along with availability of sufficiently pure **1**,[6] encouraged us to apply it for oxidation of **1**, and Table 1 summarizes the results. In view of the tendency that initially formed monobasic acid **2** was oxidized more readily than starting **1**, probably due to their solubility differences in the aqueous reaction medium, the dichromate oxidation should more advantageously be utilized for selective synthesis of dicarboxylic acid **3**. This was realized by the use of three molar amounts of the oxidant affording **3** in fairly good yield (Run 5). The synthesis of **3** via oxidation of **1** is not new; as long ago as 1937 Coulson used aqueous potassium permanganate as the oxidant.[7,8] However, the procedure has suffered seriously from the concomitant formation of a significant amount of 2-hydroxyisophthalic acid which requires tedious separation from **3**.[7,9] It should be pointed out here that **3** itself is of potential importance as the building block for not only biaryls[7,8] but also diarylamines including acridones of pharmaceutical interest,[11] but that only limited success in the preparation of **3** seems to have restricted its wide use.

As the synthetically passable route to **2**, we eventually resorted to the stepwise oxidation of **1** (Scheme 1) which is essentially an extention of the method used by Bergmann and Szmuszkovicz,[12] and Hall and Turner[13] for transformation of **4** to **5**. Upon treatment with slightly excess amounts of *N*-bromosuccinimde (NBS) almost all of **1** reacted, indicating that preferential bromination of both of the methyl substituents did not so much matter. Crude 2-bromo-3-(bromomethyl)toluene (**6**) was converted to hexamethylenetetramine (hexamine) adduct, which was then hydrolyzed to 2-bromo-3-methylbenzaldehyde (**7**) as needles on standing the reaction mixture (the Sommelet reaction). Conversion of **7** to **2** was effected well with potassium permanganate according to the method of Hall and Turner with slight modifications.[13]

The above procedure was repeated several times with

Table 1. Oxidation of **1** with Aqueous $Na_2Cr_2O_7$ Under CO_2[a]

Run	$Na_2Cr_2O_7$/**1** mol/mol	T/°C	t/h	Yield[b]/% **2**	Yield[b]/% **3**	Recovered[c] **1**/%
1	0.8	230	8	15	13	28
2	1.0	230	8	12	14	21
3	1.0	260	5	1.0	1.4	3.1
4	1.5	230	8	8.2	37	12
5	3.0	230	5	1.3	58	11

a) Reaction conditions: **1**, 26—30 mmol; H_2O, 90 ml; initial CO_2 press., 20 atm. b) Isolated by crystallization. c) Isolated by bulb-to-bulb distillation of the nonacidic components.

slightly changing the reaction variables giving the overall yields of **2** ranging from 25 to 42% based on starting **1**. As frequently encountered in the Sommelet reaction,[14] the low yield in the hydrolysis step is one limiting factor, but the straightforward and simple reaction sequence provides a considerable improvement over the conventional preparation of **2**.[2]

Experimental

Preparation of 3 (Run 5 in Table 1). A mixture of **1** (5.38 g, 0.0291 mol), $Na_2Cr_2O_7 \cdot 2H_2O$ (26.0 g, 0.0872 mol), and 90 ml of water placed in a 300 ml autoclave was allowed to react[4] under the conditions cited in Table 1. After the reaction, acidic products were taken into ether and treated as usual. Removal of the solvent left white solid, which was heated at reflux in 100 ml of toluene and filtered hot. The solid was then recrystallized from 2 M HCl (1 M=1 mol dm^{-3}) to give **3** as colorless needles (4.15 g, 0.0169 mol); mp 218—220 °C (lit,[7] mp 218 °C); δ (acetone-d_6) 7.3—7.9 (3H, m, ring-Hs) and 11.0 (2H, br, -COOH); IR (KBr) 1710 and 1685 cm^{-1} (νCO). Anal. ($C_8H_5BrO_4$) C, H, Br.

The toluene filtrate was concentrated to about 20 ml volume. After precipitated solid had been filtered off (70 mg, mp 216—220 °C), the solvent was removed from the filtrate and then crystallization from H_2O-EtOH gave **2** (80 mg, 0.37 mmol), mp 133—136 °C.

Preparation of 2. A mixture of **1** (25.8 g, 0.139 mol), NBS (25.8 g, 0.145 mol), and 0.1 g of benzoyl peroxide was refluxed in 75 ml of CCl_4 for 3 h. The cool reaction mixture was filtered, and evaporation of the solvent left crude **6** as a pale yellow oil; δ (CCl_4) 2.35 (3H, s, $-CH_3$), 4.50 (2H, s, $-CH_2Br$), and 7.0—7.4 (3H, m, ring-Hs).

To the mechanically stirred **6** in 180 ml of $CHCl_3$ was added 24.4 g of hexamethylenetetramine (0.174 mol). After 1 h heating at reflux, the amine adduct was filtered and dried under reduced pressure. The adduct was boiled in 280 ml of 50% aqueous AcOH for 2 h, and then for further 1 h after adding 30 ml of concd HCl. The mixture was allowed to stand overnight at room temperature to give **7** as needles[15] (13.7 g, 49.4% based on **1**); mp 53—54 °C; δ ($CDCl_3$) 2.40 (3H, s, $-CH_3$), 7.2—7.8 (3H, m, ring-Hs), and 10.4 (1H, s, -CHO); IR (KBr) 1680 cm^{-1} (νCO). Combustion analysis suggested the presence of about 5—6% of 2-bromoisophthalaldehyde (Found: C, 46.57; H, 3.38; Br, 38.45%. C_8H_7BrO requires C, 48.27; H, 3.54; Br, 40.14%).

To a boiling solution of **7** (13.2 g, 66.3 mmol) in 420 ml of acetone was added dropwise a $KMnO_4$ solution (13.8 g, 87.3 mmol) in 250 ml of water for 1/2 h, and the heating was continued for another 1 h. Sulfur dioxide was passed through the cool, dark brown mixture until it became clear solution, to which was added 2 l of water and 200 ml of 28% NH_3. The mixture was passed through a short silica-gel column to remove brown precipitates, acidified with concd HCl, and extracted with ether. After the usual work-up, the solvent was evaporated, and the residue was recrystallized from H_2O-EtOH to give **2** as colorless needles (12.2 g, 85.6% based on **7** and 42.3% based on **1**), mp 135—137 °C (lit,[2a] mp 135—137 °C); δ ($CDCl_3$) 2.40 (3H, s, $-CH_3$), 7.0—7.8 (3H, m, ring-Hs), and 11 (1H, br, -COOH); IR (KBr) 1690 cm^{-1} (νCO). Anal. ($C_8H_7BrO_2$) C, H, Br.

The present work was partially supported by a Grant-in-Aid for Scientific Research No. 60550599 from the Ministry of Education, Science and Culture.

References

1) S. Miyano, S. Handa, K. Shimizu, K. Tagami, and H. Hashimoto, *Bull. Chem. Soc. Jpn.*, **57**, 1943 (1984).
2) a) J. F. Bunnett and M. M. Rauhut, *Org. Syhth.*, Coll. Vol. 4, 114 (1963); b) Idem, *J. Org. Chem.*, **21**, 934 (1956).
3) Cf. D. Peltier, *Bull. Soc. Chim. France*, **1958**, 994.
4) S. Miyano, H. Inagawa, S. Handa, and H. Hashimoto, *Chem. Ind. (London)*, **1985**, 236.
5) J. Yamashita, K. Kurashima, and S. Kato, *Yuki Gosei Kagaku Kyokai Shi*, **20**, 277 (1962).
6) Available from, for example, Aldrich Chem Co. and Tokyo Kasei Kogyo Co.
7) E. A. Coulson, *J. Chem. Soc.*, **1937**, 1298.
8) G. Helmchen and V. Prelog, *Helv. Chim. Acta*, **55**, 2599 (1972).
9) Mn(II) seems to promote hydrolytic displacement of bromine from **3** to 2-hydroxyisophthalic acid, while Cr(III) to be inactive.[10]
10) a) K. A. Cirigottis, E. Ritchie, and C. W. Taylor, *Aust. J. Chem.*, **27**, 2209 (1974); b) A. Bruggink and A. McKillop, *Tetrahedron*, **31**, 2607 (1975).
11) Cf. G. W. Rewcastle and W. A. Denny, *Synthesis*, **1985**, 217.
12) E. D. Bergmann and J. Szmuszkovicz, *J. Am. Chem. Soc.*, **73**, 5153 (1951).
13) D. M. Hall and E. E. Turner, *J. Chem. Soc.*, **1955**, 1242.
14) S. J. Angyal, *Organic Reactions*, **8**, 197 (1954).
15) In cases where crystallization was incomplete accompanying deposition of pale yellow viscous oil, the mixture was extracted with benzene.

A Convenient Method for Conversion of Allylic Chlorides to α,β-Unsaturated Aldehydes

Shigeaki SUZUKI,† Takashi ONISHI,† Yoshiji FUJITA,† Hiromitsu MISAWA, and Junzo OTERA*
†Central Research Laboratories, Kuraray Co., Ltd., Sakazu, Kurashiki, Okayama 710
Department of Applied Chemistry, Okayama University of Science, Ridai-cho, Okayama 700
(Received May 15, 1986)

Synopsis. Tertiary amine *N*-oxides were found to be effective for converting allylic chlorides to α,β-unsaturated aldehydes.

Oxidation of allylic chlorides provides a convenient method for synthesizing α,β-unsaturated aldehydes. Unfortunately, however, only a few successful results have been reported which had recourse to dimethyl sulfoxide oxidation[1,2] or a potassium salt of 2-*aci*-nitropropane-tetrakis(triphenylphosphine)palladium system[3] whereas allylic bromides proved to be oxidized by a potassium salt of 2-*aci*-nitropropane[4] or potassium chromate.[5,6] In our continuing efforts to develop an efficient method to synthesize α,β-unsaturated compounds as a raw material for the vitamin A synthesis,[7] we have now disclosed that tertiary amine *N*-oxides (**1**) effect a smooth conversion of allylic chlorides into α,β-unsaturated aldehydes.

Various tertiary amine *N*-oxides were reported to oxidize benzylic halides successfully.[8-10] We have found that treatment of primary allylic chlorides **2** with 3 equiv of *N*-ethylmorpholine *N*-oxide (**1a**) in DMF at 50°C for 4 h affords the desired α,β-unsaturated aldehydes **3** in excellent yields according to Eq. 1 (Table 1, Entries 1—5) (Method A). Other tertiary amine *N*-oxides derived from *N*-methylmorpholine, *N*-methylpyrrolidine, *N*-methylpiperidine, trimethylamine, *N*,*N*-dimethylcyclohexylamine, *N*,*N*-dicyclohexylmethylamine, and *N*,*N*-diethylcyclohexylamine gave rise to lower yields of **3**.

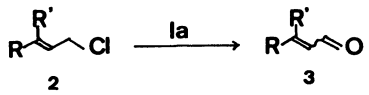

2 3 (1)

When this reaction was applied to secondary allylic chlorides **5**, no satisfactory results were obtained. The difficulty was overcome, however, by conducting the reaction in the presence of an alkali metal iodide such as lithium iodide (Table 1, Entries 6 and 7) (Method B) or in the presence of a catalytic amount of copper (I) chloride (Table 1, Entry 8) (Method C). Since **5** can be readily prepared by the ene-type chlorination of the corresponding alkenes **4**,[11] the effective method for converting **4** into **6** has been established (Eq 2). The

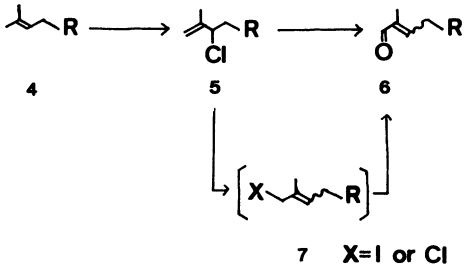

(2)

Table 1. Oxidation of Allylic Chlorides by Tertiary Amine *N*-Oxides (**1**)

Entry	Allyl chloride	Method	α,β-Unsaturated aldehyde[a]	Yield/%	*E*/*Z*[b]
1	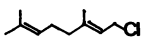	A	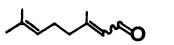	88[c]	70/30
2	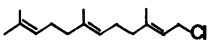	A	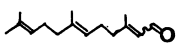	82[d]	53/47
3	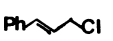	A		97[c]	100/0
4	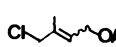	A	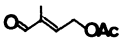	88[d]	100/0
5	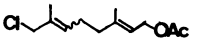	A	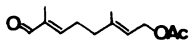	90[d]	100/0
6	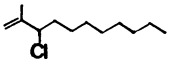	B	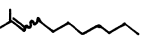	47(89)[d,e]	77/23
7	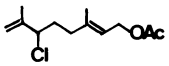	B	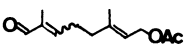	71[d]	68/32
8		C		61[d]	100/0

a) All products were confirmed by comparison with authentic samples. b) Determined by means of GLC or ^{1}H NMR spectra. c) Isolated yield after distillation. d) Isolated yield after column chromatography. e) The starting material was recovered (47%). The value in the parenthesis indicates the yield based on the consumed starting material.

reaction can be viewed as proceeding via initial formation of the primary allylic halides **7**.[12]

Experimental

Reaction of Primary Allylic Chlorides with *N*-Ethylmorpholine *N*-Oxide (1a): Method A (Typical Procedure). A DMF solution (3 cm^3) of geranyl chloride (346 mg, 2 mmol) and **1a** (787 mg, 6 mmol) was stirred at room temperature for 1 h and at 50 °C for additional 4 h under an argon atmosphere. The reaction mixture was combined with 2.5% H_2SO_4 (10 cm^3) and ethyl acetate (10 cm^3). The organic layer was washed successively with 2.5% H_2SO_4, saturated $NaHCO_3$, and 10% Na_2SO_3 solutions. Drying ($MgSO_4$) followed by evaporation afforded a crude oil which was distilled to give 3,7-dimethyl-2,6-octadienal (268 mg, 88%, *E*/*Z*=70:30, bp 93 °C/400 Pa, .Kugelrohr bath temperature).

Reaction of Secondary Allylic Chlorides with Tertiary Amine *N*-Oxide: Method B (Typical Procedure). A DMF solution (3 cm^3) containing (*E*)-6-chloro-3,7-dimethyl-2,7-octadienyl acetate[11] (461 mg, 2 mmol), **1a** (787 mg, 6 mmol), and $LiI \cdot 2H_2O$ (680 mg, 4 mmol) was stirred at room temperature for 1 h and at 50 °C for additional 4 h. Workup as described above and column chromatogrpahy of the crude oil on silica gel (10:1 hexane-ethyl acetate) gave 8-acetoxy-2,6-dimethyl-2,6-octadienal (298 mg, 71%, 2*E*/2*Z* 68:32).

Method C: A dioxane solution (5 cm^3) containing (*E*)-6-chloro-3,7-dimethyl-2,7-octadienyl acetate (2.17 g, 9.41 mmol), triethylamine *N*-oxide (**1b**) (3.47 g, 29.6 mmol), and copper(I) chloride (92 mg, 0.93 mmol) was stirred at 50 °C for 10 h. Workup and chromatographic purification as described above gave (2*E*,6*E*)-8-acetoxy-2,6-dimethyl-2,6-octadienal (1.21 g, 61%). In this reaction, **1a** gave rise to a lower yield.

References

1) B. Ganem and R. K. Boeckman, Jr., *Tetrahedron Lett.*, **1974**, 917.
2) J. H. Babler, M. J. Coghlan, M. Feng, and P. Fries, *J. Org. Chem.*, **44**, 1716, (1979).
3) S. Suzuki, T. Onishi, Y. Fujita, and J. Otera, *Synth. Commun.*, **15**, 1123 (1985).
4) M. Montavon, H. Lindlar, R. Marbet, R. Ruegg, G. Ryser, G. Saucy, P. Zeller, and O. Isler, *Helv. Chim. Acta.*, **40**, 1250, (1957).
5) G. Cardillo, M. Orena, and S. Sandri, *J. Chem. Soc., Chem. Commun.*, **1976**, 190.
6) G. Cardillo, M. Orena, and S. Sandri, *Tetrahedron Lett.*, **1976**, 3985.
7) J. Otera, H. Misawa, T. Mandai, T. Onishi, S. Suzuki, and Y. Fujita, *Chem. Lett.*, **1985**, 1883.
8) W. Feely, W. L. Lehn, and V. Boekelheide, *J. Org. Chem.*, **22**, 1135 (1957).
9) V. Franzen and S. Otto, *Chem. Ber.*, **94**, 1360 (1961).
10) G. Bernhardt, E. N. Peresen, and G. Daum, Ger. Offen. 2948058 (1981).
11) J. Otera, M. Kishi, K. Kanehira, S. Suzuki, M. Shiono, and Y. Fujita, *Synth. Commun.*, **14**, 347 (1984).
12) R. H. Dewolfe and W. G. Young, "The Chemistry of Alkenes," ed by S. Patai, Interscience Publishers, London (1964), p. 681.

Synthesis of 1,3,6,8-Tetrakis(dimethylamino)pyrene Having Low Oxidation Potential

Naomi UEDA, Yoshiteru SAKATA,* and Soichi MISUMI
The Institute of Scientific and Industrial Research, Osaka University, Mihoga-oka, Ibaraki, Osaka 567
(Received May 23, 1986)

Synopsis. 1,3,6,8-Tetrakis(dimethylamino)pyrene (**1**) was synthesized starting from the corresponding tetranitro compound. The first oxidation potential of **1** shows the lowest value ($E^1_{1/2}$=−0.12 V vs SCE) among those of aromatic amines reported so far.

It is well known that the substitution of olefinic or aromatic protons with dimethylamino groups results in lowering the oxidation potential. Typical examples are tetrakis(dimethylamino)ethylene[1] and 1,4-bis(dimethylamino)benzene,[2] whose oxidation potentials ($E^1_{1/2}$) are −0.75 V and 0.04 V vs SCE, respectively. The former value is the lowest among those of all organic compounds so far reported. Our previous study[3] on the synthesis of 2,7-bis(dimethylamino)pyrene ($E^1_{1/2}$= 0.37 V) and -tetrahydropyrene ($E^1_{1/2}$=0.14 V) with fairly low oxidation potentials prompted us to prepare 1,3,6,8-tetrakis(dimethylamino)pyrene (**1**) with a view to powerful donor.

1: R = -NMe_2
2: R = -NO_2
3: R = -NH_2·HCl

Results and Discussion

1,3,6,8-Tetranitropyrene (**2**), prepared by nitration of pyrene according to the literature,[4] was reduced with tin powder in 6M HCl to give **3** in 87% yield. Because of the instability of free amine, **3** was used for the subsequent reaction without further purification. Methylation of **3** was carried out with dimethyl sulfate to give the desired compound **1** in 37% yield. Although **1** is very sensitive to oxygen, **1** can be kept for several months at ordinary temperature under inert atmosphere.

Figure 1 shows a cyclic voltammogram for 1 mM (mmol dm^{-3}) of **1** in 0.1 M tetraethylammonium perchlorate in acetonitrile, recorded with a scan rate of 50 mV s^{-1}. It exhibits two reversible redox waves. Judging from the peak separation (ca. 30 mV) two electron-transfer process is involved in each wave. In agreement with the initial expectation, the oxidation potentials of **1** are very low ($E^1_{1/2}$=−0.12 V, $E^2_{1/2}$=−0.05 V vs SCE). It is noteworthy that the value of $E^1_{1/2}$ is less than that of 1,4-bis(dimethylamino)benzene, which is the lowest among those of aromatic amines so far reported.

1 forms charge-transfer complex with iodine.

Experimental

All the melting points are uncorrected. The IR, NMR, MS, and electronic spectra were measured on a Hitachi EPI-G2 and a Hitachi 345, a JEOL JNM-FX-100, a Hitachi RMU-7, and a Hitachi EPS-3T spectrometer, respectively. The cyclic voltammetry was carried out at room temperature under argon using the combination of a generator of Hokuto HB-107 A and a potentiostat of Hokuto HA-104. A glassy carbon electrode (Yanagimoto P-13) was used as the anode, and platinum wire was used as the counter electrode.

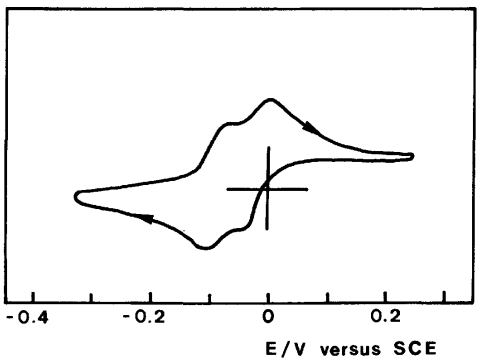

Fig. 1. Cyclic voltammogram of **1** in acetonitrile.

1,3,6,8-Tetrakis(dimethylamino)pyrene (1). To a suspension of 1,3,6,8-tetranitropyrene (**2**) (200 mg 0.52 mmol) in 15 ml of 6M hydrochloric acid was added tin powder (372 mg, 3.13 mmol) in small portions under nitrogen and the mixture was warmed at 50—60 °C for 3.5 d. After cooling, precipitates of ammonium salt **3** were collected, washed with 6M HCl and dried to give 184 mg (87%) of **3**, which was used for the next step without further purification [**3**: MS 262 (M^+); IR (nujol mull) 3570, 3475, 3200—2300, and 1605 cm^{-1}].

To a stirred aqueous solution (5 ml) of crude **3** (184 mg, 0.45 mmol) was added an aqueous solution (6 ml) of sodium hydrogencarbonate (1.818 g, 21.64 mmol) and dimethyl sulfate (908 mg, 7.21 mmol) under nitrogen at room temperature. Stirring was continued at room temperature for 1 h and then at 50—60 °C for 4 h. After cooling, 2-aminoethanol (3 ml) was added and the mixture was heated at 120—130 °C for 3 h with stirring. After cooling, yellow precipitates of **1** were collected, washed with water and dried to give 102 mg of crude **1**. Purification by sublimation gave 62 mg (37%) of **1**: Yellow prisms, mp 212—213 °C; ^{1}H NMR ($CDCl_3$) δ=3.02 (24H, s), 7.43 (2H, s), and 8.17 (4H, s); IR (KBr disk) 1585 cm^{-1}; UV (CH_3CN) 228 (ε 4.10×10^4), 302 (2.25×10^4), and 414 nm (3.04×10^4). Found: C, 76.69; H, 8.11; N, 15.18%. Calcd for $C_{24}H_{30}N_4$: C, 76.97; H, 8.07; N, 14.96%.

Complexation of 1 with Iodine. Under nitrogen atmosphere, a solution of **1** (10 mg, 0.03 mmol) in benzene (2 ml) and a solution of iodine (33 mg, 0.15 mmol) in the same solvent(3 ml) were mixed at room temperature. Precipitated dark purple microcrystals were filtered, washed with benzene, and dried to give 8 mg (80% yield based on **1**) of **1**-I_2: black fine crystals, decomp>180 °C; IR (KBr disk) 1550 cm^{-1}: UV (CH_3CN) 220 (sh, ε 5.33×10^4), 256 (4.26×10^4), 296 (1.28×10^5). 368 (6.39×10^4), 456 (2.79×10^4), and 532 nm (1.06×10^4). Found: C,19.16; H,2.01; N, 3.73; I, 74.66%. Calcd for $C_{24}H_{30}N_4$·4.4I_2: C, 18.93; H, 2.10; N, 3.84; I, 74.33%.

References

1) K. Kuwata and D. H. Geske, *J. Am. Chem. Soc.*, **86**, 2101 (1964).
2) L. Michaelis, M. P. Schubert, and S. Granick, *J. Am. Chem. Soc.*, **61**, 1981 (1939).
3) N. Ueda, B. Natsume, K. Yanagiuchi, Y. Sakata, T. Enoki, G. Saito, H. Inokuchi, and S. Misumi, *Bull. Chem. Soc. Jpn.*, **56**, 775 (1983).
4) H. Vollmann, H. Becker, M. Corell, and H. Streeck, *Justus Liebigs Ann. Chem.*, **531**, 1 (1937).

^{17}O- and ^{33}S-Hyperfine Splittings for Aromatic RCONSAr Radicals. Complete Evaluation of ESR Parameters[1)]

Yozo MIURA,* Yoshitaka SHIBATA, and Masayoshi KINOSHITA
Department of Applied Chemistry, Faculty of Engineering, Osaka City University, Sumiyoshi-ku, Osaka 558
(Received March 27, 1986)

Synopsis. ^{17}O- and ^{33}S-Hyperfine splitting constants for aromatic RCONSAr radicals have been determined and the spin density distribution has been elucidated on the basis of the ESR parameters.

N-(Arylthio)acylaminyl radicals (RCONSR′) have interesting structures in which both an electron-accepting (C=O) and an electron-donating substituent (SR′) attach directly to the radical center. In an earlier paper,[2)] we showed that in the radicals the unpaired electron resides mainly on the nitrogen and the phenylthio group on the basis of large a_N and a_H values (due to the phenylthio benzene ring protons). However, owing to a lack of the a_{17O} and a_{33S} values, we could not fully elucidate the unpaired-electron distribution pattern. We report herein the a_{17O} and a_{33S} values for the radicals.

Results and Discussion

Type-**2** radicals were generated at room temperature by the photolysis of solutions of the corresponding *N*-(arylthio)amides **1** in 1:4 (v/v) di-*t*-butyl peroxide–benzene using a 1 kW xenon lamp. Under these experimental conditions we could unequivocally detect ^{33}S-hyperfine splittings (hfs) without any enrichment of the ^{33}S atoms in each wing of the ESR spectra obtained at high gain (see Fig. 2). On the other hand, ^{17}O-hfs's could only be detected (see Fig. 1) when the radical was enriched by ^{17}O-atoms (5.9 atom%). The experimentally obtained intensity ratios of the ^{17}O (0.96%) and ^{33}S (0.20%) satellite lines to the parent peaks coincided satisfactorily with the theoretical values (^{17}O, 0.98%; ^{33}S, 0.19%), respectively. The ESR parameters obtained are listed in Table 1.

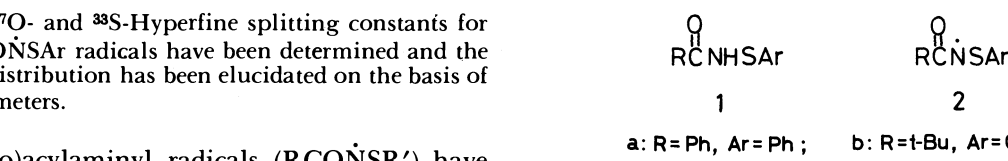

Type-**2** radicals can be represented by the following four possible canonical structures (A, B, C, and D) as reported in an earlier paper.[2)] However, the very low a_{17O} value obtained for **2a** reveals clearly that the canonical structure D is much less important. The π-

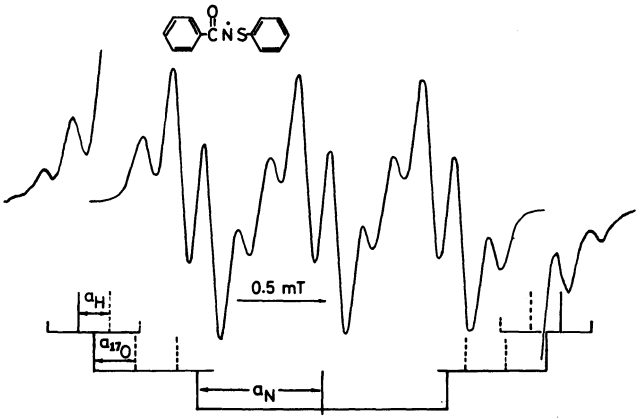

Fig. 1. ESR spectrum of ^{17}O-enriched (5.9%) **2a** recorded during photolysis of a solution of ^{17}O-enriched (5.9%) **1a** in 1:4 (v/v) di-*t*-butyl peroxide–benzene at 17°C. The wings are shown at high gain (20 times). The stick diagram represents a part of the theoretical reconstruction of the splittings due to ^{14}N, ^{1}H, and ^{17}O. The experimentally observed satellite lines due to ^{17}O are shown by the full lines.

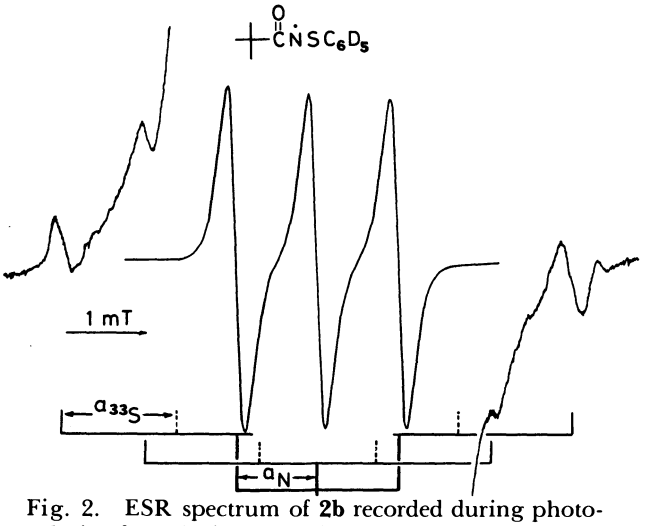

Fig. 2. ESR spectrum of **2b** recorded during photolysis of a solution of **1b** in 1:4 (v/v) di-*t*-butyl peroxide–benzene at 17°C. The wings are shown at high gain (100 times). The stick diagram represents a part of the theoretical reconstruction of the splittings due to ^{14}N and ^{33}S. The experimentally observed satellite lines due to ^{33}S are shown by the full lines.

Table 1. ESR Parameters for Aromatic RCONSAr Radicals[a–c)]

Radical	a_N	a_H[d)]	a_{other}	g
2a	0.709[e)]	0.168 (3)[e,f)]	1.06 (^{33}S), 0.225 (^{17}O),[g)]	2.0081[e)]
2b	0.745		1.07 (^{33}S)	2.0082
t-BuCONSPh	0.749[e)]	0.169 (3)[e)]		2.0082[e)]

a) Hyperfine splitting constants are given in mT. b) Solvent 1:4 (v/v) di-*t*-butyl peroxide–benzene. c) Temperature 17±1°C. d) Numbers in parentheses refer to the number of equivalent protons. e) Taken from Ref. 2. f) The ortho and para protons on the phenylthio benzene ring. g) The value obtained for the ^{17}O-enriched (5.9 atom%) **2a**.

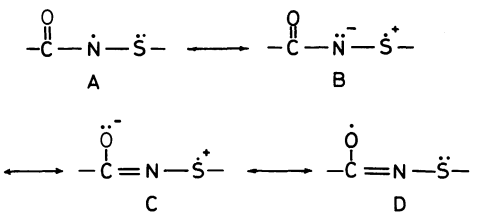

orbital spin density ($\rho_{o\pi}$) on the oxygen can be derived by using Silver's equation,[3,4] where the contribution to a_{17O} from $\rho_{c\pi}$ of the carbonyl carbon is neglected. The $\rho_{o\pi}$ value obtained is only 0.055.

$$\rho_o^\pi = a_{17O}/Q_o = a_{17O}/-4.1\ \text{mT}$$

On the other hand, the a_{33S} values (1.06 and 1.07 mT) are much higher than the a_{17O} value and is strongly indicative of a high π-orbital spin density ($\rho_{s\pi}$) on the sulfur. Consequently, it can be concluded on the basis of the large a_N and a_{33S} values that in **2** the unpaired electron resides mainly on the nitrogen and sulfur. Accordingly, type-**2** radicals can be best represented by three canonical structures: A, B, and C.

Furthermore, we note that the a_{33S} values for **2** are substantially higher than those (0.46—0.74 mT) for the radicals of the type RNSR′ (R, R′=alkyl, aryl).[5,6] The only radical having a comparable magnitude of a_{33S} among the thioaminyls studied is **3**,[7] in which both an electron-accepting (SO_2) and an electron-donating substituent (SAr) attach directly to the radical center in a manner similar to **2**. The somewhat higher a_N and a_{33S} values for **3** can be accounted for by the fact that there is no ability of the sulfonyl group to delocalize an unpaired electron.[8]

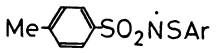

3

$a_N = 0.79-0.894$ mT

$a_{33S} = 1.19-1.23$ mT

In an earlier paper,[5] we showed that the π-orbital spin density ($\rho_{s\pi}$) on the sulfur in RNSR′ radicals can be derived from the a_{33S} values by using the following established equation through an investigation of the ^{33}S-hfs's of a variety of RNSR′ radicals. From

$$\rho_S^\pi = a_{33S}/Q_S = a_{33S}/2.3\ \text{mT}$$

this equation we can estimate the $\rho_{s\pi}$ value for **2** to be 0.47. On the other hand, the $\rho_{s\pi}$ values for the RNSR′ radicals derived from the a_{33S} values of 0.46—0.74 mT are 0.20—0.32. This increased $\rho_{s\pi}$ value for **2** can be readily rationalized in terms of the contribution of canonical structure C; that is, it can be interpreted as a consequence of a synergetic effect of the electron-accepting carbonyl group and the electron-donating arylthiyl group. Therefore, we are interested in this result in connection with the hypothesis concerning captodative stabilization of radicals.[9] Further investigations are under way.

Experimental

Melting points, and IR and ^{1}H NMR spectra were taken as previously reported.[10] Benzenesulfenyl chloride,[11] deuterated benzenesulfenyl chloride,[11] and ^{17}O-enriched (5.9 atom%) benzamide[1,12] were prepared by the previously described procedures.

***N*-(Phenylthio)benzamide (1a).** This amide was prepared by the previously reported procedure,[2] with some modifications. To a solution of 200 mg (1.65 mmol) of benzamide in 15 cm^3 of dry THF was added 79 mg (2.0 mmol) of NaH (60 wt%) and the mixture was stirred for 3 h at room temperature. To this mixture was added, in one portion, at 0—5 °C with stirring a solution of 290 mg (2.0 mmol) of freshly distilled benzenesulfenyl chloride in 1 cm^3 of dry hexane. After 2 h of stirring at room temperature, 0.5 cm^3 of Et_3N was added and the resultant mixture was stirred for an aditional 0.5 h. Filtration, evaporation, column chromatography (alumina, Merck Art 1097, column size 3×10 cm, 1:100 ethanol-benzene), and crystallization (benzene-hexane) gave **1a** in 67% yield (260 mg, 1.1 mmol); mp 123—124 °C (lit,[2] 122—124 °C).

^{17}O-Enriched **1a** was prepared by the same method; mp 123—123.5 °C.

***N*-(Phenylthio-d_5)pivalamide (1b).** To a stirred solution of 2.02 g (20 mmol) of pivalamide and 4 cm^3 of Et_3N in 300 cm^3 of dry ether was added dropwise at 0—5 °C a solution of 3.59 g (24 mmol) of benzenesulfenyl-d_5 chloride in 20 cm^3 of dry ether. After being stirred for 3 h at the same temperature, the mixture was filtered, evaporated, and chromatographed as described above. Crystallization from hexane gave colorless needles in 21% yield (0.91 g, 0.42 mmol); mp 98—99 °C; IR (KBr) 3250 (NH), 1670 (C=O) cm^{-1}; ^{1}H NMR ($CDCl_3$) δ=1.16 (s, *t*-Bu, 9H), 7.91 (s, NH, 1H). Anal. ($C_{11}H_{10}D_5NOS$) C, H, N.

ESR Measurements. A 10—20 mg portion of amide **1** and 0.40 cm^3 of 1:4 (v/v) di-*t*-butyl peroxide-benzene were placed in an ESR cell. The cell was then degassed by three freeze-pump-thaw cycles using a high-vacuum system and sealed off. Type-**2** radicals were generated in the cavity of an ESR instrument by direct irradiation using a 1-kW xenon lamp (Wacom UV-10X). The ESR spectra were recorded during irradiation on a JEOL JES-FE-2XG spectrometer equipped with an X-band microwave unit and 100-kHz field modulation. Hyperfine-splitting constants and *g* values were determined by a comparison with Fremy's salt in K_2CO_3 aqueous solution (a_N=1.309 mT, *g*=2.0057).

References

1) ESR studies of nitrogen-centered free radicals 28. Part 27, Y. Miura, Y. Shibata, and M. Kinoshita, *J. Org. Chem.*, **51**, 1239 (1986).

2) Y. Miura, Y. Katsura, and M. Kinoshita, *Bull. Chem. Soc. Jpn.*, **51**, 3004 (1978).

3) E. Melamud and B. L. Silver, *J. Phys. Chem.*, **77**, 1896 (1973).

4) ^{17}O-Hyperfine splitting constants are known to take the negative sign; see Ref. 3.

5) Y. Miura, H. Asada, M. Kinoshita, and K. Ohta, *J. Phys. Chem.*, **87**, 3450 (1983).

6) Y. Miura, M. Isogai, and M. Kinoshita, *Bull. Chem. Soc. Jpn.*, **58**, 751 (1985).

7) Y. Miura, T. Kunishi, and M. Kinoshita, *J. Org. Chem.*, **50**, 5862 (1985).

8) P. M. Carton, B. C. Gilbert, H. A. H. Laue, R. O. C. Norman, and R. C. Sealy, *J. Chem. Soc., Perkin Trans. 2*, **1975**, 1245.

9) H. G. Viehe, Z. Janousek, R. Merényi, and L. Stella, *Acc. Chem. Res.*, **18**, 148 (1985).

10) Y. Miura, T. Kunishi, M. Isogai, and M. Kinoshita, *J. Org. Chem.*, **50**, 1627 (1985).

11) Y. Miura and M. Kinoshita, *J. Org. Chem.*, **49**, 2724 (1984).

12) M. L. Bender, *J. Am. Chem. Soc.*, **73**, 1626 (1951); M. L. Bender and R. D. Ginger, *ibid.*, **77**, 348 (1955).

Synthesis of Phosphirane Oxide Derivatives Promoted by Introduced Phenylsulfinyl Groups and Their Pummerer Reaction

Tatsuo OSHIKAWA* and Mitsuji YAMASHITA
Department of Synthetic Chemistry, Faculty of Engineering, Shizuoka University, Hamamatsu 432
(Received October 7, 1985)

Synopsis. Phosphirane oxide derivatives were first successfully synthesized in good yield under mild conditions wherein carbon-carbon bond formation was promoted by two phenylsulfinyl groups on the α and α' carbons of the phosphorus atom. A structure determination of the formed phosphirane oxide derivatives as well as the stereochemistry of the Pummerer reaction product revealed a trans geometry for the phosphirane oxide.

In the field of three-membered heterocycles, many papers concerning aza and thia analogues have been published; however, little is known about the syntheses of phosphiranes via reactions of phosphides with epoxides[2] and via the formation of two carbon-phosphorus bonds were reported.[3] This paper describes the first attempt to introduce activating groups, such as phenylsulfinyl groups, on the α and α' carbons of phosphorus atom in order to promote regioselectivity in a coupling reaction leading to phosphirane oxides via carbon-carbon bond formation.

Results and Discussion

Compound **1** was prepared by a reaction of phenylphosphonous dichloride with a Grignard reagent of chloromethyl phenyl sulfide. Phosphine **1** was oxidized with hydrogen peroxide to give compound **2**, the bromonation of which was then carried out with an *N*-bromosuccinimide/bromine/pyridine system[4] to afford α-bromophosphine oxide **3**. Compound **3** consisted of diastereomers, being used for a further transformation without separation. The treatment of **3** with a variety of bases, such as DBU and triethylamine, in tetrahydrofuran at room temperature brought about dehydrobromination to afford a phosphirane oxide **4**. When DBU, a strong dehydrobromination reagent, was used an olefinic product **5** was obtained as the major product (yield of **4** and **5** were 3 and 73%, respectively).

Phosphiranes have been known to be unstable towards bases and heat; therefore, it may be difficult to produce phosphirane as the sole product.[1,2] The amount of the olefinic product which was formed as the by-product depended on the base, since the base catalyzed a ring opening of the phosphirane oxide **4** to open the three-membered ring. Therefore, the major product was an olefinic type when a strong dehydrobromination reagent such as DBU was used. On the other hand, triethylamine remarkably improved the formation of phosphirane oxide **4** by a 1,3-elimination of hydrogen bromide (yield of **4** and **5** were 75 and 3%, respectively). Quast and Heuschmann[5] obtained a single stereoisomer of a phosphirane oxide having a configuration where the C-H vs. C-H was syn and P=O vs. C-H was an anti form from the diastereomeric α-bromo precursor. Four isomers can possibly exist for the phosphirane oxide **4**; however, the substituent R's (PhSO) should be anti to each other, as shown in the Scheme since only the Z-isomer **5** was produced in the ring-opening transformation of the phosphirane oxide **4**. The vinyl proton of compound **5** showed small values for the H-P coupling constant[6] in the ^{1}H NMR spectrum (J_{HCCP}=15.0 Hz), indicating a Z-geometry (as cis for H-C=C-P or R-C=C-R bond) compared with the large coupling constant for the E-isomer.[6] Since the cleavage of the carbon-phosphorus bond of phosphirane oxide 4 having trans R's proceeds in a conrotatory fashion from the Woodward-Hoffmann rule (as shown in the literature[7]) the cis-geometry for the phenylsulfinyl groups on the carbon-carbon double bond to form the Z-isomer **5** should be brought about in consequence of the three-membered ring opening.

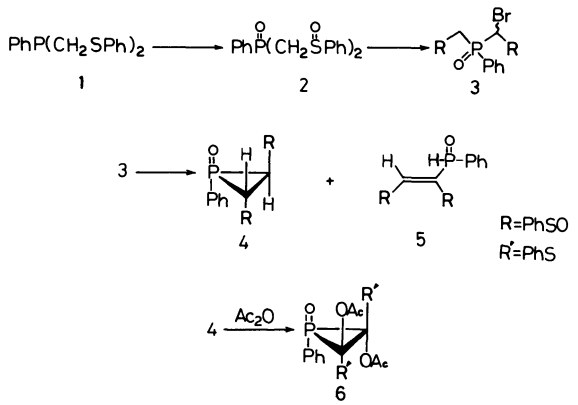

Scheme.

The product of a Pummerer reaction[8] of the phosphirane oxide **4** (i.e., compound **6**) gave additional strong information regarding the structure of compound **4**. If the Pummerer reaction product **6** has a trans configuration for two acetoxyl groups or for two phenylthio groups, the two methyl protons of the acetoxyl groups should be observed separately from the two singlet signals in the ^{1}H NMR spectrum. On the other hand, if the configuration of **6** is cis for these two groups, the two methyl protons should be observed as one singlet, owing to the symmetry. The treatment of compound **4** with acetic anhydride afforded a crystalline phosphirane oxide derivative **6** which had two acetoxyl groups on the α and α' positions of the phosphorus atom. The ^{1}H NMR spectrum of compound **6** clearly showed two kinds of acetoxyl signals at δ 3.00 and 3.32 (three protons each). These observations clearly established the structure of phosphirane oxide **4** to be either (2*S*, 3*S*) or (2*R*, 3*R*) as shown in the scheme. The sp^3 α and α' carbon signals of the phosphorus atom were observed downfield (69.5 and 73.6 ppm) compared with various publish-

ed reports[2,5] regarding ^{13}C NMR spectrum, since the carbon atoms are connected to oxygen and sulfur atoms.

Experimental

Apparatus. The IR spectra were measured on a Japan Spectroscopic Co., Ltd. JASCO A-3 spectrophotometer; the ^1H NMR spectra were run on a Hitachi R-24B (60 MHz) spectrameter; the mass spectra were measured by a Hitachi RMU, DMG, GC-MS spectrometer; the high-performance liquid chromatography was carried out using a Japan Spectroscopic Co., Ltd. UNIFLOW-211 and melting points were measured on a Yanagimoto Seisakusho micro melting-point apparatus.

Synthesis of Bis(phenylthiomethyl)phenylphosphine (1). A Grignard reagent was prepared from chloromethyl phenyl sulfide (3.7 g, 23.4 mmol) and magnesium metal (0.57 g, 23.4 mg atom) in freshly distilled tetrahydrofuran or ether (30 ml) under a dry nitrogen atmosphere. Phenylphosphonous dichloride (2.0 g, 11.2 mmol) in tetrahydrofuran (20 ml) was added to a solution of the Grignard reagent and the resulting solution was stirred for 5 h at room temperature. An aqueous solution of ammonium chloride (20 ml) was added to the reaction mixture; then, the solution was extracted with ether (3×30 ml). The organic layer was washed with water (3×10 ml). and dried over anhydrous sodium sulfate; the solvent was then evaporated. The residue was separated by column chromatography on silica gel (eluent: hexane) to afford compound **1** as colorless crystals in 45% yield, mp 71—72°C (from ethanol). ^1H NMR ($CDCl_3$) δ=2.92 (s, 4H, $2CH_2$) and 6.98 (br s, 15H, 3Ph).

Found: C, 74.54; H, 5.96%. Calcd for $C_{20}H_{19}PS$: C, 74.51; H, 5.94%.

Synthesis of Bis(phenylsulfinylmethyl)phenylphosphine Oxide (2). A 30% aqueous solution of hydrogen peroxide (0.37 g) was added to a solution of compound **1** (0.5 g, 1.55 mmol) in acetic acid (10 ml) and was stirred for 1 h at 0°C. The reaction mixture was allowed to warm to room temperature and was stirred for an additional 0.5 h, followed by the usual work-up. Isolation of the product by column chromatography on silica gel (eluent: benzene/ethyl acetate=1/1 in v/v) afforded compound **2** as a white crystalline material in 80% yield, mp 125—127°C. ^1H NMR ($CDCl_3$) δ=2.92 and 3.20 (s×2, 4H, $2CH_2$), and 7.36—7.43 (m, 15H, 3Ph). IR (ν_{max}^{KBr}) cm^{-1}, 1100 (P=O) and 1150 (S=O).

Found: C, 64.82; H, 5.15%. Calcd for $C_{20}H_{19}PSO_3$: C, 64.85; H, 5.17%.

Synthesis of 3. After the addition of a dichloromethane (20 ml) solution of bromine (0.25 g, 1.59 mmol), *N*-bromosuccinimide (0.14 g, 0.76 mmol), and pyridine (1 ml) to a solution of compound **2** (0.28 g, 0.76 mmol) in dichloromethane (10 ml), the mixture was stirred for 3 h at room temperature. The reaction mixture was poured into water (30 ml) and the organic layer was separated, washed with water, dried over anhydrous sodium sulfate, and then the solvent was evaporated. The separation of the product by thin-layer chromatography on silica gel afforded a crystalline compound **3** in 60% yield, mp 119—124°C. Compound **3** was a mixture of diastereoisomers which were detected by an HPLC retention time of 4.2 and 4.4 min (eluent: chloroform/methanol=20/1 in v/v) at the ratio of 1.5 to 1.0, respectively. ^1H NMR ($CDCl_3$) δ=3.09—3.81 (m, 2H, CH_2), 4.81—5.30 (m, 1H, CH-Br), and 7.43—7.85 (m, 15H, 3Ph); IR (ν_{max}^{KBr}) cm^{-1}, 1100 (P=O), 1160 (S=O), and 690 (C-Br); MS, *m/z*, 480 (M^+) and 482 (M^++2).

Found: C, 49.57: H, 3.69%. Calcd for $C_{20}H_{18}PS_2BrO_3$: C, 49.90; H, 3.77%.

Synthesis of 1-Phenyl-2,3 -bis(phenylsulfinyl)phosphirane 1-Oxide (4). A solution of compound **3** (0.1 g, 0.21 mmol) and an excess amount of triethylamine (3 ml) in tetrahydrofuran 5 ml) was stirred for 12 h at room temperature. The solvent was evaporated and the residue was separated by thin-layer chromatography on silica gel (eluent: benzene/ethyl acetate=1/1 in v/v) to afford the phosphirane oxide, **4**, and the olefinic product, **5**, in 75 and 3% yields, respectively. The phosphirane oxide, **4**, (syrup): ^1H NMR ($CDCl_3$) δ=4.34 (dd, J_{PCH}=7.5 Hz, 2H, 2CH) and 7.55—7.93 (m, 15H, 3Ph); IR (ν_{max}^{KBr}) cm^{-1}, 1450 (P-C_{arom}), 1130 (P=O), 1050 (S=O), and 700 (P-C); MS *m/z*, 400 (M^+).

Found: C, 60.11; H, 4.31%. Calcd for $C_{20}H_{17}O_3PS_2$: C, 59.99; H, 4.28%.

The olefinic product,**5**,(syrup): ^1H NMR ($CDCl_3$) δ=6.10 (d, J_{HCCP}=15.0 Hz, 1H, $P\diagdown C{=}C\diagup H$), 7.00 (d, J_{HP}=444.0 Hz, 1H, PH), and 7.2—7.6 (m, 15H, 3Ph); IR (ν_{max}^{neat}) cm^{-1}, 2350 (P-H), 1580 and 840 (C=C); MS *m/z*, 400 (M^+).

Pummerer Reaction of Phosphirane Oxide Derivative 4 with Acetic Anhydride. A solution of phosphirane oxide **4** (0.1 g, 0.25 mmol), acetic anhydride (0.06 g, 0.55 mmol), and a trace of *p*-toluenesulfonic acid in dichloromethane (5 ml) was stirred for 12 h at room temperature; then, the solvent was evaporated. The isolation of the crude product by thin-layer chromatography on silica gel afforded (2*S*, 3*S* or 2*R*, 3*R*)-1-phenyl-2,3-diacetoxy-2,3-bis(phenylthio)phosphirane 1-oxide (**6**) in 85% yield, mp 135—136°C. ^1H NMR ($CDCl_3$) δ=3.00, 3.32 (s, 6H, 2OAc), and 7.52 (m, 15H, 3Ph); ^{31}P NMR ($CDCl_3$) δ_P=−62.7 ppm (from 85% H_3PO_4); ^{13}C NMR ($CDCl_3$) δ=34.2 (s, CH_3), 34.5 (s, CH_3), 69.5 (d, J_{CP}=37.8 Hz, C^{α}), 73.6 (d, J_{CP}=35.2 Hz,$C^{\alpha'}$, 127.4 (P-arom), 128.1 (P-arom), 129.3 (P and S arom), 129.5 (S-arom), 130.4 (S-arom), 140.9 (S-arom), 143.3 (P-arom), 226.3 (s, C=O), 230.3 (s, C=O); IR (ν_{max}^{KBr}) cm^{-1}, 1590 (C=O), 1450 (P-Ph), 1150 (P=O), 750 (C-S-C), and 690 (C-P); MS *m/z*, 484 (M^+).

Found: C, 59.52; H, 4.34%. Calcd for $C_{24}H_{21}O_5PS_2$: C, 59.50; H, 4.37%.

The authors wish to express their thanks to Dr. Masaaki Yoshifuji for his kind discussions and measurements of the NMR spectra.

References

1) a) R. I. Wagner, L. D. Freemann, H. Goldwhite, and D. G. Rowsell, *J. Am. Chem. Soc.*, **89**, 1102 (1967); b) S. Chan, H. Goldwhite, H. Kreyser, D. G. Rowsell, and R. Tang, *Tetrahedron*, **25**, 1097 (1969).

2) M. Yoshifuji, K. Toyota, and N. Inamoto, *Chem. Lett.*, **1985**, 441.

3) T. Oshikawa and M. Yamashita, *Synthesis*, **1985**, 290.

4) G. Tsuchihashi and K. Ogura, *Bull. Chem. Soc. Jpn.*, **44**, 1726 (1971).

5) a) H. Quast and M. Heuschmann, *Angew. Chem. Int. Ed. Engl.*, **17**, 867 (1978); b) *Idem, Liebigs Ann. Chem.*, **1981**, 977.

6) a) H. Quast and M. Heuschmann, *J. Chem. Soc., Chem. Commun.*, **1979**, 390; b) J. P. Albrand, D. Gagnaier, M. Picard, and J. B. Robert, *Tetrahedron Lett.*, **1970**, 4593.

7) R. B. Woodward and R. Hoffmann, "The Conservation of Orbital Symmetry," Verlag Chemie GmbH and Academic Press, Inc, Weinheim and New York (1970).

8) S. Glue, I. T. Kay, and M. R. Kipps, *J. Chem. Soc., Chem. Commun.*, **1970**, 1158.

Chromotropisms of Imidazole Derivatives. III.[1,2] Crystal Structure of 4,5-Bis(4-methoxyphenyl)-2-(4-nitrophenyl)-1*H*-imidazole

Yoshinobu INOUYE* and Yoshiko SAKAINO†
Department of Chemistry, University of Tsukuba, Sakura-mura, Niihari-gun, Ibaraki 305
†Department of Chemistry, Faculty of Education, Gunma University, Maebashi 371
(Received April 30, 1986)

Synopsis. The molecular and crystal structure of the title compound was determined by the single-crystal X-ray analysis. The crystal is orthorhombic with a space group *Pbca*, a=15.161 (9), b=25.805 (5), c=9.948 (1) Å, and Z=8. The 4-nitrophenyl ring is nearly on a same plane with the imidazole ring, while the other two benzene rings make angles of 26.5° and 47.7°.

In the course of our study on the chromotropic behavior of the dimers of 2,4,5-triarylimidazolyl radicals obtained by the oxidation of 2,4,5-triaryl-1*H*-imidazole,[3] we have recently found that 4,5-bis(4-methoxyphenyl)-2-(4-nitrophenyl)-1*H*-imidazole (**I**) crystallized in several colored states under different conditions. Crystallization of **I** from aqueous acetic acid gave an orange-yellow imidazolium acetate dihydrate (**I**), which exhibits sensitive color change from orange-yellow to red by drying, trituration, or heating.[1] The crystal structure of **I** showed that the solvents of crystallization played an essential role in crystal packing.[2] On the other hand, crystallization from dry benzene gave initially red needles (**II**), which changed their color and crystal form to light orange prisms (**III**) when the solution containing **II** had been allowed to stand for several days at room temperature. When exposed to AcOH-H_2O vapor, pulverized **III** changed to **I** after three days.

In order to clarify the relation between the color and the structure, a single-crystal X-ray analysis of **III** has been carried out.

Experimental

Data Collection. **III**; $C_{23}H_{19}N_3O_4$, F. W. 401.42, D_m= 1.35 g cm^{-3} (aqueous KI), D_x=1.37 g cm^{-3}, μ (Mo$K\alpha$)=1.02 cm^{-1}. The unit-cell dimensions were refined on a Rigaku automated four-circle diffractometer with graphite monochromated Mo$K\alpha$ radiation (50 kV, 160 mA). The diffraction intensities were measured for a single crystal with approximate dimensions of 0.25×0.20×0.12 mm^3 on the diffractometer by the ω—2θ scan technique at room temperature. The intensities of three standard reflections, measured after every 56 reflections, were stable within a 1% fluctuation. In the range of 2θ values up to 45°, 1252 independent structure factors ($|F_o|>3\sigma(F_o)$) were used for the structure determination. The intensities were corrected for Lorentz and polarization effects but not for absorption. All calculations were carried out on a FACOM M-380 computer at the Science Information Processing Center, University of Tsukuba.

Structure Dtermination. The structure was solved by the direct method (MULTAN 80).[4] All the 30 non-hydrogen atoms were found on the first E map calculated with 320 $|E|$'s greater than 1.54. The atomic parameters were refined by the full-matrix least-squares method.[5] The atomic scattering factors, given by Cromer and Mann[6] for C, N, or O, and listed[7] on the table for H were used.

Refinement with isotropic temperature factors for C, N, O lowered the R factor to 0.216. One reflection 020 had $|F_o|$ abnormally lower than $|F_c|$. As it seemed to suffer the secondary extinction, the subsequent refinements were carried out without this reflection. Refinement with anisotropic temperature factors for non-hydrogen atoms reduced the R value to 0.093. All the hydrogen atoms were revealed on a difference Fourier map, which were included in the refinement with isotropic temperature factors. Finally the R value reduced to 0.037 (R_w=0.041). The residuals in the difference map were within in the range of +0.47—−0.22 e Å^{-3}. The atomic parameters[8] are listed in Table 1 (for the numbering diagram, see Fig. 1).

Results and Discussion

The selected bond distances and angles are shown in

Table 1. Atomic Coordinates of the Non-Hydrogen Atoms (×10^4) and Equivalent Isotropic Temperature Factors with e.s.d.'s in Parentheses

Atom	x	y	z	B_{eq}/Å^2	Atom	x	y	z	B_{eq}/Å^2
O(1)	5106(2)	112(1)	3463(3)	5.5	C(16)	3333(3)	3872(1)	4190(4)	3.7
O(2)	5112(2)	532(1)	1608(3)	7.7	C(17)	3117(3)	4344(1)	3617(4)	4.1
N(3)	4972(2)	502(1)	2805(3)	4.2	C(18)	2266(2)	4523(1)	3732(3)	3.5
C(4)	4649(2)	967(1)	3506(4)	3.2	C(19)	1649(3)	4245(1)	4446(3)	3.3
C(5)	4251(2)	915(1)	4744(4)	3.4	C(20)	1867(2)	3774(1)	5005(3)	3.0
C(6)	3930(2)	1356(1)	5361(3)	3.2	O(21)	1977(2)	4977(1)	3179(3)	5.1
C(7)	4016(2)	1841(1)	4753(3)	2.7	C(22)	2465(5)	5182(2)	2098(6)	6.6
C(8)	4459(2)	1877(1)	3537(4)	3.3	C(23)	2190(2)	2944(1)	7679(3)	2.8
C(9)	4766(2)	1438(1)	2894(4)	3.5	C(24)	2223(2)	3440(1)	8210(3)	3.4
C(10)	3582(2)	2290(1)	5338(3)	2.8	C(25)	1699(2)	3579(2)	9297(4)	3.8
N(11)	3151(2)	2306(1)	6504(3)	3.0	C(26)	1143(2)	3220(2)	9855(3)	4.1
C(12)	2752(2)	2789(1)	6545(3)	2.8	C(27)	1104(2)	2724(2)	9348(3)	4.2
C(13)	2960(2)	3068(1)	5406(3)	2.7	C(28)	1619(2)	2587(2)	8265(4)	3.7
N(14)	3494(2)	2745(1)	4664(3)	2.9	O(29)	598(2)	3322(1)	10929(3)	6.1
C(15)	2718(2)	3578(1)	4190(4)	2.7	C(30)	718(4)	3803(4)	11596(7)	8.8

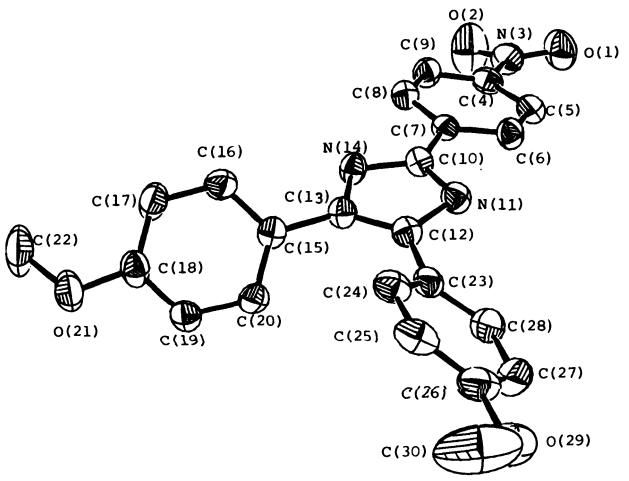

Fig. 1. A perspective view (ORTEP)[9] of the molecule with the atom numbering scheme. Non-hydrogen atoms are represented by thermal ellipsoids at 50% probability level.

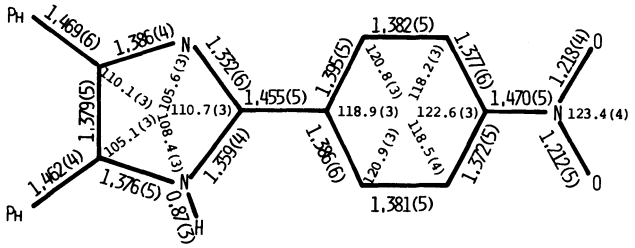

Fig. 2. Selected bond lengths and angles with estimated standard deviation in parentheses.

Fig. 2. Neither unusual bond distances nor angles in the molecule were observed. The molecular geometry of **III** is similar to that of **I**. The conformation of the molecule is illustrated in Fig. 1. The imidazole ring and the 4-nitrophenyl ring are nearly on a same plane. The dihedral angle [15.1°] between both rings is slightly larger than that [9.1°] in **I**. The other two benzene rings in **III** makes angles of 26.5° and 47.7° with the imidazole ring, while in **I** of 39.9° and 40.4°, respectively. This discrepancy is due to the presence of the solvents of crystallization in **I** and, by those, the benzene ring were forced to twist as to minimize the steric interaction between the ring and the water molecules.

Molecular packing of both compounds, on the other hand, are quite different with each other. The solvents of crystallization played an essential role in molecular packing in **I** and the molecules were packed in sheet parallel to the *ac* plane by the three-dimensional hydrogen-bonding network.[2] In **III**, as shown in Fig. 3, only a weak intermolecular hydrogen bonding was observed: N(11)(x,y,z)···H(14)–N(14)(x, $1/2-y,1/2+z$) 3.190(5)Å and N(11)···1H(14) 2.46(3)Å, H(14)–N(14) 0.87(3)Å, and ϕ [N(11)–H(14)–N(14)] 141.8°. Other intermolecular atomic contacts are usual van der Waals distances and the shortest one is O(1)(x, y,z)···O(1) ($1-x,-y,1-z$) 3.129(5)Å.

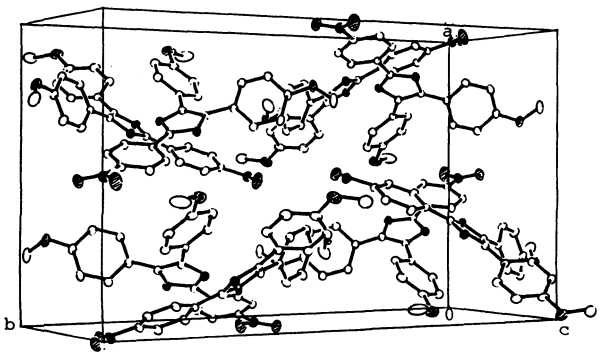

Fig. 3. The molecular packing diagram. O: Carbon, ●: nitrogen, ⊘: oxygen.

As no significant π–π interaction between molecules was estimated from the crystal packing, the orange color of **III** is due to the absorption of the chromophore of **I** itself. This is consistent with the similarity of the longest UV maximum in solution (EtOH, 405 nm) to that in solid state (in Nujol, 410 nm).

References

1) Part I. Y. Sakaino, T. Takizawa, Y. Inouye, and H. Kakisawa, *J. Chem. Soc., Perkin Trans. 2*, in press.

2) Part II.Y. Inouye and Y. Sakaino, *Acta Crystallogr., Sect. C*, **41**, 1106 (1985).

3) Y. Sakaino, H. Kakisawa, K. Arita, M. Kouno, and H. Morishima, *Tetrahedron*, **29**, 1185 (1973).

4) P. Main, S. J. Fiske, S. E. Hull, L. Lessinger, G. Germain, J.-P. Declercq, and M. M. Woolfson, "A System of Computer Programs for the Authomatic Solution of Crystal Structures from X-Ray Diffraction Data, *MULTAN* 80," University of York (1980).

5) L. W. Finger, "A System of Fortran IV Computer Programs for Crystal Structure Computations, *RFINE* 2," Geophysical Laboratory, Carnegie Institute, Washington, DC (1969). The program modified by H. Horiuchi was used.

6) D. T. Cromer and J. B. Mann, *Acta Crystallogr.*, **A24**, 321 (1968).

7) "International Tables for X-Ray Crystallography," Kynoch Press, Birmingham (1974), Vol. 4, p. 99.

8) Final F_o—F_c table and lists of hydrogen-atom coordinates, and least-squares planes are deposited at Chem. Soc. Jpn., Document No. 8645.

9) C. K. Johnson, *ORTEP* II, Report ORNL-5138, Oak Ridge National Laboratory, Tennessee, USA (1976).

Imidazolium Dichromate. A New Reagent for the Oxidation of Alcohols to Carbonyl Compounds

Sunggak KIM* and Dong Chul LHIM
Department of Chemistry, Korea Advanced Institute of Science and Technology, Seoul 131, Korea
(Received September 21, 1985)

Synopsis. Imidazolium dichromate, a stable yellow crystalline compound, is found to be a mild selective reagent for the oxidation of allylic and benzylic alcohols to the corresponding carbonyl compounds.

Among many useful and reliable oxidation methods available in the literature,[1] the use of chromium(VI) reagents is the most convenient and efficient. Chromium trioxide–pyridine complex,[2] pyridinium chlorochromate,[3] and pyridinium dichromate,[4,5] have been widely utilized as oxidizing agents in most cases.

We have had occasion to study chromium trioxide–imidazole complex as an oxidizing agent and found that imidazolium dichromate (IDC) is very useful and reliable for the oxidation of allylic and benzylic alcohols to the corresponding carbonyl compounds in high yields under mild conditions.

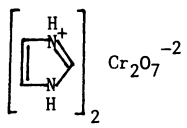

IDC

IDC is conveniently prepared by the addition of imidazole to a solution of an equimolar amount of chromium trioxide in a minimum of water and obtained in 80% yield as a nonhygroscopic and air-stable yellow crystals. IDC is readily soluble in *N,N*-dimethylformamide and dimethyl sulfoxide, while very slightly soluble in dichloromethane, chloroform, and acetone.

The choice of solvent in the oxidation of alcohols with IDC appeared to be important. The oxidation of 1-phenylethanol with 2 equiv of IDC in dichloromethane at room temperature for 16 h gave 35% of acetophenone along with the recovery 55% of the original alcohol, while the reaction in *N,N*-dimethylformamide under the same conditions was complete, yielding acetophenone in 83% yield. Thus, remaining reactions were carried out with 2 equiv of IDC in *N,N*-dimethylformamide at room temperature.

Table 1 includes several experimental results and shows the efficiency, the applicability, and the scope of this method. Under the present conditions, allylic alcohols such as cinnamyl alcohol and carveol were rapidly oxidized to α,β-unsaturated carbonyl compounds in high yields. The oxidation of geraniol to geranial resulted in isomerization of double bond to some extent. GLC analysis indicated the 6% E→Z isomerization at double bond took place. The oxidation of benzylic alcohols was somewhat slower than that of allylic alcohols and required 4—16 h for completion of the reaction.

The oxidation of saturated aliphatic alcohols occurred very slowly. For example, when the oxidation of 1-undecanol was carried out with 2 equiv of IDC in *N,N*-dimethylformamide at room temperature for 24 h, undecanal was obtained in 38% yield along with the recovery of the starting material in 53% yield. Similar results were realized with several saturated aliphatic alcohols, though relatively sterically-hindered cyclohexanol derivatives such as 2-*t*-butylcyclohexanol and 3,3,5-trimethylcyclohexanol were cleanly and completely oxidized to the corresponding carbonyl compounds in high yields under the same conditions.

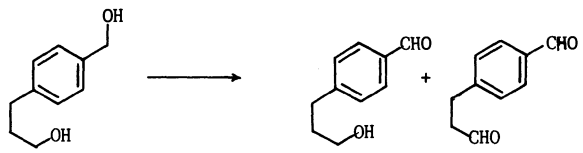

Since the possibility of selective oxidation of benzylic and allylic alcohols in the presence of saturated aliphatic alcohols was indicated by the oxidation results obtained herein, the oxidation of an equimolar mixture of isophorol (3,5,5-trimethyl-2-cyclohexen-1-ol) and 1-nonanol with 2 equiv of IDC was carried out in *N,N*-dimethylformamide at room temperature for 1 h. GLC analysis indicated the presence of a 98:11 mixture of isophorone and nonanal. Even better selectivity was obtained with *p*-(3-hydroxypropyl)benzyl alcohol. Reaction of *p*-(3-hydroxypropyl)benzyl alcohol with 2 equiv of IDC in *N,N*-dimethylformamide at room temperature for 4 h gave *p*-(3-hydroxypropyl)-benzaldehyde in 68% yield along with less than 3% of the corresponding dialdehyde. The selectivity achieved with IDC is comparable to 4-(dimethylamino)pyridinium chlorochromate.[5]

In conclusion, the use of imidazolium dichromate as an oxidizing agent offers some distinct advantages such as easy preparation and stability of the reagent, the selective oxidation of allylic and benzylic alcohols, and mild conditions.

Experimental

Preparation of Imidazolium Dichromate. Imidazole (13.6 g, 0.2 mol) was slowly added to a cooled solution of chromium trioxide (20.0 g, 0.2 mol) in water (16 ml). After 0.5 h, the reaction mixture was diluted with acetone (20 ml) and cooled to −20 °C. The yellow crystals were collected, washed with acetone (40 ml), and dried in vacuo at room temperature to give imidazolium dichromate (28.3 g, 80%). Mp 130—131 °C (decomp); NMR (DMSO-d_6) δ=7.50 (s, 2H), 8.96 (s, 1H), 12.37 (s, 2H); IR (KBr) 930, 890, 765 cm^{-1}. Found: C, 20.80; H, 2.90; N, 16.19%. Calcd for $C_6H_{10}O_7N_4Cr_2$: C, 20.35; H, 2.85; N, 15.82.

Table 1. Oxidation of Alcohols to Carbonyl Compounds with IDC in DMF at Room Temperature[a)]

Alcohol	Time/h	Yield/%[b)]	Alcohol	Time/h	Yield/%[b)]
t-C_6H_5-CH=CH-CH_2OH	1	91	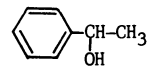	16	83
t-C_6H_5-CH=CH-CH(OH)CH_3	1	94			
Geraniol	2	82 [c)]	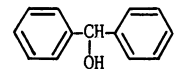	12	93
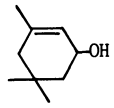	2	88			
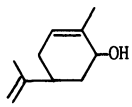	2	91	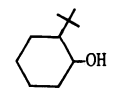	24	84
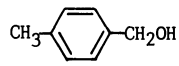	6	75	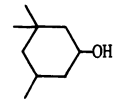	24	87
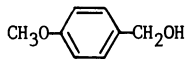	6	75	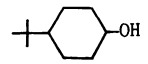	24	58(25)
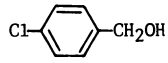	6	71	$CH_3CH(OH)(CH_2)_8CH_3$	24	77(13)
			$CH_3(CH_2)_9CH_2OH$	24	38(53)

a) The reaction was carried out with 2 equiv of IDC. b) The yields refer to isolated products. The numbers in parentheses indicate the isolated yields of the recovered starting materials. c) 6% E→Z isomerization was detected by GLC.

General Procedure for Oxidation of Alcohols. To a solution of an alcohol (2 mmol) in *N,N*-dimethylformamide (5 ml) was added imidazolium dichromate (4 mmol) and the reaction mixture was stirred at room temperature. After completion of the reaction, water (30 ml) was added to the reaction mixture and the product was extracted three times with diethyl ether. The ether extracts were washed with water and aqueous $NaHCO_3$, dried over anhydrous $MgSO_4$, and evaporated to dryness. The crude product was purified by distillation with a Kugelrohr apparatus or crystallization. The oxidation products obtained here were known products in all cases and were readily available compounds in most cases.

Selective Oxidation of *p*-(3-Hydroxypropyl)benzyl Alcohol. To a solution of *p*-(3-hydroxypropyl)benzyl alcohol (165 mg, 1 mmol) in *N,N*-dimethylformamide (3 ml) was added imidazolium dichromate (705 mg, 2 mmol) and the mixture was stirred at room temperature for 4 h. After usual workup as described above, the crude product was subjected to silica-gel column chromatography with dichloromethane–ethyl acetate (4:1) as an eluant to yield *p*-(3-hydroxypropyl)-benzaldehyde (112 mg, 68%) and 3-(4-formylphenyl)propanal (4 mg, 3%). *p*-(3-Hydroxypropyl)benzaldehyde: NMR ($CDCl_3$) δ=1.80—2.30 (m, 2H), 2.77 (s, 1H), 2.93 (t, 2H, J=6 Hz), 3.80 (t, 2H, J=6 Hz), 7.40—7.98 (m, 4H), 10.10 (s, 1H). IR (film) 1700 cm^{-1}. 3-(4-Formylphenyl)propanal: ^1H NMR ($CDCl_3$) δ=2.45—3.21 (m, 4H), 7.31—7.85 (m, 4H), 9.81 (s, 1H), 9.95 (s, 1H).

We thank Korea Advanced Institute of Science and Technology for financial support.

References

1) L. J. Chinn, "Selection of Oxidants in Synthesis," Marcel Dekker, New York (1971); J. G. Moffatt, "Oxidation," Marcel Dekker, New York (1971), Vol. 2; H. O. House, "Modern Synthetic Reactions," 2nd ed. W. A. Benzamin, Inc., New York (1972); K. Omura and D. Swern, *Tetrahedron*, **34**, 1651 (1978).

2) J. C. Collins, W. W. Hess, and F. J. Frank, *Tetrahedron Lett.*, **1968**, 3363.

3) E. J. Corey and J. W. Suggs, *Tetrahedron Lett.*, **1975**, 2647.

4) E. J. Corey and G. Schmidt, *Tetrahedron Lett.*, **1979**, 399.

5) For recently developed chromium(VI) reagents, see: F. S. Guziec and F. A. Luzzio, *Synthesis*, **1980**, 691; F. S. Guziec and F. A. Luzzio, *J. Org. Chem.*, **47**, 1787 (1982); M. N. Bhattacharjee, M. K. Chaudhuri, H. S. Dasgupta, N. Roy, and D. T. Khathing, *Synthesis*, **1982**, 588; X. Huang and C. Chan, *Synthesis*, **1982**, 1091; J. Herscovici, M-J. Egron, and K. Antonakis, *J. Chem. Soc., Perkin Trans. 1*, **1982**, 1967; J. M. Aizpurua and C. Palomo, *Tetrahedron Lett.*, **24**, 4367 (1983).

Electrochemical Properties of Adriamycin Adsorbed on Pyrolytic Graphite Electrodes Modified by Phospholipid Monomolecular Membranes

Tomonori KONSE, Kenji KANO, Rika KANO, and Tanekazu KUBOTA*
Gifu Pharmaceutical University, 6-1 Mitahora-higashi, 5-Chome, Gifu 502
(Received February 24, 1986)

Synopsis. Electrochemical equilibrium and kinetic parameters have been determined by means of numerical simulation of d.c. voltammograms based on the theory of a two-step surface-redox reaction for the case of the redox system of adriamycin adsorbed on a basal-plane pyrolytic graphite electrode (BPGE) which is modified by a phospholipid monomolecular membrane. Comparison of these parameters with those obtained at a bare BPGE has shown that the semiquinone formation reaction is thermodynamically favorable and that the electron transfer rate constant decreases in these lipid membranes.

The toxic mechanism of adriamycin (anticancer drug), especially its cardiotoxicity, is not yet fully understood. The most acceptable mechanism is due to the bioreductive formation of the adriamycin semiquinone free radical as an intermediate catalyzed by NADPH-cytochrome P-450 reductase,[1] which is a membrane-bound enzyme. In addition, it is noted that the affinity of adriamycin for the phospholipid membrane is high.[2] These circumstances suggest that the elucidation of the redox property of adriamycin in the lipid membrane is fundamentally very important. In previous papers,[3,4] we have proposed a technique based on a numerical simulation of the quasi-reversible d.c. cyclic voltammograms in order to determine the electrochemical equilibrium and kinetic parameters pertinent to a two-step surface-redox reaction; $O_{ad}+e \rightleftarrows S_{ad}$ and $S_{ad}+e \rightleftarrows R_{ad}$. Here O_{ad}, S_{ad}, and R_{ad} stand for the oxidized, semiquinone, and reduced species in the adsorbed form, respectively.

In this study using the above analytical technique, we report the redox behavior of the quinone moiety in an adriamycin molecule adsorbed on a BPGE modified by two kinds of phospholipid monomolecular membranes, i.e., lecithin (phosphatidylethanolamine) and cardiolipin. The electrochemical equilibrium and kinetic parameters thus obtained are then compared with those determined at a bare BPGE.

Experimental

Chemicals. Adriamycin hydrochloride was kindly supplied by Kyowa Hakko Co. and used as received. Soybean lecithin (Wako Pure Chemical) and bovine heart cardiolipin (Sigma Chemical), both commercially available, were employed as received. Other chemicals were of reagent grade quality.

Preparation of BPGE Modified by a Phospholipid Monomolecular Membrane. BPGE's were prepared as described in a previous paper.[4] The phospholipid monomolecular layer was obtained according to the simplified Blodgett method.[5] The cleaned surface of triply-distilled water in a vessel was divided into two parts by a nylon thread. Upon the one part of the surface, a benzene solution of phospholipid was added dropwise and extended. On the other part, distilled rapeseed oil was extended as a piston oil.[6] The new plane surface of the BPGE was horizontally contacted to the phospholipid monomolecular layer. After the adhesion the modified electrode surface was sonicated for ca. 30 s in distilled water, and then air-dried at room temperature.

Electrochemical Measurement. The phospholipid membrane modified electrode was immersed in 3 ml of an acetate buffer (0.2 mol dm^{-3}, pH 4.5, ionic strength I=0.5) containing 3×10^{-5} mol dm^{-3} of adriamycin for 30 s under stirring. After the electrode had been washed by triply-distilled water, it was ultrasonically washed in distilled water and air-dried at room temperature. This electrode was immersed into a de-aerated electrolysis solution (0.2 mol dm^{-3} acetate buffer, pH 4.5, I=0.5) without adriamycin, and the voltammograms were then recorded. All other electrochemical measurements were described in previous papers.[3,4,7]

Results and Discussion

Lecithin-Monomolecular-Layer Modified BPGE (LT-BPGE). Adriamycin adsorbed or bound strongly on an LT-BPGE shows a reversible surface redox wave at a sweep rate v=10 mV s^{-1}. The peak potential, E_p^{rev}, and the half-peak width, $\Delta E_{p/2}^{rev}$, of these reversible waves are −0.500 V vs. SCE and 77—82 mV, respectively. These waves can be ascribed to the redox reaction of the quinone moiety in the adriamycin[7] and are analyzed on the basis of the theory regarding a two-step one-electron surface-redox reaction.[3,8] Assuming that the surface activity coefficients of O_{ad}, S_{ad}, and R_{ad} of adriamycin are equal, the semiquinone formation constant, K, is defined as:

$$K = [S_{ad}]^2/[O_{ad}][R_{ad}] = \exp[F(E'_{o1}-E'_{o2})/RT], \quad (1)$$

where $[j_{ad}]$'s (j=O, S, R) are the surface concentrations of j_{ad}, and E'_{o1} and E'_{o2} are the standard surface redox potentials of the couples O_{ad}/S_{ad} and S_{ad}/R_{ad}, respectively. The K value was estimated to be 2.2—2.8 from $\Delta E_{p/2}^{rev}$.[7,8]

At large v such as 1 V s^{-1} a typical quasi-reversible voltammogram is recorded as shown in Fig. 1A (solid line). Here we observed that the cathodic and anodic peak currents and also the cathodic and anodic half-peak widths are respectively almost the same within an experimental error. The average of the anodic and cathodic peak potentials is equal to E_p^{rev}. In other words, this quasi-reversible wave is symmetrical about the point of $E=E_p^{rev}$ and i=0. These results confirm the following two assumptions[3,4]: a) the apparent rate constants, k_{sap}, of the first and the second single electron transfer steps at E'_{o1} and E'_{o2} are equal and b) the transfer coefficient for the electron transfer of each step is 0.5. Under these conditions, the current (i)-potential (E)-surface concentration (Γ) characteristics can be expressed by the Butler-Volmer equation:[3,8]

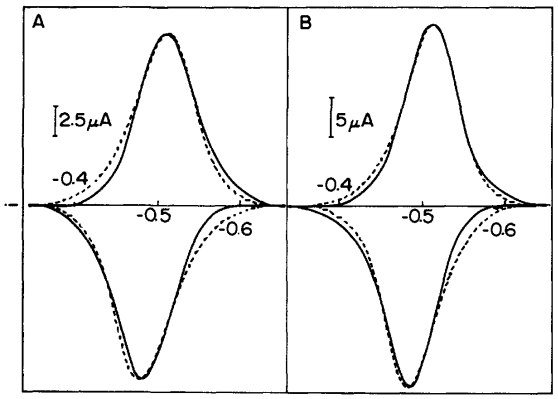

Fig. 1. Background-corrected cyclic d.c. voltammograms of adriamycin adsorbed on A) LT-BPGE and B) CL-BPGE. Voltage scanning was done with v=1 V s^{-1}. The solid lines and broken lines represent the experimental and the regression curves, respectively. See text for the parameters used for calculation.

$$i = FAk_{sap}\{\Gamma_S[(\rho/\sqrt{K})^{0.5} - (\rho\sqrt{K})^{-0.5}] - \Gamma_O(\rho/\sqrt{K})^{-0.5} + \Gamma_R(\rho\sqrt{K})^{0.5}\} \quad (2)$$

where Γ_j's (j=O, S, R) are the surface concentrations of j species, and A is the surface area. The standard surface redox potential of the O_{ad}/R_{ad} couple is given by E'_o [$=(E'_{o1}+E'_{o2})/2=E_p^{rev}$], and $\rho=\exp[F(E-E'_o)/RT]$. Other symbols have their usual meanings. Using Eq. 2 and the other fundamental equations with regard to the cyclic voltammetry on the surface-redox reaction, we can draw a quasi-reversible current-potential curve by the technique of numerical calculations.[3]

We have now analyzed the voltammogram shown in Fig. 1A by applying the technique of numerical simulation using two parameters,[3,4] k_{sap} and K, at E'_o=−0.500 V and the electricity Q=1.29 μC, here $Q=2FA\Gamma_t$, Γ_t being the sum of Γ_O, Γ_S, and Γ_R. The refined parameters are k_{sap}=65.7±5.0 s^{-1} and K=2.61±0.29. The resultant regression curve is depicted in Fig. 1A as a broken line. The K value obtained is in agreement with those estimated from the reversible voltammogram (K=2.2—2.8). The analysis of the voltammograms at various Q's shows that, within the experimental error, the values of K and k_{sap} are independent of Q in the range of 1.3 to 2.6 μC[9] that is in the possible limit of the present experiment. The average K value evaluated in this Q range is 2.32, and the k_{sap} is 62.4 s^{-1} in the same Q range. Alternatively, we calculated the theoretical current-potential curves[3] at v=100 and 200 mV s^{-1} by using the above average values of K and k_{sap}. These theoretical curves well reproduce the experimental one. These results indicate that the electrochemical behavior of adriamycin adsorbed on an LT-BPGE can be well interpreted on the base of the theory of a two-step one-electron surface-redox reaction, and that these refined parameters would be considered to be physically significant.

Cardiolipin-Monomolecular-Layer Modified BPGE (CL-BPGE). The electrochemical redox behavior of adriamycin adsorbed on a CL-BPGE was fundamentally the same as that observed on an LT-BPGE. In Fig. 1B the solid line shows an observed quasi-reversible wave at v=1 V s^{-1} and Q=2.00 μC (solid line), and the regression curve is given by the broken line. The refined parameters are k_{sap}=73.7±4.8 s^{-1} and K=1.75±0.17. The K value is equivalent to 73 mV of $\Delta E_{p/2}^{rev}$,[7,8] which agrees well with the experimental value (71—76 mV) of the reversible wave recorded at v=10 mV s^{-1}. It was also observed that the K and k_{sap} values at this electrode are independent of Q within an experimental error in the range of the experimentally obtainable Q (1.5—2.0 μC), and the average values are 1.69 and 77.9 s^{-1} for K and k_{sap}, respectively, in the above Q range. The reliability of the parameters was supported by the same method as in the case of LT-BPGE.

Table 1. Electrochemical Data of Adriamycin on a Bare BPGE and Two Kinds of Phospholipid Membrane Modified Electrodes

	E'_o	k_{sap}	K	$\Delta G°$
	V vs. SCE	s^{-1}		kJ mol^{-1}
Bare-BPGE	−0.497	115[a]	0.21	+3.85
LT-BPGE	−0.500	62	2.32	−2.10
CL-BPGE	−0.500	78	1.69	−1.30

a) The value at θ_A (the surface coverage of adriamycin)→1 is used.

Comparison with the Behavior at Bare BPGE. Table 1 summarizes the electrochemical data of the adriamycin adsorbed on the two types of phospholipid membrane modified BPGE as well as those on a bare BPGE. The E'_o values are almost the same in all three cases. However, it is to be noted that the K values at the phospholipid membrane modified electrodes are almost ten times larger than that at the bare one, and the free energy changes, $\Delta G°(=-RT\ln K)$, of the semiquinone radical formation equilibrium ($O_{ad}+R_{ad} \rightleftarrows 2S_{ad}$) are lower by about 5—6 kJ mol^{-1} than that at the bare one. In other words, the semiquinone radical is stabilized in the hydrophobic environment in the phospholipid membranes. On the other hand, the k_{sap} values at the phospholipid membrane modified electrodes are about one-half the value of that obtained at the bare electrode. The above decrease in k_{sap} may be attributed in part to the attructive interaction between adriamycin and the phospholipid molecule,[3,8,10] and in part to the slow rate of the proton transfer in phospholipid membranes immediately following the electron transfer.

The aforementioned properties of adriamycin in phospholipid membranes are important from the viewpoint of the cardiotoxicity of this drug. It is evident that the toxicity is associated with the inhibition of mitochondrial electron transport in the lipid bilayer and with the generation of oxyradicals, such as superoxide anion radical, by an auto-oxidation of the semiquinone radical intermediate.[11] It has been suggested that the adriamycin-mediated oxyradicals are responsible for the adriamycin-caused DNA and enzyme damage and also for the adriamycin-enhanced

peroxidation of unsaturated phospholipids.[12] The high stability of the semiquinone radical in lipid membranes and the high affinity of adriamycin for the membranes may bring about the increase of the semiquinone-related cardiotoxicity.

The authors wish to express their many thanks to Kyowa Hakko Kogyo Co. for the kind gift of adriamycin hydrochloride. This work was supported in part by a Grant-in-Aid for Scientific Research (No. 59390012) from the Ministry of Education, Science and Culture.

References

1) S. Pan, L. Pedersen, and N. R. Bachur, *Mol. Pharmacol.*, **19**, 184 (1981); N. R. Bachur, J. L. Gordon, M. V. Gee, and H. Kon, *Proc. Natl. Acad. Sci. U.S.A.*, **76**, 954 (1979).

2) T. G. Burke and T. R. Tritton, *Biochemistry*, **24**, 1768 (1985); D. Cheneval, M. Müller, R. Toni, S. Ruetz, and E. Carafoli, *J. Biol. Chem.*, **260**, 13003 (1985); E. Goormaghtigh, P. Chatelain, J. Caspers, and J. M. Ruysschaert, *Biochim. Biophys. Acta*, **597**, 1 (1980).

3) K. Kano, T. Konse, and T. Kubota, *Bull. Chem. Soc. Jpn.*, **58**, 1879 (1985).

4) T. Konse, K. Kano, and T. Kubota, *Bull. Chem. Soc. Jpn.*, **59**, 265 (1986).

5) K. B. Blodgett, *J. Am. Chem. Soc.*, **56**, 1007 (1935).

6) Surface pressure of the rapeseed oil is 10.5×10^{-3} N m^{-1}. See also: I. Langmuir and V. J. Schaefer, *Chem. Rev.*, **24**, 181 (1939).

7) K. Kano, T. Konse, N. Nishimura, and T. Kubota, *Bull. Chem. Soc. Jpn.*, **57**, 2383 (1984); K. Kano, T. Konse, and T. Kubota, *Bull. Chem. Soc. Jpn.*, **58**, 424 (1985).

8) T. Kakutani and M. Senda, *Bull. Chem. Soc. Jpn.*, **53**, 1942 (1980).

9) These Q values correspond to 0.074—0.148 in the surface coverage of adriamycin by taking account of the maximum $\Gamma_t=7.21\times10^{-10}$ mol cm^{-2} at a bare BPGE.[3]

10) B. B. Damaskin, O. A. Petrii, and V. V. Batrakov, "Adsorption of Organic Compounds on Electrodes," Plenum Press, New York (1971).

11) N. R. Bachur, S. L. Gordon, and M. V. Gee, *Mol. Pharmacol.*, **13**, 901 (1977); J. Goodman, P. Hochstein, *Biochem. Biophys. Res. Chem.*, **77**, 797 (1977); B. Kalyanaraman, E. Perez-Reyers, and R. P. Mason, *Biochim. Biophys. Acta*, **630**, 119 (1980); J. H. Doroshow, *J. Pharmacol. Exp. Ther.*, **218**, 206 (1981); T. Komiyama, T. Kikuchi, and Y. Sugiura, *Biochem. Pharmacol.*, **31**, 3651 (1982).

12) E. G. Mimnaugh, K. A. Kennedy, M. A. Trush, and B. K. Sinha, *Cancer Res.*, **45**, 3296 (1985); E. G. Mimnaugh, M. A. Trush, M. Bhatnagar, and T. E. Gram, *Biochem. Pharmacol.*, **34**, 847 (1985); and references cited therein.

Photocatalytic Decomposition of Formic Acid on Platinized n-Type Silicon Powder in Aqueous Solution

Hiroshi YONEYAMA,* Nobuyuki MATSUMOTO, and Hideo TAMURA
Department of Applied Chemistry, Faculty of Engineering, Osaka University, Yamada-oka 2-1, Suita, Osaka 565
(Received March 15, 1986)

Synopsis. Photocatalytic decomposition of aqueous formic acid was successfully achieved by using platinized n-type silicon powder as a photocatalyst under the conditions that the photocatalyst was spread on the bottom of a reaction cell.

Light-induced heterogeneous reactions at semiconductor photocatalysts in solution have recently gained popularity especially from the viewpoint of solar energy utilization in chemical synthesis. The semiconductors used as a medium for solar energy conversion should be matched well to the solar spectrum. In this respect, CdS,[1-6] CdS–CdSe solid solutions,[7] and CdS–ZnS composites,[8,9] have been employed as the photocatalysts.

Silicon is one of the best materials suitable for solar energy conversion. Our interests lie in the use of this material as photocatalysts in aqueous solution systems, because a variety of synthetic reactions involving hydrogen evolution and hydrogenation of organic substances are conceivable in the presence of water. It is well-known, however, that silicon is easily passivated in aqueous solutions, requiring stabilization prior to use as photocatalysts. In a previous paper,[10] it was shown that platinum-coated n-type silicon single crystal wafers served as photocatalysts for decomposition of formic acid in aqueous solutions. The covered platinum films in that case were 1—2 nm in thickness. The photocatalytic activity appeared under conditions that platinum-coated smooth etched surfaces were illuminated and platinum-coated damaged back surfaces were in the dark. It is expected that silicon powder has both defect-free surface and defective surface in individual particle. Platinization of n-type silicon powder particles will then attach activities and stabilities to the powder as photocatalysts. The present paper will demonstrate the validity of such an idea with the use of decomposition of formic acid as a photocatalytic reaction. It will be shown that the conversion efficiency obtained was low, and main causes for this will be briefly discussed referring to preliminary results on other synthetic reactions such as decomposition of alcohols.

Experimental

The n-type silicon powder was prepared with the same manner as described previously.[11] After etched in 48% HF for 15 min, the powder was suspended in a 0.2 mol dm^{-3} H_2PtCl_6 methanol solution, the volume of which was chosen to give a desired amount of platinum coating. The methanol was then evaporated under reduced pressure, and the resulting H_2PtCl_6-loaded silicon powder was heated in a hydrogen stream at 150 °C for 1 h, followed by heating at 400 °C for 15 min under 1.3×10^{-3} Pa. Hydrogen and carbon dioxide as the reaction products were determined by means of gas chromatography. Molecular sieve 5A was used as a column for the former, while Porapak Q for the latter.

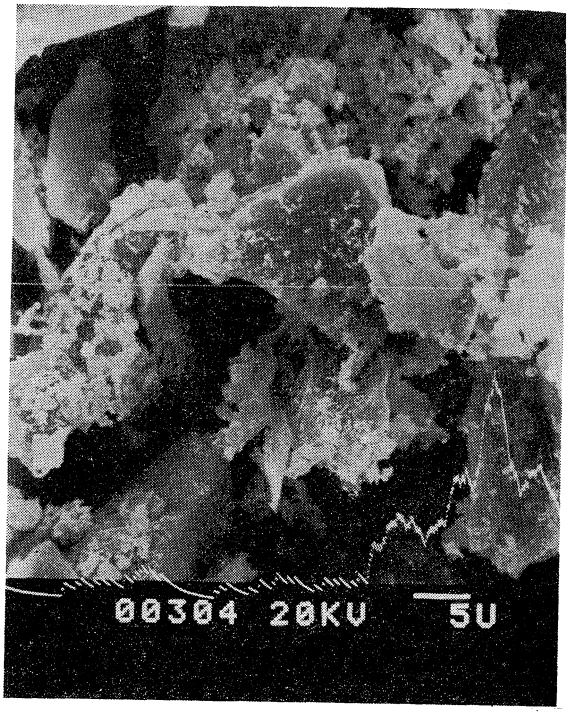

Fig. 1. SEM photograph of Pt-coated Si powder (10 wt% Pt) used as the photocatalyst and a distribution profile of the coated Pt given by a rugged white line in a lower part of the figure for microanalysis of the line direction shown in the center of the figure.

Photocatalytic decomposition of formic acid was studied using an Erlenmyer flask as a reaction cell. The top of the cell was equipped with a gas inlet and an outlet in a concentric position, and a port for sampling gases was also contained in the side wall of the cell. The platinized silicon powder (10 wt% platinum) of 110 mg was spread on the bottom of the cell and 20 ml of a 2.7 mol dm^{-3} formic acid solution was poured into the cell. Before illumination of the photocatalysts from the bottom of the cell, nitrogen was flushed for 30 min to purge the solution of disolved oxygen, and then the cell was closed with stopcocks. A 500 W high pressure mercury arc lamp was used as a light source and light from the lamp was passed through a Toshiba UV-39 filter to eliminate light of wavelengths shorter than 390 nm. The light intensity at the bottom of the cell was 0.2 W cm^{-2}.

Results and Discussion

Observations by a scanning electron microscope (SEM) of platinum-loaded silicon (10 wt%) powder particles shown in Fig. 1 revealed that platinum covered the powder surface rather inhomogeneously. Some parts of the surface were covered with relatively thick platinum, and the other parts were covered with thin platinum, as shown by a distribution profile with a rugged white line in a lower part of the figure.

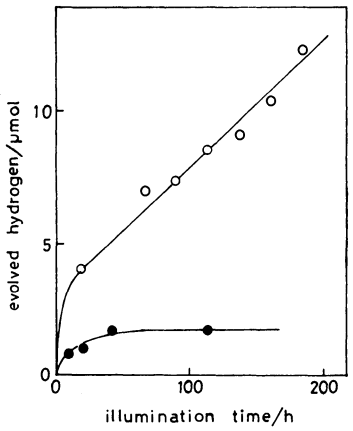

Fig. 2. The amount of evolved H_2 from 2.7 mol dm^{-3} formic acid as a function of illumination time. Photocatalyst: (○) Pt-coated n-type Si (10 wt% Pt), (●) Pt-coated insulating n-type Si (10 wt% Pt). For details, see text.

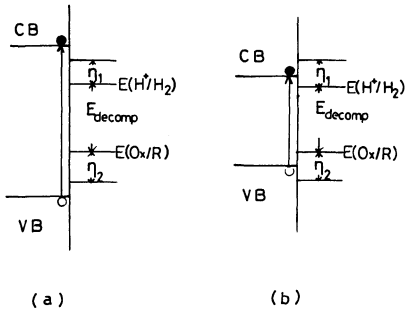

Fig. 3. Energy correlations which allow (a) and does not allow (b) photocatalytic decomposition of an organic substance to give hydrogen evolution. η_1: overvoltage needed for hydrogen evolution, η_2: overvoltage needed for oxidation of an organic substance. $E(H^+/H_2)$: hydrogen electrode potential, $E(Ox/R)$: redox potential of an organic substance. E_{decomp}: theoretical decomposition voltage. CB: conduction bands, VB: valence bands.

Hydrogen evolution occurred with the time course shown in Fig. 2. It is known that formic acid is decomposed by a thermal process in the presence of platinum. The contribution of this possibility was then examined by employing photoinactive catalysts. The photoinactive catalysts were prepared by heating the n-type silicon powder in air at 800 °C for 3 h to give an insulating oxide layer on the powder surface and then by depositing platinum on this surface with the same procedures as used in the preparation of platinized n-type silicon photocatalysts. Results obtained at this photocatalyst are also included in Fig. 2. It is confirmed from this figure that not the covered platinum alone but photoexcitation of the silicon powder plays a key role in evolving hydrogen under our experimental conditions. The photogenerated electrons and positive holes move to the covered platinum at defective surfaces and at smooth surfaces, respectively, with the energetics discussed previously for silicon single crystal photocatalysts,[10] leading to decomposition of formic acid. In the case of platinized oxide-covered n-type silicon, the photogenerated charge carriers cannot reach the covered platinum owing to the presence of the insulating oxide between the semiconductor substrate and the covered platinum.

The achievement of photocatalytic decomposition of formic acid was confirmed by determining both hydrogen and carbon dioxide produced; evolution of 7.8 μmol hydrogen was accompanied with 6.0 μmol carbon dioxide. The quantum efficiency for the hydrogen evolution was 0.02%, as determined by a 25 mW He-Ne laser as a light source.

It is desired from the viewpoint of perfect utilization of irradiated photons that experiments are performed using well-suspended photocatalysts. Photocatalytic experiments were then conducted by magnetically stirring the photocatalyst in the formic acid solution. The rate of hydrogen evolution obtained in that case was more than ten times of that achieved when the photocatalyst was spread on the bottom of the reaction cell. It was found, however, that evolution of carbon dioxide did not take place in the suspension system. Observations by SEM of morphology of the photocatalyst before and after the photocatalytic experiments for 100 h revealed that silicon particles were finely ground by the stirring during the course of the experiments. These results on the suspension system lead to the conclusion that hydrogen evolution in that case mainly came from anodic oxidation of bare surfaces of the particles that were created when the powder particles were ground. Thus, the covered platinum on the smooth surfaces of silicon did not significantly contribute to the anodic sites of the photocatalysts in that case.

The activities of the photocatalysts observed were quite low, as described above. It was found that activities were null for hydrogen evolution from aqueous ethanol, 2-propanol, and oxalic acid, adjusted pH to that of the formic acid solution, when the photocatalysts were palced on the bottom of the reaction cell. Current-potential measurements showed that the onset potentials of anodic photocurrents due to oxidation of these organic substances at platinum-covered smooth electrodes under illumination were more positive than those of cathodic currents due to hydrogen evolution at platinum-covered damaged electrodes in the dark. The observed correlation of the onset potentials does not allow the photocatalytic hydrogen evolution,[12] as observed.

The observed inactivity seems to reflect the situation that the bandgap (E_g) of the semiconductor photocatalyst (1.1 eV) is short of the sum of the theoretical decomposition voltage of each photocatalytic reaction and overvoltages of an anodic and a cathodic process of the photocatalytic reaction. As shown in Fig. 3, a light-induced hydrogen evolution occurs under conditions that positive holes have potentials more positive than the redox potential of an organic substance ($E(Ox/R)$) plus the overvoltage for the oxidation reaction and photogenerated electrons have potentials more negative than the hydrogen electrode potential plus the overvoltage for hydrogen evolution. The larger the bandgap of semiconductors used as photocatalysts are, the more easily the energy requirements are fulfilled. This view is supported by the results previously reported by

other investigators. Fujii et al.[13] found that CdS (E_g=2.4 eV), SiC (E_g=3.0 eV), TiO_2 (E_g=3.0 eV), Fe_2O_3 (E_g=2.2 eV), and In_2O_3 (E_g=2.7 eV) showed remarkable activities for hydrogen evolution from aqueous ethanol, but GaAs (E_g=1.4 eV), CdSe (E_g=1.68 eV), MoS_2 (E_g=1.2 eV), WO_3 (E_g=2.8 eV), and CdO (E_g=2.1 eV) did not. The latter two materials should be treated as exceptions, because not hydrogen evolution but hydrogen insertion into the semiconductor occurs at WO_3[14] and reduction of oxide itself rather than hydrogen evolution seems likely to occur at CdO. Furthermore, Kambe et al.[7] reported that activities of platinized CdS-CdSe solid solutions for hydrogen evolution from aqueous methanol and ethanol decreased with decreasing the bandgaps from 2.4 eV (CdS) to 1.68 eV (CdSe).

The theoretical decomposition voltages of formic acid, methanol, ethanol, 2-propanol, and oxalic acid to give hydrogen evolution are −0.2, 0.19, 0.19, 0.15, and −0.49 V, respectively. The minus sign means that the decomposition reaction is thermodynamically feasible. Anyway overvolatges, especailly that for oxidation of these organic substances seem to be large, resulting in inactivities of platinized silicon except for the reaction of fromic acid decomposition. Considering this overvoltage problem, semiconductors having good matching to solar spectrum does not necessarily suitable for photochemical synthesis using solar energy.

This work was supported by Grant-in-Aid for Energy Research from the Ministry of Education, Science and Culture.

References

1) M. Matsumura, H. Hashimoto, T. Iehara, and H. Tsubomura, *J. Phys. Chem.*, **88**, 248 (1984).
2) N. Bühler, K. Meier, and J.-F. Reber, *J. Phys. Chem.*, **88**, 3261 (1984).
3) N. M. Dimitrijevic, S. Li, and M. Grätzel, *J. Am. Chem. Soc.*, **106**, 7359 (1984).
4) Y.-M. Tricot and J. H. Fendler, *J. Am. Chem. Soc.*, **106**, 7359 (1984).
5) A. J. Frank, Z. Goren, and I. Willner, *J. Chem. Soc., Chem. Commun.*, **1985**, 1029.
6) T. Sakata, *J. Photochem.*, **29**, 205 (1985).
7) S. Kambe, M. Fujii, T. Kawai, S. Kawai, and F. Nakahara, *Chem. Phys. Lett.*, **109**, 105 (1984).
8) A. Ueno, N. Kakuta, K. H. Park, M. F. Finlayson, A. J. Bard, A. Campion, M. A. Fox, S. E. Weber, and J. M. White, *J. Phys. Chem.*, **89**, 3828 (1985).
9) K. Kitaguchi, H. Tsuiki, A. Ueno, and Y. Kotera, *Chem. Lett.*, **1985**, 1029.
10) H. Yoneyama, N. Matsumoto, and H. Tamura, *Langmuir*, **2**, 377 (1986).
11) Y. Taniguchi, H. Yoneyama, and H. Tamura, *Chem. Lett.*, **1983**, 269.
12) H. Yoneyama, Y. Toyoguchi, and H. Tamura, *J. Phys. Chem.*, **72**, 3460 (1972); M. Miyake, H. Yoneyama, and H. Tamura, *Bull. Chem. Soc. Jpn.*, **50**, 1492 (1977); A. J. Bard, *Science*, **207**, 139 (1980).
13) M. Fujii, T. Kawai, and S. Kawai, *Chem. Phys. Lett.*, **106**, 517 (1984).
14) M. Fujii, T. Kawai, H. Nakamatsu, and S. Kawai, *J. Chem. Soc., Chem. Commun.*, **1983**, 1428.

An Electron Spin Resonance Study of 1,2,3,4-Tetrahydro-3-methyl-2,4-dioxo-1-quinazoliyloxyl Radical

Yoshimi SUEISHI* and Norio NISHIMURA
Department of Chemistry, School of Science, Okayama University, Okayama 700
(Received March 31, 1986)

Synopsis. The ESR spectra of the title radical have been obtained in various solvents, and the assignments have been made. It is found that the solvent effects on the hyperfine coupling constants(hfc) for hydrogens on the benzene ring were small, while the nitrogen hfc ($a_{N(1)}$) remarkably increased in polar solvents. The solvent dependence of the nitrogen hfc has been explained in terms of a substantial contribution of dipolar resonance structures through the N-O bond.

Oxidation with lead dioxide converts 1-hydroxy-3-methyl-2,4(1*H*,3*H*)-quinazolinedione (**1**) into its *N*-oxyl radical (**2**) which has the half-life of about 1.5 h at room temperature in solution. The ESR spectrum of this radical consists of nine lines (Fig. 1). Baldock et al.[1] have ascribed the stability of the radical to the canonical resonance structures (**2a** and **2b**) in Scheme 1.

They assigned the spectrum to the two nitrogen atoms. However, this is questionable since the simulated spectrum on the basis of their hfc-values does not reproduce the observed one at all.

It has been recognized that the stability of free radicals is controlled by both mesomeric and steric

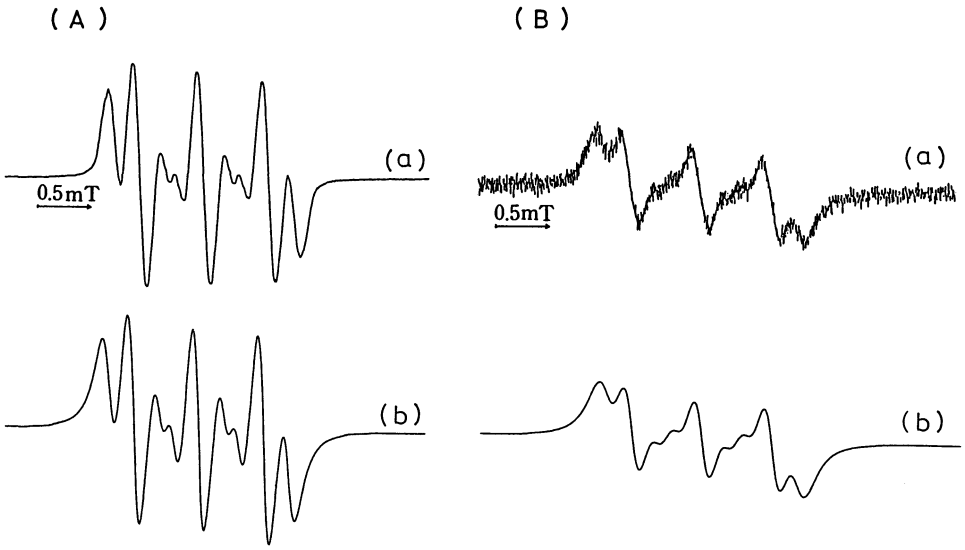

Fig. 1. ESR spectra of *N*-oxyl radical **2** in CCl_4 (A) and acetonitrile (B). (a): experimental spectra, (b): spectra simulations using parameters given in Table 1.

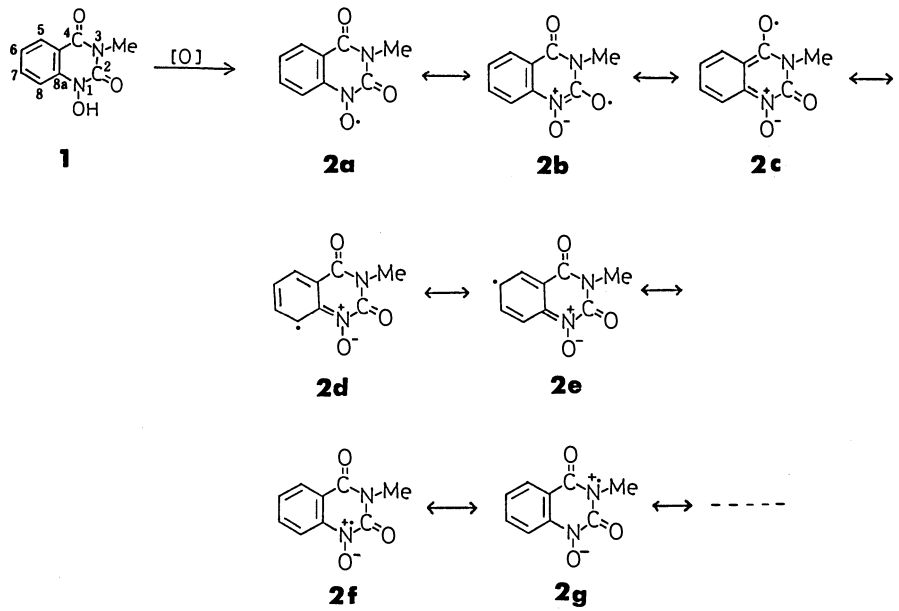

Scheme 1.

factors.[2] Knauer and Napier[3] have shown that the linear correlation between the E_T-value and the nitrogen hfc of aliphatic nitroxide radicals in various solvents exists, and the hfc variation is a useful empirical solvent polarity parameter. In cases where molecules in question have polarized resonance structures, it seems necessary to take into account special interactions between solute and solvent molecules in order to explain the solvent dependency of hfc.

In this paper, we would like to report a modified assignment of **2** and the solvent dependency of the hfc.

Experimental

Materials. The reagent grade solvents were purified and distilled in the usual manner just before use. The solvents were purged with nitrogen. The substance **1** was prepared according to the method by Baldock et al.[1] and recrystallized from ethanol; mp 246—247 °C (lit,[1] 254—257 °C). The product was checked by IR and NMR spectra.

Procedure. Radical **2** was prepared by oxidation of **1** (ca. 10^{-4} mol dm^{-3}) with PbO_2 in various solvents. ESR spectra were obtained with a JEOL JES-FE 3XG equipped with a 100 kHz field modulator. The magnetic field sweep was calibrated using Fremy's salt.[4] Computer-simulated spectra were obtained according to an attached program by using a DEC RT-11 computer. The accuracy of the coupling constants obtained from these simulations was within 4 μT.

Results and Discussion

The ESR spectra of **2** in CCl_4 and acetonitrile are shown in Fig. 1. Since the dielectric loss for acetonitrile is large and **1** is sparingly soluble in acetonitrile, the spectrum was very weak and not well-resolved. The spectra in other solvents are rather similar to that in CCl_4. As may be seen in Fig. 1, the spectrum consists of nine lines. Baldock et al.[1] assumed the planar structure for this molecular skeleton, and showed two canonical forms **2a** and **2b**. They ascribed the nine-line spectrum to the two nitrogen atoms (a=612, 210 μT), hydrogen atoms causing only broadening. If these hyperfine coupling constants are used, a nine-line spectrum with the same intensity and approximately the same peak-to-peak distance could be expected. The spectra in Fig. 1 are, however, quite different.

We have inspected these spectra and simulations have been made so as to reproduce the observed spectra best. Representative computer simulated spectra are shown in Fig. 1. The hfc values of N(1), H(6,8), and H(5,7) are given in Table 1. From these data, some interesting points may be noticed. (1) The hfc $a_{N(1)}$ increases as the solvent polarity increases, and the value is considerably small compared with those of similar nitroxide radicals.[3,5] (2) The dependencies of the hfc of the hydrogen atoms in the benzene ring on the solvent polarity are small compared with that of the nitrogen. However, there is a trend that $a_{H(6,8)}$ increases, while $a_{H(5,7)}$ decreases as the solvent polarity increases. (3) The hyperfine structure due to N(3) was not observed. Here, we wish to comment the above findings.

If radical **2** is planar (as could be presumed by the CPK model), a considerable flow of lone-pair electrons to the benzene rings would be expected and we could write down various types of polar structures besides **2a** and **2b**, as shown in Scheme 1. Botrel and coworkers[6] have calculated the electron densities of 4-[2-(1-methyl-4-pyridino)ethyl]phenolate by means of the CNDO/SCI method in which solvation is taken into account. They have shown that polar structures are favored in polar solvents. By applying McRae's formula, we have also shown that solvent-induced solute polarization plays an important role in the cis-trans thermal isomerization of push-pull azobenzenes, recently.[7] In Fig. 2, the nitrogen and hydrogen hfc's are plotted against the E_T-value which could be regarded as a measure of solvent polarity parameter. The $a_{N(1)}$ clearly shows a trend to increase with the increase in the E_T-value. If the contributions of the canonical polar structures such as **2b** and **2c**

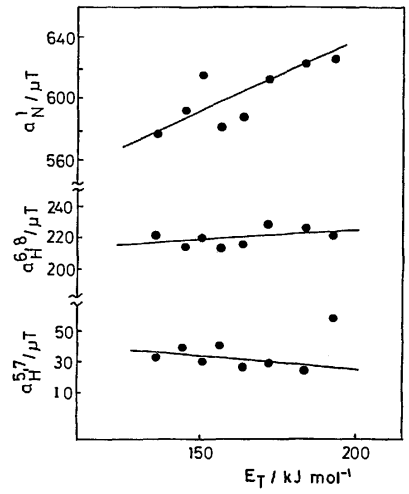

Fig. 2. Relationship between the nitrogen and hydrogen coupling constants and solvent polarity parameters, E_T.

Table 1. Nitrogen and Hydrogen Coupling Constants (in μT) for **2** in Various Solvents at 25 °C

Solvent	$E_T(30)$[a]	$a_{N(1)}$	$a_{H(6,8)}$	$a_{H(5,7)}$
CCl_4	136	577	222	33
Benzene	145	592	216	40
Dioxane	151	616	218	30
Chlorobenzene	157	581	213	41
Chloroform	164	587	216	27
Dichloromethane	172	613	230	29
N,*N*-Dimethylformamide	184	623	227	25
Acetonitrile	193	627	223	58

a) kJ mol^{-1}.

are dominant as proposed,[1] the reverse should be true. Therefore, the proposed canonical resonance structures alone cannot give a resonable explanation for the solvent dependency. It would be natural to consider that, among the canonical forms in Scheme 1, **2f** plays the most important role. Then, the solvent dependency on $a_{N(1)}$ could be understood well.

The hfc $a_{N(1)}$ for **2** (≈600 μT) is considerably small compared with those of similar nitroxide radicals. For example, a_N is ca. 1500 μT, 1000 μT, and 900 μT, for di-*t*-butyl nitroxide radical[3] diphenyl nitroxide radical,[5] and phenyl nitroxide radical,[9] respectively. The remarkably small value of $a_{N(1)}$ can be ascribed to the contibution of **2b** and possibly **2c** for which the unpaired electron moves to the adjacent carbonyl oxygen.[8] It should be noted that the hfc due to the N(3) atom has not been observed. This indicates that the contribution of **2g** is negligibly small. There is a possibility that the hetero-ring is not coplanar, or that sp^2 hybridizations are imperfect(decrease of s-character). This might be responsible for the small value of $a_{N(1)}$, and $a_{N(3)}=0$. According to our view, however, the steric hindrance is not so severe for **2** that the mesomeric stabilization through coplanar structure will overwhelm the steric factor, and **2a—f** will play an important role, thus accounting for our results. Negligible contribution of **2g** could be ascribed to the strong electron-attracting carbonyl groups adjacent to the N(3) atom rather than to the imperfect sp^2-hybridization.

On the assumption that the hybridization of the nitrogen atom in the phenyl nitroxide radical is sp^2, Kikuchi and Someno[9] estimated the spin densities on the benzene ring (0.128 for the 2,4-positions and 0.043 for the 3 position) and compared these with the calculated values on the basis of McLachlan's method. By referring to their results, we have assumed that $a_{H(6)} \approx a_{H(8)} \gg a_{H(5)} \approx a_{H(7)}$. This assumption may be valid because of the contribution of **2d** and **2e**. Applying the relationship $a_H = Q^H_{CH} \cdot \rho_c$,[10] where Q^H_{CH} (=2250 μT) is a constant, and using the data in Table 1, we have estimated the spin densities $\rho_{C(6,8)}=0.096$ and $\rho_{C(5,7)}=0.018$. As stated above, there are trends that $a_{H(6,8)}$ increases, while $a_{H(5,7)}$ decreases with an increase in the solvent polarity. Mukai et al.[5] reported similar results for the 2,6-di-*t*-butyl-4-methylphenoxyl radical and explained trends in terms of a variation in the π-electron spin density due to an electrostatic interaction between the radical and the solvent molecules. The $a_{H(5,7)}$-value in acetonitrile clearly deviates upward even if the large experimental uncertainty, as pointed out above, is taken into account, and this exceptionally large $a_{H(5,7)}$ causes to change the pattern of the ESR spectrum compared with that in other solvents (Fig. 1). The reason is not clear; however, we can say that a specific solvation of acetonitrile to the 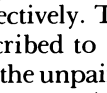 group might be operating and might modify the spin density on H(5) and H(7), as has been discussed by Leach and Tabner.[11]

The authors wish to thank Professor Keiji Kuwata of Osaka University for his helpful discussion.

References

1) R. W. Baldock, P. Hudson, A. R. Katritzky, and F. Soti, *J. Chem. Soc., Perkin Trans. 1*, **1974**, 1423.
2) R. Istratoiu, I. Pascaru, and A. T. Balaban, *Z. Naturforsch.*, **28b**, 543 (1973) and references therein.
3) B. R. Knauer and J. J. Napier, *J. Am. Chem. Soc.*, **98**, 4395 (1976).
4) G. E. Pake, J. Townsend, and S. I. Weissman, *Phys. Rev.*, **85**, 682 (1952).
5) K. Mukai, H. Nishiguchi, K. Ishizu, Y. Deguchi, and H. Takaki, *Bull. Chem. Soc. Jpn.*, **40**, 2731 (1967).
6) A. Botrel, A. Le Beuze, P. Jacques, and H. Strub, *J. Chem. Soc., Faraday Trans. 2*, **80**, 1235 (1984).
7) Y. Sueishi, M. Asano, S. Yamamoto, and N. Nishimura, *Bull. Chem. Soc. Jpn.*, **58**, 2729 (1985).
8) H. G. Aurich and Trösken, *Chem. Ber.*, **106**, 3483 (1973).
9) O. Kikuchi and K. Someno, *Bull. Chem. Soc. Jpn.*, **40**, 2549 (1967).
10) E. W. Stone and A. H. Maki, *J. Chem. Phys.*, **39**, 1935 (1963).
11) C. J. Leach and B. T. Tabner, *J. Chem. Soc., Perkin Trans. 2*, **1985**, 653.

Ground and Excited States of Hematoporphyrin and Its Derivatives

Yoshifumi TANIMOTO,* Masanari TAKAYAMA, Ikuyo INOKUCHI, Michiya ITOH, Norio MIYOSHI,† and Haruo HISAZUMI†
Faculty of Pharmaceutical Sciences, Kanazawa University, Takara-machi, Kanazawa 920
†School of Medicine, Kanazawa University, Takara-machi, Kanazawa 920
(Received April 9, 1986)

Synopsis. Hematoporphyrin and two derivatives in aqueous solution undergo the molecular association to form each dimer. The association constant of 8(3)-(1-hydroxyethyl)-3(8)-vinyldeuteroporphyrin isomers is much larger than that of hematoporphyrin. No significant difference has been observed in the photophysical properties of their excited singlet and triplet states.

With regard to tumor phototherapy, much attention has been paid to the photochemistry and photophysics of hematoporphyrin (HP) and its derivatives, as reviewed by Kessel.[1] The use of a mixture of chemically treated HP, called "hematoporphyrin derivative (HPD)," has currently been recommended for clinical purposes. It is suggested that the predominant pathway of tumor phototherapy using HPD is attributable to the singlet oxygen generated by energy transfer from excited triplet HPD to ground-state molecular oxygen.[2,3] The superiority of HPD over HP may be understood from the following points of view: The first is high affinity of HPD with tumor cell, and the second is the efficiency for generating cytotoxic molecular singlet oxygen. To verify these questions, we have examined the photophysical properties of three porphyrins which are the main components of HPD,[4] by absorption and emission spectroscopic techniques.

Experimental

Hematoporphyrin (HP, Sigma) was purified by preparative thin layer chromatography. *O,O'*-Diacetylhematoporphyrin (HPdiAc) and the mixture of 8(3)-(1-hydroxyethyl)-3(8)-vinyldeuteroporphyrin isomers (HVD), supplied by Hamari Yakuhin Co. Ltd., were used as received.

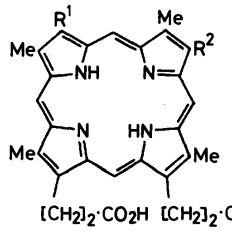

HP : $R^1 = R^2 = CH(OH)Me$
HVD : $R^1 = CH{=}CH_2$; $R^2 = CH(OH)Me$
or
$R^1 = CH(OH)Me$; $R^2 = CH{=}CH_2$
HPdiAc: $R^1 = R^2 = CH(OAc)Me$

Spectrograde methanol was used as received. Distilled water used was further deionized. Porphyrins were dissolved in a phosphate buffer (pH 7.2) solution with vigorous stirring. Sample solutions were deaerated by freeze-pump-thaw cycles, when necessary.

Absorption spectra were measured with Hitachi 224 spectrophotometer using quartz cells of 0.1, 0.5, 1.0, 2.0, and 2.5 cm path length. The fluorescence lifetime was determined by a time-correlated single-photon counting system (Ortec) with a D_2 nanosecond light pulser (PRA model 510) and a cut-off filter (Toshiba R-60, ≥600 nm). The transient absorption lifetime was determined by an excimer laser (Lambda Physik EMG-50E, 308 nm) and a monitoring xenon arc lamp system. All the measurements were carried out at room temperature.

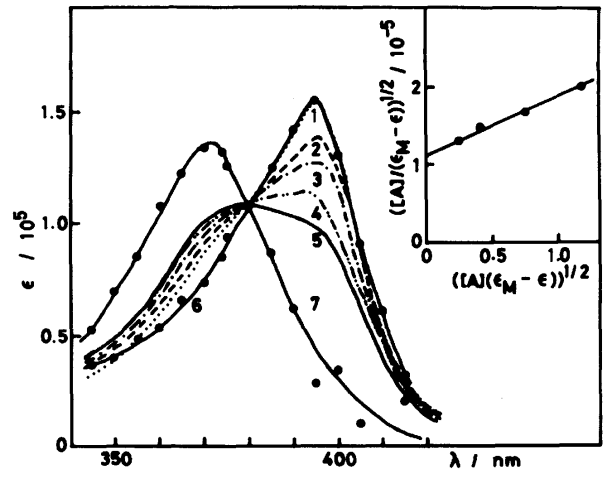

Fig. 1. Soret-band absorption spectra of HP in aqueous buffer solution, pH 7.2; 1, 1.6×10^{-6} M; 2, 3.1×10^{-6} M; 3, 6.3×10^{-6} M; 4, 1.3×10^{-5} M; 5, 2.5×10^{-5} M. 6 and 7 are the calculated absorption spectra of the monomer and the dimer, respectively. Insert: Plot of Eq. 1 for ε's at 394 nm, where ε_M is assumed to be 155000.

Results and Discussion

Ground-State Monomer-Dimer Equilibrium. Figure 1 shows the concentration dependence of absorption spectra (the Soret band) for HP. At low HP concentration the band appears at 394 nm, and a new band appears around 375 nm with increasing concentration, suggesting that the molecular association of HP takes place. To estimate the aggregation number of HP, the absorption intensity at 394 nm was analysed by the Zanker's method, which was successfully applied to the analysis of aggregation of organic dyes.[5,6] The analysis gave the mean aggregation number of two. This fact strongly indicates that the spectral changes in Fig. 1 are attributable to the monomer-dimer equilibrium. Thus, we further analysed the data according to the procedure proposed by Tipping et al.[7] The following equation should hold for the dimerization,

$$\left\{\frac{[A]}{\varepsilon_M-\varepsilon}\right\}^{1/2}=\frac{2}{2\varepsilon_M-\varepsilon_D}\{[A](\varepsilon_M-\varepsilon)\}^{1/2}+\left\{\frac{1}{K_D(2\varepsilon_M-\varepsilon_D)}\right\}^{1/2}. \quad (1)$$

Table 1. Fluorescence Lifetime of HP, HPdiAc, and HVD[a]

	Buffer solution		Methanol solution		
	Deaerated	Aerated	Deaerated	Aerated	k_q[b]
	ns	ns	ns	ns	$10^{10}\,M^{-1}\,s^{-1}$
HP	16.0	15.6	18.1	12.4	1.2
HPdiAc	16.1	15.9	18.4	12.3	1.3
HVD	16.4	15.9	18.5	12.3	1.3

a) Concentrations are 10^{-5} M. b) Quenching rate constants by oxygen, estimated by assuming that oxygen concentration in aerated methanol is 2.12×10^{-3} M.[15]

Here, $[A]$ represents the total concentration of hematoporphyrin in terms of monomer, ε is the observed molar extinction coefficient, ε_M and ε_D are the molar extinction coefficients of the monomer and dimer, respectively, and K_D is the monomer-dimer association constant. The plot of $\{[A]/(\varepsilon_M-\varepsilon)\}^{1/2}$ against $\{[A](\varepsilon_M-\varepsilon)\}^{1/2}$ gives a straight line. The intercept and slope can be used to calculate K_D and ε_D. Insert of Fig. 1 shows the plot of Eq. 1 for HP. The linear relationship in the figure strongly supports the formation of HP dimer in this concentration region, giving the association constant K_D of 0.3×10^5 M^{-1} (M=mol dm^{-3}).

Similar spectral changes were observed for other derivatives and analysed according to the preceding procedure. The K_D's obtained were $0.7\times10^5\,M^{-1}$ (HPdiAc) and 1.8×10^5 M^{-1} (HVD). The association constant of HVD is about six times larger than that of HP.

The aggregation of porphyrins in an aqueous solution was reported by Brown et al.[8] They suggested that dimerization occurs at a very low concentration ($\leqslant4\times10^{-6}$ M) and that the spectral changes in higher concentration region is attributable to "micellarization," i.e., the generation of large aggregates of unknown size. On the other hand, Tipping et al.[7] reported that the absorption-spectral changes of HP caused by the monomer-dimer equilibrium were observed in the concentration range of $0-200\times10^{-6}$ M. The present result agrees with that of the latter authors.

Excited Singlet States. The position of fluorescence spectra of porphyrins in methanol appearing in 600—700 nm region is insensitive to the side-group substitution of porphyrin ring. The fluorescence decays exponentially at a concentration of 10^{-5} M in both methanol and aqueous solution as shown in Table 1. Lifetime values of HP in aerated methanol and aqueous solution agree with those of HP monomer reported by Andreoni et al.[9] The absence of any shorter component due to the dimer in aqueous solution is attributable to wide pulse width of the excitation light source (2—3 ns) in the present study. The quenching rate constants (k_q) of the excited singlet porphyrins by oxygen estimated in methanol are given in Table 1. The rate seems to be diffusion-controlled. No significant difference has been shown in the photophysical properties of the excited singlet porphyrins.

Excited Triplet States. Photophysical properties of the excited triplet porphyrins were studied by laser flash photolysis. In the laser flash photolysis of HP in methanol, a transient absorption band appears in 430—600 nm region, which is assigned to the triplet-triplet absorption of HP with reference to the reported data.[10-12] Since the decay curves of the intense triplet-triplet absorption at 450 nm are strongly influenced by the laser excitation intensity, the lifetime of porphyrins was determined at a low laser intensity where the decay is exponential. The results are shown in Table 2. The lifetime values for three porphyrins are similar to each other. The triplet lifetime of HP was reported to be about 20 μs in acetone and 90% methanol/water mixture.[11] This short lifetime seems to be due to the effect of the triplet-triplet annihilation caused by intense laser excitation used.

Table 2. Triplet Lifetime of HP, HPdiAc, and HVD in Methanol[a]

	Deaerated	Aerated	k_q'[b]
	μs	μs	$10^9\,M^{-1}\,s^{-1}$
HP	77.8	0.30	1.6
HPdiAc	61.8	0.27	1.7
HVD	76.3	0.21	2.2

a) Concentrations are 10^{-5} M. b) Quenching rate constants by oxygen, estimated by assuming that oxygen concentration in aerated methanol is 2.12×10^{-3} M.[15]

In an aerated solution, the lifetime becomes shorter, where the quenching rate constants of the excited triplet porphyrins by oxygen were in the order of 10^9 $M^{-1}\,s^{-1}$. These values are about one order of magnitude smaller than those for the quenching in excited singlet states. Although molecular oxygen quenches both the excited singlet and triplet states efficiently, molecular singlet oxygen is exclusively generated via the excited triplet energy-transfer process as was discussed by Turro.[13] The relative yield of singlet oxygen for these porphyrins is similar to each other.

From the results mentioned above, the monomer-dimer association constant of HVD in the ground-state is larger than those of HP and HPdiAc, while there are no significant difference in the photophysical properties of their excited states. The molecular association (dimer formation) of porphyrins in aqueous solution is relevant to hydrophobicity of the compounds. On the other hand, affinity of porphyrins to tumor cell relates to their hydrophobicity, since photo-induced damage has been reported to occur at the cell membrane which is highly hydrophobic.[14] It is likely, therefore, that the dimer association constant of porphyrins reflects their affinity to tumor cell.

The present results showing similar yields of singlet oxygen for three porphyrins indicate that the affinity of porphyrins to tumor cell is one of determinants for the efficiency of phototherapy.

References

1) D. Kessel, *Photochem. Photobiol.*, **39**, 851 (1984).
2) K. R. Weishaupt, C. J. Gomer, and T. J. Dougherty, *Cancer Res.*, **36**, 2326 (1976).
3) C. J. Gomer, D. R. Doiron, S. Dunn, N. Rucker, N. Razum, and S. Fountain, *Photochem. Photobiol.*, **37S**, S91 (1983).
4) R. Bonnett, R. J. Ridge, P. A. Scourides, and M. C. Bereenbaum, *J. Chem. Soc., Perkin Trans., 1*, **1981**, 3135.
5) V. Zanker, *Z. Physik. Chem.* **200**, 250 (1952).
6) N. Mataga, *Bull. Chem. Soc. Jpn.*, **30**, 375 (1957).
7) E. Tipping, B. Ketterer, and P. Koskelo, *Biochem. J.*, **169**, 509 (1978).
8) S. B. Brown, M. Shillcock, and P. Jones, *Biochem. J.*, **153**, 279 (1976).
9) A. Andreoni, R. Cubeddu, S. De Silvestri, and P. Laporta, *Chem. Phys. Lett.*, **88**, 33 (1982).
10) R. Bonnett, C. Lambert, E. J. Land, P. A. Scourides, R. S. Sinclair, and T. G. Truscott, *Photochem. Photobiol.*, **38**, 1 (1983).
11) S. M. Murgia, A. Pasqua, and A. Poletti, *Chem. Phys. Lett.*, **98**, 179 (1983).
12) E. Reddi, G. Jori, M. A. Rodgers, and J. D. Spikes, *Photochem. Photobiol.*, **38**, 639 (1983).
13) N. J. Turro, "Modern Molecular Photochemistry," Benjamin/Cummings Publishing, Manlo Park (1978) p. 579.
14) A. W. Girotti, *Biochem. Biophys. Res. Commun.*, **72**, 1367 (1976).
15) S. L. Murov, "Handbook of Photochemistry," M. Dekker, New York (1973), p. 89.

A Convenient One-Pot Synthesis of Acenaphthenequinones from 1-Acenaphthenones by NBS–DMSO Oxidation

Jiro TATSUGI,* Shigeo OKUMURA, and Yasuji IZAWA
Department of Applied Chemistry, Aichi Institute of Technology, Yakusa, Toyota 470-03
(Received February 3, 1986)

Synopsis. Acenaphthenequinone was obtained in 95% yield when the reaction of 1-acenaphthenone with *N*-bromosuccinimide was carried out in dimethyl sulfoxide at room temperature. Under similar conditions, several acenaphthenequinones were prepared from the corresponding 1-acenaphthenones in good yields.

Acenaphthenequinones are interesting with regard to photochemistry,[1] synthetic photochemistry,[2] and versatile synthetic intermediates to polycyclic hydrocarbons[3] and heterocyclic compounds.[4] The most widely used methods for the preparation of acenaphthenequinones are the oxidation of acenaphthenes with various oxidizing agents[5] and the Friedel–Crafts reaction of naphthalenes with oxalyl dichloride.[6] However, the yields of acenaphthenequinones by these methods are low due to the formation of by-products such as naphthalic anhydrides and 1,1′-biacenaphthylidene-2,2′-diones. In the course of our studies on the chemistry of 1-acenaphthenones, we found that the reaction of 1-acenaphthenones with *N*-bromosuccinimide (NBS) in dimethyl sulfoxide (DMSO) gave the corresponding acenaphthenequinones in good yields. We now report on a convenient preparation of acenaphthenequinones using NBS in DMSO.

1-Acenaphthenones (**1**) and NBS were dissolved in anhydrous DMSO. The mixture was stirred at room temperature under nitrogen atmosphere until all the substrate had been consumed to give the corresponding acenaphthenequinones (**2**) in good yields. The oxidation products were identified by their melting points, and by IR, ^{1}H NMR, and MS spectra.

The reaction of **1** with NBS in DMF gave only 5-bromo-1-acenaphthenone in 84% yield and with *N*-chlorosuccinimide (NCS) in DMF gave only 5-chloro-1-acenaphthenone in 47% yield. By contrast, 5-halo-1-acenaphthenone could not be isolated at all when the reaction was carried out in DMSO at room temperature. The results of the reaction of **1** with several halogenating agents, such as NBS, *N*-bromoacetamide (NBA), 2-oxopyrrolidinium tribromide (OB), phenyltrimethylammonium perbromide (PTAB), pyridinium tribromide (PB), 2,4,4,6-tetrabromo-2,5-cyclohexadien-1-one (TCD), iodine, bromine, and NCS in DMSO at room temperature are summarized in Table 1. As shown in Table 1, the reactions gave **2** in good to excellent yields except for that with NCS. The chlorination of DMSO took place exclusively when the reaction of **1** with NCS was carried out in DMSO at room temperature. This result suggests that NCS reacts with DMSO faster than with **1**.[7] The reactions of **1** with various molar ratios of NBS were carried out in order to find the most suitable reaction conditions for the preparation of **2**. The results are summarized in Table 2. The optimum yield was achieved when the reaction was carried out using an equivalent of NBS to **1** at room temperature for 24 h. The oxidation of some substituted 1-acenaphthenones (**1a—l**) to the corresponding acenaphthenequinones (**2a—l**) was carried out under similar conditions. The results are summarized in Table 3. As shown in Table 3, the compounds **1a—l** were oxidized into **2a—l** in good yields. In the cases of **1j**, **1k**, and **1l**, however, the corresponding 1,1′-biacenaphthyliden-2-ones were produced as by-products in 22, 5, and 6% yields, respectively.

Table 1. Raction of 1-Acenaphthenone with Several Halogenating Agents in DMSO at Room Temperature

Halogenating agents	Yield[a] of **2**/%
NBS	95
NBA	95
OB[b]	96
PTAB[c]	94
PB[d]	98
TCD[e]	77
I_2	82
Br_2	93
NCS	0

a) Isolated yield. b) 2-Oxopyrrolidinium tribromide. c) Phenyltrimethylammonium perbromide. d) Pyridinium tribromide. e) 2,4,4,6-Tetrabromo-2,5-cyclohexadien-1-one.

Table 2. Reaction of 1-Acenaphthenone with Various Molar Ratios of NBS in DMSO

1	NBS	Reaction		Yield[a] of **2**/%
mmol	mmol	Temp/°C	Time/h	
5	5	r.t	24	95
5	2.5	r.t	48	88
5	1.25	r.t	110	21
5	1.25	50	24	75
5	1.25	100	5	81
5	0.63	r.t	110	6

a) Isolated yield.

To ascertain the reaction pathways leading to the quinones, the DMSO–oxidation of 2-bromo-1-acenaphthenone was carried out. The reaction of **1** with NBS in dichloromethane gave 2-bromo-1-acenaphthenone[12] in 59% yield, and the reaction of the resulting 2-bromo-1-acenaphthenone with DMSO at room temperature for 24 h afforded **2** in quantitative yield. On the basis of these facts and the results for related reactions,[13] it is clear that the course of the reaction involves α-bromination of **1** with NBS and then oxidation[14] of the resultant 2-bromo-1-acenaphthenones with DMSO to (2-oxo-1-acenaphthenyloxy)sulfonium bromides which then decomposes to give **2** and dimethyl sulfide as shown in Scheme 1.

Table 3. Reaction of 1-Acenaphthenones with NBS in DMSO at Room Temperature

1	R^1	R^2	R^3	Yield[a] of 2/%	Mp(θ_m/°C) (lit,)
a	H	H	H	95	259—260 (260—261)[5]
b	CH_3	H	H	85	204—206
c	H	CH_3	H	74	192—194
d	C_2H_5	H	H	75	128—129
e	H	H	C_2H_5	77	131—132 (117—119)[8]
f	H	Cl	H	90	216—217 (212—213)[9]
g	H	H	Cl	88	216—217 (212—213)[9]
h	H	Br	H	93	244—246 (246)[10]
i	H	H	Br	94	244—246 (246)[10]
j	H	NO_2	H	67	214—215 (218)[11]
k	H	CN	H	83	258—260
l	H	H	CN	84	258—260

a) Isolated yield.

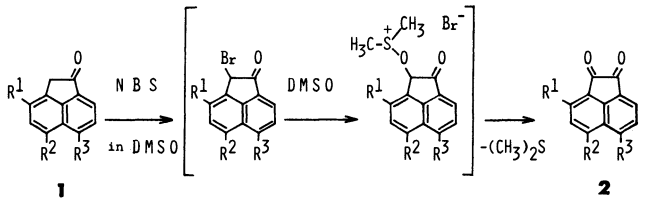

1 2

Scheme 1.

In conclusion, the advantages of the present preparation of **2** using NBS in DMSO are: 1) the yields of 2 are satisfactory, 2) the experimental set up and work up are exceedingly simple, 3) the reactions are performed under mild conditions, 4) the reagents are easy to handle and are commercially available, and 5) there is no need to isolate the α-bromo ketone intermediate, which is somewhat unstable, from the reaction mixture.

Experimental

Melting points are uncorrected. IR, ^{1}H NMR, and MS spectra were recorded on a shimadzu IR-440, a JEOL JNM-PMX 60SI, and a Hitachi M-80B spectrometers, respectively.

Materials. DMSO was fractionated over CaH_2. NBS was purified by recrystallization from water. 1-Acenaphthenone (**1a**),[15] 3-methyl-1-acenaphthenone (**1b**),[16] 5-methyl-1-acenaphthenone (**1c**),[16] 3-ethyl-1-acenaphthenone (**1d**),[17] 5-bromo-1-acenaphthenone (**1h**),[18] 6-bromo-1-acenaphthenone (**1i**),[18] and 5-nitro-1-acenaphthenone (**1j**)[19] were prepared as described in the literature. 6-Ethyl-1-acenaphthenone (**1e**) and 6-chloro-1-acenaphthenone (**1g**) were prepared from the corresponding 5-substituted acenaphthenes by a similar method to the preparation of **1i**.[18]

1e: 35% yield; mp 67—68 °C. (petroleum ether); IR (KBr) 1710 (C=O), 1603, 1495, 835, 765, and 660 cm^{-1}; ^{1}H NMR ($CDCl_3$) δ=1.37 (t, 3H, *J*=7.6 Hz), 3.11 (q, 2H, *J*=7.6 Hz), 3.69 (s, 2H), and 7.3—7.9 (m, 5H); MS *m/z* 196 (M^+). **1g**: 32% yield; mp 142—143 °C (EtOH); IR (KBr) 1725 (C=O), 1485, 840, 763, and 663 cm^{-1}; ^{1}H NMR ($CDCl_3$) δ=3.72 (s, 2H), and 7.2—8.3 (m, 5H); MS *m/z* 202 (M^+) and 204 (M^++2). 5-Chloro-1-acenaphthenone (**1f**) was prepared from **1a** and NCS in DMF at room temperature for 2 d. **1f**: 47% yield; mp 173—174 °C (EtOH); IR (KBr) 1705 (C=O), 1390, 825, and 760 cm^{-1}; ^{1}H NMR ($CDCl_3$) δ=3,77 (s, 2H), and 7.3—8.4 (m, 5H), MS *m/z* 202 (M^+) and 204 (M^++2). 5-Cyano-1-acenaphthenone (**1k**) and 6-cyano-1-acenaphthenone (**1l**) were prepared via the corresponding cyano-1-acenaphthenols which were obtained by Rosenmund-von Braun synthesis.[20] **1k**: 30% yield (based on 5-bromo-1-acenaphthenol); mp 263—265 °C (EtOH), IR (KBr) 2210 (CN), 1718 (C=O), 1495, 1385, 820, and 770 cm^{-1}; ^{1}H NMR (DMSO-d_6) δ=3.98 (s, 2H), and 7.7—8.4 (m, 5H); MS *m/z* 193 (M^+). **1l**: 37% yield (based on 6-bromo-1-acenaphthenol); mp 157—158 °C (EtOH); IR (KBr) 2210 (CN), 1720 (C=O), 850, 785, and 660 cm^{-1}; ^{1}H NMR (DMSO-d_6) δ=3.93 (s, 2H), and 7.6—8.7(m, 5H); MS *m/z* 193 (M^+).

General Procedure. A mixture of 1-acenaphthenone (**1**) (5 mmol), NBS (5 mmol) and anhydrous DMSO (5 ml) was stirred at room temperature under nitrogen atmosphere. The progress of the reaction was monitored by TLC on silica gel using dichloromethane as eluent. After disappearance of **1**, 100 ml of water was added to the resultant mixture, and the precipitates were collected by filtration and then washed with water. The product was recrystallized from dichloromethane.

Spectral data of acenaphthenequinones are as follows.

3-Methylacenaphthenequinone (2b). IR (KBr) 1720 and 1738 cm^{-1}, (C=O); ^{1}H NMR ($CDCl_3$) δ=2.73 (s, 3H), and 6.8—8.0 (m, 5H); MS *m/z* 196 (M^+).

5-Methylacenaphthenequinone (2c). IR (KBr) 1720 and 1735 cm^{-1} (C=O); ^{1}H NMR ($CDCl_3$) δ=2.83 (s, 3H), and 7.3—8.4 (m, 5H); MS *m/z* 196 (M^+).

3-Ethylacenaphthenequinone (2d). IR (KBr) 1720 and 1735 cm^{-1} (C=O); ^{1}H NMR ($CDCl_3$) δ=1.37 (t, 3H, *J*=8 Hz), 3.33 (q, 2H, *J*=8 Hz), and 7.6—8.3 (m, 5H); MS *m/z* 210 (M^+).

5-Ethylacenaphthenequinone (2e). IR (KBr) 1720 and 1737 cm^{-1} (C=O); ^{1}H NMR ($CDCl_3$) δ=1.37 (t, 3H, *J*=8 Hz), 3.07 (q, 2H, *J*=8 Hz), and 7.4—8.2 (m, 5H); MS *m/z* 210 (M^+).

5-Cyanoacenaphthenequinone (2k). IR (KBr) 1730, 1745 (C=O), and 2250 cm^{-1} (CN); ^{1}H NMR (DMSO-d_6–$CDCl_3$) δ=8.0—8.7 (m, 5H); MS *m/z* 207 (M^+).

This work was supported by the Nitto Kohgyoh Foundation for the promotion of science, which is gratefully acknowledged.

References

1) Tai-Shan Fang and L. A. Singer, *J. Am. Chem. Soc.*, **100**, 6276 (1978); Ja-Young Koo and G. B. Schuster, *J. Org. Chem.*, **44**, 847 (1979).

2) H. Takeshita, A. Mori, M. Funakura, and H. Mametsuka, *Bull. Chem. Soc. Jpn.*, **50**, 315 (1977).

3) H. W. Whitlock Jr., *J. Org. Chem.*, **29**, 3129 (1964); A. Minsky and M. Rabinovitz, *Synthesis*, **1983**, 497.

4) Recent examples: S. Mataka, K. Takahashi, T. Imura, and M. Tashiro, *J. Heterocyclic Chem.*, **19**, 1481 (1982); J. A.-Builla, G. G. Trigo, J. Ezquerra, and M. E. Fombella, *ibid.*, **22**, 681 (1985); J. J. Hlavka, P. Bitha, Y. Lin, and T. Strohmeyer, *ibid.*, **22**, 1317, (1985).

5) C. F. H. Allen and J. A. VanAllan, *Org. Synth.*, Coll.

Vol., III, 1 (1955).
6) R. Lesser and G. Gad, *Ber.*, **60**, 243 (1927); J. Cason, A. Weiss, and S. A. Monti, *J. Org. Chem.*, **33**, 3404 (1968).
7) G. Tsuchihashi and K. Ogura, *Bull. Chem. Soc. Jpn.*, **44**, 1726 (1971).
8) H. E. Nursten, and A. T. Peters, *J. Chem. Soc.*, **1950**, 2389.
9) S. K. Guha, *Chem. Ber.*, **95**, 1569 (1962).
10) F. Dewhurst and P. K. J. Shah, *J. Chem. Soc. (C)*, **1970**, 1737.
11) F. M. Rowe and J. S. H. Davies, *J. Chem. Soc.*, **117**, 1344 (1920).
12) S. Hauptmann, M. Scholz, I. Stopp, and U. Stopp, *Z. Chem.*, **7**, 351 (1967).
13) E. Schipper, M. Cinnamon, L. Rascher, Y. H. Chiang, and W. Oroshnik, *Tetrahedron Lett.*, **1968**, 6201; N. Furukawa, T. Akasaka, T. Aida, and S. Oae, *J. Chem. Soc., Perkin Trans. 1*, **1977**, 372.
14) N. Kornblum, J. W. Powers, G. J. Anderson, W. J. Jones, H. O. Larson, O. Levand, and W. M. Weaver, *J. Am. Chem. Soc.*, **79**, 6562 (1957); N. Kornblum, W. J. Jones, and G. J. Anderson, *ibid.*, **81**, 4113 (1959).
15) L. F. Fieser and J. Cason, *J. Am. Chem. Soc.*, **62**, 432 (1940).
16) I. D. Entwistle and R. A. W. Johnstone, *J. Chem. Soc. (C)*, **1968**, 1818; G. Lock, and R. Schneider, *Chem. Ber.*, **91**, 1770 (1958).
17) W. E. Bachmann and J. C. Sheehan, *J. Am. Chem. Soc.*, **63**, 2598 (1941).
18) G. Kalopissis, *J. Recherches Centre Natl. Recherche Sci., Labs. Bellevue (Paris)*, **22**, 1 (1953).
19) Y. V. Samusenko, V. I. Magda, A. P. Karishin, G. F. Dzhurka, and N. F. Grineva, *Zh. Khim.*, **1979**, 1971.
20) L. Friedmann and H. Shechter, *J. Org. Chem.*, **26**, 2522 (1961).

Synthesis of the Cyclotetrasilanes of the Type[(PhRSi)$_4$] (R=*t*-Bu; *t*-BuCH$_2$)

Hideyuki MATSUMOTO,* Atsushi SAKAMOTO, Masahiko MINEMURA, Kenji SUGAYA, and Yoichiro NAGAI*
Department of Chemistry, Gunma University, Kiryu, Gunma 376
(Received March 13, 1986)

Synopsis. The cyclotetrasilanes of the type [(PhRSi)$_4$] (R=*t*-Bu; *t*-BuCH$_2$) were prepared by the reductive coupling of the corresponding dichlorosilanes (PhRSiCl$_2$) with lithium.

As part of our continuing study of the chemistry of small-membered cyclopolysilanes bearing bulky alkyl substituents, we attempted to prepare alkylphenylcyclotetrasilanes of the type [(PhRSi)$_4$]. The cyclotetrasilanes so far obtained are limited to rings such as (Me$_2$Si)$_4$,[1] (Et$_2$Si)$_4$,[2] (*i*-Pr$_2$Si)$_4$,[3-5] (*s*-Bu$_2$Si)$_4$,[5] (*i*-Bu$_2$Si)$_4$,[5] [(*t*-BuCH$_2$)$_2$Si]$_4$,[6] [(Me$_3$SiCH$_2$)$_2$Si]$_4$,[7] [(Me$_3$Si)$_2$Si]$_4$,[8] (*t*-BuMeSi)$_4$,[9] (EtMeSi)$_4$,[10] [*t*-Bu(n-Pr)Si]$_4$,[5] [(*t*-BuCH$_2$)$_2$Si]$_2$(*i*-Pr$_2$Si)$_2$,[11] [(*t*-BuCH$_2$)$_2$Si]$_2$ (*t*-BuMeSi)$_2$,[11] (Ph$_2$Si)$_4$,[12] and [(*p*-MeC$_6$H$_4$)$_2$Si]$_4$.[13] We report here the synthesis of the novel cyclotetrasilanes, (*t*-BuPhSi)$_4$, **1**, and [(*t*-BuCH$_2$)PhSi]$_4$, **2**.

The cyclotetrasilane **1** was prepared by the reaction of *t*-BuPhSiCl$_2$, **3**, with lithium (Eq. 1). The yield of the

$$4\,t\text{-BuPhSiCl}_2(\mathbf{3}) + 8\,\text{Li} \longrightarrow (t\text{-BuPhSi})_4(\mathbf{1}) + 8\,\text{LiCl} \quad (1)$$

cyclotetrasilane strongly depended upon the choice of reaction conditions. Optimum conditions involve the treatment of **3** with 3 equiv of lithium at 0°C for 0.5 h in THF. Under these conditions, the cyclotetrasilane **1** was formed in 45% yield, as shown by a GLC analysis. The usual workup and recrystallization from MeOH/EtOH (1/1) led to the isolation of **1** in 36% yield. The reaction of the dichlorosilane **3** with sodium was also examined (toluene, 60—70°C, 3h), but no trace of the desired compound was obtained.

The first step in the reductive coupling of the dichlorosilane **3** seems to be the formation of Cl(*t*-Bu)PhSiSiPh(Bu-*t*)Cl, **4**, which would then react with lithium to give the cyclic tetramer **1**. The formation of peralkylcyclotetrasilanes from 1,2-dichloro-1,1,2,2-tetraalkyldisilanes has been reported previously.[5,6,10] The observation that if the dichlorosilane **3** is treated with a deficiency of lithium, the reaction mixture contains the dichlorodisilane **4** as its major component, is in agreement with this view.

To explore the scope of the present approach further, (*t*-BuCH$_2$)PhSiCl$_2$, **5**, was also allowed to react with lithium. In this case, the use of a 1:1 mixture of THF and benzene as the solvent led to a higher yield of the tetraneopentyltetraphenylcyclotetrasilane **2** than did the use of THF alone. Thus, stirring a mixture of the dichlorosilane **5** with 2.4 equiv. of lithium at 0°C for 2 h in the mixed solvent resulted in the formation of the cyclic tetramer **2** in 54% yield, as shown by the GLC analysis. The same cyclotetrasilane was also prepared by the reaction of Cl(*t*-BuCH$_2$)PhSiSiPh(CH$_2$Bu-*t*)Cl, **6**, with lithium (a slight excess) in 57% yield under nearly the same conditions.

Both **1** and **2** are air-stable, evidently owing to a steric protection by the *t*-butyl and neopentyl substituents, respectively. The UV absorption spectra of these four-membered rings are shown in Fig. 1. The longest wavelength bands for these rings at ca. 315 nm are slightly lower in energy than the corresponding absorptions for peralkylcyclotetrasilanes [e.g., 300 nm for (*t*-BuMeSi)$_4$[9] and 286 nm for [(*t*-BuCH$_2$)$_2$Si]$_4$[6]], presumably due to perturbation of the electronic structures of the Si$_4$ frameworks by the phenyl substituents.[14] In the mass spectra, good agreement is found between the observed isotope ratios for the parent clusters and those calculated, in support of the assignments for **1** and **2**.

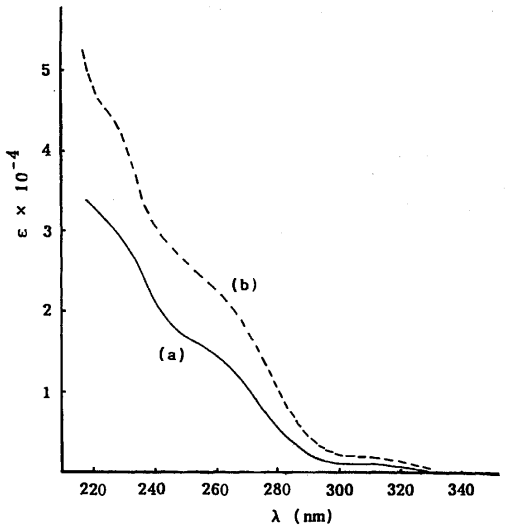

Fig. 1. UV absorption spectra for 1,2,3,4-tetraalkyl-1,2,3,4-tetraphenylcyclotetrasilane: (a): **1**, (b): **2**.

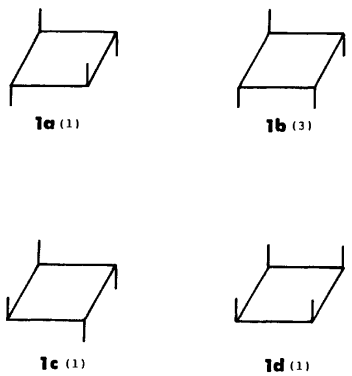

Fig. 2. The possible geometrical isomers of the cyclotetrasilane **1** in planer conformations and the number of expected β-methyl NMR resonances of the *t*-butyl substituents.

The presence of the two different substituents on each silicon atom should give rise to the four isomers. For example, the possible isomers for **1** and the number of expected β-methyl resonaces of the *t*-butyl groups in the NMR are shown in Fig. 2.[9,10] Both ^{1}H and

$^{13}C\{^1H\}$NMR show six β-methyl signals, respectively, suggesting the presence of all four isomers **1a—d**. Further work to determine the isomeric distribution of the products is in progress.

In short, the present reductive couplings can provide a useful route to the novel 1,2,3,4-tetraalkyl-1,2,3,4-tetraphenylcyclotetrasilanes **1** and **2**, which might be latent sila-functional cyclotetrasilanes since it has been shown by Hengge and coworkers that phenylcyclopolysilanes can be converted to the corresponding halocyclopolysilanes via the dephenylation with hydrogen halides.[15]

Experimental

Melting and boiling points were uncorrected. ^1H (90 MHz) and ^{13}C (22.64 MHz) NMR spectra were recorded on a Hitachi R-90H spectrometer. IR spectra were recorded on a JASCO A102 spectrometer. UV spectra were taken on a Hitachi 200-10 spectrometer. Mass spectra were recorded on a JEOL DX-300 spectrometer. GLC analyses were carried out using an Ohkura 103 gas chromatograph equipped with 1 m×0.4 cm Pyrex glass columns packed with 10% Silicone SE-30 and 10% Silicone KF-96 on Celite 545 SK (60—80 mesh).

Benzene and THF were distilled from sodium benzophenone ketyl prior to use. All reactions were carried out under an atmosphere of dried nitrogen.

The dichlorosilane **3** was prepared according to literature direction.[16] (t-BuCH$_2$)PhSiCl$_2$, **5**, and Cl(t-BuCH$_2$)PhSiSiPh(CH$_2$Bu-t)Cl, **6**, were prepared by the methods shown (Eqs. 2 and 3).[17,18]

$$PhSiCl_3 \xrightarrow{t\text{-}BuCH_2Li} \mathbf{5}\ (73\%) \qquad (2)$$

$$PhHSiCl_2 \xrightarrow{t\text{-}BuCH_2Li} (t\text{-}BuCH_2)PhHSiCl\ (69\%) \xrightarrow{Li} H(t\text{-}BuCH_2)PhSiSiPh(CH_2Bu\text{-}t)H\ (\mathbf{7})\ (56\%) \xrightarrow[PdCl_2]{CCl_4} \mathbf{6}\ (77\%) \qquad (3)$$

For **5**: Bp 113—115 °C (32 mmHg); ^1H NMR (CCl_4) δ=1.03 (s, 9H, t-Bu), 1.21 (s, 2H, -CH$_2$-), and 7.3—7.7 (m, 5H, Ph). Found: C, 53.50; H, 6.53%. Calcd for $C_{11}H_{16}SiCl_2$: C, 53.44; H, 6.52%.

For **7**: Bp 135—138 °C (0.20 mm Hg); IR (neat) principal absorptions, 2130, 1420, 1260, and 1110 cm^{-1}; ^1H NMR (CCl_4) δ=0.88 (s, 9H, t-Bu), 0.93 (s, 9H, t-Bu), 1.23 (s, 4H, -CH$_2$-), 4.41 (m, 2H, SiH), and 7.25 (m, 10H, Ph); Found: C, 74.28; H, 9.76%. Calcd for $C_{22}H_{34}Si_2$: C,74.50; H, 9.66%.

For **6**: Bp 149—155 °C (0.15 mmHg); IR (neat) principal absorptions, 1425, 1260, 1230, 1115, and 1100 cm^{-1}; ^1H NMR (CCl_4) δ=0.80 (s, 9H, t-Bu), 0.94 (s, 9H, t-Bu), 1.21 (s, 2H, -CH$_2$-), 1.38 (s, 2H, -CH$_2$-), and 7.2—7.8 (m, 10H, Ph); Found: C, 62.41; H, 7.54%. Calcd for $C_{22}H_{32}Si_2Cl_2$: C, 62.38; H, 7.62%.

Reaction of t-BuPhSiCl$_2$, 3, with Lithium: A 200 ml flask equipped with a magnetic stirrer and a nitrogen inlet was charged with lithium cut (0.60 g, 87 mg-atom) and THF (60 ml). The flask was cooled to 0 °C by an ice-water bath, and the dichlorosilane **3** (7.0 g, 30 mmol) was added dropwise over 5 min. The mixture was stirred for an additional 0.5 h and filtered. A GLC analysis showed that (t-BuPhSi)$_4$, **1**, had been produced in 45% yield. Approximately 100 ml of cyclohexane was added, and the solution was washed with water and dried over anhydrous MgSO$_4$. Evaporation of the solvents yielded a half-solid that was recrystallized from MeOH/EtOH (1/1) to give 1.9 g (36% yield) of **1** as fine colorless powders.

In another run, a mixture of **3** (4.63 g, 20 mmol), lithium (0.14 g, 20 mg-atom), and THF (48 ml) was stirred at 0 °C for 7 h. A GLC analysis showed that 68% of **3** had been consumed and that Cl(t-Bu)PhSiSiPh(Bu-t)Cl, **4**, had been produced in 27% yield together with a trace amount of **1**.

For **1**: Mp 280—310 °C; IR (KBr disk) principal absorptions, 1415, 1260, and 1095 cm^{-1}; ^1H NMR ($CDCl_3$) δ=0.77 (s, 4.5H, t-Bu), 0.81 (s, 3.1H, t-Bu), 0.98 (s, 5.2H, t-Bu), 1.03 (s, 11.4H, t-Bu), 1.42 (s, 8.9H, t-Bu), 1.51 (s, 2.9H, t-Bu), and 6.74—7.89 (m, 20H, Ph); $^{13}C\{^1H\}$NMR ($CDCl_3$) δ=21.13, 21.56, 22.62, 23.20, 23.63, 24.42 (Me$_3$C), 30.21, 30.58, 31.07, 31.28, 32.07, 32.44 (CH$_3$), 125.98—123.39 (phenyl carbons), and 135.57—139.12 (phenyl carbons); MS (70 eV) m/z (isotope ratios for parent clusters) Obsd: 696 (100), 697 (67), 698 (41), 699 (21). Calcd: 696 (100), 697 (67), 698 (34), 699 (16); UV$_{max}$ (cyclohexane) 233 (ε 28000), 263 (ε 14200), and 317 nm (ε 522). Found: C, 73.95; H, 9.02%. Calcd for $C_{24}H_{72}Si_4$: C, 74.03; H, 8.70%.

For **4**: ^1H NMR (CCl_4) δ=0.85 (s, 18H, t-Bu) and 7.28—7.75 (m, 10H, Ph); exact mass for M$^+$ measd 394.1101. Calcd 394.1106, dev 0.5 mmu.

Reaction of (t-BuCH$_2$)PhSiCl$_2$, 6, with Lithium: A 300 ml flask was charged with lithium cut (0.94 g, 135 mg-atom), THF (65 ml), and benzene (65 ml). The flask was cooled to 0 °C by ice-water bath, and **5** (14.5 g, 59 mmol) in THF (10 ml) and benzene (10 ml) was added dropwise over 1 h. The mixture was stirred for an additional 1 h and filtered. A GLC analysis showed that the cyclotetrasilane **2** had been produced in 54% yield. The filtrate was washed with water and dried over anhydrous MgSO$_4$. Evaporation of the solvents and recrystallization from MeOH/EtOH (3/1) afforded 1.12 g (28% yield) of **2** as colorless powders.

For **2**: IR (KBr disk) principal absorptions, 1420, 1355, 1250, 1090, 720, 695 cm^{-1}; ^1H NMR ($CDCl_3$) δ=0.70 (s, 2.0H, t-Bu), 0.74 (s, 4.7H, t-Bu), 0.79 (s, 16.0H, t-Bu), 0.81 (s, 2.0H, t-Bu), 0.90 (s, 7.7H, t-Bu), 0.99 s, 3.6H, t-Bu), 1.35—1.58 (m, 8H, -CH$_2$-), and 6.70—7.90 (m, 20H, Ph); $^{13}C\{^1H\}$NMR ($CDCl_3$) δ=30.73—31.97 (Me$_3$C and -CH$_2$-), 32.07, 32.14, 32.99, 33.10, 33.26, 33.32 (CH$_3$), 126.7—128.2 (phenyl carbons), and 136.8—137.4 (phenyl carbons); MS (70 eV) m/z (isotope ratios for the parent clusters) Obsd: 704 (100), 705 (71), 706 (40), 707 (16). Calcd: 704 (100), 705 (71), 706 (38), 707 (14); UV$_{max}$ (cyclohexane) 230 (ε 42600), 264 (ε 22500), 313 nm (ε 1900). Found: C, 74.86; H, 9.14%. Calcd for $C_{44}H_{64}Si_4$: C, 74.93; H, 9.14%.

Reaction of the Dichlorodineopentyldiphenyldisilane 6 with Lithium: A mixture of **6** (0.25 g, 0.55 mmol), lithium cut (9.0 mg, 1.3 mg-atom), THF (1.4 ml), and benzene (1.4 ml) was stirred at 0 °C for 2 h. A GLC analysis showed that the cyclotetrasilane 2 had been produced in 57% yield together with a trace amount of the dihydrodisilane **7**.

We thank Professor Nobumasa Kamigata, Tokyo Metropolitan University, for mass spectral analysis.

References

1) M. Ishikawa and M. Kumada, *J. Chem. Soc., Chem. Commun.*, **1970**, 612; **1971**, 507.

2) C. W. Carlson and R. West, *Organometallics*, **2**, 1792 (1983).

3) H. Watanabe, T. Muraoka, M. Kageyama, and Y. Nagai, *J. Organomet. Chem.*, **216**, C45 (1981).

4) H. Watanabe, J. Inose, K. Fukushima, Y. Kougo, and Y. Nagai, *Chem. Lett.*, **1983**, 1711.

5) H. Watanabe, T. Muraoka, M. Kageyama, K. Yoshizumi, and Y. Nagai, *Organometallics*, **3**, 141 (1984).

6) H. Matsumoto, M. Minemura, K. Takatsuna, Y. Nagai, and M. Goto, *Chem. Lett.*, **1985**, 1005.

7) H. Watanabe, M. Kato, H. Kuwabara, H. Shinoyama,

Y. Nagai, and M. Goto, 50th National Meeting of the Chemical Society of Japan, Tokyo, April 1985, Abstr., No. 4K27.

8) Y.-S. Chen and P. P. Gaspar, *Organometallics*, **1**, 1410 (1982).

9) M. Biernabaum and R. West, *J. Organomet. Chem.*, **77**, C13 (1974); C. J. Hurt, J. C. Calabrese, and R. West, *ibid.*, **91**, 273 (1975); M. Biernbaum and R. West, *ibid.*, **131**, 179 (1977); R. J. Helmer and R. West, *Organometallics*, **1**, 1458, 1463 (1982).

10) A. Katti, C. W. Carlson, and R. West, *J. Organomet. Chem.*, **271**, 353 (1984).

11) H. Matsumoto, K. Takatsuna, M. Minemura, Y. Nagai, and M. Goto, *J. Chem. Soc., Chem. Commun.*, **1985**, 1366.

12) A. W. P. Jarvie, H. J. S. Winkler, D. J. Peterson, and H. Gilman, *J. Am. Chem. Soc.*, **83**, 1921 (1961).

13) M. F. Lemanski and E. P. Schram, *Inorg. Chem.*, **15**, 2515 (1976).

14) C. G. Pitt, *J. Am. Chem. Soc.*, **91**, 6613 (1969).

15) E. Hengge and H. Markertz, *Monatsh. Chem.*, **101**, 528 (1970); E. Hengge, D. Kovar, and H. P. Sollradl, *ibid.*, **110**, 805 (1979).

16) L. H. Sommer and L. J. Tyler, *J. Am. Chem. Soc.*, **76**, 1030 (1954).

17) P. Boudjouk and B. H. Han, *Tetrahedron Lett.*, **22**, 3813 (1981).

18) Y. Nagai, H. Matsumoto, T. Yagihara, and K. Morishita, *Kogyo Kagaku Zasshi*, **71**, 1112 (1968).

A Convenient Synthesis of *N*-Substituted Formamidines by Desulfurization of the Corresponding Thioureas

Choji KASHIMA,* Masao SHIMIZU, Takeshi ETO, and Yoshimori OMOTE
Department of Chemistry, University of Tsukuba, Sakura-mura, Niihari-gun, Ibaraki 305
(Received March 17, 1986)

Synopsis. *N,N'*-Di- and *N,N,N'*-trisubstituted thioureas were easily desulfurized by Raney nickel to yield the corresponding formamidines, while *N*-monosubstituted thioureas gave *N,N'*-disubstituted formamidines.

Amidines are important compounds for the syntheses of heterocycles as well as their pharmaceutical chemistries owing to their biological activities.[1] Although amidines are generally prepared by the condensation of nitriles and amines, or the substitution of imidates with amines, the syntheses of formamidines require special methods, such as the treatment of amines with chloroimines or imidates,[1] and the treatment of isonitriles and amines with Co(I) catalysis.[2]

The desulfurization of carbon–sulfur bonds using Raney nickel is known as a convenient method for the syntheses of various organic compounds.[3] However, the desulfurization of thioureas with Raney nickel has scarcely been reported and consistent results can not be found. For example, unsubstituted thiourea afforded formamidine hydrochloride in the presence of ammonium chloride[4] or as a mixture of methane, ammonia, and methylamine[5]; *N*-benzylthiourea gave a mixture of methane, ammonia, and toluene[6]; and *N*-(*o*-tolyl)thiourea gave *o*-toluidine.[7] Although Ashworth reported that *N,N'*-diarylthioureas afforded the corresponding formamidines, he did not describe in detail such matters as yeilds and the activities of Raney nickel. Furthermore, in the case of *N*-(*p*-chlorophenyl)thiourea, he obtained only an unidentified basic liquid.[8]

In this paper, we wish to describe the convenient synthesis of many types of substituted formamidines by the desulfurization of the corresponding thioureas as well as and the scope and the limitations of the Raney nickel desulfurization of thioureas.

First, the desulfurization of *N*-monosubstituted thioureas was reinvestigated. When *N*-phenylthiourea was treated with Raney nickel in methanol, the ^{1}H NMR spectrum exhibited a new singlet at δ=7.63 which is characteristic of the formyl proton. Actually, when picric acid was added to the reaction mixture prior to purification, *N*-phenylformamidine picrate was successfully isolated in 15% yield after recrystallization. However, the chromatographic purification of the crude reaction product could not afford the expected *N*-phenylformamidine. The isolated products were *N,N'*-diphenylformamidine and formanilide. By the same treatment of some *N*-monosubstituted thioureas, the corresponding *N,N'*-disubstituted formamidines were obtained (Table 1). Yields resulted in one mole of formamidines **2** formed from two mole of thioureas **1**; also, one mole of the formamide derivatives **3** was formed from one mole of thioureas **1**.

Table 1. Desulfurization of *N*-Monosubstituted Thioureas

	R	Yield/%	
		2	**3**
1a	C_6H_5	41	7
1b	p-$CH_3C_6H_4$	60	34
1c	p-$CH_3OC_6H_4$	47	6
1d	$C_6H_5CH_2$	0	27

Since Roberts[9] and McNab[10] noted an amine exchange reaction involving *N*-(*p*-methylphenyl)-*N'*-phenylformamidine with aniline or *p*-toluidine, the exchange reaction proceeded even in the case of *N*-phenylformamidine; volatile ammonia was given off from the system. Therefore, *N,N'*-disubstituted formamidines were secondary products from an amine exchange reaction between the *N*-monosubstituted formamidines and the anilines which were generated by the hydrolysis of *N*-monosubstituted formamidines owing to air moisture during the work-up. Actually, when **1a** was treated with Raney nickel in the presence of methylamine hydrochloride and diethylamine, *N*-methyl-*N'*-phenyl- and *N,N*-diethyl-*N'*-phenylformamidine were obtained in 46 and 41% yields, respectively. These facts support the idea that amine exchange reaction occurs between an unsubstituted amino group and the secondary mediated amine. Moreover, it was suggested that the desulfurization of unsubstituted thiourea might afford *N,N'*-disubstituted formamidine in the presence of amines. Actually, by the desulfurization of thiourea in the presence of *p*-toluidine, *N,N'*-bis(*p*-methylphenyl)formamidine was isolated. However, its yield was low (9%) since there was almost no separation between the desired formamidine and *p*-toluidine.

Next, the desulfurizations of various *N,N'*-di- or *N,N,N'*-trisubstituted thioureas were investigated. In these series, the corresponding formamidines were respectively obtained without amine exchange reactions. The results are shown in Table 2. *N,N'*-Disubstituted formamidines were obtained in better yields than that for *N,N,N'*-trisubstituted. When the desulfurization of cyclic *N,N,N'*-trisubstituted thioureas was carried out in the same manner, the corresponding cyclic formamidines were obtained (Table 3).

Consequently, although *N,N'*-di- or *N,N,N'*-trisubstituted thioureas gave the corresponding formamidines by desulfurization with Raney nickel, *N*-monosubstituted thioureas afforded *N,N'*-disubstituted formamidines via an amine exchange reaction on account of the instability of the primary *N*-monosubstituted formamidines.

Table 2. Desulfurization of Di- or Trisubstituted Thioureas

	R^1	R^2	R^3	Yield/%	Product	Mp[Bp](°C)
5a	C_6H_5	H	C_6H_5	85	**2a**	136[a]
5b	p-$CH_3C_6H_4$	H	C_6H_5	50	**6b**	88—89[b]
5c	C_6H_5	H	CH_3	47	**6c**	85—87[c]
5d	p-$CH_3C_6H_4$	H	CH_3	23	**6d**	135—139[d]
5e	$C_6H_5CH_2$	H	$C_6H_5CH_2$	75	**6e**	136—137[e]
5f	C_6H_5	C_2H_5	C_2H_5	27	**6f**	[99—110/5 mmHg †][f]
5g	C_6H_5	C_6H_5	CH_3	27	**6g**	156—159[d]
5h	CH_3	$C_6H_5CH_2$	$C_6H_5CH_2$	23	**6h**	118—119[d]

a) 137—138°C (reported[8]). b) 86°C (reported[12]). c) 88—89°C (reported[13]). d) Of picrate. e) 135°C (reported[14]). f) 143—144°/15 mmHg† (reported[15]).
† 1 mmHg=133.322 Pa.

Table 3. Desulfurization of 3,4,5,6-Tetrahydropyrimidine-2(1*H*)-thiones

	R^1	R^2	Product	Yield/%	Mp[a](°C)
7a	C_6H_5	H	**8a**	77	141—142
7b	C_6H_5	CH_3	**8b**	45	157—158
7c	p-$CH_3OC_6H_4$	CH_3	**8c**	65	148—149
7d	m-ClC_6H_4	CH_3	**8d**	28	149—150

a) Of picrate.

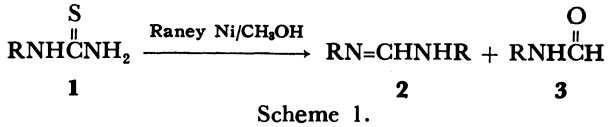

Scheme 1.

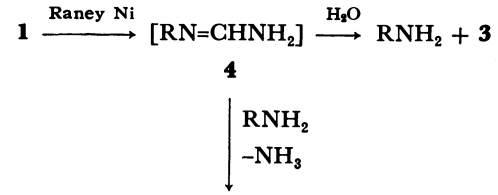

Scheme 2.

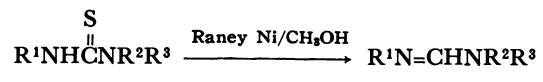

Scheme 3.

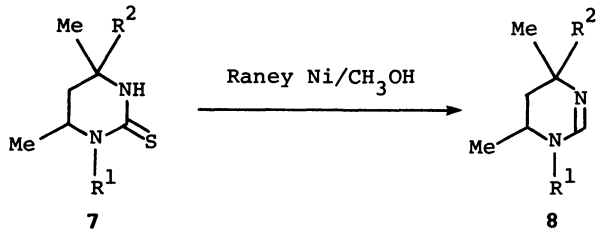

Scheme 4.

Experimantal

Melting points were measured on a Yanagimoto micro melting point apparatus and are uncorrected. IR spectra were measured on a Jasco IRA-1 infrared spectrophotometer. ^1H and ^{13}C NMR spectra were recorded on Hitachi R-24 and JEOL-100 spectrometer, respectively, using tetramethylsilane as an internal standard.

Preparation of Active Raney Nickel. Sodium hydroxide pellets (2.0 g) were added to nickel-aluminum alloy (Wako Pure Chemical Industries Ltd., 50%, 1.6 g) in distilled water (20 mL) with vigorous stirring at room temperature. After 15 min, the reaction mixture was immersed in an oil bath (bath temperature 70°C) for 20 min, and then the alkaline solution was decanted. The nickel was washed four times by suspension in distilled water and underwent decantation. The washing procedure was repeated four times with methanol.

Desulfurization of Thioureas; Typical Procedures. The mixture of thiourea (2 mmol) and the activated Raney nickel (prepared from 1.6 g nickel-aluminum alloy) in methanol (20 mL) was warmed at 50°C for 1 h and then refluxed for 2 h. After removing the catalyst by filtration, the filtrate was diluted with water and extracted with dichloromethane. It was then dried over anhydrous magnesium sulfate. After evaporating the solvent, the crude product was chromatographed on silica gel with a mixture of hexane-acetone-diethylamine (13:6:1) or benzene-ethyl acetate (3:1). Picrate was prepared as follows. To a solution of formamidine (2 mmol) in ethanol (5 mL), the solution of picric acid (2 mmol) in ethanol was added. After standing for 15 h, the resulting precipitate was recrystallized from ethanol.

Desulfurization of *N*-Phenylthiourea in the Presence of Amines. To a mixture of *N*-phenylthiourea (**1a**, 2 mmol) and methylamine hydrochloride or diethylamine (10 mmol), Raney nickel (0.8 g) was added in a sealed tube and then warmed at 50°C for 1 h and at 80°C for 2 h. The following procedure is the same as that described above.

***N*-Phenylformamidine (4).** ^1H NMR ($CDCl_3$) δ=3.81 (s, 2H, NH_2), 6.6—7.3 (m, 5H, Ar), 7.63 (s, 1H, =CH). Picrate: Mp 198—200°C. (lit,[11] 191°C). Found: C, 44.49; H, 3.18; N, 20.02%. Calcd for $C_{13}H_{11}N_5O_7$: C, 44.70; H, 3.17; N, 20.05%.

***N,N'*-Diphenylformamidine (2a).** Mp 136°C (lit,[8] 137—138°C). ·IR($CHCl_3$) 1640, 3380 cm^{-1}. ^1H NMR ($CDCl_3$) δ=6.9—7.5 (m, 10H, Ar), 8.20 (s, 1H, =CH), 9.4 (br s, 1H, NH).

^{13}C NMR ($CDCl_3$) δ=119.1 (d), 123.2 (d), 129.3 (d), 145.3 (s), 149.7 (d).

***N,N'*-Bis(*p*-methylphenyl)formamidine (2b).** Mp 140—141 °C (lit,[10] 139—140 °C). IR ($CHCl_3$) 1680, 3400 cm^{-1}. ^{1}H NMR ($CDCl_3$) δ=2.30 (s, 6H, CH_3), 6.9—7.2 (m, 8H, Ar), 8.14 (s, 1H,=CH), 9.1 (br s, 1H, NH). ^{13}C NMR ($CDCl_3$) δ=20.7 (q), 119.0 (d), 129.8 (d), 132.6 (s), 142.9 (s), 149.6 (d).

***N,N'*-Bis(*p*-methoxyphenyl)formamidine (2c).** Mp 112—113 °C. IR (KBr) 1670, 3150 cm^{-1}. ^{1}H NMR ($CDCl_3$) δ=3.77 (s, 6H, CH_3), 6.4—7.4 (m, 8H, Ar), 8.02 (s, 1H, =CH), 8.9 (br s, 1H, NH). Found: C, 70.36; H, 6.33; N, 10.95%. Calcd for $C_{15}H_{16}N_2O_2$: C, 70.29; H, 6.29; N, 10.92%.

***N*-(*p*-Methylphenyl)-*N'*-phenylformamidine (6b).** ^{1}H NMR ($CDCl_3$) δ=2.27 (s, 3H, $ArCH_3$), 6.7—7.4 (m, 9H, Ar), 8.4 (br s, 1H, NH), 8.08 (s, 1H, =CH).

***N*-Methyl-*N'*-phenylformamidine (6c).** ^{1}H NMR ($CDCl_3$) δ=2.95 (s, 3H, CH_3), 5.5 (br s, 1H, NH), 6.7—7.4 (m, 5H, Ar), 7.47 (s, 1H, =CH).

***N*-Methyl-*N'*-(*p*-methylphenyl)formamidine (6d).** IR (KBr) 1640, 3300 cm^{-1}. ^{1}H NMR ($CDCl_3$) δ=2.30 (s, 3H, Ar-CH_3), 2.94 (s, 3H, CH_3), 5.0 (br s, 1H, NH), 6.6—7.4 (m, 4H, Ar), 7.62 (s, 1H, =CH). Picrate: found: C, 47.64; H, 3.94; N, 18.61%. Calcd for $C_{15}H_{15}N_5O_7$: C, 47.74; H, 4.00; N, 18.56%.

***N,N'*-Dibenzylformamidine (6e).** IR ($CHCl_3$) 1630, 3280 cm^{-1}. ^{1}H NMR ($CDCl_3$) δ=4.29 (s, 4H, Ar-CH_2), 6.7—7.8 (m, 10H, Ar), 7.98 (s, 1H, =CH).

***N,N,*-Diethyl-*N'*-phenylformamidine (6f).** IR ($CDCl_3$) 1620 cm^{-1}. ^{1}H NMR ($CDCl_3$) δ=1.17 (t, 6H, J=7 Hz, CH_2CH_3), 3.30 (q, 4H, 4H, J=7 Hz, CH_2CH_3), 6.7—7.3 (m, 5H, Ar), 7.37 (s, 1H, =CH).

***N*-Methyl-*N,N'*-diphenylformamidine (6g).** IR ($CHCl_3$) 1620 cm^{-1}. ^{1}H NMR ($CDCl_3$) δ=3.41 (s, 3H, CH_3), 6.8—7.5 (m, 10H, Ar), 8.00 (s, 1H, =CH). Picrate: Found: C, 54.44; H, 3.86; N, 15.94%. Calcd for $C_{20}H_{17}N_5O_7$: C, 54.67; H, 3.90; N, 15.94%.

***N,N*-Dibenzyl-*N'*-methylformamidine (6h).** IR ($CHCl_3$) 1645 cm^{-1}. ^{1}H NMR ($CDCl_3$) δ=3.16 (s, 3H, CH_3), 4.29 (s, 4H, CH_2Ar), 6.8—7.5 (m, 10H, Ar), 7.61 (s, 1H, =CH). Picrate: Found: C, 56.52; H, 4.52; N, 14.98%. Calcd for $C_{22}H_{21}N_5O_7$: C, 56.56; H, 4.49; N, 14.99%.

1,4,5,6-Tetrahydro-4,6-dimethyl-1-phenylpyrimidine (8a). IR ($CHCl_3$) 1620 cm^{-1}. ^{1}H NMR ($CDCl_3$) δ=1.03 (d, 3H, J=6.0 Hz, 6-CH_3), 1.26 (d, 3H, J=6.0 Hz, 4-CH_3), 1.4—2.3 (m, 2H, 5-CH_2), 3.1—4.1 (m, 2H, 4,6-CH), 7.0—7.6 (m, 6H, Ar and =CH). Picrate: Found: C, 51.70; H, 4.53; N, 16.52%. Calcd for $C_{18}H_{19}N_5O_7$: C, 51.79; H, 4.58; N, 16.77%.

1,4,5,6-Tetrahydro-4,4,6-trimethyl-1-phenylpyrimidine (8b). IR ($CHCl_3$) 1620 cm^{-1}. ^{1}H NMR ($CDCl_3$) δ=1.06 (d, 3H, J=5.4 Hz, 6-CH_3), 1.21 (s, 3H, 4-CH_3), 1.27 (s, 3H, 4-CH_3), 1.4—2.2 (m, 2H, 5-CH_2), 3.6—4.2 (m, 1H, 6-CH), 6.9—7.6 (m, 6H, Ar and =CH). Picrate: Found: C, 52.77; H, 4.84; N, 16.21%. Calcd for $C_{19}H_{21}N_5O_7$: C, 52.89; H, 4.92; N, 16.24%.

1,4,5,6-Tetrahydro-1-(*p*-methoxyphenyl)-4,4,6-trimethylpyrimidine (8c). IR ($CHCl_3$) 1620 cm^{-1}. ^{1}H NMR ($CDCl_3$) δ=1.02 (d, 3H, J=6.6 Hz, 6-CH_3), 1.21 (s, 3H, 4-CH_3), 1.23 (s, 3H, 4-CH_3), 1.4—2.2 (m, 2H, 5-CH_2), 3.3—3.9 (m, 1H, 6-CH), 3.75 (s, 3H, OCH_3), 6.7—7.0 (m, 4H, Ar), 7.03 (s, 1H, =CH). Picrate: Found: C, 52.00; H, 5.05; N, 15.13%. Calcd for $C_{20}H_{23}N_5O_8$: 52.05; H, 5.02; N, 15.17%.

1-(*m*-Chlorophenyl)-1,4,5,6-tetrahydro-4,4,6-trimethylpyrimidine (8d). IR ($CHCl_3$) 1620 cm^{-1}. ^{1}H NMR ($CDCl_3$) δ=1.08 (d, 3H, J=6.0 Hz, 6-CH_3), 1.20 (s, 3H, 4-CH_3), 1.27 (s, 3H, 4-CH_3), 1.4—2.2 (m, 2H, 5-CH_2), 3.6—4.2 (m, 1H, 6-CH), 6.8—7.6 (m, 5H, Ar and =CH). Picrate: Found: C, 49.16; H, 4.33; N, 14.88%. Calcd for $C_{19}H_{20}ClN_5O_7$: C, 48.98; H, 4.32; N, 15.03%.

References

1) "The Chemistry of the Amidines and Imidates," ed by S. Patai, John Wiley & Sons, London (1975).

2) T. Saegusa, I. Murase, and Y. Ito, *J. Org. Chem.*, **36**, 2876 (1971); and references therein.

3) J. S. Pizey, "Synthetic Reagents," John Wiley & Sons, London (1975), Vol. 2, p. 275.

4) D. J. Brown, *J. Appl. Chem. (London)*, **2**, 202 (1952); *Chem. Abst.* **48**, 557 (1954).

5) J. Bougault, E. Cattelain, and P. Chabrier, *Bull. Soc. Chim. France*, **7**, 781 (1940); *Chem. Abst.* **36**, 2198 (1942).

6) J. Bougault, E. Cattelain, and P. Chabrier, *Compt. Rend.*, **208**, 657 (1939); *Chem. Abst.* **33**, 4580 (1939).

7) C. D. Hurd and B. Rudner, *J. Am. Chem. Soc.*, **73**, 5157 (1951).

8) R. Ashworth, *J. Chem. Soc.*, **1948**, 1716.

9) R. M. Roberts, *J. Am. Chem. Soc.*, **72**, 3603 (1950).

10) H. McNab, *J. Chem. Soc., Perkin Trans. 1*, **1980**, 2200.

11) G. Fodor, *Acta Chim. Acad. Sci. Hung.*, **5**, 375 (1955); *Chem. Abst.* **50**, 10113 (1956).

12) H. L. Wheeler and T. B. Johnson, *Ber.*, **32**, 36 (1899).

13) P. Jakobsen and S. Treppendahl, *Acta Chem. Scand. [B]*, **31**, 92 (1977).

14) W. Tentzch, *Ber.*, **97**, 2755 (1964).

15) A. Larizza, G. Brancaccio, and G. Lettieri, *J. Org. Chem.*, **29**, 3699 (1964).

Synthesis of 2-Methylazuleno[1,2-*d*]thiazoles

Kunihide FUJIMORI,* Hiroyuki KITAHASHI, Satoshi KOYAMA, and Kameji YAMANE
Department of Chemistry, Faculty of Science, Shinshu University, Asahi, Matsumoto 390
(Received April 1, 1986)

Synopsis. 2-Methylazuleno[1,2-*d*]thiazoles were synthesized from diethyl 2-mercapto-1,3-azulenedicarboxylate, which was prepared by a treatment of diethyl 2-(2-methoxycarbonylethylthio)-1,3-azulenedicarboxylate with sodium ethoxide in five steps.

Among the two possible isomers of azulenothiazoles which are formed by a condensation of thiazole with azulene at the 1,2-position, azuleno[2,1-*d*]thiazole (**I**) as well as its 2-amino and 2-methyl derivatives have been synthesized.[1)]

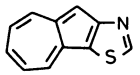

I

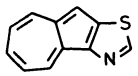

II

We now wish to report the synthesis of azuleno[1,2-*d*]thiazoles (**II**). The reaction of diethyl 2-chloro-1,3-azulenedicarboxylate (**1**)[2)] with methyl 3-mercaptopropionate in pyridine gave diethyl 2-(2-methoxycarbonylethylthio)-1,3-azulenedicarboxylate (**3**) in 93% yield. When the ester **3** was treated with sodium ethoxide in dry ethanol, diethyl 2-mercapto-1,3-azulenedicarboxylate (**4**), a reversal Michael's addition reaction product, was obtained in 96% yield, and methyl acrylate was also detected. The IR and ^{1}H NMR spectra of **4** show an absorption band at 2434 cm^{-1} and a signal at δ=7.71 due to the mercapto group, respectively. Compound **4** has also been obtained by a reaction of **1** with thioacetic acid or hydrogen sulfide in the presence of sodium ethoxide.[3)] However, the present method is unaccompanied by the formation of other by-products, such as thioether or disulfide, and is preferred as a method for the preparation of **4**.

Heating **4** with 100% phosphoric acid at 90°C resulted in deethoxycarbonylation giving ethyl 2-mercapto-1-azulenecarboxylate (**5**) in an almost quantitative yield. Further, the treatment of **5** with acetic anhydride gave 2-(acetylthio)azulene derivative **6** in 91% yield. The nitration of **6** with nitric acid in acetic anhydride at −30°C gave ethyl 2-acetylthio-3-nitro-1-azulenecarboxylate (**7**) in 44% yield. Compound **7**, upon treatment with zinc dust in acetic acid and acetic anhydride at room temperature, gave a mixture of ethyl 2-acetylthio-3-acetylamino-1-azulenecarboxylate (**8**) and ethyl 3-acetylamino-1-azulenecarboxylate (**9**). Compound **8** was treated with a potassium hydroxide solution in tetrahydrofuran–ether, followed by a treatment with hydrochloric acid by cooling with ice under an inert atmosphere to give ethyl 2-methylazuleno[1,2-*d*]thiazole-9-carboxylate (**10**). Furthermore, the demethoxycarbonylation of **10** by heating with 100% phosphoric acid gave 2-methylazuleno[1,2-*d*]thiazole (**11**) in 87% yield. The difference between the vicinal coupling constants, $\Delta J = J_{7,8} - J_{4,5}$, in ^{1}H NMR of **11** is 1.3 Hz, indicating that the 7-membered ring exhibits some bond alternation in analogy with azuleno[2,1-*d*]thiazole.[1)]

The electronic spectra of **10**, **11**, and 2-methylazuleno[2,1-*d*]thiazole[1)] are shown in Fig. 1.

Experimental

Melting points are uncorrected. ^{1}H NMR spectra were record-

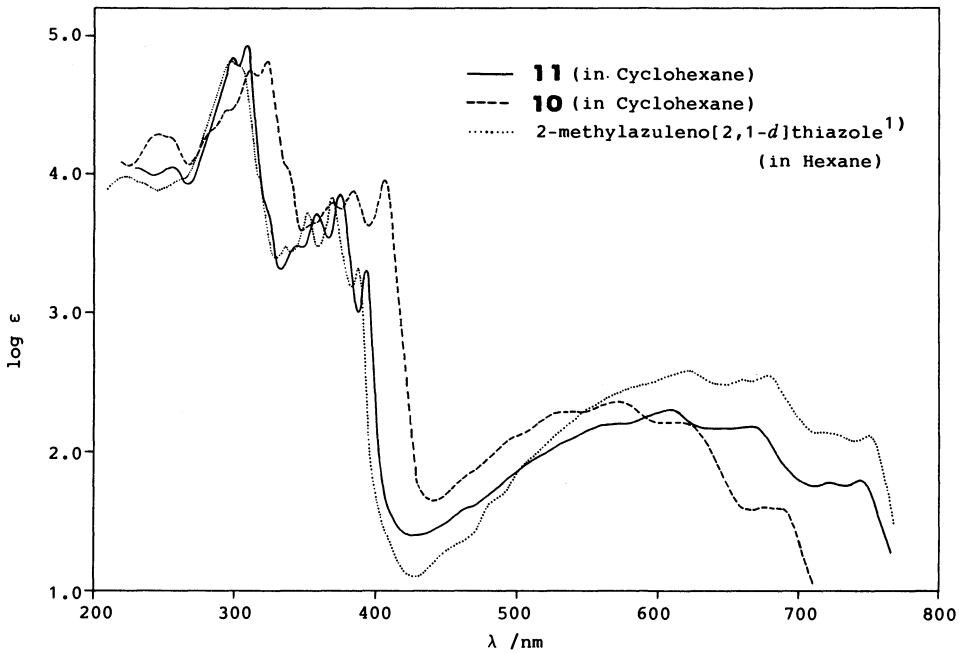

Fig. 1. Electronic spectra of **10**, **11**, and 2-methylazuleno[2,1-*d*]thiazole.

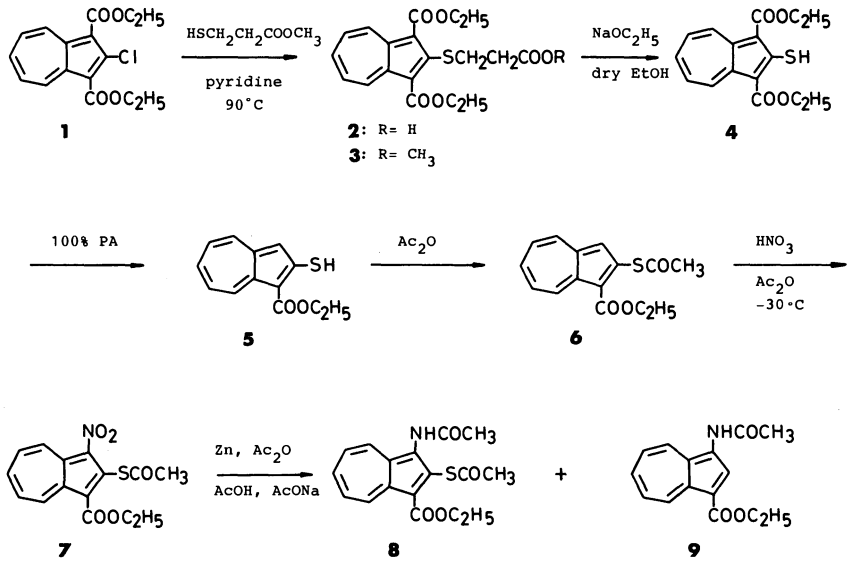

Fig. 2.

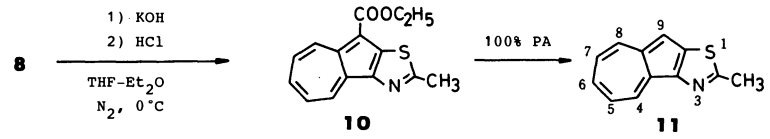

Fig. 3.

ed with a JEOL 90Q spectrometer using tetramethylsilane as an internal standard. The IR spectra were taken on a Hitachi 345 infrared spectrometer and the electronic absorption spectra were measured with a Hitachi 200-20 spectrometer.

Diethyl 2-(2-Methoxycarbonylethylthio)-1,3-azulenedicarboxylate (3). A mixture of diethyl 2-chloro-1,3-azulenedicarboxylate (**1**) (600 mg) and methyl 3-mercaptopropionate (310 mg) in pyridine (30 ml) was heated at 90°C for 1 h. After cooling, the reaction mixture was poured into water and extracted with dichloromethane. The dichloromethane layer was washed with 3M sulfuric acid and water, dried over anhydrous sodium sulfate, and evaporated under reduced pressure. The residue was chromatographed on a silica-gel column with benzene. The red effluent was freed from the solvent to give **3** (711 mg, 93%) as red micro needles; mp 70.5—71 °C; ^{1}H NMR (90 MHz, in $CDCl_3$) δ=1.49 (6H, t, J=7.2 Hz, $COOCH_2C\underline{H}_3$), 2.61 (2H, t, J=7.7 Hz, $SCH_2C\underline{H}_2COOMe$), 3.34 (2H, t, J=7.7Hz, $SC\underline{H}_2CH_2COOMe$), 3.64 (3H, s, $SCH_2CH_2COOC\underline{H}_3$), 4.51 (4H, q, J=7.2 Hz, $COOC\underline{H}_2CH_3$), 7.4—7.9 (3H, m, H-5,6,7), and 9.17 (2H, dm, J=9.6 Hz, H-4,8). Found: C, 61.35; H, 5.56; S, 8.24%. Calcd for $C_{20}H_{22}O_6S$: C, 61.52; H, 5.68; S, 8.21%. The second red effluent gave a trace of diethyl 2-(2-carboxyethylthio)-1,3-azulenedicarboxylate (**2**) as a red solid; ^{1}H NMR (90 MHz, in $CDCl_3$) δ=1.50 (6H, t, J=7.2 Hz, $COOCH_2C\underline{H}_3$), 2.66 (2H, t, J=7.7 Hz, $SCH_2C\underline{H}_2COOH$), 3.33 (2H, t, J=7.7 Hz, $SC\underline{H}_2CH_2COOH$), 4.51 (4H, q, J=7.2 Hz, $COOC\underline{H}_2CH_3$), and 10.7 (1H, bs, $COO\underline{H}$).

Diethyl 2-Mercapto-1,3-azulenedicarboxylate (4). Into a solution of **3** (6.25 g) in anhydrous ethyl alcohol (100 ml), a sodium ethoxide solution which was prepared from sodium metal (583 mg) and anhydrous ethanol (50 ml) was added. The mixture was stirred for 2 h at room temperature. The reaction mixture was diluted with water, neutralized with 2M hydrochloric acid (1 M=1 mol dm^{-3}), and extracted with benzene. The extract was washed with water, dried over anhydrous sodium sulfate, and evaporated under reduced pressure. The residue was chromatographed on a silica-gel column. From the benzene effluent, **4** was obtained as orange needles (4.69 g, 96%); mp 88.5—89°C (lit, 3, 85—86°C); ^{1}H NMR (90 MHz, in $CDCl_3$) δ=1.53 (6H, t, J=7.2 Hz, $COOCH_2C\underline{H}_3$), 4.51 (4H, q, J=7.2 Hz, $COOC\underline{H}_2CH_3$), 7.71 (1H, s, S$\underline{H}$), 7.5—7.8 (3H, m, H-5,6,7), and 9,3—9.5 (2H, m, H-4,8); IR (KBr) 2434 cm^{-1} (SH). (Found: C, 63.38; H, 5.39; S, 10.36%).

Ethyl 2-Mercapto-1-azulenecarboxylate (5). A mixture of **4** (3.93 g) and 100% phosphoric acid (50 ml) was heated for 30 min at 90°C. After cooling, the reaction mixture was poured into water and extracted with benzene. The extract was washed with water, dried, and evaporated. The residue was chromatographed on a silica-gel column with benzene-hexane (1:1). The red effluent was freed from the solvent to give **5** (3.00 g, ca. 100%) as red oil; ^{1}H NMR (90 MHz, in $CDCl_3$) δ=1.49 (3H, t, J=7.2 Hz, $COOCH_2C\underline{H}_3$), 4.47 (2H, q, J=7.2 Hz, $COOC\underline{H}_2CH_3$), 5.35 (1H, s, S$\underline{H}$), 7.30 (1H, s, H-3), 7.1—7.7 (3H, m, H-5,6,7), 8.02 (1H, dm, J=9.8 Hz, H-4), and 9.24 (1H, dm, J=9.8 Hz, H-8). Found: C, 67.00, H, 5.10; S, 13.85%. Calcd for $C_{13}H_{12}O_2S$: C, 67.24; H, 5.17; S, 13.81%. From the purple effluent, a trace of 2-mercaptoazulene[3] was obtained as bluish purple crystals; mp 112—113°C; IR (KBr) 2538 cm^{-1} (SH); ^{1}H NMR (90 MHz, in $CDCl_3$) δ=3.87 (1H, s, S$\underline{H}$), 7.11 (2H, s, H-1,3), 6.9—7.6 (3H, m, H-5,6,7), and 8.04 (2H, dm, J=9.7 Hz, H-4,8); ^{13}C NMR (22.5 MHz, in $CDCl_3$) δ=116.8, 124.5, 133.1, 135.4, 140.7, and 140.9.

Ethyl 2-Acetylthio-1-azulenecarboxylate (6). A mixture of **5** (3.00 g) and acetic anhydride (55 ml) was heated for 30 min at 90°C. The reaction mixture was evaporated under reduced pressure, and the residue was diluted with water. The solution was then neutralized with a aqueous sodium carbonate solution and extracted with benzene. The benzene layer was dried over anhydrous sodium sulfate and evaporated under reduced pressure. The residue was chromatographed on a silica-gel column with benzene-hexane (1:1). The purple

effluent gave **6** (3.22 g, 91%) as dark purple prisms; mp 72—73°C; ^{1}H NMR (90 MHz, in $CDCl_3$) δ=1.48 (3H, t, J=7.2 Hz, $COOCH_2C\underline{H}_3$), 2.56 (3H, s, $SCOC\underline{H}_3$), 4.47 (2H, q, J=7.2 Hz, $COOC\underline{H}_2CH_3$), 7.2—7.8 (3H, m, H-5,6,7), 8.26 (1H, dm, J=9.8 Hz, H-4), and 9.46 (1H, dm, J=9.8 Hz, H-8). Found: C, 65.60; H, 5.15; S, 11.57%. Calcd for $C_{15}H_{14}O_3S$: C, 65.67; H, 5.14; S, 11.69%.

Ethyl 2-Acetylthio-3-nitro-1-azulenecarboxylate (7). Into a solution of **6** (500 mg) in acetic anhydride (240 ml) which had been cooled at −30°C, nitric acid was added, drop by drop; the solution was then stirred for 8 h. The reaction mixture was diluted with water, neutralized with a 6M sodium hydroxide aqueous solution, and extracted with dichloromethane. The extract after being dried and freed from solvent yielded a residue. The residue was chromatographed on a silica-gel column with benzene. The effluent gave **7** (258 mg, 44%) as dark red prisms; mp 144.5—145°C; ^{1}H NMR (90 MHz, in $CDCl_3$) δ=1.46 (3H, t, J=7.2 Hz, $COOCH_2C\underline{H}_3$), 2.56 (3H, s, $SCOC\underline{H}_3$), 4.44 (2H, q, J=7.2 Hz, $COOC\underline{H}_2CH_3$), 7.7—8.2 (3H, m, H-5,6,7), and 9.5—9.7 (2H, m, H-4,8). Found: C, 56.48; H, 4.08; N, 4.13; S, 9.99%. Calcd for $C_{15}H_{13}NO_5S$: C, 56.41; H, 4.07; N, 4.42; S, 10.04%. From purple effluent, **6** (175 mg, 35%) was recovered.

Ethyl 3-Acetylamino-2-acetylthio-1-azulenecarboxylate (8) and Ethyl 3-Acetylamino-1-azulenecarboxylate (9). A mixture of **7** (300 mg), acetic anhydride (75 ml), sodium acetate (5.28 g), and zinc dust (10.7 g) in acetic acid (75 ml) was stirred for 21 h at room temperature. The reaction mixture was diluted with water and unchanged zinc dust was removed by filtration. The filtrate was neutalized with potassium carbonate and extracted with dichloromethane. The extract was dried and the solvent was removed. The resulting residue was chromatographed on a silica-gel column. **8** (109 mg, 35%, purple needles, mp 113—114°C); IR (KBr) 3264, 1711, 1684, 1644, and 1528 cm^{-1}; ^{1}H NMR (90 MHz, in $CDCl_3$) δ=1.45 (3H, t, J=7.2 Hz, $COOCH_2C\underline{H}_3$), 2.26 (3H, s, $NHCOC\underline{H}_3$), 2.52 (3H, s, $SCOC\underline{H}_3$), 4.45 (2H, q, J=7.2 Hz, $COOC\underline{H}_2CH_3$), 6.90 (1H, bs, $N\underline{H}COCH_3$), 7.1—7.9 (3H, m, H-5,6,7), 8.30 (1H, dm, J=9.6 Hz, H-4), and 9.49 (1H, dm, J=9.6 Hz, H-8). Found: C, 61.50; H, 5.15; N, 4.20; S, 9.65%. Calcd for $C_{17}H_{17}O_4NS$: C, 61.61; H, 5.17; N, 4.23; S, 9.68%. **9** (66 mg, 27%, greenish blue micro needles, mp 181—181.5°C); IR (KBr) 3266, 1695, 1659, and 1541 cm^{-1}; ^{1}H NMR (90 MHz, in $CDCl_3$) δ=1.40 (3H, t, J=7.2 Hz, $COOCH_2C\underline{H}_3$), 2.25 (3H, s, $NHCOC\underline{H}_3$), 4.36 (2H, q, J=7.2 Hz, $COOC\underline{H}_2CH_3$), 7.0—7.8 (3H, m, H-5,6,7), 7.97 (1H, dm, J=9.6 Hz, H-4), 8.47 (1H, s, H-2), and 9.49 (1H, dm, J=9.6 Hz, H-8); ^{13}C NMR (22.5 MHz, in $CDCl_3$) δ=14.6, 23.7, 59.9, 114.6, 124.0, 125.4, 127.3, 133.3, 133.9, 134.5, 137.9, 138.1, 139.5, 165.2, and 169.2. Found: C, 70.28; H, 5.91; N, 5.52%. Calcd for $C_{15}H_{15}NO_3$: C, 70.02; H, 5.88; N, 5.44%.

Ethyl 2-Methylazuleno[1,2-*d*]thiazole-9-carboxylate (10). To a solution of **8** (78 mg) in tetrahydrofuran (7 ml) and ether (14 ml) which had been cooled in an ice bath, a solution of potassium hydroxide (148 mg) in water (7 ml) was added, drop by drop, under an atmosphere of nitrogen, after which the solution was stirred for 20 min. Further, hydrochloric acid (7 ml) was added and then the solution was stirred for 12 h at room temperature. The reaction mixture was diluted with water and extracted with dichloromethane. The extract was washed with water, and evaporated. The residue was chromatographed on a silica-gel column with benzene–ethyl acetate (9:1). The purple effluent was freed from the solvent to give **10** (42 mg, 41%) as purple prisms; mp 107.5—108°C; IR (KBr) 1683, 1437, 1417, and 1196 cm^{-1}; ^{1}H NMR (90 MHz, in $CDCl_3$) δ=1.51 (3H, t, J=7.2 Hz, $COOCH_2C\underline{H}_3$), 2.96 (3H, s, $C\underline{H}_3$-2), 4.52 (2H, q, J=7.2 Hz, $COOC\underline{H}_2CH_3$), 7.4—8.0 (3H, m, H-5,6,7), 8.97 (1H, dm, J=9.0 Hz, H-4), and 9.68 (1H, dm, J=10.3 Hz, H-8); ^{13}C NMR (22.5 MHz, in $CDCl_3$) δ=14.7, 20.5, 60.3, 106.4, 127.6, 128.2, 131.6, 133.7, 137.2, 138.6, 142.2, 146.8, 148.6, 164.2, and 168.2. Found: C, 66.68; H, 4.80; N, 5.23; S, 11.95%. Calcd for $C_{15}H_{13}NO_2S$: C, 66.40; H, 4.83; N, 5.16; S, 11.82%.

2-Methylazuleno[1,2-*d*]thiazole (11). A mixture of **10** (23 mg) and 100% phosphoric acid (5 ml) was heated for 1 h at 90°C. After cooling, the reaction mixture was diluted with water and extracted with benzene. The dried extract was evaporated to give a residue. The residue was chromatographed on a silica-gel column with benzene. The blue effluent was from the solvent to give **12** (15 mg, 87%) as deep blue prisms; mp 139—139.5°C; IR (KBr) 1574, 1514, 1378, 1146, and 786 cm^{-1}; ^{1}H NMR (90 MHz, in $CDCl_3$) δ=2.90 (3H, s, $C\underline{H}_3$-2), 7.0—7.7 (3H, m, H-5,6,7), 7.33 (1H, s, H-9), 8.22 (1H, dm, J=10.3 Hz, H-8), and 8.81 (1H, dm, J=9.0 Hz, H-4); ^{13}C NMR (22.5 MHz, in $CDCl_3$) δ=20.6, 105.7, 122.8, 123.5, 128.0, 131.9, 136.5, 136.8, 140.4, 144.2, 150.1, and 166.0. Found: C, 72.55; H, 4.47; N, 6.72; S, 16.20%. Calcd for $C_{12}H_9NS$: C, 72.32; H, 4.55; N, 7.03, S, 16.09%.

The present work was partially supported by a Grant-in-Aid for Scientific Research No. 00547021 from the Ministry of Education, Science and Culture.

References

1) K. Yamane, K. Fujimori, and S. Ichikawa, *Chem. Lett.*, **1982**, 707; K. Yamane, K. Fujimori, S. Ichikawa, S. Miyoshi, and K. Hashizume, *Heterocycles*, **20**, 1263 (1983).

2) R. N. McDonald and J. M. Richimond, *J. Org. Chem.*, **40**, 1689 (1975).

3) A. Sato, Doctoral Thesis, Tohoku University, Sendai 1962.

Reactions of Schiff Bases with Superoxide Ion in Acetonitrile

Katsuyoshi SHIBATA,* Yoshiyuki SAITO, Katsuyoshi URANO, and Masaki MATSUI
Department of Industrial Chemistry, Faculty of Engineering, Gifu University, Yanagido, Gifu 501-11
(Received April 2, 1986)

Synopsis. The reactions of Schiff bases such as *N*-benzylideneanilines with superoxide ion in acetonitrile under mild conditions gave the cyanomethyl adducts, 3-arylamino-3-arylpropionitriles, as the main products in relatively good yields. In the case of *N*-(4-nitrobenzylidene)aniline, the adduct was further oxidized to β-anilino-4-nitrocinnamonitrile. No oxidative products such as amides were obtained except in the reactions of *N*-(4-chloro- and 4-nitrobenzylidene)aniline.

Although superoxide ion reacted with many organic compounds as oxidant, reductant, nucleophile, base, or radical,[1] there have been only a few reports on carbon–nitrogen double-bonds with superoxide ion. These reports have been on the oxidations of iminium fluorosulfates and nitrones to the corresponding amide and hydroxamic acids respectively;[2] the reaction of hydrazine to azine,[3] and the reactions of oximes to *O,O'*-methylenebis(oxime)s in the presence of Pd(II) and dichloromethane.[4]

We found that *N*-benzylideneanilines (**1**) with a C=N bond reacted with superoxide ion and acetonitrile in the presence of dicyclohexano-18-crown-6(DCC), resulting in the formation of 3-anilino-3-phenylpropionitriles (**2**) as the main product. This paper will describe the reactions of the various Schiff bases with superoxide ion in acetonitrile.

Results and Discussion

Substituted *N*-benzylideneanilines (**1**) and DCC were dissolved in dry acetonitrile, after the addition of powdered KO_2, the mixture was stirred for 1 h under an argon atmosphere at room temperature. Then the solution was treated with water to decompose the unreacted KO_2, and extracted with ether. The results are summarized in Scheme 1 and Table 1. Cyanomethyl adducts (**2a—d**, **2f—i**) to the C=N bond of **1** were obtained as the main products in 32—71% yields. In addition, benzaldehydes (**4**), anilines (**5**), *trans*- and *cis*-cinnamonitriles (**6** and **7**), and benzyl alcohols (**8**) were obtained in low yields. In these cases of R_1=Cl and NO_2 (**1d** and **1e**), the **3d** and **3e** amides, derived from the oxidation of the C=N bond with superoxide ion, were obtained in about 15% yields. No 3-anilino-3-(4-nitrophenyl)propionitrile (**2e**) was afforded from 4-nitrobenzylideneaniline (**1e**). It can be assumed that **2e** was further dehydrogenated by superoxide ion to form

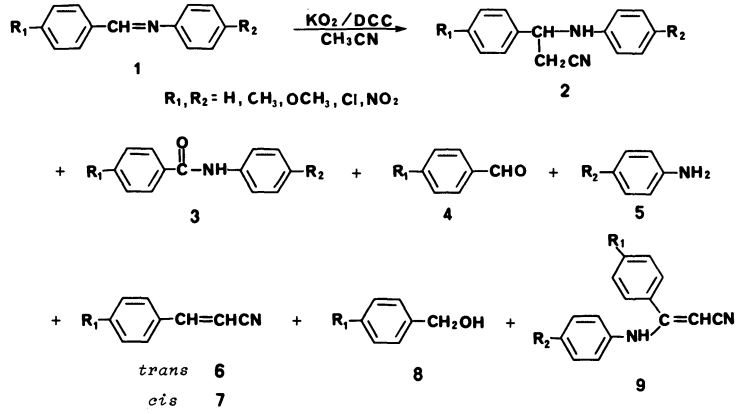

Scheme 1.

Table 1. Reactions of *N*-Benzylideneanilines (**1a—i**) with Superoxide Ion in Acetonitrile (room temp, 1 h)

	Substituent		Conv	Yield[a]/%							
	R_1	R_2	%	**2**	**3**	**4**	**5**	**6**	**7**	**8**	**9**
1a	H	H	84	71	—	Trace	8	2	Trace	2	—
1b	Me	H	47	55	—	6	13	6	Trace	—	—
1c	MeO	H	54	68	—	Trace	11	2	2	—	—
1d	Cl	H	41	58	17	16	17	Trace	—	Trace	—
1e	NO_2	H	53	—	16	2	6	—	—	—	31
1f	H	Me	30	54	—	Trace	10	3	Trace	Trace	—
1g	H	MeO	32	72	—	3	16	6	Trace	Trace	—
1h	H	Cl	100	32	—	—	42	8	Trace	—	—
1i	H	NO_2	100	48	—	Trace	34	15	3	—	—

a) Yields were determined by GLC analysis and based on converted substrates.

Table 2. Cyanomethylations of Various Schiff Bases

$$R_3\text{-}CH{=}N\text{-}R_4 \xrightarrow[CH_3CN]{KO_2/DCC} R_3\text{-}\underset{\displaystyle CH_2CN}{\underset{|}{CH}}\text{-}NH\text{-}R_4$$

	Substituent		Time	Temp	Conv	Adduct	Yield[a]
	R_3	R_4	h	°C	%		%
10	Cyclohexyl	Ph	1	60	43	**11**	12
12	Ph	Cyclohexyl	20	60	12	—	—
13	Ph	1-Naphthyl	1	rt	94	**14**	34
15	Ph	2-Naphthyl	1	rt	97	**16**	48
17	1-Naphthyl	Ph	1	rt	95	**18**	90
19	2-Naphthyl	Ph	1	rt	95	**20**	73
21	1-Naphthyl	1-Naphthyl	1	rt	98	**22**	41

a) GLC analysis.

Table 3. Melting Points and Analytical Data of 3-Arylamino-3-arylpropionitriles (**2a—d**, **2f—i**) and β-Anilino-4-nitrocinnamonitrile (**9e**)

Compd No.	Mp	IR(KBr)	MS	^{1}H NMR δ($CDCl_3$)	Found(Calcd)/%		
	θ_m/°C	cm^{-1}	$m/z(M^+)$	ppm	C	H	N
2a	81.5—82.5 (lit,[7] 80—82)	3350 2275	222	2.89 (2H, dd, J=5.9, 1.8 Hz, CH_2), 4.20 (1H, br s, NH), 4.76 (1H, t, J=6.0 Hz, CH)			
2b	70—71	3320 2260	236	2.34 (3H, s, CH_3), 2.89 (2H, dd, J=6.0, 0.9 Hz, CH_2), 4.18 (1H, s, NH), 4.71—4.75 (1H, m, CH),[a] 6.6—7.3 (9H, m, Ar)	81.57 (81.32	6.90 6.83	11.74 11.85)
2c	108.5—109	3350 2250	252	2.84 (2H, d, J=6.2 Hz, CH_2), 3.78 (3H, s, OCH_3), 4.18 (1H, s, NH), 4.70 (1H, t, J=7.3 Hz, CH), 6.6—7.3 (9H, m, Ar)	76.01 (76.16	6.27 6.39	11.34 11.15)
2d	109—110	3380 2250	256	2.87 (2H, dd, J=5.9, 2.9 Hz, CH_2), 4.18 (1H, br s, NH), 4.73 (1H, t, J=5.9 Hz, CH), 6.6—7.4 (9H, m, Ar)	70.02 (70.17	4.99 5.10	10.77 10.91)
2f	64.5—65	3360 2240	236	2.21 (3H, s, CH_2), 2.88 (2H, dd, J=6.0, 1.7 Hz, CH_2), 4.07 (1H, br s, NH), 4.73 (1H, t, J=6.0 Hz, CH), 6.5—7.4 (9H, m, Ar)	81.49 (81.32	6.97 6.83	11.69 11.85)
2g	111—112	3370 2240	252	2.84 (2H, dd, J=6.2, 2.2Hz, (CH_2), 3.70 (3H, s, CH_3O), 4.66 (1H, t, J=6.2 Hz, CH), 6.5—7.4 (9H, m, Ar)	76.37 (76.16	6.46 6.39	11.02 11.15)
2h	54—56	3370 2250	256	2.89 (2H, dd, J=7.3, 6.2 Hz, CH_2), 4.25 (1H, br s, NH), 4.72 (1H, t, J=5.9 Hz, CH), 6.5—7.4 (9H, m, Ar)	70.08 (70.17	5.02 5.10	10.99 10.91)
2i	109—110	3360 2260	267	2.97 (2H, dd, J=6.6, 5.9 Hz, CH_2), 4.8—4.95 (1H, m, CH), 5.28 (1H, br s, NH), 6.5—8.0 (9H, m, Ar)	67.21 (67.40	4.79 4.90	15.87 15.72)
9e	145—146	3270 2200	265	4.79 (1H, s, CH), 6.02 (1H, br s, NH), 7.2—8.4 (9H, m, Ar)	67.80 (67.95	4.12 4.18	15.97 15.85)

a) This signal was varied from m to t by the addition of D_2O.

the olefin **9e**. Compound **1** might be decomposed to **4** and **5** by base (O_2^- or HO_2^-). Compound **4a** reacts with superoxide ion in acetonitrile to yield **6a—8a**.[5] We also observed the formations of **6a—8a** under the same conditions as the reaction of **1a**.

Shrader has obtained **2a** in a 54% yield by photo-ring-opening reaction of 1,5-diphenyl-2-pyrazoline under 22 h irradiation.[6] On the other hand, the method using superoxide ion, (**2a**) has given a better yield (71%) in a shorter reaction time (1 h).

Similar reactions were carried out with cyclohexyl-, 1-naphthyl-, and 2-naphthyl-substituted compounds instead of the phenyl group of **1**. The results are summarized in Table 2. When *N*-(hexahydrobenzylidene)aniline (**10**) reacted with superoxide ion for 1 h at 60°C, the cyanomethyl adduct (**11**) was obtained in a 12% yield: however, no cyanomethyl adduct was afforded from *N*-benzylidenecyclohexylamine (**12**) even 20 h at 60°C. In the cyanomethylations of naphthyl-substituted Schiff bases, no difference in reactivity was observed between 1-naphthyl- and 2-naphthyl-substituted Schiff bases. *N*-Naphthyl-substituted Schiff bases (**13**, **15**, **21**) gave cyanomethyl adducts (**14**, **16**, **22**) in lower yields than C-substituted ones (**17**, **19**). The physical properties of cyanomethyl adducts are summarized in Tables 3 and 4.

On the basis of the results mentioned above, the formation of **2** is explained by Scheme 2. In the reaction of **1**, superoxide ion abstracts the hydrogen atom from acetonitrile, thus giving cyanomethyl radical. This cyanomethyl radical attacks the carbon of the C=N bond and gives cyanomethyl adducts (**2**) via radical

Table 4. Melting Points and Analytical Data of 3-Anilino-3-cyclohexylpropionitrile (**11**) and 3-Aryl-3-(arylamino)propionitriles (**14**, **16**, **18**, **20**, **22**)

Compd No.	Mp	IR(KBr)	MS	^{1}H NMR δ($CDCl_3$)	Found(Calcd)/%		
	θ_m/°C	cm^{-1}	$m/z(M^+)$	ppm	C	H	N
11	62—62.5	3340 2210	228	1.0—2.0 (11H, m, C_6H_{11}), 2.64 (2H, dd, J= 11.9, 4.9 Hz, CH_2), 3.4—3.55 (1H, m, CH), 3.64 (1H, br s, NH), 6.6—7.3 (5H, m, Ar)	79.08 (79.25	8.22 8.43	12.39 12.32)
14	113.5—114	3405 2260	272	3.03 (2H, d, J=6.2 Hz, CH_2), 4.83 (1H, br s, NH), 4.95 (1H, t, J=6.0 Hz, CH), 6.5—8.0 (12H, m, Ar)	83.91 (83.79	5.98 5.92	10.18 10.29)
16	125.5—126	3440 2260	272	2.97 (2H, d, J=5.9 Hz, CH_2), 4.52 (1H, br s, NH), 4.90 (1H, t, J=6.0 Hz, CH), 6.7—7.7 (12H, m, Ar)	83.72 (83.79	5.79 5.92	10.27 10.29)
18	114—114.5	3380 2260	272	3.08 (2H, ddd, J=51.3, 16.9, 5.9 Hz, CH_2), 4.37 (1H, s, NH), 5.57 (1H, t, J=5.9 Hz, CH), 6.6—8.0 (12H, m, Ar)	83.88 (83.79	5.82 5.92	10.32 10.29)
20	134—134.5	3415 2245	272	2.99 (2H, dd, J=5.9, 3.3 Hz, CH_2), 4.31 (1H, s, NH), 4.93 (1H, t, J=6.0 Hz, CH), 6.6—7.9 (12H, m, Ar)	83.62 (83.79	5.74 5.92	10.41 10.29)
22	149.5—150.5	3360 2240	322	3.32 (2H, dd, J=28.6, 5.9 Hz, CH_2), 5.05 (1H, br s, NH), 5.77 (1H, t, J=5.9 Hz, CH), 6.4—8.1 (14H, m, Ar)	87.58 (87.54	4.77 4.90	7.72 7.56)

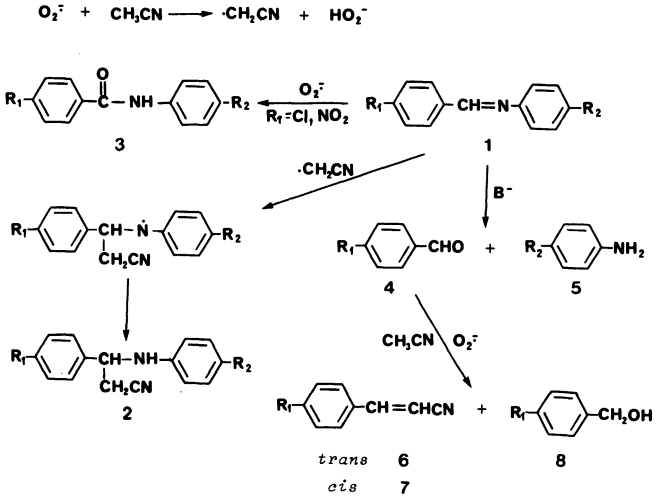

Scheme 2.

intermediates. Oae et al. have reported that diaryl sulfide reacted with superoxide ion in acetonitrile to yield bis(arylthio)acetonitrile as the main product; its formation mechanism might be via the cyanomethyl radical.[7] When R_1=NO_2 and Cl, the electron density of the carbon of the C=N bond is decreased, and **3** are obtained by the nucleophilic attack of superoxide ion. In the case of R_1=NO_2, the resulting adduct is further oxidized to **9e**. On the other hand, **1** are decomposed to **4** and **5** by bases, and **4** further reacts with acetonitrile and superoxide ion to yield **6**—**8**.

Experimental

Melting points are uncorrected. NMR spectra were measured by the use of a JEOL GX-270 Spectrometer in a $CDCl_3$ solution; the chemical shifts were expressed in units from the internal Me_4Si. Mass spectra were measured by means of a Hitachi M-52 Spectrometer (20 eV). IR spectra were recorded over KBr disks with a JASCO A-302 Spectrometer. Gas chromatography was performed on a Shimadzu 4C-PF Gas chromatograph (2% OV-1 or 5% FFAP).

Materials. *N*-Benzylideneanilines (**1**) and the various Schiff bases were prepared from the corresponding aldehydes and amines. The resulting Schiff bases were recrystallized from ethanol. Pottasium superoxide (Alfa) was crushed and pulverized in a dry atmosphere. The acetonitrile was purified by distillation in the presence of P_2O_5 and stored Molecular Sieves (3A, 1/16). Dicyclohexano-18-crown-6 (Tokyo Kasei) was used as received.

General Procedure. *N*-Benzylideneaniline (**1a**) (300 mg, 1.65 mmol) and DCC (300 mg, 0.81 mmol) were dissolved in dry acetonitrile (50 cm^3). After powdered KO_2 (500 mg, 7.04 mmol) has been added to the solution, the mixture was stirred under an argon atmosphere. After 1 h, water (50 cm^3) was slowely added to decompose the residual KO_2. The mixture was extracted with ether in the presence of NaCl. The ether layer was dried over $MgSO_4$ and evaporated (rotary). The extract was separated by thin-layer chromatography (Merck, Silica Gel 60 PF_{254}; hexane:dichloromethane=1:2).

References

1) a) E. Lee-Ruff, *Chem. Soc. Rev.*, **6**, 195 (1977); b) D. T. Sawyer, *Acc. Chem. Res.*, **14**, 393 (1981); c) A. A. Frimer, *Superoxide Dismutase*, **2**, 83 (1982).

2) A. Picot, P. Milliet, M. Cherest, and X. Lushinchi, *Tetrahedron Lett.*, **18**, 3811 (1977).

3) C. I. Chern and J. S. Filippo, Jr., *J. Org. Chem.*, **42**, 178 (1978).

4) T. Hosokawa, T. Ohta, Y. Okamoto, and S. Murahashi, *Tetrahedron Lett.*, **21**, 1259 (1980).

5) M. J. Gibian, D. T. Sawyer, T. Ungermann, R. Tangpoonpholvivat, and M. M. Morrison, *J. Am. Chem. Soc.*, **101**, 640 (1979).

6) L. Schreder, *Tetrahedron Lett.*, **12**, 2977 (1971).

7) S. Oae, T. Takata, and Y. H. Kim, *Bull. Chem. Soc. Jpn.*, **54**, 2712 (1981).

Synthesis of 5*H*-Cyclohepta[4,5]pyrrolo[2,3-*b*]indoles[1]

Kameji YAMANE,* Hiroshi YAMAMOTO,*,† (the late)Akira SATOH, Yuhji TAMURA, and Tetsuo NOZOE††,§

Department of Chemistry, Faculty of Science, Shinshu University, Matsumoto 390
†Department of Chemistry, Faculty of Science, Okayama University, Okayama 700
††Department of Chemistry, Faculty of Science, Tohoku University, Sendai 980

(Received April 28, 1986)

Synopsis. The title compounds (indolo[2,3-*b*][1]azaazulenes) were synthesized from 2-hydrazino-1-azaazulene and cyclohexanone utilizing Fischer's indole synthesis, followed by dehydrogenation of the *N*-acetylated tetrahydro precursor with DDQ. Structures of the neutral and cationic species of these compounds were discussed on the basis of the spectral data.

We have prepared several troponoid compounds fused with an indole ring.[2] We now wish to report herein the synthesis of the first examples of 1-azaazulene[3] fused with a pyrrole or an indole ring.

Condensation of 2-hydrazino-1-azaazulene (**1**)[4] with various ketones and an aldehyde readily gave the corresponding hydrazones: i.e. **2** (with cyclohexanone), **3** (with cycloheptanone), **4** (with acetone), **5** (with ethyl methyl ketone), and **6** (with phenylacetaldehyde). Among these hydrazones, only **2** was managed to be led to the pyrrolo[2,3-*b*][1]azaazulene derivative (**7**) by the application of Fischer's indole synthesis, whereas on employing the similar procedures the conversion of other hydrazones **3**—**6** into the corresponding pyrrolo-[2,3-*b*][1]azaazulenes has remained unsuccessful because of the profound decomposition of the starting materials accompanied by the formation of many complex products.

Attempts of dehydrogenation of **7** with chloranil or DDQ (2,3-dichloro-5,6-dicyano-*p*-benzoquinone) failed mainly due to the exclusive precipitation of an unidentified, dark blue solid, from which no desired product was liberated. However, treatment of its *N*-acetyl derivative **8** with DDQ yielded the dehydrogenated *N*-acetyl compound (**9**), which in turn was led to the parent title compound (indolo[2,3-*b*][1]-azaazulene, **10**) on acid or alkaline hydrolysis.

Physical data for the structural proof for all these compounds are given in the Experimental section. Usful ^{1}H NMR parameters of the pryyolo- and indolo-1-azaazulenes **7**—**10** are summarized in Table 1. The position (N-5) of the acetyl group of **8** and **9** are derived from the evidence of the considerable down-field shifts (0.5 and 1.2 ppm) of H-4 signals of these compounds (compared with those of **7** and **10**, respectively) apparently due to an anisotropic effect of the *N*-acetyl group.[5] Moreover, since the UV spectra of **7** and **10** closely resemble those of **8** and **9**, respectively, these compounds are considered to exist predominantly in 5*H*-cyclohepta[4,5]pyrrolo[2,3-*b*]indole forms (**7** and **10**) rather than in their tautomeric 6*H*-forms. An appreciable down-field shift (0.6 ppm) observed for H-1 signal of **10** (in $CDCl_3$, when compared with that of H-4) can be explained by an anisotropic effect caused by the ring current of the 1-azaazulene moiety that is situated in the vicinity.[6] The divergences of the vicinal coupling constants suggests some degree of bond alternation in the seven-membered ring of **7**—**10**, as was observed in the case of azuleno[1,2-*b*]thiophene.[7]

The signals of the seven-membered ring protons of **7**

§Present address: 811-1-5-2 Kamiyoga, Setagaya-ku, Tokyo 158.

Table 1. ^{1}H NMR Parameters for Cyclohepta[4,5]pyrrolo[2,3-*b*]indoles in $CDCl_3$

Compd	Chemical shifts, δ									
	H-1	H-2	H-3	H-4	R-5	H-7	H-8	H-9	H-10	H-11
7[a]	2.97[b]	1.98[b]	1.98[b]	2.97[b]	9.5[c]	8.55	7.60	7.74	7.68	8.61
7[a,d]	3.02[b]	2.07[b]	2.07[b]	2.89[b]	11.0[c]	8.66	8.11	8.23	8.15	8.92
8[a]	3.21[b]	2.22[b]	2.22[b]	3.51[b]	3.44[e]	8.62	7.67	7.88	7.79	8.74
9[f]	8.01	7.45	7.44	8.73	3.23[e]	8.71	7.84	7.90	7.79	8.82
10[f]	8.14	7.36	7.41	7.57	9.44[c]	8.64	7.85	7.83	7.79	8.84
10[d,f]	8.05	7.47	7.51	7.56	11.65[c]	8.65	8.15	8.23	8.24	8.95

	Coupling constants/Hz[g]												
	$J_{1,2}$	$J_{1,3}$	$J_{1,4}$	$J_{2,3}$	$J_{2,4}$	$J_{3,4}$	$J_{7,8}$	$J_{7,9}$	$J_{8,9}$	$J_{8,10}$	$J_{8,11}$	$J_{9,10}$	$J_{9,11}$	$J_{10,11}$
7							9.5	1.0	10.2	1.0	0.5	9.4	1.0	10.0
7[d]							9.5	1.0	10.3	1.0	0.5	9.4	1.0	10.2
8							9.5	1.0	10.3	1.0	0.5	9.4	1.0	10.2
9	8.0	1.2	0.5	7.5	1.2	7.6	9.5	1.0	10.2	1.0	0.5	9.4	1.0	10.0
10	8.0	1.2	0.5	7.5	1.0	7.6	9.5	1.0	10.0	1.0	0.5	9.4	1.0	10.0
10[d]	8.0	1.2	0.5	7.5	1.0	8.0	9.5	1.0	10.3	1.0	0.5	9.4	1.0	10.2

a) At 100 MHz. b) A multiplet (2H) centered at this value. c) R=H, broad singlet. d) In CF_3COOD. e) R=$COCH_3$, singlet. f) At 400 MHz. g) Values confirmed by double resonance and simulation analysis.

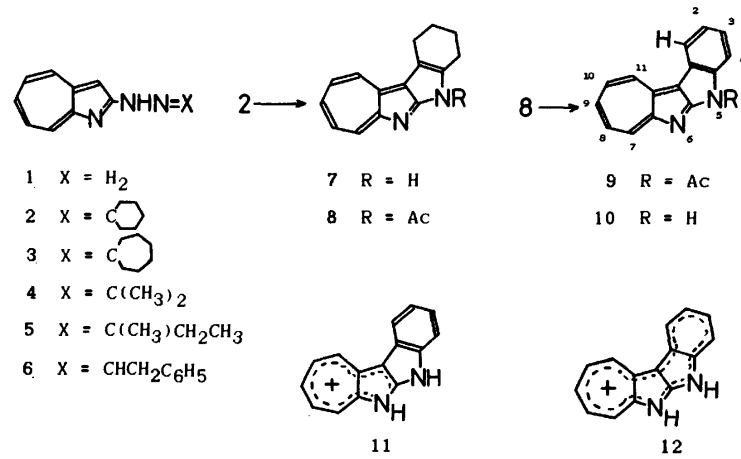

and **10** in trifluoroacetic acid-*d* show a down-field shift of 0.2—0.55 ppm (when compared with the corresponding compounds measured in $CDCl_3$, whereas those of the benzene ring protons of **10** show an almost negligible shift (ca. 0.1 ppm) in the acid (see Table 1). This suggests that the positive charge of the cation derived from **10** in trifluoroacetic acid is delocalized mostly over the 1-azaazulene ring (as in **11**) rather than over the 18π peripheral tetracyclic ring system **12**.

Experimental†

Melting points were determined with a Yanagimoto MP-S3 and are uncorrected. Column chromatography was performed with Wako C-200 silica gel. UV and IR spectra were taken on Hitachi 345 and Shimadzu Multipurpose MPL 50L spectrophotometers, respectively. NMR spectra were recorded with a JEOL JNM-4H-100 (100 NHz at 30 °C) or JEOL GX400 (400 MHz, for **9** and **10**) with TMS as an internal standard. The assignments of all signals were made by employing a first-order analysis with the aid of decoupling technique and the parameters were confirmed by a computer-assisted simulation analysis using an NEC 9801F Personal Computer[8]; those values are summarized in Table 1. Mass spectra were taken on a Hitachi RMS-4 low-resolution instrument at 70 eV, and are given in terms of *m/z* (rel intensity).

Cyclohexanone Cyclohepta[*b*]pyrrol-2-ylhydrazone (2). A solution of 4.5 g (27 mmol) of **1**[4] and 3.9 g (40 mmol) of cyclohexanone in 86 cm^3 of ethanol was refluxed for 15 min. The solvent and excess cyclohexanone was evaporated in vacuo and the residue was recrystallized from acetonitrile to give **2** as dark brown plates (4.9 g, 76%): mp 152—153 °C; UV (MeOH) 279, 288, 316, 435, and 490 sh nm (log ε 4.43, 4.40, 4.22, 4.07, and 3.52); IR (KBr) 3185 (NH), 1620 sh, and 1600 cm^{-1} (C=N, C=C); ^1H NMR ($CDCl_3$) δ=1.5—2.0 (6H, m, 2H-3',4',5'), 2.3—2.6 (4H, m, 2H-2',6'), 6.85 (1H, brs, H-3), 7.1—7.5 (3H, m, H-5,6,7), and 7.7—8.0 (3H, m, H-4,8, NH); MS *m/z* 239 (M^+, 100), 196 (76), 144 (90), 116 (40), and 41 (79).

Found: C, 75.47; H, 7.26; N, 17.32%. Calcd for $C_{15}H_{17}N_3$: C, 75.28; H, 7.16; N, 17.56%.

Cycloheptanone Cyclohepta[*b*]pyrrol-2-ylhydrazone (3). Similar procedures for **2** were followed. Thus 3.7 g (23 mmol) of **1** and 2.6 g (23 mmol) of cycloheptanone in refluxing ethanol (75 cm^3, for 45 min) gave **3** as dark brown plates (4.3 g, 74%): mp 121—122 °C (from hexane); UV (EtOH) 280, 288, 324, 385, 398, 444, 463 sh, and 495 sh nm (log ε 4.43 4.40, 4.18, 4.03, 4.01, 3.83, 3.75, and 3.33); IR (KBr) 3165 (NH), 1620 sh, and 1600 cm^{-1} (C=N, C=C); ^1H NMR ($CDCl_3$) δ=1.4—2.1 (8H, m, 2H-3',4',5',6'), 2.4—2.8 (4H, m, 2H-2',7'), 7.00 (1H, brs, H-3), 7.2—7.6 (3H, m, H-5,6,7), and 7.8—8.3 (3H, m, H-4,8, NH); MS *m/z* 253 (M^+, 100), 252 (47), 196 (55), 144 (81), and 116 (27).

Found: C, 75.74; H, 7.51; N, 16.57%. Calcd for $C_{16}H_{19}N_3$: C, 75.85; H, 7.56; N, 16.59%.

Acetone Cyclohepta[*b*]pyrrol-2-ylhydrazone (4). Similar procedures for **2** were followed. Thus 100 mg of **1** and 30.4 mg of acetone in refluxing ethanol (20 cm^3, for 60 min) gave **4** as dark amber plated (86 mg, 69%): mp 147—147.5 °C (from hexane); UV (EtOH) 280, 288, 325, 386, 400, 444, and 495 sh nm (log ε 4.51, 4.46, 4.18, 4.02, 4.01, 3.84, and 3.32); IR (KBr) 3170 (NH), 1608, and 1600 cm^{-1} (C=N, C=C); ^1H NMR ($CDCl_3$) δ=1.93 (3H, s, Me), 2.09 (3H, s, Me), 7.00 (1H, brs, H-3), 7.2—7.6 (3H, m, H-5,6,7), 7.8—8.1 (2H, m, H-4,8), and 8.85 (1H, m, NH); MS *m/z* 199 (M^+, 73), 184 (100), 143 (40), 116 (51), and 89 (30).

Found: C, 72.45; H, 6.64; N, 21.14%. Calcd for $C_{12}H_{13}N_3$: C, 72.34; H, 6.58; N, 21.09%.

Ethyl Methyl Ketone Cyclohepta[*b*]pyrrol-2-ylhydrazone (5). Similar procedures for **2** were followed. Thus 100 mg of **1** and 38 mg of ethyl methyl ketone gave **5** as dark amber needles (90 mg, 67%) after purification by chromatography in a column of alumina with CH_2Cl_2 as an eluant: mp* 113.5—114 °C (from hexane); UV* (EtOH) 280, 288, 322, 332, 382, 400, 447, 464 sh, and 496 sh nm (log ε 4.48, 4.44, 4.18, 4.17, 4.02, 4.00 3.81, 3.73, and 3.31); IR* (KBr) 3160 (NH), 1605, and 1595 cm^{-1} (C=N, C=C); ^1H NMR* ($CDCl_3$) δ=1.17 (3H, t, J=6.5 Hz, CH_3-CH_2-), 1.89 (3H, s, Me), 2.38 (2H, q, J=6.5 Hz, CH_2), 7.03 (1H, brs, H-3), 7.2—7.6 (3H, m, H-5,6,7), 7.8—8.1 (2H, m, H-4,8), and 8.95 (1H, m, NH), besides these, there exist signals due to a small proportion (ca. 15%) of **5** (presumably in the Z-form) at δ=1.08 (t). 2.06 (s), and 2.30 (q); MS* *m/z* 213 (M^+, 35), 184 (100), 144 (27). 143 (27), and 116 (36).

Found*: C, 73.10; H, 6.85; N, 19.60%. Calcd for $C_{13}H_{15}N_3$: C, 73.21; H, 7.09; N, 19.70%.

Phenylacetaldehyde Cyclohepta[*b*]pyrrol-2-ylhydrazone (6). Similar procedures for **2** were followed. Thus 120 mg of **1** and 75.5 mg of phenylacetaldehyde in refluxing ethanol (25 cm^3, for 30 min) gave **6** as dark brown needles (125 mg,

†We are greatly indebted to Mr. H. Kuwano, Dr. T. Kinoshita, and Mr. K. Ono, the Sankyo Co., Ltd., for the measurements of the 400 MHz NMR, mass spectra, and the elemental analysis.

*For specimen consisting of a ca. 85 : 15 mixture of E- and Z-form (by NMR), because their separation could not be achieved by recrystallization or chromatography.

63%): mp 143.5—144°C (from benzene–hexane); UV (EtOH) 278, 287, 317, 380, 398, 440, 462 sh, and 495 sh nm (log ε 4.47, 4.47, 4.22, 4.01. 3.95, 3.83, 3.76, and 3.31); IR (KBr) 3170 (NH) and 1610 cm^{-1} (C=N, C=C); ^1H NMR ($CDCl_3$) δ= 3.80 (2H, d, J=4.5 Hz, CH_2), 6.80 (1H. brs, H-3), 7.1—7.9 (12H, m, H-4,5,6,7,8, CH, C_6H_5, NH); MS m/z 261 (M^+, 18), 170 (100), 144 (22), 116 (18), and 91 (17).

Found C, 78.09; H, 5.73; N, 15.96%. Calcd for $C_{17}H_{15}N_3$: C, 78.13; H, 5.79; N, 16.08%.

1,2,3,4-Tetrahydro-5*H*-cyclohepta[4,5]pyrrolo[2,3-*b*]indole (7). A solution of 4.9 g of **2** in 247 cm^3 of 1 M sulfuric acid (1 M=1 mol dm^{-3}) was refluxed for 5 h. After cooling, the mixture was diluted with cold water, brought to pH 9—10 with 2 M NaOH, and extracted with benzene. The organic layer was dried (Na_2SO_4), treated with active carbon, and evaporated in vacuo. The residue was recrystallized from ethanol to give **7** as dark red needles (1.64 g, 36%): mp 243—244°C; UV (MeOH) 233, 258, 312, 340, 417, 522, and 560 sh nm (log ε 4.16, 4.34, 4.63, 4.22, 3.75, 2.69, and 263), (MeOH+0.1 M HCl) 230, 259, 265, 322, and 350 sh nm (log ε 4.31, 4.38, 4.35, 4.19, and 4.35); IR (KBr) 3100 (NH), 2930, 2840 (CH_2), and 1605 cm^{-1} (C=N and C=C); ^1H NMR, see Table 1.

Found: C, 80.67; H, 6.07; N, 11.92%. Calcd. for $C_{15}H_{14}N_2$: C, 81.05; H, 6.35; N, 11.60%.

5-Acetyl-1,2,3,4-tetrahydro-5*H*-cyclohepta[4,5]pyrrolo[2,3-*b*]indole (8). A mixture of 1.0 g of **7** and 10 g of acetic anhydride was gently refluxed for 2 h. After cooling, it was diluted with water and brought to pH 8—9 with a saturated aqueous $NaHCO_3$. The ppt was filtered off and the filtrate was extracted with $CHCl_3$. The organic layer was evaporated in vacuo. The residue combined with the above ppt was chromatographed in a column of silica gel with chloroform as an eluant, giving **8** as red-violet needles (1.2 g, 70%): mp 133—135°C. (from cyclohexane): UV (MeOH) 232, 258, 313, 341, 417, 510, and 550 sh nm (log ε 4.14, 4.32, 4.59, 4.17, 3.71, 2.61, and 2.55); IR (KBr) 2930, 2850 (CH_2) and 1700 cm^{-1} (C=O); ^1H NMR, see Table 1.

Found: C, 77.03; H, 6.02; H, 10.74%. Calcd for $C_{17}H_{16}N_2O$: C, 77.25; H, 6.10; N, 10.60%.

5-Acetyl-5*H*-cyclohepta[4,5]pyrrolo[2,3-*b*]indole (9). A solution of 0.5 g (1.9 mmol) of **8** and 0.9 g (4 mmol) of DDQ in 80 cm^3 of dry benzene was refluxed for 5 h. After cooling, the ppt was filtered off and the filtrate was evaporated in vacuo. The residue and the above ppt were combined and triturated with $CHCl_3$. The combined $CHCl_3$ solution was washed with saturated aqueous $NaHCO_3$ and concentrated in vacuo. The residue was chromatographed over silica gel with $CHCl_3$ as an eluant, giving **9** as red-violet needles (0.34 g, 69%): mp 200—202°C (from benzene); UV (MeOH) 241, 284, 297, 325, 480, 500, and 545 sh nm (log ε 4.27, 4.28, 4.29, 4.56, 3.12, 3.11, and 2.83); IR (KBr) 1695 cm^{-1} (C=O); ^1H NMR, see Table 1; MS m/z 260 (M^+, 39), 218 (100), 190 (14), and 164 (5).

Found: C, 78.22; H, 4.44; N, 10.79%. Calcd for $C_{17}H_{12}N_2O$: C, 78.44; H, 4.65; N, 10.76%.

5*H*-Cyclohepta[4,5]pyrrolo[2,3-*b*]indole (10). A solution of 0.1 g of **9** in 10 cm^3 of 6 M HCl was refluxed for 5 h and then, after cooling, diluted with 10 cm^3 of water. The ppt was filtered off and recrystallized from ethanol, giving **10** as red-brown needles (0.084 g, 100%): mp>300°C (decomp); UV (MeOH) 240, 284, 296, 325, 472, 495, and 545 sh nm (log ε 4.30, 4.33, 4.32, 4.57, 3.17, 3.16, and 2.84), (MeOH+0.1 M HCl) 263, 282, 335, and 415 sh, nm (log ε 4.30, 4.31, 4.25, and 3.94); IR (KBr) 3050 (NH), 1620, and 1605 cm^{-1} (C=N, C=C); ^1H NMR, see Table 1; MS m/z 218 (M^+, 100), 190 (16), 164 (5), and 109 (4).

Found: C, 82.73; H, 4.65; N, 12.87%. Calcd for $C_{15}H_{10}N_2$: C, 82.54; H, 4.62; N, 12.84%.

Hydrolysis of **9** with 2 M NaOH similarly gave **10** in a quantitative yield.

We are grateful to Professor Toyonobu Asao and Dr. Tadayoshi Morita (Tohoku University) for valuable discussions, and to Mr. Shuji Ohmichi and Professor Seiichi Hirakawa (Shinshu University) for their kind cooperation in preparing some of the hydrazones and measuring the mass spectra.

References

1) Partly described in Ph. D. Thesis of A. Satoh, Tohoku University, 1963.

2) K. Yamane and K. Fujimori, *Bull. Chem. Soc. Jpn.*, **45**, 267 (1972); K. Fujimori and K. Yamane, *ibid.*, **47**, 1951 (1974); T. Nozoe, J.-K. Sin, K. Yamane, and K. Fujimori, *ibid.*, **48**, 314 (1975); K. Yamane and K. Fujimori, *ibid.*, **49**, 1101 (1976); K. Fujimori and K. Yamane, *ibid.*, **51**, 3579 (1978).

3) For synthesis of 1-azaazulenes, see K. Yamane, K. Fujimori, J.-K. Sin, and T. Nozoe, *Bull. Chem. Soc. Jpn.*, **50**, 1184 (1977) and references cited therein.

4) T. Nozoe, S. Seto, S. Matsumura, and T. Terasawa, *Chem. Ind.*, **1954**, 1357: mp 165°C decomp (Found: C, 67.85; H, 5.58; N, 26.52%).

5) Such an anisotropic effect is frequently observed for many *N*-acetylated aniline derivatives as exemplified by the δ values of the *o*-proton signals of acetanilide (ca. 7.2) and aniline (6.4): see C. J. Pouchert and J. R. Campbell, "The Aldrich Library of NMR Spectra," Aldrich Chemical Company, Inc., Milwaukee, Wisconsin (1974), Vol. 5, 37A and Vol. 7, 66A.

6) An inspection of the molecular model of **10** suggests that the H-1 is situated at a distance of ca. 2.8—3.0 Å from the C-11 and C-11b of the 1-azaazulene nucleus.

7) K. Fujimori, T. Fujita, K. Yamane, M. Yasunami, and K. Takase, *Chem. Lett.*, **1983**, 1731.

8) H. Yamamoto and K. Satake, "The Application of Microcomputer to Chemistry and Pharmaceutical Sciences," ed by Y. Tanaka and U. Mikawa, Nankodo, Tokyo (1985), Chap. 2, pp. 31—68.

Asymmetric Reduction of Aromatic Ketone in a Continuous Flow System

Shinichi ITSUNO,* Koichi ITO, Toshihiro MARUYAMA,† Naoki KANDA,†
Akira HIRAO,† and Seiichi NAKAHAMA†
School of Materials Science, Toyohashi University of Technology, Tempaku-cho, Toyohashi 440
†Department of Polymer Science, Tokyo Institute of Technology, Ohokayama, Meguro-ku, Tokyo 152
(Received May 16, 1986)

Synopsis. When THF-borane (1/1) and aromatic ketone were supplied continuously to the column containing polymer-supported (*S*)-(−)-2-amino-3-(*p*-hydroxyphenyl)-1,1-diphenyl-1-propanol, the chiral product, secondary benzylic alcohol, could be obtained successfully (>90% ee). Large quantities of highly optically pure alcohol could be produced by the continuous flow system by the use of only a small amount of polymeric auxiliary.

Though many procedures have been known for syntheses of optically active alcohols by the asymmetric induction in solutions,[1] there are relatively few methods involving the use of the chiral polymer-supported reagent.[2] We have reported that polymer-supported (*S*)-(−)-2-amino-3-(*p*-hydroxyphenyl)-1,1-diphenyl-1-propanol (**1**) was an excellent chiral auxiliary reagent for asymmetric reduction of ketones with BH_3·THF.[3] This insoluble cross-linked polystyrene gel

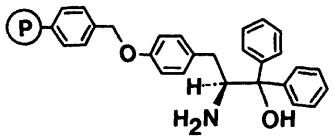

1

supporting chiral amino alcohol, which was prepared from L-tyrosine, could be readily recovered as its hydrochloride by simple filtration after acidic hydrolysis of the reaction mixture. Recovered polymer-supported hydrochloride was neutralized and could be reused. Chiral product secondary alcohol was obtained from the filtrate quantitatively with high enantioselectivity (>90% ee). Indeed the high chemical and enantiomeric yields were reproducible during several recyclings.[3,4]

During studies for the asymmetric reduction with polymer-supported chiral amino alcohol **1**-borane complex, an interesting fact was observed. After reduction of ketone with the polymeric reagent, careful filtration of the reaction mixture under a dry nitrogen stream without hydrolytic process gave the THF solution, which was successively hydrolyzed to yield the optically active secondary alcohol quantitatively with high enantioselectivity. Even after the filtration the chiral polymer containing the amino alcohol-borane complex had the ability to induce chirality in the ketone reduction with borane. Thus, if borane and substrate ketone are supplied continuously to the polymer complex, the chiral product may be obtained successively.

In a preliminary experiment, repeated asymmetric reduction in the batch system was attempted. Glassware being made up of two flasks (**A**, **B**) and glass filter was used for this system (Fig. 1). A THF solution of the chiral product yielded in the asymmetric reduction in the flask **A** was filtered into the flask **B**. Table 1 lists the results obtained from the batch system in the asymmetric reduction of valerophenone with **1**-BH_3 complex. In the first run valerophenone was reduced asymmetrically (90% ee) with the reagent prepared from **1** and 2 equiv of BH_3. Reaction was completed within a few minutes in THF at ambient temperature. After separation of the product by filtration under nitrogen 2 equiv of borane and 0.8 equiv of valerophenone were added again (flask **A**). Another optically active 1-phenyl-1-pentanol was obtained in 82% ee from the filtrate (Batch No. 2). In this batch system optical yields were reproducible on five repeated runs. Accumulated yield of isolated optically active alcohol was about 2.4 times the molar quantity of the chiral auxiliary reagent **1** after five repetitions. Although the conversion of ketone to alcohol was 100% by GC analysis, isolated yield was somewhat low owing to handling loss during the purification by distilling a small amount of the product in each fraction. Asymmetric reduction of some other alkyl phenyl ketones was performed. Large amount of optically active purified alcohols were isolated in this system. Results are summarized in Table 2.

The fact that the product was not bonded covalently to the polymeric chiral complex and optically active alcohol was obtained from the filtrate successively by hydrolysis implies this reaction could be conducted

Table 1. Asymmetric Reduction of Valerophenone in Batch System

Batch No.	Optical yield[a]/% (Config)	[Isolated yield]/[**1**] (Accumulated)
1	90(*R*)	0.42
2	82(*R*)	0.97
3	84(*R*)	1.40
4	92(*R*)	2.00
5	81(*R*)	2.37

a) Values for maximum rotation and confguration taken from Ref. 7).

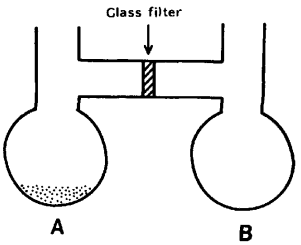

Fig. 1. Glassware for batch system.

Table 2. Asymmetric Reduction of Alkyl Phenyl Ketones in Batch System

Ketone	Number of repetition	[Isolated yield]/[1] (Accumulated)	Optical yield/% (Average)	Configuration
CH_3COPh	14	5.8	66[a]	*R*
C_2H_5COPh	16	8.6	72[b]	*R*
C_4H_9COPh	14	6.1	90	*R*

a) Value for maximum rotation taken from U. Nagai, T. Shishido, R. Chiba, and H. Mitsuhashi, *Tetrahedron*, **21**, 1701 (1965). b) Value for maxmum rotation taken from H. Kwart and D. P. Hoster, *J. Org. Chem.*, **32**, 1867 (1967).

Table 3. Asymmetric Reduction of Valerophenone Using Continuous Flow System[a]

Fraction No.	Rate of injection		1-Phenyl-1-pentanol		
	BH_3/THF [ml/min(mmol/min)]	Ketone/THF [ml/min(mmol/min)]	Optical yield/% (Config)	Isolated yield/mg (Accumulated)	[Isolated yield] [1]
1	0.31 (0.14)	0.06 (0.11)	87 (*R*)	455	0.65
2	0.47 (0.21)	0.09 (0.17)	93 (*R*)	741	1.06
3	0.63 (0.27)	0.12 (0.23)	91 (*R*)	899	1.28
4	0.31 (0.14)	0.06 (0.11)	86 (*R*)	1196	1.70
5[b]	—	—	83 (*R*)	1502	2.14
6[c]	—	—	85 (*R*)	1824	2.60

a) 2.49 g (4.27 mmol) of **1** was used. b) Only eluent (THF) was made to flow. c) 1-Phenylpentanol remained in gel.

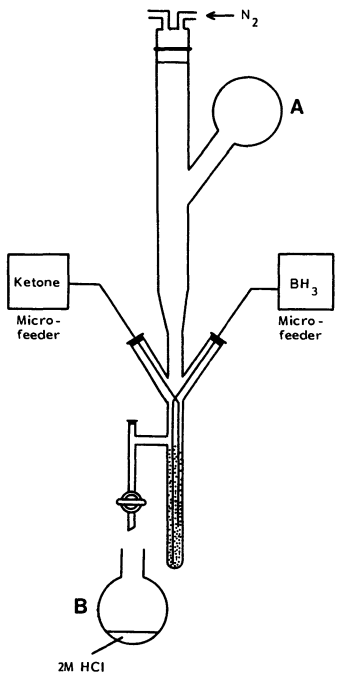

Fig. 2. Apparatus for conducting continuous flow reaction.

by a continuous flow system which avoids the repetition of a batch system process. Thus, large quantities of the highly optically pure product could be yielded through the continuous flow system by the use of only a small amount of polymeric chiral auxiliary **1**.

The procedure found to be most effective involves the two slow injections of 0.8:1.0 molar ratio of valerophenone and borane in THF to the bottom of a THF-presaturated column containing polymeric **1**–BH_3 complex through a syringe needle (Fig. 2). The polymeric **1**–BH_3 complex was prepared in the flask **A** prior to use this system. The flow rate and the ratio of borane and the ketone was controlled by means of microfeeder. The overflowed THF solution was collected in the flask **B** in which alkoxyborane was hydrolyzed with 2M HCl (1 M=1 moldm^{-3}) to give the optically active alcohol continuously in high enantioselectivity (83—93% ee, Table 3). Optically active alcohol of 2.6 equiv to the chiral auxiliary **1** was obtained from six fractions. Rate of injection seems not to be an important factor for the asymmetric reduction in this system (Fraction No. 1—3).

A noteworthy feature of the continuous flow method is the absence of destruction of the chiral gel since no stirring was required. The chiral gel column method reported in this note offers several advantages over alternative modes, especially with regard to the extreme tractability of the reaction and the yield of large quantities of optically active alcohol by the use of the small amount of chiral auxiliary. Such a procedure as well as high enantioselectivity would be required for the practical asymmetric synthesis.

Experimental

All reactions were carried out under an atmosphere of nitrogen. Tetrahydrofuran (THF) was heated under reflux over sodium metal and distilled from lithium aluminum hydride in a nitrogen atmosphere. Valerophenone, acetophenone, and propiophenone commercially purchased were dried and distilled over calcium hydride and checked for purity by GLPC and ^1H NMR. Borane was prepared by the reaction of sodium borohydride with trifluoroborane–diethyl ether (1/1) according to the procedure of Brown.[5] (*S*)-Tyrosyne (from Kyowa Hakko Co.) was used without purification. Polymer-supported (*S*)-(−)-2-amino-3-(*p*-hydroxyphenyl)-1,1-diphenyl-1-propanol (**1**) was prepared from chloromethylated polystyrene gel (2% cross linking, 2.92 meq Cl/g) by method described previously.[3,6] GLPC analysis was performed on a Yanaco G180 instrument with a stain-

less steel analytical column (3 mm×3 m) packed with PEG20M on Diasolid L. ^{1}H NMR spectra were recorded by a JEOL JNM PMX-60 spectrometer. Optical rotations were measured with a microcell. IR spectra were recorded by JASCO A-3 instrument for Nujol mulls. TLC was run on silica gel 60F-254 precoated plates with chloroform as mobile phase.

Repeated Asymmetric Reduction of Valerophenone with Polymer-Supported Chiral Amino Alcohol (1)-Borane Complex in Batch System. In the flask **A** (Fig. 1) the asymmetric reducing agent was prepared from **1** (1.6 meq amino alcohol/g, 3.0 g) and 2 equiv of borane (9.6 mmol) at first by the method described previously.[3] After addition of THF solution of valerophenone (0.6 g, 3.7 mmol) reaction was checked by TLC. When no ketone was detected by TLC the polymer was filtered through glass filter under nitrogen. THF solution collected in the flask **B** was hydrolyzed with 2M HCl and THF was evaporated. The ether extract was washed with saturated NaCl (2×10 ml), dried ($MgSO_4$) and evaporated to give a colourless oil. The conversion was checked by GLPC (100%). The crude product was then distilled by bulb-to-bulb distillation to give 1-phenyl-1-pentanol (0.33 g); α_D^{20} +1.80° (neat, l=1.0 cm), corresponding to an enantiomeric excess of 90% ee.[7] To the polymer kept in the flask **A** THF (10 ml), borane (9.6 mmol), and valerophenone (3.7 mmol) was added again. After ketone was reduced the same work up as above was used to give (*R*)-1-phenyl-1-pentanol of 82% ee.

Asymmetric Reduction of Valerophenone Using Continuous Flow System. The polymer-supported chiral reagent prepared in the flask **A** (Fig. 2) from **1** (1.71 meq of amino alcohol/g, 2.49 g) and 2 equiv of borane (8.5 mmol) by the method described previously, was transfered into the column by turning the apparatus upside down. The column (the inside diameter of 1 cm) was filled with a 14 cm of the column of the chiral gel. Borane (0.14 mmol min^{-1}) and ketone (0.11 mmol min^{-1}) were injected at the bottom of the column through the syringe needle by means of microfeeder. The overflow was collected in the flask **B** containing 2M HCl. After 30 min collected fraction was worked up according to the procedure outlined above to give (*R*)-1-phenyl-1-pentanol of 87% ee. After four fractions were collected only eluent (THF) was made to flow to give the same alcohol of 83% ee (Fraction No. 5). by means of hydrolysis of the chiral gel taken out of the column, the another fraction of the same alcohol was obtained in 85% ee (Fraction No. 6).

References

1) See: "Asymmetric Synthesis," ed by J. D. Morrison, Academic Press Inc., London (1983), Vol. 2.

2) a) T. Yamashita, H. Mitsui, H. Watanabe, and N. Nakamura, *Makromol. Chem.*, **181**, 2563 (1980); b) S. Shinkai, H. Tsuji, and O. Manabe, *J. Polym. Sci., Polym. Lett. Ed.*, **19**, 17 (1981); c) A. Akelah and D. C. Sherrington, *Polym. Commun.*, **24**, 147 (1983); d) J. H. Liu, K. Kondo, and K. Takemoto, *Makromol. Chem.*, **184**, 1547 (1983).

3) S. Itsuno, M. Nakano, K. Ito, A. Hirao, M. Owa, N. Kanda, and S. Nakahama, *J. Chem. Soc., Perkin Trans. 1*, **1985**, 2615.

4) S. Itsuno, M. Nakano, K. Miyazaki, K. Ito, A. Hirao, and S. Nakahama, *J. Chem. Soc., Perkin Trans. 1*, **1985**, 2039.

5) H. C. Brown, "Organic Syntheses via Boranes," John Wiley and Sons, New York (1975).

6) S. Itsuno, K. Ito, A. Hirao, and S. Nakahama, *J. Chem. Soc., Perkin Trans. 1*, **1984**, 2887.

7) A. Horeau, J. P. Guette, and R. Weiolmann, *Bull. Soc. Chim. Fr.*, 3513 (1966).

Synthesis of New 1-Alkoxycarbonylamino-3-sulfonylpyrroles by Reaction of (Alkoxycarbonylazo)alkenes with β-Keto Sulfones

Orazio ATTANASI,* Paolino FILIPPONE, Amedeo MEI, Stefania SANTEUSANIO, and Franco SERRA-ZANETTI
Cattedra di Chimica Organica della Facoltá di Scienze, Universitá di Urbino, Piazza della Repubblica 3, 61029 Urbino, Italy
(Received October 15, 1985)

Synopsis. A mild, simple, and direct method for the synthesis of some new 1-alkoxycarbonylamino-3-sulfonylpyrrole derivatives by reaction of (alkoxycarbonylazo)alkenes with β-keto sulfones is reported.

The chemistry of the pyrrole ring received considerable attention by several authors, mainly due to the fact that this heterocycle is present in some natural products. In addition, several pyrrole derivatives manifested to have attractive biological and pharmacological activities.[1]

Considering this wide interest, during the last few years we particularly intended to a detailed and systematic elaboration of a synthetic strategy able to provide a large number of unknown 1-aminopyrrole derivatives containing various functional groups both at the carbon atoms of the pyrrole ring and, especially, on the amino group linked to the nitrogen heteroatom. The direct preparative procedure of 1-aminopyrrole derivatives investigated in our laboratories is in general based on the nucleophilic attack by an activated methylene group on the heterodiene system of a conjugated azoalkene, affording the formation of the 1,4-adduct intermediate. This preliminary 1,4-conjugate addition (Michael-type) may be followed by an intramolecular condensation between the C=N nitrogen atom and a ketonic carbonyl group in δ-position (esteric carbonyl group showing to be inactive), producing the pyrrole ring closure. In rather different way for each case, these reactions were frequently observed to more satisfactorily take place under copper(II) ions catalysis,[2] affording interesting 1-aminopyrrole derivatives that should result to be with difficulty synthesized by other methods.[1,3] NMR spectra,[4] X-ray crystal structures,[5] and biological activities[6] in part have been already examined and in part are presently in progress. Since the synthesis of variously functionalized 1-aminopyrroles appears to be largely dependent on the nature of conjugated azoalkenes, also the preparation of new classes of these latter derivatives have been extensively studied.[7] By these studies, conjugated azoalkenes demonstrated to represent versatile products and useful intermediates in organic chemistry.

Continuing these investigations, in this paper we report the synthesis of new 1-alkoxycarbonylamino-3-sulfonylpyrroles (**4**) by reaction of (alkoxycarbonylazo)alkenes (**1**) with β-keto sulfones (**2**). These reactions easily proceed at room temperature under magnetic stirring, often showing at first the 1,4-adduct intermediate (**3**) formation. This adduct is unambigously revealed by NMR spectra, exhibiting two doublets at δ=4—5 and δ=5.5—6.5 ppm ascribable to the two CH vicinal protons, in accordance with our previous findings on this matter.[2] The subsequent conversion of this 1,4-adduct intermediate (**3**) into related 1-alkoxycarbonylamino-3-sulfonylpyrrole is then observed, and these latter compounds are isolated in good yields without complicated procedures.

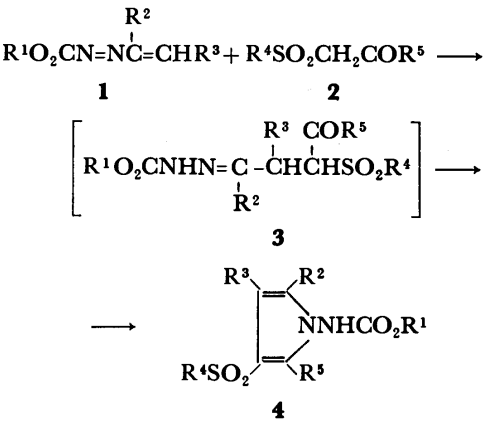

R^1	R^2	R^3	R^4	R^5
CH_3	CH_3	CO_2CH_3	CH_3	CH_3
CH_3	CH_3	$CO_2C_2H_5$	p-$CH_3C_6H_4$	CH_3
C_2H_5	CH_3	CO_2CH_3	C_6H_5	C_6H_5
C_2H_5	CH_3	$CO_2C_2H_5$		
$C(CH_3)_3$	CH_3	CO_2CH_3		
$C(CH_3)_3$	CH_3	$CO_2C_2H_5$		

Experimental

Materials and Methods. Yields are of pure isolated products (see Table 1). The reaction times are reported in Table. Melting points were determined in capillary tubes with a Büchi apparatus, and are uncorrected (see Table 1). The products often decompose at melting point. IR spectra were recorded in Nujol mull on a Perkin-Elmer 298 spectrophotometer, and values are expressed in cm^{-1}. ^1H NMR spectra were measured in deuteriochloroform with tetramethylsilane (TMS) as internal standard, using a Varian EM-360L spectrometer at 60 MHz. The chemical shifts are expressed in ppm in respect to TMS, and the coupling constants J in hertz (Hz). The abbreviations used are as follows: s, singlet; d, doublet; t, triplet; q, quartet; m, multiplet; br, broad; D_2O ex, D_2O exchange. Kieselgel 60 was used for chromatography. All the compounds obtained showed a satisfactory elemental analysis. (Alkoxycarbonylazo)alkenes (**1**) were prepared as previously reported.[2] The β-keto sulfones (**2**) were commercial materials, and were used without further purification.

Preparation of 1-Alkoxycarbonylamino-3-sulfonylpyrroles (4a—j). General Procedure. The (alkoxycarbonylazo)alkene (**1**) (2.0 mmol) and β-keto sulfone (**2**) (2.0 mmol) were

Table 1. Preparation of 1-Alkoxycarbonylamino-3-sulfonylpyrroles (**4**)

Pyrrole 4	R^1	R^2	R^3	R^4	R^5	Time h	Yield %	Mp[a] θ_m/°C
4a	CH_3	CH_3	CO_2CH_3	CH_3	CH_3	85	67	197—200
4b	CH_3	CH_3	CO_2CH_3	*p*-$CH_3C_6H_4$	CH_3	75	51	238—240
4c	CH_3	CH_3	CO_2CH_3	C_6H_5	C_6H_5	50	75	67
4d	CH_3	CH_3	$CO_2C_2H_5$	CH_3	CH_3	120	73	157—159
4e	C_2H_5	CH_3	CO_2CH_3	*p*-$CH_3C_6H_4$	CH_3	22	73	168—171
4f	C_2H_5	CH_3	$CO_2C_2H_5$	*p*-$CH_3C_6H_4$	CH_3	24	72	138—141
4g	$C(CH_3)_3$	CH_3	CO_2CH_3	*p*-$CH_3C_6H_4$	CH_3	30	71	108—110
4h	$C(CH_3)_3$	CH_3	CO_2CH_3	C_6H_5	C_6H_5	60	70	80—82
4i	$C(CH_3)_3$	CH_3	CO_2CH_3	*p*-$CH_3C_6H_4$	C_6H_5	48	76	78—82
4j	$C(CH_3)_3$	CH_3	$CO_2C_2H_5$	C_6H_5	C_6H_5	72	63	61—65

a) Melting points are uncorrected and occur with decomposition.

dissolved in tetrahydrofuran (2 ml) and the reaction was allowed to stand at room temperature under magnetic stirring (for reaction time see Table 1) until the reaction is complete (monitored by TLC silica gel). In some cases the formation of the 1,4-adduct intermediate (**3**) was at first observed, and then its conversion into related 1-aminopyrrole (**4**) was revealed. Sometimes the precipitated product (**4**) was isolated in satisfactory purity by filtration, or otherwise tetrahydrofuran was removed under reduced pressure obtaining the crude product (**4**) as residue (for yield see Table 1). The products (**4a—j**) can be further purified by recrystallization from dichloromethane–petroleum ether (40—60 °C) or tetrahydrofuran–pentane (for melting point see Table 1). In some cases, a preliminary purification of the crude product (**4**) by column chromatography on silica gel may be necessary (at first elution with cyclohexane and then with cyclohexane–ethyl acetate mixtures, gradually increasing the amount of ethyl acetate to a 80/20 (v/v) ratio).

Following compounds were prepared by this procedure.

1-Methoxycarbonylamino-2,5-dimethyl-3-methoxycarbonyl-4-(methylsulfonyl)pyrrole (4a). IR: 3275 (NH), 1750, and 1715 (COO), 1290, and 1145 (SO_2). ^{1}H NMR δ=2.27 (6H, s, 2Me), 3.32 (3H, s, SO_2Me), 3.77 (3H, s, COOMe), 3.83 (3H, s, COOMe), 8.91 (1H, s, br, NH, D_2O ex). Found: C, 43.65; H, 5.01; N, 9.02%. Calcd for $C_{11}H_{16}N_2O_6S$: C, 43.42; H, 5.30; N, 9.21%.

1-Methoxycarbonylamino-2,5-dimethyl-3-methoxycarbonyl-4-(*p*-tolylsulfonyl)pyrrole (4b). IR: 3270 (NH), 1765 and 1710 (COO), 1600 (Ar), 1290 and 1150 (SO_2). ^{1}H NMR δ=2.25 (3H, s, Me), 2.4 (3H, s, Me), 2.47 (3H, s, Ar<u>Me</u>), 3.66 (3H, s, COOMe), 3.83 (3H, s, COOMe), 7.52 (4H, q, Ar, J=8.7 Hz), 8.73 (1H, s, br, NH, D_2O ex). Found: C, 53.51; H, 5.42; N, 7.43%. Calcd for $C_{17}H_{20}N_2O_6S$: C, 53.68; H, 5.30; N, 7.37%.

1-Methoxycarbonylamino-2-methyl-3-methoxycarbonyl-4-(phenylsulfonyl)-5-phenylpyrrole (4c). IR: 3275 (NH), 1755 and 1720 (COO), 1600 and 1585 (Ar), 1290 and 1140 (SO_2). ^{1}H NMR δ=2.23 (3H, s, Me), 3.52 (3H, s, COOMe), 3.67 (3H, s, COOMe), 7.13—7.92 (10H, m, Ar), 8.28 (1H, s, br, NH, D_2O ex). Found: C, 59.01; H, 4.69; N, 6.38%. Calcd for $C_{21}H_{20}N_2O_6S$: C, 58.88; H, 4.71; N, 6.54%.

1-Methoxycarbonylamino-2,5-dimethyl-3-ethoxycarbonyl-4-(methylsulfonyl)pyrrole (4d). IR: 3260 (NH), 1760 and 1710 (COO), 1290 and 1150 (SO_2). ^{1}H NMR δ=1.37 (3H, t, COOEt), 2.28 (6H, s, 2Me), 3.33 (3H, s, SO_2Me), 3.82 (3H, s, COOMe), 4.32 (2H, q, COOEt), 8.95 (1H, s, br, NH, D_2O ex). Found: C, 45.03; H, 5.69; N, 9.02%. Calcd for $C_{12}H_{18}N_2O_6S$: C, 45.28; H, 5.70; N, 8.80%.

1-Ethoxycarbonylamino-2,5-dimethyl-3-methoxycarbonyl-4-(*p*-tolylsulfonyl)pyrrole (4e). IR: 3280 (NH), 1755 and 1710 (COO), 1600 (Ar), 1295 and 1145 (SO_2). ^{1}H NMR δ=1.3 (3H, t, COOEt), 2.27 (3H, s, Me), 2.37 (3H, s, Me), 2.47 (3H, s, C_6H_4<u>Me</u>), 3.67 (3H, s, COOMe), 4.23 (2H, q, COOEt), 7.5 (4H, q, Ar, J=8.9 Hz), 8.82 (1H, s, br, NH, D_2O ex). Found: C, 54.99; H, 5.47; N, 7.00%. Calcd for $C_{18}H_{22}N_2O_6S$: C, 54.82; H, 5.62; N, 7.10%.

1-Ethoxycarbonylamino-2,5-dimethyl-3-ethoxycarbonyl-4-(*p*-tolylsulfonyl)pyrrole (4f). IR: 3290 (NH), 1755 and 1715 (COO), 1600 (Ar), 1290 and 1150 (SO_2). ^{1}H NMR δ=0.92—1.52 (6H, m, 2COOEt), 2.27 (3H, s, Me), 2.37 (3H, s, Me), 2.47 (3H, s, C_6H_4<u>Me</u>), 3.87—4.5 (4H, m, 2COOEt), 7.5 (4H, q, Ar, J=8.8 Hz), 8.87 (1H, s, br, NH, D_2O ex). Found: C, 55.69; H, 6.06; N, 6.93%. Calcd for $C_{19}H_{24}N_2O_6S$: C, 55.88; H, 5.92; N, 6.86%.

1-(*t*-Butoxycarbonylamino)-2,5-dimethyl-3-methoxycarbonyl-4-(*p*-tolylsulfonyl)pyrrole (4g). IR: 3330 (NH), 1750 and 1730 (COO), 1600 (Ar), 1290 and 1150 (SO_2). ^{1}H NMR δ=1.52 (9H, s, CMe_3), 2.25 (3H, s, Me), 2.37 (3H, s, Me), 2.45 (3H, s, C_6H_4<u>Me</u>), 3.63 (3H, s, COOMe), 7.47 (4H, q, Ar, J=9.0 Hz), 8.46 (1H, s, br, NH, D_2O ex). Found: C, 56.69; H, 6.47; N, 6.69%. Calcd for $C_{20}H_{26}N_2O_6S$: C, 56.87; H, 6.20; N, 6.63%.

1-(*t*-Butoxycarbonylamino)-2-methyl-3-methoxycarbonyl-4-phenylsulfonyl-5-phenylpyrrole (4h). IR: 3295 (NH), 1755 and 1725 (COO), 1600 and 1585 (Ar), 1275 and 1150 (SO_2). ^{1}H NMR δ=1.3 (9H, s, CMe_3), 2.23 (3H, s, Me), 3.65 (3H, s, COOMe), 7.17—8.0 (10H, m, Ar and NH; 1H, D_2O ex). Found: C, 61.45; H, 5.63; N, 5.69%. Calcd for $C_{24}H_{26}N_2O_6S$: C, 61.27; H, 5.57; N, 5.95%.

1-(*t*-Butoxycarbonylamino)-2-methyl-3-methoxycarbonyl-4-(*p*-tolylsulfonyl)-5-phenylpyrrole (4i). IR: 3290 (NH), 1745 and 1725 (COO), 1600 (Ar), 1300 and 1150 (SO_2). ^{1}H NMR δ=1.3 (9H, s, CMe_3), 2.27 (3H, s, Me), 2.37 (3H, s, C_6H_4<u>Me</u>), 3.68 (3H, s, COOMe), 6.93—7.9 (10H, m, Ar and NH; 1H, D_2O ex). Found: C, 62.15; H, 5.86; N, 5.98%. Calcd for $C_{25}H_{28}N_2O_6S$: C, 61.98; H, 5.83; N, 5.78%.

1-(*t*-Butoxycarbonylamino)-2-methyl-3-ethoxycarbonyl-4-phenylsulfonyl-5-phenylpyrrole (4j). IR: 3280 (NH), 1740 and 1715 (COO), 1600 and 1585 (Ar), 1300 and 1150 (SO_2). ^{1}H NMR δ=1.13—1.5 (12H, s, CMe_3 and COOEt), 2.28 (3H, s, Me), 4.22 (2H, q, COOEt), 7.17—7.97 (11H, m, Ar and NH; 1H, D_2O ex). Found: C, 61.87; H, 5.69; N, 5.61%. Calcd for $C_{25}H_{28}N_2O_6S$: C, 61.98; H, 5.83; N, 5.78%.

This work was supported by financial assistance from the Ministero della Pubblica Istruzione (Roma).

References

1) A. R. Katritzky and C. W. Rees, "Comprehensive Heterocyclic Chemistry," Pergamon Press, London (1984).

2) O. Attanasi, P. Bonifazi, E. Foresti, and G. Pradella, *J. Org. Chem.*, **47**, 684 (1982); O. Attanasi, P. Bonifazi, and F.

Buiani, *J. Heterocycl. Chem.*, **20**, 1077 (1983); O. Attanasi and S. Santeusanio, *Synthesis*, **1983**, 742; O. Attanasi, P. Filippone, A. Mei, and S. Santeusanio, *ibid.*, **1984**, 671; O. Attanasi, P. Filippone, A. Mei, and S. Santeusanio, *ibid.*, **1984**, 873; O. Attanasi and F. R. Perrulli, *ibid.*, **1984**, 874; O. Attanasi, P. Filippone, A. Mei, S. Santeusanio, and F. Serra-Zanetti, *ibid.*, **1985**, 157; O. Attanasi, F. R. Perrulli, and F. Serra-Zanetti, *Heterocycles*, **23**, 867 (1985); O. Attanasi, M. Grossi, and F. Serra-Zanetti, *Org. Prep. Proced. Int.*, **18**, 1 (1986); O. Attanasi, P. Filippone, A. Mei, and F. Serra-Zanetti, *Synth. Commun.*, **16**, 343 (1986).

3) R. A. Jones and G. P. Bean, "The Chemistry of Pyrroles," Academic Press, London (1977); J. M. Patterson, *Synthesis*, **1976**, 281; A. Gossauer, "Die Chemie der Pyrrole," Springer-Verlag, Berlin (1974); G. P. Gardini, *Adv. Heterocyclic Chem.*, **15**, 67 (1973); R. A. Jones, *ibid.*, **11**, 383 (1970); A. H. Corwin, "Heterocyclic Compounds," New York (1970); H. H. Inhoffen, J. W. Buchler, and P. Jäger, *Fortschr. Chem. Org. Naturst.*, **26**, 284 (1968); R. E. Willette, *Adv. Heterocyclic Chem.*, **9**, 27 (1968).

4) O. Attanasi, S. Santeusanio, G. Barbarella, and V. Tugnoli, *Magn. Res. Chem.*, **23**, 383 (1985).

5) G. Giuseppetti, C. Tadini, O. Attanasi, M. Grossi, and F. Serra-Zanetti, *Acta Crystallogr.*, **C41**, 450 (1985).

6) Some data are the results of screening performed under the auspices of the Developmental Therapeutics Program, Division of Cancer Treatment, National Cancer Institute, Bethesda, Maryland, USA. Other data are the results of screening performed by a chemical corporation and are communicated for our confidential use only.

7) O. Attanasi, M. Grossi, and F. Serra-Zanetti, *Org. Prep. Proced. Int.*, **17**, 385 (1985); O. Attanasi, P. Filippone, A. Mei, and F. Serra-Zanetti, *J. Heterocycl. Chem.*, **23**, 25, (1986).

Electrocatalysis of the Heat-Treated (5,10,15,20-Tetraphenylporphyrinato)-manganese(III) Halides for Cathodic Reduction of Oxygen

Osamu IKEDA,* Toyosei KOJIMA, and Hideo TAMURA
Department of Applied Chemistry, Faculty of Engineering, Osaka University, Yamadaoka, Suita, Osaka 565
(Received December 20, 1985)

Electrocatalysis of the heat-treated (5,10,15,20-tetraphenylporphyrinato)manganese(III) halides (Mn^{III}(TPP)X, X:F^-, Cl^-, Br^-, I^-) for the O_2 reduction in an alkaline solution has been studied by rotating ring-disc electrode technique, and the result was correlated with properties of the heat-treated Mn^{III}(TPP)X, such as magnetic moment and electrical resistivity. The axial ligand X showed noticeable effect on the catalytic activity. The catalytic activity estimated from the overpotential changed in the following order: $F^->Cl^->Br^->I^-$. The catalytic activity for reducing oxygen to OH^- was low, but the same order of activity as the above applies. The order was interpreted by the σ-donating ability of halide ion X to d_{z^2} orbital. The active site of the Mn^{III}(TPP)X heat-treated at 700 °C for O_2 reduction is ascribed to the metal ion, coordinated to slightly degraded or perfect N_4 center, but not degradation products of the relevant compounds.

Many transition metal complexes with macrocycles such as porphyrin, phthalocyanine, and tetraaza-annulene show catalytic activity for the cathodic reduction of oxygen. When these metallomacrocycles are applied to practical electrocatalyst for O_2 reduction, however, many of them are unstable in strong acid and alkaline electrolytes. Jahnke et al.[1] showed that this defect is overcome by the heat treatment in an inert atmosphere, and that the catalytic activity improved by the treatment. The disclosure accelerated the study on the heat treatment of metallomacrocycles for the cathodic reduction of oxygen.[2-15] However, the active site and the electrocatalysis of the heat-treated metallomacrocycles have not been fully elucidated. The active site suggested so far is (i) metal ion in the N_4 center,[7,16] (ii) carbonaceous substance formed by the degradation of N_4 center,[4] and (iii) an intermediate between (i) and (ii), namely, metal ion coordinated to partially degraded N_4 center.[13] The finely dispersed metal such as β-cobalt, which is formed by the heat treatment of cobalt(II) porphyrins, is examined.[11]

Recently, we studied the cathodic reduction of oxygen on unheated Mn^{III}(TPP)X, whose various properties are influenced by the axial ligand because of the strong π-mixing between metal and porphyrin ring.[17-20] It follows that the catalytic activity for O_2 reduction strongly depends on the axial ligand.[21] The porphyrins seem to be suitable to investigate active site and the electrocatalysis of heat-treated metallo-porphyrins for O_2 reduction, because the axial ligand affects the electrocatalysis, if the metal ion is the active site.

Experimental

Materials. In analogy with octaethylporphyrinatoiron-(III) halides,[22] Mn^{III}(TPP)X (X:F^-, Cl^-, Br^-, I^-) were prepared by the ligand-exchange reaction of Mn^{III}(TPP)($OCOCH_3$) with aqueous NaX as described elsewhere.[21] Plates (10×10 mm^2) and rods (6 mmϕ) of glassy carbon (G.C., Tokai Carbon, GC20) were used as the base electrode, onto which one of the Mn^{III}(TPP)X was coated. These G.C. electrodes were polished to a mirror surface with alumina powder, and washed in an ultrasonic bath to remove alumina powder. 1 M(=mol dm^{-3}) KOH was used as the electrolyte, which was saturated with pure oxygen at the cathodic reduction experiments. Pt net and Hg/HgO electrode in 1 M KOH were used as counter and reference electrodes, the potential of the latter against normal hydrogen electrode (NHE) being +0.098 V.

Heat Treatment. The chloroform solution of each Mn^{III}(TPP)X was coated onto the G.C. plate (1 cm^2) and top surface of the rod (0.28 cm^2) using a microcyringe, and the coating amount was fixed to 3×10^{-7} mol cm^{-2}. After drying in air, the electrodes were placed in a quarz tube, and then filled with highly pure Ar (O_2<1—2 ppm) by alternate degassing and filling. The Mn^{III}(TPP)X-coated G.C. in the tube was heated in an electric furnace for 10 min at each temperature and cooled in air. Electrochemical data for heat-treated Mn^{III}(TPP)X varied with the amount of coating, probably due to imperfect coating and sublimation up to less than 1×10^{-7} mol cm^{-2}. However, the data became nearly constant at the coating over 1×10^{-7} mol cm^{-2}.

The heat treatment of Mn^{III}(TPP)X powder, for the measurement of bulk properties, was carried out by the same manner as described above by putting the powder in a small quarz beaker.

Electrochemical Measurements. The G.C. rod coated with heat-treated Mn^{III}(TPP)X was used as the ring (Pt)-disc electrode. The Pt ring was cleaned by a potential sweep cycling between O_2 and H_2 generation potentials in 0.5 M H_2SO_4 before use. In the cathodic reduction of oxygen, the ring potential was fixed to +0.25 V (vs. Hg/HgO in 1 M KOH), where the diffusion limiting current for HO_2^- oxidation was observed.

The G.C. plate coated with heat-treated Mn^{III}(TPP)X was installed into a Teflon holder with a window of 0.5 cm^2 open to the electrolyte solution, and was used in the cyclic voltammetry to evaluate catalytic activity and stability.

Other Measurements. The mass magnetic susceptibility

* Present address: Laboratory of Chemistry, College of Liberal Arts, Kanazawa University, 1-1 Marunouchi, Kanazawa 920.

χ_g of heat-treated $Mn^{III}(TPP)X$ was measured by Gouy method using a magnetic balance (Shimadzu, MB-11) at room temperature, usually 25 °C. The χ_g was corrected for ferromagnetic impurities by extrapolating the plot of (mass magnetization)/(magnetic field strength) $[(M)/(H)]$ against $(1/H)$ to $(1/H)=0$. The molar magnetic susceptibility χ_M was evaluaded by determining the molecular weight (M.W.) of the porphyrin unit per manganese ion, using the relation: $\chi_M=\chi_g\times$M.W. Thermogravimetry (TG) and differential thermal analysis (DTA) for $Mn^{III}(TPP)X$ were carried out by means of Rigaku DG-ClH Thermoflex, at a heating rate of 5 °C min^{-1} in Ar stream. Electrical resistivity of heat-treated $Mn^{III}(TPP)X$ was measured by the two-probe method for powdered sample pressed between metal rods in a thick glass tube.

Results and Discussion

Thermal Behavior of $Mn^{III}(TPP)X$. Thermal reactions taking place during the heat treatment were elucidated from the DTA and TG curves. The results for four $Mn^{III}(TPP)X$ ($X:F^-$, Cl^-, Br^-, I^-) examined are shown in Fig. 1. The DTA curve of each porphyrin has two endo/exothermic peaks at nearly same temperature regions: The first is between 400° and 500 °C, and the second around 850 °C. An obvious weight loss was observed in TG curves at the first DTA peak, but not at the second DTA peak. The first thermal reaction between 400° and 500 °C is speculated to be the condensation reaction due to release of phenyl groups and hydrogen, indicating formation of an extended π-electron system, because the resistivites of $Mn^{III}(TPP)X$ decreased from $>10^9\ \Omega$ cm to 10^5—$10^4\ \Omega$ cm with this reaction. The second thermal reaction seems to be the degradation of porphyrin skeleton, because manganese monoxide (MnO) was detected by X-ray diffraction in the samples heated above 850 °C.

The following analyses examine the changes in the heat treatment of $Mn^{III}(TPP)X$. Some properties of $Mn^{III}(TPP)X$ heat-treated at 700 °C were compared, where the catalytic activity for O_2 reduction is maximum.

Molecular Weight. Since $Mn^{III}(TPP)X$ heat-treated above 500 °C are insoluble in organic solvents, the molecular weight per manganese ion was evaluated by determining Mn ion in the ashed samples on heating in air. Table 1 summarizes the results. The accuracy of this measurement is ±3% from the results for unheated $Mn^{III}(TPP)X$. The molecular weight decreased with the heat treatment at 700 °C by 60—90. This suggests a release of one phenyl group during the heat treatment. Release of hydrogen atoms on phenyl groups may occur at 700 °C, because the condensation products show no solubility in organic solvents and have low resistivity of about $10^2\ \Omega$ cm.

Atomic Ratio. In order to examine the stability of N_4 center during the heat treatment, the atomic ratio of N to Mn was evaluated using the manganese content and the nitrogen content obtained from the elemental analysis. Figure 2 shows the results as a function of the heat-treatment temperature. The N/Mn ratio for unheated $Mn^{III}(TPP)X$ was about 4,

Table 1. Molecular Weight Per Manganese Ion for Unheated and Heat-Treated $Mn^{III}(TPP)X$

X	Heat-treatment temperature/°C			
	unheated	500	700	900
F^-	670	630	600	580
Cl^-	720	—	630	—
Br^-	760	—	700	—
I^-	800	—	740	—

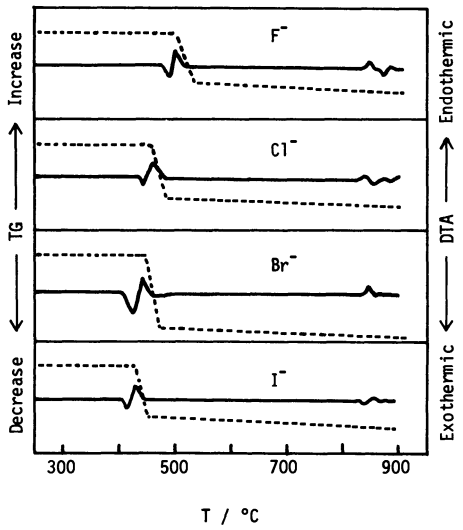

Fig. 1. Differential thermal analysis (——) and thermogravimetry (----) curves for $Mn^{III}(TPP)X$ (X: F^-, Cl^-, Br^-, I^-) in Ar stream. Heating rate, 5 °C min^{-1}.

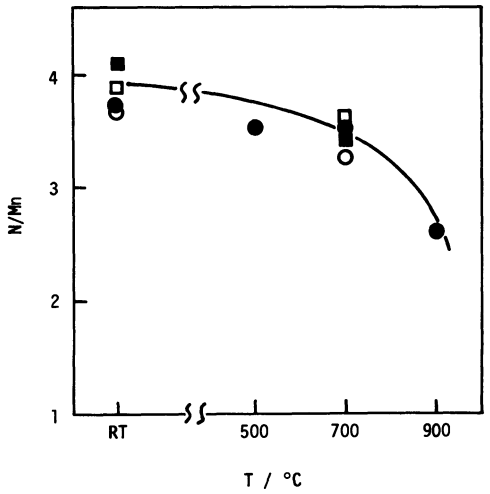

Fig. 2. Variation of N/Mn ratio with the heat-treatment temperature for $Mn^{III}(TPP)X$. X: (●) F^-; (■) Cl^-; (□) Br^-; (○) I^-. RT(room tempereature) means the unheated $Mn^{III}(TPP)X$.

while the ratio gradually decreased to 3.5 with the heat treatment up to 700 °C, and greatly fell to 2.6 at 900 °C. The results suggest that the N_4 center is maintained up to 700 °C, but it is degraded at 900 °C where the second DTA peak appears and MnO is detected by X-ray diffraction.

Next, we determined the ratio of X to Mn to estimate the stability of Mn–X bond in the heat treatment, using the molecular weight per manganese ion and the X content from the elemental analysis. The X/Mn ratio for $Mn^{III}(TPP)X$ heat-treated at 700 °C, except for $Mn^{III}(TPP)F$ whose elemental analysis for F was impossible, was 0.8—0.9. This suggests that most of the manganese sites are coordinated by the axial ligand even after the heat treatment at 700 °C.

Magnetic Moment. Magnetic moment for $Mn^{III}(TPP)X$ heat-treated at 700 °C was evaluated to estimate the spin state of central manganese ion. The effective magnetic moment μ_{eff} was calculated by the following relation for magnetically diluted substances: $\mu_{eff}=2.84\sqrt{\chi_M T}$, where T is the temperature at the measurement. The μ_{eff} for all $Mn^{III}(TPP)X$ (X: F^-, Cl^-, Br^-, and I^-) heat-treated at 700 ° were in the range of 5.0—5.3 μ_B (Bohr Magneton) and were in good agreement with the values of 5.0—4.8 μ_B for unheated $Mn^{III}(TPP)X$ (X: Cl^-, Br^-, and I^-), a fact indicating high-spin $Mn^{III}(d^4)$ complex which has the theoretical μ_{eff} of 4.9 μ_B. The μ_{eff} of unheated $Mn^{III}(TPP)F$ was 3.8 μ_B. The result indicates that an intermediate-spin changed to the high-spin complex by the heat treatment, as can be seen from Fig. 3. We confirmed previously that the unheated $Mn^{III}(TPP)F$ has the highest π-mixing with ring orbitals among $Mn^{III}(TPP)X$.[21] Extended π-electron system due to the heat treatment seems to weaken the π-mixing, resulting in high-spin state.

Electrocatalysis for O_2 Reduction. We have discussed the electrocatalysis of heat-treated $Mn^{III}(TPP)X$ based on two methods to examine the catalytic activity: One is the overpotential and the other the capability of reducing oxygen to OH^- or the so-called 4-electron reducibility.

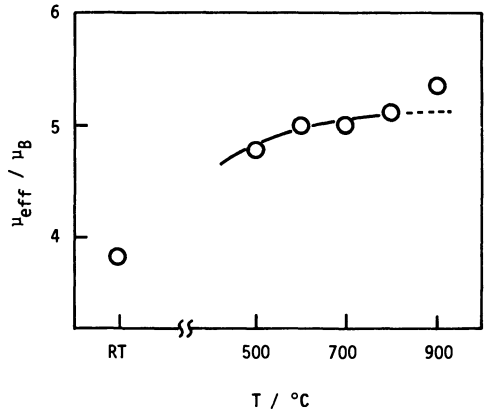

Fig. 3. Variation of the effective magnetic moment (μ_{eff}) of $Mn^{III}(TPP)F$ with heat-treatment temperature. RT(room temperature) means the unheated $Mn^{III}(TPP)F$.

Figure 4 shows the voltammograms of $Mn^{III}(TPP)F$ heat-treated at different temperatures for the O_2 reduction by rotating disc electrode. The catalytic activity based on the overpotential or the current at a constant potential showed a complicated change with the heat-treatment temperature: It decreased with the temperature up to 600 °C, and then increased showing a maximum at 700 °C. The same change was also observed in the cyclic voltammograms by use of plate electrode. The catalytic activity fluctuated at 800 °C: Low reproducility at 800 ° seems to be related with that the temperature is in the vicinity of the degradation temperature of N_4 center. The low catalytic activity of $Mn^{III}(TPP)F$ heat-treated at 900 °C is caused by the degradation of N_4 center. The diffusion limiting current for O_2 reduction became lower by the heat treatment, indicating the change in reduction pathway from the 4-electron pathway ($O_2+2H_2O+4e^-\rightarrow 4OH^-$) to the 2-electron pathway ($O_2+H_2O+2e^-\rightarrow HO_2^-+OH^-$), as will be discussed later.

Figure 5 shows the cyclic voltammograms of $Mn^{III}(TPP)X$ heat-treated at 700 °C. Under more negative potentials, the reduction peak in the cyclic voltammogram was observed for $Mn^{III}(TPP)Br$, but unobservable for $Mn^{III}(TPP)I$. However, the catalytic

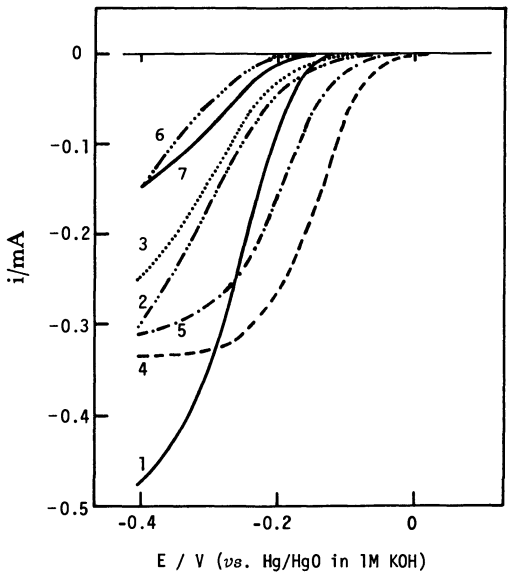

Fig. 4. Voltammograms at the rotating disc(glassy carbon coated with $Mn^{III}(TPP)F$) electrode for the cathodic reduction of oxygen in O_2-saturated 1M KOH. Heat-treatment temperature of $Mn^{III}(TPP)F$: (1) unheated; (2) 500 °C; (3) 600 °C; (4) 700 °C; (5) 800 °C; (6) 900 °C; (7) bare G.C. Sweep rate, 20 mV s^{-1}; rotation rate, 1000 r.p.m.; surface area of the disc, 0.28 cm^2.

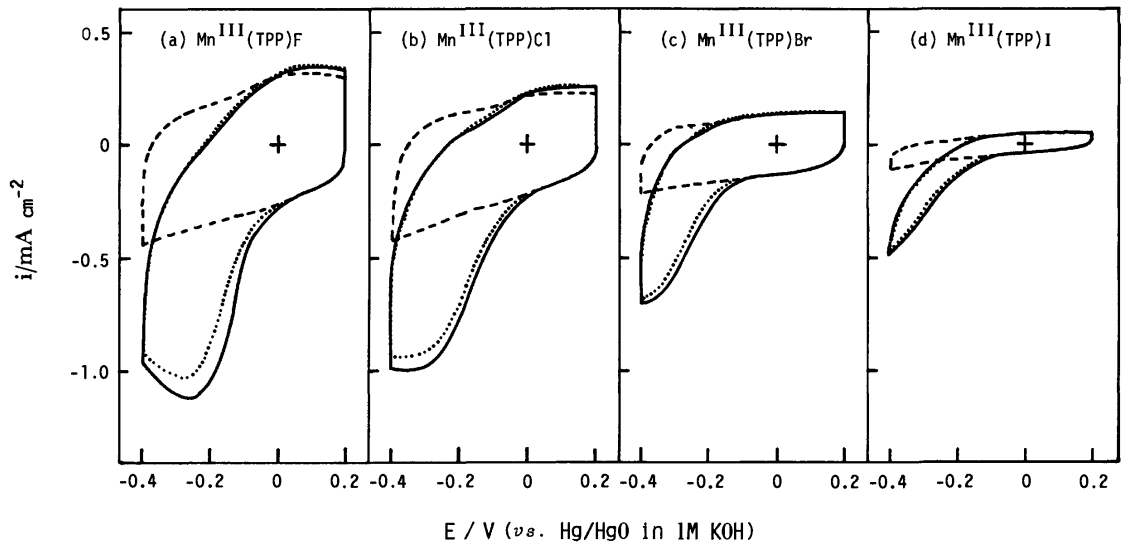

Fig. 5. Cyclic voltammograms at the plate(glassy carbon coated with Mn^{III}(TPP)X heat-treated at 700 °C) electrode for the cathodic reduction of oxygen in O_2-saturated 1 M KOH. X: (a) F^-; (b) Cl^-; (c) Br^-; (d) I^-. The broken line is for N_2-saturated 1 M KOH. The solid and dotted lines for O_2-saturated 1 M KOH are the voltammograms at the first cycle and after 1000 cycles, respectively. Sweep rate, 100 mV s^{-1}; electrode area, 0.5 cm^2.

activity estimated from the overpotential was in the order: $F^->Cl^->Br^->I^-$. Stability of the catalysts was improved by the heat treatment, because there appeared only a small change in the cyclic voltammograms at the first and 1000 cycles (Fig. 5). Since the instability of unheated Mn^{III}(TPP)X depends upon the ligand exchange of X with OH^-,[21] the improved stability suggests the formation of a dense structure without pores which prevents from penetrating of electrolyte.

Figure 6 shows the voltammograms at the rotating ring (Pt)-disc (G.C. coated with Mn^{III}(TPP)X heat-treated at 700 °C) electrode. The lower curves represent the disc currents for O_2 reduction and the upper curves the ring currents for the oxidation of HO_2^- as a reduction intermediate of O_2.

In order to elucidate the 4-electron reducibility of the heat-treated Mn^{III}(TPP)X for oxygen, the apparent number of electrons consumed in the O_2 reduction (n_{app}) was evaluated using the ring and disc currents around −0.3 V in Fig. 6. In the evaluation of n_{app}, it was assumed that the O_2 reduction at the disc consists of a mixed reaction of the 2-electron pathway ($O_2+H_2O+2e^-\rightarrow HO_2^-+OH^-$) and the 4-electron pathway ($O_2+2H_2O+4e^-\rightarrow 4OH^-$). Thus n_{app} was estimated by the next relation:[15,23] $n_{app}=4I_{Disc}/(I_{Disc}+I_{Ring}/N_{corr})$, where N_{corr} is the collection efficiency for HO_2^-, corrected for a deviation from the coplanality between the Pt ring and the Mn^{III}(TPP)X-coated disc, which is about 0.1 for various ring-disc electrodes.

The result for Mn^{III}(TPP)X heat-treated at 700 °C is shown in Fig. 7. Also, the result for Mn^{III}(TPP)F heat-treated at different temperatures is shown in Fig. 8. As can be seen from Fig. 7, the n_{app} shows some

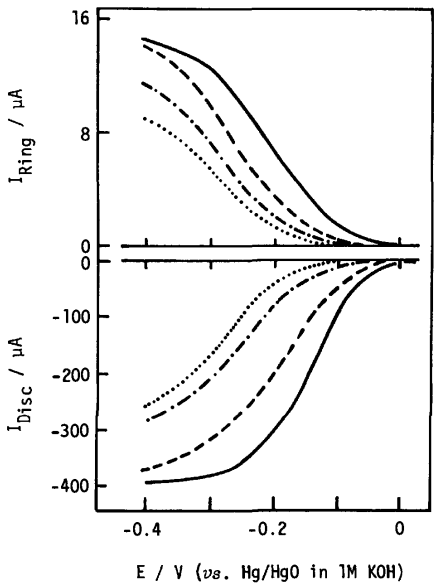

Fig. 6. Voltammograms at the rotating ring(Pt)-disc (glassy carbon coated with Mn^{III}(TPP)X heat-treated at 700 °C) electrode for the cathodic reduction of oxygen in O_2-saturated 1 M KOH. X: (——) F^-; (– – –) Cl^-; (—·—) Br^-; (·····) I^-. Ring potential, 0.25 V (vs. Hg/HgO in 1 M KOH); sweep rate at the disc, 20 mV s^{-1}; rotation rate, 1000 r.p.m.; surface area of the disc, 0.28 cm^2.

dependence on the axial ligand, and the n_{app} value decreases from 2.3 for F^- to 2.0 for I^-. On the other hand, it is observed from Fig. 8 that the high 4-electron reducibility of unheated Mn^{III}(TPP)F is considerably lost by the heat treatment.

Effect of Axial Ligand on Electrocatalysis. The catalytic activity of heat-treated Mn^{III}(TPP)X, based

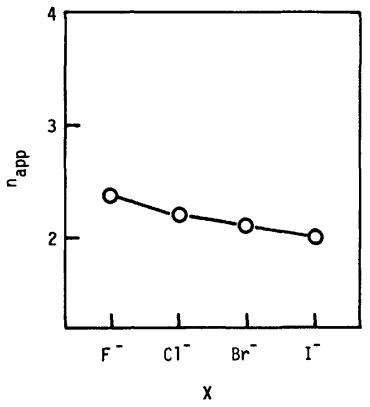

Fig. 7. Variation of the apparent number of electrons consumed in O_2 reduction (n_{app}) with the axial ligand of $Mn^{III}(TPP)X$ heat-treated at 700 °C.

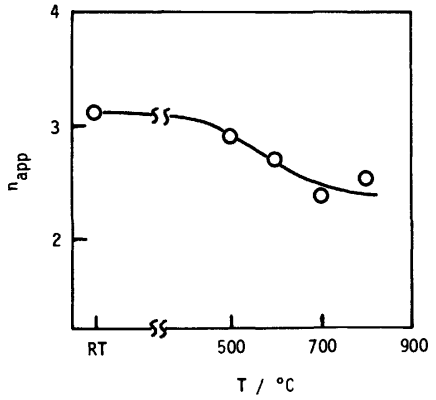

Fig. 8. Variation of the apparent number of electrons consumed in O_2 reduction (n_{app}) with the heat-treatment temperature for $Mn^{III}(TPP)F$. RT(room temperature) is for the unheated $Mn^{III}(TPP)F$.

on the overpotential and the 4-electron reducibility, depends markedly on the axial ligand. As for the property of the axial ligand affecting the catalytic activity, the most probable one seems to be the electron-donating ability of X, which influences on interaction with O_2 molecule on manganese site through a change in the d-electron population.

The coordination mode of oxygen to metal has been considered to be an important factor for the catalysis or the reaction pathway in the cathodic reduction of oxygen. The end-on coordination (Pauling model[24]) leads to the 2-electron pathway, while the side-on coordination (Griffith model[25]) leads to the 4-electron pathway. Therefore, the d-electron configuration leading to the 4-electron pathway is considered to be empty d_{z^2} orbital which accepts electrons of oxygen $1\pi_u$ to form σ-bond, and filled d_{xz} and d_{yz} (d_π) orbitals which enable the back donation to oxygen $1\pi_g^*$ orbital.[26]

Figure 9 represents (a) the low-spin and (b) the high-spin d-electron configuration for a manganese(III) porphyrin, respectively.[27] Though the high-spin

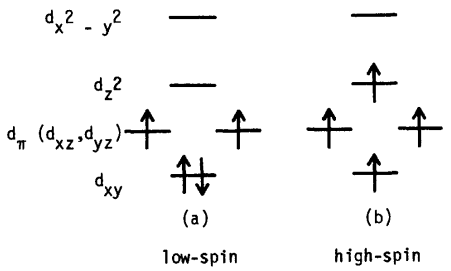

Fig. 9. The d-electron configurations for (a) low-spin and (b) high-spin d^4 manganese(III) porphyrin.

$Mn^{III}(TPP)X$ has half-filled d_π orbitals, the O_2 reduction on it occurs virtually through the 2-electron pathway. The presence of unpaired electron on d_{z^2} orbital seems to form predominantly the end-on coordination of oxygen through an interaction with $1\pi_g^*$ orbital, leading to the 2-electron pathway. The high 4-electron reducibility of unheated $Mn^{III}(TPP)F$ is ascribed to the intermediate spin, i.e., periodical or partial formation of the low-spin state with high affinity with the side-on coordination of oxygen. The 4-electron reducibility lowered by the heat treatment can be accounted for by the alteration into the high-spin state (Figs. 3 and 8). Irrespective of the high-spin state, the σ-donation by axial ligand onto d_{z^2} orbital seems to favor slightly the 4-electron reducibility because the character of unpaired electron of the d_{z^2} orbital is diluted by the donated electrons. In this context, the order of the electron-donating ability of X[17] ($F^- > Cl^- > Br^- > I^-$) explains the change in the 4-electron reducibility of heat-treated $Mn^{III}(TPP)X$ with X (Fig. 7).

The electron-donating ability of X thus explains the catalytic activity based on the overpotential (Fig. 5), because the increased population of electron on d_{z^2} orbital facilitates the interaction with O_2 molecule, as in the case of [tetrakis(methoxyphenyl)porphyrinato]-cobalt(II) with electron-donating methoxy groups.[28]

A particular phenomenon observed for heat-treated $Mn^{III}(TPP)X$ was the occurrence of large background current in Fig. 5. Moreover, the magnitude of the background current appears to represent the catalytic activity. This current is considered to be a capacitive current, as has already been confirmed for thick cobalt-phthalocyanine film,[29] which presumably has a characteristic surface state. As the surface state in the heat-treated $Mn^{III}(TPP)X$, delocalized π-electron in the extended π-system or metal may be conceivable. It has been noted for hydrophobic iron-porphyrin[23] that only the outermost layer of multiple layer on the electrode is effective on the electrocatalysis. Accordingly, the surface state described above will assist the electron transfer to oxygen molecule coordinated on the metal.

References

1) H. Jahnke, M. Schönborn, and G. Zimmerman, *Fortschr. Chem. Forsch.*, **61**, 133 (1976).

2) V. S. Bagozky, M. M. Tarasevich, K. A. Radyushkina, O. A. Levina, and S. I. Andrusyova, *J. Power Sources*, **2**, 233 (1977/78).

3) K. Wiesener and A. Fuhrman, *Z. Phys. Chem. (Leipzig)*, **261**, 411 (1980).

4) A. Fuhrman, K. Wiesener, I. Iliev, S. Gamburzev, and A. Kaisheva, *J. Power Sources*, **6**, 69 (1981).

5) J. A. R. van Veen, J. F. van Baar, C. J. Kroese, J. G. F. Coolegem, N. de Wit, and H. A. Colijn, *Ber. Bunsenges. Phys. Chem.*, **85**, 693 (1981).

6) J. A. R. van Veen and H. A. Colijn, *Ber. Bunsenges. Phys. Chem.*, **85**, 700 (1981).

7) J. A. R. van Veen, J. F. van Baar, and K. J. Kroese, *J. Chem. Soc., Faraday Trans. 1*, **77**, 2827 (1981).

8) A. Kaisheva, S. Gamburtsev, and I. Iliev, *Elektrokhimiya*, **18**, 139 (1982).

9) S. Gamburtsev, I. Iliev, and A. Kaisheva, *Elektrokhimiya*, **18**, 1602 (1982).

10) K. Okabayashi, O. Ikeda, and H. Tamura, *Chem. Lett.*, **1982**, 1659.

11) K. Wiesener, *Elektrokhimiya*, **18**, 758 (1982).

12) I. Iliev, S. Gamburtsev, A. Kaisheva, A. Fuhrman, and K. Wiesener, *J. Power Sources*, **13**, 217 (1984).

13) E. Yeager, *Electrochim. Acta.*, **29**, 1527 (1984).

14) O. Ikeda, H. Fukuda, and H. Tamura, *J. Chem. Soc., Chem. Commun.*, **1984**, 567.

15) O. Ikeda, H. Fukuda, and H. Tamura, *J. Chem. Soc., Faraday Trans. 1*, **82**, 1561 (1986).

16) R. W. Joyner, J. A. R. van Veen, and W. M. H. Sachtler, *J. Chem. Soc., Faraday Trans. 1*, **78**, 1021 (1982).

17) G. N. La Mar and F. A. Walker, *J. Am. Chem. Soc.*, **97**, 5103 (1975).

18) R. R. Gaughan, D. F. Shriver, and L. J. Boucher, *Proc. Nat. Acad. Sci. U.S.A*, **72**, 433 (1975).

19) L. J. Boucher, *Ann. N. Y. Acad. Sci.*, **205**, 409 (1973).

20) L. J. Boucher, *J. Am. Chem. Soc.*, **92**, 2725 (1970).

21) O. Ikeda, T. Kojima, and H. Tamura, *J. Electroanal. Chem. Interfacial Electrochem.*, **200**, 323 (1986).

22) H. Ogoshi, E. Watanabe, Z. Yoshida, J. Kincaid, and K. Kawamoto, *J. Am. Chem. Soc.*, **95**, 2845 (1973).

23) K. Shigehara and F. C. Anson, *J. Phys. Chem.*, **86**, 2776 (1982).

24) L. Pauling, *Nature*, **203**, 182 (1964).

25) J. S. Griffith, *Proc. R. Soc. London, Ser. A*, **235**, 23 (1956).

26) J. S. Valentine, *Chem. Rev.*, **73**, 235 (1973).

27) A. P. Hansen and H. M. Goff, *Inorg. Chem.*, **23**, 4519 (1984).

28) H. Alt, H. Binder, W. Lindner, and G. Sandstede, *J. Electroanal. Chem. Interfacial Electrochem.*, **31**, App. 19 (1961).

29) F. van den Brink, W. Visscher, and E. Barendrecht, *J. Electroanal. Chem. Interfacial Electrochem.*, **157**, 283 (1983).

 © 1986 The Chemical Society of Japan Bull. Chem. Soc. Jpn., 59, 3341—3346 (1986)

A Molecular Dynamical Study of the Mutual Diffusion Coefficient and Cooperative Motion in a 2-Dimensional Aqueous Solution

Yosuke KATAOKA
Department of Chemistry, Faculty of Science, Kyoto University, Kyoto 606
(Received December 24, 1985)

Constant-temperature constant-pressure molecular dynamics simulations of a two-dimensional aqueous solution-like system are performed at many temperatures under a constant pressure. The total number of molecules in the system is 576, and the mole fraction of the solute is 0.5. The mutual diffusion coefficient, the kinetic diffusion coefficient, and the velocity correlation between different molecules are thus obtained. The reduced kinetic diffusion coefficient has a maximum at an intermediate temperature under a constant pressure. This feature is consistent with the temperature dependence of the mean-square-concentration fluctuations. The lifetime of the local structure is estimated from the cross-correlation function of displacement, which is computed from the time-averaged configurations, where the average period is several times longer than the velocity-autocorrelation time. The correlation length of the local concentration fluctuations is obtained and compared with the snapshots of the configurations at several temperatures. The dynamical properties are qualitatively in agreement with those of an alcohol–water mixture.

Local fluctuations of concentration afford information which is useful for understanding the mixing of liquids from a molecular point of view.[1] In order to discuss the state of mixing from a dynamical standpoint, the lifetime of local structures should be taken into account.[1] For these reasons, quasi-elastic light scattering, NMR, and Rayleigh–Brillouin scattering experiments are performed in order to determine the mean-square-concentration fluctuations, the mutual diffusion coefficients, and the correlation length.[1–25] In such studies, solutions with a lower critical solution temperature are often examined because many thermodynamical quantities of such solutions show a prominent temperature- and concentration-dependence. Binary mixtures of an alcohol and water are typical examples. For the present, it is difficult to simulale such systems with a sufficient number of molecules by either the Monte Carlo or molecular dynamics (MD) method using realistic models at many temperatures and concentrations for a systematic study, although some works have been published reporting on work at a few temperatures and concentrations.[26–29]

In a previous paper,[30] a Monte Carlo study of a 2-dimensional (2-D) aqueous solution-like system was carried out by making use of the 2-D water-like model.[31] This solution model was designed to simulate binary mixtures of an alcohol and water. This is suitable for the systematic Monte Carlo calculation and molecular dynamics of solutions. The mean-square-concentration fluctuation was calculated as a function of the temperature, the density and the concentration. The mean-square-concentration fluctuation has a maximum at an intermediate temperature. This feature is similar to those of solutions with upper and lower critical solution temperatures.[30] The concentration dependence of the thermodynamic properties at low temperatures is qualitatively in agreement with that of an alcohol–water mixture.[30] We perform molecular dynamical calculations on the same model in this work.

The purpose of the present study is to see dynamical properties of a system where the concentration fluctuates to a considerable extent and to obtain the mutual diffusion coefficient, the velocity correlation between different molecules, and the lifetime of the local structure.

We adopt the 2-dimensional (2-D) aqueous solution-like model.[30] The solvent is a 2-D water-like model, which reproduces the well-known anomalous behavior of liquid water.[31,32] The water-solute interaction is anisotropic. The solute–solute interaction is assumed to be of the Lennard–Jones type for the sake of simplicity.

The merits of low dimensions are as follows. (i) We can save computing time and memory size. This point is important because we are going to perform many simulations at various temperatures. (ii) The linear dimension of the basic cell in the simulation is larger than that of a three-dimensional cell (3-D) ($576=24^2\simeq 8.3^3$) provided that the total number of molecules is fixed. Thus, the effect of the periodic boundary condition would be smaller in the case of 2-D than that in the 3-D calculation with the same number of molecules. Despite theoretical predictions that transport coefficients in a 2-D system will diverge, a computer simulation of a small system can be used to study the transport properties.[33] The shortcoming of our simulation on a 2-D solution is that there are no experimental results on any 2-D aqueous-like solution and that our results must, therefore, be qualitatively compared with experimental results; we shall use reduced units.[31]

The constant-temperature and constant-pressure MD(T-P-MD) method is used, because this method is more convenient for obtaining the temperature dependence of the system. By T-P-MD, the mutual diffusion coefficient D[35,36] is calculated for the system with 576 molecules in a square cell. As the mean-square-concentration fluctuation of the system has a maximum around $x_s=0.5$ (x_s is the mole fraction of

the solute),[30] the mole fraction of the solute is 0.5 in this work. The kinetic diffusion coefficient, L, is derived from the mutual diffusion coefficient D and the mean-square-concentration fluctuation. We want here to discuss the temperaure dependence of the kinetic diffusion coefficient L. The kinetic diffusion coefficient L includes the L_0 term, which equals L when the velocity correlation between different molecules can be neglected. As this term L_0 also depends on the temperature, the temperature dependence of L will be discussed by means of the reduced quantities L/L_0. Its temperature dependence will be qualitatively compared with that in an alcohol-water mixture.[21]

In order to estimate the lifetime of the local structure, the cross-correlation function of translation will be studied using the time-averaged positions of molecules, where the average period is several times longer than the velocity-autocorrelation time.[32] From the analysis of the cross-correlation of translation, the size of the "moving unit" will also be estimated; the "moving unit" is a group of molecules which move together for a time much longer than the velocity-autocorrelation time.[1] This size will be compared with the static correlation lenght of the local-concentration fluctuations. It will be shown that these are consistent with the snapshots of the configurations at several temperatures.

Molecular Dynamics Method

The 2-D model of an aqueous solution-like system was described in the previous paper.[30] The constant-temperature constant-pressure MD method was shown in another paper.[32] Therefore, the model and the MD method will be described only briefly here.

The pair potential U_{AB} between molecules A and B is given as follows (the suffixes A and B will be used to express water or a solute, unless otherwise stated):

$$U_{WW} = U_{LJ}^{WW}(R_{WW}) + U_{ANISO}^{WW}(R_{WW}, \varphi_{W1}, \varphi_{W2}), \quad (1)$$

$$U_{WS} = U_{LJ}^{WS}(R_{WS}) + U_{ANISO}^{WS}(R_{WS}, \varphi_{W}, \varphi_{S}), \quad (2)$$

$$U_{SS} = U_{LJ}^{SS}(R_{SS}). \quad (3)$$

Here, U_{WW} is the water-water interaction energy,[31] R_{AB} denotes the distance between two molecules A and B, and φ_A and φ_B, the orientation of the respective molecules, as is shown in Fig. 1 in Ref. 30. The first terms in Eqs. 1—3 $U_{LJ}^{AB}(R_{AB})$ are the Lennard-Jones potential functions. The parameter of these functions and the anisotropic interaction between water and a solute U_{ANISO}^{WS} are given in Ref. 30.

The mass M_A and the moment of inertia I_A of the A molecule are assumed as follows for the sake of simplicity:

$$M_W = M_S = 18 \text{ (in units of atomic weight)} \quad (4)$$

$$I_W = I_S = 3.34 \times 10^{-44} \text{ gm}^2. \quad (5)$$

We use the following reduced units.[31] The energy E is measured in units of ε_0=24.68 kJ mol^{-1}, ($-\varepsilon_0$ is the absolute minimum of the pair potential energy U_{WW}); the temperature in units of ε_0/k_B (k_B is the Boltzmann constant,) and the length, in units of R_0=0.276 nm which is the hydrogen-bond length in U_{WW}. The pressure P is measured in units of ε_0/R_0^2.

The T-P-MD simulations of the system mentioned above[30] are performed at many temperatures under a constant pressure (P=0.17 ε_0/R_0^2). This value of the pressure is a representative one in the 2-D aqueous solution.[30] The system consists of 576 molecules in a square unit cell with the periodic boundary condition. The mole fraction of the solute x_S is 0.5 in this work, since a solution with this concentration is interesting because of the large mean-square-concentration fluctuation.[30] The dynamical equations are integrated with the time increment:

$$\Delta t = 0.435 \times 10^{-15} \text{ s} \quad (6)$$

by the predictor-corrector method. In our standard run, 60000 steps are spent for the aging of the system. After this, the 60000-step run is performed twice a least; from these runs the statistical averages are obtained.

The constant-temperature MD mehod by Nosé[34] is used, combined with the constant-pressure MD method of Andersen.[37] Some things special to these methods has heen described elsewhere.[32]

Mutual Diffusion Coefficient

In a binary liquid system there are three diffusion coefficients, viz. the two self diffusion coefficients and the mutual diffusion coefficient. The former are calculated from the mean-square displacement or from the velocity autocorrelation[35] in the MD simulation. The latter is interesting in solutions with local concentration fluctuations.[1] The mutual diffusion coefficient can be obtained from the mean-square displacement of the center of mass of all water molecules $\langle R_{WCM}(t)^2 \rangle$ as follows:[35]

$$D = \frac{Q}{4Nc_W c_S}\left[\left(\frac{M_W}{M_S}\right)c_W + c_S\right]^2 \lim_{t\to\infty} \frac{\partial}{\partial t}\langle R_{WCM}(t)^2 \rangle, \quad (7)$$

where c_A is the concentration (number density) of the species A, the velocity of the center of the mass of the system is fixed as 0, N is the total number of molecules in the system and M_A is the mass of the species A. The quantity Q is often called the thermodynamic factor and is defined as:

$$Q = \frac{x_W x_S}{N\langle(\Delta x)^2\rangle}, \quad (8)$$

where x_A is the mole fraction of the species A and where $\langle(\Delta x)^2\rangle$ is the mean-square-concentration fluctuation.[30] The mean-square-concentration fluc-

Table 1. Thermodynamic and Transport Properties of the 2-D Aqueous Solution Using Micro Canonical MD and Constant-Temperature Constant-Pressure MD

	Micro canonical MD			T-P-MD		
	Run 1	Run 2	Av.	Run 1	Run 2	Av.
$T/\varepsilon_0 k_B^{-1}$	0.230	0.231	0.230	0.229	0.229	0.229
$P/\varepsilon_0 R_0^{-2}$	0.130	0.137	0.134	0.131	0.131	0.131
A/NR_0^2	1.296	1.296	1.296	1.302	1.332	1.317
$E/N\varepsilon_0$	−0.605	−0.608	−0.606	−0.601	−0.592	−0.596
$N\langle(\Delta x)^2\rangle$	1.19	1.29	1.24	1.36	1.35	1.36
$D_W/10^{-7}$ m^2 s^{-1}	0.355	0.313	0.334	0.319	0.341	0.330
$D_S/10^{-7}$ m^2 s^{-1}	0.311	0.337	0.324	0.348	0.417	0.383
$D/10^{-7}$ m^2 s^{-1}	0.204	0.156	0.180	0.211	0.137	0.174

T is the temperature, P is the pressure, A is the total area of the system, E is the potential energy, $\langle(\Delta x)^2\rangle$ is the mean square concentration fluctuation, D_W and D_S are the self diffusion coefficients of the water and the solute, and D is the mutual diffusion coefficient. The mole fraction of solute $x_S=0.5$, the total number of molecules in the system $N=576$.

tuation is calculated using the radial-distribution function.[30]

Although it has been proved that the sufficient averages of the static quantities are the same in micro canonical MD and in T-P-MD,[34,38] nothing is known about the mutual diffusion coefficient. For this reason, typical examples of calculations in the two methods are compared in Table 1. The results are not very different from each other for the micro canonical MD and T-P-MD.

As the mutual diffuion coefficient D has the thermodynamic factor Q, the kinetic diffusion coefficient L is more directly related to velocity correlation functions between different molecules:[39]

$$D = QL, \tag{9}$$

with:

$$L = L_0 + x_W x_S(D_{WW} + D_{SS} - 2D_{WS}) \tag{10}$$

$$L_0 = x_S D_W + x_W D_S, \tag{11}$$

$$D_{AB} = \frac{N}{2}\int_0^\infty \langle v_{Ai}(t)\cdot v_{Bj}(0)\rangle dt, \qquad (i \neq j) \tag{12}$$

where v_{Ai} is the velocity of an i-th molecule of the species A. D_A is the self-diffusion coefficient of the species A. By the use of Eq. 10, the trend of the cooperative translation in the binary mixture can be seen from the comparison of L with L_0, because the second term in Eq. 10 comes from the velocity correlations between different molecules. At the same time, we would like to discuss the temperature dependence of L by means of the reduced quantity L/L_0 since the first term L_0 in Eq. 10 also depends on the temperature. The temperature dependence of L/L_0 is shown in Fig. 1. The reduced kinetic diffusion coefficient L/L_0 has a maximum value around $T=0.24\ \varepsilon_0/k_B$. The mean-square-concentration fluctuation also has a maximum value around the same temperaure (Fig. 7 in Ref. 30). The second

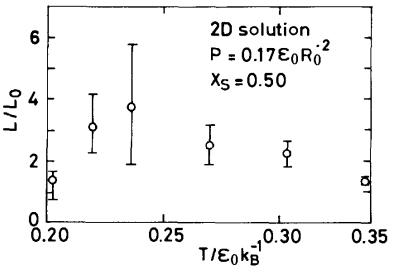

Fig. 1. Plot of the reduced kinetic diffusion coefficient L/L_0 vs. temperature T, at $P=0.17\ \varepsilon_0/R_0^2$, $x_S=0.5$.

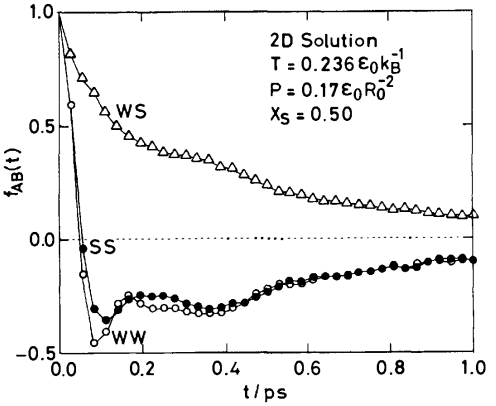

Fig. 2. The correlation function of velocity $f_{AB}(t)$ vs. time t. $T=0.236\ \varepsilon_0/k_B$, $P=0.17\ \varepsilon_0/R_0^2$, $x_S=0.5$.

point to be mentioned about Fig. 1 is that the value of L/L_0 is larger than 1.

The experimental values in a binary solution of t-butyl alcohol and water are as follows: L/L_0= about 2 at 24 °C and about 5 at 63 °C.[21] The order of magnitude of L/L_0 shown in Fig. 1 is comparable to the experimental results.[21] The temperature dependence below about $0.24\ \varepsilon_0/k_B$ in Fig. 1 is qualitatively in agreement with such results.[21]

As the value of L/L_0 is larger than 1, the general

tendency for the same species to move in the same direction is seen in this solution. In order to see this more directly, the correlation functions of velocities between the different molecules are shown in Fig. 2. The correlation functions of velocities $f_{AB}(t)$ are defined as follows:

$$f_{AB}(t) = \frac{\langle \boldsymbol{v}_{Ai}(t)\cdot\boldsymbol{v}_{Bj}(0)\rangle}{\langle \boldsymbol{v}_{Ai}(0)\cdot\boldsymbol{v}_{Bj}(0)\rangle}, \quad (i \neq j). \tag{13}$$

The normalization constants at temperature T=0.236 ε_0/k_B are given below:

$$\left.\begin{aligned} \langle \boldsymbol{v}_{Wi}(0)\cdot\boldsymbol{v}_{Wj}(0)\rangle &= -0.7\times10^6\ \mathrm{m^2\,s^{-2}},\\ \langle \boldsymbol{v}_{Wi}(0)\cdot\boldsymbol{v}_{Sj}(0)\rangle &= -0.8\times10^6\ \mathrm{m^2\,s^{-2}},\\ \langle \boldsymbol{v}_{Si}(0)\cdot\boldsymbol{v}_{Sj}(0)\rangle &= -0.7\times10^6\ \mathrm{m^2\,s^{-2}}. \end{aligned}\right\} \tag{14}$$

From Eqs. 12—14 and Fig. 2 it may be seen that D_{WW} and D_{SS} are positive, while D_{WS} is negative. The tendency mentioned above for the same species generally to move in the same direction may be seen again in Fig. 2.

There are two time constants in the correlation functions in Fig. 2. They are 0.05 ps and 1 ps. As these time constants are derived from all the pairs in the system they are not adequate for an examination of the lifetime of the local structure. For this reason, the lifetime will be studied in a different way in the next section.

Lifetime of the Local Structure

In this section, we will estimate the lifetime of the local structure due to fluctuations in the concentration. An oscillatory motion of water molecules is seen at low temperatures and densities, as is shown in Ref. 32. Therefore, we use the time-averaged configuration in order to obtain the lifetime of the local structure.[32] The configuration is averaged over a period of 0.13 ps which is several times longer than the velocity autocorrelation time. We calculate the cross-correlation of displacement as in the case of the estimation of the lifetime of the hydrogen-bonded local structure in 2D water.[32] When the position $\boldsymbol{r}_i$ of i-th molecule at time t=0 is denoted as $\boldsymbol{r}_i^0$, the displacement of the molecule i is $\boldsymbol{r}_i-\boldsymbol{r}_i^0$. Figure 3 shows the cross-correlation of the displacement of the molecules i and j $\langle(\boldsymbol{r}_i-\boldsymbol{r}_i^0)\cdot(\boldsymbol{r}_j-\boldsymbol{r}_j^0)\rangle$ where the following conditions, with the molecular distance R_{ij} set at t=0:

$$\left.\begin{aligned} &1.5R_0<R_{ij}(0)<2.5R_0 \quad (\text{i.e. } R_{ij}(0)\text{—}2R_0),\\ &3.5R_0<R_{ij}(0)<4.5R_0 \quad (\text{i.e. } R_{ij}(0)\text{—}4R_0),\\ &5.5R_0<R_{ij}(0)<6.5R_0 \quad (\text{i.e. } R_{ij}(0)\text{—}6R_0). \end{aligned}\right\} \tag{15}$$

The linear part of the cross-correlation function extends up to 3×10 ps in the case of $R_{ij}(0)$—$2R_0$. The tangent of this linear part is about 25% as large as that in the case of i=j. Thus, this figure shows that the molecules i and j with R_{ij}—$2R_0$ at t=0 move collectively in nearly the same direction over a period

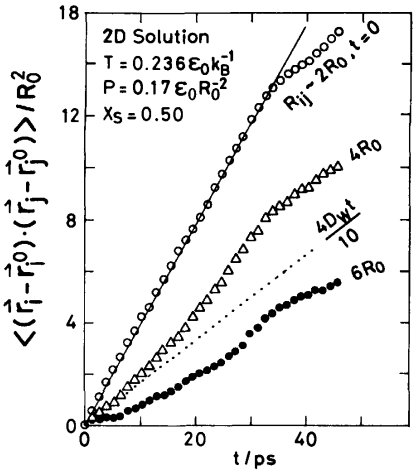

Fig. 3. The cross correlation function $\langle(\boldsymbol{r}_i-\boldsymbol{r}_i^0)\cdot(\boldsymbol{r}_j-\boldsymbol{r}_j^0)\rangle$ vs. time t. The initial conditions in statistics are indicated in the figure. T=0.236 ε_0/k_B, P=0.17 ε_0/R_0^2, x_S=0.5.

of about 3×10 ps.

As the molecular distance at t=0 increases, the cross-correlation decreases, as is shown in Fig. 3. We tentatively use one-tenth of the correlation in the case of i=j (the dotted line in Fig. 3) as the criterion to determine whether or not the cross-correlation is sufficiently large. By this criterion, we see that the correlation length of translation is about $4R_0$ in Fig. 3.

The cross-correlation time and the length of the solute-solute pair are about the same as those of the water-water pair at T=0.236 and 0.270 ε_0/k_B. At low temperatures, the length of the MD run was not enough to determine the correlation length. The temperature dependence of the cross-correlation time τ and length ξ_{trans} are as follows:

$$\left.\begin{aligned} &\tau(T=0.202\,\varepsilon_0/k_B) = 9\times10\ \mathrm{ps}, \quad \text{run length} = 131\ \mathrm{ps},\\ &\tau(T=0.236\,\varepsilon_0/k_B) = 3\times10\ \mathrm{ps}, \quad \xi_{trans}=4R_0,\\ &\qquad\qquad\qquad\qquad\qquad\qquad \text{run length} = 131\ \mathrm{ps},\\ &\tau(T=0.270\,\varepsilon_0/k_B) = 4\ \mathrm{ps}, \quad \xi_{trans}=3R_0,\\ &\qquad\qquad\qquad\qquad\qquad\qquad \text{run length} = 104\ \mathrm{ps}, \end{aligned}\right\} \tag{16}$$

where the length of the MD run used in the analysis is also shown. The value of the correlation time at T=0.202 ε_0/k_B listed above is only a tentative one, because the MD run was not long enough to determine such a long correlation time (9×10 ps).

Correlation Length of Concentration Fluctuation

In the preceding section, the cross-correlation length of translation was estimated. Now we are going to obtain the static correlation length of the local fluctuation of concentration.

There are many definitions of the correlation length in a solution.[25] We define the following function using radial-distribution functions:

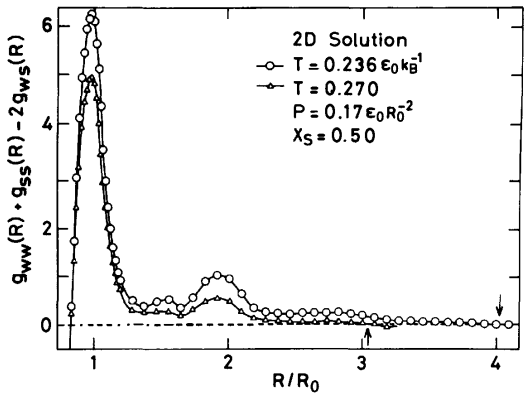

Fig. 4. The distribution function $\Delta g(R)$ defined in Eq. 17, at T=0.236 and 0.270 ε_0/k_B, P=0.17 ε_0/R_0^2, x_S=0.5.

$$\Delta g(R) = g_{ww}(R) + g_{ss}(R) - 2g_{ws}(R) \tag{17}$$

because the integration of this function with respect to the molecular distance R is proportional to the excess mean-square fluctuation in the concentration (cf. Eqs. 2.12, 2.19 in Ref. 30):

$$N\langle(\Delta x)^2\rangle = x_w x_S + \frac{N}{\langle A\rangle}(x_w x_S)^2\int_0^\infty \Delta g(R)\mathrm{d}^2R, \tag{18}$$

where A is the total area of the system.

This function $\Delta g(R)$ is plotted at T=0.236 and 0.270 ε_0/k_B in Fig. 4. At the point shown by an arrow, the function is 0. As the function $\Delta g(R)$ is positive in the $0.8R_0<R<4R_0$ range at T=0.236 ε_0/k_B, we can see that, in this case, the same species have a tendency to gather in the region where the molecular distance is less than $4R_0$. This length $4R_0$ is identified with the static correlation length of the local-concentration fluctuation in this work. The correlation length at T=0.270 ε_0/k_B is $3R_0$. It was difficult to estimate the correlation length at low temperatures by this method because the radial-distribution functions oscillate frequently with a large amplitude (cf. Fig. 18 in Ref. 30).

In order to confirm the correlation length mentioned above, typical configurations at several temperatures are shown in Fig. 5. Circles with a rectangular indication are water molecules; circles without a rectangular indication mean solutes. The stable pair with a pair energy larger than 0.55 ε_0 is connected by a straight line.

There are many water-rich regions and solute-rich regions at T=0.236 ε_0/k_B, and the characteristic radius of these regions is about $4R_0$. The radius of these regions at T=0.270 ε_0/k_B is seen as about $3R_0$. These values are in agreement with the correlation length determined by $\Delta g(R)$. The radius of the water-rich region at a low temperature (T=0.202 ε_0/k_B) is read as 5 ± 1 R_0 while that of the solute-rich region is about 3 ± 1 R_0.

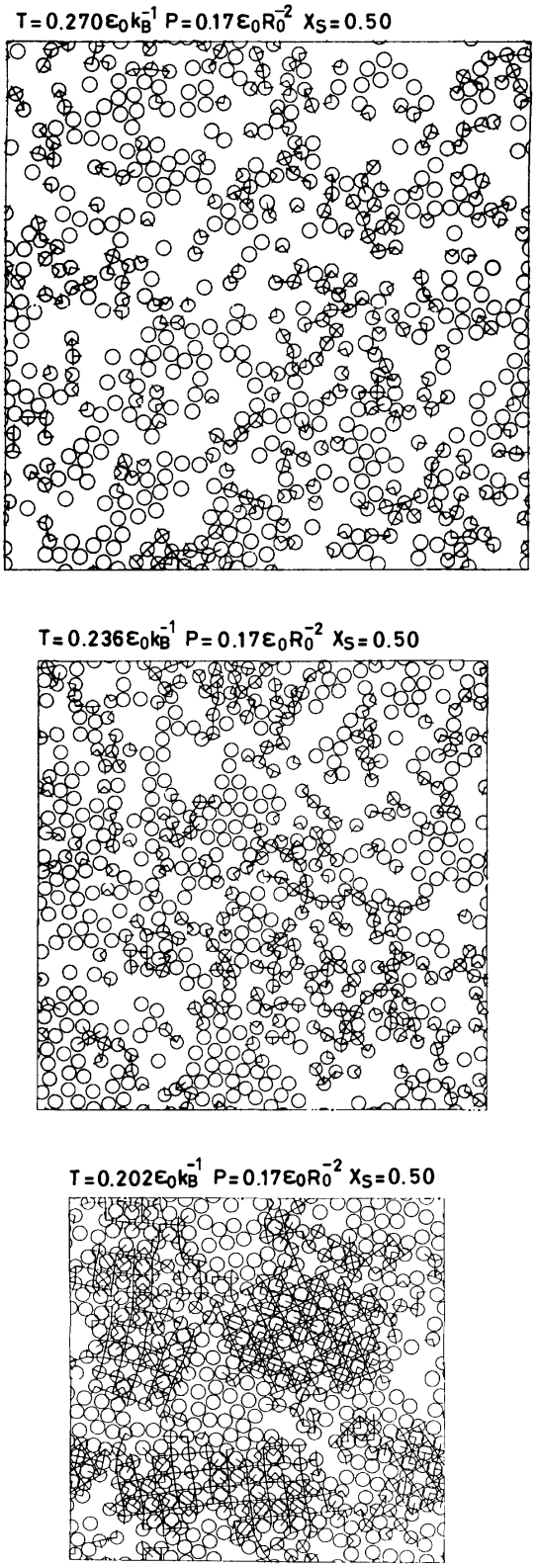

Fig. 5. Some examples of configurations. Circles with a rectangular indication are water molecules, where the diameter is the Lennard-Jones parameter σ_{ww} (=0.212 nm). Circles without a rectangular indication mean solute and the diameter is σ_{ss}(=0.228 nm). The stable pair with bond energy larger than 0.55 ε_0 is connected by a straight line. P=0.17 ε_0/R_0^2, x_S=0.5.

Although the present model is too simple, let us compare the correlation length obtained with that in the real system, as we have no experimental results on any 2-D aqueous-like solution. The correlation length observed in a 2-butoxyethanol-water mixture at 23 °C is about 2 nm.[25] The order of magnitude of our correlation length ($5R_0 \simeq 1$ nm) is in agreement with such an experimental result.[25]

A few configurations are shown in Fig. 5 because it is easier to see some examples of configurations in a 2-D solution than in a 3-D solution. However, it should be noted that the configurations shown in Fig. 5 are special, as they depend on the model assumed. The present model has a tendency toward phase separation at an intermediate temperature (around $T=0.236\ \varepsilon_0/k_0$) This feature is seen by the temperature dependences of the mean-square-concentration fluctuation, the reduced kinetic diffusion coefficient, and the free energy.[30] The temperature dependence of the mean-square-concentration fluctuation is as follows:

$$\left.\begin{aligned} N\langle(\Delta x)^2\rangle &= 0.55 \pm 0.05, \quad T = 0.202\ \varepsilon_0/k_B, \\ N\langle(\Delta x)^2\rangle &= 1.3 \pm 0.3, \quad T = 0.236\ \varepsilon_0/k_B, \\ N\langle(\Delta x)^2\rangle &= 0.67 \pm 0.08, \quad T = 0.270\ \varepsilon_0/k_B, \end{aligned}\right\} \tag{19}$$

where pressure $P=0.17\ \varepsilon_0/R_0^2$.

The author would like to thank Dr. Tadashi Kato, Tokyo Metropolitan University for his valuable discussions. He also thank Mr. Mitsuhiro Matsumoto for reading the manuscript carefully. This work was supported in part by a grant in aid for Science Research (Nos. 59340025, 60129031, 60121013) from the Ministry of Education, Science and Culture, and also by the Kyoto University Data Processing Center. The author thank the Computer Center of the Institute for Molecular Science, for the use of the HITAC M-200H computer. The computations were also done by the FACOM VP-100 and M-382 computer at the Kyoto University Data Processing Center.

References

1) T. Kato, N. Ito, and T. Fujiyama *Bull. Chem. Soc. Jpn.*, **53**, 2167 (1980).
2) D. W. McCall and D. C. Douglass *J. Phys. Chem.*, **71**, 987 (1967).
3) D. G. Miller, *Faraday Discuss. Chem. Soc.*, **64**, 295 (1977).
4) D. G. Miller, *J. Phys. Chem.*, **85**, 1137 (1981).
5) D. G. Miller, J. A. Rard, L. B. Eppstein, and J. G. Albright, *J. Phys. Chem.*, **88**, 5739 (1984).
6) H. G. Hertz, *Ber Bunsenges. Phys Chem.*, **81**, 656 (1977).
7) H. G. Hertz and R. J. Mills, *J. Phys. Chem.*, **82**, 952 (1978).
8) A Geiger, H. G. Hertz, and R. J. Mills, *J. Solution Chem.*, **10**, 83 (1981).
9) H. J. Schonert, *J. Phy. Chem.*, **88**, 3359 (1984).
10) L. A. Woolf, *J. Phys. Chem.*, **82**, 959 (1978).
11) L. A. Woolf and K. R. Harris, *J. Chem. Soc., Faraday Trans. I*, **74**, 933 (1978).
12) D. C. Douglass and H. L. Frisch, *J. Phys. Chem.*, **73**, 3039 (1969).
13) R. Mills and H. G. Hertz, *J. Phys. Chem.*, **84**, 220 (1980).
14) H. L. Freedman and R. Mills, *J. Solution Chem.*, **10**, 395 (1981).
15) T. Kato, S. Hyodo, and T. Fujiyama, *J. Phys. Chem.*, **82**, 1010 (1978).
16) K. Iwasaki and T. Fujiyama, *J. Phys. Chem.*, **83**, 463 (1979).
17) T. Kato, K. Yano, and T. Fujiyama, *Bull. Chem. Soc. Jpn.*, **53**, 53 (1980).
18) T. Kato, T. Nakanishi, and T. Fujiyama, *Bull. Chem. Soc. Jpn.*, **53**, 2173 (1980).
19) N. Ito, K. Saito, T, Kato, and T. Fujiyama, *Bull. Chem. Soc. Jpn.*, **54** 991 (1981).
20) T. Kato, M. Yudasaka, and T. Fujiyama, *Bull. Chem. Soc. Jpn.*, **54**, 1632 (1981).
21) N. Ito, T. Kato, and T. Fujiyama, *Bull. Chem. Soc. Jpn.*, **54**, 2573 (1981).
22) T. Kato, T. Fujiyama, and H. Nomura, *Bull. Chem. Soc. Jpn.*, **55**, 3368 (1982).
23) N. Ito, T. Fujiyama, and Y. Udagawa, *Bull. Chem. Soc. Jpn.*, **56**, 379 (1983).
24) N. Ito and T. Kato, *J. Phys. Chem.*, **88**, 801 (1984); T. Kato, *ibid.*, **88**, 1248 (1984)
25) T. Kato, *J. Phys. Chem.*, **89**, 5750 (1985).
26) G. Alagona and A. Tani, *J. Chem. Phys.*, **74**, 3980 (1981); *Chem. Phys. Lett.*, **87**, 337 (1982).
27) S. Okazaki, K. Nakanishi, and H. Touhara, *J. Chem. Phys.*, **78**, 454 (1983).
28) K. Nakanishi, K. Ikari, S. Okazaki, and H. Touhara, *J. Chem. Phys.*, **80**, 1656 (1984); S. Okazaki, H. Touhara, and K. Nakanishi, *J. Chem. Phys.*, **81**, 890 (1984).
29) H. Tanaka, K. Nakanishi, and H. Touhara, *J. Chem. Phys.*, **81**, 4065 (1984).
30) Y. Kataoka, *J. Chem. Phys.*, **80**, 4470 (1984).
31) K. Okazaki, S. Nosé, Y. Kataoka, and T. Yamamoto, *J. Chem. Phys.*, **75**, 5864 (1981).
32) Y. Kataoka, *Bull. Chem. Soc. Jpn.*, **57**, 1522 (1984); **59**, 1425 (1986).
33) W. G. Hoover, W. T. Ashurst, and R. J. Olness, *J. Chem, Phys.*, **60**, 4043 (1974); D. J. Evans, *Phys. Rev.*, **A22**, 290 (1980); T. E. Wainwright, B. J. Alder, and D. M. Gass, *Phys. Rev.*, **A4**, 233 (1971); S. Toxvaerd, *Mol. Phys.*, **29**, 373 (1975).
34) S. Nosé, *Mol. Phys.*, **52**, 255 (1984); *J. Chem. Phys.*, **81**, 511 (1984).
35) D. L. Jolly and R. J. Bearman, *Mol. Phys.*, **41**, 137 (1980).
36) M. Schoen and C. Hoheisel, *Mol. Phys.*, **52**, 33 (1984); **52**, 1029 (1984).
37) H. C. Andersen, *J. Chem. Phys.*, **72**, 2384 (1980).
38) D. Brown and J. H. R. Clarke, *Mol. Phys.*, **51**, 1243 (1984).
39) See Eq. 35 in Ref. 2 or Eq. 10 in Ref. 25.

 © 1986 The Chemical Society of Japan Bull. Chem. Soc. Jpn., 59, 3347—3349 (1986)

Removal of Some Alkali Salts from Aqueous Solution by Active-Charcoal Electrode

Masao Ichinose, Takashi Yasuoka,* Shunmei Mitsuzawa, and Tsunetaka Sasaki
Department of Chemistry, Faculty of Science, Tokai University,
Kitakaname, Hiratsuka 259-12
(Received February 18, 1986)

An electrolytic removal of potassium and sodium sulfates from aqueous solutions was worked out by using an active-charcoal cathode and a platinum anode with a porous porcelain septum between them. Maximum removal of nearly 99% was attained for these salts. The mechanism of removal was confirmed to be based on the facts that potassium and sodium ions are entrapped and concentrated as hydroxides in the pores of the active-charcoal cathode while sulfate ions are removed from the solution and concentrated as sulfuric acid in the anode chamber.

As regards the removal of inorganic salts in aqueous solutions using an active charcoal, a simple adsorption method is not available, since the amount of adsorption is generally too small of the order of 0.01 to 0.5 mmol g^{-1} from 0.01 to 0.1 mol dm^{-3} aqueous solutions,[1] and the method of electrolysis using charcoal as an electrode has been reported[2,3] or patented[4]. However these studies mainly concern with the removal by the electrolytic formation of the substance of low solubility resulting in gas evolution or precipitation. In the present study, a method was devised to remove electrolytes by the electrolysis which locally concentrated and immobilized cations in pores of the active-charcoal cathode and entrapped anions in the anode chamber.

Experimental

Materials. The potassium and sodium sulfates used were commercial products of a guaranteed grade which were used without further purification. The active charcoal used as an electrode was the product of Wako special grade, charcoal activated, granulated. The active charcoal together with the porous porcelain tube used as a septum was carefully washed with distilled water until it showed no increase in electric conductance after washing.

Apparatus and Procedure. The apparatus used consisted of three parts, an electrode chamber, a circulation pump, and a reservoir, as shown in Fig. 1. The anode was a platinum wire coiled around the porous porcelain tube of 4 cm in diameter and 15 cm in height, while the cathode consisted of a poly(vinylidene dichloride) bag which contained a central graphite rod surrounded by the active charcoal.

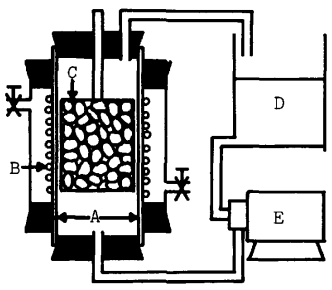

Fig. 1. Apparatus for the removal of electrolyte.
A: Porous porcelain tube (diameter 4 cm, height 15 cm), B: Platinum wire anode, C: Active-charcoal cathode with central graphite rod, D: Reservoir, E: Circulation pump (rate of circulation 3.2 dm^3 min^{-1}).

To carry out the removal experiment, 1 dm^3 of 1.25×10^{-4} mol dm^{-3} potassium or sodium sulfate was introduced in the apparatus and was circulated at the rate of 3.2 dm^3 min^{-1}. A direct current was then applied and the voltage was controlled so as to keep the current constant to 50 mA. During the electrolysis, small portions of the solution were withdrawn from the reservoir at the time interval of 20 min, and the concentrations of cations and anions were measured by the atomic absorption spectrophotometry using Hitachi 508 type Atomic Absorption Spectrophotometer and by the ion chromatography using Shimadzu LC-5A Liquid Chromatograph, respectively. The weight percentage of removal of each ions was then calculated. Conductance and pH measurements were further made to trace the removal of the electrolyte.

In order to study the mechanism of the electrolytic removal of electrolyte, measurements were made in addition for potassium sulfate under the same conditions as mentioned above excepting the following conditions: 1 without electrolysis, 2 without active charcoal, 3 with active charcoal placed outside the electric field, 4 without the circulation of the solution.

Results and Discussion

The percentage of removal obtained under various experimental conditions was plotted against the time of electrolysis as shown in Fig. 2. In the case of measurement 4, only one plot was made for the solution circulated after 100 min's electrolysis. As seen in this figure, the measurements 1 through 4 showed no removal of potassium ions. Compared with these results, nearly 99% of potassium and sulfate ions were found to be removed from the solution under circulation by 100 min's electrolysis at 50 mA using active-charcoal cathode. Conductance measurement also showed a decrease from 45 μs cm^{-1} for initial potassium sulfate solution to 1.6 μs cm^{-1} for the solution after 100 min's electrolysis, the latter being equal to the value for distilled water after sufficient electrolysis. A slight increase of pH observed during electrolysis of the solution which could be noticed also

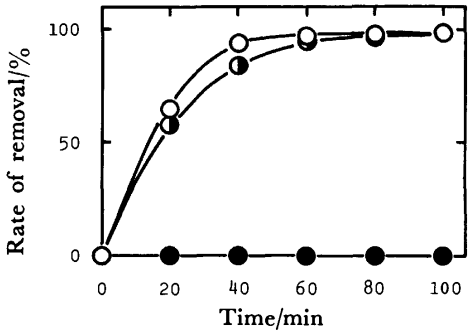

Fig. 2. Rate of removal of potassium and sulfate ions.
Initial concn of potassium sulfate: 1.25×10^{-4} mol dm^{-3}.
Rate of circulation: 3.2dm³ min^{-1}, Current: 50mA.
Rate of removal of ○: Potassium ions, ◑: Sulfate ions, ●: Potassium ions measured under conditions of 1, 2, 3, 4 (see the text).

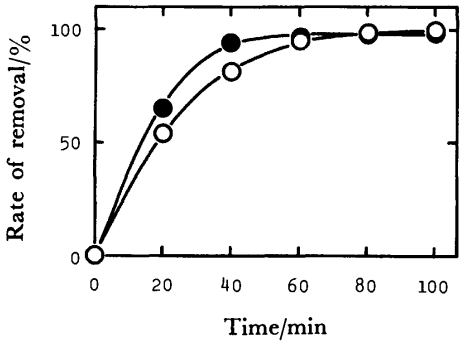

Fig. 3. Rate of removal of potassium ions using active-charcoal electrodes of single and multilayer of particles.
○: Single layer of particles, ●: Multilayer of particles.

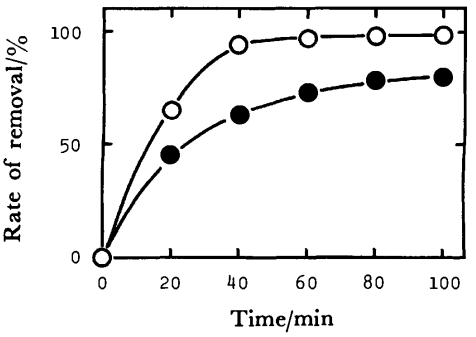

Fig. 4. Rate of removal of potassium ions with and without porous porcelain tube.
○: With porous porcelain tube, ●: Without porous porcelain tube.

for the electrolysis of distilled water may be due to the removal of dissolved carbon dioxide. Thus it was confirmed that the electrolysis under the circulation of the solution using active-charcoal cathode and platinum anode with porous porcelain septum between them effectively removed the potassium sulfate from an aqueous solution.

As regards the mechanism of the removal of the electrolyte, sulfate ions were considered to be exclusively removed by concentrating in the anode chamber as sulfuric acid as was confirmed by the coincidence of the initial amount of sulfate ions with the decrease of pH observed in the anode chamber assumed to be due to the formation of sulfuric acid and by the absence of sulfate ions in the circulating solution after electrolysis.

As for the mechanism of the removal of potassium ions, up-take by charcoal as potassium hydroxide is expected, since electrolysis of an aqueous potassium sulfate is known to result in the evolution of hydrogen and the formation of potassium hydroxide at a cathode.

To confirm this possibility, the active-charcoal electrode after being used for 100 min's electrolysis was placed in distilled water together with a platinum wire electrode, then the current was flowed in the reverse direction to the case of the removal experiment and the amount of potassium ions released, if any, from the charcoal was measured. The amount of hydroxide ions taken up was measured by the titrations of the active charcoal with hydrochloric acid.

The results of these measurements showed that the amounts of potassium and hydroxide ions taken up by the active-charcoal electrode were found to be nearly equivalent, being 1:1.08 in mol ratio. This fact together with the fact that graphite cathode without active charcoal could not remove potassium sulfate as shown in Fig. 2 confirmed the mechanism of removal that potassium ions are concentrated and entrapped as potassium hydroxide in the pores or cavities of the active-charcoal electrode.

As regards the active-charcoal electrode, the action of so called bipolar electrode has been reported,[3,5] according to which both ends of all particles of charcoal electrode act as anodes and cathodes. When we apply this mechanism in our case, inner and outer parts of charcoal electrode should equally contribute to the removal of potassium ions. To check the contribution of this bipolar action in the present experiment, potassium ions taken up by the outermost layer of active-charcoal electrode after being used for the removal of potassium sulfate were extracted by treating the charcoal with concentrated hydrochloric acid. The amount of potassium ions thus obtained was measured and was expressed as the percentage of the total amount of potassium ions removed. The value of 88% was obtained which confirmed the fact that the surface layer of active charcoal mainly acted to remove electrolytes and bipolar action played a minor role. In this connection, the removal of potassium ions by using a graphite cathode surrounded by a single layer of active charcoal particles was attempted. The result is shown in Fig. 3, together with the result

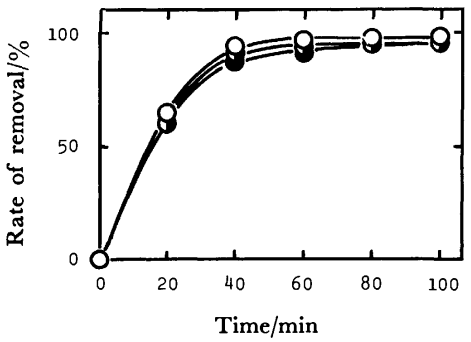

Fig. 5. Rate of removal of potassium ions using active charcoal of different origin.
Commercial products of ○: Wako Pure Chemical Co., Ltd., ◑: Kanto Chemical Co., Ltd., ●: Nakarai Chemicals, Ltd.

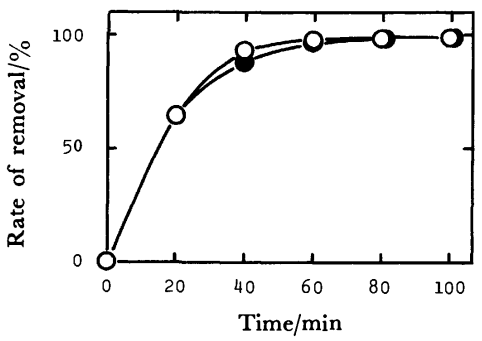

Fig. 6. Rate of removal of sodium and sulfate ions.
Initial concn of sodium sulfate: 1.25×10^{-4} mol dm^{-3}.
Rate of circulation: 3.2dm^3 min^{-1}, Current: 50mA
Rate of removal of ○: Sodium ions, ●: Sulfate ions.

obtained by using the apparatus shown in Fig. 1 for comparison. The removal of potassium ions was only slightly less in the former case as was expected. This may suggest the effective and economical use of active charcoal.

With regard to the action of porous porcelain tube it is considered to hinder the sulfuric acid formed at the anode from mixing with circulating solution, as is evident from the comparison of the removal experiments using the apparatuses with and without the porous porcelain tube as shown in Fig. 4.

The rate of removal of potassium ions was further measured by using several active-charcoal of different origin as cathodes. The results are shown in Fig. 5. As seen, the nature of the active charcoal did not influence the efficiency of the removal of potassium ions as far as the present study was concerned. This may suggest that for the removal of electrolyte according to the present method, any porous substance having an electric conductance can be effectively used as the cathode irrespective of its nature.

The present studies were mainly made for potassium sulfate, but similar results could be obtained for several other salts, an instance of which is shown for sodium sulfate in Fig. 6. The maximum removal of 99% was also attained.

Finally it may be mentioned that in the case of the practical application of the present method for the removal of electrolytes, the reproduction of charcoal for the repeated use is the problem which cannot be disregarded. But the electrolytic removal of potassium ions mentioned above might be expected to facilitate the reproduction.

References

1) H. Freundlich, "Kapillarchemie," Bd I, Akademische Verlag, Leipzig (1930), p. 291.

2) K. Hosokawa and Y. Tsuru, *Kyushu Kogyo Daigaku Kenkyuhokoku (Kogaku)*, **37**, 79 (1978); T. Nishiwaki and S. Yonekura, *Tokyo Kogyo Shorei Kanpo*, No. 19, 72 (1968).

3) S. Yoshizawa, Y. Miyazaki, and A. Katagiri, *Nippon Kagaku Kaishi*, **1977**, 19.

4) M. Tarjanyi, M. P. Strier, and H. D. Siegerman, U.S. Patent, 3730864, (1973); C. H. Roy, Brit. Patent, 1362704, (1974).

5) T. Z. Fahidy, *Can. J. Chem. Eng.*, **51**, 521 (1973).

 © 1986 The Chemical Society of Japan Bull. Chem. Soc. Jpn., 59, 3351—3356 (1986)

Molecular and Crystal Structure of an Azobenzene-Linked Amphiphile, $C_{33}H_{54}N_3O_3Br$

Kenji OKUYAMA,* Hitoshi WATANABE, Masatsugu SHIMOMURA, Kiyoshi HIRABAYASHI, Toyoki KUNITAKE,† Tisato KAJIYAMA,† and Noritake YASUOKA††
Faculty of Technology, Tokyo University of Agriculture and Technology, Koganei, Tokyo 184
†Faculty of Engineering, Kyushu University, Fukuoka 812
††Institute for Protein Research, Osaka University, Suita, Osaka 565
(Received February 12, 1986)

Azobenzene-linked, single-chain ammonium amphiphile ($C_{12}AzoC_5N^+Br^-$), $C_{33}H_{54}N_3O_3Br$, was crystallized from their solutions in water and ethanol. The crystals are triclinic with the space group $P\bar{1}$, $Z=2$, $a=3.4243(6)$, $b=0.8525(1)$, $c=0.6073(1)$nm, $\alpha=73.45(1)$, $\beta=88.03(1)$, and $\gamma=93.32(1)°$. The structure was solved by the direct method and refined anisotropically by the block-diagonal least-squares procedure: $R=0.06$ for 2917 observed reflections ($2\theta<105°$, Cu $K\alpha$, $\lambda=0.154184$ nm). The crystal structure consists of regularly stacking bimolecular layers in which $C_{12}AzoC_5N^+Br^-$ molecules incline about 30° to the layer surface. As expected from spectroscopic analyses, the azobenzene chromophore shows a head-to-tail (J-like) aggregation between adjacent molecules. The pronounced planarity of the azobenzene chromophore found in this crystal structure enables parallel stacking of phenyl groups in the J-like aggregation.

Biological membranes are organized assemblies consisting mainly of proteins and lipids. Their gross organization has been proposed by Singer and Nicolson[1] in the form of a fluid mosaic model, in which lipid molecules are assembled in the bilayer form. For better understanding of structural details of biological membranes and their relation to specific functions, it is essential to accumulate structural information about various lipid bilayers on the atomic level. However, it has been difficult to obtain single crystals of amphipathic lipids suitable for X-ray diffraction, which could provide the most detailed information about their preferred molecular conformations and interactions. Such information has been obtained so far only for a few amphipathic lipids.[2]

In order to establish the physicochemical basis of the biological membrane and to develop membrane-related chemical processes, one of the authors (T. K) has studied the formation of the bilayer structure using a large variety of amphiphiles containing a single,[3] double,[4] and triple[5] alkyl chains as the hydrophobic tail part. It has been shown that many of these compounds form stable molecular (monolayer and bilayer) membranes spontaneously when dispersed in water. Furthermore, in the case of dialkyldimethylammonium bromides with alkyl chain lengths of $n=18$ and 16, single crystals suitable for X-ray diffraction could be provided[6] and detailed structure analyses are now in progress. In the case of single-chain ammonium amphiphiles containing azobenzene chromophore (abbreviated as $C_nAzoC_mN^+Br^-$, hereafter, the general formula shown in Fig. 1), a

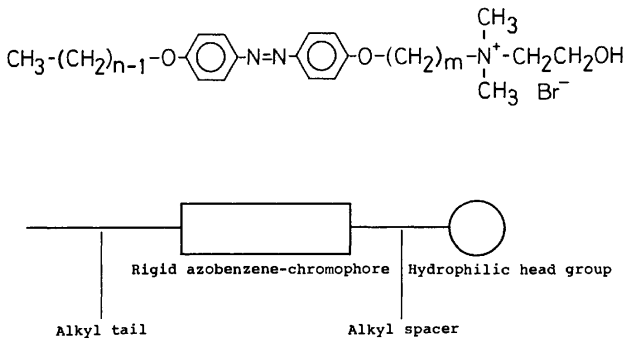

Fig. 1. Chemical formula and its schematic illustration for azobenezene-linked single chain amphiphiles (abbreviated as $C_nAzoC_mN^+Br^-$). n and m represent a number of carbons in the alkyl tail and spacer parts, respectively.

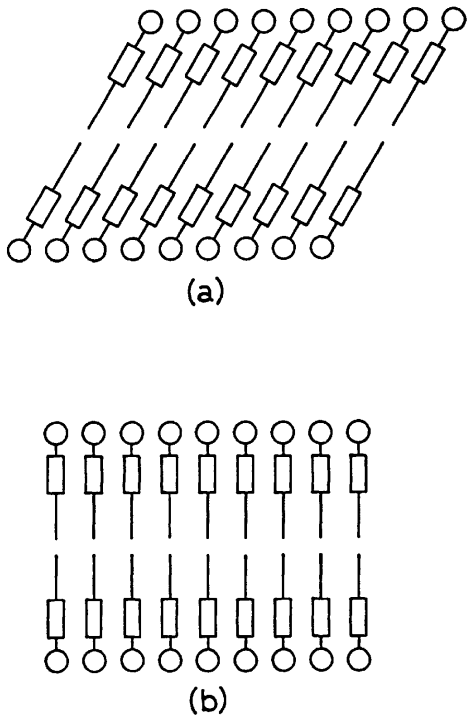

Fig. 2. Schematic illustration of two aggregation forms for $C_nAzoC_mN^+Br^-$ amphiphiles in crystalline bilayer. (a) J-like aggregate showing head-to-tail chromophore orientation. (b) H-aggregate showing highly parallel chromophore orientation.

Table 1. Fractional Coordinates and Equivalent Isotropic Temperature Factors[26] for Non-Hydrogen Atoms of $C_{12}AzoC_5N^+Br^-$ with Estimated Standard Deviations in Parentheses

Atom	x	y	z	$B_{eq}\times10^2$ / nm^2
Br	0.9335(1)	0.3596(1)	0.9798(1)	501
O(1)	0.9976(1)	0.1844(6)	1.3215(8)	473
O(2)	1.1856(1)	−0.3977(6)	1.4408(8)	446
O(3)	1.2892(1)	−1.4853(6)	0.7964(9)	501
N(1)	1.0639(2)	0.2391(6)	1.6589(9)	359
N(2)	1.2245(2)	−0.8960(7)	1.0696(10)	405
N(3)	1.2497(2)	−0.9864(7)	1.1669(10)	426
C(1)	0.9935(2)	0.2223(8)	1.5329(12)	405
C(2)	1.0276(2)	0.3271(8)	1.5728(12)	401
C(3)	1.0949(2)	0.3704(10)	1.6658(16)	602
C(4)	1.0550(3)	0.1249(10)	1.8946(13)	561
C(5)	1.0784(2)	0.1469(8)	1.4971(11)	342
C(6)	1.1140(2)	0.0520(9)	1.5642(13)	422
C(7)	1.1223(2)	−0.0506(8)	1.4025(12)	387
C(8)	1.1533(2)	−0.1695(8)	1.4867(12)	389
C(9)	1.1604(2)	−0.2743(8)	1.3297(12)	393
C(10)	1.1940(2)	−0.5175(8)	1.3424(12)	357
C(11)	1.1772(2)	−0.5383(8)	1.1469(12)	408
C(12)	1.1888(2)	−0.6634(9)	1.0641(12)	421
C(13)	1.2213(2)	−0.6222(9)	1.4485(12)	414
C(14)	1.2319(2)	−0.7474(8)	1.3646(12)	392
C(15)	1.2154(2)	−0.7695(18)	1.1677(11)	360
C(16)	1.2588(2)	−1.1121(8)	1.0688(12)	384
C(17)	1.2419(2)	−1.1387(8)	0.8737(11)	378
C(18)	1.2533(2)	−1.2617(9)	0.7899(12)	426
C(19)	1.2861(2)	−1.2167(9)	1.1712(12)	428
C(20)	1.2979(2)	−1.3436(9)	1.0883(13)	450
C(21)	1.2805(2)	−1.3669(8)	0.8953(12)	390
C(22)	1.3172(2)	−1.6003(9)	0.8913(13)	484
C(23)	1.3201(2)	−1.7104(9)	0.7407(13)	474
C(24)	1.3506(2)	−1.8361(9)	0.8027(14)	521
C(25)	1.3520(2)	−1.9418(10)	0.6437(15)	566
C(26)	1.3826(3)	−2.0654(11)	0.6831(16)	670
C(27)	1.3819(3)	−2.1693(11)	0.5178(17)	695
C(28)	1.4135(3)	−2.2886(11)	0.5411(16)	674
C(29)	1.4124(3)	−2.3877(11)	0.3704(18)	726
C(30)	1.4424(3)	−2.5098(12)	0.3962(18)	752
C(31)	1.4419(3)	−2.6113(12)	0.2334(19)	859
C(32)	1.4725(4)	−2.7331(13)	0.2605(23)	1045
C(33)	1.4713(4)	−2.8371(16)	0.0966(24)	1243

Table 2. Torsion Angles for Various Azobenzene-Linked Compounds

Compound	Torsion angles**		
	$\theta1$/°	$\theta2$/°	$\theta3$/°
$C_{12}AzoC_5N^+Br^-$	−177.7	−179.0	−179.9
trans-Azobenzene[15]*	−163.3	163.3	180.0
	−173.1	173.1	180.0
4,4′-Dimethylazobenzene[12]*	−170.6	170.6	180.0
	−174.5	174.5	180.0
4-Amino-2′,3-dimethyl-azobenzene[13]	−177.1	−173.9	177.7
1,4-Bis(phenylazo)benzene[14]	178.4	178.9	179.0
2,2′,4,4′,6,6′-Hexamethyl-azobenzene[18]*	161.2	−161.2	180.0
2,2′,4,4′,6,6′-Hexa-*t*-butyl-azobenzene[19]	−132.9	−119.5	161.6
2,2′,4,4′,6,6′-Hexaisopropyl-azobenzene[20]*	−155.5	155.5	180.0
2-Thiocyanatoazobenzene[21]	−123.4	−118.7	−171.7

* Molecule has an inversion symmetry at the center of azobenzene moiety. ** Torsion angles are defined as follows:

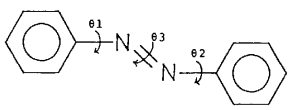

series of compounds were synthesized to investigate the relationship between their aggregation behavior and the alkyl chain length in the tail(n) and spacer(m) portions.[7] In terms of absorption spectroscopy, their molecular aggregation states were classified into four types. They are the monomeric chromophore in micelles and in molecularly dispersed solutions, the dimeric chromophore in the liquid crystalline bilayer, and the H-aggregate and the J-like aggregate in the crystalline bilayer (Table 5 in Ref. 7). The latter two aggregates are particularly interesting because of their chromophore orientations. The H-aggregate implies the highly parallel chromophore orientation and the J-like aggregate implies the head-to-tail orientation (Fig. 2). We already investigated the structure of the H-aggregate in a cast film of $C_8AzoC_{10}N^+Br^-$ by the X-ray diffraction technique.[8]

In this paper, we discuss the detailed structure of the J-like aggregate in a single crystal of $C_{12}AzoC_5N^+Br^-$ on the basis of the structure obtained by X-ray crystal analysis. Since this is the first analysis of a totally synthetic amphiphile on the atomic level, the results will be useful for the better understanding of the biological membrane. Furthermore, it will also play an important part in the elucidation of the energy transfer mechanism, which occurs characteristically in the azobenzene-linked amphiphiles with J-like chromophore orientation.

Experimental and Structure Determination

$C_{12}AzoC_5N^+Br^-$ (25 mg) was dissolved in a boiling solution (30 ml) of water and ethanol (water/ethanol=1/1 by volume rotio). Yellow, plate-like crystals with thickness of about 0.02 mm were obtained by keeping the solution for a week or two at room temperature. However, these plate-like crystals were usually multiple crystals with the common axis normal to the plate surface. Needle-like crystals were also obtained by storing the solution in a refrigerator. In this case crystals were very thin (about 0.01 mm) and small

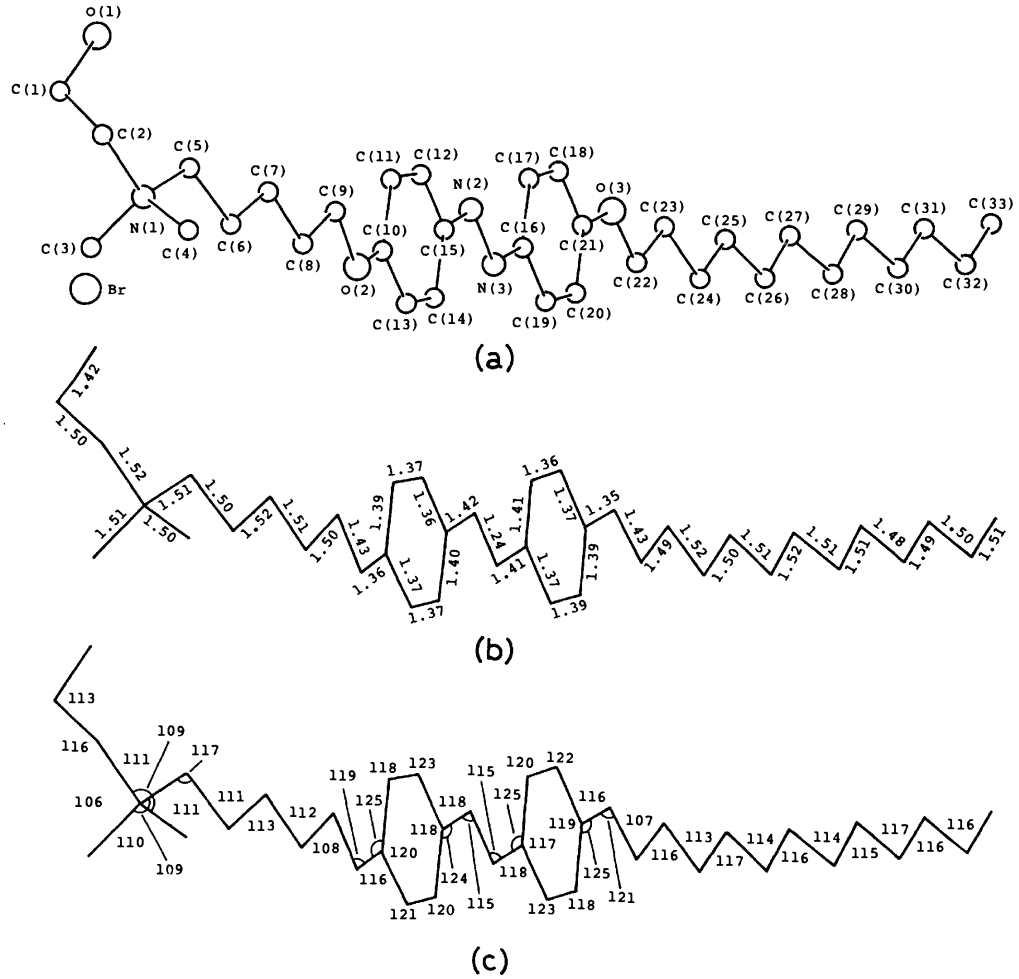

Fig. 3. Atomic labelling (a) and bond lengths (1×10/nm) (b) and angles (ϕ/°) in $C_{12}AzoC_5N^+Br^-$. Maximum estimated standard deviations for bond lengths and angles are 0.002 nm and 1°, respectively.

in width (about 0.1 mm) but long (2—3 mm). Diffraction experiments showed that these two types of crystals have identical lattice constants and intensity distribution. One of the latter type of crystals was used for the intensity measurements.

Lattice parameters and diffraction intensities were measured on a Rigaku four-circle diffractometer with Ni-filtered Cu $K\alpha$ radiation (λ=0.154184 nm). The lattice parameters were refined by the least-squares fit using 25 reflections in the 2θ range of 15—66°. By using the ω-scan mode at a scan rate of 6°/min, intensities of 4423 reflections were measured up to 105° in 2θ. The scan width was $\Delta\omega=(2.8+0.15\tan\theta)°$. Three reference reflections monitored every 50 reflections showed no significant intensity deterioration during the data collection. Corrections were made for the Lorentz and polarization factors, but not for absorption and extinction effects. A total of 2917 reflections greater than $3\sigma(F_o)$ were used in the following analysis, where $\sigma(F_o)$ is the standard deviation estimated from the counting statistics.

Crystal Data: $C_{33}H_{54}N_3O_3Br$, $F.W.$=620.7, triclinic, space group $P\bar{1}$, Z=2, a=3.4243(6), b=0.8525(1), c=0.6073(1) nm, α=73.45(1), β=88.03(1), γ=93.32(1)°, V=1.6941(4) nm^3, D_x=1.215, D_m=1.21 gcm^{-3}.

Determination and Refinement of the Structure

The direct method with the *MULTAN* 78 program[9] was applied for $P1$ and $P\bar{1}$ space groups. Only for the latter space group, a rigid azo moiety and two planar zigzag alkyl chains could be readily discerned. The vector between two bromide ions related by the centrosymmetric operation was clearly appeared in the three-dimensional Patterson map, which also supported the $P\bar{1}$ space group for the $C_{12}AzoC_5N^+Br^-$ crystal. After several cycles of block-diagonal least-squares refinement starting from the atomic coordinates obtained by the direct method, difference Fourier syntheses revealed the remaining two carbon atoms in the alkyl chain and a terminal oxygen atom in the hydrophilic head group. After an anisotropic refinement of non-hydrogen atoms, hydrogen atoms located on their calculated positions with isotropic temperature factors were included in the refinement. The quantity minimized was $\sum w(|F_o|-|F_c|)^2$ with w=1.0 for all reflections. After several cycles some hydrogen atoms with unacceptable geometry were

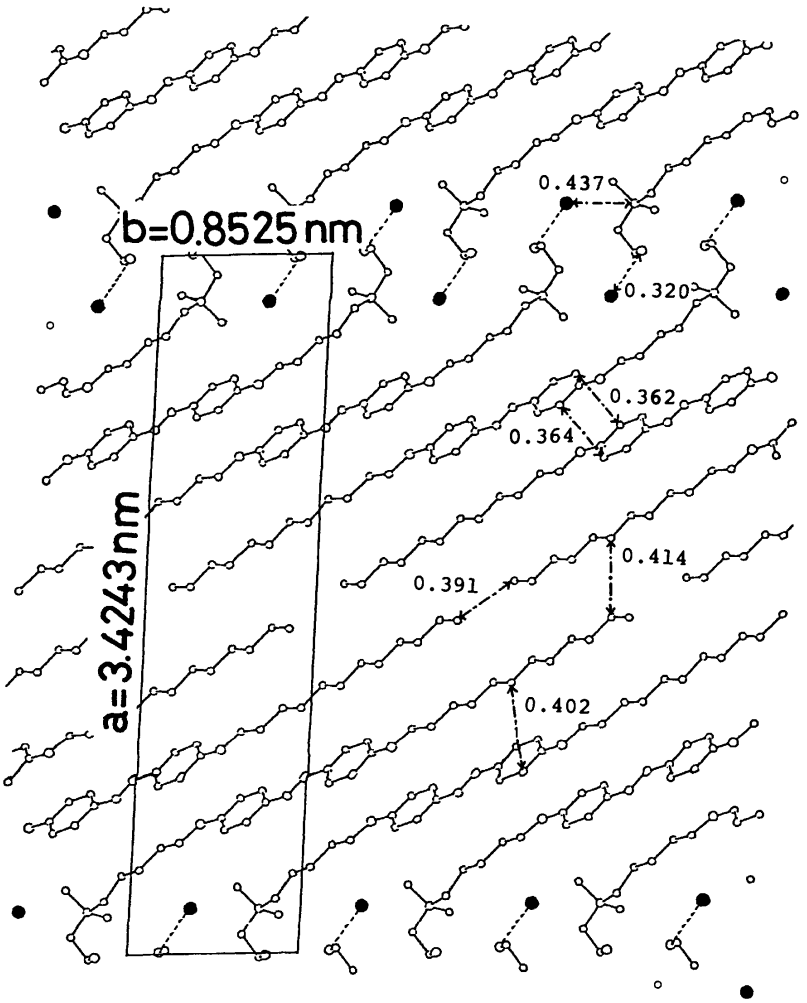

Fig. 4. Packing of $C_{12}AzoC_5N^+Br^-$ projected onto the *c*-plane. Hydrogen bonds between bromide anions and hydroxyl groups are indicated by broken lines (ORTEP[22] drawing).

excluded from further calculations. At the final stage of refinements the full-matrix least-squares calculation was carried out but no significant improvement was obtained. The final R value was 0.059 (R_w=0.060) for all nonhydrogen atoms and 51 hydrogen atoms. The final atomic parameters for non-hydrogen atoms are given in Table 1.[10]

The atomic scattering factors were taken from International Tables for X-Ray Crystallography, Vol. IV.[11] Computations were done on an ACOS 700S computer at the Crystallographic Research Center, Institute for Protein Research, Osaka University and on a HITAC M-280H computer at the Computer Center, University of Tokyo.

Results and Discussion

Molecular Structure of $C_{12}AzoC_5N^+Br^-$. Bond distances and angles are shown in Fig. 3, together with its atomic labelling. The average bond length between carbon atoms in the benzene rings is 0.138 nm. Judging from the bond distances in Fig. 3, there are no evidence for the quinonoid character in both benzene rings, unlike in 4,4′-dimethylazobenzene[12] and 4-amino-2′,3-dimethylazobenzene.[13] The C(11)-C(10)-O(2), C(14)-C(15)-N(2), C(17)-C(16)-N(3) and C(20)-C(21)-O(3) bond angles deviate by 4—5° from the standard value (120°) for sp^2 carbon atoms, presumably in order to relieve the close approach between the C(9) and C(11), C(14) and N(3), C(17) and N(2), and C(20) and C(22) atoms, respectively. This type of deviation has been found in many other compounds,[12-15] in which substituent groups are located approximately in the benzene ring plane. The mean C-C bond distance and C-C-C bond angle in the alkyl spacer and tail parts are 0.150(1) nm and 115(1)°, respectively. They are in good agreement with values previously found in other amphiphilic compounds with long hydrocarbon chains.[16,17]

The most striking feature of the $C_{12}AzoC_5N^+Br^-$ molecule is the planarity of the azobenzene chromophore. Table 2 shows two torsion angles (θ_1 and θ_2) between the azo group and the benzene rings, and at the azo group itself (θ_3) for various compounds. In

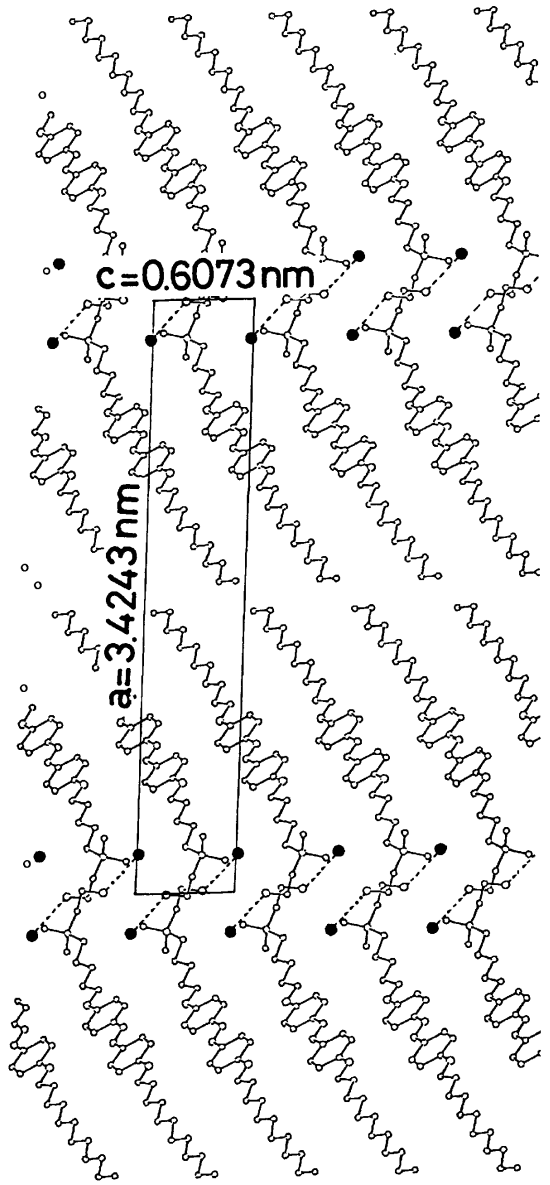

Fig. 5. Packing of $C_{12}AzoC_5N^+Br^-$ projected onto the *b*-plane (ORTEP[22]).

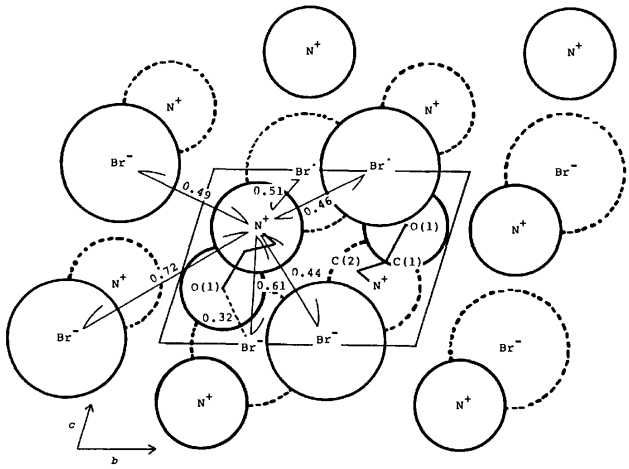

Fig. 6. Schematic illustration of hydrophillic layer of $C_{12}AzoC_5N^+Br^-$ projected onto the *a*-plane. Solid and broken circles represent atoms on the upper and lower side of the hydrophillic layer, respectively. Distances (*l*/nm) are indicated.

many cases, the deviation from the planar conformation is more than 6°, while in the $C_{12}AzoC_5N^+Br^-$ case the deviation is less than 2.3°. So far, this kind of planarity for an azobenzene chromophore has been found only in the case of 1,4-bis(phenylazo) benzene,[14] where adjacent molecules along the *b*-axis had very strong interactions and are separated by only 0.325 nm. Another example of the comparatively good planarity has been found in 4-amino-2′,3-dimethylazobenzene where there is delocalization of π-electrons between phenyl groups and an azo moiety.[13] The pronounced planarity of the azobenzene moiety in the $C_{12}AzoC_5N^+Br^-$ crystal enables parallel stacking of head and tail phenyl rings in the J-like aggregation (Fig. 4). Furthermore, the zigzag planes of the spacer alkyl and the tail alkyl parts of $C_{12}AzoC_5N^+Br^-$ are linked to the azobenzene plane with small torsion angles, 7.3° and 4.1°, respectively. Consequently, the whole molecule is like a long thin plate (Figs. 4 and 5).

Crystal Structure of $C_{12}AzoC_5N^+Br^-$. The crystal structure of $C_{12}AzoC_5N^+Br^-$ can be considered as a structure regularly stacked by the bimolecular layers along the *a* direction (Figs. 4 and 5). Within the bimolecular layer, two molecules related by the inversion symmetry face each other in the tail-to-tail fashion with the contact distance of 0.391 nm and their molecular axes inclined by about 30° to the layer surface (Fig. 4). The structure also can be seen as an alternation of the hydrophobic and hydrophilic layers stacked along the *a* direction. The hydrophilic layer, consisted of ammonium cations, bromide anions and terminal hydroxyl groups from both sides of bimolecular layers, coincides in position with the (100) plane of the crystal (Figs. 4 and 5). In particular, ammonium cations and bromide anions make a plane parallel to the (100) plane within the deviation of 0.004 nm. Two such planes are contained in one hydrophilic layer. This type of planarity among charged atoms in an amphiphilic salt crystal have been found in many other cases.[23,24] Figure 6 shows one of the planes composed of charged atoms and 2-hydroxyethyl groups. A nitrogen cation is surrounded by six bromide anions (four on the same plane and two on the other plane in the same hydrophilic layer). Terminal atoms, $N(1)^+$, C(2), C(1), and O(1) are nestled near the center of four equivalent bromides. A nitrogen cation locates at the point with long distances (0.61 and 0.72 nm) from bromide anions on the same side as O(1) atom. The distances from the other side of bromides are rather short (0.44—0.51 nm). The terminal hydroxyl group, which is the

only one potential hydrogen bonder in the $C_{12}AzoC_5N^+Br^-$ molecule, takes part in the hydrogen bond formation with bromide anion. Hydrogen bond distance (0.32 nm) and angle ($\angle OHBr^-=160.7°$) are those of commonly observed. In addition to this hydrogen bond, electrostatic interactions between ammonium cations and bromide anions stabilize the hydrophilic phase and link the neighboring bimolecular layers tightly, while hydrophobic alkyl chains and azobenzene moieties are stabilized only by the van der Waals interactions.

The cross-section of the benzene ring, S_B which is the largest part in the hydrophobic chain, could be estimated as 0.234 nm^2 by using van der Waals radii 0.18 and 0.12 nm for atoms C and H, respectively. While it is possible to calculate the molecular area, S_M, at the bilayer surface from the lattice constants: $S_M=0.497$ nm^2($=bc\times\sin\alpha$). In order to balance the cross-sections of the hydrophilic and hydrophobic part, molecules have to incline by 62° ($=\cos^{-1}(S_B/S_M)$) from the layer normal. Thus, the azobenzene chromophores are obliged to form J-like aggregate (head-to-tail orientation). On the other hand, hydrophobic chains from both sides interdigitate each other in the bilayer of the cast film of $C_8AzoC_{10}N^+Br^-$.[8] This is another stable aggregation (H-aggregate), since the cross-section of the interdigitated hydrophobic chain, 2 S_B is comparable to the molecular area S_M.

Some short interatomic distances between the neighboring azobenzene chromophores are shown in Fig. 4 together with those between alkyl tail parts. Absorption spectra of azobenzene in J-like aggregates of $C_nAzoC_mN^+Br^-$ show a shift to longer wavelength (red shift) than those of the molecularly dispersed azobenzene chromophores. This shift has been attributed to the intermolecular interactions between azobenzene chromophores in J-like aggregates.[7] The distance about 0.36 nm between overlapped phenyl groups seems to be short enough for red shift by reference to theoretical calculations for dye molecules in J-aggregates.[25] In order to clarify the relationship between a molecular and/or packing structure and spectroscopic behavior, further analyses for several compounds with different n and m of $C_nAzoC_mN^+Br^-$ are now carring on.

References

1) S. J. Singer and G. L. Nicolson, *Science*, **175**, 720 (1972).

2) H. Hauser, I. Pascher, R. H. Peason, and S. Sundell, *Biochim. Biophys. Acta*, **650**, 21 (1981).

3) T. Kunitake and Y. Okahata, *J. Am. Chem. Soc.*, **102**, 549 (1980).

4) T. Kunitake and Y. Okahata, *J. Am. Chem. Soc.*, **99**, 3860, (1977).

5) T. Kunitake, N. Kimizuka, N. Higashi, and N. Nakashima, *J. Am. Chem. Soc.*, **106**, 1978 (1984).

6) K. Okuyama, Y. Soboi, K. Hirabayashi, A. Harada, A. Kumano, T. Kajiyama, M.Takayanagi, and T. Kunitake, *Chem. Lett.*, **1984**, 2117, (1984).

7) M. Shimomura, R. Ando, and T. Kunitake, *Ber. Bunsenges. Phys. Chem.*, **87**, 1134 (1983).

8) T. Kunitake, M. Shimomura, T. Kajiyama, A. Harada, K. Okuyama, and M. Takayanagi, *Thin Solid Films*, **121**, L89 (1984).

9) P. Main, S. E. Hull, L. Lessinger, G. Germain, J. P. Declercq, and M. M. Woolfson, *MULTAN 78*. "A System of Computer Programs for the Automatic Solution of Crystal Structures from X-ray Diffraction Data," Univs. of York, England, and Louvain, Bergium (1978).

10) Tables of anisotropic thermal parameters, coordinates of hydrogen atoms, and observed and calculated structure factors are kept at the Chemical Society of Japan, Document No. 8647.

11) International Tables for X-ray Crystallography, Vol. IV, Kynoch Press, Birmingham (1974), p. 71.

12) C. J. Brown, *Acta Crystallogr.*, **21**, 153 (1966).

13) S. Kurosaki, S. Kashino, and M. Haisa, *Acta Crystallogr., Sect. B*, **32**, 3160 (1976).

14) R. D. Gilardi and I. L. Karle, *Acta Crystallogr., Sect*, **B28**, 1635, (1972).

15) J. A. Bouwstra, A. Schouten, and J. Kroon, *Acta Crystallogr., Sect.* **C39**, 1121 (1983).

16) S. Abrahamsson, B. Dahlen, and I. Pascher, *Acta Crystallogr., Sect.* **B33**, 2008 (1977).

17) I. Pascher and S. Sundell, *Chem. Phys. Lipids*, **20**, 175 (1977).

18) E. J. Gabe, Y. Wang, L. R. C. Barclay, and J. M. Dust, *Acta Crystallogr., Sect.* **B37**, 978 (1981).

19) Y. L. Page, E. J. Gabe, Y. Wang, L. R. C. Barclay, and H. L. Holm, *Acta Crystallogr., Sect.* **B36**, 2846 (1980).

20) Y. L. Page, E. J. Gabe, L. R. C. Barclay, and J. M. Dust, *Acta Crystallogr., Sect.* **B37**, 976 (1981).

21) K. K. Kakati and B. Chandhuri, *Acta Crystallogr., Sect.* **B24**, 1645 (1968).

22) C. K. Johnson, ORTEP 11, Report ORNL-5138, Oak Ridge National Laboratory, Tennessee (1976).

23) J. H. Dumbleton and T. R. Lomer, *Acta Crystallogr.*, **19**, 301 (1965).

24) V. Vand, T. R. Lomer, and A. Lang, *Acta Crystallogr.*, **2**, 214 (1949).

25) V. Czikkely, H. D. Forsterling, and H. Kuhn, *Chem. Phys. Lett.*, **6**, 11 (1970).

26) W. C. Hamilton, *Acta Crystallogr.*, **12**, 609 (1959).

 © 1986 The Chemical Society of Japan Bull. Chem. Soc. Jpn., 59, 3357—3361 (1986)

Dichroism Analysis of Oriented Polyenes Produced in Poly(vinyl alcohol) Film

Kazunori MARUYAMA and Yoshié TANIZAKI*
Department of Materials Science and Technology, Technological University of Nagaoka, Nagaoka, Niigata 940-21
(Received March 14, 1986)

Dichroic spectra of polyenes $-(CH=CH)_n-$ produced in heat-treated poly(vinyl alcohol) [PVA] film were determined for two cases; stretch (at 85 °C) after heat (120 °C), (Δ,S), and heat after stretch, (S,Δ). The dichroic ratios Rd_n of component polyenes (n=2—6) were estimated by means of simulation. In both cases (Δ,S) and (S,Δ), the relation of Rd_n vs. Rs (stretch ratio) kept the theoretical equation of the dichroism analysis. The relative angles among the transition moments μ_n (n=2—6) were in accordance with those obtained by drawings of *trans*-polyenes. The idea of an azimuth vector in the stretched PVA substrate was justified. The relation of $Rd_n(\Delta,S)>Rd_n(S,\Delta)$ was always observed at any Rs. This was explained by the thermal orientation-relaxation of polymer chains.

Stretched PVA film colored by heating is utilized as a polarizing film.[1] In such a film, various kinds of π electron systems must be produced and oriented to the stretched direction. Therefore, the whole dichroism has to be dependent upon the respective polarization characteristics of the π electron systems. But the detailed analysis of the dichroism has not been investigated yet, though the dichroic ratio of the stretched and heat-treated PVA film has been reported.[2]

Up to date, the conventional dichroism analysis by the technique of stretching the PVA film[3] has succeeded in explaining the correlation between the transition moment and the geometrical structure of many molecules.[4] This analysis is based on a distribution function of an azimuth vector postulated for the PVA substrate.[3]

Previously, we have made assignments for the polyenes produced in heat-treated PVA film[5] and have further attempted to estimate the concentrations of the polyenes by simulations.[6]

When the dichroism analysis is combined with the method of simulation, it is expected that the correlation between the whole and the component dichroisms of the polyenes in a stretching state can be analyzed. Since the polyenes should be formed along the polymer chains in this case, the orientation aspect of the polyenes is regarded to be the same as that of the polymer chains. In other words, the orientation vector of the polyenes as an absorption species is the same as the azimuth vector of the substrate. This is important because, in the conventional dichroism analysis, it is assumed that an orientation vector of a guest molecule acts with the same behavior as the azimuth vector concomitant with the substrate itself. For that reason, the respective orientation directions of polyenes must be identical with a single direction which is common to all. This will be checked by the geometrical relation between the common azimuth direction and the molecular structure of the polyene.

The purpose of the present study is the following. The first is to seperate the total dichroism of polyenes into the component dichroisms by simulation and then to determine the relative directions of the transition moments μ_n. The second is to verify the justification of an azimuth vector, for which the distribution function is fundamental to the conventional dichroism analysis.

Experimental

PVA films treated with $NaBH_4$ according to the method reported previously[5] were digested in 0.05 M HCl solution (1 M=1 mol dm^{-3}) or 0.05 M H_2SO_4 solution for 3 h and dried for 1 d at room temperature. Further, they were treated by the following processes (A) or (B).

(A) After the film was heated at 120 °C to turn it red, it was digested in distilled water for 1 d, dried at room temperature for 1 d, and then stretched. The stretched film was fixed on a metal holder.

(B) At first the film was stretched and fixed on a metal holder. Then it was heated at 120 °C for about 15 min.

In order to distinguish between (A) and (B) by the sequence of heating (Δ) and stretching (S), the notations (Δ,S) and (S,Δ) will be used, respectively.

The film was uniaxially stretched at 85±5 °C and the stretch ratio (Rs) was defined in the same way as reported previously.[3] That the stretched film is ideally deformed was checked by assuring that the dimensional requirement for the theory of dichroism analysis was satisfied with respect to the length, width and thickness of film before and after stretching.[7] The heat treatment of the sample film was carried out in a heating compartment under conditions of 0.5 dm^3 min^{-1} flow of nitrogen.

The absorption spectra were measured using a Shimadzu UV-360 Spectrophotometer equipped with a rotatory Rochon-type prism. The net absorption of the sample film was obtained by compensation for the absorption of a colorless PVA film before heating. The dichroic ratio Rd is defined as $A_\parallel/A_\perp$, where $A_\parallel$ and $A_\perp$ are the absorbances for the incident polarized light, of which the electric vector is parallel and perpendicular to the stretching direction of film, respectively. The Rd curves were obtained by a data processor, Sapcom-1, attached to the spectrophotometer.

Theoretical

When a PVA film undergoes an ideal uniaxial stretching, the width and thickness of the film shrink at the same rate. In this case, the following relation must hold,

$$A = k(A_{\parallel} + 2A_{\perp}) \tag{1}$$

where A is the absorbance before stretching and k is a constant depending on the film dimensions deformed. Equation 1 also holds in the case of respective polyenes. Using the same constant k, the absorbance of n-polyene -(CH=CH)$_n$- is given by

$$A_n = k(A_{n\parallel} + 2A_{n\perp}) = \varepsilon_n C_n d \tag{2}$$

where ε_n and C_n are the extinction coefficient and the concentration of n-polyene, and d is the film thickness. The dichroic ratio is defined as usual:

$$Rd_n = A_{n\parallel}/A_{n\perp} \tag{3}$$

From Eqs. 2 and 3, the $A\parallel$ and $A\perp$ spectra of the whole system can be represented as follows,

$$\left.\begin{aligned} A_{\parallel} &= \sum_n A_{n\parallel} = (d/k)\sum_n \varepsilon_n C_n (1+2/Rd_n)^{-1} \\ A_{\perp} &= \sum_n A_{n\perp} = (d/k)\sum_n \varepsilon_n C_n (2+Rd_n)^{-1} \end{aligned}\right\} \tag{4}$$

Therefore, the following relation between Rd and Rd_n is obtained.

$$Rd = \frac{\sum_n \varepsilon_n C_n (1+2/Rd_n)^{-1}}{\sum_n \varepsilon_n C_n (2+Rd_n)^{-1}} \tag{5}$$

Strictly speaking, on account of the molecular vibration, the ratio of $A_{n\parallel}$ to $A_{n\perp}$ of the dichroic spectra of A_n depends on the wavelength, namely, Rd_n is not constant over the whole absorption region. But, its variation in the main part is generally small. At the present stage, therefore, all of Rd_n are assumed to be invariable in the respective absorption regions.

By simulation of the absorption spectra of polyenes produced in PVA film,[6] the concentrations C_n of Eq. 2 can be estimated, using the known ε_n, from the simulated spectrum A of Eq. 1 together with the relation $A=\sum_n A_n$. From these and the observed Rd values, Rd_n of respective polyenes can be determined so as to satisfy Eq. 5.

According to the theory of dichroism analysis using uniaxially stretched PVA film,[3] the anisotropy of the substrate can be described by a distribution function $f(Rs)$ of an azimuth vector (OD vector) for the stretching direction. And the dichroic ratio Rd_n is derived from $f(Rs)$. An important point to be noticed here is that the direction which keeps the distribution $f(Rs)$ is not the transition vector μ_n itself but the projective part (μ_{na}) of μ_n upon the direction of OD. For that reason, the Rd_n equation involves Rs and a parameter r_n, $Rd_n=F(Rs, r_n)$, where r_n is defined as

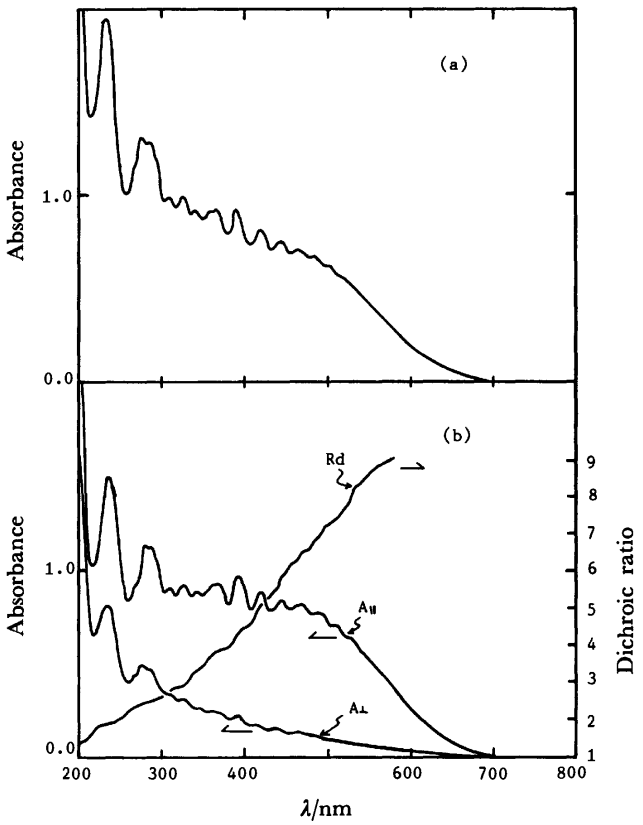

Fig. 1. Isotropic (a) and polarized absorption spectra (b) of PVA film for the case of (Δ,S), which is stretched (Rs=5.7) after heating at 120 °C for 15 min. Rd is dichroic ratio. Film thickness is 195 μm (a) and 110 μm (b).

$r_n=|\mu_{na}/\mu_{nb}|$, and μ_{na} and μ_{nb} are the components of μ_n along OD and its normal direction, respectively.

Finally, Rd_n is expressed by Rs and r_n as follows.[3]

$$\left.\begin{aligned} Rd_n &= \frac{2+2(r_n^2-1)T}{(2r_n^2+1)-(2r_n^2-1)T} \\ \text{where} \\ T &= \frac{Rs^2}{Rs^2-1}\left[1-\left\{\frac{\pi}{2}\tan^{-1}(Rs^2-1)^{-1/2}\right\}(Rs^2-1)^{-1/2}\right]. \end{aligned}\right\} \tag{6}$$

The inclination of μ_n for OD can be given by

$$\alpha_n = \cot^{-1} r_n \tag{7}$$

where α_n is called the orientation angle of μ_n.

Results

Figure 1(a) shows the absorption spectrum of a PVA film heated to red, and Fig. 1(b) the dichroic spectra and the Rd curve of the same film stretched to Rs=5.7. The spectrum A calculated by Eq. 1 using $A\parallel$ and $A\perp$ of Fig. 1(b) coincided with that of Fig. 1(a) when k=0.66. This indicates that the deformation of PVA substrate was ideal and that the absorption species did not change chemically by stretching.

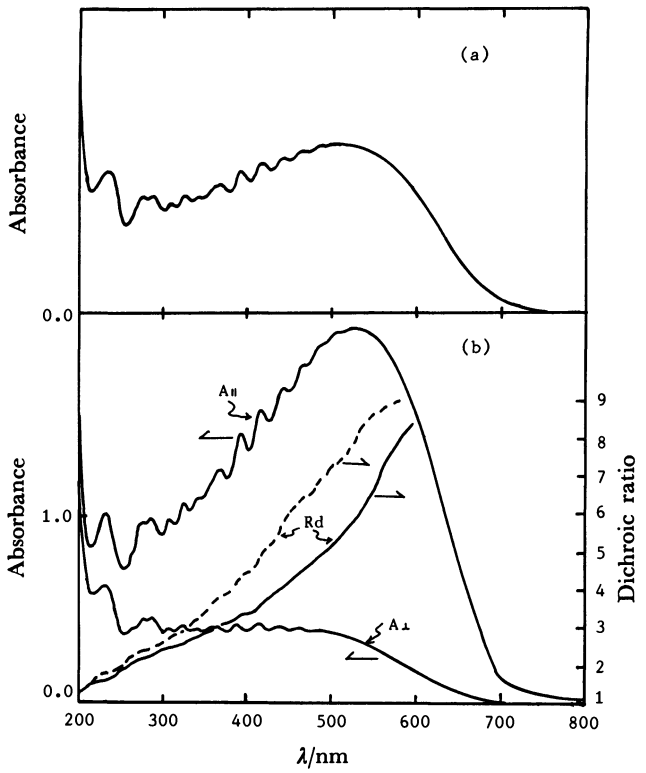

Fig. 2. Isotropic (a) and polarized absorption spectra (b) of PVA film for the case of (*S*,*Δ*), which is heated at 120 °C for 15 min after stretching (*R*s=6.2). Fig. (a) is obtained from $(A_{\parallel}+2A_{\perp})/3$ of Fig. (b). Film thickness is 98 μm. Broken line in (b) indicates *R*d curve in Fig. 1(b).

Figure 1(b) is for the case of (*Δ*,*S*). In contrast to this, the film for (*S*,*Δ*) is reddish purple and its dichroic spectra at *R*s=6.2 are measured as shown in Fig. 2(b). Figure 2(a) shows the isotropic spectrum *A* determined by Eq. 1 using $A_{\parallel}$ and $A_{\perp}$ of Fig. 2(b).

From the comparison of Figs. 1(a) and 2(a), it is clear that the absorption spectrum of a film is changed by reversing the procedure, heat (*Δ*) and stretch (*S*); the relative intensities in the short and long wavelength regions are exchanged. The absorption in the long wavelength region is more intensive for the case of (*S*,*Δ*) than for (*Δ*,*S*).

The *R*d curve rises toward the long wavelength in either case (Figs. 1(b) and 2(b)), but the *R*d value at each wavelength is smaller for (*S*,*Δ*) (solid line in Fig. 2(b)) than for (*Δ*,*S*) (broken line), though *R*s of the former is larger than that of the latter.

The concentrations C_n of Eq. 2 were obtained using litetature values of ε_n.[8] The Rd_n values at *R*s=5.7 were calculated from the data of Fig. 1(b), in such a way that *R*d of Eq. 5 becomes equal to the observed *R*d. The Rd_n values thus determined at the wavelength corresponding to the 1←0 transition of *n*-polyenes are listed in Table 1 together with the *R*d values at the same wavelengths. In Table 1, only the results of *n*=2—7 are presented, being left out those of $n \geqq 8$,

Table 1. Simulated Rd_n and Observed *R*d at 1←0 Transitions of *n*-Polyenes[a]

n	Rd_n	*R*d
2	1.9	1.9 (234)
3	2.3	2.3 (274)
4	2.6	2.8 (310)
5	3.1	3.3 (342)
6	4.2	3.9 (366)
7	4.3	4.5 (390)

a) Observed *R*d is the case of *R*s=5.7 (Fig. 1(b)). ( ) indicates wavelength of 1←0 transition of *n*-polyene.

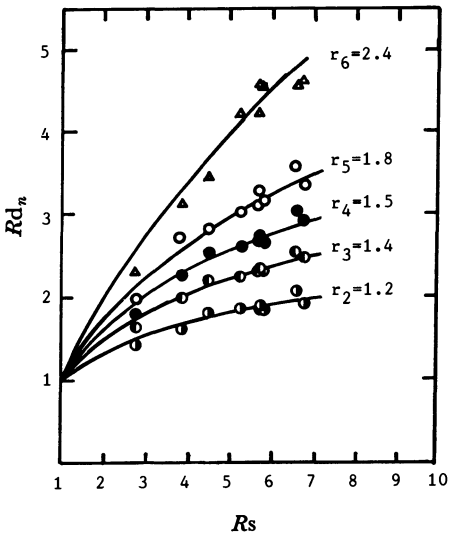

Fig. 3. Relationship of Rd_n(*Δ*,*S*) vs. *R*s for *n* which is the number of double bonds of *n*-polyene. Marks are experimental and lines are obtained from Eq. 6 using the parameters r_n listed in Table 2. ◑: *n*=2, ◐: *n*=3, ●: *n*=4, ○: *n*=5, △: *n*=6.

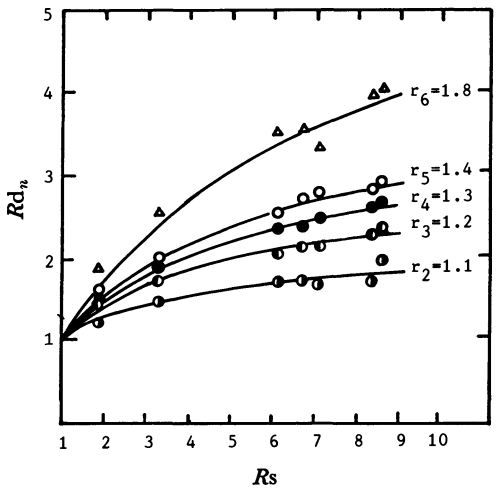

Fig. 4. Relationship of Rd_n(*S*,*Δ*) vs. *R*s for *n* which is the number of double bonds of *n*-polyene. Marks are experimental and lines are obtained from Eq. 6 using the parameters r_n listed in Table 2. ◑: *n*=2, ◐: *n*=3, ●: *n*=4, ○: *n*=5, △: *n*=6.

Table 2. r_n and Orientation Angle of n-Polyene[a)]

n	(Δ, S)			(S, Δ)		
	r_n	α_n°	α_n	r_n	α_n°	α_n
2	1.2	41°	41°	1.1	44°	44°
3	1.4	36°	36°	1.2	39°	39°
4	1.5	33°	33°	1.3	37°	36°
5	1.8	29°	31°	1.4	35°	34°
6	2.4	22°	30°	1.8	29°	33°

a) Orientation angle: α_n° is observed, α_n is from drawing (see Fig. 6).

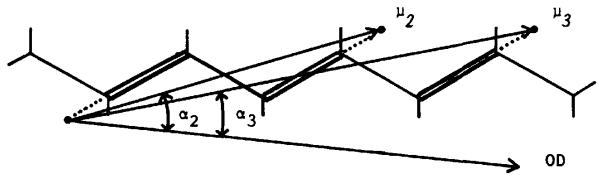

Fig. 6. Drawing of $\mu_n(n=2, 3)$ and OD for polyene skeleton. Terminals of transition vector μ_n are at two points taken at halves as long as the terminal bond on the outer extension lines. α_n is the orientation angle of μ_n against OD (orientation direction) of polymer chain.

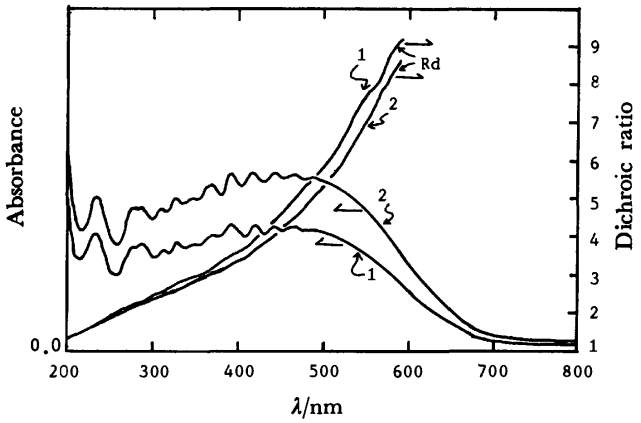

Fig. 5. Absorption spctra of PVA film for the case of (S,Δ), stretched (Rs=6.8) and heated at 120 °C for 16 min (curve 1) and 20 min (curve 2). Film thickness is 68 μm.

because these concentrations computed are not dependable.[6)]

In the same way as above, the Rd_n values at various Rs were determined. The relation Rd_n vs. Rs is plotted in Fig. 3 for individual polyenes. The curves drawn in Fig. 3 are those obtained theoretically by Eq. 6 using the parameters which fit for the Rd_n-Rs plot. Figure 4 shows the same relation for the case (S,Δ), where the heating times were kept at 15 min, because the Rd value was dependent upon the length of the heating period (see Fig. 5). The r_n values of Figs. 3 (Δ,S) and 4 (S,Δ), and the orientation angles α_n° obtained from Eq. 7 are listed in Table 2.

Figure 5 shows the absorption spectra and the Rd curves for the different heating times (1:16 min, 2:20 min) of a film for the case of (S,Δ), in which the spectra are derived from Eq. 1 using the observed $A\parallel$ and $A\perp$. Figure 5 reveals an interesting phenomenon that the longer the heating time, the stronger the absorption and at the same time the lower the Rd values.

Discussion

Orientation Angles of Polyenes. As shown in Figs. 3 and 4, the Rd_n values agree well with the theoretical curves. This means that μ_{na} is acting with the same behavior as the OD vector which is common to all polyenes. For that reason, the inclinations of μ_n can be compared by the orientation angles α_n° against only one OD vector.

Table 2 shows that α_n° becomes smaller with increase of n in both cases, (Δ,S) and (S,Δ). This indicates that the OD vector points to a certain lengthwise direction close to the zigzag chain of polyene skeleton.

In order to investigate α_n° in Table 2 by a molecular diagram, the transition directions of μ_n with respect to the same geometry of polyene-skeleton were made in the following way. The direction of μ_n is regarded as the direction through the two points which are respectively half as long as the C-C bond on the outer extension line of each of the terminal double bonds of n-polyene as shown in Fig. 6. Assuming that an angle α_2 between μ_2 and OD by drawing is equal to α_2°, other α_n are obtained as listed in the right columns of (Δ,S) and (S,Δ) in Table 2.

In both cases, (Δ,S) and (S,Δ), the experimental α_n° are in good agreement with the drawing α_n in the range n=2—5. This fact indicates that the distribution of the OD vector agrees with the theoretical distribution function and that the concept of an azimuth vector is justified.

Relaxation Phenomenon of Orientation. Inspecting the same n, the following relations are recognized: $\alpha_n^\circ(\Delta,S)<\alpha_n^\circ(S,\Delta)$ in Table 2 and $Rd_n(\Delta,S)>Rd_n(S,\Delta)$ at any Rs in Figs. 3 and 4. The latter relation may correspond to some reduction of $Rs(S,\Delta)$ by heating after stretching. However the film was fixed tightly on a metal holder during the heat treatment and any appreciable deformation of film could not be observed by heating, accordingly the reduction of the Rs of the film itself cannot be considered. Therefore, the apparent reduction of Rs by heating may be due to some orientation-relaxation by the thermal motion of the polyene chains.

If the reduction of apparent Rs is regarded as a relaxation phenomenon, a stationary state of orientation must exist at a given temperature. Let f_1 and f_2 be the distribution functions for stationary states at temperature T_1 and T_2 ($T_1<T_2$), respectively, the time

dependent change from f_1 to f_2 may be described as follows,

$$f(t) = f_2 + (f_1 - f_2)\exp(-t/\tau) \quad (8)$$

where τ is the relaxation time.

Since the orientation relaxation is induced by thermal motion, the change of Eq. 8 should be directed towards the isotropic state. Consequently, Rd must be lowered with the period of heating time. In fact, as shown in Fig. 5, the Rd curve in the whole wavelength region is lowered with the heating time. This is considered evidence for the relaxation phenomenon of orientation.

Stretching Effect on Polyenes Formation. In spite of the equal heating temperature (120 °C), the relative intensity of absorption in the long wavelength region was greater for the stretched film (Fig. 2(a)) than for the unstretched one (Fig. 1(a)). This stretching effect on polyenes formation, however, cannot be analyzed at the present stage.

References

1) E. H. Land and H. G. Logers, U. S. Patent, 2173304 (1939); C. A. Finch, "Poly Vinyl Alcohol," John Wiley & Sons, New York (1973), p. 505.

2) Y. Nishijima, Y. Onogi, and T. Asai, *J. Polymer Sci.*, **C-15**, 237 (1966).

3) Y. Tanizaki, *Bull. Chem. Soc. Jpn.*, **38**, 1978 (1965); *ibid.*, **32**, 75 (1959).

4) As one of the most recent reports: M. Kobayashi, T. Hoshi, J. Okubo, H. Hiratsuka, T. Harazono, M. Nakagawa, and Y. Tanizaki, *Bull. Chem. Soc. Jpn.*, **57**, 2905 (1984).

5) K. Maruyama, H. Akahoshi, M. Kobayashi, and Y. Tanizaki, *Chem. Lett.*, **1983**, 1863; *Bull. Chem. Soc. Jpn.*, **58**, 2923 (1985).

6) K. Maruyama, M. Také, N. Fujii, and Y. Tanizaki, *Bull. Chem. Soc. Jpn.*, **59**, 13 (1986).

7) Y. Tanizaki, T. Kobayashi, and N. Ando, *Bull. Chem. Soc. Jpn.*, **32**, 1362 (1959).

8) F. Sondheimer, D. A. Ben-Efrain, and R. Molovsky, *J. Am. Chem. Soc.*, **83**, 1675 (1961).

 © 1986 The Chemical Society of Japan Bull. Chem. Soc. Jpn., 59, 3363—3366 (1986)

Adsorption of Tetrachloro-*p*-benzoquinone from Various Solvents on Metal Oxides

Kunio Esumi,* Kazuaki Miyata, Fumio Waki, and Kenjiro Meguro
Department of Applied Chemistry and Institute of Colloid and Interface Science, Science University of Tokyo, Kagurazaka, Shinjuku-ku, Tokyo 162
(Received March 17, 1986)

Adsorption of tetrachloro-*p*-benzoquinone(chloranil) from basic and acidic solvents on metal oxides, such as alumina and titania was carried out to understand the acid-base interaction at the interface. The amount of chloranil adsorbed decreases with an increase of acid-base interaction between the basic solvent and chloranil and also decreases with an increase of acid-base interaction between the acidic solvent and electron donor sites of the metal oxides for both metal oxides. Furthermore, the change in concentration of chloranil radicals formed on their metal oxides by the adsorption is correlated with the acid-base interaction at the interfaces.

Recently, the acid-base theory has been applied to colloidal systems. Fowkes et al.[1,2] have studied the interactions between inorganic solids and basic adsorbates by using the Drago correlation of the heats of acid-base interaction and have determined the Drago parameters for several solids, such as silica, rutile, and magnetite. Esumi et al.[3,4] have examined the adsorption of a strong electron acceptor such as tetracyanoquinodimethane from various solvents on metal oxides and they have demonstrated that the acid-base interaction is an important factor for the adsorption.

In this work, further to confirm the importance of acid-base interaction at solid-liquid interface, the adsorption of chloranil similar to TCNQ on metal oxides was performed.

Experimental

Materials. Alumina and titania were used as metal oxides. These metal oxides were prepared as follows: excess aqueous methanol (water:methanol=4:1 in weight) was vigorously added to a 1-butanol solution of each alkoxide. Stirring was continued for 5 h at about 90°C. The precipitate obtained was separated by centrifuging, washed with methanol, finely ground, and then evacuated at 100°C. Finally, the dried products were calcined for 2 h at 500°C, and used as samples.

Chloranil was obtained from Tokyo Kasei Ltd., and purified by repeated recrystallization from toluene. The solvents used in this study were dried by the use of molecular sieves.

Procedure. The metal oxide was placed in an L-type test tube and a solution of chloranil in an organic solvent was then poured in. After the tube had subsequently been shaken for 2 h at 25°C, the metal oxide was collected by centrifuging and dried at room temperature in vacuo. The dried sample was then used for an ESR measurement.

The ESR spectra were measured by means of a Japan Electrons Optics Laboratory ESR spectrometer (JES-FE3X) operating with an X-band microwave 100 kHz field modulation. The radical concentrations were estimated by comparing the area under the absorption curves for the sample and for standard solutions of 2,2-diphenyl-1-picrylhydrazyl in benzene.

The amount of chloranil adsorbed was determined from the difference in concentrations before and after the adsorption. The absorbance of chloranil was measured by means of an UV spectrophotometer (Hitachi 220A). The maximum absorption wavelengths of the absorption band of chloranil in three basic solvents were 367 nm in acetonitrile, 365 nm in ethyl acetate, and 286 nm in 1,4-dioxane while the maxima of the two acidic solvents were 372 nm in dichloromethane and 375 nm in chloroform.

The specific surface areas of the samples were determined with a Sorptograph, Model ADS-1B(Shimadzu Seisakusho Co., Ltd.): alumina, 227.4 $m^2 g^{-1}$ and titania, 54.7 $m^2 g^{-1}$.

Results and Discussion

The amount of chloranil in solutions adsorbed on the surfaces of alumina and titania was determined from three basic and two acidic solvents. The adsorption isotherms of chloranil are shown in Fig. 1; it is seen that their isotherms are of the Langmuir type for both metal oxides. Table 1 gives the saturated amounts of chloranil adsorbing on the metal oxides estimated from the Langmuir plots. In order to interpret this adsorption result in terms of the acid-base theory, the Drago equation[5] is employed:

$$-\Delta H^{ab} = C_A C_B + E_A E_B$$

where E and C are the Drago constants for the acidic compound(A) and the basic compound(B). It has been demonstrated[5] for the above equation that ΔH^{ab} values can be predicted within 3%. Furthermore, a useful approach for relating the interfacial inter-

Table 1. Data of Chloranil Adsorption

Sample	Saturated amount($\times 10^4$ mmol m^{-2})		
	Acetonitrile	Ethyl acetate	1,4-Dioxane
Alumina	3.82	1.49	1.05
Titania	5.33	0.32	0
	Dichloromethane		Chloroform
Alumina	3.59		2.85
Titania	1.97		1.80

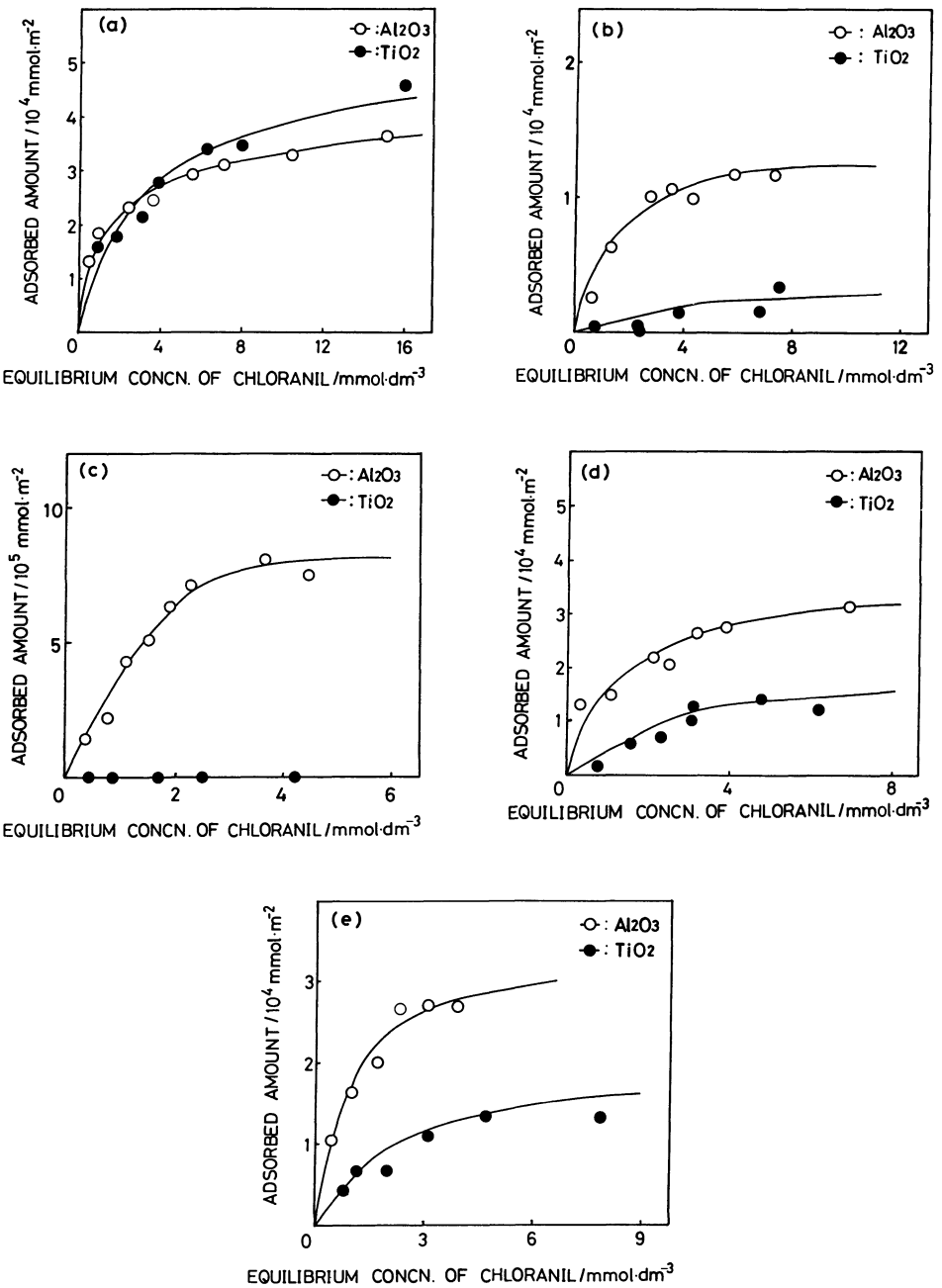

Fig. 1. Adsorption isotherms for Chloranil adsorbing on metal oxides from three basic and two acidic solvents. (a): Acetonitrile, (b): Ethyl acetate, (c): 1,4-Dioxane, (d): Dichloromethane, (e): Chloroform.

actions quantitatively has been the Drago equation of enthalpy changes in acid-base complexation. To apply the Drago equation to this work, the E and C values for the solvents and chloranil should be known, the former is available, but the latter is not reported in the literature.[5] However, from the enthalpy values[6,7] of chloranil and some electron donor solvents, the E and C values of chloranil can be calculated using the Drago equation. The Drago constants and their enthalpy values are listed in Table 2. Figure 2 shows that the saturated amounts of chloranil adsorbed on both metal oxides decrease with an increase of acid-base enthalpy between chloranil and their basic solvents. The behavior of the saturated amounts of chloranil adsorbed in the system of the acidic solvents is similar to that for the basic solvent systems; the saturated amounts of chloranil adsorbed decrease also with an increase of acid-base enthalpy between the acidic solvents and the electron donor sites of metal oxides. In addition, the adsorption results show that the saturated amount of chloranil on alumina is considerably larger than that on titania for both basic

Table 2. Acid-Base Parameters

Solvent	C_B	E_B	C_A	E_A	ΔH^{ab} with *Chloranil or Acetone (Kjoule/mol)
Acetonitrile	2.74	1.812	—	—	11.19
Ethyl acetate	3.56	1.994	—	—	13.61
1,4-Dioxane	4.87	2.23	—	—	17.35
Dichloromethane	—	—	0.02	3.40	6.96
Chloroform	—	—	0.307	6.77	15.13

*Chloranil(C_A=2.39, E_A=2.56), Acetone(C_B=4.77, E_B=2.019).

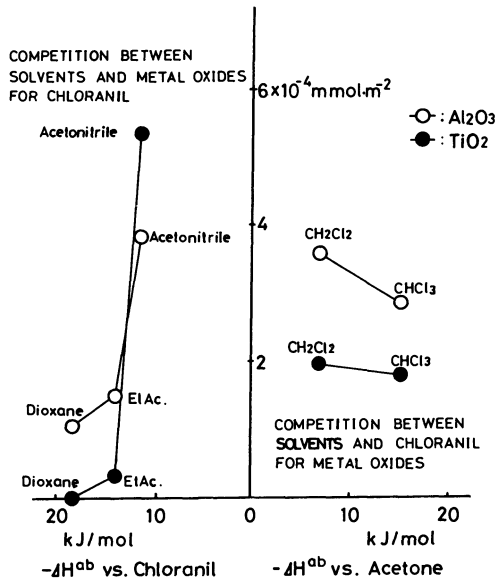

Fig. 2. The Change in the saturated amount of Chloranil on metal oxides as a function of the basicity or acidity of the solvent.

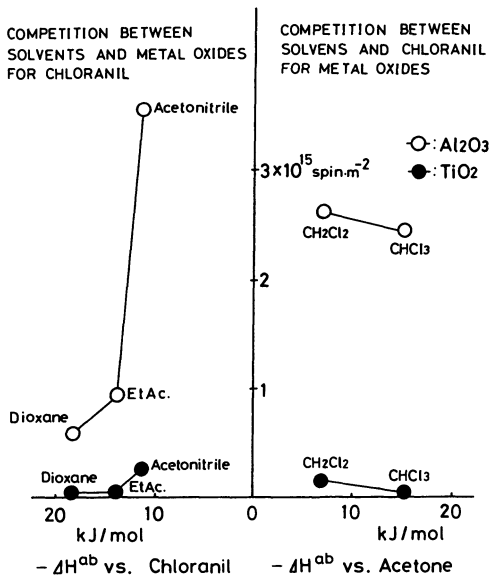

Fig. 3. The Change in the Chloranil radical concentration on metal oxides as a function of the basicity or acidity of the solvent.

and acidic solvent systems.

When chloranil is adsorbed on the metal oxides from the basic and acidic solvents, the surfaces develop characteristic colors; the colors for both alumina and titania were violet, whereas the color strength was dependent on the kind of solvent. It has been reported[8–10] that the colored oxide samples obtained by adsorption of electron acceptors exhibit ESR signals indicating the presence of the free anion radicals of their acceptors. In the present study, the colored samples obtained by the adsorption of chloranil gave an unresolved ESR spectra having a g-value of 2.011.[11] To compare the concentration of the chloranil anion radicals formed on the surfaces as a function of acid-base enthalpy, their concentrations obtained at corresponding to the half-value of the saturated amounts, are given in Fig. 3. It is apparent that the concentrations of chloranil anion radicals decrease with an increase of the acid-base interaction between basic solvents and chloranil or between acidic solvents and electron donor sites on their oxides. Furthermore, it is noteworthy that the concentrations of these radicals formed on alumina are higher than those on titania in all the solvent systems, implying that the electron donor sites on alumina provide a higher electron donicity than those on titania, for which the result is in good agreement with previous data.[3]

Thus, the results obtained from the adsorption of chloranil show a similar trend to those from the adsorption of TCNQ for the acid-base interaction.

For the electron donor sites for both metal oxides, surface hydroxide ions are responsible, because they exist at a relatively low activation temperature. Further, Flockhart et al.[12,13] have confirmed that such hydroxide ions are formed below 500°C which are correlated with electron donicity. Also, Che et al.[14] have reported that electron donor sites for titania at relatively low temperature (<500 °C) are assigned to surface hydroxide ions.

References

1) F. M. Fowkes, ACS Proceedings: Division of Polymeric Materials Science and Engineering, **53**, 560 (1985).

2) F. M. Fowkes, "Physico-chemical Aspects of Polymer Surfaces," Vol. 2, Plenum Press (1983), p. 583.

3) K. Esumi, K.Miyata, and K. Meguro, *Bull. Chem. Soc., Jpn.*, **58**, 3524 (1985).

4) K. Esumi, K. Miyata, F. Waki, and K. Meguro, *Colloids Surfaces*, **20**, 81 (1986).

5) R. S. Drago, L. B. Parr, and C. S. Chamberlain, *J. Am. Chem. Soc.*, **99**, 3203 (1977).

6) G. Briegleb, J. Czekalla, and G. Reuss, *Z. Physik. Chem. N. F.*, **30**, 333 (1961).

7) G. Briegleb and J. Czekalla, *Z. Elecktrochem.*, **58**, 249 (1954).

8) A. J. Tench and R. L. Nelson, *Trans. Faraday Soc.*, **63**, 2254 (1967).

9) H. Hosaka, T. Fujiwara, and K. Meguro, *Bull. Chem. Soc. Jpn.*, **44**, 2616 (1971).

10) K. Esumi and K. Meguro, *J. Colloid Interface Sci.*, **66**, 192 (1978).

11) K. Esumi and K. Meguro, *J. Japan Colour Material*, **48**, 539 (1975).

12) B. D. Flockhart, J. A. N. Scott, and R. C. Pink, *Trans. Faraday Soc.*, **62**, 730 (1966).

13) B. D. Flockhart, I. R. Leith, and R. C. Pink, *Trans. Faraday Soc.*, **63**, 2254 (1967).

14) M. Che, C. Naccache, and B. Imelik, *J. Catal.*, **24**, 328 (1972).

 © 1986 The Chemical Society of Japan Bull. Chem. Soc. Jpn., 59, 3367—3373 (1986)

Phase Transition of Unsymmetric Bis(quaternary alkyl bromide) Salts of 1,4-Diazabicyclo[2.2.2]octane, C_{10}-DABCO-C_n-Br_2 ($11 \leqq n \leqq 22$)

Jun SHIMIZU, Kengo IMAMURA, Takashi NOGAMI,* and Hiroshi MIKAWA†
Department of Applied Chemistry, Faculty of Engineering, Osaka University, Yamada-oka, Suita, Osaka 565
(Received April 23, 1986)

Phase transitions of unsymmetric bis(quaternary alkyl bromide) salts of 1,4-diazabicyclo[2.2.2]octane (DABCO)(C_{10}-DABCO-C_n-Br_2, $11 \leqq n \leqq 22$) were studied on the basis of measurements of differential scanning calorimetries, infrared absorption spectroscopy, and bromide-anion conductivities. The DSC measurements showed two transition temperatures (T_{c1} and T_{c2}, $T_{c1} > T_{c2}$); this exhibits the existence of the metastable phase for the DABCO salts (C_{10}-DABCO-C_n-Br_2, $12 \leqq n \leqq 22$). The metastable phase was converted to the stable phase within several days except for C_{10}-DABCO-C_n-Br_2 (n=12, 22). The temperature dependence of the infrared absorption spectra revealed that the band progressions due to two different alkyl chains disappeared at T_{c1} and appeared again at T_{c2}. This shows that the *trans*-zigzag conformation of the alkyl chains in the low temperature phase is destroyed by the conformational change above T_{c1} and then recovered again below T_{c2}. Abrupt increases in the bromide-anion conductivities by 100—1380 times were observed at around T_{c2} for the samples annealed beforehand above T_{c1}. However, the virgin samples showed much broader increases in the conductivities below T_{c1}; no conductivity jump was observed. The conductivity increase was caused by the conformational change in the alkyl groups. The concomitant formations of the voids facilitate the bromide-anion transport.

As an extension of the studies of the halide-anion conductivities of crown ether–metal halide complexes,[1] cryptand 222-metal halide complexes,[2] quaternary tetraalkylammonium halides,[3] and quaternary tetraalkylphosphonium halides,[4] we have studied the halide-anion conductivities of the symmetric bis(quaternary alkyl halide) salts of 1,4-diazabicyclo[2.2.2]octane (DABCO).[5] A first order solid-solid phase transition was observed for the DABCO salts, with concomitant increases in the halide-anion conductivities by two to three orders of magnitude. The phase transition was also studied by means of DSC, IR absorption spectroscopy, and powdered X-ray diffraction. The temperature dependence of the IR absorption spectra of the DABCO salts exhibited the abrupt disappearance of the band progressions above the transition temperatures.[6] Thus, the phase transition was found to be caused by the conformational change in the alkyl groups. Powdered X-ray diffraction revealed a reversible change in the crystal structure at the transition temperature.[5] Unlike the case of the symmetric salts, the existence of the metastable phase was clarified for the unsymmetric bis(quaternary alkyl bromide) salts of DABCO by means of DSC and a study of the IR absorption spectra.[7] The unsymmetric DABCO bromide salts studied previously possess two alkyl groups; the difference in their carbon numbers was fixed at two.[7] Since the unsymmetric salts exhibited different phenomena from the symmetric salts for the phase transition, it seemed interesting to see how the phase transition would be modified for the unsymmetric salts by changing the difference in the carbon numbers of two alkyl groups attached to DABCO nitrogens. The unsymmetric DABCO bromide salts in this study possess two alkyl groups; one is fixed to the decyl group, while the other is changed systematically from n-$C_{11}H_{23}$ to n-$C_{22}H_{45}$. The materials studied are shown in Fig. 1. The names of the materials are abbreviated by the numbers of alkyl carbons. For example, *N*-decyl-*N'*-tetradecyl-1,4-diazoniabicyclo[2.2.2]octane dibromide is abbreviated as C_{10}-DABCO-C_{14}-Br_2. Thus, the materials in Fig. 1 can be described generally as C_{10}-DABCO-C_n-Br_2 ($11 \leqq n \leqq 22$).

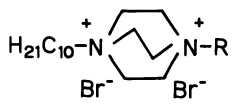

R = $C_{11}H_{23}$. $C_{12}H_{25}$. $C_{13}H_{27}$
$C_{14}H_{29}$. $C_{15}H_{31}$. $C_{16}H_{33}$
$C_{17}H_{35}$. $C_{18}H_{37}$. $C_{22}H_{45}$

Fig. 1. Unsymmetric bis(quaternary alkyl bromide) salts of DABCO.

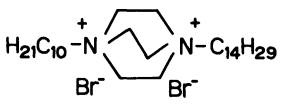

C_{10}-DABCO-C_{14}-Br_2

Experimental

Materials. All of the materials and the solvents were purified before the synthesis of the quaternary DABCO salts, as has been described previously.[6,7]

† Present address: Department of Environment and Safety Engineering, Faculty of Engineering, Fukui Institute of Technology, Gakuen-cho, Fukui 910.

Syntheses of Unsymmetric Bis(quaternary Alkyl Bromide) Salts of DABCO. The syntheses of mono(quaternary alkyl bromide) salts of DABCO were described in a previous paper.[7] The unsymmetric bis(quaternary alkyl bromide) salt of DABCO was synthesized by the reaction of the mono(quaternary salt) with alkyl bromide. The synthesis of unsymmetric salts will be described for C_{10}-DABCO-C_{14}-Br_2 as a typical example. The methanol (20 ml) solution of *N*-decyl-1-aza-4-azoniabicyclo[2.2.2]octane bromide (2 g, 6 mmol) and tetradecyl bromide (1.66 g, 6 mmol) was refluxed for 48 h. After it had then been cooled to room temperature, it was poured into diethyl ether (500 ml) to obtain a white precipitate. The crude product was recrystallized three times from the mixed solvent of ethyl acetate and ethanol (5:1). Essentially the same reaction conditions were adopted for the other materials. The solvents of recrystallization are acetonitrile for C_{10}-DABCO-C_n-Br_2 (n=11, 12, 13, 15, 16, 17, 18) and a mixed solvent of ethyl acetate and ethyl alcohol (5:1) for C_{10}-DABCO-C_n-Br_2 (n=14, 22) respectively.

Measurements. The measurements of the bromide-anion conductivities, DSC, and IR spectra were made by the methods described before.[5,6]

Results and Discussion

DSC Measurements. The DSC measurements were made while changing the temperature by 5 °C min^{-1}. Most of the virgin samples (C_{10}-DABCO-C_n-Br_2, $n \geqq 13$) showed single and reproducible endothermic signals (the values are designated as $\Delta H_{en,1}$) at the transition temperatures (designated as T_{c1}) when they were heated from room temperature. When they were cooled after they had once been heated above T_{c1}, much smaller exothermic signals ($\Delta H_{exo,1}$) were observed at much lower temperatures (T_{c2}) than T_{c1}; i.e., $\Delta H_{en,1} > \Delta H_{exo,1}$, and $T_{c1} > T_{c2}$. The succeeding heating-cooling cycles showed reproducible endothermic ($\Delta H_{en,2}$) and exothermic ($\Delta H_{exo,1}$) signals at around T_{c2}. The absolute values of $\Delta H_{en,2}$ were close to those of $\Delta H_{exo,1}$. Figure 2 shows the observed result of C_{10}-DABCO-C_{18}-Br_2 as a typical example of the above observations (T_{c1}=86 °C, T_{c2}=34 °C). However, when most of the samples ($13 \leqq n \leqq 18$) were kept at room temperature after they had once been heated above T_{c1}, the transition temperatures (T_{c2}) tended to increase slowly. After several days, the sample was converted to the original phase; it showed the endothermic signal ($\Delta H_{en,1}$) at T_{c1}. These facts can be explained by the free energy (F)-temperature (T) relation shown in Fig. 3. When the sample was heated from room temperature across the transition temperature, and then cooled, it followed the F-T curve by the sequence of 1→2→3→4→5 shown in Fig. 3. A detailed explanation of this F-T relation was given in the previous paper.[7] C_L, C_M, and C_H in Fig. 3 are the low temperature phase, the metastable phase, and the high-temperature phase respectively. The most important characteristic of the present materials is the existence of the metastable phase. The metastable phase was found to be converted to the stable phase (C_L) by keeping the sample at room temperature for several days. The gradual increase in the transition temperature can be explained as follows. When the C_M phase was left at room temperature, it was converted to another metastable phase ($C_{M'}$)[8] (Fig. 3). When a DSC measurement is made for the resultant $C_{M'}$ phase, its transition temperature ($T_{c2'}$) should be found between T_{c2} and T_{c1}; $T_{c2} < T_{c2'} < T_{c1}$. As the metastable phase approaches the C_L phase, the transition temperature increases until it is converted to the C_L phase where the phase transition takes place at T_{c1}. Thus, the greatest difference in the present systems (C_{10}-DABCO-C_n-Br_2, $13 \leqq n \leqq 18$) from the previous systems (C_n-DABCO-C_{n+2}-Br_2) is that the metastable phase can be converted to the stable phase in the former systems, whereas the conversion rate is too slow to be followed in the latter systems.[7] The larger the difference in the carbon numbers of the two alkyl groups, the faster was the conversion rate from

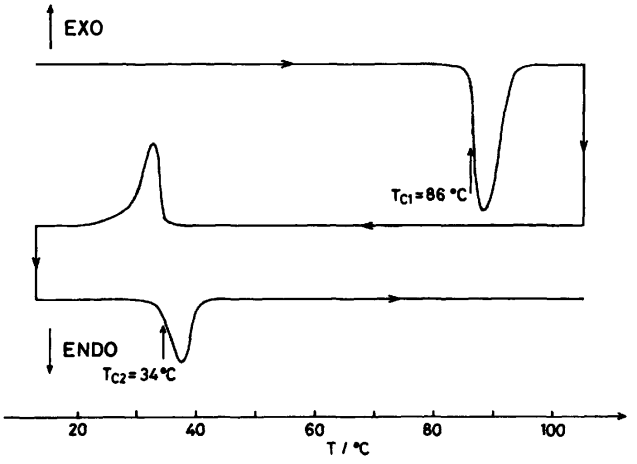

Fig. 2. DSC thermogram of C_{10}-DABCO-C_{18}-Br_2.

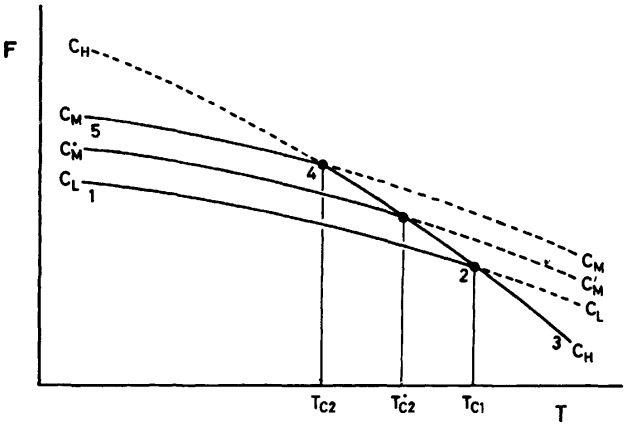

Fig. 3. Free energy (F)-temperature (T) relation of the unsymmetric bis(quaternary alkyl bromide) salts of DABCO. C_L, C_M, and C_H denote low temperature phase, metastable phase, and high temperature phase. respectively. C_M' denotes another metastable phase.

C_M to C_L.[9] For example, the conversion rates of C_{10}-DABCO-C_{14}-Br_2 and C_{10}-DABCO-C_{18}-Br_2 were one week and 1 d respectively. However, the C_M phases of C_{10}-DABCO-C_n-Br_2 (n=12, 22) did not go back to the C_L phases. C_M was not observed for C_{10}-DABCO-C_{11}-Br_2, which is similar to the cases of the symmetric bis(quaternary alkyl halide) salts of DABCO.[6]

Part of Table 1 shows some materials, T_{c1}, $\Delta H_{en,1}$, $\Delta S_1(=\Delta H_{en,1}/T_{c1})$, T_{c2}, $\Delta H_{en,2}$, and $\Delta S_2(=\Delta H_{en,2}/T_{c2})$. Here ΔS_1 and ΔS_2 denote the transition entropies at T_{c1} and T_{c2} respectively. The transition temperatures were obtained by the onsets of the endothermic peaks. The characteristic points of the salts are discussed below. Figure 4 plots T_{c1} and T_{c2} against the carbon

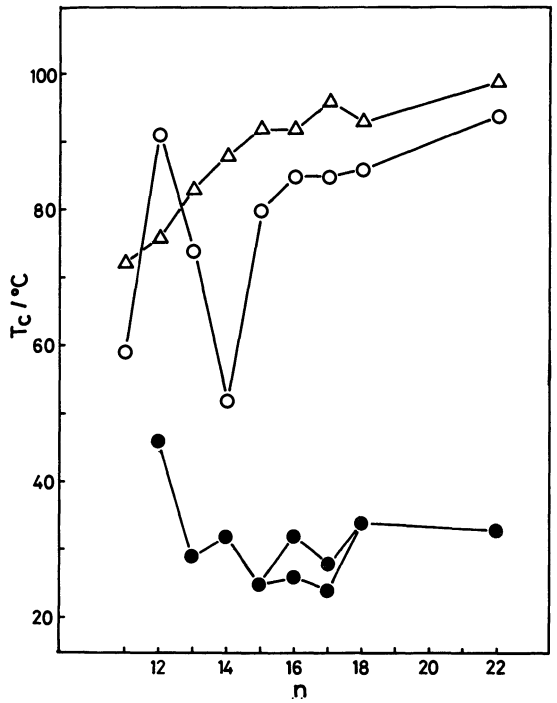

Fig. 4. The plots of the transition temperatures against the carbon numbers of alkyl groups.
○: T_{c1} for C_{10}-DABCO-C_n-Br_2, △: T_c for C_n-DABCO-C_n-Br_2, ●: T_{c2} for C_{10}-DABCO-C_n-Br_2.

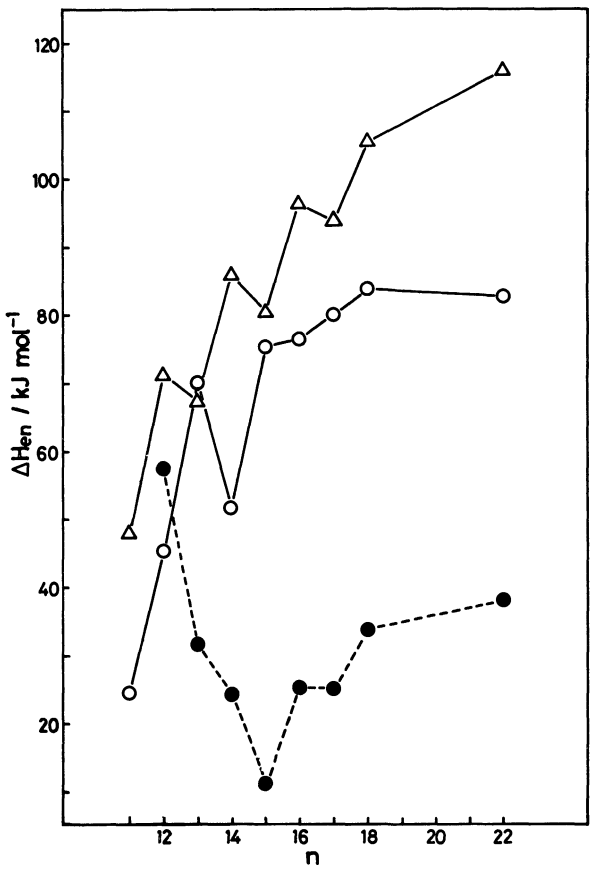

Fig. 5. The plots of the transition enthalpies against the carbon numbers of alkyl groups.
○: $\Delta H_{en,1}$ for C_{10}-DABCO-C_n-Br_2, △: ΔH for C_n-DABCO-C_n-Br_2, ●: $\Delta H_{en,2}$ for C_{10}-DABCO-C_n-Br_2.

Table 1. Transition Temperatures (T_{c1} and T_{c2}), Transition Enthalpies ($\Delta H_{en,1}$ and $\Delta H_{en,2}$), and Transition Entropies (ΔS_1 and ΔS_2) of C_{10}-DABCO-C_n-Br_2, and Ratios of the Conductivities Before (σ_l) and After (σ_h) the Transition at T_{c2}

Material	T_{c1} / °C	$\Delta H_{en,1}$ / kJ mol^{-1}	ΔS_1 / J/(mol deg)	T_{c2} / °C	$\Delta H_{en,2}$ / kJ mol^{-1}	ΔS_2 / J/(mol deg)	σ_h/σ_l
C_{10}-DABCO-C_{11}-Br_2	59	24.7	74	a)	a)	a)	a)
C_{10}-DABCO-C_{12}-Br_2	91	45.4	125	46	57.5	180	770
C_{10}-DABCO-C_{13}-Br_2	74	70.1	202	29	31.8	105	340
C_{10}-DABCO-C_{14}-Br_2	52	51.8	159	32	24.3	80	260
C_{10}-DABCO-C_{15}-Br_2	80	75.4	214	25	11.5	38	120
C_{10}-DABCO-C_{16}-Br_2	85	76.5	214	26, 32	25.3[b]	c)	190
C_{10}-DABCO-C_{17}-Br_2	85	80.0	222	24, 28	25.2[b]	c)	100
C_{10}-DABCO-C_{18}-Br_2	86	83.8	233	34	34.0	111	340
C_{10}-DABCO-C_{22}-Br_2	94	82.7	225	33	38.1	125	150

a) No phase transition occurred at T_{c2}. b) This value is a summation of the transition enthalpies at the two transition temperatures. The two signals could not be separated because of the proximity of the two transition temperatures. c) No correct ΔS_2 could be obtained.

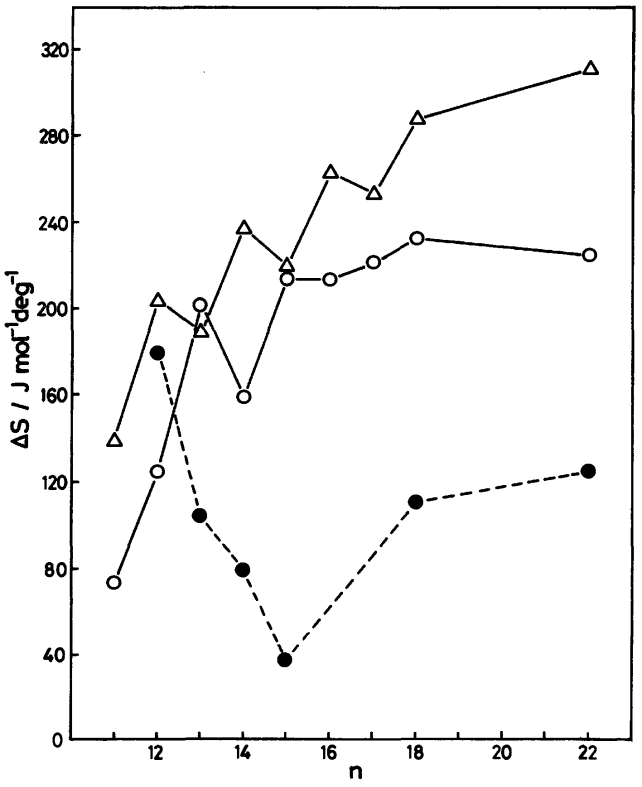

Fig. 6. The plots of the transition entropies against the carbon numbers of alkyl groups.
○: ΔS_1 of C_{10}-DABCO-C_n-Br_2, ●: ΔS_2 of C_{10}-DABCO-C_n-Br_2, △: ΔS of C_n-DABCO-C_n-Br_2.

numbers of the alkyl groups. This figure also shows the transition temperatures of the symmetric salts (C_n-DABCO-C_n-Br_2)[6] for the sake of comparison. Although complex behavior was observed for the T_{c1} of C_{10}-DABCO-C_n-Br_2 ($11 \leqq n \leqq 14$), the T_{c1}'s of C_{10}-DABCO-C_n-Br_2 ($15 \leqq n \leqq 22$) have a parallel relation to those of the symmetric salts; the former are slightly lower than the latter. The parallel relation suggests that the transition at T_{c1} is mainly governed by the longer alkyl chain of the two. On the other hand, T_{c2} decreases with the increase in the alkyl-chain length and levels off at around 30 °C for the DABCO salts, which possess longer alkyl chains than C_{12}. The differences between T_{c1}'s and T_{c2}'s were found to be in the range of 20—61 °C. Figures 5 and 6 plot the transition enthalpies ($\Delta H_{en,1}$ and $\Delta H_{en,2}$) and transition entropies (ΔS_1 and ΔS_2) respectively. These figures also show the transition enthalpies and transition entropies of the symmetric salts[6] for the sake of comparison. Since $\Delta H_{en,2}$ and ΔS_2 correspond to the transition enthalpy and the transition entropy from the metastable phase to the high temperature phase, the observed values are connected with dotted lines in these figures. $\Delta H_{en,2}$ and ΔS_2 are much smaller than $\Delta H_{en,1}$ and ΔS_1 respectively for C_{10}-DABCO-C_n-Br_2 ($n \geqq 13$). However, they are close to each other for C_{10}-DABCO-C_{12}-Br_2. The above results lead to the following assumptions for the phase transitions. The virgin sample (C_L)[10] possesses a close-packed crystal structure. This is confirmed by the IR absorption spectra, as will be described later. Therefore, T_{c1} is high, and $\Delta H_{en,1}$ and ΔS_1 are large, as a result of the considerable change in the crystal and molecular structures at the transition temperature. When it was once annealed[10] above T_{c1} and then cooled to room temperature, the conformational change in the alkyl chain and possibly the translational shift and rotational change of the molecule, all of which had been produced in the C_H phase, remained to some extent in the C_M phase at room temperature. This gave rise to a large number of disorders which facilitate the conformational, translational, and rotational movements of the molecule. Thus, when C_M was heated again, the phase transition due to these movements occurred at much lower temperatures (T_{c2}) than T_{c1}. From the Boltzmann relation, $\Delta S = R \ln W$, the ratios of the numbers of sites (W) before and after the phase transition can be estimated. W are estimated to be in the range of 10^6—10^{12} for the transitions at T_{c1} and in that of 10^2—10^9 for the transitions at T_{c2}. The fact that the former are much larger than the latter also exhibits how the metastable phase contains the above-mentioned disorder. In other words, the structural change from C_L to C_H is much larger than that from C_M to C_H. This results in the smaller enthalpy and entropy changes at T_{c2} than at T_{c1}.

Infrared Absorption Spectroscopy. The temperature dependence of the IR absorption spectra was measured for the KBr pellet sample in order to obtain more information on the phase transition and on the metastable phase. We have already reported the temperature dependences of the IR spectra of C_{14}-DABCO-C_{14}-Br_2[6] and C_{14}-DABCO-C_{16}-Br_2[7] as typical examples of the symmetric and unsymmetric DABCO salts respectively. In the former case, an abrupt change in the IR spectra was observed at the transition temperature. The spectral change was reversible, which was consistent with the DSC measurements. The band progressions in the low-temperature phase disappeared completely at the transition temperature. This was explained by the conformational change in the alkyl groups above the transition temperature. In the latter case, the band progressions disappeared at T_{c1} and were recovered again at lower temperatures (T_{c2}) than T_{c1}; $T_{c2} < T_{c1}$. These observations show the existence of the metastable phase in the latter case. Thus, the change in the IR spectra of the symmetric bis(quaternary salt) was quite different from that of the unsymmetric bis(quaternary salt). In order to see the effect of the difference in the carbon numbers of the two alkyl groups on the IR spectra, we measured the temperature dependence of the IR spectra of C_{10}-DABCO-C_{22}-Br_2, which possesses the largest difference in the

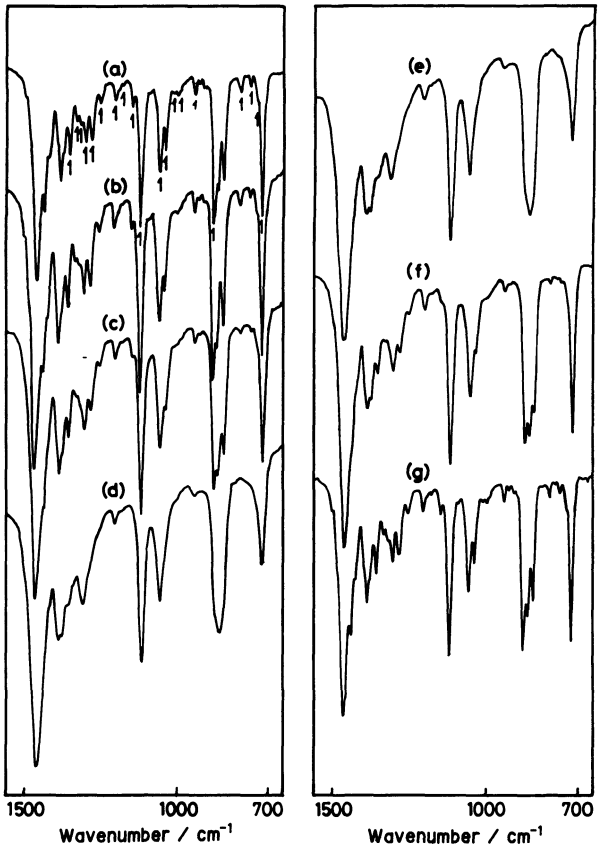

Fig. 7. Temperature dependence of the IR absorption spectra of C_{10}–DABCO–C_{22}–Br_2 for KBr disk sample obtained by heating the sample from room temperature to 94 °C, and then by cooling from 94 °C to 23 °C. The arrows in the spectrum (a) show the band progressions of the two alkyl groups.
(a): 29 °C, (b): 71 °C, (c): 90 °C, (d): 94 °C, (e): 70 °C, (f): 23 °C, (g): kept overnight at room temperature.

carbon numbers of the two alkyl groups.

Figure 7 shows the temperature dependence of the IR absorption spectra of C_{10}–DABCO–C_{22}–Br_2 for the KBr disk sample when the sample was heated from room temperature to 94 °C and then cooled to room temperature. The resulting IR spectra are shown sequentially from the upper left to the lower right. The IR spectra of the virgin sample[10] at 29 °C (a) exhibited the several structures shown by the arrows. The absorption positions of these structures were compared with the band progressions of n-$C_{11}H_{24}$ and n-$C_{23}H_{48}$,[11] which have the same numbers of CH_2 units as the alkyl groups of C_{10}–DABCO–C_{22}–Br_2. The good coincidence leads to the conclusion that the structures in Fig. 7 may be assigned to the band progressions of the two alkyl groups. The band progressions originating from 720 cm^{-1} are known as the CH_2-rocking mode. Since a single absorption was observed at 720 cm^{-1}, the molecules of the DABCO salts seem to possess a parallel-packed layered structure in the crystal.[12]

The absorption spectra at 29 °C (a) and 71 °C (b) were not very different. When the temperature of the sample approached T_{c1}, all of the absorptions were broadened (see Spectrum (c) at 90 °C), but the band progressions could still be seen. However, all of the band progressions disappeared at T_{c1} (94 °C) (d). This shows that the *trans*-zigzag conformation of the alkyl group of the low-temperature phase is destroyed at T_{c1}. When the temperature of the sample was lowered after it had once been raised above T_{c1}, no band progression appeared between T_{c1} and T_{c2}. For example, the IR Spectra (b) and (e) were measured at almost the same temperature, but they were quite different; Spectrum (b) exhibited the band progressions, but (e) did not show them. This is consistent with the free energy-temperature relation shown in Fig. 3, because Spectra (b) and (e) correspond to the C_L and C_H phases respectively. The *trans*-zigzag conformation of the alkyl chain is still destroyed in Spectrum (e). Only after the temperature had been lowered below T_{c2} (33 °C) did the band progressions appear again (see Spectrum (f)). Comparing Spectrum (a) with (f), however, the latter are broader than the former. This suggests that the conformational disorder still exists in (f). When the sample was left overnight at room temperature, the spectrum gradually became shaper to give Spectrum (g), which can not be differentiated from Spectrum (a). Thus, it is clear that the conformational change in the alkyl chain takes place slowly at room temperature. This is a distinct difference from C_n–DABCO–C_{n+2}–Br_2 ($10 \leqq n \leqq 16$), reported previously.[7] The band progressions recovered quickly below T_{c2} for these systems after they had once been heated above T_{c1}. Although Spectra (a) and (g) could not be differentiated from each other, their DSC results were quite different; the annealed sample[10] was converted to the metastable phase, but exceptionally, it did not go back to the stable phase.[9] A similar change in the IR absorption spectra was also observed for the other materials (C_{10}–DABCO–C_n–Br_2, $13 \leqq n \leqq 18$). However, the metastable phases of these materials are converted slowly to the stable phase by keeping the sample at room temperature. The conversion process could not be followed by IR spectroscopy, because the two phases possess identical IR absorption spectra. The powdered X-ray diffraction gave a distinct difference between the stable and metastable phases; the former gave sharp diffraction patterns, but the latter gave broader ones. Thus, the crystallinity of the latter is lower than that of the former.

Bromide-anion Conductivities. All of the samples have already been confirmed as bromide-anion conductors.[5,6,7] Ionic conductivities were measured for the compressed pellet samples by an AC method.[5,6] The temperature dependences of the bromide-anion conductivities were measured while raising the

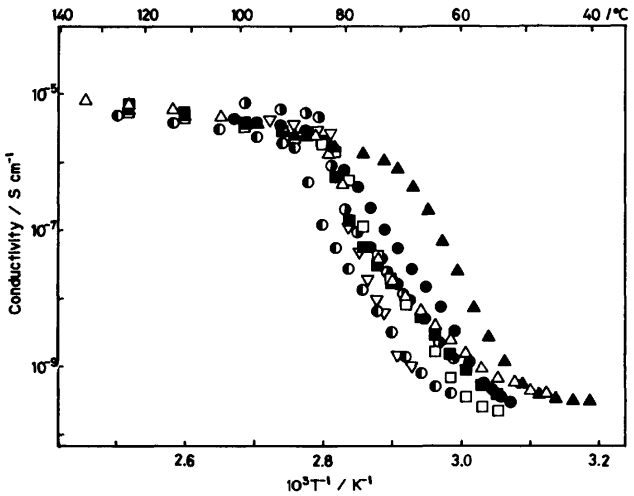

Fig. 8. Temperature dependences of the bromide-anion conductivities of the virgin samples (C_{10}-DABCO-C_n-Br_2).
●: n=12, △: n=13, ▲: n=14, □: n=15, ■: n=16, ◐: n=17, ◑: n=18, ▽: n=22.

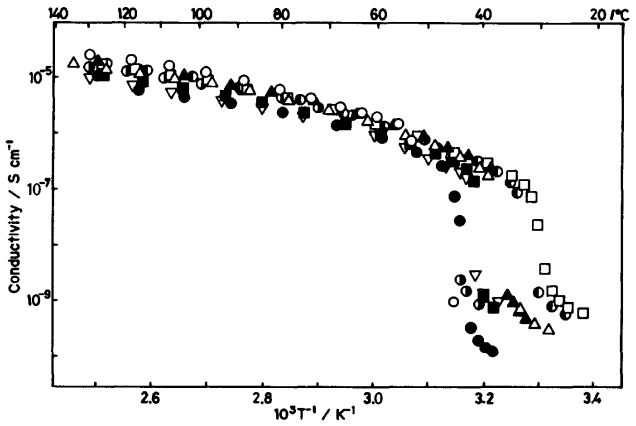

Fig. 9. Temperature dependences of the bromide-anion conductivities of the annealed samples (C_{10}-DABCO-C_n-Br_2).
○: n=11, ●: n=12, △: n=13, ▲: n=14, □: n=15, ■: n=16, ◐: n=17, ◑: n=18, ▽: n=22.

temperature of the sample slowly (0.5 °C min^{-1}) from room temperature. Conductivities less than 10^{-9} S cm^{-1} are below the limit of our measurements. Since the materials (C_{10}-DABCO-C_n-Br_2, $n \geqq 12$) exhibited phase transitions at T_{c1} and T_{c2}, we focused our attention mainly on the conductivity changes at these transition temperatures. The conductivity changes at around T_{c1} were measured for the virgin samples[10] dried in a vacuum overnight at room temperature. On the other hand, the conductivity changes at around T_{c2} were measured for the samples dried in a vacuum overnight above T_{c1}. Thus, the samples had already been converted to the metastable phase before the measurements. The proton conduction due to moisture seems to be negligible after the complete drying procedure.

Figure 8 shows the temperature dependences of the bromide-anion conductivities of the virgin samples.[10] Most of them consist of gradual increases in the conductivities in the low-temperature range and slow increases in the high-temperature range. Conductivity jumps like C_n-DABCO-C_n-Br_2,[6] C_n-DABCO-C_{n+2}-Br_2,[7] and the present materials in the metastable phase (see below) were not observed except for C_{10}-DABCO-C_{11}-Br_2. Thus, the conductivity change below the transition temperature is much broader than in the previous systems. The behavior in the low-temperature range was classified phenomenologically into two cases for C_{10}-DABCO-C_n-Br_2: (1) a considerable increase in the conductivity occurs below T_{c1} (n=12, 15, 16, 17, 18, 22), and (2) T_{c1} is located in the temperature range of the gradual increase in the conductivity (n=13, 14). At any rate, gradual increases in the conductivities occurred over wide temperature ranges. This suggests that the local movement of the alkyl chain sets in more than twenty degrees below T_{c1} for the virgin samples. Regarding the high-temperature phase, a considerable conformational movement of the alkyl group occurs. Thus, the activation energy of the conductivity was low (about 30 kJ mol^{-1}) as a result of the formation of a large number of transport channels of the bromide anion.

Figure 9 shows the temperature dependence of the bromide-anion conductivities of the annealed samples.[10] Unlike the case of the virgin samples,[10] an abrupt increase in the bromide-anion conductivities was observed at around T_{c2}. Part of Table 1 shows the ratios of the conductivities before (σ_l) and after (σ_h) the phase transitions; i.e., σ_h/σ_l. The σ_h/σ_l values were found to be in the range of 100—1380. Thus, they are smaller than those of C_n-DABCO-C_n-Br_2[6] and C_n-DABCO-C_{n+2}-Br_2.[7] If we define T_{c2}* as the middle point of the conductivity jump,[14] the following relations are obtained: T_{c2}*<T_{c2} for n=11, 12, and T_{c2}<T_{c2}* for $13 \leqq n \leqq 22$. The differences between T_{c2} and T_{c2}* were found to be in the range of 3—11 °C. The above relations suggest that the conductivity jumps begin before the considerable structural change for n=11, 12, and do after the change for $13 \leqq n \leqq 22$. It is noteworthy that the conductivities above T_{c1} of the virgin sample and those above T_{c2} of the annealed sample lie on the same σ-T curve. Figure 10 shows the temperature dependences of the bromide-anion conductivities of C_{10}-DABCO-C_{18}-Br_2 for the virgin sample and for the annealed sample as a typical example of this observation. Thus, the F-T relation in Fig. 3 is clearly demonstrated by Fig. 10. Since the ratios of the sites (W) before and after the phase transition are very large, as has been described before, the conformational change in the alkyl group seems to occur at every site of the CH_2 units. This gives rise to a large number of voids, which facilitate the bromide-anion transport above the transition temperature.

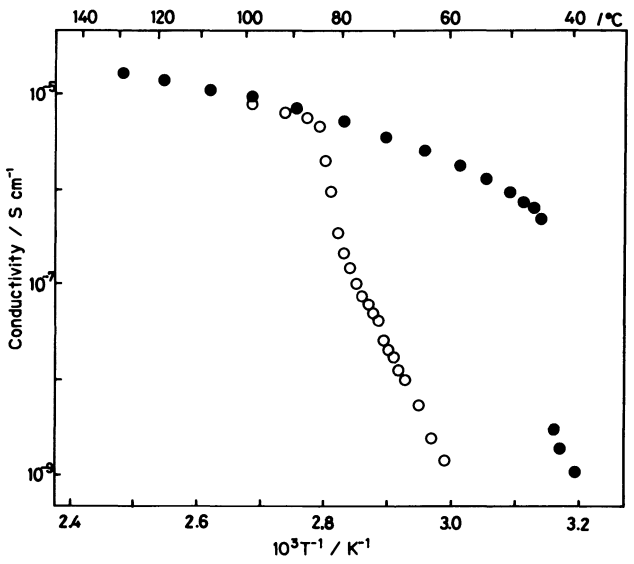

Fig. 10. Temperature dependences of the bromide-anion conductivities of C_{10}–DABCO–C_{18}–Br_2 for the virgin and annealed samples.
○: Virgin sample, ●: annealed sample.

Summary. Phase transitions of the unsymmetric bis(quaternary alkyl bromide) salts of DABCO (C_{10}–DABCO–C_n–Br_2, $11 \leqq n \leqq 22$) were studied by means of the measurements of the DSC, the IR absorption spectra, and the bromide-anion conductivities. The DSC measurements revealed the existence of a metastable phase. The metastable phase was found to be converted gradually to the stable phase for $13 \leqq n \leqq 18$ when the sample was kept at room temperature. The larger the difference in the carbon numbers of the two alkyl groups, the faster the conversion rate. The stable phase was not recovered from the metastable phase for $n=12$ and 22. The temperature dependence of the IR absorption spectra showed that the band progressions in the low-temperature phase disappeared above T_{c1} and appeared again at T_{c2}. The band progressions of the annealed sample became sharper when it was kept at room temperature. These facts can be explained by the conformational change in the alkyl group above the transition temperature, by the existence of the metastable phase, and by the slow recovery of the stable conformation at room temperature. Abrupt increases in the bromide-anion conductivities by two to three orders of magnitude were found at around T_{c2} for the annealed samples. The conductivity jump could be explained by the formation of voids attributable to conformational disorder above the transition temperature. On the other hand, the virgin sample did not show any conductivity jump. Instead, they exhibited broad conductivity changes below T_{c1}.

We are grateful to Professor Shigekazu Kusabayashi and Dr. Shunsuke Takenaka, Faculty of Engineering, Osaka University, for the use of the DSC apparatus.

References

1) D. S. Newman, D. Hazlett, and K. F. Mucker, *Solid State Ionics*, **3/4**, 389 (1981); M. Fujimoto, T. Nogami, and H. Mikawa, *Chem. Lett.*, **1982**, 547.

2) M. Fujimoto, T. Nogami, and H. Mikawa, *Solid State Ionics*, **11**, 313 (1984).

3) J. Shimizu, T. Nogami, and H. Mikawa, *Solid State Ionics*, **14**, 153 (1984).

4) K. Imamura, T. Nogami, and H. Mikawa, *Solid State Ionics*, **17**, 77 (1985).

5) J. Shimizu, T. Nogami, and H. Mikawa, *Solid State Commun.*, **54**, 1009 (1985).

6) J. Shimizu, K. Imamura, T. Nogami, and H. Mikawa, *Bull. Chem. Soc. Jpn.*, **59**, 1443 (1986).

7) K. Imamura, J. Shimizu, and T. Nogami, *Bull. Chem. Soc. Jpn.*, **59**, 2699 (1986).

8) There are a large number of metastable phases ($C_{M'}$, $C_{M''}$, $C_{M'''}$, ··· etc) between C_L and C_M. They differ mainly in the conformation of the alkyl groups and in their crystallinity.

9) One exception to this rule was C_{10}–DABCO–C_{22}–Br_2. The conversion rate from C_M to C_L was too slow to be followed for this material.

10) The virgin sample and the annealed sample are defined as the DABCO salts synthesized and the DABCO salts which have been heated above T_{c1} at least once respectively.

11) R. G. Snyder, *J. Mol. Spectrosc.*, **4**, 411 (1960); R. G. Snyder and J. H. Schachtschneider, *Spectrochim. Acta*, **19**, 85 (1963).

12) If the adjacent molecules are located in different orientations along the long axes of the molecules in the solid, crystal-field splitting must be observed at around 720 cm^{-1} (see Ref 13).

13) R. F. Holland and J. R. Nielsen, *J. Mol. Spectrosc.* **8**, 383 (1962).

14) The T_{c2}*'s of C_{10}–DABCO–C_n–Br_2 are as follows: 49 °C (n=11); 43 °C (n=12); 36 °C (n=13); 37 °C (n=14); 30 °C (n=15); 40 °C (n=16); 32 °C (n=17); 45 °C (n=18); 42 °C (n=22).

 © 1986 The Chemical Society of Japan Bull. Chem. Soc. Jpn., 59, 3375—3382 (1986)

Theoretical Studies on the Catalytic Oxidation of Carbon Monoxide on Nickel Clusters

A. K. Srivastava,† Isao Kojima,†† and Eizo Miyazaki*
Department of Chemistry, Tokyo Institute of Technology, Ookayama, Meguro-ku, Tokyo 152
(Received April 25, 1986)

Complete neglect of differential overlap (CNDO) molecular orbital calculations using the method of Anno and Sakai for the evaluation of the valence orbital ionization potential (VOIP) were performed with the aim of studying the oxidation of carbon monoxide on nickel clusters. A cluster surface was assumed to be preadsorbed with oxygen and the variation of various bond energies with the approach of a carbon monoxide molecule was studied for different models. Various possibilities for the reaction path are discussed in the light of the theoretical findings and it is suggested that at a low coverage of oxygen the reaction may follow a Langmuir-Hinshelwood path, whereas at a high coverage, an Eley-Rideal path might be more probable.

A catalytic reaction on a solid surface is not simple, but comprises several reaction steps in which a reaction cycle must be formed, starting from an initial chemisorption process of reactants to a closing process by desorbing final products from the surface. Under such requirements for a catalytic reaction, the most stable chemisorbed state among the several possible states is not always the most effective one for completing the catalytic reaction, since this kind of chemisorbed state occasionally remains persistently on the surface without desorbing into the gas phase. The above-mentioned concept should be important for studying, as a whole, a reaction mechanism on heterogeneous catalysts. In order to do so, calculations of all the bond energies as well as the total energies involved in the catalytic cycle are required. In the present paper, we have attempted a new approach to this problem through, as an example, an oxidation reaction of carbon monoxide on a Ni surface using the CNDO molecular-orbital method.

The oxidation of carbon monoxide over active metal catalysts (e.g. Pt, Pd, Rh, Ru, and Ni) has been investigated by numerous workers under well defined conditions with single crystals[1-11] as well as with polycrystalline surfaces.[12-16] The individual steps which are possibly involved in the oxidation of carbon monoxide can be given as follows:

$$CO \rightleftharpoons CO_{ad} \quad (1)$$

$$O_2 \longrightarrow 2O_{ad} \quad (2)$$

$$O_{ad} + CO_{ad} \longrightarrow CO_2 \quad (3)$$

$$O_{ad} + CO(g) \longrightarrow CO_2 \quad (4)$$

$$O_2(g) + 2CO_{ad} \longrightarrow 2CO_2 \quad (5)$$

A dissociative adsorption of oxygen is well established above 100 K as can be concluded from isotopic exchange experiments[17] and also from the absence of features in the UPS spectrum that could be assigned to adsorbed molecules;[18,19] hence, the reaction steps involving O_{2ad} need not be taken into consideration. Step (3) represents a Langmuir-Hinshelwood path, which predicts a reaction between both the reactants in a chemisorbed state. Steps (4) and (5) represent an Eley-Rideal mechanism in which one of the reactants is in its normal chemisorbed state(O_{ad}) and the second reacts either through a direct collision from the gas phase or from a weakly held physisorbed or molecular state. At present it is widely believed that the oxidation of CO on noble metal surfaces (such as Pd and Pt) follows a predominantly Langmuir-Hinshelwood type machanism; evidence for this was earlier obtained from nonstationary studies[2,4,6] and its dominance has been mainly proposed by recent molecular-beam experiments.[7,8] However, in addition to these extreme possibilities a precursor mechanism including an Eley-Rideal like path has also been suggested by many authors.[20-22]

The formation of carbon dioxide through a catalytic oxidation of carbon monoxide is of significant practical importance, particularly in connection with pollution problems. Thus, one must also consider the fact that although recently a wide variety of theoretical techniques such as EHT (extended Hückel theory),[23-25] CNDO,[26-33] DV(discrete variational)-Xα-SCF,[34-37] LCMTO(linear combination of muffin-tin orbital),[38,39] Localized orbital approach[40,41] and ab initio[42-44] have been applied for studying complex phenomenon on solid surfaces, most of these were aimed at obtaining a clear understanding of the chemisorption process in which the chemical reaction could be well described by the splitting of one bond and the formation of other bonds. The changes in various bond energies may, therefore, throw some interesting light on the disruption(weakening) and formation of various bonds; hence, the CNDO method as described here might become a good technique for studying simple reactions on metal surfaces, particularly since the bond energy is explicitly defined within its framework.

† Permanent address: Chemistry Department, University of Allahabad, Allahabad, India.

†† Present address: National Chemical Laboratory for Industry, Yatabe, Ibaraki 305.

Method of Calculation

Semiempirical methods like CNDO are flexible and convenient because of their inherent parametrized treatment; however, the involvement of many parameters makes them somewhat tedious and of lesser importance for systems containing transition metals. In the present paper the local core matrix elements U's have been estimated from atomic data using the following expressions:

$$U_{ii} = -I_p(i) - (N-1)\gamma_{ss} - M\gamma_{sd} \quad (i=s \text{ or } p)$$

and

$$U_{dd} = -I_p(d) - (M-1)\gamma_{dd} - N\gamma_{sd}.$$

Here, I_p is the valence-state ionization potential, N denotes the total number of electrons in the valence "s" and "p" orbitals and M represents the number of electrons in "d" orbitals. The I_p's have been calculated by using the method of Anno and Sakai,[45] where the valence orbital ionization potential (VOIP) was calculated with the help of the quadratic equation,

$$\text{VOIP} = A_0 + A_1Z + A_2Z^2. \quad (7)$$

Here, Z is the atomic number. A_0 and A_1 were evaluated with the help of

$$A_0 = a_0 + a_1M + a_2M^2 \quad (8)$$

and

$$A_1 = b_0 + b_1M. \quad (9)$$

The values of a_0, a_1, a_2, b_0, and b_1 were taken from Ref. 45. The exchange integral H_{ij} were calculated with the help of the Wolfsberg-Helmholtz approximation:[46]

$$H_{ij} = KS_{ij}\,(H_{ii}+H_{jj})/2. \quad (10)$$

An electronic configuration of $3d^M4s4p$ was assumed for the ground state of the Ni atom. Veigele[47] orbital exponents were used for Ni and Slater values were used for C and O. Thus, in the present calculation only K (=1.50) was empirically chosen. The total energy was calculated from

$$E_t = 1/2 \sum_{r,s} P_{rs}\,(H_{rs}+F_{rs}) + \sum_{A<B} Z_AZ_BR_{AB}. \quad (11)$$

The bond energies between atoms A and B have been evaluated by the following equation:

$$E_{AB} = \sum_{r}^{A}\sum_{s}^{B}(2P_{rs}\beta_{rs} - 1/2P_{rs}^2\gamma_{AB}) + (Z_AZ_BR_{AB}^{-1} - P_{AA}V_{AB} - P_{BB}V_{BA} + P_{AA}P_{BB}\gamma_{AB}). \quad (12)$$

In the above equations P_{rs} represents the density matrix, Z_A and Z_B represent the charge on nucleus A and B, respectively, V terms represent the potential integrals, R_{AB} represents the internuclear seperation, β_{rs} is the resonance integral and γ_{AB} represents interelectronic repulsion between any electron on atom A and any electron on atom B.

Results and Discussion

1. Reaction of Carbon Monoxide and Oxygen Atom. The aim of this section is to at least show the qualitative utility of the present method when it is applied to study a simple chemical reaction. The reaction of an oxygen atom with carbon monoxide has been studied in detail with the frontier orbital concept and is known to proceed as

$$O + :C{\equiv}O \longrightarrow O{=}C{=}O. \quad (13)$$

This reaction should cause a strong stabilization in the energy of the 3σ orbital of CO. In fact, the photoelectron spectra of CO and CO_2 show that the first σ orbital of CO_2 ionizes at 18 eV, whereas the 3σ of CO ionizes at 14 eV,[48] consequently, the 3σ of CO is stabilized by about 4 eV. In the present calculations the ionization potential for the first σ orbital of CO_2 was found to be 17.9 eV and the energy of the 3σ orbital for CO came out to be 13.25 eV, which gives a stabilization energy of about 4.6 eV. This is in fairly good agreement with the experimental results.

The C-O_a ("a" denotes the oxygen atom of CO) bond length was assumed to have a fixed value of 1.15 or 1.19 Å and the approaching oxygen atom O_b was

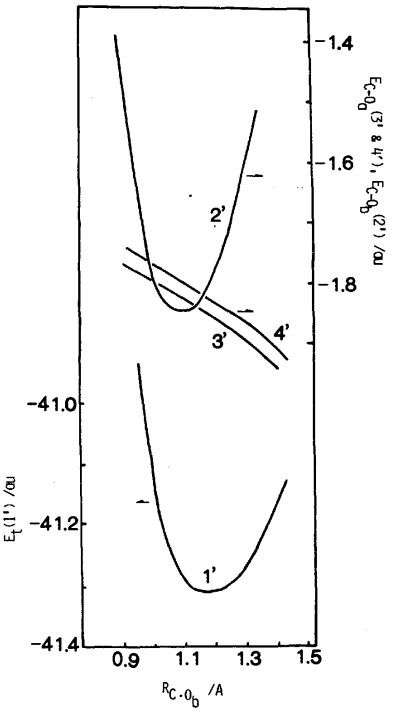

Fig. 1. Evaluation of total energy (E_t) at $R_{C\text{-}O_a}$= 1.15 Å and bond energies ($E_{C\text{-}O}$) as a function of the bond length, $R_{C\cdot O}$ at fixed bond lengthes of C–O_a. 1': E_t, 2': $E_{C\cdot O_b}$, 3': $E_{C\text{-}O_a}$ at $R_{C\cdot O_a}$=1.15 Å and 4': $E_{C\text{-}O_a}$ at $R_{C\cdot O_a}$=1.19 Å.

considered to exist along a linear path for calculating the total energy E_t, the bond energy of the C-O_b bond (the new bond being formed, i.e. $E_{C\text{-}O_b}$) and the bond energy of the C-O_a bond (i.e. $E_{C\text{-}O_a}$).

Figure. 1 contains plots of E_t, $E_{C\text{-}O_b}$, and $E_{C\text{-}O_a}$ against $R_{C\text{-}O_b}$ (the distance between C and O_b). The total-energy curve 1′ shows a minimum at 1.18 Å whereas the bond-energy curve 2′ has a minimum at 1.13 Å. Both of these equilibrium distances are in fairly good agreement with the experimental bond length 1.16 Å for CO_2.

The reaction path to form the CO_2 product (i.e. the formation of a new bond C-O_b) is clearly depicted by curve 2′; however, curves 3′ or 4′ represent a weakening of the C-O_a bond due to the approaching O_b. This is caused by a delocalization of p_π electrons of the approaching oxygen atom into the LUMO of CO, resulting in a simultaneous strengthening of the C-O_b bond. It should be mentioned here that even for a different value of the C-O bond length (1.19 Å), the curves for the total energy E_t and the bond energy $E_{C\text{-}O_b}$ were found to be almost identical and showed very little change. However, as expected, curve 4′ for $E_{C\text{-}O_a}$ is slightly different but runs almost parallel to the earlier curve 3′. This makes it clear that even if the bond length in CO is held constant, the curves representing the changes in various bond energies are capable of showing a weakening of the C-O_a bond as well as the formation of a new bond between C and the approaching O atom.

Studies on this simple reaction have shown both qualitatively and quantitatively satisfactory results and have also made it very clear that the bond energy not only follows the pattern of the total energy of the system, but is also capable of depicting the weakening as well as the strengthening of various bonds.

In the next section the present method is applied to the CO oxidation on two types of clusters of nickel containing two and five atoms, respectively. Throughout this paper a value of 2.50 Å is used for the Ni-Ni distance (the same as that in bulk Ni) and 1.15 Å for the bond length of a CO molecule.

2. Oxidation of CO on Ni_2 Cluster. For Ni_2, two different positions were considered for the preadsorbed O, namely: SYMMETRICAL and UNSYMMETRICAL. As shown in Fig. 2, in the first case two different sites were chosen for the coadsorption of CO (labeled as ON TOP (Model 1) and ADJACENT VERTICAL (Model 4)). However, in addition to the perpendicular models a slightly angular (ϕ=30°) approach of CO (labeled as ADJACENT BENT (Model 3)) was included in the calculations. In the second case, the three similar types were also considered (Models 2, 5, 6). CO was supposed to be ON TOP (Model 2); an ADJACENT VERTICAL (Model 5) and an angular approach were also considered (ϕ=30°, Model 6). In the models 5 and 6, CO was supposed to be on top of

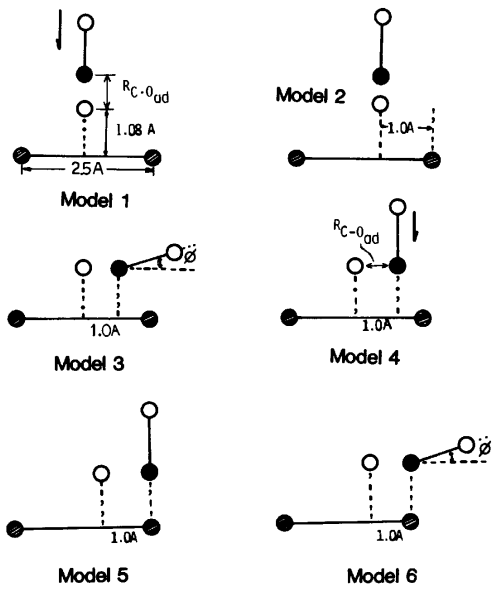

Fig. 2. Models for Ni_2-O_{ad} and Ni_2-O-CO.
1: Symmetrical on top, 2: Unsymmetrical on top, 3: Symmetrical adjacent bent, 4: Symmetrical abjacent vertical, 5: Unsymmetrical adjacent vertical and 6: Unsymmetrical adjacent bent.
●: C, ●: Ni and ○: O atoms.

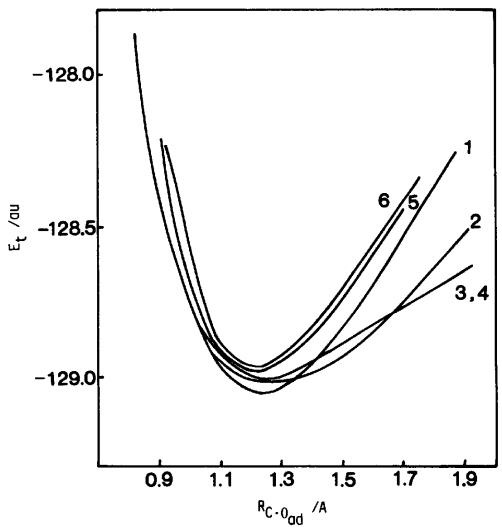

Fig. 3. Plots of E_t vs. $R_{C\text{-}O_{ad}}$.
Notations of curves correspond to the numbers of models in Fig. 2.

one Ni atom, which models arise from the conclusion by Li and Tong by analysis of the LEED patterns of CO adsorption on Ni(100) surface.[49]

A plot of the total energy of the system E_t as a function of $R_{C\text{-}O_{ad}}$ is given in Fig. 3; it can be said that the total energy of the system remains almost the same for all the models under study.

Figure 4 contains plots of $E_{C\text{-}O_{ad}}$ as a function of $R_{C\text{-}O_{ad}}$ and a comparative study of the various curves shows that for the bond formation between C and O_{ad} three favourable arrangements are:

(1) O preadsorbed symmetrically and CO on top,
(2) O preadsorbed at an unsymmetrical site with CO lying on top,
and
(3) O preadsorbed symmetrically and CO adsorbed at an adjacent site in a bent form (ϕ=30°). An increase or decrease in this angle by 10—15° was found to have an adverse effect on bond formation.

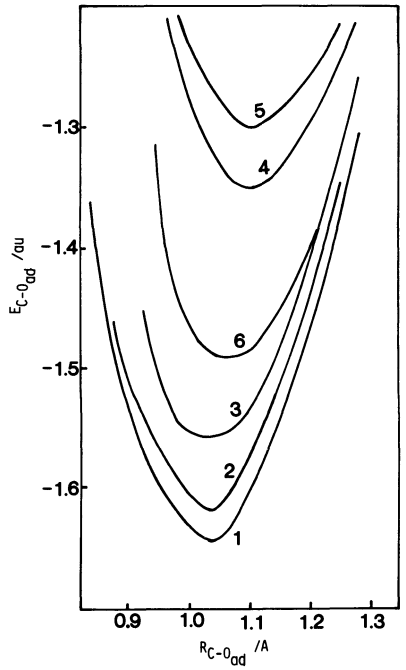

Fig. 4. Plots of $E_{C-O_{ad}}$ vs. $R_{C-O_{ad}}$.
Notations of curves correspond to the numbers of models in Fig. 2.

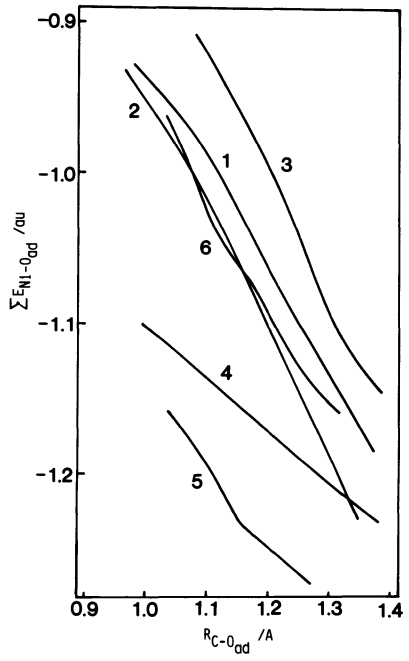

Fig. 5. Plots of $E_{Ni-O_{ad}}$ vs. $R_{C-O_{ad}}$.
Notations of curves correspond to the numbers of models in Fig. 2.

Figure 5 shows the plots of the total bond energies between two Ni atoms and O_{ad}: $\Sigma E_{Ni-O_{ad}}$ against $R_{C-O_{ad}}$. All of the curves shown here clearly indicate a weakening of the Ni–O_{ad} bond, one of the requirements for the formation of a catalytic cycle. However, evidently this weakening is a maximum when O is symmetrically adsorbed and CO is adsorbed at an adjacent site in a bent form; the next best choice seems to be a symmetrical site for preadsorbed O with CO lying on top of it.

Plots of ΣE_{Ni-C} vs. $R_{C-O_{ad}}$ are given in Fig. 6. It can be inferred from the nature of the various curves that CO may be attacking from the gas phase when it lies on top of either symmetrically or unsymmetrically adsorbed O; in other cases it seems to be adsorbed rather strongly.

In order to evaluate the possibility of a desorption of CO_2, the total energy of all the Ni–O_{ad} and Ni–C bonds has been plotted against $R_{C-O_{ad}}$ (Fig.7) and the nature of the curves suggests that the desorption of CO_2 should be easiest when O is symmetrically preadsorbed and CO lies on top of it, followed by unsymmetrical-on-top and symmetrical-adjacent-bent models.

3. Oxidation of CO on Ni_5 Cluster. The Ni_5 cluster model contains four atoms in the first layer; the fifth atom lies below in the second plane (Fig. 8). In all the cases, oxygen was supposed to be preadsorbed at a multi-center symmetrical site which lies on top of

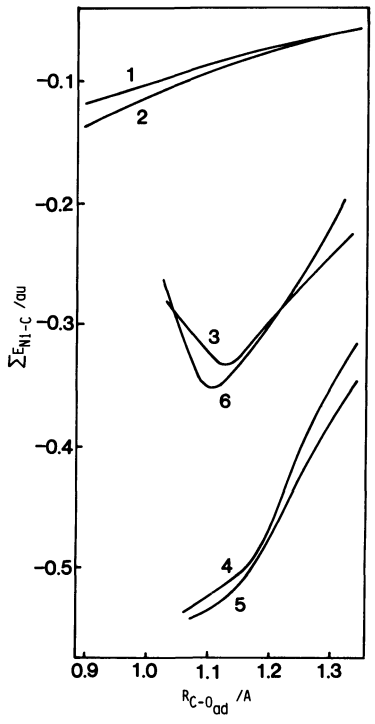

Fig. 6. Plots of E_{Ni-C} vs. $R_{C-O_{ad}}$.
Notations of curves correspond to the numbers of models in Fig. 2.

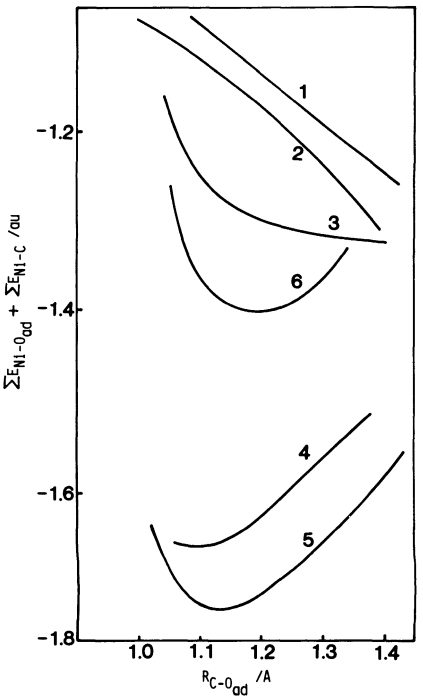

Fig. 7. Plots of $\Sigma E_{Ni-C} + \Sigma E_{Ni-O_{ad}}$ vs. $R_{C-O_{ad}}$.
Notations of curves correspond to the numbers of models in Fig. 2.

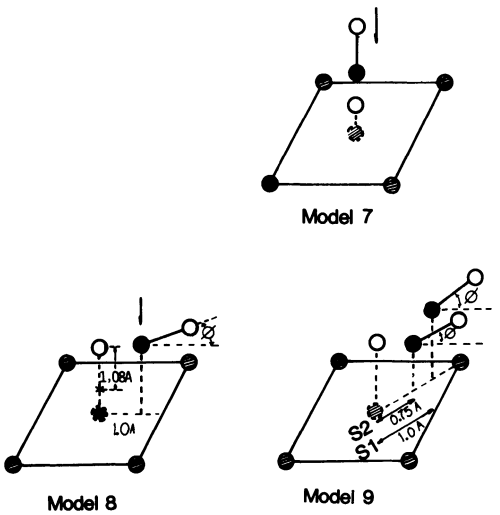

Fig. 8. Models for Ni_5 cluster and Ni_5–O–CO.
7: On top, 8: on bridge, 9: on diagonal. Note that two different site labeled S1 and S2 for the model 9 are distinguished for the adsorption site of CO.
●: surface Ni, ○: second layer Ni, ●: C and ○: 0 atoms.

the fifth Ni atom. For CO, however, in addition to a site on top of O_{ad} (Model 7), two other sites were also chosen:
(a) CO adsorbed at an adjacent BRIDGE site as shown in Model 8. (b) CO adsorbed at a site on the DIAGONAL (Model 9).. However, in this case in order to study the effect of the preadsorbed O on the adsorption of CO, two different sites were selected

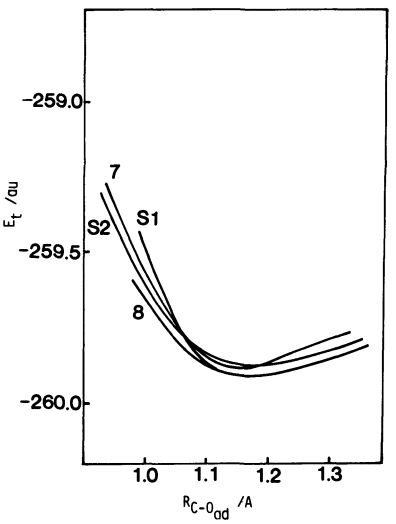

Fig. 9. Plots of E_t vs. $R_{C-O_{ad}}$.
Curves 7,8, S1, and S2 correspond to models 7,8,9-S1 and 9-S2 in Fig. 8, respectively.

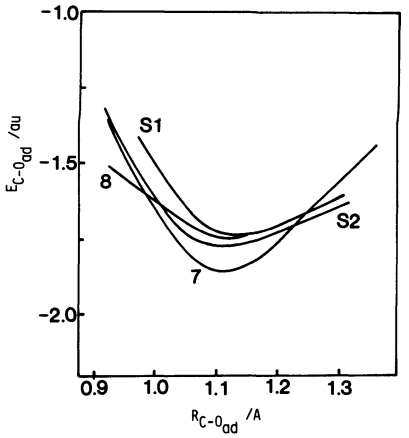

Fig. 10. Plots of $E_{C-O_{ad}}$ vs. $R_{C-O_{ad}}$.
Notations of curves are the same to those in Fig. 9.

which are denoted as S1 and S2, respectively, in Model 9. Relying on our previous experience with Ni_2 where the bent approach was found to be more appropriate for the formation as well as desorption of CO_2, we decided to consider only the angular approach of CO for adsorption (ϕ=30°).

Figure 9 shows plots of E_t as a function of $R_{C-O_{ad}}$, from which it becomes evident that the total energy of the system dose not differ appreciably for different models.

Figure 10 contains different curves for a plot of $E_{C-O_{ad}}$ as a function of $R_{C-O_{ad}}$ and a comparative study suggests that an on-top site may be slightly more favourable for the formation of CO_2.

Figure 11 represents a plot of $\Sigma E_{Ni-O_{ad}}$ against $R_{C-O_{ad}}$. Although no clear-cut observation can be made since in all the cases the Ni–O_{ad} bond shows a tendency of becoming weaker with the approach of CO the DIAGONAL-S2 site for CO adsorption may be

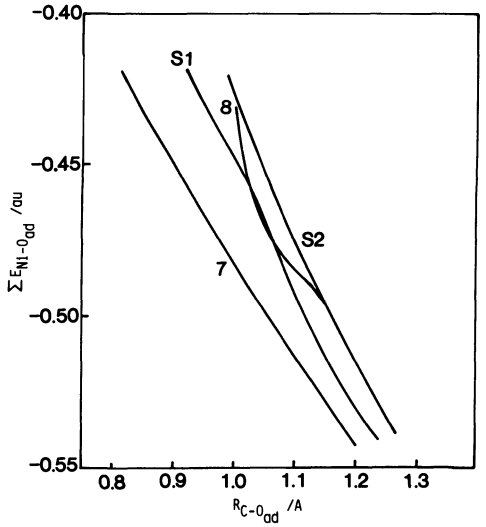

Fig. 11. Plots of $\Sigma E_{Ni-O_{ad}}$ vs. $R_{C-O_{ad}}$.
Notations of curves are the same to those in Fig. 9.

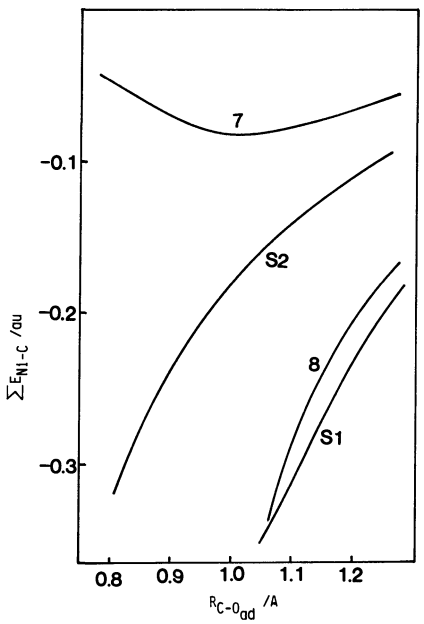

Fig. 12. Plots of ΣE_{Ni-C} vs. $R_{C-O_{ad}}$.
Notations of curves are the same to those in Fig. 9.

slightiy more favorable for such a weakening.

Figure 12 shows plots of ΣE_{Ni-C} against $R_{C-O_{ad}}$; these curves show some interesting features regarding the adsorption of CO on Ni preadsorbed with O. A comparison of curves S1 and S2 shows that as CO moves closer to the preadsorbed O, the strength of Ni–C bond decreases considerably. The effect of preadsorbed electronegative atoms on the adsorption of CO and H_2 has been studied by Kiskinova[50] using thermal desorption, LEED and AES. It was found that the presence of electronegative atoms causes a reduction in the adsorption rate, the adsorption bond strength and the capacity of the Ni surface for CO and H_2 adsorption. The same conclusion was reached by Madix[51] for the case of iron. Our theoretical results

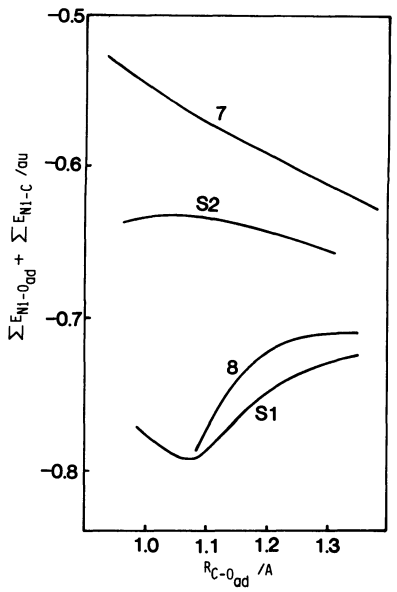

Fig. 13. Plots of $\Sigma E_{Ni-O_{ad}} + \Sigma E_{Ni-C}$ vs. $R_{C-O_{ad}}$.
Notations of curves are the same to those in Fig. 9.

are in agreement with these results, clearly indicating a predominant role for the preadsorbed O.

Figure 13 contains plots of the sum of ΣE_{Ni-C} and $\Sigma E_{Ni-O_{ad}}$ against $R_{C-O_{ad}}$. On the basis of these curves it is suggested that ON BRIDGE and ON DIAGONAL-S1 which are comparatively far from the O_{ad} may not be suitable for the desorption of CO_2, which is otherwise known to desorb immediately from the surface at usual catalytic temperatures (>100°C[52]). The remaining two possibilities (namely ON TOP and ON DIAGONAL-S2) are, perhaps, good adsorption sites as far as the desorption of CO_2 is concerned. In order to evaluate the effect of neighbouring O_{ad} atoms, it was considered appropriate to include four such nearest-neighbour O_{ad} atoms in one calculation set for both on-top and on-diagonal sites. It was also found that the various bond energies remain almost unaffected, probably due to the large distance.

On the basis of the qualitative studies presented in this paper it is suggested that the reaction of CO and O_2 on nickel might consist of the following stages:

(1) **Preadsorption of Ni with Oxygen:** Engel et al.[53] have observed that the chemisorbed oxygen is the primary surface species formed by an interaction of O_2 with the surface of platinum metals and that this species generally exihibits a higher reactivity towards CO. They further suggest that as long as the actual concentration of oxygen under a steady-state condition is low it may be safely concluded that if the temperature is not extremely high the chemisorbed atomic oxygen is the only species that enters into the catalytic oxidation of CO. Our studies of Ni_2 clusters suggest that the symmetrical site is more suitable both for the formation and desorption of CO_2; this is in agreement with the findings based upon LEED

studies.

(2) Oxidation of Carbon Monoxide at Low Coverage of Oxygen: It has been concluded by Engel[53] that if both kinds of particles (i.e. CO and O) are present on the surface, the CO can be regarded as moving within an essentially fixed matrix of O_{ad} atoms. On the basis of the present studies regarding both Ni_2 and Ni_5, it is suggested that at a low coverage of oxygen, CO might be adsorbed at an adjacent site and that in the transition state this adsorbed mobile species assumes a bent configuration which has been found to be more favorable for the formation (as well as desorption) of CO_2. The possibility of an angular form of adsorbed CO in the transition state has also been suggested by Anderson[54] while describing the mechanism of CO oxidation on Pt. Obviously, the oxidation of CO at low coverage of oxygen can be assumed to follow the Langmuir-Hinshelwood path.

(3) Oxidation of Carbon Monoxide at High Coverage of Oxygen: Behm et al.[55] have noted that for a reaction of preadsorbed oxygen during exposure to CO on Pt(100) at 355 K and at pressures upto 1×10^{-4}Pa the CO coverage is negligibly small as long as $\theta_0>0.05$. With respect to the relative rates of adsorption, reaction and desorption, this means that the latter two processes must be at least as fast as CO adsorption. It has also been found that the lifetime of a chemisorbed CO adjacent to a chemisorbed O on Pt is $\approx10^{-4}$ s. It has reaction probability of unity for each chemisorbed CO; however, at a high coverage of O_{ad} or in the case of CO_{ad} exposed to O_2, the CO_{ad} is held by a matrix of surrounding oxygen atoms and such islands of the two species can coexist on the surface for hundreds of seconds with very little reaction probability for CO_2 formation. The theoretical results on Ni_2 and Ni_5 in the present paper suggest that under such conditions there is a high probability of a reaction between adsorbed oxygen and CO from the gas phase follwing an Eley-Rideal type mechanism including a "precursor state."

One of the authors (A. K. S.) would like to express sincere thanks to Ministry of Education, Japan and UNESCO for being awarded a fellowship. Thanks are also due to Dr. K. Shimokoshi for his help in computations and his fruitful discussions. The computations were performed at the computer center of Tokyo Institute of Technology, as well as the Institute for Molecular Science at Okazaki.

References

1) G. Ertl and P. Rau, *Surface Sci.*, **15**, 443 (1969).
2) H. Conrad, G. Ertl, and G. Küppers, *Surface Sci.*, **76**, 323 (1978).
3) G. Ertl and J. Koch, *Z. Phys. Chem.*, **69**, 323, (1970).
4) G. Ertl and J. Koch, "Adsorption Desorption Phenomenon," Academic Press N. Y. (1972).
5) G. Ertl and J. Koch, "Proceeding of 5th Intern. Congr. Catalysis, Florida (1972)," p. 969.
6) G. Ertl and Neumann, *Z. Phys. Chem.*, **90**, 127 (1974).
7) T. Engel and G. Ertl, *Chem. Phys. Lett.*, **54**, 95 (1978).
8) T. Engel and G. Ertl, *J. Chem. Phys.*, **69**, 1267 (1978).
9) A. M. Horgan and D. A. King, *Trans. Farad. Soc.*, **67**, 2145 (1971).
10) T. H. Lindstrom and T. T. Tsotsis, *Surface Sci.*, **150**, 487 (1985).
11) T. H. Lindstrom and T. T. Tsotsis, *Surface Sci.*, **147**, 647 (1984).
12) J. S. Close and J. M. White, *J. Catal.*, **36**, 185 (1975).
13) T. Matsushima and J. M. White, *J. Catal.*, **39**, 265 (1975).
14) T. Matsushima, D. B. Almy, D. C. Foyt, J. S. Close, and J. M. White, *J. Catal.*, **39**, 277 (1975).
15) T. Matsushima, D. B. Almy, D. C. Foyt, J. S. Close, and J. M. White, *J. Catal.*, **40**, 334 (1975).
16) T. Matsushima, D. B. Almy, D. C. Foyt, J. S. Close, and J. M. White, *J. Catal.*, **41**, 397 (1976).
17) M. Wilf and P. T. Dawson, *Surface Sci.*, **65**, 399 (1975).
18) J. Küppers and A. Plagge, *J. Vacuum Sci. Technol.*, **13**, 259 (1976).
19) J. W. Davenport, *Phys. Rev. Lett.*, **36**, 945 (1976).
20) J. Harris and .Kasemo, *Surface Sci.*, **105**, L281 (1981).
21) J.Harris and B. Kasemo, *Surface Sci.*, **105**, L288 (1981).
22) E. G. Keim, F. Labohm, O. L. J. Gizeman, G. A. Bootsma, and J. W. Geus, *Surface Sci.*, **112**, 52 (1981).
23) R. C. Baetzold, *Inorg. Chem.*, **20**, 52 (1981).
24) R. C. Baetzold, M. G. Mason, and J. F. Hamilton, *J. Chem. Phys.*, **72**, 366 (1980).
25) R. C. Baetzold, *Advan. Catal.*, **25**, 1 (1976).
26) G. Blyholder, *J. Chem. Soc., Chem. Commun.*, **1973**, 625.
27) G. Blyholder, *J. Chem. Phys.*, **62**, 3193 (1975).
28) G. Blyholder, *J. Phys. Chem.*, **79**, 756 (1975).
29) G. Blyholder, *J. Vacuum Sci. Technol.*, **11**, 865 (1974).
30) G. Blyholder, *Surface Sci.*, **42**, 249 (1974).
31) H. Kobayashi., H. Kato, K. Tarama, and F. Fukui, *J. Catal.*, **49**, 294 (1977).
32) J. Spanget-Larsen, *Theoret. Chim. Acta*, **55**, 165 (1980).
33) R. C. Baetzold, *J. Chem. Phys.*, **68**, 555 (1978).
34) E. Miyazaki, M. Tsukada, and H. Adachi, *Surface Sci.*, **131**, L390 (1983).
35) K. H. Johnson, *Ann. Rev. Phys. Chem.*, **26**, 39 (1975).
36) D. R. Salahub and R. P. Messemer, *Phys. Rev.*, **B16**, 2526 (1977).
37) G. Seifert, E. Mrosan, and H. Mueller, *Phys. Status Solidi*, **B89**, 553 (1978).
38) R. V. Kasowski, *Surface Sci.*, **63**, 370 (1977).
39) R. V. Kasowski and E .Caruthers, *Phys. Rev.*, **B21**, 3200 (1980).
40) D. W. Bullett, *Surface Sci.*, **68**, 149 (1977).
41) D. W. Bullett and E .P. O. Reilly, *Surface Sci.*, **89**, 274 (1979).
42) H. Stoll and H. Preuss, *Phys. Status Solidi*, **B64**, 103 (1974).
43) C. W. Bauschlicher, P. S. Bagus, and H. F. Schaefer, *I. B. M. J. Res. Develop.*, **22**, 213 (1978).
44) C. F. Melius, T. H. Upton, and W. A. Goddard, *(III), Solid. State. Commun.*, **28**, 501 (1978).
45) T. Anno and. Y. Sakai, *Theoret. Chim. Acta*, **18**, 208 (1970).

46) M. Wolfsberg and C. Helmholtz, *J. Chem. Phys.*, **20**, 837 (1952).
47) W. J. Veigele, D. E. Stevenson, and E. M. Henry, *J. Chem. Phys.*, **50**, 208, (1969).
48) R. L. DeKock and H. B. Gray, Chemical Structure and Bonding, Benjamin Inc., (California (1980)). p. 321.
49) C. H. Li, S. Y. Tong, *Phys. Rev. Lett.*, **43**, 360 (1979).
50) M. Kisikinova and D. W. Goodmann, *Surface Sci.*, **108**, 64 (1981).
51) J. Benziger and R. J. Madix, *Surface Sci.*, **94**, 119 (1980).
52) T. Engel and G. Ertl, "The Chemical Physics of Solid Surfaces and Heterogeneous Catalysis," Elisvier, N. Y. (1982), Vol. 4, p. 78.
53) T. Engel and G. Ertl, *Adv. Catal.* **28**, 1 (1979).
54) N. K. Rya and A. B. Anderson, *Surface Sci.*, **119**, 35 (1982).
55) R. J. Behm, P. A. Thiel, P. R. Norton, and P. E. Binder, *Surface Sci.*, **147**, 143 (1984).

 © 1986 The Chemical Society of Japan Bull. Chem. Soc. Jpn., 59, 3383—3387 (1986)

A ^2H NMR Study of [*Ser*-3,3-$^2H_2$]- and [*Ala*-3,3,3-$^2H_3$]- Silk Fibroins in the Solid State. Role of Side-Chain Moiety in Stabilization of Secondary Structure

Hazime SAITÔ,* Ryoko TABETA, Akio KUZUHARA,† and Tetsuo ASAKURA*,†
Biophysics Division, National Cancer Center Research Institute,
Tsukiji 5-Chome, Chuo-ku, Tokyo 104
†Department of Polymer Engineering, Tokyo University of Agriculture and Technology,
Nakamachi 2-Chome, Koganei, Tokyo 184
(Received May 10, 1986)

An attempt was made to prepare [*Ser*-3,3-$^2H_2$]- and [*Ala*-3,3,3-$^2H_3$]-fibroins by feeding respective amino acids DL-[3,3-$^2H_2$]-serine (Ser) and [3,3,3-$^2H_3$]-alanine (Ala), respectively, to silkworms, *Bombyx mori* and *Philosamia cynthia ricini* together with daily artificial diet. We recorded ^2H powder-pattern NMR spectra of [*Ser*-3,3-$^2H_2$]- and [*Ala*-3,3,3-$^2H_3$]-cocoons and fibroins (10—20% deuteration) by means of the quadrupole echo method. It was found that separation of the ^2H quadrupole splittings is 125 and 39 kHz, respectively, for [*Ser*-3,3-$^2H_2$]- and [*Ala*-3,3,3-$^2H_3$]-cocoons and fibroins, respectively. Accordingly, it was concluded that side-cain reorientation of Ser residue is virtually frozen irrespective of differences in conformations of silk I and silk II, suggesting that the hydroxyl groups in these cases might be hydrogen-bonded to C=O or NH groups in intra or interchain. On the other hand, side-chain methyl group of Ala residue in [*Ala*-3,3,3-$^2H_3$]-fibroin turned out to undergo rapid three-fold rotation about the C_α-C_β axis, as viewed from data of the quadrupole splittings.

Silk fibroin from *Bombyx mori* is a fibrous protein whose major amino acid composition consists of Gly, Ala, and Ser residues (over 85%) and its ratio Gly:Ala:Ser is 3:2:1.[1-4] Lucas et al.[5,6] showed the presence of the following long hexapeptide sequence for the crystalline fraction (C_p fraction) obtained as precipitate (60% of the original material) after digestion by chymotrypsin: Ser-Gly-Ala-Gly-Ala-Gly. Accordingly, X-ray powder diffraction patterns of this hexapeptide and its polymer were found to be similar to those obtained in powdered cocoon samples.[7,8] This model could be further simplified to repetition of Ala-Gly sequence, if the difference of side chains in Ala and Ser were ignored. To support this view, secondary structure of silk I and silk II from *B. mori* fibroin turned out to be very similar to that of forms II and I of poly(alanylglycine), respectively, on the basis of X-ray powder diffraction studies.[2,3,9] We further confirmed this conclusion on the basis of the similarity of ^{13}C chemical shifts of Gly and Ala residues between corresponding forms of silk and poly(alanylglycine),[10] because displacement of the ^{13}C chemical shifts due to a conformational change are found to be very useful as a novel means to examine conformational features of a variety of peptides, polypeptides, and proteins.[11-18]

Nevertheless, it seems important to clarify the role of side chains in Ser residues in stabilization of these secondary structures in the solid state, because half of Ala residues is replaced by Ser in *B. mori* fibroin. If the amount of Ser residues is smaller than this ratio, α-helix form is stabilized instead of silk I form, as in *P. c. ricini* fibroin. To gain insight into the manner of side-chain orientation, it has been demonstrated that analysis of the quadrupole splittings in ^2H NMR spectra of ^2H-labeled samples provides one unequivocal means to assess molecular reorientation or motions.[19-21]

In the present paper, we aimed to analyze the manner of side-chain reorientation in Ser residues of silk fibroins as compared to that of Ala residues, on the basis of ^2H NMR spectra of [^2H]-labeled fibroins from *B. mori* and *P. c. ricini* which were prepared by incorporation of deuterated amino acids, DL-[3,3-$^2H_2$]-serine (Ser) and L-[3,3,3-$^2H_3$]-alanine (Ala), to artificial diet. We found from analysis of ^2H NMR spectra that reorientation of side chains in Ser residues is virtually frozen, for any form of fibroin (silk I, silk II and α-helix), as a result of plausible involvement of OH groups in hydrogen bonds which cause stabilization of these individual conformations. On the contrary, separation of the motionally averaged quadrupole-splittigs of Ala residue is 39 kHz due to the presence of the three-fold rotation of the methyl groups and is found to be identical among various types of backbone conformations such as silk I, silk II and α-helix forms.

Experimental

Silkworms of *Bombyx mori*, a hybrid between strains Nichi 140 and Shi 140, were reared with an artificial diet. During the period of 5 d before maturation, 2.5% DL-[3,3,-$^2H_2$]Ser (98 atom%, Sigma Chemical Company, USA; Lot No. 985-H) or L-[3,3,3-$^2H_3$]Ala (99.4 atom%, Sigma Chemical Company, USA; Lot No. 2010-I) were fed with an artificial diet (Silkmate 2M, Nippon Nosan Kogyo, Tokyo). Selectively deuterated cocoons thus obtained were degummed twice, to remove sericin, with 0.5% Marseilles soap solution at 100 °C, for 30 min. and washed by distilled water. Silk II sample thus obtained was dissolved in 9M LiBr aqueous solution (40 °C) and dialyzed against distilled water for 4 h and lyophilized (Silk I sample). Prior to measurements of ^2H NMR spectra of the individual forms,

these structural modifications were monitored by examination of infrared or high-resolution ^{13}C solid-state NMR spectra.

[*Ala*-3,3,3-$^2H_3$]-cocoon and fibroin from *P. c. ricini* were prepared by feeding 2.5% (w/w) L-[3,3,3-$^2H_3$]Ala to the silkworms together with an artificial diet during 5 d before maturation. At the same time, silkworms fed with [3,3,3-$^2H_3$]-Ala were excised and liquid silk was directly removed from the middle silk gland portion of *P. c. ricini*. The liquid silk thus obtained was dried gently over film of poly(vinyldene chloride).

Infrared spectra were obtained with a Shimadzu IR-435 spectrometer. 75.46 MHz high-resolution solid-state ^{13}C NMR spectra were recorded on a Bruker CXP-300 spectrometer by cross polarization-magic angle spinning (CP-MAS) method. Samples were contained in an Andrew-Beams type rotor machined from perdeuterated poly(methyl methacrylate) and spun as fast as 3—4 kHz by compressed air. In some instances, spinning side bands from quaternary carbons were suppresed by means of pulse sequence of the total side-band suppression (TOSS) by Dixon.[22] Chemical shifts were calibrated by the peak position of benzene at 128.5 ppm from TMS.

46.06 MHz high-power ^2H NMR spectra[19-21] were recorded on a Bruker CXP-300 spectrometer utilizing the quadrupole-echo pulse-sequence, 90°_x-t-90°_y-t-echo.[23] The experiments were done on resonance so that negative frequencies of the symmetry spectrum are folded over on top of the positive frequencies on transformation. Samples were contained in a 10 mm sample tube placed in a transverse solenoid coil. Duration of 90° pulse was usually 4 μs. Spectral width, spacing of the two 90° pulses t, and data points were 250 kHz (125 kHz×2), 40—60 μs, and 2 K, respectively. Repetition time was 0.5 s. Spectra were usually accumulated more than 120000 times.

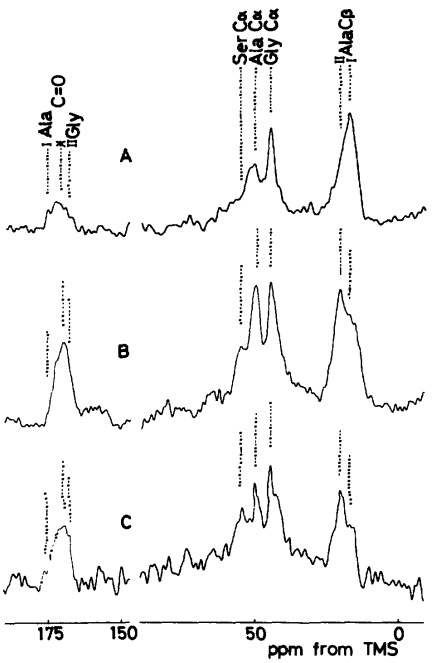

Fig. 1. 75.46 MHz ^{13}C CP-MAS NMR spectra of [*Ser*-3,3-$^2H_2$]cocoon and fibroin taking a variety of crystalline forms. The asterisked peak is ascribed to the carbonyl carbons other than silk I peak of Ala residue and silk II of Gly residue. A. silk I, B. silk II and C. cocoon.

Results

We obtained [*Ser*-3,3-$^2H_2$]- and [*Ala*-3,3,3-$^2H_3$]-cocoons and fibroin samples from biosynthesis by feeding respective deuterated amino acids to silkworms and resultant degumming procedure, as described in the previous section.[24] Before recording individual ^2H NMR spectra of each samples, we first examined change of spectral features due to structural modifications by the ^{13}C CP-MAS NMR spectra, as demonstrated in Fig. 1. The ^{13}C CP-MAS NMR spectra of [*Ser*-3,3-$^2H_2$]cocoon or fibroin are not strongly different from those of undeuterated samples previously recorded,[10,14] because degree of deuteration at Ser C_β carbon is at most 10—20%, as estimated by examination of high-resolution ^{13}C NMR spectra in aqueous solution. Apparently, expected conformational modification of the present samples was effectively achieved, because each silk I and silk II samples contain the respective forms as major components (≈80%), as manifested from the ^{13}C NMR peak-positions of Ala C_β or C=O peaks.

Figure 2 illustrates ^2H powder-pattern NMR spectra of corresponding [*Ser*-3,3-$^2H_2$]-cocoon and fibroin

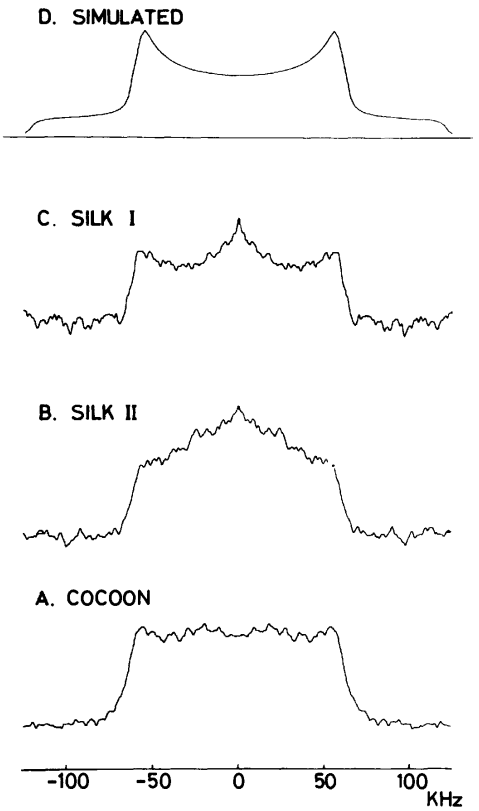

Fig. 2. 46.06 MHz ^2H NMR spectra of [*Ser*-3,3-$^2H_2$]-cocoon and fibrion. A. cocoon, B. silk II, C. silk I, and D. calculated spectrum with e^2qQ/h=180 kHz.

samples from *Bombyx mori* taking silk I and silk II forms. Obviously, these ^{2}H NMR spectra arose from superposition of at least two kinds of powder patterns, the wider and narrow components. It appears that no appreciable change in the spectral patterns of the wider components was noted among cocoon, silk I and silk II samples. In principle, any difference in spectral feature between the cocoon and silk II samples could be ascribed to the presence or absence of sericin which is a protein consisting of a large proportion of Ser residue. Therefore, it is now clear that there exists no appreciable change in the ^{2}H NMR spectra of side-chain orientation as seen from the wider component in the deuterated fibroin and sericin. The spectral feature and the separation of peaks (D_q) due to the quadrupole splittings (125 kHz) were well reproduced by spectral simulation[33,34] assuming the quadrupole coupling constant e^2qQ/h as 180 kHz, as shown in the top trace. In particular, the separation of peaks in the doublet signals is[19]

$$D_q = 3/4\,(e^2qQ/h) \qquad (1)$$

It is difficult, however, to record correctly the outer edges portion with separation of $2D_q$ (250 kHz) because of experimental limitation (spectral width 250 kHz).

On the contrary, we observed ^{2}H powder-pattern NMR spectra with reduced spectral separation as large as 39 kHz for [3,3,3-$^2H_3$]Ala(A), silk II(cocoon; B) and silk I (C) of *Bombyx mori*, α-helical sample obtained as dried liquid silk removed from the middle silk gland (D) and cocoon (E) from *P. c. ricini* (Fig. 3). Conformational feature of dried liquid silk sample from *P. c. ricini* is rather heterogeneous because of the presence of both the α-helix (about 30%[35]) and random coil form (about 70%) (Fig. 4). Nevertheless, it is obvious that Ala residues are mainly involved in the α-helix form, as far as the peak positions of the ^{13}C CP-MAS NMR spectra are concerned (Fig. 5).[36] Consistent with our previous finding,[17] the peak positions of the ^{13}C NMR peaks in Ala C_α, C_β and C=O carbons of [*Ala*-3,3,3-$^2H_3$]-fibroin in the solid state are in good agreement with those obtained from $(Ala)_n$ taking α-helix form.

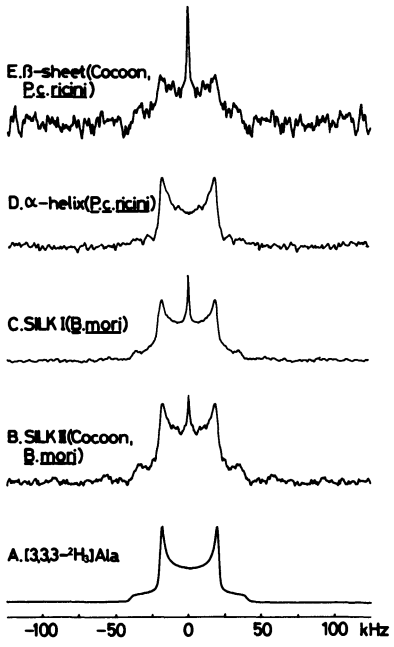

Fig. 3. 46.06 MHz ^{2}H NMR spectra of [*Ala*-3,3,3-$^2H_3$]-cocoons and fibroins from *Bombyx mori* and *P. c. ricini*. A. [3,3,3-$^2H_3$]alanine, B. cocoon from *Bombyx mori*, C. silk I from *B. mori*, D. α-helical portin of dried liquid silk from *P. c. ricini*, and E. cocoon of *P. c. ricini*.

Discussion

It is conceivable that side-chain moiety of Ser in silk fibroins, CD_2OH group, might participate in stabilization of secondary conformation in the solid state, because OH group has ability to form hydrogen bonding with C=O group of the same molecular

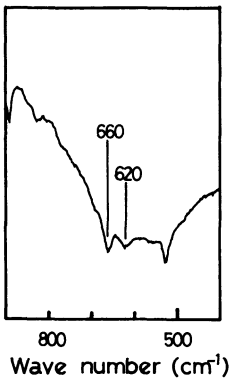

Fig. 4. Infrared spectrum of dried liquid silk from *P. c. ricini*.

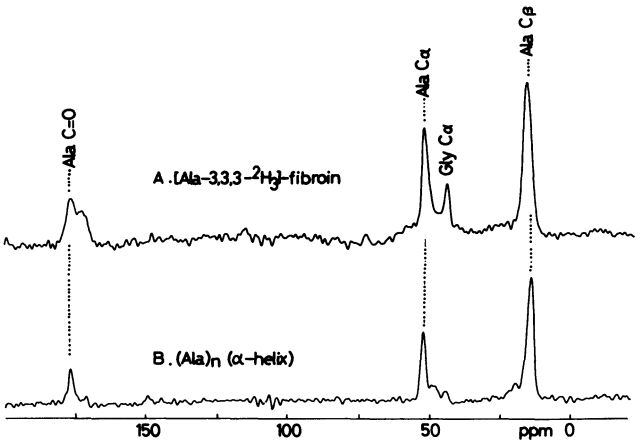

Fig. 5. ^{13}C CP-MAS NMR spectra of dried liquid silk [*Ala*-3,3,3-$^2H_3$]-fibroin from *P. c. ricini* and α-helical $(Ala)_n$. Spinning side bands were suppressed by the pulse sequence of TOSS.

chain. On the basis of survey of X-ray diffraction data on 19 or 43 globular proteins, Janin et al.[37] or Gray and Matthews[38] respectively, showed that approximately 70% of serine residue have their O_γ atom within hydrogen-bonding distance (3.5 Å) of at least one carbonyl group, with an acceptable angular geometry for OH··O bond. They showed that the χ_1 angle distribution of Ser side chain is almost equal among g^- (38%), t (28%), and g^+ (34%), suggesting the lesser steric hindrance created by the hydroxyl group, which in turn results in a smaller barriers for the rotation about the C_α-C_β bond.[37,38] Nevertheless, most of these observed hydrogen bonds involve a main chain carbonyl group as acceptor (83%), though side chain to side chain bonds may coexist with side chain to main chain bonds. It is further obvious that these hydrogen bonds are determined by the conformation of the main chain which fixes the position and orientation of the acceptor oxygens. In the case of the β-sheet form, intramolecular hydrogen bond can occur either between OH and C=O of the preceding (i-1) residue or of the same residue (i).[37] In the case of the α-helix, similar hydrogen bond can be formed between the OH of i th residue and C=O of i-4 residue.

It is now obvious that ^{2}H NMR spectra of side-chain methylene (CD_2) group of Ser residues can be analyzed as static and the separation of the quadrupole splittings was also unchanged among the cocoon, silk II and silk I samples. This finding implies that side chain reorientation of Ser residue is virtually frozen irrespective of differences in backbone conformations (silk II (β-sheet) or silk I). Undoubtedly, the β-sheet or silk II form could be further stabilized by taking the above-mentioned intrachain hydrogen bonds. As to a silk I model of *B. mori* silk fibroin in the solid state, crankshaft-type model has been proposed by Lotz et al.[3,9] and later, three kinds of revised loose helix models have been reported.[39] Therefore, we examined any possibility of forming intramolecular hydrogen bonds between the OH group of given Ser residue and backbone carbonyl groups in the chain of partial sequence Ala-Gly-Ser-Gly-Ala-Gly-Ala taking several conformations for models of silk I form. Basically, it was found by model-building that most of these models are feasible to form intramolecular hydrogen bonds (<3.5 Å) between the OH hydrogen and the C=O oxygen of the Gly residue in the preceding (i-1) residue in a similar manner to the case of the β-sheet form.

Therefore, it is natural to consider that almost all of side-chain hydroxyl group of Ser residue in fibroin could participate in the formation of intra- or interchain hydrogen bonds. In addition, it appears that in cocoons side chain hydroxyl groups of Ser in sericin are mostly hydrogen-bonded to proton acceptors of fibroin in cocoon, as inferred from the data of Fig. 2. This view might be important in connection with understanding of a manner of sericin-fibroin interaction in the cocoons. Further, it is worthwhile to point out that there appears no difference in the dynamic aspect of these main chains, because particular motions, if any, could significantly influence the ^{2}H NMR spectral features.

As illustrated in Fig. 3, however, the quadrupole splittings of [3,3,3-$^2H_3$]Ala and [*Ala*-3,3,3-$^2H_3$]-cocoon and fibroins were equally reduced to 39 kHz, as a result of motionally averaged reduction in the quadrupole interaction of the methyl group. Apparently, these spectral patterns arose from the presence of axially symmetric field gradient. Therefore, the simplest such a motion is the three-fold rotation about the C_α-C_β axis. The separation of the doublet peaks due to the quadrupole interaction is then reduced to

$$D_q' = 3/8\,(e^2qQ/h)(3\cos^2\alpha - 1) \qquad (2)$$

where α is the angle between the C-D vector and C_α-C_β axis. The calculated quadrupole splitting D_q' from this case is obtained as 42.6 kHz by using α= 109° 44′ and this value is slightly larger than the observed value (39 kHz).[21] In other systems, the quadrupole splittings of deuterated methyl groups are in the range of 35 kHz for palmitic acid[40] and nonadecane.[41] Again, there appears no variation in the above-mentioned value among alanine monomer and fibroins of α-helix, β-sheet, and silk I forms, reflecting the absence of major change in the dynamic state of main chains in these systems.

In conclusion, we successfully recorded powder-pattern ^{2}H NMR spectra of [*Ser*-3,3-$^2H_2$]- and [*Ala*-3,3,3-$^2H_3$]-cocoons and fibroins taking various types of secondary structure. The quadrupole splitting for CD_2OH side chain of Ser residue was found to be 125 kHz, indicating the presence of static side chain, whereas the splitting of the CD_3 side chain of Ala residue was reduced to 39 kHz, as a result of fast three-fold rotation. Accordingly, it is plausible that the hydroxyl groups of the side chains in Ser residue might participate in the formation of the intrachain hydrogen bonds which are effective in stabilization of particular forms irrespective of differences in backbone conformation in the cocoon, silk I, and silk II forms. Then, it is expected that the present approach might be useful as a new means to gain insight into molecular organization of fibroin samples as related to several kinds of physical properties of fibroins.

We are grateful to Dr. Takeshi Yamanobe and Professor Isao Ando of Tokyo Institute of Technology for use of their computer program for simulation of powder pattern. This work was supported, in part, by a Grant-in-Aid from the Ministry of Education, Science and Culture.

References

1) F. Lucas and K. M. Rudall, "Comprehensive Biochemistry," 26B, ed by M. Florkin and E. Scotz, Elsevier, Amsterdam (1968), Chap. 7.

2) R. D. Fraser and T. P. MacRae, "Conformation of Fibrous Proteins and Related Synthetic Polypeptides," Academic Press, New York (1973), Chap. 13.

3) B. Lotz and F. C. Cesari,*Biochimie*, **61**, 205 (1979).

4) "Zoku Kenshi no Kozo (Structure of Silk fibroins)," ed by N. Hojo, Shinshu University, Ueda, Japan (1980).

5) F. Lucas, J. T. B. Shaw, and S. G. Smith, *Nature*, **179**, 906 (1957).

6) F. Lucas, J. T. B. Shaw, and S. G. Smith, *Adv. Protein Chem.*,**13**, 107 (1958).

7) J. O. Warwicker, *Acta Crystallogr.*, **7**, 565 (1954).

8) E. Schnabel and H. Zahn, *Justus Liebig Ann. Chem.*, **614**, 141 (1958).

9) B. Lotz and H. D. Keith, *J. Mol. Biol.*, **61**, 201 (1971).

10) H. Saitô, R. Tabeta, T. Asakura, Y. Iwanaga, A. Shoji, T. Ozaki, and I. Ando, *Macromolecules*, **17**, 1405 (1984).

11) H. Saitô, R. Tabeta, A. Shoji, T. Ozaki, I. Ando, and T. Asakura, "Magnetic Resonance in Biology and Medicine," ed by G. Govil, C. L. Kheterapal, and A. Saran, Tata McGraw-Hill, New Delhi (1985), p. 195.

12) H. Saitô, Magn. Res. Chem. in press.

13) H. Saitô, Y. Iwanaga, R. Tabeta, M. Narita, and T. Asakura, *Chem. Lett.* **1983**, 431.

14) T. Asakura, A. Kuzuhara, R. Tabeta, and H. Saitô, *Macromolecules*, **18**, 1841 (1985).

15) T. Taki, S. Yamashita, S. Satoh, A. Shibata, T. Yamashita, R. Tabeta, and H. Saitô, *Chem. Lett.* **1981**, 1803.

16) H. Saitô, R. Tabeta, A. Shoji, T. Ozaki, and I. Ando, *Macromolecules*, **16**, 1050 (1983).

17) H. Saitô, R. Tabeta, I. Ando, T. Ozaki, and A. Shoji, *Chem. Lett.*, **1983**, 1437.

18) H. Saitô, R. Tabeta, A. Shoji, T. Ozaki, I. Ando, and T. Miyata, *Biopolymers*, **23**, 2279 (1984).

19) H. H. Mantsch, H. Saitô, and I. C. P. Smith, *Prog. NMR Spectrosc.*, **11**, 211 (1977).

20) L. W. Jelinski, C. E. Sullivan, and D. A. Torchia, *Nature*, **284**, 531 (1980).

21) L. S. Batchelder, C. H. Niu, and D. A. Torchia, *J. Am. Chem. Soc.*, **105**, 2228 (1983).

22) W. T. Dixon, *J. Chem. Phys.*, **77**, 1800 (1982).

23) J. H. Davis, K. R. Jeffrey, M. Bloom, M. I. Valic, and T. P. Higgs, *Chem. Phys. Lett.*, **42**, 390 (1976).

24) It is already known that there is a possibility of conversion of fed deuterated serine or alanine to other amino acids such as glycine, alanine or serine within a body of silkworm (Ref. 25—29). It appears that the extent of amino-acid conversion is not larger than 10% for alanine and glycine, as inferred from our previous experience on biosynthetic experiment utilizing [1-^{13}C]-labeled amino acids (Ref. 30). However, it is well known that serine is the most important source of glycine biosynthesis in mammalian system (Ref. 31). In a similar manner, Muramatsu et al. showed that radioactivity of glycine rose to nearly 60% of that of [1-^{14}C]-serine by 20 min after injection to *B. mori* silkworms (Ref. 29). They showed that radioactivity from [1-^{14}C]-serine is retained only in the carboxyl carbons. This finding is consistent with that the conversion of serine to glycine in insect is catalyzed by serine hydroxymethylase in the presence of tetrahydrofolic acid (Ref. 32). In this connection, deuterium atoms from deuterated hydroxymethyl group in the side chain of serine are thus not any more retained in converted glycine by this reaction. By contrast, conversion of serine to alanine was very low (2%) and no other amino acids were synthesized from serine (Refs. 25 and 29). Accordingly, we neglected, in this paper, a plausible contribution from any converted amino acid residues. Further, it is emphasized that the present conclusion as to the orientation of side-chains in serine to be described later remains unchanged, even if deuterium atoms are incorporated into glycine to some extent by an unidentified mechanism from the deuterated serine (see text).

25) T. Fukuda, *J. Biochem.* **47**, 581 (1960).

26) T. Fukuda, *J. Biochem.* **43**, 137 (1956).

27) T. Fukuda, *J. Biochem.* **47**, 720 (1960).

28) T. Ito, "Kasan Seikagaku (Biochemistry of Bombyx Mori)," Shokabo (1984).

29) M. Muramatsu, H. Nagayama, and K. Shimura, *J. Biochem.* **49**, 55 (1961).

30) T. Asakura, Y. Watanabe, and T. Itoh, *Macromolecules*, **17**, 2421 (1984).

31) H. R. V. Arnstein and V. Stankovic, *Biochem. J.*, **62**, 190 (1956).

32) D. E. Metzler, "Biochemistry, The Chemical Reactions of Living Cells," Academic Press, New York (1977), p. 837.

33) N. Bloembergen and J. A. Rowland, *Acta Met.*, **1**, 731 (1953).

34) M. Mehring, "Principle of High Resolution NMR in Solids," Second Edition, Springer-Verlag, Berlin and New York (1983).

35) T. Asakura and T. Murakami, *Macromolecules*, **18**, 2614 (1985).

36) Note that in Fig. 5 Ser C_α peak is superimposed on the Ala C_α peak in the silk I form, although these peaks are separated into two peaks in the silk II form (Ref. 13). It is also pointed out that the peak-intensities of Ala C_β signal are suppressed to some extent by the TOSS experiment.

37) J. Janin, S. Wodak, M. Levitt, and B. Maigret, *J. Mol. Biol.*, **125**, 357 (1978).

38) T. Gray, and B. W. Matthews, *J. Mol. Biol.*, **175**, 75 (1984).

39) T. Asakura, "Proceedings of the 7th International Wool Textile Research Conference, Tokyo," ed by M. Sakamoto, The Society of Fiber Science and Technology, Japan (1985), Vol. 1, p. 354.

40) H. Saitô, Y. Sugimoto, R. Tabeta, S. Suzuki, G. Izumi, M. Kodama, S. Toyoshima, and C. Nagata, *J. Biochem.*, **94**, 1877 (1983).

41) M. G. Taylor, E. C. Kelusky, I. C. P. Smith, H. L. Casal and D. G. Cameron, *J. Chem. Phys.*, **78**, 5108 (1983).

 © 1986 The Chemical Society of Japan Bull. Chem. Soc. Jpn., 59, 3389—3392 (1986)

Temperature Effect on the Association of Aqueous Europium and Sulfate Ions from Luminescence Decay Measurement

Fujio TANAKA,* Yoshiko KAWASAKI, and Shigeru YAMASHITA
College of Integrated Arts and Sciences, University of Osaka Prefecture,
Mozu-umemachi, Sakai, Osaka 591
(Received May 14, 1986)

The luminescence lifetime for $Eu_2(SO_4)_3$ and $EuCl_3$ in H_2O and D_2O has been measured at 0.01 and 0.001 mol dm^{-3} of Eu^{3+} and at various temperatures from 5 to 45 °C. The average number of water molecules coordinated to Eu^{3+} ion, q, is evaluated from the difference of the luminescence decay constants in the H_2O and D_2O solutions. By using the q value of 8.3 for aquaeuropium(III) ion in $EuCl_3$ solutions, q values for $Eu_2(SO_4)_3$ solutions were determined as a function of concentration and temperature. The average number of water molecules released from the primary hydration sphere by the inner-sphere complexation between Eu^{3+} and SO_4^{2-} ions is given as $\Delta q=8.3-q$, and Δq value increases with concentration and temperature. From the values of Δq and the known equilibrium constants on the overall complexation, it is revealed that for both the unis(sulfato) and bis(sulfato) complexation the ratio of inner-sphere complex to outer-sphere complex increases with temperature and that about one water molecule is released from the inner hydration sphere surrounding Eu^{3+} ion on the formation of an inner-sphere unis(sulfato) complex. The coordination state of the unis(sulfato) complex and the thermodynamic quantities for the equilibrium between outer- and inner-sphere complexes are discussed.

The ion-association is one of the most important problems in the chemistry of electrolyte solutions. In addition to conventional methods, modern techniques have been used to clarify this phenomenon. Ion complexes are classified into two types: inner- and outer-sphere complexes. It is rather difficult to identify them and, therefore, conflicting conclusions have frequently been reported. Some of the spectroscopic methods reflect not only inner-sphere interaction but also outer-sphere interaction. Thermodynamic data are useful for the examination of average characteristics of the complexes.

Recently, the luminescence decay measurement has been utilized in various fields as a method to investigate the coordination state of Eu^{3+} ion.[1-4] This method is based on the fact that the difference between the observed luminescence decay constants for H_2O and D_2O solutions is proportional to the number of inner-sphere water molecules surrouding Eu^{3+} ion. The information acquired by this method reflects only the inner-sphere interaction. In a previous work we showed the formation of an inner-sphere complex between Eu^{3+} and SO_4^{2-} ions by this method.[5] For revealing the details of ion-association in this system more quantitatively, the luminescence lifetime for H_2O and D_2O solutions of $Eu_2(SO_4)_3$ and $EuCl_3$ has been measured as a function of temperature. The combination of the present result with the known equilibrium constants for the overall complexation[6] will provide new information on the equilibrium between outer- and inner-sphere complexes.

Experimental

$EuCl_3 \cdot 6H_2O$ and $Eu_2(SO_4)_3 \cdot 8H_2O$ were prepared by dissolving Eu_2O_3 into HCl and H_2SO_4, respectively, as described previously.[5] Deuterated salts were obtained from hydrated salts by repeating D_2O addition and evaporation. D_2O of 99.95% grade(Merck) was used. A few modifications were made in the previous procedure and instrument for the lifetime measurement.[5] 1-Acetylnaphthalene was used as a photosensitizer instead of 2-acetylnaphthalene, because the fluorescence of the former was much weaker than that of the latter and so optical and electric interference due to the fluorescence from sensitizer reduced significantly. A transient memory(10 bits, Kawasaki Electronica TMR-10) was used. Data were analyzed by the least-squares method by means of a microcomputer system. Temperature was controlled by circulating thermostated water inside the cell holder.

Results and Discussion

Luminescence decay constants of Eu^{3+} ion in H_2O and D_2O, k^{H_2O} and k^{D_2O}, are related to the number of inner-sphere water molecules, q, as follows:[1-3,5]

$$\Delta k = k^{H_2O} - k^{D_2O} = A \cdot q, \quad (1)$$

Table 1. Luminescence Decay Constants(s^{-1})[a] for $EuCl_3$ and $Eu_2(SO_4)_3$ in H_2O and D_2O

$[Eu^{3+}]$	T	$EuCl_3$			$Eu_2(SO_4)_3$		
mol dm^{-3}	°C	k^{H_2O}	k^{D_2O}	Δk	k^{H_2O}	k^{D_2O}	Δk
0.001	5	8928	290	8638	8472	283	8189
	15	8951	313	8638	8471	306	8165
	25	8996	337	8659	8390	328	8062
	35	9077	367	8710	8373	356	8017
	45	9190	411	8779	8372	423	7949
0.01	5	8828	260	8567	8168	268	7900
	15	8940	266	8674	8173	281	7892
	25	9010	278	8732	8148	294	7854
	35	9100	292	8808	8109	312	7797
	45	9219	315	8904	8058	354	7704

a) ±20 for k^{H_2O} and ±5 for k^{D_2O}.

Table 2. Average Number of Water Molecules in the Primary Coordination Sphere, q, and Average Loss of Coodinated Water Molecules Caused by Inner-Sphere Complexation, Δq, and Fractions of Complexed Eu^{3+} Ions, f's, for $Eu_2(SO_4)_3$ Solutions

$[Eu_2(SO_4)_3]$ / mol dm^{-3}	T / °C	q [a]	Δq [b]	$f_{EuSO_4^+}$ [c]	$f_{Eu(SO_4)_2^-}$ [c]	$\Delta q/f$ [d]
5×10^{-4}	5	7.86	0.44	0.519	0.006	0.838
	15	7.84	0.46	0.577	0.010	0.783
	25	7.72	0.58	0.630	0.015	0.899
	35	7.64	0.66	0.682	0.022	0.937
	45	7.51	0.79	0.725	0.030	1.046
5×10^{-3}	5	7.65	0.65	0.719	0.046	0.849
	15	7.55	0.75	0.743	0.067	0.925
	25	7.46	0.84	0.756	0.091	0.991
	35	7.34	0.96	0.761	0.118	1.092
	45	7.18	1.12	0.756	0.149	1.237

a) Calculated by using the value of 8.3 as the hydration number of aquaeuropium(III) ion. b) $\Delta q=8.3-q$. c) Including both outer- and inner-sphere complexes. Estimated according to Ref. 6. d) $f=f_{EuSO_4^+}+f_{Eu(SO_4)_2^-}$.

Table 3. Formation Constants for Europium Unis(sulfato) Complex, K's, and Number of Water Molecules Released from the Primary Hydration Sphere by the Formation of One Inner-Sphere Complex, l, in the 5×10^{-4} mol dm^{-3} Solution of $Eu_2(SO_4)_3$

T / °C	K^T [a] / mol^{-1} dm^3	$\mathring{a}$ [b] / Å	K^{out} [c] / mol^{-1} dm^3	K^{lo} [d]	l [e]
5	1132	6	266	3.25	1.10
15	1555		292	4.32	0.98
25	2129		323	5.59	1.08
35	3002		362	7.29	1.10
45	4171		407	10.2	1.19
5		7	155	6.30	0.98
15			168	8.25	0.89
25			172	11.3	1.08
35			204	13.7	1.03
45			226	17.4	1.15

a) Ref. 6.[10] b) Distance of closest approach of ions which was assumed for the outer-sphere complex. c) Estimated by the Fuoss equation. d) Obtained by Eq. 2. e) Calculated by Eq. 6.

where A is the proportionality constant, which corresponds to the rate constant of nonradiative deactivation caused by one molecule of H_2O. Luminescence decay constants measured for $EuCl_3$ and $Eu_2(SO_4)_3$ in H_2O and D_2O are shown in Table 1. It shows that at different Eu^{3+} concentrations and temperatures Δk is smaller for $Eu_2(SO_4)_3$ than for $EuCl_3$ and that at both the concentrations Δk increases for $EuCl_3$ and decreases for $Eu_2(SO_4)_3$ with the rise of temperature. It has been known that inner-sphere complexes are not formed in $EuCl_3$ solutions under the present conditions and the inner coordination sphere surrounding Eu^{3+} ion is occupied solely by water molecules.[5,7,8] The hydration number of aquaeuropium(III) ion has been determined to be 8.3 by X-ray diffraction for the $EuCl_3$ solution of 3.23 mol kg^{-1}.[7] Apart from its absolute value, we reported previously by the luminescence lifetime measurement that the hydration number for $EuCl_3$ solutions is nearly constant over a wide range of concentration.[5] We, therefore, use the q value of 8.3 for $EuCl_3$ solutions irrespective of concentration and temperature, and the values of A at each of conditions are obtained from Eq. 1. Subsequently, q values for $Eu_2(SO_4)_3$ solutions are determined by using these A values.[9] The q values shown in Table 2 are smaller than 8.3, indicating that water molecules are partially removed from the primary hydration sphere of Eu^{3+} ion by the formation of inner-sphere sulfato complexes. As predicted from the chemical equilibrium, the value of q for 5×10^{-3} mol dm^{-3} is smaller than that for 5×10^{-4} mol dm^{-3} at respective temperatures.

Hale and Spedding investigated this system in detail by the UV absorption method.[6] They suggested that their data were related to the equilibrium of overall complexation including both the outer-sphere and inner-sphere complexes. By using their data, we have calculated the fractions of unis(sulfato) and bis(sulfato) europium ions to total europium ions,[10] fractions being denoted by $f_{EuSO_4^+}$ and $f_{Eu(SO_4)_2^-}$, respectively. On the other hand, the average loss of inner-sphere water molecules caused by the inner-sphere complexation is obtained from the relation, $\Delta q=8.3-q$. The values of f's and Δq are given in Table 2. The values of Δq and f's, and the ratio of Δq to the sum of fractions ($f_{EuSO_4^+}+f_{Eu(SO_4)_2^-}$) increase with the rise of temperature.

The temperature effect on the ion-association between various cations and the sulfate ion were studied by electrical conductivity and spectroscopic methods. The enthalpy change for the overall ion-association has a positive value in most cases.[11-14] The enthalpy changes(ΔH) for formation of unis(sulfato) europium complex obtained by Hale and Spedding are 17.1 and 22.5 kJ mol^{-1} at 25 °C for the ionic strength of 0.045 mol kg^{-1} and infinite dilution, respectively.[6] They also gave ΔH of 25.9 kJ mol^{-1} at 25 °C and the ionic strength of 0.045 mol kg^{-1} for the formation of bis(sulfato) complex.[6]

We now consider the equlibrium between outer- and inner-sphere complexes by using the values of f's and Δq. The effect of temperature on the equilibrium can be expressed qualitatively by the value of $\Delta q/f$, where f denotes the sum of $f_{EuSO_4^+}$ and $f_{Eu(SO_4)_2^-}$. This

Table 4. Enthalpy and Entropy Changes[a] for Unis(sulfato) Complexation of Eu^{3+} Ion at 25 °C in the Infinite Dilution

$\mathring{a}$	ΔH^{out} [b]	ΔH^{io}	ΔS^{out} [b]	ΔS^{io}	ΔH^{T} [c]	ΔS^{T} [c]
6 Å	6.2	19.2	74.8	78.6		
					22.5	146.3
7 Å	5.3	18.7	67.2	82.8		

a) In kJ mol^{-1} and $J\,mol^{-1}\,K^{-1}$ for ΔH and ΔS, respectively. b) By the Fuoss equation. c) Ref. 6.

value seems to be relevant to the ratio of inner-sphere complexes to the total complexes. The fact that the value of $\Delta q/f$ increases with temperature makes it conceivable to conclude that for both the unis(sulfato) and bis(sulfato) complexes the temperature elevation shifts the equilibrium between outer- and inner-sphere complexes toward the inner-sphere complex.

For the formation of the unis(sulfato) complex the following equations are derived.

$$K^{T} = \frac{[EuSO_4^+]_{out}+[EuSO_4^+]_{in}}{[Eu^{3+}][SO_4^{2-}]} = K^{out}(1+K^{io}) \quad (2)$$

$$K^{out} = \frac{[EuSO_4^+]_{out}}{[Eu^{3+}][SO_4^{2-}]} \quad (3)$$

$$K^{io} = \frac{[EuSO_4^+]_{in}}{[EuSO_4^+]_{out}} \quad (4)$$

K^{out} can be estimated by the Fuoss equation,[15]

$$K = \frac{4\pi N_A \mathring{a}^3 e^b}{3000} \quad \text{and} \quad b = \frac{|z_i z_j| e^2}{\varepsilon k T \mathring{a}}, \quad (5)$$

where N_A=Avogadro's number, $\mathring{a}$=distance of closest approach of ions, ε=dielectric constant, k=Boltzmann constant, z=charge on the ion, and e=charge on the electron. Using the complex $[Eu(H_2O)SO_4]^+$, in which two ions are separated by one water molecule, as a model of the outer-sphere complex, we have calculated K^{out} at infinite dilution by Eq. 5 with two $\mathring{a}$ values of 6 Å and 7 Å.[16] K^{out} at the equilibrium ionic strength was evaluated by the Eq. 12 of Ref. 6, and K^{io} by Eq. 2 using calculated K^{out} and K^{T} given by Hale and Spedding.[10] On the other hand, in the 5×10^{-4} mol dm^{-3} solution, where the formation of the bis(sulfato) complex is almost negligible, K^{io} is correlated with Δq as follows:

$$K^{io} = \frac{[EuSO_4^+]_{in}}{[EuSO_4^+]_{out}} = \frac{(1/l)\cdot\Delta q}{f_{EuSO_4^+}-(1/l)\cdot\Delta q}, \quad (6)$$

where l represents the number of water molecules released from the inner hydration sphere by the inner-sphere coordination of sulfate ion to Eu^{3+} ion. The values of l calculated from Δq, $f_{EuSO_4^+}$, and K^{io} by Eq. 6 are shown in Table 3 along with K^{T}, K^{out}, and K^{io} values.

The l values are close to 1, the result meaning that one water molecule is released from the inner hydration sphere on the formation of inner-sphere unis(sulfato) complex. If the average coordination number of Eu^{3+} ion is invariant in the aqua ion and the inner-sphere complex, the sulfate ion seems to act as a unidentate ligand. Further, it is postulated that aquaeuropium(III) ion exists as an equilibrium mixture of $[Eu(H_2O)_8]^{3+}$ and $[Eu(H_2O)_9]^{3+}$. The average hydration number of 8.3 assessed by X-ray diffraction indicates that the ratio of $[Eu(H_2O)_8]^{3+}$ to $[Eu(H_2O)_9]^{3+}$ is approximately 2.[7] The result that l is unity suggests that the inner-sphere complex $[Eu(H_2O)_7SO_4]^+$ is formed from a bidentate sulfate ion and an octaaqua europium(III) ion. Since the l values estimated are reasonable, dividing of K^{T} into K^{out} and K^{io} in Eq. 2, followed by application of the Fuoss equation, is considered to be appropriate.

Finally, it is interesting from the thermodynamic viewpoint to compare ΔH and ΔS corresponding to K^{out} and K^{io}. ΔH^{out} and ΔS^{out} at infinite dilution are calculated by the Fuoss equation. ΔH^{io} was calculated from ΔH^{T} and ΔH^{out} according to a relation based on Eq. 2, $\Delta H^{T}=\Delta H^{out}+[K^{io}/(1+K^{io})]\cdot\Delta H^{io}$, and ΔS^{io} was obtained by $\Delta S^{io}=\Delta H^{io}/T+R\ln K^{io}$. The results at 25 °C are listed in Table 4, together with Hale and Spedding's ΔH^{T} and ΔS^{T}. It indicates that the predominance of inner-sphere complex in this system is ascribed to the fairly large value of ΔS^{io}.

References

1) W. D. Horrocks, Jr. and D. R. Sudnick, *J. Am. Chem. Soc.*, **101**, 334 (1979).

2) W. D. Horrocks, Jr. and D. R. Sudnick, *Acc. Chem. Res.*, **14**, 384 (1981).

3) W. D. Horrocks, Jr. and M. Albin, "Progress in Inorganic Chemistry," ed by J. Lippard, Wiley, New York (1984), Vol. 30, pp. 1—104.

4) S. P. Sinha, "Systematics and the Properties of the Lanthanides," ed by S. P. Sinha, D. Reidel, Holland (1983), pp. 451—500.

5) F. Tanaka and S. Yamashita, *Inorg. Chem.*, **23**, 2044 (1984).

6) C. F. Hale and F. H. Spedding, *J. Phys. Chem.*, **76**, 1887 (1972).

7) A. Habenshuss and F. H. Spedding, *J. Chem. Phys.*, 73, 442 (1980).

8) P. J. Breen and W. D. Horrocks, Jr., *Inorg. Chem.*, **22**, 536 (1983).

9) We have assumed that the A value is dependent on temperature and concentration. It is probable that the hydration number of aquaeuropium(III) ion is dependent on these conditions and the A value is constant. However, the small difference caused by the two different treatments does not substantially influence on the following discussion.

10) The complex formation constants are calculated by using the equations in Ref. 6. For the unis(sulfato) complexation, the equation on the temperature dependence of k_1° and Eq. 12 with the value of D=0.6 were used. For the bis(sulfato) complexation, the values of K_2 and ΔH_2 at ionic

strength of 0.045 mol kg^{-1} and Eq. 12 with the value of D=0.3 were used. By repeating the calculation for Eq. 12, K's and f's were evaluated at respective concentrations and temperatures.

11) R. M. Izatt, D. Eatough, J. J. Christensen, and C. H. Bartholomew, *J. Chem. Soc., A*, **1969**, 47.

12) S. Katayama, *J. Sol. Chem.*, **5**, 241 (1976).

13) A. Dadger, D. Khorsandle, and G. Atkinson, *J. Phys. Chem.*, **86**, 3829 (1982).

14) R. G. D. Carvalho and G. R. Choppin, *J. Inorg. Nucl. Chem.*, **29**, 737 (1967).

15) R. M. Fuoss, *J. Am. Chem. Soc.*, **80**, 5059 (1958).

16) The Eu^{3+}–H_2O distance for a Eu^{3+} aquo-ion is 2.45 Å,[7] and the S–O distance for SO_4^{2-} is 1.49 Å. The distance between SO_4^{2-} and H_2O is estimated from 2.7 Å for the H···O distance in the O–H···O hydrogen bonding.

 © 1986 The Chemical Society of Japan Bull. Chem. Soc. Jpn., 59, 3393—3397 (1986)

Equilibrium and Kinetic Studies of the Dimerization of Acridine Orange and Its 10-Alkyl Derivatives

Kiyofumi MURAKAMI,* Katsumi MIZUGUCHI, Yukio KUBOTA, and Yasuo FUJISAKI
Department of Chemistry, Faculty of Science, Yamaguchi University,
Yoshida 1677-1, Yamaguchi 753
(Received May 15, 1986)

The thermodynamics and kinetics of the dimerization of Acridine Orange (AO, 3,6-bis(dimethylamino)-acridinium chloride) and its 10-alkyl derivatives in 0.1 M NaCl solution have been studied by spectrophotometry and temperature-jump method. Dimerization constants, which were determined spectrophotometrically, become large with an increase in the length of the introduced alkyl chain; this behavior is the same as that in water and a dilute HCl solution. The association and dissociation rate constants determined from the temperature-jump measurements also depend on the length of the alkyl chain. Especially, the rate constants for methyl-AO are unexpectedly small. Both the effect of added salt on the thermodynamic parameters and the kinetic results are discussed in view of the structure of hydration water surrounding dye molecules. ^{1}H NMR data for AO and methyl-AO suggest that the planes of two component molecules in a dimer are parallel to each other. This result is consistent with the spectrophotometric and kinetic data.

Aggregation of metachromatic dyes in aqueous solution has extensively been studied as the most fundamental model system for the self-aggregation of biomolecules and the interaction between small molecules and biological macromolecules. Among these, Acridine Orange (AO) has particularly attracted many interests[1-15] because of its bacteriostatic and mutagenic activities as well as the ability of binding with nucleic acids.

In recent years, equilibrium studies on the dimerization of 10-alkyl derivatives of AO have been performed to elucidate the role of hydrophobic interaction.[11,13] As a result, the dimerization constant, the enthalpy and entropy changes for the dimerization were found to become large with an increase in the length of the introduced alkyl chain; the behavior has been interpreted in terms of the enhanced hydrophobic interactions. Kinetic studies for AO[3,7], 10-octyl- and 10-decyl-AO[8] have also shown that the greater stabilities of dimer for the long alkyl chain derivatives are realized by the small dissociation rate constants.

However, the mechanism of the dimerization is still not completely elucidated. The present paper describes the details of the thermodynamics and kinetics of the dimerization, using various 10-alkyl derivatives of AO. Our goal is to establish a plausible reaction mechanism for the dimerization.

Experimental

Materials. AO (3,6-bis(dimethylamino)acridinium chloride) and D_2O (99.8 atom% in deuterium) were purchased from Merck. The 10-alkyl derivatives of AO (methyl-AO, ethyl-AO, propyl-AO, pentyl-AO, and octyl-AO), shown in Fig. 1, were synthesized according to the method of Miethke and Zanker.[16] All dyes were purified by column chromatography on alumina, using methanol as an eluent; no trace of impurity was detected by the method of thin-layer chromatography for each dye. All other chemicals used were reagent grade and water was glass-redistilled. Spectrophotometric and kinetic experiments were conducted in 0.1 M† NaCl and 5 mM phosphate buffer solution (ionic strength I=0.11; pH=6.9).

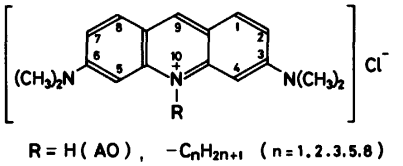

Fig. 1. Structural formulas of AO and its 10-alkyl derivatives.

Method. Spectrophotometric measurements were carried out with a Shimadzu UV-200S spectrophotometer. ^{1}H NMR spectra of AO and methyl-AO were recorded using a 200-MHz JOEL FX-200 Fourier transform spectrometer. The measurements were performed in the concentration range 10^{-2} M to 5×10^{-4} M. The sample solutions were prepared in D_2O so as to contain a small amount of internal reference sodium 2,2-dimethyl-2-silapentane-5-sulfonate(DSS). Kinetic experiments were performed with a Unisoku TF-102 fluorescence temperature-jump spectrophotometer. This equipment is one of joule-heating type. The light source was a 250 W halogen lamp and the path length of the cell was 5 mm. The time cource of temperature rise could be approximated by an exponential function and its time constant (τ_r) was in the range of 4—5 μs, depending on temperature and concentration of salt. Data were obtained at the temperature rise of 5 °C. Since the relaxation times (τ) for the present systems were close to τ_r, especially at high temperatures and high concentrations of dye, they were determined by the deconvolution method.[17] The relaxation curve observed by an imposition of an exponential type perturbation can be expressed by

$$X(t) = X_0\left\{\frac{\tau}{\tau-\tau_r}\exp(-t/\tau) - \frac{\tau_r}{\tau-\tau_r}\exp(-t/\tau_r)\right\} \quad (1)$$

† 1 M=1 mol dm^{-3}.

where X and X_0 are an observable and its relaxation amplitude, respectively. τ was evaluated using a nonlinear regression analysis. All the calculations were carried out on an NEC ACOS-850 computer system.

Results

Equilibrium constants and Thermodynamic Parameters of Dimerization. Figure 2 shows typical absorption spectra observed for methyl-AO in 0.1 M NaCl solution. Similar spectral changes were also obtained with AO and other 10-alkyl derivatives. The presence of clear isosbestic points (475 and 518 nm) in the absorption spectra indicates an equilibrium between two spectral species, monomer and dimer (Fig. 2). Hence, the data were analyzed on the basis of monomer-dimer equilibrium.

$$2D \overset{K_D}{\longleftarrow} D_2 \tag{2}$$

The apparent molar extinction coefficient (ε) at a given wavelength can be expressed by

$$\varepsilon = \varepsilon_M\alpha + \varepsilon_D(1-\alpha) = (\varepsilon_M-\varepsilon_D)\alpha + \varepsilon_D, \tag{3}$$

where ε_M and ε_D are the molar extinction coefficients per monomer unit in the monomer and dimer forms, respectively, and α is the fraction of dye present in the monomer form. α can be estimated from the dimerization constant K_D and the total concentration of dye C_T as

$$\alpha = \frac{(1+8K_DC_T)^{1/2}-1}{4K_DC_T}. \tag{4}$$

The value of K_D was determined by the reiteration method. First an arbitrary K_D is chosen and then the corresponding values of α for several concentrations are calculated using Eq. 4. For each wavelength, the best straight-line fit of ε vs. α is found by linear least-squares method. The procedure is repeated to self-consistency. Dimer and monomer spectra were obtained from the intercepts of the straight lines at α=0 and α=1. Assuming that the planes of two component molecules in a dimer are parallel to each other, intermolecular distance R was estimated according to the method of Monahan and Blossey.[18] From temperature dependence of K_D, standard enthalpy and entropy changes of dimerization were also determined. These results are summarized in Table 1.

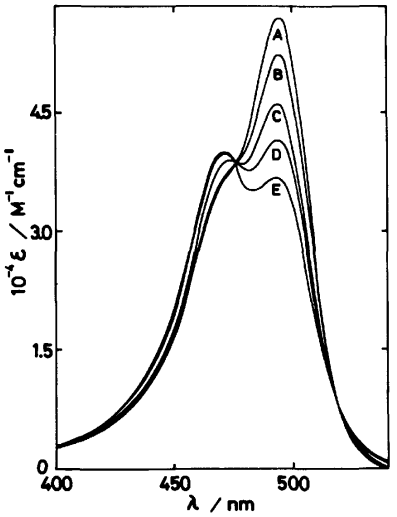

Fig. 2. Absorption spectra of methyl-AO in 0.1 M NaCl and 5 mM phosphate buffer solution (I= 0.11; pH=6.9) at 25 °C.
A: 4.1×10^{-6} M, B: 7.2×10^{-6} M, C: 1.4×10^{-5} M, D: 2.38×10^{-5} M, E: 3.6×10^{-5} M.

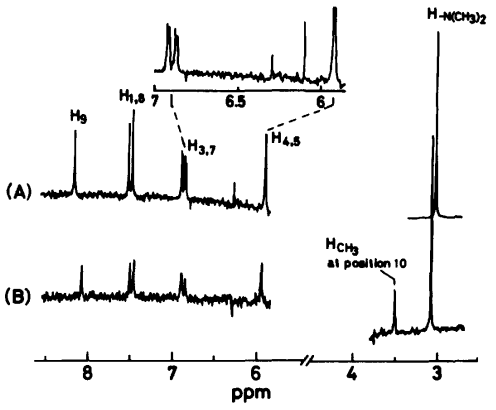

Fig. 3. ^{1}H NMR spectra of (A) AO (5×10^{-4} M) and (B) methyl-AO (5×10^{-4} M) in D_2O.

Table 1. Equilibrium and Thermodynamic Parameters for Dimerization of AO and Its 10-*N*-alkyl Derivatives at 25 °C, I=0.11

	$10^{-4}K_D$ / M^{-1}	$-\Delta H°$ / kJ mol^{-1}	$-\Delta S°$ / J K^{-1} mol^{-1}	R / Å
AO	1.60 (1.0[a], 1.08[c])	56.9 (37.4[a], 28.7[c])	111 (41.3[a], 19.0[c])	6.1
Methyl-AO	1.70 (0.71[b], 1.08[c])	57.0 (29.7[b], 29.0[c])	110 (26.0[b], 20.0[c])	6.4
Propyl-AO	2.65 (0.85[b], 1.65[c])	57.3 (29.3[b], 29.0[c])	108 (23.0[b], 16.5[c])	6.8
Pentyl-AO	3.03 (1.07[b], 2.22[c])	58.6 (28.6[b], 28.6[c])	110 (19.0[b], 12.7[c])	6.8
Octyl-AO	2.90 (1.89[b])	— (24.3[b])	— (0.0[b])	—

a) 1 mM phosphate buffer (pH=6.9) at 25 °C.[6,7] b) Water, at 25 °C.[13] c) 1 mM HCl, at 20 °C.[10,11] Listed values for K_D at 25 °C were calculated from $\Delta H°$ and $\Delta S°$ using the equation $K_D=\exp\{-(\Delta H°-T\Delta S°)/RT\}$.

Configuration of AO and Methyl-AO Dimers. Figure 3 shows ^1H NMR spectra of AO and methyl-AO in D_2O. In agreement with the assignment reported by Blears and Danyluk,[14] the NMR spectrum of AO was assigned, in order of decreasing field, to resonances due to methyl protons (3.02 ppm), 4,5-protons (5.92 ppm), 2,7-protons (6.89 ppm), 1,8-protons (7.51-ppm), and 9-proton (8.19 ppm). A clear splitting due to long-range coupling between 2,7- and 4,5-protons was also observed (Fig. 3). In the case of methyl-AO, an additional resonance due to the methyl protons at the position 10 was observed at 3.51 ppm (Fig. 3). Concentration dependence of the spectra shows similar dilution shifts to low field as observed for AO by Blears and Danyluk.[14] Table 2 lists the dilution shift of each resonance, given in terms of the difference between two concentrations 10^{-2} M and 5×10^{-4} M.

Kinetic Parameters. The square of the reciprocal relaxation time for the dimerization reaction (Eq. 2) can be expressed by[19]

$$\tau^{-2} = 8k_F k_B C_T + k_B^2, \quad (5)$$

where k_F and k_B are the forward and backward rate constants, respectively. Figure 4 shows plots of τ^{-2} vs. C_T for AO and its five 10-alkyl derivatives, indicating that the linear relationship does hold for the present system in agreement with Eq. 5. The rate constants and K_D ($=k_F/k_B$) obtained from these plots are listed in Table 3. This table also summarizes thermodynamic parameters (ΔH^0 and ΔS^0) determined kinetically and activation parameters determined according to Eyring's absolute rate theory. Activation enthalpy for the forward reaction ΔH_F^* has the value nearly equal to zero for all dyes ($\Delta H_F^* \sim 0\pm6$ kJ mol^{-1}), while that for the backward reaction ΔH_B^* has the value in the range 60—70 kJ mol^{-1} (Table 3). The forward and backward activation entropies were found to be $\Delta S_F^* = -40$—-80 JK^{-1} mol^{-1} and $\Delta S_B^* = 60$—95 JK^{-1} mol^{-1}, respectively (Table 3). The experimental error for the rate constants was estimated to be ±10—20%, while that for the thermodynamic parameters was ±20—30%. Considering this point, it seems likely that both kinetically and spectrophotometrically determined thermodynamic parameters are in agreement with each other.

Table 2. Observed Dilution Shifts for AO and 10-Methyl-AO, and Ring Current Shielding

Proton	Dilution shift of AO in ppm	Dilution shift of 10-methyl-AO in ppm	Ring current shielding in ppm
H_1	0.34	0.33	0.25
H_2	0.32	0.29	0.21
H_4	0.49	0.46	0.34
H_9	0.42	0.37	0.31
$H_{-N(CH_3)_2}$	0.18	0.18	
H_{CH_3}[a]		0.41	

a) Methyl proton at position 10.

Discussion

Constantino et al.[11] and Septinus et al.[13] found that the values of K_D, ΔH^0, and ΔS^0 for the dimerization of 10-alkyl derivatives of AO in water and a dilute HCl solution have a tendency to become large with an increase in the length of the alkyl chain (Table 1). They attributed this tendency to the increase of

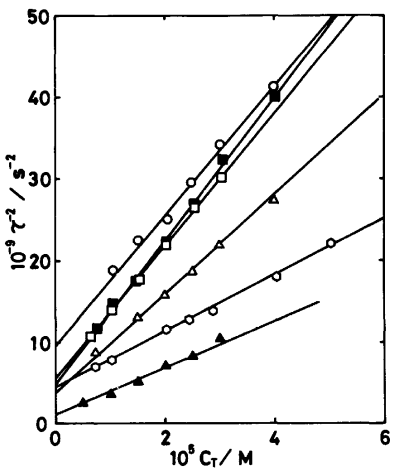

Fig. 4. Plots of τ^{-2} vs. C_T. ○: AO, ⬡: methyl-AO, □: ethyl-AO, ■: propyl-AO, △: pentyl-AO, ▲: octyl-AO.

Table 3. Summary of Kinetic Results

	$10^{-4}K_D$ / M^{-1}	$10^{-9}k_F$ / $M^{-1}s^{-1}$	$10^{-4}k_B$ / s^{-1}	$-\Delta H^\circ$ / kJ mol^{-1}	ΔH_F^* / kJ mol^{-1}	ΔH_B^* / kJ mol^{-1}	$-\Delta S^\circ$ / JK^{-1} mol^{-1}	$-\Delta S_F^*$ / JK^{-1} mol^{-1}	ΔS_B^* / JK^{-1} mol^{-1}
AO	1.0 (1.8[a])	1.0 (1.0[a])	9.8 (5.6[a])	65			140		
Methyl-AO	0.97	0.65	6.7	65			140		
Ethyl-AO	1.8	1.3	7.5	57	≈0	60—70	110	40—80	60—95
Propyl-AO	2.3	1.6	7.0	59			110		
Pentyl-AO	2.0	1.2	6.2	64			130		
Octyl-AO	3.4 (2.2[b])	1.0 (0.77[b])	3.2 (3.4[b])	—			—		

a) 1 mM phosphate buffer and 0.1 M NaCl at 23 °C and pH = 6.9.[7] b) 0.05 M NaF at 23 °C.[8]

hydrophobic interactions, that is, to the stabilization of water structure surrounding the introduced alkyl group. Septinus et al.[13] also pointed out that the longer the alkyl chain becomes, the more the tendency is pronounced. The values of ΔH^0 and ΔS^0 in 0.1 M NaCl solution (Table 1) exhibit no clear dependence on the length of the alkyl chain, whereas the K_D value clearly shows that the stabilization of dimer due to the introduction of alkyl chain takes place as in the case of water and a dilute HCl solution. Furthermore, the comparison of the present results with those in water and a dilute HCl solution shows that the presence of salt leads to the increase of K_D. This can be interpreted in terms of the stabilization of dimer by the electrostatic screening of positive charges.[6] Table 1 also shows that NaCl has a significant effect upon ΔH^0 and ΔS^0. The change in ΔH^0 by the presence of NaCl is compensated by the corresponding change in ΔS^0 to minimize the change in ΔG^0. Such enthalpy-entropy compensation has scarecely been reported for the dimerization of dye molecules. By comparison of two reports concerning the dimerization of proflavine,[20,21] however, one can find the same behavior; $\Delta H^0=-23$ kJ mol^{-1} and $\Delta S^0=-25$ JK^{-1} mol^{-1} in 0.05 M acetate buffer solution[20] and $\Delta H^0=-60$ kJ-mol^{-1} and $\Delta S^0=-150$ JK^{-1} mol^{-1} in 0.2 M KCl solution.[21] The marked decrease in ΔH^0 and ΔS^0 upon addition of salt suggests an alteration in the hydration structure surrounding dye molecules. In this connection, it should be noted that Cl^-, which forms a negative charge cloud around dye molecules, is well-known as an order-destroying ion of water structure.[22] The effect of Cl^- upon water structure may be responsible for the change in the thermodynamic parameters. The origin of this effect is at present unclear but is being explored in our laboratory.

As can be seen in Table 2, the dilution shifts of proton resonances of AO and methyl-AO show almost the same behavior, suggesting the same dimer configuration. Using the theory of Johnson and Bovey[23] and assuming that the dye molecules are arranged in parallel so that the centers of adjacent acridine rings are exactly superimposed or they are laterally displaced,[14] the shielding due to the ring currents of adjacent rings was estimated as a function of the interplanar distance (R) and the distance by which adjacent rings are off-center with respect to each other (B). The relative shifts[14] of proton resonance were found to agree well with the ring current schieldings calculated for the configuration in which ring nitrogens of adjacent dye molecules are in opposite direction and R=6 Å and B=0.5 Å (Table 2). This interplanar distance (6 Å) coincides with the values obtained from the spectrophotometric analysis (Table 1). Furthermore, the magnitude of the dilution shifts for 10-methyl protons is several times larger than that for dimethylamino protons, showing that the 10-methyl group is placed at a position where the protons are readily exposed to the field due to the ring currents of adjacent rings. Such a position can be attained by the lateral displacement between the centers of adjacent rings; this is in harmony with the above dimer configuration.

Table 3 shows that the association and dissociation rate constants vary, in a complex manner, with increasing length of the introduced alkyl chain. To understand this behavior in more detail, it is necessary to examine the following general mechanism for the dimer formation.

$$D + D \underset{k_{-1}}{\overset{k_1}{\longleftrightarrow}} D, \quad D \underset{k_{-2}}{\overset{k_2}{\longleftrightarrow}} D_2. \tag{6}$$

The first step is the diffusion-controlled formation of an outer-sphere complex. The second step is the formation of a stable dimer accompanying a rearrangement of dye monomers and ejection of water molecules. Applying the steady-state assumption to the outer-sphere complex, the observed rate constant can be expressed by

$$k_F = \frac{k_1 k_2}{k_{-1}+k_2}, \qquad k_B = \frac{k_{-1}k_{-2}}{k_{-1}+k_2}. \tag{7}$$

The diffusion controlled-rate constants k_1 and k_{-1} for AO can be theoretically calculated[24] to be $k_1=4.5\times10^9$ M^{-1} s^{-1} and $k_{-1}=5.3\times10^9$ s^{-1}, assuming that the diffusion coefficient of AO is 5×10^{-10} m^2 s^{-1}[17] and the encounter distance is 9 Å; the encounter distance was

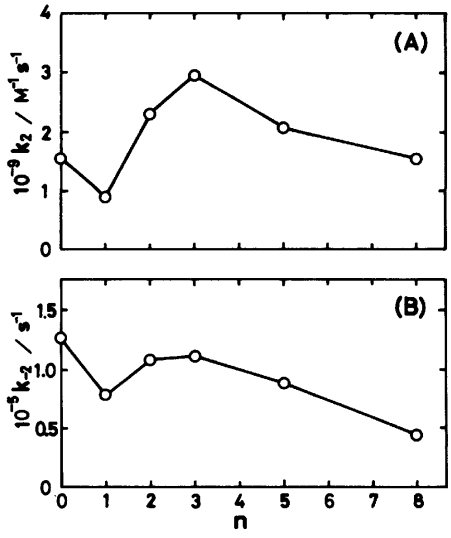

Fig. 5. The dependence of the rate constants associated with the second step in Eq. 8 on the length of the introduced alkyl chain. Abscissa shows the number of carbon atoms in the alkyl chain. (A): forward rate constant, (B): backward rate constant.

estimated as the sum of the interplanar distance in dimer (6 Å) and the diameter of water molecule (2.8 Å). Substituting these values and the values of k_F and k_B (Table 3) into Eq. 7, the rate constants associated with the second step can be determined. The rate constants for other dyes can also be estimated in the same manner by using the diffusion coefficients evaluated with the Stokes-Einstein relation for a spherical model. The evaluation of the diffusion coefficients may not be strictly valid. However, the uncertainty is unlikely to affect the conclusions of the present paper. Figure 5 indicates that both k_2 and k_{-2} vary with the length of the alkyl chain in a similar manner as k_F and k_B (Table 3). In the case of methyl-AO, the relatively slow rates can be ascribed either to a high-energy activated state, or to the stabilization of the outer-sphere complex and the dimer, or to both. The dimer configuration determined from the ^{1}H NMR spectra suggests that an alteration in the hydration structure rather than a direct interaction between the introduced methyl groups plays a significant role. The rate constants for ethyl- and propyl-AO have somewhat larger values, suggesting that the alkyl chains containing two or three carbon atoms make the activated configuration be easily accessible. For AO-derivatives having more longer alkyl chains, the rate decrease with an increase in the chain length. This effect may be attributed to the stabilization of both the outer-sphere complex and the dimer by direct hydrophobic interactions between hydrocarbon chains.[13] Dewey et al.[25,26] have shown that specific solvent-solute interactions play an important role in the kinetics of the dimerization of proflavine and thionine in aqueous alcohol solutions. In the case of methyl-AO, such interactions may be responsible for the relatively slow rates.

The authors wish to express their thanks to Mr. Yoshiaki Ishida, Mr. Masakatsu Hatakenaka, and Mr. Tsuyoshi Arai of Department of Analytical Chemistry Corporate Research and Development UBE Industries for their supports in NMR measurements. We also would like to thank Dr. Kohto Migita for his helpful discussions.

References

1) V. Zanker, *Z. Phys. Chem. (Leipzig)*, **199**, 225 (1952).
2) M. E. Lamm and D. M. Neville, Jr., *J. Phys. Chem.*, **69**, 3872 (1965).
3) G. G. Hammes and C. D. Hubbard, *J. Phys. Chem.*, **70**, 1615 (1966).
4) R. E. Ballard and C. H. Park, *J. Chem. Soc. (A)*, **1970**, 1340.
5) R. Larsson and B. Norden, *Acta Chem. Scand.*, **24**, 2583 (1970).
6) B. H. Robinson, A. Loffler, and G. Schwarz, *J. Chem. Soc., Faraday Trans. 1*, **69**, 56 (1973).
7) B. H. Robinson, A. Seeling-Loffler, and G. Schwarz, *J. Chem. Soc., Faraday Trans. 1*, **71**, 815 (1975).
8) A. D. James and B. H. Robinson, *Adv. Mol. Relax. Interact. Proc.*, **8**, 287 (1976).
9) C. A. Brignoli and H. Devoe, *J. Phys. Chem.*, **82**, 2570 (1978).
10) V. Vitagliano, L. Constantino, N. Staiano, O. Ortona, and S. Wurzburger, *Adv. Mol. Relax. Interact. Proc.*, **12**, 251 (1978).
11) L. Constantino, O. Ortona, R. Sartorio, L. Silvestri, and V. Vitagliano, *Adv. Mol. Relax. Interact. Proc.*, **20**, 191 (1981).
12) V. P. Hampe and D. Fassler, *Z. Phys. Chem. (Leipzig)*, **263**, 111 (1982).
13) M. Septinus, W. Seiffert, and H. W. Zimmermann, *Histochemistry*, **79**, 443 (1983).
14) D. J. Blears and S. S. Danyluk, *J. Am. Chem. Soc.*, **89**, 21 (1967).
15) A. N. Veselkov, L. N. Djimant, L. S. Karawajew, and E. L. Kulikov, *Stud. Biophys.*, **106**, 171 (1985).
16) E. Miethke and V. Zanker, *Z. Phys. Chem. (Frankfurt am Main)*, **18**, 375 (1958).
17) C. F. Bernasconi, "Relaxation Kinetics," Academic Press, New York (1976), p. 130.
18) A. R. Monahan and D. F. Blossey, *J. Phys. Chem.*, **74**, 4014 (1970).
19) C. F. Bernasconi, "Relaxation Kinetics," Academic Press, New York (1976), p. 15.
20) G. R. Haugen and W. H. Melhuish, *Trans. Faraday Soc.*, **60**, 386 (1964).
21) D. D. F. Shiano and J. M. Sturtevant, *Biochemistry*, **8**, 4910 (1969).
22) R. W. Gurney, "Ionic Process in Solution," McGraw-Hill Book Company, Inc, New York (1953), p. 177.
23) C. E. Johnson and F. A. Bovey, *J. Chem. Phys.*, **29**, 1012 (1958).
24) H. Strehlow and W. Knoche, "Fundamentals of Chemical Relaxation," in "Monographs in Modern Chemistry," ed by H. F. Ebel, Verlag Chemie, New York (1977), Vol. 10, pp. 101—105.
25) T. G. Dewey, P. S. Wilson, and D. H. Turner, *J. Am. Chem. Soc.*, **100**, 4550 (1978).
26) T. G. Dewey, D. A. Raymond, and D. H. Turner, *J. Am. Chem. Soc.*, **101**, 5822 (1979).

 © 1986 The Chemical Society of Japan Bull. Chem. Soc. Jpn., 59, 3399—3403 (1986)

Stopped-Flow Kinetic Study of the Complex Formation between Pyridoxal 5′-Phosphate and Bovine Serum Albumin

Kiyofumi MURAKAMI,* Yukio KUBOTA, Yasuo FUJISAKI, and Takayuki SANO†
Department of Chemistry, Faculty of Science, Yamaguchi University,
Yoshida 1677-1, Yamaguchi 753
†Department of Chemistry, Faculty of Science, Hiroshima University,
Higashisenda-machi, Naka-ku, Hiroshima 730
(Received May 15, 1986)

The complex formation between pyridoxal 5′-phosphate (PLP) and bovine serum albumin at pH=7.0 and 25 °C was characterized by four relaxation processes. The dependence of the reciprocal relaxation times upon reactant concentrations was found to be consistent with a mechanism in which a rapid bimolecular binding step is followed by three sequential isomerization steps. The eight rate constants for this mechanism were determined and then combined to calculate an overall equilibrium constant which is in agreement with the literature value. Absorption spectra of the complexes formed by the two faster steps were determined from absorbance changes associated with them; the spectrum corresponding to the first complex has two bands at 330 nm and 360 nm and an additional 410 nm band, while the spectrum corresponding to the second complex has a large single band at 375 nm. Comparing these spectra with those reported for other PLP-enzyme systems, we speculate that four steps in the proposed mechanism may correspond to the rapid formation of a carbinolamine, which is in very rapid equilibrium with a Schiff base form, followed by the deprotonation of the ring nitrogen, the formation of an ionic hydrogen-bonded Schiff base, and the final formation of a nonionic hydrogen-bonded Schiff base.

Pyridoxal 5′-Phosphate (PLP), which is an important cofactor of many enzymes, has been found to be transported in plasma by albumin molecules.[1] Dempsey and Christensen[2] have studied the binding of PLP with bovine serum albumin (BSA) and have shown that there are at least two kinds of strong binding sites, i.e., the primary site characterized by the 332 nm absorption band and the association constant $K_{ass}>10^6\ M^{-1}$ †† and the secondary site characterized by the 415 nm band and $K_{ass}\sim10^5\ M^{-1}$. The bindings occur at ε-amino lysine groups of the protein. On the basis of the irreducibility by $NaBH_4$ and the abundance of lysyl residues in the neighborhood of the primary binding site, Dempsey and Christensen[2] and Anderson et al.[3] have suggested that the structure of PLP bound to the primary site is not a Schiff base but a substituted aldimine. On the other hand, recent polarographic[4] and circular dichroism[5] studies have claimed that a nonionic hydrogen-bonded Schiff base structure is responsible for the primary complex. Although this structure seems to be plausible, the process of its formation has not been well elucidated.

The present study describes the kinetics of the interaction of PLP with BSA. Our goal is to establish an overall reaction mechanism for the binding of PLP to the primary site.

Experimental

Materials. Albumin (fraction V from bovine serum) was purchased from Wako Pure Chemical Industries and used without further purification. The dimer content was about 5%. The molar concentration of BSA was determined from the absorbance at 280 nm ($E^{1\%}_{1\,cm}=6.6$[6]), assuming its molecular weight of 67000. Pyridoxal 5′-phosphate was purchased from Tokyo Kasei and used without further purification. All the sample solutions were prepared in 0.1 M phosphate buffer at pH=7.00±0.02.

Methods. Absorption spectra were measured with a Union Giken SM401 Spectrophotometer. Kinetic measurements were performed using a Union Giken stopped-flow apparatus (RA401 and RA1100). In order to investigate the binding to the primary site all the measurements were carried out at P_0/L_0 (protein to ligand ratio)≧1. The temperature was controlled to be 25±0.2 °C.

Results and Discussion

Relaxations and Their Characteristics. The stopped-flow and spectrophotometric measurements revealed that the binding of PLP to BSA occurs through four distinct relaxations. Typical traces observed are shown in Fig. 1. Among these, the two slower relaxations have already been reported by Dempsey and Christensen.[2] They showed that an increase of absorbance around 415 nm within 100 s is followed by a very slow increase of that at 332 nm with a loss of the 415 nm band, exhibiting an apparent isosbestic point at 350 nm. However, the two faster relaxations have not been reported so far.

The relaxation time (τ) for each relaxation was determined from a semi-logarithmic plot of the trace. Figures 2—5 show the concentration dependence of the reciprocal relaxation times. As can be seen in Figs. 4(A) and 5(A), the concentration dependence of τ^{-1} at $L_0=5\times10^{-5}$ M for each of the two slower relaxations exhibits a sharp increase within a narrow range of the protein concentration above $P_0=5\times10^{-5}$ M. Only with these data it is difficult to perform an accurate determination of kinetic parameters. Hence, the concentration dependence of τ^{-1} at $P_0/L_0=1$ (Figs.

†† 1 M=1 mol dm^{-3}.

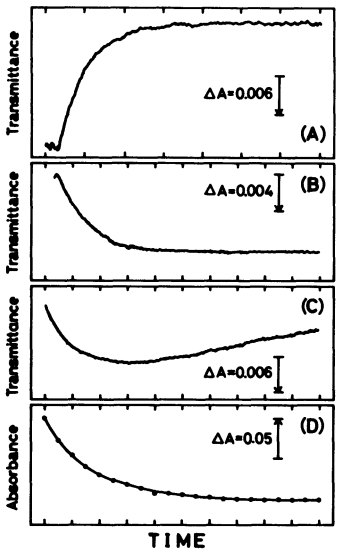

Fig. 1. Typical traces of the reaction observed after the mixing of PLP (1×10^{-4} M) and BSA (1×10^{-4} M). (A): Transmittance change at 390 nm. (B): Transmittance change at 390 nm. (C): Transmittance change at 415 nm. (D): Absorbance change at 415 nm. The abscissa scale is (A) 2.5 ms per division, (B) 100 ms per division, (C) 100 s per division, and (D) 1 h per division. The three faster relaxations were observed by the stopped-flow method, while the fourth one by spectrophotometry. The arrow designated for each trace shows the magnitude and the direction of the positive absorbance change.

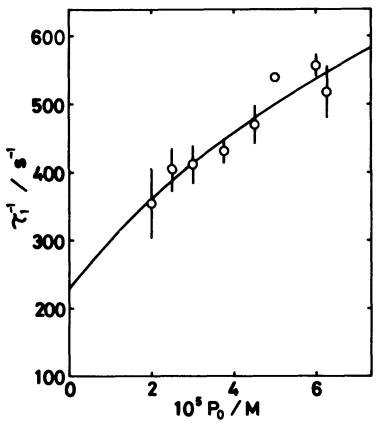

Fig. 2. Concentration dependence of τ_1^{-1} at P_0/L_0 (protein to ligand ratio)=1. The abscissa indicates the initial concentration after mixing. The solid line represents the theoretical curve calculated using the equilibrium and rate constants listed in Table 1. Legends are also the case for Figs. 3—5.

4(B) and 5(B)), which exhibits a more gradual increase with protein concentration, was also measured and analyzed together with the previous data. τ_1^{-1} increases progressively with an increase in the protein concentration, while τ_2^{-1}, τ_3^{-1}, and τ_4^{-1} increase at low concentrations but tend toward constant values at

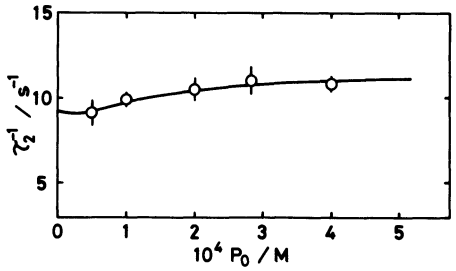

Fig. 3. Concentration dependence of τ_2^{-1} at $L_0=5\times10^{-5}$ M.

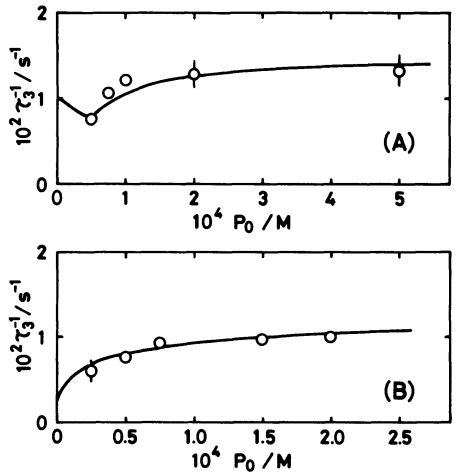

Fig. 4. Concentration dependence of τ_3^{-1}. (A) Concentration dependence at $L_0=5\times10^{-5}$ M. (B) Concentration dependence at $P_0/L_0=1$.

high concentrations. This behavior suggests a reaction scheme that a bimolecular rapid binding step is followed by three sequential isomerization reaction steps.

Reaction Scheme. In order to interpret the concentration dependence of the reciprocal relaxation times, the following model is examined.

$$\mathbf{L}+\mathbf{P} \underset{k_{-1}}{\overset{K_1\ k_1}{\rightleftarrows}} \mathbf{C}_1 \underset{k_{-2}}{\overset{K_2\ k_2}{\rightleftarrows}} \mathbf{C}_2 \underset{k_{-3}}{\overset{K_3\ k_3}{\rightleftarrows}} \mathbf{C}_3 \underset{k_{-4}}{\overset{K_4\ k_4}{\rightleftarrows}} \mathbf{C}_4, \tag{1}$$

where **L**, **P**, and **C** denote free ligand, free protein and complex species, respectively, and K_i, k_i, and k_{-i} are the equilibrium constant, the forward and backward rate constants of the ith step. This mechanism predicts four relaxation times, defined by

$$\tau_1^{-1} = k_1(L+P) + k_{-1}, \tag{2}$$

$$\tau_2^{-1} = k_2\frac{K_1(L+P)}{1+K_1(L+P)} + k_{-2}, \tag{3}$$

$$\tau_3^{-1} = k_3\frac{K_1K_2(L+P)}{1+K_1(1+K_2)(L+P)} + k_{-3}, \tag{4}$$

$$\tau_4^{-1} = k_4\frac{K_1K_2K_3(L+P)}{1+K_1\{1+K_2(1+K_3)\}(L+P)} + k_{-4}, \tag{5}$$

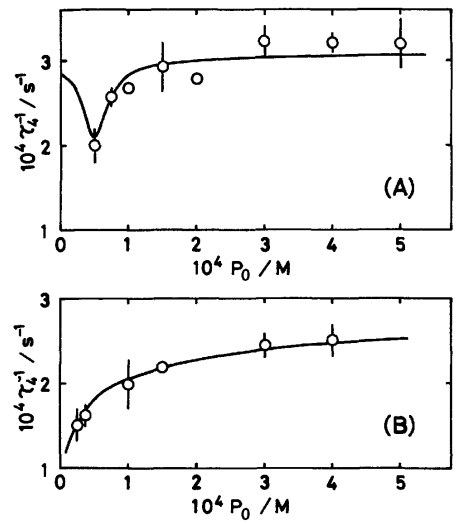

Fig. 5. Concentration dependence of τ_4^{-1}. (A) Concentration dependence at $L_0=5\times10^{-5}$ M (B) Concentration dependence at $P_0/L_0=1$.

where L and P, respectively, denote free ligand and free protein concentrations at the end of each step and where the rapid equilibrium of the preceding step has been assumed in each case, since the relaxation times observed for the present system are well separated each other (Fig. 1).

The data of Figs. 2—5 were fitted to Eqs. 2—5 by linear or nonlinear regression analysis, using the following protocol. First, an arbitrary K_1 was chosen to calculate the equilibrium concentrations, L and P, at the end of the first step. Then the best straight-line fit of τ_1^{-1} vs. $(L+P)$ was found to obtain k_1, k_{-1}, and K_1. The procedure was iterated until all the parameters converge. The estimate of K_1 was used with Eq. 3 to fit the data of Fig. 3 and to obtain k_2, k_{-2}, and K_2. The estimated values for K_1 and K_2 were used with Eq. 4 to obtain k_3, k_{-3}, and K_3 from the data of Fig. 4. Finally, k_4, k_{-4}, and K_4 were determined using Eq. 5 and the data of Fig. 5. The solid lines in Figs. 2—5 indicate the best least-squares fits, and the kinetic parameters obtained are summarized in Table 1.

The overall association constant for Scheme 1 is given by

$$K_{ass} = K_1(1+K_2+K_2K_3+K_2K_3K_4). \quad (6)$$

From the kinetic data of Table 1, we calculate an overall association constant of 5.27×10^6 M^{-1}. This value is consistent with the prediction by Dempsey and Christensen[2] that K_{ass} for the primary site should be larger than 1×10^6 M^{-1}. Independently of the first step, K_1 can be estimated by nonlinear regression analysis using Eq. 3 and the data of Fig. 3. The result is $K_1=2.02\times10^4$ M^{-1}, a value in excellent agreement with the estimate of K_1 in Table 1. The agreement of these values lends considerable confidence to the validity of Scheme 1 as a plausible reaction scheme.

Table 1. Equilibrium and Rate Constants Associated with the Mechanism of Eq. 1

Step	K_i	k_i	$\frac{k_{-i}}{s^{-1}}$
1	1.94×10^4 M^{-1}	4.41×10^6 M^{-1} s^{-1}	227
2	0.702	4.77 s^{-1}	6.80
3	13.5	3.03×10^{-2} s^{-1}	2.25×10^{-3}
4	27.5	3.49×10^{-4} s^{-1}	1.27×10^{-5}

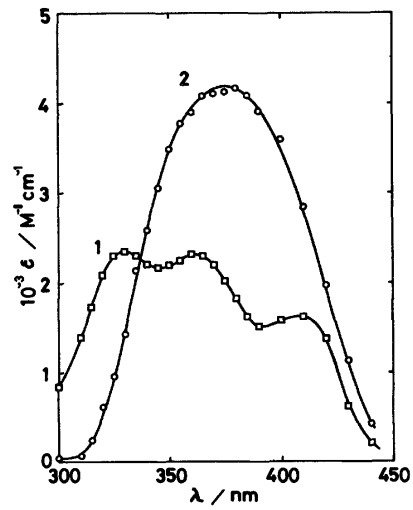

Fig. 6. Absorption spectra of C_1 (curve 1) and C_2 (curve 2).

Structures of the Intermediate Species. To investigate the structures of the intermediate species in Scheme 1, the molar extinction coefficients were determined as follows. At the end of the first step, the absorbance of the sample at a given wavelength can be expressed by

$$A_1 = \varepsilon_L L + \varepsilon_P P + \varepsilon_1 C_1, \quad (7)$$

where ε_L, ε_P, and ε_1 are molar extinction coefficients of the free ligand, the free protein and the first complex, respectively. Using the change in absorbance associated with the first step (ΔA_1), A_1 can also be expressed as

$$A_1 = A_0 + \Delta A_1, \quad (8)$$

where A_0 is the absorbance of the sample after mixing but before initiation of the reaction. Combining Eqs. 7 and 8, ε_1 becomes

$$\varepsilon_1 = \frac{A_0+\Delta A_1-\varepsilon_L L-\varepsilon_P P}{C_1}. \quad (9)$$

In this equation, ε_L, ε_P, and A_0 can be estimated from spectrophotometric data for the reactants, and the concentrations L, P, and C_1 can be calculated with the value of K_1 in Table 1. ΔA_1 was determined taking into account the dead time of the apparatus. Sub-

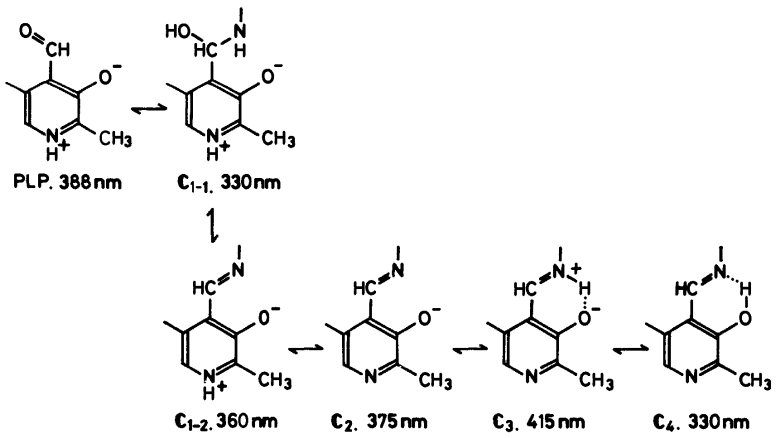

Fig. 7. Mechanism for the isomerization of PLP at the primary site.

stitution of these values into Eq. 9 yields the molar extinction coefficient of C_1 (ε_1). The molar extinction coefficient of C_2 (ε_2) was also determined in a similar manner. The absorption spectra of C_1 and C_2 thus obtained are displayed in Fig. 6. The absorption spectra of C_1 (curve 1) has two maxima at 330 nm and 360 nm and a small peak around 410 nm, suggesting the existence of more than one spectral species, while that of C_2 (curve 2) exhibits a single strong band having a peak at 375 nm. These 360 and 375 nm bands have not been reported for the PLP-albumin system.

Considering the present kinetic data and other results reported so far, we propose a mechanism for the complex formation at the primary site (Fig. 7). Three possible structures, i.e., substituted aldimine,[2,7] carbinolamine[2] and nonionic hydrogen-bonded Schiff base,[4,5,8] have been proposed for 330 nm band. Among these the carbinolamine (C_{1-1}) is the most suitable structure for the 330 nm band in curve 1 of Fig. 6 because it is an intermediate structure[9] for a subsequent Schiff base formation. The 360 nm band, which has been observed as a stable species for PLP-aspartate β-decarboxylase[10] and PLP-aspartate aminotransferase[11-15] systems, is now generally recognized as due to a Shiff base structure (C_{1-2}). Considering that the relaxation time for the formation of C_{1-1} was indistinguishable from that of C_{1-2}, it seems reasonable to conclude that these structures are in very rapid equilibrium with each other.

Matsushima and Martell[16] have observed a single strong band for pyridoxylidenevaline (373 nm) and pyridoxal phosphate valine Schiff base (350 nm) in alkaline methanol solutions, and assigned the band to the π_1 band of the anionic form of the Schiff base. The resemblance of the present absorption spectrum (curve 2 in Fig. 6) to those bands suggests that the anionic Schiff base structure is responsible for C_2.

The 415 nm band is attributed to an ionic hydrogen bonded Schiff base structure (C_3), with or without protonation of the ring nitrogen.[3,4,16,17] Considering that the ring nitrogen is already deprotonated in the previous step ($C_{1-2} \rightarrow C_2$), it is reasonable to expect that the ring nitrogen of C_3 is deprotonated rather than protonated.[8] The appearance of the band around 410 nm in curve 1 of Fig. 6 implies the existence of another path of the rapid formation of an ionic hydrogen-bonded Schiff base at a different site, which may correspond to the secondary site.

Based on the irreducibility of the complex by $NaBH_4$ and the presence of three lysyl residues in the neighborhood of the primary binding site, Dempsey and Christensen[2] and Anderson et al.[3] have suggested a substituted aldimine, in which the ring nitrogen is protonated, for the final and stable complex (330 nm band). However, the mechanism shown in Fig. 7 suggests that the nonionic hydrogen-bonded Schiff base in hydrophobic environment rather than the substituted aldimine is plausible for C_4. It is likely that the hydrophobic environment causes the irreducibility of the Schiff base by $NaBH_4$. This structure is consistent with the conclusion obtained from polarographic studies[4] and circular dichroism and spectrophotometric investigations.[5,8] The proposed mechanism (Fig. 7) indicates that the structure of bound PLP changes, step by step, from the polar form to the nonpolar one. Perhaps PLP first binds to a polar site at the surface of the protein and migrates to a more hydrophobic region.

The authors wish to express their thanks to Professor Tatsuya Yasunaga of Kinki University for his helpful discussions.

References

1) L. Lumeng, R. E. Brashear, and Y.-K. Li, *J. Lab. Clin. Med.*, **84**, 334 (1974).

2) W. B. Dempsey and H. N. Christensen, *J. Biol. Chem.*, **237**, 1113 (1962).

3) J. A. Anderson, H.-F. W. Chang, and C. J. Granjean, *Biochemistry*, **10**, 2408 (1971).

4) M. Cortijo, J. S. Jimenez, and J. Llor, *Biochem. J.*, **171**, 497 (1978).
5) S. Shimomura and T. Fukui, *J. Biochem.*, **81**, 1781 (1977).
6) E. J. Cohn, W. L. Huges, Jr., and J. H. Weare, *J. Am. Chem. Soc.*, **69**, 1753 (1947).
7) A. B. Kent, E. G. Krebs, and E. H. Fischer, *J. Biol. Chem.*, **232**, 549 (1958).
8) M. C. Hilak, B. J. M. Harmsen, J. J. M. Joordens, and G. A. J. Van Os, *Int. J. Peptide Protein Res.*, **7**, 411 (1975).
9) D. S. Auld and T. C. Bruice, *J. Am. Chem. Soc.*, **89**, 2083 (1967).
10) E. M. Wilson and A. Meister, *Biochemistry*, **5**, 1166 (1966).
11) W. T. Jenkins and I. W. Sizer, *J. Am. Chem. Soc.*, **79**, 2655 (1957).
12) Y. N. Breusov, V. I. Ivanov, M. Y. Karpeisky, and Y. V. Morozov, *Biochim. Biophys. Acta*, **92**, 388 (1964).
13) M. Martinez-Carrion, D. C. Tiemeier, and D. L. Peterson, *Biochemistry*, **9**, 2574 (1970).
14) S. M. Bonsib, R. C. Harruff, and W. T. Jenkins, *J. Biol., Chem.*, **250**, 8635 (1975).
15) D. E. Metzler, *Adv. Enzymol. Relat. Areas. Mol. Biol.*, **50**, 1 (1979).
16) Y. Matsushima and A. E. Martell, *J. Am. Chem. Soc.*, **89**, 1322 (1967).
17) G. F. Johnson, J.-I. Tu, M. L. S. Bartlett, and D.J. Graves, *J. Biol. Chem.*, **245**, 5560 (1970).

Fluorescence and Nonradiative Relaxation from Vibronic Levels of S_1 Pyrimidine: Effects of Molecular Rotation and Intramolecular Vibrational Redistribution

Osamu Sekiguchi,† Nobuhiro Ohta, and Hiroaki Baba*
Division of Chemistry, Research Institute of Applied Electricity, Hokkaido University, Sapporo 060
(Received May 19, 1986)

Emission characteristics of pyrimidine vapor which were measured after excitation into various S_1 vibronic levels with relatively low excess vibrational energies (ΔE) below 2650 cm^{-1} were found to depend markedly upon ΔE. The emission from a vibronic level with $\Delta E<1000$ cm^{-1} (e.g., $6a^1$ or 1^1) is sharp and attributable to the fluorescence from the initially prepared vibronic level (IPL), and that from a vibronic level with $\Delta E>1000$ cm^{-1} (e.g., 12^1, $6a^2$, or 12^2) involves broad fluorescence besides the IPL fluorescence. At low pressure, the broad fluorescence consists of fast and slow components with lifetimes comparable to those for the corresponding components of the IPL fluorescence. The broad fluorescence exhibits another slow component which is characterized by a less tendency to undergo collisional quenching. The quantum yield of the slow component of the IPL fluorescence clearly depends upon molecular rotation, whereas that of the broad fluorescence appears to show little or no rotational-level dependence. On the basis of these observations, the broad fluorescence is assigned to the one originating from S_1 vibronic levels that can be reached directly from the IPL through intramolecular vibrational redistribution (IVR) or indirectly via triplet levels. There exists no evidence to show that the IVR is affected by molecular rotation.

When an isolated molecule is optically excited, the excitation energy may be transferred nonradiatively from the initially prepared vibronic level to the other isoenergetic levels through redistribution of the vibrational energy.[1-4] Understanding of this sort of intramolecular vibrational redistribution (IVR) is important not only in elucidating intramolecular dynamics but also in exploring the possibility of state selective chemistry. The IVR phenomena have been investigated extensively within the first excited singlet state (S_1) under bulk gas conditions at room temperature or ultracold supersonic jet conditions.[3,4] Most of these investigations were performed with aromatic hydrocarbons and their alkyl or halogen derivatives,[3,4] all of which belong to the statistical limit case in radiationless electronic relaxation.

The IVR process is known to occur usually at vibronic levels with relatively high excess vibrational energies, ΔE. Thus, IVR occurs at $\Delta E=3000$ cm^{-1} in benzene itself[5] and at $\Delta E=2000$ cm^{-1} in *p*-difluorobenzene and *p*-fluorotoluene,[6] though IVR can be recognized at a small ΔE value of 530 cm^{-1} in substituted benzenes with a long side chain.[4,7] The times required for IVR range from sub-picosecond to microsecond, but those reported in recent papers are mostly of the order of picosecond.[8] The anharmonic interaction is considered to induce IVR, but the Coriolis coupling is sometimes regarded as responsible for IVR. Recently, Riedle et al. showed that the Coriolis coupling plays an important role in IVR in the third channel region of benzene.[9]

Pyrimidine is known to have an intermediate-case level structure and gives fast and slow components of fluorescence under collision-free conditions.[10,11] It has been established that, so far as the fluorescence resulting from excitation at the 0-0 absorption band or a lower vibronic band is concerned, the characteristics of the slow fluorescence component of an intermediate-case molecule undergo considerable variation across the rotational contour.[12-15] On the other hand, little attention has been directed to IVR in the intermediate-case molecules except for the work by Lim and his collaborators, who observed the IVR induced by excitation at the 12_0^2 absorption band of pyrimidine.[16]

In the present study, fluorescence and nonradiative relaxation in pyrimidine vapor have been observed after exciting the molecule into various S_1 vibronic levels with relatively low excess vibrational energies ranging from 600 to 2650 cm^{-1}. The purpose of the study is twofold. First, attention is given to the change in the effect of molecular rotation on electronic or vibrational relaxation with excess energy. Second, an attempt is made to elucidate the kinetic mechanism of the occurrence of IVR. It will be shown in this paper that, in the case of pyrimidine, IVR appears to take place at vibronic levels whose energies are much lower than usually expected.

Experimental

Pyrimidine obtained from Aldrich Chemical Co. was purified by repeated vacuum sublimation. Commercially available sulfur hexafluoride (SF_6) from Seitetsu Chemicals was used as an inert foreign gas without further purification. The pressure of pyrimidine was determined by measuring the absorption intensity or by using a capacitance manometer (MKS Baratron type 170).

All the optical measurements were carried out at room temperature. Absorption and fluorescence spectra, fluores-

† Present address: Department of Industrial Chemistry, Faculty of Engineering, Shinshu University, Nagano 380.

cence excitation spectra, and fluorescence decays were measured with a laser spectrophotometric system.[17] The procedures for these measurements are essentially the same as those reported in previous papers.[13,17] In the spectrophotometric system, a pulsed dye laser (Molectron DL 14) is pumped by a nitrogen laser (Molectron UV 22). The frequency of the dye laser is doubled by a KDP crystal to generate UV laser pulses, which are used for exciting the sample. The UV laser pulses have a linewidth of 0.5 cm^{-1} and a duration of 3 ns. Emission measurements were made with a 3.5 cm cubic quartz cell. Absorption spectra and fluorescence-excitation spectra were measured simultaneously. The excitation spectra were obtained by monitoring the fluorescence emission dispersed by a grating monochromator (Nikon G250) and were corrected for fluctuation of the laser intensity. A relative quantum yield spectrum is derived as a ratio of a corrected excitation spectrum to the corresponding absorption spectrum. No correction was made for the spectral sensitivity of the detecting system. Fluorescence decays were measured with a single photon counting lifetime apparatus equipped with a time-to-amplitude converter. The lifetimes of the fast fluorescence of pyrimidine were determined by the convolution method.

Results

The emission spectrum of pyrimidine vapor changes markedly in shape with the excess vibrational energy (ΔE) of the S_1 vibronic level excited. Figure 1 shows the emission spectra from 0^0, $6a^2$, and $6a^1 12^2$ levels of S_1 pyrimidine at a low pressure of 80.8 mTorr.† See Table 1 for the values of ΔE for the individual levels.[18,19] When ΔE is small (Fig. 1(a)), the emission spectrum consists of sharp fluorescence bands which are due to vibronic transitions starting from the initially prepared vibronic level (IPL). As ΔE increases, the intensity of the IPL fluorescence decreases, and a broad, structureless emission appears instead at longer wavelengths (Fig. 1(b)). From now on, the latter emission will be referred to as "broad fluorescence." It is seen in Fig. 1(c) that the emission from the $6a^1 12^2$ level having a large ΔE value consists almost solely of the broad fluorescence.

Thus, according to the results of the present study, the fluorescence from vibronic levels with $\Delta E < 1000$ cm^{-1} is attributable solely to the IPL fluorescence, while that from vibronic levels with $\Delta E > 1000$ cm^{-1} involves the broad fluorescence in addition to the IPL fluorescence. The features of the fluorescence and nonradiative relaxation from some representative vibronic levels in S_1 pyrimidine will be described in the following.

$6a^1$ Level (ΔE=613 cm^{-1}) and 1^1 Level (ΔE=941 cm^{-1}). Absorption, fluorescence excitation, and fluorescence quantum yield spectra at a low pressure are shown in Fig. 2(a) for the rotational contour of the $6a_0^1$ absorption band. It was found that the excitation spectrum does not change in shape and position with the fluorescence band monitored. The quantum yield

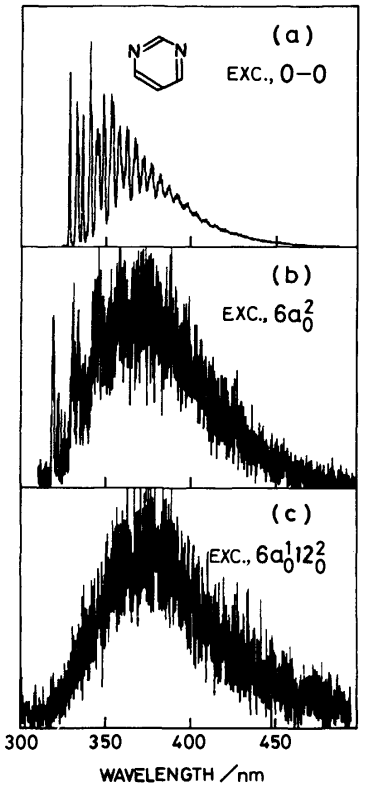

Fig. 1. Emission spectra of pyrimidine at 80.8 mTorr. Excitation bands: (a) 0—0; (b) $6a_0^2$; (c) $6a_0^1 12_0^2$. Spectral resolution is 0.6 nm in every case.

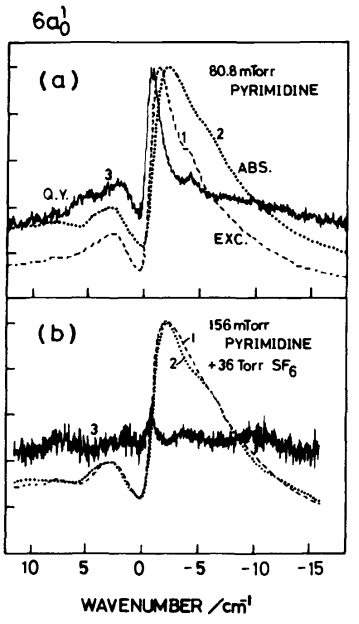

Fig. 2. Spectra for the $6a_0^1$ band of pyrimidine: (1,----) fluorescence excitation spectrum; (2,·····) absorption spectrum; (3,——) fluorescence quantum yield spectrum. Sample vapors: (a) 80.8 mTorr of pyrimidine; (b) 156 mTorr of pyrimidine plus 36 Torr of SF_6. The band origin is denoted by 0.

† 1 Torr≈133.322 Pa.

spectrum gives a prominent peak for excitation frequencies near the band origin, that is, for low values of the total rotational angular momentum quantum number J', the prime referring to the excited state S_1; furthermore, the yield is found to decrease with increasing J'. As is seen in Fig. 2(b), at high pressure, the excitation and absorption spectra agree with each other, giving a flat fluorescence quantum yield spectrum.

Experimental results similar to those given in Figs. 2(a) and 2(b) have been obtained with the 1_0^1 absorption band. Thus, with respect to the rotational-level dependence of fluorescence, the situation in the $6a_0^1$ and 1_0^1 bands is essentially the same as that in the 0-0 band.[13] Note that $\Delta E<1000\,cm^{-1}$ for the $6a^1$ and 1^1 levels.

$6a^2$ Level (ΔE=1291 cm^{-1}). The fluorescence characteristics change in many respects when ΔE becomes higher than $1000\,cm^{-1}$. Figures 3(a) and 3(b) show fluorescence spectra obtained by excitation at two different positions within the rotational contour of the $6a_0^2$ absorption band of pyrimidine at a low pressure of 80.8 mTorr. In either case, both the IPL and the broad fluorescence appear. However, the fluorescence intensity distribution in Fig. 3(b) is different from the one in Fig. 3(a). In fact, the relative contribution of the IPL fluorescence is larger in Fig. 3(b) than in Fig. 3(a).

Reflecting the change in intensity distribution of the fluorescence spectrum with the rotational level excited, the excitation spectrum at low pressure changes in shape with the region of the fluorescence monitored, as illustrated in Fig. 4. The excitation spectrum in Fig. 4(b), which is related (mainly) to the broad fluorescence, resembles the absorption spectrum more closely than does the excitation spectrum in Fig. 4(a) related to the IPL fluorescence.

The quantum yield spectra for the IPL and broad fluorescence, shown in Figs. 4(a) and 4(b) respectively, vary across the rotational contour of the $6a_0^2$ band with a peak near the band origin. However, the variation of the quantum yield is obviously small in the case of the broad fluorescence. The IPL fluorescence is considered to be involved, to some extent, in the emission at 390 nm, i.e., at the monitoring wavelength in Fig. 4(b). Then the variation of the quantum yield for the broad fluorescence alone should be even smaller than what is seen in Fig. 4(b). It may thus be said that the actual quantum yield of the broad fluorescence will show little or no rotational-level dependence.

Extrapolating spectral data at low pressures, including those given in Fig. 4, to zero pressure, we have reached the conclusion that the broad fluorescence exists even at zero pressure; in other words, the

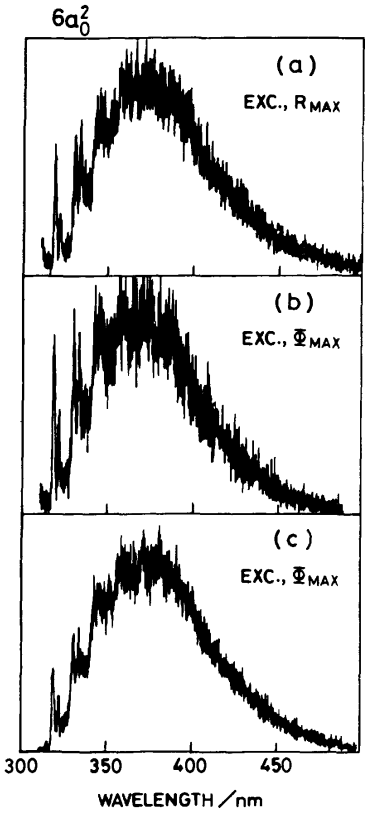

Fig. 3. Fluorescence spectra from the $6a^2$ level of pyrimidine. Sample vapors: (a, b) 80.8 mTorr of pyrimidine; (c) 156 mTorr of pyrimidine plus 36 Torr of SF_6. Excitation positions in the $6a_0^2$ band: (a) maximum of the R branch (R_{max}); (b, c) maximum of the quantum yield spectrum (Φ_{max}).

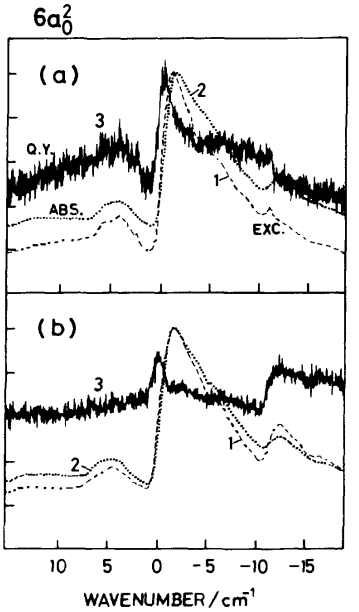

Fig. 4. Spectra for the $6a_0^2$ band of pyrimidine at 80.8 mTorr: (1,----) fluorescence excitation spectrum; (2,·····) absorption spectrum; (3,——) fluorescence quantum yield spectrum. Excitation and quantum yield spectra: (a) obtained by monitoring selectively the IPL fluorescence at 321 nm; (b) obtained by monitoring mainly the broad fluorescence at 390 nm. The band origin is denoted by 0.

broad fluorescence occurs as an intramolecular phenomenon.

Let us now turn to pyrimidine vapor at high total pressure. Figure 3(c) shows the fluorescence spectrum excited at the $6a_0^2$ absorption band of pyrimidine (156 mTorr) in the presence of 36 Torr of SF_6. Here the excitation position corresponds to the maximum of the quantum yield spectrum; it should be noted, however, that the fluorescence spectrum was found to be independent of excitation position within the $6a_0^2$ band. It is seen in Fig. 3(c) that the broad fluorescence appears at high pressure also. The excitation spectra at high pressure (Fig. 5) obtained by monitoring the fluorescence at 321 and 390 nm agree fairly well with the absorption spectrum, so that in both cases the quantum yield spectra are nearly flat over the rotational contour.

Figures 6(a) and 6(b) show the decays of the IPL and broad fluorescence following excitation within the $6a_0^2$ band at a pressure of 80.8 mTorr. The decay curves of Figs. 6(b) and 6(c) were obtained under the same conditions except for the time scales. It is seen from Fig. 6(b) that the broad fluorescence also involves fast and slow components which are analogous to the fast and slow components of the IPL fluorescence found in Fig. 6(a). In each of the IPL and broad fluorescence emissions, the fast and slow components will be called component I and component II, respectively, for the sake of simplicity. Note that, with the time resolution employed in the case of Fig. 6, the photoelectron pulses corresponding to the fast component of fluorescence fall on the first and second channels in (a) and (b), and on the first channel in (c).

The lifetime of the slow component II (τ_{II}) at 80.8 mTorr is found to be 72 ns from Fig. 6(a) for the IPL fluorescence and 81 ns from Fig. 6(b) for the broad fluorescence. Allowing for experimental error, however, the two lifetime values should be regarded as practically equal to each other (vide infra).

The broad fluorescence is thus similar to the IPL fluorescence in the lifetime of component II and also in the ratio of the amount of component I to that of component II. However, as is seen in Fig. 6(c), the broad fluorescence involves another slow component, which will be referred to as component III. The lifetime of component III (τ_{III}) at 80.8 mTorr is about 470 ns, which is much longer than τ_{II} at the same pressure.

The reciprocal lifetimes (τ^{-1}) for components II and III of the broad fluorescence as well as that for component II of the IPL fluorescence are plotted against pressure in Fig. 7. Allowing for experimental error, in the pressure range concerned, one cannot find any appreciable difference in lifetime between

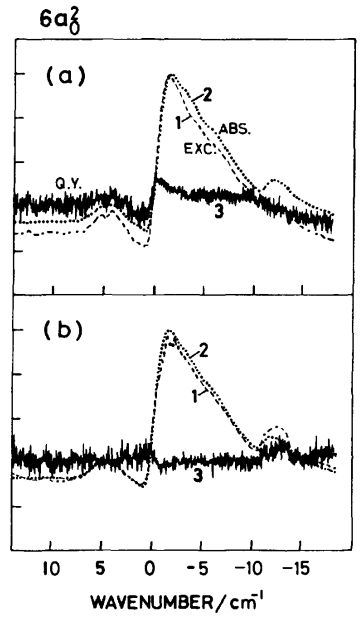

Fig. 5. Spectra for the $6a_0^2$ band of pyrimidine at 156 mTorr in the presence of 36 Torr of SF_6: (1,——) fluorescence excitation spectrum; (2,·····) absorption spectrum; (3,——) fluorescence quantum yield spectrum. Excitation and quantum yield spectra: (a) obtained by monitoring selectively the IPL fluorescence at 321 nm; (b) obtained by monitoring mainly the broad fluorescence at 390 nm. The band origin is denoted by 0.

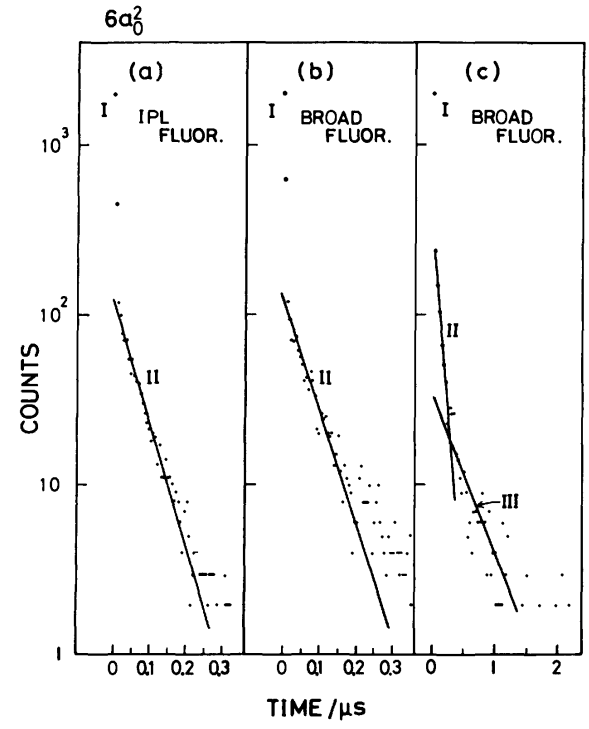

Fig. 6. Fluorescence decays for pyrimidine at 80.8 mTorr after excitation at the maximum of the R branch of the $6a_0^2$ band: (a) obtained by monitoring selectively the IPL fluorescence at 319.5 nm; (b, c) obtained by monitoring mainly the broad fluorescence at 390 nm under the same conditions except for the time scales.

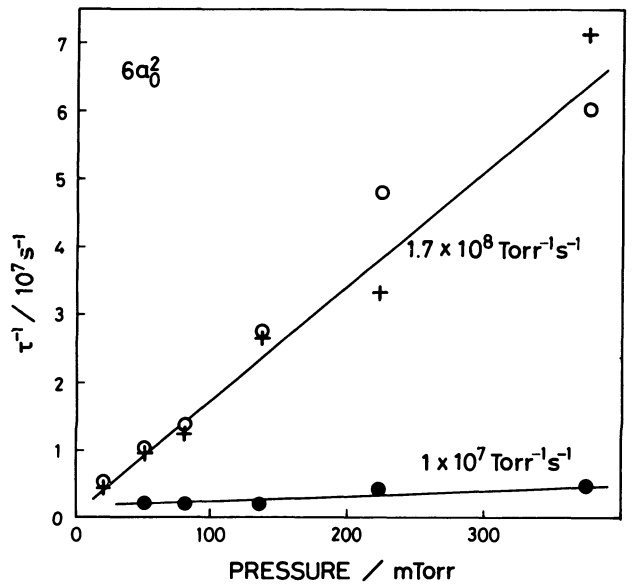

Fig. 7. Plots of τ^{-1} against pressure for $6a^2$ of pyrimidine: O, component II of the IPL fluorescence; +, component II of the broad fluorescence; ●, component III of the broad fluorescence.

components II of the IPL and broad fluorescence, and these two kinds of components II are quenched in essentially the same manner with increasing pressure. Thus, in either case, the quenching rate constant is evaluated to be about 1.7×10^8 Torr^{-1} s^{-1}, which is more than one order of magnitude larger than the hard sphere collision rate constant ($k_{hsc}\approx1\times10^7$ Torr^{-1} s^{-1}). This indicates that the quenching of components II results from a long-range, weak collision leading to rotational relaxation, as in the case of the slow fluorescence from the 0^0 level.[13]

Component III of the broad fluorescence, on the other hand, is quenched with a rate constant of 1×10^7 Torr^{-1} s^{-1}, which is equal to k_{hsc}. It can thus be said that, among the slow fluorescence components, component III is characterized by a less tendency to undergo collisional quenching. It is to be noted that the lifetime values for components II and III of the broad fluorescence are fairly close to each other at pressures lower than 10 m Torr.

It may be noted here that the occurrence of component I in the decay of the broad fluorescence (Fig. 6) is consistent with the observation that the broad fluorescence exists even at such high pressures that the slower components, II and III, are almost fully quenched.

12^1 Level (ΔE=1012 cm^{-1}). The ΔE value for this level is smaller than that for the $6a^2$ level, but is larger than 1000 cm^{-1}. Figure 8 shows excitation, absorption, and quantum yield spectra for the 12_0^1 band. Actually, the band appears to consist of two overlapping vibronic bands. This situation is clearer in the excitation spectrum obtained under supersonic

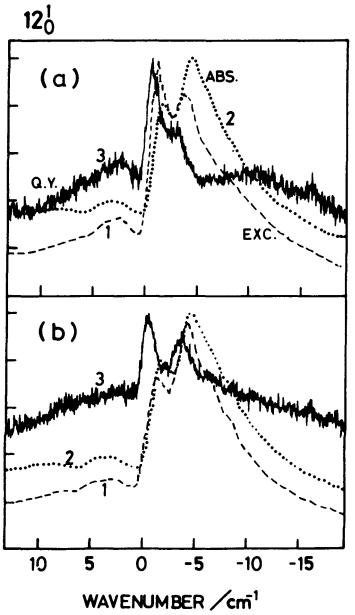

Fig. 8. Spectra for the 12_0^1 band of pyrimidine at 80.8 mTorr: (1,----) fluorescence excitation spectrum; (2,·····) absorption spectrum; (3,——) fluorescence quantum yield spectrum. Excitation and quantum yield spectra: (a) obtained by monitoring selectively the IPL fluorescence at 321 nm; (b) obtained by monitoring mainly the broad fluorescence at 390 nm. The band origin is denoted by 0.

jet conditions.[20] It is seen from Fig. 8(a) that the quantum yield for the IPL fluorescence varies greatly across the rotational contour. As in the case of the $6a_0^2$ band, the variation of the quantum yield for the broad fluorescence (Fig. 8(b)) is small compared with that for the IPL fluorescence.

The fluorescence decay after excitation into the 12^1 level is similar in nature to the decay after excitation into the $6a^2$ level. The IPL fluorescence and the broad fluorescence decay in similar manners, and both involve components I and II. The lifetimes of components II of the two types of fluorescence are nearly equal to each other at any pressure concerned in the present study. On the other hand, in the case of the 12^1 excitation, component III which is characterized by a less tendency to undergo collisional quenching makes only a negligibly small contribution to the broad fluorescence.

12^2 Level (ΔE=2025 cm^{-1}). Figures 9(a) and 9(b) show, respectively, decay curves for the IPL and broad fluorescence at two different pressures after excitation within the 12_0^2 band. It is seen that the IPL fluorescence consists of components I and II. The broad fluorescence also consists of fast and slow components. The former corresponds to component I. On the other hand, inspection of the decay curves given in Figs. 9(a) and 9(b) clearly shows that the slow component of the broad fluorescence is less liable to be quenched by collisions than component II of the IPL fluorescence,

indicating that the slow component of the broad fluorescence corresponds to component III. Although a small amount of component II can be detected in a decay curve of the broad fluorescence obtained at a higher time resolution, it may be said that the broad fluorescence resulting from excitation into the 12^2 level consists mainly of components I and III. One can thus conclude that the contribution of component III to the broad fluorescence notably increases with increasing ΔE.

The lifetimes of the fast component (component I),

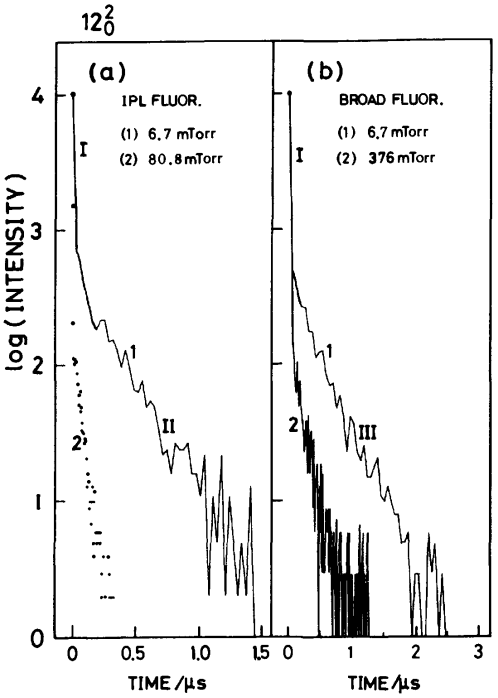

Fig. 9. Fluorescence decays for pyrimidine after excitation at the maximum of the 12_0^2 band: (a) obtained by monitoring the IPL fluorescence at 308.6 nm for (1) 6.7 and (2) 80.8 mTorr of pyrimidine vapor; (b) obtained by monitoring the broad fluorescence at 390 nm for (1) 6.7 and (2) 376 mTorr of pyrimidine vapor.

Table 1. Excess Vibrational Energies (ΔE), Lifetimes of the Fast Component (τ_I) of the IPL and Broad Fluorescence, and k_{SU} for Various Vibronic Levels in S_1 Pyrimidine

Vibronic level	ΔE[a] / cm^{-1}	τ_I/ns IPL	τ_I/ns Broad	k_{SU} / 10^8 s^{-1}
0^0	0			
$6a^1$	613			
1^1	941			
12^1	1012	1.5	2.0	1.7
$6a^2$	1291	0.9	1.3	3.4
$6a^112^1$	1629	1.2	1.4	1.2
12^2	2025	0.8	1.4	5.4
$6a^112^2$	2642			

a) From Refs. 11, 18, and 19.

τ_1, were obtained from decay curves for high-pressure samples by the convolution method. The results are summarized in Table 1 for the IPL and broad fluorescence emitted from some vibronic levels including 12^1, $6a^2$, and 12^2. For any level listed in Table 1, the value of τ_1 for the broad fluorescence is larger than the corresponding τ_I value for the IPL fluorescence.

Discussion

The results of the present experiments indicate that the fluorescence of pyrimidine vapor optically excited into an S_1 vibronic level with $\Delta E > 1000$ cm^{-1} involves broad fluorescence besides the IPL fluorescence. Each of the two types of fluorescence gives fast and slow components, I and II. The broad fluorescence gives another slow component, III, which is less liable to undergo collisional quenching than component II; the ratio of the yield of component III to that of component II increases with increasing ΔE.

In the following discussion, we shall give special attention to the mechanism by which the broad fluorescence is generated. It has turned out that general treatment of this subject is mathematically too difficult. Therefore, we first treat three simplified and rather extreme cases on the basis of kinetic schemes shown in Fig. 10. Here, solid and wavy arrows represent radiative (R) and nonradiative (NR) processes, respectively. S is the initially prepared vibronic level (IPL) belonging to S_1. U denotes the emitting levels of the broad fluorescence; it is assumed that these levels also belong to S_1, as will be shown

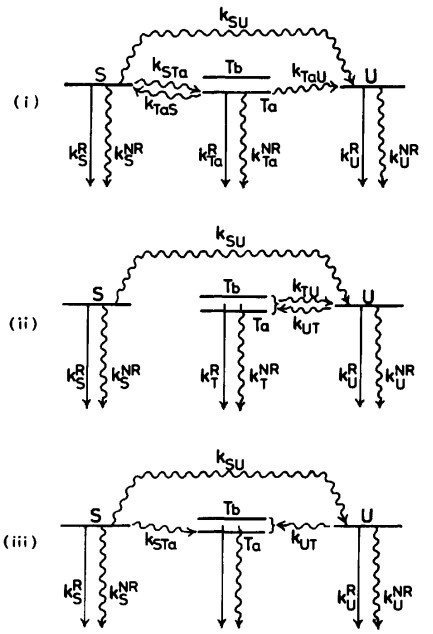

Fig. 10. Kinetic schemes and various rate constants (k) for pyrimidine. R and NR refer to radiative and nonradiative processes, respectively. See text for other symbols.

later. Ta stands for the triplet levels coupled directly to S, and Tb stands for the other triplet levels that are quasidegenerate with S and U. Note that the number of the levels of Ta may be much smaller than the total number of the triplet levels isoenergetic with S and U. The rate constants associated with the individual processes are also given in the figure. For levels with $\Delta E<1000\,\mathrm{cm}^{-1}$, the broad fluorescence is absent, so that we are concerned only with S and Ta.

Case (i). This corresponds to scheme (i) in Fig. 10. In this case, k_{SU} is assumed to be much smaller than k_{STa}. Hence, the population of U will be small in at least the early stage of relaxation, so that the processes U ⇝ Ta, U ⇝ Tb, and Tb ⇝ U are neglected in scheme (i). It is to be noted, however, that the nonradiative rate constant k_U^{NR} is assumed here to include the value of the rate constant which would be associated with U ⇝ T (=Ta+Tb).

According to scheme (i), the concentrations of the molecule existing in the S and U levels, denoted by [S] and [U] respectively, are found to be given, as a function of time t, by

$$[S] = [S]_0\left\{\frac{k_S-\lambda_2}{\lambda_1-\lambda_2}\exp(-\lambda_1 t)+\frac{\lambda_1-k_S}{\lambda_1-\lambda_2}\exp(-\lambda_2 t)\right\}, \tag{1}$$

$$\begin{aligned}[U] = {}& [S]_0\frac{(k_S-\lambda_2)k_{SU}-k_{TaU}k_{STa}}{(\lambda_1-\lambda_2)(k_U-\lambda_1)}\exp(-\lambda_1 t)\\ &+ [S]_0\frac{k_{SU}(k_{Ta}-k_U)+k_{TaU}k_{STa}}{(k_U-\lambda_1)(k_U-\lambda_2)}\exp(-k_U t)\\ &+ [S]_0\frac{(\lambda_1-k_S)k_{SU}+k_{TaU}k_{STa}}{(\lambda_1-\lambda_2)(k_U-\lambda_2)}\exp(-\lambda_2 t),\end{aligned} \tag{2}$$

where

$$\left.\begin{aligned}\lambda_{1,2} &= \frac{1}{2}\{(k_S+k_{Ta})\pm\sqrt{(k_S-k_{Ta})^2+4k_{TaS}k_{STa}}\},\\ k_S &= k_S^R + k_S^{NR} + k_{STa} + k_{SU},\\ k_U &= k_U^R + k_U^{NR},\\ k_{Ta} &= k_{Ta}^R + k_{Ta}^{NR} + k_{TaS} + k_{TaU},\end{aligned}\right\} \tag{3}$$

and $[S]_0$ means [S] at $t=0$; note that $\lambda_1>\lambda_2$. The quantum yield of the IPL fluorescence (Φ_{IPL}) and that of the broad fluorescence (Φ_{broad}) are then expressed as

$$\Phi_{IPL} = \frac{k_S^R k_{Ta}}{k_S k_{Ta}-k_{STa}k_{TaS}} = G^{-1}k_S^R(k_{Ta}^R+k_{Ta}^{NR}+k_{TaS}+k_{TaU}) \tag{4}$$

with

$$\begin{aligned}G = {}& (k_S^R+k_S^{NR}+k_{STa}+k_{SU})(k_{Ta}^R+k_{Ta}^{NR}+k_{TaU})\\ &+ k_{TaS}(k_S^R+k_S^{NR}+k_{SU}),\end{aligned}$$

$$\Phi_{broad} = \frac{k_U^R}{k_U}\left(\frac{k_{SU}}{k_S^R}\Phi_{IPL}+\frac{k_{TaU}}{k_{Ta}^R}\Phi_{Ta}\right) \tag{5}$$

with

$$\Phi_{Ta} = \frac{k_{Ta}^R k_{STa}}{k_S k_{Ta}-k_{STa}k_{TaS}} = G^{-1}k_{Ta}^R k_{STa}. \tag{6}$$

Case (ii). This corresponds to scheme (ii) in Fig. 10. In this case, it is assumed that $k_{STa} \ll k_{SU}$, and the interaction between S and Ta is neglected accordingly. The nonradiative rate constant k_S^{NR}, however, is assumed here to include the value of the rate constant which would be associated with S ⇝ Ta. Note that in scheme (ii) U is considered to interact with both Ta and Tb. Thus, in Fig. 10, T represents collectively all the triplet levels belonging to Ta and Tb.

According to scheme (ii), [S] and [U] are given by

$$[S] = [S]_0\exp(-k_S t), \tag{7}$$

$$\begin{aligned}[U] = {}& [S]_0\frac{\alpha}{k_{UT}}\left\{(k_T-k_S)\exp(-k_S t)\right.\\ &+ \frac{(k_T-\gamma_1)(\gamma_2-k_S)}{\gamma_1-\gamma_2}\exp(-\gamma_1 t)\\ &\left.+ \frac{(k_T-\gamma_2)(k_S-\gamma_1)}{\gamma_1-\gamma_2}\exp(-\gamma_2 t)\right\},\end{aligned} \tag{8}$$

where

$$\left.\begin{aligned}\gamma_{1,2} &= \frac{1}{2}\{(k_U+k_T)\pm\sqrt{(k_U-k_T)^2+4k_{UT}k_{TU}}\},\\ k_S &= k_S^R + k_S^{NR} + k_{SU},\\ k_T &= k_T^R + k_T^{NR} + k_{TU},\\ k_U &= k_U^R + k_U^{NR} + k_{UT},\\ \alpha &= \frac{k_{UT}k_{SU}}{(k_S-\gamma_1)(k_S-\gamma_2)}.\end{aligned}\right\} \tag{9}$$

Note that $\gamma_1>\gamma_2$.

Case (iii). This corresponds to scheme (iii) in Fig. 10. In this case, processes Ta ⇝ S and T ⇝ U are neglected.

According to scheme (iii), [S] and [U] are given by

$$[S] = [S]_0\exp(-k_S t), \tag{10}$$

$$[U] = [S]_0\frac{k_{SU}}{k_S-k_U}\{-\exp(-k_S t)+\exp(-k_U t)\} \tag{11}$$

Here, only the fast fluorescence emissions occur. The quantum yields for the fast components of the IPL fluorescence and broad fluorescence, denoted by Φ_{IPL}^I and Φ_{broad}^I respectively, are given by

$$\Phi_{IPL}^I = k_S^R/k_S, \tag{12}$$

$$\Phi_{broad}^I = \frac{k_U^R}{k_U}\frac{k_{SU}}{k_S}. \tag{13}$$

In Eqs. 10—13, k_S and k_U are defined as

$$\left.\begin{aligned}k_S &= k_S^R + k_S^{NR} + k_{STa} + k_{SU},\\ k_U &= k_U^R + k_U^{NR} + k_{UT}.\end{aligned}\right\} \tag{14}$$

Interpretation of Experimental Results at Low Pressure. Using the kinetic schemes presented in Fig. 10, we first discuss the results of experiments made at low pressure.

Let us first consider case (i). According to Eq. 1, the IPL fluorescence gives fast and slow components, I

and II, with lifetimes $1/\lambda_1$ and $1/\lambda_2$, respectively. It may be noted that $1/\lambda_1<1/\lambda_2$, since $\lambda_1>\lambda_2$. Let us assume here that in Eq. 2

$$\lambda_1>k_U>\lambda_2. \tag{15}$$

It can then be shown that in Eq. 2 the preexponential factor for $\exp(-\lambda_1 t)$ is negative, but that the factors for $\exp(-k_U t)$ and $\exp(-\lambda_2 t)$ are both positive. Therefore, Eq. 2 indicates that the broad fluorescence should give a biexponential decay preceded by a rise. It is natural to consider that $1/k_U$ is the lifetime of component I. The third term on the right hand side of Eq. 2 decays with a lifetime of $1/\lambda_2$ which is equal to the lifetime of component II of the IPL fluorescence, so that the third term in question can be assigned to component II of the broad fluorescence. Thus, the dynamics of pyrimidine excited into the 12^1 level corresponds closely to case (i). The behavior of pyrimidine after excitation into the $6a^2$ level can be described by case (i), except that component III appears weakly upon $6a^2$ excitation. It may be noted that component III does not occur in case (i); it results from reversible intersystem crossing between U and T(=Ta+Tb), as seen in scheme (ii) of Fig. 10. To sum up, aside from component III mentioned above, case (i) accounts for our observations that (1) the broad fluorescence resulting from the excitation into $6a^2$ or 12^1 level shows at least approximately a biexponential decay similar to the one of the IPL fluorescence and (2) the lifetimes of components II of the broad fluorescence and the IPL fluorescence agree with each other. However, we could not detect the rise portion in the change in intensity of the broad fluorescence with time. It may be noted that the assumption of inequalities (15) is considered to be valid, because $\lambda_1>k_S$ and moreover k_U would be smaller than k_S by a value corresponding to k_{SU} (see Table 1), and because λ_2 is of the order of the reciprocal lifetime of the triplet state.

Most of the fluorescence properties of pyrimidine that are observed after 12^1_0 or $6a^2_0$ excitation can be explained, at least approximately or qualitatively, in terms of case (i) by assuming that only the rate constant k_{TaS} depends on the rotational level excited. It is reasonable to consider that, in Eq. 4, $k_{STa} \gg k_S^R+k_S^{NR}+k_{SU}$ and that k_{TaS} is comparable in magnitude to $k_{Ta}^R+k_{Ta}^{NR}+k_{TaU}$. The factor G will then be insensitive to the variation of k_{TaS}. One may thus expect that Φ_{IPL} given by Eq. 4 is an approximately linear function of k_{TaS}. According to Eq. 6, on the other hand, Φ_{Ta} is insensitive to the variation of k_{TaS}, so that it follows from Eq. 5 that there is a linear relation between Φ_{broad} and k_{TaS}. Owing to the existence of the constant term, $k_U^R k_{TaU}\Phi_{Ta}/k_U k_{Ta}^R$, Φ_{broad} varies with k_{TaS} to a lesser extent than does Φ_{IPL}. Thus, the rotational level dependence of the quantum yield of the broad fluorescence (Φ_{broad}) at low pressure would be small compared with that of the IPL fluorescence (Φ_{IPL}) in agreement with our observation.

We now proceed to the fluorescence emissions from the 12^2 and $6a^112^2$ levels at low pressure. Suppose here that case (ii) holds true. Then it follows from Eq. 7 that the IPL fluorescence lacks component II. Further, since one can assume that $k_{SU} \gg k_S^R+k_S^{NR}$, Φ_{IPL} should be much smaller than Φ_{broad}. On the assumption that

$$k_S>\gamma_1>k_T>\gamma_2, \tag{16}$$

it can readily be verified that the broad fluorescence is characterized by a rise due to $-\exp(-k_S t)$, a fast decay (component I) due to $\exp(-\gamma_1 t)$ and a slow decay due to $\exp(-\gamma_2 t)$ (see Eq. 8). This slow decay is attributable to component III, since the quenching rate constant of component III is expected to be much smaller than that of component II, as will be seen later. It is to be noted that component III associated with case (ii) results from reversible intersystem crossing between U and T which includes the triplet levels uncoupled to S (see γ_2 in Eq. 9). On the other hand, component II of the broad fluorescence associated with case (i) results from reversible intersystem crossing between S and Ta which is directly coupled to S (see λ_2 in Eq. 3). Thus, in case (ii), the broad fluorescence consists of components I and III without involving component II.

The foregoing considerations indicate that the dynamics of pyrimidine excited into the $6a^112^2$ level just corresponds to case (ii). For excitation into the 12^2 level, the dynamics appears to be close to case (ii), but the observed IPL fluorescence from 12^2 includes component II as well as I (Fig. 9(a)). Therefore, the relaxation processes from 12^2 cannot fully be explained by case (ii).

Interpretation of Experimental Results at High Pressure. At high pressures where the slower components II and III are fully quenched, leaving the fast component I free from the collisional perturbation, the recurrence from Ta and/or Tb to S and/or U can be neglected, because the collision-induced vibrational relaxation in the triplet state is to be very fast. Consequently, for any initially excited level leading to the broad fluorescence, the situation at high pressure may be described in terms of case (iii).

According to Eq. 10, the IPL fluorescence shows an exponential decay due to $\exp(-k_S t)$, which is associated with the fast component I. Equation 11 indicates that the broad fluorescence also shows an exponential decay due to $\exp(-k_U t)$, associated with component I; in this case, however, the decay is preceded by a rise due to $-\exp(k_S t)$.

As will be mentioned later, U is assigned to rovibronic levels belonging to S_1 and isoenergetic with S. It may then be assumed, though very roughly, that

$$k_S^R + k_S^{NR} + k_{STa} \approx k_U^R + k_U^{NR} + k_{UT}. \tag{17}$$

It follows from Eqs. 14 and 17 that

$$k_S - k_U \approx k_{SU}. \quad (18)$$

As expected from this relation, the observed lifetime of component I (τ_I) of the IPL fluorescence, $1/k_S$, is shorter than the corresponding lifetime of the broad fluorescence, $1/k_U$, for all the excited vibronic levels studied (see Table 1). These lifetime data enable one to obtain approximate values of k_{SU} from Eq. 18. The resulting k_{SU} values are given in Table 1, from which it is seen that k_{SU} ranges in magnitude from 10^8 to 10^9 s^{-1} in the ΔE range 1000—2000 cm^{-1}. It may be noted that the rise of the broad fluorescence, which is predicted from Eq. 11, could not be detected with the present time resolution.

Behavior of Component III. As has been mentioned in the section of results, there is a substantial difference in rate of collisional quenching between component II and component III. In fact, the quenching rate constants for components II of the IPL fluorescence and broad fluorescence are ten times as large as k_{hsc}, whereas that for component III of the broad fluorescence is nearly equal to k_{hsc}. It is to be recalled here that the slow component of the (IPL) fluorescence from lower vibronic levels of intermediate-case molecules,[13,14] including pyrimidine, is known to have a quenching rate constant much larger than k_{hsc}.

According to a quantum-mechanical treatment of the behavior of intermediate-case molecules,[10,11,21] the slow fluorescence components, II and III, are emitted from mixed levels that result from coupling of singlet and triplet levels. In terms of the kinetic model, the same coupling is described by reversible conversion between the singlet and triplet levels,[21] as shown in Fig. 10 with forward and backward wavy arrows. Note that U is here assumed to represent singlet levels.

Let us first consider the collisional quenching of component II of the IPL fluorescence. This component originates from S-Ta mixed levels. At a lower vibronic level S, prepared initially, the singlet rovibronic level density is low. Hence a weak collision can transfer pyrimidine molecule from the S-Ta mixed levels to pure triplet rovibronic levels, which are not coupled to any singlet level, resulting in quenching of the IPL fluorescence.[11] At a high vibronic level S, such as 12^2 or $6a^112^2$, the singlet rovibronic level density is very high. Hence, there is a large probability that a weak collision will transfer the molecule from the S-Ta mixed levels to triplet rovibronic levels which are coupled to singlet levels. However, even if the latter rovibronic levels may give emission, the emission must be different from the IPL fluorescence. Accordingly, in this case also, the IPL fluorescence itself is quenched by a weak collision. It should be noted in this connection that, when we were concerned with the behavior of the IPL fluorescence, we measured its intensity by monitoring selectively an appropriate peak in the IPL fluorescence spectrum. From the foregoing discussion it can be concluded that, whether the initially prepared vibronic level S is low or high, the IPL fluorescence is quenched very efficiently with a rate much greater than that of the hard sphere collision.

Since component II of the broad fluorescence is closely associated with component II of the IPL fluorescence (see scheme (i) in Fig. 10), the former component II is also expected to undergo efficient collisional quenching as in the case of the latter.

Now, component III, which originates from U-T mixed levels, appears in the broad fluorescence from the pyrimidine molecule excited into its higher vibronic levels, such as 12^2 and $6a^112^2$. At these levels, the singlet rovibronic level density is so high that only a hard collision that can remove an energy of hundreds of cm^{-1} will transfer the molecule from the U-T mixed levels to pure triplet levels and thereby will quench component III. This accounts for the observation that, unlike component II, component III has as small a collisional quenching constant as k_{hsc}. In the above argument, the following has been assumed implicitly: When the pyrimidine molecule undergoes collisional transfer (owing to a weak collision) from the U-T mixed levels to other triplet levels with singlet character, the fluorescence from the latter levels is similar in spectral shape and position to, and hence indistinguishable from, component III of the broad fluorescence emitted from the U-T mixed levels; apparently, therefore, the collisional transfer in question does not lead to quenching of component III.

Mention should be made here of a study by Spears and El-Manguch[11] on the dual fluorescence of pyrimidine vapor. On the basis of the pressure dependence of the fluorescence decay, these authors reported that the collisional quenching constant of the slow component of fluorescence is remarkably smaller for higher vibronic levels (12^2 and $6a^112^2$) than for lower levels (0^0, $6a^1$, 12^1, and $6a^112^1$), and that the higher levels have quenching constants close (or equal) to k_{hsc}. They interpreted these experimental results in terms of the energy level dependence of the singlet level density in much the same way as we have done in our discussion. In the study by Spears and El-Manguch, however, the total fluorescence was monitored, with no attention being given to the fact that the fluorescence from pyrimidine vapor may contain not only the IPL fluorescence but also the broad fluorescence in our definition. In their experiments on the higher levels (12^2 and $6a^112^2$), the observed slow emission should be regarded as consisting largely of component III of the broad fluorescence.

Spears and El-Manguch[11] reported also that the

behavior of pyrimidine fluorescence observed when the pressure is increased up to 0.5 Torr is unusual. On excitation to vibronic levels higher than $6a^1$, they observed varying degrees of nonexponential decay for the slow component of fluorescence in the pressure range 0.1—0.5 Torr. Especially for excitation to the 12^2 and $6a^112^2$ levels, the increase in pressure to 0.5 Torr causes the appearance of a large background that appears to be flat over the time scale of the experiment.

The above observations by Spears and El-Manguch can readily be understood by taking account of component III of the broad fluorescence. As the pressure is increased, component II is quenched to a far greater extent than is component III, so that the amount of III may become comparable or superior to the amount of II. This leads to the nonexponential decay of the slow fluorescence or to the appearance of the background, which can be assigned naturally to component III.

Intramolecular Vibrational Redistribution (IVR). It was suggested in our previous papers[14,22] that in the case of 1,3,5-triazine the emitting levels of the broad fluorescence, U, are those vibronic levels which belong not only to S_1 but also to another singlet electronic state. This is rationalized by the observation that the radiative rate constant of the 1,3,5-triazine molecule increases with increasing excess vibrational energy.[22] On the contrary, in pyrimidine the radiative rate constant is largest for the 0^0 level and it decreases roughly monotonically with increasing excess energy.[19] One may thus reasonably assign U to S_1 vibronic levels which are isoenergetic with S. In other words, the conversion from S to U corresponds to the IVR, which is considered to occur in pyrimidine vapor not only directly from S but also via triplet levels.

For the fluorescence from the 12^2 level of pyrimidine, Lim et al.[16] reported experimental results similar to ours. On the basis of their experiments on the bulk gas and on a supersonic jet,[16] they pointed out that the fluorescence spectrum of pyrimidine vapor excited into its 12^2 level consists of a subspectrum with a sharp spectral feature and a subspectrum with a broad feature. The former was attributed to resonance fluorescence from the 12^2 level and the latter to fluorescence from levels which are populated through IVR. Furthermore, they found, as we did, that the excitation spectra with respect to the two fluorescence subspectra are different from each other in shape. This, along with temperature dependence of the characteristics of the subspectra, led them to the conclusion that the IVR process shows rotational level dependence which is to be predicted from the Coriolis interaction. Thus, their conclusion agrees with ours in the sense that the broad fluorescence is emitted from levels populated through IVR, but it is discrepant from our view concerning the nature of the IVR.

The data available in the present experiments indicate that, at high pressure, the quantum yields of the IPL and broad fluorescence emissions obtained by excitation at a vibronic band are independent of the rotational level excited. This means that $\Phi^{\mathrm{I}}_{\mathrm{IPL}}$ and $\Phi^{\mathrm{I}}_{\mathrm{broad}}$ are constant irrespective of the rotational level, since only the fast fluorescence components survive at high pressure. The quantum yields of the fast components, $\Phi^{\mathrm{I}}_{\mathrm{IPL}}$ and $\Phi^{\mathrm{I}}_{\mathrm{broad}}$, are given by Eqs. 12 and 13. For any vibronic level, the radiative rate constants $k^{\mathrm{R}}_{\mathrm{S}}$ and $k^{\mathrm{R}}_{\mathrm{U}}$ can reasonably be regarded as independent of the rotational level. Then the constancy of $\Phi^{\mathrm{I}}_{\mathrm{IPL}}$ ensures that k_{S} is independent of the rotational level (Eq. 12). This along with the constancy of $\Phi^{\mathrm{I}}_{\mathrm{broad}}$ indicates that $k_{\mathrm{SU}}/k_{\mathrm{U}}$ also is independent of the rotational level (Eq. 13). The rate constant k_{U} defined by Eq. 14 seems to be independent of the rotational level. Furthermore, it is hardly conceivable that k_{SU} and k_{U} vary with the rotational level in the same manner so that the ratio $k_{\mathrm{SU}}/k_{\mathrm{U}}$ may become constant. It can be concluded, therefore, that k_{SU} as well as k_{U} does not depend appreciably on the rotational level excited.

In their work already mentioned,[16] Lim et al. interpreted their observation of rotational contour dependence of the fluorescence of pyrimidine by presuming that Coriolis coupling plays an important role in IVR. According to these authors, the rate constant of IVR is governed by a factor $\sqrt{J(J+1)-K(K+1)}$, which appears in the matrix element of the second-order Coriolis interaction. Note that the pyrimidine molecule is here regarded as a symmetric top, and that J and K are the rotational quantum numbers. In other words, the rate constant k_{SU} (in our notation) should depend strongly on the rotational level belonging to S in marked contrast to our conclusion.

We have already shown in Fig. 9 the fluorescence decays of pyrimidine after excitation at the 12^2_0 band. It is seen in Fig. 9(a) that the IPL fluorescence contains the slow component, II. The content of component II is found to be about 15 percent of the total IPL fluorescence at 80.8 mTorr, which pressure is close to the one employed by Lim et al. in their experiment on the bulk gas. If we take account of this observation and of the fact that the yield of the slow component of the IPL fluorescence varies with the rotational level excited, then on the assumption that k_{SU} is independent of the rotational level we are able to explain most of the experimental results reported by Lim et al. We, therefore, believe that the rate of the IVR does not depend on the rotational level; in other words, the Coriolis coupling plays no significant role in the IVR process.

Up to now, the occurrence of IVR has been noticed

for many molecules.[1-4] Almost all of these molecules, however, belong to the statistical limit case, where the fluorescence is characterized by a single exponential decay. Except for 1,3,5-triazine,[14,22] pyrimidine is the first example of the intermediate case molecule in which IVR has been found to occur. It is worthy of note that the IVR in pyrimidine is observed even for levels with small excess vibrational energies ($\approx$1000 cm^{-1}). In a statistical limit case molecule with a size similar to benzene and with no side chain, IVR is observed usually for levels with excess energies of more than $\approx$2000 cm^{-1}.[5,6] For some alkylbenzenes[4,7] the IVR is observed for levels with very small excess energies such as 530 cm^{-1}. However, these molecules have low frequency modes like the torsion or the bending of the alkyl chain, so that the situation in alkylbenzenes is different from that in pyrimidine. Using the vibrational frequencies in the literature,[18] the vibronic state density of pyrimidine at ΔE=1000 cm^{-1} in S_1 was found to be as small as $\approx$0.06 cm from the Haarhoff formula.[23] It should be reasonable, therefore, to consider that the rotational levels will cause the effective state density to increase and thereby will be involved in the IVR occurring in S_1 pyrimidine.

This work was partly supported by a Grant-in-Aid for Cooperative Research (58340028) from the Ministry of Education, Science and Culture.

References

1) K. F. Freed and A. Nitzan, *J. Chem. Phys.*,**73**, 4765 (1980), and references cited therein.

2) P. R. Stannard and W. M. Gelbert, *J. Phys. Chem.*,**85**, 3592 (1981), and references cited therein.

3) C. S. Parmenter, *J. Phys. Chem.*, **86**, 1735 (1982), and references cited therein.

4) R. E. Smalley, *J. Phys. Chem.*, **86**, 3504 (1982), and references cited therein.

5) M. Sumitani, D. V. O'Connor, Y. Takagi, N. Nakashima, K. Kamogawa, Y. Udagawa, and K. Yoshihara, *Chem. Phys.*, **93**, 359 (1985).

6) R. A. Coveleskie, D. A. Dolson, and C. S. Parmenter, *J. Chem. Phys.*, **72**, 5774 (1980); D. A. Dolson, C. S. Parmenter, and B. M. Stone, *Chem. Phys. Lett.*, **81**, 360 (1981).

7) J. B. Hopkins, D. E. Powers, S. Mukamel, and R. E. Smalley, *J. Chem. Phys.*, **72**, 5049 (1980).

8) J. B. Hopkins, D. E. Powers, and R. E. Smalley, *J. Chem. Phys.*, **73**, 683 (1980); H. T. Jonkman and D. A. Wiersma, *Chem. Phys. Lett.*, **97**, 261 (1983); S. A. Schwartz and M. R. Topp, *Chem. Phys.*, **86**, 245 (1984).

9) E. Riedle, H. J. Neusser, and E. W. Schlag, *J. Phys. Chem.*, **86**, 4847 (1982); E. Riedle, H. J. Neusser, E. W. Schlag, and S. H. Lin, *J. Phys. Chem.*, **88**, 198 (1984).

10) K. Uchida, I. Yamazaki, and H. Baba, *Chem. Phys. Lett.*, **38**, 133 (1976); *Chem. Phys.*, **35**, 91 (1978).

11) K. G. Spears and M. El-Manguch, *Chem. Phys.*, **24**, 65 (1977).

12) H. Baba, M. Fujita, and K. Uchida, *Chem. Phys. Lett.*, **73**, 425 (1980).

13) H. Baba, N. Ohta, O. Sekiguchi, M. Fujita, and K. Uchida, *J. Phys. Chem.*, **87**, 943 (1983), and references cited therein.

14) N. Ohta and H. Baba, *Chem. Phys.*, **82**, 41 (1983).

15) D. M. Bartels and K. G. Spears, *J. Phys. Chem.*, **86**, 5180 (1982); H. Saigusa and E. C. Lim, *Chem. Phys. Lett.*, **88**, 455 (1982); *J. Chem. Phys.*, **78**, 91 (1983).

16) B. E. Forch, K. T. Chen, H. Saigusa, and E. C. Lim. *J. Phys. Chem.*, **87**, 2280 (1983); K. T. Chen, B. E. Forch, and E. C. Lim, *Chem. Phys. Lett.*, **99**, 98 (1983); B. E. Forch and E. C. Lim, *Chem. Phys. Lett.*, **110**, 593 (1984).

17) H. Baba, M. Fujita, N. Ohta, and Y. Shindo, *J. Spectrosc. Soc. Jpn.*, **29**, 387 (1980).

18) A. E. W. Knight, C. M. Lawburgh, and C. S. Parmenter, *J. Chem. Phys.*, **63**, 4336 (1975).

19) I. Yamazaki, M. Fujita, and H. Baba, *Chem. Phys.*, **57**, 431 (1981).

20) O. Sekiguchi, N. Ohta, and H. Baba, unpublished data.

21) F. Lahmani, A. Tramer, and C. Tric, *J. Chem. Phys.*, **60**, 4431 (1974).

22) N. Ohta and H. Baba, *Chem. Phys. Lett.*, **106**, 382 (1984); **112**, 212 (1984).

23) P. C. Haarhoff, *Mol. Phys.*, **7**, 101 (1963).

 © 1986 The Chemical Society of Japan Bull. Chem. Soc. Jpn., 59, 3417—3421 (1986)

^{129}I Mössbauer Spectroscopic Studies of Tetrathiafulvalene-Iodine Charge-Transfer Salts

Hiroshi SAKAI,* Manabu MIZOTA,† and Yutaka MAEDA
Research Reactor Institute, Kyoto University,
Kumatori-cho, Sennan-gun, Osaka 590-04
(Received May 19, 1986)

The Mössbauer effect of ^{129}I has been applied to investigate tetrathiafulvalene-iodine (TTF-I_n) charge-transfer salts at 16 K. The electrically conductive TTF-$I_{0.71}$ salt shows a broad single-line with the isomer shift of -0.36 mm s^{-1}, suggesting that the iodine atoms on the average are not completely ionic ($I^{-1.0}$) but are negatively charged by about 0.9 ($I^{-0.9}$) in the low temperature phase. This is due to the weak interactions of the iodine atoms with the sulfur atoms of the TTF molecules. This fact is consistent with the crystallographic data and the electron spin resonance spectra of the salt. This salt is recognized as a partially oxidized mixed-valence compound. The spectrum of the TTF-I_3 salt consists of two sets of quadrupole octets, corresponding to the central and terminal iodine atoms of the slightly distorted I_3^- ion. The charge density localized on each iodine atom of the I_3^- ion is close to that of the isolated I_3^- ion. That is, the salt is regarded as a simple ionic compound, for which a high electrical conductivity can not be expected. It is confirmed that a small amount of the TTF-I_2 salt coexists in the TTF-$I_{0.71}$ phase obtained from the solution of excess TTF and iodine. In the salt the iodine atoms exist as polyiodides consisting predominantly of I_3^- units.

Tetrathiafulvalene (TTF) is a good π-electron donor which forms highly conductive charge-transfer complexes (or salts) with various electron acceptors. The high electrical conductivity arises from the segregated donor and/or acceptor stacks and the incomplete charge-transfer from the donor to the acceptor. In the TTF-iodine system three phases have been confirmed by X-ray diffraction: TTF-$I_{0.71}$ (monoclinic),[1,2] TTF-I_2 (orthorhombic),[3] and TTF-I_3 (monoclinic).[4] However, the crystal structure of the TTF-I_2 phase is not yet established in detail. In the monoclinic TTF-$I_{0.71}$ salt, the dc conductivity at room temperaure is observed to be $\approx$400 S cm^{-1} along the needle c-axis, which is comparable to that of TTF-TCNQ (TCNQ, tetracyano-*p*-quinodimethane).[3,5] The salt exhibits a phase transition near 210 K between the metallic (high temperature) phase and the semiconductive (low temperature) phase. The crystallographic data of the salt in the metallic phase suggest that the TTF molecules form segregated stacks along the c-axis with an intermolecular separation of about 3.56 Å and the iodine atoms, probably iodide ions I^-, occupy the channels between the TTF stacks.[1,2] Preliminary X-ray results of the salt at low temperature reveal no major change in crystal structure.[3] According to Ref. 3, the room-temperature conductivity for the orthorhombic TTF-I_2 salt is found to be $\approx 10^{-3}$ S cm^{-1} along the TTF stacking axis. The iodine atoms seem to exist as small polyiodide species, probably predominately triiodide ion I_3^-. In the monoclinic TTF-I_3 salt,[4] the TTF molecules do not form segregated stacks but exist as completely oxidized $(TTF)^+$ dimers interspersed between pairs of triiodide ions. The electrical conductivity of the salt is observed to be $\approx 10^{-9}$ S cm^{-1} at room temperature, as one would expect from the crystal structure.

It is important to estimate the degree of charge-transfer and interactions between the TTF molecules and the iodine atoms in order to understand the electrical properties of these TTF-iodine salts. The ^{129}I Mössbauer spectroscopy is a powerful method for this purpose. The Mössbauer parameters such as the quadrupole coupling constant (e^2Qq), the asymmetry parameter (η), and the isomer shift (δ), are directly related to the charge distribution and the charge density of the iodine atom. Previously ^{129}I Mössbauer spectroscopy has been successfully applied to iodine complexes or salts exhibiting high electrical conductivity: perylene-iodine,[6,7] metal glyoximate-iodine,[8,9] metal phthalocyanine-iodine,[8,10] and oligoaniline-iodine.[11] The Mössbauer spectrum of the TTF-$I_{0.71}$ salt has been measured, but the detailed analysis and discussion are not given.[8] In this paper we report the results of the ^{129}I Mössbauer spectroscopic study of the TTF-$I_{0.71}$ and TTF-I_3 salts. The Mössbauer data of the TTF-I_2 salt coexisting in the TTF-$I_{0.71}$ phase are also presented.

Experimental

Materials. The commercially available TTF (Aldrich Chemical Co.) was recrystallized from cyclohexane. The radioisotope ^{129}I, in the standard from of Na ^{129}I in a Na_2SO_3 solution (New England Nuclear Co.), was oxidized with 3 mol dm^{-3} H_2SO_4 and 10% H_2O_2, and the resulting molecular iodine ($^{129}I_2$) was extracted with benzene. The iodine solution was thoroughly washed with water and passed through a Teflon filter to eliminate any slight amount of water. The ^{129}I-labeled TTF-iodine salts were prepared on a small scale by mixing together benzene

† Present address: Mitsubishi Fusion Center, Mitsubishi Denki Bldg, 2-3, Marunouchi 2-Chome, Chiyoda-ku, Tokyo 100.

solutions of TTF and iodine ($^{129}I_2$) with the prescribed mole ratios. A precipitate obtained from the solution with a composition of TTF:I=1:0.71 contains the TTF-$I_{0.71}$ salt and small amounts of another salt, probably TTF-I_2. Therefore, the precipitate was recrystallized from acetonitrile. The iodine contents of the TTF-iodine salts were checked on nonradioactive (natural iodine) preparation samples by elemental analysis: Found; C, 24.52; H, 1.28; I, 30.38%. Calcd for TTF-$I_{0.71}$:C, 24.48; H, 1.37; I, 30.60%. Found: C, 11.79; H, 0.67; I, 66.31%. Calcd for TTF-I_3:C, 12.32; H, 0.69; I, 65.07%. No pure TTF-I_2 salt could be isolated by recrystallization from acetonitrile.

Measurements. A single-line $^{66}Zn^{129}Te$ Mössbauer source was prepared by irradiating 140 mg $^{66}Zn^{128}Te$ at a thermal neutron fluence rate of 2×10^{13} n $cm^{-2}s^{-1}$ for 1 h in the Kyoto University Reactor (KUR). The source was checked by the spectrum against a single-line Cu ^{129}I absorber (10 mg ^{129}I cm^{-2}). The line width at half maximum was found to be 1.12 mm s^{-1} for the single absorption peak. The isomer shift of Cu ^{129}I was −0.42 mm s^{-1} for the source, which is in good agreement with the literature.[12] Measurements were carried out in a transmission geometry by cooling the source and the absorber to 16 K in the same way as reported previously.[11]

Results and Discussion

^{129}I Mössbauer spectra of the recrystallized TTF-$I_{0.71}$ (absorber thickness; 12 mg ^{129}I cm^{-2}) and TTF-I_3 (13 mg ^{129}I cm^{-2}) salts at 16 K are shown in Fig. 1(a) and (c), respectively. The former shows only a single absorption peak (no quadrupole hyperfine splitting), while the latter consists of two kinds of quadrupole octets. Figure 1(b) shows the spectrum of a precipitate (29 mg ^{129}I cm^{-2}) obtained from the benzene solution with a composition of TTF:I=1:0.71. The spectrum evidently consists of one singlet and two different quadrupole octets. These spectra were analyzed by the least-squares method. The solid curves in the figure represent the best-fitted Lorentzian spectra and the dashed curves indicate their components. Table 1 gives the Mössbauer parameters obtained such as the quadrupole coupling constant (e^2Qq) and its sign, the asymmetry parameter (η), the isomer shift (δ), and the line width (2Γ). Included inTable 1 for comparison are results of the isolated I_3^- ions in the [Ru(η-$C_5H_5)_2$I]I_3[13] and β-carotene-I_3[14] complexes and of I_3^- chains in the *N,N'*-diphenyl-*p*-phenylenediamine-iodine (DPPD-I_x) and *N,N'*-diphenylbenzidine-iodine (DPB-I_x) complexes.[11]

TTF-$I_{0.71}$ Salt. The single-line spectrum of TTF-$I_{0.71}$ with the small δ value suggests that the iodine atom exists almost as an ionic I^- ion. This result is in good agreement with that of Marks.[8] However, the δ value (=−0.36±0.05 mm s^{-1}) for this salt is slightly larger than that for the typical I^- ion in the KI crystal (δ =−0.51±0.025 mm s^{-1}).[15] This implies that a slight amount of covalency is present between the I^- ion and the TTF molecules. According to the detailed crystallographic data of the salt,[2] each iodine atom has four sulfur neighbors and there are two characteristic coordination geometries; a distorted tetrahedron and a distorted square planar. The I···S bond distances for both coordination geometries are in the range of 3.56 to 3.79 Å, less than the sum of the respective van der Waals radii (4.0 Å). Furthermore, the presence of the interaction between the iodine and the sulfur atoms has been suggested from the *g* value and the line width of the ESR spectra of the salt.[16]

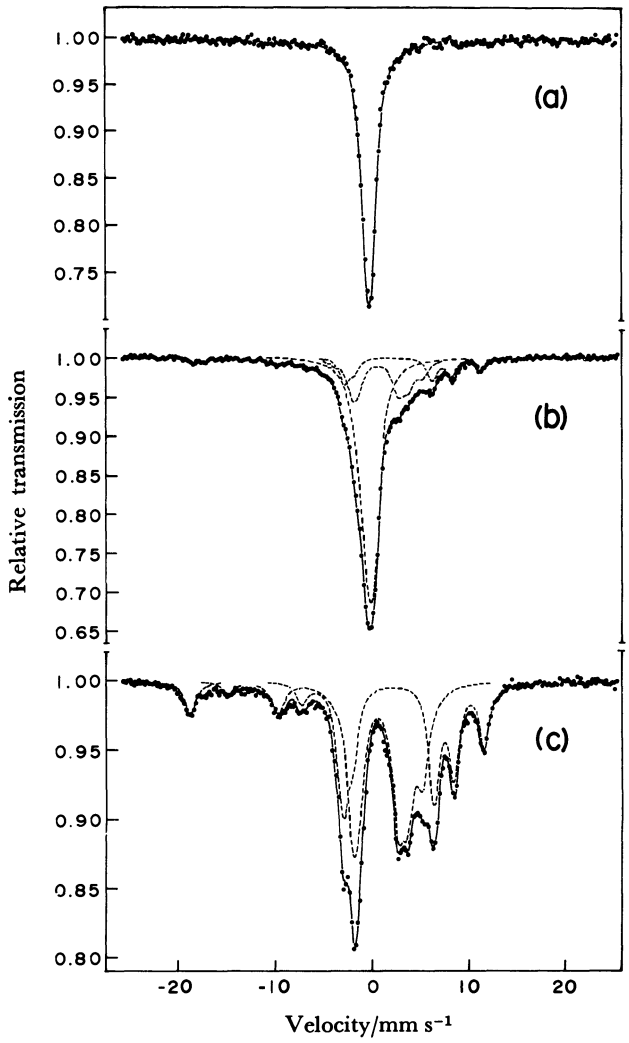

Fig. 1. ^{129}I Mössbauer spectra at 16 K of (a) the TTF-$I_{0.71}$ salt recrystallized from acetonitrile, (b) the precipitate obtained from the benzene solution with composition of TTF: I=1 : 0.71 (shows the presence of the TTF-$I_{0.71}$ and TTF-I_2 salts), and (c) the TTF-I_3 salt.

The charge density on the iodine atom can be evaluated from the semiempirical relation as follows;[12]

$$\delta(\text{mm s}^{-1}) = -9.2\,h_s + 1.5\,h_p - 0.54 \quad \text{(for ZnTe source)}, \qquad (1)$$

where h_s and h_p are the numbers of 5s- and 5p-electron holes, respectively, in the $5s^25p^6$ configuration. Therefore, the h_p is expressed as

Table 1. ^{129}I Mössbauer Parameters for the Tetrathiafulvalene-Iodine Charge-Transfer Salts, $[Ru(\eta\text{-}C_5H_5)_2I]I_3$, β-Carotene-$I_3$, and the Oligoaniline-Iodine Complexes

		e^2Qq[a] / MHz	η	δ[b] / mm s^{-1}	2Γ / mm s^{-1}	Area[c] Ratio	U_p[d]	h_p[e]	Ref.
TTF-$I_{0.71}$		+ 130±25[f]	—	−0.36±0.05	1.12[f]		0.05	0.12	*
TTF-I_2	I_c	−2285±25	0.06±0.04	1.18±0.05	1.41±0.10	1.0	1.00	1.15	*
	I_t	−1060±25	0.05±0.04	0.15±0.05	1.64±0.10	1.6	0.46	0.46	*
TTF-I_3	I_c	−2336±25	0.05±0.04	1.32±0.05	1.31±0.10	1.0	1.02	1.24	*
	I_t	−1153±25	0.06±0.04	0.18±0.05	1.48±0.10	1.6	0.50	0.48	*
$[Ru(\eta\text{-}C_5H_5)_2I]I_3$	I_c	−2460±25	0.06±0.04	1.48±0.05	0.83±0.08	1.0	1.07	1.35	13
	I_t	−1152±25	0.06±0.04	0.25±0.05	0.85±0.08	1.6	0.50	0.53	
β-Carotene-I_3	I_c	−2445±20	0.05±0.04	1.59±0.04	1.04±0.10	1.0	1.07	1.42	14
	I_t	−1152±20	0.06±0.04	0.23±0.04	1.20±0.10	1.4	0.50	0.51	
DPPD-$I_{2.4}$	I_c	−2347±20	0.05±0.04	1.32±0.04	1.00±0.06	1.0	1.02	1.24	11
	I_t	−1183±20	0.04±0.04	0.25±0.04	0.93±0.06	1.6	0.52	0.53	
DPB-$I_{2.7}$	I_c	−2282±20	0.10±0.04	1.35±0.04	1.09±0.06	1.0	1.00	1.26	11
	I_t	−1166±20	0.06±0.04	0.22±0.04	1.60±0.06	1.7	0.51	0.51	

a) The e^2Qq values are converted to the ^{127}I nucleus. b) The δ values are relative to the ZnTe source.
c) The ratios are normalized with respect to the I_c atom. d) $U_p=-e^2Qq_{obsd}/e^2Qq_{atom}$, $e^2Qq_{atom}=2292.7$ MHz.
e) $\delta=1.5\,h_p-0.54$ (mm s^{-1}). f) The e^2Qq value is obtained by analysis with a fixed line width (1.12 mm s^{-1}).
* The errors quoted in this work include estimated systematic errors.

$$h_p = 6 - (N_x+N_y+N_z), \quad (2)$$

where N_x, N_y, and N_z are the populations of the 5p-electrons in the x, y, and z orbitals, respectively. If only 5p-electrons take part in bond formation, the h_p value is calculated to be 0.12 from the δ value. This implies that the iodine atom on the average is negatively charged by 0.88 in the TTF-$I_{0.71}$ salt. The average covalency per I···S bond is, therefore, found to be 3%. The e^2Qq value is affected only a little by the slight covalency. In the tetrahedral coordination geometry the e^2Qq value would be zero, regardless of the extent of covalency. In the case of the square planar geometry, the contribution of the covalency to e^2Qq may be calculated on the basis of the Townes and Dailey approximation as follows;[12]

$$U_p = -e^2Qq_{obsd}/e^2Qq_{atom} = -N_z + (N_x+N_y)/2, \quad (3)$$

where U_p is the number of unbalanced p-electrons and e^2Qq_{atom}, the atomic iodine quadrupole coupling constant. The latter is equal to 2292.7 MHz for the ^{127}I nucleus. Since the z principal axis (V_{zz}) of the electric field gradient (EFG) tensors lies along the four-fold axis in the square planar coordination, the 5pz orbital has two nonbonded electrons, i.e., N_z=2.00. Substituting the values of h_p and N_z into Eq.2, one obtains N_x=N_y=1.94. If all iodine atoms are surrounded in a square planar configuration by four sulfur atoms, the covalency of 3% for each I···S bond leads to +138 MHz for e^2Qq from Eq. 3. However, the crystallographic results of the salt suggest that about 40% of the iodine atoms have a distorted square planar coordination and the residual 60% have a distorted tetrahedral coordination.[2] Therefore, the spectrum of the salt should have two components corresponding to two kinds of iodine atoms, one in a distorted square planar arrangement and the other in a distorted tetrahedron. Unfortunately, since the resolution of the Mössbauer spectrum of ^{129}I is not very high, it may be difficult to distinguish between them.

The line width of the spectrum is apparently broad compared with that of Cu ^{129}I with nearly the same absorber thickness. The broadening is mainly due to the slight covalency of the I···S bonds described above. When the spectrum was analyzed with the fixed line width (1.12 mm s^{-1}) determined from the single-line spectrum of Zn^{129}Te vs. Cu^{129}I and with the theoretical intensity ratios obtained from the square of the Clebsch-Gordan coefficient $|CG|^2$, the e^2Qq value was found to be 130 MHz. If a larger line width, due to the saturation effect, is used for the analysis, this value would further decrease. The e^2Qq value obtained from the broadening of the line-width is in good agreement with that predicted from the δ value within experimental error. It is concluded that on the average the iodine atom in the TTF-$I_{0.71}$ salt is not completely ionic ($I^{-1.0}$), but is negatively charged by about 0.9 ($I^{-0.9}$) in the low temperature (semiconductive) phase (16 K). The average covalency per I···S bond is estimated to be 3%, which is likely from the I···S bond distances. The ^{129}I Mössbauer spectrum in the high temperature (metallic) phase of the salt is important and interesting in order to understand the phase transition near 210 K. Unfortunately, because of a significant decrease in the Mössbauer resonance absorption, the measurement of the spectrum could not be performed above 210 K.

TTF-I_3 Salt. The Mössbauer spectrum of the TTF-I_3 salt is similar to those of the linear triiodide anions observed in the β-carotene-I_3,[14] DPPD -I_x, and

DPB-I_x complexes.[11] The crystallographic data of the salt have revealed that the iodine atoms exist as a slightly distorted triiodide anion.[4] The bond distances between the iodine atoms in the asymmetric triiodide anion are 2.907 and 2.953 Å, respectively, while the bond angle ∠I-I-I of 175.40° deviates slightly from linearity. The distances between two terminal iodine atoms and sulfur atoms of the TTF molecules are in the range of 3.636 to 3.989 Å, suggesting weak intermolecular interactions. By analogy with the Mössbauer spectra of the other I_3^- ions, it is appropriate to assign the iodine with the larger quadrupole splitting to the central iodine atom (I_c), and the other splitting to the two terminal iodine atoms (I_t). A slight broadening of the line width has been observed for I_t compared with that for I_c, suggesting that the charge densities on the two I_t atoms are slightly different from each other, i.e., the I_3^- ion is slightly asymmetric. This is consistent with the result of the crystal structure. Therefore, the values of e^2Qq, η, and δ given in Table 1 are the means of those for two I_t atoms. The absorption area ratio of I_t and I_c was found to be 1.6:1, which is close to the values obtained for the other I_3^- ions in the $[Ru(\eta\text{-}C_5H_5)_2I]I_3$ and β-carotene-I_3 complexes, as shown in Table 1. The deviation from the composition ratio of 2:1 in the I_3^- ion is due to the differences in the recoilless fraction and in the saturation effect, as discussed in our previous paper.[11] The small η value for the I_c atom is in accord with the fact that the I_3^- ion is almost linear. The bond angle of 175.40° leads to only 0.01 for η, assuming that two I_t atoms are equivalent. In this case e^2Qq for I_c is negative in sign and the z principal axis (V_{zz}) of the EFG tensors lies along the direction of the bonding axis. The small η value for the I_t atoms implies that the interaction is little present between the I_t atoms and the sulfur atoms of the TTF molecules.

The charge density of 5p-electrons localized on each iodine atom can be estimated from the values of δ and e^2Qq using Eqs. 1—3. The U_p value is close to the h_p value on the average for two I_t atoms of the asymmetric I_3^- ion. This suggests that the bonding of I_t is mainly due to $5p_\sigma$-electrons. If $5p_\pi$-electrons take part in an intra- or intermolecular bond formation, the relationship $U_p < h_p$ is generally observed. Therefore, the I_t atoms are unlikely to be interacting with sulfur atoms of the TTF molecules, consistent with the small η value. The I_t atom of the salt is negatively charged by about 0.50 e^- on the average due to the values of U_p and h_p. This charge density on the terminal iodine atom is in good agreement with that of the usual isolated I_3^- ion. For the I_c atom the h_p value is larger than the U_p value, which is always found in the I_c atoms of the other I_3^- ions, as shown in Table 1. This phenomenon has been successfully explained on the basis of the contribution of the core $4d_\sigma$-electrons, on the I_c atom, to the linear I_3^- bond formation, in addition to the delocalized three-center four-electron bonding scheme.[11,17] Consequently the charge density localized on the I_c atom of the I_3^- ion is computed to be +0.01 e^- from the values of δ and e^2Qq using Eqs. 4 and 5 of Ref. 17. The charge density is close to that on the I_c atom of the successive I_3^- chain in the DPPD-$I_{2.4}$ complex rather than to that on the isolated I_3^- ion. This seems to be attributed to the fact that the I_3^- ion in the TTF-I_3 salt is slightly asymmetric and bent. It is concluded that the iodine atoms of the TTF-I_3 salt exist as an almost isolated I_3^- ion and the interaction of the I_3^- ion with sulfur atoms of the TTF molecules is extremely weak. Since the TTF-I_3 salt is regarded as a simple ionic compound, a high electrical conductivity is not expected for the salt, consistent with the observed conductivity ($\approx 10^{-9}$ S cm^{-1}).[4]

TTF-I_2 Salt. A precipitate obtained from the solution with a composition of TTF:I=1:0.71 showed a complicated spectrum consisting of one broad singlet and small amounts of two different quadrupole octets, as shown in Fig. 1(b). If the broad single-line spectrum corresponds to the iodine of the TTF-$I_{0.71}$ salt, the δ value actually agrees well with that of TTF-$I_{0.71}$, the residual two quadrupole octets must arise from iodine species of another TTF-I_n salt. The Mössbauer parameters of the iodine species are evidently different from those of the TTF-I_3 salt, though of lower precision because of the weak intensities and the broad line widths of the iodine species. Warmack et al.[3,18] have reported that two different types of charge-transfer crystals are formed by slow diffusion of TTF and iodine in acetonitrile: monoclinic TTF-$I_{0.71}$ (needles) and orthorhombic TTF-I_2 (flat platelets). In the latter TTF-I_2 form the iodine columns seem to contain small polyiodide species, probably predominantly I_3^-. It is reasonable to assume that the unknown iodine species corresponds to the I_3^- unit of the TTF-I_2 salt. That is, the iodine with the larger quadrupole splitting can be assigned to the central iodine atom (I_c) of the I_3^- unit, whereas the other to the two terminal iodine atoms (I_t), in analogy with the I_3^- ion of the TTF-I_3 salt. However, the values of e^2Qq and δ for the I_3^- unit of TTF-I_2 are considerably different from those for the isolated I_3^- ion of TTF-I_3, as shown in Table 1. Further, the line widths are very broad for the I_3^- unit. The optical data for the salt have suggested the presence of monomers (I^-) and dimers (I_2) in the iodine columns, in addition to the trimers (I_3^-).[18] Accordingly, the I_3^- units in the polyiodides containing the I_3^-, I_2, and I^- species are presumably distorted significantly compared with the *symmetric* isolated I_3^- ion. Furthermore, the spectrum of the dimer (for free iodine molecule, $e^2Qq = -2250 \pm 30$ MHz, $\delta = +0.94 \pm 0.05$ mm s^{-1} [19]) present in the poly-

iodide may be superimposed on that of the I_c atom in the I_3^- unit. The spectrum of the monomer, of course, can not be distinguished from that of the coexisting TTF-$I_{0.71}$ salt. These effects may complicate the spectrum of the I_3^- unit present in the TTF-I_2 salt, and then the spectrum may not permit a quantitative discussion of the charge density of the iodine species. It is concluded that the TTF-I_2 salt is formed from the benzene solution of excess TTF and iodine, in addition to the TTF-$I_{0.71}$ salt. The iodine atoms in the iodine columns of TTF-I_2 exist as polyiodides consisting predominantly of I_3^- units. These results are consistent with the crystallographic data and the optical data of the TTF-I_2 salt.

We are very grateful to Prof. Takenobu Higashimura (Research Reactor Institute, Kyoto University) for his useful discussion and encouragement. This work was supported by the grant in aids of special research project on properties of molecular assemblies (No. 59212018, No. 60104002) from the Ministry of Education, Science and Culture.

References

1) J. J. Daly and F. Sanz, *Acta Crystallogr., Sect. B*, **31**, 620 (1975).
2) C. K. Johnson and C. R. Watson, Jr., *J. Chem. Phys.*, **64**, 2271 (1976).
3) R. J. Warmack, T.A.Callcott, and C. R. Watson, *Phys. Rev., B*, **12**, 3336 (1975).
4) R. C. Teitelbaum, T. J. Marks, and C. K. Johnson, *J. Am. Chem. Soc.*, **102**, 2986 (1980).
5) R. B. Somoano, A. Gupta, V.Hadek, T. Datta, M. Jones, R.Deck, and A. M. Hermann, *J. Chem. Phys.*, **63**, 4970 (1975).
6) R. C. Teitelbaum, S. L. Ruby, and T. J. Marks, *J. Am. Chem. Soc.*, **101**, 7568 (1979).
7) H. Sakai, T. Matsuyama, H. Yamaoka, and Y. Maeda, *Bull. Chem. Soc. Jpn.*, **56**, 1016 (1983).
8) T. J. Marks, *Ann. N. Y. Acad. Sci.*, **313**, 594 (1978).
9) M. Cowie, A. Gleizes, G. W. Grynkewich, D. W. Kalina, M. S. McClure, R. P. Scaringe, R. C. Teitelbaum, S. L. Ruby, J. A. Ibers, C. R. Kannawurf, and T. J. Marks, *J. Am. Chem. Soc.*, **101**, 2921 (1979).
10) J. L. Peterson, C. S. Schramm, D. R. Stojakovic, B. M. Hoffman, and T. J. Marks, *J. Am. Chem. Soc.*, **99**, 286 (1977).
11) H.Sakai and Y.Maeda, *Bull. Chem. Soc. Jpn.*, **59**,1311 (1986).
12) H. DeWaard, "Mössbauer Effect Data Index 1973," ed by J. G. Stevens and V. E. Stevens, IFI/Plenum Press, New York (1974), p. 447.
13) M. J. Potasek, P. G. Debrunner, W. H. Morrison, Jr., and D. N. Hendrickson, *J. Chem. Phys.*, **60**, 2203 (1974).
14) T. Matsuyama, H. Sakai, H. Yamaoka, and Y. Maeda, *J. Chem. Soc., Dalton Trans.*, **1982**, 229.
15) D. W. Hafemeister, G. DePasquali, and H. DeWaard, *Phys. Rev., B*, **135**, 1089 (1964).
16) T. Sugano and H. Kuroda, *Chem. Phys. Lett.*, **47**, 92 (1977).
17) H. Sakai, Y. Maeda, S. Ichiba, and H. Negita, *J. Chem. Phys.*, **72**, 6192 (1980).
18) R. J. Warmack and T. A. Callcott, *Phys. Rev., B*, **14**, 3238 (1976).
19) S. Bukshpan, C. Goldstein, and T. Sonnino, *J. Chem. Phys.*, **49**, 5477 (1968).

Electrochemical Study on the Initial Stages of the Electropolymerization of 1-Pyrenamine in Acetonitrile

Takeo Ohsaka, Kazuhiko Hirabayashi, and Noboru Oyama*
Department of Applied Chemistry for Resources, Tokyo University of Agriculture and Technology, Koganei, Tokyo 184
(Received May 20, 1986)

The kinetic study of the mechanism for the reaction of the initial stages of the electropolymerization of 1-pyrenamine (PA) in an acetonitrile solution was carried out by cyclic voltammetry (CV) and double potential-step chronoamperometry (DPSCA). The experiments were conducted at various time windows (i.e., at various scan rates of CV and various potential-step widths of DPSCA) and under the conditions of the presence or absence of the basic or acidic additives (pyridine, 2,6-lutidine, trifluoroacetic acid). As a result, it was found that the mechanism of the reaction of the initial stages of the electropolymerization of PA is an "ECE" mechanism, and that the chemical reaction interposed between successive electron transfers is considered as the radical-radical coupling reaction rather than the radical-parent monomer coupling reaction. The second-order rate constant for the radical-radical coupling reaction was estimated to be $(1.0\pm 0.8)\times 10^5\ M^{-1}\ s^{-1}$ (1 M=1 mol dm^{-3}). The cyclic voltammetric responses for the oxidation of PA were varied by the presence or absence of the basic or acidic additives. This can be explained considering the basicity of the additives and their influences in the deprotonation reactions following the heterogeneous electron-transfer step.

One of the most active areas in a recent electrochemical research deals with "electropolymerization."[1-60] The attractiveness of electropolymerization stems not only from its potentiality in the synthesis[27-44] of new organic conducting, semiconducting or nonconducting polymers, but also from the point of the modification of electrode surfaces.[1-26] A number of recent papers[1-60] on electropolymerization are concerned with the preparation of polymeric compounds, the characterization of their electrochemical, electrical, physicochemical, spectroscopic and other kinds of properties, and the applications of "composite electrode materials" produced by the modification of electrode surfaces by electropolymerization. In contrast, there have been only a few papers[38,45,46,55,61-63] concerning the studies of the mechanism of electropolymerization.

It seems to be quite difficult (or impossible) to elucidate quantitatively the whole mechanism of the electropolymerization of a given monomer, since in general many reaction steps are involved in the chemical polymerization reaction, as being apparent from the fact that it can be regarded as "chain reactions." However, the electropolymerization occurs at and/or in the vicinity of electrode surface and at least the first step of the polymerization (i.e., dimerization) can be considered as "follow-up chemical reaction" from a viewpoint of the mechanism of electrode reaction.[65] In other words, in the initial step of electropolymerization the initiators for polymerization (they are usually radical ions) are first produced at electrode surface by the heterogeneous electron-transfer reaction of parent monomers and then dimerization and any higher polymerization proceed at and/or in the vicinity of electrode surface. Many electrochemical methods which are suitable for the study of such chemical reactions coupled to the heterogeneous electron-transfer have been ever developed.[66]

In this paper, we report the kinetic study of the mechanism of the reaction of the initial stages in the electropolymerization of 1-pyrenamine (PA, Fig. 1) in an acetonitrile solution by means of cyclic voltammetry (CV) and double potential-step chronoamperometry (DPSCA) which have proved to be useful for the study of the chemical reactions which are associated with heterogeneous electron-transfer reaction proper.[66-69] Recently, we[36] have reported the preparation of poly(1-pyrenamine) (PPA) film by the electropolymerization of PA, the characterization of its electrochemical, physicochemical and electrical properties,and the spectroscopic identification of the structure of the PPA film. The electrochemical responses obtained for the initial step of the electropolymerization of PA seem to be simple compared with other monomers (e.g., aniline and pyrrole). This is the first reason why we chose PA as the first candidate for the examination of the mechanism of electropolymerization. The second reason is that the first dimerization reaction, regarded as a follow-up chemical reaction, is not so fast and thus DPSCA can be applied to the determination of the rate constant of the dimerization reaction. In addition, the third reason is that no study has been reported on the mechanism of the initial-step

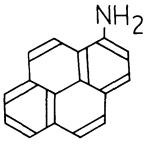

Fig. 1. Structure of 1-pyrenamine.

reactions in the electropolymerization of PA. It will be shown that the mechanism of the reaction of the initial stages in the electropolymerization of PA is an "ECE" mechanism, and that the chemical reaction interposed between successive electron transfers is considered as the radical-radical coupling reaction rather than the radical-parent monomer coupling reaction.

Experimental

Materials. 1-Pyrenamine (PA) (Aldrich Chemical Co.) was purified by the procedure described previously.[36] Acetonitrile (Wako Pure Chemical Industries, LTD) was distilled by ordinary technique after dehydration on molecular sieves (5A 1/16, Wako). Pyridine (Wako) of reagent grade was twice distilled under reduced pressure. Tetrabutylammonium tetrafluoroborate ($(n\text{-}C_4H_9)_4NBF_4$, $TBABF_4$) (Tokyo Kasei Co.) was of reagent grade. The basal-plane pyrolytic graphites (BPG) (Union Carbide Co.) were used as electrodes.[36] All other chemicals were of reagent grade and were used as received without further purification.

Apparatus and Procedures. A standard three-electrode electrochemical cell was used for all electrochemical experiments. The electrode assembly consists of a BPG disk electrode (area; 0.20 cm^2) as working electrode, a sodium chloride saturated calomel electrode (SSCE) as reference electrode and a spiral platinum wire as counter electrode. The compositions of the electrolytic solutions were 0.2 M $TBABF_4$+1—10 mM PA+0—25 mM pyridine (or CF_3COOH or 2,6-lutidine) in acetonitrile.

For cyclic voltammetry and double potential-step chronoamperometry (DPSCA), a home-made instrument was employed. The experiments of DPSCA were conducted according to the previously described procedure.[69] The width (τ) of the applied potential pulse was varied from 0.5 to 100 ms. An IR compensation was employed. The current-time responses of DPSCA were monitored and stored on a Nicolet 3091 oscilloscope and then the enlarged current-time curves were displayed on an X-Y recorder (Graphtec Co. WX 4403). The analysis of DPSCA's data was carried out according to the procedure originally suggested by Schwarz and Shain[70].

All experiments were run under nitrogen atmosphere at laboratory temperature (25±1°C). Potentials were measured and are quoted with respect to SSCE.

Results

Cyclic Voltammetry. The typical cyclic voltammograms obtained at a BPG disk electrode in an acetonitrile solution containing 0.2 M $TBABF_4$+5 mM PA are shown in Fig. 2, where to prepare a fresh electrode surface the BPG electrode was cut parallel to the eletrode surface with a scalpel each measurement. In the first forward potential scan at 10 V s^{-1} the anodic peak can be observed at ca. 0.65 V vs. SSCE. This peak is considered to correspond to the oxidation of PA to the corresponding cation radical (PA^+).[84] When the electrode potential was scanned to more positive potentials than 0.65 V vs. SSCE, additional anodic peaks were obtained.[36] From the viewpoint of polymer formation, the potential application of about 0.8 V vs. SSCE to the working electrode is enough to lead to the electropolymerization of PA at electrode surface. When the electrode potential was turned to negative, the cathodic peak corresponding to the anodic peak at 0.65 V vs. SSCE was observed at 0.55 V vs. SSCE, though the peak current is much smaller than the anodic one due to the consumption of the electrogenerated PA^+ by the follow-up chemical reaction. Furthermore, the cathodic peak at ca. 0.3 V corresponds to the reduction of the oxidized forms of the dimeric, oligomeric, and/or polymeric products which can be considered to be formed from the electrogenerated PA^+'s and/or PA's during the period (ca. several tens ms) of the potential scan from ca. 0.5 V to 0.8 V and then to ca. 0.5 V at 10 V s^{-1}. During the second forward scan, the new anodic peak is observed at ca. 0.4 V and corresponds to the cathodic peak at 0.3 V. In the further potential cycling between −0.5 and 0.8 V, two anodic peaks and two cathodic ones are obtained as shown in Fig. 2A. The peak currents at 0.55 and 0.65 V tend to decrease with the potential cycling, while the peak currents at 0.3 and 0.4 V tend to increase with the cycling of electrode potential. This suggests that the electroactive products deposite onto the electrode surface and at the same time the diffusion of PA monomers to the electrode surface through the deposited product layer becomes more difficult.[36]

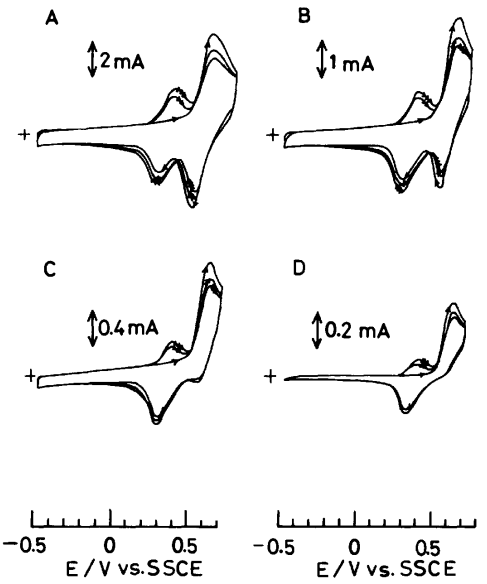

Fig. 2. Scan rate dependence of cyclic voltammograms obtained at a BPG disk electrode in an acetonitrile solution containing 0.2 M $TBABF_4$ and 5.0 mM PA. Scan rate: (A): 10, (B): 5.0, (C): 1.0, and (D): 0.2 Vs^{-1}. Electrode area: 0.20 cm^2.

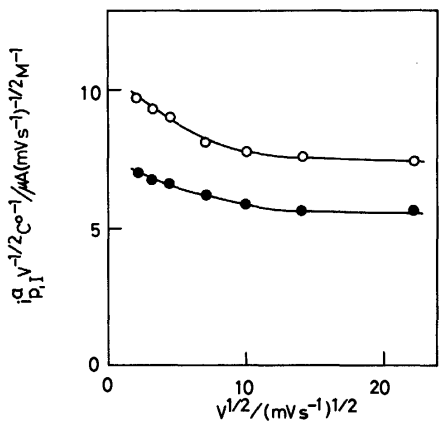

Fig. 3. Dependence of $i^a_{p,I}/v^{1/2}C^o$ on potential scan rate ($v^{1/2}$) at different concentrations of PA. Concentration of PA (C^o): (○): 1.0 mM, (●): 5.0 mM. Other experimental conditions are the same as in Fig. 2.

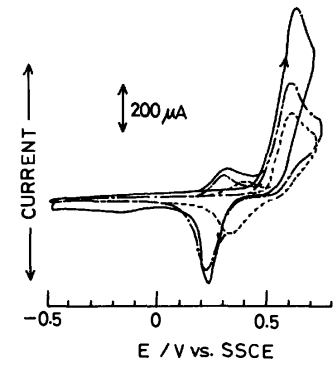

Fig. 4. Cyclic voltammograms of PA and PA-pyridine mixtures. Concentration of PA: 5.0 mM. Concentration of pyridine: (——): 25.0, (— — —): 2.5, and (----): 0 mM. Scan rate: 100 mV s^{-1}. Other experimental conditions are the same as in Fig. 2.

Furthermore, it is apparent from Fig. 2 that the peak current ratio of the cathodic peak current ($i^c_{p,I}$) corresponding to the reduction of PA^+ to the anodic peak current ($i^a_{p,I}$) corresponding to the oxidation of PA decreased with decreasing the potential scan rate (v) and at v=0.2 V s^{-1} the $i^c_{p,I}$ was not substantially observed. Also, the values of $i^a_{p,I}/C^o v^{1/2}$ (C^o: concentration of PA) decreased with $v^{1/2}$ in a way which is dependent on C^o (Fig. 3). This behavior is taken as an indication that the chemical complication that follows the electron transfer may have a higher than first-order kinetics. These results suggest that the follow-up chemical reactions which consume the electrogenerated PA^+'s occur at and/or in the vicinity of the electrode surface on the time scale of this experiment.

Figure 4 shows the effect of the addition of various amounts of pyridine into the electrolytic solution upon the cyclic voltammetric response of PA. An increase of pyridine concentration produces an increase in $i^a_{p,I}$ towards a value corresponding to a two-electron electrode reaction. A similar result was obtained when 2,6-lutidine was used instead of pyridine. The effect of an acidic medium was also studied by addition of anhydrous CF_3COOH to the electrolytic solutions. The results are shown in Fig. 5. Increasing amounts of CF_3COOH produced a decrease in $i^a_{p,I}$, while the peak potential ($E^a_{p,I}$) shifted to more positive values. This was expected, since in an acidic medium the free amine forms a protonated species which is electrochemically inactive.

Double Potential-Step Chronoamperometry (DPSCA). Figure 6 shows the typical current-time curve obtained in the DPSCA's experiment of the PA system. In this case, the electrode potential (E_1) was first set at the potential region where no oxidation of PA occurs substantially and then the potential was stepped to the potential (E_2) at which the oxidation of PA is

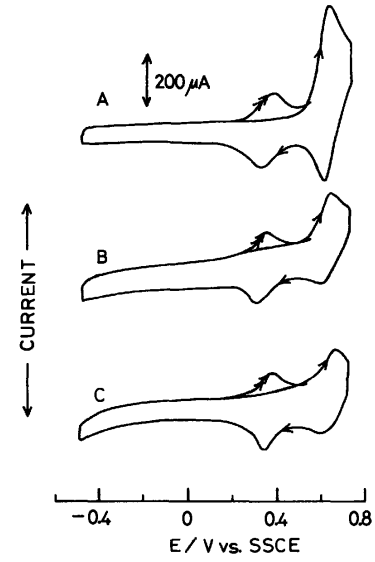

Fig. 5. Cyclic voltammograms of PA in the presence and absence of CF_3COOH. Concentration of PA: 1.0 mM. Concentration of CF_3COOH: (A): 0, (B): 1.0, and (C): 10.0 mM. Scan rate: 1 V s^{-1}. Other experimental conditions are the same as in Fig. 2.

diffusion-controlled and for a given period (τ) the electrode potential was held at this potential, and after that the electrode potential was re-stepped to the potential (E_3) at which the reduction of the electrogenerated PA^+ is diffusion-controlled. Typically, E_1=−0.2 V, E_2=0.7 V, and E_3=0.4 V vs. SSCE. However, it is not easy to choose appropriately the potentials E_2 and E_3, as can be seen from the cyclic voltammograms shown in Fig. 2. The reasons are as follows: (i) the potential regions corresponding to E_2 and E_3 are narrow due to the occurrence of the succeeding oxidation or reduction process and (ii) the peak potentials ($E^c_{p,I}$ and $E^a_{p,I}$) corresponding to $i^c_{p,I}$ and $i^a_{p,I}$ shift to more cathodic and anodic potentials, respectively, with shortening the time window of the

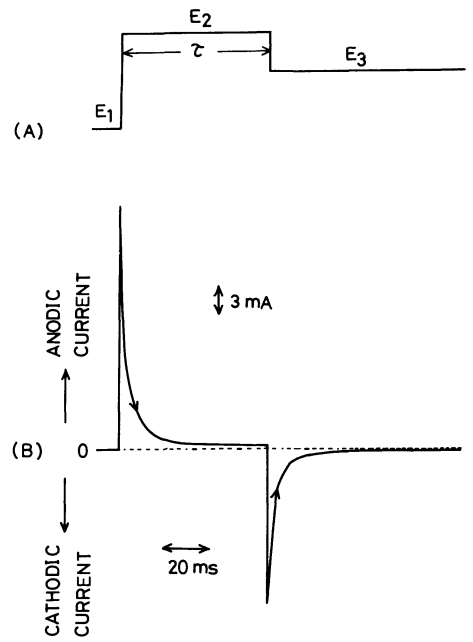

Fig. 6. (A) Typical potential-step mode used in the DPSCA measurement of the PA system. $E_1=-0.2$, $E_2=0.7$, and $E_3=0.4$ V vs. SSCE. Potential-step width (τ): 60 ms. (B) The current-time curve obtained for the potential-step application shown in A. Solution composition: 0.2 M $TBABF_4$+1.0 mM PA in acetonitrile. Electrode area: 0.20 cm^2.

measurement (i.e., τ). The latter phenomenon is apparent from Fig. 2 and is due to the fact that the electrode reaction of the PA/PA^+ redox couple is not completely reversible on the time scale of the measurement. To overcome these problems, the cyclic voltammogram of PA was observed at the scan rate which corresponds to the time scale of each DPSCA's experiment and then on the basis of the obtained cyclic voltammogram the most reasonable E_2 and E_3 potentials were chosen. Furthermore, by changing slightly the E_2 and E_3 potentials, the DPSCA's measurement was repeated. The current-time response obtained for the forward potential step, during which the oxidation of PA to PA^+ occurs, was found to nearly obey the chronoamperometric Cottrell equation, that is, a plot of i vs. $t^{-1/2}$ was almost linear and passed the origin.[66]

From the cyclic voltammetric behavior shown in Fig. 2, we assumed that the mechanism of the reaction of the initial stages of the electropolymerization of PA is apparently the "ECE" mechanism, that is, the oxidation reaction of PA to PA^+ (E), the follow-up chemical reaction consuming PA^+ (C) and the reduction (and oxidation) of the product (i.e., dimer) produced by the follow-up chemical reaction (E) occur continuously. We can assume various mechanisms for such chemical reactions interposed between successive electron transfers.[66,67] In this study, the mechanisms of the most popular two types were suggested for the follow-up chemical reaction; "radical-radical coupling" reaction and "radical-parent monomer coupling" reaction. Thus, the following two ECE mechanisms were assumed for the initial stages of the electropolymerization of PA.

Mechanism I:

$$A \overset{E_1^{0\prime}}{\rightleftharpoons} B \quad (1)$$

$$2B \xrightarrow{k} C \quad (2)$$

$$C \overset{E_2^{0\prime}}{\rightleftharpoons} D \quad (3)$$

Mechanism II:

$$A \overset{E_1^{0\prime}}{\rightleftharpoons} B \quad (1)$$

$$A + B \xrightarrow{k} C \quad (2')$$

$$C \overset{E_2^{0\prime}}{\rightleftharpoons} D \quad (3)$$

where Eqs. 1 and 3 show the heterogeneous electron-transfer reactions of the A/B couple and the C/D couple, respectively, the formal oxidation-reduction potentials of which are $E_1^{0\prime}$ and $E_2^{0\prime}$, respectively and $E_2^{0\prime}<E_1^{0\prime}$, and Eqs. 2 and 2′ indicate the chemical reactions which proceed at and/or in the vicinity of electrode surface. In the present case, A, B, C, and D correspond to PA, PA^+, $(PA)_2$ and $(PA)_2^+$, respectively, where $(PA)_2$ and $(PA)_2^+$ are the dimer of PA and its cation radical, respectively.

The distinction between Mechanism I and Mechanism II is possible by analyzing the dependence of the current ratio $i^c(t=2\tau)/i^a(t=\tau)$ on $\log(kC^\circ\tau)$,[67] where $i^c(t=2\tau)$ and $i^a(t=\tau)$ show the cathodic current (at $t=2\tau$) for the reduction of PA^+ to PA and the anodic current (at $t=\tau$) for the oxidation of PA to PA^+, respectively, in the DPSCA's current-time curves, τ is the potential-step width, and k is the apparent rate constant of the reactions expressed by Eqs. 2 and 2′. The theoretical curves[67] representing the relations between $i^c(t=2\tau)/i^a(t=\tau)$ and $\log(kC^\circ\tau)$ for Mechanisms I and II are shown in Fig. 7 together with the experimental plots. As can be expected from these theoretical curves,[67] the examination of the dependences of $i^c(t=2\tau)/i^a(t=\tau)$ on $\log(kC^\circ\tau)$ at larger values of $\log(kC^\circ\tau)$ allowed us to determine which of the two mechanisms more suitably applies to the initial stages of the follow-up chemical reaction. The experimentally available quantity $i^c(t=2\tau)/i^a(t=\tau)$ is plotted vs. $\log(C^\circ\tau)$. By overlaying the experimental and theoretical plots and by appropriately shifting the experimental plot along the abscissa and ordinate of the theoretical plot, the two can be superimposed. The relative location of the experimental and theoretical axes permits the evaluation of the rate constant, k.

The resulting plots of $i^c(t=2\tau)/i^a(t=\tau)$ vs. $\log(C^\circ\tau)$ seem to fall on a continuous curve which represents

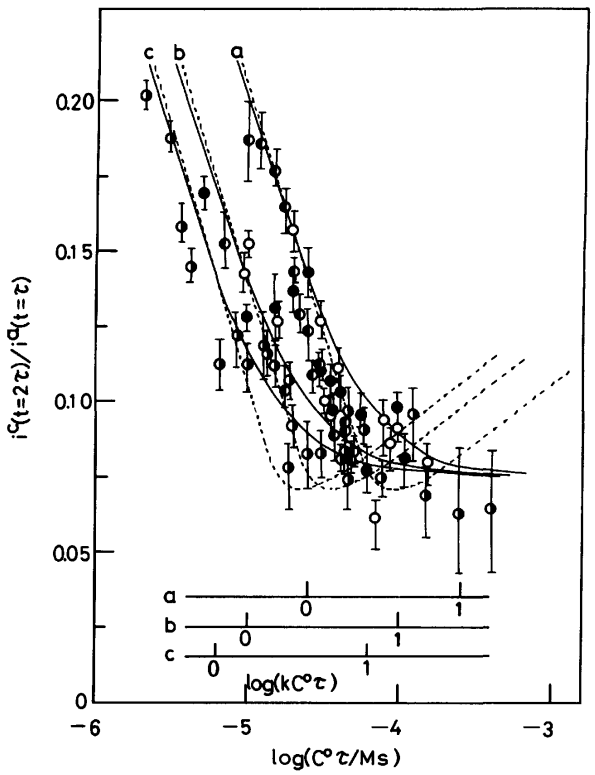

Fig. 7. Polts of $i^c(t=2\tau)/i^a(t=\tau)$ vs. $\log(C^\circ\tau)$. Solid and dashed curves indicate the theoretical $i^c(t=2\tau)/i^a(t=\tau)-\log(kC^\circ\tau)$ curves for Mechanism I and Mechanism II, respectively. The curves a, b, and c correspond to $k=0.4\times10^5$, 1.0×10^5, and 1.6×10^5 $M^{-1}s^{-1}$, respectively. Closed circles indicate the experimental data. Supporting electrolyte: 0.2 M $TBABF_4$. Concentration of PA: (●): 0.5, (○): 1.0, (◑): 5.0, and (◐): 10.0 mM. Widths of error bars indicate uncertainties in the measurements of $i^c(t=2\tau)/i^a(t=\tau)$.

the $i^c(t=2\tau)/i^a(t=\tau)-\log(kC^\circ\tau)$ relation for Mechanism I rather than that for Mechanism II, irrespective of the used values of C° and τ. In this case, the C°'s used were 0.50, 1.0, 5.0, and 10.0 mM, and the τ's were arbitrarily changed in the range of ca. 0.5 to 100 ms. Using the overlay matching technique just described the experimental points were matched with the theoretical curve. From the comparison of these experimental and theoretical curves, the value of k was estimated to be $(1.0\pm0.8)\times10^5$ $M^{-1}s^{-1}$.

Discussion

From the data obtained above, one can see that the initial-stage process of the electropolymerization of PA is symbolized as an ECE type of mechanism, and that the chemical reaction interposed betweeen successive electron transfers is the radical-radical coupling (PA^+-PA^+ coupling) reaction rather than the radical-parent monomer coupling (PA^+-PA coupling) reaction. Further, from the previous paper,[36] the coupling of PA^+'s is considered to occur at the 1- and 6- positions and/or the 1- and 8- positions. The mechanistic scheme for an electropolymerization via such a radical-radical coupling seems to be familiar in the electropolymerization of many aromatic compounds.[41,45,46,55,61,64,72,73] In the case of these electropolymerization, when the electrode oxidation reaction occurs, the radical cation concentration at the anode surface is high, whereas the concentration of parent monomer is low, rendering reactions between radical cations more probable than their reactions with parent monomers. This may be due to the fact that the radical-radical coupling reaction is likely to be faster than the diffusion of the parent monomer into the vicinity of the electrode. Therefore, the situation under consideration is very different from typical polymerization reactions occurring in the bulk of a solution, where the concentration of parent monomer is always much higher than those of the reactive intermediates (such as radical ions).

Two types of electrochemical polymerizations have seemed to be recently accepted;[55,74-77] one is the electrochemically initiated polymerization[75-77] and the other is the stoichiometric electrochemical polymerization.[55,74] In the former case, the initiators of polymerization are formed by the heterogeneous electron-transfer reaction of parent monomers and then the propagation reaction, chain-transfer reaction, termination reaction, etc. are thought to occur as in usual chemical polymerization reactions. In the latter case, on the other hand, the reactive intermediates are formed by the heterogeneous electron-transfer reactions of parent monomers as well as the products (the aromatic dimer, the higher molecular weight oligomers, etc.) and the electropolymerization via the reactions between them proceeds. The stoichiometric electrochemical polymerization was first described with polypyrrole by the IBM research group[55,74] and since then, it has been reported that it is applicable to the heterocyclic compounds such as pyrrole, thiophene, indole and benzo[*b*]thiophene,[38,55,72-74] the nonbenzenoid aromatic hydrocarbons such as azulene,[55,78] and the polycyclic aromatic hydrocabons such as pyrene and fluorene.[37-39,55] The electrochemical polymerization of PA is also regarded as a stoichiometric electrochemical polymerization. In general, such a stoichiometric electrochemical polymerization is symbolized as $E(CE)_n$ on the basis of an extension of customary electrochemical abbreviation.[55,65] In the present study, the initial stages of the electropolymerization of PA were elucidated as an ECE mechanism. Of course, note that further reactions proceed actually as can be seen from the fact that the degree of the polymerization of PA is ca. 8.[36]

Further, it is remarkable that the cyclic voltammetric responses for the oxidation of PA were varied by the presence or absence of the basic or acidic additives. An increase of pyridine (or 2,6-lutidine)

concentration produces an increase in $i^a_{p,I}$ towards about twice the $i^a_{p,I}$ value in the absence of pyridine (or 2,6-lutidine). These additives are stronger bases than PA in acetonitrile and would replace it as proton acceptor. Then, the overall reaction corresponding to the first anodic peak may be considered as a two-electron process, as being previously suggested for the anodic oxidation of 1-naphthylamine in acetonitrile[80,81] and would thus be represented by the following equation:

$$2PA + B \rightleftarrows D^{2+} + 2BH^+ + 4e^- \quad (4)$$

where B is the basic additives, BH^+ is the protonated form of B and D^{2+} is the dicationic dimer of PA. In contrary, the addition of the acidic additives such as CF_3COOH to the electrolytic solution of PA caused a decrease in $i^a_{p,I}$ and a shift of $E^a_{p,I}$ to more anodic values. This may be understood considering that if PA is protonated in an acidic medium, it becomes electroinactive. The similar behaviors have been reported for the anodic oxidation of the other aromatic compounds (e.g., 2-fluorenamine,[79] 1-naphthylamine,[80,81] *o*- and *p*-phenylenediamine,[64,82] and aniline[83]) in nonaqueous solutions. From a viewpoint of the preparation of the poly(1-pyrenamine) film on electrode surfaces, it is preferable to electrolyze PA in the presence of basic additives, as reported previously.[36]

Finally, we demonstrate that the DPSCA technique used in this study would be successfully applicable to the kinetic study (e.g., the determination of mechanistic pathways and associated chemical rate) of the initial stages of the electropolymerization of many aromatic compounds other than PA.

This work was partially supported by Grant-in-Aid for Scientific Research No. 60211011, for Noboru Oyama, from the Ministry of Education, Science, and Culture and the Nissan Science Foundation.

References

1) A. Volkov, G. Tourillon, P. C. Lacaze, and J. E. Dubois, *J. Electroanal. Chem.*, **115**, 279 (1980).
2) R. A. Bull, R. R. Fan, and A. J. Bard, *J. Electrochem. Soc.*, **130**, 1636 (1983).
3) T. Skotheim, I. Lundström, and J. Prajza, *J. Electrochem. Soc.*, **128**, 1625 (1981).
4) R. Noufi, A. J. Nozik, J. White, and L. F. Warren, *J. Electrochem. Soc.*, **129**, 2261 (1982).
5) P. G. Pickup and R. W. Murray, *J. Electrochem. Soc.*, **131**, 833 (1984).
6) J. E. Dubois, P. C. Lacaze, and M. C. Pham, *J. Electroanal. Chem.*, **177**, 233 (1981) and references therein.
7) F. Garnier, G. Tourillon, M. Gazard, and J. E. Dubois, *J. Electroanal. Chem.*, **148**, 299 (1983).
8) T. Kobayashi, H. Yoneyama, and H. Tamura, *J. Electroanal. Chem.*, **161**, 419 (1984).
9) A. J. Heeger, "Electroactive Polymers," Part 1, Ecole d'Hiver, Font-Romeu, France (1982), p. 3.
10) P. Burgmayer and R. W. Murray, *J. Electroanal. Chem.*, **147**, 339 (1983).
11) Y. Ohnuki, H. Matsuda, T. Ohsaka, and N. Oyama, *J. Electroanal. Chem.*, **158**, 55 (1983).
12) N. Oyama, Y. Ohnuki, K. Chiba, and T. Ohsaka, *Chem. Lett.*, **1983**, 1759.
13) N. Oyama, T. Ohsaka, and T. Shimizu, *Anal. Chem.*, **57**, 1526 (1985).
14) T. Ohsaka, T. Okajima, and N. Oyama, *J. Electroanal. Chem.*, **200**, 159 (1986).
15) T. Ohsaka, K. Chiba, and N. Oyama, *Nippon Kagaku Kaishi*, **1986**, 457.
16) N. Oyama, T. Ohsaka, and M. Nakanishi, *J. Macromol. Sci.-Chem.*, in press.
17) M. Kaneko, K. Okuzumi, and A. Yamada, *J. Electroanal. Chem.*, **183**, 407 (1985).
18) S. Glenis, G. Tourillon, and F. Garnier, *Thin Solid Films*, **122**, 9 (1984).
19) M. Josowicz and J. Janata, *Anal. Chem.*, **58**, 514 (1986).
20) G. Horowitz and F. Garnier, *J. Electrochem. Soc.*, **132**, 634 (1985).
21) F-R. F. Fan and A. J. Bard, *J. Electrochem. Soc.*, **133**, 301 (1986).
22) O. Inganäs and I. Lundström, *J. Electrochem. Soc.*, **130**, 1129 (1984).
23) H. Yoneyama, K. Wakamoto, and H. Tamura, *J. Electrochem. Soc.*, **132**, 2414 (1984).
24) G. P. Kittlesen, H. S. White, and M. S. Wrighton, *J. Am. Chem. Soc.*, **106**, 7389 (1984).
25) W. R. Heineman, H. J. Wieck, and A. M. Yacynych, *Anal. Chem.*, **52**, 345 (1980).
26) A Kitani, J. Yano, and K. Sasaki, *Chem. Lett.*, **1984**, 1565.
27) R. J. Waltman, J. Bargon, and A. F. Diaz, *J. Phys. Chem.*, **87**, 1459 (1983).
28) G. Tourillon and F. Garnier, *J. Electroanal. Chem.*, **135**, 173 (1982).
29) P. Mourcel, M. C. Pham, P. C. Lacaze, and J. E. Dubois, *Electroanal. Chem.*, **145**, 467 (1982).
30) P. G. Pickup and R. A. Osteryoung, *J. Am. Chem. Soc.*, **106**, 2294 (1984).
31) P. K. Ghosh and T. G. Spiro, *J. Electrochem. Soc.*, **128**, 1281 (1981).
32) J. M. Calvert, R. H. Schmehl, B. P. Sullivan, J. S. Facci, T. J. Meyer, and R. W. Murray, *Inorg. Chem.*, **22**, 2151 (1983).
33) C. D. Ellis, L. D. Margerum, R. W. Murray, and T. J. Meyer, *Inorg. Chem.*, **22**, 1283 (1983).
34) T. Ohsaka, Y. Ohnuki, N. Oyama, G. Katagiri, and K. Kamisako, *J. Electroanal. Chem.*, **161**, 399 (1984).
35) Y. Ohnuki, H. Matsuda, and N. Oyama, *Nippon Kagaku Kaishi*, **1984**, 1801.
36) N. Oyama, K. Hirabayashi and T. Ohsaka, *Bull. Chem. Soc. Jpn.*, **59**, 2071 (1986).
37) R. J. Waltman, A. F. Diaz, and J. Bargon, *J. Electrochem. Soc.*, **131**, 740 (1984).
38) R. J. Waltman and A. F. Diaz, *J. Electrochem. Soc.*, **132**, 631 (1985).
39) R. J. Waltman and J. Bargon, *J. Electroanal. Chem.*, **194**, 49 (1985).
40) A. Desbene-Monvernay, J. E. Dubois, and P. C.

Lacaze, *J. Electroanal. Chem.*, **189**, 51 (1985).
41) E. Tsuchida, H. Nishida, and T. Maekawa, *J. Macromol. Sci.-Chem.*, **A21**, 1081 (1984).
42) M. Kaya, A. Kitani, and K. Sasaki, *Chem. Lett.*, **1986**, 147.
43) R. M. Penner and C. R. Martin, *J. Electrochem. Soc.*, **133**, 310 (1986).
44) T. Komori, T. Nonaka, and T. Fuchigami, *Chem. Lett.*, **1986**, 11.
45) D. M. Mohilner, R. N. Adams, and W. J. Argersinger, Jr., *J. Am. Chem. Soc.*, **84**, 3618 (1962).
46) E. M. Genies, G. Biden, and A. F. Diaz, *J. Electroanal. Chem.*, **149**, 101 (1983).
47) K. K. Kanazawa, A. F. Diaz, R. H. Geiss, W. D. Gill, K. F. Kwak, and J. A. Logan, *J. Chem. Soc., Chem. Commun.*, **1979**, 854.
48) M. Lapkowski, J. Zak, and J. W. Strojek, *J. Electroanal. Chem.*, **145**, 173 (1983).
49) I. Rubinstein, *J. Electrochem. Soc.*, **130**, 1506 (1983).
50) H. O. Finklea and R. S. Vithange, *J. Electroanal. Chem.*, **161**, 283 (1984).
51) G. Tourillon, P. C. Lacaze, and J. E. Dubois, *J. Electroanal. Chem.*, **100**, 247 (1979).
52) A. F. Diaz, J. I. Castillo, K. K. Kanazawa, and J. A. Logan, *J. Electroanal. Chem.*, **133**, 233 (1982).
53) A. F. Diaz and J. I. Castillo, *J. Chem. Soc., Chem. Commun.*, **1980**, 397.
54) G. Tourillon and F. Garnier, *J. Electroanal. Chem.*, **161**, 407 (1984).
55) J. Bargon, S. Mohmand, and R. J. Waltman, *IBM J. Res. Dev.*, **27**, 330 (1983).
56) A. F. Diaz and B. Hall, *IBM J. Res. Dev.*, **27**, 342 (1983).
57) A. Kitani, J. Izumi, J. Yano, Y. Hiromoto, and K. Sasaki, *Bull. Chem. Soc. Jpn.*, **57**, 2254 (1984).
58) A. F. Diaz and J. A. Logan, *J. Electroanal. Chem.*, **111**, 111 (1980).
59) K. Murano and K. Suzuki, *J. Chem. Soc., Chem. Commun.*, **1984**, 238.
60) O. Niwa, M. Hikita, and T. Tamamura, *Appl. Phys Lett.*, **46**, 444 (1985).
61) F. Bruno, M. C. Pham, and J. E. Dubois, *Electrochim. Acta*, **22**, 451 (1977).
62) D. Laurin and G. Pdarravano, *J. Polym. Sci.*, Part C, 103 (1968).
63) B. L. Funt and T. J. Blain, *J. Polym. Sci., Part A-1*, **8**, 3339 (1970).
64) V. Solis, T. Iwasita, and M. C. Giordano, *J. Electroanal. Chem.*, **105**, 169 (1979).
65) R. N. Adams, *Acc. Chem. Res.*, **2**, 175 (1969).
66) For example; A. J. Bard and L. R. Faulkner, "Electrochemical Methods, Fundamentals and Applications," Wiley, New York (1980).
67) M. K. Hanafey, R. L. Scott, T. H. Ridgway, and C. N. Reilley, *Anal. Chem.*, **50**, 116 (1978).
68) C. Amatore, M. Gareil, and J. M. Savéant, *J. Electroanal. Chem.*, **147**, 1 (1983).
69) T. Ohsaka, T. Sotomura, H. Matsuda, and N. Oyama, *Bull, Chem. Soc. Jpn.*, **56**, 3065 (1983).
70) W. M. Schwarz and I. Shain, *J. Phys. Chem.*, **69**, 30 (1965).
71) L. S. Marcoux, J. M. Fritsch, and R. N. Adams, *J. Am. Chem. Soc.*, **89**, 5766 (1967).
72) R. J. Waltman, A. F. Diaz, and J. Bargon, *J. Electrochem. Soc.*, **131**, 1452 (1984).
73) R. J. Waltman, A. F. Diaz, and J. Bargon, *J. Phys. Chem.*, **88**, 4343 (1984).
74) A. F. Diaz and K. K. Kanazawa, "Extended Linear Chain Compounds," ed by J. Miller, Plenum Press, New York (1982), vol. 3, p. 417.
75) G. Parravano in "Organic Electrochemistry," ed by M. N. Baizer, Marcel Dekker, New York (1973), p. 947.
76) B. L. Funt and J. Tanner, *Tech. Chem. (N.Y.)*, **5**, 599 (1975).
77) R. V. Subramanian and J. J. Jakubowski, *J. Polym. Eng. Sci.*, **18**, 590 (1978).
78) J. Bargon, S. Mohmand, and R. J. Waltman, *Molec. Cryst. Liq. Cryst.*, **93**, 279 (1983).
79) K. Yasukouchi, I. Taniguchi, H. Yamaguchi, K. Miyaguchi, and K. Horie, *Bull. Chem. Soc. Jpn.*, **52**, 3208 (1979).
80) N. Vettorazzi, J. J. Silber, and L. Sereno, *J. Electroanal. Chem.*, **158**, 89 (1983).
81) N. Vettorazzi, J. J. Silber, and L. Sereno, *J. Electroanal. Chem.*, **125**, 459 (1981).
82) V. Solis, T. Iwasita, and M. C. Giordano, *J. Electroanal. Chem.*, **73**, 91 (1976).
83) S. Wawzonek and T. W. McIntyre, *J. Electrochem. Soc.*, **114**, 1025 (1967).
84) At the present stage, we have no direct evidence for the formation of the cation radical ($PA^{\ddagger}$) by the first anodic oxidation of PA, but according to a number of studies[37-39,45,46,52,55,64,71-74,78,80-82,85-89] concerning the electrochemical oxidation of aromatic hydrocarbons with or without functional groups such as amino and hydroxyl groups, the formation of $PA^{\ddagger}$ seems not to be unexpected.
85) B. Speiser and A. Rieker, *J. Electroanal. Chem.*, **147**, 205 (1983).
86) E. T. Seo. R. F. Nelson, J. M. Fritsch, L. S. Marcoux, D. W. Leedy, and R. N. Adams, *J. Am. Chem. Soc.*, **88**, 3498 (1966).
87) M. E. Peover and B. S. White. *J. Electroanal. Chem.*, **13**, 93 (1967).
88) E. S. Pysh and N. C. Yang, *J. Am. Chem. Soc.*, **85**, 2124 (1963).
89) M. J. Drews, P. S. Wong, and P. R. Jones, *J. Am. Chem. Soc.*, **94**, 9122 (1972).

 © 1986 The Chemical Society of Japan Bull. Chem. Soc. Jpn., 59, 3431—3437 (1986)

High-Temperature Reaction of NH_3-N_2O System in Shock Waves

Nobuyuki FUJII, Syuji UCHIDA, Hisaaki SATO, Shiro FUJIMOTO† and Hajime MIYAMA*
Department of Materials Science and Technology, The Technological University of Nagaoka, Kamitomioka, Nagaoka 940-21
(Received May 21, 1986)

The high-temperature reaction of NH_3 with N_2O in shock waves was investigated by measuring ultaviolet absoption of NH_3 and OH, and infrared emission of N_2O, in the temperature range of 1700—2300 K on the mixture of NH_3-N_2O diluted with large amount of argon. A comparison of the observed decays of NH_3 and N_2O and the formation of OH with those obtained by computer simulation behind the incident shock wave was carried out. From the comparison, the rate constants of the following elementary reactions were determined: $NH_3+O\rightarrow NH_2+OH[k_4=10^{12.5}\exp(-25.5\,kJ/RT)\,cm^3\,mol^{-1}\,s^{-1}]$; $NH_3+OH\rightarrow NH_2+H_2O[k_5=10^{12.5}\exp(-8.4\,kJ/RT)\,cm^3\,mol^{-1}\,s^{-1}]$.

The high-temperature oxidation of NH_3 has been studied by many researchers,[1-4] and it was reported that NH_2 radicals play important roles.[1] Among the formation reaction of NH_2, the most important reactions in the initial stage of the reaction, $NH_3+O\rightarrow NH_2+OH$ and $NH_3+OH\rightarrow NH_2+H_2O$ have been investingted by several reserchers and their rate constants have been recommended.[5,6] However, larger values of the rate constants have also been reported.[4,7-9]

The objective of the present work is to examine the above two rate constants precisely by measuring spectroscopically the concentrations of NH_3, N_2O, and OH in the high-temperature reaction of NH_3-N_2O system in shock waves. Since the high temperature dissociation of N_2O is the initiation reaction of above reaction system and its rate constants have been determined exactly,[8,10,11] the decomposition of N_2O was studied in the incident shock waves at first. Simulatin of the reaction was carried out and the results were compared with the experiments. After confirming the accuracy of this experimental technique by the comparison, reaction of NH_3-N_2O was studied in the incident shock waves.

Experimental

The shock tube used in this study is made of stainless steel tubing of 46 mm internal diameter, consisting of a test section of 3.6 m long, a high-pressure section of 2 m long and a dump tank located at the end of the test section. The shock tube had a leak rate less than 5×10^{-4} Torr min^{-1} (1 Torr=133.322 Pa) and was evacuated to less than 2×10^{-4} Torr before each experiment. Polyester diaphragms were pressure burst using H_2 driver gas. The incident shock wave velocity was measured by four piezo-electric gauges located at intervals of 200 mm and a time counter, and the shock parameters were calculated from the shock velocity. An observation section is installed at 3.1 m down stream from the diaphragm. The time history of NH_3 was monitored by measuring the ultraviolet absorption of NH_3 at 200 nm by using an optical system consisting of a D_2 lamp, a monochromator, and a photomultiplier. N_2O time history was monitored by the infrared emission of N_2O at 4.52 μm with an InSb detector through an interference filter (half width: 0.18 μm). Also at the same location, the pressure profile was measured by a piezoelectric gauge. On the other hand, simultaneously with measurement of NH_3, the formation of OH radical was observed by resonant absorption at 306 nm by using OH lamp powered by a microwave discharge in a flow of H_2O vapor. Calibration of OH absorption was carried out by the exeriment of shock heated H_2-O_2-Ar mixtures. These signals were displayed on a digital storage oscilloscope. Experiments were carried out on mixtures of N_2O (1%) and argon (99%) and of NH_3 (1—2%), N_2O (0.3—1%) and argon (97.6—98.7%). The experimental conditions were; 1700—2300 K and 0.9—2.1 atm as summarized in Table 1.

Results and Discussion

Dissociation of N_2O. High-temperature decom-

Table 1. Experimental Conditions

Mixture	N_2O %	NH_3 %	Ar %	T_{20} K	p_{20} atm
I	1.0	0	99.0	1690—2010	1.89—2.04
II	0.3	1.0	98.7	1690—2310	1.78—2.04
III	1.0	1.0	98.0	2000—2260	2.04—2.14
IV	0.4	2.0	97.6	1860—2290	0.91—1.05
V	1.0	1.0	98.0	1770—2040	1.92—2.14

1 atm=101325 Pa.

† Present address: Department of Chemistry, National Defense Academy, Hashirimizu, Yokosuka 239.

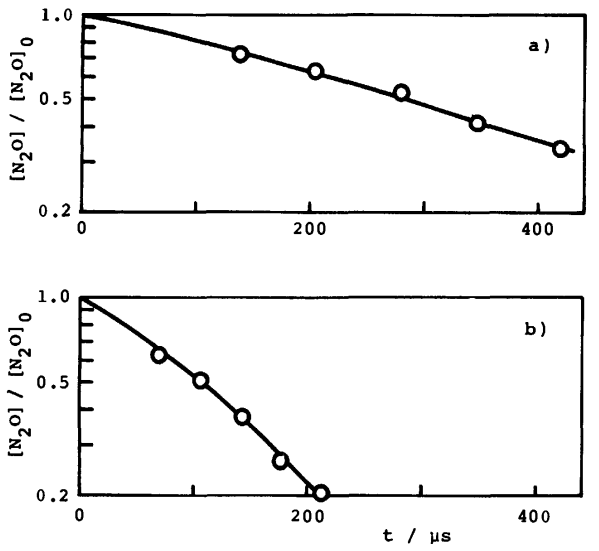

Fig. 1. Examples of the comparison of the experimentally measured N_2O first order decays in mixture I (symbols) with simulated ones (lines). a): $T_0=1855$ K, $p_0=2.01$ atm, b): $T_0=2010$ K, $p_0=1.93$ atm.

position of N_2O has been studied by many researchers[8,10,11] and its reaction scheme is well-established. That is, the following elementary reactions (1)—(3) are important at the inital stage of the reaction;

(1) $N_2O + M \longrightarrow O + N_2 + M$,
(2) $N_2O + O \longrightarrow NO + NO$,
(3) $N_2O + O \longrightarrow N_2 + O_2$.

When the O atoms are in the steady state, the decomposition rate of N_2O is given by the following equation;[8,10]

$$d[N_2O]/dt = -2k_1[N_2O][M], \quad (1)$$

where [M] is the concentration of the third body. Accordingly, the rate constant of the dissociation of N_2O is obtained as follows by integrating Eq. 1;

$$k_1 = (2[M]t)^{-1}\ln([N_2O]_0/[N_2O]), \quad (2)$$

where subscript 0 shows the initial condition.

In the present experiment, the decay profile of N_2O infrared emission intensity measured behind the incident shock wave deviated from the first-order rate law as the reaction proceeded. Examples of the decay of N_2O are shown in Fig. 1. From the initial slope of the emission, the rate constants for the dissociation of N_2O were obtained according to Eq. 2. They are listed with the experimental conditions in Table 2. The Arrhenius plot of k_1 is shown in Fig. 2, together with the values recommended by Baulch et al.,[10] by Just,[11] and by Hanson et al.[8] Agreement between the values obtained in the present experiment and the recommended values are very good. From the plot of Fig. 2, the following Arrhenius expression was obtained;

Table 2. Experimental Results for Mixture I

Run	T_{20} / K	p_{20} / atm	$[M]_{20}$ / mol cm^{-3}	k_1 / cm^3 mol^{-1} s^{-1}
1	1550	2.05	1.61×10^{-5}	3.64×10^{6}
2	1580	1.89	1.44	4.43×10^{6}
3	1680	1.92	1.39	1.38×10^{7}
4	1690	1.93	1.40	1.87×10^{7}
5	1800	2.02	1.38	5.02×10^{7}
6	1855	2.01	1.33	9.58×10^{7}
7	1929	1.89	1.20	1.74×10^{8}
8	2010	1.93	1.18	2.94×10^{8}

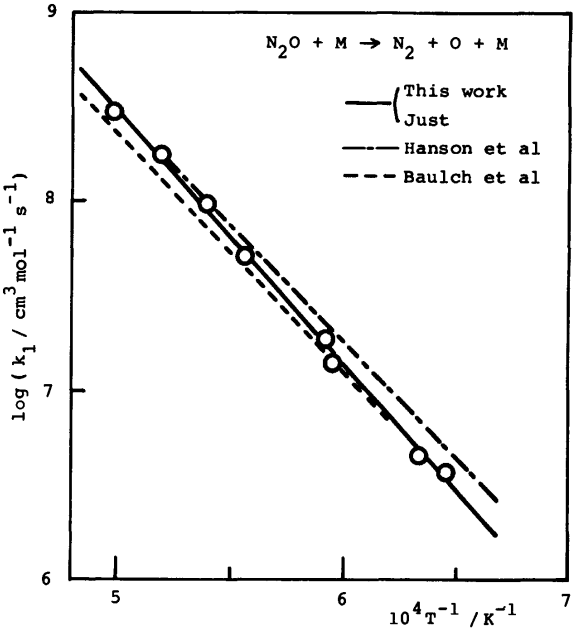

Fig. 2. Arrhenius plots of k_1.

$$k_1 = 10^{15.21}\exp(-257.7\ \text{kJ}/RT)\ \text{cm}^3\ \text{mol}^{-1}\ \text{s}^{-1}.$$

Then, the decay of N_2O was calculated by computer simulation by using elementary reactions (1)—(3) and their reverse reactions. In this calculation, the rate constant of Reaction (1) obtained in this experiment was used and values recently recommended by Hanson et al.[8] for Reactions (2) and (3) were adopted. In this simulation the heat of reaction and the correction for the nonideality of shocked flow caused by the boundary layer behind the incident shock front[12,13] were taken into account. The calculated decay profiles of N_2O agreed with the experiments as shown in Fig. 1. From the results, it was confirmed that the shock tube technique coupled with the above mentioned computer simulation had a good accuracy in the present experiment.

Reaction of NH_3 with N_2O. Reaction mechanism: The reaction of NH_3 with N_2O at high temperatures is initiated by the decomposition of N_2O and the main

Table 3. Reaction Schemes and Rate Parameters[a)]

Reaction	Mechanism A[6)]			Mechanism B[7)]		
	log A	B	E/kJ	log A	B	E/kJ
1. $N_2O + M \rightarrow N_2 + O + M$	15.21		257.7	23.84	−2.5	272.0
2. $N_2O + O \rightarrow NO + NO$	13.84		111.7			
3. $N_2O + O \rightarrow N_2 + O_2$	14.00		117.2			
4. $NH_3 + O \rightarrow NH_2 + OH$	12.49		25.5	13.34		37.2
5. $NH_3 + OH \rightarrow NH_2 + H_2O$	12.50		8.4	13.91		35.2
6. $NH_3 + NH_2 \rightarrow N_2H_3 + H_2$	11.90	0.5	90.4			
7. $N_2H_3 + M \rightarrow NH_2 + NH + M$	12.80		41.8			
8. $NH_2 + O \rightarrow NH + OH$	11.96	0.5	0	14.07	−0.5	0
9. $NH_2 + O \rightarrow HNO + H$				14.82	−0.5	0
10. $NH_2 + OH \rightarrow NH + H_2O$				11.70	0.5	8.3
11. $HNO + M \rightarrow H + NO + M$				16.25		203.7
12. $H + N_2O \rightarrow N_2 + OH$				13.88		63.2
13. $H + NH_3 \rightarrow NH_2 + H_2$				14.30		97.4

a) $k = AT^B\exp(-E/RT)$ in units of $cm^3\ mol^{-1}\ s^{-1}$.

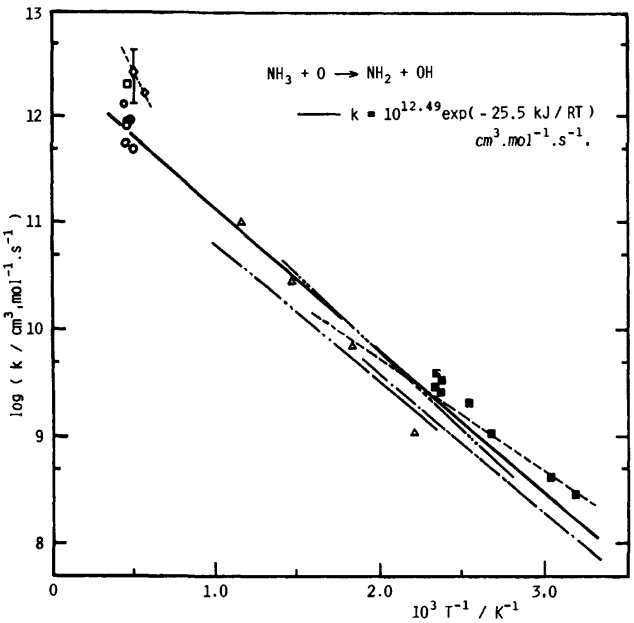

Fig. 3. Arrhenius plots of k_4. Solid line: this work, other lines : from Baulch et al.,[10)] ○: Fujii et al.,[6)] ◇: Salimian et al.,[7)] □: Saito et al.,[14)] ■: Kirchner et al.,[15)] △: Perry.[16)]

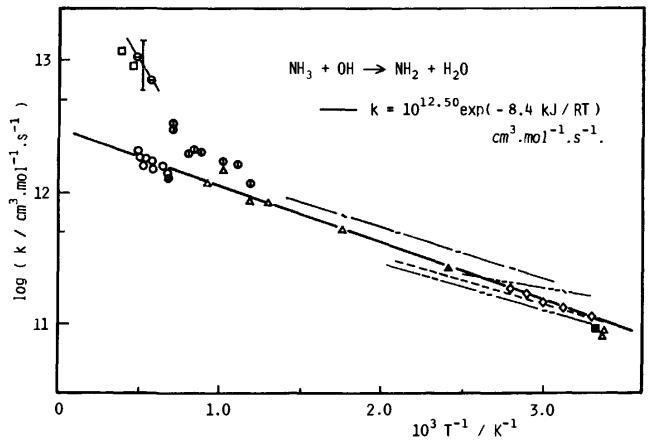

Fig. 4. Arrhenius plots of k_5. Solid line: this work, other lines, ●, △, ▲, ■: from Fujii et al.,[5)] ○: Fujii et al.,[5)] ⊖: Salimian et al.,[7)] □: Zabielski et al.,[9)] ◇: Stephens,[17)] ⓘ: Jeffries et al.[18)]

subsequent reactions are;

(4) $NH_3 + O \longrightarrow NH_2 + OH$, $\Delta H = 28.5\ kJ\ mol^{-1}$,

(5) $NH_3 + OH \longrightarrow NH_2 + H_2O$, $\Delta H = -42.6\ kJ\ mol^{-1}$.

The reaction scheme in the initial stage of this system, presented by Fujii et al. (Mechanism A)[6)] is shown in Table 3. Here, Reactions (1)—(3) are those of the decomposition of N_2O, Reactions (4)—(6) are main reactions for the consumption of NH_3 and Reactions (7) and (8) are the subsequent reactions. Also the scheme reported by Salimian et al. (Mechanism B)[7)] is shown in the table. In this scheme, Reaction (9) is included as the reaction of NH_2 with O, then H atom plays an imporant role for the formation of OH. Also, Salimian el al.[4)] reported the kinetic model including 60 reactions of the N-O, N-H, N-H-O, and O-H system (Mechanism B′). However, the rate constants of many of these reactions were not accurately known and their values were estimated for the simulation.

As for the rate constants k_4 and k_5, Fujii et al.[5)] obtained k_4 by measuring ultraviolet absorption of NH_3 in NH_3-H_2-O_2-Ar mixtures. Also, Fujii et al.[6)] obtained k_5 by measuring ultraviolet absorption of NH_3 and infrared emission of N_2O in NH_3-N_2O-Ar mixtures. On the other hand, Salimian et al.[7)] measured ultraviolet absorption of OH and infrared emission of NH_3 in NH_3-N_2O-Ar mixtures and obtained k_4 and k_5 simultaneously. Zabielski et al.[9)] mea-

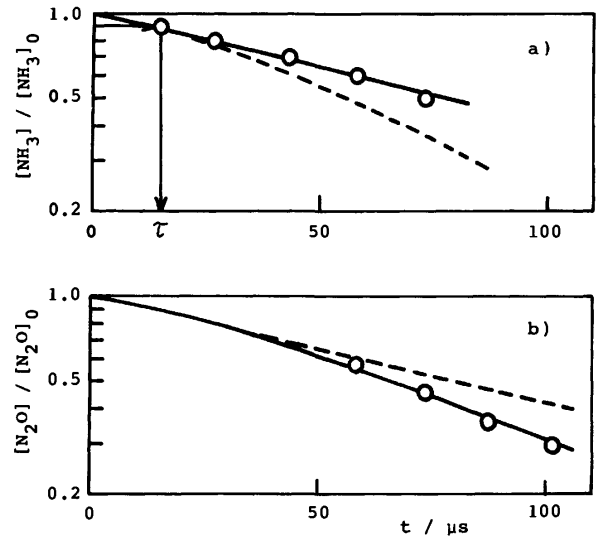

Fig. 5. Examples of the comparison of the experimentally obtained first order decays of NH_3 and N_2O in mixture III (symbols) with simulated ones (lines) T_0=2110 K, p_0=2.13 atm, a): NH_3, b): N_2O.

sured concentration profiles of NH_3, OH, and O in a low-pressure CH_4-O_2-Ar flat flame containing small amounts of NH_3 and obtained k_5 using k_4 given by Salimian et al.[7] The values of k_4 and k_5 by Salimian et al.[7] and k_5 by Zabielski et al.[9] were about 5 times as large as those recommended by Fujii et al.[5,6] Jefferies and Smith[18] measured k_5 over the range 840—1425 K by using an infrared laser pyrolysis technique (10.6 μm) with laser-induced fluolescence detection of OH. The values of k_5 at 1425 K were about 2 times larger than those by Fujii et al.[5] The Arrhenius plots of these rate constants are shown in Figs. 3 and 4, together with the values reported by other researchers. For the experimental data at high and low temperatures, nonlinear-Arrhenius expressions were adopted for k_4 by Salimian et al.[7] and for k_5 by Salimian et al.,[7] Zabielski et al.[9] and Jefferies et al.[18] In order to justify the experimental curved-Arrhenius expression, they calculated the rate constants by the transition state theory using some assumptions. The rate constants of other Reactions (6)—(8) have not yet been measured accurately.

Consumption of NH_3 and N_2O: The concentration of NH_3 decayed almost according to the first order rate law in NH_3-N_2O system. The concentration of N_2O decayed also according to the first-order rate law and the rate of the decay in the equimolar mixture of NH_3 and N_2O was almost similar to that of the decomposition of N_2O. Examples of the first order decays of NH_3 and N_2O are shown in Fig. 5.

In order to examine the contribution of each elementary reaction to the decay rate of NH_3, the sensitivity checks described previously[1] were applied as follows. The decay of NH_3 was computed using

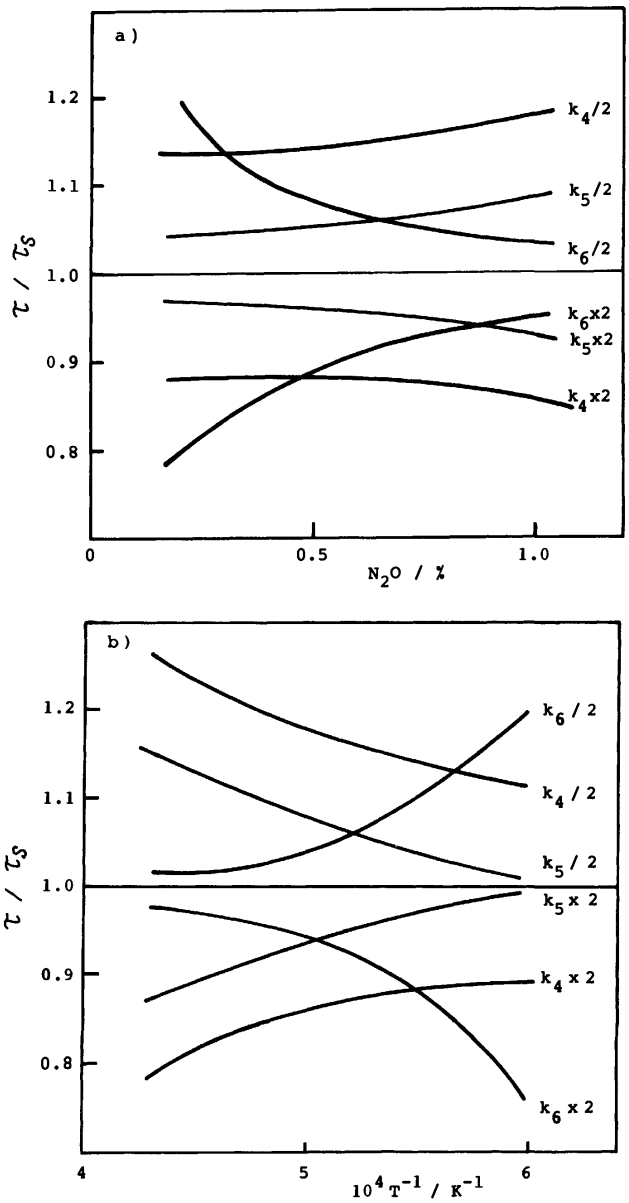

Fig. 6. Sensitivity check of the elementary reactions of (4), (5), and (6) for NH_3 consumption in NH_3-N_2O-Ar mixture. τ_s: Calculated reaction time obtained using the standard rate constants cited in Table 3. τ: Calculated reaction time obtained using the doubled ($k\times2$) or halved ($k/2$) value of the standard rate constant of Reaction (4), (5), or (6), and the standard values for other reactions. a) N_2O concentration dependence of τ/τ_s, NH_3=1%, T=2000 K, p=2 atm. b) Temperature dependence of τ/τ_s, NH_3: N_2O: Ar=1 : 1 : 98, p=2 atm.

Mechanism A, by either halving or doubling the standard rate constant of each elementary reaction shown in Table 3, and keeping other rate constants unchanged. The computed reaction time required for 10% consumption of NH_3, τ in Fig. 5, was found to be very sensitive to the change in the rate constants of Reactions (1) and (4)—(6), but not sensitive to those of

Table 4. Experimental Results for Mixture III

Run	T_{20} / K	p_{20} / atm	τ / μs	$k_4 \times 10^{-11}$ / $cm^3\ mol^{-1}\ s^{-1}$
31	2000	2.06	28±2	4.8±1.5
32	2060	2.14	17±2	10.0±2.0
33	2110	2.05	18±2	7.2±2.0
34	2110	2.13	15±2	9.1±2.0
35	2190	2.15	12±2	5.7±3.0
36	2260	2.09	8±2	13.0±5.0

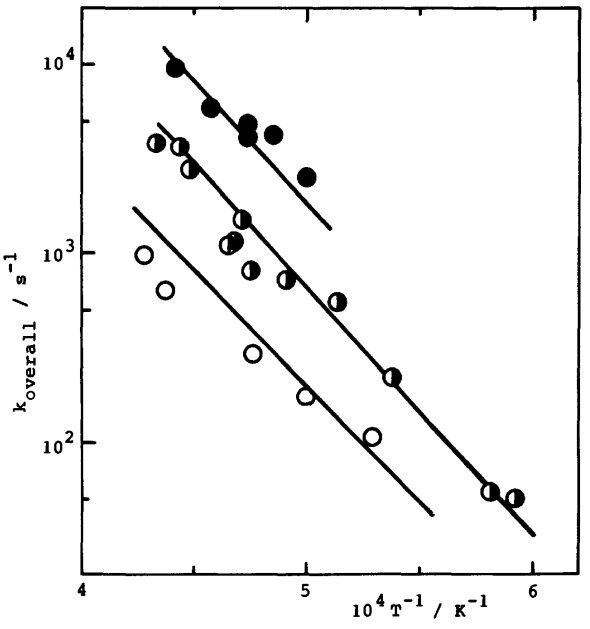

Fig. 7. Comparison of the measured overall rate constants for NH_3 (symbols) with calculated ones (lines). ○: Mixture II, ●: mixture III, ◑: mixture IV.

other elementary reactions. Examples of these results of the sensitivity checks comparing the effects by Reactions (4)—(6) are shown in Figs. 6 a) and b). From the figures, it is shown that the calculated reaction time τ is not sensitive to the rate constant of Reaction (6), when the N_2O concentration is higher than 1% (when NH_3 is 1%) and the temperature is higher than 2000 K. Therefore, mixtures I and II were omitted for the simulation to determine the value of k_4 without using reaction (6). Also, when the N_2O concentration is higher than that of NH_3, it is considered that the subsequent Reaction (12) becomes important. Therefore, N_2O rich mixtures was not examined in the present simulation to determine k_4 without using reaction (12). Based on the discussion, the mixture III was used for the simulation at first, in which only three Reactions (1), (4), and (5) were used.

The rate constant of Reaction (4) was determined by fitting the simulated τ value of NH_3 decay to the experimental one, where the rate constant k_1 determined in this experiment and k_5 of Fujii et al.[5] were

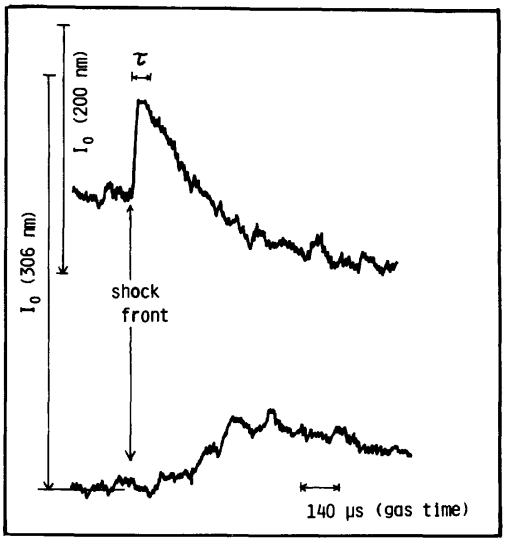

Fig. 8. Typical experimental records of NH_3 decay (upper trace) and OH formation (lower trace), NH_3: N_2O : Ar=1 : 1 : 98, T_0=1853 K, p_0=2.26 atm.

used. The rate constants of Reaction (4) obtained are shown in Table 4 and Fig. 4.

The decays of NH_3 and N_2O calculated by using reactions (1), (4), and (5) are shown by the dotted lines in Fig. 5. They agreed with the experimental values in the initial stage of the reaction. The deviation of the calculated curves from the experimental ones after the reaction time τ were improved by adding the subsequent Reactions (2), (3), and (6)—(8) to the reaction scheme, as shown by the solid lines in Fig. 5.

Computer simulatons using reactions (1)—(8) shown in Table 3 were also carried out for the mixtures II and IV, which were omitted for the simulation using reactions (1), (4), and (5) as described above. The time histories of NH_3 concentration obtained by the simulation almost agreed with the experimental ones, as well as in the case of III shown in Fig. 5. The overall rate constant for the first order decay of NH_3 was obtained according to the following equation;

$$-d[NH_3]/dt = k_{overall}[NH_3] \quad (3)$$

The comparison of the overall first order rate constant obtained by the simulation using Mechanism A with those obtained by the experiments are shown in Fig. 7.

From the results of the present study, it was found that the high temperature reaction of NH_3 with N_2O can be explained by the Reactions (1)—(8) shown in Table 3.

Formation of OH: The formation of OH were measured simultaneously with the decay of NH_3 in shock heated NH_3-N_2O equimolar mixtures. Typical experimental records of NH_3 and OH are shown in Fig. 8. Since the detection limit of OH absorption was about 5×10^{-10} mol cm^{-3}, high noise level prevented to

Table 5. Experimental Results of NH_3 Consumption and OH Formation for Mixture V

Run	T_{20} / K	p_{20} / atm	$\tau^{a)}$ / μs	$[OH]_{t=100}$ / mol cm^{-3}
51	1770	2.00	78±5	4.0×10^{-10}
52	1802	1.92	110±5	4.6
53	1841	2.10	84±5	8.0
54	1854	2.02	62±5	7.8
55	1876	2.14	54±5	8.3
56	1883	2.06	70±5	8.8
57	1953	2.00	42±5	8.2
58	1956	1.99	39±5	9.1
59	1953	2.02	38±5	1.1×10^{-9}
60	1990	2.00	28±5	2.0
61	2040	2.12	25±5	2.8

a) τ for 10% consumption of NH_3.

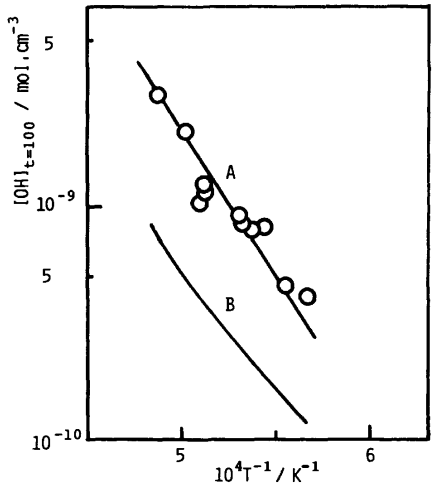

Fig. 9. Comparison of the experimental OH concentrations at $t=100$ μs (symbols) with those obtained by Mechanisms A and B (lines), NH_3 : N_2O : Ar= 1 : 1 : 98.

examine the OH formation in the very initial stage of the reaction. In order to evaluate the rate of OH formation, concentration of OH at $t=100$ μs, $[OH]_{t=100}$, were taken from the experimental record of OH. The value is shown in Table 5, together with τ value of NH_3 consumption.

In order to examine the rate constants of Reactions (4) and (5), calculations were performed using the above described two mechanisms A and B. A comparison of the experimental concentrations of OH at $t=100$ μs with calculated values are shown in Fig. 9. In this figure, the values calculated by Mechanism A agree well with the experiments, but those by Mechanism B are much lower than the experiments. Also, the changes of the computed concentrations of NH_3 and OH were compared with the experiments in the period of about 50% NH_3 consumption. Figures. 10 (I) and (II) show examples of comparison of the

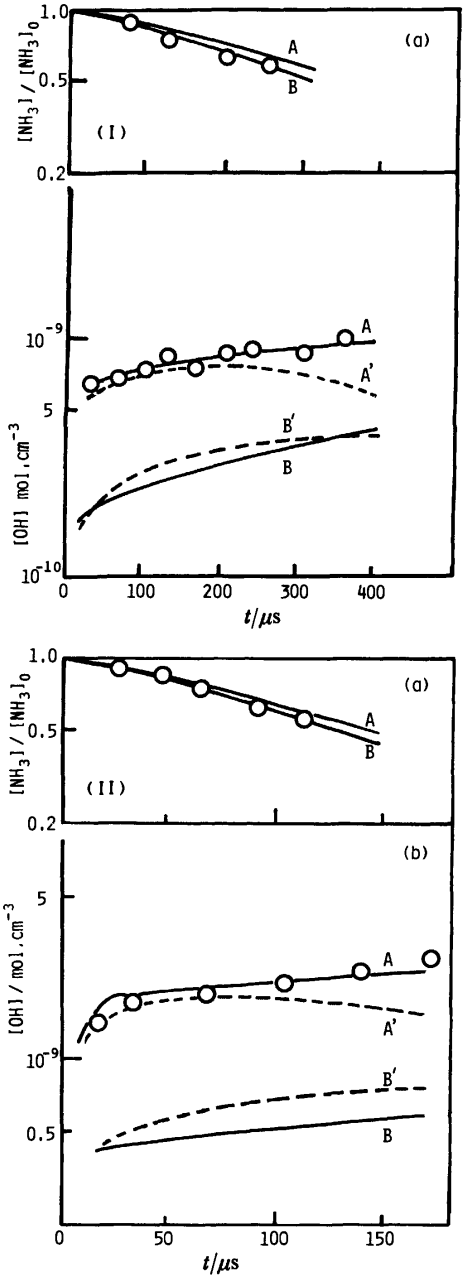

Fig. 10. Comparison of the experimental profiles (symbols) of (a) NH_3 (b) OH with those obtained by calculations (lines). Solid lines A and B are those calculated by Mechanisms A and B respectively. Broken lines A′ and B′ are those calculated by Mechanisms A′ and B′, respectively.
(I) NH_3 : N_2O : Ar=1 : 1 : 98, $T_0=1854$ K; $p_0=2.25$ atm, (II) $T_0=1990$ K; $p_0=2.08$ atm.

experimental profiles of NH_3 and OH with calculated ones. As shown in the figures, consumption of NH_3 calculated by Mechanism B are faster than those by Mechanism A, however both values are not very different from the experimental values. For those of OH formation, the profiles calculated by Mechanism A are much closer to the experimental profiles than those by Mechanism B as shown in the figures.

In addition, a calculation based on Mechanism A using the k_4 and k_5 values reported by Salimian et al.[7] and a calculation based on Mechanism B using the k_4 and k_5 values reported by Fujii et al.[5,6] were carried out. The former results were not very different from the results of the calculation based on Mechanism B listed in Table 3, while the latter results were similar to those of Mechnism A listed in Table 3, in the initial stage of the reaction.

The effects of the subsequent reactions on NH_3 consumption and OH formation were also calculated. As the subsequent reactions of Mechanism A, 54 reactions from the report by Salimian et al. (Mechanism B')[4] were adopted. The results of the calculation using 62 reactions and their reverse reactions (Mechanism A') were compared with the experiments. Examples of the calculated profiles of NH_3 consumption and OH formation by Mechanisms A' and B' are shown by broken lines A' and B' in Figs. 10 (I) and (II). They do not deviate appreciably from the original profiles A and B, respectively, in the initial stage of the reaction, inspite of including many reactions of which rate constants are not known accurately.

From the comparisons described above, it was found that the calculated OH profiles by Mechanism A are much closer to the experiments than those by Mechanism B, and the effects of the subsequent reactions on OH formation can be ignored in the initial stage of the reaction. Thus, the rate constans k_4 and k_5 determined from Mechanism A in the initial stage of the reaction are reasonable and those obtained by Salimian et al.[7] seem to have been overestimated.

It was reported that the amount of adsorbed NH_3 on the wall of stainless steel was several times the value calculated by assuming monomolecular layer adsorption.[19] In the experiments by Salimian et al., the concentration of NH_3 introduced into the shock tube was about 4×10^{-9} mol cm^{-3} at 300 K. In such a low concentration, the adsorption of NH_3 cannot be ignored. Since in the experiments of Jefferies et al.[18] the mixture was irradiated by a TEA CO_2 laser at 10.6 μm, there is a possibility that NH_3 molecules themselves decomposed by the laser irradiation and the decomposed products accelerate the consumption of OH. This might give higher k_5 value. Also, the curved Arrhenius plots calculated by the transition state theory were based upon the arbitrary selection of parameters.[7,9,18] From those reasons, linear expressions were preferred to the curved ones for Arrhenius plots of k_4 and k_5.

In conclusion, the linear Arrhenius expressions for the rate constants of Reactions (4) and (5) combining the values at low temperatures[5,6,16,17] are proposed as follows:

(4) $NH_3 + O \longrightarrow NH_2 + OH$

$$k_4 = 10^{12.5\pm0.4}\exp(-25.5\pm2.3\ \mathrm{kJ}/RT)\ \mathrm{cm^3\ mol^{-1}\ s^{-1}}$$

(5) $NH_3 + OH \longrightarrow NH_2 + H_2O$

$$k_5 = 10^{12.5\pm0.1}\exp(-8.4\pm0.1\ \mathrm{kJ}/RT)\ \mathrm{cm^3\ mol^{-1}\ s^{-1}}$$

This work was partially supported by a Research Grant from Tanikawa Foundation, to which the authors wish to express their thanks.

References

1) N. Fujii, H. Miyama, M. Koshi, and T. Asaba, "Eighteenth Symposium (International) on Combustion," The Combustion Institute, Pittsburgh (1981), p. 873.

2) A. M. Dean, J. E. Hardy, and R. K. Lyon, "Nineteenth Symposium (International) on Combustion," The Combustion Institute, Pittsburgh (1983), p. 97.

3) A. M. Dean, M. Chou, and D. Stern, *Int. J. Chem. Kinet.*, **16**, 633 (1984).

4) S. Salimian, R. K. Hanson, and C. H. Kruger, *Combust. Flame*, **56**, 83 (1984).

5) N. Fujii, H. Miyama, and T. Asaba, *Chem. Phys. Lett.*, **80**, 355 (1981).

6) N. Fujii, H. Sato, S. Fujimoto, and H. Miyama, *Bull. Chem. Soc. Jpn.*, **57**, 277 (1984).

7) S. Salimian, R. K. Hanson, and C. H. Kruger, *Int. J. Chem. Kinet.*, **16**, 725 (1984).

8) R. K. Hanson and S. Salimian, "Combustion Chemistry," ed by W. C. Gardiner, Jr., Springer Verlag (1984), p. 361.

9) M. F. Zabielski and D. J. Seery, *Int. J. Chem. Kinet.*, **17**, 1191 (1985).

10) D. L. Baulch, D. D. Drysdale, D. G. Horne, and A. C. Lloyd, "Evaluated Kinetic Data for High Temperature reactions," Butterworths, London (1973), Vol. 2.

11) T. Just, "Shock waves in Chemistry," ed by A. Lifshitz, Marcel Dekker, Inc., New York (1981), p. 279.

12) N. Fujii, M. Koshi. H. Ando, and T. Asaba. *Int. J. Chem. Kinet.*, 11, 285 (1979).

13) W. C. Gardiner, Jr., B. F. Walker, and C. B. Wakefield, "Shock Waves in Chemistry," ed by A. Lifshitz, Marcel Dekker, Inc., New York (1981), p. 319.

14) K. Saito and J. N. Bradley, unpublished data.

15) K. Kirchner, N. Merget, and C. Schmidt, *Chem. Ing. Tech.*, **46**, 661 (1974).

16) R. A. Perry, *Chem. Phys. Lett.*, **106**, 223 (1984).

17) R. D. Stephens, *J. Phys. Chem.*, **88**, 3308 (1984).

18) J. B. Jeffries and G. P. Smith, *J. Phys. Chem.*, **90**, 487 (1986).

19) M. Yumura, T. Asaba, Y. Matsumoto, and H. Matsui, Int. *J. Chem. Kinet.*, **12**, 439 (1980).

Reflection Spectra of $(DBTTF)_4 \cdot (BF_4)_2 \cdot EtOH$ Complex

Masashi TANAKA
Department of Chemistry, College of General Education, Nagoya University, Chikusa-ku, Nagoya 464
(Received May 26, 1986)

The polarized reflection spectra of the crystal of $(DBTTF)_4 \cdot (BF_4)_2 \cdot EtOH$ complex were measured and the optical parameters were determined by the simulation of the observed reflection spectra. The theoretical analysis of the observed spectra shows that the electronic structure of DBTTF cation molecules is typical of the island type configuration. The 4000 and 11500 cm^{-1} bands polarized parallel to the stacking axis were assigned to the CT_2 and CT_1 bands, and the parameters U and t of the Hubbard Hamiltonian were estimated to be U=8950 cm^{-1} and t=1250 cm^{-1}.

There has been considerable interest recently in organic conductors which have highly abnisotropic electrical, optical and magnetic properties. Tetrathiafulvalene-tetracyanoquinodimethane (TTF-TCNQ) is one of them which received the most detailed attention. After the discovery of the TTF-TCNQ complex, many compounds with fulvalene rings were synthesized to obtain the radical salts with highly electrical conductivity. Dibenzotetrathiafulvalene (DBTTF) is one of those compounds[1] and the direct oxidation of DBTTF by halogens and metal halides were reported to yield radical salts such as $(DBTTF)_2I_3$,[2] $(DBTTF)_8(SnCl_6)_3$,[3] and $(DBTTF)_3(SnBr_6)$,[3] $(DBTTF)_2(Cu_2Cl_6)$,[4] and $(DBTTF)_2(Cu_2Br_6)$.[5] The employment of tetrafluoroborate as an oxidant was reported to yield the ion-radical salt $(DBTTF)(BF_4)_{0.8}$ showing a high conductivity up to 180 K.[6] We repored the crystal structure of another complex $(DBTTF)_4(BF_4)_2$ EtOH.[7] In the present paper, the reflection spectra of the crystal of $(DBTTF)_4 \cdot (BF_4)_2 \cdot EtOH$ complex are reported and the results of the theoretical analysis are presented by using the Hubbard approximation.

Experimental

The crystal of $(DBTTF)_4 \cdot (BF_4)_2 \cdot EtOH$ complex was prepared in an ethanol solution. The reflection spectra of the single crystal at the normal incidence were measured over the range of 5000—25000 cm^{-1} by means of a reflection spectrophotometer made in our laboratory. All calculations for the analysis of the experimental data were made on a FACOM M382 computer of Nagoya University.

Theoretical

For the island type system[8] of $[(DBTTF)_3]^{2+}$ cations the Hamiltonian H may be given by the Hubbard Hamiltonian as follows,

$$H = -t \sum_i \sum_{\sigma=\alpha,\beta} (a^+_{i,\sigma} a_{i+1,\sigma} + a^+_{i+1,\sigma} a_{i,\sigma}) + U \sum_i n_{i,\alpha} n_{i,\beta} \quad (1)$$

where $a^+_{i,\sigma}$ and $a_{i,\sigma}$ are the creation and anihilation operators of the π-electron occupying HOMO of the DBTTF molecule at the i-th site, σ represents the spin of π-electron, $n_{i,\sigma}=a^+_{i,\sigma}a_{i,\sigma}$ is the number of π-electron on the i-th site, t is the electron transfer integral and U the intramolecular Coulomb integral. Then, the ground and lower excited configuration functions for the singlet state are taken into account for the calculation of the electronic states of the island type system.[8]

$$\Phi^{1,2} = \frac{1}{\sqrt{2}}(a_{1,\beta}a_{2,\alpha} - a_{1,\alpha}a_{2,\beta})\Phi_{HF} \quad (2)$$

$$\Phi^{2,3} = \frac{1}{\sqrt{2}}(a_{2,\beta}a_{3,\alpha} - a_{2,\alpha}a_{3,\beta})\Phi_{HF} \quad (3)$$

$$\Phi^{1,3} = \frac{1}{\sqrt{2}}(a_{1,\beta}a_{3,\alpha} - a_{1,\alpha}a_{3,\beta})\Phi_{HF} \quad (4)$$

$$\Phi^{CT}_1 = a_{3,\alpha}a_{3,\beta}\Phi_{HF} \quad (5)$$

$$\Phi^{CT}_2 = a_{1,\alpha}a_{1,\beta}\Phi_{HF} \quad (6)$$

$$\Phi^{CT}_3 = a_{2,\alpha}a_{2,\beta}\Phi_{HF} \quad (7)$$

Here, Φ_{HF} means the Hartree-Fock wave function of the neutral trimer of DBTTF. The energy of the island type system is calculated by diagonalizing the secular determinant for the symmetrical and the antisymmetrical states as is shown in the next equations,

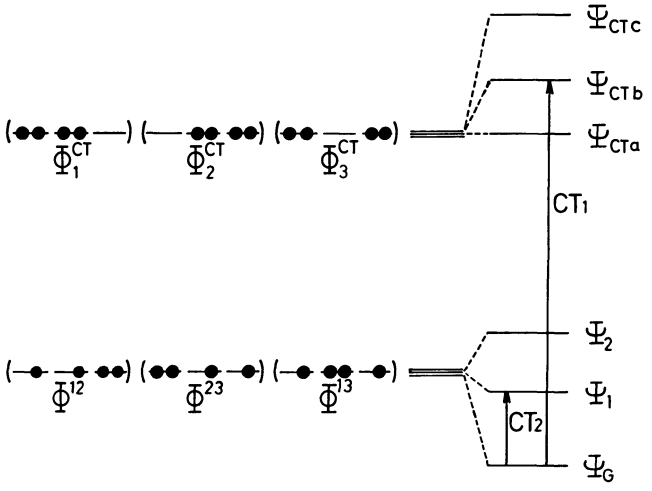

Fig. 1. Energy diagram of the island trimer type configuration.

$$\begin{array}{l|ccc} \Phi^{1,3} & 0 & \sqrt{2}t & 0 \\ \frac{1}{\sqrt{2}}(\Phi^{1,2}+\Phi^{2,3}) & \sqrt{2}t & 0 & -\sqrt{6}t \\ \frac{1}{\sqrt{2}}(\Phi_1^{CT}+\Phi_2^{CT}+2\Phi_3^{CT}) & 0 & -\sqrt{6}t & U \end{array}, \tag{8}$$

and

$$\begin{array}{l|ccc} \frac{1}{\sqrt{2}}(\Phi^{1,2}-\Phi^{2,3}) & 0 & \sqrt{2} & 0 \\ \frac{1}{\sqrt{2}}(\Phi_1^{CT}-\Phi_2^{CT}) & \sqrt{2}t & U & 0 \\ \frac{1}{\sqrt{3}}(\Phi_1^{CT}+\Phi_2^{CT}-\Phi_3^{CT}) & 0 & 0 & U \end{array}. \tag{9}$$

Then, the eigenvalues and eigenfunctions are obtained as follows and the energy diagram of the cation trimer system is depicted in Fig. 1.

$$\Psi_G = c_0\left\{\frac{1}{2}(\Phi^{1,2}+\Phi^{2,3}-\sqrt{2}\Phi^{1,3}) + \frac{\sqrt{3}t}{U-\sqrt{2}t}\frac{1}{\sqrt{6}}(\Phi_1^{CT}+\Phi_2^{CT}+2\Phi_3^{CT})\right\},$$
$$E_G = -\sqrt{2}t - \frac{3t^2}{U+\sqrt{2}t}, \tag{10}$$

$$\Psi_1 = \frac{b_1}{\sqrt{2}}(\Phi^{1,2}-\Phi^{2,3}) + \frac{b_2}{\sqrt{2}}(\Phi_1^{CT}-\Phi_2^{CT}),$$
$$E_1 = \frac{U-\sqrt{U^2+8t^2}}{2}, \tag{11}$$

$$\Psi_2 = c_1\left\{\frac{1}{2}(\Phi^{1,2}+\Phi^{2,3}+\sqrt{2}\Phi^{1,3}) + \frac{\sqrt{3}t}{U-\sqrt{2}t}\frac{1}{\sqrt{6}}(\Phi_1^{CT}+\Phi_2^{CT}+2\Phi_3^{CT})\right\},$$
$$E_2 = \sqrt{2}t - \frac{3t^2}{U-\sqrt{2}t}, \tag{12}$$

$$\Psi_{CT,a} = \frac{1}{\sqrt{3}}(\Phi_1^{CT}+\Phi_2^{CT}+\Phi_3^{CT}),$$
$$E_{CT,a} = U, \tag{13}$$

$$\Psi_{CT,b} = -\frac{b_2}{\sqrt{2}}(\Phi^{1,2}-\Phi^{2,3}) + \frac{b_1}{\sqrt{2}}(\Phi_1^{CT}-\Phi_2^{CT}),$$
$$E_{CT,b} = \frac{U+\sqrt{U^2+8t^2}}{2}, \tag{14}$$

$$\Psi_{CT,c} = c_2\left\{\frac{1}{\sqrt{6}}(\Phi_1^{CT}+\Phi_2^{CT}+2\Phi_3^{CT}) - \frac{\sqrt{3}t}{U+\sqrt{2}t}\frac{1}{2}(\Phi^{1,2}+\Phi^{2,3}-\sqrt{2}\Phi^{1,3}) - \frac{\sqrt{3}t}{U-\sqrt{2}t}\frac{1}{2}(\Phi^{1,2}+\Phi^{2,3}+\sqrt{2}\Phi^{1,3})\right\},$$
$$E_{CT,c} = U + \frac{3t^2}{U+\sqrt{2}t} + \frac{3t^2}{U-\sqrt{2}t}. \tag{15}$$

Here, c_0, c_1, c_2, b_1, and b_2 are given by the following equations,

$$c_0 = \left\{1+\frac{3t^2}{(U+\sqrt{2}t)^2}\right\}^{-1/2},$$
$$c_1 = \left\{1+\frac{3t^2}{(U-\sqrt{2}t)^2}\right\}^{-1/2},$$
$$c_2 = \left\{1+\frac{3t^2}{(U+\sqrt{2}t)^2}+\frac{3t^2}{(U-\sqrt{2}t)^2}\right\}^{-1/2},$$
$$b_1 = \left\{\frac{1}{2}\left(1+\frac{U}{\sqrt{U^2+8t^2}}\right)\right\}^{-1/2},$$

and

$$b_2 = -\left\{\frac{1}{2}\left(1-\frac{U}{\sqrt{U^2+8t^2}}\right)\right\}^{-1/2}. \tag{16}$$

The optically allowed transitions are the CT_2 transition from Φ_G to Φ_1 and the CT_1 transition from Φ_G to $\Phi_{CT,b}$, and their transition energies are given by

$$\Delta E_{CT_2} = E_1 - E_G = \frac{U-\sqrt{U^2+8t^2}}{2} + \sqrt{2}t + \frac{3t^2}{U+\sqrt{2}t}, \tag{17}$$

and

$$\Delta E_{CT_1} = E_{CT,b} - E_G = \frac{U+\sqrt{U^2+8t^2}}{2} + \sqrt{2}t + \frac{3t^2}{U+\sqrt{2}t}. \tag{18}$$

The transition moments of these two bands may be expressed as follows,

$$\langle\Psi_G|M|\Psi_1\rangle = c_0\left\{\frac{b_1}{\sqrt{2}} - \frac{2tb_2}{U+\sqrt{2}t}\right\}\boldsymbol{R}, \tag{19}$$

and

$$\langle\Psi_G|M|\Psi_{CT,b}\rangle = c_0\left\{-\frac{b_2}{\sqrt{2}} - \frac{2tb_1}{U+\sqrt{2}t}\right\}\boldsymbol{R}, \tag{20}$$

were $\boldsymbol{R}$ is the vector between the nearest neighboring DBTTF molecules. Then, the oscillator strengths of the CT_2 and CT_1 bands are given by the next equations,

$$f_{CT_2} = 3 \times 1.09 \times 10^{11} \times \Delta E_{CT_2} \times |\langle\Psi_G|M|\Psi_1\rangle|^2, \tag{21}$$

and

$$f_{CT_1} = 3 \times 1.09 \times 10^{11} \times \Delta E_{CT_1} \times |\langle\Psi_G|M|\Psi_{CT,b}\rangle|^2. \tag{22}$$

Here U and t are in cm^{-1} and $\boldsymbol{R}$ is in cm.

The optical reflectivity R can be expressed by the following equation

$$R = \frac{1+|\varepsilon|-\sqrt{2(|\varepsilon|+\varepsilon_1)}}{1+|\varepsilon|+\sqrt{2(|\varepsilon|+\varepsilon_1)}}. \tag{23}$$

and the dielectric function $\varepsilon(\omega)$ are approximated by the semiclassical Lorentz model,

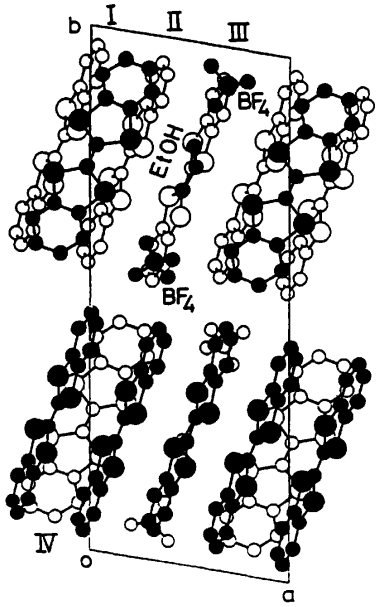

Fig. 2. The projection of the structure of $(DBTTF)_4\cdot(BF_4)_2\cdot EtOH$ along the c axis.

$$\varepsilon(\omega) = \varepsilon_{core} + \sum_j \frac{\Omega_j^2}{\omega_j^2-\omega^2-i\omega\gamma_j} = \varepsilon_1(\omega) + i\varepsilon_2(\omega), \quad (24)$$

where $\varepsilon_1(\omega)$ and $\varepsilon_2(\omega)$ are the real and imaginary parts of the dielectric function of the DBTTF cation trimers, and $|\varepsilon|=\sqrt{\varepsilon_1^2(\omega)+\varepsilon_2^2(\omega)}$. The oscillator strength f is determined by using the equation,

$$f = \frac{m_e}{4\pi Ne^2}\Omega_j^2. \quad (25)$$

Here, m_e is the electron mass and N is the number density of DBTTF molecule. By fitting the above-mentioned equations of the reflectivity R to the observed values, the optical parameters of the complexes $(DBTTF)_4\cdot(BF_4)_2\cdot EtOH$ may be obtained and their energy structure can be determined.

Results and Discussion

$(DBTTF)_4\cdot(BF_4)_2\cdot EtOH$ crystallizes in the form of the dark blue needle and the space group is monoclinic $C2/m$.[7] The projection of the structure along the c axis is shown in Fig. 2. The structure consists of two crystallographically independent stacks. The DBTTF molecules (I, II, and III) are stacked parallel to each other in columns along the a axis. The angles between the mean planes of these DBTTF molecules and the a axis are almost equal and the mean interplanar spacing is 3.6A. The fourth DBTTF (IV) and ethanol and two BF_4^- anions form another sheet along the same direction. The molecular plane of DBTTF (IV) is almost perpendicular to the column of the other three DBTTF (I, II, and III) molecules.

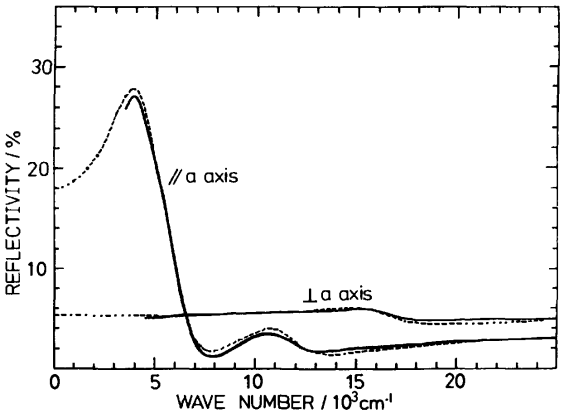

Fig. 3. Observed and calculated reflection spectra of the crystal of $(DBTTF)_4\cdot(BF_4)_2\cdot EtOH$ on the ac plane. (——: obsd, ----: calcd)

Table 1. Dielectric Parameters of the Lorentz Fits of Reflectivity Data for $(DBTTF)_4\cdot(BF_4)_2\cdot EtOH$

	$//a$ spectrum		$\perp a$ spectrum
ε_{core}	2.1		2.5
Ω_j/cm^{-1}	7500	5000	5000
ω_j/cm^{-1}	3800	11500	16500
γ_j/cm^{-1}	2500	3000	4000
f	0.32	0.14	0.14

Table 2. Hubbard Parameters (t and U) Determined by the Analysis of the Reflection Spectra of Various DBTTF Crystals[11,12]

Type	Compound	t/cm^{-1}	U/cm^{-1}
Alternant	$(DBTTF)_3(SnBr_6)$	2000	
Dimer	$(DBTTF)_2(Cu_2Cl_6)$	2200	6500
	$(DBTTF)_2(Cu_2Br_6)$	2300	7700
Island	$(DBTTF)_4(BF_4)_2EtOH$	1250	8950

On the other hand, Raman spectra of the complex shows that the DBTTF ν_5 band (totally symmetric streching vibrational mode of the central C=C bond) are observed at three Raman frequencies of 1540, 1442, and 1400 cm^{-1}.[9] The ν_5 band at 1540 cm^{-1} corresponds to that of the neutral DBTTF molecule and another one at 1400 cm^{-1} to the fully ionized cation radical $DBTTF^+$. The third band (ν_5=1442 cm^{-1}) is located intermediately between those of the neutral and cation molecules.

The above consideration suggests that the molecule (IV) is neutral and the other three molecules (I, II, and III) are ionized. Then, the island type model may be used to the analysis of the reflection spectra. The reflection spectra were observed for the polarizations

parallel and perpendicular to the a axis on the ac plane as is shown in Fig. 3. The 4000 cm^{-1} band in the a axis spectrum can be assigned to the CT_2 band and the 11000 cm^{-1} band to the CT_1 band. The 16000 cm^{-1} in the $\perp a$ axis spectrum are assigned to the short axis component of the LE band of $DBTTF^+$ cation radical.[10]

The best fit of Eq. 23 to the observed reflectivity is obtained and the calculated reflection spectra are depicted in Fig. 3 in order to compare with the observed ones. The obtained parameters Ω_j, ω_j, γ_j, and ε_{core} are shown in Table 1 together with the oscillator strength determined by Eq. 25. Then, the experimental data (ΔE_{CT_1}=11500 cm^{-1}, f_{CT_1}=0.14, ΔE_{CT_2}=3800 cm^{-1}, f_{CT_2}=0.32, and R=3.6 A) give U=8950 cm^{-1} and t=1250 cm^{-1} which correspond to the calculated values (ΔE_{CT_1}=11500 cm^{-1}, f_{CT_1}=0.04, ΔE_{CT_2}=1900 cm^{-1} and f_{CT_2}=0.41). The obtained parameters (t and U) are shown in Table 2 together with those estimated by the analysis of other crystals ($(DBTTF)_3(SnBr_6)$,[11] $(DBTTF)_2(Cu_2Cl_6)$,[12] and $(DBTTF)_2(Cu_2Br_6)$[12]). In these crystals, the interplanar distances between DBTTF's are almost same (3.6 A) but the stacking behaviors are different. Therefore, the smaller t and the larger U values for $(DBTTF)_4 \cdot (BF_4)_2 \cdot EtOH$ may be explained by the comparison of the overlap integrals between the HOMO's of DBTTF in the crystals.

References

1) M. L. Khidekel and E. I. Zhilyaeva, *Synthetic Metal*, **4**, 1 (1981).
2) R. P. Shibaeva, L. P. Rozenberg, M. Z. Aldoshina, R. N. Lubovskaya, and M. L. Khidekel, *Zh. Strukt., Khim.*, **20**, 486 (1979).
3) R. P. Shivaeva, L. P. Rozenberg, and R. N. Lubovskaya, *Kristallografiya*, **25**, 507 (1980).
4) M. Honda, C. Katayama, J. Tanaka, and M. Tanaka, *Acta Crystallogr., Sec. C.*, **41**, 197 (1985).
5) M. Honda, C. Katayama, J. Tanaka, and M. Tanaka, *Acta Crystallogr., Sec. C.*, **41**, 688 (1985).
6) I. V. Krivoshei, V. P. Babiyczvk, I. M. Guella, I. F. Golovkina, N. V. Mansia, V. A. Starodub, and S. A. Chueva, *Phys. Status Solidi*, **A. 50**, K197 (1978).
7) M. Tanaka, M. Honda, C. Katayama, and J. Tanaka, *Acta Crystallogr., Sec. C.*, **41**, 1635 (1985).
8) J. Tanaka, M. Tanaka, T. Kawai, T. Takaba, and O. Maki, *Bull. Chem. Soc. Jpn.*, **49**, 2358 (1976).
9) M. Tanaka, M. Shimizu, Y. Saito, and J. Tanaka, *Chem. phys. Lett.*, **125**, 594 (1986).
10) C. Tanaka, J. Tanaka, K. Dietz, C. Katayama, and M. Tanaka, *Bull. Chem. Soc. Jpn.*, **56**, 405 (1983).
11) M. Tanaka, K. Kamiya, J. Tanaka, and S. Murata, *Bull. Chem. Soc. Jpn.*, **57**, 2258 (1984).
12) M. Tanaka, *Bull. Chem. Soc. Jpn.*, **59**, 775 (1986).

 © 1986 The Chemical Society of Japan Bull. Chem. Soc. Jpn., 59, 3443—3450 (1986)

The Precipitation of Monodispersed α-Iron(III) Oxide Particles from Iron(III) Chloride-Glycine System in Aqueous and 2-Propanol/Water Media

Shuichi HAMADA,* Shin NIIZEKI, and Yoshiyuki KUDO
Department of Applied Chemistry, Faculty of Science, and Institute of Colloid and Interface Science, Science University of Tokyo, Kagurazaka, Shinjuku-ku, Tokyo 162
(Received May 31, 1986)

Monodispersed α-iron(III) oxide (hematite) particles were prepared by aging iron(III) chloride solutions in the presence of glycine at elevated temperatures, 98—100 °C. An aqueous solution of glycinatoiron (III) complex directly gave monodispersed double spheres of hematite, ≈4 μm in size, under the specified conditions, for example, 2.0×10^{-2} mol dm^{-3} $FeCl_3$, 0.60 mol dm^{-3} glycine, and 0.46 mol dm^{-3} HCl for 96 h. The hematite particles grew up through the polynuclear layers mechanism. By the forced hydrolysis in 2-propanol/water mixed solution of 30% by volume, monodispersed cuboidal hematite particles, 0.06—0.43 μm in size, were also obtained through the conversion of β-iron(III) hydroxide oxide previously deposited. The nucleation rate was markedly affected by acidity at the latter case. The formation processes of these monodispersed hematite particles are discussed.

The preparation of monodispersed (hydrous) metal oxide particles has been studied extensively.[1-10] Monodispersed α-iron(III) oxide (hematite) particles have also been produced by the forced hydrolysis of iron(III) salt solutions under a limited set of conditions.[2,4-6,8,9] In this process, iron(III) hydroxide oxide is usually produced first and then transforms into hematite. However, monodispersed double spheres of hematite have been directly prepared from an iron(III) chloride-glycine aqueous system[6] without precipitation of β-iron(III) hydroxide oxide, while glycinatoiron(III) complex acts as a reservoir of hydroxo complexes. In the present work, the preparation process of the monodispersed hematite particles was studied in both the aqueous and 2-propanol/water mixed solutions containing glycine.

Experimental

Materials. All of reagents used in this work were of a guaranteed grade and employed without further purification. A stock solution of iron(III) chloride was previously passed through a membrane filter, of 0.2 μm pore size, before use. The solution thus obtained (≈3 mol dm^{-3}) did not show any visual change over one month. An aliquot of the stock solution was diluted to the fixed concentration of 2.0×10^{-2} mol dm^{-3} together with desired amounts of glycine and hydrochloric acid with doubly distilled water or 2-propanol/water mixed solvent of 30% by volume.

Procedures. A freshly prepared mixed solution was tightly sealed in a screw-capped glass tube and then aged for 24—96 h at 100±1 °C in a thermostated air oven. After the reaction, the particles were centrifuged at 1700 g and then washed repeatedly with doubly distilled water. The morphology and size of the particles were observed with scanning and transmission electron microscopes.

To reveal the formation process of the monodispersed hematite particles, the iron(III) chloride-glycine aqueous solution was aged in a flask equipped with a condensor at 98±0.5 °C in an oil bath. The concentration of iron species remaining in a supernatant solution was followed colorimetrically using 1,10-phenanthroline at regular time intervals, after the solids had been centrifuged at 45000 g. The supernatant solution thus obtained did not show any Tyndall cone. The concentration of iron(II) species was determined in the presence of iron(III) species using absorbances at different wavelengths. The amount of iron(III) species was estimated from the difference between those of iron(II) and the total iron species: the latter value was determined after the iron(III) species had been completely reduced to the iron(II) state.

When the hematite particles were produced through the conversion of β-iron(III) hydroxide oxide in the 2-propanol/water system, changes in their amounts were also followed spectrophotometrically, after they had been separated by repeated centrifugation at 500, 1300, and 45000 g, followed by solution in hydrochloric acid.

The amounts of monomeric and polymeric iron(III) complexes were determined spectrophotometrically on the basis of reactivity to 8-quinolinol.[11] The total iron(III) concentration was determined after the polymeric species had been depolymerized in 0.1 mol dm^{-3} hydrochloric acid at 80 °C for 10 min. The 8-quinolinatoiron(II) complex was previously confirmed not to exhibit absorbance over the wavelength between 380 and 600 nm.

Results

Concentration Changes of Soluble Iron(III) and (II) Species during Deposition of Monodispersed Hematite Particles in Aqueous Solution. The monodispersed doubly spherical hematite particles have been prepared under a limited set of conditions by the forced hydrolysis of the aqueous iron(III) chloride solution including glycine.[6] Figure 1 displays an example of monodispersed hematite particles prepared by aging a solution of 2.0×10^{-2} mol dm^{-3} $FeCl_3$, 0.60 mol dm^{-3} glycine, and 0.46 mol dm^{-3} HCl at 100 °C for 96 h. An average size of the particles was estimated as 4.1 μm with relative standard deviation of 0.08. The particles were attributable to aggregates of well-crystallized fine hematite particles, according to their X-ray powder diffraction pattern[12] and morphology.

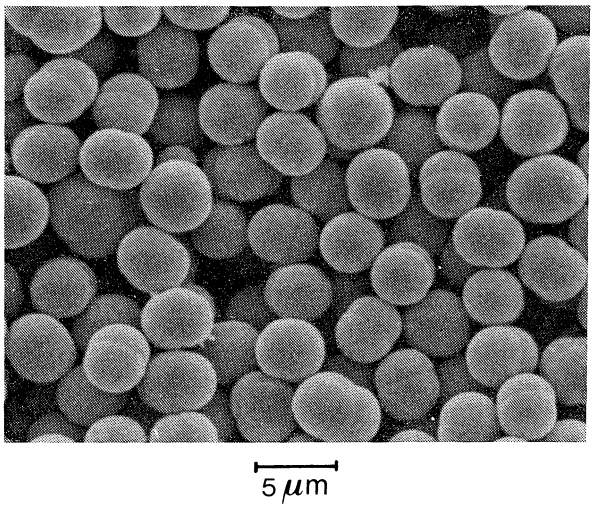

Fig. 1. Doubly spherical hematite particles obtained by hydrolysis at 100 °C for 96 h. Aging conditions: $[FeCl_3]=2.0\times10^{-2}$, [HCl]=0.46, and [Gly]=0.60 mol dm^{-3}.

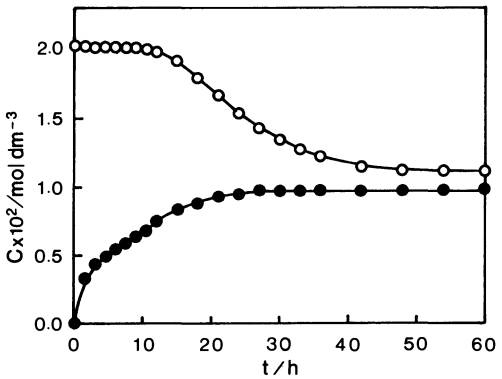

Fig. 2. Concentration changes in total and Fe(II) species in supernatnat solution during hydrolysis at 98 °C. Symbols: ○: total iron, ●: Fe(II).

The forced hydrolysis gave excellent monodispersed hematite particles only over a narrow composition range of the solution between 0.40 and 0.60 mol dm^{-3} for glycine and from 0.39 to 0.50 mol dm^{-3} for HCl under the fixed iron(III) chloride concentration of 2.0×10^{-2} mol dm^{-3}.[6] The pH of the solutions initially ranged between 1.5 and 1.8 and scarcely changed after the reaction because of the buffer action of the glycine.

Iron(III) nitrate and sulfate solutions containing glycine and the corresponding acid gave only irregularly shaped hematite or α-iron(III) hydroxide oxide particles.

In order to reveal the formation process of monodispersed hematite particles, the concentrations of iron species in the supernatant solution were followed at 98±0.5 °C up to 60 h. A starting solution was prepared similar to that shown in Fig. 1. The

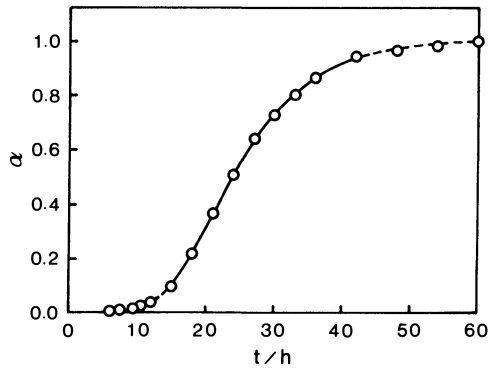

Fig. 3. Change in reaction degree during hydrolysis at 98 °C. ○: Observed, —: Calculated.

particles appeared after an induction period of around 10 h and then developed, while the iron(III) species were partially reduced into iron(II) state by glycine present, as shown in Fig. 2. Finally, the total iron concentration reached 1.1×10^{-2} mol dm^{-3} after 50 h. The concentration of iron(II) species became almost constant as 1.0×10^{-2} mol dm^{-3} after 30 h. Thus, effective concentrations of iron(III) for producing the hematite equal those between the upper and lower curves. The difference in the concentrations, C_s, between the total iron and iron(II) species at the final state corresponds to the solubility of hematite under the given conditions.

Growth Process of Double Spheres of Hematite. The reaction degree, α, is defined as:

$$\alpha = (C_0-C)/(C_0-C_s-C_{Fe(II)}) \quad (1)$$

where C_0 is the initial concentration of iron(III), C the total concentration of iron species at reaction time t, and $C_{Fe(II)}$ that of iron(II), respectively. Based on the results in Fig. 2, the reaction degree, α, was estimated as shown in Fig. 3.

According to Nielsen,[13] the radial growth rate is expressed as Eq. 2 when the particles developed through a polynuclear layers mechanism.

$$dr/dt = 0.60\, dJ'^{1/3}R'^{2/3} \quad (2)$$

where J' and R' are the nucleation and growth rates of two-dimensional surface nuclei. Both terms are given as:

$$J' = k_m C_r^m \quad [C_r=C-C_s-C_{Fe(II)}] \quad (3)$$

$$R' = d^2DC_r \quad (4)$$

where d is the height of the surface nuclei, k_m the apparent rate constant of surface nucleation, and D the diffusion coefficient, respectively. On the other hand, the radius of the monodispersed particles at t can be given as:

$$r = r_f\alpha^{1/3} \quad (5)$$

where r_f is the final radius of the particle. On the basis

of differentiation of Eq. 5, the following equation is obtained as:

$$dr/dt = 0.33\, r_f \alpha^{-2/3} d\alpha/dt \quad (6)$$

Finally, Eq. 7 can be derived by combining Eq. 6 with Eq. 1 as:

$$d\alpha/dt = KC_r^{(m+2)/3}\alpha^{2/3} \quad (7)$$

where

$$K = 1.8\, k_m^{1/3} d^{7/3} D^{2/3} r_f^{-1} \quad (8)$$

However, Eq. 7 was not integrable because the concentration of iron(II) changed continuously in this system; accordingly a numerical method was employed. At first, the parameters, m and K, were estimated as 1.22 and 22.6[14] by the least squares method using the logarithmic values of $d\alpha/dt$, C_r, and α. Equation 7 was integrated by the Runge–Kutta method using these values. The solid curve shown in Fig. 3 displays the reaction degree thus calculated, which agreed well with the experimental values over a wide range of the reaction degree from around 0.1 to 0.9. Similar studies were also made on the diffusional and mononuclear layer mechanisms,[13] but neither of them fitted the experimental values. These results indicated that the double spheres of hematite developed through the polynuclear layers mechanism including condensation and polymerization of hydroxoiron(III) complexes on the surface of particles, as suggested by Flynn.[15]

Hydroxoiron(III) Complexes in Iron(III) Chloride-Glycine Aqueous System. To reveal a role of the monomeric and polymeric hydroxoiron(III) complexes on the formation of hematite particles, the fractions of these species in the solution were examined spectrophotometrically during the forced hydrolysis. Murphy et al.[16] have mentioned that only unpolymerized iron(III) species were reactive to 8-quinolinol. Furthermore, Iwase et al.[11] have specified that monomeric and dimeric species, Fe^{3+}, $[FeOH]^{2+}$, and $[Fe_2(OH)_2]^{4+}$, were extractable in chloroform as 8-quinolinate by shaking for 10 s, in addition to monomeric sulfatoiron(III) complex.

According to the above facts, the polymerization of iron(III) ions was examined first as follows: The pH values of 1.0×10^{-2} and 2.5×10^{-3} mol dm^{-3} iron(III) perchlorate solutions were adjusted in the range from 1.70 to 2.20 and from 1.98 to 2.43 respectively. After standing the solutions at 25±0.5° C for 24 h, 8-quinolinatoiron(III) complex was extracted in 10 cm^3 chloroform by vigorous shaking for 10 s. Figure 4 displays the fractions of extractable iron(III) species as a function of pH. These results clearly indicate that the hydroxoiron(III) complexes were drastically polymerized at pH 2.2 and 2.4, respectively, in spite of no precipitation, depending upon the total concentration of iron(III) species.

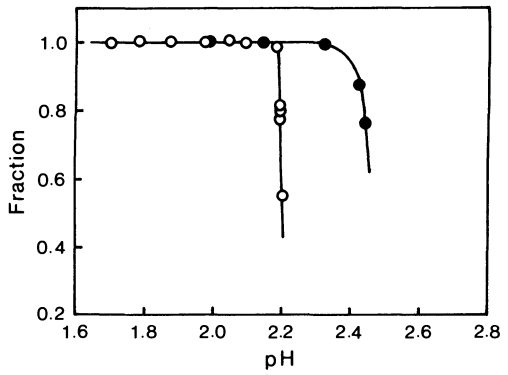

Fig. 4. Fractions of extractable Fe(III) species at 25 °C and I=0.5. Conditions: $[Fe(ClO_4)_3]=1.0\times10^{-2}$ (○) and 2.5×10^{-3} (●) mol dm^{-3}.

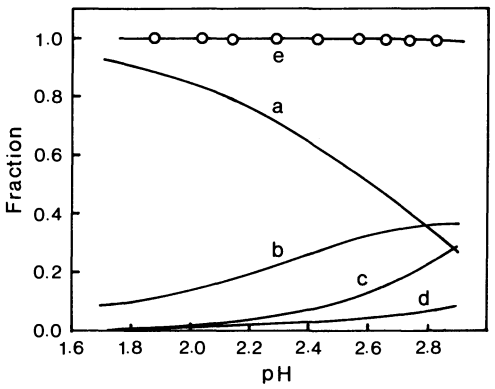

Fig. 5. Fractions of extractable Fe(III) species and respective species at 25 °C and I=0.5. Conditions: $[Fe(ClO_4)_3]=5.0\times10^{-4}$ mol dm^{-3}, a: Fe^{3+}, b: $[FeOH]^{2+}$, c: $[Fe(OH)_2]^{+}$, d: $[Fe_2(OH)_2]^{4+}$, and e: total.

On the other hand, a much diluted solution (5.0×10^{-4} mol dm^{-3}) scarcely showed any polymerization in the pH range between 1.87 and 2.82, as shown in Fig. 5. The circles in Fig. 5 stand for the fractions of extractable iron(III) species. Furthermore, the solid curves a—d indicate the fractions of Fe^{3+}, $[FeOH]^{2+}$, $[Fe(OH)_2]^{+}$, and $[Fe_2(OH)_2]^{4+}$ which were calculated by the Newton–Raphson method using the formation constants for the respective hydroxo complexes at 25 °C and ionic strength of 0.5.[17–20] The curve e displays the sum of above fractions, which agrees well with the experimental values. The fraction of $[Fe_3(OH)_4]^{5+}$ was confirmed to be negligible in this diluted solution. Thus, the results suggest that $[Fe(OH)_2]^{+}$ is also extractable as the 8-quinolinatoiron(III) complex.

On the basis of above results, the behavior of the polymeric iron(III) species in the iron(III) chloride–glycine aqueous solution was examined in the following way. A solution with the same composition shown in Fig. 1 was aged for desired periods at 98±0.5 °C. After the reaction, the solids formed were

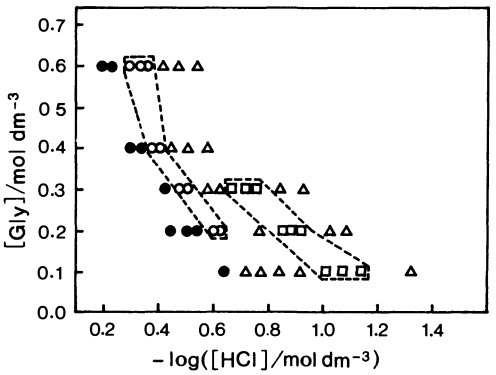

Fig. 6. Concentration domain of glycine and HCl for making hematite particles by hydrolysis at 100 °C for 48 h in 2-propanol/water mixture. Coditions: $[FeCl_3]=2.0\times10^{-2}$ mol dm^{-3}, 2-propanol; 30% by volume, Symbols: ○: double sphere, □: cube, △: irregular, and ●: no precipitation.

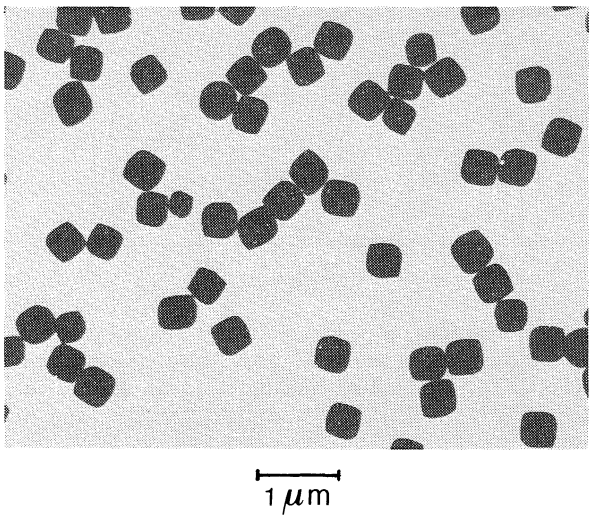

Fig. 7. Cuboidal hematite particles obtained by forced hydrolysis at 100 °C for 56 h in 2-propanol/water mixed solution. Conditions: $[FeCl_3]=2.0\times10^{-2}$, [HCl]=0.16, and [Gly]=0.20 mol dm^{-3}, 2-prpanol: 30% by volume.

completely removed by centrifugation at 45000 g. As mentioned above, iron(III) ions were partially reduced into the iron(II) state, so that the actual total iron(III) concentration was separately determined after depolymerizing the polymeric species. The presence of chloride ions and glycine in the solution did not have any influence on the determination with 8-quinolinol. However, the total fraction of the monomeric and dimeric iron(III) species remained constant as $1.00\pm0.00_6$ during the course of aging up to 48 h at intervals of 6 h. In addition, no polymeric iron(III) species was observed in the solution before aging.

Formation of Monodispersed Hematite Particles in 2-Propanol/Water System. Figure 6 shows the

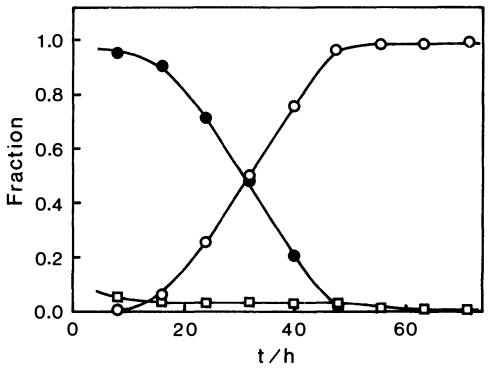

Fig. 8. Conversion of β-FeOOH during hydrolysis at 100 °C in 2-propanol/water mixed solution. Conditions: $[FeCl_3]=2.0\times10^{-2}$, [HCl]=0.14, and [Gly] =0.20 mol dm^{-3}, Symbols: ●: β-FeOOH, ○: hematite, □: Fe(III) species in supernatant solution.

domain of hydrochloric acid and glycine concentrations for making hematite particles by the forced hydrolysis at 100 °C for 48 h under the fixed concentration of 2.0×10^{-2} mol dm^{-3} iron(III) chloride in 2-propanol/water mixed solutions of 30% by volume. The solutions with the composition indicated by the symbol ○ directly gave the monodispersed double spheres of hematite as in the aqueous solutions.

In addition, monodispersed cuboidal hematite particles were obtained in the region shown by the symbol □, in contrast to the former case. In this process, β-iron(III) hydroxide oxide[21] appeared first and then transformed into cubes of hematite. Iron(III) ions are much more hydrolyzable in alcohol/water mixtures than in aqueous solutions.[22,23] Therefore, the β-iron(III) hydroxide oxide would result from much higher supersaturation of hydroxoiron(III) complexes at an initial stage of the forced hydrolysis in rather dilute acid. Thus, a mixture of hematite and fine hydroxide oxide particles was obtained by the forced hydrolysis. It was, however, easy to separate them by repeated slow and high speed centrifugation. Figure 7 shows the cuboidal particles thus separated. The symbols ● indicate the region in which no precipitation occurred even after 100 h.

Conversion of β-Iron(III) Hydroxide Oxide to Hematite in 2-Propanol/Water System. In order to examine the conversion process, the respective amounts of β-iron(III) hydroxide oxide and hematite were followed at regular time intervals during the forced hydrolysis, in addition to that of the soluble iron species in the supernatant solution. A solution was prepared as $[FeCl_3]=2.0\times10^{-2}$, [HCl]=0.14, and [Gly]=0.20 mol dm^{-3} in the 2-propanol/water mixture of 30% by volume. The solution was aged at 100±0.5 °C in an oil bath. After the reaction, the precipitates were first separated by centrifugation at 45000 g and then the extremely fine β-iron(III)

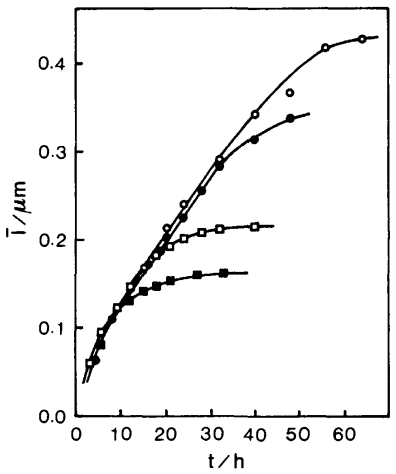

Fig. 9. Growth of cuboidal hematite particles at 100 °C in 2-propanol/water mixed solution. Conditions: $[FeCl_3]=2.0\times10^{-2}$, [Gly]=0.20, [HCl]=0.12 (■), 0.13(□), 0.15 (●), and 0.16(○) mol dm^{-3}, 2-propanol: 30% by volume.

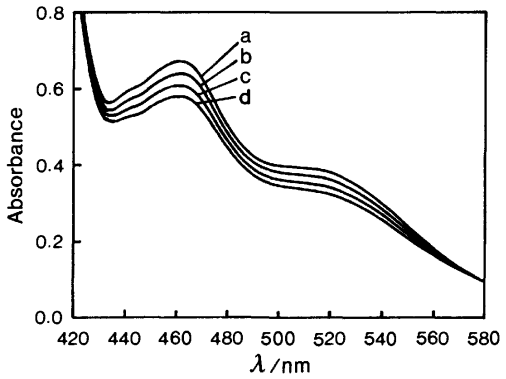

Fig. 10. Spectra of $Fe(ClO_4)_3$-glycine aqueous solution at $I=0.5$. Conditions: $[Fe(ClO_4)_3]=1.9\times10^{-2}$, $[HClO_4]=0.45$, and [Gly]=0.80 mol dm^{-3}, temperature: a: 15, b: 20, c: 25, and d: 30 °C, cell length: 1 cm.

hydroxide oxide particles were isolated from the solid phase by repeated slow and fast centrifugation. The amounts of iron(III) in the each phase were determined spectrophotometrically using 1,10-phenanthroline.

Figure 8 displays the fractions of the β-iron(III) hydroxide oxide, hematite, and soluble iron(III) species as a function of the reaction time. The rate of appearance of the hematite was the same as that of the disappearance of the β-iron(III) hydroxide oxide and the conversion continued until all the β-iron(III) hydroxide oxide had disappeared. This fact clearly indicated that the cuboidal hematite particles developed through the conversion of β-iron(III) hydroxide oxide. The total concentration of hydroxo, chloro, and glycinato complexes of iron(III) in the supernatant solution remained constant (6.0×10^{-4} mol dm^{-3}) throughout the conversion. The soluble iron (III) species were scarcely reduced to the iron(II) state by glycine in this process, in contrast to the aqueous system.

The results in Fig. 8 indicate that the soluble iron(III) species were continuously supplied by the dissolution of β-iron(III) hydroxide oxide and the supersaturation of hydroxoiron(III) complexes was appropriately maintained during the growth of the monodispersed hematite particles.

Growth of Cuboidal Hematite Particles. Figure 9 shows the growth of the cubes at 100±0.5 °C as a function of aging time. A starting solution was prepared similar to that shown in Fig. 8 except for the acid concentration. The relative standard deviation of the particle size remained almost constant in the range 0.11—0.13 in 0.15 mol dm^{-3} hydrochloric acid during the growth from 12 to 40 h. The size of the cuboidal particles reached a plateau at which the β-iron(III) hydroxide oxide was completely consumed.

Though the growth rate of the particles was almost identical ($\approx6.7\times10^{-3}$ μm h^{-1} in the linear part), the final particle size significantly increased with the acid concentration even in a narrow range from 0.12 to 0.16 mol dm^{-3} (pH 2.0—1.6). According to the final size and the consumption time of the β-iron(III) hydroxide oxide, the nucleation rate of the hematite was greatly enhanced with increasing pH even at the same concentrations of iron(III) and glycine.

Excellent monodispersed cuboidal hematite particles have also been obtained through a similar conversion process in alcohol/water mixed solutions without glycine.[4,5] In this case, the particles developed to around 4 μm through slow nucleation even at the same concentration of iron(III) chloride.

Discussion

The hematite particles have been recognized to form through the transformation of β-iron(III) hydroxide oxide in acidified iron(III) chloride solutions at elevated temperatures.[4,5,21,24] Highly-polymerized cationic hydroxoiron(III) complexes have been confirmed to form at an initial stage of hydrolysis of iron(III) chloride solution, followed by their precipitation as β-iron(III) hydroxide oxide.[25,26] However, Atkinson et al.[24] have observed that rather low-molecular-weight hydroxoiron(III) complexes would act as the precursor of hematite. Actually, the aqueous solutions of iron(III) chloride-glycine system did not show the presence of any polymeric iron(III) species before and after aging, from which the monodispersed hematite particles directly originated.

Figure 10 displays the spectra of an iron(III) perchlorate-glycine aqueous solution at different temperatures. The absorption bands ranged between around 435 and 580 nm were charasteristic of the glycinatoiron(III) complex.[27] A decrease in the

absorbance was clearly shown as the temperature increased, which indicated that the glycinatoiron(III) complex was dissociated at higher temperatures in spite of the negative enthalpy change of protonation of glycine anions (-45.0 ± 0.2 kJ mol^{-1}).[28,29] Thus, the enthalpy change of the formation of glycinatoiron(III) complex would be negative: this consideration can be reasonable because the formation of glycinatometal complexes is mostly exothermic except for indium and lanthanoids.[30]

By the use of the formation constants for hydroxo,[17-20] chloro,[31,32] and glycinato[27] complexes of iron(III) and the dissociation constants of glycine,[33] the sum of the fractions of chloro and glycinato complexes was numerically estimated as 0.84 at 25 °C under the conditions given in Fig. 1. According to the enthalpy changes of the formation of the respective species (36 kJ mol^{-1} for $Fe^{3+}+H_2O=[FeOH]^{2+}+H^+$,[17] -33 kJ mol^{-1} for $2[FeOH]^{2+}=[Fe_2(OH)_2]^{4+}$,[19] 72 kJ mol^{-1} for $Fe^{3+}+2H_2O=[Fe(OH)_2]^{+}+2H^+$,[17] 21 kJ mol^{-1} for $Fe^{3+}+Cl^-=[FeCl]^{2+}$,[31] and 5.0 kJ mol^{-1} for $[FeCl]^{2+}+Cl^-=[FeCl_2]^+$,[34] the amounts of $[FeOH]^{2+}$ and $[Fe(OH)_2]^+$ would increase much more than those of chloro complexes at higher temperatures by the degradation of glycinato complex. Although it is uncertain which hydroxoiron(III) complex is the actual precursor of hematite paricles, the glycinatoiron(III) complex was obviously indicated to participate as the soluble reservoir of hydroxo complex for originating the monodispersed hematite particles.

The monodispersed double spheres of hematite obtained in the 2-propanol/water mixed solution would be produced through a process similar to that in the aqueous solution.

When β-iron(III) hydroxide oxide, which was separately prepared and washed, was treated at 100 °C in the same solution given in Fig. 8 but without iron(III) chloride, the dissolution of hydroxide oxide quickly reached an equilibrium state in around 15 min. On the basis of the mass balance during the dissolution of hydroxide oxide and the deposition of hematite, it was concluded that the total concentration of the iron(III) species was not controlled by the dissolution rate of the β-iron(III) hydroxide oxide but by the solubility of the hydroxide oxide. Thus, the suspension of β-iron(III) hydroxide oxide would give an appropriate supersaturation of hydroxoiron(III) complexes to form the monodispersed hematite particles under the conditions suitably adjusted.

In addition, the formation mechanism of monodispersed cuboidal hematite particles in the presence of glycine would be basically the same as that in the alcohol/water mixtures without glycine.[5] However, the final size of the particles was greatly reduced by the presence of glycine even under the same concentrations of total iron(III) chloride, depending on the acid concentration. As the size distribution was kept

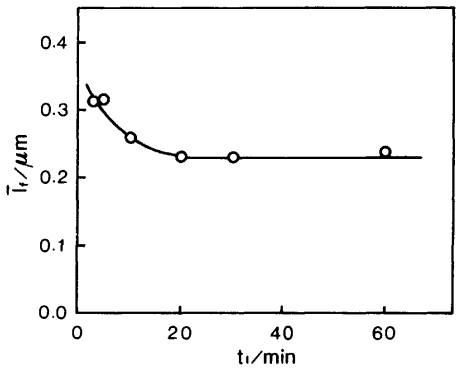

Fig. 11. Influence of acid concentration changed at t_1 on final size of cuboidal hematite particles at 100 °C. Conditions: $[HCl]_i=0.13$ and $[HCl]_f=0.15$ mol dm^{-3}.

almost constant (the relative standard deviation of 0.11—0.13 for 40 h) throughout the forced hydrolysis, the nucleation of the hematite particles would be completed at an early stage of the conversion. The dependence of acid concentration on the final size of hematite particles was also examined by a different way as follows: A solution contained 0.13 mol dm^{-3} hydrochloric acid and the same concentrations of iron(III) chloride and glycine as shown in Fig. 8 was aged at 100±0.5 °C for specified periods, t_1, from 3 to 60 min. The solution was then quenched to room temperature and its acidity was immediately changed to 0.15 mol dm^{-3} by adding hydrochloric acid, followed by repeated heating for 48—60 h.

Figure 11 displays the final size of the hematite particles as a function of t_1. The particles grew larger when the acidity was increased only at very early stages of aging. As shown in Fig. 9, the solution gave the final sizes of 0.22 and 0.35 μm at 0.13 and 0.15 mol dm^{-3} of hydrochloric acid respectively. Thus, these facts indicated that the final size was scarcely affected by the acidity applied after completion of the nucleation.

On the other hand, the cuboidal hematite particles can be also obtained when β-iron(III) hydroxide oxide particles were separately prepared and then aged in a solution without iron(III) ions under suitable conditions. In order to examine the dependence of the nature of β-iron(III) hydroxide oxide on the final size of hematite particles, three kinds of the hydroxide oxide were prepared under the conditions shown in Table 1. These were centrifuged and washed ten times with distilled water. These particles, as the iron(III) concentration of 2.0×10^{-2} mol dm^{-3}, were aged under the conditions shown in Table 2. The final sizes of the hematite particles thus prepared are also given in Table 2. The samples B and C gave hematite particles with final sizes of 0.22—0.37 μm which depended merely on the initial pH for preparing β-iron(III) hydroxide oxide, regardless of the original size of the

Table 1. Preparing Conditions for β-FeOOH at 100 °C[a)]

Sample	$[FeCl_3]\times 10$ / mol dm^{-3}	[Gly] / mol dm^{-3}	$[HCl]\times 10^2$ / mol dm^{-3}	pH[b)]	$\bar{l}\times 10^{2}$ [c)] / μm
A	2.0		0.25	1.58	7.2
B	0.20	0.20	13	2.14	6.0
C	0.20	0.20	16	1.93	24

a) 2-Propanol: 30% by volume. b) Observed at 25 °C before aging. c) Average size of acicular β-FeOOH particles.

Table 2. Aging Conditions and Final Size of Cuboidal Hematite Particles Obtained from β-FeOOH Suspension at 100 °C[a)]

Sample	[Gly] / mol dm^{-3}	$[HCl]\times 10^2$ / mol dm^{-3}	pH[b)]	$\bar{l}_f$ / μm
A	0.20	17	2.12	0.85[c)]
B	0.20	17	2.11	0.22
B		4.5	1.52	0.23
C	0.20	20	2.10	0.34
C	0.20	17	1.80	0.37

a) $[Fe(III)]=2.0\times 10^{-2}$ mol dm^{-3} as β-FeOOH, 2-propanol: 30% by volume. b) Observed at 25 °C before aging. c) The reaction did not complete even for 120 h.

hydroxide oxide, the presence of glycine, and the pH at aging. Contrary to the above results, the sample A, obtained from the solution without glycine, yielded much larger hematite particles in spite of the almost identical size of the original β-iron(III) hydroxide oxide and the aging conditions.

These facts imply that the nature of the hematite nuclei would depend definitively on the initial conditions in producing β-iron(III) hydroxide oxide. The nuclei would originate on the surfaces of the hydroxide oxide, probably by epitaxial nucleation, at the beginning of the reaction and tightly bind to the original hydroxide oxide. In the pH range applied in this work, the fraction of glycine anions is of the order of 10^{-9}, so that the adsorption of the anions would be negligible. If glycine anions adsorbed on the surfaces and reduced an interfacial energy of hematite particles, the growth rate should be also strongly affected by the acidity even in the narrow range of pH similar to the nucleation rate. Actually, little adsorption was observed even at pH 4.

However, glycine anions would combine strongly with embryos of hematite prior to the formation of stable nuclei even at low pH, because of a large excess surface energy of the embryos. In such a situation, the interfacial energy of the embryos would be significantly reduced, depending on the amount of adsorbed glycine anions, i.e., the acidity, which enhances the nucleation rate. Actually, the aging of the solutions without glycine gave much slower nucleation rates.[4,5)]

References

1) J. H. L. Watson, R. R. Cardell, Jr., and W. Heller, *J. Phys. Chem.*, **66**, 1757 (1962).
2) E. Matijević, *Acc. Chem. Res.*, **14**, 22 (1981).
3) K. Miyata and K. Nakahara, *Shikizai Kyokaishi*, **49**, 349 (1976).
4) S. Hamada and E. Matijević, *J. Colloid Interface Sci.*, **84**, 274 (1981).
5) S. Hamada and E. Matijević, *J. Chem. Soc., Faraday Trans. 1*, **78**, 2147 (1982).
6) S. Hamada, T. Hanami, and Y. Kudo, *Nippon Kagaku Kaishi*, **1984**, 1065.
7) S. Hamada, K. Bando, and Y. Kudo, *Nippon Kagaku Kaishi*, **1984**, 1068.
8) E. Matijević, *Ann. Rev. Mater. Sci.*, **15**, 483 (1985).
9) E. Matijević and P. Scheiner, *J. Colloid Interface Sci.*, **63**, 509 (1978).
10) S. Hamada, K. Bando, and Y. Kudo, *Bull. Chem. Soc. Jpn.*, **59**, 2063 (1986).
11) M. Iwase, T. Yotsuyanagi, and M. Nagayama, *Nippon Kagaku Kaishi*, **1985**, 2271.
12) V. Kastalsky and M. F. Wescott, *Aust. J. Chem.*, **21**, 1061 (1968).
13) A. E. Nielsen, "Kinetics of Precipitation," Pergamon Press, Oxford (1964), p. 53.
14) The dimension of K is dm^3 mol^{-1} h^{-1} assuming that m equals unity.
15) C. M. Flynn, Jr., *Chem. Rev.*, 84, 31 (1984).
16) P. J. Murphy, A. M. Posner, and J. P. Quirk, *Aust. J. Soil Res.*, **13**, 189 (1975).
17) R. S. Sapieszko, R. C. Patel, and E. Matijević, *J. Phys. Chem.*, **81**, 1061 (1977).
18) G. Wada and K. Kobayashi, *Bull. Chem. Soc. Jpn.*, **48**, 2451 (1975).
19) R. M. Milburn, *J. Am. Chem. Soc.*, **79**, 537 (1957).
20) C. F. Baes, Jr. and R. E. Mesmer, "The Hydrolysis of Cations", John Wiley and Sons, New York (1976), p. 235.
21) A. L. MacKay, *Mineral. Mag.*, **32**, 545 (1960).
22) E. J. Bowers and H. D. Weaver, Jr., *Proc. Indiana Acad. Sci.*, **17**, 101 (1961).
23) K. Bridger, R. C. Patel, and E. Matijević, *J. Phys. Chem.*, **87**, 1192 (1983).
24) R. J. Atkinson, A. M. Posner, and J. P. Quirk, *Clays Clay Minerals*, **25**, 49 (1977).
25) P. J. Murphy, A. M. Posner, and J. P. Quirk, *J. Colloid Interface Sci.*, **56**, 298 (1976).
26) P. J, Murphy, A. M. Posner, and J. P. Quirk, *J. Colloid Interface Sci.*, **56**, 312 (1976).
27) D. D. Perrin, *J. Chem. Soc.*, **1958**, 3120.

28) K. P. Anderson, W. O. Greenhalgh, and R. M. Izatt, *Inorg. Chem.*, **5**, 2106 (1966).
29) K. P. Anderson, W. O. Greenhalgh, and E. A. Butler, *Inorg. Chem.*, **6**, 1056 (1967).
30) J. J. Christensen and R. M. Izatt, "Handbook of Metal Ligand Heats," Marcel Dekker, New York (1983), p. 293.
31) N. Sutin, J. K. Rowley, and R. W. Dodson, *J. Phys. Chem.*, **65**, 1248 (1961).
32) E. Robinowitch and W. H. Stockmayer, *J. Am. Chem. Soc.*, **64**, 335 (1942).
33) E. J. King, *J. Am. Chem. Soc.*, **73**, 155 (1951).
34) U. Strahm, R. C. Patel, and E. Matijević, *J. Phys. Chem.*, **83**, 1689 (1979).

 © 1986 The Chemical Society of Japan Bull. Chem. Soc. Jpn., 59, 3451—3457 (1986)

Exciplexes in Perfluorohydrocarbon. Charge-Transfer Interaction between Exciplexes and Perfluorohexane

Koji KANO,* Masaru YANAGIMOTO, and Shizunobu HASHIMOTO
Department of Applied Chemistry, Faculty of Engineering, Doshisha University, Kamikyo-ku, Kyoto 602
(Received June 3, 1986)

The rate constants for photochemical processes of pyrene in perfluorohexane (PFH) and hexane containing *N,N*-dimethylaniline (DMA) have been determined by analyzing the rise and decay curves of the pyrene-DMA exciplex to study the interaction between electronically polar exciplex and an extremely nonpolar solvent, PFH. In PFH, the dissociation of the exciplex to the original pyrene in the excited singlet state and DMA was decelerated and the radiationless deactivation of the exciplex to the ground states was accelerated. In the case of the naphthalene-triethylamine exciplex system, the radiationless deactivation of the exciplex was also much faster in PFH than in hexane. These results suggest charge-transfer interactions between the polar exciplexes and PFH. The negative charges of the exciplexes may transfer to the strongly electronegative fluorine atom(s) of PFH. The deceleration of the back reaction and the acceleration of the radiationless deactivation seem to lead the efficient fluorescence quenching of pyrene and naphthalene by amines in PFH.

Solvation plays an essentially important role to dominate physical properties and chemical reactivities of molecules in solutions. Several studies have demonstrated very weak solute-solvent interactions in perfluorohydrocarbons. The absorption and fluorescence emission spectra of benzene in perfluorinated alkanes are very similar to those in vapor phase.[1-3] The vibronic bands of the electronic spectra of 9*H*-xanthene-9-thione and its related thiones in perfluorohexane (PFH) are well-resolved compared with those in 3-methylpentane glass at 77 K.[4,5] These spectral data clearly indicate a very weak perturbation of the electronic states of solute molecules by perfluorohydrocarbon solvents. The fluorescence intensities of the vibronic bands of the pyrene monomer are known to be sensitive toward solvent polarity. This probe molecule also indicates extremely weak dipole-dipole interaction between pyrene and perfluorohydrocarbons.[6,7] A Kamlet-Taft's π^* value is one of the measures of the ability of a solvent to interact with solute through dipole-dipole interaction.[8,9] Table 1 shows the π^* values of various perfluorohydrocarbons together with the dielectric constants (ε) and the refractive indexes (n_D). The Kamlet-Taft's π^* values of perfluorohydrocarbons are large and negative, indicating very weak solute-solvent interactions in these solvents. Fluorine atom is so electronegative that perfluorohydrocarbon solvents show extremely low polarizabilities leading to weak van der Waals interactions.

Table 1. Dielectric Constants (ε), Refractive Indexes (n_D), and Kamlet-Taft's π^* Values for Perfluorohydrocarbons

	ε	n_D	π^*
Perfluoro(dimethyldecalin)	1.94[a]	1.312[a]	−0.33[a]
Tris(perfluorobutyl)amine	1.90[a]	1.291[a]	−0.36[a]
Perfluorooctane	1.85[a]	1.271[a]	−0.41[a]
Perfluoroheptane	1.765[a]	1.258[a]	−0.39[a]
Perfluorohexane	1.679[b]	1.251[c]	−0.40[d]

a) Ref. 9(b). b) This work. c) N. Ishikawa, *Petrotech*, **6**, 761 (1983). d) Ref. 8 e).

In spite of these physical aspects, we scarecely know chemical reactivities in perfluorohydrocarbons. Since perfluorinated alkanes are less active toward triplet carbonyl compounds than corresponding hydrocarbons, they are suitable solvents for phosphorescence measurements at room temperature.[10] Metal pentacarbonyls ($M(CO)_5$, M=Cr, Mo, and W) generated by the photolysis of the metal hexacarbonyls are very reactive toward carbon monoxide, cyclohexane, and nitrogen in perfluoro(methylcyclohexane) (PFMCH) because $M(CO)_5$ is free from solvation in PFMCH.[11] In some cases, perfluorohydrocarbons act as electron acceptors. The fluorescence emissions of triethylamine[12] and hydrocarbons such as cyclohexane, decalin, and 2,3-dimethylbutane[13] are quenched by perfluorohydrocarbons through charge-transfer interactions.

The present study deals with the solvent effects of perfluorohexane (PFH) on exciplex formation and dissociation. PFH shows the smallest ε and π^* values among the perfluorohydrocarbons listed in Table 1. The exciplex states have been well-known to be very sensitive toward solvent polarity because of their polar structures.[14] The exciplex, therefore, may be useful as a probe to study the interaction of polar solutes with extremely nonpolar solvents, perfluorohydrocarbons.

Experimental

Materials. Naphthalene was purified by sublimation. Pyrene was chromatographed on silica gel with cyclohexane and recrystallized from cyclohexane. Anthracene (Nakarai, 99.9%), triethylamine (TEA, Nakarai, reagent grade), and PFH (PCR Research Chemicals) were used without further

purification. Reagent grade of *N,N*-dimethylaniline (DMA, Nakarai) was purified by distillation prior to use. Spectral grades of hexane and cyclohexane (Nakarai) were used.

Measurements. Fluorescence emission and excitation spectra were taken on a Hitachi 650—60 spectrofluorometer (emission and excitation bandwidths=2 nm). Fluorescence quantum yields of naphthalene and pyrene (Φ_X) were determined by measuring the corrected fluorescence spectra of very dilute sample solutions. The optical densities of the samples were arranged to be less than 0.05 at excitation wavelengths. We used the reported fluorescence quantum yields (Φ_{ST}) of naphthalene (0.21)[15] and pyrene (0.60)[6] in cyclohexane as standards. Both sample and standard solutions were excited at the same wavelength. Φ_X, therefore, can be represented as

$$\Phi_X = \Phi_{ST}(FA_X/FA_{ST})(A_{ST}/A_X)(n_X^2/n_{ST}^2), \quad (1)$$

where FA is the spectral area, A is the optical density at the excitation wavelength, and n is the refractive index. The fluorescence decay curves were taken using an Ortec-PRA single photon counting apparatus and analyzed by a Simplex method using an NEC 9801 microcomputer. All samples were degassed by five freeze-pump-thaw cycles.

Dielectric constant (ε) of PFH was kindly measured at 25 °C by Professor Shimizu and Mr. Tsuchihashi of this university by using a Shibayama dielectric constant measurement apparatus SS207-B.

Results

Figure 1 shows the fluorescence spectra of pyrene in PFH containing various amounts of DMA. Upon addition of DMA, the fluorescence intensities of the pyrene and anthracene monomers decreased and new broad fluorescence bands due to the exciplexes appeared at longer wavelengths in nonpolar solvents. The exciplex emission was also observed for the naphthalene–TEA system. The fluorescence maxima (λ_{max}) of these exciplexes are listed in Table 2. The peak of the fluorescence band of the anthracene–DMA exciplex was obscure in hexane and cyclohexane due to overlap with the monomer fluorescence band. In each system, the fluorescence maximum of the exciplex in PFH was observed at the shortest wavelength. A good linear relationship between the energy of the pyrene–DMA exciplex emission band (ν_E) and the solvent polarity parameter ($f(\varepsilon,n)$) was observed for the pyrene–DMA system:[16]

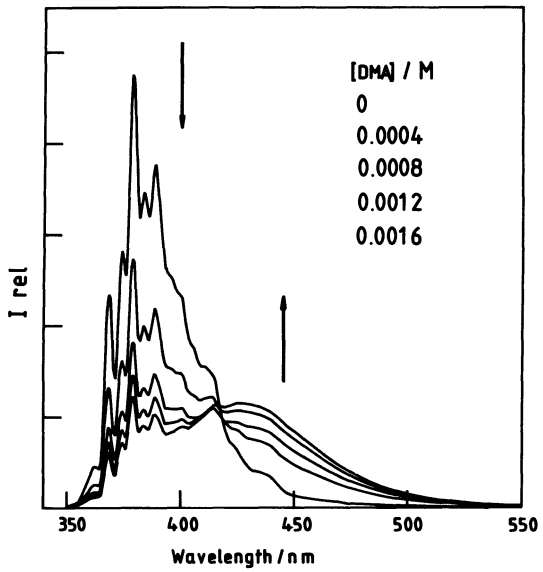

Fig. 1. Fluorescence spectra of pyrene (1×10^{-6} M) in degassed PFH in the absence and the presence of DMA at 25 °C. Pyrene was excited at 328 nm.

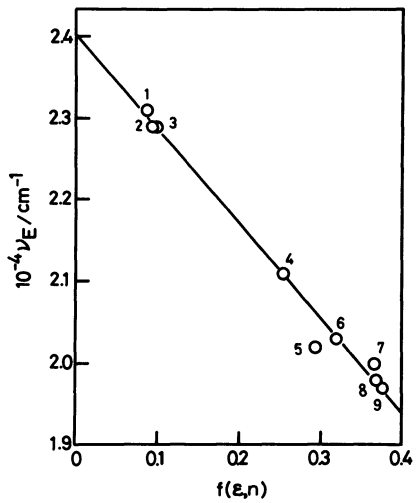

Fig. 2. Plot of the energy of the fluorescence maximum of the pyrene–DMA exciplex (ν_E) vs. the solvent polarity parameter $f(\varepsilon, n)$: 1: PFH, 2: hexane, 3: cyclohexane, 4: diethyl ether, 5: ethyl acetate, 6: dichloromethane, 7: isopropyl alcohol, 8: propyl alcohol, 9: ethanol.

Table 2. Fluorescence Maxima (λ_{max}) of Exciplexes of Pyrene and DMA, Anthracene and DMA, and Naphthalene and TEA in Various Solvents at 25 °C

	ε	λ_{max}, nm		
		Pyrene–DMA	Anthracene–DMA	Naphthalene–DMA
Perfluorohexane	1.679	432	458	402
Hexane	1.89	436	460—470	408
Cyclohexane	2.02	437	460—470	409
Ethyl acetate	6.12	494	516	473

Table 3. Fluorescence Quenching of Pyrene, and Naphthalene by DMA or TEA in PFH, Hexane, and Cyclohexane at 7 °C and 25 °C

Solvent	τ_0/ns	K_{SV}/M^{-1}	$10^{-9}k_q$/M^{-1} s^{-1}
	Pyrene-DMA (7 °C)		
Perfluorohexane	399	4940	12.4
Hexane	464	1014	2.2
	Pyrene-DMA (25 °C)		
Perfluorohexane	389	1827	4.7
Hexane	398	448	1.1
Cyclohexane	401	615	1.5
	Anthracene-DMA (7 °C)		
Perfluorohexane	7.1	244 (113)[a]	34.4 (15.9)[a]
Hexane	5.2	102	19.6
	Anthracene-DMA (25 °C)		
Perfluorohexane	7.0	156 (126)[a]	22.3 (17.9)[a]
Hexane	5.4	72	13.3
Cyclohexane	5.1	44	8.6
	Naphthalene-TEA (25 °C)		
Perfluorohexane	99	366	3.7
Hexane	120	132	1.1
Cyclohexane	117	187	1.6

a) The K_{SV} and k_q values in the parentheses were determined from the Stern-Volmer plots for fluorescence lifetime of anthracene.

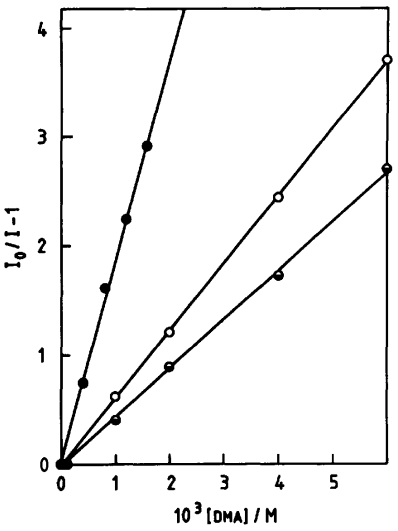

Fig. 3. Stern-Volmer plots for the fluorescence quenching of pyrene (1×10^{-6} M) by DMA in degassed PFH (●), hexane (◒), and cyclohexane (○) at 25 °C. Pyrene was excited at 328 nm in PFH, 334 nm in hexane, and 335 nm in cyclohexane. The fluorescence intensities (I) were followed at 378 nm in PFH and 382 nm in hexane and cyclohexane.

$$f(\varepsilon, n) = 2(\varepsilon-1)/(2\varepsilon+1) - (n^2-1)/(2n^2+1). \quad (2)$$

The plot of ν_E vs. $f(\varepsilon,n)$ is shown in Fig. 2. A plot for PFH does not deviate from the straight line. The same linear relationship between ν_E and $f(\varepsilon,n)$ has been observed for the naphthalene-TEA system.[17]

A simple Stern-Volmer relationship could be applied for the fluorescence quenching of pyrene, anthracene, and naphthalene by amines (Fig. 3) and the results are summarized in Table 3. The fluorescence quenching parameters, the Stern-Volmer constants (K_{SV}) and the rate constants of fluorescence quenching (k_q), determined for the pyrene-DMA system in hexane and for the anthracene-DMA system in cyclohexane are in good agreement with those reported by Ware and his coworkers.[18,19] In each system, both K_{SV} and k_q values obtained for the fluorescence quenching in PFH were significantly larger than those in hexane and cyclohexane. In order to understand the reasons for very efficient fluorescence quenching in PFH, we determined the all rate constants of photochemical processes shown in the following scheme:

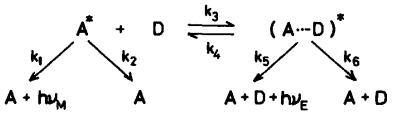

The fluorescence decays of monomer and exciplex can be written as Eqs. 2 and 3, respectively:[20,21]

$$I_M(t) = a_1\exp(-\lambda_1 t) + a_2\exp(-\lambda_2 t), \quad (3)$$

$$I_E(t) = a_3[\exp(-\lambda_1 t) - \exp(-\lambda_2 t)], \quad (4)$$

where

$$\lambda_{1,2} = 1/2[k_1 + k_2 + k_3[Q] + k_4 + k_5 + k_6 \mp \{(k_1+k_2+k_3[Q]-k_4-k_5-k_6)^2+4k_3k_4[Q]\}^{1/2}]. \quad (5)$$

From Eq. 3, linear correlations between $(\lambda_1+\lambda_2)$ and $\lambda_1\lambda_2$ and [Q] can be expected:

$$\lambda_1 + \lambda_2 = k_1 + k_2 + k_3[Q] + k_4 + k_5 + k_6 \quad (6)$$

$$\lambda_1\lambda_2 = (k_1+k_2)(k_4+k_5+k_6) + (k_5+k_6)k_3[Q] \quad (7)$$

The k_3 and (k_5+k_6) values are determined from the slopes of the plots of $(\lambda_1+\lambda_2)$ vs. [Q] and of $\lambda_1\lambda_2$ vs. [Q], respectively. Since (k_1+k_2) can be obtained from the fluorescence decay of a fluorophore in the absence of quencher, k_4 is determined from the intercept of the plot of $(\lambda_1+\lambda_2)$ vs. [Q]. The k_1 and k_2 values are presented from the fluorescence lifetime (τ_0) and quantum yield (Φ_{M0}) of a fluorophore in the absence of quencher:

$$\tau_0 = (k_1+k_2)^{-1} \quad (8)$$

$$\Phi_{M0} = k_1/(k_1+k_2) \quad (9)$$

In the presence of quencher, the ratio of the fluorescence quantum yield of exciplex to that of monomer (Φ_E/Φ_M) is represented as

$$\Phi_E/\Phi_M = (k_5/k_1)\{k_3[Q]/(k_4+k_5+k_6)\}. \quad (10)$$

From the slope of the plot of Φ_E/Φ_M vs. [Q], one can get k_5. We obtained Φ_E/Φ_M value at each quencher concentration by measuring spectral areas of monomer and exciplex emissions:

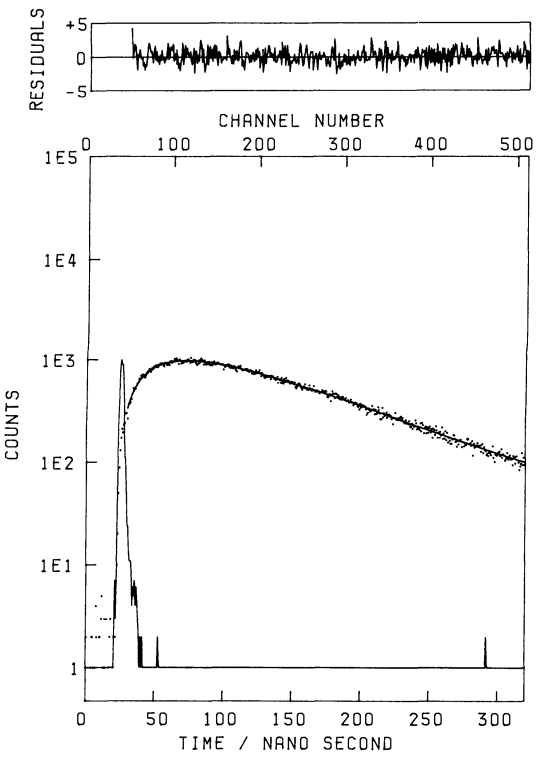

Fig. 4. Fluorescence decay curve of the pyrene–DMA exciplex in degassed PFH at 7 °C. The concentrations of pyrene and DMA were 1×10^{-6} and 1.5×10^{-3} M, respectively. Pyrene was excited at 328 nm and the exciplex emission was passed through a Toshiba glass filter VY-45 to eliminate the monomer emission. The best fit provided the rise and decay times of 29.5 and 91.8 ns, respectively ($\chi_\nu^2=1.09$).

$$\frac{\Phi_E}{\Phi_M} = \frac{\int I_E(\nu)d\nu}{\int I_M(\nu)d\nu} \quad (11)$$

The λ_1 and λ_2 values were determined from the fluorescence rise and decay curve of the exciplex. A typical example of the rise and decay curve of the pyrene–DMA exciplex in PFH is shown in Fig. 4. The plots of $(\lambda_1+\lambda_2)$ and of $\lambda_1\lambda_2$ vs. [DMA] are given in Figs. 5 and 6, respectively. The results shown in Figs. 5 and 6 were treated statistically by using a microcomputer to determine k_3 and (k_5+k_6). We had large experimental errors for determining λ_1 and λ_2 from the monomer fluorescence decay curve. The fluorescence quantum yields of naphthalene and pyrene in PFH

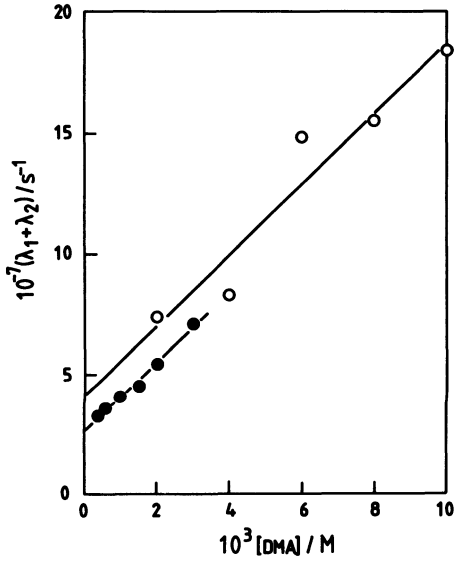

Fig. 5. Dependence of $(\lambda_1+\lambda_2)$ on the DMA concentration for the pyrene–DMA system in PFH (●) and hexane (○) at 7 °C.

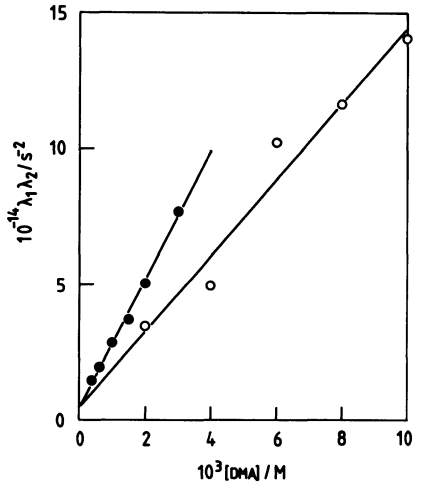

Fig. 6. Dependence of $\lambda_1\lambda_2$ on the DMA concentration for the pyrene–DMA system in PFH (●) and hexane (○) at 7 °C.

Table 4. Fluorescence Quantum Yields (Φ_{M0}) of Naphthalene and Pyrene in Degassed PFH and Hexane in Absence of Quencher

Fluorophore	Solvent	T/°C	Φ_{M0}
Naphthalene	Perfluorohexane	25	0.20
Naphthalene	Hexane	25	0.21
Pyrene	Perfluorohexane	25	0.33
Pyrene	Hexane	25	0.49
Pyrene	Perfluorohexane	7	0.35
Pyrene	Hexane	7	0.51

Table 5. Rate Constants for Photochemical Processes of Pyrene-DMA System in Degassed PFH and Hexane at 7 °C

	PFH	Hexane
$10^{-6}k_1$ s^{-1}	0.88±0.05	1.1±0.1
$10^{-6}k_2$ s^{-1}	1.6±0.1	1.1±0.1
$10^{-10}k_3$ M^{-1} s^{-1}	1.5±0.1	1.5±0.1
$10^{-7}k_4$ s^{-1}	0.69±0.17	3.0±1.6
$10^{-6}k_5$ s^{-1}	2.3±0.2	2.5±1.1
$10^{-6}k_6$ s^{-1}	13.0±1.0	7.0±2.0

and hexane are listed in Table 4. From the results listed in Tables 3 and 4, the k_1 and k_2 values were evaluated. The determined rate constants for the photochemical processes of the pyrene-DMA system are summarized in Table 5.

In the case of the naphthalene-TEA system, the rise time of the exciplex emission at 25 °C was so short that the λ_1 and λ_2 values could not be determined accurately. Although large errors might be included, we evaluated the $(k_4+k_5+k_6)$ values by extrapolating λ_2 to the zero TEA concentration. The λ_2 values were determined by fitting the experimentally obtained decay curves with trial single-exponential decay functions at larger t. Figure 7 shows the plots of λ_2 vs. [TEA] in PFH and hexane. The slope of the plot of Φ_E/Φ_M vs. [TEA] gives $(k_3k_5/k_1)/(k_4+k_5+k_6)$ (see Eq. 10). Since the k_1 value can be known from the fluorescence lifetime and quantum yield of naphthalene in the absence of quencher, the k_3k_5 value can be evaluated. The rate constant for fluorescence quenching is represented as

$$k_q = k_3(k_5+k_6)/(k_4+k_5+k_6). \quad (12)$$

From Eq. 12, we could get the k_3k_6 value. Table 6 summarizes the results.

Table 6. Rate Constants for Photochemical Processes of Naphthalene-TEA System in PFH and Hexane at 25 °C

	PFH	Hexane
$10^{-6}k_1$ s^{-1}	2.1	1.8
$10^{-6}k_2$ s^{-1}	8.5	6.6
$10^{-15}k_3k_5$ s^{-2} M^{-1}	2.5	1.6
$10^{-16}k_3k_6$ s^{-2} M^{-1}	7.2	0.94
k_6/k_5	29	6

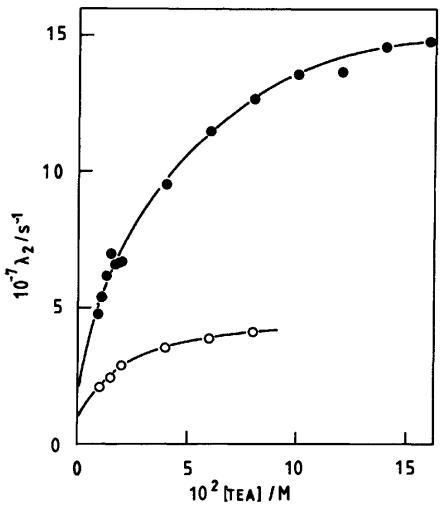

Fig. 7. Plots of λ_2 vs. [TEA] for the pyrene-DMA exciplex in PFH (●) and hexane (○) at 7 °C.

Discussion

The photochemical processes of the fluorophores such as pyrene, anthracene, and naphthalene in the presence of aromatic or aliphatic amines have been well known to be dependent on solvent polarity.[14] In nonpolar solvents, these fluorophores in the excited singlet states form the exciplexes in collision with amines while direct electron transfers from amines to photoexcited fluorophores occur without exciplex formation in strongly polar solvents. If an exciplex is fluorescent, the emission maximum of the exciplex shifts to longer wavelength with increasing solvent polarity because the exciplex having an electronically polar structure is solvated to a large extent by polar solvent. These characteristics of exciplex seem to be suitable for investigating the interaction between photoexcited solute and perfluorocarbon solvent. Especially, exciplexes may be very interesting probes for studing interaction of electronically polar solute with perfluorinated solvent, which has not been examined.

Fluorescence Quenching. The fluorescence quenching of pyrene and anthracene by DMA and of naphthalene by TEA was carried out in PFH, hexane, and cyclohexane. As indicated in Fig. 3 and Table 3, the fluorescence quenching in PFH proceeds much faster than that in hexane and cyclohexane. In the case of pyrene, the k_q values obtained at 7 °C are considerably larger than those at 25 °C. This should be due to the back reaction of the pyrene-DMA

exciplex to the original precursors, pyrene in the excited singlet state and DMA in the ground state. The back reaction is accelerated at higher temperature.[18] Very efficient fluorescence quenching occurred in the anthracene-DMA system in PFH, the k_q values being $3.44\times10^{10}\,M^{-1}\,s^{-1}$ (1 M=1 mol dm^{-3}) at 7 °C and $2.23\times10^{10}\,M^{-1}\,s^{-1}$ at 25 °C. Since the viscosity (η) of PFH at 20 °C is 0.7 cP (1 P=0.1 Pas), the diffusion-controlled rate constant (k_{diff}) is calculated to be $1.4\times10^{10}\,M^{-1}\,s^{-1}$ using Stokes-Einstein-Smoluckowski's equation, $k_{diff}=8RT/(2000\eta)$. The k_q values are much larger than the calculated k_{diff} value. Then we measured the fluorescence lifetime of the anthracene monomer at each DMA concentration to obtain k_q for dynamic quenching. The Stern-Volmer plots for the fluorescence lifetimes provided the k_q values of $1.59\times10^{10}\,M^{-1}\,s^{-1}$ at 7 °C and $1.79\times10^{10}\,M^{-1}\,s^{-1}$ at 25 °C, which are very close to the calculated k_{diff} value. These results indicate the occurrence of a static quenching in this system. Although the mechanism of the static quenching is not clear, one possibility is the formation of ground-state aggregates of anthracene and DMA due to low solubilities of these solute molecules in PFH. In the case of the pyrene-DMA system, however, the fluorescence decay curve (see Fig. 4) indicates that the exciplex forms dynamically. The efficient fluorescence quenching of pyrene by DMA in PFH, therefore, cannot be interpreted in terms of the ground-state aggregates.

Pyrene-DMA System. We determined the rate constants for the photochemical processes of the pyrene-DMA system according to the procedures described in detail by Cheung and Ware.[18] The results are summarized in Table 5. Since the fluorescence rise time of the pyrene-DMA exciplex was so short in PFH at 25 °C that the measurements were undertaken at 7 °C. The exciplex formation for the pyrene-DMA system has been verified to be diffusion-controlled process.[18,22] The k_3 values in cyclohexane at 20 °C and in hexane at 7.6 °C have been reported to be 9.8×10^9 and $1.37\times10^{10}\,M^{-1}\,s^{-1}$, respectively.[18,22] The k_3 value ($1.5\times10^{10}\,M^{-1}\,s^{-1}$) in hexane at 7 °C obtained in the present study is in good agreement with the reported value. The k_3 value in PFH is the same as that in hexane. As mentioned above, the Stokes-Einstein-Smolukowski's equation predicts that k_{diff} in PFH is $1.4\times10^{10}\,M^{-1}\,s^{-1}$ at 20 °C which is very close to k_3 obtained in this study.

The large difference between PFH and hexane was found in the k_4 and k_6 values. The fluorescence quenching rate constant, k_q, is represented as Eq. 12. The large k_q value in PFH, therefore, is ascribed to the smaller k_4 and larger k_6 values compared with the case in hexane. If the solute-solvent interaction in PFH is very weak as predicted from ε and π^* values (Table 1), the back reaction of the exciplex (k_4) in PFH should be faster than that in hexane because of the smaller stabilization of the pyrene-DMA exciplex in PFH. The experimental result, however, is opposite from the assumption. Therefore, we have to consider the interaction between the exciplex and surrounding PFH molecules. Alford et al. have found that the fluorescence of TEA is efficiently quenched by perfluorohydrocarbons such as PFMCH, octafluorocyclobutane, and perfluoro-2-butene in both vapor and liquid phases.[12] In cyclohexane, k_q for the fluorescence quenching of TEA by PFMCH is $1.3\times10^{10}\,M^{-1}\,s^{-1}$. Alford et al. assumed a charge-transfer (CT) interaction as the fluorescence quenching mechanism. Similarly, the fluorescence of hydrocarbons such as cyclohexane, decalin, and 2,3-dimethylbutane is also quenched by perfluorohydrocarbons such as PFMCH and perfluorodecalin.[13] Choi and Lipsky proposed a quenching mechanism involving charge transfer from photoexcited hydrocarbons to perfluorohydrocarbons.[13] In the case of pyrene, the fluorescence quantum yield (Φ_{M0}) and lifetime (τ_0) of the pyrene monomer in PFH without quencher are somewhat smaller than those in hexane (see Tables 3 and 4). Although CT interaction between photoexcited pyrene and PFH may be accounted for the smaller Φ_{M0} in PFH, the quenching by PFH was not so remarkable. Meanwhile, since the pyrenyl moiety of the exciplex is negatively charged and is expected to have a lower ionization potential compared with photoexcited pyrene, it can be expected to transfer the negative charge of the pyrenyl moiety to the strongly electronegative fluorine atom(s) of PFH:

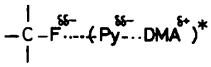

The CT interaction between the exciplex and PFH may decelerate the back reaction of the exciplex and accelerate the radiationless deactivation of the exciplex leading to smaller k_4 and larger k_6. If the CT interaction stabilizes the exciplex, the fluorescence maximum of the exciplex may shifts to longer wavelength in PFH. No novel behavior of PFH, however, was observed in the plot of ν_E vs. $f(\varepsilon,n)$ as shown in Fig. 2. In the present stage, we do not have any experimental data to explain the fluorescence maximum of the pyrene-DMA exciplex in PFH. Presumably, the Franck-Condon ground state of the exciplex should be considered to answer this problem. The Franck-Condon ground state may still interact with PFH because PFH interacting with the exciplex can be regarded microscopically as a sort of a polar solvent. Another plausible mechanism for the smaller k_4 value in PFH is the self association of the exciplex. It can be assumed that the activation energy due to weak association of the exciplex causes the deceleration of the back reaction of the exciplex. However, this mechanism should be excluded by the fact that the

fluorescence quenching of pyrene in PFH obeys a simple Stern-Volmer linear relationship (see Fig. 3).

Naphthalene-TEA System. In this system, we could not determined all rate constants for the photochemical processes because of a very fast rise of the exciplex emission intensity. However, we could evaluate the k_6/k_5 values as mentioned in the Results Section. As Table 6 shows, the k_6/k_5 value in PFH is much larger than that in hexane. Judging from the results obtained for the pyrene-DMA system, it may be reasonable to assume that the k_5 value for PFH does not differ largely from that for hexane. The radiationless deactivation of the exciplex in PFH, therefore, should be much faster than that in hexane as the case of the pyrene-DMA system. The CT interaction between the polar naphthalene-TEA exciplex and PFH may accelerate the radiationless deactivation.

This work was supported by Grant-in-Aid for Scientific Research No. 59550560 from the Ministry of Education, Science and Culture.

References

1) C. W. Lawson, F. Hirayama, and S. Lipsky, *J. Chem. Phys.*, **51**, 1596 (1968).

2) H. Mauser and R. Kretschmer, *Z. Phys. Chem. (Frankfurt am Main)*, **21**, 80 (1972).

3) K. Kano, S. Yamamori, M. Yanagimoto, and S. Hashimoto, *Chem. Lett.*, **1984**, 379.

4) A. Maciejewcki and R. P. Steer, *Chem. Phys. Lett.*, **100**, 540 (1983).

5) A. Maciejewcki and R. P. Steer, *J. Am. Chem. Soc.*, **105**, 6738 (1983).

6) K. Kalyanasundaram and J. K. Thomas, *J. Am. Chem. Soc.*, **99**, 2039 (1977).

7) K. Hara and W. R. Ware, *Chem. Phys.*, **51**, 61 (1980).

8) a) M. J. Kamlet and R. W. Taft, *J. Am. Chem. Soc.*, **98**, 377 (1976); b) R. W. Taft and M. J. Kamlet, *ibid.*, **98**, 2886 (1976); c) M. J. Kamlet, J. L. Abboud, and R. W. Taft, *ibid.*, **99**, 6027 (1977); d) M. J. Kamlet, J. M. Abboud, M. H. Abraham, and R. W. Taft, *J. Org. Chem.*, **48**, 2877 (1983); e) J. M. Abboud, G. Guiheneuf, M. Essfar, R. W. Taft, and M. J. Kamlet, *J. Phys. Chem.*, **88**, 4414 (1984).

9) a) J. E. Brady and P. W. Carr, *J. Phys. Chem.*, **86**, 3053 (1982); b) J. E. Brady and P. W. Carr, *Anal. Chem.*, **54**, 1751 (1982).

10) a) C. A. Parker and T. A. Joyce, *Chem. Commun.*, **1968**, 749; b) C. A. Parker and T. A. Joyce, *ibid.*, **1968**, 1421; c) C. A. Parker and T. A. Joyce, *Trans. Faraday Soc.*, **65**, 2823 (1969).

11) J. M. Kelly, C. Long, and R. Bonneau, *J. Phys. Chem.*, **87**, 3344 (1983).

12) P. C. Alford, C. G. Cureton, R. A. Lampert, and D. Phillips, *Chem. Phys. Lett.*, **55**, 100 (1978).

13) H. T. Choi and S. Lipsky, *J. Phys. Chem.*, **85**, 4089 (1981).

14) N. Mataga and M. Ottolenghi, "Molecular Association," ed by R. Foster, Academic Press, London (1971), Vol. 2, Chap. 1.

15) C. Parker and T. A. Joyce, *Trans. Faraday Soc.*, **62**, 2758 (1966).

16) E. Lippert, *Z. Naturforsch. A*, **10**, 541 (1955); E. Lippert, *Electrochem.*, **61**, 962 (1957); N. Mataga, Y. Kaifu, and M. Koizumi, *Bull. Chem. Soc. Jpn.*, **28**, 690 (1955); N. Mataga, Y. Kaifu, and M. Koizumi, *ibid.*, **29**, 465 (1956).

17) K. Kano, S. Hashimoto, A. Imai, and T. Ogawa, *J. Inclusion Phenomena*, **2**, 737 (1984).

18) S. T. Cheung and W. R. Ware, *J. Phys. Chem.*, **87**, 466 (1983).

19) M. Hui and W. R. Ware, *J. Am. Chem. Soc.*, **98**, 4718 (1976).

20) J. B. Birks, D. J. Dyson, and I. H. Munro, *Proc. R. Soc. London, Ser. A*, **275**, 575 (1963).

21) W. R. Ware and H. P. Richter, *J. Chem. Phys.*, **48**, 1595 (1968).

22) K. Yoshihara, T. Kasuya, A. Inoue, and S. Nagakura, *Chem. Phys. Lett.*, **9**, 469 (1971).

 © 1986 The Chemical Society of Japan Bull. Chem. Soc. Jpn., 59, 3459—3464 (1986)

Isotachophoretic Analysis of Quaternary Ammonium Ions by Using α-Cyclodextrin as Complex-Forming Agent

Masato TAZAKI,† Takashi HAYASHITA,†† Yasumitsu FUJINO, and Makoto TAKAGI*
Department of Organic Synthesis, Faculty of Engineering, Kyushu University, Higashi-ku, Fukuoka 812
(Received January 23, 1986)

The isotachophoretic behavior of aromatic nucleus-containing quaternary ammonium ions was studied in the presence of a neutral ligand, α-cyclodextrin. Due to the interaction of cyclodextrin with the hydrophobic aromatic nucleus, isomeric ammonium ions containing, e.g., an *o*-, *m*-, or *p*-disubstituted benzene ring, were satisfactorily separated. In the absence of cyclodextrin, the separation of the isomers was poor. A theoretical approach was also used in order to evaluate the binding equilibrium constant (K) between the analyte ion and α-cyclodextrin through an isotachophoretic measurement. The binding constants (log K) with (*o*-, *m*-, and *p*-methylbenzyl)trimethylammonium ions were found to be 0.8, 1.1, and 1.6, respectively.

During the past twenty years, substantial progress has been made concerning isotachophoresis, both in regard to theory and instrumentation, making it an important physicochemical tool for the analysis of ionic species in solution. In this technique, ion separation is based on a difference in the ionic mobilities under an electrical potential gradient. Therefore, the most important task in isotachophoresis is to control or modify the effective mobility of analyte ions in order to expand its analytical applications.

Several approaches have been made to modify the mobility of ionic species: (i) a pH adjustment of the leading solution, (ii) a change in the solvent polarity, and (iii) the use of complex-forming equilibria with counter ions.[1-10] As a new approach, we have recently proposed a system in which an electrically-neutral ligand is used to bind ionic species and to alter their effective ionic mobility.[11] For example, by adding an appropriate amount of crown ethers to the leading solution, some alkali and alkaline earth metal ions (which otherwise did not form electrophoretically resolved zones) could be mutually separated.

On the other hand, cyclodextrins are known to have specific interactions with various aromatic compounds in aqueous solution.[12] This type interaction has recently been successfully used for improving the chromatographic separation of aromatic compounds and amino acids.[13-16] Further, the separation of optical isomers has been attained by taking advantage of the chiral nature of cyclodextrins.[17,18] Such interactions of cyclodextrins with aromatic compounds should be directly applicable to an isotachophoretic system; in fact, we have found that the separation of bulky (lipophilic) inorganic anions can be improved by adding α-cyclodextrin (α-CD).[11]

During the present study, we looked at the effect of α-CD on the isotachophoretic separation of quaternary ammonium ions. These ions, especially those in isomeric forms, are difficult to separate under conventional isotachophoretic conditions. The addition of α-CD greatly improved the separation. The study was also extended to an evaluation of the binding constant between the analyte ammonium ion and α-CD.

Experimental

Apparatus A Shimadzu IP-2A isotachophoretic analyzer was combined and used with a potential gradient detector (model PGD-1). The ion-migration current and the temperature were set at 50 μA and 25 °C, respectively. The length of the analyzing capillary tube (PTFE; i. d. 0.5 mm) was 15 cm.

Reagents. Ten mM (1 M=1 mol dm^{-3}) of hydrochloric acid or 10 mM of an acetic acid-potassium acetate (1:1) buffer solution was used as the leading solution. The solution also contained 0.01 wt% poly (vinyl alcohol) (PVA) and an appropriate amount of α-CD. A terminating solution was prepared by dissolving 5 mM of (*p*-methylbenzyl)trimethylammonium bromide or 5 mM of 1-naphthylamine hydrochloride in water. The quaternary ammonium salts used as analyte ions were synthesized by a conventional reaction between tertiary amines and substituted benzyl halides in methanol or in ethanol. After recrystalization from ethanol-ether, the structure and purity of the product was confirmed by ^{1}H NMR, melting points and an elemental analysis.

Results and Discussion

Mobility of Analyte Ions. In isotachophoresis, each electrophoretic zone migrates at a constant velocity

$$v = \bar{m}_L E_L = \bar{m}_A E_A = \bar{m}_T E_T, \quad (1)$$

where $\bar{m}$ and E are the effective mobility and the (electric) potential gradient, respectively. The suffixes denote the quantities related to leading (L), analyte (A) and terminating (T) zones or ions. In our

† Present address: Department of Industrial Chemistry, Kumamoto Institute of Technology, Ikeda 4-22-1, Kumamoto 860.

†† Present address: Department of Applied Chemistry, Faculty of Engineering, Kanagawa University, Kanagawa-ku, Yokohama 221.

measurements, the potential gradient at each zone was obtained from an isotachopherogram. The mobility of the ion corresponding to each zone was then calculated by using Eq. 1 once the isotachopherogram was calibrated against ions of a known ionic mobility. In doing this, we had to be careful that the potential gradient read on isotachopherogram as a step height (cm) was not an absolute, but rather a relative value. Also, the observed step height could possibly contain a detector-drift term. Therefore, in order to determine the correct mobility of analyte ions from an isotachopherogram, several internal standard ions (calibration ions) of known mobility were required. They were subjected to the same isotachophoresis along with the analyte ions.

In the present study, K^+, Na^+, Li^+, and tetraethylammonium (TEA^+) were used as calibration ions. Figure 1 shows the potential gradient (step height) observed for these calibration ions as well as an analyte ion, (*p*-methylbenzyl)trimethylammonium ion (which is used in this case as a terminating ion). The calibration ions were such that no interaction was reported or could be expected to take place with the α-CD. The observed potential gradient of these ions, however, steadily increased as the α-CD concentration in the leading solution was increased.

In order to analyze the effect of α-CD on the calibration ions, the observed potential gradient (step height) for those ions was plotted against the reciprocals of the mobility of the ions (Fig. 2). Since this depends on their ionic atmosphere or the salt concentration in the solution, an appropriate correction was made to the absolute ionic mobility (the value at infinite dilution) by using the Debye-Hückel-Onsager equation.[19] The ionic concentration in each electrophoretic zone was calculated according to the regulating function derived from isotachophoretic equilibrium.[1]

As shown in Fig. 2, the plots resulted in good straight lines. This could be expected from Eq. 1, except that the observed potential-gradient values contained a drift term as indicated by the intersection of the lines with the ordinate. This is consistent with the experimental observation that when isotachopherogram was recorded from the start of sample-ion electrophoresis, the potential gradient of the leading zone began to drift upward at around the middle of the leading zone and then again became constant (flat) just before the analyte zones appeared. This detector-drift was quite reproducible, but could not be eliminated in spite of the extensive effort made during this study.

Figure 2 further shows that the slopes of the lines increased as the concentration of the α-CD in the leading solution was increased. This α-CD effect is associated with a decrease in the mobility of calibration ions in the presence of α-CD. The complexation of these calibration ions by α-CD might decrease their effective mobilities, but the well-defined straight lines shown in Fig. 2 can hardly be explained by such a bimolecular complexation. On the other hand, since α-CD is a rather large molecule, a change in the physical property of a bulk solution can be expected, even at a relatively low molar α-CD concentration.

According to Stokes' law, the ionic mobility is reciprocally proportional to the viscosity of the medium. This and Eq. 1 predict that if the viscosity of a solution increases with the addition of α-CD, the slopes of the lines in Fig. 2 increase with the increase in the α-CD concentration while retaining their straightness. Therefore, the mobility-lowering effect by α-CD must be entirely due to the change in the viscosity. This conclusion is also in line with the results shown in Fig. 1. Thus, the calibration ions unanimously show only a slight and an almost linear

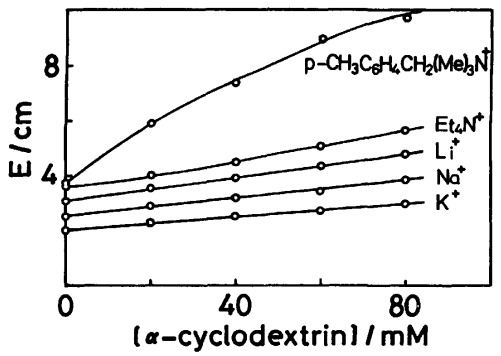

Fig. 1. Isotachophoresis of calibration ion in the presence of α-CD. Relation between potential gradient and α-CD concentration in leading solution. E: potential gradient as measured by step height (cm) in isotachopherogram. Leading solution, 10 mM HCl containing α-CD and 0.01 wt% PVA; terminating solution, 5 mM (*p*-methylbenzyl)trimethylammonium bromide; analyzing capillary tube (PTFE; i.d., 0.5 mm), 15 cm; ion migration current, 50 μA; 25 °C.

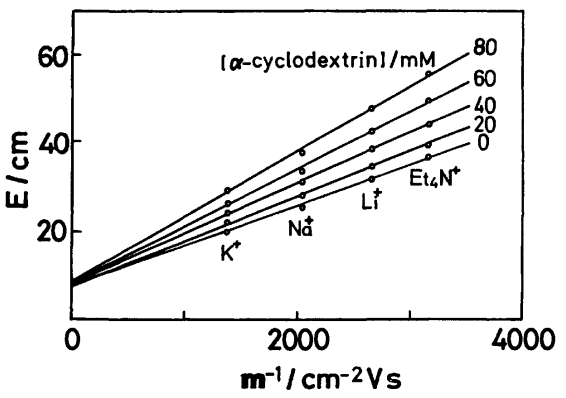

Fig. 2. Relation between potential gradient (E) and reciprocal ionic mobility (m^{-1}) of calibration ions at various α-CD concentrations. Calibration lines. For ionic mobility, see Eq. 2. For E and migrating conditions, see Fig. 1.

increase in potential gradient upon increasing the α-CD concentration. On the other hand, the (*p*-methylbenzyl)trimethylammonium ion, which is expected to make a specific (bimolecular) interaction with α-CD, shows a marked potential-gradient increase. The general behavior, therefore, is quite different.

In order to quantitatively extract the (purely) complexing effect of α-CD from the observed potential-gradient data, it was necessary to either cancel out or to make calibrations for both the detector signal-drift and the viscosity effect of α-CD. For this purpose, a calibration line (the same as that shown in Fig.2) was prepared for each α-CD concentration and was used to correlate the observed potential gradient and the mobility (reciprocal mobility) of the analyte ions. With the aid of such a calibration line, we could obtain the mobility of any analyte ion at any α-CD concentration by simply measuring the corresponding step height on the isotachopherogram.

Another way of looking at this is that the mobility of the analyte ion obtained from such a calibration method is not a real but, rather, an ideal or abstracted one since the contribution from the viscosity effect is artificially eliminated. According to Stokes' law, the above-mentioned mobility m_i and the actual mobility m_i are related by

$$m_i = \frac{\eta_{[CD]>0}}{\eta_{[CD]=0}} \times m_i, \tag{2}$$

where η is the viscocity of the medium.

Isotachophoresis of Quaternary Ammonium Ions and Complexation with α-CD. Figure 3 illustrates an isotachophoretic separation of analyte cations (A^+ and B^+) in the presence of an electrically-neutral ligand (N). L^+ and T^+ indicate the leading and terminating cations, respectively. Q^- represents the counter anion.

The binding constants or association constants of ligand N with A^+ and B^+ are defined by Eqs. 3 and 4. Then, the effective mobilities of A^+ and B^+ ($\bar{m}_A$ and $\bar{m}_B$: mobilities which are observed experimentally) in their sample zones in the presence of ligand N can be expressed by Eqs. 5 and 6. The latter equations indicate that cations A^+ and B^+ can be separated from each other even when they have the same ionic mobilities ($m_A=m_B$) if the binding constants with N are appreciably different ($K_{AN} \neq K_{BN}$):

$$K_{AN} = \frac{[AN^+]_A}{[A^+]_A[N]_A} \tag{3}$$

$$K_{BN} = \frac{[BN^+]_B}{[B^+]_B[N]_B} \tag{4}$$

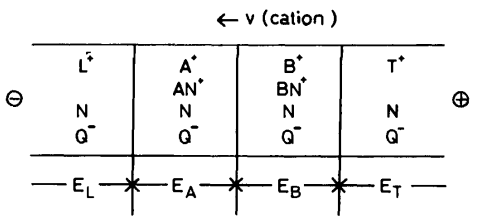

Fig. 3. Isotachophoretic separation of cations in the presence of neutral ligand. E_i: potential gradient in the *i*-th zone, *v*: migration velocity of cation, L^+: leading ion, A^+: B^+: analyte ions, T^+: terminating ion, N: neutral ligand, Q^-: counter ion.

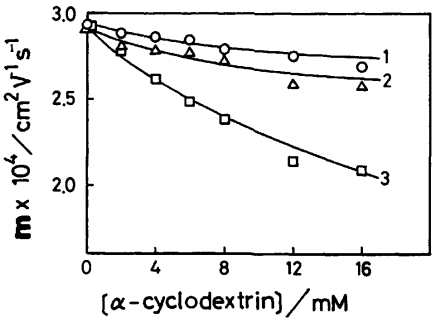

Fig. 4. Complexing effect of α-CD on the mobility of (*o*-, *m*-, and *p*-methylbenzyl)trimethylammonium ions. For ***m***, see Eq. 2. Terminating solution, 5 mM 1-naphthylamine hydrochloride. Other conditions are the same as those in Fig. 1.

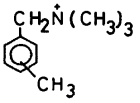

1 (*o*-, ○), **2** (*m*-, △), **3** (*p*-, □)

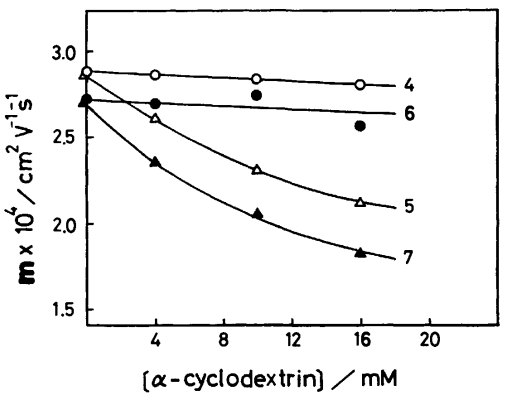

Fig. 5. Complexing effect of α-CD on the mobility of (substituted benzyl)trimethylammonium ions. For ***m***, see Eq. 2. Leading solution, 10 mM acetic acid-potassium acetate (1 : 1) buffer solution containing α-CD and 0.01 wt% PVA; terminating solution, 5 mM 1-naphthylamine hydrochloride; analyzing capillary tube (PTFE; i.d., 0.5 mm), 15 cm; ion migration current, 50 μA; 25 °C.

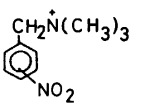

4 (*o*-, ○), **5** (*p*-, △)

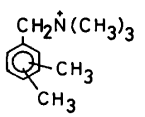

6 (*m*-, *p*-, ●), **7** (*o*-, *p*-, ▲)

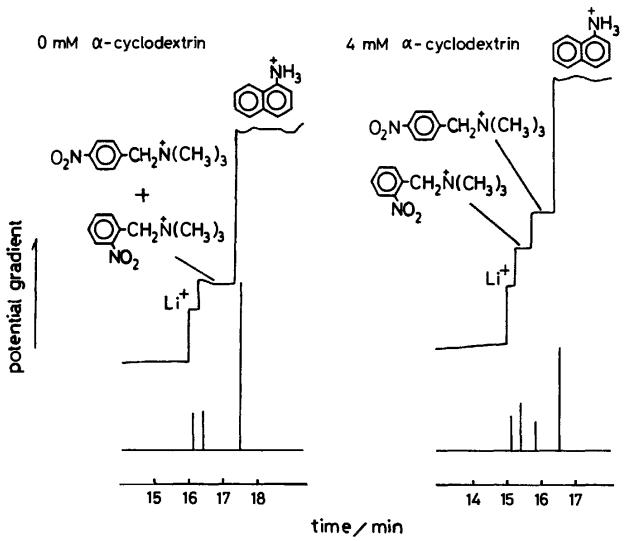

Fig. 6. Isotachophoretic separation of (*o*- and *p*-nitrobenzyl)trimethylammonium ions. See Fig. 5 for conditions.

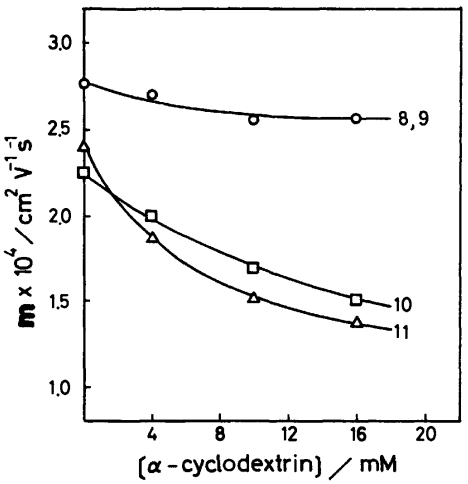

Fig. 7. Complexing effect of α-CD on the mobility of some quaternary pyridinium ions. For ***m***, see Eq. 2. Migration conditions are the same as those in Fig. 5.

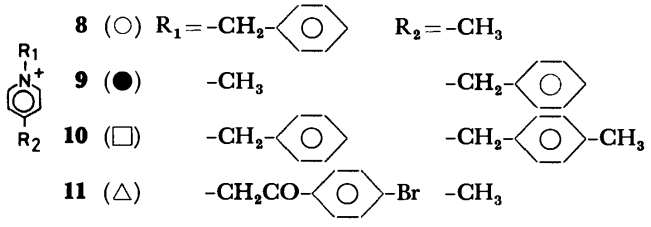

$$\bar{m}_A = \frac{m_A[A^+]_A + m_{AN}[AN^+]_A}{[A^+]_A + [AN^+]_A} = \frac{m_A + m_{AN}K_{AN}[N]_A}{1 + K_{AN}[N]_A} \quad (5)$$

$$\bar{m}_B = \frac{m_B[B^+]_B + m_{BN}[BN^+]_B}{[B^+]_B + [BN^+]_B} = \frac{m_B + m_{BN}K_{BN}[N]_B}{1 + K_{BN}[N]_B}. \quad (6)$$

Figures 4 and 5 summarize the effect of α-CD on the mobilities of (substituted benzyl) trimethylammonium ions. Figure 6 shows one of the typical isotachopherograms obtained in these studies. It can be seen that the isomeric ammonium ions showed no indication of a mutual separation in the absence of α-CD. These (quaternary) ammonium ions are not acids nor bases in ordinary pH range (i.e., their electrophoretic behavior is not dependent on pH); therefore, the pH change in the medium can not help their separation. A change of medium from aqueous to organic does not show much promise either. The addition of α-CD brought about a clear separation (indicated in Figs. 4—6). Obviously, the separation was caused by complexation with α-CD (implicated by Eqs. 5 and 6). In fact, it is conceivable that this is the only way to achieve a separation of this type of organic ions by isotachophoresis, since the means are quite scarce for assuring a specific interaction with such isomeric quaternary ammonium ions.

One can see in Figs. 4 and 5 that the complexation characteristics of α-CD is clearly reflected in the mobility change of isomeric ammonium ions. α-CD is a cylinder-like molecule with an internal hydrophobic cavity which fits the size and the polarity of aromatic (benzene) derivatives. When inclusion complexes are formed with disubstituted benzenes, it is generally accepted that o- and m-isomers suffer steric hindrance from the wall of the cavity while p-isomers do not. Among *o*-(**1**), *m*- (**2**), and *p*-(**3**) methyl-substituted benzyl isomers, the p-isomer (**3**) shows the most pronounced mobility decrease upon an addition of α-CD. This indicates that the p-isomer formed the most stable inclusion complex. Because of its high molecular weight, the α-CD complex exhibits a much lower mobility than that of the uncomplexed ammonium ion ($m_A = m_B > m_{AN} = m_{BN}$). If the complex formation (binding) constant of isomer A is larger than that of isomer B ($K_{AN} > K_{BN}$ in Eqs. 3 and 4), the observed (effective) mobility of isomer A becomes smaller than that of isomer B ($\bar{m}_A < \bar{m}_B$ in Eqs. 5 and 6).

A distinct difference in the migration behavior was observed when α-CD was added to isomeric (nitrobenzyl) trimethylammonium ions (**4** and **5**; Fig. 5). The p-substituted isomer indicated a much stronger interaction with α-CD. For trisubstituted aromatic compounds **6** and **7**, however, a simplified consideration can not be made regarding the preference of complexation among the isomers. However, the analytical importance of cyclodextrin complexation is obvious if one looks at the separation achieved by applying only 5 mM α-CD to the leading solution.

Figure 7 shows the effect of α-CD on the mobility of some quaternary pyridinium ions. An inspection of the figure suggests that pyridinium moieties are too hydrophilic to be effectively bound in the hydrophobic cavity of cyclodextrin. It was rather discouraging that the mixture of isomers **8** and **9** could not be resolved. Compounds **10** and **11**, which carry more

lipophilic (larger) substituents on the pyridinium ring, showed a substantial decrease in mobility upon the addition of α-CD.

Estimation of Binding Constant. A theoretical treatment of the present isotachophoretic system is simple since the complexation of analyte ions (cations) only takes place with an electrically neutral ligand (α-CD).

First, a mass balance is taken for counter ions (anion) in the leading (L) and its neighboring analyte (A) zones. This gives

$$-m_Q E_A[Q^-]_A + m_Q E_L[Q^-]_L = v([Q^-]_A - [Q^-]_L), \quad (7)$$

where Q^- stands for a counter anion and the suffixes A, L, and Q denote the quantities related to these ionic species or their zones.

Since the neutral ligand in zone A exists in both free (N) and charged (AN^+) forms, it can move under the potential gradient in the zone. The effective mobility of the ligand in zone A is given by

$$\bar{m}_{N,A} = \frac{m_{AN}[AN^+]_A}{[AN^+]_A + [N]_A}. \quad (8)$$

Then, the mass balance for neutral ligand in the leading and its neighboring analyte zones is given by

$$\bar{m}_{N,A} E_A C_{N,A} = v(C_{N,A} - C_{N,L}), \quad (9)$$

where $C_{N,A}$(=$[AN^+]_A$+$[N]_A$) and $C_{N,L}$ are the concentrations of the neutral ligand in the analyte (A) zone and the leading solution, respectively.

Finally, Eqs. 10 and 11 are obtained from the electrical neutrality of each zone:

$$[A^+]_A + [AN^+]_A = [Q^-]_A \quad (10)$$

and

$$C_L = [Q^-]_L, \quad (11)$$

where C_L is the concentration of leading cation in the leading zone (=concentration of the leading electrolyte).

From these equations, coupled with Eqs. 1 and 3—6, the parameters could be eliminated (except for m_L, m_A, m_{AN}, m_Q, C_L, $C_{N,L}$, $[N]_A$, and K_{AN}). This afforded the following equation, which is a cubic function with respect to $[N]_A$:

$$m^*_{AN}K_{AN}^2[N]_A^3 + (m^*_A + m^*_{AN} - m^*_{AN}K_{AN}C_{N,L})K_{AN}[N]_A^2 + \{m^*_A + (m^*_A - m^*_{AN})m^*_L/m_L K_{AN}C_L - (m^*_A + m^*_{AN})K_{AN}C_{N,L}\} \times [N]_A - m^*_A C_{N,L} = 0 \quad (12)$$

where,

$$m^*_i = m_i + m_Q \ (i=L, A, AN).$$

To solve Eq. 12, the viscosity effect of α-CD must be considered. The mobility of individual ionic species at any α-CD concentration can be expressed as indicated before by Eq. 2, where m_i is the mobility of the ionic species free from the viscosity effect of α-CD and η is the viscosity of a medium containing α-CD at a specific concentration. By using Eq. 2, $\bar{m}_i$ and m_i can be replaced by $\bar{m}_i$ and m_i, respectively, in Eqs. 1 as well as 5-12. The resulting equations, as they appear, indicate only a simple replacement of $\bar{m}_i$ and m_i by $\bar{m}_i$ and m_i, respectively, and a replacement of E_i by $E_i \times (\eta_{[CD]=0}/\eta_{[CD]>0})$. This means that, even if numerical viscosity data is not available, Eq. 12 can be solved for $[N]_A$ by using the mobility data in the presence and the absence of α-CD after calibrating for the viscosity effect of α-CD.

The mobility of uncomplexed analyte ions could be experimentally determined during the present study. On the other hand, the mobility of α-CD-complexed analyte ions (m_{AN} or m_{AN}) could not be experimentally obtained, since complexation never went to completion under our isotachophoresis conditions. Now, a relationship between the relative mobility U (m_{TEA}=1.00) and the molecular weight is known to exist which follows the phenomenological equation:[20]

$$U/Z = 14.7/\sqrt{Mw} - 0.29, \quad (13)$$

where Z is an ionic charge and Mw is a molecular weight. By using this equation we could estimate the absolute mobility of α-CD-bound quaternary ammonium ions (complexed cation) with reasonable accuracy. The value (4.94×10^{-5} $cm^2 V^{-1} s^{-1}$ for (methyl-substituted benzyl)trimethylammonium-α-CD complex; Mw=972.85+164.27=1137.12), thus obtained, was used in Eq. 12. Then, we could numerically calculate the concentration of the free neutral ligand in the analyte zone ($[N]_A$) as a function of the binding constant (K_{AN}), where the concentration of the ligand in the leading zone was set as a parameter. Once $[N]_A$ was known, we could readily obtain $\bar{m}_A$ from Eq. 5; these $\bar{m}_A$ values were compared with the experimentally-obtained $\bar{m}_A$ value in order to check the validity of the value of parametrically-chosen K_{AN} values (see below).

A computer-assisted calculation was performed by using the Newton-Raphson method for solving cubic functions (Eq. 12) and by using an iterative method for approximating the ionic-strength modification to the absolute mobility (m_{0i}) using the Debye-Hückel-Onsager equation. Figure 8 summarizes the result of the theoretical calculation, where the effective mobility of the analyte ion is plotted as a function of the binding constant with α-CD. The effect of the α-CD concentration is also included in the figure.

The profiles in Fig. 8 indicate that as the K_{AN} value decreases or the α-CD concentration becomes lower, the effective mobility of the analyte ion approaches that of the free ion. On the other hand, as the K_{AN} value increases or the α-CD concentration increases, the effective mobility of the analyte ion approaches that of the α-CD-bound (complexed) analyte ion.

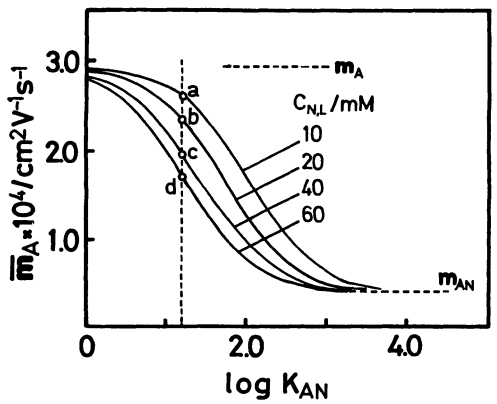

Fig. 8. Mobility change of (methyl-substituted benzyl) trimethylammonium ion (A) as a function of its binding constant (K_{AN}) with α-CD (N). Theoretical calculation. Parameters used are as follows. Absolute mobility m_{0i} ($cm^2\ V^{-1}\ s^{-1}$): $m_{0L}=362.5\times10^{-5}$, $m_{0Q}=79.08\times10^{-5}$, $m_{0A}=31.55\times10^{-5}$, $m_{0AN}=4.94\times10^{-5}$. Concentration (M): $C_L=0.0102$, $C_{N,L}=0.010$, 0.020, 0.040, 0.060.

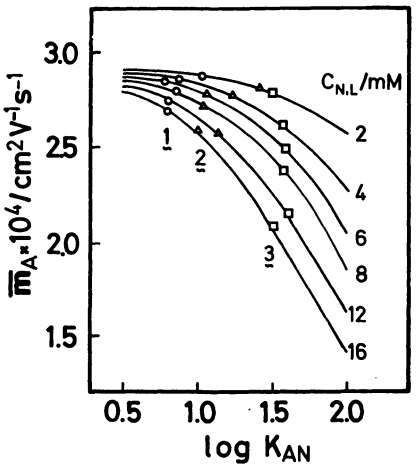

Fig. 9. Comparison of calculated and experimentally-obtained mobility. Determination of binding constant (K_{AN}) of (*o*-, *m*-, and *p*-methylbenzyl)trimethylammonium ions with α-CD. Experimental and calculation conditions are the same as those in Figs. 4 and 8.

Such behavior is in good accordance with our intuitive chemical picture and is quite reasonable.

The series of theoretical lines in Fig. 8 are useful for experimentally evaluating the binding constant between the analyte ions and α-CD. Consider that one carried out isotachophoresis of a certain analyte ion in the presence of 10, 20, 40, and 60 mM α-CD and obtained mobility data at each α-CD concentration. If the assumptions that were made in preparing the theoretical lines in Fig. 8 are correct, the observed mobility data should fall on a single vertical line crossing the four theoretical lines at experimental points a, b, c, and d. The intersect of the vertical line with the abscissa defines the required binding constant K_{AN}.

Figure 9 includes the mobility data obtained for (*o*-, *m*-, and *p*-methylbenzyl)trimethylammonium ions along with some theoretical mobility lines at various α-CD concentrations. Though experimental points are somewhat scattered at low α-CD concentrations, the data define fairly reasonable vertical lines, affording binding constants ($\log K_{AN}$) of 0.8, 1.1, and 1.6 for o-, m-, and p- isomers, respectively. Such low binding constants are usually accessible only by methods which involve multi-stage interactions, such as liquid chromatography. The present method using isotachophoresis is obviously characterized by a similar feature and is considered to be generally useful both for detecting and quantitatively treating weak interactions between an ion and an uncharged ligand.

References

1) H. Miyazaki and K. Kato, "Tosoku-Denki-Eido-Ho (Isotachophoresis)," Kodansha-Scientific, Tokyo (1980).
2) F. M. Everaerts, J. L. Beckers, and Th. P. E. M. Verheggen, "Isotachophoresis," Elsevier, Amsterdam, Oxford, and New York (1976).
3) P. Boček, I. Miedziak, M. Deml, and J. Janák, *J. Chromatogr.*, **137**, 83 (1977).
4) D. Kaniansky and F. M. Everaerts, *J. Chromatogr.*, **148**, 441 (1978).
5) H. Yoshida, I. Nukatsuka, and S. Hikime, *Bunseki Kagaku*, **28**, 382 (1979).
6) I. Nukatsuka and H. Yoshida, *J. Chromatogr.*, **237**, 506 (1982).
7) I. Nukatsuka, M. Taga, and H. Yoshida, *J. Chromatogr.*, **205**, 95 (1981).
8) I. Nukatsuka, M. Taga, and H. Yoshida, *Bull. Chem. Soc. Jpn.*, **54**, 2629 (1981).
9) T. Hirokawa and Y. Kiso, *J. Chromatogr.*, **242**, 227 (1982); **248**, 341 (1982).
10) P. Gebauer and P. Boček, *J. Chromatogr.*, **242**, 245 (1982).
11) M. Tazaki, M. Takagi, and K. Ueno, *Chem. Lett.*, **1982**, 639.
12) M. L. Bender and M. Komiyama, "Chemistry of Cyclodextrin," Springr Verlag, Bertin (1978).
13) W. L. Hinze and D. W. Armstrong, *Anal. Lett.*, **13**, 1093 (1980).
14) D. W. Armstrong, *J. Liq. Chromatogr.*, **3**, 895 (1980).
15) M. Tanaka, Y. Mizobuchi, T. Kuroda, and T. Shono, *J. Chromatogr.*, **219**, 108 (1981).
16) Y. Kawaguchi, M. Tanaka, M. Nakae, K. Funazo, and T. Shono, *Anal. Chem.*, **55**, 1852 (1983).
17) K. G. Feitsma, B. F. H. Drenth, and R. A. de Zeeuw, *J. High. Resolt. Chromatogr., Chromatogr. Commun.*, **7**, 147 (1984).
18) I. Tabushi and E. Shinkai, *Bunseki*, **1985**, 162.
19) H. S. Harned and B. B. Owen, "The Physical Chemistry of Electrolytic Solutions," 3rd Ed., Reinhold, New York, Amsterdam, and London (1958), p. 179.
20) V. Jokl, *J. Chromatog.*, **13**, 454 (1964).

 © 1986 The Chemical Society of Japan Bull. Chem. Soc. Jpn., 59, 3465—3468 (1986)

Synthesis of Copper(II)-Dithiooxamide Complex in Zirconium Phosphate[1)]

Yoshitsugu HASEGAWA,* Midori KAMIKAWAJI, and Kaname SASAKI
Department of Industrial Chemistry, Faculty of Technology, Tokyo University of Agriculture and Technology, Nakamachi, Koganei, Tokyo 184
(Received April 12, 1986)

Copper(II)-dithiooxamide (rubeanic acid) complex was synthesized in the interlayer region of zirconium phosphate. The product, called ZP-CuLra, was chracterized by chemical analysis, thermal analysis, infrared spectroscopy, and X-ray diffractometry. The chemical composition of ZP-CuLra was represented as $ZrCu(H_2NCS)_2(PO_4)_2 \cdot H_2O$ or $ZrCu(HNCS)_2(HPO_4)_2 \cdot H_2O$. The interlayer distance of ZP-CuLra was found to be 9.0 Å. By analogy with Cu(II)-rubeanic acid complex prepared in a solution, a structural model of ZP-CuLra was proposed.

Zirconium phosphates have been studied most extensively as inorganic ionexchangers.[2)] Of these the α-from, $Zr(HPO_4)_2 \cdot H_2O$, is crystalline and its crystal structurc has been determined.[3)] Hence, the interrelation between the ion-exchange reaction and the change in the structure has been investigated for many cations. Also, α-zirconium phosphate behaves as a host when an organic molecule intercalates into the interlayer space.[4)] Recently, the application of α-zirconium phosphate to new materials has been examined.[2)]

Dithiooxamide, $(NH_2CS)_2$, (so-called to rubeanic acid (RA)), has been used in analytical chemistry.[5)] When RA is added to a solution containing Cu(II), a black precipitate (Cu-ra complex) is formed. It has been found that this Cu-ra complex exhibits semiconductivity and antiferromagnetism.[6)] The complex is considered to be a coordination polymer. Since it is amorphous, its physicochemical properties have not been explained theoretically. Abboudi et al. have studied large-angle X-ray scattering of the amorphous compound and proposed a structural model.[7)]

Montmorillonite, a typical clay mineral, has a layered structure similar to α-zirconium phosphate. Many attempts have been made to control tacticity using this clay as a template. Son et al. prepared the Cu-ra complex in an interlayer space of montmorillonite and found that the complex was monomeric and oriented in such a way that the molecular plane of the ligand was parallel to the silicate layer.[8)] They suggested that because the distance between Cu(II) in montmorillonite was too large to bridge with rubeanic acid molucules, only a monomeric compound was formed.[9)] The ion-exchange capacity of the clay used was 0.95 meq g^{-1}. Since α-zirconium phosphate has a larger ion-exchange capacity than montmorillonite, it can be expected that the distance between Cu(II) in the interlayer space will be shorter than that in montmorillonite. Consequently, if Cu(II) can be made to react with rubeanic acid in α-zirconium phosphate layer, a polymeric compound can be formed.

The present study established a preparative method for the Cu-ra complex in α-zirconium phosphate (the product obtained is referred to as ZP-CuLra) and ZP-CuLra was characterized by chemical analysis, infrared spectroscopy, and thermal analysis.

Experimental

Reagents. Rubeanic acid (Tokyo Kasei Co., Ltd.) was recrystallized from ethanol, and then dissolved in acetone. The rubeanic acid was recovered after evaporating the acetone. The other reagents were used without further purification.

Preparation of ZP-CuLra. All ion-exchange reaction was carried out by a batch method. The α-zirconium phosphate was prepared by the direct precipitation method.[10)] It was then converted into the half-exchanged sodium ion form, $ZrNaH(PO_4)_2 \cdot 5H_2O$(ZrNaH).[11)] Copper(II) ion was exchanged by adding ZrNaH to the solution of 0.03 mol dm^{-3} Cu(II) acetate. The mixture was shaken continuously for 48 h at 25 °C in order to prevent the solution from decomposing at elevated temperatures. After the reaction, the solid was centrifuged from the solution, and washed with distilled water. An X-ray diffraction pattern was obtained for the solid, and the sodium ion in the supernatant was determined by atomic absorption spectrometry. The solid was again immersed in Cu(II) acetate solution, and the same procedure repeated. The X-ray diffraction pattern was identical to the copper exchanged form, but the sodium ion was still detected. Since the large amount of the sodium and hydrogen ions in the solid phase was almost exchaned with Cu(II), a solution of 0.03 mol dm^{-3} Cu(II) nitrate was employed and the third ion exchange was carried out. To ensure the exchange, the solid was contacted with 0.01 mol dm^{-3} Cu(II) acetate in the fourth run. The Cu(II) form of the zirconium phosphate (ZP-Cu) was identified by X-ray diffractometry. The ZP-Cu was stored over silica gel in a desiccator.

In order to intercalate the Cu-ra complex in α-zirconium phosphate, the ZP-Cu was immersed in an ethanol solution containing rubeanic acid (0.56 g/120 ml) for 7 days with intermittent shaking. The product was separated by centrifugation, and washed with acetone several times. It was then dried in air at room temperature.

Analytical Procedure. The chemical analysis of ZP-CuLra was carried out as follows. A weighed sample was

heated in a crucible at about 900 °C, and weight loss was determined. A part of the ignited sample was then weighed and decomposed according to the previous method.[12] The precipitate was separated by filtration and dissolved in hydrochloric acid. Zirconium was separated as mandelate and determined according to the literature.[13] Copper was titrated with a standardized EDTA solution, using 1-(2-pyridylazo)-2-naphthol (PAN) as an indicator. Phosphorus was determined gravimetrically as $Mg_2P_2O_7$.[14] Determinations of carbon, hydrogen, nitrogen, and sulfur were carried out by elemental analysis.

X-Ray powder patterns were measured with a Rigaku Geigerflex RAD-2B. The infrared (IR) spectra were measured on an A-302 infrared spectrophotometer (Japan Spectroscopic Co. Ltd.,). The thermogravimetric (TG) and differential thermal analysis (DTA) curves were obtained with a Shimadzu thermal analyzer at a heating rate of 10 °C min^{-1} in static atomosphere.

Results and Discussion

Chemical Composition of ZP-CuLra. Alluli et al. have reported that ZP-Cu can be prepared by the column method.[15] Since the α-zirconium phosphate used was too fine to apply in a column, a batch method was emploed. The X-ray diffraction pattern of ZP-Cu and the loss on ignition agreed well with values reported.[15]

The chemical composition of ZP-CuLra is shown in Table 1. Thermal analysis showed that ZP-CuLra was monohydrate (see later). When Cu(II) salt (for example, nitrate) reacts with rubeanic acid in an ethanol solution, Cu(II) rubeanate is precipitated and an acid (nitric acid) released. Between the interlayer region of zirconium phosphate the counter ion of Cu(II), namely phosphate, is fixed. It is not likely that Cu(II) can form the salt directly in the region. Consequently, the following two formulae must be considered; $ZrCu(NH_2CS)_2(PO_4)_2 \cdot H_2O$(Type I), and $ZrCu(NHCS)_2(HPO_4)_2 \cdot H_2O$(Type II). In Type I a molecule of rubeanic acid coordinates to Cu(II). The rubeanate of Cu(II) is sandwiched between zirconium phosphate layer in Type II. In each case the ZP-CuLra has the same elemental composition. The molar ratio of copper to rubeanic acid or rubeanate and to the water of hydration were in agreement with those obtained for the amorphous compound.[7]

Thermal Analysis. Figure 1 shows TG and DTA curves of ZP-CuLra. Thermal decomposition occurred in three steps. In the first step an endothermic reaction took place in the temperature range of 50—120 °C. Then the second step followed until about 380°C. Though the TG curve indicates that this step consisted of two successive reactions, these reactions can not be separated clearly in the DTA curve. The reactions at this step appears exothermic. It can be considered that the decomposition products are oxidized at the surface of the platinum crucible, and converted to oxides, for example water. At higher temperature (600°C-) the third reaction occurred.

The X-ray diffraction pattern of the solid after heating was identical to that obtained from ZP-Cu. The facts show that the water of hydration and the ligand were removed by heating. The whole process is described as follows:

$$\text{ZP-CuLra} \xrightarrow[\text{step I}]{} \text{anhydrous ZP-CuLra} \xrightarrow[\text{step II}]{} \text{intermediate} \xrightarrow[\text{step III}]{} ZrCu(PO_4)_2.$$

The weight loss at the first step was 4.9% which corresponds to dehydration. The total weight loss of the second and the third step was 23.6%. This is almost equal to the calculated value.

IR Studies. The IR spectra of ZP-CuLra, ZP-Cu, and Cu-ra prepared in a solution are shown in Fig. 2. The spectrum of ZP-CuLra can be considered to be composed of those of ZP-Cu and Cu-ra.

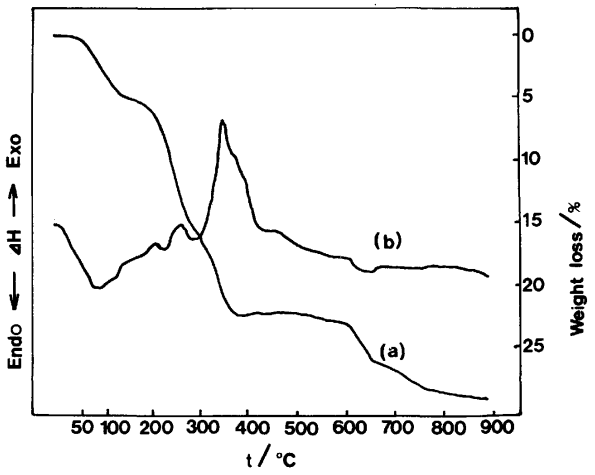

Fig. 1. TG(a) and DTA curve (b) of ZP-CuLra.

Table 1. Chemical Composition of ZP-CuLra/%

	Zr	Cu	PO_4	H	C	N	S
Found	18.11	13.72	37.60	1.27	4.75	5.50	11.14
	(1.00)	(1.08)	(1.99)	(6.35)	(1.99)	(1.98)	(1.75)
Calcd	18.89	13.16	39.33	0.83	4.97	5.80	13.28
	(1.00)	(1.00)	(2.00)	(6.00)	(2.00)	(2.00)	(2.00)

The values in parentheses are the molar ratios of each element to zirconium.

In order to determine Type I or II, it is important to examine the spectra in the region of 3500—3000 cm^{-1}, because the N-H bond gives an absorption band in this region. However, the O-H bond can also be assigned in the same region. According to Horsly et al., the absorption band at 3280 cm^{-1} was assigned to OH in P-OH, and bands at about 3500 and 1620 cm^{-1} to OH in the hydrated water in α-zirconium phosphate.[16] The absorption bands around 3460 and 1620 cm^{-1} disappeared in the IR spectrum after ZP-CuLra was heated in an air-bath at 150 °C. This fact suggests that these bands can be assigned to the hydrated water, and that the water was present in a similar manner as in α-zirconium phosphate.

On the other hand, the absorption bands at 3230 and 1520 cm^{-1} were still present after heating. Taking account of the above observation and the assignment of the spectrum for ZP-CuLra,[17] these bands can be assigned to -NH in $\overset{H}{Cu}\!>\!N-$.

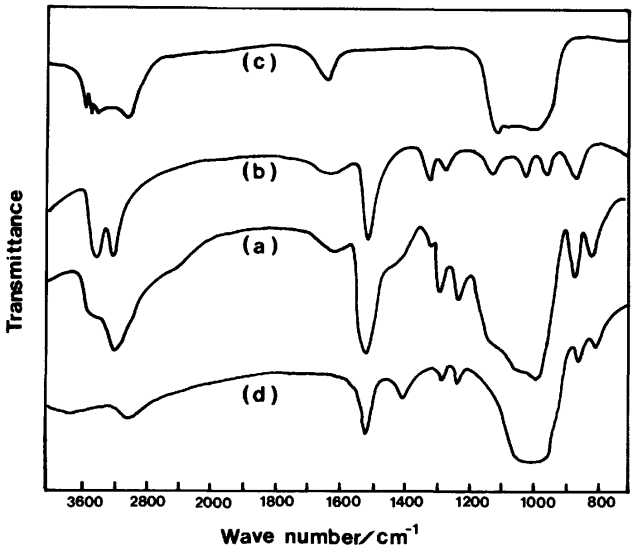

Fig. 2. IR spectrum of (a)ZP-CuLra, (b)Cura, and (c) ZP-Cu. The curve (d) is the spectrum of the sample obtained by heating of ZP-CuLra.

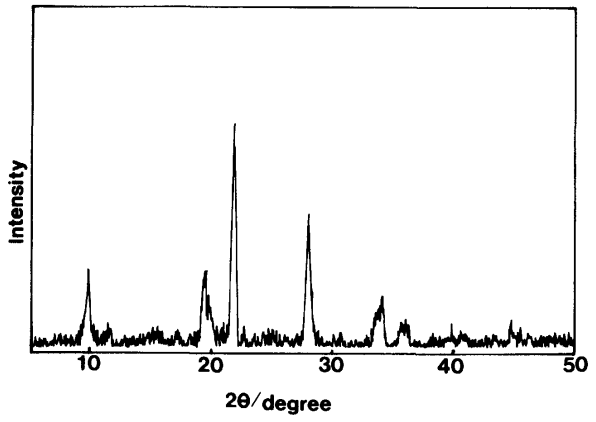

Fig. 3. X-Ray powder pattern of ZP-CuLra.

X-Ray Studies. It is well known that α-zirconium phosphate and its salt forms have a layered structure, and that the interlayer spacing is dependent on the cations present.[2] Hence, the change in an interlayer distance can be estimated from the lowest angle reflection in an X-ray diffractogram.

The X-ray powder pattern of ZP-CuLra is shown in Fig. 3. The interlayer distance of the exchanger phases was changed as follows.

α-$Zr(HPO_4)_2 \cdot H_2O$ 7.6 Å, $ZrNaH(PO_4)_2 \cdot 5H_2O$ 12.1 Å,
$ZrCu(PO_4)_2 \cdot 4H_2O$ 9.7 Å, ZP-CuLra 9.0 Å.

It is noteworthy that the interlayer spacing of ZP-CuLra was smaller than that of ZP-Cu. The molecular structure of rubeanic acid was known to be a planar form and the molecular dimensions were given.[18] The bond angle of HNH and CNH and the bond length of NH were not reported in the literature.[18] The molecular structure of rubeanic acid can be posturated by assuming that these are almost equal to those in thioformamid, $HSCNH_2$, that is, the angle HNH 122°, CNH 118—120°, and the length 1.01 Å.[19] The molecular size of rubeanic acid is estimated as shown in Fig. 4. The width of molecular plane is equal to be 3.60 Å.

.The copper complex can be arranged between the layers of zirconium phosphate in three manners, namely, parallel, perpendicular and inclined to the layers. If the plane of the rubeanic acid is parallel to

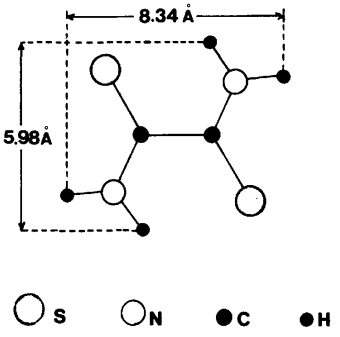

Fig. 4. Molecular size of rubeanic acid.

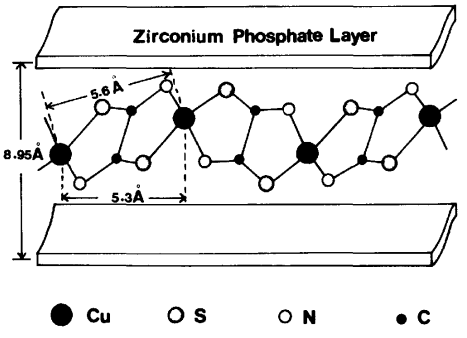

Fig. 5. Proposed model of CuLra complex between the zirconium phosphate layers.

that of the zirconium phosphate, the interlayer distance of ZP-CuLra will be shorter than that observed. When the plane of the acid is perpendicular to that of the exchanger, the distance will be longer. In the third case, the distance is dependent on the slant of the complex plane to the zirconium phosphate layer.

According to Alberti and Costantino,[4] the arrangement of the fixed charge in α-zirconium phosphate is an hexagonal array and the distance between them is equal to be 5.3 Å. It is possible to consider that the projective distance between Cu(II) in the copper form is 5.3 Å. On the other hand, the distance between Cu(II) in Cu-ra prepared in a solution is 5.6 Å according to the structural model proposed by Abboudi et al.[7]

The crystal structure of the salt form of zirconium phosphate has not been analyzed except for the ammonium form. Since the ammonium form has essentially a similar structure to α-zirconium phosphate,[20] it is possible to infer that the crystal structure of ZP-CuLra also is similar to α-zirconium phosphate.

Though the position of the hydrated water molecule was not determined, it is thought that the water molecule is involved in hydrogen bonding with hydrogen atoms over the oxygen atoms in phosphates (see IR Studies).

Assuming that the molecular structure of Cu-ra is persistent in the exchanger phase, the following model is proposed (Fig. 5). The ligand is coordinated to Cu(II) through the nitrogen and sulfur atoms. Between the zirconium phosphate layers the complex forms a polymeric zigzag chain composed of $Cu(NHCS)_2 \cdot H_2O$ as an unit, and the plane of the complex is slightly twisted to the layers of the exchanger.

The authors wish to express their thanks to Prof. Isao Tomita, Tokyo University of Fisheries, for the measurement of thermal analysis.

References

1) A part of this work was presented at the 52nd National Meeting of the Chemical Society of Japan, Kyoto, April, 1986, Abstr. No. 3H16.

2) A. Clearfield, "Inorganic Ion Exchange Materials," ed by A. Clearfield, CRC Press Inc., Boca Raton, Florida (1982), Chap. 1, pp. 1—74.

3) a) A. Clearfield and G. D. Smith, *Inorg. Chem.*, **8**, 431 (1969); b) J. M. Troup and A.Clearfield, *Inorg. Chem.*, **16**, 3311 (1977).

4) G. Alberti and U. Costantino, "Intercalation Chemistry," ed by M. S. Whittingham and A. J. Jacobson, Academic Press, New York (1982), Chap. 5. pp. 147—180.

5) P. Ray and J. Xavier, *J. Indian Chem. Soc.*, **38**, 535 (1961).

6) a) S. Kanda, *Nippon Kagaku Zasshi*, **83**, 560 (1972); b) S. Kanda, K. Ito, and T. Nogaito, *J. Polym. Sci., Part C*, **17**, 151 (1967).

7) M. Abboudi, A. Mosset, and J. Galy, *Inorg. Chem.*, **24**, 209 (1985).

8) S. Son, S. Ueda, F. Kanamaru, and M. Koizumi, *J. Phys. Chem.*, **80**, 1780 (1976).

9) S. Son, T. Maeda, S. Ueda, F. Kanamaru, and M. Koizumi, *J. Inorg. Nucl. Chem.*, **42**, 367 (1980).

10) Y. Hasegawa and M. Kuwayama, *Bull. Chem. Soc. Jpn.*, **51**, 3485 (1978).

11) Y. Hasegawa and I. Tomita, *Bull. Chem. Soc. Jpn.*, **43**, 3011 (1970).

12) Y. Hasegawa and G. Yamamine, *Bull. Chem. Soc. Jpn.*, **56**, 3765 (1976).

13) G. W. C. Milmer and P. J. Phennah, *Analyst*, **79**, 475 (1954).

14) I. M. Kolthoff ans E. B. Sandell, "Textbook of Quantitative Inorganic Analysis," 3rd ed, McMillan, New York (1952), pp. 377—382.

15) S. Alluli, C. Ferragina, A. La Ginestra, M. A. Massucci, N. Tomassini, and A. A. G. Tomlinson, *J. Chem. Soc.*, 1976, 2115.

16) S. E. Horsley, D. V. Nowell, and D. T. Stewart, *Spectrochim. Acta*, **30A**, 535 (1974).

17) J. R. Barcelo, *Spectrochim. Acta*, **10**, 245 (1958).

18) P. J. Wheatley, *J. Chem. Soc.*, **1965**, 396.

19) "Kagaku Binran" 3rd ed, ed by the Chemical Society of Japan, Maruzen, Tokyo (1984), p. II-657.

20) A. Clearfield and J. M. Troup, *J. Phys. Chem.*, **77**, 243 (1973).

Interfacial Phenomena in the Extraction Kinetics of Nickel(II) with 2′-Hydroxy-5′-nonylacetophenone Oxime

Hitoshi WATARAI,* Manabu TAKAHASHI, and Kiyoji SHIBATA
Department of Chemistry, Faculty of Education, Akita University, Akita 010
(Received April 24, 1986)

The interfacial adsorption of (*E*)-2′-hydroxy-5′-nonylacetophenone oxime and its role in the extraction kinetics of the nickel(II) ion with the oxime were investigated in heptane/aqueous phase systems by means of a high-speed stirring apparatus. The interfacial oxime concentration was correlated to the organic phase concentration, obeying the Langmuir isotherm. The interfacial activity of the oxime was also measured by means of interfacial tension measurements. The initial extraction rate of nickel(II) ion was linearly proportional to the interfacial concentration of the oxime (rather than to the bulk-phase concentration), to the nickel-ion concentration, and inversely to the hydrogen-ion concentration. These results supported the mechanism that the rate-determining step in the extraction is the 1:1 complex formation at the interface.

Recently, one of the present authors has pointed out the importance of interfacial reaction in the extraction kinetics of zinc(II) and nickel(II) with alkyl-substituted dithizones by means of the high-speed stirring method.[1] The advantages of the new method are (a) that an extraction rate is measured with a high accuracy, even in liquid-liquid dispersions generated by vigorous stirring, and (b) that the amount of extractant adsorbed at the interface in the same dispersed system is determined.[2,3] Therefore, this method is very promising for studies of interfacial phenomena in solvent-extraction kinetics.

In the present study, the role of the interface in the extraction of nickel(II) with (*E*)-2′-hydroxy-5′-nonylacetophenone oxime (HL), the active species of the commercial extractant SME 529, was investigated by means of the high-speed stirring apparatus.

Although the mechanism of the extraction kinetics of nickel(II) with β-hydroxy oxime has recently been discussed,[4,5] the assignment of the location, whether an interface or an aqueous phase, of the rate-determining reaction in a highly agitated extraction system has been remained ambiguous.

Experimental

The oxime was isolated from SME 529 donated by the Shell Chemical Co. and purified by the copper-complex method[6] and silica-gel chromatography. The fraction of the *E*-form in the purified oxime was not less than 0.98. Heptane, Wako G.R., was purified by distillation and used as an organic-phase solvent. The ionic strengths of all the aqueous phases were adjusted to 0.1 by the use of sodium perchlorate, and the pH of the aqueous phase was controlled by employing the acetate buffer (0.002 M, 1 M=1 mol dm^{-3}) and the phosphate buffer (0.002 M).

The high-speed stirring apparatus used in the present study is shown in Fig. 1. Although the principle of this apparatus is the same as that of a previous one,[3] the reproducibility of the stirring conditions, the stability of the spectrophotometric measurement, and the accuracy of the data analysis are much improved by the use of an Ono Sokki HT-431 digital tachometer and a Jasco UVIDEC 430 double-beam spectrophotometer interfaced by means of RS-232C with a NEC PC microcomputer system.

The amount of the oxime adsorbed at the interface in the stirred liquid-liquid system was determined at 25±0.1 °C by employing an equal volume (50 ml) of an organic solution of the oxime and an aqueous solution. When stirring was begun at 4700 rpm, the absorbance of the organic phase observed with a cell with an optical length of 1 cm decreased and reached a constant value. When it was stopped, the absorbance was restored to the initial state. The change in the absorbance was continuously recorded on the chart recorder. Figure 2 shows some typical results of the reversible absorbance decrease caused by stirring. The absorbance decrement, ΔA, defined as the difference between the equilibrium absorbance under no stirring, A, and the one under stirring, A', is considered to be proportional to the interfacial amount of the oxime or to the interfacial concentration, provided that the interfacial area remains constant.[2,6-8] A strong influence of the stirring rate on the magnitude of ΔA was observed in the range of 1000—4000 rpm, suggesting a contribution from the interfacial area, but it was diminished above 4500 rpm.[6] In the present study, 4700 rpm was adopted as the stirring rate.

The extraction rate of nickel(II) was measured at

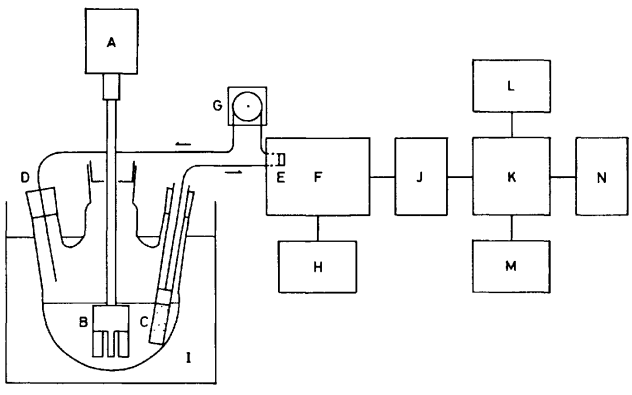

Fig. 1. Schematic diagram of the computer-assisted extraction kinetics measurement system. (A): Electric motor, (B): Teflon stirring bar, (C): Teflon phase separater, (D): sample inlet, (E): flow cell, (F): spectrophotometer, (G): peristaltic pump, (H):chart recorder, (I): thermostated water bath, (J): controlled device with RS-232C interface, (K): microcomputer, (L): printer, (M): dual-floppy disk drive, (N): CRT.

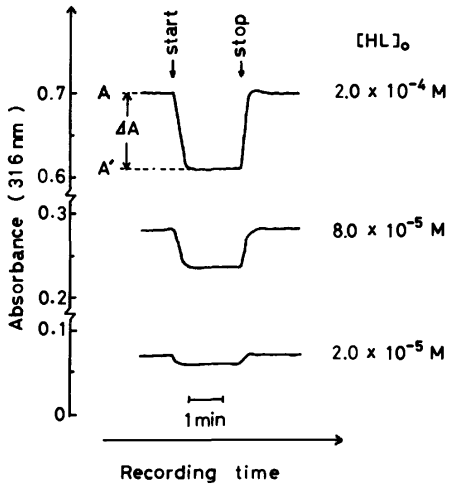

Fig. 2. Reversible change in the organic phase absorbance resulting from stirring at 4700 rpm, pH= 3.01.

25±0.1 °C by means of a microcomputer-assisted system (Fig. 1). Fifty ml of a heptane solution of oxime and 45 ml of an aqueous buffer solution were poured into the three-necked flask, and stirring was begun at 4700 rpm. The organic phase was pumped out through a Teflon phase-separator (Kokuboseiki Co.) and circulated through the flow cell (8 μl; 0.25 cm in optical length) at the flow rate of 16 ml min^{-1}. Extraction was started by injecting 5 ml of a nickel(II) stock solution through a glass syringe into the dispersed mixture. The absorbance of the organic phase was read by the computer at the acquisition rate of 1 data/sec, and it was displayed graphically on CRT as a function of the time. Soon after the termination of the data acquisition, the absorbance data, stored on a floppy disk, were analyzed according to the first-order rate law. The extraction rate constant, k_{obsd}, was calculated by the use of the following equation;

$$\ln \frac{A_f - A_o}{A_f - A_t} = k_{obsd} \cdot t \qquad (1)$$

where A_o, A_t, and A_f correspond to the absorbances of the nickel(II) complex in the organic phase at the start of extraction, at a certain time t, and at the extraction equillibrium. Some typical results of kinetic measurement are shown in Fig. 3. From the observed extraction rate constant, the observed initial extraction rate (in absorbance units), r°_{obsd}, was calculated by the use of this relation;

$$r^{\circ}_{obsd} = (A_f - A_o)k_{obsd}. \qquad (2)$$

In several experiments, the agreement of r°_{obsd} calculated by Eq. 2 and of r°_{obsd} directly obtained from $r^{\circ}_{obsd}=(dA_t/dt)_{t=0}$, which is the definition of r°_{obsd}, was confirmed.

The acid dissociation constant (K_a) of the oxime was estimated as $10^{-9.79\pm0.09}$ from the apparent dissociation constants, $10^{-10.28}$, $10^{-10.45}$, and $10^{-10.76}$, which were obtained in 30, 40, and 50% ethanolic aqueous solution by means of spectrophotometry.

The experiments on the distribution equilibrium of the oxime and the extraction equilibrium of nickel(II) with the

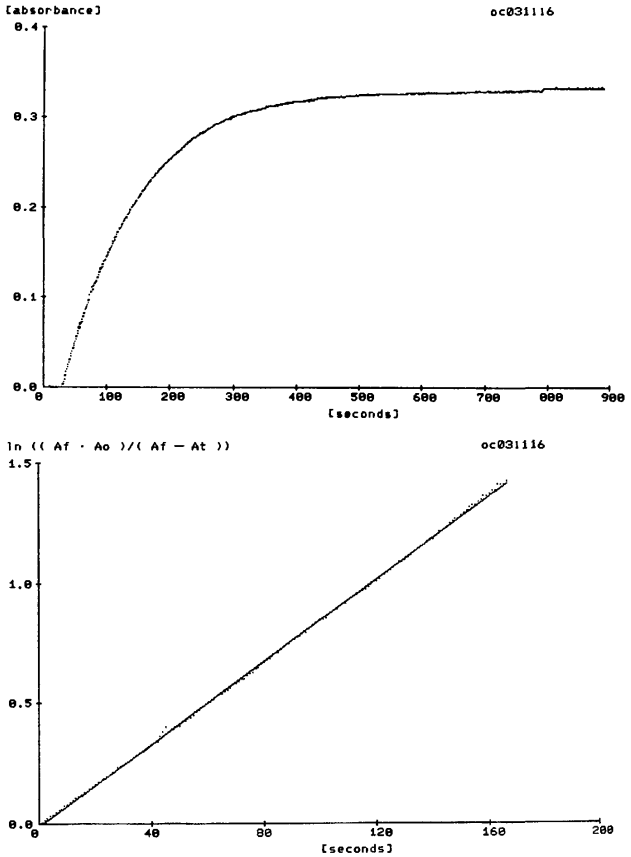

Fig. 3. Typical results of a recorded extraction kinetic run (upper) and a first-order kinetic analysis (lower). $[Ni^{2+}]_{Inlt}=1.0\times10^{-2}$ M, $[HL]_{0,Inlt}=1.0\times10^{-3}$ M, pH=4.52. $k_{obsd}=(8.57\pm0.01)\times10^{-3}$ s^{-1}.

oxime were done by means of the conventional batch method and by means of spectrophotometry at 25±1 °C. The distribution constant (K_D) was calculated as $10^{3.99\pm0.21}$ from the distribution ratio determined in the alkaline region and the acid dissociation constant. The extraction equilibrium of;

$$Ni^{2+} + 2HL_o \rightleftharpoons NiL_{2,o} + 2H^+ \qquad (3)$$

was confirmed and the extraction constant of $10^{-3.99\pm0.41}$ was determined from a slope analysis of the distribution ratio plotted against the pH.

The interfacial tension in heptane/water systems containing the oxime was measured by means of the drop-volume method at 25±0.1 °C, applying the Harkins-Brown correction.[9,10]

Results and Discussion

Interfacial Adsorption of the Oxime. The reversible absorbance decrease caused by stirring was measured while varying the concentration of the oxime. Figure 4 shows the concentration effect as a plot of ΔA against A'. As may be noted in this figure, ΔA approaches a saturated value with the increase in A', which means that the saturation in the interfacial amount of the oxime occurs at a higher-organic-phase

concentration than 10^{-3}M. The effect of the pH on ΔA was not observed under the acidic and neutral conditions (pH=3—6) where the kinetic experiments were conducted.

The interfacial tension in the heptane/water system decreased with an increase in the oxime concentration, as is shown in Fig. 5, demonstrating an interfacial activity of the neutral form of the oxime. Also, Fig. 5 indicates that the heptane/water interface is saturated by oxime when the oxime concentration becomes as concentrated as 10^{-3} M, corresponding to the result observed in the stirring experiment (Fig. 4).

The mechanism of interfacial adsorption in the vigorously stirred systems can be understood in terms of the following discussion. The total amount of oxime in the dispersed system is represented by;

$$[HL]_{init}V_o \simeq [HL]_oV_o + [HL]_iS10^3, \quad (4)$$

where $[HL]_{init}$, $[HL]_o$, and $[HL]_i$ refer to an initial organic-phase concentration before contact with the aqueous phase, an organic-phase concentration under stirring, and an interfacial concentration (mol cm^{-2}) in the dispersed liquid-liquid system, V_o, to the volume (ml) of the organic phase, and S, to the total interfacial area (cm^2) of the dispersed system. If the Langmuir isotherm is assumed to be the adsorption equilibrium of the oxime, $[HL]_i$ is represented by;

$$[HL]_i = \frac{ab[HL]_o}{1+b[HL]_o}, \quad (5)$$

where a corresponds to a saturated interfacial concentration, and ab, to an adsorption equilibrium constant at an infinite dilution, K', itself defined by;

$$ab = K' = \lim_{[HL]_o \to 0} \frac{[HL]_i}{[HL]_o}. \quad (6)$$

From Eqs. 4—6 and the Lambert-Beer equations of;

$$\Delta A = \varepsilon([HL]_{init} - [HL]_o)$$
$$A' = \varepsilon[HL]_o, \quad (7)$$

the following equation can be derived upon the relationship between $1/\Delta A$ and $1/A'$:

$$\frac{1}{\Delta A} = \left(\frac{1}{a} + \frac{\varepsilon}{K'}\frac{1}{A'}\right)\frac{V_o}{\varepsilon S10^3} \quad (8)$$

where ε refers to the molar absorptivity of the oxime in heptane, ε (316 nm)=3.49×10^3 M^{-1} cm^{-1}.

The straight line shown in Fig. 6 confirmed the proposed relationship of Eq. 8, and its slope and intercept gave these two parameters: $K'S$=1.0×10^{-2} l and a S=3.9×10^{-6} mol. Employing a=2.0×10^{-10} mol cm^{-2}, which was determined from Fig. 5 by applying the Gibbs equation,[6] S=2.0×10^4 cm^2 was estimated; by its use, K'=5.1×10^{-7} l cm^{-2} was then calculated. The value of S is consistent with that obtained previously.[8]

Extraction Mechanism of Nickel(II). The dependence of r°_{obsd} on the oxime concentration was examined at a constant pH; the results are shown in Fig. 7. The plot of r°_{obsd} against $[HL]_o$ was curved, and

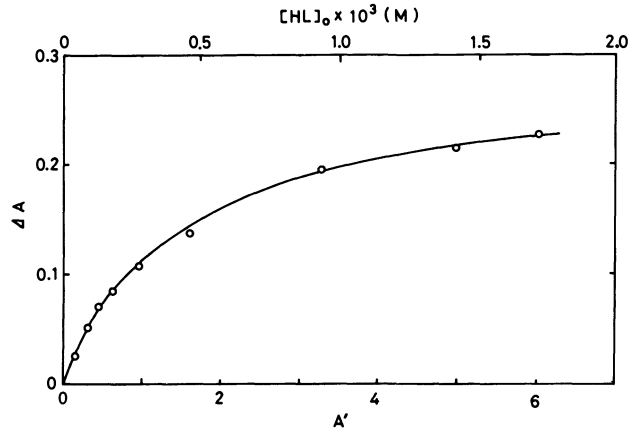

Fig. 4. Dependence of the absorbance decrement, ΔA, on the organic phase absorbance, A,' under stirring. $[HL]_{o,init}$=2.0×10^{-5} M—2.0×10^{-3} M, pH=3.0—6.2, λ=316 nm, 4700 rpm.

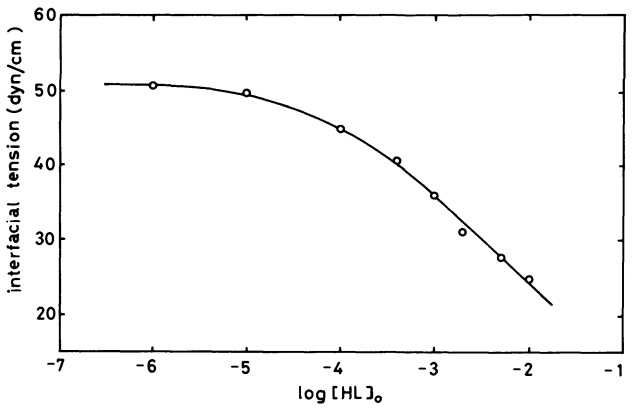

Fig. 5. Lowering of the interfacial tension with increase of the oxime concentration in the heptane/water system.

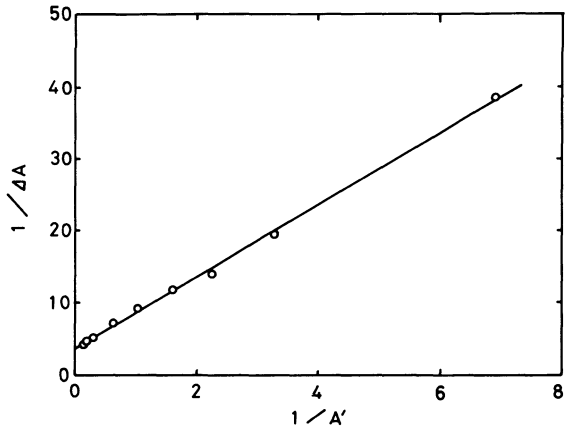

Fig. 6. Linear correlation between $1/\Delta A$ and $1/A'$.

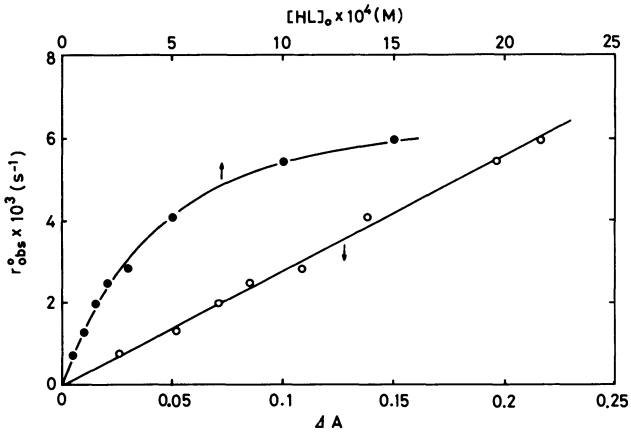

Fig. 7. Linear dependence of the initial extraction rate on ΔA, and nonlinear one on the bulk phase concentration of the oxime. $[HL]_{o,init}=1.0\times10^{-4}$ M—1.5×10^{-3}M, $[Ni^{2+}]_{init}=9.85\times10^{-3}$ M, pH=5.61.

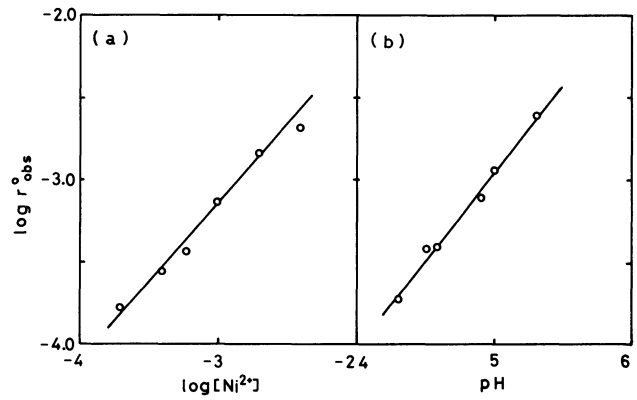

Fig. 8. First-order dependences of the initial extraction rate on nickel concentration (a), and on $[H^+]^{-1}$ (b).

no linear relationship was obtained between them. On the other hand, the plot of r°_{obsd} against ΔA gave a good linearity indicating that r°_{obsd} is proportional to $[HL]_i$, and not to $[HL]_o$. The effects of the nickel-ion concentration and the hydrogen-ion concentration on r°_{obsd} are shown in Figs. 8(a) and 8(b) respectively. In either figure, a linear plot was obtained, and the relation of $r^\circ_{obsd} \propto [Ni^{2+}]/[H^+]$ was experimentally concluded.

If the rate-determining step is 1 : 1 chelate formation in the aqueous phase, as has been reported for other nickel(II)-extraction systems,[11] r°_{obsd} will be represented by;

$$r^\circ_{obsd} = k_1 \frac{K_a}{K_D} \frac{[Ni^{2+}][HL]_o}{[H^+]} \varepsilon_c l, \tag{9}$$

where k_1 refers to the formation-rate constant of NiL^+; ε_c, to the molar absorptivity of NiL_2 in heptane, ε_c (387 nm)=4.53×10^4 M^{-1} cm^{-1}, and l, to the optical length of the flow cell. Although Eq. 9 proposes the relation of $r^\circ_{obsd} \propto [HL]_o$, this is inconsistent with the experimental results (Fig. 7). Furthermore, the magnitude of r°_{obsd} calculated from Eq. 9 under the probable conditions of $k_1=10^5$ M^{-1} s^{-1}, pH=5, $[HL]_o=10^{-3}$ M, and $[Ni^{2+}]=10^{-2}$ M was of an order of 10^{-6} s^{-1} and 10^3 times less than the observed value of r°_{obsd} under the corresponding conditions.

All of the experimental results and the above discussions seems to be favorable for the interfacial reaction mechanism rather than the aqueous-phase reaction mechanism. If the rate-determining step is the formation of a 1 : 1 complex at the interface, the following scheme can be assumed;

$$HL_o \rightleftharpoons HL_i \quad ; \text{ Langmuir isotherm} \tag{10}$$

$$HL_i \rightleftharpoons L_i^- + H^+ \quad ; K_a' \tag{11}$$

$$Ni^{2+} + L_i^- \longrightarrow NiL_i^+ \quad ; k_i \tag{12}$$

where K_a' is the acid dissociation constant at the interface defined by $K_a'=[L^-]_i[H^+]/[HL]_i$ and where k_i is the formation-rate constant of NiL^+ at the interface. The final complex of NiL_2 did not show any significant interfacial adsorption in the stirring experiment. From the scheme, the following equation can be derived for the observed initial extraction rate;

$$r^\circ_{obsd} = k_i[Ni^{2+}][L^-]_i \frac{10^3 S}{V_o} \cdot \varepsilon_c l$$

$$= k_i K_a' \frac{[Ni^{2+}]}{[H^+]} \cdot \frac{\varepsilon_c l}{\varepsilon} \cdot \Delta A. \tag{13}$$

Equation 13 is consistent with the observed relationships between r°_{obsd} and $[Ni^{2+}]$, $[H^+]$ and ΔA, shown in Figs. 7 and 8. Consequently, the proposed mechanism of Eqs. 10—12 is considered to be reasonable. The slope of the line in Fig. 7 and the intercepts of Figs. 8(a) and 8(b) gave the combined parameter of $k_iK_a'=(2.18\pm0.09)\times10^{-5}$ s^{-1} as an averaged value. Although the value of K_a' in the present system has not been determined, if $K_a' \simeq K_a$ is assumed, as has been observed in LIX65N,[8] k_i can be estimated as 1.3×10^5 M^{-1} s^{-1}. The value of k_i is apparently close to the formation-rate constant of the mono(8-quinolinethiol)nickel(II) complex in the aqueous phase.[11]

As has been concluded in the present study, the primary step of an extraction reaction is the adsorption of an extractant at the interface when the extractant has a large distribution constant and, more or less, an interfacial activity. Therefore, the experimental determination of the interfacial concentration of an extractant is very important in evaluating the contribution of an interfacial reaction to the mechanism of extraction kinetics. Also, the utility of the high-speed stirring apparatus for the study of interfacial phenomena was demonstrated. Further studies of the interfacial phenomena in other chelate-extraction systems and ion-association extraction systems are in progress.

The authors wish to thank the Shell Chemical Co., Ltd., for supplying the samples of SME 529 and Dr. Y. Honma of Akita University for his help in making the Teflon stirring bar. This work was financially supported by a Grant-in-Aid for Scientific Research from the Ministry of Education, Japan (No. 59540353-1984).

References

1) H. Watarai and H. Freiser, *J. Am. Chem. Soc.*, **105**, 187 (1983).
2) H. Watarai and H. Freiser, *J. Am. Chem. Soc.*, **105**, 191 (1983).
3) H. Watarai, L. Cunningham, and H. Freiser, *Anal. Chem.*, **54**, 2390 (1982).
4) K. Akiba and H. Freiser, *Sep. Sci. Technol.*, **17**, 745 (1982).
5) K. Inoue, S. Tomita, and T. Maruuchi, *J. Chem. Eng. Jpn.*, **18**, 445 (1985).
6) H. Watarai, *J. Phys. Chem.*, **89**, 384 (1985).
7) H. Watarai, *Talanta*, **32(8B)**, 817 (1985).
8) H. Watarai and K. Sasabuchi, *Solv. Extn. Ion Exchange*, **3**, 881 (1985).
9) W. D. Harkins and F. E. Brown, *J. Am. Chem. Soc.*, **41**, 499 (1919).
10) J. L. Lando and H. T. Oakley, *J. Colloid Interface Sci.*, **25**, 526 (1967).
11) K. Haraguchi and H. Freiser, *Anal. Chem.*, **55**, 656 (1983) and the references cited therein.

Mechanism of Chiral Recognition of Octahedral Metal Complexes Effected by Bis(μ-*d*-tartrato)-diantimonate(III) Anion in Solution. I. Association Models and Their Application to Some $[Co(N)_6]^{3+}$-Type Complexes

Katsuhiko Miyoshi, Shinji Izumoto, and Hayami Yoneda*
Department of Chemistry, Faculty of Science, Hiroshima University,
Higashi-senda-machi, Naka-ku, Hiroshima 730
(Received May 6, 1986)

An association model has been proposed which accounts for how bis(μ-*d*-tartrato)-diantimonate(III) anion, $[Sb_2(d\text{-tart})_2]^{2-}$ ion recognizes the chirality of $[Co(en)_3]^{3+}$ (en=ethylenediamine) and some related cation complexes in solution. In this model, two oxygen atoms of the chiral anion, i.e., the carboxylic oxygen atom (coordinated to the Sb atom) of one *d*-tartrate moiety and the alcoholic oxygen atom (coordinated to the same Sb atom) of the other *d*-tartrate moiety, are hydrogen-bonded to the two amine protons in $[Co(en)_3]^{3+}$ which are directed along either the C_3 or C_2 axis. When these hydrogen bonds are formed along the C_3 axis (C_3 association), $[Sb_2(d\text{-tart})_2]^{2-}$ ion forms a more favorable ion pair with Λ-$[Co(en)_3]^{3+}$, whereas it does with Δ-$[Co(en)_3]^{3+}$ if the two amine protons directed along the C_2 axis are utilized for hydrogen bonding to it (C_2 association). This model is successfully applied to the interpretation of chromatographic behavior of some $[Co(N)_6]^{3+}$-type complexes as well as of their related complexes with amine or phosphine ligands.

It is well-known that bis(μ-*d*-tartrato)-diantimonate(III) anion, $[Sb_2(d\text{-tart})_2]^{2-}$ ion serves as an effective eluent in chromatographic resolution of various octahedral complex cations.[1-3] We have already proposed a so-called L-J model[4] which explains conceptually how the chiral anion recognizes the chirality of a series of $[Co(N)_6]^{3+}$-type complexes. However, this model does not tell us anything about the actual interaction prevailing between $[Sb_2(d\text{-tart})_2]^{2-}$ and $[Co(N)_6]^{3+}$ ions. In addition, several new experimental results have been accumulated which are not easily interpreted within the framework of the L-J model. In the present study, we propose a concrete association model in which $[Sb_2(d\text{-tart})_2]^{2-}$ ion interacts with $[Co(N)_6]^{3+}$-type complexes through intermolecular hydrogen bonding.

Association Models

Experimental Observations. We have at least two experimental results which are quite informative to construct an association model between $[Sb_2(d\text{-tart})_2]^{2-}$ and $[Co(N)_6]^{3+}$ ions. The first is concerned with the effect of added $[Sb_2(d\text{-tart})_2]^{2-}$ ion on the circular dichroism (CD) spectrum of $[Co(en)_3]^{3+}$ in solution; its A_2 component at the first ligand field band is enhanced upon the addition of the chiral anion.[5] Since the A_2 transition is polarized along the C_3 axis, this CD-spectral change implies that the chiral anion approaches the complex predominantly along its C_3 axis to perturb the rotational strength of the A_2 transition.[6] Another observation relevant to the present study is that $[Co(Me_2\text{-en})(en)_2]^{3+}$ (Me_2-en=*N*,*N*′-dimethylethylenediamine) having axial methyl groups almost parallel to the pseudo C_3 axis, i.e., a mixture of its Λ(RR) and Δ(SS) isomers, is eluted considerably slower than $[Co(en)_3]^{3+}$ on the SP-Sephadex column with $[Sb_2(d\text{-tart})_2]^{2-}$ ion employed as an eluent.[7] Furthermore, the degree of optical resolution attained is much lower for $[Co(Me_2\text{-en})(en)_2]^{3+}$. Similar difference in chromatographic behavior has been found between $[Co(sar)(en)_2]^{2+}$ (sar=sarcosinate anion) and its parent complex $[Co(gly)(en)_2]^{2+}$ (gly=glycinate anion).[8] These observations suggest that the axial NH protons directed along the (pseudo) C_3 axis are utilized in the hydrogen-bonding interaction with some oxygen atoms in $[Sb_2(d\text{-tart})_2]^{2-}$ anion.

C_3 Association Model. When the molecular structure of $[Sb_2(d\text{-tart})_2]^{2-}$ ion (shown in Fig. 1) is examined in detail, a pair of oxygen atoms are found whose lone-pair electrons are nicely disposed to interact with two of the three axial NH protons directed along the C_3 axis of $[Co(en)_3]^{3+}$. They are the alcoholic oxygen atom of one *d*-tartrate moiety which is coordinated to the Sb atom and the carboxylic oxygen atom of another *d*-tartrate moiety which is coordinated to the same Sb atom. $[Sb_2(d\text{-tart})_2]^{2-}$ ion

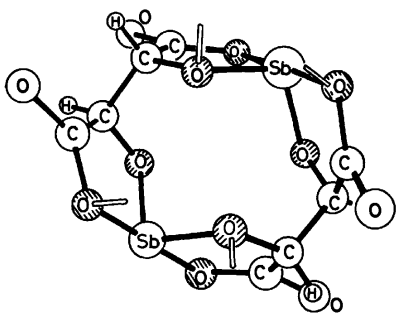

Fig. 1. Molecular structure of $[Sb_2(d\text{-tart})_2]^{2-}$ ion. Two shaded oxygen atoms coordinated to the same Sb atom are used for double hydrogen bonding.

has evidently four such pairs, which may be partly responsible for its high recognition efficiency as compared with *d*-tartrate ion.[9]

In Fig. 2 is depicted the C_3 association model which accomodates the above-mentioned experimental results, taking $[Co(en)_3]^{3+}$ as an example. In this model, the two oxygen atoms of $[Sb_2(d\text{-tart})_2]^{2-}$ ion participates in the double hydrogen bonding to two of the three axial NH protons directed along the C_3 axis, and the remaining part of the chiral anion is disposed opposite to the third NH group free from hydrogen bonding. If a bulky or negatively charged group is present in place of the third NH group, it will impose a steric or electrostatic repulsion on the carboxylic oxygen atom hydrogen-bonded to the complex. Since the double hydrogen bonds are formed along the C_3 axis, this model is called as the C_3 association model.

It is seen in Fig. 2 that the distal carboxylato group of $[Sb_2(d\text{-tart})_2]^{2-}$ ion is situated between the two en chelate rings in the C_3 association with Λ-$[Co(en)_3]^{3+}$ (left model) and a favorable ion pair is thus formed between the two ions, whereas the carboxylato group, particularly its C=O group experiences a steric hindrance from one en chelate ring in the C_3 association with Δ-$[Co(en)_3]^{3+}$ (right model), as indicated by an arrow. In this way, the C_3 association model predicts that $[Sb_2(d\text{-tart})_2]^{2-}$ ion associates more smoothly with the Λ complex than with the Δ complex, in accordance with the experimental result.[5] Since two axial NH protons are utilized in the C_3 association, it follows that six equivalent interaction sites are present in $[Co(en)_3]^{3+}$. Interaction sites are counted similarly for other $[Co(N)_6]^{3+}$-type complexes. Even if a complex is devoid of a true C_3 axis, it may have some C_3 interaction sites; if a set of three NH protons are present on a triangular facet[10] of a complex, they serve as interaction sites equivalent to true C_3 interaction sites. Furthermore, the C_3 interaction is possible even when only two NH protons are present on the triangular facet, provided that the third group is electrically neutral and/or is not bulky (see later).

Another C_3 association is conceivable in which all of the three axial NH protons of $[Co(en)_3]^{3+}$ are simultaneously hydrogen-bonded to three oxygen atoms of $[Sb_2(d\text{-tart})_2]^{2-}$ ion. The three oxygen atoms appropriately disposed in the chiral anion are two oxygen atoms of one carboxylato group in one *d*-tartrate moiety, and the alcoholic oxygen atom on the asymmetric carbon atom to which the other carboxylato group in the same *d*-tartrate moiety as above is directly attached; $[Sb_2(d\text{-tart})_2]^{2-}$ ion has apparently four sets of such three oxygen atoms, each *d*-tartrate moiety providing the two sets. A molecular model consideration reveals that the chiral recognition is similarly effected in this alternative C_3 association model through the steric repulsion imposed stereoselectively by the chelate ring of the Δ complex on the distal carboxylato group. However, this C_3 model is applicable only to those complexes which have three NH protons on the triangular facet. For example, complete chromatographic resolution of $[Co(phen)(en)_2]^{3+}$ and $[Co(acac)(en)_2]^{2+}$ (phen=1,10-phenanthroline and acac=acetylacetonate anion)[3] is not reasonably interpreted by this C_3 model in which triple hydrogen bonds are required. Consequently, we abandon this C_3 model and adopt the aforementioned C_3 model, to interpret the chromatographic behavior of various types of octahedral metal complexes throughout the present study.

C_2 Association Model. Since two NH protons in $[Co(en)_3]^{3+}$ are required for the interaction with $[Sb_2(d\text{-tart})_2]^{2-}$ ion, those NH protons which are directed along the C_2 axis can also be utilized for the double hydrogen bonding. This interaction is called as the C_2 association and its model is depicted in Fig. 3, taking *cis*-$[Co(X)_2(en)_2]^+$ (X=anion ligand) as an example. Here, $[Sb_2(d\text{-tart})_2]^{2-}$ ion approaches the complex along the C_2 axis from the side opposite to X so as to avoid an electrostatic repulsion from X, and

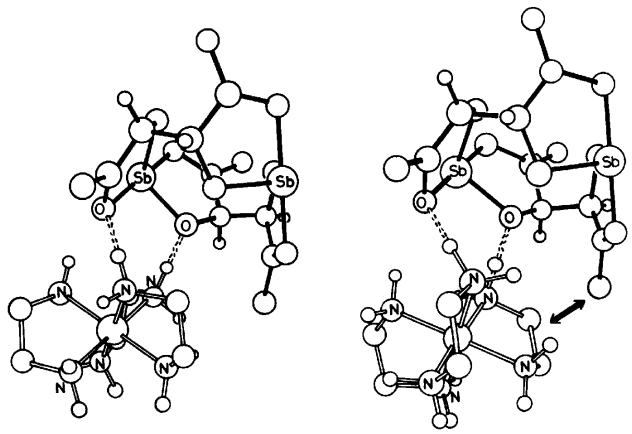

Fig. 2. C_3 Association models for Λ-$[Co(en)_3]^{3+}$-$[Sb_2(d\text{-tart})_2]^{2-}$ (left) and Δ-$[Co(en)_3]^{3+}$-$[Sb_2(d\text{-tart})_2]^{2-}$ (right).

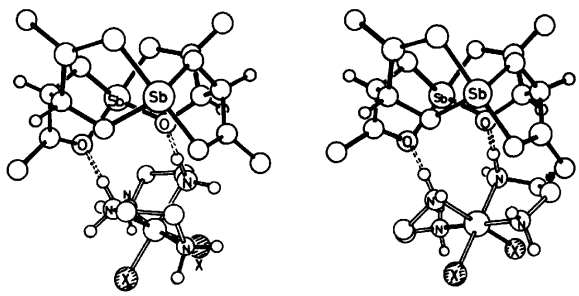

Fig. 3. C_2 Association models for Δ-*cis*-$[Co(X)_2(en)_2]^+$-$[Sb_2(d\text{-tart})_2]^{2-}$ (left) and Λ-*cis*-$[Co(X)_2(en)_2]^+$-$[Sb_2(d\text{-tart})_2]^{2-}$ (right).

the double hydrogen bonds are formed to the two NH protons directed along the C_2 axis. It is evident in Fig. 3 that the distal carboxylato group suffers a steric hindrance from one en chelate ring when the complex has a Λ configuration (right model). On the other hand, a smooth association is possible with *Δ-cis*-$[Co(X)_2(en)_2]^+$ (left model),[11] since the distal carboxylato group is disposed between the two en chelate rings like in the C_3 association with *Δ*-$[Co(en)_3]^{3+}$. Therefore, $[Sb_2(d\text{-tart})_2]^{2-}$ ion forms a more favorable ion pair with the Δ complex in the C_2 association. In fact, $[Sb_2(d\text{-tart})_2]^{2-}$ ion elutes the Δ isomer faster on an ion-exchange column for most of *cis*-$[Co(X)_2(en)_2]^+$-type complexes[12] which adopt the C_2 association predominantly. It should be noted, however, that the C_2 association is possible also for $[Co(N)_6]^{3+}$-type complexes. For example, $[Co(en)_3]^{3+}$ has three C_2 interaction sites in addition to six C_3 interaction sites.

Comparison with Experimental Results

$[Co(N)_6]^{3+}$-Type Complexes. Now, it is possible to count the C_3 and C_2 interaction sites for respective $[Co(N)_6]^{3+}$-type complexes. For simplicity, those sites are neglected here in which the distal carboxylato group suffers a steric hindrance from the chelate ring, viz., no smooth association is possible. For example, *Δ*-$[Co(en)_3]^{3+}$ has six favorable C_3 interaction sites but has no favorable C_2 site. By contrast, *Δ*-$[Co(en)_3]^{3+}$ has no C_3 site but has three favorable C_2 sites. For $[Co(Me_2\text{-}en)(en)_2]^{3+}$ and $[Co(Me\text{-}en)(en)_2]^{3+}$ (Me-en=*N*-methylethylenediamine) having methyl group(s) almost parallel to the pseudo C_3 axis, interaction sites are counted on the assumption that the methyl group does not interfere with the C_3 interaction. Numbers of favorable interaction sites counted in this way agree perfectly with the numbers of L-shaped channels defined in the previous work for $[Co(N)_6]^{3+}$-type complexes.[4] This means that the conceptual L-J model is automatically incorporated into the C_3 association model, but the C_2 association mode has been ignored in the L-J model. Numbers of C_3 and C_2 interaction sites *N* are given for respective $[Co(N)_6]^{3+}$-type complexes in Table 1. It is naturally expected that a complex having a greater difference in *N* between its Λ and Δ enantiomers should be resolved more effectively by ion-exchange chromatography.

In Table 1 are also given the separation factors α, a measure of efficiency of optical resolution attained for respective complexes, when available. It is confirmed in Table 1 that the above expectation is actually fulfilled as far as the C_3 interaction mode is concerned. This suggests that the C_2 interaction mode which has not been taken into account in the L-J model, does not contribute appreciably to chiral recognition of $[Co(N)_6]^{3+}$-type complexes.

Even for the complexes α values of which are not known, the elution order in chromatography is at least in good agreement with the prediction of our association models. The two complexes, *cis* α-$[Co(trien)(NH_3)_2]^{3+}$ (trien=triethylenetetramine) and *fac,fac,mer*-$[Co(tetren)(NH_3)]^{3+}$ (tetren=tetraethylenepentamine) need to examine somewhat in detail. The former complex has eight C_3 sites both for the Λ and Δ isomers; no practical resolution is expected. However, for the Λ isomer, a secondary amine proton is involved

Table 1. Number of Favorable Interaction Sites *N*, Separation Factor α, and Elution Order for $[Co(N)_6]^{3+}$-Type Complexes

Complex	*N*				α	Enantiomer Eluted Faster		Ref.
	C_3		C_2					
	Λ	Δ	Λ	Δ		Obsd	Predic.	
$[Co(en)_3]^{3+}$	6	0	0	3	1.45	Λ	Λ	4
$[Co(en)_2(Me\text{-}en)]^{3+}$(*ΔR,ΔS*)	4	0	0	3(1)		Λ	Λ	3
$[Co(en)_2(Me_2\text{-}en)]^{3+}$(*ΔRR,ΔSS*)	2	0	0	3(2)		(Λ)[a]	Λ	7
cis-$[Co(en)_2(NH_3)_2]^{3+}$	10	8	0	1		Λ	Λ	3
$[Co(en)_2(phen\text{ or }bpy)]^{3+}$	2	0	0	1		Λ[b]	Λ	3
cis α-$[Co(trien)(en)]^{3+}$	4(2)	0	0	2	1.37	Λ	Λ	4, 15
cis β-$[Co(trien)(en)]^{3+}$(*ΔSS,ΔRR*)	3	0	1(1)	2(1)	1.28	Λ	Λ	4, 15
cis β-$[Co(trien)(en)]^{3+}$(*ΔSR,ΔRS*)	3	0	1(1)	2(1)		Λ	Λ	15
cis α-$[Co(trien)(NH_3)_2]^{3+}$	8(2)	8	0	0		Λ	Λ	14
cis β-$[Co(trien)(NH_3)_2]^{3+}$(*ΔSS,ΔRR*)	7(1)	6(1)	0	0		Λ	Λ	14
cis β-$[Co(trien)(NH_3)_2]^{3+}$(*ΔSR,ΔRS*)	7(1)	6(1)	0	0		Λ	Λ	14
unsym-fac-$[Co(dien)_2]^{3+}$	4	2	1(1)	2(2)	1.20	Λ	Λ	4
unsym-fac-$[Co(dien)(en)(NH_3)]^{3+}$	6(1)	4(1)	2	3(1)		Λ	Λ	15
fac,mer,fac-$[Co(tetren)(NH_3)]^{3+}$	4(2)	2(2)	0	0		Λ	Λ	15
fac,fac,mer-$[Co(tetren)(NH_3)]^{3+}$(*ΔS,ΔR*)	3(1)	4	1	0		Λ	—	15

Numbers in parentheses denote numbers of interaction sites at which a secondary amine proton is involved in double hydrogen bonding (see the text). a) Partial resolution. b) Partial resolution for bpy complex.

in the double hydrogen bonding at two of the eight C_3 sites. Since a secondary amine proton is generally more acidic than a primary one, a stronger hydrogen bond is formed with the former proton,[10,13] other conditions being equal. In short, interaction sites associated with a secondary amine proton contribute more to the interaction with $[Sb_2(d\text{-tart})_2]^{2-}$ ion than those with a primary amine proton. Since all of the interaction sites of the Δ isomer are associated with primary amines only, the Λ isomer is expected to interact with $[Sb_2(d\text{-tart})_2]^{2-}$ ion more strongly than the Δ isomer for *cis* α-$[Co(trien)(NH_3)_2]^{3+}$.[14]

For *fac,fac,mer*-$[Co(tetren)(NH_3)]^{3+}$, the Δ isomer has a greater N than the Λ isomer; the Δ isomer may be eluted faster. However, the Λ isomer has three C_3 interaction sites one of which is associated with a secondary amine, while only primary amines are involved in the double hydrogen bonding at all of the four C_3 interaction sites for the Δ isomer. Furthermore, one favorable C_2 site adds to the Λ isomer. In practice, *Λ(S)-fac,fac,mer*-$[Co(tetren)(NH_3)]^{3+}$ has been eluted faster.[15] This implies that a secondary amine proton contributes much more to the total hydrogen-bonding interaction with $[Sb_2(d\text{-tart})_2]^{2-}$ ion than a primary amine proton.[13] Then, the partial resolution of $[Co(Me_2\text{-en})(en)_2]^{3+}$ may be attributed to the fact that the Λ isomer has two usual C_3 sites only, but the Δ isomer has three C_2 sites two of which are associated with a secondary amine.

As is evident from the above discussions, the C_3 association model leads to a general prediction that *Λ*-$[Co(N)_6]^{3+}$-type complexes interact with $[Sb_2(d\text{-tart})_2]^{2-}$ ion more favorably than their antipodes. However, some complexes are known which behave oppositely to the above prediction. For example, Δ isomers are eluted faster in ion-exchange chromatography for a series of $[Co(en)_x(tn)_y(tmd)_z]^{3+}$ complexes when $x=0$[16] (tn=trimethylenediamine and tmd=tetramethylenediamine). In addition, *Λ-cis*-$[Co(tn)_2(NH_3)_2]^{3+}$ is eluted faster, but the elution order is reversed if tn ligands are replaced with tmd ligands.[17,18] These exceptional elution orders are not easily rationalized by our association models, but they may be attributed to conformational lability of these complexes. That is, since axial NH protons are not fixed in these higher-membered chelate complexes, the C_3 mode will not effectively contribute to chiral recognition for these flexible complexes. If the contribution of the C_3 mode is reduced to the extent that the C_2 mode predominates over the C_3 mode, Δ isomers should be eluted faster.

***cis(O)*-$[Co(O)_2(N)_4]^+$-Type Complexes.**[19] When negatively charged donor atom(s) are present in a complex, a care must be taken in counting the C_3 and C_2 interaction sites. For example, $[Co(gly)(en)_2]^{2+}$ has two triangular facets along the pseudo C_3 axis, one composed of three NH protons and the other of two NH protons and one oxygen atom of gly. They are shown schematically in Fig. 4. The former facet provides three normal C_3 sites for the Λ isomer (Fig. 4(a)), but the latter provides only one C_3 site which is expected to suffer an electrostatic repulsion from the negatively charged oxygen atom present nearby (Fig. 4(b)). Since this C_3 site is electrostatically handicapped, it contributes less than the normal C_3 site and is designated as the C_3* site to differentiate it from the normal one. Similar allowance has been made in the ranked L–J model,[19] and should be also made in counting the C_2 sites; *Λ*-$[Co(gly)(en)_2]^{2+}$ has two C_2 sites one of which (C_2*) suffers an electrostatic repulsion from the oxygen atom of gly (Fig. 5). Numbers of interaction sites thus counted for *cis(O)*-$[Co(O)_2(N)_4]^+$-type and related complexes are given in Table 2, where starred numbers in parentheses denote the numbers of such handicapped sites out of all the possible C_3 or C_2 interaction sites.

Three points are mentioned in Table 2. The first is that our association models predict a correct elution order even for *cis(O),trans(N),cis(NH₃)*-$[Co(gly)_2(NH_3)_2]^+$ which is exceptional in that its Δ isomer is eluted faster.[19] The second point is that the elution order is not rationalized for C_2-$[Co(gly)_2(en)]^+$ if the C_3* site is neglected. Thus, the C_3* interaction should be taken into account, particularly when other rival interactions are not possible. Anyway, C_2-$[Co(gly)_2(en)]^+$ should not be resolved effectively.[19] Similarly,

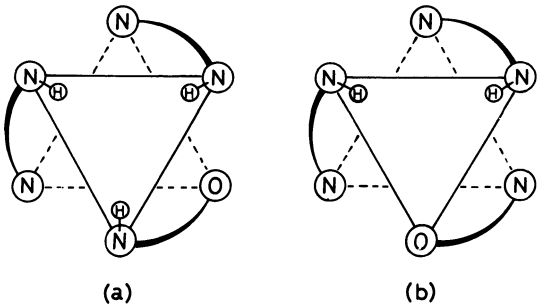

Fig. 4. Triangular facets providing C_3 (a) and C_3* (b) interaction sites in *Λ*-$[Co(gly)(en)_2]^{2+}$.

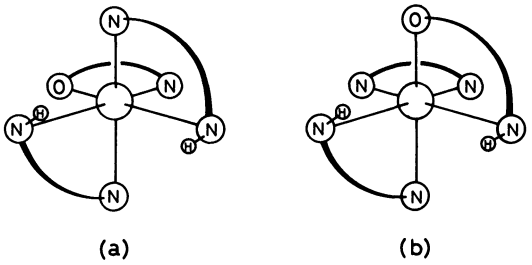

Fig. 5. C_2 (a) and C_2* (b) interaction sites in *Λ*-$[Co(gly)(en)_2]^{2+}$.

no effective resolution is expected for *trans(O)*-[Co(gly)$_2$(en)]$^+$.

Finally, the last two complexes, *fac(NH$_3$)*-[Co(X)(gly)(NH$_3$)$_3$]$^+$ and [Co(X)(gly)(tacn)]$^+$ (X=anion ligand and tacn=1,4,7-triazacyclononane) have been prepared and resolved by ion-exchange chromatography.[20,21] These complexes have a chirality different from those defined by helical rearrangements of chelate rings. Schematic structures of their two enantiomers (a) and (b) are shown in Fig. 6. Shibata et al.[20,21] have found that the (a) enantiomer is eluted faster for the ammine complex, while the (b) enantiomer is for the tacn complex. Our association models predict a correct elution order straightforwardly for the former, while the elution order of the latter complex is not rationalized unless the C_3* mode predominates over the C_2* mode. This will happen since the C_3 mode generally predominates over the C_2 mode.

Complexes with Phosphine Chelates. Recently, Fujita and co-workers have prepared and resolved a number of octahedral Co(III) complexes with phosphine chelates. Since these complexes have invariably some substituents on the phosphorus donor atom(s), they provide us a chance to examine the steric effect of substituents on the C_3 and C_2 interactions.

When the C_3 and C_2 interaction sites are counted for phosphine complexes, an assumption is made that a methyl or phenyl group on the triangular facet prohibits the C_3 interaction involving the two NH protons on the same facet. For example, [Co(en)$_2$(edmp or edpp)]$^{3+}$ (edmp=(2-aminoethyl)dimethylphosphine and edpp=(2-aminoethyl)diphenylphosphine) has two triangular facets, one of which has an axial methyl or phenyl group on the P atom, and thus the C_3 mode is sterically prohibited on this facet. As a result, the Λ isomer has three C_3 sites on the other facet, and the Δ isomer has two C_2 sites. Interaction sites are counted similarly for *fac(N)*-[Co(en)(edmp)$_2$]$^{3+}$ and *fac(N)*-[Co(edmp)$_3$]$^{3+}$. The results given in Table 3 predict correct elution orders for these complexes.[24]

For [Co(en)$_2$(dmpe or dppe)]$^{3+}$ (dmpe=1,2-(dimethylphosphino)ethane and dppe=1,2-(diphenylphosphino)ethane), and *trans(P,P)*-[Co(edmp)$_2$(dmpe)]$^{3+}$, no C_3 interaction is possible. Instead, one C_2 site is present in the Δ isomers, which thus should be eluted faster.[25] On the other hand, [Co(en)(dmpe or dppe)$_2$]$^{3+}$, *trans(P,N)*- and *trans(N,N)*-[Co(edmp)$_2$(dmpe)]$^{3+}$, and [Co(dmpe or dppe)$_3$]$^{3+}$ have no NH protons available for the double hydrogen bonding to the chiral eluent anion, so that practical resolution is not attained for these complexes.[25] In this way, elution orders are correctly predicted for most of the phosphine complexes listed in Table 3 on the assumption that no C_3 interaction is possible on the triangular facet on which an axial methyl or phenyl group is attached to the P atom. In the preceding section, however, interaction sites are counted for *N*-methylated complexes by assuming that an axial methyl group on the N donor atom does not interfere with the C_3 interaction. If the methyl group also prohibits the C_3 interaction, our models fail to predict a correct elution order for [Co(Me$_2$-en)(en)$_2$]$^{3+}$. Thus, a methyl group should be regarded as a steric obstacle to the C_3 interaction only when it is attached to the P

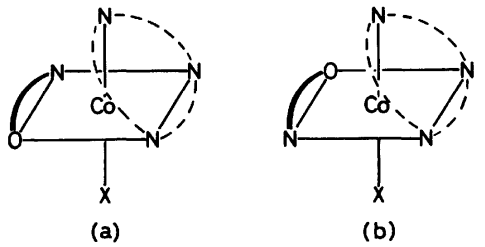

Fig. 6. Schematic structures of two possible enantiomers (a) and (b) for *fac(NH$_3$)*-[Co(X)(gly)(NH$_3$)$_3$]$^+$ and [Co(X)(gly)(tacn)]$^+$.

Table 2. Interaction Sites *N* and Elution Orders for *cis(O)*-[Co(O)$_2$(N)$_4$]$^+$-Type and Related Complexes

Complex	*N* C_3 Λ	C_3 Δ	C_2 Λ	C_2 Δ	Enantiomer Eluted Faster Obsd	Predic.	Ref.
[Co(gly or β-ala)(en)$_2$]$^{2+}$	4(1*)	0	0	2(1*)	Λ	Λ	22
cis(O),cis(N),cis(NH$_3$)-[Co(gly)$_2$(NH$_3$)$_2$]$^+$	6(1*)	5(1*)	0	0	(Λ)[d]	Λ	19
cis(O),trans(N),cis(NH$_3$)-[Co(gly)$_2$(NH$_3$)$_2$]$^+$	5(1*)	7(1*)	0	0	Δ	Δ	19
C_1-[Co(gly)$_2$(en)]$^+$	3	0	0	1(1*)	Λ	Λ	19
C_2-[Co(gly)$_2$(en)]$^+$	2(2*)	0	0	2(2*)	(Λ)[d]	—	19
trans(O)-[Co(gly)$_2$(en)]$^+$	2(2*)	0	0	1(1*)	c)	—	—
fac-[Co(amino acidato)$_3$]	3	0	0	0	Λ	Λ	23
fac(NH$_3$)-[Co(X)(gly)(NH$_3$)$_3$]$^+$	8(2*)[a]	7(2*)[b]	0[a]	0[b]	a	a	20
[Co(X)(gly)(tacn)]$^+$	0[a]	1(1*)[b]	1(1*)[a]	0[b]	b	—	21

Starred numbers in parentheses denote the numbers of handicapped C_3* or C_2* interaction sites (see the text). a, b) a and b correspond to absolute configurations shown in Fig. 6(a) and 6(b) respectively. c) Not known. d) Partial resolution.

Table 3. Interaction Sites *N* and Elution Orders for Phosphine Complexes

Complex	*N*				Enantiomer Eluted Faster		Ref.
	C_3		C_2				
	Λ	Δ	Λ	Δ	Obsd	Predic.	
$[Co(en)_2(edmp \text{ or } edpp)]^{3+}$	3	0	0	2	Λ	Λ	24
fac(*N*)-$[Co(en)(edmp)_2]^{3+}$	3	0	0	1	Λ	Λ	24
fac(*N*)-$[Co(edmp)_3]^{3+}$	3	0	0	0	Λ	Λ	24
$[Co(en)_2(dmpe \text{ or } dppe)]^{3+}$	0	0	0	1	Δ	Δ	25
$[Co(en)(dmpe \text{ or } dppe)_2]^{3+}$	0	0	0	0	(Δ)[a,e]	—	25
trans(*P,P*)-$[Co(edmp)_2(dmpe)]^{3+}$	0	0	0	1	b)	Δ	27
trans(*P,N*)-$[Co(edmp)_2(dmpe)]^{3+}$	0	0	0	0	b)	—	27
trans(*N,N*)-$[Co(edmp)_2(dmpe)]^{3+}$	0	0	0	0	b)	—	27
$[Co(dmpe \text{ or } dppe)_3]^{3+}$	0	0	0	0	—[c,e]	—	25
$[Co(acac)(en)_2]^{2+}$	2*	0	0	1	Λ	Λ	12
$[Co(ox)(en)_2]^{+}$	0	0	0	1	(Δ)[a]	Δ	12
fac(*N*)-$[Co(acac)(en)(edmp \text{ or } edpp)]^{2+}$	1*	0	0	1	(Λ)[a,d]	Λ	28
fac(*N*)-$[Co(ox)(en)(edmp \text{ or } edpp)]^{+}$	0	0	0	1	b)	Δ	—
trans(*P,N*)-$[Co(acac)(edmp \text{ or } edpp)_2]^{2+}$	1*	0	0	0	Λ[d]	Λ	29
trans(*P,N*)-$[Co(ox)(edmp \text{ or } edpp)_2]^{+}$	0	0	0	0	(Λ)[a,d]	—	29
trans(*P,P*)-$[Co(acac)(edpp)_2]^{2+}$	0	0	0	1	Λ	Δ	29
trans(*P,P*)-$[Co(ox)(edpp)_2]^{+}$	0	0	0	1	(Λ)[a]	Δ	29
$[Co(acac)(en)(dmpe \text{ or } dppe)]^{2+}$	0	0	0	0	(Λ)[a]	—	25, 29
$[Co(ox)(en)(dmpe \text{ or } dppe)]^{+}$	0	0	0	0	—[c]	—	29
$[Co(acac)(dmpe \text{ or } dppe)_2]^{2+}$	0	0	0	0	—[c]	—	25
$[Co(acac)_2(edmp \text{ or } edpp)]^{+}$	0	0	0	0	(Λ)[a]	—	30
$[Co(acac)_2(dmpe \text{ or } dppe)]^{+}$	0	0	0	0	(Λ)[a]	—	25, 30

Starred numbers denote the numbers of handicapped interaction sites (see the text). a) Partial resolution. b) Not known. c) No resolution. d) Elution order for edpp complex. e) Elution order for dmpe complex.

donor atom. Since a P atom is much bigger in size than an N atom, the above claim seems reasonable. A phenyl group is, on the other hand, so bulky that it will always serve as an obstacle whether it is on the P atom or on the N atom, and will exert an additional influence on the C_2 interaction (see later).

Finally, our attention is focused on phosphine complexes with negatively charged ligand(s) such as acetylacetonate (acac) or oxalate (ox) anion. Before they are examined, interaction sites are counted for the two parent complexes, $[Co(acac)(en)_2]^{2+}$ and $[Co(ox)(en)_2]^{+}$. They have two triangular facets composed of two NH protons and one oxygen atom. If an electrostatic repulsion due to the negatively charged oxygen atom of acac or ox is taken into account, they have no C_3 site but have one C_2 site. As a result, the Δ isomer should be eluted faster. In fact, *Δ*-$[Co(ox)(en)_2]^{+}$ is eluted faster as expected, but *Δ*-$[Co(acac)(en)_2]^{2+}$ is eluted *later*.[12] This means, according to our models, that the C_3* interaction is possible for $[Co(acac)(en)_2]^{2+}$. Since the oxygen atom of acac carries a formal charge of −0.5, its electrostatic field is not as strong[26] as that of ox^{2-} or gly^{-} which bears a formal charge of −1.0 on the oxygen atom. In fact, we assumed before that such an electrostatically handicapped C_3* interaction comes into play even for $[Co(gly)_2(en)]^{+}$-type complexes, when other interaction modes do not contribute appreciably. Thus, interaction sites are counted in the following complexes on a fairly valid assumption that the triangular facet composed of two NH protons and one oxygen atom of acac provides one C_3* site, but that of two NH protons and one oxygen atom of ox (or gly) does not. However, the latter facet may contribute if other rival interaction sites are not present or do not contribute appreciably, like in C_2-$[Co(gly)_2(en)]^{+}$, *trans*(*O*)-$[Co(gly)_2(en)]^{+}$, and *trans*(*P,N*)-$[Co(ox)(edmp \text{ or } edpp)_2]^{+}$ (see later). Detailed discussions on the C_3* interaction will be presented elsewhere in connection with the interpretation of chromatographic resolution of *cis*-$[Co(X)_2(en)_2]^{+}$-type complexes.

Now, it is confirmed in Table 3 that our association models afford a satisfactory prediction of the elution order for most of the phosphine complexes with an acac or ox ligand. For example, the Λ isomer should be eluted faster for *fac*(*N*)-$[Co(acac)(en)(edmp \text{ or } edpp)]^{2+}$,[28] since it has one C_3* site besides one C_2 site, whereas the elution order is reversed for the corresponding ox complex, since the C_3* interaction is prohibited but one C_2 site survives in the ox complex. For *trans*(*P,N*)-$[Co(acac)(edmp \text{ or } edpp)_2]^{2+}$ which has one C_3* site, the Λ isomer should be eluted faster. By contrast, no effective resolution is expected for the corresponding ox complex, since it has neither the C_3

(or C_3*) nor the C_2 site.

For *trans*(*P*,*P*)-$[Co(acac)(edpp)_2]^{2+}$ and *trans*(*P*,*P*)-$[Co(ox)(edpp)_2]^{+}$, the Λ isomers are eluted unexpectedly faster, though both of the two *trans*(*P*,*P*) complexes have one C_2 site only. In order to rationalize these anomalous elution orders, the steric influence of a bulky phenyl group must be taken into account. It is true that two phenyl groups are situated in these complexes such that the distal carboxylato group experiences a steric repulsion from either of them in the C_2 interaction with the Δ isomer, while they do not impose any steric hindrance on the antipode. Then, if the steric repulsion due to the phenyl group in the C_2 interaction with the Δ isomer predominates over the usual repulsion due to the P–N chelate ring in the C_2 interaction with the Λ isomer, the Λ isomer should form a relatively stable ion pair with $[Sb_2(d\text{-tart})_2]^{2-}$ ion as compared with the Δ isomer. If the methyl group on the P atom is not bulky enough to serve as a steric obstacle to the C_2 interaction, the Δ isomer should be eluted faster, as our models predict, for the corresponding edmp complexes, *trans*(*P*,*P*)-$[Co(acac)(edmp)_2]^{2+}$ and -$[Co(ox)(edmp)_2]^{+}$. Similarly, the Δ isomer should be eluted faster for *trans*(*P*,*P*)-$[Co(edmp)_2(dmpe\text{ or }dppe)]^{3+}$, whereas the elution order should be reversed for the corresponding edpp complex, *trans*(*P*,*P*)-$[Co(edpp)_2(dmpe\text{ or }dppe)]^{3+}$. Anyway, experimental data are not enough to decide whether the methyl group on the P atom exerts a similar steric effect on the C_2 interaction.

Any of other complexes listed in Table 3 have neither the C_3 (or C_3*) nor the C_2 interaction site, so that no practical resolution is expected for them. However, for *trans*(*P*,*N*)-$[Co(ox)(edmp\text{ or }edpp)_2]^{+}$, one electrostatically handicapped C_3* interaction is conceivable which has been neglected and is shown in Fig. 4(b), and it will come into play because of complete absence of other interactions. Consequently, optical resolution, though it may be partial, is potentially possible with the Λ isomer eluted faster.[29]

The reason is not known why $[Co(en)(dmpe)_2]^{3+}$, $[Co(acac)(en)(dmpe\text{ or }dppe)]^{2+}$, $[Co(acac)_2(dmpe\text{ or }dppe)]^{+}$, and $[Co(acac)_2(edpp)]^{+}$ have been partially resolved by ion-exchange chromatography with $[Sb_2(d\text{-tart})_2]^{2-}$ ion employed as an eluent. Interaction modes other than the C_3 and C_2 hydrogen-bonding interactions must be invoked. Since the SP-Sephadex column is used for the resolution of these complexes, its chirality might be in part responsible.

Hydrophobic Complexes with Aromatic Ligands. It is note worthy that $[Sb_2(d\text{-tart})_2]^{2-}$ ion can recognize the chirality of some hydrophobic complexes with aromatic ligands such as phen or bpy (phen=1,10-phenanthroline and bpy=2,2′-bipyridine). For example, $[Cr(phen\text{ or }bpy)_2(bpdo)]^{3+}$ (bpdo=2,2′-bipyridine *N*,*N*′-dioxide),[31] $[Cr(acac)_2(bpdo)]^{+}$,[32] $[Cr(bpy)(phen)(bpdo\text{ or }mbdo)]^{3+}$ (mbdo=3,3′-dimethyl-2,2′-bipyridine *N*,*N*′-dioxide),[33] $[Co(acac)(en)(bpy)]^{2+}$, *mer*(*N*)-$[Co(acac)(empp\text{ or }edpp)(bpy)]^{2+}$ (empp=(2-aminoethyl)methylphenylphosphine),[28] and $[Ru(bpy)_n(Hpda)_{3-n}]^{2+}$ (Hpda=di-2-pyridylamine)[34] have been resolved by ion-exchange chromatography with $[Sb_2(d\text{-tart})_2]^{2-}$ ion employed as an eluent. Furthermore, complete chromatographic resolution has been attained for some Co(III) complexes with 2,2′-biimidazole[35] and its related ligands,[36] and the Pfeiffer effect has been detected for $[M(phen\text{ or }bpy)_3]^{2+}$ in the presence of $[Sb_2(d\text{-tart})_2]^{2-}$ ion.[37] Since the above complexes have no NH protons available for the double hydrogen bonding to the chiral anion, they associate with it through some interactions other than hydrogen bonding. Though a so-called hydrophobic interaction is one of the plausible interactions, its detailed nature is out of the scope of the present study.

The present work was partially supported by a Grant-in-Aid for Scientific Research No. 60470047 from the Ministry of Education, Science and Culture.

References

1) H. Yoneda, *J. Liq. Chromatogr.*, **2**, 1157 (1979).
2) H. Yoneda, *J. Chromatogr.*, **313**, 59 (1984).
3) Y. Yoshikawa and K. Yamasaki, *Coord. Chem. Rev.*, **28**, 205 (1979).
4) H. Nakazawa and H. Yoneda, *J. Chromatogr.*, **160**, 89 (1978).
5) U. Sakaguchi, A. Tsuge, and H. Yoneda, *Inorg. Chem.*, **22**, 3745 (1983).
6) A. Drake, R. Kuroda, and S. F. Mason, *J. Chem. Soc., Dalton Trans.*, **1979**, 1095.
7) K. Miyoshi, unpublished work.
8) M. Fujita, Y. Yoshikawa, and H. Yamatera, *Bull. Chem. Soc. Jpn.*, **50**, 3209 (1977).
9) T. Taura, H. Nakazawa, and H. Yoneda, *Inorg. Nucl. Chem. Lett.*, **13**, 603 (1977); U. Sakaguchi, A. Tsuge, and H. Yoneda, *Inorg. Chem.*, **22**, 1630 (1983).
10) K. Sakakibara, Y. Yoshikawa, and H. Yamatera, *Bull. Chem. Soc. Jpn.*, **52**, 2725 (1979).
11) The same interaction mode as proposed here has been actually found in the crystal structure of *Δ-cis*-$[Co(NO_2)_2(en)_2]_2[Sb_2(d\text{-tart})_2]\cdot 2H_2O$, A. Miyanaga, Y. Kushi, and H. Yoneda, 27th Symposium on Coordination Chemistry, Matsumoto, October 1977, Abstr., No. 1B06.
12) H. Nakazawa, C. H. Oh, K. Miyoshi, and H. Yoneda, *Bull. Chem. Soc. Jpn.*, **53**, 273 (1980).
13) G. H. Searle, *Aust. J. Chem.*, **30**, 2625 (1977).
14) S. Utsuno, Y. Yoshikawa, and Y. Tahata, *Inorg. Chem.*, **24**, 2724 (1985).
15) Y. Yoshikawa, N. Kato, Y. Kimura, S. Utsuno, and G. N. Natu, *Bull. Chem. Soc. Jpn.*, **59**, 2123 (1986).
16) M. Kojima, H. Yamada, H. Ogino, and J. Fujita, *Bull. Chem. Soc. Jpn.*, **50**, 2325 (1977).
17) M. Sano, M. Fujita, K. Sasaki, Y. Yoshikawa, and H. Yamatera, *Bull. Chem. Soc. Jpn.*, **54**, 2823 (1981).

18) M. Kojima, K. Morita, and J. Fujita, *Bull. Chem. Soc. Jpn.*, **54**, 2947 (1981).
19) H. Nakazawa, U. Sakaguchi, and H. Yoneda, *J. Chromatogr.*, **213**, 323 (1981).
20) S. Fujinami, A. Hattori, and M. Shibata, *Bull. Chem. Soc. Jpn.*, **56**, 2420 (1983).
21) S. Simba, S. Fujinami, and M. Shibata, *Bull. Chem. Soc. Jpn.*, **53**, 2523 (1980).
22) M. Kojima, H. Takayanagi, and J. Fujita, *Bull. Chem. Soc. Jpn.*, **50**, 1891 (1977).
23) S. Yamazaki, T. Yukimoto, and H. Yoneda, *J. Chromatogr.*, **175**, 317 (1979); T. Yukimoto and H. Yoneda, *J. Chromatogr.*, **210**, 477 (1981).
24) I. Kinoshita, K. Kashiwabara, J. Fujita, K. Matsumoto, and S. Ooi, *Bull. Chem. Soc. Jpn.*, **54**, 2683 (1981).
25) T. Ohishi, K. Kashiwabara, and J. Fujita, *Bull. Chem. Soc. Jpn.*, **56**, 3441 (1983); *Chem. Lett.*, **1981**, 1371.
26) U. Sakaguchi, H. Nakazawa, and H. Yoneda, *J. Chem. Soc., Chem. Commun.*, **1979**, 356.
27) T. Ohishi, S. Ohba, K. Kashiwabara, Y. Saito, and J. Fujita, *Bull. Chem. Soc. Jpn.*, **57**, 877 (1984).
28) M. Takata, K. Kashiwabara, H. Ito, T. Ito, and J. Fujita, *Bull. Chem. Soc. Jpn.*, **58**, 2247 (1985).
29) M. Atoh, I. Kinoshita, K. Kashiwabara, and J. Fujita, *Bull. Chem. Soc. Jpn.*, **55**, 3179 (1982); M. Atoh, K. Kashiwabara, and J. Fujita, *Bull. Chem. Soc. Jpn.*, **58**, 3492 (1985).
30) K. Kashiwabara, I. Kinoshita, T. Ito, and J. Fujita, *Bull. Chem. Soc. Jpn.*, **54**, 725 (1981).
31) H. Kanno, K. Kashiwabara, and J. Fujita, *Bull. Chem. Soc. Jpn.*, **53**, 2881 (1980).
32) H. Kanno, S. Utsuno, and J. Fujita, *Bull. Chem. Soc. Jpn.*, **57**, 3443 (1984).
33) H. Kanno, S. Utsuno, and J. Fujita, *Bull. Chem. Soc. Jpn.*, **59**, 1293 (1986).
34) T. Fukuchi, K. Mizumachi, and K. Shimizu, 33rd Symposium on Coordination Chemistry, Osaka, October 1983, Abstr., No. 1PA06.
35) H. Kanno, S. Manriki, S. Utsuno, and J. Fujita, 32nd Symposium on Coordination Chemistry, Nagasaki, October 1982, Abstr., No. 2A16.
36) H. Kanno, H. Nagata, H. Miyagi, T. Natsume, T. Kondoh, S. Utsuno, and J. Fujita, 34th Symposium on Coordination Chemistry, Nagaoka, October 1984, Abstr., No. 1PA07.
37) L. Mayer and R. C. Brasted, *J. Coord. Chem.*, **3**, 85 (1973).

 © 1986 The Chemical Society of Japan Bull. Chem. Soc. Jpn., 59, 3483—3488 (1986)

High-Spin($^5T_2$) ⇌ Low-Spin($^1A_1$) Transition in Mixed Ligand Complex [Fe(2,2′-bipyridine)(1,10-phenanthroline)(NCS)$_2$]

Hidenari INOUE,* Hiroko NAKAJIMA, Takeshi TAKAHASHI, Hiroshi UCHIDA
Tsuneo SHIRAI, and Ekkehard FLUCK†
Department of Applied Chemistry, Faculty of Science and Technology, Keio University,
3-14-1, Hiyoshi, Kohoku-ku, Yokohama 223
†Gmelin-Institut der Max-Planck-Gesellschaft, Varrentrappstrasse 40/42,
D-6000 Frankfurt am Main 90, FRG
(Received May 14, 1986)

A new type of the mixed ligand complex [Fe(bpy)(phen)(NCS)$_2$] (bpy=2,2′-bipyridine and phen=1,10-phenanthroline) has been prepared by two different methods. The influence of the mixed ligand coordination of bpy and phen to a central iron(II) ion is studied by measurements of the temperature variation of magnetic moments and Mössbauer parameters. It has been demonstrated that the mixed coordination tends to make the $^5T_2$(high-spin) ⇌ $^1A_1$(low-spin) transition more gradual. The spin-crossover transition temperature depends on the electronic property as well as the structure of the ligand coordinated to the central iron(II) ion.

A wide variety of bidentate ligands has been studied in an attempt to prepare iron(II) complexes which exhibit the spin-crossover transition $^5T_2$(high-spin) ⇌ $^1A_1$(low-spin). Almost all spin-crossover iron(II) complexes contain 1,10-phenanthroline (phen), 2,2′-bipyridine (bpy) or their derivatives as bidentate ligands because the ligand field strength of these diamines is intermediate and can afford both high-spin and low-spin states. A few iron(II) complexes of biimidazole and pyridine derivatives are also known to give rise to the spin-crossover transition.[1] A number of topics concerning the spin-crossover transition in iron(II) complexes has already been fully reviewed in recent articles.[2] These articles pointed out that the spin-crossover behavior observed for the electronic configuration $3d^6$ is affected by some factors such as ligand substitution,[3] metal dilution,[4] nature of crystal solvent and anion,[5] and isotopic substitution.[6] In spite of much attention to spin-crossover phenomena there have been relatively few reports on the spin-crossover transition of iron(II) complexes with mixed ligands. Exceptionally Spacu et al.[7] reported the spin-crossover transition of the mixed ligand complex [Fe(py)$_2$(phen)(NCS)$_2$], which stimulated our interest in the preparation of a new mixed-ligand complex for studying the influence of the mixed coordination on spin-crossover behavior.

In the present work we have prepared a new type of the mixed ligand iron(II) complex [Fe(bpy)(phen)(NCS)$_2$] by two different methods. The first method is based on the addition of a methanol solution of iron(II) thiocyanate to a mixed solution of bpy and phen in methanol. The second one is based on stepwise replacing two pyridine ligands of the starting material [Fe(py)$_4$(NCS)$_2$] with a phen, followed by further replacement of the residual two pyridine ligands by a bpy. These two synthetic methods are likely to be very useful in preparing a variety of novel mixed-ligand iron(II) complexes which display the spin-crossover transition $^5T_2$(high-spin) ⇌ $^1A_1$(low-spin). In order to examine the thermally induced spin-crossover transition, we have measured the temperature variation of magnetic susceptibilities and ^{57}Fe Mössbauer spectra of the mixed ligand iron(II) complex [Fe(bpy)(phen)(NCS)$_2$]. Our particular interest is to learn how the mixed coordination of bpy and phen to a central iron(II) ion influences transition temperature, hysteresis effect, and mechanism of spin-transitions.

Experimental

Materials. All reagents were of reagent grade and used without further purification. Tetrakis(pyridine)bis(thiocyanato)iron(II) [Fe(py)$_4$(NCS)$_2$][8] and bis(pyridine)(1,10-phenanthroline)bis(isothiocyanato)iron(II) [Fe(py)$_2$(phen)(NCS)$_2$][7] were prepared according to the literature methods.

Preparation. The mixed ligand complex [Fe(bpy)(phen)(NCS)$_2$] was prepared by the following two methods. Method I: A 50 cm^3 solution of 0.49 g (5.00 mmol) KSCN in methanol was added to a 6 cm^3 solution of 0.70 g (2.50 mmol) $FeSO_4 \cdot 7H_2O$ in water. The resulting precipitate of K_2SO_4 was filtered off with a G4 glass filter. To the filtrate was dropwise added a solution of 0.39 g (2.50 mmol) bpy and 0.45 g (2.50 mmol) phen in 50 cm^3 of methanol with vigorous stirring. After the mixed solution was allowed to stand overnight, red purple crystals obtained were filtered, washed with methanol and dried over silica gel. Found: C, 54.7; H, 3.3; N, 15.4%. Calcd for [Fe(bpy)(phen)(NCS)$_2$]: C, 56.70; H, 3.17; N, 16.53%. Method II: A 20 cm^3 solution of 0.31 g (2.00 mmol) bpy in pyridine was slowly added to a 500 cm^3 solution of 1.02 g (2.00 mmol) [Fe(py)$_2$(phen)(NCS)$_2$] in pyridine. The reaction mixture was stirred at 80 °C for 20 h, then evaporated to 50 cm^3 under reduced pressure. After the solution was cooled to room temperature, red purple crystals obtained were collected by filtration, washed with methanol and dried over silica gel. Found: C, 56.3; H, 3.2; N, 15.5%. Calcd for [Fe(bpy)(phen)(NCS)$_2$]: C, 56.70; H, 3.17; N, 16.53%. All manupulations were performed in a nitrogen-filled glovebox to prevent oxidation of iron(II) compounds.

Physical Measurements. The X-ray diffraction powder patterns were taken at room temperature with a Rigaku-

Denki Geigerflex RAD-IIA X-ray diffractometer using graphite-monochromated Cu $K\alpha$ radiation (λ=0.1542 nm). Infrared spectra were recorded on a Hitachi Perkin-Elmer Model 225 grating infrared spectrophotometer using KBr pellets. The calibration of wavenumbers was carried out using polystyrene film. Magnetic susceptibilities were measured in the temperature range between 77 and 300 K by the Bozorth method with $Hg[Co(SCN)_4]$ as a calibrant.[9] The molar susceptibilities were corrected for diamagnetism using the following corrections: Fe^{2+}, −13; bpy, −105; phen, −128; NCS^-, −35 (in units of 10^{-6} cm^3 mol^{-1}).[10,11] Mössbauer spectra were obtained with a 10 mCi ^{57}Co source in Pd foil (The Radiochemical Centre, Amersham, England) using a Wissel constant-acceleration transducer coupled with a Canberra OMEGA-1 multichannel analyzer. The absorber temperature was varied between 77 and 300 K with a Torisha cryostat. The spectra were fitted to Lorentzian curves with an iterative least-square computer program. The isomer shifts were referred to natural iron foil at 293 K.

Results and Discussion

Preparation of Mixed Ligand Complexes. Thermodynamic data are not available for the prediction whether the mixed ligand complex $[Fe(bpy)(phen)(NCS)_2]$ can be synthesized or not. When the target mixed ligand complex is prepared by Method I, one or more than two unfavorable products such as $[Fe(phen)_2(NCS)_2]$ $[Fe(bpy)_2(NCS)_2]$, $[Fe(phen)_3(NCS)_2]$ or $[Fe(bpy)_3](NCS)_2$ are expected to yield under the present experimental conditions. Of these complexes both $[Fe(phen)_3](NCS)_2$ and $[Fe(bpy)_3](NCS)_2$ are easily distinguishable from $[Fe(phen)_2(NCS)_2]$, $[Fe(bpy)_2(NCS)_2]$, and $[Fe(phen)(bpy)(NCS)_2]$ by elemental analysis or Mössbauer spectroscopy. The formation of $[Fe(bpy)_2(NCS)_2]$ is also ignored because it is synthesized only under more rigorous experimental conditions, e.g. by elimination of bpy from $[Fe(bpy)_3](NCS)_2$.[11] One might still suspect that a mixture of $[Fe(bpy)(phen)(NCS)_2]$ and $[Fe(phen)_2(NCS)_2]$ is formed by Method I. Therefore, we undertook Method II in which the pyridine ligands of $[Fe(py)_4(NCS)_2]$ are stepwise replaced by a bidentate phen or bpy. Since the complete substitution of the two remaining pyridine ligands in $[Fe(py)_2(phen)(NCS)_2]$ was supposed to be the most difficult step of the successive substitution reactions, the reaction mixture was heated for a prolonged period (20 h). In spite of somewhat tedious procedures, the successive substitution method employed in Method II was demonstrated to be an excellent method for preparing a variety of mixed ligand complexes. The preparation of some mixed ligand complexes analogous to $[Fe(bpy)(phen)(NCS)_2]$ is in progress in our laboratory.

Identification of Mixed Ligand Complexes. The identity of the mixed ligand complexes prepared by the above two different methods was confirmed by a comparison of the X-ray diffraction powder patterns as well as the infrared spectra. The X-ray diffraction powder patterns of the mixed ligand complex $[Fe(bpy)(phen)(NCS)_2]$ are shown in Fig. 1. The diffraction powder pattern of $[Fe(phen)_2(NCS)_2]$ is also presented for comparative purposes, although the X-ray diffraction data are already reported on this complex.[12] The diffraction pattern of $[Fe(bpy)(phen)(NCS)_2]$ prepared by Method I agrees with that by Method II, indicating that the mixed ligand complexes prepared by the two different methods are identical. The intensities observed for $[Fe(bpy)(phen)(NCS)_2]$ prepared according to Method I and II are appreciably different from those of $[Fe(phen)_2(NCS)_2]$, while the peak positions are very similar to each other. This means that $[Fe(bpy)(phen)(NCS)_2]$ is isomorphous with $[Fe(phen)_2(NCS)_2]$ and the lattice parameters of the former are also quite similar to those of the latter.

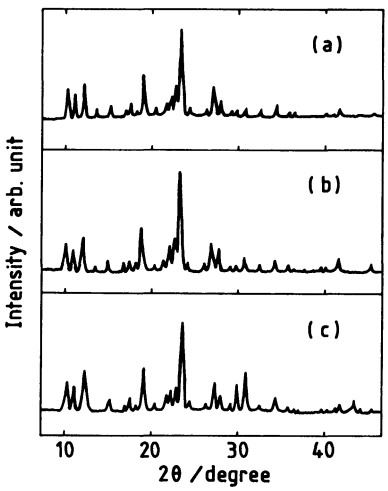

Fig. 1. Comparison of X-ray diffraction powder patterns. (a): $[Fe(bpy)(phen)(NCS)_2]$ prepared by Method I, (b): $[Fe(bpy)(phen)(NCS)_2]$ prepared by Method II, (c) $[Fe(phen)_2(NCS)_2]$.

Table 1. Infrared Absorption Frequencies of Thiocyanato Ligands in $[Fe(bpy)(phen)(NCS)_2]$

Compound	Absorption frequencies/cm^{-1}		
	ν_1(CN str.)	ν_2(SCN bend.)	ν_3(CS str.)
$[Fe(bpy)(phen)(NCS)_2]$[a]	2055	473	800
$[Fe(bpy)(phen)(NCS)_2]$[b]	2055	475	798
$[Fe(phen)_2(NCS)_2]$[c]	2060	(483, 473)	(809)

a) Prepared by Method I. b) Prepared by Method II. c) Taken from 10).

The infrared absorption frequencies observed for [Fe(bpy)(phen)(NCS)$_2$] are listed in Table 1 along with those for [Fe(phen)$_2$(NCS)$_2$]. Three fundamental modes of the thiocyanato ligand are referred to as ν_1(C-N str.), ν_2(N-C-S bend.), and ν_3(C-S str.). The absorption frequencies of these three fundamental modes provide information on whether the central iron(II) ion is coordinated through the nitrogen end or through the sulfur end of the thiocyanato ligand. A comparison of the three frequencies in [Fe(bpy)(phen)-(NCS)$_2$] to those in [Fe(phen)$_2$(NCS)$_2$] which are already reported[10] reveals that the coordination atom of the thiocyanato ligand to the central iron(II) ion is nitrogen in [Fe(bpy)(phen)(NCS)$_2$] prepared by Method I and II. In addition, the range of the absorption frequencies observed for the three fundamental modes clearly indicates that the mixed ligand complexes [Fe(bpy)(phen)(NCS)$_2$] are both in the high-spin state at room temperature. The infrared spectra of mixed ligand complexes are generally very useful in verifying the coordination of different kinds of ligands to a central metal ion. In the present case the absorption positions of bpy are too similar to those of phen to clarify the mixed coordination of both ligands to an iron(II) ion.

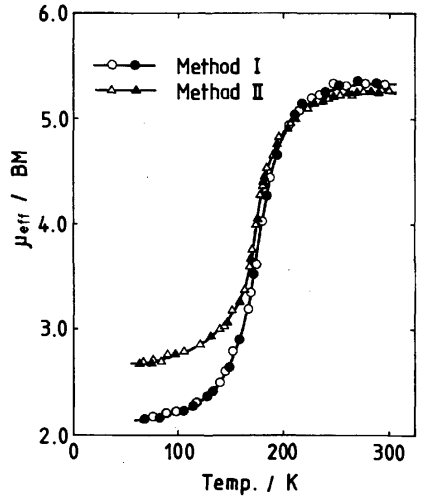

Fig. 2. Temperature dependence of μ_{eff} in [Fe(bpy)-(phen)(NCS)$_2$]. ○: Prepared by Method I, △: prepared by Method II. Open and full symbols represent cooling and heating runs respectively.

Influence of Mixed Coordination on Spin-Crossover Behavior. The variation of the effective magnetic moment μ_{eff} of [Fe(bpy)(phen)(NCS)$_2$] with temperature is shown in Fig. 2. The cooling curve of the temperature dependence of the magnetic moment agrees with the heating one and hence no hysteresis effect is observed for [Fe(bpy)(phen)(NCS)$_2$] within experimental errors. The magnetic moments of [Fe(bpy)(phen)(NCS)$_2$] prepared by Method I and II are deflected suddenly at 179 and 175 K, respectively, each of which is here defined as transition temperature. The marked change in magnetic moments within a narrow temperature range indicates that the present mixed ligand complexes do not belong to the spin-equilibrium type but to the spin-transition one. The rather sharp transition is comparable to a reversible quintet-singlet transition observed for [Fe(phen)$_2$-(NCS)$_2$],[13] in which a cooperative transition mechanism is predominant.

The magnetic moments observed at 77 and 293 K are summarized in Table 2 together with the transition temperature. The magnetic moments of [Fe(bpy)-(phen)(NCS)$_2$] are rather independent of the preparative methods in the high-temperature range 220 to 300 K. In contrast, the complex prepared by Method I gives lower magnetic moments than that by Method II in the low-temperature range below 120 K. The so-called residual paramagnetism depends on the preparative method employed. The disagreement of the residual paramagnetic moments in the low-temperature range is probably due to the difference in topography of crystalline particles, e.g. boundary surface and size of fine crystals.[14] In fact, it is reported that an increase of surface area by grinding and doping fine crystals results in an increase of the residual paramagnetic moments in the low-temperature range.[15] It is to be noted that the residual paramagnetism observed for almost all spin-crossover complexes will be studied because no clearcut explanation has been given to this strange phenomenon. The theoretical interpretation of the temperature dependence of magnetic moments is made more difficult mainly due to the following two reasons: 1)

Table 2. Magnetic Moment and Transition Temperature

Compound	Magnetic moment (BM)		Transition temperature
	High-spin($^5T_2$)	Low-spin($^1A_1$)	
	293 K	77 K	K
[Fe(bpy)(phen)(NCS)$_2$][a]	5.26	2.16	179
[Fe(bpy)(phen)(NCS)$_2$][b]	5.20	2.79	175
[Fe(phen)$_2$(NCS)$_2$][c]	5.17	0.65	174
[Fe(bpy)$_2$(NCS)$_2$][c]	5.20	0.94—1.39	215

a) Prepared by Method I. b) Prepared by Method II. c) Taken from 10) and 11).

The $^5T_2$(high-spin) $\rightleftarrows$ $^1A_1$(low-spin) transition is accompanied by a discontinuous change in metal-ligand distances and 2) the magnetic moments observed in the low-temperature range depend to some extent on the preparative method employed. We believe that the high-spin ($^5T_2$) $\rightleftarrows$ low-spin ($^1A_1$) transition in [Fe(bpy)(phen)(NCS)$_2$] is thermodynamically of first order, although the present complex does not exhibit any hysteresis effect in the experimental time scale of our magnetic measurements.[16] Of course, the conclusive demonstration should be made by heat capacity measurements, particularly because the transition observed in the magnetic moments is almost discontinuous.

Change in Electronic Structure with Spin-Crossover Transition. The Mössbauer spectra obtained at three different temperatures are shown in Fig. 3. Only the spectra of [Fe(bpy)(phen)(NCS)$_2$] prepared by Method II are given as representative ones because the spectral patterns are similar to those by Method I. A quadrupole-splitting doublet characteristic of iron(II) complexes in the high-spin $^5T_2$ state was observed at 298 K. When the absorber temperature was lowered around 190 K, a quadrupole-splitting doublet assignable to the low-spin $^1A_1$ state began to appear in the Mössbauer spectra. As seen from Fig. 3, the absorption intensity, i.e. the area of the quadrupole splitting doublet is much smaller in the high-spin state than in the low-spin state. This indicates that the recoil-free fraction of the iron nucleus in the high-spin state is extremely small as compared with that in the low-spin state. This should be taken into consideration when the high-spin fraction in [Fe(bpy)(phen)(NCS)$_2$] is estimated from the area of the quadrupole splitting doublet.[17] Thus, almost all the high-spin phase seems to be annihilated in the Mössbauer spectra at 77 K, although there are high-spin molecules of [Fe(bpy)(phen)(NCS)$_2$] at least on the surface of microcrystals and/or at the boundary between magnetic domains. Indeed, measurements of temperature variation in magnetic susceptibilities also show that there exist appreciable paramagnetic species even at 77 K.[18]

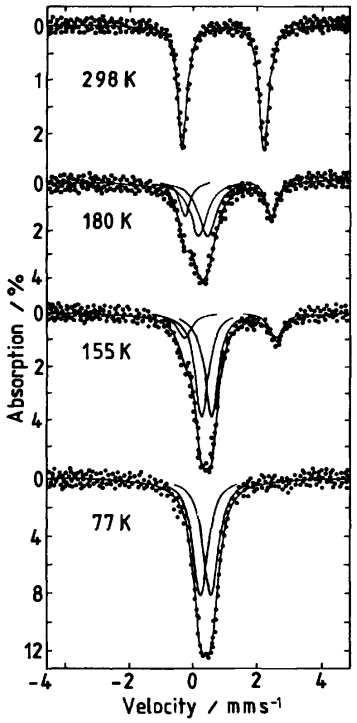

Fig. 3. Mössbauer spectra of [Fe(bpy)(phen)(NCS)$_2$] prepared by Method II.

The Mössbauer parameters obtained at 77 and 293 K are summarized in Table 3, where the parameters of closely related complexes are also listed for comparison. It is noteworthy that the isomer shift as well as the quadrupole splitting decreases on changing from the high-spin to the low-spin state. The thermally induced transition from the high-spin state to the low-spin state is accompanied by an increase in the back donation of 3d electrons to the π^* orbital of the bpy, phen or thiocyanato ligands; the lowering of the 3d electron density around the central iron(II) ion decreases the shielding of the s electron density at the iron nucleus and thereby gives rise to a negative isomer shift. For d^6 iron(II) complexes, the transfer of two electrons from the e_g and t_{2g} orbitals is known to

Table 3. Comparison of Mössbauer Parameters Observed for [Fe(bpy)(phen)(NCS)$_2$] and Related Complexes

Compound	Temp / K	Isomer shift / mms^{-1}	Quadrupole splitting / mms^{-1}
[Fe(bpy)(phen)(NCS)$_2$][a]	293	0.99_3	2.50_9
	77	0.42_3	0.36_9
[Fe(bpy)(phen)(NCS)$_2$][b]	293	0.94_5	2.49_6
	77	0.40_1	0.35_4
[Fe(phen)$_2$(NCS)$_2$][c]	293	1.00	2.67
	77	0.36	0.34
[Fe(bpy)$_2$(NCS)$_2$][c]	293	1.06	2.15
	77	0.36	0.49

a) Prepared by Method I. b) Prepared by Method II. c) Taken from 10) and 11).

cause a considerable reduction in the metal-ligand bond length. Thus, the cell volume generally contracts on going from the high-spin to low-spin state.[19] On transition from the $^5T_2$ state to the $^1A_1$ state, the tendency of phen or bpy to reduce the electron density on the iron is enhanced by the larger overlap of the iron t_{2g} orbitals and the antibonding π^* orbitals of bpy or phen. Consequently, the increased back donation from the central iron(II) ion to the antibonding π^* orbitals of the ligands causes the shortening of Fe-N bond length.

In the high-spin state, the isomer shifts observed for [Fe(bpy)(phen)(NCS)$_2$] are slightly smaller than those for [Fe(bpy)$_2$(NCS)$_2$] and [Fe(phen)$_2$(NCS)$_2$] while the quadrupole splittings lie between both complexes. On the other hand, in the low-spin state the isomer shifts of [Fe(bpy)(phen)(NCS)$_2$] are somewhat larger than those of [Fe(bpy)$_2$(NCS)$_2$] and [Fe(phen)$_2$(NCS)$_2$]. This suggests that the back donation from the t_{2g} orbitals of the iron(II) ion to the antibonding π° orbitals of bpy, phen, and thiocyanato ligands is smaller in [Fe(bpy)(phen)(NCS)$_2$] than in [Fe(bpy)$_2$(NCS)$_2$] or [Fe(phen)$_2$(NCS)$_2$].

The Mössbauer parameters of [Fe(bpy)(phen)-(NCS)$_2$] prepared by Method II are shown as a function of temperature in Fig. 4. In the high-spin temperature range the quadrupole splitting increases with decreasing temperature, while in the low-spin temperature range it is almost independent of temperature. The mixed ligand complex [Fe(bpy)-(phen)(NCS)$_2$] prepared by Method I showed a quite similar tendency in the temperature-dependence of its Mössbauer parameters to that prepared by Method II. The temperature variation of the quadrupole splitting in the high-spin temperature range is ascribed to the Boltzmann distribution of 3d electrons among the sublevels in the distorted octahedral ligand field. On the other hand, the isomer shift increases with decreasing temperature both in the high-spin and in the low-spin temperature ranges. This increasing tendency in the isomer shift is due to the so-called second-order Doppler shift. A dramatic change around 180 K in both the isomer shift and the quadrupole splitting demonstrated that the electronic configuration of the central iron(II) ion abruptly changes around this transition temperature. This discontinuous change in Mössbauer parameters is in good accord with the abrupt $^5T_2$(high-spin) $\rightleftarrows$ $^1A_1$ (low-spin) transition observed for the temperature dependence of magnetic moments.

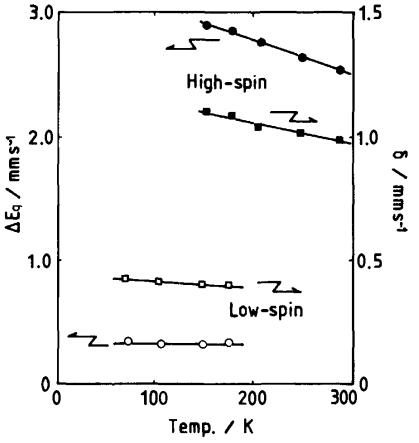

Fig. 4. Temperature dependence of Mössbauer parameters in [Fe(bpy)(phen)(NCS)$_2$] prepared by Method II.

References

1) J. Ensling, J. Fleisch, P. Gütlich, and B. W. Fitzsimmons, *Chem. Phys. Lett.*, **45**, 22 (1977); E. König, G. Ritter, S. K. Kulshreshtha, and S. M. Nelson, *Inorg. Chem.*, **21**, 3022 (1982).

2) H. A. Goodwin, *Coord. Chem. Rev.*, **18**, 293 (1976); J. R. Ferraro, *Coord. Chem. Rev.*, **29**, 1 (1979); P. Gütlich, *Struct. Bonding (Berlin)*, **44**, 83 (1981).

3) E. König, G. Ritter, K. Madeja, and W. H. Böhmer, *Ber. Bunsenges. Phys. Chem.*, **76**, 393 (1972); E. König, G. Ritter, W. Irlert, and B. Kanellakopulos, *J. Phys. C*, **10**, 603 (1977).

4) P. Gütlich, R. Link, and H. G. Steinhäuser, *Inorg. Chem.*, **17**, 2509 (1978); P. Ganguli and P. Gütlich, *J. Phys. (Paris), Colloq.*, **41**, C1-313 (1980); P. Ganguli, P. Gütlich, and W. Müller, *Inorg. Chem.*, **21**, 3429 (1982).

5) E. König and K. Madeja, *Inorg. Chem.*, **6**, 48 (1967); M. Sorai, J. Ensling, K. M. Hasselbach, and P. Gütlich, *Chem. Phys.*, **20**, 197 (1977); E. König, G. Ritter, and K. Madeja, *J. Inorg. Nucl. Chem.*, **43**, 2273 (1981); E. König, G. Ritter, S. K. Kulshreshtha, J. Waigel, and L. Sacconi, *Inorg. Chem.*, **23**, 1241 (1984).

6) P. Gütlich, *J. Phys. (Paris)*, **40**, C2-378 (1979).

7) P. Spacu, M. Teodorescu, and D. Ciomártan, *Rev. Roum. Chim.*, **12**, 145 (1967); P. Spacu, M. Teodorescu, G. Filotti, and P. Telnic, *Z. Anorg. Allg. Chem.*, **392**, 88 (1972).

8) D. J. McIvor and R. J. Magee, *J. Inorg. Nucl. Chem.*, **37**, 2031 (1975).

9) B. N. Figgis and R. S. Nyholm, *J. Chem. Soc.*, **1958**, 4190.

10) E. König and K. Madeja, *Inorg. Chem.*, **6**, 48 (1967).

11) E. König, K. Madeja, and K. J. Watson, *J. Am. Chem. Soc.*, **90**, 1146 (1968).

12) W. A. Baker, Jr. and H. M. Bobnich, *Inorg. Chem.*, **3**, 1184 (1964).

13) P. Gütlich, H. Koppen, R. Link, and H. G. Steinhäuer, *J. Chem. Phys.*, **70**, 3977 (1979).

14) Our efforts to recrystallize the mixed ligand complexes [Fe(bpy)(phen)(NCS)$_2$] obtained by Method I and II were unsuccessful because they are hardly soluble in solvent such as pyridine.

15) M. S. Haddad, W. D. Federer, M. W. Lynch, and D. N. Hendrickson, *Inorg. Chem.*, **20**, 131 (1981); E. Köing, G. Ritter, and S. K. Kulshreshtha, *Inorg. Chem.*, **23**, 1144 (1984).

16) E. Müller, H. Spiering, and P. Gütlich, *Chem. Phys. Lett.*, **93**, 567 (1982); E. König, G. Ritter, S. K.

Kulshreshtha, J. Waigel, and H. A. Goodwin, *Inorg. Chem.*, **23**, 1896 (1984).

17) E. König, G. Ritter, W. Irler, and H. A. Goodwin, *J. Am. Chem. Soc.*, **102**, 4681 (1980).

18) The high-spin fractions of [Fe(bpy)(phen)$(NCS)_2$] prepared by Method I and II are estimated to be ca. 16.9 and 28.8% from their corresponding magnetic susceptibilities at 77 K. In spite of the fairly large amount of high-spin fractions no quadrupole-splitting doublet attributable to residual paramagnetism has been appreciably observed for their Mössbauer spectra at 77 K.

19) E. König and K. J. Watson, *Chem. Phys. Lett.*, **6**, 457 (1970); M. Mikami, M. Konno, and Y. Saito, *Acta Crystallogr., Sect. B*, **36**, 275 (1980).

 © 1986 The Chemical Society of Japan Bull. Chem. Soc. Jpn., 59, 3489—3494 (1986)

Preparation, Characterization, and Some Reactions of Cationic Hydrido-Carboxylato Complexes of Molybdenum(IV), $[MoH_2(O_2CR)(dppe)_2]^+$

Takashi Ito,* Akihiko Takahashi, and Shigeyoshi Tamura
Department of Materials Chemistry, Faculty of Engineering, Yokohama National University, Tokiwadai, Hodogaya-ku, Yokohama 240
(Received May 20, 1986)

Cationic carboxylatodihydridomolybdenum(IV) complexes, $[MoH_2(O_2CR)(dppe)_2]BPh_4$ (R=CH_3, C_2H_5, CH_2=CH, and CH_2=C(CH_3); dppe=$Ph_2PCH_2CH_2PPh_2$), were prepared by treating $[MoH_4(dppe)_2]$ with RCOOH followed by anion exchange with $NaBPh_4$, and characterized spectroscopically. A possible pathway of the reaction is discussed on the basis of the experiment using CH_3COOD. Light irradiation of the EtOH solution of the cationic acetato complex in the presence and absence of CO afforded the known *cis*-$[Mo(CO)_2(dppe)_2]$ and the neutral hydridoacetato complex, $[MoH(O_2CCH_3)(dppe)_2]$, respectively.

Although molybdenum complexes with the carboxylato ligands bridging singly or multiply bonded two metal centers have been extensively studied,[1] only a few well defined mononuclear carboxylato complexes of molybdenum have been reported.[2-7] Furthermore a very limited number of the carboxylato complexes of molybdenum containing tertiary phosphine ligands have been reported, i.e., $[MoH_2(O_2CCF_3)_2(PMePh_2)_3]$,[3] $[MoH(O_2CR)(PMe_3)_4]$ (R=H, CH_3, and CF_3),[6] $[Mo(O_2CCF_3)_2(dppe)_2]$,[2] and the cationic $[Mo(O_2CCF_3)(dppe)_2]BPh_4$.[2] As an extension of our continuing studies on the preparation of group 6a metal complexes possessing functionally substituted ligands,[7,8] reactions of carboxylic acids, including unsaturated carboxylic acids, with tetrahydridomolybdenum(IV) complex, $[MoH_4(dppe)_2]$ (**1**), are investigated in this study. The analogous Mo(IV) complex with unidentate phosphine ligands, $[MoH_4(PMePh_2)_4]$, has been known to be protonated with some protonic acids such as CF_3COOH and *p*-$CH_3C_6H_4SO_3H$ to give products in which some of the phosphine ligands were dissociated.[3] Recently Caulton et al. have shown that the acidolysis of $[MoH_4(PMe_2Ph)_4]$ with HBF_4 in MeCN yielded dicationic $[MoH_2(PMe_2Ph)_4(MeCN)_2]^{2+}$,[9] whereas the similar reaction in THF (tetrahydrofuran) yielded fluorine-bridged dinuclear cation $[\{(PMePh_2)_3H_2Mo\}_2(\mu\text{-}F)_3]^+$.[10] Here we found that **1** was easily protonated with carboxylic acid RCOOH to give carboxylatodihydridomolybdenum cation of the type $[MoH_2(O_2CR)(dppe)_2]^+$ and H_2.

Results and Discussion

Preparation of the Complexes. On stirring the mixture of yellow crystals of $[MoH_4(dppe)_2]$ (**1**) and acetic acid in vacuo at room temperature for several hours, a purple homogeneous solution resulted with accompanying release of two molar equivalents of H_2. Evaporating the solvent off from the solution left deep purple oil, which was solidified into red powder (**2a**) by triturating it in hexane. The product **2a** turned purple powder on treatment it with $NaBPh_4$ in ethanol and vermilion needles (**3a**) were obtained by recrystallization of the purple powder from acetone. The products **2a** and **3a** were characterized as $[MoH_2(O_2CCH_3)(dppe)_2]CH_3CO_2$ and its anion-exchanged compound, $[MoH_2(O_2CCH_3)(dppe)_2]BPh_4 \cdot 0.5(CH_3)_2CO$, respectively, on the basis of analytical (for **3a**) and spectral evidence (vide infra). The analogous carboxylatodihydridomolybdenum cations, $[MoH_2(O_2CR)(dppe)_2]A$ [A=RCO_2 (**2**) and BPh_4 (**3**)], were obtained similarly for propionic, acrylic, and methacrylic acids (Table 1).

$$\underset{(\mathbf{1})}{[MoH_4(dppe)_2]} + 2RCOOH \longrightarrow \underset{(\mathbf{2})}{[MoH_2(O_2CR)(dppe)_2]RCO_2} + 2H_2 \quad (1)$$

Table 1. Reactions of $[MoH_4(dppe)_2]$ (**1**) with Carboxylic Acids, RCOOH.[a]
$[MoH_4(dppe)_2]$ (**1**) + 2RCOOH ⟶ $[MoH_2(O_2CR)(dppe)_2]RCOO$ (**2**) + $2H_2$
$[MoH_2(O_2CR)(dppe)_2]RCOO$ (**2**) + $NaBPh_4$ ⟶ $[MoH_2(O_2CR)(dppe)_2]BPh_4$ (**3**) + RCOONa

RCOOH			**1**	Time	$NaBPh_4$	Products (mol/mol of **1**)		
	R	ml	mmol	h	mmol	H_2	**2**[b]	**3**
(**a**)	CH_3	20	1.62	3	3.63	1.89	0.85[c]	0.72
(**b**)	CH_3CH_2	20	0.65	20	0.85	1.69	0.82	0.38
(**c**)	CH_2=CH	10	0.86	4	1.41	1.95	d)	0.76
(**d**)	CH_2=C(CH_3)	10	1.05	120	1.53	1.83	d)	0.73

a) At room temperature. b) Crude yield. c) Yield estimated in a separate run. d) Not measured.

$$\mathbf{2} + NaBPh_4 \xrightarrow{EtOH} [MoH_2(O_2CR)(dppe)_2]BPh_4\ (\mathbf{3}) + RCOONa \quad (2)$$

R = CH_3(**a**), CH_2CH_3(**b**), CH_2=CH(**c**), CH_2=C(CH_3)(**d**)

Since purification of the carboxylate derivatives **2** is usually more difficult as compared with that of **3** due to their poor tendencies to be crystallized, their characterizations were achieved mainly spectroscopically, although the latter have been fully analyzed as shown in Table 2. Considerable low values of the observed molecular weight in acetone as compared with the calculated values and the conductivity measurements of their acetone solution (Λ, these values are compared with the observed value of 92.5 S cm^2 mol^{-1} for $NaBPh_4$ under similar conditions) as shown in Table 2 strongly support their proposed ionic formulation.

In order to obtain some mechanistic information of the reaction (1), the similar reaction of **1** with acetic acid-*d* was examined and the formation of dideuteride analogue of **2a** with the accompanying evolution of H_2 and D_2 (molar ratio of 1.0/4.2, total amount 2.1 mol/mol of **1**) was observed. The mechanistic aspect will be discussed in the later section.

$$[MoH_4(dppe)_2]\ (\mathbf{1}) + 2CH_3COOD \longrightarrow [MoD_2(O_2CCH_3)(dppe)_2]CH_3CO_2\ (\mathbf{2a}\text{-}d_2) + 0.4H_2 + 1.7D_2 \quad (3)$$

Identification of the dideuteride **2a**-d_2 was achieved by confirming the disappearance of the Mo–H signals in the ^{1}H NMR spectrum of the isolated tetraphenylborate derivative, $[MoD_2(O_2CCH_3)(dppe)_2]BPh_4$ (**3a**-d_2), in $CDCl_3$. Furthermore, the absence of an H–D exchange process between the cationic acetatodihydrido complex **2a** and acetic acid-*d* was suggested by confirming that there was no difference in the ^{1}H NMR spectra taken in $CDCl_3$ before and after treatment of **2a** with excess CH_3COOD at room temperature for 3 days.

IR Spectra of the Complexes. Carboxylatodihydridomolybdenum cations **2** showed weak Mo–H stretching absorption bands at around 1880 cm^{-1}. In addition, moderately strong absorptions at around 1460 cm^{-1} and fairly weak ones at around 1380 cm^{-1} were observed, which were assigned to asymmetric and symmetric CO_2 stretchings, respectively, of the coordinated carboxylato ligand.[11] The relatively low

Table 2. Analytical Data for Complexes $[MoH_2(O_2CR)(dppe)_2]BPh_4 \cdot n(CH_3)_2CO$ (**3**)

	R	n	Analysis[a] C/%	Analysis[a] H/%	mol wt[a,b]	Conductivity, Λ[c] S cm^2 mol^{-1}
(**3a**)	CH_3–	0.5	73.1 (73.6)	6.0 (5.8)	900 (1273)	102
(**3b**)	CH_3CH_2–	1.0	72.8 (73.2)	6.1 (6.1)	d)	d)
(**3c**)	CH_2=CH–	0.5	73.1 (73.6)	6.0 (5.8)	816 (1314)	78
(**3d**)	CH_2=C(CH_3)–	0.5	73.4 (73.7)	6.0 (5.9)	867 (1328)	79

a) Calculated values are given in parentheses. b) Measured by vapor pressure osmometry in acetone at 25 °C. c) Measured in acetone at 18 °C. d) Not measured.

Table 3. Selected IR and ^{1}H NMR Data for Complexes $[MoH_2(O_2CR)(dppe)_2]BPh_4$ (**3**)

Complex		IR[a]			^{1}H NMR[b]	
	R	ν(Mo-H)	$\nu(OCO)_a$	$\nu(OCO)_s$	δ(Mo-H)[c]	δ(RCOO)[d]
(**3a**)	Me	1880 w, br	1470 m	1410 w	−4.08 (pq, 40.5, **2**)	0.03 (t, [1.4], **3**, CH_3)
(**3b**)	$MeCH_2$	1880 w, br	1475 s	1375 w	−4.04 (pq, 43.0, **2**)	0.01 (t, 6.15, **3**, CH_3), 0.20 (m, **2**, CH_2)
(**3c**)	CH_2=CH	1880 w, br	1455 m	1370 w	−3.94 (pq, 40.5, **2**)	ca. 4.8 (m, **3**, CH_2=CH)
(**3d**)	CH_2=CMe	1885 w, br	1455 m	1370 w	−3.84 (pq, 40.5, **2**)	0.78 (s, **3**, CH_3), 4.59 (s, **1**, =CH_2), 4.85 (s, **1**, =CH_2)

a) Measured as KBr disk; values in cm^{-1}. b) 90 MHz in $CDCl_3$. Given as chemical shift δ in ppm, downfield positive from tetramethylsilane as an internal reference. Signals due to dppe ligand, BPh_4 anion and solvated acetone are omitted for brevity. Multiplicity abbreviations are: pq = pseudo quintet, t = triplet, m = multiplet. c) In parentheses are multiplicity, ^2J(P-H) in Hz, and **relative intensity**. d) In parentheses are multiplicity, J(H-H), [J(P-H)] in Hz, **relative intensity**, and assignment where necessary.

values of the separation between these two ν(OCO) bands (60—100 cm^{-1}) suggest that the carboxylato ligands in these complexes coordinate to the metal bidentately.[11,12]

NMR Spectra of the Complexes. As shown in Table 3 and Fig. 1, ^1H NMR spectra of carboxylato complexes **3** showed a characteristic pseudo quintet signal [apparent J(PH)=ca. 40 Hz] assignable to hydride protons at around δ −4, which is not so much different from the parent neutral tetrahydride **1** [δ(Mo–H)=−3.64 in chlorobenzene].[13] The pseudo quintet pattern of the signal may be analyzed as $A_2M_2X_2$ spin system where A_2 are hydride protons, and M_2 and X_2 are pairs of two equivalent phosphorus atoms. The deviation of the signal pattern from the typical 1:4:6:4:1 quintet suggests that the values of J(AX) and J(AM) differ slightly each other. Methyl protons of the acetato ligand in **3a** resonated at δ 0.03 as a triplet which was higher than the corresponding free acetic acid by δ 2.1.[14] The similar trends were observed for the protons attached to α-carbon of the propionato ligand of the complex **3b** in accordance with the reported results for hydridocarboxylato complexes of ruthenium.[15] Measurement of the phosphorus-decoupled ^1H NMR for complexes **3a** and **3b** revealed that both the pseudo quintet signals of Mo–H and the triplet signals of the protons attached to the α-carbon changed to singlets (Fig. 1), indicating that these splittings originated from the coordinated phosphines.

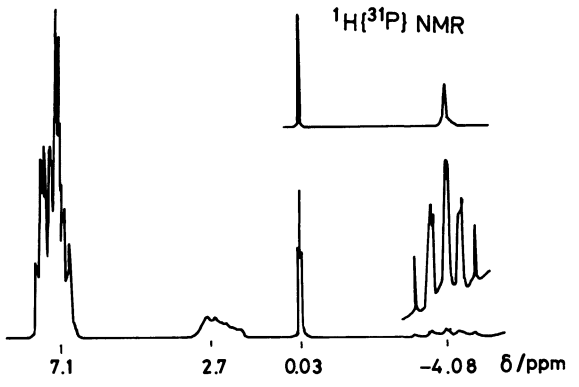

Fig. 1. ^1H NMR spectra of $[MoH_2(O_2CCH_3)(dppe)_2]BPh_4$ (**3a**), (100 MHz in $CDCl_3$ at room temperature).

In the ^{13}C NMR spectra of complexes **3**, carbonyl carbon of the carboxylato ligand resonated at δ 181—191 (Table 4). The signals due to carboxylato ligands were observed at the reasonable positions as judged from their corresponding ^1H NMR signals.

$^{31}P\{^1H\}$ NMR spectra of the complexes **3a—d** (Table 4) consisted of double triplets appearing at about δ 81 and 61, respectively, downfield from the external PPh_3 reference, which suggests that there are two pairs of magnetically unequivalent phosphorus nuclei, each consisting of two equivalent phosphori. The ^{31}P NMR spectra did not show any change at the temperature range from 20 to 70 °C.

Structure of the Complexes. On the basis of the spectral evidences described above, the bicapped octahedral structure, either I or II, seems to be most conceivable for the present octacoordinate cationic complexes **3**, although a square antiprism and a dodecahedron arrangements have been known to occur most commonly in the octacoordinate complexes.[16] The $A_2M_2X_2$ pattern of the hydride signal of the ^1H NMR spectra is elucidated by assigning A to the hydrides, M to the equatorial phosphori P_2 and P_3, and X to the axial P_1 and P_4, respectively. Of the two triplets of ^{31}P NMR signals, the signals at 61 ppm may be assigned to the mutual trans axial phosphorus atoms P_1 and P_4, and those at 81 ppm to equatorial P_2 and P_3.[15b] Of the two possible structures, structure I in which two hydride caps are directed toward the side occupied with phosphine ligands seems to be more preferable to II in view of the steric congestion around the hydrogen atoms. The pentagonal bipyramidal structure has been determined recently for the related

Table 4. $^{13}C\{^1H\}$ and $^{31}P\{^1H\}$ NMR Data for $[MoH_2(O_2CR)(dppe)_2]BPh_4$ (**3**)

Complex	^{13}C NMR[a]			^{31}P NMR[b]		
R	MoO_2C	α-C	β-C	P_E	P_A	J(P-P)/Hz[c]
(**3a**) Me	188.73	23.35		80.88	61.61	5.86
(**3b**) $MeCH_2$	191.54	29.88	6.74	81.12	61.24	6.35, 6.31
(**3c**) CH_2=CH	181.02	d)	d)	81.24	61.81	5.86
(**3d**) CH_2=CMe	182.24	d) 15.08 (α-*Me*)	d)	81.08	61.45	5.86

a) 22.5 MHz in $CDCl_3$. Given as chemical shift δ in ppm, downfield positive from tetramethylsilane as an internal reference. Signals due to dppe ligand, BPh_4 anion and solvated acetone which appeared at the ordinary region are omitted for brevity. All signals listed appeared as a singlet unless stated otherwise. b) 36.2 MHz in $CDCl_3$. Given as chemical shift δ in ppm, downfield positive from triphenylphosphine in CH_2Cl_2/C_6D_6 as an external reference. All signals are observed as triplet. c) For those there are two figures each of which corresponds to P_E and P_A respectively, and these differences may be originated from the second order couplings between various phosphori. d) Obscured due to overlapping with dppe and BPh_4 signals.

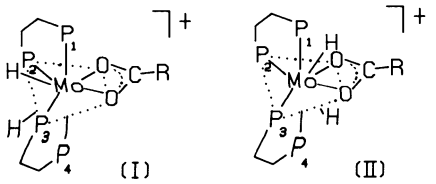

(I) (II)

neutral, seven-coordinate, hydridocarboxylatomolybdenum complex in which the hydride ligand resides in a pentagonal plane flanked with two equatorial phosphorus nuclei.[6]

Properties and Some Reactions of the Complexes. Carboxylatodihydridomolybdenum(IV) complexes **2** and **3** are moderately stable to air in the solid state and even in the solution in the dark. Furthermore, they are thermally stable: The solid acetato complex **3a** was found to be stable in vacuo up to 150 °C. The complexes bearing carboxylate anions **2** were soluble in chloroform, dichloromethane, ethanol, and acetone and slightly soluble in benzene and toluene, whereas those with BPh_4 anions **3** were soluble only in acetone and the halogenated solvents. When the solution of **3a** in $CHCl_3$ was heated at 60 °C for 2 h in the dark, 14% of CH_2Cl_2 on the basis of **3a** was formed. Subsequently, by allowing the resulting solution to leave under the exposure of the sunlight for 10 days, the formation of CH_2Cl_2 in 85% yield was observed. These results suggest that the cation which is thermally stable is easily activated by the light irradiation.

$$\mathbf{3a} + CHCl_3 \xrightarrow{h\nu} CH_2Cl_2 + \text{yellow complex} \quad (4)$$

Although complexes **2a** and **3a** were found to be inert to CO, alkenes (e.g. 1-heptene), alcohols (e.g. 2-propanol), and phenol even heating at 60 °C, complex **2a** released one mole of acetic acid on irradiation in ethanol with high pressure mercury lamp for 5 h to yield the neutral monohydrido acetato complex **4a** (21%).[17]

$$\mathbf{2a} \xrightarrow{h\nu,\,EtOH} [MoH(O_2CCH_3)(dppe)_2] + CH_3COOH \quad (5)$$
$$(\mathbf{4a})$$

The reaction was accompanied by the side reaction to form H_2 in 70% yield and acetaldehyde (32%) together with the orange complex which was tentatively assigned to $[Mo(O_2CCH_3)_2(dppe)_2]$ (12%) on the basis of its IR spectrum (see Experimental).

$$\mathbf{2a} + CH_3CH_2OH \xrightarrow{h\nu} [Mo(O_2CCH_3)_2(dppe)_2] + CH_3CHO + 2H_2 \quad (6)$$

The mechanism of the oxidation of ethanol to aldehyde with **2a** is not clear at the present stage.

Under the Hg-lamp irradiation, **2a** reacted with 1 atm of CO in EtOH to yield, after 37 h, a small amount of the known dicarbonylmolybdenum complex together with the uncharacterized carbonyl complexes.

$$\mathbf{2a} + CO \xrightarrow{h\nu,\,EtOH} cis\text{-}[Mo(CO)_2(dppe)_2] + \text{Mo-carbonyls} \quad (7)$$

Finally, the carboxylato ligands of the cationic carboxylatodihydrido complexes **3** were found to be thermally labile in the presence of carboxylic acid to exhibit ligand exchange. Thus, by heating the acetato complex **3a** in acetone in the presence of excess methacrylic acid at 60 °C for 7 h, the methacrylato complex **3d** was obtained in a quantitative yield as is judged from the ^1H NMR spectrum of the isolated compound. The formation of equimolar amount of acetic acid in this reaction was confirmed by the GLC measurement. Conversely, complex **3d** was converted into acetato complex **3a** by stirring **2d** in acetone at 60 °C for 17 h in the presence of acetic acid.

$$[MoH_2(O_2CCH_3)(dppe)_2]^+ + CH_2{=}C(Me)COOH \rightleftharpoons [MoH_2(O_2CC(Me){=}CH_2)(dppe)_2]^+ + CH_3COOH \quad (8)$$
$$(\mathbf{3a}) \qquad\qquad (\mathbf{3d})$$

Discussion as to the Formation of the Cation $[MoH_2(O_2CR)(dppe)_2]^+$ (2). The first stage of the reaction between tetrahydrido complex **1** and carboxylic acid RCOOH to form carboxylatodihydrido cation **2** may be the protonation of **1** to give intermediate pentahydrido cation (**A**) (Scheme). Although this intermediate species was not able to be observed in the present system, the corresponding tungsten pentahydride has been prepared by the reaction between $[WH_4(PMePh_2)_4]$ and trifluoroacetic acid.[3] The selective evolution of D_2 gas when **1** was allowed to react with CH_3COOD [equation (3)] suggests that the equilibrium between **1** and the protonated molybdenum cation (**A**) as shown in the Scheme may be attained rapidly followed by a fairly slow reductive elimination of D_2. This process may be accompanied by the transfer of the acetate anion from the outer sphere to the inner sphere to yield the neutral 18-electron intermediate species (**B**).

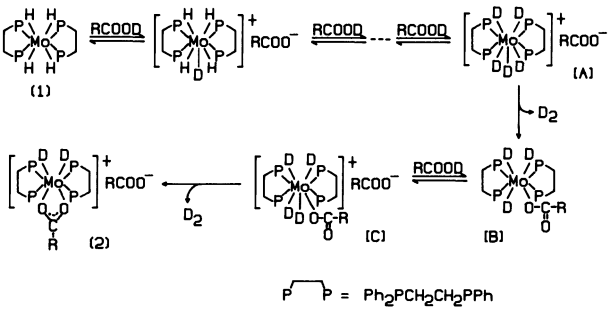

P⌒P = $Ph_2PCH_2CH_2PPh$

Scheme

The trideuterido intermediate possessing the unidentately coordinated acetato ligand (**B**) may be protonated by another mole of acetic acid to give the cationic intermediate (**C**), which releases D_2 with the concomitant transfer of the acetato ligand from the unidentate to the bidentate fashion to attain 18-electrons of the metal center in the final product **2a**. The alternative path from (**B**) to **2a** which involves intermediary formation of monohydride **4a** by reductive elimination of H_2 from (**B**) was ruled out since **4a** was found to be inert to RCOOH.[17] The evolution of a small amount of H_2 in the reaction of **1** with CH_3COOD suggests that there exists, in addition to that shown in the Scheme, a minor process where H_2 is released prior to the deuteriation of **1** leading to (**A**). The dihydridomolybdenum(II) intermediate thus formed may be rapidly converted into (**B**) by reversible protonation with RCOOD as is judged from the absence of an HD component in the evolved gas.

Experimental

Most manipulations were carried out either under dry, oxygen-free nitrogen or argon or in vacuo with Schlenk-type flasks. Solvents were dried, purified in the usual manner, and stored under an atmosphere of argon. Commercial carboxylic acids were degassed and introduced into the reaction flask by a trap to trap method in order to avoid contamination with oxygen and moisture.

Infrared spectra were recorded on a JASCO A-202 spectrometer using KBr disks prepared under an inert atmosphere. Nuclear magnetic resonance spectra were measured on JEOL JNM-PMX-60 (^1H, 60 MHz) and JNM-FX-90Q (^1H, 90 MHz; ^{13}C, 22.5 MHz; ^{31}P, 36.2 MHz) spectrometers. $^1H\{^{31}P\}$ NMR spectra were recorded on a JEOL JNM-FX-100 (100 MHz) spectrometer. The molecular weight was measured in acetone at 25 °C using Mechrolab Vapor Pressure Osmometer Model 302. The electric conductivity of the complex solution was measured in acetone at 18 °C with TOA CM-5B conductivity meter. The organic products formed in the reactions were quantitatively analyzed by GLC using internal standard. GLC was recorded on a Shimadzu GC-7APTF or GC-3BT gas chromatography using PEG-20M, SDC-410, and/or SDC-550 columns and helium as carrier gas. Non-condensable gas evolved through the reaction was measured by a Toepler pump and analyzed by a mass spectrometer (Hitachi Model M-80) and GLC using Molecular Sieve 5A column. $[MoH_4(dppe)_2]$ (**1**) was prepared as previously reported.[18] Acetic acid-*d* was prepared from acetic anhydride and D_2O.

Preparation of Acetatodihydridobis[1,2-bis(diphenylphosphino)ethane]molybdenum(IV) Tetraphenylborate (3a). To $[MoH_4(dppe)_2]$ (**1**) (1.45 g, 1.62 mmol) was added 20 ml of acetic acid by means of a trap-to-trap method. The mixture was stirred in vacuo at room temperature for 3 h to give a purple solution. Evolution of H_2 (3.06 mmol) by the reaction was observed in the flask. Unreacted acetic acid was evaporated off from the solution in vacuo to leave a deep purple sticky solid which was dissolved in 75 ml of EtOH, and the solution was filtered. To the red filtrate was added 1.24 g (3.63 mmol) of $NaBPh_4$ to give purple precipitate, which was filtered and washed with EtOH. Recrystallization of the purple product from acetone afforded vermilion needles of $[MoH_2(O_2CCH_3)(dppe)_2]BPh_4\cdot\frac{1}{2}(CH_3)_2CO$ (**3a**) (1.41 g, 72%). Analytical results for **3a** are listed in Table 2. Inclusion of half mole of acetone as crystallization solvent in **3a** was also confirmed by the intensity measurement of its ^1H NMR spectrum.

In a separate experiment which aimed at the isolation of acetatodihydridobis[1,2-bis(diphenylphosphino)ethane]molybdenum(IV) acetate (**2a**), 1.13 g (1.26 mmol) of $[MoH_4(dppe)_2]$ (**1**) was allowed to react with 16 ml of acetic acid at room temperature under argon for 1 h to give a purple solution. After excess acetic acid being evaporated off from the solution, the resulting sticky solid was triturated in hexane at −50 °C or in Et_2O at room temperature to give red precipitate, which was filtered off, washed well with Et_2O and dried in vacuo to give red powder of $[MoH_2(O_2CCH_3)(dppe)_2]CH_3CO_2$ (**2a**) [ν(MoH)=1890 w, br; ν(OCO) of $CH_3CO_2^-$=1710 s; $\nu(OCO)_{asym}$=1465 m; $\nu(OCO)_{sym}$=1407 w cm^{-1}] (1.09 g, 85%).

The other carboxylato complexes **2** and **3** were obtained similarly. Reaction conditions of each synthesis are listed in Table 1. Complexes **3** were found to contain half (**3c** and **3d**) or one equivalent (**3b**) of acetone as crystallization solvent as is judged from their elemental analyses and ^1H NMR spectra (see Table 2).

Photodegradation of 2a. $[MoH_2(O_2CCH_3)(dppe)_2]CH_3CO_2$ (**2a**) (0.500 g, 0.494 mmol) in 120 ml of EtOH was irradiated with 100 W high pressure mercury lamp at room temperature under N_2 for 5 h to cause the color change of the solution from purple to brown. Evolution of 0.3 mmol (70%) of H_2 in the vapor phase was detected by the GLC analysis. A volatile component, in which acetic acid (0.31 mmol, 63%) and acetaldehyde (0.16 mmol, 32%) were observed to present by its GLC analysis, was removed in vacuo to leave brown powder, which was fractionally crystallized from Et_2O to give orange crystals of $[MoH(O_2CCH_3)(dppe)_2]$[17] (**4a**) (0.101 g, yield 21.4%) and yellow powder. The latter was tentatively assigned to $[Mo(O_2CCH_3)_2(dppe)_2]$ [$\nu(CO_2)$=1618 s, 1580 w, 1360 m, and 1297 vs cm^{-1}] (0.061 g, 12%).

Authors are indebted to Drs. F. Ozawa and Y. Nakamura of Tokyo Institute of Technology for the measurement of mass and $^1H\{^{31}P\}$ NMR spectroscopy, respectively, and to Mr. T. Saito of the same Institute for elemental analyses. They also acknowledge to Dr. H. Suezawa of Yokohama National University for the NMR measurement with an FX-90Q instrument.

References

1) See for example: F. A. Cotton and J. G. Norman, Jr., *J. Coord. Chem.*, **1**, 161 (1971); J. S. Flippo, Jr. and H. J. Sniadoch, *Inorg. Chem.*, **15**, 2209 (1976); M. L. H. Green, G. Parkin, J. Bashkin, J. Fail, and K. Prout, *J. Chem. Soc., Dalton Trans.*, **1982**, 2519; J. D. Arenivar, V. V. Mainz, H. Ruben, R. A. Andersen, and A. Zalkin, *Inorg. Chem.*, **7**, 2649 (1982); G. S. Girolami, V. V. Mainz, and R. A. Andersen, *J. Am. Chem. Soc.*, **104**, 2041 (1982); P. Agaskar and F. A.

Cotton, *Inorg. Chim. Acta*, **83**, 33 (1984).
2) T. Ito and A. Yamamoto, *J. Chem. Soc., Dalton Trans.*, **1975**, 1398.
3) E. Carmona-Guzman and G. Wilkinson, *J. Chem. Soc., Dalton Trans.*, **1977**, 1716.
4) F. A. Cotton, D. J. Darensbourg, and B. W. S. Kolthammer, *J. Am. Chem. Soc.*, **103**, 398 (1981).
5) B. J. Brisdon and A. Day, *J. Organomet. Chem.*, **3**, 279 (1981).
6) D. Lyons, G. Wilkinson, M. Thornton-Pett, and M. B. Hursthouse, *J. Chem. Soc., Dalton Trans.*, **1984**, 695.
7) T. Ito and T. Nakano, *J. Chem. Soc., Chem. Commun.*, **1984**, 98, and references cited therein.
8) T. Ito, H. Tosaka, S. Yoshida, K. Mita, and A. Yamamoto, *Organometallics*, **5**, 735 (1986).
9) L. F. Rhodes, J. D. Zubkowski, K. Folting, J. C. Huffman, and K. G. Caulton, *Inorg. Chem.*, **21**, 4185 (1982).
10) R. H. Crabtree, G. G. Hlatky, and E. M. Holt, *J. Am. Chem. Soc.*, **105**, 7302 (1983).
11) K. Nakamoto, "Infrared and Raman Spectra of Inorganic and Coordination Compounds," 3rd ed, John Wiley & Sons, Inc., New York (1978), p. 232.
12) S. D. Robinson and M. F. Uttley, *J. Chem. Soc., A*, **1973**, 1972.
13) P. Meakin, L. J. Guggenberber, W. G. Peet, E. L. Muetterties, and J. P. Jesson, *J. Am. Chem. Soc.*, **95**, 1467 (1973).
14) C. J. Pouchert, "The Aldrich Library of NMR Spectra," 2nd ed, Aldrich Chemical Company, Inc., Milwaukee (1975).
15) See for example: a) D. Rose, J. D. Gilbert, R. P. Richardson, and G. Wilkinson, *J. Chem. Soc., A*, **1969**, 2610; b) R. J. Young and G. Wilkinson, *J. Chem. Soc., Dalton Trans.*, **1976**, 719.
16) F. A. Cotton and G. Wilkinson, "Advanced Inorganic Chemistry," 4th ed, John Wiley & Sons, New York (1980), p. 53.
17) Recently we prepared this type of neutral carboxylatomonohydrido complexes, $[MoH(O_2CR)(dppe)_2]$, via different photochemical routes, which, together with their characterization, will be reported in detail elsewhere.
18) F. Pennela, *Inorg. Synth.*, **15**, 42 (1974).

 © 1986 The Chemical Society of Japan Bull. Chem. Soc. Jpn., 59, 3495—3499 (1986)

Synthesis, and Crystal and Molecular Structure of Bis(*N*-methylformamide)tetrakis(thiocyanato)cobalt(II)mercury(II), $CoHg(SCN)_4(HCONHCH_3)_2$

Hisashi KINOSHITA* and Akira OUCHI†
Department of Chemistry, Faculty of Liberal Arts, Shizuoka University, Ohya, Shizuoka 422
†Department of Chemistry, College of Arts and Sciences, The University of Tokyo, Komaba, Meguro-ku, Tokyo 153
(Received May 28, 1986)

The title complex was synthesized and its crystal and molecular structures were determined by the single-crystal X-ray diffraction technique. The crystal is orthorhombic with a space group $P2_1nb$, a=14.953(4), b=15.955(4), c=7.6838(9) Å. The structure was solved by means of the heavy-atom method and the final R value was 0.059. The mercury atom is in the tetrahedral geometry, coordinated with four sulfur atoms of the thiocyanate (SCN) ions, and the cobalt atom is in the octahedral geometry, coordinated with four nitrogen atoms of SCN ion and two oxygen atoms of *N*-methylformamide which occupy the *cis* positions. Each pair of different kinds of metal atoms is bridged by an SCN ion and are in a three-dimensional network. Twenty-four membered rings of $Co_3Hg_3(SCN)_6$, where the metal atoms are arranged hexagonally in a chair-form, are condensed two-dimensionally approximately parallel to the (1 0 0) plane. All mercury atoms on one plane are bridged by SCN ions to the cobalt atoms of the polymeric plane next to the [1 0 0] direction, while the cobalt atoms are linked by SCN ions to the mercury atoms on the next plane of the opposite side. The mfa ligands take their positions in the vacancy of the network.

The cobalt(II) mercury(II) thiocyanate (**1**) was found to have a diamond-like three-dimensional polymeric structure,[1] where both kinds of the metal atoms are in the tetrahedral geometry, and each pair of the different kind of metal atoms are bridged by one thiocyanate (SCN) ion. In **1**, a twenty-four membered ring containing three mercury and three cobalt atoms and six thiocyanate ions is formed as the unit where the six metal atoms are in a chair-form hexagonal arrangement. The units are condensed and linked three-dimensionally in a crystal comprising a diamond-like structure.

The pyridine (py) and *N*,*N*-dimethylformamide (dmf) adducts of **1**, $CoHg(SCN)_4py_2$ (**2**),[2] and $CoHg(SCN)_4dmf_2$ (**3**),[3] were obtained and their structures were elucidated; they are in the respective characteristic three-dimensional polymeric structures. Since the types of the networks of **1**, **2**, and **3** are different from each other, it is expected that if another kind of the Lewis-base adduct of **1** is obtained, it may have a different type of the three-dimensional network structure. Previously, the present authors studied and determined the crystal structures of some adducts of **1**.[4-6] Among them, relatively bulky amide molecules, such as *N*,*N*-dimethylacetamide (dma)[5] and *N*-methyl-2-pyrrolidone (mpd),[6] were shown to form a kind of inclusion compound of the type $CoHg(SCN)_4(H_2O)_2\cdot 2L$ (where L=dma or mpd).

Along this line of research, the title complex has been synthesized, where the added Lewis base, *N*-methylformamide (mfa) is smaller in size than dma or mpd (and even py or dmf). Its crystal and molecular structure has been determined by the X-ray diffraction method using its single-crystal.

Experimental

Synthesis of Bis(*N*-methylformamide)tetrakis(thiocyanato)-cobalt(II)mercury(II) (4). A crystalline powder of **1** (1.0 g, 2.0 mmol) was dissolved into mfa (20 cm^3), and 3 cm^3 of water was added to the solution. It was left standing for several days and crystals of **4** were deposited. The red-violet crystals were filtered off and dried over silica-gel. Yield: 0.65 g, 54%. Found: Co, 9.63; C, 15.45; H, 1.57; N, 14.00%. Calcd for $CoHgC_8N_6O_2S_4$: Co, 9.66; C, 15.75; H, 1.65; N, 13.78%.

Intensity-Data Collection. A crystal shaped into a sphere[a] (ϕ=0.21 mm) was used for the intensity data measurement. Crystallographic data are: $CoHgC_8H_{10}N_6O_2S_4$ F.W.=609.99, orthorhombic, with the space group of $P2_1nb$, a=14.953(4), b=15.955(4), c=7.6838(9) Å, U=1833.2(7) Å^3, Z=4, D_m=2.21(3) Mg m^{-3}, D_x=2.21 Mg m^{-3}, μ(Mo $K\alpha$)=9.94 mm^{-1}. Reflections within a range of $3°<2\theta<60°$ were collected on a Rigaku AFC-6A automated four-circle X-ray diffractometer with graphite-monochromated Mo $K\alpha$ radiation. The ω—2θ scan technique was employed (scan speed, 4° min^{-1} in 2θ; scan width, 1.12+0.5tanθ°(θ)). Of the 3072 independent reflections measured, 1707 $|F_o|>3\sigma(|F_o|)$ reflections were used for the structure determinaion. The intensities were corrected for Lorentz and polarization factors as well as for absorption. The latter correction was made using a numerical Gaussian integration.[7]

Structure Determination. The structure was solved by the heavy atom method. The positions of the mercury and cobalt atoms were deduced from a three-dimensional Patterson map, while the other non-hydrogen atoms were located by means of succesive Fourier syntheses. Their positional and thermal parameters (first isotropic and finally anisotropic) were refined by a block-diagonal least-squares method.

a) The crystal was shaped by rolling it on the fine particle sand-paper while pressing very weakly.

During the final refinement step, the shift of the all the parameters was less than $\sigma/3$'s. At the step, two spots remained at positions about 2.1 Å from the mercury atom on the differential synthesis map. A calculation of the structure analysis was repeated using new intensity data obtained from another crystal, but the spot remained, although the intensity of the both spots were about 3 electrons Å^{-3}. As these spots were about 2.1 Å from the thiocyanate nitrogen atoms, their positions were too near to be thought of as those of the coordinated water oxygen atoms. Actually, the infrared spectra of the complex, as well as the element analysis did not show the existence of water in the crystal. The adopted space group was also found to be the correct one from Weissenberg and oscillation photographs. Therefore, the spots are now thought to be due to a termination effect owing to the large mercury atom; such a phenomenon was sometimes found around a heavy atom. The final R value obtained by applying anisotropic temperature parameters was 0.059.[8] As the R value for structure with an inversed chirality was 0.064, the structure was not adopted.

All calculations were carried out on a HITAC M-280H computer apparatus at the Computer Center of the University of Tokyo using a local version of the UNICS program system.[9] The atomic scattering factors were taken from Ref. 10.

Other Measurement. The magnetic moment of the solid sample was measured at 20 °C using a Gouy balance.

Table 1. Final Atomic Coordinates ($\times 10^3$) and Equivalent Isotropic Temperature Factors (B_{eq}/Å^2), with Estimated Standard Deviations in Parentheses

Atom	x	y	z	B_{eq}/Å^2 a)
Hg	500.0	435.4(1)	548.3(1)	3.27
Co	306.6(2)	127.9(2)	477.7(3)	2.31
S(1)	332.0(4)	440.4(4)	528.0(9)	3.82
S(2)	550.3(5)	302.8(4)	701.3(11)	4.64
S(3)	568.4(4)	548.7(4)	749.4(9)	3.49
S(4)	554.5(5)	458.5(5)	239.5(10)	4.93
N(1)	304.6(13)	552.3(11)	797(2)	2.96
N(2)	407.6(14)	205.6(11)	587(3)	3.19
N(3)	708.0(13)	447.0(13)	859(3)	3.74
N(4)	405.1(11)	552.6(12)	130(3)	3.12
C(1)	316.1(15)	507.1(13)	690(3)	2.51
C(2)	463.8(15)	244.0(12)	630(3)	2.82
C(3)	651.3(15)	488.4(13)	814(3)	2.66
C(4)	464.2(14)	515.8(13)	174(3)	2.40
O(11)	212.3(11)	206.0(11)	595(2)	3.67
O(21)	308.1(13)	210.5(9)	260.3(19)	3.34
N(11)	120.2(15)	317.8(11)	613(3)	3.98
N(21)	303(2)	242.7(19)	−30(3)	6.07
C(11)	185.9(17)	273.3(14)	541(4)	3.42
C(12)	74(3)	296(2)	760(6)	9.73
C(21)	299(2)	184.5(16)	104(3)	5.22
C(22)	317(4)	328(2)	5(5)	7.82

a) The isotropic temperature factors were computed using the following expressions: $B_{eq}=4/3(B_{11}a^2+B_{22}b^2+B_{33}c^2)$. The B_{ij}'s are defined by: $T=\exp[-(h^2B_{11}+k^2B_{22}+l^2B_{33}+2hlB_{13}+2hkB_{12}+2klB_{23})]$.

Results and Discussion

The final atomic parameters of the non-hydrogen atoms are listed in Table 1, while the selected bond-lengths, bond-angles, and some interatomic distances are shown in Table 2.[11] Perspective drawings of the complex around the mercury and the cobalt atoms are given in Figs. 1 and 2, together with the numbering

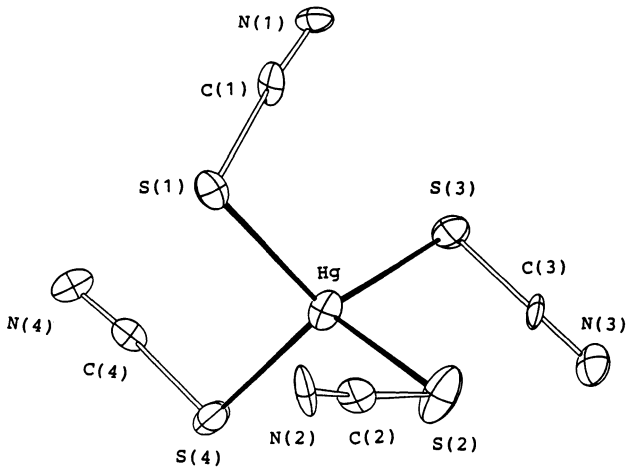

Fig. 1. The perspective drawing of the complex around a mercury atom.

Table 2. Selected Bond Lengths and Bond Angles with Estimated Standard Deviations in Parentheses

Bond length	l/Å	Bond length	l/Å
Hg-S(1)	2.518(6)	Hg-S(2)	2.535(7)
Hg-S(3)	2.588(7)	Hg-S(4)	2.537(9)
Co-N(1^{i})	2.113(19)	Co-N(2)	2.13(2)
Co-N(3^{ii})	2.11(2)	Co-N(4^{iii})	2.073(19)
Co-O(11)	2.087(17)	Co-O(21)	2.128(16)
S(1)-C(1)	1.66(2)	C(1)-N(1)	1.11(3)
S(2)-C(2)	1.69(2)	C(2)-N(2)	1.09(3)
O(11)-C(11)	1.22(3)	O(21)-C(21)	1.28(3)
C(11)-N(11)	1.33(3)	C(21)-N(21)	1.38(4)
Hg···Co	5.722(3)	Hg···Co^{i}	5.573(3)
Hg···Co^{ii}	5.738(3)	Hg···Co^{iii}	5.842(3)
Bond angle	ϕ/°	**Bond angle**	ϕ/°
S(1)-Hg-S(2)	110.5(2)	S(1)-Hg-S(3)	114.2(2)
S(1)-Hg-S(4)	105.0(2)	S(2)-Hg-S(3)	100.9(2)
N(1^{i})-Co-N(2)	91.1(8)	N(2)-Co-N(3^{ii})	177.5(8)
N(2)-Co-N(4^{iii})	89.4(8)	N(2)-Co-O(11)	87.8(7)
N(2)-Co-O(21)	86.6(7)	O(11)-Co-O(21)	88.7(6)
Hg-S(1)-C(1)	96.7(8)	Hg-S(2)-C(2)	94.9(8)
Co-N(1^{i})-C(1^{i})	168.3(19)	Co-N(2)-C(2)	173.6(19)
Co-O(11)-C(11)	126.9(16)	Co-O(21)-C(21)	122.5(16)
S(1)-C(1)-N(1)	179(2)	S(2)-C(2)-N(2)	179(2)

Key to the symmetry operations: i, x, $-0.5+y$, $1.5-z$; ii, $-0.5+x$, $0.5-y$, $-0.5+z$; iii, x, $-0.5+y$, $0.5-z$

scheme of the atoms. A crystal-packing diagram of the unit cell is shown in Fig. 3.

Each mercury atom is coordinated with four thiocyanate sulfur atoms and has a tetrahedral geometry. The average Hg-S length is 2.545 Å (maximum Hg-S(3), 2.588(7) and minimum Hg-S(1), 2.518(6) Å) which is about the same as the sum of the Pauling's radii, 2.52 Å (r_{Hg}=1.48, r_S=1.04 Å).[12] The average angles of S-Hg-S and Hg-S-C are 109.5 and 95.5°, respectively. These bond lengths and angles about the mercury atoms of these complexes are normal compared with several mercury thiocyanates whose structures are crystallographycally known.[1,13-15]

The cobalt atom is hexa-coordinated and is in an octahedral geometry, where two amide oxygen atoms are ligated in a *cis*-orientation, and four thiocyanate nitrogen atoms are bonded to the rest positions. The average Co-N and Co-O bond-lengths are 2.104, and 2.108 Å, respectively. Although they are a little longer than the respective sums of the Pauling radii, 2.02 and 1.98 Å (where r_{Co}=1.32, r_N=0.70, r_O=0.66 Å), such Co-O[16-18] and Co-N[19-21] lengths are found in many octahedral cobalt(II) complexes. The bond angles N-Co-N′ are; N(2)-Co-N(3^{ii})=177.5(8)°, and the other five angles are 90.15° on the average. Including the bond angles around the cobalt atoms, such as O-Co-N and O-Co-O, it was thought that the octahedral geometry of the cobalt core is not much deformed from the ideal one. The bond angle Co-N-C is 172° on the average (maximum Co-N(4^{iii}),

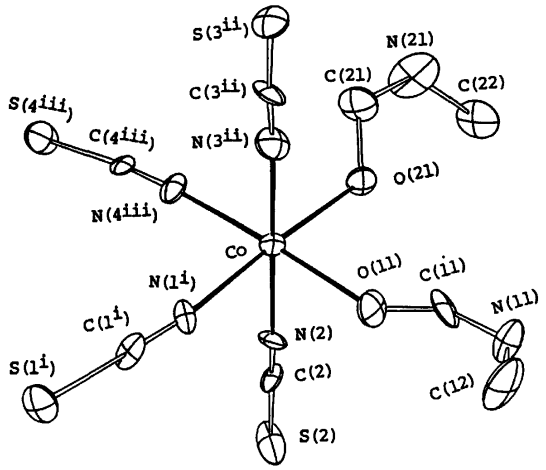

Fig. 2. The perspective drawing of the complex around a cobalt atom.

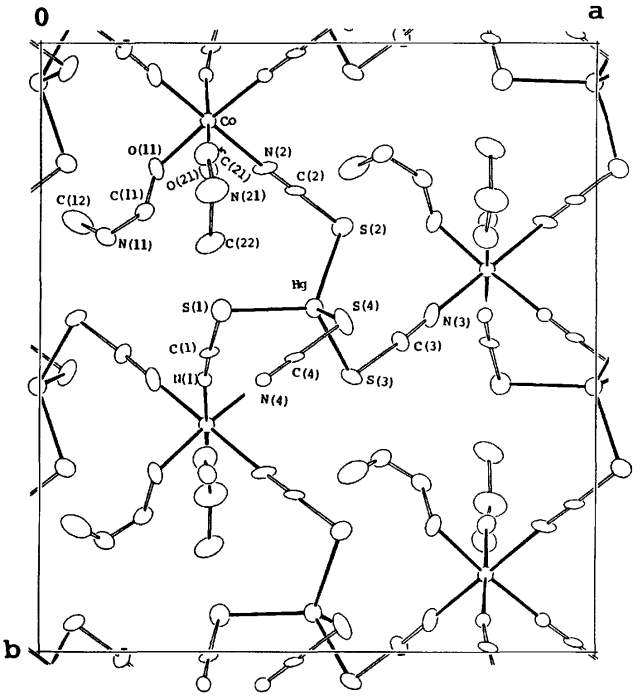

Fig. 3. The projection of the unit cell of the complex to the (0 0 1) plane.

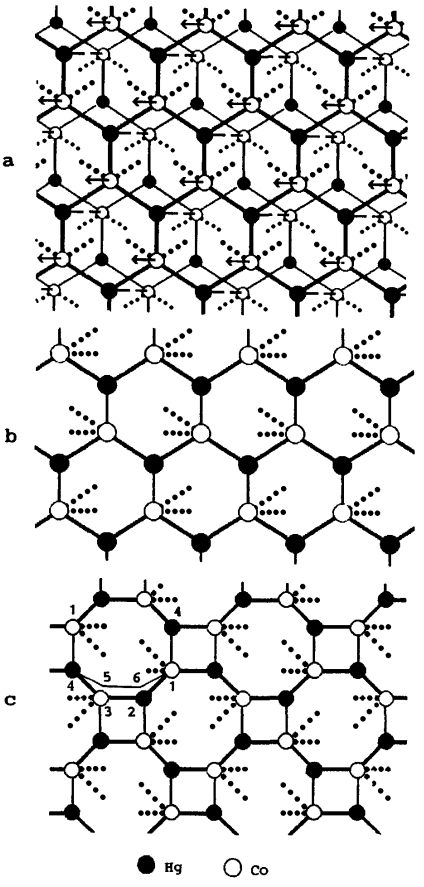

Fig. 4. The schematic presentation of the projection of the metal atomic arrangements of the complexes.
a: $CoHg(SCN)_4(mfa)_2$ projected to (1 0 0) plane,
b: $CoHg(SCN)_4(mfa)_2$ projected to (0 0 1) plane,
c: $CoHg(SCN)_4(dmf)_2$ projected to an appropriate plane.
Each solid line indicates the thiocyanato bridge. The broader lines show respective polymeric planes parallel(a) or perpendicular(b and c) to the projected plane. The dotted lines indicate the Lewis base molecules.

174(2); minimum Co-N(1^{i})-C(1^{i}), 168(2)°), being deformed only slightly from 180°.

Each pair of mercury and cobalt atoms are bridged by a thiocyanate ion (where the sulfur atom is ligated to the mercury and the nitrogen atom to the cobalt atom).

The projection of the metal atoms of **4** onto the (1 0 0) plane is shown schematically in Fig 4-a, where each bridging thiocyanate ion between the metal atoms is abbreviated as a straight line, in place of the real one which is broken at the sulfur atom position in about right angle. As shown in the figure, there are two kinds of two-dimensional networks (shown by broad and narrow lines) piled up alternatively. Both of them consist of condensed twenty-four membered rings where each three mercury and cobalt atoms are arrayed hexagonally in a chair form, and their average plane is parallel to (1 0 0). The dotted lines indicate mfa molecules. Each mercury atom in the plane is bridged by a thiocyanate ion to the cobalt atoms on the parallel next polymer plane on one side, (shown by the broken line), while each cobalt atom is linked to the mercury atom on the plane of the other side (shown by the arrow), respectively. All such interlayer bridging SCN ions are the S(3)-C(3)-N(3) types.

As shown in Fig. 4-b, which is a schematic presentation of the projection of the network to the (0 0 1) plane, there are other kinds of twenty-four membered rings represented by the hexagons of their metal atomic positions. However, projections of the hexagons are not very deformed. They are very different from the exact chair forms since the up and down deviations of the respective metal atomic positions from the average plane are irregular. Thus the three-dimensional network of complex 4 is regarded as consisting of a unit cage surrounded by two chair forms (up and down face parallel to (1 0 0) plane), and three deformed (side ones) twenty-four membered rings. The cages are arranged three-dimensionally and mfa ligands take positions in them.

A type of cage consisting of twenty-four membered rings was also found in **1**,[1] but all the hexagons of the metal-atom positions of all the rings were in the chair form. The metal atoms were arrayed like the carbon atoms in a diamond crystal.

According to Udupa's data of **3**,[3] two dmf oxygen atoms are ligated to a cobalt atom in a cis orientation, but its bridging structure is much different from that of **4** (written as follows). As schematically shown in Fig. 4-c, which is the projection to an appropriate plane, there are the same types of the twenty-four membered ring units; the hexagons indicating the metal-atom positions are condensed and linked to form a planar-type polymer which are spread perpendicular to the paper plane (one such hexagon is shown schematically as 1—6 in the figure). All the hexagons are in a boat form; the concave and convex types are arrayed alternatively. Their planar networks are shown by the broad lines in the figure. The metal atoms at the head and tail (1 and 4) positions of one hexagon unit are also bridged to the respective different kind of metal atoms at the 4 or 1 positions of another ring on a parallel next plane by the thiocyanate ions, while the other four metal atoms (2,3,5, and 6 position ones) are linked to the respective other kind of metal atoms on the next parallel plane of the opposite side. Thus, in **3** there are two kinds of cages (large and small ones) and as shown in the figure the side wall of the large one consists of two thirty-two membered rings (including, each, four mercury and cobalt atoms as well as eitht thiocyanate ions). Thus, the crystal of **3** has the vacant small cages other than the large cages to accomodate large dmf ligands in them; it is expected to have a less compact structure than that of **4**; the density of **3** and **4** are 2.01[3] and 2.21, respectively.

According to Beauchamp,[2] in **2**, two py nitrogen atoms are axially ligated to a cobalt atom, and four thiocyanate nitrogen atoms equatorially; its unit cage comprises two thirty-two membered rings ($Co_4Hg_4(SCN)_8$) and four sixteen-membered rings ($Co_2Hg_2(SCN)_4$) and the shape of the unit cage is much different from that of **1** or **4**.

From these comparisons of the framework, in **4** the mfa ligand can be included into the network of **1** with a relatively minor modification of the network, although the diamond-like structure of **1** is lost.

On the other hand, as py and dmf consist of six and five non-hydrogen atoms, respectively, they are relatively large in size compared with mfa which has only four non-hydrogen atoms. Therefore, the frameworks of **2** and **3** are too much different from those of **1** and **4** to take in these additional ligands.

The magnetic moment of 4 is about 5.02 BM (1 BM=$9.274078(36)\times10^{-24}$ JT^{-1}) at 20 °C. The value is almost the same as that of the related adducts, such as **2** or **3**, and which is the typical value for cobalt(II) complexes in an octahedral geometry.

The authors are greatly obliged to Dr. Mamoru Shimoi, Assistant Professor of Tohoku University, for his helpful discussions during this study.

References

1) J. W. Jeffery and K. M. Rose, *Acta Crystallogr., Sect B*, **24**, 653 (1968).

2) A. L. Beauchamp, L. Pazdernik, and R. Rivest, *Acta Crystallogr., Sect B*, **32**, 650 (1976).

3) M. R. Udupa and B. Krebs, *Inorg. Chim. Acta*, **42**, 37 (1980).

4) H. Kinoshita, M. Shimoi, and A. Ouchi, *Bull. Chem. Soc. Jpn.*, **58**, 1304 (1985).

5) H. Kinoshita, M. Shimoi, A. Ouchi, and S. Sato, *Bull.*

Chem. Soc. Jpn., **58**, 2782 (1985).

6) H. Kinoshita, M. Shimoi, and A. Ouchi, *Bull. Chem. Soc. Jpn.*, **59**, 1253 (1986).

7) W. R. Busing and H. A. Levy, *Acta Crystallogr.*, **10**, 180 (1957).

8) $R=\sum||F_o|-|F_c||/\sum|F_o|$.

9) "The Universal Crystallographic Computation Program-System (UNICS)," ed by T. Sakurai, Crystallographic Society of Japan, Tokyo (1967).

10) "International Tables for X-ray Crystallography," Kynoch Press, Birmingham (1974), Vol. IV, pp. 72, 150.

11) The final atomic and thermal parameters, and the final F_o-F_c tables are deposited as Document No. 8648 at the Office of the Editor of Bull Chem. Soc. Jpn.

12) L. Pauling, "The Nature of the Chemical Bond," 3rd ed, Cornell University Press, N. Y. (1960), pp. 246, 256.

13) R. C. Makhija, A. L. Beauchamp, and R. Rivest, *J. Chem. Soc., Dalton Trans.*, **1973**, 2447.

14) R. C. Makhija, A. L. Beauchamp, and R. Rivest, *J. Chem. Soc., Chem. Commun.*, **1972**, 1043.

15) D. Grdenic, *Quart. Rev.*, **19**, 303 (1965).

16) H. Lynton and P. Y. Siew, *Can. J. Chem.*, **51**, 227 (1973).

17) J. A. Bertrand and T. C. Hightower, *Inorg. Chem.*, **12**, 206 (1973).

18) A. Vegas, *Acta Crystallogr., Sect B*, **37**, 1916 (1981).

19) H. Hartl and S. Steidl, *Z. Naturforsch., B*, **32**, 6 (1977).

20) B. Buss, P. G. Jones, R. Mews, M. Noltemeyer, and G. M. Sheldrick, *Acta Crystallogr., Sect B*, **36**, 141 (1980).

21) H. Hartl and I. Brudgam, *Acta Crystallogr., Sect B*, **36**, 162 (1980).

 © 1986 The Chemical Society of Japan Bull. Chem. Soc. Jpn., 59, 3501—3504 (1986)

Selective Modification of the Two Type I Copper Sites in Human and Bovine Ceruloplasmin with the Action of Azide and L-Cysteine

Takeshi SAKURAI* and Akitsugu NAKAHARA
Institute of Chemistry, College of General Education, Osaka University,
Toyonaka, Osaka 560
(Received May 31, 1986)

The two type I copper sites of human and bovine ceruloplasmin (CP) were indirectly modified through the binding of N_3^- to types II and III copper ions. Based on the fact that the activities of CP's modified with N_3^- were 85 and 47% for human and bovine CP, respectively, it was disclosed that the electronic and steric states of the "fast" type I Cu or "CuA" which is coupled with the types II and III copper ions was changed reversibly, whilst the "slow" type I Cu or "CuB" which is not coupled with the types II and III copper ions was changed to a type II copper ion and/or irreversibly reduced. On the other hand, the reaction of a limited amount of L-cysteine with CP gave the absorption and electron paramagnetic resonance spectra of CP whose CuB was selectively reduced. The treatment of this CP with 4,7-diphenyl-2,9-dimethyl-1,10-phenanthroline-4′,4″-disulfonate did not result in the selective removal of CuB.

Ceruloplasmin (CP) is one of the serum globulins possessing oxidase activity towards Fe(II) and some aromatic amines and phenols.[1] Like the other multicopper oxidases, laccase,[2] and ascorbate oxidase,[3] CP contains three kinds of copper(II) ions besides one or more copper(I) ions, i.e. two type I coppers characterized by the intense absorption at 610 nm and very small hyperfine coupling constants in the electron paramagnetic resonance (EPR) spectrum, one type II copper with EPR hyperfine parameter similar to that found in usual tetragonal copper(II) complexes and a pair of type III copper ions which are antiferromagnetically coupled and exhibit relatively strong absorption at around 330 nm.[1] It has been revealed that the two type I coppers of human and bovine CP's are oxidized at different rates:[4,5] The "fast" one or "CuA" has been elucidated to be coupled with the types II and III copper ions, constituting the active site, whilst the "slow" one or "CuB" is isolated from the active site.[5] Many studies on the effect of anions like N_3^-, SCN^-, OCN^-, F^- on human CP(HCP) have reached the conclusion that only one of the two type I coppers is indirectly affected by the anions in the light of the absorption change at 610 nm.[6,7] However, in the previous work on bovine CP(BCP) we disclosed both the type I coppers are affected by these anions: The steric and electronic structure of one of the two type I coppers is reversibly changed, whereas the other is irreversibly reduced and/or changed to a type II copper.[8] In the present paper, we report the discrimination of the two type I coppers both of which are indirectly perturbed by N_3^-. Further, we furnish the absorption and EPR spectra of CP whose CuB is selectively reduced.

Experimental

HCP was purchased from Green Cross Corp. and BCP was prepared from bovine serum as described previously.[5,8] The absorption ratio of A_{610}/A_{280} was 0.041 and 0.044 for HCP and BCP, respectively. All reagents used were of analytical grade. Absorption spectra were obtained on a Union Giken SM-401 high sensitivity spectrophotometer and circular dichroic (CD) spectra on a JASCO J-500A spectropolarimeter. EPR spectra were recorded on a JEOL FE-1X spectrometer at 77 K. The amount of EPR detectable Cu^{2+} was estimated based on an EPR signal intensity of ethylenediaminetetraacetatocopper(II) as a standard. Total copper content of CP was determined using a Jarrell-Ash AA-1 atomic absorption spectrometer.

Results and Discussion

The absorbance at 610 nm of HCP treated with 1720

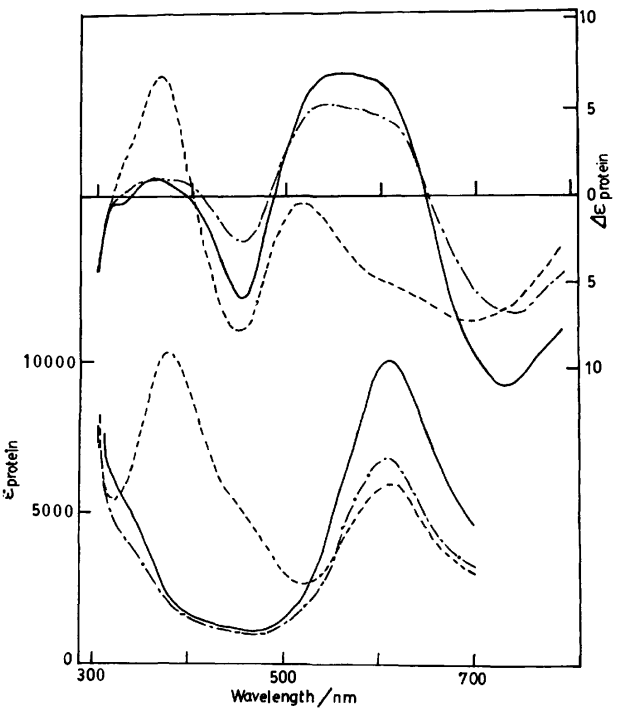

Fig. 1. Absorption and CD spectra of native (——), N_3^--treated (×1720, incubated for 2 d) (----), and dialyzed (——) human ceruloplasmin (protein concentration 2.9×10^{-5} mol dm^{-3}, pH 6.5, 0.1 mol dm^{-3} Na-phosphate buffer).

fold excess of N_3^- for 2 days decreased to 60% of the original intensity. Concomitantly, new band appeared at 381 and at 450 nm (Fig. 1). In the CD spectra, the sign of the band at about 660 nm arising from the charge transfer, S^-(cysteine)→Cu inverted from positive to negative because of the change of the steric and electronic states of one type I copper: The steric structure has been supposed to change from tetrahedrally distorted tetragon to trigonal pyramid.[9] The ellipticity of the negative CD band at 448 nm coming from the charge transfer, N(histidine)→Cu became greater, being accompanied by a development of a positive band at 370 nm due to the charge transfer, N_3^-→Cu (types II and III coppers). Simultaneously, the band at about 330 nm arising from the type III coppers almost lost its intensity. However, the CD spectral pattern returned to the original one after N_3^- was removed by dialysis against buffer solution. Each band showed a smaller intensity (Fig. 1) in accordance with the absorbance decrease of the band centered at 610 nm, although 9% recovery of the absorption intensity was observed. In the EPR spectra, the type II copper signal changed significantly: $g_{//}$=2.26, $A_{//}$=0.019 cm^{-1} for native HCP and $g_{//}$=2.26, $A_{//}$=0.015 cm^{-1} for N_3^--treated HCP (Fig. 2). The spin Hamiltonian parameters of one type I copper also changed slightly: $g_{//}$=2.21, $A_{//}$=0.0072 cm^{-1} for native HCP and $g_{//}$=2.18, $A_{//}$=0.0076 cm^{-1} for N_3^--treated HCP. Another possibility is that the type I copper which has the former parameter was reduced and/or changed to a type II copper. However, in the simulation study the following parameters were given for the two type I coppers of HCP: $g_{//}$=2.21, $A_{//}$=0.0074 cm^{-1} and $g_{//}$=2.22 and $A_{//}$=0.0095 cm^{-1}.[10] The former set of values are similar to those observed in our study. But the signal containing the latter parameters have not been observed in the present study. The whole feature of EPR spectrum returned to that similar to the native HCP after dialysis, while the increase of the type II copper signal(s) was noticeable. The amount of EPR detectable Cu^{2+} was estimated to be 3.0, 2.7, and 2.9 for native, N_3^--treated, and N_3^--treated and succeedingly dialyzed HCP. This result indicates that one type I copper was changed mostly to a type II copper through the binding of N_3^- to the type II and III copper ions even taking into consideration that the estimation error of EPR detectable Cu^{2+} is 10% or even more.

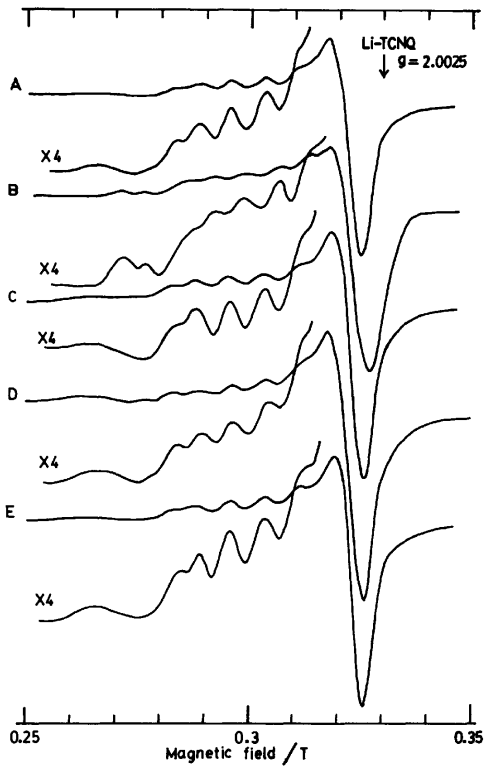

Fig. 2. X-band EPR spectra of native(A), N_3^-(×1720)-treated(B), dialyzed as (B)(C), DDP-treated after cysteine-treatment(D), and dialyzed as (D)(E) human ceruloplasmin; microwave frequency 9.21 GHz, microwave power 5 mW, modulation 0.8 mT at 100 kHz, amplitude 630 or 1000.

The activity[11] of the dialyzed HCP after N_3^--treatment for oxidizing 1,4-benzenediamine was 85%

Table 1. Characterization of Modified HCP and BCP

State of CP	Total Cu	EPR detectable Cu^{2+}	Relative oxidase activity/%	Relative absorbance at 610 nm/%
Native HCP	6.8	3.0	100	100
N_3^--treated HCP	—	2.7	—	60
Dialyzed HCP after N_3^--treatment	6.8	2.9	85	69
Cysteine-treated HCP	—	2.2	88	66
Dialyzed HCP after cysteine-treatment	6.9	2.7	87	77
Native BCP	6.7	3.0	100	100
N_3^--treated BCP	—	3.1	—	59
Dialyzed BCP after N_3^--treatment	6.7	3.7	47	45
Cysteine-treated BCP	—	2.0	98	54
Dialyzed BCP after cysteine-treatment	6.3	2.6	74	—

of that of the native HCP in spite of the 31% decrease of the absorbance at 610 nm (Table 1). The two type I coppers have been differentiated from the different rate of reoxidation, i.e. the "fast" one or "CuA" and the "slow" one or "CuB".[5] The former has been believed to be coupled with the types II and III coppers to constitute the active site, while the latter is not.[6,7] In addition, CuA has been supposed to be affected irreversibly by several anions such as N_3^-, since this anion binds with types II and III coppers to exert the fatal perturbation on protein structure. However, the fact that the dialyzed HCP after N_3^--treatment still reserved the activity indicated that CuA is the type I copper which is reversibly modified by the treatment with N_3^-. On the other hand, CuB is supposed to be changed mainly to a type II copper irreversibly owing to its reduction by the S^- group of the cysteine residue, the succeeding disruption of the Cu-S (cysteine) bond and the final automatic reoxidation.

A similar behavior was also observed for BCP (spectra are not shown). Although BCP is especially unstable, the dialyzed BCP after N_3^--treatment showed 45% activity as compared with that of the native enzyme (Table 1). The conservation of the oxidase activity indicates again that CuA was reversibly modified by N_3^- as was observed in the case of HCP. The amount of EPR detectable Cu^{2+} increased from 3 to 3.7 probably because the destruction of the active site including the type III site had occurred during the treatment of this enzyme with N_3^-.

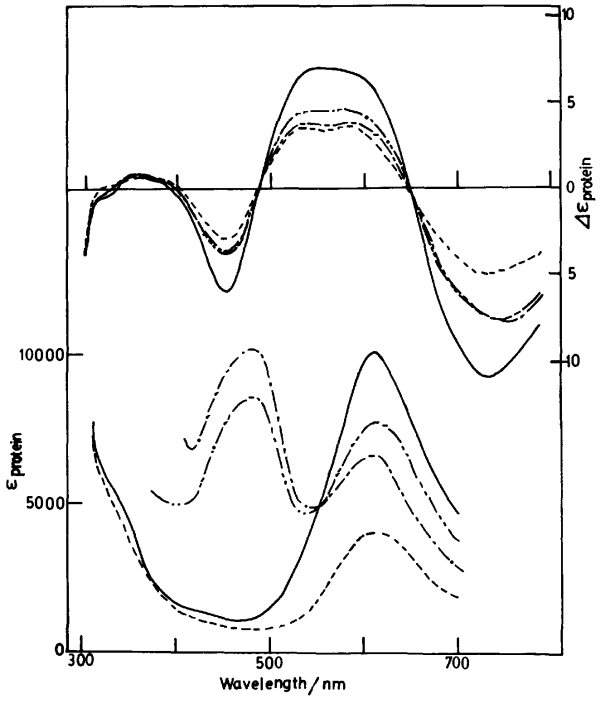

Fig. 3. Absorption and CD spectra of native (——), cysteine-treated (----), DDP-treated after cysteine-treatment (——), and dialyzed (——) human ceruloplasmin.

Native HCP was treated in three steps with two moles of L-cysteine. The resulting HCP gave absorption and CD spectra whose all bands were reduced to almost half of the native enzyme. Since CuA is coupled with the types II and III coppers, electrons afforded to this copper site were intramolecularly transferred to the type II copper and finally to the type III coppers where O_2 received them to give $2H_2O$. This intramolecular electron-transfer process is so rapid that electrons received by CuA are consumed in a few minutes.[12] However, the electron received by CuB is not transferred to other coppers because this type I copper is isolated from the active site. Accordingly CuB is autooxidized rather slowly, although the rate is not so slow as the autooxidation rate of the type I copper of simple blue copper proteins like plastocyanin, azurin, stellacyanin, plantacyanin, nitrite reductase, and amicyanin.[13] Thus the resulting absorption, CD and EPR spectra of the cysteine-treated HCP was not affected by CuB. This means that those spectra correspond to those of laccase which has the intrinsic one type I, one type II, and a pair of type III copper ions. It is not unexpected that the whole feature of the EPR spectrum was rather similar to that of the native enzyme (Fig. 2), even if the amount of EPR detectable Cu^{2+} was really decreased from 3.0 to 2.0. A rigorous EPR simulation study for the native enzyme should be performed again very carefully, since the former simulation study[10] suggested that the two type I coppers gave apparently different EPR parameters (vide supra).

In order to remove CuB selectively, 4,7-diphenyl-2,9-dimethyl-1,10-phenanthroline-4′,4″-disulfonate (DDP) was acted on a cysteine treated-HCP. A strong new band, which does not contribute to the CD spectrum, appeared at 485 nm. The absorption did not become pale appreciably after dialysis against buffer solution, since the Cu(I)-complex was firmly bound on the protein surface. The EPR detectable amount of Cu^{2+} increased from 2.3 for the cysteine-treated state to 2.7 for the dialyzed state. The corresponding absorptions at 610 nm were 66 and 77% of that of the native HCP, respectively, indicating that CuB was mainly changed to a type II copper irreversibly and was partly reduced and succeedingly autooxidized during dialysis. The net decrease of 0.3 Cu^{2+} may arise from the exclusion of CuB by the chelating reagent. Alternatively, since the experimental error in estimating the EPR detectable amount of Cu^{2+} is usually 10% or more, CuB may not be removed at all and the copper source of the 485 nm band might be copper(I) ions bound on protein surface. The activity of cysteine treated HCP did not change appreciably (Table 1),[14] indicating that CuB does not contribute to the appearance of the oxidase activity of

HCP. A similar result was also obtained in the case of BCP (Table 1)(spectra are not shown).

As a conclusion, it was confirmed that the type I CuA is assembled together with the types II and III copper ions to form the active site, but the type I CuB is isolated from the active site. Both the type I coppers are affected indirectly by the action of N_3^- on CP. Then, unexpectedly, CuB is mainly altered to a type II copper irreversibly, whereas CuA is reversibly modified in its steric and electronic states.

The present work was partly supported by a Grant-in-Aid for Scientific Research No. 61740348 from the Ministry of Education, Science and Culture.

References

1) L. Ryden, "Copper Proteins and Copper Enzymes," ed by R. Lontie, CRC Press, Boca Raton, Florida (1984), Vol. 3, pp. 37—100.

2) R. Malkin and B. G. Malmstrom, *Adv. Enzymol.*, **33**, 177 (1970).

3) T. Sakurai, S. Sawada, S. Suzuki, and A. Nakahara, *Biochem. Biophys. Res. Commun.*, **131**, 647 (1985); **135**, 644 (1986).

4) R. J. Carrico, B. G. Malmstrom, and T. Vanngard, *Eur. J. Biochem.*, **22**, 127 (1971).

5) T. Sakurai and A. Nakahara, *Inorg. Chim. Acta*, **123**, 217 (1986).

6) K.-E. Falk and B. Reinhammar, *Biochim. Biophys. Acta*, **285**, 84 (1972).

7) W. Byers, G. Curzon, K. Garbett, B. E. Speyer, S. N. Young, and R. J. P. Williams, *Biochim. Biophys. Acta*, **310**, 38 (1973).

8) T. Sakurai and A. Nakahara, *J. Inorg. Biochem.*, **27**, 85 (1986).

9) T. Sakurai, S. Suzuki, A. Nakahara, M. Masuko, and H. Iwasaki, *Chem. Lett.*, **1985**, 1297.

10) P.-O. Gunnarsson, U. Nylen, and G. Pettersson, *Eur. J. Biochem.*, **37**, 47 (1973).

11) E. W. Rice, *Anal. Biochem.*, **3**, 452 (1962).

12) R. Branden and J. Deinum, *Biochim. Biophys. Acta*, **524**, 297 (1978).

13) T. Sakurai, H. Okamoto, K. Kawahara, and A. Nakahara, *FEBS Lett.*, **147**, 220 (1982).

14) M. V. Chidambaram, A. Zgirski, and E. Friden, *J. Inorg. Biochem.*, **21**, 227 (1984).

 © 1986 The Chemical Society of Japan Bull. Chem. Soc. Jpn., 59, 3505—3510 (1986)

Inversion at Selenium in the Bis(β-diketonato)[2-(methylseleno)-ethylamine]cobalt(III) Ion

Kiyohiko NAKAJIMA, Masaaki KOJIMA, and Junnosuke FUJITA*
Department of Chemistry, Faculty of Science, Nagoya University,
Chikusa-ku, Nagoya 464
(Received June 10, 1986)

The selenide (selenoether) complexes, $[Co(\beta\text{-dik})_2(CH_3SeCH_2CH_2NH_2)]^+$ (β-dik: acac=2,4-pentanedionate, Clacac=3-chloro-2,4-pentanedionate, Meacac=3-methyl-2,4-pentanedionate, and dbme=1,3-diphenyl-1,3-propanedionate) were prepared and separated into two racemic pairs of the diastereomers (Δ(*R*)Λ(*S*) and Δ(*S*)Λ(*R*) isomers). The complexes in solution epimerize by inversion at the selenium atom, and the rates were followed by high-performance liquid chromatography in the temperature range of 30.3—55.0 °C in 0.05 mol dm^{-3} Na_2SO_4 (acac, Clacac, and Meacac complexes) or in methanol (dbme complex). The $\Delta G^{\ddagger}_{25\,°C}$ values for inversion of $[Co(\beta\text{-dik})_2(CH_3SeCH_2CH_2NH_2)]^+$ decrease in the order β-dik=Clacac(108)>acac(106)>dbme(104)>Meacac(100 kJ mol^{-1}), and the decrease in $\Delta G^{\ddagger}_{25\,°C}$ comes mainly from a decrease in $\Delta H^{\ddagger}$. The effect of substituents is electronic and the Hammett relationship was found to hold for the inversion rates of the acac, Clacac, and Meacac complexes.

The selenium atom of a selenide (RSeR′) ligand becomes chiral on coordination to a metal ion. It has been reported that inversion at a coordinated selenide site is too rapid for the resolution in such complexes as Pt^{II}, Pt^{IV}, and Pd^{II}.[1] In a previous paper, however, we reported that inversion at selenium in $[M^{III}(RSeCH_2CH_2NH_2)(tren)]^{3+}$ (M^{III}=Co, Rh; R=CH_3, CH_3CH_2, $C_6H_5CH_2$; tren=tris(2-aminoethyl)amine=$N(CH_2CH_2NH_2)_3$) is so slow that they can be resolved by conventional methods, and that the inversion rates are dependent on the steric crowding around the Se-R group of the complexes.[2]

In order to investigate the electronic effect on the inversion rate, we have prepared a series of $[Co(\beta\text{-dik})_2(CH_3SeCH_2CH_2NH_2)]^+$ (β-dik: Clacac=3-chloro-2,4-pentanedionate, Meacac=3-methyl-2,4-pentanedionate, and dbme=1,3-diphenyl-1,3-propanedionate) and studied the inversion kinetics.

A part of this study has been reported briefly.[3,4]

Experimental

$[Co(acac)_2(CH_3SeCH_2CH_2NH_2)]ClO_4$. This complex was prepared from $[Co(acac)_2(H_2O)_2]$ and $CH_3SeCH_2CH_2NH_2$ by the same method as that for $[Co(acac)_2(CH_3SeCH_2CH_2NH_2)]PF_6$[3] except that $LiClO_4$ was used instead of NH_4PF_6. Yield: 42%. Found: C,31.71; H, 4.83; N, 2.27%. Calcd for $C_{13}H_{23}NClCoO_8Se$: C, 31.56; H, 4.69; N, 2.83%.

$[Co(Clacac)_2(CH_3SeCH_2CH_2NH_2)]ClO_4$. This complex was prepared by chlorination of $[Co(acac)_2(CH_3SeCH_2CH_2NH_2)]ClO_4$ with *N*-chlorosuccinimide by a method similar to that for $[Co(Clacac)(en)_2](ClO_4)_2$.[5] To a methanol solution (15 cm^3) of *N*-chlorosuccinimide (0.041 g, 3.07×10^{-4} mol) was added $[Co(acac)_2(CH_3SeCH_2CH_2NH_2)]ClO_4$ (0.050 g, 1.01×10^{-4} mol), and the solution was stirred for ca. 4 h at room temperature. The reaction mixture was diluted with water (20 cm^3) and applied on a column (φ 1.1 cm×6 cm) of SE-Toyopearl HW-40 (fine).[6] The adsorbed product was washed with water and eluted with 0.05 mol dm^{-3} Na_2SO_4. The column showed two green bands. The faster-moving band (minor product) seemed to contain $[Co(Clacac)(acac)(CH_3SeCH_2CH_2NH_2)]^+$ on the basis of the absorption spectrum, but this complex was not isolated. The eluate containing the slower-moving band (major product) was collected and mixed with $LiClO_4$ (ca. 5 g), and the complex was extracted with chloroform (50 cm^3×3). The chloroform layer was dried with anhydrous $MgSO_4$ and evaporated under reduced pressure to dryness. The deep green residue was dissolved in acetone (0.4 cm^3)–water (1.6 cm^3), and the solution was evaporated slowly in a desiccator over P_2O_5 to yield deep green crystals, which were collected by filtration, washed with cold water, and air dried. Yield: 0.03 g (53%). Found: C, 27.71; H, 3.76; N, 2.49%. Calcd for $C_{13}H_{21}NCl_3CoO_8Se$: C, 27.96; H, 3.53; N, 2.20%.

$[Co(Meacac)_2(CH_3SeCH_2CH_2NH_2)]ClO_4$. To a cold aqueous solution (7 cm^3) of NaOH (0.70 g, 1.75×10^{-2} mol) was slowly added 3-methyl-2,4-pentanedione[7] (2.0 g, 1.75×10^{-2} mol). The solution was then added dropwise to an aqueous solution (10 cm^3) of $CoCl_2\cdot 6H_2O$ (2.1 g, 8.83×10^{-3} mol). A yellow powder precipitated was collected quickly by filtration. This product was believed to be crude $[Co(Meacac)_2(H_2O)_2]$ and was used without purification. It is not stable even in the solid state; the color changes from yellow to green. To a hot (ca. 50 °C) ethanol solution (20 cm^3) containing $CH_3SeCH_2CH_2NH_2\cdot HCl$ (0.10 g, 5.73×10^{-4} mol) and LiOH (0.014 g, 5.8×10^{-4} mol) was added freshly prepared $[Co(Meacac)_2(H_2O)_2]$ (0.20 g, 6.2×10^{-4} mol). The color of the solution turned deep green immediately. The mixture was heated at 50 °C with stirring for 30 min. After cooling to room temperature, the solution was mixed with 3 mol dm^{-3} $LiClO_4$ (10 cm^3), and the complex was extracted with chloroform (200 cm^3×2). The chloroform layer was evaporated to dryness under reduced pressure, the deep green residue was dissolved in water, and then the solution was applied on a column (φ 2.2 cm×8 cm) of SP-Sephadex C-25. After washing the column with water the adsorbed product was eluted with 0.05 mol dm^{-3} Na_2SO_4. The column showed a green and a brown band. From the eluate containing the faster-moving green band the complex was isolated as the perchlorate by the same method as that for the Clacac complex, and recrystallized from water. Yield: 0.063 g (21%). Found: C, 34.80; H, 5.47; N, 2.89%. Calcd for $C_{15}H_{27}NClCoO_8Se$: C, 34.47; H, 5.21; N, 2.68%.

$[Co(dbme)_2(CH_3SeCH_2CH_2NH_2)]ClO_4\cdot H_2O$. To an eth-

anol solution (10 cm^3) of LiOH (0.12 g, 5.0×10^{-3} mol) was added slowly 1,3-diphenyl-1,3-propanedione (1.125 g, 5.0×10^{-3} mol). The resulting yellow suspension was added dropwise to an ethanol solution (6 cm^3) of $CoCl_2\cdot6H_2O$ (0.595 g, 2.5×10^{-3} mol). The mixture containing a yellow-orange precipitate was mixed with water (10 cm^3), stirred for 30 min at room temperature, and then the precipitate was collected by filtration. It was dissolved in hot ethanol (65 cm^3)–chloroform (35 cm^3), and the solution was evaporated to a volume of ca. 30 cm^3 and cooled to give fine orange crystals, which were collected by filtration and air dried. Yield: 1.30 g. This product was believed to be $[Co(dbme)_2(H_2O)_2]$ and was used to prepare $[Co(dbme)_2(CH_3SeCH_2CH_2NH_2)]^+$ without analysis. To an *N*,*N*-dimethylformamide (DMF) solution (40 cm^3) of $[Co(dbme)_2(H_2O)_2]$ (1.00 g, 1.85×10^{-3} mol) was added a DMF solution (10 cm^3) containing $CH_3SeCH_2CH_2NH_2\cdot HCl$ (0.322 g, 1.85×10^{-3} mol) and triethylamine (0.187 g, 1.85×10^{-3} mol). Acetic acid (2 cm^3) and PbO_2 (0.221 g, 9.25×10^{-4} mol) were added to the solution, the mixture was stirred for about 30 min at 30—40 °C, and then filtered. The filtrate was mixed with 0.5 mol dm^{-3} $NaClO_4$ (200 cm^3) with vigorous stirring to yield a green precipitate, which was recrystallized from chloroform by adding hexane. Yield: 1.04 g (74%). Found: C, 52.19; H, 3.97; N, 2.00%. Calcd for $C_{33}H_{33}NClCoO_9Se$: C, 52.09; H, 4.37; N, 1.84%.

$[Co(Bracac)_2(CH_3SeCH_2CH_2NH_2)]ClO_4$. This complex was obtained from the acac complex by a method similar to that for the corresponding Clacac complex using *N*-bromosuccinimide instead of *N*-chlorosuccinimide. Yield: 30%. Found: C, 23.91; H, 3.13; N, 2.25%. Calcd for $C_{13}H_{21}NBr_2ClCoO_8Se$; C, 23.93; H, 3.24; N, 2.15%. This complex is stable in the solid state but decomposes gradually in aqueous solution (ca. 5% in a day at room temperature).

$[Co(NO_2acac)_2(CH_3SeCH_2CH_2NH_2)]ClO_4$. This complex was prepared by nitration of $[Co(acac)_2(CH_3SeCH_2CH_2NH_2)]ClO_4$ in a manner similar to that for $[Co(NO_2acac)_3]$.[8] Yield: 42%. The complex is not stable even in the solid state and was not analyzed; the color of the complex changed from purple to brown on storage in a vial. The complex in water was estimated to decompose by ca. 10% in a day on the basis of the absorption spectrum.

Separation of the Diastereomers. The complexes $[Co(Clacac)_2(CH_3SeCH_2CH_2NH_2)]^+$ and $[Co(Meacac)_2(CH_3SeCH_2CH_2NH_2)]^+$ were separated into two racemic pairs of the diastereomers ($\Delta(R)\Lambda(S)$ and $\Delta(S)\Lambda(R)$) by column chromatography on SE-Toyopearl (eluent: 0.05 mol dm^{-3} Na_2SO_4) in the same manner as that for $[Co(acac)_2(CH_3SeCH_2CH_2NH_2)]^+$.[3] The column showed two green bands, but the diastereomers were not isolated because they are likely to epimerize. Each eluate was kept in a freezer at ca. −20 °C for kinetic studies. The diastereomers do not interconvert detectably over a period of at least 1 month under the given conditions.

$[Co(dbme)_2(CH_3SeCH_2CH_2NH_2)]^+$ was separated into the diastereomers by fractional crystallization of the perchlorate salt. $[Co(dbme)_2(CH_3SeCH_2CH_2NH_2)]ClO_4\cdot H_2O$ (0.14 g, 1.84×10^{-4} mol) was dissolved in chloroform (3 cm^3), and hexane (4 cm^3) was added dropwise. After cooling the solution in an ice bath, the crystals which deposited were collected. Almost pure (purity>95%) $\Delta(S)\Lambda(R)$ isomer (0.05 g) was obtained by repeated (4 times) recrystallization from chloroform–hexane by the same method as above. The purity was checked by a high-performance liquid chromatographic method (vide infra). The $\Delta(S)\Lambda(R)$ isomer (purity>95%) was also obtained by slow evaporation of a methanol solution of the perchlorate salt at room temperature.

Partial Resolution of $[Co(dbme)_2(CH_3SeCH_2CH_2NH_2)]^+$. Partial resolution of $[Co(dbme)_2(CH_3SeCH_2CH_2NH_2)]^+$ was achieved by column chromatography. About 5 mg of $[Co(dbme)_2(CH_3SeCH_2CH_2NH_2)]ClO_4\cdot H_2O$ dissolved in a small amount of methanol was applied on a column of D-TA(ES)-Toyopearl[6] (ϕ1.7 cm×30 cm; eluent: 0.02 mol dm^{-3} sodium (*R*,*R*)-tartrate in 70% methanol-30% water). A recycling chromatographic technique was employed. After three times of recycling, the first and the last fractions of the band showed CD spectra almost mirror image of each other in the region of 340—600 nm, indicating partial resolution of the complex.

Kinetic Studies. Kinetics of epimerization of $[Co(dbme)_2(CH_3SeCH_2CH_2NH_2)]^+$ was studied by a method similar to those for $[Co(acac, Clacac, or Meacac)_2(CH_3SeCH_2CH_2NH_2)]^+$.[3,4] Since the complex is insoluble in water, methanol was used as the solvent. Portions of the reaction mixture were withdrawn at intervals, and chromatographed with a column (ϕ 0.46 cm×15 cm) of JASCO Finepack SIL $C_{18}S$ and 0.1 mol dm^{-3} sodium dodecyl sulfate in 72.5% CH_3CN–27.5% H_2O as the eluent. The chromatography was carried out with a JASCO TRI ROTAR V system at a flow rate of 1.0 cm^3 min^{-1}, the $\Delta(R)\Lambda(S)$ isomer being eluted faster. The two isomers ($\Delta(R)\Lambda(S)$ and $\Delta(S)\Lambda(R)$) were detected at 315 nm where they give the same molar absorption coefficient and no detectable change in absorbance was observed during the epimerization reaction.

Measurements. Absorption and circular dichroism (CD) spectra were recorded on a Hitachi 323 spectrophotometer and a JASCO J-40CS spectropolarimeter, respectively. ^1H NMR spectra in $CDCl_3$ solutions were measured with a JEOL PMX-60 spectrometer using TMS as an internal reference.

Results and Discussion

Preparation and Characterization of the Complexes. Metal-acac complexes are known to be susceptible to electrophilic substitutions such as halogenation, nitration, or acetylation at the central methine of the acac chelate.[9] The $[Co(acac)_2(CH_3SeCH_2CH_2NH_2)]^+$ complex was halogenated (chlorinated, brominated) and nitrated, respectively, by *N*-halosuccinimide and a mixture of copper(II) nitrate and acetic anhydride. The ^1H NMR spectra verified the substitutions at the methine of the acac ligand. The resonances due to the methine protons in the spectrum of the parent complex disappeared completely on halogenation or nitration. The Bracac and NO_2acac complexes were unstable in solution, and the kinetics of epimerization reactions could not be studied. $[Co(Meacac or dbme)_2(CH_3SeCH_2CH_2NH_2)]^+$ was prepared by oxidizing a mixture of $[Co(Meacac or dbme)_2(H_2O)_2]$ and $CH_3SeCH_2CH_2NH_2$. The Meacac complex was easily

oxidized on exposure to the air, while the dbme complex was not formed under similar conditions and PbO_2 was used as an oxidizing agent.

Four stereoisomers, $\Delta(R)$, $\Delta(S)$, $\Lambda(R)$, and $\Lambda(S)$ are possible for the present complexes (Fig. 1). The complexes were separated into two isomers (racemic pairs of the diastereomers), $\Delta(R)\Lambda(S)$ and $\Delta(S)\Lambda(R)$, by column chromatography on SE-Toyopearl or by fractional crystallization. The structures of the isomers were assigned on the basis of the ^1H NMR spectra. Table 1 lists the ^1H NMR spectral data. In the $\Delta(R)\Lambda(S)$ isomer, the Se-methyl group is placed over one of the two acac chelate rings and the methyl protons will be shielded by the acac ring. Thus, the isomer whose Se-methyl signal is observed at a higher magnetic field is assigned to the $\Delta(R)\Lambda(S)$ isomer.

The absorption spectral data for [Co(acac, Clacac, Meacac, or dbme)$_2$($CH_3SeCH_2CH_2NH_2$)]$^+$ are given in Table 2, and the spectra are shown in Fig. 2. The spectral difference between the isomers is very small in each complex.

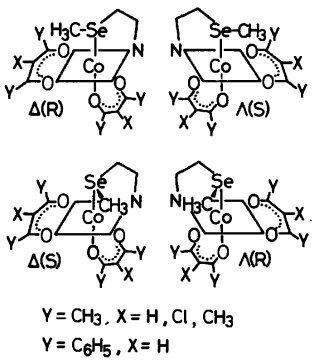

Fig. 1. The four stereoisomers of [Co(β-dik)$_2$($CH_3SeCH_2CH_2NH_2$)]$^+$.

Table 1. ^1H NMR Data for [Co(β-dik)$_2$($CH_3SeCH_2CH_2NH_2$)]$^+$ in $CDCl_3$

β-dik	Assignment	Chemical shift (Se-methyl, δ)
acac	$\Delta(R)\Lambda(S)$	1.63
	$\Delta(S)\Lambda(R)$	1.94
Clacac	$\Delta(R)\Lambda(S)$	1.60
	$\Delta(S)\Lambda(R)$	1.96
Bracac	$\Delta(R)\Lambda(S)$	1.61
	$\Delta(S)\Lambda(R)$	1.98
Meacac	$\Delta(R)\Lambda(S)$	1.53
	$\Delta(S)\Lambda(R)$	1.90—2.00[a]
dbme	$\Delta(R)\Lambda(S)$	1.49
	$\Delta(S)\Lambda(R)$	1.93
NO_2acac	$\Delta(R)\Lambda(S)$	1.71
	$\Delta(S)\Lambda(R)$	2.08

a) Overlapping with the *C*-methyl signals.

The absorption spectra of the acac, Clacac, and Meacac complexes are similar to that of [Co(acac)$_2$(en)]$^+$[10,11] (en=ethylenediamine) except a strong band at 32000—33000 cm^{-1} assignable to an Se-to-Co^{III} charge transfer transition.[2,12,13] The present complexes show the first absorption band, $^1A_{1g}\rightarrow{}^1T_{1g}$ (O_h) around 17000 cm^{-1}, and a shoulder in the region of 23000—24000 cm^{-1}. [Co(acac)$_2$(en)]$^+$ also shows a shoulder at ca. 24000 cm^{-1} and it has been assigned to the second d-d absorption band, $^1A_{1g}\rightarrow{}^1T_{2g}$ (O_h).[10,11] The first d-d absorption band of [Co(β-dik)$_2$($CH_3SeCH_2CH_2NH_2$)]$^+$ shifts to lower energies as β-dik is changed from acac (17100 cm^{-1}) through Clacac (16800 cm^{-1}) to Meacac (16600 cm^{-1}). It has been reported that the intensities of the first absorption band of cobalt(III)-acac complexes increase on halogenation.[5] [Co(acac)$_2$($CH_3SeCH_2CH_2NH_2$)]$^+$ is the case.

The bands observed at energies higher than 32000 cm^{-1} in the spectra of the acac, Clacac, and

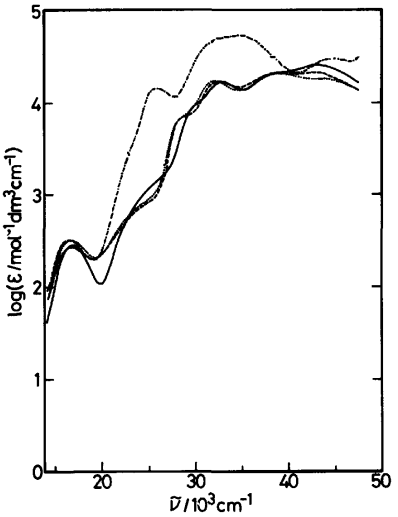

Fig. 2. Absorption spectra of [Co(β-dik)$_2$($CH_3SeCH_2CH_2NH_2$)]$^+$, β-dik=acac(——, in H_2O), Clacac(····, in H_2O), Meacac(– – –, in H_2O), and dbme(—·—, in CH_3OH).

Table 2. Absorption Spectral Data for [Co(β-dik)$_2$($CH_3SeCH_2CH_2NH_2$)]$^+$

β-dik	$\tilde{\nu}_{max}/10^3$ cm^{-1} (log (ε/mol^{-1} dm^3 cm^{-1}))
acac[a]	17.1(2.46) 24(sh, 2.93) 30(sh, 3.97) 32.9(4.23) 39.2(4.32) 43.3(4.40)
Clacac[a]	16.8(2.51) 23(sh, 2.79) 29(sh, 3.87) 32.1(4.23) 38.9(4.30) 44(sh, 4.25)
Meacac[a]	16.6(2.52) 23(sh, 2.75) 29(sh, 3.86) 32.6(4.24) 38.6(4.31) 42.7(4.32)
dbme[b]	16.8(2.43) 23(sh, 3.48) 25.9(4.16) 32(sh, 4.68) 34.5(4.73) 44.8(4.48)

Solvent, a): H_2O, b): CH_3OH.

Meacac complexes can be assigned to the π-π^* transitions of the β-diketonate ligand[14,15] and an N-to-Co^{III} charge transfer transition. $[Co(dbme)_2(CH_3SeCH_2CH_2NH_2)]^+$ shows the first d-d absorption band at nearly the same position as that for the Clacac complex. The absorption bands observed at energies higher than 22000 cm^{-1} for the dbme complex are more intense than those for the other complexes probably because of overlapping of the intense phenyl group transitions.

Inversion at the Coordinated Selenium Atom. In a previous paper,[3] we have shown that the epimerization of $[Co(acac)_2(CH_3SeCH_2CH_2NH_2)]^+$ is caused by the inversion at the selenium atom. The related complexes, Clacac and Meacac complexes, are expected to epimerize by the same way, and the dbme complex is also suggested to epimerize in a similar way on the basis of the CD spectrum. The dbme complex was partially resolved into the enantiomers by column chromatography. The CD spectra changed only slightly during epimerization. In general, the optical activity of a metal complex is explained by the superposition of the configurational (chiral arrangement of ligands around the metal ion) and the vicinal (chiral ligand) effects, the former being larger.[16,17] These observations suggest that the small CD change is caused by inversion at the selenium atom and that the configuration around the cobalt(III) ion remains unchanged. Thus, all the complexes studied here are believed to epimerize by selenium inversion.

The epimerization of $[Co(\beta\text{-dik})_2(CH_3SeCH_2CH_2NH_2)]^+$ was studied in the temperature range of 30.3—55.0 °C. $\Delta(S)\Lambda(R)$-$[Co(acac, Clacac, or Meacac)_2(CH_3SeCH_2CH_2NH_2)]^+$ was epimerized in 0.05 mol dm^{-3} Na_2SO_4, and $\Delta(S)\Lambda(R)$-$[Co(dbme)_2(CH_3SeCH_2CH_2NH_2)]^+$ was done in methanol since the complex is insoluble in water. The rates were followed by high-performance liquid chromatography. This method has the great advantages of a short elution time and micro quantities of samples. Figure 3 shows a typical set of elution curves obtained at intervals after $\Delta(S)\Lambda(R)$-$[Co(dbme)_2(CH_3SeCH_2CH_2NH_2)]ClO_4$·$H_2O$ had been dissolved in methanol at 40.0 °C. The area of band I ($\Delta(R)\Lambda(S)$ isomer) increases whereas that of band II ($\Delta(S)\Lambda(R)$ isomer) decreases with time as the result of epimerization:

$$\Delta(R)\Lambda(S) \underset{k_{-1}}{\overset{k_1}{\rightleftharpoons}} \Delta(S)\Lambda(R)$$

where k_1 and k_{-1} denote the forward and reverse rate constants, respectively. In each kinetic run, the plot of $\ln[S_t^{II}/(S_t^I+S_t^{II})-S_\infty^{II}/(S_\infty^I+S_\infty^{II})]$ vs. time gave a straight line for at least three half-lives (S_t^I, S_t^{II}, S_∞^I, and S_∞^{II}

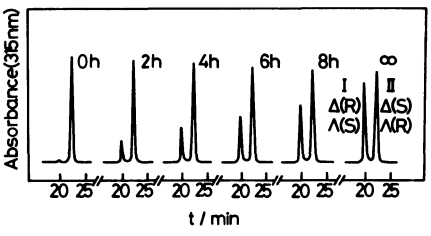

Fig. 3. Change in the elution curve during the epimerization of $\Delta(S)\Lambda(R)$-$[Co(dbme)_2(CH_3SeCH_2CH_2NH_2)]ClO_4$·$H_2O$ in methanol at 40.0 °C. Chromatographic conditions: column, JASCO Finepack SIL $C_{18}S$, ϕ0.46 cm × 15 cm; eluent, 0.1 mol dm^{-3} sodium dodecyl sulfate in 72.5% CH_3CN–27.5% H_2O; flow rate, 1.0 cm^3 min^{-1}; UV detection, 315 nm.

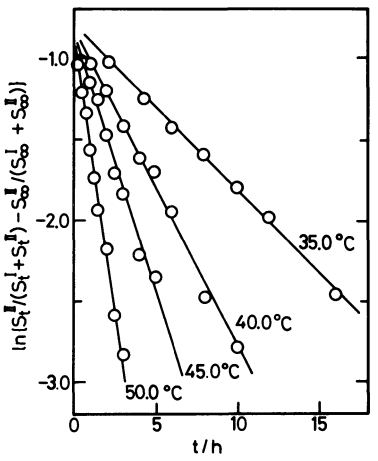

Fig. 4. The plots of $\ln[S_t^{II}/(S_t^I+S_t^{II})-S_\infty^{II}/(S_\infty^I+S_\infty^{II})]$ against time for the epimerization of $\Delta(R)\Lambda(S)$-$[Co(dbme)_2(CH_3SeCH_2CH_2NH_2)]^+$ at 35.0, 40.0, 45.0, and 50.0 °C (S_t^I, S_t^{II}, S_∞^I, and S_∞^{II} denote the areas of bands I and II at time t and at infinite time).

Table 3. Rate Constants for Epimerization of $[Co(\beta\text{-dik})_2(CH_3SeCH_2CH_2NH_2)]^+$ and Equilibrium Constants of the Isomers

$\Delta(R)\Lambda(S) \underset{k_{-1}}{\overset{k_1}{\rightleftharpoons}} \Delta(S)\Lambda(R)$ $k_{obsd}=k_1+k_{-1}$ $K_{eq}=k_1/k_{-1}$

β-dik (K_{eq})	t/°C	$k_{obsd}/10^{-5}$ s^{-1}	$k_1/10^{-5}$ s^{-1}	$k_{-1}/10^{-5}$ s^{-1}
acac[a]	40.0	3.39±0.09	1.78±0.06	1.61±0.06
(K_{eq}=1.1)	45.5	7.18±0.14	3.76±0.10	3.42±0.10
	50.4	14.2 ±0.04	7.44±0.03	6.76±0.03
	55.0	25.8 ±0.06	13.5 ±0.04	12.3 ±0.04
Clacac[a]	35.0	0.63±0.03	0.39±0.02	0.24±0.02
(K_{eq}=1.6)	40.0	1.29±0.05	0.80±0.03	0.50±0.03
	45.0	2.67±0.09	1.64±0.06	1.03±0.06
	50.0	6.01±0.15	3.70±0.11	2.31±0.11
Meacac[a]	30.3	5.87±0.16	3.56±0.11	2.31±0.11
(K_{eq}=1.5)	35.1	11.01±0.19	6.68±0.14	4.33±0.14
	40.2	20.03±0.31	12.14±0.22	7.89±0.22
	45.2	37.60±0.74	22.80±0.53	14.80±0.53
dbme[b]	35.0	2.79±0.07	1.53±0.05	1.26±0.05
(K_{eq}=1.2)	40.0	5.38±0.14	2.94±0.10	2.43±0.10
	45.0	8.80±0.27	4.82±0.19	3.98±0.19
	50.0	18.48±0.39	10.12±0.28	8.36±0.28

Solvent, a): 0.05 mol dm^{-3} Na_2SO_4, b): CH_3OH.

denote the areas of bands I and II at time t and at infinite time). The slope gave the first-order rate constant, k_{obsd} (Fig. 4). The rate constants for the epimerization were calculated from the equilibrium constant, K_{eq}, and the observed rate constant:

$$K_{eq} = k_1/k_{-1} = S_\infty^{II}/S_\infty^{I}$$
$$k_{obsd} = k_1 + k_{-1}.$$

The K_{eq} value was constant for each complex in the temperature range of 30.3—55.0 °C. The values of k_1 and k_{-1} are given in Table 3.

The racemization of $[Co(CH_3SeCH_2CH_2NH_2)(tren)]^{3+}$ and related complexes has been suggested to take place intramolecularly by pyramidal inversion at the selenium atom which proceeds via a trigonal intermediate.[2] The epimerization of $[Co(\beta\text{-dik})_2(CH_3SeCH_2CH_2NH_2)]^+$ also seems to proceed intramolecularly, since the rates are independent of pH.

Eyring treatments of $\ln(k_1/T)$ and $\ln(k_{-1}/T)$ vs. T^{-1} (Fig. 5) yielded activation parameters given in Table 4. The $\Delta G^{\ddagger}_{25\,°C}$ values for inversion of $[Co(\beta\text{-dik})_2(CH_3SeCH_2CH_2NH_2)]^+$ decrease in the order β-dik=Clacac>acac>dbme>Meacac. This order coincides with the decreasing order of $\Delta H^{\ddagger}$ values. The decrease in $\Delta G^{\ddagger}_{25\,°C}$ values comes mainly from a decrease in $\Delta H^{\ddagger}$, the $\Delta S^{\ddagger}$ values making relatively small contributions. Examination of molecular models indicates that the substituents (Cl, Me, Ph) on a β-diketonate chelate ring do not induce a large steric effect on the inversion at the selenium atom. Thus the enthalpy change associated with the inversion seems to arise from the electronic influence of the substituents on β-diketonate chelate rings. This view is supported by the Hammett correlation shown in Fig. 6, where logarithms of the observed rate constants at 40 °C for the Clacac and Meacac complexes relative to that for the acac complex are plotted against the Hammett σ_p values. The aromatic character of the coordinated acac is known.[18] The data follow a straight line with a slope equal to −2.9. The result shows that the Cl (or Me) substituent of the Clacac (or Meacac) complex, which is at the para position to the central metal, withdraws (or releases) the electron on the selenium atom via the central metal to decrease (or increase) the rate. For the inversion rates at sulfur of organic sulfonium ions, it is well-known that substituents more electronegative than carbon slow the rate.[19] The Hammett relationship was also reported to hold for the proton-exchange rate of ethylenediamine of $[Co(acac, Bracac, or NO_2acac)_2(en)]^+$.[20]

If we take the pK_a value of a substituted Hacac in the enol form (Hacac: 8.23, HMeacac: 9.2, Hdbme: 9.1)[21] as a measure of the electronic effect of the substituent, then the order of $\Delta G^{\ddagger}_{25\,°C}$ and $\Delta H^{\ddagger}$ values should be related to that of the pK_a values. The $\Delta G^{\ddagger}_{25\,°C}$ and $\Delta H^{\ddagger}$ values of $[Co(\beta\text{-dik})_2(CH_3SeCH_2CH_2NH_2)]^+$ decrease in the order β-dik=acac>dbme>Meacac. The order is in accord with that of electron-

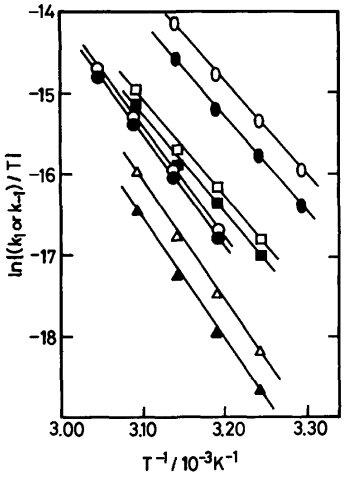

Fig. 5. Eyring treatments of $\ln(k_1/T)$ vs. T^{-1} and $\ln(k_{-1}/T)$ vs. T^{-1} for $[Co(\beta\text{-dik})_2(CH_3SeCH_2CH_2NH_2)]^+$, β-dik=acac(○,●) Clacac (△,▲), Meacac(0,◐), and dbme(□,■).

Table 4. Thermodynamic Parameters for Epimerization of $[Co(\beta\text{-dik})_2(CH_3SeCH_2CH_2NH_2)]^+$

$$\Delta(R)\Lambda(S) \underset{(2)\ k_{-1}}{\overset{(1)\ k_1}{\rightleftharpoons}} \Delta(S)\Lambda(R)$$

β-dik		$\Delta H^{\ddagger}$/kJ mol^{-1}	$\Delta S^{\ddagger}$/J mol^{-1} K^{-1}	$\Delta G^{\ddagger}_{25\,°C}$/kJ mol^{-1}
acac	(1)	113.2±1.8	25.2±5.6	105.7±2.5
	(2)	113.3±1.8	25.1±5.7	105.8±2.5
Clacac	(1)	121.3±2.2	44.8±6.9	107.9±3.0
	(2)	121.3±2.1	40.9±6.7	109.1±2.9
Meacac	(1)	96.9±1.9	−10.8±6.0	100.1±2.6
	(2)	97.0±2.5	−14.0±7.9	101.2±3.4
dbme	(1)	99.3±2.9	−15.2±9.1	103.8±4.0
	(2)	99.4±2.9	−16.3±9.1	104.3±4.0

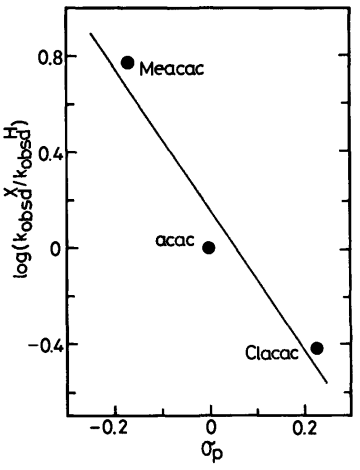

Fig. 6. Hammett's relationship for the inversion rate of $[Co(acac, Clacac, or Meacac)_2(CH_3SeCH_2CH_2NH_2)]^+$.

withdrawing tendency of the substituents predicted from the pK_a values. That the dbme and Meacac ligands increase electron density on the selenium atom via the central metal is also suggested by ^1H NMR spectra; for example, the CH_3Se- signal of the dbme complex is observed at a higher field than that of the acac complex (Table 1). Thus, the difference in inversion rate among the present complexes is explained by the difference in electron density on the selenium atom which is induced by the substituent on the β-diketonate skeleton. The inversion rate of $[Co(NO_2acac)_2(CH_3SeCH_2CH_2NH_2)]^+$, which has highly electron-withdrawing NO_2- groups (σ_p=0.78), is expected to be very slow. Unfortunately, the complex was so unstable that we could not determine the rate.

The present work was partially supported by a Grant-in-Aid for Scientific Research No. 58470032 from the Ministry of Education, Science, and Culture.

References

1) E. W. Abel, S. K. Bhargava, and K. G. Orrell, *Prog. Inorg. Chem.*, **32**, 1 (1984) and the references cited therein.
2) K. Nakajima, K. Tozaki, M. Kojima, and J. Fujita, *Bull. Chem. Soc. Jpn.*, **58**, 1130 (1985).
3) K. Nakajima, M. Kojima, M. Fujita, and J. Fujita, *J. Chromatogr.*, **301**, 241 (1984).
4) K. Nakajima, M. Kojima, and J. Fujita, *J. Chromatogr.*, **362**, 281 (1986).
5) K. Kuroda, K. Yoshitani, K. Kunigita, Y. Kamiiba, and K. Watanabe, *Bull. Chem. Soc. Jpn.*, **49**, 2445 (1976).
6) M. Fujita, Y. Yoshikawa, and H. Yamatera, *Chem. Lett.*, **1982**, 437.
7) A. W. Johnson, E. Markham, and R. Prince, *Org. Synth.*, Coll. Vol. V, 785 (1973).
8) J. P. Collman and W. L. Young, III, *Inorg. Synth.*, VII, 205 (1963).
9) J. P. Collman, "Transition Metal Chemistry," ed by R. L. Carlin, Marcel Dekker, Inc., Vol. 2, New York (1966), p. 35, and the references cited therein.
10) L. J. Boucher, *Inorg. Chem.*, **9**, 1202 (1970).
11) Y. Ouyang, M. Kojima, and J. Fujita, *Bull. Chem. Soc. Jpn.*, **57**, 3574 (1984).
12) T. Konno, K. Okamoto, and J. Hidaka, *Bull. Chem. Soc. Jpn.*, **57**, 3104 (1984).
13) T. Konno, K. Okamoto, H. Einaga, and J. Hidaka, *Bull. Chem. Soc. Jpn.*, **58**, 1119 (1985).
14) C. A. Fleming and D. A. Thornton, *J. Mol. Struct.*, **25**, 271 (1975).
15) I. Hanazaki, F. Hanazaki, and S. Nagakura, *J. Chem. Phys.*, **50**, 265 (1969); D. W. Barnum, *J. Inorg. Nucl. Chem.*, **22**, 183 (1961).
16) C. T. Liu and B. Douglas, *Inorg. Chem.*, **3**, 1356 (1964); B. Douglas, *ibid.*, **4**, 1813 (1965).
17) K. Ogino, K. Murano, and J. Fujita, *Inorg. Nucl. Chem. Lett.*, **4**, 351 (1965).
18) J. P. Collman, R. L. Marchall, and W. L. Young, III, *Chem. Ind. (London)*, **1962**, 1380.
19) J. B. Lambert, *Top. Stereochem.*, **6**, 19 (1971).
20) K. Ito, H. Isono, E. Iwamoto, and Y. Yamamoto, *Inorg. Chem.*, **23**, 850 (1984).
21) M. P. Rumph and R. L. Riviere, *C. R. Acad. Sci. Paris*, **244**, 902 (1957).

 © 1986 The Chemical Society of Japan Bull. Chem. Soc. Jpn., 59, 3511—3514 (1986)

The Crystal and Molecular Structure of 6-Bromo[2.2]paracyclo-(4,8)[2. 2]metaparacyclophane

Yosuke Koizumi, Hisanori Horita, Tetsuo Otsubo, Nobutami Kasai,*,† and Soichi Misumi*

The Institute of Scientific and Industrial Research, Osaka University, Ibaraki, Osaka 567

†Department of Applied Chemistry, Faculty of Engineering, Osaka University, Suita, Osaka 565

(Received February 20, 1986)

The molecular structure of the title compound has been determined by means of X-ray diffraction. $C_{26}H_{25}Br$, M 417.4, orthorhombic, space group $P2_12_12_1$, a=12.713(1), b=14.998(1), c=10.156(1) Å, V=1936.3(1) Å^3, D_m=1.43 g cm^{-3}, D_c=1.432 g cm^{-3} for Z=4.

Novel skeletal rearrangement of triple-layered [2.2]paracyclophane (**1**) to triple-layered [2.2]metaparacyclophanes (**2**—**4**) with several Friedel-Crafts acids has been reported by Misumi and coworkers.[1]

Structures of [2.2]metacyclo(4,7)[2.2]paracyclophane (**2**) and [2.2]paracyclo(4,6)[2.2]metaparacyclophane (**3**) were determined by PMR and alternative syntheses,[2]

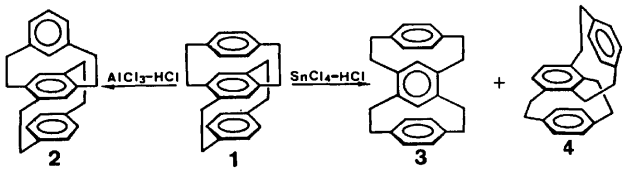

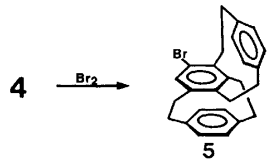

and molecular structures of **2** and **3** have been reported recently.[3] This paper deals with the molecular structure of **5** which was derived from the third rearranged isomer, [2.2]paracyclo(4,8)[2.2]metaparacyclophane (**4**) in quantitative yield. A preliminary result of the structure has been reported.[1]

Experimental.

Colorless bipyramidal crystal, recrystallized from benzene-ethyl acetate, with approximate dimensions of 0.5× 0.5×0.5 mm was mounted on a Rigaku automated, four-circle diffractometer. Unit cell dimensions and integrated intensities were measured on the diffractometer with Zr-filtered Mo $K\alpha$ radiation (λ=0.71069 Å). Intensity data were collected by the θ—2θ scan technique: The 2θ scan rate was 2° min^{-1}, and the scan width was from $\{2\theta(\alpha_1)-0.9\}$ to $\{2\theta(\alpha_2)+0.9\}$°. Backgrounds were measured for 10 s at both ends of a scan. Five standard reflections were measured after every 50 reflections, which showed no intensity decrease during the experiment. In total, 2833 reflections out of 3416 were observed. Usual Lorentz and polarization corrections were applied but an absorption correction was ignored [μ(Mo $K\alpha$)=23.7 cm^{-1}].

Structure Solution and Refinement

The structure was solved by the heavy atom method, and refined anisotropically by the block-diagonal least-squares procedure (*HBLS* V).[4] The function minimized was $\sum w(\Delta F)^2$. Hydrogen atoms were located on the calculated positions, which were confirmed on the difference Fourier map. They were refined isotropically. The R value converged to 0.080 for non-zero (0.117 for all) reflections. The weighting schemes used were $w=(F_{max}/|F_o|)^2$ for $|F_o| \geqq F_{max}$, w=1 for $|F_o| < F_{max}$, and w=0.1 for $|F_o|$=0. Atomic parameters are listed in Table 1.††

Table 1. Final Atomic Coordinates of Non-Hydrogen Atoms with Equivalent Isotropic Temperature Factors[5] Estimated Standard Deviations in Parentheses

Atom	x	y	z	B_{eq}/Å^2
BR	0.28342(7)	0.46252(7)	0.42830(11)	5.4
C(1)	0.5080(6)	0.4725(5)	0.5654(8)	3.5
C(2)	0.4652(8)	0.5049(6)	0.7041(8)	4.5
C(3)	0.4748(7)	0.6051(6)	0.7129(7)	4.1
C(4)	0.5717(7)	0.6450(6)	0.7329(7)	4.0
C(5)	0.5953(8)	0.7286(6)	0.6794(8)	4.3
C(6)	0.5188(7)	0.7708(5)	0.6027(7)	3.7
C(7)	0.4174(7)	0.7399(6)	0.6076(8)	4.1
C(8)	0.3949(6)	0.6580(6)	0.6622(7)	4.0
C(9)	0.5514(8)	0.8316(5)	0.4902(9)	4.1
C(10)	0.5956(7)	0.7717(5)	0.3744(8)	3.5
C(11)	0.5337(5)	0.6863(4)	0.3598(7)	2.5
C(12)	0.4383(6)	0.6846(5)	0.2867(7)	3.1
C(13)	0.3691(6)	0.6138(6)	0.3043(8)	3.4
C(14)	0.3922(5)	0.5485(5)	0.3943(7)	2.9
C(15)	0.4885(5)	0.5415(5)	0.4571(7)	2.6
C(16)	0.5635(4)	0.6078(4)	0.4280(7)	2.3
C(17)	0.6797(5)	0.5919(5)	0.4611(7)	3.0
C(18)	0.7360(6)	0.5350(6)	0.3540(9)	4.1
C(19)	0.6946(6)	0.5626(6)	0.2199(8)	3.9
C(20)	0.6069(6)	0.5186(5)	0.1676(8)	3.5
C(21)	0.5361(7)	0.5621(5)	0.0866(8)	3.9
C(22)	0.5503(7)	0.6516(5)	0.0590(7)	3.8
C(23)	0.6483(8)	0.6893(6)	0.0854(8)	4.4
C(24)	0.7197(8)	0.6450(6)	0.1653(9)	4.5
C(25)	0.4546(8)	0.7102(6)	0.0358(8)	4.2
C(26)	0.4172(8)	0.7505(5)	0.1736(8)	4.0

†† Tables of anisotropic temperature factors, coordinates of hydrogen atoms, and observed and calculated structure factors are kept at the Chemical Society of Japan, Document No. 8646.

Atomic scattering factors used were taken from International Tables for X-Ray Crystallography.[6] Calculations were done mainly on a NEAC 2200—500 computer at the Computation Center, Osaka University, and at the final stage an ACOS 850 computer was used at the Crystallographic Research Center, Institute for Protein Research, Osaka University.

Results and Discussion

Molecular Structure. Structure of the molecule[7] is shown in Fig. 1. Bond distances and bond angles are given in Fig. 2. Both the upper and lower layer benzene rings are in boat form. The deformation angles[3] p_1 and q_1 at the C(3) atom (Fig. 3) are 11.6 and 16.4°, p_2 and q_2 at the C(6) 12.7 and 14.9°, p_3 and q_3 at the C(19) 11.7 and 16.0°, and p_4 and q_4 at the C(22) 13.6 and 13.7°. These benzene rings have normal bond distances [av. 1.387 and 1.390 Å]. Among the bond angles in these rings, the inner angles at the bow and stern of the boat form show a tendency to have the smaller angles than 120°, though it is not fully significant: C(4)-C(3)-C(8)=117.3(8), C(5)-C(6)-C(7)=118.7(8), C(20)-C(19)-C(24)=116.7(8), and C(21)-C(22)-C(23)=118.1(8)°.

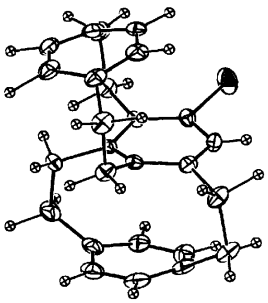

(a)

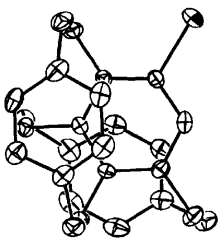

(b)

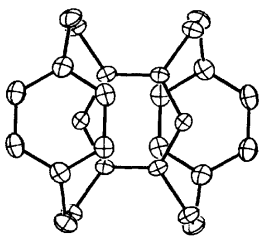

(b′)

Fig. 1. Molecular structure[7] of 6-bromo[2.2]paracyclo(4,8)[2.2]metaparacyclophane.
Non-hydrogen atoms are expressed by thermal ellipsoids with 30% probability level.
(a): A perspective view, Hydrogen atoms are expressed as spheres with $B=1.0$ Å^2 (b): Projected onto the plane defined by the C(11), C(12), C(14), and C(15) atoms, Hydrogen atoms are omitted for clarity. (b′): Similar projection as (b) of [2.2]paracyclo(4,6)[2.2]metaparacyclophane.[3]

The central four-bridged benzene ring is twisted. The dihedral angle between the plane made by the C(11), C(12), C(13) atoms and that by the C(14), C(15),

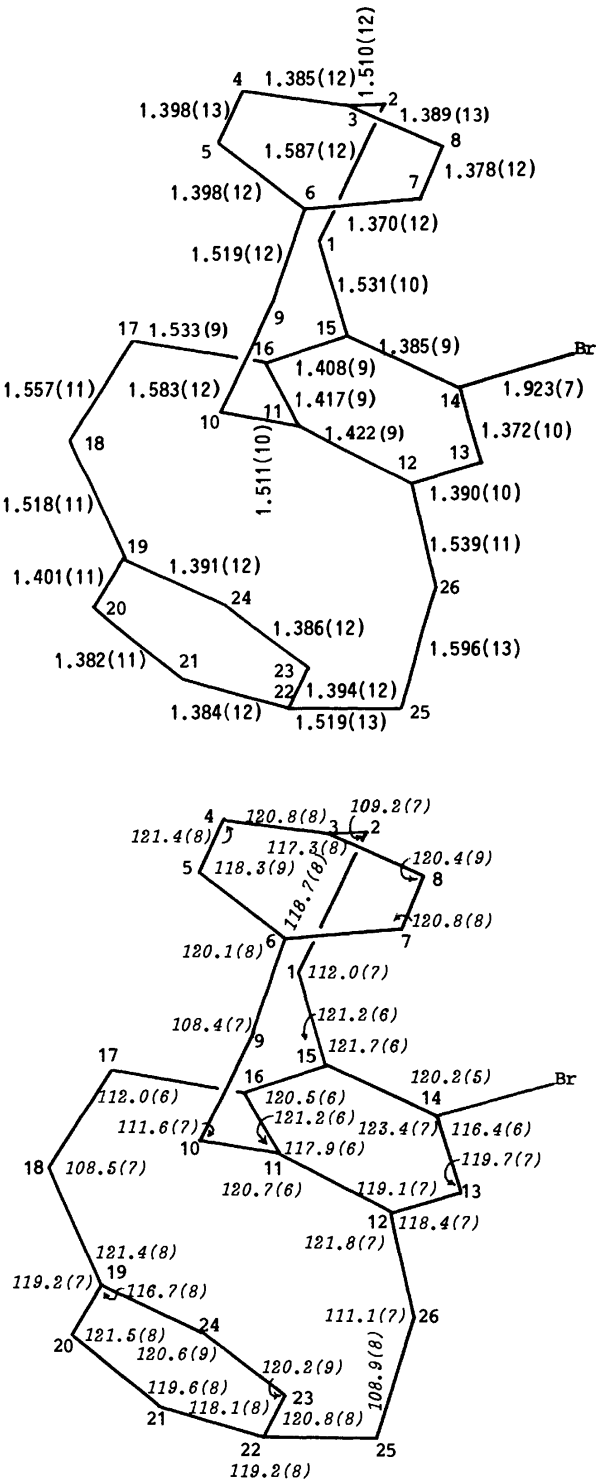

C(2)-C(3)-C(8) 119.2(8), C(14)-C(15)-C(16) 116.6(6)
C(7)-C(6)-C(9) 119.2(8), C(11)-C(16)-C(17) 119.6(6)
C(15)-C(16)-C(17) 119.7(6)

Fig. 2. Bond distances [l/Å] and bond angles [ϕ/°] with estimated standard deviations in parentheses.

and C(16) is 7.3°. The bending angles[3] of q_5 at the C(15) [6.4°] and q_6 at the C(12) [8.2°] are much larger then those of q_7 at the C(11) [4.8°] and q_8 at the C(16) [1.3°]. The Br-C(14) bond makes an angle of 1.3° with the plane formed by the C(13), C(14), and C(15) atoms.

In the four ethylene bridges between the outer and central benzene rings, four central C-C bonds [1.587(12), 1.583(12), 1.557(11), and 1.596(13) Å) can be compared with the corresponding distances in two triple-layered metaparacyclophanes [1.579(4) and 1.572 (4) Å and 1.558(8) and 1.572(6) Å].[3] Torsional angles around the C(1)-C(2) and C(25)-C(26) bonds [32.1 and 32.8°] are equal, which are much smaller than those around the C(9)-C(10) and C(17)-C(18) [38.1 and 38.0°]. It seems that the C(1)-C(2)-C(3), C(6)-C(9)-C(10), C(17)-C(18)-C(19), and C(22)-C(25)-C(26) angles [109.2(7), 108.4(7), 108.5(7), and 108.9(8)°] of the outer ring sides are smaller than the C(2)-C(1)-C(15), C(9)-C(10)-C(11), C(16)-C(17)-C(18), and C(12)-C(26)-C(25) [112.0(7), 111.6(7), 112.0(6), and 111.1(7)°, respectively]. The overlapping of three benzene rings (Fig. 1(b)) is larger than that of [2.2]paracyclo-(4,6)[2.2]metaparacyclophane (Fig. 1(b′)).[3] The shortest atomic contact between the upper and central benzene rings is C(3)···C(15) [2.773(10) Å] and that between the lower and central rings is C(12)···C(22) [2.760(11) Å].

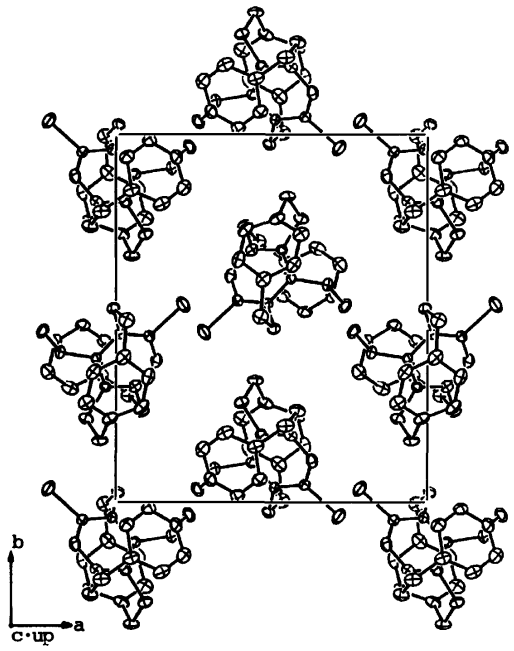

Fig. 4. Crystal structure projected along the *c* axis.[7] Non-hydrogen atoms are expressed as thermal ellipsoids with 30% probability level. Hydrogen atoms are omitted for clarity.

Crystal Structure. The packing mode of molecules in the crystal is drawn in Fig. 4. Molecules are packed rather loosely in the a and b directions, whereas very closely in the c direction: Shortest intermolecular atomic contacts are C(4)····C(22)(x, y, 1+z)=3.325(12) and C(4)····C(25)(x, y, 1+z)=3.555(13) Å.

The authors wish to express their deep thanks to Miss Nobuko Kanehisa for computations at the final stage and *ORTEP* drawings.

References

1) H. Horita, Y. Koizumi, T. Otsubo, Y. Sakata, and S. Misumi, *Bull. Chem. Soc. Jpn.*, **51**, 2668 (1978).

2) N. Kannen, T. Otsubo, Y. Sakata, and S. Misumi, *Bull. Chem. Soc. Jpn.*, **49**, 3307 (1976).

3) Y. Koizumi, T. Toyoda, N. Kasai, and S. Misumi, *Bull. Chem. Soc. Jpn.*, **58**, 3158 (1985).

4) T. Ashida, *HBLS* V, "The Universal Crystallographic Computing System-Osaka," The Computation Center,

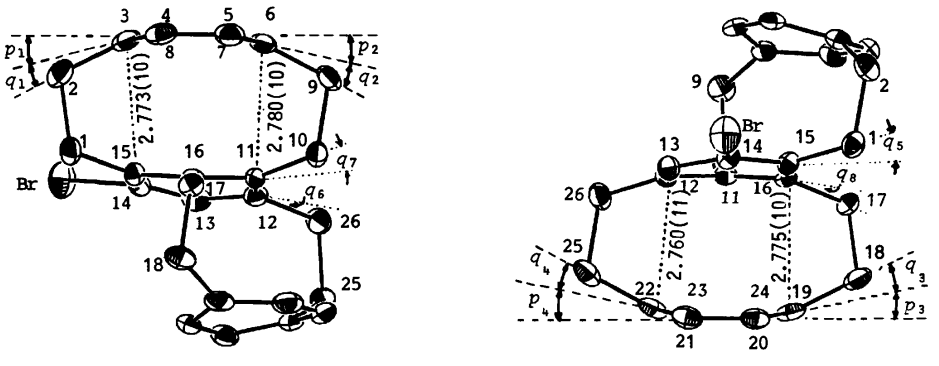

Fig. 3. Side views of the molecule.[7]
Non-hydrogen atoms are expressed as thermal ellipsoids with 30% probability level. Hydrogen atoms are omitted for clarity.
(a): Projected along the C(4)···C(8) and parallel to the plane defined by the C(5), C(6), C(7), and C(8) atoms (b): Projected along the C(20)···C(24) and parallel to the plane defined by the C(20), C(21), C(23), and C(24) atoms.

Osaka Univ. (1978), p. 55.
5) W. C. Hamilton, *Acta Crystallogr.*, **12**, 609 (1959).
6) International Tables for X-Ray Crystallography, Kynoch Press, Birmingham, Vol. IV (1974), p. 71.
7) C. K. Johnson, *ORTEP* II, Report ORNL-5138, Oak Ridge National Laboratory, Tennessee, 1976.

 © 1986 The Chemical Society of Japan Bull. Chem. Soc. Jpn., 59, 3515—3518 (1986)

Regio- and Stereochemistry of Bromochlorinations of Alkynes with Molecular Bromine Chloride and Dichlorobromate(1−) Ion

Takeshi NEGORO* and Yoshitsugu IKEDA
Department of Chemistry, Faculty of Education, Wakayama University,
Sakaedani, Wakayama 640
(Received April 15, 1986)

The bromochlorination of phenyl- and alkyl-substituted acetylenes with tetrabutylammonium dichlorobromate(1−) (**1**) in dichloromethane was found to be *anti*-stereospecific and nonregiospecific (regiospecific in the case of phenylacetylene). Whereas the addition of molecular bromine chloride (**2**) to phenyl-substituted acetylenes was found to give nonstereospecific and regiospecific adducts, the reaction of alkyl-substituted acetylenes gave *anti*-stereospecific and nonregiospecific adducts. These results suggest that the addition of **1** involves an attack of chloride ion to a three-centered π-complex in the product-forming stage, and that the addition of **2** to phenyl-substituted acetylenes involves a vinyl cation intermediate (but a bridged bromonium ion intermediate in the case of alkyl-substituted acetylenes).

The stereochemistry of bromine addition to alkynes has been known to markedly depend both on reaction conditions and on the structure of alkynes.[1,2] *Anti*-stereospecific addition was observed for the bromination of alkynes in the presence of bromide ion.[1,2] However, only a few scattered data have been made available on the bromochlorination of alkynes. The reaction of diphenylacetylene,[3] ethyl 3-butynoate,[4] or 1-hexyne[5] with molecular bromine chloride (**2**) has been reported to give the corresponding bromo chloro adducts in an *anti*-stereospecific manner. We have reported that tetrabutylammonium dichlorobromate-(1−) (**1**) reacted with phenyl- or alkyl-substituted ethylenes to give bromo chloro adducts in nearly quantitative yields, and that the addition took place in an *anti*-stereospecific manner,[6,7] while that the regio- and stereochemistries of the bromochlorination of alkenes[6,7] or dienes[8] with **1** are strikingly different from those with **2**. As a continuation of our studies, we have studied on the regio- and stereochemistries of the reaction of **1** and **2** with various alkynes.

Results and Discussion

The reaction of 1-phenylpropyne (**3a**), 1-hexyne (**3c**), or 2-hexyne (**3d**) with tetrabutylammonium dichlorobromate(1−) (**1**) in CH_2Cl_2 gave a mixture of (*E*)-Markownikoff and (*E*)-*anti*-Markownikoff adducts (**4a**, **c**, and **d** and **5a**, **c**, and **d**, respectively) in nearly quantitative yields (Scheme 1 and Table 1).

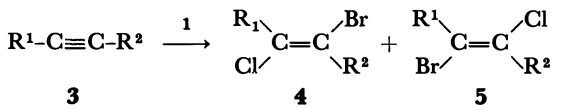

3 **4** **5**

a: R^1=Ph, R^2=Me **c**: R^1=*n*-Bu, R^2=H
d: R^1=*n*-Pr, R^2=Me

Scheme 1.

Similarly, treatments of symmetrical alkynes such as diphenylacetylene (**3e**: R^1=R^2=Ph) and 3-hexyne (**3f**: R^1=R^2=Et) with **1** also gave the corresponding bromo chloro adducts (**4e** and **4f**, respectively) in an *anti*-stereospecific manner (Table 1).

On the other hand, the reaction of phenylacetylene (**3b**: R^1=Ph, R^2=H) with **1** gave a mixture of (*E*)-2-bromo-1-chloro-1-phenylethene (**4b**) and 1-bromo-2-phenylethyne (**6b**) (Scheme 2 and Table 1).

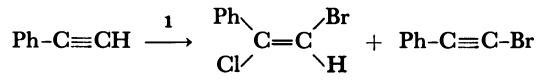

3b **4b** **6b**

Scheme 2.

The formation of **6b** cannot be ascribed to the subsequent secondary reaction of **4b**, since prolonged reaction time did not cause any change in the ratio of the products. Further, the bromo chloro adduct **4b** was stable under the reaction conditions. Formation

Table 1. Regio- and Stereochemistries of the Bromochlorination of Alkynes with **1**[a]

Alkynes	Product composition/%[b]			Yield/%[c]
	(*E*)-M[d]	(*E*)-*a*M[d]	(*Z*)	
3a	89.2	10.8	0	76(97)
3b	100	0	0	42[e]
3c	86.5	13.5	0	81(97)
3d	50.2	49.8	0	81(98)
	(*E*)		(*Z*)	
3e	100		0	93
3f	100		0	80(96)

a) Reactions were carried out with 20 mmol of **1**, 20 mmol of **3**, and 50 ml of CH_2Cl_2 at 20 °C. b) Percentages are normalized to 100%. Determined by ^{1}H NMR analysis. c) Isolated yield. Yields in parentheses were determined by ^{1}H NMR using 1,2-dibromo-1-phenylethane as the internal standard. d) M=Markownikoff adduct (**4**). *a*M=*anti*-Markownikoff adduct (**5**). e) The other product was 1-bromo-2-phenylethyne (**6b**, 58%). Determined by GLC analysis.

of 1-bromo-2-phenylethyne (**6b**) has already been reported for the reaction of **3b** with bromine.[2]

Although attempts to separate two regioisomers (**4** and **5**) were unsuccessful, the orientation of halogen atoms was elucidated mainly on the basis of the chemical shifts of the protons in the ^{1}H NMR spectra of the adducts. The structures of **4** and **5** have been determined by a comparison of their ^{1}H NMR or ^{13}C NMR spectra with those of the corresponding dibromo and dichloro adducts. It has been known that the proton β to a bromine atom is deshielded relative to the one β to a chlorine atom, and that the proton α to a chlorine atom is deshielded relative to the one α to a bromine atom.[5,9] Thus, the methyl protons of **4a** give δ=2.56 but those of **5a** δ=2.45, in agreement with the observation that the methyl protons (δ=2.60) of (*E*)-1,2-dibromo-1-phenylpropene are deshielded relative to those (δ=2.41) of (*E*)-1,2-dichloro-1-phenylpropene. Similarly, the methyl protons (=C-CH_3) of **4d** give δ=2.38 but those of **5d** δ=2.27 (Experimental). Control experiments revealed that all the bromo chloro adducts are stable under the reaction conditions.

Treatments of alkynes (**3a** and **3b**) with molecular bromine chloride (**2**) in CH_2Cl_2 gave the corresponding (*E*)- and (*Z*)-Markownikoff adducts (**4** and **4'**) in a regiospecific and nonstereospecific manner (Scheme 3 and Table 2).

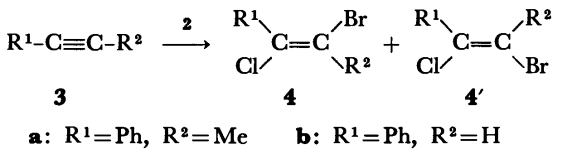

3 **4** **4'**

a: R^1=Ph, R^2=Me **b**: R^1=Ph, R^2=H

Scheme 3.

Table 2. Regio- and Stereochemistries of the Bromochlorination of Alkynes with **2**[a]

Alkynes	Product composition/%[b]			Yield/%[c]
	(*E*)-M[d]	(*Z*)-M[d]	(*E*)-*a*M[d]	
3a	78.1 (77.9)	21.9 (22.1)	0	69
3b	62.8	37.2	0	70
3c	90.9	0	9.1	71
3d	47.5[e]	0	52.5[e]	73
	(*E*)	(*Z*)		
3e	100	0		20[f]
3f	(100)	(0)		75

a) Reactions were carried out with 10 mmol of **2**, 20 mmol of **3**, and 50 ml of CH_2Cl_2 at 20 °C. b) Percentages are normalized to 100%. Determined by ^{1}H NMR analysis. Yields in parentheses were determined by GLC analysis. c) Determined by GLC analysis. d) M=Markownikoff adduct. *a*M=*anti*-Markownikoff adduct. e) Determined by ^{13}C NMR analysis. f) Ref. 3. Isolated yield.

As with the reaction with **1**, the reaction of alkyl-substituted acetylenes (**3c** and **3d**) with **2** gave a mixture of (*E*)-Markownikoff and (*E*)-*anti*-Markownikoff adducts (**4** and **5**) in a nonregiospecific and *anti*-stereospecific manner, and the reaction of 3-hexyne (**3f**) gave the *anti*-stereospecific adduct (**4f**) (Table 2). The yields of the bromo chloro adducts were lower than those in the reaction of **1** because dibromo- and dichloroalkenes were formed as by-products in every case.

An inspection of the data in Tables 1 and 2 clearly reveals that the regio- and stereochemistries of the bromochlorinations of alkynes depend greatly both on the structure of alkynes and on the bromochlorinating agents employed. Therefore, the electronic structure of the intermediate in the product-forming step must depend both on the substituent on the acetylene linkage and on the bromochlorinating agents.

Regio- and Stereochemistries of the Reaction of 3 with 2. As shown in Table 2, the addition of molecular bromine chloride (**2**) to phenyl-substituted alkynes such as **3a** and **3b** is nonstereospecific and regiospecific. This result can be explained by assuming a mechanism involving the attack of chloride ion on an open vinyl cation intermediate **7**, in which the cationic character of the phenyl-substituted carbon atom is stabilized by overlap of *p*-orbitals of the phenyl group; a similar reaction intermediate has been suggested for the bromination of these alkynes with molecular bromine.[1,2]

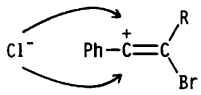

(7)

On the other hand, the addition of **2** to alkyl-substituted acetylenes **3c**, **3d**, and **3f** gave only *trans*-bromo chloro adducts (Table 2). Such an *anti*-stereospecific addition of **2** to these alkynes are fully in accordance with the mechanism involving a bridged bromonium ion intermediate **8**.[2]

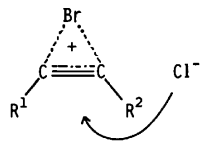

(8)

Meanwhile, the addition of **2** to monoalkyl-substituted acetylene **3c** gave the Markownikoff adduct **4c** as the major product. This implies that the attack of chloride ion on the intermediate **8** occurs at the alkyl-substituted carbon atom. Thus, the orientation of the addition of **2** would be due to the electronic effect of the alkyl substituent which stabilizes the developed cationic character on the alkyl-substituted carbon atom in the intermediate **8**.[5]

Regio- and Stereochemistries of the Reaction of 3 with 1. In contrast to the addition of **2** to alkynes, the

addition of **1** is in an *anti*-stereospecific manner irrespective of substituents on the acetylene linkage (Table 1). Thus, the addition of **1** to phenyl-substituted alkynes **3a** and **3b** gave only the *anti*-stereospecific adducts. This result cannot be explained on the basis of the mechanism involving an open vinyl cation intermediate **7** for the addition of **2** to **3a—b** as described above. We would like to suggest another possible mechanism which involves the attack of chloride ion on a three-centered π-complex intermediate **9** in a product-forming step with a very little charge development on the unsaturated carbon; a similar intermediate has been suggested for the addition of **1** to alkenes and dienes.[6-8]

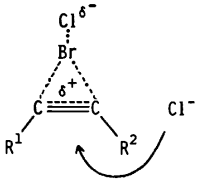

(9)

Meanwhile, the addition of **1** to phenylacetylene (**3b**) gave only the regiospecific Markownikoff adduct **4b**. The addition to 1-phenylpropyne (**3a**) was in a regioselective Markownikoff manner. These results imply that the attack of chloride ion on the intermediate **9** occurs on the phenyl-substituted carbon atom. Thus, the orientation of the bromochlorination with **2** would depend on the electronic effect of phenyl substituent which stabilizes the developed cationic character on the phenyl-substituted carbon atom in the intermediate **9**. The addition of **1** to 1-hexyne (**3c**) gave the regioselective Markownikoff adduct **4c**. Thus, the orientation of addition with **1** can be influenced also by the electronic effect of the alkyl substituent.

Experimental

All the melting points and boiling points are uncorrected. NMR spectra were recorded on a JEOL JNM FX-60Q and a JEOL C-60HL spectrometer, with TMS as the internal standard. Mass spectra were recorded on a JMS-D-300 mass spectrometer. GLC analyses were performed on a Yanako G-180 gas chromatograph with a Silicone SE-30(10%)-Chromosorb WAW DMCS (2 m) column, with helium as the carrier gas. All the organic starting materials, including the solvents, were distilled just before use.

Tetrabutylammonium dichlorobromate(1−) (**1**) was prepared by the known procedure.[10] Bromine chloride (**2**) was prepared by adding an equimolar amount of bromine to a chlorine-carbon tetrachloride solution.

Reaction of Alkynes with 1. General Procedure: To a solution of **3** (20 mmol) in dichloromethane (50 ml) was added **1** (7.87 g, 20 mmol) at 20 °C over 20 min with stirring. After the yellow color disappeared, the reaction mixture was washed with water and dried over Na_2SO_4. After the solvent was removed by evaporation, the products were purified by distillation. The results are shown in Table 1. Although attempts to separate **4** and **5** were unsuccessful, these structures were determined by a comparison of their ^1H NMR spectra (^{13}C NMR spectra in some cases) with those of the corresponding dibromo and dichloro analogs.

A Mixture of (*E*)-2-Bromo-1-chloro- and (*E*)-1-Bromo-2-chloro-1-phenylpropenes (4a and 5a) from 1-Phenylpropyne (3a): Bp 78—79 °C/2 mmHg (1 mmHg=133.322 Pa); MS *m/z* (rel intensity) 230 (M^+; 100), 232 (135), and 234 (32). Found: *m/z* 229.9488. Calcd for C_9H_8BrCl: M, 229.9498. ^1H NMR ($CDCl_3$) (an asterisk indicates **5a**) δ=2.45,* 2.56 (3H, s, CH_3), and 7.30—7.40 (5H, m, C_6H_5). These assignments were supported for the dibromo and dichloro analogs as follows: (*E*)-1,2-dibromo-1-phenylpropene, ^1H NMR ($CDCl_3$) δ=2.60 (3H, s, CH_3) and 7.20—7.40 (5H, m, C_6H_5); (*E*)-1,2-dichloro-1-phenylpropene, ^1H NMR ($CDCl_3$) δ=2.41 (3H, s, CH_3) and 7.20—7.50 (5H, m, C_6H_5).

(*E*)-2-Bromo-1-chloro-1-phenylethene (4b) and 1-Bromo-2-phenylethyne (6b) from Phenylacetylene (3b): **4b**: bp 85—90 °C/6 mmHg; MS *m/z* (rel intensity) 216 (M^+; 100), 218 (128), and 220 (32). Found: *m/z* 215.9310. Calcd for C_8H_6BrCl: M, 215.9342. ^1H NMR ($CDCl_3$) δ=6.56 (1H, s, CH) and 7.30—7.67 (5H, m, C_6H_5). **6b**: bp 76—78 °C/6 mmHg (lit,[11] bp 40—41 °C/0.1 mmHg); MS *m/z* (rel intensity) 180 (M^+; 100) and 182 (100). Found: *m/z* 179.9550. Calcd for C_8H_5Br: M, 179.9575. ^1H NMR ($CDCl_3$) δ=7.28—7.53 (m, C_6H_5). The ^1H NMR spectrum of **4b** corresponds well with that reported in the literature.[12]

A Mixture of (*E*)-1-Bromo-2-chloro- and (*E*)-2-Bromo-1-chloro-1-hexenes (4c and 5c): Bp 55—56 °C/25 mmHg; MS *m/z* (rel intensity) 196 (M^+; 100), 198 (132), and 200 (32). Found: *m/z* 195.9648. Calcd for $C_6H_{10}BrCl$: M, 195.9655. ^1H NMR ($CDCl_3$) (an asterisk indicates **5c**) δ=0.75—1.10 (3H, br. t), 1.15—1.90 (4H, m), 2.40—2.80 (2H, m), 6.20, and 6.27* (1H, 2s); ^{13}C NMR ($CDCl_3$) (an asterisk indicates **5c**) δ=13.8, 21.6, 21.7,* 28.5,* 29.2, 34.5, 34.9,* 101.1,* 114.8, 127.0, and 136.9.* The ^1H and ^{13}C NMR of a mixture (**4c** and **5c**) correspond well with those reported in the literature.[5]

A Mixture of (*E*)-2-Bromo-3-chloro- and (*E*)-3-Bromo-2-chloro-2-hexenes (4d and 5d) from 2-Hexyne (3d): Bp 35—36 °C/5 mmHg; MS *m/z* (rel intensity) 196 (M^+; 100), 198 (133), and 200 (32). Found: *m/z* 195.9650. Calcd for $C_6H_{10}BrCl$: M, 195.9655. ^1H NMR ($CDCl_3$) (an asterisk indicates **5d**) δ=0.93 (3H, t, *J*=7.3 Hz), 1.18—1.79 (2H, m), 2.27,* 2.38 (3H, 2s), and 2.43—2.74 (2H, m); ^{13}C NMR ($CDCl_3$) (an asterisk indicates **5d**) δ=13.0,* 13.1, 20.3, 20.9,* 25.8,* 25.9, 39.6,* 40.1, 115.9, 121.7,* 125.4,* and 130.5. These assignments were supported for the dibromo and dichloro analogs as follows: (*E*)-2,3-dibromo-2-hexene: ^1H NMR ($CDCl_3$) δ=0.94 (3H, t, *J*=6.7 Hz), 1.28—1.85 (2H, m), 2.41 (3H, s), and 2.65 (2H, t, *J*=7.2 Hz); ^{13}C NMR ($CDCl_3$) δ=13.0, 20.8, 28.8, 42.4, 115.2, and 121.8. (*E*)-2,3-dichloro-2-hexene: ^1H NMR ($CDCl_3$) δ=0.93 (3H, t, *J*=6.7 Hz), 1.26—1.88 (2H, m), 2.00 (3H, s), and 2.52 (2H, t, *J*=7.2 Hz); ^{13}C NMR ($CDCl_3$) δ=13.1, 20.2, 23.2, 37.5, 124.9, and 129.9.

(*E*)-1-Bromo-2-chloro-1,2-diphenylethene (4e) from Diphenylacetylene (3e): Mp 170—172 °C (lit,[3] 173—175 °C); ^1H NMR ($CDCl_3$) δ=7.30—7.66 (m, $2C_6H_5$); ^{13}C NMR ($CDCl_3$) δ=117.7, 128.2, 128.8, 129.0, and 129.1.

(*E*)-3-Bromo-4-chloro-3-hexene (4f) from 3-Hexyne (3f): Bp 55—57 °C/25 mmHg; MS *m/z* (rel intensity) 196 (M^+;

100), 198 (130), and 200 (33). Found: *m/z* 195.9649. Calcd for $C_6H_{10}BrCl$: M, 195.9655. ^1H NMR ($CDCl_3$) δ=1.10 (6H, t, J=7.3 Hz) and 2.41—2.83 (4H, m); ^{13}C NMR ($CDCl_3$) δ=11.4, 12.2, 31.7, 32.2, 122.1, and 130.8.

Reaction of Alkynes (3) with Bromine Chloride (2). To a solution of **3** (20 mmol) in CH_2Cl_2 (50 ml) was added 5.5 ml of BrCl (**2**) solution in CCl_4 (1.8 mol dm^{-3}) at 20 °C over 5 min with stirring. After the reaction completed, the solvent and unreacted alkyne were removed under reduced pressure and the residues were analyzed by GLC and ^1H NMR or ^{13}C NMR. The results are given in Table 2. In all cases, GLC analyses showed the presence of 11—15% of the dichloro adduct and 12—17% of the dibromo adduct as by-products.

The reaction of 1-phenylpropyne (**3a**) with **2** gave a mixture of (*E*)-2-bromo-1-chloro- and (*Z*)-2-bromo-1-chloro-1-phenylpropenes (**4a** and **4a'**, 69%) (**4a**:**4a'**=78:22) with dichloro and dibromo adducts (31%) by GLC analysis. After the bromo chloro adducts were separated by distillation, a column chromatography (silica gel, with hexane as the eluent) of the mixture of **4a** and **4a'** gave almost pure **4a** and **4a'**. **4a**: MS *m/z* (rel intensity) 230 (M^+; 100), 232 (132), and 234 (32). Found: *m/z* 229.9487. Calcd for C_9H_8BrCl: M, 229.9498. ^1H NMR ($CDCl_3$) δ=2.56 (3H, s, CH_3) and 7.30—7.40 (5H, m, C_6H_5). **4a'**: MS *m/z* (rel intensity) 230 (M^+; 100), 232 (133), and 234 (30). Found: *m/z* 229.9485. Calcd for C_9H_8BrCl: M, 229.9498. ^1H NMR ($CDCl_3$) δ=2.32 (3H, s, CH_3) and 7.30—7.40 (5H, m, C_6H_5).

The reaction of phenylacetylene (**3b**) with **2** gave a mixture of (*E*)-2-bromo-1-chloro- and (*Z*)-2-bromo-1-chloro-1-phenylethenes (**4b** and **4b'**, 70%) (**4b**:**4b'**=63:37 by ^1H NMR analysis) with dichloro and dibromo adducts (26%) and a small amount of 1-bromo-2-phenylethyne (**6b**, 4%) by GLC analysis. Although the isolation of **4b** and **4b'** was not carried out, the retention time of GLC and the ^1H NMR (δ=6.56, vinyl proton of **4b** and δ=6.82, vinyl proton of **4b'**) agreed with those of a sample prepared by the reaction of **3b** with copper(II) chloride and bromine.[12]

The authors sincerely wish to thank Professor Shigeru Oae of Okayama University of Science for his kind guidance.

References

1) J. A. Pincock and Y. Yates, *J. Am. Chem. Soc.*, **90**, 5643 (1968).
2) J. A. Pincock and Y. Yates, *Can. J. Chem.*, **48**, 3332 (1970).
3) R. E. Buckles, J. L. Forrester, R. L. Burham, and T. W. McGee, *J. Org. Chem.*, **25**, 24 (1960).
4) J. Tendil, M. Verney, and R. Vassiere, *Tetrahedron*, **30**, 579 (1974).
5) V. L. Heasley, D. F. Shellhamer, J. A. Iskikian, D. L. Street, and G. E. Heasley, *J. Org. Chem.*, **43**, 3139 (1978).
6) T. Negoro and Y. Ikeda, *Bull. Chem. Soc. Jpn.*, **57**, 2111 (1984).
7) T. Negoro and Y. Ikeda, *Bull. Chem. Soc. Jpn.*, **57**, 2116 (1984).
8) T. Negoro and Y. Ikeda, *Bull. Chem. Soc. Jpn.*, **58**, 3655 (1985).
9) R. M. Silverstein and G. C. Bassler, "Spectrometric Identification of Organic Compounds," 2nd ed, Wiley, New York (1967).
10) A. I. Popov and R. E. Buckles, *Inorg. Synth.*, Vol. V, 172 (1957).
11) S. I. Miller, G. R. Ziegler, and R. Wieleseck, *Org. Synth.*, Coll. Vol. V, 921 (1973).
12) S. Uemura, H. Okazaki, A. Onoe, and M. Okano, *J. Chem. Soc., Perkin Trans. 1*, **1979**, 548.

 © 1986 The Chemical Society of Japan Bull. Chem. Soc. Jpn., 59, 3519—3522 (1986)

Bromochlorination of Alkenes with Dichlorobromate(1−) Ion. V. Regio- and Stereochemistry for the Bromochlorination of Styrene Derivatives with Dichlorobromate(1−) Ion in Protic Solvents

Takeshi NEGORO* and Yoshitsugu IKEDA
Department of Chemistry, Faculty of Education, Wakayama University, Sakaedani, Wakayama 640
(Received April 24, 1986)

The bromochlorination of styrene derivatives with tetrabutylammonium dichlorobromate(1−) (**1**) in such protic solvents as acetic acid and methanol gives the corresponding bromo chloro adducts along with substantial amounts of solvent-incorporated products in a regiospecific manner (regioselective in the case of 3-nitro- or 2-chlorostyrenes). The reaction of 1-phenylpropenes with **1** gives nonstereospecific but regiospecific adducts. These results suggest that the addition of **1** to styrene derivatives in protic solvents involves an attack of chloride ion or solvent molecule to a bromonium ion intermediate.

In this series of studies, we have reported that the regiochemistry of the bromochlorination of alkenes with tetrabutylammonium dichlorobromate(1−) (**1**) is very sensitive to the structure of alkenes.[1-4] Meanwhile, the regio- and stereochemistries of the reaction of phenyl-substituted alkenes with **1** have been reported to be independent of the solvent polarity when the reaction is carried out in aprotic solvents.[1,2] However, only a few studies have been carried out on the addition of **1** to these alkenes in protic solvents.[1] As a continuation of our studies, the present work was initiated to examine the effect of protic solvents on the regio- and stereochemistries of the addition of **1** to styrene derivatives.

Results and Discussion

The reaction of $(n\text{-}C_4H_9)_4NBrCl_2$ (**1**) with styrene derivatives **2a—f** in acetic acid gave the corresponding bromo chloro compounds **3a—f** along with substantial amounts of solvent-incorporated products **4a—f** in good yields (Scheme 1 and Table 1).

$$\underset{\mathbf{2}}{XC_6H_4CH{=}CH_2} + \mathbf{1} \longrightarrow \underset{\mathbf{3}}{XC_6H_4CHClCH_2Br} + \underset{\mathbf{4}}{XC_6H_4CH(OCOCH_3)CH_2Br}$$

a: X=H **b**: X=4-CH_3
c: X=4-F **d**: X=4-Cl
e: X=3-Cl **f**: X=4-Br

Scheme 1.

Table 1. Bromochlorination of **2** with **1** in Acetic Acid[a]

Alkene	Product composition/%[b]		
2	**3**	**3′**	**4**
2a	66.7(65.4)	0	33.3(34.6)
2b	72.2(70.0)	0	27.8(30.0)
2c	72.4(71.4)	0	27.6(28.6)
2d	69.8(70.0)	0	30.2(30.0)
2e	72.7(71.2)	0	27.3(28.8)
2f	72.9(71.6)	0	27.1(28.4)
2g	66.3	2.0	31.7
2h	71.8	6.8	21.4
2i	64.8[c]	0	35.2
2j	66.7[d]	0	33.3

a) Reactions were carried out with 10 mmol of **1**, 10 mmol of **2**, and 20 ml of acetic acid at 20 °C. b) Determined by ^1H NMR analysis. Figures in parentheses represent the product compositions determined by GLC analysis. Percentages are normalized to 100%. Total yields were found to be more than 80% in all runs. c) A mixture of **3i** (89.5%) and **3j** (10.5%). d) A mixture of **3i** (11.5%) and **3j** (88.5%).

On the other hand, the reaction of 2-chloro- and 3-nitrostyrenes (**2g** and **2h**) with **1** gave a mixture of two regioisomers, **3g** and **3h** and **3g′** and **3h′**, and **4g** and **4h**, respectively (Scheme 2 and Table 1).

$$\underset{\mathbf{2}}{XC_6H_4CH{=}CH_2} + \mathbf{1} \longrightarrow \underset{\mathbf{3}}{XC_6H_4CHClCH_2Br} + \underset{\mathbf{3'}}{XC_6H_4CHBrCH_2Cl} + \underset{\mathbf{4}}{XC_6H_4CH(OCOCH_3)CH_2Br}$$

g: X=2-Cl **h**: X=3-NO_2

Scheme 2.

The solvent-incorporated products **4** were found to be formed in a completely regiospecific Markownikoff manner from all the styrene derivatives.

The reaction of *trans*-1-phenylpropene (**2i**) with **1** in acetic acid gave a mixture of *erythro*- and *threo*-2-bromo-1-chloro-1-phenylpropanes (**3i** and **3j**) along with a substantial amount of *erythro*-1-acetoxy-2-bromo-1-phenylpropane (**4i**). When *cis*-1-phenylpropene (**2j**) was allowed to react with **1**, a mixture of **3i**, **3j**, and *threo*-1-acetoxy-2-bromo-1-phenylpropane (**4j**) was obtained (Scheme 3 and Table 1).

$$PhCH{=}CHCH_3 + \mathbf{1} \longrightarrow PhCHClCHBrCH_3 + PhCH(OCOCH_3)CHBrCH_3$$

2i	**3i**, 58.0%	**4i**, 35.2%
	3j, 6.8%	
2j	**3i**, 7.7%	**4j**, 33.3%
	3j, 59.0%	

Scheme 3.

The formation of the solvent-incorporated products **4** cannot be ascribed to the subsequent secondary reaction of the bromo chloro compounds **3** with acetic acid, since prolonged reaction did not cause any change in the isomer ratio of the products.

We have previously reported that the reaction of **2d—h** with **1** in chloroform occurred in a nonregiospecific manner, although the Markownikoff adducts were formed mainly.[4] The reactions of *trans*- and *cis*-1-phenylpropenes (**2i** and **2j**) with **1** have been found to proceed in an *anti*-stereospecific and nonregiospecific manner in aprotic solvents.[2] Therefore, we have suggested that the addition of **1** to alkenes in aprotic solvents involves a rate- and product-determining attack of chloride ion on a three-center bound π-complex **6**.

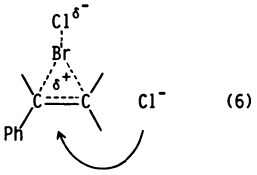

(6)

As shown in Table 1, the regio- and stereochemistries of the reaction of **2** with **1** in acetic acid are very different from those of the previous reaction in aprotic solvents.[2,4] Obviously, a different product-determining step is involved in the reaction in acetic acid.

Furthermore, in order to determine the effect of solvent on the regiochemistry of the addition, the reactions of **2e** or **2h** with **1** have been investigated in various solvents. Table 2 presents the data on the effect of solvents on the regiochemistry of bromo chloro adducts obtained from the reactions of **2e** or **2h** with **1**. No change in the regiochemistry has been observed with the reactions in the aprotic solvents. Similar regiochemical results have been observed previously for the reactions of **2i** and **2j**.[2]

On the other hand, the reaction of 3-chlorostyrene (**2e**) in methanol gave a solvent-incorporated product, 2-bromo-1-(3-chlorophenyl)-1-methoxyethane (**5e**, 78%) as the major product. In analogy with the reaction in acetic acid, the resulting bromo chloro adduct **3e** (22%) was found to be formed in a regiospecific Markownikoff manner. Similarly, the reaction of 3-nitrostyrene (**2h**) in methanol also gave 2-bromo-1-methoxy-1-(3-nitrophenyl)ethane (**5h**, 73%) along with a mixture of **3h** and **3h'** (**3h**:**3h'**=93:7) (Table 2).

As shown in Table 2, the reaction in protic solvents proceeded in a more regioselective (or regiospecific) manner than the reaction in aprotic solvents. The effect of protic solvents on the regiochemistry cannot be related to the dielectric constant of the medium, since in both acetic acid and ethyl acetate having similar dielectric constants, the regiochemistry was different, whereas chloroform and acetic anhydride have different dielectric constants but gave similar regiochemical results.

Table 2. Regiochemistry of Bromo Chloro Adducts Obtained from the Reactions of **2e** or **2h** with **1** in Various Solvents[a]

Solvent	Dielectric constant[c]	Product composition/%[b] from **2e**		from **2h**	
		3e	**3e'**	**3h**	**3h'**
$CHCl_3$	4.81	87.6	12.4	71.3	28.7
$CH_3COOC_2H_5$	6.02	87.2	12.8	69.1	30.9
CH_2Cl_2	9.08	87.0	13.0	71.7	28.3
$(CH_3CO)_2O$	20.7	87.7	12.3	70.0	30.0
CH_3COOH[d]	6.19	100	0	91.3	8.7
CH_3OH[e]	32.6	100	0	93.1	6.9

a) At 0 °C. b) Determined by ^1H NMR analysis. Percentages are normalized to 100%. c) J. A. Riddick and E. E. Toops, "Technique of Organic Chemistry," ed by A. Weissberger, Interscience, New York (1955), Vol. VII. d) At 20 °C. From the data of Table 1. e) The yield of **3e** was 22%. The yield of a mixture of **3h** and **3h'** was 27%.

Two different mechanisms can account for the role of such protic solvents as acetic acid and methanol. They are indicated in Schemes 4 and 5.

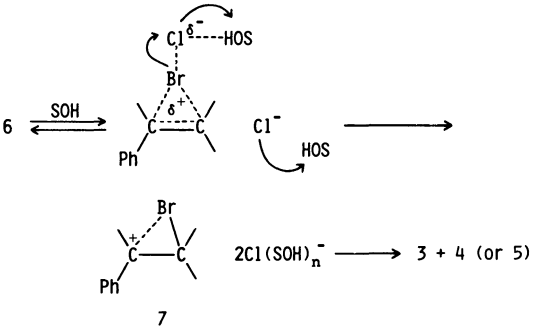

Scheme 4.

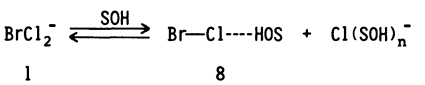

Scheme 5.

According to Scheme 4, the major role of protic solvent is assumed to be the solvation of the external chloride ion (Cl^-) in a three-center bound π-complex **6**, and promoting the ionization of **6** by stabilizing the negatively polarized chlorine atom ($Br^{\delta+}\cdots Cl^{\delta-}$) via hydrogen bonding. The solvent molecule may then assist catalytically the bromine-chlorine bond cleavage, followed by the formation of the cationic intermediate **7**. Evidence for such a specific role of the solvent has been observed by Dubois et al.[5] for the bromination of 1-pentene in methanol.

In Scheme 5, we assume the initial formation of solvated BrCl **8** and chloride ion by the solvation of $BrCl_2^-$ (**1**) in protic solvent. The solvated BrCl **8** thus formed is assumed to react with alkene (**2**) to give the cationic intermediate **7**, which is in turn attacked by chloride ion or solvent molecule to form a mixture of **3** and **4** (or **5**). Although we cannot decide by which mechanism the reactions proceed, the present results clearly show that the addition of **1** to alkenes in protic solvent proceeds via a cationic intermediate **7** prior to the product-determining step.

The regiochemical results in protic solvents (Tables 1 and 2) show that all the styrene derivatives (except **2g** and **2h**) were attacked by chloride ion exclusively on the phenyl-substituted carbon atom of the double bond. Furthermore, the addition of 1-phenylpropenes (**2i** and **2j**) was nonstereospecific, although the trans-addition product was formed mainly (Scheme 3). These results would be taken as evidence supporting that such a cationic intermediate resembles a weakly bridged benzylic carbonium ion intermediate **7**.[6] In the case of the reaction of **2h**, the formation of *anti*-Markownikoff adduct **3h′** would suggest that the intermediate resembles a fully bridged bromonium ion. A similar intermediate has been suggested for the bromination of 3-nitro- and 4-nitrostyrenes in acetic acid.[7] In the case of 2-chlorostyrene (**2g**), a small amount of *anti*-Markownikoff adduct **3g′** was also isolated in the reaction in acetic acid (Table 1). Probably, the formation of this product is due to the combination of polar and steric effects.

Experimental

NMR spectra were recorded on a JEOL JNM FX-60Q and a JEOL C-60HL spectrometer, using TMS as the internal standard. GLC analyses were performed on a Yanako G-180 gas chromatograph with a Silicone SE-30(2.5%)-Chromosorb WAW DMCS (2 m) column, with helium as the carrier gas. All the organic starting materials, including the solvents, were distilled before use. Tetrabutylammonium dichlorobromate(1−) (**1**) was prepared by the known procedure.[8]

Reaction of 2a—j with 1 in Acetic Acid. General Procedure: To a solution of **2** (10 mmol) in acetic acid (20 ml) was added **1** (3.93 g, 10 mmol) at 20 °C over 5 min with stirring. After the yellow color disappeared, the product was isolated by pouring the reaction mixture into a cold saturated aq NaCl solution, followed by extraction with ether (200 ml) and washing with aq $NaHCO_3$ and then with water. The ethereal extract was dried over $MgSO_4$ and concentrated. The crude products were subjected to GLC and NMR. All the results are given in Table 1. Furthermore, the crude products were separated by column chromatography (silica gel) with hexane-ether as the eluent. The structures of the bromo chloro adducts **3** and **3′** were determined by a comparison of their GLC and NMR spectra with those of the authentic samples prepared by the reaction of **1** with styrene derivatives **2** in chloroform.[4] The spectral data of each bromo chloro adduct have been reported in the previous papers.[2,4] The structures of the acetoxy bromide (**4**) were determined by a comparison of their GLC and NMR spectra with those of the authentic samples prepared by the reaction of **2** with bromine in acetic acid.[9] The spectral data are as follows.

1-Acetoxy-2-bromo-1-phenylethane (4a): ^1H NMR ($CDCl_3$) δ=2.12 (3H, s, $OCOCH_3$), 3.61, 3.62 (2H, 2d, J=5.9 and 7.0 Hz, CH_2Br), 5.97 (1H, approx. t, CH), and 7.34 (5H, s, C_6H_5); ^{13}C NMR ($CDCl_3$) δ=20.9, 34.2, 74.7, 126.4, 128.5, 128.6, 137.5, and 169.6.

1-Acetoxy-2-bromo-1-(4-methylphenyl)ethane (4b): ^1H NMR ($CDCl_3$) δ=2.11 (3H, s, $OCOCH_3$), 2.33 (3H, s, CH_3), 3.59, 3.60 (2H, 2d, J=5.9 and 7.3 Hz, CH_2Br), 5.95 (1H, approx. t, CH), and 7.26 (4H, s, C_6H_4); ^{13}C NMR ($CDCl_3$) δ=21.0, 21.2, 34.2, 74.8, 126.5, 129.3, 134.7, 138.6, and 169.7.

1-Acetoxy-2-bromo-1-(4-fluorophenyl)ethane (4c): ^1H NMR ($CDCl_3$) δ=2.12 (3H, s, $OCOCH_3$), 3.58, 3.59 (2H, 2d, J=6.1 and 7.2 Hz, CH_2Br), 5.94 (1H, approx. t, CH), and 6.9—7.6 (4H, m, C_6H_4); ^{13}C NMR ($CDCl_3$) δ=20.9, 34.1, 74.1, 114.9, 116.4, 128.1, 128.7, 133.4, 133.6, 154.5, 169.6, and 170.9.

1-Acetoxy-2-bromo-1-(4-chlorophenyl)ethane (4d): ^1H NMR ($CDCl_3$) δ=2.12 (3H, s, $OCOCH_3$), 3.57, 3.58 (2H, 2d, J=5.9 and 6.7 Hz, CH_2Br), 5.93 (1H, approx. t, CH), and 7.31 (4H, s, C_6H_4); ^{13}C NMR ($CDCl_3$) δ=20.8, 33.8, 74.0, 127.9, 128.8, 134.6, 136.1, and 169.6.

1-Acetoxy-2-bromo-1-(3-chlorophenyl)ethane (4e): ^1H NMR ($CDCl_3$) δ=2.14 (3H, s, $OCOCH_3$), 3.58 (2H, d, J=6.3 Hz, CH_2Br), 5.93 (1H, t, J=6.3 Hz, CH), and 7.28 (4H, br. s, C_6H_4); ^{13}C NMR ($CDCl_3$) δ=20.9, 33.8, 74.0, 124.8, 126.6, 128.9, 129.9, 134.5, 139.6, and 169.5.

1-Acetoxy-2-bromo-1-(4-bromophenyl)ethane (4f): ^1H NMR ($CDCl_3$) δ=2.12 (3H, s, $OCOCH_3$), 3.58 (2H, d, J=6.3 Hz, CH_2Br), 5.91 (1H, t, J=6.3 Hz, CH), and 7.13—7.68 (4H, m, C_6H_4); ^{13}C NMR ($CDCl_3$) δ=20.8, 33.7, 74.0, 122.7, 128.2, 131.8, 136.6, and 169.4.

1-Acetoxy-2-bromo-1-(2-chlorophenyl)ethane (4g): ^1H NMR ($CDCl_3$) δ=2.17 (3H, s, $OCOCH_3$), 3.63, 3.68 (2H, 2d, J=6.9 and 4.4 Hz, CH_2Br), 6.36 (1H, q, 6.9 and 4.4 Hz, CH), and 7.20—7.70 (4H, m, C_6H_4); ^{13}C NMR ($CDCl_3$) δ=20.8, 33.1, 71.4, 127.0, 127.4, 129.7, 132.2, 135.3, and 169.3.

1-Acetoxy-2-bromo-1-(3-nitrophenyl)ethane (4h): ^1H NMR ($CDCl_3$) δ=2.18 (3H, s, $OCOCH_3$), 3.65 (2H, d, J=6.2 Hz, CH_2Br), 6.04 (1H, t, J=6.2 Hz, CH), and 7.70—8.30 (4H, m, C_6H_4); ^{13}C NMR ($CDCl_3$) δ=20.9, 33.5, 73.4, 121.5, 123.6, 129.6, 132.8, 139.6, 148.3, and 169.4.

***erythro*-1-Acetoxy-2-bromo-1-phenylpropane (4i):** ^1H NMR ($CDCl_3$) δ=1.64 (3H, d, J=6.7 Hz, CH_3), 2.15 (3H, s, $OCOCH_3$), 4.15—4.57 (1H, m, CHBr), 5.95 (1H, d, J=5.3 Hz, CH), and 7.34 (5H, s, C_6H_5); ^{13}C NMR ($CDCl_3$) δ=20.8, 20.9, 50.0, 78.2, 127.0, 128.3, 128.4, 137.1, and 169.5.

threo-1-Acetoxy-2-bromo-1-phenylpropane (4j): ^{1}H NMR ($CDCl_3$) δ=1.53 (3H, d, J=6.7 Hz, CH_3), 2.11 (3H, s, $OCOCH_3$), 4.08—4.56 (1H, m, CHBr), 5.82 (1H, d, J=7.8 Hz, CH), and 7.34 (5H, s, C_6H_5); ^{13}C NMR ($CDCl_3$) δ=21.0, 22.4, 50.5, 79.2, 127.1, 128.5, 128.6, 137.1, and 169.5.

Reaction of 2e and 2h with 1 in Aprotic Solvents. To a solution of the alkene (10 mmol) in the solvent (20 ml) was added 10 mmol of **1** at 0 °C over 5 min with stirring. After the yellow color disappeared, the mixture was washed with water and dried over Na_2SO_4. The product of the reaction in acetic anhydride was isolated by pouring the reaction mixture into water, followed by extraction with ether (200 ml) and washing with aq $NaHCO_3$ and then with water. After the solvent was evaporated, the residues were analyzed by ^{1}H NMR. The relative amounts of products were determined from the ratio of the peak areas of the methylene protons of the bromo chloro adducts **3** and **3'**.[4] The results are given in Table 2.

Reaction of 2e and 2h with 1 in Methanol. To a solution of the alkene (10 mmol) in methanol (20 ml) was added **1** (10 mmol) at 0 °C over 5 min with stirring. The solvent was removed by evaporation and ether (200 ml) was added to the residue. The ether solution was washed with aq $NaHCO_3$ and then with water. The ethereal extract was dried over Na_2SO_4 and concentrated. In the case of **2e**, the ^{1}H NMR spectrum of the residue showed a 78:22 mixture of **5e** and **3e** (by integration of the methine protons). In the case of **2h**, the ^{1}H NMR spectrum of the residue showed a 73:27 mixture of **5h** and **3h** with a trace amount of **3h'**.

A column chromatography of the residue (2.12 g) from the reaction of **2e** on silica gel with hexane–ether as the eluent gave 1.50 g of **5e** and 0.4 g of **3e**. The spectral data for 2-bromo-1-(3-chlorophenyl)-1-methoxyethane (**5e**) are as follows: ^{1}H NMR ($CDCl_3$) δ=3.32 (3H, s, OCH_3), 3.46, 3.47 (2H, 2d, J=5.9 and 6.7 Hz, CH_2Br), 4.36 (1H, approx. t, CH), and 7.26—7.35 (4H, m, C_6H_4); ^{13}C NMR ($CDCl_3$) δ=35.7, 57.4, 82.7. 125.0, 126.8, 128.6, 129.9, 134.6, and 141.1. The ^{1}H and ^{13}C NMR spectra of **5e** correspond well with those of the authentic sample prepared by the reaction of **2e** with N-bromosuccinimide (NBS) in methanol.[10] The data for 2-bromo-1-chloro-1-(3-chlorophenyl)ethane (**3e**) have been reported in the previous paper.[4]

Similarly, a column chromatography of the residue (2.13 g) from the reaction of **2h** gave 1.30 g of **5h** and 0.45 g of a mixture of **3h** and **3h'**. The spectral data for 2-bromo-1-methoxy-1-(3-nitrophenyl)ethane (**5h**) are as follows: ^{1}H NMR ($CDCl_3$) δ=3.36 (3H, s, OCH_3), 3.53 (2H, d, J=5.9 Hz, CH_2Br), 4.51 (1H, t. J=5.9 Hz, CH), and 7.67—8.22 (4H, m, C_6H_4); ^{13}C NMR ($CDCl_3$) δ=35.3, 57.6, 82.1, 121.8, 123.4, 129.6, 132.8, 141.4, and 148.4. The ^{1}H and ^{13}C NMR spectra of **5h** correspond well with those of the authentic sample prepared by the reaction of **2h** with NBS in methanol.[10] The ^{1}H NMR spectrum of the isolated bromo chloro adducts showed a 93:7 mixture of **3h** and **3h'**. The data for 2-bromo-1-chloro- and 1-bromo-2-chloro-1-(3-nitrophenyl)ethanes (**3h** and **3h'**) have been reported in the previous paper.[4]

The authors sincerely wish to thank Professor Shigeru Oae of Okayama University of Science for his kind guidance.

References

1) T. Negoro and Y. Ikeda, *Bull. Chem. Soc. Jpn.*, **57**, 2111 (1984).
2) T. Negoro and Y. Ikeda, *Bull. Chem. Soc. Jpn.*, **57**, 2116 (1984).
3) T. Negoro and Y. Ikeda, *Bull. Chem. Soc. Jpn.*, **58**, 3665 (1985).
4) T. Negoro and Y. Ikeda, *Bull. Fac. Edu. Wakayama Univ. Nat. Sci.*, **35**, 15 (1986).
5) F. Garnier, R. H. Donnay, and J. E. Dubois, *J. Chem. Soc., Chem. Commun.*, **1971**, 829.
6) J. H. Rolston and K. Yates, *J. Am. Chem. Soc.*, **91**, 1477 (1969); G. E. Heasley, J. M. Bundy, V. L. Heasley, S. Arnold, A. Gipe, D. McKee, R. Orr, S. L. Rodgers, and D. F. Shellhamer, *J. Org. Chem.*, **43**, 2793 (1978).
7) J. H. Rolston and K. Yates, *J. Am. Chem. Soc.*, **91**, 1483 (1969).
8) A. I. Popov and R. E. Buckles, *Inorg. Synth.*, Vol. **V**, 172 (1957).
9) J. H. Rolston and K. Yates, *J. Am. Chem. Soc.*, **91**, 1469 (1969).
10) V. L. Heasley, R. A. Skidgel, G. E. Heasley, and D. Strickland, *J. Org. Chem.*, **39**, 3953 (1974).

Synthetic Approach toward Antibiotic Ezomycins. II. Synthesis of 5-Amino-3,7-anhydro-5-deoxy-octofuranose-(1,4) Derivatives

Osamu Sakanaka, Takashi Ohmori, Shuji Kozaki, and Tetsuo Suami*
Department of Applied Chemistry, Faculty of Science and Technology, Keio University, Hiyoshi, Yokohama 223
(Received May 1, 1986)

A conversion of 5-acetamido-5-deoxy-1,2:7,8-di-*o*-isopropylidene-3-*o*-methylthiomethyl-β-L-*erythro*-D-allo-octofuranose-(1,4) and -L-talooctofuranose-(1,4) to 5-amino-3,7-anhydro-5-deoxyoctofuranose-(1,4) derivatives has been investigated as a preliminary study for a synthesis of the octose moiety of ezomycins.

Nucleoside antibiotic ezomycins were discovered in a fermentation broth of a strain which was similar to Streptomyces Kitazawaensis.[1] They exhibit antimicrobial activity against limited species of phytopathogenic fungi, such as Sclerotinia and Botritis. Ezomycins A, B, and C comprise a unique bicyclic trans-fused octose derivative,[2-4] which is a target of our present studies. Although several studies related to synthesis of 3,7-anhydrooctofuranose-(1,4) derivatives have been described,[5-7] any derivatives with all functional groups have not yet been synthesized.

In the preceding paper,[8] a synthesis of 5-acetamido-5-deoxyoctofuranose-(1,4) derivatives has been described. A KF-catalyzed Henry reaction between 5-nitro-D-ribose derivative (**1**) and L-glyceraldehyde derivative (**2**) and successive hydrogenation followed by *N*-acetylation afforded three diastereomeric isomers (**3a**, **3b**, and **3c**). Also their absolute configurations of the newly introduced chiral centers on C-5 and C-6 have been established. The configurations of the major product **3a** were found to be identical with those of the octose part of ezomycins.

In the present article, we wish to report a synthesis of 5-amino-3,7-anhydro-5-deoxyoctofuranose-(1,4) derivatives from **3a** and **3b**.

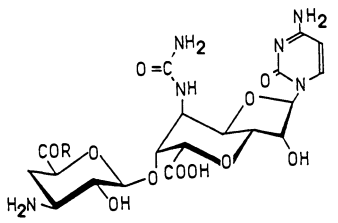

Ezomycin

A_1

R = NHCHCH$_2$CH$_2$SCH$_2$CHNH$_2$ (COOH, COOH)

A_2

R = OH

Scheme 1.

Results and Discussion

O-Benzylation of an intact mixture (67% from 1) of **3a** and **3b**, which could not be separated chromatographically, with benzyl bromide and sodium hydride in *N*,*N*-dimethylformamide (DMF) gave the corresponding benzyl ethers (**4a** and **4b**), which could be isolated readily in 49 and 30% yield respectively.

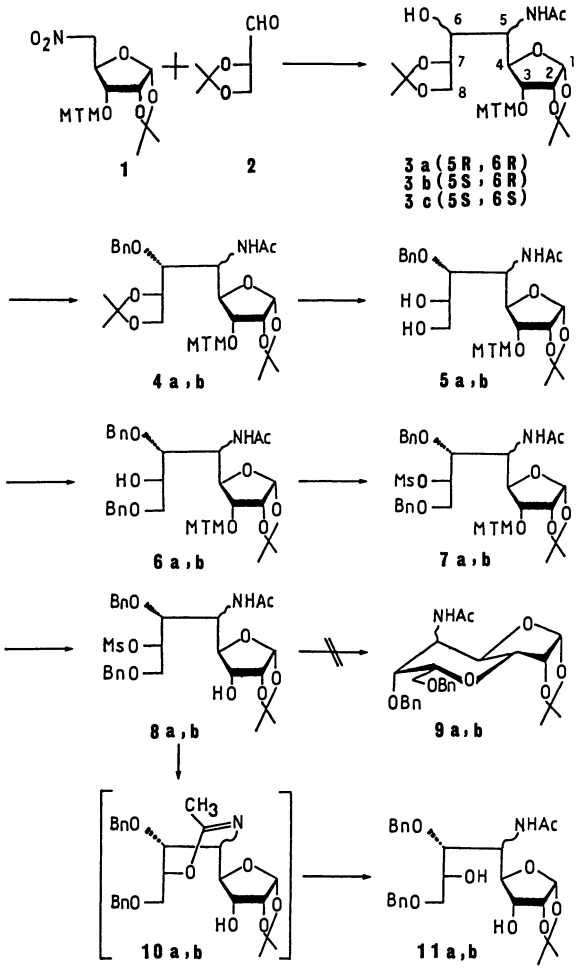

Bn benzyl
Ms methylsulfonyl
MTM methylthiomethyl

Scheme 2.

Selective removal of 7,8-*O*-isopropylidene group in **4a** with aqueous acetic acid afforded a diol (**5a**). Preferential 8-*O*-benzylation of **5a** with benzyl bromide and sodium hydride in tetrahydrofuran (THF) gave 6,8-di-*O*-benzyl compound (**6a**) in 49% yield. *O*-Mesylation of **6a** with methanesulfonyl chloride in pyridine afforded a mesylate (**7a**) in 78% yield. Treatment of **7a** with iodomethane in the presence of sodium hydrogencarbonate in aqueous acetone[9] gave 3-*O*-deprotected compound (**8a**) in 53% yield. Another benzyl ether (**5b**) was also converted to the corresponding compound (**8b**) by the analogous procedure. Cyclization of **8a** to a 3,7-anhydride with a base (NaH or *t*-BuOK) in various solvent systems have been attempted, but in vain. The product was treated with acetic anhydride in pyridine to give a diacetate, which was not an acetylated derivative of **5a**. Therefore, it was thought that an epimerization was caused by a participation of 5-acetamido group. The product derived from **8b** was also an epimerized diol (**9b**). Although a benzyloxycarbonyl or a phthaloyl group was used as protective group of the 5-amino group, a satisfactory result was not obtained.

Then, a 2,4-dinitrophenyl group was used as protective group. Hydrolysis of **6a** with sodium hydroxide in aqueous 2-methoxyethanol and successive treatment of the resultant amine with 2,4-dinitrofluorobenzene and triethylamine in THF afforded dinitrophenylamino compound (**12a**) in 75% yield. *O*-Mesylation of **12a** with methanesulfonyl chloride in pyridine yielded a mesylate (**13a**) quantitatively. Treatment of **13a** with iodomethane and sodium hydrogencarbonate in aqueous acetone gave 3-*O*-deprotected compound (**14a**) in 72% yield. Compound **6b** was also converted to the corresponding compound (**14b**) by the analogous procedure. Treatment of **14b** with NaH in DMF afforded the desired 3,7-anhydride (**15**) in 59% yield. However, attemps to cyclize **14a** with a base (NaH or *t*-BuOK) in various solvent systems were unsuccessful. The ^{1}H NMR spectrum of the main product showed a characteristic doublet at δ 6.64 (J=14 Hz), possibly a trans-olefin signal, and a doublet at δ 3.08 (J=6 Hz) assignable to 3-OH. Accordingly, the product is thought to have a structure **16**. The structure is also reasonable for all other signals. The other products were unable to isolate. The conformation of 7-mesyloxy group in **14a** might be unfavorable to a nucleophilic attack of a 3-oxido anion.

Therefore, the epimer of **14a** at C-7 was prepared as follows. Treatment of **7a** with NaH in DMF resulted in an attack of 5-acetamido group to C-7 as above-mentioned and successive acidic workup with silica gel afforded an epimeric product (**17**) in 92% yield. Compound **17** was converted to a mesylate (**20**) by the analogous procedure as described already. Treatment

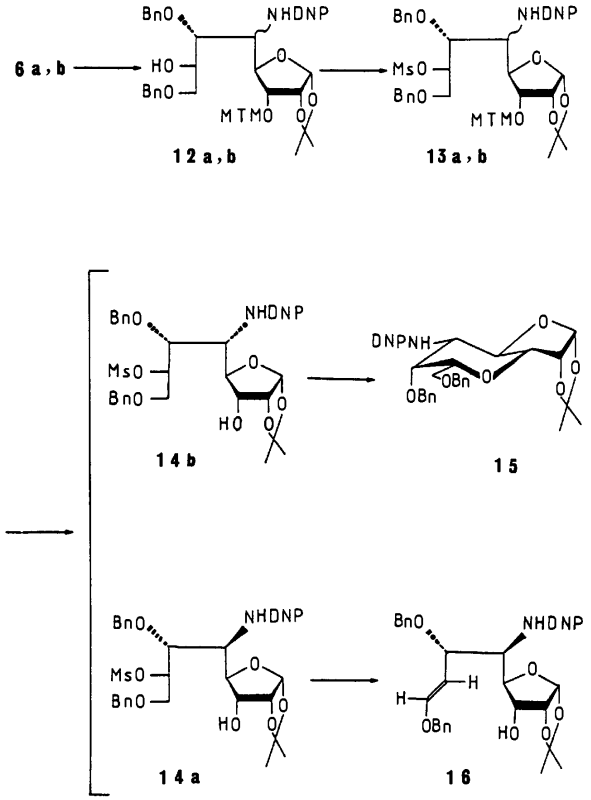

DNP 2,4-dinitrnphenyl

Scheme 3.

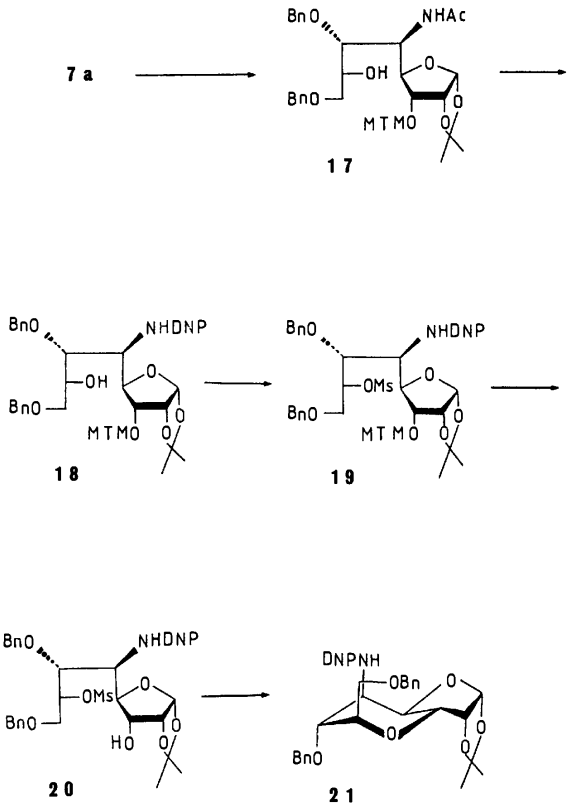

Scheme 4.

of **20** with NaH in dimethyl sulfoxide (DMSO) afforded a bicyclic 3,7-anhydride (**21**) in 66% yield as expected. Since an attack of a 3-oxido anion to C-7 is an S_N2 type reaction, the stereochemistry is non-natural. However, if **21** can be oxidized to an uronic acid, it is expected that the configuration of C-7 can be reversed because of α-position of carboxyl function.

Experimental

Melting points were determined on a Büchi 510 capillary melting point apparatus and are uncorrected. Optical rotations were measured with a Jasco DIP-4 polarimeter. IR spectra were recorded on a Hitachi 225 spectrometer. ^{1}H NMR spectra were recorded on a Varian EM-390 (90 MHz), a JEOL FX-200 (200 MHz), or a JEOL GX-400 (400 MHz) spectrometer with a reference to tetramethylsilane as an internal standard. Mass spectra were recorded on a Hitachi M-80B spectrometer. Solutions were dried over anhydrous sodium sulfate and concentrated below 35 °C. TLC was carried out on glass plates coated with Kieselgel 60 F_{254} (Merck Art. 5715), and compounds were detected by spraying with an H_2SO_4 followed by heating. Chromatography was performed on a silica gel (Merck Kieselgel 60 Art. 7734) column.

5-Acetamido-6-*O*-benzyl-5-deoxy-1,2-*O*-isopropylidene-3-*O*-methylthiomethyl-β-L-*erythro*-L-talooctofuranose-(1,4) (5b). Compound **4b** (104 mg) was dissolved in 70% aqueous acetic acid (2 ml) and the solution was allowed to stand for 14 h at room temperature. Coevaporation with toluene gave a pale yellow syrupy residue, which was chromatographed (chloroform–methanol (v/v) 30:1) to afford **5b** in an almost quantitative yield (95 mg) as crystals: R_f=0.35 on TLC (chloroform–methanol (v/v) 15:1); mp 136—138 °C; $[\alpha]_D^{21}$ +17.2° (*c* 1.06, $CHCl_3$); IR (KBr) 1650 cm^{-1} (NHCO); ^{1}H NMR (90 MHz, $CDCl_3$) δ=1.32, 1.45 (3H×2, s×2, CMe_2), 1.97 (3H, s, NHAc), 2.14 (3H, s, SMe), 3.15 (1H, bs, OH), 5.77 (1H, d, *J*=4 Hz, H-1), 6.26 (1H, d, *J*=10 Hz, NH), 7.30 (5H, m, Ph).

Found: C, 55.78; H, 6.97; N, 3.13; S, 6.59%. Calcd for $C_{22}H_{33}NO_8S$: C, 56.04; H, 7.05; N, 2.97; S, 6.80%.

5-Acetamido-6,8-*O*-di-*O*-benzyl-5-deoxy-1,2-*O*-isopropylidene-3-*O*-methylthiomethyl-β-L-*erythro*-L-talooctofuranose-(1,4) (6b). To a chilled solution (−15 °C) of **5b** (163 mg) in anhydrous THF (4 ml) were added sodium hydride (60% dispersion in mineral oil, 16 mg) and benzyl bromide (45 μl), and the mixture was stirred for 2 h under ice cooling. The mixture was chilled to −15 °C again, and sodium hydride (7 mg) and benzyl bromide (12 μl) were added. The mixture was stirred for 12 h at 5 °C. Coevaporation with ethanol gave a pale yellow syrup, which was chromatographed (chloroform–methanol (v/v) 30:1) to afford 109 mg (56%) of **6b** as a colorless syrup: R_f=0.44 on TLC (ethyl acetate); ^{1}H NMR (90 MHz, $CDCl_3$) δ=1.32, 1.46 (3H×2, s×2, CMe_2), 1.91 (3H, s, NHAc), 2.13 (3H, s, SMe), 2.85 (1H, d, *J*=4 Hz, OH), 5.76 (1H, d, *J*=4 Hz, H-1), 5.84 (1H, d, *J*=10 Hz, NH), 7.15—7.54 (10H, m, Ph×2). Although contaminated with 6,7-di-*O*-benzyl compound (<1/10, judged from NMR spectrum), the product was used in the next step without further purification. Both isomers had a similar mobility in a column chromatography.

6,8-Di-*O*-benzyl-5-deoxy-5-(2,4-dinitrophenylamino)-1,2-*O*-isopropylidene-3-*O*-methylthiomethyl-β-L-*erythro*-L-talooctofuranose-(1,4) (12b). A mixture of **6b** (146 mg), sodium hydroxide (270 mg) and 95% aqueous 2-methoxyethanol (3 ml) was heated for 75 min under reflux. The mixture was partitioned between water and ethyl acetate. The organic layer was washed twice with water, dried and concentrated to dryness. The pale brown syrupy residue was dissolved in THF (3 ml), and to the solution were added triethylamine (68 μl) and 2,4-dinitrofluorobenzene (98 mg). The mixture was stirred for 18 h at room temperature, and partitioned between water and ethyl acetate. The organic layer was washed twice with water, dried and concentrated to dryness. The syrupy residue was chromatographed (toluene–ethyl acetate (v/v) 6:1) to give 141 mg (79%) of **12b** as yellow amorphous solids: R_f=0.47 on TLC (toluene–ethyl acetate (v/v) 2:1); $[\alpha]_D^{22}$ +33.7° (*c* 1.21, $CHCl_3$); IR (KBr) 1520 cm^{-1} (NO_2); ^{1}H NMR (90 MHz, $CDCl_3$) δ=1.33, 1.52 (3H×2, s×2, CMe_2), 1.99 (3H, s, SMe), 2.76 (1H, d, *J*=4 Hz, OH), 5.88 (1H, d, *J*=4 Hz, H-1), 7.06 (1H, d, *J*=10 Hz, H-6′), 7.19—7.42 (10H, m, Ph×2), 7.99 (1H, dd, *J*=10, 3 Hz, H-5′), 9.03 (1H, d, *J*=3 Hz, H-3′).

Found: C, 58.06; H, 5.95; N, 5.88; S, 4.67%. Calcd for $C_{33}H_{39}N_3O_{11}S$: C, 57.80; H, 5.73; N, 6.13; S, 4.67%.

6,8-Di-*O*-benzyl-5-deoxy-5-(2,4-dinitrophenylamino)-1,2-*O*-isopropylidene-7-*O*-methylsulfonyl-3-*O*-methylthiomethyl-β-L-*erythro*-L-talooctofuranose-(1,4) (13b). To a solution of **12b** (150 mg) in dry pyridine (3 ml) was added methanesulfonyl chloride (70 μl) under ice cooling, and the mixture was stirred for 2 h. After 1 h at room temperature additionally, the mixture was partitioned between 3% aqueous sodium hydrogencarbonate and ethyl acetate. The organic layer was washed with water, dried and concentrated to dryness. The syrupy residue was chromatographed (toluene–ethyl acetate (v/v) 8:1) to give 146 mg (88%) of **13b** as yellow amorphous solids: R_f=0.62 on TLC (toluene–ethyl acetate (v/v) 2:1); $[\alpha]_D^{22}$ +11.6° (*c* 1.35, $CHCl_3$); IR (KBr) 3320 (NH), 1525, 1515 (NO_2) cm^{-1}; ^{1}H NMR (90 MHz, $CDCl_3$) δ=1.33, 1.52 (3H×2, s×2, CMe_2), 1.92 (3H, s, SMe), 2.96 (3H, s, SO_2Me), 5.85 (1H, d, *J*=4 Hz, H-1), 6.89 (1H, d, *J*=10 Hz, H-6′), 7.24—7.43 (10H, m, Ph×2), 7.86 (1H, dd, *J*=3, 10 Hz, H-5′), 8.72 (1H, d, *J*=10 Hz, NH), 8.99 (1H, d, *J*=3 Hz, H-3′).

Found: C, 53.32; H, 5.47; N, 5.21; S, 8.25%. Calcd for $C_{34}H_{41}N_3O_{13}S_2$: C, 53.46; H, 5.41; N, 5.50; S, 8.39%.

6,8-Di-*O*-benzyl-5-deoxy-5-(2,4-dinitrophenylamino)-1,2-*O*-isopropylidene-7-*O*-methylsulfonyl-β-L-*erythro*-L-talooctofuranose-(1,4) (14b). To a mixture of **13b** (146 mg), sodium hydrogencarbonate (81 mg) and 90% aqueous acetone (2.4 ml) was added iodomethane (0.25 ml) three times at intervals of 2 h under reflux, and then furthermore the mixture was refluxed for 2 h. The reaction mixture was diluted with ethyl acetate, dried and concentrated to dryness. The syrupy residue was chromatographed (toluene–ethyl acetate (v/v) 8:1) to afford 86 mg (64%) of **14b** as yellow amorphous solids: R_f=0.30 on TLC (toluene–ethyl acetate (v/v) 3:1); $[\alpha]_D^{20}$ −68.9° (*c* 2.11, $CHCl_3$); IR (KBr) 1525, 1520 cm^{-1} (NO_2); ^{1}H NMR (90 MHz, $CDCl_3$) δ=1.35, 1.52 (3H×2, s×2, CMe_2), 2.34 (1H, d, *J*=12 Hz, OH), 2.98 (3H, s, SO_2Me), 5.87 (1H, d, *J*=4 Hz, H-1), 6.91 (1H, d, *J*=10 Hz, H-6′), 7.24—7.44 (10H, m, Ph×2), 7.92 (1H, dd, *J*=3, 10 Hz, H-5′), 8.62 (1H, d, *J*=10 Hz, NH), 9.02 (1H, d, *J*=3 Hz,

H-3′).

Found: C, 54.61; H, 5.51; N, 5.71; S, 4.52%. Calcd for $C_{32}H_{37}N_3O_{13}S$: C, 54.62; H, 5.30; N, 5.97; S, 4.56%.

3,7-Anhydro-6,8-di-*O*-benzyl-5-deoxy-5-(2,4-dinitrophenylamino)-1,2-*O*-isopropylidene-α-D-*threo*-L-talooctofuranose-(1,4) (15). To a solution of **14b** (31.8 mg) in anhydrous DMF (0.3 ml) was added sodium hydride (8 mg) under ice cooling, and the mixture was stirred for 3 h at room temperature. The mixture was partitioned between water and ethyl acetate. The organic layer was washed with water repeatedly, dried and concentrated to dryness. The syrupy residue was chromatographed (toluene-ethyl acetate (v/v) 5:1) to give 16.2 mg (59%) of **15** as yellow amorphous solids: R_f=0.51 on TLC (toluene-ethyl acetate (v/v) 2:1); $[\alpha]_D^{21}$ −39.7° (*c* 0.79, $CHCl_3$); IR (KBr) 3450 (NH), 1525, 1520 (NO_2) cm^{-1}; ^1H NMR (200 MHz, $CDCl_3$) δ=1.33, 1.57 (3H×2, s×2, CMe_2), 3.29 (1H, dd, *J*=3, 9 Hz, H-3), 3.68—3.97 (4H, H-5, 7, 8), 4.09 (1H, d, *J*=2 Hz, H-6), 4.23 (1H, dd, *J*=9, 9 Hz, H-4), 4.44—4.60 (2H, CH_2Ph), 4.65—4.78 (3H, H-2, CH_2Ph), 5.79 (1H, d, *J*=4 Hz, H-1), 7.02 (1H, d, *J*=10 Hz, H-6′), 7.18—7.39 (10H, m, Ph×2), 8.16 (1H, dd, *J*=3, 10 Hz, H-5′), 9.03 (1H, d, *J*=10 Hz, NH), 9.05 (1H, d, *J*=3 Hz, H-3′).

Found: C, 61,03; H, 5.55; N, 6.70%. Calcd for $C_{31}H_{33}N_3O_{10}$: C, 61.28; H, 5.47; N, 6.92%.

5-Acetamido-6,8-di-*O*-benzyl-5-deoxy-1,2-*O*-isopropylidene-3-*O*-methylthiomethyl-β-L-*erythro*-D-allooctofuranose-(1,4) (6a). To a solution of **5a** (509 mg) in anhydrous THF (5 ml) were added sodium hydride (108 mg) and benzyl bromide (0.14 ml) under ice cooling, and the mixture was stirred for 12 h at 5 °C. The reaction mixture was partitioned between water and ethyl acetate. The organic layer was dried and concentrated to dryness. The syrupy residue was chromatographed (toluene-ethyl acetate (v/v) 3:2) to afford 294 mg (48.6%) of **6a** as crystals: R_f=0.50 on TLC (ethyl acetate); mp 130—132 °C; $[\alpha]_D^{20}$ +9.32° (*c* 1.03, $CHCl_3$); IR (KBr) 1630 cm^{-1} (NHCO); ^1H NMR (90 MHz, $CDCl_3$) δ=1.34, 1.54 (3H×2, s×2, CMe_2), 1.97 (3H, s, NHAc), 2.17 (3H, s, SMe), 5.79 (1H, d, *J*=4 Hz, H-1), 7.29, 7.35 (5H×2, s×2, Ph×2).

Found: C, 62.29; H, 7.01; N, 2.33; S, 5.57%. Calcd for $C_{29}H_{39}NO_8S$: C, 62.29; H, 7.00; N, 2.49; S, 5.71%.

6,8-Di-*O*-benzyl-5-deoxy-5-(2,4-dinitrophenylamino)-1,2-*O*-isopropylidene-3-*O*-methylthiomethyl-β-L-*erythro*-D-allooctofuranose-(1,4) (12a). A solution of **6a** (0.47 g) and sodium hydroxide (0.4 g) in 95% aqueous 2-methoxyethanol (5 ml) was heated for 6 h under reflux. The mixture was partitioned between water and ethyl acetate. The organic layer was washed twice with water, dried and concentrated to dryness. The residue was dissolved in THF (5 ml), and to the solution were added triethylamine (0.18 ml) and 2,4-dinitrofluorobenzene (190 mg). After 12 h at room temperature the mixture was partitioned between water and ethyl acetate. The organic layer was washed with water, dried and concentrated to dryness. The residue was chromatographed (toluene-ethyl acetate (v/v) 3:1) to give 433 mg (75%) of **12a** as yellow amorphous solids: R_f=0.37 on TLC (toluene-ethyl acetate (v/v) 4:1); $[\alpha]_D^{25}$ −103 °C (*c* 2.91, $CHCl_3$); IR (KBr) 1520 cm^{-1} (NO_2); ^1H NMR (90 MHz, $CDCl_3$) δ=1.32, 1.46 (3H×2, s×2, CMe_2), 1.86 (3H, s, SMe), 2.48 (1H, d, *J*=5 Hz), 5.78 (1H, d, *J*=4 Hz, H-1), 7.35 (10H, bs, Ph×2), 8.20 (1H, dd, *J*=3, 10 Hz, H-5′), 9.02 (1H, d, *J*=8 Hz, NH), 9.11 (1H, d, *J*=3 Hz, H-3′).

Found: M, 685. Calcd for $C_{33}H_{39}N_3O_{11}S$: *m/z*, 685.

6,8-Di-*O*-benzyl-5-deoxy-5-(2,4-dinitrophenylamino)-1,2-*O*-isopropylidene-7-*O*-methylsulfonyl-3-*O*-methylthiomethyl-β-L-*erythro*-D-allooctofuranose-(1,4) (13a). To a solution of **12a** (128 mg) in dry pyridine (3 ml) was added methanesulfonyl chloride (43 μl) under ice cooling, and the mixture was allowed to stand overnight in a refrigerator. The reaction mixture was partitioned between saturated aqueous sodium hydrogencarbonate and ethyl acetate. The organic layer was washed with water repeatedly, dried and concentrated to dryness. The residue was chromatographed (toluene-ethyl acetate (v/v) 10:1) to afford 132 mg (93%) of **13a** as yellow amorphous solids: R_f=0.44 on TLC (toluene-ethyl acetate (v/v) 4:1); $[\alpha]_D^{26}$ −47.1° (*c* 1.05, $CHCl_3$); IR (KBr) 3330 (NH), 1525, 1515 (NO_2) cm^{-1}; ^1H NMR (90 MHz, $CDCl_3$) δ=1.33, 1.48 (3H×2, s×2, CMe_2), 1.95 (3H, s, SMe), 2.89 (3H, s, SO_2Me), 5.78 (1H, d, *J*=4 Hz, H-1), 7.08 (1H, d, *J*=8 Hz, H-6′), 7.32, 7.37 (5H×2, s×2, Ph×2), 8.18 (1H, dd, *J*=3, 8 Hz, H-5′), 9.12 (1H, d, *J*=3 Hz, H-3′).

6,8-Di-*O*-benzyl-5-deoxy-5-(2,4-dinitrophenylamino)-1,2-*O*-isopropylidene-7-*O*-methylsulfonyl-β-L-*erythro*-D-allooctofuranose-(1,4) (14a). To a mixture of **13a** (107 mg), sodium hydrogencarbonate (59 mg) and 90% aqueous acetone (2 ml) was added iodomethane (0.18 ml) three times at intervals of 1 h under reflux, and furthermore the mixture refluxed for 2 h. The reaction mixture was diluted with ethyl acetate, dried and concentrated to dryness. The syrupy residue was chromatographed (toluene-ethyl acetate (v/v) 3:1) to give 52 mg (53%) of **14a** as yellow amorphous solids: R_f=0.15 on TLC (toluene-ethyl acetate (v/v) 4:1); $[\alpha]_D^{26}$ −43.2° (*c* 1.08, $CHCl_3$); IR (KBr) 3460 (OH), 3330 (NH), 1525, 1515 (NO_2); ^1H NMR (90 MHz, $CDCl_3$) δ=1.34, 1.47 (3H×2, s×2, CMe_2), 2.34 (1H, bs, OH), 2.91 (3H, s, SO_2Me), 5.78 (1H, d, *J*=4 Hz, H-1), 7.09 (1H, d, *J*=10 Hz, H-6′), 7.34, 7.38 (5H×2, s×2, Ph×2), 8.16 (1H, dd, *J*=3, 10 Hz, H-5′), 9.11 (1H, d, *J*=3 Hz).

A Reaction of 14a with NaH. To a solution of **14a** (23.8 mg) in anhydrous DMF (0.5 ml) was added sodium hydride (5.7 mg) under ice cooling, and the mixture was stirred for 3.5 h at room temperature. The mixture was partitioned between water and ethyl acetate. The organic layer was washed twice with water, dried and concentrated to dryness. The residue was chromatographed (toluene-ethyl acetate (v/v) 8:1) to afford 5.2 mg (25%) of an olefinic compound **16** as yellow amorphous solids: R_f=0.37 on TLC (toluene-ethyl acetate (v/v) 4:1); $[\alpha]_D^{26}$ +20.0° (*c* 0.52, $CHCl_3$); IR (KBr) 3480 (OH), 3350 (NH), 1515, 1505 (NO_2) cm^{-1}; ^1H NMR (90 MHz, $CDCl_3$) δ=1.30, 1.52 (3H×2, s×2, CMe_2), 3.08 (1H, d, *J*=6 Hz, OH), 5.57 (1H, d, *J*=5 Hz, H-1), 6.64 (1H, d, *J*=14 Hz, H-8), 7.00 (1H, d *J*=10 Hz, H-6′), 7.25, 7.28 (5H×2, s×2, Ph×2), 8.09 (1H, dd, *J*=3, 10 Hz, H-5′), 8.95 (1H, d, *J*=7 Hz, NH), 9.03 (1H, d, *J*=3 Hz, H-3′).

Found: M, 607. Calcd for $C_{31}H_{33}N_3O_{10}$: *m/z*, 607.

5-Acetamido-6,8-di-*O*-benzyl-5-deoxy-1,2-*O*-isopropylidene-7-*O*-methylsulfonyl-3-*O*-methylthiomethyl-β-L-*erythro*-D-allooctofuranose-(1,4) (7a). To a solution of **6a** (1.14 g) in dry pyridine (11 ml) was added methanesulfonyl chloride (0.47 ml) under ice cooling, and the mixture was stirred for 2 h at room temperature. The reaction mixture was coevaporated with toluene, and the residue was partitioned between water and ethyl acetate. The organic layer was

washed with water repeatedly, dried and concentrated to dryness. The residue was chromatographed (toluene–ethyl acetate (v/v) 3:1) to give 1.01 g of **7a** as a colorless syrup: R_f=0.50 on TLC (toluene–ethyl acetate (v/v) 1:1); $[\alpha]_D^{19}$ +11.7° (*c* 1.23, $CHCl_3$); IR ($CHCl_3$) 3390 (NH), 1670 (NHCO), 1350, 1170 (SO_2Me) cm^{-1}; ^1H NMR (90 MHz, $CDCl_3$) δ=1.33, 1.54 (3H×2, s×2, CMe_2), 1.91 (3H, s, NHAc), 2.19 (3H, s, SMe), 3.01 (3H, s, SO_2Me), 5.73 (1H, d, *J*=4 Hz, H-1), 7.30, 7.33 (5H×2, s×2, Ph×2).

5-Acetamido-6,8-di-*O*-benzyl-5-deoxy-1,2-*O*-isopropylidene-3-*O*-methylthiomethyl-α-D-*threo*-D-allooctofuranose-(1,4) (17). To a solution of **7a** (905 mg) in anhydrous DMF (9 ml) was added sodium hydride (227 mg) under ice cooling, and the mixture was stirred for 40 min at room temperature. The reaction mixture was partitioned between water and ethyl acetate. The organic layer was washed with water repeatedly, dried and concentrated to dryness. The syrupy residue was dissolved in a small amount of toluene, and a silica-gel column was charged with the solution. After 3 h elution (toluene–ethyl acetate (v/v) 1:2) afforded 733 mg (92.3%) of **17** as a colorless syrup: R_f=0.66 on TLC (ethyl acetate); $[\alpha]_D^{21.5}$ +24.2 (*c* 1.01, $CHCl_3$); IR ($CHCl_3$) 1670 cm^{-1} (NHCO); ^1H NMR (90 MHz, $CDCl_3$) δ=1.33, 1.53 (3H×2, s×2, CMe_2), 1.92 (3H, s, NHAc), 2.19 (3H, s, SMe), 2.52 (1H, d, *J*=3 Hz, OH), 5.75 (1H, d, *J*=4 Hz, H-1), 7.35 (10H, s, Ph×2).

Found: C, 62.06; H, 6.97; N, 2.47; S, 5.87%. Calcd for $C_{29}H_{39}NO_8S$: C, 62.01; H, 7.00; N, 2.49; S, 5.71%.

6,8-Di-*O*-benzyl-5-deoxy-5-(2,4-dinitrophenylamino)-1,2-*O*-isopropylidene-3-*O*-methylthiomethyl-α-D-*threo*-D-allooctofuranose-(1,4) (18). A mixture of **17** (565 mg), sodium hydroxide (452 mg) and 95% aqueous 2-methoxyethanol (5.7 ml) was heated for 1.5 h under reflux. The reaction mixture was partitioned between water and chloroform. The organic layer was washed twice with water, dried and concentrated to dryness. The pale brown syrup was dissolved in THF (5.6 ml) and to the solution were added triethylamine (0.21 ml) and 2,4-dinitrofluorobenzene (225 mg). After 12 h at room temperature the reaction mixture was partitioned between water and ethyl acetate. The organic layer was washed twice with water, dried and concentrated to dryness. The deep yellow syrupy residue was chromatographed (toluene–ethyl acetate (v/v) 3:1) to give 548 mg (79.3%) of **18** as a yellow syrup: R_f=0.18 on TLC (toluene–ethyl acetate (v/v) 5:1); $[\alpha]_D^{20}$ +18.6° (*c* 1.07, $CHCl_3$); IR ($CHCl_3$) 1520, 1330 cm^{-1} (NO_2); ^1H NMR (90 Hz, $CDCl_3$) δ=1.32, 1.50 (3H×2, s×2, CMe_2), 2.00 (3H, s, SMe), 2.48 (1H, d, *J*=3 Hz, OH), 5.72 (1H, d, *J*=4 Hz, H-1), 6.91 (1H, d, *J*=10 Hz, H-6′), 7.32 (10H, s, Ph×2), 8.02 (1H, dd, *J*=3, 10 Hz, H-5′), 9.05 (1H, d, *J*=3 Hz, H-3′).

Found: C, 58.07; H, 5.89; N, 5.90; S, 4.43%. Calcd for $C_{33}H_{39}N_3O_{11}S$: C, 57.80; H, 5.73; N, 6.13; S, 4.68%.

6,8-Di-*O*-benzyl-5-deoxy-5-(2,4-dinitrophenylamino)-1,2-*O*-isopropylidene-7-*O*-methylsulfonyl-3-*O*-methylthiomethyl-α-D-*threo*-D-allooctofuranose-(1,4) (19). To a solution of **18** (554 mg) in dry pyridine (5.5 ml) was added methanesulfonyl chloride (0.19 ml) under ice cooling, and the mixture was stirred overnight at room temperature. The mixture was coevaporated with toluene, and the residue was partitioned between water and ethyl acetate. The organic layer was washed with water repeatedly, dried and concentrated to dryness. The syrupy residue was chromatographed (toluene–ethyl acetate (v/v) 10:1) to give 537 mg (86.9%) of **19** as yellow amorphous solids: R_f=0.43 on TLC (toluene–ethyl acetate (v/v) 5:1); $[\alpha]_D^{21.5}$ +23.8° (*c* 0.88, $CHCl_3$); IR (KBr) 1520 (NO_2), 1170 (SO_2Me) cm^{-1}; ^1H NMR (90 MHz, $CDCl_3$) δ=1.33, 1.50 (3H×2, s×2, CMe_2), 2.02 (3H, s, SMe), 2.93 (3H, s, SO_2Me), 5.78 (1H, d, *J*=4 Hz, H-1), 6.87 (1H, d, *J*=10 Hz, H-6′), 7.40 (10H, s, Ph×2), 8.09 (1H, dd, *J*=3, 10 Hz, H-5′), 9.09 (1H, d, *J*=3 Hz, H-3′).

Found: C, 53.26; H, 5.40; N, 5.43; S, 8.28%. Calcd for $C_{34}H_{41}N_3O_{13}S_2$: C, 53.46; H, 5.41; N, 5.51; S, 8.39%.

6,8-Di-*O*-benzyl-5-deoxy-5-(2,4-dinitrophenylamino)-1,2-*O*-isopropylidene-7-*O*-methylsulfonyl-α-D-*threo*-D-allooctofuranose-(1,4) (20). To a mixture of **19** (485 mg), sodium hydrogencarbonate (267 mg) and 90% aqueous acetone (5 ml) was added iodomethane (0.8 ml) nine times at intervals of 1 h under reflux. Furthermore, the mixture was refluxed for 6 h. The reaction mixture was poured into water and the mixture was extracted with ethyl acetate. The organic layer was washed with water, dried and concentrated to dryness. The residue was chromatographed (toluene–ethyl acetate (v/v) 5:1) to yield 338 mg (86.7%) of **20** as yellow amorphous solids: R_f=0.68 on TLC (toluene–ethyl acetate (v/v) 3:1); $[\alpha]_D^{22}$ +21.2° (0.965, $CHCl_3$); IR ($CHCl_3$) 1520, 1340 (NO_2), 1300, 1170 (SO_2Me) cm^{-1}; ^1H NMR (90 MHz, $CDCl_3$) δ=1.31, 1.48 (3H×2, s×2, CMe_2), 2.92 (3H, s, *SO₂Me*), 5.73 (1H, d, *J*=4 Hz, H-1), 6.80 (1H, d, *J*=10 Hz, H-6′), 7.40 (10H, s, Ph×2), 8.02 (1H, dd, *J*=3, 10 Hz, H-5′), 9.05 (1H, d, *J*=3 Hz, H-3′).

Found: C, 54.33; H, 5.35; N, 5.70; S, 4.33%. Calcd for $C_{32}H_{37}N_3O_{13}S$: C, 54.61; H, 5.30; N, 5.97; S, 4.56%.

3,7-Anhydro-6,8-di-*O*-benzyl-5-deoxy-5-(2,4-dinitrophenylamino)-1,2-*O*-isopropylidene-β-L-*erythro*-D-allooctofuranose-(1,4) (21). To a solution of **20** (154 mg) in anhydrous DMSO (1.5 ml) was added sodium hydride (35 mg) under ice cooling, and the mixture was stirred for 2 h at room temperature. The mixture was partitioned between water and chloroform. The organic layer was washed with water repeatedly, dried and concentrated to dryness. The residue was chromatographed (toluene–ethyl acetate (v/v) 10:1) to afford 92 mg (66%) of **21** as yellow amorphous solids: R_f=0.49 on TLC (toluene–ethyl acetate (v/v) 5:1); $[\alpha]_D^{23}$ +182° (*c* 0.585, $CHCl_3$); IR (KBr) 1520, 1330 cm^{-1} (NO_2); ^1H NMR (400 MHz, $CDCl_3$) δ=1.38, 1.66 (3H×2, s×2, CMe_2), 3.61—3.70 (2H, m, H-8), 3.80 (1H, dd, *J*=10.5, 4.0 Hz, H-3), 3.92 (1H, m, H-6), 4.26 (1H, m, H-5), 4.31 (1H, d, *J*=12.5 Hz, CH_2Ph), 4.42 (1H, m, H-7), 4.54 (1H, dd, *J*=4.5, 10.5 Hz, H-4), 4.55 (1H, d, *J*=12.5 Hz, CH_2Ph), 4.71 (1H, dd, *J*=3.5, 4.0 Hz, H-2), 4.77 (1H, d, *J*=12.5 Hz, CH_2Ph), 5.79 (1H, d, *J*=3.5 Hz, H-1), 6.24 (1H, d, *J*=9.5 Hz, H-6′), 7.02—7.42 (10H, m, Ph×2), 7.86 (1H, dd, *J*=3.0, 9.5 Hz, H-5′), 8.68 (1H, d, *J*=6.0 Hz, NH), 8.96 (1H, d, *J*=3.0 Hz, H-3′). The assignment was established by a spectrum of two dimensions.

Found: C, 61.51; H, 5.42; N, 6.82%. Calcd for $C_{31}H_{33}N_3O_{10}$: C, 61.28; H, 5.47; N, 6.92%.

We thank Mrs. Emi Yano and Mr. Shoji Zushi for recording the NMR spectra, Miss Shigeko Miki, Meiji Seika Kaisha, Ltd., for recording the mass spectra, and Mr. Saburo Nakada for his elemental analyses.

References

1) K. Takaoka, T. Kuwayama, and A. Aoki, Japan Patent, 1971, 615332.

2) K. Sakata, A. Sakurai, and S. Tamura, *Agric. Biol. Chem.*, **37**, 697 (1973); **38**, 1883 (1974); **39**, 885 (1975); **40**, 1993 (1976); *Tetrahedron Lett.*, **1974**, 1533; **1974**, 4327; **1975**, 3191.

3) K. Sakata and J. Uzawa, *Agric. Biol. Chem.*, **41**, 413 (1977).

4) K. Sakata, *Nippon Nogei Kagaku Kaishi*, **49**, R51 (1975).

5) K. Anzai and T. Saita, *Bull. Chem. Soc. Jpn.*, **50**, 169 (1977).

6) S. Hannesian, T. J. Liak, and D. M. Dixit, *Carbohydr. Res.*, **88**, C14 (1981); *Pure Appl. Chem.*, **53**, 129 (1981).

7) K. S. Kim and W. A. Szarek, *Can. J. Chem.*, **59**, 878 (1981); *Carbohydr. Res.*, **100**, 169 (1982).

8) O. Sakanaka, T. Ohmori, S. Kozaki, T. Suami, T. Ishii, S. Ohba, and Y. Saito, *Bull. Chem. Soc. Jpn.*, **59**, 1753 (1986).

9) P. M. Pojer and S. J. Angyal, *Aust. J. Chem.*, **31**, 1031 (1978).

Infrared C-D Stretching and ^{2}H NMR Spectra of Isopropyl-2-*d* 1-(*p*-Substituted Phenyl)ethyl Ketones. Evidence for the Hydrogen Bond-Like Interaction between C-D Group and Aromatic π-Electrons

Makoto KARATSU, Hiroko SUEZAWA, Kazuhisa ABE, Minoru HIROTA,* and Motohiro NISHIO†
Department of Applied Chemistry, Faculty of Engineering, Yokohama National University, Hodogaya-ku, Yokohama 240
†Central Research Laboratories, Meiji Seika Kaisha Ltd., Kohoku-ku, Yokohama 222
(Received May 9, 1986)

Isopropyl-2-*d* 1-(*p*-X-phenyl)ethyl ketones (where, X=H, NO_2, Br, Cl, C_2H_5, CH_3, and NH_2) were shown to have two absorption bands in the C-D stretching region. The absorption band at the higher frequency (ca. 2177 cm^{-1}) is assigned to the C-D···π approached conformer, and the high frequency shift is ascribed to the effect of steric compression. Weak C-D···π hydrogen bond was shown to occur by the measurement of the substituent effect on the formation constant and the relative enthalpy of the C-D···π approached conformer.

Through the recent investigations of ours[1-5] and several other authors,[6,7] it has been clarified that an alkyl group often prefers to take a position close to an aromatic ring in certain molecules. Thus, 2-alkyl-1-arylethanes Ar-CHR-CHXR′ generally take preferably a conformation in which the aryl (Ar) and the alkyl (R′) groups are gauche to each other.[2,3,8] In addition, 1-arylethyl *t*-butyl sulfides and sulfoxides have similar preferred conformations. To account for the preferred conformations of these compounds, weak attractive force is assumed to operate between the aryl and the alkyl groups and named sometimes CH···π interaction, while the nature of the weak interaction remains to be explored. At first, the authors[9,10] tentatively explained this as being originated from weak hydrogen bonding between CH group and aromatic π-electrons similar to the intermolecular interaction between chloroform and benzene.[11,12] However, this interpretation is hypothetical and nothing renders a confident support on it. Alternatively, the observed conformational preferences were reproduced nearly quantitatively by molecular force field calculations.[8,13] The preference for alkyl/aryl approached (gauche) conformations in the series of $ArCH_2CHXR'$ cannot be rationalized without taking into account an attractive interaction between aryl and alkyl groups. Dispersion force is the only general attractive force included in the calculation. Therefore, the CH···π interaction should be ascribed to dispersive force to a large extent.

In spite of this conclusion, presence of weak CH···π hydrogen bonding cannot be excluded completely. On the contrary, the minor contribution of CH···π hydrogen bonding to the stabilization of the alkyl/aryl gauche conformers of 1-aryl-2-alkylethanes is suggested from LIS measurements on this series of compounds.[2-4] Ab initio (4—31G) calculation on 1-phenyl-2-propanol gives small but definitely positive bond population between methyl hydrogen atom and aromatic carbon atoms.[14] However, the absolute values of the bond populations are about one tenth of those for OH···π interaction ((O)-H···C bond populations). If the hydrogen bond-like CH···π interaction does exist, the interaction is expected to become strong when the C-H group is linked to an electronegative atom. Thus, the possibility of such an interaction was examined in the series of 1-phenylalkyl ketones. In order to observe the behavior of the particular hydrogen atom participating in CH···π hydrogen bonding separately, isopropyl-2-*d* 1-(substituted phenyl)ethyl ketones in which the hydrogen atom is replaced by deuterium were prepared, and their infrared and ^{2}H NMR spectra were measured and discussed.

Experimental

Preparation of 1-Aryl Isopropyl-2-*d* Ketones. Appropriately substituted 2-phenylpropionaldehyde was prepared by the method reported by Nerdel and Frohlich[15,16] and reacted with (isopropyl-2-*d*)magnesium bromide in ether. The alcohol obtained as the product was then oxidized by sodium dichromate-sulfuric acid mixture to give the ketone **2**. Other ketones (**3—9**) were also prepared by a similar method. Nitro ketone **2b** was prepared by nitrating ketone **2a**. Reduction of **2b** gives amino ketone **2g**.

All ketones and intermediate alcohols were identified by comparing their boiling points with the reported boiling points of unlabeled ketones[16] and also by their NMR, infrared, and mass spectra.

Measurement of Spectra. ^{2}H NMR spectra were recorded on a JEOL FX 90Q spectrometer in acetone or dimethyl sulfoxide solutions. Infrared spectra were recorded on a Hitachi 225 spectrophotometer using an NaCl cell of 2 cm optical path length in carbon tetrachloride or chloroform solutions. Temperature studies were performed with the carbon tetrachloride solutions.

Results and Discussion

Infrared C-D Stretching Absorptions and Their Assignment. The C-H stretching absorption of methine (isolated C-H) group is known to be very weak in comparison with those of CH_2 and CH_3

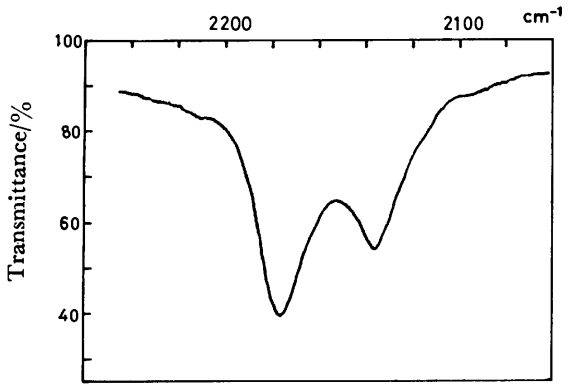

Fig. 1. Infrared C-D stretching absorption of isopropyl-2-*d* 1-phenylethyl ketone in CCl_4 solution.

groups,[17] which would make the recognition of the C-H band of isopropyl group extremely difficult. In fact, the C-H band of isopropyl group could not be identified in the spectrum of isopropyl 1-phenylethyl ketone (**1**) probably because of the interference caused by stronger overlapping bands. Thus, the deuterium-labeled analogs, isopropyl-2-*d* 1-(substituted phenyl)-ethyl ketones **2a**—g, were prepared and their infrared spectra in the C-D stretching frequency region (2300—2000 cm^{-1}) were measured.

As shown in Fig. 1, ketone **2a** has two absorption maxima at 2177 and 2136 cm^{-1} in this frequency region. The absorption bands can be characterized in spite of their very low intensity, since both the ketone and the solvent (carbon tetrachloride or chloroform) do not absorb the light of this frequency region.

Since the ketone **2a** has only a C-D bond, two absorption bands should be assigned to two different isomers, most probably rotamers in this case. Fermi resonance and related vibrational couplings might not operate in these circumstances, though they cannot be excluded completely. Temperature dependence measurement decribed later will support the conclusion, showing the presence of two energetically unequal isomers rapidly converting to each other. The sterical structures of the two conformers were estimated by molecular mechanics (MM2) calculations,[8] and the two conformers were tentatively assigned to the most and the next stable conformations (I and II, respectively) from the calculations.

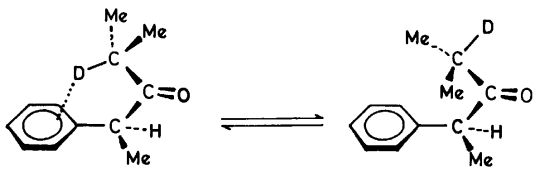

(I) (II)

Table 1. C-D Stretching Absorptions of Isopropyl-2-*d* Ketones R-C-CD(CH_3)$_2$

No.	R	ν/cm^{-1}	No.	R	ν/cm^{-1}
3	Ph	2191	**6**	CMe_3	2195
		2156			2182
2a	PhCHMe	2177	**7**	$CDMe_2$	2182
		2136			2154
4	$PhCH_2$	2153	**8**	CH_2CH_3	2168
					2130
5	$PhCH_2CH_2$	2157	**9**	CH_3	2167
		2130			2130

The absorption frequencies of the two bands are rather higher than estimated from the reported methine C-H frequency 2890±10 cm^{-1}.[18] This frequency can be converted to 2121 cm^{-1} in the C-D stretching region if we assume the band to arise from a pure C-H (or C-D) stretching mode of molecular vibration. As revealed by examining the molecular models and more confidently by the C-H···C(Ar) distance in the most stable conformation(I) estimated from MM2 calculations on ketone **1**, some compression of the C-H bond length is expected to occur with the isopropyl methine group of ketone **1** due to the steric congestion around the bond.[18,19] Therefore, the high frequency shift of the C-D bands of ketones **2a**—g are ascribable to the shortening of the C-D bonds due to the steric compression.

In order to prove the effect of steric compression experimentally, the C-D stretching absorptions of several isopropyl-2-*d* ketones $RCOCDMe_2$ (**3**—**9**) were measured and given in Table 1. In cases of methyl and ethyl ketones (**8** and **9**), as well as 2-phenylethyl ketone (**5**), no steric congestion was expected around the C-D bond in problem. The C-D absorption frequencies of the two series of ketones in Table 1 clearly shows that the high frequency shift is caused by the steric crowdedness, the most crowded *t*-butyl and phenyl ketones (**3** and **6**, respectively) absorbing at the highest frequency in both series. In line with the prediction from MM2 calculations, the C-D bond in one conformer (which absorbs at 2177 cm^{-1} of **2a** is suspected from its high absorption frequency to suffer a considerable compression sterically.[20,21] MM2 calculations further revealed that the C-D bond is located very close and nearly perpendicular to the plane of the aromatic ring of 1-phenylethyl group in this conformer(I), and the nonbonded H(D)·····C_{Ar} distance was calculated to be as close as 2.65 A. The distance is too close to have an optimum van der Waals contact with each other and results in a weak repulsive nonbond interaction between H(D) and C_{Ar}. In accord with the above reasonings, the band at the higher frequency (2177 cm^{-1}) was tentatively assigned to the C-D···π approached conformation(I) and the one at the lower frequency to the conformation(II)

Table 2. C-D Stretching Absorptions of the Ketones *p*-XC$_6$H$_4$CHMeCOCDMe$_2$ (**2**) in CCl_4. (2 cm NaCl Cell; Concentration, ca. 0.05 mol dm^{-3})

No.	X	ν_I/cm^{-1}	ε_I/l mol^{-1} cm^{-1}	ν_{II}/cm^{-1}	ε_{II}/l mol^{-1} cm^{-1}	$\varepsilon_I/\varepsilon_{II}$
2b	NO_2	2174	4.94	2135	4.99	1.10
2c	Br	2174	5.26	2135	4.07	1.29
2d	Cl	2175	6.48	2136	4.59	1.41
2a	H	2177	6.54	2136	4.12	1.59
2e	C_2H_5	2176	5.07	2136	3.30	1.54
2f	CH_3	2176	6.34	2136	3.98	1.59
2g	NH_2	2175	5.65	2135	3.44	1.64

which is estimated to be the next stable from the MM2 calculations.

Possibility of Intramolecular C-D···π Hydrogen Bonding. In turn, C-D···π hydrogen bonding is expected to be favorably formed in the C-D···π approached conformation(I). Ab initio calculations on a more simplified model compound $PhCH_2CH$-(OH)Me also gave a small but definitely positive bond populations between the methyl H and aromatic C atoms opposing in close distances (CH_3 and C_1 or C_2 of phenyl group in a conformer).[14]

Both the unusually short distance from MM2 and the positive bond populations from ab initio MO suggest the occurrence of an intramolecular hydrogen bond-like interaction between the CH and the aromatic π system. If such an interaction is assumed to be present, the formation constant of the intramolecular hydrogen bond could be estimated from the ratio of the absorption intensities (ε_I and ε_{II}) of the two C-D bands assigned to the conformations I and II by Eq. 1.

$$K = a\frac{\varepsilon_I}{\varepsilon_{II}} \text{ or } a\frac{\varepsilon_{int}}{\varepsilon_{free}} \quad (1)$$

As the intrinsic molar extinction coefficients of the C-D···π interacted and the free (non-interacted) conformers (ε_I^0 and ε_{II}^0, respectively) are not necessarily equal, proportionality constant a which is equal to their ratio was introduced. Here, ε_I and ε_{II} are appearent extinction coefficients and related to the intrinsic extinction coefficients by $\varepsilon_I = X_I\varepsilon_I^0$ and $\varepsilon_{II} = X_{II}\varepsilon_{II}^0$, where X_I and X_{II} are molar fractions of conformers I and II.

Since the more electron-rich π system acts as a stronger hydrogen acceptor in forming hydrogen bond, negative slope is expected with the logarithm of the formation constant vs. σ plot for a series of isopropyl-2-*d* 1-(substituted phenyl)ethyl ketones (**2a**—**2g**). Thus the $\log(\varepsilon_I/\varepsilon_{II})$ vs. σ plot was drawn by employing the intensities in Table 2. As expected, the slope of the plot (in Fig. 2) becomes negative, and the above assignment was supported experimentally.

In general, intramolecular hydrogen bonds are cleaved when a stronger hydrogen-donating solvent coexists. Therefore, the spectra of these ketones were measured in chloroform-*d* which is known as a typical C-H hydrogen donor in C-H···π hydrogen bonding.[11,12,22]

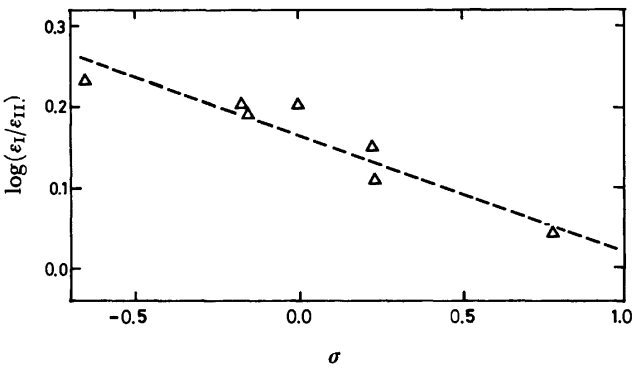

Fig. 2. Substituent effect on the ratios of absorption intensities of the two C-D bands. The $\varepsilon_I/\varepsilon_{II}$ vs. σ plot.

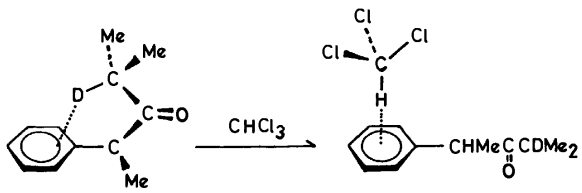

(I) (III)

The results are shown in Table 3. The observed $\varepsilon_I/\varepsilon_{II}$ ratios in Table 3 are significantly smaller than those in carbon tetrachloride. This reveals the fact that conformer I has been converted to the associated species III due to the solvation by forming intermolecular C-H···π hydrogen bond in chloroform. At present, we have no experimental evidence on whether the associated species III takes a conformation similar to the conformer II or not. However, the C-D bond of the associated species must not be very congested judging from its absorption frequency. Thus, the solvent effect on $\varepsilon_I/\varepsilon_{II}$ ratio again supports the above assignment of the C-D stretching bands and the presence of intramolecular hydrogen bonds.

Table 3. C-D Stretching Absorptions of the Ketones p-$XC_6H_4CHMeCOCDMe_2$ (**2**) in $CDCl_3$. (2 cm NaCl Cell; Concentration, ca. 0.05 mol dm^{-3})

No.	X	ν_I/cm^{-1}	$\varepsilon_I/l\ mol^{-1}\ cm^{-1}$	ν_{II}/cm^{-1}	$\varepsilon_{II}/l\ mol^{-1}\ cm^{-1}$	$\varepsilon_I/\varepsilon_{II}$
2b	NO_2	2167	3.00	2131	3.42	0.88
2d	Cl	2163	2.24	2133	3.00	0.75
2a	H	2163	2.84	2132	3.74	0.76
2f	CH_3	2163	2.25	2131	2.92	0.77

Table 4. ^2H NMR Spectra of the Ketones p-XC_6H_4-$CHMeCOCDMe_2$ (**2**) in Acetone[a)]

No.	X	δ_D(ppm) from $CDCl_3$
2b	NO_2	−5.298
2c	Br	−5.357
2d	Cl	−5.357
2a	H	−5.367
2e	C_2H_5	−5.371
2f	CH_3	−5.378

a) A small amount of LiBr for internal lock signal and $CDCl_3$ for reference were added.

Another evidence comes from ^2H NMR spectra of the ketones **2a**—g. The deuterium atom is located just above and very close to the plane of aromatic ring in conformer I and expected to resonate at a higher frequency than the one in conformer II due to the anisotropy effect of strongly diamagnetic aromatic ring. This implies that the electron-donating substituent on the aromatic ring favors the conformation I and, hence, causes a high field shift of the ^2H chemical shift. ^2H NMR of ketones **2** are given in Table 4. Due to the limitations from the solubility of LiBr for internal locking (since LiBr is sparingly soluble in CCl_4), the measurements were carried out in acetone containing a small amount of chloroform-d as an internal reference. As anticipated, the ^2H chemical shifts tend to move towards high fields in the order of decreasing electron-withdrawing ability and increasing electron-donating ability of the substituent, i.e., in the order of decreasing σ value.[23,24)]

In conclusion, the C-D bond is sterically enforced to oppose the aromatic ring to have a considerable overlap of its antibonding orbital with the aromatic π-MO and is favorable in forming a C-D···π hydrogen bond. Judging from the substituent electronic effect and the solvent effect discussed above, the existence of the intramolecular hydrogen bonding between the isopropyl methine group and π-electrons on the aromatic ring becomes confident.

Substituent Effect on the Enthalpy of the C-D···π Interacted Conformer. As is remarked briefly in relation to the assignment of the C-D stretching bands, the intensities of the two C-D absorption bands

Table 5. Temperature Dependence of the C-D Absorption Intensities of p-$XC_6H_4CHMeCOCDMe_2$

X	T/K	$\varepsilon_I/\varepsilon_{II}$	ΔH/kJ mol^{-1}
NO_2	291.1	1.095	1.26
	300.4	1.110	
	310.0	1.126	
	320.1	1.145	
	329.0	1.162	
Br	293.5	1.289	0.92
	300.7	1.303	
	302.9	1.308	
	310.1	1.308	
	314.1	1.320	
	318.7	1.321	
	324.2	1.334	
	330.1	1.345	
Cl	297.6	1.413	0.88
	304.0	1.427	
	311.8	1.438	
	317.4	1.441	
	319.2	1.453	
	329.8	1.461	
H	293.7	1.586	0.80
	301.4	1.593	
	310.8	1.618	
	321.0	1.634	
	323.2	1.634	
	329.6	1.642	
C_2H_5	293.6	1.553	0.67
	303.2	1.546	
	313.1	1.565	
	320.3	1.582	
	329.9	1.595	
CH_3	292.4	1.594	0.55
	300.5	1.612	
	311.3	1.617	
	319.7	1.629	
	330.3	1.638	
NH_2	291.4	1.639	0.42
	301.4	1.640	
	307.4	1.657	
	317.4	1.650	
	329.1	1.673	

are temperature dependent. This provides us with a clue to elucidate the nature of the intramolecular interaction, since we can estimate the relative enthalpies of the C-D···π interacted conformers by measuring the formation constant K (given by Eq. 1) as a function of temperature. The measurements were carried out with carbon tetrachloride solutions of ketones **2a**—g, and the results are given in Table 5. The differences in enthalpy between the two conformers (ΔH) were calculated by Eq. 2 from the slope of $\log K$ vs. T^{-1} plots obtained by least squares calculation.[25]

$$\log K = -(\Delta H/R)T^{-1} + \Delta S/R \quad (2)$$

Here, K could be substituted by $\varepsilon_I/\varepsilon_{II}$ since a (in Eq. 1) affects only the entropy term in Eq. 2.

The relative enthalpies ΔH ($=H_I-H_{II}$) in Table 5 showed that the C-D···π interacted conformer(I) is not the most stable. This conclusion on the conformational preference does not agree with the prediction from MM2. However, the difference in enthalpy is less than 2 kJ mol^{-1} (or 0.5 kcal† mol^{-1}) which is known to be the maximal deviation from the experiment in MM2 calculations on hydrocarbons.[26]

If we assume that the substituent on the aromatic ring does not affect the stability of the free conformer(II), the relative enthalpy (ΔH) should give the relative stability of the C-D···π interacted conformer(I). The assumption seems entirely reasonable since the C-D bond is separated by a saturated carbon and a carbonyl carbon atoms from the aromatic ring, and the electronic effect is not likely to be transmitted through them. After all, the ΔH value can be a measure of the enthalpy of the C-D···π hydrogen-bond formation.

The C-D···π hydrogen bond is expected to be strengthened in the increasing order of π-electron density on the aromatic carbon atoms. Hence, electron-donating substituent on the aromatic ring should favor the hydrogen bond and stabilize the C-D···π interacted conformer. This leads to the conclusion that the ΔH should be lower when the substituent is more electron-donating. As easily seen from the ΔH vs. σ plot in Fig. 3, the relative enthalpies in Table 5 are in line with the theoretical consequences on the substituent effect, giving a straight line with a positive ρ value (ρ=+0.605 kJ mol^{-1}). In other words, the C-D···π interacted conformer becomes more stabilized with ketone 2 carrying an electron-donating substituent and less stabilized with ketone 2 carrying an electron-withdrawing substituent. Without an exception, hydrogen-bonded system previously investigated were shown to behave similarly towards the effect of polar substituents.[27] Thus, the substituent effect on the ΔH's renders another support on the C-D···π hydrogen bonding in isopropyl-2-*d* 1-arylethyl ketones (**2**).

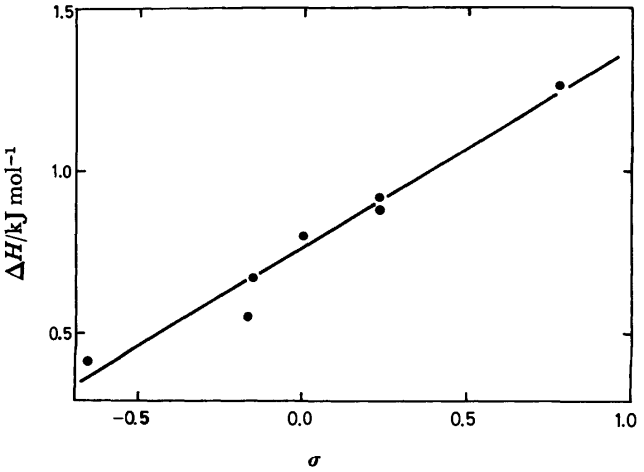

Fig. 3. Substituent effect on the relative enthalpies of the C-D···π interacted conformers. The ΔH vs. σ plot.

This research was partly supported by a Grant-in-Aid for Scientific Research from the Ministry of Education, Science and Culture to which the authors are grateful.

References

1) Y. Kodama, K. Nishihata, M. Nishio, and Y. Iitaka, *J. Chem. Soc., Perkin Trans. 2*, **1976**, 1490.
2) M. Hirota, Y. Takahashi, M. Nishio, and K. Nishihata, *Bull. Chem. Soc. Jpn.*, **51**, 2358 (1978).
3) J. Uzawa, S. Zushi, Y. Kodama, Y. Fukuda, K. Nishihata, K. Umemura, M. Nishio, and M. Hirota, *Bull. Chem. Soc. Jpn.*, **53**, 3623, 3631 (1980).
4) S. Zushi, Y. Kodama, K. Nishihata, M. Nishio, M. Hirota, and J. Uzawa, *Bull. Chem. Soc. Jpn.*, **54**, 2113 (1981).
5) N. Kunieda, H. Endo, M. Hirota, Y. Kodama, and M. Nishio, *Bull. Chem. Soc. Jpn.*, **56**, 3110 (1983).
6) K. K. Chiu, H. H. Huang, and L. H. L. Chia, *J. Chem. Soc., Perkin Trans. 2*, **1972**, 286.
7) R. E. Carter and P. Stibs, *J. Am. Chem. Soc.*, **98**, 7515 (1976).
8) M. Hirota, T. Sekiya, K. Abe, H. Tashiro, M. Karatsu, M. Nishio, and E. Osawa, *Tetrahedron*, **39**, 3091 (1983).
9) M. Nishio, *Kagaku No Ryoiki*, **31**, 834, 928 (1977).
10) Y. Kodama, K. Nishihata, M. Nishio, and N. Nakagawa, *Tetrahedron Lett.*, **1977**, 2105.
11) T. Ledaal, *Tetrahedron Lett.*, **1968**, 1683.
12) M. F. Rettig and R. S. Drago, *J. Am. Chem. Soc.*, **88**, 2966 (1966).
13) M. Hirota, K. Abe, T. Sekiya, H. Tashiro, and E. Osawa, *Chem. Lett.*, **1981**, 685.
14) K. Abe, M. Hirota, and K. Morokuma, *Bull. Chem. Soc. Jpn.*, **58**, 2713 (1985).
15) C. F. H. Allen and J. VanAllan, *Org. Synth.*, Coll. Vol.

† 1 cal=4.184 J.

3, 727 (1965).
16) F. Nerdel and H. Frohlich, *Ber.*, **85**, 171 (1952).
17) L. J. Bellamy, "The Infra-red Spectra of Complex Molecules," 3rd ed., Chapman & Hall, London (1975), Vol. 1, p. 16.
18) J. J. Fox and A. E. Martin, *Proc. Roy. Soc.*, **A175**, 208, 234 (1940).
19) E. L. Saier and N. D. Coggeshall, *Anal. Chem.*, **20**, 812 (1948).
20) D. Kivelson, S. Winstein, P. Bruck, and R. L. Hansen, *J. Am. Chem. Soc.*, **83**, 2938 (1961).
21) L. DeVries and P. R. Ryason, *J. Org. Chem.*, **26**, 621 (1961).
22) G. C. Pimentel and A. L. McClellan, "The Hydrogen Bond," Freeman & Co., San Francisco (1960).
23) L. P. Hammett, *J. Am. Chem. Soc.*, **59**, 96 (1937).
24) D. H. McDaniel and H. C. Brown, *J. Org. Chem.*, **23**, 420 (1958).
25) Details in variable temperature measurement are given in our previous paper: M. Ōki and M. Hirota, *Bull. Chem. Soc. Jpn.*, **36**, 290 (1963); *Nippon Kagaku Zasshi*, **86**, 115 (1965).
26) D. H. Wertz and N. L. Allinger, *Tetrahedron*, **35**, 3 (1979).
27) Examples of substituent effect on hydrogen bond energies are found in the following papers; a) M. Ōki and K. Mutai, *Bull. Chem. Soc. Jpn.*, **39**, 809 (1966); b) Ref. 25.

 © 1986 The Chemical Society of Japan Bull. Chem. Soc. Jpn., 59, 3535—3539 (1986)

Synthesis and Biological Activities of Acetylenic Fatty Acids and Their Esters

Munehiro NAKATANI,* Yuji FUKUNAGA, Hiroyuki HARAGUCHI,† Makoto TANIGUCHI,† and Tsunao HASE

Department of Chemistry, Faculty of Science, Kagoshima University, Korimoto 1-Chome, Kagoshima 890

†Department of Biology, Faculty of Science, Osaka City University, Sugimoto-cho, Sumiyoshi-ku, Osaka 558

(Received May 12, 1986)

Eight terminal acetylenic fatty acids from 5-hexynoic to 12-tridecynoic acids and their methyl, ethyl, and isopropyl esters were synthesized via *o*-nitrophenyl selenides. These acids and esters all showed inhibitory effect on lettuce seed germination and seedling growth. The effect was dependent on the number of carbon atoms in acetylenic chain. 8-Nonynoic acid showed potent activity, and its methyl ester was the most effective among the test compounds. In addition, the acids showed antifungal activity which increased as the number of carbon atoms increased.

There have been some attempts to relate the chemical structure of fatty acids to inhibition of seed and pollen germination. In a series of straight-chain saturated monocarboxylic acids, Raynolds showed that the inhibitory activity on lettuce seed germination increased with the number of carbon atoms of the acids and that the main structure-activity correlation was lipophilic in nature.[1,2] Orito et al. studied the effects of a variety of monocarboxylic acids with and without hydroxy substituent at the 2- or 3-positions on pollen germination in *Camellia sinensis*.[3] They showed that the intensity of inhibition was related not only to the carbon number of the acid but also to the degree of unsubstitution of the carbon chain. We recently reported the isolation of 8-nonynoic (**1d**) and 9-decynoic (**1e**) acids and their methyl esters (**2d**) and (**2e**) from the stem bark of *Hibiscus rosa-sinensis*.[4] These metabolites were found to be inhibitors of the germination of lettuce seeds. The acid (**1d**) showed higher activity than **1e**, and the esters (**2d**) and (**2e**) were more active than the corresponding free acids. Thereupon, considerable attention was devoted to the correlation of inhibitory activity with number of carbon atoms in terminal acetylenic fatty acids and esters.

In this research, eight acids from 5-hexynoic (**1a**) to 12-tridecynoic (**1h**) acids and their methyl (**2a**—h), ethyl (**3a**—h) and isopropyl (**4a**—**h**) esters were prepared via ω-(*o*-nitrophenylseleno) esters and their effects on lettuce seed germination and seedling growth were studied. Further, the antimicrobial properties of the acids (**1a**—**h**) were examined, since acetylenic fatty acids 7-octynoic (**1c**), 8-nonynoic (**1d**), 10-undecynoic (**1f**), and 11-dodecynoic (**1g**) acids have been described to inhibit the growth of some fungi.[5-8]

Results and Discussion

Synthesis. Seven acids from 5-hexynoic (**1a**) to 12-tridecynoic (**1h**) acids were prepared from the corresponding terminal diols via the *o*-nitrophenyl selenides (Scheme 1), except that **1f** was prepared from commercially available 10-undecenoic acid. Primary alkyl phenyl selenides obtained from bromides or alcohols were shown to produce terminal olefins in good yield,[9,10] which were easily converted into acetylenes by a typical method. From the terminal diols (n=3—10), 1,6-hexanediol to 1,13-tridecanediol, except 1,11-undecanediol, the corresponding bromo esters (**5**) were prepared in three steps in ca. 35% yield by monobromination with hydrobromic acid followed by oxidation and methylation. Treatment of the esters (**5**) with *o*-nitrophenyl selenocyanate in the presence of sodium borohydride under nitrogen in ethanol at room temperature[9] gave *o*-nitrophenyl selenides (**7**) in 75—80% yields. The structures of **7** were comfirmed by elemental analysis, ^{1}H NMR and mass spectra (Table 1). In their ^{1}H NMR spectra, the methylene protons attached to selenium atom appeared at about δ 2.9. The EI-MS of each selenide displayed a $(M+1)^+$ ion and a characteristic M−201 peak which was apparently due to the fission of -CH_2-Se- bond. It also contained to more prominent peaks indicating further successive loss of methanol and carbon monoxide. On the other hand, the alcohols (**4d**) and (**4e**), obtained by hydrolysis of the bromo esters (**5d**) and (**5e**), were also converted into the selenides (**7d**)

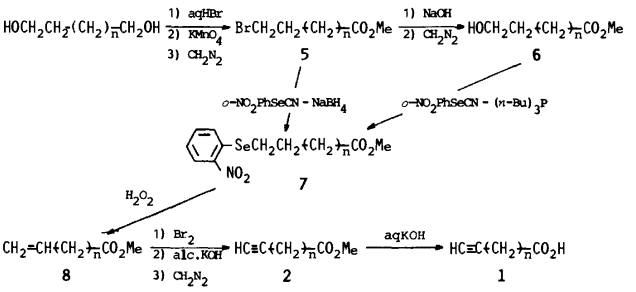

Scheme 1.

Table 1. Yields and Physicochemical Properties of Phenyl Selenides **7**

Compound	Yield %	Mp θ_m/°C	^{1}H-NMR δ ppm(Hz) PhSe-C$\underline{H}_2$-	Ms *m/z*(rel. int.)	Formula	Analysis Found(Calcd) C (%)	H (%)	N (%)
7a	68	25.0—26.0	2.95 (t, J=7.2)	69(100), 97(97) 129(15), 331(19)	$C_{13}H_{17}NO_4Se$	47.22 (47.13)	5.17 (5.14)	4.22 (4.06)
7b	73	33.0—33.5	2.88 (t, J=7.5)	83(100), 111(81) 143(20), 345(26)	$C_{14}H_{19}NO_4Se$	48.96 (48.70)	5.56 (5.51)	4.01 (4.06)
7c	75	37.5—38.0	2.88 (t, J=7.5)	97(80), 125(100) 157(15), 359(34)	$C_{15}H_{21}NO_4Se$	50.39 (50.14)	5.90 (5.85)	3.91 (3.90)
7d	79	61.5—62.5	2.90 (t, J=7.3)	111(15), 139(93) 171(12), 373(40)	$C_{16}H_{23}NO_4Se$	51.65 (51.61)	6.23 (6.23)	3.75 (3.76)
7e	76	44.0—44.5	2.96 (t, J=7.5)	125(11), 153(58) 185(11), 387(45)	$C_{17}H_{25}NO_4Se$	52.77 (52.89)	6.61 (6.53)	3.65 (3.63)
7g	75	52.0—53.0	2.92 (t, J=7.5)	153(9), 181(20) 213(10), 415(50)	$C_{19}H_{29}NO_4Se$	54.98 (54.94)	7.08 (6.99)	3.35 (3.37)
7h	75	57.0—57.5	2.90 (t, J=7.3)	167(9), 195(19) 227(10), 529(53)	$C_{20}H_{31}NO_4Se$	55.88 (55.94)	7.24 (7.23)	3.13 (3.26)

Table 2. Inhibitory Effect of Acetylenic Fatty Acids and Ester Derivatives on Lettuce Seed Germination

		Number of carbon atom in acid	Concentration/mM[a)] Acid **1**	Me ester **2**	Et ester **3**	Isopropyl ester **4**
5-Hexynoic	**a**	6	0.99	3.2	2.9	6.5
6-Heptynoic	**b**	7	0.92	2.8	2.5	6.0
7-Octynoic	**c**	8	0.78	0.49	2.3	5.5
8-Nonynoic	**d**	9	0.13	0.030	0.41	0.77
9-Decynoic	**e**	10	0.24	0.055	1.00	0.83
10-Undecynoic	**f**	11	0.41	0.38	1.43	4.5
11-Dodecynoic	**g**	12	0.44	0.90	1.08	4.2
12-Tridecynoic	**h**	13	0.48	0.98	1.19	4.0

a) Concentrations at which percentage germination of the seeds at 25 °C is 50% of the control value.

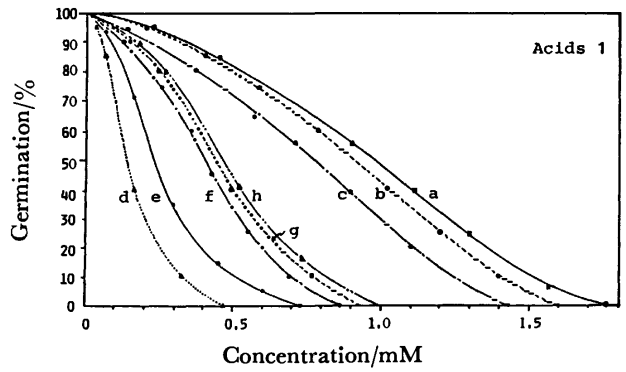

Fig. 1. Relationship between the concentration of the acid (**1a**—**h**) and the percentage of seed germination.

and (**7e**) in 73 and 78% yields, respectively, by using *o*-nitrophenyl selenocyanate with tributylphosphine in tetrahydrofuran at room temperature.[10] Decomposition of these selenides (**7**) by 30% hydrogen peroxide produced the corresponding olefins (**8**) in ca. 85% yields.

The synthesis was completed by converting **8** into the corresponding acetylenes (**1**), by bromination with bromine and subsequent dehydrobromination with ethanolic potassium hydroxide under reflux, in ca. 80% yields. In this simple method, the formation of allene compounds was minimal. The purification of these (**1a**—**h**) acids was done by column chromatography after methylation into **2a**—**h**. The ethyl (**3a**—**h**) and isopropyl (**4a**—**h**) esters were obtained from **1** by treatment with concentrated sulfuric acid under reflux in absolute ethanol and 2-propanol, respectively.

Activity on Seed Germination. To assess the effect of the variation in number of carbon atoms and ester substituents on the acetylenic fatty acids and their derivatives, the inhibitory activity of eight synthetic acids (**1a**—**h**) and their methyl (**2a**—**h**), ethyl (**3a**—**h**), and isopropyl (**4a**—**h**) esters on lettuce seed germina-

Table 3. Inhibitory Effect of Acetylenic Fatty Acids and Ester Derivatives on Hypocotyl Growth of Lettuce Seedlings

Compd	Concentration[a] mM	Compd	Concentration[a] mM
1b	1.2	**2d**	0.089
1d	0.13	**3d**	0.16
1f	0.55	**4d**	0.38
1h	0.35		

a) Concentrations at which hypocotyl is 50% of the control value.

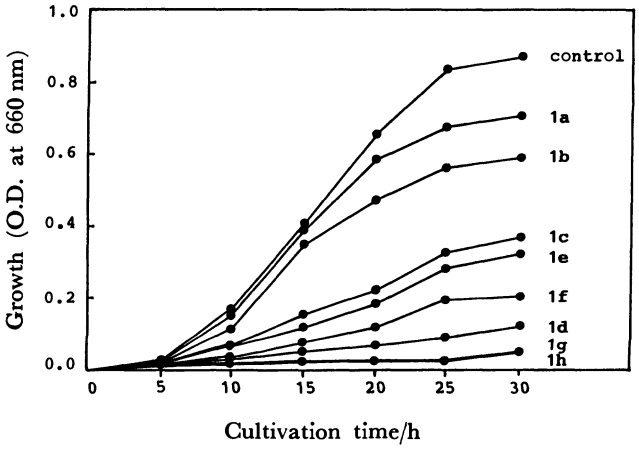

Fig. 2. Inhibitory effect of the acid (**1a**—**h**) on growth of *Hansenula anomala*.

tion were compared. Figure 1 presents the relationship between the concentration of the acids and the percentage of germination. The millimolar concentration producing 50% inhibition of germination is obtained from each curve. The inhibitory activity of all test compounds at a given concentration is shown in Table 2.

Among the acids tested, 8-nonynoic acid (**1d**) was the most potent and showed 50% inhibition at 0.13 mM (1 M=1 mol dm^{-3}). The activity of **1d** was much greater than that of nonanoic and 8-nonenoic acids so far reported.[1,4] Thus, it is apparent that the introduction of a terminal acetylenic group in the fatty acids increase inhibitory activity. As with the case of the acids, the activity of each set of methyl, ethyl and isopropyl esters was dependent on the number of carbon atoms in acetylenic chain with maximum activity at carbon number 9. The ester moiety also affected activity, a bulky one causing a decrease in activity. These results suggest that the lipophilicity-hydrophilicity balance of the compound is a fundamental requirement for the expression of marked inhibitory activity. In general, free acids showed greater activity than the corresponding esters. However, naturally occurring methyl 8-nonynoate (**2d**) and methyl 9-decynoate (**2e**) showed greater activity than the free acids (**1d**) and (**1e**). Their activities are comparable to those of well-known inhibitors, 3-indoleacetic acid[2] and abscisic acid.[11]

Activity on Seedling Growth. Four acids and three esters were selected among the synthetic compounds based on the above results of germination test and their activity tested on the hypocotyl growth in lettuce seedlings. As shown in Table 3, the acids showed similar inhibitory activity to the germination test, In which 8-nonynoic acid (**1d**) exhibited greater activity than the other acids. Its methyl ester (**2d**) was the most effective. It is interesting to note that these terminal acetylene compounds are also observed to inhibit a photosynthetic path.[12]

Antimicrobial Activity. The acids (**1g**) and (**1h**) showed weak and broad antifungal activity. The minimum inhibitory concentrations against almost all yeasts and filamentous fungi tested were 20—200 μg ml^{-1} (data not shown). Bacteria were insensitive to both **1g** and **1h**. The other acids (**1a**—**f**) were little antifungal. However, they inhibited in some degree, the growth of *Hansenula anomala* as shown in Fig. 2. In general, the inhibitory activity increased as the number of carbon atoms in the acids increased. Interestingly, **1d** was exceptionally active.

The structural significance of 8-nonynoic acid and its ester derivatives on the biological activity in microorganisms and plants remains to be elucidated.

$HC{\equiv}C{-}(CH_2{-})_n{-}CO_2R$

	n	R		*n*	R		*n*	R		*n*	R
1a:	3	H	**2a**:	3	Me	**3a**:	3	Et	**4a**:	3	*i*-Pr
1b:	4	H	**2b**:	4	Me	**3b**:	4	Et	**4b**:	4	*i*-Pr
1c:	5	H	**2c**:	5	Me	**3c**:	5	Et	**4c**:	5	*i*-Pr
1d:	6	H	**2d**:	6	Me	**3d**:	6	Et	**4d**:	6	*i*-Pr
1e:	7	H	**2e**:	7	Me	**3e**:	7	Et	**4e**:	7	*i*-Pr
1f:	8	H	**2f**:	8	Me	**3f**:	8	Et	**4f**:	8	*i*-Pr
1g:	9	H	**2g**:	9	Me	**3g**:	9	Et	**4g**:	9	*i*-Pr
1h:	10	H	**2h**:	10	Me	**3h**:	10	Et	**4h**:	10	*i*-Pr

Experimental

Mps are uncorrected. UV spectra were measured in methanol (MeOH) with a Shimadzu UV-210A spectrometer and IR spectra recorded on a Shimadzu IR-408 spectrometer. ^{1}H NMR spectra in chloroform-*d* with TMS as internal standard (δ=0) were measured at 60 (JEOL MH-60), 100 (JEOL MH-100), and 360 MHz (by Dr. Iwashita at Suntory Institute for Bioorganic Research). EI-Mass spectra were measured with a JEOL JMS-D300 apparatus and FD-mass spectra by Dr. Naoki at Suntory Institute for Bioorganic Research.

Bromo Esters from Terminal Diols. Commercially available terminal diols of 1,6-hexanediol to 1,10-decanediol and 1,12-dodecanediol, and 1,13-tridecanediol obtained from 1,13-tridecanedioic acid by methylation with diazomethane (CH_2N_2) and lithium aluminium hydride (LAH) reduction, were converted to the corresponding bromo esters by the following general procedure. A terminal diol (0.03 mol) was treated in a soln of 48% hydrobromic acid (HBr) (8.7 g) and concd sulfuric acid (H_2SO_4) (1.5 ml) for 3 h under reflux. A crude product extracted with ether was oxidized with potassium permanganate ($KMnO_4$) (2.5 g) in 20% H_2SO_4 (28 ml) at 15—20 °C. After methylation with CH_2N_2, the crude product was chromatographed over silica gel to give the bromo ester (**5**).

Bromo Ester 5. **5a** (oil): Yield 33%; IR (neat) 1740 cm^{-1}; ^{1}H NMR δ=2.36 (2H, t, J=7 Hz), 3.42 (2H, t, J=6.5 Hz), 3.70 (3H, s). **5b** (oil): Yield 33%. **5c** (oil): Yield 35%. **5d** (oil): Yield 36%. **5e** (oil): Yield 37%. **5g** (oil): Yield 37%. **5h** (oil): Yield 39%.

Methyl 9-Hydroxynonanoate (6d) and Methyl 10-Hydroxydecanoate (6e). The bromo esters (**5d**) and (**5e**) were hydrolyzed with 20% aq sodium hydroxide (NaOH) at 50 °C and the products were methylated with CH_2N_2 to give **6d** and **6e** in 93 and 91% yields, respectively. **6d**, mp 56.5—57.5 °C: IR (neat) 3400, 1740 cm^{-1}; ^{1}H NMR δ=2.27 (2H, t, J=7 Hz), 3.33 (2H, t, J=6 Hz), 3.69 (3H, s). **6e**, mp 59.5—60.5 °C: IR (neat) 3350, 1740 cm^{-1}; ^{1}H NMR δ=2.31 (2H, t, J=7 Hz), 3.32 (2H, t, J=6 Hz), 3.67 (3H, s).

Preparation of Selenides 7. 1) **From Bromide.** To a cooled (0 °C) suspension of *o*-nitrophenyl selenocyanate (1.43 g, 6.3 mmol) in abs ethanol (EtOH) (20 ml) under nitrogen (N_2), sodium borohydride ($NaBH_4$) (0.28 g, 7.4 mmol) was added with stirring. A bromo ester (**5**) (5.7 mmol) was added and the soln stirred at room temp for 13 h. After removal of EtOH, the crude product was chromatographed over silica gel to give **7**, a yellow crystalline compound. ii) **From Alcohol.** A soln of **6** (2.4 mmol) in tetrahydrofuran (THF) (8 ml) containing *o*-nitrophenyl selenocyanate (2.9 mmol) under N_2 was treated dropwise with tributylphosphine (2.9 mmol) at room temp. After being stirred for 30 min, the solvent was removed in vacuo. The crude product was purified by chromatography.

***o*-Nitrophenyl Selenides 7.** **7a**, mp 25.0—26.0 °C: IR (Nujol) 1730, 1590, 1560 cm^{-1}; ^{1}H NMR δ=2.35 (2H, t, J=7 Hz), 2.95 (2H, t, J=7.5 Hz), 3.70 (3H, s), 7.37—7.73 (3H, m), 8.47 (1H, d, J=8 Hz). Table 1.

Olefins 8 from Selenides 7. Into a cooled (0 °C) soln of a selenide **7** (3 mmol) in THF (30 ml), 30% aq hydrogen peroxide (H_2O_2) (8 ml) was added dropwise. The ice bath was removed and the soln was stirred for additional 24 h. The reaction mixture was diluted with water (H_2O) and extracted with hexane to give **8**, a very smelly oil.

Terminal Olefins 8. **8a**: Yield 68%; EIMS m/z 128 (M$^+$); IR (neat) 3070, 1740, 1640 cm^{-1}; ^{1}H NMR δ=2.35 (2H, t, J=7 Hz), 3.66 (3H, s), 4.78 (1H, br d, J=8 Hz), 4.88 (1H, br d, J=15 Hz), 5.41—6.11 (1H, m). **8b**: Yield 72%; EIMS m/z 142 (M$^+$). **8c**: Yield 80%; EIMS m/z 156 (M$^+$). **8d**: Yield 85%: EIMS m/z 170 (M$^+$). **8e**: Yield 84%; EIMS m/z 184 (M$^+$). **8g**: Yield 82%; EIMS m/z 198 (M$^+$). **8h**: Yield 80%; EIMS m/z 212 (M$^+$).

Acetylenic Esters 2 from Olefins 8. To a soln of olefin **8** (2 mmol) in chloroform ($CHCl_3$) (10 ml), excess bromine (Br_2) was added and the soln was stirred for 1 h at room temp. After being treated in the usual way, the product was made to react with potassium hydroxide (KOH) (1.7 g) in abs EtOH under reflux for 3 h. After being acidified, the product was extracted with hexane and methylated with CH_2N_2 to give **2**, a smelly oil, which was purified by chromatography over silica gel.

Acetylenic Esters 2. **2a**: Yield 68%; EIMS m/z 126 (M$^+$), 94, 81, 74, 68; IR (neat) 3300, 2100, 1730 cm^{-1}; UV 206 nm (ε 150); ^{1}H NMR δ=1.98 (1H, t, J=2.8 Hz, HC≡C-), 2.17 (2H, dt, J=2.8 and 7.0 Hz, ≡C-CH$_2$-), 2.28 (2H, t, J=7.0 Hz, -CH$_2$CO-), 3.73 (3H, s, -CO$_2$CH$_3$). **2b**: Yield 65%; EIMS m/z 140 (M$^+$), 108, 81, 74, 68. **2c**: Yield 70%; EIMS m/z 156 (M$^+$), 94, 81, 74, 68. **2d**: Yield 75%; EIMS m/z 168 (M$^+$), 137, 94, 81, 74, 68, 54. **2e**: Yield 78%; EIMS m/z 182 (M$^+$), 151, 108, 87, 74, 68, 54. **2f**: Yield 75%; EIMS m/z 196 (M$^+$), 165, 108, 87, 81, 74, 68. **2g**: Yield 73%; EIMS m/z 210 (M$^+$), 179, 108, 87, 81, 74, 68. **2h**: Yield 74%; EIMS m/z 224 (M$^+$), 193, 108, 87, 81, 74, 68.

Acetylenic Acids 1. Methyl ester **2** was gently refluxed in a small amount of 30% aq KOH for 30 min and the soln acidified with dil hydrochloric acid (HCl) to give **1**. **1a** (oil)[13]: UV 206 nm (ε 430); IR (neat) 3300, 3200—2500, 2100, 1705 cm^{-1}. **1b** (oil)[13]: UV 206 nm (ε 450). **1c** (oil): UV 206 nm (ε 450). **1d**, mp 22—23 °C: UV 206 nm (ε 490). **1e**,[14] mp 24.5—25.5 °C: UV 206 nm (ε 510). **1f**,[15] mp 29.5—30.0 °C: UV 206 nm (ε 540). **1g**, mp 33—34 °C: UV 206 nm (ε 780). **1h**, mp 40—41 °C: UV 206 nm (ε 860).

Ethyl and Isopropyl Esters 3 and 4. Ethyl and isopropyl esters **3** and **4** were obtained from the acids (**1**) by treatment with concd H_2SO_4 in abs EtOH and *i*-PrOH under reflux, respectively.

Ethyl Esters 3. **3a** (oil)[13]: Yield 70%; EIMS m/z 140 (M$^+$), 94, 88, 81, 68. UV 206 nm (ε 170); IR ($CHCl_3$) 3300, 2100, 1735 cm^{-1}; ^{1}H NMR δ=1.26 (3H, t, J=7.5 Hz, -CO$_2$CH$_2$CH$_3$), 1.94 (1H, t, J=3 Hz, HC≡C-), 2.24 (2H, dt, J=3 and 7 Hz, ≡C-CH$_2$-), 2.38 (2H, t, J=7 Hz, -CH$_2$-CO-), 4.20 (2H, q, J=7.5 Hz, -CO$_2$CH$_2$CH$_3$). **3b** (oil)[13]: Yield 70%; EIMS m/z 154 (M$^+$), 108, 88, 81, 68; UV 206 nm (ε 170). **3c** (oil): Yield 75%; EIMS m/z 168 (M$^+$), 108, 94, 88, 68; UV 206 nm (ε 204). **3d** (oil): Yield 74%; EIMS m/z 182 (M$^+$), 167, 108, 81, 68; UV 206 nm (ε 270). **3e** (oil)[14]: Yield 74%; EIMS m/z 196 (M$^+$), 108, 88, 81, 68; UV 206 nm (ε 470). **3f** (oil): Yield 72%; EIMS m/z 210 (M$^+$), 94, 88, 81, 68; UV 206 nm (ε 470). **3g** (oil): Yield 75%; EIMS m/z 224 (M$^+$), 94, 88, 81, 68; UV 206 nm (ε 830). **3h** (oil): Yield 72%; EIMS m/z 238 (M$^+$), 108, 88, 81, 68; UV 206 nm (ε 950).

Isopropyl Esters 4. **4a** (oil): Yield 68%; EIMS m/z 154 (M$^+$), 112, 94, 81, 68; UV 205 nm (ε 150); IR ($CHCl_3$) 3300, 2100, 1735 cm^{-1}; ^{1}H NMR δ=1.21 (6H, d, J=6 Hz, -CO$_2$CH-(CH$_3$)$_2$), 1.97 (1H, t, J=3 Hz, HC≡C-), 2.27 (2H, dt, J=3 and 7 Hz, ≡C-CH$_2$-), 2.39 (2H, t, J=7 Hz, -CH$_2$CO-), 4.09 (1H,

sept, J=6 Hz, $-CO_2C\underline{H}Me_2$). **4b** (oil): Yield 69%; EIMS m/z 168 (M^+), 108, 94, 81, 68; UV 205 nm (ε 170). **4c** (oil): Yield 70%; EIMS m/z 182 (M^+), 94, 81, 80, 68; UV 205 nm (ε 190). **4d** (oil): Yield 70%; EIMS m/z 196 (M^+), 102, 94, 81, 68; UV 205 nm (ε 190). **4e** (oil): Yield 72%; EIMS m/z 210 (M^+), 108, 102, 94, 81; UV 205 nm (ε 830). **4f** (oil): Yield 72%; EIMS m/z 224 (M^+), 122, 102, 81, 68; UV 205 nm (ε 1400). **4g** (oil): Yield 71%; EIMS m/z 238 (M^+), 136, 102, 94, 81; UV 205 nm (ε 1700). **4h** (oil): Yield 70%; EIMS m/z 252 (M^+), 150, 102, 81, 68; UV 205 nm (ε 1700).

Seed Germination Test. Twenty seeds of lettuce (*Lactuca sativa*, L., cv. Grand Rapids) were placed on 2 layers of filter paper in a 9-cm Petri dish containing 4 ml of test solution. The dish was incubated at 23 °C in the dark room. After 3 d, the percentage germination was determined. The test was repeated three times and the mean values calculated.

Seedling Growth Test. Lettuce seeds were germinated on filter paper moistened with distilled water for 2 d. Twenty seedlings were selected for size uniformity and planted on 2 layers of filter paper in a 9-cm Petri dish containing 4 ml of test solution. Seedlings were grown for another 3 d at 23 °C in the dark, and then hypocotyl length was measured.

Antimicrobial Test. Test organisms: fungus; *Mucor mucedo* IFO 0136, *Rh. chinensis* IFO 4745, *Asp. niger* ATCC 6275 and *P. crustosum* Thom: Yiest; *S. cerevisiae* IFO 0203, *C. utilis* ATCC 42402, *Schiz. pombe* IFO 0342 and *H. anomala* IFO 0136: bacteria; *S. aureus* NCTC 8530, *B. subtilis* K-49, *E. coli* IFO 3545 and *Ps. aeruginosa* IAM 1007. Minimum inhibitory concentration of test compound was determined by a two-fold dilution method reported previously.[16] Effect on yeast growth was evaluated turbidimetrically as follows. *Hansenula anomala* IFO 0136 was cultured in 5 ml malt wort containing a test compound at 100 μg/ml in a test tube at 25 °C. The growth was periodically examined as the optical density at 660 nm.

We are grateful to Dr. Hiroyuki Akita (The Institute of Physical and Chemical Research) and Professor Koji Hasegawa (Kagoshima University) for helpful discussion and suggestions. Our thanks are also due to Dr. Hideo Naoki and Dr. Takashi Iwashita (Suntory Institute for Bioorganic Research) for FD-mass and ^1H NMR (360 MHz) and to Dr. Kozo Shibata (Osaka City University) for elemental analysis.

References

1) T. Reynolds, *Ann. Botany*, **39**, 797 (1975).
2) T. Reynolds, *Ann. Botany*, **41**, 637 (1977); **42**, 419 (1978).
3) K. Orito, T. Iwadare, and Y. Iwanami, *Phytochemistry*, **22**, 2316 (1983).
4) M. Nakatani, T. Yamachika, T. Tanoue, and T. Hase, *Phytochemistry*, **24**, 39 (1985).
5) E. S. Hudak, B. D. Mercer, and J. H. Wotiz, *J. Am. Pharm. Assoc.*, **45**, 327 (1956).
6) R. G. Binder, B. G. Chan, and C. A. Elliger, *Agric. Biol. Chem.*, **43**, 2467 (1979).
7) J. Reisch, W. Sptzner, and K. E. Schalte, *Arzneim. Forsch*, **17**, 816 (1967).
8) J. J. Kobara, R. Vrable, and M. S. F. Lie Ken Jie, *Lipids*, **12**, 753 (1977).
9) K. B. Sharpless and M. W. Young, *J. Org. Chem.*, **40**, 947 (1975).
10) P. A. Grieco, S. Gilman, and M. Nishizawa, *J. Org. Chem.*, **41**, 1485 (1976).
11) V. I. Kefeli, "Natural Plant Growth Inhibitors and Phytohormones," The Hagve, Boston (1978), p. 6.
12) Y. Kobayashi; unpublished data. A detailed study is now in progress.
13) G. Eglinton and M. C. Whiting, *J. Chem. Soc.*, **1953**, 3052.
14) H. K. Black and B. C. L. Weedon, *J. Chem. Soc.*, **1953**, 1785.
15) N. Rabjohn, *Org. Synth.*, Coll. Vol. IV, 969 (1963).
16) M. Taniguchi and Y. Satomura, *Agric. Biol. Chem.*, **36**, 2169 (1972).

 © 1986 The Chemical Society of Japan Bull. Chem. Soc. Jpn., 59, 3541—3546 (1986)

Structures of Yadanziosides K, M, N, and O, New Quassinoid Glycosides from *Brucea javanica* (L.) MERR[1)]

Toshiro SAKAKI, Shin YOSHIMURA, Takahiko TSUYUKI,* Takeyoshi TAKAHASHI,*
Tadashi HONDA,† and Toshihiro NAKANISHI†
Department of Chemistry, Faculty of Science, The University of Tokyo,
Hongo, Bunkyo-ku, Tokyo 113
†Suntory Institute for Biomedical Research, Wakayamadai,
Shimamotocho, Mishimagun, Osaka 618
(Received May 15, 1986)

Four new bitter quassinoid glycosides, yadanziosides K, M, N, and O were isolated from *Brucea javanica* (L.) MERR and their structures were determined by spectral measurement and chemical means. The aglycone of yadanzioside O was found to exhibit a significant antitumor activity against the murine P388 lymphocytic leukemia and this aglycone could be prepared from brusatol.

"Ya-dan-zi," seed of *Brucea javanica* (L.) MERR has been used as a Chinese medicine for the treatment of cancer, and the main components with antileukemic activity have been investigated.[2)] We examined the minor components of "Ya-dan-zi," and reported structure elucidation of sixteen new bitter principles.[3)] Further investigation led to the isolation of four new quassinoid glycosides, yadanziosides K, M, N, and O (**1**—**4**). This paper describes structure determination of these bitter principles (**1**—**4**) and a preparation and antileukemic activity of the aglycone of yadanzioside O (**4**).

The methanol extract of defatted seeds of *B. javanica* was partitioned between dichloromethane and water. The organic layer was subjected to separation by a silica-gel column chromatography, followed by a Lobar column Lichroprep RP-8, Toyopearl HW-40S, or silicic acid column chromatography to afford yadanzioside K (**1**; ca. 0.001% yield), yadanzioside M (**2**; ca. 0.0005% yield), yadanzioside N (**3**; ca. 0.0001% yield), and yadanzioside O (**4**; ca. 0.0002% yield).

Yadanzioside K (**1**) crystallized from methanol, mp 214.5—216.5 °C and showed the presence of three tertiary methyl, two vinyl methyl, an acetoxyl, and a methoxycarbonyl groups and an olefinic proton in the ^{1}H NMR spectrum (Table 1), and the presence of an α,β-unsaturated carbonyl group was shown by the UV spectrum. The molecular formula, $C_{36}H_{48}O_{18}$, was inferred from ^{13}C NMR spectrum (Table 2) together with a peak at *m/z* 769 ($[M+H]^+$) in the secondary ion mass spectrometry (SI-MS) and hydrolysis with β-glucosidase to give bruceantinol (**5**)[4)] as the major aglycone. The glycosylation shifts of signals due to C-3 and C-4 were $\Delta\delta$+2.1 and +18.3 ppm, respectively (Table 2), and the signal due to the $C_{(4)}$-CH_3 was observed at δ 2.04 as a singlet in the ^{1}H NMR spectrum of **1**. Thus the structure of yadanzioside K (**1**) was determined to be 3-*O*-(β-D-glucosyl)bruceantinol.

Yadanzioside M (**2**) was obtained as amorphous powder from acetone-hexane, mp 208—213 °C (decomp). The EI-MS showed a peak at *m/z* 542 ($[M-C_6H_{10}O_5]^+$) and the SI-MS afforded a peak at *m/z* 727 ($[M+Na]^+$). Enzymatic hydrolysis of **2** with β-glucosidase afforded bruceantarin (**6**)[5)] as the major aglycone. These observations suggest the molecular formula, $C_{34}H_{40}O_{16}$, for **2**. The ^{1}H NMR spectrum of **2** showed the presence of a doublet signal (J=7 Hz) due to $C_{(4)}$-CH_3 at δ 1.18 and a singlet signal at δ 7.26 assignable to $C_{(1)}$-H. This fact suggests the bruceantarin moiety enolizes into a 2-hydroxy-3-keto-1-ene structure, which forms the β-glucoside linkage through the oxygen atom on C-2 of the aglycone.[3b)] The configuration of the $C_{(4)}$-CH_3 of **2** was inferred to be α-equatorial from the structural similarity to bruceoside A.[2c)] The structure (**2**) is, therefore, proposed for yadanzioside M.

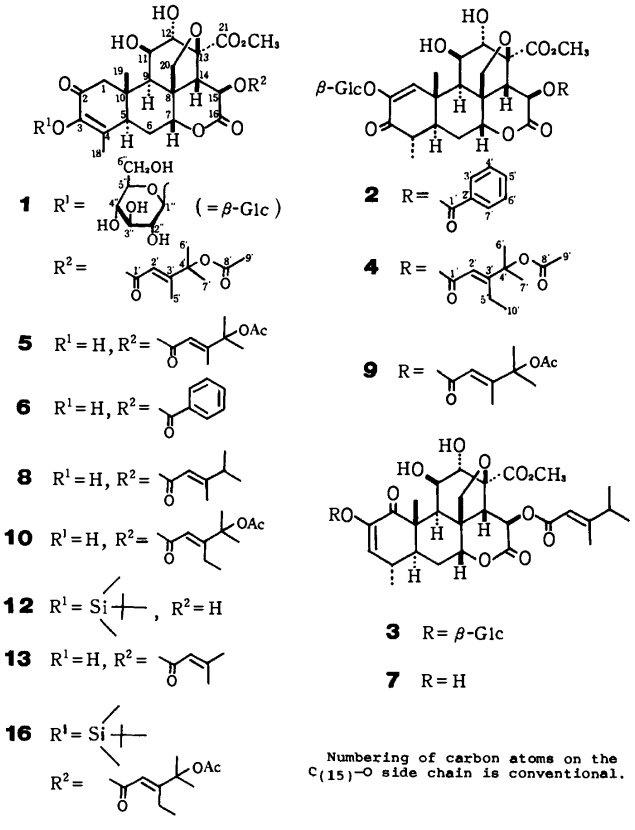

Table 1. ^{1}H NMR Spectra[a] of Yadanziosides K (**1**), M (**2**), N (**3**), and O (**4**) and Some Aglycones

	K (**1**)[b]	M (**2**)[b]	N (**3**)[c]	O (**4**)[d]	**7**[e]	**10**[e]
1-H	f)	7.26 s	—	7.27 s	—	f)
3-H	—	—	6.10 d (2.2)	—	5.74 d (2.4)	—
4-H	—	f)	2.24 brt	2.42 m	f)	—
5-H	f)	f)	0.98 dd (9.5, 6.6)	f)	f)	f)
6α-H	f)	f)	2.15 brd	f)	2.25 brtd (2.9, 14.8)	f)
6β-H	f)	f)	1.56 brt (13)	f)	1.94 brt (11.1)	f)
7-H	f)	f)	5.13 brs	4.96 brs	4.66 brs	4.82 brs
9-H	f)	f)	2.95 d (4.0)	2.50 d (5.4)	f)	f)
11-H	f)	f)	6.20 d (4.4)	5.13 d (5.4)	5.44 br	4.26 brd (4.3)
12-H	f)	f)	4.90 brs	5.08 brs	4.29 brs	4.22 brs
15-H	6.85 d (13)	f)	f)	f)	f)	f)
20-H	f)	f)	5.12 d (7.7)	5.05 d (8.1)	4.70 d (7.9)	4.73 d (7.6)
4-Me	2.04 brs	1.18 d (7)	0.87 d (8.8)	1.16 d (8.1)	1.11 d (7.0)	1.85 d (2.2)
10-Me	1.68 s	1.64 s	1.87 s	1.63 s	1.62 s	1.40 s
CO_2Me	3.89 s	3.56 s	3.77 s	3.86 s	3.78 s	3.81 s
2′-H	6.06 s		5.89 s	6.10 s	5.66 brs	5.78 s
3′-Me	2.26 s		2.18 s		2.14 d (1.1)	—
4′-Me	1.42 s		0.85 d (7.0)	1.49 s	1.06 d (6.8)	1.57 s
	1.47 s			1.51 s		
4′-OAc	1.98 s		—	1.94 s	—	2.03 s
5′-H	—		—	2.67 m	—	2.59 q (7.2)
				2.78 m		
5′-Me	—		—	1.24 t (8.1)	—	1.13 t (7.3)
1″-H	f)	f)	5.47 d (7.0)	5.28 d (8.1)		
6″-H	f)	f)	4.57 d (11)	4.42 dd (10.8, 2.7)		

a) Coupling constants in Hz in parentheses. b) 90 MHz, C_5D_5N. c) 400 MHz, C_5D_5N. d) 270 MHz, C_5D_5N. e) 270 MHz, $CDCl_3$. f) Not measured.

Yadanzioside N (**3**), mp 175—180 °C, showed a doublet signal due to an anomeric proton at δ 5.47 (J=7.0 Hz) in the ^{1}H NMR spectrum, a peak at m/z 733 ($[M+Na]^+$) in SI-MS, and a peak at m/z 548 ($[M-C_6H_{10}O_5]^+$) in EI-MS. These spectral data together with ^{13}C NMR spectrum (Table 2) indicate that **3** is a hexoside with the molecular formula, $C_{34}H_{46}O_{16}$. Yadanzioside N (**3**) was hydrolyzed with 1.5 M (1 M=1 mol dm^{-3}) sulfuric acid in boiling methanol to afford an aglycone (**7**) and D-glucose, the latter of which was identified by GLC after trimethylsilylation. The aglycone (**7**), mp 180—183 °C, was shown to have the molecular formula, $C_{28}H_{36}O_{11}$, by high-resolution mass spectrum (HR-MS), and a peak at m/z 111 in EI-MS suggested the presence of a heptenoyl group ($C_6H_{11}CO$) in the side chain. Since the ^{1}H NMR spectrum revealed the presense of an isopropyl group and a vinyl methyl group (δ 1.06 d (J=6.8 Hz) and 2.14 d (J=1.1 Hz), respectively) in the side chain and the shift values of signals due to these groups are similar to those of bruceantin (**8**)[6] in ^{1}H and ^{13}C NMR spectra, the side chain might be 3,4-dimethyl-2-pentenoyl group. The UV absorption maxima appeared at 220 and 267 nm in ethanol solution, and the latter was shifted to 314 nm on addition of alkali, indicating the presence of a diosphenol moiety.[7]

In the ^{1}H NMR spectrum of **3**, a doublet signal due to $C_{(11)}$–H appeared at δ 6.20, which is lower than that of bruceantin (**8**).[6] On irradiation of a broad triplet signal due to $C_{(4)}$–H at δ 2.24, signals at δ 0.87 due to $C_{(4)}$–CH_3 and at δ 6.10 due to $C_{(3)}$–H became sharp. On the other hand, the aglycone (**7**) showed a doublet signal due to $C_{(4)}$–CH_3 at δ 1.11 and a doublet signal due to an olefinic proton at C-3 at δ 5.74 with a coupling constant, J=2.4 Hz. These spectral features suggest that the configuration of $C_{(4)}$–CH_3 is α-equatorial and that A-ring of the aglycone (**7**) is the same as that of norquassin.[7] From these observations and ^{1}H and ^{13}C NMR spectral comparison with bruceantin (**8**), the aglycone (**7**) was shown to be an isomer with 1-keto-2-ene structure of bruceantin (**8**). Since no bathochromic shift of the UV absorption maxima of **3** was observed on addition of alkali, the glycoside linkage was shown to be formed through an oxygen atom on C-2 of the aglycone (**7**). The structure of yadanzioside N (**3**) was, therefore, determined to be methyl 2-(β-D-glucopyranosyloxy)-13β,20-epoxy-15β-

Table 2. ^{13}C NMR Spectra of Yadanziosides K (**1**), M (**2**), N (**3**), and O (**4**), Bruceantin (**8**), and Some Aglycones

No. of carbon	K (**1**) [a]	M (**2**) [a]	N (**3**) [a]	O (**4**) [a]	(**5**) [a]	(**7**) [b]	(**8**) [c]	(**10**) [b]
1	51.1 t	129.4 d	199.6 s	129.6 d	50.0 t	201.0 s	48.7 t	48.6
2	193.6 s	148.8 s	146.4 s	148.8 s	192.9 s	143.7 s	192.2 s	192.1
3	148.0 s [d]	194.5 s	125.5 d	194.6 s	145.9 s	121.3 d	144.2 s	144.1
4	146.6 s [d]	43.9 d	31.6 d	43.9 d	128.3 s	30.7 d	127.9 s	127.8
5	43.4 d	40.8 d	36.9 d	40.4 d	42.5 d	36.5 d	41.2 d	44.1
6	29.3 t	30.1 t	28.8 t	30.0 t	29.6 t	28.5 t	29.2 t	29.1
7	83.4 d	83.7 d	83.0 d	83.4 d	83.6 d	82.4 d	82.4 d	82.6
8	46.0 s	46.9 s	46.7 s	46.6 s	46.2 s	46.1 s	45.5 s	45.4
9	41.9 d	41.4 d	44.2 d	41.4 d	42.1 d	43.9 d	41.9 d	41.9
10	40.8 s	39.7 s	48.9 s	39.6 s	41.4 s	47.3 s	41.2 s	41.1
11	73.0 d	73.5 d	75.1 d	73.5 d	73.1 d	72.9 d	71.1 d	71.0
12	75.9 d	76.1 d	76.3 d	76.0 d	75.9 d	76.1 d	75.9 d	75.7
13	82.6 s	82.7 s	83.0 s	82.6 s [l]	82.7 s	81.2 s	81.4 s	81.3
14	50.2 d	50.7 d	50.9 d	50.3 d	50.4 d	51.6 d	51.7 d	51.5
15	68.4 d	69.3 d	68.8 d	68.6 d	68.6 d	66.7 d	66.0 d	66.2
16	168.0 s	168.0 s	168.2 s	168.0 s [m]	168.0 s	168.2 s	167.0 s	166.9
18	15.2 q	12.6 q	14.5 q	12.5 q	13.3 q	14.8 q	13.3 q	13.3
19	15.8 q	18.0 q	18.9 q	18.0 q	15.7 q	19.0 q	15.5 q	15.5
20	73.5 t	73.8 t	73.7 t	73.6 t	73.7 t	73.6 t	74.1 t	74.1
21	171.2 s	171.2 s	171.1 s	171.1 s	171.2 s	171.6 s	171.8 s	171.8
OMe	52.5 q	52.3 q	52.3 q	52.6 q	52.5 q	52.8 q	52.9 q	53.4
1′	165.7 s	165.3 s	166.0 s	165.2 s	165.7 s	165.2 s	165.0 s	164.2
2′	113.5 d	130.4 s [f]	113.6 d	113.8 d	113.6 d	111.8 d	111.8 d	112.0
3′	169.5 s	130.2 d [g]	167.2 s	169.5 s	169.5 s	169.6 s	169.6 s	169.6
4′	82.3 s	128.7 d [h]	38.1 d	82.7 s [l]	82.4 s	38.3 d	38.4 d	82.4
5′	14.3 q	133.6 d [i]	16.7 q	22.0 t	14.5 q	17.1 q	17.0 q	22.1
6′	25.8 q	128.7 d [h]	20.7 q	26.2 q	26.4 q	20.8 q	20.8 q	26.5
7′	26.3 q	130.2 d [g]	20.7 q	26.5 q	25.9 q	20.8 q	20.8 q	26.5
8′	163.4 s			168.6 s [m]	163.3 s			170.9
9′	21.4 q			21.7 q	21.4 q			21.9
10′				14.6 q				14.2
1″	104.8 d	102.0 d	100.9 d	102.0 d				
2″	75.6 d	74.7 d	74.7 d	74.6 d				
3″	78.5 d [e]	78.8 d [j]	78.9 d [k]	78.8 d [n]				
4″	71.5 d	71.4 d	71.5 d	71.3 d				
5″	78.3 d [e]	78.5 d [j]	78.6 d [k]	78.4 d [n]				
6″	62.8 t	62.4 t	62.5 t	62.4 t				

a) 22.5 MHz, C_5D_5N. b) 67.5 MHz, $CDCl_3$. c) 22.5 MHz, $CDCl_3$. d) The assignment of signals may be reversed. e) and j)—n) are the same as d). f) Aromatic carbon atom adjacent to the carbonyl carbon. g) Carbon atom at *o*-position. h) Carbon atom at *m*-position. i) Carbon atom at *p*-position.

[(2*E*)-3,4-dimethyl-2-pentenoyloxy]-11β,12α-dihydroxy-1,16-dioxo-2-picrasen-21-oate, which is a new type bruceoside with a quassin-type A-ring.

Yadanzioside O (**4**), mp 183—188 °C, was found to be a hexose with the same skeleton as yadanzioside G (**9**)[3b] except for an additional triplet signal (δ 22.0) due to a methylene group from the comparison of ^{13}C NMR spectra (see Table 2). The ^1H NMR spectrum of **4** also revealed the presence of an acetoxyl, an ethyl, and two methyl groups assignable to the side chain together with an olefinic proton. Therefore the structure of the side chain could be formulated as 15-*O*-(4-acetoxy-3-ethyl-4-methyl-2-pentenoyl), and geometry of the double bond was assigned to be 2*E* by the following difference NOE measurement of **4** at 400 MHz. Irradiation of the signal due to $C_{(2')}$-H at δ 6.10 resulted in an enhancement of the signals at δ 1.49 and 1.51 due to the geminal methyl group at C-4′.

Yadanzioside O (**4**) was hydrolyzed with β-glucosidase to yield an aglycone (**10**), mp 138—143 °C, which gave no molecular ion but a fragment ion at *m/z* 560 due to a loss of acetic acid in the EI-MS. The ^1H and ^{13}C NMR spectra of **10** were very similar to those of bruceantinol (**5**)[4] except for signals due to the

additional methylene group in the side chain. This fact implies that A-ring of **10** possesses 3-hydroxy-3-en-2-one structure; the signal due to $C_{(4)}$-CH_3 appeared at δ 1.85 as a doublet signal with a small coupling constant (J=2.2 Hz). An anomeric proton was observed at δ 5.28 as a doublet signal (J=8.1 Hz) and a signal due to $C_{(4)}$-CH_3 appeared at δ 1.16 as a doublet signal (J=8.1 Hz) in the ^{1}H NMR spectrum of **4**. Since these spectral features are almost the same as those for yadanzioside G (**9**) and also yadanziosides A,[3b] C,[3b] F,[3a] and J,[3a] the structure of yadanzioside O (**4**) was determined to be methyl 2-(β-D-glucopyranosyloxy)-13β,20-epoxy-15β-[(2*E*)-4-acetoxy-3-ethyl-4-methyl-2-pentenoyloxy]-11β,12α-dihydroxy-3,16-dioxo-1-picrasen-21-oate. Yadanzioside O (**4**) is a bruceoside with the largest carbon number in the 15-*O* side chain so far in nature.

The structure (**10**) proposed for the aglycone of yadanzioside O was confirmly established by the partial synthesis, which was achieved by the reaction of (2*E*)-4-acetoxy-3-ethyl-4-methyl-2-pentenoic acid (**11**) with 3-*O*-(*t*-butyldimethylsilyl)bruceolide (**12**) derived from brusatol (**13**).

Methyl (2*E*)-3-ethyl-4-hydroxy-4-methyl-2-pentenoate (**14**) was prepared by the Wittig-Honer reaction[8] of 2-hydroxy-2-methyl-3-pentanone (**15**)[9] with a Wittig reagent derived from dimethyl (methoxycarbonylmethyl)phosphonate using sodium hydride as a base in dimethoxyethane (DME). The reaction did not occur at room temperature, but took place at boiling temperature to afford the reaction product (**14**) together with a considerable amount of undesirable by-products. Separation of **14** from the reaction mixture was attained by preparative liquid chromatography to afford **14** in 27% yield. Geometry of the double bond of **14** was determined after hydrolysis and acetylation. Although a double bond isomer, the starting material (**15**), and unidentified by-products were obtained from the reaction mixture, neither further purification nor identification for these products was carried out. Hydrolysis of **14** with alkali followed by acetylation yielded 4-acetoxy-3-ethyl-4-methyl-2-pentenoic acid (**11**) in 95% yield from **14**. The synthetic unsaturated acid (**11**) showed a singlet signal due to the olefinic proton at δ 5.85, which was almost the same as the shift value (δ 5.78) observed for yadanzioside O aglycone (**10**). Thus the double bond geometry of **11** was concluded to be 2*E*.

The derivation of the skeletal part and introduction of the side chain into $C_{(15)}$-OH are as follows; brusatol (**13**) was treated with *t*-butyldimethylsilyl chloride in the presence of imidazole in DME to afford 3-*O*-(*t*-butyldimethylsilyl)brusatol in 94% yield, which, on hydrolysis with potassium methoxide in dry methanol, gave 3-*O*-(*t*-butyldimethylsilyl)bruceolide (**12**) in 65% yield.[10] The esterification of the acid (**11**) with **12** was effected in the presence of dicyclohexylcarbodiimide (DCC) in dichloromethane,[11] and the reaction product (**16**) was subjected to deprotection by a treatment with 5% hydrofluoric acid-acetonitrile or with tetrabutylammonium fluoride in tetrahydrofuran (THF) at 0 °C. The synthetic specimen was found to be completely identical with yadanzioside O aglycone (**10**).

Yadanzioside O aglycone (**10**) exhibited a significant antitumor activity against the murine P388 lymphocytic leukemia[12] and the ILS values for the natural specimen were 8.2, 37.1, and 47.2% at 1, 2, and 4 mg/kg/d dose levels, respectively. The ILS values for the synthetic one were 42.3 and 46.4% at 4 and 6 mg/kg/d dose levels, respectively, but a toxicity was observed at 8 mg/kg/d dose level.

Experimental[13]

Extraction and Separation. Pulverized seeds (49.5 kg) of *B. javanica*, "Ya-dan-zi" were defatted with hexane (100 l) twice and then with extracted with methanol (100 l) twice. The methanol extract was concentrated in vacuo to give a syrup, to which the equal volume of water was added. The aqueous solution was completely defatted with hexane (7 l) three times and then extracted with dichloromethane five times. The organic layer was concentrated to give an oily residue (158 g), which was subjected to the following separation.

Column A. The residue (158 g) was dissolved in chloroform and absorbed on silica gel (335 g). After the solvent was removed in vacuo, the silica gel was placed on the top of a column of silica gel (2.5 kg) and elution was performed with the following solvents; benzene (frs 1—3, each 1.5 l), benzene-ethyl acetate (2:1, frs 4—10; 1:1, frs 11—19; 1:2, frs 20—23, each 1.5 l), ethyl acetate (frs 24—30, each 1.5 l), 10% methanol in ethyl acetate (frs 31—35, each 2 l), and 20% methanol in ethyl acetate (frs 36—40, each 2 l).

Column B. The fractions 35—37 of Column A were combined to give a residue (73 g), a part (10.7 g) of which was chromatographed on silica gel (850 g) eluted with lower layer of chloroform-methanol-water in the following ratio; frs 1—6 (25:4:1), frs 7—11 (20:4:1), and frs 11—24 (16:4:1) in 400 ml fraction each.

Column C. A part (55.3 g) of the fractions 35—37 of Column A was separated by column chromatography on silica gel (2.5 kg) eluted with lower layer of chloroform-methanol-water (25:4:1). Thirty fractions (each 500 ml) were collected.

Column D. The fraction 21 of Column C gave a residue (3.8 g), a part (500 mg) of which was separated by reversed phase chromatography using Lobar column Lichroprep RP-8 size B. Elution (each fraction, 10 g) was performed with methanol-water (4:6—5:5). Fractions 55—63 gave yadanzioside O (**4**; 16 mg).

Column E. A part (826 mg) of the fraction 24 (2.2 g) of Column C was subjected to separation using Lobar column eluted with methanol-water (4:6). Eighty-two fraction (each 10 g) were collected. Fractions 62—65 gave yadanzioside M (**2**; 25 mg).

Column. F. Tne fraction 27 (1.2 g) of Column C was separated using Lobar column eluted with methanol-water

(4:6—5:5). Seventy-six fractions (each 10 g) were collected. Fractions 70—76 gave yadanzioside N (**3**; 25 mg).

Column G. The fractions 12 and 13 of Column B were combined and evaporated to afford a residue (5.2 g), a part (1.5 g) of which was separated using Lobar column. Elution (each 10 g) was performed with methanol-water (4:6) and 142 fractions were collected.

Column H. The fractions 64—74 (89 mg) of Column G were combined and separated by gel chromatography using Toyopearl HW-40S. Elution with methanol (each 10 g) gave yadanzioside M (**2**; 22 mg) in fractions 56—62.

Column I. The fractions 127—142 of Column G gave a residue (17 mg), which was separated using Toyopearl HW-40S. Elution (each 10 g) with methanol gave yadanzioside O (**4**; 5 mg).

Column J. The fraction 14 (932 mg) of Column B was purified by partition chromatography on silicic acid (400 g) pretreated with water (270 ml). Elution (each 250 ml) was performed with 0, 3, 6, ···, 24% ethanol in chloroform (each 1 l).

Column K. The fractions 16 and 17 of Column J were combined (524 mg) and chromatographed using a Lobar column. Elution (each 10 g) was performed with methanol-water.

Column L. The fractions 17—24 of Column K were combined and evaporated to afford a residue (291 mg), which was separated using Toyopearl HW-40S. Elution (each 10 g) with methanol gave yadanzioside K (**1**; 24 mg) from fractions 41 and 42.

Yadanzioside K (1). $[\alpha]_D^{23}$ +15° (*c* 1.0, EtOH); $[\alpha]_D^{18}$ −31° (*c* 0.9, C_5H_5N); IR (KBr) 3450, 1740, 1645, and 1065 cm^{-1}; UV (EtOH) 222 nm (ε 17000) and 252 nm (ε 9000); ^1H NMR (Table 1); ^{13}C NMR (Table 2); EI-MS *m/z* (%) 546 ([M−162−60]$^+$: 1.4), 438 (3), 420 (1.4), 402 (1.9), 392 (1.8), 149 (18), 109 (90), 83 (70), 60 (100), and 57 (82); SI-MS *m/z* 769 ([M+H]$^+$); HR-MS (EI) *m/z* 546.2100. Calcd for $C_{28}H_{34}O_{11}$: *m/z* 546.2100.

Enzymatic Hydrolysis of 1. Yadanzioside K (**1**; 67 mg) in water (5 ml) was treated with β-glucosidase (20 mg) at 37 °C for 2 weeks and the usual work-up afforded bruceantinol (**5**; 17 mg) together with the starting material (**1**; 35 mg).

Yadanzioside M (2). $[\alpha]_D^{26}$ +39° (*c* 1.3, EtOH); IR (KBr) 3450, 1740, 1680, 1640, 1075, 1050, and 720 cm^{-1}; UV (EtOH) 231 nm (ε 16000) and 255 nm (ε 9000); ^1H NMR (Table 1); ^{13}C NMR (Table 2); EI-MS *m/z* (%) 542 ([M−162]$^+$; 3.8), 438 (6.6), 420 (3.5), 402 (3.4), 392 (2.4), 374 (2), 369 (2), and 105 (100); SI-MS *m/z* 727 ([M+Na]$^+$); HR-MS (EI) *m/z* 542.1804. Calcd for $C_{28}H_{30}O_{11}$: *m/z* 542.1789.

Enzymatic Hydrolysis of 2. Yadanzioside M (**2**; 60 mg) in water (6 ml) was hydrolyzed with β-glucosidase (28 mg) under the same conditions as before to yield bruceantarin (**6**; 11 mg) and the unchanged material (**2**; 24 mg).

Yadanzioside N (3). $[\alpha]_D^{24}$ +7.6° (*c* 1.8, EtOH); IR (KBr) 3420, 1740, 1680, 1640, 1080, 1045, and 1020 cm^{-1}; UV (EtOH) 222 nm (ε 13400) and 255 nm (ε 5100); ^1H NMR (Table 1); ^{13}C NMR (Table 2); EI-MS *m/z* (%) 548 ([M−$C_6H_{10}O_5$]$^+$; 0.1), 530 (0.8), 438 (0.6), 420 (0.9), 402 (5), 372 (4), 345 (3), 315 (4), and 111 (100); SI-MS *m/z* 733 ([M+Na]$^+$), 549, 531, 439, 421, 185, and 111; HR-MS (EI) *m/z* 548.2264. Calcd for $C_{28}H_{36}O_{11}$: *m/z* 548.2258.

Acid Hydrolysis of 3. A solution of yadanzioside N (**3**; 35 mg) in 1.5 M sulfuric acid-methanol (14 ml) was heated under reflux for 4 h. The reaction product, after removal of the solvent, was extracted with dichloromethane and divided into an organic layer and an aqueous layer. The usual work-up of the organic layer gave a residue, which was purified by column chromatography on silica gel (1 g). Elution with 5% methanol in chloroform yielded an aglycone (**7**; 11 mg), mp 180—183 °C; $[\alpha]_D^{24}$ +30° (*c* 0.7, EtOH); IR (KBr) 3460, 1750, 1685, 1645, 1050, and 1010 cm^{-1}; UV (EtOH) 220 nm (ε 16100) and 267 nm (ε 5500); on addition of potassium hydroxide, the latter maximum shifted to 314 nm (ε 4000); ^1H NMR (Table 1); ^{13}C NMR (Table 2); EI-MS *m/z* (%) 548 (M$^+$; 0.3), 530 (3), 512 (0.2), 420 (1), 402 (10), 372 (6), 345 (4), 315 (4), and 111 (100); HR-MS *m/z* 548.2282. Calcd for $C_{28}H_{36}O_{11}$: M, 548.2257. The aqueous layer, obtained from the acid hydrolysis of **3**, was passed through a short column of anion-exchange resin (Amberlite IRA-400, hydroxide form) and the eluate was evaporated in vacuo to give a residue. The residue was identified as D-glucose by GLC after trimethylsilylation.

Yadanzioside O (4). $[\alpha]_D^{21}$ +20° (*c* 2.0, EtOH); IR (KBr) 3430, 1740, 1680, 1640, 1065, 1050, and 1020 cm^{-1}. UV (EtOH) 224 nm (ε 14900) and 254 nm (ε 8000); ^1H NMR (Table 1); ^{13}C NMR (Table 2); EI-MS *m/z* (%) 560 ([M−$C_6H_{10}O_5$−AcOH]$^+$; 0.7), 438 (3), 420 (0.8), 402 (1), 392 (0.9), 141 (8), 123 (29), and 60 (100); SI-MS *m/z* 805 ([M+Na]$^+$), 561, 439, and 421.

Enzymatic Hydrolysis of 4. Yadanzioside O (**4**; 72 mg) was hydrolyzed with β-glucosidase (20 mg) to afford an aglycone (**10**; 13 mg) together with the starting material (**4**; 33 mg). **10**: Mp 138—143 °C; $[\alpha]_D^{27}$ +23° (*c* 0.6, EtOH); IR (KBr) 3450, 1740, 1640, and 1060 cm^{-1}; UV (EtOH) 222 nm (ε 14800) and 278 nm (ε 7000); ^1H NMR (Table 1); ^{13}C NMR (Table 2); EI-MS *m/z* 560 ([M−AcOH]$^+$; 1.5), 438 (4), 420 (3), 402 (4), 392 (6), 354 (18), 278 (36), 140 (56), 123 (68), 111 (82), and 60 (100); HR-MS *m/z* 560.2258. Calcd for $C_{29}H_{36}O_{11}$: *m/z* 560.2258.

Methyl (2*E*)-3-Ethyl-2-hydroxy-4-methyl-2-pentanoate (14). A Wittig reagent was prepared from dimethyl (methoxycarbonylmethyl)phosphonate (3.4 ml; 4 equiv) and sodium hydride (750 mg; 4 equiv) in DME (60 ml) at room temperature for 1 h under nitrogen atmosphere in a three-necked flask and then the solution was heated under reflux. To the solution 2-hydroxy-2-methyl-3-pentanone (**15**; 500 mg, 4.3 mmol) in DME (10 ml) was added and the heating was continued for 4 h. The usual work-up gave a residue, which was subjected to separation by preparative LC (Liquid Chromatograph LC-08, Japan Analytical Industry, column: JAIGEL-1H and 2H; solvent: chloroform) to afford methyl (2*E*)-3-ethyl-4-hydroxy-4-methyl-2-pentenoate (**14**; 203 mg) as an oil, IR (neat) 3460, 1710, 1640, and 750 cm^{-1}; ^1H NMR (90 MHz, $CDCl_3$) δ=1.13 (3H, t, *J*=8 Hz), 1.39 (6H, s), 2.57 (2H, q, *J*=8 Hz), 3.68 (3H, s), and 6.03 (1H, s); ^{13}C NMR (22.5 MHz, $CDCl_3$) δ=14.8q, 22.4t, 29.0q, 29.0q, 50.9q, 77.4s, 112.7d, 167.3s, and 170.6s; EI-MS *m/z* (%) 157 ([M−15]$^+$; 33), 154 (94), 139 (28), 129 (100), 122 (57), 111 (20), 97 (91), and 85 (65).

(2*E*)-4-Acetoxy-3-ethyl-4-methyl-2-pentenoic Acid (11). Methyl (2*E*)-3-ethyl-4-hydroxy-4-methyl-2-pentenoate (**14**; 468 mg) was treated with 5% potassium hydroxide solution (15 ml) at 80 °C for 10 h. Acidification by addition of 0.25 M sulfuric acid and the usual work-up afforded (2*E*)-3-ethyl-4-hydroxy-4-methyl-2-pentenoic acid as an oil quantitatively,

IR (film) 3450, 3300—2500, 1700, and 1640 cm^{-1}; ^1H NMR (90 MHz, $CDCl_3$) δ=1.13 (3H, t, J=8 Hz), 1.43 (6H, s), 2.56 (2H, q, J=8 Hz), and 6.07 (1H, s); EI-MS m/z (%) 143 ($[M-15]^+$; 22), 140 (39), 125 (28), 115 (100), and 97 (38).

The carboxylic acid (430 mg) above obtained was acetylated with acetic anhydride (1 ml) in the presence of triethylamine (5 ml) and 4-dimethylaminopyridine (DMAP, 330 mg) at room temperature for 3 h with stirring. To the cooled solution was added 2 M hydrochloric acid (50 ml) and the reaction product was extracted with ether (30 ml×3). The extracts were combined and washed with 2 M hydrochloric acid (30 ml) and then with water. The usual work-up gave a residue, which was purified by column chromatography on silica gel (25 g). Elution with 0—2% methanol in chloroform yielded (2*E*)-4-acetoxy-3-ethyl-4-methyl-2-pentenoic acid (**11**; 95% yield) as an oil, IR (neat) 3500—2500, 1740, 1700, and 1640 cm^{-1}. ^1H NMR (90 MHz, $CDCl_3$) δ=1.13 (3H, t, J=8 Hz), 1.59 (6H, s), 2.62 (2H, q, J=8 Hz), 2.02 (3H, s), and 5.85 (1H, s); ^{13}C NMR (22.5 MHz, $CDCl_3$) δ=14.4q, 21.9q, 21.9q, 26.6q, 26.6q, 82.9s, 113.9d, 169.1s, 169.6s, and 171.0s; EI-MS m/z (%) 158 ($[M-42]^+$; 5), 140 (100), 125 (81), 122 (33), 112 (38), 97 (85), 60 (23), and 43 (56).

Reaction of 3-*O*-(*t*-Butyldimethylsilyl)bruceolide (12) with 11. 3-*O*-(*t*-Butyldimethylsilyl)bruceolide (**12**; 970 mg),[10] DMAP (21 mg), and DCC (362 mg) were dissolved in dry dichloromethane (15 ml) under nitrogen atmosphere and the acid (**11**; 351 mg) in dichloromethane (15 ml) was added. The mixture was stirred at 25 °C overnight and filtered through a column of Celite. The filtrate was washed with water (50 ml), 5% acetic acid (50 ml), and then water (50 ml). The usual work-up gave a residue, which was purified by column chromatography on silica gel (50 g). Elution with 1% methanol in chloroform afforded a 3-*O*-(*t*-butyldimethylsilyl) derivative (**16**; 469 mg) of the aglycone (**10**) together with the starting material (**12**; 579 mg). **16**: Mp 281.5—283 °C, colorless needles from chloroform-acetone; IR (KBr) 3560, 3380, 1745, 1680, 1650, 1060, and 1020 cm^{-1}; ^1H NMR (90 MHz, $CDCl_3$) δ=0.13 (3H, s), 0.17 (3H, s), 0.97 (9H, s), 1.13 (3H, t, J=7 Hz), 1.39 (3H, s), 1.56 (6H, s), 1.85 (3H, brs), 2.01 (3H, s), 3.78 (3H, s), 4.22 (2H, br), 4.62 (1H, d, J=8 Hz), 4.80 (1H, brs), 5.78 (1H, s), and 6.20 (1H, d, J=13 Hz); EI-MS m/z (%) 677 ($[M-(CH_3)_3C]^+$; 6), 659 (4), 635 (14), 617 (92), 598 (16), 537 (47), 495 (8), 478 (27), 424 (16), 326 (13), 123 (100), and 60 (58); HR-MS (EI) m/z 677.2656. Calcd for $C_{33}H_{45}O_{13}Si$: m/z 677.2629.

Deprotection of 3-*O*-(*t*-Butyldimethylsilyl) Group of 16. i) A solution of 3-*O*-(*t*-butyldimethylsilyl) derivative (**16**; 50 mg) in acetonitrile-47% hydrofluoric acid (10:1, 3 ml) was stirred at room temperature for 4 h. After addition of dichloromethane and water, the organic layer was separated. The aqueous layer was extracted with dichloromethane twice and the organic layers were combined. The usual work-up gave a residue, which was chromatographed on silica gel (5 g). Elution with 1% methanol in chloroform yielded yadanzioside O aglycone (**10**; 21 mg). ii) To a solution of 3-*O*-(*t*-butyldimethylsilyl) derivative (**16**; 244 mg) in THF (5 ml) was added tetrabutylammonium fluoride (230 mg) in THF (5 ml) at 0 °C under nitrogen atmosphere. The solution was stirred for 30 min at the same temperature and chloroform (100 ml) was added. The organic solution was washed with a saturated sodium hydrogencarbonate solution. The washings were extracted with chloroform (50 ml×2) and the organic solution and the extracts were combined and worked up as usual. Column chromatographic separation on silica gel (15 g, eluted with 3% methanol in chloroform) afforded yadanzioside O aglycone (**10**; 206 mg).

The authors wish to thank Mr. Hideo Naoki of Suntory Institute for Bioorganic Research for measurement of SI-MS.

References

1) A part of this work was reported in a preliminary form: T. Sakaki, S. Yoshimura, T. Tsuyuki, T. Takahashi, T. Honda, and T. Nakanishi, *Tetrahedron Lett.*, **27**, 593 (1986).

2) a) J. Polonsky, Z. Baskévitch, A. Gaudemer, and B. C. Das, *Experientia*, **23**, 424 (1967); b) K. Y. Sim, J. J. Sims, and T. A. Geissman, *J. Org. Chem.*, **33**, 429 (1968); c) K. H. Lee, Y. Imakura, Y. Sumida, R.-Y. Wu, and I. H. Hall, *ibid.*, **44**, 2180 (1979).

3) a) S. Yoshimura, T. Sakaki, M. Ishibashi, T. Tsuyuki, T. Takahashi, and T. Honda, *Bull. Chem. Soc. Jpn.*, **58**, 2673 (1985); b) T. Sakaki, Y. Yoshimura, M. Ishibashi, T. Tsuyuki, T. Takahashi, T. Honda, and T. Nakanishi, *ibid.*, **58**, 2680 (1985).

4) a) J. D. Phillipson and F. A. Darwish, *Planta Med.*, **41**, 209 (1981); b) J. Polonsky, J. Varenne, T Prangé, and C. Pascard, *Tetrahedron Lett.*, **21**, 1853 (1980).

5) S. M. Kupchan, R. W. Britton, J. A. Lacadie, M. F. Ziegler, and C. W. Sigel, *J. Org. Chem.*, **40**, 648 (1975).

6) S. M. Kupchan, R. W. Britton, M. F. Ziegler, and C. W. Siegel, *J. Org. Chem.*, **38**, 178 (1973).

7) T. Murae, T. Tsuyuki, T. Ikeda, T. Nishihama, S. Masuda, and T. Takahashi, *Tetrahedron*, **27**, 1545 (1971).

8) The hydroxy ketone (**15**) was prepared by the Grignard reaction of acetone cyanohydrin 2-ethoxyethyl derivative with ethylmagnesium bromide.

9) a) W. S. Wadsworth, Jr. and W. D. Emmons, *J. Am. Chem. Soc.*, **83**, 1733 (1961); b) J. Boutagy and R. Thomas, *Chem. Rev.*, **74**, 87 (1974); c) K. H. Dahm, B. M. Trost, and H. Röller, *J. Am. Chem. Soc.*, **89**, 5292 (1967).

10) Suntory Ltd., Jpn. Kokai Tokkyo Koho JP 59 67,287 (84 67,287) (cl. C07D493/08) 16Apr 1984, Appl. 82/178,210 09 Oct 1982; 16pp.

11) A. Hassner and V. Alexanian, *Tetrahedron Lett.*, **1978**, 4475.

12) In vivo activity was assayed according to the standard National Cancer Institute procedure.

$$\text{ILS}(\%) = \left(\frac{\text{Mean survival time(day) of the test group}}{\text{Mean survival time(day) of the control group}} - 1\right) \times 100$$

The ILS value of bruceantin (**8**) was 70.1% at 2 mg/kg/d dose level and a toxicity was observed at 4 mg/kg/d dose level.

13) General procedures are the same as those described in lit, 3a.

 © 1986 The Chemical Society of Japan Bull. Chem. Soc. Jpn., 59, 3547—3552 (1986)

The Ability of the Proline Residue to Promote Successive-Intramolecular Hydrogen Bonds in Oligopeptides[1)]

Mitsuaki NARITA, Shizuko ISOKAWA, Masamitsu DOI, and Ryuhei WAKITA
Department of Industrial Chemistry, Faculty of Technology, Tokyo University of Agriculture and Technology, Koganei 184
(Received May 15, 1986)

In order to investigate the ability of the Pro residue to promote helical folding in oligopeptides, the IR spectroscopic conformational study of the oligo(Leu)s containing the Pro residue was performed in dichloromethane. Their IR difference spectra suggested the occurrence of successive-intramolecular hydrogen bonds just like incipient α-helical structures formed by one, two, three, and so forth $i \rightarrow i-4$ hydrogen-bonding patterns, alluding to the ability of the Pro residue to promote helical folding in the peptides. However, the intensities of hydrogen-bonded absorption bands in the amide A region of each peptide strongly suggested that conformations of the peptides investigated were also contributed by other intramolecularly hydrogen-bonded folded structures, which had lower absorption coefficients. The initiation mechanism of successive-intramolecular hydrogen bonding in the peptides is apparently attributed to the disturbance of the β-sheet formation by the rotation of the tertiary peptide bond plane (Leu-Pro), that is, the restriction of the values of the backbone dihedral angles ϕ and ψ of the Pro residue due to the low flexibility of the pyrrolidine ring.

In connection with the design of the synthetic route for peptides and proteins based on the solubility prediction method,[2-5)] it is of particular importance to investigate the nucleation site of helical folding in peptide intermediates since the β-sheet→helical conformational transformation gives rise to the great improvement on solubility of peptide intermediates.[6-8)] The investigation of the initiation mechanism of helical folding in proteins is also one of the quite interesting problems for understanding the mechanism of protein folding and also for predicting protein folding from amino acid sequences. However, it has been well recognized that the determination of nucleation sites of helical folding in peptides and proteins is quite difficult.[9)] In our recent papers,[6-8)] we demonstrated the great ability of the Aib residue to promote helical folding in peptides and subsequently proposed that the restriction of the backbone dihedral angles ϕ and ψ of an amino acid residue to the helical region is one of important initiation mechanisms of helical folding in natural proteins. Therefore, it is of particular interest to investigate the ability of the Pro residue to promote helical folding in peptides since the most frequently observed conformations for the Pro residue lie in the region of the backbone dihedral angles $\phi=-60\pm10°$ and $\psi=-30\pm20°$ (helical region), and $\phi=-60\pm10°$, $\psi=120\pm20°$ due to the low flexibility of the pyrrolidine ring in the Pro residue.[10)]

Thus, in this paper, we give attention to the Pro residue, which is hitherto emphasized to be a strong helix and β-sheet breaker.[11-14)] As for conformations of oligo(Leu)s containing the Pro residue,[14)] in the solid state, the insertion of the Pro residue into homooligo(Leu)s caused the disturbance of the β-sheet structure by the rotation of the tertiary peptide bond plane (Leu-Pro). On the other hand, in methanol, the CD patterns of the oligo(Leu)s containing the Pro residue suggested the existence of a detectable amount of the α-helical structure. In this paper, we investigate the ability of the Pro residue to promote helical folding in oligo(Leu)s containing the Pro residue using IR difference spectra in dichloromethane and discuss the role of the Pro residue in remarkable improvement on solubility of peptide intermediates containing the Pro residue.

Experimental

The samples of Boc-Leu$_2$-OBzl **1**, Boc-Leu$_3$-OBzl **2**, Boc-Leu$_4$-OBzl **3**, and Boc-Leu$_5$-OBzl **4** were prepared by the method described in the previous paper.[14)] The other peptides **5**—**10** examined in this study were also prepared by the essentially same method described previously for

Table 1. Elemental Analysis of the Peptides **5**—**10**

Compound	Formula	Found (Calcd)		
		C (%)	H (%)	N (%)
5	$C_{45}H_{83}N_7O_{10}\cdot H_2O$	60.23 (60.04)	9.48 (9.52)	11.03 (10.89)
6	$C_{35}H_{56}N_4O_7$	65.31 (65.19)	8.71 (8.75)	8.93 (8.69)
7	$C_{41}H_{67}N_5O_8$	64.95 (64.97)	8.95 (8.91)	9.29 (9.24)
8	$C_{47}H_{78}N_6O_9$	64.52 (64.80)	9.07 (9.03)	9.66 (9.65)
9	$C_{53}H_{89}N_7O_{10}\cdot H_2O$	63.51 (63.51)	8.77 (9.15)	9.71 (9.78)
10	$C_{59}H_{100}N_8O_{11}\cdot 0.5H_2O$	64.04 (64.04)	9.22 (9.20)	10.02 (10.13)

		Boc-Leu$_2$-Aib-Leu$_4$-OH	5
Boc-Leu$_2$-OBzl	1	Boc-Leu-Pro-Leu$_2$-OBzl	6
Boc-Leu$_3$-OBzl	2	Boc-Leu-Pro-Leu$_3$-OBzl	7
Boc-Leu$_4$-OBzl	3	Boc-Leu-Pro-Leu$_4$-OBzl	8
Boc-Leu$_5$-OBzl	4	Boc-Leu$_2$-Pro-Leu$_4$-OBzl	9
		Boc-Leu$_3$-Pro-Leu$_4$-OBzl	10

Fig. 1. The peptides **1**—**10** examined in this study.

Boc-Leu$_4$-Aib-Leu$_4$-OBzl[6] and Boc-Leu$_3$-Pro-Leu$_3$-OBzl.[14] The data of elemental analysis of the peptides **5**—**10** are assembled in Table 1 and they are in good agreement with the calculated values. Each peptide also gave a single peak on HPLC. The IR spectra in dichloromethane of the peptides **1**—**10** were recorded at room temperature with a JEOL JIR-100 FT-IR spectrophotometer over a wide range

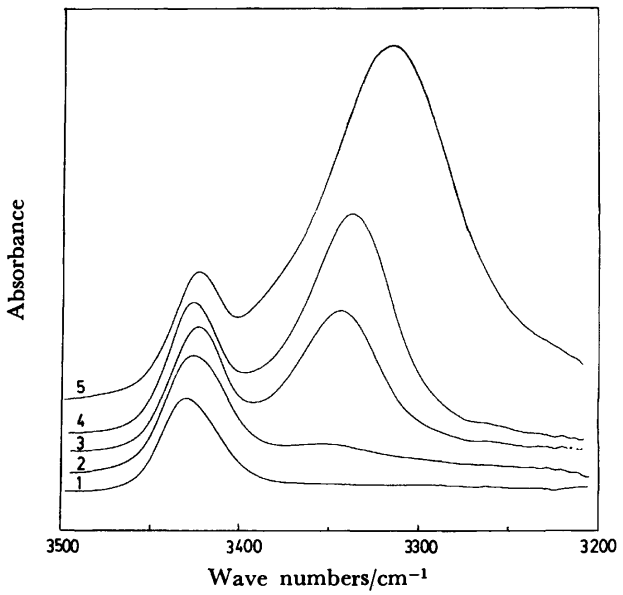

Fig. 2. IR absorption spectra in the amide A region of the peptides **1**—**5** in dichloromethane (1.0 mM).

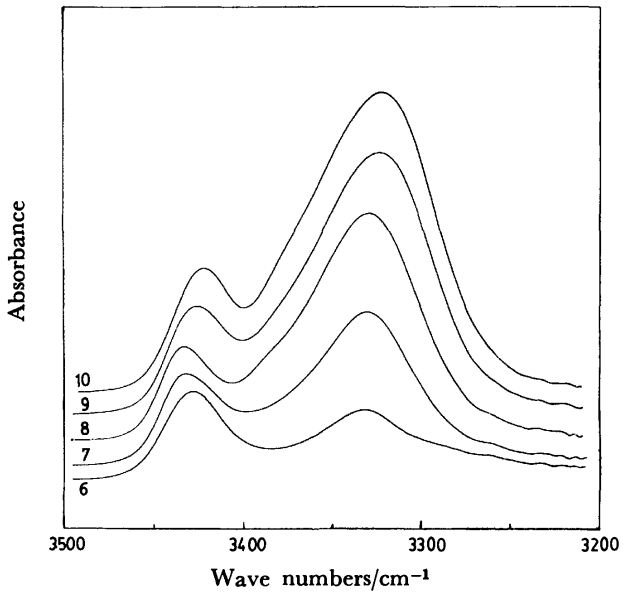

Fig. 3. IR absorption spectra in the amide A region of the peptides **6**—**10** in dichloromethane (1.0 mM).

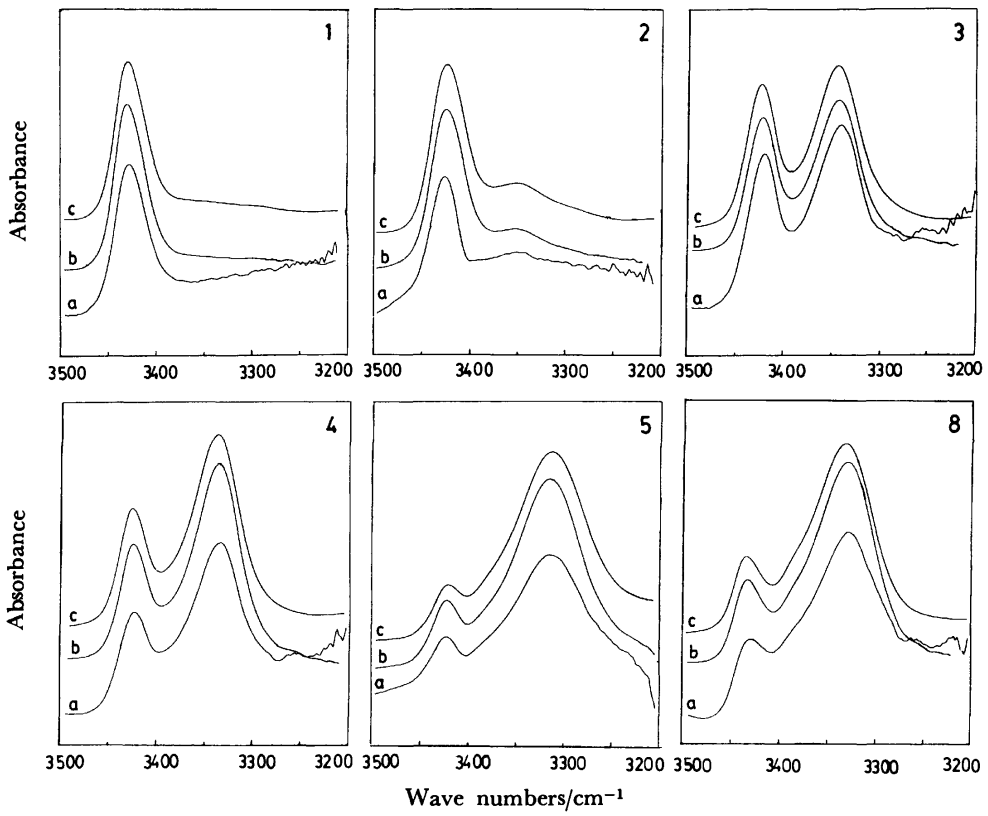

Fig. 4. IR absorption spectra in the amide A region of the peptides **1**—**4** and **8** in dichloromethane over the wide range of concentrations (0.10—10 mM). a: 0.10 mM, b: 1.0 mM, c: 10 mM.

of concentrations by employing 0.5 mm- and 5 mm-path length cells with potassium bromide windows.

Results and Discussion

The peptides **1**—**10** examined in this study are listed in Fig. 1. The IR spectra in the N-H stretching region of the peptides **1**—**5** and **6**—**10** in dichloromethane (1.0 mM (1 M=1 mol dm^{-3})) are shown in Figs. 2 and 3, respectively. The spectra in Figs 2, 3, 5, 7, and 9 are shown with the same scale of absorbance. The spectra in Figs. 2 and 3 show two distinct bands at 3430—3420 and 3350—3320 cm^{-1} although the latter band of the dipeptide **1** is negligible. The bands at 3430—3420 cm^{-1} are clearly due to the free urethane and peptide N-H stretching vibration, and the bands at 3350—3320 cm^{-1} can arise from the hydrogen-bonded N-H groups.[5,15-18] Figure 4, as typical examples, shows the IR spectra of the peptides **1**—**5** and **8** over the wide range of concentrations (0.10—10 mM). Intensity ratios of the hydrogen-bonded N-H absorption to the free N-H absorption (A_H/A_F) for each peptide do not vary much with concentration, indicating that, especially at concentrations lower than 1.0 mM, the hydrogen-bonded N-H absorptions are due almost exclusively to intramolecularly hydrogen-bonded folded species as reported for Boc-Leu_n-OCH_3 (n=3—6).[17]

For the purpose of elucidating intramolecularly hydrogen-bonded folded species, the IR difference spectra between the dipeptide **1** and the peptides **6** through **9** are examined in the amide A region. As shown in Fig. 5, the absorptions of the free urethane and peptide N-H groups in the peptides **6**—**9** are almost clearly compensated with those absorptions in the peptide **1**. When we presume that the absorption coefficients of the free urethane and peptide N-H groups in the unordered structure for the dipeptide **1** are nearly equal to those absorption coefficients in the α-helical structures for the peptides **6**—**9**, the results in Fig. 5 suggest the occurrence of incipient α-helices formed by one, two, three, and four $i \rightarrow i-4$ hydrogen-bonding patterns in the peptides **6**—**9**, respectively, as shown in Fig. 6 schematically. These conformational

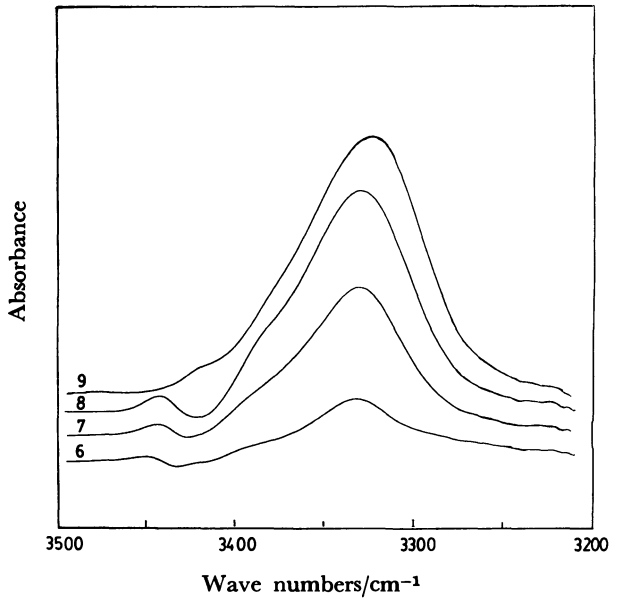

Fig. 5. IR difference spectra between the dipeptide **1** and the peptides **6** through **9** in the amide A region (1.0 mM).

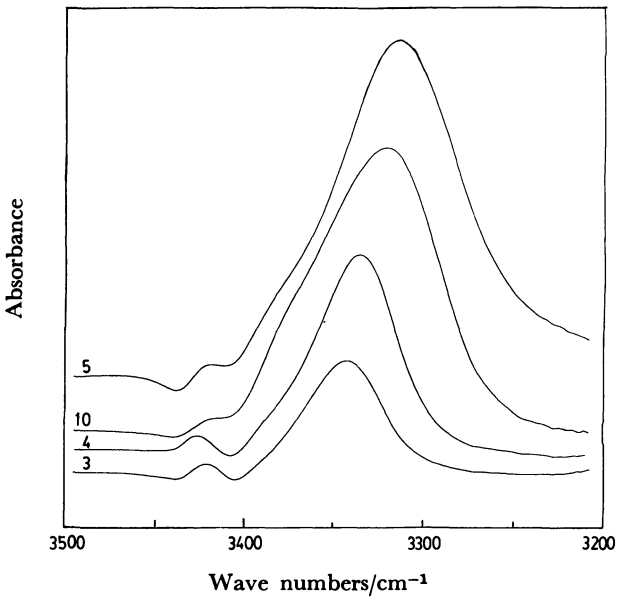

Fig. 7. IR difference spectra between the tripeptide **2** and the peptides **3**—**5** and **10** in the amide A region (1.0 mM).

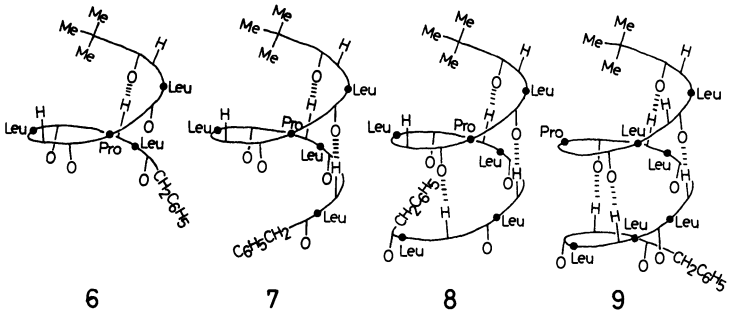

Fig. 6. α-Helical structures for the peptides **6**—**9**.

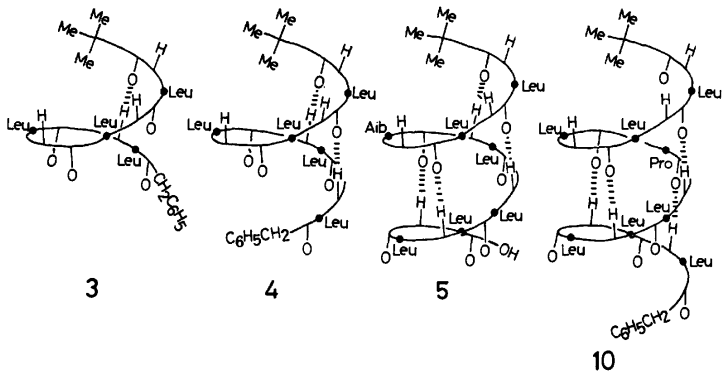

Fig. 8. α-Helical structures for the peptides **3**—**5** and **10**.

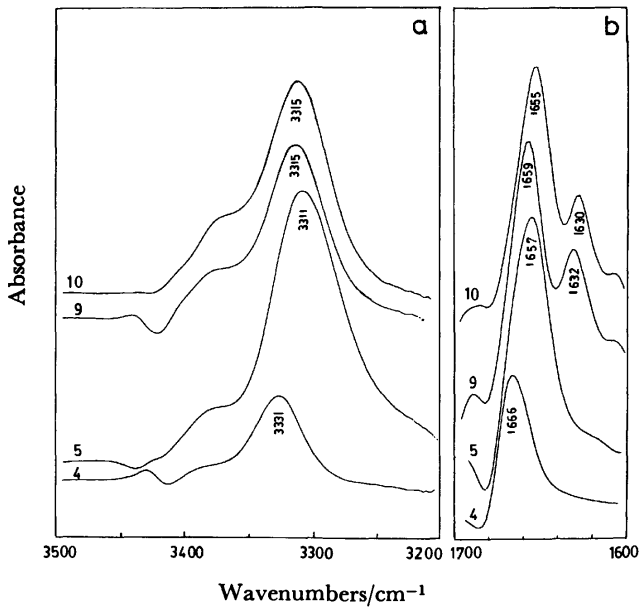

Fig. 9. IR difference spectra between the tetrapeptide **3** and the peptides **4**, **5**, **9**, and **10** (1.0 mM). a: The amide A region, b: the amide I region.

behaviors are just the same with those of the oligo(Leu)s containing the Aib residue as reported previously.[6,7] Furthermore, although the tripeptide **2** possesses low amounts of intramolecularly hydrogen-bonded folded species, the IR difference spectra between the tripeptide **2** and the peptides **3**—**5** and **10** are also examined in the amide A region (Fig. 7). When we also presume the α-helical structures for the peptides **3**—**5** and **10** (Fig. 8), the three free N-H groups in the helical structures for each peptide look like to be almost compensated with the three N-H groups of the peptide **2**. Small positive and negative peaks around 3440 and 3420 cm^{-1} in Figs. 5 and 7 are probably caused by the difference in the band positions of the free N-H groups.

In the α-helical structures for the peptides **3**—**10** in Figs.6 and 8, three peptide carbonyl groups and one C-terminal ester carbonyl group are free from hydrogen bonding. Therefore, the IR difference spectra between the tetrapeptide **3** and the peptides **4**, **5**, **9**, and **10** are useful to investigate the absorption bands assigned to hydrogen-bonded peptide carbonyl groups. Figures 9a and 9b show their IR difference spectra in the amide A and amide I regions, respectively. Except for the peptide **9**, the three free N-H groups in the presumed α-helices for the peptides **4**, **5**, and **10** are again almost compensated with the free N-H groups in the presumed α-helix for the peptide **3** (Fig. 9a). On the other hand, the peptide **9** has only two free N-H groups in the α-helical structure, and the IR difference spectrum between the peptides **3** and **9** shows a negative band at 3420 cm^{-1}. Shoulder bands around 3370 cm^{-1} in Fig. 9a are probably explained by the difference in the band positions of the hydrogen-bonded N-H groups or the contribution of other intramolecularly hydrogen-bonded folded-structures. In Fig. 9b, the strong intensity bands at 1666—1655 cm^{-1} in the amide I region also suggest the α-helical structures.[15-18] The bands at 1632—1630 cm^{-1} are probably assigned to the hydrogen-bonded Pro carbonyl groups in the peptides **9** and **10**. The tendency that the hydrogen-bonded absorption bands in the amide A and amide I regions for the peptides **4**, **9**, and **10** shift to lower frequencies with increasing peptide chain length is quite resembled with that for oligo(Leu)s containing the Aib residue[6,7] and the homopeptides Z-Aib_n-OBu^t (n=3—11),[19] which have 3_{10}-helical structures. With respect to the heptapeptide **5** having the Aib residue, the ^1H NMR study also suggests that it has the α-helix in $CDCl_3$.[20]

The conformational analysis of the peptides **3**—**10** mentioned above is based on the assumption that the absorption coefficients in the amide A region of the free urethane and peptide N-H groups in the unordered structures for the peptides **1** and **2** are nearly equal to those absorption coefficients in the α-helical structures for the peptides **3**—**10**. However, the fully developed, stable α-helical structures in Figs. 6 and 8 are not supported by the intensities of

hydrogen-bonded N-H groups (Figs. 5 and 7). In Table 2, the relative intensities for hydrogen-bonded N-H groups of each peptide are summarized when we presume the α-helical structures for the peptides **3**—**10**. With respect to the homopeptides Z-Aib$_n$-OBu^t (n=3—11),[19] it was reported that a fully-developed, stable 3_{10}-helix was formed at about the octamer level. Therefore, we estimated the percentages[21] of α-helical structures for each peptide using the data of the A_H/A_F ratios for Z-Aib$_n$-OBu^t (n=8—11).[19] The results are also summarized in Table 2. The data strongly suggest that each peptide does not exist only in the fully-developed, stable α-helical structure but coexists in intramolecularly hydrogen-bonded folded-structures which have lower absorption coefficients. Since the assumption is probably not suitable that the absorption coefficients in the amide A region of the free urethane and peptide N-H groups in the unordered structures for the peptides **1** and **2** are nearly equal to those absorption coefficients in the α-helical structures for the peptides **3**—**10**, we should assume that conformations of the peptides **3**—**10** are contributed by the α-helical structures, other successively intramolecularly hydrogen-bonded folded-structures, and the unordered structures free from hydrogen bonding. This conclusion may be in compatible with the ^{1}H NMR result of the peptide **5** that its α-helical structure is not so tight around the C-terminal.[20]

High solubility in dichloromethane of the hexapeptide **8** and the higher oligopeptides **5**, **9**, and **10** is in remarkable contrast with the fact that homologous oligo(Leu) counterparts are practically insoluble in dichloromethane due to their β-sheet structures in the solid state.[5,14] The Pro residue in the peptide **10**, for example, clearly disturbs the development of the β-sheet aggregation by the rotation of the tertiary peptide bond plane (Leu-Pro), facilitating solvation of the peptide chain to cause helical folding. Thus, the ability of the Pro residue to promote helical folding in dichloromethane of the octapeptide **10** is attributed to the disturbance of the β-sheet aggregation, that is, the restriction of the values of the backbone dihedral angles ϕ and ψ of the Pro residue due to the low flexibility of the pyrrolidine ring. The fact that the Pro residue promotes helical folding in the peptides **6**—**10** suggests that the Pro residue included in the N-terminal, four amino acid residues of a helical region plays the role of the nucleation site in helical folding in natural proteins. Undoubtedly, the Pro residue can play the role of the nucleation site in helical folding only when the Pro residue is included in the sequence having high potential for helical formation. In fact, it is well recognized that the Pro residue is frequently found in N-terminal portions of helical regions in natural proteins.[11]

Furthermore, in connection with the design of the synthetic route for peptides and proteins based on the solubility prediction method,[2-5] the fact that the Pro residue promotes successive-intramolecular hydrogen bonds in oligopeptides is of particular interest since helical folding in peptide intermediates, which gives rise to the remarkable solubility improvement, is of quite importance for the design of the synthetic route for peptides and proteins. For example, we assume to be able to design successfully the synthetic route for globin proteins which contain several Pro residues in N-terminal portions of helical regions.

Table 2. Relative Intensities and Wave Numbers of Hydrogen-Bonded N-H Absorption Bands and Helical Contents of Each Peptide

Compound	Relative intensities of hydrogen-bonded N-H absorption bands[a]	Helical content/%[a,b]	Wavenumbers of hydrogen-bonded N-H absorption bands/cm^{-1} [c]
3	0.87	64	3344
4	0.84	62	3336
5	1.00	75	3315
6	0.56	42	3332
7	0.73	54	3331
8	0.80	59	3331
9	0.77	57	3325
10	0.85	63	3323

a) Relative intensities of R/n in Figs. 5 and 7, where R is the area of each N-H absorption bands, and n is the number of intramolecular hydrogen bonds of the α-helices formed by each peptide in Figs. 6 and 7. b) Calculated from the equation, helical content/% = R×100/5.5nA, where A is the half area of the free N-H absorption band of the peptide **1** in Fig. 2, and the coefficient, 5.5, is obtained as $2A_H/A_F/n'$ in Fig. 5 of Ref. 19. c) The band positions of each peptide in Figs. 2 and 3.

References

1) Design of the Synthetic Route for Peptides and Proteins. IV. For part III of this series, see M. Narita, T. Ogura, K. Sato, and S. Honda, *Bull. Chem. Soc. Jpn.*, **59**, 2445 (1986). Abbreviations used are the following: Pro, L-proline residue; Leu, L-leucine residue; IR, infrared; CD, circular dichroism; Aib, α-aminoisobutyric acid residue; Boc, *t*-butoxycarbonyl; OBzl, benzyl ester; HPLC, high-performance liquid chromatography; NMR, nuclear magnetic resonance; Z, benzyloxycarbonyl; OBu^t, *t*-butyl ester.

2) M. Narita, K. Ishikawa, J.-Y. Chen, and Y. Kim, *Int. J. Peptide Protein Res.*, **24**, 580 (1984).

3) M. Narita, T. Ogura, K. Sato, and S. Honda, *Bull. Chem. Soc. Jpn.*, **59**, 2433 (1986).

4) M. Narita, T. Ogura, K. Sato, and S. Honda, *Bull. Chem. Soc. Jpn.*, **59**, 2439 (1986).

5) M. Narita, T. Ogura, K. Sato, and S. Honda, *Bull. Chem. Soc. Jpn.*, **59**, 2445 (1986).

6) M. Narita, M. Doi, H. Sugasawa, and K. Ishikawa, *Bull. Chem. Soc. Jpn.*, **58**, 1473 (1985).

7) M. Narita, K. Ishikawa, H. Sugasawa, and M. Doi, *Bull. Chem. Soc. Jpn.*, **58**, 1731 (1985).

8) M. Narita, J.-Y. Chen, H. Sato, and Y. Kim, *Bull. Chem. Soc. Jpn.*, **58**, 2494 (1985).

9) G. E. Schulz and R. H. Schirmer, "Principles of Protein Structure," Springer-Verlag GmbH & Co. KG (1979).

10) D. F. De Tar and N. Luthra, *J. Am. Chem. Soc.*, **99**, 1232 (1977); V. Madison, *Biopolymers*, **16**, 2671 (1977); B. V. V. Prasad, H. Balaram, and P. Balaram, *ibid.*, **21**, 1261 (1982).

11) P. Y. Chou and G. D. Fasman, *Biochemistry*, **13**, 211, 222 (1974); P. Y. Chou and G. D. Fasman, *Adv. Enzymology*, **47**, 45 (1978).

12) S. Lifson and C. Sander, *Nature*, **282**, 109 (1979).

13) C. Toniolo, G. M. Bonora, M. Mutter, and V. N. R. Pillai, *Makromol. Chem.*, **182**, 1997, 2007 (1981).

14) M. Narita, T. Fukunaga, A. Wakabayashi, K. Ishikawa, and H. Nakano, *Int. J. Peptide Protein Res.*, **23**, 306 (1984); M. Narita, K. Ishikawa, H. Nakano, and S. Isokawa, *ibid.*, **24**, 14 (1984).

15) M. Narita, Y. Tomotake, S. Isokawa, T. Matsuzawa, and T. Miyauchi, *Macromolecules*, **17**, 1903 (1984) and references cited therein.

16) Ch. P. Rao, P. Balaram, and C. N. R. Rao, *Biopolymers*, **22**, 2091 (1983); V. N. R. Pillai and M. Mutter, *Acc. Chem. Res.*, **14**, 122 (1981), and references cited therein.

17) C. Toniolo, G. M. Bonora, M. Palumbo, E. Peggion, and E. S. Stevens, *Biopolymers*, **17**, 1713 (1978).

18) T. Miyazawa and E. R. Blout, *J. Am. Chem. Soc.*, **83**, 712 (1961).

19) C. Toniolo, G. M. Bonora, V. Barone, A. Bavoso, E. Benedetti, B. D. Blasio, P. Grimaldi, F. Lelj, V. Pavone, and C. Pedone, *Macromolecules*, **18**, 895 (1985).

20) The ^{1}H NMR study will be reported elsewhere.

21) The percentages of α-helical structures for each peptide are obtained presuming the equilibrium between the fully developed α-helix and unordered structures.

 © 1986 The Chemical Society of Japan Bull. Chem. Soc. Jpn., 59, 3553—3557 (1986)

Conformations in the Solid State and Solubility Properties of Protected Homooligopeptides of Glycine and β-Alanine[1)]

Mitsuaki NARITA,* Masamitsu DOI, Koji KUDO, and Yusuke TERAUCHI
Department of Industrial Chemistry, Faculty of Technology, Tokyo University of Agriculture and Technology, Koganei 184
(Received May 23, 1986)

IR spectroscopic conformational analyses of Boc-Gly$_n$-OBzl (n=3—7) and Boc-(β-Ala)$_n$-OBzl (n=3—8) were performed in the solid state, suggesting the occurrence of the β-sheet structure in the higher oligomers (n=5—8). Solubility data indicate that insolubilities of Boc-Gly$_n$-OBzl and Boc-(β-Ala)$_n$-OBzl in high-polar solvents begin at hexa- and heptapeptide levels, respectively. Insolubility of protected homooligopeptides of Gly and β-Ala was estimated to be caused by β-sheet aggregation. The high potential for the β-sheet formation of Boc-Gly$_n$-OBzl and Boc-(β-Ala)$_n$-OBzl ($n\geqq5$) could clearly be attributed to the great freedom of the peptide backbone dihedral angles of each of the Gly and β-Ala residues in the β-sheet structure. The implications of a replacement of a few Gly residues with β-Ala residues in surface regions of proteins are also discussed.

The solubility prediction method proposed by us is principally based on the hypothesis that the insolubility of protected peptide intermediates is essentially caused by a β-sheet aggregation consisting of peptide chains equal to or larger than an octapeptide sequence level;[2)] it provides the scope of the design of synthetic routes for peptides and proteins.[2-4)] In the solubility prediction method, the coil conformation parameters, P_c, for each amino acid residue are used for estimating the potential for the β-sheet formation. Here, the value of P_c for the Gly residue is 1.50, which is similar to the value of P_c for the Pro residue, 1.59. These P_c values represent the fact that in globular proteins Gly residues appear in coil conformation regions[5)] as frequently as Pro residues, and that Gly-rich peptides are readily soluble in organic solvents. On the other hand, considering the high flexibility of the peptide backbones of the Gly-rich peptides,[6)] peptides larger than a certain peptide size appear to be insoluble in high-polar solvents due to the β-sheet aggregation.

Therefore, in this work, an investigation of the relationship between the conformation and solubility of protected homooligopeptides of Gly and β-Ala was carried out to confirm the generality of the above hypothesis. The second purpose in this study was to demonstrate that protected homooligopeptides of Gly and β-Ala have a high potential for β-sheet formation due to the great freedom of the peptide backbone dihedral angles of each of Gly and β-Ala residues in the β-sheet structure. In relation to the creation of novel proteins with improved properties, which can not be produced by a recombinant DNA method,[7)] we have discussed the effect of the replacement of a few Ala residues with Aib residues; these have the ability to promote helical folding in helical regions of proteins.[8)] The final purpose in this study was to discuss the possibility and implications of the replacement of the Gly residue with the β-Ala residue in proteins through the investigation of the similarity of conformational behaviors between the Gly and β-Ala residues.

Experimental

General. Uncorrected capillary melting points will be reported. Analytical instruments and conditions were described in a previous paper.[8)]

Synthesis of the Peptides 1—6. The tripeptides **1a** and **1b** were prepared by the usual stepwise elongation, starting with H-Gly-OBzl and H-β-Ala-OBzl as amino components, respectively, in the conditions described before for the preparation of oligopeptides.[8)] The higher oligopeptides **2**—**6** were prepared by fragment condensation in dichloromethane or DMF using DCC activation in the presence of HOBt as described before for fragment condensation.[8)] Procedures for the removal of the Boc group from the peptides (n=2—4) and of the Bzl group from the peptides (n=2—4) were essentially the same to those described previously.

IR Measurements. The IR absorption spectra of the solid samples were recorded with a Jasco Model DS-701G spectrometer in a nujol mull.

Results

Synthesis and Solubility Properties of Protected Homooligopeptides of Gly and β-Ala. The synthetic route for Boc-Gly$_n$-OBzl (n=3—7) and Boc-(β-Ala)$_n$-OBzl (n=3—8) is set out in the Scheme. The tripeptides **1a** and **1b** (n=3) were prepared by the usual stepwise elongation, starting with H-Gly-OBzl and H-β-Ala-OBzl as amino components, respectively.

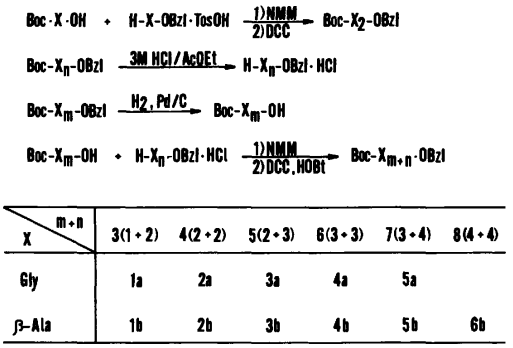

X \ m+n	3(1+2)	4(2+2)	5(2+3)	6(3+3)	7(3+4)	8(4+4)
Gly	1a	2a	3a	4a	5a	
β-Ala	1b	2b	3b	4b	5b	6b

Scheme

Table 1. Synthetic Results and Physical Properties of the Peptides **1**—**6**

Compound	Yield/%[a]	Recrystallization Solvent	Mp θ_m/°C
1a	84	AcOEt/Hexane (1/1)	122—124
2a	76	EtOH/Water (3/1)	177—180
3a	80	b)	Over 200
4a	84	b)	Over 200
5a	78	b)	Over 200
1b	89	EtOH/Water (2/1)	120—121
2b	65	EtOH/Water (1/1)	168—171
3b	66	EtOH/Water (3/2)	Over 200
4b	88	b)	Over 200
5b	83	b)	Over 200
6b	65	b)	Over 200

a) Coupling yields in final steps. b) Purified by washing with hot MeOH.

Both amino components were obtained from the corresponding TosOH salts with an equivalent of NMM. The stepwise elongation was performed in dichloromethane using DCC activation.[9] For the preparation of the higher oligopeptides **2**—**6**, the removal of the Boc group[10] from the peptides (n=2—4) was performed in 3 M HCl/AcOEt (1 M=1 mol dm^{-3}), and removal of the Bzl group,[11] in AcOH/MeOH by hydrogenolysis in the presence of Pd/C as catalyst, respectively. The higher oligopeptides **2**—**6** were obtained by fragment condensation in dichloromethane or DMF using DCC activation in the presence of HOBt.[12] The peptides **1**—**6** were purified by repeated recrystallization or by washing with hot MeOH. The synthetic results and elemental analyses of the peptides **1**—**6** are given in Tables 1 and 2. Their solubility properties are also shown in Table 3.

Table 2. Elemental Analyses of the Peptides **1**—**6**

Compound	Formula	Found (Calcd)		
		C/%	H/%	N/%
1a	$C_{18}H_{25}N_3O_6$	56.94 (56.98)	6.59 (6.64)	11.06 (11.07)
2a	$C_{20}H_{28}N_4O_7$	54.93 (55.04)	6.40 (6.47)	12.73 (12.84)
3a	$C_{22}H_{31}N_5O_8 \cdot 0.5H_2O$	52.37 (52.58)	6.21 (6.42)	14.03 (13.94)
4a	$C_{24}H_{34}N_6O_9 \cdot 0.5H_2O$	51.78 (51.51)	6.05 (6.30)	15.26 (15.01)
5a	$C_{26}H_{37}N_7O_{10} \cdot H_2O$	49.90 (49.92)	6.14 (6.28)	15.70 (15.67)
1b	$C_{21}H_{31}N_3O_6$	59.98 (59.82)	7.60 (7.40)	10.00 (9.97)
2b	$C_{24}H_{36}N_4O_7$	58.73 (58.50)	7.56 (7.38)	11.34 (11.37)
3b	$C_{27}H_{41}N_5O_8$	57.55 (57.53)	7.45 (7.33)	12.39 (12.43)
4b	$C_{30}H_{46}N_6O_9 \cdot 1.5H_2O$	54.34 (54.45)	7.23 (7.46)	12.59 (12.70)
5b	$C_{33}H_{51}N_7O_{10} \cdot 0.5H_2O$	55.51 (55.45)	7.31 (7.33)	13.77 (13.72)
6b	$C_{36}H_{56}N_8O_{11} \cdot 9/4H_2O$	52.74 (52.90)	7.01 (7.46)	13.97 (13.71)

Table 3. Solubility Properties[a] of the Peptides **1**—**6** (c=1.0 g dl^{-1})

Compound	Solvent						
	High-polar solvent[b]	MeOH EtOH	$CHCl_3$	AcOEt	CH_2Cl_2	Acetone	CCl_4
1a	A	A	A	A	A	B	D
2a	A	A	B	B	B	B	D
3a	A	D	D	D	D	D	D
4a	D, C[c]	D	D	D	D	D	D
5a	D	D	D	D	D	D	D
1b	A	A	A	A	A	D	B
2b	A	A	A	A	B	B	D
3b	A	B	B	D	B	C	D
4b	B, A[c]	D	D	D	D	D	D
5b	D, C[c]	D	D	D	D	D	D
6b	D, C[c]	D	D	D	D	D	D

a) Solubility: A, soluble at room temperature; B, soluble at 80° or refluxing temperature; C, partially soluble at 80° or refluxing temperature; D, practically insoluble at 80° or refluxing temperature. b) DMF, NMP, DMA, DMSO, and HMPA. c) Solubility in NMP and HMPA.

IR Absorption Study in the Solid State of Protected Homooligopeptides of Gly and β-Ala. The IR absorption spectra in the amide A and amide I regions of the peptides **1a—5a** and **1b—6b** in the solid state are presented in Figs. 1 and 2, respectively. The assignments of the various bands of the peptides **1—6** were made on the basis of theoretical and experimental data for oligopeptides.[13-16] The peptides **1** and **2** (n=3 and 4) in Figs. 1 and 2 show strong bands around 3290 cm^{-1} and a few bands in the amide A region, indicating a predominant conformation with hydrogen bonds, most probably of the interchain type, but quite different from the usual antiparallel β-sheet structure, as assumed on Boc-Gly_n-OPEG (n=3 and 4).[15] However, details of the IR absorption frequencies of Boc-Gly_n-OPEG (n=3 and 4) are different from those of Boc-Gly_n-OBzl (n=3 and 4) due to the effect of the bulky and bifunctional PEG. In the case of the peptide **1b**, the absorption band of the ester carbonyl group shifts around 1715 cm^{-1}, indicating its hydrogen bonding with a N-H group. When n=5 the peptides **3a** and **3b** have a strong band around 3290 cm^{-1} in the amide A region and weak and strong bands around 1685 cm^{-1} and 1630 cm^{-1}, respectively, in the amide I region, accompanied by a shoulder around 1655—1645 cm^{-1}. These bands indicate the predominant antiparallel β-sheet and other coexistent conformations.[15] These results are quite different from the ternary helix conformation reported on CH_3CO-Gly_n-NHC_2H_5 (n=1—4) and poly$(Gly)_n$,[16] which have strong characteristic absorption bands at 3285 cm^{-1} in the amide A region, 1646 cm^{-1} in the amide I region, and 1560 cm^{-1} in the amide II region. The peptides **4—6** having n=6—8 assume predominantly the antiparallel β-sheet structure as reported on Boc-Gly_n-OPEG (n=7—9),[15] although the broad bands around 1640—1630 cm^{-1} suggests the coexistence of other conformations. Through an IR conformational analysis in the solid state of the peptides **1—6**, the conformational behaviors of each oligo(β-Ala) are very close to those of the corresponding oligo(Gly).

Discussion

By using the IR absorption spectra in the solid state of the peptides **1—6**, the occurrence of the β-sheet structure was actually established for Boc-Gly_n-OBzl (n=5—7) and Boc-$(\beta\text{-Ala})_n$-OBzl (n=5—8), and insolubilities in high-polar solvents of Boc-Gly_n-OBzl and Boc-$(\beta\text{-Ala})_n$-OBzl begin at hexa- and heptapeptide levels, respectively. As in the case of protected homooligo-L-leucines,[17] protected oligopeptides having various hydrophobic side chains,[8] and protected oligopeptides having various polar side chains,[3] insolubility of the homooligopeptides of Gly and β-Ala was estimated to be mainly caused by β-sheet aggregation. Boc-Gly_n-OBzl (n=6 and 7) and Boc-$(\beta\text{-Ala})_n$-OBzl (n=7 and 8) are practically insoluble even in the high-polar solvents such as DMF, DMA, NMP, DMSO, and HMPA (Table 3). Smaller critical sizes for the insolubility of Boc-Gly_n-OBzl and Boc-$(\beta\text{-Ala})_n$-OBzl than protected other oligopeptides[3,8,17] are probably due to the high symmetry of peptide backbones of homooligopeptides of Gly and β-Ala.

According to the solubility prediction method based on the $\langle P_c \rangle$ values of the average coil conformation

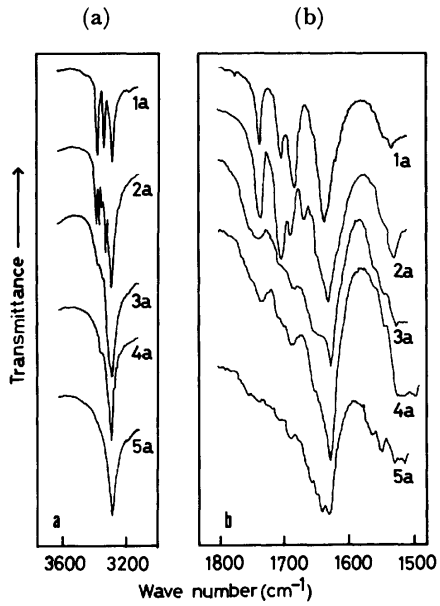

Fig. 1. IR absorption spectra of the peptides **1a—5a**. a: The amide A region; b: the amide I region.

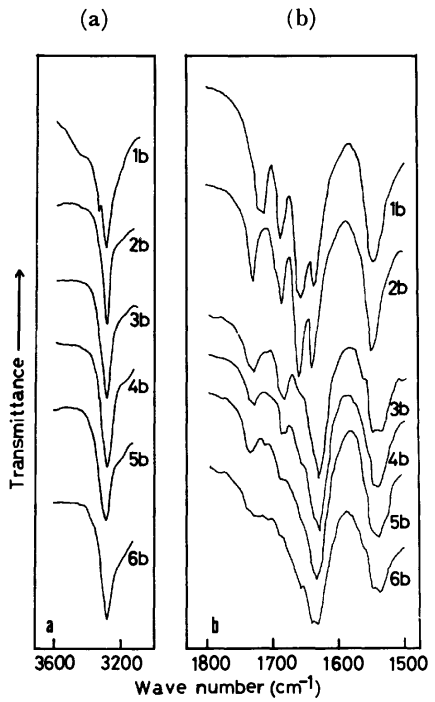

Fig. 2. IR absorption spectra of the peptides **1b—6b**. a: The amide A region; b: the amide I region.

parameters of protected homooligo(Gly)s, they are predicted to be easily soluble due to the great freedom of the backbone dihedral angles ϕ and ψ of the Gly residue.[2] Actually, the Gly residue can explore a large conformational space,[6] thus inducing a high flexibility to the peptide chain. The great freedom of the backbone dihedral angles ϕ and ψ of the Gly residue is essentially attributed to the fact that there is no substituent on the C^{α} atom of the Gly residue. The great freedom is just due to the release in the Gly residue of the steric hindrance between O_{i-1} and C^{β}_{i} (postulated C^{β} atom on C^{α}_{i}), between N_{i+1} and C^{β}_{i}, and between H_{i+1} and C^{β}_{i} as illustrated in Fig. 3a. This fact results in the large value of W_{free}, which leades the peptide chain to various conformations:

$$\Delta S_{\beta\text{-sheet}} = S_{\beta\text{-sheet}} - S_{free} = R \ln W_{\beta\text{-sheet}} - R \ln W_{free}, \quad (1)$$

where $S_{\beta\text{-sheet}}$ is the entropy value in the β-sheet structure and S_{free} that in the free structure.[18] R is the gas constant, $W_{\beta\text{-sheet}}$ the probability of a β-sheet structure and W_{free} that of the free structure. On the other hand, the high potency for a β-sheet formation of Boc-Gly_n-OBzl ($n \geqq 5$) represents the large value of $\Delta S_{\beta\text{-sheet}}$ in Eq. 1, thus inducing the large value of $W_{\beta\text{-sheet}}$ in Eq. 1. The large value of $W_{\beta\text{-sheet}}$ corresponds to the great freedom in the β-sheet structure of the backbone dihedral angles ϕ and ψ of each Gly residue of Boc-Gly_n-OBzl. If the value of $W_{\beta\text{-sheet}}$ in the β-sheet structure of Boc-Gly_n-OBzl is as small as the values of W of various other conformations, Boc-Gly_n-OBzl inevitably has various conformations, resulting in coil conformation structures. The conformational behavior of Boc-(β-Ala)$_n$-OBzl is, essentially, quite similar to that of Boc-Gly_n-OBzl. The freedom of the peptide backbone of Boc-(β-Ala)$_n$-OBzl is much greater than that of Boc-Gly_n-OBzl due to an additional release in the β-Ala residue of the steric hindrance between O_{i-1} and O_i, between O_{i-1} and C^{β}_{i}, between O_{i-1} and N_{i+1}, between H_{i+1} and O_{i-1}, and between H_i and H_{i+1} as illustrated in Fig. 3b. Due to the fact that there is no substituent on the C^{α} and C^{β} atoms of the β-Ala residue, each β-Ala residue in the β-sheet structure can explore the large conformational space, inducing the high flexibility to the peptide chain in the β-sheet structure. Using the CPK models of the antiparallel β-sheet structures of Boc-Gly_7-OBzl and Boc-(β-Ala)$_7$-OBzl, we can actually confirm the great freedom of the methylene groups in the antiparallel β-sheet structures of Boc-Gly_7-OBzl and Boc-(β-Ala)$_7$-OBzl.

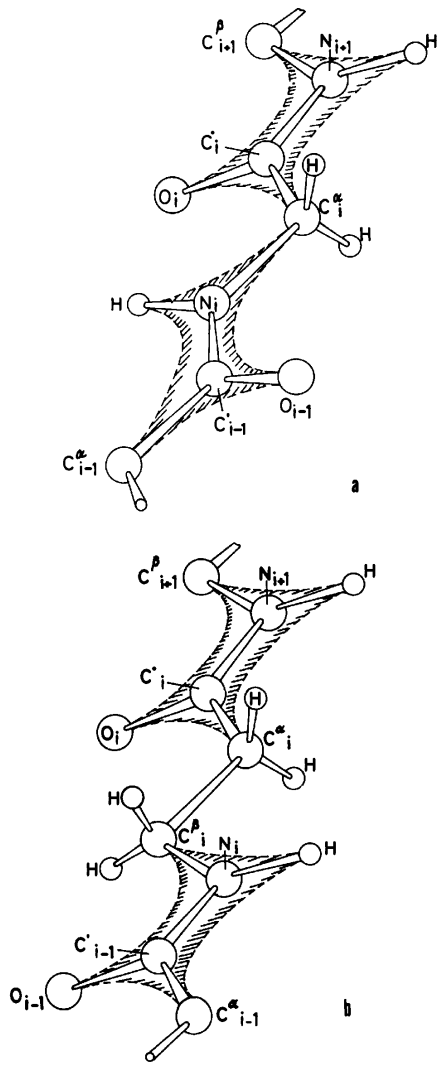

Fig. 3. Release of steric hindrance (a) in the Gly residue and (b) in the β-Ala residue.

The large value of W_{free} of the Gly residue compared with other amino acid residues corresponds to the fact that Gly residues in globular proteins have various values of the backbone dihedral angles ϕ and ψ, as shown by X-ray diffraction studies of globular proteins. Thus, the Gly residue often appears in turn structures,[19] that is, in surface regions of globular proteins. Since the β-Ala residue has a value of W_{free} that is larger than the Gly residue, it is estimated that we can suitably replace the Gly residue with the β-Ala residue in surface regions of globular proteins without changing the protein structures essentially. Moreover, active sites of proteins are usually located on the surface regions of the proteins, especially clefts or crevices, and the packing density in the active sites is usually low.[6] These facts mean that the active sites have a greater freedom than the other regions. Therefore, the replacement of a few Gly residues with β-Ala residues in surface regions of proteins offers the prospect for creating novel proteins which can not be produced by the recombinant DNA method.[7] The replacement techniques also offer the potential for altering protein functions in ways not possible by any other method, just as mentioned in protein engineering pioneered by genetic technology.[20]

References

1) Design for the Synthetic Route of Peptides and Proteins. V. For part IV of this series, see M. Narita, S. Isokawa, M. Doi, and R. Wakita, *Bull. Chem. Soc. Jpn.*, **59**, 3547 (1986). Abbreviations used are the following: Gly, glycine residue; β-Ala, β-alanine residue; Boc, *t*-butoxycarbonyl; Bzl, benzyl; IR, infrared; Aib, α-aminoisobutyric acid residue; DNA, deoxyribonucleic acid; DCC, dicyclohexylcarbodiimide; DMF, *N*,*N*-dimethylformamide; HOBt, 1-hydroxy-1*H*-benzotriazole; MeOH, methanol; TosOH, *p*-toluenesulfonic acid; NMM, *N*-methylmorpholine; AcOEt, ethyl acetate; AcOH, acetic acid; DMA, *N*,*N*-dimethylacetamide; NMP, *N*-methylpyrrolidone; DMSO, dimethyl sulfoxide; HMPA, hexamethylphosphoric triamide; PEG, polyethylene glycol.

2) M. Narita, K. Ishikawa, J.-Y. Chen, and Y. Kim, *Int. J. Peptide Protein Res.*, **24**, 580 (1984).

3) M. Narita, T. Ogura, K. Sato, and S. Honda, *Bull. Chem. Soc. Jpn.*, **59**, 2433 (1986); **59**, 2439 (1986), **59**, 2445 (1986).

4) M. Narita, S. Isokawa, M. Doi, and R. Wakita, *Bull. Chem. Soc. Jpn.*, **59**, 3547 (1986).

5) Coil conformation regions in this definition include β-turn regions.

6) G. E. Schulz and R. H. Schirmer, "Principles of Protein Structure" Springer-Verlag GmbH & Co. KG (1979).

7) K. Itakura, T. Hirose, R. Crea, and A. D. Riggs, *Science*, **198**, 1056 (1977).

8) M. Narita, M. Doi, H. Sugasawa, and K. Ishikawa, *Bull. Chem. Soc. Jpn.*, **58**, 1473 (1985); M. Narita, K. Ishikawa, H. Sugasawa, and M. Doi, *Bull. Chem. Soc. Jpn.*, **58**, 1731 (1985); M. Narita, J.-Y. Chen, H. Sato, and Y. Kim, *Bull. Chem. Soc. Jpn.*, **58**, 2494 (1985).

9) J. C. Sheehan and G. P. Hess, *J. Am. Chem. Soc.*, **77**, 1067 (1955); H. G. Khorana, *Chem. Rev.*, **53**, 145 (1953).

10) F. C. McKay and W. F. Albertson, *J. Am. Chem. Soc.*, **79**, 4686 (1957).

11) E. Abderhalden and S. Suzuki, *Hoppe-Seyler's Z. Physiol. Chem.*, **176**, 101 (1958).

12) W. König and R. Geiger, *Chem. Ber.*, **103**, 788 (1970).

13) T. Miyazawa and E. R. Blout, *J. Am. Chem. Soc.*, **83**, 712 (1961); Yu. N. Chirgadze and N. A. Nevskaya, *Biopolymers*, **15**, 627 (1976); V. N. R. Pillai and M. Mutter, *Acc. Chem. Res.*, **14**, 122 (1981), and references cited therein.

14) M. Narita, S. Isokawa, Y. Tomotake, and S. Nagasawa, *Polymer J.*, **15**, 25 (1983), and references cited therein.

15) C. Toniolo, G. M. Bonora, V. N. R. Pillai and M. Mutter, *Macromolecules*, **13**, 772 (1980).

16) M. Avignon and C. Garrigou-Lagrange, *Spectrochim. Acta*, Part A, **27**, 297 (1971).

17) M. Narita, T. Fukunaga, A. Wakabayashi, K. Ishikawa, and H. Nakano, *Int. J. Peptide Protein Res.*, **23**, 306 (1984).

18) The free structure represents all of the conformations allowed.

19) P. Y. Chou and G. D. Fasman, *Biochemistry*, **13**, 222 (1974); P. Y. Chou and G. D. Fasman, *Adv. Enzymol.*, **47**, 45 (1978).

20) K. M. Ulmer, *Science*, **219**, 666 (1983).

A Novel and Highly Efficient Asymmetric Synthesis of Optically Active Anthracyclinones[1)]

Michiyo SUZUKI, Yoshikazu KIMURA, and Shiro TERASHIMA*
Sagami Chemical Research Center, Nishi-Ohnuma, Sagamihara, Kanagawa 229
(Received May 21, 1986)

The bromolactonization of the optically active acetals derived from 2-acetyl-5,8-dimethoxy-3,4-dihydronaphthalene and (*R,R*)-*N,N*:*N'*,*N'*-tetraalkyltartaramide was found to proceed highly diastereoselectively, giving mixtures of the seven-membered bromo lactones and the bromohydrins. The predominantly produced bromo lactones could be effectively converted to (*R*)-2-acetyl-5,8-dimethoxy-1,2,3,4-tetrahydro-2-naphthol, the AB ring synthon of optically active 11-hydroxyanthracyclinones, >95% ee, in one pot reaction. Application of the explored synthetic scheme to 2-acetyl-5,12-dimethoxy- and 2-acetyl-5-methoxy-3,4-dihydro-6,11-naphthacenedione similarly gave (*R*)-2-acetyl-2,5,12-trihydroxy- and (*R*)-2-acetyl-2,5-dihydroxy-1,2,3,4-tetrahydro-6,11-naphthacenedione, the advanced key synthetic intermediates of optically active 4-demethoxy- and 11-deoxy-4-demethoxyanthracyclinones, 94% ee and >99% ee, respectively, by way of mixtures of the seven- and six-membered bromo lactones.

The anthracycline antibiotics, adriamycin (**1a**) and daunorubicin (**1b**), hold leading positions of anticancer agents because of their prominent activity against various types of human cancers.[2)] While various undesirable side effects, the most notable and serious of which is dose-related cardiotoxicity,[2,3)] restrict their wide utilization for cancer chemotherapy, more improved therapeutic indices can be expected for recently discovered natural 11-deoxyanthracyclines (**1e,f**)[4)] and synthetically explored unnatural 4-demethoxy-[5)] and 11-deoxy-4-demethoxyanthracyclines[6)] (**1c,d** and **1g,h**).

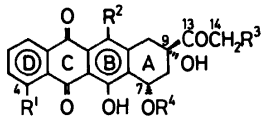

1 : R^4 = 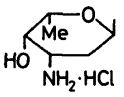

2 : R^4 = H

	R^1	R^2	R^3		R^1	R^2	R^3
a:	OMe	OH	OH	e:	OMe	H	OH
b:	OMe	OH	H	f:	OMe	H	H
c:	H	OH	OH	g:	H	H	OH
d:	H	OH	H	h:	H	H	H

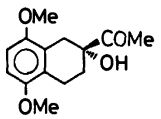

(R) - 3

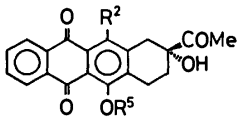

dl- or (R) - 4

	R^2	R^5
d:	OH	H
h:	H	H
i:	OMe	Me
j:	H	Me

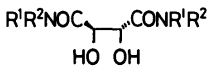

5

	R^1	R^2
a:	Me	Me
b:	$-(CH_2)_4-$	

Syntheses of optically active natural and unnatural 11-hydroxyanthracyclinones (**2a—d**),[7)] the aglycones of **1a—d**, have been achieved by employing asymmetric syntheses[8-13)] or optical resolutions[5a-c,14-23)] as key processes for producing optically active compounds. However, a synthetic scheme which is generally applicable not only to optically active **2a—d** but also to their 11-deoxy congeners (**2e—h**), seems to be still lacking.[24)]

By selecting (*R*)-2-acetyl-5,8-dimethoxy-1,2,3,4-tetrahydro-2-naphthol ((***R***)-**3**) as a model target compound, an efficient synthetic method being generally applicable to the whole family of optically active anthracyclinones (**2a—h**) was sought. As for (***R***)-**3** which is anticipated to be one of the most versatile AB ring synthons for the chiral synthesis of **2a—d**,[7)] numerous synthetic methods have so far been explored by employing asymmetric synthesis[8-11,13)] or optical resolution.[5a-c,14,22)]

Previously, the authors reported the asymmetric synthesis of (***R***)-**3** in which the bromolactonization of (*S*)-*N*-(α,β-unsaturated acyl)proline derivatives constitutes the key diastereoselective reaction.[8)] We succeeded in obtaining (***R***)-**3** of 97% ee by sequential manipulation of the formed bromo lactone by way of (*R*)-2-hydroxy-5,8-dimethoxy-1,2,3,4-tetrahydro-2-naphthoic acid. However, this asymmetric synthesis was found to be less practical and to lack generality because of long synthetic steps for obtaining the reaction substrates, requirement of a stoichiometric amount of expensive (*S*)-proline as a chiral source, and failure of construction of the α-hydroxy ketone functionality from the optically active α-hydroxy acid moiety involved in the 1,2,3,4-tetrahydro-6,11-naphthacenedione system.[25)]

We have now explored another efficient asymmetric synthesis of (***R***)-**3** by featuring the bromolactonization of the optically active acetal (**8**) prepared from readily available 2-acetyl-5,8-dimethoxy-3,4-dihydronaphthalene (**6**) and (*R,R*)-*N,N*:*N'*,*N'*-tetraalkyltartaramide (**5**).[26)] Moreover, it appears that this asymmetric

synthesis can be similarly employed for producing highly optically active (*R*)-2-acetyl-2,5,12-trihydroxy- and (*R*)-2-acetyl-2,5-dihydroxy-1,2,3,4-tetrahydro-6,11-naphthacenedione ((*R*)-7-deoxy- and (*R*)-7,11-dideoxy-4-demethoxydaunomycinone) ((***R***)-**4d**,**h**) from the tetracyclic 2-acetyl-3,4-dihydro-6,11-naphthacenedione derivatives (**21**). These optically active tetracyclic α-hydroxy ketones (***R***)-**4d**,**h** are usable as the advanced key synthetic intermediates of unnatural 4-demethoxy and 11-deoxy-4-demethoxyanthracyclinones (**2c**,**d** and **2g**,**h**).[6,7,9,15,23]

This report details the exploration of this novel asymmetric synthesis which is considered to be more practical and general than the previously reported methods.[8-13]

Asymmetric Synthesis of Optically Active (*R*)-2-Acetyl-5,8-dimethoxy-1,2,3,4-tetrahydro-2-naphthol ((*R*)-3). The starting material (**6**) of the asymmetric synthesis could be prepared from 5,8-dimethoxy-2-tetralone[27] by addition of ethynylmagnesium bromide and Rupe rearrangement of the formed propargylic alcohol.[9] However, modification of the method reported by Russell et al.[28] was found to be more promising for obtaining a large quantity of **6**. Thus, treatment of 4a,5,8,8a-tetrahydro-1,4-naphthoquinone[29] with acetic anhydride and potassium hydroxide, followed by isomerization of the $C_{6,7}$-double bond of 1,4-diacetoxy-5,8-dihydronaphthalene catalyzed with pentacarbonyliron(0), Friedel-Crafts acetylation of 1,4-diacetoxy-5,6-dihydronaphthalene, alkaline hydrolysis of the diacetates, and methylation of the two phenolic hydroxyl groups, readily produced **6**.

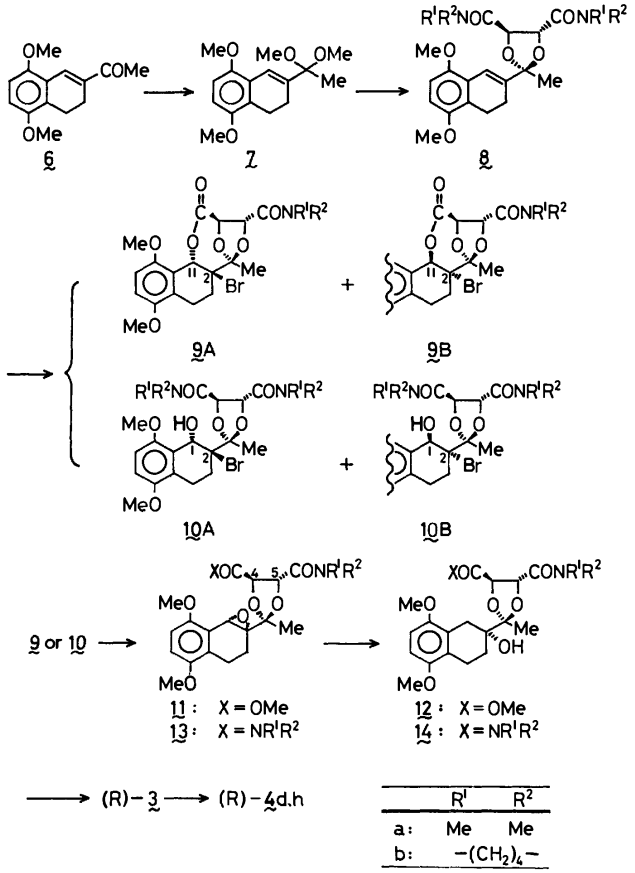

Chart 1.

While the direct acetalization of **6** with **5** was found to be sluggish, preparation of the optically active acetals **8** could be effectively accomplished by successive acetalization and transacetalization as shown in Chart 1. Thus, acetalization of **6** with trimethoxymethane in the presence of *dl*-10-camphorsulfonic acid (CSA) followed by transacetalization of the formed dimethylacetal (**7**) with (*R*,*R*)-*N*,*N*:*N'N'*-tetramethyltartaramide (**5a**)[30] gave **8a** in 92% overall yield.

After numerous unsuccessful attempts,[31,32] it was finally found that when **8a** was treated with *N*-bromoacetamide in a mixture of *N*,*N*-dimethylformamide (DMF) and water (100:1)[33] at 0 °C for 15.5 h, a mixture of the bromo lactone (**9a**) and the bromohydrin (**10a**) could be obtained in 83 and 7% yields, respectively. Separation of **9a** and **10a** was readily accomplished by column chromatography. The bromo lactone obtained as a mixture of the two diastereomers (**9aA** and **9aB**) (vide infra) showed mp 140 °C (decomp) and $[\alpha]_D^{20}$ −110° (chloroform). The formation ratio of **9aA** to **9aB** was estimated to be more than 97.5:2.5 based on the optical purity of (***R***)-**3** derived from this sample. Recrystallization of the mixture of **9aA** and **9aB** from a mixture of dichloromethane and ether gave the predominantly formed bromo lactone **9aA** in a pure form, mp 140—140.5 °C and $[\alpha]_D^{20}$ −114° (chloroform). The structures of **9aA** and **9aB** could be assigned as (2S,11S)- and (2R,11R)-configurations, by assuming that the bromolactonization and epoxide formation (vide infra)

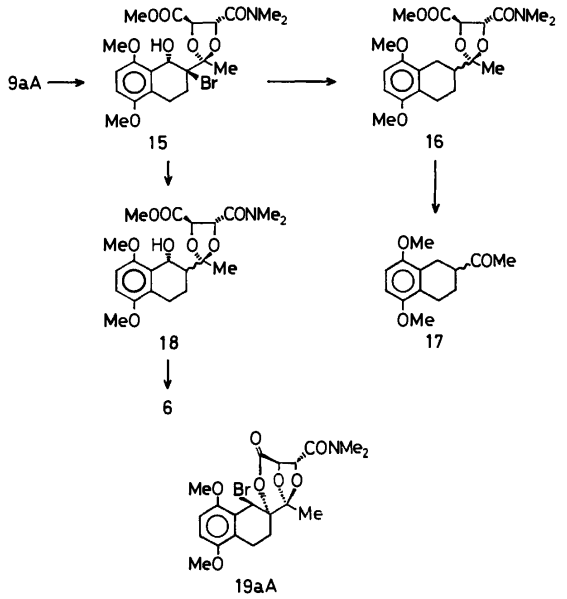

Chart 2.

proceed in a trans fashion and an S_N2 manner, respectively. The bromohydrin (**10a**) isolated as a caramel, also consisted of the two diastereomers (**10aA** and **10aB**). The formation ratio could be similarly estimated to be 85.5:14.5 by converting this mixture to (***R***)-**3**. By assuming that the epoxide formation proceeds in an S_N2 manner, **10aA** and **10aB** were anticipated to belong (1S,2S)- and (1R,2R)-configurations, respectively.

In order to establish rigorously the seven-membered bromo lactone structure of **9a**, some chemical transformations were next examined using predominantly formed **9aA**. As shown in Chart 2, **9aA** was treated with methanol in the presence of triethylamine to give the methyl ester (**15**) as a colorless caramel, $[\alpha]_D^{20}$ +35.8° (chloroform), in a quantitative yield. The C_{11}-proton of **9aA**, which appeared as a doublet at δ 5.87, moved to δ 5.47 in the NMR spectrum of **15**. This spectral feature may strongly support the seven-membered structure of **9aA**. Catalytic reduction of **15** over palladium on carbon under a hydrogen atmosphere produced the acetal (**16**) as a diastereomeric mixture. Without separation of the two diastereomers, hydrolysis of **16** with concd hydrochloric acid gave 2-acetyl-5,8-dimethoxy-1,2,3,4-tetrahydro-naphthalene (**17**)[34] in 94% overall yield from **15**. On the other hand, debromination of **15** with tributyltin hydride followed by acidic removal of the chiral acetal group regenerated **6** with concomitant dehydration of the primarily formed β-hydroxy ketone. Since these chemical transformations should afford (***R***)-**3** if **9aA** has the six-membered bromo lactone structure (**19aA**), the successful preparation of **17** and **6** clearly discloses the seven-membered bromo lactone structure of **9aA**. The similarity of the NMR spectrum of the mixture of **10aA** and **10aB** to that of **15** unambiguously supports the bromohydrin structure of **10a**.

The bromo lactone **9aA** was elaborated to (***R***)-**3** by the following three successive operations. As shown in Chart 1, treatment of **9aA** with anhyd potassium carbonate in methanol gave an 80% yield of the epoxide (**11a**). Catalytic hydrogenation of **11a** over palladium on carbon quantitatively produced the alcohol (**12a**), which on acidic hydrolysis yields (***R***)-**3**, mp 127.5—129 °C and $[\alpha]_D^{20}$ −48.4° (chloroform), 100% ee,[35] in 89% yield. Recrystallization of this sample from ether gave analytically pure (***R***)-**3**, mp 129.5—130.5 °C, $[\alpha]_D^{20}$ −48.7° (chloroform). On the other hand, when the mixture of **9aA** and **9aB** directly obtained from the bromolactonization, was successively treated in methanol under the conditions for epoxide formation, catalytic hydrogenation, and acidic hydrolysis without isolation of the intermediates **11a** and **12a** (one pot reaction), (***R***)-**3**, mp 129.5—130.5 °C and $[\alpha]_D^{20}$ −49.0° (chloroform), >95% ee,[35] could be obtained in 75% overall yield. The same successive treatments of the mixture of **10aA** and **10aB** as described (for above mixture of **9aA** and **9aB**), gave (***R***)-**3**, mp 111—126.5 °C and $[\alpha]_D^{20}$ −32.4° (chloroform), 71% ee,[35] in 38% overall yield by way of the epoxide **13a** and the alcohol **14a**. Based on these results, the formation ratio of **9aA** to **9aB** and that of **10aA** to **10aB** could be firmly established as described above.

Taking into account the chemical yields and formation ratios, separation of **9a** and **10a** seems to be unneccessary for a large scale preparation of (***R***)-**3**. Namely, it is desirable to immediately subject the crude reaction products of the bromolactonization reaction to the three sequential operations in a single flask to yield highly optically active (***R***)-**3**.

In place of **5a**, (*R,R*)-*N,N*:*N'*,*N'*-bis(tetramethylene)tartaramide (**5b**) was similarly usable as a chiral source of the asymmetric synthesis. The enone **6** was converted to **8b** in 85% overall yield by the similar manner to that described for **8a**. The bromolactonization of **8b** under the same conditions as described for **8a** gave **9b** and **10b** in 78 and 8% yields, respectively. The bromo lactone produced as a mixture of **9bA** and **9bB** showed mp 150.5 °C (decomp) and $[\alpha]_D^{20}$ −114° (chloroform). The mixture of the bromohydrins **10bA** and **10bB** was obtained as a caramel. The formation ratio of **9bA** and **9bB** could be estimated as more than 97.5:2.5 by the optical purity of (***R***)-**3** derived from this mixture. However, since the mixture of **10bA** and **10bB** was not subjected to further chemical elaborations, their formation ratio could not be determined. Recrystallization of the mixture of **9bA** and **9bB** readily gave the major bromo lactone **9bA** in a pure state, mp 149.5—150.5 °C (decomp) and $[\alpha]_D^{20}$ −116° (chloroform). Similarly to the case for **9a**, three successive treatments of the mixture **9bA** and **9bB** afforded (***R***)-**3**, mp 129.5—130 °C and $[\alpha]_D^{20}$ −47.6° (chloroform), >95% ee,[35] in 81% overall yield.

The highly diastereoselective bromolactonization may be explained in terms of the kinetically controlled mechanism. As shown in Chart 3, the two diastereomeric bromonium ions (**20A** and **20B**) are anticipated as intermediates for the formation of the

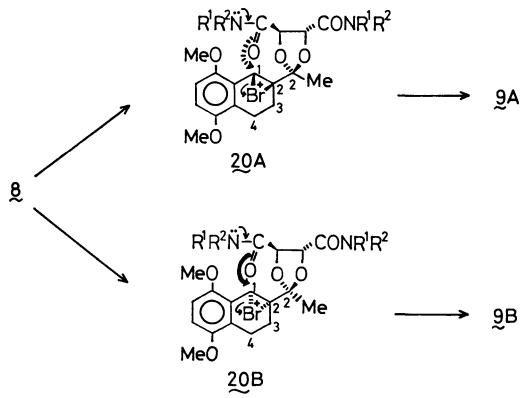

Chart 3.

major and the minor bromo lactones (**9A** and **9B**). Examinations using molecular models disclose that the bond angle between the C_2—C_3 bond and the C_2-CH_3 bond is clearly smaller in **20A** than in **20B**. That is, the C_2-methyl group should be involved in the plane of the 3,4-dihydronaphthalene ring in the conformer of **8** leading to **20A**. On the other hand, the conformer of **8** giving rise to **20B** should have the C_2-methyl group below the plane of the 3,4-dihydronaphthalene ring. Accordingly, less steric interaction between the incoming bromonium ion (Br^+) and the C_2-methyl group may be expected for **20A**, resulting in the formation of **9A** as a kinetically more favored product.

The formation of **10** may be reasonably explained by assuming that the intermediate bromonium ions **20A** and **20B** are opened by the intermolecular nucleophilic attack of water instead of the intramolecular oxygen atom of the amide group. Similar steric interaction between the bromonium ion (Br^+) and the C_2-methyl group may well account for the observed preferential production of **10A** being derived to (***R***)-**3**.

As mentioned above, the highly efficient asymmetric synthesis of (***R***)-**3** was explored by featuring the bromolactonization as a key diastereoselective reaction. While partial racemization is accompanied, Friedel-Crafts reaction of (***R***)-**3** with phthalic anhydride in the presence of aluminium chloride can give rise to the optically active tetracyclic α-hydroxy ketone ((***R***)-**4d**),[9,14] the advanced key intermediate of **2c,d**. Aiming to overcome the inefficient partial racemization and to explore practicality and generality of the developed synthetic scheme, application of the asymmetric synthesis to the preparation of (***R***)-**4d,h** was attemped. This is the subject of the next section.

Asymmetric Synthesis of Optically Active (*R*)-2-Acetyl-2,5,12-trihydroxy- and (*R*)-2-Acetyl-2,5-dihydroxy-1,2,3,4-tetrahydro-6,11-naphthacenedione ((*R*)-7-Deoxy- and (*R*)-7,11-Dideoxy-4-demethoxydaunomycinone) ((*R*)-4d,h). In the field of the asymmetric synthesis of optically active anthracyclinones,[8-13] no general methods which are applicable to both the bicyclic AB and the tetracyclic ABCD ring systems have been explored. Accordingly, application of the developed asymmetric synthesis of (***R***)-**3** to optically active (*R*)-2-acetyl-2,5,12-trihydroxy-1,2,3,4-tetrahydro-6,11-naphthacenedione ((*R*)-7-deoxy-4-demethoxydaunomycinone) ((***R***)-**4d**) was first attempted. Since the methods for stereoselectively introducing the $C_{7\alpha}$-hydroxyl group into (***R***)-**4d** and for converting the C_{14}-position into a hydroxymethyl group have been explored,[15] the ready access to (***R***)-**4d** holds a pivotal position in the synthesis of optically active **2c,d**.

The starting tetracyclic enone (**21i**) required for the asymmetric synthesis of (***R***)-**4d** could be readily produced from ***dl*-4d**.[14,23] Namely, dehydration of ***dl*-4d** with trifluoroacetic anhydride and collidine[36] gave 2-acetyl-5,12-dihydroxy-3,4-dihydro-6,11-naphthacenedione(77%), which on methylation with dimethyl sulfate under phase-transfer conditions afforded **21i** in 82% yield.[37] The dehydrated product of ***dl*-4d** can be also synthesized according to the reported method.[18]

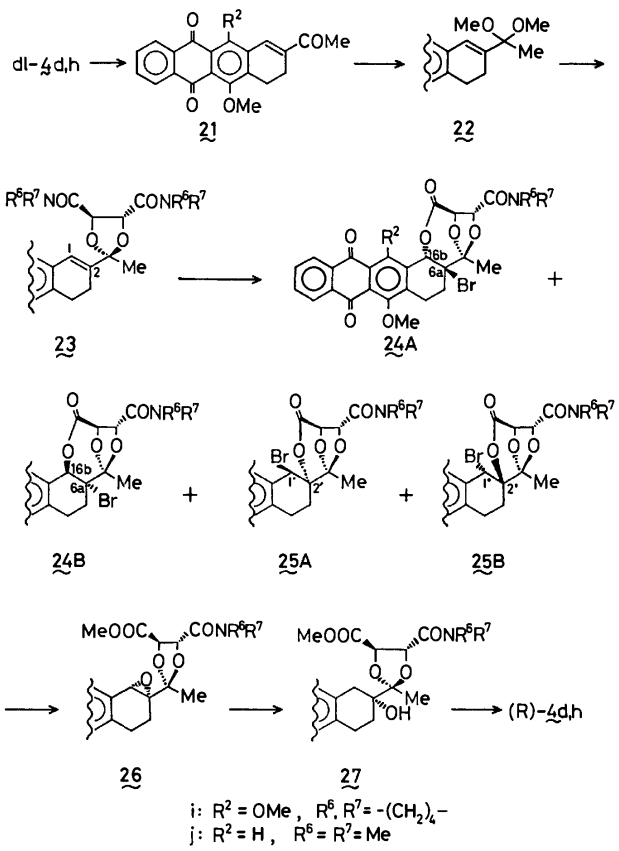

Chart 4.

Acetalization of **21i** with trimethoxymethane followed by transacetalization of the crude dimethyl acetal (**22i**) with **5b** gave the optically active acetal (**23i**) in 89% overall yield. Treatment of **23i** under the same bromolactonization conditions as that employed for **8** produced a mixture of the bromo lactones (**24i** and **25i**) in 78% combined yield. Recrystallization of the mixture with a mixture of chloroform and ether gave the predominantly formed diastereomer of the seven-membered bromo lactone (**24iA**) as a yellow powder, mp 217—219 °C and $[\alpha]_D^{20}$ −263° (chloroform). The minor six-membered bromo lactone (**25iA**) could be also isolated in a pure state as an unstable yellow solid by concentration of the mother liquor of recrystallization in vacuo followed by column chromatography. Structures of **24iA** and **25iA** were tentatively assigned based on their spectral data and successful preparation of highly optically active (***R***)-**4d** from this bromo lactone mixture (vide infra). The NMR spectrum of the bromo lactone mixture (**24i** and **25i**) clearly disclosed that no detectable amounts of the undesired bromo lactones **24iB** and **25iB** were involved in the bromo lactone mixture **24i** and **25i** (<5%). The

formation ratio of **24iA** to **25iA** could be roughly estimated as 6:1 by integral intensity of the C_{16b} and $C_{1'}$-methine signals observed in the NMR spectrum: **24iA**, δ 6.04 (J=2.0 Hz); **25iA**, δ 5.60 (J=2.1 Hz).

Being different from the case for **8**, no bromohydrins corresponding to **10** could not be detected in the crude reaction products. This may be explained by stability of the cationic species at the benzylic position (the C_1-position), which transiently develops during the bromolactonization reaction. The cationic species at the C_1-position produced from **8** can be effectively stabilized by the two methoxyl groups present in the adjacent aromatic ring. Accordingly, the mixture of **9** and **10** can be produced by the intra- and intermolecular nucleophilic attacks at the C_1-position, respectively, in the bromolactonization of **8**. On the other hand, the generation of the cationic species at the benzylic C_1-position should be less favored for **23i** than for **8** by the presence of two carbonyl groups at the $C_{6,11}$-positions. Therefore, the six-membered bromo lactone **25i** resulting from the intramolecular nucleophilic attack at the C_2-tertiary carbon atom, could be obtained in addition to the common seven-membered bromo lactone **24i**. The bromohydrins similar to **10**, which could be produced by the intermolecular trap of the cationic species at the benzylic C_1-position with water, was not detected in the bromolactonization of **23i**.

Smilarly to the preparation of (***R***)-**3** from **9a**, direct treatment of the mixture of **24i** and **25i** with anhyd potassium carbonate in methanol yields the epoxide **25i**, which without isolation was hydrogenated over palladium on carbon to give the alcohol **27i**. Removal of the chiral acetal group with concd hydrochloric acid in ethanol followed by demethylation of the phenolic dimethyl ethers with aluminum chloride in benzene, produced (***R***)-**4d**, mp 215—218.5 °C and $[\alpha]_D^{20}$ −90.4° (chloroform), 94% ee,[35] in 68% overall yield. Recrystallization of this sample readily gave optically pure (***R***)-**4d**, mp 219—220.5 °C and $[\alpha]_D^{20}$ −90.9° (chloroform), $[\alpha]_D^{20}$ −20.0° (chloroform-methanol 1:1).

The same reaction scheme was further applied to the asymmetric synthesis of (*R*)-2-acetyl-2,5-dihydroxy-1,2,3,4-tetrahydro-6,11-naphthacenedione ((*R*)-7,11-dideoxy-4-demethoxydaunomycinone) ((***R***)-**4h**). While 11-deoxy-4-demethoxyanthracyclinones (**1g,h**) have been reported to show notable anticancer activity,[6] no methods have been developed for preparing optically active (***R***)-**4h** which is usable as a versatile synthetic intermediate of their aglycones (**2g,h**).

The substrate **21j** was prepared from ***dl*-4h** synthesized according to the reported method.[38] Sequential methylation of the ***dl*-4h** with dimethyl sulfate in the presence of anhyd potassium carbonate and dehydration of the formed methyl ether ***dl*-4j** with thionyl chloride in pyridine gave **21j**.[39] The yields of the two steps were 87 and 50%, respectively. The enone **21j** was treated by the similar manner to that described for **21i** except for the use of **5a** in place of **5b**, giving **23j** in 77% overall yield. Subjection of **23j** to the bromolactonization conditions gave rise to a mixture of the bromo lactones **24j** and **25j** in 85% combined yield. The predominantly formed diastereomer of the seven-membered bromo lactone **24jA** could be separated in a pure form by recrystallization from a mixture of chloroform and ether, mp 238—239.5 °C and $[\alpha]_D^{20}$ −103° (chloroform). The structures of **24j** and **25j** were assigned by comparing their spectral data with those of **24i** and **25i**, respectively, and by the successful conversion to highly optically acitive (***R***)-**4h** (vide infra). The formation ratio of **24j** to **25j** was similarly estimated as 6:1 based on the NMR spectrum. The undesired bromo lactones **24jB** and **25jB** being diastereomeric to **24jA** and **25jA**, were not detected by means of the NMR of the crude reaction products (<5%).

The same successive treatments of the bromolactone mixture mainly consisting of **24jA** and **25jA**, as those described for the 11-hydroxy series produced (***R***)-**4h**, mp 202.5—204.5 °C and $[\alpha]_D^{20}$ −32.7° (chloroform), >99% ee,[35] by way of **26j** and **27j** in 49% overall yield.

The bromolactonization reactions of **23i,j**, which preferentially produce **24A** and **25A**, can be best explained by the mechanism similar to that proposed for the asymmetric synthesis of (***R***)-**3**.

Following various notable merits are recognizable for the explored asymmetric synthesis: 1) the reaction substrates **6** and **21** are readily available, 2) inexpensive **5**, readily available from natural (*R,R*)-(+)-tartaric acid by way of its diester, can be used as a chiral source, 3) conversion of **6** and **21** to the corresponding optically active α-hydroxy ketones ((***R***)-**3** and (***R***)-**4d,h**) can be accomplished using readily available cheap reagents in one-pot reaction and in good overall yields, 4) (***R***)-**3** and (***R***)-**4d,h** whose optically purity is equal to or more than 95% ee can be regularly produced, 5) all reactions can be performed above 0 °C and strictly anhydrous conditions are not required. Due to these reasons, the asymmetric synthesis developed herein is anticipated to be one of the most practical and general synthetic methods of various structural types of optically active anthracyclinones.

Experimental

General. All melting points were determined with a Yamato MP-21 melting point apparatus and were uncorrected. IR spectral measurements were carried out with a JASCO A-202 diffraction grating infrared spectrometer. NMR spectra were recorded with a Varian EM-390 spectrometer (90 MHz), a Hitachi R-90H spectrometer (90 MHz), and a Bruker AM-400 spectrometer (400 MHz). All signals were expressed as ppm downfield from TMS

used as an internal standard (δ value). Mass spectra were taken with a Hitachi RMU-6MG mass spectrometer. Measurements of optical rotations were performed with a Horiba SEPA-200 automatic digital polarimeter. Wakogel C-200 was used as an adsorbent for column chromatography. All reactions were carried out using anhydrous solvents. Especially, tetrahydrofuran and ether freshly distilled from sodium benzophenone ketyl, and dichloromethane, acetone, pyridine, and *N,N*-dimethylformamide freshly distilled from calcium hydride were used. Following abbreviations are used for solvents and reagents; acetone (Me_2CO), α,α'-azobis(isobutyronitrile) (AIBN), benzene (C_6H_6), *N*-bromoacetamide (NBA), *dl*-10-camphorsulfonic acid (CSA), chloroform ($CHCl_3$), dichloromethane (CH_2Cl_2), *N,N*-dimethylformamide (DMF), dimethyl sulfate (Me_2SO_4), ethanol (EtOH), ether (Et_2O), ethyl acetate (EtOAc), hexane (C_6H_{14}), methanol (MeOH), pyridine (C_5H_5N), tetrahydrofuran (THF), triethylamine (Et_3N), trimethoxymethane ($CH(OMe)_3$).

2-Acetyl-5,8-dimethoxy-3,4-dihydronaphthalene (6). a) Preparation from 5,8-Dimethoxy-2-tetralone: Similarly to the reported methods,[9] successive addition of ethynylmagnesium bromide to 5,8-dimethoxy-2-tetralone[27] and Rupe rearrangement of formed *dl*-2-ethynyl-5,8-dimethoxy-1,2,3,4-tetrahydro-2-naphthol gave **6** after purification on column chromatography (CH_2Cl_2 then CH_2Cl_2–Et_2O 9:1). NMR spectrum of this sample were identical with that previous reported.[9]

b) Preparation from 4a,5,8,8a-Tetrahydro-1,4-naphthoquinone: According to the reported method,[28] potassium hydroxide (35 g, 0.62 mol) and acetic anhydride (70 mL, 0.74 mol) were successively added to an acetone solution (300 mL) of crude unstable 4a,5,8,8a-tetrahydro-1,4-naphthoquinone[29] (30 g, 0.18 mol) cooled in an ice bath. The mixture was stirred in an ice bath for 3 h, then at room temperature for 1.5 h. After filtration, the filtrate was concentrated in vacuo to give a residue, which was purified by column chromatography (C_6H_6–EtOAc 10:1) to afford 1,4-diacetoxy-5,8-dihydronaphthalene as a solid. Recrystallization from MeOH gave a pure sample as colorless crystals (20.9 g, 46%), mp 131.5—133.5 °C. IR (KBr) 2900, 1760, 1475, 1370, 1235, 1220, 1195, 1185, 1040, 895, 680, 615, 600 cm^{-1}. ^1H NMR ($CDCl_3$) δ=2.29 (6H, s, $CH_3CO\times2$), 3.19 (4H, br s, C_5–H_2 and C_8–H_2), 5.83 (2H, m, C_6–H and C_7–H), 6.92 (2H, s, aromatic protons). Found: C, 67.91; H, 5.67%. Calcd for $C_{14}H_{14}O_4$: C, 68.28; H, 5.73%.

A mixture of 1,4-diacetoxy-5,8-dihydronaphthalene (20.9 g, 85 mmol) and pentacarbonyliron(0) (0.5 mL, 3.8 mmol, 0.04 equiv) was heated in a sealed tube at 135—140 °C for 6.75 h. After further amount of pentacarbonyliron(0) (1.0 mL, 7.6 mmol, total 1.5 mL, 11.4 mmol, 0.13 equiv) was added, the heating in a sealed tube was continued at the same temperature for 12 h. After cooling, the mixture was directly subjected to column chromatography (CH_2Cl_2 then EtOAc) to give 1,4-diacetoxy-5,6-dihydronaphthalene as a pale yellow solid (16.5 g, 79%). Recrystallization from MeOH gave a pure sample as colorless crystals, mp 140—141 °C (lit.,[28] mp 137—138 °C).

Sequential Friedel-Crafts acetylation of 1,4-diacetoxy-5,6-dihydronaphthalene (13.9 g, 56 mmol), hydrolysis of formed 2-acetyl-5,8-diacetoxy-3,4-dihydronaphthalene, and in situ methylation according to the same method as that reported[28] gave **6** (7.6 g, 58%) after purification by column chromatography (C_6H_6–EtOAc 10:1). Recrystallization from Et_2O afforded a pure sample as pale brown crystals, mp 106—106.5 °C (lit.,[9] mp 106—107 °C). NMR spectrum of this sample was identical with that of the authentic sample obtained in a).

c) Preparation from 15: A mixture of **15** (49.1 mg, 0.10 mmol), tributyltin hydride (123 mg, 0.42 mmol), and AIBN (0.2 mg, 0.001 mmol) in C_6H_6 (1.5 mL) was stirred at 65 °C for 3 h under an argon atmosphere. After further amount of AIBN (0.2 mg, 0.001 mmol) was added, the stirring was continued for 3 h. The mixture was concentrated in vacuo, and the residue was purified by column chromatography (C_6H_6–Et_2O then EtOAc) to give **18** as a caramel (23.8 mg, 57%). IR (KBr) 3525, 1755, 1660, 1490, 1260, 1095 cm^{-1}. ^1H NMR ($CDCl_3$) δ=1.57 (3H, s, C_2–CH_3), 1.7—3.2 (6H, m, C_2–H, C_3–H_2, C_4–H_2, and OH), 3.00, 3.14 (6H, two s, $N(CH_3)_2$), 3.78, 3.83 (9H, three s, $OCH_3\times3$, integration ratio of the two signals was 2:1), 4.84 (1H, d, J=6.6 Hz, C_4–H), 5.37 (1H, d, J=6.6 Hz, C_5–H), 5.0—5.5 (1H, m, C_1–H), 6.69 (2H, s, aromatic protons). The NMR spectrum clearly shows that this sample solely consists of the (2R)- or (2S)-isomer and not of a mixture of these two isomers. MS *m/z*: 424, 423 (M^+), 216.

A mixture of **18** (23.8 mg, 0.056 mmol) and concd HCl (0.5 mL) in EtOH (2.0 mL) was heated at reflux for 2 h. After cooling, the whole was diluted with EtOAc (50 mL), and the organic mixture was washed successively with H_2O and satd NaCl. After drying over anhyd $MgSO_4$, filtration and concentration in vacuo followed by separation on column chromatography (C_6H_6–EtOAc 10:1), gave **6** as colorless crystals (9.3 mg, 71%), mp 103.5—105 °C. IR and NMR spectra of this sample were identical with those of the authentic sample obtained in a).

(*R,R*)-(+)-*N,N*:*N′,N′*-Tetramethyltartaramide (5a). This was prepared from commercially available (*R,R*)-(+)-diethyl tartrate according to the reported method.[30] A sample recrystallized from a mixture of CH_2Cl_2 and Et_2O showed mp 184.5—188.5 °C and $[\alpha]_D^{20}$ +44.3° (*c* 1.06, EtOH) (lit,[30] mp 189—190 °C and $[\alpha]_D^{20}$ +43° (*c* 3.0, EtOH)).

(*R,R*)-(+)-*N,N*:*N′,N′*-(+)-Bistetramethylenetartaramide (5b). A mixture of commercially available (*R,R*)-(+)-diethyl tartrate (10.0 g, 49 mmol) and pyrrolidine (10.0 g, 0.14 mol) was stirred at room temperature for 18 h. After concentration in vacuo, the residue was purified by filtration through a short column (EtOAc then EtOAc–MeOH 9:1), to give **5b** as a pale yellow solid (11.6 g, 93%). Recrystallization of this solid from CH_2Cl_2–Et_2O gave an analytical sample of **5b** as colorless crystals, mp 132.5—135 °C and $[\alpha]_D^{20}$ +34.2° (*c* 1.02, EtOH). IR (KBr) 3450, 3400, 1645, 1630, 1460, 1385, 1110, 1090 cm^{-1}. ^1H NMR ($CDCl_3$) δ=1.6—2.2 (8H, m, $NCH_2C\underline{H}_2C\underline{H}_2CH_2N\times2$), 3.3—3.8 (8H, m, $NC\underline{H}_2CH_2CH_2C\underline{H}_2N\times2$), 4.20 (2H, d, J=7 Hz, $OH\times2$), 4.50 (2H, d, J=7 Hz, $C\underline{H}OH\times2$). Found: C, 56.00; H, 7.88; N, 10.85%. Cacld for $C_{12}H_{20}N_2O_4$: C, 56.24; H, 7.87; N, 10.93%.

(−)-5,8-Dimethoxy-2-[(4*R*,5*R*)-2-methyl-4,5-bis(dimethylcarbamoyl)-1,3-dioxolan-2-yl]-3,4-dihydronaphthalene (8a). A mixture of **6** (698 mg, 3.0 mol), CSA (15.9 mg, 0.07 mmol), and $CH(OMe)_3$ (1.0 mL, 9.1 mmol) in MeOH (15 mL) was stirred at 0 °C for 12 h, then poured onto satd $NaHCO_3$ (40 mL) cooled in an ice bath. The aqueous

mixture was extracted with EtOAc. The combined organic extracts were washed successively with H_2O and satd NaCl, then dried over anhyd $MgSO_4$. Filtration and concentration in vacuo gave crude **7** as an oil, which was immediately subjected to the next transacetalization.

The diamide **5a** (1.23 g, 6.0 mmol) dissolved in C_6H_6 (25 mL) was added to crude **7** prepared above, and the mixture was heated at reflux for 1.25 h using a Dean-Stark apparatus packed with molecular sieves 3A to remove a small amount of H_2O. After cooling, CSA (20 mg, 0.09 mmol) was added to the reaction mixture, the reflux was further continued for 1.25 h. The whole mixture was poured onto satd $NaHCO_3$ (50 mL) after being cooled, and was extracted with EtOAc. The combined extracts were washed successively with satd $NaHCO_3$, H_2O, and satd NaCl, then dried over anhyd $MgSO_4$. Filtration and concentration in vacuo followed by purification on column chromatography (EtOAc then EtOAc-MeOH 19:1) gave pure **8a** as a colorless caramel (1.16 g, 92%), $[\alpha]_D^{20}$ −4.0° (*c* 0.99, $CHCl_3$). IR (KBr) 1650, 1490, 1260, 1105, 1045, 870, 800, 720, 675 cm^{-1}. ^1H NMR ($CDCl_3$) δ=1.60 (3H, s, CH_3), 2.1—2.4 (2H, m, C_3-H_2), 2.6—3.0 (2H, m, C_4-H_2), 2.90, 2.97, 3.20, 3.24 (12H, four s, NCH_3×4), 3.77 (6H, two s, OCH_3×2), 5.19, 5.30 (2H, two d, *J*= each 6.6 Hz, C<u>H</u>CON×2), 6.59, 6.69 (2H, two d, *J*= each 9.3 Hz, aromatic protons), 6.90 (1H, m, C_1-H). MS *m/z*: 419, 418 (M^+), 187, 116, 72. Found: C, 62.40; H, 7.22; N, 6.52%. Calcd for $C_{22}H_{30}N_2O_6 \cdot 0.25H_2O$: C, 62.47; H, 7.27; N, 6.62%.

(−)-5,8-Dimethoxy-2-[(4*R*,5*R*)-2-methyl-4,5-bis(1-pyrrolidinylcarbonyl)-1,3-dioxolan-2-yl]-3,4-dihydronaphthalene (8b). The diamide **5b** (1.15 g, 4.5 mmol) in C_6H_6 (30 mL) was added to crude **7** similarly prepared from **6** (518 mg, 2.2 mmol), and the resulting benzene solution was heated at reflux for 1.25 h using a Dean-Stark apparatus packed with molecular sieves 3A to remove a small amount of H_2O. After cooling, CSA (17 mg, 0.07 mmol) was added to the reaction mixture, and the reflux was further continued for 2 h. After being cooled, the reaction mixture was worked up in the same manner as that described for the preparation of **8a**, giving **8b** as a colorless solid (892 mg, 85%) after purification on column chromatography (EtOAc then EtOAc-MeOH 19:1). Recrystallizatoion from EtOAc-Et_2O-C_6H_{14} gave an analytical sample of **8b** as colorless crystals, mp 163.5—164.5 °C and $[\alpha]_D^{20}$ −21.1° (*c* 1.03, $CHCl_3$). IR (KBr) 1665, 1635, 1490, 1440, 1260. 1105, 1045, 800, 705 cm^{-1}. ^1H NMR ($CDCl_3$) δ=1.61 (3H, s, CH_3), 1.7—2.1 (8H, m, $NCH_2C\underline{H}_2$-$C\underline{H}_2CH_2N$×2), 2.1—2.4 (2H, m, C_3-H_2), 2.6—2.9 (2H, m, C_4-H_2), 3.3—4.0 (8H, m, $NC\underline{H}_2CH_2CH_2C\underline{H}_2N$×2), 3.76 (6H, two s, OCH_3×2), 5.04, 5.17 (2H, two d, *J*= each 6.9 Hz, C<u>H</u>CON×2), 6.59, 6.70 (2H, two d, *J*= each 9.0 Hz, aromatic protons), 6.92 (1H, m, C_1-H). MS *m/z*: 470 (M^+). Found: C, 66.22; H, 7.46; N, 5.88%. Calcd for $C_{26}H_{34}O_6N_2$: C, 66.36; H, 7.28; N, 5.95%.

(1*R*,2*S*,11*S*,14*R*,15*R*)-(−)-2-Bromo-15-dimethylcarbamoyl-6,9-dimethoxy-1-methyl-12,16,17-trioxatetracyclo[12.2.1.0^{2,11}.0^{5,10}]-heptadeca-5,7,9-trien-13-one (9aA), (1*S*,2*S*)-2-Bromo-5,8-dimethoxy-2-[(4*R*,5*R*)-2-methyl-4,5-bis(dimethylcarbamoyl)-1,3-dioxolan-2-yl]-1,2,3,4-tetrahydro-1-naphthol (10aA), and Their (2*R*,11*R*)- and (1*R*,2*R*)-Isomers (9aB and 10aB). Bromolactonization of 8a: *N*-Bromoacetamide (718 mg, 5.2 mmol) was added to a solution of **8a** (724 mg, 1.7 mmol) in a mixture of DMF-H_2O (100:1) (15 mL), and the mixture was stirred at 0 °C for 15.5 h. After further amount of NBA (239 mg, 1.7 mmol, total 6.9 mmol, 4.0 equiv) was added, the stirring was continued at the same temperature for 6 h. The reaction mixture was diluted with 10% $Na_2S_2O_3$ (30 mL), and extracted with EtOAc (×3) and CH_2Cl_2 (×2). The organic extracts were combined, washed successively with 10% $Na_2S_2O_3$, H_2O, and satd NaCl, then dried over anhyd $MgSO_4$. Filtration and concentration in vacuo gave a residue (876 mg), a part of which (799 mg) was separated by column chromatography (EtOAc) to give a mixture of **9aA** and **9aB** as a colorless solid (615 mg, 83%), mp 140 °C (decomp) and $[\alpha]_D^{20}$ −110° (*c* 1.02, $CHCl_3$), and a mixture of **10aA** and **10aB** as a colorless caramel (55.8 mg, 7%). IR and NMR spectra of the mixture of **9aA** and **9aB** were identical with those of pure **9aA** (vide infra). Recrystallization of the mixture of **9aA** and **9aB** from CH_2Cl_2-Et_2O gave pure **9aA** as colorless crystals, mp 140—140.5 °C and $[\alpha]_D^{20}$ −114° (*c* 1.00. $CHCl_3$). IR (KBr) 1750, 1645, 1495, 1265, 1240, 1220, 1100, 1090, 1080, 960, 800, 650 cm^{-1}. ^1H NMR ($CDCl_3$) δ=1.95 (3H, s, C_1-CH_3), 2.0—3.3 (4H, m, C_3-H_2 and C_4-H_2), 3.00, 3.17 (6H, two s, NCH_3×2), 3.78, 3.81 (6H, two s, OCH_3×2), 5.23, 5.38 (2H, two d, *J*= each 2.0 Hz, C_{14}-H and C_{15}-H), 5.87 (1H, d, *J*=1.9 Hz, C_{11}-H), 6.70, 6.80 (2H, two d, *J*= each 9.6 Hz, aromatic protons). MS *m/z*: 473, 471, 470, 469 (M^+), 467. Found: C, 51.01; H, 5.10; N, 2.94; Br, 17.05%. Calcd for $C_{20}H_{24}NO_7Br$: C, 51.08; H, 5.14; N, 2.98; Br, 16.99%. The mixture of **10aA** and **10aB** exhibited the following spectra. IR (KBr): 3450, 1650, 1490, 1260, 1100, 1050 cm^{-1}. ^1H NMR ($CDCl_3$) δ=1.87 (3H, s, C_2-CH_3), 2.1—3.3 (5H, m, C_3-H_2, C_4-H_2, and OH), 3.00, 3.02, 3.18, 3.26 (12H, four s, NCH_3×4), 3.80, 3.86 (6H, two s, OCH_3×2), 5.16, 5.24 (1H, two d, *J*=7.2 Hz and 6.6 Hz, C_4-H or C_5-H), 5.52, 5.67 (1H, two d, *J*=7.2 and 6.6 Hz, C_5-H or 4_4-H), 5.53 (1H, br s, C_1-H), 6.76 (2H, s, aromatic protons). The integration ratio of the two doublets at 5.16 and 5.24 ppm, or at 5.52 and 5.67 ppm was found to be 5.4:1. This value appeared to be consistent with the formation ratio of **10aA** to **10aB** determined by the optical purity of (***R***)-**3** derived from this sample (vide infra). MS *m/z*: 516, 514 (M^+), 496, 418, 229, 189, 187. The formation ratio of **9aA** to **9aB** and that of **10aA** to **10aB** could be determined as more than 97.5:2.5 and 85.5:14.5, respectively, based on the optical purity of (***R***)-**3** derived from these samples (vide infra).

(1*R*,2*S*,11*S*,14*R*,15*R*)-(−)-2-Bromo-15-(1-pyrrolidinylcarbonyl)-6,9-dimethoxy-1-methyl-12,16,17-trioxatetracyclo[12.2.1.0^{2,11}.0^{5,10}]-heptadeca-5,7,9-trien-13-one (9bA), (1*S*,2*S*)-2-Bromo-5,8-dimethoxy-2-[(4*R*,5*R*)-2-methyl-4,5-bis(1-pyrrolidinylcarbonyl)-1,3-dioxolan-2-yl]-1,2,3,4-tetrahydro-1-naphthol (10bA), and Their (2*R*,11*R*)- and (1*R*,2*R*)-Isomers (9bB and 10bB). Bromolactonization of 8b: *N*-Bromoacetamide (372 mg, 2.7 mmol, 3.0 equiv) was added to a solution of **8b** (419 mg, 0.89 mmol) in a mixture of DMF-H_2O (100:1) (7.5 mL) cooled at 0 °C, and the mixture was stirred at the same temperature for 18 h. After 10% $Na_2S_2O_3$ (20 mL) was added, the mixture was worked up in the same manner as that for the bromolactonization of **8a**, giving a mixture of **9bA** and **9bB** as colorless crystals (347 mg, 78%), mp 150.5 °C (decomp) and $[\alpha]_D^{20}$ −114° (*c* 1.04, $CHCl_3$), and a mixture of **10bA** and **10bB** as a caramel (41.3 mg, 8%), after separation by column chromatography (EtOAc then EtOAc-MeOH 95:5). IR and NMR spectra of the mixture of **9bA** and **9bB** were identical with those of pure **9bA** (vide infra). Recrystallization of the

mixture of **9bA** and **9bB** from EtOAc–Et_2O gave pure **9bA** as colorless crystals, mp 149.5—150.5 °C (decomp) and $[\alpha]_D^{20}$ −116° (*c* 1.04, $CHCl_3$). IR (KBr) 1750, 1650, 1495, 1450, 1265, 1225, 1105, 1095, 965, 955 cm^{-1}. ^1H NMR ($CDCl_3$) δ=2.00 (3H, s, C_1-CH_3), 1.7—2.1 (4H, m, $NCH_2C\underline{H}_2C\underline{H}_2CH_2N$), 2.1—3.1 (4H, m, C_3-H_2 and C_4-H_2), 3.4—3.8 (4H, m, $NC\underline{H}_2CH_2CH_2C\underline{H}_2N$), 3.80, 3.83 (6H, two s, OCH_3×2), 5.10, 5.29 (2H, two d, *J*= each 2.0 Hz, C_{14}-H and C_{15}-H), 5.88 (1H, d, *J*=1.7 Hz, C_{11}-H), 6.74, 6.77 (2H, two d, *J*= each 8.7 Hz, aromatic protons). Found: C, 53.30; H, 5.21; N, 2.74; Br, 16.18%. Calcd for $C_{22}H_{26}O_7NBr$: C, 53.24; H, 5.28; N, 2.82; Br, 16.10%. The mixture of **10bA** and **10bB** showed the following spectra. IR (KBr): 3450, 1645, 1490, 1450, 1260, 1100 cm^{-1}. ^1H NMR ($CDCl_3$) δ=1.83 (3H, s, C_2-CH_3), 1.5—2.2 (8H, m, $NCH_2C\underline{H}_2C\underline{H}_2CH_2N$×2), 2.2—3.1 (5H, C_3-H_2, C_4-H_2, and OH), 3.2—4.0 (8H, m, $NC\underline{H}_2CH_2CH_2C\underline{H}_2N$×2), 3.77, 3.82 (6H, two s, OCH_3×2), 4.96, 5.34 (2H, two d, *J*= each 7.1 Hz, C_4-H and C_5-H), 5.51 (1H, br s, C_1-H), 6.69 (2H, s, aromatic protons). MS *m/z*: 551, 550, 549, 548. The formation ratio of **9bA** to **9bB** could be determined as more than 97.5:2.5 based on the optical rotation of (***R***)-**3** derived from the mixture of **9bA** and **9bB**. However, the formation ratio of **10bA** to **10bB** could not be determined since the mixture of **10bA** and **10bB** was not derived to optically active **3**.

(1*S*,2*S*)-(+)-2-bromo-5,8-dimethoxy-2-[(2*R*,4*R*,5*R*)-4-methoxycarbonyl-2-methyl-5-dimethylcarbamoyl-1,3-dioxolan-2-yl]-1,2,3,4-tetrahydro-1-naphthol (15). A mixture of **9aA** (98.0 mg, 0.21 mmol) and Et_3N (0.05 mL, 0.68 mmol) in MeOH (2.0 mL) was stirred at 0 °C for 0.25 h under an argon atmosphere. Concentration of the mixture in vacuo followed by purification on column chromatography (EtOAc), gave pure **15** as a colorless caramel (106 mg, 100%), $[\alpha]_D^{20}$ +35.8° (*c* 1.02, $CHCl_3$). IR (KBr) 3500, 1745, 1655, 1490, 1260, 1100 cm^{-1}. ^1H NMR ($CDCl_3$) δ=1.83 (3H, s, C_2-CH_3), 2.1—3.1 (4H, m, C_3-H_2 and C_4-H_2), 3.01, 3.15 (6H, two s, $N(CH_3)_2$), 3.21 (1H, d, *J*=3.6 Hz, OH), 3.79, 3.81, 3.83 (9H, three, s, OCH_3×3), 4.97, 5.39 (2H, two d, *J*= each 7.3 Hz, C_4-H and C_5-H), 5.47 (1H, d, *J*=3.6 Hz, C_1-H), 6.72 (2H, s, aromatic protons). The doublet at δ 3.21 disappeared on treatment with D_2O. Irradiation of the doublets at δ 3.21 and 4.97 changed the doublets at δ 5.47 and 5.39 into singlets, respectively. Accordingly, the doublet at δ 5.47 was rigorously assigned to the C_1-proton. MS *m/z*: 504, 503, 502, 501 (M^+), 270, 268. Found: C, 50.05; H, 5.62; N, 2.70; Br, 15.61%. Calcd for $C_{21}H_{28}NO_8Br$: C, 50.21; H, 5.62; N, 2.79; Br, 15.91%.

2-Acetyl-5,8-dimethoxy-1,2,3,4-tetrahydronaphthalene (17). A mixture of **15** (49.3 mg, 0.098 mmol) and 5% Pd/C (20 mg) in MeOH (20 mL) was stirred under a hydrogen atmosphere at room temperature for 16.5 h. After further amount of 5% Pd/C (20 mg) was added, the mixture was stirred under the same conditions for 48 h. Insoluble materials were removed by filtration and washed with EtOAc. The combined filtrate and washings were concentrated in vacuo. The residue was purified by column chromatography (C_6H_6–EtOAc 4:1) to give **16** as a colorless oil. IR (neat) 1760, 1740, 1660, 1485, 1255, 1100, 755 cm^{-1}. ^1H NMR ($CDCl_3$) δ=1.44 (3H, s, C_2-CH_3), 1.8—3.2 (7H, C_1-H_2, C_2-H, C_3-H_2, and C_4-H_2), 3.00, 3.14 (6H, two s, $N(CH_3)_2$), 3.77 (9H, three s, OCH_3×3), 4.79, 4.83 (1H, two d, *J*= each 6.6 and 6.2 Hz, integration ratio ca. 2:1, C_4-H), 5.33, 5.34 (1H, two d, *J*= each 6.2 and 6.6 Hz, integration ratio ca. 1:2, C_5-H), 6.60 (2H, s, aromatic protons). Based on the NMR spectrum, this sample was found to consist of the two isomers concerning the C_2-position in a ratio of ca. 2:1. MS *m/z*: 409, 408, 407 (M^+). The total amount of **16** was immediately subjected to the next hydrolysis. Concd hydrochloric acid (0.25 mL) was added to a solution of **16** in EtOH (1.0 mL), and the mixture was heated at reflux for 1 h. After dilution with EtOAc, the organic solution was washed successively with H_2O and satd NaCl. After drying over anhyd $MgSO_4$, filtration and concentration in vacuo followed by separation on column chromatography (C_6H_6–EtOAc 30:1), gave **17** as colorless crystals (21.6 mg, 94% overall yield from **15**), mp 79—83.5 °C (lit,[34] mp 81—82 °C for ***dl*-17**) and $[\alpha]_D^{20}$ +5.0° (*c* 0.12, $CHCl_3$).[40] IR and NMR spectra of this sample were identical with those reported for ***dl*-17**).[34]

(1*S*,2*S*)-(−)-1,2-Epoxy-5,8-dimethoxy-2-[(2*R*,4*R*,5*R*)-4-methoxycarbonyl-2-methyl-5-dimethylcarbamoyl-1,3-dioxolan-2-yl]-1,2,3,4-tetrahydronaphthalene (11a). Anhyd potassium carbonate (16 mg, 0.12 mmol) was added to a suspension of **9aA** (50.6 mg, 0.11 mmol) in MeOH (1.5 mL) under an argon atmosphere, and the mixture was stirred in an ice bath for 0.5 h, then at room temperature for 4 h.[41] After cooling in an ice bath, H_2O (10 mL) was added to the mixture, and the aqueous mixture was extracted with EtOAc. The combined extracts were washed successively with H_2O and satd NaCl, then dried over anhyd $MgSO_4$. Filtration and concentration in vacuo followed by purification on column chromatography (EtOAc), gave **11a** as a colorless caramel (36.2 mg, 80%), $[\alpha]_D^{20}$ −132° (*c* 1.02, $CHCl_3$). IR (KBr) 1760, 1735, 1660, 1495, 1260, 1095, 875, 715 cm^{-1}. ^1H NMR ($CDCl_3$) δ=1.57 (3H, s, C_2-CH_3), 1.6—3.3 (4H, m, C_3-H_2 and C_4-H_2), 3.00, 3.20 (6H, two s, $N(CH_3)_2$), 3.75, 3.77, 3.79 (9H, three s, OCH_3×3), 4.41 (1H, s, C_1-H), 5.21 (2H, s, C_4-H and C_5-H), 6.70 (2H, m, aromatic protons). MS *m/z*: 422, 421 (M^+), 217, 216. Found: C, 59.62; H, 6.45; N, 3.28%. Calcd for $C_{21}H_{27}NO_8$: C, 59.85; H, 6.46; N, 3.32%.

(2*R*)-(−)-5,8-Dimethoxy-2-[(2*R*,4*R*,5*R*)-4-methoxycarbonyl-2-methyl-5-dimethylcarbamoyl-1,3-dioxolan-2-yl]-1,2,3,4-tetrahydro-2-naphthol (12a). A mixture of **11a** (129 mg, 0.31 mmol) and 5% Pd/C (33 mg) in THF (5.0 mL) was stirred at room temperature for 21.5 h under a hydrogen atmosphere. The mixture was filtered through a pad of Celite and the Celite layer was washed with CH_2Cl_2. The combined filtrates were concentrated in vacuo. The residue was purified by column chromatography (EtOAc) to give **12a** as a colorless caramel (129 mg, 99%) $[\alpha]_D^{20}$ −58.1° (*c* 1.01, $CHCl_3$). IR (KBr) 3500, 1745, 1660, 1655, 1485, 1260, 1100 cm^{-1}. ^1H NMR ($CDCl_3$) δ=1.46 (3H, s, C_2-CH_3), 1.5—2.2 (2H, m, C_3-H_2), 2.4—3.2 (5H, m, C_1-H_2, C_4-H_2, and OH), 2.99, 3.14 (6H, two s, $N(CH_3)_2$), 3.73, 3.77 (9H, three s, OCH_3×3), 5.00, 5.35 (2H, two d, *J*= each 6.3 Hz, C_4-H and C_5-H), 6.59 (2H, s, aromatic protons). MS *m/z*: 423 (M^+), 217, 216, 207, 206. Found: C, 59.43; H, 6.83; N, 3.19%. Calcd for $C_{21}H_{29}NO_8$: C, 59.56; H, 6.90; N, 3.31%.

(*R*)-(−)-2-Acetyl-5,8-dimethoxy-1,2,3,4-tetrahydro-2-naphthol ((*R*)-3). a) Preparation from 12a: Concd hydrochloric acid (0.5 mL) was added to a solution of **12a** (94.5 mg, 0.22 mmol) in EtOH (2.0 mL), and the mixture was stirred under reflux for 2 h. After cooling, the mixture was diluted with H_2O (10 mL) and extracted with EtOAc. The combined organic extracts were washed successively

with H_2O and satd NaCl, then dried over anhyd $MgSO_4$. Filtration and concentration in vacuo followed by purification on column chromatography (C_6H_6-EtOAc 4:1), gave (***R***)-**3** as a colorless solid (49.7 mg, 89%), mp 127.5—129 °C and $[\alpha]_D^{20}$ −48.4° (*c* 0.977, $CHCl_3$). This sample showed identical IR and NMR spectra with those of the authentic sample.[8,9] Optical purity of this sample was determined to be 100% ee by measuring the NMR spectrum in the presence of tris[3-(heptafluoropropylhydroxymethylene)-*d*-camphorato]europium[III] (Eu(hfc)$_3$) in a similar manner to that previously reported.[9] Recrystallization of this sample from Et_2O gave pure (***R***)-**3** as colorless needles, mp 129.5—130.5 °C and $[\alpha]_D^{20}$ −48.7° (*c* 0.368, $CHCl_3$) (lit,[8] mp 128—129 °C and $[\alpha]_D^{20}$ −48.2° (*c* 0.982, $CHCl_3$); lit,[9] mp 128—128.5 °C and $[\alpha]_D^{20}$ −47.1° (*c* 1.11, $CHCl_3$); lit,[14] mp 128—128.5 °C and $[\alpha]_D^{20}$ −46.3° (*c* 0.54, $CHCl_3$).

b) Preparation from the Mixture of 9aA and 9aB: Anhyd Potassium carbonate (55 mg, 0.40 mmol) was added to a suspension of the mixture of **9aA** and **9aB** (179 mg, 0.38 mmol) in MeOH (4.0 mL), and the mixture was stirred at room temperature under an argon atmosphere for 10.5 h. After further amount of anhyd K_2CO_3 (10 mg, 0.07 mmol, total 0.47 mmol) was added, the stirring was continued for 13 h to completely produce the epoxide. 5% palladium on carbon (50 mg) was directly added to the reaction mixture, and the whole mixture was stirred at room temperature under a hydrogen atmosphere for 8.5 h to cleave the epoxide. After concd HCl (1.0 mL) was added, the mixture was heated at reflux for 2 h to effect hydrolysis of the chiral acetal. Concd hydrochloric acid (1.0 mL) was added after 2 h reaction, and the reflux was further continued for 2 h. The reaction mixture was cooled, and the insoluble materials were removed by filtration an washed with EtOAc. The combined filtrates and washings were diluted with H_2O (10 mL), and extracted with EtOAc. The organic extracts were combined, washed successively with H_2O and satd NaCl, then dried over anhyd $MgSO_4$. Filtration and concentration in vacuo followed by purification on column chromatography (C_6H_6-EtOAc 4:1), gave (***R***)-**3** as a colorless solid (71.0 mg, 75%), mp 129.5—130.5 °C and $[\alpha]_D^{20}$ −49.0° (*c* 0.988, $CHCl_3$). This sample showed the IR and NMR spectra identical with those of the authentic sample.[8,9] The optical purity of this sample was similarly calculated to be more than 95% ee by measuring the NMR spectrum in the presence of Eu(hfc)$_3$.[9] Accordingly, the formation ratio of **9aA** and **9aB** could be firmly determined as more than 97.5:2.5. Recrystallization from Et_2O gave pure (***R***)-**3** as colorless needles, mp 130—131 °C and $[\alpha]_D^{20}$ −48.6° (*c* 0.987, $CHCl_3$) (for the reported values, see a)).

c) Preparation from the Mixture of 10aA and 10aB: Treatment of the crude mixture of **10aA** and **10aB** (55.8 mg, 0.11 mmol) with anhyd K_2CO_3 (23 mg, 0.17 mmol) in MeOH (2.0 mL), followed by hydrogenation over 5% Pd/C (23 mg) in MeOH (2.0 mL) and hydrolysis with concd HCl (2.0 mL) in EtOH (2.0 mL) in a similar manner to that described for the preparation of (***R***)-**3** from a mixture of **9aA** and **9aB**, gave (***R***)-**3** as a colorless solid (10.4 mg, 38% overall yield), mp 111—126.5 °C and $[\alpha]_D^{20}$ −32.4° (*c* 1.04, $CHCl_3$) (for the reported values, see a)). This was identified by comparing its IR and NMR spectra with those of the authentic sample.[8,9] Measurement of the NMR spectrum in the presence of Eu(hfc)$_3$ clearly disclosed that the optical purity of this sample was 71% ee. Based on this value, the formation ratio of **10aA** to **10aB** could be calculated as 85.5:14.5.

d) Preparation from the Mixture of 9bA and 9bB: The same successive treatments of the mixture of **9bA** and **9bB** (201 mg, 0.40 mmol) as those described for the preparation of (***R***)-**3** from the mixture of **9aA** and **9aB** gave (***R***)-**3** as a colorless solid (82.4 mg, 81%), mp 129.5—130 ° and $[\alpha]_D^{20}$ −47.6° (*c* 1.02, $CHCl_3$) (for the reported value, see a)). IR and NMR spectra of this sample were identical with those of the authentic sample.[8,9] Measurement of the NMR spectrum in the presence of Eu(hfc)$_3$ disclosed that the optical purity of this sample and the formation ratio of **9bA** to **9bB** were more than 95% ee and 97.5:2.5, respectively.[9]

2-Acetyl-5,12-dimethoxy-3,4-dihydro-6,11-naphthacenedione (21i). a) Preparation of 2-Acetyl-5,12-dihydroxy-3,4-dihydro-6,11-naphthacenedione: Trifluoroacetic anhydride (2.0 mL, 14 mmol) was added to a mixture of ***dl*-4d**[14,23] (137 mg, 0.39 mmol) and collidine (4.0 mL) cooled in an ice bath under an argon atmosphere. After being stirred in an ice bath for 0.5 h and at room temperature for 1 h, the reaction mixture was diluted with H_2O (1.0 mL). The reaction mixture was stirred for 5 min, then poured onto ice-water (50 mL). A solid separated was collected by filtration, and washed successively with H_2O, MeOH, and Et_2O. After drying in vacuo, the crude product obtained as a red solid weighed 99.4 mg (77%), mp 225—236.5 °C. Recrystallization from $CHCl_3$-EtOH gave an analytical sample as red crystals, mp 245—246 °C (lit,[18] mp 235—237 °C). IR (KBr) 1665, 1620, 1590, 1400, 1370, 1335, 1290, 1270, 1260, 1220, 1010, 800, 770, 735 cm^{-1}. ^1H NMR ($CDCl_3$) δ=2.52 (3H, s, CH_3), 2.5—2.85 (2H, m, C_3-H_2), 2.85—3.2 (2H, m, C_4-H_2), 7.7—8.0 (2H, m, aromatic protons), 7.89 (1H, s, C_1-H), 8.3—8.5 (2H, m, aromatic protons), 13.23, 13.56 (2H, two s, phenolic OH×2). Found: C, 71.80; H, 4.33%. Calcd for $C_{20}H_{14}O_5$: C, 71.85; H, 4.22%.[37]

b) Preparation of 21i: Tetrahydrofuran (20 mL) was added to a mixture of 2-acetyl-5,12-dihydroxy-3,4-dihydro-6,11-naphthacenedione (102 mg, 0.31 mmol) and sodium hydride (50% oil dispersion) (36 mg, 0.75 mmol) cooled at −78 °C, and the mixture was degassed in vacuo. Then, the mixture was stirred at room temperature for 0.5 h and at 50 °C for 1 h under an argon atmosphere. After tetrabutylammonium bromide (242 mg, 0.75 mmol) was added, the mixture was stirred at 50 °C for 0.25 h. Dimethyl sulfate (0.25 mL, 2.6 mmol) was added to the resulting mixture, and the whole was stirred at 50 °C for 5 h. After cooling, the mixture was diluted with 1.5 M† HCl and extracted with CH_2Cl_2. The combined extracts were washed with H_2O, and dried over anhyd $MgSO_4$. Filtration and concentration in vacuo followed by purification on column chromatography (CH_2Cl_2-EtOAc 20:1), gave **21i** as a yellow solid (90.8 mg, 82%). Recrystallization from $CHCl_3$-MeOH gave an analytical sample of **21i** as yellow crystals, mp 202.5—204 °C. IR (KBr) 1670, 1325, 1275, 1255, 1035 cm^{-1}. ^1H NMR ($CDCl_3$) δ=2.53 (3H, s, CH_3), 2.4—2.7 (2H, m, C_3-H_2), 2.8—3.2 (2H, m, C_4-H_2), 3.92, 3.99 (6H, two s, OCH_3×2), 7.6—7.9 (2H, m, aromatic protons), 7.80 (1H, s, C_1-H), 8.1—8.3 (2H, m, aromatic protons). Found: C, 72.95;

† 1 M=1 mol dm^{-3}.

H, 4.96%. Calcd for $C_{22}H_{18}O_5$: C, 72.92; H, 5.01%.

2-Acetyl-5-methoxy-3,4-dihydro-6,11-naphthacenedione (21j). a) Preparation of *dl*-4j: A mixture of ***dl*-4h**[38] (506 mg, 1.5 mmol), Me_2SO_4 (596 mg, 4.7 mmol), and anhyd K_2CO_3 (624 mg, 4.5 mmol) in Me_2CO (20 mL) was heated at reflux for 8.5 h. After cooling, insoluble materials were separated and washed with CH_2Cl_2. The combined organic layer was washed with satd $NaHCO_3$ and dried over anhyd $MgSO_4$. Filtration and concentration followed by column chromatography (C_6H_6-EtOAc 4:1) gave ***dl*-4j** as a yellow solid (458 mg, 87%). An analytical sample was prepared as yellow crystals by recrystallization from $CHCl_3$-MeOH, mp 209—209.5 °C. IR (KBr) 3500, 1710, 1675, 1585, 1335 1270 cm^{-1}. ^1H NMR ($CDCl_3$) δ=1.9—2.1 (2H, m, C_3-H_2), 2.37 (3H, s, $COCH_3$), 2.7—3.5 (4H, m, C_1-H_2 and C_4-H_2), 3.77, 3.93 (6H, two s, OCH_3×2), 7.6—7.9 (2H, m, aromatic protons), 7.83 (1H, C_{12}-H), 8.1—8.4 (2H, m, aromatic protons). Found: C, 71.41; H, 5.23%. Calcd for $C_{21}H_{18}O_5 \cdot 1/6H_2O$: C, 71.38; H, 5.23%.

b) Preparation of 21j: Thionyl chloride (0.15 mL, 2.1 mmol) was added dropwise to a suspension of ***dl*-4j** (481 mg, 1.4 mmol) in C_5H_5N (10 mL) at room temperature under an argon atmosphere, and the mixture was stirred at the same temperature for 0.5 h. After being cooled in an ice bath, the mixture was diluted with H_2O (30 mL), and extracted with CH_2Cl_2. The combined extracts were washed with H_2O, dried over anhyd $MgSO_4$, then concentrated in vacuo. The residue was purified by column chromatography (CH_2Cl_2 then C_6H_6-EtOAc 10:1), giving **21j** as a yellow solid (230 mg, 50%). Recrystallization from $CHCl_3$-MeOH gave an analytical sample of **21j** as yellow crystals, mp 241.5—243 °C. IR (KBr) 1670, 1580, 1330, 1310, 1280 cm^{-1}. ^1H NMR ($CDCl_3$) δ=2.49 (3H, s, $COCH_3$), 2.3—2.8 (2H, m, C_3-H_2), 2.9—3.2 (2H, m, C_4-H_2), 3.93 (3H, s, OCH_3), 7.43 (1H, m, C_1-H), 7.6—7.9 (2H, m, aromatic protons), 8.00 (1H, s, C_{12}-H), 8.1—8.4 (2H, m, aromatic protons). Found: C, 75.43; H, 4.73%. Calcd for $C_{21}H_{16}O_4 \cdot 1/8H_2O$: C, 75.38; H, 4.89%.

(−)-5,12-Dimethoxy-2-[(4*R*,5*R*)-2-methyl-4,5-bis(1-pyrrolidinylcarbonyl)-1,3-dioxolan-2-yl]-3,4-dihydro-6,11-naphthacenedione (23i). A mixture of **21i** (254 mg, 0.70 mmol), $CH(OMe)_3$ (1.0 mL, 9.1 mmol), and CSA (21.5 mg, 0.093 mmol) in MeOH (25 ml) was stirred at room temperature for 5.5 h under an argon atmosphere. After cooling in an ice bath, the mixture was diluted with satd $NaHCO_3$ (15 mL) and extracted with CH_2Cl_2. The organic extracts were combined, washed with dil $NaHCO_3$, then dried over anhyd $MgSO_4$. Filtration and concentration in vacuo gave crude **22i** as a red solid. ^1H NMR ($CDCl_3$) δ=1.43 (3H, s, C_2-CH_3), 2.2—2.5 (2H, m, C_3-H_2), 2.8—3.1 (2H, m, C_4-H_2), 3.26 (6H, two s, $C(OCH_3)_2$), 3.90, 3.93 (6H, two s, OCH_3×2), 7.15 (1H, t, J=1.5 Hz, C_1-H), 7.6—7.8 (2H, m, aromatic protons), 8.1—8.3 (2H, m, aromatic protons). The total amount of **22i** was immediately subjected to the next transacetalization.

A mixture of crude **22i** and **5b** (358 mg, 1.4 mmol) in C_6H_6 (30 mL) was heated at reflux for 0.5 h using a Dean-Stark apparatus packed with molecular sieves 3A to removed a small amount of H_2O. After CSA (22 mg, 0.095 mmol) was added, the reflux was further continued for 1 h. After being cooled, the mixture was poured onto satd $NaHCO_3$ (50 mL) cooled in an ice bath, and extracted with CH_2Cl_2. The organic extracts were combined, washed with dil $NaHCO_3$, then dried over anhyd $MgSO_4$. Filtration and concentration in vacuo followed by purification on column chromatography (EtOAc-MeOH 19:1), gave almost pure **23i** as a yellow caramel (375 mg, 89% overall yield from **21i**). This was recrystallized from $CHCl_3$-Et_2O to give pure **23i** as a yellow powder, mp 148.5—150.5 °C and $[\alpha]_D^{20}$ −20.4° (*c* 1.02, $CHCl_3$).[42] IR (KBr) 1675, 1645, 1450, 1330, 1275, 1255, 1155, 1045, 995 cm^{-1}. ^1H NMR ($CDCl_3$) δ=1.67 (3H, s, C_2-CH_3), 1.7—2.2 (8H, m, $NCH_2CH_2CH_2CH_2N$×2), 2.2—2.5 (2H, m, C_3-H_2), 2.8—3.1 (2H, m, C_4-H_2), 3.3—4.0 (8H, m, $NCH_2CH_2CH_2CH_2N$×2), 3.89, 3.90 (6H, two s, OCH_3×2), 5.11, 5.18 (2H, two d, J= each 7.2 Hz, C_4-H and C_5-H), 7.05 (1H, m, C_1-H), 7.6—7.8 (2H, m, aromatic protons), 8.1—8.3 (2H, m, aromatic protons). Found: C, 67.75; H, 6.00; N, 4.60%. Calcd for $C_{34}H_{36}N_2O_8$: C, 67.99; H, 6.04; N, 4.66%.

(−)-5-Methoxy-2-[(4*R*,5*R*)-2-methyl-4,5-bis(dimethylcarbamoyl)-1,3-dioxolan-2-yl]-3,4-dihydro-6,11-naphthacenedione (23j). A mixture of **21j** (244 mg, 0.73 mmol), $CH(OMe)_3$ (1.0 mL, 9.1 mmol), and pyridinium *p*-toluenesulfonate (PPTS) (39 mg, 0.16 mmol) in a mixture of MeOH (5.0 mL) and CH_2Cl_2 (20 mL) was stirred at 45 °C for 17.5 h under an argon atmosphere. Similar treatments of the reaction mixture to that described for the preparation of **22i** gave crude **22j** after concentration of the combined organic extracts (256 mg, 100%). ^1H NMR ($CDCl_3$) δ=1.40 (3H, s, C_2-CH_3), 2.2—2.5 (2H, m, C_3-H_2), 2.8—3.1 (2H, m, C_4-H_2), 3.23 (6H, two s, $C(OCH_3)_2$), 3.85 (3H, s, C_5-OCH_3), 6.77 (1H, m, C_1-H), 7.5—7.8 (2H, m, aromatic protons), 7.73 (1H, s, C_{12}-H), 8.0—8.3 (2H, m, aromatic protons). This was directly used for the next transacetalization.

A mixture of crude **22j** (256 mg, 0.73 mmol) and **5a** (308 mg, 1.5 mmol) in C_6H_6 (20 mL) was heated at reflux for 0.5 h using a Dean-Stark apparatus packed with molecular sieves 3A to remove a small amount of H_2O. After PPTS (16.2 mg, 0.06 mmol) was added, the mixture was further heated at reflux for 0.5 h. Work-up of the reaction mixture in the same manner as that described for the preparation of **23i** gave as a yellow caramel (294 mg, 77%) after purification on column chromatography (Florisil, EtOAc). This was dissolved in Et_2O (10 mL), and the ethereal solution was stirred in an ice bath to afford an analytical sample of **23j** as a yellow powder, mp 132.5—135.5 °C and $[\alpha]_D^{20}$ −14.6° (*c* 1.03, $CHCl_3$). IR (KBr) 1665, 1630, 1580, 1330, 1280 cm^{-1}. ^1H NMR ($CDCl_3$) δ=1.64 (3H, s, C_2-CH_3), 2.2—2.5 (2H, m, C_3-H_2), 2.8—3.1 (2H, m, C_4-H_2), 2.97, 3.02, 3.24, 3.27 (12H, four s, $N(CH_3)_2$×2), 3.90 (3H, s, OCH_3), 5.29, 5.31 (2H, two d, J= each 7.0 Hz, C_4-H and C_5-H), 6.68 (1H, m, C_1-H), 7.6—7.9 (2H, m, aromatic protons), 7.79 (1H, s, C_{12}-H), 8.1—8.4 (2H, m, aromatic protons). Found: C, 67.24; H, 5.94; N, 5.35%. Calcd for $C_{29}H_{30}N_2O_7$: C, 67.17; H, 5.83; N, 5.40%.

(3*R*,4*R*,6*R*,6a*S*,16b*S*)-6a-Bromo-3,6-epoxy-9,16-dimethoxy-6-methyl-4-(1-pyrrolidinylcarbonyl)-3,4,6a,7,8,16b-hexahydro-2*H*,6*H*-naphthaceno[1,2-b][1,5]dioxocin-2,10,15-trione (24iA), (1*R*,1′*R*,2*S*,5*R*,6*R*)-1′-Bromo-5′,12′-dimethoxy-1-methyl-6-(1-pyrrolidinylcarbonyl)-3′,4′-dihydro-3,7,8-trioxaspiro[bicyclo-[3.2.1]octane-2,2′(1′*H*)-naphthacene]-4,6′,11′-trione (25iA), and Their (6a*R*,16b*R*)- and (1′*S*,2*R*)-Isomers (24iB and 25iB). Bromolactonization of 23i: *N*-Bromoacetamide (100 mg, 0.73 mmol) was added to a solution of **23i** (213 mg, 0.35 mmol) in a mixture of DMF-H_2O (100:1) (5.0 mL), and the mixture was stirred at room temperature for 8 h under an

argon atmosphere. After further amount of NBA (49 mg, 0.36 mmol, total 1.1 mmol, 3.0 equiv) was added, the stirring was continued for 3 h. The mixture was cooled in an ice bath, diluted with 10% $NaHSO_3$ (10 mL), and extracted with CH_2Cl_2. The organic extracts were combined, washed successively with 10% $NaHSO_3$ and H_2O, then dried over anhyd $MgSO_4$. Filtration and concentration in vacuo followed by purification on column chromatography (EtOAc), afforded a pale yellow solid which mainly consisted of **24iA** and **25iA** (174 mg, 78%). The formation ratio of **24i** to **25i** was roughly estimated as 6:1 based on the NMR spectrum showing the C_{16b} and $C_{1'}$-protons as two sets of doublets at δ 6.04 and 5.60. Recrystallization of the mixture of **24i** and **25i** from $CHCl_3$-Et_2O gave pure **24iA** as a yellow powder, mp 217—219 °C and $[\alpha]_D^{20}$ −263° (*c* 0.104, $CHCl_3$). IR (KBr) 1755, 1675, 1645, 1450, 1340, 1250, 1225, 1045, 955 cm^{-1}. ^1H NMR ($CDCl_3$) δ=1.99 (3H, s, C_6-CH_3), 1.7—2.3 (4H, m, $NCH_2C\underline{H}_2C\underline{H}_2CH_2N$), 2.3—2.9 (2H, m, C_7-H_2), 3.0—3.3 (2H, m, C_8-H_2), 3.3—3.9 (4H, m, $NC\underline{H}_2CH_2CH_2C\underline{H}_2N$), 3.96, 4.03 (6H, two s, OCH_3×2), 5.13, 5.44 (2H, two d, *J*= each 2.0 Hz, C_3-H and C_4-H), 6.04 (1H, d, *J*=2.0 Hz, C_{16b}-H), 7.6—7.9 (2H, m, aromatic protons), 8.1—8.4 (2H, m, aromatic protons). MS *m/z*: 628, 627, 626, 625 (M^+). Found: C, 56.87; H, 4.51; N, 2.14%. Calcd for $C_{30}H_{20}NO_9Br \cdot 0.5H_2O$: C, 56.70; H, 4.60; N, 2.20%.

Concentration of the mother liquor from the recrystallization in vacuo gave a solid (27 mg) in which **25iA** was enriched. This was further separated by column chromatography (C_6H_6-EtOAc 2:1) to give pure **25iA** as a pale yellow solid (7.8 mg), mp 143—184.5° (decomp) and $[\alpha]_D^{20}$ +295° (*c* 0.124, $CHCl_3$). IR (KBr) 1770, 1675, 1455, 1340, 1265, 1040 cm^{-1}. ^1H NMR ($CDCl_3$) δ=1.95—2.14 (4H, m, $NCH_2C\underline{H}_2C\underline{H}_2CH_2N$), 2.11 (3H, s, C_1-CH_3), 2.40 (1H, dddd, *J*=14.0, 7.6, 2.1, and 1.1 Hz, $C_{3'-eq}$-H), 2.60 (1H, ddd, *J*=14.0, 11.2, and 7.4 Hz, $C_{3'-ax}$-H), 3.06 (1H, ddd, *J*=18.9, 11.2, and 7.6 Hz, $C_{4'-ax}$-H), 3.34 (1H, ddd, *J*=18.9, 7.4, and 1.1 Hz, $C_{4'-eq}$-H), 3.50—3.63 (4H, m, $NC\underline{H}_2CH_2CH_2C\underline{H}_2N$), 3.94, 4.06 (6H, s, OCH_3×2), 4.81, 5.15 (2H, two s, C_5-H and C_6-H), 5.60 (1H, d, *J*=2.1 Hz, $C_{1'}$-H), 7.72—7.80 (2H, m, aromatic protons), 8.17—8.25 (2H, m, aromatic protons). MS *m/z*: 627, 625 (M^+). High resolution MS: Found: 627.0902 and 625.0881. Calcd for $C_{30}H_{28}NO_9Br$: 627.0925 and 625.0946.

Although the pale yellow solid obtained by the bromolactonization was expected to involve small amounts of **24iB** and **25iB**, these undesired isomers could not be detected by the NMR spectrum. Based on the optical purity of (***R***)-**4d** derived from the mixture of **24i** and **25i**, the total amount of **24iB** and **25iB** should be less than 5%. Since **25i** being a sort of benzyl bromide, seemed to be fairly unstable, the mixture of **24i** and **25i** was immediately subjected to the next reaction.

(3*R*,4*R*,6*R*,6a*S*,16b*S*)-6a-Bromo-3,6-epoxy-9-methoxy-6-methyl-4-(dimethylcarbamoly)-3,4,6a,7,8,16b-hexahydro-2*H*,6*H*-naphthaceno[1,2-*b*][1,5]dioxocin-2,10,15-trione (24jA), (1*R*,1′*R*,2*S*,5*R*,6*R*)-1′-Bromo-5′-methoxy-1-methyl-6-(dimethylcarbamoyl)-3′,4′-dihydro-3,7,8-trioxaspiro[bicyclo[3.2.1]-octane-2,2′(1′*H*)-naphthacene]-4,6′,11′-trione (25jA), and Their (6a*R*,16b*R*)- and (1′*S*,2*R*)-Isomers (24jB and 25jB). Bromolactonization of 23j: *N*-Bromoacetamide (205 mg, 1.5 mmol) was added to a solution of **23j** (254 mg, 0.49 mmol) in a mixture of DMF-H_2O (100:1) (7.0 mL), and the mixture was stirred at room temperature under an argon atmosphere for 7 h. After further amount of NBA (67 mg, 0.49 mmol, total 2.0 mmol, 4.0 equiv) was added, the stirring was continued for 3 h. Work-up of the reaction mixture in the same manner as that described for the bromolactonization of **23i** gave a pale yellow solid which mainly consisted of **24jA** and **25jA** (239 mg, 85%). The formation ratio of **24j** to **25j** was estimated as 6:1, based on the NMR spectrum showing the C_6 and C_1-methyl groups as two singlets at δ 1.98 and 2.05. This solid was recrystallized from $CHCl_3$-Et_2O to give **24jA** as a yellow powder, mp 238—239.5 °C (decomp) and $[\alpha]_D^{20}$ −103° (*c* 0.105, $CHCl_3$). IR (KBr) 1750, 1680, 1640, 1590, 1275, 1255, 1245, 1220 cm^{-1}. ^1H NMR ($CDCl_3$) δ=1.98 (3H, s, C_6-CH_3), 2.36 (1H, dddd, *J*=14.8, 7.5, 1.8, and 1.4 Hz, C_{7-eq}-H), 2.65 (1H, ddd, *J*=14.8, 10.6, and 6.9 Hz, C_{7-ax}-H), 3.06, 3.23 (6H, two s, $N(CH_3)_2$), 3.08 (1H, ddd, *J*=19.1, 10.6, and 7.5 Hz, C_{8-ax}-H), 3.30 (1H, ddd, *J*=19.1, 6.9, and 1.4 Hz, C_{8-eq}-H), 3.98 (3H, s, OCH_3), 5.32, 5.47 (2H, two d, *J*= each 1.9 Hz, C_3-H and C_4-H), 7.74—7.83 (2H, m, aromatic protons), 8.13 (1H, s, C_{16}-H), 8.23-8.30 (2H, m, aromatic protons). Found: C, 56.70; H, 4.29; N, 2.38; Br, 14.11%. Calcd for $C_{27}H_{24}NO_8Br$: C, 56.86; H, 4.24: N, 2.46; Br, 14.01%.

Concentration of the mother liquor from the recrystallization in vacuo gave a solid in which the amount of **25jA** was increased. The NMR spectrum of this sample showed the followed signals assignable to **25jA** in addition to those of **24j**. ^1H NMR ($CDCl_3$) δ=2.05 (3H, s, C_1-CH_3), 2.42 (1H, dddd, *J*=14.1, 7.6, and 1.9 Hz, another coupling constant could not be determined due to overlapping, $C_{3'-eq}$-H), 2.54 (1H, ddd, *J*=14.1, 11.3, and 7.0 Hz, $C_{3'-ax}$-H), 3.03, 3.20 (6H, two s, $N(CH_3)_2$), 3.98 (3H, s, OCH_3), 4.98 (1H, s, $C_{1'}$-H, C_5-H, or C_6-H), 5.28 (2H, s, two protons of $C_{1'}$-H, C_5-H, and C_6-H), 7.70—7.84 (2H, m, aromatic protons), 8.08 (1H, s, $C_{12'}$-H), 8.23—8.30 (2H, m, aromatic protons).

While the pale yellow solid obtained by the bromolactonization was anticipated to contain small amounts of **24jB** and **25jB**, these undesired isomers could not be detected by the NMR spectrum. Based on the optical purity of (***R***)-**4h** derived from this sample, the total amount of these isomers should be less than 5%. The mixture of **24j** and **25j** was immediately subjected to the next reaction.

(*R*)-(−)-2-Acetyl-2,5,12-trihydroxy-1,2,3,4-tetrahydro-6,11-naphthacenedione ((*R*)-(−)-7-deoxy-4-demethoxydaunomycinone) ((*R*)-4d). A methanolic suspension (7.5 mL) containing the mixture of **24i** and **25i** (**24i**:**25i** 6:1) (177 mg, 0.28 mmol) and anhyd K_2CO_3 (80 mg, 0.58 mmol) was stirred at room temperature under an argon stmosphere for 3.5 h to produce the epoxide. After 5% Pd/C (30 mg) was added to the resulting suspension, the mixture was stirred under a hydrogen atmosphere for 23 h to cleave the epoxide. Insoluble materials were removed by filtration, and the filtrate was concentrated in vacuo. Ethanol (2.0 mL) and concd HCl (1.0 mL) were added to the concentration residue, and the mixture was heated at reflux for 1 h to hydrolyse the chiral acetal group. After concd HCl (1.0 mL) was added, the reflux was further continued for 1 h. The mixture was cooled, diluted with H_2O (20 mL), and extracted with CH_2Cl_2. The organic extracted were combined, washed with H_2O, then dried over anhyd $MgSO_4$. Filtration and concentration in vacuo gave crude (***R***)-**4i** as a yellow solid. A benzene solution (15 mL) of crude (***R***)-**4i** and anhyd $AlCl_3$

(408 mg, 3.1 mmol) was stirred at 50 °C for 2 h under an argon atmosphere to cleave the two phenolic methyl ethers. After cooling, the mixture was diluted with satd oxalic acid solution (40 mL), and extracted with CH_2Cl_2. The organic extracts were combined, washed with H_2O, then dried over anhyd $MgSO_4$. Filtration and concentration in vacuo followed by purification on column chromatography (C_6H_6–EtOAc 10:1), gave (***R***)-**4d** as orange crystals (67.9 mg, 68% overall yield from the mixture of **24i** and **25i**), mp 215—218.5 °C and $[\alpha]_D^{20}$ −90.4° (*c* 0.104, $CHCl_3$), $[\alpha]_D^{20}$ −20.1° (*c* 0.189, $CHCl_3$–MeOH 1:1) (lit,[9] mp 218—219 °C and $[\alpha]_D^{20}$ −87.0° (*c* 0.115, $CHCl_3$); lit,[14] mp 218—219.5 °C and $[\alpha]_D^{20}$ −90.0° (*c* 0.106, $CHCl_3$); lit,[15] mp 217—219 °C and $[\alpha]_D^{20}$ −90.3° (*c* 0.106, $CHCl_3$); lit,[43] $[\alpha]_D^{20}$ −95.2° (*c* 0.13, $CHCl_3$) and $[\alpha]_D^{20}$ −20.0° (*c* 0.18, $CHCl_3$–MeOH 1:1)). IR and NMR spectra of this sample were superimposable on those of the authentic sample.[9] Methylation of this sample with Me_2SO_4 and anhyd K_2CO_3 in Me_2CO according to the reported procedure[9] reproduced (***R***)-**4i** as a yellow solid in 98% yield after purification on column chromatography (C_6H_6–EtOAc 3:1). The optical purity of (***R***)-**4i** was rigorously determined as 94% ee by measuring the NMR spectrum in the presence of Eu(hfc)$_3$ following the same manner as that reported.[9] Accordingly, the optical yield of (***R***)-**4d** produced from the mixture of **24i** and **25i** was estimated as 94% ee.

(*R*)-2-Acetyl-2,5-dihydroxy-1,2,3,4-tetrahydro-6,11-naphthacenedione ((*R*)-7,11-dideoxy-4-demethoxydaunomycinone) ((*R*)-4h). The same four successive treatments of the mixture of **24j** and **25j** (**24j**:**25j** 6:1) (188 mg, 0.33 mmol) as those described for the preparation of (***R***)-**4d** gave (***R***)-**4h** as yellow crystal (53.8 mg, 49% overall yield from the mixture of **24j** and **25j**), after purification on column chromatography (CH_2Cl_2–EtOAc 7:1), mp 202.5—204.5 °C and $[\alpha]_D^{20}$ −32.7° (*c* 0.104, $CHCl_3$), $[\alpha]_D^{20}$ +17.3° (*c* 0.104, $CHCl_3$–MeOH 1:1). A part of (***R***)-**4h** was recrystallized from C_6H_6 to give an analytical sample as yellow crystals, mp 204.5—206.5 °C and $[\alpha]_D^{20}$ −35.3° (*c* 0.102, $CHCl_3$), $[\alpha]_D^{20}$ +16.0° (*c* 0.100, $CHCl_3$–MeOH 1:1). IR (KBr) 3475, 1705, 1670, 1630, 1590, 1360, 1290 cm^{-1}. ^{1}H NMR ($CDCl_3$) δ=1.8—2.1 (2H, m, C_3-H_2), 2.37 (3H, s, $COCH_3$), 2.75, 3.30 (2H, two d, *J*= each 18.0 Hz, C_1-H_2), 2.6—3.1 (2H, m, C_4-H_2), 3.70 (1H, s, OH), 7.47 (1H, s, C_{12}-H), 7.7—7.9 (2H, m, aromatic protons), 8.1—8.4 (2H, m, aromatic protons), 12.95 (1H, s, phenolic OH). Found: C, 70.90; H, 4.74%. Calcd for $C_{20}H_{16}O_5 \cdot 1/6H_2O$: C, 70.79; H, 4.85%.

In order to determine the optical purity of (***R***)-**4h**, the sample (20.2 mg, 0.06 mmol) obtained from the column chromatography was methylated according to the same procedure as that described for (***R***)-**4i**. Purification of the crude product by column chromatography (C_6H_6–EtOAc 4:1) gave (***R***)-**4j** as a yellow solid (18.5 mg, 88%), mp 140—141 °C and $[\alpha]_D^{20}$ +64.7° (*c* 0.102, $CHCl_3$), $[\alpha]_D^{20}$ +43.0° (*c* 0.107, $CHCl_3$–MeOH 1:1). This sample showed the identical NMR spectrum with that of ***dl*-4j**. The NMR spectrum of ***dl*-4j** measured in the presence of Eu(hfc)$_3$ exhibited two sets of two singlets at δ 4.01, 4.24 and 9.18, 9.47. The former two singlets could be assigned to the acetyl group and the latter to the C_{12}-proton. Two singlets at δ 4.24 and 9.47 were only observed in the NMR spectrum of (***R***)-**4j** measured under the same conditions as that for the racemic compound. Accordingly, the optical yield of (***R***)-**4h** produced from the mixture of **24j** and **25j** was determined as more than 99% ee.

References

1) Part of this work has been the subject of two preliminary communications. a) M. Suzuki, Y. Kimura, and S. Terashima, *Chem. Lett.*, **1985**, 367; b) M. Suzuki, Y. Kimura, and S. Terashima, *Tetrahedron Lett.*, **26**, 6481 (1985).

2) F. Arcamone, *Lyoydia*, **40**, 45 (1977); F. Arcamone, "Topics in Antibiotic Chemistry," ed by P. G. Sammes, Ellis Horwood, Chichester, England (1978), Vol. 2, pp. 98—239; F. Arcamone, "Anticancer Agents Based on Natural Product Models," ed by J. M. Cassady and J. D. Douros, Academic Press, New York (1980), pp. 1—41; F. Arcamone, "Doxorubicin Anticancer Antibiotics," Academic Press, New York (1981); M. B. Naff, J. Plowman, and V. L. Narayanan, "Anthracycline Antibiotics," ed by H. S. El Khadem, Academic Press, New York (1982), pp. 1—57.

3) T. Oki, *Hakko To Kogyo*, **37**, 1187 (1979); K. Ohta and Ohkuma, *Saishin Igaku*, **36**, 1060 (1981); T. Oki and T. Takeuchi, *Yuki Gosei Kagaku Kyokai Shi*, **40**, 2 (1982).

4) F. Arcamone, G. Cassinelli, F. DiMatteo, S. Fronza, M. C. Ripamonti, G. Rivola, A. Vigevani, J. Clardy, and T. McCake, *J. Am. Chem. Soc.*, **102**, 1462 (1980).

5) a) F. Arcamone, L. Bernardi, P. Giardino, B. Patelli, A. DiMarco, A. M. Cassaza, G. Pratesi, and P. Reggiani, *Cancer Treat. Rep.*, **60**, 829 (1976); b) F. Arcamone, L. Bernardi, B. Patelli, P. Giardino, A. DiMarco, A. M. Cassaza, C. Soranzo, and G. Pratesi, *Experientia*, **34**, 1255 (1978); c) F. Arcamone, L. Bernardi, B. Patelli, and A. DiMarco, *Ger. Offen.*, 2601785 (1976); d) B. Patelli, L. Bernardi, F. Arcamone, and A. DiMarco, Japan Patent, JP-58-40557; e) F. Arcamone, L. Bernardi, P. Giardino, and A. DiMarco, *ibid.*, JP-57-36919; f) F. Arcamone, L. Bernardi, B. Patelli, and A. DiMarco, *ibid.* JP-59-231037, JP-59-231038, and JP-59-231098.

6) H. Umezawa, Y. Takeuchi, M. Kinoshita, H. Naganawa, K. Tatsuta, and T. Takeuchi, *J. Antibiot.*, **33**, 1518 (1980).

7) T. R. Kelly, *Ann. Rep. Med. Chem.*, **14**, 288 (1979); S. Terashima, *Yuki Gosei Kagaku Kyokai Shi*, **40**, 20 (1982); M. J. Broadhurst, C. H. Hassall, and G. J. Thomas, *Chem. Ind. (London)*, **1985**, 106.

8) S-s. Jew, S. Terashima, and K. Koga, *Chem. Pharm. Bull.*, **27**, 2351 (1979).

9) N. Tanno and S. Terashima, *Chem. Pharm. Bull.*, **31**, 811, 821 (1983).

10) R. A. Russell, P. S. Gee, R. W. Irvine, and R. N. Warrener, *Aust. J. Chem.*, **37**, 1709 (1984).

11) R. A. Russell, A. S. Krauss, R. W. Irvine, and R. N. Warrener, *Aust. J. Chem.*, **38**, 179 (1985).

12) R. C. Gupta, R. A. Harland, and R. J. Stoodly, *Tetrahedron*, **40**, 4657 (1984).

13) M. Sodeoka, T. Iimori, and M. Shibasaki, *Tetrahedron Lett.*, **26**, 6497 (1985).

14) K. Tamoto and S. Terashima, *Chem. Pharm. Bull.*, **32**, 4328 (1984).

15) K. Tamoto, M. Sugimori, and S. Terashima, *Tetrahedron*, **40**, 4617 (1984).

16) M. J. Broadhurst, C. H. Hassall, and G. J. Thomas, *J. Chem. Soc., Perkin Trans. 1*, **1982**, 2249.

17) D. Dominguez, R. J. Ardecky, and M. P. Cava, *J. Am. Chem. Soc.*, **105**, 1608 (1983).

18) D. Dominguez and M. P. Cava, *J. Org. Chem.*, **48**, 2820

(1983).

19) A. S. Kende, Y-g. Tsay, and J. E. Mills, Japan Patent, JP-59-10648.

20) R. B. Garland, U. S. Patent, 4496485 (1985).

21) J. S. Swenton, J. N. Freskos, G. W. Morrow, and A. D. Sercel, *Tetrahedron*, **40**, 4625 (1984).

22) A. V. R. Rao, J. S. Yadav, K. B. Reddy, and A. R. Mehendale, *Tetrahedron*, **40**, 4643 (1984).

23) Y. Kimura, M. Suzuki, T. Matsumoto, R. Abe, and S. Terashima, *Bull. Chem. Soc. Jpn.*, **59**, 415 (1986).

24) Synthesis of 11-deoxyanthracyclinones such as aklavinone and 11-deoxydaunomycinone have been accomplished using an asymmetric cross aldol reaction. See, a) J. M. McNamara and Y. Kishi, *Tetrahedron*, **40**, 4685 (1984); b) H. Sekizaki, M. Jung, J. M. McNamara, and Y. Kishi, *J. Am. Chem. Soc.*, **104**, 7372 (1982).

25) (*R*)-(+)-2-Hydroxy-5,12-dimethoxy-1,2,3,4-tetrahydro-6,11-dioxo-2-naphthacenecarboxylic acid (**i**) produced from 5,12-dimethoxy-3,4-dihydro-6,11-dioxo-2-naphthacenecarboxylic acid by the asymmetric bromolactonization, could not be derived to (***R***)-**4i** by treating with methyllithium.[8] However, we have recently explored that sequential treatments of (*R*)-2,5,12-trihydroxy-1,2,3,4-tetrahydro-6,11-dioxo-2-naphthacenecarboxylic acid (**ii**) with *N,N'*-carbonyldiimidazole, trimethylsilyl trifluoromethanesulfonate, and methylmagnesium bromide efficiently afford (***R***)-**4d**. The acid (**ii**) could be readily obtained from **i** or independently prepared from 5,12-dihydroxy-1,2,3,4-tetrahydro-2,6,11-naphthacenetrione. See ref. 23 and references cited therein.

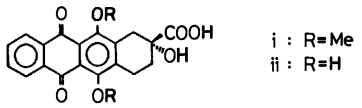

26) The C_2-symmetric nature of optically active tartaric acid derivatives has been introduced as efficient chiral templates in asymmetric synthesis. For example, P. A. Bartlett, W. S. Johnson, and J. D. Elliott, *J. Am. Chem. Soc.*, **105**, 2088 (1983), and N. Ikeda, I. Arai, and H. Yamamoto, *ibid.*, **108**, 483 (1986). Recently, **5a** has been nicely utilized as a chiral source in the asymmetric nucleophilic addition of organoaluminum reagents to chiral α,β-unsaturated acetals. See, J. Fujiwara, Y. Fukutani, M. Hasegawa, K. Maruoka, and H. Yamamoto, *J. Am. Chem. Soc.*, **106**, 5004 (1984).

27) C. A. Grob and W. Jundt, *Helv. Chim. Acta*, **35**, 2111 (1952).

28) R. A. Russell, G. J. Collin, P. S. Gee, and R. N. Warrener, *J. Chem. Soc., Chem. Commun.*, **1983**, 994.

29) a) O. Diels and K. Alder, *Ber.*, **62**, 2337 (1929); b) J. Alexander and L. A. Mitscher, *Tetrahedron Lett.*, **1978**, 3403.

30) D. Seebach, H-O. Kalinowski, W. Langer, G. Grass, and E-M. Wilkam, *Org. Synth.*, **61**, 24 (1983).

31) At the outset of this work, (2*R*,3*R*)-2,3-butanediol (**iii**), (2*S*,3*S*)-1,4-dimethoxy-2,3-butanediol (**iv**), (2*R*,3*R*)-1,4-bis(benzyloxy)-2,3-butanediol (**v**), and (2*R*,3*R*)-1,4-bis(4-chlorobenzyloxy)-2,3-butanediol (**vi**) were employed as chiral sources. When the acetals (**vii**) prepared from **6** and the chiral diols (**iii**—**vi**) were treated with *N*-bromoacetamide and barium hydroxide in a mixture of tetrahydrofuran and water, diastereomeric mixtures of the bromohydrins similar to **10** could be obtained as sole reaction products in almost quantitative yields. These bromohydrins were converted to optically active **3**, 10% ee [(***R***)-**3**, **iii** as a chiral source], 17% ee [(***S***)-**3**, **iy** as a chiral source], 19% ee [(***R***)-**3**, **v** as a chiral source], and 17% ee [(***R***)-**3**, **vi** as a chiral source], by the same sequential treatments as those emplyed for the preparation of (***R***)-**3** from the mixture of **10aA** and **10aB**. On the other hand, the diastereoselective epoxidation of **vii** with *m*-chloroperbenzoic acid, *t*-butyl hydroperoxide-oxobis(acetylacetonato)vanadium(iv), hydrogen peroxide-sodium tangstate, etc., were all found to be fruitless and simply recovered the starting material (**vii**). By accumlating these numerous unsuccessful results, the novel bromolactonization reaction reported herein was finally explored.

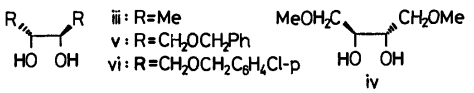

32) When (R,R)-(+)-dimethyl tartrate was used in place of **5**, the same successive acetalization and transacetalization gave the chiral acetal (**viii**) in 80% overall yield. Treatment of the bis(triethylamine) salt (**ix**) derived from **viii**, under the conditions for bromolactonization produced the bromo lactone which was presumed to mainly consist of **x**. Since **x** was found to be unstable, it was immediately derived to the bromohydrin (**xi**) in 79% yield from **viii** by methanolysis and esterification. Successive epoxide formation, catalytic hydrogenation, and acidic hydrolysis in the same manner as that described for **9** and **10**, afforded (***R***)-**3**, mp 126.5—127.5 °C and $[\alpha]_D^{20}$ −45.8° (*c* 0.94, $CHCl_3$), 96% ee,[35] in 47% overall yield from **xi** (M. Suzuki, Y. Kimura, and S. Terashima, unpublished results). This asymmetric synthesis of (***R***)-**3** is considered to be less practical than that reported herein because of the complex multi-step operations and the lower overall yield.

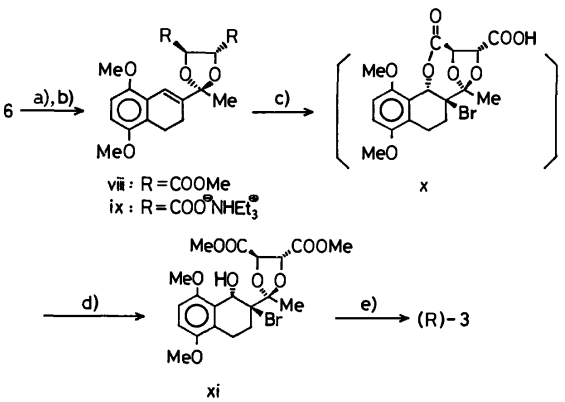

a) (i) $CH(OMe)_3$-CSA in MeOH, (ii) (+)-Dimethyl (2*R*,3*R*)-tartrate-CSA-MS3A in C_6H_6. b) Et_4N-H_2O. c) $CH_3CONHBr$(4.0 equiv) in DMF, 0 °C, 45.5 h. d) (i) Et_3N-MeOH, (ii) CH_2N_2. e) (i) K_2CO_3 in MeOH, (ii) H_2-5%Pd/C, (iii) concd HCl.

33) Presence of a small amount of water in the reaction medium was found to be necessary for effecting the successful formation of **9a** and **10a** from **8a**. Considering the fact that the bromolactonization of the bis(triethylamine) salt (**ix**) proceeds in anhyd DMF (see, Ref. 32), the role of

water is considered to promote hydrolysis of the intermediary immonium salt (**xii**) during the bromolactonization.

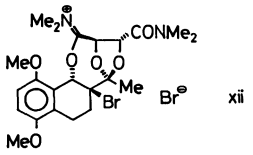

xii

34) C. M. Wong, D. Popien, R. Schwenk, and J. Teraa, *Can. J. Chem.*, **49**, 2712 (1971).

35) The optical yield of this sample was determined by measuring the NMR spectrum, directly or after converting to the methyl ether, in the presence of the chiral shift reagent. See the experimental section.

36) G. Cassinelli and F. Arcamone, *Ger. Offen*, 2757101 (1978).

37) By the same method as that described herein, 2-acetyl-5,12-dimethoxy-3,4-dihydro-6,11-naphthacenedione could be also prepared from partially optically active (*S*)-**4d** which was available in a large quantity by the optical resolution of *dl*-**4d**.[14,15]

38) A. V. R. Rao, A. R. Mehendale, and K. B. Reddy, *Tetrahedron Lett.*, **24**, 1093 (1983); N. Tanno, M. Muramatsu, H. Sato, and K. Ishizumi, Japan Patent, JP-58-198435.

39) Attempted dehydration of *dl*-**4h** with trifluoroacetic anhydride and collidine simply recovered the starting materials. The methyl ether (*dl*-**4j**) was found to be dehydrated more effectively than *dl*-**4h** under the reaction conditions.

40) Considering the ratio of the two isomers of **16**, the optical purity of this sample could be estimated as ca. 30%.

41) When **9aA** (200 mg, 0.43 mmol) was treated with sodium methylate (1.3 mmol) in MeOH for 32 h, a mixture of **11a** and its (4S)-epimer (the formation ratio 20:1) separable by column chromatography, could be obtained in 84% yield.

42) The TLC and NMR spectral analyses showed that this sample was contaminated with a small amount of the $C_{3,4}$-dehydro isomer of **23i** (M. Suzuki, Y. Kimura, and S. Terashima, unpublished results).

43) R. A. Russell, R. W. Irvine, and A. S. Krauss, *Tetrahedron Lett.*, **25**, 5817 (1984).

 © 1986 The Chemical Society of Japan Bull. Chem. Soc. Jpn., 59, 3573—3579 (1986)

Dehydrooligopeptides. VII. Convenient Synthesis of Various Dehydrodi- and tripeptide Esters by Using *N*-Carboxy α-Dehydroamino Acid Anhydride[1)]

Chung-gi SHIN,* Yasuchika YONEZAWA, and Masahiro IKEDA
Laboratory of Organic Chemistry, Faculty of Technology, Kanagawa University, Rokkakubashi, Kanagawa-ku, Yokohama 221
(Received May 22, 1986)

The one-pot syntheses of *N*-protected Δ^1- and Δ^2-dehydrodipeptide esters by the coupling of *N*-carboxy α-dehydroamino acid anhydride (ΔNCA) with several kinds of C- or N-protected L-α-amino acids are described. In addition, it was found that a similar coupling of ΔNCA with both C- and N-protected α-amino acids also took place to give Δ^2-dehydrotripeptide derivatives, involving eight kinds of important C-terminal segments of antrimycins and cirratiomycins. The configurational confirmation of the α-dehydroisoleucine residue of the antibiotics is also discussed.

Recently, much attention is being given to the synthesis of dehydrooligopeptides (DHP) from not only pharmacological interests but also regarding its usefulness for asymmetric hydrogenation. Although a number of important results and facts regarding the syntheses and properties of α-dehydroamino acid (DHA) and DHP have been reported by many workers,[2-4)] we also reported a few synthetic methods for DHA and DHP.[5,6)] In particular, the application of *N*-carboxy α-dehydroamino acid anhydride (ΔNCA; **2**), derived from benzyloxycarbonyl (Cbz)-DHA (**1**), to the synthesis of DHP has been briefly reported.[7-10)]

Most recently, some interesting peptide antibiotics, e.g., antrimycins[11-13)] (cirratiomycins)[14)] and lavendomycin,[15,16)] have been discovered and determined structurally. The two kinds of the antibiotics have dehydrohepta- and hexapeptide sequences, containing a dehydrovaline (ΔVal) or a dehydroisoleucine (ΔIle) and a 2-amino-2-butenoic acid (ΔAbu) residue, respectively.

In this paper, we wish to report fully on the synthesis of various kinds of N-protected Δ^1- and Δ^2-dehydrodi- and tripeptide esters,[17)] by a new peptide synthetic method, i.e., the ΔNCA method. Moreover, the synthesis and configuration of all the C-terminal dehydrotripeptide segments of antrimycins are also described.

Results and Discussion

Syntheses of Δ^1- and Δ^2-Dehydrodipeptides. In a preceding paper,[8b)] as is shown in Scheme 1, the synthesis of DHA (**1**) and the corresponding ΔNCA [**2**: **a**; R=R^1=H (ΔAla),[18)] **b**; R=H, R^1=CH$_3$ (ΔAbu), **c**; R=R^1=CH$_3$ (ΔVal), **d**; R=H, R^1=*i*-C$_3$H$_7$ (ΔLeu), **e**; R=H, R^1=C$_6$H$_5$ (ΔPhe)], except for the *N*-carboxy α-dehydroisoleucine anhydride (ΔIle·NCA, **2f**), was reported. Here, according to a previously reported method,[8b,19)] the condensation of 3-methyl-2-oxopentanoic acid with benzyl carbamate was also carried out to give Cbz-α-dehydroisoleucine (**1f**), which was subsequently cyclized to give **2f** in a 90% yield. While the configuration of all the compounds **2** used here except **2f** has a (Z)-geometry, in the case of ΔIle, both the DHA (**1f**) and ΔNCA (**2f**), thus obtained, were found to comprise a mixture of (E)- and (Z)-geometric isomers by ca. a 3:2 ratio. Interestingly, however, it was found that the repeated recrystallization of **2f** from cyclohexane gave only the (E)-isomer.

Generally, by a comparison with the chemical shifts of γ-methylene proton between the (E)- and (Z)-isomers of DHA, the geometry of each isomer could be readily determined. It is well-known that γ-proton of the (E)-isomer of DHA shifts in a lower magnetic field than that of the (Z)-isomer, according to the available criterion reported previously.[20-22)] In the ^{1}H NMR spectrum of **1f** and **2f**, the γ-methylene protons of ethyl groups of (E)-isomer certainly resonate at a lower magnetic field (at δ 2.42 and at δ 2.70) than that of the (Z)-isomer (at δ 2.10 and at δ 2.26): Δδ 0.32 and Δδ 0.44, respectively.

Subsequently, in order to obtain N-protected Δ^1-dehydrodipeptide esters, compounds **2** were subjected to acylation, followed by couplings with L-α-amino acid (AA) esters. After the acylation of **2** with acetyl chloride (Ac-Cl), trifluoroacetic acid anhydride [(Tfa)$_2$O], or di-*t*-butyl carbonate [(Bu^{t}OCO)$_2$O] in the presence of triethylamine or pyridine in tetrahydrofuran (THF) by the usual method, the corresponding *N*-acylated ΔNCA intermediates (**3**, **4**, and **5**), thus

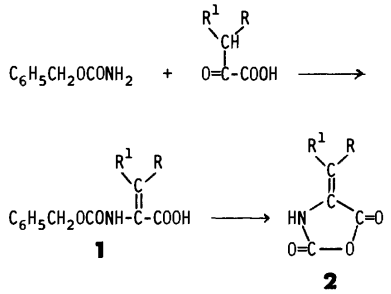

1 **2**

Scheme 1.

formed, were coupled in situ with an appropriate H-L-AA-OMe at room temperature within 1 h to give the desired acyl-Δ^1-(z, L)-dehydrodipeptide-OMe (**6**, **7**, and **8**) in good yields, respectively, as shown in Scheme 2.

On the other hand, to synthesize Δ^2-dehydrodipeptide esters, which seem to be regio-geometric isomers of **6**—**8**, the ΔNCAs (**2**) were similarly acylated with chloride of phthaloyl(Pht)-L-AA-OH and then the resulting Pht-L-AA-ΔNCA intermediates (**9**) yielded were treated in situ with water, methanol, or ethanol to give Pht-Δ^2-dehydrodipeptide-OH (**10**) and their esters (**11**; Me and Et) in ca. 75% yields, respectively. As a result, the acylation of **2** by the acid chloride method was found to be successful. In addition, it was of much interest to explore whether or not the coupling of **2** with N-protected L-AA-OH could proceed using the other peptide synthetic method.

Attempts at conventional coupling of **2** with Boc- or Cbz-L-AA-OH in the presence of dicyclohexylcarbodiimide (DCC) alone have failed. However, fortunately, it was found that a similar reaction readily took place in the presence of pyridine in addition to DCC at pH 5.5—6.0 to form Boc- and Cbz-L-AA-ΔNCA (**9**). The subsequent treatment of the intermediates (**9**) with methanol or ethanol in one-pot gave the expected Boc- and Cbz-Δ^2-(L, z)-dehydrodipeptide-OZ (**12** and **13**; Z=Me and Et) in good yields, respectively, as illustrated in Scheme 3.

The yields, physical constants, the ^{1}H NMR spectral data of all the new dehydrodipeptide derivatives

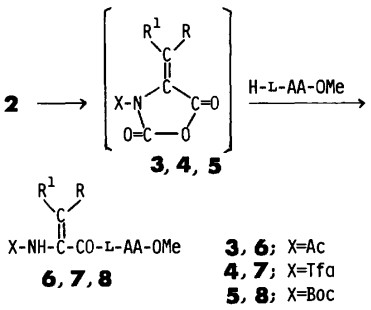

Scheme 2.

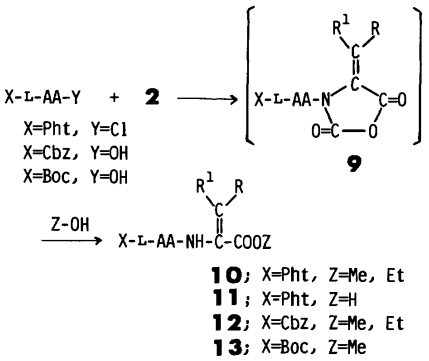

Scheme 3.

Table 1. Acyl-Δ^2-Dehydrodipeptide Methyl Esters (**6** and **7**)

Compound[a]	Yield %	Mp θ_m/°C	^{1}H NMR (δ, $CDCl_3$) R-CH= (J/Hz)	^{1}H NMR (δ, $CDCl_3$) -NHCHCO- (J/Hz)	$[\alpha]_D^{25}$ (c 1.00°, MeOH)
Ac-ΔAbu-L-Leu-OMe	72	148—150[b]	6.38 q (7.0)	4.45 dt (7.5, 6.0)	−24.3
Ac-ΔAbu-L-Tyr-OMe	79	Syrup	5.77 q (7.0)	4.45 dt (7.5, 7.0)	10.2
Ac-ΔAbu-L-Ser-OMe	65	Syrup	6.44 q (7.0)	4.56 m	7.5
Ac-ΔAbu-L-Pro-OMe	70	118—120[b]	5.50 q (7.0)	4.60 t (7.0)	−22.5
Ac-ΔAbu-L-Met-OMe	70	110—112[b]	6.44 q (7.0)	4.64 dt (7.5, 7.0)	−19.8
Ac-ΔAbu-L-Trp-OMe	65	183—185[b]	6.36 q (7.0)	4.60 m[d]	−2.4
Ac-ΔAbu-L-Glu-OMe (OEt)	75	88—90[c]	6.47 q (7.0)	6.54 dt (7.5, 6.0)	−16.5
Tfa-ΔLeu-L-Phe-OMe	89	103—104[c]	6.19 d (10.0)	4.83 dt (8.0, 5.7)	−15.6
Tfa-ΔPhe-L-Thr-OMe	65	Syrup	7.15—7.29 (+Ph)	4.43 dd (8.5, 3.0)	29.0
Tfa-ΔLeu-L-Orn-OMe (Cbz)	70	Syrup	6.21 d (10.0)	4.58 m	−7.5

a) All compounds were analyzed for C, H, and N, and the results were within ±0.3% of theoretical values. b) Colorless needles from chloroform-diisopropyl ether. c) Colorless needles from hexane. d) Measured in DMSO-d_6.

(**6—8** and **10—13**) are summarized in Tables 1—3. In the ^{1}H NMR spectra, no characteristic differences could be observed between the olefin proton signals of the two types of Δ^1- and Δ^2-dehydrodipeptide esters.

From the above results, the possibility of consecutive reactions of **2** with N-protected AA-OH and then H-AA-OZ (Z=Me and Et) instead of alcohols is expected. Furthermore, similar couplings of **2** with appropriate peptides are also anticipated.

Synthesis of Δ^2-Dehydrotripeptides. So far, it has been difficult to synthesize Δ^2-dehydrotripeptide esters, containing a DHA residue in center, by the conventional coupling of Δ^1- or Δ^2-dehydrodipeptide with

Table 2. Boc-Δ^1-Dehydrodipeptide Methyl Esters (**8**)

Compound[a]	Yield %	Mp[b] θ_m/°C	^{1}H NMR (δ, $CDCl_3$) -CH=	^{1}H NMR (δ, $CDCl_3$) -NHC$\underline{H}$CO- (J/Hz)	$[\alpha]_D^{23}$ (c 1.00°)[d]
Boc-ΔPhe-Gly-OMe	70	156—157	7.14 s	4.14 d (8.0)	—
Boc-ΔPhe-L-Leu-OMe	75	99—101	7.12 s	4.68 dt (8.0, 8.0)	−41.8
Boc-ΔPhe-L-Phe-OMe	65	127—128	7.04 s	4.90 dt (6.0, 7.0)	−3.6
Boc-ΔLeu-L-Ser-OMe	60	Syrup	6.25 d (10.0)	4.66 dt (3.5, 7.0)	−11.9
Boc-ΔnVal-L-Tyr-OMe[c]	70	Syrup	6.39 t (7.0)	4.80 dt (7.0, 8.0)	−11.7

a) All compounds were analyzed for C, H, and N, and the results were within ±0.3% of theoretical values. b) Colorless needles from chloroform-diisopropyl ether. c) nVal is normal valine residue. d) Measured in methanol.

Table 3. *N*-Blocked-Δ^2-Dehydrodipeptide Derivatives (**10, 11, 12,** and **13**)

Compound[a]	Yield %	Mp θ_m/°C	^{1}H NMR (δ, $CDCl_3$) R-CH=	^{1}H NMR (δ, $CDCl_3$) -NHC$\underline{H}$CO- (J/Hz)	$[\alpha]_D^{24}$ (c 1.00°, MeOH)
Pht-DL-Phe-ΔnVal-OH	73[b]	148—150[d]	6.76 t (7.0)	5.20 dt[h] (8.0, 5.5)	—
Pht-Gly-ΔPhe-OMe	86[b]	160—161[e]	7.46—7.26 m (+Ph)	4.43 s	—
Pht-L-Ala-ΔAbu-OEt	85[b]	133—135[d]	6.76 q (7.0)	5.06 q (7.0)	0.9
Cbz-L-Ala-ΔAbu-OMe	52[c]	137—138[f]	6.76 q (7.0)	4.43 m	−10.5 (c 0.65)
Cbz-Gly-ΔAbu-OEt	13[b] 74[c]	Syrup	7.02 q (7.0)	3.87 d (6.0)	—
Cbz-Gly-ΔPhe-OMe	82[c]	107—108[f]	7.25—7.53 m (+Ph)	3.91 d (7.0)	—
Boc-L-Ala-ΔAbu-OMe	55	116—117[g]	6.80 q (7.0)	4.40 m	−25.7
Boc-L-Val-ΔAbu-OMe	63	110—111[g]	6.82 q (7.0)	4.10 m	−25.4
Boc-L-Leu-ΔAbu-OMe	58	Syrup	6.64 q (7.0)	4.18 m	−19.2
Boc-L-Phe-ΔAbu-OMe	75	96—98[f]	6.73 q (7.0)	4.58 dt (8.0, 7.0)	−15.0
Boc-Gly-ΔAbu-OMe	51	103—104[g]	6.84 q (7.0)	3.98 d (6.0)	—
Boc-L-Leu-ΔPhe-OMe	76	91—93[g]	7.24—7.50 m (+Ph)	4.28 m	41.5
Boc-L-Phe-ΔPhe-OMe	82	116—118[g]	6.54 d (10.0)	4.54 dt (8.0, 7.0)	−15.5

a) All compounds were analyzed for C, H, and N, and the results were within ±0.3% of theoretical values. b) Yield by acid chloride method. c) Yield by DCC-pyridine method. d) Colorless needles from chloroform-hexane. e) Colorless needles from benzene. f) Colorless needles from ethyl acetate-hexane. g) Pale yellow needles from diisopropyl ether. h) Measured in DMSO-d_6.

two kinds of C- and N-protected L-α-amino acids, respectively. Accordingly, the ⊿NCA method mentioned above was expected to facilitate the coupling of **2** with the above two kinds of α-amino acids in one-pot. At first the acylation of an equimolar **2** with chloride of Pht-L-AA-OH in the presence of triethylamine in THF at 5—10 °C for 1 h was performed, followed by a treatment with H-L-AA-OMe at room temperature for 1.5 h. As a result, it is interesting to note that the above successive reactions were also completely accomplished in only one-pot to give Pht-⊿²-(L, Z, L)-dehydrotripeptide-OMe (**14**) in good yields.

Furthermore, instead of the acid chloride method, the usual DCC method was also utilized for the synthesis of ⊿²-dehydrotripeptides using **2**. A similar coupling of **2** with Boc- or Cbz-L-AA-OH in the presence of DCC and pyridine in THF or CH_2Cl_2 and then with H-L-AA-OMe gave the expected Boc- and Cbz-⊿²-(L, Z, L)-dehydrotripeptide-OMe (**15** and **16**) via Boc- and Cbz-L-AA-⊿NCA as intermediates in good yields, respectively, as illustrated in Scheme 4. On the other hand, on the contrary, after treating **2** with an amino acid ester in THF, the subsequent treatment of the resulting solution with a N-protected amino acid was found not to be effective. In addition, the simultaneous treatment of **2** with two kinds of C- and N-protected amino acids was also unsuccessful.

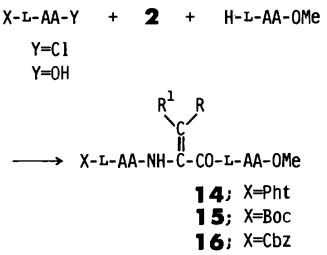

Scheme 4.

From the above versatile information, the ⊿NCA method can be firmly believed to be promising for the synthesis of antrimycins as well as the C-terminal ⊿²-dehydrotripeptide moieties. The dehydrotripeptide sequences were composed of L-AA [Ala, Abu, nVal (normal valine), and Leu], DHA (⊿Val and ⊿Ile), and Ser residues in turn, which were variously combined to afford eight kinds of antrimycins. The syntheses of all the partial skeletons have already been briefly reported.[10] However, since the yields were comparatively low, here, the procedures were modified. Consequently, similar reactions of **2c** or **2f** with the four kinds of Boc-L-AA-OH listed above for 12 h (then in situ with H-L-Ser-OMe) were carried out to give the expected Boc-⊿²-dehydrotri-

Table 4. Pht-⊿²-Dehydrotripeptide Methyl Esters (**14**)

Compound[a]	Yield %	Mp[b] θ_m/°C	^{1}H NMR (δ, $CDCl_3$) R-CH= (J/Hz)	-NHCHCO- (J/Hz)		$[\alpha]_D^{25}$ (c 1.00°)[c]
Pht-Gly-⊿Abu-L-Phe-OMe	58	175—176	6.43 q (7.0)	4.74 dt (7.5, 7.0)	4.28 s	−24.9
Pht-Gly-⊿Abu-L-Leu-OMe	76	161—162	6.59 q (7.0)	4.52 dt (7.0, 7.0)	4.44 s	−42.8
Pht-Gly-⊿Leu-L-Val-OMe	74	204—205	6.33 d (10.0)	4.44 m		−24.6
Pht-Gly-⊿Phe-L-Phe-OMe	68	175—176	6.92—7.30 m	4.64 dt (7.5, 7.0)	4.24 s	−64.6 (c 0.50)
Pht-Gly-⊿Leu-L-Phe-OMe	78	193—194	6.25 d (10.0)	4.80 dt (7.5, 7.0)	4.40 s	−20.2
Pht-L-Ala-⊿Abu-L-Phe-OMe	55	161—162	6.48 q (7.0)	4.92 q (7.0)	4.62 dt (7.0, 6.5)	12.9
Pht-L-Leu-⊿Abu-L-Phe-OMe	71	151—152	6.46 q (7.0)	5.00 dd (11.0, 5.0)	4.66 dt (7.0, 7.0)	−4.5
Pht-Gly-⊿Phe-L-Val-OMe	77	215—216	7.17 s	4.26 dd (7.5, 7.0)	4.50 s	−20.5
Pht-Gly-⊿nVal-L-Phe-OMe	72	169—171	6.36 t (7.0)	4.80 dt (7.0, 7.0)	4.42 s	−18.9
Pht-L-Leu-⊿nLeu-L-Phe-OMe	56	53—55	6.46 t (7.0)	5.02 dd (11.0, 5.0)	4.72 dt (7.5, 6.0)	−7.0
Pht-L-Phe-⊿Abu-Gly-OMe	77	100—101	6.56 q (7.0)	5.20 dd (10.5, 5.5)	3.90 d (6.0)	−113.4
Pht-L-Phe-⊿Leu-L-Ser-OMe	58	179—180	6.21 d (10.0)	5.30 dd (11.0, 5.0)	4.38 m	−59.1

a) All compounds were analyzed for C, H, and N, and the results were within ±0.3% of theoretical values. b) Colorless needles from chloroform–hexane. c) Measured in methanol.

peptide-OMe (**15**). The yields reached to ca. 65% within 1 h. As a result, in the case of **2f**, even if a pure (E)-isomer was used, it was found that geometric isomerization took place during stepwise couplings to give a 3:2 mixture of the (Z)- and (E)-isomers of **15**.

The yields, physical constants, and the ^{1}H NMR spectral data of **14—16**, involving C-terminal dehydrotripeptides of antrimycins, are summarized in Tables 4—6. From the ^{1}H NMR spectra of the (E)-isomers of **15**, the chemical shifts of CH_3 (δ 1.75s) and $CH_3C\underline{H}_2$ (δ 2.42q) in ΔIle residue and of two CH_3 (δ 1.75s and 2.05s) in ΔVal residue were found to be very similar to those (δ 1.78s, 2.46q, 1.81s, and 2.10s, respectively) of antrimycins.[13] Consequently, the naturally occurring products could be unambiguously determined to have (E)-isomeric structures.

In conclusion, it is worth noting that not only the synthesis of all the C-terminal Δ^2-dehydrotripeptides of antrimycins in one pot but also the configuration of the DHA residues could be readily confirmed.

Table 5. Boc- and Cbz-Δ^2-Dehydrotripeptide Methyl Esters (**15** and **16**)

Compound[a]	Yield %	Mp[b] θ_m/°C	^{1}H NMR (δ, $CDCl_3$) R-CH=	-NHC$\underline{H}$CO- (J/Hz)		$[\alpha]_D^{25}$ (c 1.00°, MeOH)
Cbz-Gly-ΔPhe-L-Ser-OMe	60	Syrup	7.06 s	3.84 m	4.60 m	−21.9
Boc-L-Ala-ΔAbu-L-Ser-OMe	51	Syrup	6.63 q (7.0)	4.20 dd (7.0, 7.0)	4.61 dt (8.0, 4.0)	−31.9
Boc-L-Val-ΔAbu-L-Ser-OMe	52	Syrup	6.62 q (7.0)	4.02 m	4.62 m	−22.9
Boc-L-Ala-ΔnVal-L-Ser-OMe	56	Syrup	6.57 t (7.0)	4.20 dd (7.0, 7.0)	4.60 dt (8.0, 4.0)	−34.5
Boc-Gly-ΔPhe-L-Met-OMe	74	160—162	7.12 s	3.70 d (6.0)	4.51 dt (8.0, 7.0)	−50.9
Boc-Gly-ΔPhe-L-Leu-OMe	75	188—189	7.16 s	3.70 d (5.5)	4.40 dt (8.0, 4.5)	−26.2
Boc-L-Phe-ΔAbu-L-Ala-OMe	85	190—191	6.65 q (7.5)	4.36 dq (8.0, 5.5)	4.59 m	−26.4
Boc-L-Ala-ΔLeu-L-Phe-OMe	83	121—122	6.29 d (10.0)	4.21 m	4.86 dq (7.5, 5.0)	−35.8
Boc-L-Leu-ΔLeu-L-Ala-OMe	77	126—127	6.36 d (10.0)	4.19 m	4.62 dq (7.5, 5.0)	−60.8

a) All compounds were analyzed for C, H, and N, and the results were within ±0.3% of theoretical values.
b) Colorless needles from chloroform-diisopropyl ether.

Table 6. C-Terminal Dehydrotripeptide Sequences of Antrimycins (**15**)

Compound[a]	Yield[b] %	^{1}H NMR (δ, $CDCl_3$) $CH_3C\underline{H}_2$- [J=7.5 Hz]	CH_3-	-NHC$\underline{H}$CO- (J/Hz)	
Boc-L-Ala-ΔIle-L-Ser-OMe	84	(*E*) 2.40 q (*Z*) 2.10 q	1.72 s 2.04 s	4.16 dq (7.0, 7.0)	4.60 m
Boc-L-Abu-ΔIle-L-Ser-OMe	72	(*E*) 2.44 q (*Z*) 2.08 q	1.76 s 2.04 s	4.08 m	4.68 m
Boc-L-nVal-ΔIle-L-Ser-OMe	53	(*E*) 2.40 q (*Z*) 2.08 q	1.76 s 2.04 s	4.12 m	4.64 m
Boc-L-Leu-ΔIle-L-Ser-OMe	58	(*E*) 2.42 q (*Z*) 2.08 q	1.76 s 2.04 s	4.14 m	4.60 m
Boc-L-Ala-ΔVal-L-Ser-OMe	82		(*E*) 2.04 s (*Z*) 1.72 s	4.16 dq (7.0, 7.0)	4.58 m
Boc-L-Abu-ΔVal-L-Ser-OMe	61		(*E*) 2.06 s (*Z*) 1.76 s	4.08 m	4.68 m
Boc-L-nVal-ΔVal-L-Ser-OMe	59		(*E*) 2.04 s (*Z*) 1.76 s	4.12 m	4.64 m
Boc-L-Leu-ΔVal-L-Ser-OMe	53		(*E*) 2.04 s (*Z*) 1.74 s	4.20 m	4.64 m

a) All compounds were analyzed for C, H, and N, and the results were within ±0.3% of the theoretical values.
b) Colorless needles from ethyl acetate.

Experimental

General. Melting points were determined with a Yamato (Model Mp-21) micro melting-point apparatus, and were not corrected. IR spectra were recorded with a Hitachi EPI-G2 grating spectrometer. ^{1}H NMR spectra were measured with a JEOL JMN PS-100 spectrometer in a $CDCl_3$ solution with tetramethylsilane as the internal standard. The specific rotations were measured in a 0.5-dm tube using a JASCO DIP-4 polarimeter (Japan Spectroscopic Co., Ltd.).

Cbz-Dehydroisoleusine (1f). A solution of 3-methyl-2-oxopentanoic acid (0.50 mol) and benzyl carbamate (0.55 mol) in the presence of *p*-toluenesulfonic acid (0.10 mmol) in dry benzene (800 ml) was refluxed for 6 h, removing water by means of water-separator. The reaction solution was extracted three times with a saturated $NaHCO_3$ aqueous solution; then, the combined aqueous extracts were acidified to pH 1—2 with concentrated HCl. The deposited crystals were collected and then recrystallized from benzene to give Cbz-ΔIle-OH (**1f**) as colorless needles. Yield 60% as a mixture of (E)- and (Z)-isomers by 3:2 ratio, mp 141—142 °C. IR (KBr): 3280 (NH), 1700, 1520 (NHCO) cm^{-1}. ^{1}H NMR (DMSO-d_6): δ=1.76 (s, 3H, CH_3-), 2.04 (s, 3H, CH_3-), 2.10 (q, 2H, J=7.0 Hz, $CH_3C\underline{H}_2$-), 2.42 (q, 2H, J=7.0 Hz, $CH_3C\underline{H}_2$-), 8.56 (bs, 1H, -NH-). Found: C, 68.02; H, 6.90; N, 5.61%. Calcd for $C_{14}H_{17}NO_3$: C, 67.99; H, 6.93; N, 5.66%.

***N*-Carboxy-α-dehydroisoleusine Anhydride (2f).** A solution of **1f** (20 mmol) in acetyl chloride (3 ml) and thionyl chloride (9 ml) was stirred at room temperature for 2 h. After removal of the solvent under reduced pressure, dry carbon tetrachloride (30 ml) was added to the crystalline residue and then the resulting solution was concentrated. This procedure was repeated three times. The residual crystals were recrystallized from cyclohexane to give ΔIle·NCA (**2f**) as colorless needles. Yield 90% as a mixture of (E)- and (Z)-isomers by 3:2 ratio, mp 69—101 °C. The mixture was recrystallized repeatedly to give only (E)-isomer, which melting point was 122—123 °C. IR (KBr): 3200 (NH), 1820, 1780 (-O-C=O) cm^{-1}. ^{1}H NMR (DMSO-d_6): (E)-isomer; δ=1.96 (s, 3H, CH_3-), 2.70 (q, 2H, J=7.0 Hz, $CH_3C\underline{H}_2$-). 9.44 (s, 1H, -NH-). (Z)-isomer; δ= 2.24 (s, 3H, CH_3-), 2.26 (q, 2H, J=7.0 Hz, $CH_3C\underline{H}_2$-), 9.44 (s, 1H, -NH-). Found: C, 54.21; H, 5.88; N, 9.07%. Calcd for $C_7H_9NO_3$: C, 54.19; H, 5.85; N, 9.03%.

Ac-Δ^1-Dehydrodipeptide Methyl Esters (6). To a solution of an appropriate **2** (10 mmol) in THF (5 ml) was added acetyl chloride (12 mmol). The resulting solution was approximately neutralized under cooling by adding triethylamine and then stirred at room temperature for 1 h. After concentrating the solution, the residue, thus obtained, was suspended in THF (5 ml) and then with a solution of an appropriate L-α-amino acid ester (12 mmol) in THF (5 ml). with stirring, at room temperature for 1 h. The solvent was removed and the obtained residue was dissolved in chloroform (50 ml); the resulting solution was successively washed twice with 1 M HCl (1 M=1 mol dm^{-1}) and water and then dried over anhydrous Na_2SO_4. After removing the chloroform, the residual crystals or syrup was purified by recrystallization from a mixture of chloroform–diisopropyl ether or hexane and by chromatography on a silica-gel column using a mixture of chloroform and acetone (20:1 v/v) as the eluent. See Table 1.

Tfa-Δ^1-Dehydrodipeptide Methyl Esters (7). To a solution of **2** (10 mmol) in CH_2Cl_2 (5 ml) trifluoroacetic acid anhydride (12 mmol) was added dropwise at 0 °C and the resulting prepared solution was made acidic to pH 5—6 by adding pyridine. After stirring at room temperature for 5 h, an appropriate L-α-amino acid methyl ester (11 mmol) was added to the resultant solution. After stirring continuously for 1 h, CH_2Cl_2 (50 ml) was further added to the reaction solution and then solution, thus prepared, was successively washed twice with 1 M HCl and water and then dried over anhydrous Na_2SO_4. The removal of the solvent gave a residual syrup, which was purified on a silica-gel column using a mixture of benzene and ethyl acetate (20:1 v/v) as the eluent to give **7** as a viscous syrup or as colorless needles from hexane. See Table 1.

Boc-Δ^1-Dehydrodipeptide Methyl Esters (8). To a solution of **2** (10 mmol) in THF (5 ml) was added $(Bu^tOCO)_2O$ (12 mmol) and a few drops of pyridine; the resulting solution was stirred at room temperature for 6 h. A solution of an appropriate L-α-amino acid methyl ester (11 mmol) in THF (5 ml) was added to the solution prepared above, which was then stirred continuously for 1 h. After removing the solvent, the residual syrup was dissolved in ethyl acetate (100 ml) and the resulting solution was successively washed twice with 10% citric acid, a saturated NaCl aqueous solution, and water and then dried over anhydrous $MgSO_4$. The concentration of the solution gave a viscous syrup, which was purified on a silica-gel column using a mixture of benzene and ethyl acetate (5; 1 v/v) as the eluent to give **8** as a colorless viscous syrup or as colorless needles from a mixture of chloroform and diisopropyl ether. See Table 2.

Pht-Δ^2-Dehydrodipeptides (10 and 11). To a solution of **2** (10 mmol) and chloride of phthaloyl-L-α-amino acid (11 mmol) in THF (5 ml) was added dropwise triethylamine until reaching pH 6 under cooling. After stirring at room temperature for 1 h, the resulting solution was treated with methanol or ethanol (10 ml) and then made basic to pH 8—9 by adding triethylamine. After further stirring for 1 h and then removing the solvent under reduced pressure, the residual syrup was dissolved in ethyl acetate (100 ml). The resultant solution was washed twice, successively, with 1 M HCl and water and then dried over anhydrous Na_2SO_4. The concentration of the solution gave a crude syrup which was then purified on a silica-gel column using a mixture of benzene and ethyl acetate (10:1 v/v) as the eluent to give **10** as a colorless viscous syrup or needles.

In a similar manner, a treatment of **2** with Pht-L-AA-Cl in water instead of alcohol was worked up to give **11** as colorless needles. See Table 3.

Cbz- and Boc-Δ^2-Dehydrodipeptide Esters (12 and 13). To a solution of Cbz-L-α-amino acid (11 mmol) and **2** (10 mmol) in THF (5 ml) was added DCC (11 mmol) portionwise at −10 °C. After stirring for 20 min, the resulting solution was made acidic to pH 6 by adding pyridine and then stirred at 0 °C for 1 h. After cooling to stand at room temperature, the stirring was continued for 12 h.

The prepared solution was treated with alcohol (10 ml) and then made basic to pH 9 by adding *N*-methylmorpholine and stirred continuously for 1 h. After removing the solvent under reduced pressure, the residue, thus obtained, was dissolved in ethyl acetate (50 ml) and the resultant solution was allowed to stand under cooling for 1 h. The deposited *N,N'*-dicyclohexylurea was filtered off and the filtrate was further diluted in ethyl acetate (50 ml) and then successively washed twice with 10% citric acid and water and finally dried over anhydrous Na_2SO_4. The evaporation of the solvent gave a syrup or crystalline substance, which was purified on a silica-gel column using a mixture of chloroform and acetone (20:1 v/v) as the eluent to give **12** as a colorless viscous syrup or needles.

In a similar manner, the treatment of **2** with Boc-L-α-amino acid in alcohol was worked up to give **13** as a colorless viscous syrup or needles. See Table 3.

Pht-Δ^2-Dehydrotripeptide Methyl Esters (14). To a solution of **2** (10 mmol) and Pht-L-α-AA-Cl (11 mmol) in THF (5 ml) was added dropwise triethylamine under cooling. When the pH of the solution became to 6, the resulting solution was stirred at room temperature for 1 h and was then treated with an appropriate L-α-amino acid methyl ester (11 mmol) and finally made basic to pH 8—9 by adding triethylamine. After stirring for an additional 1 h and removing the solvent, the residual crystalline substance was dissolved in ethyl acetate (100 ml). The solution, thus obtained, was successively washed twice with 1 M HCl and water and then dried over anhydrous Na_2SO_4. The evaporation of the solvent gave crude crystalline materials, which were purified on a silica-gel column using a mixture of benzene and ethyl acetate (10:1 v/v) as the eluent to give **14** as colorless needles. See Table 4.

Boc- and Cbz-Δ^2-Dehydrotripeptide Methyl Esters (15 and 16). To a solution of Boc-L-α-amino acid (11 mmol) and **2** (10 mmol) in CH_2Cl_2 (5 ml) was added portionwise DCC (11 mmol) at −10 °C. After stirring for 20 min, the resultant solution was made slightly acidic to pH 6 by adding pyridine and then stirring below 0 °C for 1 h. The prepared solution was continuously stirred at room temperature for 12 h and treated with L-α-amino acid methyl ester (11 mmol) and then made basic to pH 9 by adding *N*-methylmorpholine, with stirring for 1 h. After removing the solvent under reduced pressure, the residue, thus obtained, was dissolved in ethyl acetate (50 ml) and the solution was allowed to stand under cooling for 1 h. Deposited *N,N'*-dicyclohexylurea was filtered off and the filtrate was further diluted in ethyl acetate (50 ml) and then successively washed twice with 10% citric acid and water and finally dried over anhydrous Na_2SO_4. The concentration of the solution gave a crystalline product, which was purified on a silica-gel column using a mixture of chloroform and acetone (20:1 v/v) as the eluent to give **15** as a colorless viscous syrup or needles. See Table 5.

In a similar manner, a treatment of **2** with Cbz-Gly-OH and H-L-Ser-OMe was worked up to give **16** as a colorless syrup.

In addition, a similar treatment of **2** with Boc-L-AA-OH and H-L-Ser-OMe gave C-terminal dehydrotripeptide sequences of antrimycins (**15**). See Table 6.

References

1) Part VI. Y. Yonezawa, A. Kisuno, and C. Shin, *Bull. Chem. Soc. Jpn.*, in press.

2) Y. Shimohigashi and N. Izumiya, *Yuki Gosei Kagaku Koykai Shi*, **36**, 1023 (1978).

3) U. Schmidt, J. Häusler, E. Öhler, and H. Poisel, *Fortschr. Chem. Org. Naturst.* **37**, 300 (1979).

4) C. H. Stammer, "Chemistry and Biochemistry of Amino Acid, Peptide and Proteins," ed by B. Weinstein, Marcel Dekker Inc., N. Y. (1982), Vol. 6, 34.

5) C. Shin, *Yuki Gosei Kagaku Koykai Shi*, **37**, 830 (1979).

6) C. Shin and Y. Yonezawa, *Yuki Gosei Kagaku Koykai Shi*, **41**, 1181 (1983).

7) Y. Yonezawa, T. Yamada, and C. Shin, *Chem. Lett.*, **1982**, 1567.

8) a) C. Shin, T. Yamada, and Y. Yonezawa, *Tetrahedron Lett.*, **24**, 2175 (1983); b) C. Shin, Y. Yonezawa, and T. Yamada, *Chem. Pharm. Bull.*, **32**, 3934 (1984).

9) C. Shin and Y. Yonezawa, *Chem. Lett.*, **1985**, 519.

10) C. Shin, M. Ikeda, and Y. Yoneazawa, *Agric. Biol. Chem.*, **49**, 2243 (1985).

11) N. Shimada, K. Morimoto, H. Naganawa, T. Takita, M. Hamada, K. Maeda, T. Takeuchi, and H. Umezawa, *J. Antibiot.*, **34**, 1613 (1981).

12) K. Morimoto, N. Shimada, H. Naganawa, T. Takita, and H. Umezawa, *J. Antibiot.*, **34**, 1615 (1981).

13) K. Morimoto, N. Shimada, H. Naganawa, T. Takita, H. Umezawa, and H. Kambara, *J. Antibiot.*, **35**, 378 (1982).

14) T. Shiroza, N. Ebisawa, K. Furihata, T. Endo, H. Seto, and N. Otake, *Agric. Biol. Chem.*, **46**, 865, 1891 (1982).

15) T. Komori, M. Ezaki, E. Kino, M. Kohsaka, H. Aoki, and H. Imanaka, *J. Antibiot.*, **38**, 691 (1985).

16) I. Uchida, N. Shigematsu, M. Ezaki, and M. Hashimoto, *Chem. Pharm. Bull.*, **33**, 3053 (1985).

17) Δ^1, Δ^2, the position number of a double bond of the DHA residues from the N-terminus in sequence.

18) S. Sakakibara, *Bull. Chem. Soc. Jpn.*, **32**, 814 (1959).

19) C. Shin, Y. Yonezawa, and J. Yoshimura, *Chem. Lett.*, **1981**, 1635.

20) A. Srinivasan, K. D. Richards, and R. K. Olsen, *Tetrahderon Lett.*, **1976**, 891.

21) D. Hoppe and R. Hollemann, *Chem. Ber.*, **109**, 3062 (1976).

22) C. Shin, M. Hayakawa, T. Suzuki, A. Ohtsuka, and J. Yoshimura, *Bull. Chem. Soc. Jpn.*, **51**, 550 (1978).

 © 1986 The Chemical Society of Japan Bull. Chem. Soc. Jpn., 59, 3581—3587 (1986)

Syntheses of New Optically Active Organosilanes and Their Applications for the Optical-Purity-Determining Agents

Daiyo TERUNUMA,* Masato KATO, Masanao KAMEI, Hidekatsu UCHIDA, Satoshi UENO, and Hiroyuki NOHIRA
Department of Applied Chemistry, Faculty of Engineering, Saitama University, Urawa, Saitama 338
(Received May 23, 1986)

New optically active organosilicon compounds such as (benzylmethylphenylsilyl)acetic acid (**1**) and (ethylmethylphenylsilyl)acetic acid (**2**) were synthesized. Application of these acids as the optical purity determining agents for chiral amines and alcohols were successfully carried out. In addition, it was also revealed that optically active (benzylmethylphenylsilyl)methylamine (**3**) and [benzylmethyl(*o*-tolyl)silyl]methylamine (**4**) are able to be used as the optical purity determining agents for chiral carboxylic acids.

It is well-known that the method of optical purity determination of chiral organic compounds by using NMR spectrometer is one of the most convienient methods. A variety of agents for this purpose have been proposed.[1] One of the most useful agents is α-methoxy-α-trifluoromethylphenylacetic acid, Mosher agent.[2] These agents, however, do not always have a suitable group which shows a par of diastereomeric peaks in its ^{1}H NMR spectrum. In that case, the possibility for determining the optical purity has to depend on the structure of the chiral substrate to be estimated.

On the other hand, in the course of our studies on the syntheses of new optically active carbon-functional organosilanes, it was found that some of them were suitable for the enantiomer-ratio-determining agents.[3]

The advantages of these carbon-functional optically active organosilanes as optical-purity-determining agents over the agents which have been developed for this purpose are;

a) One of the most convienient analytical instruments, ^{1}H NMR spectrometer, can be used.

b) The Si-Me signal in the ^{1}H NMR spectra appears in the region of δ 0.1—0.4, where any other signal of ordinary organic compounds rarely appears.

c) The shape of the Si-Me signal is always observed as a sharp singlet.

d) These carbon-functional organosilicon compounds never reacemize during leading them to a pair of diastereomers.

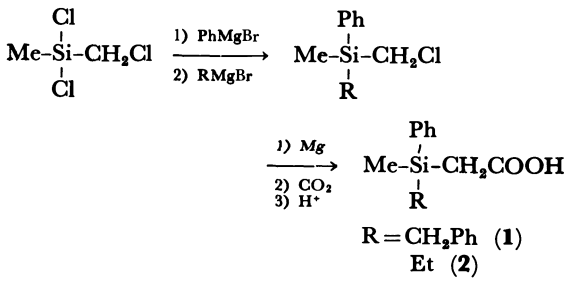

Scheme 1.

Results and Discussion

Synthesis and Resolution. Racemic silylacetic acid derivatives **1** and **2** were obtained by the three steps of Grignard reactions starting from dichloro(chloromethyl)methylsilane in a good yield (Scheme 1).

Resolution of **1** was carried out by the fractional crystallization using 1-phenylethylamine(PEA) as a resolving agent (Fig. 1). Optically pure (+)-**1** was obtained by four times recrystallization of the diastereomer salt of **1** with (+)-PEA from appropriate ratio of benzene-hexane mixed solvent. Then (−)-rich **1** salt was recovered from the filtrates, and the acid was liberated. The acid recovered was treated with (−)-PEA and the diastereomer salt was recrystallized from

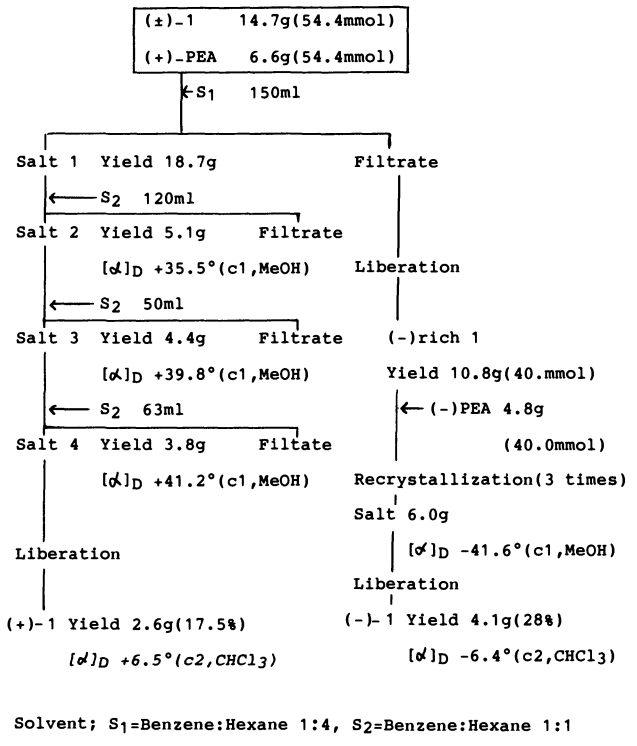

Fig. 1. Optical resolution of **1** using (+)- or (−)-PEA as a resolving agent.

the same solvent descrived above.

Optically active (+)- and (−)-**2** were obtained by using optically active PEA as a resolving agent in a similar manner to that descrived above. It is noted that optically pure **1** can be obtained rather easier than **2**.

Optically active silylmethylamine derivatives **3** and **4** were obtained by a modified method descrived in the previous paper.[4] Then these optically active amines were converted into salts with hydrochloric acid in order to make them easier to be dealt with (Scheme 2).

The physical properties of optically active **1**, **2**, **3′**, and **4′** are listed in Table 1.

Application of the Enantiomer-Ratio-Determining Agent for a Amine. Optically pure (+)-**1** was treated with (±)- and (−)-PEA in the presence of a condensation agent, 2-chloro-1-methyl-pyridinium iodide,[5] to give the corresponding diastereomeric amides (Scheme 3).

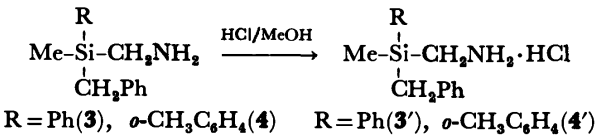

Scheme 2.

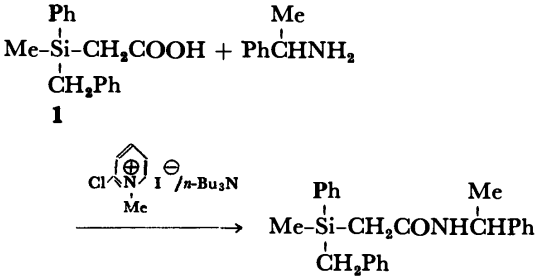

Scheme 3.

Proton NMR spectrum of the amide of (+)-**1** with racemic PEA shows two equivalent Si-Me peaks at δ 0.30 and 0.34, but that of with (−)-PEA shows only one peak at δ 0.34 (Fig. 2). These data suggest that optically active **1** is able to be used as an optical-purity-determining agent for the chiral amine. In the diastereomeric amide method, one of the most important points is that the two NMR peaks of an amide derived from racemic amine may not appear in equal intensity, mainly due to the difference in the diastereomeric selectivity of the reaction between the optically active determining agent and the chiral amine. If it happens, the NMR peaks of the diaster-

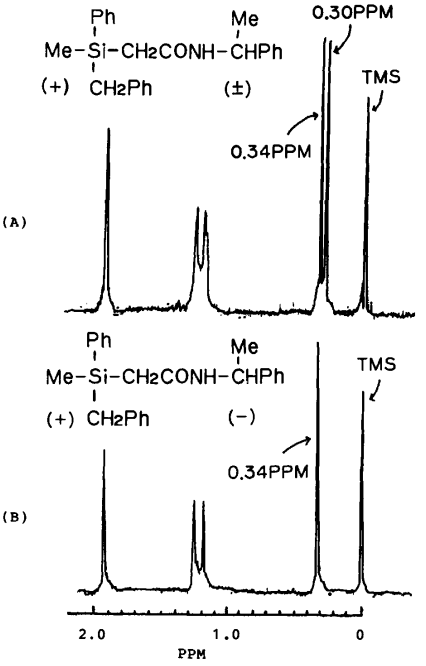

Fig. 2. ^{1}H-NMR spectra of the amides of (+)-**1** with (±)-PEA(A) and with (−)-PEA(B) measured at 90 MHz.

Table 1. The Physical Properties of Optically Active **1**, **2**, **3′**, and **4′**

Compound	Mp(Bp)(°C/Torr†)	Specific Rotation
Ph Me-Si-CH$_2$COOH (**1**) CH$_2$Ph	69—70	$[\alpha]_D$ +6.5° (*c* 2, $CHCl_3$)
Ph Me-Si-CH$_2$COOH (**2**) Et	(154—157/0.9)	$[\alpha]_D$ +7.9° (*c* 1, MeOH)
Ph Me-Si-CH$_2$NH$_2$·HCl (**3′**) CH$_2$Ph	166.5—167	$[\alpha]_D$ +45.0° (*c* 1, MeOH)
o-tolyl Me-Si-CH$_2$NH$_2$·HCl (**4′**) CH$_2$Ph	186—186.5	$[\alpha]_D$ +35.2° (*c* 1, MeOH)

†1 Torr=133.322 Pa.

eomeric amide never reflect the correct enantiomer compositions of the chiral amine. In order to check this point, appropriate grade samples of optically active PEA were prepared, and the values of optical purity measured by a Polarimeter were compared with those calculated from the NMR method (Fig. 3). These results indicate that the correlation between both methods is fairly good. Although the balance of the diastereotopic Si-Me chemical shifts($\Delta\delta$ 0.04) is rater small, it is clear that the estimation of the optical purity of the amine can be done in a significant accuracy based on the unique characters of Si-Me peak: the peak appears in a paticular region and the shape is always sharp singlet, in the NMR spectra.

Then the diastereomeric amides of (+)-**1** with a number of racemic and optically active amines were prepared, and the chemical shifts of Si-Me of the diastereomeric amides were investigated. These results are summarized in Table 2.

In a similar manner, Si-Me chemical shifts of the diastereomeric amides of (+)-**2** with a number of

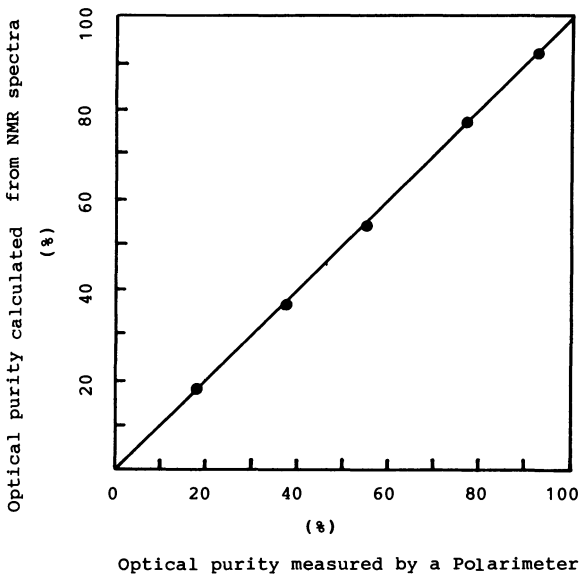

Fig. 3. Correlation of the values of optical purity measured by a polarimeter and calculated from the NMR method.

Table 2. Chemical Shifts of Si-Me of Diastereomeric Amides of (+)-**1** and (+)-**2** with Chiral Amines

Amine Structure		Chemical Shift of the Amide of (+)-**1** (PPM)			Chemical Shift of the Amide of (+)-**2** (PPM)		
$R_1R_2CHNH_2$		(+)-(+)	(+)-(−)	$\Delta\delta$[a]	(+)-(+)	(+)-(−)	$\Delta\delta$[a]
R_1	R_2						
Ph	Me	0.30	0.34	−0.04	0.39	0.33	+0.06
Me-C$_6$H$_4$-	Me	0.38	0.35	+0.03	—	—	—
MeO-C$_6$H$_4$-	Me	0.32	0.35	−0.03	—	—	—
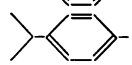	Me	0.30/0.35[b]		(0.05)	—		—
Ph	Et	0.23/0.31[b]		(0.08)	0.26/0.38[b]		(0.11)
Ph	*n*-Pr	0.26/0.33[b]		(0.09)	0.26/0.38[b]		(0.09)
Ph	*i*-Pr	0.23/0.32[b]		(0.09)	0.27/0.37[b]		(0.10)
Ph	Allyl	0.29/0.33[b]		(0.04)	0.32/0.38[b]		(0.06)
Ph	Cl-C$_6$H$_4$-CH$_2$-	0.21/0.23[b]		(0.02)	—		—
$PhCH_2$	CH_2OH	(0.28/0.32)[c]		—	—		—
Me_2CHCH_2	COOMe	(0.35/0.38)[c]		—	—		—
Me	Et	(0.36)[d]		—	—		—
$R_1R_2CHCH_2NH_2$							
R_1	R_2						
Ph	*i*-Pr	0.24	0.21	+0.03	0.24	0.27	−0.03
Me-C$_6$H$_4$-	*i*-Pr	0.25	0.21	+0.03	0.25	0.28	−0.03
MeO-C$_6$H$_4$-	*i*-Pr	0.25	0.22	+0.04	0.25	0.28	−0.03
Cl-C$_6$H$_4$-	*i*-Pr	0.25	0.22	+0.03	0.25	0.28	−0.03
Br-C$_6$H$_4$-	*i*-Pr	0.24	0.21	+0.03	0.25	0.28	−0.03
F-C$_6$H$_4$-	*i*-Pr	0.25	0.21	+0.04	0.25	0.28	−0.03
1-Np	*i*-Pr	0.11	0.14	−0.03	—	—	—

a) The balance of the chemical shifts of the diasteromeric amides of the same and the opposite sign of rotation. b) The data used only racemic amines. c) The separation of the Si-Me peaks was observed after the addition of a little amount of $Eu(fod)_3$. d) The separation of the Si-Me peaks was not observed.

chiral amines were investigated. These results are also summarized in Table 2.

As listed in Table 2, it is clear that most of the pairs of diastereomeric amides of (+)-**1** and (+)-**2** with chiral amines have different chemical shifts. These results suggest that these silylacetic acid derivatives are useful as optical-purity-determining agents for these chiral amines, except for *s*-butylamine.

If the separation of the Si-Me chemical shifts is not observed, addition of a little amount of shift agent, i. e. $Eu(fod)_3$, is often effective, although somewhat broadening of the Si-Me peak result.

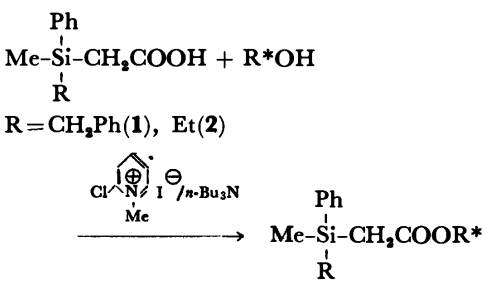

Scheme 4.

The values of the separation degree ($\Delta\delta$) were calculated from differences in the chemical shifts of the diastereomeric amides obtained from (+)-**1** and (+)-amines, and those of the amides obtained from (+)-**1** and (−)-amines. It seems that the signs of the separation degree have a definite tendency dependent on the structures of (+)-**1** or (+)-**2** and chiral amines. It is of interest to investigate the correlations between the absolute configurations of the amines and the signs of the separation degrees, although we do not have enough data yet.

The diastereomeric esters of chiral alcohols with (+)-**1** and (+)-**2** were prepared (Scheme 4).

Although the differences in the chemical shifts of the Si-Me of these esters are rather smaller than those of diasteromeric amides, determination of optical purity of these chiral alcohols seems to be possible (Table 3). Actually the optical purity of 2-(2-chlorophenyl)-3-methyl-1-butanol, a new optically active alcohol, was successfully estimated by using (+)-**1**.[6]

Another silylacetic acid derivatives as shown in

Table 3. Chemical Shifts of Si-Me of Diastereomeric Esters of (+)-**1** and (+)-**2** with Chiral Alcohols

Alcohol Structure		Chemical Shift of the Esters of (+)-**1** (PPM)			Chemical Shift of the Esters of (+)-**2** (PPM)		
R_1R_2CHOH		(+)-(+)	(+)-(−)	$\Delta\delta$[a]	(+)-(+)	(+)-(−)	$\Delta\delta$[a]
R_1	R_2						
Ph	Me	0.29/0.31[b]		(0.02)	0.32/0.35[b]		(0.03)
Ph	Et	0.26/0.29[b]		(0.03)	0.30/0.33[b]		(0.33)
Ph	*n*-Bu	0.26/0.28[b]		(0.02)	0.30/0.32[b]		(0.02)
$PhCH_2$	*n*-Bu	0.32/0.33[b]		(0.01)	—		—
o-$CH_3C_6H_4$	*n*-C_5H_{11}	0.28/0.30[b]		(0.02)	0.32/0.34[b]		(0.02)
n-C_5H_{11}	Et	(0.35)[c]		—	—		—
$R_1R_2CHCH_2OH$							
R_1	R_2						
	i-Pr	0.19	0.18	+0.01	—		—

a) The balance of the chemical shifts of the diastereomeric esters of the same and the opposite sign of rotation. b) The data used only racemic alcohol. c) The separation of the peaks was not observed.

Table 4. Chemical Shifts of Si-Me of Diastereomeric Amides of (±)-PEA with Racemic Chiral Organosilanes

R_1 Me-Si-CH_2COOH R_2		Chemical Shift of the Amide of PEA (PPM)		R_1 Me-Si-CH_2COOH R_2		Chemical Shift of the Amide of PEA (PPM)	
R_1	R_2		$\Delta\delta$[a]	R_1	R_2		$\Delta\delta$[a]
Ph	*n*-Pr	0.34/0.40	0.06	*o*-$CH_3C_6H_4$	*n*-Pr	0.39/0.45	0.06
Ph	*n*-Bu	0.34/0.41	0.07	*p*-$CH_3C_6H_4$	Et	0.32/0.37	0.05
$PhCH_2$	Et	0.03/0.05	0.02	*o*-$CH_3OC_6H_4$	Et	0.31/0.38	0.07
$PhCH_2$	*n*-Pr	0.03/0.05	0.02	*o*-$CH_3OC_6H_4$	Allyl	0.34/0.39	0.05
o-$CH_3C_6H_4$	Et	0.39/0.45	0.06	1-Naphtyl	Et	0.35/0.60	0.07

a) The balance of the chemical shifts of the diastereomeric amides.

Table 4, were synthesized. The Si-Me chemical shifts of the diastereomeric amides of these acids with racemic PEA were investigated. The chemical shifts differences of some of these amides reveal rather larger than those of **1** and **2**, but, unfortunately, we have not found out the adequate resolving agent for these acids. The investigation of optical resolution of these acids are in progress.

Application of the Enantiomer-Ratio-Determining Agent for a Carboxylic Acid. The diasteromeric amides of **3'** and **4'** with a number of chiral caboxylic acids were prepared in a similar manner to that described above (Scheme 5).

The chemical shifts of Si-Me of these diastereomeric amides were also measured (Table 5). The most of the Si-Me chemical shifts of the two pairs of diastereomeric amides were separated. It is clear that both **3** and **4** have high potentials enough to estimate the enantiomer ratio of a number of chiral carboxylic acids.

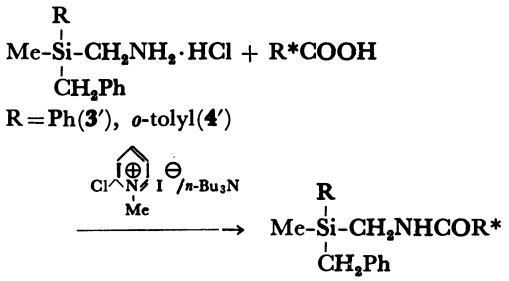

Scheme 5.

Experimental

The melting points and boiling points are uncorrected. The IR spectra were determined with JASCO IR-A 302 spectrometer. The NMR spectra were determined at 60MHz and 90MHz with a JEOL 60Si and FX90Q spectrometer, in $CDCl_3$ using TMS as an internal standard. The optical rotations were measured with a JASCO DIP-360 polarimeter. All the reactions of the Grignard reagents and the preparations of amides and esters were carried out under dry nitrogen atmosphere. All optically active amines and carboxylic acids were prepared by the procedures described in the literatures.[7]

(Benzylmethylphenylsilyl)acetic Acid (1). In a two-necked flask, equipped with a reflux condenser and an additional funnel, magnesium (3.3 g, 0.14 mol) and dry tetrahydrofuran(THF)(90 ml) were placed. A solution of (benzylmethylphenylsilyl)methyl chloride[3] (30.0 g, 0.12 mol) in THF (20 ml) was added to the solution slowly. An exothermic reaction took place. The reaction mixture was refluxed for 3 h after the addition was completed. The reaction mixture was poured into a excess amount of Dry Ice, and then the mixture was allowed to stand at room temperature until the chips of the Dry Ice disappeared. To the mixture, dil. HCl was added and the organic layer was separated from the aqueous solution. The aqueous layer was extracted with ether (30 ml×2). The combined organic and ether layer was washed with water, and then extracted with 10% aq K_2CO_3 (50 ml×3). The alkaline layer was

Table 5. Chemical Shifts of Si-Me of Diastereomeric Amides of (+)-**3** and (+)-**4** with Chiral Carboxylic Acids

Carboxylic Acid Structure		Chemical Shift of the Amide of (+)-**3** (PPM)			Chemical Shift of the Amide of (+)-**4** (PPM)		
$R_1R_2CHCOOH$		(+)-(+)	(+)-(−)	$\Delta\delta$[a]	(+)-(+)	(+)-(−)	$\Delta\delta$[a]
R_1	R_2						
Ph	OH	0.20	0.17	+0.03	0.23	0.21	+0.02
Ph	*i*-Pr	0.17	0.15	+0.02	0.22	0.17	+0.05
p-$CH_3C_6H_4$	*i*-Pr	0.18	0.16	+0.02	0.23	0.19	+0.04
F-C$_6$H$_4$	*i*-Pr	0.20	0.16	+0.04	0.25	0.18	+0.07
Cl-C$_6$H$_4$	*i*-Pr	0.20	0.17	+0.03	0.25	0.18	+0.07
Br-C$_6$H$_4$	*i*-Pr	0.20	0.17	+0.03	0.25	0.16	+0.09
Me	Cl	(0.59/0.62)[b]		—	(0.72/0.80)[b]		—
Et	Cl	(0.56/0.60)[b]		—	(0.52/0.55)[c]		—
Ph-C(CF$_3$)(OMe)-COOH		(0.18/0.22)[b]			0.33	0.30	+0.03
cis 2-NHCOPh-cyclohexyl-COOH		0.27	0.28	−0.01	0.33	0.30	+0.03

a) The balance of the chemical shifts of the diastereomeric amides of the same and opposite sign of rotation.
b) The separation of the Si-Me peaks was observed after the addition of a little amount of $Eu(fod)_3$.

washed with ether (50 ml), and 3 M†† HCl was added to the solution until the solution changes to acidic. The resulted carboxylic acid was extracted with ether (50 ml×3). The combined extracts was dried over Na_2SO_4, and subsequent evaporation gave **1** in 26.3 g (80%) yield. Mp 36—38 °C. IR (neat) 2900 cm^{-1} (s, COOH), 1680 cm^{-1}. ^1H NMR δ=0.38 (s, 3, Si-CH_3), 2.12 (s, 2, -CH_2C=O), 2.43 (s, 2, -CH_2Ph), 6.7—7.6 (m, 10, Ph), 9.0 (s, 1, COOH). Found: C, 71.33; H, 6.81%. Calcd for $C_{16}H_{18}O_2Si$: C, 71.07; H, 6.71%.

(Ethylmethylphenylsilyl)acetic Acid (2). The phenylmagnesium bromide and the ethylmagnesium bromide were prepared from magnesium (3.3 g, 0.14 mol) and bromobenzene(19.2 g, 0.12 mol) in dry ether (50 ml), and from magnesium (3.3 g, 0.14mol) and bromoethane (13.3 g, 0.12 mol) in dry ether (50 ml), respectively. The phenyl Grinard reagent was added to a solution of (dichloromethylsilyl)methyl chloride[3] (20.0 g, 0.12 mol) in dry ether (30 ml). The mixture was refluxed for 4 h with stirring. Then, the ethyl Grinard reagent was added to the reaction mixture, and it was refluxed for 4 h with stirring. Saturated NH_4Cl was added to the reaction mixture with external cooling. The organic layer was separated and the aqueous layer was extracted with ether (30 ml×2). The combined organic layer was dried (Na_2SO_4). Subsequent evaporation and distillation gave (ethylmethylphenylsilyl)methyl chloride in 17.8 g (73%) yield. Bp 130—135 °C/20 Torr (1 Torr =133.322 Pa). ^1H NMR δ=0.37 (s, 3, Si-CH_3), 1.0—1.2 (m, 5, Et), 2.86 (s, 2, CH_2Cl), 7.1—7.6 (m, 5, Ph).

In a two-necked flask, equipped with a condeser and an additional funnel, magnesium (3.1 g, 0.13 mol) and THF (35 ml) was placed. A solution of (ethylmethylphenylsilyl) methyl chloride (17.0 g, 0.89 mol) in THF (35 ml) was added to the flask. An exothermic reaction took place. After the addition was completed, the reaction mixture was refluxed for 4 h with stirring. The reaction mixture was allowed to stand at room temperature until the chips of Dry Ice disappeared. Workup of the reaction mixture in the similar manner descrived above, and subsequent distillation gave **2** in 12.3 g (69%) yield. Bp 154—157°C/0.9 Torr. IR (neat) 2990 cm^{-1} (s, COOH), 1680 cm^{-1} (s, C=O). ^1H NMR δ=0.41 (s, 3, Si-CH_3), 0.94—1.0 (m, 5, Et), 2.15 (s, 2, CH_2C=O), 7.2—7.5 (m, 5, Ph), 9.6 (broad s, 1, COOH). Found: C, 63.42; H, 7.74%. Calcd for $C_{11}H_{16}O_2Si$: C, 63.30, H, 7.60%.

Another Silylacetic Acid Derivatives. All silylacetic acid derivatives listed in Table 4 were prepared in the similar manner described above. The yield and boiling points of the (alkylarylmethylsilyl)methyl chlorides are as follows; Compound; Yield(%), BP(°C/Torr): MePh(*n*-Pr)$SiCH_2Cl$; 73, 145—150/20: *n*-BuMePhSiCH_2Cl; 82, 130/13: BzEtMeSiCH_2-Cl; 89, 117—119/5: BzMe(*n*-Pr)$SiCH_2Cl$; 87, 95/3: EtMe(*o*-$CH_3C_6H_4$)$SiCH_2Cl$; 72, 108/3: Me(*n*-Pr)(*o*-$CH_3C_6H_4$)$SiCH_2Cl$; 84, 106/2: EtMe(*p*-$CH_3C_6H_4$)$SiCH_2Cl$; 76, 95/3: EtMe(*o*-$CH_3OC_6H_4$)$SiCH_2Cl$; 70, 110/1: AllylMe(*o*-$CH_3C_6H_4$)$SiCH_2Cl$; 76, 120/4: Et(1-Np)MeSiCH_2Cl; 73, 140/3.

The yield and NMR spectra data of the silylacetic acid derivatives are as follows; Compound; Yield(%), Bp(°C/Torr): MePh(*n*-Pr)$SiCH_2COOH$; 51, -, ^1H NMR δ=0.40 (s, 3, Si-CH_3), 0.8—1.3 (m, 7, Pr), 2.15 (s, 2, CH_2), 7.0—7.5 (m, 5, Ph), 12.0 (broad s, 1, COOH): *n*-BuMePhSiCH_2COOH; 18, -, ^1H NMR δ=0.40 (s, 3, Si-CH_3), 0.7—1.5 (m, 9, Bu), 2.10 (s, 2, CH_2), 7.0—7.5 (m, 5, Ph), 11.0 (broad s, 1, COOH): BzEtMeSiCH_2COOH; 75, -, ^1H NMR δ=0.06 (s, 3, Si-CH_3), 0.6—1.4 (m, 5, Et), 1.80 (s, 2, CH_2C=O), 2.16 (s, 2, CH_2Ph), 6.7—7.3 (m, 5, Ph), 12.0 (broad s, 1, COOH): BzMe(*n*-Pr)$SiCH_2COOH$; 65, -, ^1H NMR δ=0.06 (s, 3, Si-CH_3), 0.5—1.7 (m, 7, Pr), 1.80 (s, 2, CH_2C=O), 2.16 (s, 2, CH_2Ph), 6.8—7.3 (m, 5, Ph), 11.5 (broad s, 1, COOH): EtMe(*o*-$CH_3C_6H_4$)-$SiCH_2COOH$; 71, 170/0.6, ^1H NMR δ=0.45 (s, 3, Si-CH_3), 0.99 (s, 5, Et), 2.15 (s, 2, CH_2), 2.45 (s, 3, CH_3), 6.9—7.5 (m, 4, Ar), 12.5 (broad s, 1, COOH); Me(*n*-Pr)(*o*-$CH_3C_6H_4$)-$SiCH_2COOH$; 38, -, ^1H NMR δ=0.45 (s, 3, Si-CH_3), 0.8—1.6 (m, 7, Pr), 2.10 (s, 2, CH_2), 2.45 (s, 3, CH_3), 6.9—7.5 (m, 4, Ar), 11.5 (broad s, 1, COOH): EtMe (*p*-$CH_3C_6H_4$)-$SiCH_2COOH$; 49, 155/0.3, ^1H NMR δ=0.40 (s, 3, Si-CH_3), 0.9—1.1 (m, 5, Et), 2.05 (s, 2, CH_2), 2.35 (s, 3, CH_3), 6.9—7.5 (m, 4, Ar), 11.5 (broad s, 1, COOH): (*o*-$CH_3OC_6H_4$)-EtMe$SiCH_2COOH$; 53, -, ^1H NMR δ=0.36 (s, 3, Si-CH_3), 0.95 (s, 5, Et), 2.10 (s, 2, CH_2), 3.75 (s, 3, O-CH_3), 6.5—7.5 (m, 4, Ar), 11.5 (broad s, 1, COOH): Allyl (*o*-$CH_3OC_6H_4$)-$MeSiCH_2COOH$; 19, -, ^1H NMR δ=0.35 (s, 3, Si-CH_3), 1.90 (d, 2, CH_2), 2.05 (s, 2, CH_2C=O), 3.74 (s, 3, O-CH_3), 4.6—5.0 (m, 2, =CH_2), 5.2—6.2 (m, 1, CH=), 6.5—7.5 (m, 4, Ar), 10.5 (broad s, 1, COOH): EtMe(1-Np)$SiCH_2COOH$; 44, -, ^1H NMR δ=0.59 (s, 3, Si-CH_3), 1.0—1.2 (m, 5, Et), 2.85 (s, 2, CH_2), 7.2—8.0 (m, 7, Ar), 11.5 (broad s, 1, COOH).

Optical Resolution of 1. A solution of (+)-PEA (6.6 g, 54.4 mmol) in a mixed solvent (benzene:hexane 1:4, 50 ml) was added to a solution of (±)-**1**(14.7 g, 54.4 mmol) in the same mixed solvent (100 ml). The solution was allowed to stand over night at room temperature. The salt precipitated was collected by filtration (Salt **1**, yield 18.7 g). The salt **1** was recrystallized from a mixed solvent(benzene-hexane 1:1, 120 ml)(Salt **2**, yield 5.1 g). Further twice recrystallizations were carried out by using the same solvent (Salt **3**, yield 4.4 g) (Salt **4**, yield 3.8 g, $[\alpha]_D$ +41.2° (*c* 1, MeOH)). (+)-**1** was liberated from (+)-PEA and extracted with ether (30 ml×2). The ether solution was dried over Na_2SO_4. Evaporation gave optically pure (+)-**1** in 2.6 g (17.5%) yield. Mp 68—69.5 °C. $[\alpha]_D$ +6.5°(*c* 2, $CHCl_3$).

The first and second filtrates were collected and (−)-rich **1**, was liberated from the solution. (−)-Rich **1** was treated with an equimolar amount of (−)-PEA, and subsequent four times fractional crystallization were carried out. Optically pure salt was obtained in 6.0 g (28%) yield. $[\alpha]_D$ −41.6° (*c* 1, MeOH). Subsequent liberation of the acid, extraction, and evaporation gave optically pure (−)-**1** in 4.1 g (28%) yield. Mp 69—70.5 °C. $[\alpha]_D$ −6.4° (*c* 2, $CHCl_3$).

Optical Resolution of 2. A solution of (+)-PEA in a mixed solvent (benzene-hexane 1:4, 50 ml) was added to a solution of (±)-**2** in the same solvent (100 ml). The solution was allowed to stand over night at room temperature. The precipitated crystalls were collected by filtration. Yield 20.1 g (72%). $[\alpha]_D$ +4.9° (*c* 1, MeOH). The crystalline solid was recrystallized from a mixed solvent (benzene-hexane 1:1). Yield 13.6 g (68%). $[\alpha]_D$ +6.2° (*c* 1, MeOH). It was recrysallized from the same mixed solvent (136 ml). Yield 9.1 g (71%). $[\alpha]_D$ +7.0° (*c* 1, MeOH). It was further recrystallized from the same solvent (180 ml). Yield 7.5 g (55%). $[\alpha]_D$ +7.9° (*c* 1, MeOH). Then, it was recrystallized from benzene (75 ml). Yield 5.8 g (77%). $[\alpha]_D$ +8.0° (*c* 1, MeOH). The salt was recrystallized from benzene (86 ml)

†† 1 M=1 mol dm^{-3}.

again. Yield 4.3 g (75%). $[\alpha]_D$ +8.0° (*c* 1, MeOH). Liberation and subsequent usual work-up gave (+)-**2** in 2.7 g (14%) yield. $[\alpha]_D$ +7.9° (*c* 1, MeOH). Optical purity of this (+)-**2** was estimated as 99% by NMR method using optically pure (+)-PEA.

The enantiomer of **2**, which has oppsite sign of rotation, was recovered from the filtrates. Optically pure (−)-**2** was obtained in a similar manner described above, by several times fractional crystallization of its (−)-PEA salt from appropriate solvents.

Optically Active (Benzylmethylphenylsilyl)methylamine Hydrochloride Salt (3'). To a solution of optically active (+)-**3** (1.0 g, 4.1 mmol), $[\alpha]_D$ +12.6° (*c* 1, Et_2O) in MeOH (5 ml), 3 M HCl (5 ml) was added. The mixture was evaporated and the residue was recrystallized from a mixed solvent (benzene–hexane 2:1, 90 ml). White crystalline salt was obtained in 1.2 g (99%) yield. Mp 166.5—167 °C. $[\alpha]_D$ +45.0° (*c* 1, MeOH). ^{1}H NMR δ=0.50 (s, 3, Si-CH_3), 2.57 (m, 4, $SiCH_2N$, $SiCH_2Ph$), 7.0—7.5 (m, 10, Ph), 9.0 (broad s, 3, NH_3).

Optically Active (Benzylmethyl-*o*-tolylsilyl)methylamine Hydrochloride Salt(4'). To a solution of (+)-**4** (1.0 g, 3.9 mmol), $[\alpha]_D$ +4.3° (*c* 4, Et_2O) in MeOH (5 ml), 3 M HCl (5 ml) was added. The solvent was evaporated and the residue was recrystallized from benzene (50 ml). The salt of (+)-**4** was obtained in 1.0 g (89%) yield. Mp 186.5—187 °C. $[\alpha]_D$ +35.2° (*c*1, MeOH). ^{1}H NMR δ=0.55 (s, 3, Si-CH_3), 2.36 (s, 3, Ph-CH_3), 2.47—2.65 (m, 4, CH_2-N, CH_2ph), 7.0–8.0 (m, 9, Ar), 8.2 (broad s, 3, NH_3).

Preparation of the Diastereomeric Amide of (+)-1 with (±)-PEA. In a flask, equipped with a condenser, a solution of 2-chloro-1-methylpridinium iodide (56 mg, 0.22 mmol) in dry dichloromethane (0.5 ml) was placed. A mixture of (+)-**1** (51 mg, 0.19 mmol), (±)-PEA(22 mg, 0.19 mmol), and tributylamine (82 mg, 0.44 mmol) in dry dichloromethane (0.5 ml) was added to the solution. The reaction mixture was refluxed for 1 h with stirring. Subsequent evaporation and purification by TLC(benzene–ethylacetate 5:1, R_f=0.6) gave the diastereomeric amide in 57 mg (80%) yield. ^{1}H NMR δ=0.34 (two s, 3, Si-CH_3), 1.21, 1.22, 1.28, 1.29 (a pair of d, 3, CH_3), 1.96 (s, 2, CH_2C=O), 2.44 (s, 2, CH_2Ph), 4.6—5.2 (a pair of q, 1, CH), 5.12 (broad s, 1, NH), 7.0—7.5 (m, 15, Ph).

All the amides listed in Tables 2 and 4 were prepared in a similar manner described above. Most of the amides were obtained in the range from 50 to 80% yields.

Preparation of Diastereomeric Ester of (+)-2 with (±)-1-Phenylethanol. In a flask, equipped with a condenser, a solution of 2-chloro-1-methylpyridinium iodide (112 mg, 0.44 mmol) in dry dichloromethane (1 ml) was placed. A mixture of (+)-**2** (83 mg, 0.4 mmol), (±)-1-phenylethanol (49 mg, 0.4 mmol) and tributylamine (160 mg, 0.88 mmol) was added to the flask. The reaction mixture was refluxed for 3 h with stirring. Evaporation and purification by TLC (bnzene, R_f=0.5—0.6) gave the ester in 60 mg (48%) yield. ^{1}H NMR δ=0.32, 0.35 (two s, 3, Si-CH_3), 0.85—1.0 (m, 5, Et), 1.36, 1.37, 1.43, 1.45 (a pair of d, 3, CH_3), 2.15 (s, 2, CH_2), 7.0—7.5 (m, 10, Ph).

All the esters listed in Table 3 were prepared in a similar manner described above. Most of the esters were obtained in the range of 40 to 70% yields.

Preparation of Diastereomeric Amide of (+)-3 with (±)-2-(4-Methylphenyl)-3-methylbutanoic Acid. In a flask, equipped with a condenser, a solution of 2-chloro-1-methylpyridinium iodide (31 mg, 0.12 mmol) in dichloromethane (1 ml) was placed. A mixture of (benzylmethylphenylsilyl) methylamine hydrochloride (28 mg, 0.10 mmol), tributylamine (60 mg, 0.32 mmol), and (±)-2-(4-methylphenyl)-3-methylbutanoic acid (20 mg, 0.10 mmol) was added to the flask. The reaction mixture was refluxed for 1 h with stirring. Evaporation and purification by TLC (dichloromethane, R_f=0.6—0.7) gave the diastereomeric amide in 20.6 mg (50%) yield. ^{1}H NMR δ=0.16, 0.18 (two s, 3, Si-CH_3), 0.60, 0.67, 0.87, 0.94 (a pair of d, 6, CH_3). 2.30 (s, 3, Ar-CH_3), 2.35 (s, 2, Ph-CH_2), 2.1—2.4 (m, 2, CH), 2.9—3.0 (m, 2, CH_2N), 6.9—7.4 (m, 14, Ar).

All diastereomeric amides listed in Table 5 were prepared in a similar manner described above. Most of the amides were obtained in the range of 50—80% yields.

The authors wish to thank the Shin-etsu Chemical Industry Co. for the gift of dichlorodimethylsilane.

References

1) S. Yamaguchi, *Asymmetric Synthesis*, **1**, 125 (1983); M. Raban and K. Mislow, *Top. Stereochem.*, **2**, 199 (1967).

2) J. A. Dale, D. L. Dull, and H. S. Mosher, *J. Org. Chem.*, **34**, 2543 (1969); J. A. Dale and H. S. Mosher, *J. Am. Chem. Soc.*, **95**, 512 (1973).

3) D. Terunuma, M. Kato, M. Kamei, H. Uchida, and H. Nohira, *Chem. Lett.*, **1985**, 13.

4) D. Terunuma, K. Murakami, M. Kokubo, K. Senda, and H. Nohira, *Bull. Chem. Soc. Jpn.*, **53**, 789 (1980).

5) K. Saigo, M. Usui, K. Kikuchi, E. Shimada, and T. Mukaiyama, *Bull. Chem. Soc. Jpn.*, **50**, 1863 (1977).

6) Unpublished data.

7) N. Miyakado, N. Ohno, Y. Okuno, N. Hirano, K. Fujimoto, and H. Yoshioka, *Agric. Biol. Chem.*, **39**, 267 (1976); H. Nohira, M. Kai, M. Nohira, J. Nishikawa, T. Hoshiko, and K. Saigo, *Chem. Lett.*, **1981**, 951; H. Nohira, D. Terunuma, S. Kobe, I. Asakura, A. Miyashita, and T. Ito, *Agric. Biol. Chem.*, **50**, 675 (1986); P. Newman, "Optical Resolution Procedures for Chemical Compounds," Optical Resolution Information Center, Manhattan College, New York (1978).

Photocatalytic Behavior of Di- and Triferrocenylbenzenes on Reduction of Methyl Viologen and Photochemical Hydrogen Evolution from Methanol under Visible Light

Takeo Akiyama,* Yukihiko Kawaharada, Akira Kondo, Masatsugu Kajitani, Akira Endo, Kunio Shimizu, and Akira Sugimori
Department of Chemistry, Faculty of Science and Technology, Sophia University, Kioi-cho 7-1, Chiyoda-ku, Tokyo 102
(Received May 26, 1986)

1,4- and 1,3-Diferrocenylbenzenes (**1a** and **1b**), 1,2,4- and 1,3,5-triferrocenylbenzenes (**1c** and **1d**) can act as photocatalysts for photochemical hydrogen evolution from methanol in the **1**-methyl viologen MV^{2+}-triethanolamine-colloidal Pt-catalyst system under the irradiation with visible light. The order of the photocatalytic activities of **1** is **1d**>**1c**>**1a**>**1b**. The catalytic activities of **1** can be correlated to the $E_{1/2}$ values. **1** acts as a photocatalyst in the wavelength region of λ>440 nm, whereas it acts as a quencher for the formation of MV^{+} in the wavelength region of λ<440 nm. The highest quantum yield of the formation of MV^{+} catalyzed by **1**(**1d**: $Q_{MV^{+}}$=0.028, at 480 nm) was obtained in the wavelength region where the intensity of the solar light is the largest.

The photochemical evolution of hydrogen from water is of interest[1] because of the need to convert of solar energy into chemical forms. The systems containing a photocatalyst, methyl viologen (MV^{2+}), platinum catalyst, and a sacrificial reductant have been intensively investigated.[1b-f,2] The most popular photocatalysts used in these systems are tris(2,2′-bipyridine)ruthenium(II) chloride[1b-f] and several zinc porphyrin complexes.[2] No ferrocene derivative has been investigated in view of photochemical hydrogen evolution, although ferrocene is known to undergo electron transfer in its excited state when a suitable electron acceptor is present,[3] and the synthetic methods of the ferrocene derivatives have been extensively investigated.[4]

Recently, we reported the photocatalytic behavior of bis(η^5-indenyl)iron(II) on the reduction of MV^{2+} [5] and the photochemical evolution of hydrogen catalyzed by diferrocenylbenzenes in methanol solutions.[6] In this paper we wish to report the full details of the photocatalytic behavior of polyferrocenylbenzenes on the hydrogen evolution under irradiation with visible light and a mechanistic study on the excited state of polyferroenylbenzenes which participate in the reduction of methyl viologen.

Experimental

Materials. 1,4-Diferrocenylbenzene (**1a**) was synthesized from ferrocene (Aldrich Chemical Co., mp 174—176 °C) and 1,4-benzenebis(diazonium tetrafluoroborate) which was prepared by diazotization of *p*-phenylenediamine (Kanto Chemical Co., E.P.) according to the method in the literature:[7] mp 176—179 °C. The ^{1}H NMR spectra of **1a** ($CDCl_3$) δ=7.38 (4H, s, C_6H_4), 4.66 (4H, t, C_5H_4-), 4.32 (4H, t, C_5H_4-), and 4.08 (10H, s, C_5H_5) were identical with those reported.[8]

1,3-Diferrocenylbenzene (**1b**) was prepared similarly from ferrocene and 1,3-benzenebis(diazonium tetrafluoroborate) prepared by diazotization of *m*-phenylenediamine (Kanto Chemical Co., E.P.): mp 188—189 °C (lit,[7] 189—191 °C).

1,2,4-Triferrocenylbenzene (**1c**) was prepared according to the reported method[9] by cyclotrimerization of ethynylferrocene in dioxane in the presence of $Co_2(CO)_8$ as a catalyst: mp 248—250 °C (lit,[9] 246—249 °C); ^{1}H NMR ($CDCl_3$) δ=7.67 (3H, m, C_6H_3), 4.77 (2H, t, C_5H_4-), 4.38 (2H, t, C_5H_4), and 4.12—3.95 (23H, m, C_5H_5×3, 8H from C_5H_4-). These ^{1}H NMR spectral data were identical with those reported by Schlögl and Soukup.[9]

1,3,5-Triferrocenylbenzene (**1d**) was prepared by the acid (HCl)-catalyzed cyclotrimerization of acetylferrocene in the presence of triethyl orthoformate (Wako Junyaku Co., E.P.) according to the method reported by Sasaki and Pittman[10a] and Schlögl and Soukup:[10b] mp 265—265.5 °C (lit,[10] 265—266 °C); ^{1}H NMR ($CDCl_3$) δ= 7.47 (3H, s, C_6H_3), 4.76 (6H, t, C_5H_4-), 4.39 (6H, t, C_5H_4-) and 4.13 (15H, s, C_5H_5). The ^{1}H NMR data were identical with those reported.[10]

Ethynylferrocene was prepared from acetylferrocene (mp 84—86 °C) in the presence of phosphoryl chloride (Wako Junyaku Co., G.R.) and DMF (Wako Junyaku Co., G.R.) and then with sodium hydroxide under the reflux in dioxane according to the method reported by Schlögl and Steyrer[11a]: mp 53.5—55.0 °C (lit,[11] 55—56 °C).

Methyl viologen dichloride hydrate (83%)(Wako Junyaku Co., G.R.) was used as received.

Colloidal platinum catalyst was prepared from dihydrogen hexachloroplatinate(IV) hexahydrate (Wako Junyaku Co., G.R.)(0.20 g) and poly(vinyl alcohol) (Wako Junyaku Co., G.R.)(degree of polymerization=500, 0.160 g) in a methanol-water (50 cm^3, 1/1, v/v) solution according to the method reported by Toshima et al.[12]

Methanol (Wako Junyaku Co., E.P.) was purified by refluxing for 2 h in the presence of calcium hydride and then distilled.

Acetonitrile (Wako Junyaku Co., G.R.) was dried overnight with molecular sieves (Wako Junyaku Co., Molecular Sieves 4A, 1/16). Calcium hydride was added and the mixture was stirred until the gas evolution ceased. This acetonitrile was refluxed for 3—4 h in the presence of anhydrous phosphorus pentaoxide and then distilled under a stream of Ar.

Dioxane (Wako Junyaku Co., Dotite Spectrosol) was used as received.

N,*N*-Dimethylformamide (Wako Junyaku Co., G.R.) was dried over molecular sieves (Wako Junyaku Co., 4A, 1/16) and then distilled under Ar.

Measurements. UV spectra were recorded on a Hitachi 228 UV-Vis spectrophotometer. IR spectra were obtained by use of a Hitachi 260—50 grating spectrophotometer. ^{1}H NMR spectra were taken on a Hitachi R-22 (90 MHz) spectrometer. Gas chromatography for the evolved gas was performed by use of a Shimadzu GC-5A (column: molecular sieves 13X, 30—60 mesh, 2 m; temp: 20 °C; carrier gas: Ar). The gas sample was sucked from the gas buret attached to the cell by using a syringe.

Cyclic voltammetry was carried out for **1a**, **1b**, **1c**, **1d**, ferrocene and tris(2,2′-bipyridine)ruthenium(II) chloride by using a platinum disk electrode (ϕ=2.0 mm)(reference electrode: Ag|0.1 mol dm^{-3} $AgClO_4$ in acetonitrile) in an acetonitrile-tetraethylammonium perchlorate (0.1 mol dm^{-3}) solution.

Irradiation. (a) Hydrogen Evolution. The sample solutions (methanol): 12 cm^3, **1a**: 7.8×10^{-5} mol dm^{-3}, **1b**: 1.4×10^{-4} mol dm^{-3}, **1c**: 2.2×10^{-5} mol dm^{-3}, **1d**: 2.5×10^{-5} mol dm^{-3}, $[Ru(bpy)_3]Cl_2$: 1.40×10^{-5} mol dm^{-3}; MV^{2+}: 4.3×10^{-2} mol dm^{-3}; TEOA: 8.9×10^{-2} mol dm^{-3}; Pt: 1.32×10^{-6} mol) were prepared under a stream of Ar in a quartz vessel (2.5×2.5×6 cm^3) equipped with a gas buret and were irradiated with a 150 W tungsten lamp attached to a slide projector for 2 h. In the cases of ferrocene and phenylferrocene the sample solutions (methanol-dioxane=9:1, v/v, 12 cm^3, ferrocene: 1.1×10^{-4} mol dm^{-3}, phenylferrocene: 9.0×10^{-4} mol dm^{-3}; MV^{2+}: 4.3×10^{-2} mol dm^{-3}; TEOA: 8.9×10^{-2} mol dm^{-3}; Pt: 1.92×10^{-6} mol) were irradiated with a 500 W Xe lamp for 10 min. Comparisons of the catalytic activities of **1** and $[Ru(bpy)_3]Cl_2$ were carried out by comparing the amounts of the evolved gas based on that of the blank system (without metal complex) at 30 min, when the linear correlation between the amount of the evolved hydrogen and the irradiation time was obtained (this relationship was not linear after 30 min). The volume of the evolved hydrogen gas was measured by the gas buret.

(b) Reduction of Methyl Viologen. The sample solutions containing **1**, MV^{2+}, and TEOA (**1a**: 3.4—6.8×10^{-5} mol dm^{-3}, **1b**: 0.6—1.7×10^{-4} mol dm^{-3}, **1c**: 2.3—4.6×10^{-5} mol dm^{-3}, **1d**: 2.2—5.0×10^{-5} mol dm^{-3}, phenylferrocene: 8.4×10^{-4} mol dm^{-3}; MV^{2+}: 1.29×10^{-2} mol dm^{-3}; TEOA: 6.0×10^{-2} mol dm^{-3}; methanol (for **1a** and **1b**): 5 cm^3; methanol-dioxane (9/1, v/v)(for **1c** and **1d**): 5 cm^3) were prepared under a stream of Ar in a quartz cell (1 cm×1 cm) equipped with a stopcock and were irradiated with monochromatic light (light source: Osram HBO 200 W, monochromator: Shimadzu-Bausch & Lomb grating monochromator, dispersion: 7.4 nm mm^{-1}; slit width: 1.5 mm). The quantitative analysis was carried out by measuring the absorbance at 603 nm (molar absorption coefficient of $MV^{+\cdot}$: 13800 mol^{-1} dm^3 cm^{-1})[13] which is characteristic of $MV^{+\cdot}$.

Actinometry. Actinometry was carried out for 313, 355, 400, 440, 480, 500, 546, and 580 nm light by using potassium trioxalatoferrate(III) according to the method in the literature.[14]

Effect of Additives on the Yield of $MV^{+\cdot}$. (i) To the sample solutions (methanol-dioxane(9:1, v/v) 5 cm^3) containing MV^{2+}(1.29×10^{-2} mol dm^{-3}) and TEOA (6×10^{-2} mol dm^{-3}) was added *trans*-1,3-pentadiene (1.2—5×10^{-4} mol dm^{-3}). The solutions were irradiated with 313 nm light for 3 min and the ratios of the yield of $MV^{+\cdot}$ were calculated. (ii) To the methanol-dioxane(9:1, v/v) solutions containing MV^{2+}(1.29×10^{-2} mol dm^{-3}) and TEOA (6×10^{-2} mol dm^{-3}) was added **1d** (2.5—5×10^{-4} mol dm^{-3}). The solutions were irradiated with 313 nm light for 3 min and $Q_{MV^{+\cdot}}$ values were calculated. (iii) The sample solutions containing **1d**, MV^{2+}, TEOA, and azulene (**1d**: 4.36×10^{-4} mol dm^{-3}, MV^{2+}: 1.29×10^{-2} mol dm^{-3}, TEOA: 6×10^{-2} mol dm^{-3}, azulene: 2.1—8.4×10^{-3} mol dm^{-3}) were irradiated with 480 nm light for 3 min.

Results and Discussion

For the ferrocene derivatives in which several ferrocenyl groups attached to benzene rings can interact with each other through the π-electron system of the benzene ring, the following two important properties of the photocatalyst are expected: (i) a higher light harvesting ability and (ii) a higher electron-donating ability than ferrocene. We thus prepared four ferrocene derivatives of this kind; 1,4-diferrocenylbenzene (**1a**), 1,3-diferrocenylbenzene (**1b**), 1,2,4-triferrocenylbenzene (**1c**), and 1,3,5-triferrocenylbenzene (**1d**), as illustrated below.

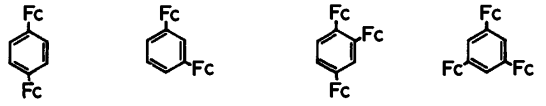

(1a) (1b) (1c) (1d)

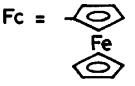

The electronic absorption spectra of **1a—1d** and those of ferrocene are shown in Fig. 1. These absorption spectra show that **1a—1d** have 10 fold as high light harvesting abilities as that of ferrocene in the wavelength region of 280—500 nm and they have slopes of absorption even at 600 nm. For the utilization of visible or solar light, **1a—1d** are better than ferrocene itself.

Photochemical Hydrogen Evolution Catalyzed by Di- and Triferrocenylbenzenes. The irradiation of the system consisting of **1** (2.2—14×10^{-5} mol dm^{-3}), MV^{2+} (4.30×10^{-2} mol dm^{-3}), triethanolamine (TEOA)(8.9×10^{-2} mol dm^{-3}), colloidal Pt-catalyst (1.32×10^{-6} mol), and methanol (12 cm^3) with a 150 W tungsten lamp for 2 h gave hydrogen gas. The results of the photochemical evolution of hydrogen for **1**-MV^{2+}-TEOA-Pt-MeOH system and for $[Ru(bpy)_3]Cl_2$-MV^{2+}-TEOA-Pt-MeOH system are shown in Fig. 2 and Table 1.

As seen from Fig. 2, **1a**, **1c**, and **1d** show rather high activities for the evolution of hydrogen compared to $[Ru(bpy)_3]Cl_2$, while **1b**, ferrocene, and phenylferrocene show low activity.

The comparisons of the photocatalytic activities of **1** were done by comparing the amount of the evolved hydrogen after the irradiation of 30 min, where a linear correlation between the amount of the evolved

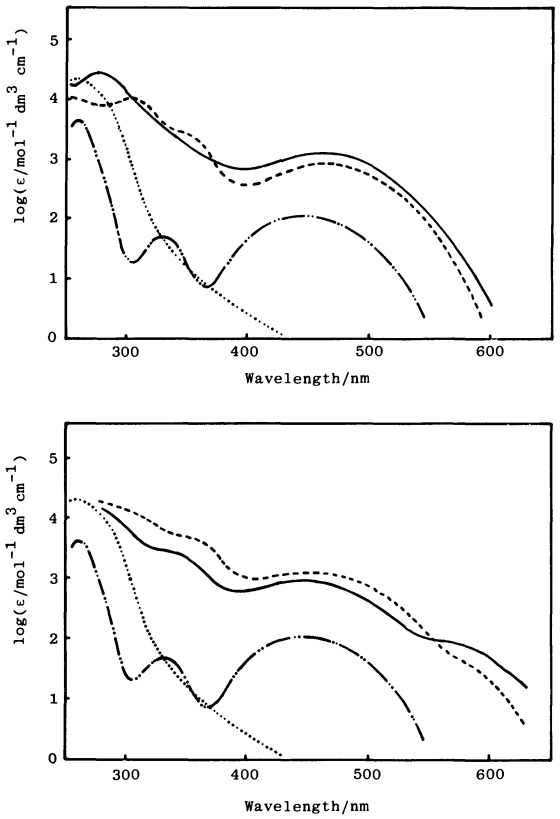

Fig. 1. Absorption spectra of 1,4-diferrocenylbenzene (**1a**) (above, ----), 1,3-diferrocenylbenzene(**1b**)(above, ——), 1,2,4-triferrocenylbenzene(**1c**)(below, ----), 1,3,5-triferrocenylbenzene(**1d**) (below, ——), ferrocene-(—·—·—), and methyl viologen(·····) in methanol solutions.

hydrogen and the irradiation time is obtained (Table 1). In the third and fourth column of Table 1 are shown the fraction of light absorbed by the complex at 440 and 480 nm.

The data given in Table 1 show that (i) **1a** produces hydrogen about a half the amount of the case of

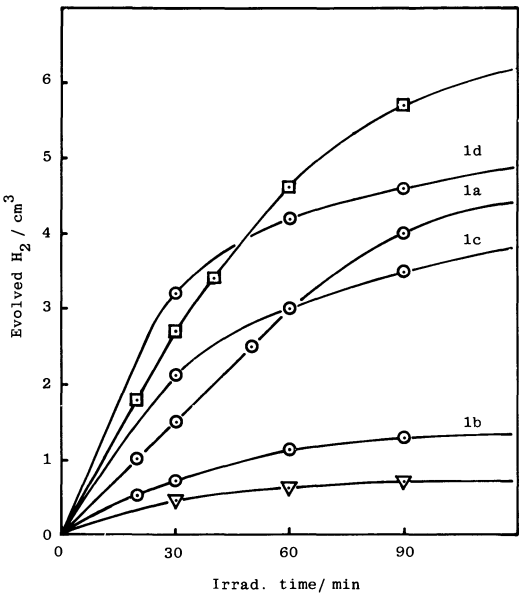

Fig. 2. Hydrogen evolution catalyzed by di- and triferrocenylbenzenes under the irradiation with a tungsten lamp (150 W).
(—⊙—): Ferrocenylbenzenes(**1a**—**d**), (—▣—): [Ru(bpy)$_3$]Cl$_2$, (—▽—): Blank(MV^{2+}–TEOA–Pt catalyst system).

Table 1. Hydrogen Evolution Catalyzed by Di- and Triferrocenylbenzenes under the Irradiation with Visible Light[a)]

[Complex]×10^{-5} mol dm^{-3}		H_2[b)]×10^{-5} mol/30 min	Fraction of light absorbed by complex[c)] 440 nm	480 nm	Turnover number[d)]	$E_{1/2}$[e)] V
1a	7.8	4.35 (47)	27.4 (48)	24.6 (58)	47	0.025(1), 0.110(1)
1b	14.0	0.84 (9)	75.0(131)	53.3(131)	5	0.070(2)
1c	2.2	6.13 (66)	13.6 (24)	11.9 (28)	232	0.017(1), 0.133(2)
1d	2.5	10.74(115)	12.4 (22)	8.7 (21)	358	0.025(3)
Fc-H[f)]	11.0	0 (0)	6.1 (11)	5.4 (13)	0	0.070(1)
Fc-Ph[f)]	90.0	0 (0)	63.6(111)	56.3(133)	0	—
[Ru(bpy)$_3$]Cl$_2$	1.4	9.33(100)	57.1(100)	42.2(100)	555	0.906

a) [MV^{2+}]: 4.3×10^{-2} mol dm^{-3}, [TEOA]: 8.9×10^{-2} mol dm^{-3}, Pt: 1.32×10^{-6} mol, Solvent: methanol, 12 cm^3, Light source: 150 W tungsten lamp, Irradiation time: 30 min. b) The amount of evolved hydrogen gas was based on that of blank experiment. The values in parentheses are percentage of the amount of hydrogen based on that obtained in the case of [Ru(bpy)$_3$]Cl$_2$. c) Fraction of light absorbed by metal complex in 2.5 cm cell ($F=(1-10^{-(2.5)\varepsilon c})\times 100$). The values in parentheses are percentage of the F value based on that obtained in the case of [Ru(bpy)$_3$]Cl$_2$. d) Turnover number$=\dfrac{\text{Amount of evolved hydrogen(mol)}}{\text{Amount of metal complex used(mol)}}$. e) $E_{1/2}=\dfrac{1}{2}(E_p^a+E_p^c)$, where E_p^a and E_p^c are anodic and cathodic peak potentials against Ag|0.1 mol dm^{-3} AgClO$_4$ in acetonitrile. The values in parentheses are the charge numbers of electrode reaction. f) The amount of evolved hydrogen gas was based on that of blank obtained in the same set of experiments which were carried out under the irradiation with a 500 W Xe lamp for 10 min. Fc- represents (C_5H_5)Fe(C_5H_4-).

$[Ru(bpy)_3]Cl_2$ with light absorption of about 50% of $[Ru(bpy)_3]Cl_2$(48% at 440 nm, 58% at 480 nm), (ii) **1c** produces hydrogen 66% of the case of $[Ru(bpy)_3]Cl_2$ with light absorption of 24—28% of that of $[Ru(bpy)_3]Cl_2$, (iii) **1d** produces hydrogen 115% of the case of $[Ru(bpy)_3]Cl_2$ with light absorption of 21—22% of $[Ru(bpy)_3]Cl_2$, (iv) **1b** produces hydrogen 9% of the case of $[Ru(bpy)_3]Cl_2$ with 31% higher light absorption than $[Ru(bpy)_3]Cl_2$, and (v) ferrocene and phenylferrocene do not show any positive effect on the production of hydrogen.

The turnover number (the amount of the evolved hydrogen (mol) per the amount of the metal complex used(mol)) for **1** and $[Ru(bpy)_3]Cl_2$ at 30 min are shown in the fifth column of Table 1. The fact that the turnover numbers of **1a—1d** are all greater than 1 indicates that **1a—1d** act as a catalyst for the photochemical evolution of hydrogen. The order of the catalytic activities of **1** in terms of the amount of the evolved hydrogen is **1d>1c>1a>1b**. It is noteworthy that **1a—1d** show photocatalytic activities, whereas phenylferrocene does not have any catalytic activity. This suggests that more than one ferrocenyl group in a benzene ring is necessary for the appearance of the photocatalytic activity. In the last column in Table 1 are shown redox potentials($E_{1/2}$) of **1** and $[Ru(bpy)_3]Cl_2$ obtained by cyclic voltammetry. **1a—1d** show reversible waves under the experimental conditions. **1a**, **1c**, and **1d** have first oxidation potentials of 0.026, 0.025, and 0.017 V, respectively; these values are all lower than that of **1b** (0.070 V). These electrochemical properties of **1** are roughly parallel to the catalytic activity of **1**; that is, **1** with the lower oxidation potential has the higher photocatalytic activity. That the oxidation potential of **1b** was higher than that of **1a** was ascribed earlier to the inefficiency of the interaction of two ferrocenyl groups through resonance stabilization in the benzene ring.[6] However, the oxidation potential of **1d** is as low as that of **1a**, in spite of having three ferrocenyl groups at positions of benzene ring similar to those for **1b**. The relationship between the electrochemical behavior of **1** and the position of the ferrocenyl groups in the benzene ring still remains unclear and is now under investigation in our laboratory.

Photoreduction of Methyl Viologen Catalyzed by Polyferrocenylbenzenes in Methanol Solutions. In order to obtain evidence that the hydrogen evolution is initiated by the excited state of **1**, followed by an electron transfer from **1** to MV^{2+}, the modified quantum yields (Q_{MV^+}) in terms of the amount of light absorbed by **1** were obtained at various wavelengths.

The modified quantum yield (Q_{MV^+})was calculated based on the amount of the cation radical (MV^+) formed by the contribution of **1** per amount of light absorbed only by 1, as shown in the following equation:

$$Q_{MV^+} = \frac{\text{Amount of } MV^+ \text{ formed by the contribution of } \mathbf{1}}{\text{Amount of light absorbed by } \mathbf{1}(=I\times t)}$$

Two different cases should be considered as to the absorption of the incident light by **1** and MV^{2+}, since the MV^+ is also formed when MV^{2+} only is excited with the light of wavelength shorter than 440 nm. In the case that most of incident light is absorbed by the system (λ<440 nm), Q_{MV^+} can be defined as the following equation:

$$Q_{MV^+} = \frac{[MV^+]_{1+MV^{2+}} - [MV^+]_{MV^{2+}}\times L}{(1-L)} \times \frac{1}{I_0 t}$$

where $[MV^+]_{1+MV^{2+}}$, and $[MV^+]_{MV^{2+}}$, are the amounts of MV^+(mol) in the system consisting of **1** and MV^{2+} and of MV^{2+} only; L is the fraction of light absorbed by MV^{2+} and is defined as:

$$L = \frac{(C_{MV^{2+}})(\varepsilon_{MV^{2+}})}{C_1\varepsilon_1 + (C_{MV^{2+}})(\varepsilon_{MV^{2+}})},$$

where $C_{MV^{2+}}$ and C_1 are the concentrations of MV^{2+} and **1**; $\varepsilon_{MV^{2+}}$ and ε_1 are the molar absorption coefficients of MV^{2+} and **1**; and I_0 is the amount of light quanta(mol) absorbed by the system at wavelength λ per second; t is the irradiation time.

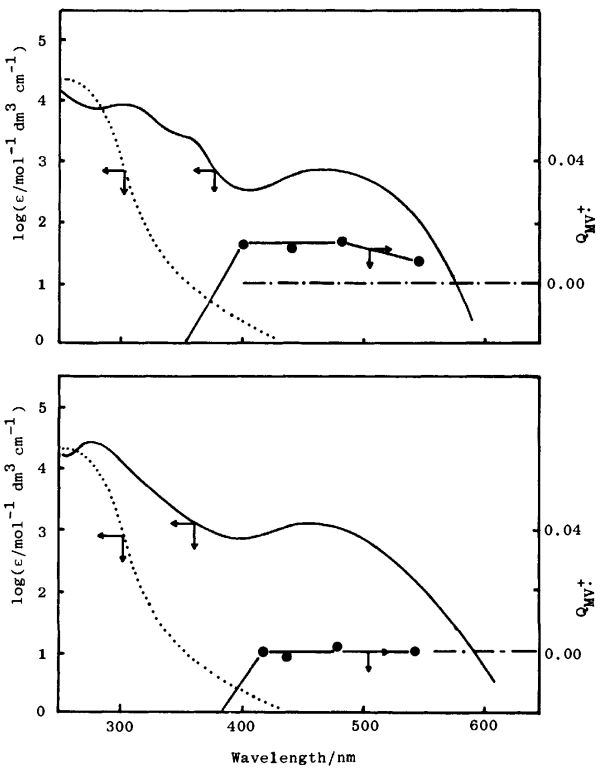

Fig. 3. Wavelength dependences of the quantum yield (Q_{MV^+}) of photoreduction of MV^{2+} catalyzed by 1,4-diferrocenylbenzene(**1a**, above) and 1,3-diferrocenylbenzene(**1b**, below).
(—●—): Q_{MV^+}, (——): Absorption spectra of **1**, (·····): Absorption spectra of methyl viologen.

In the case that most of the incident light is passed through the system and the light is absorbed only by **1** (λ>440 nm), Q_{MV^+} can be defined as the following equation:

$$Q_{MV^+} = \frac{[MV^+]_{1+MV^{2+}} - [MV^+]_{MV^{2+}}}{I \times t},$$

where $[MV^+]_{1+MV^{2+}}$, $[MV^+]_{MV^{2+}}$, and t are the same as defined above; I is the amount of light quanta(mol) absorbed solely by **1** per second. The amount of MV^+ is calculated for the irradiation of 10 min, when the linear relationship between the amount of formed MV^+ and the irradiation time is obtained. However, in the case of the irradiation with 313 nm light, the amount of formed MV^+ at 10 min was obtained by extrapolation of that obtained for 4 min irradiation since the irradiation after 4 min did not follow a linear relationship.

Wavelength dependences of Q_{MV^+} for **1a—d** were obtained as shown in Figs. 3 and 4. These results indicate that: (i) **1a**, **1c**, and **1d** promote the formation of MV^+ in the wavelength region longer than 440 nm where only **1** absorbs light, whereas in the shorter wavelength region, where both MV^{2+} and **1** absorb light competitively, **1** inhibits the formation of MV^+; (ii) the highest Q_{MV^+}(0.028) is obtained in the **1d**-MV^{2+}-TEOA system under the irradiation with 480 nm light, so, **1d** is a suitable photocatalyst for the photochemical hydrogen evolution with solar light, whose intensity is maximum at 480 nm; and (iii) **1b** shows a small promotion effect in the wavelength region longer than 440 nm, but an inhibiting effect similar to that of **1d** was observed in the wavelength region of λ<440 nm.

The inhibiting effect of **1** on the formation of MV^+ in the wavelength region shorter than 440 nm can be accounted for by the quenching of the excited triplet state of MV^{2+}(E_T=299 kJ mol^{-1})[15] by the ground state of **1** (cf. ferrocene: E_T=179 kJ mol^{-1}).[16] In Fig. 5 are shown the Stern-Volmer plots for the effect of a typical triplet quencher, *trans*-1,3-pentadiene(E_T=248 kJ mol^{-1})[17] and **1d**, on the formation of MV^+ under the irradiation with 313 nm light. That the linear correlation in the Stern-Volmer plots was obtained in the cases of both *trans*-1,3-pentadiene and **1d** indicates that the excited triplet state of MV^{2+} is quenched by **1d** by energy transfer process and that this results in the inhibition of the formation of MV^+. Similar results were obtained in the cases of **1a**, **1b**, and **1c**. Recently, Hoffman and Jones II[18] reported that MV^{2+} forms a charge-transfer(CT) complex with TEOA in the ground state and that the excitation of this CT-complex gives MV^+(Φ=0.0018—0.010, at pH 8.7). The results shown in Fig. 5 may thus be explained by the quenching of the excited triplet state of the CT-complex,$^3(MV^{2+}\cdots TEOA)^*_{CT}$ by **1** although the absorption band which originated from the CT-complex was

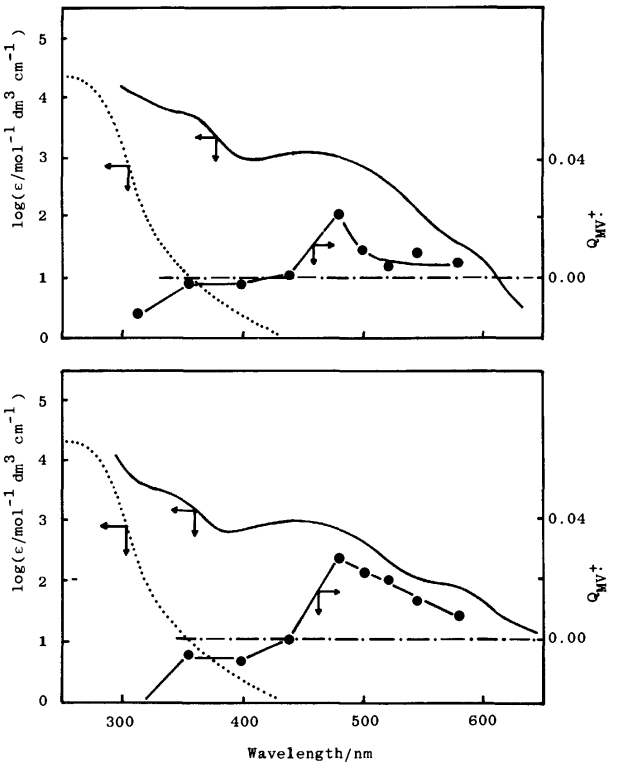

Fig. 4. Wavelength dependences of the quantum yield (Q_{MV^+}) of photoreduction of MV^{2+} catalyzed by 1,2,4-triferrocenylbenzene(**1c**, above) and 1,3,5-triferrocenylbenzene(**1d**, below).
(—●—): Q_{MV^+}, (——): Absorption spectra of **1**, (·····): Absorption spectra of methyl viologen.

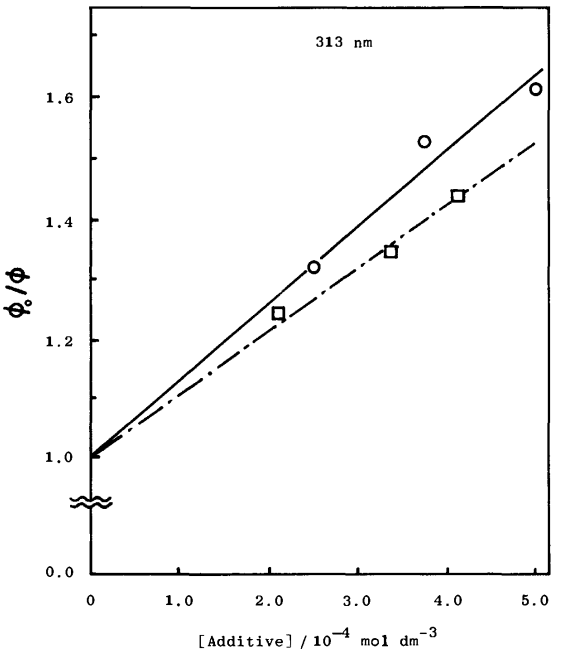

Fig. 5. Stern-Volmer plots for quenching of photoreduction of MV^{2+} under the irradiation with 313 nm light.
(—○—): MV^{2+}-TEOA-1,3-pentadiene system,
(—□—): MV^{2+}-TEOA-1,3,5-triferrocenylbenzene(**1d**) system.

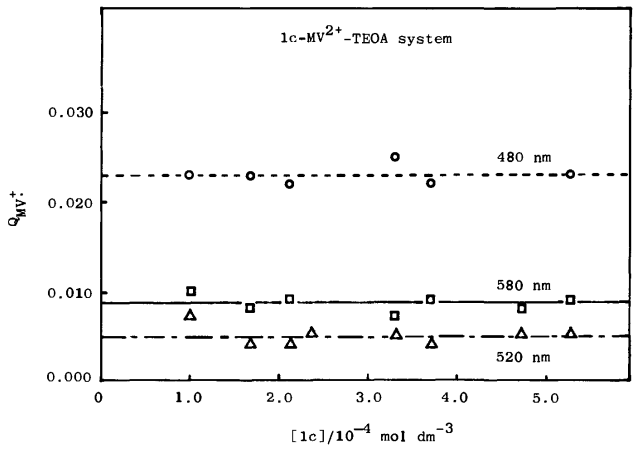

Fig. 6. Dependence of Q_{MV^+} on concentration of 1,2,4-triferrocenylbenzene(**1c**).
(—○—): Irradiation with 480 nm light, (—△—): Irradiation with 520 nm light, (—□—): Irradiation with 580 nm light.

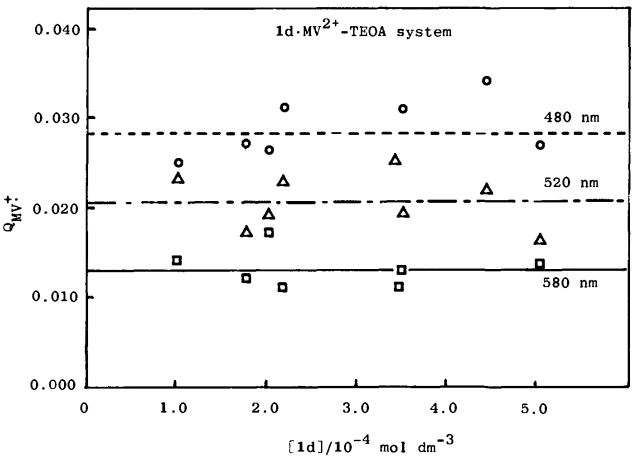

Fig. 7. Dependence of Q_{MV^+} on concentration of 1,3,5-triferrocenylbenzene(**1d**).
(—○—): Irradiation with 480 nm light, (—△—): Irradiation with 520 nm light, (—□—): Irradiation with 580 nm light.

not observed in our case.

The effects of the concentration of **1** (**1c** and **1d**) on Q_{MV^+} under the irradiation with 480, 520, and 580 nm are shown in Figs. 6 and 7. The Q_{MV^+} values are independent of the concentrations of **1**. In Fig. 8 is shown the effect of concentrations of MV^{2+} on Q_{MV^+} values. It is clear that the Q_{MV^+} values are proportional to the concentration of MV^{2+}. The results in Figs. 6—8 show that (i) the photoreduction of MV^{2+} proceeds in first order with respect to the excited state of **1** (Figs. 6 and 7) and (ii) the photoreduction is first order with respect to MV^{2+} under the irradiation with the light of wavelength longer than 440 nm.

Information on the excited state of **1** involved in the photoreduction was gained by another quenching

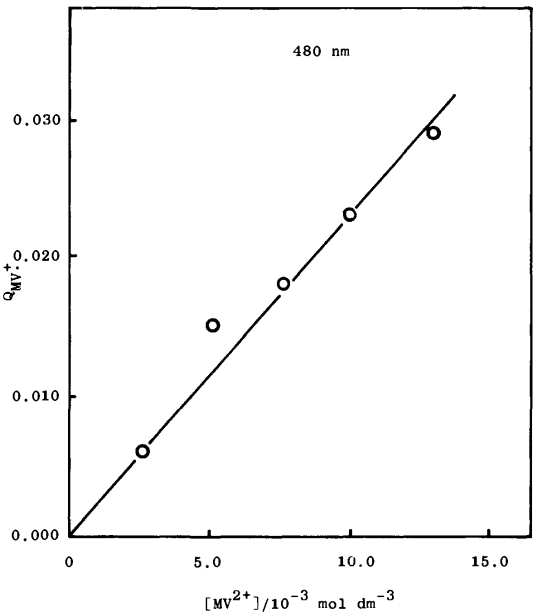

Fig. 8. Dependence of Q_{MV^+} on concentration of methyl viologen (MV^{2+}) under the irradiation with 480 nm light.

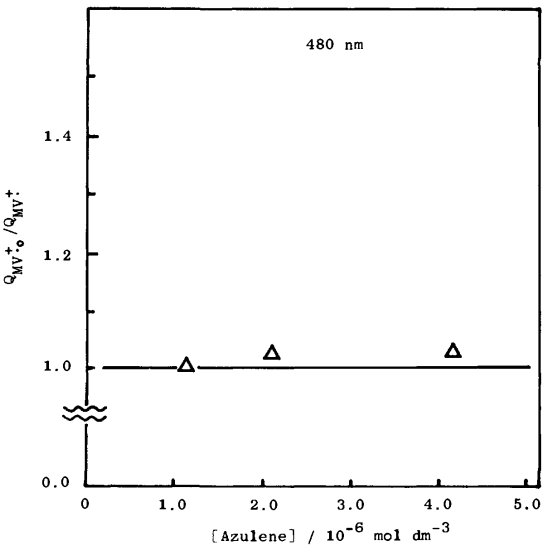

Fig. 9. Stern-Volmer plots for $Q_{MV^+}{}^{\circ}/Q_{MV^+}$ under the irradiation with 480 nm light.

experiment using azulene; its triplet energy level (E_T=163.6 kJ mol^{-1})[19] is lower than ferrocene. The Stern-Volmer plots are shown in Fig. 9. The absence of any effect of added azulene on Q_{MV^+} indicates that the reduction of MV^{2+} is initiated by the excited singlet state of **1**, followed by the electron transfer from ^{1}(**1**)* to MV^{2+} under the irradiation with light of wavelength longer than 440 nm.

The Excited State of 1 Involved in the Photoreduction of Methyl Viologen. The assignments of the absorption bands of di- and triferrocenylbenzenes have not been reported, but those of ferrocene were reported

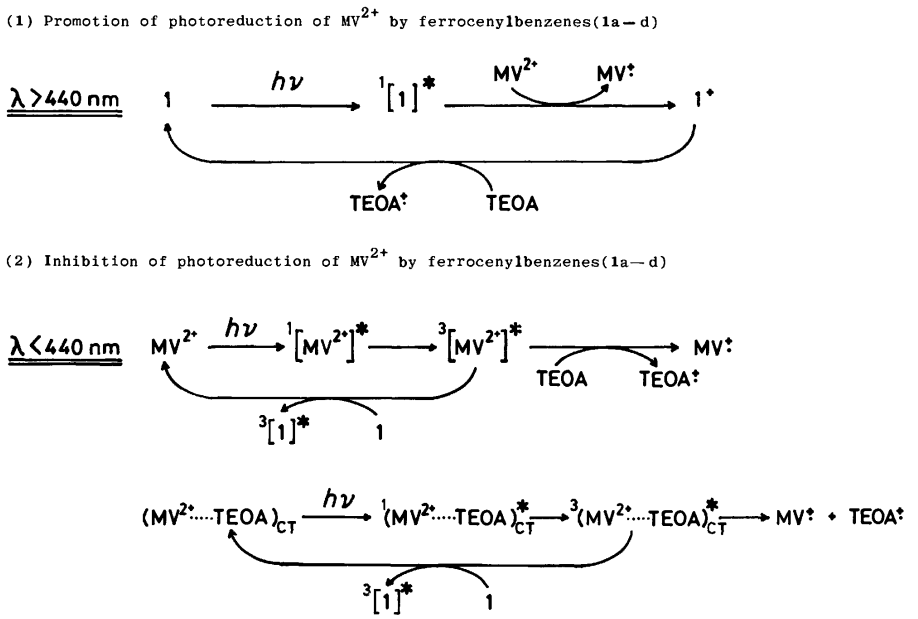

Scheme 1.

by several workers.[20,21,22] According to Sohn[20] and Gordon,[22] the bands at 440 and 324 nm have d-d character and the bands at 265 nm has LMCT character.[22] In the cases of ferrocene and phenylferrocene the irradiation with the light of wavelength longer than 440 nm gave Q_{MV^+} values of zero. Therefore, the excited state involved in the reduction of MV^{2+} can be considered to have some LMCT character. These red shifts of LMCT-band might be accounted for by the intramolecular interaction of ferrocenyl groups through π-electron systems.

The reaction mechanism for the photoreduction of MV^{2+} catalyzed by **1** is shown in Scheme 1.

The authors gratefully acknowledge the financial support of this work by the Grant-in-Aid for Scientific Research (Special Project Research on Energy, No 56045116, 57045106, 58045141, 59040005, and 60040004) from the Ministry of Education, Science and Culture.

References

1) a)V. Balzani, L. Moggi, M. F. Manfrin, F. Boletta, and M. Gleria, *Science*, **189**, 852 (1975); b) J.-M. Lehn and J.-P. Sauvage, *Nouv. J. Chim.*, **1**, 449 (1977); c) K. Kalyanasundaram, J. Kiwi, and M. Grätzel, *Helv. Chim. Acta*, **61**, 2720 (1978); d) A. Moradpour, E. Amouyal, P. Keller, and H. B. Kagan, *Nouv. J. Chim.*, **2**, 547 (1978); e) M. Kirch, J.-M. Lehn, and J.-P. Sauvage, *Helv. Chim. Acta*, **62**, 1345 (1979); f) P.-A. Brugger, P. Cuendet, and M. Grätzel, *J. Am. Chem. Soc.*, **103**, 2923 (1981); g) M. Grätzel, *Acc. Chem. Res.*, **14**, 376 (1981); h) J. Kiwi, "Examples for Photogeneration of Hydrogen and Oxygen from Water" in "Energy Resources through Photochemistry and Catalyst," ed by M. Grätzel, Academic Press, Inc., New York, N. Y. (1983), Chapt. 9, pp. 297—330.

2) a) K. Kalyanasundaram and M. Grätzel, *Helv. Chim. Acta*, **63**, 478 (1980); b) K. Monserrat and M. Grätzel *J. Chem. Soc., Chem. Commun.*, **1981**, 183, c) I. Tabushi and A. Yazaki, *J. Org. Chem.*, **46**, 1899 (1981), d) A. Harriman, G. Porter, and M.-C. Richoux, *J. Chem. Soc., Faraday Trans. 2*, **77**, 833 (1981); *ibid.*, **77**, 1939 (1981); *ibid.*, **78**, 1955 (1982); e) A. Harriman and G. Porter, *ibid.*, **78**, 1937 (1982).

3) a) O.Traverso and F. Scandola, *Inorg. Chim. Acta*, **4**, 493 (1970); b) T. Akiyama, A. Sugimori, and H. Hermann, *Bull. Chem. Soc. Jpn.*, **46**, 1855; c) J. A. Powell and S. R. Logan, *J. Photochem.* **3**, 189 (1974).

4) For example; D. E. Bublitz and K. I. Rinehart, Jr., "The Synthesis of Substituted Ferrocenes" in "Organic Reactions," ed by W. G. Dauben, John Wiley, New York, N. Y. (1964), Vol. 17, pp. 1—68 and E. G. Perevalova and T. V. Nikitina, "Reactions of Bis(π-cyclopentadienyl) transition Metal Compounds" in "Organometallic Reactions," ed by E. I. Becker and M. Tsutsui, Wiley Interscience, New York, N. Y. (1972), Vol. 4, pp. 168—309.

5) T. Akiyama, A. Kondo, M. Omata, M. Kajitani, and A. Sugimori, *Chem. Lett.*, **1985**, 301.

6) T. Akiyama, A. Kondo, Y. Kawaharada, M. Kajitani, A. Endo, K. Shimizu, and A. Sugimori, *Chem. Lett.*, **1985**, 1071.

7) W. F. Little, B. Nielsen, and R. Williams, *Chem. Ind. (London)*, **1964**, 195.

8) H. Kottelwesch and U. Kruerke, Gmelin's "Handbuch der Anorganische Chemie," Ergenzungswerk zur achten Auflage, Teil A, Ferrocen 6, ed by U. Kruerke and A. Slawisch, Springer Verlag, Berlin-Heidelberg (1977), p. 130.

9) K. Schlögl and H. Soukup, *Monatsh. Chem.*, **99**, 927 (1968).

10) a) Y. Sasaki and C. U. Pittman, Jr., *J. Org. Chem.*, **38**, 3723 (1973); b) K. Schlögl and H. Soukup, *Tetrahedron Lett.*, **1967**, 1181.

11) a) K. Schlögl and W. Steyrer, *Monatsh. Chem.*, **96**, 1520 (1965); b) K. Schlögl and H. Egger, *ibid.*, **94**, 376 (1963).

12) N. Toshima, M. Kariyama, Y. Yamada, and H. Hirai, *Chem. Lett.*, **1981**, 793.

13) T. Watanabe and K. Honda, *J. Phys. Chem.*, **86**, 2617 (1982).
14) C. G. Hatchard and C. A. Parker, *Proc. R. Soc. London, Ser. A*, **235**, 518 (1956).
15) P. Hyde and A. Ledwith, *J. Chem. Soc., Perkin Trans. 2*, **1974**, 1768.
16) K. Kikuchi, H. Kokubun, and M. Kikuchi, *Bull. Chem. Soc. Jpn.*, **48**, 1378 (1975).
17) S. Murov, "Handbook of Photochemistry," Marcel Dekker Inc., New York, N. Y. (1973), p. 29.
18) M. Z. Hoffman, D. R. Prasad, G. Jones, II, and V. Malba, *J. Am. Chem. Soc.*, **105**, 6360 (1983).
19) W. G. Herkstroeter, *J. Am. Chem. Soc.*, **97**, 4161 (1975).
20) Y. S. Sohn, D. N. Hendrickson, and H. B. Gray, *J. Am. Chem. Soc.*, **93**, 3603 (1971).
21) M. M. Rohmer, A. Veillard, and M. H. Wood, *Chem. Phys. Lett.*, **54**, 575 (1974).
22) K. R. Gordon and K. D. Warren, *Inorg. Chem.*, **17**, 987 (1978).

 © 1986 The Chemical Society of Japan Bull. Chem. Soc. Jpn., 59, 3597—3603 (1986)

Restricted Rotation Involving the Tetrahedral Carbon. LIX. Stereodynamics of Singly *peri*-Substituted 9-(3,5-Dimethylphenoxy)triptycene Derivatives[1)]

Gaku YAMAMOTO* and Michinori ŌKI
Department of Chemistry, Faculty of Science, The University of Tokyo,
Bunkyo-ku, Tokyo 113
(Received May 26, 1986)

Five singly *peri*-substituted derivatives of 9-(3,5-dimethylphenoxy)triptycene with F, OCH_3, CH_3, Br, and $C(CH_3)_3$ as the *peri*-substituent were synthesized and their dynamic NMR behavior was studied. In any of the compounds, two *m*-methyl groups in the phenoxyl moiety were anisochronous at low temperatures and the signals coalesced into a single peak on raising the temperature. Lineshape analysis afforded the energy barriers to the rate process ranging from 10.1 kcal mol^{-1} (1 cal_{th}=4.184 J) for the F compound to 17.6 kcal mol^{-1} for the $C(CH_3)_3$ one. Molecular mechanics calculations (MM2) were performed on closely related model compounds to obtain the relative steric energies of the ground states and the possible transition states. The results from the dynamic NMR and the molecular mechanics studies suggest the following: When the *peri*-substituent is small (F and OCH_3), the complete gear rotational circuit with the passing of the aryl group over the *peri*-substituent as the rate-determining step is the lowest-barrier process, while when the *peri*-substituent is bulky (CH_3, Br, and $C(CH_3)_3$), the "isolated" rotation of the aryl group at the *ap* site has a lower barrier and is responsible for the observed dynamic NMR behavior. In the 1,3-di-*t*-butyl derivative, restricted rotation of the 1-*t*-butyl group was observed below −75 °C, the free energy of activation being 9.5 kcal mol^{-1}.

Gear rotation or correlated disrotation of two groups (chemical rotors) attached to a common central atom is a topic of recent interest. Bis(9-triptycyl)-X compounds **1** are chemical bevel gears consisting of a pair of three-toothed wheels.[2)] In these compounds, two wheels are tightly meshed and energy barriers to gear rotation are extremely low, being below the detection limit by dynamic NMR spectroscopy, while those to slippage of the gear are very high when X is oxygen or methylene, giving rise to isolable "phase" isomers.[2a)] Diaryl-X compounds may be regarded as a bevel gear system composed of a pair of two-toothed wheels. Static and dynamic stereochemical behavior of these compounds, however, seems diverse depending on the substituents on the aryl and the X moieties.[3)] Recently, correlated disrotation was clearly proved in 2,2-bis(2,4,6-trimethylphenyl)ethenol (**2**).[3b)]

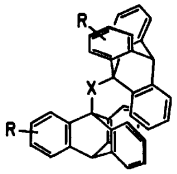

1

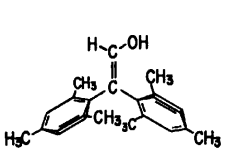

2

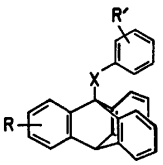

3

During the course of our studies on rotational isomerism in 9-substituted triptycene derivatives, we have been interested in the stereodynamics of 9-(arylmethyl)triptycenes (**3**: X=CH_2). These compounds adopt a conformation reminiscent of a bevel gear consisting of a two-toothed wheel and a three-toothed one, an edge of the aryl group being inserted into the notch of the triptycene skeleton.[4a-d)] A rate process which corresponds to either meshed gear rotation or gear slippage can be of low barrier depending on the substitution pattern on both the aryl and the triptycene moieties. We have extended the studies to 9-aryloxytriptycenes (**3**: X=O) by replacing the methylene group by a divalent oxygen and found that 9-(2-alkylphenoxy)-1,4-dimethyltriptycenes behave as dynamic gears, the meshed gear rotation being the lowest-barrier process.[4e,f)] The presence of a substituent at the ortho position of the aryloxyl moiety is an important factor for raising the gear slippage barrier and thus rendering the gear rotation solely detectable.

We describe in this paper the dynamic ^1H NMR and molecular mechanics studies on the stereodynamics of singly *peri*-substituted 9-(3,5-dimethylphenoxy)triptycenes (**4a—e**) which lack an *o*-substituent in the aryloxyl moiety and discuss the results in comparison with those on the carbon counterparts. We also report an almost unprecedented observation of restricted rotation of a *t*-butyl group bonded to a benzene ring found during this investigation.

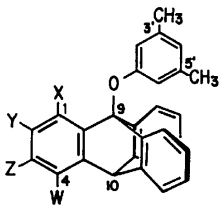

	X	Y	Z	W
4a	F	F	F	F
4b	OCH_3	H	H	OCH_3
4c	CH_3	H	H	CH_3
4d	Br	Br	Br	Br
4e	$C(CH_3)_3$	H	$C(CH_3)_3$	H

Figure 1 shows six conformers corresponding to energy minima and possible interconversion processes among them. Three rotameric sites, *ap*, $+sc$, and $-sc$, are conceivable about the C_9-O bond, and in each site $CH_3{}^A$ may look outwards (subscript 1) or inwards (subscript 2). Interconversion between ap_1 and $\pm sc_2$ and between ap_2 and $\pm sc_1$ occurs by gear rotation in which the aryl group passes over a *peri*-hydrogen

(GR(H)), while that between $\pm sc_1$ and $\mp sc_2$ occurs by gear rotation of the aryl group over the *peri*-substituent (GR(X)). Another possible process is "isolated" rotation (IR) in which the aryl group rotates by 180° without changing the rotameric site with respect to the C_9–O bond. This process corresponds to slippage of the gear and can occur either at the *ap* site (IR(*ap*)) or at the $\pm sc$ sites (IR(*sc*)).

Results and Discussion

Syntheses. 9-(3,5-Dimethylphenoxy)anthracene (**5**) was prepared in 36% yield by Ullmann reaction of 9-bromoanthracene with 3,5-dimethylphenol.[5] **5** was also obtained by acid-catalyzed condensation of anthrone[6] with 3,5-dimethylphenol but the yield was low (21%). Reactions of **5** with appropriate benzynes gave the triptycenes **4a—e**. 3,5-Di-*t*-butylbenzyne added to **5** to give **4e** and the corresponding 2,4-di-*t*-butyl derivative in ca. 3:1 ratio. Preferential formation of the more crowded regioisomer in the Diels-Alder reaction of benzynes is not unprecedented and has been discussed.[7]

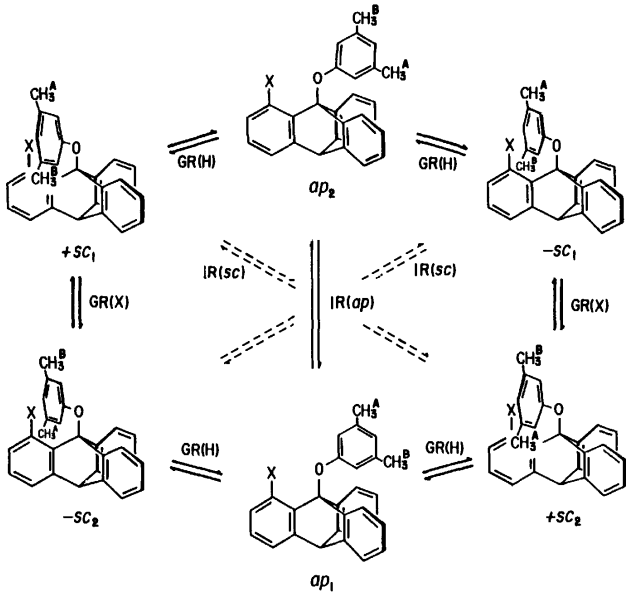

Fig. 1. Conformers of 1-substituted 9-(3,5-dimethylphenoxy)triptycenes and possible interconversion processes among them.

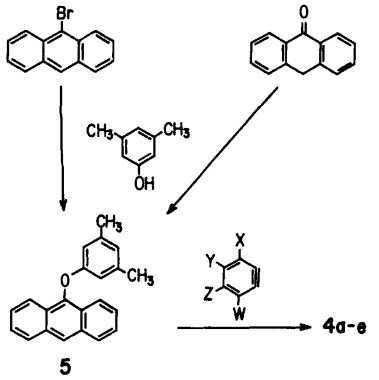

Dynamic NMR Studies. Variable temperature ^{1}H NMR study of the triptycenes **4a—e** revealed a common feature of the temperature dependence of the spectra. In any of the compounds, the signals derived from the *m*-methyl groups in the aryloxyl moiety appear as two equally intense singlets at low temperatures (Table 1) and they broaden and coalesce into a single peak upon raising the temperature. The lineshape change was analyzed as a coalescing AB spin system without mutual coupling using the DNMR3 program.[8] The kinetic parameters obtained are given in Table 2. By the same token, the *o*-protons in the aryloxyl moiety are anisochronous at low temperatures and isochronous at high temperatures. The substituents at 1 and 4 positions in **4b** and **4c** as well as the 3-*t*-butyl group in **4e** give rise to a sharp singlet for each throughout the temperature range

Table 1. Low Temperature ^{1}H chemical Shifts at 400 MHz[a]

Compd	Temp °C	Solvent	3′,5′-CH_3	10-H	1-X	3-Z or 4-W	2′,6′-H	4′-H
4a	−80	CD_2Cl_2	2.148 2.395	5.940			6.395 7.022	6.778
4b	−56	$CDCl_3$	2.087 2.414	5.952	3.205	3.876	6.340 7.074	6.663
4c	−56	$CDCl_3$	2.032 2.430	5.694	2.854	2.463	6.087 7.119	6.673
4d	−40	$CDCl_3$	2.055 2.386	6.142			6.041 7.108	6.680
4e	−96	CD_2Cl_2	1.923 2.437	5.507	1.489[b] 1.815[b]	1.264	5.673 ~7.19[c]	6.669

a) Aromatic protons in the triptycene moiety are omitted. Chemical shifts are given in δ. All the signals shown in the table are singlets although 2′-, 4′-, and 6′-H are slightly broad. b) See text. c) Overlapped with other aromatic signals.

examined. The 1-*t*-butyl signal in **4e** behaves differently, which will be discussed later in detail. The two *o*-benzeno bridges carrying no substituent are magnetically equivalent in the whole temperature range in any compound.

The spectral feature observed at low temperatures suggests that the molecules exist either solely in *ap* conformation or as a rapidly interconverting mixture of *ap* and $\pm sc$, preserving the diastereotopicity of the *m*-methyl groups in the aryloxyl moiety.

The two *m*-methyl groups should remain diastereotopic so far as the *ap* and $\pm sc$ rotamers rapidly interconvert by to-and-fro gear rotation via GR(H), $+sc_1 \rightleftarrows ap_2 \rightleftarrows -sc_1$ or $+sc_2 \rightleftarrows ap_1 \rightleftarrows -sc_2$. As discussed in the later section, compounds **4a—d** are thought to exist as a mixture of rotamers with respect to the C_9-O bond, while **4e** exists solely as the *ap* rotamer. Observation of only a single pair of methyl signals in **4a—d** in spite of the presence of both *ap* and $\pm sc$ rotamers should mean that GR(H) processes are too fast for the rotamers to be separately observed even at the lowest temperature examined.

Coalescence of the *m*-methyl signals occurs when either the GR(X) or the IR process becomes fast on the NMR time scale. However, which of these processes is the lowest-barrier one responsible for the observed dynamic NMR behavior is neither a priori evident nor is concluded by the NMR analysis.

Molecular Mechanics Calculations. In order to solve the above problem, we planned to resort to molecular mechanics calculations employing the MM2 program.[9] For simplifying the calculations, we adopted compounds **6a—e** as the respective models of **4a—e**; *m*-methyl groups in the aryloxyl moiety and 3- and 4-substituents in **4b**, **4c**, and **4e** were omitted by assuming that the buttressing effects of these groups against the neighboring hydrogen atoms are negligibly small, but halogen atoms at 2, 3, and 4 positions in **4a** and **4d** were included because the possible buttressing effect should be adequately considered.

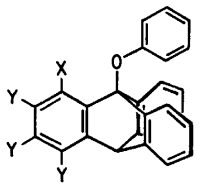

6

	X	Y
6a	F	F
6b	OCH_3	H
6c	CH_3	H
6d	Br	Br
6e	$C(CH_3)_3$	H

Calculated steric energies of the ground states, *ap* and $\pm sc$, and of the transition states for the possible dynamic processes, GR(H), GR(X), IR(*ap*), and IR(*sc*), are given in Table 3. We did not make efforts to construct the whole energy surface. In calculating the GR(X) and IR(*ap*) transition states, we assumed geometries of C_s symmetry; the substituted *o*-benzeno bridge coincides with the mirror plane and the phenoxyl benzene ring is perpendicular to it.

The *ap* ground state in any compound is shown to have C_s symmetry; the C_9-O-$C_{1'}$-$C_{6'}$ dihedral angle is 0°, giving rise to a static meshed gear. The $\pm sc$ isomer also resides in a meshed gear conformation, the C_9-O-$C_{1'}$-$C_{6'}$ angle being ca. −5° for the $+sc$ forms of **6a—d** and −19° for $+sc$-**6e**. The $\pm sc$ form is calculated to be less stable than *ap* in any compound, and the detailed discussion on this point is given in the later section.

Table 2. Dynamic NMR Data

Compd	Solvent	Freq / MHz	Temp Range[a] / °C	T_c[b] / °C	ΔH^* / kcal mol^{-1}	ΔS^* / cal mol^{-1} K^{-1}	ΔG^*_{300K} / kcal mol^{-1}
4a	CD_2Cl_2	400	−80.7—−34.6	−58	10.0$_6$±0.02	−0.9±0.1	10.3
4b	$CDCl_3$	400	−34.7—5.0	−18	11.8±0.2	−0.9±0.7	12.1
4c	$CDCl_3$	60	−4.0—36.0	24	15.4±0.6	0.6±2.0	15.2
4d	$CDCl_3$	400	25.0—50.4	48	14.3±0.3	−3.4±1.0	15.3
4e	C_2Cl_4	60	51.4—100.6	75	17.6±0.2	−0.2±0.5	17.6

a) The range in which rate constants were obtained. b) Coalescence temperature.

Table 3. Relative Steric Energies by MM2 Calculations[a]

Compd	X	Y	Ground States		Transition States			
			ap	±*sc*	GR(H)	GR(X)[b]	IR(*ap*)[b]	IR(*sc*)
6a	F	F	0	0.61	8.9	11.9	16.4	18.6
6b	OCH_3	H	0	0.52	9.0	14.0	16.5	c)
6c	CH_3	H	0	2.48	10.6	21.4	16.3	c)
6d	Br	Br	0	2.70	11.6	25.4	15.5	23.7
6e	$C(CH_3)_3$	H	0	7.78	14.3	33.1	15.3	c)

a) Values relative to that of *ap* for each compound are shown in kcal mol^{-1}. b) Geometry of C_s symmetry is assumed. c) Not calculated.

Steric energies of the transition states as given relative to that of the most stable ground state are nothing but the energy barriers to the respective processes. Dependence of the calculated barriers on the bulkiness of the *peri*-substituents is compatible with what comes from the intuitive considerations on the molecular models of the compounds: The GR barriers as well as the IR(*sc*) one are highly dependent on the *peri*-substituent but the IR(*ap*) one is rather insensitive to the size of the *peri*-substituent. We must note that, although a bromo group is usually thought to be smaller than a methyl group,[10] the 1-bromo group in **4d** is effectively bulkier than the 1-methyl group in **4c** because of the buttressing effect in **4d**.

The GR(H) barriers calculated for **6a—d** are small enough to be consistent with the fact that slowing down of this process is not observed in the ^{1}H NMR spectra of **4a—d**.

The IR(*sc*) barrier is inferred to be much higher than the IR(*ap*) one in any compound, although the calculations were made only for **6a** and **6d**, bacause the increased degrees of rotational freedom of the 1-substituent prevented the ready calculation of the IR(*sc*) transition states for **6b**, **6c**, and **6e**. Therefore the IR(*sc*) process may be disregarded as an actually occurring process.

The GR(X) barrier is calculated to be lower than the IR(*ap*) one in **6a** and **6b**, but the situation is reversed in **6c—e**. Although the inaccuracy of the absolute values of the barrier heights should be allowed for, the following deduction would be reasonable. In **4a** and **4b**, the rate process observed by dynamic NMR corresponds to GR(X), while the IR(*ap*) process is responsible for the dynamic NMR behavior in **4c—e**. Therefore, the full gear rotational circuit involving GR(X) as the rate-determining step is the lowest-barrier process when the *peri*-substituent is small (F and OCH_3), but the gear slippage occurs more easily than the full gear rotation when the *peri*-substituent is bulkier (CH_3, Br, and $C(CH_3)_3$). The calculation underestimates the IR(*ap*) barrier in **6e** but the origin is uncertain.

Previously we reported that, in 1-methoxy-9-(3,5-dimethylbenzyl)triptycene (**7**), the free energy barrier to the *ap*→±*sc* conversion at −28 °C is 12.4 kcal mol^{-1} while the one to the exchange of the *m*-methyl groups is roughly estimated to be 12.6 kcal mol^{-1}.[4b] The former process corresponds to GR(H) and the latter to either GR(X) or IR(*ap*). Assuming that the GR(X) barrier should be considerably higher than the GR(H) one, we can assign IR(*ap*) to the process responsible for the *m*-methyl exchange.

A comparison of the data for **4b** with those for **7** reveals the effects of the central group (CH_2 or O) on the barriers to gear rotation and gear slippage. Here the effect of the 4-methoxyl group in **4b** is assumed to be negligible. The GR(H) barrier in **4b** is

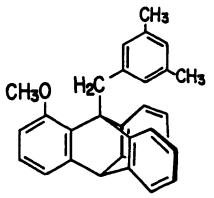

7

undetectably low, being calculated as 9.0 kcal mol^{-1} for **6b**, and thus is considerably lower than that in **7**. This may be explained in terms of the large valency effect (tetravalent in C and divalent in O) and the bond length effect partially cancelling the former, as discussed in detail in the previous paper.[4f] The IR(*ap*) barrier is far lower in **7** than in **4b** as calculated for **6b**, suggesting the importance of the bond length effect which causes tighter meshing of the gear in the oxygen compound **4b**. A similar trend in the gear slippage barriers has been observed in bis(9-triptycyl)-X compounds (**1**: X=CH_2 vs. O).[2a]

Rotamer Equilibria. No direct information on the rotamer distributions in **4a—e** is experimentally obtained because the rotamers interconvert rapidly even at the lowest temperature examined. However some information is indirectly obtained by careful examination of the NMR data. The chemical shift difference between the two *m*-methyl signals observed at low temperatures varies from 0.25 ppm for **4a** to 0.51 ppm for **4e** (Table 1), which may reflect the rotamer distribution between *ap* and ±*sc*. As the observed value is the difference between the chemical shift of CH_3^A averaged over the rotamers and that of CH_3^B also averaged over the rotamers and it should be very small if the two rotamers populate comparably and the larger it will be the more the equilibrium shifts to one side. In 9-(3,5-dimethylbenzyl)triptycene derivatives, where the rotamers were separately observed in the NMR spectra, the chemical shift differences between the *m*-methyl groups were 0.45—0.57 ppm.[11b] If the similar values of chemical shift differences are assumed for 9-(3,5-dimethylphenoxy)-triptycene rotamers, it is inferred that the rotamer equilibrium is moderately shifted to one side in **4a—d** and is almost exclusively one-sided in **4e**.

Similar inference can be made from the temperature dependence of the chemical shift difference: It decreases almost linearly with the temperature in **4a—d**, the increment being −0.40, −0.20, −0.33, and −0.27 Hz/deg, respectively, reflecting the increasing population of the minor rotamer at higher temperatures. The chemical shift differences in **4e** is almost independent of the temperature (+0.05 Hz/deg), and thus it is reasonable to conclude that **4e** exists solely as a single rotamer.

The next question to answer is to which side the equilibrium is shifted. The above reasoning together

with the results of molecular mechanics calculation concludes that **4e** exists solely as the *ap* rotamer. As for **4b** and **4c**, the chemical shifts of the 1-substituent give some information. The 1-methoxyl proton signal in **4b** appears at a considerably high field of δ 3.21 at −56 °C and shifts slightly downfield upon raising the temperature (δ 3.24 at 24 °C). The facts are consistent with the reasoning that the ±*sc* rotamer, in which the 1-methoxyl group is located in the shielding region of the aryl group, is predominant and the population of the less stable *ap* rotamer increases with temperature. In various 1-methoxy-9-(arylmethyl)triptycene derivatives ever examined,[11] the 1-methoxyl group gives its signal at δ 2.89—2.95 in the ±*sc* rotamers and at δ 3.78—3.85 in *ap*. The Winstein-Holnes relation using these values suggests that about two thirds of **4b** exists as ±*sc*. Predominance of the ±*sc* rotamer in **4b** is in line with the behavior observed in the 1-methoxy-9-(arylmethyl)-triptycene derivatives.[11] The population of the *ap* rotamer in 1,4-dimethyl-9-phenoxytriptycene was previously suggested to be about 80% at room temperature from the 1-methyl chemical shift[4f] and the similar value may also be applicable to **4c**.

The population of *ap* of 33 and 80% at room temperature corresponds to the energy difference ($E_{\pm sc}-E_{ap}$) of 0.0 and 1.24 kcal mol^{-1}, respectively, if the statistical factor of 2 for ±*sc* is assumed to be the sole contributor to the entropy term. As the MM2 calculation (Table 3) gives the energy differences of 0.52 and 2.48 kcal mol^{-1} for **6b** and **6c**, respectively, it somewhat overestimates the relative instability of the ±*sc* rotamers. The discrepancies between the NMR and MM2 results may be at least partly ascribed to the insufficiency of the force field used in the calculation as discussed before.[4f]

Restricted Rotation of the 1-*t*-Butyl Group in 4e.[12] In the 400 MHz ^{1}H NMR spectrum of **4e** at ambient temperature, the singlet at δ 1.715 due to the 1-*t*-butyl group appears considerably broader than the one at δ 1.247 assigned to the 3-*t*-butyl group. On lowering the temperature, the low-field signal further broadens and below −75 °C it splits into two peaks. At −96.2 °C, they appear as a three-proton singlet at δ 1.489 and a six-proton singlet at δ 1.815, while the high-field signal remains a sharp nine-proton singlet at δ 1.264. The phenomenon should be ascribed to the restricted internal rotation of the 1-*t*-butyl group. Lineshape analysis of the spectra at −83 to −56 °C using the DNMR3 program[8] gave the following activation parameters: $\Delta H^{\ddagger}=9.2\pm0.6$ kcal mol^{-1}, $\Delta S^{\ddagger}=-1.7\pm2.9$ cal mol^{-1} K^{-1}, $\Delta G^{\ddagger}_{200K}=9.5$ kcal mol^{-1}.

This high energy barrier to rotation of a *t*-butyl group bonded to an sp^2-hydridized carbon atom is unprecedented.[13] Several attempts at observing the restricted rotation of C_{sp^2}–Bu^t bonds by NMR spectroscopy were unsuccessful.[14] The failure might

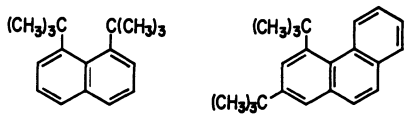

8 **9**

result from the fact that the presence of a supposedly rotation-hindering group raised not only the transition state energy but also the ground state one. An apparent exception may be 1,8-di-*t*-butylnaphthalene (**8**) derivatives, where an energy barrier of 6.5 kcal mol^{-1} was reported for the internal rotation of the *t*-butyl groups,[15a] although the geometry around the 1- and 8-carbons is far from what is expected for the normal sp^2-hybridization.[15b]

The ORTEP drawing[17] of the lowest-energy conformation of **6e** obtained by the MM2 calculation is shown in Fig. 2. Compound **4e** should reasonably adopt a similar conformation as **6e**. The molecule has a plane of symmetry and two enantiotopic methyl groups (CH_3^A) in the 1-*t*-butyl group face the oxygen atom and the other methyl (CH_3^B) eclipses C-2. The geometrical features that the benzene ring carrying the *t*-butyl group is completely planar, that the C_1–Bu^t bond shows no out-of-plane deformation in spite of the large in-plane distortion, and that the C_9–O bond is also in plane of the benzene ring, are in sharp contrast with those observed in the 1,8-di-*t*-butylnaphthalenes[15b] and 2,4-di-*t*-butylphenanthrene (**9**),[16] where significant distortion from planarity has been noticed. This rigidity of the triptycene skeleton together with the rather small oxygen atom as the obstacle to rotation should cause the high energy barrier to rotation of the 1-*t*-butyl group: The transition state for rotation is effectively raised while the ground state is not raised too much. It will be

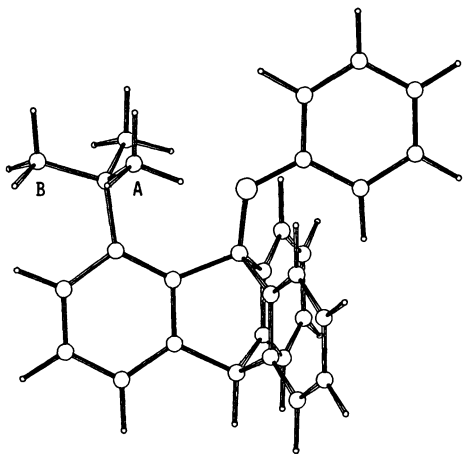

Fig. 2. ORTEP drawing of the most stable conformation of 1-*t*-butyl-9-phenoxytriptycene (**6e**) obtained by the MM2 calculation.

interesting to examine whether 9-substituted 1-*t*-butyltriptycenes generally have high energy barrier to rotation of the 1-*t*-butyl group, and further studies on this point is in progress.

Judging from the relative signal intensities, the CH_3^A protons resonate at a lower field than the CH_3^B protons. The anisotropy and/or the field effect of the oxygen atom as well as the ring current effect of the phenoxyl benzene ring might cause the deshielding of the CH_3^A protons, which should exceed the deshielding effect of the *o*-benzeno ring carrying the *t*-butyl group on the protons of the in-plane CH_3^B group.

Below −90 °C, the CH_3^B signal showed further broadening probably because of the slow-down of the internal rotation of this methyl group, although no discrete splitting of the signal was observed down to −111 °C. The staggered conformation of the methyl group and the presence of the 2-hydrogen atom as the effective obstacle might be responsible for the high rotational barrier of the methyl group.

Experimental

General Methods. ^{1}H NMR spectra at ambient temperature were obtained on a Varian EM-390 spectrometer at 90 MHz in the CW mode and on a JEOL GX-400 spectrometer at 399.65 MHz in the pulse FT mode. Variable temperature ^{1}H NMR spectra were recorded either on a Hitachi R-20B spectrometer at 60 MHz in the CW mode or on GX-400. With R-20B, temperatures were calibrated with a methanol or ethylene glycol sample[18] while they were read as digital outputs and are not corrected with GX-400. ^{19}F NMR spectra were obtained on EM-390 at 84.67 MHz. ^{1}H NMR data given in the Experimental section are those obtained on GX-400 at 21—24 °C, unless otherwise stated.

Preparative gel permeation chromatography was performed on an LC-08 Liquid Chromatograph of Japan Analytical Industry Co., Ltd. using a series of JAIGEL 1H and 2H columns and chloroform as the eluent.

Theoretical spectra for the dynamic NMR simulations were obtained on a HITAC M-280H computer system at the Computer Center of the University of Tokyo (CCUT) using the DNMR3 program.[8]

Molecular mechanics calculations were performed on the M-280H system using the MM2 program in the CCUT Program Library with some modifications of the parameters as described before.[4f,19] In obtaining the transition state energies, the C_{9a}–C_9–O–$C_{1'}$ and C_9–O–$C_{1'}$–$C_{6'}$ bonds were driven near the supposed transition state geometries and the saddle points of energy were sought. In cases of GR(X) and IR(*ap*) transition states, the geometries of C_s symmetry were assumed, although such geometries are not necessarily a prerequisite for the transition states.[20]

9-(3,5-Dimethylphenoxy)anthracene (5). (A) A mixture of 5.14 g (20 mmol) of 9-bromoanthracene, 12.2 g (100 mmol) of 3,5-dimethylphenol, 2.8 g of potassium hydroxide, and 1.0 g of copper powder was heated at 230 °C for 2 h. The cooled mixture was extracted with benzene-water. The benzene layer was washed successively with aqueous sodium hydroxide and water, and dried over magnesium sulfate. After evaporation of the solvent, the residue was chromatographed on alumina with hexane-dichloromethane as the eluent. A fraction containing 1.11 g (6.2 mmol) of anthracene eluted first, followed by a fraction containing **5**. Recrystallization of the eluate from tetrahydrofuran-hexane gave 2.12 g (36%) of **5**, mp 174—175 °C. Found: C, 88.79; H, 6.02%. Calcd for $C_{22}H_{18}O$: C, 88.56; H, 6.08%. ^{1}H NMR ($CDCl_3$, 90 MHz, 35 °C) δ=2.15 (6H, s), 6.45 (2H, s), 6.61 (1H, s), 7.2—7.5 (4H, m), 7.8—8.2 (4H, m), 8.31 (1H, s).

(B) A solution of 5.82 g (30 mmol) of anthrone and 7.33 g (60 mmol) of 3,5-dimethylphenol in 100 mL of toluene containing 1.0 mL of concentrated sulfuric acid was heated with a Dean-Stark water collector for 140 h. The solution was washed successively with aqueous sodium hydroxide and water, dried over magnesium sulfate, and concentrated. Column chromatography of the residue on alumina gave 1.86 g (21%) of **5**.

1,2,3,4-Tetrafluoro-9-(3,5-dimethylphenoxy)triptycene (4a). To a chilled (−78 °C) solution of 0.5 mL (ca. 4.3 mmol) of chloropentafluorobenzene in 30 mL of diethyl ether was added 2.0 mL (ca. 3.1 mmol) of a 10% (w/v) solution of butyllithium in hexane and the solution was stirred for 2 h at −78 °C. To this solution was added 448 mg (1.5 mmol) of **5** and the mixture was allowed to warm up to room temperature with stirring, stirred at room temperature for 2 h and heated under reflux for 2 h. The reaction mixture was washed with water, dried over magnesium sulfate and concentrated. The residue was heated under reflux overnight with 0.5 g (ca. 5 mmol) of maleic anhydride in 10 mL of acetonitrile. After evaporation of the solvent, the residue was chromatographed on alumina with hexane-dichloromethane as the eluent, affording 33 mg (5%) of **4a**, mp 250—252 °C. Found: C, 75.09; H, 4.15%. Calcd for $C_{28}H_{18}F_4O$: C, 75.33; H, 4.06%. ^{1}H NMR ($CDCl_3$) δ=2.241 (6H, s), 5.783 (1H, d, J=1.5 Hz), 6.657 (2H, s), 6.691 (1H, s), 7.00—7.10 (4H, m), 7.40—7.50 (4H, m). ^{19}F NMR ($CDCl_3$, ppm downfield from internal hexafluorobenzene) 3.13 (dd, J=19 and 21 Hz, 2-F), 3.81 (ddd, J=3, 19, and 21 Hz, 3-F), 13.10 (dd, J=15 and 21 Hz, 4-F), 20.39 (br m, 1-F).

1,4-Dimethoxy-9-(3,5-dimethylphenoxy)triptycene (4b). To a boiling solution of 298 mg (1.0 mmol) of **5** in 20 mL of 1,2-dimethoxyethane(DME) was added a solution of 986 mg (5.0 mmol) of 3,6-dimethoxyanthranilic acid[21] in 20 mL of DME and a solution of 1.0 mL (ca. 7.4 mmol) of isopentyl nitrite in 10 mL of DME during the course of 2 h so that excess of isopentyl nitrite always existed in the reaction mixture. The mixture was heated under reflux for 0.5 h and concentrated. The residue was chromatographed on alumina with hexane-dichloromethane as the eluent, affording 70 mg (16%) of **4b**, mp 264—265 °C after recrystallization from tetrahydrofuran-hexane. Found: C, 82.79; H, 5.95%. Calcd for $C_{30}H_{26}O_3$: C, 82.92; H, 6.03%. ^{1}H NMR ($CDCl_3$) δ=2.221 (6H, br s), 3.236 (3H, s), 3.859 (3H, s), 5.898 (1H, s), 6.509 and 6.611 (2H, AB-q, J=8.9 Hz), 6.608 (1H, s), 6.668 (2H, br s), 6.90—7.05 (4H, m), 7.35—7.60 (4H, m).

1,4-Dimethyl-9-(3,5-dimethylphenoxy)triptycene (4c). Similar reaction as above of **5** with 3,6-dimethylanthranilic acid[22] gave **4c**, mp 261—262 °C, in 58% yield. Found: C, 89.33; H, 6.56%. Calcd for $C_{30}H_{26}O$: C, 89.51; H, 6.51%. ^{1}H NMR ($CDCl_3$) δ=2.031 (3H, br s), 2.372 (3H, br s), 2.440 (3H, s), 2.792 (3H, s), 5.622 (1H, s), 6.154 (1H, br s), 6.628

(1H, s), 6.640 and 6.667 (2H, AB-q, J=7.2 Hz), 6.85—7.05 (5H, m), 7.25—7.45 (4H, m).

1,2,3,4-Tetrabromo-9-(3,5-dimethylphenoxy)triptycene (4d). Similar reaction as above of **5** with tetrabromoanthranilic acid[23] gave **4d**, mp 330—332 °C (decomp), in 11% yield. Found: C, 48.62; H, 2.67; Br, 46.80%. Calcd for $C_{28}H_{18}Br_4O$: C, 48.73; H, 2.63; Br 46.32%. ^{1}H NMR ($CDCl_3$) δ=2.054 (3H, br s), 2.344 (3H, br s), ca. 6.1 (1H, br), 6.100 (1H, s), 6.654 (1H, s), 6.95—7.15 (5H, m), 7.30—7.55 (4H, m).

1,3-Di-*t*-butyl-9-(3,5-dimethylphenoxy)triptycene (4e). Similar reaction as above of **5** with 3,5-di-*t*-butylanthranilic acid[7b] gave a ca. 3:1 mixture of **4e** and the isomeric 2,4-di-*t*-butyl-9-(3,5-dimethylphenoxy)triptycene. Separation of the regioisomers was performed by gel permeation chromatography. Even after 20 recycles, complete baseline separation of the isomers was not attained. **4e** was isolated in ca. 18% yield, mp 203—205 °C. Found: C, 88.62; H, 7.58%. Calcd for $C_{36}H_{38}O$: C, 88.84; H, 7.87%. ^{1}H NMR ($CDCl_3$) δ=1.227 (9H, s), 1.722 (9H, s), 1.905 (3H, s), 2.429 (3H, s), 5.322 (1H, s), 5.720 (1H, s), 6.601 (1H, s), 6.8—7.5 (11H, m). The 2,4-di-*t*-butyl compound was isolated in ca. 6% yield, mp 238—239 °C. Found: C, 88.90; H, 7.59%. ^{1}H NMR ($CDCl_3$, 90 MHz, 35 °C): δ=1.14 (9H, s), 1.58 (9H, s), 2.23 (6H, s), 6.14 (1H, s), 6.65 (1H, s), 6.73 (2H, s), 6.8—7.1 (5H, m), 7.3—7.5 (5H, m).

References

1) Part LVIII: Ref. 12.

2) a) H. Iwamura, *J. Mol. Struct.*, **126**, 401 (1985); Y. Kawada and H. Iwamura, *J. Am. Chem. Soc.*, **105**, 1449 (1983); H. Iwamura, T. Ito, H. Ito, K. Toriumi, Y. Kawada, E. Ōsawa, T. Fujiyoshi, and C. Jaime, *ibid.*, **106**, 4712 (1984); b) H.-B. Bürgi, W. D. Hounshell, R. B. Nachbar, Jr., and K. Mislow, *ibid.*, **105**, 1427 (1983); A. Guenzi, C. A. Johnson, F. Cozzi, and K. Mislow, *ibid.*, **105**, 1438 (1983).

3) a) D. Gust and K. Mislow, *J. Am. Chem. Soc.*, **95**, 1535 (1973) and references cited therein; b) D. A. Nugiel, S. E. Biali, and Z. Rappoport, *ibid.*, **106**, 3357 (1984); c) cf. B. F. Bononi, L. Grossi, L. Lunazzi, and D. Macchiantelli, *J. Org. Chem.*, **51**, 517 (1986).

4) a) G. Yamamoto, *J. Mol. Struct.*, **126**, 413 (1985); b) G. Yamamoto and M. Ōki, *Chem. Lett.*, **1979**, 1251; G. Yamamoto and M. Ōki, *Bull. Chem. Soc. Jpn.*, **54**, 473 (1981); c) G. Yamamoto and M. Ōki, *Chem. Lett.*, **1979**, 1255; G, Yamamoto and M. Ōki, *Bull. Chem. Soc. Jpn.*, **54**, 491 (1981); d) G. Yamamoto and M. Ōki, *J. Org. Chem.*, **48**, 1233 (1983); e) G. Yamamoto and M. Ōki, *Chem. Lett.*, **1984**, 92; f) G. Yamamoto and M. Ōki, *Bull. Chem. Soc. Jpn.*, **56**, 1953 (1985).

5) cf. W. Theilacker, U. Berger-Brose, and K.-H. Beyer, *Chem. Ber.*, **93**, 1658 (1960).

6) cf. W. H. Pirkle and J. M. Finn, *J. Org. Chem.*, **48**, 2779 (1983).

7) a) G. Yamamoto, M. Suzuki, and M. Ōki, *Bull. Chem. Soc. Jpn.*, **56**, 306 (1983); b) R. W. Franck and E. G. Leser, *J. Org. Chem.*, **35**, 3932 (1970); c) J. E. Anderson, R. W. Franck, and W. L. Mandella, *J. Am. Chem. Soc.*, **94**, 4608 (1972).

8) D. A. Kleier and G. Binsch, *QCPE*, No. 165.

9) N. L. Allinger and Y. H. Yuh, *QCPE*, No. 395.

10) L. Pauling, "The Nature of the Chemical Bond," 3rd ed., Cornell University Press, New York (1960), p. 260; G. Bott, L. D. Field, and S. Sternhell, *J. Am. Chem. Soc.*, **102**, 5618 (1980). See also: W. D. Hounshell, L. D. Iroff, D. J. Iverson, R. J. Wrozynski, and K. Mislow, *Isr. J. Chem.*, **20**, 65 (1980).

11) a) F. Suzuki and M. Ōki, *Bull. Chem. Soc. Jpn.*, **48**, 596 (1975); b) G. Yamamoto and M. Ōki, *ibid.*, **54**, 473 (1981); c) G. Yamamoto and M. Ōki, *ibid.*, **54**, 481 (1981).

12) Preliminary results have been reported: G. Yamamoto and M. Ōki, *Tetrahedron Lett.*, **27**, 49 (1986).

13) Restricted rotation of a trimethylsilyl group attached to an sp^2-hybridized carbon atom has been reported: J.-C. Clinet, E. Dunach, and K. P. C. Vollhardt, *J. Am. Chem. Soc.*, **105**, 6710 (1983); H. Butenschön, M. Winkler, and K. P. C. Vollhardt, *J. Chem. Soc., Chem. Commun.*, **1986**, 388.

14) M. Ōki and N. Nakamura, *Bull. Chem. Soc. Jpn.*, **44**, 1880 (1971); B. Miller and K.-H. Lai, *Tetrahedron Lett.*, **1971**, 2957.

15) a) J. E. Anderson, R. W. Franck, and W. L. Mandella, *J. Am. Chem. Soc.*, **94**, 4608 (1972); b) J. Handal, J. G. White, R. W. Franck, Y. H. Yuh, and N. L. Allinger, *ibid.*, **99**, 3345 (1977); **101**, 5456 (1979).

16) The 4-*t*-butyl proton signal of 2,4-di-*t*-butylphenanthrene (**9**) does not split down to −90 °C and the X-ray crystal structure of this compound shows considerable distortion of the 4-*t*-butyl group as well as the phenanthrene ring itself: H. J. Lindner, H. Scherübl, and A. Mannschreck, unpublished results. We are grateful to Professor Mannschreck for informing us the results.

17) C. K. Johnson, ORNL-3794, Oak Ridge National Laboratory, Oak Ridge, Tenn. (1965).

18) A. L. Van Geet, *Anal. Chem.*, **40**, 2227 (1968).

19) G. Yamamoto and M. Ōki, *Bull. Chem. Soc.*, **56**, 1690 (1985).

20) L. Salem, J. Durup, G. Bergeron, D. Cazes, X. Chapuisat, and H. Kagan, *J. Am. Chem. Soc.*, **92**, 4472 (1970).

21) M. Ōki, Y. Tanaka, G. Yamamoto, and N. Nakamura, *Bull. Chem. Soc. Jpn.*, **56**, 302 (1983).

22) S. Gronowitz and G. Hansen, *Arkiv Kemi*, **27**, 145 (1967).

23) H. Heaney, K. G. Mason, and J. M. Sketchley, *J. Chem. Soc., C*, **1971**, 567.

 © 1986 The Chemical Society of Japan Bull. Chem. Soc. Jpn., 59, 3605—3610 (1986)

Dynamic NMR as a Nondestructive Method for the Determination of Rates of Dissociation. X. Rates of Dissociation of the C-N Bond in Substituted 1-(1,3-Dithiolan-2-yl)pyridinium Perchlorates[1,2]

Toshiari Morita and Michinori Ōki*
Department of Chemistry, Faculty of Science, The University of Tokyo,
Bunkyo-ku, Tokyo 113
(Received June 6, 1986)

Rates of dissociation of the C-N bond in substituted 1-(1,3-dithiolan-2-yl)pyridinium ions in the perchlorate forms were obtained by the dynamic NMR technique in nitromethane-d_3 and for one case in acetonitrile-d_3. The study of the substituent effects on the rates of dissociation revealed that the rates were linearly correlated with the pK_a values of the substituted pyridines. The mechanism of the dissociation was postulated to be of S_N2 type, the perchlorate ion acting as a nucleophile, from the kinetic data.

Dynamic NMR techniques are unique in that the rates of dissociation of molecular species can be studied in nonpolar aprotic solvents without destruction of the molecule. The so-called topomerization[3] is the key step in this methodology. The method had been originally applied to organometallic compounds[4] and then the method has now been extended to the dissociation of organic halides,[5] ammonium ions derived from tertiary amines and acids,[6] and amine ligands of some coordination compounds.[7] The method is capable of producing the rates of dissociation which exceed the limit obtainable by the classical kinetic method.

Since quaternary ammonium salts can be considered as composed of a tertiary amine and a carbocation, the dissociation of this group of compounds must be on an extrapolation map of the above-mentioned ammonium salts or coordination compounds. From the standpoint of organic chemistry, there are varieties of reactions of quaternary ammonium salts which involve dissociation of the C-N bond in them.[8] Hence it will be interesting to find examples of ammonium salts which give suitable rates of dissociation for the dynamic NMR technique. This will also give information which is useful in understanding the dissociation processes in aprotic solvents.

The crucial point is that we must search a group of compounds which give suitable rate constants of dissociation for the dynamic NMR technique. Our experience showed that the pyridinium salt which was derived from benzyl α-chlorobenzyl sulfide and pyridine exhibited too low rates of dissociation for the dynamic NMR. Thus we explored compounds which could produce more stable carbocation than the α-(benzylthio) benzyl cation. The natural choice was to introduce two sulfur atoms alpha to the cation.

1,3-Dithiolan-2-yl cation was expected to be a good candidate for the system in question. Various attempts to identify the suitable compounds, including the pyridinium compounds derived from 2-chloro-1,3-dithiolane, led to a finding that 1-(1,3-dithiolan-2-yl)pyridinium salts were suitable for the investigation. Perchlorate salts were selected because of their stability and the ease of syntheses.

The compounds were prepared by treating 1,3-dithiolane with triphenylmethyl perchlorate and then with substituted pyridines in acetonitrile. The compounds were rather unstable and were especially moisture-sensitive, if the substituent was electron-withdrawing. In spite of the easy deterioration in the air, they could be purified by recrystallization from acetonitrile-ether, if we handled them carefully, under dry conditions.

The 400 MHz NMR spectra of the compounds were determined as nitromethane-d_3 solutions except for one case, when acetonitrile-d_3 was used. The use of the polar solvent was necessary because their solubilities in nonpolar aprotic solvents were very low. The compounds exhibited either complex AA'BB' patterns or a broad signal for the ring protons of the 1,3-dithiolane, the former giving broadening of the signals at high temperatures and the latter showing AA'BB' signals at low temperatures. The rate process becomes slow as the 4-substituent on the pyridine ring becomes electron-donating. Although we have made various pyridinium salts of this type, which carry electron-withdrawing substituents, their rates of hydrolysis were too large to obtain pure samples. Thus, although the trend in the rate processes mentioned above is apparent, we wish to present the results with the samples only which gave correct elemental analyses in this paper.

The change in the line shapes of the NMR spectra is indicative of the presence of a dynamic process. The site exchange is most reasonably explained by assuming the dissociation of the C-N bond of the pyridinium salts followed by association to the covalent species, when topomerization takes place (Eq. 1). If the basicity of a pyridine compound is high, the C-N bond in question must be stronger than the case of a weak base, because it is the acid-base combination. The above results conform to this expectation, if we assume the dissociation of the C-N bond in the pyridinium ions.

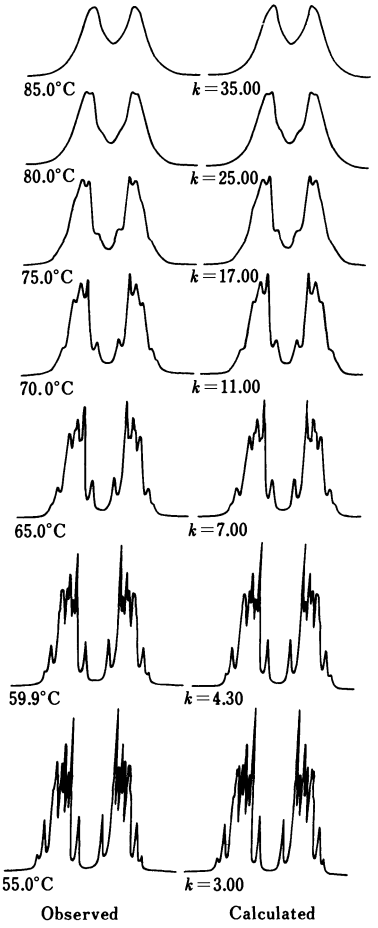

Fig. 1. Observed and calculated AA'BB' ^{1}H NMR spectra of 4-methoxy-1-(1,3-dithiolan-2-yl)pyridinium perchlorate at various temperatures.

Table 1. Equations Correlating the Chemical Shift Differences and Temperature and Coupling Constants of AA'BB' Systems in Substituted 1-(1,3-Dithiolan-2-yl)pyridinium Perchlorates

Substituent	$f(T)$[a]	J_{gem}/Hz	J_{cis}/Hz	J_{trans}/Hz
4-CH_3O	106.12—0.18T	−11.9	5.2	6.8
4-CH_3	100.02—0.18T	−11.9	5.3	6.8
H	88.13—0.15T	−11.9	5.3	6.8
3-CH_3O	88.32—0.16T	−11.9	5.3	6.8

a) $f(T)$ for $\Delta\nu$/Hz=$f(T)$/K.

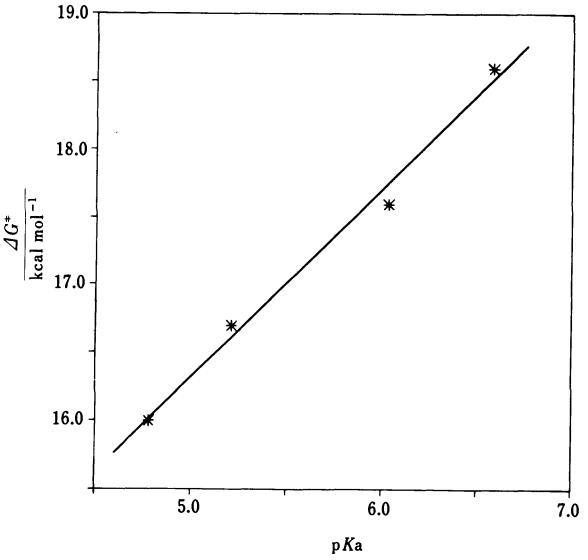

Fig. 2. Relationship between the pK_a values of pyridine bases and the free energy of activation for dissociation of the C–N bond in 1-(1,3-dithiolan-2-yl)-pyridinium perchlorates.

Table 2. Rate Constants (k) and Transverse Relaxation Times (T_2) at Various Temperatures as Obtained by Simulation of the NMR Line Shapes

Substituent	k/s^{-1} (T_2/s, Temperature/°C)
4-CH_3O	3.0 (0.47, 55.0), 4.3 (0.45, 59.9), 7.0 (0.47, 65.0), 11.0 (0.41, 70.0), 17.0 (0.45, 75.0), 25.0 (0.41, 80.0), 35.0 (0.45, 85.0)
4-CH_3	3.7 (0.57, 40.0), 5.5 (0.66, 45.0), 8.8 (0.65, 50.0), 14.0 (0.52, 55.0), 21.5 (0.50, 60.0), 32.5 (0.49, 65.1)
H	3.7 (0.22, 25.1), 6.4 (0.32, 30.7), 9.1 (0.24, 35.0), 13.4 (0.18, 40.0), 19.5 (0.13, 45.0), 29.0 (0.15, 50.0)
3-CH_3O	2.6 (0.36, 10.2), 4.3 (0.36, 14.8), 6.8 (0.35, 20.0), 11.0 (0.36, 24.9), 18.0 (0.31, 30.1), 28.0 (0.29, 35.0)

Table 3. Activation Parameters for the Dissociation of the C–N Bond in Substituted 1-(1,3-Dithiolan-2-yl)pyridinium Perchlorates

Substituent	Correlation[a] Coecfficient	$\Delta H^{\ddagger}$ [b] / kcal mol^{-1}	$\Delta S^{\ddagger}$ / cal mol^{-1} K^{-1}	$\Delta G^{\ddagger}_{298}$ / kcal mol^{-1}	k_{298} / s^{-1}	pK_a[c]
4-CH_3O	0.9993	19.0±0.8	1.2±2.4	18.6	0.142	6.58
4-CH_3	0.9995	17.8±0.8	0.9±2.3	17.6	0.804	6.03
H	0.9995	15.0±0.7	−5.6±1.7	16.7	3.79	5.21
3-CH_3O	0.9998	15.9±0.5	−0.3±1.6	16.0	11.2	4.78

a) In the least squares treatment. b) 1 cal=4.184 J. c) Ref. 10.

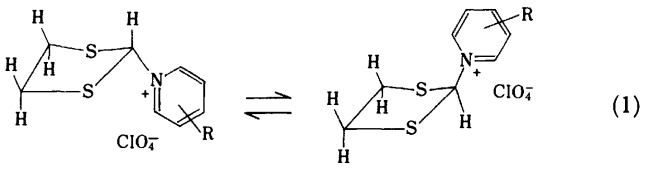

1a 1b (1)

Typical line shapes at various temperatures together with the simulated spectra of 4-methoxy-1-(1,3-dithiolan-2-yl)pyridinium perchlorate are given in Fig. 1. The spectral parameters of the AA'BB' patterns were obtained by simulation with the use of the LAOCN III program stored in the Computer Center of this University. The simulation was performed for the spectra at various temperatures where the rates of the exchange were negligibly small. This operation confirmed that the coupling constants were temperature-independent, while chemical shift differences for the A and B protons were temperature-dependent. The drift of the chemical shift differences could be linearly correlated with temperature. The correlation of the chemical shift differences with temperature together with coupling constants are compiled in Table 1 for the nitromethane-d_3 solutions. Thus the chemical shift differences at a given temperature could be calculated by these equations and were used for the simulation.

The rate constants of topomerization at various temperatures were obtained by simulation of the line shapes with the use of DNMR3 program.[9] The rate constant k and the transverse relaxation time T_2 were treated as variables. In spite of this practice, thanks to the complicated line shapes, the variation of k gives a different trend in modification of the line shape from that in T_2, thus enabling us to determine unique values of k and T_2. The values k and T_2 are given in Table 2. The agreement of the calculated spectra with the observed was satisfactory, as is shown in Fig. 1.

Putting the rate constants and temperatures into the Eyring equation, we obtained the kinetic parameters which are shown in Table 3. A trend is apparent: The more basic is the pyridine derivative, the higher is the enthalpy of activation. Indeed, the pK_a values of the pyridine bases and the free energy of activation for the dissociation gives a good straight line, as is shown in Fig. 2, the slope and the correlation coefficient being 4.8 and 0.995, respectively. The linearity is not necessarily held between the base strengths toward the proton and carbon acids,[11] but the increase in the hardness of the carbocation in this case due to the presence of two alpha sulfur atoms will be the key factor for this linearity between the proton and carbocation acids. The results clearly indicate that the bond dissociation is the key step in the observed topomerization processes. Thus we are able to show examples of self dissociation of ammonium salts which can be observed by the dynamic NMR technique. Further application of this technique in this area will certainly contribute to the understanding of the S_N1 type substitution reactions of the ammonium salts which have been known for some time.

The entropies of activation are interesting: They are all close to zero. Although the reliability of entropy of activation obtained by the dynamic NMR method had been questioned, a concensus has now been established that it is reproducible and reliable, when the total line shape analyses are performed on complex line shapes.[4b,12] The observed entropies of activation make a striking contrast with the other cases we have examined so far. It has been shown that, if a covalent species dissociates to form ion pairs, the entropy of activation is large negative, whereas it is large positive, if an ion pair colapses to form a covalent species on dissociation.[5,6] Since the case studied here is the dissociation of an ion pair to covalent species, the simple application of the above generalization to the present case tells that entropy of activation should be large positive because the disorderedness of solvent molecules should increase at the transition state of the reaction.[13] Yet the observed entropy of activation is close to zero.

We should like to take this fact as indicative of the reaction mechanism and the rate determining step. In principle, the bond dissociation of the C-N can occur either in S_N1 (Eq. 2) or in S_N2 (Eq. 3) fashion.

If the dissociation is of S_N1 type, 1, 3-dithiolan-2-yl cation and a pyridine molecule are partially formed at the transition state. The net electric charge is invariant, whereas a new particle is being formed. This transition state should give positive entropy of activation. The results in Table 3 are not in conformity with this expectation.

In the S_N2 type reactions, the perchlorate anion must be the nucleophile. This is unusual but not without precedence. Perchlorate esters are known[14] and perchlorate anion shows nucleophilic nature in some instances.[15] It is possible, therefore, that the reaction proceeds in the S_N2 fashion. However, in the S_N2 type reactions, the electric charges are to be extinguishing and this contributes to the increase in the entropy of activation. Thus there must be good reasons why the observed entropy of activation is close to zero, if we postulate the rate-determining step of the reaction to be of S_N2 type.[16,17]

We believe the followings are the explanations for the observation. In the ground state of the reaction, perchlorate anion will be rotating freely with having interactions through its four equivalent oxygens, bearing the negative charge, with the cationic center. In the transition state, a partial covalent bond is to be formed, thereby losing the freedom of motion of the perchlorate ion. This should contribute to the

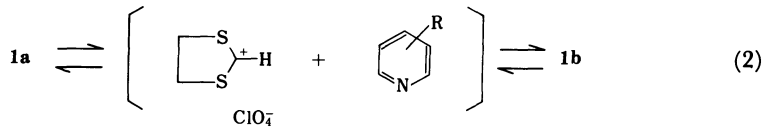

(2)

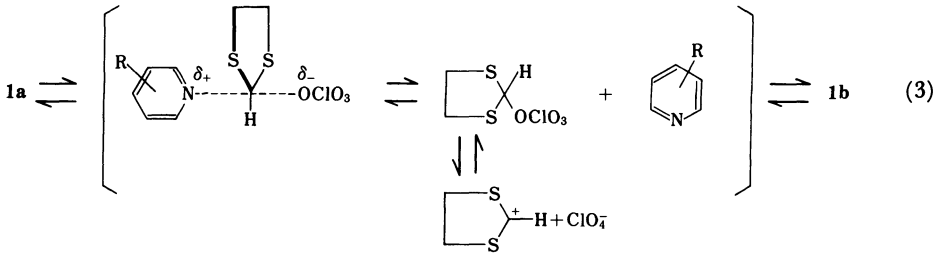

(3)

decrease in entropy. The decrease in entropy due to the loss of freedom of motion of the anion and the increase in entropy due to the increase in the freedom of motion of the solvent molecules may compensate to make the absolute values of the entropy of activation very small. There are examples of this sort: Whereas proton transfer reactions from an ammonium ion to chloride ion exhibits a large positive entropy of activation, that between an ammonium ion and sulfonate anion proceeds with nearly zero entropy of activation.[19] Therefore, we conclude that the bond dissociation reaction in the 1-(1,3-dithiolan-2-yl)-pyridinium ions takes place with the S_N2 type mechanisms.

Table 4. ^{1}H NMR Data and Kinetic Parameters for the Dissociation of 1-(1,3-Dithiolan-2-yl)pyridinium Perchlorates in CD_3CN

$\Delta\nu$/Hz vs. Temperature/K Correlation	$\Delta\nu = 66.46 - 0.10T$
J_{gem}/Hz, J_{cis}/Hz, J_{trans}/Hz	−11.9, 5.4, 6.8
k/s^{-1} (T_2/s, Temperature/°C)	4.0 (0.30, 25.1), 6.4 (0.33, 30.3), 9.2 (0.30, 35.4), 13.3 (0.25, 40.0), 19.3 (0.18, 45.0), 28.0 (0.17, 50.0)
Correlation Coefficient	0.9997
$\Delta H^{\ddagger}$/kcal mol^{-1}	14.2±0.5
$\Delta S^{\ddagger}$/cal mol^{-1} K^{-1}	−8.1±1.6
$\Delta G^{\ddagger}_{298}$/kcal mol^{-1}	16.4

Since the perchlorate ester which is transiently formed is very unstable due to the fact that the cation is stabilized by the presence of two alpha sulfur atoms, it rapidly dissociates to an ion pair which subsequently topomerizes and then recombines to form the topomer of the starting material. This series of reactions completes the observed process.

The dissociation reaction of 1-(1,3-dithiolan-2-yl)-pyridinium perchlorate can also be detected in acetonitrile-d_3. The NMR data as well as kinetic parameters are listed in Table 4. The chemical shift differences are small in acetonitrile relative to those in nitromethane. This causes coalescence of the signals at lower temperature in acetonitrile than in nitromethane. However, the kinetic parameters for the dissociation in the two solvents are very close with each other. This may be rationalized by the fact that the polarity of the solvents is similar. Because of the similarity of the results, no further measurements were carried out for other compounds in acetonitrile.

Table 5. Melting Points and Elemental Analyses of Substituted 1-(1,3-Dithiolan-2-yl)pyridinium Perchlorates

Substituent	Mp (θ_m/°C)	Analysis					
		C/%		H/%		N/%	
		Calcd	Found	Calcd	Found	Calcd	Found
4-CH_3O	96—114[a]	34.45	34.21	3.86	3.83	4.47	4.32
4-CH_3	64—66	36.30	36.05	4.06	4.25	4.71	4.68
H	140—149[a]	33.86	33.74	3.55	3.46	4.94	4.80
3-CH_3O	86—87	34.45	34.14	3.86	4.27	4.47	4.34

a) With decomposition.

Table 6. ^{1}H NMR Data of Substituted 1-(1,3-Dithiolan-2-yl)pyridinium Perchlorates in CD_3NO_2 at 400 MHz

Substituent	Temperature °C	Chemical Shifts (δ)				
		1,3-Dithiolane		Pyridine		Others
		3,4-H	1-H	3,5-H	2,6-H	
4-CH_3O	10	3.68 (m)	7.25 (s)	7.52 (dd)	8.97 (dd)	4.27 (s)
4-CH_3	10	3.72 (m)	7.34 (s)	7.06 (dd)	9.04 (dd)	2.75 (s)
H	10	3.73 (m)	7.43 (s)	8.18 (td)	9.26 (dd)	8.67 (td)[a]
3-CH_3O	0	3.73 (m)	7.40 (s)	b)	9.83[c]	4.14 (s)[d]

a) 4-H of the pyridine ring. b) 5-H gives a signal at δ 8.08 (q). c) Apparent triplet for 2-H. d) 4-H and 6-H give signals at δ 8.18 (q) and 8.90 (apparent d), respectively.

Experimental

The compounds examined here are easily hydrolyzable with water in the air or in solvents. Special care was exercised to remove trace of water from the solvents and to avoid contact with air. Nitromethane-d_3 and acetonitrile-d_3 were dried over Molecular Sieves 3A, the method being recommended by a literature for acetonitrile.[20] Acetonitrile for the syntheses of the compounds was distilled from its mixture with phosphorus pentaoxide and dried over Molecular Sieves 3A. Ether was distilled from its mixture with lithium tetrahydridoaluminate.

Substituted 1-(1,3-Dithiolan-2-yl)pyridinium Perchlorates. The whole operations were carried out under dry argon. Triphenylmethyl perchlorate[21] (0.44 g or 1.3 mmol) was dissolved in 5 mL of acetonitrile. To this solution was added 0.15 g (1.4 mmol) of 1,3-dithiolane[22] in one portion and the mixture was stirred for 10 min at room temperature, and then 30 mL of dry ether was added to form yellow precipitates. The solvent was removed by filtration and the solid was washed with ether for several times. The solid was then dissolved in acetonitrile and mixed with 1.3 mmol of an appropriate pyridine derivative. Ether was added to the mixture until slight turbidity was observed at room temperature and the whole was cooled to −40~−50 °C. The precipitate was collected by filtration and recrystallized from acetonitrile-ether. The melting points and analytical data are given in Table 5 and the ^{1}H NMR data in Table 6.

Dynamic NMR Spectral Study. The spectral measurement was carried out with either a JEOL GX400 machine installed in Nippon Kayaku Company, Ltd., or that in Institute for Molecular Science. Samples were dissolved in nitromethane-d_3 or in acetonitrile-d_3 to make up a solution of ca. 200 mmol L^{-1}. Temperature was read by a thermocouple. For measurements of the dependence of the chemical shift differences on temperature, the spectra were obtained at 4—5 points of temperatures where the exchange of sites of magnetic spins was negligibly slow. The straight line was drawn by the least squares method. Fitting of the calculated spectra with the observed was carried out visually.

We wish to thank Dr. G. Izumi of Nippon Kayaku Co., Ltd., for measuring the ^{1}H NMR spectra at various temperatures and Institute for Molecular Science for the permission of using the NMR spectrometer. This work was supported by a Grant-in-Aid for Scientific Research of the Ministry of Education, Science and Culture, to which our thanks are due.

References

1) For Part IX of the series, see Ref. 7.
2) A preliminary note has been published: M. Ōki and T. Morita, *Chem. Lett.*, **1984**, 989.
3) G. Binsch, E. L. Eliel, and H. Kessler, *Angew. Chem. Int. Ed. Engl.*, **10**, 570 (1971).
4) a) G. M. Whitesides, M. Witanowski, and J. D. Roberts, *J. Am. Chem. Soc.*, **87**, 2854 (1965); M. Ōki, "Applications of Dynamic NMR Spectroscopy to Organic Chemistry," VCH Publishers, Deerfield Beach (1985), pp. 394—397.
5) A. Shimizu, Y. Sakamaki, K. Azuma, H. Kihara, N. Nakamura. and M. Ōki, *Bull. Chem. Soc. Jpn.*, **54**, 2774 (1981).
6) M. Ōki, M. Ohira, Y. Yoshioka, T. Morita, H. Kihara, and N. Nakamura, *Bull. Chem. Soc. Jpn.*, **57**, 2224 (1984).
7) M. Ōki and M. Ohira, *Bull. Chem. Soc. Jpn.*, **57**, 3117 (1984).
8) J. H. Brewster and E. L. Eliel, *Org. React.*, **7**, 99 (1953).
9) G. Binsch, *Top. Stereochem.*, **3**, 97 (1968).
10) A. Fischer, W. J. Galloway, and J. Vaughan, *J. Chem. Soc.*, **1964**, 3591.
11) "Hard and Soft Acids and Bases," ed by R. G. Pearson, Dowden, Hutchinson and Ross, Stroudsburg, Pennsylvania (1973); T.-L. Ho, *Chem. Rev.*, **75**, 1 (1975).
12) G. Binsch and H. Kessler, *Angew. Chem. Int. Ed. Engl.*, **19**, 41 (1980).
13) J. W. Moore and R. G. Pearson, "Kinetics and Mecanism," 3rd ed, John-Wiley, New York (1981), p. 256.
14) D. N. Kevill and H. S. Posselt, *J. Chem. Res. Synop.*, **1983**, 264 and earlier papers.
15) N. S. Zefirov, A. S. Koz'min, V. V. Zhdankin, V. N. Kirin, N. M. Yur'eva, and V. D. Sorokin, *Chem Scr.*, **22**, 195 (1983); N. S. Zefirov, V. V. Zhdankin, and A. S. Koz'min, *Tetrahedron Lett.*, **27**, 1845 (1986); N. S. Zefirov and A. S. Koz'min, *Acc. Chem. Res.*, **18**, 154 (1985).
16) Ordinary S_N2 reactions are known to proceed with negative entropy of activation.[18] However, this is due to the fact that the reaction occurs from a free nucleophile and a substrate in solution and is different from the case discussed here, where the reaction occurs from tight ion pairs or solvent-separated ion pairs. This assumption is consistent

with the fact that ammonium chlorides and a bromide give large positive entropy of activation for their dissociation.[6,19]

17) In Eq. 3, it is not meant that the reaction to afford the topomerized product proceeds with S_N2 mechanism between the perchlorate ester and the pyridine, but that a reaction between the pyridine and the perchlorate ester and/or the ion pair takes place. The necessary information for the diagnosis of the contribution of the two possible routes cannot be obtained because this step is not rate-determining. At any rate, a simple S_N2 reaction between the formed perchlorate ester and the pyridine does not account for the topomerization: It gives back the original topomer. The ester must dissociate to the ion pair in which topomerization takes place.

18) R. A. Y. Jones, "Physical and Mechanistic Organic Chemistry," 2nd ed, Cambridge University Press, Cambridge (1984), p.297.

19) M. Ōki and M. Ohira, *Bull. Chem. Soc. Jpn.*, **57**, 3025 (1984).

20) D. R. Burfield, K. -H. Lee, and R. H. Smithers, *J. Org. Chem.*, **42**, 3060 (1977).

21) H. J. Dauben, Jr., L. R. Honnen, and K. M. Harmon, *J. Org. Chem.*, **25**, 1442 (1960).

22) 1,3-Dithiolane was prepared by a method described for the synthesis of 1, 3-dithiane [E. J. Corey and D. Seebach, *Org. Synth.*, **50**, 72 (1970)], starting from 1, 2-ethanedithiol and dimethoxymethane, bp 97.7 °C/62 mmHg (1 mmHg= 133.322 Pa), in 78% yield. Lit,[23] bp 77 °C/23 mmHg.

23) B. C. Newman and E. L. Eliel, *J. Org. Chem.*, **35**, 3641 (1970).

The Preparation and Some Properties of 1,4,7-Trithia[7]- and 1,5,9-Trithia[9]ferrocenophanes and Their Copper(I), Silver(I), Mercury(II), and Palladium(II) Complexes

Masaru SATO,* Kaoru SUZUKI, and Sadatoshi AKABORI†
Chemical Analysis Center, Saitama University, Urawa, Saitama 338
†Department of Chemistry, Faculty of Science, Toho University, Funabashi, Chiba 274
(Received May 27, 1986)

1,5,9-Trithia[9]ferrocenophane was prepared by the reaction of 1,1′-bis(3-chloropropylthio)ferrocene with sodium sulfide. The complexes of 1,5,9-trithia[9]ferrocenophane, along with 1,4,7-trithia[7]ferrocenophane, with copper(I), silver(I), mercury(II), and palladium(II) salts were prepared. Some interaction between the iron atom and the metal atoms coordinated to the thia-crown moiety was suggested from their spectral data in the solution for the complexes of 1,4,7-trithia[7]ferrocenophane with mercury(II) and palladium(II) salts and the complex of 1,5,9-trithia[9]ferrocenophane with silver(I) tetrafluoroborate.

Much attention was focused on the metal-metal interaction existing between metallocenes and metal cations from the viewpoints of biochemical and catalytic interests.[1,2] Ferrocene has been known to form an unstable complex with mercury(II) salts,[3] while [2]Ferrocenophanes, in which the two cyclopentadienyl rings are tilted by 20° because of their shorter bridging, can form more stable 1:1 complexes with mercury(II) chloride[4] and tin(IV) chloride,[5] since a direct metal-metal interaction is present as revealed by their Mössbauer spectra. Recently, dative Fe–Pd and Fe–Pt bonds have been confirmed by X-ray analyses of (1,1′-ferrocenedithiolato-S,S,Fe)(triphenylphosphine) palladium(II)[6] and platinum(II).[7] In regard to these results, we now report on the preparation and various properties of 1,4,7-trithia[7]- (**1**) and 1,5,9-trithia[9]-ferrocenophanes (**2**) and their copper(I), silver(I), mercury(II), and palladium(II) complexes.

Results and Discussion

Synthesis of 1,5,9-Trithia[9]ferrocenophane (2). It has been reported that 1,4,7-trithia[7]ferrocenophane was prepared by the reaction of 1,1′-bis(2-chloroethylthio)ferrocene with sodium sulfide.[8] In a similar manner, 1,5,9-trithia[9]ferrocenephane (**2**) was prepared in 53% yield by refluxing a mixture of 1,1′-bis(3-chloropropylthio)ferrocene and sodium sulfide in ethanol–tetrahydrofuran (THF). The structure was determined by an elemental analysis and spectral data. Thus, the molecular formula of **2** was deduced to be $C_{16}H_{20}S_3Fe$ by an elemental analysis and by the mass spectrum (M^+ m/z 364). In the ^1H NMR spectrum of **2**, the α- and β-ring protons of the cyclopentadienyl rings (Cp-rings) appeared as a singlet (8H) at δ 4.23, while the methylene protons next to the sulfur atoms resonated as two triplets at δ 3.10 and 2.82 and the other methylene protons as a quintet at δ 2.02. The ^{13}C NMR spectrum of **2** showed a bridge-head carbon as well as α- and β-carbons at 88.8, 71.8, and 68.3 ppm, respectively. Specific spectral behavior observed in the electronic and ^{13}C NMR spectra of 1,4,7-trithia[7]-ferrocenophane (**1**)[9] was not observed in the present ferrocenophane.

Copper(I) Complexes. A solution of **1** and $(CH_3CN)_4CuBF_4$ was refluxed in acetonitrile for 1 h and then diluted with diethyl ether to give the copper(I) complex **3a** in good yield. The copper(I) perchlorate complex **3b** was similarly obtained by a reaction of **1** with $(CH_3CN)_4CuClO_4$ in acetonitrile. An elemental analysis showed that **3a** was a 1:1 complex of **1** with $CuBF_4$, containing one equivalent of acetonitrile in the crystal. The IR spectrum of **3a** showed the absorption characteristic of a coordinated

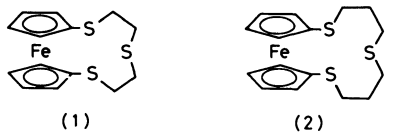

Fig. 1.

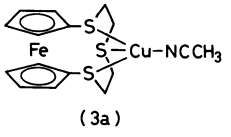

Fig. 3.

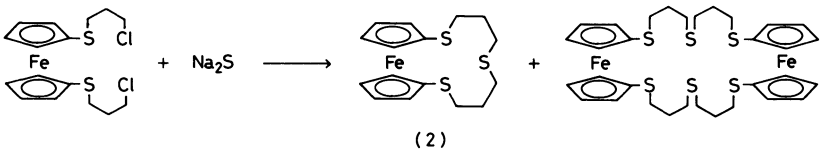

Fig. 2.

cyano group at 2256 cm^{-1}. From the IR spectrum of the perchlorate complex **3b**, it appears that an intermediate between a free and covalently bounded perchlorate anion was present owing to the appearance of three well-defined maxima in the region between 1200 and 1000 cm^{-1}.[10] Upon considering a stereo-model of **1** it was found that the size of the ferrocenothiacrown ring is too small to allow the inclusion of the Cu(I) ion (r_{ion} 0.96 Å)[11] into the center of the trithia-macrocycle. Moreover, it was confirmed by an X-ray analysis that the Cu(I) ion in the 1,4,8,11-tetrathiacyclotetradecane with $CuClO_4$ had a tetrahedral configuration.[12] From these facts and the IR spectra, it is suggested that the copper(I) ion in complex **3** is coordinated by the three sulfur atoms of ligand **1** and the nitrogen atom of acetonitrile or the oxygen atom of a perchlorate anion in the crystal of complex **3**. On the other hand, in the ^1H NMR spectrum of **3a**, the signals of the Cp-rings and the methylene protons appeared as multiplets centered at δ 4.37 and 3.13, respectively, indicating the presence of a symmetrical structure. This view was supported by the ^{13}C NMR spectrum of **3a**, which showed only three Cp-ring carbon signals at 91.1 (C_b), 69.8 (C_α), and 69.0 (C_β). The appearance of symmetrical signals for the Cp-rings in a solution of **3** seems to be due to a rapid dissociative equilibrium to afford an averaged spectra. Small changes in the IR, ^{13}C NMR ($\Delta\delta$ −1.9 and +0.2 ppm in α- and β-carbons, respectively), and electronic spectral data [hypsochromic shift ($\Delta\lambda$ 14 nm) and a decreased absorbance ($\Delta\varepsilon$ 155) in the 440 nm-band] when going from the free ligand **1** to the metal complex **3a** may suggest that the ferrocene moiety of complex **3** is little influenced by the Cu(I) ion coordinated to the sulfur atoms of the thia-crown moiety. Such a small perturbation was also observed in the tetrathia[*n*]ferrocenophane series.[13]

Table 1. Visible Spectral Data of **1**—**9** in Acetonitrile

Compd	λ_{max} (ε)
1	462 (349)
3a	448 (194)
3b	448 (211)
4	450 (246)
6	458 (280)
8	558 (403), 410 (832)
2	446 (211)
5	448 (226)
7	449 (170)
9	552 (809), 388 (2200)

Ag(I) Complexes. A solution of **1** in acetonitrile was added to a solution of silver(I) tetrafluoroborate in acetonitrile; the solution was then diluted with anhydrous diethyl ether to give the 1:1 complex **4** in good yield. In a similar manner, the 1:1 complex **5** was obtained from **2** and $AgBF_4$. An elemental analysis confirmed that **5** contained one equivalent of acetonitrile in its crystal form. The IR spectrum showed a C≡N stretching vibration at 2260 cm^{-1}. In the ^1H NMR (Table 2) and the electronic spectra (Table 1), negligible differences were observed between ligand **1** and complex **4**. In the ^{13}C NMR spectrum of **4**, rather small up-field shifts of the α- ($\Delta\delta$ 2.1) and β-carbons ($\Delta\delta$ 0.2) of the Cp-rings were observed. These spectral data suggest two possible coordinations: (i) the silver(I) ion is coordinated to only the sulfur atom (S-4) farthest from the ferrocene nucleus of ligand **1**; (ii) complex **4** is in a rapid equilibrium with the free ligand **1** and $AgBF_4$ in acetonitrile. In any case, the interaction between the ferrocene nucleus and the Ag(I) ion in **4** was negligible. Also, complex **5** exhibited similar features regarding the electronic spectrum, but showed a specific behavior regarding the ^1H NMR spectrum. That is, the H-3 and H-7 signals appeared at δ 2.83 as multiplets and the H-4 and H-6 signals at δ 1.74 as multiplets. These chemical shifts are nearly comparable with the corresponding values of the free ligand **2**. However, the signals of the Cp-ring protons

Table 2. ^1H NMR Spectral Data of **1**—**9** in CD_3CN

Compd	Ring-H	SCH_2	CH_2
1	4.33 (t, J = 1.3 Hz, 4H), 4.25 (t, J = 1.3 Hz, 4H)	3.5—2.9 (A_2B_2 pattern, 8H)	
3a	4.37 (m, 8H)	3.13 (m, 8H)	
3b	4.37 (m, 8H)	3.14 (s, 8H)	
4	4.37 (broad s, 8H)	3.18 (m, 8H)	
6[a]	ca. 5.3 (extremely broad, 12H)	2.81 (m, 4H)	
8[b]	4.81 (m, 2H), 4.60 (m, 2H), 4.43 (m, 4H)	3.0—3.7 (m, 8H)	
2	4.23 (s, 8H)	3.10 (t, J = 7.1 Hz), 2.82 (t, J = 6.8 Hz, 4H)	2.02 (m, 4H)
5	ca. 6.3 (extremely broad, 8H)	2.83 (m, 4H)	1.74 (m, 4H)
7[c]	4.32 (broad s, 8H)	3.23 (t, J = 7.4 Hz, 4H), 2.85 (t, J = 6.8 Hz, 4H)	2.04 (m, 4H)
9[b]	4.85 (m, 1H), 4.50 (m, 3H), 4.28 (m, 4H)	2.7—3.3 (m, 8H), 1.9—2.5 (m, 4H)	

a) at 70 °C, b) in DMSO-d_6, c) at 60 °C.

and H-2 and H-8 shifted down-field (δ ca. 6.3) and collapsed to become extremely broad. This phenomenon can be understood as resulting from the scanty appearance of the unpaired electrons on the Cp-ring carbons as well as the C-2 and C-8 by means of a partial electron transfer from the iron atom of the ferrocene nucleus to the coordinated Ag(I) ion in intermediate **5a**, which may lie in the rapid equilibrium (Scheme 1). In a solution of **5** in acetonitrile, at least, the silver(I) ion seemed to be incorporated into the center of the thia-crown or located near the iron atom of the ferrocene nucleus of **5**.

Hg(II) Complexes. A solution of mercury(II) chloride in anhydrous diethyl ether was added to a solution of **1** in anhydrous diethyl ether to give the 1:1 complex **6** as dark-red crystals in good yield. In the same manner, a 1:1 complex **7** was obtained from **2** and $HgCl_2$ as red-orange cubes in good yield. As can be seen in Tables 1 and 3, the electronic and IR spectra of **6** and **7** are similar to those of the free ligands **1** and **2**, respectively. The octahedral coordination of the Hg(II) ion in a 1:1 complex of 1,4,8,11-tetrathiacyclotetradecane with $HgCl_2$ was suggested from its IR spectrum;[14] an X-ray analysis has confirmed that the coordination about the Hg(II) atom is approximately tetrahedral in the 1:2 complex of 1,4,8,11-tetrathiacyclotetradecane with $HgCl_2$.[15] The Hg(II) ion (r_{ion} 1.10 Å)[10] does not seem to be incorporated into the smaller thia-macrocycle of **6** and **7** than that of 1,4,8,11-tetrathiacyclotetradecane. Therefore, a structure in which the Hg(II) atom coordinates to only the sulfur atoms attached to a ferrocene nucleus in the thia-maclocycle is suggested. In the ^1H NMR spectrum (70 °C) of **7** in acetonitrile-d_3, the Cp-ring protons appeared as a symmetrically broad singlet and shifted down-field ($\Delta\delta$ 0.09), suggesting the same reason given for the Ag(I) complexes. On the other hand, the ^1H NMR spectrum (60 °C) of **6** in CD_3CN showed features that were similar to those observed in a silver(I) complex **5**: The Cp-ring protons and H-2 and H-6 collapsed and shifted down-field (δ ca. 6.3). This suggests some type of interaction between the iron atom and the Hg(II) atom coordinated to the thia-macrocycle moiety in the solution, as described for complex **5**.

Palladium(II) Complexes. Compound **1** reacted with dichlorobis(acetonitrile)palladium(II) in hot acetonitrile to give the 1:1 complex **8** as black crystalline powder in good yield. Compound **2**, on the other hand, gave two products: black crystals **9** and black violet powder **10** in a similar manner. The former was confirmed to be a 1:1 complex by an elemental analysis. The IR spectra of **8**—**10** showed absorption at 330—315 cm^{-1}, the region for *cis*-$PdCl_2$ moieties.[16] The ^1H NMR spectrum of **8** in DMSO-d_6 showed three multiplets at δ 4.81 (2H), 4.61 (2H), and

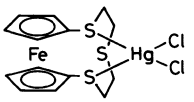

(6)

Fig. 4.

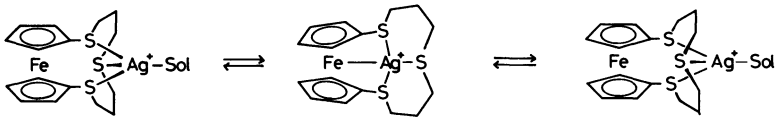

Scheme 1.

Table 3. IR Spectral Data of **1**—**10** (KBr disk)

Compd	ν_{max}/cm^{-1}
1	3100, 2924, 1418(s), 1160, 1050, 1024, 890, 846, 810(s), 524, 502, 472(s)
3a	3088, 3060, 2944, 2912, 2256(w), 1424(s), 1414(s), 1158, 1140—1030(vs), 940(w), 890(s), 840(s), 806(s), 540, 512, 490, 480
3b	3084, 3060, 2944, 2912, 1414(s), 1144(vs), 1116(vs), 1082(vs), 1030, 890(s), 940, 840, 832, 816, 804, 624(s), 540, 510, 488, 480
4	3092, 2924, 2904, 1430(s), 1420(s), 1160, 1120—1030(vs), 892, 806(s), 526(s), 498, 480
6	3096, 2924, 1416(s), 1160, 1032, 1020, 884(w), 808(s), 508(s), 474(s)
8	3084, 2924, 1432, 1414, 1406, 1162, 1154, 1032, 1020, 888, 820(s), 526, 488, 480, 342(w), 306(s)
2	3088, 2920, 2900, 1430(s), 1420(s), 1264, 1160, 1026, 892, 806(s), 798(s), 526(s), 498(s), 480(s)
5	3088, 2920, 2260(vw), 1418(s), 1160, 1120—1020(vs), 892, 882, 810(s), 526(s), 514(s), 496, 482
7	3120, 3100, 2924, 1412(s), 1262, 1158, 1026(s), 890, 880, 812(s), 514(s), 480(s)
9	3076, 2984, 2948, 1444(m), 1436(m), 1386, 1030, 1020, 880, 840, 828(s), 818(s), 520(s), 490, 476(s), 338, 320(s), 298
10	3088, 2924, 1620, 1416(s), 1254, 1164, 1030(s), 888, 826(s), 516(s), 480(s), 358, 319

Table 4. Mössbauer Parameters of **2**—**9**

Compd	*IS*	*QS*
2	0.43	2.36
3	0.44	2.31
4	0.43	2.33
5	0.44	2.34
6	0.47	2.44
7	0.46	2.39
8	0.45	2.29
9	0.42	2.34

Fig. 5.

4.43 (m, 4H) for the Cp-ring protons, indicating a strong coordination of $PdCl_2$ to the sulfur atoms at 1 and 7 positions on one side of the thiamacrocycle in **1** and no intervention of the dissociative equilibrium in the solution observed in the Cu(I), Ag(I), and Hg(II) complexes. On the other hand, in the ^1H NMR spectrum of **9** in DMSO-d_6, the Cp-ring protons appeared at δ 4.85 (m, 1H), 4.50 (m, 3H), and 4.28 (m, 4H). This pattern of the Cp-ring protons can probably be rationalized by the coordination of a $PdCl_2$ moiety to the sulfur atoms at 1 (or 9) and 5 positions in **9**. Compounds **8** and **9** were very insoluble in most organic solvents. As the complexes of 1,1′-bis(alkylthio)ferrocene with $PdCl_2$ are soluble in a polar solvent,[17] a possibility that the present $PdCl_2$ complexes have a polymeric structure cannot be ruled out. Complex **10** gave an unsatisfactory elemental analysis as a 1 : 1 complex and a rather broad IR spectrum, suggesting a polymeric product.

Mössbauer Spectra. ^{57}Fe Mössbauer spectral data can give useful information about the state of an iron atom in various complexes. The IS and *QS* values of the free ligand **2** and the metal complexes **4**—**9** are summarized in Table 4. A large change in the *QS* value was observed in complexes of [2]ferrocenophanes with mercury(II)[4] and tin(IV) chlorides,[5] in which a direct interaction between the iron atom of a ferrocene nucleus and the metal atoms was suggested on the basis of their Mössbauer spectra. The negligible change observed here is within the limits of the difference in the packing mode of the crystal, suggesting that the metal atoms coordinated to the polythia-crown moiety in the trithia[*n*]ferrocenophanes **1** and **2** exert little interaction on the iron atom of a ferrocene nucleus in the solid state. A similar change was also observed in the metal complexes of tetrathia[*n*]ferrocenophanes[13] and the complex of 1,1′-bis(diphenylphosphino)ferrocene with $HgCl_2$.[18]

Experimental

The melting points are uncorrected. The IR spectra were taken on a Hitachi 270-50 Infrared Spectrometer. The ^1H and ^{13}C NMR spectra were measured on a JEOL FX-90Q Spectrometer, TMS being chosen as the standard material. The electronic spectra were taken on a Hitachi 340 spectrometer. The Mass spectra were measured on a Hitachi M-80B spectrometer.

Materials. 1,4,7-Trithia[7]ferrocenophane (**1**) was previously reported.[8] Mercury(II) chloride, silver(I) tetrafluoroborate, and copper(II) tetrafluoroborate hydrate were commercially available. Tetrakis(acetonitrile)copper(I) perchlorate[19] and dichlorobis(acetonitrile)palladium(II)[20] were prepared according to methods described in the literature.

1,5,9-Trithia[9]ferrocenophane (2). Sodium sulfide nonahydrate (3.6 g, 15 mmol) was dissolved in ethanol (650 cm^3). To the solution was added a solution of 1,1′-bis(3-chloropropylthio)ferrocene[8] (2.0 g, 5 mmol) in tetrahydrofuran (120 cm^3). The mixture was refluxed for 24 h under a nitrogen atmosphere. After evaporation under reduced pressure, the residue was dissolved in water. The mixture was extracted with benzene and the extract was dried over anhyd sodium sulfate. After evaporation under reduced pressure, the residue was chromatographed on silica gel by the elution of hexane-toluene (1:1) and, subsequently, toluene. The following products were separated.

1,5-Dithia[5]ferrocenophane.[9] Yield 28 mg (1.9%).

1,5,9-Trithia[9]ferrocenophane (2). Red orange crystals, mp 69—70 °C (recrystallization from cyclohexane). Yield 0.96 g (53%). Found: C, 52.74; H, 5.74%. Calcd for $C_{16}H_{20}S_3Fe$: C, 52.74; H, 5.53%. MS: *m/z* 364 (M^+). ^{13}C NMR ($CDCl_3$) 87.5 (C_b), 71.2 (C_α), 67.7 (C_β), 33.9 (SCH_2), 31.1 (SCH_2), and 29.6 (CH_2).

1,5,9,21,25,29-Hexathia[9.9]ferrocenophane. Yellow orange needles, mp 102—103 °C (recrystallization from benzene). Yield 0.32 g (8.6%). Found: C, 52.77; H, 5.60%. Calcd for $C_{32}H_{40}S_6Fe_2$: C, 52.74; H, 5.53%. MS: *m/z* 728 (M^+). IR (KBr): 3080, 1418, 1190, 1022, and 810 cm^{-1}. ^1H NMR ($CDCl_3$) δ=4.34 (t, *J*=1.6 Hz, 4H), 4.28 (t, *J*=6.8 Hz, 4H), 2.74 (t, *J*=6.8 Hz, 4H), 2.63 (t, *J*=7.5 Hz, 4H), and 1.83 (p, 4H).

(1,4,7-Trithia[7]ferrocenophane)copper(I) Perchlorate (3b). To a solution of **1** (34 mg, 0.1 mmol) in hot anhyd acetonitrile (2 cm^3) was added tetrakis(acetonitrile)copper(I) perchlorate (33 mg, 0.1 mmol). After tetrakis(acetonitrile)-copper(I) perchlorate had been dissolved, the solution was filtered. The filtrate was diluted with anhyd diethyl ether (5 cm^3) to form orange crystals. After the mixture had been kept for 2 h in a refrigerator, the crystals were collected by filtration. Orange needles. Yield 36 mg (72%). This compound was very explosive on heating. ^{13}C NMR ($CDCl_3$) 69.8 (C_α), 69.2 (C_β), 37.0 (SCH_2), and 34.9 (SCH_2).

(1,4,7-Trithia[7]ferrocenophane)copper(I) Tetrafluoroborate (3a). Copper(II) tetrafluoroborate hydrate (18 mg, 0.075 mmol) and excess copper powder were refluxed in anhyd acetonitrile (5 cm^3) for 1 h under nitrogen and then the mixture was filtered. To the filtrate was added **1** (50 mg, 0.15 mmol) and the mixture was refluxed for 0.5 h. After being cooled to room temperature, the solution was diluted

with anhyd diethyl ether (20 cm^3) to form orange crystals. The mixture was kept overnight in a refrigerator, and the resulting crystals were collected by filtration. Orange needles (63 mg, 86.4%), mp ~230 °C (decomp). Found: C, 36.56; H%, 3.53%. Calcd for $C_{14}H_{16}BF_4S_3FeCu \cdot CH_3CN$: C, 36.42; H, 3.63%. ^{13}C NMR (CD_3CN) 91.1 (C_b), 69.8 (C_α), 69.0 (C_β), 36.9 (SCH_2), and 35.0 (SCH_2).

(1,4,7-Trithia[7]ferrocenophane)silver(I) Tetrafluoroborate (4). To a hot solution of **1** (34 mg, 0.1 mmol) in acetonitrile (2 cm^3) was added to a hot solution of silver(I) tetrafluoroborate (20 mg, 0.1 mmol) in acetonitrile (1 cm^3). The resulting solution was filtered and the filtrate was diluted with anhyd diethyl ether (10 cm^3). The solution was kept overnight in a refrigerator. The title compound **4** (43 mg, 81%) was obtained as yellow orange needles, mp 195 °C (decomp). Found: C, 31.61 H, 2.99%. Calcd for $C_{14}H_{16}BF_4S_3FeAg$: C, 31.67; H, 3.04%. ^{13}C NMR (CD_3CN) 91.3 (C_b), 69.6 (C_α), 68.6 (C_β), 35.3 (SCH_2), and 32.5 (SCH_2).

(1,5,9-Trithia[9]ferrocenophane)(acetonitrile)silver(I) Tetrafluoroborate (5). To a solution of **2** (100 mg, 0.27 mmol) in anhyd acetonitrile (7 cm^3) was added a solution of silver(I) tetrafluoroborate (53 mg, 0.27 mmol) in anhyd acetonitrile (3 cm^3). The resulting dark red-brown solution was filtered and then diluted with anhyd diethyl ether (35 cm^3). After the solution had been kept in a refrigerator, the resulting crystals were collected by filtration. The complex **5** (108 mg, 66%) was obtained as yellew plates, mp 115 °C (decomp). Found: C, 36.06; H, 3.97%. Calcd for $C_{16}H_{20}BF_4FeAg \cdot C_2H_3N$: C, 36.03; H, 3.86%.

Dichloro(1,4,7-Trithia[7]ferrocenophane)mercury(II) (6). To a solution of **1** (68 mg, 0.2 mmol) in anhyd diethyl ether (4 cm^3) was added a solution of mercury(II) chloride (55 mg, 0.2 mmol) in anhyd diethyl ether (4 cm^3). The solution was stirred for 15 min. The resulting crystals were collected by filtration. Light orange crystals (104 mg, 85%), mp 121 °C (decomp). Found: C, 28.02; H, 2.58%. Calcd for $C_{14}H_{16}Cl_2S_3FeHg$: C, 27.67; H, 2.65%.

Dichloro(1,5,9-trithia[9]ferrocenophane)mercury(II) (7). To a solution of **2** (200 mg, 0.55 g) in anhyd diethyl ether (25 cm^3) was added a solution of mercury(II) chloride (136 mg, 0.5 mmol) in anhyd diethyl ether (20 cm^3). The solution was refluxed for 30 min and then kept overnight in a refrigerator. The title compound **7** (257 mg, 81%) was obtained as red fine crystals, mp 115—116 °C (decomp). Found: C, 30.29; H, 3.46%. Calcd for $C_{16}H_{20}Cl_2FeHg$: C, 30.22; H, 3.17%.

Dichloro(1,4,7-trithia[7]ferrocenophane)palladium(II) (8). To a solution of **1** (36 mg, 0.1 mmol) in hot acetonitrile (5 cm^3) was added a solution of dichlorobis(acetonitrile)-palladium(II) (26 mg, 0.1 mmol) in hot acetonitrile (5 cm^3). The solution was kept for 1 h at room temperature. The resulting crystals were collected by filtration. Greenish black crystals (41 mg, 80%), mp~300 °C. Found: C, 32.95; H, 3.15%. Calcd for $C_{14}H_{16}Cl_2S_3FePd$: C, 32.74; H, 3.15%.

Dichloro(1,5,9-trithia[9]ferrocenophane)palladium(II) (9). To a solution of **2** (180 mg, 0.5 mmol) in hot acetonitrile (20 cm^3) was added a solution of dichlorobis(acetonitrile)-palladium(II) (130 mg, 0.5 mmol). The solution was kept overnight in a refrigerator. The resulting violet fine powder (**10**) was collected by filtration. Yield: 105 mg (39%). Mp ~250 °C. Found: C, 33.77; H, 3.65%. Calcd for $(C_{16}H_{20}Cl_2S_3FePd)_n$: C, 35.48; H, 3.72%.

The filtrate was kept for several days in a freezer. The resulting black-brown crystals were filtered and washed with acetonitrile. Yield 102 mg (38%). Mp 235 °C (decomp). Found: C, 35.71; H, 3.72%. Calcd for $C_{16}H_{20}Cl_2S_3FePd$: C, 35.48; H, 3.71%.

We thank Prof. Izumi Motoyama and Prof. Motomi Katada for measurement of Mössbauer spectra. The present work was supported by a Grant-in-Aid for Science Research (No. 61540362) from the Ministry of Education, Science and Culture.

References

1) M. I. Bruce, *J. Organomet. Chem.*, **242**, 147 (1983).
2) W. R. Cullen and J. D. Woollins, *Coord. Chem. Rev.*, **39**, 1 (1981).
3) R. M. G. Roberts, J. Silver, and I. G. Harrison, *J. Organomet. Chem.*, **209**, 385 (1981).
4) M. Watanabe, H. Ichikawa, I. Motoyama, and H. Sano, *Bull. Chem. Soc. Jpn.*, **56**, 3291 (1983).
5) M. Watanabe, H. Ichikawa, I. Motoyama, and H. Sano, *Chem. Lett.*, **1983**, 1009.
6) D. Seyferth, B. W. Hames, T. G. Rucker, M. Cowie, and R. S. Dickson, *Organometallics*, **2**, 472 (1983).
7) S. Akabori, T. Kumagai, T. Shirashige, S. Sato, K. Kawazoe, C. Tamura, and M. Sato, unpublished data.
8) M. Sato, H. Watanabe, S. Ebine, and S. Akabori, *Chem. Lett.*, **1982**, 1753; M. Sato, S. Tanaka, S. Ebine, and S. Akabori, *Bull. Chem. Soc. Jpn.*, **57**, 1929 (1984).
9) M. Sato, S. Tanaka, S. Ebine, K. Morinaga, and S. Akabori, *J. Organomet. Chem.*, **282**, 247 (1985).
10) B. J. Hathaway and A. E. Underhill, *J. Chem. Soc.*, **1961**, 3091.
11) F. A. Cotton and G. Willkinson, "Advanced Inorganic Chemistry," Interscience Publishers, New York (1966), p. 44.
12) E. R. Dockal, L. L. Diaddario, M. D. Glick, and D. B. Rorabacker, *J. Am. Chem. Soc.*, **99**, 4530 (1977).
13) M. Sato, S. Tanaka, and S. Akabori, *Bull. Chem. Soc. Jpn.* **59**, 1515 (1986).
14) D. Sevdic and H. Meider, *J. Inorg. Nucl. Chem.*, **39**, 1409 (1977).
15) N. W. Alcock, N. Herron, and P. Moore, *J. Chem. Soc., Dalton Trans.*, **1978**, 394.
16) G. E. Coats and C. Parkins, *J. Chem. Soc.*, **1963**, 421.
17) B. McCulloch, D. L. Ward, J. D. Woolins, and C. H. Brubacker, Jr., *Organometallics*, **4**, 1428 (1985).
18) K. P. Mann, W. H. Morrison, and D. N. Hendrickson, *Inorg. Chem.*, **13**, 1180 (1974).
19) P. Hemmerich and C. Sigwart, *Experimentia*, **19**, 488 (1963).
20) F. R. Hartley, S. G. Murray, and C. A. McAuliffe, *Inorg. Chem.*, **18**, 1394 (1979).

 © 1986 The Chemical Society of Japan Bull. Chem. Soc. Jpn., 59, 3617—3620 (1986)

Selenium and Tellurium Tetrachlorides as Reagents for the Conversion of Alcohols to Alkyl Chlorides and Tellurium Tetrachloride as a Lewis Acid Catalyst for Aromatic Alkylation

Takayoshi YAMAUCHI, Kaneaki HATTORI, Shoichi MIZUTAKI, Kentaro TAMAKI, and Sakae UEMURA*,†

Research & Development Laboratory, Sakai Plant, Kyowa Hakko Kogyo Co., Ltd., 1-1-53, Takasu-cho, Sakai, Osaka 590

†Institute for Chemical Research, Kyoto University, Uji, Kyoto 611

(Received May 29, 1986)

Selenium tetrachloride($SeCl_4$) reacts smoothly with alcohols in various nonpolar solvents to give the corresponding alkyl chlorides in 44—97% yield. Similar reaction also proceeds with tellurium tetrachloride ($TeCl_4$), while the treatment of benzyl, 1-phenylethyl, and *t*-butyl alcohols with $TeCl_4$ in aromatic solvents results in a high yield formation of alkylated aromatics instead of alkyl chlorides. Such Friedel-Crafts aromatic alkylation hardly occurs in the $SeCl_4$ case. The chlorinating species is not chlorine which might be evolved by dissociation of $SeCl_4$ or $TeCl_4$, but the metal chloride itself. The conversion of optically active (*R*)-(+)-1-phenylethanol to 1-phenylethyl chloride proceeds with nearly complete racemization.

During a search for direct aryl migration method of 2-hydroxypropiophenones to 2-arylpropionic acids by various sulfur, selenium, and tellurium reagents[1] we came across the replacement of hydroxyl group by chlorine when the ketones were treated with selenium or tellurium tetrachloride ($SeCl_4$ or $TeCl_4$). Although $SeCl_4$ has been known as chlorinating agent of olefins,[2] acetylenes,[3] and isocyanides,[3] there is no precedent for the use of $TeCl_4$ as chlorinating agent as well as the reactions of each reagent with alcohols to our knowledge.[4] In order to know the scope and limitation of this replacement reaction the reactions of typical primary, secondary, and tertiary alcohols with $SeCl_4$ or $TeCl_4$ were carried out in various solvents. It is worthwhile to note that selenium tetrafluoride is known to react with alcohols to give the corresponding alkyl fluorides in good yields.[5] During this study we also disclosed that $TeCl_4$, but not $SeCl_4$, works as a mild Lewis acid catalyst for aromatic alkylation. We report here the details of our new findings.

Results and Discussion

Conversion of Alcohols to Alkyl Chlorides by $SeCl_4$ or $TeCl_4$. Treatment of 1- and 2-phenylethanols, diphenylmethanol, triphenylmethanol, and 1- and 2-octanols with $SeCl_4$ in toluene, dichloromethane, or 1,2-dichloroethane as solvent at 25—60 °C for 1.5—15 h afforded the corresponding alkyl chlorides respectively in 44—97% yield. The addition of amine sometimes improved the product yield. Selenium tetrafluoride-pyridine complex is known to be a good fluorinating agent of alcohols.[5] Similar treatment with $TeCl_4$ also gave alkyl chlorides in 65—86% yield, but the addition of triethylamine or pyridine resulted in lowering the product yield probably because of the

Table 1. Conversion of Alcohols to Alkyl Chlorides Using $SeCl_4$ or $TeCl_4$

R in **1** (2 mmol)	$SeCl_4$ or $TeCl_4$ (2.4 mmol)	Base (equiv)[a]	Solvent (4 ml)	Temp/°C	Time/h	Products/%[b]	
						2	**1**
$PhCH_2CH_2$	$SeCl_4$[$TeCl_4$]		Toluene	50	4	44[65]	24[20]
$PhCH_2CH_2$	$SeCl_4$	Et_3N(1.0)	Toluene	50	4	71[0]	25[94]
Ph_2CH	$SeCl_4$		Toluene	50	4	90	0
Ph_2CH	$TeCl_4$		DMF-Toluene[c]	25	3	85	0
Ph_2CH	$SeCl_4$[$TeCl_4$]	Et_3N(1.5)	Toluene	25	3	97[8]	2[90]
$PhCHCH_3$[d]	$SeCl_4$		Toluene	25	6	96[e]	—[f]
$PhCHCH_3$[d]	$TeCl_4$		CH_2Cl_2	−50	3.5	86[e]	—[f]
$PhCHCH_3$[d]	$SeCl_4$[$TeCl_4$]	Et_3N(1.0)	CH_2Cl_2	25	1.5	96[e][39][e]	—[f][7][e]
Ph_3C	$SeCl_4$[$TeCl_4$]		CH_2Cl_2	25	15	95[77]	3[3]
Ph_3C	$SeCl_4$[$TeCl_4$]	C_5H_5N(1.2)	CH_2Cl_2	25	15	92[22]	2[64]
1-C_8H_{17}	$SeCl_4$[$TeCl_4$]		$ClCH_2CH_2Cl$	60	2	92[2]	0[98]
2-C_8H_{17}	$SeCl_4$[$TeCl_4$]		$ClCH_2CH_2Cl$	60	2	49[71]	22[0]

a) Equivalent to $SeCl_4$ or $TeCl_4$. b) GLC yield based on **1** charged unless otherwise stated. c) *N*,*N*-Dimethylformamide-toluene (2 ml-2 ml). d) **1** (30 mmol), $SeCl_4$ or $TeCl_4$ (36 mmol), and solvent (60 ml) were used. e) Isolated yield. f) Not determined.

formation of too stable adducts between $TeCl_4$ and the amine.[6] Applicability of the reaction with $TeCl_4$ for this conversion seems to be more limited than that with $SeCl_4$ from the following observations: 1) Primary alcohols such as 1-octanol and 1-butanol were almost recovered intact, 2) secondary alcohols sometimes reacted very slowly; e.g., 2-butanol gave *s*-butyl chloride in less than 20% yield even under somewhat severe conditions, and 3) in toluene as solvent aromatic alkylation often predominated (vide infra). Typical results are shown in Table 1.

$$\underset{1}{R\text{-}OH} \xrightarrow[\text{solvent}]{SeCl_4 \text{ or } TeCl_4} \underset{2}{R\text{-}Cl}$$

It is knwon that $SeCl_4$ is almost completely dissociated to lower chlorides and chlorine in the vapor, while there is little such dissociation in the case of $TeCl_4$.[7] In order to know whether a true chlorinating species is $SeCl_4$ itself or chlorine evolved by dissociation in the liquid phase, the reaction of 1-phenylethanol with $SeCl_4$ in dichloromethane was compared with that with chlorine gas. As a result it was revealed that in the chlorine case the reaction is slow and always accompanied by the formation of 1-chloroacetophenone (**3**), while only the expected 1-phenylethyl chloride, **2** (R=PhCHCH$_3$), is obtained quantitatively in the $SeCl_4$ case (Table 2). These results show $SeCl_4$ itself to be a reactive species for this conversion in accord with the observation obtained so far in the liquid-phase chlorination of various olefins with $SeCl_4$.[2]

$$\underset{\substack{\text{1(R=PhCHCH}_3\text{)}}}{\text{PhCHOH}\ (\text{CH}_3)} \xrightarrow[CH_2Cl_2]{SeCl_4 \text{ or } Cl_2} \underset{\substack{\text{2(R=PhCHCH}_3\text{)}}}{\text{PhCHCl}\ (\text{CH}_3)} + \underset{\substack{\mathbf{3}}}{\text{PhCCH}_2\text{Cl}\ (\text{O})}$$

Next, the stereochemistry of this conversion to alkyl chlorides was investigated using almost optically pure (*R*)-(+)-1-phenylethanol as follows. Treatment of the alcohol with $SeCl_4$ in toluene at 25 °C for 6 h afforded 1-phenylethyl chloride in 90% isolated yield which did not show any optical activity. The reaction of the alcohol with $TeCl_4$ in dichloromethane at −50 °C for 6 h produced the chloride in 89% isolated yield, optical rotation $[\alpha]_D^{20}$ of which being −0.5° (optical purity, 0.5%; inversion), while similar reaction at 25 °C for 48 h in the presence of pyridine gave the chloride of $[\alpha]_D^{20}$ +1.6° in 18% isolated yield (optical purity, 1.5%; retention). These results show that the replacement of hydroxyl group by chlorine with either $SeCl_4$ or $TeCl_4$ proceeds with nearly complete racemization in the case of 1-phenylethanol.

From experimental observations described above an S_Ni like reaction scheme may be conceivable for this chlorination at least in the cases of secondary and tertiary alcohols as exemplified using 1-phenylethanol as a substrate as follows.

$$\text{PhCHOH}\ (\text{CH}_3) \xrightarrow[-HCl]{MCl_4} \left[\text{PhCH}(\text{CH}_3)\text{-O}(MCl_3)\right] \xrightarrow{-MOCl_3^-} \left[\text{PhCH}^+(\text{CH}_3)\right] \xrightarrow[-MOCl_2]{MOCl_3^-} \text{PhCHCl}\ (\text{CH}_3)$$

(M=Se,Te)

Friedel-Crafts Alkylation Catalyzed by $TeCl_4$. When the reaction of 1-phenylethanol with $TeCl_4$ was carried out in toluene as solvent at 25 °C, the product was not the expected 1-phenylethyl chloride but an isomeric mixture of 1-phenyl-1-tolylethanes (**4**) in a sharp contrast to the reaction with $SeCl_4$ under similar conditions. On the other hand, the same reaction at −50 °C afforded mainly 1-phenylethyl chloride. This fact suggests that the alkyl chloride initially produced further reacts with aromatic solvent at higher temperature and $TeCl_4$ works as a Lewis acid catalyst. In fact, this was confirmed by a separate experiment using 1-phenylethyl chloride and a catalytic amount of $TeCl_4$ which revealed the formation of **4** of the same isomer ratio as that obtained directly from 1-phenylethanol. Namely, $TeCl_4$ worked as a reagent for the conversion of alcohols to alkyl chlorides and then as a catalyst for aromatic alkylation. Similar phenomenon was also observed in the reactions using *t*-butyl alcohol and *t*-butyl chloride as substrates, an equivalent and a catalytic amount of $TeCl_4$ being required in the former and the latter case respectively. The alkylation using 1-phenylethanol could be applied to other aromatic compounds such as benzene, *p*-xylene, and anisole to produce 1-phenylethylated aromatics, **7**—**10**, in moderate yields. One of the characteristic features of the reaction is the formation of only o- and p-isomers from toluene and

Table 2. Chlorination of **1**(R=PhCHCH$_3$) with $SeCl_4$ or Cl_2

1(R=PhCHCH$_3$) (mmol)	Reagent (equiv)[a]	Solvent CH_2Cl_2/ml	Temp/°C	Time/h	Products/%[b]		
					2(R=PhCHCH$_3$)	**3**	**1**(R=PhCHCH$_3$)
30	Cl_2(1.4)	30	−50	4.5	2	16	75
30	Cl_2(1.4)	30	25	15	77	12	trace
8	$SeCl_4$(1.2)	12	−50	4	99	0	0
8	$SeCl_4$(1.2)	12	25	4	98	0	0

a) Equivalent to **1**. b) Isolated yield in the case of Cl_2 and GLC yield in the case of $SeCl_4$, respectively, based on **1** charged.

anisole, none of m-isomer being produced. In the case of benzene as solvent the initially formed product, 1,1-diphenylethane (**7**), was far more reactive than benzene itself and alkylated further to give dialkylated benzene **8** highly selectively. Typical results are summarized in Table 3. The catalytic activity of $TeCl_4$ seems to be not so strong, as alkylation proceeded only with very reactive (benzyl, 1-phenylethyl, *t*-butyl etc.) alcohol or chloride and even *s*-butyl chloride did not alkylate toluene under similar conditions. It has been known that $TeCl_4$[8] and tellurium(IV) oxide(TeO_2)[9] work as a mild catalyst for aromatic acylation and alkylation respectively. However, no data are so far available on the catalytic activity of $TeCl_4$ for Friedel-Crafts aromatic alkylation. We are sure that this is a first example of $TeCl_4$ working as Friedel-Crafts alkylation catalyst, though its activity is mild.

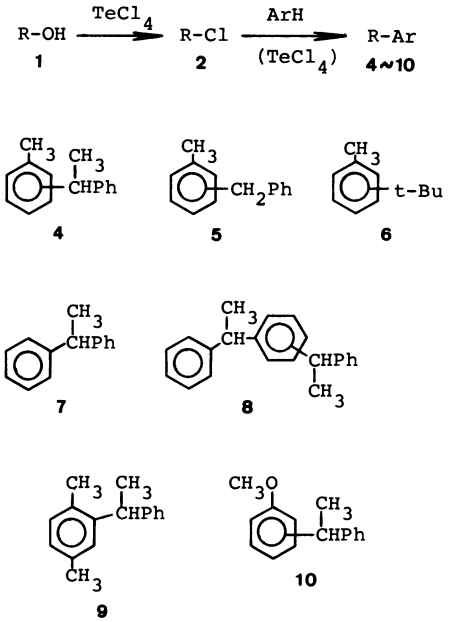

Experimental

General. ^1H NMR spectra were recorded with JEOL FX-90Q (90 MHz) instrument on solutions in $CDCl_3$ with Me_4Si as an internal standard. GLC analyses were carried out with a Shimadzu 4CMPF apparatus using Thermon-1000(5% or 0.5%)-Chromosorb-W(3 mm×3 m or 1.5 m), SILAR-10C(5%)-Chromosorb-W(3 mm×1 m), PEG 20 M(10%)-Chromosorb-W(3 mm×2 m), Silicone CBP 5-M-25-025(0.2 mm×25 m), and Silicone OV-101(0.24 mm×30 m) columns (N_2 as carrier gas). Optical rotations were measured on a UNION PM-201 automatic polarimeter. All organic and inorganic materials were commercial products of the purest grade and used without further purification. Authentic samples of **2** were all commercially available for GLC analyses.

Conversion of Alcohols to Alkyl Chlorides by $SeCl_4$ or $TeCl_4$ (Table 1). A typical experimental procedure is as follows. To a solution of 2-phenylethanol, [**1**(R=$PhCH_2CH_2$)], (0.244 g, 2 mmol) in toluene (4 ml) was added selenium tetrachloride (0.533 g, 2.4 mmol) and the resulting mixture was stirred at 50 °C for 4 h. After being cooled down to room temperature, the mixture was added with water (6 ml) and stirred for 0.5 h. The precipitated red-brown solids were filtered off. The organic layer was separated, washed with brine (3 ml), and dried ($MgSO_4$). GLC analysis using Thermon-1000(5%)-Chromosorb-W(3 mm×3 m) column and propiophenone as an internal standard revealed the presence of 2-phenylethyl chloride, [**2**(R=$PhCH_2CH_2$)], (0.88 mmol, 44%) and unreacted 2-phenylethanol (0.48 mmol, 24%). The reactions with $TeCl_4$ were similarly carried out. In the case of 1-phenylethanol the experiment of 15 times scale was carried out and the product 1-phenylethyl chloride was isolated by distillation.

Reaction of 1-Phenylethanol[1(R=$PhCHCH_3$)] with Chlorine (Table 2). To a solution of chlorine (3.06 g, 43.2 mmol) in dichloromethane (30 ml) was added 1-phenylethanol[**1**(R=$PhCHCH_3$)] (3.67 g, 30 mmol) at −50 °C and the mixture was stirred at the same temperature for 4.5 h. After the addition of 10% aqueous sodium thiosulfate (20 ml) the resulting solution was stirred at room temperature for 0.5 h. The organic layer was separated, washed with brine (10 ml×2), and dried ($MgSO_4$). Evaporation of the solvent left an oily residue which was subjected to column chromatography on SiO_2 [hexane-ethyl acetate (20:1) as eluent] to give 1-phenylethyl chloride [**2**(R=

Table 3. Aromatic Alkylation Using $TeCl_4$

1 or **2** (30 mmol)	$TeCl_4$ (equiv)[a]	Solvent (30 ml)	Temp/°C	Time/h	Product/%[b] (o/p ratio)[c]
1(R=$PhCHCH_3$)	1.2	Toluene	25	3	**4** 83(12/88)[d]
1(R=$PhCHCH_3$)	1.2	Toluene	−50	4	**2**(R=$PhCHCH_3$) 62[e], **4** 7
2(R=$PhCHCH_3$)	0.1	Toluene	25	3	**4** 93(11/89)[d]
1(R=$PhCH_2$)	1.2	Toluene	25	4	**5** 87(35/65)
1(R=*t*-Bu)	1.2	Toluene	80	5	**6** 34(1/99)
2(R=*t*-Bu)	0.2	Toluene	25	20	**6** 71[e] (1/99)[d]
1(R=$PhCHCH_3$)	1.2	Benzene	5	1	**7** 3, **8** 44(24/76)
1(R=$PhCHCH_3$)	1.2	*p*-Xylene	25	24	**9** 40
1(R=$PhCHCH_3$)	1.2	Anisole	25	24	**10** 59(17/83)

a) Equivalent to **1** or **2**. b) Isolated yield based on **1** or **2** charged. c) Determined by NMR unless otherwise stated. d) Determined by GLC. e) GLC yield based on **1** or **2** charged.

$PhCHCH_3$)] (0.10 g, 0.71 mmol, 2.4% yield), 1-chloroacetophenone (**3**) (0.73 g, 4.72 mmol, 15.7% yield) and the starting **1**(R=$PhCHCH_3$) (2.74 g, 22.5 mmol, 74.9% yield), respectively.

Treatment of Optical Active Alcohol with $SeCl_4$ or $TeCl_4$. A typical example is as follows. To a solution of commercially available optical active (*R*)-(+)-1-phenylethanol($[\alpha]_D^{20}$ +42°, 1.00 g, 8.19 mmol) in dichloromethane (10 ml) was added tellurium tetrachloride (2.65 g, 9.84 mmol) at −50 °C; the reported maximum optical rotation of the alcohol is $[\alpha]_D^{25}$ +43.4°.[10] The resulting mixture was stirred at the same temperature for 6 h. The mixture was then added with water (20 ml) and stirred at room temperature for 10 min. The precipitated white solids were filtered off. The organic layer was separated, washed with brine (20 ml) and dried ($MgSO_4$). Evaporation of the solvent left an oily residue which was distilled in vacuo to give 1-phenylethyl chloride (1.02 g, 7.26 mmol, 88.6% yield) at bp 64 °C/8 mmHg (1 mmHg=133.322 Pa). It shows the optical rotation of $[\alpha]_D^{20}$ −0.5°, the value corresponding to the optical purity of 0.5% calculated from $[\alpha]_D^{20}$ +109° of optically pure (*R*)-(+)-1-phenylethyl chloride.[11]

Friedel-Crafts Aromatic Alkylation Catalyzed by $TeCl_4$ (Table 3). A typical experimental procedure starting from alcohol is as follows. To a solution of 1-phenylethanol, **1**(R=$PhCHCH_3$), (3.7 g, 30 mmol) in toluene (30 ml) was added slowly tellurium tetrachloride (9.7 g, 36 mmol) keeping the reaction temperature at 25 °C (exothermic reaction). Small amounts of white precipitates appeared immediately and then the color of the mixture turned dark-brown in a few minutes. The mixture was stirred for 3 h and then quenched with water (20 ml). The organic layer was separated, washed with brine (20 ml×2) and dried ($MgSO_4$). Evaporation of the solvent left an oily residue which was distilled in vacuo to afford a mixture of 1-phenyl-1-tolylethanes (**4**)(4.9 g, 25 mmol, 83.3% yield) at bp 117—128 °C/1 mmHg. GLC analysis of **4** using Silicone OV-101 (0.24 mm×30 m) capillary column at 100→260 °C (4 °C min^{-1}) revealed the presence of two isomers of ortho/para=12/88: ^1H NMR, para-isomer, δ=1.57 (d, J=7 Hz, 3H), 2.26 (s, 3H), 4.07 (q, J=7 Hz, 1H), 7.05 (m, 4H), 7.18 (m, 5H); ortho-isomer, 2.19 (s, 3H). Found: C, 91.92; H, 8.08%. Calcd for $C_{15}H_{16}$: C, 91.78; H, 8.22%.

Analytical data of other alkylated aromatics are as follows.

Benzyltoluenes (5): A colorless liquid of o/p=35/65 by ^1H NMR; ^1H NMR, para-isomer, δ=2.40 (s, 3H), 4.02 (s, 2H), 7.14—7.28 (m, 9H); ortho-isomer, 2.35 (s, 3H), 4.06 (s, 2H).

***t*-Butyltoluenes (6):** A colorless liquid, bp 38 °C/1 mmHg; ^1H NMR δ=1.25 (s, 9H), 2.24 (s, 3H), 6.98 (d, 2H), 7.17 (d, 2H). The isomer ratio (o/p) was determined by GLC using Silicone OV-101 capillary column as 1/99.

1,1-Diphenylethane (7): A colorless liquid isolated by column chromatography on SiO_2 (hexane as eluent); ^1H NMR δ=1.57 (d, 3H), 4.03 (q, 1H), 6.92—7.32 (m, 10H).

Bis(1-phenylethyl)benzenes (8): A colorless liquid isolated by column chromatography on SiO_2 (hexane as eluent), o/p=24/76 by ^1H NMR; ^1H NMR, para-isomer, δ=1.65 (d, 6H), 4.87 (q, 2H), 6.88—7.24 (m, 14H); ortho-isomer, 1.46 (d, 6H), 3.95 (q, 2H).

1,4-Dimethyl-2-(1-phenylethyl)benzene (9): A colorless liquid, bp 129 °C/2 mmHg; ^1H NMR, δ=1.55 (d, 3H), 2.13 (s, 3H), 2.47 (s, 3H), 4.22 (q, 1H), 6.80—7.24 (m, 8H).

(1-Phenylethyl)anisoles (10): A colorless liquid of o/p=17/83 by ^1H NMR, bp 156 °C/5 mmHg; ^1H NMR, para-isomer, δ=1.58 (d, 3H), 3.71 (s, 3H), 4.05 (q, 1H), 6.68—7.20 (m, 9H); ortho-isomer, 1.55 (d, 3H).

References

1) T. Yamauchi, K. Hattori, K. Nakao, and K. Tamaki, *Synthesis*, in press.

2) S. Uemura, A. Onoe, and M. Okano, *Bull. Chem. Soc. Jpn.*, **48**, 3702 (1975); **50**, 1078 (1977); A. Onoe, S. Uemura, and M. Okano, *ibid.*, **49**, 345 (1976); S. Uemura, A. Onoe, H. Okazaki, M. Okano, and K. Ichikawa, *ibid.*, **49**, 1437 (1976).

3) S. Uemura, unpublished data.

4) For the reactivity of $TeCl_4$, see for example, K. J. Irgolic, "The Organic Chemistry of Tellurium," Gordon and Breach, New York, N. Y. (1974).

5) G. A. Olah, M. Nojima, and I. Kerekes, *J. Am. Chem. Soc.*, **96**, 925 (1974).

6) See for example, Ref. 4, p. 35.

7) See for example, K. W. Bagnall, "Comprehensive Inorganic Chemistry," ed by J. C. Bailar et al., Vol. 2, pp. 958—959, Pergamon, Oxford (1973).

8) O. C. Dermer, D. M. Wilson, F. M. Johnson, and V. H. Dermer, *J. Am. Chem. Soc.*, **63**, 2881 (1941).

9) C. H. Fisher and A. Eisner, *J. Org. Chem.*, **6**, 169 (1941).

10) A. McKenzie and G. W. Clough, *J. Chem. Soc.*, **103**, 687 (1913).

11) R. L. Burwell, A. D. Shields, and H. Hart, *J. Am. Chem. Soc.*, **76**, 908 (1954).

 © 1986 The Chemical Society of Japan Bull. Chem. Soc. Jpn., 59, 3621—3624 (1986)

Enzymatic Esterolysis of Polymers Containing 2-Biphenylyl Ester Bonds in Side Chains

Tomomichi Ishikawa,* Makoto Otsuki, and Toshiaki Iwatsuki
Department of Industrial Chemistry, Fucalty of Technology, Tokyo Metropolitan University, Fukasawa, Setagaya-ku, Tokyo 158
(Received June 4, 1986)

The preparation and α-chymotrypsin-catalyzed esterolysis of polymeric substrates anchoring fungicidal biphenyl-2-ol are described. In order to obtain information regarding the influence of one type of polymeric backbone and the distance between a cleavable bond and a polymer main chain, poly(2-biphenylyl acrylate), poly(2-biphenylyl methacrylate), and poly(methacryloylamino acid 2-biphenylyl ester)s were studied. The esterolysis were evaluated by means of Michaelis constant K_m and the catalytic reaction rate constant $k_{cat.}$ Poly(2-biphenylyl methacrylate) was a more suitable substrate than poly(2-biphenylyl acrylate). Poly[6-(methacryloylamino)hexanoic acid 2-biphenylyl ester] was the most suitable substrate in a series of polymers containing amino acid side chains with 2-biphenylyl ester terminal groups. The release rate of biphenyl-2-ol could also be controlled by using copolymers with an appropriate comonomer.

The use of polymers in drug delivery systems has recently received a great deal of attention.[1-5] The mildew defacement of water-soluble paints and their coatings has been a serious problem in the paint industry and for keeping of a good life environment. In connection with this problem, Pittman and co-workers[6,7] examined the biological properties of film-forming polymers with chemically attached biocides using microbiological accelerated fungus-growth tests. In a previous paper[8] we reported on the kinetics of the chymotrypsin-catalyzed hydrolytic cleavage of free biphenyl-2-ol (fungicides, abbreviated to BPOL) from ester groups in the side chains of homopolymer and copolymers with various comonomers in order to simulate microbiological degradation. Kopecek and co-workers[9] also reported on the kinetics of the enzymatic cleavage for the copolymers of various 4-nitroanilides of methacryloylamino acids or origopeptides with *N*-(2-hydroxypropyl)methacrylamide. On the other hand, Kloss and Schröder[10] reported on the hydrolysis of 51 kinds of peptides alkyl esters by chymotrypsin and trypsin. These results suggest that one type of carboxylic acid which forms cleavable ester bonds affects the enzymatic cleavage rates. Therefore, this paper describes the influence of the structure of a polymer main chain and the distance between a cleavable bond and the main chain upon the kinetics of the enzymatic cleavage of polymers **1**, **2**, and **3a—c**.

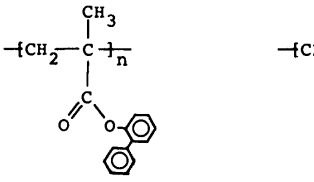

1

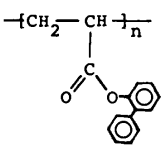

2

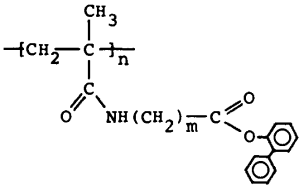

3a m = 1
3b m = 2
3c m = 5

Experimental

Materials. Methacryloyl chloride was distilled prior to use. BPOL and dicyclohexylcarbodiimide (DCC) were purified by distillation. Solvents were dried by the usual methods and distilled. The α-chymotrypsin was the same as in a previous paper,[8] and its activity was checked at the bigining of the experiments. Other chemicals were of reagent grade.

Monomer Preparation. 2-Biphenylyl acrylate (BPA) was prepared according to a method described in a previous paper.[11]

2-Biphenylyl methacryloylaminoacetate (BPMAA-1) was prepared by the esterification of *N*-methacryloylglycine[9,10] with BPOL in the presence of DCC in a way similar to that of a known procedure.[12] Yield 12.3%; mp 131.5—132.9 °C; IR (KBr) 3310 (NH), 1765 (C=O), 1650 (C=O), 1610 (C=C), 760, 730, and 700 cm^{-1}; ^1H NMR (DMSO-d_6) δ=1.90 (3H, s, CH_3), 4.02 (2H, d, CH_2), 5.39 (H, s, CH=), 5.83 (H, s, CH=), 7.30—7.75 (9H, m, Aromatic) and 8.54 (H, broad, NH).

2-Biphenylyl 3-(methacryloylamino)propionate(BPMAA-2) was prepared by the esterification of 3-(methacryloylamino)propionic acid with BPOL in the presence of DCC.[12] Yield 16.3%; mp 88—88.5 °C; IR (KBr) 3340 (NH), 1740 (C=O), 1645 (C=O), 1610 (C=C), 770, 740, and 700 cm^{-1}; ^1H NMR (DMSO-d_6) δ=1.81 (3H, s, CH_3), 2.53 (2H, t, CH_2), 3.39 (2H, q, CH_2), 5.15 (H, s, CH=), 5.45 (H, s, CH=), 6.00 (H, broad, NH) and 7.00—7.40 (9H, s, Aromatic).

2-Biphenylyl 6-(methacryloylamino)hexanoate(BPMAA-5) was prepared by the esterification of BPOL with 6-(methacryloylamino)hexanoic acid[9] in the presence of DCC.[12] Yield 57.1%; mp 64.7—66.0 °C; IR (KBr) 3350 (NH), 1710 (C=O), 1650 (C=O), 1600 (C=C), 750 and 700 cm^{-1}; ^1H NMR (DMSO-d_6) δ=0.90—1.80 (6H, m, $3CH_2$), 1.83 (3H, s, CH_3), 2.23 (2H, t, CH_2), 3.05 (2H, q, CH_2), 5.25 (H, s, CH=), 5.61 (H, s, CH=), 7.10—7.60 (9H, m, Aromatic) and 8.13 (H, broad, NH).

General Procedure for Polymerization. All polymerization experiments were carried out in a hot oil bath at 60 °C using a solution-polymerization technique (in toluene) in the presence of 1 mol% AIBN. The mixtures were poured into methanol. The obtained polymers were dissolved in toluene and precipitated into methanol. The precipitation was repeated, and the polymer was dried in a vaccum oven at 40 °C.

Synthesis of Model Compounds. 2-Biphenylyl propionate (BPP) was obtained by a reaction of BPOL with propionyl chloride.[8]

2-Biphenylyl isobutyrate(BPIB) was obtained by the reaction of BPOL with isobutyryl chloride.[8] Yield 19.0%; bp 155—160 °C (665 Pa); ^{1}H NMR (DMSO-d_6) δ=0.99 (6H, d, 2CH$_3$), 2.41 (1H, m, CH) and 6.95—7.50 (9H, m, Aromatic).

2-Biphenylyl pivalate (BPPV) was obtained by the reaction of BPOL with pivaloyl chloride.[8] Yield 69.3%; bp 114.0 °C (133 Pa); ^{1}H NMR ($CDCl_3$) δ=1.11 (9H, s, 3CH$_3$), 7.00—7.60 (9H, m, Aromatic).

Rate of Esterolysis with α-Chymotrypsin. An esterolysis of monomeric and polymeric substrates was carried out in 50 cm^3 of a buffer solution (0.08 mol dm^{-3} 2-amino-2-hydroxymethyl-1,3-propanediol (Tris) and 0.1 mol dm^{-3} $CaCl_2$ adjusted with HCl to pH=8.0) in the presence of 2.8 mg α-chymotrypsin. For each experiment a substrate converted into 0.15—1.0 mmol dm^{-3} BPOL was used. The reactions were carried out at 25 °C with a regulated water bath. The reaction mixture was continuously shaken. After a given time, some part of this mixture was removed and then the detection of released BPOL was performed by UV at 240.0 nm. The degree of conversion was evaluated by observing the difference between the absorbance at time zero and t.

Results and Discussion

Polymeric substrates anchoring BPOL were obtained by the polymerization of vinyl monomers in proportion to the structure of their polymer units. In order to observe the influence of the structure of a polymer backbone on the rate of esterolysis of a 2-biphenylyl ester bond in a side chain, polymer **2** was obtained by the polymerization of BPA,[11] and its reactivity during esterolysis was compared with that for polymer **1**.[8] On the other hand, it is known that the hydrolysis rate for a cleavable bond at the end of a side chain is affected by the distance between the cleavable site and the polymer backbone.[9,13] Therefore, some methacryloylamino acid 2-biphenylyl esters were synthesized and polymerized; then their polymers were hydrolyzed. We chose an amino acid such as glycine, 3-aminopropionic acid, and 6-aminohexanoic acid as a spacer of side chains in polymeric substrates. Some monomeric model compounds were also synthesized for a comparison with the polymeric substrates. The abbreviation of the monomers and model compounds are shown in Fig. 1.

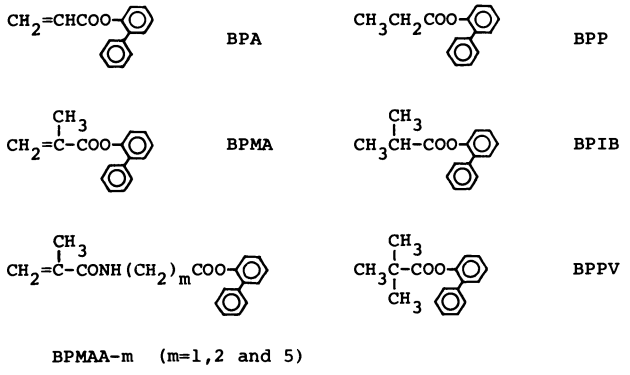

Fig. 1. Abbreviation of 2-biphenylyl esters.

The monomeric and polymeric substrates were hydrolyzed with α-chymotrypsin in a Tris-buffer solution (pH 8). The amount of released BPOL was periodically determined using UV.[8] It is well-known that a chymotrypsin-catalyzed reaction can be expressed by the equation of Michaelis-Menten[14]; thus, the Michaelis constant K_m and the maximum reaction rate V_{max} were determined by a method of Lineweaver and Burk[15] from the relation between the initial reaction rate and the initial concentration of the substrate.

The results for polymer **1** and **2** and the model compounds are summarized in Table 1. It is quite evident from Table 1 that the values of K_m and k_{cat} for the model compounds are in the order BPIB>BPP>BPPV. The order of BPIB and BPP agree with those of the Hammett-Taft's σ^* values. However, no systematic structural correlation was found between BPPV and the others. The small values of K_m and k_{cat} for the BPPV indicate that an enzyme-substrate complex formed is more stable in comparison with those for the others. This can be attributed to the significantly large hydrophobic and steric properties of the t-butyl group. The enzyme was also inactivated

Table 1. α-Chymotrypsin-Catalyzed Esterolysis of Monomeric and Polymeric Substrates

Substrate	Yield / %	K_m 10^3 / mol dm^{-3}	V_{max} 10^5 / mol dm^{-3} h^{-1}	k_{cat}[a] / h^{-1}	k_{cat}/K_m / l mol^{-1} h^{-1}
BPP	64.0	0.89	74	330	370000
BPIB	19.0	1.2	83	370	310000
BPPV	69.3	0.14	9.4	42	300000
1[b]	61.9	1.9	1.7	7.4	3800
2	64.0	1.3	0.82	3.7	2800
3a	12.3		No change		
3b	95.3	0.93	1.0	4.5	4800
3c	57.1	0.63	7.2	32.1	51000

a) Calculated by using a value of 25000 as the molecular weight of α-chymotrypsin. b) Reported in the previous paper (Ref. 8).

owing to a so-called product inhibition[16,17] of pivalic acid which was formed while hydrolyzing BPPV. This result suggests that the reactivity of the substrates is affected by the alkyl groups adjoining to the cleavable bond. As shown in Table 1, both K_m and k_{cat} for polymer **1** is larger than those for polymer **2**, and that the reactivity of the polymeric substrates with α-chymotrypsin varies with the structure of the polymeric main chain. Both K_m and k_{cat} indicate that the formation of the enzyme-polymer **2** complex is easier than that for the polymer **1**; however, the reactivity of the polymer **2**-complex is lower than that of the polymer **1**-complex. When the kinetic parameters for the polymeric substrates is compared with those for the monomeric substrates, the former gave almost the same K_m value as with the latter; a remarkably large difference was observed in the k_{cat} values. The reactivity of chymotrypsin-catalyzed hydrolysis can be estimated by a k_{cat}/K_m value.[18] The high k_{cat}/K_m value for polymer **1** indicates that this polymeric structure is more useful than that of polymer **2**.

The results of the enzymatic hydrolysis of the polymeric substrates containing amino acid side chains with 2-biphenylyl ester terminal groups are also presented in Table 1. It can be seen from Table 1 that no BPOL is released from the glycine 2-biphenylyl ester terminals in polymer **3a**. This is in agreement with the resistance of glycine ethyl ester,[10] *N*,*N*-succinylglycine 4-nitroanilide and the polymer with glycine 4-nitroanilide terminals.[9] Although the k_{cat} values are in the order of polymer **3b**<**1**<**3c**, the values of K_m and k_{cat}/K_m indicate that the general influence of the spacer become greater with an increase in the number of methylene groups. From these results, it seems that the reactivity of the substrates depends on the stability of enzyme-substrate complexes. In the polymeric substrates, the complex of polymer **3c** with enzyme is easily formed and shows a high reactivity: Namely, that the Michaelis constant K_m is the lowest and the reaction rate constant k_{cat} is the highest value of the series. Kopecek and coworkers[9] examined the necessity of a spacer having a certain length for the cleavage of polymers with amino acid 4-nitroanilide terminals. He concluded that in the case of chymotrypsin the spacer must be at least 6-atoms long. In this study the result for polymer **3d** was in agreement with their conclusion.

Table 2. Additional Effect of 3-(Methacryloylamino)-propionic Acid (MAA-2) in Esterolysis of BPMAA-2

BPMAA-2 / mol dm^{-3}	MAA-2 / mol dm^{-3}	v_0 / mol dm^{-3} h^{-1}
9.99×10^{-4}	5.01×10^{-4}	0.370×10^{-4}
9.86×10^{-4}	—	1.79×10^{-4}
3.96×10^{-4}	11.0×10^{-4}	0.216×10^{-4}
4.09×10^{-4}	—	1.43×10^{-4}
2.78×10^{-4}	—	1.16×10^{-4}
1.36×10^{-4}	13.6×10^{-4}	0.105×10^{-4}
1.55×10^{-4}	—	0.709×10^{-4}

The substrates anchoring BPOL through the amino acid residues are competitively degraded in both the amide and the ester bonds with α-chymotrypsin. Therefore, some mixtures of the BPMAA-2 and 3-(methacryloylamino)propionic acid were hydrolyzed in order to obtain information on the influence of amides regarding the esterolysis rate. All the experiments were carried out under the conditions of the same initial concentration on the amide group. The results are shown in Table 2. It is evident from Table 2 that all the initial rates for the mixtures were slower than that for a single substrate, BPMAA-2. In the case of mixtures, values of K_m=0.52×10^{-3} mol dm^{-3} and k_{cat}=20 h^{-1} were obtained. The K_m and k_{cat} values for BPMAA-2 were 0.52×10^{-3} mol dm^{-3} and 143 h^{-1}, respectively. These results suggest that 3-(methacryloylamino)propionic acid acts as a so-called noncompetitive inhibitor, because the Michaelis constant K_m for the mixture gives the same value as that for mixture, whereas the maximum reaction rate V_{max} decrease with an increase in the content of the amide groups. If the cleavage of the ester and amide bonds proceeds competitively, the K_m value for the mixture ought to be different from that for the substrate BPMAA-2. Therefore, the same K_m value for the mixture and for the BPMAA-2 can be assumed to be caused by a very slow cleavage rate of the amide bonds with α-chymotrypsin.

Generally, water-soluble paints are prepared from vinyl acetate (VAc) and methyl methacrylate (MMA). Film-forming polymers with chemically attached BPOL can be used as a vehicle for fungicidal paints. Therefore, copolymers of BPMAA-2 with VAc or

Table 3. Preparation and Esterolysis of Copolymers of BPMAA-2 with VAc and MMA[a]

Comonomer	Molar fraction BPMAA-2 in monomer	Time / h	Yield[b] / %	Molar fraction BPMAA-2 in polymer[c]	$[\eta]$[d] / dm^3 g^{-1}	$K_m\ 10^3$ / mol dm^{-3}	k_{cat} / h^{-1}	k_{cat}/K_m / l mol^{-1} h^{-1}
—	1.000	44	95.3	1.000	0.12	0.93	4.5	4800
VAc	0.700	71	51.6	0.650	0.05	1.2	9.8	8170
MMA	0.500	43	86.8	0.456	0.22	0.81	23.6	29100

a) Reacted in toluene at 60 °C in the presence of AIBN(1—1.4 mol%). b) Reprecipitated with hexane. c) Determined by ^{1}H NMR. d) Measured in $CHCl_3$ at 25 °C.

MMA were also prepared, and hydrolyzed with α-chymotrypsin. The results are given in Table 3. As shown in Table 3, a small difference between the homopolymer and the copolymers was observed in the K_m values, whereas the k_{cat} values were apparently in the order of polymer **3b**<VAc-BPMAA-2 copolymer< MMA-BPMAA-2 copolymer. On the other hand, we have reported in a previous paper[7] that the reaction rate of a VAc-BPMA copolymer is slower than that of a BPMA homopolymer, and that the K_m value for both the homopolymer and the copolymer was equal to 1.9 mol dm^{-3}. The contrast between the two cases could readily be explained in terms of differences in a steric conditions at the cleavable bond, which is surrounded with acetoxyl groups. In the case of a VAc-BPMAA-2 copolymer, the 2-biphenylyloxycarbonyl groups that are sensitive to chymotrypsin attack a row of acetoxyl groups and can easily form a complex with the enzyme. In contrast to this case, the 2-biphenylyloxycarbonyl groups on the VAc-BPMA copolymer are buried into the acetoxyl groups. Azori and co-workers[19] examined the chymotrypsin catalyzed hydrolysis in the range 1 to 20 mol% for side chains containing *p*-nitroaniline bound to poly(*N*-vinyl-2-pyrrolidone-co-maleic anhydride), and reported that the maximum reaction rate V_{max} varies with the mole fraction of the side chains. These results indicate that the release rate of BPOL from the polymers can be controlled by using copolymers with an appropriate comonomer. Although the hydrolysis rate constant k_{cat} for the MMA-BPMAA-2 copolymer showed a considerably large value among the polymeric substrates used in this work, only 4% of total BPOL was released during a four-hour period. However, the conversion of the same substrate in hydrolysis without chymotrypsin was 0.9% during a four-day period.

References

1) H. Lingsdorf, *J. Polymer Sci., Symposium*, **51**, 135 (1975).
2) C. G. Gebelein, *Polymer News*, **4**, 163 (1978).
3) J. Feijen, D. Gregonis, C. Anderson, R. V. Petersen, and J. Anderson, *J. Pharm. Sci.*, **69**, 871 (1980).
4) S. K. Chandrasekaran, Editer, *Am. Inst. Chem. Eng., Symposium Series*, No. 206, vol. **77** (1981).
5) T. Hayashi, Y. Tabata, and A. Nakajima, *Rep. Pro. Polym. Phys. Jpn.*, **26**, 578 (1983).
6) C. U. Pittman, Jr., G. A. Stahl, and H. Winters, *J. Coatings Tech.*, **50**, 49 (1978).
7) C. U. Pittman, Jr., *J. Coatings Tech.*, **48**, 31 (1976); A. Stahl, and C. U. Pittman, Jr., *J. Coatings Tech.*, **50**, 62 (1978).
8) T. Ishikawa, and Y. Tanaka, *Bull. Chem. Soc. Jpn.*, **58**, 1182 (1985).
9) J. Drobnik, J. Kopecek, J. Labasky, P. Rejmanova, J. Exner, V. Saudek, and J. Kalal, *Makromol. Chem.*, **177**, 2833 (1976).
10) G. Kloss and E. Schröder, *Hoppe-Seyler.*, **336**, 248 (1964).
11) T. Ishikawa and S. Asai, *Bull. Chem. Soc. Jpn.*, **56**, 2177 (1983).
12) P. Rejmanova, J. Labsky, and J. Kopecek, *Makromol. Chem.*, **178**, 2159 (1977); H. D. Jakubke, and A. Voigt, *Chem. Ber.*, **99**, 2948 (1966).
13) J. Pato, M. Azori, K. Ulbrich, and J. Kopecek, *Makromol. Chem.*, **185**, 231 (1984).
14) L. Michaelis and M. L. Menten, *Biochem. Z.*, **49**, 333 (1913).
15) H. Lineweaver and D. Burk, *J. Am. Chem. Soc.*, **56**, 658 (1934).
16) W. W. Cleland, *Biochem. Biophys. Acta*, **67**, 173 (1963).
17) R. Y. Hsu, W. W. Cleland, and L. Anderson, *Biochem.*, **5**, 799 (1966).
18) F. E. Brot and M. L. Bender, *J. Am. Chem. Soc.*, **91**, 7187 (1969).
19) M. Azori, J. Pato, F. Fehervari, and F. Tudos, *Makromol. Chem.*, **187**, 303 (1986).

α-Fluorination of Sulfides with *N*-Fluoropyridinium Triflates

Teruo UMEMOTO* and Ginjiro TOMIZAWA
Sagami Chemical Research Center, Nishi-Ohnuma 4-4-1, Sagamihara, Kanagawa 229
(Received June 4, 1986)

The reaction of sulfides possessing α-hydrogen with various *N*-fluoropyridinium salts was examined. While the fluorinating power increased in the order of *N*-fluoro-2,4,6-trimethylpyridinium triflate **1**<*N*-fluoropyridinium triflate **2**<*N*-fluoro-3,5-dichloropyridinium triflate **3**, the yield of an α-fluoro sulfide decreased in the order of **1**>**2**, and **3** no longer produced the α-fluoro sulfide. Triflate **1** was more reactive than the corresponding tetrafluoroborate **4**. Thus, it was shown that **1** satisfactorily fluorinated various kinds of sulfides under very mild conditions, giving α-fluoro sulfides. A two-step mechanism, oxidative fluorination of sulfur and Pummerer-type rearrangement, was proposed for the fluorination. The corresponding α-fluoro sulfoxide or sulfones were easily prepared from the sulfides by successive fluorination-oxidation procedure.

In recent years, introduction of fluorine into organic molecules is of increasing importance in the biological and pharmaceutical fields because it can alter the biological activity of the molecules or make them specific irreversible enzyme inhibitors with high possibility.[1] Therefore the methodologies for preparing the fluoro-compounds are being investigated actively.[1,2] Among them, α-fluorination of sulfides is of importance since some of sulfides are biologically active compounds such as β-lactam antibiotics[3] and amino acids[4] or since the resulting α-fluoro sulfides can serve as useful synthetic intermediates for the biologically active fluoro-compounds.[5] The reported methods for the preparation of α-fluoro sulfides are as follows; (1) direct fluorination of sulfides with xenon difluoride,[6] (2) replacement reaction of α-chloro sulfides with rigorously dried potassium fluoride and 18-crown-6,[7] and (3) conversion of sulfoxides to α-fluoro sulfides with diethylaminosulfur trifluoride (DAST).[8] However, xenon difluoride is very expensive and difficult to handle, and in order to prepare acid-labile α-fluoro sulfides, the special technique using bis (trimethylsilyl) amine is needed to remove hydrogen fluoride resulting from the reaction.[6b,c] The latter two methods required two steps from sulfides and severe reaction conditions for the fluorination because of the use of very hygroscopic potassium fluoride or thermally unstable and moisture-sensitive DAST.

We developed *N*-fluoropyridinium salts as easily handled fluorinating agents with variable fluorinating power[9] and found that the reaction of sulfides having α-hydrogen with the reagents resulted in the easy formation of α-fluoro sulfides. In this paper, α-fluorination of the sulfides with various *N*-fluoropyridinium salts was examined.

Results and Discussion

The reactivity of *N*-fluoropyridinium triflates **1**—**3** to the sulfide **5** was examined and the results are shown in Table 1. It was found that, while the fluorinating power increased in the order of **1** < **2** < **3**,[9] the yield of an α-fluoro sulfide **6** decreased in the order of **1** > **2** and **3** no longer produced **6**. It has been demonstrated that the fluorinating power is variable depending on the electron density at the positive nitrogen site.[9] The least reactive **1** mildly reacted with **5** in dichloromethane at room temperature to produce the α-fluoro sulfide **6** in a high yield (Eq. 1). On the other hand, the most reactive **3** underwent rapid and exothermic reaction with **5**, but the fluoro sulfide **6** and any other organic fluorides were not detected in

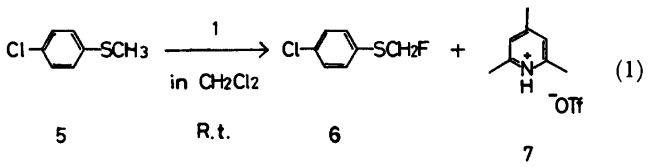

(1)

the ^{19}F-NMR spectrum of the resulting reaction solution. **2** afforded **6** in a moderate yield (48%) under

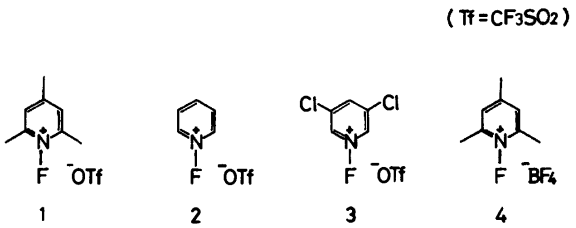

Scheme 1.

Table 1. α-Fluorination of Sulfide **5** with *N*-Fluoropyridinium Salts

Run[a]	Salt	Temp	Time/h	Yield/%[b] of **6**
1	**1**	R.t.	8	87 (76)
2	**2**	R.t.	7.5	(48)
3[c]	**3**	R.t.	—	0
4	**4**	R.t.	11	No reaction
5	**4**	Reflux	4.5	75

a) Dichloromethane was used as a solvent. b) ^{19}F NMR yields. The values in parentheses are isolated yields. c) An exothermic reaction occurred immediately.

the similar conditions. As seen from Eq. 1, the reaction of **1** proceeded under almost neutral conditions because triflic acid liberated during the reaction was trapped by collidine simultaneously liberated. This is of great benefit to the preparation of acid-labile α-fluoro sulfides. Accordingly, the relatively low Yield and the unproductiveness of the fluoro sulfide **6** using **2** and **3** should be concerned with their relatively acidic conditions because of low and very low basicity of pyridine and 3,5-dichloropyridine liberated, respectively, compared to collidine. Of course, it cannot be excluded that the high oxidation power, particularly, of **3** is reponsible for it.

A tetrafluoroborate **4** which was expected to have the same fluorination power as triflate **1**[9a] exhibited the great difference in the reactivity. **4** did not react with the sulfide **5** under the same conditions as **1**, but **4** reacted at an elevated temperature to give the fluoro sulfide **6** in a 75% yield (Table 1, Run 5). The low reactivity of **4** is probably due to the low solubility compared to **1**. But another reason cannot entirely be excluded that the reactivity is somewhat dependent on the nature of the counter anions.

Furthermore, the reaction of *N*-fluoropyridinium salts was greatly dependent on the solvents. It was found from the ^{19}F NMR spectra of the resulting reaction solutions that no α-fluoro sulfides were produced in the polar solvents such as tetrahydrofuran (THF) and acetonitrile though the reagents were consumed (Table 2, Runs, 6, 11, and 12). The cause of the great solvent dependence is not clear. The *N*-fluoropyridinium salts do not fluorinate THF and acetonitrile.

Table 2 shows the results about α-fluorination of several kinds of sulfides including ones having functional groups such as alkoxycarbonyl and amido with triflate **1** or **2**. Alkyl aryl sulfides were converted to α-fluoroalkyl aryl sulfides in high yields. More acid-labile α-fluoroalkyl alkyl sulfides were also prepared by the present method though their yields were generally moderate. Since the more labile fluoro sulfides decomposed during the post-treatment, they were determined by ^{19}F NMR and their structures were confirmed by oxidizing them to stable α-fluoro sulfones which were characterized.

An unsymmetrical dialkyl sulfide, methyl dodecyl sulfide, afforded fluoromethyl dodecyl sulfide only. Ethyl methylthioacetate gave the product resulting from the fluorination at activated hydrogen site only. Benzyl methyl sulfide gave a mixture of benzyl fluoromethyl sulfide and α-fluorobenzyl methyl sulfide (3:4). Thus, the present method using **1** has been shown to be very useful and broadly applicable to the preparation of α-fluoro sulfides because of stable and nonhygroscopic crystals of **1**, mildness of the reaction conditions, and the simplicity of the procedure.

The above-mentioned selectivity of the α-fluorination with *N*-fluoropyridinium salts is very similar to that of Pummerer rearrangement which converted sulfoxides to α-acetoxy sulfides.[10] We propose the following two-step mechanism, oxidative fluorination of sulfur and Pummerer-type rearrangement, for

Table 2. α-Fluorination of Sulfides

Run	Sulfide	Salt	Solv.	Temp/°C	Time/h	α-Fluoro sulfide	Yield/%[a]	^{19}F NMR[b]
1	$PhSCH_3$	**1**	CH_2Cl_2	R.t.	4	$PhSCH_2F$	85 (49)	180.3 (t, J=54 Hz)
2	$PhSCH_3$	**2**	CH_2Cl_2	R.t.	6	$PhSCH_2F$	56	—
3	Cl-C$_6$H$_4$-SCH_3	**1**	CH_2Cl_2	R.t.	8	Cl-C$_6$H$_4$-SCH_2F	87 (76)	182.8 (t, J=52.5 Hz)
4	Cl-C$_6$H$_4$-SCH_3	**2**	CH_2Cl_2	R.t.	7.5	Cl-C$_6$H$_4$-SCH_2F	48	—
5	n-$C_{12}H_{25}SCH_3$	**1**	CH_2Cl_2	R.t.	17.5	n-$C_{12}H_{25}SCH_2F$	44	184.2 (t, J=52 Hz)
6	n-$C_{12}H_{25}SCH_3$	**1**	CH_3CN	R.t.	18	Non[c]	—	—
7	CH_3SCH_2COOEt	**1**	CH_2Cl_2	R.t.	8	$CH_3SCHFCOOEt$	46	167.3 (d, J=54 Hz)
8	$PhSCH_2COOMe$	**1**	CH_2Cl_2	R.t.	23	$PhSCHFCOOMe$	45 (38)	158.4 (d, J=52 Hz)
9	$PhCH_2SCH_3$	**1**	CH_2Cl_2	R.t.	0.5	$PhCHFSCH_3$ 4) $PhCH_2SCH_2F$ 3)	77	152.0 (d, J=56 Hz) 187.2 (t, J=51 Hz)
10	$PhCH_2SCH_3$	**1**	CH_2Cl_2	0	3	$PhCHFSCH_3$ 4) $PhCH_2SCH_2F$ 3)	48	—
11	$PhCH_2SCH_3$	**1**	THF	0→R.t.	50	Non[c]	—	—
12	$PhCH_2SCH_3$	**2**	THF	R.t.	11	Non[c]	—	—
13	$CH_3SCH_2CH_2CHCOOMe$ $NHCOCF_3$	**1**	CH_2Cl_2	R.t.	7.5	$FCH_2SCH_2CH_2CHCOOMe$ $NHCOCF_3$	39	183.8 (t, J=51 Hz)
14	$CH_3SCH_2CH_2CHCOOMe$ $NHCOCF_3$	**1**	CH_2Cl_2	Reflux	2	$FCH_2SCH_2CH_2CHCOOMe$ $NHCOCF_3$	41	—

a) See b) in Table 1. b) Chloroform-*d* was used as a solvent for Run 1, 2, 8, and 13, and dichloromethane for Runs 5, 7, and 9. c) No α-fluoro sulfides were detected.

the α-fluorination (Scheme 2). Marat and Janzen suggested a similar mechanism for the α-fluorination with xenon difluoride.[5b] McCarthy et al. proposed Pummerer-type rearrangement as the mechanism for the conversion of sulfoxides to α-fluoro sulfides with DAST.[8]

Our attempt to detect intermediate S-F compounds on ^{19}F NMR spectra was unsuccessful. In the α-fluorination of methyl phenyl sulfide, the ^{19}F-peak corresponding to the α-fluoro sulfide appeared with the consumption of triflate **1**, indicating that the intermediates are very unstable. M. Zupan also failed to detect the intermediate S-F compounds by ^{19}F NMR technique in the reaction with xenon difluoride.[6a]

Furthermore, we tried to detect a ^{19}F-peak corresponding to S-F in the reaction of **1** with diphenyl sulfide without α-hydrogen in order to demonstrate the transfer of a fluorine atom from the positive nitrogen to the sulfur site. The reaction of **1** with diphenyl sulfide in dichloromethane was carried out at room temperature in a NMR-tube and followed by NMR measurement. A new singlet peak at −3.25 ppm was definitely observed after 19 h. It was found that the peak slightly shifted to downfield with time and reached to −5.25 ppm after 4 d. The reaction mixture became completely homogeneous in 5 d and addition of water into the solution resulted in immediate disappearence of the peak. The subsequent usual

$$\text{Ph-S-Ph} \xrightarrow{\mathbf{1}} \xrightarrow{H_2O} \text{Ph-SO-Ph} \qquad (2)$$

workup gave diphenyl sulfoxide in a 34% yield. Although the slight shift with time cannot be explained at the present stage, the chemical shift of the new peak is very close to the ^{19}F-chemical shift (−5.43 ppm) of diphenylsulfur difluoride[6b] which was easily hydrolyzed to diphenyl sulfoxide. The above results indicated that the new peak corresponded to a S-F compound and supported that the α-fluorination of sulfides occurred via the oxidative fluorination of sulfur followed by the rearrangement of fluorine to α-carbon. But we have no full data for determining the exact structures of the intermediate S-F compounds.

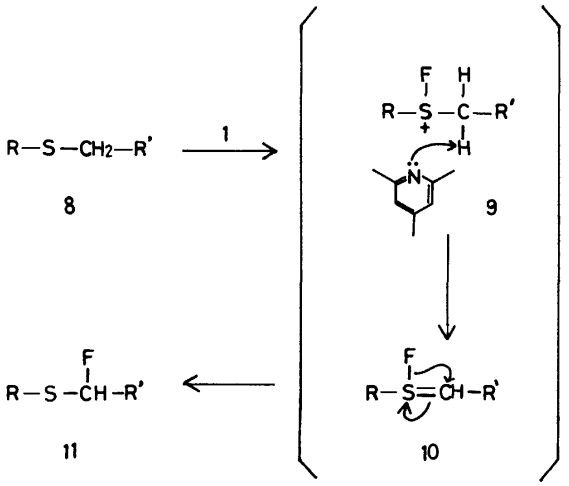

Scheme 2.

The mechanism is in agreement with that of the other α-halogenation of sulfides with chlorine, bromine, sulfuryl chloride, or *N*-chloro- or bromosuccinimide.[11] However, the present α-fluorination should be essentially different in the mechanism of the initial transfer of fluorine to sulfur site from the case of the other α-halogenation, because the N^+-F bond is very firm[9a] due to extreme difficulty in the formation of a fluorine cation in contrast to the case of the other halogen atoms.[12] Although a stepwise mechanism by a one-electron transfer for the initial fluorine transfer may be suggested, the detailed mechanism is not clear at the present stage.

α-Fluoro sulfoxide[7,8] or sulfones[8] were easily prepared by the fluorination, followed by oxidation with *N*-bromosuccinimide-water or *m*-chloroperbenzoic acid (Table 3). The successive fluorination-oxidation were conveniently carried out by one-pot

Table 3. One-Pot Preparation of α-Fluoro sulfoxide or Sulfones from Sulfides

$$\text{R-S-CH}_2\text{R}' \xrightarrow[\text{R.t. in } CH_2Cl_2]{\mathbf{1}} \xrightarrow{[O]} \text{R-}\overset{(O)_n}{\overset{\|}{S}}\text{-CHFR}' \quad (n=1,\ 2)$$

Run	Sulfide	Oxidation Conditions	Product	Yield/%[a]
1	$PhSCH_3$	NBS[b] (1.5 eq), r.t., 0.5 h in CH_2Cl_2-MeOH-H_2O	$PhSOCH_2F$	66
2	$PhCH_2SCH_3$	MCPBA[c] (2.5 eq), r.t., 2 h in CH_2Cl_2	$PhCHFSO_2CH_3$ (4), $PhCH_2SO_2CH_2F$ (3)	77
3	n-$C_{12}H_{25}SCH_3$	MCPBA[c] (2.5 eq), r.t., 4 h in CH_2Cl_2	n-$C_{12}H_{25}SO_2CH_2F$	37
4	CH_3SCH_2COOEt	MCPBA[c] (2.5 eq), r.t., 10 h in CH_2Cl_2	$CH_3SO_2CHFCOOEt$	48
5	$CH_3SCH_2CH_2CHCOOMe$ (NHCOCF₃)	MCPBA[c] (2.5 eq), r.t., 10 h in CH_2Cl_2	$FCH_2SO_2CH_2CH_2CHCOOMe$ (NHCOCF₃)	34

a) Isolated yields. b) *N*-Bromosuccinimide. c) *m*-Chloroperbenzoic acid.

method. Since most of α-fluoro sulfides decompose partly or completely during the post-treatment, our one-pot procedure is very advantageous for praparing the α-fluoro sulfoxides or sulfones from sulfides.

Experimental

General. Melting points were uncorrected. ^{1}H NMR spectra were determined with a Varian HA-100 NMR spectrometer or a Varian EM 390 NMR spectrometer. ^{19}F NMR spectra were determined with a Varian XL-100 A NMR spectrometer or a Hitachi R-20 B NMR spectrometer. ^{19}F NMR chemical shifts are given in ppm upfield from trichlorofluoromethane as an internal standard. IR spectra were measured on a Jasco A-202 diffraction grating infrared spectrophotometer. Dichloromethane used was dried by treatment with calcium chloride followed by distillation on calcium hydride.

Materials. *N*-Fluoropyridinium salts **1**—**4** were prepared according to our methods reported previously.[9a]

α-Fluorination of Sulfides. A Typical Procedure: *p*-Chlorophenyl methyl sulfide (158 mg, 1 mmol) was added into a mixture of triflate **1** (290 mg, 1 mmol) and dry dichloromethane (3 ml) at room temperature under argon atmosphere and the reaction mixture was stirred for 8 h. The reaction was followed by checking the oxidation power with aq KI solution. After **1** completely disappeared, anhydrous sodium carbonate (0.5 g) was added and the organic layer was thin-layer chromatographed on silica gel by using a mixture of hexane and triethylamine (100:1) as an eluent to give *p*-chlorophenyl fluoromethyl sulfide as an oily product (133 mg, 76%).

Spectral date of fluoromethyl phenyl sulfide and *p*-chlorophenyl fluoromethyl sulfide are in good agreement with the reported data.[7] Although the products of Runs 5, 7, 9, 10, 13 and 14 in Table 2 were detected by ^{19}F NMR analysis, they completely decomposed during the post-treatment using chromatography on silica gel. Therefore the labile α-fluoro sulfides were converted to the easily isolated fluoro sulfones.

Methyl Phenylthio Fluoroacetate: Oil, ^{1}H NMR ($CDCl_3$) δ=3.70 (3 H, s, CH_3), 6.08 (1 H, d, J_{H-F}=52.5 Hz, CHF), 7.20—7.70 (5 H, m, Ar); ^{19}F NMR ($CDCl_3$) 158.4 (d, J_{H-F}=52.5 Hz); IR (neat, cm^{-1}) 1760 (CO); MS (*m/z*) 200 (M^+). Found: C, 53.97; H, 4.46%. Calcd for $C_9H_9FO_2S$: C, 53.99; H, 4.53%.

One-Pot Synthesis of Fluoromethyl Phenyl Sulfoxide from Methyl Phenyl Sulfide. α-Fluorination of methyl phenyl sulfide (124 mg, 1 mmol) by using **1** (290 mg, 1 mmol) and dry dichloromethane (3 ml) as a solvent was carried out in the same manner as the above. The reaction time was 4 h. After that, methanol (1 ml), water (0.1 ml) and then *N*-bromosuccinimide (270 mg, 1.5 mmol) were added into the resulting reaction mixture under cooling with ice bath and it was stirred at room temperature for 0.5 h. The reaction mixture was washed with aq sodium thiosulfate and the aq layer was extracted with ethyl acetate. The combined organic layer was washed with aq sodium hydrogen carbonate solution, 10% hydrochloric acid, and then aq sodium chloride solution. The organic layer was dried over magnesium sulfate, filtered and concentrated. The residue was column-chromatographed on silica gel by using a mixture of hexane and ethyl acetate (2:1) as an eluent to give fluoromethyl phenyl sulfoxide (105 mg, 66%). The spectral data of the sulfoxide was in good agreement with the reported.[7]

One-Pot Synthesis of α-Fluoro Sulfones from Sulfides. A Typical Procedure: α-Fluorination of dodecyl methyl sulfide (216 mg, 1 mmol) by using **1** (290 mg) and dry dichloromethane (2 ml) was carried out in the same manner as the above. The reaction time was 4 h. Then, 80—90%

Table 4. Properties of α-Fluoro Sulfones

α-Fluoro sulfones		Mp θ_m/°C	^{19}F NMR[a]/ppm (CHF)	^{1}H NMR[a]/δ (CHF)	IR/cm^{-1} [Method]	Mass/*m/z*	Anal./% (Calcd)
$PhCHFSO_2CH_3$	**12**	78—79	176.0 (d, J=48 Hz)	5.96 (1H, J=48 Hz)	1320 (SO_2) [KBr]	190 ($M^+-CH_3SO_2$)	C, 51.25 (51.05) H, 4.82 (4.81)
$PhCH_2SO_2CH_2F$	**13**	Oil	212.3 (t, J=47 Hz)	4.86 (2H, t, J=47 Hz)	1320 (SO_2) [Neat]	180 (M^+)	C, 50.76 (51.05) H, 4.83 (4.82)
n-$C_{12}H_{25}SO_2CH_2F$	**14**	62—63	212.6 (t, J=48 Hz)	5.06 (2H, t, J=48 Hz)	1325 (SO_2) [KBr]	266 (M^+)	C, 58.37 (58.61) H, 10.00 (10.22)
$CH_3SO_2CHFCOOC_2H_5$	**15**	Oil	183.4 (d.q, J=48 Hz J=2.4 Hz)	5.53 (1H, d, J=48 Hz)	1760 (CO) 1380 (SO_2) [Neat]	185 (M^++1) 156	C, 32.75 (32.61) H, 5.00 (4.93)
$FCH_2SO_2CH_2CH_2CHCOOCH_3$ $\quad\quad\quad

m-chloroperbenzoic acid (540 mg, about 2.5 mmol) was added into the resulting reaction mixture under cooling with ice bath and then the mixture was stirred at room temperature for 4 h. The same workup as the above gave dodecyl fluoromethyl sulfone (99.4 mg, 37%). The spectral data and elemental analysis of new α-fluoro sulfones are shown in Table 4.

References

1) a) "Biomedical Aspect of Fluorine Chemistry," ed by R. Filler and Y. Kobayashi, Kodansha Ltd., Tokyo (1982); b) F. A. Smith, *CHEMTECH*, 422, July, 1973; c) N. Ishikawa, *Kagaku No Ryoiki*, **35**, 441 (1981).

2) a) M. R. C. Gerstenberger and A. Haas, *Angew. Chem. Int. Ed. Engl.*, **20**, 647 (1981); b) M. Schlosser, *Tetrahedron*, **34**, 3 (1978); c) N. Ishikawa, *Kagaku No Ryoiki*, **37**, 6 (1983).

3) P. G. Sammes, *Chem. Rev.*, **76**, 113 (1976).

4) P. Hermann, "Organic Sulfur Chemistry," ed by R. Kh. Freidlima and A. E. Skorova, Pergamon Press, Oxford (1981), pp. 51—67.

5) a) M. Inbasekaran, N. P. Peet, J. R. McCarthy, and M. E. LeTourneau, *J. Chem. Soc., Chem. Commun.*, **1985**, 678; b) V. Reutrakul and V. Rukachaisirikul, *Tetrahedron Lett.*, **24**, 725 (1983).

6) a) M. Zupan, *J. Fluorine Chem.*, **8**, 305 (1976); b) R. K. Marat and A. F. Janzen, *Can. J. Chem.*, **55**, 3031 (1977); c) A. F. Janzen, P. M. C. Wang, and A. E. Lemire, *J. Fluorine Chem.*, **22**, 557 (1983).

7) K. M. More and J. Wemple, *Synthesis*, **1977**, 791.

8) J. R. McCarthy, N. P. Peet, M. E. LeTourneau, and M. Inbasekaran, *J. Am. Chem. Soc.*, **107**, 735 (1985).

9) a) T. Umemoto and K. Tomita, *Tetrahedron Lett.*, **27**, 3271 (1986); b) T. Umemoto, K. Kawada, and K. Tomita, *Tetrahedron Lett.*, **27**, 4465 (1986).

10) a) R. Pummerer, *Chem. Ber.*, **43**, 1401 (1910); b) L. Horner, *Justus Liebigs Ann. Chem.*, **631**, 198 (1960); c) A. Ohno, "Yûki Gôsei ni okeru Iô Kagôbutsu no Yakuwari," ed by Shigeru Oae, Sankyo Shuppan, Tokyo (1981), pp. 124—132.

11) a) G. E. Wilson, Jr., *Tetrahedron*, **38**, 2597 (1982); b) G. E. Wilson, Jr., and M. G. Huang, *J. Org. Chem.* **35**, 3002 (1970); c) W. Takagi, K. Kikukawa, K. Ando, and S. Oae., *Chem. Ind. (London)*, **1964**, 1624.

12) R. C. Weast, "Handbook of Chemistry and Physics,' CRC Press (1980), Vol. 61, p. E-69.

 © 1986 The Chemical Society of Japan Bull. Chem. Soc. Jpn., 59, 3631—3635 (1986)

Stereoselective Cycloadditions of Pyridinium or Isoquinolinium Methylides with Olefinic Dipolarophiles and Subsequent Cycloadditions of the Cycloadducts with Nitrile Oxides

Otohiko TSUGE,* Shuji KANEMASA, and Shigeori TAKENAKA
Research Institute of Industrial Science, and Department of Molecular Science and Technology, Interdisciplinary Graduate School of Engineering Sciences, Kyushu University, Kasugakoen, Kasuga 816
(Received June 7, 1986)

Pyridinium or isoquinolinium methylides undergo highly stereo- and regioselective cycloadditions with olefinic dipolarophiles to form unstable tetrahydroindolizine derivatives. One of the two double bonds existing in the dihydro heteroaromatic ring of the cycloadducts reacts with nitrile oxides, in the same flask, in stereo-, regio-, and periselective fashions to lead to stable isoxazole-fused tetrahydroindolizines in good yields.

Although the cycloadditions of heteroaromatic *N*-ylides such as pyridinium, quinolinium, isoquinolinium, pyridazinium, thiazolium, and triazolium methylides with electron-deficient olefins take place in a highly diastereoselective manner to give fused heterocycles which bear a nitrogen atom at the point of fusion,[1-13] the cycloadducts are not always thermally stable. This instability is mainly due to the loss of aromaticity of the heteroaromatic ring of ylides in the step of cycloaddition. The cycloadducts frequently undergo retro cycloaddition[1,2] or carbon–carbon bond cleavage into betaine intermediates,[2,14-16] both of which are encouraged by the recovery of aromaticity.

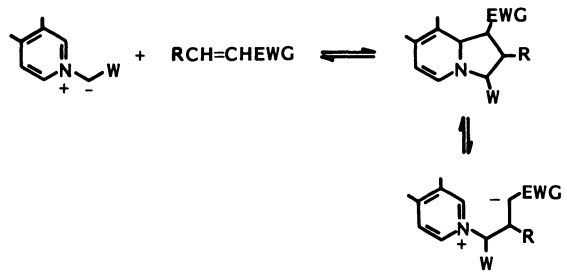

The cycloadducts derived from pyridinium methylides contain a fused dihydropyridine ring. Therefore, formal reduction of one of the two double bonds involved in the dihydropyridine skeleton should be effective for isolation of the cycloadducts as stable products. A cycloaddition and desilylation sequence of 4-silyloxypyridinium methylides is a successful example along this line.[17] In the present article, another method was applied for the formal reduction of these instability-causing double bonds: a cycloaddition method of such unstable cycloadducts with nitrile oxides.

Results and Discussion

Pyridinium **1** and isoquinolinium methylides **2** were generated in situ from the corresponding pyridinium and isoquinolinium halides by treatment with triethylamine in dichloromethane and used for subsequent reactions without isolation (Scheme 1). More than two equivalent amounts of triethylamine were employed in general. One equivalent was for the ylide generation and the rest for the nitrile oxide generation which is to be carried out in the same flask as shown later.

These ylides **1** and **2** were first allowed to react with olefinic dipolarophiles to form diastereoselective cycloadducts **3**—**10**, though only **3** and **4** could be isolated and assigned as endo cycloadducts to the anti form of **1a** (Scheme 2 and Table 1).[1] The other cycloadducts **5**—**10** were too labile to be isolated, but their structures were readily deduced on the basis of the exclusive diastereoselectivity observed in the reaction of isoquinolinium phenacylide with unsymmetrical olefins such as methyl acrylate and acrylonitrile.[18] High regioselectivity (or periselec-

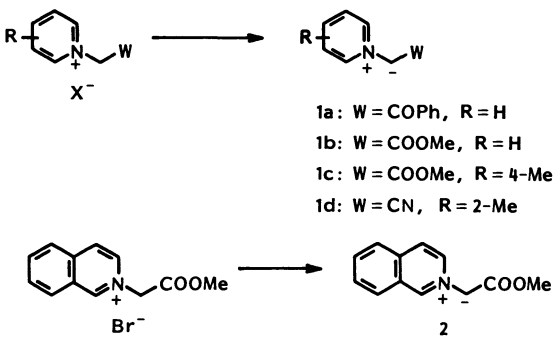

Scheme 1.

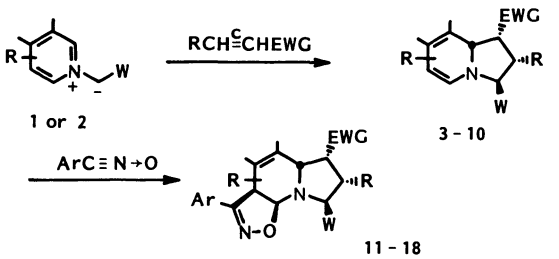

Scheme 2.

tivity) in favor of the 5-methyl derivative **9** is also consistent with the previously observed selectivity.[1]

The diastereoselective cycloadducts **3**—**10** formed in situ as thermally unstable products were next subjected to react with nitrile oxides (Scheme 2). Thus, *N*-(α-chloro-*p*-methoxybenzylidene)hydroxylamine was added to the reaction mixture which consisted of **3** and the remaining triethylamine. After 1 h at room temperature, nitrile oxide cycloadduct **11** was obtained as a single stereo- and regioisomer in an almost quantitative yield (based on the ylide precursor). Similar reactions of other unstable tetrahydroindolizines **4**—**7** with benzonitrile oxide or *p*-methoxybenzonitrile oxide gave also single isomers **12**—**15** of nitrile oxide cycloadducts (Scheme 2 and Table 1). Substitution on the fused dihydropyridine ring of **8**—**10** did not affect the cycloaddition with nitrile oxides, similar products **16**—**18** being produced.

It is clear that nitrile oxide cycloadducts **11**—**18** are all those formed through regioselective cycloaddition across the carbon–carbon double bond adjacent to the fused nitrogen. In every case, the newly formed methine carbon carrying an oxygen and a nitrogen substituent (10a-C in **11** and **12**, 9a-C in **13**—**17**, and 3a-C of **18**) appeared as low as 92—98 ppm, and the methine hydrogen on this carbon was observed around 5.8—6.0 ppm as a doublet.

Stereochemistry of the fused pyrrolidine ring of **11**—**18** should be the same with that of the initial cycloadducts **3**—**10**, respectively. Thus, the endo fusion of the maleimide ring and the exo configuration of 9-benzoyl of **11** were confirmed by the coupling constants J_{8a-9} and J_{5a-5b} (the same to **12**). The 6-endo (or 7-endo) and 8-exo (or 5-exo) substitution of **13**—**17** (or **18**) was assigned on the basis of the coupling patterns of **17** as well as the magnetic shielding of ester methyl at the 7-endo position of **18** (Fig. 1).

Table 1. Cycloaddition of Ylides **1** or **2** with Olefins and Then with Nitrile Oxides[a]

Ylide	Dipolarophile[b]	Cycloadduct		Nitrile oxide precursor[c]	Product		Yield/%[d]
1a	*N*-methylmaleimide rt, 10 min	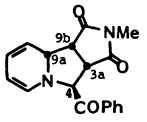	**3**	*p*-MeOC$_6$H$_4$C(Cl)=NOH, rt, 1 h	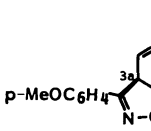	**11**	97
1a	*N*-phenylmaleimide rt, 1 h	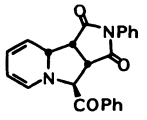	**4**	PhC(Cl)=NOH, −85 °C, 1h	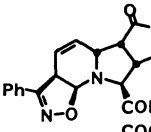	**12**	96
1a	CH$_2$=CHCOOMe rt, 50 min	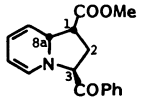	**5**	PhC(Cl)=NOH, rt, 1 h	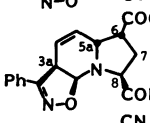	**13**	45
1a	CH$_2$=CHCN rt, 20 min	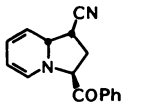	**6**	*p*-MeOC$_6$H$_4$C(Cl)=NOH, rt, 10 min	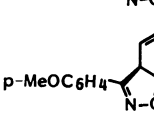	**14**	55
1b	CH$_2$=CHCOOMe reflux, 1 h	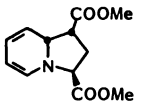	**7**	PhC(Cl)=NOH, reflux, 4 h	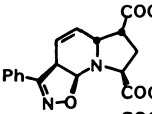	**15**[e]	51
1c	CH$_2$=CHCOOMe reflux, 6 h	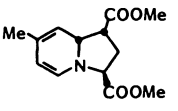	**8**	PhC(Cl)=NOH, reflux, 3 h	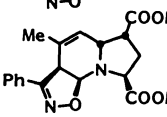	**16**	50
1d	CH$_2$=CHCOOMe reflux, 1 h	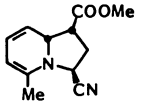	**9**	PhC(Cl)=NOH, reflux, 5 h	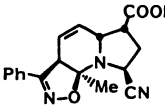	**17**	45
2	CH$_2$=CHCOOMe rt, 1 h	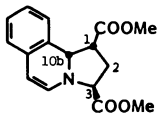	**10**	PhC(Cl)=NOH, rt, 10 h	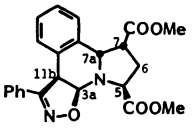	**18**	62

a) All reactions were carried out in dichloromethane. b) One equivalent amounts of ylide precursor and dipolarophile were allowed to react in the presence of 2—4 equivalents of triethylamine. c) Nitrile oxide precursor was added at room temperature and the reactions were continued under the conditions shown in this table. d) Isolated yield based on ylide precursor. e) After treatment with a catalytic amount of trifluoroacetic acid.

Although stereochemistry of the fused isoxazoline ring of **11—18** could not be determined only by a spectroscopic analysis, these cycloadducts were tentatively assigned to have exo-fused isoxazolines on the basis of the following discussion: The reaction of stereoselective cycloadduct **7** with benzonitrile oxide provided, after chromatographic work-up over silica gel, a 1 : 1 mixture of two stereoisomers of nitrile oxide cycloadducts **15** and **15′**. When treated with a catalytic amount of trifluoroacetic acid in chloroform at room temperature, **15′** was converted into **15** in a quantitative yield. Thus, **15** and **15′** were assigned as thermodynamically controlled exo and kinetically controlled endo cycloadducts, respectively. Acid-catalyzed isomerization of **15′** into **15** was easily rationalized with a mechanism via iminium **A** and dienamine intermediate B (Scheme 3).

Experimental

General Methods. Melting points were determined on a Yanagimoto micro melting point apparatus and are uncorrected. IR spectra were taken with a JASCO A-702 spectrometer. ^{1}H NMR spectra were recorded on a Hitachi R-40 or a JEOL FX-100 instrument and ^{13}C NMR on a JEOL FX-100 spectrometer at 25.05 MHz. Chemical shifts are expressed in parts per million downfield from tetramethylsilane. Mass spectra were measured with a JEOL JMS-O1SG-2 spectrometer at 70 eV of ionization energy. Elemental analyses were performed on a Hitachi 026 CHN micro analyzer. Thin-layer chromatography (TLC) was accomplished on 0.2 mm precoated plates of silica gel 60 F-254 (Merck). Visualization was accomplished with ultraviolet light (254 and 365 nm) and iodine. Silica gel 60 (70—230 mesh or 230—400 mesh, Merck) or Wakogel C-200 (100—200 mesh) was used for preparative column chromatography. Micro vacuum distillation was performed with a Shibata GTO-250 R Kugelrohr distilling apparatus. Solvents were evaporated with a Tokyo Rikakikai rotary evaporator type V.

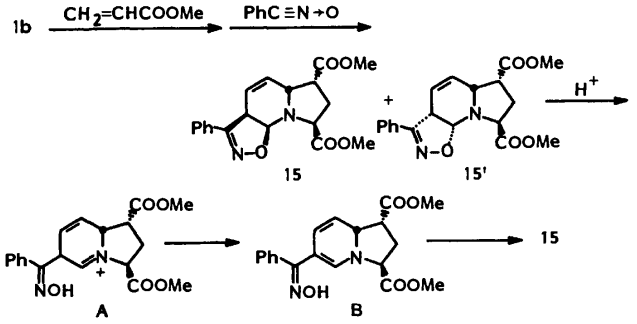

Scheme 3.

Ylide Precursors: The precursors for pyridinium methylides **1** and isoquinolinium methylide **2** were prepared from the reactions of substituted pyridines or isoquinoline with alkyl halides in dry acetone or dry ether at room temperature. The precursor salts precipitated were collected on a filter and washed with dry ether: 1-Phenacylpyridinium bromide:[19] Mp 204—206 °C; 96% (1 h in acetone). 1-(Methoxycarbonylmethyl) pyridinium chloride:[20] Mp 170—173 °C; 78% (24 h in acetone). 1-(Methoxycarbonylmethyl)-4-methylpyridinium bromide: Colorless prisms; mp 175—176 °C (decomp); 63% (54 h at 0 °C in ether); Found: C, 44.12; H, 4.95; N, 5.57%. Calcd for $C_9H_{12}NO_2Br$: C, 43.90; H, 4.88; N, 5.69%. 1-Cyanomethyl-2-methylpyridinium bromide: Colorless prisms; mp 194—197 °C (decomp); 49% (17 h in ether); Found: C, 44.90; H, 4.31; N, 12.96%. Calcd for $C_8H_9N_2Br$: C, 45.07; H, 4.23; N, 13.15%. 2-(Methoxycarbonylmethyl)isoquinolinium bromide:[21] Mp 158—160 °C; 62% (51 h in ether).

General One-pot Procedure for Cycloadditions of Ylides 1 or 2 with Olefins and Subsequent Cycloadditions of Cycloadducts 3—10 with Nitrile Oxides Leading to 11—18. An equimolar mixture of ylide precursor and olefin in dry dichloromethane (10—25 ml for 1 mmol of the precursor) was stirred in the presence of 2—4 equivalents of triethylamine at room temperature or under reflux (see Table 1). After the mixture was cooled to room temperature, 1 equivalent amount of an imidoyl chloride as nitrile oxide precursor was added. The mixture was allowed to react under the conditions listed in Table 1 and poured into ice water. The dichloromethane separated was dried over anhydrous magnesium sulfate and evaporated in vacuo. The residue was chromatographed over silica gel with hexane-ethylacetate (5-1 : 1) to give **11—18**. The yields are summarized in Table 1.

11: Colorless prisms (ethyl acetate-hexane); mp 210 °C; IR (KBr) 1770, 1700, and 1680 cm^{-1}; ^{1}H NMR (CD_3CN) δ=2.87 (3H, s, NMe), 3.42 (1 H, dd, J=7.6 and 0.8 Hz, 8a-H), 3.51 (1H, t, J=7.6 Hz, 5b-H), 3.77 (3H, s, p-MeO), 3.9—4.1 (1H, m, 3a-H), 4.2—4.3 (1H, m, 5a-H), 5.32 (1H, d,

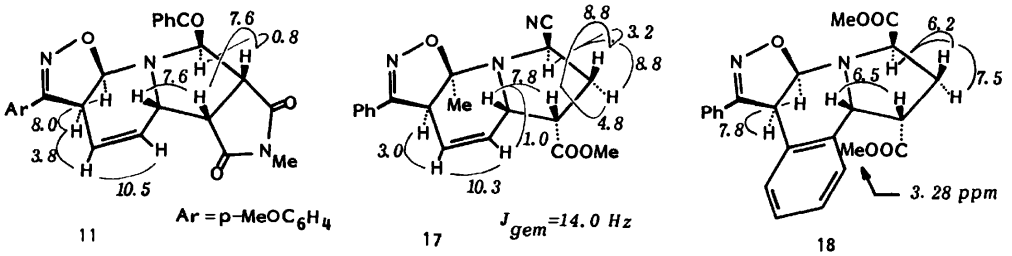

Fig. 1. Stereostructures of isooxazole-fused cycloadducts **11**, **17**, and **18** and their ^{1}H NMR spectral data.

J=0.8 Hz, 9-H), .5.67 (1 H, ddd, J=10.5, 3.8, and 2.5 Hz, 4-H), 5.85 (1H, d, J=8.0 Hz, 10a-H), 6.29 (1 H, br d, J=10.5 Hz, 5-H), 6.8—7.0 (2 H, m, Ar), 7.4—7.8 (5H, m, Ar), and 8.0—8.2 (2 H, m, Ar); ^{13}C NMR ($CDCl_3$) δ=25.35 (q, NMe), 44.71, 47.89 (each d, 5b- and 8a-C), 50.12 (d, 3a-C), 55.42 (q, *p*-MeO), 56.77 (d, 5a-C), 68.36 (d, 9-C), 92.71 (d, 10a-C), 114.48, 118.54 (each d), 121.42 (s), 124.54, 128.18, 129.13, 129.24, 134.01 (each d), 134.48, 159.89, 161.42 (each s), 175.89, 178.42 (each s, CON), and 195.43 (s, PhCO); MS *m/z* (rel intensity, %) 457 (M^+, 5), 353 (21), 352 (base peak), 240 (30), 203 (27), 196 (18), 105 (24), and 77 (23).

Found: C, 67.99; H, 5.14; N, 8.98%. Calcd for $C_{26}H_{23}N_3O_5$: C, 68.26; H, 5.07; N, 9.19%.

12: Colorless prisms (ethyl acetate-hexane); mp 238—240 °C (decomp); IR (KBr) 1780, 1713, 1687, 1595, 1387, and 1192 cm^{-1}; ^{1}H NMR ($CDCl_3$) δ=3.62 (1H, t, J=8.8 Hz, 5b-H), 3.95 (1H, dd, J=8.8 and 1.5 Hz, 8a-H), 3.8—4.0 (1H, m, 3a-H), 4.2—4.4 (1H, m, 5a-H), 5.53 (1H, d, J=1.5 Hz, 9-H), 5.62 (1H, dt, J=10.4, 2.8, and 2.8 Hz, 4-H), 5.83 (1H, d, J=6.8 Hz, 10a-H), 6.24 (1H, ddd, J=10.4, 3.2, and 2.3 Hz, 5-H), 7.2—7.7 (13 H, m, Ar), and 8.0—8.2 (2H, m, Ar); MS *m/z* (rel intensity, %) 384 (M^+—PhCO, 78), 291 (26), 105 (base peak), and 77 (71).

Found: C, 73.36; H, 4.90; N, 8.60%. Calcd for $C_{30}H_{23}N_3O_4$: C, 73.60; H, 4.74; N, 8.58%.

13: Pale yellow prisms (ethyl acetate-hexane); mp 174—175 °C; IR (KBr) 1740 and 1690 cm^{-1}; ^{1}H NMR ($CDCl_3$) δ=2.0—2.4 (1H, m, one of 7-H), 2.5—3.0 (2H, m, the other of 7-H and 6-H), 3.67 (3H, s, COOMe), 3.7—4.0 (1H, m, 3a-H), 4.1—4.3 (1H, m, 5a-H), 5.01 (1H, dd, J=10.0 and 6.8 Hz, 8-H), 5.87 (1H, ddd, J=9.8, 4.0, and 2.8 Hz, 4-H), 5.92 (1H, d, J=8.0 Hz, 9a-H), 6.28 (1H, dt, J=9.8, 1.5, and 1.5 Hz, 5-H), 7.3—7.8 (8H, m, Ar), and 7.9—8.1 (2H, m, Ar); MS *m/z* (rel intensity, %) 402 (M^+, 1), 298 (19), 297 (base peak), 197 (40), 196 (49), 178 (37), 151 (48), 118 (22), 105 (21), 99 (32), and 77 (49).

HRMS Found: *m/z* 402.1597. Calcd for $C_{24}H_{22}N_2O_4$: M, 402.1580.

14: Colorless needles (ethyl acetate-hexane); mp 230 °C (decomp); IR (KBr) 2240, 1680, 1605, and 1515 cm^{-1}; ^{1}H NMR ($CDCl_3$) δ=2.36 (1H, ddd, J=13.6, 6.4, and 2.5 Hz, one of 7-H), 2.5—2.8 (1H, m, the other of 7-H), 3.26 (1H, ddd, J=8.2, 6.0, and 2.5 Hz, 6-H), 3.81 (3H, s, *p*-MeO), 3.8—4.1 (1H, m, 3a-H), 4.1—4.4 (1H, m, 5a-H), 4.90 (1H, dd, J=10.0 and 6.4 Hz, 8-H), 5.90 (1H, d, J=8.2 Hz, 9a-H), 5.8—6.3 (2H, m, 4- and 5-H), 6.8—7.0 (2H, m, Ar), 7.3—7.7 (5H, m, Ar), and 7.9—8.1 (2H, m, Ar); MS *m/z* (rel intensity, %) 399 (M^+, 4), 295 (20), 294 (base peak), 197 (25), 196 (28), and 77 (16).

Found: C, 72.41; H, 5.26; N, 10.38%. Calcd for $C_{24}H_{21}N_3O_3$: C, 72.16; H, 5.30; N, 10.52%.

15 and 15′: The above general procedure was applied to the reaction of **1b** with methyl acrylate and then with benzonitrile oxide to give a mixture of 3a,5a-trans isomer **15** and 3a,5a-cis isomer **15′** (51%, 1 : 1 by ^{1}H NMR) after chromatographic separation. When this mixture in deuteriochloroform was treated with a catalytic amount of trifluoroacetic acid at room temperature, **15′**was found to completely isomerize into **15** (^{1}H NMR). The isomer **15** was isolated by column chromatography over silica gel. **15**: Pale yellow prisms (diethyl ether); mp 116—117 °C; IR (KBr) 1753, 1730, and 1597 cm^{-1}; ^{1}H NMR ($CDCl_3$) δ=2.2—3.0 (3H, m, 6-H and 7-H), 3.6—3.9 (1H, m, 3a-H), 3.69, 3.75 (each 3H, s, COOMe), 4.12 (1H, dd, J=9.2 and 5.8Hz, 8-H), 4.1—4.3 (1H, m, 5a-H), 5.73 (1H, ddd, J=10.0, 4.4, and 2.3 Hz, 4-H), 6.02 (1H, d, J=9.0 Hz, 9a-H), 6.22 (1H, dt, J=10.0, 1.0, and 1.0 Hz, 5-H), 7.2—7.5 (3H, m, Ar), and 7.5—7.8 (2H, m, Ar); ^{13}C NMR ($CDCl_3$) δ=31.35 (t, 7-C), 44.42, 45.89 (each d, 3a- and 6-C), 52.18 (2×C, q, COOMe), 55.12 (d, 5a-C), 58.30 (d, 8-C), 91.95 (d,9a-C), 122.07, 126.79, 128.95 (each d), 129.48 (s), 130.18, 131.24 (each d), 158.60 (s, 3-C), and 172.93 (2×C, s, COOMe); MS *m/z* (rel intensity, %) 356 (M^+, 8), 237 (25), 236 (23), 222 (25), 151 (base peak), and 93 (17). Found: C, 63.84; H, 5.66; N, 7.81%. Calcd for $C_{19}H_{20}N_2O_5$: C, 64.03; H, 5.66; N, 7.86%. **15′**: Available only as a mixture with its stereoisomer **15**. ^{1}H NMR ($CDCl_3$) δ=3.30 (1H, ddd, J=8.1, 7.0, and 4.8 Hz, 6-H), 3.64, 3.79 (each 3H, s, COOMe), and 4.08 (1H, dd, J=8.3 and 4.5 Hz, 8-H); ^{13}C NMR ($CDCl_3$) δ=29.77 (t, 7-C), 42.36, 46.12 (each d, 3a- and 6-C), 51.47, 52.24 (each q, COOMe), 53.89 (d, 5a-C), 61.83 (d, 8-C), 93.00 (d, 9a-C), 121.30, 126.60, 128.77, 129.24, 129.95, 158.37 (s, 3-C), 173.07, and 173.77 (each s, COOMe); MS *m/z* (rel intensity, %) 356 (M^+, 5) and 151 (base peak). HRMS Found: *m/z* 356.1353. Calcd for $C_{19}H_{20}N_2O_5$: M, 356. 1336.

16: Colorless viscous liquid; IR (neat) 1751, 1733, 1670, and 1647 cm^{-1}; ^{1}H NMR (CD_3CN) δ=1.50 (3H, br s, 4-Me), 2.2—2.8 (3H, m, 6- and 7-H), 3.63 (1H, m, 3a-H), 3.66, 3.69 (each 3H, s, COOMe), 3.98 (1H, dd, J=9.0 and 6.2 Hz, 8-H), 4.17 (1H, br d, J=8.5 Hz, 5a-H), 5.92 (1H, br s, 5-H), 5.95 (1H, d, J=8.1 Hz, 9a-H), 7.3—7.5 (3H, m, Ar), and 7.5—7.7 (2H, m, Ar); MS *m/z* (rel intensity, %) 370 (M^+, 6), 278 (16), 251 (53), 250 (31), 236 (20), 165 (base peak), 132 (33), 107 (72), and 76 (32).

HRMS Found: *m/z* 370.1529. Calcd for $C_{20}H_{22}N_2O_5$: M, 370.1529.

17: Colorless prisms (ethyl acetate-hexane), mp 122—124 °C; IR (KBr) 2250, 1751, 1741, and 1167 cm^{-1}; ^{1}H NMR ($CDCl_3$) δ=1.57 (3H, s, 9a-Me), 2.35 (1H, ddd, J=14.0, 8.8, and 3.2 Hz, 7-H$_{exo}$) 2.78 (1H, ddd, J=14.0, 8.8, and 4.8 Hz, 7-H$_{endo}$). 3.29 (1H, ddd, J=8.8, 7.8, and 4.8 Hz, 6-H), 3.66 (3H, s, COOMe), 3.70 (1H, m, 3a-H), 4.10 (1H, m, 5a-H), 4.47 (1H, dd, J=8.8 and 3.2 Hz, 8-H), 5.72 (1H, ddd, J=10.3, 3.0, and 2.0 Hz, 4-H), 5.97 (1H dt, J=10.3, 1.0, and 1.0 Hz, 5-H), 7.3—7.5 (3H, m, Ar), and 7.5—7.8 (2H, m, Ar); ^{13}C NMR ($CDCl_3$) δ=23.83 (q, 9a-Me), 32.24 (t, 7-C), 44.47, 45.89 (each d, 6- and 8-C) 50.24 (d, 3a-C),52.00 (q, COOMe), 55.30 (d, 5a-C), 98.36 (s, 9a-C), 120.13 (s, CN), 122.48, 126.54, 127.13, 129.07 (each d), 129.42 (s), 130.30 (d), 158.30 (s, 3-C), and 172.65 (s, COOMe); MS *m/z* (rel intensity, %) 337 (M^+, 8), 218 (35), 203 (23), 165 (13), 132 (base peak), and 92 (20).

Found: C, 67.51; H, 5.64; N, 12.20%. Calcd for $C_{19}H_{19}N_3O_3$: C, 67.64; H, 5.68; N, 12.46%.

18: Colorless solid; IR (KBr) 1730 cm^{-1}; ^{1}H NMR (CD_3CN) δ=2.2—2.6 (2H, m, 6-H), 3.28 (3H, s, 7-COOMe), 3.73 (3H, s, 5-COOMe), 3.4-3.7 (1H, m, 7-H), 4.17 (1H, dd, J=7.5 and 6.2 Hz, 5-H), 4.73 (1H, d, J=7.8 Hz, 11b-H), 4.83 (1H, d, J=6.5 Hz, 7a-H), 5.94 (1H, d, J=7.8 Hz, 3a-H), and 5.9—7.6 (9H, m, Ar); ^{1}H NMR ($CDCl_3$) δ=2.3—2.6 (2H, m, 6-H), 3.27 (3H, s, 7-COOMe), 3.75 (3H, s, 5-COOMe), 3.4—3.7 (1H, m, 7-H), 4.20 (1H, dd, J=7.0 and 6.0 Hz, 5-H), 4.50 (1H, d, J=9.0 Hz, 11b-H), 4.86 (1H, d, J=6.0 Hz, 7a-H), 5.90 (1H, d, J=9.0 Hz, 3a-H), and 6.8—7.6 (9H, m, Ar); MS *m/z* (rel intensity, %) 406 (M^+, 9) and 76 (base peak).

Found: C, 67.47; H, 5.35; N, 6.71%. Calcd for $C_{23}H_{22}N_2O_5$: C, 67.96; H, 5.46; N, 6.89%.

References

1) O. Tsuge, S. Kanemasa, and S. Takenaka, *Bull. Chem. Soc. Jpn.*, **58**, 3137 (1985).

2) O. Tsuge, S. Kanemasa, and S. Takenaka, *Bull. Chem. Soc. Jpn.*, **58**, 3320 (1985).

3) B. E. Landberg and L. W. Lown, *J. Chem. Soc., Perkin Trans. 1*, **1975**, 1326.

4) K. T. Potts, D. R. Choudhury, and T. R. Westby, *J. Org. Chem.*, **41**, 187 (1976).

5) M. Petrovanu, I. Drŭta, and M. V. Tri, *Rev. Roum. Chim.*, **23**, 781 (1978).

6) M. Petrovanu, C. Luchian, G. Suprăteanu, and V. Barboiu, *Rev. Roum. Chim.*, **24**, 733 and 1053 (1979).

7) O. Tsuge, H. Shimoharada, and M. Noguchi, *Heterocycles*, **15**, 807 (1981).

8) O. Tsuge, Y. Shimizu, H. Shimoharada, and S. Kanemasa, *Heterocycles*, **19**, 2259 (1982).

9) G. A. Kraus and J. O. Nagy, *Tetrahedron Lett.*, **24**, 3427 (1983).

10) O. Tsuge, S. Kanemasa, and S. Takenaka, *Heterocycles*, **20**, 1907 (1983).

11) G. Suprăteanu and A. Lablache-Combier, *Heterocycles*, **22**, 2079 (1984).

12) Z. Bende, L. Töke, L. Weber, G. Tóth, F. Janke, and G. Csonka, *Tetrahedron*, **40**, 369 (1984).

13) O. Tsuge, S. Kanemasa, and S. Takenaka, *Chem. Lett.*, **1985**, 355.

14) O. Tsuge, S. Kanemasa, S. Kuraoka, and S. Takenaka *Chem. Lett.*, **1984**, 281.

15) O. Tsuge, S. Kanemasa, S. Takenaka, and S. Kuraoka, *Chem. Lett.*, **1984**, 465.

16) Y. Miki, H. Hachiken, and S. Takemura, *Heterocycles*, **22**, 701 (1984).

17) O. Tsuge, S. Kanemasa, and S. Takenaka, *J. Org. Chem.*, **51**, 1853 (1986).

18) The only cycloadduct formed was 3-*exo*-benzoyl-1-*endo*-methoxycarbonyl(or 1-*endo*-cyano)-1,2,3,10b-tetrahydropyrrolo[2, 1-*a*]isoquinoline. See Ref. 2.

19) C. A. Henrick, E. Ritchie, and W. C. Taylor, *Aust. J. Chem.*, **20**, 2441 (1967).

20) C. Leonte and I. Zugrăvescu, *Tetrahedron Lett.*, **1972**, 2029.

21) D. G. Farnum, R. J. Alamo, and J. M. Duston, *J. Org. Chem.*, **32** 1130 (1967).

 © 1986 The Chemical Society of Japan Bull. Chem. Soc. Jpn., 59, 3637—3642 (1986)

Preparation and Characterization of a Resin-Supported Palladium Catalyst

Takayoshi UEMATSU,* Masao UMINO, Shogo SHIMAZU, Masatoshi MIURA, and Hidehisa HASHIMOTO
Department of Synthetic Chemistry, Faculty of Engineering, Chiba University, Yayoi-Cho, Chiba 260
(Received February 26, 1986)

The process of the ligand release and the reduction of $[Pd(NH_3)_4]$-form sulfonic resin has been studied by chemical analysis, X-ray photoelectron spectroscopy and adsorption techniques. The removal of ammonia ligands remarkably increased with hydrogen treatment above 353 K, and was complete at around 393 K. It is suggested that the released ammonia partly transfers to $-SO_3^-$ groups to form $-SO_3NH_4$ groups as the reduction proceeds. The dispersion of the metal particles prepared by hydrogen reduction ranged from 0.11 to 0.31 depending on the loading concentration of the palladium cation. The metal particles are considered to be entrapped in the pores of the resin. The formation of cationic palladium sites by the low temperature reduction is also suggested.

During our study on the nature of active sites of polymer anchored complex catalysts, we found that the various types of active sites can be prepared on ion-exchange resins by varying the pretreatment methods of cation-form resins. Several reports have been focussed on the differences in the catalytic nature of the active sites prepared on commercialy available ion-exchange resins.[1-4] In our trial, starting from cation-form sulfonic resins, two different types of active sites were prepared on the resin,[5] one of which is active for the isomerization and the other for the hydrogenation of butenes.

In the present study, we tried to scrutinize the process of active site formation by ligand removal from $[Pd(NH_3)_4]$-form sulfonic resin. The active sites thus prepared on the resin are characterized by means of chemical analysis, X-ray photoelectron spectroscopy (XPS), and adsorption of CO, NH_3, and acetylene. The catalytic activity was tested over these sites for the hydrogenation of ethylene. Further detailed catalytic behavior will be reported in a succeeding paper.

Experimental

Tetraamminepalladium complex cation, $[Pb(NH_3)_4]^{2+}$, was supported on Na-form sulfonic resin, denoted as AMNa (Amberlyst-15, Room & Haas; surface area: 51.3 $m^2 g^{-1}$; ion-exchange capacity for Na^+ ion: 4.02 mmol g^{-1}-Na-form dry resin) according to the following ion-exchange process, viz.,

$$\left\{\begin{matrix}-SO_3\text{-}Na\\ \\ -SO_3\text{-}Na\end{matrix}\right. + [Pd(NH_3)_4]^{2+} \longrightarrow \left\{\begin{matrix}-SO_3\\ \\ -SO_3\end{matrix}\right.\!\!\!

Table 1. Chemical Analysis of Pretreated Palladium-Form Sulfonic Resin

	Treatment	Content/mmol g^{-1}					
		S	Pd	N(anal)	N(s)	N(Pd)	N(Pd)/Pd
1	Evac Room Temp	4.06	0.080	0.625	0.305	0.320	4.00
2	Evac 373 K 2 h H_2 353 K	3.96	0.082	0.568	0.305	0.263	3.21
3	Evac 373 K 2 h H_2 383 K	4.10	0.078	0.525	0.305	0.220	2.82
4	Evac 373 K 2 h H_2 393 K	4.00	0.082	0.506	0.305	0.201	2.45
5	Evac 373 K 2 h H_2 473 K (Flow)	3.99	0.082	0.418	0.305	0.113	1.38
6	HCHO-treat. 333 K	4.02	0.082	0.400	0.305	0.095	1.16

N(anal) is the total nitrogen by chemical analysis. N(s) and N(Pd) indicate the number of NH_4 on $-SO_3^-$ and NH_3 on the palladium, respectively. See text.

the amount of the ammonium ion originally bound to sulfonic groups was calculated as N(s)=0.305 mmol g^{-1} by substraction of the stoichiometrically coordinated ammonia ligands to the palladium, N(Pd)= 0.320 mmol g^{-1}, from the total ammonia which was given by nitrogen chemical analysis as N(anal)=0.625 mmol g^{-1} for Pd-Comp/AMNa evacuated at room temperature.

Since ammonium sulfonate is stable and N(s) was considered to be constant for all samples treated by H_2 below 493 K, the values of N(Pd) for the variously treated Pd-Comp/AMNa were determined, in turn, from the differences between N(anal) and N(s). The ammonia coordination number to the palladium, N(Pd)/Pd, was also calculated. These values are listed in Table 1.

The coordination number for Pd-Comp/AMNa (Pd: 0.08 mmol g^{-1}) decreased from 4 to 2.45 when the hydrogen treatment temperature was increased up to 393 K. The reduction at a higher temperature of 473 K (No. 5) led to a marked decrease in nitrogen content, N(anal), and only 0.113 mmol g^{-1} of ammonia ligand was left on the palladium. The reduction in the formaldehyde solution (No. 6) gave rise to a similar dramatic decrease in N(Pd) to 0.095 mmol g^{-1}. However, these values still correspond to the residual coordination number of N(Pd)/Pd=1.38 and 1.16 respectively.

The weight loss due to the ammonia release during pretreatment was also studied as shown in Fig. 1. The hydrogen treatment at 353 K was only sufficient to remove 10% of the ammonia from the palladium. The treatment at higher temperatures facilitated the ligand removal and 50% of ammonia release, NH_3(des), was attained at 433 K. It is noticeable that further elevation of the reduction temperature up to 453 K had no effect on the residual ammonia on the resin.

Figure 2 shows the effect of the hydrogen treatment on the oxidation state of the palladium studied by

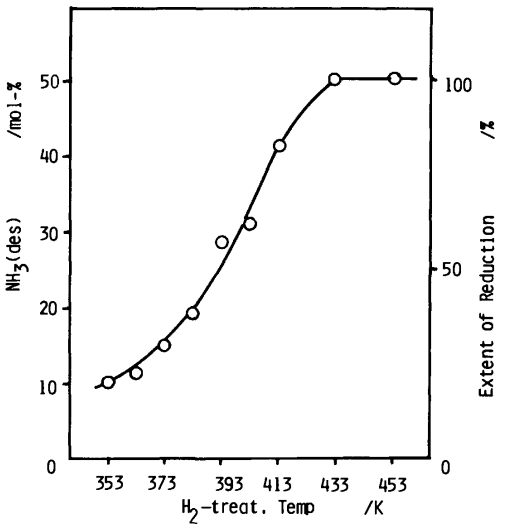

Fig. 1. Removal of ammonia ligand by H_2-treatment Pd-Comp/AMNa(Pd: 0.519 mmol g^{-1}): evacuated at 373 K for 2 h and subjected to hydrogen treatment for 1 h at $P(H_2)$=26.6 KPa.

XPS. Pd-Comp/AMNa (Pd: 0.519 mmol g^{-1}) was first evacuated in the preparation chamber over night at 1.33×10^{-6} Pa. The peak due to Pd^{2+} (3d-5/2) was detected at a binding energy B. E. of 339.2 eV, but gradually shifted to 337.2 eV on increasing the hydrogen treatment temperature up to 433 K. The latter peak was ascribed to palladium metal, Pd^0 (3d-5/2) on the sulfonic resin. The hydrogen treatment at 453 K appeared to complete the reduction of the palladium cations. Refluxing in a formaldehyde solution at 353 K seemed also to reduce them completely to the metal.

However, as shown in Table 1, the complete reduction with H_2 or formaldehyde did not necessarily result in the decrease in the total nitrogen to zero. The reason for this may well be explained in terms of "ammonia transfer" from the palladium to

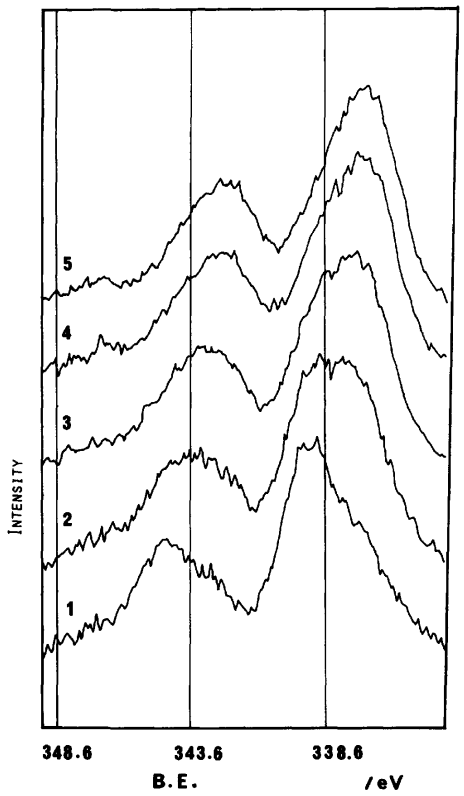

Fig. 2. XPS spectra for H_2-treated palladium-form sulfonic resin.
Sample: Pd-Comp/AMNa(Pd: 0.519 mmol g^{-1}). 1: evacuated at 353 K in the preparation chamber over night at 1.33×10^{-10} Pa, 2: H_2-treated at 358 K for 60 min after 1, 3: H_2-treated at 398 K for 20 min after 2, 4: H_2-treated 433 K for 20 min after 3, 5: H_2-treated at 453 K for 20 min after 4. The binding energy was referred to C(1s): 284.9 eV, Pd metal on Na-form sulfonic resin: 336.5 eV and Pd metal(Solid): 335.0 eV.

the sulfonic groups during the reduction; this was previously proposed in an analogous system of a palladium ammine complex cation on zeolites,[6] viz.,

$$\left\{\begin{matrix}-SO_3\\-SO_3\end{matrix}\right\}[Pd(NH_3)_4] + H_2 \longrightarrow \left\{\begin{matrix}-SO_3NH_4\\-SO_3NH_4\end{matrix}\right\} + Pd^\circ + 2NH_3 \quad (2)$$

If this is the case, the extent of reduction is directly related to the removal of ammonia ligands from the palladium. As shown in Fig. 1 the weight loss due to the ammonia release was almost complete at 433 K, where 50% removal of ammonia from Pd-Comp/AMNa was attained. This suggests that Eq. 2 is also valid for Pd-Comp/AMNa and the 100% reduction was accomplished as indicated also by the XPS study. An Arrehenius plot for the ammonia release gave an activation energy of 74 KJ mol^{-1}.

Re-adsorption of ammonia was studied over the hydrogen treated Pd-Comp/AMNa (Pd: 0.519 mmol g^{-1}) and the result is shown in Fig. 3. After the

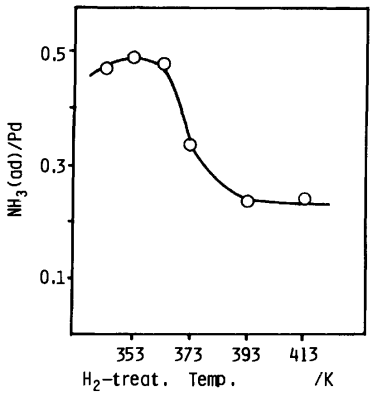

Fig. 3. Re-adsorption of NH_3 over H_2-treated palladium-form sulfonic resin
Pd-Comp/AMNa(Pd: 0.519 mmol g^{-1}) was evacuated at 373 K for 2 h and subjected to H_2-treatment for 1 h under $P(H_2)=26.6$ KPa. Adsorption: 303 K, $P(NH_3)=399$ Pa.

hydrogen treatment at 353 K, the ammonia re-adsorption amounted to about NH3(ad)/Pd=0.5. This value is close to that of ammonia previously removed, 0.4, during the hydrogen treatment. This suggests that the coordination and the release of ammonia are quite reversible over the samples treated at this low temperature region. However, after the treatment above 373 K the amount of ammonia re-adsorption decreased remarkably to give the ratio, NH3(ad)=0.25. Thus, the ammonia was removed irreversibly when the Pd-Comp/AMNa was once reduced at high temperatures.

Carbon monoxide has been widely used as a probe to characterize catalytic sites of supported metal catalysts.[7,8] The effect of hydrogen treatment on CO adsorption are shown in Figs. 4 and 5. In the case of Pd-Comp/AMNa (Pd: 0.519 mol g^{-1}), the amount of adsorbed CO was increased on raising the hydrogen treatment temperature from 353 K to 393 K and reached a constant level of CO(ad)/Pd=0.28. The further elevation of temperature did not change the value.

Figure 5 shows similar results for Pd-Comp/AMNa with different palladium concentrations and for Pd-Comp/SiO_2. The temperature where the ratio, CO(ad)/Pd, attained constant values almost coincided with each other at about 393 K, irrespective of the different supports and different loading concentrations applied. Moreover, the amount of CO adsorbed on Pd-Comp/SiO_2 decreased little on further elevation of the treatment temperature up to 673 K.

A similar trend was obtained for the adsorption of acetylene. Figure 6 shows that the amount of adsorption increased with the hydrogen treatment temperature up to 403 K and reached a constant value, which may be related to the completion of the reduction.

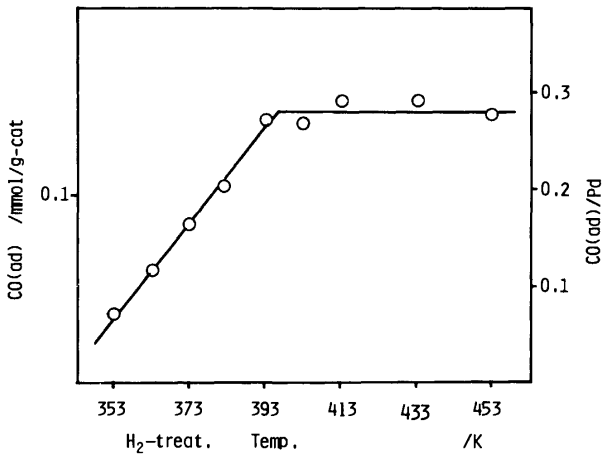

Fig. 4. Effect of H_2-treatment on CO adsorption Pd-Comp/AMNa (Pd: 0.519 mmol g^{-1}) was evacuated at 373 K for 2 h and subjected to H_2-treatment for 1 h. Adsorption of CO at 303 K, under $P(CO)=399$ Pa.

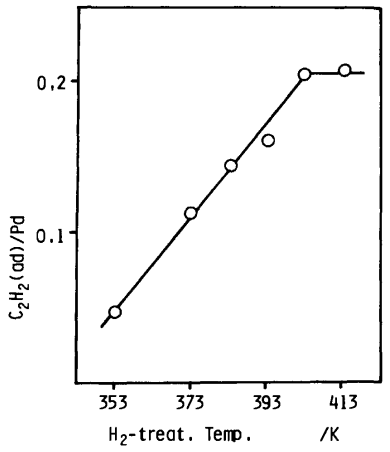

Fig. 6. Effect of H_2-treatment on C_2H_2 adsorption Pd-Comp/AMNa (Pd: 0.519 mmol g^{-1}) was evacuated at 373 K for 2 h and subjected to H_2-treatment at T K for 1 h.

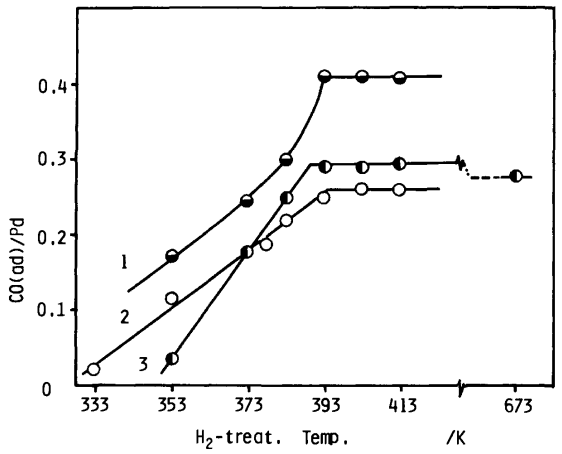

Fig. 5. Effect of CO adsorption on palladium-form sulfonic resin and silica supported palladium.
Samples were evacuated at 373 K for 2 h and subjected to H_2 hydrogen treatment at T K for 1 h. Adsorption was carried out at 273 K at $P(CO)=399$ Pa. 1: Pd-Comp/AMNa (Pd: 0.0904 mmol g^{-1}). 2: Pd-Comp/AMNa (Pd: 0.12 mmol g^{-1}). 3: Pd-Comp/SiO_2. (Pd: 1.00 mmol g^{-1}).

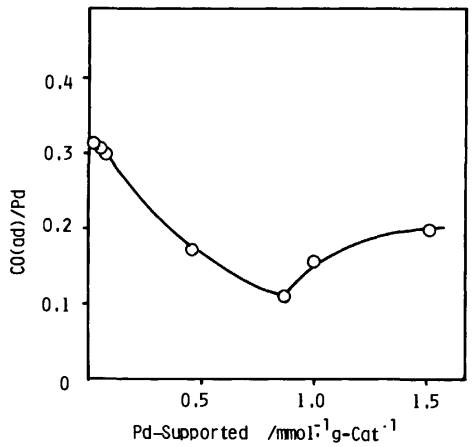

Fig. 7. Effects of palladium loading concentration on CO adsorption.
Pd-Comp/AMNa (Pd: 0.519 mmol g^{-1}) was evacuated at 373 K for 2 h and subjected to H_2 treatment at 403 K for 1 h. Adsorption at 273 K at $P(CO)=399$ KPa.

If the reduction of palladium was once completed, the number of CO adsorption sites would not increase any more by further elevation of the reduction temperature. Moreover, the values of CO(ad)/Pd would decrease if the sintering proceeded. However, the observed values were almost constant from 393 to 453 K for Pd-Comp/AMNa (Pd: 0.519 mmol g^{-1}) and to 673 K for Pd-Comp/SiO_2, and thus, it may be said that the palladium metal particles are highly stable over the widespread temperature range.

In view of the different behavior between ammonia and CO adsorption in Figs. 3, 4, and 5, the adsorption sites produced by the treatments can be ascribed respectively to palladium cations with unsaturated ligands and the metal sites. The isomerization of butenes takes place over the cation site,[5] while the adsorption of CO and acetylene (Fig. 6) can be attributed to the metal sites formed by the high temperature reduction according to Eq. 2.

The effect of the loading concentration on the dispersion of palladium is given in Fig. 7. In this case, the palladium cations were completely reduced to the metal by hydrogen treatment at 403 K. The dispersion of the metal particles is defined by D=Pd(surface)/Pd(total),[9] where Pd(surface) was determined by CO adsorption. The average particle sizes were estimated from the equation, $d=1.23/D$ nm.[10] The maximum dispersion, 0.31, and the minimum, 0.11 correspond respectively to d=3.97 and 11.2 nm. The formation of these fine particles may be facilitated by the retardation of the diffusion and the sintering of palladium by anchoring on $-SO_3^-$ groups.

Table 2. Dispersion and Particle Size of Palladium Metal Prepared by Reduction with Formaldehyde

Sample	Pd loaded /mmol g^{-1}	Dispersion D=CO/Pd	Diameter d/nm
1 Pd-Comp/AMNa(F)	0.090	0.075	16.5
2 Pd-Comp/AMNa(F)	1.11	0.020	62.0

Pd-Comp/AMNa(F): Pd-Comp/AMNa was reduced by refluxing in a formaldehyde solution at 358 K for 5 min.

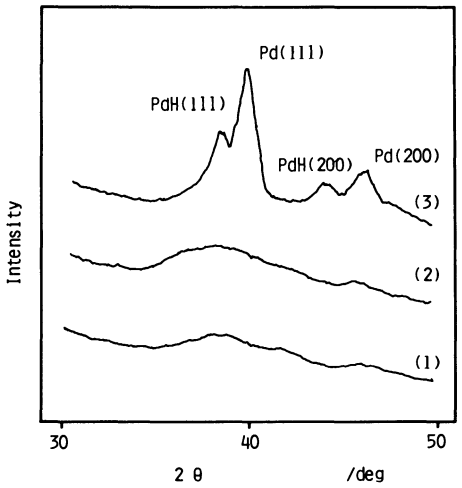

Fig. 8. XRD spectra for palladium-form sulfonic resin Pd-Comp/AMNa(Pd: 0.519 mmol g^{-1}).
1: H_2-treated at 353 K. 2: H_2-treated at 393 K. 3: formaldehyde treated at 358 K.

The mean pore diameter measured by the mercury penetration method was 24.8 nm for the support AMNa which agreed well with the reported value of 25.6 nm.[11] The total amount of palladium complex contained in a pore can be estimated from the loading concentration and the BET surface area. A pore of average diameter of 24.8 nm has a surface area of 1.93×10^3 nm^2 where the palladium cations anchored are 1.98×10^3 and 1.25×10^4, respectively for Pd-Comp/AMNa (Pd: 0.08 mmol g^{-1}) and Pd-Comp/AMNa (Pd: 0.519 mmol g^{-1}).

Based on a cubo-octahedral crystal model,[12] the expected dispersions of the metal particles in the pore was estimated to be about D=0.32 and 0.19 which are very close respectively to the observed values of 0.31 and 0.18 in Fig. 7. This fact suggests that the particle size of the metal palladium was controlled by entrapment within each pore in the resin.

While the reduction by formaldehyde resulted in a smaller dispersion as given in Table 2. A highly loaded Pd-Comp/AMNa (Pd: 1.1 mmol g^{-1}) gave larger particles than that for the mean pore size. They might grown outside of the pore due to the increase in the sintering probability and the particle sizes.

The X-ray diffraction spectra for a formaldehyde-treated Pd-Comp/AMNa(F) in Fig. 8 shows clear patterns of palladium metal. The crystallite diameter obtained by Scherre's equation was about 12 nm. The formation of palladium hydride, $PdH_{0.706}$ was also indicated in the spectra.

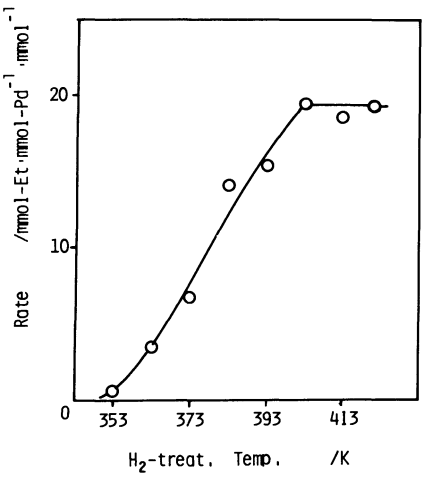

Fig. 9. Catalytic activity for the hydrogenation of ethylene over H_2-treated Pd-Comp/AMNa.
Pd-Comp/AMNa (Pd: 0.519 mmol g^{-1}): evacuated at 373 K for 2 h and subjected to H_2-treatment at T K for 1 h. The reaction was carried out at 313 K with 1 : 1 mixture of C_2H_4 and H_2.

The evidence of the formation of catalytic sites due to metallic palladium is given in Fig. 9. The catalytic activity for the hydrogenation of ethylene changed almost in parallel with the numbers of the metal sites for CO and acetylene adsorption sites (Figs. 4, 5, and 6). Thus, it may be conclusively said that the partial reduction takes place gradually from low temperature hydrogen treatment and the complete reduction is accomplished above 393 K where the catalytic activity also the reached a constant level. The results by XPS study also supports this observation.

Conclusion

Fine metal palladium can be prepared on a sulfonic resin by the reduction of $[Pd(NH_3)_4]$-form resin. The particle size can be controlled by changing the loading concentration and the reducing condition. The metal particles may be formed in the pores by the effect of the entrapment, when the loading concentration was kept low. The low temperature treatment may also produce cationic sites with vacant ligands by removing the ammonia ligands.

References

1) W. O Haag and D. D. Whitehurst, *Belg. Pat.*, 721, 686 (1962); *Proc. Intern. Congr. Catal.*, **5**, 465 (1972).
2) H. Dolibor, *Chem. Ber.*, **91**, 1955 (1958).
3) T. Uematsu, T. Kondo, S. Saitoh, and H. Hashimoto, *J. Catal.*, **62**, 275 (1980).

4) M. S. Jarell and B. C. Gates, *J. Catal.*, **40**, 225 (1975).
5) T. Uematsu, N. Egashira, and H. Hashimoto, unpublished Data.
6) W. Rogan, *J. Catal.*, **69**, 89 (1981).
7) R. P. Eishens and W. A. Pliskin, *Adv. Catal.*, **10**, 1 (1958).
8) F. M. Hoffmann and A. M. Bradshaw, *J. Catal.*, **44**, 328 (1976).
9) J. R. Anderson and N. R. Avery, *J. Catal.*, **5**, 466 (1966).
10) S. Y. Wang, S. H. Moon, and M. A. Vannice, *J. Catal.*, **71**, 167 (1981).
11) Room & Haas Technical Note.
12) R. van Hardeveld and F. Hartog, *Surface Sci.*, **15**, 189 (1969).

 © 1986 The Chemical Society of Japan Bull. Chem. Soc. Jpn., 59, 3643—3648 (1986)

Catalytic Effects of $MoCl_3$- and $NiCl_2$-Containing Molten Salts for Hydroliquefaction of Morwell Brown and Taiheiyo Subbituminous Coals

Chunshan Song and Masakatsu Nomura*
Department of Applied Chemistry, Faculty of Engineering, Osaka University, Yamada-oka, Suita, Osaka 565
(Received April 24, 1986)

The catalytic effects of $MoCl_3$-LiCl-KCl and $NiCl_2$-LiCl-KCl molten salts were studied for the hydroliquefaction of Morwell brown and Taiheiyo subbituminous coals at 400 °C for 1 h in a batch reactor with an initial hydrogen pressure of 9.8 MPa. The conversion to pyridine-soluble materials and the yield of hexane-soluble materials (HS) with the $MoCl_3$ catalyst were 82 and 42% for Morwell coal, and 84 and 61% for Taiheiyo coal, respectively. The conversion and HS yield with the $NiCl_2$ catalyst were 87 and 43% for Morwell coal, and 82 and 56% for Taiheiyo coal, respectively. The HS yield of the catalytic runs was about 2.6—3.2 times higher than that of noncatalytic runs. This finding established the effectiveness of the two new catalysts for the hydroliquefaction of brown and subbituminous coals. Detailed analyses of the reaction products have revealed that these catalysts promoted a depolymerization of the coals and strongly catalyzed the hydrocracking of polynuclear aromatic structures of heavy products into hydroaromatic and aromatic structures with smaller ring sizes. Most of these smaller hydroaromatic and aromatic structures did not undergo much further ring-opening reactions. This accounts for the high HS selectivity of the catalysts.

One of the most promising approaches to the development of coal liquefaction processes is the development of new and novel catalytic systems.[1] We have previously found[2] that $MoCl_3$- and $NiCl_2$-LiCl-KCl molten salts acted as excellent hydrocracking catalysts for the hydroliquefaction of an Australian subbituminous coal (Wandoan). Since different ranks of coal generally show different reactivities toward hydroliquefaction, it is necessary to examine the effectiveness of these new catalysts for the hydroliquefaction of other coals different from Wandoan coal.

Two coals, Morwell brown coal (Australia) and Taiheiyo subbituminous coal (Japan), which have lower carbon contents and higher oxygen contents compared with Wandoan coal, were used in the present work. This paper reports on the hydroliquefaction of Morwell and Taiheiyo coals over $MoCl_3$-LiCl-KCl and $NiCl_2$-LiCl-KCl molten salt catalysts; their catalysis is characterized by a detailed analytical study of the reaction products.

Experimental

Reagents and Materials. Morwell brown and Taiheiyo subbituminous coals were used in the present work. The coals were pulverized to <74 μm and then stored under an N_2 atmosphere. Proximate and ultimate analyses of the coals are listed in Table 1. For each experiment the required quantity of coal was dried at 105 °C in vacuo for 1.5 h before use. The examined catalysts were $MoCl_3$-LiCl-KCl (molar composition, 12:51:37; eutectic temperature, 387 °C) and $NiCl_2$-LiCl-KCl (14:54:36; 360 °C) ternary molten salts. $MoCl_3$ was synthesized according to a procedure proposed by Mallock,[3] except that resulting $MoCl_3$ was further purified by washing with distilled methanol. The X-ray diffraction pattern of thus-purified $MoCl_3$ is very consistent with that of literature.[4] The $MoCl_3$ and guaranteed reagent-grade $NiCl_2$, LiCl, and KCl were used as salt constituents of the catalysts. For each experiment the required quantity of catalyst was dried at 140 °C in vacuo for 6 h before use. Guaranteed reagent-grade hexane, benzene and pyridine were used as received.

Hydroliquefaction Procedures. Hydroliquefaction reactions were carried out in a 200 ml batch autoclave (SUS 316) that was shaken horizontally. In a typical run, coal was impregnated with the same weight of catalyst by immersing the coal into a methanol solution or a suspension in methanol followed by drying at 105 °C in vacuo for more than 6 h. Thus-treated coal was placed into an autoclave. Hydroliquefaction was carried out at 400 °C for 1 h with an initial hydrogen pressure (cold) of 9.8 MPa (100 kg cm^{-2}). After the reaction, products were separated into gases consisting of C_1–C_4 hydrocarbons and COx ($CO+CO_2$), hexane-soluble fraction (HS), hexane-insoluble and benzene-soluble fraction (BS), benzene-insoluble and pyridine-soluble fraction (PyS) and pyridine-insoluble fraction (PyI). The HS, BS, and PyS fractions are denoted as oil, asphaltene and preasphaltene, respectively. Details of the procedures have been described elsewhere.[2] The yield of products,

Table 1. Representative Analyses of Coals

Coal	Morwell	Taiheiyo
Proximate (wt%)		
Volatile matter	41.4	45.5
Fixed carbon	37.4	33.9
Ash	1.6	14.5
Moisture	19.6	6.1
Ultimate (wt%, daf)		
Carbon	67.4	76.1
Hydrogen	5.0	6.7
Nitrogen	0.5	1.5
Sulfur	0.3	0.2
Oxygen (by difference)	26.8	15.5

conversion and amount of hydrogen consumed were calculated on a d.a.f. coal basis.

Analytical Method of Products. The HS and BS fractions obtained from the hydroliquefaction of the two coals were subjected to elemental and ^{1}H NMR analyses. The ^{1}H NMR spectra were measured in a $CDCl_3$ solution with tetramethylsilane as an internal standard using a JNM-PS-100 spectrometer operating at 100 MHz. Deuterium oxide was added to some of the solutions of HS and BS fractions in order to identify the phenolic OH resonance; contribution from overlapping signals was then subtracted. The integrated intensity from all the hydrogen was divided into several parts, which could be assigned to the hydrogen of different chemical environments. A distribution of hydrogen types was calculated as the numbers of hydrogen atoms per 100 carbon atoms from the ^{1}H NMR data and elemental analysis. The average structural parameters of the HS and BS fractions were calculated based on Brown-Ladner equations[5] from the data of ^{1}H NMR and elemental analyses.

Results

Hydroliquefaction of Coals. Table 2 gives conversion and H_2 consumption values and Fig. 1 shows the product distribution of the hydroliquefaction of Morwell brown and Taiheiyo subbituminous coals. Without a catalyst, the hydroliquefaction of Morwell and Taiheiyo coals gave relatively low conversions (66.0—67.8%) with low H_2 consumptions (0.7—0.9%). The use of both $NiCl_2$-LiCl-KCl and $MoCl_3$-LiCl-KCl catalysts considerably increased the coal conversion and H_2 consumption, indicating the great effectiveness of these catalysts for converting brown and subbituminous coals.

The increases in the conversion and H_2 consumption with the $MoCl_3$ and $NiCl_2$ catalysts (Table 2) were accompanied by pronounced changes in the product distribution (Fig. 1); the important features of the catalytic runs compared with noncatalytic runs are considerably decreased PyI and PyS yields and greatly increased HS yield. The net production of HS was, as would be expected,[6-7] lower with Morwell brown coal than with Taiheiyo subbituminous coal.

Table 2. Hydroliquefaction of Morwell and Taiheiyo Coals

Run No.	Coal	Catalyst	Conversion[a] (wt%, daf)	H_2 consumed (wt%, daf)
1	Morwell	None	66.0	0.7
2	Morwell	$NiCl_2$-LiCl-KCl	86.8	3.6
3	Morwell	$MoCl_3$-LiCl-KCl	82.4	5.5
4	Taiheiyo	None	67.8	0.9
5	Taiheiyo	$NiCl_2$-LiCl-KCl	82.3	4.0
6	Taiheiyo	$MoCl_3$-LiCl-KCl	84.0	4.7

a) Conversion = (1-PyI/coal) × 100%.

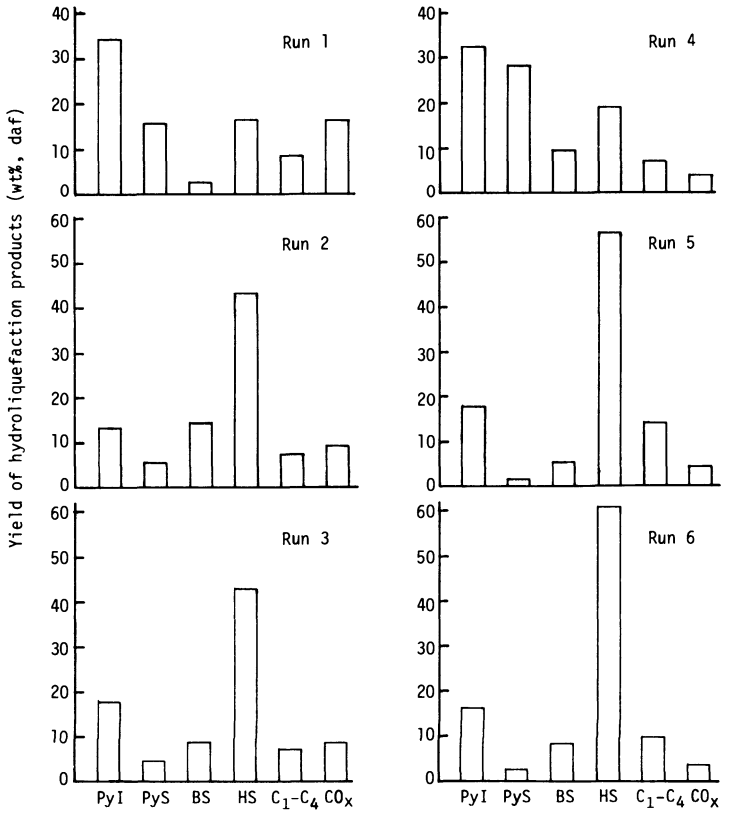

Fig. 1. Product distribution of hydroliquefaction of Morwell and Taiheiyo coals. See Table 2 for run number.

However, it should be noted that relative to noncatalytic runs of the two coals, both the $MoCl_3$ and $NiCl_2$ catalysts selectively enhanced the production of the HS yield without a significant change in the C_1-C_4 gas yield.

Elemental Analysis. Table 3 shows the results of an elemental analysis of the HS and BS fractions. The HS of the catalytic runs had a little higher carbon content, a lower hydrogen content and a lower H/C atomic ratio than that of noncatalytic runs. The content of heteroatoms (N+O+S) of the former was lower or similar to that of the latter. In runs involving Morwell coal, nitrogen was completely removed from the HS by the use of both catalysts. On the other hand, more heteroatoms were retained in the BS of catalytic runs, as compared with its corresponding HS.

^{1}H NMR Spectroscopy. Table 4 gives assignments of ^{1}H NMR spectra bands of HS and BS. The assignments are based on both the chemical shifts of the model compounds[8] containing structures that are believed to be present in coal-derived products and some other assignments found in the literature.[9-12]

Table 3. Elemental Analysis of HS and BS from Morwell and Taiheiyo Coals

Run No.	Product	C	H	N	O+S[a]	H/C
		wt%				
1	HS	85.3	9.0	0.4	5.3	1.25
	BS	85.0	6.7	0.7	7.6	0.94
2	HS	87.9	8.9	—	3.2	1.20
	BS	86.7	6.6	1.0	5.7	0.91
3	HS	87.4	8.7	—	3.9	1.19
	BS	83.4	6.4	0.9	9.3	0.92
4	HS	85.2	10.2	0.4	4.2	1.43
	BS	87.6	6.9	1.3	4.2	0.94
5	HS	86.3	8.9	0.3	4.5	1.23
	BS	83.9	6.9	1.6	7.7	0.98
6	HS	87.2	9.4	—	3.4	1.29
	BS	76.8	6.6	1.3	15.4	1.03

a) By difference.

The major separation was between the aromatic (9.20—6.00 ppm) and aliphatic (5.00—0.20 ppm) hydrogen resonances; the aliphatic region was further divided into six subgroups because the aliphatic region of the spectrum gave highly characteristic structural data regarding coal-derived products.[9] The chemical shift of the phenolic OH proton was variable and its resonance was observed at between 8.50—4.00 ppm. The contribution of phenolic OH was small and made little difference in both the trends and conclusions deduced from the analytical data reported here. However, where applicable, we have subtracted its contribution based on an examination of the D_2O addition.

Tables 5 and 6 show the hydrogen distribution per 100 carbon atoms and the average structural parameters of HS and BS from Morwell and Taiheiyo coals, respectively. For a comparison, Table 7 gives the analytical data of HS and BS derived from the hydroliquefaction of Wandoan coal,[2] among which all the data of BS and hydrogen distribution data of HS have not been previously reported. Important structural differences between the products from catalytic and noncatalytic runs (Tables 5—7) are cited as follows. The HS fractions of noncatalytic runs of Morwell and Taiheiyo as well as Wandoan coals have the highest $H_{\alpha 2}$, $H_{\beta 2}$, H_γ (except Morwell coal), and

Table 4. Assignments of Bands in ^{1}H NMR Spectra of HS and BS

Chemical shift δ (ppm from TMS)	Symbol	Assignments of hydrogen type
9.20—6.00	H_{ar}	Aromatics
5.00—3.40	H_F	CH_2 α to two aromatic rings
3.40—2.35	$H_{\alpha 1}$	CH_2 α to an aromatic ring
2.35—2.00	$H_{\alpha 2}$	CH_3 α to an aromatic ring
2.00—1.60	$H_{\beta 1}$	CH_2 β to an aromatic ring
1.60—1.05	$H_{\beta 2}$	CH_3 β to an aromatic ring CH_2 γ or further from an aromatic ring
1.05—0.20	H_γ	CH_3 γ or further from an aromatic ring

Tabe 5. Hydrogen Distribution and Structural Parameters of HS and BS from Morwell Coal

Run No.	Product	Hydrogen distribution per 100 carbon atoms							Structural parameters[a]		
		H_{ar}	H_F	$H_{\alpha 1}$	$H_{\alpha 2}$	$H_{\beta 1}$	$H_{\beta 2}$	H_γ	f_a	σ	H_{aru}/C_{ar}
1	HS	29.4	2.1	23.4	15.5	7.9	35.5	11.2	0.57	0.38	0.84
	BS	31.9	6.5	16.2	5.6	4.5	22.0	7.3	0.71	0.29	0.64
2	HS	25.6	5.0	24.6	12.0	10.1	29.9	12.8	0.58	0.41	0.81
	BS	28.4	5.4	17.8	7.2	8.0	16.9	7.3	0.71	0.33	0.60
3	HS	27.8	6.2	26.5	11.3	9.4	26.6	11.2	0.58	0.42	0.82
	BS	27.1	4.4	18.2	8.0	8.6	15.9	9.8	0.71	0.34	0.58

a) f_a: aromaticity; σ: degree of substitution in aromatic systems; H_{aru}/C_{ar}: ratio of the number of aromatic hydrogen atoms to the number of aromatic carbon atoms for a hypothetical unsubstituted aromatic system.

Table 6. Hydrogen Distribution and Structural Parameters of HS and BS from Taiheiyo Coal

Run No.	Product	Hydrogen distribution per 100 carbon atoms							Structural parameters		
		H_{ar}	H_F	$H_{\alpha 1}$	$H_{\alpha 2}$	$H_{\beta 1}$	$H_{\beta 2}$	H_γ	f_a	σ	H_{aru}/C_{ar}
4	HS	21.5	1.1	19.2	13.3	8.0	57.7	22.2	0.45	0.40	0.80
	BS	29.3	6.6	20.1	5.8	6.1	18.2	7.9	0.70	0.34	0.64
5	HS	24.1	2.8	21.5	10.2	9.9	38.8	15.7	0.55	0.39	0.73
	BS	21.2	5.1	13.2	5.1	8.1	30.5	14.8	0.65	0.34	0.50
6	HS	22.4	2.8	23.7	11.4	10.7	41.9	16.1	0.51	0.43	0.77
	BS	21.9	7.0	18.9	8.0	9.9	26.2	11.1	0.63	0.42	0.60

Table 7. Hydrogen Distribution and Structural Parameters of HS and BS from Wandoan Coal

Run No.[a)]	Product	Hydrogen distribution per 100 carbon atoms							Structural parameters		
		H_{ar}	H_F	$H_{\alpha 1}$	$H_{\alpha 2}$	$H_{\beta 1}$	$H_{\beta 2}$	H_γ	f_a	σ	H_{aru}/C_{ar}
7	HS	21.3	3.8	21.0	11.0	8.5	57.9	20.5	0.44	0.45	0.88
	BS	26.8	6.1	19.4	9.7	7.1	36.1	9.8	0.59	0.37	0.73
8	HS	25.9	4.3	24.1	9.2	10.0	35.8	12.7	0.54	0.40	0.82
	BS	25.2	4.2	17.0	6.7	8.3	16.5	7.1	0.72	0.34	0.53
9	HS	24.7	4.4	24.7	9.8	11.3	38.1	14.0	0.53	0.42	0.81
	BS	23.0	7.7	16.9	7.4	10.1	20.1	10.8	0.67	0.39	0.57

a) Catalyst: run 7, none; run 8, $NiCl_2$-LiCl-KCl; run 9, $MoCl_3$-LiCl-KCl.

H_{aru}/C_{ar} values. The values of H_F, $H_{\alpha 1}$, $H_{\beta 1}$ and f_a of HS from the catalytic runs are higher than those of HS from noncatalytic runs.

A somewhat surprising observation is that the trends of differences in hydrogen distribution between the HS of noncatalytic and catalytic runs were quite clear and were the same for the three kinds of coals, regardless of the different nature of the coals (Tables 5—7). Generally, a BS showed a higher f_a value and lower $H_{\alpha'\beta'\gamma'}$, σ and H_{aru}/C_{ar} values than its corresponding HS. The values of H_{ar} and H_{aru}/C_{ar} of BS from catalytic runs were lower than those of the BS from noncatalytic runs, the $H_{\beta 1}$ value of the former being higher than that of the latter.

Discussion

Catalytic Effects of $MoCl_3$- and $NiCl_2$-LiCl-KCl Molten Salts. In direct coal hydroliquefaction, the initial step is a thermal fragmentation (depolymerization) of coal organic materials to produce large quantities of fragments which are extremely reactive.[13-14] A thermogravimetric examination (in N_2) of the coal impregnated with catalysts indicated that the $MoCl_3$ and $NiCl_2$ catalysts effectively enhanced the initial thermal fragmentation of the coal.[2] The coal-derived reactive fragments must be stabilized by the hydrogen of the coal, itself, through an autogeneous hydrogen-transfer mechanism[14] and by the hydrogen from such external hydrogen sources as a hydrogen-donor solvent and/or gas-phase hydrogen; otherwise, they would promptly recombine or repolymerize to form insoluble organic materials.[14-16]

It has been commonly recognized that in this stabilizing step, molecular hydrogen is much less effective than a hydrogen donor solvent such as tetralin.[17] Taking our reaction conditions into consideration, the considerably decreased PyI yield of catalytic runs (Fig. 1) and our previous results[2,18-23] suggest that in the initial reaction stage the molten-salt catalysts not only promote coal depolymerization but also act to reduce repolymerization by stabilizing the reactive fragments and permitting them to be capped by gas-phase hydrogen.

After the initial fragmentation and stabilization steps, these salts function as hydrocracking catalysts[2] for the hydrocracking of stabilized heavy products such as PyS and BS. As shown in Table 2 and Fig. 1, for each run of the two coals, the increasing extent of the HS yield with the catalysts is much higher than that of conversion. Therefore, the high H_2 consumption during catalytic runs (Table 2) is probably mainly associated with the hydrocracking of PyS and BS to give a light HS product. These results reinforced our previous conclusion[2] derived from results with Wandoan subbituminous coal: the $MoCl_3$ and $NiCl_2$ catalysts have a high hydrocracking ability and also show a high catalytic activity and HS selectivity.

It should be noted that the selectivity of a coal-liquefaction catalyst is probably more important than its activity.[1] The high HS selectivity of the new catalysts is both of scientific and practical interest since HS is the most desirable oil product of coal hydroliquefaction.

Characteristics of Catalysis by $MoCl_3$- and $NiCl_2$-LiCl-KCl Molten Salts. It has been indicated[24] that

the best procedure for characterizing catalytic effects during coal liquefaction is to pay maximum attention to the liquid-oil part (HS) of the coal products. Yoshida et al.[25] have concluded that during the hydroliquefaction of coal, a cleavage of its ether bonds mainly contributes to the formation of PyS (preasphaltene); however the scission of CH_2 bridges and some naphthenic CH_2 bonds mainly contributes to the formation of HS (oil). As shown in Tables 5—7, ^1H NMR analysis indicated that among all the HS of catalytic and noncatalytic runs, HS of noncatalytic runs of the three coals had the lowest content of hydrogens α to two aromatic rings (H_F). This might be due to a cleavage of the ring-joining methylene bridges (Ar-CH_2-Ar), being consistent with highest content of methyl hydrogens in α-CH_3 (Ar-CH_3) ($H_{\alpha 2}$) of HS of noncatalytic runs. Moreover, the fact that the HS of noncatalytic runs has the highest amounts of hydrogens in β-CH_3 and γ-CH_2 ($H_{\beta 2}$) and γ-CH_3 (H_γ) together with its highest content of hydrogens in α-CH_3 ($H_{\alpha 2}$) suggests that many bridge structures like Ar-$(CH_2)_n$-Ar ($n \geq 2$) which are rich in coal[26-27] and some naphthenic CH_2 bonds which are thermally sensitive,[25-26] have been cleavaged.

Interestingly, all the HS of catalytic runs had an even higher content of hydrogens in CH_2 α to two aromatic rings (H_F) than those of noncatalytic runs (Tables 5—7). Probably this was mainly the result of an increase of CH_2 hydrogen existing in structures like 9,10-dihydroanthracene and fluorene types. This is because the formation of these type compounds is reasonable[9] and their CH_2 hydrogens also resonate in the region of H_F.[8-9] Secondly, all the HS of catalytic runs contain larger amounts of hydrogens in α-CH_2 ($H_{\alpha 1}$) and β-CH_2 ($H_{\beta 1}$) than all of the HS of noncatalytic runs, indicating an increase in CH_2 hydrogens in hydroaromatic structures such as 9,10-dihydrophenanthrene,[9] tetralin and indan types.[12] With regard to the high HS yield, these results suggest that large amounts of polynuclear aromatic structures of the heavy products from these coals were considerably hydrocracked into relatively smaller hydroaromatic and aromatic structures as well as some alkyl aromatic structures, which accounts for the high activity of the catalysts.

Furthermore, all the HS of the catalytic runs contained smaller amounts of hydrogens in β-CH_3 and γ-CH_2 ($H_{\beta 2}$) and in γ-CH_3 (H_γ)(except Morwell coal) and showed higher f_a and lower H_{aru}/C_{ar} values than those of noncatalytic runs. These results, together with the relatively low yield of C_1-C_4 hydrocarbons of the catalytic runs, suggest that most of the newly formed smaller hydroaromatic and aromatic structures did not undergo much further ring-opening reactions. Therefore, the detailed structural study of HS has rationalized the high HS selectivity and activity of the $MoCl_3$ and the $NiCl_2$ catalysts.

It can be seen from Tables 5—7 that the structural differences between the BS of catalytic and noncatalytic runs are not as clear as those observed in HS. This suggests that the structural features of HS can not be directly correlated with those of BS, presumably because HS might also be formed directly from the thermal cracking and hydrocracking of BS and PyS as well as the coal.[28] Nevertheless, all the BS from catalytic runs contained smaller amounts of H_{ar}, larger amounts of $H_{\beta 1}$ and show a lower H_{aru}/C_{ar} value than all the BS of noncatalytic runs. This suggests that the relatively larger polynuclear aromatic compounds contained in coal and PyS were converted into BS by using the catalysts.

Through the present study, we have established the effectiveness of $MoCl_3$-LiCl-KCl and $NiCl_2$-LiCl-KCl molten salt catalysts for the hydroliquefaction of subbituminous and brown coals (especially subbituminous coals). Also, the characteristics of hydroliquefaction catalysis of these new catalysts was clarified. We believe that the analytical methods presented in this paper are useful in characterizing the catalytic effects of a catalyst for the hydrocracking of coal and coal-related materials.

The authors would like to thank Mr. Hiroshi Maki for his assistance in preparation of this manuscript.

References

1) E. S. Lee, "Coal Conversion Technology," ed by C. Y. Wen and E. S. Lee, Addison-Wesley Publishing Company, Massachusetts (1979), pp. 489—538; K. Tanabe and H. Hattori, *Energy and Resources*, **2**, 570 (1981).

2) C. Song, M. Nomura, and M. Miyake, *Fuel*, **65**, 922 (1986); C. Song, Y. Kawakami, M. Miyake, and M. Nomura, 50th National Meeting of the Chemical Society of Japan, Tokyo, April 1985, Abstr. No. 1F47.

3) A. K. Mallock, "Inorganic Synthesis," ed by R. W. Parry, McGraw-Hill, New York (1970), Vol. XII, p. 178.

4) D. E. Couch and A. Brenner, Journal of Research of the National Bureau of Standard-A., *Physics and Chemistry*, **63A**, 185 (1959).

5) J. K. Brown and W. R. Ladner, *Fuel*, **39**, 87 (1960).

6) A feature of brown coal liquefaction compared with that of subbituminous coal is lower oil yield and higher yields of CO_x and water. see Ref. 7 and 20.

7) Y. Kamiya, *Nenryo Kyokai Shi*, **65**, 154 (1986).

8) ALDRICH, "The Aldrich Library of NMR Spectra," (1982); F. A. Bovery, "NMR Data Tables for Organic Compounds," Interscience Publishers, New York (1967).

9) C. E. Snape, W. R. Ladner, and K. D. Bartle, "COAL LIQUEFACTION PRODUCTS," NMR Spectroscopic Characterization and Production Processes, ed by H. D. Schultz, John Wisley & Sons, New York (1983), Vol. 1, p. 73; H. D. Schultz, *ibid.*, p. 149.

10) Y. J. Maekawa, *Sekiyu Gakkaishi*, **18**, 28 (1975); I. Mochida, E. Nakamura, K. Maeda, and K. Takeshita, *Carbon*, **14**, 123 (1976); H. Tsukashima, T. Kato, H. Wakita,

T. Kuruma, and N. Nei, *Nenryo Kyokai Shi*, **55**, 254 (1976).
11) J. W. Clarke, T. D. Rantell, and C. E. Snape, *Fuel*, **61**, 707 (1982); Z. J. Stompel and K. D. Bartle, *Fuel*, **62**, 900 (1983).
12) P. J. Collin, R. J. Tyler, and M. Wilson, *Fuel*, **59**, 479 (1980).
13) D. D. Whitehurst, "Coal liquefaction Fundamentals," ACS Symposium Series 139, ACS, Washington (1980), p. 134.
14) R. C. Neavel, *Fuel*, **55**, 237 (1976).
15) K. W. Han and C. Y. Wen, *Fuel*, **58**, 779 (1979).
16) L. M. Stock, "Chemistry of Coal Conversion," ed by R. H. Schlosberg, Plenum Press, New York (1985), p. 253; R. P. Skowronski, J. J. Ratto, I. B. Goldberg, and L. A. Heredy, *Fuel*, **63**, 440 (1984).
17) J. A. Kleinpeter, in Ref. 9, p. 9.
18) M. Nomura, M. Miyake, H. Sakashita, and S. Kikkawa, *Fuel*, **61**, 19 (1982); M. Nomura, H. Sakashita, M. Miyake, and S. Kikkawa, *ibid.*, **62**, 73 (1983).
19) M. Nomura, K. Kimura, and S. Kikkawa, *Fuel*, **61**, 1119 (1982).
20) M. Nomura, T. Yoshida, and Z. Morita, *Ind. Eng. Chem. Prod. Res. Dev.*, **23**, 215 (1984).
21) M. Nomura, Y. Ikkaku, Y. Nakatsuji, and S. Kikkawa, *J. Japan Petrol. Inst.*, **26**, 303 (1983).
22) M. Nomura, H. Kawakami, Y. Kawakami, "The Latest Advances on Geochemistry, Chemistry and Geology of Coal," ed by S. S. Augustithis, Theophrastus Publications S. A., to be published.
23) M. Miyake, T. Kagajyo, and M. Nomura, *Fuel Processing Technology*, **9**, 293 (1984).
24) L. M. Polinski, V. U. S. Rao, and J. M. Stencel, "The Science and Technology of Coal and Coal Utilization," ed by B. R. Cooper and W. A. Ellingson, Plenum Publishing Corporation, New York (1984), p. 459.
25) T. Yoshida, K. Tokuhashi, and Y. Maekawa, *Fuel*, **64**, 890 (1985).
26) B. M. Benjamin, V. F. Raaen, P. H. Maupin, L. L. Brown, and C. J. Collins, *Fuel*, **57**, 269 (1978); P. Bredael and T. H. Vinh, *Fuel*, **58**, 211 (1979).
27) D. F. McMillen, W. C. Ogier, and D. S. Ross, *J. Org. Chem.*, **46**, 3322 (1981).
28) H. Itoh and K. Ouchi, *Shokubai*, **22**, 71 (1980).

Effect of CH_2Br_2-Addition upon Direct Oxidative Dehydrogenation of Butane into 1,3-Butadiene over Fe-Sb-O Composite Catalyst

Hitoshi SAITOH, Satoshi SATOH, Toshiaki SODESAWA, and Fumio NOZAKI*
Department of Industrial Chemistry, Faculty of Engineering, Chiba University, Yayoi-cho, Chiba 260
(Received February 27, 1986)

Synopsis. Effect of CH_2Br_2-addition upon direct oxidative dehydrogenation of butane into 1,3-butadiene has been investigated in a conventional flow apparatus. The activity and selectivity of Fe-Sb-O catalyst were much improved by the addition of CH_2Br_2 to butane in the mole ratio, CH_2Br_2/n-C_4H_{10}, of 0.03 to 0.10 at temperatures near 450 °C.

The dehydrogenation of paraffinic hydrocarbons such as butane (hereafter referred to as n-C_4H_{10}) is endothermic, so that high temperature is required to facilitate the reaction. The oxidative dehydrogenation has no such difficulty; however, catalytic selectivity is often poor.

The oxidative dehydrogenation of olefin such as 1-butene (1-C_4H_8) is selectively achieved by the use of composite catalysts such as Fe-Sb-O[1] and Bi-Mo-O.[2] On the other hand, the oxidative dehydrogenation of n-C_4H_{10} using oxygen or air as the oxidant gives preferentially a large amount of CO_2 and the selectivity to form butenes (C_4H_8) or 1,3-butadiene (C_4H_6) is generally lowered. It is well known that the addition of small amounts of halogen (I_2, Br_2, etc.) or halogen compound (HBr, HCl, KBr, etc.) is effective for the dehydrogenation or oxidative dehydrogenation of paraffinic hydrocarbons or ethylbenzene.[3-5] In addition, attempts to use COS[6] or N_2O[7] as the oxidant for the dehydrogenation of C_4H_{10} or ethane have recently been made. In these studies, however, a large portion of the dehydrogenated products was C_4H_8 or olefinic hydrocarbons such as propylene and ethylene, and the extent of C_4H_6 formation was usually very small.

We have previously reported on the oxidative dehydrogenation of 1-C_4H_8 to C_4H_6 over Fe-Sb-O catalyst.[1] In this paper, we describe a promoting action of CH_2Br_2 for the direct oxidative dehydrogenation of n-C_4H_{10} to C_4H_6 over Fe-Sb-O catalyst. It should also be noted that CH_2Br_2 is chosen as a promoter because of its appropriate magnitude of vapor pressure and its low cost.

Experimental

The catalytic tests were conducted in a conventional tubular-flow reactor operating at atmospheric pressure. The reaction products were analyzed by the gas chromatography on a 4 m column of VZ-7 (Gasukuro-kogyo Co.) operated at room temperature. The conversion of n-C_4H_{10} (expressed by x), the selectivity to C_4H_6 (S_{C_4}), C_4H_8 (S_{C_4}), etc. were calculated by the usual procedure on the mole basis of n-C_4H_{10} fed.

The method of preparation of the Fe-Sb-O catalyst was similar to that previously reported[1]: $Fe(NO_3)_3$ and Sb_2O_3 were used as the starting materials for the preparation of $FeSb_2O_4$ composite catalyst. In order to compare the activity of the Fe-Sb-O catalyst with other catalysts, Cr_2O_3(7.5 wt%)/Al_2O_3 and Fe_2O_3(30 wt%)/SiO_2 were also used in the catalytic tests. These two materials were commercially supplied from Nissan-Girdler Co., Ltd.

Results and Discussion

The results of catalytic tests obtained by three kinds of catalysts, Fe-Sb-O, Cr_2O_3/Al_2O_3, and Fe_2O_3/SiO_2, are summarized in Table 1. Table 1 indicates that an addition of small amounts of CH_2Br_2 to the reactant mixture is effective for the oxidative dehydrogenation of n-C_4H_{10} to give C_4H_6. Especially in the case of the Fe-Sb-O catalyst, the high conversion and selectivity (x=67%, S_{C_4}=59%) were obtained with the addition of CH_2Br_2.

The detailed behavior of the promoting action of

Table 1. Conversion and Selectivities Obtained by Use of Various Catalysts in Oxidative Dehydrogenation of n-C_4H_{10} with and without Addition of CH_2Br_2
Reaction temperature: 450 °C, Catalyst weight: 3.0 g, Total gas feeding rate: 130 ml min^{-1}
Reactant concentration(mole) n-C_4H_{10}/Air = 1/12

Catalyst	Without the Addition of CH_2Br_2						With the Addition of CH_2Br_2[a]					
	%						%					
	x	S_{C_4}	S_{C_4}	S_{CO_2}	S_{C_4}	S_{C_4}	x	S_{C_4}	S_{C_4}	S_{CO_2}	S_{C_4}	S_{C_4}
Fe-Sb-O	11	8	b)	92	b)	b)	67	59	5	36	b)	b)
Cr_2O_3/Al_2O_3	32	5	18	77	b)	b)	40	19	16	58	2	5
Fe_2O_3/SiO_2	38	3	2	89	6	b)	48	11	20	65	b)	4
None	17	7	9	49	21	14	6	13	67	17	3	b)

a) The catalytic reaction was carried out with the mole ratio n-C_4H_{10}/Air/CH_2Br_2 = 1/12/0.12. b) The mark indicates that the numerical value is less than about 1%.

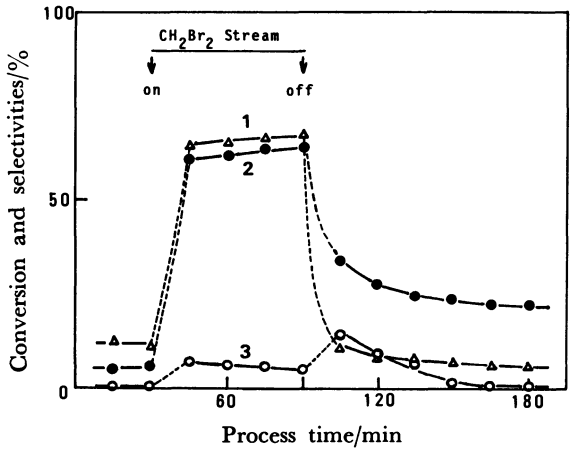

Fig. 1. Influence of CH_2Br_2-addition upon the reaction. 1: Conversion of n-C_4H_{10}, 2: Selectivity to C_4H_6 (Sc), 3: Selectivity to C_4H_8(Sc)
Catalyst: Fe–Sb–O, W: 3.0 g, t: 450 °C, F: 130 ml min^{-1}, Mole ratio n-C_4H_{10}/Air/CH_2Br_2: 1/12/0.12.

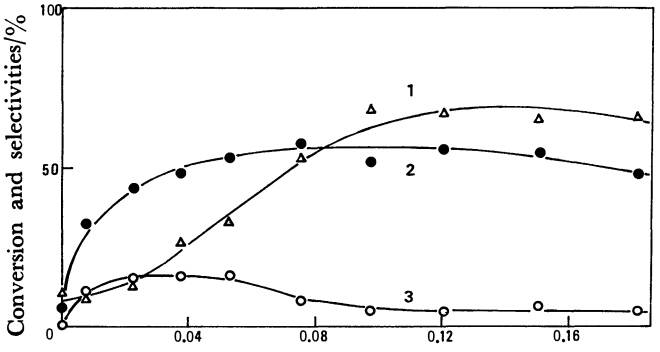

Fig. 2. Influence of CH_2Br_2/n-C_4H_{10} ratio upon the reaction. The reaction conditions and the symbols are the same as for Fig. 1.

CH_2Br_2 for the Fe–Sb–O catalyst is further illustrated in Fig. 1. Figure 1 depicts clearly that the oxidative dehydrogenation to form C_4H_6 continues to occur so long as CH_2Br_2 is fed into the reaction. When the introduction of CH_2Br_2 is stopped, the enhanced activity gradually decreases and tends to resume the original activity.

The influence of CH_2Br_2 concentration upon the catalytic reaction is shown in Fig. 2. The conversion of n-C_4H_{10} (curve 1) is increased with an increase of the CH_2Br_2 concentration and then levels off when the mole ratio of CH_2Br_2 to n-C_4H_{10} becomes approximately 1:10. The selectivity to C_4H_6 or C_4H_8 (curve 2 or 3) is much improved even at a low CH_2Br_2 concentration (CH_2Br_2/n-C_4H_{10}=0.03—0.05).

The activity and selectivity of the Fe–Sb–O catalyst enhanced by the addition of CH_2Br_2 stayed at the same level for as long as CH_2Br_2 was being supplied. The changes in the conversion and selectivity with reaction temperature and contact time were also investigated. The results indicated that the reaction temperature near 450 °C was the best for the formation of C_4H_6, and its yield decreased with a decreasing contact time.

No reaction occurred between n-C_4H_{10} and CH_2Br_2 without air over the Fe–Sb–O catalyst. This fact suggests that oxygen is essential for the dissociation of CH_2Br_2 to Br_2 and for the formation of C_4H_6 and C_4H_8. As was shown in Table 1, the dehydrogenation of n-C_4H_{10} into C_4H_8 took place to a certain extent even in the absence of the Fe–Sb–O catalyst.

In accordance with the above findings and with other information, we have tentatively speculated the reaction pathways as follows:

$$\left.\begin{aligned} &CH_2Br_2 + 3/2O_2 \longrightarrow CO_2 + H_2O + Br_2 \\ &Br_2 \rightleftarrows 2Br\cdot \end{aligned}\right\} \quad (1)$$

$$\left.\begin{aligned} &C_4H_{10} + Br\cdot \longrightarrow C_4H_9\cdot + HBr \\ &C_4H_9\cdot + Br\cdot \longrightarrow C_4H_8 + HBr \end{aligned}\right\} \quad (2)$$

$$C_4H_8 + 1/2O_2 \xrightarrow{\text{Fe-Sb-O cat.}} C_4H_6 + H_2O \quad (3)$$

$$\left.\begin{aligned} &FeSb_2O_{4-y} + 2HBr \longrightarrow FeSb_2Br_2O_{3-y} + H_2O \\ &FeSb_2Br_2O_{3-y} + 1/2O_2 \longrightarrow FeSb_2O_{4-y} + Br_2 \end{aligned}\right\} \quad (4)$$

(here, $FeSb_2O_{4-y}$ shows the partially reduced state of the Fe–Sb–O catalyst).

The bromine radical Br· generated by Eq. 1[8] probably plays an important role in the formation of C_4H_8. The resulting C_4H_8 is oxidatively dehydrogenated to C_4H_6 by the subsequent reaction step, Eq. 3, over the Fe–Sb–O catalyst.[1]

In addition, it can be speculated that the resulting HBr is converted into Br_2 by the redox mechanism of the Fe–Sb–O catalyst, as is shown by Eq. 4. This is probably responsible for the experimental fact that such a high conversion and selectivity as x=60—70%, Sc≅ 60% have been attained even at the low CH_2Br_2/n-C_4H_{10} ratio.

However, the more definitive reaction scheme must remain to be the subject for a further study.

References

1) M. Shimamura and F. Nozaki, *Nippon Kagaku Kaishi* **1982**, 1879.

2) For example: Ph. A. Batist and G. C. A. Schuit et al., *J. Catal.*, **12**, 45 (1968).

3) P. S. Nangia and S. W. Benson, *J. Am. Chem. Son.*, **86**, 2773 (1964); Shell International, B. P. 1004, 393 (1965).

4) D. B. Fox and E. H. Lee, CHEMTECH March 1973, 186.

5) K. Fujimoto and T. Kunugi, *Ind. End. Chem., Prod. Res. Dev.*, **20**, 319 (1981).

6) M. Akimoto, T, Sakatani, and E, Echigoya., *Bull. Chem. Soc. Jpn.*, **56**, 3503 (1983).

7) M. Iwamoto, T. Taga, and S. Kagawa, *Chem. Lett.*, **1982**, 1469.

8) $Log_{10} K_p$ for the reaction $Br_2 \rightarrow 2Br$ has been estimated to be about −7.9 at 450 °C by the use of data listed in "JANAF Thermochemical Tables," 2nd ed., p. 290 and p. 318 (National Bureau of Standards). The low value of log K_p appears to be unfavorable to the proposed mechanism; however, a small amount of Br can be formed and it can initiate the subsequent reaction steps represented by Eqs. 2—4.

Nonexistence of Hydration Number Change of Cd^{2+} Ions in Aqueous $Cd(NO_3)_2$ Solution

Hitoshi KANNO
Department of Chemistry, The National Defence Academy,
Hashirimizu, Yokosuka, Kanagawa 239
(Received May 13, 1986)

Synopsis. Raman spectra for the Cd^{2+}–OH_2 stretching vibration (ν_1 band) were measured for aqueous $Cd(NO_3)_2$ solutions of R=15 and 40 (R: moles of water/moles of salt). Contrary to the results reported by Kuznetsov et al.,[5] it is concluded that the hydration number of Cd^{2+} ions does not change with salt concentration in the $Cd(NO_3)_2$ solution.

In recent years, inner-sphere hydration numbers have been determined by X-ray diffraction method for many metal cations in aqueous electrolyte solutions.[1-4] Most divalent cations are reported to have six water molecules in their inner-coordination spheres.[1,2] However, the recent X-ray diffraction study by Kuznetsov et al.[5] asserts that the hydration number of Cd^{2+} ions changes from four in an aqueous $Cd(NO_3)_2$ solution (R=40) to six in the R=25 solution where R is the molar ratio of water to salt in the solution. If this is the case, it should be the first experimental evidence for the hydration number change with variation of salt concentration for divalent cations and has a significant implication for our understanding of aqueous electrolyte solutions. Valeev et al.[6] have very recently reported that the Cd^{2+} ions in the R=10 solution are tetrahedrally coordinated with two water molecules and two nitrate ions. When ligands other than water molecules constitute a part of the coordination sphere, geometrical factors such as size and the manner of coordination (monodentate or bidentate) of the ligands have a large effect on the coordination number so that comparison between the coordination number of an all-aquated metal ion and that of a partially-aquated metal ion should be made with care.

On the other hand, Bol et al.[7] determined the coordination number of Cd^{2+} ions in aqueous $Cd(NO_3)_2$ solution ($R\simeq55$) by X-ray diffraction method and reported that the hydration number of Cd^{2+} ions is six. The X-ray diffraction study by Ohtaki et al.[8] of aqueous $Cd(ClO_4)_2$ solution ($R\simeq19$) also reports that it is about six. With these experimental data, it is evident that Cd^{2+} ions are octahedrally coordinated in concentrated Cd-salt solutions ($R\lesssim25$). However, there is a clear discrepancy between the two reports by Kuznetsov et al.[5] and Bol et al.[7] in rather dilute $Cd(NO_3)_2$ concentration range (R=40—55). Therefore, it is important to determine whether the hydration number change really occurs with decreasing salt concentration in aqueous $Cd(NO_3)_3$ solution.

In this work, we examined the possibility of hydration number change of Cd^{2+} ions in aqueous $Cd(NO_3)_2$ solution by Raman spectroscopy. As a symmetric M–OH_2 stretching vibration (a ν_1 band) of aquated metal ions (M: metal cation) is sensitive in frequency to the constituents of the coordination spheres of the cations, it can serve as a sensitive probe for the hydration number change, if any, in aquated Cd^{2+} ions. We measured the ν_1 spectra for the aqueous $Cd(NO_3)_2$ solutions of R=15 and 40 and the ν_4 spectra of the NO_3^- ions in the solutions. Raman measurements were carried out in the same way as previously reported.[9]

Results and Discussion

The ν_1 spectra are shown in Fig. 1. We see only a small frequency change ($\Delta\nu_1=6\pm2\,cm^{-1}$) from the R=15 solution to the R=40 solution. From the ν_4 spectra shown in Fig. 2, we know that some nitrate ions are coordinated to cadmium ions in the R=15 solution because the coordinated NO_3^- ions give a higher ν_4 frequency (about 738 cm^{-1}) than 718 cm^{-1} (the ν_4 frequency for non-coordinated NO_3^- ions).[10] In the R=40 solution, the $\approx$738 cm^{-1} peak is much weaker than that in the R=15 solution, indicating that the inner-coordination sphere around a Cd^{2+} ion consists mostly of water molecules in the R=40 solu-

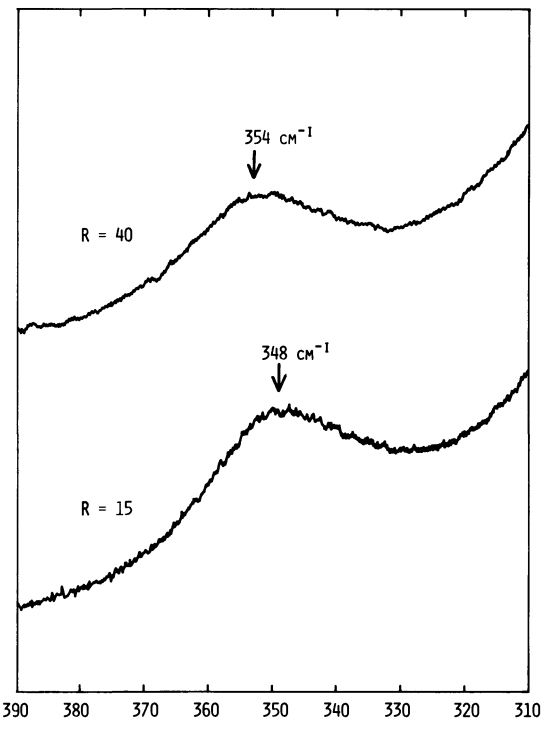

Fig. 1. Raman spectra of the Cd^{2+}–OH_2 stretching vibration for aqueous $Cd(NO_3)_2$ solutions of R=15 and 40.

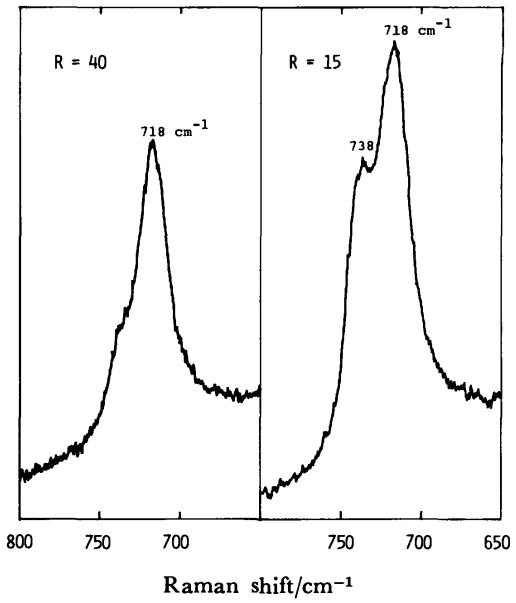

Fig. 2. Raman spectra of the ν_4 band of the NO_3^- ions in aqueous $Cd(NO_3)_2$ solutions of $R=15$ and 40.

tion. It is a well-known fact that a ligand other than water molecules enters into an inner-coordination sphere of an aquated cation, the frequency of a ν_1 band gets lower than that for all-aquated cations.[10,11] In other words, the overall effects of increasing in mole fraction of a aquated Cd^{2+} ions partially substituted with nitrate ion(s) such as $[Cd(NO_3)(OH_2)_n]^+$ ion are a steady decrease in the total ν_1 frequency. Therefore, the frequency change $\Delta\nu_1=6\pm2\ cm^{-1}$ between the $R=15$ and 40 solutions is mainly ascribable to the difference of the average constituents of the innersphere coordinations: The mole fraction of nitrate ions complexed to Cd^{2+} ions is larger in the $R=15$ solution than in the $R=40$ solution. In the Raman study by Davis and Plane,[12] it is reported that the nitrate ions coordinated to Cd^{2+} ions are acting as a monodentate ligand and that no evidence for complex species higher than $[Cd(NO_3)(OH_2)_n]^+$ was found. The smallness of the ν_1 frequency change from $R=40$ to $R=15$ indicates that the mole fraction of nitrate ions coordinatig to Cd^{2+} ions is not large. This is also confirmed by the Raman ν_4 spectrum for the $R=15$ solution.

There have been a few examples[13,14] which can be a guide for the estimation of the frequency change when the hydration number change really takes place in aqueous $Cd(NO_3)_2$ solution. The conversion from an octahedral to a tetrahedral configuration of a metal halide gives rise to an increase in the frequency of the symmetric stretching vibrations (a ν_1 band): e.g.,

$$[InCl_6]^{3-}(\nu_1:\ 275\ cm^{-1}) \longrightarrow [InCl_4]^-(\nu_1:\ 366\ cm^{-1})$$

and

$$[SnCl_6]^{2-}(\nu_1:\ 301\ cm^{-1}) \longrightarrow [SnCl_4](\nu_1:\ 360\ cm^{-1}).^{13}$$

Hydration number change of rare earth ions from 9 to 8 results in the ν_1 frequency change of about 25 cm^{-1}, e.g., $[Eu(OH_2)_9]^{3+}(\nu_1:\ 369\ cm^{-1}) \rightarrow [Eu(OH_2)_8]^{3+}(\nu_1:\ 394\ cm^{-1})$.[14] Thus, the hydration number change, if it really occurs in an aqueous $Cd(NO_3)_2$ solution between $R=15$ and 40, should give rise to a ν_1 frequency change of more than 30 cm^{-1}. However, the observed ν_1 frequency shift is much smaller than the one expected from the hydration number change. Accordingly, we conclude that the hydration number change, at least the one proposed by Kuznetsov et al.,[5] does not takes place in aqueous $Cd(NO_3)_2$ solution between $R=15$ and 40. From the ν_1 results shown in Fig. 1 and the X-ray diffraction results by Bol et al.,[7] it is considered that the coordination number of all-aquated Cd^{2+} ions in an aqueous $Cd(NO_3)_2$ solution remains six in all concentration ranges ($15 \lesssim R \lesssim 55$). This is supported by the observation[15] that the ν_1 band is at $356\pm3\ cm^{-1}$ in an aqueous $Cd(ClO_4)_2$ solution ($R=15$), in which all Cd^{2+} ion are octahedrally hydrated according to the X-ray diffraction study by Ohtaki et al.[8]

Raman measurements were carried out in National Chemical Laboratory for Industory, for which the author is thankful to Dr. K. Tanabe.

References

1) J. E. Enderby and G. W. Neilson, "Water: a Comprehensive Treatise," ed by F. Franks, Plenum Press, New York (1979) Vol. 6, Chap. 1 and references therein.
2) H. Ohtaki, *Rev. Inorg. Chem.* **4**, 103 (1982) and references therein.
3) T. Yamaguchi, O. Lindqvist, T. Claeson, and J. B. Boyce, *Chem. Phys. Lett.*, **93**, 528 (1982).
4) R. Caminiti, D. Atzei, P. Cucca, A. Anedda, and G. Bongiovanni, *J. Phys. Chem.*, **90**, 238 (1986).
5) V. V. Kuznetsov, V. N. Trostin, and G. A. Krestov, *Izv. Vyssh. Uchebn. Zavd., Khim. Kim. Tekhnol.*, **25**, 954 (1982).
6) A. Kh. Valeev, V. V. Kuznetsov, V. N. Trostin, and G. A. Krestov, *Dokl. Akad. Nauk. SSSR*, **285**, 911 (1986).
7) W. Bol, G. J. A. Gerrits, and C. L. V. P. van Eck, *J. Appl. Crystallogr.* **3**, 486 (1970).
8) H. Ohtaki, M. Maeda, and S. Ito, *Bull. Chem. Soc. Jpn.*, **47**, 2217 (1974).
9) H. Kanno and J. Hiraishi, *J. Phys. Chem.*, **87**, 3664 (1983).
10) D. E Irish and M. H. Brooker, "Advances in Infrared and Raman Spectroscopy," ed by R. J. H. Clark and R. E. Hester, Heyden, New York (1976), Vol. 2, Chap. 6.
11) H. Kanno and J. Hiraishi, *J. Raman Spectrosc.*, **12**, 224 (1982).
12) A. R Davis and R. A. Plane, *Inorg. Chem.*, **7**, 2565 (1968).
13) L. A. Woodward and M. J. Taylor, *J. Chem. Soc.*, **1960**, 4473.
14) H. Kanno and J. Hiraishi, *Chem. Phys. Lett.*, **75**, 553 (1980); *J. Phys. Chem.*, **86**, 1488 (1982).
15) H. Kanno, *J. Raman Spectrosc.*, in press.

Solvent Effects on the Unimolecular Dissociation of Radical Anions Studied by Pulse Radiolysis

Norio KIMURA* and Setsuo TAKAMUKU
The Institute of Scientific and Industrial Research, Osaka University,
8-1 Mihogaoka, Ibaraki, Osaka 567
(Received May 26, 1986)

Synopsis. The rate constants of the unimolecular dissociation of radical anions formed by one-electron reduction of chloroacetophenone isomers in dipolar aprotic solvents were measured by a pulse radiolysis technique. The reactivities of these isomers were affected by the polarity of the solvent used.

Solvent effects on chemical reactivity are commonly found in a wide variety of reactions involving electron-transfer reactions which are currently attracting the interest of chemists.[1,2] However, only a few investigations have been reported about solvent effects on the further reactions of radical anions formed by one-electron reduction.[3] For example, radical anions of aromatic halides are well-known to undergo unimolecular dissociation producing an aryl radical and halide ion,[3-7] but the rate constants reported spread over a wide range, probably due to the effect of the solvent used.[4,7] Therefore, the present purpose is to clarify the solvent effects on the unimolecular dissociation of radical anions of chloroacetophenone isomers (*o*-, *m*-, and *p*-CAP) and also to elucidate the reaction mechanism by use of a pulse radiolysis technique.

Experimental

Chemicals. Chloroacetophenone isomers (Wako Pure Chemical and Aldrich) and *o*-chlorobenzaldehyde (Wako Pure Chemical) were purified by distillation. *N,N*-dimethylacetamide (DMA), *N,N*-dimethylformamide (DMF), dimethyl sulfoxide (DMSO), *N*-methyl-2-pyrrolidone (NMePy), and hexamethylphosphoric triamide (HMPA) used as solvents were distilled over calcium hydride. Solutions were prepared freshly before irradiation and were degassed under high vacuum.

Apparatus. The electron pulse from Osaka Univ. linear accelerator was used. The energy was 28-MeV and the pulse width was 8-ns. The dose was 1 kGy per pulse. A 450W xenon pulse lamp (OPG-450, Osram), a monochromator (Nikon G-250), and a photomultiplier (R-928) were used. The output of the photomultiplier was monitored by a programable transient digitizer (Tektronix 7912AD) with 7A29 plug-in and stored for display in a Melcom 70/25 computer (Mitsubishi Electric Co.).

Results and Discussion

Transient absorption spectra obtained by the pulse radiolysis of *o*-CAP in HMPA are shown in Fig. 1. The spectra with λ_{max} at 330 and 490 nm are assigned to the radical anion of *o*-CAP on the basis of the similarity to that of acetophenone which was measured in this work under the same reaction conditions (λ_{max} 330 and 490 nm).[8] The decay of the 330-nm band followed first order kinetics and the rate, 5.3×10^{6} s^{-1}, was independent of the concentration of *o*-CAP (1×10^{-2}—1×10^{-3} mol dm^{-3}). This fact is consistent with the unimolecular dissociation of the radical anion. Similar spectra were observed with *m*- and *p*-CAP. The decay rate of 330-nm bonds of *m*- and *p*-CAP were 9.6×10^{4} and 2.8×10^{5} s^{-1}, respectively. These rates are much slower than that of *o*-CAP.

The chemical reactivities of radical anions of these CAP isomers were also examined in other dipolar aprotic solvents such as DMA, DMF, DMSO, and NMePy. The spectral features of the radical anions formed in these solvents were not different from that in HMPA. However, the rate constants were dependent on the nature of solvents used. A good correlation between the rate constants (log k) and an acceptor number (AN) of the solvent[9] which is an empirical parameter reflecting the electrophilic properties of solvent was obtained as shown in Fig. 2.

In the cases of *m*- and *p*-CAP, an increase of solvent polarity resulted in an increase in the rate. In general, an acceleration of the rate is induced in such a case where the solvation is stronger in the transition state than in the initial state. In the present reactions, therefore, the negative charge of the radical anion must be localized in a molecule at the transition state which makes the solvation more tight. Indeed, the negative charge may be present initially at the delocalized π-orbital of an acetophenone moiety since the absorption spectra of the CAP radical anions are

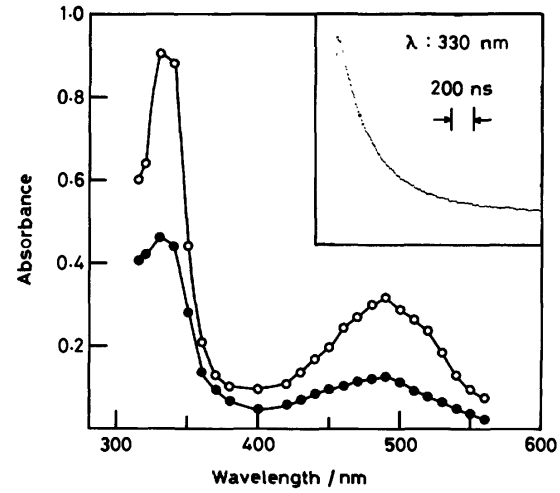

Fig. 1. Transient absorption spectra observed at immediately (○) and 200 ns (●) after an 8-ns pulse irradiation of a degassed HMPA solution of *o*-CAP (1×10^{-2} mol dm^{-3}) at room temperature. Absorption dose was 1 kGy/pulse. Insert: Decay curve of the 330-nm band.

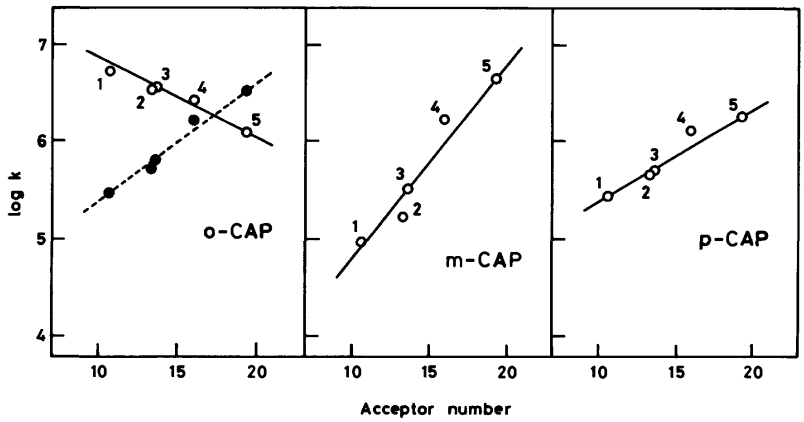

Fig. 2. Plot of log $k(s^{-1})$ vs. the acceptor number of the following solvents: 1, HMPA, 2, NMePy; 3, DMA; 4, DMF; 5, DMSO. The dotted line (--●--) indicates the result for *o*-chlorobenzaldehyde.

similar to that of acetophenone itself. The negative charge migrates to a C-Cl σ^* orbital at the transition state and finally localizes at a dissociated chlorine atom. Such an intramolecular electron-transfer mechanism has been proposed for the dissociation of aromatic halides by Neta and Behar[5] as shown in Eq. 1. The present observation is compatible with this mechanism.

$$\underset{\text{(I)}}{\overset{\cdots\overset{\cdot}{\cdot}\cdots}{CH_3COC_6H_4\text{-}Cl}} \rightleftharpoons \underset{\text{(II)}}{CH_3COC_6H_4\text{-}\overset{\cdot}{Cl}} \longrightarrow \underset{\text{(III)}}{CH_3COC_6H_4\cdot} + Cl^- \quad (1)$$

The slope of the straight line for the plot of log k vs. AN reflects the relative extent of solvation to the initial state and the transition state. The larger slope for *m*-CAP than for *p*-CAP as shown in Fig. 2 is explained by the fact that the negative charge at the C-Cl σ^* orbital in the transition state is more delocalized in *p*-CAP than in *m*-CAP simply due to the presence of an electron-withdrawing group at the para position. This delocalization of the negative charge at the transition state decreases the solvation and reduces the rate.

On the other hand, a negative slope was obtained in the case of *o*-CAP, that is, an increase of solvent polarity resulted in a decrease in the rate. This means that the extent of solvation decreased in the transition state. In the case of *o*-CAP, two conformers (IV and V)

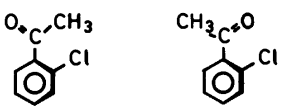

(IV) (V)

exist and the C-CO-C plane is rotated from that of the phenyl ring on the basis of the strong steric interaction between the chlorine atom and oxygen atoms or methyl groups.[10] Consideration of steric and electrostatic factors indicated that an antiperiplanar-conformation, IV, is more favored than V. This argument concerning the stable conformation is also applicable to the radical anion. Therefore, the solvation of the negative-charged C-Cl bond at the transition state of the radical anion will be subject to steric hindrance by the proximately faced methyl group which leads to the abnormal solvent effect. The validity of such an explanation is supported by the findings that a normal behavior is observed for *o*-chlorobenzaldehyde in which such an intense steric effect as *o*-CAP cannot be expected as shown in Fig. 2 (dotted line).

In conclusion, we have demonstrated that the unimolecular dissociation of radical anions is subject to a remarkable solvent effect; normally an increase of solvent polarity results in an increase in the rate in consistent with the dissociation mechanism. Works along these lines are currently in progress.

References

1) A. Parker, *Chem. Rev.*, **69**, 1 (1969).
2) C. Reichardt, "Solvent Effects in Organic Chemistry," Verlag Chemie, Weinheim (1979).
3) V. D. Parker, *Acta Chem. Scand.*, **B35**, 595 (1981).
4) P. Neta and D. Behar, *J. Am. Chem. Soc.*, **103**, 103 (1981).
5) D. Behar and P. Neta, *J. Am. Chem. Soc.*, **103**, 2280 (1981).
6) D. Behar and P. Neta, *J. Phys. Chem.*, **85**, 690 (1981).
7) F. M'Halla, J. Pinson, and J. M. Saveant, *J. Am. Chem. Soc.*, **102**, 4120 (1980).
8) T. Shida and W. H. Hamill, *J. Am. Chem. Soc.*, **88**, 3683 (1966).
9) V. Gutmann, *Electrochim. Acta*, **21**, 661 (1976).
10) C. L. Chemg, R. J. W. Le Fevre, G. L. Ritchie, P. A. Goodman, and P. H. Gore, *J. Chem. Soc. (B)*, **1971**, 1198.

Polystyrene Resin-Supported Aluminium Copper(I) Chloride as Selective Ethylene Adsorbent

Hidefumi HIRAI,* Masahiro NAKAMURA, Susumu HARA, and Makoto KOMIYAMA
Department of Industrial Chemistry, Faculty of Engineering, The University of Tokyo, 7-3-1, Hongo, Bunkyo-ku, Tokyo 113
(Received June 13, 1986)

Synopsis. Solid adsorbents for ethylene are prepared by stirring copper(I) chloride, aluminium chloride, and a macroreticular type polystyrene resin in carbon disulfide, followed by removal of the liquid phase. The adsorbents effectively adsorb ethylene at 20 °C under 1 atm, and exhibit no measurable adsorptions of nitrogen, hydrogen, and methane.

Ethylene, one of the most important raw materials in chemical industry, is usually obtained as gas mixtures with nitrogen, hydrogen, methane, carbon monoxide, and others. Thus, ethylene must be separated from the gas mixtures prior to utilization.[1]

Previously, the authors have reported that toluene solutions of aluminium silver chloride[2] and the macroreticular type polystyrene resin-supported aluminium silver chloride[3] reversibly and selectively absorb ethylene under mild conditions.

This paper reports preparation of solid adsorbents for ethylene from copper(I) chloride, aluminium chloride, and a macroreticular type polystyrene resin. The ethylene adsorbing and desorbing abilities as well as selectivities of the ethylene adsorptions with respect to the adsorptions of other gases are described.

Experimental

A macroreticular type polystyrene resin, purchased from Bio-Rad Laboratories (Bio-Beads SM-2; divinylbenzene content, 20 mol%; diameter, 296—740 μm; average pore diameter, 9 nm; surface area, 300 m^2/g),[4] was successively washed with aqueous hydrochloric acid solution (6 mol dm^{-3}), with aqueous sodium hydroxide solution (4 mol dm^{-3}), with water, with methanol, and with dichloromethane, and then was dried in vacuo at 80 °C for 12 h. Aluminium chloride was purified by sublimation. Copper(I) chloride was reprecipitated using concentrated aqueous hydrochloric acid solution-water system, was washed with ethanol and diethyl ether, and was dried in vacuo at 80 °C for 12 h. Ethylene, nitrogen, hydrogen, methane, and carbon monoxide were passed through columns of molecular sieve 3A immediately before use.

The adsorbents were prepared by refluxing copper(I) chloride, aluminium chloride, and the polystyrene resin in carbon disulfide under dry nitrogen for 6 h. The charged molar ratios of copper(I) chloride and the aromatic residue of the polystyrene resin, respectively, to aluminium chloride were 1.0 and 1.2. Then the liquid phase was removed at 4 mmHg, where the temperature was gradually elevated from 20 to 60 °C. The adsorbents were obtained as orange colored beads.

Adsorptions of gases by the adsorbents were carried out at 20 °C under 1 atm, and were followed by the gas uptake using a gas burette. Gas compositions were determined by gas chromatography (Ohkura Model 701; column, Porapak Q; column temperature, 80 °C; carrier gas, helium).

Results and Discussion

The open circles in Fig. 1 depict the adsorption of ethylene at 20 °C under 1 atm by the adsorbent prepared from copper(I) chloride, aluminium chloride, and the macroreticular type polystyrene resin. The adsorption is rapid, and the equilibrium molar ratio of adsorbed ethylene to the charged copper(I) chloride is 1.40. The amount of ethylene adsorbed by 1 g of the adsorbent is 89 cm^3 (standard temperature and pressure).

Then, desorption of the adsorbed ethylene has been carried out by subjecting the adsorbent to a reduced pressure (8 mmHg) at 20 °C for 10 min. In the second adsorption, shown by the closed circles in Fig. 1, the equilibrium molar ratio of the adsorbed ethylene to the charged copper(I) chloride is 0.29. Both the time courses of the adsorptions and the equilibrium molar ratios in the third, the fourth, and the fifth adsorptions are identical with those in the second adsorption within experimental error. Reversible adsorption of ethylene is successfully achieved by use of the present adsorbent.

The difference between the molar ratio (1.40) of the adsorbed ethylene to the charged copper(I) chloride in the first adsorption and that (0.29) in the second and the later adsorptions corresponds to the amount of ethylene, which is not desorbed under the desorption conditions employed (8 mmHg, 20 °C for 10 min).

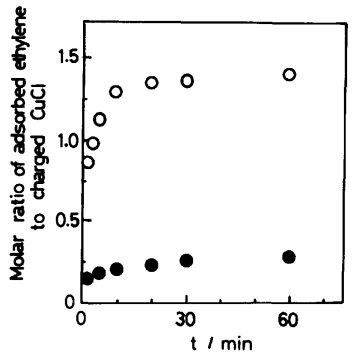

Fig. 1. Adsorption of ethylene under 1 atm at 20 °C by the polystyrene resin-supported aluminium copper (I) chloride: The first adsorption (○); the second adsorption (●) by the adsorbent which was subjected to a reduced pressure (8 mmHg) at 20 °C for 10 min after the first adsorption; the adsorbent was prepared from 2.57 g (26.0 mmol) of copper(I) chloride, 3.47 g (26.0 mmol) of aluminium chloride, and 3.24 g (31.1 milliequivalents in phenyl residue) of the macroreticular type polystyrene resin by use of 30 cm^3 of carbon disulfide.

The desorption of the ethylene adsorbed by the present adsorbent was also effectively carried out by heating the adsorbent to 90 °C under 1 atm for 10 min. The molar ratio of the desorbed ethylene to the charged copper(I) chloride was 0.47, as followed by the gas burette. In the following adsorption, the molar ratio of adsorbed ethylene to the charged copper(I) chloride was 0.47, which was exactly identical with the value for the ethylene desorbed in the foregoing desorption.

When the desorption of adsorbed ethylene was carried out under 8 mmHg at 142 °C for 10 min, the molar ratio of the desorbed ethylene to the charged copper(I) chloride was 0.87.

The present adsorbents exhibited no measurable adsorptions of nitrogen, hydrogen, and methane under 1 atm at 20 °C.

Separation of ethylene from ethylene–carbon monoxide mixture was examined by use of the adsorbent prepared from 12.0 mmol of copper(I) chloride, 12.0 mmol of aluminium chloride, and 1.50 g of the resin. Here, 1050 cm^3 of ethylene–carbon monoxide mixture having initial molar fraction 0.47 of ethylene was contacted with the adsorbent at 20 °C under 1 atm. The adsorbent rapidly adsorbed both ethylene and carbon monoxide[5] from the gas mixture, and the equilibrium amounts of adsorbed ethylene and adsorbed carbon monoxide were 9.0 mmol and 1.8 mmol, respectively. These values were evaluated by use of both the molar fraction (0.35) of ethylene in the gas phase after the contact with the adsorbent, measured by gas chromatography, and the total amount (264 cm^3) of the adsorbed gas, determined by a gas burette. Thus the amount of adsorbed ethylene was 5 times as large as that for carbon monoxide.

The efficient adsorptions of ethylene by the present adsorbents are ascribed to coordination of ethylene to the aluminium copper(I) chloride, which is formed from copper(I) chloride and aluminium chloride and is highly dispersed in the polystyrene resin.[5] The aluminium copper(I) chloride forms molecular complexes with carbon monoxide[5] and with various aromatic compounds.[6,7] The adsorbing capacity of the adsorbent, prepared from copper(I) chloride and the polystyrene resin in the absence of aluminium chloride, is minimal: the molar ratio of adsorbed ethylene to the charged copper(I) chloride is only 0.03.

Rather low price of copper(I) chloride, in comparison with the price of silver chloride used for the preparation of the polystyrene resin-supported aluminium silver chloride as selective ethylene adsorbent,[3] is an advantage of the present adsorbents from the viewpoints of practical applications.

In conclusion, solid adsorbents for ethylene are prepared from copper(I) chloride, aluminium chloride, and a macroreticular type polystyrene resin. The adsorbents are applicable to selective separation of ethylene from gas mixtures containing ethylene together with nitrogen, hydrogen, methane, and carbon monoxide.

References

1) "Encyclopedia of Chemical Technology," 1st ed, ed by R. E. Kirk and D. F. Othmer. The Interscience Encyclopedia Inc., New York (1950), Vol. 5, p. 894.

2) H. Hirai, S. Hara, and M. Komiyama, *Chem. Lett.*, **1986**, 257.

3) H. Hirai, S. Hara, and M. Komiyama, *Angew. Makromol. Chem.*, **130**, 207 (1985).

4) "Materials, Equipment, and Systems for Chromatography, Electrophoresis, Immunochemistry, and HPLC," Catalog G, Bio-Rad Laboratories Ltd., (1981), p. 28.

5) H. Hirai, S. Hara, and M. Komiyama, *Bull. Chem. Soc. Jpn.*, **59**, 1051 (1986).

6) R. W. Turner and E. L. Amma, *J. Am. Chem. Soc.*, **88**, 1877 (1966).

7) H. Hirai, M. Nakamura, and M. Komiyama, *Bull. Chem. Soc. Jpn.*, **56**, 2519 (1983).

High Stereoselectivity of Tris[4-(*l*-menthyloxy)-1-(*p*-tolyl)-1,3-butandionato]lanthanoid(III)[1)]

Hisashi Ōkawa,* Michio Nakamura, Yūko Shuin, and Sigeo Kida†
Department of Chemistry, Faculty of Science, Kyushu University,
33, Hakozaki, Higashi-ku, Fukuoka 812
(Received May 30, 1986)

Synopsis. Tris[4-(*l*-menthyloxy)-1-(*p*-tolyl)-1,3-butanedionato]lanthanoid(III), [Ln(*l*-moba-Me)$_3$](Ln=La, Pr, Nd, Eu, Gd, Dy, Ho, Er, Tm), showed a high stereoselectivity effected by intramolecular noncovalent interactions, giving rise to the cis-Δ form.

We have shown that interligand noncovalent interactions operate within a complex molecule and cause a high stereoselectivity of metal complexes to give rise to one of the possible stereoisomers.[2)] In the case of tris[4-(*l*-menthyloxy)-1-phenyl-1,3-butanedionato]metal(III) [M(*l*-moba)$_3$] (M=Co, Cr, Mn, Ln-(lanthanoid ions)) the cis-Δ form is predominantly formed.[3,4)] Further, it was found that tris[4-(*l*-menthyloxy)-1-(*p*-tolyl)-1,3-butanedionato]metal(III) [M(*l*-moba-Me)$_3$] (M=Co, Cr, Mn) showed a higher stereoselectivity compared with [M(*l*-moba)$_3$].[5)] The configurational analysis for [Co(*l*-moba-Me)$_3$] by means of high resolution NMR spectroscopy has demonstrated that this complex is in pure cis-Δ form.[6)] For our ultimate object to develope new stereoselective reactions by use of sterically-controlled lanthanoid complexes, it is desired to prepare new complexes of higher stereoselectivity. This paper deals with the synthesis and stereoselectivity of lanthanoid complexes with H(*l*-moba-Me).

Experimental

Preparations. H(*l*-moba-Me) was prepared by the method described previously.[5)]

[Ln(*l*-moba-Me)$_3$]. H(*l*-moba-Me) (1×10^{-3} mole) and NaOH (1×10^{-3} mole) in ethanol (30 cm^3) were stirred for 30 min. To the resulted gelatinous solution was added lanthanoid(III) chloride (3.3×10^{-4} mole), and the mixture was stirred for 3 h. The reaction mixture was filtered, and the solvent was evaporated to dryness. The oily substance thus obtained was crystallized from ethanol.

Measurements. Electronic and circular dichroism spectra were recorded in benzene on a Shimadzu UV-215 Spectrophotometer and a JASCO J-500 Spectropolarimeter, respectively. Molecular weights were determined with a Hitachi Perkin-Elmer 115 Apparatus in benzene. The elemental analyses were obtained at the Elemental Analysis Service Center, Kyushu University.

Results and Discussion

The elemental analyses for the complexes (Table 1) suggest that all the complexes obtained can be described by the general formula [Ln(*l*-moba-Me)$_3$]. The molecular weight (1150) of [Eu(*l*-moba-Me)$_3$] determined at the 0.13 wt% concentration in benzene

† Present address: Coordination Chemistry Laboratories, Institute for Molecular Science, Okazaki National Research Institutes, Myodaiji, Okazaki 444.

Table 1. Elemental Analyses of Complexes

	Found(%)		Calcd(%)	
	C	H	C	H
[Pr(*l*-moba-Me)$_3$]	66.54	7.71	67.01	7.77
[Nd(*l*-moba-Me)$_3$]	66.97	7.87	66.81	7.74
[Eu(*l*-moba-Me)$_3$]	66.48	7.77	66.36	7.69
[Gd(*l*-moba-Me)$_3$]	65.80	7.70	66.05	7.65
[Dy(*l*-moba-Me)$_3$]	65.82	7.65	65.75	7.62
[Ho(*l*-moba-Me)$_3$]	65.49	7.69	65.61	7.60
[Er(*l*-moba-Me)$_3$]	65.20	7.71	65.48	7.59
[Tm(*l*-moba-Me)$_3$]	65.17	7.63	65.38	7.57

Table 2. Electronic and Circular Dichroism Spectral Data for Complexes

	AB	CD	
	wavelength /nm (ε)	wavelength/nm (Δε×10^3)	
[Pr(*l*-moba-Me)$_3$]	444 (5.81)	446 (−6.46)	
	448 (6.38)	447 (−4.87)	
	472 (5.18)	472 (−4.87)	
	486 (2.28)	489 (−3.56)	
	580 (0.87)	589 (−1.32)	
	594 (1.52)		
[Nd(*l*-moba-Me)$_3$]	512 (3.19)		
	528 (7.61)	525 (−2.73)	
	572 (27.3)	571 (−5.46)	
	582 (42.9)	577 (−7.59)	587 (+5.82)
		587 (−8.50)	
	680 (0.44)		
[Eu(*l*-moba-Me)$_3$]	463 (3.20)		
	433 (0.40)	438 (−2.30)	
[Dy(*l*-moba-Me)$_3$]	452 (0.77)	449 (+4.10)	452 (+3.28)
		455 (−5.17)	
[Ho(*l*-moba-Me)$_3$]	451 (89.5)	450 (+35.1)	
	460 (28.5)	458 (+12.0)	464 (−10.1)
	468 (8.14)	467 (+5.29)	
	473 (6.78)	470 (−6.74)	
	484 (7.46)		
	537 (20.3)	533 (+1.69)	538 (−2.41)
[Er(*l*-moba-Me)$_3$]	488 (2.14)	485 (−1.07)	
	520 (33.0)	518 (+10.1)	
	523 (25.7)	522 (+8.26)	528 (+0.93)
	542 (0.69)	542 (+0.93)	
[Tm(*l*-moba-Me)$_3$]	685 (2.26)	683 (−1.93)	
	662 (0.50)	660 (−0.43)	

ε: Extinction coefficient given in the unit dm^3 mole^{-1} cm^{-1}

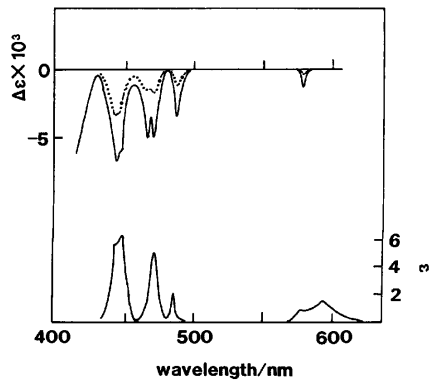

Fig. 1. Difference absorption and circular dichroism spectra of [Pr(*l*-moba-Me)$_3$] (——) and [Pr(*l*-moba)$_3$] (……). The absorption spectrum of [Pr(*l*-moba)$_3$] is essentially the same as that of [Pr(*l*-moba-Me)$_3$].

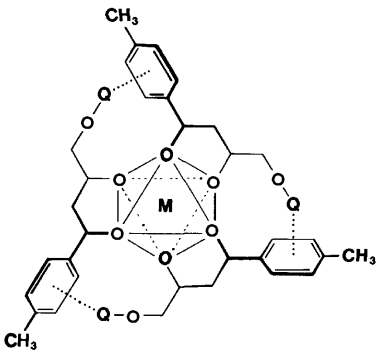

Fig. 2. Schematical representation of interligand interaction in [M(*l*-moba-Me)$_3$].

well agrees with the value (1140.4) for this composition, whereas the molecular weight (1260) at the 0.87 wt% is slightly larger. It is likely that [Ln(*l*-moba-Me)$_3$] dimerizes at a higher concentration, as demonstrated for the complexes with H(*l*-moba)[4] and other lanthanoid complexes with 1,3-diketones.[7] However, such a tendency to dimerize is much low compared with the *l*-moba complexes[4] as judged from the molecular weight measurements, and [Ln(*l*-moba-Me)$_3$] may be assumed to be practically monomeric in the concentration range ($\approx 10^{-2}$ M (1 mol dm^{-3})) for the electronic and circular dichroism spectral measurements.

In Table 2 are given spectral and circular dichroism spectral data in benzene. Electronic and circular dichroism spectra for [Pr(*l*-moba-Me)$_3$] are shown in Fig. 1 together with the circular dichroism spectrum of [Pr(*l*-moba)$_3$]. The Pr, Nd, Eu, Dy, Ho, Er, and Tm complexes show circular dichroism at the f-f transition bands. The CD intensities are significantly high and comparable to those of the L-amino acidato complexes.[8,9] This fact indicates that the optical activities observed are due to the configurational effect (disymmetry around the metal) but not the vicinal effect from the *l*-menthyl moiety. It is likely that the noncovalent interligand interaction occuring between the *l*-menthyl and *p*-tolyl groups leads to a controlled disposition of the *l*-moba-Me$^-$ molecules about the metal (Fig. 2). The preferred configuration of the complexes is assumed as cis-Δ by analogy with the case of [Co(*l*-moba-Me)$_3$] and [Cr(*l*-moba-Me)$_3$].[5]

As is seen in Fig. 1, the CD bands of f-f transitions of [Pr(*l*-moba-Me)$_3$] are more intense than those of [Pr(*l*-moba)$_3$].[4] The same trend was observed for the Nd, Dy, Eu, Ho, and Tm complexes with *l*-moba and *l*-moba-Me (the comparison can not be made for the Gd and Er complexes because Gd complexes show no f-f band (and thence no CD) below 310 nm[10] and the Er complex of *l*-moba has not been obtained). This trend is the same as that found for the transition metal homologs.[5] Thus, it is revealed that the interligand *l*-menthyl/*p*-tolyl interaction is more effective than the *l*-menthyl/phenyl interaction also for lanthanoid complexes in causing the stereoselectivity of the complexes.

This work was supported by the joint Studies Program (1980—1981) of the Institute for Molecular Science.

References

1) Noncovalent Interactions in Metal Complexes. Part 13. Part 12: H. Ōkawa, M. Nakamura, and S. Kida, *Inorg. Chim. Acta*, **120**, 185 (1986).

2) H. Ōkawa and S. Kida, *Kagaku No Ryoiki*, **37**, 276 (1983).

3) H. Ōkawa, K. Ueda, and S. Kida, *Inorg. Chem.*, **21**, 1594 (1982).

4) M. Nakamura, H. Ōkawa, S. Kida, and S. Misumi, *Bull. Chem. Soc. Jpn.*, **57**, 3147 (1984).

5) M. Nakamura, H. Ōkawa, and S. Kida, *Bull. Chem. Soc. Jpn.*, **58**, 3377 (1985).

6) M. Nakamura, M. Kato, H. Ōkawa, T. Itoh, and S. Kida, submitted to publication.

7) H. G. Brittain, *Coord. Chem. Rev.*, **48**, 243 (1983).

8) S. Misumi, S. Kida, T. Isobe, Y. Nishida, and H. Furuta, *Bull. Chem. Soc. Jpn.*, **42**, 3433 (1969).

9) S. Misumi, S. Kida, and T. Isobe, *Spectrochim. Acta*, **24A**, 271 (1966).

10) G. H. Dieke, "Spectra and Energy Levels of Rare Earth Ions in Crystals," Intersci., New York (1968), p. 249.

Molecular Structure of a Reductive Dimer of Pulegone

Mitsuko KIKUCHI* and Zenei TAIRA†
Department of Industrial Chemistry, College of Engineering, Nihon University, Koriyama, Fukushima 963-11
†Department of Pharmacology, Tokushima Bunri University, Tokushima 770
(Received March 24, 1986)

Synopsis. The molecular structure of "bishydropulegone," a reductive dimer of pulegone, was determined as (1*R*,3′a*R*,4*R*,6′*R*,7′a*S*)-7-′a-hydroxy-2′,2′,3′,3′,4,6′-hexamethylspiro[cyclohexane-1,1′-indan]-2-one by X-ray crystallographic analysis.

After "bishydropulegol" $C_{20}H_{36}O_2$ had been isolated by Pascual et al. as one of the dimeric products of the reduction of (*R*)-(+)-pulegone with sodium,[1] a systematic investigation of this reduction was carried out by the same group.[2-15] They isolated five hydroxy ketones and the diols as the reductive dimer and elucidated their structures by chemical degradation and spectral studies. Furthermore, many derivatives of these products were also synthesized for the structural elucidation of these dimers. Among their work, the most prominent results obtained were the classification of the five ketols into two groups acording to the orientation of the carbonyl group in the ring B[9] and a determination of the absolute configurations of the spiro-carbons of two hydroxy ketones ("bishydropulegone" and "isobishydropulegone") and the relative stereochemistries of the hydroxyl and carbonyl groups of these and other hydroxy ketones.[14] However, the stereochemistry at the C05 and C09 positions of these products has not yet been elucidated.

In this paper, we describe the molecular structure of bishydropulegone (Fig. 1) determined by an X-ray crystallographic analysis.

Experimental

Melting points were determined with a Mitamura melting point apparatus (No. 8209) and are uncorrected. IR spectra were recorded on a JEOL JIR 100 FT-IR spectrophotometer in CCl_4. ^1H NMR spectra were recorded on a JEOL FX-90Q (90 MHz) instrument in $CDCl_3$, unless otherwise stated. Coupling constants (*J*) are given in hertz.

(*R*)-(+)-pulegone was supplied by Takasago Perfumery Industrial Co., Ltd.: Bp 94—95 °C/10 mmHg (1 mmHg= 133.322 Pa); n_D^{20} 1.4875; d_4^{20} 0.9351; $[\alpha]_D^{20}$ +20.2° (*c* 1.01, $CHCl_3$).

Bishydropulegone was prepared through the oxidation of bishydropulegol, which was obtained by a modified Pascual procedure as follows.[1] Small pieces of Sodium (ca. 9 g) were gradually added to a solution of (*R*)-(+)-pulegone (10.4 g, 68.4 m mol) in ether (20 ml) in an ice bath. The whole mixture was stirred at room temperature for 24 h. Then, unreacted sodium pieces were removed and wet ether (50 ml) was added to the reaction mixture. Water (each 5 ml) was added three times over 3 d. The product was extracted with ether and the extract was washed with water and saturated brine and then dried (anhydrous sodium sulfate). The removal of the solvent left an oil (10.3 g), which was distilled to give a fraction (6.35 g, 61.5%) boiling at 90—144 °C (bath temperature/15—12 mmHg) and a residual oil (3.97 g, 38.5%). The residue was passed through a sillica-gel column by eluting with hexane-AcOEt (5:1) to give a soft mass (2.34 g). The mass was further purified using a sillica-gel column chromatography by eluting with hexane-AcOEt (10:1) to give bishydropulegol (1.20 g, 51.2% of the residue) as an amorphous soft mass. To a stirred solution of bishydropulegol (230 mg, 0.75 m mol) in acetic acid (1.6 ml) was added dropwise a 10% CrO_3-CH_3COOH solution (ca. 16 ml). After being stirred at room temperature for 24 h, the mixture was diluted with water (3.3 ml) and extracted with benzene. The extract was washed with water and saturated brine and dried (anhydrous sodium sulfate). The removal of the solvent afforded an oil (214 mg), which was purified by sillica-gel column chromatography using hexane-AcOEt (10:1) as the solvent to give bishydropulegone (124 mg, 54.3%) as crystals, mp 100 °C, recrystallized from petroleum ether-EtOH (10:1); $[\alpha]_D^{19}$ +72.1° (*c* 1.06, $CHCl_3$); IR (CCl_4) 3474 (intramolecularly hydrogen-bonded OH), 1678 (C=O) cm^{-1}; ^1H NMR ($CDCl_3$) δ=0.86 (3H, d, *J*=6.4 Hz, Me), 1.01 (3H, d, *J*=6.4 Hz, Me), 0.87 (3H, s, Me), 0.98 (3H, s, Me), 1.09 (3H, s, Me), 1.25 (3H, s, Me), 4.97 (1H, d, *J*=2.1 Hz, OH). Anal. Calcd for $C_{20}H_{34}O_2$: C, 78.37; H, 11.18%. Found: C, 78.64; H, 11.57%.

X-Ray diffraction analysis of bishydropulegone. For the X-ray experiments, a single crystal (0.4×0.4×0.4 mm) was mounted on a Rigaku automatic four-circle diffractometer AFC-6B using graphite monoclomated Mo $K\alpha$ radiation (λ=0.71069 Å). Crystal data: Orthorhombic; space group $P2_12_12_1$; *a*=11.765(3), *b*=14.392(4), *c*=10.833(3) Å; *U*=1834.3 Å^3; D_x=1.110 g cm^{-3} for *Z*=4; μ(Mo $K\alpha$)=0.745 cm^{-1}.

Intensity data with a range $2°<2\theta<50°$ were collected by the ω scan method at a rate of 4° min^{-1}. The data were corrected for Lorentz, polarization factors and background effects, but not corrected for the absorption. The independent reflections (1729) were observed under the criterion $|F|>6\sigma_F$ and were used in subsequent calculations.

The crystal structure was solved by a direct method using the program MULTAN.[16] Refinements of the structure were performed by block-diagonal least-squares calculations with anisotropic thermal parameters for non-hydrogen atoms. The hydrogen atoms were located on a difference map and included only structure-factor calculations which assumed the isotropic thermal parameters of the binding non-hydrogen atoms. The final refinement yielded an *R* value of 0.089 and an R_w of 0.103 (used unit weight).

The atomic scattering factors used were those from the literature.[17]

The absolute configuration was elucidated in the relation with (*R*)-(+)-pulegone[18] used as the reactant.

All crystallographic calculations were performed on the PANAFACOM U-1400 computer in Tokushima Bunri University (RASA and X-STANP program package) and at the computer center in Tokushima University (MULTAN program package).

Results and Discussion

The molecule is depicted in Fig. 2 (drawn by ORTEP).[19] The absolute configuration of the spiro-carbon atom of bishydropulegone was unequivocally established as *R*.[14] The configuration of the 4-methyl

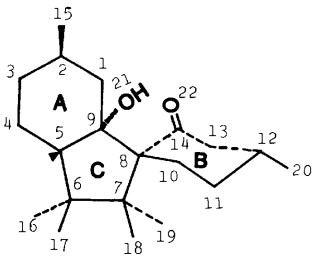

Fig. 1.

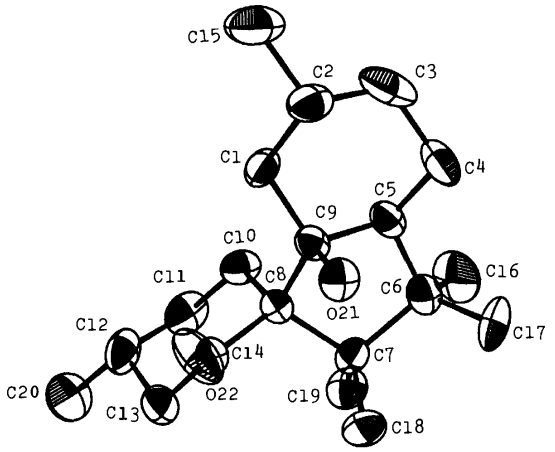

Fig. 2. ORTEP drawing of the molecular structure of bishydropulegone. Hydrogen atoms are omitted for clarity.

group relative to C06 and C07 is syn; also, the carbonyl group is syn with respect to the hydroxyl group. There is an intramolecular hydrogen bond between the hydroxyl group 021-H and the ketone 022 as shown by the short contact 2.635(8) Å[021···022]. This was also confirmed by measurements of the IR spectra with an FT-IR spectrometer in highly diluted solutions (2.5×10^{-3} mol dm^{-3}) of bishydropulegone (3474 and 1678 cm^{-1}).

The above results were completely the same as the conclusions obtained by Pascual et al.[14] As a new result, we showed that the ring fusion in perhydroindene is trans.

As a characteristic structural feature of bishydropulegone, the bond distances C06 and C07 [1.629 Å (11)] and C08 and C07 [1.615 Å (10)] were unusually extended. This may be due to four bulky tertiary methyl groups at C06 and C07.

In conclusion, the whole stereochemistry of bishydropulegone was determined to be (1*R*,3′a*R*,4*R*,-6′*R*,7′a*S*)-7′a-hydroxy-2′,2′,3′,3′,4,6′-hexamethylspiro[cyclohexane-1,1′-indan]-2-one.

We thank professor Akira Yoshikoshi of Tohoku University, and Professor Yoshinori Asakawa of Tokushima Bunri University for their helpful discussions. We also thank Dr. Shinji Onodera of Tohoku University for FT-IR measurements and Takasago Perfumery industrial Co., Ltd. for kindly supplying the (*R*)-(+)-pulegone.

The list of the structure factor, table of atomic parameters, bond distances, bond angles and torsion angles data has been deposited as Document No. 8649 at the Office of the Editor of Bull. Chem. Soc. Jpn.

References

1) F. Camps, A. Esquefa, H. Ferrer, F. Magrans, J. Pascual, and J. Sust, *An. R. Soc. Esp. Fis. Quim., Ser B*, **57**, 791 (1961).
2) J. Bartual, J. Ferrer, J. Pascual, and M. Vendrell, *An. R. Soc. Esp. Fis. Quim., Ser B*, **62**, 829 (1966).
3) J. Bartual, F. Camps, J. Pares, and J. Pascual, *An. Quim.*, **1968**, 64, 157.
4) A. Perales, S. Maetinez-Carrera, and S. Garcia-Blanco, *Acta Crystallogr., Sect. B*, **25**, 1817 (1969).
5) J. Bartual and J. Pascual, *An. Quim.*, **1970**, 66, 693.
6) F. Cistero and Jose M, *Rev. Real Acad. Cienc. Exactas, Fis, Natur. Madrid* **1972**, 66, 455.
7) J. Bartual, J. M. Font, E. Forne, J. Pascual, and J. Roque, *An. Quim.*, **1972**, 68, 483.
8) J. M. Font-Cistero and J. Pascual, *An. Quim.*, **1974**, 70, 90.
9) J. M. Font-Cistero, E. Forne, and J. Pascual, *An. Quim.*, **1974**, 70, 1004.
10) J. M. Franco, S. Martinez-Carrera, and S. Garcia-Blanco, *Acta Crystallogr., Sect. B*, **30**, 415 (1974).
11) E. F. Felip, *Rev. R. Acad. Cienc. Exactas, Fis. Natur Madrid*, **1974**, 68, 209.
12) P. Camps and J. Pascual, *An. Quim.*, **1976**, 72, 1032.
13) V. Pascual and D. Jose, *Mem. R. Acad. Clenc. Artes Barcelona*, **1977**, 43, 385.
14) E. Forne and J. Pascual, *J. Chem. Soc., Perkin Trans. 1*, **1978**, 288.
15) F. Munoz-Madrid and J. Pascual, *An. Quim.*, **1978**, 74, 1270.
16) G. Germain, P. Main, and M. M. Woolfson, *Acta Crystallogr., Sect. A*, **1971**, 27, 368.
17) "International Tables for X-ray Crystallography" Kynoch Press, Birmingham, England (1974), Vol. IV.
18) A. J. Birch, *Ann. Reports on Progr. Chem.*, **47**, 191 (1950).
19) C. K. Johnson, ORTEP. Report ORNL-3794. Oak Ridge National Laboratory, Tennessee.

Interaction of Iron(III) Chloride with D-Fructose in an Acidic Solution

Koji ARAKI* and Shinsaku SHIRAISHI*
Institute of Industrial Science, The University of Tokyo,
7-22-1 Roppongi, Minato-ku, Tokyo 106
(Received June 13, 1986)

Synopsis. Complex formation between Fe(III) and D-fructose in an acidic solution was studied by electronic and CD spectroscopy, and the role of the complex in the photochemically-induced oxidation of D-fructose by Fe(III) was discussed.

An Fe(III)–monosaccharide complex was suggested to play an essential role in the photochemically-induced oxidation of monosaccharides by $FeCl_3$.[1-3] The reaction was assumed to proceed via an Fe(III)–D-fructose complex, and irradiation of near-UV light caused oxidative cleavages of C–C bonds of monosaccharides with high specificity.[1] Though interactions between monosaccharides and a variety of metal ions have been the subject of intense studies,[4-6] only a little has been known as to the interaction of Fe(III) with monosaccharides in solutions.[6,7] Because of the physiological importance of the Fe(III)–monosaccharide systems,[3,8] we report here the interaction of Fe(III) with D-fructose in an acidic solution and clarify further the role of the Fe(III)–D-fructose complex in the photooxidation of D-fructose.

Experimental

Photoirradiation was carried out according to the method described previously.[1,3] Electronic and CD spectra (path length 10 mm) were recorded with JASCO UVIDEC-505 and J-20 spectrophotometers, respectively.

Results and Discussion

An aqua complex of Fe(III) shows a strong ligand-to-metal charge-transfer (LMCT) band in near-UV region.[9] Upon addition of D-fructose to an acidic $FeCl_3$ solution, the initial brown solution becomes reddish with concomitant decrease in pH. Difference spectra of the $FeCl_3$ solutions before and after addition of D-fructose showed appearance of the absorption band at 300—350 nm along with the band at 280 nm due to an acyclic form of D-fructose (Fig. 1).[10] The absorption at 300—350 nm in the difference spectra increased as the D-fructose concentration increased, though D-fructose alone had no absorption in this range. Therefore, this absorption band is ascribed to the Fe(III)–D-fructose complex. CD spectra of an $FeCl_3$–D-fructose solution further supported this assignment (Fig. 2). In addition to a strong positive absorption at 280 nm presumably due to the acyclic form of D-fructose, the CD spectra showed a weak negative absorption at 320 nm. The presence of the CD absorption at 320 nm indicated the contirbution of D-fructose to this absorption band, confirming the formation of the Fe(III)–D-fructose complex. Thus, the band observed at 300—350 nm in the difference spectra is ascribed to the LMCT band of the Fe(III)–D-fructose complex. Upon photoirradiation, the CD absorption at 320 nm disappeared (Fig. 2b). As the highest quantum yield for the photooxidation of D-fructose was observed at around 330 nm,[1] the result presented here confirmed that the reaction proceeded by the excitation of the LMCT band of the Fe(III)–D-fructose complex.

Apparent stability constants (K_{app}) of the Fe(III)–D-fructose complex in aqueous acidic solutions (pH 1—3) at 20 °C were determined from the electronic (380 nm) and CD (337 nm) spectra by the Benesi-Hildebrand and Rose-Drago methods.[11,12] The plots obtained by assuming a formation of the 1:1 complexes (Eq. 1) in the presence of a large excess amount of D-fructose gave satisfactory results. Typical Benesi-Hildebrand plots are shown in Fig. 3, and

$$\text{Fe(III)} + \text{D-fructose} \overset{K_{app}}{\rightleftharpoons} \text{complex};$$
$$K_{app} = \frac{[\text{complex}]}{[\text{Fe(III)}][\text{D-fructose}]} \quad (1)$$

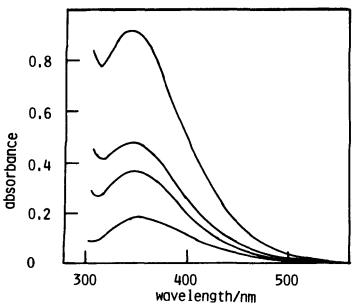

Fig. 1. Difference spectra of of $FeCl_3$(1×10^{-3} mol dm^{-3} solutions before and after addition of D-fructose; D-fructose concentrations are 0.4, 0.8, 1, and 2 mol dm^{-3}, respectively.

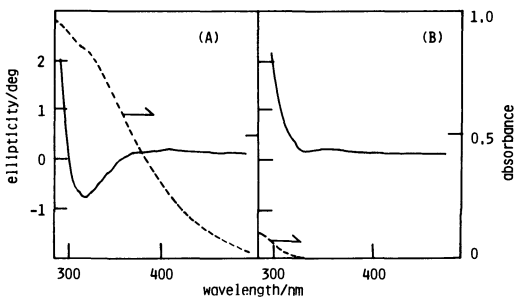

Fig. 2. CD(——) and electronic (----) sectra of $FeCl_3$ (1×10^{-3} mol dm^{-3})–D-fructose(0.4 mol dm^{-3}) solution (A) before and (B) after irradiation of Pyrex-filtered light at 20 °C.

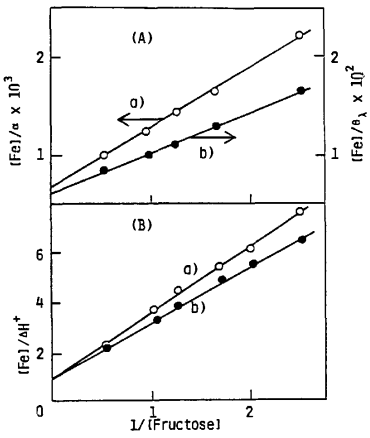

Fig. 3. Benesi-Hildebrand plots ([Fe]/absorbance vs. 1/[Fructose], where [Fructose]≫[Fe]) for the complex formation between Fe(III) and D-fructose at 20 °C. (A) Applied for the (○) electronic (380 nm) and (●) CD (337 nm) spectra of the $FeCl_3$(5×10^{-4} mol dm^{-3})-D-fructose solutions at pH 2.82; (B) Applied for the amounts of H^+ liberated upon addition of D-fructose to (○) $FeCl_3$ and (●)$Fe(NO_3)_3$ solutions (4×10^{-3} mol dm^{-3}) at pH 2.50.

the results are summarized in Table 1. When pH of a solution was below 2, the absorption bands due to the complex was too small to determine the K_{app} values, and a rough estimation was made only from the electronic spectra. The stability constants could also be estimated from the amounts of H^+ liberated ($\Delta[H^+]$) on addition of D-fructose to $FeCl_3$ solutions. The $\Delta[H^+]$ values were estimated from pH decreases of freshly-prepared $FeCl_3$ solutions on addition of a large excess amount of D-fructose. If we assume that n H^+ are liberated upon formation of the 1 : 1 complex, the concentration of the complex is expressed as $\Delta[H^+]/n$ and the Benesi-Hildebrand plot can be applied by replacing absorbance and molar extinction coefficient with $\Delta[H^+]$ and n, respectively.[11] The plot gave a linear line yielding $1/(n\,K_{app})$ as a slope and $1/n$ as an intercept (Fig. 3), and the K_{app} values obtained here were in good agreement with those obtained from the electronic and CD spectra (Table 1). Therefore, formation of the complex can be written as follows (Eq. 2), and log K_s is estimated to be −2.8.

$$\text{Fe(III)} + \text{D-fructose} \overset{K_s}{\rightleftharpoons} \text{complex} + H^+ \qquad (2)$$

$$K_s = \frac{[\text{complex}][H^+]}{[\text{Fe(III)}][\text{D-fructose}]}$$

Table 1. Apparent Stability Constants (K_{app}) at 20 °C.

pH	Fe(III) salt	K_{app}
2.82	$FeCl_3$	1.03(UV); 1.04(CD)
2.50	$FeCl_3$	0.4(UV); 0.4(CD); 0.40(pH)
	$Fe(NO_3)_3$	0.37(pH)
1.20	$Fe(NO_3)_3$	0.03(UV)

K_{app} values were estimated from (UV): the electronic spectra (380 nm), (CD): the CD spectra (337 nm), and (pH): the amounts of H^+ liberated.

We previously reported that the quantum yield of the reduction of Fe(III) in the photochemically-induced oxidation of D-fructose (0.5 mol dm^{-3}) by Fe(III) (2×10^{-3} mol dm^{-3}) was 0.061 at 338 nm.[1] Since the action spectrum of the reaction coincided well with the absorption spectrum of the complex,[1] the reaction was assumed only to proceed by the light absorption of the complex but not by that of free Fe(III). Proportion of the light absorbed by the complex was determined from the electronic and difference spectra, and concentration of the complex was estimated from the K_s value obtained here. Thus, the quantum yield for the photoreactivity of the complex was estimated to be 0.3, showing that the excitation of the LMCT band of the complex efficiently induced reduction of Fe(III) with concomitant oxidation of D-fructose.

References

1) K. Araki, M. Sakuma, and S. Shiraishi, *Chem. Lett.*, **1983**, 665; *Bull. Chem. Soc. Jpn.*, **57**, 997 (1984).
2) K. Araki and S. Shiraishi, *Chem. Lett.*, **1984**, 267.
3) K. Araki and S. Shiraishi, *Bull. Chem. Soc. Jpn.*, **59**, 229 (1986).
4) J. Briggs, P. Finch, M. C. Matulewicz, and H. Weigel, *Carbohydr. Res.*, **97**, 181 (1981).
5) H. A. Tajmir-Riahi, *J. Inorg. Biochem.*, **26**, 23 (1986).
6) P. J. Charley, B. Sarkar, C. F. Stitt, and P. Saltman, *Biochem. Biophys. Acta*, **69**, 313 (1963).
7) S. A. Barker, P. J. Somers, and J. Stevenson, *Carbohydr. Res.*, **36**, 331 (1974).
8) J. S. G. Cox, R. E. King, and G. F. Reynolds, *Nature*, **207**, 1202 (1965).
9) F. A. Cotton, G. Wilkinson, "Advanced Inorganic Chemistry," John Wiley & Sons, Inc., New York, N. Y. (1966).
10) L. A. T. Verhaar and J. M. H. Dirkx, *Carbohydr. Res.*, **62**, 197 (1978).
11) H. A. Benesi and J. H. Hildebrand, *J. Am. Chem. Soc.*, **71**, 2703 (1949).
12) N. J. Rose and R. S. Drago, *J. Am. Chem. Soc.*, **81**, 6138 (1959).

Viscosity *B* Coefficients for *N,N'*-Polymethylenebis-(trialkylammonium) Dibromides in Aqueous Solutions

Kunio TAMAKI,* Goro HORII, Takashi CHIDA, Keiko OCHIAI, and Yoshiyuki KADOKURA
Department of Chemistry, Yokohama City University, Kanazawa-ku, Yokohama 236
(Received May 14, 1986)

Synopsis. The viscosity *B* coefficients for aqueous solutions of *N,N'*-polymethylenebis(trialkylammonium) dibromides $[(C_mH_{2m+1})_3N(CH_2)_nN(C_mH_{2m+1})_3]Br_2$ (m=2—4, n=3—6, 8, 10, and 12) and, for comparison, of $C_nH_{2n+1}N(C_mH_{2m+1})_3Br$ (m=2, n=1—6; m=3,4, n=2—6) have been determined at 25 and 35 °C. The effect of structural changes in the solvent water upon the dissolution of these homologous electrolytes is discussed.

The physicochemical properties of aqueous solutions of tetraalkylammonium salts have been studied by many investigators in terms of the structural changes in liquid water caused by these hydrophobic solutes.[1] However, the solubilities of tetrapentylammonium salts and the higher homologs of this series are too small for precise measurements. On the other hand, bis(quaternary ammonium) salts are highly soluble in water, and it seems that bis(quaternary ammonium) salts can be expected to exhibit the characteristics of large hydrophobic solutes in water. In order to elucidate the balance of the ionic hydration and the hydrophobic hydration of *N,N'*-polymethylenebis(trialkylammonium) dibromides in water, we have extended the measurements of the viscosity *B* coefficients for these electrolytes in water. In a previous paper,[2] the results of *N,N'*-polymethylenebis-(trimethylammonium)dibromides (to be abbreviated as MeC_nMe) and, for comparison, of alkyltrimethylammonium bromides (to be abbreviated as C_nMe) were reported. This paper will describe the experimental results for three homologous series of electrolytes; *N,N'*-polymethylenebis(triethylammonium) dibromides (to be abbreviated as EtC_nEt), *N,N'*-polymethylenebis(tripropylammonium) dibromides (to be abbreviated as PrC_nPr) and *N,N'*-polymethylenebis-(tributylammonium) dibromides (to be abbreviated as BuC_nBu). For comparison, the viscosity *B* coefficients of the corresponding alkyl compounds with a single terminal quaternary ammonium group, alkyltriethylammonium bromides (to be abbreviated as C_nEt), alkyltripropylammonium bromides (to be abbreviated as C_nPr) and alkyltributylammonium bromides (to be abbreviated as C_nBu), have also been studied.

Experimental

Materials. EtC_nEt, PrC_nPr, and BuC_nBu were prepared by refluxing the α,ω-dibromoalkanes with an excess of the respective trialkylamines in ethanol or acetonitrile.[3,4,5] After the solvent had been removed, the salts were purified several times by recrystallization from suitable solvents: acetone–ethanol solutions for EtC_nEt and ethyl acetate–ethanol solutions for PrC_nPr and BuC_nBu. $PrC_{12}Pr$, BuC_8Bu, $BuC_{10}Bu$, and $BuC_{12}Bu$ were found to be fairly difficult to obtain as solid samples from reaction mixtures, so they were precipitated from reaction mixtures by means of the repeated extraction of the unreacted or impure materials with dry ethyl acetate at −20 °C. C_nEt (except for C_1Et), C_nPr, and C_nBu were prepared by refluxing the alkyl bromides with an excess of the respective trialkylamines in ethanol. C_1Et was prepared by the reaction of *N,N*-diethylmethylamine with ethyl bromide in ethanol. The salts were recrystallized several times from suitable solvents: ethyl acetate–ethanol solutions for C_nEt, ethyl acetate–acetone solutions for C_nPr and C_2Bu, and ethyl acetate for C_3Bu, and C_4Bu. C_5Bu and C_6Bu were found to be fairly difficult to obtain as solid samples from reaction mixtures. C_5Bu and C_6Bu were precipitated by the repeated extraction of the unreacted or impure materials with butyl acetate and isopentyl acetate respectively. All the salts were dried in vacuo at room temperature for several days and then analyzed for bromide ion by means of argentrometric titration. The salts were found to have a purity greater than 99.5%. Water was triply distilled.

Viscosity Measurements. The viscosities were measured at 25 and 35 °C using an automatic viscometer of the Shibayama Scientific Co., Ltd. The densities were measured using a vibrating-tube densimeter, twin-type SS-D-200 of the Shibayama Scientific Co., Ltd. The detailed procedure was described in a previous paper.[6] The electric conductivities were measured with a Yokogawa audio-frequency bridge using a frequency of 1000 Hz.

Results and Discussion

The Viscosity *B* Coefficients of Electrolytes. Jones and Dole[7] showed that the viscosity of dilute electrolyte solutions, η, can be related to the following equation:

$$\eta = \eta_0(1 + Ac^{1/2} + Bc), \quad (1)$$

where η_0 is the viscosity of the solvent, c is the molar concentration, and A and B are the characteristic constants of the solute. In a previous work[2] for MeC_nMe and C_nMe, it was found that the viscosities can be represented by Eq. 1 for concentrations up to about 0.1 mol dm^{-3}. However, successive studies of organic electrolytes with large values of viscosity *B* coefficients such as are used in this work revealed that the viscosities even in fairly dilute solutions cannot be described by Eq. 1; therefore the extended Jones-Dole equation with an extra term in c^2 was applied:

$$\eta = \eta_0(1 + Ac^{1/2} + Bc + Dc^2), \quad (2)$$

where D is a constant, whose significance is not completely understood. The A coefficient was interpreted theoretically by Falkenhagen and Vernon[8]; it can be calculated using the data of the limiting equivalent conductivities of the salt, the cation, and the anion. The electric conductivities of the aqueous solutions for bis(quaternary ammonium) salts as used in this work were interpreted in terms of 2-1

electrolytes by Fuoss and Chu[9] and Evans et al.[3,10] The A coefficient is fairly small numerically, and the contribution of the $Ac^{1/2}$ term to the viscosity is relatively small, in the solutions of such organic electrolytes with large B coefficients as are used in this work. The B coefficients are related to the ion-solvent interactions and to the size and shape of the ions, and are highly specific for the electrolytes and the temperature.

Equation 2 may be converted to:

$$(\eta/\eta_0 - 1 - Ac^{1/2})/c = B + Dc. \quad (3)$$

When the left-hand side of Eq. 3 is plotted against c, the viscosity B coefficient is obtained as the intercept

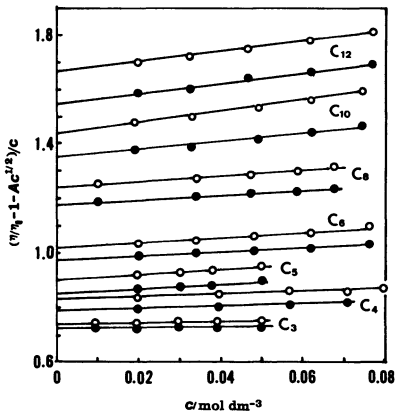

Fig. 1. Plots of $(\eta/\eta_0 - 1 - Ac^{1/2})/c$ against c for EtC_nEt. ○: 25 °C, ●: 35 °C.

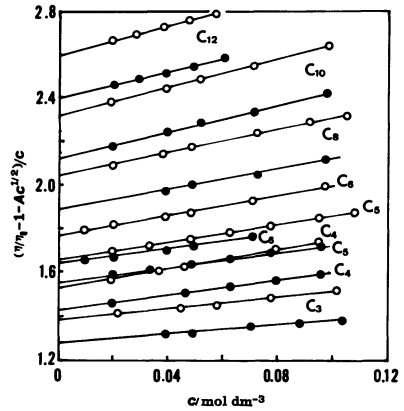

Fig. 2. Plots of $(\eta/\eta_0 - 1 - Ac^{1/2})/c$ against c for PrC_nPr. ○: 25 °C, ●: 35 °C.

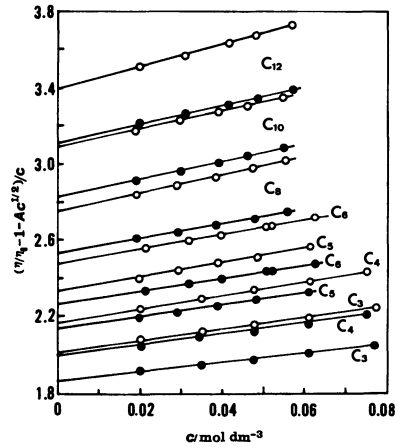

Fig. 3. Plots of $(\eta/\eta_0 - 1 - Ac^{1/2})/c$ against c for BuC_nBu. ○: 25 °C, ●: 35 °C.

Table 1. The Values of A and B

n	A / dm$^{3/2}$ mol$^{-1/2}$		B / dm^3 mol^{-1}	
T/°C	25	35	25	35
	EtC_nEt			
3	0.0162	0.0167	0.740	0.728
4	0.0165	0.0170	0.826	0.794
5	0.0168	0.0173	0.905	0.857
6	0.0171	0.0176	1.018	0.968
8	0.0174	0.0178	1.242	1.168
10	0.0176	0.0180	1.440	1.348
12	0.0178	0.0183	1.660	1.542
	PrC_nPr			
3	0.0177	0.0179	1.347	1.273
4	0.0181	0.0186	1.530	1.433
5	0.0187	0.0191	1.652	1.541
6	0.0190	0.0193	1.770	1.636
8	0.0194	0.0197	2.045	1.890
10	0.0196	0.0199	2.313	2.120
12	0.0198	0.0200	2.602	2.398
	BuC_nBu			
3	0.0183	0.0191	2.015	1.860
4	0.0188	0.0195	2.162	1.998
5	0.0192	0.0199	2.330	2.142
6	0.0197	0.0203	2.472	2.272
8	0.0205	0.0212	2.770	2.538
10	0.0208	0.0217	3.090	2.827
12	0.0212	0.0221	3.410	3.107
	C_nEt			
1	0.0070	0.0072	0.275	0.261
2	0.0072	0.0073	0.337	0.316
			0.333[12]	0.322[12]
			0.339[11]	
3	0.0074	0.0075	0.426	0.393
4	0.0075	0.0077	0.518	0.472
5	0.0077	0.0078	0.608	0.553
6	0.0079	0.0080	0.698	0.622
	C_nPr			
2	0.0079	0.0080	0.643	0.594
3	0.0082	0.0084	0.745	0.675
			0.760[11]	
4	0.0085	0.0086	0.837	0.761
5	0.0087	0.0089	0.938	0.845
6	0.0088	0.0090	1.055	0.938
	C_nBu			
2	0.0083	0.0085	0.955	0.864
3	0.0086	0.0088	1.066	0.971
4	0.0088	0.0090	1.162	1.057
			1.148[11]	
5	0.0090	0.0091	1.280	1.148
6	0.0092	0.0092	1.378	1.240

of a straight line. For example, Figs. 1—3 show the results of plotting Eq. 3 for EtC_nEt, PrC_nPr, and BuC_nBu respectively. The values of A and B for the electrolytes are summarized in Table 1. The B values for C_2Et, C_3Pr, and C_4Bu are in reasonable agreement with the literature values.[11,12] The B values for six homologous series of compounds increase approximately linearly with the number of carbon atoms in the polymethylene or alkyl group, n, respectively.

The Solute-Solvent Interaction. The temperature dependence of the B values is a factor of the solute-solvent interaction; the B values increase with the temperature for a solvent-structure-breaking salt, and decrease with the temperature for a solvent-structure-making solute.[13] For all the organic electrolytes used in this work, it may be seen in Table 1 that the B values decrease as the temperature is raised from 25 to 35 °C; therefore they may be considered to behave as structure-making salts in water.

Figure 4 shows the changes in the viscosity B coefficients which occur as the temperature is raised from 25 to 35 °C, ΔB, as a function of n for all the homologous series used in this work. The results for the MeC_nMe and C_nMe series reported in a previous paper[2] are also included in Fig. 4. It is found that the ΔB values generally decrease with n for each homologous series of electrolytes, and that the ΔB values for both bis(quaternary ammonium) compounds and the corresponding terminal mono-(quaternary ammonium) compounds with the same number of n are in these orders: $BuC_nBu<PrC_nPr<EtC_nEt<MeC_nMe$ and $C_nBu<C_nPr<C_nEt<C_nMe$ respectively. If we take one-half the ΔB values for $[(C_mH_{2m+1})_3N(CH_2)_nN(C_mH_{2m+1})_3]Br_2$, the ΔB values for a series of $-(CH_2)_nN(C_mH_{2m+1})_3Br$ can be estimated. The ΔB vs. n relations thus obtained are plotted as dotted lines in Fig. 4. It may be seen that, for the same number of n, the ΔB values for $-(CH_2)_nN(CH_3)_3Br$ are larger than those of ΔB for C_nMe. This fact indicates the hydrophobic character of the polymethylene chain in MeC_nMe is considerably diminished as compared with that of the alkyl chain in C_nMe with the same number of n. Analogous results are still observed by a comparison of the ΔB values for the EtC_nEt and C_nEt series; the ΔB values for $-(CH_2)_nN(C_2H_5)_3Br$ are larger than those of C_nEt. It seems that two terminal $(C_2H_5)_3N^+$- groups situated at opposite ends of a chain may interfere with the interaction of a polymethylene group with water.

On the other hand, it may be seen from Fig. 4 that, for the same number of n, the ΔB values of $-(CH_2)_nN(C_3H_7)_3Br$ and $-(CH_2)_nN(C_4H_9)_3Br$ are nearly the same as those of C_nPr and C_nBu, respectively. In these cases, the hydrophobic hydration of propyl or butyl groups attached to the charge-bearing nitrogen atoms surpass the ionic hydration due to the ionic parts. Therefore, it seems that the hydrophobic characteristics of the polymethylene groups of the PrC_nPr and BuC_nBu series are comparable to those of the alkyl group of the corresponding mono(quaternary ammonium) salts.

The Viscosity *B* Coefficients of Ions. The viscosity

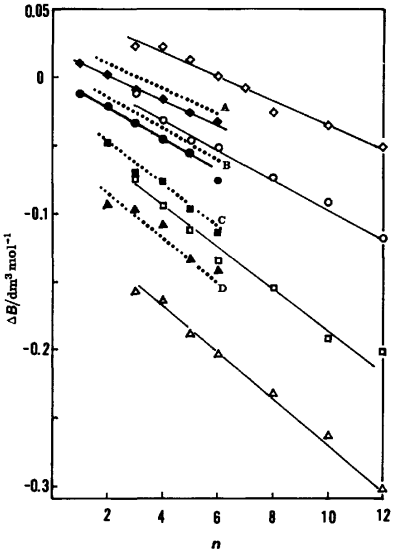

Fig. 4. Plots of ΔB against n.
◇: MeC_nMe, ◆: C_nMe, ○: EtC_nEt, ●: C_nEt, □ PrC_nPr, ■: C_nPr, △: BuC_nBu, ▲: C_nBu.
A: $-(CH_2)_nN(CH_3)_3Br$, B: $-(CH_2)_nN(C_2H_5)_3Br$, C: $-(CH_2)_nN(C_3H_7)_3Br$, D: $-(CH_2)_nN(C_4H_9)_3Br$.

B coefficients of electrolytes are considered to be determined by adding the individual contribution of the solute constituent ions. The ionic B values for the Br^- ion, derived according to the convention of Gurney[14] that the ionic B values for K^+ and Cl^- ions are equal, are -0.40 and -0.26 dm³ mol⁻¹ at 25 and 35 °C respectively.[12] Therefore, the values of ΔB for all the organic ions used in this work become more negative than those of the corresponding salts, and the organic ions may also be classified as structure-making ions.

References

1) W-Y. Wen, "Water and Aqueous Solutions, Structure, Thermodynamics, and Transport Processes," ed by R. A. Horne, Wiley-Interscience, New York (1972), p. 613.
2) K. Tamaki and A. Fujiwara, *Bull. Chem. Soc. Jpn.*, **58**, 3367 (1985).
3) T. L. Broadwater and D. F. Evans, *J. Phys. Chem.*, **73**, 3985 (1969).
4) J. A. Burns and R. E. Verrall, *J. Solution Chem.*, **2**, 489 (1973).
5) H. Nakayama, *Bull. Chem. Soc. Jpn.*, **52**, 52 (1979).
6) K. Tamaki, Y. Ohara, M. Inabe, T. Mori, and F. Numata, *Bull. Chem. Soc. Jpn.*, **56**, 1930 (1983).
7) G. Jones and M. Dole, *J. Am. Chem. Soc.*, **51**, 1950 (1929).
8) H. Falkenhagen and E. L. Vernon, *Z. Physik.*, **33**, 140 (1932).
9) R. M. Fuoss and V. R. H. Chu, *J. Am. Chem. Soc.*, **73**, 949 (1951).
10) J. Thomas and D. F. Evans, *J. Phys. Chem.*, **74**, 3812 (1970).
11) J. E. Desnoyers and G. Perron, *J. Solution Chem.*, **1**, 199 (1972).
12) D. J. P. Out and J. M. Los, *J. Solution Chem.*, **9**, 19 (1980).
13) R. L. Kay, T. Vituccio. C. Zawoyski, and D. F. Evans, *J. Phys. Chem.*, **70**, 2336 (1966).
14) R. W. Gurney, "Ionic Processes in Solution," McGraw-Hill, New York (1953), p. 159.

A Kinetic Study of the Thermal Conversion of 1′,3′,3′-Trimethylspiro-[2*H*-1-benzopyran-2,2′-indoline]-8-carboxylic Acid

Yoshimi Sueishi, Masanobu Ohcho, Shunzo Yamamoto, and Norio Nishimura*
Department of Chemistry, School of Science, Okayama University, Tsushima, Okayama 700
(Received May 26, 1986)

Synopsis. The rate of the thermal conversion of 1′,3′,3′-trimethylspiro[2*H*-1-benzopyran-2,2′-indoline]-8-carboxylic acid (8-COOH-SP) from its spiro form to its merocyanine form has been measured in several solvents at high pressures. Small solvent- and pressure-dependencies of the rate were observed. These results suggest that the electronic structure of the transition state of this reaction is nonpolar and that it is similar to that previously observed for the thermal conversion of so-called 6-nitrospiropyran from its merocyanine form to its spiro form.

It is a matter of interest, when an isomerization is accompanied by a π- or σ-bond fission, what kind of bond fission (homolytic or heterolytic?) is involved. Hitherto, we have investigated the cis-trans thermal isomerizations of azobenzenes,[1-3] acetylindigos,[4] and formazans[5] from such a point of view. The isomerization of the so-called spiropyrans has attracted much attention because of their reversible photochromic and thermochromic behavior. In a previous paper,[6] we have studied the solvent and pressure effects on the rate of the thermal conversion of 1′,3′,3′-trimethyl-6-nitro[2*H*-1-benzopyran-2,2′-indoline](6-NO_2-SP) and suggested that the observed results are more consistent with the mechanism involving the homolytic fission of the C_{spiro}-O bond than with that involving the heterolytic fission (Scheme 1). In contrast to 6-NO_2-SP, it was shown[7] that the spiro (SP) form of 8-COOH-SP is less stable than its merocyanine (MC) form; an intramolecular hydrogen bonding for the latter may be responsible for this. Therefore, the SP form thermally isomerizes to the MC form. In spite of this, it seems natural to consider that the thermal isomerizations of the two compounds proceed via the same reaction path or the same type of transition state. In order to confirm our previous view, we have now examined the kinetic solvent and pressure effects on the thermal conversion (SP→MC) of 8-COOH-SP.

Experimental

Materials. The 8-COOH-SP was generously supplied by Nippon Kanko Shikiso Kenkyusho (Japanese Research Institute for Photosensitizing Dyes, Co., Ltd.), and it was recrystallized from acetone: mp 244—245 °C (lit,[7] 245 °C). The reagent-grade solvents were purified and distilled in the usual manner.

Apparatus and Procedure. The high-pressure apparatus and procedure for the kinetic measurements were identical with those described elsewhere.[6] The solvents were deaerated by means of N_2 bubbling. The sample solution (ca. 10^{-4} mol dm^{-3}) was irradiated with a 650W projection lamp through a filter of a $CuCl_2$ solution. The absorption maximum (λ_{max} 530 nm) was monitored by means of a Hitachi 139 spectrophotometer, and the absorbance was recorded as a function of the time.

Results and Discussion

It was found that the first-order kinetics holds for this reaction. The rate constants obtained in several solvents and at various pressures are given in Table 1, together with the activation parameters. In such nonpolar solvents as hexane, the solubilities are very poor; this made the estimation of the rate constant impossible in nonpolar solvents.

Solvent Effects. For the thermal conversion of 8-COOH-SP, there are two possible routes: the conversion via the C_{spiro}-O bond stretching to produce either homopolar or dipolar transition states (Scheme 1). If the conversion proceeds via the dipolar transition state, a very large kinetic solvent effect can be expected, as has been observed in Menschutkin reactions.[7] However, as may be seen in Table 1, no systematic solvent effects are observed. In DMSO, the rate is remarkably smaller than in other solvents. In spite of this, the activation energy is roughly compensated for by the activation entropy (Fig. 1). This suggests that a simple interaction mechanism[8] is involved in this reaction, too, as in the case of 6-NO_2-

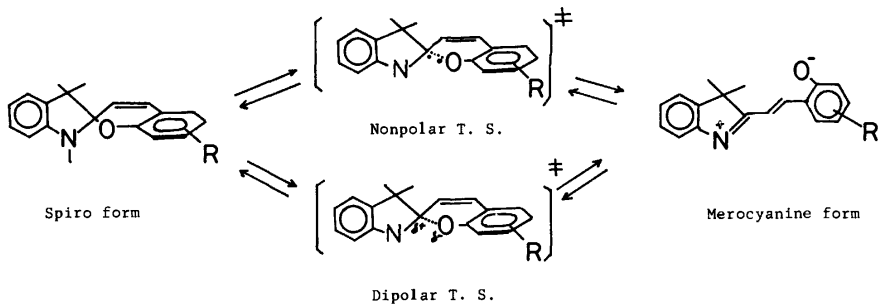

Scheme 1.

Table 1. Rate Constants and Activation Parameters for the Thermal Conversion of 8-COOH-SP at 30 °C (Probable errors in parentheses)

Solvent	10^3 k/s^{-1}				ΔV^*	E_a [b]	$\Delta S^*_{303\,K}$ [b]
P/kg cm^{-2} [a]	1	400	800	1200	cm^3 mol^{-1}	kJ mol^{-1}	J K^{-1} mol^{-1}
Chloroform	60.8(0.2)	58.8(0.3)	58.5(0.4)	55.7(0.6)	1.2	88.1(0.7)	14.1(2.2)
Ethyl acetate	38.9(0.3)	36.7(0.2)	32.6(0.9)	30.2(0.8)	4.7	75.1(12.7)	−29.8(42.4)
Dichloroethane	48.1(0.2)	46.9(0.3)	45.9(0.9)	45.7(1.8)	2.1	89.6(0.4)	17.1(1.4)
Acetone	18.3(0.3)	17.9(0.2)	16.2(0.1)	14.6(0.1)	1.4	79.6(1.3)	−24.4(4.3)
Acetonitrile	27.2(0.2)	26.9(0.1)	26.4(0.4)	26.0(0.3)	0.8	78.9(3.4)	−23.7(0.9)
Dimethyl sulfoxide	1.45(0.01)	1.35(0.02)	1.30(0.01)	1.24(0.02)	4.6	104(1)	35.5(2.1)

a) 1 kg cm^{-2}=0.9807 10^5 Pa. b) Estimated from the rate constants at 20—40 °C.

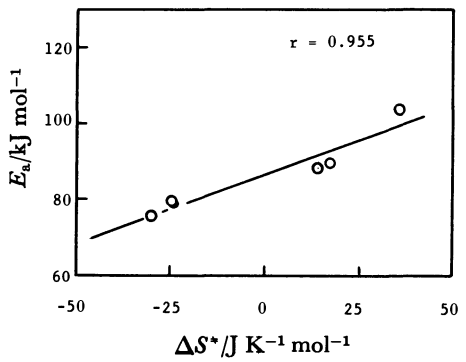

Fig. 1. $E_a-\Delta S^*$ relationship for the thermal conversion of 8-COOH-SP.

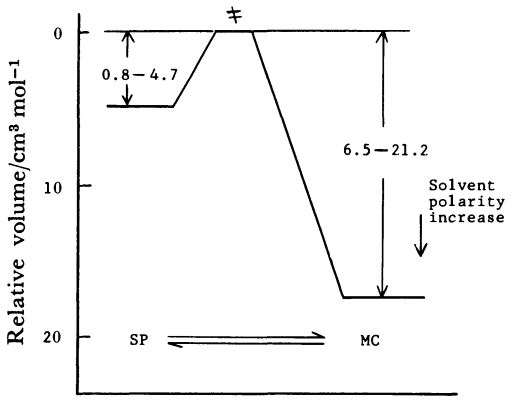

Fig. 2. Approximate volume profile for the SP⇄MC isomerization of spiropyrans.

SP. In the present case, what kind of interaction is operative has not yet been clarified. However, it would be hard to explain the kinetic solvent effect, at least, in terms of solvent-polarity parameters or a special solvent-solute interaction, since the plots do not line up in the order of changing solvent polarities. As a whole, the above findings suggest that the nonpolar transition state is more likely than the dipolar or ionic one.

Pressure Effects. In order to confirm the above view, the rate was followed under high pressures. The pressure dependence on the rate constants was appoximated by a quadratic equation (Eq. 1), while the activation volume (ΔV^*) at atmospheric pressure were estimated according to Eq. 2:

$$\ln k = a + bP + cP^2 \quad (1)$$

$$\Delta V^* = -RT(\partial \ln k/\partial P)_{T,P=1} \approx -bRT \quad (2)$$

If the reaction proceeds by the heterolytic mechanism, ΔV^* may be expected to be negative and its absolute value ($|\Delta V^*|>20$ cm^3 mol^{-1}) will decrease with an increase in the solvent polarities, as exemplified by Menschutkin reactions.[7] In the present case, however, the thermal conversion are slightly retarded by external pressures and the activation volumes take small positive values, virtually independent of the solvent polarity. This also supports the idea presented above.

The volume of activation could be explained in terms of the intrinsic volume alone. The stretching of the C_{spiro}-O bond upon activation must cause a small increase in volume. On the assumption that the stretching of the bond is 30%[9] of its original length, and that the thickness of the spiro ring is kept constant (34 nm),[10] the increment of the van der Waals volume due to the expansion of the ring is estimated to be 1.7 cm^3 mol^{-1}. Since the partial molar volume is about twice as large as its van der Waals volume,[11] ΔV^* would be about 3.4 cm^3 mol^{-1}. If this is compared with the experimental ΔV^*- values, the homolytic fission is judge to be more likely.

Approximate Energy and Volume Profiles. For the MC→SP conversion of 6-NO_2-SP, the activation energies and activation volumes are in the ranges of 71—105 kJ mol^{-1} and 6.5—21.2 cm^3 mol^{-1} respectively in solvents of different polarities. It was found that there is a trend for both E_a and ΔV^* to be greater in polar solvents than in nonpolar solvents. In the case of the SP→MC conversion of 8-COOH-SP, the E_a's are in the range 75—104 kJ mol^{-1} and the ΔV^*'s are 0.8—4.7 cm^3 mol^{-1}. In this case, no trend relating them to the solvent-polarity parameters could be observed. The above findings can be regarded as reasonable when one remembers the difference in the electronic structures between the MC and SP forms (Scheme 1).

Using the activation volume data of 6-NO_2—SP and 8-COOH-SP, we obtained the approximate volume profile shown in Fig. 2. Judging from the volume profile, the transition state is shifted to the SP form.

This implies that the bond breaking does not proceed very far at the transition state if the reaction is started from the SP form. The reverse is true if the reaction is started from the MC form.

It has been reported that some kinds of spiropyrans are in equilibrium with their MC form in solutions.[12] If we use such species and estimate ΔV and $\Delta V^{\neq}$, a more precise volume profile can be drawn. Along this line of thought, work is now under way.

A Comment on the Existence of Intermediates for the SP ⇌ MC Isomerization. From the NMR study of some kinds of spiropyrans at various temperatures, to account for their experimental facts Toppet et al.[12] suggested that an open-ring cis-isomer exists as the intermediate for the SP⇌MC thermal isomerization (Scheme 2):

$$\text{SP} \rightleftharpoons \text{X(open-ring cis-isomer)} \rightleftharpoons \text{MC trans-isomer}$$

Scheme 2.

By using the picosecond-flash photolysis method, Krysanov and Alfimov[13] observed a transient spectrum with a very short lifetime during the photoisomerization of 6-NO_2-SP. They assigned the band peaking at 440 nm to the intermediate nonplanar cis configuration with the broken C-O bond of the pyran ring. This isomer corresponds to that suggested by Toppet et al.

Meanwhile, Inoue et al.[14] reported colorless intermediates were observed in the photo-decoloration process of 8-COOH-SP derivatives. They therefore considered that an energy minimum exists along the reaction coordinate. For unsubstituted 8-COOH-SP, however, they could not detect any such intermediate. It would be natural to assume the existence of such intermediate cis-isomer just after the breaking of the C_{spiro}-O bond. The intermediates observed by Inoue et al. are fairly stable and have activation energies as large as 80 kJ mol^{-1} for the reactions producing SP and MC isomers. Therefore, these can not correspond to the cis-isomer in Scheme 2. Incidentally, Zerbetto et al.[15] reported that no minimum was found in the ground-state potential curves computed by the NMDO method for the ring-opening reactions of chromens, which can be regarded as model compounds of spiropyrans. If we take these situations into account, it may be concluded that the transition state is involved in the formation process of X, followed by the rapid conversion to the MC trans isomer (Scheme 2).

References

1) N. Nishimura, S. Kosako, and Y. Sueishi, *Bull. Chem. Soc. Jpn.*, **57**, 1617 (1984).
2) N. Nishimura, T. Tanaka, and Y. Sueishi, *J. Chem. Soc., Chem. Commun.*, **1985**, 903.
3) T. Tanaka, Y. Sueishi, S. Yamamoto, and N. Nishimura, *Chem. Lett.*, **1985**, 203.
4) Y. Sueishi, K. Ohtani, and N. Nishimura, *Bull. Chem. Soc. Jpn.*, **58**, 810 (1985).
5) Y. Sueishi and N. Nishimura, *Bull. Chem. Soc. Jpn.*, **56**, 2598 (1983).
6) Y. Sueishi, M. Ohcho, and N. Nishimura, *Bull. Chem. Soc. Jpn.*, **58**, 2608 (1985).
7) Y. Kondo, M. Uchida, and N. Tokura, *Bull. Chem. Soc. Jpn.*, **41**, 992 (1968), and the references cited therein.
8) J. E. Leffler, *J. Org. Chem.*, **31**, 533 (1966).
9) "Kagakusosetsu," ed by Nippon Kagaku Kai, No. 22 (1972), Chap. 4, pp. 59—60.
10) L. Pauling, "The Nature of the Chemical Bond," ed by Cornell Univ. (1960), Chap. 7.
11) Y. Yoshimura, J. Osugi, and M. Nakahara, *J. Am. Chem. Soc.*, **105**, 5414 (1983).
12) S. Toppet, W. Quintens, and G. Smets, *Tetrahedron*, **31**, 1957 (1975).
13) S. A. Krysanov and M. V. Alfimov, *Laser Chem.*, **4**, 129 (1984).
14) E. Inoue, H. Kokado, I. Shimizu, H. Kobayashi, and Y. Takahashi, *Bull. Chem. Soc. Jpn.*, **45**, 1951 (1972).
15) F. Zerbetto, S. Monti, and G. Orlandi, *J. Chem. Soc., Faraday Trans. 2*, **80**, 1513 (1984).

Orthogonal Approximation and Classification of Molecules for Zero-Point Energy Shifts Due to H/D Isotope Substitutions

Takao Oi* and Takanobu Ishida†
Department of Chemistry, Sophia University, 7-1 Kioicho, Chiyodaku, Tokyo 102
†Department of Chemistry, State University of New York, Stony Brook, New York 11794, U.S.A
(Received June 17, 1986)

Synopsis. Dozens of hydrogenous molecules have been classified for the approximation of the H/D isotope shifts in zero-point energies. The classification, based on their molecular structures, has yielded relative approximation errors of better than one percent with a few predictable exceptions. A further refinement of the classification has been suggested.

The zero-point energy (ZPE) of a molecule can be expressed in terms of the traces of the vibrational $\boldsymbol{H}$ ($\equiv\boldsymbol{GF}$) and $\boldsymbol{H}^2$ matrices in a second-order orthogonal approximation[1]

$$\text{ZPE} \simeq \frac{\hbar}{2}[b_0 f + b_1 \text{Tr}(\boldsymbol{H}) + b_2 \text{Tr}(\boldsymbol{H}^2)], \quad (1)$$

where f is the internal degrees of freedom, $\text{Tr}(\boldsymbol{A})$ is the trace of a square matrix $\boldsymbol{A}$ and b_0, b_1, and b_2 are approximation coefficients and are simple functions of approximation parameters involved. The precision of the approximation depends on the choice of the values of approximation parameters, which have been determined by minimizing a weighted integral of the square of the approximation error taken over the range of vibrational eigenvalue λ between zero and its largest value $\lambda_{\max}$. The weighting function $w(\lambda)$ used has the form of

$$w(\lambda) = (k+1)\lambda^k/\lambda_{\max}^{k+1}, \quad (2)$$

where k is the weighting parameter and the approximation parameters have been calculated in the range of $k \geq 0$. Parameter values thus determined are to optimize the approximation for the ZPE itself rather than the approximation for the difference between two ZPE's such as differences between the ZPE's of two isotopic molecules and those between the ZPE's of a molecule in two phases.

In a recent paper,[2] we developed another second-order approximation for the ZPE and on the basis of the approximation established a theoretical foundation for the additivity of the ZPE. In the new approximation, the zeroth-order term, which is the ZPE of an imaginary molecule consisting of completely uncoupled oscillators, i.e., consisting only of diagonal elements of $\boldsymbol{F}$ and $\boldsymbol{G}$ matrices, $\frac{\hbar}{2}\Sigma(f_{ii}g_{ii})^{1/2}$, has been singled out. The approximation parameters in the new approximation were determined by minimizing the weighted integral of the square of the derivative of the error. The weighting function used was the same as that of Eq. 2 in form and parameters were determined in the range of $k > -1/2$. The parameter values thus obtained were expected to give better approximation for ZPE differences than for the ZPE itself since they are designed to optimize the differential ZPE.

In this paper, we report on results of the approximation for the ZPE shifts due to deuterium-for-hydrogen substitutions, using the approximation form of Eq. 1 with parameters obtained in the new approximation. A scheme of classification of molecules based on their molecular structures is presented for satisfactory H/D ZPE shift approximations.

Computation

From Eq. 1, the isotopic difference in the ZPE, δ(ZPE), can be expressed as

$$\delta(\text{ZPE}) \simeq \frac{\hbar}{2}[\beta_1 \delta\text{Tr}(\boldsymbol{H}) + \beta_2 \delta\text{Tr}(\boldsymbol{H}^2)], \quad (3)$$

where $\delta\text{Tr}(\boldsymbol{A})$=Tr($\boldsymbol{A}$)(lighter isotope)−Tr($\boldsymbol{A}$)(heavier isotope), and β_1 and β_2 are the approximation coefficients which were determined in the new procedure for ZPE approximation[2] and are unique at a given k value. The values of the approximation coefficients have been tabulated for various k values.[2]

We examined dozens of hydrogenous molecules. All the isotopic pairs studied were grouped according to the molecular geometries around the site of the H/D substitutions. In a somewhat trial-and-error manner, we first determined the best k value, k_o, at which the error in the δ(ZPE) is almost zero for each pair. We then obtained a group average of k_o's, $\bar{k}_o$ for each group, and calculated percent errors of δ(ZPE) by using the same $\bar{k}_o$ value for all isotopic pairs of the molecules belonging to the same group.

Grouping of molecules is important. We have already shown in a previous paper[3] that for a very limited set of sample molecules the best k value for the approximation of H/D isotope shifts in ZPE can be well correlated with the number of H-X bonds and H-X-Y angles, where X is the site of isotopic substitutions and H is the substituted hydrogen atom (SHA), and with the number of torsional and other plane-wagging motions involving the SHA.

Results and Discussion

The molecular species studied were classified as shown in the first two columns of Table 1. In the second column of the table, (Y), (Z), and (W) represent polyatomic moieties of a species while those letters without parentheses denote single atoms ($\neq$H). Also, X-Y means a direct bonding, which may be a multiple bond, while X···(Y) indicates that there may be more than one bond between X and (Y). The values of $\bar{k}_o$'s are listed in the third column. In the fourth through seventh columns are listed the k_o values and % errors of

Table 1. Classification of Molecules for H/D Isotope Shifts in Zero-Point Energies[a)]

Group	Description	$\bar{k}_o$[b)]	Representative molecule				
			molecule	pair	k_o	% error at $\bar{k}_o$	Ref.
Ia	HX-Y [Linear]	0.277	HCN	d_0/d_1	0.259	−0.72	4
	HX-Y-Z [Linear]:						
Ib1	(Z=H)	0.264	C_2H_2	d_0/d_1	0.266	0.07	5
				d_0/d_2	0.262	−0.07	
Ib2	(Z≠H)	0.197	HCCF	d_0/d_1	0.206	0.37	5
Ic	HX-Y [Bent]	0.427	HOCl	d_0/d_1	0.442	0.40	6
Id	HX···(Y) [Planar]	0.278	C_6H_6	d_0/d_1	0.269	−0.35	7
Ie	HX···(Y) [Nonplanar][d)]	0.322 (0.278)	CHF_3	d_0/d_1	0.409	2.78	8
			$CHCl_3$	d_0/d_1	0.299	−0.90 (0.86)[f)]	5
			$CHBr_3$	d_0/d_1	0.257	−2.56 (−0.84)[f)]	5
IIa	H_2X	1.052	H_2O	d_0/d_1	1.005	−0.28	9
IIb	H_2X-Y [Planar]	0.718	H_2CO	d_0/d_1	0.742	0.31	10
IIc	H_2XY_2 [Nonplanar]	0.441	CH_2F_2	d_0/d_2	0.498	1.38	11
	H_2X-YZ_2 [Planar]:						
IId1	(Z=H)	0.398	CH_2CH_2	CH_2/CD_2	0.401	0.08	12
IId2	(Z≠H)	0.272	CH_2CF_2	d_0/d_2	0.276	0.16	5
IIe	H_2X···(Y) [Nonplanar][g)]	0.400	CH_3CH_2Cl	d_0/d_2	0.390	−0.30	5
			$CH_3CH_2CH_3$	CH_2/CD_2	0.410	0.26	5
IIIa	H_3X	0.723	NH_3	d_0/d_1	0.677	−0.64	13
IIIb	H_3X-Y [Nonplanar][d)]	0.462 (0.437)[e)]	CH_3F	d_0/d_3	0.537	1.69	14
			CH_3Cl	d_0/d_3	0.463	0.46 (0.65)[f)]	5
			CH_3Br	d_0/d_3	0.432	−0.76 (−0.13)[f)]	5
			CH_3I	d_0/d_3	0.415	−1.21 (−0.58)[f)]	5
IIIc	H_3X-Y-Z···(W) [X-Y-Z Linear]	0.528	CH_3CCH	d_0/d_3	0.574	0.91	5
IIId	H_3X-Y···(Z) [Around Y nonlinear][g)]	0.419	CH_3CH_2Cl	CH_3/CD_3	0.436	0.46	5
			$CH_3CH_2CH_3$	CH_3/CD_3	0.442	0.63	5
IV	H_4X	0.686	CH_4	d_0/d_1	0.733	0.64	15
				d_0/d_3	0.646	−0.59	

a) Case B approximation. See Ref. 2 for details. b) The group average of the optimum k. See text. c) The first-named isotopic species is the reference molecules from which λ_{max} was obtained. d) With no possibility of torsion involving the H atom being substituted. e) Alternate $\bar{k}_o$ value obtained by excluding fluoro compounds. f) The numbers in the parentheses are the percent errors obtained by using the alternate $\bar{k}_o$ listed in the parentheses in the third column. g) With possibility of torsions involving the H atom being substituted.

δ(ZPE) at the $\bar{k}_o$ for isotopic pairs of representative molecules of each group. Each group contains more isotopic pairs than listed, but we limit the presentation of the results to the molecules that are used in the discussion hereafter, thus avoiding a lengthy listing of numerical results. In the last column of the table, the origin of the used frequency data is shown.

With a few exceptions, the k_o values within any given group are similar and consequently, the relative errors obtained by using the group average of the k_o's are less than one percent. Any larger error suggests a further subdivision of the classification when it occurs. For instance, Group Ie should be further divided into fluoro compounds and others. Figures 1(a) and 1(b) compare the patterns of the eigenvalue shifts upon the H/D substitutions in fluoroform and chloroform. The high electronegativity of F induces relatively high stretching and bending force constants in CHF_3, which in turn causes the higher frequencies for CHF_3 than for $CHCl_3$, especially in the region below ρ ($\equiv\lambda/\lambda_{max}$)~0.2. Thus one needs different weighting parameters for CHF_3 and for other haloforms. The results of using $\bar{k}_o$=0.278 for the other haloforms are shown in the parentheses in the 7th

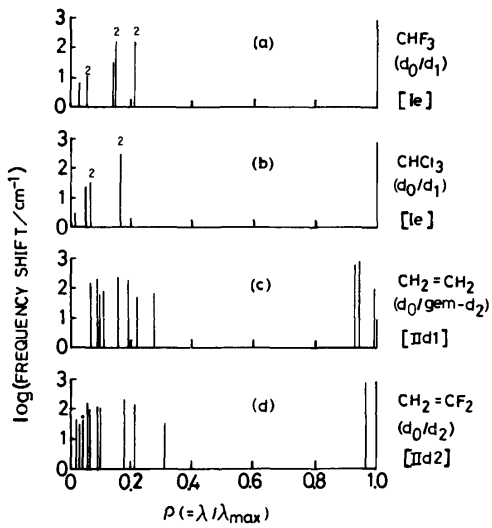

Fig. 1. Examples of differences in eigenvalue shift patterns; (a) vs. (b) for fluoro vs. other halo compounds and (c) vs. (d) for H vs. heavier atoms at β position. A vertical line is positioned at the eigenvalue of the lighter molecule, and its height shows the magnitude of the red-shift in the corresponding frequency due to the indicated H/D substitution. A number at the top of the shift line denotes the degeneracy of the shift.

column of Table 1. Group IIIb is another example of the potential advantage of decoupling fluoro compounds from other halo compounds.

The reason for the necessity for distinguishing between hydrogen atom and non-hydrogen atoms in Group Ib (Ib1 and Ib2) and IId (IId1 and IId2) is illustrated in Figs. 1(c) and 1(d). The substitution of H's by heavy atoms such as F not only reduces the number of H-Y stretching vibrations into half, thus affecting the high frequency population, but also does it decrease the frequencies of angle-bending and out-of-plane vibrations.

In general, the number of hydrogen atoms at the α and β positions relative to the site of H/D substitutions significantly affect the shift pattern. The expectation that molecular structure beyond the β positions would have been negligible effects on δ(ZPE) is in good agreement with the cut off procedure[16] and the general fact that the hydrogen isotope effects are well localized.[17]

As illustrated in acetylene (Ib1) and methane (IV), multiple H/D substitutions at the equivalent hydrogen positions do not significantly affect k_o. On the other hand, the substitutions at nonequivalent positions, such as methylene and methyl hydrogen, do require different k_o values as exemplified by CH_3CH_2Cl and $CH_3CH_2CH_3$ (cf: IIe and IIId).

The evidently satisfactory results obtained on the basis of the present scheme of classification are, in a sense, surprising especially because 1) this classification scheme has been based only on the molecular geometries and has given no consideration to the possible effects of intramolecular forces (except for the discussion on fluorine vs. other halogens), and 2) δ(ZPE) for the H/D effect has been approximated as a difference between two large numbers.

The present groups do not cover all hydrogenous molecules. However, the geometrical aspect of the classification is not far from being complete. Effects of substituents and bond orders can be incorporated in further refinements of the classification without qualitative knowledge of intramolecular forces. The prospect of such a classification is in that an appropriate parameter value may be obtained directly from a molecular structure, which in turn enables one to write δ(ZPE) as an explicit function of the elements of $\boldsymbol{F}$ and $\boldsymbol{G}$ matrices even before knowing the $\boldsymbol{F}$ matrix. Furthermore, coupled with the analytical method for δ(ZPE) presented in a previous paper,[18] the present classification scheme would provide a means for a deeper insight into correlation of the isotopic ZPE shifts with molecular structure and molecular forces.

This research has been supported in part by the Office of Basic Energy Sciences, U. S. Department of Energy, Under Contract No. DE-AC08-80ER10612.

References

1) T. Oi and T. Ishida, *J. Phys. Chem.*, **87**, 1067 (1983).
2) T. Oi, A. Popowicz, and T. Ishida, *J. Phys. Chem.*, **90**, 3080 (1986).
3) T. Oi and T. Ishida, *J. Phys. Chem.*, **88**, 2057 (1984).
4) H. C. Allen, Jr., E. D. Tidwell, and E. K. Plyler, *J. Chem. Phys.*, **25**, 302 (1956).
5) S. R. Hartshorn and V. J. Shiner, Jr., *J. Am. Chem. Soc.*, **94**, 9002 (1972).
6) I. Schwager and A. Arkell, *J. Am. Chem. Soc.*, **89**, 6006 (1967).
7) B. L. Crawford, Jr. and F. A. Miller, *J. Chem. Phys.*, **17**, 249 (1949): F. A. Miller and B. L. Crawford, Jr., *J. Chem. Phys.*, **14**, 282 (1946).
8) A. Popowicz, T. Oi, J. Shulman, and T. Ishida, *J. Chem. Phys.*, **76**, 3732 (1982).
9) D. Papousek and J. Pliva, *Collect. Czech. Chem. Commun.*, **29**, 1973 (1964).
10) W. Spindel, M. J. Stern, and E. U. Monse, *J. Chem. Phys.*, **52**, 2022 (1970).
11) I. Suzuki and T. Shimanouchi, *J. Mol. Spectrosc.*, **46**, 130 (1973).
12) M. J. Stern, W. A. Van Hook, and M. Wolfsberg, *J. Chem. Phys.*, **39**, 3179 (1963).
13) J. C. Whitmer, *J. Chem. Phys.*, **56**, 1050 (1972).
14) T. Oi, J. Shulman, A. Popowicz, and T. Ishida, *J. Phys. Chem.*, **87**, 3153 (1983).
15) J. Bigeleisen, C. B. Cragg, and M. Jeevanandam, *J. Chem. Phys.*, **47**, 4335 (1967).
16) M. J. Stern and M. Wolfsberg, *J. Chem. Phys.*, **45**, 4105 (1966).
17) For instance, see J. Bigeleisen and T. Ishida, *J. Chem. Phys.*, **62**, 80 (1975).
18) T. Oi and T. Ishida, *Bull. Chem. Soc. Jpn.*, **59**, 373 (1986).

Magnetic Properties of Dimeric Copper(II) 2,2-Dimethylpropanoate Complexes

Yoneichiro MUTO,* Nobuchika HIRASHIMA, Tadashi TOKII, Michinobu KATO,† and Ikuo SUZUKI††
Department of Chemistry, Faculty of Science and Engineering, Saga University, Saga 840
†Aichi Prefectural University, Mizuho-ku, Nagoya 467
††Department of Electrical and Computer Engineering, Nagoya Institute of Technology, Showa-ku, Nagoya 466
(Received January 13, 1986)

Synopsis. Dimeric copper(II) 2,2-dimethylpropanoate complexes, $[Cu(Me_3CCOO)_2 \cdot L]_2$, where L is pyridine, acridine, quinaldine, 2-picoline, 4-picoline, and 2,6-lutidine, have been prepared. Magnetic data show that the singlet-triplet separation ($-2J$) ranges from 319 to 397 cm^{-1}. Strong antiferromagnetic interaction observed for the acridine adduct ($-2J$=397 cm^{-1}) is discussed on the basis of weak Cu-N(acridine) bond. The magnetic behavior of the non-adduct compound $[Cu(Me_3CCOO)_2]_2$ ($-2J$=403 cm^{-1}) is explained with respect to its non-polymeric structure.

A large number of dimeric copper(II) carboxylate adducts, $[Cu(RCOO)_2 \cdot L]_2$, have been studied to elucidate the factors affecting the magnetic properties of these compounds. In particular, effects of the carboxylate substituent R and of apical ligand L on the strength of antiferromagnetic interaction have been extensively investigated.[1,2] The X-ray diffraction and magnetic measurement by Kirillova et al.[3] on the dimeric copper(II) 2,2-dimethylpropanoate adduct with acridine, $[Cu(Me_3CCOO)_2(ac)]_2$, showed that the dimeric molecule has copper(II) acetate monohydrate structure. The singlet-triplet separation ($-2J$) of 340 cm^{-1}, which is considerably larger than those reported for the well-characterized dimeric copper(II) acetate adducts (284—325 cm^{-1}),[1] was attributed to electron-releasing properties of *t*-butyl substituents in the carboxylato bridges. A structural characteristic of the acridine adduct is the Cu-N distance of 2.371(5) Å, which is longer than those found for other dimeric copper(II) carboxylate adducts with pyridine analogues (2.10—2.20 Å).[1,2] The anomalies made us investigate the influence of apical ligand on magnetic interaction. We prepared purposely six copper(II) 2,2-dimethylpropanoate complexes, $Cu(Me_3CCOO)_2$ and $Cu(Me_3CCOO)_2 \cdot L$, where L denotes pyridine (py), quinaldine (qu), 2-picoline (2-pic), 4-picoline (4-pic), and 2,6-lutidine (2,6-lu), to compare their magnetic properties with that of acridine adduct.

Rakitin et al.[4] reported magnetic properties of some of these complexes. They suggested that the molar magnetic susceptibility, χ_A, depends only weakly on the apical ligand.

Experimental

Syntheses. $Cu(Me_3CCOO)_2$: A solution of 2,2-dimethylpropanoic acid (12 mmol) in 0.25 M sodium hydroxide (100 ml (1 M=1 mol dm^{-3})) was filtered and neutralized with dilute nitric acid with phenolphthalein indicator. Addition of a solution of copper(II) nitrate (6 mmol) in water (25 ml) to the above solution with stirring gave green crystals. The crystals were recrystallized from acetone with a small amount of 2,2-dimethoxypropane.

$Cu(Me_3CCOO)_2 \cdot L$ (L=py, qu, ac, 2-pic, 4-pic, and 2,6-lu): Mixtures of $Cu(Me_3CCOO)_2$ (2 mmol) and L (3 mmol) in benzene (50 ml) were stirred for about 30 min at room temperature. The resultant solution was filtered and concentrated to one-third of the volume. When petroleum ether was added to the solution, green crystals precipitated, which were washed with petroleum ether and dried in vacuo at room temperature.

The results of the elemental analyses are given in Table 1.

Physical Measurements. Magnetic susceptibility in the temperature range of 80—300 K was determined by the Faraday method. The correction for diamagnetic contribution was made by use of Pascal's constants.[5] The cryomagnetic data were applied to the modified Bleaney-Bowers equation,

$$\chi_A = \frac{Ng^2\beta^2}{3kT}\left[1+\frac{1}{3}\exp\left(\frac{-2J}{kT}\right)\right]^{-1} \times (1-P) + \frac{Ng_i^2\beta^2}{4kT}\cdot P + N\alpha, \quad (1)$$

where P is the mole fraction of the noncoupled copper(II) impurity and g_i is the average g factor for the impurity. The values of g_i of 2.2 and $N\alpha$ of 60×10^{-6} cgs emu (1 cgs emu=$4\pi\times10^{-6}$ m^3) were used throughout the present study. The best-fit parameters of $-2J$, g, and P were obtained by a nonlinear least-squares fitting procedure. The quantity of fit was estimated by means of a discrepancy index,

$$\sigma_{dis} = \left[\frac{\Sigma(\chi_{obsd}-\chi_{calcd})^2}{\Sigma\chi_{obsd}^2}\right]^{1/2}. \quad (2)$$

Table 1. Analytical Data

Complex	Found(Calcd) (%)			
	C	H	N	Cu
$Cu(Me_3CCOO)_2$	44.83	6.93		23.91
	(45.19)	(6.83)		(23.91)
$Cu(Me_3CCOO)_2(py)$	52.20	6.69	4.04	18.53
	(52.24)	(6.72)	(4.06)	(18.42)
$Cu(Me_3CCOO)_2(ac)$	61.90	6.17	3.07	14.46
	(62.08)	(6.12)	(3.15)	(14.28)
$Cu(Me_3CCOO)_2(qu)$	58.86	6.76	3.42	15.53
	(58.73)	(6.65)	(3.42)	(15.54)
$Cu(Me_3CCOO)_2(2\text{-pic})$	53.65	6.95	3.79	17.76
	(53.54)	(7.02)	(3.90)	(17.70)
$Cu(Me_3CCOO)_2(4\text{-pic})$	53.59	7.03	3.91	17.61
	(53.54)	(7.02)	(3.90)	(17.70)
$Cu(Me_3CCOO)_2(2,6\text{-lu})$	54.72	7.19	3.69	17.03
	(54.75)	(7.30)	(3.76)	(17.04)

Table 2. Magnetic Parameters and Magnetic Moments

Complex	$\frac{-2J}{cm^{-1}}$	g	$P\times10^2$	$\sigma_{dis}\times10^3$	$\frac{\mu_{eff}}{B.M.^{a)}}$	T/K
$Cu(Me_3CCOO)_2$	403	2.27	0.51	7.25	1.26	302
$Cu(Me_3CCOO)_2(py)$	366	2.29	0.50	5.05	1.34	299
$Cu(Me_3CCOO)_2(ac)$	397	2.30	1.51	9.11	1.28	295
$Cu(Me_3CCOO)_2(qu)$	393	2.29	0.40	7.70	1.29	301
$Cu(Me_3CCOO)_2(2\text{-pic})$	371	2.29	0.49	4.15	1.32	293
$Cu(Me_3CCOO)_2(4\text{-pic})$	319	2.23	1.40	4.87	1.38	289
$Cu(Me_3CCOO)_2(2,6\text{-lu})$	379	2.29	0.29	6.37	1.29	289

a) 1 B.M. $=9.27\times10^{-24}$ A m^2.

Effective magnetic moments at room temperature were calculated from the equation,

$$\mu_{eff} = 2.83\sqrt{(\chi_A - N\alpha)\cdot T}. \quad (3)$$

The values of $-2J$, g, P, σ_{dis}, and μ_{eff} are summarized in Table 2.

Polycrystalline powder EPR spectrum of $Cu(Me_3CCOO)_2$ in Fig. 1 was recorded by Jeolco JES-ME 2 spectrometer in the X-band range.

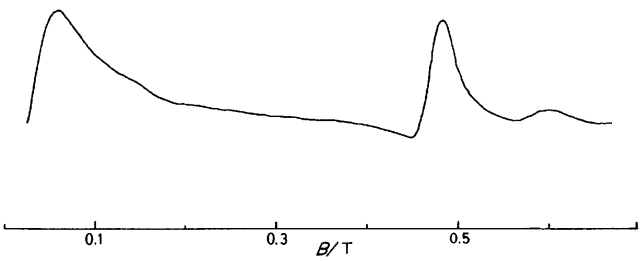

Fig. 1. Room-temperature polycrystalline powder EPR spectrum of $Cu(Me_3CCOO)_2$ at X-band frequency.

Results and Discussion

The magnetic susceptibility data of the complexes are well represented by Eq. 1, indicating that all complexes have a copper(II) acetate type dimeric structure. The $-2J$ value of 397 cm^{-1} observed for the acridine adduct prepared in the present study differs from the previously reported value of 340 cm^{-1};[3] this difference may partially be attributed to different fitting procedures of experimental χ_A values to those calculated from Eq. 1.

The $-2J$ value of acridine adduct is largest among values of adducts examined in the present study (cf. Table 2). Since the coordination bond between N of acridine and Cu seems to be weak as is indicated by long bond length (2.371 Å),[3] this result will be an evidence of the previous conclusion[6,7] that the antiferromagnetic interaction in dimeric copper(II) carboxylate adducts, $[Cu(RCOO)_2\cdot L]_2$, becomes stronger as the σ electron donation from L to copper becomes weaker. Weaker donation resulting in stronger Cu-O covalent bonds in CuO_4 basal planes enhances the spin-spin coupling between unpaired electrons of metal ions by superexchange interaction through bridging carboxylato ligands. This mechanism may be further supported by the following facts. First, the $-2J$ values of the adducts with quinaldine and 2,6-lutidine, both of which have substituents at 2- and 6-positions of pyridine ring, are larger than those of other adducts with apical ligands which have no or only one substituent at the ortho-position of pyridine ring (cf. Table 2). The apical ligation is hindered by the ortho-substituents as in the case of acridine in $[Cu(Me_3CCOO)_2(ac)]_2$[3] and, consequently, the N-Cu bonds in both the adducts must be weak. Secondly, as shown in Table 2, the $-2J$ value of 4-picoline adduct is much smaller than those of other adducts. Since 4-picoline has no substituent at ortho-position of the donor site and the basicity is higher than other pyridine bases examined in this study, except for 2,6-lutidine, the N-Cu bond in the 4-picoline adduct is considered to be much stronger than in other adducts. Thus, in contrast with the acridine adduct, the smallest $-2J$ value of 319 cm^{-1} found for 4-picoline adduct can be ascribed to strong Cu-N bond.

The $-2J$ value of 403 cm^{-1} found for the non-adduct compound, $Cu(Me_3CCOO)_2$, is larger than those of any other adducts in the present study. This fact differs from the general tendency that for many dimeric copper(II) carboxylates the $-2J$ values for non-adducts are smaller than those for the corresponding adducts.[8-10] In addition, the X-band EPR spectral pattern of $Cu(Me_3CCOO)_2$ is quite different from that of many non-adduct copper(II) carboxylates. In many cases, the EPR spectra of non-adduct copper(II) carboxylates show a single broad line in the 0.2—0.4 T region and this fact has been regarded as a sign of the existence of a polymeric chain structure consisting of dimeric molecules.[11-13] The EPR spectral feature of the present non-adduct compound shown in Fig. 1 is fundamentally the same as that usually observed for dimeric copper(II) carboxylates with axial ligands.[14] The obtained EPR parameters are: $g_\perp$ 2.139, $g_{//}$ 2.415, g_{av} 2.235, and D 0.340 cm^{-1}. The relation commonly observed for dimeric copper(II) carboxylates is held; i.e., D (0.340 cm^{-1})$>H_0$ (0.316 cm^{-1}).[14,15] These facts suggest that the strong antiferromagnetic interaction in $Cu(Me_3CCOO)_2$ is due to absence of (or very weak) coordination at the apical positions.

References

1) R. J. Doedens, *Prog. Inorg. Chem.*, **21**, 209 (1976).
2) M. Melník, *Coord. Chem. Rev.*, **42**, 259 (1982).
3) N. I. Kirillova, Yu. T. Struchkov, M. A. Porai-Koshits, A. A. Pasynskii, A. S. Antsyshkina, L. Kh. Minacheva, G. G. Sadikov. T. Ch. Idrisov, and V. T. Kalinnikov, *Inorg. Chim. Acta*, **42**, 115 (1980).
4) Yu. V. Rakitin, V. T. Kalinnikov, V. M. Novotortsev, G. M. Larin, A. A. Pasynskii, T. Ch. Iddisov, and A. V. Philatov, *Koord. Khim.*, **3**, 807 (1977).
5) P. W. Selwood, "Magnetochemistry," Interscience Publishers, New York (1956), pp. 78, 91.
6) Y. Muto, T. Tokii, K. Chijiwa, and M. Kato, *Bull. Chem. Soc. Jpn.*, **57**, 1008 (1984).
7) M. Nakashima, M. Mikuriya, and Y. Muto, *Bull. Chem. Soc. Jpn.*, **58**, 968 (1985).
8) R. W. Jotham, S. F. A. Kettle, and J. A. Marks, *J. Chem. Soc., Dalton Trans.*, **1972**, 428.
9) J. Lewis, F. E. Mabbs, L. K. Royston, and W. R. Smail, *J. Chem. Soc., A*, **1969**, 291.
10) Y. Muto, A. Sasaki, T. Tokii, and M. Nakashima, *Bull. Chem. Soc. Jpn.*, **58**, 2572 (1985).
11) V. V. Gavrilov, Yu. V. Yablokov, L. N. Milkova, and A. B. Ablov, *Phys. Stat. Sol.*, **B45**, 603 (1971).
12) F. Cariati, L. Erre, G. Micera, L. Menabue, M. Saladini, and P. Prampolini, *Inorg. Chem. Acta*, **63**, 85 (1982).
13) J. Mroziński and E. Heyduk, *J. Coord. Chem.*, **13**, 291 (1984).
14) J. R. Wasson, C. I. Shyr, and C. Trapp, *Inorg. Chem.*, **7**, 469 (1968).
15) J. H. Price, J. R. Pilbrow, K. S. Murray, and T. D. Smith, *J. Chem. Soc., A*, **1970**, 968.

Stabilities of the Copper(II) Complexes with Quadridentate Derivatives of L-Prolinamide and L-Proline Methylamide

Tasuku MURAKAMI* and Koichi CHIBA
Faculty of Education, Iwate University, Ueda, Morioka 020
(Received March 29, 1986)

Synopsis. The stability constants of the copper(II) complexes with potentially quadridentate derivatives of L-prolinamide and L-proline methylamide (see text) have been determined by potentiometric titrations. The amide-proton dissociations from the complexes have also been estimated. These were then discussed in terms of the ligand structure and the complex geometry.

Chelating ligands with amide groups have been of considerable interest in connection with the biological signification that the amide group has a character essentially identical with those of peptide bonds in proteins.[1] This work is concerned with the stability of the copper(II) complexes with the potentially quadridentate ligands (shown in Chart 1) which have two L-prolinamide and L-proline methylamide moieties linked by ethylene and trimethylene. Some of the complexes with neutral or anionic amide ligands have exhibited unique absorption, circular dichroism (CD), and ESR spectra very different from those usually observed for ordinary square-planar copper(II) complexes; hence, unusual complex geometries have been postulated for such complexes.[2,3] Therefore, it seemed that it would be worthwhile to estimate the stability of these complexes, to study the ease of the proton dissociation of the amide groups, and to connect them with the ligand structure.

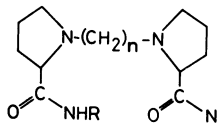

$n=2$	R=H	H_2epa
$n=2$	R=CH_3	H_2epma
$n=3$	R=H	H_2tpa
$n=3$	R=CH_3	H_2tpma

Chart 1. Structure and abbreviations of quadridentate derivatives of L-prolinamide and L-proline methylamide.

Experimental

Reagents. The synthesis and nomenclature of the diamides in Chart 1 have been described in previous papers.[4,5] The stock solutions of the diamides were prepared by the addition of twice equimolar amounts of HCl prior to titration. The $Cu(NO_3)_2$ solution was standardized by chelatometry with edta. The ionic strengths of the sample solutions were adjusted to 0.1 M (1 M=1 mol dm^{-3}) with KNO_3.

pH Titrations. The potentiometric titrations were carried out with a TOA HM-50AT auto pH meter, equipped with a TOA GC-125C multiple electrode and a temperture probe, and a TOA ADT-1 automatic dispenser synchronized with the pH meter. The apparent ion product of water was 0.719×10^{-14} M^2 at I=0.1 M. Solutions (1×10^{-3} M) of ligands only and of copper(II) and each ligand (molar ratio 1:1) were titrated with 0.1 M of NaOH at 25±0.1 °C under moistened N_2. Each titration was run at least three times. Some typical titration curves are shown in Fig. 1.

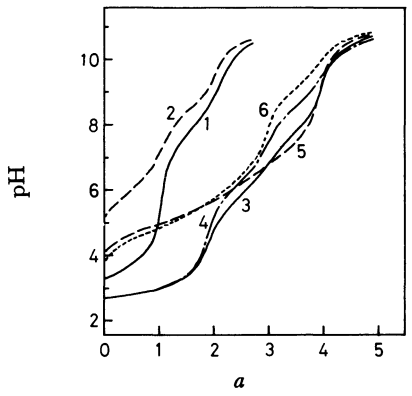

Fig. 1. Typical titration curves for proton-ligand and 1 : 1 Cu(II)-ligand systems. Curves: 1: H_4epa^{2+}, 2: H_4tpa^{2+}, 3: Cu(II)–H_4epa^{2+}, 4: Cu(II)–H_4epma^{2+}, 5: Cu(II)–H_4tpa^{2+}, 6: Cu(II)–H_4tpma^{2+}. a represents moles of NaOH added per mole of ligand.

Calculations. The proton-dissociation process of the protonated ligands occurs in two steps (the charges are omitted for the sake of clarity):

$$H_4L \rightleftarrows H_3L + H \qquad K_{a_1} = \frac{[H_3L][H]}{[H_4L]}$$

$$H_3L \rightleftarrows H_2L + H \qquad K_{a_2} = \frac{[H_2L][H]}{[H_3L]}$$

where H_2L represents neutral ligands. The copper(II) ion reacts with the neutral ligands to form Cu (H_2L):

$$Cu + H_2L \rightleftarrows Cu(H_2L) \qquad K = \frac{[Cu(H_2L)]}{[Cu][H_2L]}$$

Since these ligands possess two amide groups, two protons can be released step-by-step from Cu (H_2L):

$$Cu(H_2L) \rightleftarrows Cu(HL) + H \qquad K_{a_3'} = \frac{[Cu(HL)][H]}{[Cu(H_2L)]}$$

$$Cu(HL) \rightleftarrows Cu(L) + H \qquad K_{a_4'} = \frac{[Cu(L)][H]}{[Cu(HL)]}$$

All these constants were calculated by the method of linear least-squares by means of a micro computer.[6]

Results and Discussion

Table 1 lists the obtained data, and also those for 3,7-diazanonanedioic acid diamide (H_2DANA) and its bis-(diethylamide) (H_2 DANEA),[7] which are open-

R-NHCOCH$_2$NHCH$_2$CH$_2$CH$_2$NHCH$_2$CONH-R

R=H: H_2DANA R=C_2H_5: H_2DANEA

chain analogues of H_2tpa and H_2tpma, and for *N,N'*-dimethylethylenediamine(dmen)[8] and *N,N'*-dimethyl-1,3-propanediamine(dmtn).[7]

Table 1. Proton-Dissociation Constants and Stability Constants at 25 °C and $I=0.1$ M(KNO_3)[a]

Ligand	pK_{a_1}	pK_{a_2}	log K	$pK_{a_3'}$	$pK_{a_4'}$
H_2epa	3.46(1)	7.75(1)	8.03(3)	6.06(1)	7.77(1)
H_2epma	3.31(2)	7.57(1)	7.75(1)	6.50(1)	7.84(2)
H_2tpa	5.31(1)	7.68(2)	6.49(2)	6.44(1)	7.59(2)
H_2tpma	5.70(1)	8.02(1)	7.41(1)	6.74(3)	8.42(3)
H_2DANA[b]	6.55	8.40	10.23	7.14	8.38
H_2DANEA[b]	6.54	8.38	10.73	7.75	11.72
dmen[c]	7.30	10.17	10.09		
dmtn[b]	9.10	10.80	8.38		

a) Values in parentheses denote errors in the last figures, calculated from three different titrations. b) From Ref. 7 ($I=0.5$ M KCl). c) From Ref. 8 ($I=0.5$ M KNO_3).

Table 2. Stabilizing Effect in the Linear Relationship between Ligand Basicities and Complex Stabilities

Ligand	ΔpK[a]	Δ_R[b]
H_2epa	3.18	0.05
H_2epma	3.13	
H_2tpa	6.50	0.19
H_2tpma	6.31	
H_2DANA	4.72	0.53
H_2DANEA	4.19	
dmen	7.38	
dmtn	11.52	

a) $\Delta pK=pK_{a_1}+pK_{a_2}-\log K$. b) Δ_R represents the stabilizing effect by the inductive effect of alkyl substituents on the amide group.

Proton Dissociation of Ligand. The K_{a_1} and K_{a_2} values of H_2tpa and H_2tpma are larger than those of H_2DANA and H_2DANEA. This indicates that the steric effect of the methylene groups hindering the proton association on the tertiary amino group is superior to their electron-donating inductive effect, as is commonly observed in going from a secondary to a tertiary amine.

Formation of Cu(H_2L). The inspection of the linear relationship between the proton-dissociation and complex-formation constants of structurally similar ligands[9] often reveals the factor favoring complex formation.[7] Table 2 gives the values of $\Delta pK=pK_{a_1}+pK_{a_2}-\log K$ for the systems studied. A small ΔpK value implies that the stabilizing effect for the complex is more than would be expected from the ligand basicity. For example, the ΔpK values of Cu(H_2DANA)$^{2+}$ and Cu(H_2DANEA)$^{2+}$ are smaller than that of Cu(dmtn)$^{2+}$ by about 7 log units, which indicates a strong stabilizing effect attributable to the noticeable carbonyl coordination forming a 5,6,5-membered trifused chelate.[7] In addition, the inductive effect of the ethyl substituent which increases the electron density on the carbonyl group properly makes Cu(H_2DANEA)$^{2+}$ more stable than Cu(H_2DANA)$^{2+}$ (see Table 2).

Table 2 also shows that Cu(H_2tpa)$^{2+}$ and Cu(H_2tpma)$^{2+}$ have an instability factor of 2 log units compared with Cu(H_2DANA)$^{2+}$ and Cu(H_2DANEA)$^{2+}$. This may be a result of the steric restriction of the pyrrolidine rings, which makes the planar geometry unfavorable[10,11] and, consequently, the carbonyl coordination weaker. The small difference in ΔpK between Cu(H_2tpa)$^{2+}$ and Cu(H_2tpma)$^{2+}$ is other evidence that the carbonyl coordination is weak. The view that these ligands containing pyrrolidine rings act essentially as bidentate in aqueous solutions is supported also by the fact that the stabilizing effect in H_2epa-type complexes is larger than that in H_2tpa-type complexes, just as in the case of the dmen and dmtn complexes. In methanol, however, these neutral ligands seem to act as quadridentate rather than as bidentate[2,3] as a result of the change in the coordination ability of the solvent.

Proton Dissociation from Cu(H_2L). The $pK_{a_3'}$ value corresponding to the first amide-proton dissociation is smaller for the complexes with alkyl-substituted amide groups (Table 1). The electron-donating property of alkyl groups suppresses the proton dissociation.

The second proton dissociation from Cu(Htpa)$^+$ is easier than that from Cu(Htpma)$^+$ because of the ability of dianionic tpa to form a stable planar chelate. For dianionic tpma, the large repulsion between the *N*-methyl groups, in addition to the steric effect of the pyrrolidine rings, forces it to take a non-planar geometry, an unsymmetric cis form.[2,3] Thus, the second amide-proton dissociation takes place in a rather high pH region, corresponding to the inflection at $a=3.5$ in the titration curve. The tpma complex exhibits the spectral features typical for the tetragonal ligand-field, with a strong apical coordination.[2,3]

Although, in DANEA, the steric repulsion between the amide groups would be almost the same as in tpma, there is no reason why this linear ligand should favor any cis form containing an apical coordination of the ionic amide group.[12,13] Therefore, it is much harder for the second proton dissociation corresponding to $K_{a_4'}$ to occur, and this dissociation has been assigned to a coordinated water.[7]

The complexes with dianionic epa and epma, on the other hand, have been considered, on the basis of their visible and ESR spectra,[2,3] to have a similar

geometry, one highly distorted, probably to a tetrahedral form, from a squre-planar geometry. Whether or not the amide group is methyl-substituted seems to be insignificant for the proton release leading to such a distorted geometry.

The present work was partially supported by a Grant-in-Aid for Scientific Research No. 59540381 from the Ministry of Education, Science and Culture.

References

1) H. Sigel and R. B. Martin, *Chem. Rev.*, **82**, 385 (1982), and the references cited therein.
2) T. Murakami and M. Hatano, *Chem. Lett.*, **1981**, (1667).
3) T. Murakami and M. Hatano, *Inorg. Chim. Acta*, **125**, 111 (1986).
4) S. Kitagawa, T. Murakami, and M. Hatano, *Chem. Lett.*, **1974**, (925); *Inorg. Chem.*, **14**, 2347 (1975).
5) T. Murakami and M. Hatano, *Inorg. Chem.*, **15**, 2119 (1976).
6) The validity of the calculating method used here was confirmed by the treatments of other complexes with stabilities known in advance.
7) T. A. Kaden and A. D. Zuberbühler, *Helv. Chim. Acta*, **57**, 286 (1974).
8) R. Barbucci, L. Fabbrizzi, P. Paoletti, and A. Vacca, *J. Chem. Soc., Dalton Trans.*, **1972**, 740.
9) M. Calvin and K. W. Wilson, *J. Am. Chem. Soc.*, **67**, 2003 (1945).
10) T. Murakami and M. Hatano, *Bull. Chem. Soc. Jpn.*, **49**, 3037 (1976).
11) M. Strasak and F. Bachraty, *J. Coord. Chem.*, **13**, 105 (1984).
12) H. Gampp, H. Sigel, and A. D. Zuberbühler, *Inorg. Chem.*, **21**, 1190 (1982).
13) H. Gampp, D. Haspra, M. Maeder, and A. D. Zuberbühler, *Inorg. Chem.*, **23**, 3724 (1984).

Photolytic Formation of a Uranium(V)-DMSO Complex and the Paramagnetic Shift of DMSO by Uranium(V)

Hiroshi FUKUTOMI* and Toshie HARAZONO
Research Laboratory for Nuclear Reactors, Tokyo Institute of Technology,
O-okayama, Meguro-ku, Tokyo 152
(Received June 2, 1986)

Synopsis. A U(V)-DMSO complex (DMSO=dimethyl sulfoxide) formed by photoreduction of $[UO_2(dmso)_5]^{2+}$ was stable in acid-free DMSO and a small quantum yield of U(V) was attributed to the difficulty in electron transfer from ligands to U(VI). The paramagnetic shift of DMSO by U(V) indicates that only the pseudo-contact shift is induced.

Uranium(V)[1] ions are known to be extremely unstable in aqueous solution owing to its rapid disproportionation.[2,3] Therefore, the absorption spectrum of U(V) was only roughly obtained as that of an intermediate in aqueous solution[2,4] and in rigid methanol matrix.[5] Gritzner and Selbin obtained the absorption spectrum of U(V) by electrolytic reduction of $UO_2(NO_3)_2$ in DMSO solution.[6] Miyake et al. observed the absorption and ESR spectra of U(V) in photo- and electrolytic reduction processes of $[UO_2(dmf)_5](ClO_4)_2$ in DMF (=*N*,*N*-dimethylformamide).[7] Recently, photoreduction of U(VI) in nonaqueous solutions was found to be a better method for U(V) preparation.[8-10] On the other hand, chemical properties of U(V) having electron configuration of $5f^1$ became a subject of great interest, but only a few of information are available about its absorption spectra in solid state,[11] in eutectic mixture,[12] and in rigid matrix,[5] and about magnetic property in solution.[9] In the present paper, we report the results of photoreduction of $[UO_2(dmso)_5](ClO_4)_2$ in DMSO and the paramagnetic shift of DMSO by the resulting U(V).

Experimental

The $[UO_2(dmso)_5](ClO_4)_2$[13] and $[U(dmso)_8](ClO_4)_4$[14] complexes were prepared by the same method as reported previously. Acetone was purified as described previously.[14] Dimethyl sulfoxide was distilled twice in vacuo and stored over 3A molecular sieves. Analytical grade benzene and acetone-d_6 (Merck 99%) were used without further purification. NMR shift reagent Pr(fod)$_3$ (Dojin, fod=6,6,7,7,8,8,8-heptafluoro-2,2-dimethyl-3,5-octanedionate) was dried over phosphorus pentaoxide under vacuum. Sample solutions for the measurements of UV-visible, luminescence, NMR and ESR spectra were degassed under vacuum. The UV-visible spectra were measured at 25±0.1 °C on a Shimadzu UV-210A spectrophotometer. Luminescence spectra were recorded by using a JASCO FP-550A fluorescence spectrophotometer at room temperature. NMR measurements were carried out on a JEOL JNM-FX 100 FT-NMR spectrometer. Acetone-d_6 was used as an internal lock for the measurement of paramagnetic shifts, and D_2O and benzene were used as an external lock and an internal standard, respectively, for the measurement of magnetic susceptibility. The DMSO solution of $[UO_2(dmso)_5](ClO_4)_2$ was irradiated with the light from a 500 W ultrahigh-pressure mercury lamp (Ushio USH-500D) through a filter (Corning 052) which cut off the wavelengths shorter than 365 nm. ESR spectra were recorded on a JEOL JES-FX3 spectrometer during the light irradiation.

Results and Discussion

The molar extinction coefficient of $[UO_2(dmso)_5](ClO_4)_2$ in DMSO was 34.8 M^{-1} cm^{-1} (M=mol dm^{-3}) at 430 nm. The luminescence of the uranyl ion was not observed in DMSO at room temperature, but observed in acetone. Figure 1a shows spectral changes of 0.04 M $[UO_2(dmso)_5]^{2+}$ in DMSO during the light irradiation, where a different absorption peak at 770 nm appeared at the beginning of the irradiation, and further irradiation induced another absorption spectrum with two peaks at 558 and 657 nm. The 770 nm peak disappeared immediately with addition of a small amount of perchloric acid under nitrogen atmosphere, and the two peaks at 558 and 657 nm became more intense. *Addition of concentrated perchloric acid to the DMSO solution should be carried out with great caution to avoid a possible explosion.* The appearance of the peak at 770 nm suggests the

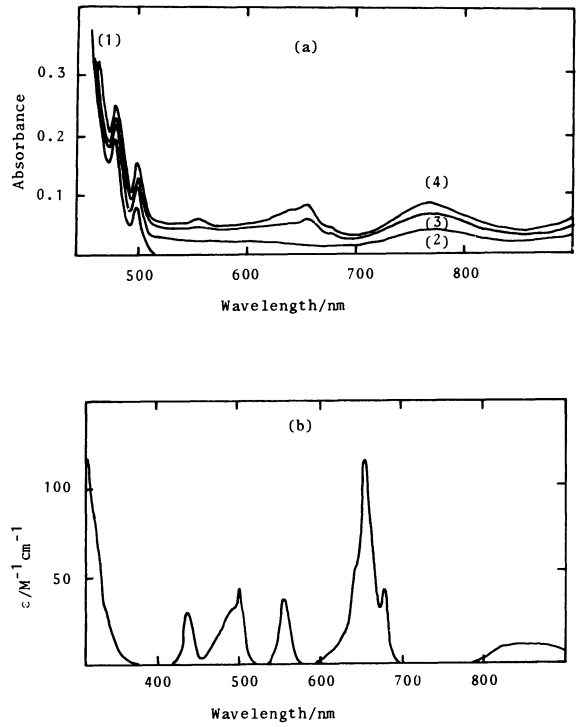

Fig. 1. (a): Spectral changes of 0.04 M $[UO_2(dmso)_5]^{2+}$ in DMSO irradiated with the light (>365 nm) at 25 °C. (1), 0 h; (2), 3 h; (3), 4.5 h; (4), 6 h. (b): Absorption spectrum of $[U(dmso)_8]^{4+}$ in DMSO.

formation of a new cmplex(I), and the absorption spectrum with the two peaks after further irradiation implies the formation of another complex(II). The latter two peaks are well consistent with those of $[U(dmso)_8](ClO_4)_4$ in DMSO (ε=115.2±2.0 M^{-1} cm^{-1} at 657 nm) as shown in Fig. 1b. Therefore, complex II was assigned to the U(IV)-DMSO complex. On the other hand, complex I was identified as the U(V)-DMSO complex which rapidly disproportionated with addition of perchloric acid as follows:

$$2UO_2^+ + 4H^+ \longrightarrow UO_2^{2+} + U^{4+} + 2H_2O$$

The concentration of U(V) was determined from the resulting U(IV) by using a relation, [U(V)]=2[U(IV)], after adding an appropriate amount of perchloric acid to the solution containing U(V). The absorption spectrum of the U(V)-DMSO complex is shown in Fig. 2, and the value of the molar extinction coefficient at 770 nm was determined to be 59.0±3.2 M^{-1} cm^{-1}. This spectrum is almost the same as that of the U(V)-DMSO complex prepared by electrolytic reduction of $UO_2(NO_3)_2$ in DMSO, which has the absorption maximum at 773 nm,[8] and very similar to those of U(V)-DMF[9] and U(V)-DMA (DMA=*N*,*N*-dimethylacetamide) complexes,[10] both of which were obtained by photoreduction of U(VI).

The quantum yield of the U(V)-DMSO complex was estimated to be 1.5×10^{-3}, which is very small compared with the values (0.3—0.4) for U(V)-DMF and U(V)-DMA complexes. This might be due to the difference in structure of ligands. The light irradiation of $[UO_2(dmf)_5]^{2+}$[14] and $[UO_2(dma)_5]^{2+}$[10] at −170 °C yielded the radicals $HCON(CH_3)CH_2\cdot$ and $CH_3CON(CH_3)CH_2\cdot$ respectively, while $[UO_2(dmso)_5]^{2+}$ gave no radical formation. As was reported in an earlier paper,[15] electron transfer from ligands to the excited uranyl ion leads to the formation of radicals and U(V) as follows:

$$UO_2L_5^{2+} \xrightarrow{h\nu} (UO_2L_5^{2+})^* \longrightarrow$$

$$(\overset{e^-}{\frown}UO_2LL_4^{2+})^* \longrightarrow UO_2L_4^+ + L\cdot + H^+,$$

where L represents a ligand. In DMF and DMA, all the atoms of $O{=}C{-}N{<}\begin{matrix}C\\C\end{matrix}$ lie on the same plane, and π orbitals of C=O and $-N<$ overlap pseudo π orbitals of two methyl groups. This favors transfer of electrons from ligands to the uranyl ion on excitation by light irradiation. On the other hand, DMSO has a trigonal pyramidal structure and no overlap of the π orbital of S=O with the pseudo π orbitals of two methyl groups. This structure of DMSO seems to be unfavorable to electron transfer from ligand dmso to the excited uranly ion, which results in no release of radicals and a rather small quantum yield of U(V).

The paramagnetic susceptibility of U(V) was determined by Evans' method[16] which was employed in a previous study.[17] It has been known that benzene, which was used as the internal standard, forms an excited complex with the uranyl ion, but does not contribute to chemical reactions except deactivation of the excited uranyl ion.[18,19] The results are shown in Table 1. The value of molar magnetic susceptibility ($10^6\chi_M$ emu mol^{-1}) of the U(V)-DMSO complex is well consistent with values of so far reported U(V)-TEP complex (2014, TEP=triethyl phosphate),[8] U(V)-DMF complex (2140)[17] and U(V)-DMA complex (2230—2330).[17]

The ^1H and ^{13}C NMR measurements for the paramagnetic shifts were carried out for bulk DMSO in the presence and absence of the U(V) complex. The

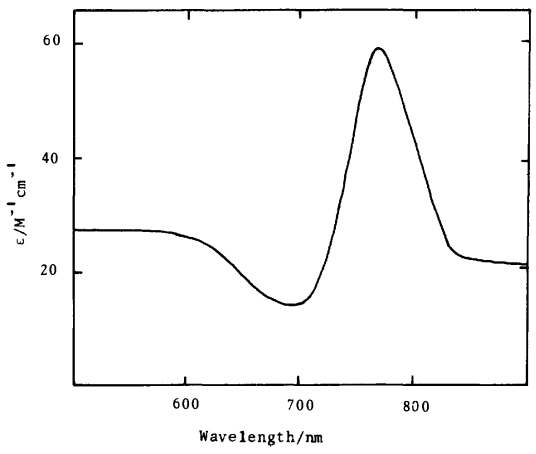

Fig. 2. Absorption spectrum of the U(V)-DMSO complex formed by photoreduction of $[UO_2(dmso)_5]^{2+}$ in DMSO at 25 °C.

Table 1. Molar Magnetic Susceptibility of the U(V)-DMSO Complex at 25 °C

[U(V)][a]	$\Delta\nu(C_6H_6)$[b]	$\Delta\nu(C_6H_6)$[c]	χ_M
10^{-2} M	Hz	Hz	10^{-6} emu mol^{-1}
0.73	3.17	435	2080
0.68	3.66	540	2580

a) $[UO_2(dmso)_5](ClO_4)_2$ concentration=0.302 M. b) Shift values of benzene in Hz. c) Reduced values at [U(V)]=1 M.

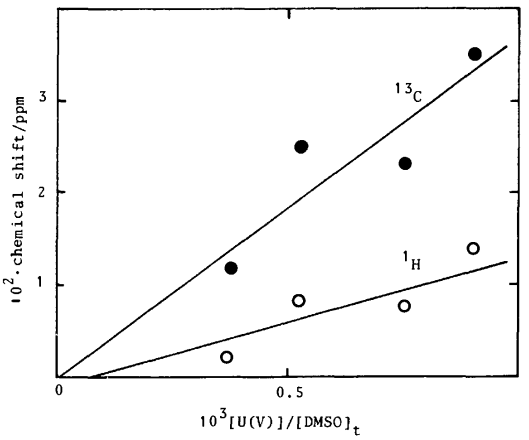

Fig. 3. Plots of ^1H and ^{13}C chemical shifts of DMSO vs. [U(V)]/[DMSO]$_t$ at 25 °C. $[UO_2(dmso)^{2+}]$= 0.40 M, $[DMSO]_t$=10.52 M.

NMR spectra of the bulk DMSO gave each single signal for ^{1}H and ^{13}C, and exhibited the paramagnetic shift to the higher field by U(V). The paramagnetic shift depends on the U(V) concentration, and the plots of the ^{1}H and ^{13}C chemical shifts of DMSO against $[U(V)]/[DMSO]_t$ at 25 °C, where t denotes total, give straight lines as seen in Fig. 3. The value of the slope is expressed as nS, where n is the number of ligands coordinated to U(V). The ratio of nS for ^{1}H and ^{13}C of DMSO was obtained as 0.42, where the complex formation shift (CFS) was neglected from the following reason. The CFS correction was estimated by using diamagnetic $[UO_2(dmso)_5]^{2+}$ in the mixture of DMSO and acetone-d_6. The value of correction was 0.84 ppm which was negligibly small compared with 14 ppm of the paramagnetic shift observed at $[U(V)]/[DMSO]_t=1$.

The value of $S(^{1}H)/S(^{13}C)$ by $Pr(fod)_3$ was 0.48. A satisfactory agreement between these two values indicates that the pseudocontact shift (PCS) is mainly responsible for the paramagnetic shifts of DMSO induced by U(V) and the contribution of contact shift is negligible, because the PCS is of major importance for Pr(III). This conclusion is compatible with the fact that the quantum yield of U(V) is very small on account of a lack of orbital overlap in the DMSO complex.

The present work was partially supported by a Grant-in-Aid for Scientific Research No. 57470035 from the Ministry of Education, Science and Culture.

References

1) For the sake of simplicity, U(VI), U(V), and U(IV) are used for UO_2^{2+}, UO_2^{+}, and U^{4+}, respectively.
2) T. W. Newton and F. B. Baker, *Inorg. Chem.*, **4**, 1166 (1965).
3) H. Kaneki and H. Fukutomi, *Bull. Res. Lab. Nucl. Reactor (Tokyo Inst. Tech.)*, **5**, 27 (1980).
4) A. Ekstrom, *Inorg. Chem.*, **13**, 2237 (1974).
5) T. Harazono, S. Nakamura, T. Kojima, and H. Fukutomi, *Bull. Res. Lab. Nucl. Reactor (Tokyo Inst. Tech.)*, **8**, 1 (1983).
6) G. Gritzner and J. Selbin, *J. Inorg. Nucl. Chem.*, **30**, 1799 (1968).
7) C. Miyake, Y. Yamana, S. Imoto, and H. Ohya-Nishiguchi, *Inorg. Chim. Acta*, **95**, 17 (1984).
8) G. Cauzzo, G. Gennari, G. Giacometti, G. C. Agostini, and A. Gambaro, *Inorg. Chim. Acta*, **32**, 45 (1979).
9) T. Harazono, H. Tomiyasu, and H. Fukutomi, *Chem. Lett.*, **1983**, 1173.
10) T. Harazono, T. Kojima, and H. Fukutomi, *Nippon Kagaku Kaishi*, **1984**, 213.
11) J. Selbin and J. D. Ortego, *Chem. Rev.*, **69**, 657 (1969).
12) D. A. Wentz, M. D. Adams, and R. K. Steunenberg, *Inorg. Chem.*, **3**, 989 (1964).
13) H. Doine, Y. Ikeda, H. Tomiyasu, and H. Fukutomi, *Bull. Chem. Soc. Jpn.*, **57**, 1021 (1984).
14) H. Fukutomi, T. Harazono, and T. Kojima, *Bull. Chem. Soc. Jpn.*, **59**, 2387 (1986).
15) T. Harazono, S. Sato, and H. Fukutomi, *Bull. Chem. Soc. Jpn.*, **57**, 768 (1984).
16) O. F. Evans, *J. Chem. Soc.*, **1959**, 2003.
17) T. Harazono and H. Fukutomi, *Bull. Chem. Soc. Jpn.*, **59**, 2129 (1986).
18) S. Sakuraba and R. Matsushima, *J. Am. Chem. Soc.*, **93**, 7143 (1971).
19) R. Matsushima, *J. Am. Chem. Soc.*, **94**, 6010 (1972).

Determination of a Small Amount of a Biological Constituent by Use of Chemiluminescence. VIII. Effect of Heating on the Determination of Protein

Tadashi HARA,* Kazuhiko TSUKAGOSHI, Akihiro ARAI, and Takeshi IHARADA
Department of Chemical Engineering, Faculty of Engineering, Doshisha University, Karasuma Imadegawa, Kamigyo-ku, Kyoto 602
(Received June 2, 1986)

Synopsis. The effect of heating on the determination of protein by chemiluminescence was examined by estimating the apparent coupling constant of a copper(II)-protein complex after treatment of a solution at 25 °C or 95 °C and by comparing the values with each other. The values obtained for two proteins were as follows: 1.3×10^{8} mol^{-1} dm^3—2.1×10^{11} (mol^{-1} dm^3)$^{1.5}$ at 25 °C and 4.3×10^{17} (mol^{-1} dm^3)$^{2.3}$—1.9×10^{18} (mol^{-1} dm^3)$^{2.2}$ at 95 °C. These values suggest that heating makes a copper(II)-protein complex more stable and improves the concentration range for the determination of protein.

New methods for the determination of protein by chemiluminescence (CL) reaction between 5-amino-2,3-dihydro-1,4-phthalazinedione(luminol) or 1,10-phenanthroline(phen) and hydrogen peroxide (H_2O_2) were reported by the authors in the previous papers.[1,2] The determination is based on the measurement of the decreasing catalytic activity of copper(II) (Cu(II)) for CL reaction in the presence of protein. Both the concentration range of determinable protein and the detection limit were improved by heating a Cu(II)-protein complex sample solution.[1] This seemed to be attributed to the formation of a more stable Cu(II)-protein complex by heating. However, no attempt to confirm this has been carried out in detail. The present study deals with the estimation of an apparent ratio of Cu(II) to protein and a coupling constant of a Cu(II)-protein complex after treatment of a sample solution at 25 °C or 95 °C. The values obtained were compared and discussed.

Experimental

A phen solution, a H_2O_2 solution, a Cu(II) catalyst solution, and a buffer solution were prepared as in the previous paper.[2] The 1.2×10^{-4} mol dm^{-3} phen solution contained 4.0×10^{-3} mol dm^{-3} ethylhexadecyldimethylammonium bromide, 2.0×10^{-7} mol dm^{-3} tetraethylenepentamine, and 1.0×10^{-1} mol dm^{-3} sodium hydroxide. A 5.0 wt% H_2O_2 solution was prepared by diluting 30 wt% H_2O_2 with water. A Cu(II) catalyst solution was prepared by diluting a 2.0×10^{-2} mol dm^{-3} Cu(II) stock solution with a buffer solution (pH 10.2) consisting of 1.0×10^{-1} mol dm^{-3} boric acid and 1.0×10^{-1} mol dm^{-3} potassium hydroxide. This solution also contained L-aspartic acid (its concentration is 1.2×10^{3} times of Cu(II)) instead of tartrate in a biuret reagent.

All reagents were of commercially available special grade. Ion-exchange water was distilled before use. Bovine serum albumin (BSA) and human serum albumin (HSA) from NAKARAI CHEMICAL, LTD were prepared by diluting them with a buffer solution. A definite volume of Cu(II) solution was added to a sample solution containing protein and the resulting solution was heated for a definite period.

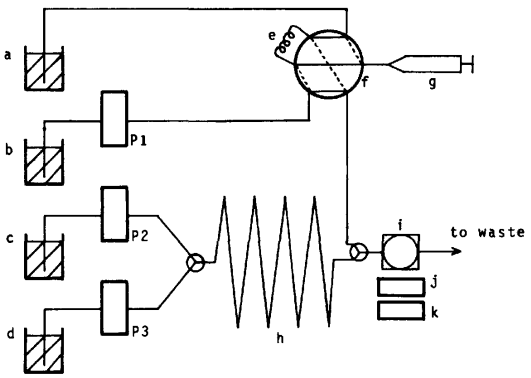

Fig. 1. Flow-injection system.
a: Sample solution, b: buffer solution, c: hydrogen peroxide solution, d: 1,10-phenanthroline solution, e: sampling loop, f: six-way cock, g: sylinge, h: mixing coil, i: flow cell, j: photon counter, k: recorder, and P1, P2, P3: pump.

After the solution was cooled to room temperature, an aliquot of the solution was injected into the flow-through system.

The schematic diagram of the apparatus which was set up for flow-injection analysis is shown in Fig. 1. All the tubes and connectors used were made of Teflon. A buffer solution(b), a H_2O_2 solution(c), and a phen solution (d) were delivered at the flow rate of 1.6 cm^3 min^{-1} with the corresponding pumps: (p_1), (p_2), (p_3)-(PERISTA MINI PUMP SJ-1211). A phen solution and a H_2O_2 solution were first mixed using a mixing coil(h) (346 cm, 0.5 mm i.d.) and the resulting mixture was combined with a buffer solution. A definite amount (50 mm^3) of the sample solution was injected into the line of a buffer solution. A poly(vinyl chloride) tube (45 cm, 0.8 mm i.d.) was spirally wound and was then used as the cell(i). The CL intensity of the solution passing through the cell was measured by a photon counter-(j) (HAMAMATSU, C1230) and recorded on a recorder(k) (National. PEN RECORDER). The net CL intensity of a sample solution was obtained by subtracting the background (the CL intensity of the solution containing no sample) from the intensity obtained.

Results and Discussion

After a Cu(II) catalyst solution was held at 25 °C or 95 °C for a definite period and then cooled at room temperature, the catalytic activity of Cu(II) for CL was measured. The calibration curve thus obtained was linear for 1×10^{-9}—1×10^{-7} mol dm^{-3} Cu(II) (Fig. 2).

The relationship between reaction time and the CL intensity in the presence of 1.0×10^{-7} mol dm^{-3} Cu(II) and BSA as a model protein was examined at 25 °C and 95 °C, respectively. The reaction between Cu(II)

Table 1. The Concentration of Species at Equilibrium for BSA at 25 °C

Initial Cu(II) concd / mol dm^{-3}	CL intensity / kcps	Free Cu(II) concn[a] / mol dm^{-3}	Bound Cu(II) concd / mol dm^{-3}
7.50×10^{-8}	4.83	2.70×10^{-8}	4.80×10^{-8}
8.00×10^{-8}	5.55	3.10×10^{-8}	4.90×10^{-8}
1.00×10^{-7}	8.70	4.80×10^{-8}	5.20×10^{-8}
1.25×10^{-7}	12.40	6.90×10^{-8}	5.60×10^{-8}

Initial BSA concd $=6.1\times10^{-8}$ mol dm^{-3}. a) Estimated from Fig. 2.

Table 2. An Apparent Coupling Ratio and Coupling Constant at 25 and 95 °C

Protein	25 °C		95 °C	
	Coupling ratio (Cu(II) : Protein)	Coupling constant	Coupling ratio (Cu(II) : Protein)	Coupling constant
BSA	1 : 1	1.3×10^{8} mol^{-1} dm^{3}	2.3 : 1	1.9×10^{18} (mol^{-1} dm^{3})$^{2.3}$
HSA	1.5 : 1	2.1×10^{11} (mol^{-1} dm^{3})$^{1.5}$	2.2 : 1	4.3×10^{17} (mol^{-1} dm^{3})$^{2.2}$

Protein concd $=6.1\times10^{-8}$ mol dm^{-3}. Cu(II) concd $=7.50\times10^{-8}$—1.50×10^{-7} mol dm^{-3}. Ionic strength $\fallingdotseq 0.1$ mol dm^{-3}.

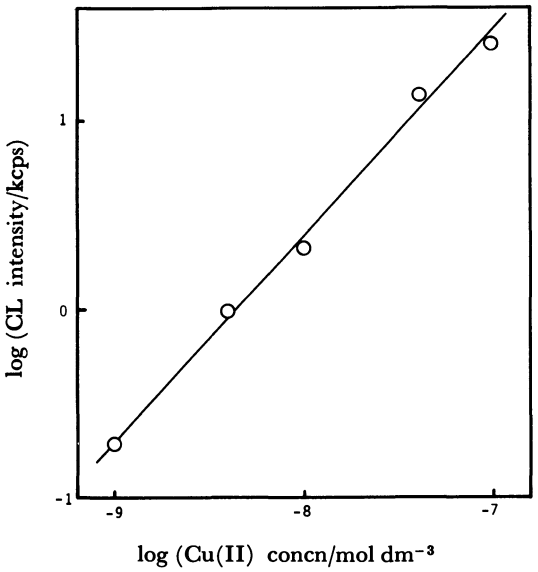

Fig. 2. Calibration curve of Cu(II) catalyst solution.

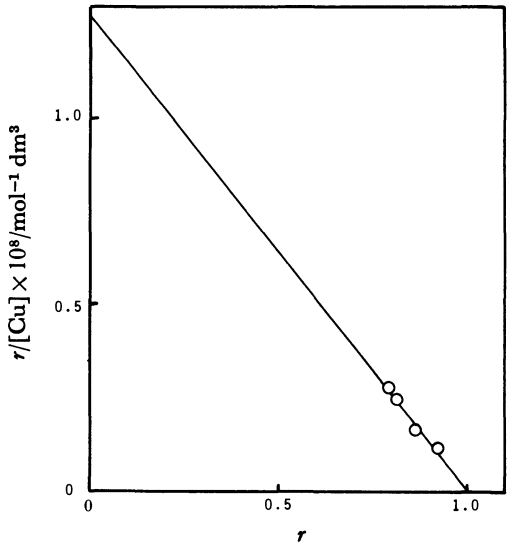

Fig. 3. Relationship between r and r/[Cu] at 25 °C for BSA.

catalyst and BSA went to completion in 30 min at 25 °C and in 45 min at 95 °C. These reaction times contain the times required for a sample solution to reach the individual temperature from room temperature. In the following experiment, the CL intensity of a protein solution was examined in 45 min at 25 °C and 60 min at 95 °C.

The reaction between Cu(II) and protein is assumed to proceed as follows (Eq. 1).

$$x[\mathrm{Cu}] + [\mathrm{Prot}] \rightleftharpoons [\mathrm{Cu}\,x\cdot\mathrm{Prot}] \quad (1)$$

where [Cu], [Prot], [Cu x·Prot], and x are the concentration of free Cu(II), free protein, and associated complex, and an apparent coupling ratio, respectively. An apparent coupling constant K is defined by Eq. 2.

$$K=\frac{[\mathrm{Cu}\,x\cdot\mathrm{Prot}]}{[\mathrm{Cu}]^{x}[\mathrm{Prot}]} \quad (2)$$

From Eq. 2, Eq. 3 is derivered.

$$r/[\mathrm{Cu}]^{x} = xK - rK \quad (3)$$

where r means the mole ratio of bound Cu(II) to total protein. The free Cu(II) concentration is estimated from the CL intensity and the bound Cu(II) concentration is obtained by subtracting the free Cu(II) concentration from the initial Cu(II) concentration. Thus r is found from the bound Cu(II) and total protein concentration.

The value of x was determined so as to satisfy Eq. 3 by the use of the experimental data, and the plot of r/[Cu]^{x} to r was obtained. The value of K was found from the slope of a straight line in the plot. Table 1

and Fig. 3 show the data and the plot for BSA at 25 °C. An apparent coupling ratio and coupling constant were Cu(II):protein=1:1 and 1.3×10^{8} mol^{-1} dm^{3} respectively under the following conditions: initial Cu(II) concentration 7.50×10^{-8}—1.25×10^{-7} mol dm^{-3} and ionic strength about 0.1 mol dm^{-3}. An apparent coupling ratio and coupling constant for two proteins (BSA and HSA) were estimated similarly as above at 25 °C and 95 °C, respectively (Table 2). A molecular weight of 66000 was assumed for these proteins for the calculation.

On the basis of these data the effect of heating on the determination of protein by the use of CL can be understood. Though heating made a Cu(II)–protein complex more stable and improved the concentration range for the determination of protein, the reaction mechanism between Cu(II) and protein still remains unknown.

The authors wish to thank Mr. Masakatsu Imaki (Horiba Ltd.) for providing the apparatus necessary for the present study.

References

1) T. Hara, M. Toriyama, and K. Tsukagoshi, *Bull. Chem. Soc. Jpn.*, **57**, 1551 (1984).

2) T. Hara, T. Ebuchi, A. Arai, and M. Imaki, *Bull. Chem. Soc. Jpn.*, **59**, 1833 (1986).

Determination of a Small Amount of a Biological Constituent by Use of Chemiluminescence. IX. Effect of a Ligand on a Peak Shape

Tadashi HARA,* Akihiro ARAI, and Takeshi IHARADA
Department of Chemical Engineering, Faculty of Engineering, Doshisha University, Karasuma Imadegawa, Kamigyo-ku, Kyoto 602
(Received June 6, 1986)

Synopsis. The chemiluminescence intensity of a 1,10-phenanthroline-hydrogen peroxide system was systematically examined in the presence of various types of copper(II) chelate-forming ligands. There was a good relation between the peak shape on a recorder chart and the types of ligands; they could be classified into four groups as follows: A) Both bidentate and tridentate ligands gave positive and negative peaks. B) The ligand having more than four donor atoms, as in a quadridentate ligand or protein, gave a single negative peak. C) A liberated porphine ring gave a single sharp negative peak. D) Some metal organic compounds such as vitamine B-12 and ferritin gave broader positive and negative peaks in comparison with those in A). These unique peak shapes were applicable to the estimation of the type of ligand. α-Fetoprotein as a tumor marker could be also easily detected with a detection limit of 250 pg and with a typical coefficient of variation of 3.8%.

In order to establish a new analytical method by which several proteins can be sensitively and rapidly determined without labeling, the flow-injection method using the fact that the catalytic activity of copper(II) for the chemiluminescence (CL) reaction between 1,10-phenanthroline (phen) and hydrogen peroxide (H_2O_2) decreased in the presence of protein has been reported by the authors.[1]

As pointed out in the previous paper, the peak shape of the CL intensity changed, depending upon the type of ligand. The relationship between the type of ligand (e.g. uni-, bi-, tri-, and quadri-dentate ligands) and the peak shape has been systematically investigated in the present paper.

Furthermore, such ligands as α-fetoprotein (AFP), ferritin, and polyamines which are well-known as cancer markers were also investigated.

Experimental

All chemicals used were reagent grade. A phen solution, a H_2O_2 solution, and a copper(II) catalyst solution were prepared as in the previous paper. The sample solution of AFP (human placental) from The Green Cross Co., and ferritin (TYPE IV, human liver) from Sigma Chemical Co., and polyamines (sperminetetrahydrochloride, spermidine, and putrescine), and all other samples were prepared by diluting them in a buffer solution (pH 10.2) consisting of 0.1 mol dm^{-3} boric acid and 0.1 mol dm^{-3} potassium hydroxide.

The experiment was carried out using the same apparatus as in the previous paper.

Results and Discussion

According to the previous paper, the injection of an α-amino acid solution into the copper(II)-tartrate catalyst solution flow showed a first positive peak and then a second negative peak based on the formation of a copper(II)-amino acid complex compound. Since this result appeared to have a close relation with the composition of a copper(II) complex compound, an investigation was systematically carried out for various ligands, and the results obtained are shown in Table 1.

The effect of an unidentate ligand such as ammonia and pyridine on a peak shape was small. Neither positive nor negative peaks were observed until the mole ratio of ligand to copper(II) ([ligand]/[copper(II)]=r) exceeded 10^5.

Both positive and negative peaks were observed for a bidentate or a tridentate ligand such as in Group A. This was explained on the assumption that the positive peak corresponding to the positive catalytic activity was obtained first due to the formation of a

Table 1. Observed Peak Shape for Various Ligands

Group	Ligand	Donor atoms	Positive peak	Negative peak
A	α-Amiao acid[a]	2-(5)	○	○
	2,2′-Bipyridine	2	○	○
	Ethylenediamine	2	○[d]	○
	Diethylenetriamine	3	○[e]	○
	Peptide[b]	3-(6)	○[f]	○
	Spermine	4	○	○
	Spermidine	3	○	○
B	Triethylenetetramine	4	×	○
	Tetraethylenepentamine	5	×	○
	EDTA	6	×	○
	Diethylenetriamine-pentaacetic acid	8	×	○
	Protein[c]		×	○
	α-Fetoprotein		×	○
C	TCPP	4	×	○
	TPPS	4	×	○
	Hematoporphyrin	4	×	○
D	Ferritin		○	○
	Vitamine B-12		○	○

a) L-Aspartic acid, L-glutamic acid, L-glycine, L-alanine, L-proline, L-lysine hydrochloride, L-arginine hydrochloride, and L-histisine hydrochloride. b) glycylglycine, glycyl-L-phenylalanine, glycyl-L-proline, and glycylglycylglycine. c) bovine serum albumin, bovine serum γ-globulin, human serum albumin, human serum γ-globulin, and ovalbumin. d) $r<10^6$. e) $r<10^3$. f) $r<10^6$.

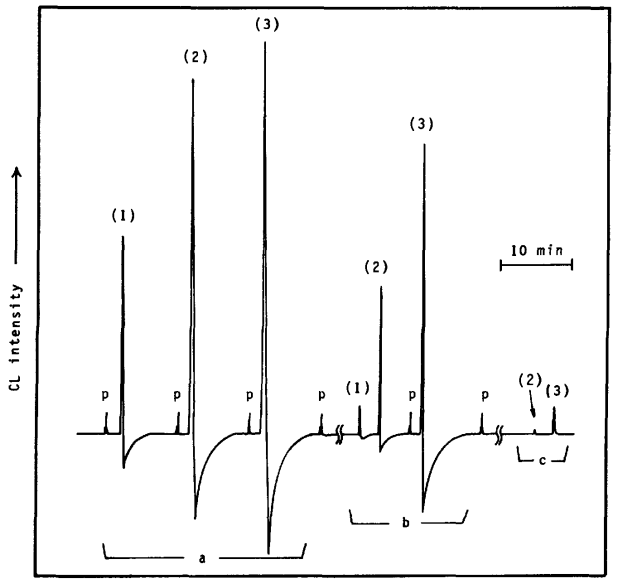

Fig. 1. Observed signals of polyamines.
a: Spermine, b: spermidine, c: putrescine, p: periodical shock peak accompanying with a reciprocation of the pump piston, (1): 1.0×10^{-6} mol dm^{-3}, (2): 1.0×10^{-5} mol dm^{-3}, and (3): 1.0×10^{-4} mol dm^{-3}.
Conditions: 5.0×10^{-5} mol dm^{-3} phen(4.0×10^{-3} mol dm^{-3} ethylhexadecyldimethylammonium bromide (EHDAB), 2.0×10^{-7} mol dm^{-3} tetraethylenepentamine (TEPA), 1.0×10^{-1} mol dm^{-3} sodium hydroxide(NaOH)), 5% H_2O_2, and 1.0×10^{-7} mol dm^{-3} copper(II) (5.0×10^{-5} mol dm^{-3} L-arginine hydrochloride(Arg)).

1:1 copper(II)-ligand complex compound, followed by the negative peak corresponding to the inactivation of the catalyst due to the complete occupation of the four coordination sites of copper(II) by the ligand. These results are consistent with the fact that the negative peak area increased with an increase of the *r* value.

A ligand which had more than four donor atoms, as in a quadridentate ligand, strongly linked with all four coordination sites in a planar square by way of a chelate effect, in which case a negative peak alone was obtained (Group B).

In addition, such liberated porphine ring as 5,10,15,20-tetrakis(4-carboxyphenyl)porphine (TCPP), 5,10,15,20-tetraphenylporphinesulfonic acid (TPPS) (Dojindo Laboratories.), and hematoporphyrin (Porphyrin Products.) (Group C) showed sharp negative peaks which were different from the peak shape of Group B and proteins. These results suggest that the center of the porphin molecule was rapidly occupied by copper(II), and that the catalytic activity of copper(II) was lowered rapidly.

The present method was further applied to other compounds which were of importance in clinical diagnostics as a tumor marker. The peaks obtained for polyamines such as sperminetetrahydrochloride, spermidine, and putrescine are shown in Fig. 1. Considerably large positive and negative peaks were obtained for both spermine and spermidine while a small positive peak alone was obtained for putrescine.

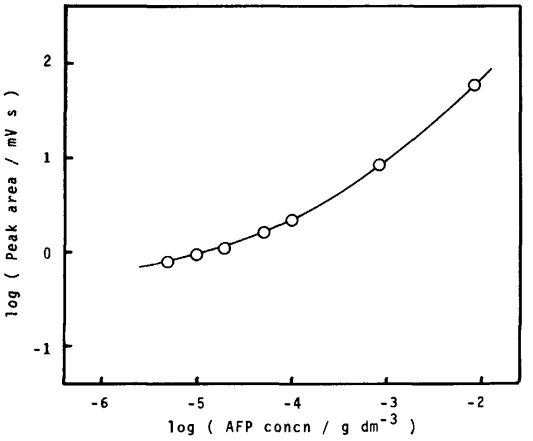

Fig. 2. Calibration curve of AFP.
Conditions: 5.0×10^{-5} mol dm^{-3} phen(4.0×10^{-3} mol dm^{-3} EHDAB, 2.0×10^{-7} mol dm^{-3} TEPA, 1.0×10^{-1} mol dm^{-3} NaOH), 5% H_2O_2, and 1.0×10^{-7} mol dm^{-3} copper(II) (5.0×10^{-5} mol dm^{-3} Arg).

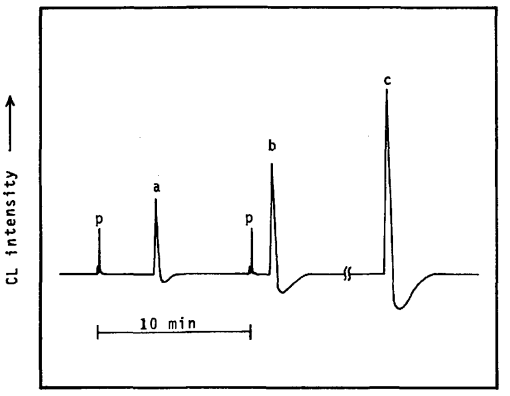

Fig. 3. Observed signals of ferritin.
a: 2×10^{-5} g dm^{-3}, b: 1×10^{-4} g dm^{-3}, c: 4×10^{-4} g dm^{-3}, and p: periodical shock peak accompanying with a reciprocation of the pump piston.
Conditions: 5.0×10^{-5} mol dm^{-3} phen(4.0×10^{-3} mol dm^{-3} EHDAB, 2.0×10^{-7} mol dm^{-3} TEPA, 1.0×10^{-1} mol dm^{-3} NaOH), 5% H_2O_2, and 1.0×10^{-7} mol dm^{-3} copper(II) (5.0×10^{-5} mol dm^{-3} Arg).

This was reasonably understood by considering the following complex formations: two six-membered chelate rings for spermine; one six-membered chelate ring for spermidine; and one single seven-membered chelate ring for putrescine.

The calibration curve of AFP which is well-known as a tumor marker is shown in Fig. 2. The AFP as a glycoprotein also formed a stable complex compound with copper(II) and showed a single negative peak. Using the present detector, the detection limit of AFP was 250 pg with the coefficient of variation of 3.8% for five measurements of 1×10^{-4} g dm^{-3} AFP. This sensitivity is satisfactory for practical use from the standpoint that the criterion of hepatoma is approximately 20 ng.

The peaks of ferritin which are also utilized as a marker for lung cancer and another malignant tumor including a blood disease are also shown in Fig. 3.

Judging from the molecular structure containing iron(III) at the central position, the positive peak was assumed to be due to the existence of iron(III) as a CL catalyst, while the negative peak to be due to the existence of protein. Vitamine B-12 containing a cobalt(II)–porphine complex structure was experimentally confirmed to act as a catalyst similarly to ferritin. The detection limit of ferritin corresponding to the negative peak was 200 pg, while the diagnostic significance of ferritin is regarded as "abnormaly large value" for more than 25 ng.

To sum up, there were good relations between the peak shape and the type of ligands that formed stable complex compounds with copper(II). The peak shapes were available for the estimation of the type of a ligand. According to the present study, several cancer markers are also sensitively determinable though their peak shapes differ from one another.

Reference

1) T. Hara, T. Ebuchi, A. Arai, and M. Imaki, *Bull. Chem. Soc. Jpn.*, **59**, 1833 (1986).

Potentiometric Study of Copper(II) Complexes with β-Diketone in Micellar Solution Using a Copper(II) Ion-Selective Electrode

Makoto AIHARA,* Kyoko SUGI, and Yumiko GOYA
Laboratory of Inorganic Chemistry, Faculty of Home Life Science, Fukuoka Women's University, Higashi-ku, Fukuoka 813
(Received June 5, 1986)

Synopsis. The distribution of copper(II) complexes with thenoyltrifluoroacetone, pivaloyltrifluoroacetone and 3-phenyl-2,4-pentanedione between micellar and bulk phases in aqueous solution containing nonionic surfactant was investigated by potentiometry with a copper(II) ion-selective electrode. The apparent equilibrium constants for the copper(II) complexes in micellar solution were determined.

The spectrophotometric method using β-diketone in aqueous solution containing nonionic surfactant is usefull for the determination of metal ions.[1-6] The method is based on solubilizing metal complexes to aqueous solution containing nonionic surfactant and it is simple and rapid method compared with solvent extraction-spectrophotometric determination of metal ions.[7-10]

On the other hand, ion-selective electrodes have been used for complex formation studies in aqueous solutions.[11-14] The solid membrane ion-selective electrode could be employed effectively for study of complex formation in micellar solution, too.

In the present paper, the distribution behavior of copper(II) complexes with thenoyltrifluoroacetone (abbreviated as TTA), pivaloyltrifluoroacetone (PTA) and 3-phenyl-2,4-pentanedione(3-phenylacetylacetone, PAA) in aqueous solutions containing trideca (oxyethylene) dodecyl ether, $CH_3(CH_2)_{11}$-O-$(CH_2$-CH_2-$O)_{13}$-H (Emulgen 120) were investigated by potentiometry with a copper(II) ion-selective electrode and the apparent equilibrium constants for the systems were obtained.

Experimental

Materials. A standard solution of copper(II) was prepared by dissolving reagent grade copper(II) chloride to dilute hydrochloric acid. The concentration of copper(II) ion was determined by EDTA titration. A 1×10^{-2} M (1 M=1 mol dm^{-3}) chelating agent (TTA, PTA, or PAA) solution was prepared by dissolving a known amount of the reagent (Dojin Co., Ltd.) in 5 W/V% Emulgen 120 (Kao-Atlas Co., Ltd.), which was purified with ion-exchange resin (Bio Rad; AG501-X8(D), analytical grade mixed bed resin). All other chemicals used were of an analytical reagent grade.

Copper membrane disks were supplied by Denki Kagaku Keiki Co., Ltd. The preparation of a copper(II) ion-selective electrode was described in previous paper.[15]

Procedure. Direct potentiometry in the solution containing copper(II) ion and 0.5% Emulgen 120 was perfomed by usual method.

Known amounts of copper(II) and a chelating agent containing 0.5% Emulgen 120 were placed in a titration vessel. Dilute hydrochloric acid solution was added to the above solution. After equilibrium was reached, the value of pH was measured and the potential of copper(II) ion-selective electrode was measured to determine the concentration of free copper(II) ion in the system. Each system was allowed to attain equilibrium (±0.1 mV). All measurements were carried out in a 0.1 M sodium perchlorate at 25±0.1 °C.

Results and Discussion

It was recognized by a spectrophotometric method that most of TTA or PTA exists outside the micelle, i.e. in the bulk phase.[4-6] PAA is also anticipated to be exist outside the micelle. On the other hand, metal-β-diketone complex could not be dissolved in an aqueous solution at the low concentration of nonionic surfactant.

The complex CuL_n (HL; TTA, PTA, and PAA) is presummed to be formed by the following equilibrium.

$$Cu^{2+}_{(b)} + nHL_{(b)} = CuL_{n(m)} + nH^{+}_{(b)} \quad (1)$$

the subscripts (b) and (m) refering to mutually equilibrated bulk and micellar phases, respectively.

The equilibrium constant, K, and distribution ratio, D, are defined by

$$K = \frac{[CuL_n]_{(m)}[H^+]^n_{(b)}}{[Cu^{2+}]_{(b)}[HL]^n_{(b)}} \quad (2)$$

$$D = \frac{[CuL_n]_{(m)}}{[Cu^{2+}]_{(b)}} \quad (3)$$

From Eqs. 2 and 3, Eq. 4 was derived

$$\log D = -n\log[H^+]_{(b)} + n\log[HL]_{(b)} + \log K \quad (4)$$

The following relationship for copper(II) concentration can be expected to hold

$$(V_{(b)}+V_{(m)})\sum Cu = V_{(b)}[Cu^{2+}]_{(b)} + V_{(m)}[CuL_n]_{(m)} \quad (5)$$

where $\sum$ Cu is total concentration of copper ion, $V_{(b)}$ and $V_{(m)}$ are volume of bulk and micellar phases, respectively. Then making use of one approximation,

$$V_{(b)} \gg V_{(m)} \quad (6)$$

Eq. 5 will be written in the form

$$V_{(b)}\sum Cu = V_{(b)}[Cu^{2+}]_{(b)} + V_{(m)}[CuL_n]_{(m)} \quad (7)$$

Combination of Eqs. 3 and 7 results in the Eq. 8

$$D = \frac{\sum Cu - [Cu^{2+}]_{(b)}}{[Cu^{2+}]_{(b)}} \cdot \frac{V_{(b)}}{V_{(m)}} \quad (8)$$

$$= D_{app} \cdot \frac{V_{(b)}}{V_{(m)}} \quad (9)$$

Apparent distribution ratio, D_{app} is determined by potentiometry with a copper(II) ion-selective electrode

for each system. Thus, log D_{app} is expressed by

$$\log D_{app} = n\mathrm{pH} + n\log [\mathrm{LH}]_{(b)} + \log K_{app} \quad (10)$$

where $K_{app}=K\times V_{(m)}/V_{(b)}$. The value of n is obtained as follows

$$\frac{d\log D_{app}}{d\mathrm{pH}} = n \quad (11)$$

The concentration of free copper(II) in the bulk, $[Cu^{2+}]_{(b)}$, were obtained from the measurement of free ion concentration with a Cu(II) ion-selective electrode and the value of D_{app} were calculated.

Figure 1 shows the calibration curves for copper(II) ions in 0.5% Emulgen 120 solutions at the different pH. The copper(II) ion selective electrode responds very well to copper(II) concentration of 10^{-6} M. Nernstian response was observed in each 0.5% Emulgen 120 solution.

The determination of free copper(II) ion concentration was made in the solution containing copper(II) and β-diketone in 0.5% Emulgen 120. The values of D_{app} at each system of TTA, PTA, and PAA were calculated from the experimental data.

Figure 2 shows the variation of log D_{app} as a function of pH at 15 and 25 °C. These plots are found to be linear and each value of log D_{app}/dpH was nearly equal to two. These show that the formation of [Cu(tta)$_2$], [Cu(pta)$_2$], and [Cu(paa)$_2$] complexes occur in micellar solution. The results are in agreement with the previous results by spectrophotometric method.[2] The facts described above indicate that the equilibrium (Eq. 1) is set up between bulk and micellar phases. But, it appears to necessary to explain also the equilibrium by dependence of log D_{app} on the concentration of the β-diketone. It will be a subject for further study.

The apparent equilibrium constants were calculated from the data for Fig. 2 by Eq. 10. The results are summarized in Table 1. The orders of apparent equilibrium constants are [Cu(tta)$_2$]>[Cu(pta)$_2$]>[Cu(paa)$_2$].

These data indicate that the formation reaction of [Cu(tta)$_2$] is endothermic and those of [Cu(pta)$_2$] and [Cu(paa)$_2$] are exothermic. But the dependence of the equilibrium constant on the temperature is small. The distribution behavior of the complexes in micellar solutions will be cleared by further study.

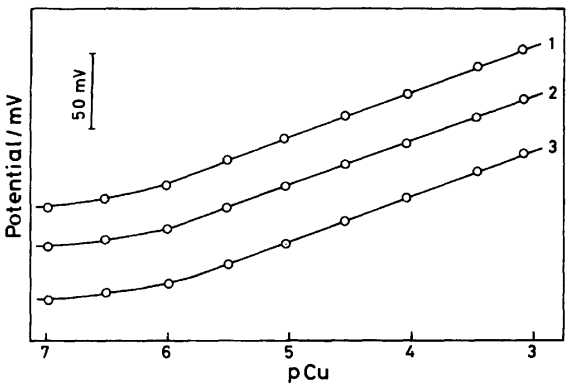

Fig. 1. Calibration curves for copper(II) ions in 0.5% Emulgen 120 solutions at the different pH.
(1): pH=4.00, (2): pH=4.50, (3): pH=5.00.

The authors are grateful to Professor Tomitsugu Taketatsu of Kyushu University for valuable discussion.

References

1) T. Taketatsu, M. Aihara, and K. Kimoto, *Bunseki Kagaku*, **30**, 328 (1981).

Table 1. The Equilibrium Constants for the Complex Formation of Cu(β-diketone)$_2$

β-Diketone	t / °C	$\frac{d\log D_{app}}{d\mathrm{pH}}$	log K_{app}
TTA	15	2.0	−1.50±0.02
	25	2.1	−1.27±0.01
PTA	15	2.1	−2.34±0.02
	25	2.0	−2.41±0.01
PAA	15	1.9	−3.00±0.01
	25	2.0	−3.38±0.03

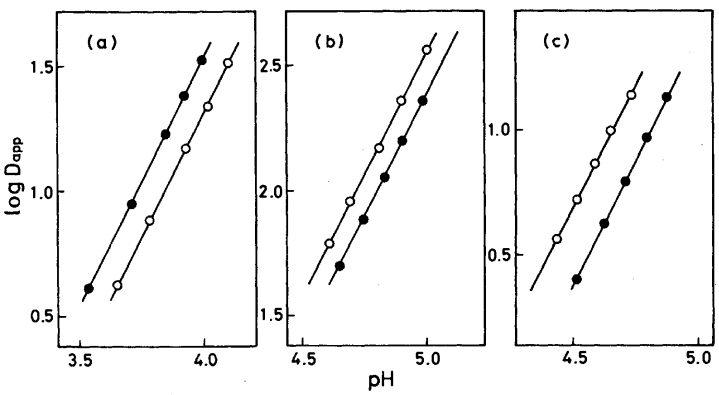

Fig. 2. Variation of log D_{app} as a function of pH at 15 °C (○) and 25 °C (●).
(a): Cu(II)-TTA system, (b): Cu(II)-PTA system, (c): Cu(II)-PAA system.

2) M. Aihara, Y. Omori, and T. Taketatsu, *Bull. Fac. Home Life Sci., Fukuoka Women's University*, **14**, 53 (1983).
3) M. Aihara, Y. Miwa, and T. Taketatsu, *Bull. Fac. Home Life Sci., Fukuoka Women's University*, **16**, 21 (1985).
4) T. Takatatsu and A. Sato, *Bull. Chem. Soc. Jpn.*, **53**, 3713 (1980).
5) T. Taketatsu and A. Sato, *Anal. Chim. Acta*, **108**, 429 (1979).
6) T. Taketatsu, *Talant*, **29**, 397 (1982).
7) A. M. Poskanzer and B. M. Foreman, *J. Inorg. Nucl. Chem.*, **16**, 323 (1961).
8) S. M. Khopkar and A. K. De, *Z. Anal. Chem*, **171**, 241 (1959).
9) A. K. De and MD. S. Rahaman, *Anal. Chem.*, **35**, 159 (1963).
10) A. J. Fishman, H. L. Finston, and D. E. Golgberg, *J. Inorg. Nucl. Chem.*, **35**, 2497 (1973).
11) K. Ohzeki, M. Saruhashi, and T. Kambara, *Bull. Chem. Soc., Jpn.*, **53**, 2548 (1980).
12) S. Ramamoorthy, *J. Inorg. Nucl. Chem.*, **34**, 1651 (1972).
13) W. A. E. McBride, *J. Inorg. Nucl. Chem.*, **35**, 4193 (1973).
14) G. Nakagawa, H. Wada, and T. Hayakawa, *Bull. Chem. Soc. Jpn.*, **48**, 424 (1975).
15) M. Aihara, S. Kanetake, and Y. Fukuda, *Bull. Chem. Soc. Jpn.*, **58**, 1617 (1985).

Catalytic and Electrocatalytic Hydrogenation of Benzylideneazlactone and Benzylidenehydantoin

Tomokazu MATSUE, Tsukasa YAMADA, Hiroko TAKAHASHI, and Tetsuo OSA*
Pharmaceutical Institute, Tohoku University, Aobayama, Sendai 980
(Received March 3, 1986)

Synopsis. The electrocatalytic hydrogenatoin of benzylideneazlactone and 5-benzylidenehydantoin with Raney-nickel cathode proceeded smoothly to afford *N*-acetylphenylalanine and 5-benzylhydantoin, respectively. In addition, refluxing the electrolyte solution after the electrolysis finally yielded phenylalanine with satisfactory chemical yields and current efficiencies. This electrocatalytic process showed slightly higher reactivity than the ordinary catalytic hydrogenation.

The previous studies[1-5] have demonstrated that Raney-nickel (R-Ni) powder acts as an effective cathode for electrocatalytic hydrogenation of various reducible compounds. The electrocatalytic hydrogenation has several unique characteristics in comparison with direct, uncatalyzed electroreduction or ordinary catalytic hydrogenation, as described previously.[4,5] In this paper, we report the hydrogenation of benzylideneazlactone and 5-benzylidenehydantoin aimed at preparing finally phenylalanine by using the electrocatalytic and ordinary catalytic processes. The present results have shown that the electrocatalytic process has slightly higher reactivity than the ordinary catalytic one.

Results and Discussion

The Erlenmeyer method[6] via benzylideneazlactone (**1**) as an intermediate has been widely used for preparing α-amino acids, especially phenylalanine derivatives (Scheme 1). This method contains several reaction steps involving one for catalytic hydrogenation of 2-acetamide-3-phenyl-2-propenoic acid (**2**). The most widely adopting method for this step is the catalytic hydrogenation with platinum catalysts such as PtO_2 under a hydrogen pressure of about 3×10^5 Pa.[6] We have applied the electrocatalytic hydrogenation with R-Ni powder cathode to this step. The results are summarized in Table 1.

The electrocatalytic hydrogenation of **2** produced *N*-acetylphenylalanine (**3**) with satisfactory isolating yields and current efficiencies. The present hydrogenation proceeds smoothly under mild conditions (atmospheric pressure and room temperature). The isolating yield and the current efficiency were dependent on the electrolysis time. The long electrolysis time assures a high chemical yield but turns out a low current efficiency. The electrochemical process of the present electrolysis is the discharge of proton in the electrolyte solution to form active hydrogen at the R-Ni cathode surface. This active hydrogen is then transferred to a substrate to give a hydrogenation product. If the concentration of the substrate is not sufficiently high, two active hydrogens combine each other to form hydrogen gas. This is a main side reaction. The decrease in the current efficiency with the electrolysis time is caused by

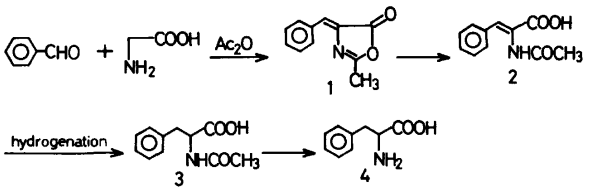

Scheme 1.

Table 1. Hydrogenation of **2** to **3**

Run	Method	W_R[a]	Condition	Reaction time/h	Yield %	Q[b] 96500C/mol	CE[c] %
1	EC[d]	0.5	2.0 M NaOH aq	3.7	78	2.6	60
2		0.5	1.0 M $NaOH/H_2O$: MeOH (1 : 1)	2.6	50	1.8	56
3		0.5	1.0 M $NaOH/H_2O$: MeOH (1 : 1)	4.3	72	3.0	48
4		0.5	2.0 M NaOMe/MeOH	4.3	70	3.0	47
5		0.5	1.0 M $NaClO_4/H_2O$: MeOH (1 : 1)		63		
6		0.25	2.0 M NaOMe/MeOH	5.7	78	4.0	39
7		0.13	2.0 M NaOMe/MeOH	5.7	71	4.0	36
8		0.08	2.0 M NaOMe/MeOH	6.4	70	4.5	31
9	C[e]	0.5	2.0 M NaOH aq, H_2 3.8×10^5 Pa	12	55		
10		0.5	MeOH, H_2 3.0×10^5 Pa	4.5	62		
11		0.25	MeOH, H_2 3.0×10^5 Pa	12	63		
12		0.08	MeOH, H_2 3.0×10^5 Pa	12	5		
13		0.08	2.0 M NaOMe/MeOH, H_2 3.0×10^5 Pa	12	69		

a) Weight ratio of R-Ni to **2**. b) Charge passed. c) Current efficiency. d) Electrocatalytic hydrogenation. e) Catalytic hydrogenation. M = mol dm^{-3}

formation of hydrogen gas due to the lowering the concentration of substrate in the solution. Indeed, the bubble formation became noticeable as the electrolysis proceeded. The ordinary catalytic hydrogenation also produced **3**. However, the yields observed in the latter hydrogenation are slightly lower than those observed in the former.

The relative amount of the R-Ni to the substrate affected the hydrogenation. Table 1 also lists the W_R values (the weight ratio of the R-Ni to the substrate) used in this hydrogenation. In both types of the hydrogenation, the decrease in the W_R value reduces the reactivity as is shown by the prolonged reaction time to obtain satisfactory isolating yields. The influence of the W_R ratio is serious on the catalytic hydrogenation (Runs 10, 11, and 12). On the other hand, the electrocatalytic hydrogenation proceeded fairly smoothly even at W_R=0.08 and afforded a satisfactory chemical yield and a current efficiency (Run 8). It is ovbious from the table that the electrocatalytic process has higher reactivity than the ordinary catalytic process.

The use of a base as a supporting electrolyte showed good chemical yields and current efficiencies since basic solution enhanced the reactivity of R-Ni.[7] Perchlorate salts such as $NaClO_4$ also acted as a supporting electrolyte, but the chemical yield was relatively low. The effect of the basic atmosphere is eminent in the catalytic hydrogenation. The hydrogenation of **2** at W_R=0.08 in methanol (Run 12) proceeded very slowly and the chemical yield of **3** was only ca. 5% even after 12 h of the reaction time. However, the addition of NaOH to the methanol solution accelerated the hydrogenation more than 10 times (Run 13). In this case, the isolating yield of **3** was 69%, comparable to that observed in the electrocatalytic hydrogenation.

Since the present electrolysis was usually conducted in a basic solution, the use of **1** as a starting material burings about concurrent opening of the lactone ring during the electrolysis besides hydrogenation of the carbon–carbon double bond. Thus, the hydrogenation of **1** yielded **3** (Table 2). There is no significant difference in reactivity between **1** and **2**. The both substrates afforded **3** with almost same isolating yields and current efficiencies. The ordinary catalytic hydrogenation of **1** also gave **3**. However, the isolating yield was slightly low compared with that obtained in the electrocatalytic hydrogenation under the same conditions (Runs 14 and 21). In this case, use of water:ethanol (1:1 in volume) as a solvent showed good results. When the reaction solution was basic enough to hydrolyze the amide linkage of **3**, the reflux of the reaction solution after the hydrogenation gave phenylalanine (**4**), the final product, without isolating intermediates (Runs 20, 21, and 24).

The Wheeler method[8] via 5-benzylidenehydantoin (**5**) is also a typical method for preparing **4** (Scheme 2). This method contains a hydrogenation step. As shown in Table 3, the ordinary catalytic hydrogenation of **5** in ethanol at 5×10^6 Pa (Run 29) of hydrogen pressure gave 5-benzylhydantoin (**6**) with a high yield, whereas no hydrogenation proceeded at 2.6×10^5 Pa of hydrogen pressure (Run 28). On the other hand, the electrocatalytic hydrogenation under the equivalent conditions (Run 26) afforded **6** with a 57% chemical yield. In this case, the hydrogenation proceeded solwly and the current efficiency was quite unsatisfactory. The addition of NaOH to the solution facilitated the reaction to proceed due to the enhancement of the catalytic activity by the basic atmosphere.[7] This effect is pronounced on the ordinary catalytic hydrogenation (Runs 28 and 30). This is also true in the electrocatalytic hydrogenation.

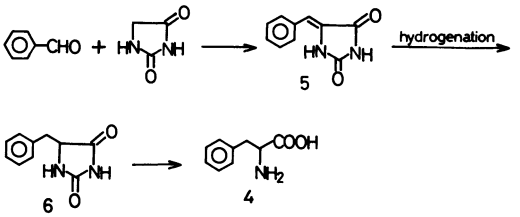

Scheme 2.

Table 2. Hydrogenation of **1**[a]

Run	Method	Condition	Reaction time/h	Product	Yield %	Q 96500C/mol	CE %
14	CE	2.0 M NaOH aq	4.0	**3**	77	2.8	55
15		1.0 M $NaOH/H_2O$: EtOH (2 : 1)		**3**	70		
16		1.0 M $NaOH/H_2O$: MeOH (1 : 1)	4.3	**3**	70	3.0	47
17		1.0 M $NaClO_4/H_2O$: MeOH (1 : 1)		**3**	51		
18		2.0 M NaOMe/MeOH	4.3	**3**	75	3.0	50
19		2.0 M $NaOH/H_2O$: THF (5 : 1)	3.9	**3**	75	2.7	56
20		2.0 M NaOMe/MeOH, reflux[b]	4.3	**4**	70	3.0	47
21		2.0 M $NaOH/H_2O$: THF (5 : 1), reflux[b]	7.2	**4**	68	5.0	27
22	C	2.0 M NaOH aq, H_2 3.8×10^5 Pa	24	**3**	60		
23		1.0 M $NaOH/H_2O$: EtOH (1 : 1), H_2 3.0×10^5 Pa	2	**3**	66		
24		1.0 M $NaOH/H_2O$: EtOH (1 : 1), H_2 2.8×10^5 Pa, reflux[b]	3	**4**	64		

a) W_R=0.5. b) Reaction solution was refluxed for 10 h after the hydrogenation.

Table 3. Hydrogenation of 5[a)]

Run	Method	Condition	Reaction time/h	Product	Yield %	Q 96500 C/mol	CE %
25	EC	2.0 M NaOH aq	3.6	**6**	90	2.5	72
26		1.0 M $NaClO_4$/EtOH	11.5	**6**	57	8.0	14
27		2.0 M NaOH aq, reflux	3.3	**4**	74	2.3	64
28	C	EtOH, H_2 2.6×10^5 Pa	12	No reaction			
29		EtOH, H_2 5×10^6 Pa	5	**6**	94		
30		2.0 M NaOH aq, H_2 2.6×10^5 Pa	12	**6**	80		

a) $W_R=0.5$.

The use of NaOH as a supporting electrolyte resulted in a reduction of the reaction time as well as an improvement of the chemical yield and the current efficiency (Runs 25 and 26). If the electrolyte solution was basic enough, reflux of the solution after the electrolysis gave **4** (Run 27).

In the hydrogenation of **5**, the electrocatalytic hydrogenation showed slightly higher yields than the ordinary process. Similar trend was also observed in the hydrogenation of **1** or **2** as described above. These phenomena may be accounted for by the following argument. As pointed out previously,[5)] the concentration of the active hydrogen on the R-Ni surface could be higher in the electrocatalytic hydrogenation than that in the ordinary catalytic one. The present electrocatalytic process will produce 8×10^{-8} mol of hydrogen in an apparent unit area (1 cm^2) in every second under the present conditions if a substrate is absent. If we dare to caluculate roughly by using the diffusion coefficient of hydrogen of 3.6×10^{-5} cm^2 s^{-1},[9)] the concentration of hydrogen in an aqueous system is estimated to be ca. 1×10^{-2} M (mol dm^{-3}) in the vicinal region from the cathode under the nonequilibrium state. On the other hand, the concentration is calculated to be ca. 8×10^{-4} M in the ordinary catalytic hydrogenation under the hydrogen pressure of around 3×10^5 Pa since the absorption coefficient is 0.018.[10)] Thus, the calculated concentration of hydrogen is ca. 13 times higher in the electrocatalytic process than that in the ordinary catalytic one. Although the effective concentration of dissolved hydrogen may be low due to the bubble formation in the electrocatalytic process, it is probably still higher than that in the ordinary catalytic hydrogenation. This in turn indicates high surface concentration of the active hydrogen at the cathode. Another considerable important factor is the basicity of the electrolyte solution near the R-Ni cathode. The discharge of proton makes the solution basic and thus the R-Ni is activated by the basic atmosphere, resulting in high chemical yields and short reaction time.

In conclusion, the hydrogenation of **1**, **2**, and **5** was accomplished by the electrocatalytic and ordinary catalytic hydrogenation with R-Ni powder. The addition of a base into the solution facilitated the hydrogenation to proceed and the reflux of the reaction mixture after the hydrogenation afforded **4** without isolating intermediates. In this hydrogenation, the electrocatalytic process showed slightly higher reactivity than the ordinary catalytic one.

Experimental

Electrolysis was carried out with a conventional H-type cell equipped with a R-Ni cathode and a Pt gauze anode under a constant current density (16 mA cm^{-2}). The preparation of R-Ni cathode was described previously.[4,5)] The electrolyte consisted of 2.0 g of a substrate dissolved in a solution (60 cm^3) described in Tables 1—3. After the electrolysis, the R-Ni cathode was filtered off from the solution. The solution was acidified, extracted with ethyl acetate three times, and dried over magnesium sulfate for a day. The products were obtained as crystalline forms by concentration of the solution. The products were identified by ir and mass spectroscopies. In order to evaluate the electrocatalytic hydrogenation, the ordinary catalytic hydrogenation was also carried out with a Burgess-Parr instrument under the hydrogen pressure of around 3×10^5 Pa with the basically same solution and R-Ni as used in the electrocatalytic hydrogenation.

This work was supported in part by Grant-in-Aids for Scientific Research (Nos. 59470070 and 60219003) from the Ministry of Education.

References

1) B. Sakurai and T. Arai, *Bull. Chem. Soc. Jpn.*, **28**, 93 (1962).
2) T. Chiba, M. Okimoto, H. Nagai, and Y. Takata, *Bull. Chem. Soc. Jpn.*, **56**, 719 (1983).
3) M. Fujihira, A. Yokozawa, H. Kinoshita, and T. Osa, *Chem. Lett.*, **1982**, 1089.
4) T. Osa, T. Matsue, A. Yokozawa, and T. Yamada, *Denki Kagaku*, **52**, 629 (1984).
5) T. Osa, T. Matsue, A. Yokozawa, T. Yamada, T. Osa, and M. Fujihira, *Denki Kagaku*, **53**, 104 (1985).
6) R. M. Herbst and D. Shemin, *Org. Synth.*, II, 1 (1943); H. B. Gillespie and H. R. Snyder, *ibid.*, II, 491 (1943).
7) H. E. Ungnade and D. V. Niphtingale, *J. Am. Chem. Soc.*, **66**, 1218 (1944); M. Paty, *Compt. Rend.*, **220**, 827 (1945).
8) E. T. Borrows, J. C. Clayton, and B. A. Hems, *J. Chem. Soc., Suppl. Issue* No. 1, 185 (1949); W. J. Boyd and W. Robson, *Biochem. J.*, **29**, 2256 (1935).
9) W. Jost, "Diffusion in Solids, Liquids, Gases," Academic Press, New York (1960), p. 475.
10) J. A. Dean, "Lange's Handbook of Chemistry," Mcgraw Hill, New York (1973), Section 10.

Reactions of Alkyl Isothiocyanates with Dianions of Cyclic Thioureas

Noboru MATSUMURA,* Masaaki TOMURA, Ritsuo MANDO, Yuko TSUCHIYA, and Shigeo YONEDA*

Department of Applied Chemistry, College of Engineering, University of Osaka Prefecture, Sakai, Osaka 591

(Received March 22, 1986)

Synopsis. The reactions of methyl (or ethyl) isothiocyanate with dianions (**4**, **5**, and **6**), which are readily derived from available cyclic thioureas (**1**, **2**, and **3**) with butyllithium, gave ring fused 1,3-disubstituted 1,3,5-triazine-2,4(1*H*,3*H*)-dithiones (**7**) and/or thiocarbamoyl derivative (**8**) as major products.

Recently we have reported that the bromomagnesium thioureide acts effectively as a carbon dioxide carrier in the carboxylation of active methylene compounds under mild conditions.[1] In our continuing investigation on the properties of the dianions, which are readily derived from available cyclic thioureas with butyllithium, we have found the formation of 7,8-dihydro-1,3-dimethyl-6*H*-pyrimido[1,2-*a*][1,3,5]-triazine-2,4(1*H*,3*H*)-dithione (**7b**) and 3,4-dimethyl-1,6-propano-1*H*,6*H*-**3a**-thia(S^{IV})-1,3,4,6-tetraazapentalene-2,5(3*H*,4*H*)-dithione (**10a**) by the reaction of methyl isothiocyanate with dianion (**5**). The reaction behavior of dianions of cyclic thioureas has not been well investigated so far.[2] This paper reports the reaction of alkyl isothiocyanates with dianions (**4**, **5**, and **6**). The reactions were carried out in tetrahydrofuran (THF) at room temperature for 24 h under argon. When the RNCS:dianion molar ratio was 3:1, **7** was obtained in relatively good yield. The outline of the reaction pathway is shown in Scheme 1.

Reactions of alkyl isothiocyanates with dianions **4**, **5**, and **6** gave ring fused 1,3-disubstituted 1,3,5-triazine-2,4(1*H*,3*H*)-dithione (**7**), thiocarbamoyl de-

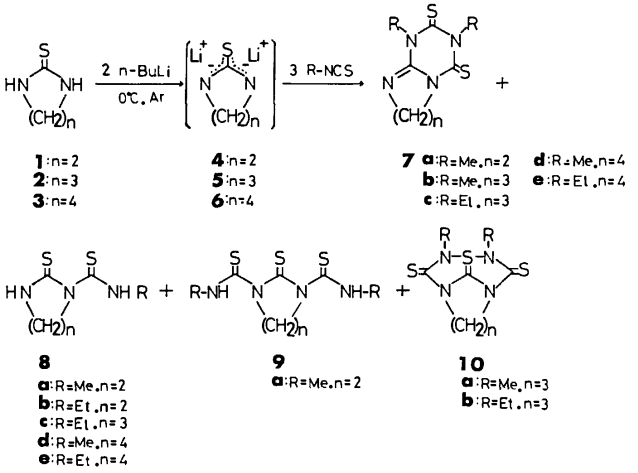

Scheme 1.

Table 1. Reactions of Alkyl Isothiocyanates with Dianions[a]

Dianion	R-NCS R	Product yield/%[b] 7	8	9	10
4	Me	10 (**7a**)[c]	38 (**8a**)	48 (**9a**)	—
4	Et	—	53 (**8b**)	—	—
5	Me	61 (**7b**)	—	—	15 (**10a**)
5	Et	36 (**7c**)	19 (**8c**)	—	10 (**10b**)
6	Me	22 (**7d**)	48 (**8d**)	—	—
6	Et	13 (**7e**)	40 (**8e**)	—	—

a) All reactions were carried out at room temperature for 24 h. b) Isolated yields. c) Isolated products are designated in parentheses.

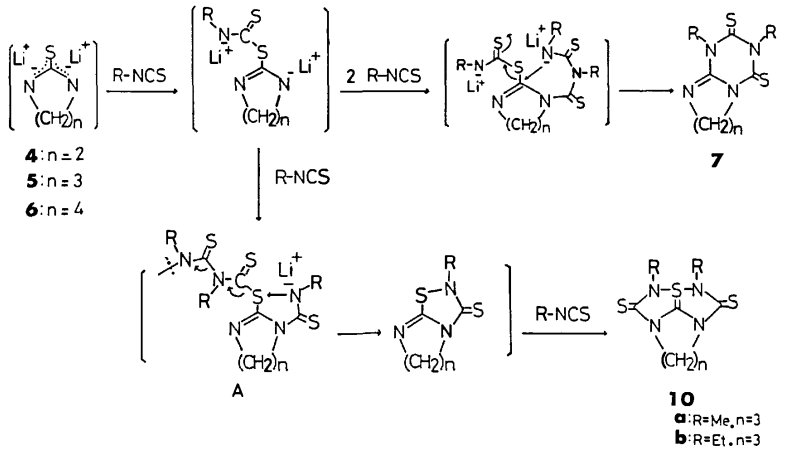

Scheme 2.

rivative (**8**), bis(thiocarbamoyl) derivative (**9**), and heteropentalene derivative (**10**). The yields are summarized in Table 1. The yields of products depended on the ring size of cyclic thiourea, the alkyl group of alkyl isothiocyanate, and reaction conditions. The dianions, **5**, and **6**, reacted with alkyl isothiocyanate to give the ring fused compound **7** in good yields, whereas the dianion **4** to give **7** in poor yields. A possible mechanism for the formation of **7** is given in Scheme 2.

The reaction of methyl (or ethyl) isothiocyanate with dianion **5** at room temperature for 24 h under argon afforded heteropentalene derivative **10** as a minor product together with ring fused compound **7**. The compound **10**, **3a**-thia(S^{IV})pentalene system containing π-hypervalent sulfur, is of interest from the structural point of view. The structure of **10** was determined by IR, Mass, ^{1}H NMR, ^{13}C NMR, and elemental analysis. Our mechanistic interpretation for the formation of **10** is outlined in Scheme 2. When the dianions **4** and **6** were used, heteropentalene derivatives were not obtained. For these results there are two possible explanations. One is that the intermediates A derived from the dianions **4** and **6** have unfavorable configurations for the attack of N atom to S atom compared with the intermediate A derived from the dianion **5**. The other is that the strain of heteropentalene derivative with five- or seven-membered ring is larger than that of **10**.

Next, we have examined the reaction of alkyl isothiocyanate with the dianion of acyclic thiourea.

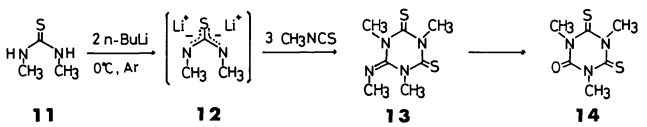

11 **12** **13** **14**

When the reaction of methyl isothiocyanate with dianion (**12**), which is derived from *N,N'*-dimethylthiourea (**11**) with butyllithium, was carried out at room temperature for 24 h under argon, 5,6-dihydro-1,3,5-trimethyl-6-methylimino-1,3,5-triazine-2,4-(1*H*,3*H*)-dithione (**13**) was obtained as a crude product in 84% yield. The structure of **13** was determined by the following spectral data: IR (KBr) 1682 cm^{-1} (C=N); MS (70 eV) *m/z*, 216 (M$^+$); ^{1}H NMR ($CDCl_3$) δ=3.25 (s, 3H), 3.60 (s, 6H), and 3.90 (s, 3H). When the crude product **13** was chromatographed on preparative TLC (silica gel using dichloromethane as an eluent), it was converted into the 3,4,5,6-tetrahydro-1,3,5-trimethyl-4,6-dithioxo-1,3,5-triazin-2(1*H*)-one (**14**) in quantitative yield.

Experimental

Melting points were determined on a Yanagimoto melting point apparatus and were uncorrected. Proton magnetic resonance (^{1}H NMR) spectra were obtained using a Hitachi Perkin-Elmer R-24 spectrometer (60 MHz), JEOL FX-90Q (90 MHz), and JEOL JNM-GX270 (270 MHz). ^{13}C NMR spectra were obtained using a JEOL FX-90Q and JEOL JNM-GX270. Chemical shifts are reported in ppm form TMS as an internal standard and are given in δ units. The IR spectra were determined on a Hitachi 215 Grating infrared spectrometer. Mass spectra were obtained with a SHIMADZU-LKB 9000 instrument equipped with a solid injector; the ionizing voltage was 70 eV.

General Procedure for the Reaction of Alkyl Isothiocyanate with Dianions, (4, 5, and 6). To a cooled THF solution (0 °C) of 3,4,5,6-tetrahydro-2(1*H*)-pyrimidinethione (**2**, 2.0 mmol) was added a hexane solution of butyllithium (4.4 mmol) with stirring at 0 °C under argon, and the mixture was stirred for 1 h under same conditions. To the resulting dianion (**5**) was added dropwise a THF solution of methyl isothiocyanate (6.0 mmol). The solution immediately became orange, and the mixture was stirred for 24 h under argon. After THF was evaporated, the residue was poured into an aqueous ammonium chloride. The solution was extracted with chloroform, and the extract was washed with water, dried over Na_2SO_4, and condensed under reduced pressure. The residue was chromatographed on a silica-gel column or preparative TLC (dichloromethane as an eluent) to give products, **7b** (61%) and **10a** (15%). All compounds were recrystallized from hexane–chloroform to give colorless solid.

6,7,8,8a-Tetrahydro-1,3-dimethylimidazo[1,2-*a*][1,3,5]triazine-2,4(1*H*,3*H*)-dithione (7a). Mp 128—129 °C; IR (KBr) 1677 (C=N) cm^{-1}; ^{1}H NMR ($CDCl_3$) δ=3.68 (s, 3H, CH_3), 4.03 (s, 3H, CH_3), and 3.7—4.4 (m, 4H, NCH_2CH_2N); MS *m/z* 214 (M$^+$). Found: C, 39.47; H, 4.78; N, 26.21%. Calcd for $C_7H_{10}N_4S_2$: C, 39.23; H, 4.70; N, 26.42%.

7,8-Dihydro-1,3-dimethyl-6*H*-pyrimido[1,2-*a*][1,3,5]triazine-2,4(1*H*,3*H*)-dithione (7b). Mp 143—145 °C (lit,[3] 141—142 °C).

7,8-Dihydro-1,3-diethyl-6*H*-pyrimido[1,2-*a*][1,3,5]triazine-2,4(1*H*,3*H*)dithione (7c). Mp 92—94 °C; IR (KBr) 1600 (C=N) cm^{-1}; ^{1}H NMR ($CDCl_3$) δ=1.22 (t, 3H, *J*=7.0 Hz, CH_2CH_3), 1.32 (t, 3H, *J*=7.0 Hz, CH_2CH_3), 1.90 (m, 2H, $NCH_2CH_2CH_2N$), 3.50 (t, 2H, *J*=6.0 Hz, $C=NCH_2$), 4.15 (t, 2H, *J*=6.0 Hz, NCH_2), 4.50 (q, 2H, *J*=7.0 Hz, CH_2CH_3), and 4.96 (q, 2H, *J*=7.0 Hz, CH_2CH_3); MS *m/z* 256 (M$^+$). Found: C, 47.08; H, 6.34; N, 21.80%. Calcd for $C_{10}H_{16}N_4S_2$: C, 46.85; H, 6.29; N, 21.85%.

6,7,8,9-Tetrahydro-1,3-dimethyl-1,3,5-triazino[1,2-*a*][1,3]diazepine-2,4(1*H*,3*H*)-dithione (7d). Mp 97—98 °C; IR (KBr) 1682 (C=N) cm^{-1}; ^{1}H NMR ($CDCl_3$) δ=2.00 (m, 4H, $NCH_2CH_2CH_2CH_2N$), 3.65 (s, 3H, CH_3), 3.75 (t, 2H, *J*=7.0 Hz, $C=NCH_2$), 4.00 (s, 3H, CH_3), and 4.35 (t, 2H, *J*=7.0 Hz, NCH_2); ^{13}C NMR ($CDCl_3$) δ=22.56, 24.46, 38.49, 43.31, 137.74, and 175.82; MS *m/z* 242 (M$^+$). Found: C, 44.35; H, 5.78; N, 22.84%. Calcd for $C_9H_{14}N_4S_2$: C, 44.60; H, 5.82; N, 23.12%.

6,7,8,9-Tetrahydro-1,3-diethyl-1,3,5-triazino[1,2-*a*][1,3]diazepine-2,4(1*H*,3*H*)-dithione (7e). Mp 67—70 °C; IR (KBr) 1650 (C=N) cm^{-1}; ^{1}H NMR ($CDCl_3$) δ=1.22 (t, 3H, *J*=7.0 H, CH_2CH_3), 1.35 (t, 3H, *J*=7.0 Hz, CH_2CH_3), 1.9 (m, 4H, $NCH_2CH_2CH_2CH_2N$), 3.7 (t, 2H, *J*=5.5 Hz, $C=NCH_2$), 4.23 (t, 2H, *J*=5.5 Hz, NCH_2), 4.4 (q, 2H, *J*=7.0 Hz, CH_2CH_3), and 4.8 (q, 2H, *J*=7.0 Hz, CH_2CH_3); MS *m/z* 270 (M$^+$). Found: C, 48.90; H, 6.89; N, 20.55%. Calcd for $C_{11}H_{18}N_4S_2$: C, 48.86; H, 6.71; N, 20.72%.

1-(Methylthiocarbamoyl)-2-imidazolidinethione (8a). Mp 205—206 °C; IR (KBr) 3170 (NH) cm^{-1}; ^{1}H NMR ($CDCl_3$) δ=3.16 (d, 3H, *J*=4.3 Hz, CH_3), 3.60 (d, of t, 2H, *J*=1.2 and 8.9 Hz, $HNCH_2$), 4.67 (t, 2H, *J*=8.9 Hz, NCH_2), 6.5 (br, 1H, NH), and 11.9 (br, 1H, NH); ^{13}C NMR ($CDCl_3$) δ=32.63, 40.12, 52.25, 179.24, and 180.70; MS *m/z* 175 (M$^+$). Found: C, 34.09; H, 5.23; N, 23.80%. Calcd for $C_5H_9N_3S_2$: C, 34.26; H, 5.18; N, 23.97%.

1-(Ethylthiocarbamoyl)-2-imidazolidinethione (8b). Mp 171—172 °C; IR (KBr) 3250 (NH) cm^{-1}; ^{1}H NMR ($CDCl_3$) δ=1.31 (t, 3H, *J*=7.3 Hz, CH_2CH_3), 3.59 (d of t, 2H, *J*=0.8

and 9.1 Hz, $HNC\underline{H}_2$), 3.67 (d of q, 2H, J=5.0 and 7.3 Hz, $C\underline{H}_2CH_3$), 4.66 (t, 2H, J=9.1 Hz, NCH_2), 6.6 (br, 1H, NH), and 11.9 (br, 1H, NH); MS m/z 189 (M^+). Found: C, 38.21; H, 5.94; N, 22.28%. Calcd for $C_6H_{11}N_3S_2$: C, 38.07; H, 5.86; N, 22.20%.

1-(Ethylthiocarbamoyl)perhydropyrimidine-2-thione (8c). Mp 152—154 °C; IR (KBr) 3180 (NH) cm^{-1}; ^1H NMR ($CDCl_3$) δ=1.33 (t, 3H, J=7.3 Hz, $CH_2C\underline{H}_3$), 2.11 (m, 2H, $NCH_2C\underline{H}_2CH_2N$), 3.35 (d of t, 2H, J=2.4 and 6.4 Hz, $HNC\underline{H}_2$), 3.70 (d and q, 2H, J=4.9 and 7.3 Hz, $C\underline{H}_2CH_3$), 4.40 (t, 2H, J=5.5 Hz, NCH_2), 7.3 (br, 1H, NH), and 11.2 (br, 1H, NH); MS m/z 203 (M^+). Found: C, 41.15; H, 6.44; N, 20.50%. Calcd for $C_7H_{13}N_3S_2$: C, 41.35; H, 6.44; N, 20.67%.

1-(Methylthiocarbamoyl)perhydro-1,3-diazepine-2-thione (8d). Mp 138—140 °C; IR (KBr) 3170 (NH) cm^{-1}; ^1H NMR ($CDCl_3$) δ=1.5—2.2 (m, 4H, $NCH_2C\underline{H}_2C\underline{H}_2CH_2N$), 3.15 (d, 3H, J=5.0 Hz, CH_3), 3.35 (d of t, 2H, J=6.0 and 7.0 Hz, $HNC\underline{H}_2$), 4.25 (t, 2H, J=7.0 Hz, NCH_2), 8.25 (br, 1H, NH), and 8.95 (br, 1H, NH); ^{13}C NMR ($CDCl_3$) δ=25.11, 26.30, 32.53, 47.54, 53.17, 182.43, and 189.10; MS m/z 203 (M^+). Found: C, 41.07; H, 6.61; N, 20.48%. Calcd for $C_7H_{13}N_3S_2$: C, 41.35; H, 6.44; N, 20.67%.

1-(Ethylthiocarbamoyl)perhydro-1,3-diazepine-2-thione (8e). Mp 102—104 °C; IR (KBr) 3170 (NH) cm^{-1}; ^1H NMR ($CDCl_3$) δ=1.26 (t, 3H, J=7.3 Hz, $CH_2C\underline{H}_3$), 1.64—2.06 (m, 4H, $NCH_2C\underline{H}_2C\underline{H}_2CH_2N$), 3.35 (d of t, 2H, J=4.8 and 5.6 Hz, $HNC\underline{H}_2$), 3.65 (d of q, 2H, J=4.8 and 7.3 Hz, $C\underline{H}_2CH_3$), 4.22 (t, 2H, J=6.0 Hz, NCH_2), 7.8 (br, 1H, NH), and 9.1 (br, 1H, NH); MS m/z 277 (M^+). Found: C, 43.98; H, 7.05; N, 19.50%. Calcd for $C_8H_{15}N_3S_2$: C, 44.21; H, 6.96; N, 19.33%.

1,3-Bis(methylthiocarbamoyl)-2-imidazolidinethione (9a). Mp 152—154 °C; IR (KBr) 3150 (NH) cm^{-1}; ^1H NMR ($CDCl_3$) δ=3.28 (d, 6H, J=5.0 Hz, 2×CH_3), 4.4 (s, 4H, NCH_2CH_2N), and 11.1 (br, 2H, 2×NH); ^{13}C NMR ($CDCl_3$) δ=33.04, 48.38, 174.23, and 180.91; MS m/z 248 (M^+). Found: C, 33.70; H, 4.94; N, 22.48%. Calcd for $C_7H_{12}N_4S_3$: C, 33.85; H, 4.87; N, 22.56%.

3,4-Dimethyl-1,6-propano-1*H*,6*H*-3a-thia(S^{IV})-1,3,4,6-tetraazapentalene-2,5(3*H*,4*H*)-dithione (10a). Mp 201—203 °C (decomp); IR (KBr) 2920, 1580, 1540, 1500, 1245, 1195, and 1120 cm^{-1}; ^1H NMR ($CDCl_3$) δ=2.36 (m, 2H, $NCH_2C\underline{H}_2CH_2N$), 3.24 (s, 6H, 2×$CH_3$), and 4.4 (t, 4H, J=6.0 Hz, 2×NCH_2); ^{13}C NMR ($CDCl_3$) δ=19.91, 30.91, 44.72, 155.78, and 169.48; MS m/z 187 (M^+-CH_3NCS). Found: C, 36.44; H, 4.43; N, 21.18%. Calcd for $C_8H_{12}N_4S_3$: C, 36.90; H, 4.64; N, 21.52%.

3,4-Diethyl-1,6-propano-1*H*,6*H*-3a-thia(S^{IV})-1,3,4,6-tetraazapentalene-2,5(3*H*,4*H*)-dithione (10b). Mp 217—220 °C (decomp); IR (KBr) 2960, 2910, 1570, 1530, 1490, 1230, 1180, and 1120 cm^{-1}; ^1H NMR ($CDCl_3$) δ=1.33 (t, 6H, J=7.0 Hz, 2×$CH_2C\underline{H}_3$), 2.36 (m, 2H, $NCH_2C\underline{H}_2CH_2N$), 3.78 (q, 4H, J=7.0 Hz, 2×$C\underline{H}_2CH_3$), and 4.41 (t, 4H, J=6.0 Hz, 2×NCH_2); ^{13}C NMR ($CDCl_3$) δ=13.82, 20.01, 39.93, 44.61, 156.11, and 168.65; MS m/z 201 ($M^+-CH_3CH_2NCS$). Found: C, 41.52; H, 5.56; N, 19.55%. Calcd for $C_{10}H_{16}N_4S_3$: C, 41.64; H, 5.59; N, 19.42%.

3,4,5,6-Tetrahydro-1,3,5-trimethyl-4,6-dithioxo-1,3,5-triazin-2(1*H*)-one (14). Mp 112—113 °C; IR (KBr) 1720 (C=O) cm^{-1}; ^1H NMR ($CDCl_3$) δ=3.7 (s, 6H, 2×CH_3) and 4.2 (s, 3H, CH_3); MS m/z 203 (M^+). Found: C, 35.61; H, 4.55; N, 20.74%. Calcd for $C_6H_9N_3OS_2$: C, 35.45; H, 4.46; N, 20.67%.

The authors are grateful to Dr. Masaki Nakamura for collecting NMR data with JEOL FX-90Q.

References

1) a) N. Matsumura, N. Asai, and S. Yoneda, *Nippon Kagaku Kaishi*, **1985**, 310; b) N. Matsumura, N. Asai, and S. Yoneda, *J. Chem. Soc., Chem. Commun.*, **1983**, 1487.

2) a) H. J. M. Dou, M. Ludwikow, P. Hassanaly, J. Kister, and J. Matzger, *J. Heterocyclic Chem.*, **17**, 393 (1980); b) M. Yokoyama and T. Takeshima, *Tetrahedron Lett.*, **21**, 635 (1980); c) M. Yokoyama, K. Hosi, and T. Imamoto, *Synthesis*, **1981**, 908.

3) F. D'Angeli, C. DiBello, and V. Giormani, *Gazz. Chim. Ital.*, **94**, 1342 (1964).

Dehydrooligopeptides. VI. Facile Transformation of α-Phosphoranylideneamino-α-alkenoates to Δ^2-Dehydrodipeptide Derivatives[1)]

Yasuchika YONEZAWA, Atsushi KISUNO, and Chung-gi SHIN*
Laboratory of Organic Chemistry, Faculty of Technology, Kanagawa University, Rokkakubashi, Kanagawa-ku, Yokohama 221
(Received April 12, 1986)

Synopsis. Arbusov reaction of alkyl α-phosphoranylideneamino-α-alkenoates with several halides gave the corresponding α-phosphinylamino-α-alkenoates and Δ^2-dehydrodipeptide derivatives.

In connection with the synthesis of α-dehydroamino acids (DHAs) and dehydropeptides (DHPs), we briefly reported that the an Arbusov-type reaction of alkyl 2-triethoxyphosphoranylideneamino-2-alkenoates (**2**) gave the corresponding diethoxyphosphinyl (Dep) derivatives and that a similar reaction of **2** with phthaloyl (Pht)-Leu-Cl also gave Pht-(Dep)-Δ^2-dehydrodipeptide derivatives.[2-4)]

This paper deals with the utilization of **2** and alkyl 2-triphenylphosphoranylideneamino-2-alkenoates (**3**),[2)] derived from alkyl (*Z*)-2-azido-2-alkenoates (**1**) and $P(OEt)_3$ or $P(C_6H_5)_3$ respectively, to the synthesis of DHA and DHP derivatives. In order to further extend the reaction of **2** and **3**, we chose several halides, including Pht-(L)-α-amino acid (AA) chlorides as reagents.

According to the method reported,[3)] a similar reaction of (*Z*)-**2** with chloroacetyl chloride gave alkyl 2-(*N*-chloroacetyl)-2-diethoxyphosphinylamino-2-alkenoates (**5**). From the results, it was found that after an addition of acyl chloride to the N=P bond of **2** (**4**), an Arbusov reaction of **4** immediately took place, giving **5**, as is illustrated in Scheme 1.

Furthermore, when **2** was treated with alkyl iodide or methyl iodoacetate, a similar reaction readily proceeded to give alkyl 2-[*N*-(alkyl)diethoxyphosphinylamino]-2-alkenoates (**6**). As a result, alkyl halides as well as acyl chlorides were found to be sensitive to the 2-triethoxyphosphoranylideneamino function. In addition, a reaction of **2** with Pht-Gly-Cl or Pht-(L)-Leu-Cl was attempted under similar conditions as those mentioned above to give the expected Pht-(Dep)-Δ^2-(L,Z)-dehydrodipeptide esters (**7** and **8**).

Subsequent treatments of **7** and **8**, respectively, with 25% HBr in acetic acid gave deblocked Pht-Δ^2-(L,Z)-dehydrodipeptide esters (**9** and **10**). However, it was found that the other deprotection of **7** and **8** with HCl in MeOH, HCl in benzene, and with CF_3COOH, respectively, did not take place, even under heating. On the other hand, interestingly, a treatment of **3** with Pht-Gly-Cl in benzene under reflux, and then that of the resulting solution with $NaHCO_3$ aqueous solution, directly gave **9**; however, a similar reaction of **2** did not proceed. Moreover, even a one-pot reaction of **1** with Pht-Gly-Cl and $P(C_6H_5)_3$, **9** was also obtained (see Scheme 2). The results, thus obtained, are summarized in Tables 1—4.

Table 1. Properties of Products (**5** and **6**)

Compd[a)] No.	Yield %	Bp[b)] (θ_b/°C)mmHg[c)]	^{1}H NMR (δ) -CH= (*J*, Hz)
5a	60	Syrup	7.16 dq (2.0, 7.0)
5b	80	Syrup	7.02 dt (2.0, 7.0)
5c	73	Syrup	7.04 dt (2.0, 7.0)
5d	75	Syrup	6.84 dd (1.9, 11.0)
6a	95	98—100/0.14	7.06 dq (2.1, 7.0)
6b	90	108—110/0.09	6.80 dt (2.1, 7.0)
6c	92	110—112/0.08	6.63 dd (2.0, 10.5)
6d	92	102—104/0.09	6.62 dd (2.0, 10.5)
6e	90	120—125/0.05	6.60 dd (2.0, 10.5)
6f	88	Syrup	6.52 dd (2.0, 11.0)
6g	86	Syrup	6.70 dd (2.0, 11.0)

a) All the compounds were analyzed for C, H and N and gave analytical values within 0.3% of the theoretical ones. b) Colorless. c) 1 mmHg = 133.322 Pa.

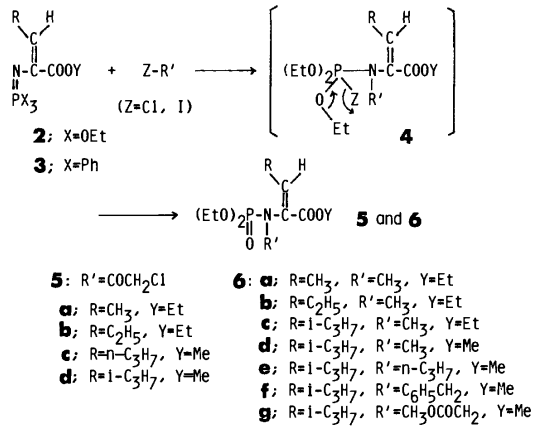

Scheme 1.

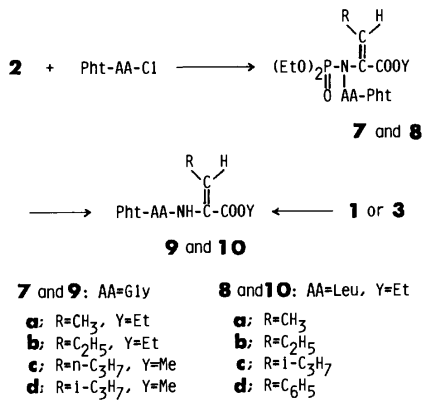

Scheme 2.

Table 2. Properties of Products (**7** and **8**)

Compd[a] No.	Yield %	Mp[b] θ_m/°C	^{1}H NMR (δ) -CH= (J,Hz)	$[\alpha]_D^{25}$ (c 0.2)[c]
7a	70	61—62	7.20 dd (2.0, 7.0)	
7b	67	99—100	7.06 dt (2.0, 7.0)	
7c	83	89—90	7.10 dt (2.0, 7.0)	
7d	74	98—99	6.90 dd (2.0, 11.0)	
8a	70	59—60	7.02 dq (2.0, 7.0)	−21.5°
8b	66	79—80.5	6.90 dt (2.0, 7.0)	−60.2°
8c	64	Syrup	6.75 dd (2.2, 11.0)	−45.3°
8d	60	119—120	7.35— 7.84m (C_6H_5+H)	−40.4°

a) See footnote a) in Table 1. b) Colorless prisms from cyclohexane. c) Measured in methanol.

Table 3. Yields of **9** from **1**, **3**, and **7**

Compd. No.	From **1**	From **3**	From **7**	Mp(θ_m/°C[a])
9a	48	51	97	177—179 (180.5—181.5[b])
9b	43	50	86	173—175 (173—173.5[b])
9c	43	48	72	174—175[c]
9d	41	45	71	164—165 (162—165[b])

a) Colorless needles. b) Lit,[5]. c) See footnote a) in Table 1.

Based on the spectral data as well as a satisfactory elemental analysis, the structures of all the new compounds could be readily determined. The NMR spectra of the products showed long-range coupling between β-olefinic, γ-methyl or γ-methylene protons and the phosphorus atom. In the case of **6**, in addition to the above long-range couplings, another coupling between *N*-alkyl protons and phosphorus also appeared.

As is summarized in the Tables, the characteristic olefin proton signals of **6** shifted at the δ 7.06—6.52 ($J_{3,4}$=7.0—11.0 Hz) region, whereas those of **5**, **7**, and **8** resonated at a slightly lower magnetic field at the δ 7.60—6.75 region with a similar coupling constant ($J_{3,4}$=7.0—11.0). On the other hand, the coupling constants between the β-olefinic proton and phosphorus in **6** were also found to be almost the same ($J_{3,P}$=1.9—2.2 Hz) as that of **5**, **7**, and **8**. In addition, the methyl and methylene protons at the nitrogen coupled with phosphorus and was observed as a doublet (J=7.5—10.0 Hz). Consequently, all the signals and the coupling constants of the new compounds obtained could be assigned.

Furthermore, in the IR spectrum of the products, the characteristic absorption bands of ester carbonyl, C=C, -P=O, and =P-O-CH_2- functions appear at 1715—1760 (strong; s), 1615—1660 (medium), 1260—1280 (s), and 1020—1040 (s) cm^{-1}, respectively.

In closing, since **9** was in accordance with the authentic samples[5] and **10** was prepared independently by a reaction of Pht-(L)-Leu-Cl with ethyl 2-amino-2-alkenoates or *N*-carboxy α-dehydroamino acid anhydrides,[6] the structures could be readily determined as alkyl 2-phthaloylglycyl-and-(L)-leucyl-amino-2-alkenoates, respectively.

Table 4. Properties of Products (**10**)

Compd[a] No.	Yield %	Mp[b] θ_m/°C	^{1}H NMR (δ) -CH= (J, Hz)	$[\alpha]_D^{25}$ (c 0.2)[c]
10a	60	90—91	6.54 d (8.0)	−20.2°
10b	60	169—170	6.44 d (8.0)	−52.5°
10c	55	117—119	6.41 d (10.0)	−55.8°
10d	65	164—165	7.22— 7.50m (Ph+H)	−49.6°

a) See footnote a) in Table 1. b) Colorless needles from ethyl acetate and cyclohexane. c) Measured in methanol.

Experimental

All the boiling and melting points are uncorrected. The IR spectra were recorded with a Hitachi EPI-G3 spectrometer. The NMR spectra were measured with a JEOL JNM-PS-100 spectrometer in a $CDCl_3$ solution with tetramethylsilane as the internal standard.

Preparation of 5. To a solution of **2** (25 mmol) in dry benzene (30 ml) was added chloroacetyl chloride (50 ml) with stirring under cooling. The resulting solution was continuously stirred at room temperature for 2.5 h. After removing the solvent, the obtained residual syrup was purified on a silica-gel column using a mixture of benzene-ethyl acetate (4:1 v/v) as the eluent to give **5**.

Preparation of 6. A reaction of **2** (15 mmol) with an appropriate alkyl iodide or methyl iodoacetate (45 mmol) was similarly worked up under reflux for 4 h to give a residual syrup, which was distilled in vacuo or purified on a silica-gel column using a mixture of benzene-ethyl acetate (5:1 v/v) as the eluent to give **6**.

Preparation of 7 and 8. A treatment of **2** (10 mmol) with Pht-(L)-AA-Cl (11 mmol) was similarly worked up at room temperature for 12 h to give a reaction solution which was washed with saturated $NaHCO_3$ solution and water and then dried over anhydrous Na_2SO_4. The removal of the solvent under reduced pressure gave a crude syrup, which was purified on a silica-gel column using a mixture of benzene-ethyl acetate (4:1 v/v) as the eluent to give **7** and **8** as a syrup or crystals.

Preparation of 9. a) A solution of **7** (3 mmol) in 25% HBr in acetic acid (5 ml) was stirred at room temperature for 3h and then the excess solvent was removed to give crystals. Recrystallization from EtOH gave **9**.

In a similar manner, a treatment of **8** with 25% HBr in acetic acid was worked up to give **10**.

b) A solution of an equimolar **3** (10 mmol) and Pht-Gly-Cl in dry benzene (30 ml) was refluxed for 5 h. The resulting solution was washed five times with a saturated $NaHCO_3$ solution and then three times with water and finally dried over anhydrous Na_2SO_4. The removal of the solvent gave residual crystals, which were recrystallized from EtOH to give **9**.

c) Into a solution of **1** (10 mmol) in dry benzene (30 ml) $P(C_6H_5)_3$ (10 mmol) was added with stirring, portionwise, under cooling. After stirring at room temperature for 1 h, Pht-Gly-Cl (10 mmol) was added to the

resulting solution and then refluxed for 5 h. Finally, the reaction solution was similarly worked up to give **9**.

References

1) Part V: C. Shin, Y. Yonezawa, and T. Yamada, *Chem. Pharm. Bull.*, **32**, 3934 (1984).
2) C. Shin, Y. Yonezawa, K. Watanabe, and J. Yoshimura, *Bull. Chem. Soc. Jpn.*, **54**, 3811 (1981).
3) Y. Yonezawa, C. Shin, M. Kiyohara, and J. Yoshimura, *Tetrahedron Lett.*, **1979**, 3851.
4) In this paper, the symbol Δ^2 indicates the position of double bond of DHA residue from the N-terminus in sequence.
5) C. Shin, M. Hayakawa, T. Suzuki, A. Ohtsuka, and J. Yoshimura, *Bull. Chem. Soc. Jpn.*, **51**, 550 (1978).
6) Unpublished data.

Formation of 2-Substituted 1,3-Diphenylindenes by an *N*-Bromosuccinimide Prompted Dehydrocyclization of 2-Substituted 1,3,3-Triphenyl-1-propenes

Kimiaki YAMAMURA,* Hideyoshi MIYAKE, and Akira SERA†
Department of Chemistry, College of General Education, Kobe University, Tsurukabuto, Nada, Kobe 657
†Department of Chemistry, Faculty of Science, Kobe University, Rokkodai, Nada, Kobe 657
(Received April 23, 1986)

Synopsis. The reactions of a series of 2-substituted 1,3,3-triphenyl-1-propenes with *N*-bromosuccinimide (NBS) afforded the corresponding 2-substituted 1,3-diphenylindenes in moderate yields. A reaction mechanism involving a novel free-radical intramolecular ring-closure reaction is suggested.

N-Bromosuccinimide (NBS) has been extensively used both in the bromination of the allylic and benzylic positions and in the oxidation of many classes of organic compounds.[1] This article details an NBS-prompted conversion of a series of 2-substituted 1,3,3,-triphenyl-1-propene derivatives (**1**) to the 2-substituted 1,3-diphenylindenes (**2**) by means of a novel free-radical intramolecular ring-closure reaction. The starting 2-substituted 1,3,3-triphenyl-1-propenes (**1**) were readily obtainable by the phenylation of the corresponding 2-substituted 1-phenyl-1-propenes using palladium(II) salts as previously reported.[2]

The reactions of **1** with NBS in the presence of benzoyl peroxide unexpectedly gave 2-substituted 1,3-diphenylindenes(**2**); no corresponding benzylic bromination product was detected. The results are shown in Table 1. Thus, ethyl (*E*)-α-(diphenylmethyl)cinnamate ((*E*)-**1a**) reacted with NBS in refluxing benzene or carbon tetrachloride to give 2-ethoxycarbonyl-1,3-diphenylindene (**2a**) as the sole crystalline product in 66—69% yields (Runs 1 and 2). Similar reactions of (*E*)-**1a** by the use of *N*-bromocaprolactam or *N*-bromoacetamide also yielded **2a**, though the yields were somewhat unsatisfactory. In these reactions some of the starting (*E*)-**1a** was recovered together with its isomer ((*Z*)-**1a**). The (*Z*)-isomer ((*Z*)-**1a**) also underwent a similar reaction with NBS to afford **2a** in 63% yield (Run 3). In the same manner, α-(diphenylmethyl)cinnamic acid (**1b**), α-(diphenylmethyl)chalcone (**1c**), 1,2,3,3-tetraphenyl-1-propene (**1d**) and 2-(*p*-methoxyphenyl)-1,3,3-triphenyl-1-propene (**1e**) reacted with NBS to produce the corresponding 2-substituted 1,3-diphenylindene derivatives, **2b—d**, and **2e**, respectively (Run 4—10). The structures of **2a—e** were determined by spectroscopic and elemental analyses. Compound **2d** was identified by a comparison of its melting point and NMR spectrum with those reported in the literature.[3] Furthermore, the hydrogenation of **2d** on Pd–C afforded known *r*-1, *c*-2, *c*-3-triphenylindan, whose structure was identified by comparing its physical data with that from the literature.[4]

However, an attempted conversion of the nitro derivative (**1f**) into 2-nitro-1,3-diphenylindene (**2f**) was unsuccessful. The starting material was recovered unchanged (Run 11). The reaction, under forced conditions, gave an intractable product mixture.

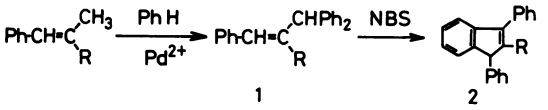

1 2

Table 1. Dehydrocyclization of **1** with NBS

	R	1	Solvent	Reaction Time/h	Product	Yield[a] %
1	CO_2Me	(*E*)-**1a**	C_6H_6	6	**2a**	66
2		(*E*)-**1a**	CCl_4	6	**2a**	68
3		(*Z*)-**1a**	C_6H_6	4	**2a**	63
4	CO_2H	(*E*)-**1b**	C_6H_6	5	**2b**	51
5		(*Z*)-**1b**	C_6H_6	5	**2b**	53
6	COC_6H_5	(*E*)-**1c**	C_6H_6	4	**2c**	60
7	C_6H_5	(*E*)-**1d**	C_6H_6	6	**2d**	11
8		(*E*)-**1d**	CCl_4	4	**2d**	42
9		(*Z*)-**1d**	CCl_4	4	**2d**	40
10	C_6H_4-OMe(*p*)	(*E*)-**1e**	CCl_4	4	**2e**	40
11	NO_2	(*E*)-**1f**	CCl_4	8	—[b]	
12	H	(*Z*)-**1g**	C_6H_6	6	**7**[c]	56

a) Isolated yields of the pure products. b) Recovered unchanged. c) The formation of **2g** was not detected.

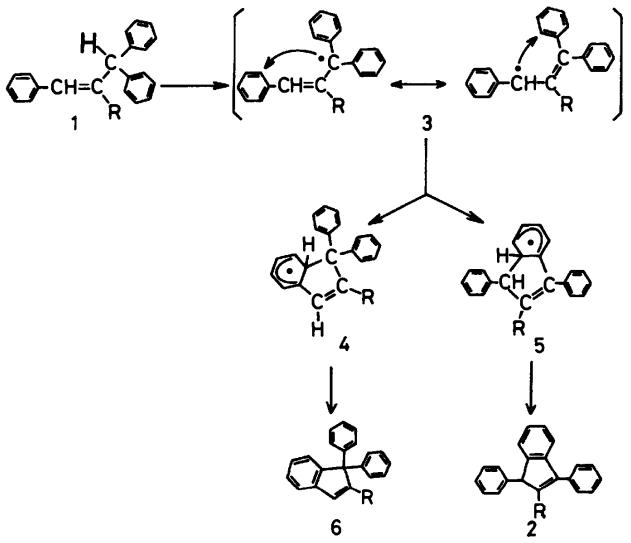

Scheme 1.

The formation of **2** can best be rationalized by the mechanism given in Scheme 1. The boldfaced hydrogen atom in **1**, being both allylic and benzylic, is readily abstracted by NBS to give a resonance-stabilized substituted cinnamyl radical (**3**). In general a cinnamyl radical generated in solutions tends to give products which result from an intramolecular attack; thus, indene was produced.[5,6] The formation of indene was observed solely during the gas-phase pyrolysis of cinnamyl ester.[7] A kinetic isotope effect suggested an intervention of a reversible process of the cinnamyl radical to a cyclic radical intermediate (Ar_2-5 mechanism) and a following rate-determining aromatization step.[7] These results are in contrast to the present observation where the indene derivatives were produced from 1,2,3-trisubstituted cinnamyl radicals. The radical could cyclize either through a cyclized radical (**4**) to give 1,1-diphenylindene derivative (**6**), or through another cyclized radical (**5**) to **2**, or could couple to give a dimer. The absence of the coupling process is best rationalized by taking account of steric hindrance near the reaction sites. The same steric factor also gives an explanation for the failure of a cyclization of the radical to the intermediate radical (**4**).

As mentioned before, the nitro derivative (**1f**) did not afford the corresponding indene (**2f**) (Run 11). The presence of the nitro group on the carbon atom next to the benzylic carbon atom is responsible for the innertness of **1f** under the present reaction conditions.[1c] By the same token, 1,1-diphenyl-2-nitroethane, which has a similar structural feature, also resisted hydrogen abstraction by NBS.

The reaction of 1,3,3-triphenyl-1-propene (**1g**)[8] with NBS did not afford the expected product, 1,3-diphenylindene (**2g**). Instead, a dimeric product, 1,3-diphenyl-2-(1,3,3-triphenyl-2-propenyl)indene (**7**),[9] was obtained (Run 12). This observation suggests that the initially formed **2g** is capable of being attacked by an intermediate 1,3,3-triphenyl-2-propenyl radical (**3g**) at the unsubstituted 2-position of **2g** (Scheme 2).

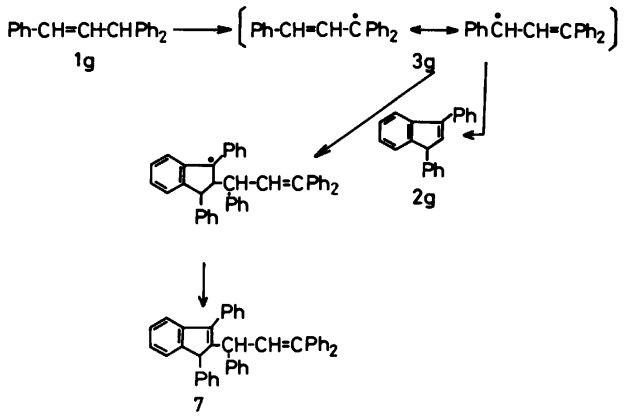

Scheme 2.

Indene itself was, in fact, supposed to be added by radicals to yield unidentified polymeric materials.[6] However, similar attacks by rather bulky 2-substituted 1,3,3-triphenyl-2-propenyl radicals were highly restricted in the reactions of **1a—e**; hence, 1,2,3-trisubstituted indenes survived under the present reaction conditions.

In summary, although NBS has been known to be an effective reagent for the dehydrogenation of allylic and benzylic positions, such an intramolecular dehydrocyclization between allyl and phenyl groups is almost unprecedented. Also, the diphenylation of the 2-substituted 1-phenyl-1-propenes and subsequent cyclization reaction may serve as a synthetic route to a series of 2-substituted 1,3-diphenylindene derivatives.

Experimental

All melting points were uncorrected. ^1H NMR spectra were determined with a Hitachi R-24A spectrometer in $CDCl_3$ using tetramethylsilane as an internal reference.

General Procedure for the Dehydrocyclization of 1,3,3-Triphenyl-1-propenes (1). A mixture of the 2-substituted 1,3,3-triphenyl-1-propene (1 mmol), *N*-bromosuccinimide (1.2 mmol) and a catalytic amount of benzoyl peroxide in 30 ml of benzene or carbon tetrachloride was refluxed with stirring for the stated period of time, cooled, and partitioned between benzene and water. The benzene extracts were dried over anhydrous magnesium sulfate, and the solvent was removed under reduced pressure. The residue was purified by column chromatography (silica gel) and recrystallization to give **2**. The physical properties of **2** are given below.

2a: Colorless prisms, mp 75 °C, ^1H NMR δ=7.36 (s, 4H, phenyl), 7.16 (s, 5H, phenyl), 7.09 (s, 5H, phenyl), 4.96 (s, 1H, methine), 3.43 (s, 3H, methyl), Found: C, 84.36, H, 5.51%. Calcd for $C_{23}H_{18}O_2$: C, 84.64, H, 5.56%.

2b: Colorless microcrystals, mp 194 °C, ^1H NMR δ=7.38 (s, 4H, phenyl), 7.28 (s, 5H, phenyl), 7.11 (s, 5H, phenyl), 4.96 (s, 1H, methine), 3.43 (s, 3H, methyl), Found: C, 84.69, H, 5.10%. Calcd for $C_{22}H_{16}O_2$: C, 84.59, H, 5.16%.

2c: Colorless prisms, mp 154 °C, ^1H NMR δ=7.50—6.90 (m, 19H, phenyl), 7.28 (s, 5H, phenyl), 7.11 (s, 5H, phenyl), 4.94 (s, 1H, methine), Found: C, 90.42, H, 5.70%. Calcd for $C_{28}H_{20}O$: C, 90.29, H, 5.41%.

2d: Colorless needles, mp 136 °C, ^1H NMR δ=7.30 (s, 4H, phenyl), 7.25 (s, 4H, phenyl), 7.05 (s, 5H, phenyl), 6.98 (s, 5H, phenyl), 5.03 (s, 1H, methine), Found: C, 94.02, H, 5.99%. Calcd for $C_{27}H_{20}$: C, 94.15, H, 5.85%.

2e: Colorless needles, mp 95 °C, ^{1}H NMR δ=7.29 (s, 4H, phenyl), 7.10—6.40 (m, 14H, phenyl), 4.96 (s, 1H, methine), 3.56 (s, 3H, methyl), Found: C, 89.99, H, 5.84%. Calcd for $C_{28}H_{22}O$: C, 89.81, H, 5.92%.

The authors are indebted to Miss Masuko Nishinaka for mass spectral measurements and elemental analyses.

References

1) a) R. Filler, *Chem. Revs.*, **63**, 21 (1963); b) R. S. Skell and J. C. Day, *Acc. Chem. Res.*, **11**, 381 (1978); c) J. S. Pizey, "Synthetic Reagents," Ellis Horwood Ltd., Chichester, (1974), Vol. 2.

2) K. Yamamura, *J. Chem. Soc., Perkin Trans. 1*, **1975**, 988.

3) R. Maroni, G. Melloni, and G. Modena *J. Chem. Soc., Perkin Trans. 1*, **1974**, 353.

4) G. Melloni and F. Marcuzzo, *J. Chem. Res. (S).*, **1979**, 184.

5) H. P. Koch, *J. Chem. Soc.*, **1948**, 1111.

6) P. D. Bartlett and R. R. Hiatt, *J. Am. Chem. Soc.*, **80**, 1398 (1958).

7) W. S. Trahanovsky and C. C. Ong, *J.Am. Chem. Soc.*, **92**, 7174 (1970).

8) Compound **lg** was prepared from **lf** by removal of the nitro group; N. Ono, S. Kawai, K. Tanaka, and A. Kaji, *Tetrahedron Lett.*, **1979**, 1733.

9) D. W. Jones, *J. Chem. Soc. (c)*, **1966**, 1026; T. Greibrokk, *Acta. Chem. Scad.*, **27**, 2252 (1973).

A Convenient Synthesis of Cholesta-1,5,7-trien-3β-ol

Yoji TACHIBANA
Central Research Laboratory, Nisshin Flour Milling, Co., Ltd.,
Tsurugaoka, Ooimachi, Iruma-gun, Saitama 354
(Received May 7, 1986)

Synopsis. Cholesta-4,6-dien-3β-ol (**4**) was obtained selectively by the dehydrobromination of 7-bromocholesterol with a base in the presence of a catalytic amount of tetrabutylammonium bromide. The oxidation of **4** with 2,3-dichloro-5,6-dicyano-p-benzoquinone gave cholesta-1,4,6-trien-3-one (**7**). Treatment of **7** with isopropenyl acetate under acidic conditions afforded 3-acetoxy-1,3,5,7-cholestatetraene, which was reduced with calcium borohydride to yield cholesta-1,5,7-trien-3β-ol (**2**).

The synthesis of cholesta-5,7-diene-1α,3β-diol (**1**), the photoprecursor of the physiologically active 1α-hydroxyvitamin D_3, has been reported by many research groups.[1-13] Kaneko et al.[5] reported the synthesis of cholesta-1,5,7-trien-3β-ol (**2**), a key intermediate for the preparation of **1**, by the base-catalyzed rearrangement of cholesta-1,4,6-trien-3-one (**7**)[14,15] followed by the reduction of the formed cholesta-1,5,7-trien-3-one. This method is interesting and attractive, but generally gives a poor yield of **2**. Thus, it is desirable to prepare **2** in higher yield. In the present paper, an improved method for the preparation of cholesta-4,6-dien-3-one (**6**)[16] and its conversion to **2** are described.

Lappordt et al.[17] reported the selective synthesis of cholesta-4,6-dien-3-β-ol (**4**) through the dehydrobromination of 7-bromocholesterol (**3**) derivative[18,19] in the presence of a combination of a large excess of tetrabutylammonium bromide and 2,4,6-trimethylpyridine in tetrahydrofuran. In contrast to their results, we have found that at higher temperature, the dehydrobromination of **3** by a base proceeded smoothly in the presence of a catalytic amount of tetrabutylammonium bromide (Table 1).

The 4,6-dien-3-ol (**4**) was oxidized by various oxidizing agents to give the corresponding 4,6-dien-3-one (**6**) in 50—85% yields (Table 2). Treatment of **4** with 2,3-dichloro-5,6-dicyano-*p*-benzoquinone[20,21] afforded **7** in one stage without isolation of **6**.

It is well-known that the steroidal 1,4-dienone and 1,4,6-trienone undergo rearangement to give the phenol derivatives under acidic conditions.[22,23] However it was found that the enol acetylation of the 1,4,6-trien-3-one (**7**) with isopropenyl acetate in the presence of p-toluenesulfonic acid successfully yielded 3-acetoxy-1,3,5,7-cholestatetraene (**8**)[12] in a fairly good yield. The tetraenyl acetate (**8**) was reduced with calcium borohydride to afford the 1,5,7-trien-3-ol (**2**)

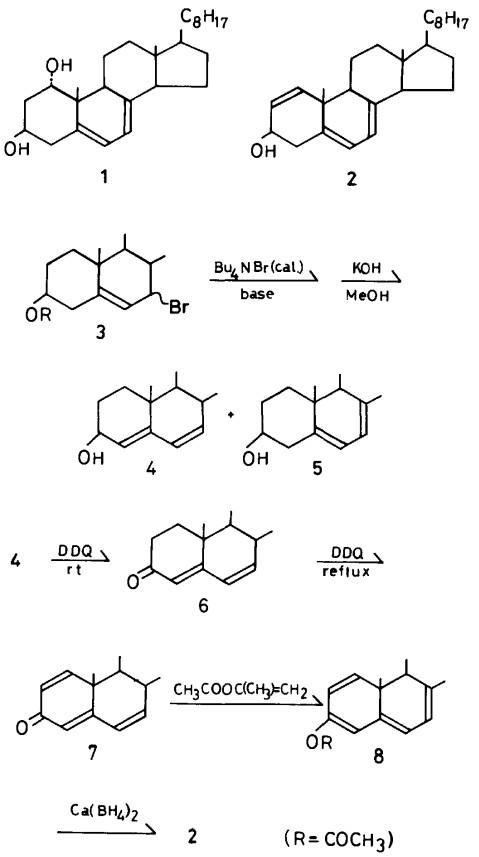

Table 1. Yields of Cholesta-4,6-dien-3β-ol (**4**) in the Dehydrobromination of 7-Bromocholesteryl Acetate (**3**)[1]

Bu_4NBr/**3**	Base	Temp °C	Time min	Yield[2] %	4/5[4]
0.1	2,4,6-Trimethylpyridine	100	20	60	7.4
0.1	2,4,6-Trimethylpyridine	125	10	62	6.8
0.1	2,4,6-Trimethylpyridine	65	70	18[3]	9.5
1.0	2,4,6-Trimethylpyridine	125	10	68	8.3
1.0	2-Methylquinoline	125	10	44	5.9

1) 7-Bromocholesteryl acetate was prepared by the reaction of cholesteryl acetate with *N*-bromosuccinimide and employed without further purification. 2) Isolated yield. 3) Tetrahydrofuran was used as a solvent. 4) The formation ratio was determined on the basis of UV spectra.

Table 2. Oxidation of Cholesta-4,6-dien-3β-ol (**4**) into Cholesta-4,6-dien-3-one (**6**) under Various Conditions

Oxidizing agent	Time h	Solvent	Temp °C	Yield[1] %
DDQ[2]	20	Dioxane	rt[3]	85
DDQ	20	Toluene	rt	74
PDC[4]	6	Dichloro-methane	rt	75
PCC[5]	20	Dichloro-methane	rt	58
$Al(OPr^i)_3$-*p*-benzoquinone	20	Toluene	rt	72
$Al(OPr^i)_3$-*p*-benzoquinone	20	Toluene	110	70
RuO_2-$NaIO_4$	48	Trichloro-ethylene/ methanol/H_2O	rt	50

1) Isolated yield. 2) 2,3-Dichloro-5,6-dicyano-*p*-benzoquinone. 3) Room temperature. 4) Pyridinium dichromate. 5) Pyridinium chlorochromate.

quantitatively. The 1,5,7-trien-3-ol (**2**) was converted to **1** by the method described in the literatures.[5,12-13]

Since cholesta-1,5,7-trien-3β-ol (**2**) is obtainable readily from cholesterol as described above, the present study provides a simple and efficient method for the preparation of 1α-hydroxyprovitamin D_3 (**1**).

Experimental

Melting points are uncorrected. UV spectra were taken on a Hitachi 320 spectrometer. Optical rotations were determined with JASCO DIP-4 polarimeter.

Cholesta-4,6-dien-3β-ol (4). A hexane solution of cholesteryl acetate (42.8 g), *N*-bromosuccinimide (21.0 g) and a catalytic amount of benzoyl peroxide was allowed to react under reflux for 40 min. The hexane solution was filtered to remove succinimide and the filtrate was evaporated to dryness under reduced pressure at below 40 °C. The residue was dissolved in butyl acetate (150 ml). Tetrabutylammonium bromide (3.2 g) and 2,4,6-trimethylpyridine (14.5 g) were added to the butyl acetate solution. The mixture was refluxed for 20 min. The solution was washed with dil. hydrochloric acid, water, dried over sodium sulfate and concentrated to a semi-crystalline residue under reduced pressure. To the residue, methanolic potassium hydroxide solution (KOH 6.2 g, methanol 200 ml) was added and the mixture was refluxed for 10 min. The methanol solution was allowed to stand overnight at room temperature. The crude cholesta-4,6-dien-3β-ol (**4**) was collected by filtration. The crude product was purified by silica-gel column chromatography (eluted with chloroform) to give **4**. 23.8 g (62%): Mp 116—117 °C (lit,[15] mp 119—120 °C); λ_{max} 239 nm (ε=25,000, EtOH).

Cholesta-4,6-dien-3-one (6). A typical procedure for the preparation of cholesta-4,6-dien-3-one (**6**) from cholesta-4,6-dien-3β-ol (**4**) is described in the following. A mixture of **4** (3.8 g) and 2,3-dichloro-5,6-dicyano-p-benzoquinone (DDQ) (2.9 g) in dioxane (20 ml) was allowed to react at room temperature for 18 h. After the formed hydroquinone was filtered off, the filtrate was condensed to dryness at reduced pressure. The residue was chromatographed on silica gel using hexane-ethyl acetate (9/1) as eluent. Crystallization from acetone gave cholesta-4,6-dien-3-one (**6**). 3.2 g (85%): Mp 81—82 °C (lit,[17] mp 80.5—81.5 °C); λ_{max} 284 nm (ε=28,700, EtOH).

Cholesta-1,4,6-trien-3-one (7). A dioxane solution containing the 4,6-dienol (**4**) (7.7 g) and DDQ (5.2 g) was treated with stirring at room temperature for 18 h. After the hydroquinone was removed by filtration, a further DDQ (4.4 g) was added to the filtrate. The dioxane solution was refluxed for 2 h. After filtration and removal of the solvent under reduced pressure, the resulting residue was chromatographed on silica gel. Elution with hexane-ethyl acetate (9/1) and crystallization from acetone gave the 1,4,6-trienone (**7**). 4.9 g (65%): Mp 89—90 °C (lit,[14] mp 82—83 °C; λ_{max} 300 nm (ε=13,400, EtOH).

Cholesta-1,5,7-trien-3β-ol (2). A mixture of the 1,4,6-trien-3-one (**7**) (38.0 g), *p*-toluenesulfonic acid (19.0 g) in butyl acetate (500 ml) and isopropenyl acetate (400 ml) was refluxed for 7 h. The butyl acetate solution was washed with water and dried over sodium sulfate. The solution was concentrated to dryness under reduced pressure. The residue was crystallized from acetone to give 3-acetoxy-1,3,5,7-cholestatetraene (**8**) as yellow needles. 27.0 g (64%): Mp 123—124 °C (lit,[12] mp 122—124 °C); $[\alpha]_D^{25}$ −507° (*c* 0.6, $CHCl_3$).

The ether solution of the tetraene (**8**) (15.0 g) was added dropwise at −10 °C to a stirred solution of calcium borohydride in ethanol-methanol (calcium chloride (30.0 g) in methanol (250 ml) and sodium borohydride (15.0 g) in ethanol (250 ml)).[5] The mixture was stirred at 0 °C for 3 h and standed overnight. After addition of 50% acetic acid to dissolve the resulted precipitate, the product was extracted with ether. The extract was washed with aq sodium hydrogencarbonate, water and dried over sodium sulfate. The ether was evaporated to dryness under reduced pressure and the residue was chromatographed on silica gel. The product, which was eluted with hexane-ethyl acetate (4/1) was crystallized from acetone to give **2**. 12.8 g (94%): Mp 126—127 °C (lit,[5] mp 128—129 °C); λ_{max} 282 nm (ε=10,900, EtOH).

References

1) M. F. Holich, F. J. Semmler, H. K. Schnoes, and H. F. Deluca, *Science*, **180**, 190 (1973).

2) D. H. R. Barton, R. H. Hesse, M. M. Pechet, and E. Rizzardo, *J. Am. Chem. Soc.*, **95**, 2748 (1973).

3) A. Fürst, L. Labler, W. Meier, and K.-H. Pfoertner, *Helv. Chim. Acta*, **56**, 1708 (1973).

4) C. Kaneko, S. Yamada, A. Sugimoto, M. Ishikawa, S. Sasaki, and T. Suda, *Tetrahedron Lett.*, **1973**, 2339.

5) C. Kaneko, A. Sugimoto, Y. Eguchi, S. Yamada, and M. Ishikawa, *Tetrahedron*, **30**, 2701 (1974).

6) C. Kaneko, S. Yamada, A. Sugimoto, Y. Eguchi, M. Ishikawa, T. Suda, M. Suzuki, S. Kakuta, and S. Sasaki, *Steroids*, **23**, 75 (1974).

7) M. Morisaki, K. Bannai, N. Ikekawa, *Chem. Pharm. Bull.*, **21**, 1853 (1973).

8) M. Morisaki, A. Saika, K. Bannai, M. Sawamura, J. R. Lightbourn, and N. Ikekawa, *Chem. Pharm. Bull.*, **23**, 3272 (1975).

9) M. Morisaki, K. Bannai, and N. Ikekawa, *Chem. Pharm. Bull.*, **24**, 1948 (1976).

10) D. Freeman, A. Acher, and Y. Mazur, *Tetrahedron Lett.*, **1975**, 261.

11) T. Sato, H. Yamauchi, Y. Ogata, M. Tsuji, T. Kunii, K. Kogai, S. Toyoshima, and T. Kobayashi, *Chem. Pharm. Bull.*, **26**, 2933 (1978).

12) A. Emke, D. Hands, J. M. Midgley, W. B. Whalley, and R. Ahmad, *J. Chem. Soc., Perkin Trans. 1*, **1977**, 820.

13) D. W. Guest and D. H. Williams, *J. Chem. Soc., Perkin Trans. 1*, **1979**, 1695.

14) C. Djerassi, G. Rosenkrantz, J. Romo, J. Pataki, and St. Kaufmann, *J. Am. Chem. Soc.*, **72**, 4540 (1950).
15) F. Sondheimer, C. Amendolla, and C. Rosenkrantz, *J. Am. Chem. Soc.*, **75**, 5932 (1953).
16) A. L. Wilds and C. Djerassi, *J. Am. Chem. Soc.*, **68**, 1712 (1946); L. Mandell, *J. Am. Chem. Soc.*, **78**, 3199 (1956); K. M. Baker and B. R. Davis, *J. Chem. Soc., (C)*, **1968**, 2743.
17) M. P. Lappoldt, O. Hoogendoorn, and L. F. Pauli, "Vitamin D: Chemical and Clinical Endocrinology of Calcium Metabolism," ed by A. M. Norman, K. Schaefer, D. V. Herrath, and H. G. Grigoleit, Walter de Gruyter & Co., New York (1982), pp. 1133—1135.
18) K. Ziegler, A. Späth, E. Schaaf, W. Schumann, and E. M. Winkelmann, *Justis Liebigs Ann. Chem.*, **551**, 80 (1942).
19) R. Jaworska and M. Kocór, *Tetrahedron Lett.*, **1968**, 4341; A. E. Bide, H. B. Henbest, E. R. H. Jones, R. M. Peevers, and P. A. Wilkinson, *J. Chem. Soc.*, **1948**, 1783.
20) D. Burn, D. M. Kirk, and V. Petrov, *Proc. Chem. Soc.*, **1960**, 4; A. B. Turner, *J. Chem. Soc., (C)*, **1968**, 2568.
21) M. M. Nitra, A. M. Norman, and W. H. Okamura, *J. Org. Chem.*, **39**, 2931 (1974).
22) St. Kaufmann, J. Pataki, G. Rosenkrantz, J. Romo, and C. Djerassi, *J. Am. Chem. Soc.*, **72**, 4531 (1950).
23) A. G. Avent, J. R. Hanson, L. Yang-Zhi, and I. H. Sadler, *J. Chem. Soc., Perkin Trans. 1*, **1985**, 2129.

Carbon Dioxide-Promoted Telomerization of 1,2- and 1,3-Dienes with Benzenesulfinate Catalyzed by Palladium(0)*

Yoshio INOUE* and Harukichi HASHIMOTO
Department of Applied Chemistry, Faculty of Engineering, Tohoku University, Aoba, Aramaki, Sendai 980
(Received May 12, 1986)

Synopsis. The telomerization of 1,2- and 1,3-dienes with benzenesulfinate dihydrate catalyzed by palladium(0) has been promoted by the presence of carbon dioxide.

Palladium complexes catalyze the dimerization of 1,3-butadiene with incorporation of nucleophiles such as alcohols, phenols, carboxylic acids, amines, enamines and active methylene compounds to form 1-substituted 2,7-octadiene and 3-substituted 1,7-octadiene.[1]

$$2CH_2{=}CHCH{=}CH_2 + YH \xrightarrow{Pd} CH_2{=}CH(CH_2)_3CH{=}CHCH_2Y + CH_2{=}CH(CH_2)_3CH(Y)CH{=}CH_2$$

Allene reacts similarly to afford 2,3-dialkyl-1,3-butadiene derivatives.[1]

$$2CH_2{=}C{=}CH_2 + YH \xrightarrow{Pd} CH_2{=}C(CH_3)C(CH_2Y){=}CH_2$$

In certain cases, introduction of carbon dioxide profoundly alters the properties of the catalyst. For example, formation of 2,7-octadien-1-ol has been accomplished from the reaction of water with two moles of 1,3-butadiene in the presence of a considerable amount of carbon dioxide.[2] In the absence of carbon dioxide, the formation of the alcohol is very sluggish. The telomerization of 1,3-dienes with arenesulfinic acids or sodium arenesulfinates in acetic acid has been carried out in the presence of palladium catalysts to afford high yields of allylic sulfones.[3]

In the course of the study on the CO_2-promoted reactions,[4] we have discovered that 1,2- and 1,3-dienes react with sodium benzenesulfinate dihydrate in the presence of a palladium(0) catalyst to give allylic sulfones under CO_2 atmosphere.

The results are shown in Table 1. The reaction of sodium benzenesulfinate dihydrate with 3.8 equiv of 1,3-butadiene (**1a**) in *N*,*N*-dimethylformamide (DMF) at 80 °C for 2 h under the pressure of CO_2 in the presence of [$Pd(PPh_3)_3$] gave the 1:1 addition product, 2-butenyl pheny sulfone (**2a**), in 20% yield (*E*:*Z*=2:1) together with the 1:2 addition product, (*E*)-2,7-octadienyl phenyl sulfone, in 78% yield. The effect of CO_2 was remarkable because the addition reaction did not take place at all in the absence of CO_2.

Isoprene (**1b**) afforded exclusively the 1:1 addition product 3-methyl-2-butenyl pheny sulfone (**2b**).

$$CH_2{=}CHC(CH_3){=}CH_2 + PhSO_2Na{\cdot}2H_2O \xrightarrow[CO_2]{Pd} PhSO_2CH_2CH{=}C(CH_3)_2$$

Table 1. Reaction of Dienes with Sodium Benzenesulfinate Dihydrate[a]

Diene	Reaction temp/time °C/h	Product	Yield %
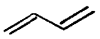 **1a**	80/2	**2a**	20 (*E*:*Z*=2:1)
		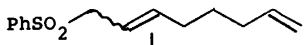	78 (*E*:*Z*=6:1)
1b	80/2	**2b**	94
1c	100/4	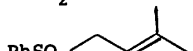 **2c**	67
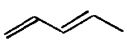 **1d**	110/4	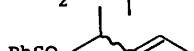 **2d**	31[b] (*E*:*Z*=19:1)
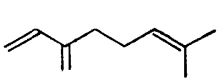 **1e**	80/2	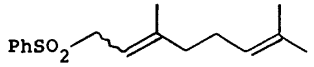 **2e**	48 (*E*:*Z*=3:1)
3	80/2	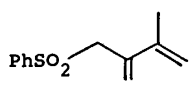 **4**	44

a) $PhSO_2Na{\cdot}2H_2O$ 9.1 mmol, 1,3-diene 10—34 mmol, [$Pd(PPh_3)_3$] 0.2 mmol, DMF 10 cm³, CO_2 15 kg/cm². For the 1,2-diene **3**, see the experimental part. b) 2-Pentenyl phenyl sulfone was also formed in 11% yield.

* The term "telomerizartion" is meant here to imply formation of adducts between one or more dienes and a second substance.

These results contrasted sharply with those reported earier,[3] where the reaction of dienes with arenesulfinic acid or sodium arenesulfinate in acetic acid gave allylic sulfones containing large proportion of the more substituted isomer. 2,3-Dimethyl-1,3-butadiene (**1c**) gave predominantly 2,3-dimethyl-2-butenyl phenyl sulfone (**2c**) in a moderate yield at the reaction temperature of 100 °C. The reaction of (*E*)-1,3-pentadiene (**1d**) with the sulfinate was sluggish at the reaction temperature of 80 °C. Under forced conditions (110 °C, 4 h), the diene afforded 1-methyl-2-butenyl phenyl sulfone (**2d**) in 31% yield. Myrcene (**1e**) underwent the addition reaction at 80 °C to give mainly geranyl phenyl sulfone. 1,4-Disubstituted 1,3-dienes such as 1,3-cyclooctadiene and methyl sorbate did not take part in this reaction.

Allene (**3**) underwent smoothly the 2:1 addition reaction to afford 3-methyl-2-methylene-3-butenyl phenyl sulfone (**4**) selectively under the pressure of CO_2 in the presence of the palladium catalyst.

$$2CH_2{=}C{=}CH_2 + PhSO_2Na{\cdot}2H_2O \xrightarrow[CO_2]{Pd} PhSO_2CH_2C(=CH_2)C(=CH_2)CH_3$$

We point out here one of possible roles of CO_2 in the telomerization reaction. Benzenesulfinic acid may be formed from its sodium salt as follows.

$$PhSO_2Na{\cdot}2H_2O + CO_2 \rightleftharpoons PhSO_2H{\cdot}H_2O + NaHCO_3$$

Although the equilibrium is declined to the left due to the strong acidity of the free sulfinic acid (pK_a ca. 2), the sulfinic acid thus formed may, in turn, begin to undergo telomerization with dienes in the presence of a palladium catallyst.[3]

The intermediate has been supposed to be a π-allylpalladium species, which is attacked by benzenesulfinate to afford allylic sulfones.[3] There are several preceedings concerning the attack of sulfinate on an in situ-generated π-allyl palladium complex.[5] Usually thermodynamically-controlled products were reported to be predominated. The observations coincide well with our results.

As free sulfinic acid is unstable having a tendency to undergo disproportionation into thiosulfonic *S*-ester and sulfonic acid,[6] the employment of CO_2 and a sulfinic acid salt, that is stable, instead of free sulfinic acid may be a choice in the diene telomerization reaction.

Experimental

Materials. The dienes (1,2- and 1,3-) were used as received except myrcene. Myrcene was distilled under reduced pressure before use. [$Pd(PPh_3)_3$] was prepared according to the reported method.[7]

General Procedure for the Telomerization of Dienes with Benzenesulfinate Dihydrate. A mixture of sodium benzenesulfinate dihydrate (1.82 g, 9.1 mmol), a diene, and [$Pd(PPh_3)_3$] (179 mg, 0.2 mmol) in 10 cm^3 of DMF was stirred in an autoclave under CO_2 pressure (15 kg cm^{-2}) under the conditions described in Table 1. After the teaction was completed, the whole content was poured into water. The products were extracted with diethyl ether and the organic layer was dried on $MgSO_4$. After the solvent was evaporated, the residue was subjected to column chromatography on silica gel eluting with hexane–ethyl acetate.

Reaction of 1,3-Butadiene (1a) with Benzenesulfinate. Reaction of **1a** (1.86 g, 34.4 mmol) in the usual way as above gave an oil after column chromatography (hexane/ethyl acetate=2/1). Yield 2.13 g. GLC analysis (OV-1, 3 m, 3%, 194 °C) showed the formation of 2-butenyl phenyl sulfone (**2a**) and 2,7-octadienyl phenyl sulfone in a 1:4 ratio. The products were isolated by GLC and characterized spectroscopically (IR, ^{1}H NMR, Mass).[3] The *E*/*Z* ratios of **2a** and 2,7-octadienyl phenyl sulfone were determined by ^{1}H NMR spectroscopy to be 2:1 and 6:1, respectively.

Reaction of Isoprene (1b) with Benzenesulfinate. Reaction of **1b** (1.36 g, 20 mmol) in the usual way gave 3-methyl-2-butenyl phenyl sulfone (**2b**) as a pale yellow oil after column chromatography (hexane/ethyl acetate=2/1). Yield 1.79 g (8.52 mmol, 94%). Spectroscopic (IR, ^{1}H and ^{13}C NMR, Mass) and elemental analysis supported the structure.

Reaction of 2,3-Dimethyl-1,3-butadiene (1c) with Benzenesulfinate. Reaction of **1c** (0.8 g, 10 mmol) at 100 °C for 4 h in the usual way gave 2,3-dimethyl-2-butenyl phenyl sulfone (**2c**)[8] after column chromatography (hexane/ethyl acetate=3/1). Yield 1.36 g (6.1 mmol, 67%). Recrystallization from toluene/hexane (1/3) afforded pure material as white needles: mp 98—99 °C. IR (KBr) 1285, 1135, 750, 580 cm^{-1}. ^{1}H NMR ($CDCl_3$) δ=1.24 (s, 3H), 1.60 (s, 3H), 1.74 (s, 3H), 3.80 (s, 2H), 7.40—7.92 (m, 5H). Found: C, 64.27; H, 7.31. Calcd. for $C_{12}H_{16}O_2S$: C, 64.29; H, 7.14.

Reaction of (*E*)-1,3-Pentadiene (1d) with Benzenesulfinate. Reaction of **1d** (0.77 g, 10.3 mmol) at 110 °C for 4 h in the usual way gave an oil after kugelrohr distillation at 140 °C (4 mmHg) (1 mmHg=133.322 Pa). Yield 796 mg (42%). Found: C, 63.10; H, 7.01. Calcd. for $C_{11}H_{14}O_2S$: C, 62.83; H, 6.71. IR (neat) 1300, 1140, 965, 720, 680 cm^{-1}. GLC analysis (OV-1, 2 m, 3%, 150 °C) of the product showed two peaks in the ratio of 77:23. The major portion, which was isolated by GLC, was composed of (*E*)- and (*Z*)-1-methyl-2-butenyl phenyl sulfone (**2d**). (*E*)-Isomer: ^{1}H NMR ($CDCl_3$) δ=1.36 (d, *J*=7 Hz, 3H), 1.58 (d, *J*=5 Hz, 3H), 3.40—3.90 (m, 1H), 5.24—5.60 (m, 2H), 7.30—7.96 (m, 5H). The absorption of the (*Z*)-isomer occurred differently at δ=1.40 (d, *J*=7 Hz) instead of δ=1.36 in the (*E*)-isomer. The *E*/*Z* ratio was determined by ^{1}H NMR to be 19:1. The minor portion, which was also isolated by GLC, was composed of (*E*)- and (*Z*)-2-pentenyl phenyl sulfone. (*E*)-Isomer: ^{1}H NMR ($CDCl_3$) δ=0.84 (t, *J*=8 Hz, 3H), 1.60—2.00 (m, 2H), 3.68 (d, *J*=6 Hz, 2H), 5.24—5.65 (m, 2H), 7.35—7.90 (m, 5H). The absorption of the (*Z*)-isomer occurred at δ=3.78 (d, *J*=9 Hz) instead of δ=3.68 in the (*E*)-isomer. The *E*/*Z* ratio was determined by ^{1}H NMR to be 9:1.

Reaction of Myrcene (1e) with Benzenesulfinate. Reaction of **1e** (1.36 g, 10 mmol) in the usual way gave 3,7-dimethyl-2,6-octadienyl phenyl sulfone[5] as an oil on chromatography (hexane/ethyl acetate=2/1) followed by kugelrohr distillation at 165 °C (3 mmHg). Found: C, 69.08; H, 7.72. Calcd for $C_{16}H_{22}O_2S$: C, 69.03; H, 7.97. The *E*/*Z* ratio was determined by GLC (OV-1, 2 m, 3%, 200 °C) to be 3:1. IR (neat) 1445, 1310, 1150 cm^{-1}. ^{1}H NMR ($CDCl_3$) δ=1.28 (s, 3H), 1.56 (s, 3H), 1.64 (s, 3H), 1.80—2.24 (m, 4H), 3.78 (d, *J*=8 Hz, 2H), 4.80—5.40 (m, 2H), 7.20—8.00 (m, 5H).

Reaction of Allene (3) with Benzenesulfinate. $PhSO_2Na{\cdot}2H_2O$ (3.64 g, 20 mmol) and **3** (0.70 g, 17.5 mmol) were reacted in an autoclave at 80 °C for 2 h in the presence of [$Pd(PPh_3)_3$] (179 mg, 0.2 mmol) in DMF (20 cm^3) under CO_2 pressure (15 kg cm^{-2}). Isolation as above by column

chromatography on silica gel (hexane/ethyl acetate=3/2) gave 3-methyl-2-methylene-3-butenyl phenyl sulfone as a pale yellow oil. Yield 860 mg (3.87 mmol, 44%). An analytical sample was obtained by kugelrohr distillation at 150 °C (4 mmHg). This compound polymerized partially during the distillation. ^{1}H NMR ($CDCl_3$) δ=1.83 (s, 3H), 4.08 (s, 2H), 4.96 (s, 1H), 5.02 (s, 1H), 5.06 (s, 1H), 5.36 (s, 1H), 7.20—7.96 (m, 5H). ^{13}C NMR ($CDCl_3$) δ=140.585 (s), 138.730 (s), 136.102 (s), 133.467 (d), 128.789 (d), 128.399 (d), 120.949 (t), 115.003 (t), 60.133 (t), 20.710 (q). IR (neat) 1722, 1300, 1145, 895, 775 cm^{-1}. Mass (70 eV) *m/z* 222 (M^+), 143, 81, 79, 77, 53. Found: C, 64.71; H, 6.24. Calcd. for $C_{12}H_{14}O_2S$: C, 64.84, H, 6.35.

References

1) For reviews, see J. Tsuji, "Organic Synthesis with Palladium Compounds," Springer Verlag, Berlin (1980); B. M. Trost, *Tetrahedron*, **33**, 2615 (1977).

2) K. E. Atkins, W. E. Walker, and R. M. Manyik, *J. Chem. Soc., Chem. Commun.*, **1971**, 330.

3) M. Julia, M. Nel, and L. Saussine, *J. Organomet. Chem.*, **181**, C17 (1979); M. Julia, M. Nel, A. Righini, and D. Uguen, *J. Organomet. Chem.*, **235**, 113 (1982); U. M. Dzhemilev, R. V. Kunakova, R. L. Gaisin, and G. A. Tolstikov, *Izv. Akad. Nauk SSSR, Ser. Khim.*; **1979**, 2702; *Chem. Abstr.*, **92**, 128509 q (1980).

4) Y. Inoue, M. Sato, M. Satake, and H. Hashimoto, *Bull. Chem. Soc. Jpn.*, **56**, 637 (1983); Y. Inoue, Y. Ohtsuka, and H. Hashimoto, *Bull. Chem. Soc. Jpn.*, **57**, 3345 (1984); Y. Inoue, R. Ohashi, M. Toyofuku, and H, Hashimoto, *Nippon Kagaku Kaishi*, **1985**, 523.

5) K. Inomata, T. Yamamoto, and H. Kotake, *Chem. Lett.*, **1981**, 1357; B. M. Trost, N. R. Schmuff, and M. J. Miller, *J. Am. Chem. Soc.*, **102**, 5979 (1980); N. Ono, I. Hamamoto, T. Kawai, A. Kaji, R. Tamura, and M. Kakihana, *Bull. Chem. Soc. Jpn.*, **59**, 405 (1986); G. P. Boldrini, D. Savoia, E. Tagliavini, C. Trombini, and A. U.-Ronchi, *J. Organomet. Chem.*, **268**, 97 (1984).

6) L. Horner and H. Basedow, *Justus Liebigs Ann. Chem.*, **612**, 108 (1958); H. Bredereck, A. Wagner, E. H. Beck, H. Herlinger, and K. G. Kottenhahn, *Angew. Chem.*, **70**, 268 (1958); J. L. kice and K. W. Bowers, *J. Am. Chem. Soc.*, **84**, 605 (1962); J. L. Kice and N. E. Powlowski, *J. Org. Chem.*, **28**, 1162 (1963).

7) P. Giannoccaro, A. Sacco, and G. Vasapallo, *Inorg. Chim. Acta*, **37**, L455 (1979).

8) Y. Gaoni, A. Tomažič, and E. Potgieter, *J. Org. Chem.*, **50**, 2943 (1985).

A Supercritical Carbon Dioxide Extraction from Mackerel (Scomber Japonicus) Powder: Experiment and Modeling

Yutaka IKUSHIMA,* Norio SAITO, Kiyotaka HATAKEDA, Shota ITO, Takashi ASANO, and Tomio GOTO
Government Industrial Research Institute, Tohoku, Nigatake 4-Chome, Sendai 983
(Received March 12, 1986)

The extraction of some organic substances from freezed-dried mackerel powder was performed using supercritical carbon dioxide (SC-CO_2) at 4.9—24.5 MPa and 313 K in a fixed-bed flow extractor. It was found that the rate of extraction was enhanced by raising the pressure. The overall yield of the SC-CO_2 extraction was comparable to that of a hot-hexane-extraction from the same material. The SC-CO_2 extraction produced glycerides of pharmacologic significance such as icosapentaenoic acid (IPA) and docosahexaenoic acid (DHA) from mackerel. In addition, a kinetic model for extraction with supercritical fluids is described, and is applied to correlate our results obtained in the SC-CO_2 extraction of mackerel. This model could express the transport within the solid in the supercritical fluid extraction process.

Recently much attention has been drawn to the separation process using a supercritical fluid (SCF). As compared with usual extraction procedure performed at relatively high temperature, the SCF extraction has several advantages. For example, it can yield thermolabile materials without denaturalization because of its low operating temperature. The feature of SCF techniques has previously been described and discussed in detail.[1-4] In some industries, the SCF has effectively separated the desired materials from natural products.[5-8]

We have been studying supercritical carbon dioxide (SC-CO_2) extraction of mackerel powder to obtain unsaturated fatty acids of pharmacologic value such as icosapentaenoic acid (IPA) and docosahexaenoic acid (DHA). These two acids have recently been reported to be efficacious against arteriosclerois.[9,10] The present study concerns the effective utilization of natural resources rich in our area where over one million tons of mackerel are caught every year for domestic use. Therefore, it should make possible the extraction of such high-valued substances as IPA and DHA from this inexpensive material.

In the present work, we carried out SC-CO_2 extraction from freezed-dried mackerel powder in a fixed bed extractor at pressures of 4.9—24.5 MPa and a temperature of 313 K. The pressure dependence of the extraction effectiveness of SC-CO_2 is discussed. The composition of the SC-CO_2-extracted oil is analyzed and compared with that of a hot hexane-extracted oil. We also present a kinetic model for the SCF extraction and attempt to use it to correlate our results of the SC-CO_2 extraction. For the practical design of SCF extraction plants, it is highly desirable to kinetically express the extraction process in order to optimize process parameters. For this not only knowledge of phase equilibria but also a kinetic analysis of the processes involved is essential. For the latter, however, little consideration has been made so far in the literature.

A Model of SCF Extraction

A mass transfer model is used to express the SCF extraction process. We regard the extraction process as a reaction such that one molecule of a solute, B, associates with j molecules of a SCF, A, with the formation of a complex, BA_j, $B+jA \rightarrow BAj$, and use a kinetic and diffusional model of solid-gas reaction. In the application of this model to the extract of mackerel, we will suppose the oils to be extracted to consist of a single component, as described later.

At first, the mass transfer for a single spherical extract is considered. Then the results are applied to a fixed bed of spheres. The model for solid-gas reactions proposed by Ishida and Wen[11] is used for a single spherical extract. Ishida et al. presented a kinetic and diffusional model for solid-gas reaction occurring in a spherical particle. We apply this model for the extraction of a solute from a solid with SCF. In applying this model to a fixed bed of spheres in the extractor, we make some modifications as mentioned later. The extraction process in a single spherical particle with SCF will be described in the following manner. Since the extraction near the surface is faster, the solute in this region is completely extracted after a certain time. That is to say, as the extraction progresses, a so-called raffinate layer is formed in the outside of the extract. Here, the stage of extraction prior to the formation of the raffinate layer is regarded as the first stage and the following stage as the second stage. Two models, 1

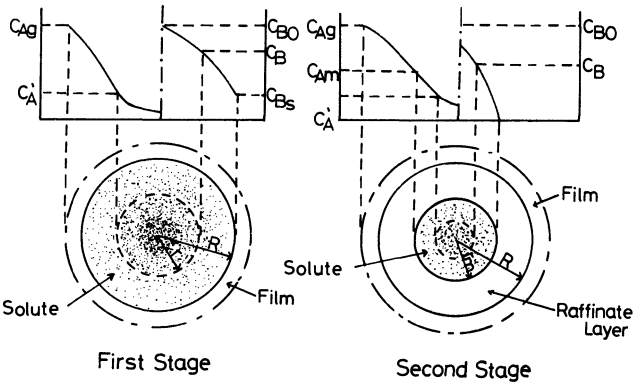

Fig. 1. Schematic diagram of the concentration profile in the first and second stage.

and 2, are presented for the first and second stages, respectively. Schematic diagram for these two stages are shown in Fig. 1. The following assumptions are employed:

—A steady state approximation for the transfer of SCF,A, holds.

—The rate of extraction is independent of the extract concentration in the solid.

—The fixed bed consists of spherical particles of uniform size which remain unchanged during the extraction.

Model 1: The mass balance and boundary conditions for gas A and solute B are given by

$$0 = D'(d^2C_A'/dr^2+2/r\, dC_A'/dr) - jk_VC_{B0}(C_A'-C_A^*), \quad (1)$$

$$dC_B/dt = - k_VC_{B0}(C_A-C_A^*), \quad (2)$$

$$D'dC_A'/dr = k_g(C_{Ag}-C_A^*) \quad \text{at } r = R, \quad (3)$$

$$dC_A'/dr = 0 \quad \text{at } r = 0, \quad (4)$$

where C_A' is the concentration of component A in solid B, C_A^* is C_A' at equilibrium, C_{Ag} is the concentration of component A in gas, C_B is the concentration of solid extract B, C_{B0} is the initial concentration of solid extract B, D' is the effective diffusivity of component A in the extraction layer, j is a stoichiometric coefficient, k_g is the mass transfer coefficient of component A, k_V is the extraction rate constant based on volume, r is a distance from the center of the sphere, R is a particle radius, t is a time.

The concentration profile of solute B can be obtained

$$C_B = C_{B0} - \int_0^t k_VC_{B0}(C_A'-C_A^*)dt \quad (5)$$

as

$$C_B/C_{B0} = 1 - (\sinh(\phi'\xi)/(\xi \sinh\phi')(\theta_V/\theta_{Vc}), \quad (6)$$

where ξ is a dimensionless radius, $\phi'$is a Thile modulus based on D', θ_v is a dimensionless time, θ_{vc} is θ_v at the end of the first stage as defined respectively by

$$\xi = r/R, \quad (7)$$

$$\phi' = R(jk_VC_{B0}/D')^{1/2}, \quad (8)$$

$$\theta_V = k_V(C_{Ag}-C_A')t, \quad (9)$$

$$\theta_{Vc} = 1 + (\phi' \coth\phi' - 1)/N_{sh}', \quad (10)$$

$$N_{sh}' = k_gR/D', \quad (11)$$

where N_{sh}' is a Sherwood number. Further, the degree of extraction X is given as follows.

$$X = 1 - \left[\int_0^R 4\pi r^2C_B dr/\int_0^R 4\pi r^2C_{B0}dr\right] \quad (12)$$

as

$$X = 3/(\phi')^2[\phi'\coth\phi' - 1]\theta_V/\theta_{Vc} \quad (13)$$

At the end of the first stage, the degree of extraction X can be obtained upon substituting $\theta_v=\theta_{vc}$ in Eq 13 as follows.

$$X = 3/(\phi')^2[\phi'\coth\phi' - 1] \quad (14)$$

The concentration profile of gas A in the solid is obtained from Eqs. 1, 3, and 4 as

$$(C_A'-C_A^*)/(C_{Ag}-C_A^*) = \sinh(\phi'\xi)/\theta_{Vc}\xi \sinh\phi', \quad (15)$$

Model 2: As the extraction progresses, the solute is completely extracted at an outer layer, the raffinate layer is gradually formed as a new diffusion resistance for the gaseous solvent, but the extraction still occurs inside the raffinate layer. The mass balance and boundary conditions for gas A and solute B are then given as follows. In the inner core (extraction region), the mass balance and boundary conditions are identical to Eqs. 1, 2, and 4. In the raffinate layer, as extraction dose not occur, the mass balance for gas A can be obtained by

$$0 = D(d^2C_A/dr^2+r/2\, dC_A/dr), \quad (16)$$

$$C_B = 0 \quad \text{at } r = R, \quad (17)$$

$$DdC_A/dr=k_g(C_{Ag}-C_A) \quad \text{at } r = R, \quad (18)$$

where D is the effective diffusivity of component A in raffinate layer. Further, at the boundary between the extraction region and the raffinate layers,

$$C_A' = C_A \quad (19)$$

$$D'dC_A'/dr = DdC_A/dr. \quad (20)$$

The concentration profile of the solid extract can be obtained from

$$C_B = C_{Bm} - \int_{tc}^t k_VC_{B0}(C_A'-C_A^*)dt \quad (21)$$

as

$$C_B/C_{B0} = 1 - \sinh(\phi'\xi)/\xi \sinh\phi' - \sinh(\phi'\xi)/\xi\left[\int_{\theta_{Vc}}^{\theta_V}[\xi_m/\sinh(\phi'\xi_m)]d\theta_V/[1+D'/D\,[1-\xi_m+\xi_m/N_{sh}][\phi'\xi_m\coth(\phi'\xi_m) - 1]]\right], \quad (22)$$

where C_{Bm} is C_B at the end of the first stage, $N_{sh}=k_gR/D$, $\xi_m=r_m/R$, r_m is r at the boundary between the extraction region and the raffinate layer. The time required for the raffinate layer to reach r_m is obtained as

$$\theta_V = \theta_{Vc} + \int_1^{\xi_m}(d\theta_V/d\xi_m)d\xi_m \quad (23)$$

θ_v can be obtained from Eqs. 22 and 23 as follows.

$$\theta_V = 1 + (1-D'/D)\ln[\xi_m\sinh\phi'/\sinh(\phi'\xi_m)]+\phi^2(1-\xi_m)^2(1+2\xi_m)/6+D'/D(1-\xi_m)[\phi'\xi_m\coth(\phi'\xi_m)-1] + \phi^2(1-\xi_m^3)/3N_{sh} + \xi_m[\phi'\xi_m\coth(\phi'\xi_m)-1]/N_{sh}'. \quad (24)$$

When we substitute Eq. 24 into Eq. 22, the concentration profile for the solid extract is obtained as

$$1 - C_B/C_{B0} = \xi_m\sinh(\phi'\xi)/\xi\sinh(\phi'\xi_m). \quad (25)$$

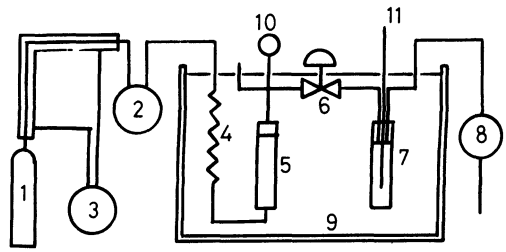

Fig. 2. Schematic diagram of supercritical CO_2 extraction apparatus. 1: CO_2 Cylinder, 2: High pressure pump, 3: Cooling circulator, 4: Preheater, 5: Extractor, 6: Back pressure regulator, 7: Receiver, 8: Flow totalizer, 9: Constant temperature bath, 10: Pressure gauge, 11: Thermocouples.

Thus, the degree of extraction X_2 can be obtained from Eq. 25 as

$$X_2 = 1 - \xi_m^3 + 3\xi_m[\phi'\xi_m \coth(\phi'\xi_m) - 1]/(\phi')^2. \quad (26)$$

Experimental

Materials. Mackerel were obtained commercially. They were freezed-dried and sieved in the range of about 32 to 64 mesh. The average diameter of the mackerel particles was 10^{-5} m. The amount of water contained was 7.3 wt%. Commercial-grade carbon dioxide was used as solvent.

Extraction Procedures. A flow diagram of the extraction apparatus used is shown in Fig. 2. Liquid carbon dioxide is charged into a Hitachi high pressure liquid pump through a 1/16 inch tube and a check valve, and compressed to the desired pressure. The pump can deliver the solvent at a constant flow rate of 1 NL min^{-1} (1 NL=1 L of gas at 293 K and 101.3 kPa). The pressure is controlled by a back pressure regulator. The extraction pressure is measured with a Bourdon-type pressure gauge. Fluctuations in pressure due to the pump are less than ± 1 Kg cm^{-2} below 300 Kg cm^{-2}. The temperature is controlled within ± 0.1 K.

A 25 g sample of mackerel particles is placed in a 0.1 L extractor and extracted at pressures of 4.9—24.5 MPa and 313 K. The extracted solution is flashed to atmospheric pressure across a heated back pressure regulator and the component is collected in a receiver. The amount collected is determined by weighing and the corresponding total volume of CO_2 used is measured with a flow totalizer.

Further, mackerel particles were extracted with hexane for 5 h in a Soxhlet for comparison.

Analytical Methods. Extracted glycerides were changed into methyl esters of fatty acids according to the usual method. The esters were identified by GC-MS and gas chromatography. Phosphorus was analyzed colorimetrically.[12]

Results and Discussion

In Fig. 3, the yield of extracted oil is plotted against the total amount of CO_2 consumed under the conditions that carbon dioxide was forced to flow at a rate of 1 NL min^{-1} at 19.6 MPa and 313 K. The linear portion of the curve indicates that steady-state extraction conditions are readily established at the beginning of the extraction. The extraction rate is maintained

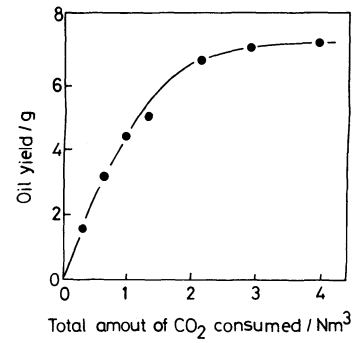

Fig. 3. Oil yield from freezed-dried mackerel powder during supercritical CO_2 extraction at 19.6 MPa and 313 K.

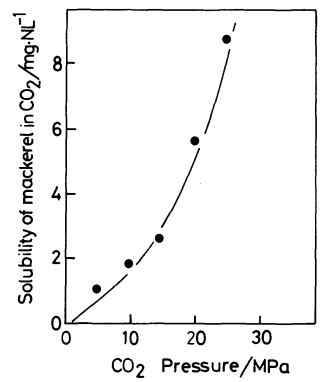

Fig. 4. Effect of pressure on the solubility of mackerel in CO_2 during the initial 6 h at 313 K.[13]

at about 0.27 g h^{-1} until an oil yield of 6.7 g is obtained. The overall yield is comparable to 85% of that obtained by the hot hexane extraction.

The solubility at 313 K between 4.9—24.5 MPa is given in Fig. 4. The initial solubility of mackerel oil in CO_2 was determined from the slope of the plot of oil yield-to-total amount of CO_2 consumed (as shown in Fig. 3, for example).[13] The solubility at 313 K increased greatly with the pressure. For example, the amount of the oil extracted at 24.5 MPa is about 4.6 times that at 9.8 MPa. This is considered to be associated with an increased solute holding power. Previously, Yamaguchi[14] reported that 14.4 g of oil per 100 g of mackerel could be extracted at 39.2 MPa, 313 K and a flow rate of 10 kg h^{-1}.

Table 1 provides an analytical characterization of SC-CO_2-extracted and hot hexane-extracted oils from the same mackerel particles. In this Table are listed the kinds of fatty acid components and the amounts of phosphorus contained in both SC-CO_2- and hexane-extracted mackerel oils. Under these conditions, the oils obtained by SC-CO_2 extraction contains both IPA and DHA and the amounts of fatty acid components compete with those obtained by the hot hexane extraction.[13] Furthermore, SC-CO_2-extracted oil has significantly less phosphorus than hexane-extracted oil. The

hexane-extracted oil is red brown and turbid whereas the SC-CO_2-extracted oil is yellow and clear. The method used to estimate the phosphatide content is to multiply the percent elemental phosphorus by 25.4.[12] The phosphatide content calculated on this basis is 1% for the hexane-extracted oil and 0.023% for the SC-CO_2-extracted oil. These values are reflected in a significant difference in the refining loss on the removal of the phosphatide content in the purification process between the SC-CO_2- and hexane-extracted oils. Therefore, the oil extracted with SC-CO_2 has the advantage of being essencially comparable to a degummed, hexane-extracted crude oil. In addition, it was reported[15] that oil extracted from soybeans with SC-CO_2 had less phosphorus than hexane-extracted oil. That is to say, with SC-CO_2, phosphatide free oil not only from plant seed but from fish is shown to be extracted.

The Application of the Kinetic Models. The results obtained for a single sphere in the models 1 and 2 using the Ishida's model[11] are transfered to a fixed bed of spheres by correcting the Sherwood number. In the model 1, we present the modification of the Sherwood number N_{sh}' as follows.

Table 1. Compositions of SC-CO_2- and Hexane-Extracted Mackerel Oils[13]

Fatty acid	Hexane	SC-CO_2
	%	%
Myristoreic	4.8	6.3
Palmitic	20.4	21.8
Palmitoleic	5.7	7.3
Stearic	2.3	1.1
Oleic	33.4	32.2
Linoleic	—	1.9
Icosenoic	5.4	2.0
Icosapentaenoic	7.8	5.8
Erucic	0.5	0.6
Docosahexaenoic	11.7	8.1
Lignoceric	0.4	—
	Hexane	SC-CO_2
	ppm	ppm
Phoshorous	405	3
	Hexane	SC-CO_2
Oil description	Yellow oil	Red brown oil

$$N_{sh}^* = N_{sh}'\psi, \tag{27}$$

where N_{sh}^* is the Sherwood number for a fixed bed of spheres. In the model 2, we regard the correction factor ψ as a function of the dimensiomless radius ξ_m of the extraction region as follows.

$$\psi = \exp(-K/\xi_m), \tag{28}$$

where K is a constant, which is treated here as an adjustable parameter.

The results calculated from the above two models employing Eqs. 27 and 28 are compared with the experimental results in Fig. 5. Table 2 summarizes the parameters used in the present calculations. The stoichiometric coefficient was estimated from the components of each fatty acids of the SC-CO_2-extracted mackerel oils shown in Table 1 and the solubility constant of triglycerides in SC-CO_2 studied by Chrastll.[16] The initial concentration of the mackerel oil was determined as follows. The weight of the mackerel oil obtained from 25 g of mackerel powder with n-hexane in a Soxhlet was 8.8 g. We assumed that it was the total yield contained in the powders and that the oil consisted of triglycerides. From the analytical results shown in Table 1, 25 g of mackerel powder contained 9.9×10^{-3} mol (=0.01 mol) of the oil. Since the bulk density of the mackerel powder was 0.25, the initial concentraion was about 100 mol m^{-3}. The effective diffusivity D' and D were estimated in the following manner. First, for D', we applied the equation of Grigull.[17]

$$m/m_c = C_q(1-\exp(-EF_o)), \tag{29}$$

where F_o is the Fourier number, C_q and E are coefficients (C_q=0.6079, E=9.8696), m is the remaining quantity of SC-CO_2-extracted oil, m_c is the initial quantity of mackerel oil. Further, F_o was defined as

$$F_o = D't/R^2, \tag{30}$$

where R is the radius of the sphere. D' was determined from Eqs. 29 and 30. Next, in the second stage, the mass transfer coefficient k_g was considered as follows.

$$1/k_g = 1/\beta_i + 1/\beta_a, \tag{31}$$

where β_i is the mass transfer coefficient in the extraction layer, β_a is the mass transfer coefficient in the raffinate layer. Since $\beta_a \gg \beta_i$,

Table 2. Parameters Used in the Model Calculations for Extraction of Mackerel Oil with SC-CO_2

Diameter of the equivalent sphere	$d=10^{-4}$/m
Initial concentration of the solute	$C_{BO}=100$/mol Nm^{-3}
Effective diffusivity of the solvent in the extraction region	$D'=4\times10^{-7}/m^2\,h^{-1}$
Effective diffusivity of the solvent in the raffinate layer	$D=9\times10^{-5}/m^2\,h^{-1}$
Pressure	P=19.6/MPa
Temperature	T=313/K
Volumetric flow of the solvent	F=60/NL h^{-1}
Stoichiometric coefficient	$j=4$
Thiele modulus	$\phi'=2.5$, $\phi'=0.17$
Correction constant	$K=3.2$

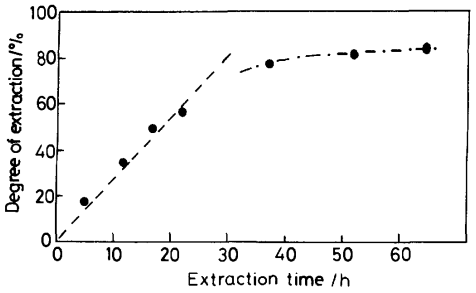

Fig. 5. Degree of extraction of mackerel oil at 19.6 MPa and 313 K.
●: Exp., ——: Model 1, —·—: Model 2.

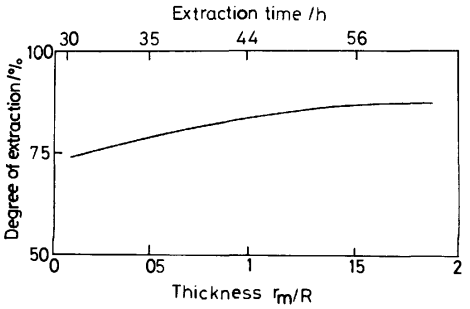

Fig. 6. Calculated relation between the degree of extraction and the thickness of raffinate layer in the second stage.

$$k_g \simeq \beta_1. \tag{32}$$

Schlunder proposed the following equation.[18]

$$\beta_1 R/D = (10.82^2 + 4/\pi F_0)^{1/2}. \tag{33}$$

In addition, Brauer[19] assumed that if F_0 was larger than 0.4,

$$\beta_1 \sim 1/t. \tag{34}$$

Therefore, D was estimated from Eqs. 32, 33, and 34. The optimal Thile modulus and the correction constant K were determined so as to minimize the difference between the experimental results in Fig. 3 and the estimates using the models.

As shown in Fig. 5, the overall extraction process can be represented by these models well, the initial stage being by model 1 while the latter stage by model 2. Furthermore, using the parameters in Table 2 and the results in Fig. 5, the overall yield in the first stage from Eq. 14 and the duration for it is shown to be about 74% and 28 h, respectively. This means that beyond this extraction region, the solvent CO_2 rapidly becomes more difficult to diffuse into the particle because under these conditions, the raffinate layer begins to form.

In model 2, the ralationship between the thickness of the raffinate layer and the degree of extraction derived from Eqs. 24 and 26 is shown in Fig. 6. The formation rate of the raffinate layer decreases with the extraction time. As the raffinate layer thickens, the degree of extraction gradually decreases and attains a steady value such that the thickness of the raffinate layer is over about 10% of the whole extraction region. That is to say, the raffinate layer acts as a diffusion resistance for the extraction and decrease the degree of extraction. Estimating from the above calculated results, the extraction occurs near the surface of the mackerel particle and large amounts of the materials contained remain unextracted. Therefore, the diffusion of the gas in the particle must progress in order to improve the degree of extraction. This may be attained by the adjustment of the extraction pressure and temperature. Finally, we would like to note that the addition of a suitable third substance to the CO_2 enhances the extraction efficiency.[20,21]

References

1) L. G. Randall, *Sep. Sci. Tech.*, **17**, 1 (1982).
2) S. Saito, *Petrotech*, **5**, 115 (1982).
3) K. Nagahama, *Bunrigizyutsu*, **11**, 23 (1981).
4) S. Peter and S. G. Brunner, "Extraction with Supercritical Gases," ed by G. M. Schneider, E. Stahl, and G. Wilke, Verlag Chemie, Weinheim (1980).
5) Brit. Patent, 133651.
6) U. S. Patent, 3843824.
7) Brit. Patent, 1388581.
8) Japan Patent, 55-45391.
9) T. O. Lossonczy, *Am. J. Clin. Nutr.*, **31**, 1340 (1978).
10) A. Hirai, T. Hamazaki, T. Terano, T. Nishikawa, A. Tamura, A. Kumagai, and J. Sajiki, *Lacent*, **11**, 1132 (1980).
11) M. Ishida and C. Y. Wen, *AIChE, J.*, **14**, 311 (1968).
12) "Kizjun Yushi Bunseki Shikenho," The Japan Oil Chemists' Society (1981).
13) N. Saito, *Shokuhin Kogyo*, **28**, 1 (1985).
14) K. Yamaguchi, 8th Technical Seminar, The Society of Chemical Engineering, Japan (1985), p. 59.
15) J. P. Friedrich, G. R. List, and A. J. Heakin, *J. Am. Oil Chem. Soc.*, **59**, 288 (1982).
16) J. Chrastll, *J. Phys. Chem.*, **86**, 3016 (1982).
17) U. Grigull, "Temperaturausgleich in Einfachen Korpern, Springer," Berlin (1964).
18) E. U. Schlunder, "Einfuhrung in die Warmeubertertragung, Vieweg," Braunschweig (1981).
19) H. Brauer, Stoffaustausch einschlieβlich Chemischer Reaktion, Sauelander," Aaraw (1971).
20) Y. Ikushima, N. Saito, K. Hatakeda, S. Ito, T. Asano, and T. Goto, *Chem. Lett.*, **1985**, 1789.
21) To be submitted.

An Analysis of the Voltammetric Adsorption Waves of Methyl Viologen

Katsuyoshi KOBAYASHI,* Fumiaki FUJISAKI, Toshifumi YOSHIMINE, and Katsumi NIKI
Department of Electrochemistry, Faculty of Engineering, Yokohama National University, Tokiwadai, Hodogaya-ku, Yokohama 240
(Received March 14, 1986)

The electrochemical behavior of 1,1′-dimethyl-4,4′-bipyridinium dichloride (methyl viologen, MV) is complicated with the strong adsorption of both the oxidized (MV^{2+}) and the reduced ($MV^{+\cdot}$) forms of MV on a mercury electrode. MV^{2+} adsorbs on the electrode with a flat orientation at more positive potentials than the potential of zero charge of the mercury electrode. $MV^{+\cdot}$ adsorbs on the electrode with a vertical orientation at more negative potentials than the formal potential of the $MV^{2+/+\cdot}$ couple, $(E^{0'})_{MV}$. It is probable that the change in the orientation of the adsorbed $MV^{+\cdot}$ from flat to vertical with the increase in the $MV^{+\cdot}$ concentration in the vicinity of the $(E^{0'})_{MV}$ leads to a strongly attractive interaction between the adsorbed $MV^{+\cdot}$ molecules and a sharp voltammetric adsorption peak results at higher concentrations of MV^{2+}.

Methyl viologen has been widely used as one of the active herbicides, the "paraquat" family.[1] This herbicidal activity originates from the formation of the cation radical of methyl viologen.[2,3]

MV^{2+} is reduced in two steps. The first step is a reversible one-electron transfer with a very negative half-wave potential, −(0.68—0.69) V vs. a saturated calomel electrode (SCE).[4,5] The reduction of MV^{2+} to the methyl viologen cation radical, which is relatively stable in an oxygen-free solution,[6-8] causes a marked color change. MV acts as a good electron-transfer mediator for biological systems.[5,9] These properties lead to the applications of MV to photoelectrodes,[10-14] electrochromisms,[15-19] and electrocatalyses.[20-24]

The electrochemical behavior of MV itself is complicated by the strong adsorption of both MV^{2+} and $MV^{+\cdot}$ molecules on a mercury electrode. Pospisil et al.[3,25] and Grachev et al.[8] have reported on the analysis of the adsorption waves of MV by means of classical d.c. and a.c. polarographic techniques. Recently, resonance and surface enhanced Raman scattering spectroscopies[26,27] and UV-visible reflectance spectroscopy[28] have been used for in situ studies of the redox behavior of adsorbed methyl viologen molecules on silver and platinum electrodes. However, the conformation of both the adsorbed MV^{2+} and $MV^{+\cdot}$ molecules at the electrode surface has not yet been discussed in detail.

Wopshall and Shain[29] showed in the simulation of cyclic voltammograms that a sharp adsorption wave appears when the adsorption coefficient varies with the electrode potential. In many redox systems, similar sharp adsorption waves have been reported.[30-35] In classical d.c. polarograms of Methylene Blue, the half-wave potential ($E_{1/2}$) of the single adsorption wave depends upon its concentration, while the $E_{1/2}$ of the prewave has a constant value when a double wave is observed.[36] Laviron[37] has shown that the dependence of $E_{1/2}$ on the concentration of the reactant is due to the interaction between the adsorbed redox molecules, provided that the adsorption coefficient is large enough. Flanagan et al.[38,39] discussed the effects of reactant and product adsorption in the digital simulation of pulse polarograms.

In the present work, we have found several unusual adsorption phenomena of methyl viologen using the normal pulse (NPP), differential pulse (DPP), and a.c. polarographic techniques. That is, in NPP, 1) a single wave is observed at concentrations lower than 0.5 mM, and a sharp prewave appears at concentrations higher than 0.5 mM for the forward scan. However, a sharp postwave appears over the whole concentration range investigated for the reverse scan. 2) The half-wave potential of the single wave ($E_{1/2,s}$) is about 0.2 V more positive than the $(E^{0'})_{MV}$ and depends upon both the sampling time (t_s) and the initial potential (E_{in}) of NPP. 3) The cathodic prewave on the forward scan always appears at a more negative potential than the anodic postwave on the reverse scan. At concentrations lower than 0.5 mM, the $E_{1/2,s}$ on the forward scan is much more positive than the peak potential (E_p) of the postwave on the reverse scan. 4) On the forward scan, the $E_{1/2,s}$ in the lower concentration range of (0.01—0.5) mM shifts toward negative potentials with the increase in the MV^{2+} concentration in contrast to the positive shift of the E_p of the prewave in the higher concentration range (>0.5 mM). On the reverse scan, the E_p of the postwave always shifts toward positive potentials with an increase in the MV^{2+} concentration.

The surface concentrations of adsorbed MV^{2+} and $MV^{+\cdot}$ molecules, as determined by the present potential-step chroncoulometry, indicate that the orientation of MV^{2+} molecules adsorbed on a mercury electrode is different from that of $MV^{+\cdot}$ molecules.

The peculiar adsorption behavior of methyl viologen can be explained by considering an orientation change in the adsorbed redox species.

Experimental

Materials. The 1,1′-dimethyl-4,4′-bipyridinium dichloride (BDH Chemical, Ltd) and 4,4′-bipyridyl (Tokyo Kasei Kogyo Co.) were of a reagent grade and were used without further purification. The phosphate buffer solution (pH 7.0) was 0.1 M (M=mol dm^{-3}) and was prepared from chemicals of the pH standard grade from Wako Pure Chemical Industries, Ltd. All the solutions were prepared from triply

distilled water.

Apparatus and Procedures. The d.c. polarographic measurements (classical d.c., tast, normal pulse, and differential pulse polarographies) were carried out with a Fuso Polarograph (Fuso and Co., Model 312) and the cyclic voltammetric measurements with a Fuso Potentiostat (Model 311) and a Fuso Potential Scanning Unit (Model 321). The a.c. polarographic measurements were carried out with a Fuso Potentiostat (Model 311), a Fuso Phase-sensitive Detector (Model 332), and a RC Oscillator (Matsushita Communication Industrial Co., Ltd, Model VP 722A). The potential-step chronocoulometric measurements were carried out with a Transient Converter (Riken Denshi Co., Ltd, Model TCA 1000) and a Fuso Potentiostat (Model 311 S2). The concentration of MV in the stock solution was determined spectrophotometrically (molar absorption coefficient at 605 nm, ε_{605}=12400 $M^{-1}cm^{-1}$)[5] with a UV-visible Recording Spectrophotometer (Shimadzu Corporation, Model UV2).

A two-compartment water-jacketed electrochemical cell was used; the compartments were separated by porous Vycor glass so that the contamination of oxygen could be minimized. The working electrode used was a dropping mercury electrode (DME), and the flow rate of mercury was 1.335 mg s^{-1} at an open circuit in a 0.1 M phosphate buffer solution (pH 7.0). The working electrode in the cyclic voltammetry was a Metrohm hanging mercury drop electrode (25.6×10^{-3} cm^2). The counter electrode was a mercury pool in the working electrode compartment. The reference electrode was a saturated calomel electrode which was separated from the working electrode compartment by porous Vycor glass. The reference electrode was coupled with a platinum wire (0.3 mm diameter) electrode in the working electrode compartment through a 0.1 μF capacitor in order to improve the response at higher frequencies in the a.c. polarographic measurements. The solution was deaerated by bubbling purified argon through the solution. All the experiments were carried out at (25±0.5) °C.

Results

Cyclic Voltammetry. Figure 1 shows some cyclic voltammograms of 1 mM MV^{2+} in 0.1 M of a phosphate buffer solution at pH 7.0. The i_p of the main wave was linear with respect to $v^{1/2}$, and the plot passed through the point of the origin, where i_p was the peak current and v the rate of the potential scan. The ratio of cathodic to anodic peak currents was almost unity. The peak-to-peak separation was about 60 mV, and the midpoint potential was −0.68 V. That is, the electrode reaction of MV in the bulk is a diffusion-controlled reversible electrode process. The prepeak shifted toward positive potentials with an increase in the concentration of MV^{2+}. The anodic postpeaks were sharper and higher than the cathodic prepeaks.

Classical d.c. Polarography. A small prewave was followed by the main wave. The $E_{1/2}$ of the main wave was −0.68 V in the concentration range of (0.4—5) mM MV^{2+}. The prewave observed at −0.62 V in 5 mM of a MV^{2+} solution shifted toward negative potentials with the decrease in the MV^{2+} concentration and merged into the main wave at concentrations below 0.25 mM.

Differential Pulse Polarography. Figure 2 shows

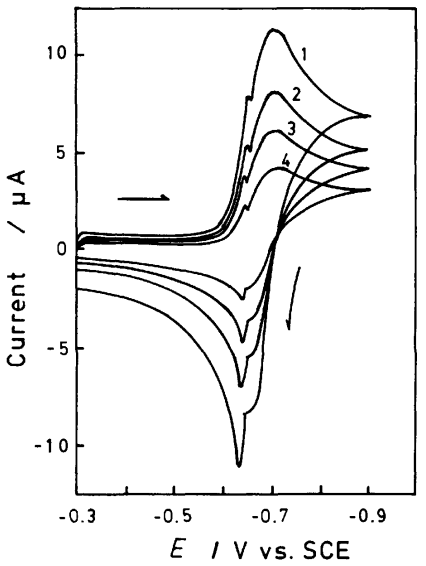

Fig. 1. Cyclic voltammograms of 1 mM MV^{2+} in a 0.1 M phosphate buffer solution (pH 7.0). Scan rates are (1): 200 mV s^{-1}, (2): 100 mV s^{-1}, (3): 50 mV s^{-1}, and (4): 20 mV s^{-1}.

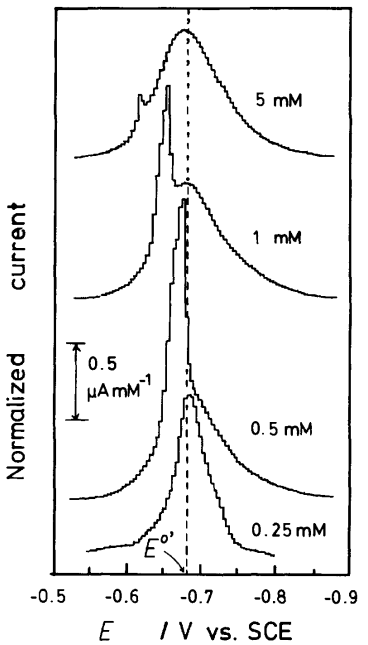

Fig. 2. Concentration dependence of differential pulse polarograms of methyl viologen in a 0.1 M phosphate buffer solution (pH 7.0). The concentrations are given on polarograms. The scan rate is 2 mV s^{-1}, the drop time 2 s, the sampling time 30 ms, and the modulation amplitude 10 mV.

the concentration dependence of the differential pulse polarograms of MV. At 0.1 mM, a single asymmetric peak was observed at −0.7 V, and the width of the peak at half height ($W_{1/2}$) was about 60 mV. At 0.25 mM, a single asymmetric peak was at −0.68 V, and $W_{1/2}$ was about 50 mV. At concentrations higher than 0.5 mM, a very sharp prepeak ($W_{1/2}$<20 mV) was separated from the main wave ($W_{1/2}$=90 mV, E_p=−0.68 V), and the

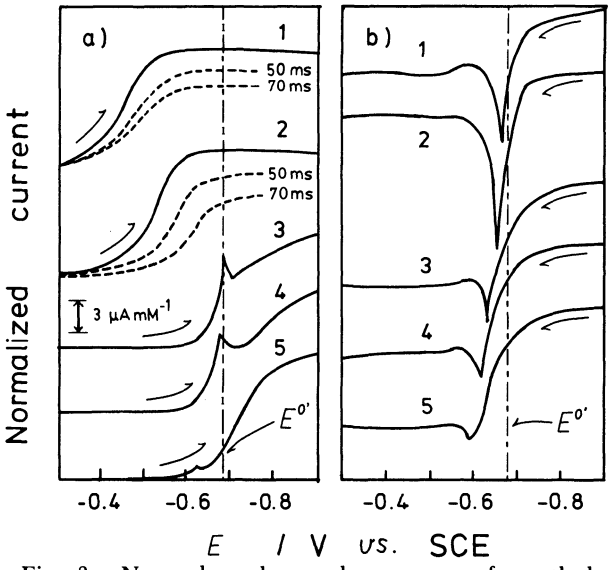

Fig. 3. Normal pulse polarograms of methyl viologen in a 0.1 M phosphate buffer solution (pH 7.0). a) On the forward scan with E_{in}=−0.3 V, and b) on the reverse scan with E_{in}=−0.9 V. The concentrations are (1): 0.1 mM, (2): 0.25 mM, (3): 0.75 mM, (4): 1 mM, and (5): 5 mM. (-----): Measured at the sampling times of 50 ms and 70 ms. t_d=2 s and t_s=30 ms.

potentials of the prepeak shifted toward positive potentials with an increase in the concentration of MV^{2+}. In the concentration range of (0.1—5) mM, the E_p of the prepeak on DPP was almost independent of the drop time (t_d) and the sampling time.

Normal Pulse Polarography. The adsorption waves of normal pulse polarograms varied with the concentration, the initial potential, the sampling time, and the direction of the potential scan. Figure 3 shows the concentration dependence of the NPP of MV.

Forward Scan: Above 0.5 mM, a sharp prewave appeared with the main wave, and the peak potential of the prewave shifted toward positive potentials with the increase in the MV^{2+} concentration. Below 0.5 mM, the prewave disappeared and a single wave was observed. The limiting current of the main wave or the single wave was proportional to $h^{1/2}$ and $t_s^{-1/2}$ throughout the concentration range of (0.01—5) mM, where h is the height of the mercury column. Below 0.25 mM, $E_{1/2,s}$ shifted by about 0.2 V toward the positive potential from $(E^{0'})_{MV}$, while at concentrations higher than 0.4 mM, the $E_{1/2,s}$ and the E_p of the prewave were not far from $(E^{0'})_{MV}$. The dependence of $E_{1/2,s}$ on E_{in} was observed only in the concentration range of (0.1—0.3) mM, in the range of E_{in} at −(0.3—0.5) V, and with a short t_s (Table 1). The drop time did not affect $E_{1/2,s}$ (Table 1).

Reverse Scan: A sharp postwave appeared throughout the measured concentration range, and the peak potential of the postwave shifted toward positive potentials with an increase in the concentration of MV^{2+}. The peak potential of the postwave on the reverse scan was always more positive than that of the

Table 1. Dependence of $E_{1/2,s}$ on E_{in}, t_d, and t_s[a)]

E_{in}	t_d	$E_{1/2,s}$ / mV		
V	s	t_s / ms		
		30	50	70
0	1	—	−667	—
0	2	−585	−667	−680
0	4	−587	−666	−680
−0.1	4	−588	−663	−680
−0.2	4	−595	−667	−680
−0.3	2	−630	−677	−680
−0.3	4	−630	−677	−680
−0.3	8	−630	—	—
−0.4	4	−672	−677	−680
−0.5	4	−677	−677	−680

a) The solution is 0.28 mM MV^{2+} in 0.1 M of a phosphate buffer solution (pH 7.0). The scan rate is 2 mV s^{-1}.

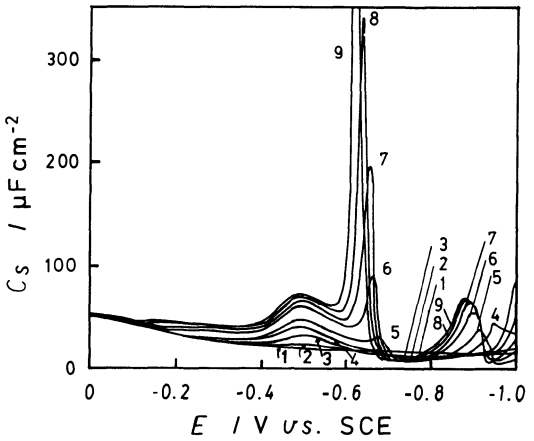

Fig. 4. Differential capacities of methyl viologen at mercury electrode in a 0.1 M phosphate buffer solution (pH 7.0). The concentrations are (1): 0 M, (2): 10 μM, (3): 50 μM, (4): 0.1 mM, (5): 0.25 mM, (6): 0.5 mM, (7): 1 mM, (8): 2 mM, and (9): 5 mM. The scan rate is 2 mV s^{-1}, the drop time 4 s, the a.c. frequency 1 kHz, and the amplitude of a.c. voltage 5 mV.

prewave on the forward scan, and the potential difference between these peaks increased with the decrease in the MV^{2+} concentration. The peak potential of the postwave was independent of t_s and t_d.

a.c. Polarography. Figure 4 shows the differential capacity (C_s) of the mercury electrode in various concentrations of MV^{2+}. Figure 5 shows the variation in C_s with respect to the a.c. frequency. The height of the C_s peak in the vicinity of $(E^{0'})_{MV}$ increased rapidly with the increase in the MV^{2+} concentration and with the decrease in the a.c. frequency. This C_s-peak potential shifted toward positive potentials with an increase in the concentration of MV^{2+}. A broad and symmetric C_s peak ($W_{1/2}$=about 120 mV) was observed at −0.49 V throughout the measured concentration range of (0.01—5) mM. The height of the C_s peak at −0.49 V

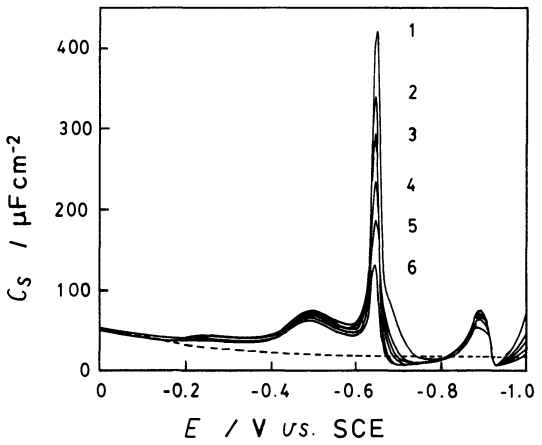

Fig. 5. Frequency dependence of differential capacities of 1 mM MV^{2+} in a 0.1 M phosphate buffer solution (pH 7.0). a.c. frequencies are (1): 100 Hz, (2): 200 Hz, (3): 300 Hz, (4): 500 Hz, (5): 1 kHz, and (6): 2 kHz. (-----): A 0.1 M phosphate buffer solution at 1 kHz (C_s is independent of the a.c. frequency). Other conditions are given in Fig. 4.

Table 2. Amounts of Adsorbed MV^{2+} and $MV^{+\cdot}$ on a Mercury Electrode

Concentration[a] mM	$\Gamma_{MV^{2+}}$[b] 10^{-10} mol cm^{-2}		$\Gamma_{MV^{+\cdot}}$[b] 10^{-10} mol cm^{-2}	
	t_d / s		t_d / s	
	2	4	2	4
2.3	1.3	1.3	4.0	4.0
1.0	0.93	0.99	3.9	4.0
0.75	0.81	0.84	3.8	3.9
0.5	0.61	0.59	3.8	4.0
0.25	0.47	0.48	3.7	3.9
0.15	0.43	0.45	—	3.8
0.1	0.39	0.45	2.9	3.5

a) Concentrations of methyl viologen in 0.1 M of a phosphate buffer solution (pH 7.0). b) $\Gamma_{MV^{2+}}$ and $\Gamma_{MV^{+\cdot}}$ are the amounts of the adsorbed MV^{2+} and $MV^{+\cdot}$ molecules which were determined by means of potential-step chronocoulometry from −0.3 V to −0.8 V and from −0.8 V to −0.3 V, respectively.

varied slightly with the a.c. frequency and approached a saturation value at concentrations higher than 5 mM. The peak potential at −0.49 V was almost independent of both the concentration of MV^{2+} and the a.c. frequency. The increase in the MV^{2+} concentration led to the depression of C_s in the potential range of −(0.7—0.8) V, and C_s reached a minimum value of 8 μF cm^{-2} in the concentration range of (0.2—1) mM.

The resistive component of the alternating current (R_s) also depended markedly on the concentration of MV^{2+} and the a.c. frequency in the vicinity of $(E^{0'})_{MV}$. At −0.49 V, R_s was almost independent of the concentration of MV^{2+} and the a.c. frequency, and R_s was almost equal to R_{sol}, where R_{sol} was the solution resistance. At −0.65 V in 1 mM of the MV^{2+} solution, the phase angle of the faradaic impedance plot obtained by using the Randles-Ershler equivalent circuit exceeded 45°.

Potential-Step Chronocoulometry. The amounts of MV^{2+} and $MV^{+\cdot}$ adsorbed on the mercury electrode at −0.3 and −0.8 V were evaluated by means of potential-step chronocoulometry.[40]

The amounts of the adsorbed redox species were calculated by the use of

$$(Q_{total})_{t=0} = n_e FS\Gamma + Q_{dl}, \quad (1)$$

where $(Q_{total})_{t=0}$ was the intercept of Q_{total} vs. the $t^{1/2}$ plot; Q_{total}, the total electric charge from time $t=0$ to t; n_e, the number of electrons involved in the redox reaction; S, the area of the electrode; Γ, the surface concentration of adsorbed redox species, and Q_{dl}, the capacitive charge of the double layer. The interfacial capacitance of the electrode covered by methyl viologen, Q_{dl}, was assumed to be equal to that covered by 4,4′-bipyridyl, which is electrochemically stable in the stepped potential range ($E_{1/2}$=−1.06 V)[41] and which has a structure analogous to that of methyl viologen. Table 2 shows the amounts of MV^{2+} and $MV^{+\cdot}$ molecules adsorbed on the mercury electrode, as calculated from Eq. 1.

Discussion

Formal Potential and Diffusion Coefficient of Methyl Viologen. The formal potentials of the $MV^{2+/+\cdot}$ couple in 0.1 M of a phosphate buffer solution at pH 7.0, as obtained by cyclic voltammetry, classical d.c. polarography, and differential pulse polarography, were −(0.680±0.005) V, −(0.682±0.002) V, and −(0.683±0.007) V, respectively. These values were in agreement with the formal potentials of methyl viologen reported in the literatures.[4,5]

Both the diffusion coefficients of MV^{2+} and $MV^{+\cdot}$ which were calculated by the Cottrell equation from NPP, were 4.4×10^{-6} cm^2 s^{-1}.

Adsorption of MV^{2+} Molecules. In the analysis of C_s vs. E curves of methyl viologen obtained by a.c. polarography, Pospisil et al.[3,25] and Grachev et al.[8] have reported that the C_s peak at about −0.49 V is attributable to an adsorption-desorption process of MV^{2+}, for this peak is greatly stretched out along the potential axis, the peak potential is much more positive than $(E^{0'})_{MV}$, and no faradaic wave is observed at about −0.49 V in classical d.c. polarograms. As is shown in Table 2, however, the amount of MV^{2+} molecules adsorbed at −0.3 V is about 1×10^{-10} mol cm^{-2} in 1 mM of a MV^{2+} solution. That is, MV^{2+} has already been adsorbed on a mercury electrode at the foot of the positive side of this C_s peak. The height of the C_s peak is practically independent of the a.c. frequency, and R_s in the vicinity of −0.49 V is equal to R_{sol}. Since the faradaic impedance of a reversible surface redox reaction of the adsorbed species is inde-

pendent of the a.c. frequency,[35,42-44] it is probable that the C_s peak at −0.49 V is attributable to the reversible redox reaction of the adsorbed species and that a repulsive interaction between the adsorbed redox species gives rise to a broad peak.[45,46] In the present NPP study, on the forward scan below 0.25 mM, we have found a diffusion-controlled faradaic wave with a half-wave potential close to −0.49 V, the value at which the broad C_s peak was observed in a.c. polarograms. These results strongly suggest that the C_s peak at −0.49 V is not an adsorption-desorption peak, but the faradaic pseudo-capacitive peak due to the adsorbed MV^{2+} and the adsorbed $MV^{+\cdot}$.

It is probable that the adsorption of MV^{2+} on a positively charged mercury electrode is due to the π-electron interaction between adsorbed molecules and a mercury electrode, which has been reported by Frumkin and Damaskin,[47] and others.[48-56] Moreover, it has been reported that aromatic cations can also be adsorbed on electrodes at more positive potentials than the potential of zero charge of the mercury electrode by means of the π-electron interaction.[8,32,36,57,58]

C_s Peak in the Vicinity of $(E^{0'})_{MV}$. Grachev et al.[8] surmised that, in a.c. polarograms of MV, the C_s peak in the vicinity of $(E^{0'})_{MV}$ was observed only in the narrow concentration range of (0.1—0.2) mM because the first reduction step of MV^{2+} becomes irreversible because of the inhibition by both the adsorbed MV^{2+} molecules in the MV^{2+} concentrations lower than 0.1 mM and the adsorbed $MV^{+\cdot}$ molecules in the MV^{2+} concentrations higher than 0.2 mM. However, both the present and previous studies[2-5,11] have proved that the first reduction step of MV^{2+} is not irreversible, even at the concentrations higher than 0.2 mM. As is shown in Fig. 6, the C_s peak potential in the vicinity of $(E^{0'})_{MV}$ in a.c. polarograms is almost identical with the potential of the prewave in classical d.c. and differential pulse polarograms. It is clear in Fig. 4 that the C_s peak in the vicinity of $(E^{0'})_{MV}$ did not disappear, but shifted toward positive potentials with an increase in the concentration of MV^{2+}.

Orientation of MV^{2+} and $MV^{+\cdot}$. Pospisil et al.[3,25] reported that the marked depression of C_s over −(0.7—0.8) V is caused by a complete coverage of the mercury electrode by $MV^{+\cdot}$ and that the C_s peak at −0.9 V is due to the reorientation of the adsorbed $MV^{+\cdot}$ from flat to vertical.

As is shown in Table 2, the maximum surface concentration of adsorbed $MV^{+\cdot}$ molecules, as determined by potential-step chronocoulometry at −0.8 V, was $(4.0\pm0.1)\times10^{-10}$ mol cm^{-2}. Figure 7 shows the structure of methyl viologen. The area occupied by one molecule adsorbed on an electrode (S_{ad}) can be estimated from the van der Waals radii. If methyl viologen is oriented vertically on the electrode, and if the methyl group of MV can rotate freely around the C-N sigma-bond axis,[59] S_{ad} is estimated to be 34 Å^2 per molecule. If hexagonal array is considered in addition

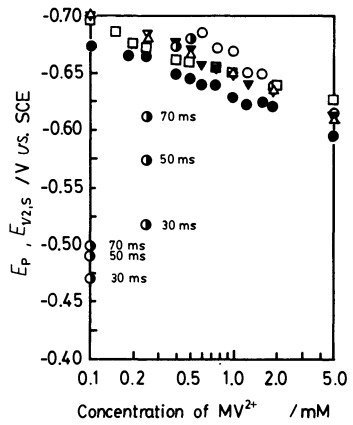

Fig. 6 Concentration dependence of E_p and $E_{1/2,s}$ of methyl viologen. The values of E_p are plotted as (○) for NPP on the forward scan, (●) for NPP on the reverse scan, (□) for a.c. polarograms, (△) for DPP, and (▼) for classical d.c. polarograms. The values of $E_{1/2,s}$ are plotted as (◑) for NPP on the forward scan and (▽) for classical d.c. polarograms. The conditions of measurements are given in Fig. 2—4.

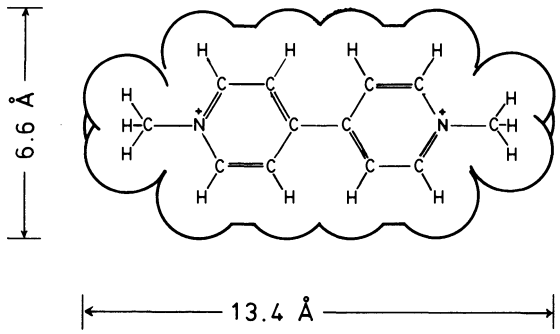

Fig. 7. Structure of methyl viologen.

to a vertical orientation, S_{ad} becomes 38 Å^2 per molecule, which corresponds to 4.4×10^{-10} mol cm^{-2} for the maximum surface concentration (Γ_m). If methyl viologen is oriented flat on an electrode, S_{ad} becomes 88 Å^2 per molecule, which corresponds to 1.9×10^{-10} mol cm^{-2} for Γ_m. If the twisting by 37.2° between two pyridyl rings is considered in addition to a flat orientation, S_{ad} becomes 84 Å^2 per molecule, which corresponds to 2.0×10^{-10} mol cm^{-2} for Γ_m. The good agreement between the measured and the calculated maximum surface concentrations suggests that adsorbed $MV^{+\cdot}$ molecules are oriented vertically, at least in the potential region of −(0.7—0.8) V (cf. Fig. 4). On the other hand, the maximum surface concentration of MV^{2+} has not yet been attained at −0.3 V, as is shown in Table 2 (probably because of a repulsive interaction between adsorbed MV^{2+} molecules) and the orientation of the MV^{2+} molecules adsorbed at a positively charged electrode by means of π-electron interaction is considered to be flat rather than vertical.[43,44,47-58]

Orientation Change of Adsorbed $MV^{+\cdot}$ Molecules. The findings that the C_s peak with the symmetric

shape[37,46] at −0.49 V is independent of the a.c. frequency and that the resistive component at −0.49 V is equal to the solution resistance[44] suggest a surface redox reaction between the adsorbed MV^{2+} molecules and the adsorbed $MV^{+\cdot}$ molecules without the reorientation of the adsorbed species in the vicinity of −0.49 V. If $MV^{+\cdot}$ molecules with a flat orientation are adsorbed on the mercury electrode much more strongly than MV^{2+} molecules (that is, if the ratio of the adsorption coefficient of $MV^{+\cdot}$ to that of MV^{2+} is higher than 10^3), it would be expected that a faradaic prewave would appear at a potential about 0.2 V more positive than $(E^{0'})_{MV}$.

The potential step from the initial potential at which only MV^{2+} molecules have been adsorbed to about −0.49 V gives rise to the formation of adsorbed $MV^{+\cdot}$ at the electrode. A faradaic current and consequently, the $E_{1/2,s}$ are determined by the interfacial concentration gradient and by the surface concentration change of the redox species at the time when the current is sampled.[39] That is, the $E_{1/2,s}$ depends on the t_s, the bulk concentration, and the adsorption states of the redox species at E_{in}. In NPP with a short sampling time at lower concentrations of MV^{2+}, an adsorption wave which is diffusion-controlled can be observed. In NPP at higher concentrations of MV^{2+} and with a long sampling time, and in the differential pulse and the tast polarographic techniques where the electrode potential is kept practically at the sampling potential during the drop time, the amount of the adsorbed $MV^{+\cdot}$ at −0.49 V approaches the value at the adsorption equilibrium or the saturation value. Consequently, the interfacial concentration would be rehomogenized[35] and the adsorption current would decay and would be apt to be overlooked when the current is sampled. On the other hand, in a.c. polarography, a faradaic pseudo-capacitive peak due to the adsorbed MV^{2+} and the adsorbed $MV^{+\cdot}$ molecules can be observed, and also, in cyclic voltammetry, an adsorption peak can be observed provided that the eletrode potential where the $MV^{+\cdot}$ molecules are not adsorbed is chosen for the initial potential.

At concentrations higher than 0.5 mM, as the electrode potential approaches $(E^{0'})_{MV}$, the surface concentration of the adsorbed $MV^{+\cdot}$ molecules increases so abruptly that a reorientation of adsorbed $MV^{+\cdot}$ molecules from flat to vertical takes place.[53,54] The vertical orientation makes possible an attractive interaction between adsorbed $MV^{+\cdot}$ molecules, which causes the further adsorption of $MV^{+\cdot}$ and leads to a sharp adsorption peak. The increase in the bulk concentration of MV^{2+} gives rise to the increase in the interfacial concentration of $MV^{+\cdot}$ after the reduction by a potential step, and the surface concentration of the adsorbed $MV^{+\cdot}$ molecules will be sufficient to change the orientation from flat to vertical at a more positive potential than the potential where the reorientation takes place at lower concentrations of MV^{2+}. It is probable that the positive shift of the peak potential with an increase in the MV^{2+} concentration shown in Fig. 6 is to be attributed to the concentration dependence of the potential at which the reorientation of adsorbed $MV^{+\cdot}$ molecules occurs.

Parry and Parsons[50] have reported that the orientation of *p*-toluenesulfonate adsorbed on a mercury electrode changes from flat at lower concentrations to vertical at higher concentrations, and that the flat orientation accelerates a repulsive interaction between adsorbed *p*-toluenesulfonate molecules, and the vertical orientation, an attractive interaction. Similar discussions of the relation between an orientation and the interaction constants of redox species have been reported by Ershler et al.[60] and others.[48,49,55,56,61,62] Laviron[32] has reported that, in cyclic voltammetry, *trans*-1,2-di(4-pyridyl)ethylene adsorbed on a mercury electrode displays a similar orientation change with the concentration and that the vertical orientation of the redox molecules at the electrode surface causes an attraction force between them which leads to a sharp adsorption peak.

The abrupt change in the orientation of the adsorbed $MV^{+\cdot}$ molecules at the electrode surface leads to the strong frequency dependence of the sharp C_s peak in the vicinity of $(E^{0'})_{MV}$ (Fig. 5). In Fig. 5, the main C_s peak is not observed because of the mergence with the larger adsorption C_s peak. At 6.4 Hz, the appearance of a shoulder corresponding to the main faradaic C_s peak on the negative potential side of a larger C_s peak has been reported.[3] At concentrations lower than 50 μM, no C_s peak appears in the vicinity of $(E^{0'})_{MV}$ because the interfacial concentration of the redox species is negligible compared to the surface concentration of these species because of the depletion of the interfacial concentration as a result of the strong adsorption of the redox species.

In the reverse scan of NPP, the surface concentration of $MV^{+\cdot}$ molecules pre-adsorbed at the initial potential is so high that the adsorbed $MV^{+\cdot}$ molecules are already oriented vertically, even at 0.1 mM (cf. Table 2). The potential step from the initial potential, where the adsorbed $MV^{+\cdot}$ molecules are oriented vertically, to the anodic potential always leads to an orientation change from vertically adsorbed $MV^{+\cdot}$ molecules to flat adsorbed MV^{2+} molecules. This orientation change leads to the situation in which a sharp postpeak always appears over the measured concentration range and the postpeak potential always shifts toward positive potentials with an increase in the concentration.

In the forward scan of NPP, the direction of the shift of the $E_{1/2,s}$ with the concentration in the lower concentration range (<0.5 mM) is opposite to the shift of the prepeak potential with the concentration in the higher concentration range (>0.5 mM). This is probably caused by the change in the orientation of the adsorbed $MV^{+\cdot}$ at the electrode surface and the change in the interaction between adsorbed $MV^{+\cdot}$ molecules. The

potential difference between the prepeak for the forward scan and the postpeak for the reverse scan which is observed at concentrations higher than 0.5 mM probably originates from both the sigmoid-type adsorption isotherm with the strongly attractive interaction between the adsorbed $MV^{+\cdot}$ molecules and the difference between the S_{ad} values of MV^{2+} and $MV^{+\cdot}$ molecules, as has been discussed by Laviron.[37] The peculiar adsorption behavior of methyl viologen is simulated by the digital simulation of the normal pulse polarograms based on the Frumkin-type Flory-Huggins isotherm, which will be published in a subsequent paper.

The present work was supported by a Grant-in-Aid for Scientific Research No. 5670031 from the Ministry of Education, Science and Culture.

References

1) C. L. Bird and A. T. Kuhn, *Chem Soc. Rev.*, **10**, 49 (1981).
2) J. Volke, *Collect. Czech. Chem. Commun.*, **33**, 3044 (1968).
3) L. Pospisil, J. Kuta, and J. Volke, *J. Electroanal. Chem. Interfacial Electrochem.*, **58**, 217 (1975).
4) R. M. Elofson and R. L. Edsberg, *Can. J. Chem.*, **35**, 646 (1957).
5) E. Steckhan and T. Kuwana, *Ber. Bunsenges. Phys. Chem.*, **78**, 253 (1974).
6) E. M. Kosower and J. L. Cotter, *J. Am. Chem. Soc.*, **86**, 5524 (1964).
7) H. T. Van Dam and J. J. Ponjee, *J. Electrochem. Soc.*, **121**, 1555 (1974).
8) V. N. Grachev, S. I. Zhdanov, and G. S. Supin, *Sov. Electrochem.*, **14**, 1180 (1978).
9) G. Hauska, "Photosynthesis 1. Artificial Acceptors and Donors," in "Encyclopedia of Plant Physiology, New Series," Springer-verlag (1977), Vol. 5, Chap. 15.
10) A. B. Bocarsly, D. C. Bookbinder, R. N. Dominey, N. S. Lewis, and M. S. Wrighton, *J. Am. Chem. Soc.*, **102**, 3683 (1980).
11) K. Kobayashi and K. Niki, *Chem. Lett.*, **1982**, 829.
12) Y. M. Tricot, D. N. Furlong, W. H. F. Sasse, P. Daivis, I. Snook, and W. Van Megen, *J. Colloid Interface Sci.*, **97**, 380 (1984).
13) P. Cuendet, M. Gratzel, and M. L. Pelaprat, *J. Electroanal. Chem. Interfacial Electrochem.*, **181**, 173 (1984).
14) W. J. Albery and A. J. Mcmahon, *J. Electroanal. Chem. Interfacial Electrochem.*, **182**, 1 (1985).
15) I. F. Chang, B. L. Gilbert, and T. I. Sun, *J. Electrochem. Soc.*, **122**, 955 (1975).
16) D. J. Barclay, C. L. Bird, and D. H. Martin, *J. Electronic Materials*, **8**, 311 (1979).
17) M. Yamana and T. Kawada, *Nippon Kagaku Kaishi*, **1977**, 941.
18) S. Fletcher, L. Duff, and R. G. Barradas, *J. Electroanal. Chem. Interfacial Electrochem.*, **100**, 759 (1979).
19) J. Bruinink and P. van Zanten, *J. Electrochem. Soc.*, **124**, 1232 (1977).
20) M. Ito and T. Kuwana, *J. Electroanal. Chem. Interfacial Electrochem.*, **32**, 415 (1971).
21) F. Rauwel and D. Thevenot, *J. Electroanal. Chem. Interfacial Electrochem.*, **75**, 579 (1977).
22) S. D. Varfolomeev, A. I. Yaropolov, I. V. Berezin, M. R. Tarasevich, and V. A. Bogdanovskaya, *Bioelectrochem. Bioenerg.*, **4**, 314 (1977).
23) J. F. Stargardt, F. M. Hawkridge, and H. L. Landrum, *Anal. Chem.*, **50**, 930 (1978).
24) B. Zinger and L. L. Miller, *J. Electroanal. Chem. Interfacial Electrochem.*, **181**, 153 (1984).
25) L. Pospisil and J. Kuta, *J. Electroanal. Chem. Interfacial Electrochem.*, **90**, 231 (1978).
26) C. A. Melendres, P. C. Lee, and D. Meisel, *J. Electrochem. Soc.*, **130**, 1523 (1983).
27) R. Rossetti, S. M. Beck, and L. E. Brus, *J. Am. Chem. Soc.*, **106**, 980 (1984).
28) B. Beden, O. Enea, F. Hahn, and C. Lamy, *J. Electroanal. Chem. Interfacial Electrochem.*, **170**, 357 (1984).
29) R. H. Wopshall and I. Shain, *Anal. Chem.*, **39**, 1514 (1967).
30) G. C. Barker and J. A. Bolzan, *Z. Anal. Chem.*, **216**, 215 (1966).
31) A. M. Hartley and G. S. Wilson, *Anal. Chem.*, **38**, 681 (1966).
32) E. Laviron, *J. Electroanal. Chem. Interfacial Electrochem.*, **52**, 355 (1974).
33) D. R. Canterford, *J. Electroanal. Chem. Interfacial Electrochem.*, **52**, 144 (1974).
34) G. Piccardi, F. Pergola, M. L. Foresti, and R. Guidelli, *J. Electroanal. Chem. Interfacial Electrochem.*, **84**, 235 (1977).
35) E. Laviron, "Voltammetric Methods for the Study of Adsorbed Species," in "Electroanalytical Chemistry," ed by A. J. Bard, Marcel Dekker, New York and Basel (1982), Vol. 12, Chap. 2.
36) M. Heyrovsky, S. Vavricka, and R. Heyrovska, *J. Electroanal. Chem. Interfacial Electrochem.*, **46**, 391 (1973).
37) E. Laviron, *J. Electroanal. Chem. Interfacial Electrochem.*, **63**, 245 (1975).
38) J. B. Flanagan, K. Takahashi, and F. C. Anson, *J. Electroanal. Chem. Interfacial Electrochem.*, **81**, 261 (1977).
39) J. B. Flanagan, K. Takahashi, and F. C. Anson, *J. Electroanal. Chem. Interfacial Electrochem.*, **85**, 257 (1977).
40) F. C. Anson, *Anal. Chem.*, **38**, 54 (1966).
41) A. B. Zahlan and R. H. Linnel, *J. Am. Chem. Soc.*, **77**, 6207 (1955).
42) H. A. Laitinen and J. E. B. Randles, *Trans. Faraday Soc.*, **51**, 54 (1955).
43) A. N. Frumkin and B. B. Damaskin, "Modern Aspect of Electrochemistry," ed by J. O'M Bockris and B. E. Conway, Butterworths, Washington (1964), Vol. 3, Chap. 3.
44) B. B. Damaskin, O. A. Petrii, and V. V. Batrakov, "Adsorption of Organic Compounds on Electrodes," Plenum Press, New York and London (1971), Chap. 2.
45) T. Kakutani and M. Senda, *Bull. Chem. Soc. Jpn.*, **52**, 3236 (1979).
46) E. Laviron, *J. Electroanal. Chem. Interfacial Electrochem.*, **105**, 25 (1979).
47) A. N. Frumkin and B. B. Damaskin, *Pure Appl. Chem.*, **15**, 263 (1967).
48) B. E. Conway and R. G. Barradas, *Electrochim. Acta*, **5**, 319 (1961).
49) R. G. Barradas and B. E. Conway, *Electrochim. Acta*, **5**, 349 (1961).

50) J. M. Parry and R. Parsons, *J. Electrochem. Soc.*, **113**, 992 (1966).
51) R. Parsons, *Rev. Pure Appl. Chem.*, **18**, 91 (1968).
52) E. Blomgren, J. O'M Bockris, and C. Jesch, *J. Electrochem. Soc.*, **65**, 2000 (1961).
53) B. B. Damaskin, *J. Electroanal. Chem. Interfacial Electrochem.*, **21**, 149 (1969).
54) B. B. Damaskin, A. A. Sulvila, S. Ya. Vasina, and A. I. Fedorova, *Sov. Electrtochem.*, **3**, 729 (1967).
55) E. A. Mambetkaziev, S. I. Zhdanov, and B. B. Damaskin, *Sov. Electrochem.*, **8**, 1607 (1972).
56) N. K. Akhmetov, R. I. Kaganovich, E. A. Mambetkaziev, and B. B. Damaskin, *Sov. Electrochem.*, **13**, 236 (1977).
57) R. I. Kaganovich, B. B. Damaskin, and M. A. Suranova, *Sov. Electrochem.*, **7**, 1109 (1971).
58) B. B. Damaskin, *Sov. Electrochem.*, **5**, 561 (1969).
59) D. Guerin-euler, C. Nicollin, C. Sieiro, and C. Lamy, *Mol. Phys.*, **34**, 161 (1977).
60) A. B. Ershler, G. A. Tedoradze, and E. M. Podgaetskii, *Sov. Electrochem.*, **7**, 1041 (1971).
61) E. A. Mambetkaziev, A. M. Shaldybaeva, V. N. Statsyuk, and S. I. Zhdanov, *Sov. Electrochem.*, **11**, 1643 (1975).
62) N. K. Akhmetov, R. I. Kaganovich, B. B. Damaskin, and E. A. Mambetkaziev, *Sov. Electrochem.*, **14**, 1534 (1978).

 © 1986 The Chemical Society of Japan Bull. Chem. Soc. Jpn., 59, 3723—3727 (1986)

Pressure and Temperature Effects on the Excess Conductance of the Hydroxide Ion in Water

Masakatsu UENO,* Yasushi SAKATA, Noriaki TSUCHIHASHI, and Kiyoshi SHIMIZU
Department of Applied Chemistry, Faculty of Engineering, Doshisha University, Karasuma Imadegawa, Kamigyo-ku, Kyoto 602
(Received March 27, 1986)

The limiting molar conductances, Λ°, of sodium hydroxide were determined at 15, 25, and 40 °C as a function of the pressure up to 1500 kgf cm^{-2} (1 kgf cm^{-2}=0.9807×10^5 Pa) from the conductances measured in a dilute concentration range (1×10^{-3}—2×10^{-2} M, 1 M=1 mol dm^{-3}). The excess conductances at an infinite dilution, λ°_E, of the hydroxide ion, as estimated by [$\lambda^\circ_E(OH^-)=\Lambda^\circ(NaOH)-\Lambda^\circ(NaCl)$], were found to increase with an increase in the pressure and temperature, as well as those of the oxonium ion, $\lambda^\circ_E(H_3O^+)$. However, there was a significant difference in the magnitude of λ°_E, itself, and a slight difference in the magnitude of the pressure and temperature dependences of λ°_E between hydroxide and oxonium ions. These results may be related to a difference between the proton-jump mechanisms of the hydroxide and oxonium ions.

In our previous papers,[1,2] the oxonium ion was used as a probe to study the variation of the solvent structure in hydrogen-bonded solvents with the pressure, temperature, and ethanol content, since protons are transferred through the hydrogen-bonded networks in addition to the hydrodynamic migration, resulting in a high mobility of the oxonium ion. The high mobility of the hydroxide ion in aqueous solutions can also be attributed to a proton-jump mechanism. There is, however, a significant difference between the proton-jump mechanisms of hydroxide and oxonium ions. According to the theory of Conway et al.,[3] the rate-determining step in the proton-jump mechanism is a rotation of hydrogen-bonded water molecules as dipoles near the ions, necessary to make possible the next proton jump. In the case of the oxonium ion, the driving force for the rotation is a repulsion between the two OH groups facing each other as a result of the proton jump in addition to an ion-dipole interaction. The force causing the rotation arises principally from an ion-dipole interaction in the case of the hydroxide ion. This difference between the ions may be reflected by the variation in their excess conductances due to a proton jump with the pressure and temperature. So far, only a few papers[4-6] have been published on the conductances of alkaline solutions at high pressures and at moderate temperatures. Here, the pressure and temperature effects on the excess conductances of the hydroxide ion are reported, and are compared with those of the oxonium ion.

Experimental

Chemicals, Solutions, and Properties of Water. Conductivity water was prepared by passing distilled water through a mono-bed ion-exchange resin; it was stored in a stainless-steel tank under a nitrogen atmosphere. Its conductivity, κ_S, was about 4.3×10^{-7} S cm^{-1} at 25 °C and at 1 atm as is shown in Table 1. Table 1 also summarizes such properties of water used in the data analysis as the density, ρ,[7,8] the static dielectric constant, ε,[10,11] and the viscosity, η.[13,14]

The aqueous solutions of sodium hydroxide were prepared by the same method as Darken and Meier.[15] All the dilute solutions of NaOH were prepared gravimetrically by diluting a stock solution (about 2×10^{-2} M) made from a saturated solution at 0 °C. The saturated solution was prepared from the analytical-grade sodium hydroxide supplied by Merck. The concentration of the stock solution was determined by titration with oxalic acid solutions, using a phenolphthalein indicator. The titrations were performed with a micro burette; the reproducibility was about one part in one thousand. The concentrations of the dilute NaOH solutions at 25 °C and at 1 atm were determined by using the densities, ρ(NaOH), of the stock solution and dilute solutions, which were measured at 25 °C and at 1 atm by means of a digital vibrating densimeter (SS-D-200 twin-type) manufactured by the Shibayama Scientific Co., Ltd. The following equation was obtained:

$$\rho(\mathrm{NaOH}) = 0.9970_6 + 0.046_0 c, \quad (1)$$

where ρ(NaOH) is in g cm^{-3} and c is the concentration of the solution in M. The above equation is in very good agreement with the one described in Ref. 15. The concentrations of the solutions at other pressures and temperatures were calculated by assuming that the ratios of densities between

Table 1. Physical Properties of Water as a Function of the Pressure and Temperature, and the Corrrection Factors for the Cell Constant of the Teflon Cell at 40 °C

P / kgf cm^{-2}	ρ / g cm^{-3}	ε	η / cP	$10^7\kappa_s$ / S cm^{-1}	$f^{(p)}$
		15 °C			
1	0.9991	82.1	1.137	3.5	
500	1.0208	83.9	1.113	4.4	
1000	1.0405	85.6	1.107	5.5	
1500	1.0584	87.2	1.119	7.1	
		25 °C			
1	0.9970	78.5	0.8937	4.3	
500	1.0181	80.2	0.8865	5.4	
1000	1.0372	81.9	0.8897	6.8	
1500	1.0546	83.5	0.9034	8.7	
		40 °C			
1	0.9922	73.2	0.657	5.3	1.0000
500	1.0127	74.9	0.661	6.7	0.9871
1000	1.0312	76.5	0.676	8.4	0.9807
1500	1.0483	77.9	0.693	10.7	0.9758

Table 2. Molar Conductances (Λ/S cm^2 mol^{-1}) at Various Concentrations, Limiting Molar Conductances ($\Lambda°$/S cm^2 mol^{-1}), Ion-Size Parameters ($\mathring{a}$/Å), and Standard Deviations of Λ (σ_Λ/S cm^2 mol^{-1}) of NaOH in Compressed Water at 15, 25, and 40 °C

P/kgf cm^{-2}	Λ							$\Lambda°$	$\mathring{a}$	σ_Λ
				15 °C						
	1.151[a]	3.079[a]	6.164[a]	9.248[a]	18.15[a]					
1	204.3	202.2	200.6	199.4	196.8			207.4	3.3	0.15
500	208.4	206.3	204.7	203.4	200.8			211.6	3.2	0.13
1000	210.4	208.4	206.8	205.4	203.0			213.6	3.2	0.06
1500	210.9	209.0	207.5	206.0	203.7			214.0	3.3	0.14
				25 °C						
	1.421[a]	2.237[a]	4.326[a]	8.597[a]	10.92[a]	14.03[a]	17.14[a]			
1	245.6	244.8	242.9	239.8	238.6	237.5	235.7	250.4	2.4	0.26
500	249.2	248.3	246.5	243.5	242.5	241.1	239.6	253.9	2.6	0.22
1000	250.5	249.6	248.0	245.0	244.0	242.7	241.2	255.2	2.7	0.26
1500	250.3	249.5	248.0	245.1	244.2	242.7	241.3	255.0	2.7	0.31
				40 °C						
	3.522[a]	5.278[a]	10.56[a]	14.10[a]	20.84[a]					
1	309.0	307.0	303.7	301.4	297.6			318.6	2.5	0.52
500	309.2	307.1	304.2	302.5	298.8			318.3	2.9	0.59
1000	309.3	307.3	304.7	302.8	299.4			318.2	3.0	0.59
1500	308.9	306.6	304.3	302.3	299.0			317.4	3.0	0.64

a) Concentrations (10^{-3} M) at atmospheric pressure.

the solutions under various conditions were equal to those of pure water under the corresponding conditions. All the solutions were treated in a dry box under a nitrogen atmosphere.

Apparatus. Two kinds of conductivity cells with lightly platinized electrodes were employed: a glass cell (capacity, 10 cm^3)[16] at 15 and 25 °C, and a Teflon cell (capacity, 12 cm^3)[2] at 40 °C. The resistances of NaOH aqueous solutions in the glass cell did not change at 15 and 25 °C for at least 5 h required for one run. The resistances, however, increased with time at 40 °C because of a reaction involving hydroxide ions with glass. Thus, the Teflon cell was used, though it has several disadvantages compared with a glass cell: the walls are very tenacious retainers of gas-bubbles and the cell constant varies greatly with the pressure. The cell constants at 1 atm and at each temperature were determined from the conductances of a 0.01 M KCl aqueous solution.[17-20] They were assumed to be invariant with the pressure for the glass cell; for the Teflon cell, the correction factors, $f^{(P)}=K_{cell}^{(P)}/K_{cell}^{(1)}$, in which $K_{cell}^{(P)}$ and $K_{cell}^{(1)}$ are the cell constant at pressure P and 1 atm respectively, were determined by comparing the conductances of 5×10^{-3} and 1×10^{-2} M KCl aqueous solutions obtained by the glass cell with those by the Teflon cell, as have been described in a previous paper.[2] The values of $f^{(P)}$, thus determined, are also listed in Table 1.

The procedure and the apparatus used here for conductance measurements at high pressures were the same as those described in a previous paper.[16]

Results and Discussion

Table 2 shows the molar conductances, Λ, of NaOH at various concentrations at 15, 25, and 40 °C as a function of the pressure. The molar conductances, Λ, were reproducible within ±0.15%. The Fuoss-Onsager equation of conductance for unassociated electrolytes:[21,22]

$$\Lambda = \Lambda° - Sc^{1/2} + Ec\log c + Jc, \quad (2)$$

where c is the concentration (M), and S, E, and J have the usual meanings, was employed to determine the limiting molar conductance, $\Lambda°$, at each pressure and temperature. The limiting molar conductances, $\Lambda°$, thus obtained, are listed in Table 2, together with their related quantities: the ion-size parameter, $\mathring{a}$, and the standard deviation of Λ, σ_Λ. The present values of $\Lambda°$(NaOH)/S cm^2 mol^{-1} at 1 atm (207.4 at 15 °C, 250.4 at 25 °C, and 318.6 at 40 °C) are larger by about (0.3—0.8)% than the literature ones (205.65[23] at 15 °C, 249.33[23] and 248.85[15] at 25 °C, and 317.66[23] at 40 °C). However, no high-pressure data are available for a comparison. As is shown in Table 2, $\Lambda°$(NaOH) increases monotonously with an increase in the pressure up to 1500 kgf cm^{-2} at 15 °C; it then appears to have a maximum at about 1500 kgf cm^{-2} at 25 °C, but slightly decreases with pressure at 40 °C.

The limiting ionic molar conductances, $\lambda°$, of the hydroxide ion under various conditions were determined by Kohlrausch's law regarding the independent migration of ions, using the values of $\Lambda°$(NaOH), $\Lambda°$(NaCl),[24-26] $\Lambda°$(KCl),[27,28] and the limiting cation-transference number for KCl, $t°(K^+)$;[16,29-31] those of the oxonium ion, $\lambda°(H_3O^+)$, were also obtained from the data on $\Lambda°$(HCl).[2,33] The values of the $\lambda°$'s of hydroxide and other ions, thus obtained, are listed in Table 3. Table 3 shows that the values of $\lambda°(OH^-)$ are about 2.5-times larger than those of $\lambda°(Cl^-)$ at each pressure and temperature, and that compared with the $\lambda°$'s of other ions, $\lambda°(OH^-)$ increases with an increase in the pressure as well as $\lambda°(H_3O^+)$, irrespective of the pressure dependence of the solvent viscosity, although the rate of the increase in $\lambda°(OH^-)$ with the pressure

Table 3. Limiting Ionic Molar Conductances (λ°/S cm^2 mol^{-1}) and Excess Conductances (λ°_E/S cm^2 mol^{-1}) in Compressed Water at 15, 25, and 40 °C

P	λ°					λ°_E	
kgf cm^{-2}	Na^+	K^+	Cl^-	OH^-	H_3O^+	OH^-	H_3O^+
			15 °C				
1	39.7	59.7	61.4	167.7	300.6	106.3	240.9
500	39.7	60.4	63.9	171.9	319.9	108.0	259.2
1000	39.7	60.5	64.9	173.9	330.0	109.0	269.5
1500	39.2	60.0	65.2	174.8	337.4	109.6	277.4
			25 °C				
1	50.1	73.5	76.4	200.3	349.8	123.9	276.3
500	50.2	73.9	77.9	203.7	360.4	125.8	286.5
1000	49.5	73.3	78.9	205.7	367.8	126.8	294.5
1500	48.9	72.6	78.8	206.1	374.2	127.3	301.6
			40 °C				
1	67.6	95.8	100.5	251.0	419.5	150.5	323.7
500	66.8	95.4	101.3	251.5	427.2	150.2	331.8
1000	66.1	94.4	101.1	252.1	434.2	151.0	339.8
1500	65.2	92.9	100.2	252.2	440.9	152.0	348.0

is much smaller than that in $\lambda^\circ(H_3O^+)$. It is apparent that these features are closely related to the proton-jump mechanism of hydroxide and oxonium ions.

The excess conductance due to the proton-jump mechanism, λ°_E, was estimated according to:

$$\lambda^\circ_E(OH^-) = \lambda^\circ(OH^-) - \lambda^\circ(Cl^-) = \Lambda^\circ(NaOH) - \Lambda^\circ(NaCl), \quad (3)$$

where the translational mobility of the OH^- ion was approximated by that of the Cl^- ion since their sizes are similar. There is only one literature data compared with the present values. The present values of $\lambda^\circ_E(OH^-)$ at 25 °C shown in Table 3 are a little larger than those obtained by Hamann and Strauss[4] from the equation: $[\lambda^\circ_E(OH^-)=\Lambda^\circ(KOH)-\Lambda^\circ(KCl)]$; their values are 123, 124, and 125 S cm^2 mol^{-1} at 1, 1000, and 2000 atm, respectively. As is shown in Table 3, $\lambda^\circ_E(OH^-)$ increases with the pressure and temperature as well as $\lambda^\circ_E(H_3O^+)$, as estimated by $[\lambda^\circ_E(H_3O^+)=\lambda^\circ(H_3O^+)-\lambda^\circ(K^+)]$, and the rate of the increase in the relative excess conductance, $\lambda^\circ_{E(P)}/\lambda^\circ_{E(1)}$, with the pressure becomes larger with a decrease in the temperature as is shown in Fig. 1. These results qualitatively correspond to the pressure and temperature dependences of the reorientational relaxation time of water molecules studied by the NMR method,[34] and those of the dielectric relaxation time.[35] That is, the rotation of water molecules is accelerated by an increase in the pressure and/or temperature; at lower temperatures it is more accelerated by the pressure. Molecular dynamics simulations[36,37] have suggested that the hydrogen bonds between water molecules become more distorted in compressed water. The things mentioned above confirm the proton-jump mechanism of Conway et al.[3] which proposes that the rate-determining step in the proton-jump mechanism is the rotation of hydrogen-bonded water molecules near the hydroxide or the oxonium ion.

From Table 3, the contribution of the proton-jump mechanism to the conductance of hydroxide and oxonium ions, $\lambda^\circ_E/\lambda^\circ$, can be calculated; the average values of $\lambda^\circ_E/\lambda^\circ$ are about 0.63 at 15 °C, 0.62 at 25 °C, and 0.60 at 40 °C for the hydroxide ion, and 0.81 at 15 °C, 0.80 at 25 °C, and 0.78 at 40 °C for the oxonium ion. The difference in $\lambda^\circ_E/\lambda^\circ$ between the ions is about 0.18 at each pressure and temperature. Table 3 also shows that the values of $\lambda^\circ_E(OH^-)$ are about (0.40—0.47)-times those of $\lambda^\circ_E(H_3O^+)$. These results would suggest that there is a significant difference between the proton-jump mechanisms of hydroxide and oxonium ions. The driving force for rotation is a repulsion between the two OH groups facing each other as a result of the proton jump in addition to an ion-dipole interaction in the case of the oxonium ion. In the case of the hydroxide ion, the driving force arises principally from an ion-dipole interaction owing to a proton deficience of the OH^- ion. Conway et al.[3] have shown from their model that the average hydroxide ion-dipole force is approximately 1/4-times the total force causing the rotation in the oxonium ion case, and that since the time of the rotation is inversely proportional to the square root of the driving force, the excess conductance of the hydroxide ion is about 1/2-times that of the oxonium ion; this can be seen in Table 3.

When the pressure and temperature dependences of λ°_E were examined in greater detail, it was found that there is a slight difference between the hydroxide and oxonium ions regarding the rate of the increase in the relative excess conductance with the pressure and temperature (Figs. 1 and 2). The pressure dependence of the relative excess conductance of the hydroxide ion was smaller than that of the oxonium ion, while the reverse tendency was found regarding the temperature

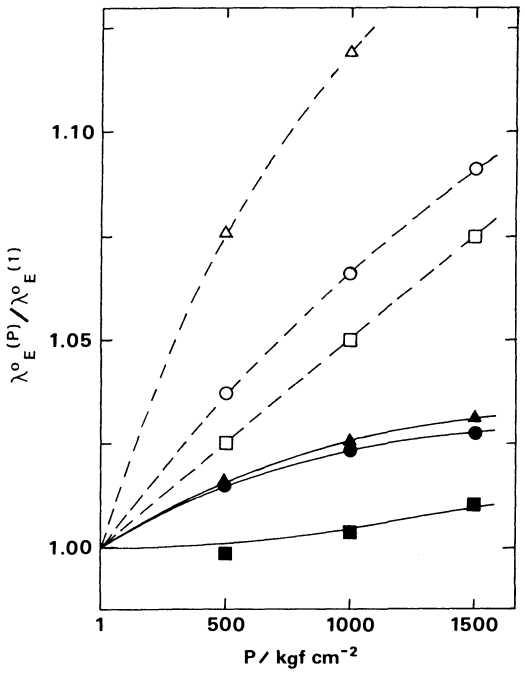

Fig. 1. Pressure dependence of the relative excess conductances of the OH^- and H_3O^+ ions at various temperatures.
▲: 15 °C, ●: 25 °C, ■: 40 °C for the OH^- ion;
△: 15 °C, ○: 25 °C, □: 40 °C for the H_3O^+ ion.

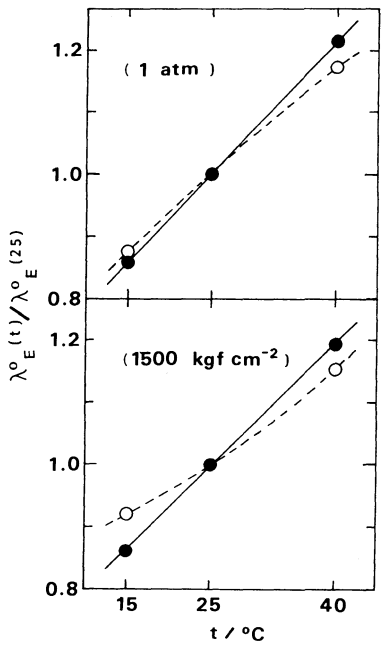

Fig. 2. Temperature dependence of the relative excess conductances of the OH^- and H_3O^+ ions at 1 atm and 1500 kgf cm^{-2}.
●: OH^-, ○: H_3O^+.

dependence. The apparent activation volume for λ°_E, $\Delta V^* = -RT(\partial \ln \lambda^\circ_E / \partial P)_T$, at 1 atm and at 25 °C is about -0.9 cm^3 mol^{-1} for the hydroxide ion and -2.0 cm^3 mol^{-1} for the oxonium ion, and the values of ΔV^* for both ions decrease with a decrease in the temperature. The apparent activation energy for λ°_E, $E^* = RT^2(\partial \ln \lambda^\circ_E / \partial T)_P$, at 1 atm and at 25 °C is about 11 kJ mol^{-1} for the hydroxide ion and 8.9 kJ mol^{-1} for the oxonium ion, and the values of E^* for both ions decrease with an increase in the pressure. The difference in ΔV^* and E^* between hydroxide and oxonium ions may be based on the difference in the proton-jump mechanism between the ions; however, a more thorough interpretation of the results shown in Figs. 1 and 2 would require more detailed microscopic information concerning the structure and the potential-energy profile of the nearest hydration shell around the ions in dilute solutions at high pressures and over a wide range of temperatures. Neutron diffraction[38] and computer simulation studies concerning these systems are, therefore, hoped to be extended to high pressures.

References

1) M. Ueno, M. Nakahara, and J. Osugi, *J. Solution Chem.*, **8**, 881 (1979).
2) M. Ueno, K. Ito, N. Tsuchihashi, and K. Shimizu, *Bull. Chem. Soc. Jpn.*, **59**, 1175 (1986).
3) B. E. Conway, J. O'M. Bockris, and H. Linton, *J. Chem. Phys.*, **24**, 834 (1956).
4) S. D. Hamann, "Physico-Chemical Effects of Pressure," Butterworths, London (1957), Chap. 7; S. D. Hamann and W. Strauss, *Trans. Faraday Soc.*, **51**, 1684 (1955).
5) R. A. Horne, B. R. Myers, and G. R. Frysinger, *J. Chem. Phys.*, **39**, 2666 (1963).
6) D. A. Lown and H. R. Thirsk, *Trans. Faraday Soc.*, **67**, 132 (1971).
7) C. T. Chen, R. A. Fine, and F. J. Millero, *J. Chem. Phys.*, **66**, 2142 (1977).
8) The values above 1000 kgf cm^{-2} are obtained by the extrapolation based on a given formula,[7] and they agree sufficiently well with those measured by Burnham et al.[9]
9) C. W. Burnham, J. R. Holloway, and N. F. Davis, *Am. J. Sci.*, **267A**, 70 (1969).
10) K. R. Srinivasan and R. L. Kay, *J. Chem. Phys.*, **60**, 3645 (1974).
11) The values at 15 °C are obtained by assuming that the logarithmic form of the quantity is expressed by a linear function of the temperature[12] at high pressure as well as at 1 atm.
12) R. L. Kay, G. A. Vidulich, and K. S. Pribadi, *J. Phys. Chem.*, **73**, 455 (1969).
13) J. B. Cappi, Ph. D. Thesis, London University, 1964; K. E. Bett and Cappi, *Nature*, **207**, 620 (1965).
14) The values at 15 and 40 °C are obtained by the interpolation of the data.[13]
15) L. S. Darken and H. F. Meier, *J. Am. Chem. Soc.*, **64**, 621 (1942).
16) M. Ueno, N. Tsuchihashi, and K. Shimizu, *Bull. Chem. Soc. Jpn.*, **58**, 2929 (1985).
17) G. C. Benson and A. R. Gordon, *J. Chem. Phys.*, **13**, 473 (1945).
18) J. F. Lind, Jr., J. J. Zwolenik, and R. M. Fuoss, *J. Am. Chem. Soc.*, **81**, 1557 (1959).
19) B. B. Owen and H. Zeldes, *J. Chem. Phys.*, **18**, 1083 (1950).
20) The values of the conductances of 0.01 M KCl aqueous

solutions are cited from Ref. 17 at 15 °C and Ref. 18 at 25 °C, and the value at 40° is obtained by expressing the data[17-19] in the form of a third-order polynomial in temperature.

21) R. M. Fuoss and F. Accascina, "Electrolytic Conductance," Interscience Pub., New York (1959), Chap. 15.

22) P. C. Carman, *J. Phys. Chem.*, **74**, 1653 (1970).

23) K. N. Marsh and R. H. Stokes, *Aust. J. Chem.*, **17**, 740 (1964).

24) R. L. Kay, *J. Am. Chem. Soc.*, **82**, 2099 (1960).

25) A. R. Gancy and S. B. Brummer, *J. Chem. Eng. Data*, **16**, 385 (1971).

26) The values at 1 atm are taken from Ref. 24, and the ratios between Λ°(NaOH) at pressure P and at 1 atm are from Ref. 25. The values at 40° are obtained by the interpolation of these data.

27) K. Shimizu and N. Tsuchihashi, *Rev. Phys. Chem. Jpn.*, **49**, 18 (1979).

28) The values of Λ°(KCl) are obtained by recalculating the data[27] with the aid of Eq. 2.

29) M. Ueno, S. I, and K. Shimizu, *Bull. Chem. Soc. Jpn.*, **56**, 846 (1983).

30) Y. Matsubara, K. Shimizu, and J. Osugi, *Nippon Kagaku Kaishi*, **1979**, 1817.

31) The values of $t^{\circ}(K^{+})$ at 15 and 40° are obtained with the aid of the Kay-Dye equation[32] as is described in a previous paper.[16]

32) R. L. Kay and J. L. Dye, *Proc. Natl. Acad. Sci. U. S. A.*, **49**, 5 (1963).

33) M. Nakahara and J. Osugi, *Rev. Phys. Chem. Jpn.*, **47**, 1 (1977).

34) J. Jonas, T. Defries, and D. J. Wilber, *J. Chem. Phys.*, **65**, 582 (1976).

35) R. Pottel and E. Aselborn, *Ber. Bunsenges. Phys. Chem.*, **83**, 29 (1979).

36) F. H. Stillinger and A. Rahman, *J. Chem. Phys.*, **61**, 4973 (1974).

37) G. Pálinkás, P. Bopp, G. Jancsó, and K. Heinzinger, *Z. Naturforsch*, **39a**, 179 (1984).

38) N. Ohtomo, K. Arakawa, M. Takeuchi, T. Yamaguchi, and H. Ohtaki, *Bull. Chem. Soc. Jpn.*, **54**, 1314 (1981).

 © 1986 The Chemical Society of Japan Bull. Chem. Soc. Jpn., 59, 3729—3733 (1986)

Adsorption of Organic Halides on Amine-Impregnated Silica Gels

Tatsuo ISHIKAWA,* Naoki YAMAGAMI, and Seiichi KONDO
School of Chemistry, Osaka University of Education, 4-88 Minamikawahori-cho, Tennoji-ku, Osaka 543
(Received April 1, 1986)

The adsorption behaviors of methyl and propyl iodides, propyl chloride and chlorobenzene were examined on silica gels impregnated with 1,4-diazabicyclo[2.2.2]octane (DABCO), pyperazine (PPZ), hexamethylene tetramine (HMTA), and modified with (3-aminopropyl)triethoxysilane (ATS) and dimethoxybis[3-(methylamino)-propyl]silane (DAS). The irreversibly adsorbed amount of these halides except chlorobenzene was proportional to the amount of impregnated amines. The molar ratios of irreversible adsorption of the halides to the impregnated amine were less than 2 and in the order of DABCO>PPZ>HMTA>ATS>DAS. The former three amine compounds are less stable than the last two materials against thermal pretreatment.

Organic halides such as trichloromethane in city water, organic chlorides from waste plastics and solvents, 2,3,7,8-tetrachlorodibenzo[*b*,*e*][1,4]dioxin (dioxin) in insecticides and methyl iodide from nuclear reactors are serious environmental pollutants. Therefore, it is very important to find effective ways of removing these pollutants. From this point of view, silver-impregnated silica gels were found to adsorb organic halides effectively.[1] Silver-impregnated molecular sieves are used to remove organic iodides in waste gases from nuclear reactors.[2] However, in order to expect a good performance, a rather careful procedure of pretreatment of these materials seems to be necessary. Also, activated carbons impregnated with 1,4-diazabicyclo[2.2.2]octane triethylene diamine (DABCO) are used as an adsorbent to analyze atmospheric alkyl iodides.[3]

In the present paper, the adsorption behaviors of methyl and propyl iodides, propyl chloride and chlorobenzene were described in detail on well-characterized mesoporous silica gels impregnated with DABCO, piperazine (PPZ), hexamethylene tetramine (HMTA) and modified with (3-aminopropyl)triethoxysilane (ATS) and dimethoxybis[3-(methylamino)propyl]silane (DAS). The mechanism of adsorption is clarified in view of thermodynamic properties and ir spectra.

Experimental

Materials. Thin and transparent plates of mesoporous silica gels suitable for spectroscopic measurement were synthesized by hydrolyzing tetraethoxysilane according to the method mentioned elsewhere.[4] The BET specific surface area, pore volume and mean pore radius of this material obtained from the N_2 adsorption isotherm are 705 $m^2 g^{-1}$, 0.60 $ml g^{-1}$ and 1.7 nm respectively. These gels were impregnated with DABCO, PPZ, and HMTA by immersing them in methanol solutions of each of these amines of various concentrations at 298 K for 10 h and then evaporating methanol in the samples in vacuo at room temperature. The impregnated amounts were determined by CN elemental analysis. Free silanol groups on silica surface were modified with ATS and DAS by immersing gels in toluene solutions of ATS and DAS of various concentrations at 323 K for 5 h and washing with acetone and then drying at room temperature. The amounts of ATS and DAS reacted were determined

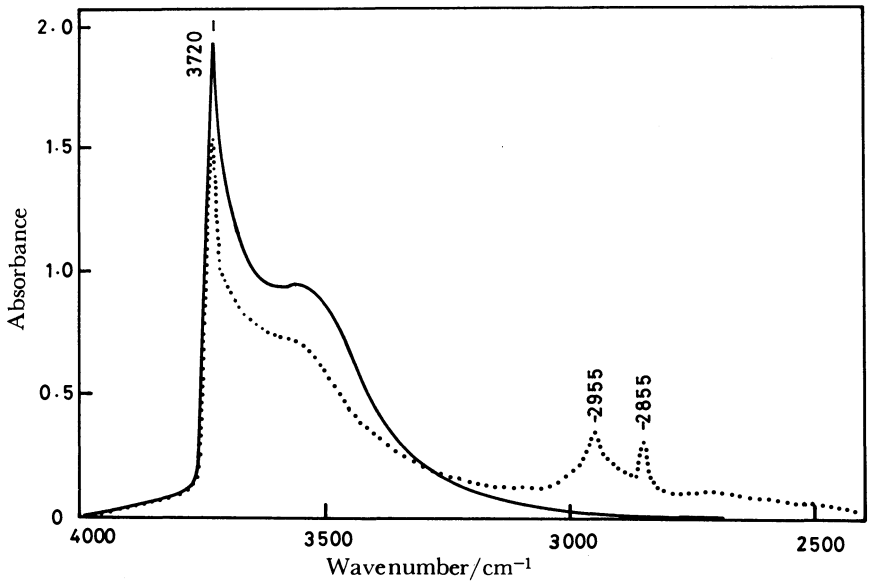

Fig. 1. IR spectra of silica gels before and after impregnating DABCO of 0.331 mmol g^{-1}. The full line, before impregnation; the dotted line, after impregnation.

by CN elemental analysis.

Methods of Measurements. The adsorption isotherms of methyl and propyl iodides, propyl chloride and chlorobenzene were measured at 298 K by means of a computer-operated quartz spring balance using a diaphragm manometer (BARATRON, 170M-6C). These samples were pretreated at desired temperatures under 10^{-3} Pa for 2 h. The adsorbates were dried with molecular sieves 3A and then distilled into a reservoir of the adsorption apparatus in the same vacuum system without exposing to air.

IR spectra were measured with a dispersion-type IR spectrophotometer (Hitachi-Perkin Elmer) and a FT-NIR spectrometer (Digilab, FTS-15E). A vacuum and high-temperature cell[5] was used to measure spectra at room temperature after pretreating the sample at 423 K unless otherwise stated.

Results and Discussion

In Fig. 1, the IR spectrum of silica gels before impregnating DABCO (a full line) has a sharp 3720 cm^{-1} and a broad 3500 cm^{-1} absorption bands which are assigned to the stretching vibration of free and hydrogen-bonded silanol groups respectively. After impregnating 0.331 DABCO mmol g^{-1} SiO_2 (about 0.3 DABCO molecules nm^{-2} of the original surface), the intensity of 3720 cm^{-1} band decreased to about 80% and two bands assigned to assymmetric and symmetric C-H vibrations of methylene groups of DABCO appeared at 2955 and 2855 cm^{-1} as is shown by a dotted line in this figure. Since there are about three free silanol groups per nm^2 on this mesoporous silica gels[6] and 0.6 free silanol groups (about 20% of total silanol groups) adsorbed DABCO, one DABCO molecule seems to be adsorbed on two free silanol groups by hydrogen bond.

The adsorption isotherms of methyl iodide on pure silica gels at 288 K (a full line) and on silica gels impregnated with 1.00 DABCO mmol g^{-1} SiO_2 and pretreated at 303 K for 2 h in vacuo (a dotted line) are shown in Fig. 2. No hysteresis was observed in the former isotherm, but the latter material shows a remarkable irreversible desorption in the low pressure range after evacuation at the temperature of adsorption, the amount of which at $P/P_0=0$ is shown by W_{ir} molecules nm^{-2} in Table 1. The same kind of hysteresis was observed on the adsorption isotherms of methyl iodide to the PPZ- and HMTA-impregnated samples pretreated at 303 K in vacuo. The monolayer adsorption capacities, W_m molecules nm^{-2} obtained by applying BET equation to the isotherms of the halides except chlorobenzene increased on impregnating these amines as is shown in Table 1. The adsorption behav-

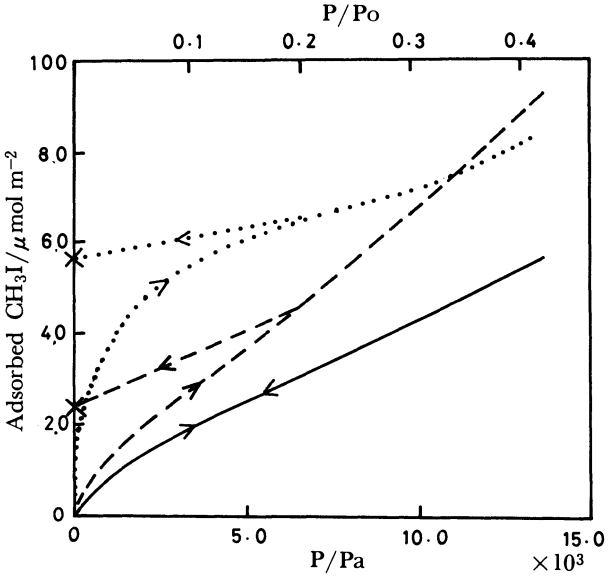

Fig. 2. The adsorption isotherms of methyl iodide on DABCO and ATS-impregnated samples which were pretreated at 303 and 373 K in vacuo for 2 h respectively. The impregnated amounts of DABCO and ATS are 1.00 and 1.21 mmol g^{-1} respectively. The full line, pure silica gels; the dotted line, DABCO-impregnated sample; the broken line, ATS-impregnated sample; X, the amount of irreversible adsorption.

Table 1. The Monolayer Adsorption Capacity (W_m) and the Amount of Irreversible Adsorption (W_{ir}) of Organic Halides on Silica Gels Impregnated with 1,4-Diazabicyclo[2,2,2]octan (DABCO), Pyperazine (PPZ), Hexamethylene Tetramine (HMTA), and (3-Aminopropyl)-triethoxysilane (ATS). DABCO-, PPZ-, and HMTA-Impregnated Samples were Pretreated at 303 K in vacuo for 2 h. ATS-Impregated Sample was Pretreated at 373 K

Impregnated		Pure	DABCO	PPZ	HMTA	ATS
Surface area ($m^2 g^{-1}$)		705	360	430	378	377
Impregnated amount ($mmol^{-1}$)		—	1.00	1.31	1.06	1.21
W_m (molecules nm^{-2})	CH_3I	2.34	3.18	3.40	3.53	3.87
	n-C_3H_7I	2.42	2.89	2.92	2.56	3.62
	n-C_3H_7Cl	2.20	4.64	2.20	2.26	3.07
	C_6H_5Cl	3.71	3.63	2.49	3.08	2.81
W_{ir} (molecules nm^{-2})	CH_3I	0	3.44	2.40	1.77	1.52
	n-C_3H_7I	0	1.20	0.07	1.25	0.44
	n-C_3H_7Cl	0	0.69	0.03	0	0.16
	C_6H_5Cl	0	0	0	0	0

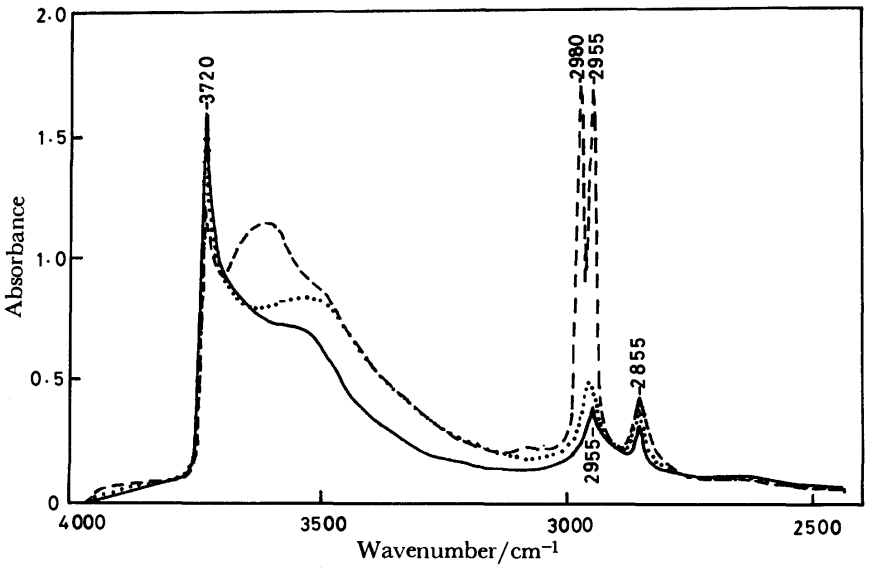

Fig. 3. The influence of adsorption and desorption of methyl iodide on the IR spectrum of DABCO-impregnated silica gels. The full line, before adsorption; the broken line, after adsorption; the dotted line, after desorption.

iors of propyl iodile and propyl chloride were similar to that of methyl iodide. On the other hand, the adsorption and desorption of chlorobenzene was reversible on pure and amine-impregnated samples. W_m in this case was larger for pure material than these with amines.

A full, a broken and a dotted lines in Fig. 3 show the IR spectrum of original DABCO-impregnated sample, that after the adsorption of methyl iodide at 1.3×10^4 Pa, and that after desorption by evacuation at room temperature respectively. After methyl iodide adsorption, the intensity of the 3720 cm^{-1} band decreased by the hydrogen-bond adsorption of methyl iodide, and the 2980 and 2955 cm^{-1} bands assigned to C-H vibrations of methyl groups of the adsorbate appeared. When evacuating this sample at 298 K, these C-H bands disappeared and the 3720 cm^{-1} band revived. These changes indicate the reversible desorption of most of methyl iodide molecules adsorbed. There is no positive evidence of irreversible adsorption in these spectra because the amount of irreversible adsorption was very small. However, there may exist an irreversible adsorption as follows. Methyl iodide is known to react easily with DABCO at room temperature by the reaction.[7]

$$N(CH_2CH_2)_3N + 2CH_3I \rightarrow I^-[H_3CN^+(CH_2CH_2)_3N^+CH_3]I^- \quad (1)$$

The IR spectrum of this resultant compound shown in Fig. 4 has two bands at 2945 and 2871 cm^{-1} which may be assigned to assymmetric and symmetric C-H vibrations of the methyl radicals of the resultants in Eq. 1. The bands mentioned above are different from those of methyl groups of methyl iodide molecules, because the molecular orbitals of these radicals would be different

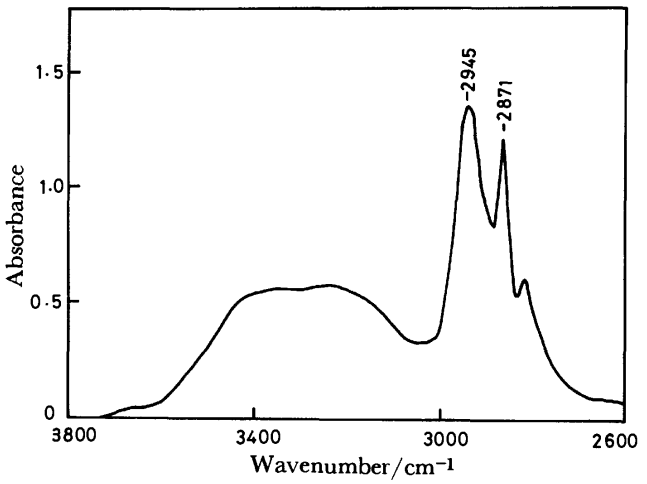

Fig. 4. The IR spectrum of the resultant of reaction of methyl iodide with DABCO in tetrachloromethane at room temperature.

from sp^3 hybrid orbitals of methyl groups by the Reaction (1). Since the irreversible amount of adsorption is rather small and the wave numbers of the bands of radicals are close to those of impregnated amines, it was not possible to identify the existence of the bands of methyl radicals in the spectrum after desorption in Fig. 3 under the present experimental error. Therefore, it may be plausible to postulated Reaction (1) for the present irreversible adsorption.

The amount of irreversible adsorption, W_{ir}, in Table 1 is in the order of methyl iodide>propyl iodide >propyl chloride>chlorobenzene for each amine impregnated. This is because the Reaction (1) can take place more easily for larger ionicity of carbon-halogen bonds which can be estimated from the nuclear quad-

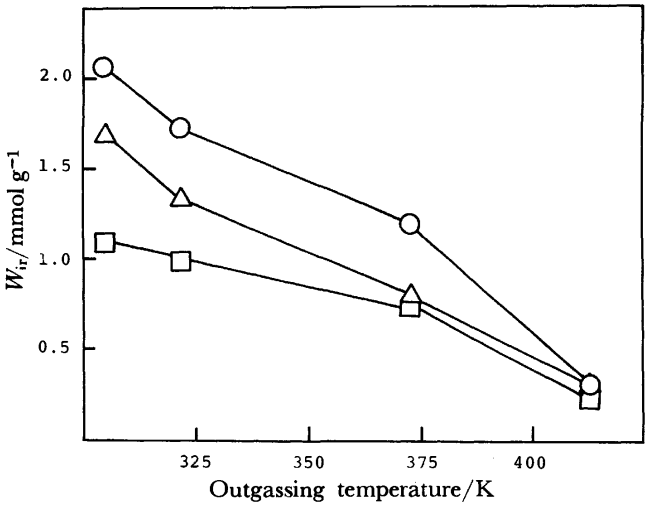

Fig. 5. The relations between the amount of irreversible adsorption of methyl iodide and pretreatment temperature. O: DABCO-impregnated sample, △: PPZ-impregnated sample, □: HMTA-impregnated sample.

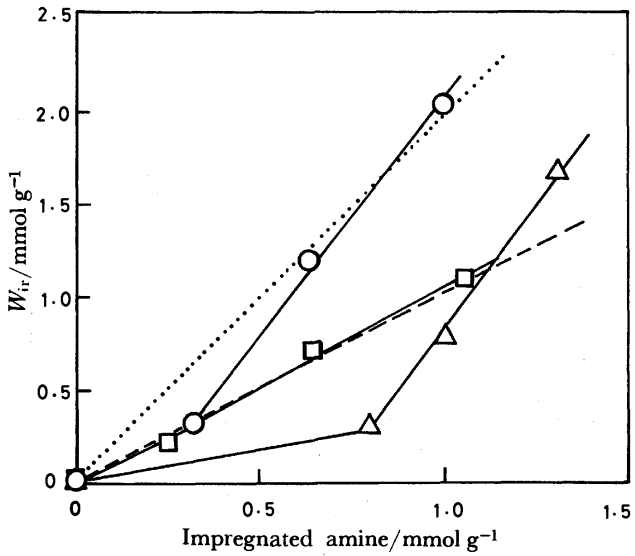

Fig. 6. The relations between the amount of irreversible adsorption of methyl iodide and the amount of amines impregnated. The dotted and broken lines show that the molal ratios of adsorbed methyl iodide to impregnated amine are 2 and 1 respectively. O: DABCO, △: PPZ, □: HMTA.

rupole moments.[8] In Fig. 5, W_{ir} of all the amine impregnated samples decreased as the pretreatment temperature was raised. This is because the impregnated amines are removed by evacuating samples above 303 K as confirmed by CN elemental analysis.

Figure 6 shows the relations between W_{ir} of methyl iodide and the amount of impregnated amines. The molar ratios of adsorbed methyl iodide to impregnated DABCO and that to HMTA are 2 and 1 respectively as is shown by the dotted and broken lines in Fig. 6 respectively, suggesting that two nitrogen atoms of a

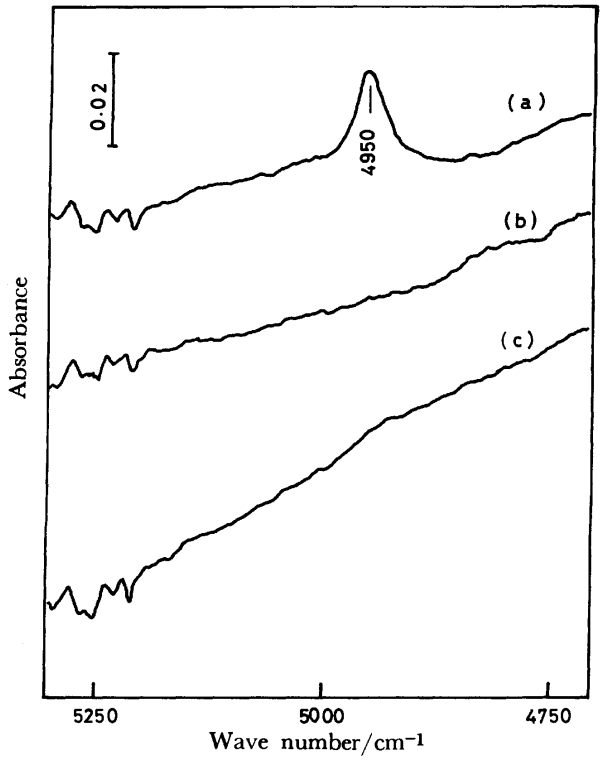

Fig. 7. The influence of adsorption and desorption of methyl iodide on NIR spectra of ATS modified sample. (a): Before adsorption, (b): after adsorption, (c): after desorption.

DABCO molecule react with two methyl iodide molecules. This result supports the postulated Reaction (1). On the other hand, only one nitrogen atom of HMTA molecule having four nitrogen atoms reacts with one methyl iodide molecule, the reason for which lies perhaps in the lower basicity of HMTA than that of DABCO. The molar ratio of PPZ-impregnated sample is 2 above 0.8 PPZ mmol g^{-1} SiO_2, and, below this amount, this molar ratio is very small as is seen in Fig. 6. The reason for this difference can be interpreted as follows. Below 0.8 PPZ mmol g^{-1}, molecules are likely to lie on the surface with their molecular plane parallel to the surface and with two nitrogen atoms in the molecule are hydrogen-bonded to the surface silanol groups. This impregnated amount corresponds to the monolayer adsorption capacity estimated with the cross sectional area of PPZ molecules as equal to that of molecular plane. Therefore, these nitrogen atoms may not react with methyl iodide. The steep increase of W_{ir} above this amount can be interpreted as that both nitrogen atoms of PPZ molecules on the second layer may be free to capture methyl iodide molecules. The molar ratios of adsorbed propyl iodide to impregnated DABCO, PPZ, and HMTA are always less than unity, probably because C-I bond of propyl iodide has less ionicity than that of methyl iodide.

Most of impregnated amines are removed by outgassing at 423 K and hence W_{ir} decreases by heating

as is seen in Fig. 5. In order to increase W_{ir}, amino groups were fixed on the surface of mesoporous silica gels by substituting free silanol groups to ethoxy and methoxy groups of ATS and DAS, and thus the surface density of substituted amino groups was about 1/nm^2. CN elemental analysis indicated more thermal stability of ATS than the above mentioned amines till 673 K. The adsorption isotherm of methyl iodide on ATS-modified sample shown by a broken line in Fig. 2 is irreversible like these of amine-impregnated samples. W_{ir} in this case did not decrease on heating, and was in the order of methyl iodide>propyl iodide> propyl chloride>chlorobenzene. One methyl iodide molecule is adsorbed to about one nitrogen atom of ATS. NIR spectra of this sample before methyl iodide adsorption in Fig. 7 has a combination vibration band of N-H bond of ATS molecule at 4950 cm^{-1}. This band diminished after methyl iodide adsorption and did not recover on heating in vacuo, suggesting the irreversible adsorption of methyl iodide by amino groups. The 4950 cm^{-1} band diminished after propyl chloride adsorption, but revived almost after desorption. W_{ir} of DAS-modified sample was very little, perhaps because dimethylamino groups interact with free silanol groups on the surface as will be reported soon.

References

1) T. Ishikawa, S. Kondo, H. Yamaoka, and M. Muroya, *Adsorption Sci. Techn.*, **1**, 93 (1984).

2) D. A. Collins, L. R. Tailor, and R. Tailor, TRG-1300 (B) (1967).

3) M. Kikuchi, K. Funahashi, H. Yusa, and Y. Takashima, *Radioanal. Lett.*, **45**, 279 (1980).

4) S. Kondo, K. Tomoi, and C. Pak, *Bull. Chem. Soc. Jpn*, **52**, 2046 (1979).

5) S. Kondo, M. Muroya, and H. Fujii, *Bull. Chem. Soc. Jpn*, **47**, 553 (1974).

6) S. Kondo, H. Fujiwara, H. Okazaki, and T. Ichii, *J. Colloid Interface Sci.*, **75**, 328 (1980).

7) G. M. Loudon, "Organic Chemistry," Addison-Wesley Publishing Co.,London (1984), p. 1193.

8) E. A. C. Lucken, "Nuclear Quadrupole Coupling Constants," Academic Press, New York and London (1969), p. 167.

 © 1986 The Chemical Society of Japan Bull. Chem. Soc. Jpn., 59, 3735—3739 (1986)

Temperature-Programmed Desorption of Ammonia on Zeolites. Influence of the Experimental Conditions on the Acidity Measurement

Miki NIWA,* Masakazu IWAMOTO,† and Koh-ichi SEGAWA††
Department of Synthetic Chemistry, Faculty of Engineering, Nagoya University, Furo-cho, Chikusa-ku, Nagoya 464
†Department of Industrial Chemistry, Faculty of Engineering, Nagasaki University, Nagasaki 852
††Department of Chemistry, Sophia University, 7-1 Kioicho, Chiyoda-ku, Tokyo 102
(Received April 17, 1986)

The Influence of the experimental conditions of the TPD (Temperature-Programmed Desorption) of ammonia on the measurement of acidity of mordenites and Y zeolites was studied. The results were applicable to the measurements of the strength and the number of acid sites of zeolites. For contact times of the carrier gas from 10^{-2} to 10^{-6} g min ml^{-1} defined as W/F (W, sample weight; F, flow rate of the carrier gas), the peak maximum temperature was related to the parameter (W/F). The relationship was explained on the basis of a theoretical equation derived by Cvetanović and Amenomiya under the conditions of readsorption. Ammonia is readsorbed on zeolites under these conditions, and one has to use the experimental conditions of the same contact time in order to evaluate the acid strength of zeolite from the peak maximum temperature. On the other hand, the ratio of intensity of low temperature peak (l-peak) to that of the high temperature peak (h-peak) increased with increasing the contact time of the carrier gas. This relation suggested that the l-peak intensity depended upon the degree of evacuation of the weakly-held ammonia. The l-peak is ascribable to very weakly or physically adsorbed ammonia on zeolites, and only the h-peak has to be accounted for to measure the number of acid sites.

Currently, much attention is focused on the activity and selectivity of catalytic reactions over acid-type zeolites. Because the acidity as well as the structure strongly affects the catalytic activity, it is of extreme importance to characterize the zeolite catalyst from the viewpoint of the acidity. Usually, the acidity of zeolite can not be measured by the titration method using Hammett indicators, because the diffusion of base molecules may be strictly retarded due to the small pores of the zeolite. Temperature-programmed desorption (TPD) of ammonia[1-3] and the microcalorimetry of differential heat of adsorption of ammonia[4] have been recommended.

One of the authors has already reported the usefulness of TPD of ammonia for the measurement of the acidity, and has compared the strength and number of acid sites of various zeolites.[1] This method is preferable to others because of the rapidness of the experiment. However, some problems remain unsolved. Firstly, the experimental conditions including sample weight, flow rate of carrier gas, rate of increasing temperature, partial pressure within the cell, etc., have to be examined in more detail to determine the acidity precisely. Although some criteria were proposed theoretically to design the conditions,[5] no experimental confirmations were attempted. Secondly, the identification of desorption peaks is still a matter of controversy: the origin of the l-peak (desorbed at ca. 323 K) is not clearly known, although the h-peak (another peak desorbed at a higher temperature) is attributed to an IR absorption band at 3600 cm^{-1}.[1,2]

We started a project on the TPD of ammonia under the organization of the Catalysis Society of Japan, committee of reference catalysts. Five kinds of acid-type mordenite and Y zeolites were distributed to research groups in universities and industrial companies. Each group measured the acidity of zeolites using TPD of ammonia by their own procedures, some of the conditions being unified. Results thus obtained were compared and discussed. As a result of the cooperative work, important conclusions were obtained about the acidity measurement using the TPD of ammonia. In this communication, we will report on the influence of experimental conditions on the measurement of acidic strength and amount of zeolites.

Experimental

Zeolites Reference Catalysts (JRC-Z) were supplied by the Catalysis Society of Japan: Some properties are shown in Table 1. All of them had been converted into the decationized form before distribution, and no pretreatment except for the evacuation was performed before the measurements.

Only the following experimental conditions were unified:

(1) pretreatment: evacuation at 773 K for 1 h.

(2) adsorption of ammonia, at 373 K.

(3) increase of bed temperature, at a rate of 10 K min^{-1} from 373 K.

Other experimental conditions were chosen individually, as shown in Table 2. Experimental methods were divided into those of vacuum and of flow. Intensity of desorbed ammonia was detected by thermal conductivity detector (tcd), mass spectroscopy (ms), gravimetry, or vacuum gauge. The carrier gas, helium, was made to flow into the zeolite bed with or without pumping, or the zeolite was pumped to evacuate the desorbed ammonia.

The strength and amount of acidic sites were measured by the peak maximum temperature and the desorbed amount.

Results and Discussion

Dependence of Desorption Temperature on Experimental Conditions. The TPD spectra obtained were characteristic of two desorption peaks (l- and h-peaks at low and high temperatures, respectively) on not only mordenite but also Y-zeolite (Fig. 1), which was in agreement with in the previous study.[1] The resolu-

Table 1. List of Zeolites Used in This Study[a)]

Name	Structure	(SiO_2/Al_2O_3) ratio	(%) of H^+ exch.	Surf. Area ($m^2 g^{-1}$) Total	Ext.[b)]	Crystal Habit
JRC-Z-HM10	Mordenite	9.9	98	187	9.8	Rod
JRC-Z-HM15	Mordenite	14.9	99	309	13.5	
JRC-Z-HM20	Mordenite	19.9	99	299	15.2	Cube
JRC-Z-HY4.8	Y	5.2	99	646	17.0	
JRC-Z-HY5.6	Y	5.6	72	634	10.6	

a) Prepared by ion exchange with corresponding Na-form zeolites in a NH_4Cl solution, followed by calcination at 673 K for 2 h. b) Measured by the benzene-filled pore method, see Ref. 6.

Table 2. List of Measurement Conditions

No.	Method	Detector	Samp. Wt. (W) (g)	Flow Rate/f[a)] (ml(STP) min^{-1})	Cell Press. (p)[b)] (Torr)	W/F[c)] g min ml^{-1}
1	Vacuum	gauge	0.15	Unknown	Unknown	—
2	Flow	gravimetry	0.1	100	Ambient	1.0×10^{-3}
3	Flow	ms	0.005	40	380	6.3×10^{-5}
4	Flow	tcd	0.5	30	Ambient	1.7×10^{-2}
5	Flow	tcd	0.1	30	50	2.2×10^{-4}
6	Flow	ms	0.05	50	Ambient	1.0×10^{-3}
7	Flow	ms	0.0018	10	495	1.2×10^{-4}
8	Flow	tcd	0.5	80	360	3.0×10^{-3}
9	Flow	tcd	0.2	60	30	1.3×10^{-4}
10	Flow	tcd	0.01—0.5	20—60	35	7.6×10^{-6}—9.2×10^{-4}

a) Measured in ambient pressure. b) The pressure in the TPD cell was below the ambient pressure when the carrier gas was pumped. c) F=760 f/p. d) 1 Torr=133.3 Pa.

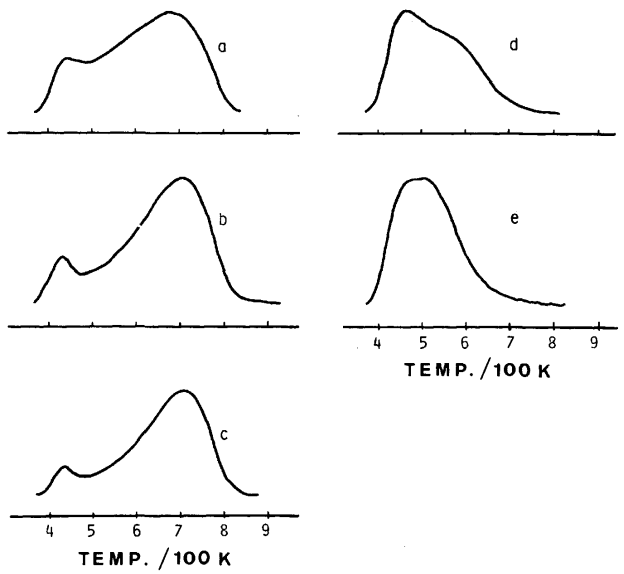

Fig. 1. Typical example of TPD spectra on Zeolites HM-10 (a), HM-15 (b), HM-20 (c), HY-4.8 (d), and HY-5.6 (e) obtained in the W/F of 7.7×10^{-5} g min ml^{-1}. Spectrum intensity was shown in an arbitrary units divided by grams of zeolite. Temperatures for the h-peak maximum were 680 (a), 703 (b), 705 (c), ca. 590 (d), and ca. 490 K (e).

tion of double peaks was good in cases of mordenites, but imperfect in those of Y-zeolites. The acid strength of these zeolites could be summarized due to the comparison between peak maximum temperatures of the h-peak. The comparison consistently afforded the following sequence for the acidity strength:

$$\text{HM-15} \geq \text{HM-20} > \text{HM-10} \gg \text{HY-4.8} > \text{HY-5.6}$$

However, the desorption temperatures did not agree at all, when comparisons were made between those obtained by various groups. For example, the peak temperature on the HM-15 was distributed from 673 to 883 K. In order to understand such a large difference, we examined experimental conditions relevant to the desorption temperature. Although various experimental methods were included in these experiments, such a large difference could not be understood only by differences in apparatus or in measuring the temperature.[7] It was thus found that the desorption temperature was correlated with the contact time of the carrier gas W/F, where W and F denoted the zeolite weight and the flow rate of carrier gas. If the carrier gas was pumped, F should be replaced by a corrected flow rate 760 f/p, where p was the pressure in the TPD cell in Torr (1 Torr=133.3 Pa), and f was the flow rate measured in atmospheric pressure, because the carrier gas was made to flow at a faster rate than under atmospheric conditions. The relationship in the case of the HM-15 is shown in Fig. 2; the peak temperature gradually increased with increasing the contact time W/F in the range of 10^{-2} to 10^{-6} g min ml^{-1}.

According to the kinetical analysis of the TPD spec-

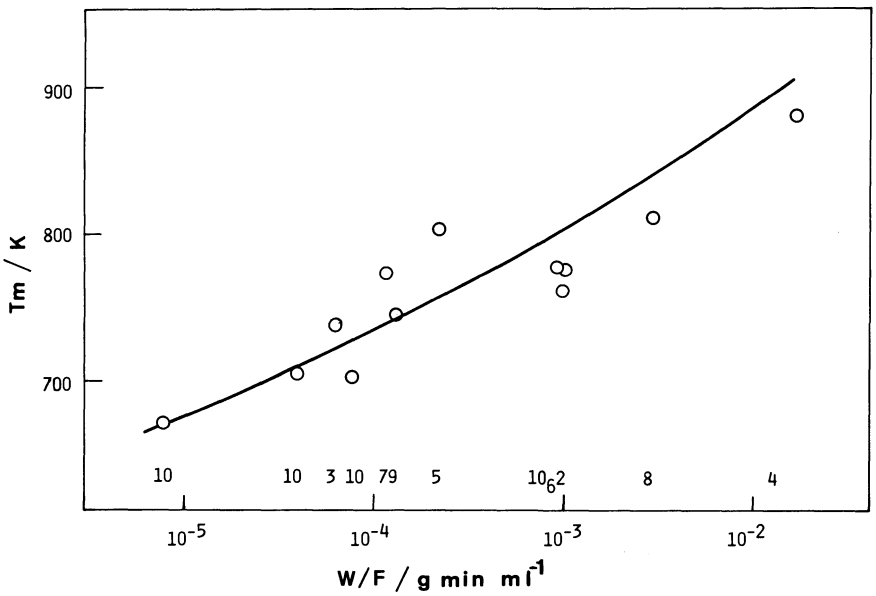

Fig. 2. Correlation between the peak maximum temperature and the W/F on HM-15. The theoretical curve was simulated for the parameters. β: 10 ($K\,min^{-1}$), ΔH: 1.5×10^5 ($J\,mol^{-1}$), θ: 0.35, ρ: 0.5, R: 8.31 ($J\,K^{-1}\,mol^{-1}$). Experimental run numbers in this Figure are referred to in Table 2.

tra by Cvetanović and Amenomiya,[8] the conditions of the TPD experiment are divided into three limiting cases: (a) When the readsorption of a desorbed molecule does not occur, (b) when the readsorption occurs freely, and (c) when the diffusion controls the desorption. The correlation found in this study indicates that the present experiments are carried out under the readsorption conditions, because, in case (b), the peak maximum temperature (Tm) is theoretically correlated with the contact time:

$$2\log T_m - \log\beta = \Delta H/2.303RT_m + \log Q$$
$$Q = (1-\theta)^2 V\Delta H/FAR$$
$$V = W/\rho$$

Here β and θ show the rate of temperature increase and the coverage at peak maximum, ΔH and R are heat of adsorption and gas constant, and V and ρ are the volume and density of solid. Parameter A is equal to $\exp(\Delta S/R)$, where ΔS is the increase of entropy upon desorption. After the values of parameters were assumed, theoretical relations could be calculated, as shown in Fig. 2. When A is assumed to be 2.86×10^5, the simulated curve follows the relation between the peak temperature and W/F. One can thus conclude that ammonia was freely readsorbed on these zeolites in the TPD experiment, and the peak temperature depends on the contact time of the carrier gas.

The conclusion is in agreement with the theoretical consideration by Gorte[5]: He showed that the desorption temperature was changed by several hundreds K due to the effect of the readsorption on the porous catalyst. Additionally, Demmin and Gorte[5] reported on the influence of the crystal size on the desorption temperature. According to their analysis, a temperature gradient exists along the catalyst bed, when the $Fr^2\rho/3WD$ is larger than 0.1, where r is the radius of the crystal and D is the diffusion constant. In such a case, the desorption temperature will be affected by the diffusion of molecules inside the pore, and the peak maximum temperature will not correspond to the strength of the acid sites. When these parameters are assumed: r=1 μm; $D=10^{-5}$ $cm^2\,s^{-1}$, their proposed conditions are satisfied only in less than 2.7×10^{-5} g min ml^{-1} of W/F, and almost all the present experiments are carried out under different conditions. Furthermore, it was found experimentally that the sequence of zeolites in order of the acid strength did not change throughout these experiments. Therefore, the influence of crystal size on the judgment of the acid strength may be disregarded, as far as the present experiments are concerned. Measurements on larger crystals seems to be required for the confirmation of the influence of crystal size.

This method has recently been used frequently by many researchers. However, these measurements are utilized only for a relative comparison of the acidities of their own zeolites, but not for comparisons with findings reported elsewhere. However, the present conclusion indicates the possibility of comparison of the strength of zeolite acidities which were obtained by TPD of ammonia, if only some parameters such as A and ΔH are given. Therefore, from now on, the experimental conditions of contact time of carrier gas must be described together with the experimental results.

Identification of Low Temperature Peak. Desorbed amounts of ammonia measured by various groups distributed significantly. For example, the desorbed amounts from HM-15 were 1.09—3.18 and 0.21—1.87

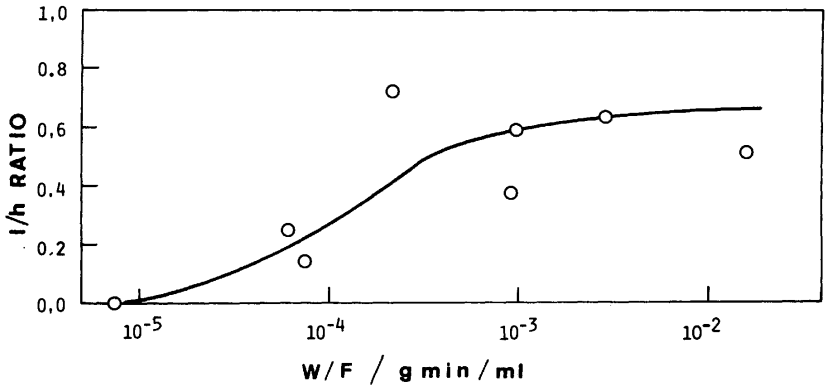

Fig. 3. Correlation between the peak intensity ratio (l-/h-peaks) and the W/F.

(mmol g^{-1}) in the h- and l-peaks, respectively. The distribution in the h-peak was not, however, related with any experimental conditions or measurement method. Experimental errors were probably included in measuring the desorbed amount. On the other hand, the intensity ratio of the l- to h-peaks which was used in order to compensate for the experimental errors in the quantitative measurements was related with the contact time W/F, as shown in Fig. 3. The intensity of l-peak was almost negligible at the small contact time, and the intensity relative to that of h-peak increased with increasing the contact time. This trend indicates that the l-peak does not depend on the catalyst property, but on the experimental conditions.

Furthermore, it was found that the Na-mordenite possessed only the l-peak, whose amount was much greater than that on the decationized one (Fig. 4). The appearance of the desorption spectrum at this temperature has been already reported on non-acidic zeolite by Kanazirev,[9] who measured the TPD for the study of diffusion processes.

These findings indicate that the l-peak of the mordenite does not originate from molecules adsorbed on the weak-acid site but from physically or very weakly chemisorbed molecules. The dependence of the l- to h-peak ratio on the contact time may be caused by the degree of the removal of the weakly-held ammonia. Under the conditions of the large contact time, i.e. slow flow rate of the carrier gas and/or large amount of zeolites, the weakly-held ammonia is difficult to remove by evacuation, and some molecules remain undesorbed. Those remaining molecules may be desorbed as the l-peak upon increase of the bed temperature. In other words, the l-peak could be regarded as the *remainder* of the desorbable ammonia. Therefore, it is concluded that only the h-peak has to be accounted for to measure the acidity of zeolites.

The method of removal of gaseous ammonia was not strictly determined. However, it is practical to require that the removal of gaseous ammonia should be done until the detector reaches the base level. In these conditions, small amounts of desorbed ammonia

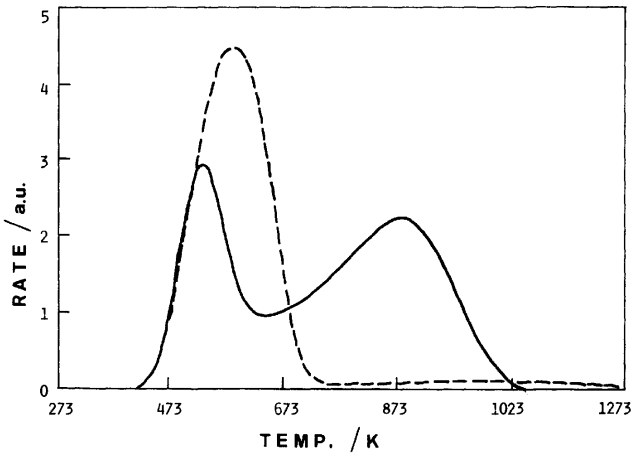

Fig. 4. Comparison between spectra on HM-15 (solid line) and on M-15 (Na-mordenite)(dotted line). These were obtained in the W/F of 1.7×10^{-2} (g min ml^{-1}).

may be undetectable, and a desorption peak will be readily found as the l-peak. The completely evacuation of ammonia is difficult and impractical, because it requires a long time, and the extent of evacuation is not properly decided.

On the other hand, the NaY-zeolite showed only a smaller intensity of the l-peak than the HY, unlike the mordenite. For example, in the experiment of run number 1 (see Table 2), the amount of ammonia desorbed from Y-4.8 (NaY type) was 0.08 (mmol g^{-1}), while that from HY-4.8 was 1.87 (mmol g^{-1}). Although it is difficult to analyze precisely the components of the TPD spectra on the HY-zeolite because of the poor resolution, the peak appearing in the low temperature seems to be easily evacuated due to the large pore size of the Y-zeolites.

Prof. Yasuhiko Kurusu of Sophia Univ., Prof. Yuan Nai-Ju of Qinghua Univ., Mr. Makoto Nakamura, Mr. Yoshimasa Inoue, Dr. Yukuaki Mitarai, and Dr. Yasuo Takami of Sumitomo Metal Mining, Mr. Tetsuya Imai, and Mr. Kozo Iida of Mitsubishi Heavy Ind., Mr. Masahiro Tajima, and Prof. Shuichi Kagawa of

Nagasaki Univ., Mr. Sotaro Nakamura, Mr. Masao Ishii, and Mr. Kiyonari Matsuoka of Shindaikyowa Petrochemical Ind., Mr. Hiroshi Sato, Mr. Ken-ichi Hirose, and Mr. Hiroshi Ichihashi of Sumitomo Chemical, Mr. Masaru Ushio, and Mr. Takeshi Ishii of Nippon Oil, Mr. Takahiro Kawamura, Mr. Shigeo Baba, and Mr. Toshio Shimizu of Cosmo Oil, Prof. Yuukei Takasaki, and Mr. Takemi Shibuya of Utsunomiya Univ., and Mr. Masahiko Sawa of Nagoya Univ. are thanked for supplying experimental data and helpful discussions.

References

1) C. V. Hidalgo, H. Itoh, T. Hattori, M. Niwa, and Y. Murakami, *J. Catal.*, **85**, 362 (1984).

2) N-Y. Topsφe, K. Pedersen, and E. G. Derouane, *J. Catal.*, **70**, 41 (1981).

3) J. G. Post and J. H. C. van Hooff, *Zeolites*, **4**, 9 (1984).

4) A. Auroux, V. Bolis, P. Wierzchowski, P. G. Gravelle, and J. C. Vedrine, *J. Chem. Soc., Faraday Trans. 1*, **75**, 2544 (1979).

5) a) R. J. Gorte, *J. Catal*, **75**, 164 (1982); b) R. A. Demmin, and R. J. Gorte, *ibid.*, **90**, 32 (1984).

6) M. Inomata, M. Yamada, S. Okada, M. Niwa, and Y. Murakami, *J. Catal.*, **100**, 264 (1986).

7) a) Design of the TPD cell, for example, the size of cell diameter or the preheating of the carrier gas could affect the measurement of temperature; b) Metal pipes and connectors should be avoided, if possible, since ammonia could interact with the metal.

8) R. J. Cvetanović and Y. Amenomiya, *Advan. Catal.*, **17**, 103 (1967).

9) V. Kanazirev and N. Borisova, *Zeolites*, **2**, 23 (1982).

 © 1986 The Chemical Society of Japan Bull. Chem. Soc. Jpn., 59, 3741—3746 (1986)

The Regulation of Emulsion Polymerization of Styrene with Anionic-Nonionic Emulsifier Mixtures

Kazufumi KATO,* Harumi KONDO, Kunio ESUMI, and Kenjiro MEGURO
Department of Applied Chemistry and Institute of Colloid and Interface Science, Science University of Tokyo, Kagurazaka, Shinjuku-ku, Tokyo 162
(Received April 24, 1986)

The emulsion polymerization of styrene was carried out in the presence of mixtures of a nonionic surfactant (poly(oxyethylene) hexadecyl ether; BC-20) and an anionic surfactant (sodium dodecyl sulfate; SDS or lithium perfluorooctanesulfonate; LiFOS). The polymerization rate changed with the hydrophile-lypophile balance (HLB) of the BC-*n* series. The polymerization rate considerably increased on the addition of SDS or LiFOS. However, the further addition of LiFOS caused a gradual depression of the polymerization rate. The polymerization rate was not dependent on the amount of styrene solubilized in the mixed emulsifier solution. The particle sizes decreased remarkably on adding SDS. The molecular weights of polystyrene in latex synthesized in mixed emulsifier solutions were larger than those in a single emulsifier solution. The molecular-weight distributions of polystyrene formed in mixed emulsifier solutions were wider than those of polystyrene formed in a single emulsifier solution. These results may be attributed to properties such as the composition and the charge density of the mixed micelles, and to the solubilized amount of styrene monomer in the mixed nonionic-anionic emulsifier solutions.

There are many reports concerning the physical properties of mixed surfactant solutions, such as, size, form, aggregation number, composition of components and surface charge of the mixed micelles.[1-3] Mixtures of emulsifiers have been also used for emulsion polymerization. There are also some reports about the effect of mixtures of emulsifiers on the emulsion polymerization process, compared with that of a single emulsifier.[4-6] The emulsifiers play important roles: for example, their micelles offer sites for polymerization and they stabilize the synthesized latex in the process of emulsion polymerization.[7-9]

In our previous paper, the emulsion polymerization of styrene in the presence of a mixture of anionic fluorocarbon-anionic hydrocarbon emulsifiers was studied.[10] And it has been confirmed that the fluorocarbon surfactant has the effect of slowing down the polymerization rate. The addition of a fluorocarbon emulsifier reduced the particle number concentration of the latex and the molecular weight of the polystyrene latex formed. It also caused an increase in the size of the latex particles.

In this work, the emulsion polymerization of styrene was carried out using a mixture of a nonionic emulsifier and an anionic emulsifier (sodium dodecyl sulfate; SDS, or lithium perfluorooctanesulfonate; LiFOS). The effect of the mixture of nonionic-anionic emulsifiers on the emulsion polymerization process was investigated by measuring the polymerization rate, the particle size, the molecular weight and their distribution.

Experimental

Materials. Poly(oxyethylene) hexadecyl ethers ($RO-(C_2H_4O)_nH$; BC-*n*) were used as nonionic emulsifiers. As anionic emulsifiers, sodium dodecyl sulfate ($C_{12}H_{25}OSO_3Na$; SDS) and lithium perfluorooctanesulfonate($C_8F_{17}SO_3Li$; LiFOS) were used. LiFOS was prepared by the same synthesis described in the previous paper.[10] SDS was marketed for biochemical use (Wako Pure Chem. Ind. Ltd.) and was purified by recrystallization twice from ethanol. The purities of the SDS and LiFOS were confirmed by elemental analysis and the absence of a minimum in the surface tension measurement. BC-*n* (Nikko Chemical Co.) were used without further purification.

The styrene monomer was distilled under a nitrogen atmosphere, and was stored in a refrigerator under nitrogen before use. For an initiator potassium peroxodisulfate ($K_2S_2O_8$) of analytical grade supplied by Wako Pure Chemical Ind. Ltd. was used. Water was purified by Milli-Q Reagent Grade Water System (Millipor Ltd.) until its specific conductivity fell below 0.1 $\mu S\,cm^{-1}$.

Procedure. Each run of emulsion polymerization was done using a batch process in a one-liter glass reactor fitted with a metal screw, thermometer and facilities for charging and sampling. A typical polymerization recipe is shown in Table 1. The main conditions of the emulsifiers using in the polymerization process were as follows.

a) HLB in BC-*n* series are varied. Each hydrophile-lypophile balance (HLB) of BC-*n* series is summarized in Table 2.

b) The amounts of BC-20 (HLB; 17) are varied.

c) Mixing ratios of anionic-nonionic emulsifiers are varied. The changes in the mixing conditions were done in two ways; one of them was made up by adding various quantities of SDS or LiFOS to a definite quantity of BC-20 (5.0 g), and the other was made up by varing the mixed ratios of each emulsifier (SDS-BC-20, LiFOS-BC-20).

At first, the water and emulsifier were added to the reactor at room temperature. The styrene monomer was then added. The reactor was immersed in a constant temperature bath adjusted to 60±1°C under a nitrogen atmosphere, and the mixture was stirred at 250 rpm. When the temperature reached 60°C, the aqueous solution of potassium peroxodisulfate (0.2 g/50 cm^3) was added to the contents in the reactor to initiate the polymerization.

The 5 cm^3 of emulsion samples for determination of the conversion ratio in the polymerization process was withdrawn with pipettes at fixed intervals. The samples were poured into 5 cm^3 of *p*-benzoquinone methanol solution (1.5

Table 1. Emulsion Polymerization Recipe

Ingredients	Grams
Styrene	50
Water	250
Potassium peroxodisulfate	0.2
Emulsifier	Poly(oxyethylene) hexadecyl ether (BC) BC-20 (H.L.B.: 17) Sodium dodecyl sulfate (SDS) Lithium perfluorooctane sulfonate (LiFOS)

Table 2. Hydrophile-Lypophile Balance (HLB) of Poly(oxyethylene) Hexadecyl Ether (BC-*n*) Series

BC-*n*	H.L.B.
n:10	13.5
n:15	15.5
n:20	17.0
n:23	18.0
n:25	18.5
n:30	19.5
n:40	20.0

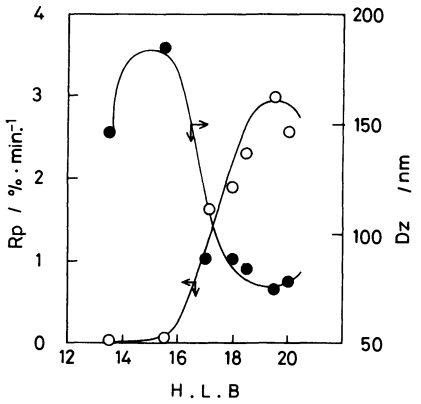

Fig. 1. The effect of hydrophile-lypophile balance (HLB) of poly(oxyethylene) hexadecyl ethers (BC-*n*) on polymerization rate (Rp) and particle size (Dz). Amount of BC-*n*; 10.0g.

g dm^{-3}) as an inhibitor to terminate the polymerization reaction. Then, the unreacted styrene monomer, methanol and water were evaporated at 70°C. The percent conversions of styrene to polystyrene were estimated by measuring the ratios: (polymer/total monomer) on the assumption that the (monomer+polymer)/water was constant throughout the reaction.

In order to determine the particle sizes and the molecular-weight distributions of the latex particles after 90 min of reaction time, the samples were cooled rapidly in cold water (0°C). The particle sizes and the size distributions were determined by a submicron particle sizer (AUTOSIZER MODEL-700; Malvern Instruments Ltd.). This was carried out at 25.0°C by assuming that the refractive index of the latex-suspended solution was 1.33 and its viscosity $8.909*10^{-4}$ Pas.[11,12] Their polydispersity indexes (Pusey'Q factor) which gave an indication of the breadth of the size distribution were determined.

The molecular-weight distributions of polystyrene latex samples were measured by using a gel permeation chromatograph (GPC) fitted with a packed column (Showa Denko Co. A-80M). The weight-average molecular weights (M_w) and their molecular-weight distributions (M_w/M_n) were calculated with a Shimadzu Chromatopac C-R2AX.

The amounts of ethylbenzene solubilized in the mixed emulsifier solutions were determined spectrophotemetrically by measuring the absorbance of ethylbenzene at a wavelength of 262.6 nm at 25°C. It was assumed that the solubilized amount of ethylbenzene was similar to that of styrene in several emulsifier solutions.

Results and Discussion

In general, emulsifiers play important roles in the good running of emulsion polymerization. Especially, nonionic emulsifiers have a high selectivity toward the emulsification of the monomer and the stabilization of emulsion droplets and polymer particles. Greth has systematically studied the suitabilities of nonionic emulsifiers for several monomers, such as, styrene and vinyl acetate. He has also reported that the solubility of a monomer for water is correlated with the HLB of nonionic emulsifiers, which give good stability to the latex.[4]

In our report, the emulsion polymerization of styrene was carried out by using BC-*n* series as nonionic emulsifiers which have various different HLB. The time-conversion curves were first obtained and the polymerization rates (%min^{-1}) were calculated from their initial slopes. The effects of HLB of BC-*n* on the polymerization rate and on the particle size are shown in Fig. 1. It can be seen that the polymerization rate has a maximum value in the range of 17—20 of the HLB. The polymerization rate is dependent on the HLB of the BC-*n*. The particle size was also changed with the HLB. The change of particle size will be caused by the change of the number of latex particles accompanying the change of the polymerization rate with HLB.

It was confirmed in the first stage that the latex formed by using the nonionic emulsifiers (BC-*n*) of its HLB ranged at 17—20 was stable. In the next stage, the effect of the concentration of BC-20 (HLB; 17) on the polymerization rate and on the size of latex particle was examined. The changes of the polymerization rate (Rp) and the particle size of the latex formed with the change of the concentration of BC-20 are shown in Fig. 2. From this figure, it is evident that an exponential increase in polymerization rate accompanies an arith-

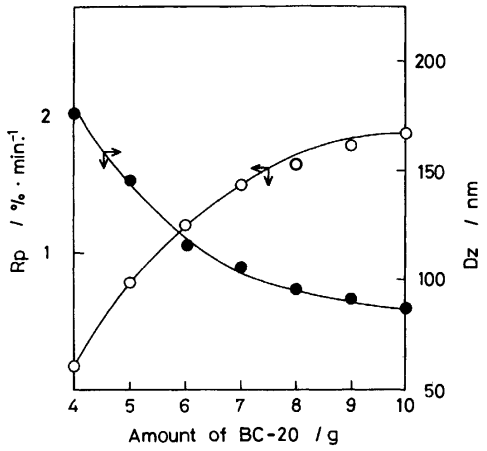

Fig. 2. The change of polymerization rate (Rp) and particle size (Dz) with amount of BC-20 (g).

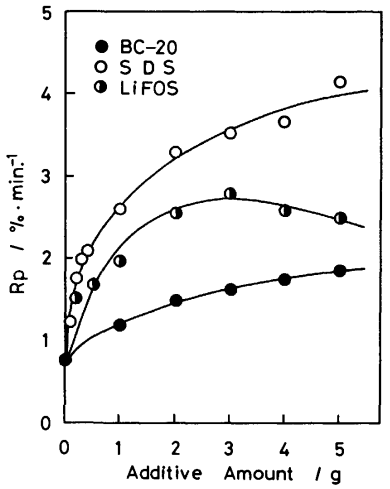

Fig. 3. Polymerization rate (Rp) as a function of additive amount of SDS(○), LiFOS(◑), BC-20(●) to BC-20 (5.0g).

metic increase in the concentration of BC-20 [BC-20]. Indeed, this relationship can be mathematically expressed as;

$$Rp \propto [BC\text{-}20]^{0.17}$$

The mechanism of particle formation in emulsion polymerization has been studied by many workers. According to the micellar nucleation theory of Smith-Ewart,[7] the number concentration (N) and the polymerization rate can be expressed as follows; when a homogeneous nucleation occurred in the emulsion polymerization of a water-insoluble monomer such as a styrene;

$$N \propto [I]^{2/5}[S]^{3/5}$$

$$Rp \propto (N/2)[M]$$

where [I] is the initiator concentration, [S] the emulsifier concentration and [M] the monomer concentration. These expressions have been proven to be valid only for the emulsion polymerization of a water-insoluble monomer in an aqueous solution of an anionic emulsifier above its cmc. However, when the nonionic emulsifiers were used in emulsion polymerization, the Smith-Ewart theory does not often coincide with the polymerization process, owing to the change of several factors; HLB, solubilized amount and their affinity for the monomer.[4,6]

In this study, the polymerization rate increased in proportion to the BC-20 concentration of 0.17 power. This power value is further changeable with temperature, mixing process, mixed ratio of water to monomer and conversion. Therefore, it was confirmed that the Smith-Ewart theory was inapplicable to this emulsion polymerization system of styrene in the presence of BC-20.

Figure 3 shows the change of the polymerization rate when various quantities of SDS or LiFOS are added to a definite quantity of BC-20, whereas the total amount of the mixed emulsifiers is different in each

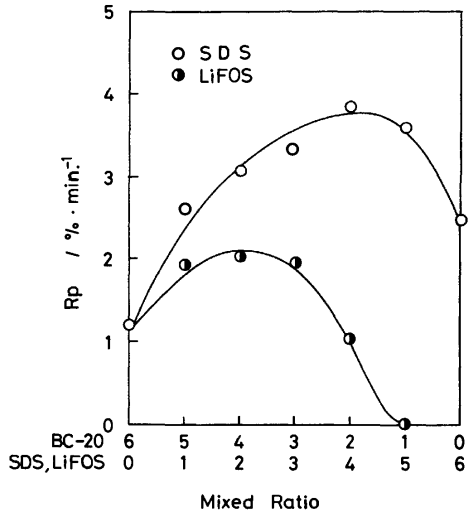

Fig. 4. The change of polymerization rate (Rp) with mixed ratio of (BC-20–SDS) or (BC-20–LiFOS) at the total concentration of 6.0g 250cm^{-3}.

reaction system. Figure 4 shows the change of the polymerization rate with various mixed ratios in the emulsifier mixtures, by keeping the total amount of emulsifiers constant. It can be seen from Fig. 3 that the polymerization rate increases with increase of the additive amount of SDS or LiFOS. Especially, only a small addition of anionic emulsifier to the system caused a steep increase of the polymerization rate. Figure 4 indicates that the polymerization rate in the mixture of (SDS-BC-20) or (LiFOS-BC-20) is much larger than that using each single emulsifier (BC-20, SDS or LiFOS).

In this work, it was assumed that the solubilized amount of ethylbenzene was equal to that of styrene in the emulsifier solutions. The solubilized amount of ethylbenzene is shown in Fig. 5 as a function of the additive amount of each emulsifier being adjusted by

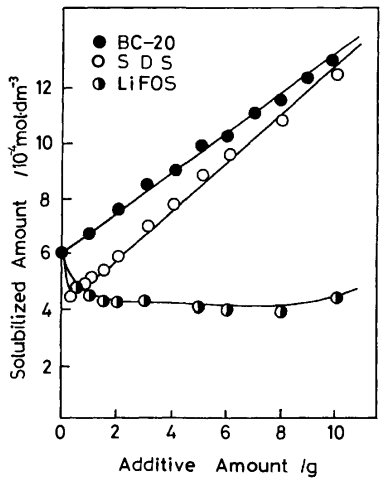

Fig. 5. Solubilized amount of ethylbenzene in mixed emulsifier aqueous solution as a function of additive amount of emulsifiers; SDS(○), LiFOS(◑), BC-20(●) to BC-20, at temperature 25°C.

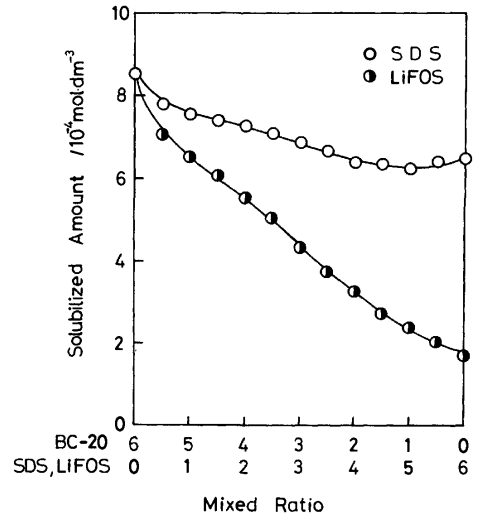

Fig. 6. Solubilized amount of ethylbenzene in mixed emulsifier aqueous solution as a function of mixed ratio of (BC-20-SDS) or (BC-20-LiFOS) at temperature 25°C.

the same amounts of emulsifiers as used in Fig. 3. The solubilized amount of ethylbenzene is also shown in Fig. 6 as a function of the mixed ratio of (SDS-BC-20) or (LiFOS-BC-20) being adjusted as indicated in Fig. 4. By the addition of the emulsifier, the solubilized amount of ethylbenzene increased in proportion to the concentration of BC-20 and this increase of the solubilized amount was higher than that in the case of a nonionic-anionic emulsifier mixture. The solubilized amount of ethylbenzene in the mixed solutions by adding a little amount of SDS to BC-20 became smaller than that in the case of single nonionic emulsifier. However, on the further addition of SDS, the solubilized amount of ethylbenzene increased. This amount was always smaller than that of the solubilized amount in the same concentration of BC-20.

It is known that the polymerization rate is proportional to the solubilizing power of various emulsifiers.[13] By a comparison between Figs. 3 and 5, while the solubilized amount of ethylbenzene in the mixed emulsifier solution, (BC-20-SDS) or (BC-20-LiFOS), was smaller than that in the single BC-20 solution, the polymerization rate in the former solution was larger than in the latter. In Fig. 4, the polymerization rate is seemed to increase with mixing the emulsifiers more than in the case of a single emulsifier, while the solubilized amount of styrene is reduced in the mixed emulsifier solutions. This would be expected from the same effect in the solubilized amount of ethylbenzene as shown in Fig. 6. These results confirmed that the polymerization rate was not much associated with the solubilized amount in nonionic-anionic emulsifier mixtures.

In general, it is difficult to predict the properties of mixed nonionic-anionic surfactant solutions theoretically,[2,3] such as the micelle size, the aggregation number and the composition in their mixed micelles. This is because of the specific difference in the interaction among hydrophilic polar groups of their molecules in the mixed micelles, compared with that in single micelles. Therefore, emulsion polymerization with nonionic-anionic emulsifier mixture cannot be directly attributed to the solubilized amount in mixed emulsifier solutions.

In the mixture of BC-20-LiFOS, the polymerization rate increased with increase of the addition of LiFOS. But the further addition of LiFOS caused the polymerization rate to decrease in spite of an increase in the total amount of the emulsifiers. In a previous paper,[10] it was confirmed that LiFOS has a repressive effect on the polymerization rate. According to Suzuki et al.[14] it was also reported that the addition of a fluorocarbon surfactant is effective to expel any materials solubilized in the micelles of a hydrocarbon surfactant by forming mixed micelles. From the above consideration, it is also supported that the deacceleration of the polymerization rate occurs due to the expulsive effect of LiFOS. The added LiFOS expels styryl radicals from the micelles in aqueous emulsifier solutions, resulting in a depression of the polymerization rate. However, this effect was slight in this nonionic-anionic emulsifier mixture.

The particle number concentration in synthesized latex per cubic meter of the aqueous phase (N) was calculated from the z-average diameter and the conversion ratio, and the diagram of the particle number concentration plotted against the addition of emulsifiers is shown in Fig. 7. The increase of the number of latex particle is seemed to be caused by the increase of the number of micelles and the increase in the number of emulsion particle with the total amount of emulsifier in the reaction solution. The increase of the particle number concentration caused by the addition of SDS or LiFOS is much larger than that with BC-20, while further addition of LiFOS causes a gradual

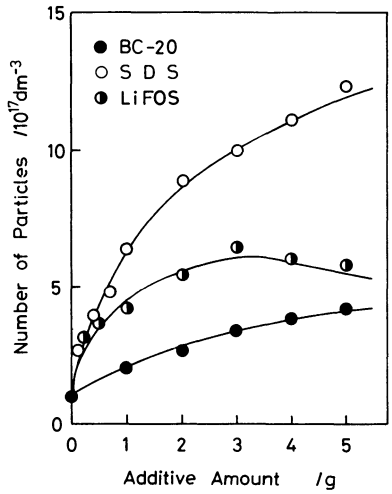

Fig. 7. Particle number concentration as a function of additive amount of SDS(○), LiFOS(◑), BC-20(●).

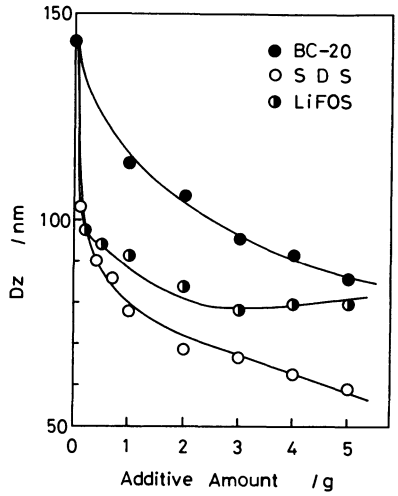

Fig. 8. Particle size (Dz) as a function of additive amount of emulsifiers; SDS(○), LiFOS(◑), BC-20(●).

decrease in the particle number concentration. These results can be explained by the same reason as mentioned about the change of the polymerization rate, for example, the variation of the composition in nonionic-anionic emulsifier micelles and the change of the solubilized amount of monomer in mixed emulsifier solutions.

The change in the latex particle size with the addition of BC-20, SDS, LiFOS to BC-20 (5.0 g) is shown in Fig. 8. Each particle size became smaller with increasing the addition of emulsifiers. The explanation for this result is based on the number of latex particles with the addition of the emulsifier, resulting in the increase of the polymerization rate. That is to say, as the particle number increases, the amount of monomer which is supplied for one latex particle decreases. In other words, since the polymerization of water-insoluble monomer proceeds in micelles containing

Table 3. Weight-Average Molecular Weight (M_w) and Molecular-Weight Distribution (M_w/M_n) of Formed Polystyrene Latex

Mixed Ratio	Molecular Weight	
BC-20 : SDS	M_w (×10⁶)	M_w/M_n
6 : 0	1.29	3.85
5 : 1	1.63	4.15
4 : 2	1.65	4.55
3 : 3	1.64	4.40
2 : 4	1.67	4.60
1 : 5	1.43	4.93
0 : 6	0.77	3.19
BC-20 : LiFOS	M_w (×10⁶)	M_w/M_n
6 : 0	1.29	3.85
5 : 1	1.39	4.55
4 : 2	1.29	4.57
3 : 3	1.37	5.05
2 : 4	0.99	4.50
1 : 5	0.55	1.75
0 : 6	—	—

monomer, the slower the polymerization rate is, the longer is the time in which the polymer particles and emulsion droplets coexist. As a result, the latex particle sizes are continuously increasing up to the depletion of monomer droplets. Furthermore, the particle size decreases with only a small addition of the anionic emulsifier, compared with the corresponding addition of BC-20. The remarkable decrease of particle sizes may occur because of the considerable increase in the number of latex particles. As an anionic is added to a nonionic emulsifier, the composition of the mixed micelles changes and the charge density of the anionic head group in the mixed micelles' surface increases. This increase of surface charge may bring about the increase in the repulsion between styryl oligomeric radical and the micelles. Actually, it has been established that the surface properties of a mixed micelle are remarkably changed upon a small addition of an anionic to a nonionic surfactant. This has been shown by measuring the surface potential,[1] and self-diffusion coefficients and line width at half height by NMR.[3]

The molecular-weight of the polystyrene latex formed was measured by GPC after being dissolved in tetrahydrofuran. These samples were the same ones used for the particle size measurement. The weight-average molecular weights (M_w) and their molecular weight distributions (M_w/M_n) are shown in Table 3 as a function of mixed ratio of (BC-20-SDS) or (BC-20-LiFOS). It was found that the breadth of the molecular-weight distribution of the polystyrene formed in a latex by using the mixed emulsifiers was rather broadened compared with that by using each single emulsifier. These results demonstrate that the compositions of emulsions and micelles in the mixed emulsifier solutions have a much wider distribution than that in a single emulsifier solution. The M_w of polystyrene latex formed with mixed emulsifiers increased more

than that of polystyrene latex formed with each single emulsifier. The increase of M_w on adding SDS was higher than that on adding LiFOS. These results depend on the change of the polymerization rate and the particle number concentration with the mixed ratio of emulsifiers.

References

1) M. Nakagaki, S. Yokoyama and I. Yamamoto, *Nippon Kagaku Kaishi*, **1982**, 1865.
2) N. Nishikido, *J. Colloid Interface Sci.*, **60**, 242 (1977).
3) P. G. Nilsson and B. Lindman, *J. Phys. Chem*, **88**, 5391 (1984).
4) G. G. Greth and J. E. Wilson, *J. Appl. Polym. Sci.*, **5**, 135 (1961).
5) S. Muroi, *Kogyo Kagaku Zasshi*, **68**, 1785 (1965).
6) S. S. Medvedev, I. A. Gritskova, A. V. Zuikov, L. I. Sedakova and G. D. Berejnol, *J. Macromol. Sci. Chem.*, **A7**, 715 (1973).
7) W. V. Smith and R. H. Ewart, *J. Chem. Phys.*, **16**, 592 (1948).
8) R. N. Haward, *J. Polym. Sci*, **4**, 273 (1949).
9) F. K. Hansen and J. Ugelstad, *J. Polym. Sci. Polym. Chem. Ed*, **16**, 1953 (1978).
10) K. Kato, K. Esumi, and K. Meguro, *Bull. Chem. Soc. Jpn.*, **59**, 249 (1986).
11) P. N. Pussey, "Indusrial Polymer; Characterization by Molecular Weights," ed by Green and Dietz, Transcripta Books, London (1973).
12) S. W. Provencher, J. Hendrix, L. D. Maeyer, and N. Paulussen, *J.Chem.Phys.*, **69**, 4273 (1978).
13) I. M. Kolthoff, E. J. Meehan and C. W. Car, *J. Polym. Sci.*, **6**, 73 (1951).
14) T. Suzuki, K. Esumi, and K. Meguro, *J. Colloid Interface Sci.*, **93**, 205 (1983).

Stopped-Flow Small-Angle X-Ray Scattering Study on the Acid-Denaturation of Taka-Amylase A

Tatsuya HOZAKI,† Mitsunori KATO,† Mamoru SATO,* Nobuo TANAKA, Yukio MORIMOTO, Yasuo HATA, Yukiteru KATSUBE, and Nobutami KASAI†
Institute for Protein Research, Osaka University
†Department of Applied Chemistry, Faculty of Engineering, Osaka University, Suita, Osaka 565
(Received May 21, 1986)

A stopped-flow small-angle X-ray scattering method was applied to study the structural change of Taka-amylase A by acid-denaturation. The structural change could be described by two successive steps. The first step is described by a change in the eccentricity of a prolate ellipsoid from 2.0 to 2.4; this was estimated by a comparison between the observed scattering profile and the theoretical scattering function of the prolate ellipsoid. The second step supposes that the X-ray scatterer in a solution comprises two kinds of particles with large and small radii of gyration. The X-ray scatterer with a large radius expands with time. By contrast, the radius of gyration of the small scatterer corresponds to that of a native Taka-amylase A monomer and it remains unchanged. These facts imply that in the denaturation of Taka-amylase A the molecule is prolonged by a partial unfolding of the polypeptide chain and then aggregates with each other.

Taka-amylase A (EC 3.2.1.1,α-1,4-glucan-4-glucano hydrolase) is an α-amylase that catalyzes the hydrolysis of α-1,4-glucosidic linkages in polysaccharides. Many studies have been undertaken on Taka-amylase A since Akabori and Okahara extracted the enzyme from *Aspergillus oryzae*.[1] The enzyme is monomeric, composed of a single polypeptide chain (478 amino acid residues[2]) and has a molecular weight of 51000. The three-dimensional structure of Taka-amylase A has been determined at a 3.0-Å resolution by an X-ray crystal structure analysis,[3] and the mechanism of its enzymatic activity has been proposed.[4]

Takagi et al. have studied the renaturation of Taka-amylase A from an acid- or a urea-denaturated molecule by such means as optical rotatory dispersion, pH titration, and sedimentation velocity.[5-7] They have suggested that through acid-denaturation the hydrogen bonds between the side-chain groups are completely cleaved and most of the peptide hydrogen bonds are retained to maintain the structure of the helical region, though the urea-denaturation results in unfolded molecules devoid of secondary and tertiary structures. It has also been reported that the acid-denaturation of Taka-amylase A proceeds very slowly at pH 3.3 with a time resolution of 1 min.[5] For studies concerning the slow change in the structure, it is useful to analyze the structural change with a small-angle X-ray scattering method with a stopped-flow mixing device and a position-sensitive detector. From these points of view, the present paper concerns a study of the time-resolved structural change of Taka-amylase A by acid-denaturation at pH 3.3 by means of stopped-flow small-angle X-ray scattering.

Experimental

Sample Preparation for X-Ray Experiments. Taka-amylase A was isolated from Takadiastase Sankyo according to the method of Akabori et al.,[8] and purified with chromatography on a DEAE-cellulose column. The eluent from the column was desalted by ultrafiltration with a Diaflo YM-30 membrane followed by a repeated addition of distilled water. At the end of the desalting process, the purified protein solution was concentrated to more than 70 mg ml^{-1} by ultrafiltration. The protein concentration of the purified Taka-amylase A, which was determined spectrophotometrically by UV absorption at 279 nm by using $E^{1\%}_{1cm}$=22.1, was then adjusted to be 20.0 mg ml^{-1} by diluting the solution with distilled water. The protein solution was mixed with a 0.1-M glycine/NaCl-HCl (1 M=1 mol dm^{-3}) buffer in the stopped-flow mixing device. The pH of the buffer was determined so that the pH of the mixed solution might be 3.3 (tested at each temperature before X-ray experiments).

Stopped-Flow Mixing Device. A stopped-flow mixing device was constructed by Union Giken Co. Ltd.. Equal volumes of two solutions were mixed in a jet mixer and transferred into a 1.0-mmφ thin-walled quartz capillary using the pressure difference of nitrogen gas; this was also used for draining the mixed solution. The irradiated area was modified so that line-collimated X-rays could completely irradiate the capillary. The temperature in the device was controlled by circulating water with a constant temperature. The temperature of the mixed solution was detected by a copper-constantan thermocouple located beside the capillary and was monitored on a recorder. The dead time between the transmission of the signal and the filling of the tube with the mixed solution was about 100 ms. No meaningful difference was found between the scattering intensity distribution of the distilled water obtained from one time accumulation of 200-s measured data and that obtained from 2000 accumulations of 100-ms measured data. This shows that no mixing artifact was observed during the experiments. About 100 μl of a mixed solution was consumed per shot. The capillary was washed out with two shots of immediately mixed solution just before each measurement was started. All operations for the stopped-flow mixing device were controlled with a microcomputer connected with an X-ray detector.

X-Ray Measurements. The X-ray source was a 0.4×8 mm spot on the copper anode of a Philips fine-focus X-ray tube operated with a Rigaku Denki D9C X-ray generator run at 40 KV, 30 mA. A line focus was used to obtain sufficiently intense scattered X-rays. The spot was foreshortened to 0.04×8 mm at a glancing angle of 6°. The nickel-filtered (10 μm in thickness) X-rays were collimated with a 0.3×10

mm slit, and then reflected and focussed by a nickel-coated glass mirror[9] through two kinds of limiting slits. One was located immediately after a mirror holder to collimate reflected X-rays; the other was located just before a stopped-flow mixing device to reduce the parasitic scattering originating from the edge of the former slit. The scattered X-rays were recorded on a one-dimensional position-sensitive proportional detector (delay-line type). The flowing gas (11 mm in thickness) used was a mixture of 90% argon and 10% methane. The width of the detector window was 10 mm. The detector length was 50 mm and was divided into 256 channels on a multichannel analyzer. The sample-to-detector distance was 310.0 mm. The scattered X-rays were collected in the range of the scattering angles from 3.8×10^{-3} to 7.7×10^{-2} rad. The X-ray path from the stopped-flow mixing device to the detector was evaculated to avoid air scattering. All the X-ray camera units were located in the small chamber with the temperature controlled to be 5 °C (with a cooling unit) in order to prevent dew from appearing on and in the stopped-flow mixing device during low-temperature experiments. X-Ray experiments were performed at 0, 5, 10, and 15 °C, respectively. These temperatures were kept within ±0.1 °C by circulating water with a constant temperature within the device. For each experiment, 32 frames of scattering profiles of 256 points were sequentially stored in the process memory of the multichannel analyzer in the following time pattern: 10 frames of 60 s accumulation with a time gap of 1 s; 6 frames of 60 s accumulation with a time gap of 10 s; 5 frames of 60 s accumulation with a time gap of 60 s; 5 frames of 60 s accumulation with a time gap of 120 s; and 6 frames of 60 s accumulation with a time gap of 240 s. Ten cycles of these measurements were summed and saved on the floppy disk of a microcomputer.

Data Reduction. The scattering intensities recorded on both sides of the primary beam were averaged at equivalent points after subtracting background intensities. The center of the primary beam (zero-angle scattering) was precisely searched so as to realize the best coincidence of the scattering intensities at the equivalent points on both sides of the zero-angle. The coincidences expressed by a reliability factor R_{sym}[10] were all good. The scattering intensity $I(s)$ was then obtained by a deconvolution (desmearing) for the beam-height effects according to the method of O. Glatter.[11] The scattering parameter s is defined by $s=4\pi\sin\theta/\lambda$, where 2θ is the scattering angle and λ the wavelength (λ=1.5418 Å).

Results

Radius of Gyration and Zero-Angle Scattering Intensity. The radius of gyration R_g and zero-angle scat-

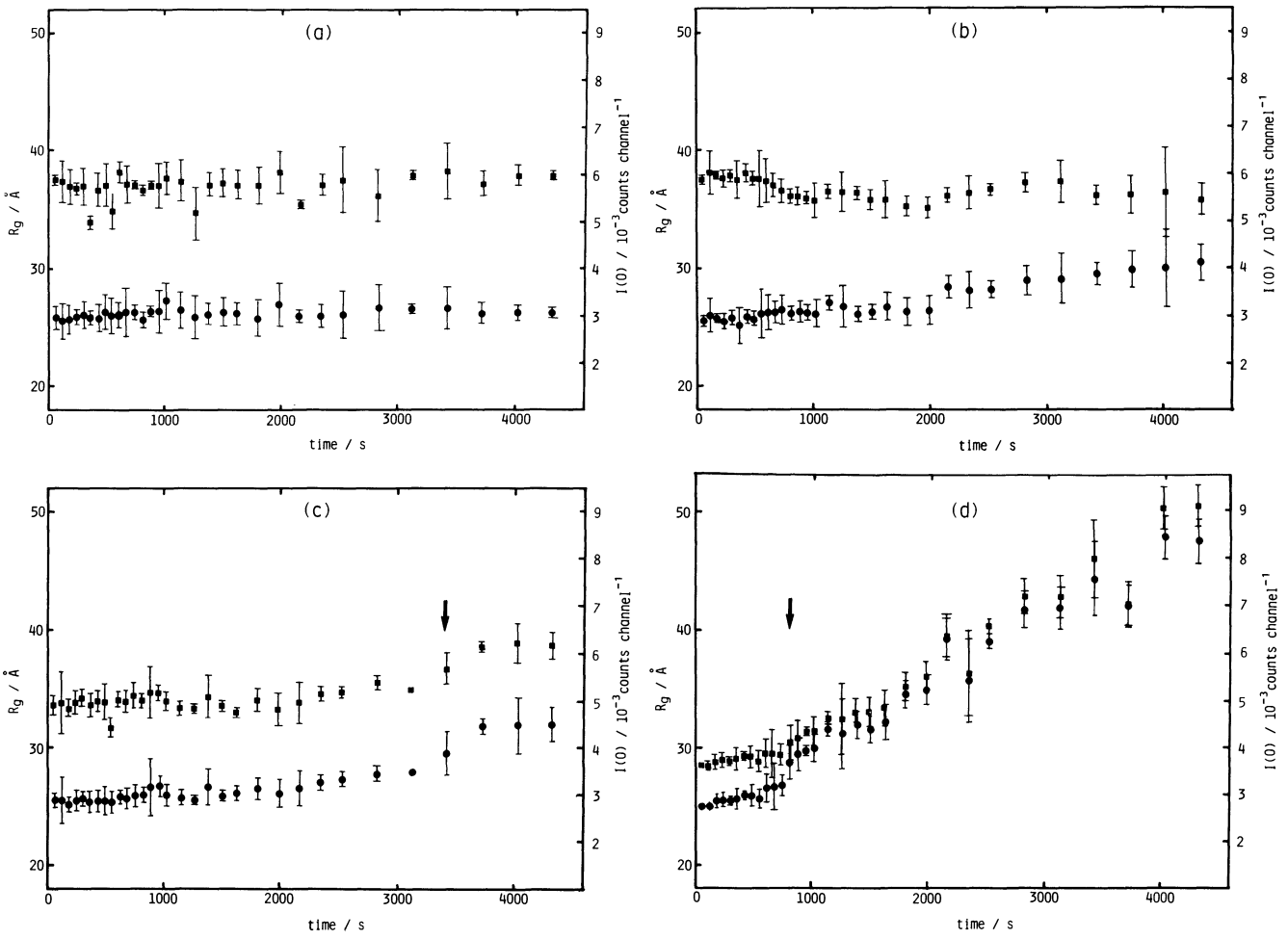

Fig. 1. Time courses of radius of gyration, R_g(●) and zero-angle scattering intensity, $I(0)$(■): (a) at 0°C, (b) at 5°C, (c) at 10°C, and (d) at 15°C. Error bar is drawn by 3σ, where σ is the standard deviation obtained from the least-squares method.

tering intensity $I(0)$ were derived from a Guinier plot[12] of the small-angle scattering profile by a least-squares method. The time courses of R_g and $I(0)$ at each temperature are plotted in Fig. 1. At 15 °C, R_g and $I(0)$ increase appreciably after about 800 s, within the time during which R_g gradually increases and $I(0)$ remains unchanged. This phenomenon was also observed at 10 °C; however the time at which the large increases of R_g and $I(0)$ were observed was retarded to about 3400 s. At 5 °C, only the phenomenon of a gradual increase of R_g and an almost constant $I(0)$ was observed over the whole range of the time course. However, neither R_g nor $I(0)$ changed at 0 °C. These results show that the acid-denaturation of Taka-amylase A can be explained by two steps of a structural change from the time courses of R_g and $I(0)$. Also, its rate is strongly dependent on the temperature. The arrow in Fig. 1 shows the time between the first and second steps. A further analysis regarding the respective steps resulted in the following two paragraphs.

The Time Courses of Structural Parameters in the First Step. The X-ray crystal structure analysis has clarified that the Taka-amylase A molecule is an ellipsoid with approximate dimensions of 35×45×80 Å.[13] Since the ellipsoid was considered to be a prolate ellipsoid of revolution with a semi-axis length of a=20 Å and an eccentricity of w=2.0, the observed scattering profile for each frame was compared with the theoretical scattering function of a prolate ellipsoid (Fig. 2). This comparison was performed in a time range in which $I(0)$ was nearly constant, because the increase of $I(0)$ corresponds to that of the molecular mass.[12] The time courses of the semi-axis lengths, a and b (b=a×w), of the ellipsoid are plotted in Fig. 3. The structural parameters of the initial and the final stages in the first step are summarized in Table 1. Taking account of the hydration in solution and/or the experimental errors, the structural parameters (a, b and R_g) of the initial stage were all in good agreement with those obtained from the X-ray crystal structure analysis[13] (a=20 Å, b=40 Å) and from the ellipsoidal model with a=20 Å and b=40 Å (R_g=22 Å), respectively. These parameters changed with time. As shown in Fig. 3, the eccentricity w of the ellipsoid increased from 2.0 to 2.4 and the semi-axis length a did not change. However, neither a nor w changed at 0 °C. These findings indicate that the native Taka-amylase A elongates with time during the first step of the acid-denaturation.

The Time Courses of Structural Parameters in the Second Step. As described above, the increase of $I(0)$ may be attributed to an aggregation of a Taka-amylase A molecule. Figure 4 depicts Guinier plots of the small-angle scattering profiles at 15 °C. Time frames of 1, 18, 24, and 29 are plotted. The single straight line just after mixing (Fig. 4(1)) can be approximated by two lines (Fig. 4(2)—(4)) with time. The slope of the Guinier plots in the smaller-angle region gradually increases, whereas that in the larger-angle region remains unchanged. This behavior (of the Guinier plot) suggests that the X-ray scatterer in solution is composed of two kinds of particles with different sizes.[14]

Jellinek and Fankuchen have proven that in a polydispersed solution, R_g of each X-ray scatterer can be estimated from the small-angle scattering profile.[15] Figure 5 shows the R_g' s of the two X-ray scatterers derived from the method of Jellinek and Fankuchen using scattering profiles at 15 °C. From the figure it was found that the R_g of the large X-ray scatterer increased with time, and that of the small one remained unchanged and corresponded to that of a Taka-amylase A monomer. This is because the R_g of the ellipsoidal model of Taka-amylase A was estimated to be 27 Å.

The distance distribution function $P(r)$[16] was also calculated by a Fourier transform of the scattering profile at 15 °C. The maximal dimension D_{max} of the particle, which was approximated at an r where $P(r)$ decreases to zero, corresponds to that of the larger particle of the two X-ray scatterers in the present system. The D_{max} becomes larger with time as the R_g of the large X-ray scatterer.

Discussion

As shown in Fig. 1, the time courses of R_g and $I(0)$ could be described by two steps: one a gradual increase in R_g and almost constant $I(0)$, and the other a large increases in both R_g and $I(0)$. Since $I(0)$ corresponds to the square of the number of excess electrons in the X-ray scatterer (for details regarding $I(0)$, see the next stage), the nearly constant $I(0)$ throughout the time means that the morphological change (such as the aggregation or dissociation of X-ray scatterer) was not brought about by acid-denaturation. Therefore, the gradual increase in R_g implies that the internal structure of the X-ray scatterer changes without aggregation or dissociation. On the other hand, the large increase in $I(0)$ indicates that X-ray scatterers aggregate with each other through acid-denaturation; this simultaneously causes a large increase in R_g. In addition, the higher the temperature, the faster they aggregate. The details of the structural changes in the two steps are discussed in the following paragraphs, respectively.

Structural Change in the First Step. The small-angle X-ray scattering method does not give as many structural parameters as does an analysis in the crystalline state. This indicates that a unique structural model could not be constructed in some cases in spite of the recent development of such analytical method as the contrast variation.[16,17] Therefore, the structural change was analyzed regarding the shape of a native Taka-amylase A molecule as a prolate ellipsoid. It was ascertained by X-ray crystal structure analysis. This analysis is supported by the fact that the values of the

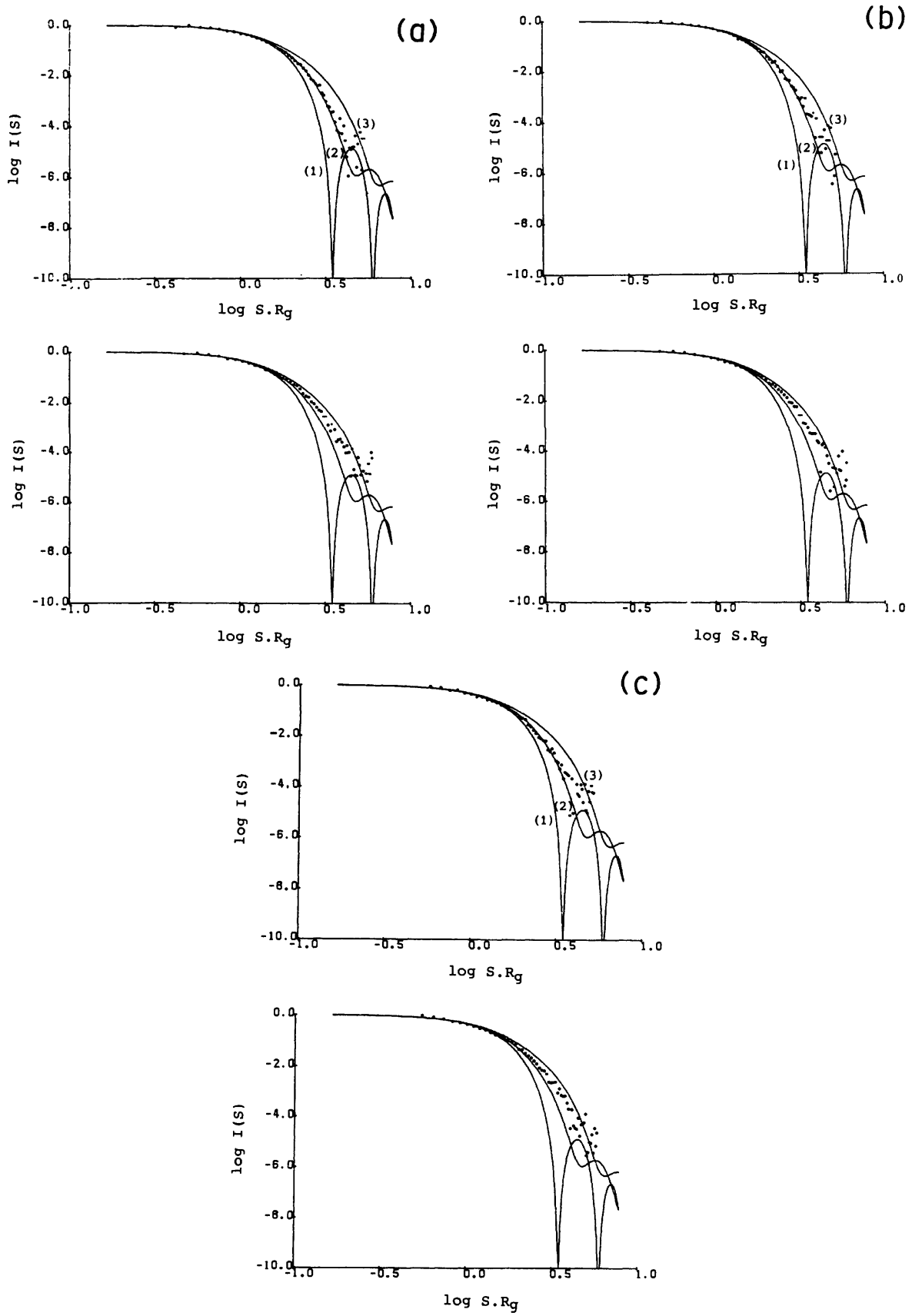

Fig. 2. Log $I(s)$-log s plot of the observed scattering intensities (●). (a), (b), and (c) are the plots at 5, 10, and 15°C, respectively. In (a), (b), and (c), top corresponds to the time frame 1 at each temperature and bottom corresponds to the time frame 32 at 5°C, 29 at 10°C and 13 at 15°C. Superimposed are the theoretical scattering functions (soild lines) of the prolate ellipsoids with the eccentricities, w of (1) w=1.0, (2) w=2.0 and (3) w=3.0.

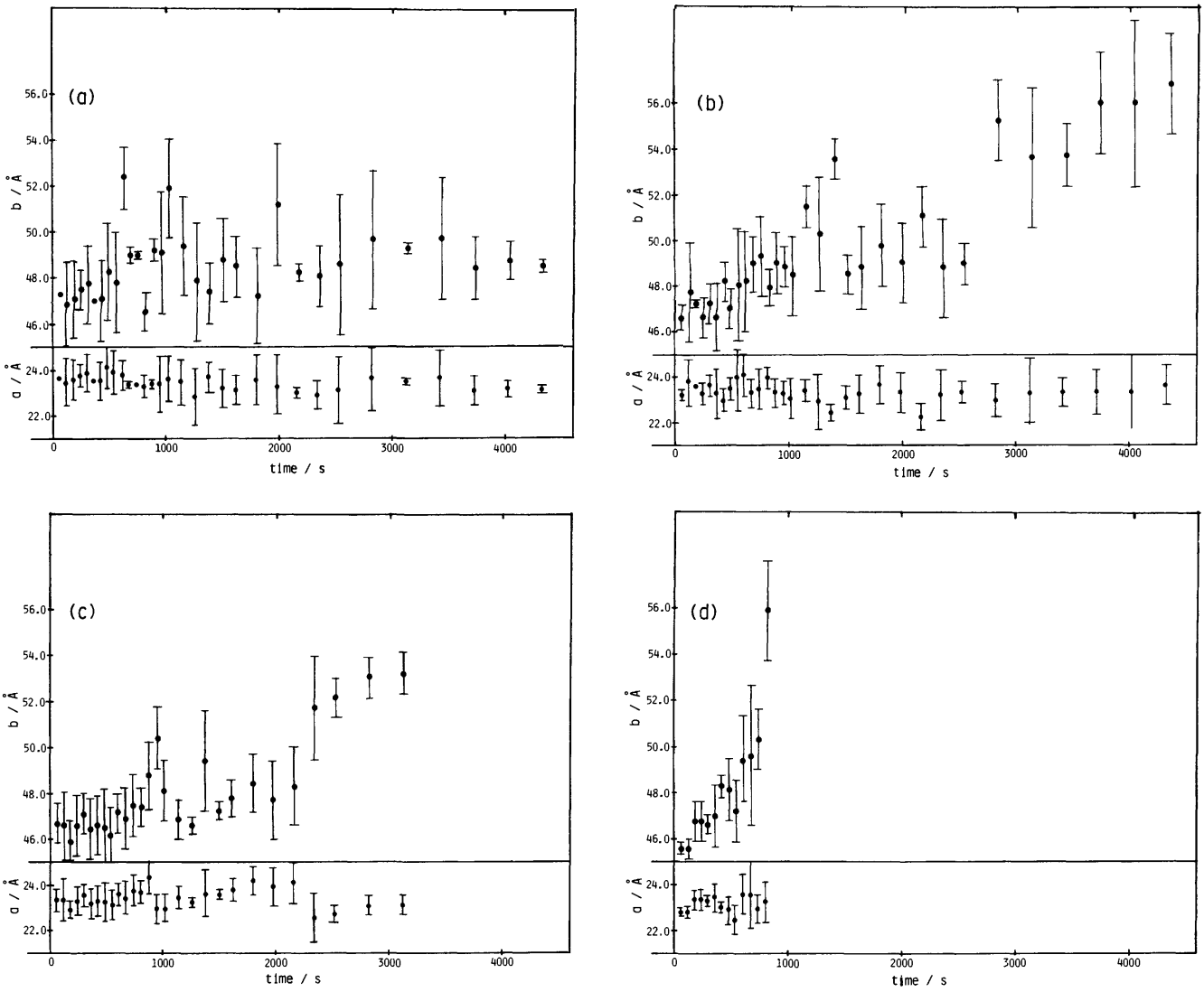

Fig. 3. Time courses of semi-axis lengths, a and b ($b=a\times w$) of a prolate ellipsoid. (a) at 0°C, (b) at 5°C, (c) at10°C, (d) at 15°C. Error bar is drawn by 3σ, where the σ is the standard deviation obtained from the least-squares method.

Table 1. The Structural Parameters of the Initial Stage (Time 1) and the Final Stage (Time 2) in the First Step

t/°C	Time 1/s			Time 2/s		
	R_g/Å	a/Å	b/Å	R_g/Å	a/Å	b/Å
0		60			4320	
	25.9	23.7	47.3	26.2	23.1	48.5
5		60			4320	
	25.5	23.3	46.6	30.2	23.7	56.8
10		60			3420	
	25.6	23.4	46.7	29.6	23.3	53.7
15		60			810	
	25.0	22.8	45.6	29.0	23.3	55.9

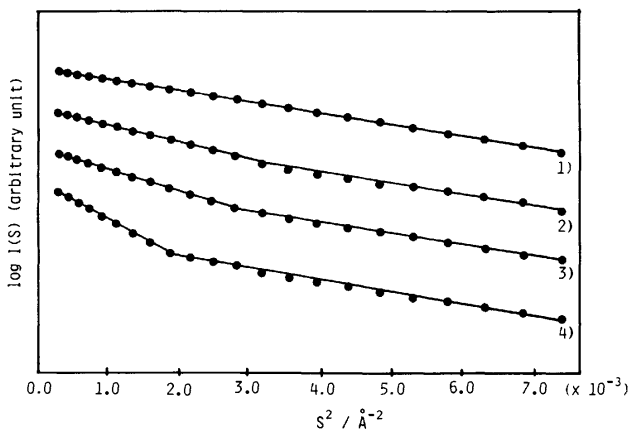

Fig. 4. Guinier plots of the small-angle scattering profiles at 15°C. Time frames 1 (1), 18 (2), 24 (3), and 29 (4) are plotted.

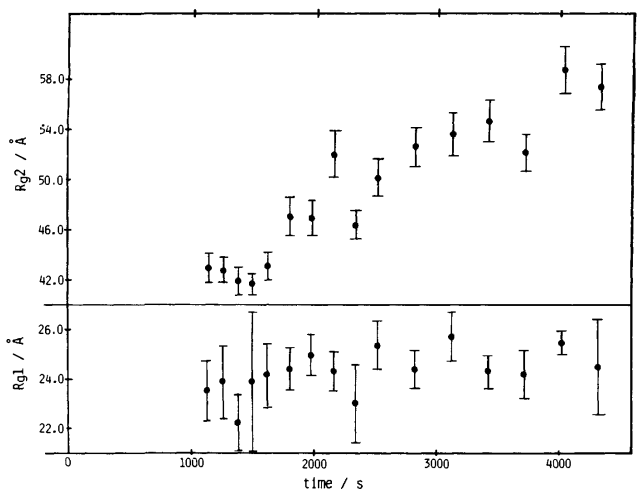

Fig. 5. Time courses of radii of gyration of a small X-ray scatterer, R_g1 and a large X-ray scatterer, R_g2 at 15°C. Error bar is drawn by 3σ, where σ is the standard deviation obtained from the least-squares method.

radius of gyration and the semi-axis lengths (a and b) of the ellipsoid just after mixing (*Time1* in Table 1.) are all in good agreement with those from the X-ray crystal structure analysis. As can be seen in Fig. 3, the eccentricity of native Taka-amylase A gradually increases to about 2.4 until 800 s at 15 °C, 3400 s at 10 °C and 4300 s or more at 5 °C. The semi-axis length a was constant throughout all time. These results show that a Taka-amylase A molecule extends along the b-axis. However, since this extension of the molecule reduces the difference between the average electron densities of the molecule and the solvent, $I(0)$ must gradually decrease, because $I(0)$ is directly proportional to the square of the number of excess electrons in the molecule (sum of the electron density difference over the molecule). The actual state in which $I(0)$ is almost constant may arise from an experimental error in $I(0)$.

Takagi and Toda[6] have indicated that by acid-denaturation the hydrogen bonds between side-chain groups were completely cleaved and most of the peptide hydrogen bonds were retained to maintain a helical region; that is, most helical structures of a Taka-amylase A molecule remain during acid-denaturation. The fact that the eccentricity of the prolate ellipsoid gradually increases and the semi-axis length a is unchanged may arise from a cleavage of the hydrogen bonds between the side-chain groups. This is because a complete destruction of secondary and tertiary structures is expected to provide more drastic changes in the structural parameters. The CD spectra of acid-denaturated Taka-amylase A also showed little difference regarding the α-helix content between native Taka-amylase A and the acid-denaturated one.

The X-ray crystal structure analysis[3] has also clarified the fact that native Taka-amylase A is composed of two large domains (main domain and C-terminal domain) with a narrow cleft between them. These domains are linked by a single polypeptide chain and stabilize each other with some hydrogen bonds. Therefore, the cleavage of the hydrogen bonds by acid-denaturation is expected to cause an increase in the molecular eccentricity; this is because a domain is supposed to be the folding unit of a protein[18] and most of the hydrogen bonds are more stable than those between the two domains. A $(\beta\alpha)_8$ super-secondary structure (β-barrel), similar to those of triose phosphate isomerase,[19] pyruvate kinase[20] or aldolase[21] is found in the main domain of the native Taka-amylase A. The β-barrel contains the active site and protects against the destruction of the large cleft located in the main domain. The destruction of the cleft by the cleavage of the hydrogen bonds is also considered to be one of the factors which cause an elogation in the native molecule.

The small-angle X-ray scattering method, however, does not give much information concerning the internal structure of a molecule. As a result, no direct experimental evidence for the cleavage of the hydrogen bonds between the domains and the destruction of the β-barrel structure has been obtained in the present analysis. It is necessary to analyze the middle- and high-angle scattering intensities which give information about the internal structure. The correlation of the middle- and high-angle scattering intensities with secondary and tertiary structures of protein is now being investigated in our laboratory.

Structural Change in the Second Step. As shown in Fig. 4, the Guinier plot of the small-angle scattering profile at 15 °C became biphasic with time. This phenomenon indicates that the X-ray scatterer in a solution comprises two kinds of particles with different sizes. Using analyses by the method of Jellinek and Fankuchen as well as the distance distribution function, it was elucidated that the large particle further expanded with time and the small one remained unchanged. The R_g of the small particle showed a good coincidence with that of Taka-amylase A monomer. These results indicate that Taka-amylase A molecules aggregate with each other and the X-ray scatterer in solution consists of a large aggregate and a small elongated molecule transformed from native Taka-amylase A by a partial unfolding of the polypeptide chain.

It was, however, shown from a sedimentation velocity study that acid-denaturated Taka-amylase A molecules became highly aggregated with each other to different degrees.[6] However, this may result from the differences in the times at which the X-ray scattering intensities and the sedimentation patterns of Taka-amylase A were measured. In the present X-ray analysis, Taka-amylase A molecules started to aggregate with each other at 800 s after the molecules began to be denaturalized at 15 °C. However, in the sedimentation

velocity study, the sedimentation patterns were measured in an acid-denaturated Taka-amylase A solution dialyzed against a 0.02-M glycine-HCl buffer (pH 2.2) for one day after the enzyme solution was acidified to pH 2.2.[6]

We thank Professor Masao Kakudo for his interest, valuable discussions, and warm encouragement throughout this study.

References

1) S. Akabori and K. Okahara, *Bull. Chem. Soc. Jpn.*, **12**, 55 (1937).
2) H. Toda, K. Kondo, and K. Narita, *Proc. Jpn. Acad.*, **58B**, 202 (1982).
3) Y. Matsuura, M. Kusunoki, W. Harada, N. Tanaka, Y. Iga, N. Yasuoka, H. Toda, K. Narita, and M. Kakudo, *J. Biochem.*, **87**, 1555 (1980).
4) Y. Matsuura, M. Kusunoki, W. Harada, and M. Kakudo, *J. Biochem.*, **95**, 697 (1984).
5) T. Takagi and T. Isemura, *J. Biochem.*, **49**, 43 (1961).
6) T. Takagi and H. Toda, *J. Biochem.*, **52**, 16 (1962).
7) T. Takagi and T. Isemura, *J. Biochem.*, **52**, 314 (1962).
8) S. Akabori, T. Ikenaka, and B. Hagihara, *J. Biochem.*, **41**, 577 (1954).
9) A. Franks, *Proc. Phys. Soc. London, Sect. B.*, **68**, 1054 (1955).
10) T. L. Blundel and L. N. Johnson, "Protein Crystallography," Academic Press, London (1976), pp. 318—319.
11) O. Glatter, *J. Appl. Crystallogr.*, **7**, 147 (1974).
12) A. Guinier and G. Fournet, "Small Angle Scattering of X-Rays," John Wiley and Sons Ltd., New York (1955), pp. 24—28.
13) Y. Matsuura, M. Kusunoki, W. Date, S. Harada, S. Bando, N. Tanaka, and M. Kakudo, *J. Biochem.*, **86**, 1773 (1979).
14) A. Guinier, "Theorie et Technique de la Radiocristallographie," Dunod, Paris (1964).
15) M. H. Jellinek and I. Fankuchen, *Ind. Eng. Chem.*, **37**, 158 (1945).
16) O. Glatter and O. Kratky, "Small Angle X-ray Scattering," Academic Press, New York (1982), pp. 130—131.
17) H. B. Stuhrmann and A. Miller, *J. Appl. Crystallogr.*, **11**, 325 (1978).
18) G. E. Schulz and R. H. Schirmer, "Principles of Protein Structure," Springer-Verlag, New York (1978), Chap. 5.
19) D. W. Banner, A. C. Bloomer, G. A. Petsko, D. C. Phillip, C. I. Pogson, and I. A. Wilson, *Nature*, **255**, 609 (1975).
20) D. I. Stuart, M. Levine, H. Muirhead, and D. K. Stammers, *J. Mol. Biol.*, **134**, 109 (1979).
21) J. S. Richardson, *Biochem. Biophys. Res. Commum.*, **90**, 285 (1979).

 © 1986 The Chemical Society of Japan Bull. Chem. Soc. Jpn., 59, 3755—3759 (1986)

The Arrhenius Parameters for the Reactions of $N(2^4S_{3/2})$ with Halogen Molecules

Hironobu UMEMOTO,* Teruo UCHIDA, Seiko NAKAGAWA, Shigeru TSUNASHIMA, and Shin SATO†
Department of Applied Physics, Tokyo Institute of Technology, Ookayama, Meguro-ku, Tokyo 152
†Research Laboratory for Nuclear Reactors, Tokyo Institute of Technology, Ookayama, Meguro-ku, Tokyo 152
(Received May 23, 1986)

The temperature dependence of the rate constants for the reactions of ground-state atomic nitrogen with halogens were measured by means of a pulse radiolysis-resonance absorption technique. The rate constants for iodine and bromine were well expressed by the following Arrhenius expressions below 410 K: $k(N+I_2)=1.1\times10^6 \exp(-1170/T)$; $k(N+Br_2)=1.1\times10^5 \exp(-1490/T)$, in units of $m^3\,mol^{-1}\,s^{-1}$. The rate constant for the reaction with chlorine was found to be 1.1×10^3 $m^3\,mol^{-1}\,s^{-1}$ at 411 K. Below this temperature, the rate constants for $N+Cl_2$ were too small to be measured. The preexponential factors for the I_2 and Br_2 reactions were found to be much smaller than the semiempirically calculated ones. These small preexponential factors suggest that the reactions between $N(^4S)$ and halogens proceed via nonadiabatic routes.

Ground-state atomic nitrogen, $N(2^4S_{3/2})$, is unreactive to stable molecules which do not have unpaired electrons. For example, the rate constants for the reactions of atomic nitrogen with unsaturated hydrocarbons are too small to be measured by ordinary techniques,[1,2] although ground-state atomic hydrogen and oxygen react with unsaturated hydrocarbons once in every ten or one hundred gas kinetic collisions at room temperature.[3,4] The situation is similar in the cases of inorganic species with even-numbered electrons, such as oxygen, ozone, and phosphine.[5,6] The halogen molecules are not exceptions. In the 1960's Phillips and his co-workers measured the rate constants for the reactions of $N(^4S)$ with halogens near room temperature and found that they are several orders of magnitude smaller than that for gas kinetic collisions.[7,8] In our recent work, we also measured the rate constant for the reaction with molecular iodine at 302 K and found it to be 2.4×10^4 $m^3\,mol^{-1}\,s^{-1}$.[1] The slow reaction rates for the addition of $N(^4S)$ to unsaturated hydrocarbons have been explained by the concept of the simple spin-conservation rule.[1] However, the unreactiveness to halogens, as well as to oxygen and ozone,[5] cannot be explained by this concept, because there are spin-allowed and energetically accessible exit channels—for example, the formation of triplet-state nitrogen halide and atomic halogen. In other words, there must be large potential barriers or entropies of activation for these exit channels. Therefore, in order to ascertain why $N(^4S)$ is unreactive, it is necessary to determine the preexponential factors and the activation energies separately. In the present work, we measured the temperature dependence of the rate constants for the reactions of $N(^4S)$ with chlorine, bromine, and iodine, by employing a pulse-radiolysis resonance-absorption technique. The preexponential factors were then compared with those predicted by the semiempirical LEPS (London-Eyring-Polanyi-Sato) and BEBO (Bond Energy-Bond Order) calculations.

Experimental

The experimental apparatus and the procedure were similar to those described in previous publications.[1,9] Atomic nitrogen was produced by the irradiation of a pulsed electron beam generated by a Febetron 706 apparatus. The pseudo-first-order decay in the concentration of $N(^4S)$ atoms was measured by means of the resonance absorption around 120 nm. The temperature of the reaction vessel was controlled by winding it with a nichrome heater or by introducing cold nitrogen gas from boiling liquid nitrogen into the surrounding copper tubing. A temperature controller (Sanyo Rikagaku SR-4000) was used to reduce the fluctuation in temperature within ±2 K. The relationship between the gas temperature in the chamber and the temperature of the outside wall of the chamber was measured prior to the experiments, and the gas temperature for each run was estimated by measuring the wall temperature with a copper-constantan thermocouple. The halogen pressures were measured with a capacitance manometer (MKS Baratron). After measuring the halogen pressure, an excess amount of nitrogen gas was introduced into the vessel. In general, considerable care is required in the measurement of the gas pressure when the temperature of the reaction zone and that of the pressure gauge are different. Under the conditions of viscosity flow, normally when the pressure is over 100 Pa, the pressure at the gauge, P_0, agrees with that at the reaction zone, P. On the other hand, under the conditions of molecular flow, below 0.1 Pa, the ratio of the pressure at the reaction zone to that at the gauge, P/P_0, is equal to the square root of the ratio of the temperature of the reaction zone, T, to that of the gauge, T_0. In the present experiments, the pressures of halogens were in the intermediate region: 0.8—4.0 Pa for I_2 and 3—20 Pa for Br_2 and Cl_2. In other words, P should be between P_0 and $P_0(T/T_0)^{1/2}$. Therefore, at high temperatures and at low pressures, the error in the estimation of the pressures should be around 10 %. However, since the above error decreases with the increase in the pressure, the error in the estimation of the second-order rate constants as well as the Arrhenius parameters should be much smaller than this. Therefore, the rate constants were estimated with using P_0 without corrections.

The sources and purities of N_2, He, I_2, and Cl_2 were the same as those reported previously.[1,9] Br_2 was separated from its aqueous solution (Koso Chemical Co.) and used after repeated trap-to-trap distillation and drying with P_2O_5.

Results

Evaluation of the Arrhenius Parameters. Figure 1

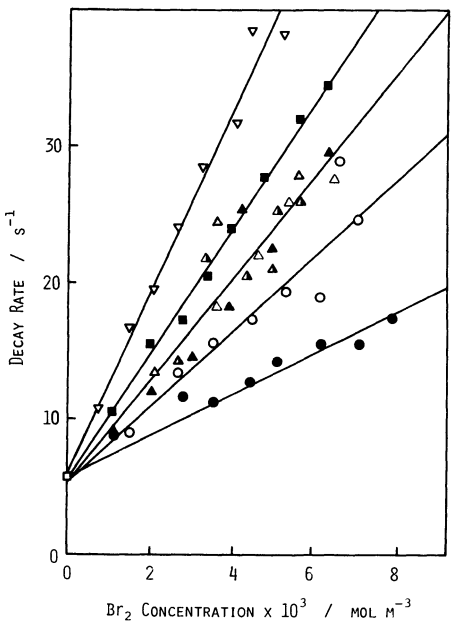

Fig. 1. The decay rate of N(⁴S) as a function of the Br_2 concentration. The temperatures and the total pressures are 410 K and 93 kPa(▽), 387 K and 93 kPa(■), 365 K and 93 kPa(▲), 365 K and 53 kPa(▲), 365 K and 133 kPa(△), 330 K and 93 kPa(○), and 293 K and 93 kPa(●). The symbol □ stands for the average of 24 runs measured in the absence of halogens.

illustrates the dependence of the pseudo-first-order decay rates of N(⁴S) on the Br_2 concentration at several temperatures. As has been observed for the N+I_2 reaction,[1] no total pressure dependence could be observed in this case, either. This suggests that termolecular processes are not important. Similar linear relationships could also be obtained for the cases of I_2 and Cl_2. The intercepts of such linear plots correspond to the decay in the absence of halogens. This value was found to be temperature-independent and to be 6.2± 1.7 s^{-1} (average of 24 runs). In a previous paper, we reported this value to be 3.2 s^{-1}.[1] This change is due to the difference in the reaction vessel. The decay of N(⁴S) in the system of pure nitrogen is considered to be the sum of the homogeneous and heterogeneous recombination of atomic nitrogen. The rate for the homogeneous loss is supposed to be independent of the size of the reaction vessel, while that for the heterogeneous loss may depend on the size. In the present work, we used a smaller vessel in order to obtain better temperature control; this may be the cause of the difference. It should be noted that the room temperature experiments with iodine showed that the slope of the plots was independent of the size of the reaction vessel.

From the slopes of the plots, such as are shown in Fig. 1, the rate constants could be obtained. In a previous paper, we proposed the following reaction scheme for the N_2+I_2 system in order to explain the nonlinear relationship between the decay rate of N(⁴S) and the I_2 pressure in the presence of ethene:[1]

Table 1. Rate Constants for the Reactions of N(⁴S) with Halogens

Reactant	T/K	$k\times10^{-4}$/m³ mol⁻¹ s⁻¹
I_2	410	6.28 ±0.45
	366	3.93 ±0.38
	325	2.95 ±0.17
	302	2.39 ±0.15[a]
	275	1.37 ±0.13
Br_2	410	0.330±0.010
	387	0.226±0.003
	365	0.182±0.010
	330	0.136±0.010
	293	0.070±0.003
Cl_2	411	0.105±0.013
	387	<0.07

a) Ref. 1.

$$N(^4S) + I_2 \longrightarrow NI(X^3\textstyle\sum^-) + I, \quad (1)$$

$$N + NI \longrightarrow N_2(\text{or } N_2^*) + I, \quad (2)$$

$$NI + I_2 \longrightarrow NI_2 + I, \quad (3)$$

$$N + NI_2 \longrightarrow \text{Products}, \quad (4)$$

If NI and NI_2 are not reactive with N(⁴S), the apparent decay rate of N(⁴S) should agree with that for Reaction 1. However, it seems unreasonable to assume that Reactions 2 and 4 are slow. Their rate constants should be of the same order as those for the N+OH, N+CN, and N+NH_2 reactions, which have been measured to be very fast.[10] If NI and NI_2 react with N(⁴S) rapidly, the apparent decay rate should be twice that for Reaction 1. As has been mentioned in a previous paper, the addition of ethyne and 1,3-butadiene, which have been considered to be reactive with NI, to the N_2+I_2 system has halved the apparent decay rate of N(⁴S). This strongly suggests that Reaction 1 is rate-determining and that the apparent decay rate of N(⁴S) in the N_2+I_2 system can be regarded as twice that for Reaction 1. It should also be pointed out that the concentrations of NI and NI_2 are considered to be much less than that of N(⁴S) and that such processes as NI+NI may be neglected. Similar reaction mechanisms may also be assumed for the cases of Br_2 and Cl_2. As for the system of N_2+Cl_2, a reaction similar to Reaction 3, NCl+Cl_2→NCl_2+Cl, has been proposed by Combourieu et al.[11] Table 1 summarizes the rate constants for the reactions of N(⁴S) with halogens calculated by the least squares method at various temperatures. The error limits are the standard deviations. As for Cl_2, the reaction rates were too small to be measured precisely below 387 K. All the data for I_2 and Br_2 are well characterized by Arrhenius equations; the Arrhenius plots are shown in Fig. 2, together with the results of Phillips and his co-workers.[7,8] The Arrhenius parameters, as determined by the weighted least-squares method,[12] are listed in Table 2.

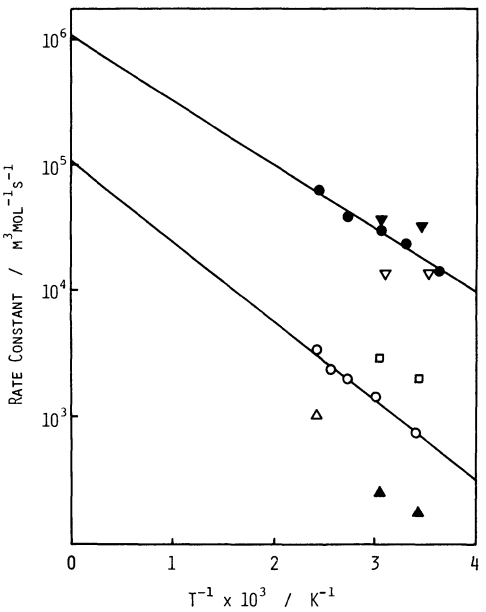

Fig. 2. Arrhenius plots for the reactions of N+I_2(●), N+Br_2(○), and N+Cl_2(△). Results reported by Phillips for N+I_2(▽), and by Grigor and Phillips for N+I_2(▼), N+Br_2(□), and N+Cl_2(▲) are also shown.[7,8]

Table 2. Arrhenius Parameters for the Reactions of N(⁴S) with I_2 and Br_2

Reactant	$A\times10^{-6}$/m³ mol⁻¹ s⁻¹	E_a/kJ mol⁻¹
I_2	1.08 ±0.26	9.7±0.6
Br_2	0.110±0.029	12.4±0.8

Semiempirical Calculations of the Preexponential Factors. The LEPS and BEBO calculations were performed. The general procedures for these calculations have been reviewed by Johnston.[13] In the LEPS calculation, Sato's empirical parameters were adjusted to give the experimental activation energies. The Morse parameters were evaluated from the molecular constants listed in the table of Huber and Herzberg, except for NI.[14] As for those of NI, since the molecular constants were not listed in that table, they were extrapolated from the NF/NCl/NBr series. For a given Sato parameter, the calculated activation energy was the lowest at the linear symmetric configuration in both cases. The force constants for the bending vibrations at the transition states were calculated to be in the order of 10^3 J mol⁻¹ rad⁻². As has been discussed by Mayer et al., the conventional transition state theory should not be used to calculate the rate constants when the bending force constant is less than 10^4 J mol⁻¹ rad⁻², because the amplitude of the vibration becomes too large.[15,16] Therefore, the rate constants were evaluated by the hard-sphere collision treatment.[15,16] From the Arrhenius plots of the calculated rate constants from 280 to 420 K, the preexponential factors were estimated to be 2.5×10^8 and 2.4×10^8 m³ mol⁻¹ s⁻¹ for the N+I_2 and N+Br_2 reactions respectively.

As for the BEBO calculation, many modifications of its original form have been presented.[16-21] Mayer et al. have demonstrated that the anti-Morse function for the repulsion potential must be modified for reactions which involve transfers of atoms other than hydrogen.[17] It has also been suggested that the anti-Morse function should be scaled in some cases.[16-18] In the present work, we not only employed the modification by Mayer et al., but also parametrized the factor of the anti-Morse function to give the experimentally obtained activation energy. The modification to change the Pauling constant, which has been proposed by Gilliom,[20] was also employed, but it was found to have little effect on the final results. The molecular constants of the noble gas clusters which originate from the recent crossed molecular beam-scattering experiments and which are recommended by Bérces and Dombi[22] were used for the calculation. The conventional transition-state theory with unit transmission coefficients was employed to evaluate the preexponential factors. The results are 6.0×10^7 m³ mol⁻¹ s⁻¹ in the cases of both N+I_2 and N+Br_2.

Both of the semiempirical calculations predict the presence of early potential barriers, loose transition states, and, consequently, fairly large preexponential factors for the reactions of N(⁴S) with halogens.

Discussion

Comparison with Literature Values. Figure 2 compares the present results with those of Phillips and his co-workers.[7,8] In Ref. 7, Phillips has mentioned that he performed the experiments on N+I_2 under conditions in which the homogeneous loss of NI is negligible and that the rate constant for Reaction 1 is 1.4×10^4 m³ mol⁻¹ s⁻¹ at room temperature. However, the rate constant cited from this paper by Grigor and Phillips (Ref. 8) is 3.3×10^4 m³ mol⁻¹ s⁻¹. We cannot judge which is more reliable. Therefore, both results are plotted in Fig. 2. At any rate, the present results are not greatly different from those of Phillips. Phillips estimated the activation energy for N+I_2 to be around 0.3 kJ mol⁻¹. This value is much smaller than the present one, and we think their temperature range, 283—323 K, is too small to estimate activation energies. As for Cl_2, the very small rate constants reported by Grigor and Phillips near room temperature are consistent with the present results if the activation energy is in the order of 10 kJ mol⁻¹. In this case, the preexponential factor for N+Cl_2 should be less than that for Br_2. The unreactiveness of N(⁴S) to Cl_2 has also been reported by Iannuzzi and Kaufman.[23] The rate constants for N+Br_2 obtained in the present work are much smaller than those reported by Grigor and Phillips. We have no idea of how to account for this discrepancy.

Comparison with the Semiempirically Calculated Values. As has been mentioned in the Results section, the agreement between the calculated and the observed

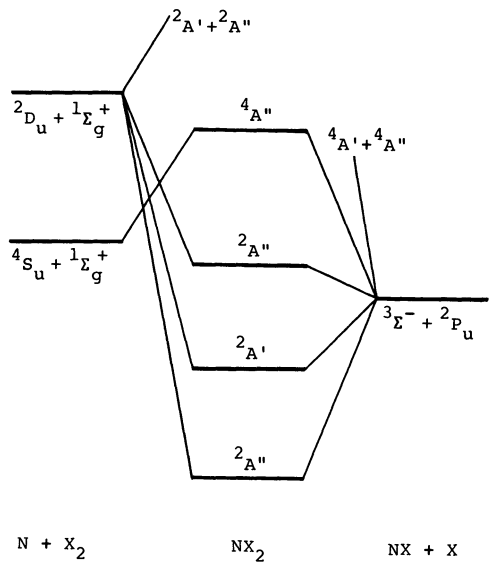

Fig. 3. Schematic correlation diagram connecting the states of N+X_2 and NX+X.

preexponential factors is very poor, especially for the N+Br_2 reaction. The experimental ones are two or three orders of magnitude smaller than the calculated ones. The LEPS method has originally been developed for the system of three hydrogen atoms.[24] Although the LEPS method has been applied to many systems, it is not necessarily accurate enough to evaluate the reaction rates, especially in the systems with p-electrons. The BEBO method has also been developed for the H-atom-transfer reactions. It is also questionable if the conventional transition-state theory is applicable.[25] However, the disagreement between the experimental and the calculated values seems beyond the uncertainty in the experiments or the calculations. In the next section, we would like to discuss the reason why.

Correlation between N+X_2 and NX+X. The reaction between N(^{4}S) and X_2 (X represents halogen atoms) presumably proceeds via a collision complex, N-X-X, in the C_s symmetry. Although the LEPS calculation suggests that the transition state is collinear, this should not be considered to be conclusive, for the LEPS calculation predicts that the geometry of the transition state for the reaction of N+O_2 is also linear, while the more reliable ab initio calculations suggest that it is bent.[26] As is shown in Table 38 of Ref. 27, the ground state and the first and the second excited states of NF_2 in C_{2v} symmetry are doublets. By analogy with the case of NH_2, the energy of the lowest quartet state should be fairly high.[28] This situation will not change in the case of C_s symmetry, or in the cases of the other nitrogen dihalides. On the other hand, the intermediate state which can be correlated with N(^{4}S)+X_2 is a quartet. Therefore, under the assumption of weak spin-orbit coupling, there must be a crossing between the quartet and the doublet surfaces. A schematic correlation diagram is shown in Fig. 3. In such a case, the activation energy for the adiabatic route is very high; the only path to the product state, NX+X, is the non-adiabatic one via a doublet surface, and the preexponential factor should be much smaller than the theoretical one. On the other hand, under the approximation of strong spin-orbit coupling, the level crossings which appear in Fig. 3 are avoided and the reaction can proceed adiabatically. In conclusion, the extremely small preexponential factors for the N+Br_2 and N+I_2 reactions can be explained by considering that the reactions are non-adiabatic, while the increase in the preexponential factor from Br_2 to I_2 may be accounted for in terms of the increase in the degree of the spin-orbit interaction. The preexponential factors for the N+Cl_2 and N+F_2 reactions should be even smaller. Now, we are trying to measure the reaction rates for the N+HI reaction, which is also expected to have a small preexponential factor.

References

1) H. Umemoto, S. Nakagawa, S. Tsunashima, and S. Sato, *Bull. Chem. Soc. Jpn.*, **59**, 1449 (1986).
2) J. V. Michael, *Chem. Phys. Lett.*, **76**, 129 (1980).
3) Y. Ishikawa, M. Yamabe, A. Noda, and S. Sato, *Bull. Chem. Soc. Jpn.*, **51**, 2488 (1978).
4) K. Sugawara, Y. Ishikawa, and S. Sato, *Bull. Chem. Soc. Jpn.*, **53**, 1344 (1980).
5) D. L. Baulch, R. A. Cox, R. F. Hampson, Jr., J. A. Kerr, J. Troe, and R. T. Watson, *J. Phys. Chem. Ref. Data*, **9**, 295 (1980); D. L. Baulch, R. A. Cox, P. J. Crutzen, R. F. Hampson, Jr., J. A. Kerr, J. Troe, and R. T. Watson, *ibid.*, **11**, 327 (1982); D. L. Baulch, R. A. Cox, R. F. Hampson, Jr., J. A. Kerr, J. Troe, and R.T. Watson, *ibid.*, **13**, 1259 (1984).
6) P. A. Hamilton, T. P. Murrells, *J. Chem. Soc., Faraday Trans. 2*, **81**, 1531 (1985).
7) L. F. Phillips, *Can. J. Chem.*, **43**, 369 (1965).
8) M. R. Grigor and L. F. Phillips, 11th Symp. Combust., Berkeley, California, U.S.A. 1966, 1171 (1967).
9) H. Umemoto, K. Sugiyama, S. Tsunashima, and S. Sato, *Bull. Chem. Soc. Jpn.*, **58**, 3076 (1985).
10) M. J. Howard and I. W. Smith, *J. Chem. Soc., Faraday Trans. 2*, **77**, 997 (1981); A. R. Whyte and L. F. Phillips, *Chem. Phys. Lett.*, **98**, 590 (1983); A. R. Whyte and L. F. Phillips, *ibid.*, **102**, 451 (1983).
11) J. Combourieu, G. Le Bras, G. Poulet, and J. L. Jourdain, 16th Symp. Combust., Cambridge, Massachusetts, U.S.A. 1976, 863 (1976).
12) R. J. Cvetanović, R. P. Overend, and G. Paraskevopoulos, *Int. J. Chem. Kinet.*, **S1**, 249 (1975); R. J. Cvetanović and D. L. Singleton, *ibid.*, **9**, 481 (1977); R. J. Cvetanović and D. L. Singleton, *ibid.*, **9**, 1007 (1977).
13) H. S. Johnston, "Gas Phase Reaction Rate Theory," The Ronald Press Co., New York (1966).
14) K. P. Huber and G. Herzberg, "Molecular Spectra and Molecular Structure IV, Constants of Diatomic Molecules," Van Nostrand Reinhold Co., New York (1979).
15) S. W. Mayer, L. Schieler, and H. S. Johnston, *J. Chem. Phys.*, **45**, 385 (1966).
16) S. W. Mayer and L. Schieler, *J. Phys. Chem.*, **72**, 236 (1968).
17) S. W. Mayer, L. Schieler, and H. S. Johnston, 11th

Symp. Combust., Berkeley, California, U.S.A. 1966, 837 (1967).
18) R.D.H. Brown and I.W.M. Smith, *Int. J. Chem. Kinet.*, **7**, 301 (1975).
19) D. L. Singleton and R. J. Cvetanović, *Can. J. Chem.*, **56**, 2934 (1978).
20) R. D. Gilliom, *J. Chem. Phys.*, **65**, 5027 (1976); *J. Am. Chem. Soc.*, **99**, 8399 (1977).
21) I. K. Dmitrieva, V. A. Zenevich, and G. I. Plindov, *Chem. Phys. Lett.*, **123**, 541 (1986).
22) T. Bérces and J. Dombi, *Int. J. Chem. Kinet.*, **12**, 183 (1980).
23) M. P. Iannuzzi and F. Kaufman, *J. Am. Chem. Soc.*, **101**, 4002 (1979).
24) S. Sato, *J. Chem. Phys.*, **23**, 592 (1955).
25) D. G. Truhlar, W. L. Hase, and J. T. Hynes, *J. Phys. Chem.*, **87**, 2664 (1983); D. G. Truhlar and B. C. Garrett, *Ann. Rev. Phys. Chem.*, **35**, 159 (1984).
26) P. A. Benioff, G. Das, and A. C. Wahl, *J. Chem. Phys.*, **67**, 2449 (1977); G. Das and P. A. Benioff, *Chem. Phys. Lett.*, **75**, 519 (1980).
27) G. Herzberg, "Molecular Spectra and Molecular Structure III, Electronic Spectra and Electronic Structure of Polyatomic Molecules," D. van Nostrand Co., Princeton (1967), p. 345.
28) S. D. Peyerimhoff and R. J. Buenker, *Can. J. Chem.*, **57**, 3182 (1979).

 © 1986 The Chemical Society of Japan Bull. Chem. Soc. Jpn., 59, 3761—3764 (1986)

Oxygen-17 NMR Study of the Uranyl Ion. III.[1] Factors Influencing ^{17}O Chemical Shifts of Uranyl Oxygens in Aqueous Perchlorate Media

Woo-Sik Jung, Hiroshi Tomiyasu, and Hiroshi Fukutomi*
Research Laboratory for Nuclear Reactors, Tokyo Institute of Technology, O-okayama, Meguro-ku, Tokyo 152
(Received May 29, 1986)

Effects of concentrations of perchlorate ion, nitrate ion, uranyl ion, and acid, isotopic substitutions, and temperature on ^{17}O chemical shifts of oxygen in the uranyl ion (uranyl oxygens hereafter) have been studied in aqueous perchlorate media. Insensitivity of the ^{17}O chemical shifts to $[ClO_4^-]$ leads to the conclusion that the perchlorate ion is not coordinated to the uranyl ion. The stability constant (0.10 ± 0.04 m^{-1} at 25 °C and ionic strength 5.0 m; m=mol kg^{-1}) of a $UO_2NO_3^+$ complex has been obtained from the dependence of the ^{17}O chemical shifts on $[NO_3^-]$. The ^{17}O resonances shift toward the lower field with increasing concentrations of uranyl ion and acid, indicating the possibilities of the dimer formation of the uranyl ion and the protonation of uranyl oxygen atoms in concentrated solution, respectively. Isotope shifts in ^{17}O nuclear magnetic shielding in the uranyl ion are interpreted in terms of the change of mean separation between the ground and lowest excited electronic states upon oxygen and uranium isotopic substitutions. Temperature dependence of ^{17}O chemical shifts is discussed in connection with the isotope effects.

The aqueous solution chemistry of a uranyl ion (UO_2^{2+}) is fundamental and important in understanding chemical and physical properties of the uranyl ion. In spite of many studies on the aqueous solution chemistry, there remain several unsolved problems in the uranyl ion in aqueous solution, e.g. whether or not a counter ion (perchlorate or nitrate ion) is coordinated to the uranyl ion, or whether uranyl oxygen atoms are chemically inert. ^{17}O chemical shifts of uranyl oxygens were reported to be sensitive to the base strength of ligands in the equatorial plane.[1] The ^{17}O chemical shifts were correlated with the reciprocal of the lowest electronic transition energies of uranyl complexes in nonaqueous solvents. ^{17}O NMR spectroscopy plays an important role in studying the uranyl ion because of the sensitivity of ^{17}O chemical shifts to chemical surroundings and the electronic structure of the uranyl ion. In order to pursue the above-mentioned problems in aqueous solution chemistry of the uranyl ion, we have investigated effects of concentrations of perchlorate ion, nitrate ion, uranyl ion, and acid on ^{17}O chemical shifts of uranyl oxygens in aqueous perchlorate solution.

The oxygen isotope effect on ^{17}O NMR spectra of uranyl oxygens reported in previous papers[1,2] will be interpreted on the basis of spectroscopic information which is currently available for the uranyl ion. Temperature dependence of ^{17}O chemical shifts of uranyl oxygens is measured and discussed in connection with the isotope effects in ^{17}O chemical shifts.

Experimental

The uranyl complex and acid used were uranyl perchlorate pentahydrate $UO_2(ClO_4)_2\cdot5H_2O$[2] and 60% perchloric acid (Wako Pure Chemical Ind., Ltd.), respectively. Sodium perchlorate(Wako) and sodium nitrate (Wako) were recrystallized twice from aqueous solution before use. The ionic strength was adjusted by using sodium perchlorate. Procedure for preparation of ^{17}O-enriched uranyl oxygens is described in the previous paper.[2] A 5 mm o.d. NMR sample tube was immersed in a 10 mm o.d. NMR tube containing $(CD_3)_2CO$ (Merck). Measurements of ^{17}O NMR spectra were carried out at 13.46 MHz on a JEOL JNM-FX 100 FT-NMR spectrometer equipped with a JNM-VT-3B temperature controller. Typical spectral settings for the measurements of ^{17}O NMR spectra are as follows: 8 K data points, 90° pulse angle corresponding to ca. 10 μs pulse width, 10 or 20 kHz spectral width (leading to 2.44 or 4.88 Hz digital resolution), and normally 2000 scans.

Results and Discussion

Effects of Concentrations of Perchlorate Ion, Nitrate Ion, Uranyl Ion, and Acid. Addition of $NaClO_4$ (up to 1.5 m) to the solution, where $[UO_2^{2+}]=0.02$ m and $[H^+]=0.06$ m, did not change ^{17}O chemical shifts of uranyl oxygens, while ^{17}O resonance of solvent H_2O shifted toward the higher field by the addition.[3] The former result indicates that the perchlorate ion is not coordinated to the uranyl ion in solution[4,5] as in the solid state.[6] In contrast to the result on the effect of the perchlorate ion, the addition of $NaNO_3$ to the solution, where $[UO_2^{2+}]=0.11$ m and $[H^+]=0.08$ m at ionic strength 5.0 m, increased ^{17}O chemical shifts of uranyl oxygens relative to $(CD_3)_2CO$ at 25 °C, as shown in Fig. 1. This result can be explained by the formation of a $UO_2NO_3^+$ complex:

$$UO_2^{2+} + NO_3^- \overset{K_1}{\rightleftharpoons} UO_2NO_3^+ \quad (1)$$

Assuming that $[NO_3^-]\gg[UO_2^{2+}]$ and the equilibrium reaction is very fast, the observed ^{17}O chemical shifts $\delta(^{17}O)_{obsd}$ is given by

$$\delta(^{17}O)_{obsd} = \delta(^{17}O) + \frac{\Delta\delta K_1[NO_3^-]}{1+K_1[NO_3^-]} \quad (2)$$

or

$$\frac{1}{\delta(^{17}O)_{obsd}-\delta(^{17}O)} = \frac{1}{\Delta\delta}\left(1+\frac{1}{K_1[NO_3^-]}\right), \quad (3)$$

where $\delta(^{17}O)$ is the ^{17}O chemical shift of the UO_2^{2+} ion and $\Delta\delta$ is the difference in ^{17}O chemical shift between UO_2^{2+} and $UO_2NO_3^+$ ions. The positive value of $\Delta\delta$ is

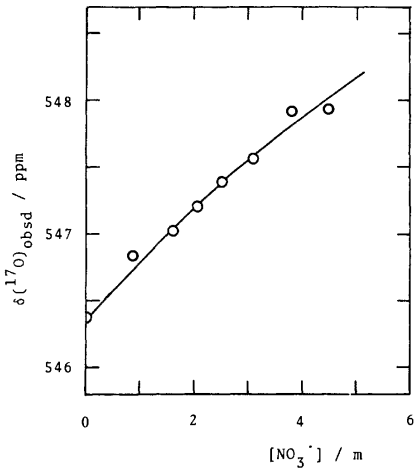

Fig. 1. Dependence of ^{17}O chemical shifts of uranyl oxygens on $[NO_3^-]$ at 25°C and ionic strength 5.0 m. $[UO_2^{2+}]$=0.11 m and $[H^+]$=0.08 m. The ^{17}O chemical shift is referred to external $(CD_3)_2CO$.

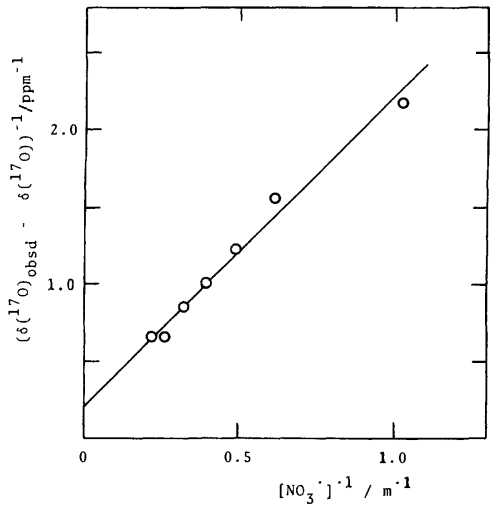

Fig. 2. A plot of $1/(\delta(^{17}O)_{obsd}-\delta(^{17}O))$ vs. $1/[NO_3^-]$ at 25°C and ionic strength 5.0 m. $[UO_2^{2+}]$=0.11 m and $[H^+]$=0.08 m.

expected from the bathochromic shift of electronic absorption bands by the complexation of NO_3^- ion.[1,7] Figure 2 shows a linear relationship between $1/(\delta(^{17}O)_{obsd}-\delta(^{17}O))$ and $[NO_3^-]^{-1}$, as expected from Eq. 3. The formation constant K_1 of (0.10±0.04) m^{-1} was calculated from the slope and intercept in Fig. 2. This value is comparable to the literature values: 0.15 M^{-1} (M=mol dm^{-3}) at ionic strength 6.25 M[4] and 0.21 M^{-1} at ionic strength 5.38 M.[8] The value of $\Delta\delta$ was determined to be (4.9±2.1) ppm at 25 °C.

The $\delta(^{17}O)$ values relative to $(CD_3)_2CO$ at 25 °C increased linearly with increasing concentration of the uranyl ion up to 1.5 m in acidic solution ($[H^+]$=0.06 m), i.e. $d\delta(^{17}O)/d[UO_2^{2+}]$=(0.57±0.11) ppm m^{-1}. This may suggest the possibility of the dimer formation of the uranyl ion

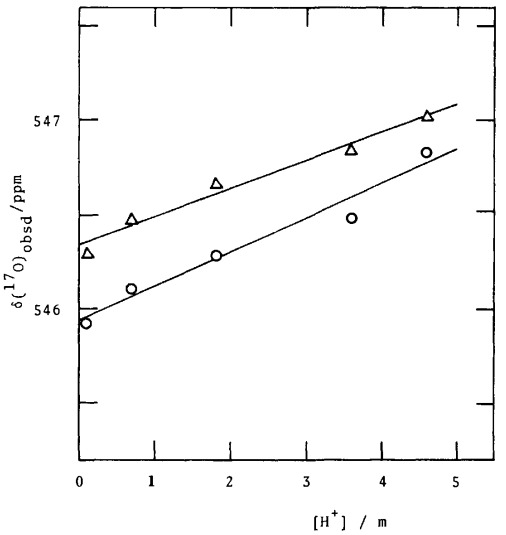

Fig. 3. Dependence of ^{17}O chemical shifts of uranyl oxygens on the acid concentration at 25(○) and 39(△)°C. $[UO_2^{2+}]$=0.1 m and ionic strength=5.0 m. The ^{17}O chemical shift is referred to external $(CD_3)_2CO$.

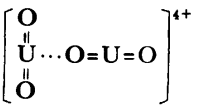

with increasing concentration of the uranyl ion. The coordination ability of uranyl oxygen atoms is well known for UO_2(β-diketonate)$_2$ complexes.[9] The fact that the hydration number of the uranyl ion decreases with lowering H_2O/UO_2^{2+} mole ratios may not be due to the inner-sphere coordination of ClO_4^- as indicated by Åberg et al.,[5] but be due to the dimer formation.

Figure 3 shows that ^{17}O chemical shifts of uranyl oxygens increase with increasing acid concentration. This can be explained by the following fast equilibrium reaction.[10,11]

$$UO_2^{2+} + H^+ \overset{K_2}{\rightleftharpoons} UO_2H^{3+} \quad (4)$$

Assuming that $K_2[H^+] \ll 1$, the observed ^{17}O chemical shift $\delta(^{17}O)_{obsd}$ is given by $\delta(^{17}O)+\{\delta'(^{17}O)-\delta(^{17}O)\}K_2[H^+]$, where $\delta'(^{17}O)$ and $\delta(^{17}O)$ are ^{17}O chemical shifts of uranyl oxygens in the protonated and unprotonated uranyl ion, respectively. Thus the slopes in Fig. 3 correspond to $\{\delta'(^{17}O)-\delta(^{17}O)\}K_2$, whose values are determined to be (0.18±0.02) and (0.15±0.02) ppm m^{-1} at 25 and 39 °C, respectively.

Isotope Shifts. We reported in the previous paper[1] that chemical shifts for the signals of $[^{17}O=U=^{17}O]^{2+}$ and $[^{18}O=U=^{17}O]^{2+}$ isotopomers were observed to be −0.059 and −0.117 ppm, respectively, relative to $[^{16}O=U=^{17}O]^{2+}$. To our knowledge, these isotope shifts are the first finding with respect to two-bond isotope shifts in ^{17}O NMR spectroscopy, and we have attempted to elucidate the origin of these shifts.

The nuclear magnetic shielding is the sum of diamagnetic (σ_d) and paramagnetic (σ_p) terms. The latter

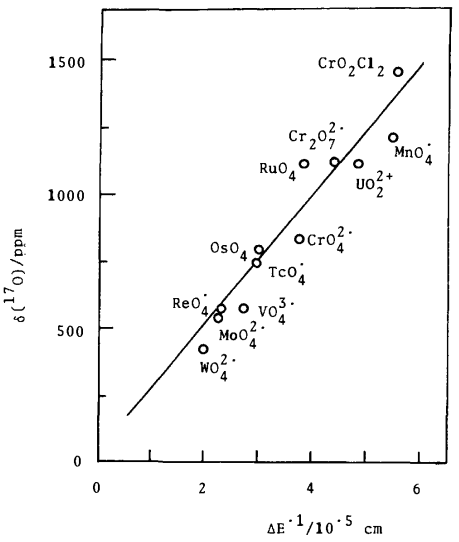

Fig. 4. A plot of ^{17}O chemical shifts vs. the reciprocal of the lowest electronic transition energies for compounds containing oxygen bonded to transition metals. ^{17}O chemical shifts are reported downfield from external water.

Table 1. Vibrational Frequencies (cm^{-1}) of Isotopomers of the $^{238}UO_2^{2+}$ Ion in Aqueous Solution

Isotopomer	ω_{01}	ω_{02}	ω_{03}
$[^{16}O=U=^{16}O]^{2+}$	881[a]	210[b]	963[c]
$[^{16}O=U=^{17}O]^{2+}$	868	207	950
$[^{17}O=U=^{17}O]^{2+}$	855	204	938
$[^{18}O=U=^{17}O]^{2+}$	843	202	926

a) Y. Tanaka, Y. Fujii, and M. Okamoto, *J. Phys. Chem.*, **86**, 1015 (1982). b) F. A. Hart and J. E. Newbery, *J. Inorg. Nucl. Chem.*, **30**, 318 (1968). c) Ref. 17

Table 2. Isotope Shifts in ^{17}O Nuclear Magnetic Shielding

Compound	Isotope shift/ppm	Ref.
$[^{17,18/16}O=U=^{17}O]^{2+}$	0.059, 0.117	1
$[^{16}O=^{235/238}U=^{17}O]^{2+}$	-2×10^{-3}	This work
$^{101/99}Ru^{16}O_3{}^{17}O$	0.02	23
$^{13/12}C^{17}O$	0.110	24
$^{16}O=^{13/12}C=^{17}O$	0.143	24
$D_2{}^{17}O/H_2{}^{17}O$[a]	3.08	25

a) In liquid phase.

term is proportional to the reciprocal of the mean transition energy (ΔE) between the ground and excited electronic states,[12] which is obtained by averaging over the vibrational levels of these states. Benedek et al.[13] investigated the dependence of ΔE upon the vibrational frequencies, ω_0 and ω_1, in the ground and excited states. In the temperature range studied ($\omega_{0j}>kT$), the vibronic dependence of the nuclear magnetic shielding for a single excited state can be expressed by

$$\sigma = \sigma_d + \sigma_p\left\{1 + \sum_{j=1}^{p}(4\Delta E_0)^{-1}\left[1-\left(\frac{\omega_{1j}}{\omega_{0j}}\right)^2\right]\omega_{0j}\right\}, \quad (5)$$

where ΔE_0 is the separation of the ground and excited electronic states at the zero vibrational levels, and the summation is carried out over the p normal vibration mode. Since the ratio ω_{1j}/ω_{0j} will not be affected by isotopic substitution, the two-bond oxygen-isotope shift ($\Delta\sigma_{x,y}$)[14] in ^{17}O nuclear shielding of uranyl oxygens ($(^2\Delta^{17}O(^{17,18/16}O))$[15] is given by

$$\Delta\sigma_{x,y} = \sigma_{x,y} - \sigma_{16,17} = \frac{B}{4(\Delta E)^2}\sum_{j=1}^{p}\left[1-\left(\frac{\omega_{1j}}{\omega_{0j}}\right)^2\right](\omega_{0j}^{x,y}-\omega_{0j}^{16,17}). \quad (6)$$

Parameter B (-2.50×10^7ppm cm) can be obtained from the slope in Fig. 4, which shows a linear relationship between the ^{17}O chemical shifts and the reciprocal of the lowest electronic transition energies for compound containing oxygen bonded to transition metals.[16] The ω_{1j}/ω_{0j} value can be taken as $(f_1/f_0)^{1/2}$, where f_0 (7.52 mdyne Å^{-1})[17] and f_1 (6.54 mdyne Å^{-1})[18] are force constants in the ground and lowest excited states, respectively. If three vibrations in the UO_2 unity are assumed to be harmonic and the force constants are unchanged by isotopic substitutions, the effect of isotopic substitutions on vibrational frequencies can be calculated theoretically.[19] The calculated vibrational frequencies in the ground states for various isotopomers are listed in Table 1. The values for a $[^{16}O=U=^{16}O]^{2+}$ isotopomer are those obtained experimentally for the uranyl ion in aqueous solution. The calculated $\Delta\sigma_{17,17}$ and $\Delta\sigma_{18,17}$ from Eq. 6 are 0.063 and 0.12 ppm, respectively, which agree surprisingly with the experimental results, when considered the assumptions involved in deriving Eq. 6 and estimating the parameters. The calculated difference (1.9 cm^{-1}) in the lowest electronic transition energies between $[^{16}O=U=^{17}O]^{2+}$ and $[^{18}O=U=^{17}O]^{2+}$ isotopomers for the hydrated uranyl ion is of the same order as that (5.0 cm^{-1}) obtained experimentally for $Cs_2UO_2Cl_4$.[20]

The one-bond uranium isotope shift in ^{17}O nuclear shielding ($(^1\Delta^{17}O(^{235/238}U))$,[15] which is defined by $\sigma([^{16}O=^{235}U=^{17}O]^{2+})-\sigma([^{16}O=^{238}U=^{17}O]^{2+})$, can be estimated in a similar way. The estimated isotope shift of -2×10^{-3} ppm is too small compared with the linewidth (ca. 1 Hz) of ^{17}O resonance of uranyl oxygens. This might make it difficult to observe the uranium isotope effect in the ^{17}O NMR spectrum. It is noted that no uranium isotope effect was observed in ^{19}F nuclear shielding for UF_6.[21] Isotope shifts in ^{17}O nuclear shieldings so far reported are summarized in Table 2, which shows that the isotope shift becomes larger with increasing fractional change in mass upon isotopic substitution.[22]

Temperature Dependence. We investigated the temperature dependence of ^{17}O chemical shift of uranyl oxygens and the results are shown in Fig. 5. The ^{17}O resonances of the uranyl oxygens shift toward the lower field with increasing temperature ((0.087 ± 0.002) ppm $°C^{-1}$), whereas the ^{17}O resonances of solvent H_2O

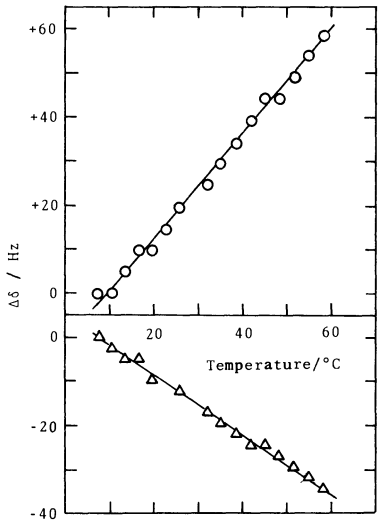

Fig. 5. Temperature dependence of ^{17}O resonances of uranyl oxygens (O) and solvent H_2O (△). The positive sign means the shift to the lower field. $[UO_2^{2+}]$=0.32 M and $[H^+]$=0.01 M.

shift toward the higher field with temperature ((−0.050±0.001) ppm °C^{-1}). The latter is due to the increasing fraction of broken hydrogen bonds with temperature.[3] The former result is in accord with that for temperature dependence of magnetic susceptibility, i.e. the uranyl ion becomes more paramagnetic as the temperature increases.[26] Bell and Biggers[27] resolved the overlapping bands in the absorption spectrum of the uranyl ion in aqueous solution and studied the temperature dependence of position of each band. They showed that the positions of all the bands shift linearly toward the red with increasing temperature. This result consists with that for the temperature dependence of ^{17}O chemical shifts in view of the fact that ^{17}O chemical shifts of uranyl oxygens for uranyl complexes in nonaqueous solvents increase as absorption bands of the complexes shift toward the red.[1]

Changes in ^{17}O nuclear shielding of uranyl oxygens with temperature can arise from the following effects: (1) variation of effective separation between the ground and excited states because of thermal statistical occupancy of the ground vibrational levels[13]; (2) thermal expansion of U=O bond length with increasing temperature, where the energy separation between the ground and excited states is calculated to increase with decreasing U=O bond length.[28]

Effects of temperature and isotopic substitutions on ^{17}O nuclear shielding of uranyl oxygens may be also explained by using Jameson's model,[29] where the nuclear shielding is considered as an electronic property which depends on the relative positions of nuclei. The heavier isotopomer has smaller amplitude of motion than a lighter one on the same potential surface, while the average amplitude of vibrational motion increases with temperature. Thus the average U=O bond length is expected to vary with isotopic substitution and temperatue, resulting in the change in ^{17}O nuclear shielding.

References

1) Part II: W.-S. Jung, H. Tomiyasu, and H. Fukutomi, *Bull. Chem. Soc. Jpn.*, **58**, 938 (1985).
2) W.-S. Jung. Y. Ikeda, H. Tomiyasu, and H. Fukutomi, *Bull. Chem. Soc. Jpn.*, **57**, 2317 (1984).
3) Z. Luz and G. Yagil, *J. Phys. Chem.*, **70**, 554 (1966).
4) M. H. Brooker, C. -H. Huang, and J. Sylwestrowitz, *J. Inorg. Nucl. Chem.*, **42**, 1431 (1980).
5) M. Åberg, D. Ferri, J. Glaser, and I. Grenthe, *Inorg. Chem.*, **22**, 3986 (1983).
6) N. W. Alock and S. Esperås, *J. Chem. Soc., Dalton Trans.*, **1977**, 893.
7) M. D. Marcantonatos, M. Deschaux, and F. Celardin, *Chem. Phys. Lett.*, **69**, 144 (1980).
8) R. H. Betts and R. K. Michels, *J. Chem. Soc. Suppl.*, **1949**, S286.
9) A. Ekstrom, H. J. Hurst, C. H. Randall, and H. Loeh, *J. Phys. Chem.*, **84**, 2626 (1980); B. V. Sidroenko, R. B. Dushin, E. K. Legin, and D. N. Suglobov, *Radiokhimiya*, **24**, 75 (1982); J. C. Taylor, A. Ekstrom, and C. H. Randall, *Inorg. Chem.*, **17**, 3285 (1978).
10) S. Sakuraba and R. Matsushima, *Bull. Chem. Soc. Jpn.*, **44**, 2915 (1971).
11) A. A. Nemodruk, *Radiokhimiya*, **14**, 843 (1972).
12) N. F. Ramsey, *Phys. Rev.*, **78**, 699 (1950).
13) G. B. Benedek, R. Englman, and J. A. Armstrong, *J. Chem. Phys.*, **39**, 3349 (1963).
14) Notations $\sigma_{x,y}$ and $\omega^{x,y}$ refer to the values for a $[^xO=U=^yO]^{2+}$ isotopomer.
15) Gombler's notation: W. Gombler, *J. Am. Chem. Soc.*, **104**, 6616 (1982).
16) B. N. Figgis, R. G. Kidd, and R. S. Nyholm, *Proc. R. Soc. London, Ser. A*, **269**, 469 (1962).
17) W.-S. Jung, H. Tomiyasu, H, Fukutomi, and J.-S. Kim, *Bull. Korean Chem. Soc.*, **6**, 318 (1985).
18) S. De Jaegere and C. Görller-Walrand, *Spectrochim. Acta*, **25A**, 559 (1969).
19) G. Herzberg, "Molecular Spectra and Molecular Structure," Vol. II, D. Van Nostrand, Princeton (1945), p. 228.
20) J. R. G. Thorne, R. G. Denning, T. J. Barker, and D. I. Grimley, *J. Lumin.*, **34**, 147 (1985).
21) K. Sepplet and N. Barlett, *Z. Anorg. Allg. Chem.*, **436**, 122 (1977).
22) H. Batiz-Hernandez and R. A. Bernheim, *Prog. Nucl. Magn. Reson. Spectrosc.*, **3**, 63 (1967).
23) C. Brevard and P. Granger, *J. Chem. Phys.*, **75**, 4175 (1981).
24) R. E. Wasylishen, J. O. Friedrich, S. Mooibroek, and J. B. Macdonald, *J. Chem. Phys.*, **83**, 548 (1985).
25) O. Lutz and H. Oehler, *Z. Naturforsch., A*, **32a**, 131 (1977).
26) S. Freed and C. Kasper, *J. Am. Chem. Soc.*, **52**, 4671 (1950).
27) J. T. Bell and R. E. Biggers, *J. Mol. Spectrosc.*, **187**, 247 (1965).
28) M. Boring, J. H. Wood, and J. W. Moskowitz, *J. Chem. Phys.*, **63**, 638 (1975).
29) C. J. Jameson, *J. Chem. Phys.*, **66**, 4983 (1977); C. J. Jameson, *Bull. Magn. Reson.*, **3**, 3 (1980).

The Dynamical Structure of Normal Alcohols in Their Liquids as Determined by the Viscosity and Self-Diffusion Measurements

Makio Iwahashi,* Yoko Ohbu, Tadashi Kato,† Yumi Suzuki, Kazuhiro Yamauchi, Yoshimi Yamaguchi, and Mitsuo Muramatsu

Department of Chemistry, Faculty of Hygienic Sciences, Kitasato University, Sagamihara, Kanagawa 228
†Department of Chemistry, Faculty of Science, Tokyo Metropolitan University, Setagaya-ku, Tokyo 158

(Received June 4, 1986)

The conformation of molecules of normal alcohols in their pure liquids is estimated through an analysis of their self-diffusion coefficients, viscosities, and molar volumes. The conformation of molecules of shorter chained alcohols (C_1-C_3) is approximately of sphere, while that for longer chains is of rodlike shape. In pure liquids of alcohols, rigid rod molecules whose free rotating motions along their rod axes seem to be restricted, are randomly orientated and entangled with one another. The self-diffusion of long-chain alcohols involves a longitudinal translation of rodlike molecules. Large apparent hydrodynamic radii suggest that the transport unit of normal alcohol is a dimer (on an average) of alcohol molecules.

A linear macromolecule in its solution is known to have many conformations such as a rod and a flexibly coiled shape[1] owing to interaction between solute and solvent molecules. However, the conformation of a small alcohol molecule in pure liquid state has scarcely been investigated probably because of theoretical and experimental difficulties. The present study has thus been made for estimating the rigidity and conformation of molecules of normal alcohol homologs (C_1—C_8) by use of data from viscosity, self-diffusion, and density experiments at 298 K.

Experimental

Materials. Purest grade samples (>99%) of methanol, ethanol, 1-propanol, 1-butanol, 1-pentanol, 1-hexanol, 1-heptanol, and 1-octanol, from Wako Pure Chemical Industries, Ltd., were used without further purification. The water used was triply distilled one. Deuterium oxide (99.75%) from E. Merck AG was used without further purification.

Viscosity. The viscosity of alcohol was measured with two Ostwald capillary viscometers (characterized by times 1 and 3 min required for a given volume of water to flow through their capillaries) in a thermostat with an accuracy of ±0.2 K. Pure water (0.8902 mPa s at 298.15 K)[2] was used for calibrating the viscosity.

Self-Diffusion Coefficient. The self-diffusion coefficient of alcohol was obtained by the pulsed-gradient FT-NMR method.[3,4,5] All measurements were made on protons at 99.6 MHz, with internal D_2O lock, at an ambient temperature of 298±0.5 K on a JEOL FX-100 Fourier transform NMR spectrometer.** A spin echo was produced by a 90°—τ—180° pulse. The gradient was turned on before and after a 180° pulse. The magnitude of gradient, G, can be varied from 0 to about 0.5 T m^{-1}. The absolute magnitude of G was calibrated against the value of the diffusion coefficient of pure water at 298.15 K, 2.30×10^{-9} m^2 s^{-1}.[6]

The diffusional attenuation of a signal for the component i, at the time of echo, is given by[7]

$$\ln\frac{M(G)}{M(0)} = -\gamma^2G^2D_i\delta^2(\Delta-\delta/3), \quad (1)$$

where $M(G)/M(0)$ is the ratio of the echo amplitude in the presence of the gradient to that in its absence, γ the gyromagnetic ratio (2.675×10^{-8} T^{-1} s^{-1} for ^{1}H), δ the duration of each gradient pulse, and Δ the time between two gradient pulses. In our experiments, G was about 0.087 T m^{-1}. The value of Δ was kept constant at 50 ms and δ was varied from 4 to 12 ms. Each sample was placed in a 1 mm-dia. tube inserted in a 5 mm-dia. tube containing D_2O (for NMR lock) for avoiding the saturation of signal. All spectra were obtained with a high signal-to-noise ratio by one pulse sequence. Self-diffusion coefficients were obtained from gradients of ln $M(G)/M(0)$ vs. $\delta^2(\Delta-\delta/3)$ plots.

Molar Volume. Molar volumes for normal alcohols were obtained from their densities.[8] Theoretical molar volumes were calculated by use of the CPK molecular model[9] and by assuming a hexagonal close-packed structure of rods rotating along the axis or pilelike packing of rectangular solids for longer chain alcohols (C_4—C_8) and a face-centered cubic packed structure of spheres for shorter ones (C_1—C_3).

Results and Discussion

Table 1 summarizes values of molar weight, density,[8] viscosity, and self-diffusion coefficient for normal alcohol homologs.

For a moving spherical particle almost equal in size to surrounding solvent molecules under the slip boundary condition, Stokes' equation for frictional coefficient,[5,10,11] f, is given by

$$f = 4\pi\eta a, \quad (2)$$

where π is the ratio of the circular constants, η the viscosity of the solvent, and a the radius of the spherical particle.

Let us apply this equation to a flow of a pure normal alcohol. By assuming a hypothetical sphere with an equivalent radius a_0 for a linear alcohol molecule, the a_0 is expressed as

$$a_0 = \left[\frac{3M}{4\pi\rho N}\right]^{1/3}, \quad (3)$$

where M is the molar weight of the alcohol, ρ the density of the alcohol at 298.15 K, and N the Avogadro number. By substituting a_0 in Eq. 3 for a in Eq. 2, the

**PGNMR measurements were carried out at the Instrument Center of Institute for Molecular Science.

Table 1. Molar Weight (M), Density (ρ), Viscosity (η), and Self-diffusion Coefficient (D) for Normal Alcohol Homologs

	$M/10^{-3}$ kg	$\rho/10^{-9}$ kg m^{-3}	$\eta/10^{-3}$ N sm^{-2}	$D/10^{-10}$ m^2 s^{-1}
Methanol	32.04	0.78664[8]	0.5573 0.5445[8]	23.2[18]
Ethanol	46.07	0.78504[8]	1.056 1.078[8]	10.1[18]
1-Propanol	60.10	0.79975[8]	1.887	5.52[19]
1-Butanol	74.12	0.8060[8]	2.479	4.16 4.26[19]
1-Pentanol	88.15	0.8115[8]	3.519 3.347[8]	2.96
1-Hexanol	102.18	0.8159[8]	4.551 4.592[8]	2.18
1-Heptanol	116.21	0.8189[8]	5.897	1.72
1-Octanol	130.23	0.8221[8]	7.450	1.42 1.38[19]

frictional coefficient, f_0, for the hypothetical sphere is given by

$$f_0 = 4\pi\eta\left[\frac{3M}{4\pi\rho N}\right]^{1/3}. \quad (4)$$

On the other hand, from Einstein's equation for diffusion, the frictional coefficient is expressed by

$$f = kT/D, \quad (5)$$

where k is the Boltzmann constant, T the absolute temperature, and D the diffusion coefficient.

Combining Eqs. 4 and 5, we obtain

$$f/f_0 = kT/[4\pi\eta D(3M/4\pi\rho N)^{1/3}]. \quad (6)$$

The ratio f/f_0 should be unity when the actual molecule is a sphere. For most rod-shaped or prolate macromolecules including proteins in an organic solvent or in an aqueous solution, the frictional ratio is in general greater than unity.[12]

Figure 1 shows a plot of the ratio against the number of carbon atoms for normal alcohols. The ratios for the short-chained alcohols (C_1—C_3) are almost unity, while, for those with longer chains, they decrease with increasing hydrocarbon chain. This suggests that the molecule of a short-chain alcohol (C_1—C_3) can be regarded as a sphere and that a molecule with a longer chain is deformed more from a spherical shape.

Let us estimate the shape of a long-chained molecule in its pure liquid. By combining Eqs. 2 and 5, the apparent hydrodynamic radius, a, is given by

$$a = kT/(4\pi\eta D). \quad (7)$$

This is the Stokes-Einstein formula under the slip boundary condition.[5,10,11]

In Fig. 2, the Stokes-Einstein radii, a, of the normal alcohols (open circles) are plotted against the hydrocarbon chainlengths, together with the hypothetical radii (filled ones) obtained by substituting the value of the density of normal alcohol into Eq. 3. The latter radii increase monotonously with increase in the chain-length, whereas the former increase up to 1-propanol and saturate at 1-butanol giving a constant value of ca. 3.2×10^{-10} m., which suggests a sphere for the molecules of the short-chained alcohols and a rod with a

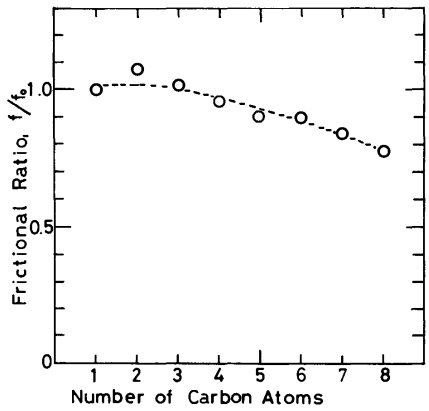

Fig. 1. Frictional ratio, f/f_0, of n-alcohol against the number of carbon atoms at 298.15 K.

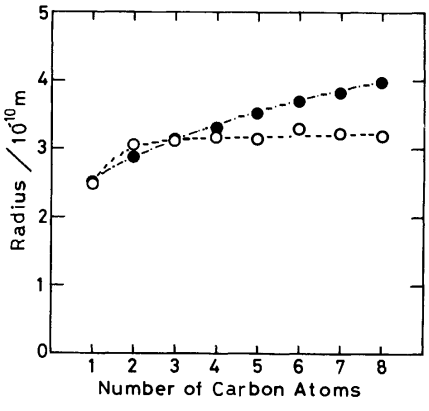

Fig. 2. Molecular radius of normal alcohol against the number of carbon atoms at 298.15 K. Open circles indicate the apparent hydrodynamic radius (the Stokes-Einstein radius), while filled ones were obtained from the density of the normal alcohol according to Eq. 3.

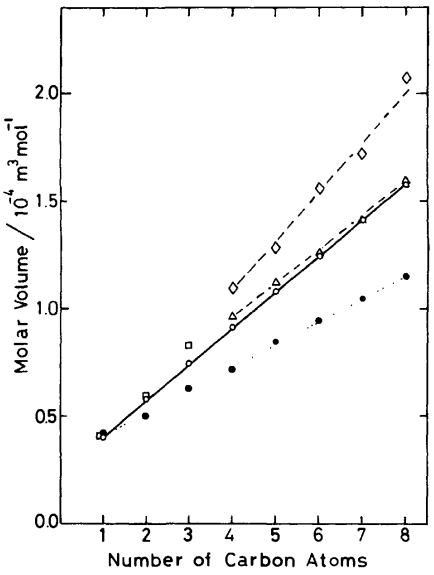

Fig. 3. Effects of the number of carbon atoms in the normal alcohol molecule upon the molar volumes based on the density data,[8] O, and on the CPK model with assumptions of the hexagonal close packing of the rotating rods with a radius of 3.2×10^{-10} m, ◇, the hexagonal close-packing of the rotating rods with a radius of 2.4×10^{-10} m, △, the face-centered cubic packing of the sphere with radii of 2.4×10^{-10} m (methanol), 2.63×10^{-10} m (ethanol) and 2.96×10^{-10} m (1-propanol), □, and the pile-like packing of rectangular rods with a corss sectional area of $3.6\times4.0\times10^{-20}$ m^2, ●.

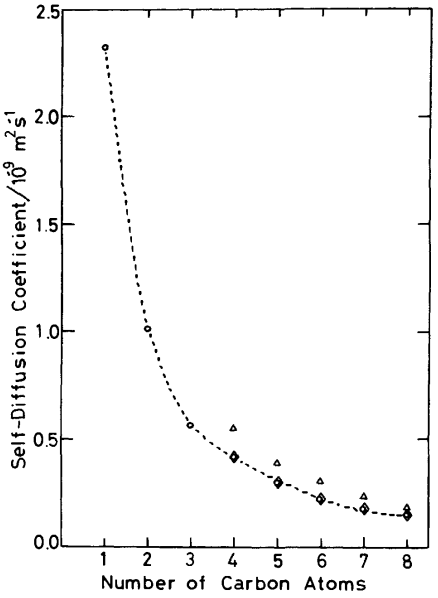

Fig. 4. Self-diffusion coefficient of normal alcohol against the number of carbon atoms at 298.15 K. O, experimental results; △ and ◇, calculated by Eq. 7 using the hydrodynamic radii of 2.4×10^{-10} m, and 3.2×10^{-10} m, respectively.

constant crosssection for the alcohol molecules having longer hydrocarbon chains than 1-butanol.

In order to confirm the validity of the value 3.2×10^{-10} m, which is larger than expected for the crosssection of a hydrocarbon chain in its solid state,[13] the experimental molar volumes based on the density data[8] for the normal alcohols were compared with those based on the CPK molecular model.[9] In Fig. 3 are shown effects of the number of carbon atoms in the normal alcohol molecules on the molar volumes based on various calculations. The sphere molecule model (open rectangles) for the short-chained alcohols, except 1-propanol, gives a molar volume almost equal to that based on the density data[8] (open circles). The molecules of methanol and ethanol can therefore be perfectly spherical in their shape, while the 1-propanol molecule deviates more or less from the spherical shape. For the alcohols having longer carbon chains than 1-propanol, the molar volume values (open circles) are always larger than those based on the pilelike packed model (filled circles) with a value of $3.6\times4.0\times10^{-20}$ m^2*** for the crosssectional area of a rectangular rod, and also too small to be compared with those based on the hexagonal close-packed model (open diamonds) with a value of 3.2×10^{-10} m for the radius of the helically coiled hydrocarbon chain. For the rotating rods whose radii are commonly 2.4×10^{-10} m (a half of the diagonal length for the above rectangular rod), the calculated values (open triangles) are almost comparable with those based on the density data.

If, however, the pure liquid of the normal alcohol consists of the above rotating rods orientated in the hexagonal close-packed structure, optical anisotropy should be observed for the pure liquid of the normal alcohol as if it were a liquid crystal. However, no optical anisotropies such as streaming birefringence have ever been observed for pure liquids of short-chained normal alcohols. The alcohol molecules would therefore be randomly orientated and the free rotating motion along the rodaxis should be restricted, which conditions are in support of the experimental molar volumes. The gradual decrease in the self-diffusion coefficients (open circles in Fig. 4) from 1-butanol to 1-octanol may support the above argument; the straight rodlike molecules entangle with one another and the rotational (end-over-end), as well as transverse,[14] motion of each rod may be severely restricted. The self-diffusion of the long-chained alcohols, therefore, must involve the longitudinal rather than transverse motion of the rodlike molecules.[14]

In Fig. 4 are compared the experimental values of self-diffusion coefficient with the theoretical ones calculated by Eq. 7 with a value of 2.4×10^{-10} m (open triangles) or 3.2×10^{-10} m (open diamonds) for the hydrodynamic radius a. The open diamonds agree exactly with the experimental values. The value of the

***The theoretical cross section of hydrocarbon chain in solid state was obtained by use of the CPK molecular model. The value is in fair agreement with the reference value by X-ray diffraction measurement.[13]

radius (3.2×10^{-10} m), however, does not satisfy the molar volume based on the density data as mentioned above. This discrepancy may be reconciled in terms of dimerization of alcohol molecules through hydrogen bonding of their hydroxyl groups.[15,16] Consequently, the self-diffusion coefficient of such a dimer becomes inversely proportional to the root of the mass for two molecules of monomeric alcohol, when one assumes a hard sphere model[12,17] for the self-diffusion of the alcoholic systems. Thus the hypothetical value of the self-diffusion coefficient for the monomer alcohol gives 2.25×10^{-10} m as the apparent hydrodynamic radius, which seems reasonable for the cross-section of hydrocarbon chain.[13] The values of the apparent hydrodynamic radii of methanol, ethanol, and 1-propanol have been similarly calculated as 1.77×10^{-10}, 2.15×10^{-10}, and 2.20×10^{-10} m, respectively. The significantly small value of methanol results from the extremely large value of its experimental self-diffusion coefficient as compared with those of the other alcohols (see Fig. 4); dimers of methanol molecules seem to be too short to entangle with one another and can translate not only longitudinally but also transversely.

References

1) K. E. Van Holde, "Physical Biochemistry," Prentice-Hall, Inc., New Jersey (1971), p. 33.
2) "Kagaku Binran," Maruzen Co., Ltd., Tokyo (1984), Vol. 2, p. 42.
3) J. Kida and H. Uedaira, *J. Magn. Reson.*, **27**, 253 (1977).
4) P. Stilbs and M. E. Moseley, *Chem. Ser.*, **15**, 176 (1980).
5) T. Kato, *J. Phys. Chem.*, **89**, 5750 (1985).
6) R. Mills, *J. Phys. Chem.*, **69**, 3116 (1965).
7) E. O. Stejskal and J. E. Tanner, *J. Chem. Phys.*, **42**, 288 (1965).
8) J. A. Riddick and W. B. Bunger, "Organic Solvents," Wiley-Interscience, New York (1970).
9) "Jikken Kagaku Guide Book," Maruzen Co., Ltd., Tokyo (1984), p. 902.
10) F. Perrin, *J. Phys., Radium*, **5**, 497 (1934).
11) W. Steel, "Transport Phenomena in Fluids," ed by H. J. M. Hanley, Marcel Dekker, New York (1969), p. 230.
12) C. Tanford, "Physical Chemistry of Macromolecules," John Wiley & Sons, Inc., New York (1961), pp. 358, 359, 361.
13) A. W. Ralston, "Fatty Acids and Their Derivatives," John Wiley & Sons, Inc., New York (1948), p. 330.
14) M. Doi and S. F. Edwards, *J. Chem. Soc., Faraday Trans. 2*, **74**, 560 (1978).
15) U. Liddel and E. D. Becker, *Spectro. Acta*, **10**, 70 (1959); W. C. Coburn, Jr. and E. Grunwald, *J. Am. Chem. Soc.*, **80**, 1318 (1958).
16) G. Paschina and G. Piccaluga, *J. Chem. Phys.* **77**, 2051 (1982).
17) H. Yamakawa, "Modern Theory of Polymer Solution," Harper & Row Publisher, New York (1971), p. 252.
18) R. E. Rathbun and A. L. Babb, *J. Phys. Chem.*, **65**, 1072 (1961).
19) D. W. McCall and D. C. Douglass, *J. Chem. Phys.*, **32**, 1876 (1960).

 © 1986 The Chemical Society of Japan Bull. Chem. Soc. Jpn., 59, 3775—3779 (1986)

The Epitaxial Growth of the Methyl Triacontanoate Crystal

Yasukiyo UEDA
Department of Industrial Chemistry, Faculty of Engineering, Kobe University, Rokko, Nada, Kobe 657
(Received June 4, 1986)

Methyl triacontanoate (MT) was deposited on the cleavage face of the KCl crystal in vacuo. The MT film was composed of V-shaped crystals growing along two directions crossing at 32°, and these crystals intersected at right angles to each other. The bisectional direction of the V-shaped crystals corresponds to the [110] direction of the substrate crystal. The electron-diffraction pattern from the film consisted of the reflection spots corresponding to the $(hkl)_s$ planes of the subcell and the series of $00l$ reflections in the small-angle region. The crystal structure of the deposited MT crystal was monoclinic in form. The (110) plane of the MT crystal was oriented parallel to the substrate (001) plane, and its c-axis was parallel to the [110] direction of the substrate crystal. The V-shaped crystal was explained by the molecular arrangement in the epitaxial growing crystals. When the substrate was kept at a higher temperature than the melting point of MT, the deposit coagulated to disk-like crystals whose c-axis was perpendicular to the substrate.

Recently organic thin films have attracted a good deal of attention for use in new systems which enable one to draw out various functions by the design of the molecular construction and various combinations. Their electronic, photoelectronic, and optical properties can be expected to improve those of metals and inorganic compounds. These properties are probably controlled by the molecular arrangement in the films. The techniques for preparing organic films can be divided into two types of processes: dry and wet. The Langmuir-Blodgett (L-B) method has been well developed as a wet process, and the properties of L-B films have been reported by many workers.[1] However, the L-B method can be applied only to amphiphilic molecules. In the case of vacuum-evaporation as a dry process, on the contrary, there have been many reports on the structures and nucleation mechanisms of metals and inorganic compounds, but few reports on those of organic compounds.[2-5]

Ashida and his co-workers have studied the epitaxial growth from the vapor phase of polycyclic aromatic[6-8] and linear molecules, such as paraffins,[9] polyethylene[10] and polypropylene.[11] Paraffin molecules took two orientations on the cleavage surface of alkali halide, depending on the evaporation conditions. The films deposited on the cleavage face of alkali halide crystals kept at room temperature were found to be composed of raft-like crystallites. The (110) plane of these crystals was oriented parallel to the substrate (001) plane, and their fiber axes were parallel to the [110] direction of the substrate crystal. When paraffins were deposited on the substrate kept at temperatures near or above their melting points, the films were composed of discrete disk-like crystals and their fiber axes were oriented perpendicular to the substrate. The linear polymers, such as polyethylene and polypropylene, were decomposed thermally to compounds of a low molecular weight during the evaporation process; these compounds also took an orientation similar to that of the paraffin crystals. The crystals composed of linear molecules probably exhibit a distinguished anisotropy of electrical and mechanical properties as a result of interaction between long-chain molecules. It is well-known that these crystals exhibit polymorphs depending on the crystallization temperature. It is interesting to investigate the effect of end group on the morphology and orientation of linear molecular crystals. In this work, the epitaxial overgrowth of methyl triacontanoate (MT) film evaporated on the potassium chloride (001) surface was studied by using an electron micrograph and electron diffraction.

Experimental

MT ($C_{29}H_{59}COOCH_3$, mp, 71.0 °C) was obtained from the Tokyo Chemical Industry Co., Ltd.. The purity of the MT was 99.5%. The single crystal of potassium chloride used as the substrate was cleaved in air and immediately placed in the evaporation chamber. After the substrate had been baked out at 200 °C for one hour in 1.33×10^{-3} Pa, the MT was evaporated vertically from a quartz crucible heated with a tungsten coil onto the substrate surface, which was kept at a temperature between 20 and 90 °C. The average thickness of the deposited film, monitored by means of a quartz crystal microbalance, was 100 nm. The specimen used for electron microscopy was prepared by the dissolution of the substrate in water after the film had been reinforced with evaporated carbon film. The orientation of the deposited crystal related to the substrate crystal was determined by shadowcasting the chromium metal along the [100] direction of the substrate crystal. Thallium(I) chloride prepared by evaporation was used as a standard calibration material for the spacing measurements.

Results and Discussion

The features and orientation of the deposited crystallites depend on the evaporation conditions. The crystalline size increases generally with an elevation of the substrate temperature, whereas the crystal shape and the molecular orientation have a close relation to the substrate treatment, mainly the bake-out procedure of the substrate. When MT was evaporated onto a cleavage surface of potassium chloride without heat treatment, the film was composed of randomly-oriented granules about 100 nm in diameter. When, on the other hand, the substrate was heated at 200 °C

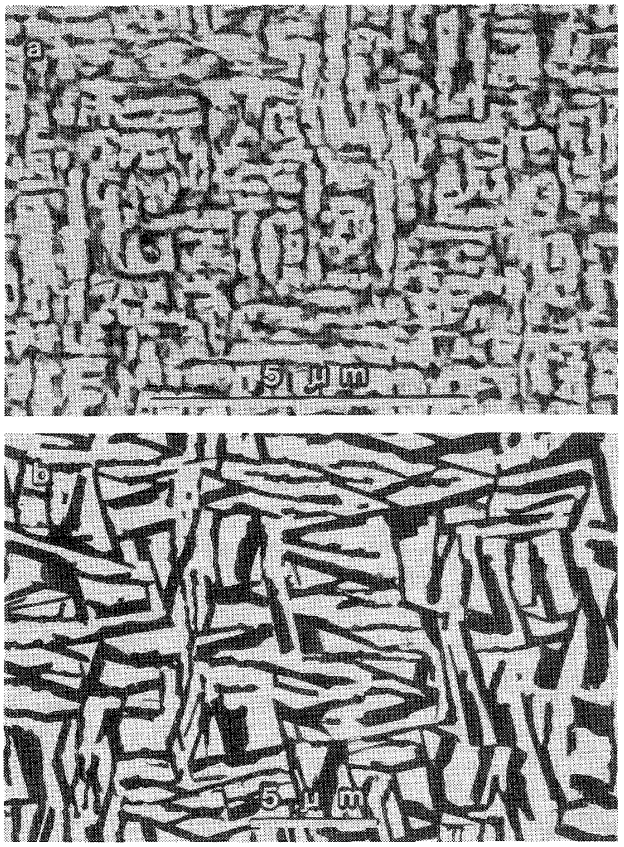

Fig. 1. Electron micrographs of MT films vacuum-deposited on the (001) plane of KCl kept at 20°C (a) and 30°C (b) after being preheated at 200°C.

for 1 h in advance and then kept at about 20 °C, the MT film vacuum-deposited on the substrate was composed of string-like crystals, as is shown in Fig. 1 (a). Although these crystals appeared to cross each other at right angles, careful observation showed that each string-like crystal was composed of many small rod-like crystals. A slight elevation of the substrate temperature to 30 °C caused a considerable growth of the crystallites, as is shown in Fig. 1 (b). The film was composed of V-shaped crystals growing along two directions crossing at 32°, and the [110] direction of the substrate crystal corresponded to the bisectional direction of the V-shaped crystals. These crystals intersected at right angles to each other. Figure 2 shows the electron-diffraction pattern from the film. This diffraction pattern as well as the intensity appeared identical to the diffraction pattern from hexatriacontane film reported in a previous paper.[9] Although the crystal structure of MT has not been reported, it seems that the evaporated films of MT and paraffin are similar in crystal structure and take the same orientation. In order to generalize the similarity detected among the crystal structures of chain molecules, Vand has introduced the concept of a subcell determined by the positions of the methylene groups.[12] The most widely encountered type of subcell is the orthorhombic paraffin cell. The crystals, composed of chain molecules, have long spacings which are defined as the distance between the basal planes of the crystal lattice passing through the end groups of the chain molecules. These distances are of the order of a chain length of one molecule. Francis and Piper have measured the long spacings of a series of methyl esters of fatty acids containing carbon atoms from 16 to 38.[13] The long spacings of these esters fall accurately on two individual straight lines corresponding to their carbon number. The line for the esters containing an odd number of carbon atoms lies about 0.5 Å above the line of the even. Malkin found that methyl esters containing an even number of carbon atoms have only one crystal form, in which the chains are tilted 63° relative to the basal plane.[14] Because the MT molecule contains 30 carbon atoms, it seems that the MT crystal belongs to the same crystal form as those crystals with even carbon atoms and that its long spacing is 150 Å. Among the homologous series of methyl esters with the even number of carbon atoms, the crystal structure of methyl stearate (C_{18}) is investigated in detail. The crystal form is monoclinic, with dimensions of $a=5.61$, $b=7.33$, $c=106.6$ Å, and $\beta=116°\ 47'$.[15] The carbon chains are arranged in an orthorhombic packing, $O\perp(101)$, and the subcell dimensions are $a_s=5.07$, $b_s=7.33$, $c_s=2.53$ Å, and $\beta_s=89°$, the suffix s indicates the subcell lattice. On the basis of these results, it is assumed that the crystal dimensions of MT are $a=5.61$, $b=7.33$, $c=150$ Å, and $\beta=116°\ 47'$, including the subcell of $a_s=5.07$, $b_s=7.33$, $c_s=2.53$ Å, and $\beta_s=89°$. The relationship between the unit cell and the subcell is represented schematically in Fig. 3. The (001) plane of the unit cell corresponds to the (101) plane of the subcell, and the (110) plane is held in common between the unit cell and the subcell. The electron-diffraction

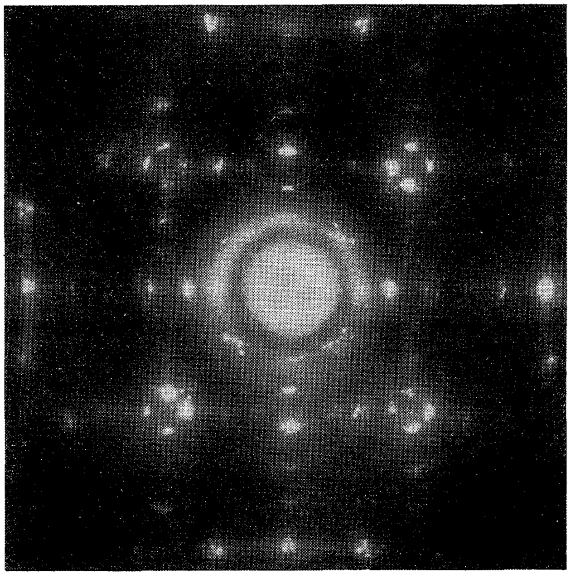

Fig. 2. Electron diffraction pattern of MT film shown in Fig. 1 (b).

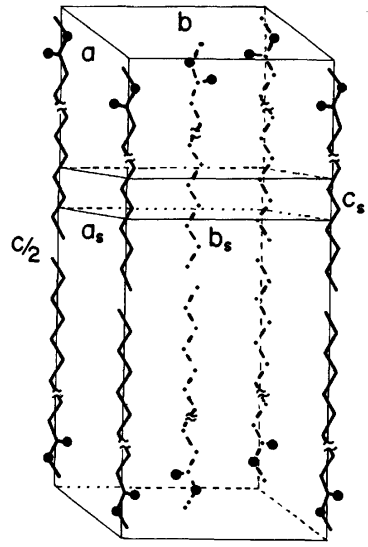

Fig. 3. The relationship between the subcell and the unit cell of MT crystal. Closed circles indicate the oxygen atoms.

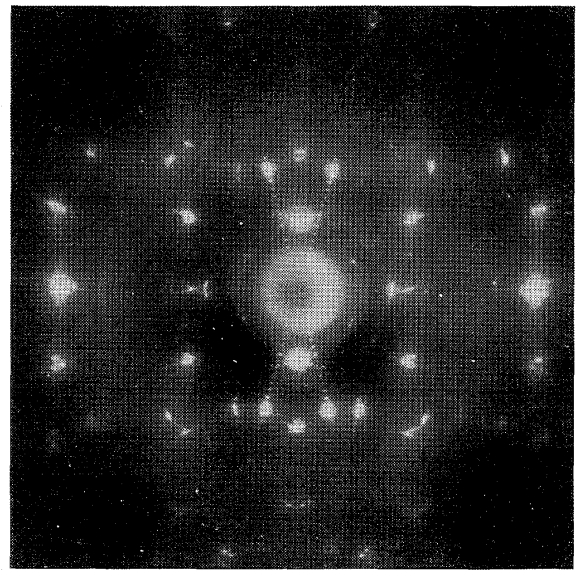

Fig. 5. Electron diffraction pattern of MT film tilted about 23° around c_u-axis of the B-set crystals.

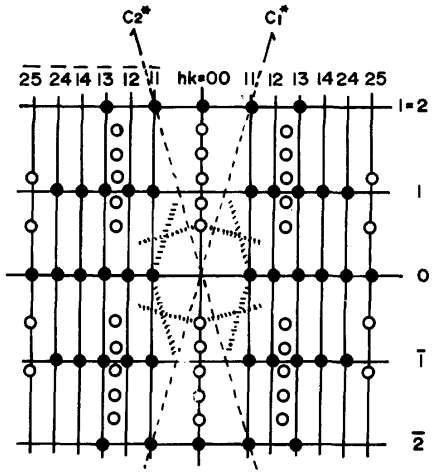

Fig. 4. The interpretation of the diffraction pattern shown in Fig. 2. Closed circles are representation of the basic single crystal pattern. The dotted lines indicate the reciprocal c_u*-axis of the crystals.

pattern shown in Fig. 2 showed the reflection spots corresponding to hkl_s of the sublattice and a series of $00l$ reflections in the small-angle region. On the basis of the subcell dimensions, the reflection spots in Fig. 2 were indexed as is shown in Fig. 4, in which the closed circles represent the basic single-crystal pattern. The total pattern is overlapped by rotating the pattern at 90°. All the crystals are classified as A- or B-set, corresponding to the reflection spots indicated by the closed and the open circles. As a result of the finite thickness of the layers, the reflection spots are elongated in the direction perpendicular to the layer surface. They intersect at the points and/or in the elongated intensity regions of the reciprocal lattice with the Ewald sphere. From a consideration of the observed and calculated spacing as well as the intensities, the reciprocal lattice points, 250_s and 002_s, were found to lie directly on the Ewald sphere. The direction of the c_S-axis corresponds to the [110] direction of the substrate crystal. Consequently, the a_s-, b_s-, and c_s-axes of the subcell lattice are inclined to the normal of the substrate surface at angles of about 30°, 120°, and 90° respectively. On the other hand, the normal of the (110) plane is inclined to the a_s-, b_s-, and c_s-axes at angles of about 34°, 124°, and 90° respectively. When the two sets of angles are compared, it is found that the (110) plane of the MT crystal is oriented parallel to the substrate (001) plane and that its c-axis lies parallel to the [110] direction of the substrate crystal. From a consideration of the molecular arrangement, these findings indicate that the close-packed layer of molecules lies parallel to and adjacent to the substrate face and that the chain molecules are aligned along the lines of the same charge in the substrate [110] direction. The $00l$ reflection spots of hexatriacontane crystals were clearly observed on the line between the point of origin and the 001_s reflection spot; they divide the space into half the number of its carbon atoms, as has been described in a previous paper.[9] In the case of the MT crystal, the lines of the $00l$ reflection spots intersect the equator by an angle of about 74°, the spot intensities on the line through the point of origin are very weak, while those on the line through the 110_s reflection spot are relatively strong. The crossing angle between c_u*- and c_s*-axes, in which the suffix u indicates the unit lattice, is calculated to be about 16° when these axes are projected on the (110) plane. Therefore, the direction of the $00l$-reflection-spots line corresponds to the direction of the reciprocal c_u*-axis of the crystal, indicated by a dotted line in Fig. 4.

In order to determine the molecular orientation of

MT, the film was tilted against the incident beam. When the film was tilted about 23° around the [110] axis of the substrate crystal, that is, the c_u-axis of the B-set crystals, so that the incident beam became perpendicular to the reciprocal c_u*-axis of the A-set crystals, $00l$ reflection spots clearly appeared on the line through the point of origin and intersected the equator at about 74°, as is shown in Fig. 5. Because the order of $00l$ reflection spots appeared to be more than 50th, it seems that the crystallinity of the evaporated MT film is very high. The reflection spots were indexed as is shown in Fig. 6. The diffraction pattern from the A-set crystals contained hkl_s spots of the sublattice and the series of $00l$ reflection spot crossing each other at about 32°, while that from the B-set crystals shows the net pattern of 110_s and 001_s reflection spots. The reflection spots of the A-set crystals show a mirror symmetry, whose mirror plane corresponds to the (110) plane of the substrate crystal. Therefore, two MT crystals (A_1- and A_2-sets), related with mirror symmetry, and oriented so as to cross each other at about 32°. The long spacing was found to be 75.0 Å by the measurement of the distance of the $00l$ reflection spots. Because of the symmetry of the MT crystal, $00l$ reflections are absent when l is odd. The observed intensities of the $00l$ reflection spots are strong when l is $4n$, while they are very weak when l is $2n$. The calculated values of the structure factor of the $00\cdot 4n$ reflection are several times higher than those of the $00\cdot 2n$ reflection. This phenomenon was also observed in the methyl stearate crystal.[15] These facts suggest that the longer the aliphatic chain length, the less the effect of the end groups on the structure factor. Considering the rule of the absent reflection, the long spacing ($=c\sin\beta$) of the MT crystal is determined to be 150.0 Å. This value agrees well with the one calculated as has been described in a previous section. Since the $12l$ and its higher-order reflection spots from the A-set crystals appeared strongly, the reciprocal lattice points, 120_s and 001_s, were found to lie nearly on the Ewald sphere. The intersection angle between the normal of the (110) plane and the zone axis [210] of the $(001)_s$ and $(120)_s$ planes is calculated to be about 21°. This value coincides well with the tilting angle of the film against the incident beam.

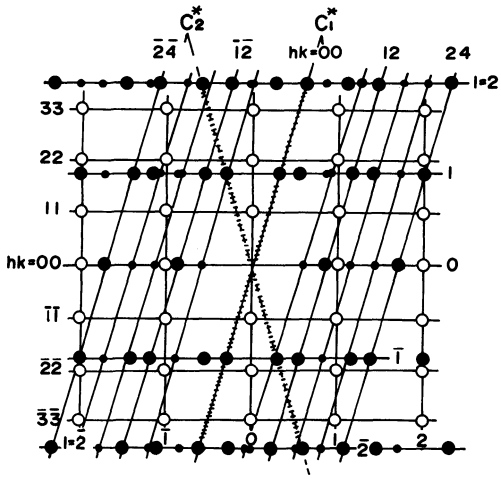

Fig. 6. The interpretation of the diffraction pattern shown in Fig. 5.

On the other hand, the diffraction pattern from the B-set crystals shows the single net pattern of the higher-order reflections of 110_s and 001_s. Each reflection spot has a very strong intensity and shows a streak to the reciprocal c_u*-axis of the crystal. Figure 7 shows schematically the relationship of the B-set reflection

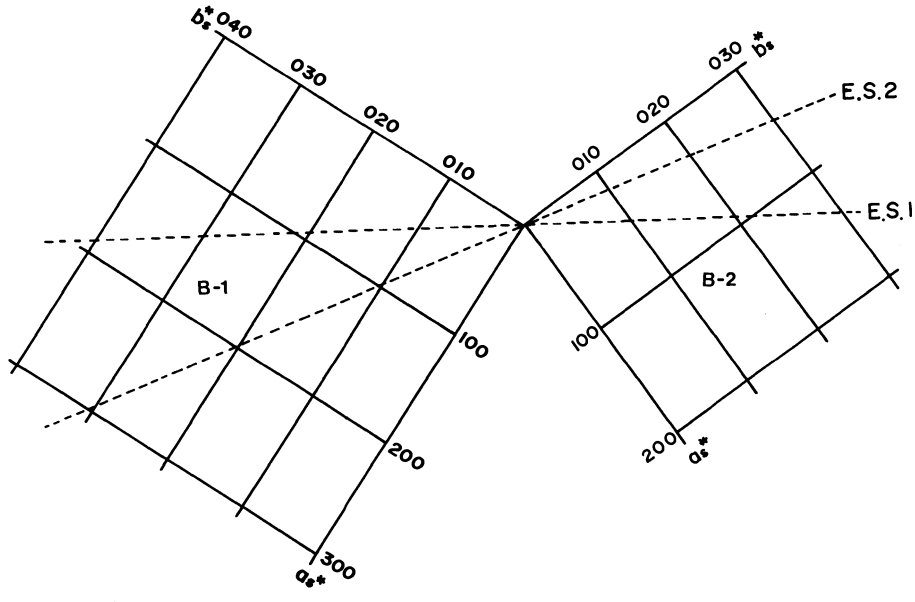

Fig. 7. Schematic diagram of the reciprocal B-set lattice points and Ewald spheres corresponding to Figs. 2 and 5. The lines of E.S.1 and E.S.2 represent the cross sections of Ewald sphere before and after tilting the film.

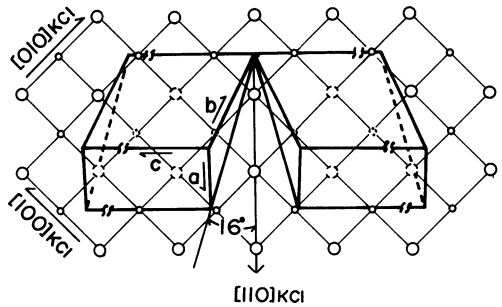

Fig. 8. Schematic diagram of the relative orientation of MT crystals and KCl (001) surface.

spots before and after tilting the film by 23°. The lines of E.S.1 and E.S.2 represent the cross-sections of the Ewald sphere before and after tilting the film. Before tilting the film, the 120_s and 130_s lattice points of the crystals related to the mirror symmetry in the B-set (B_1-and B_2-sets) and situated near the E.S.1. After tilting the film, on the other hand, 110_s and its higher-order reflection spots of the B_1-set crystal came to lie directly on the E.S.2.

The epitaxial overgrowth of MT crystals on the surface of potassium chloride is represented schematically in Fig. 8. The (110) planes of the two crystals related by mirror symmetry, whose mirror plane corresponds to the (110) plane of potassium chloride, are oriented parallel to the substrate surface. Their *c*-axes are parallel to the [110] direction of potassium chloride. Consequently, the [110] direction of the MT crystals crosses the [110] direction of the substrate crystal at 16°. The longitudinal directions of the deposited MT crystals cross at 32°, corresponding to such a molecular orientation. Therefore, the morphology of the deposited MT is V-shaped and these V-shaped crystals grow epitaxially, crossing each other orthogonally corresponding to the C_{4v} symmetry of the substrate crystal.

When the substrate was kept at a temperature between 80 and 90 °C, the MT vacuum-deposited on the substrate formed discrete, disk-like crystals, as is shown in Fig. 9 (a). The electron-diffraction pattern from these crystals shows the single net pattern of higher-order reflections of 100_s and 010_s, as is shown in Fig. 9 (b), which indicates that the *c*-axes of the crystals are perpendicular to the substrate surfaces. This diffraction pattern is similar to the pattern obtained from solution-grown crystallites of linear molecules. It is well-known that the crystals of linear molecules containing MT grow in lamellae from organic solutions. This fact suggests that this crystal habit of linear molecules is the most stable form thermodynamically.

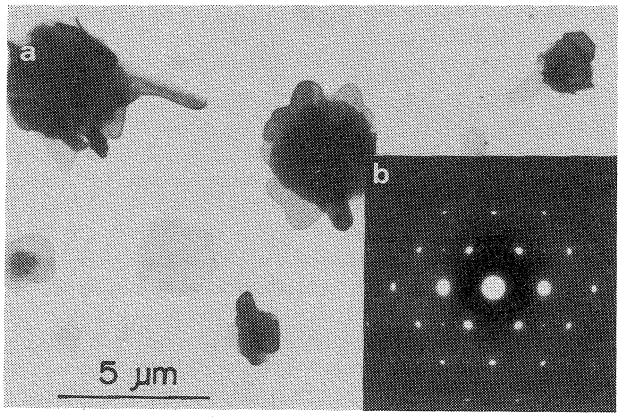

Fig. 9. Electron micrograph (a) and electron diffraction (b) of MT crystals deposited on KCl at 80°C.

When the substrate is kept at a higher temperature than the melting point of MT, the deposit melts completely on the substrate and crystallizes independently of the molecule-substrate interaction on cooling.

The author wishes to express his thanks to Professor Michio Ashida of his helpful discussions. Thanks are also due to Mr. Hisao Yanagi for his assistance.

References

1) *Thin Solid Films*, **99**, Nos, 1—3 (1983).
2) N. Uyeda, M. Ashida, and E. Suito, *J. Appl. Phys.*, **36**, 1453 (1965).
3) Y. Murata, T. Kobayashi, N. Uyeda, and E. Suito, *J. Crystal Growth*, **26**, 187 (1984).
4) T. Kobayashi, Y. Fujiyoshi, and N. Uyeda, *Acta Crystallogr., Sect. A*, **38**, 356 (1982).
5) M. Mitsuya, Y. Taniguchi, and M. Akagi, *J. Colloid Interface Sci.*, **92**, 291 (1983).
6) M. Ashida and T. Watanabe, *Bull. Chem. Soc. Jpn.*, **45**, 2312 (1972).
7) M. Ashida, *Bull. Chem. Soc. Jpn.*, **39**, 2625 (1966).
8) M. Ashida, *Bull. Chem. Soc. Jpn.*, **39**, 2632 (1966).
9) Y. Ueda and M. Ashida, *J. Electron Microscopy*, **29**, 38 (1980).
10) Y. Hattori, M. Ashida, and T. Watanabe, *Nippon Kagaku Kaishi*, **1975**, 496.
11) M. Ashida, Y. Ueda, and T. Watanabe, *J. Polym. Sci., Polym. Phys. Ed.*, **16**, 179 (1978).
12) V. Vand, *Acta Crystallogr.*, **4**, 465 (1951).
13) F. Francis and S. H. Piper, *J. Am. Chem. Soc.*, **61**, 577 (1939).
14) T. Malkin, *J. Chem. Soc.*, **133**, 2796 (1931).
15) S. Aleby and E. von Sydow, *Acta. Crystallogr.*, **13**, 487 (1960).

 © 1986 The Chemical Society of Japan Bull. Chem. Soc. Jpn., 59, 3781—3789 (1986)

How Do Proton Chemical Shifts Reflect Aromaticity ? Graph Theory of the Secondary Magnetic Field Due to Ring Currents

Jun-ichi AIHARA
Department of Chemistry, Faculty of Science, Shizuoka University, Oya, Shizuoka 422
(Received June 7, 1986)

A secular determinant for a polycyclic conjugated molecule, combined with a test dipole, is definable as a function of the applied magnetic field. It was found that this determinant can be expanded graph-theoretically into a characteristic polynomial. A secondary magnetic field is brought about by so-called ring currents. A new formula for evaluating the secondary field was derived by applying Newton's method to this polynomial. This formula indicates that the secondary field at any point in the molecular plane is given exactly as a sum of the contributions of all π-electron circuits. The contribution of each π-electron circuit is expressible in terms of a pure geometric factor and an aromatic stabilization energy assigned to the circuit. The secondary field and then the proton chemical shifts can thus be related to aromaticities of individual π-electron circuits. Magnetotropism of most polycyclic conjugated molecules can be rationalized in this manner. π-Electron circuits which share the conjugated atom nearest to a given proton dominate the chemical shift. In general, a peripheral π-electron circuit contributes modestly to the overall thermodynamic stability of a molecule, but contributes much to the secondary fields at attached protons.

It is well-known that ring currents are induced in an aromatic hydrocarbon on application of an external magnetic field.[1,2] Ring currents are equivalent to magnetic shells, and the field at an attached proton consequently differs from the applied field owing to the resultant secondary field.[3-6] A significant part of the deshielding of aromatic protons is presumed to be due to ring current effects.[3-7] The deshielding can be estimated from what we call proton chemical shifts, i.e., shifts in the magnetic resonance peaks of the protons.[6]

In 1958, the secondary magnetic field was formulated independently by Pople and McWeeny within the Hückel framework.[4-6,8,9] The problem of finding a secondary field differs somewhat from that of finding London susceptibility, i.e., magnetic susceptibility associated with ring currents.[2] Pople managed to expand London's field-dependent secular determinant[2] into a characteristic polynomial, and solved the problem.[4] McWeeny introduced an infinitesimal test dipole into an aromatic molecule placed in the magnetic field, and evaluated the coupling energy between the dipole and the induced current distribution in the molecule.[5,6,8,9] The secondary field experienced by the dipole was obtainable from it. McWeeny employed the perturbational technique of Coulson and Longuet-Higgins[10] to derive the secondary field.

In 1979 Sachs' graph theory[11-14] proved very useful for expanding the field-dependent secular determinant for an aromatic molecule straightforwardly into a characteristic polynomial. We succeeded in devising the graph-theoretical formulas of London susceptibility and ring currents for cyclic conjugated systems.[15-26] Our graph-theoretical formula of London susceptibility established the existence of a distinct relationship between aromatic stabilization and diamagnetic susceptibility exaltation.[15,20,21] Diamagnetic susceptibility exaltation is an experimental manifestation of London susceptibility.

Sachs' graph theory[11-14] can likewise be used to formulate the secondary magnetic field experienced by the test dipole in a polycyclic aromatic molecule. McWeeny's secular determinant for such a system[5] can be expanded graph-theoretically into the characteristic polynomial. The secondary field at any proton can then be deduced without using any complicated perturbational technique. In this paper we present the graph-theoretical formulas thus obtained for ring currents and secondary fields. They are expressed in terms of pure geometric factors and circuit currents[24,25] or circuit resonance energies.[20,21] As will be seen, this kind of formulation is very useful for answering the question as to why and how proton chemical shifts reflect aromatic stabilization of a cyclic conjugated system.

General Terminology and Notation

Some unfamiliar terms and symbols are surveyed beforehand. A given conjugated molecule is denoted by G, which is assumed to have N conjugated atoms. In this paper, we deal only with cyclic conjugated molecules. If G is cyclic in geometry, one or more cyclic paths can be chosen from it. Such cyclic paths are termed π-electron circuits,[25,27] which are identical with ring components in Sachs' graph theory.[11-14] All possible cyclic paths in G constitute an entire set of π-electron circuits. The tth π-electron circuit is denoted by r_t. For example, seven π-electron circuits can be chosen from the acenaphthylene conjugated system. They are two six-membered, one five-membered, one ten-membered, and two nine-membered circuits, together with one eleven-membered peripheral circuit. $G-r_t$ represents the subsystem of G, obtained by deleting from G the tth π-electron circuit and all π bonds incident to it.[11-14]

Some geometric factors are then defined to characterize the individual π-electron circuits. The origin of the coordinates is usually set at the point in the molecular plane where the secondary magnetic field is to be evaluated. The signed area of the triangle formed by the origin and the i-j π bond is denoted by s_{ij}. It is counted positive if i→j is right-handed about the unit vector normal to the molecular plane.[2,4-6] Then, the following two quantities, S_t and F_t, are defined for the tth π-electron circuit:

$$S_t = \sum_{(ij)}^{r_t} s_{ij} \tag{1}$$

$$F_t = \sum_{(ij)}^{r_t} s_{ij} f_{ij} \tag{2}$$

Here, (ij) stands for the i-j π bond. It runs over all π bonds forming the tth π-electron circuit. The absolute value of S_t is equal to the area of the tth π-electron circuit.[2,4-6] f_{ij} is defined for (ij) as follows:

$$f_{ij} = \frac{1}{d_i^3} + \frac{1}{d_j^3}, \tag{3}$$

where d_i and d_j are the distances of atoms i and j, respectively, from the origin.

The polynomial obtained by expanding the Hückel secular determinant for G is termed the characteristic polynomial for G. This polynomial is denoted by $P_G(X, B)$ because the coefficients in it depend upon the applied magnetic field B. $P_{G-r_t}(X, B)$ represents a characteristic polynomial for $G-r_t$. Roots of the equation $P_G(X, B)=0$ represent the energies of N π-electron molecular orbitals in G. They are given relative to α, in units of β, where α and β are the standard Coulomb and resonance integrals, respectively.

When the external magnetic field is absent, the resonance integral for the i-j π bond is expressed in the form:

$$\beta_{ij}^{\circ} = k_{ij}\beta, \tag{4}$$

where k_{ij} is the resonance integral parameter which depends upon the bond type and bond order. The wth largest root of the equation $P_G(X,0)=0$, i.e., the energy of the wth π-electron molecular orbital in the absence of the external field is denoted by X_w. The number of π-electrons present in the wth molecular orbital is denoted by g_w. $Q_{G-r_t}(X)$ is defined by[25]

$$Q_{G-r_t}(X) = \frac{P_{G-r_t}(X,0)}{P_G'(X,0)} \prod_{(ij)}^{r_t} k_{ij}, \tag{5}$$

where (ij) runs over all π bonds forming the tth π-electron circuit. $P_G'(X,0)$ is the first derivative of $P_G(X,0)$ with respect to X. Finally, e, c, $\hbar$, and μ_o are the standard constants with these symbols.

Graph-Theoretical Formulation of the Secondary Magnetic Field

The strength of the secondary magnetic field due to ring currents was formulated in the following manner. A given cyclic conjugated molecule G is placed in the magnetic field **B**, which is assumed to be perpendicular to the molecular plane, i.e., $\mathbf{B}=B\mathbf{n}$, where **n** is the unit vector normal to the molecular plane. An infinitesimal test dipole of moment $\mathbf{m}=m\mathbf{n}$ is introduced at a given point in the plane of G, this point being chosen as origin of the coordinates. The entire system now consists of the molecule G and the test dipole D. The resonance integral for the i-j π bond becomes[5,6]

$$\beta_{ij} = \beta_{ij}^{\circ} \exp\left[\frac{ie s_{ij}}{\hbar}\left(B + \frac{\mu_o m}{4\pi} f_{ij}\right)\right]. \tag{6}$$

It is to be noted that Eq. 6 represent the general form of off-diagonal elements of the secular determinant for this complex system. The diagonal elements remain the same as those of the secular determinant for the conjugated molecule alone.[2,6,15] Such a secular determinant can be expanded into a characteristic polynomial without difficulty.

As in the case of the system with no test dipole,[15,21] Sachs' graph theory[11-14] is applicable, and every coefficient in the polynomial is expressed as a combination of cyclic products of resonance integrals. Such cyclic products can be classified into two groups. The first group consists of cyclic products of two resonance integrals associated with individual π bonds. They take the general form $\beta_{ij}\beta_{ji}$, which in this case is associated with the i-j π bond. The second group consists of cyclic products of more than two resonance integrals associated with individual π-electron circuits. They take the general form $\beta_{op}\beta_{pq}\cdots\beta_{uv}\beta_{vo}$, which in this case is associated with a π-electron circuit formed by atoms o, p, q, ···, u, and v. This indicates that if one or more π-electron circuits can be chosen from the molecule, there always are cyclic products of more than two resonance integrals corresponding to them all.

The following two relationships can be deduced with regard to these cyclic poducts of resonance integrals:

$$\begin{aligned}\beta_{ij}\beta_{ji} &= \beta_{ij}^{\circ}\beta_{ji}^{\circ} \\ &= k_{ij}^2\beta^2\end{aligned} \tag{7}$$

$$\begin{aligned}&\beta_{op}\beta_{pq}\cdots\beta_{uv}\beta_{vo} + \beta_{ov}\beta_{vu}\cdots\beta_{qp}\beta_{po} \\ &= 2\beta_{op}^{\circ}\beta_{pq}^{\circ}\cdots\beta_{uv}^{\circ}\beta_{vo}^{\circ}\cos\left[\frac{e}{\hbar}\left(BS_t + \frac{\mu_o m}{4\pi}F_t\right)\right] \\ &= 2k_{op}k_{pq}\cdots k_{uv}k_{vo}\beta^{z_t}\cos\left[\frac{e}{\hbar}\left(BS_t + \frac{\mu_o m}{4\pi}F_t\right)\right].\end{aligned} \tag{8}$$

Here, z_t is the number of atoms constituting the tth π-electron circuit. Since the applied field and the test dipole can be treated as small perturbations, Eq. 8 can be approximated to:

$$\begin{aligned}&\beta_{op}\beta_{pq}\cdots\beta_{uv}\beta_{vo} + \beta_{ov}\beta_{vu}\cdots\beta_{qp}\beta_{po} \\ &= 2k_{op}k_{pq}\cdots k_{uv}k_{vo}\beta^{z_t}\left[1 - \frac{e^2}{2\hbar^2}\left(BS_t + \frac{\mu_0 m}{4\pi}F_t\right)^2\right].\end{aligned} \tag{9}$$

We have previously investigated the magnetic response of a conjugated molecule, not combined with a test dipole.[15-26] In this case, Eq. 7 remains unchanged, but the value of m in Eqs. 8 and 9 vanishes, so that

$$\beta_{op}\beta_{pq}\cdots\beta_{uv}\beta_{vo} + \beta_{ov}\beta_{vu}\cdots\beta_{qp}\beta_{po} = 2k_{op}k_{pq}\cdots k_{uv}k_{vo}\beta^{z_t}\left[1-\frac{e^2}{2\hbar^2}(BS_t)^2\right]. \quad (10)$$

A characteristic polynomial for the molecule alone is expressed in the form:[15,16,19]

$$P_G(X,B) = P_G(X,0) + \frac{e^2}{\hbar^2}\sum_t^G (BS_t)^2 P_{G-r_t}(X,0)\prod_{(ij)}^{r_t} k_{ij}. \quad (11)$$

It is noteworthy that Eq. 9 can be derived formally by replacing BS_t in Eq. 10 by $BS_t+(\mu_o m/4\pi)F_t$. This indicates that the characteristic polynomial for the present system can likewise be derived by replacing BS_t in Eq. 11 by $BS_t+(\mu_o m/4\pi)F_t$:

$$P_{G+D}(X,B) = P_G(X,0) + \frac{e^2}{\hbar^2}\sum_t^G\left(BS_t+\frac{\mu_o m}{4\pi}F_t\right)^2 P_{G-r_t}(X,0)\prod_{(ij)}^{r_t} k_{ij}, \quad (12)$$

where G+D stands for the whole system consisting of the molecule G and the test dipole D.

By solving the equation $P_{G+D}(X,B)=0$ by means of the Newton method, energies of the π-electron molecular orbitals in the whole system can be obtained, each as a function of the field strength B. When there are no degenerate orbitals in G, the energy of the wth π-electron molecular orbital is given in the form:

$$\varepsilon_w(B) = \alpha + X_w(B)\beta = \alpha + \beta\left[X_w^\circ - \frac{e^2}{\hbar^2}\sum_t^G\left(BS_t+\frac{\mu_o m}{4\pi}F_t\right)^2 Q_{G-r_t}(X_w^\circ)\right]. \quad (13)$$

Here, $X_w(B)$ is the wth largest root of the equation $P_{G+D}(X,B)=0$. If there are degenerate orbitals in G, $X_w(B)$ for them must be evaluated by the procedure described in Refs. 16 and 22.

Toal π-electron energy of the whole system becomes

$$E_{G+D}(B) = \sum_{w=1}^N g_w\varepsilon_w(B) = \sum_{w=1}^N g_w\left\{\alpha+\beta\left[X_w^\circ - \frac{e^2}{\hbar^2}\sum_t^G\left(BS_t+\frac{\mu_o m}{4\pi}F_t\right)^2 Q_{G-r_t}(X_w^\circ)\right]\right\}, \quad (14)$$

where g_w is the occupation number for the wth orbital.

It is readily seen that Eq. 14 contains the term linear in m. This term represents the coupling energy between the test dipole and the secondary magnetic field.[5,6] Therefore, it can be identified with $-mB'$, where B' is the secondary field at the position where the test dipole is placed. Then, the strength of the secondary magnetic field is given by

$$B' = -\left[\frac{\partial}{\partial m}E_{G+D}(B)\right]_{m=0} = \frac{\mu_o e^2 B}{2\pi\hbar^2}\beta\sum_t^G F_t S_t\sum_{w=1}^N g_w Q_{G-r_t}(X_w^\circ), \quad (15)$$

This graph-theoretical formula is in marked contrast to McWeeny's one expressed in terms of imaginary bond-bond polarizabilities,[5,6] and had an advantage in that the secondary field can be related to the molecular geometry straightforwardly.

We have previously shown that London susceptibility and ring currents can both be partitioned exactly among the constituent π-electron circuits.[16,19-26] Equation 15 clearly indicates that the secondary field can also be partitioned among the π-electron circuits. This is expressed explicitly as

$$B' = \sum_t^G \gamma_t, \quad (16)$$

where γ_t stands for the contribution of the tth π-electron circuit:

$$\gamma_t = \frac{\mu_o e^2 B}{2\pi\hbar^2}\beta F_t S_t\sum_{w=1}^N g_w Q_{G-r_t}(X_w^\circ). \quad (17)$$

As shown previously,[24,25] a bond current, i.e., a ring current flowing through a given π bond, is expressed as a sum of the contributions of π-electron circuits sharing the very π bond in common. The current contribution of the tth π-electron circuit is called the tth circuit current, which is given by[24,25]

$$I_t = -\frac{2e^2 B}{\hbar^2}\beta S_t\sum_{w=1}^N g_w Q_{G-r_t}(X_w^\circ) = \frac{9I_o S_t}{S_o}\sum_{w=1}^N g_w Q_{G-r_t}(X_w^\circ), \quad (18)$$

where I_o is the bond current induced in benzene under the same experimental condition, and S_o is the area of the benzene ring. Using this expression for circuit currents, Eq. 15 is rewritten as

$$B' = \frac{\mu_o}{4\pi}\sum_t^G I_t F_t. \quad (19)$$

The secondary field thus is a function of not only all circuit currents in G but also all F_t values. The quantity F_t is purely geometric in nature, depending merely upon the shape and the location of the tth π-electron circuit with respect to the origin, i.e., the position where the secondary field is evaluated.

In 1958, McWeeny derived the formula similar to, but not the same as, Eq. 19.[5,6,28-30] It is expressed analogously as

$$B' = \frac{\mu_o}{4\pi}\sum_{t'}^G \bar{I}_{t'}\bar{F}_{t'}, \quad (20)$$

where t' runs over all rings in G, but not over π-electron circuits, $\bar{I}_{t'}$ is the current contribution of the tth ring, and $\bar{F}_{t'}$ is the quantity analogous to $F_{t'}$, but defined for the t'th ring. Here, the term "ring" has the usual meaning in chemistry. It is used in such a

manner that the acenaphthylene conjugated system consists of one five-membered and two six-membered rings. It is worth noting that Eqs. 19 and 20 represent two different physical aspects of the secondary field. Both ring currents and secondary fields can thus be partitioned not only among the constituent rings but also among the π-electron circuits.

Relationship between the Secondary Field and Aromaticity

We have developed the graph theory of aromaticity, in which the resonance energy arising from cyclic π-electron conjugation is defined graph-theoretically.[13,21,31,32] This type of resonance energy, RE_G, has ben recognized as a reasonable index for determining the degree of aromatic stabilization. In 1981, we found that the resonance energy can be estimated as[20,21]

$$RE_G \approx \sum_t^G \rho_t, \tag{21}$$

where t runs over all π-electron circuits in G, and

$$\rho_t = -2\beta \sum_{w=1}^{N} g_w Q_{G-r_t}(X_w^\circ). \tag{22}$$

The quantity denoted by ρ_t can obviously be attributed to the tth π-electron circuit, and can be interpreted as a contribution of the tth π-electron circuit to the overall resonance energy, which we term the tth circuit resonance energy. The same quantity has previously been called the tth ring resonance energy.[20,21] Thus, the resonance energy can be partitioned among the π-electron circuits. In other words, the overall resonance energy is given approximately by adding up all the circuit resonance energies defined by Eq. 22. In general, circuit resonance energy is positive for $(4n+2)$-membered carbocyclic circuits, and negative for $(4n)$-membered carbocyclic circuits.[25,27]

By the use of Eq. 22, Eq. 15 can be rewritten as

$$B' = -\frac{\mu_0 e^2 B}{4\pi\hbar^2} \sum_t^G A_t \rho_t, \tag{23}$$

where A_t is the pure geometric factor defined by $F_t S_t$. This expression is nothing other than what we wanted to derive in this paper. It clearly shows that the secondary field at any position is associated with the resonance energy or the extra thermodynamic stability due to aromaticity. Exactly speaking, the secondary field reflects not only all geometric factors denoted by A_t but also all circuit resonance energies. Both quantities are mathematically independent to each other within a Hückel framework.

Unfortunately, the interrelation between the resonance energy and the secondary field is never straightforward. As shown in Eq. 23, the secondary field is a function of all A_t values and all circuit resonance energies. If all A_t values were equal, B' would be proportional to the overall resonance energy. However, such a situation never occurs. Therefore, the secondary field cannot be predicted easily from the resonance energy and the molecular geometry.

Every A_t value is strongly dependent upon the distance from the origin and the shape of the π-electron circuit. Since the value of A_t is large for nearby π-electron circuits, it is quite possible that for many condensed aromatic hydrocarbons the secondary field is dominated primarily by the π-electron circuits which share the carbon nearest to the origin, i.e., the carbon to which a given proton is attached.

In a previous paper,[25] we proved that $(4n+2)$-membered circuits are diatropic in nature while $(4n)$-membered circuits are paratropic in nature. In the case of alternant hydrocarbons, smaller $(4n+2)$- and $(4n)$-membered circuits sustain stronger diamagnetic and paramagnetic currents, respectively. Therefore, if one or more $(4n+2)$-membered circuits can be chosen from a given conjugated hydrocarbon, in such a manner that they contain the carbon nearest to the origin, a proton at the origin will exhibit a downfield shift in the NMR spectrum. However, if one or more $(4n)$-membered circuits can also be chosen in the same manner, a downfield shift will be suppressed to some extent, or a net upfield shift will sometimes occur. This constitutes the very reason why typical aromatic compounds exhibit large downfield shifts of the constituent protons. There are no $(4n)$-membered circuits in catacondensed benzenoid hydrocarbons, so all protons necessarily exhibit downfield shifts.

Benzene is monocyclic in geometry, so only one π-electron circuit can be chosen from the conjugated system. The circuit resonance energy defined by Eq. 22 is $-2/9\beta$ or -0.2222β for it. The value of A_t is -5.28731×10^{-10} m at any benzene proton. Accordingly, using the strength of the secondary field at benzene protons, B_0, Eq. 23 is rewritten as

$$B' = -0.85110 \times 10^{10} B_0 \sum_t^G A_t \rho_t, \tag{24}$$

where

$$B_0 = -9.3500 \times 10^{-12} \frac{\mu_0 e^2 B}{\hbar^2}. \tag{25}$$

We will use Eq. 24 in what follows.

Secondary Fields in Anthracene

Anthracene **1** and dicycloocta[1,2,3,4-*def*:1′,2′,3′,4′-*jkl*]biphenylene **2** illustrate the utility of the above

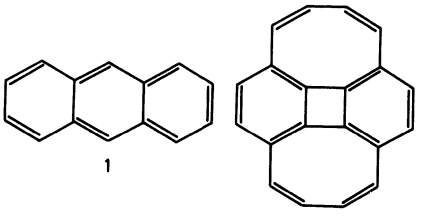

1

2

Table 1. Secondary Fields and Related Quantities for Anthracene **1**

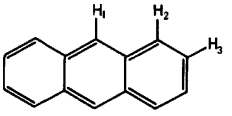

$t^{a)}$	$I_t/I_o{}^{b)}$	$\rho_t/(-\beta)^{c)}$	$A_t/10^{-10}\,m^{d)}$	$\gamma_t/B_o{}^{e)}$	$t^{a)}$	$I_t/I_o{}^{b)}$	$\rho_t/(-\beta)^{c)}$	$A_t/10^{-10}\,m^{d)}$	$\gamma_t/B_o{}^{e)}$
					3	0.3550	0.07889	−5.2873	0.3550
		Proton 1			4	0.3125	0.03472	−2.5712	0.0760
1	0.3550	0.07889	−1.0395	0.0698	5	0.3125	0.03472	−12.6536	0.3739
2	0.3617	0.08038	−5.2873	0.3617	6	0.2478	0.01836	−19.7187	0.3081
3	0.3550	0.07889	−1.0395	0.0698					
4	0.3125	0.03472	−12.6536	0.3739			Proton 3		
5	0.3125	0.03472	−12.6536	0.3739	1	0.3550	0.07889	−0.1045	0.0070
6	0.2478	0.01836	−22.0990	0.3453	2	0.3617	0.08038	−0.3747	0.0256
					3	0.3550	0.07889	−5.2873	0.3550
		Proton 2			4	0.3125	0.03472	−0.9584	0.0283
1	0.3550	0.07889	−0.2461	0.0165	5	0.3125	0.03472	−11.3241	0.3346
2	0.3617	0.08038	−1.0395	0.0711	6	0.2478	0.01836	−17.2996	0.2703

a) Circuit number. b) Circuit current defined by Eq. 9. c) Circuit resonance energy defined by Eq. 13. d) Geometric factor defined in Eq. 14. e) Contribution to the secondary field, defined by Eq. 8.

theory. In general, calculated magnetic properties are often very sensitive to the degree of sophistication of the molecular orbital (MO) method for computing them.[33] The MO model employed here is an iterative $\beta\omega'\omega''$ method,[34,35] which is a kind of self-consistent Hückel method. This method has successfully been applied to many conjugated hydrocarbons.[33-37] Compounds **1** and **2** are both alternant hydrocarbons in the neutral state, so all Coulomb integrals remain unchanged by application of this method. Resonance integrals are all functions of the bond order. The resonance integral parameter employed is of the form:[25]

$$k_{ij} = \exp(0.6327p_{ij} - 0.4218), \quad (26)$$

where p_{ij} is the bond order for the i-j π bond. MO calculations were iterated until resonance integrals were made self-consistent with the corresponding bond orders.

Anthracene **1** is a typical catacondensed aromatic hydrocarbon. Three rings in it are assumed to be regular hexagons with all edge lengths equal to the carbon-carbon bond lengths of benzene (139.65 pm).[38] All carbon-hydrogen bond lengths are set equal to 108.5 pm.[38] There are three non-identical protons and six π-electron circuits in the conjugated system. They are numbered as shown in Table 1 and Fig. 1. Positions of all non-identical protons were succesively taken as origin of the coodinates, and the secondary fields and related quantities were calculated using Eqs. 15—25. All the numerical results are presented in Table 1 and Fig. 3.

As shown in Table 1, all π-electron circuits in anthracene contribute to the increase in the secondary field at any proton. This corresponds to the fact that they are all $(4n+2)$-membered circuits. It is clear that not all π-electron circuits contribute much to the secondary field at a given proton. In general, each

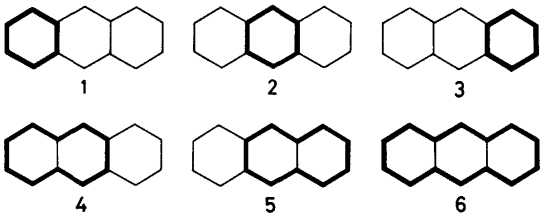

Fig. 1. π-Electron circuits in anthracene **1**.

π-electron circuit contributes much to the secondary fields at the protons located around it.

Proton 1 in anthracene is predicted to suffer the secondary field of 1.594 B_o, which is comparable to the value obtained by the simple Hückel method, 1.707 B_o.[38] This indicates that this proton must exhibit a fairly large downfield shift in the NMR spectrum as long as local anisotropic effects[7] are not very unusual. π-Electron circuits 2, 4, 5, and 6 contribute almost equally to the secondary field although the circuit resonance energy decreases in this order. The decrease in the circuit resonance energy is obviously compensated by the increase in the geometric factor. These π-electron circuits share the carbon atom to which proton 1 is attached. The contribution of the peripheral π-electron circuit is far from negligible owing to the very large geometric factor.

π-Electron circuits which do not share the carbon nearest to proton 1 have much smaller geometric factors than those of circuits 2, 4, 5, and 6. Therefore, they contribute much less to the secondary field at proton 1. It is in marked contrast to the overall resonance energy, which is determined primarily by smaller π-electron circuits. Therefore, it is obvious that the relationship between the overall resonance energy and the secondary field is considerably obscured by the geometric factors which are unrelated to the thermodynamic stability. This supports Mallion's view that

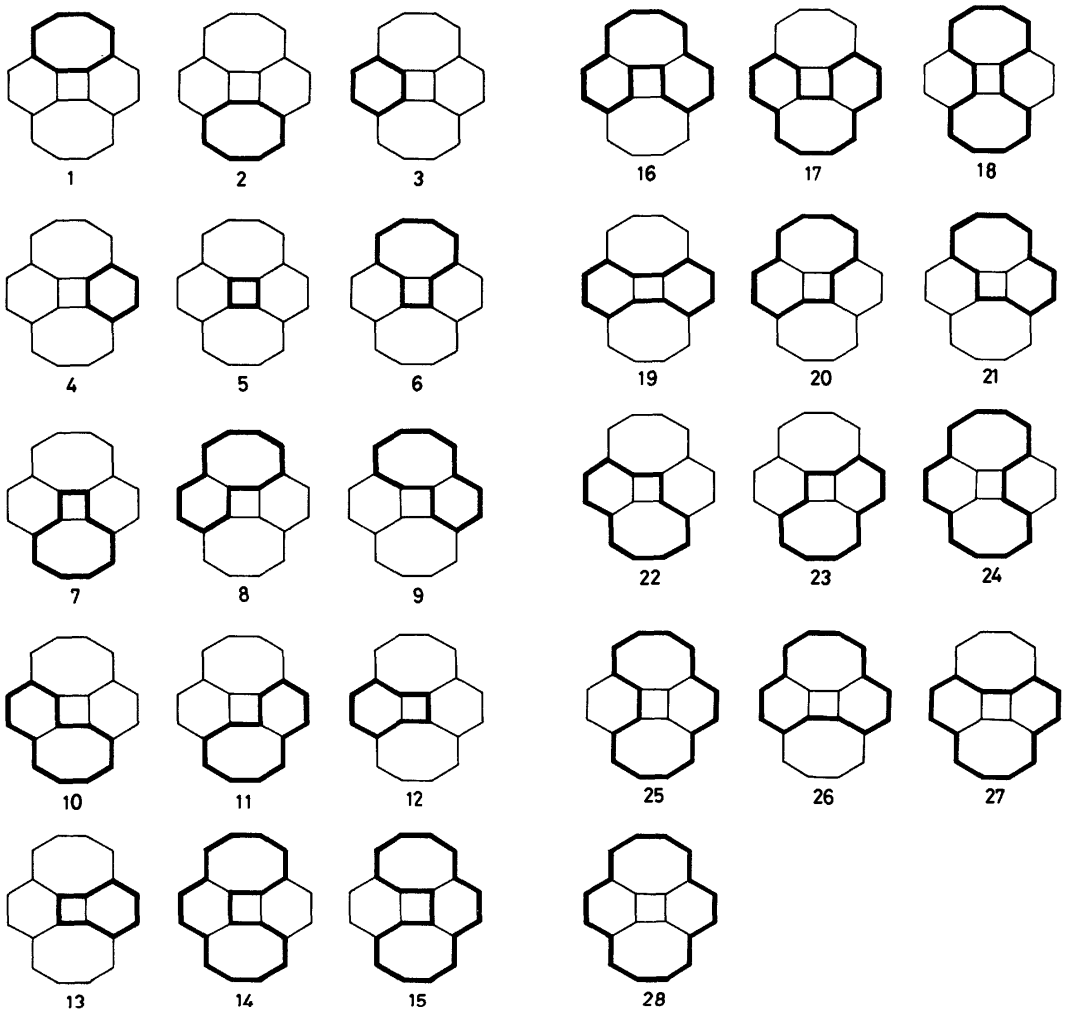

Fig. 2. π-Electron circuits in dicyclooctabiphenylene **2**.

the graph-theoretical and geometric contributions to ring-current intensities are disentangled.[9]

The situation is essentially the same for protons 2 and 3. Protons 2 and 3 are predicted to suffer the secondary fields of 1.201 B_0 and 1.021 B_0, respectively. They are also comparable to the values calculated by the simple Hückel method, 1.387 B_0 at proton **2** and 1.197 B_0 at proton 3.[38] π-Electron circuits which share the carbon atom nearest to each of these protons again contribute primarily to the secondary field.

Every circuit current is proportional to the circuit area and the circuit resonance energy defined by Eq. 22. Thus, it is not influenced by the value of A_t, and independent of the distance from the origin.

Haigh et al. obtained the following regression line between experimental proton chemical shifts and the corresponding B'/B_0 ratios for a number of condensed benzenoid hydrocarbons:[38]

$$\delta = 5.66 + 1.56\frac{B'}{B_0} \qquad (27)$$

This is based on the secondary fields calculated by the simple Hückel method. The regression line has not been obtained with the fields calculated by the iterative $\beta\omega'\omega''$ method, but Eq. 27 is not too bad to predict the proton chemical shifts from them. Protons 1, 2, and 3

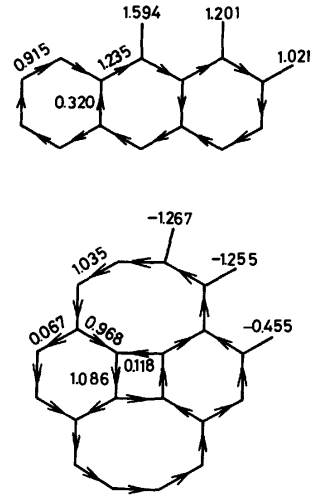

Fig. 3. Bond currents in units of I_0 and secondary magnetic fields in units of B_0: anthracene (upper) and dicyclooctabiphenylene (lower).

Table 2. Secondary Fields and Related Quantities for Dicyclooctabiphenylene **2**

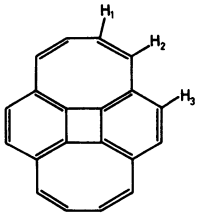

t[a]	I_t/I_o[b]	$\rho_t/(-\beta)$[c]	$A_t/10^{-10}$ m[d]	γ_t/B_o[e]	t[a]	I_t/I_o[b]	$\rho_t/(-\beta)$[c]	$A_t/10^{-10}$ m[d]	γ_t/B_o[e]
					14	0.0785	0.00384	−28.5993	0.0936
		Proton 1			15	0.0785	0.00384	−32.4166	0.1061
1	−0.1937	−0.02432	−10.7103	−0.2217	16	−0.2118	−0.01248	−26.5595	−0.2822
2	−0.1937	−0.02432	−0.3989	−0.0083	17	−0.2118	−0.01248	−5.7763	−0.0614
3	1.2461	0.27692	−0.2364	0.0557	18	−0.1441	−0.00816	−24.7661	−0.1720
4	1.2461	0.27692	−0.4605	0.1085	19	−0.2916	−0.02717	−3.4520	−0.0798
5	−0.1829	−0.10560	−0.0522	−0.0047	20	−0.0349	−0.00246	−19.6069	−0.0410
6	0.0946	0.00976	−13.3320	0.1107	21	−0.0349	−0.00246	−22.2596	−0.0466
7	0.0946	0.00976	−0.7781	0.0065	22	−0.0349	−0.00246	−2.2148	−0.0046
8	−0.2155	−0.01729	−17.4168	−0.2563	23	−0.0349	−0.00246	−4.8675	−0.0102
9	−0.2155	−0.01729	−18.0374	−0.2654	24	−0.1619	−0.00730	−32.0549	−0.1993
10	−0.2155	−0.01729	−1.2791	−0.0188	25	−0.1619	−0.00730	−36.1958	−0.2250
11	−0.2155	−0.01729	−1.8997	−0.0280	26	0.1448	0.00775	−30.1409	0.1987
12	−0.2463	−0.03952	−0.5154	−0.0173	27	0.1448	0.00775	−7.2357	0.0477
13	−0.2463	−0.03952	−0.8257	−0.0278	28	−0.0570	−0.00214	−44.7227	−0.0814
14	0.0785	0.00384	−29.5686	0.0967					
15	0.0785	0.00384	−30.5857	0.1001			Proton 3		
16	−0.2118	−0.01248	−25.4408	−0.2703	1	−0.1937	−0.02432	−2.2196	−0.0459
17	−0.2118	−0.01248	−3.4767	−0.0369	2	−0.1937	−0.02432	−0.9267	−0.0192
18	−0.1441	−0.00816	−25.1670	−0.1748	3	1.2461	0.27692	−0.1677	0.0395
19	−0.2916	−0.02717	−1.9857	−0.0459	4	1.2461	0.27692	−5.2873	1.2461
20	−0.0349	−0.00246	−20.2653	−0.0424	5	−0.1829	−0.10560	−0.0676	−0.0061
21	−0.0349	−0.00246	−20.9721	−0.0439	6	0.0946	0.00976	−3.0808	0.0256
22	−0.0349	−0.00246	−1.8850	−0.0039	7	0.0946	0.00976	−1.5067	0.0125
23	−0.0349	−0.00246	−2.5918	−0.0054	8	−0.2155	−0.01729	−3.9381	−0.0580
24	−0.1619	−0.00730	−32.7440	−0.2036	9	−0.2155	−0.01729	−18.1185	−0.2666
25	−0.1619	−0.00730	−33.8474	−0.2104	10	−0.2155	−0.01729	−1.9147	−0.0282
26	0.1448	0.00775	−28.6023	0.1885	11	−0.2155	−0.01729	−16.0951	−0.2368
27	0.1448	0.00775	−4.3957	0.0290	12	−0.2463	−0.03952	−0.4755	−0.0160
28	−0.0570	−0.00214	−42.1213	−0.0766	13	−0.2463	−0.03952	−7.5657	−0.2544
					14	0.0785	0.00384	−8.8313	0.0289
		Proton 2			15	0.0785	0.00384	−32.0725	0.1049
1	−0.1937	−0.02432	−10.2776	−0.2127	16	−0.2118	−0.01248	−25.2920	−0.2687
2	−0.1937	−0.02432	−0.5205	−0.0108	17	−0.2118	−0.01248	−22.5380	−0.2394
3	1.2461	0.27692	−0.1986	0.0468	18	−0.1441	−0.00816	−7.6661	−0.0532
4	1.2461	0.27692	−1.0395	0.2450	19	−0.2916	−0.02717	−13.4285	−0.3105
5	−0.1829	−0.10560	−0.0806	−0.0072	20	−0.0349	−0.00246	−5.0395	−0.0105
6	0.0946	0.00976	−12.9638	0.1076	21	−0.0349	−0.00246	−21.1905	−0.0443
7	0.0946	0.00976	−1.0848	0.0090	22	−0.0349	−0.00246	−2.7349	−0.0057
8	−0.2155	−0.01729	−16.6349	−0.2448	23	−0.0349	−0.00246	−18.8859	−0.0395
9	−0.2155	−0.01729	−18.9640	−0.2791	24	−0.1619	−0.00730	−10.4452	−0.0649
10	−0.2155	−0.01729	−1.3648	−0.0201	25	−0.1619	−0.00730	−35.6569	−0.2217
11	−0.2155	−0.01729	−3.6939	−0.0544	26	0.1448	0.00775	−28.6042	0.1886
12	−0.2463	−0.03952	−0.5649	−0.0190	27	0.1448	0.00775	−25.5690	0.1685
13	−0.2463	−0.03952	−1.7295	−0.0582	28	−0.0570	−0.00214	−43.8909	−0.0799

a)—e) See Table 1, footnotes a)—e).

are predicted from Eq. 27 to resonate at δ 8.15, δ 7.53, and δ 7.25, respectively. They are well compared to the experimental values, δ 8.36 for proton 1, δ 7.93 for proton 2, and δ 7.39 for proton 3.[38]

Secondary Fields in Dicyclooctabiphenylene

Secondary fields in dicyclooctabiphenylene **2** can be evaluated in the same manner. One four-membered and two six-membered rings in it are assumed to be regular in shape. Two eight-membered rings are made centrosymmetric in such a manner that they are attached closely to the biphenylene structure. All carbon-carbon bond lengths are assumed to be equal to those of benzene (139.65 pm).[38] All carbon-hydrogen bond

lengths are again assumed to be 108.5 pm.[38] There are three non-identical protons and 28 π-electron circuits in all. They are numbered as shown in Table 2 and Fig. 2. All the numerical results are also presented in Table 2 and Fig. 3.

In contrast to anthracene, not all π-electron circuits contribute to the increase in the secondary field at a given proton. Since the geometric factor of any π-electron circuit has the same sign, the sign of the contribution depends upon the sign of the circuit resonance energy. As stated before, the circuit resonance energy is positive for all $(4n+2)$-membered circuits and negative for all $(4n)$-membered circuits. There are no odd-membered π-electron circuits in dicyclooctabiphenylene. Accordingly, all $(4n+2)$-membered π-electron circuits contribute to the increase in the secondary field at all protons, while all $(4n)$-membered π-electron circuits contribute to the decrease in it.

Circuits 3, 4, 6, 7, 14, 15, 26, and 27 are the $(4n+2)$-membered ones. When these π-electron circuits share the carbon atom nearest to a given proton, they contribute much to the increase in the secondary field thereat. Other π-electron circuits are the $(4n)$-membered ones. When these π-electron circuits share the carbon atom nearest to a given proton, they generally contribute much to the decrease in the secondary field. The contribution of the peripheral π-electron circuit is not negligible owing to the very large geometric factor.

Circuits 20—23 are exceptional, in that they contribute little to the secondary field. When any of these π-electron circuits is deleted from the entire conjugated system, Kekulé structures cannot be written for the residual system. In general, such π-electron circuits have very small positive or negative resonance energy,[39] so it follows that they little contribute to the secondary field.

Circuits 2 and 4 are also exceptional in another sense. For example, circuit 4 contributes much to the secondary fields at protons 1 and 2 although these protons are not attached to this π-electron circuit. This is due to the exceptionally large circuit resonance energy. These exceptions suggest that the secondary field and the proton chemical shift cannot always be inferred from the nearby bond currents.

Protons 1 and 2 are predicted to experience the secondary fields of $-1.267\ B_0$ and $-1.255\ B_0$, respectively, which indicates that these protons must exhibit fairly large upfield shifts in the NMR spectrum. Proton 3 is predicted to suffer a secondary field of $-0.455\ B_0$, which indicates that this proton must exhibit a slightly upfield shift. This is in good agreement with experiment. According to Wilcox and Farley,[36] the two benzene rings in 2 are esssentially atropic, while the two eight-membered rings are highly paratropic.

Protons 1, 2, and 3 in dicyclooctabiphenylene are predicted from Eq. 27 to resonate at δ 3.68, δ 3.70, and δ 4.95, respectively. They are again in good agreement with the experimental values, δ 3.63 for proton 1, δ 3.59 for proton 2, and δ 4.55 for proton 3.[36] It seems that Eq. 27 is still very applicable to the results obtained by use of the iterative $\beta\omega'\omega''$ method. However, this may be due to the fact that both anthracene and dicyclooctabiphenylene happen to be alternant hydrocarbons with uniform charge distribution. Local anisotropic effects[7] appear fairly uniform over all conjugated atoms and bonds.

Concluding Remarks

It was in 1961 that Elvidge and Jackman put forward the proposal that a molecule should be defined as aromatic if it will sustain an induced diamagnetic ring current.[40] They implied that the proton chemical shifts may be taken to be a quantitative measure of aromaticity. An NMR criterion has since been established according to which downfield proton chemical shifts indicate aromaticity while upfield proton chemical shifts indicate antiaromaticity. However, it has not at all been clear why the molecules which exhibit downfield proton chemical shifts have strong conjugative stabilization.[41]

In this paper, we proved that proton chemical shifts are really related to aromatic stabilization, but clarified that proton chemical shifts of a polycyclic conjugated system are never proportional to the degree of aromatic stabilization. The calculated secondary magnetic field was a function of both the circuits resonance energies and the pure geometric factors. It is now clear that marked downfield proton chemical shifts are associated with one or more π-electron circuits which contribute much to aromatic stabilization.

Gayoso[42] and Gomes and Mallion[43] have attempted to estimate magnetic properties of cyclic conjugated hydrocarbons by means of Randić's conjugated circuit theory.[44] The present approach gives a physical basis for these attempts.

The author thanks Dr. R. B. Mallion for helpful discussions. This work was supported by the Grant-in-Aid for Scientific Research (No. 60540283) from the Ministry of Education, Science and Culture.

References

1) L. Pauling, *J. Chem. Phys.*, **4**, 673 (1936).
2) F. London, *J. Phys. Radium*, **8**, 397 (1937).
3) J. A. Pople, *J. Chem. Phys.*, **24**, 1111 (1956); H. J. Bernstein, W. G. Schneider, and J. A. Pople, *Proc. R. Soc. London, Ser. A*, **236**, 515 (1956).
4) J. A. Pople, *Mol. Phys.*, **1**, 175 (1958).
5) R. McWeeny, *Mol. Phys.*, **1**, 311 (1958).
6) C. W. Haigh and R. B. Mallion, *Progr. Nucl. Magn. Reson. Spectrosc.*, **13**, 303 (1979).
7) Strictly speaking, local anisotropic effects are partly responsible for the deshielding of aromatic protons: G. Berthier, M. Mayot, A. Pullman, and B. Pullman, *J. Phys. Radium*, **13**, 15 (1952); J. A. Pople, *Proc. R. Soc. London,*

Ser. A, **239**, 550 (1957); H. M. McConnell, *J. Chem. Phys.*, **27**, 226 (1957); J. A. Pople, *J. Chem. Phys.*, **41**, 2559 (1964); M. Barfield, D. M. Grant, and D. Ikenberry, *J. Am. Chem. Soc.*, **97**, 6959 (1975).

8) A. Veillard, *J. Chim. Phys.*, **59**, 1056 (1962); A. Boucekkine and J. Gayoso, *C. R. Hebd. Seances Acad. Sci., Ser. C*, **274**, 358 (1972).

9) R. B. Mallion, *Proc. R. Soc. London. Ser, A*, **341**, 429 (1975).

10) C. A. Coulson and H. C. Longuet-Higgins, *Proc. R. Soc. London, Ser. A.*, **191**, 39 (1979).

11) H. Sachs, *Publ. Math. (Debrecen)*, **11**, 119 (1964).

12) A. Graovac, I. Gutman, N. Trinajstić, and T. Živković, *Theor. Chim. Acta*, **26**, 67 (1972); A. Graovac, O. E. Polansky, N. Trinajstić, and N. Tyutyulkov, *Z. Naturforsch., Teil A*, **30**, 1696 (1975).

13) J. Aihara, *J. Am. Chem. Soc.*, **98**, 6840 (1976).

14) M. J. Rigby, R. B. Mallion, and A. C. Day, *Chem. Phys. Lett.*, **51**, 178 (1977); *ibid.*, **53**, 418 (1978).

15) J. Aihara, *J. Am. Chem. Soc.*, **101**, 558 (1979).

16) J. Aihara, *J. Am. Chem. Soc.*, **101**, 5913 (1979).

17) J. Aihara, *Bull. Chem. Soc. Jpn.*, **53**, 1163 (1980).

18) J. Aihara, *J. Am. Chem. Soc.*, **103**, 1633 (1981).

19) J. Aihara, *Bull Chem. Soc. Jpn.*, **54**, 1245 (1981).

20) J. Aihara, *J. Am. Chem. Soc.*, **103**, 5704 (1981).

21) J. Aihara, *Pure Appl. Chem.*, **54**, 1115 (1982).

22) J. Aihara and T. Horikawa, *Chem. Phys. Lett.*, **95**, 561 (1983).

23) T. Horikawa and J. Aihara, *Bull. Chem. Soc. Jpn.*, **56**, 1547 (1983).

24) J. Aihara and T. Horikawa, *Bull. Chem. Soc. Jpn.*, **56**, 1853 (1983).

25) J. Aihara, *J. Am. Chem. Soc.*, **107**, 298 (1985).

26) J. Aihara, *Bull. Chem. Soc. Jpn.*, **58**, 1045 (1985).

27) N. Mizoguchi, *Chem. Phys. Lett.*, **106**, 451 (1984).

28) C. W. Haigh and R. B. Mallion, *Mol. Phys.*, **18**, 767 (1970).

29) R. B. Mallion, *J. Chem. Phys.*, **75**, 793 (1981).

30) C. W. Haigh and R. B. Mallion, *J. Chem. Phys.*, **76**, 4063 (1982).

31) J. Aihara, *J. Am. Chem. Soc.*, **98**, 2750 (1976); *J. Org. Chem.*, **41**, 2488 (1976); *Kagaku No Ryoiki*, **30**, 379 (1976); *Netsu Sokutei*, **12**, 61 (1985).

32) I. Gutman, M. Milun, and N. Trinajstić, *J. Am. Chem. Soc.*, **99**, 1692 (1977).

33) C. A. Coulson and R. B. Mallion, *J. Am. Chem. Soc.*, **98**, 592 (1976); R. B. Mallion, *Pure Appl. Chem.*, **52**, 1541 (1980); J. A. N. F. Gomes and R. B. Mallion, *J. Org. Chem.*, **46**, 719 (1981).

34) J. Gayoso, J.-C. Andrieux, and V. Herault, *J. Chim. Phys.*, **66**, 1631 (1969); J. Gayoso, *ibid.*, **68**, 1091 (1971).

35) J. Gayoso and A. Boucekkine, *C. R. Hebd. Seances Acad. Sci., Ser. C*, **272**, 184 (1971); *ibid.*, **274**, 358 (1972); C. F. Wilcox, Jr., and G. D. Grantham, *Tetrahedron*, **31**, 2889 (1975).

36) C. F. Wilcox, Jr., and E. N. Farley, *J. Am. Chem. Soc.*, **105**, 7191 (1983); *ibid.*, **106**, 7195 (1984).

37) K. Tamagawa, T. Iijima, and M. Kimura, *J. Mol. Struct.*, **30**, 243 (1976).

38) C. W. Haigh, R. B. Mallion, and E. A. G. Armour, *Mol. Phys.*, **18**, 751 (1970); R. B. Mallion, *ibid.*, **25**, 1415 (1973).

39) J. Aihara, *J. Am. Chem. Soc.*, **99**, 2048 (1977).

40) J. A. Elvidge and L. M. Jackmann, *J. Chem. Soc.*, **1961**, 856.

41) R. Breslow, *Acc. Chem. Res.*, **6**, 393 (1973).

42) J. Gayoso, *C. R. Hebd. Seances Acad. Sci., Ser. C*, **288**, 327 (1979).

43) J. A. N. F. Gomes and R. B. Mallion, *Rev. Port. Quim.*, **21**, 82 (1979).

44) M. Randić, *Chem. Phys. Lett.*, **38**, 68 (1976); *J. Am. Chem. Soc.*, **99**, 444 (1977); *Tetrahedron*, **33**, 1905 (1977).

 © 1986 The Chemical Society of Japan Bull. Chem. Soc. Jpn., 59, 3791—3795 (1986)

The Microwave Spectrum and Molecular Structure of Methyl Selenocyanate

Takeshi SAKAIZUMI,* Masahiko OBATA, Katsumasa TAKAHASHI, Eiichi SAKAKI, Yaeko TAKEUCHI, Osamu OHASHI, and Ichiro YAMAGUCHI

Department of Chemistry, Faculty of Science and Technology, Sophia University, Kioi-cho, Chiyoda-ku, Tokyo 102

(Received June 13, 1986)

The microwave spectra of $CH_3{}^{80}SeCN$, $CH_3{}^{78}SeCN$, $CH_3{}^{80}Se{}^{13}CN$, $CH_3{}^{80}SeC{}^{15}N$, *sym*-$CH_2D{}^{80}SeCN$, and *asym*-$CH_2D{}^{80}SeCN$ have been observed. In order to determine the rotational constants of $^{13}CH_3{}^{80}SeCN$, we used the transition frequencies observed by Landsberg. From these spectra the complete r_s coordinates of seven atoms have been calculated using Kraitchman's equation. The structural parameters (bond lengths in Å(1Å=0.1 nm) and angles in degree) are: r(C1-H1)=1.073(4), r(C1-H2)=1.083(6), r(C1-Se)=1.954(7), r(Se-C2)=1.836(11), r(C2-N)=1.162(9), ∠H1-C1-H2=110.6(6), ∠H2-C1-H2′=111.4(3), ∠H1-C1-Se=105.4(5), ∠H2-C1-Se=109.3(6), ∠C1-Se-C2=96.0(11), and ∠Se-C2-N=179.3(15). It was found from the r_s structural parameters that the methyl group is at a staggered position with respect to the cyano group, the methyl group does not show C_{3v} symmetry, the bond length of r(Se-C2) is much shorter than that of r(Se-C1), and the chain bond of Se-C2-N is linear.

In a previous paper,[1] we reported on the microwave spectra, the rotational constants, the dipole moments, the barrier heights of the methyl internal rotation, the first excited state of the methyl torsional mode, and the r_0 structure of methyl selenocyanate (with ^{80}Se, ^{78}Se, ^{77}Se, and ^{76}Se) and methyl selenocyanate-d_3 (with ^{80}Se and ^{78}Se).

The selenocyanates are interesting molecules for several reasons. When a selenium atom is bonded to a cyano group, it is expected that the bond length of r(Se-C2) will be shorter than the normal single-bond length. The numbering of the atoms on the methyl selenocyanate is shown in Fig. 1. Another question is whether the chain bond of Se-C2-N is linear or bent.

In this research four isotopic species were newly prepared and the spectra were observed. The r_s structural parameters of methyl selenocyanate were calculated from the r_s coordinates of all atoms. The r_s structural parameters obtained are compared with those of related molecules and are discussed.

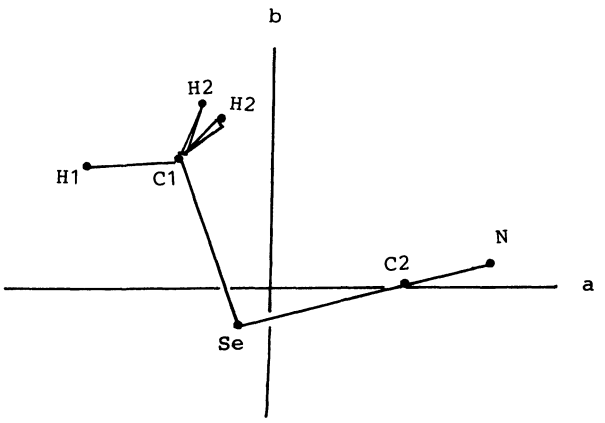

Fig. 1. The numbering of the atoms on methyl selenocyanate.

Experimental

The sample of methyl selenocyanate-*d* (CH_2DSeCN) was prepared by a reaction of methyl-*d* iodide (99% D, Merck Sharp & Dohme Canada) with potassium selenocyanate according to the method used for normal species.[1] The isotopic species of $CH_3Se{}^{13}CN$ and $CH_3SeC{}^{15}N$ were prepared by mixing potassium selenocyanate-^{13}C or potassium selenocyanate-^{15}N with methyl iodide. The potassium selenocyanate-^{13}C and potassium selenocyanate-^{15}N were synthesized by mixing potassium cyanide-^{13}C (91.6% ^{13}C, British Oxygen Co. Ltd.) or potassium cyanide-^{15}N (96.6% ^{15}N, Boxy Brown Co. Ltd.) with black selenium in ethanol.

The spectra were observed in the frequency region from 8.0 to 37 GHz with a conventional 100-kHz Stark modulation microwave spectrometer. The microwave source employed was a synthesized signal generator (HP 8672A). The absorption cell was cooled to about −20 °C with dry ice.

Results and Discussion

In order to determine as accurately as possible the rotational constants which are used to calculate the r_s coordinates of the Se atom, several a-type R-branch transitions of ^{80}Se and ^{78}Se species for which the discrepancies between the observed and the calculated frequencies were large in the previous measurement[1] were remeasured. In addition, a-type Q-branch transitions were newly assigned as listed in Table 1. The microwave spectra of $CH_3{}^{80}Se{}^{13}CN$ and $CH_3{}^{80}SeC{}^{15}N$ were newly observed and were assigned as listed in Table 2. In partially deuterated methyl selenocyanate, two conformations are possible. The symmetrical conformer (sym-species) has a plane of symmetry whereas the asymmetrical conformer (asym-species) exists in two equivalent forms. The sym-species shows the spectrum of an ordinary asymmetric rigid-rotor while the asym-species is expected to show splittings due to a tunnelling effect through the two equivalent potential wells. The observed transitions of *sym*-$CH_2D{}^{80}SeCN$ were assigned as listed in Table 3. The a-type R-branch transitions in asym-species were little affect by the tunnelling effect, but small splittings due to the tunnelling effect in a-type Q-branch transitions were observed. The center frequencies of the splittings observed in the Q-branch transitions were used to fit the rigid-rotor approximation Hamiltonian. The observed transitions of *asym*-$CH_2D{}^{80}SeCN$ were assigned as shown in Table 4. The rotational and cen-

Table 1. Observed Transition Frequencies (MHz) of CH_3SeCN in the Ground State (A-species)

Transition	$^{12}CH_3{}^{80}Se^{12}C^{14}N$		$^{12}CH_3{}^{78}Se^{12}C^{14}N$		Transition	$^{12}CH_3{}^{80}Se^{12}C^{14}N$		$^{12}CH_3{}^{78}Se^{12}C^{14}N$	
	ν_{obsd}	$\Delta\nu$[a]	ν_{obsd}	$\Delta\nu$[a]		ν_{obsd}	$\Delta\nu$[a]	ν_{obsd}	$\Delta\nu$[a]
3_{13}–2_{12}	17021.77	(−0.05)*[b]	17074.96	(−0.02)*[b]	8_{26}–8_{27}	11711.77	(−0.01)		
3_{03}–2_{02}	18043.38	(0.03)*	18098.33	(−0.07)*	9_{27}–9_{28}	16526.87	(0.12)	16482.10	(−0.02)
3_{22}–2_{21}	18345.52	(0.11)*	18398.46	(−0.15)*	10_{28}–10_{29}	22086.54	(−0.03)	22039.30	(0.06)
3_{21}–2_{20}			18699.52	(0.21)*	11_{29}–11_{210}	28250.88	(−0.03)	28206.13	(−0.04)
3_{12}–2_{11}	19573.39	(−0.03)*	19627.14	(−0.05)*	13_{310}–13_{311}	18936.08	(−0.03)	18822.12	(0.05)
4_{14}–3_{13}	22615.80	(−0.07)	22687.21	(−0.02)*	14_{311}–14_{312}	25076.00	(−0.02)	24949.55	(−0.04)
4_{04}–3_{03}	23729.26	(−0.18)*	23804.26	(−0.07)*	17_{413}–17_{414}	20262.50	(−0.03)	20066.45	(−0.01)
4_{23}–3_{22}	24400.93	(0.13)*	24472.08	(−0.07)*	18_{414}–18_{415}	26854.15	(−0.01)	26631.80	(0.07)
4_{22}–3_{21}	25132.05	(−0.03)*	25199.60	(0.09)*	21_{516}–21_{517}	20746.94	(−0.03)	20463.20	(−0.14)
4_{13}–3_{12}	25997.93	(0.07)*	26070.38	(0.11)*	22_{517}–22_{518}	27650.34	(0.21)	27321.62	(0.03)
5_{15}–4_{14}	28152.88	(−0.29)*	28242.88	(−0.13)*	25_{619}–25_{620}	20576.30	(−0.06)	20206.15	(0.02)
5_{05}–4_{04}	29201.02	(−0.02)*	29296.38	(0.02)*	26_{620}–26_{621}	27646.12	(−0.16)	27208.15	(−0.12)
5_{24}–4_{23}	30405.52	(0.09)	30495.37	(0.09)	29_{722}–29_{723}	19907.97	(0.01)	19457.71	(0.08)
5_{23}–4_{22}	31778.89	(0.09)	31862.22	(0.02)	30_{723}–30_{724}	27002.00	(0.07)	26457.68	(0.11)
5_{14}–4_{13}	32323.58	(0.15)	32415.27	(0.02)	33_{825}–33_{826}	18877.46	(0.01)	18357.90	(−0.06)
6_{15}–6_{16}	17537.79	(0.04)	17545.78	(0.02)	34_{826}–34_{827}	25861.47	(−0.01)	25219.78	(0.01)
7_{16}–7_{17}	22993.91	(0.01)	23008.85	(0.01)	38_{929}–38_{930}	24356.49	(0.01)	23631.50	(0.01)
8_{17}–8_{18}	28850.67	(−0.12)	28877.08	(−0.06)					

a) $\Delta\nu = \nu_{obsd} - \nu_{calcd.}$ b) The values marked by * are the remeasured ones for the reported values of the previous paper.[1]

Table 2. Observed Transition Frequencies (MHz) of $CH_3{}^{80}Se^{13}CN$ and $CH_3{}^{80}SeC^{15}N$ in the Ground State (A-species)

Transition	$CH_3{}^{80}Se^{13}CN$		$CH_3{}^{80}SeC^{15}N$		Transition	$CH_3{}^{80}Se^{13}CN$		$CH_3{}^{80}SeC^{15}N$	
	ν_{obsd}	$\Delta\nu$[a]	ν_{obsd}	$\Delta\nu$[a]		ν_{obsd}	$\Delta\nu$[a]	ν_{obsd}	$\Delta\nu$[a]
2_{12}–1_{11}	11260.61	(0.04)	10989.63	(0.06)	9_{27}–9_{28}	15967.17	(0.02)	14780.68	(0.09)
2_{02}–1_{01}	12021.23	(0.06)	11717.44	(−0.20)	10_{28}–10_{29}	21389.96	(0.09)	19901.72	(0.00)
2_{11}–1_{10}	12927.67	(−0.03)	12576.74	(−0.23)	13_{310}–13_{311}	18033.19	(−0.13)	16156.28	(−0.02)
3_{13}–2_{12}	16846.78	(−0.27)	16444.93	(0.07)	14_{311}–14_{312}	23981.66	(0.07)	21681.78	(−0.02)
3_{02}–2_{02}	17852.76	(−0.07)	17415.17	(0.03)	17_{413}–17_{414}	18992.20	(0.03)	16405.62	(−0.01)
3_{22}–2_{21}	18140.80	(−0.12)	17674.87	(0.22)	18_{414}–18_{415}	25322.60	(−0.04)	22159.96	(0.01)
3_{21}–2_{20}	18429.12	(−0.20)	17934.16	(−0.28)	21_{516}–21_{517}	19110.62	(−0.08)	15857.74	(−0.07)
3_{12}–2_{11}	19343.78	(0.09)	18822.51	(0.01)	22_{517}–22_{518}	25667.60	(0.01)	21655.04	(0.04)
4_{14}–3_{13}	22386.30	(−0.07)	21857.31	(−0.05)	25_{619}–25_{620}	18599.74	(−0.10)	14776.77	(0.01)
4_{04}–3_{03}	23489.63	(0.08)	22935.11	(0.00)	26_{620}–26_{621}	25224.85	(0.02)	20438.29	(−0.01)
4_{23}–3_{22}	24130.80	(−0.16)	23515.00	(0.01)	29_{722}–29_{723}	17637.16	(−0.05)	13378.07	(0.09)
4_{32}–3_{31}			23687.55	(0.20)	30_{723}–30_{724}	24178.56	(−0.05)	18748.78	(−0.05)
4_{31}–3_{30}			23707.71	(−0.01)	31_{724}–31_{725}			25338.89	(−0.01)
4_{22}–3_{21}	24829.25	(0.20)	24146.15	(−0.07)	33_{825}–33_{826}	16372.79	(−0.01)	11831.73	(−0.07)
4_{13}–3_{12}	25696.72	(0.20)	25011.74	(0.07)	34_{826}–34_{827}	22695.23	(0.11)	16792.44	(−0.04)
5_{14}–5_{15}	12391.85	(−0.15)	11810.81	(0.12)	35_{827}–35_{828}			23034.66	(0.06)
6_{15}–6_{16}	17175.81	(0.00)	16387.40	(0.05)	38_{929}–38_{930}	20922.30	(−0.07)	14737.60	(0.04)
7_{16}–7_{17}	22537.70	(−0.01)	21538.16	(−0.12)	39_{930}–39_{931}			20503.87	(−0.03)
8_{26}–8_{27}	11286.95	(−0.02)	10392.68	(0.14)					

a) $\Delta\nu = \nu_{obsd} - \nu_{calcd.}$

trifugal distortion constants obtained for normal and isotopic species are listed in Table 5 except for $^{13}CH_3{}^{80}SeCN$ species.

For the $^{13}CH_3{}^{80}SeCN$ species, Landsberg[2] has determined the rotational constants by using the frequencies of the a-type R-branch transition, but has not determined the centrifugal distortion constants. We obtained the rotational constants by using a Hamiltonian which included the centrifugal distortion effects for all of isotopic species. Therefore, in order to consider the effects for $^{13}CH_3{}^{80}SeCN$ species, we used the centrifugal distortion constants of $CH_3{}^{80}SeCN$ as those of $^{13}CH_3{}^{80}SeCN$. The rotational constants of $^{13}CH_3{}^{80}SeCN$ were calculated by using the assumed centrifugal distortion constants and the frequencies of an a-type R-branch transition observed by Landsberg.[2] The obtained rotational constants are listed in Table 5 and are in good agreement with those reported by Landsberg.[2]

The obtained values of moments of inertia and the planar moments of inertia,[3] P_c, are shown in Table 6. The values of P_c in isotopic species were close to 1.42

Table 3. Observed Transition Frequencies (MHz) of *sym*-$CH_2D^{80}SeCN$ in the Ground State

Transition	ν_{obsd}	$\Delta\nu$[a)]	Transition	ν_{obsd}	$\Delta\nu$[a)]	Transition	ν_{obsd}	$\Delta\nu$[a)]
$2_{12}-1_{11}$	11005.00	(−0.28)	$6_{15}-6_{16}$	17047.59	(0.01)	$24_{6,18}-24_{6,19}$	14788.34	(0.04)
$2_{02}-1_{01}$	11758.20	(−0.33)	$7_{16}-7_{17}$	22343.51	(−0.07)	$25_{6,19}-25_{6,20}$	20625.76	(0.11)
$3_{13}-2_{12}$	16462.98	(0.18)	$8_{17}-8_{18}$	28021.84	(0.11)	$26_{6,20}-26_{6,21}$	27607.25	(−0.01)
$3_{03}-2_{02}$	17453.68	(0.15)	$9_{27}-9_{28}$	16152.60	(−0.10)	$28_{7,21}-28_{7,22}$	14310.83	(0.03)
$3_{12}-2_{11}$	18943.91	(−0.14)	$10_{28}-10_{29}$	21565.26	(−0.05)	$29_{7,22}-29_{7,23}$	20099.78	(0.03)
$4_{14}-3_{13}$	21871.89	(−0.07)	$12_{2,10}-12_{2,11}$	33948.86	(−0.05)	$30_{7,23}-30_{7,24}$	27143.31	(0.03)
$4_{04}-3_{03}$	22949.30	(0.11)	$13_{3,10}-13_{3,11}$	18612.76	(0.07)	$32_{8,24}-32_{8,25}$	13568.10	(0.15)
$4_{23}-3_{22}$	23608.57	(−0.03)	$14_{3,11}-14_{3,12}$	24605.00	(−0.11)	$33_{8,25}-33_{8,26}$	19199.69	(−0.17)
$4_{13}-3_{12}$	25160.26	(−0.02)	$16_{4,12}-16_{4,13}$	14489.29	(−0.02)	$35_{8,27}-35_{8,28}$	34430.50	(−0.06)
$5_{15}-4_{14}$	27225.50	(−0.03)	$17_{4,13}-17_{4,14}$	20038.88	(−0.03)	$36_{9,27}-36_{9,28}$	12649.24	(−0.14)
$5_{05}-4_{04}$	28235.50	(−0.03)	$18_{4,14}-18_{4,15}$	26492.68	(0.15)	$37_{9,28}-37_{9,29}$	18034.30	(−0.15)
$5_{24}-4_{23}$	29416.69	(−0.11)	$20_{5,15}-20_{5,16}$	14891.50	(−0.18)	$38_{9,29}-38_{9,30}$	24827.43	(0.21)
$5_{23}-4_{22}$	30764.08	(0.17)	$21_{5,16}-21_{5,17}$	20653.00	(−0.10)	$39_{9,30}-39_{9,31}$	33013.00	(−0.06)
$5_{14}-4_{13}$	31279.39	(0.31)	$22_{5,17}-22_{5,18}$	27438.29	(0.12)	$40_{10,30}-40_{10,31}$	11627.79	(0.10)

a) $\Delta\nu=\nu_{obsd}-\nu_{calcd}$.

Table 4. Observed Transition Frequencies (MHz) of *asym*-$CH_2D^{80}SeCN$ in the Ground State

Transition	ν_{obsd}	$\Delta\nu$[a)]	Transition	ν_{obsd}	$\Delta\nu$[a)]	Transition	ν_{obsd}	$\Delta\nu$[a)]
$2_{12}-1_{11}$	11165.00	(0.20)	$6_{15}-6_{16}$	18014.23	(0.17)	$22_{5,17}-22_{5,18}$	12091.18	
							12092.56	(0.06)
$2_{02}-1_{01}$	11953.15	(−0.38)	$7_{16}-7_{17}$	23484.53	(−0.08)	$23_{6,17}-23_{6,18}$	17532.66	
							17534.57	(−0.01)
$2_{11}-1_{10}$	12927.64	(−0.04)	$8_{17}-7_{18}$	29244.22	(−0.15)	$24_{6,18}-24_{6,19}$	24214.34	
							24216.50	(0.12)
$3_{13}-2_{12}$	16691.86	(−0.08)	$8_{26}-8_{27}$	13182.00	(0.24)	$25_{6,19}-25_{6,20}$	31994.38	
							31997.08	(0.06)
$3_{03}-2_{02}$	17705.08	(0.11)	$9_{27}-9_{28}$	18318.50	(0.06)	$26_{6,20}-26_{6,21}$	13048.50	
							13050.00	(−0.03)
$3_{12}-2_{11}$	19330.00	(−0.07)	$10_{28}-10_{29}$	24120.00	(0.01)	$27_{7,20}-27_{7,21}$	18800.68	
							18802.89	(−0.15)
$4_{14}-3_{13}$	22160.88	(−0.08)	$11_{29}-11_{2,10}$	30392.45	(−0.02)	$30_{7,23}-30_{7,24}$	13797.30	
							13799.67	(−0.19)
$4_{04}-3_{03}$	23220.79	(−0.08)	$12_{2,10}-12_{2,11}$	36902.49		$31_{8,23}-31_{8,24}$	19801.35	
				36903.44	(0.12)		19803.36	(0.10)
$4_{23}-3_{22}$	24019.66	(0.02)	$14_{3,11}-14_{3,12}$	29251.00		$32_{8,24}-32_{8,25}$	27223.00	
				29252.00	(−0.15)		27225.62	(−0.16)
$4_{22}-3_{21}$	24891.00	(0.14)	$15_{4,11}-15_{4,12}$	14038.43		$34_{8,26}-34_{8,27}$	14363.84	
				14039.63	(−0.02)		14365.56	(−0.04)
$4_{13}-3_{12}$	25650.04	(0.03)	$16_{4,12}-16_{4,13}$	19710.51		$35_{8,27}-35_{8,28}$	20563.34	
				19711.53	(0.17)		20565.49	(−0.01)
$5_{15}-4_{14}$	27564.82	(−0.04)	$18_{4,14}-18_{4,15}$	33640.85		$36_{9,27}-36_{9,28}$	28265.28	
				33643.25	(0.12)		28268.36	(0.21)
$5_{05}-4_{04}$	28506.50	(0.06)	$19_{5,14}-19_{5,15}$	15960.50		$38_{10,28}-38_{10,29}$	14767.75	
				15962.00	(−0.03)		14769.83	(−0.02)
$5_{24}-4_{23}$	29908.83	(−0.05)	$20_{5,15}-20_{5,16}$	22173.62		$39_{10,29}-39_{10,30}$	21113.15	
				22175.45	(0.03)		21115.76	(0.29)
$5_{23}-4_{22}$	31514.75	(−0.08)	$21_{5,16}-21_{5,17}$	29395.40		$40_{10,30}-40_{10,31}$	29038.47	
				29397.50	(−0.07)		29041.62	(−0.25)
$5_{14}-4_{13}$	31845.75	(0.02)						

a) $\Delta\nu=\nu_{obsd}-\nu_{calcd}$.

uÅ² (1 uÅ²=1.66053×10⁻²⁹ kg(nm)²) except for *asym*-CH_2DSeCN. This is in conformity with the fact that the heavy atoms (C1, Se, C2, and N) and the deuterium atom in the methyl group are located in the symmetry plane. The large value (2.159 uÅ²) of P_c of *asym*-CH_2DSeCN agrees with the fact that the deuterium atom of the methyl group is located out of the plane.

The coordinates of the atoms in the principal-axis system of the normal species ($CH_3{}^{80}SeCN$), as obtained using Kraitchman's equation,[4] are listed in Table 7. The b-coordinate of C2 atom obtained from Kraitchman's equation was small (0.0898 Å) and unreliable. Therefore, the b-coordinate of C2 was calculated from the first moment equation. Although the c-coordinates(Å) of H1, C1, Se, C2, and N obtained from Kraitchman's equation were found to be either extremely small or imaginary (0.1557(121), 0.0032*i*, 0.0002*i*, 0.0272(674), and 0.0019*i*), respectively, these c-

Table 5. Observed Rotational (MHz) and Centrifugal Distortion (kHz) Constants in A-Species[a)]

Species	A	B	C	Δ_J	Δ_{JK}	Δ_K	δ_J	δ_K
$CH_3{}^{80}SeCN$	10143.93(35)	3483.665(33)	2631.619(33)	0.80(78)	14.7(23)	14.6(25)	0.425(73)	10.0(33)
$CH_3{}^{78}SeCN$	10198.33(20)	3492.634(90)	2640.404(83)	0.8[b)]	14.1(8)	14.6[b)]	0.444(13)	8.8(13)
$^{13}CH_3{}^{80}SeCN$[c)]	9725.60(60)	3454.943(20)	2586.432(18)	0.8[b)]	14.7[b)]	14.6[b)]	0.425[b)]	10.0[b)]
$CH_3{}^{80}Se^{13}CN$	10142.18(23)	3440.361(13)	2606.736(12)	0.8[b)]	14.5(10)	14.6[b)]	0.403(15)	10.2(15)
$CH_3{}^{80}SeC^{15}N$	10122.20(21)	3342.726(13)	2548.964(12)	0.8[b)]	14.2(10)	14.6[b)]	0.366(11)	9.6(11)
a-$CH_2D^{80}SeCN$	9270.81(7)	3452.336(38)	2570.825(38)	1.4(9)	13.1(2)	14.6[b)]	0.436(53)	10.0[b)]
s-$CH_2D^{80}SeCN$	9775.95(14)	3372.768(13)	2544.179(12)	0.8[b)]	10.5(7)	14.6[b)]	0.490(5)	6.1(9)

a) The values of A-species for the molecules except for mono-dueterated species are given. Figures in parentheses indicate the uncertainties attached to the last significant figures calculated from 2.5 times the standard deviation. b) The assumed values of the centrifugal distortion constants in normal species were used. c) The transition frequencies observed by Landsberg[2)] were used.

Table 6. Observed Moments of Inertia[a)] (uÅ^2) and P_c (uÅ^2)

Species	I_a	I_b	I_c	P_c
$CH_3{}^{80}SeCN$	49.8205(17)	145.0702(14)	192.0400(24)	1.4254(28)
$CH_3{}^{78}SeCN$	49.5548(10)	144.6977(37)	191.4010(60)	1.4258(54)
$^{13}CH_3{}^{80}SeCN$	51.9633(32)	146.2762(8)	195.3950(14)	1.4223(27)
$CH_3{}^{80}Se^{13}CN$	49.8291(11)	146.8962(6)	193.8731(9)	1.4261(13)
$CH_3{}^{80}SeC^{15}N$	49.9275(10)	151.1867(6)	198.2672(9)	1.4235(13)
a-$CH_2D^{80}SeCN$	54.5126(4)	146.3867(16)	196.5813(29)	2.1590(25)
s-$CH_2D^{80}SeCN$	51.6958(7)	149.8401(6)	198.6401(9)	1.4479(11)

a) Conversion factor is 505376 uÅ^{2}MHz. Figures in parentheses indicate the uncertainty attached to the last significant figures estimated from 2.5 times the standard deviations. (1 uÅ^2=1.66053×10^{-29}kg(nm)^2). b) $P_c=(I_a+I_b-I_c)/2$.

Table 7. r_s Coordinates of Atoms[a)] (in Å) (1 Å=0.1 nm)

Atom	a	b	c
H1	−2.1596(8)	1.3958(13)	0.0[b)]
H2	−0.7462(30)	1.9820(12)	0.8946(29)
H2′	−0.7462(30)	1.9820(12)	−0.8946(29)
Cl(methyl)	−1.0898(27)	1.4779(20)	0.0[b)]
Se	−0.4289(29)	−0.3611(34)	0.0[b)]
C2(cyanide)	1.3543(13)	0.0775(237)[c)]	0.0[b)]
N	2.4860(7)	0.3422(57)	0.0[b)]

a) The numbering of the atoms is shown in Fig. 1. Atomic masses taken from W. Gordy and R. L. Cook, Microwave Molecular Spectra, third ed. (John Wiley & Sons, Inc., New York, 1984) Appendix E. b) Assumed to be zero by symmetry. c) Obtained by first-moment relation, $\sum m_i b_i=0$.

Table 8. r_s Structure[a)] of Methyl Selenocyanate

r(Cl-H1) :	1.073(4)	∠H1-Cl-H2 :	110.6(6)
r(Cl-H2) :	1.083(6)	∠H2-Cl-H2′ :	111.4(3)
r(Cl-Se) :	1.954(7)	∠H1-Cl-Se :	105.4(5)
r(Se-C2) :	1.836(11)	∠H2-Cl-Se :	109.3(6)
r(C2-N) :	1.162(9)	∠Cl-Se-C2 :	96.0(11)
		∠Se-C2-N :	179.3(15)

a) Bond lengths are in Å (1 Å=0.1 nm) and angles are in degree.

coordinates are assumed to be zero because the heavy atoms and H1 atom is located in the symmetry plane. The structural parameters obtained are listed in Table 8.

Table 9. Comparison of r_s Structural Parameters of Methyl Group in CH_3SeCN and CH_3SCN (Bond Lengths in Å and Angles in degree)

	CH_3SeCN[a)]	CH_3SCN[b)]
r(Cl-H1)	1.073(4)	1.073(3)
r(Cl-H2)	1.083(6)	1.086(4)
∠H1-Cl-H2	110.6(6)	110.3(2)
∠H2-Cl-H2′	111.4(3)	111.3(2)
∠H1-Cl-M[c)]	105.4(5)	105.4(3)
∠H2-Cl-M[c)]	109.3(6)	109.7(1)

a) This work. b) Ref. 5. c) M=Se or S atom.

The r_s structural parameters of the methyl group for CH_3SeCN were compared with those for CH_3SCN[5)] as listed in Table 9. The structural parameters of the methyl group for CH_3SeCN are quite similar to those for CH_3SCN. The bond length of r(Cl-H1) for CH_3SCN has been found to be shorter by about 0.01 Å than that of r(Cl-H2).[5)] The numbering of the atoms of CH_3SCN is the same as that of CH_3SeCN, as shown in Fig. 1. Although a similar trend can be seen for CH_3SeCN, the bond length of r(Cl-H1) agrees with that of r(Cl-H2) within the limits of error. The two H-C-H angles are almost the same, but the angle of H1-Cl-Se is much smaller than that of H2-Cl-Se. Neither the methyl group of CH_3SeCN nor that of CH_3SCN shows a C_{3v} symmetry. The methyl group is staggered with respect to the cyano group.

The r_s structural parameters of CH_3SeCN were compared with those of related molecules as listed in Table

Table 10. Comparison of the Structural Parameters of CH_3SeCN with Those of Related Molecules. (Bond Lengths in Å and Angles in degree).

	r(Cl-Se)	∠Cl-Se-C2	r(Se-C2)	r(C2≡N)	∠Se-C2≡N
CH_3SeCH_3[a] (r_s)	1.943(1)	96.2(2)	1.943(1)		
CH_3SeCN[b] (r_s)	1.954(7)	96.0(11)	1.836(11)	1.162(9)	179.3(15)
$CH_3C(H)=Se$[c] (r_o)			1.758(10)		
CH_3CN[d] (r_s)				1.157(1)	
CH_3SCN[e] (r_s)	1.824(2)[f]	99.03(8)[g]	1.684(3)[h]	1.170(2)	179.8(13)[i]

a) Ref. 6. b) This work. c) Ref. 7. d) Ref. 8. e) Ref. 5. f) r(Cl-S). g) ∠Cl-S-C2. h) r(S-C2). i) ∠S-C2≡N.

10. The bond length of r(Cl-Se) is almost the same as that for a normal single bond of CH_3SeCH_3.[6] On the other hand, the bond length of r(Se-C2) comes between those of a single bond and a double bond and has the value which is shorter by about 0.1 Å than a normal single bond[6] and is longer by about 0.1 Å than a normal double bond of $CH_3C(H)=Se$.[7] This intermediate bond length arises from the back donation of electrons from the selenium atom to a cyano group. The same trend has also been seen in the bond length of r(Cl-S) and r(S-C2) of methyl thiocyanate,[5] as shown in Table 10. The bond length of r(C2-N) of methyl selenocyanate agrees with that of CH_3CN[8] within 0.01 Å. The bond angle of Cl-Se-C2 is similar to that of CH_3SeCH_3[6] but is smaller by about 3° than that of Cl-S-C2 of methyl thiocyanate.[5] Both the chain bonds of Se-C2-N of methyl selenocyanate and that of S-C2-N of methyl thiocyanate[5] were found to be linear.

It was concluded from the r_s structural parameters of methyl selenocyanate that (i) the methyl group is staggered with respect to the cyano group, (ii) the bond angle of H1-C1-Se is much smaller than that of H2-C1-Se and the methyl group does not have the C_{3v} symmetry, (iii) the bond length of r(Se-C(N)) is much shorter than that of r(Se-C(CH_3)) because of the back donation of electrons in bonding a selenium atom to a cyano group, and (iv) the chain bond of Se-C2-N is linear.

References

1) T. Sakaizumi, Y. Kohri, O. Ohashi, and I. Yamaguchi, *Bull. Chem. Soc. Jpn.*, **51**, 3411 (1978).
2) B. M. Landsberg, *Z. Naturforsch.*, **33a**, 1333 (1978).
3) W. Gordy and R. L. Cook, "Microwave Molecular Spectra," 3rd ed., John Wiley & Sons, Inc., New York (1984), Chap. 13.
4) J. Kraitchman, *Am. J. Phys.*, **21**, 17 (1953).
5) H. Dreizler, H. D. Rudolph, and M. Schleser, *Z. Naturforsch.*, **25a**, 1643 (1970).
6) J. F. Beecher, *J. Mol. Spectrosc.*, **4**, 414, (1966).
7) M. Hutchinson and H. W. Kroto, *J. Mol. Spectrosc.*, **70**, 347 (1978).
8) C. C. Costain, *J. Chem. Phys.*, **29**, 864 (1958).

 © 1986 The Chemical Society of Japan Bull. Chem. Soc. Jpn., 59, 3797—3802 (1986)

Relations between Diatomic Constants and the Features of the Potential Energy Surfaces

Noboru TANAKA
Hachinohe Institute of Technology, Hachinohe 031
(Received June 16, 1986)

The semiempirical method is used to calculate potential energy surfaces. The linear H_3 and rectangular H_4 systems have been chosen as standard surfaces in order to compare the surface features. Relationships between diatomic constants and topological features along a minimum energy path, and the height and location of the barrier, are demonstrated.

The knowledge of the relation between the effect of vibrational and translational energies on the reaction cross section and the topological features of potential energy surfaces have provided valuable information in understanding the fundamental nature of collision dynamics.[1-3] We are seeking additional insight into this relation. In this attempt, we investigate correlations between the features of the potential energy surfaces and the characters of the reactant molecules. With the understanding of the correlations, the effect of the two kinds of energies on the chemical reaction can be estimated directly from the characters of the reactant molecules.

Recently, more accurate ab initio potential energies have been calculated for many reaction systems, using fast computers. Even though the potential energies calculated by ab initio method are accurate, it is difficult to relate the potential energies with the character of reactant molecules because of the complicated calculation method. On the other hand, a semiempirical method can relate directly the potential energies with the character without complicated calculations. Commonly used semiempirical methods[4,8,10] employ the diatomic constants as the characteristics of reactant molecules.

This report investigates the relation between diatomic constants and features of potential energy surfaces, using our semiempirical method.[5] In this article, such simple models as linear H_3 and rectangular H_4 will be chosen. Varying the values of the diatomic constants which are used to calculate potential energies in the both systems, we observe the changes of the topological features along minimum energy path, and height and location of the barrier.

Theoretical

Our semiempirical method[5] to calculate potential energies (E) is based on a valence bond treatment[6] of an n-electron n-atom system. In this method, E can be obtained from the secular equation,

$$|\boldsymbol{H} - \boldsymbol{M}E| = 0 \tag{1}$$

where $\boldsymbol{H}$ is a Hamiltonian matrix and $\boldsymbol{M}$ is an overlap matrix. Each matrix element is defined as

$$H_{ij} = \sum \varepsilon_P \langle \Omega | H | P\Omega \rangle \langle \theta_i | P\theta_j \rangle,$$
$$M_{ij} = \sum \varepsilon_P \langle \Omega | P\Omega \rangle \langle \theta_i | P\theta_j \rangle, \tag{2}$$

where H is the Hamiltonian of the system, P is a permutation operator of electrons, ε_p is the parity, and θ_i is the spin function.

The matrix elements of $\boldsymbol{H}$ contain multiple exchange integrals given by

$$\Lambda_p = \langle \Omega | H | P\Omega \rangle. \tag{3}$$

We found that Λ_p is reduced to two basic types.[5] One of them is a transposition type, and the other is a cycle type. These integrals can be formulated in terms of diatomic components α_i, Q_i, and S_i, using the Mulliken approximation,[7] as follows;

$$\Lambda_P^1 \simeq \Pi S_i^2 [\sum (\alpha_i / S_i^2) + Q - \sum Q_i],$$
$$\Lambda_P^2 \simeq (1/2) \Pi S_i [\sum (\alpha_i / S_i^2) + 2Q - \sum Q_i], \tag{4}$$

where Q is a Coulomb integral, which is expressed by the diatomic Coulomb integrals Qi, and i shows pairs formed with electrons (atoms). Since the multiple exchange integral Λ_P consists of these Λ_P^1 and Λ_P^2 the calculation of Λ_P is to evaluate the diatomic components α_i, Q_i, and S_i. The first two diatomic components α_i and Q_i are evaluated from the Morse and anti-Morse functions which contain diatomic constants:[8,10] dissociative energy D, force constant α, and internuclear equilibrium distance R_e. These diatomic constants are combined with spectroscopic information on diatomic molecules.[9] The last diatomic component S_i is formulated empirically with adjustable parameters κ and λ.

$$S_i = (1 + R_i \zeta_i + \frac{1}{3} \zeta_i^2 R_i^2) \exp(-\zeta_i R_i), \tag{5}$$

where the screening parameter ζ_i is given by[10,11]

$$\zeta_i = 1.0 + \kappa \exp(-\lambda R_i). \tag{6}$$

Thus the potential energy E takes the following analytical form of coordinates of internuclear distance R as

$$E = f(\chi, \beta : R), \tag{7}$$

with the adjustable parameter β and diatomic constants χ which are abbreviations for κ, λ and for D, α, R_e, respectively.

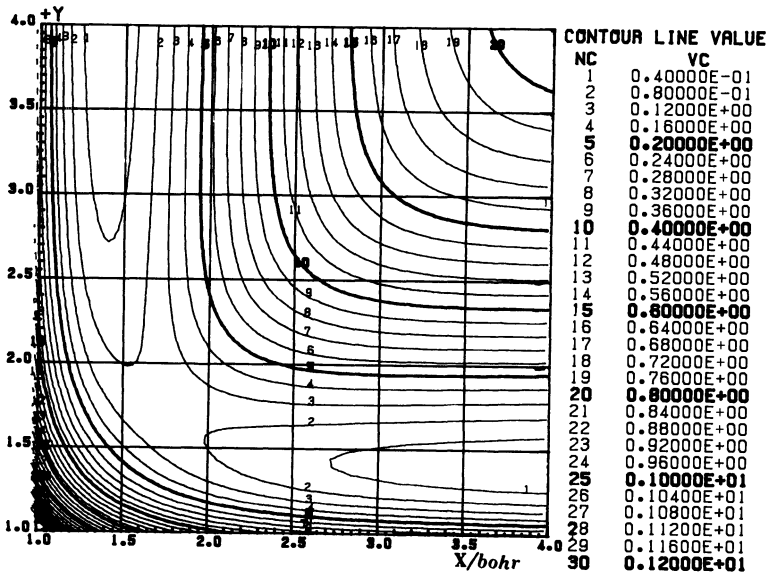

Fig. 1. Equipotential contour maps for H_3 surface corresponding to linear arrangement of the three atoms. The contour intervals are 1/25 of the H_2 dissociation energy. Number and value of the contour line are denoted by NC and VC, respectively.

In order to investigate the relationships between diatomic constants and the feature of potential energy surfaces, we define the surfaces by equipotential contour maps. The character of the surfaces are interpreted from the three following points of view;

1) Height, depth, and slope of the valley along the minimum energy path,

2) Height and location of the barrier,

3) Shape and passing positions of the minimum energy path.

Results

Equipotential contour maps for the linear H_3 and rectangular H_4 systems are presented in Figs. 1 and 4 as standard surfaces to compare the surface features. In order to assess the nature of these surfaces, we have changed the diatomic constants which are used to calculate the potential energies.[11,14] In six cases of diatomic constant change, the contour maps (a)—(f) are shown in both Figs. 3 and 5. The increase and decrease of the D, α, and R_e correspond to the cases of (a) and (b), (c) and (d), and (e) and (f), respectively. The barrier heights and the coordinates along the minimum energy path, at the starting point (entrance valley), at the saddle point (barrier), and at the ending point (exit valley), are presented in Tables 1 and 2, for each of six cases.

1) **Model of Linear H_3 System.** Figure 1 and Fig. 2 show equipotential contour maps for H_3 surfaces corresponding to a linear arrangement of the three hydrogen atoms calculated by our method[11] and the Truhlar-Horowitz method.[12,13]

The values of the diatomic constants D, α, and R_e are 0.174475 a.u., 1.05 a.u.,$^{-1}$ and 1.401 bohr, respectively. The adjustable parameters κ and λ in Eq. 6 have been so determined that the barrier height calculated by using Eq. 7 agrees with that calculated by Liu[12]; that is κ=3.20 and λ=1.202.[11] In Table 1, the values of the barrier height and coordinates of the minimum energy path are shown together with the results of Liu. Comparisons of the minimum energy path, contour

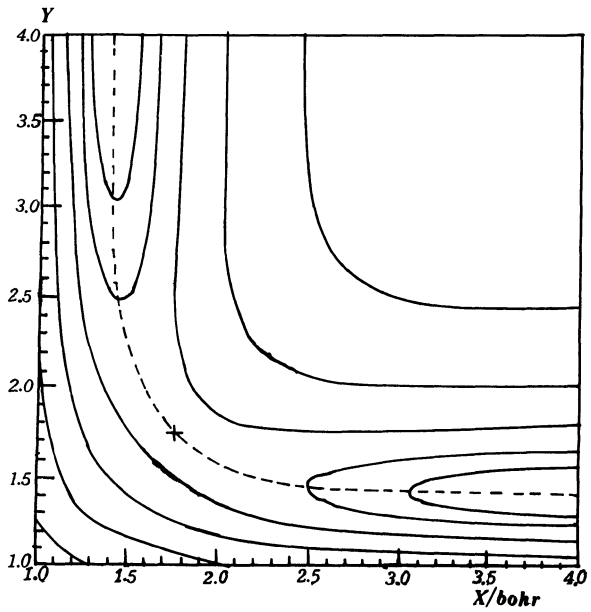

Fig. 2. Truhlar-Horowitz contour map for linear arrangement H_3 surface. The solid curves are cotours of the interaction potential corresponding to 3, 6, 12, 24, 48, 96, and 192 kcal mol^{-1}. The dashed curve is a minimum energy path and the cross is a saddle point.

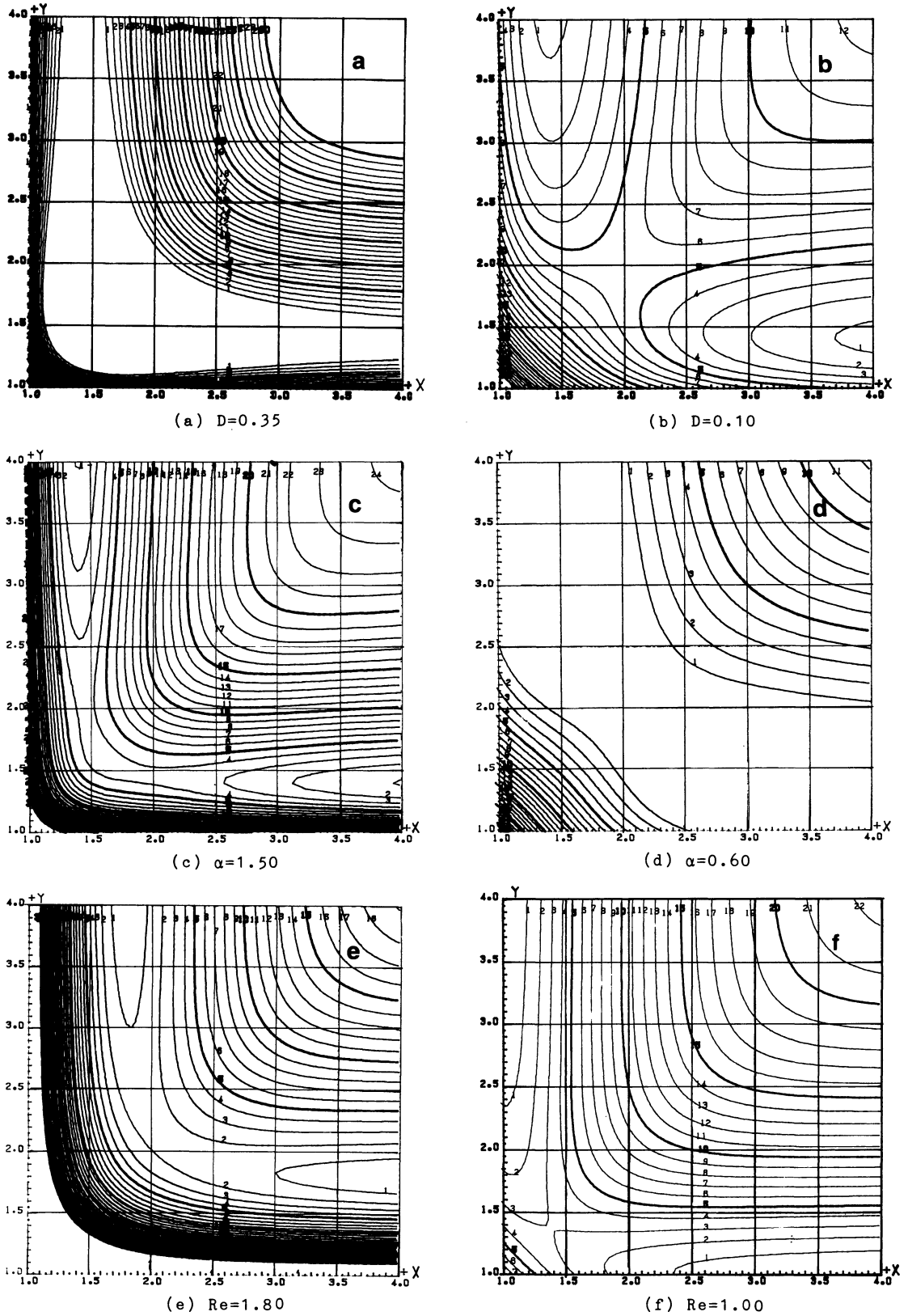

Fig. 3. Equipotential contour maps on different D, α, R_e for model of the linear H_3 system.

line, and barrier height between Figs. 1 and 2 are satisfactory.

The changes of the features of the maps can be read off from Fig. 3 and Table 1 in the case of (a)—(b) as follows;

(a) D=0.35: The valley along the minimum energy

Table 1. Barrier Height and Coordinates of the Minimum Energy Path in Six Cases[a] of the Changes of Diatomic Constants for the Model of Linear H_3 System

Case	Starting point	Saddle point	Barrier height	Ending point
	bohr	bohr	kcal/mole^{-1}	bohr
H_3[b]	(4.00, 1.40)	(1.757, 1.757)	9.802	(1.40, 4.00)
H_3[c]	(4.00, 1.40)	(1.743, 1.743)	9.802	(1.40, 4.00)
(a)	(4.00, 1.40)	(1.60, 1.60)	(−38.83)	(1.40, 4.00)
(b)	(4.00, 1.60)	(1.90, 1.90)	24.49	(1.60, 4.00)
(c)	(4.00, 1.40)	(1.60, 1.60)	15.83	(1.40, 4.00)
(d)	(4.00, 1.40)	(2.05, 2.05)	(−1.46)	(1.40, 4.00)
(e)	(4.00, 1.90)	(2.10, 2.10)	7.35	(1.90, 4.00)
(f)	(4.00, 1.275)	(1.675, 1.675)	13.12	(1.275, 4.00)

a) See the text. b) Results of this Liu; Ref. 12. c) Results of this study; Ref. 11.

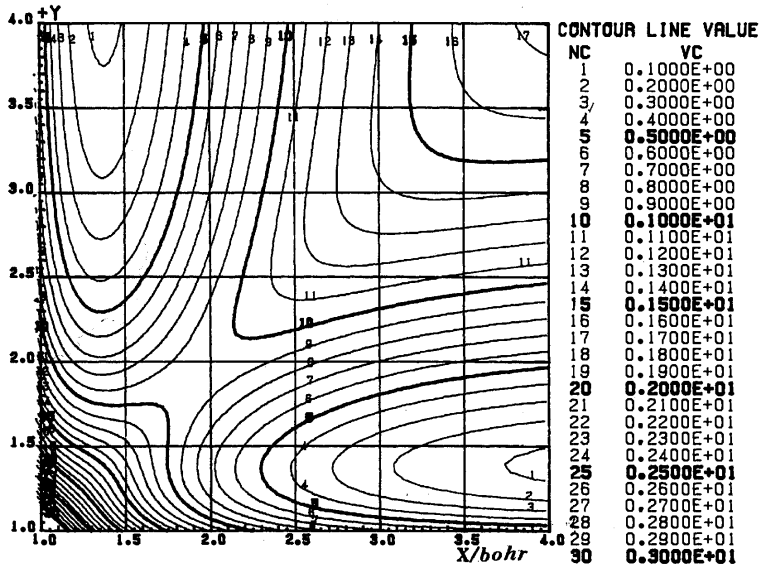

Fig. 4. Equipotential contour maps for H_4 surface corresponding to rectangular arrangement of the four atoms. The contour intervals are 1/10 of the H_2 dissociation energy. Number and value of the contour line are denoted by NC and VC, respectively.

path greatly increases in height, depth, and slope. The path moves to the inside. A deep ditch arises along the path.

(b) D=0.10: The valley along the minimum energy path decreases in height, depth, and slope, but the slope toward the barrier becomes steeper. The saddle point moves to the outside. The barrier height increases reasonably in value.

(c) α=1.50: The valley along the minimum energy path shallows but the slope becomes steep. The saddle point moves also to the inside. The basin lies between (2.0, 1.5) and (1.5, 2.0). The potential energy at the bottom in the basin is 16.87 kcal (1 cal=4.184 J) and is 15.83 kcal around the basin.

(d) α=0.60: There is no barrier but a ditch, and the slope becomes low-pitched along the minimum energy path.

(e) R_e=1.80: The depth and slopes of the valley change very little, but the minimum energy path shifts to the outside.

(f) R_e=1.00: The depth and slopes of the valley change very little, but the minimum energy path shifts to the inside.

2) **Model of rectangular H_4 System.** Figure 4 shows equipotential contour maps for H_4 surfaces corresponding to a rectangular arrangement of the four atoms calculated by our method.[14] The values of the diatomic constants D, α, and R_e are 0.174475 a.u., 1.05 a.u.$^{-1}$, and 1.401 bohr, respectively. The adjustable parameters κ and λ in Eq. 6 have been so determined that the barrier height calculated by using Eq. 7 agrees with that calculated by Bender and Schaefer III[15]; that is κ=1.00 and λ=0.40.[11] The contour maps for rectangular H_4 system were calculated from the various semiempirical methods by Silver and Brown[16]

The changes in the features of the maps can be read off from the Fig. 5 and Table 2 in the case of (a)—(b) as follows;

(a) D=0.30: The valley along the minimum energy path increases in height, depth, and slope. The saddle

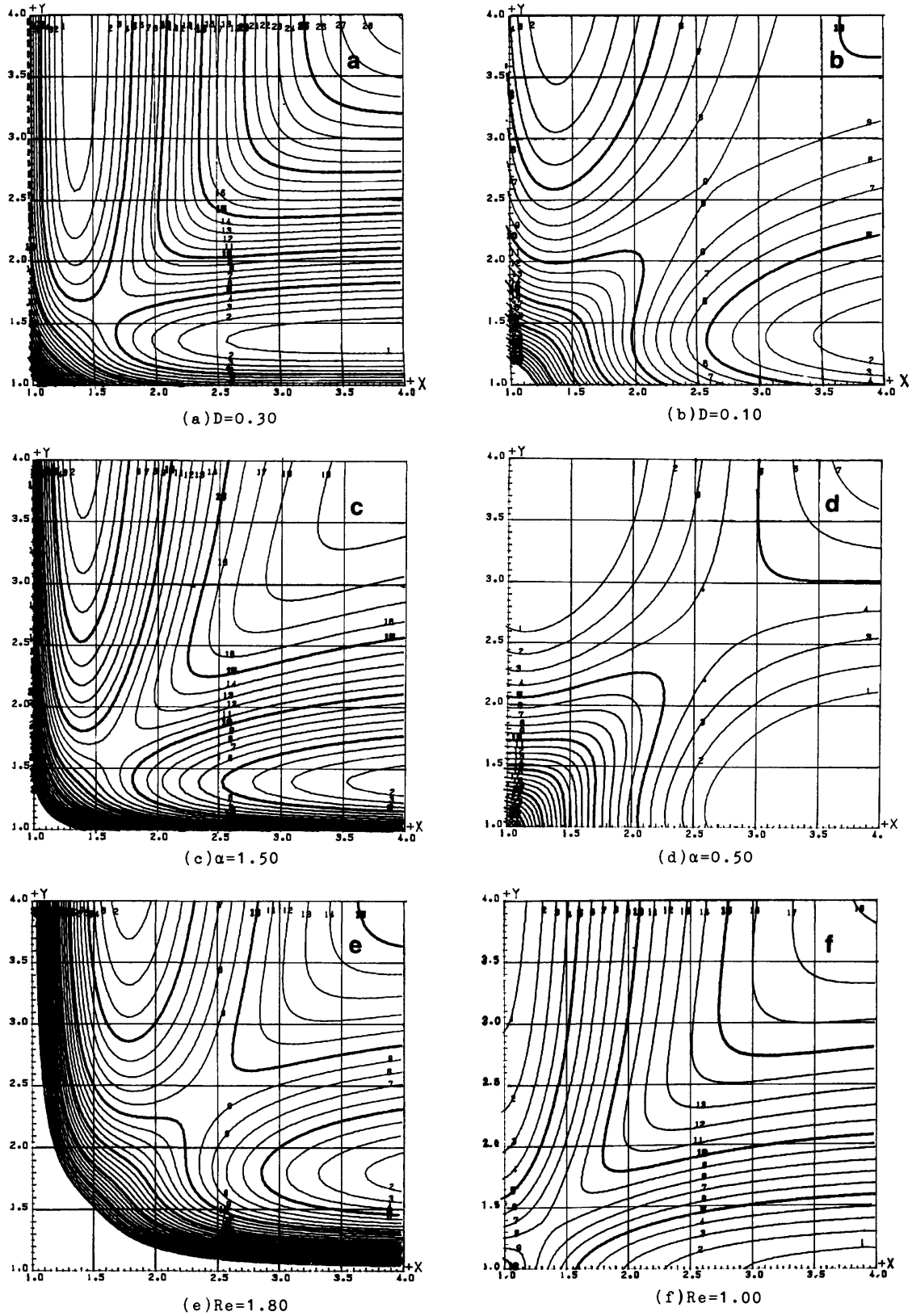

Fig. 5. Equipotential contour maps on different D, α, R_e for model of the rectangular H_4 system.

point moves to the inside. The barrier height decreases a little.

(b) D=0.10: The valley along the minimum energy path decreases in height, depth, and slope. The barrier height changes very little.

(c) α=1.50: The valley along the minimum energy

Table 2. Barrier Height and Coordinates of the Minimum Energy Path in Six Cases[a] of the Changes of Diatomic Constants for the Model of Linear H_4 System

Case	Starting point	Saddle point	Barrier height	Ending point
	bohr	bohr	kcal/mole^{-1}	bohr
H_4[b]	(4.00, 1.40)	(2.10, 2.10)	114.11	(1.40, 4.00)
(a)	(4.00, 1.40)	(1.70, 1.70)	92.58	(1.40, 4.00)
(b)	(4.00, 1.50)	(2.65, 2.65)	97.41	(1.50, 4.00)
(c)	(4.00, 1.40)	(1.80, 1.80)	145.48	(1.40, 4.00)
(d)	(4.00, 1.30)	(2.70, 2.70)	45.00	(1.30, 4.00)
(e)	(4.00, 1.80)	(2.50, 2.50)	104.90	(1.80, 4.00)
(f)	(4.00, 1.00)	(1.60, 1.60)	116.95	(1.275, 4.00)

a) See the text. b) Results this study; Ref. 14.

path shallows and the slope becomes steep. The saddle point moves also to the inside.

(d) α=0.50: The depth and width of the valley increases and their slopes become very low-pitched along the minimum energy path.

(e) R_e=1.80: The depth and slopes of the valley changes very little, but the minimum energy path shifts to the outside. The barrier height changes a little.

(f) R_e=1.00: The depth and slopes of the valley change very little, but the minimum energy path shifts to the inside. The barrier height changes a little.

Conclusions

As is evident from the Figs. 3 and 5, the diatomic constants have sensitive effects on the features of the potential energy surfaces. Except for the case (c) in Fig. 3 where the basin is formed near the saddle point, it should be noted that there appears common outcomes on both cases of the linear H_3 and the rectangular H_4 systems as follows:

(1) The binding energy D correlates remarkably well with the depth, height and slope of the valley along the minimum energy path.

(2) The force constant α correlates especially well with the slope of the valley.

(3) The internuclear equilibrium distant R_e correlates explicitly with the position of the minimum energy path.

Finally, the next step is to investigate for a more complicated system the relationships between the diatomic constants and the curvature of the minimum energy path or position of the saddle point.

The author wishes to thank Professor Takenori Suzuki of Hachinohe Institute of Technology for many helpful discussions. The numerical calculations were performed on the NEC ACOS-1000 computer at the Tohoku University Computing Center.

References

1) J. C. Polanyi and W.H. Wong, *J. Chem. Phys.*, **51**, 1439 (1969).
2) T. Tuner and Y. T. Lee, *J. Chem. Phys.*, **81**, 5638 (1984).
3) P. J. Kuntz, "Dynamics of Molecular Collision, Part B," ed by W. H. Miller, Plenum Press, New York (1976), p. 53.
4) P. J. Kuntz, E. M. Nemeth, S. D. Rosner, J. C. Polanyi, and C. E. Young, *J. Chem. Phys.*, **44**, 1168 (1966).
5) N. Tanaka and O. Nomura, *J. Chem. Phys.*, **77**, 1373 (1982).
6) R. Mcweeny and B. T. Sutcliffe, "Method of Molecular Quantum Mechanics," Acadimic Press, New York (1969).
7) R.S. Mulliken, *J. Chem. Phys.*, **46**, 497 (1967).
8) S. Sato, *J. Chem. Phys.*, **25**, 2465 (1955).
9) K. P. Huber and G. Herzberg, "Constants of Diatomic Molecules," Van Nostrand, Reinhold (1978).
10) R. N. Porter and M. Karplus, *J. Chem. Phys.*, **40**, 1105 (1964).
11) N. Tanaka, *Chem. Phys. Lett.*, **54**, 551 (1978).
12) B. Liu. *J. Chem. Phys.*, **58**, 1925 (1973).
13) D. J. Truhlar and C. J. Horowitz, *J. Chem. Phys.*, **68**, 2466 (1978).
14) Noboru Tanaka, *Bull. Chem. Soc. Jpn.*, **52**, 3477 (1979).
15) C. F. Bender and H. F. Schaefer III, *J. Chem. Phys.*, **57**, 217 (1972).
16) D. M. Silver and N. J. Brown, *J. Chem. Phys.*, **72**, 3859 (1980).

 © 1986 The Chemical Society of Japan Bull. Chem. Soc. Jpn., 59, 3803—3808 (1986)

Thermoanalytical and Calorimetric Studies on Polymorphic Behaviors of Crystalline Modifications in Aliphatic α-Amino Acids with Normal Alkyl Chains

Masayuki MATSUMOTO,* Hirofumi YAJIMA,† and (the late) Takashi HANDA†
M & A Laboratory, 428-12, Kami-asao, Asao-ku, Kawasaki 215
†Department of Applied Chemistry, Faculty of Science, Science University of Tokyo, 1-3, Kagurazaka, Shinjuku-ku, Tokyo 162
(Received February 18, 1986)

The B-A transition in DL-ABA occurs in the wide range of temperature near its decomposition temperature, and the transition pattern is similar to that of γ-α transition in glycine, whereas the pattern of α-γ transition in DL-NL is different from that in glycine, and the α-γ transition of DL-NL is of the first order. The enthalpy difference between modifications A and B of DL-ABA was nearly equal to the enthalpy of transition determined by DSC.

Much attention has been directed to polymorphic transition of aliphatic α-amino acids with normal alkyl chains, including glycine. Only the following compounds, however, have been studied. According to X-Ray diffraction and IR absorption studies, many of the aliphatic α-amino acids have crystalline modifications.[1-5] For example, glycine has 3 crystal modifications called α-, β-, and γ-forms, and the γ-form (trigonal) is transformed into the α-form (monoclinic) in the temperature range between 433 and 483 K. The enthalpy of transition is of the order of 1 kJ mol^{-1}. The transition is inferred to be due to the rearrangement of molecular layers bound with hydrogen bonds between the constituent molecules.[6-8] Iitaka and others found that the B-form of DL-2-aminobutanoic acid(DL-ABA) is transformed into the A-form at 468 K, and X-Ray analysis showed that the γ-carbon atom of the A-form DL-ABA (monoclinic) distributes among anti-position, gauche I, and gauche II with respect to nitrogen atom, whereas the γ-carbon atom in the B-form (tetragonal) is restricted to the anti-position.[6] As for polymorphic transitions of the B-form of DL-ABA and the α-form of DL-norleucine(DL-NL), it is considered that the enthalpy of transition includes contributions of rearrangement of molecular layers due to intermolecular interactions between constituent molecules and conformational change due to the rotation of carbon-carbon bonds in alkyl chains.

The thermodynamic study of phase equilibrium (or transition phenomenon) between crystal modifications seems to be useful together with the structural study of polymorphism, because the combination of structural analysis with thermodynamic study provides a significant information for polymorphism. In particular, the thermal analysis on solid-solid phase transitions between crystalline amino acids brings about suggestive information on transition phenomena of biological systems, especially of biomembranes. The objective of this work is to obtain information on polymorphic modifications of DL-ABA and DL-NL in comparison with the case of glycine by means of differential scanning calorimetry(DSC) and solution calorimetry.

Experimental

Materials. DL-2-Aminobutanoic acid(DL-ABA) and DL-norleucine(DL-NL) were purchased from Tokyo Kasei Co. and glycine from Takara Kohsan Co. All the samples used were the purest reagents commercially available: the purity of the compounds was guaranteed by each manufacturer to be 98%. The DL-NL was obtained as plate-like crystals by standing at 290 K for 24 h and the fibrous DL-ABA from a water-ethanol solution at 283 K for 48 h. By X-Ray diffraction and IR absorption, the DL-NL and DL-ABA samples were identified as α-form and B-form, respectively. The A-form DL-ABA was obtained as tabular crystals from aqueous solution by keeping at 283 K for 24 h, and the α-form glycine as tabular crystals by evaporating water. The A-form DL-ABA and α-form glycine were dried over silica gel for two months, and were dried again in vacuo for 6 h before use.

Apparatus and Procedure. Differential scanning calorimeter used in this experiment is Perkin Elmer DSC-II with Thermal Analysis Data Station(TADS). A few mg of sample was sealed in an aluminum pan, and the sample and the blank pans were set in each respective holder. The measurements of temperature and enthalpy were made in the

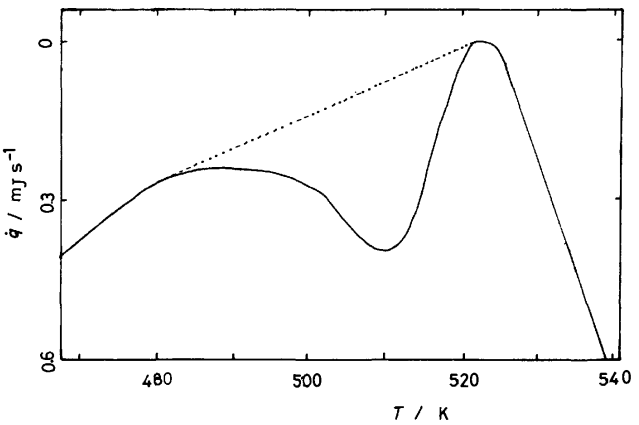

Fig. 1. DSC curve of the B-form of DL-ABA crystals heated at 5 K min^{-1} in the atmosphere of nitrogen. Sample weight: 2.64 mg.

Table 1. Thermodynamic Parameters for the Solid-Solid Transitions of Glycine and DL-2-Aminobutanoic Acid (DL-ABA)

Phase transition	Peak temperature T/K	Enthalpy change ΔH_t/kJ mol^{-1}	Entropy change ΔS_t/J mol^{-1} K^{-1}
Glycine	473(433—483)	0.92±0.08[a)]	1.95
$(\gamma\rightarrow\alpha)_{trs}$	478(459—491)	1.94±0.06	4.06
DL-ABA			
$(B\rightarrow A)_{trs}$	506(480—520)	4.91±0.29	9.70

a) Ref. 8.

range of heating rate between 0.63 and 10 K min^{-1}. The calorimeter was calibrated with indium, T_f=429.78 K and ΔH=28.5 J g^{-1}, supplied by Perkin Elmer Co. The melting point and enthalpy of fusion of indium obtained by extrapolating to null heating rate, was 429.6±0.1 K and 29.3±0.4 J g^{-1}, respectively. The apparatus for measuring enthalpy of solution was the same as described in the previous work.[9] The infrared spectra and X-Ray diffraction patterns were determined by model DR-31L of Japan Spectroscopic Co. and model JDX-8P of JEOL, respectively. Specific heat capacity measurements were carried out by model SH-3000M of Shinku-Riko Co. at heating rate of 1.5 K min^{-1}. The accuracy of the heat capacity apparatus was ±3%.[10]

Results and Discussion

DSC Measurements of DL-2-Aminobutanoic Acid(DL-ABA). The DSC result for DL-ABA is shown in Fig. 1. Phase transition from B- to A-form is observed in the temperature range between 480 and 520 K. The B-A transition of DL-ABA occurs near its decomposition temperature (577.15 K), and the transition pattern is similar to that of γ-α transition of glycine. The rate of the B-A transition of DL-ABA was slow similarly as the γ-α transition of glycine. Tsuboi et al. confirmed by means of IR spectra that the B-form was transformed into the A-form.[2] IR spetcrum of DL-ABA after transition was identical with that of A-form obtained by them. For comparison, the enthalpy of transition of glycine from γ-form to α-form was measured. The enthalpy value of transition of glycine was compared with that of DL-ABA at the same heating rate of 5 K min^{-1}. The enthalpy change of the B-A transition of DL-ABA was obtained by calculating the area between DSC curves at rise and fall (dotted line) of temperature. The results obtained are summarized in Table 1, where the enthalpy data are the average of 3 runs. Table 1 shows that the apparent entropy change of the B-A transition of DL-ABA is more than twice as that of the γ-α transition of glycine, where the entropy change was estimated by a calculation with the enthalpy change and peak temperature. Large entropy change in the B-A transition of DL-ABA seems to relate to the fact that the compound aquires the rotation around carbon-carbon bond in alkyl chain in solid state.[6] Furthermore, to confirm the value of enthalpy of transition obtained by DSC, the measurement of molar heat capacity of the B-form of DL-ABA was made. In Fig. 2, it appears that molar heat capacity, C_p, exhibits a steep peak and that enthalpy content, H, changes continuously. This feature is similar to that of specific heat capacity of $CuCl_2 \cdot 2H_2O$,[11] and seems as if C_p shows a discontinuity, that is a second-order phase transition. However, in view of the fact that the transition is accompanied by a volume change,[6] C_p and H at the transition temperature is considered to be continuous and discontinuous, respectively. Therefore, this feature makes us conclude that the transition is of the first order. As is shown in Fig. 2, the enthalpy of transition was estimated by extrapolation from both the lower and higher temperature regions to be approximately 5 kJ mol^{-1} at the transition temperature of 481 K.

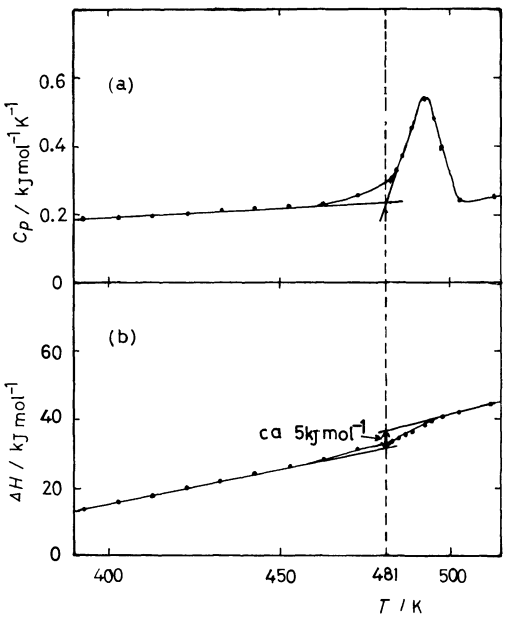

Fig. 2. Molar heat capacity (a) and enthalpy change (b) during the B-A transition in DL-ABA. Sample weight: 1.392 g. Heating rate: 1.5 K min^{-1}.

Solution Calorimetry of DL-2-Aminobutanoic Acid (DL-ABA). It is known that the A-form of DL-ABA is metastable at room temperature, whereas the B-form of DL-ABA is stable below the decomposition temperature (577.15 K). Since it is expected that the difference in the enthalpy of solution at room temperature between A and B is comparable to the enthalpy of transition of B- to A-form of DL-ABA obtained above, the

Table 2. Calorimetrically Determined Enthalpy Values of Aqueous Solutions of Glycine and DL-ABA at 298.15 K

Substance	Molality range m/mol kg^{-1}	Enthalpy of solution ΔH_s/kJ mol^{-1}	Author
α-form of	0.3	15.0±0.2	K. Sasaki[8]
Glycine	0.01	11.6±0.2	This work
γ-form of	0.3	15.8[a]	K. Sasaki[8]
Glycine	0.01	13.4±0.4	This work
A-form of	3×10^{-3}	1.56±0.01	Abraham et al.[12]
DL-ABA	5×10^{-3}	1.69±0.03	This work
B-form of	3×10^{-3}	6.92±0.08	Abraham et al.[12]
DL-ABA	5×10^{-3}	6.66±0.05	This work

a) One determination only.

Table 3. Difference in the Enthalpy of Solution between Crystalline Modifications at 298.15 K

Substance	Enthalpy difference $\Delta\Delta H_s$/kJ mol^{-1}	Author
Glycine	0.8	K. Sasaki
	1.8±0.6	This work
DL-ABA	5.36±0.09	Abraham et al.
	4.97±0.08	This work

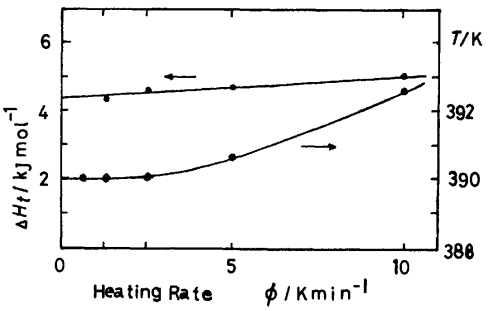

Fig. 3. Heating rate dependence of the enthalpy of transition, and of the peak temperature in the α-γ transition of DL-norleucine.

enthalpy of solution of crystal modifications of DL-ABA was measured at 298.15 K. The results obtained are given in Tables 2 and 3 together with data of preceding authors. The enthalpy of solution of glycine was measured for reference. The enthalpy of solution of both the crystal modifications in water at 298.15 K was determined by an isoperibol calorimeter. As was shown in a previous work, the systematic errror of the calorimeter was 1.4%, and the accuracy was 0.34%.[9] The enthalpy was compared between the final concentrations of glycine and DL-ABA, i.e., 1×10^{-2} and 5×10^{-3} mol kg^{-1}, respectively. The average value of enthalpy of solution for 5 determinations was used. The enthalpy data obtained agree fairly well with those of Abraham et al.[12] The difference in the enthalpy of solution between α- and γ-forms of glycine is more than twice as that obtained by Sasaki.[8] This may be due to the difference of apparatus used and purity of α-glycine used for the solution calorimetry. Sasaki pointed out that the enthalpy difference in two forms of glycine can be ascribed to the difference in intermolecular hydrogen bonds caused by rearrangement of molecular layers.[8] Assuming that the contribution of the difference in intermolecular hydrogen bonds of two forms of DL-ABA is nearly equal to that of glycine polymorphs, the difference of intermolecular hydrogen bonds is about 2 kJ mol^{-1}. The data in Table 3 suggest that the contribution due to intramolecular interactions, such as rotation around carbon-carbon bonds in alkyl chain, is predominant in the case of DL-ABA. From Tables 1 and 3, the difference in enthalpy of solution between two forms of DL-ABA appears to be nearly equal to the enthalpy of transition determined by DSC. This fact may be explained as follows. The enthalpy difference between two forms, $\Delta\Delta H_s$, is expressed as

$$\Delta\Delta H_s = \Delta H_t - \int_{T_s}^{T_t} \Delta C_p \mathrm{d}T, \quad (1)$$

where ΔC_p is the difference between molar heat capacity values at transition temparature, T_t, and at temperature of solution calorimetry, T_s. Experimental results show that $\Delta\Delta H_s$ is nearly equal to ΔH_t. The ΔC_p is negligible in the case of DL-ABA, but ΔC_p in glycine is not negligible for small quantity of enthalpy.

DSC Measurements of DL-Norleucine (DL-NL). The previous work[13] reported that a solid-solid phase transformation of crystalline DL-NL was displayed by means of DSC and X-Ray diffraction. As is shown in Fig. 3, the values of peak temperature depend on the heating rate, but the enthalpy of transition is nearly constant. The transition temperature and enthalpy of transition are estimated to be 390 K and 4.4 kJ mol^{-1}, respectively, by extrapolation to null heating rate.

On the other hand, Grunenberg et al. observed the transitions for the group of crystalline neutral apliphatic α-amino acids by means of DSC, infrared absorption spectra, and Raman spectra;[14,15] the transition of DL-NL occurs at 390 K and the enthalpy of transition is 4.41 kJ mol^{-1} at a heating rate of 10 K min^{-1}. Although the form of DL-NL was not identified as α-form by Grunenberg et al., our values are in good agreement with those by them. Therefore, the

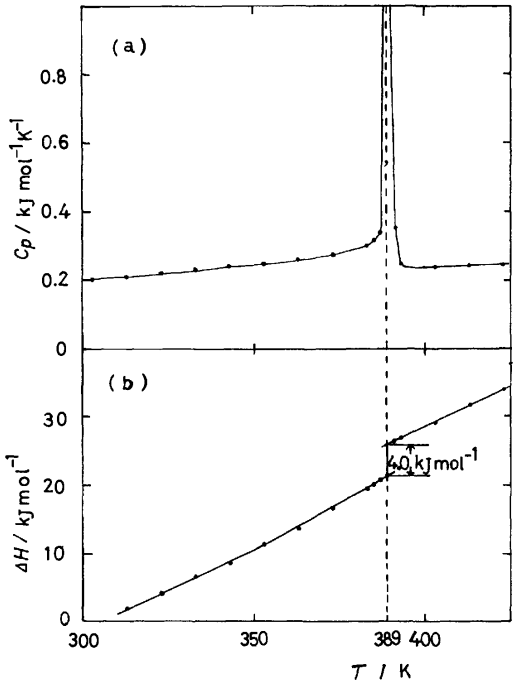

Fig. 4. Molar heat capacity (a) and enthalpy change (b) during the α-γ transition in DL-norleucine. Sample weight: 2.841 g. Heating rate: 1.5 K min^{-1}.

α-form DL-NL seems to be transformed into a new form called γ-form at 390 K.

In order to know the nature of transition of DL-NL, the specific heat capacity was measured. The sample weight was 2.841 g. As is shown in Fig. 4, the α-γ transition of DL-NL was found to be of the first order.[16] Figure 4 indicates that the transition temperature and the enthalpy of transition correspond to those by DSC measurements. The transition of DL-NL is reversible, whereas the γ-α transition of glycine and the B-A transition of DL-ABA are irreversible. Therefore, the free energy curves should intersect at the α-γ transition temperature, T_t. The entropy change in the α-γ transition of DL-NL by DSC was estimated to be 11 J mol^{-1} K^{-1}. The transition will be characterized by a large structural change similarly to the B-A transition in DL-ABA (9.70 J mol^{-1} K^{-1}, see Table 1).

Infrared Absorption Spectra and X-Ray Diffraction of DL-NL. Other physical methods such as X-Ray diffraction and IR absorption spectra were used for analysing structure change above and below the transition temperature of DL-NL.[13] The X-Ray pattern obtained was identical with that of the α-form crystals reported by Dawson and Mathieson (J.C.P.D.S. Powder Diffraction File No. 7-717).[17] Also IR spectrum of the α-form DL-NL at room temperature was identical with that of known structure.[18] The existence of polymorphism of DL-NL was suggested by Mathieson, who deduced it to be the β-form or the superlattice from the dimorphs of DL-methionine.[19-21] X-Ray diffraction result was different from the spacings either of β-form or of the superlattice. Also IR spectra of DL-NL crystals measured above and below the transition temperature are given in Fig. 5. The spectral pattern at 443 K(b) is different from that at 353 K(a). In the wavenumber range of 2000—3000 cm^{-1}, the band of the α-form (a) at 2100 and 2950 cm^{-1} were assigned to be of NH_3^+ stretching,[18] and these bands shifted to shorter wavenumbers by about 20 and 50 cm^{-1} at 443 K(b). Accordingly, it is considered that intermolecular hydrogen bond distance between NH_3^+ and COO^- groups in the γ-form is shorter than that of the α-form. Also the bands at 1470 and 925 cm^{-1} in the α-form are assigned to be of CH_3 asymmetric deformation and CH_3 rocking plus CC stretching, respectively.[18,22] The changes of the bands were observed at 443 K(b). The IR spectrum change obtained is similar to that of L-leucine reported by Bougeard.[15] The spectral change suggests that the α-γ transition in DL-NL is caused by the change of intermolecular interactions between layers accompanied by the conformational change of alkyl chains.

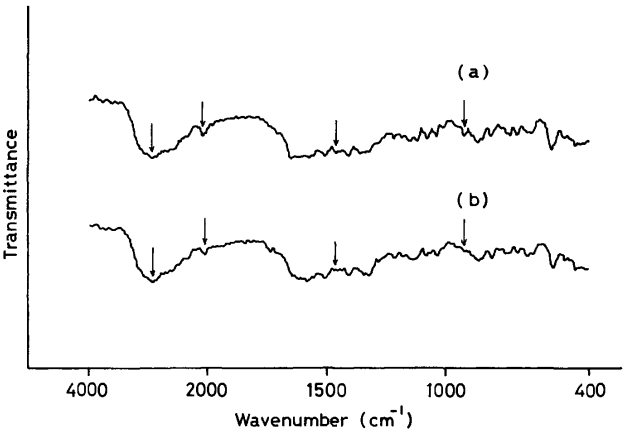

Fig. 5. Infrared absorption spectra of DL-norleucine at 353 K (a) and at 443 K (b).

Application of the Enthalpy of Solution to the Analysis of Mixtures of A- and B-Forms of DL-ABA. The enthalpy of solution of DL-ABA in water has been measured calorimetrically by some investigators, but the values obtained were different to each others.[23-25] The different solution enthalpy data can be ascribed to samples which are mixtures of A- and B-forms. Plate-like A-form crystals are easily obtained by recrystallization from water or water-ethanol mixture, but it is difficult to obtain pure B-form uncontaminated with the A-form as demonstrated by Abraham et al.[12] A sample of DL-ABA was regarded as pure B-form, because the IR spectrum of fibrous DL-ABA was identical with that given by Tsuboi et al.[2]

If the sample used is a mixture of A- and B-forms, the molar enthalpy of solution, ΔH_s^m, is expressed by

$$\Delta H_s^m = (1-x)\Delta H_s^A + x\Delta H_s^B, \quad (2)$$

where x is mole fraction of B-form in DL-ABA, and ΔH_s^A and ΔH_s^B is molar enthalpy of pure A- and B-

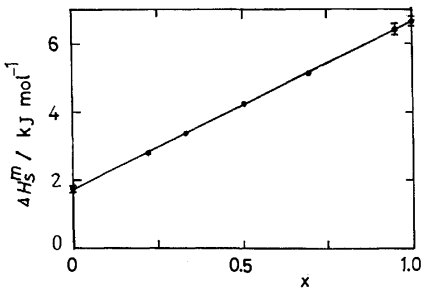

Fig. 6. Plots of the enthalpy of solution of mixture, ΔH_s^m, against mole fraction of the B-form, x, in DL-ABA at 298.15 K. It shows that Eq. 2 is found to hold as ΔH_s^m variation of arbitrary mixing ratios on mole fraction gives straight line.

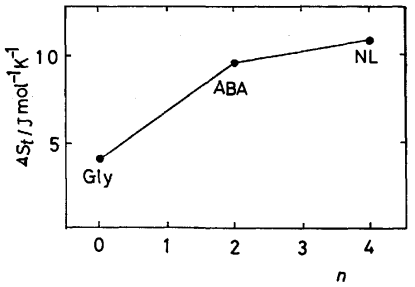

Fig. 7. Correlation between number of carbon atoms, n, in the alkyl chains of amino acids and apparent entropy of transition.

form, respectively.

To confirm whether Eq. 2 is hold, the solution calorimetry of mixing of A-form with B-form was performed at 298.15 K. Figure 6 shows linear relationship between ΔH_s^m and ΔH_s^A (or ΔH_s^B). Accordingly, we can estimate the mole fraction of a component in the mixture from the enthalpy data obtained by mixtures of known mole fractions. ΔH_s^A and ΔH_s^B values are given in Table 2.

For example, the crystallization from ethanol-water mixture at 290 K for 24 h gave ΔH_s^m of 6.43±0.14 kJ mol^{-1} at 298.15 K as the average of 3 determinations; Eq. 2 gave the result that the mixture consists of 95% B-form and 5% A-form.

Conclusion

The polymorphic transitions of DL-2-aminobutanoic acid(DL-ABA) and DL-norleucine(DL-NL) were studied by differential scanning calorimetry(DSC). The experimental results show that the B-A transition in DL-ABA occurs in the wide range of temperature near its decomposition temperature, and the transition pattern is similar to that of γ-α transition in glycine, whereas the pattern of α-γ transition in DL-NL is different from that in glycine. The DL-NL transition is of the first order. The solution calorimetry of crystalline modifications of DL-ABA was performed by an isoperibol calorimeter at 298.15 K to reveal that the enthalpy difference is nearly equal to the enthalpy of transition by DSC. The α-γ transition in DL-norleucine is accompanied with change of intermolecular interactions such as hydrogen bond and van der Waals force between layers caused by the conformational change of alkyl chains. The correlation between the number of carbon atoms in alkyl chains of amino acids and the apparent entropy of transition is shown in Fig. 7.

We are grateful to Dr. Kazuko S. Kunihisa of National Chemical Laboratory for Industry for the sample of γ-form glycine and for advice on DSC measurement. We also would like to thank Drs. Kazuo Amaya, Midori Gotoh, and Masato Mamiya of the Laboratory for advice of calorimetry, computation of X-Ray diffraction data, and IR absorption measurements, respectively.

References

1) Y. Iitaka, *Acta Crystallogr.*, **11**, 225 (1958).
2) M. Tsuboi, Y. Iitaka, S. Suzuki, and S. Mizushima, *Bull. Chem. Soc. Jpn.*, **32**, 529 (1959).
3) T. Akimoto and Y. Iitaka, *Acta Crystallogr., Sect. B*, **28**, 3106 (1972).
4) T. Ichikawa, Y. Iitaka, and M. Tsuboi, *Bull. Chem. Soc. Jpn.*, **41**, 1027 (1968).
5) K. Nakata, Y. Takaki, and K. Sakurai, *Acta Crystallogr., Sect. B*, **36**, 504 (1980).
6) a) T. Ichikawa and Y. Iitaka, *Acta Crystallogr., Sect. B*, **24**, 1488 (1968); b) J. Voogt and J. L. Derissen, *Acta Crystallogr., Sect. B.* **36**, 3175 (1980); c) J. Voogt and J. B. Hulscher, *Acta Crystallogr., Sect. B*, **36**, 3178 (1980).
7) Y. Iitaka, *Acta Crystallogr.*, **13**, 35 (1960).
8) K. Sasaki, *Rep. Nat. Chem. Lab. for Ind.*, **61**, 54 (1966).
9) M. Matsumoto and K. Amaya, *Bull. Chem. Soc. Jpn.*, **53**, 3510 (1980).
10) R. Kato, C. Uchikawa, and A. Maezono, "Proceedings of the 5th International Conference on Thermal Analysis," Kagaku-Gijutsusha (1977), p. 64.
11) S. A. Friedberg, *Physica*, **18**, 714 (1951).
12) M. H. Abraham, E. Ah-Sing, R. E. Harks, R. A. Schulz, and B. C. Stace, *J. Chem. Soc., Faraday Trans. 1*, **73**, 181 (1977).
13) M. Matsumoto and K. S. Kunihisa, *Chem. Lett.*, (**1984**), p. 1279.
14) A. Grunenberg, D. Bougeard, and B. Schroder, *Thermochimica Acta*, **77**, 59 (1984).
15) D. Bougeard, *Ber. Bunsenges. Phys. Chem.*, **87**, 279 (1983).
16) N. G. Parsonage and L. A. K. Staveley, "Disorder in Crystals," Oxford University Press (1978), p. 12.
17) B. Dawson and A. McL. Mathieson, *Acta Crystallogr.*, **4**, 476 (1951).
18) M. Tsuboi and T. Takenishi, "Infrared Spectra," Nanko-do, Tokyo (1960), Vol. 7, p. 71.
19) A. McL. Mathieson, *Acta Crystallogr.*, **6**, 399 (1953).
20) A. McL. Mathieson, *Acta Crystallogr.*, **5**, 332 (1952).
21) T. Taniguchi, Y. Takaki, and K. Sakurai, *Bull. Chem. Soc. Jpn.*, **53**, 803 (1980).
22) R. J. Koegel, R. A. McCallum, J. R. Greenstein, M. Winitz and S. M. Birnbaum, *Ann. N. Y. Acad. Sci.*, **69**, 94

(1954).
23) C. H. Spink and M. Auker, *J. Phys. Chem.*, **74**, 1742 (1970).
24) G. C. Kresheck, H. Schneider, and H. A. Scheraga, *J. Phys. Chem.*, **69**, 3132 (1965).
25) C. H. Spink and I. Wadsö, *J. Chem. Thermodyn.*, **7**, 561 (1975).

A Model of Crystal Defects in Calcite by Sodium and Potassium Uptake

Masamichi Ishikawa† and Masami Ichikuni
Department of Environmental Chemistry and Engineering, Tokyo Institute of Technology, Midori-ku, Yokohama 227
(Received April 21, 1986)

Crystal defects in calcite containing Na and K ions were investigated by means of a model based on statistical thermodynamics and measurements of thermoelectric power. The varying amount of Na and K ions in the crystal was interpreted on an assumption of ideal solution of the ions as $Ca_{1-x-y}\square_{x+y}[Na_{2x}, K_{2y}]CO_3$, where □ and [ ] means Ca-vacancy and interstitial ion, respectively. In the model, the excess charge of Na and K ions is balanced with Ca-vacancy to form interstitial-vacancy pairs ($[Na, K]_2\square$). Measurements of thermoelectric power in calcite showed the cationic transport which resulted from Na and K interstitials and/or Ca-vacancies. From the ideal mixing of Na and K ions at interstitial sites, the K/Na molar ratio in calcite was correlated with that in aqueous solution at 20 °C and pH 8.5 by the formula,

$$\frac{K_S}{Na_S} = 0.20\frac{K_L}{Na_L},$$

where S and L refer to solid- and aqueous-phase, respectively.

The study of sodium and potassium partitioning between carbonate minerals and aqueous solution has suggested the incorporation of these monovalent ions into the carbonate lattice rather than their presence as solid non-carbonate impurities or liquid inclusions.[1,2] In the partitioning of an ion with different valence from that of host carbonate ion, electroneutrality must be maintained in the crystal. The incorporation of such ions is usually accompanied with the formation of crystal defects, such as vacancies, interstitial ions, and substitutional ions.[3] The identification of crystal defects associated with impurity ions is needed to establish the partition theory of carbonate minerals. Although defect in calcite has been considered in the partitioning process of Na and K, the identification of defects has not fully been performed.

Electrical properties, such as ionic conductivity, dielectric loss and thermoelectric power, of calcium carbonate have been studied to characterize the crystal defects in the crystals.[4-6] These transport properties depend on the concentration and mobility of defects in the crystal and give direct information concerning the defect characteristics. However, it is difficult to assign the type of defect to each impurity ion, because natural and synthetic calcium carbonates contain different amounts of impurity ions. The nature of defect induced by impurity ions needs to be better understood. For the study of electrical properties, it is necessary to use samples having controlled impurity content. Further difficulty arises from the polycrystalline nature of samples. It is pointed out that the measurement of thermoelectric power of ionic crystals is not affected by the state of aggregation of samples.[7] The method, therefore, seems to be practical when we use substances not in a single-crystal form.

Statistical thermodynamics has been applied to the theoretical investigation of crystal defects in ionic crystals.[8-11] Assuming random distribution of defects in a crystal, configurational entropy is calculated to derive the equation which satisfies the condition of minimum free energy. The equation describes the equilibrium concentration of defect with respect to impurity concentration and temperature. This method requires a defect model which makes us calculate the configurational entropy and is useful for identifying the type of crystal defects.

Ishikawa and Ichikuni[2] suggested the interstitial incorporation of sodium and potassium in calcite, and assumed that the position between the carbonate ion and CaO_6 octahedron would be a possible interstitial site. Formation of Ca-vacancy in calcite was also assumed in order to explain compensation for the excess charge due to sodium and potassium. The purpose of this paper is to verify the above model based on the statistical thermodynamic calculation of sodium and potassium doping in calcite and the measurement of thermoelectric power. The model gives the formula expressing the relationship between K/Na ratio in calcite and that in aqueous phase.

Experimental

Calcite was precipitated from $Ca(OH)_2$ solution containing different amounts of NaCl and KCl by adding CO_2-saturated water. The solution was constantly stirred at 20 °C in a closed reaction vessel until an equilibrium after about 40 h. Precipitated calcite was about 1 μm in size and rhombohedral in shape. The uniform distribution of Na and K in calcite crystals was confirmed by fractional leaching in dilute HCl solution.[2] Synthetic calcite contained Cl of about 0.001 mol kg^{-1}. The content was 10^2 times lower than Na and K contents. The effect of Cl on the Na and K uptake by calcite was, therefore, disregarded in the discussion.

The measurement of thermoelectric power was made on calcite samples containing 0.13 mol kg^{-1} of Na and 0.073 mol kg^{-1} of K. The thermoelectric cell used was made of pyrophyllite preheated at 800 °C for 3 h. The arrangement of the cell was similar to that of Parravano.[7] Calcite

†Present address: Mitsubishi Research Institute, Inc., Otemachi Chiyoda-ku, Tokyo 100.

Table 1. Data on Sodium and Potassium Uptake by Calcite at pH 8.5 and 20°C. For all Experiments, $Ca^{2+}=0.6$ mM; $HCO_3^-=1.2$ mM

No.	a_{Na}^L	a_K^L	K_L / Na_L	Na_S / mol/kg^{-1}	K_S / mol/kg^{-1}	K_S / Na_S
1	0.0016	0.058	40	0.00983	0.0235	2.39
2	0.0078	0.058	8.0	0.0186	0.0246	1.32
3	0.015	0.058	4.0	0.0276	0.0224	0.812
4	0.017	0.017	1.0	0.034	0.00824	0.242
5	0.023	0.058	2.7	0.0398	0.0221	0.555
6	0.030	0.058	2.0	0.0497	0.0211	0.425
7	0.037	0.058	1.6	0.0626	0.0208	0.332
8	0.038	0.038	1.0	0.0632	0.0151	0.239
9	0.059	0.058	1.0	0.0830	0.0157	0.189
10	0.072	0.069	1.0	0.0985	0.0184	0.187
11	0.086	0.058	0.67	0.0936	0.0142	0.152
12	0.11	0.058	0.50	0.100	0.0118	0.118
13	0.14	0.058	0.43	0.105	0.0095	0.0905

a) a_{Na}^L and a_K^L represent activity values of Na and K in solution, and Na_S and K_S are contents of Na and K in precipitated $CaCO_3$.

sample was pressed at about 0.5 GPa to form a pellet of 5 mm in diameter and 7 mm thick, and was set between two platinum electrodes inside the cell. The electrodes were tightly pressed against the sample by two pyrophyllite supports, which contain chromel-alumel thermocouples and nichrome heaters near the sample. In order to reduce thermal convection current, the cell was mounted horizontally in the furnace. Supplementary heating was provided with nichrome heater to establish a temperature gradient between the electrodes.

Results

Coprecipitation of Na and K with calcite was carried out under controlled conditions where aqueous concentration of Ca^{2+} and HCO_3^- was fixed at 0.6 and 1.2 mM, respectively, at pH 8.5. Table 1 gives the amounts of coprecipitated Na and K with respect to various Na and K compositions of aqueous solutions. To investigate the relationship between contents of Na and K in calcite, the amount of coprecipitated K was determined as a function of that of Na as shown in Fig. 1, where aqueous K activity was fixed at a constant value ($a_K^L=0.058$). The result shows that K incorporation into calcite decreases with increasing Na content. The relationship between Na content and K content in calcite will be quantitatively examined in Discussion.

The thermoelectric voltage (ΔV) in samples was reversibly changed with increasing and decreasing temperature gradient (ΔT) between two electrodes. Figure 2 shows the thermoelectric power ($\Delta V/\Delta T$) as a function of temperature when ΔT was maintained at 10—15 °C. Bars in Fig. 2 show the range of the thermoelectric power of increasing and decreasing temperature. For all the samples the colder side of the sample was found to be positive in the temperature range between 360 and 570 °C and thermoelectric power showed a maximum and a minimum.

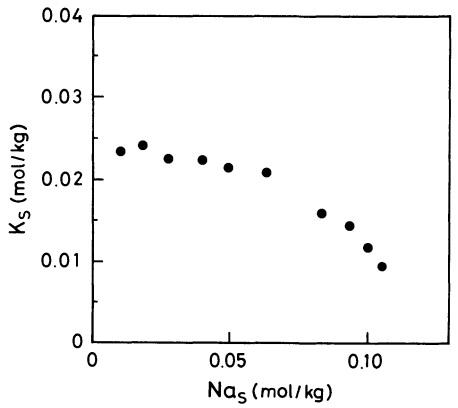

Fig. 1. Sodium and potassium uptake by calcite at pH 8.5 and 20°C. Aqueous activity of potassium is fixed at 0.058 and that of sodium ranges from 0.0016 to 0.14.

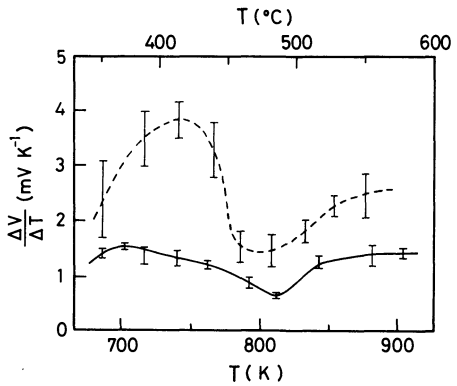

Fig. 2. Thermoelectric voltage per degree of calcite as a function of temperature. —: $Na_S=0.13$ mol kg^{-1}, ---: $K_S=0.073$ mol kg^{-1}.

Discussion

Interstitial-Vacancy Type Solid Solution. A mech-

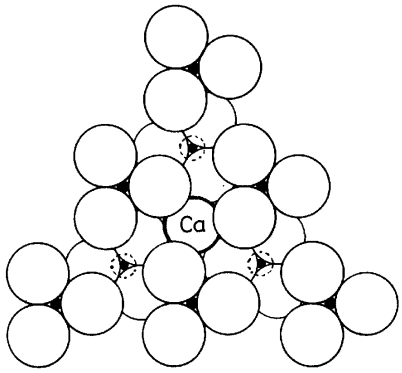

Fig. 3. Interstitial positions in the calcite lattice. The symbol ◌ represents equivalent interstitial sites around a Ca ion. Another set of three sites, found at inversion points with respect to the Ca ion, are omitted for the sake of simplicity.

anism of Na and K uptake by calcite was suggested by the present authors,[2] who assumed that Na and K are incorporated into interstitial positions in the calcite lattice. The total numbers of available interstitial sites for Na and K were 0.15 and 0.12 mol kg^{-1}, respectively, and Ca-vacancy (net charge is −2) balances with the positive charge of the ions. The interstitial sites in the calcite crystal are indicated in Fig. 3. The calculated size of the sites is about 0.89 A in radius (see Appendix), and a site is surrounded by six O^{2-} ions. Oxide ions cause a negative atmosphere around the sites.

According to the mechanism, solid solution of Na_2CO_3 and K_2CO_3 in $CaCO_3$ is formulated as,

$$(1-x-y)CaCO_3(S) + xNa_2CO_3(L) + yK_2CO_3(L) = Ca_{1-x-y}\square_{x+y}[Na_{2x}, K_{2y}]CO_3(S), \quad (1)$$

where □ and [ ] means Ca-vacancy and interstitial ion, respectively.

In order to deduce the equilibrium relationship between x and y in reaction (1), we assume as follows:

(i) Formation of interstitial-vacancy pairs ([Na, $K]_2\square$), to maintain electroneutrality in calcite.

(ii) Random distribution of the interstitial-vacancy pairs in the crystal, where dimer or trimer aggregations of the pairs are disregarded.

(iii) Ideal mixing of Na and K on the interstitial sites.

Assumptions (ii) and (iii) are introduced to simplify a calculation. As to assumption (ii), formation of dimer and trimer complexes of impurities and vacancies has been known in alkali halides at low temperature and high impurity contents.[12-14] Although this phenomenon may occur in the present case, simplicity of the model would be preferable, because any such treatments to produce an aggregation of impurity-vacancy complexes had not been done.

The dependence of K composition (y) on Na composition (x) in calcite at a constant temperature is determined by minimizing the free energy of $Ca_{1-x-y}\square_{x+y}[Na_{2x}, K_{2y}]CO_3$. To calculate the Gibbs free energy, $G=U+pV-TS$, of the solid solution, it is necessary to know the entropy term. The entropy of crystalline solids is the combination of the entropy due to thermal vibration of lattice ions (S^t) and the configurational entropy (S^c) due to mixing of ions in the crystal.

The configurational entropy among degenerate configurations is defined by the formula,

$$S^c = k \ln \Omega, \quad (2)$$

where Ω, multiplicity of thermodynamic probability of the system, is the number of distinguishable configurations that the system can adopt, and k is Boltzmann's constant. Using Eq. 2, the configurational entropy of $Ca_{1-x-y}\square_{x+y}[Na_{2x}, K_{2y}]CO_3$ is calculated as,

$$S^c = k \ln \Omega^{\text{i-v pair}} = k \ln \left[\left(\frac{N_0!}{\left(N_0 - \frac{n^T}{2}N_0\right)!\left(\frac{n^T}{2}N_0\right)!} \times \frac{\left(\frac{n^T}{2}N_0\right)!}{\left(\frac{n^T}{2}N_0 - xN_0 - yN_0\right)!(xN_0+yN_0)!} \right)_v \times \left(\frac{(2xN_0+2yN_0)!}{(2xN_0)!(2xN_0)!} \right)_i \times 3^{(xN_0+yN_0)} \right], \quad (3)$$

where i and v denotes interstitial and vacancy, respectively, and N_0 is Avogadro's number and n^T the total number of available interstitial sites in calcite. In Fig. 3, there are six equivalent interstitial sites (only three of such sites are shown) around a Ca ion just above and below the same cationic layer of the lattice. Since it results in three equivalent inversion-related [Na, $K]_2$ □ pairs with respect to one Ca-vacancy, the multiplicity increases by a factor of 3 over each interstitial-vacancy pair of a configuration. By use of Stirling's approximation, $\ln N! \simeq N \ln N - N$, Eq. 3 is transformed,

$$S^c = -kN_0 \ln \left[\left(1-\frac{n^T}{2}\right)\ln\left(1-\frac{n^T}{2}\right) + \left(\frac{n^T}{2}-x-y\right)\ln\left(\frac{n^T}{2}-x-y\right) + (x+y)\ln(x+y) + 2x\ln 2x + 2y\ln 2y - (2x+2y)\ln(2x+2y) - (x+y)\ln 3 \right]. \quad (4)$$

The difference in the free energy (ΔG) of reaction (1) is then formulated as Eq. 5, using the molar free energy of species i, $g_i=u_i+pv_i-Ts_i^t$, where u_i is the molar internal energy, v_i the molar volume, and s_i^t the molar vibrational entropy.

$$\begin{aligned}\Delta G &= [(1-x-y)g_{Ca} + (x+y)g_\square + 2xg_{Na} + 2yg_K + g_{CO_3} - TS^c] - [(1-x-y)g_{Ca} + (1-x-y)g_{CO_3} + x\mu^L_{Na_2CO_3} + y\mu^L_{K_2CO_3}] \\ &= x(2g_{Na}+g_\square+g_{CO_3}-\mu^L_{Na_2CO_3}) + y(2g_K+g_\square+g_{CO_3}-\mu^L_{K_2CO_3}) - TS^c, \end{aligned} \quad (5)$$

where μ^L is the chemical potential of Na_2CO_3 and K_2CO_3 in aqueous solution. Thus, the relationship between x and y is obtained from Eqs. 4 and 5, with the condition that at the equilibrium $\partial\Delta G/\partial y=0$ at constant x and constant temperature,

$$\left(\frac{\partial \Delta G}{\partial y}\right)_{x,T} = (2g_K + g_\square + g_{CO_3} - \mu^L_{K_2CO_3}) - T\left(\frac{\partial S^c}{\partial y}\right)_{x,T}$$
$$= (2g_K + g_\square + g_{CO_3} - \mu^L_{K_2CO_3}) + kN_0T\ln\left[\frac{(x+y)(2y)^2}{3\left(\frac{n^T}{2}-x-y\right)(2x+2y)^2}\right] = 0. \quad (6)$$

Replacing x and y by Na composition Na_S, and K composition K_S, respectively, Eq. 6 is rewritten as,

$$\ln\frac{K_S}{Na_S+K_S} = -0.5\ln\frac{Na_S+K_S}{n^T-Na_S-K_S} - 0.5\left(\frac{2g_K+g_\square+g_{CO_3}-\mu^L_{K_2CO_3}}{kN_0T} - \ln 3\right). \quad (7)$$

If aqueous activity of K_2CO_3 is fixed at a constant value, then $\mu^L_{K_2CO_3}$ becomes constant and Eq. 7 shows a linear relationship between Na_S and K_S in calcite with an inclination of -0.5.

To examine the validity of the interstitial-vacancy model described above, $\ln(K_S/[Na_S+K_S])$ is plotted against $\ln([Na_S+K_S]/[n^T-Na_S-K_S])$ in Fig. 4. As to n^T, different values of 0.15 and 0.12 mol kg^{-1} were obtained for Na and K, respectively. Since interstitial-vacancy pairs should be defined with respect to the sites available for both Na and K, 0.12 mol kg^{-1} was adopted as n^T. Other data used are given in Table 1. The empirical equation was formulated by the least-squares fit as,

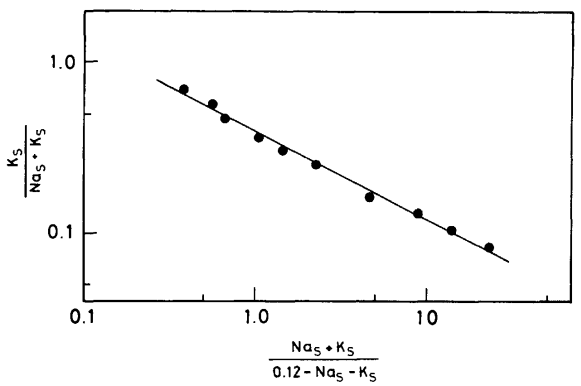

Fig. 4. Logarithmic relationship between sodium and potassium contents of calcite at 20°C and a constant activity of K_2CO_3 in aqueous solution.

$$\ln\frac{K_S}{Ka_S+K_S} = -0.51\ln\frac{Na_S+K_S}{0.12-Na_S-K_S} - 0.94. \quad (8)$$

The inclination of Eq. 8 (-0.51) is identical with the theoretical value in Eq. 7 (-0.5), showing that the interstitial-vacancy model gives an adequate explanation for Na and K mixing in calcite.

Defects associated with Na and K in calcite were investigated by measuring the thermoelectric power of the doped calcite crystal. The sign of thermoelectric power relates with the sign of dominant charge carriers in the crystal. Since charge carriers move along the temperature gradient toward the colder electrode, the positive sign indicates that the charge carrier is a cation. As shown in Fig. 2, the sign of thermoelectric power was positive in the temperature range of 360—570 °C, where defects induced by impurities dominate in calcite.[5] This result indicates the presence of charged defects which cause the transportation of cations and are attributed to interstitial cations or cation vacancies, that is, Na and K interstitials or Ca-vacancies. It has been observed in the measurements of ionic conductivity in alkali halides that the concentration of free interstitials or vacancies is increased by the dissociation of impurity-vacancy pairs in the similar temperature range.[15] The maximum and the minimum of thermoelectric power in Fig. 2 may correspond to the change in transportation mechanism induced by the dissociation of the interstitials-vacancy pairs. These results support the interstitial incorporation of Na and K, when the electroneutrality is maintained by formation of Ca-vacancies in calcite.

K/Na in Calcite as a Function of Aqueous K/Na. Natural calcites contain different amounts of Na and K depending on the origin. Table 2 summarizes the difference in K/Na molar ratio in various natural calcites. Some studies have reported a correlation of K/Na in calcites with chemical composition of natural waters from which precipitation took place.[16,17] In spite of considerable scattering of K/Na in natural calcites, however, the applicability of K/Na value as a geochemical indicator has not been established. Our study strongly suggests that K/Na in calsites can be formulated as a function of K/Na in aqueous solutions based on the mechanism of ion incorporation into the crystal.

Equilibrium partitioning of the ions between calcite

Table 2. Potassium/Sodium Molar Ratio in Marine and Freshwater Calcite

	Salinity	K_L	Ks	Nas	Ks/Nas	
	‰	Na_L	ppm	ppm	Obsd	Calcd
Marine calcite						
Shells[20]	35	0.0218	18—280	2160—6580	0.0040—0.037	0.0044
Freshwater calcite						
Travertines[17,21]	0.8—4.7	0.013—0.044	16—282	220—1410	0.034—0.40	0.0026—0.0088
Limestones[18]	0.23—0.25	0.017—0.063	3—33	19—47	0.099—0.50	0.0034—0.013

and aqueous solution is represented by Eqs. 9 and 10 for Na and K, respectively, where Na and K incorporation into the crystal is assumed to be independent of aqueous Ca and pH.[2)]

$$K_{Na} = \frac{Na_S}{\gamma_{Na} Na_L [*]_S} \quad \text{and} \tag{9}$$

$$K_K = \frac{K_S}{\gamma_K K_L [*]_S}, \tag{10}$$

in which K is the equilibrium constant of Na and K partitioning, γ is the activity coefficient of aqueous Na and K, and $[*]_S$ means the number of vacant interstitial sites in calcite. On the assumption of ideal mixing of Na and K, the activity coefficient of each ion in the crystal is unity and Eq. 11 is obtained from Eqs. 9 and 10.

$$\frac{K_S}{Na_S} = \frac{K_K \gamma_K K_L [*]_S}{K_{Na} \gamma_{Na} Na_L [*]_S} \simeq \frac{K_K}{K_{Na}} \times \frac{K_L}{Na_L}. \tag{11}$$

The proportional relationship of K/Na between calcite and aqueous solution was confirmed by the result in Fig. 5 by use of data in Table 1. The empirical equation was obtained as,

$$\frac{K_S}{Na_S} = 0.20 \frac{K_L}{Na_L}. \tag{12}$$

The K/Na ratios in marine shells, travertines, and limestones are estimated by Eq. 12 and given in Table 2. Observed values of K/Na differ by 1—2 orders of magnitude from those of marine shells to those of fresh water limestones. Calculated K/Na ratio in marine biogenic calcite (0.0044) is in the same range of observed K/Na values (0.0040—0.037). The wide range of observed values will be due to variations in physiological conditions of marine invertebrates as explained by the present authors.[2)] Travertines and freshwater limestones, however, have higher K/Na ratios (0.034—0.5) than the calculated values (0.0026—0.013). It is known that K in limestones correlates with acid-insoluble residues and is attributed to contamination from clay minerals.[18,19)] The discrepancy described above may be due to the increase in K content by the contamination.

Conclusions

The distribution of Na and K ions in calcite was formulated on an assumption of ideal mixing of the ions at interstitial sites which are associated with Ca-vacancies. The presence of the pairs composed of Na and K interstitials and Ca-vacancy was confirmed by measuring the thermoelectric power of calcites containing Na and K ions.

A model for Na and K uptake by calcite was presented to treat the partition mechanism of monovalent ions and the mechanism of formation of interstitials and vacancies. Although the theory of elemental partitioning between carbonates and natural waters has asserted the simple substitution of host ions by divalent impurities, most natural carbonates contain some mono- and trivalent ions, such as F^- an PO_4^{3-}. The partitioning of such ions has been qualitatively estimated with respect to ionic charge and radius. It should be noted that the role of crystal defects during the diagenesis of carbonate minerals is poorly understood. An extensive characterization of defects associated with various impurity ions will be fruitful in clarifying geochemical properties of sedimentary minerals.

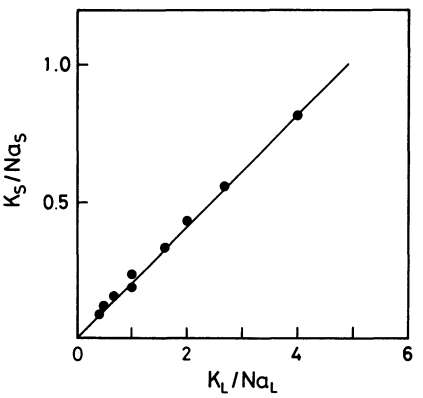

Fig. 5. Potassium/sodium molar ratio in calcite as a function of that in aqueous solution at 20°C.

The authors wish to thank Dr. Takaaki. Kobayashi for his critical comments on the study, and Dr. Kenichi Kondo for his technical assistance in the measurements of thermoelectric power.

Appendix

The calculated size of the coordination polyhedron of the presumed interstitial sites.

The interstitial site is surrounded by six oxygens. In the hexagonal system, the crystallographic coordinates of the four neighboring carbons in calcite are given by C_1 (0, 0, 1/4), C_2 (1, 1, 1/4), C_3 (0, 1, 1/4), and C_4 (1/3, 2/3, 1/12). Then those of the six oxygens will be O_1 (d, d, 1/4), O_2 (1−d, 1, 1/4), O_3 (0, 1−d, 1/4), O_4 (1/3−d, 2/3−d, 1/12), $O_{4'}$ (1/3, 2/3+d, 1/12), and $O_{4''}$ (1/3+d, 2/3, 1/12), where d corresponds to the C-O distance in CO_3^{2-} divided by the lattice parameter a, and O_4, $O_{4'}$, and $O_{4''}$ belong to the same CO_3^{2-}. The d value is calculated as 0.2568 based on the crystallographic data by Effenberger et al.[22)]

The co-ordinates of the interstitial site are given by i (1/3, 2/3, 0.1863), which is equidistant from the six oxygens. The distance r between two points (x_1, y_1, z_1) and (x_2, y_2, z_2) can be calculated by,

$$r^2 = a^2[(x_1-x_2)^2 + (y_1-y_2)^2 - (x_1-x_2)(y_1-y_2)] + c^2(z_1-z_2)^2,$$

where a and c are the lattice parameters for calcite. The distance between i and any O is then 2.1744 Å. Assuming that the O radius is equal to the C-O distance in CO_3^{2-}, we get 0.8929 Å as the radius of the interstitial site.

References

1) A. F. White, *Geochim. Cosmochim. Acta*, **41**, 613 (1977).
2) M. Ishikawa and M. Ichikuni, *Chem. Geol.*, **42**, 137 (1984).
3) W. L. McIntire, *Geochim. Cosmochim. Acta*, **27**, 1209 (1963).
4) K. S. Rao and K. V. Rao, *Z. Phys.*, **216**, 744 (1968).
5) P. W. Mirwald, *Phys. Chem. Miner.*, **4**, 291 (1979).
6) M. Ishikawa, A. Sawaoka and M. Ichikuni, *Phys. Chem. Miner.*, **8**, 247 (1982).
7) G. Parravano, *J. Chem. Phys.*, **23**, 5 (1955).
8) C. Wagner and W. Schottky, *Z. Phys. Chem.*, **B11**, 163 (1930).
9) R. H. Fowler and E. A. Guggenheim, "Statistical Thermodynamics," Cambridge Univ. (1956), p. 541.
10) C. P. Flynn, "Point Defects and Diffusion," Oxford (1972), p. 24
11) B. Y. Sukharevskii, A. M. Gavrish and A. E. Solov'eva, *Sov. Phys. Crystallogr.*, **25**, 434 (1980).
12) J. S. Cook and J. S. Dryden, *Proc. Phys. Soc.*, **80**, 479 (1962).
13) M. Dubiel, G. Berg, and F. Frölich, *Phys. Stat. Sol.*, **A55**, 153 (1979).
14) R. Capelletti, R. Fieschi, A. Gainotti, C. Mora, L. Romano, and E. Zecchi, "Defects in Insulating Crystals," ed by V. M. Tuchkevich and K. K. Shvarts, Springer, Heidelberg (1981), p. 675.
15) L. W. Barr and A. B. Lidiard, in "Physical Chemistry, an Advanced Treatise," ed by W. Jost, Academic Press, New York (1970), Vol. 10, p. 152.
16) N. Ohta, M. Terai and M. Omori, *Nippon Kagaku Zasshi*, **86**, 1254 (1965).
17) T. Araki, *Onsen Kagaku*, **24**, 20 (1973).
18) N. Sakae, T. Yokoyama, K. Yoshimura, and T. Tarutani, *J. Speleol. Soc. Jpn.*, **4**, 57 (1979).
19) G. H. Wagner, R. H. Konig, D. A. Smith, K. F. Steele and D. L. Zachry, Jr., *Chem. Geol.*, **24**, 293 (1979).
20) F. Masuda and M. Hirano, *Sci. Rep., Inst. Geosci., Univ. Tsukuba*, **B1**, 163 (1980).
21) M. Ichikuni and K. Kikuchi, *Chem. Geol.*, **9**, 13 (1972).
22) H. Effenberger, K. Mereiter, and J. Zemann, *Z. Krystallogr.*, **156**, 233 (1981).

 © 1986 The Chemical Society of Japan Bull. Chem. Soc. Jpn., 59, 3815—3820 (1986)

The Specific Effects of Tetraalkylammonium and Alkali Metal Ions on the Polarographic Reduction of Nitroalkanes and Nitrobenzenes in Acetonitrile

Masashi Hojo,* Kazukiyo Nishikawa, Yoshihiro Akita, and Yoshihiko Imai
Department of Chemistry, Faculty of Science, Kochi University, Kochi 780
(Received May 6, 1986)

The polarographic behavior of 2-methyl-2-nitropropane ($(CH_3)_3CNO_2$) was examined at DME in acetonitrile with various supporting electrolytes. The addition of Et_4N^+ or n-Bu_4N^+ caused the half-wave potential ($E_{1/2}$) of $(CH_3)_3CNO_2$ to shift negatively in the presence of a fixed concentration of $NaClO_4$. The negative shift was explained in terms of the interaction between tetraalkylammonium cations and the unreduced molecule of $(CH_3)_3CNO_2$. The formation of $(CH_3)_3CNO_2^{\cdot-}(Na^+)_2$ was also suggested, and the conditional formation constants of the species were obtained by the positive shift in the $E_{1/2}$ of $(CH_3)_3CNO_2$ with increasing concentration of Na^+ at certain concentrations of Et_4N^+ and n-Bu_4N^+. Other nitroalkanes and nitrobenzenes were also examined. The effect of water on the half-wave potentials of the first waves of the nitro compounds suggested the formation of $RNO_2^{\cdot-}(H_2O)_2$-type species.

The anion radicals of nitro compounds have attracted a number of electrochemists as well as organic chemists.[1,2] The ion-pair formation between the anion radicals and alkali metal ions in nonaqueous solutions has been suggested both by ESR[3,4] and polarography.[5-7] However, the shift in the half-wave potential of nitrobenzene in polarography has not been connected directly to the thermodynamic value of the ion-pairing.[8] Krygowski et al.[7] tried to evaluate the ion-pair formation constants between the nitrobenzene-anion radical and cations (alkali metal and tetraalkylammonium ions), using the effective ionic potential of the solvated cations in DMF. Kakutani et al.[9] discussed the effect of supporting electrolytes on kinetic paramaters in the polarographic reduction of *p*-nitrotoluene from the point of view of the double-layer theory.

We ourselves have studied polarographically ion-pair formation (or complex formation) reactions between alkali metal ions and carboxylate ions in nonaqueous solvents.[10,11] The formation of the $RCO_2^-(M^+)_2$ (M=Li and Na)-type species was clarified in acetonitrile, one of the protophobic solvents.[11]

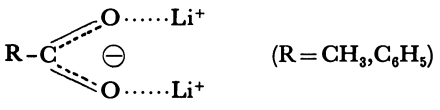

(R=CH_3,C_6H_5)

Moreover, we have found that the $RCO_2^-(M^+)_2$ species plays an important role in the polarographic reduction of carboxylic acids in pyridine solutions containing alkali metal ions as the supporting electrolyte cation.[12] Itabashi has proposed the formation of the $[CH_3COOLi_2]^+$ species in the polarographic reduction of copper(II) acetate in acetonitrile containing lithium ions.[13]

Now, let us give our attention to the similarity in the apparent structure between the carboxylate ion (RCO_2^-) and the anion radical ($RNO_2^{\cdot-}$) of a nitro compound:

In the present investigation, nitroalkanes and nitrobenzenes were examined polarographically in acetonitrile containing tetraalkylammonium (R_4N^+) and alkali metal (M^+) perchlorates as the supporting electrolytes. The specific effects of the coexistence of R_4N^+ and M^+ will be discussed. The effects of proton donors, phenol and water, will also be discussed briefly.

Experimental

Commercial nitro compounds—2-methyl-2-nitropropane ($(CH_3)_3CNO_2$, Aldrich Chemical Company, Inc.), 1-nitrobutane (Aldrich), nitroethane (Wako Pure Chemicals, EP grade), nitromethane (Wako, GR grade), nitrobenzene (Wako, GR grade), and *p*-nitrotoluene (Wako, GR grade)—were used without further purification. Lithium, sodium, tetraethylammonium, and tetrabutylammonium perchlorates were prepared by the methods mentioned previously.[14] The method of purifying acetonitrile has been described elsewhere.[15] Phenol (Wako, GR grade) was used as received.

All the polarograms were recorded with a Yanagimoto polarograph, Model P-1000, and a Watanabe X-Y recorder, Model WX-4401-L0. The rate of the potential sweep was 5 mV s^{-1}. The dropping mercury electrode had the following open-circuit characteristics: m=2.34 mg and τ=2.9 s in a 0.1 M (1 M=1 mol dm^{-3}) Et_4NClO_4–MeCN solution at h=50 cm. The drop time was regulated so as to be 1.0 s by means of a Yanagimoto P-1000-ST drop-timer, except for the potential range of −2.7 V and more negative potentials. The reference electrode was a silver-silver perchlorate electrode, Ag/0.1 M $AgClO_4$–MeCN. All the measurements were carried out at (25±0.2) °C. High-purity nitrogen gas was used for the deoxygenation.

Results and Discussion

Effect of Coexistence of Tetraalkylammonium and Alkali Metal Ions on the Reduction of Nitroalkanes.

Fiure 1 shows polarograms of 2-methyl-2-nitropropane ($(CH_3)_3CNO_2$) in acetonitrile containing various supporting electrolytes. With 0.1 M Et_4NClO_4, 2-methyl-2-nitropropane gave two cathodic waves at −2.07 and −2.85 V. These results are similar to those reported by Sayo et al.[16] with the same supporting electrolyte and solvent. The first wave is attributed to the one-electron reduction of the compound to form the monoanion radical.[16,17] With 0.1 M n-Bu_4N^+ as the supporting electrolyte cation, the second wave was hardly observed. A single wave was given in a 0.1-M $NaClO_4$ solution at a more positive potential than the potential in the tetraalkylammonium perchlorates. The positive shift may suggest interaction between the anion radical and Na^+. The wave height of the cathodic wave of the compound with 0.1 M $LiClO_4$ was larger than that with 0.1 M $NaClO_4$ by the factor of 3, as is shown in Table 1. The large wave height indicates that additional reduction is induced by the presence of Li^+.

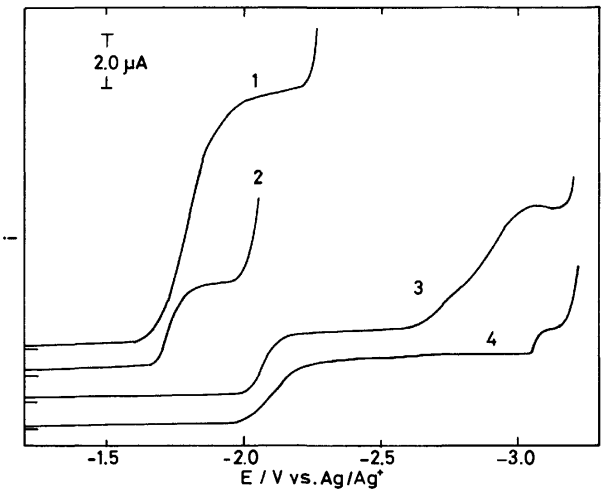

Fig. 1. Polarograms of 2-methyl-2-nitropropane in acetonitrile with various supporting electrolytes. $[(CH_3)_3CNO_2]$=0.4 mM. (1) Li^+, (2) Na^+, (3) Et_4N^+, (4) n-Bu_4N^+ of 0.1 M perchlorate.

Table 1. The Polarographic Data of Nitroalkanes and Nitrobenzenes in Acetonitrile Containing Various Supporting Electrolytes at 25 °C

Supporting electrolyte[a]	First wave			Second wave		
	$E_{1/2}$[b]/V,	I_l/μA,	Slope[c]/mV	$E_{1/2}$/V,	I_l/μA,	Slope/mV
	[2-Methyl-2-nitropropane]=0.4 mM					
n-Bu_4N^+	−2.115	2.2	105	—[d]		
Et_4N^+	−2.07	2.2	61	−2.85	4.0	184
Na^+	−1.72	2.8	35			
Li^+	−1.70	8.8	105			
	[1-Nitrobutane]=0.45 mM					
n-Bu_4N^+	−2.00	2.1	63			
Et_4N^+	−1.965	1.9	68			
Na^+	−1.585	2.5	37	−1.94[e]	3.9	97
Li^+	−1.48	7.7	61			
	[Nitroethane]=0.43 mM					
n-Bu_4N^+	−1.97	2.05	68			
Et_4N^+	−1.995	2.35	65			
Na^+	−1.58	2.6	34	−1.96[e]	4.3	93
Li^+	−1.50	8.25	72			
	[Nitromethane]=0.37 mM					
n-Bu_4N^+	−1.955	1.95	79			
Et_4N^+	−1.97	2.15	61			
Na^+	−1.58	3.2	37	−1.99[e]	2.3	79
Li^+	−1.49	6.6	66	(−1.66	2.0	66)[f]
	[Nitrobenzene]=0.35 mM					
n-Bu_4N^+	−1.52	2.1	61	−2.51	5.45	140
Et_4N^+	−1.525	2.1	59	−2.20	5.55	84
Na^+	−1.33[g]	1.85	—	(−1.49	5.0	—)[g]
Li^+	−1.15	3.5	10	−1.30	4.7	85
	[p-Nitrotoluene]=0.41 mM					
n-Bu_4N^+	−1.54	2.05	60	−2.55	4.8	145
Et_4N^+	−1.56	2.1	58	−2.215	5.5	98
Na^+	−1.36[g]	2.05	—	(−1.59	6.5	—)[g]
Li^+	−1.17	3.15	14	−1.32	5.25	84

a) 0.1 M perchlorate. b) vs. Ag/0.1 M $AgClO_4$-MeCN (+0.36 V vs. SCE). c) $-E$ vs. $\log[i/(i_d-i)]$. d) An incomplete wave was given, as is shown in Fig. 1. e) Very close to the reduction potential of the supporting electrolyte cation. f) The other wave appeared just after the first wave. g) Estimated values because of the polarographic maximum.

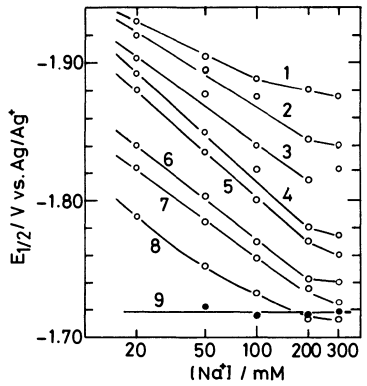

Fig. 2. Effect of Na^+ and n-Bu_4N^+ on the $E_{1/2}$ of 2-methyl-2-nitropropane. $[(CH_3)_3CNO_2]$=0.39 mM. (1) 200, (2) 100, (3) 50, (4) 20, (5) 10, (6) 5, (7) 2, (8) 1, (9) 0 mM of n-Bu_4NClO_4.

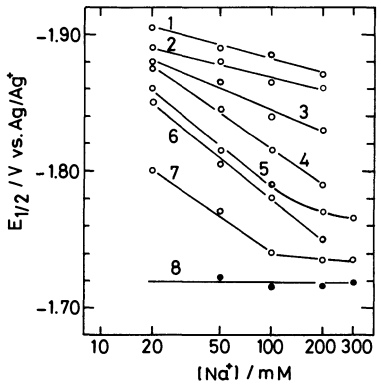

Fig. 3. Effect of Na^+ and Et_4N^+ on the $E_{1/2}$ of 2-methyl-2-nitropropane. $[(CH_3)_3CNO_2]$=0.4 mM. (1) 200, (2) 100, (3) 50, (4) 20, (5) 10, (6) 5, (7) 1, (8) 0 mM of Et_4NClO_4.

The effect of the concentration change of Na^+ on the $E_{1/2}$ of $(CH_3)_3CNO_2$ was also examined. The $E_{1/2}$ value was not significantly shifted by the increase in the concentration of $NaClO_4$ (50—300 mM) in the absence of a tetraalkylammonium salt, as is shown in Fig. 2. However, the addition of a small amount of n-Bu_4NClO_4 caused a remarkable change in $E_{1/2}$. In the presence of 10 or 20 mM n-Bu_4N^+, the $E_{1/2}$ of $(CH_3)_3CNO_2$ was shifted 110 mV to the positive by a 10-fold increase in the concentration of Na^+ ($\Delta E_{1/2}/\Delta$-log[Na^+]=110 mV). The value of $\Delta E_{1/2}/\Delta$log[Na^+] decreased to ca. 90 mV with 2 or 50 mM n-Bu_4N^+ and to smaller values with 1 or 100 mM n-Bu_4N^+. The waves were diffusion-controlled in the presence of both 10—100 mM n-Bu_4N^+ and 20—100 mM Na^+. The slope of $-E$ vs. log[$i/(i_1-i)$] was ca. 60 mV for 20—100 mM $NaClO_4$ with 5—20 mM n-Bu_4NClO_4 and for 200 mM $NaClO_4$ with more than 50 mM n-Bu_4NClO_4. The polarographic behavior with Et_4N^+ and Na^+ was quite similar to that with n-Bu_4N^+ and Na^+, except that the slope of $\Delta E_{1/2}/\Delta$log[Na^+] was, at most, 100 mV at 5 and 10 mM of Et_4N^+ (cf. Figs. 2 and 3).

The data given in Figs. 2 and 3 may be analyzed by

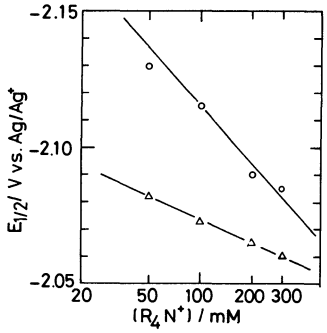

Fig. 4. Effect of the concentration of the supporting electrolyte on the $E_{1/2}$ of the first wave of 2-methyl-2-nitropropane. $[(CH_3)_3CNO_2]$=0.4 mM. (○): n-Bu_4NClO_4, (△): Et_4NClO_4.

means of the following equations, in which ion-pair formation and "complex-formation" reactions are taken into account:

$$(\Delta E_{1/2})_{R_4N^+} = \frac{0.059}{n}\log K' + \frac{0.059}{n}p\log[M^+] \quad (1)$$

$$(\Delta E_{1/2})_{M^+} = -\frac{0.059}{n}\log K'' - \frac{0.059}{n}q\log[R_4N^+] \quad (2)$$

where $(\Delta E_{1/2})_{R_4N^+}$ means the change in $E_{1/2}$ caused by the addition of M^+ at a constant concentration of R_4N^+ and where $(\Delta E_{1/2})_{M^+}$ is that caused by the addition of R_4N^+ at a constant concentration of M^+. K' and K'' are the conditional formation constants. p and q are the numbers of M^+ and R_4N^+ "coordinated" to the anion radical and the unreduced nitro compound respectively. The other conditions for Eqs. 1 and 2 are similar to those given in Ref. 11. For a fixed concentration of n-Bu_4N^+ (e.g., 10 mM), the value of p is derived as 2 from the slope of 110 mV and n=1. On the other hand, q equals ca. 1 at a constant concentration of Na^+ (e.g., 50 mM), as will be described in detail below. The fact that p=2 and q=ca. 1 for $(CH_3)_3CNO_2$ can be explained by the following scheme:

$$\begin{array}{ccc} (CH_3)_3CNO_2 & \overset{e^-}{\rightleftharpoons} & (CH_3)_3CNO_2^{\cdot-} \\ n\text{-}Bu_4N^+ \quad \Big\updownarrow K'' & & K' \Big\updownarrow \quad 2Na^+ \\ (CH_3)_3CNO_2\cdot n\text{-}Bu_4N^+ & & (CH_3)_3CNO_2^{\cdot-}(Na^+)_2 \end{array}$$

The conditional formation constant of the sodium complex was given as log (K'/M^2)=9.6 in the presence of 10 mM n-Bu_4N^+. The $E_{1/2}$ value for the case of [n-Bu_4N^+]=10 mM without Na^+ was estimated by the extrapolation from the $E_{1/2}$ values with 50—300 mM n-Bu_4N^+ (see Fig. 4). The irreversibility of the wave with n-Bu_4N^+ alone was ignored in this case. Similarly, log (K'/M^2) of 7.7 was obtained for [Et_4N^+]=10 mM from Fig. 3.

The degree of interaction between n-Bu_4N^+ and $(CH_3)_3CNO_2$ is expressed by the other conditional formation constant, K''. For a constant concentartion of Na^+ (50 mM), the $E_{1/2}$ shifted ca. 65 mV negatively

upon a 10-fold increase in the concentration of n-Bu_4N^+ (from 2 to 20 mM). In the presence of 50 mM Na^+, log (K''/M^2) was estimated to be ca. 4.4 for n-Bu_4N^+. Log (K''/M^2) was 3.8 for the interaction between Et_4N^+ and $(CH_3)_3CNO_2$ in the presence of 50 mM Na^+.

Strange to say, the half-wave potential of the first wave of $(CH_3)_3CNO_2$ shifted positively with increasing concentration of n-Bu_4N^+ or Et_4N^+ ($\Delta E_{1/2}/\Delta\log[R_4N^+]$= ca. 70 and 30 mV for n-Bu_4N^+ and Et_4N^+ respectively) without Na^+, as is shown in Fig. 4. The positive shift suggested the interaction between the R_4N^+ ion and the anion radical. The interaction between the tetraalkylammonium cations and the anion radical of nitrobenzene[7] has also been suggested by the positive shift in the $E_{1/2}$ of the reduction wave of nitrobenzene in DMF solutions. As has been shown above, the half-wave potential shifted negatively with increasing concentration of R_4N^+ in the presence of Na^+. The shifts of opposite directions between the absence and presence of Na^+ can be cleared up by the following idea: The $RNO_2^{\cdot-}$ ion as well as RNO_2 interacts with R_4N^+ in the absence of Na^+. However, the strong interaction of Na^+ with $RNO_2^{\cdot-}$ (the formation of $RNO_2^{\cdot-}(Na^+)_2$) prevents the R_4N^+ ion from interacting with $RNO_2^{\cdot-}$.

The strength of these interactions may vary with the concentration ratio between R_4N^+ and Na^+. We think that two interactions in opposite directions bring the change in the slope in Figs. 2 and 3. The minor change in the half-wave potentials with the concentration change of Na^+ in the absence of R_4N^+ can not be explained exactly at the present time, although the positive potential shift (+0.35 V) by 0.1 M $NaClO_4$, compared with 0.1 M Et_4NClO_4 (see Table 1), suggested interaction between the anion radical and Na^+. The slope of $\log[i/(i_d-i)]$ with 0.1 M $NaClO_4$ alone was rather small (35 mV). The reduction process of 2-methyl-2-nitropropane in acetonitrile seems not to be straightforward with alkali metal cations in the absence of tetraalkylammonium cations. At any rate, we have given a quantitative explanation for some typical cases in the extraordinary phenomena, without considering the other reactions or the double-layer effect.

Hyne has reported interaction between the neutral molecule of nitrobenzene and tetrabutylammonium bromide in a mixture of nitrobenzene and methanol, based on the conductivity data etc.[18] His proposal seems to support our mechanism, in which the interaction between the nitro compound and R_4N^+ is accounted.

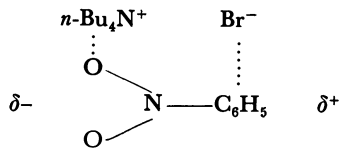

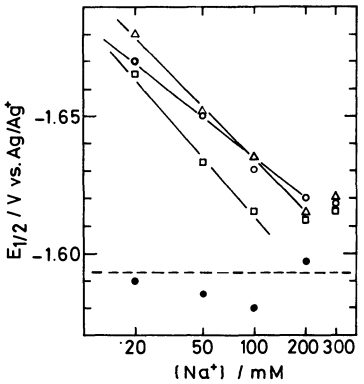

Fig. 5. Change of $E_{1/2}$ of nitroalkanes with Na^+ concentration. (○): 1-Nitrobutane, (△): nitroethane, (□): nitromethane in the presence of 10 mM n-Bu_4NClO_4, (●): 1-nitrobutane, in the absence of n-Bu_4NClO_4. The concn. of a nitroalkane is 0.4 mM.

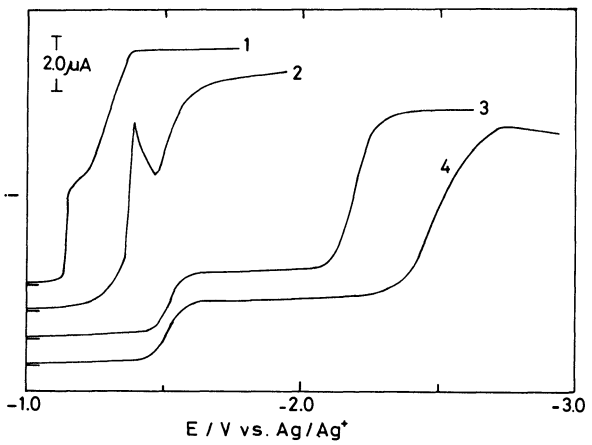

Fig. 6. Polarograms of nitrobenzene in acetonitrile with various supporting electrolytes. [Nitrobenzene]=0.4 mM. (1) Li^+, (2) Na^+, (3) Et_4N^+, (4) n-Bu_4N^+ of 0.1 M perchlorate.

Krigowsky et al. suggested the existence of two different species, $N^{\cdot-}K^+$ and $N^{\cdot-}2K^+$ ($N^{\cdot-}=C_6H_5NO_2^{\cdot-}$), in the polarographic reduction of nitrobenzene ($\Delta E_{1/2}/\Delta\log[K^+]$ of 65 and 110 mV) in DMF.[7]

As for other nitroalkanes, the values of the $\Delta E_{1/2}/\Delta\log[Na^+]$ slope were 50, 65, and 80 mV for 1-nitrobutane, nitroethane, and nitromethane respectively in the presence of 10 mM n-Bu_4N^+, as is shown in Fig. 5. These values suggest the interaction of the anion radical with a single Na^+ ion ($RNO_2^{\cdot-}Na^+$) or more in the presence of 10 mM n-Bu_4N^+. The half-wave potential of 1-nitrobutane was not so much influenced by the concentration change of $NaClO_4$ in the absence of n-Bu_4NClO_4. The increase in the concentration of n-Bu_4NClO_4 caused the half-wave potential of the first wave of 1-nitrobutane to shift positively (e.g., $E_{1/2}$=−2.02 V at 20 mM and −1.99 V at 200 mM of n-Bu_4N^+) without $NaClO_4$.

On the Reduction of Nitrobenzenes. Polarographic data of nitrobenzene and p-nitrotoluene with var-

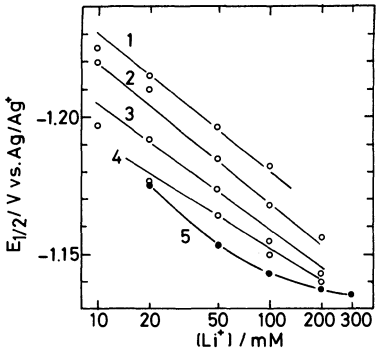

Fig. 7. Effect of Li^+ and Et_4N^+ on the $E_{1/2}$ of the first wave of nitrobenzene. [Nitrobenzene]=0.39 mM. (1) 100, (2) 50, (3) 20, (4) 5, (5) 0 mM of Et_4NClO_4.

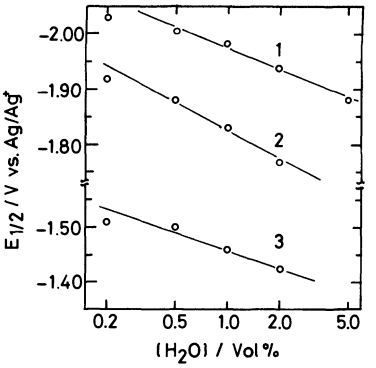

Fig. 8. Effect of H_2O on the $E_{1/2}$ of the first wave of nitroalkanes and nitrobenzene in acetonitrile solutions containing 0.1 M Et_4NClO_4. (1) 2-Methyl-2-nitropropane, (2) nitromethane, (3) nitrobenzene. The concns. of the nitro compounds are all 0.4 mM.

ious supporting electrolytes are also listed in Table 1. Nitrobenzene gave two cathodic waves with each supporting electrolyte (Fig. 6). The first wave showed a good reversibility with 0.1 M n-Bu_4N^+ or Et_4N^+. However, the slope of $-E$ vs. $\log[i/(i_d-i)]$ was extremely small (10 mV) with 0.1 M Li^+. The small slope observed with Li^+ became larger ($\approx$30 mV) upon the addition of 0.1 M n-Bu_4N^+ or Et_4N^+. The half-wave potential of nitrobenzene shifted positively ca. 50 mV ($\Delta E_{1/2}/\Delta\log[Li^+]$) with increasing concentration of $LiClO_4$ in the presence of 20—100 mM Et_4N^+, as is shown in Fig. 7. With 50 mM Et_4N^+, the highest slope (52 mV) was obtained. For p-nitrotoluene, the slope was 58 mV with a concentration change of Li^+ at 50 mM n-Bu_4N^+. From the data in Fig. 7, p=1 and q=ca. 0.5 in Eqs. 1 and 2 were derived for nitrobenzene, assuming n=1. The fact that p=1 in the presence of both Li^+ and Et_4N^+ suggests the following reaction:

$$C_6H_5NO_2^{\cdot-} + Li^+ \overset{K'}{\rightleftharpoons} C_6H_5NO_2^{\cdot-}Li^+ \qquad (3)$$

The interaction between the nitrobenzene molecule and the Et_4N^+ cation was also suggested, even though the value of q was not unity.

The difference in the number of alkali metal ions "coordinated" to the anion radicals between 2-methyl-2-nitropropane (p=2) and nitrobenzene (p=1) seems to be caused by the difference in the electron density on the nitro group. Peover and Powell described[19] that, in the anion radical of an aliphatic compound, the charge on the nitro group is virtually unity, while in that of a nitrobenzene, the charge can be delocalized into the aromatic system.

Effect of Proton Donors on the Reduction Wave of Nitro Compounds. The effect of phenol on the polarographic reduction of 2-methyl-2-nitropropane was examined. By the addition of 10 mM of phenol to a 0.4 mM $(CH_3)_3CNO_2$ solution, the two waves of $(CH_3)_3CNO_2$ without phenol merged into a single wave of $E_{1/2}$=−1.97 V. The wave height with 10 mM phenol was 3—4 times as large as the first wave height without phenol. The further addition of phenol up to 100 mM caused the half-wave potantial to shift positively, without changing the wave height.

Figure 8 shows the effect of H_2O on the half-wave potentials of 2-methyl-2-nitropropane, nitromethane, and nitrobenzene. The half-wave potentials of $(CH_3)_3CNO_2$ and nitrobenzene both shifted ca. 120 mV positively upon a 10-fold increase in the water concentration. The wave height of $(CH_3)_3CNO_2$ or nitrobenzene (the first wave) remained constant even upon the addition of water up to 2% (2.15 μA, cf. 2.1 μA without water for $(CH_3)_3CNO_2$). The waves were reversible and seemed to be diffusion controlled. Therefore, the value of 120 mV for $\Delta E_{1/2}/\Delta\log[H_2O]$ suggested that the anion radicals of $(CH_3)_3CNO_2$ and nitrobenzene interact with two molecule of water:

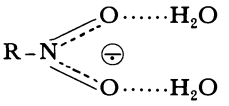

We have previously reported elsewhere[11] the interaction between the benzoate ion ($C_6H_5CO_2^-$) and two molecules of water in an acetonitrile solution.

For nitromethane, the value of $\Delta E_{1/2}/\Delta\log[H_2O]$ was 145 mV, which may also suggest the interaction between the anion radical of nitromethane and two molecules of water.

Lipsztajn et al.[20] have reported the experimental results that the slope of $\Delta E_{1/2}/\Delta\log[H_2O]$ is ca. 120 mV (0.1—1 M H_2O) for the half-wave potential of the first wave of nitrobenzene in DMF containing 0.1 M Et_4NClO_4 as the supporting elctrolyte. They[20] suggested the formation of both $NB^{\cdot-}$ Na^+ and $NB^{\cdot-}$ $2Na^+$ ($NB^{\cdot-}$=nitrobenzene anion radical) in DMF containing 1.66 M of H_2O (3% by volume).

We wish to express our thanks to Professor Toyokichi Kitagawa of Osaka City University for his helpful suggestions.

References

1) C. K. Mann and K. K. Barnes, "Electrochemical Reac-

tions in Nonaqueous Systems," Marcel Dekker, New York (1970), p. 347.
2) O. Popovych and R. P. T. Tomkins, "Nonaqueous Solution Chemistry," John Wiley and Sons, New York (1981), p. 362.
3) T. Kitagawa, T. Layloff, and R. N. Adams, *Anal. Chem.*, **36**, 925 (1964).
4) J. Oakes, J. Slater, and M. C. R. Symons, *Trans. Faraday Soc.*, **68**, 546 (1970).
5) L. Holleck and D. Becher, *J. Electroanal. Chem.*, **4**, 321 (1962).
6) L. A. Avaca and A. Bewick, *J. Electroanal. Chem. Interfacial Electrochem.*, **41**, 405 (1973).
7) T. M. Krygowski, M. Lipsztajn, and Z. Galus, *J. Electroanal. Chem. Interfacial Electrochem.*, **42**, 261 (1973).
8) T. Osa, "Denkyoku-hannō No Kiso," ed by T. Osa, Kyōritsu Shuppan, Tokyo (1973), p. 205.
9) T. Kakutani, H. Kinoshita, and M. Senda, *Review of Polarography (Japan)*, **20**, 15 (1974).
10) M. Hojo and Y. Imai, *Bunseki Kagaku*, **32**, E77 (1983).
11) M. Hojo and Y. Imai, *Bull. Chem. Soc. Jpn.*, **56**, 1963 (1983).
12) M. Hojo, Y. Akita, K. Nishikawa, and Y. Imai, *Bull. Chem. Soc. Jpn.*, in press.
13) E. Itabashi, *J. Electroanal. Chem. Interfacial Electrochem.*, **36**, 179 (1972).
14) T. Fujinaga, S. Okazaki, and M. Hojo, *Bull. Inst. Chem. Res., Kyoto Univ.*, **56**, 139 (1978).
15) T. Fujinaga, S. Okazaki, and M. Hojo, *J. Electroanal. Chem. Interfacial Electrochem.*, **113**, 89 (1980).
16) H. Sayo, Y. Tsukitani, and M. Masui, *Tetrahedron*, **24**, 1717 (1968).
17) A. K. Hoffmann, W. G. Hodgson, and W. H. Jura, *J. Am. Chem. Soc.*, **83**, 4675 (1961).
18) J. B. Hyne, *J. Am. Chem. Soc.*, **85**, 304 (1963).
19) M. E. Peover and J. S. Powell, *J. Electroanal. Chem. Interfacial Electrochem.*, **20**, 427 (1969).
20) M. Lipsztajn, T. M. Krygowski, and Z. Galus, *J. Electroanal. Chem. Interfacial Electrochem.*, **49**, 17 (1974).

 © 1986 The Chemical Society of Japan Bull. Chem. Soc. Jpn., 59, 3821—3827 (1986)

Superconductivity and Characterization of the High-Pressure Reaction Products of Carbon Diselenide, CSe_2

Akiko KOBAYASHI,* Yukiyoshi SASAKI, Tokuko WATANABE,† Seiichiro IKEHATA,†† Haruo KISHIDA,†††
Haruki KAWAMURA,†††† Reizo KATO,††††† and Hayao KOBAYASHI†††††,*
Department of Chemistry, Faculty of Science, The University of Tokyo, Hongo, Bunkyo-ku, Tokyo 113
†The University of the Air, Wakaba, Chiba 260
††Department of Physics, Faculty of Science, The University of Tokyo, Hongo, Bunkyo-ku, Tokyo 113
†††Nissei Sangyo Co., Ltd., Toranomon, Minato-ku, Tokyo 105
††††National Research Institute for Metals, Sakura, Niihari, Ibaraki 305
†††††Department of Chemistry, Faculty of Science, Toho University, Funabashi, Chiba 274
(Received May 13, 1986)

The physical properties and the structure of black solids obtained by the high-pressure reaction of CSe_2 were examined by IR, X-ray diffraction, scanning electron microscope, electron diffraction, thermal analyses and magnetic experiments. The crystalline solid, which was metallic ($\sigma(RT)\approx 50$ S cm^{-1}) at ambient pressure became superconductor above 20 GPa(T_c(onset)=6 K), while the amorphous solid was insulating. Contrary to the previously proposed one- or two-dimensional polymerization structure of $(CSe_2)_x$, it has been revealed that the metallic CSe_2 sample have a rather complex structure that is composed of the crystalline hexagonal Se, graphite and some amorphous parts. Thus, the high conductivity and the diamagnetism of the crystalline solid at ambient pressure seems to come from graphite part and the superconductivity seems to come from hexagonal Se part. The superconducting transition behavior depended on the path of the pressure-cooling steps. The superconducting state was observed only when the pressure was increased at the low temperature.

Recent discoveries of many organic superconductors based on the multi-sulfur (or selenium) π-donor or π-acceptor molecules have aroused a considerable interest in the field of synthetic metals. Contrary to the traditional organic conductors with the disadvantage of the Peierls instabilities originated from their one-dimensionalities, in these multi-sulfur compounds the two-dimensional (or three-dimensional) intermolecular close contacts of chalcogen atoms in the π-conjugated molecules play a central role for the formation of the conduction bands. Carbon diselenide is the simplest π-conjugated molecule with Se atoms.

Okamoto and Wojciechowski reported that CSe_2 was polymerized into conductive amorphous solid (10^{-3} S cm^{-1}).[1] Okamoto et al. proposed the two step reactions:

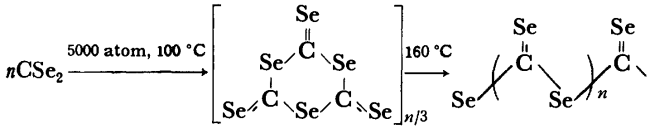

The second step appears to be analogous to the solid state polymerization of S_2N_2, into the well known inorganic polymer superconductor, $(SN)_x$.[2] Since the similar linear chain structure had been already suggested in the polymerization of CS_2 under a pressure of 30 kbar,[3] this polymerization mechanism of CSe_2 seemed to be reasonable. We tried to obtain the similar polymer. Various types of the black solids were obtained.[4,5] Most of them were amorphous but in some cases, highly conducting crystalline solids were obtained. This crystalline solid was revealed to exhibit a superconducting transition at high pressure.

Initially we proposed the two-dimensional polymerization model as to the crystalline solid,[6] because the EXAFS analysis showed that the linear chain structure model was incorrect. However, recently we have found the evidence of the existence of hexagonal Se and graphite in the conducting solid.

In this report, the electrical properties of the high pressure reaction products of CSe_2 and their characterization by X-ray diffraction, scanning electron microscope, chemical analysis, EXAFS, DSC, IR, electron microscope, electron diffraction, magnetic susceptibility and ESR experiments are described.

Experimental

Carbon diselenide, CSe_2 is a toxic, malodorus and golden-yellow liquid reagent used in the synthetic studies of the π-donor molecules with the Se atoms, which was obtained by the reaction of Se vapor with dichloromethane in the nitrogen stream and the subsequent distillation.[7] Liquid CSe_2 in the teflon cell was pressurized at about 5 kbar and heated to 80—100 °C for 2—3 h. Then the pressure was released and the cell was heated at 100—130 °C. Various types of black solids were obtained. About 0.3 ml of CSe_2 was used at a time. The degree of the crystallinity of the solid was very sensitive to the conditions of the preparation (pressure and temperature) and the reaction was hardly to controll. When the reaction temperature was too high (130—160 °C), the amorphous solid was obtained. On the contrary, when the reaction temperature was below 70 °C, nonreacted CSe_2 was remained.

The conductivity measurements were performed by the fourprobe method with silver paint within the temperature range of 1.5 K to 300 K. The high-pressure resistivity experiments were performed on the compaction sample by the two probe method using the diamond anvil high-pressure cell.

The X-ray powder patterns were measured on a Rigaku X-ray powder diffractometer. Intensities were extremely weak and those data were obtained by scanning up to 2θ=130° (Cu $K\alpha$ radiation, Ni filter, 35 kV, 15 mA) for a week running (0.72°/h).

Temperature dependence of X-band ESR spectra from 100

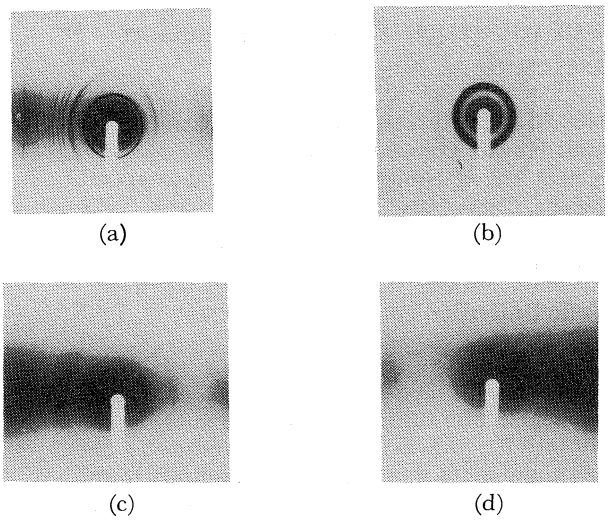

Fig. 1. X-Ray diffraction diagrams of high-pressure reaction products of CSe_2.
a): Metallic solid (50 S cm^{-1}), b): semiconducting (5 S cm^{-1}) solid, c): low-conducting solid (10^{-3} S cm^{-1}), d): insulating solid (10^{-8} S cm^{-1}).

to 300 K was examined on a JEX-FEIX ESR spectrometer with flowing liquid nitrogen gas. Skin effect of ESR was observed as to the metallic sample and the experiment was performed on the finely-ground powder sample.

Magnetic susceptibility of metallic sample was measured by a Faraday method on a powder sample of about 0.13 g over a temperature range between 2 and 296 K. A permanent magnet and electro-balance were used. The temperature of the sample was controlled through the pure helium gas at a pressure of about 3 Torr (1 Torr=133.322 Pa). The helium gas was purified by passing through a charcoal trap held at 75 K.

The measurement of the EXAFS spectra was performed at the Photon Factory of National Laboratory for High Energy Physics (KEK-PF), using EXAFS facilities at the beam line 10-B with a Si(311) channel-cut monochromator.

The IR spectra were taken of a dispersion in KBr within the range of 400 cm^{-1} to 4000 cm^{-1}.

The thermogravimetric analyses were performed on a Rigaku differential scanning calorimeter within the temperature range between 20 to 400 °C.

Electron microscope and electron diffraction experiments were performed on H-800 Hitachi Electron Microscope.

Scanning electron microscope experiments were made by using X-650 Hitachi Scanning Electron Microanalyser.

Results and Discussion

Electrical and Magnetic Properties. As described before, black solids were prepared from CSe_2. By changing the applied pressure and the heating temperature, we obtained various solids. The X-ray diffraction diagrams of the products are shown in Fig. 1. There are various solids with different crystallinities. The conductivity of the compaction sample of the crystalline solid, which gave sharp X-ray diffraction patterns (Fig. 1a), was about 50 S cm^{-1} and the resistivity ratio at 1.7 K ($\rho_{1.7}/\rho_{300}$) was 2—3 (Fig. 2a). This small resistivity ratio and almost linear temperature

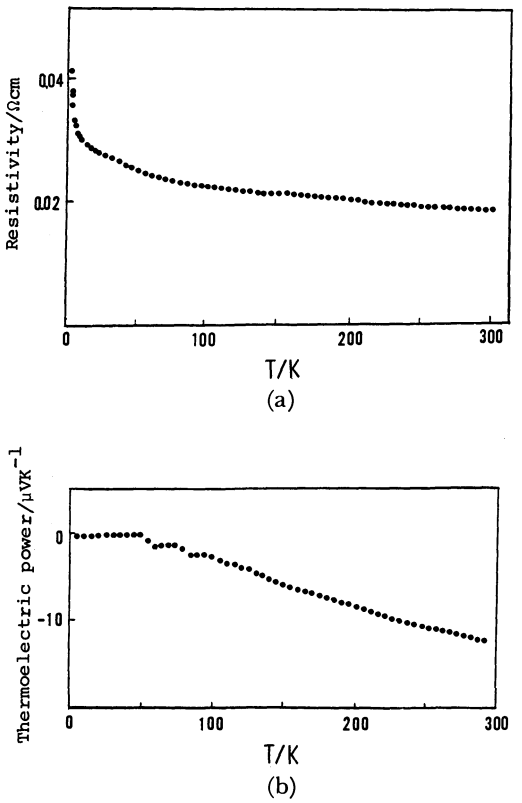

Fig. 2. a) Electrical resistivity of metallic crystalline solid. b) Thermoelectric power (S/μVK^{-1}) of metallic crystalline solid.

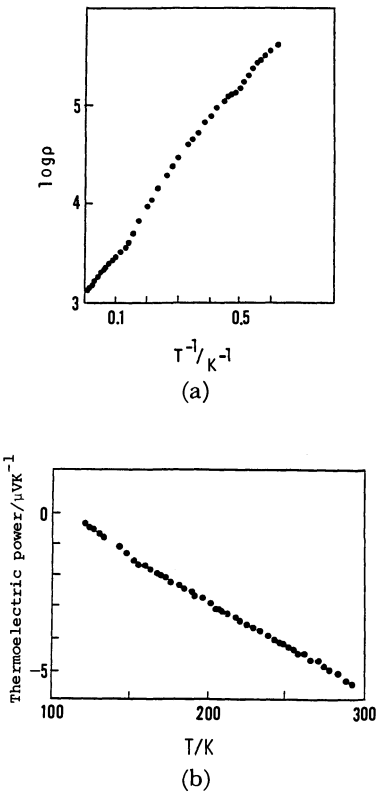

Fig. 3. a) Electrical resistivity of semiconducting solid. b) Thermoelectric power of semiconducting solid.

I	2θ	d	I	2θ	d
36.3	23.2	3.837	5.1	71.4	1.321
0.8	26.4	3.375	3.4	77.8	1.227
100.0	29.4	3.039	5.8	76.6	1.243
15.3	41.1	2.198	5.7	81.5	1.180
36.3	43,4	2.087	4.6	86.4	1.126
20.9	45.0	2.014	17.2	90.7	1.083
1.6	47.7	1.906	7.1	96.0	1.o37
19.6	51.4	1.777	2.7	105.6	0.967
20.1	55.6	1.652	3.1	106.7	0.960
17.7	61.2	1.514	4.5	121.6	0.883
11.1	65.0	1.434	2.7	122.4	0.879
3.3	68.0	1.378			

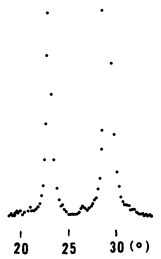

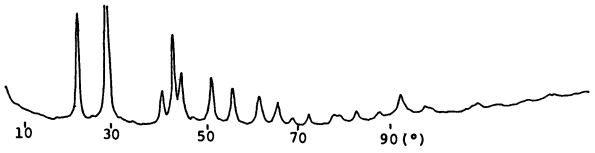

Fig. 4. Lattice spacings (d/Å^{-1}), intensities (I) and diffraction powder patterns of metallic crystalline solid. The small peak around 26° (Cu $K\alpha$) seems to be 002 reflection from graphite.

dependence of the thermoelectric power described later suggests that the highly conducting sample is essentially metallic.

Besides the highly conducting samples, there are insulating, low-conducting and semiconducting samples. The conductivity of the insulating sample, which gave amorphous X-ray halos (Fig. 1c) was less than 10^{-8} S cm^{-1} and that of the semiconducting sample was about 5 S cm^{-1} with activation energy of 0.09 eV (Fig. 3a). The semiconducting solid gave extremely broad Debye rings suggesting the heavily disordered lattices (Fig. 1b). The conductivity of the samples obtained by reheating the insulating sample up to 250 °C is ca. 10^{-3} S cm^{-1}, almost identical to the conductivity of poly(carbon diselenide) reported by Okamoto and Wojciekowski.[1] The low-conducting material was almost amorphous to X-ray diffraction (Fig. 1d). These facts indicate that the solid is metallic in an ordered crystalline state and it becomes less conductive when crystalline imperfection increases. The X-ray powder pattern of the crystalline material was measured on the X-ray diffractometer and more than twenty peaks were obtained. The lattice spacings and the X-ray powder patterns are shown in Fig. 4. The thermoelectric power of the crystalline solid was negative and as small as -12 μV/K at room temperature. The almost linear temperature dependence suggests the existence of negative free carriers (Fig. 2b).

The IR spectrum of the insulating sample showed the absorption bands at 880, 1260, and 1380 cm^{-1}. The strong band at 880 cm^{-1} was assigned to the C=Se stretching vibration. The conducting sample was opaque down to at least 400 cm^{-1} probably due to the free carrier absorption.

The Fourier transform of EXAFS spectra of the metallic sample was different from that of insulating

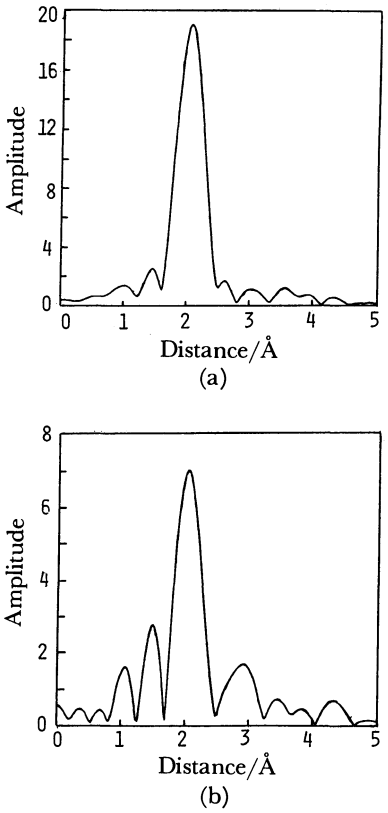

Fig. 5. Fourier transform of the EXAFS oscillation, $k^3\chi(k)$ for (a) metallic and (b) insulating solids.

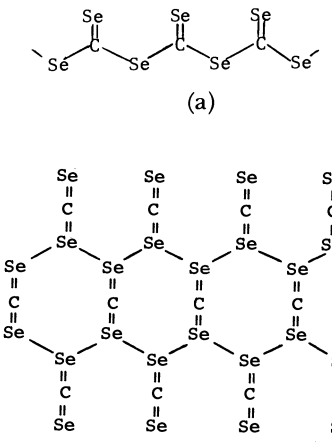

Fig. 6. Structure model of $(CSe_2)_x$ polymer.
a): Chain structure model[1] b): Two-dimensional structure model.[6]

sample but was quite similar to that of hexagonal Se powder (Fig. 5). The prominent peak in the Fourier transform of metallic sample corresponded to Se-Se bond. But no indication of Se-C or Se=C bond was found except in the insulating sample. The bond distances and coordination numbers were obtained by the curve-fitting analyses with empirical parameters. Since hexagonal Se had a helical structure of Se-Se distance of 2.37 Å, the coordination number of Se in

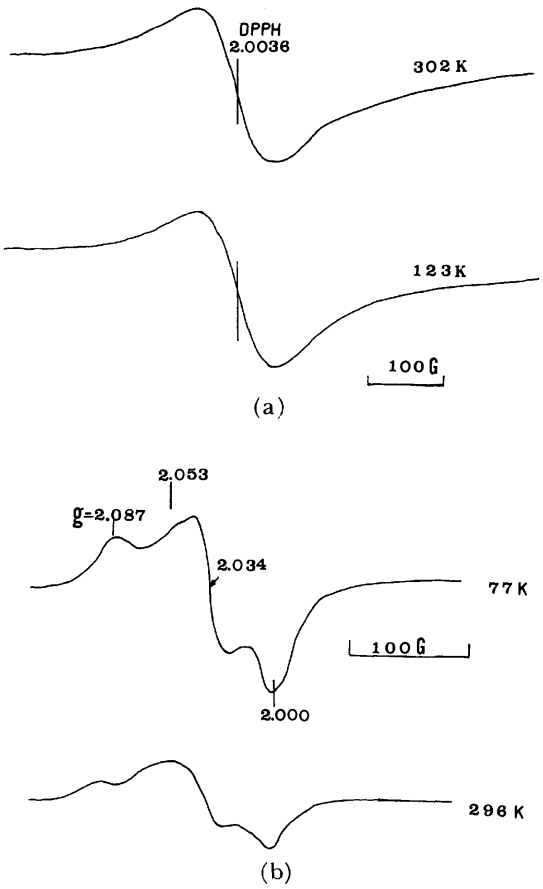

Fig. 7. ESR spectra of a) metallic and b) insulating high pressure reaction products of CSe_2.

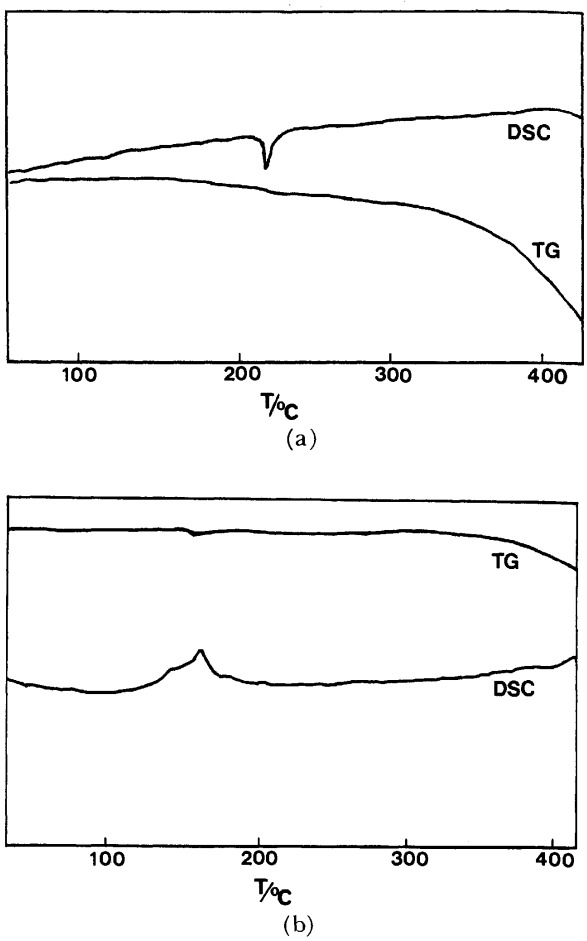

Fig. 8. DSC-TG curves of a) metallic and b) insulating solids.

hexagonal Se was fixed as 2.0. The coordination number of metallic sample was almost 2.0, which indicates that each Se atom has two neighbouring Se atom. Insulating sample had the coordination number of 0.7, but Se-Se distances were almost the same for all the samples. Since the result of EXAFS analyses indicated the existence of -Se-Se- (2.37 Å) infinite chains in the metallic sample, the chain structure model proposed by Okamoto (Fig. 6a) did not conform with the EXAFS experiments. Thus, two-dimensional structure model with -Se-Se- chains was proposed at this stage (Fig. 6b).[6] However, further characterization revealed that this structure model was not correct one, which will be mentioned later.

X-band ESR measurements of metallic and insulating powder samples of CSe_2 solid are shown in Fig. 7. The broad ESR signal (the peak-to-peak linewidth is 98 G) and the g value of 2.0038, which is very close to that of free electron (2.0023). The temperature was varied within 123—243 K at the interval of 20 K. The peak-to-peak linewidth and g-value, are almost constant within this temperature range. The lineshape was almost Lorentzian in the measured field range of four times as large as the linewidth. These results support the metallic character of the solid and the existence of the conduction electrons. For insulating sample, ESR measurements were performed at room temperature and 77 K. The g-anisotropic spectra at 77 K indicates that there are more than two radical species. The large g-shift suggests that these radical species are not C-centered radicals but Se-centered radicals. These ESR measurements indicate that in the metallic sample there exist conduction electrons and in the insulating sample there exist Se-centered radicals produced by broken Se-Se bonds.

Figure 8 shows the DSC-TG curves of the solids. For metallic sample, the endothermic reaction was observed at 220 °C. The thermogravimetric study of the insulating sample showed that three percent of the weight was lost at ca. 160 °C and the remaining was stable up to 300 °C.

In Fig. 9 the magnetic susceptibility of the crystalline sample is shown. From 5 to 296 K the magnetic susceptibility was almost constant and below 5 K the susceptibility increased gradually, which would be an effect of magnetic residuals. The effect of the oxygen molecules included in the sample was observed around 40 K. The magnetic susceptibility performed diamagnetic corrections was $\chi=-1.75\times10^{-6}$ cgsemu g^{-1}. The magnetic susceptibility of an electron gas mainly consists of the Pauli paramagnetism and the Landau-

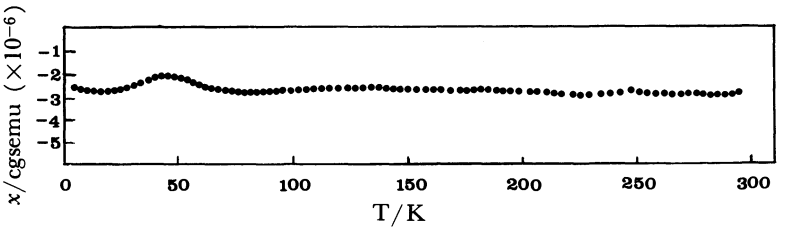

Fig. 9. Magnetic susceptibility of metallic solid.

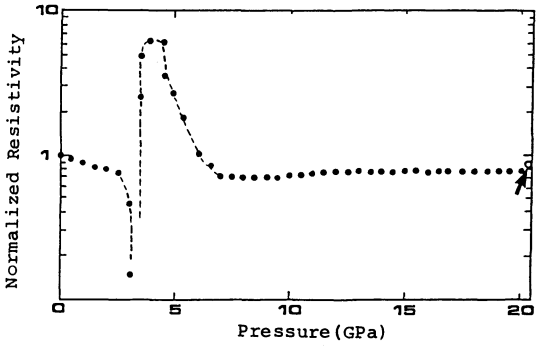

Fig. 10. The pressure dependence of the normalized room-temperature resistivity (ρ(P)/ρ(1Pa)). The open circle indicates the value at 2.1 K obtained by the measurements along the path A shown in Fig. 11.

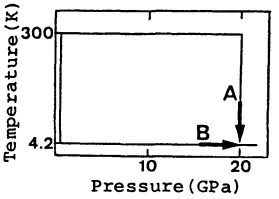

Fig. 11. Two paths (A, B) along which the resistivity measurements were performed.

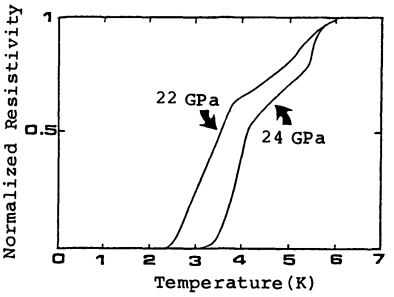

Fig. 12. Superconducting transition obtained by the measurement along the path B. The ordinate is the normalized resistivity (ρ(T)/ρ(6 K)).

Peierls diamagnetism. The contribution from Landau-Peierls-Pauli term is represented by[8]

$$\chi_{LPP} = \mu_B^2 N/3\rho\varepsilon_F(3-\langle f^2\rangle)F'\varepsilon_F/Fk T$$

where μ_B: Bohr magneton

$\langle f^2\rangle$= effective mass correction $(2m_t+m_l)/(m_t^2 m_l)^{1/3}$

χ_{LPP} becomes large negative value, when the second term of above equation is large. The second term is dependent on the anisotropy of the mass. It is well-known that in semimetallic materials such as graphite a large negative magnetic susceptibility is observed due to the large Landau-Peierls term which is derived from the two-dimensional anisotropy. Therefore, it is plausible that metallic crystalline sample has a possibility of having an anisotropic electronic structure.

Superconductivity at High Pressure. The high pressure resistivity experiments were performed on the compaction sample by the two probe method using the diamond anvil high pressure cell. The pressure dependence of the room-temperature resistivity is shown in Fig. 10. There was an anomaly around 3 GPa, where a high-conducting state appeared within a small pressure range. Above this anomaly, the solid transformed again into the less conductive state. The resistivity of this high-conducting state was about 10 times smaller than the resistivity at ambient pressure. Above 10 GPa, the pressure dependence of the resistivity became very small. Besides the hysteresis of the 3 GPa transition, the resistivity behavior was almost reversible. The temperature and pressure dependences of the resistivity were measured along two different paths shown in Fig. 11. In the path A, the pressure was increased initially to ca. 20 GPa at room temperature, then the temperature was decreased at constant pressure of ca. 20 GPa. The resistivity at high pressure (20—22 GPa) was almost temperature-independent. Any anomaly was not observed at least down to 2.1 K (the lower temperature limit of the experiment) (Fig. 10).

On the other hand, in the path B, where the temperature was lowered initially and the pressure was increased above 20 GPa with keeping the low temperature, our crystalline sample showed a decrease of the resistivity indicating the onset of the super conducting transition. The result is shown in Fig. 12. Similar dependence of the transition temperature on the measurement process has been also found in black phosphorous.[9] The superconducting transition temperature of black phosphorus measured along the path B (after temperature was decreased, pressure was increased) was much enhanced than that obtained by the path A (after pressure was increased, temperature was lowered) (T_c(25 GPa)=10 K (path B), 6 K (path A)).

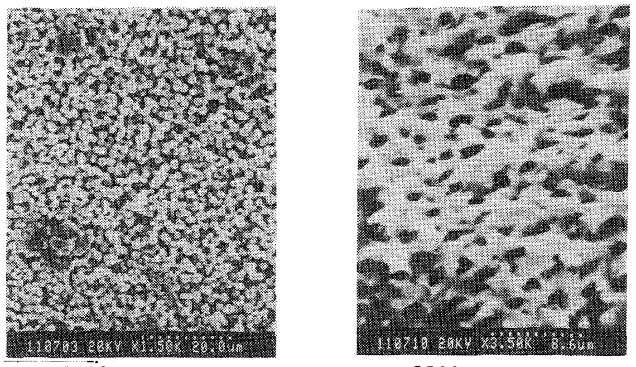

×1500 (a) ×3500 (b)

Fig. 13. Photographs of SEM. a) amorphous insulating solid (×1500) b) metallic crystalline solid (×3500).

Fig. 14. Photographs of metallic crystalline solid by the electron microscope (×1500000 magnification). Crystalline parts with lattice spacings of ≈3 Å and some amorphous or cluster regions are observed.

Black phosphorus is considered to be converted into a mixed system consisting of metallic fine threads dispersed in the semiconducting matrix. The appearance of superconductivity in the mixed system by the excitonic mechanism was suggested by Fukuyama.[10] However, the origin of the enhancement of the transition temperature remains an open questions.

In our crystalline sample, the onset of the superconducting transition was 6 K with the mid-point temperatures of 3.5 K at 22 GPa and 4.1 K at 24 GPa. The temperature range of the transition (ΔT) was fairly large, but the transition became sharp with increasing pressure (ΔT=2.7 K (22 GPa), 1.9 K (24 GPa)). This superconducting transition of the crystalline sample reminds us of those of various kinds of selenium by ordinary path A. Amorphous Se undergoes a semiconductor to metal transformation at a pressure of 13 GPa and at 7 K superconductivity was observed.[11] Monoclinic Se has a discontinuity in resistance near 15 GPa, as in amorphous Se. Superconducting transition has onsets at 7 K, but never complete.[11] Pure hexagonal Se was pressurized to about 16 GPa, no sharp semiconductor to metal transition was observed at any pressure, and at high pressure no superconductivity was found to 1.5 K.[11]

Decomposition Reaction of CSe_2. The physical properties and the structure of the black solids obtained by the high pressure reaction of CSe_2 were examined by several methods as described above. EXAFS indicated the existence of an infinite -Se-Se- chain in the metallic sample, which showed that the $(CSe_2)_x$ chain model (Fig. 6a) was not correct at least for the high conducting samples. Thus, we proposed two-dimensional structure model of $(CSe_2)_x$. However, recent examination of the metallic samples have revealed the existence of the crystals of hexagonal Se. Except for the appearance of the small peak around 26° (Cu $K\alpha$) and large intensities of the peaks around 90°, the X-ray diffraction patterns of the metallic sample (Fig. 4) are almost identical to that of hexagonal Se crystal. Since hexagonal Se is not high conductive, the metallic nature of the reaction product seems to be puzzling. However, DSC of the crystalline sample gave another evidence of the existence of hexagonal Se crystals. An endothermic peak was observed around the temperature of the m.p. (220 °C) of the hexagonal Se crystal. The photographs of SEM showed that the amorphous insulating solid was composed of the spheres with diameter of about 13000 Å, while the metallic solid appeared to be composed of the uniform black flakes (×3500) (Fig. 13). However, recent electron microscope (×1500000 magnification) and electron diffraction experiments (Fig. 14) have suggested the existence of graphite, which is consistent with the appearance of the small peak around 26° (d=3.375 $Å^{-1}$, the strongest peak of graphite crystal) in the X-ray powder diffraction. The electron microscope photographs show that the metallic solid is composed of the crystalline regions and the amorphous or cluster ones. Although the patterns of the electron diffraction and microscope photographs are not simple,[12] the conducting product could be characterized fairly satisfactorily. There are considerable amount of evidences showing the existence of hexagonal Se. Graphite powder seems to also exist. The value of magnetic susceptibility is plausible for that of graphite. If we assume magnetic susceptibility is derived from almost graphite, it will be -24.8×10^{-6} cgsemu g^{-1}. Thus we may say that the unexpected novel reaction took place. Contrary to the expected polymerization reaction, CSe_2 is decomposed into the component atoms to produce crystalline hexagonal Se with small crystal size (<500 Å), graphite and some amorphous solids or clusters. Although there exist considerably large amorphous (or cluster) regions, any conductive anomaly was not observed around the pressure where the insulating amorphous Se transform into the metallic (or superconducting) state (≈15 GPa). Therefore, it may be

unlikely that there are large amount of amorphous Se. The high conductivity and the diamagnetism seems to come from the properties of the graphite and the superconductivity from crystalline hexagonal Se. Thus our experiment seems to indicate that superconducting transition of hexagonal Se occurs at the pressure greater than 20 GPa and this may be the first observation of the superconducting transition of hexagonal Se.

However, there remain unsolved interesting features concerning the superconducting transition:

(1) Superconductivity was observed only along the path B. What is the mechenism of the enhancement of T_c? Is it plausible that the superconducting transition occurs under 2.1 K (lower limit of the experiments) along the path A and is observed at 2.5—6 K along the path B by the enhancement of the superconducting transition temperature?

(2) Why the transition occurs stepwise (Fig. 12)? The sharpning of the transition with increasing the pressure seems to indicate the increase of the onset temperature of the second step, which shows that there exist two situations of the solid which have different superconducting transition temperatures individually. Since the onset temperature of 6 K resembles that of the transition of Se, what is the origin of the transition with onset temperature of 3.5 K? Further, what is the reason of the partial occurrence of the superconducting transition of 6 K?

In this paper, we presented a novel decomposition reaction of CSe_2 and the characterization of the conducting solid product. What triggars the decomposition of CSe_2 and systematic recombination of the component atoms? What is the mechanism of the abnormal superconducting behavior? These problems are open questions.

The authors (A. K. and H. K.) are grateful to Prof. Okamoto of Polytechnic Institute of New York for helpful discussions about the possibility of the decomposition reaction of CSe_2. They are also much obliged to the members of the Application Laboratory of the Hitachi Naka Works for the assistance of the electron microscope and diffraction experiments.

References

1) Y. Okamoto and P. S. Wojciechowski, *J. Chem. Soc., Chem. Commun.*, **1982**, 386.

2) R. L. Greene, G. B. Street, and L. J. Suter, *Phys. Rev. Lett.*, **34**, 577 (1975).

3) E. Whalley, *Can. J. Chem.* **38**, 2105 (1960).

4) H. Kobayashi, T. Mori, R. Kato, A. Kobayashi, Y. Sasaki, G. Saito, and H. Inokuchi, *Chem. Lett.*, **1983**, 1407.

5) H. Kobayashi, A. Kobayashi, and Y. Sasaki, *Mol. Cryst. Liq. Cryst.*, **118**, 427 (1985).

6) A. Kobayashi, N. Sasagawa, Y. Sasaki, K. Asakura, T. Yokoyama, H. Ishii, N. Kosugi, H. Kuroda, and H. Kobayashi, *Chem. Lett.*, **1985**, 1.

7) W. Pan, and J. P. Fackler, Jr., *Inorg. Synth.*, **21**, 7 (1982).

8) W. Sasaki, and J. Kinoshita, *J. Phys. Soc. Jpn.*, **25**, 1622 (1968).

9) H. Kawamura, I. Shirotani, and K. Tachikawa, *Solid State Commun.*, **49**, 879 (1984); *ibid.*, **54**,775 (1985).

10) H. Fukuyama, *J. Phys. Soc. Jpn.*, **51**, 1709 (1982).

11) A. R. Moodenbaugh, C. T. Wu, and R. Viswanahan, *Solid State Commun.*, **13**, 1413 (1973); J. Wittig, *J. Chem. Phys.* **58**, 2220 (1973)

12) Professor Okamoto suggested the existence of $(CSe)_x$ polymer, which is very interesting from the view-point of the molecular designing. However, direct evidence of the existence of such a polymer could not be found in our experiments. Unlike the relatively simple X-ray diffraction patterns, the electron diffraction patterns show some extra reflections other than those from hexagonal Se and graphite crystals. Probably oxidation of the surface of the powdered solid will be responsible for the appearance of the complex electron diffraction patterns.

The Solvent Extraction of Palladium(II) from Hydrochloric Acid with Triisobutylphosphine Sulfide

Yoshinari BABA,* Masanori OHSHIMA, and Katsutoshi INOUE
Department of Industrial Chemistry, Faculty of Science and Engineering, Saga University, Honjo-machi, Saga 840
(Received May 22, 1986)

The equilibrium and kinetic aspects of palladium(II) extraction from hydrochloric acid with triisobutylphosphine sulfide (TIBPS) in toluene were studied, along with the aqueous solubility and interfacial adsorption equilibrium of the extractant. From the equilibrium study, palladium(II) was found to be extracted as a 1 : 1 Pd:extractant binuclear complex. The extraction rate of palladium(II) was reasonably explained by the interfacial reaction model, assuming that the elementary reactions between the extractant adsorbed at the interface and the aquatrichloro and tetrachloro complexes of palladium(II), $[PdCl_3]^-$, and $[PdCl_4]^{2-}$ in the aqueous phase are the rate-determining steps.

The solvent-extraction techniques of metals have recently become increasingly important as energy-saving and non-polluting separation and purification processes in hydrometallurgy in view of the dangers of exhausting resources and energy. While the solvent extraction of metals has so far been extensively studied with a number of commercial extractants, the majority of these have been extractants containing oxygen or nitrogen as donor atoms, such as hydroxy oximes, carboxylic acids and organophosphorus compounds. However, relatively few works have been conducted on extractants containing sulfur as the donor atom.

It is well-known that sulfur-containing extractants are highly effective and selective for palladium(II). Among the sulfur-containing extractants, dialkyl sulfides, petroleum sulfides and their oxides, and *O,O'*-dialkyl hydrogenphosphorodithioate have been extensively investigated, especially in the USSR,[1-3] though these works have not necessarily been quantitative. Actually, dialkyl sulfides are now commercially utilized for the separation of palldium(II) from platinum(IV) at the Acton precious metal refinery of INCO in the United Kingdom[4] and for the recovery of precious metals from various kinds of scrap, such as spent catalysts in Japan. However, dialkyl sulfides have a serious drawback in their slow extraction rate of palladium(II).[5]

Recently, the American Cyanamid Co. developed a new extractant for the recovery of silver(I) and palladium (II),[6] CYANEX 471, the active component of which is triisobutylphosphine sulfide. This extractant is said to have an acceptably high extraction rate of palladium (II). Following the previous investigations of the kinetics of the solvent extraction of palladium(II) from chloride media with various sulfur-containing extractants, i.e. dihexyl sulfide,[7] 1,2-bis(*t*-hexylthio)-ethane[8] and 2-(butylthio)dodecanoic acid,[9] the present authors have now conducted a quantitative investigation of the extraction kinetics of palladium(II) from hydrochloric acid with triisobutylphosphine sulfide(TIBPS) in order to elucidate its extraction mechanism. Prior to the study of the extraction kinetics, the distribution equilibrium of palladium(II), and the aqueous solubility and interfacial adsorption equilibrium of the extractant were investigated in order to obtain the fundamental information which is necessary for the analysis of the extraction kinetic data.

Experimental

Reagents. The triisobutylphosphine sulfide, abbreviated as TIBPS hereafter, used in the present study as the extractant was purified from CYANEX 471 donated by the American Cyanamid Co. by recrystallization from a water–ethanol mixture. The purity of the reagent was confirmed by elemental analysis to be as follows: Found: C, 61.3; H, 11.5%. Calcd for $C_{12}H_{27}PS$: C, 61.5; H, 11.6%. The organic phase was prepared on a gravimetric basis by diluting TIBPS with toluene of an analytical grade. The aqueous phase was prepared by dissolving palladium(II) chloride in hydrochloric acid.

Measurement of Extraction Equilibrium. As in the previous work,[7,8] it was impossible to make a precise quantitative determination of palladium(II) in the aqueous phase in the presence of a large excess concentration of the extractant because it was almost completely extracted over the whole concentration range of hydrochloric acid. Accordingly, in order to determine the mole ratio of palladium(II) to the extractant in the extracted complex under the conditions of ultimate loading, only a loading test was carried out in the presence of a large excess of the palladium(II) concentration in order to determine the mole ratio of palladium(II) extracted into the organic phase to TIBPS, in the same manner as in previous papers.[7,8]

Equal volumes (0.015 dm^3) of the organic and aqueous phases of known concentrations were vigorously shaken for 5 h in a separatory funnel using a Iwaki, V-DV-type mechanical shaker in a thermostated air bath maintained at 303 K. It had been confirmed by a preliminary experiment that the equilibrium was attained within 5 h. After the separation of the two phases, the palladium(II) concentration in the aqueous phase was determined by means of atomic absorption spectrometry using a Nippon Jarrell-Ash model AA-782 spectrophotometer. The palladium(II) concentration in the organic phase was calculated by the use of the mass balance from the aqueous palladium(II) concentrations before and after the equilibration.

Measurement of Aqueous Solubility of the Extractant. The distribution of TIBPS between the organic and aqueous phases was measured spectrophotometrically at 303 K in a method similar to that described in a previous paper.[8] A

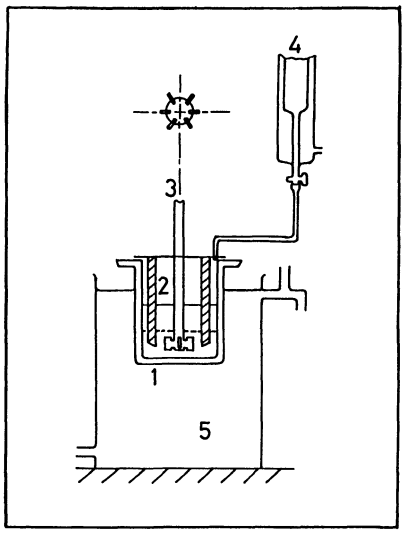

Fig. 1. Experimental apparatus.
1: Stirred glass cell, 2: baffle, 3: impeller, 4: reservoir with jacket, 5: thermostat.

toluene solution of TIBPS of a known concentration and 1 mol dm^{-3} of hydrochloric acid were shaken vigorously for 24 h with a volume ratio of the aqueous phase to the organic phase of 10 : 1 using an Iwaki mechanical shaker, V-VD-type. After phase separation, a sample of the aqueous phase (0.19 dm^3) was transferred to a separatory funnel. In order to completely convert any TIBPS dissolved in the aqueous phase to its palladium(II) complexes, 5×10^{-2} dm^3 of a 2×10^{-3} mol dm^{-3} aqueous palladium(II) chloride solution containing 0.01 mol dm^{-3} of hydrochloric acid and 1×10^{-2} dm^3 of toluene were added to the aqueous sample, and the mixture was shaken for 24 h using a mechanical shaker. The absorbance of the palladium(II) complex in toluene was measured at 329 nm against a toluene blank using a Shimadzu UV 140 spectrophotometer.

Measurement of Interfacial Adsorption Equilibrium. The interfacial tension between the organic solution and 1 mol dm^{-3} of aqueous hydrochloric acid was measured at 303 K by means of the drop-weight method in order to elucidate the interfacial adsorption equilibrium of TIBPS.

Measurement of Extraction Kinetics. The apparatus used in this study was a batch-type stirred glass cell, as is shown in Fig. 1. It is the same as that used in the previous kinetic studies of the palladium(II) extraction with 1,2-bis(*t*-hexylthio)ethane[8] or 2-(butylthio)dodecanoic acid.[9]

Equal volumes (0.3 dm^3) of hydrochloric acid containing palladium(II) and toluene solutions of TIBPS of known concentrations were carefully introduced into the cell so as not to disturb the interface. After that, stirring was initiated at a constant stirring speed and 10-cm^3 portions samples were taken out at definite time intervals. After the phase separation, the palladium(II) concentration in the aqueous phase was determined using the atomic-absorption spectrophotometer. The initial palladium(II) concentration was 1×10^{-3} mol dm^{-3} in all kinetic runs. The concentrations of the extractant and hydrochloric acid varied over the range from 8×10^{-3} to 1.6×10^{-1} mol dm^{-3} and from 1×10^{-1} to 4.7 mol dm^{-3} respectively.

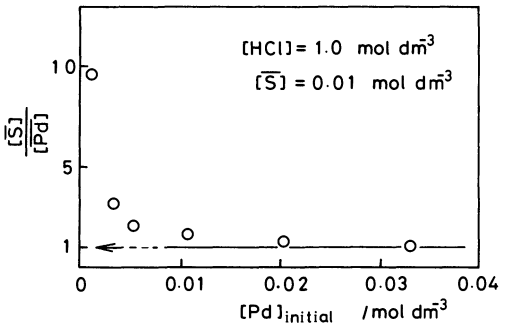

Fig. 2. Experimental results of the loading test.

Results

Distribution Equilibrium of Palladium(II). Figure 2 shows the results of the loading test. The mole ratio of TIBPS to palladium(II) in the organic phase asymptotically approaches unity with an increase in the palladium(II) concentration in the aqueous phase. This result indicates that palladium(II) is present as a metal : reagent 1 : 1 complex in the organic phase. Taking account of the coordination number of palladium(II)(=4), the stoichiometry of this extraction reaction may be expressed as follows:

$$2[PdCl_i]^{(i-2)-} + 2\overline{S} \rightleftharpoons [\overline{(PdCl_2)_2S_2}] + 2(i-2)Cl^- \quad (1)$$

where S is TIBPS and where bars denote the organic phase.

Aqueous Solubility of TIBPS. The distribution of TIBPS between the organic and aqueous solutions is expressed as follows:

$$\overline{S} \rightleftharpoons S \quad ;K_D, \quad (2)$$

where K_D is the partition coefficient of TIBPS and is expressed as follows:

$$K_D = [S]/[\overline{S}]. \quad (3)$$

The logarithm of Eq. 3 gives:

$$\log [S] = \log [\overline{S}] + \log K_D. \quad (4)$$

The partition coefficient is so small that the concentration of TIBPS in the organic phase, $[\overline{S}]$, is nearly equal to its initial concentration, C_{B0}.

The concentration of TIBPS in the aqueous phase was plotted against that in the organic phase, as is shown in Fig. 3. The points plotted in this figure appear to lie on a straight line with a slope of 1, as is to be expected from Eq. 4. From the intercept of the straight line with the ordinate, the partition coefficient, K_D, was evaluated as 5.4×10^{-6} for 1 mol dm^{-3} of hydrochloric acid.

Interfacial Tension. Figure 4 shows the plot of the interfacial tension, γ, between the organic solution containing TIBPS and 1 mol dm^{-3} of aqueous hydrochloric acid against the concentration of TIBPS. The results shown in Fig. 4 suggest that TIBPS is interfacially active and is adsorbed at the interface between

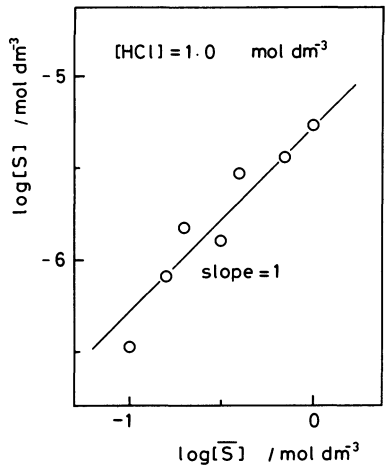

Fig. 3. Aqueous solubility of TIBPS to 1 mol dm^{-3} hydrochloric acid.

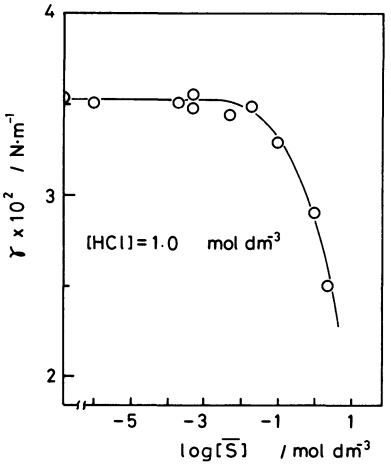

Fig. 4. Relation between interfacial tension, γ, and log [$\bar{S}$].

the two phases. The adsorption equilibrium of TIBPS is expressed as follows:

$$\bar{S} \rightleftharpoons S_{ad} \quad ;K_{ad} \tag{5}$$

where K_{ad} is the adsorption equilibrium constant defined by Eq. 6 and where the subscript "ad" denotes the adsorbed species at the interface:

$$K_{ad} = \frac{\theta_s}{[\bar{S}](1-\theta_s)} \tag{6}$$

Here, θ_s denotes the fractional coverage of the interface by TIBPS.

The combination of Gibb's adsorption isotherm and Langmuir's monolayer adsorption model gives the following relation[10] between the interfacial tension, γ, and the TIBPS concentration, [$\bar{S}$]:

$$\gamma = \gamma_0 - (RT/S_s) \ln (1+K_{ad}[\bar{S}]) \tag{7}$$

where γ_0 denotes the interfacial tension between the pure diluent and 1 mol dm^{-3} of aqueous hydrochloric acid, and where S_s denotes the interfacial area occupied

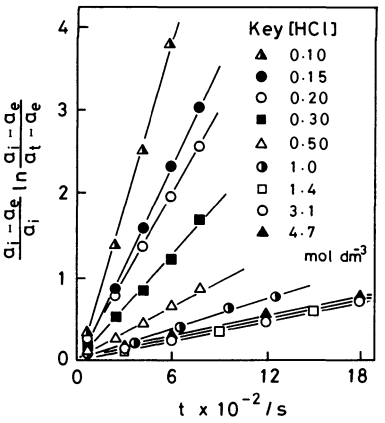

Fig. 5 A typical plot of the experimental results based on the pseudo-first-order rate expression (C_{B0} =0.01 mol dm^{-3}).

by a unit mole of TIBPS. From the experimental results shown in Fig. 4, the values of K_{ad} and S_s were evaluated by the nonlinear least-squares method based on Eq. 7 to be as follows: K_{ad}=4.4 dm^3 mol^{-1}, S_s=6.3×10^5 m^2 mol^{-1}.

The solid curve in Fig. 4 is the curve calculated from Eq. 7 using the above values. The calculated curve is in good agreement with the experimental results.

Extraction Kinetics. If it is assumed that the forward and reverse reactions are pseudo-first-order with respect to palladium(II) in the aqueous and organic phases respectively, the relation between the palladium(II) concentration(a) in the aqueous phase and the contact time(t) is expressed as follows[11]:

$$\frac{a_i-a_e}{a_i} \ln \frac{a_i-a_e}{a_t-a_e} = k_f t, \tag{8}$$

where k_f represents the observed reaction-rate constant for the forward reaction and where the quantities with the subscripts "t", "i", and "e" denote the concentrations after time t, at t=0, and at equilibrium respectively.

Figure 5 shows a typical experimental result plotted on the basis of Eq. 8. The plots in this figure give straight lines passing through the point of origin, as is to be expected from Eq. 8. This result suggests that the forward reaction rate of palladium(II) extraction is first-order with respect to palladium(II) in the aqueous phase. The apparent reaction-rate constants were obtained from the slopes of these straight lines. Since the apparent reaction-rate constant was found in the preliminary experiment to be independent of the stirring speed over the range greater than 1300 rpm, subsequent experiments were carried out at a constant stirring speed of 1500 rpm.

Figure 6 shows the effect of the chloride-ion concentration on the observed reaction rate constant. As is evident from Fig. 6, the plotted points lie on a straight line, with a slope of −1, in the low-concentration region of chloride ions and tend to approach a con-

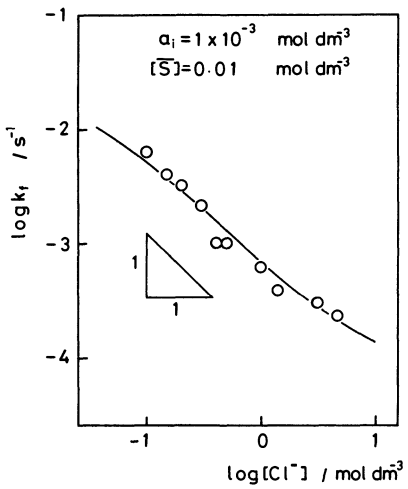

Fig. 6. Effect of chloride ion concentration on the observed extraction rate constant.

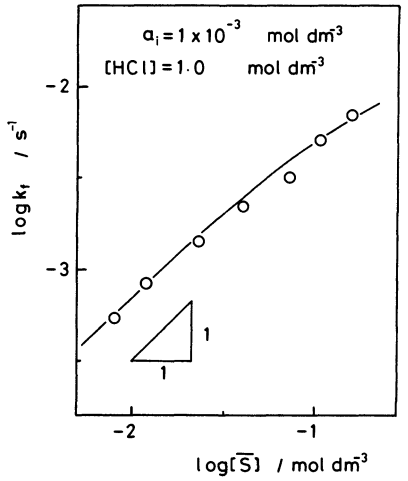

Fig. 7. Effect of TIBPS concentration on the observed extraction rate constant.

stant value in the high-concentration region. This tendency is in accordance with that observed in the extraction of palladium(II) with 1,2-bis(*t*-hexylthio)-ethane.[8] That is, it may be concluded that the extraction rate is inversely first-order with respect to the chloride ion in its low-concentration region and zeroth-order in its high-concentration region.

Similarly, the effect of the TIBPS concentration on the observed reaction rate constant is shown in Fig. 7. In this figure, the plots appear to lie on a straight line, with a slope of about 0.75. This result suggests that the extraction-reaction mechanism of this system can not be interpreted in terms of the classical homogeneous heterophase reaction mechanism.[12] Therefore, we in the following section will analyse the experimental results of the extraction kinetics based on the heterogeneous interfacial reaction model.

Discussion

The following results obtained in the present experiment suggest that a certain elementary process taking place at the interface plays an important role in the extraction mechanism: (1) The aqueous solubility of TIBPS is too low to assume that homogeneous reactions take place to any considerable extent in the aqueous phase; (2) TIBPS is adsorbed at the interface, and (3) the reaction order with respect to the extractant is less than unity. The great majority of palladium(II) exists as the tetrachloro complex, $[PdCl_4]^{2-}$, and a small amount of the aquatrichloro complex, $[PdCl_3(H_2O)]^-$, coexists in the aqueous phase over the range of chloride-ion concentrations studied. Of these, Rund,[13] in his paper on the reaction rates of palladium(II) with 1,10-phenanthroline and 2,2′-bipyridyl, reported that the latter is much more labile than the former. Taking account of these facts, the following reaction scheme was proposed to explain the extraction kinetics of palladium(II) with TIBPS:

$$[PdCl_3(H_2O)]^- + S_{ad} \xrightarrow{k_1} [PdCl_3S]^-_{ad} + H_2O \quad (9)$$

$$[PdCl_4]^{2-} + S_{ad} \xrightarrow{k_2} [PdCl_3S]^-_{ad} + Cl^- \quad (10)$$

$$[PdCl_3S]^-_{ad} + \bar{S} \rightleftharpoons \overline{[PdCl_2S_2]} + Cl^- \quad (11)$$

$$2\overline{[PdCl_2S_2]} \rightleftharpoons \overline{[(PdCl_2)_2S_2]} + 2\bar{S} \quad (12)$$

The elementary steps described by Eqs. 9 and 10 form the parallel reaction; of these steps, the former is much more rapid than the latter, as has been mentioned earlier. From the fact that the reaction order with respect to TIBPS is less than unity, the interfacial steps expressed by Eqs. 9 and 10 may be considered to be the rate-determining steps. Assuming that the parallel reactions of $[PdCl_3(H_2O)]^-$ and $[PdCl_4]^{2-}$ with TIBPS adsorbed at the interface are the rate-determining steps, the rate expression can be described as follows:

$$-\frac{da_t}{dt} = (k_1[[PdCl_3(H_2O)]^-] + k_2[[PdCl_4]^{2-}])\theta_s \quad (13)$$

where k_1 and k_2 are the forward reaction rate constants of Eqs. 9 and 10 respectively.

In case the preceding elementary step expressed by Eq. 5 is in equilibrium, θ_s is expressed by Eq. 14 from Eq. 6:

$$\theta_s = \frac{K_{ad}[\bar{S}]}{1+K_{ad}[\bar{S}]} \quad (14)$$

The substitution of Eq. 14 into Eq. 13 gives the following rate expression.

$$-\frac{da_t}{dt} = \frac{K_{ad}[\bar{S}]}{1+K_{ad}[\bar{S}]}(k_1[[PdCl_3(H_2O)]^-] + k_2[[PdCl_4]^{2-}]) \quad (15)$$

It is well known that palladium(II) gives rise to chloro complexes in hydrochloric acid as follows:

$$Pd^{2+} + iCl^- \rightleftharpoons [PdCl_i]^{(i-2)-} \quad ;\beta_i \quad (16)$$

$$\beta_i = \frac{[[PdCl_i]^{(i-2)-}]}{[Pd^{2+}][Cl^-]^i} \quad (17)$$

where β_i indicates the stability constants of the ith chloro complex of palladium(II).

The concentrations of the aquatrichloro complex, $[PdCl_3(H_2O)]^-$, and the tetrachloro complex, $[PdCl_4]^{2-}$, in Eq. 15 are expressed by Eqs. 18 and 19, using the equilibrium relations of the chloro complexes in the aqueous phase mentioned above:

$$[[PdCl_3(H_2O)]^-] = \beta_3[Cl^-]^3 a_t/\alpha \quad (18)$$

$$[[PdCl_4]^{2-}] = \beta_4[Cl^-]^4 a_t/\alpha, \quad (19)$$

where α is defined by the following equation:

$$\alpha = 1 + \sum_{i=1}^{4} \beta_i[Cl^-]^i \quad (20)$$

As has been mentioned earlier, over the chloride-ion-concentration range studied, α may be approximated as follows:

$$\alpha \simeq \beta_3[Cl^-]^3 + \beta_4[Cl^-]^4 \quad (21)$$

Consequently, Eq. 15 is ultimately expressed by Eq. 22:

$$-\frac{da_t}{dt} = \frac{K_{ad}[\bar{S}]}{1+K_{ad}[\bar{S}]}\left(\frac{k_1\beta_3 + k_2\beta_4[Cl^-]}{\beta_3+\beta_4[Cl^-]}\right)a_t \quad (22)$$

The effects on the extraction rate of varying the concentrations of each reactant species, shown in Figs. 6 and 7, can be qualitatively interpreted by means of Eq. 22, derived from the proposed interfacial reaction scheme.

The optimum values of k_1 and k_2 in Eq. 22 were evaluated by the nonlinear least-squares method from the data shown in Fig. 6, using the K_{ad} value evaluated earlier and the stability constants of the palladium(II) chloro complexes reported in the literature[14] ($\beta_3 = 2.00\times10^{10}$, $\beta_4 = 7.94\times10^{11}$) as follows: $k_1 = 6.1\times10^{-1}$ s^{-1}, $k_2 = 1.7\times10^{-3}$ s^{-1}. The solid lines shown in Figs. 6 and 7 were obtained by inserting these values into Eq. 22. The calculated lines are in fairly good agreement with the experimental results.

Conclusion

The kinetic study of the solvent extraction of palladium(II) from hydrochloric acid with triisobutylphosphine sulfide (TIBPS=S) in toluene was conducted using a stirred cell, along with studies of the aqueous solubility or the equilibrium distribution of the extractant between the organic and aqueous phases, its adsorption equilibrium at the interface, and the distribution equilibrium of palladium(II).

The experimental results on the distribution equilibrium of palladium(II) showed that palladium(II) is extracted as a Pd : extractant 2 : 2 complex, $[(PdCl_2)_2S_2]$.

From the experimental results of the equilibrium distribution and the interfacial adsorption equilibrium of the extractant, it was elucidated that TIBPS has a very low aqueous solubility and a fairly high interfacial activity, suggesting the importance of the interfacial reaction in the extraction of palladium(II) with TIBPS.

The experimental results of the extraction kinetics were quantitatively explained by the interfacial reaction model on the assumption that the ligand substitutions between the extractant adsorbed at the interface and the aquatrichloro and tetrachloro complexes of palladium(II) in the aqueous phase are the rate-determining steps. That is, the extraction rate was found to be satisfactorily expressed by the rate equation described by Eq. 22, derived from the interfacial reaction model presented above.

The authors are deeply indebted to American Cyanamid Co. for supply of the sample of CYANEX 471.

References

1) V. A. Mikhailov, V. G. Torgov, E. M. Gil'bert, L. N. Mazolov, and A. V. Nikolaev, "Proceedings of International Solvent Extraction Conference 1971," Soc. Chem. Ind., London (1971), p. 1112.

2) V. A. Mikhailov, "Proceedings of International Solvent Extraction Conference 1977," Can. Inst. Min. Metall., Montreal (1979), p. 52.

3) L. M. Gindin, "Ion Exchange and Solvent Extraction," 8, ed by J. A. Marinsky and Y. Marcus, Marcell Dekker, New York (1981), p. 311.

4) J. M. Barnes and J. D. Edwards, *Chem. Ind.*, **1982**, 151.

5) R. I. Edwards, "Proceedings of International Solvent Extraction Conference 1977," Can. Inst. Min. Metall., Montreal (1979), p. 24.

6) W. A. Rickelton, Eur. Pat. Appl., 113454 (1984).

7) Y. Baba, T. Eguchi, and K. Inoue, *J. Chem. Eng. Jpn.*, **19**, 361 (1986).

8) Y. Baba, T. Eguchi, and K. Inoue, *Bull. Chem. Soc. Jpn.*, **59**, 1321 (1986).

9) Y. Baba, A. Goto, and K. Inoue, *Solvent Extr. Ion Exch.*, **4**, 255 (1986).

10) K. Inoue, Y. Kawano, F. Nakashio, and W. Sakai, *Kagaku Kogaku*, **38**, 41 (1974).

11) D. S. Flett, D. N. Okuhara, and D. R. Spink, *J. Inorg. Nucl. Chem.*, **35**, 2471 (1973).

12) H. Freiser, *Acc. Chem. Res.*, **17**, 126 (1984).

13) J. V. Rund, *Inorg. Chem.*, **13**, 738 (1974).

14) M. I. Gelfman and N. V. Kiseleva, *Zh. Neorg. Khim.*, **14**, 502 (1969).

 © 1986 The Chemical Society of Japan Bull. Chem. Soc. Jpn., 59, 3835—3839 (1986)

Extraction Equilibria of Mercury(II) from Hydrochloric Acid with Trialkylphosphine Sulfides

Yoshinari BABA,* Yukihiro UMEZAKI, Takashi UEDA, and Katsutoshi INOUE
Department of Industrial Chemistry, Faculty of Science and Engineering, Saga University, Honjo-machi 1, Saga 840
(Received June 5, 1986)

The extraction of mercury(II) from hydrochloric acid was compared using five kinds of sulfur-containing extractants. Mercury(II) was extracted most effectively by trialkylphosphine sulfides. Subsequently, the distribution equilibria of mercury(II) from hydrochloric acid with triisobutylphosphine sulfide (TIBPS=$\bar{S}$) and trioctylphosphine sulfide (TOPS=$\bar{S}$) in toluene have been measured at 303 K in order to clarify the concentration dependencies of the reactant species. It was found that mercury(II) is extracted according to the solvation reaction by TIBPS or TOPS as a mercury(II): extractant 1:2 complex, $HgCl_2S_2$, in the range of low loading ratio of mercury(II) to the extractants, and as a 1:1 binuclear complex, $(HgCl_2)_2S_2$, in the region of high loading ratios, as follows:

$$HgCl_2 + 2\bar{S} \rightleftharpoons \overline{HgCl_2S_2} \qquad K_e$$

$$2HgCl_2 + 2\bar{S} \rightleftharpoons \overline{(HgCl_2)_2S_2} \qquad K_e'$$

The extraction equilibrium constants, K_e and K_e', were evaluated as $K_e=4.0\times10^5$ $(dm^3\ mol^{-1})^2$ and $K_e'=2.0\times10^8$ $(dm^3\ mol^{-1})^3$ for TIBPS and as $K_e=7.2\times10^6$ $(dm^3\ mol^{-1})^2$ for TOPS.

Thus far, the solvent extraction of mercury(II) has been investigated using various kinds of extractants: trioctylphosphine oxide (TOPO),[1,2] tributyl phosphate (TBP),[2] trioctylamine,[3] and trioctylmethylammonium chloride (Aliquat 336).[4] However, these extractants, containing nitrogen or oxygen as a donor atom, have only poor selectivities to mercury(II) over other metals. On the other hand, it is well-known that the extractants containing sulfur as a donor atom, such as dialkyl sulfides[5,6] and trialkyl thiophosphate,[7] are very powerful and selective extractants for mercury(II). From this point of view, in a previous work[8] we studied the extraction equilibrium of mercury(II) with 1,2-bis(hexylthio)ethane, which contains two sulfurs as donor atoms.

Recently, the American Cyanamid Co. has developed a new commercial extractant, CYANEX 471, the active species of which is triisobutylphosphine sulfide, as a selective extractant for palladium(II) and silver(I).[9] Hitchcock et al.[10] reported that tributylphosphine sulfide (TBPS) completely extracted mercury(II) from 0.1 mol dm^{-3} hydrochloric acid; however, they did not succeed in finding an effective aqueous solution for stripping. Further, no detailed studies of the extraction of mercury(II) with trialkylphosphine sulfides have been carried out to date.

In the present investigation, the authors have conducted a detailed and quantitative investigation of the distribution equilibrium of mercury(II) in extraction from hydrochloric acid with two kinds of trialkylphosphine sulfides: triisobutylphosphine sulfide and trioctylphosphine sulfide.

Prior to the detailed study of the extraction equilibrium, preliminary experiments were carried out in order to compare qualitatively the extraction behavior of trialkylphosphine sulfides with that of other sulfur-containing compounds for mercury(II).

Experimental

Reagents. Two kinds of trialkylphosphine sulfides, possessing different alkyl chains-triisobutylphosphine sulfide and trioctylphosphine sulfide-were used as the extractants. These will be abbreviated to TIBPS and TOPS respectively and denoted by S hereafter. The TIBPS was purified from a commercial extactant, CYANEX 471, donated by the American Cyanamid Co., by recrystallization from a water-ethanol mixture. The purity of the purified reagent was confirmed by elemental analysis to be as follows: Found: C, 61.34; H, 11.48%. Calcd: C, 61.49; H, 11.61%. The TOPS, which was kindly supplied by the Nippon Chemical Industry Co., was used as delivered, without further purification. The purity of this reagent was also confirmed by elemental analysis to be as follows: Found: C, 71.95; H, 12.64%. Calcd: C, 71.64; H, 12.64%. Among the extracting reagents used in the preliminary experiment for the sake of comparison, 1,2-bis-(hexylthio)ethane and 2-(butylthio)dodecanoic acid were synthesized and purified in the manners reported in previous papers,[8,11] while dihexyl sulfide was used as delivered from the Daihachi Chemical Co., Ltd. These reagents will be abbreviated as BHTE, 2-BTDA and DHS respectively hereafter. An organic phase was prepared by diluting these extractants with toluene of an analytical grade on a gravimetric basis. An aqueous phase was prepared by dissolving mercury(II) chloride in hydrochloric acid.

Procedure. Equal volumes of the aqueous and organic phases were shaken in a 0.1 dm^3 stoppered glass flask immersed in a thermostated bath maintained at 303 K—for 3 h or 1 h for TIBPS or TOPS respectively—in order to attain equilibrium. It was confirmed from a preliminary experiment that the equilibration could be attained within these times. The initial total concentration of mercury(II) was 1×10^{-3} or 5×10^{-3} mol dm^{-3} in all experiments. The total concentration of mercury(II) in the aqueous phase was determined by titration with EDTA in the presence of an excess of Mg-EDTA, using Eriochrome Black T (BT) as an indicator, or by atomic-absorption spectrochemical analysis

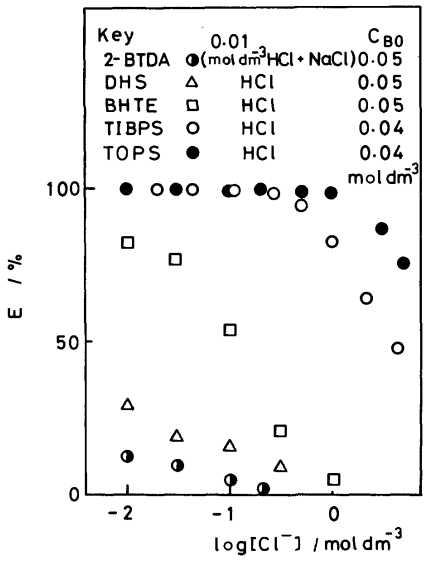

Fig. 1. Relation between % extraction of mercury(II) and log [Cl⁻] (Initial concentration of mercury(II) is 5×10^{-3} mol dm^{-3}).

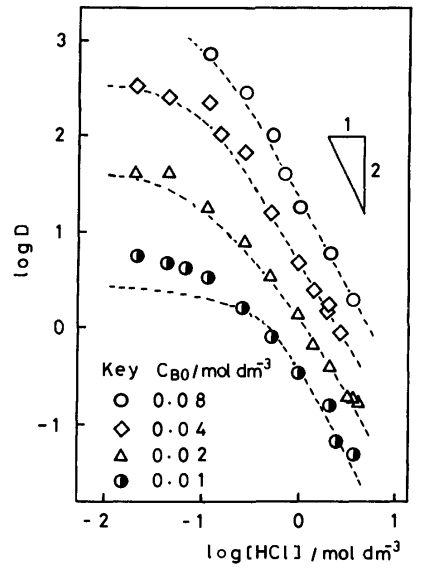

Fig. 2. Equilibrium distribution of mercury(II) from hydrochloric acid solutions with TIBPS in toluene (Initial concentration of mercury(II) is 5×10^{-3} mol dm^{-3}).

using a Nippon Jarrell-Ash model AA-782 spectrophotometer. In the range of low loading ratios, the concentration of mercury(II) in the organic phase was determined by the methods described above after stripping with a 1 and a 2 mol dm^{-3} aqueous ammonium thiocyanate solution for TIBPS and TOPS respectively. In the range of high loading ratios, it was calculated from the difference between the initial and equilibrium concentrations of mercury(II) in the aqueous phase.

Results and Discussion

Figure 1 shows the results of the preliminary experiment as the plot of the % extraction of mercury(II) by each extractant from chloride media against the chloride-ion concentration. Here, the % extraction is defined as the ratio of mercury(II) content in the organic phase after equilibration to the initial mercury(II) content in the aqueous phase. C_{B0} denotes the initial concentration of the extractants. From Fig. 1, mercury(II) is shown to be effectively extracted by TIBPS and TOPS in the range of low chloride-ion concentrations in particular; the % extractions are more than 50%, even in the high-chloride-ion-concentration region, which suggests that these extractants are very effective for the separation and recovery of mercury(II). On the other hand, DHS and 2-BTDA show only a poor extraction capacity for mercury(II) in chloride media, while BHTE shows an extraction capacity intermediate between the trialkylphosphine sulfides and DHS or 2-BTDA. Therefore, the present authors conducted a detailed and quantitative study of the extraction equilibria of mercury(II) with TIBPS and TOPS.

Figures 2 and 3 show the effects of the hydrochloric acid concentration on the distribution ratio of mercury(II) for various concentrations of the extractant in

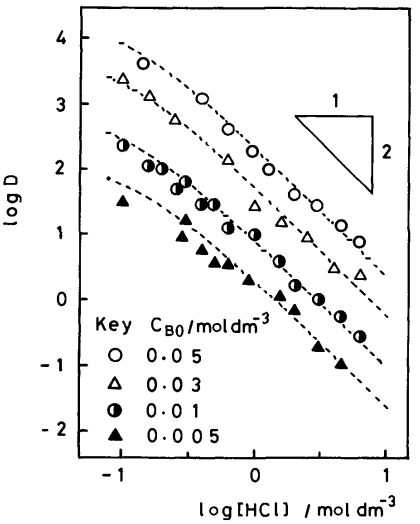

Fig. 3. Equilibrium distribution of mercury(II) from hydrochloric acid solutions with TOPS in toluene (Initial concentration of mercury(II) is 1×10^{-3} mol dm^{-3}).

the extractions with TIBPS and TOPS respectively. As is evident from these figures, the distribution ratio, D, decreases with the increase in the hydrochloric acid concentration, which is similar to the extractions of mercury(II) from hydrochloric acid with 1,2-bis-(hexylthio)ethane and 2-BTDA observed in the previous works.[8,12] Therefore, mercury(II) is considered to be extracted from hydrochloric acid according to the following solvation reaction for both the extractants:

$$HgCl_2 + n\bar{S} \rightleftharpoons \overline{HgCl_2S_n} \qquad K_e, \qquad (1)$$

where $\bar{S}$ denotes the extractant species in the organic phase. The equilibrium constant, K_e, for the above

reaction is given by Eq. 2:

$$K_e = \frac{[\overline{HgCl_2S_n}]}{[HgCl_2][\bar{S}]^n}. \quad (2)$$

It is well-known that mercury(II) gives rise to chloro complexes in the aqueous chloride solution as follows:

$$Hg^{2+} + iCl^- \rightleftharpoons HgCl_i^{(i-2)-} \quad \beta_i \ (i=1\text{–}4) \quad (3)$$

$$\beta_i = \frac{[HgCl_i^{(i-2)-}]}{[Hg^{2+}][Cl^-]^i}, \quad (4)$$

where β_i is the stability constant of the ith chloro complex of mercury(II).[13] From Eqs. 3 and 4, the concentration of the neutral complex, $[HgCl_2]$, which takes part in the extraction reaction described by Eq. 1 is expressed as follows:

$$[HgCl_2] = \alpha_2 C_{Hgw}, \quad (5)$$

where

$$\alpha_2 = \beta_2[Cl^-]^2/(1+\sum_{i=1}^{4}\beta_i[Cl^-]^i). \quad (6)$$

In the region of high chloride-ion concentrations ($[Cl^-]>1$ mol dm^{-3}), it can be approximated by Eq. 7:

$$[HgCl_2] = \alpha_2 C_{Hgw} \simeq (\beta_2/\beta_4[Cl^-]^2)C_{Hgw}. \quad (7)$$

In Eqs. 5 and 7, C_{Hgw} denotes the total concentration of mercury(II) in the aqueous phase. From Eqs. 2 and 5, the distribution ratio is expressed by Eq. 8:

$$D = \frac{[\overline{HgCl_2S_n}]}{C_{Hgw}} = K_e\alpha_2[\bar{S}]^n, \quad (8)$$

which is approximated by Eq. 9 in the regions of high concentrations of the chloride ion:

$$D \simeq K_e(\beta_2/\beta_4[Cl^-]^2)[\bar{S}]^n. \quad (9)$$

The logarithm of Eq. 9 gives:

$$\log D = -2\log[Cl^-] + a, \quad (10)$$

where

$$a = \log(\beta_2/\beta_4) + n\log[\bar{S}] + \log K_e. \quad (11)$$

In Eq. 11, the concentration of the unreacted extractant, $[\bar{S}]$, is nearly equal to its initial concentration, C_{B0}, in the region of low loading ratios.

As is evident from Figs. 2 and 3, the plotted points lie on straight lines, with a slope of −2, in the high-concentration ranges of hydrochloric acid, as is to be expected from Eq. 10. The values of a, defined by Eq. 11, were obtained from the intercepts of these straight lines with the ordinate for each C_{B0} and for each extractant. In Fig. 4, they are plotted against log C_{B0} to evaluate n and K_e. As is evident from this figure, the plotted points lie on straight lines, with a slope of 2, which suggests that n=2 in Eq. 11; that is, mercury(II) is coordinately solvated by two molecules of TIBPS or TOPS in the organic phase. Therefore, the stoichiometric relation of these extraction reactions may be expressed as follows for both the extractants:

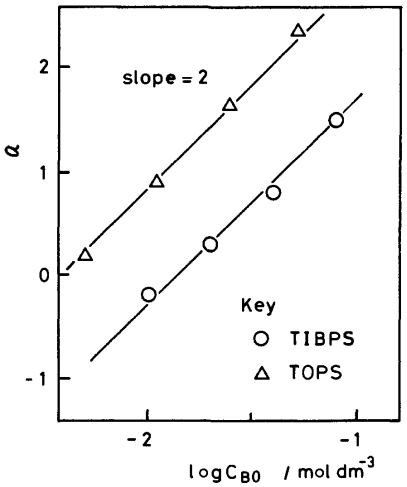

Fig. 4. Plot of a against log C_{B0} based on Eq. 11.

$$HgCl_2 + 2\bar{S} \rightleftharpoons \overline{HgCl_2S_2} \quad K_e \quad (12)$$

On the basis of Eq. 11, the extraction equilibrium constant, K_e, was evaluated as $K_e=4.0\times10^5$ (dm^3 mol^{-1})^2 for TIBPS, and as $K_e=7.2\times10^6$ (dm^3 mol^{-1})^2 for TOPS, from the intercepts of the straight lines with the ordinate in Fig. 4.

Meanwhile, in the region of high loading ratios, the mass balances with regard to the extractant and mercury(II) should be taken into consideration. The initial concentration of the extractant (C_{B0}) in the organic phase and that of mercury(II)(C_{Hg0}) in the aqueous phase are expressed as follows:

$$C_{B0} = [\bar{S}] + 2[\overline{HgCl_2S_2}] \quad (13)$$

$$C_{Hg0} = C_{Hgw} + [\overline{HgCl_2S_2}]. \quad (14)$$

Equations 8 and 14 are then combined to give Eq. 15, taking into account the fact that n=2:

$$C_{Hgw} = C_{Hg0}/(1+\gamma[[\bar{S}]^2), \quad (15)$$

where

$$\gamma = \alpha_2 K_e. \quad (16)$$

The mass balance equation of the extractant in the organic phase expressed by Eq. 13 is reduced to the cubic equation expressed by Eq. 17 with respect to the unreacted extractant concentration ($[\bar{S}]$):

$$\gamma[\bar{S}]^3 + (2\gamma C_{Hg0} - \gamma C_{B0})[\bar{S}]^2 + [\bar{S}] - C_{B0} = 0. \quad (17)$$

The distribution ratio is ultimately given by:

$$D = \frac{[\overline{HgCl_2S_2}]}{C_{Hgw}} = \frac{C_{Hg0}}{C_{Hgw}} - 1 = \gamma[\bar{S}]^2 \quad (18)$$

The dotted lines in Figs. 2 and 3 show the results calculated from Eqs. 17 and 18. The calculated curves shown in Figs. 2 and 3 are in good agreement with the experimental results except for C_{B0}=0.01 mol dm^{-3} in the extraction with TIBPS in Fig. 2.

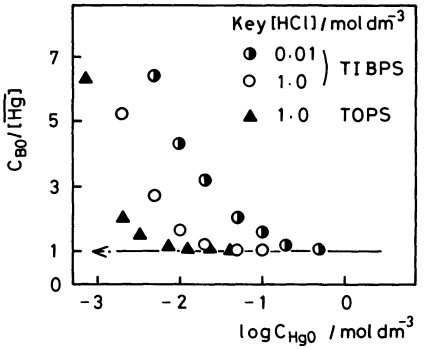

Fig. 5. Experimental results of the loading test (C_{B0}=0.01 mol dm^{-3}).

Since the calculated curve corresponding to C_{B0}=0.01 mol dm^{-3} in Fig. 2 deviates downwards from the experimental results as the mercury(II) concentration in the organic phase increases, the loading test was carried out for a constant initial concentration of the extractant in order to examine the mole ratio of mercury(II) extracted into the organic phase ($[\overline{Hg}]$) to the extractant under the conditions of excess concentrations of mercury(II), by varying the initial mercury(II) concentration (C_{Hg0}) in the aqueous phase.

In Fig. 5, the experimental results are shown as plots of the mole ratio, $C_{B0}/[\overline{Hg}]$, against C_{Hg0}, which shows that the mole ratio asymptotically approaches unity for both extractants. From these results, it is evident that mercury(II) is extracted as a 1 : 1 metal : reagent complex in the region of high loading ratios. Consequently, it may be considered to be extracted as a binuclear complex according to the extraction reaction described by Eq. 19, taking the coordination number of mercury(II)(=4) into consideration and referring to the study by Mikhailov et al.[5] on the extraction of mercury-(II) with dialkyl sulfides:

$$2HgCl_2 + 2\overline{S} \rightleftharpoons \overline{(HgCl_2)_2S_2} \qquad K_e' \qquad (19)$$

$$K_e' = \frac{[\overline{(HgCl_2)_2S_2}]}{[HgCl_2]^2[\overline{S}]^2} \qquad (20)$$

Taking account of the fact that mercury(II) is extracted according to the extraction reaction described by Eq. 19 in the region of high loading ratios, the calculated curves for the extraction with TIBPS in Fig. 2 were reconsidered. The distribution ratio, D, is described by Eq. 21 by taking account of the two reactions expressed by Eqs. 12 and 19:

$$D = \frac{[\overline{HgCl_2S_2}] + 2[\overline{(HgCl_2)_2S_2}]}{C_{Hgw}} \qquad (21)$$

The substitution of Eqs. 2, 5, and 20 into Eq. 21 gives Eq. 22, taking into account the fact that n=2:

$$D = (K_e + 2K_e'C_{Hgw}\alpha_2)\alpha_2[\overline{S}]^2 \qquad (22)$$

Further, the total concentration of the extractant in the organic phase, C_{B0}, and the initial concentration of

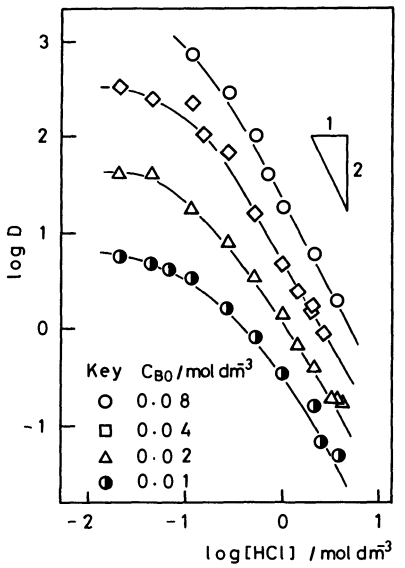

Fig. 6. Equilibrium distribution of mercury(II) from hydrochloric acid solutions with TIBPS in toluene.

mercury(II) in the aqueous phase, C_{Hg0}, are expressed as follows:

$$C_{B0} = [\overline{S}] + 2[\overline{HgCl_2S_2}] + 2[\overline{(HgCl_2)_2S_2}] \qquad (23)$$

$$C_{Hg0} = C_{Hgw} + [\overline{HgCl_2S_2}] + 2[\overline{(HgCl_2)_2S_2}] \qquad (24)$$

The subtraction of Eq. 24 from Eq. 23, followed by the substitution of Eq. 8 and taking into account the fact that n=2, yields the following quadratic equation with respect to the unreacted extractant concentration ($[\overline{S}]$):

$$K_e\alpha_2C_{Hgw}[\overline{S}]^2 + [\overline{S}] - C_{B0} + C_{Hg0} - C_{Hgw} = 0 \qquad (25)$$

The equilibrium constant for the extraction reaction described by Eq. 19, K_e', was evaluated, using the least-squares method so as to minimize the deviations between the observed and calculated results from Eqs. 22 and 25, as K_e'=2.0×10^8 (dm^3 mol^{-1})^3. The solid lines in Fig. 6 are the calculated results obtained from Eqs. 22 and 25 using the values of K_e=4.0×10^5 (dm^3 mol^{-1})^2 and K_e'=2.0×10^8 (dm^3 mol^{-1})^3. For all of the extractant concentrations, the calculated curves are in good agreement with the experimental results.

The authors are deeply indebted to American Cyanamid Co. for supply of the sample of CYANEX 471.

References

1) T. Sato and T. Nakamura, *Hydrometallurgy*, **6**, 3 (1980).

2) N. M. Rice and Michael R. Smith, *J. Appl. Chem. Biotechnol.*, **25**, 379 (1975).

3) T. Kataoka, T. Nishiki, and K. Ueyama, *J. Chem. Eng. Jpn*, **17**, 351 (1984).

4) R. W. Cattrall and H. Daud, *J. Inorg. Nucl. Chem.*, **41**, 1037 (1979).

5) V. A. Mikhailov, N. A. Korol', and D. D. Bogdanova, *Izv. Sib. Otd. Akad. Nauk SSSR, Ser. Khim.*, **1975**, 29.

6) T. Sato, I. Ishikawa, and T. Nakamura, *Solvent Extr. Ion Exch.*, **1**, 541 (1983).
7) T. H. Handley and J. A. Dean, *Anal. Chem.*, **32**, 1878 (1960).
8) Y. Baba, Y. Ikeda, and K. Inoue, *Bull. Chem. Soc. Jpn.*, **58**, 881 (1985).
9) W. A. Rickelton, Eur. Pat. Appl., 113454 (1984).
10) R. B. Hitchcock, J. A. Dean, and T. H. Handley, *Anal. Chem.*, **35**, 254 (1963).
11) Y. Baba and K. Inoue, *Solvent Extr. Ion Exch.*, **2**, 579 (1984).
12) Y. Baba and K. Inoue, *Solvent Extr. Ion Exch.*, **3**, 35 (1985).
13) L. G. Hepler and G. Olofsson, *Chem. Rev.*, **75**, 585 (1975).

 © 1986 The Chemical Society of Japan Bull. Chem. Soc. Jpn., 59, 3841—3846 (1986)

Solvation and Ionic Association of Bis(2,4-pentanedionato)-(diamine)cobalt(III) Perchlorates in 1-Propanol, Acetone, and Their Mixtures

Kazuaki Ito,†,* Etsuro Iwamoto, Shigehito Suehisa, Hiroyuki Isono, and Yuroku Yamamoto††
Department of Chemistry, Faculty of Science, Hiroshima University, Naka-ku, Hiroshima 730
(Received May 29, 1986)

The conductances of bis(2,4-pentanedionato)(diamine)cobalt(III) perchlorates ([Co(acac)$_2$(diamine)]ClO$_4$, diamine: en=ethylenediamine, pn=1,2-propanediamine, *N,N*-dmen=*N,N*-dimethylethylenediamine, *N,N'*-dmen=*N,N'*-dimethylethylenediamine, *N,N,N'*-trimen=*N,N,N'*-trimethylethylenediamine, *N,N,N',N'*-tmen=*N,N,N',N'*-tetramethylethylenediamine) were measured in isodielectric solvents, 1-propanol (*n*-PrOH), acetone (Me_2CO), and 60 and 80 mol% acetone in 1-propanol (*n*-PrOH–Me_2CO) at 25 °C. In spite of the increase in size of [Co(acac)$_2$(diamine)]$^+$ due to the introduction of *N*-methyl groups, the Walden products ($\lambda_0^+ \cdot \eta$) of the chelate cations were found to increase in all solvents. The contribution per *N*-methyl group was large in *n*-PrOH. The variation in the ionic association constants (K_a) with the number of NH protons in the chelate cations was small in all solvents. The K_a values for [Co(acac)$_2$(*N,N'*-dmen)]ClO$_4$ were larger than those for other chelate salts in all solvents. These results could be explained in terms of the solvation of the NH protons (diamine in [Co(acac)$_2$-(diamine)]$^+$) by oxygen atoms of *n*-PrOH and Me_2CO, and of oxygen atoms (acac) by the OH proton of *n*-PrOH owing to hydrogen bonding interactions and desolvation resulting from the introduction of the *N*-methyl groups. For [Co(acac)$_2$(en)]$^+$ in *n*-PrOH a solvation model to form a six-membered ring was proposed.

Our previous conductometric studies of [Co(acac)$_2$-(en)]X (X$^-$=ClO$_4^-$, I$^-$, and Br$^-$) and their *N*-methyl derivatives in nitrobenzene and 1,2-dichloroethane[1,2] indicated that NH protons in the chelate cations are solvated by the dipolar aprotic solvent nitrobenzene, and that the substitution of *N*-methyl groups for NH protons prevents solvation, leading to an increase in mobility in spite of the increasing size. The *N*-methylation results in an apparent increase in the acidity of the residual and the nearest-neighbor NH protons. These trends were not observed in 1,2-dichloroethane with a lower polarity. The association constants decrease with a decrease in the number of NH protons in both solvents and the change per proton is larger in 1,2-dichloroethane. These solvents are aprotic and weak in basicity but have different dielectric constants and polarities. Thus, it is suggested that ionic association processes of the chelate cations are affected by ion-solvent dipole interactions.

In this study, in an effort to obtain more information concerning the effects of the solvent dipole moment and the solvent acidity and basicity, the conductances of [Co(acac)$_2$(diamine)]ClO$_4$ were measured in the protic solvent 1-propanol, aprotic acetone, and their mixtures. 1-Propanol has acidic and basic sites that are effective for solvation; acetone interacts through its electron lone pair. Since the solvents have nearly the same dielectric constants, the electrostatic interaction energy between a cation and an anion is regarded as constant for a given electrolyte. Solvation of the ClO$_4^-$ ion is weak compared to that of halide ions. Thus, it is considered that specific cation-solvent interactions in ionic association process become much apparent.

Experimental

[Co(acac)$_2$(diamine)]ClO$_4$ was prepared and purified as described previously.[2] 1-Propanol was refluxed over calcium hydride for 2 d and fractionally distilled. Acetone was refluxed over Drierite after dehydration by molecular sieves (4A) for one week and fractionally distilled. The distillation was performed under a flow of N_2 gas since the solvents were relatively hygroscopic. Typical densities (d in g cm^{-3}), viscosities (η in mPa s), and specific conductances of pure solvents (κ in S cm^{-1}) at 25 °C and water contents (wc in wt%) are: for *n*-PrOH d=0.79963, η=1.952, $\kappa=2\times10^{-8}$, and $wc=8\times10^{-3}$; for Me_2CO d=0.78426, η=0.3052, $\kappa=2\times10^{-8}$, and $wc=5\times10^{-3}$.

The procedure for the conductance measurements and other measurements (viscosity and density) have been described previously.[2] The water content was measured coulometrically using a Hiranuma AQ-3 aqua counter. *n*-PrOH–Me_2CO mixtures were prepared by weight just before a conductance measurement. The dielectric constant (ε) and viscosity (η in mPa s) of the solvents used for an analysis were as follows: for *n*-PrOH ε=20.45,[3] η=1.952; for Me_2CO ε=20.45,[4] η=0.3052; for *n*-PrOH–Me_2CO (60 mol% Me_2CO) ε=18.64,[4] η=0.463; for 80 mol% Me_2CO ε=19.37,[4] η=0.361.

Results and Discussion

The measured molar conductances, Λ (S cm^2 mol^{-1}) and the corresponding electrolyte concentrations, C (mol dm^{-3}) for [Co(acac)$_2$(diamine)]ClO$_4$ in 1-propanol and acetone are given in Table 1 and those in 1-propanol–acetone mixtures (60 and 80 mol% acetone) in Table 2. The data were analyzed by the Fuoss-Hsia equation with $E=E_1\Lambda_0-2E_2$ in the form[5]

$$\Lambda = \Lambda_0 - S(C\gamma)^{1/2} + EC\gamma \log C\gamma + J_1C\gamma - J_2(C\gamma)^{3/2} - K_aC\gamma f_\pm^2\Lambda \quad (1)$$

†Present address: Department of Environmental Science, Faculty of Engineering, Hiroshima University, Saijo, Higashi-Hiroshima 724.
††Present address: Environmental and Safety Engineering Department, Fukui Institute of Technology, Gakuen, Fukui 910.

Table 1. Molar Concentrations, C/mol dm^{-3}, and Molar Conductances, Λ/S cm^2 mol^{-1} of [Co(acac)$_2$(diamine)]ClO$_4$ in 1-Propanol and Acetone at 25 °C

1-Propanol

[Co(acac)$_2$(en)]ClO$_4$		[Co(acac)$_2$(pn)]ClO$_4$		[Co(acac)$_2$(*N*,*N*-dmen)]ClO$_4$	
$C\times10^4$	Λ	$C\times10^4$	Λ	$C\times10^4$	Λ
10.224	19.505	9.5497	19.816	26.123	17.343
8.3805	20.091	7.6345	20.426	21.880	18.019
7.0600	20.556	5.9069	21.055	17.218	18.916
5.9400	21.002	4.4038	21.702	13.272	19.841
4.5408	21.640	2.9868	22.422	9.8481	20.888
3.6357	22.129	1.9922	23.062	6.9774	21.968
2.6764	22.723			4.8040	23.040
2.0269	23.184			2.7621	23.330
0.9446	24.192				

1-Propanol

[Co(acac)$_2$(*N*,*N*′-dmen)]ClO$_4$		[Co(acac)$_2$(*N*,*N*,*N*′-trimen)]ClO$_4$		[Co(acac)$_2$(*N*,*N*,*N*′,*N*′-tmen)]ClO$_4$	
$C\times10^4$	Λ	$C\times10^4$	Λ	$C\times10^4$	Λ
18.641	17.180	23.911	16.954	21.551	18.430
14.948	17.982	17.556	18.085	17.192	19.296
11.365	18.945	13.257	19.088	14.563	19.910
8.6067	19.865	10.692	19.830	11.067	20.924
6.4579	20.759	7.6271	20.941	9.2711	21.533
4.9530	21.510	5.5441	21.894	6.3357	22.742
3.1541	22.624	3.7396	22.952	4.5616	23.704
2.3229	23.297	2.4411	23.906	2.3837	25.222

Acetone

[Co(acac)$_2$(en)]ClO$_4$		[Co(acac)$_2$(pn)]ClO$_4$		[Co(acac)$_2$(*N*,*N*-dmen)]ClO$_4$	
$C\times10^4$	Λ	$C\times10^4$	Λ	$C\times10^4$	Λ
31.363	132.71	42.062	128.84	21.253	142.88
26.509	135.75	27.015	136.60	16.675	146.79
22.820	138.35	21.579	140.33	13.340	150.19
17.781	142.65	16.359	144.61	10.833	153.21
13.613	146.85	12.260	148.72	8.6943	156.25
10.152	151.08	9.1657	152.54	5.1964	162.36
6.1533	157.38	6.1154	157.19	3.3321	166.62
3.2943	163.69				

Acetone

[Co(acac)$_2$(*N*,*N*′-dmen)]ClO$_4$		[Co(acac)$_2$(*N*,*N*,*N*′-trimen)]ClO$_4$		[Co(acac)$_2$(*N*,*N*,*N*′,*N*′-tmen)]ClO$_4$	
$C\times10^4$	Λ	$C\times10^4$	Λ	$C\times10^4$	Λ
33.219	128.76	29.541	136.75	30.991	143.57
26.207	133.47	21.870	142.26	26.797	145.91
19.247	139.43	17.930	145.62	22.438	148.69
15.446	143.42	14.988	148.63	18.055	151.90
12.259	147.66	11.763	152.38	13.876	155.63
9.2749	152.22	9.0216	156.14	10.435	159.30
6.5372	157.02	5.9052	161.42	6.3053	165.10
4.1195	163.14	3.9766	165.62	3.7059	170.06

where K_a is the ionic association constant, Λ_0 is the limiting conductance, and other symbols have their usual meaning.

The conductance parameters obtained for 1-propanol and acetone are given in Table 3 and those for 1-propanol–acetone mixtures in Table 4. The limiting conductances (λ_0^+/S cm^2 mol^{-1}) and Walden products ($\lambda_0^+\cdot\eta$/S cm^2 mol^{-1} 10^{-1} Pa s) of [Co(acac)$_2$(diamine)]$^+$ are obtained from the limiting conductances of ClO_4^- (16.42[3]) and 118.35 S cm^2 mol^{-1}[4]) in 1-propanol and acetone, respectively) (Table 5).

Ionic Mobility. Figure 1 shows the variation of the

Table 2. Molar Concentrations, C/mol dm^{-3}, and Molar Conductances, Λ/S cm^2 mol^{-1} of $[Co(acac)_2(diamine)]ClO_4$ in 1-Propanol–Acetone Mixtures at 25 °C

60 (mol% Acetone)			
$[Co(acac)_2(en)]ClO_4$		$[Co(acac)_2(N,N\text{-dmen})]ClO_4$	
$C\times10^4$	Λ	$C\times10^4$	Λ
31.273	75.854	33.185	77.649
24.393	78.623	23.971	81.309
19.691	80.955	18.056	84.358
14.878	83.884	14.163	86.894
10.805	86.958	9.4644	90.732
7.7621	89.832	6.2743	94.174
5.3801	92.687	3.7910	97.727
3.3449	95.777	2.5638	99.868

60 (mol% Acetone)			
$[Co(acac)_2(N,N'\text{-dmen})]ClO_4$		$[Co(acac)_2(N,N,N',N'\text{-tmen})]ClO_4$	
$C\times10^4$	Λ	$C\times10^4$	Λ
32.162	75.095	27.439	84.765
26.544	77.468	22.923	86.714
20.531	80.527	17.154	89.695
16.227	83.286	13.512	92.072
12.413	86.215	9.5311	95.232
9.2761	89.208	7.2195	97.533
6.6941	92.237	5.3991	99.678
4.0004	96.382	3.7963	101.97

80 (mol% Acetone)			
$[Co(acac)_2(en)]ClO_4$		$[Co(acac)_2(N,N\text{-dmen})]ClO_4$	
$C\times10^4$	Λ	$C\times10^4$	Λ
41.089	98.665	36.512	102.89
33.005	101.91	28.838	106.34
25.587	105.75	22.892	109.53
19.780	109.30	17.623	113.05
14.669	113.13	14.183	115.78
10.629	117.09	10.535	119.41
6.6433	122.09	7.6902	122.85
3.8580	126.87	5.0160	126.87

80 (mol% Acetone)			
$[Co(acac)_2(N,N'\text{-dmen})]ClO_4$		$[Co(acac)_2(N,N,N',N'\text{-tmen})]ClO_4$	
$C\times10^4$	Λ	$C\times10^4$	Λ
36.095	99.126	29.046	112.28
28.375	102.99	23.603	114.97
22.211	106.76	17.865	118.52
17.202	110.48	14.133	121.25
13.539	113.83	10.209	124.84
10.241	117.53	7.7400	127.59
7.5489	121.23	5.1022	131.18
4.4823	126.76	2.8076	135.33

Walden products of $[Co(acac)_2(diamine)]^+$ with the introduction of methyl groups in 1-propanol and acetone, compared with that of tetraalkylammonium cations[3,4] for which n refers to the number of carbons in the alkyl group. For tetraalkylammonium ions which have approximately the same size as the chelate cations used here and no specific site for solvation, the Walden product decreases with increasing ionic size, as is hydrodynamically expected. It should be noted that, in contrast, the Walden product of the che-

Table 3. Conductance Results for $[Co(acac)_2(diamine)]ClO_4$ in 1-Propanol and Acetone at 25 °C

Electrolyte	Solvent	Λ_0	K_a	d[a]	σ_Λ[b]
		S cm² mol⁻¹	dm³ mol⁻¹	Å	
$[Co(acac)_2(en)]ClO_4$	*n*-PrOH	25.81±0.02	411±45	14.1	0.011
$[Co(acac)_2(pn)]ClO_4$		25.37±0.02	369± 9	20.5	0.008
$[Co(acac)_2(N,N\text{-dmen})]ClO_4$		27.86±0.02	467±11	16.2	0.016
$[Co(acac)_2(N,N'\text{-dmen})]ClO_4$		26.53±0.01	531±12	17.3	0.010
$[Co(acac)_2(N,N,N'\text{-trimen})]ClO_4$		27.31±0.03	507±36	14.3	0.006
$[Co(acac)_2(N,N,N',N'\text{-tmen})]ClO_4$		28.57±0.02	480±15	16.4	0.015
$[Co(acac)_2(en)]ClO_4$	Me_2CO	180.03±0.09	180± 4	14.0	0.06
$[Co(acac)_2(pn)]ClO_4$		178.9 ±0.1	161± 3	13.3	0.06
$[Co(acac)_2(N,N\text{-dmen})]ClO_4$		183.15±0.06	172±17	13.3	0.06
$[Co(acac)_2(N,N'\text{-dmen})]ClO_4$		184.1 ±0.2	228±34	12.8	0.17
$[Co(acac)_2(N,N,N'\text{-trimen})]ClO_4$		184.02±0.08	181± 4	14.2	0.05
$[Co(acac)_2(N,N,N',N'\text{-tmen})]ClO_4$		186.40±0.04	137± 2	13.1	0.03

a) Distance parameter with a minimum σ_Λ value in Eq. 1. b) Standard deviation ($\sigma_\Lambda=[\sum(\Lambda_{calcd}-\Lambda_{obsd})^2/(n\text{-}3)]^{1/2}$).

Table 4. Conductance Results for $[Co(acac)_2(diamine)]ClO_4$ in 1-Propanol–Acetone Mixtures at 25 °C

Electrolyte	mol% Acetone	Λ_0	K_a	d[a]	σ_Λ[b]
		S cm² mol⁻¹	dm³ mol⁻¹	Å	
$[Co(acac)_2(en)]ClO_4$	60	107.37±0.09	243±6	15.1	0.06
$[Co(acac)_2(N,N\text{-dmen})]ClO_4$		110.1 ±0.1	236±8	14.8	0.11
$[Co(acac)_2(N,N'\text{-dmen})]ClO_4$		110.41±0.07	288±5	14.8	0.05
$[Co(acac)_2(N,N,N',N'\text{-tmen})]ClO_4$		114.17±0.07	208±5	14.8	0.05
$[Co(acac)_2(en)]ClO_4$	80	142.3 ±0.1	209±4	14.1	0.09
$[Co(acac)_2(N,N\text{-dmen})]ClO_4$		144.7 ±0.1	202±6	13.6	0.07
$[Co(acac)_2(N,N'\text{-dmen})]ClO_4$		145.06±0.03	249±2	13.7	0.02
$[Co(acac)_2(N,N,N',N'\text{-tmen})]ClO_4$		147.6 ±0.1	165±5	14.8	0.09

a) and b) are the same as in Table 3.

Table 5. Ionic Mobilities and Walden Products in 1-Propanol and Acetone at 25 °C

	λ_0^+/S cm² mol⁻¹ ($\lambda_0^+\cdot\eta$/S cm² mol⁻¹ 10⁻¹ Pa s)	
	1-Propanol	Acetone
$[Co(acac)_2(en)]^+$	9.39(0.183)	61.63(0.188)
$[Co(acac)_2(pn)]^+$	8.95(0.174)	60.5 (0.185)
$[Co(acac)_2(N,N\text{-dmen})]^+$	11.44(0.223)	64.75(0.198)
$[Co(acac)_2(N,N'\text{-dmen})]^+$	10.11(0.197)	65.7 (0.201)
$[Co(acac)_2(N,N,N'\text{-trimen})]^+$	10.89(0.212)	65.62(0.200)
$[Co(acac)_2(N,N,N',N'\text{-tmen})]^+$	12.15(0.237)	68.0 (0.208)

late cations in both 1-propanol and acetone roughly increases with the *N*-methylation of NH protons in spite of the increase in the size of the cations. Similar results were also obtained in nitrobenzene which has a poor basicity and can be explained in terms of the solvation of the NH proton site by nitrobenzene through an ion-solvent dipole interaction and desolvation by *N*-methylation.[1,2]

However, this *N*-methylation effect in 1-propanol is more marked than in nitrobenzene. The difference in the Walden products between *N,N,N',N'*-tmen and en complexes in acetone, 0.020 S cm² mol⁻¹ 10⁻¹ Pa s is comparable with that in nitrobenzene; however, a large difference of 0.054 S cm² mol⁻¹ 10⁻¹ Pa s was observed in 1-propanol. A small difference of 0.003 S cm² mol⁻¹ 10⁻¹ Pa s was obtained in 1,2-dichloroethane.[2] The large variation of the Walden product with the substituted groups in diamine for the 1-propanol system is suggestive of a specific solvation of the chelate cations.

The dipole moment of acetone, 1-propanol, nitrobenzene, and 1,2-dichloroethane is 2.88, 1.68, 4.22, and 1.40 in Debye, respectively,[6] and the large variation in the Walden products in 1-propanol can not be explained by only the dipole moment.

The following two specific interactions for the solvation of chelate cations are considered: A hydrogen-bonding interaction between the NH protons in $[Co(acac)_2(diamine)]^+$ and the oxygen atom of 1-propanol and acetone which act as hydrogen bonding acceptor. The second is the hydrogen-bonding of the oxygen atom of the coordinated acac ligand with the

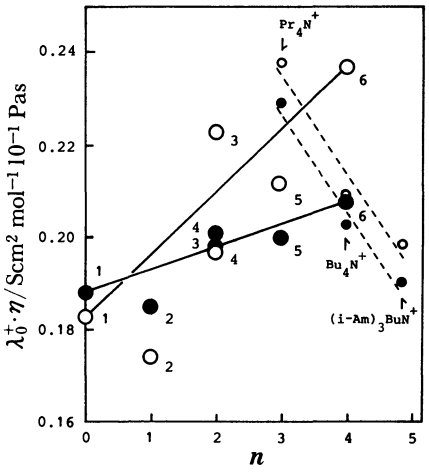

Fig. 1. Walden products of $[Co(acac)_2(diamine)]^+$ as a function of the increased carbon number, *n* compared to $[Co(acac)_2(en)]^+$. ○: in *n*-PrOH, ●: in Me_2CO. Diamine, 1: en, 2: pn, 3: *N,N*-dmen, 4: *N,N'*-dmen, 5: *N,N,N'*-trimen, 6: *N,N,N',N'*-tmen. For onium salts, *n* refers to the number of carbon in the alkyl group and the data are from Refs. 3 and 4.

OH proton of 1-propanol which acts as a hydrogen-bonding donor.

The hydrogen-bonding acceptor ability or donicity is evaluated by the Gutmann donor number. The donor numbers (DN) of acetone, nitrobenzene, and 1,2-dichloroethane are 17, 4.4, and 0.0, respectively.[7] The DN value of 1-propanol, although not available in the literature, was reasonably estimated to be around 20, since that of methanol and ethanol is 19 and 20, respectively. The ^{59}Co NMR for $[Co(en)_3]^{3+}$ was measured in several organic solvents and the signal was shifted to a higher field upon increasing the donicity of the solvents.[8] This was interpreted as the result of a donor solvent attack on the NH protons. Although an ion-dipole interaction for acetone is weaker than that for nitrobenzene, the solvation of NH protons by acetone is strengthened by its stronger donicity, resulting in a comparable difference in the Walden product between acetone and nitrobenzene.

A relatively large increase in the mobility by the *N*-methylation in 1-propanol indicates the strong solvation power of 1-propanol. The IR spectra of methanol in the carbon tetrachloride solutions of bis- and tris (2,4-pentanedionato) complexes such as $Be(acac)_2$ and $Cr(acac)_3$ showed that for $Cr(acac)_3$ hydrogen bonding occurrs between the oxygen atom of acac and the OH proton of methanol but does not occur for $Be(acac)_2$ because of a steric hindrance.[9] The ^1H NMR study of paramagnetic $Cr(acac)_3$ indicated that the OH group of methanol is closer to the central metal Cr(III) than the CH_3 group of methanol.[10] Furthermore, the X-ray study of $[Cr(acac)_2(tn)]I$ (tn=1,3-propanediamine)[11] showed that the intramolecular distance between the NH protons and oxygen atoms of the acac is 2.5 and 2.6 Å. A molecular model of $[Co(acac)_2(en)]^+$ indicates that it possesses spaces enough to accomodate the OH group of 1-propanol. Thus, it is possible that $[Co(acac)_2(en)]^+$ is solvated by 1-propanol through hydrogen bonding to form a six-membered ring.

In 1-propanol-acetone mixtures (Table 4) the mobility of the complex ions increases with the *N*-methylation in a similar manner. The differences in the Walden product between *N,N,N',N'*-tmen and en complexes are 0.031 and 0.019 S cm^2 mol^{-1} 10^{-1} Pa s in 60 and 80 mol% acetone in 1-propanol, respectively. These values are closer to the value for acetone (0.020) than that for 1-propanol (0.054), thereby suggesting that the selective solvation of $[Co(acac)_2(en)]^+$ by 1-propanol is not seen in the mixed solvents.

The methylation effect on the mobility depends on the substituted position. As can be seen for $[Co(acac)_2(pn)]^+$, the *C*-methylation leads to a decrease in the mobility. A similar result was obtained in nitrobenzene and 1,2-dichloroethane.[2] This shows that the methyl group does not prevent the solvation of NH protons, but contributes only to a decrease in mobility by increasing the size. It is interesting to compare the Walden product between $[Co(acac)_2(N,N\text{-dmen})]^+$ and $[Co(acac)_2(N,N'\text{-dmen})]^+$ in 1-propanol: the *N,N*-dmen ligand increases more the mobility than the *N,N'*-dmen ligand, compared with the ligand en. Therefore, it is likely that the mono-methylation of the two NH protons does not have a large desolvation effect; however, the doble-methylation completely prevents solvation by 1-propanol with a six-membered ring and compensates for the effect of an increasing size on mobility. This can be also seen in the decrease in the mobility from *N,N*-dmen to *N,N,N'*-trimen and an increase in the mobility from *N,N'*-dmen to *N,N,N'*-trimen and *N,N,N',N'*-tmen.

Ionic Association. The association constants of the chelate electrolytes show three features: (a) the K_a value in 1-propanol is much larger than that in acetone. (b) The variation of K_a with the number of NH protons in $[Co(acac)_2(diamine)]^+$ is small in all solvents. (c) The K_a value of $[Co(acac)_2(N,N'\text{-dmen})]^+$ is larger than that of $[Co(acac)_2(en)]^+$ in all the systems.

Observation (a) held for Bu_4NClO_4[4]: Although the dipole moment of 1-propanol (1.68 Debye) is small compared to that of acetone (2.88 Debye), the magnitude of the bulk dielectric constant of 1-propanol which is similar to that of acetone is due to the structure arising from hydrogen bonding. However, in the vicinity of the ion pairs, the structure is destroyed by the solvation of the chelate cations, leading to a diminution of the local dielectric constant. Thus, ionic association constants in 1-propanol are larger than those in acetone.

(b) The ratio of K_a for $[Co(acac)_2(en)]ClO_4$ to $[Co(acac)_2(N,N,N',N'\text{-tmen})]ClO_4$ is 0.9 and 1.3 for 1-propanol and acetone, respectively. These values are smaller than those for 1,2-dichloroethane (7.9) and

nitrobenzene (2.4).[2] The NH protons in $[Co(acac)_2(en)]^+$ associates with ClO_4^- by hydrogen bonding in 1,2-dichloroethane, leading to the larger K_a value for $[Co(acac)_2(en)]ClO_4$. In nitrobenzene, the protons are solvated due to the high polarity of the nitrobenzene molecule. However, the ion pair, $[Co(acac)_2(en)]ClO_4$ is a contact ion pair, formed by the partial exclusion of nitrobenzene molecules. On the other hand, in 1-propanol and acetone the protons are solvated owing to an acid-base interaction. Especially, the solvation is large in 1-propanol because $[Co(acac)_2(en)]^+$ is specifically solvated by the 1-propanol molecule as discussed in the preceding section. This leads to the formation of solvent-separated ion pairs and observation (b).

Previous studies showed that the trend of observation (c) was also seen in nitrobenzene and nitrobenzene-carbon tetrachloride mixtures but chloroalkane solvents such as 1,2-dichloroethane and dichloromethane, and that the results could be ascribed to a difference in polarity of the solvent.[12] For the $[Co(acac)_2(N,N'\text{-dmen})]^+$ ion in solvents which provide observation (c), the methyl substitution (CH_3-NH-) interferes with the solvation of the residual NH protons due to a steric hindrance. This leads to an increase in the acidity of the NH protons and to a larger association of $[Co(acac)_2(N,N'\text{-dmen})]ClO_4$ compared with $[Co(acac)_2(en)]ClO_4$. The K_a value of $[Co(acac)_2(N,N,N'\text{-trimen})]ClO_4$ is larger than that of $[Co(acac)_2(N,N\text{-dmen})]ClO_4$ in a similar manner. It can be said that the existence of a relatively strong specific solvation of NH protons such as solvations due to ion-dipole and hydrogen-bonding interactions gives the pattern shown in (c).

This work was supported in part by a Grant-in-Aid for Scientific Research Nos. 58740281 and 60129031 from the Ministry of Education, Science and Culture.

References

1) K. Ito, E. Iwamoto, and Y. Yamamoto, *Bull. Chem. Soc. Jpn.*, **55**, 3190 (1982).
2) K. Ito, *Inorg. Chem.*, **22**, 2872 (1983).
3) D. F. Evans and P. Gardam, *J. Phys. Chem.*, **72**, 3281 (1968).
4) D. F. Evans, J. Thomas, J. A. Nadas, and M. A. Matesich, *J. Phys. Chem.*, **75**, 1714 (1971).
5) a) R. M. Fuoss ans K. L. Hsia, *Proc. Natl. Acad. Sci., USA*, **57**, 1550 (1967); b) Fernandeź-Prini, *Trans. Faraday Soc.*, **65**, 3311 (1969).
6) R. C. West, Ed., "Handbook of Chemistry and Physics," 64th ed., CRC Press: Florida, (1983).
7) V. Gutmann, "The Donor-Acceptor Approach to Molecular Interactions," Plenum Press: New York, London, (1978).
8) G. Gonzalez, U. Mayer, and V. Gutmann, *Inorg. Nucl. Chem. Lett.*, **15**, 155 (1979).
9) T. S. Davis and J. P. Fackler, Jr., *Inorg. Chem.*, **5**, 242 (1966).
10) a) G. S. Vigee and C. L. Watkins, *Inorg. Chem.*, **16**, 709 (1977); b) S. O. Chan and D. R. Eaton, *Can. J. Chem.*, **54**, 1332 (1976).
11) K. Matsumoto and S. Ooi, *Bull. Chem. Soc. Jpn.*, **52**, 3307 (1979).
12) K. Ito, E. Iwamoto, K. Hasegawa, M. Yamamoto, and Y. Yamamoto, *Bull. Chem. Soc. Jpn.*, **58**, 1287 (1985).

 © 1986 The Chemical Society of Japan Bull. Chem. Soc. Jpn., 59, 3847—3854 (1986)

Equilibrium and Structural Studies on the Species Formed in the Extraction of Divalent Transition Metal Ions with 8-Quinolinol

Akio YUCHI,* Kenji IMAI, Hiroko WADA, Motoo SHIRO,† and Genkichi NAKAGAWA
Department of Applied Chemistry, Nagoya Institute of Technology, Gokiso-cho, Showa-ku, Nagoya 466
†Shionogi Research Laboratories, Shionogi & Co., Ltd., Fukushima-ku, Osaka 553
(Received June 9, 1986)

The equilibria were studied in the extraction of divalent transition metal ions (M^{2+}: Co^{2+}, Ni^{2+}, Zn^{2+}, Cd^{2+}) with 8-quinolinol (Hq) from aqueous solutions containing various anions (X^-) into some organic solvents. The effects of $-\log[H^+]$ and total concentrations of 8-quinolinol and metal ions on the distribution were examined in detail. Three species, $M_2q_3(Hq)_3X$, $Mq_2(Hq)$, and $M_2q_4(Hq)_2$ are responsible for the extraction. The extraction of $M_2q_3(Hq)_3X$ is favorable when hydrophobic anions and polar solvents are used. On the other hand, the extraction constants of $Mq_2(Hq)$ are almost the same for each metal ion irrespective of anions and solvents. With increasing the metal ion concentration in the organic phase, $Mq_2(Hq)$ dimerizes to form $M_2q_4(Hq)_2$. The decrease in the distribution ratio by prolonged shaking under certain conditions is reasonably ascribed to the slow precipitation of $Mq_2 \cdot 2H_2O$ which has been made supersaturated by the rapid establishment of all the equilibria except the precipitation reaction. An X-ray crystallographic study for $Ni_2q_4(Hq)_2$ showed that two nickel atoms are surrounded by three bidentate ligands with facial and meridional configurations about their oxygen atoms and these two isomers form a binuclear structure jointed by two strong hydrogen bonds.

8-Quinolinol (Hq) is one of the most familiar extracting reagents, and its behavior in the extraction of various metal ions has been repeatedly studied.[1] Among the divalent transition metal ions copper is simply extracted as Cuq_2. In contrast, the extraction equilibria of other metal ions, such as cobalt, nickel, zinc and cadmium, are rather complicated and conflicting results have been reported as shown in Table 1.[2-18] As for nickel ion, Oki and Terada have found the presence of two extracted species $Ni_2q_3(Hq)_3X$ (X^-: anion) and $Ni_2q_4(Hq)_2$,[10,11] whereas Bhatki et al. have stated the unique presence of $Niq_2(Hq)$.[12] Moreover, Sekido et al. found that the species once extracted into chloroform gradually precipitate during the prolonged shaking.[19,20] About the extracted species of the other metal ions there has also been similar confusion. Thus we made extensive equilibrium study to understand these findings altogether.

Among these proposed species, $Ni_2q_3(Hq)_3X$(X^-: I_3^- or ClO_4^-) has recently been identified by X-ray crystallographic studies.[21] We determined the crystal structure of one of the neutral extracted species $Ni_2q_4(Hq)_2$.

Table 1. Earlier Studies on the Extraction of Divalent Transition Metal Ions with 8-Quinolinol

Extracted species	$\log K_{ex}$	C_{Hq} / mol dm^{-3}	C_M / mol dm^{-3}	Medium	Method[a]	Ref.
$Coq_2(Hq)_2$	−2.16	10^{-2}—10^{-1}	—	0.1 $KClO_4$	SP, R	2
$Coq_2(Hq)_2$	−2.6	—	—	0.5	—	3
$Coq_2(Hq)$	−3.71[b]	5×10^{-2}—2×10^{-1}	2×10^{-7}, 7×10^{-5}	0.1 $NaClO_4$	SP, R	4
$Coq_2(Hq)$	—	10^{-3}—10^{-2}	—	0.1 $NaClO_4$	R	5
$Co_2q_4(Hq)_2$	−4.61	0.1	1×10^{-4}	0.1 Na_2SO_4	SP, R	6
$Co_2q_3(Hq)_3ClO_4$	2.60			0.1 $NaClO_4$		
$Coq_2(Hq)$	−3.83[b]	4×10^{-3}—6×10^{-2}	—	0.25 $NaClO_4$	R	7
$Co_2q_4(Hq)_2$[c]	—	1×10^{-1}—3×10^{-1}	2×10^{-4}—10^{-3}	0.25 $NaClO_4$	AAS	8
Niq_2	−2.18	10^{-2}—10^{-1}	—	0.1 $KClO_4$	SP	2
$Niq_2(Hq)$	−0.56[b]	10^{-2}—10^{-1}	9×10^{-7}, 8×10^{-5}	0.1 $NaClO_4$	SP, R	9
$Ni_2q_4(Hq)_2$	−0.82	10^{-2}—10^{-1}	1×10^{-4}	0.1 Na_2SO_4	SP	10
$Ni_2q_3(Hq)_3ClO_4$	7.58			0.1 $NaClO_4$		
$Ni_2q_3(Hq)_3X$	var	10^{-2}—10^{-1}	1×10^{-4}	0.1 NaX	SP	11
$Niq_2(Hq)$	−2.55[b]	5×10^{-4}—10^{-2}	6×10^{-6}	0.25 $NaClO_4$	R	12
$Znq_2(Hq)_2$	−2.41	10^{-2}—10^{-1}	—	0.1 $KClO_4$	SP, R	2
var	—	10^{-2}—3×10^{-1}	5×10^{-7}	0.1 $NaClO_4$	R	13
$Znq_2(Hq)$	−4.1[b]	10^{-2}—1.9	10^{-5}—10^{-4}	0.1 $NaClO_4$	R	14
$Znq_2(Hq)_2$	−2.66[b]	10^{-2}—10^{-1}	6×10^{-5}	0.1 $NaClO_4$	R	15
$Zn_2q_3(Hq)_3ClO_4$	1.10	10^{-1}	2×10^{-4}	0.1 $NaClO_4$	SP, R	16
$Cdq_2(Hq)_2$	−5.29	10^{-2}—10^{-1}	—	0.1 $KClO_4$	SP, R	2
$Cdq_2(Hq)_2$	−6.1	5×10^{-2}—1	8×10^{-6}	0.1 $NaClO_4$	R	17
$Cdq_2(Hq)$	−6.5[b]	3×10^{-2}—1	2×10^{-6}	1.0 $NaClO_4$	R	18

a) SP: spectrophotometry; R: radiometry; AAS: atomic absorption spectrometry. b) Converted from the constants in literature. c) Into toluene, whereas others into chloroform.

Experimental

Reagents and Equipments. Metal(II) solutions were prepared from the sulfates and standardized against a Na_2H_2 edta solution. Organic solvents were shaken successively three times with conc. sulfuric acid, 4 mol dm^{-3} potassium hydroxide solution and distilled water. Other reagents were used as received.

All experiments were carried out in a room at 25±2 °C. Absorption spectra and $-\log[H^+]$ were measured with a thermoelectric circulating bath at 25±0.5 °C. The ionic strength was maintained at 0.10 mol dm^{-3} except for sulfate medium at 0.30 mol dm^{-3}.

Hydrogen ion concentration was measured with a Radiometer pH METER 26. The solution containing 1.00×10^{-2} mol dm^{-3} perchloric acid and 9.00×10^{-2} mol dm^{-3} sodium perchlorate was used as a $-\log[H^+]$ standard. Visible absorption spectra were recorded on a Union spectrometer SM-401 and atomic absorption spectrometry was carried out with a Daini Seikosha SAS-727.

Procedure. The details of the measurement were the same as described previously.[22] A 4×10^{-5} to 4×10^{-3} mol dm^{-3} metal solution was shaken with an equal volume of an organic solvent containing 1.6×10^{-3} to 2.4×10^{-1} mol dm^{-3} 8-quinolinol. Shaking 15—30 min for nickel and 1—5 min for other metal ions at 250 strokes min^{-1} was found sufficient for equilibration. In the cases of nickel, zinc and cadmium the absorbance of the organic phase was decreased by prolonged shaking under certain conditions (see below).

After centrifugation, $-\log[H^+]$ and metal concentration were measured for the aqueous phases. The visible spectra of the organic phases were recorded with a quartz cell of 1 or 10 mm. Absorbances at 410 nm for cobalt complexes and at 400 nm for others were used for the determination of the extraction constants.

With less 8-quinolinol and at high $-\log[H^+]$ cobalt(II) is oxidized to form extractable Coq_3. In this study extraction was examined without any reducing reagents, and the data were discarded when absorption spectra indicated the formation of Coq_3.

Perchlorate ion in the organic phase was stripped into an aqueous phase buffered at $-\log[H^+]$ 7 and was determined by modifying the method in literature.[23]

Preparation of the Nickel 8-Quinolinolate Complex. The complex was prepared by two methods: One is the addition of less polar solvents to chloroform extracts of the nickel complex from sulfate solution.[10,24] The other is the reaction of Niq_2 with an excess of 8-quinolinol in refluxing benzene. These complexes were recrystallized from benzene to give greenish crystals suitable for X-ray structural determination.

The infrared spectra of these compounds were the same to each other and were also identical to those reported elsewhere.[25] Although it was assigned as $Niq_2(Hq)$,[24,25] the elemental analysis suggested the presence of water and benzene molecules. Found: C, 68.1; H, 4.1; N, 7.7%. Calcd for $Ni_2q_4(Hq)_2\cdot H_2O\cdot C_6H_6$: C, 66.7; H, 4.3; N, 7.8%.

X-Ray Analysis. Crystal data: $Ni_2q_4(Hq)_2\cdot H_2O\cdot C_6H_6$, $F.W.$=1080.5, triclinic, $P\bar{1}$, a=13.900(6), b=15.797(7), c=13.353(6) Å, α=110.82(3), β=94.84(3), γ=78.73(3)°, V=2687(2) Å^3, D_m=1.34, D_x=1.335 g cm^{-3}, Z=2, μ(Mo $K\alpha$)=0.76 mm^{-1}, $F(000)$=1120.

Approximately spherical crystal of 0.15 mm diameter was used. Three-dimensional intensity data were collected on a Rigaku AFC-5R diffractometer using graphite-monochromatized Mo $K\alpha$ radiation (λ=0.71069 Å). 6346 reflections of 9456 unique ones measured in the range of $\theta\leq25.0°$ were observed with $|F_o|>2\sigma(F_o)$. No correction was applied for absorption.

The structure was solved by conventional heavy atom method and refined by block-diagonal least-squares technique. H atoms were not located. Positional and thermal parameters, anisotropic for the non-H atoms except for benzene and isotropic for the benzene atoms, were refined to R=0.091, R_w=0.125, and S=1.04 for 6213 reflections.[26] Weights for observed reflections were estimated as $w=[\sigma^2(F_o)+0.00712|F_o|^2]^{-1}$. Very intense reflections (8) and unreliable ones with $w^{1/2}|\Delta F|\geq4.0$ (125) were rejected for the final refinement. Computations using the program of MULTAN84, PLUTO and XPACK86 SHIONOGI[27] were performed by a FACOM M-340R computer at Shionogi Research Laboratories.

Results and Discussion

Distribution data were collected under various conditions in each system. In many systems more than one species coexist in the organic phase, so the change in the distribution ratio with $-\log[H^+]$ is not straightforward. There are the conditions where only the ion-pair species is extracted in M^{2+}-ClO_4^--chloroform systems, whereas only the neutral species is extracted in M^{2+}-SO_4^{2-}-chloroform systems. The compositions of the species were determined by the slope methods with the data in these systems. The results are shown for nickel systems.

Species Extracted as an Ion-Pair. The concentration of perchlorate was determined to be half that of nickel in chloroform as reported earlier.[10] Taking into account the electroneutrality, the extraction equilibrium for a general ion-pair species, $Ni_2q_3(Hq)_m$-ClO_4, is expressed by

$$2Ni^{2+} + (3+m)(Hq)_o + ClO_4^- \rightleftharpoons (Ni_2q_3(Hq)_mClO_4)_o + 3H^+ \quad :K_{ex,1}, \tag{1}$$

where the subscript o refers to the organic phase. When D' is defined by $[Ni_2q_3(Hq)_mClO_4]_o/[Ni]^2$, we have the following relations:

$$\log D' - (3+m)\log[Hq]_o = -3\log[H^+] + \log K_{ex,1} + \log[ClO_4] \tag{2}$$

$$[Hq]_o = K_DC_{Hq}/(1/K_1[H^+] + 1 + K_2[H^+] + K_D), \tag{3}$$

where K_D is the partition constant of 8-quinolinol and K_1 and K_2 are the stepwise protonation constants of 8-quinolinolate.[28] The best linearity of the plot was obtained for m=3 as shown in Fig. 1, when various values were applied to m. Thus the extraction of the ion-pair species is expressed by[10]

$$2Ni^{2+} + 6(Hq)_o + ClO_4^- \rightleftharpoons (Ni_2q_3(Hq)_3ClO_4)_o + 3H^+. \tag{4}$$

Neutral Extracted Species. Extraction equilibrium

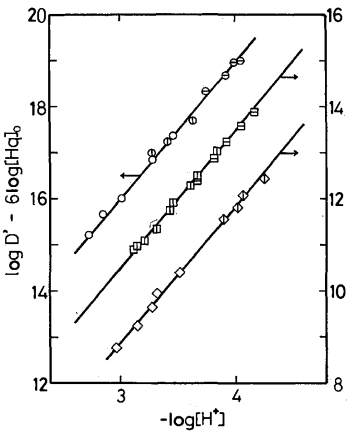

Fig. 1. Determination of the composition of the ion-pair extracted species according to Eq. 2. Ionic strength of 0.1 mol dm^{-3} $NaClO_4$. Solvent: chloroform. Metal ion: (▣, ⊟) Co^{2+}; (○, ⊕, ⊖) Ni^{2+}; (◇, ◈) Zn^{2+}. Total concentration of 8-quinolinol in the organic phase, C_{Hq}/mol dm^{-3}: (▣, ◇) 0.12; (⊟, ◈) 0.06; (○) 0.012; (⊕) 0.006; (⊖) 0.003. Solid lines: straight lines with a slope of three.

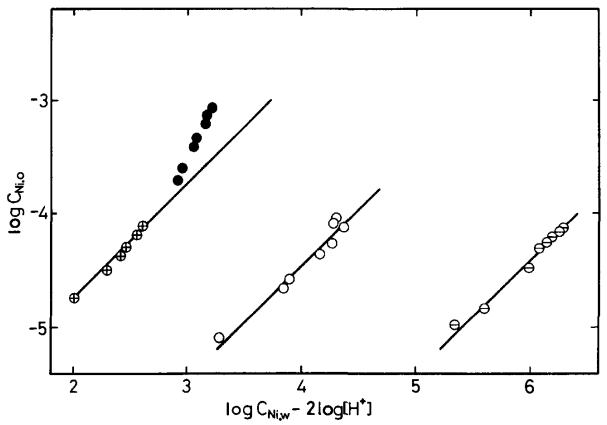

Fig. 2. Determination of the polymerization degree of neutral nickel(II) 8-quinolinolate according to Eq. 6. Ionic strength of 0.3 mol dm^{-3} Na_2SO_4. Solvent: chloroform. C_{Hq}/mol dm^{-3}: (⊕, ●) 0.05; (○) 0.013; (⊖) 0.0031. Solid lines: straight lines with a slope of unity.

of a neutral j-meric complex of the composition $Ni_jq_{2j}(Hq)_m$ is represented by[22,29]

$$j\,Ni^{2+} + (2j+m)(Hq)_o \rightleftharpoons (Ni_jq_{2j}(Hq)_m)_o + 2jH^+ \quad : K_{ex,n}. \tag{5}$$

The total concentration of nickel(II) in the organic phase, $C_{Ni,o}$ is given by

$$C_{Ni,o} = j[Ni_jq_{2j}(Hq)_m]_o = jK_{ex,n}[Ni]^j[Hq]_o^{(2j+m)}[H]^{-2j},$$

which is rewritten as a logarithmic form:

$$\log C_{Ni,o} = j(\log C_{Ni,w} - 2\log[H^+]) + (2j+m)\log[Hq]_o + \log jK_{ex,n} \tag{6}$$

If the j-meric species is responsible for the extraction,

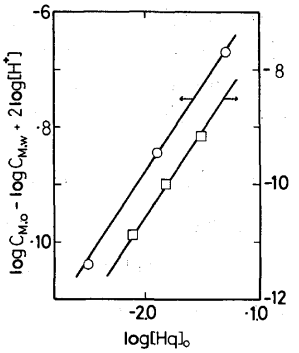

Fig. 3. Determination of the number of 8-quinolinol molecules involved in the neutral monomeric metal-(II) 8-quinolinolate. Solvent: chloroform. Metal ion: (○) Ni^{2+}; (□) Co^{2+}. Solid lines: straight lines with a slope of three.

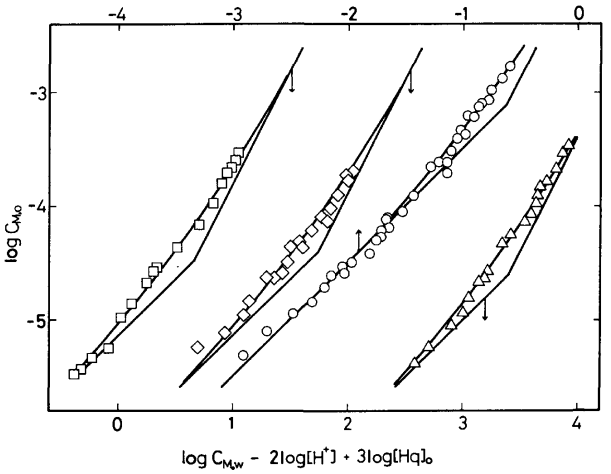

Fig. 4. Determination of the polymerization degree of neutral metal(II) 8-quinolinolate according to Eq. 8. Ionic strength of 0.3 mol dm^{-3} Na_2SO_4. Solvent: chloroform. Metal ion: (□) Co^{2+}; (○) Ni^{2+}; (◇) Zn^{2+}; (△) Cd^{2+}. Solid curves are the normalized curves, log $V(1+V)$ vs. log V. Solid lines are the asymptotes of the normalized curves.

the plot of log$C_{Ni,o}$ vs. (log$C_{Ni,w}$—2log[H^+]) would yield a straight line of slope j.

The results are shown in Fig. 2. Only monomeric species is extracted when the total concentration of nickel in the organic phase is less than 10^{-4} mol dm^{-3}, whereas at higher region some polymerized species also participate (closed circles in Fig. 2).

The number of neutral 8-quinolinol molecules in the monomeric extracted species was determined from the slope of the plot of (log $C_{Ni,o}$—log $C_{Ni,w}$+2log[H^+]) vs. log[Hq]$_o$. The actual plot falls on the straight line with a slope of 3, so m is equal to unity (Fig. 3). Thus the extraction equilibrium for the monomeric species is expressed by

$$Ni^{2+} + 3(Hq)_o \rightleftharpoons (Niq_2(Hq))_o + 2H^+ \quad : K_{ex,2}. \tag{7}$$

When the total concentration of nickel is increased, higher total concentration of 8-quinolinol is required to avoid the precipitation of $Niq_2 \cdot H_2O$ (see below).

Then nickel is extracted at lower $-\log[H^+]$ region, where $[Hq]_o$ in Eq. 6 is no longer constant to give an systematic error in such plot shown in Fig. 2. Taking account of the composition of the solid complex prepared under the same conditions, m is assumed to be equal to j. Then Eq. 6 becomes as follows:

$$\log C_{Ni,o} = j(\log C_{Ni,w} - 2\log[H^+] + 3\log[Hq]_o) + \log jK_{ex,n}. \quad (8)$$

The plot according to Eq. 8 is given in Fig. 4. At higher $\log C_{Ni,o}$ the slope of the plot tends to approach to two, which suggests the extraction of $Ni_2q_4(Hq)_2$.

$$2Ni^{2+} + 6(Hq)_o \rightleftharpoons (Ni_2q_4(Hq)_2)_o + 4H^+ : K_{ex,3} \quad (9)$$

Fitting the obtained curves with the normalized curve, $X=\log V$, $Y=\log V(1+V)$,[30] two extraction constants were obtained.

Against the previous works,[2-18] both monomeric and dimeric species prove to be responsible for the extraction. Narrow range of the total concentration of metal ion studied and unreasonable assumption of the degree of polymerization may have led to incorrect conclusion. All the reported extraction constants are too high because it was assumed that only one species was extracted instead of two (Table 1).

These two species are related by the following equation:

$$2(Niq_2(Hq))_o \rightleftharpoons (Ni_2q_4(Hq)_2)_o : K_{dim} = K_{ex,3}/(K_{ex,2})^2, \quad (10)$$

where K_{dim} is the dimerization constant. The constant is around 10^4 $mol^{-1}dm^3$ for all the metal ions except nickel. The reason for the smaller constant of nickel complexes is not clear.

Effects of Anions, Solvents and Central Metal Ions. When the total concentration of a metal ion is less than 10^{-4} mol dm^{-3}, only $M_2q_3(Hq)_3X$ and $Mq_2(Hq)$ are responsible for the extraction and the formation of $M_2q_4(Hq)_2$ is negligible. Using the absorbance vs. $-\log[H^+]$ data under these conditions (Fig. 5(a)—(i)), $K_{ex,1}$ and $K_{ex,2}$ in each system were refined to give a minimum error square sum about absorbance, $U=\sum(A_{obsd}-A_{calcd})^2$ (Table 2). The effects of anions on the distribution were examined in nickel-chloroform systems, whereas those of organic solvents in cobalt-perchlorate systems. As there formed a precipitate in hexane, carbon tetrachloride and toluene, comprehensive data were obtained in benzene, chlorobenzene and chloroform.

The extraction constant for the neutral species, $K_{ex,2}$ is almost the same for each metal ion irrespective of anions and organic solvents. Although the constants from the sulfate solution are slightly smaller than those from others, the difference is reasonably ascribed to a side reaction of metal ions with 0.1 mol dm^{-3} sulfate ion. The solvent effect on the extraction constants appears in the change of the distribution constants of the reagent and the chelate, but these influences sometimes cancel out to each other to make the effect small.[31,32] It holds also in this system.

When hydrophobic anions and polar solvents are used, the extraction is actually enhanced because of the contribution of the ion-pair species (Fig. 6). This is why polar solvents have been favorably used in the extraction with 8-quinolinol in relation to the precipitation of $Mq_2 \cdot H_2O$ (see below).

As to metal ion, all the three constants follow the well-known order, Co<Ni>Zn>Cd. Use of perchlorate medium is advantageous for the separation of cadmium ion.

Slow Reaction-Precipitation of $Mq_2 \cdot 2H_2O$. When nickel, zinc or cadmium is extracted with smaller concentration of 8-quinolinol at higher $-\log[H^+]$, decrease in absorbance of the organic phase is observed during the prolonged shaking. It has been ascribed to the precipitation of $Mq_2 \cdot 2H_2O$ by chemical analyses and infrared spectra of the precipitates,[19,20] but has not been given a sound explanation.

Figure 7 shows absorbance in Zn^{2+}-ClO_4^--chloroform system after prolonged shaking at $C_{Zn}=10^{-4}$ and $C_{Hq}=0.06$ mol dm^{-3}. If only the three extraction equi-

Table 2. Extraction and Dimerization Constants of Metal 8-Quinolinolate Complexes

Metal	Anion	Solvent	$\log K_{ex,1}$	$\log K_{ex,2}$	$\log K_{ex,3}$	$\log K_{dim}$
Co^{2+}	ClO_4^-	Chloroform	2.39	−4.43	N.d.[a]	
	ClO_4^-	Chlorobenzene	2.37	−4.57	N.d.	
	ClO_4^-	Benzene	0.47	−4.54	N.d.	
	SO_4^{2-}	Chloroform	N.f.[b]	−5.13	−6.09	4.17
Ni^{2+}	ClO_4^-	Chloroform	8.00	−2.24	N.d.	
	I^-	Chloroform	8.12	−2.12	N.d.	
	NO_3^-	Chloroform	5.97	−2.35	N.d.	
	Br^-	Chloroform	5.96	−2.34	N.d.	
	Cl^-	Chloroform	4.92	−2.22	N.d.	
	SO_4^{2-}	Chloroform	N.f.	−2.48	−2.19	2.77
Zn^{2+}	ClO_4^-	Chloroform	1.01	−4.99	N.d.	
	SO_4^{2-}	Chloroform	N.f.	−6.18	−8.26	4.10
Cd^{2+}	ClO_4^-	Chloroform	−3.22	−7.17	N.d.	
	SO_4^{2-}	Chloroform	N.f.	−8.09	−11.68	4.50

a) Not determined. b) Not found.

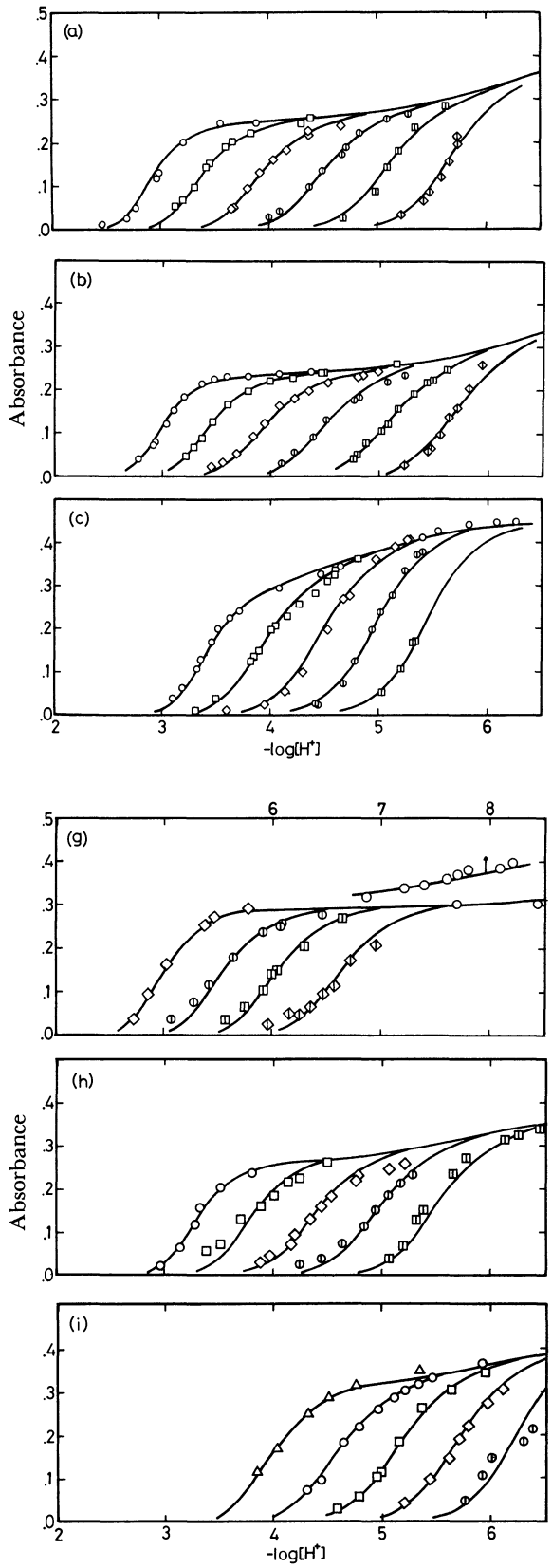

Fig. 5. Plot of absorbance vs. $-\log[H^+]$. $C_M = 1\times10^{-4}$ mol dm^{-3}. Systems, C_{Hq}/mol dm^{-3}: (a) Co^{2+}-ClO_4^--chloroform, 0.12, 0.06, 0.03, 0.015, 0.0075, 0.0038; (b) Co^{2+}-ClO_4^--chlorobenzene; (c) Co^{2+}-ClO_4^--benzene; (d) Ni^{2+}-NO_3^--chloroform, 0.05, 0.025, 0.013, 0.0062, 0.0031; (e) Ni^{2+}-Cl^--chloroform; (f) Ni^{2+}-SO_4^{2-}-chloroform, 0.05, 0.013, 0.0031; (g) Ni^{2+}-ClO_4^--chloroform, 0.013, 0.0061, 0.0032, 0.0016; (h) Zn^{2+}-ClO_4^--chloroform, 0.12, 0.06, 0.03, 0.015, 0.0075; (i) Cd^{2+}-ClO_4^--chloroform, 0.24, 0.12, 0.06, 0.03, 0.015.

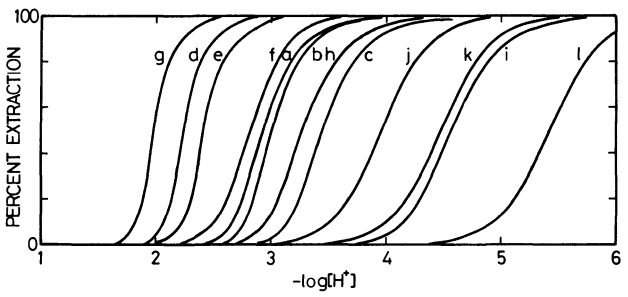

Fig. 6. Effects of anions, solvents and central metal ions on the extraction with 8-quinolinol at $C_M=10^{-4}$ and $C_{Hq}=0.12$ mol dm^{-3}. System: (a)—(i) same with Fig. 5; (j) Co^{2+}-SO_4^{2-}-chloroform; (k) Zn^{2+}-SO_4^{2-}-chloroform; (l) Cd^{2+}-SO_4^{2-}-chloroform.

libria identified above were considered, the absorbance should be as the solid line. At $-\log[H^+]$ below 4.7 the absorbance simply increased with time and the final one agreed with that given by this line. At higher $-\log[H^+]$, however, it once reached a maximum value and then slowly decreased to that shown by a circle. Table 3 tells that under these conditions the product $[Zn^{2+}][q^-]^2$ exceeds the solubility product of $Znq_2\cdot H_2O$.[33] Thus when the extraction is performed with usual procedure, all the equilibria except the precipi-

Table 3. Calculated Logarithmic Values of $[Zn^{2+}][q^-]^2$ by Assuming no Precipitation of $Znq_2 \cdot 2H_2O$[a)]

$-\log[H^+]$	C_{Hq}/mol dm^{-3}			
	0.12	0.06	0.03	0.015
3	−24.64	−25.37	−25.97	−26.53
4	−24.05	−23.81	−23.87	−24.41
5	−23.60	−23.30	−23.01	−22.81
6	−23.23	−22.93	−22.63	−22.33
7	−23.05	−22.74	−22.44	−22.14

a) $C_{Zn}=1\times10^{-4}$ mol dm^{-3}. The solubility product of zinc 8-quinolinolate is $10^{-23.34}$.[33)]

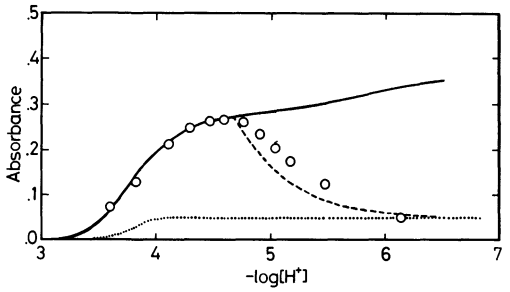

Fig. 7. Plot of absorbance vs. $-\log[H^+]$ in Zn^{2+}-ClO_4^--chloroform system after prolonged shaking. $C_{Zn}=1\times10^{-4}$ mol dm^{-3}. $C_{Hq}=0.06$ mol dm^{-3}. Solvent: chloroform. Solid line: calculated curve by considering all the equilibria except precipitation of $Mq_2 \cdot H_2O$. Broken and dotted lines: calculated curves by considering all the equilibria including the precipitation in ClO_4^- and SO_4^{2-} systems, respectively.

tation reaction are attained rapidly and Znq_2 becomes supersaturated in aqueous phase. Then $Znq_2 \cdot 2H_2O$ starts precipitating slowly with shifting other equilibria until the precipitation equilibrium holds.

When the precipitation equilibrium of $Znq_2 \cdot 2H_2O$ as well as extraction equilibria is included in the consideration, the calculated value given by a broken line well explains the experimental points. More pronounced decrease in Zn^{2+}-SO_4^{2-}-chloroform system shown by a dotted line is explained by the absence of species extracted as an ion-pair.

Crystal Structure of $Ni_2q_4(Hq)_2 \cdot H_2O \cdot C_6H_6$. The atomic coordinates and isotropic thermal parameters are listed in Table 4, and the atomic-numbering system is presented in Fig. 8. The atoms of water and benzene are represented by O(600) and C(701)—C(706), respectively.

Two crystallographically independent nickel atoms are surrounded by three bidentate ligands with facial and meridional configurations about their oxygen atoms. These two octahedra are joined by the two strong hydrogen bonds, O(11)···O(411) [2.44(1) Å] and O(111)···O(311) [2.41(1) Å], to form the binuclear unit as shown in Fig. 8. The direction of the hydrogen bonds on the oxygen atoms is reasonable: 125 for Ni(1)-O(11)-O(411), 121 for Ni(1)-O(111)-O(311), 128 for Ni(2)-O(311)-O(111) and 124° for Ni(2)-O(411)-O(11). The two equivalent units related by a center of symmetry are linked by the hydrogen bonds between the respective O(211) atoms and the water molecules, 2.93(1) and 2.81(1) Å. Only O(511) does not form any

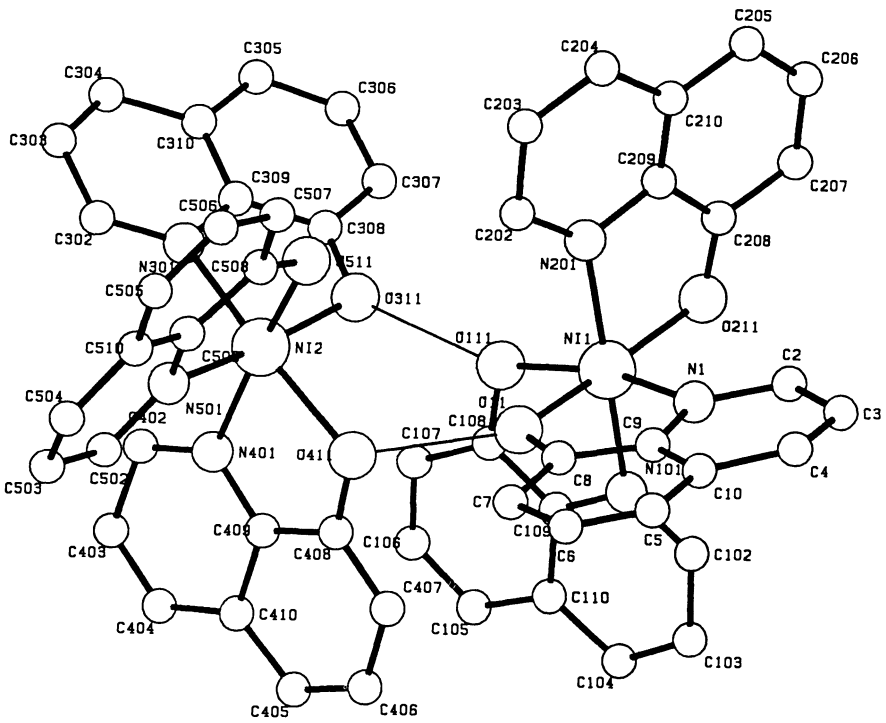

Fig. 8. Perspective drawing of binuclear structure of $Ni_2q_4(Hq)_2$.

Table 4. Fractional Coordinates ($\times 10^4$) and Isotropic Temperature Factors ($B_{eq}/Å^2 \times 10$) with e.s.d. Values in Parentheses for $Ni_2q_4(Hq)_2 \cdot H_2O \cdot C_6H_6$

Atom	x	y	z	B_{eq} or B[a)]	Atom	x	y	z	B_{eq} or B[a)]
Ni(1)	1007(1)	6966(1)	7042(1)	31(1)	C(304)	6286(5)	4472(6)	9343(6)	46(2)
N(1)	−187(4)	8019(4)	7530(4)	39(2)	C(305)	4982(6)	3656(5)	8198(6)	45(2)
C(2)	−1131(5)	7962(6)	7397(7)	53(3)	C(306)	4159(6)	3709(5)	7601(6)	45(2)
C(3)	−1880(6)	8746(7)	7786(8)	66(4)	C(307)	3681(5)	4526(5)	7446(5)	41(2)
C(4)	−1619(6)	9574(6)	8300(8)	64(3)	C(308)	4085(4)	5315(4)	7907(5)	31(2)
C(5)	−313(7)	10511(6)	8985(8)	67(3)	C(309)	4971(4)	5288(4)	8537(5)	29(2)
C(6)	641(9)	10543(6)	9082(8)	78(4)	C(310)	5426(5)	4452(5)	8697(5)	39(2)
C(7)	1410(7)	9726(5)	8683(6)	53(3)	O(311)	3693(3)	6131(3)	7812(3)	37(1)
C(8)	1108(5)	8889(4)	8180(5)	37(2)	N(401)	5247(4)	7019(4)	7281(4)	36(2)
C(9)	68(5)	8859(5)	8064(5)	41(2)	C(402)	6134(6)	6543(6)	7019(7)	52(3)
C(10)	−616(6)	9679(6)	8463(6)	55(3)	C(403)	6626(6)	6525(6)	6102(7)	58(3)
O(11)	1715(3)	8094(3)	7780(4)	38(1)	C(404)	6155(7)	7006(6)	5506(7)	59(3)
N(101)	1072(4)	7060(4)	5540(4)	36(2)	C(405)	4684(7)	8032(6)	5171(7)	61(3)
C(102)	413(6)	7498(6)	5045(6)	50(3)	C(406)	3755(8)	8503(6)	5466(7)	63(3)
C(103)	574(7)	7582(7)	4053(7)	63(3)	C(407)	3309(6)	8505(5)	6383(6)	50(3)
C(104)	1466(7)	7172(6)	3582(6)	57(3)	C(408)	3847(5)	8017(4)	6998(5)	36(2)
C(105)	3157(6)	6262(7)	3675(6)	60(3)	C(409)	4764(5)	7522(4)	6685(5)	37(2)
C(106)	3783(5)	5822(7)	4218(6)	59(3)	C(410)	5210(6)	7533(5)	5749(6)	47(2)
C(107)	3559(5)	5764(5)	5188(6)	48(2)	O(411)	3492(3)	8013(3)	7908(4)	38(1)
C(108)	2650(4)	6159(4)	5615(5)	33(2)	N(501)	5130(4)	8243(4)	9609(5)	43(2)
C(109)	1960(4)	6642(4)	5061(5)	32(2)	C(502)	5867(7)	8575(6)	9375(8)	62(3)
C(110)	2199(5)	6686(5)	4085(5)	43(2)	C(503)	6209(8)	9342(7)	10111(8)	68(4)
O(111)	2352(3)	6147(3)	6547(3)	34(1)	C(504)	5821(8)	9715(6)	11093(9)	70(4)
N(201)	1009(4)	6701(4)	8443(4)	36(2)	C(505)	4625(7)	9730(6)	12408(7)	63(3)
C(202)	1507(6)	7034(5)	9366(6)	46(2)	C(506))	3854(8)	9342(8)	12575(7)	72(3)
C(203)	1252(6)	6924(6)	10305(6)	52(3)	C(507)	3516(6)	8576(5)	11759(6)	52(3)
C(204)	494(7)	6477(6)	10291(7)	54(3)	C(508)	3937(5)	8227(5)	10752(5)	40(2)
C(205)	−779(7)	5601(7)	9227(7)	61(3)	C(509)	4726(5)	8623(4)	10585(5)	39(2)
C(206)	−1199(6)	5233(6)	8202(8)	60(3)	C(510)	5039(6)	9379(5)	11390(7)	56(3)
C(207)	−897(6)	5339(6)	7310(7)	52(3)	O(511)	3635(3)	7544(3)	9954(4)	42(2)
C(208)	−152(5)	5823(5)	7368(5)	39(2)	O(600)	1236(4)	4234(4)	5120(5)	64(2)
C(209)	293(5)	6211(5)	8402(5)	37(2)	C(701)	8043(10)	7349(10)	3712(12)	104(4)
C(210)	−6(6)	6087(5)	9310(6)	48(3)	C(702)	7388(12)	8157(11)	4014(13)	115(4)
O(211)	163(3)	5974(3)	6553(3)	42(2)	C(703)	7078(12)	8552(11)	3248(13)	112(4)
Ni(2)	4457(1)	7177(1)	8626(1)	31(1)	C(704)	7405(10)	8161(10)	2316(12)	103(4)
N(301)	5342(4)	6088(4)	8971(4)	38(2)	C(705)	7965(12)	7353(12)	1972(13)	117(4)
C(302)	6157(5)	6080(6)	9589(6)	45(2)	C(706)	8341(12)	6935(11)	2632(13)	113(4)
C(303)	6629(5)	5267(6)	9761(6)	49(3)					

a) Equivalent isotropic temperature factors for Ni(1)—O(600) were estimated as $B_{eq} = 4/3 \sum_i \sum_j \beta_{ij} \mathbf{a}_i \cdot \mathbf{a}_j$. For C(701)—C(706), isotropic ones, B, were used.

hydrogen bond.

The interatomic distances between Ni and O are 2.095(6), 2.064(5), 2.030(5), 2.063(5), 2.110(6), and 2.034(6) Å for O(11)—O(511). Oxygen atoms participating in the strong hydrogen bonds lie more distant from a nickel atom than those completely deprotonated. The Ni-N distances range from 2.057(7) to 2.098(7) Å, their average value being 2.074 Å. The bond lengths and angles in the ligand part are all comparable for the six ligands and reasonable compared with those of metal complexes with 8-quinolinol already reported.

The benzene molecules lie more than 3.35 Å apart from the metal complex and water molecules, the atoms of which undergo large thermal motion (B=10.3—11.7 Å^2). The average bond lengths and angles are 1.34 Å [1.26(3)—1.42(2) Å] and 120° [117(2)—125(2)°], respectively.

The structure of the conjugate acid complex, $Ni_2q_3(Hq)_3X$ ($X=I_3^-$ or ClO_4^-), is different in that there are three hydrogen bonds and only facial configuration about their oxygen atoms. But there is essential similarity that hydrogen atoms of free 8-quinolinol are located deep in the large hydrophobic structure.

The dimeric species can have the same structure also in the organic solvents.

References

1) J. Stary, "Critical Evaluation of Equilibrium Constants Involving 8-Hydroxyquinoline and Its Metal Chelates," IUPAC, Pergamon (1979).

2) J. Stary, *Anal. Chim. Acta*, **28**, 132 (1963).

3) N. M. Kuzmin and Yu. A. Zolotov, *Zh. Neorg. Khim.*, **11**. 2316 (1966).

4) S. Oki, *Anal. Chim. Acta*, **50**, 465 (1970).

5) H. Akaiwa, H. Kawamoto and T. Saito, *Nippon Kagaku Zasshi*, **92**, 1156 (1971).

6) E. Sekido and K. Fujita, *Bull. Chem. Soc. Jpn.*, **49**, 3073 (1976).
7) A. T. Rane and K. S. Bhatki, *Can. J. Chem.*, **57**, 580 (1979).
8) P. Guesnet and D. Bauer, *J. Chem. Research(s)*, **1981**, 127.
9) S. Oki, *Anal. Chim. Acta*, **49**, 455 (1970).
10) S. Oki and I. Terada, *Anal. Chim. Acta*, **66**, 201 (1973).
11) S. Oki and I. Terada, *Anal. Chim. Acta*, **69**, 220 (1974).
12) K. S. Bhatki, A. T. Rane, and H. Freiser, *Indian J. Chem.*, **15A**, 983 (1977).
13) G. K. Schweitzer, R. B. Neel, and F. R. Clifford, *Anal. Chim. Acta*, **33**, 514 (1965).
14) F. Chou, Q. Fernando, and H. Freiser, *Anal. Chem.*, **37**, 361 (1965).
15) S. Oki, *Bunseki Kagaku*, **18**, 822 (1969).
16) S. Oki and I. Terada, *Anal. Chim. Acta*, **61**, 49 (1972).
17) H. E. Hellwege and G. K. Schweitzer, *Anal. Chim. Acta*, **28**, 236 (1963).
18) H. E. Hellwege and G. K. Schweitzer, *J. Inorg. Nucl. Chem.*, **27**, 99 (1965).
19) E. Sekido, *Nippon Kagaku Zasshi*, **80**, 383 (1959).
20) E. Sekido, Y. Yoshimura, and Y. Masuda, *J. Inorg. Nucl. Chem.* **38**, 1183 (1976).
21) a) H. Kiriyama, T. Fukuda, Y. Yamagata, and E. Sekido, *Acta Crystallogr.*, **C41**, 1441 (1985); b) H. Kiriyama, Y. Yamagata, K. Yonetani, and E. Sekido, *Acta Crystallogr.*, **C42**, 56 (1986).
22) A. Yuchi, S. Yamada, and M. Tanaka, *Anal. Chim. Acta*, **115**, 301 (1980).
23) Y. Yamamoto, K. Kotsuji, S. Kinuwaki, and H. Sawamura, *Nippon Kagaku Zasshi*, **85**, 869 (1964).
24) A. T. Rane and V. V. Ravi, *Indian J. Chem.*, **21A**, 311 (1982).
25) A. T. Rane and V. V. Ravi, *Spectrochim. Acta*, **38A**, 937 (1982).
26) Tables of structure factors, bond lengths and angles, and thermal parameters are kept in the office of the Chemical Society of Japan (Document No. 8706).
27) *MULTAN84:* P. Main. A Computer Program for the Automatic Solution of Crystal Structures from X-Ray Diffraction Data. Univ. of York, England (1984). PLUTO: W. D. S. Motherwell and W. Clegg. Program for Plotting Molecular and Crystal Structures. Univ. of Cambridge (1978). XPACK86 SHIONOGI: H. Nakai, T. Sato and M. Shiro. Program Pack for X-ray Structure Analysis. Shionogi Res. Lab. (1986).
28) The following values are used for the calculation.[1] $\log K_D$=2.58, $\log K_1$=9.64, and $\log K_2$=4.96.
29) M. Tanaka and T. Niinomi, *J. Inorg. Nucl. Chem.*, **27**, 431 (1965).
30) L. G. Sillen, *Acta Chem. Scand.*, **10**, 186 (1956).
31) T. Omori, T. Wakahayashi, S. Oki, and N. Suzuki, *J. Inorg. Nucl. Chem.*, **26**, 2265 (1964).
32) H. Yamada and M. Tanaka, *J. Inorg. Nucl. Chem.*, **38**, 1501 (1976).
33) J. Fresco and H. Freiser, *Talanta*, **8**, 693 (1961).

 © 1986 The Chemical Society of Japan Bull. Chem. Soc. Jpn., 59, 3855—3858 (1986)

Solvent Extraction of Copper(II) with Lipoic Acid in Benzene. Evidence for the Preferential Coordination of Carboxylate

Hiromichi YAMADA,* Toshiyuki OKUDA, Yukio FUJII,
Masateru MIZUTA, and Motoharu TANAKA†
Faculty of Engineering, Gifu University, 1-1 Yanagido, Gifu 501-11
†Laboratory of Analytical Chemistry, Faculty of Science, Nagoya University, Chikusa-ku, Nagoya 464
(Received June 11, 1986)

The extraction of copper(II) was carried out with lipoic acid in benzene at 25 °C and at a constant ionic strength in the aqueous phase: 0.1 mol dm^{-3} ($NaNO_3$). The partition constant, $K_{D,HA}$ of lipoic acid between benzene and water, and the dimerization constant, $K_{2,HA}$ of lipoic acid in benzene were determined: log $K_{D,HA}$=1.17 and log $K_{2,HA}$=2.51. The dimeric copper(II) lipoate is responsible for the extraction:

$$2Cu^{2+} + 3(HA)_{2,o} \overset{K_{ex(22)}}{\rightleftharpoons} (Cu_2A_4(HA)_2)_o + 4H^+$$

with the extraction constant, log $K_{ex(22)}$=−11.00. It was proved that lipoate ion coordinates to copper(II) with the carboxylate group without a remarkable participation of the disulfide moiety in the coordination.

1,2-Dithiolane-3-pentanoic acid (lipoic acid) is widely distributed in nature in a protein-bound form, and it is an essential component of "multienzyme" units which catalyze the oxidative decarboxylation of α-keto acids. Lipoic acid has two different binding sites, that is, the carboxyl group and the disulfide linkage. The carboxylate group is known to coordinate dominantly to the biologically important metal ions, while the disulfide group is also anticipated to participate in coordination. These coordination tendencies of two groups in solution were summarized and discussed in relation to their biochemical significance by Sigel.[1,2]

Recently, some synthetic applications of lipoic acid derivatives to organic reactions utilizing their redox function were reported.[3]

It is well-known that the copper(II) carboxylates have a dimeric structure not only in the crystalline state but also in various nonsolvating solvents. It has been previously reported that only the dimeric copper(II) decanoate involving free decanoic acids, $Cu_2A_4(HA)_2$ is responsible for the extraction of copper(II) with decanoic acid in some nonsolvating solvents such as benzene and carbon tetrachloride.[4]

The present paper describes the results of the extraction of copper(II) with lipoic acid in benzene. Comparing the present results with those obtained in the extraction of copper(II) decanoate in benzene, it was found that the carboxylate group preferentially coordinates to copper(II) ions in the dimeric copper(II) lipoate, that is, the disulfide group does not participate in complex formation.

Experimental

Reagents. Lipoic Acid: Reagent grade DL-α-lipoic acid (purity: over 98%) was dissolved in benzene just before its use.

Benzene: Reagent grade benzene was washed successively with concentrated sulfuric acid, with dilute potassium hydroxide solution, with dilute perchloric acid solution, and then with distilled water. All other reagents were reagent grade and used without further purification.

Procedure. Partition was carried out in a bath thermostated at 25.0±0.2 °C. 15 cm^3 each of the aqueous and organic phases were contacted in a brown centrifuge tube. Ionic strength of the aqueous phase was adjusted to 0.1 mol dm^{-3} with sodium nitrate. Shaking for about 1 h was found sufficient for complete equilibration. After centrifugation, the aqueous phase was immediately separated from the organic phase. And then, hydrogen-ion concentration of the aqueous phase was measured with 1.00×10^{-2} mol dm^{-3} nitric acid solution (ionic strength 0.1 mol dm^{-3}) as a standard. The measured pH values were corrected for the apparent liquid junction potential. The concentration of copper in the aqueous phase was determined complexiметrically, with 4-(2-thiazolylazo)resorcinol (TAR) as an indicator.[5] In the partition of lipoic acid between water and benzene, the concentration of lipoic acid in the aqueous phase was determined by potentiometric titration. An absorption maximum at 330 nm of DL-lipoic acid was used for the determination of the lower concentration of lipoic acid in the aqueous phase.

Apparatus. For mechanical shaking in a thermostat, Taiyo Incubator M-100^N (Taiyokagaku-Kogyo Co., Tokyo) was used. The pH measurements and potentiometric titrations were carried out with a Horiba pH Analyzer F-80 (Horiba Seisakusho Ltd., Kyoto). Spectrophotometric determination was performed on a UVIDEC-430A Double Beam Spectrophotometer (Japan Spectroscopic Co. Ltd., Tokyo). KNAUER Vapor Pressure Osmometer (KNAUER Ltd., Berlin, West Germany) was used for the determination of dimerization constant of lipoic acid in benzene. A Swing Type Centrifuge Model CD-50SR (Tomy Seiko Co. Ltd., Tokyo) was used for centrifugation.

Results and Discussion

Distribution of Lipoic Acid. In studying the extraction of a metal ion with a carboxylic acid, it is indispensable to have information about the partition of the carboxylic acid between the aqueous and organic phases. Then in the present extraction system the following equilibria should be considered.

(a) The dissociation of lipoic acid HA in the aque-

ous phase:

$$HA + H_2O \rightleftharpoons H_3O^+ + A^-$$

with the dissociation constant,

$$K_a = [H_3O^+][A^-][HA]^{-1}. \quad (1)$$

(b) The partition of lipoic acid between benzene and the aqueous phase:

$$(HA)_w \rightleftharpoons (HA)_o$$

where the subscripts w and o refer to the aqueous and benzene phases, respectively. The partition constant is defined as

$$K_{D,HA} = [HA]_o[HA]_w^{-1}. \quad (2)$$

(c) The dimerization of lipoic acid in the organic phase:

$$2(HA)_o \rightleftharpoons (HA)_{2,o}$$

with $(HA)_{2,o}$ denoting the dimeric lipoic acid in the organic phase, and the dimerization constant defined as

$$K_{2,HA} = [(HA)_2]_o[HA]_o^{-2}. \quad (3)$$

Then, the distribution ratio of lipoic acid between benzene and water is written as follows:

$$D = C_{HA,o}C_{HA,w}^{-1}$$
$$= K_{D,HA}(1+2K_{2,HA}K_{D,HA}[HA]_w)(1+K_a[H^+]^{-1})^{-1}. \quad (4)$$

In the lower pH region where the dissociation of lipoic acid in the aqueous phase is negligible, that is, $1 \gg K_a/[H^+]$, Eq. 4 can be rewritten as follows:

$$D = K_{D,HA} + 2K_{2,HA}K_{D,HA}^2[HA]_w \quad (5)$$

As shown in Eq. 5, a linear relationship between the distribution ratio D of lipoic acid and the concentration of unionized lipoic acid in the aqueous phase is expected to hold. Benzene solutions of lipoic acid ranging from 0.025 to 0.7 mol dm^{-3} were equilibrated at 25 °C with 0.01 mol dm^{-3} nitric acid (I=0.1 mol dm^{-3} H, $NaNO_3$). From the results obtained, the dimerization and partition constants of lipoic acid were determined by the least-squares method according to Eq. 5: $\log K_{2,HA}$=2.51 and $\log K_{D,HA}$=1.17, respectively.

On the other hand, the dimerization constant of lipoic acid in benzene is obtained by the vapor pressure osmometry: $\log K_{2,HA}$=2.52. This value is in good agreement with that determined by the partition experiment. Thus the dimeric lipoic acid prevails in benzene.

Extraction of Copper(II) with Lipoic Acid. If a j-merized copper(II) lipoate $Cu_jA_{2j}(HA)_a$ (HA: lipoic acid) is responsible for the extraction, the extraction equilibrium can be expressed as follows:[4]

$$jCu^{2+} + 0.5(2j+a)(HA)_{2,o} \rightleftharpoons (Cu_jA_{2j}(HA)_a)_o + 2jH^+$$

with the extraction constant defined as

$$K_{ex(ja)} = [Cu_jA_{2j}(HA)_a]_o[H^+]^{2j}[Cu^{2+}]^{-j}[(HA)_2]_o^{-0.5(2j+a)}. \quad (6)$$

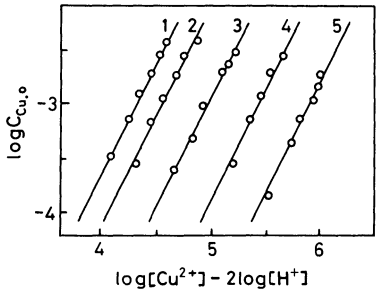

Fig. 1. Determination of the degree of polymerization of copper(II) lipoate. C_{HA}; No. 1: 1.0, No. 2: 0.7, No. 3: 0.4, No. 4: 0.2, No. 5: 0.1 mol dm^{-3}. Solid lines are the straight lines with a slope of 2.

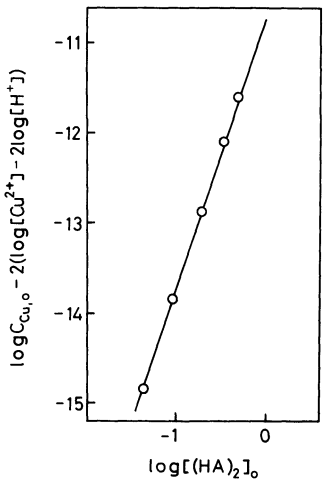

Fig. 2. Determination of the number of lipoic acid molecules involved in the dimeric copper(II) lipoate. Solid line is the straight line with a slope of 3.

When only $Cu_jA_{2j}(HA)_a$ is extracted into benzene, the total concentration of copper(II) in benzene is written as follows:

$$C_{Cu,o} = j[Cu_jA_{2j}(HA)_a]_o$$
$$= jK_{ex(ja)}[Cu^{2+}]^j[H^+]^{-2j}[(HA)_2]_o^{0.5(2j+a)} \quad (7)$$

which is rewritten as a logarithmic form:

$$\log C_{Cu,o} = j(\log[Cu^{2+}] - 2\log[H^+])$$
$$+ 0.5(2j+a)\log[(HA)_2]_o + \log j + \log K_{ex(ja)}. \quad (8)$$

According to Eq. 8, the degree of polymerization of copper(II) lipoate can be obtained from the slope of a plot of $\log C_{Cu,o}$ vs. $(\log[Cu^{2+}]-2\log[H^+])$ at a constant $[(HA)_2]_o$. The plot shown in Fig. 1, falls along the straight line with a slope of 2: only the dimeric copper(II) lipoate is responsible for the extraction under the present experimental conditions.

The number of lipoic acid molecules involved in the dimeric copper(II) lipoate is given by the slope of a plot of $\{\log C_{Cu,o}-2(\log[Cu^{2+}]-2\log[H^+])\}$ vs. $\log[(HA)_2]_o$. As shown in Fig. 2, the plot falls on the straight line with a slope of 3.0, that is, $(4+a)/2=3$ or $a=2$. Consequently, only $Cu_2A_4(HA)_2$ is extracted in

the present extraction system as in the extraction of copper(II) with decanoic acid in benzene. The extraction constant of the dimeric copper(II) lipoate, $K_{ex(22)}$ can be calculated from the intercept of the plot in Fig. 2. Then the extraction equilibrium for copper(II) lipoate can be expressed as follows:

$$2Cu^{2+} + 3(HA)_{2,o} \overset{K_{ex(22)}}{\rightleftharpoons} (Cu_2A_4(HA)_2)_o + 4H^+$$

with

$$\log K_{ex(22)} = -11.00.$$

Comparison of Lipoic with Decanoic Acids. Both the dissociation constant in the aqueous phase and the dimerization constant in benzene of lipoic acid are similar to those of decanoic acid. This would be attributed to the shielding of the electron-withdrawing effect of the disulfide group by four methylene groups.

The smaller partition constant of lipoic acid than that of decanoic acid suggests that the 1,2-dithiolane ring is more hydrophilic than the pentyl group. The extraction constant stated above is formulated as

$$K_{ex(22)} = K_{D,Cu_2A_4(HA)_2} K_{D,HA}^{-6} K_{2,HA}^{-3} \beta_{Cu_2A_4(HA)_2} K_a^4 \quad (9)$$

where $K_{D,Cu_2A_4(HA)_2}$ and $\beta_{Cu_2A_4(HA)_2}$ denote the partition constant of $Cu_2A_4(HA)_2$ between benzene and water and the overall formation constant of this complex in the aqueous phase defined, respectively as follows:

$$(Cu_2A_4(HA)_2)_w \rightleftharpoons (Cu_2A_4(HA)_2)_o$$

with

$$K_{D,Cu_2A_4(HA)_2} = [Cu_2A_4(HA)_2]_o [Cu_2A_4(HA)_2]_w^{-1}$$

and

$$2Cu^{2+} + 4A^- + 2(HA)_w \rightleftharpoons (Cu_2A_4(HA)_2)_w$$

with

$$\beta_{Cu_2A_4(HA)_2} = [Cu_2A_4(HA)_2]_w [Cu^{2+}]^{-2} [A^-]^{-4} [HA]_w^{-2}.$$

From the additive nature of the molar cohesive energy and molar volume of ligand in a complex, the partition constant of a complex MA_n can be approximately correlated to that of the ligand HA as follows[6]: $K_{D,MA_n} \simeq K_{D,HA}^n$. Since a similar relation, namely, $K_{D,Cu_2A_4(HA)_2} \simeq K_{D,HA}^6$ can be presumed to hold also for the present extraction system, the overall formation constant can be approximated as follows:

$$\beta_{Cu_2A_4(HA)_2} \simeq K_{ex(22)} K_{2,HA}^3 K_a^{-4}. \quad (10)$$

On the other hand, taking into account the electrostriction of ligands in the complex, that is, $V_{Cu_2A_4(HA)_2} = 6 \times 0.95 V_{HA}$, the partition constant of $Cu_2A_4(HA)_2$ can be approximated as follows: $\log K_{D,Cu_2A_4(HA)_2} \simeq 5.7 \log K_{D,HA}$. Then, the overall formation constant, $\beta_{Cu_2A_4(HA)_2}$ can be calculated by the following relation:

$$\beta_{Cu_2A_4(HA)_2} \simeq K_{ex(22)} K_{D,HA}^{0.3} K_{2,HA}^3 K_a^{-4}. \quad (11)$$

The results for lipoic and decanoic acids obtained from these relations are listed in Table 1 together with other constants. As can be seen from Table 1, the value of the overall formation constant of the dimeric copper(II) lipoate in the aqueous phase is close to that of the dimeric copper(II) decanoate. This suggests strongly that in the dimeric copper(II) lipoate the copper(II) ions coordinate not to the disulfide group, but to the carboxyl group of lipoic acid in the same manner as in the dimeric copper(II) decanoate.

Table 1. Comparison of Various Constants of Lipoic with Decanoic Acids

Constants	Lipoic Acid	Decanoic Acid
pK_a	4.85[a]	4.92[c,d]
$\log K_{D,HA}$	1.17[b]	2.80[c,d]
$\log K_{2,HA}$	2.51	2.41[d]
$\log K_{ex(22)}$	−11.00[b]	−11.36[c,e]
$\log \beta_{Cu_2A_4(HA)_2}$	15.93[b,f]	15.55[c,f]
	(16.28)[g]	(16.39)[g]

a) The value is estimated from the data in 50% (v/v) dioxane-water mixture.[2] b) Ionic strength 0.1 mol dm^{-3} (NO_3^-). c) Ionic strength 0.1 mol dm^{-3} (ClO_4^-). d) Ref. 7. e) Ref. 4. f) Calculated by Eq. 10. g) The values in the parentheses are evaluated by taking into account the electro-striction of ligands in the complex (Eq. 11).

In the visible region, the spectrum of copper(II) lipoate in benzene grossly resembles that of copper(II) decanoate in the presence of an excess of the respective acid, that is, copper(II) lipoate shows an absorption peak at 680 nm assigned to a so-called metal-ligand interaction. In the UV region, the spectra for copper(II) lipoate and decanoate in benzene differ from each other, because of the difference in the spectra between lipoic and decanoic acids. This result will also support that copper(II) ions coordinate to the carboxylate group in the dimeric copper(II) lipoate.

In general, soft metal ions like silver(I) ion have a tendency to coordinate to the disulfide moiety. Then we have attempted to study the extraction of silver(I) ion with lipoic acid in carbon tetrachloride. Disappointingly, silver(I) ion could not be extracted, and a white precipitate formed which would be a decomposition product of lipoate. It can be presumed that coordination of silver(I) ion to the disulfide moiety causes cleavage of the disulfide link.

To conclude, lipoate ion coordinates to copper(II) with the carboxylate group without a remarkable participation of the disulfide moiety in the coordination.

References

1) H. Sigel, *Angew. Chem. Int. Ed. Engl.*, **21**, 389 (1982).
2) H. Sigel, B. Prijs, D. B. McCormick, and J. C. H. Shin, *Arch. Biochem. Biophys.*, **187**, 208 (1978).
3) Y. Nanbu, T. Endo, and M. Okawara, *J. Syn. Org. Chem. Jpn.*, **43**, 680 (1985).
4) H. Yamada and M. Tanaka, *J. Inorg. Nucl. Chem.*, **38**, 1501 (1976).
5) H. Wada and G. Nakagawa, *Bunseki Kagaku*, **14**, 29

(1965).
6) M. Tanaka, Solvent Extr. Proc. Int. Solvent Extr. Conf., (1971), p. 16.
7) M. Tanaka, N. Nakasuka, and S. Sasane, *J. Inorg. Nucl. Chem.*, **31**, 2591 (1969).

S-Bridged Polynuclear Complexes. I. Selective Formation and Crystal Structure of (+)$^{CD}_{600}$-Bis[tris(L-cysteinato-*N,S*)cobaltate(III)-*μ*-*S*,*μ*-*S'*,*μ*-*S''*]cobalt(III) Nitrate Pentahydrate

Ken-ichi Okamoto,* Sen-ichi Aizawa, Takumi Konno, Hisahiko Einaga,[1] and Jinsai Hidaka
Department of Chemistry, University of Tsukuba, Sakura, Ibaraki 305
(Received June 18, 1986)

The crystal structure and the absolute configuration of the selectively formed title isomer, (+)$^{CD}_{600}$-[Co{Co(L-cys-*N,S*)$_3$}$_2$](NO$_3$)$_2$·5H$_2$O,[2] have been determined by X-ray diffraction. In the (+)$^{CD}_{600}$ isomer, the six L-cysteinates coordinate through the nitrogen and sulfur atoms to give two terminal [Co(L-cys-*N,S*)$_3$] moieties. The central cobalt atom spans the six sulfur atoms in these terminals to form a trinuclear structure. The (+)$^{CD}_{600}$ isomer takes selectively a $\Lambda_{LLL}\Lambda_{LLL}$ configuration, in which both of the two terminals have a Λ_{LLL}-*fac*(S) configuration, and the six sulfur donor atoms take an *R* one. The L-cysteinate chelate rings take a lel conformation along the C_3 axis and the carboxyl or carboxylato groups take the axial orientations forming the intramolecular hydrogen bonds. The (−)$^{CD}_{600}$ isomer is assigned to the $\Delta_{LLL}\Delta_{LLL}$ configuration on the basis of the electronic absorption, CD, and ^{13}C NMR spectral behaviors. The selective formation for each of the (+)$^{CD}_{600}$ and (−)$^{CD}_{600}$ isomers is discussed in relation to their reaction conditions.

2-Aminoethanetholate, aet, has a propensity to form the S-bridged polynuclear metal complexes, which have been investigated by the stereochemical and spectrochemical interests,[3-9] or by the relevance to the catalytic and biological systems.[7,8] The trinuclear cobalt(III) complexes with 2-aminoethanethiolate, [Co{Co(aet)$_3$}$_2$]$^{3+}$, have been prepared by the reaction of *fac*(S)-[Co(aet)$_3$] with Co(II) or Co(III),[4] and resolved into the optically active isomers, ΛΛ and ΔΔ.[5] In this work, the reaction of Δ_{LLL}-*fac*(S)-tris(L-cysteinato-*N,S*)cobaltate(III), Δ_{LLL}-*fac*(S)-[Co(L-cys-*N,S*)$_3$]$^{3-}$,[10-12] which has a similar framework to *fac*(S)-[Co(aet)$_3$], with Co(II) or Co(III) was investigated. This starting Δ_{LLL}-*fac*(S) complex has been selectively formed because of the preferred lel conformation of the L-cysteinate chelate rings with the equatorial carboxylato groups.[11,12] This paper deals with the stereochemistry of the (+)$^{CD}_{600}$ and (−)$^{CD}_{600}$ isomers formed selectively by the reaction mentioned above, and with the X-ray crystal analysis of the (+)$^{CD}_{600}$ isomer. Namely, each of the (+)$^{CD}_{600}$- and (−)$^{CD}_{600}$-bis[tris(L-cysteinato-*N,S*)cobaltate(III)-*μ*-*S*,*μ*-*S'*,*μ*-*S''*]cobaltate(III) isomers, (+)$^{CD}_{600}$- and (−)$^{CD}_{600}$-[Co{Co(L-cys-*N,S*)$_3$}$_2$]$^{3-}$,[2] was selectively prepared. The crystal structure of (+)$^{CD}_{600}$-[Co{Co(L-cys-*N,S*)$_3$}$_2$](NO$_3$)$_2$·5H$_2$O,[2] which is crystallized from a 4 mol dm^{-3} nitric acid, is established by the X-ray diffraction study. The absolute configurations of the two terminal [Co(L-cys-*N,S*)$_3$] moieties and the six sulfur donor atoms were also determined. The electronic absorption, CD, and ^{13}C NMR spectral behaviors of the (+)$^{CD}_{600}$ and (−)$^{CD}_{600}$ isomers are discussed in relation to their geometrical and absolute configurations.

Experimental

1) Preparation of Complexes. a) **Δ_{LLL}-*fac*(S)-Potassium Tris(L-cysteinato-*N,S*)cobaltate(III): Δ_{LLL}-*fac*(S)-K$_3$[Co(L-cys-*N,S*)$_3$]·9H$_2$O·0.5KCl.** This complex was prepared by the method of Schubert,[10] and the Δ_{LLL}-*fac*(S) isomer formed selectively.[11,12] Found: C, 14.77; H, 4.50; N, 5.74%. Calcd for $C_9H_{33}N_3O_{15}Cl_{0.5}S_3K_{3.5}Co$: C, 14.75; H, 4.54; N, 5.73%.

b) (+)$^{CD}_{600}$-Potassium Bis[tris(L-cysteinato-*N,S*)cobaltate(III)-*μ*-S,*μ*-S',*μ*-S'']cobaltate(III): (+)$^{CD}_{600}$-K$_3$[Co{Co(L-cys-*N,S*)$_3$}$_2$]·9H$_2$O.[2] To a solution containing an excess amount (0.9g, 3.78 mmol) of CoCl$_2$·6H$_2$O in 25 cm^3 of water was added a solution containing 1.0 g (1.36 mmol) of Δ_{LLL}-*fac*(S)-K$_3$[Co(L-cys-*N,S*)$_3$]·9H$_2$O·0.5KCl in 10 cm^3 of water. The color of the solution turned immediately from deep green to deep brownish green. The solution (ca. pH 9) was stirred at room temperature for 10 min. To this was added a large amount of ethanol in an ice bath. The resultant complex was recrystallized twice from water by adding ethanol in an ice bath, and washed with ethanol and ether. It was found, from the QAE-Sephadex A-25 column chromatographic technique and the absorption and CD spectral measurements, that the reaction solution contained only (+)$^{CD}_{600}$-[Co{Co(L-cys-*N,S*)$_3$}$_2$]$^{3-}$. Found: C, 18.25; H, 4.04; N, 7.29%. Calcd for $C_{18}H_{48}N_6O_{21}S_6K_3Co_3$: C, 18.46; H, 4.13; N, 7.17%.

This isomer was also prepared by the following procedure. To a solution containing 0.01 g of (−)$^{CD}_{600}$-K$_3$[Co{Co(L-cys-*N,S*)$_3$}$_2$]·6.5H$_2$O described in **1c**) (vide infra) in 10 cm^3 of water was added 1.0 g of zinc powder. After the solution was allowed to stand at room temperature for a week, the reaction solution was filtered to remove the zinc powder. The filtrate showed the identical absorption and CD spectra to (+)$^{CD}_{600}$-[Co{Co(L-cys-*N,S*)$_3$}$_2$]$^{3-}$.

The single crystal of the (+)$^{CD}_{600}$ isomer, which was used for the X-ray crystal structure analysis, was obtained as follows. (+)$^{CD}_{600}$-K$_3$[Co{Co(L-cys-*N,S*)$_3$}$_2$]·9H$_2$O was recrystallized from an 1 mol dm^{-3} warm nitric acid (ca. 40 °C). Then the crystals obtained were dissolved in a 4 mol dm^{-3} warm nitric acid (ca. 40 °C) again, and stood at room temperature for 3 d. The crystals which appeared as nitrate salt, (+)$^{CD}_{600}$-[Co{Co(L-cys-*N,S*)$_3$}$_2$](NO$_3$)$_2$·5H$_2$O,[2] were collected by filtration.

c) (−)$^{CD}_{600}$-Potassium Bis[tris(L-cysteinato-*N,S*)cobaltate(III)-*μ*-S,*μ*-S',*μ*-S'']cobaltate(III): (−)$^{CD}_{600}$-K$_3$[Co{Co(L-cys-*N,S*)$_3$}$_2$]·6.5H$_2$O. This complex was prepared selectively by a procedure similar to that used for the (+)$^{CD}_{600}$ isomer described in **1b**), using [CoCl(NH$_3$)$_5$]Cl$_2$ (0.2 g, 0.80 mmol) instead of an excess amount of CoCl$_2$·6H$_2$O. It was found, from the same manner as in **1b**), that the reaction solution contained only (−)$^{CD}_{600}$-[Co{Co(L-cys-*N,S*)$_3$}$_2$]$^{3-}$. Found: C, 19.12; H, 3.91; N, 7.49%. Calcd for $C_{18}H_{43}N_6O_{18.5}S_6K_3Co_3$: C, 19.20; H, 3.85; N,

Table 1. Position and Thermal Parameters

Atom	x	y	z	B_{eq}/Å$^{2a)}$	Atom	x	y	z	B_{eq}/Å$^{2a)}$
Co1	0.7500	0.5000	0.5000	1.61	C3	0.6760(8)	0.7241(10)	0.2879(11)	2.30
Co2	0.5181(2)	0.5888(2)	0.4850(2)	1.66	C4	0.8760(8)	0.5905(10)	0.8353(11)	2.75
Co3	0.2875(1)	0.6698(1)	0.4791(2)	1.70	C5	0.9047(7)	0.4649(12)	0.9222(12)	3.04
S1	0.6718(2)	0.7159(3)	0.4816(3)	1.85	C6	0.7497(8)	0.6306(10)	0.8177(11)	2.79
S2	0.6566(2)	0.4935(3)	0.6685(3)	2.06	C7	0.7070(8)	0.1907(9)	0.3855(11)	2.47
S3	0.5786(2)	0.4263(3)	0.3210(3)	1.99	C8	0.7310(8)	0.1645(9)	0.2332(11)	2.69
S4	0.3744(2)	0.4628(3)	0.5102(4)	2.20	C9	0.5849(8)	0.2462(9)	0.3704(12)	2.74
S5	0.3683(2)	0.6700(3)	0.2905(3)	1.85	C10	0.1559(8)	0.4068(9)	0.3032(12)	2.48
S6	0.4598(2)	0.7621(3)	0.6379(3)	2.22	C11	0.1080(7)	0.3434(9)	0.4148(12)	2.61
N1	0.8220(7)	0.5356(8)	0.3393(10)	1.94	C12	0.2855(8)	0.3652(10)	0.3237(13)	3.04
N2	0.8925(6)	0.5674(8)	0.6825(9)	2.15	C13	0.2449(7)	0.9125(9)	0.3050(11)	2.35
N3	0.7964(7)	0.2974(9)	0.4968(11)	2.43	C14	0.1462(9)	0.8685(11)	0.1520(13)	2.77
N4	0.1445(6)	0.5632(8)	0.3295(10)	2.13	C15	0.3677(8)	0.8630(9)	0.2958(11)	2.30
N5	0.2198(7)	0.8605(9)	0.4329(10)	2.33	C16	0.3226(9)	0.7405(13)	0.8120(11)	3.54
N6	0.2367(8)	0.6751(11)	0.6641(11)	2.98	C17	0.3044(10)	0.9031(14)	0.8346(13)	3.98
O1	0.9876(6)	0.7413(8)	0.4818(9)	3.02	C18	0.4494(9)	0.7017(14)	0.8127(12)	3.78
O2	0.8696(6)	0.9140(7)	0.3927(10)	3.92	NA	0.7074(10)	0.0562(11)	0.7847(14)	4.65
O3	0.9224(8)	0.3423(8)	0.8405(9)	3.63	NB	0.2022(12)	0.4353(18)	0.8983(21)	7.49
O4	0.9103(7)	0.4756(9)	1.0567(9)	4.41	OA1	0.7659(12)	0.0542(13)	0.6950(13)	7.93
O5	0.8145(8)	0.2154(10)	0.2102(11)	4.57	OA2	0.7388(11)	0.9859(10)	0.8815(12)	6.67
O6	0.6548(7)	0.0734(8)	0.1293(9)	3.89	OA3	0.6216(13)	0.1384(17)	0.7613(26)	13.04
O7	0.0520(7)	0.4129(8)	0.4864(10)	3.44	OB1	0.2682(13)	0.4112(19)	0.8103(17)	11.36
O8	0.1269(7)	0.2107(8)	0.4168(13)	5.11	OB2	0.2046(21)	0.3300(25)	0.9622(20)	17.02
O9	0.1607(6)	0.9103(9)	0.0346(9)	4.21	OB3	0.1406(13)	0.5423(25)	0.8983(23)	13.37
O10	0.0570(7)	0.8099(9)	0.1490(9)	3.98	OW1	0.9662(7)	0.1533(9)	0.0328(10)	4.67
O11	0.2208(9)	0.9547(9)	0.7505(10)	4.17	OW2	0.9744(7)	0.8813(8)	0.7793(9)	4.05
O12	0.3896(8)	0.9633(13)	0.9532(11)	6.89	OW3	0.3743(10)	0.1261(11)	0.6080(14)	7.55
C1	0.7984(8)	0.6797(9)	0.2905(11)	2.36	OW4	0.0251(7)	0.1082(9)	0.5696(11)	4.65
C2	0.8921(8)	0.7883(9)	0.3981(10)	2.13	OW5	0.3753(17)	0.2264(19)	−0.0003(20)	14.75

a) B_{eq} is the equivalent isotropic temperature factors defined by Hamilton.[20]

7.49%.

2) General Data. The electronic absorption spectra were recorded with JASCO UVIDEC-1 and UVIDEC-610 spectrophotometers, and the CD spectra with a JASCO J-20 spectropolarimeter. The infrared spectra were recorded with a JASCO IRA-2 infrared spectrophotometer using the KBr disk method. The ^{13}C NMR spectra were recorded on a JEOL JNM-FX-100 or -FX-90Q NMR spectrometer at the probe temperature in D_2O. Sodium 2,2-dimethyl-2-silapentane-5-sulfonate was used as an internal reference. The pH of the aqueous solution was measured with a Hitachi-Horiba pH meter, model F7-SS, equipped with a glass and saturated calomel electrodes. The X-ray analysis calculations were carried out on a FACOM M-380 computer at the University of Tsukuba.

3) X-Ray Characterization. Unit cell parameters and intensity data for the single crystal (ca. 0.10×0.15×0.40 mm^3) were measured on a Rigaku-denki four-circle diffractometer (AFC-5) with graphite-monochromatized Mo $K\alpha$ radiation. The unit cell parameters were determined by least-squares refinement based on 19 reflections. Crystal data: $[Co\{Co(L\text{-}cys)_3\}_2](NO_3)_2\cdot 5H_2O=Co_3S_6O_{23}N_8C_{18}H_{45}$, triclinic, space group $P\bar{1}$, M.W.=1110.76, a=12.087(8), b=9.541(4), c=9.214(4) Å, α=99.09(5), β=109.32(4), γ=87.86(5)°, V=990(1) Å^3, D_m=1.86 g cm^{-3} (by the flotation), D_x=1.863 g cm^{-3}, Z=1, and μ(Mo $K\alpha$)=1.692 mm^{-1}.

Intensity data were collected by a ω–2θ scan technique up to 2θ=50° with a scan rate of 3° min^{-1}. The intensity data were converted to F_o data in the usual manner. Absorption corrections were not applied. A total of 3677 independent reflections with $|F_o|>3\sigma(|F_o|)$ of the measured 3741 reflections were considered as 'observed' and used for the structure analysis.

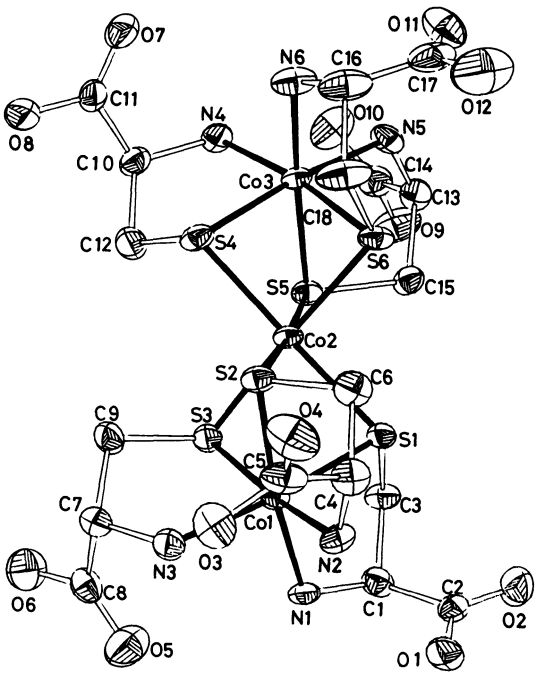

Fig. 1. Perspective view of $(+)^{CD}_{600}$-$[Co\{Co(L\text{-}cys\text{-}N,S)_3\}_2]^{2+}$ ion,[2] with the numbering scheme.

4) Determination of the Crystal Structure. The positions of three cobalt atoms were obtained from a three-

Table 2. Interatomic Distances and Bond Angles (with e.s.d.'s)

(a) Bond distances (l/Å)

Co1-S1	2.242(3)	Co1-S2	2.210(4)
Co1-S3	2.234(3)	Co1-N1	2.024(10)
Co1-N2	2.008(7)	Co1-N3	1.991(8)
Co2-S1	2.267(4)	Co2-S2	2.233(4)
Co2-S3	2.265(4)	Co2-S4	2.242(4)
Co2-S5	2.296(3)	Co2-S6	2.246(4)
Co3-S4	2.216(3)	Co3-S5	2.257(4)
Co3-S6	2.229(3)	Co3-N4	2.008(7)
Co3-N5	2.017(9)	Co3-N6	1.987(11)
S1-C3	1.816(11)	S2-C6	1.840(9)
S3-C9	1.838(10)	S4-C12	1.823(10)
S5-C15	1.834(9)	S6-C18	1.837(13)
N1-C1	1.502(13)	N2-C4	1.468(14)
N3-C7	1.508(11)	N4-C10	1.482(12)
N5-C13	1.469(15)	N6-C16	1.472(12)
O1-C2	1.269(11)	O2-C2	1.225(11)
O3-C5	1.338(13)	O4-C5	1.207(14)
O5-C8	1.228(16)	O6-C8	1.317(11)
O7-C11	1.207(14)	O8-C11	1.281(12)
O9-C14	1.275(16)	O10-C14	1.224(15)
O11-C17	1.195(14)	O12-C17	1.299(13)
C1-C2	1.536(11)	C1-C3	1.517(13)
C4-C5	1.512(16)	C4-C6	1.521(14)
C7-C8	1.507(16)	C7-C9	1.519(13)
C10-C11	1.540(17)	C10-C12	1.559(13)
C13-C14	1.524(12)	C13-C15	1.566(13)
C16-C17	1.550(18)	C16-C18	1.562(15)
NA-OA1	1.251(21)	NA-OA2	1.156(16)
NA-OA3	1.257(19)	NB-OB1	1.306(26)
NB-OB2	1.237(30)	NB-OB3	1.241(26)

(b) Bond angles (ϕ/°)

S1-Co1-S2	84.1(1)	S1-Co1-S3	83.8(1)
S1-Co1-N1	86.7(2)	S1-Co1-N2	94.9(2)
S1-Co1-N3	171.7(2)	S2-Co1-S3	84.6(1)
S2-Co1-N1	170.8(2)	S2-Co1-N2	87.5(3)
S2-Co1-N3	94.0(3)	S3-Co1-N1	93.4(2)
S3-Co1-N2	172.1(3)	S3-Co1-N3	87.9(2)
N1-Co1-N2	94.4(3)	N1-Co1-N3	94.9(4)
N2-Co1-N3	93.1(3)	S1-Co2-S2	83.0(1)
S1-Co2-S3	82.5(1)	S1-Co2-S4	175.1(1)
S1-Co2-S5	100.7(1)	S1-Co2-S6	94.5(1)
S2-Co2-S3	83.4(1)	S2-Co2-S4	92.7(1)
S2-Co2-S5	175.6(1)	S2-Co2-S6	99.2(1)
S3-Co2-S4	99.6(1)	S3-Co2-S5	94.6(1)
S3-Co2-S6	175.8(2)	S4-Co2-S5	83.7(1)
S4-Co2-S6	83.7(1)	S5-Co2-S6	83.1(1)
S4-Co3-S5	85.2(1)	S4-Co3-S6	84.7(1)
S4-Co3-N4	88.1(2)	S4-Co3-N5	172.9(3)
S4-Co3-N6	92.8(3)	S5-Co3-S6	84.4(1)
S5-Co3-N4	92.0(3)	S5-Co3-N5	87.8(3)
S5-Co3-N6	172.7(2)	S6-Co3-N4	172.2(2)
S6-Co3-N5	93.6(2)	S6-Co3-N6	88.5(3)
N4-Co3-N5	93.2(3)	N4-Co3-N6	94.9(4)
N5-Co3-N6	94.1(4)	Co1-S1-Co2	78.8(1)
Co1-S1-C3	96.3(3)	Co2-S1-C3	114.3(3)
Co1-S2-Co2	80.3(1)	Co1-S2-C6	95.0(4)
Co2-S2-C6	111.7(3)	Co1-S3-Co2	79.1(1)
Co1-S3-C9	95.4(3)	Co2-S3-C9	112.7(4)
Co2-S4-Co3	79.5(1)	Co2-S4-C12	111.5(4)
Co3-S4-C12	96.6(3)	Co2-S5-Co3	77.5(1)
Co2-S5-C15	114.8(3)	Co3-S5-C15	96.4(4)
Co2-S6-Co3	79.1(1)	Co2-S6-C18	112.1(4)
Co3-S6-C18	95.6(3)	Co1-N1-C1	114.5(6)
Co1-N2-C4	115.8(6)	Co1-N3-C7	115.9(6)
Co3-N4-C10	115.2(5)	Co3-N5-C13	115.1(6)
Co3-N6-C16	114.6(8)	N1-C1-C2	110.9(7)
N1-C1-C3	109.1(8)	C2-C1-C3	111.9(7)
O1-C2-O2	125.2(8)	O1-C2-C1	117.8(8)
O2-C2-C1	116.9(7)	S1-C3-C1	105.9(6)
N2-C4-C5	114.9(8)	N2-C4-C6	110.1(7)
C5-C4-C6	107.8(9)	O3-C5-O4	122.6(11)
O3-C5-C4	115.9(9)	O4-C5-C4	121.5(10)
S2-C6-C4	106.4(6)	N3-C7-C8	108.2(9)
N3-C7-C9	109.0(7)	C8-C7-C9	113.3(8)
O5-C8-O6	123.8(10)	O5-C8-C7	124.7(8)
O6-C8-C7	111.5(9)	S3-C9-C7	107.5(7)
N4-C10-C11	108.6(8)	N4-C10-C12	110.8(7)
C11-C10-C12	112.4(8)	O7-C11-O8	123.8(12)
O7-C11-C10	121.9(9)	O8-C11-C10	114.2(10)
S4-C12-C10	106.3(7)	N5-C13-C14	110.2(8)
N5-C13-C15	111.5(7)	C14-C13-C15	112.3(8)
O9-C14-O10	124.3(9)	O9-C14-C13	114.3(9)
O10-C14-C13	121.0(11)	S5-C15-C13	105.8(6)
N6-C16-C17	109.2(8)	N6-C16-C18	109.7(9)
C17-C16-C18	112.2(10)	O11-C17-O12	129.7(12)
O11-C17-C16	120.9(9)	O12-C17-C16	109.4(10)
S6-C18-C16	104.6(7)	OA1-NA-OA2	117.3(13)
OA1-NA-OA3	115.6(16)	OA2-NA-OA3	127.1(18)
OB1-NB-OB2	108.3(18)	OB1-NB-OB3	122.1(21)
OB2-NB-OB3	129.1(23)		

dimensional Patterson function. Difference Fourier maps, based on the three cobalt positions, revealed all the non-hydrogen atoms. The structure was refined by a full-matrix least-squares refinement of the positional and anisotropic thermal parameters of all the non-hydrogen atoms (program RFINE by L. W. Finger was used). The neutral atomic scattering factors for all the non-hydrogen atoms were taken from the literature.[13] The final R and R_w values were 0.044 and 0.057, respectively. The absolute configuration was determined on the basis of the known configuration of L-cysteinates.[14]

The final atomic parameters are given in Table 1. A list of structure factors (Table A) and anisotropic thermal parameters of non-hydrogen atoms (Table B) are kept at the Chemical Society of Japan as Document No. 8704.

Results and Discussion

Description of the Structure. A perspective drawing of the complex cation, $(+)^{CD}_{600}$-[Co{Co(L-cys-*N*,*S*)$_3$}$_2$]$^{2+}$,[2] is given in Fig. 1, together with a numbering scheme. The bond lengths and angles (with their standard deviations) in the complex cation and the nitrate anions are summarized in Table 2. Three cobalt atoms are aligned at short intervals (Co1-Co2=2.863(3) and Co2-Co3=2.849(3) Å, Co1-Co2-Co3=177.66(9)°); thus the complex cation takes a trinuclear structure. The coordination geometries around each cobalt atom are approximately octahedral. All the six L-cysteinates coordinate to two cobalt atoms (Co1 and Co3) through the nitrogen and sulfur atoms, and they form two ter-

minal [Co(L-cys-N,S)$_3$] moieties. The Col and Co2 atoms or the Co2 and Co3 ones are bridged by the sulfur atoms in the L-cysteinates, namely, the central cobalt atom, Co2, is surrounded by the six sulfur atoms.

The absolute configuration of the $(+)^{CD}_{600}$ isomer in the crystal could be confirmed on the basis of the known configuration, R, of the asymmetric carbon atom in the coordinated L-cysteinate.[14] Both of the two terminal [Co(L-cys-N,S)$_3$] moieties in the $(+)^{CD}_{600}$ isomer have Λ configuration and all the six sulfur donor atoms, which become chiral by coordination, have R one. This indicates that the reaction with $CoCl_2 \cdot 6H_2O$ causes an inversion of the absolute configuration of the starting complex, Δ_{LLL}-*fac*(S)-[Co(L-cys-N,S)$_3$]$^{3-}$, to give selectively two terminal Λ_{LLL}-*fac*(S)-[Co(L-cys-N,S)$_3$] moieties.

The average bond lengths of [Co{Co(L-cys-N,S)$_3$}$_2$]$^{2+}$ are quite similar to those of [Co{Co(aet)$_3$}$_2$]$^{3+}$;[9] Col-S and Co3-S (2.226(3) Å), Co2-S (2.258(4) Å), Co-N (2.006(9) Å), S-C (1.831(10) Å), N-C (1.484(13) Å), and C-C (1.534(14) Å). A similar trend was also observed for the bond angles; Col-S-Co2 and Co3-S-Co2 (79.0 (1)°), S-Col-S and S-Co3-S (84.5(1)°), S-Co2-S (83.2 (1)°), N-Col-N and N-Co3-N (94.1(4)°), S-Col-N and S-Co3-N (87.8(3)°), Col-S-C and Co3-S-C (95.9 (3)°), Co2-S-C (112.9(4)°), S-C-C (106.1(7)°), and C-C-N (110.2(8)°).[9] The acute S-Co2-S angle and the Co2-S distance indicate that the central cobalt atom, Co2, is trigonally distorted from regular octahedron and its distortion has the effect of lengthening the molecule along the C_3 axis through the Col, Co2, and Co3 atoms. In the terminal [Co(L-cys-N,S)$_3$] moieties, the average bond lengths and angles (given above) indicate the compressions of the S1-S2-S3 and S4-S5-S6 faces and the concomitant expansions of the N1-N2-N3 and N4-N5-N6 ones. The average bond lengths of Col-N and Co3-N in the present complex seem to be longer than those of the cobalt(III) complexes with the amino carboxylate ligands.[15-17]

The crystal structure consists of the complex cation, two nitrate anions, and five water molecules, as shown in Fig. 2. In the crystal, the hydrogen bonds are recognized between the carboxyl or carboxylato groups and water molecules: e.g., OW1-O3 (2.644(13) Å), OW1-O5 (2.825(15) Å), OW2-O1 (2.905(12) Å), OW2-O9 (2.649(9) Å), OW3-O8 (3.079(13) Å), OW4-O2 (2.627(10) Å), OW4-O8 (2.475(16) Å), and OW5-O12 (2.488(22) Å). Similar O-O bond distances to the short hydrogen bonds in this work (2.475—2.649 Å) have also been observed for the hydrogen bis(*p*-methylbenzoate) anions.[18] Taking account of the facts that only two nitrate anions exist in the unit cell and the five carboxyl groups are connected strongly to the water molecules (2.475—2.649 Å), it may be considered that the five carboxyl groups in the L-cysteinates are protonated and the one carboxylato group is not. This is supported from the result that the IR spectrum of the present $(+)^{CD}_{600}$-$\Lambda_{LLL}\Lambda_{LLL}$ isomer exhibits a strong band

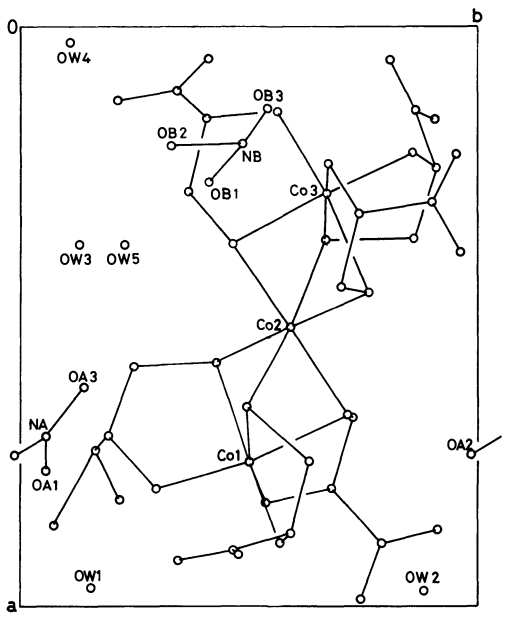

Fig. 2. The crystal packing diagram of the complex.

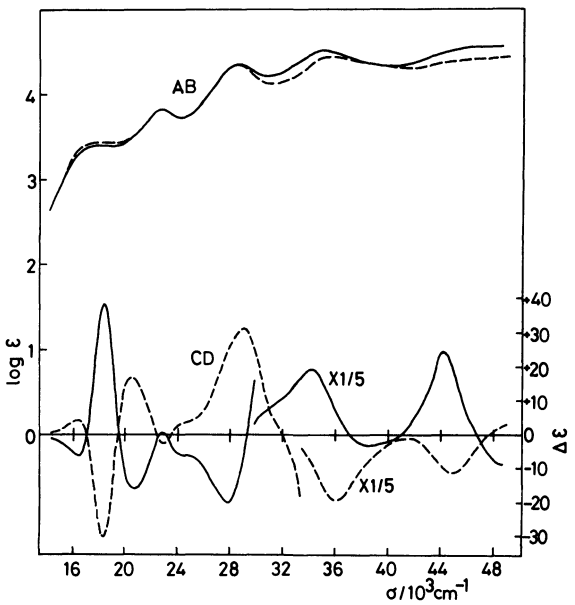

Fig. 3. Absorption and CD spectra of [Co{Co(L-cys-N,S)$_3$}$_2$]$^{3-}$;[2] the $(-)^{CD}_{600}$ isomer (——) and the $(+)^{CD}_{600}$ one (---).

at ca. 1720 cm^{-1} due to the COOH group and a week band at ca. 1625 cm^{-1} due to the COO$^-$ group.[19]

In [Co{Co(L-cys-N,S)$_3$}$_2$]$^{2+}$,[2] all of the bond distances between the oxygen atoms in the carboxyl or carboxylato groups and the nitrogen atoms in the adjacent amine groups range from 2.919 to 3.260 Å (average 3.080 Å). This indicates that they are also hydrogen bonds and incidentally, all the six L-cysteinate chelate rings take the lel conformations along the C_3 axis, which is accompanied by the axial orientations of the carboxyl or carboxylato groups.

Formation of Isomers. Three isomers, $\Lambda_{LLL}\Lambda_{LLL}$, $\Lambda_{LLL}\Delta_{LLL}$, and $\Delta_{LLL}\Delta_{LLL}$, are possible for the trinuclear

Table 3. Absorption and CD Data of $(+)^{CD}_{600}$- and $(-)^{CD}_{600}$-[Co{Co(L-cys-*N*,*S*)$_3$}$_2$]$^{3-}$

Complex	Absorption maxima $\sigma/10^3$ cm^{-1} ($\log\varepsilon$/mol^{-1} dm^3 cm^{-1})	CD extrema $\sigma/10^3$ cm^{-1} ($\Delta\varepsilon$/mol^{-1} dm^3 cm^{-1})
$(+)^{CD}_{600}$-[Co{Co(L-cys-*N*,*S*)$_3$}$_2$]$^{3-}$	17.80 (3.43)	16.23 (+4.4)
	22.53 (3.83)	18.40 (−30.0)
	28.60 (4.35)	20.43 (+17.1)
	35.53 (4.44)	23.00 (−2.8)
	45.5 (4.41 sh)	24.5 (+3.8 sh)
		29.07 (+31.8)
		36.13 (−96.5)
		44.93 (−60.5)
$(-)^{CD}_{600}$-[Co{Co(L-cys-*N*,*S*)$_3$}$_2$]$^{3-}$	17.70 (3.40)	16.39 (−6.3)
	22.62 (3.83)	18.45 (+38.7)
	28.57 (4.35)	20.62 (−15.9)
	35.09 (4.51)	22.78 (+0.7)
	47.39 (4.57)	24.09 (−6.3)
		27.86 (−19.7)
		34.25 (+94.0)
		38.53 (−15.0)
		44.05 (+95.9)

Sh denotes a shoulder.

complex, [Co{Co(L-cys-*N*,*S*)$_3$}$_2$]$^{3-}$,[2] with respect to the absolute configuration of two terminal [Co(L-cys-*N*,*S*)$_3$] moieties. The $(-)^{CD}_{600}$ isomer exhibits a quite similar absorption spectral behavior over the whole region to the $(+)^{CD}_{600}$-$\Lambda_{LLL}\Lambda_{LLL}$ isomer as shown in Fig. 3 and Table 3. Furthermore, each of the present two isomers exhibits three ^{13}C NMR resonance lines (39.0, 64.1, and 179.3 ppm for the $(+)^{CD}_{600}$-$\Lambda_{LLL}\Lambda_{LLL}$ isomer and 38.6, 67.1, and 178.3 ppm for the $(-)^{CD}_{600}$ isomer) due to the methylene, methine, and carboxylato carbon atoms in each of the six L-cysteinate ligands (Fig. 4). The ^{13}C NMR spectral behaviors point out that the present $(-)^{CD}_{600}$ isomer takes $\Delta_{l.l.l}\Delta_{l.l.l.}$ configuration having D_3 symmetry, because the $(+)^{CD}_{600}$-$\Lambda_{LLL}\Lambda_{LLL}$ isomer has approximately D_3 symmetry in the crystal (Fig. 1) but the $\Lambda_{LLL}\Delta_{LLL}$ isomer has lower than or equal to a C_3 symmetry. This assignment is supported by the fact that the $(-)^{CD}_{600}$ isomer exhibits almost enantiomeric CD spectrum over the whole region to that of $(+)^{CD}_{600}$-$\Delta_{LLL}\Delta_{LLL}$-[Co{Co(L-cys-*N*,*S*)$_3$}$_2$]$^{3-}$ (Fig. 3 and Table 3). Accordingly, the $(-)^{CD}_{600}$ isomer can be assigned to $\Delta_{LLL}\Delta_{LLL}$-[Co{Co(L-cys-*N*,*S*)$_3$}$_2$]$^{3-}$. The absorption and CD spectra of the $(-)^{CD}_{600}$-$\Delta_{LLL}\Delta_{LLL}$ isomer are also in good agreement with those of $\Delta\Delta$-[Co{Co(aet)$_3$}$_2$]$^{3+}$ whose absolute configuration was assigned on the basis of the CD spectral behavior by Brubaker and Douglas.[5] The similarity between these CD spectra suggests that the CD contribution due to the chiral carbon atom, *R*(*C*), of the coordinated L-cysteinate is minor.

The reaction of Δ_{LLL}-*fac*(*S*)-[Co(L-cys-*N*,*S*)$_3$]$^{3-}$ with [CoCl(NH$_3$)$_5$]Cl$_2$ gave only $(-)^{CD}_{600}$-$\Delta_{LLL}\Delta_{LLL}$-[Co{Co(L-cys-*N*,*S*)$_3$}$_2$]$^{3-}$. Namely, the reaction with Co(III) proceeds with retention of the absolute configuration of the starting $\Delta_{l.l.l.}$-*fac*(*S*) complex to give two terminal Δ_{LLL}-*fac*(*S*)-[Co(L-cys-*N*,*S*)$_3$] moieties. In contrast with

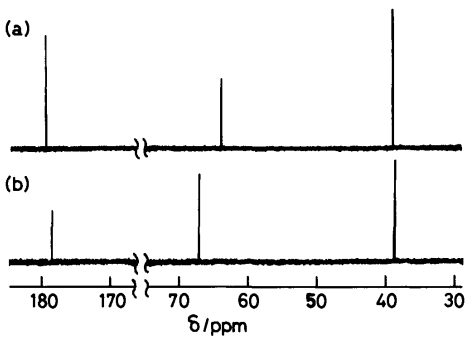

Fig. 4. ^{13}C NMR spectra of [Co{Co(L-cys-*N*,*S*)$_3$}$_2$]$^{3-}$;[2] (a) the $(+)^{CD}_{600}$ isomer and (b) the $(-)^{CD}_{600}$ one.

this reaction, the reaction (pH≈9) with an excess amount of CoCl$_2$ was accompanied by the inversion of the starting complex to give $(+)^{CD}_{600}$-$\Lambda_{l.l.l}\Lambda_{l.l.l.}$-[Co{Co(L-cys-*N*,*S*)$_3$}$_2$]$^{3-}$. Moreover, the inversion of the two terminals in the $(-)^{CD}_{600}$-$\Delta_{LLL}\Delta_{LLL}$ isomer was also observed for its reaction solution with zinc powder. These facts suggest that the Co(II) ion relates catalytically to the inversion of the starting $\Delta_{l.l.l.}$-*fac*(*S*) complex and accelerates the formation of the $(+)^{CD}_{600}$-$\Lambda_{LLL}\Lambda_{LLL}$ isomer, i.e., bridging the sulfur donor atoms of the starting complex to Co(II) ion is favorable to the labilization and inversion of the terminals. Here, an intramolecular hydrogen bonding is accompanied by the inversion. Considering from the result of the X-ray analysis of the $(+)^{CD}_{600}$-$\Lambda_{LLL}\Lambda_{LLL}$ isomer (Fig. 1), it is probable for the $\Lambda_{LLL}\Lambda_{LLL}$ isomer that in the above reaction conditions (pH≈9), the hydrogen bonds are formed between the axial carboxylato groups regulated by the lel conformation of the N-S chelate rings and the adjacent amine protons. While, the model construction of the $\Delta_{LLL}\Delta_{LLL}$ isomer reveals that this isomer prefers to the lel conformation with the equa-

torial carboxylato groups (unfavorable orientation for the hydrogen bond formation) because of the repulsion between the carboxylato groups and the lone pairs of the adjacent sulfur donor atoms. The difference in the hydrogen bond formation is probably related to the selective formation of the $(+)^{CD}_{600}$-$\Lambda_{l.l.l.}\Lambda_{l.l.l.}$ isomer.

This work was supported by a Grant-in-Aid for Scientific Research No. 60470043 from the ministry of Education, Science and Culture.

References

1) Present address: Institute of Materials Science, University of Tsukuba, Sakura, Ibaraki 305.

2) In this paper, we showed with the superscript of the chemical formula whether the L-cysteinates in the trinuclear complex take the carboxyl or carboxylato groups (they are protonated or not); that is, the five carboxyl groups are protonated in case the superscript is 2+, and all the carboxylato groups are deprotonated in case it is 3−.

3) D. C. Jicha and D. H. Busch, *Inorg. Chem.*, **1**, 872, 878 (1962).

4) D. H. Busch and D. C. Jicha, *Inorg. Chem.*, **1**, 884 (1962).

5) G. R. Brubaker and B. E. Douglas, *Inorg. Chem.*, **6**, 1562 (1967).

6) R. E. DeSimone, T. Ontko, L. Wardman, and E. L. Blinn, *Inorg. Chem.*, **14**, 1313 (1975).

7) E. L. Blinn, P. Bulter, K. M. Chapman, and S. Harris, *Inorg. Chim. Acta*, **24**, 139 (1977).

8) P. R. Bulter and E. L. Blinn, *Inorg. Chem.*, **17**, 2037 (1978).

9) M. J. Heeg, E. L. Blinn, and E. Deutsch, *Inorg. Chem.*, **24**, 1118 (1985).

10) M. P. Schubert, *J. Am. Chem. Soc.*, **55**, 3336 (1933).

11) R. D. Gillard and R. Maskill, *Chem. Commun.*, **1968**, 160.

12) M. Kita, K. Yamanari, and Y. Shimura, *Bull. Chem. Soc. Jpn.*, **55**, 2873 (1982).

13) "International Tables for X-Ray Crystallography," Kynoch Press, Birmingham (1974), Vol. IV.

14) J. P. Greenstein and M. Wintz, "Chemistry of the Amino Acids," John Wiley & Sons (1961), Vol. 3, Chap. 24.

15) K. Okamoto, T. Isago, M. Ohmasa, and J. Hidaka, *Bull. Chem. Soc. Jpn.*, **55**, 1077 (1982).

16) K. Okamoto, K. Wakayama, H. Einaga, M. Ohmasa, and J. Hidaka, *Bull. Chem. Soc. Jpn.*, **55**, 3473 (1982).

17) K. Okamoto, M. Suzuki, H. Einaga, and J. Hidaka, *Bull. Chem. Soc. Jpn.*, **56**, 3513 (1983).

18) S. Misaki, S. Kashino, and M. Haisa, *Bull. Chem. Soc. Jpn.*, **59**, 1059 (1986).

19) R. M. Silverstein, G. C. Bassler, and T. C. Morrill, "Spectrometric Identification of Organic Compounds," 3rd ed., John Wiley & Sons (1974), Chap. 3.

20) W. C. Hamilton, *Acta Crystallogr.*, **12**, 609 (1959).

 © 1986 The Chemical Society of Japan Bull. Chem. Soc. Jpn., 59, 3865—3869 (1986)

Structural Effects in the Reactions of Diazoalkanes with 2,3-Dichloro-5,6-dicyanobenzoquinone

Takumi OSHIMA* and Toshikazu NAGAI
Institute of Chemistry, College of General Education, Osaka University, Toyonaka, Osaka 560
(Received May 6, 1986)

2,3-Dichloro-5,6-dicyanobenzoquinone (DDQ) reacted with diazoethane to give stereoisomeric bicyclic diones (**3**, isomer ratio=3.4) arising from dipolar addition to the C=C bond of DDQ. DDQ reacted with phenyldiazomethane to afford also stereoisomeric bicyclic diones (**7**) in the ratio of 5 : 1, together with stilbenes (**8**). On the other hand, DDQ gave the (ethenyloxy)benzene derivative (**14**) with 1-phenyldiazoethane. The formation of **8** and **14** was interpreted by considering the participation of 1 : 1 betaines resulting from addition to the C=O bond. The added methanol captures the betaines, thus giving rise to dimethyl acetals of benzaldehyde and acetophenone, along with 2,3-dichloro-5,6-dicyanohydroquinone. These reactivities of DDQ were discussed in comparison with those of chloranil.

As one area of the addition chemistry of quinones, comprehensive studies have been made of reactions with diazoalkanes from the synthetic and mechanistic points of view.[1] Quinones behave as dipolarophiles[2] as a result of their conjugated C=C and C=O bonds, while diazoalkanes behave as 1,3-dipoles.[3] A number of reports have been concerned with the reaction of diazomethane because of its commonness and high reactivity. Diazomethane tends to add to the conjugated C=C bonds of 1,4-benzoquinone[4] and its mono-,[5] di-,[5] and trichlorinated analogues[6] to yield pyrazolines. On the other hand, the C=O bonds become active when the C=C bonds are blocked with the bulky halogens, as is exemplified in the formation of the oxirane derivative in the reaction with chloranil.[7] Recently, we extended the reaction of chloranil to phenyldiazomethane,[8] diphenyldiazomethane,[9] and 1-phenyldiazoethane,[10] and found that these diazoalkanes similarly add to the C=O bond, but variously provide stilbenes and spirooxetane, and poly(tetrachlorohydroquinone benzhydrylether), and 1-alkoxy-4-ethenyloxy-2,3,5,6-tetrachlorobenzene, respectively.

On the other hand, the reaction of diazomethane with 2,3-dichloro-5,6-dicyanobenzoquinone (DDQ) has been reported to afford bicyclic dione (**2**),[11] in contrast to the reaction with chloranil. However, we found in a previous investigation[12] that DDQ reacts with diphenyldiazomethane in a manner similar to that of chloranil. In view of the general interest in the reactions of diazoalkanes with quinones, it is desirable to extend the DDQ reaction to other diazoalkanes of structural types not previously investigated. In this paper, reactions of DDQ with diazoethane, phenyldiazomethane, 1-phenyldiazoethane, were investigated in order to gain a better understanding of the structural effects on the reactivity of diazoalkanes and to compare the results with those obtained for the corresponding chloranil reactions.

Results and Discussion

Reaction with Diazoethane. Diazoethane (**1**) reacted with 2,3-dichloro-5,6-dicyanobenzoquinone (DDQ) to provide the bicyclic dione (**3**, isomer ratio=3.4), in analogy with diazomethane,[11,13] together with a small amount of 2,3-dichloro-5,6-dicyanohydroquinone diethyl ether (**4**) (Scheme 1). In conformity with the

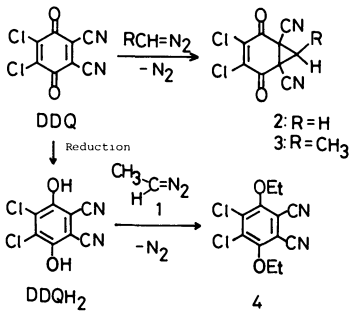

Scheme 1.

bicyclic dione structure, each isomer of **3** could be converted into the identical dimethoxycycloheptatriene derivative (**5b**) upon catalytic hydrogenation and the subsequent methylation (Scheme 2).

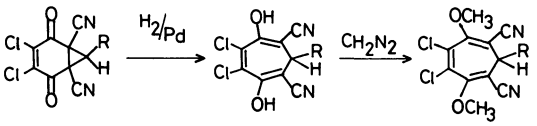

Scheme 2.

Though the ^{1}H NMR spectrum of the major isomer of **3** showed the methyl and cyclopropyl protons at a slightly higher field (0.1—0.2 ppm) than those of the minor one, it is not clear which of the two isomers corresponds to the exo or endo adduct, since both the carbonyl and cyano groups may be expected to exert magnetic anisotropy effects on the ethylidene moiety.[14] However, it may be suggested that the major **3** has an exo configuration on the basis of the estimated dihedral angles (θ) of the H-C-C-CN (134°) and H-C-C-CO (19°) fragments.[15] In fact, the fairly high isomer ratio appears to reflect the steric repulsion between the methyl group and the bulky quinone moiety.

A bicyclic dione **3** may be given by the dipolar addi-

tion of **1** to the cyano-substituted C=C bond and the subsequent release of nitrogen. Compound **4** is a usual product of the reaction of **1** and 2,3-dichloro-5,6-dicyanohydroquinone ($DDQH_2$), which indicates the reduction of DDQ during the reaction. Such a hydroquinone diether as **4** has already been obtained in a high yield by Eistert et al. in the reaction of **1** with chloranil.[16]

Unlike chloranil,[16] DDQ was found to react with **1** at the cyano-substituted C=C bond because of the reduced steric hindrance as well as the favorable LUMO energy for the dipolar addition.[17]

Reaction with Phenyldiazomethane. The reaction of DDQ with 1.6 equiv of phenyldiazomethane (**6**) mainly produced bicyclic diones (**7**, isomer ratio=5 : 1), together with stilbenes (**8**, cis/trans=0.8) (Scheme 3).

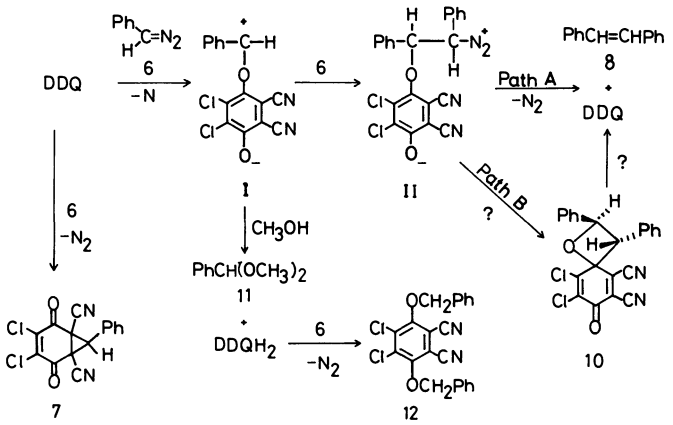

Scheme 3.

The structure of **7** was also established by the chemical conversion into the substituted cycloheptatriene (**9b**) (Scheme 2). The stereochemistry of **7** is unknown, but it is also likely that the major isomer is an exo adduct and that the much higher isomer ratio (=5) than in **3** is to be ascribed to the more enhanced steric repulsion between the phenyl group and the quinone moiety, by analogy with the case of **3**.

The formation of **8** can be explained by considering the participation of a 1 : 1 betaine intermediate, by analogy with our preceding reaction of **6** with chloranil.[8] According to the previous mechanism, the betaine I leads to the diazonium betaine(II) by the attack of another **6**, and subsequent El- and E2-type elimination (Path A) can afford **8**. On the other hand, intramolecular cyclization (Path B) is expected to build up spirooxetane (**10**). However, the DDQ reaction is somewhat different from the chloranil one in that the former gave no spirooxetane and provided more trans isomer for **8**, while the latter provided more *cis*-**8**. These phenomena may be ascribed mainly to the electronic effects of these two quinones.[18] The more electronegative DDQ moiety tends to destabilize II, thereby increasing the proportion of El elimination, mostly leading to *trans*-**8**. On the other hand, the predominant occurrence of E2-type elimination would result in the high cis to trans ratio of **8**, this is because of the steric reason mentioned previously for the chloranil reaction.[8] Moreover, the lack of spirooxetane in the present reaction must be due to its own instability, affected by the electronic factor, in the light of the relative bulkiness of these two quinones; the CN substituent of DDQ exerts less steric hindrance than the Cl substituent of chloranil.[19] Indeed, the spirooxetane of DDQ could not be obtained by the 3-h irradiation of a benzene solution (50 ml) of an equiv amount of DDQ (0.63 g, 2.8 mmol) and *trans*-**8** (0.50 g, 2.8 mmol) by using a high-pressure mercury lamp at 0 °C, though this photochemical method succeeded in providing a good yield of the *trans*-spirooxetane of chloranil.[8] Supporting the mechanistic explanation presented above, I reacted with added methanol to yield benzaldehyde dimethyl acetal (**11**) and $DDQH_2$. However, the dipolar addition to the C=C bond was not essentially affected, as is indicated by the 65% yield of **7**.

Reaction with 1-Phenyldiazoethane. The reaction of DDQ with 1-phenyldiazoethane (**13**) gave the (ethenyloxy)ethoxybenzene derivative (**14**, 92%) by a reaction sequence involving 1 : 1 betaine(III) formation, proton migration, and etherification with excess diazoalkane (Scheme 4). This reaction was accompanied

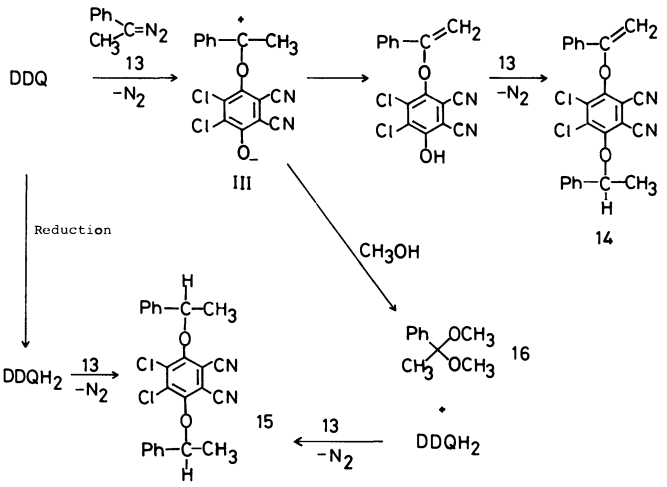

Scheme 4.

by a small amount of a product from **13** and $DDQH_2$, 2,3-dichloro-5,6-dicyanohydroquinone bis(α-methylbenzyl) ether (**15**), as in the case of diazoethane.

In contrast to phenyldiazomethane, neither bicyclic diones nor dimeric olefins were yielded in this case. The marked change in the reaction fashion must be caused by the additional methyl substituent on the diazo-carbon, which will serve to increase the steric repulsion both on the dipolar addition to the C=C bond and on the nucleophilic attack upon the cation center of III responsible for the formation of the bicyclic dione and dimeric olefin respectively. These situations resulted in the exclusive addition to the C=O bond and the following proton migration, just as in the chloranil reaction.[10] Expectedly, added methanol

Table 1. Reactivities of Diazoalkanes in the Reactions with DDQ and Chloranil[a)]

	CH_2N_2	CH_3CHN_2	$PhCHN_2$	$PhC(CH_3)N_2$	Ph_2CN_2
DDQ	C[b)]	C>R	C>O	O>R	O[c)]
Chloranil	O[d)]	R[e)]	O[f)]	O[g)]	O[h)]

a) C: C=C addition; O: C=O addition; R: Reduction. b) Ref. 11. c) Ref. 12. d) Ref. 7. e) Ref. 16. f) Ref. 8. g) Ref. 10. h) Ref. 9.

completely inhibited the proton migration and produced acetophenone dimethyl acetal (**16**) and $DDQH_2$.

In order to demonstrate that the reactions of diazoalkanes with DDQ are substantially controlled by the structural natures, we present again in the table the representative reaction features for a series of diazoalkanes in comparison with those of the comparable chloranil reactions.

Experimental

All the melting points were taken with a Laboratoty Devices Mel-Temp instrument and are uncorrected. The infrared spectra were recorded on a Hitachi 260-10 apparatus and on a Perkin Elmer 983 G spectrometer. The ^1H and ^{13}C NMR spectra were taken on a Varian EM 390 spectrometer and on a JEOL FX 90-Q spectrometer respectively. The mass spectral data were obtained with a Hitachi RMU 6E mass spectrometer.

Materials. The 2,3-dichloro-5,6-dicyanobenzoquinone (DDQ) was of commercial origin and was recrystallized from dichloromethane or chloroform. The diazoethane (**1**),[20] phenyldiazomethane (**6**),[21] and 1-phenyldiazoethane (**13**),[22] were prepared according to the procedure described in the literature. The oily **6** and **13** contained the corresponding azines formed by the spontaneous thermal decomposition in ca. 10 and 30% respectively, as detected in the ^1H NMR spectra. However, these azines remained unchanged when allowed to stand for 1 h with DDQ in benzene-d_6, as was confirmed by the NMR measurements. The benzene was refluxed over lithium aluminum hydride and was fractionated.

3,4-Dichloro-2,5-dioxo-7-methylbicyclo[4.1.0]hept-3-ene-1,6-dicarbonitrile (3) and 2,3-Dichloro-5,6-dicyanohydroquinone diethyl Ether (4). An ether solution of diazoethane was added, drop by drop, to a stirred solution of DDQ (800 mg, 3.52 mmol) in benzene (20 ml) at 25 °C until the deep orange-red color due to the CT band of DDQ and benzene disappeared. At that point, a crystalline precipitate was formed. After a further 1 h stirring, the precipitate was filtered off and washed with benzene (10 ml×3) to leave the major isomer **3** (403 mg, 45%): Mp 245—246 °C (from acetone); IR (KBr) 2269 (C≡N), 1702 (C=O), 1558 (C=C), 1260, 1178, 987, 792 cm^{-1}; ^1H NMR (acetone-d_6) δ=1.75 (d, J=6.2 Hz, 3H, CH_3), 3.77 (q, J=6.2 Hz, 1H, cyclopropyl H); ^{13}C NMR (acetone-d_6) δ=13.2 (CH_3), 39.3 (C-CH_3), 40.1 (C-CN), 111.8 (CN), 141.7 (C=C), 176.7 (C=O); MS, m/z 254 (M^+). Found: C, 47.22; H, 1.64; N, 10.94%. Calcd for $C_{10}H_4Cl_2N_2O_2$: C, 47.09; H, 1.58; N, 10.98%.

The filtrate and the washing were then combined and evaporated to dryness. The residue was column chromatographed on silica gel. Elution with petroleum ether-benzene (1 : 1) gave **4** (87 mg, 9%): Mp 101—102 °C (from petroleum ether); IR (KBr) 2237 (C≡N), 1431, 1383, 1357, 1022, 926 cm^{-1}; ^1H NMR ($CDCl_3$) δ=1.50 (t, J=7.0 Hz, 6H, 2×CH_3), 4.27 (q, J=7.0 Hz, 4H, 2×methylene); MS, m/z 284 (M^+). Found: C, 50.64; H, 3.57; N, 9.77%. Calcd for $C_{12}H_{10}Cl_2N_2O_2$: C, 50.55; H, 3.54; N, 9.83%.

Further elution with benzene subsequently yielded a second crop of the major isomer **3** (90 mg, 10%) and the minor **3** (142 mg, 16%): Mp 236—238 °C (from acetone); IR (KBr) 2260 (C≡N), 1688 (C=O), 1556 (C=C), 1253, 1168, 802 cm^{-1}; ^1H NMR (acetone-d_6) δ=1.63 (d, J=6.8 Hz, 3H, CH_3), 3.53 (q, J=6.8 Hz, cyclopropyl H); MS, m/z 254 (M^+). Found: C, 47.08; H, 1.63; N, 10.75%. Calcd for $C_{10}H_4Cl_2N_2O_2$: C, 47.09; H, 1.58; N, 10.98%. Finally, an unidentified black powder (110 mg, mp>300 °C, IR (KBr) 3440, 1625, 1524 cm^{-1}) was eluted, with benzene-acetone (1 : 1) as the eluent.

Hydrogenation of 3. 3,4-Dichloro-2,5-dimethoxy-7-methyl-1,3,5-cycloheptatriene-1,6-dicarbonitrile (5b). The major isomer **3** (150 mg, 0.59 mmol) was hydrogenated with palladium carbon (100 mg, ca. 10%) at 25 °C in 1,4-dioxane (10 ml) under a hydrogen atmosphere. After 6 h stirring, the filtration of the catalyst and the evaporation of the solvent in vacuo gave a colorless solid (140 mg) showing a strong OH band at 3220 cm^{-1}. The treatment of the crude product with excess ethereal diazomethane and the subsequent column chromatography on silica gel, with benzene-ether (10 : 1) as an eluent, provided **5b** (108 mg, 64%): Mp 136—137 °C (from petroleum ether-benzene); IR (KBr) 2220 (C≡N), 1593 (C=C), 1309, 1280, 1058, 782 cm^{-1}; ^1H NMR ($CDCl_3$) δ=1.56 (d, J=7.0 Hz, 3H, CH_3), 2.63 (q, J=7.0 Hz, 1H, methine), 3.93 (s, 6H, 2×OCH_3); MS, m/z 284 (M^+). Found: C, 50.51; H, 3.53; N, 9.74%. Calcd for $C_{12}H_{10}Cl_2N_2O_2$: C, 50.55; H, 3.54; N, 9.83%.

The same workup converted the minor isomer **3** (80 mg) into **5b** (53 mg, 59%).

3,4-Dichloro-2,5-dioxo-7-phenylbicyclo[4.1.0]hept-3-ene-1,6-dicarbonitrile (7) and Stilbene (8). To a stirred solution of DDQ (480 mg, 2.1 mmol) in benzene (10 ml), we added, drop by drop at 25 °C over a 10-min period, a solution of phenyldiazomethane (400 mg, 3.4 mmol) in benzene (5 ml). After 1 h stirring, the precipitate was filtered off and washed with benzene (10 ml×3) and ether (5 ml×2) to leave the major **7** (280 mg, 42%): Mp 215—216 °C (from methanol); IR (KBr) 2253 (C≡N), 1707 (C=O), 1559 (C=C), 1172, 834 cm^{-1}; ^1H NMR (acetone-d_6) δ=5.16 (s, 1H, cyclopropyl H), 7.1—7.6 (m, 5H, Ph); MS, m/z 316 (M^+). Found: C, 56.91; H, 1.97; N, 9.01%. Calcd for $C_{15}H_6Cl_2N_2O_2$: C, 56.81; H, 1.91; N, 8.83%.

The filtrate and the washing were then combined, and the solvent was evaporated. A slight amount of the residue was submitted to HPLC analysis in order to determine the cis to trans ratio of **8** according to the previous procedure.[23] The rest of the residue was chromatographed on silica gel. Elution with petroleum ether-benzene (5 : 1) gave a mixture of *cis* and *trans*-**8** (78 mg, 25%, based on the **6** used). The increasing benzene content provided, successively, benzaldehyde azine, a second crop of the major isomer **7** (110 mg, 17%), and the minor isomer **7** (80 mg, 12%): Mp 208—209 °C

(from methanol); IR (KBr) 2256 (C≡N), 1699 (C=O), 1548 (C=C), 1182, 836 cm^{-1}; ^1H NMR (acetone-d_6) δ=5.03 (s, 1H, cyclopropyl H), 7.4—7.7 (m, 5H, Ph); MS, m/z 316 (M^+). Found: C, 57.12; H, 1.91; N, 8.75%. Calcd for $C_{15}H_6Cl_2N_2O_2$: C, 56.81; H, 1.91; N, 8.83%.

Hydrogenation of 7. 3,4-Dichloro-2,5-dimethoxy-7-phenyl-1,3,5-cycloheptatriene-1,6-dicarbonitrile (9b). The major isomer **7** (230 mg, 0.73 mmol) was hydrogenated with palladium carbon (100 mg) at 25 °C in 1,4-dioxane (20 ml) under a hydrogen atmosphere. After 6 h stirring, the catalyst was filtered off and the solvent was evaporated. We were unsuccessful in our attempt to crystallize **9a**, so the hydrogenated product was methylated with diazomethane and column chromatographed on silica gel, with benzene–ether (10 : 1) as the eluent, to give **9b** (175 mg, 69%): Mp 158—160 °C (petroleum ether); IR (KBr) 2190 (C≡N), 1591 (C=C), 1291, 946 cm^{-1}; ^1H NMR ($CDCl_3$) δ=3.93 (s, 6H, 2×OCH_3), 4.40 (s, 1H, methine), 7.27 (s, 5H, Ph); MS, m/z 346 (M^+). Found: C, 58.76; H, 3.47; N, 8.03%. Calcd for $C_{17}H_{12}Cl_2N_2O_2$: C, 58.80; H, 3.48; N, 8.07%.

Benzaldehyde Dimethyl Acetal (11) and 2,3-Dichloro-5,6-dicyanohydroquinone Dibenzyl Ether (12). To a stirred solution of DDQ (480 mg, 2.1 mmol) in benzene (10 ml) containing methanol (0.50g, 16 mmol), we added, drop by drop at 25 °C over a 10-min period, a solution of phenyldiazomethane (**6**) (400 mg, 3.4 mmol) in benzene (5 ml). After 1 h stirring, a precipitate was filtered off and washed with benzene (10 ml×3) and ether (5 ml×2). The crystalline product was assigned to the major isomer **7** (280 mg, 42%) on the basis of the IR analysis. The evaporation of the combined filtrate and washing in vacuo gave an pasty residue, the ^1H NMR spectrum of which showed the presence of benzaldehyde dimethyl acetal (**11**) (10%, as determined by the integral ratios, with 1,1,1,2-tetrachloroethane as the internal standard). This acetal was easily degradated to benzaldehyde and methanol on 1 d standing in the NMR tube, as confirmed by the disappearance of the acetal signal: ($CDCl_3$) δ=3.30 (s, 6H, 2×OCH_3) and 5.37 (s, 1H, methine). The column chromatographic treatment of the residue, with petroleum ether–benzene (20 to 100%) as eluents, gave, successively, benzaldehyde (16 mg, 7%), benzaldehyde azine, **12** (110 mg, 13%), the second crop of the major isomer **7** (80 mg, 12%), and the minor isomer **7** (70 mg, 11%). Compound **12** had a mp of 192—194 °C (from benzene): IR (KBr) 2228 (C≡N), 1421, 1355, 993 cm^{-1}; ^1H NMR ($CDCl_3$) δ=5.28 (s, 4H, methylene), 7.2—7.6 (m, 10H, 2×Ph); MS, m/z 408 (M^+). Found: C, 64.51; H, 3.44; N, 7.09%. Calcd for $C_{22}H_{14}Cl_2N_2O_2$: C, 64.56; H, 3.45; N, 6.85%.

2,3-Dichloro-5,6-dicyano-1-(1-phenylethenyloxy)-4-(1-phenylethoxy)benzene (14) and 2,3-Dichloro-5,6-dicyanohydroquinone bis(α-methylbenzyl) Ether (15). To a stirred solution of DDQ (0.50 g, 2.2 mmol) in benzene (10 ml), we added, drop by drop at 25 °C and over a 10-min period, a solution of 1-phenyldiazoethane (0.80 g, 6.1 mmol) in benzene (10 ml). After 6 h stirring, the evaporation of the solvent gave a brown solid. The ^1H NMR spectrum of this residue showed the formation of **14** and **15** in yields of 92 and 4% respectively, as determined by using 1,1,1,2-tetrachloroethane as the internal standard. Column chromatography on silica gel gave, successively, **15** and **14** by using petroleum ether–benzene (1 : 2). Compound **14** had a mp of 126—127 °C (from petroleum ether–benzene); IR (KBr) 2238 (C≡N), 1637 (C=C), 1420, 1268, 699 cm^{-1}; ^1H NMR ($CDCl_3$) δ=1.82 (d, J=6.3Hz, 3H, CH_3), 3.77 (d, J=4.3Hz, 1H, olefinic H), 4.90 (d, J=4.3Hz, 1H, olefinic H), 5.80 (q, J=6.3Hz, 1H, methine), 7.2—7.8 (m, 10H, 2×Ph); MS, m/z 434 (M^+). Found: C, 65.99; H, 3.91; N, 6.47%. Calcd for $C_{24}H_{16}Cl_2N_2O_2$: C, 66.22; H, 3.71; N, 6.44%.

Compound **15** was identified by a comparison of its IR spectrum with that of an authentic specimen prepared by the treatment of 1-phenyldiazoethane with $DDQH_2$, having a mp of 119—120 °C (from benzene); IR (KBr) 2236 (C≡N), 1420, 1242, 1057, 700 cm^{-1}; ^1H NMR ($CDCl_3$) δ=1.73 (d, J=6.3 Hz, 6H, 2×CH_3), 5.65 (q, J=6.3 Hz, 2H, 2×methine), 7.37 (s, 10H, 2×Ph); MS, m/z 332 (M^+−$PhCH{=}CH_2$). Found: C, 65.95; H, 4.09; N, 6.37%. Calcd for $C_{24}H_{28}Cl_2N_2O_2$: C, 65.91; H, 4.15; N, 6.41%.

Acetophenone Dimethyl Acetal (16). To a stirred solution of DDQ (1.0 g, 4.4 mmol) in benzene (20 ml), we added, drop by drop, at 25 °C and over a 10-min period, a solution of 1-phenyldiazoethane (0.70 g, 5.3 mmol) and methanol (1.0 g, 31 mmol) in benzene (10 ml). After 1 h stirring, the solvent was evaporated to dryness and the yield of **16** (69%) was determined by the integration of the methoxyl signals at δ 3.13 by using 1,1,1,2-tetrachloroethane as a standard in the ^1H NMR spectrum. Though the signals assignable to **15** were also observed, the two characteristic olefinic doublets (δ=3.77 and 4.90) attributable to **14** were not found, which is consistent with the complete inhibition of the proton migration process (see Scheme 4). The crude reaction mixture was extracted with pentane (20 ml×3) and the combined pentane solution was washed with 5% aqueous sodium carbonate (5 ml×3) and with NaCl saturated water (5 ml×2), dried over sodium sulfate, and concentrated in vacuo to give a pale yellow oil. Column chromatography on alumina, using pentane–benzene (9 : 1) as the eluent, gave **16** (260 mg, 36%): colorless oil; IR (film) 1277, 1148, 1044, 701 cm^{-1}; ^1H NMR ($CDCl_3$) δ=1.50 (s, 3H, CH_3), 3.13 (s, 6H, 2×OCH_3), 7.2—7.6 (m, 5H, Ph). Found: C, 72.47; H, 8.57%. Calcd for $C_{10}H_{14}O_2$: C, 72.26; H, 8.49%.

We wish to thank Dr. S. Itoh (Osaka University) for the ^{13}C NMR measurements.

References

1) a) C. D. Gutsche, *Org. React.*, **8**, 364 (1954); b) K. T. Finley, "The Chemistry of the Quinonoid Compounds," ed by S. Patai, John Wiley & Sons (1974), Chap. 17; c) D. S. Wulfman, G. Linstrumell, and C. F. Cooper, "The Chemistry of Diazonium and Diazo Groups," ed by S. Patai, John Wiley & Sons (1978), Chap. 18; d) F. M. Dean, L. E. Houghton, R. Nayyir-Mashir, and C. Thebtaranonth, *J. Chem. Soc., Perkin Trans. 2*, **1980**, 1994, and other papers in this series.

2) G. Bianchi, C. D. Micheli, and R. Gandolfi, "The Chemistry of Double-Bonded Functional Groups, Supplement A," ed by S. Patai, John Wiley & Sons (1977), Chap. 6.

3) a) R. Huisgen, *Angew. Chem.*, **75**, 604 (1963); b) R. Huisgen, *J. Org. Chem.*, **41**, 403 (1976).

4) H. Pechmann and E. Seel, *Ber.*, **32**, 2292 (1899).

5) a) B. Eistert, K. Pfleger, and P. Donath, *Chem. Ber.*, **105**, 3915 (1972); b) B. Eistert, J. Riedinger, G. Küffner, and W. Lazik, *Chem. Ber.*, **106**, 727 (1973).

6) T. Oshima and T. Nagai, unpublished results.

7) B. Eistert and G. Bock, *Chem. Ber.*, **92**, 1274 (1959).

8) a) T. Oshima and T. Nagai, *Tetrahedron Lett.*, **1979**, 2789; b) T. Oshima and T. Nagai, *Bull. Chem. Soc. Jpn.*, **53**, 726 (1980).

9) T. Oshima and T. Nagai, *Bull. Chem. Soc. Jpn.*, **53**, 3284 (1980).

10) T. Oshima and T. Nagai, *Tetrahedron Lett.*, **1985**, 5317.

11) H.-D. Becker, B. W. Skelton, and A. H. White, *Aust. J. Chem.*, **34**, 2189 (1981).

12) T. Oshima and T. Nagai, *Bull. Chem. Soc. Jap.*, **54**, 2039 (1981).

13) H.-D. Becker, *J. Org. Chem.*, **34**, 1203 (1969).

14) Dreiding et al. have reported that unsubstituted bicyclic dione, bicyclo[4.1.0]hept-3-ene-2,5-dione, shows only a small difference ($\Delta\delta$(exo-endo)=+0.06 ppm) in the chemical shifts of H(exo) and H(endo). However, they have also estimated the corresponding difference to be large and negative ($\Delta\delta$=−0.69 ppm) for the tetramethyl substituted system; *Helv. Chim. Acta.*, **57**, 1259 (1974).

15) The dihedral angles (θ) were calculated from the coupling constants $J(^{13}C, H)$ obtained between the cyclopropyl proton and the cyano carbon (4.87 Hz) or the carbonyl carbon (6.11 Hz) in DMSO-d_6, according to the Wasylishen and Schaefer equation; *Can. J. Chem.*, **50**, 2710 (1972). Though their equation gave two θ values for each fragment, H-C-C-CN (33 and 134°) and H-C-C-CO (19 and 143°), we have chosen the pair of 134 and 19° as estimated values because the other value (θ=33°) is too large for the *cis* arrangement of the cyclopropane-ring substituents.

16) B. Eistert, H. Fink, K. Pfleger, and G. Küffner, *Liebigs Ann. Chem.*, **735**, 145 (1970).

17) a) K. W. Houk, J. Sims, R. E. Duke, Jr., R. W. Strozier, and J. K. George, *J. Am. Chem. Soc.*, **95**, 7287 (1973); b) R. Sustmann, *Tetrahedron Lett.*, **1971**, 2717; c) J. Geitter, R. Huisgen, and R. Sustmann, *Tetrahedron Lett.*, **1977**, 881; d) R. Sustmann, E. Wenning, and R. Huisgen, *Tetrahedron Lett.*, **1977**, 877.

18) R. Foster, "Organic Charge Transfer Complexes," Academic Press (1969), Chap. 13.

19) a) T. Fujita and T. Nishioka, *Progr. Phys. Org. Chem.*, **12**, 49 (1976); b) S. H. Unger and C. Hansch, *Progr. Phys. Org. Chem.*, **12**, 91 (1976).

20) F. Arndt, *Org. Synth.*, Coll. Vol. II, p. 165.

21) G. L. Closs and R. A. Moss, *J. Am. Chem. Soc.*, **86**, 4042 (1964).

22) G. L. Closs and J. J. Coyle, *J. Org. Chem.*, **31**, 2759 (1966).

23) T. Oshima, R. Nishioka, and T. Nagai, *Bull. Chem. Soc. Jpn.*, **55**, 904 (1982).

 © 1986 The Chemical Society of Japan Bull. Chem. Soc. Jpn., 59, 3871—3876 (1986)

Reaction of β-Nitro Enamines with Isocyanates, Isothiocyanates and Dimethyl Acetylenedicarboxylate

Takao TOKUMITSU
Department of Chemistry, Faculty of Science, Yamaguchi University, Yoshida, Yamaguchi 753
(Received May 10, 1986)

β-Nitro enamines (**1**) reacted with isocyanates and isothiocyanates to give β-(substituted carbamoyl) and β-(substituted thiocarbamoyl) β-nitro enamines, respectively. The reaction of **1** with benzoyl isothiocyanate gave β-(benzoylthiocarbamoyl) β-nitro enamines (**8**) and/or a mixture of **8** and 4(1*H*)-pyrimidinethione derivatives (**9**) which were cyclization products of **8**. The isolated **8** afforded the corresponding **9** in high yields upon heating in DMF. The reaction of **1** with dimethyl acetylenedicarboxylate gave [2+2] cycloadducts (**12**) and/or a mixture of **12** and δ-nitro dienamino diesters (**13**) which were ring cleavage products of **12**. Compounds **12** afforded **13** upon heating in toluene or xylene.

β-Nitro enamines are useful synthetic intermediates, and their reactivities are of interest in connection with that of β-amino enones. In a previous paper, the author reported that the primary and secondary β-nitro enamines (**1**) reacted with electrophiles, *N*-halosuccinimides, *o*-nitrobenzenesulfenyl chloride and thiocyanogen, to give exclusively the β-substituted β-nitro enamines.[1] The reaction of electrophiles such as isocyanates and isothiocyanates with **1** also is of interest because it may occur either at the nitrogen of the amino group or at the β-carbon. However, these reactions have been little studied: it has been reported only that 2-(nitromethylene)perhydroazepine reacts with benzoyl isothiocyanate to give a pyrimidine derivative.[2] On the other hand, it is known that tertiary β-nitro enamines react at the double bond with dipolar reagents such as nitrilimines, nitrile oxides and aryl azides to give azoles, [2+3] dipolar cycloaddition products.[3,4] However, there has been no report concerning the reaction of **1** with electrophilic alkynes.

In this paper, I wish to report the results of the reaction of **1** with isocyanates, isothiocyanates and dimethyl acetylenedicarboxylate.

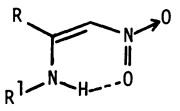

1

	R	R¹		R	R¹
a:	Me	H	**f**:	Ph	H
b:	Me	Me	**g**:	Ph	Me
c:	Me	$PhCH_2$	**h**:	Ph	$PhCH_2$
d:	Me	Ph	**i**:	Ph	Ph
e:	Me	R^1–H=$(CH_2)_5$	**j**:	Ph	R^1–H=$(CH_2)_5$

Results and Discussion

Reaction of β-Nitro Enamines (1) with Isocyanates and Isothiocyanates. The reaction of **1a—d** with phenyl isocyanate (**2**) in acetonitrile afforded β-(phenylcarbamoyl) β-nitro enamines (**3a—d**) in 29—81% yields and a small amount of the corresponding *N*-substituted ureas (**4**), which were considered to be decomposition products of an *N*-acylated product of **1**, respectively. In these reactions, tertiary β-nitro enamine, **1e**, decomposed. With methyl isocyanate, only **1b** at 90 °C in a sealed tube gave *N*-methyl-3-methylamino-2-nitro-2-butanamide (**5b**) in a 35% yield. In the reaction of **1a—e** with phenyl isothiocyanate, only

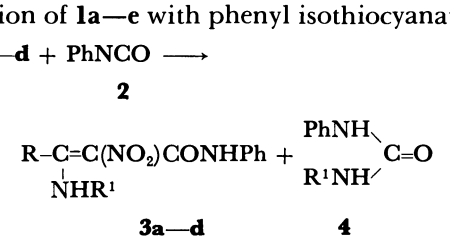

1a—d + PhNCO ⟶ **2**

R–C(NHR¹)=C(NO_2)CONHPh + $PhNH(R^1NH)C{=}O$

3a—d **4**

1b and **1e** gave β-(phenylthiocarbamoyl) β-nitro enamines (**6b**) and (**6e**), in 25 and 5% yields, respectively. These results have revealed that the electrophilic addition of isocyanates and isothiocyanate to **1** takes place predominantly on the β-carbon of **1**; this reactivity is attributable to the enamine character of **1**.[1,5] New compounds **3a—d**, **5b** and **6b,e** were identified by spectral data and elemental analyses. In the IR spectra, **3a** and **3b—d**, **5b** showed three and two weak absorptions, respectively, which were assigned to νNH. The absorptions in the carbonyl region were complex: **3a—d** and **5b** showed strong absorptions in the region 1602—1588 cm^{-1}, which may be assigned to νC=O overlapped with a ring stretching that is shifted to a lower frequency by the enamino ketone conjugation and an intramolecular hydrogen bonding strengthened by the electron-withdrawing resonance effect of α-nitro group (as described below). A strong νC=S absorption of **6b** and **6e** was found at 1168 and 1160 cm^{-1},[6] respectively. The NMR spectra of **3a—d**, **5b**, and **6b,e** showed new peaks of $NHCH_3$ or NHC_6H_5 protons with a disappearance of a =CH- proton signal near 6.5 ppm of the corresponding **1a—e**, respectively.

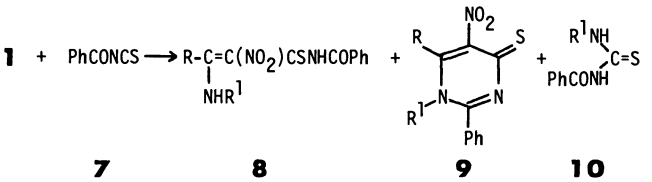

1 + PhCONCS ⟶ R–C(NHR¹)=C(NO_2)CSNHCOPh + 2-(Ph)-4-(NO_2)-5-(R)-6-(S)-1,3-pyrimidine + $R^1NH(PhCONH)C{=}S$

7 **8** **9** **10**

Table 1. Reaction of **1** with Benzoyl Isothiocyanate

	Reaction condition			Products					
	Temp/°C	Time/h	Separation[a)]	**8**	Yield/%	**9**	Yield/%	**10**	Yield/%
1a	50	100	C-CH_2Cl_2	**8a**	17	**9a**	2		8
1b	rt	48	C-CH_2Cl_2	**8b**	81	**9b**	0.5		0
1c	60	30	C-CCl_4	**8c**	0	**9c**	9		26
1d	rt	120	$CHCl_3$/CCl_4	**8d**	34	**9d**	2		0
1e	rt	30	C-CH_2Cl_2	**8e**	84	**9e**	0		1
1g	rt	100	PhH/CCl_4	**8g**	87	**9g**	0		0
1h	bp	18	C-CH_2Cl_2	**8h**	60	**9h**	17		5
1i	bp	80	C-CH_2Cl_2	**8i**	0	**9i**	16		6
1j	rt	45	C-CH_2Cl_2	**8j**	50	**9j**	0		5

a) C: Silica-gel column chromatography.

In the reaction of **1** with benzoyl isothiocyanate (**7**), **1a,b,d,h** gave a mixture of corresponding β-(benzoylthiocarbamoyl) β-nitro enamines (**8a,b,d,h**) (17—81%), 4(1*H*)-pyrimidinethione derivatives (**9a,b,d,h**) (0.5—17%) and *N*-benzoyl *N'*-R^1-thioureas (**10**) (1—26%), and **1c,i** gave a mixture of corresponding **9c, i** (9 and 16%) and **10** (26 and 6%); **1e,g,j** and **1f** gave only corresponding **8e,g,j** (50—87%) and a small amount of *N*-benzoylthiourea, respectively. deStevens et al.[5] have reported that ethyl 3-amino-2-(benzoylthiocarbamoyl)-crotonate can be converted to the corresponding 4(1*H*)-pyrimidinethione derivative upon refluxing in THF. Therefore, compounds **9** appear to be produced by a thermal *Z-E* isomerization of the initially formed β-adducts, **8**, during the reaction, followed by a ring closure and dehydration. These results are also supported by the reaction of **1h** with **7**. Namely, plots of the yields of **8h** vs. the reaction times showed a maximum (about 60%) in about 18 h, while **9h** increased with increasing time. These results are shown in Fig. 1. On the other hand, the isolated primary and secondary **8a,b,d,g,h** afforded the corresponding **9a,b,d,g,h** in 90—96% yields upon heating in DMF for 5 min at 110 °C. Compounds **10** are the decomposition products of *N*-adducts of **7**. New compounds **8a,b,d,e,g,h,j** and **9a—d, g—i** were identified by the spectral data and elemental analyses. The IR spectra for **8** showed one, two and three absorptions assigned to νNH in the region of 3500—3100 cm^{-1}, and νC=O and νC=S absorptions were observed at 1708—1706 and 1180—1162 cm^{-1}, respectively. In cyclic compounds **9b—d, g—i**, the νC=O and νNH absorptions disappeared, and **9a** showed a weak absorption of the νNH at 3400 cm^{-1}. The absorptions of νC=C+νC=N and νC=S of **9a—d, g—i** were observed at 1677—1605 and 1172—1149 cm^{-1} respectively. The NMR spectra also supported the structure of **8** and **9**, respectively.

As previously described, **3b—d** and **5b** showed two weak νNH absorptions in the regions at 3350—3270 and 3180—3150 cm^{-1}; also, a strong absorption of νC=O that overlapped with νC=C of the aromatic ring was found in the lower-frequency region of 1602—1588 cm^{-1}, respectively. 4-(Monosubstituted amino)-3-nitro-3-penten-2-one (substituent: Me, $PhCH_2$, and

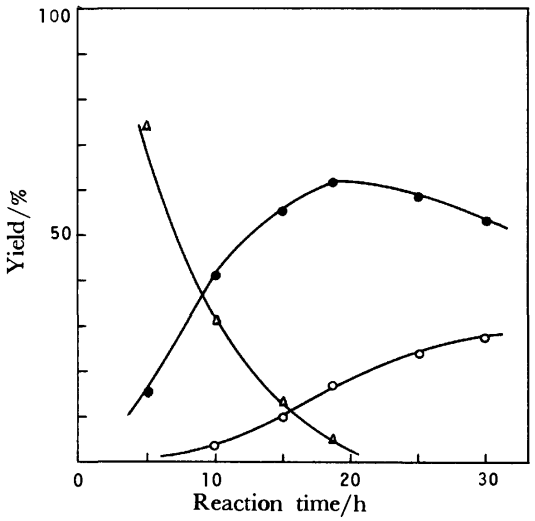

Fig. 1. Yields of **8h** and **9h** vs. reaction time in boiling benzene. ●: **8h**, ○: **9h**, △: recovered 1h.

Ph) show a strong νC=O in the lower-frequency region of 1605—1568 cm^{-1}. Such a low-frequency shift of the νC=O absorption can be attributed to a delocalization of π-electrons of the chelate ring through an intramolecular hydrogen bonding, owing to the electron-withdrawing resonance effect of the α-nitro group.[7]

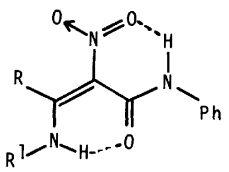

[**I**]

The peaks of two NH protons for NMR were found for a lower magnetic field at δ 13.8—12.2 and 10.5—10.4 respectively. Compound **3a** was also similar to **3b—d**. Further, the peaks of NCH_3 and NCH_2- protons for **3b,c** and **5b** split into a doublet through a spin-spin coupling with the NH proton at δ 3.16—2.87 (J=5—6 Hz) and 4.6 (J=6 Hz), respectively. From these results, **3a—d** and **5b** appear to exist in a double intramolecular hydrogen-bonded structure [**I**].

In conclusion, it has been found that **1** reacts with

Table 2. Reaction of **1** with Dimethyl Acetylenedicarboxylate

	Reaction time/h	Separation[a)]	Product			
			12	Yield/%	**13**	Yield/%
1a	9	C-CH_2Cl_2	**12a**	0	**13a**	71
1b	4	PhH	**12b**	72	**13b**	0
1d	4	C-CH_2Cl_2	**12d**	47	**13d**	25
1f	48	C-CH_2Cl_2	**12f**	64	**13f**	0
1g	7	PhH	**12g**	79	**13g**	0
1h	12	MeOH/CCl_4	**12h**	58	**13h**	16
1i	72	C-CH_2Cl_2	**12i**	26	**13i**	31
1j	100	C-CH_2Cl_2	**12j**	0	**13j**	6

a) C: Silica-gel column chromatography.

Table 3. Ring Opening Reaction of **12**

	Reaction condition				Product		
	Solvent	Temp/°C	Time/h	Separation[a)]	**13**	Yield/%	Mp(θ_m/°C)
12b	Toluene	bp	4	C-CH_2Cl_2	**13b**	49	Liquid
12d	Toluene	bp	1	C-CH_2Cl_2	**13d**	95	99—100
12f	Xylene	130	120	C-CH_2Cl_2	**13f**	50	132—133
12g	Xylene	130	8	CCl_4	**13g**	99	136—137
12h	Toluene	bp	2	CCl_4	**13h**	99	167—168
12i	Toluene	bp	3	CCl_4	**13i**	99	163—164

a) C: Silica-gel column chromatography.

isocyanates and isothiocyanates at β-carbon predominantly to give the β-adducts. With benzoyl isothiocyanate it gives 4(1*H*)-pyrimidinethiones by β-addition followed by cyclization.

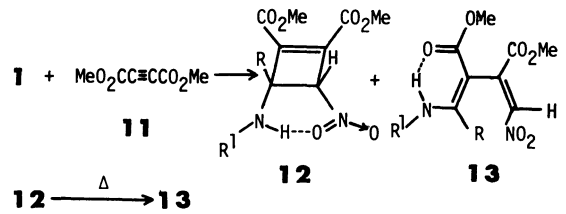

Reaction of 1 with Dimethyl Acetylenedicarboxylate (11). In a reaction of **1** with **11** in refluxing THF, **1d, h, i** gave a mixture of corresponding [2+2] cycloadducts (**12d,h,i**) and β,γ-bis(methoxycarbonyl) δ-nitro dienamines (**13d,h,i**), and **1b,f,g** gave only **12b,f,g**; **1a,j** and **1c, e** gave only the corresponding **13a, j** and decomposition products, respectively. These results are shown in Table 2. It is known that enamino ketones and esters also react similarly with **11** to give dienamino keto diesters and dienamino triesters, respectively, which are presumed to be produced via a rearrangement of unstable cyclobutene intermediates.[8] In a similar manner, **13** appears to be produced by a ring-cleavage of the initially formed cycloadducts **12**. This is also illustrated by the fact that plots of the yields of **12h** vs. the reaction times showed a maximum (58%) after about 12 h, while that of **13h** increased up to 81% with time (Fig. 2). The isolated **12** isomerized upon being heated in toluene or xylene to give the corresponding **13** in 49—99% yields. These results are summarized in Table 3. Compounds **12b,d,h,i** were

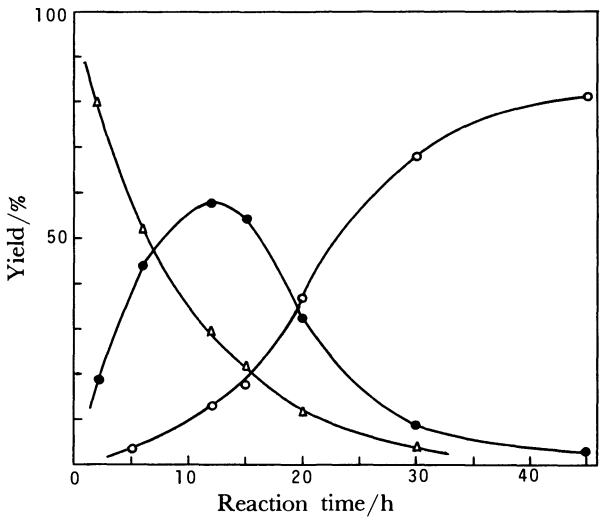

Fig. 2. Yields of **12h** and **13h** vs. reaction time in boiling THF. ●: **12h**, ○: **13h**, △: recovered 1h.

easily cleaved by refluxing in toluene to give **13b,d,h,i**, respectively. **12f,g** were stable upon prolonged heating in toluene and required a long heating period at 130 °C in xylene. Such a difference in the thermal stability of **12** is consistent with the yield of **13** for the reaction described above.

The new compounds (**12** and **13**) were identified by spectral data and elemental analyses. The IR spectra of **12b,d, f—i** all showed a weak broad νNH absorption at 3190—3120 cm^{-1}, and a strong νC=O absorption was observed in the region of 1728—1720 cm^{-1}. A weak absorption at 1639—1625 cm^{-1} region was assigned to νC=C absorption, and a strong absorption at 1603—

1561 cm^{-1} region was assigned to depend primarily on $\nu_{as}NO_2$ absorption. The NMR spectra for **12b,d,f—i** were also in agreement with the [2+2] cycloadducts, respectively, and a broad NH peak was observed at δ 12.37—9.9, respectively. These results suggested that **12b, d, f—i** have an intramolecular hydrogen-bonded structure of NH ··· O=N type. In the IR spectra of **13a,b,d,f—j** a weak broad absorption of νNH was observed in the region of 3200—3150 cm^{-1} except for **13j**, and a strong absorption of νC=O and a medium absorption of νC=C was observed at 1725—1718 and 1640—1618 cm^{-1} region, respectively. Strong absorptions of $\nu_{as}NO_2$ and ν_sNO_2 were also observed at 1614—1544 and 1376—1351 cm^{-1}, respectively. The NMR spectra were also consistent with the ring-cleavage products, respectively, and a broad NH peak was observed at δ 12.49—9.95 as observed **12**. These results suggested that **13** were δ-nitro dienamino diester and that **13a,b,d,f—j** had an intramolecular hydrogen-bonded structure of the enamino ester type. Consequently, it is considered that the compounds **13** are produced via the conrotatory ring cleavage upon heating the corresponding cyclobutenes **12**.

In conclusion, it has been found that **1** reacts with the electrophilic dimethyl acetylenedicarboxylate at the double bond, in spite of the delocalization of π-electrons as a push-pull alkene,[9] to give the [2+2] cycloadducts, and that their adducts afford the corresponding δ-nitro dienamino diesters by the ring opening reaction.

Experimental

Melting points were uncorrected. IR and UV spectra were recorded with a JASCO IRG and a Hitachi 124 spectrophotometers, respectively. NMR spectra were recorded with a Hitachi R24B (60 MHz) instrument using TMS as an internal standard. Isocyanates, isothiocyanates and dimethyl acetylenedicarboxylate were of commercial grade and used without further purification. The preparation of *N*-substituted β-nitro enamines, **1a—j**, was described in a previous paper.[7]

General Procedure for the Reaction of 1 with Isocyanates and Phenyl Isothiocyanate. A solution containing **1** (5 mmol) and phenyl isocyanate or phenyl isothiocyanate (5.5 mmol) in acetonitrile 15 ml was refluxed for 9—90 h; then, the solvent was removed by a rotary evaporator. The residue was purified by recrystallization and/or column chromatography (silica-gel, benzene/acetone 5/1) to give **3a—d** and **6b,e**. The reaction of **1** with methyl isocyanate was performed in a sealed tube at 90 °C for 48 h, and purified in a similar manner as above. The results are as follows.

***N*-Phenyl-3-amino-2-nitro-2-butenamide (3a):** Reaction time 48 h; yield 29%; mp 177—178 °C (column chromatography); IR ($CHCl_3$) 3470m, 3300w, 3130w, 1658w, 1631m, 1591s, 1530s, 1444s, and 1322s cm^{-1}; UV (EtOH) λ_{nm} ($10^{-3}\varepsilon$) 252 (14.0) and 338 (21.1); ^1H NMR (DMSO-d_6) δ=10.35 (br, 1H), 9.5 (br, 1H), 9.05 (br, 1H), 7.4 (m, 5H), and 2.11 (s, 3H). Found: C, 54.30; H, 4.98; N, 19.09%. Calcd for $C_{10}H_{11}N_3O_3$: C, 54.29; H, 5.01; N, 18.99%.

***N*-Phenyl-3-methylamino-2-nitro-2-butenamide (3b):** Reaction time 9 h; yield 81%; mp 169—170 °C (EtOH); IR ($CHCl_3$) 3270w, 3150w, 1655w, 1611m, 1591s, 1532s, 1499s, and 1324s cm^{-1}; UV (EtOH) λ_{nm} (10^{-3} ε) 249 (14.4) and 350 (13.7); ^1H NMR ($CDCl_3$) δ=12.25 (br, 1H), 10.50 (br, 1H), 7.35 (m, 5H), 3.16 (d, J=6Hz, 3H), and 2.48 (s, 3H). Found: C, 56.03; H, 5.54; N, 17.80%. Calcd for $C_{11}H_{13}N_3O_3$: C, 56.16; H, 5.57; N, 17.86%.

***N*-Phenyl-3-benzylamino-2-nitro-2-butenamide (3c):** Reaction time 24 h; yield 58%; mp 144—145 °C (CCl_4); IR ($CHCl_3$) 3270w, 3160w, 1660w, 1618m, 1591s, 1583s, 1532s, 1444s, and 1323s cm^{-1}; UV (EtOH) λ_{nm} ($10^{-3}\varepsilon$) 249 (15.6) and 352 (15.4); ^1H NMR ($CDCl_3$) δ=12.48 (br, 1H), 10.4 (br, 1H), 7.3 (m, 10H),4.6 (d, J=6Hz, 2H), and 2.47 (s, 3H). Found: C, 65.37; H, 5.47; N, 13.42%. Calcd for $C_{17}H_{17}N_3O_3$: C, 65.58; H, 5.50; N, 13.49%.

***N*-Phenyl-3-anilino-2-nitro-2-butenamide (3d):** Reaction time 18 h; yield 40%; mp 145—146 °C (CCl_4); IR ($CHCl_3$) 3300w, 3180w, 1665w, 1610m, 1588s, 1575s, 1490s, 1447s, and 1327s cm^{-1}; UV (EtOH) λ_{nm} (10^{-3} ε) 248 (14.6) and 355 (12.6); ^1H NMR ($CDCl_3$) δ=13.8 (br, 1H), 10.5 (br, 1H), 7.4 (m, 10H), and 2.45 (s, 3H). Found: C, 64.48; H, 5.05; N, 14.11%. Calcd for $C_{16}H_{15}N_3O_3$: C, 64.63; H, 5.08; N, 14.13%.

***N*-Methyl-3-methylamino-2-nitro-2-butenamide (5b):** Reaction time 48 h (at 90 °C in a sealed tube); yield 35%; mp 164—165 °C (column chromatography); IR ($CHCl_3$) 3350w, 3170w, 1602s, 1531m, and 1320s cm^{-1}; UV (EtOH) λ_{nm} (10^{-3} ε) ≈243 (≈5.3) and 350 (14.9); ^1H NMR ($CDCl_3$) δ=12.3 (br, 1H), 10.4 (br, 1H), 3.11 (d, J=5Hz, 3H), 2.87 (d, J=5Hz, 3H), and 2.44 (s, 3H). Found: C, 41.59; H, 6.36; N, 24.36%. Calcd for $C_6H_{11}N_3O_3$: C, 41.61; H, 6.40; N, 24.26%.

***N*-Phenyl-3-methylamino-2-nitro-2-butenethioamide (6b):** Reaction time 90 h; yield 25%; mp 159—160 °C (column chromatography); IR ($CHCl_3$) 3350w, 3180w, 1609s, 1595s, 1495s, 1358s, and 1168s cm^{-1}; UV (EtOH) λ_{nm} (10^{-3} ε) 316 (14.1) and 366 (11.5); ^1H NMR (DMSO-d_6) δ=12.03 (br, 1H), 10.75 (br, 1H), 7.6 (m, 5H), 3.10 (d, J=6Hz, 3H), and 2.18 (s, 3H). Found: C, 52.11; H, 5.11; N, 16.66; S, 12.75%. Calcd for $C_{11}H_{13}N_3O_2S$: C, 52.45; H, 5.20; N, 16.68; S, 12.95%.

***N*-Phenyl-2-nitro-3-piperidino-2-butenethioamide (6e):** Reaction time 10 h; yield 7%; mp 163—164 °C (CCl_4); IR ($CHCl_3$) 3160w, 1632w, 1599w, 1550s, 1445s, 1365s, 1350s, and 1160s cm^{-1}; UV (EtOH) λ_{nm} (10^{-3} ε) 334 (15.8) and 355 (15.5); ^1H NMR ($CDCl_3$) δ=12.80 (br, 1H), 7.6 (m, 5H), 3.89 (m, 4H), 2.79 (s, 3H), and 1.85 (m, 6H). Found: C, 58.76; H, 6.29; N, 13.80; S, 10.52%. Calcd for $C_{15}H_{19}N_3O_2S$: C, 58.99; H, 6.27; N, 13.76; S, 10.50%.

General Procedure for the Reaction of 1 with Benzoyl Isothiocyanate (7). A solution containing **1** (5 mmol) and **7** (5.5 mmol) in benzene 15 ml was stirred at room temperature—boiling point. The solvent was then evaporated. The residue was separated by fractional crystallization and/or column chromatography (silica-gel, CH_2Cl_2) to give β-(benzoylthiocarbamoyl) β-nitro enamines (**8**), 4(1*H*)-pyrimidinethiones (**9**) and *N*-substituted *N'*-benzoylthioureas (**5**), which was the decomposition products of the *N*-adducts. The results are summarized in Table 1.

***N*-Benzoyl-3-amino-2-nitro-2-butenethioamide (8a):** Mp 136—137 °C; IR ($CHCl_3$) 3480m, 3380w, 3180w, 1708s, 1615s, 1465s, 1321s, and 1171s cm^{-1}; UV (EtOH) λ_{nm} (10^{-3} ε) 253 (11.0), 304 (16.8), and 357 (8.0); ^1H NMR (DMSO-d_6) δ=12.65 (br, 1H), 9.7 (br, 1H), 9.2 (br, 1H), 7.7 (m, 5H), and 2.15 (s, 3H). Found: C, 49.54; H, 4.11; N, 15.70; S, 11.80%. Calcd for

$C_{11}H_{11}N_3O_2S$: C, 49.80; H, 4.18; N, 15.84; S, 12.08%.

***N*-Benzoyl-3-methylamino-2-nitro-2-butenethioamide (8b):** Mp 120—121 °C; IR ($CHCl_3$) 3370w, 3130w, 1706s, 1610s, 1600s, 1360s, and 1178s cm^{-1}; UV (EtOH) λ_{nm} (10^{-3} ε) 248 (10.0), 310 (15.4), and 377 (10.8); ^1H NMR (DMSO-d_6) δ=12.8 (br, 1H), 10.9 (br, 1H), 7.7 (m, 5H), 3.19 (d, *J*=6Hz, 3H), and 2.28 (s, 3H). Found: C, 51.51; H, 4.70; N, 14.98; S, 11.53%. Calcd for $C_{12}H_{13}N_3O_3S$: C, 51.60; H, 4.69; N, 15.04; S, 11.48%.

***N*-Benzoyl-3-anilino-2-nitro-2-butenethioamide (8d):** Mp 119—120 °C; IR ($CHCl_3$) 3380w, 3150w, 1708s, 1604s, 1582s, 1361s, and 1171s cm^{-1}; UV (EtOH) λ_{nm} (10^{-3} ε) 243 (14.0), 308 (16.8), and 386 (13.2); ^1H NMR ($CDCl_3$) δ=12.52 (br, 1H), 10.30 (br, 1H), 7.6 (m, 10H), and 2.20 (s, 3H). Found: C, 59.39; H, 4.21; N, 12.25; S, 9.39%. Calcd for $C_{17}H_{15}N_3O_3S$: C, 59.79; H, 4.43; N, 12.31; S, 9.39%.

***N*-Benzoyl-2-nitro-3-piperidino-2-butenethioamide (8e):** Mp 67—68 °C; IR ($CHCl_3$) 3140w, 1707s, 1639m, 1602m, 1525s, 1335s, and 1163s cm^{-1}; UV (EtOH) λ_{nm} (10^{-3} ε) 242 (10.0), 312 (14.8), and 397 (12.4); ^1H NMR ($CDCl_3$) δ=14.06 (br, 1H), 7.8 (m, 5H), 3.95 (m, 4H), 2.75 (s, 3H), and 1.90 (m, 6H). Found: C, 57.51; H, 5.61; N, 12.39; S, 9.45%. Calcd for $C_{16}H_{19}N_3O_3S$: C, 57.64; H, 5.74; N, 12.60; S, 9.62%.

***N*-Benzoyl-3-methylamino-2-nitro-3-phenylpropenethioamide (8g):** Mp 127—128 °C; IR ($CHCl_3$) 3370w, 3170w, 1703s, 1642m, 1598s, 1576s, 1320s, 1180s, and 1160s cm^{-1}; UV (EtOH) λ_{nm} (10^{-3} ε) 247 (12.6), 309 (11.0), 378 (10.0), and ≈400 (≈9.0); ^1H NMR (DMSO-d_6) δ=13.35 (br, 1H), 12.25 (br, 1H), 7.6 (m, 10H), and 2.91 (d, *J*=6Hz, 3H). Found: C, 59.72; H, 4.31; N, 12.40; S, 9.30%. Calcd for $C_{17}H_{15}N_3O_3S$: C, 59.79; H, 4.43; N, 12.31; S, 9.39%.

***N*-Benzoyl-3-benzylamino-2-nitro-3-phenylpropenethioamide (8h):** Mp 147—148 °C; IR ($CHCl_3$) 3360w, 3160w, 1708s, 1604w, 1590s, 1580s, 1570s, 1368s, and 1173s cm^{-1}; UV (EtOH) λ_{nm} (10^{-3} ε) 247 (15.2), 309 (14.0), 381 (11.8), and ≈400 (≈10.0); ^1H NMR (DMSO-d_6) δ=13.4 (br, 1H), 12.5 (br, 1H), 7.6 (m, 15H), and 4.65(d, *J*=6Hz, 2H). Found: C, 66.03; H, 4.35; N, 9.89; S, 7.70%. Calcd for $C_{23}H_{19}N_3O_3S$: C, 66.17; H, 4.58; N, 10.06; S, 7.68%.

***N*-Benzoyl-2-nitro-3-phenyl-3-piperidinopropenethioamide (8j):** Mp 158—159 °C; IR ($CHCl_3$) 3140w, 1707s, 1610m, 1602s, 1525s, 1330s, and 1162s cm^{-1}; UV (EtOH) λ_{nm} (10^{-3} ε) 242 (15.4), 308 (13.0), 368 (11.2), and ≈400 (≈10.0); ^1H NMR ($CDCl_3$) δ=13.0 (br, 1H), 7.7 (m, 10H), 4.0 (m, 4H), and 1.1 (m, 6H). Found: C, 63.52; H, 5.33; N, 10.64; S, 8.02%. Calcd for $C_{21}H_{21}N_3O_3S$: C, 63.78; H, 5.35; N, 10.62; S, 8.10%.

1-Benzyl-6-methyl-5-nitro-2-phenyl-4(1*H*)-pyrimidinethione (9c): Mp 224—225 °C; IR ($CHCl_3$) 1618s, 1318s, 1294s, and 1149s cm^{-1}; UV (EtOH) λ_{nm} (10^{-3} ε) ≈250 (≈7.0) and 338 (18.8); ^1H NMR (DMSO-d_6) δ=7.6 (m, 10H), 5.30 (s, 2H), and 2.20 (s, 3H). Found: C, 63.86; H, 4.44; N, 12.45; S, 9.14%. Calcd for $C_{18}H_{15}N_3O_2S$: C, 64.07; H, 4.48; N, 12.45; S, 9.50%.

5-Nitro-1,2,6-triphenyl-4(1*H*)-pyrimidinethione (9i): Mp 260—261 °C; IR ($CHCl_3$) 1615s, 1593s, 1542s, 1329s, and 1170s cm^{-1}; UV (EtOH) λ_{nm} (10^{-3} ε) 256 (10.2) and 342 (12.2); ^1H NMR ($CDCl_3$) δ=7.3 (m, 15H). Found: C, 68.08; H, 3.80; N, 10.65; S, 8.05%. Calcd for $C_{22}H_{15}N_3O_2S$: C, 68.55; H, 3.92; N, 10.90; S, 8.32%.

General Preparation of 4(1*H*)-Pyrimidinethione Derivatives (9) by the Cyclization of 8. A solution containing **8** in DMF (10 times) was heated at 110 °C for 5 min. The solvent was evaporated under reduced pressure. The residue was purified by column chromatography (silica-gel, CH_2Cl_2) to give corresponding **9**. The results are as follows.

6-Methyl-5-nitro-2-phenyl-4(1*H*)-pyrimidinethione (9a): Yield 90%; mp 238 °C; IR ($CHCl_3$) 3400w, 1675w, 1549s, 1328s, and 1155m cm^{-1}; UV (EtOH) λ_{nm} (10^{-3} ε) ≈270 (≈10.0) and 305 (12.0); ^1H NMR (DMSO-d_6) δ=7.7 (m, 5H), 6.5 (br, 1H), and 1.29 (s, 3H). Found: C, 53.32; H, 3.54; N, 16.91; S, 12.82%. Calcd for $C_{11}H_9N_3O_2S$: C, 53.41; H, 3.67; N, 17.00; S, 12.91%.

1,6-Dimethyl-5-nitro-2-phenyl-4(1*H*)-pyrimidinethione (9b): Yield 93%; mp 219—220 °C; IR ($CHCl_3$) 1619s, 1517s, 1294s, and 1153s cm^{-1}; UV (EtOH) λ_{nm} (10^{-3} ε) 251 (8.0) and 335 (18.0); ^1H NMR (DMSO-d_6) δ=7.6 (m, 5H), 3.45 (s, 3H), and 2.36 (s, 3H). Found: C, 55.15; H, 4.25; N, 15.95; S, 12.31%. Calcd for $C_{12}H_{11}N_3O_2S$: C, 55.16; H, 4.24; N, 16.08; S, 12.27%.

6-Methyl-5-nitro-1,2-diphenyl-4(1*H*)-pyrimidinethione (9d): Yield 92%; mp 252—253 °C; IR ($CHCl_3$) 1620s, 1592s, 1535s, 1320m, and 1172s cm^{-1}; UV (EtOH) λ_{nm} (10^{-3} ε) 243 (14.0), 308 (16.8), and 386 (13.2); ^1H NMR (DMSO-d_6) δ=7.6 (m, 10H) and 1.92 (s, 3H). Found: C, 63.01; H, 3.99; N, 12.78; S, 9.86%. Calcd for $C_{17}H_{13}N_3O_2S$: C, 63.14; H, 4.02; N, 12.99; S, 9.91%.

1-Methyl-5-nitro-2,6-diphenyl-4(1*H*)-pyrimidinethione (9g): Yield 96%; mp 235—236 °C; IR ($CHCl_3$) 1613s, 1589m, 1540s, 1330s, and 1153s cm^{-1}; UV (EtOH) λ_{nm} (10^{-3} ε) 245 (11.0) and 338 (19.0); ^1H NMR ($CDCl_3$) δ=7.6 (m, 10H) and 3.50 (s, 3H). Found: C, 63.00; H, 3.98; N, 13.00; S, 9.66%. Calcd for $C_{17}H_{13}N_3O_2S$: C, 63.14; H, 4.05; N, 12.99; S, 9.91%.

1-Benzyl-5-nitro-2,6-diphenyl-4(1*H*)-pyrimidinethione (9h): Yield 91%; mp 237—238 °C; IR ($CHCl_3$) 1605s, 1589s, 1552s, 1328s, and 1168s cm^{-1}; UV (EtOH) λ_{nm} (10^{-3} ε) 248 (11.0) and 340 (16.0); ^1H NMR ($CDCl_3$) δ=7.6 (m, 15H) and 4.98 (s, 2H). Found: C, 69.02; H, 4.11; N, 10.38; S, 7.95%. Calcd for $C_{23}H_{17}N_3O_2S$: C, 69.15; H, 4.29; N, 10.52; S, 8.02%.

General Procedure for the Reaction of 1 with Dimethyl Acetylenedicarboxylate (11). A solution containing **1** (5 mmol) and **11** (5.5 mmol) in THF (15 ml) was refluxed until **1** was consumed as checked by TLC. The solvent was evaporated under reduced pressure. The residue was separated by fractional crystallization and/or column chromatography on silica-gel (CH_2Cl_2) to give [2+2] cycloadducts (**12**) and their ring opening products (**13**), respectively. The results are listed in Table 2.

Dimethyl 3-Methyl-3-methylamino-4-nitro-1-cyclobutene-1,2-dicarboxylate (12b): Mp 120—121 °C; IR ($CHCl_3$) 3150w, 1720s, 1630m, 1604m, 1578s, and 1364s cm^{-1}; UV (EtOH) λ_{nm} (10^{-3} ε) ≈238 (≈5.9) and 354 (6.7); ^1H NMR ($CDCl_3$) δ=11.0 (br, 1H), 6.01 (s, 1H), 3.73 (s, 6H), 3.12 (d, *J*=6Hz, 3H), and 2.19 (s, 3H). Found: C, 46.57; H, 5.43; N, 10.80%. Calcd for $C_{10}H_{14}N_2O_6$: C, 46.51; H, 5.46; N, 10.84%.

Dimethyl 3-Anilino-3-mehtyl-4-nitro-1-cyclobutene-1,2-dicarboxylate (12d): Mp 149—150 °C; IR ($CHCl_3$) 3120w, 1723s, 1639m, 1603s, and 1361s cm^{-1}; UV (EtOH) λ_{nm} (10^{-3} ε) 230 (11.4) and 362 (12.4); ^1H NMR ($CDCl_3$) δ=12.37 (br, 1H), 7.3 (m, 5H), 6.20 (s, 1H), 3.78 (s, 6H), and 2.16 (s, 3H). Found: C, 56.02; H, 4.98; N, 8.73%. Calcd for $C_{15}H_{16}N_2O_6$: C, 56.25; H, 5.03; N, 8.74%.

Dimethyl 3-Amino-4-nitro-3-phenyl-1-cyclobutene-1,2-dicarboxylate (12f): Mp 154—155 °C; IR ($CHCl_3$) 3470w, 3290w, 3190w, 1728s, 1638m, 1599s, 1574s, and 1350s cm^{-1}; UV (EtOH) λ_{nm} (10^{-3} ε) ≈240 (≈8.6), ≈310 (≈5.2), and 355 (11.7); ^1H NMR (DMSO-d_6) δ=9.8 (br, 1H), 9.46 (br, 1H), 7.4 (s, 5H), 5.61 (s, 1H), 3.60 (s, 3H), and 3.42 (s, 3H). Found: C, 54.83; H, 4.53; N, 9.07%. Calcd for $C_{14}H_{14}N_2O_6$: C, 54.90; H,

4.60; N, 9.14%.

Dimethyl 3-Methylamino-4-nitro-3-phenyl-1-cyclobutene-1,2-dicarboxylate (12g): Mp 164—165 °C; IR ($CHCl_3$) 3180w, 1725s, 1630s, 1593s, 1572s, and 1366m cm^{-1}; UV (EtOH) λ_{nm} (10^{-3} ε) ≈240 (≈7.3) and 362 (12.0); ^1H NMR ($CDCl_3$) δ=10.92 (br, 1H), 7.40 (s, 5H), 5.50 (s, 1H), 3.75 (s, 3H), 3.55 (s, 3H), and 2.90 (d, J=6Hz, 3H). Found: C, 56.44; H, 4.87; N, 8.64%. Calcd for $C_{15}H_{16}N_2O_6$: C, 56.25; H, 5.03; N, 8.74%.

Dimethyl 3-Benzylamino-4-nitro-3-phenyl-1-cyclobutene-1,2-dicarboxylate (12h): Mp 114—115 °C; IR ($CHCl_3$) 3190w, 1724s, 1624m, 1590s, 1569s, and 1371s cm^{-1}; UV (EtOH) λ_{nm} (10^{-3} ε) ≈240 (≈7.8) and 362 (13.3); ^1H NMR ($CDCl_3$) δ=11.3 (br, 1H), 7.3 (m, 10H), 5.50 (s, 1H), 4.35 (d, J=6Hz, 2H), 3.75 (s, 3H), and 3.53 (s, 3H). Found: C, 63.39; H, 5.01; N, 7.07%. Calcd for $C_{21}H_{26}N_2O_6$: C, 63.62; H, 5.10; N, 7.07%.

Dimethyl 3-Anilino-4-nitro-3-phenyl-1-cyclobutene-1,2-dicarboxylate (12i): Mp 127—128 °C; IR ($CHCl_3$) 3190w, 1724s, 1625s, 1590s, 1569s, and 1371s cm^{-1}; UV (EtOH) λ_{nm} (10^{-3} ε) ≈231 (≈13.5), ≈310 (≈7.5), and 378 (16.0); ^1H NMR ($CDCl_3$) δ=12.25 (br, 1H), 7.3 (m, 10H), 5.50 (s, 1H), 3.80 (s, 3H), and 3.60 (s, 3H). Found: C, 62.72; H, 4.70; N, 7.12%. Calcd for $C_{20}H_{18}N_2O_6$: C, 62.81; H, 4.76; N, 7.33%.

Dimethyl 2-(1-Aminoethylidene)-3-(nitromethylene)-butanedioate (13a): Liquid; IR ($CHCl_3$) 3360w, 3272w, 3200w, 1720s, 1640m, 1614s, and 1355s cm^{-1}; UV (EtOH) λ_{nm} (10^{-3} ε) 340 (6.4); ^1H NMR ($CDCl_3$) δ=9.95 (br, 1H), 7.58 (br, 1H), 6.95 (s, 1H), 3.81 (s, 3H), 3.73 (s, 3H), and 2.22 (s, 3H). Found: C, 43.99; H, 4.87; N, 11.25%. Calcd for $C_9H_{12}N_2O_6$: C, 44.26; H, 4.95; N, 11.47%.

Dimethyl 3-Nitromethylene-2-(α-piperidinobenzylidene)-butanedioate (13j): Mp 167—168 °C; IR ($CHCl_3$) 1718s, 1618m, 1544s, and 1351s cm^{-1}; UV (EtOH) λ_{nm} (10^{-3} ε) ≈287 (≈8.2) and 404 (12.6); ^1H NMR ($CDCl_3$) δ=7.5 (m, 5H), 6.15 (s, 1H), 3.81 (s, 3H), 3.65 (s, 3H), 3.40 (m, 4H), and 2.88 (m, 6H). Found: C, 60.91; H, 5.93; N, 7.37%. Calcd for $C_{19}H_{22}N_2O_6$: C, 60.96; H, 5.92; N, 7.48%.

General Preparation of δ-Nitro Dienamino Diesters (13) by the Ring Opening Reaction of 12. A solution of **12** in toluene or xylene (10 times of **12**) was refluxed or stirred at 130 °C until **12** was consumed as revealed by TLC. The solvent was evaporated in vacuo, and the residue was recrystallized from CCl_4 or column chromatographed (silica-gel, CH_2Cl_2) to give **13** in 49—99% yields. The results are summarized in Table 3.

Dimethyl 2-[1-(Methylamino)ethylidene]-3-(nitromethylene)butanedioate (13b): IR ($CHCl_3$) 3150w, 1719m, 1608m, and 1363s cm^{-1}; UV (EtOH) λ_{nm} (10^{-3} ε) 322 (6.4); ^1H NMR ($CDCl_3$) δ=11.26 (br, 1H), 6.84 (s, 1H), 3.75 (s, 3H), 3.70 (s, 3H), 3.16 (d, J=6Hz, 3H), and 2.12 (s, 3H). Found: C, 46.23; H, 5.28; N, 10.85%. Calcd for $C_{10}H_{14}N_2O_6$: C, 46.51; H, 5.46; N, 10.84%.

Dimethyl 2-(1-Anilinoethylidene)-3-(nitromethylene)-butanedioate (13d): IR ($CHCl_3$) 3150w, 1721s, 1638m, 1605m, 1583s, and 1364s cm^{-1}; UV (EtOH) λ_{nm} (10^{-3} ε) 356 (6.6); ^1H NMR ($CDCl_3$) δ=12.49 (br, 1H), 7.4 (m, 5H), 6.98 (s, 1H), 3.80 (s, 3H), 3.75 (s, 3H), and 2.00 (s, 3H). Found: C, 56.24; H, 5.00; N, 8.80%. Calcd for $C_{15}H_{16}N_2O_6$: C, 56.25; H, 5.03; N, 8.84%.

Dimethyl 2-(α-Aminobenzylidene)-3-(nitromethylene)-butanedioate (13f): IR ($CHCl_3$) 3470w, 3280w, 3180w, 1725s, 1639m, 1601s, 1572m, and 1370s cm^{-1}; UV (EtOH) λ_{nm} (10^{-3} ε) ≈240 (≈8.6) and 350 (10.0); ^1H NMR ($CDCl_3$) δ=9.88 (br, 1H), 7.39 (m, 5H), 6.53 (s, 1H), 6.38 (br, 1H), 3.79 (s, 3H), and 3.58 (s, 3H). Found: C, 55.00; H, 4.61; N, 8.96%. Calcd for $C_{14}H_{14}N_2O_6$: C, 54.90; H, 4.60; N, 9.14%.

Dimethyl 2-[α-(Methylamino)benzylidene]-3-(nitromethylene)butanedioate (13g): IR ($CHCl_3$) 3150w, 1724s, 1639m, 1600s, and 1375s cm^{-1}; UV (EtOH) λ_{nm} (10^{-3} ε) 323 (6.6); ^1H NMR ($CDCl_3$) δ=10.95 (br, 1H), 7.30 (m, 5H), 6.50 (s, 1H), 3.78 (s, 3H), 3.68 (s, 3H), and 2.90 (d, J=5Hz, 3H). Found: C, 56.18; H, 5.05; N, 8.76%. Calcd for $C_{15}H_{16}N_2O_6$: C, 56.25; H, 5.03; N, 8.74%.

Dimethyl 2-[α-(Benzylamino)benzylidene]-3-(nitromethylene)butanedioate (13h): IR ($CHCl_3$) 3180w, 1725s, 1638m, 1592s, 1571m, and 1376s cm^{-1}; UV (EtOH) λ_{nm} (10^{-3} ε) 327 (6.1); ^1H NMR ($CDCl_3$) δ=11.19 (br, 1H), 7.3 (m, 10H), 6.50 (s, 1H), 4.33 (d, J=6Hz, 2H), 3.73 (s, 3H), and 3.63 (s, 3H). Found: C, 63.53; H, 5.01; N, 7.07%. Calcd for $C_{21}H_{20}N_2O_6$: C, 63.62; H, 5.10; N, 7.07%.

Dimethyl 2-(α-Anilinobenzylidene)-3-(nitromethylene)-butanedioate (13i): IR ($CHCl_3$) 3160w, 1725s, 1639m, 1595m, 1568s, and 1380s cm^{-1}; UV (EtOH) λ_{nm} (10^{-3} ε) ≈233 (≈12.8) and 378 (11.0); ^1H NMR ($CDCl_3$) δ=12.30 (br, 1H), 7.2 (m, 10H), 6.53 (s, 1H), 3.75 (s, 3H), and 3.55 (s, 3H). Found: C, 62.72; H, 4.73; N, 7.27%. Calcd for $C_{20}H_{18}N_2O_6$: C, 62.81; H, 4.76; N, 7.33%.

References

1) T. Tokumitsu and T. Hayashi, *J. Org. Chem.*, **50**, 1547 (1985).

2) D. Rajappa, *Heterocycles*, **7**, 507 (1977).

3) S. Maiorana, D. Pocar, and P. D. Croce, *Tetrahedron Lett.*, **1966**, 6043.

4) D. Pocar, S. Maiorana, and P. D. Croce, *Gazz. Chim. Ital.*, **98**, 949 (1968).

5) G. deStevens, B. Smolinsky, and L. Dorfman, *J. Org. Chem.*, **29**, 1115 (1964).

6) L. J. Bellamy, "Advances in Infrared Group Frequencies," Methuen & Co. Ltd., London (1968), p. 213.

7) T. Tokumitsu and T. Hayashi, *Nippon Kagaku Kaishi*, **1983**, 88.

8) K. C. Brannock, R. D. Burpitt, V. W. Goodlett, and J. G. Thweatt, *J. Org. Chem.*, **28**, 1464 (1963); G. A. Berchtold, and G. F. Uhlig, *ibid.*, **28**, 1459 (1963); C. F. Huebner, L. Dorfman, M. M. Robinson, E. Donoghue, W. G. Pierson, and P. Strachan, *ibid.*, **28**, 3139 (1963).

9) D. Lloyd and H. McNab, *Ang. Chem. Int. Ed. Engl.*, **15**, 459 (1976).

Liquid Crystal Materials with Sulfur Atoms Incorporated in the Principal Structure. VI. Optically Active New Smectic Liquid Crystal Compounds with 1,3-Oxathiane or 1,3-Dithiane Ring

Yuichiro HARAMOTO,* Yoko TOMITA, and Hiroyoshi KAMOGAWA
Department of Applied Chemistry, Yamanashi University, Takeda 4, Kofu 400
(Received May 16, 1986)

(+)-2-Methylbutyl *p*-(5-alkyl-1,3-oxathian-2-yl)benzoate and -cinnamate (**7**) were synthesized. The mesomorphic behavior of these compounds were measured. Though (+)-2-methylbutyl *p*-(5-alkyl-1,3-oxathian-2-yl)-benzoate did not exhibit any liquid-crystal phase, the corresponding 1,3-dithiane compounds (**8-1**, **8-2**, and **8-3**) and compound (**7-4**) having R' of a normal alkyl chain exhibited a smectic phase. This must originate in the wider molecular widths of compounds **7-1**, **7-2**, and **7-3**. Though cinnamate of compounds **7** and **8** exhibited an enantiotropic behavior, the corresponding benzoate did not. This must originate from an increase in the length of the conjugated system and the molecular length.

In recent years, 2,5-disubstituted 1,3-dithianes and 1,3-oxathianes have been reported as new types of liquid-crystal materials.[1-9]

In proportion to the increase in attention given to new types of liquid-crystal displays using ferroelectric liquid crystals, various optically active smectic liquid-crystal compounds have been synthesized. Thus, the basic structure of optically active new smectic liquid-crystal compounds with a 1,3-oxathiane (**7**) or a 1,3-dithiane ring (**8**) was synthesized.

This paper is related to this synthesis and the mesomorphic behavior of these compounds.

Results and Discussion

(+)-2-Methylbutyl *p*-(5-alkyl-1,3-oxathian-2-yl)benzoate and -cinnamate **7** and the corresponding 1,3-dithiane compounds **8** were synthesized via the following route.

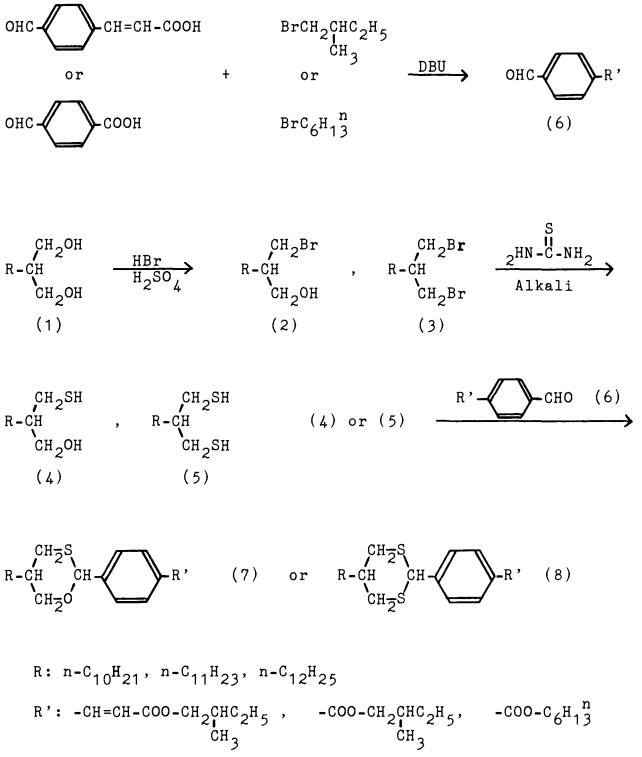

Fig. 1.

In step **1**→**2**, **3**, the reaction temperature was kept at between 80 and 85 °C so as to produce compounds **2** and **3** at nearly equal rates. A separation between **2** and **3** was not carried out. In step **2**, **3**→**4**, **5**, compounds **4** and **5** could be successfully separated by column chromatography. That is, compound **5** effused in a hexane fraction and **4** in an ether fraction. In steps **4**→**7** and **5**→**8**, cis and trans isomers were produced which differed at the C-5 position of the 1,3-oxathiane and 1,3-dithiane ring, respectively. Repeated recrystallizations (about five to seven times) were required to obtain purified trans isomers. Though for several compounds of **7** and **8**, trans isomers could not be separated by recrystallization, they were gained by using a separative TLC (hexane : ether=5 : 2). In the ^{1}H NMR data of 1,3-dithiane and 1,3-oxathiane compounds, C-2 proton signals of the 1,3-dithiane or 1,3-oxathiane ring for the trans isomer exhibited about 0.05 ppm with a different magnetic field than those for a cis isomer. For example, in compounds **8-1** and **7-4**, the trans isomer absorbs δ=5.2 (**8-1**) and 5.75 (**7-4**) but the cis isomer absorbs at δ=5.15 (**8-1**) and 5.80 (**7-4**), respectively. Therefore, the contamination of the cis isomers can be detected.

The angle of optical rotation was measured for compound **8-1** using a polarimeter; a value of +9.5° was obtained. This must mean that racemization did not occur in this reaction course.

A measurement of the mesomorphic ranges and assignment of the mesophases were carried out by means of a micro melting-point apparatus equipped with polarizers and a differential scanning calorimeter (DSC).

To determine the type of smectic phase, these smectic phases were compared with the color photographs found in the literature.[10]

A focal-conic fan texture of smectic A was observed.

Mesomorphic ranges of the synthesized 1,3-dithianes and 1,3-oxathianes are given in Table 1.

Compounds **7-1**, **7-2**, and **7-3** did not exhibit any

Table 1. Transition Temperature of Compounds **7** and **8**

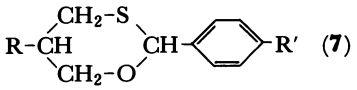

(**7**)

	R	R′	Transition temp/°C[a)]
7-1	*n*-$C_{10}H_{21}$	$-COOCH_2CHC_2H_5$ (CH$_3$)	C 35/11 I
7-2	*n*-$C_{11}H_{23}$	$-COOCH_2CHC_2H_5$ (CH$_3$)	C 45/32 I
7-3	*n*-$C_{12}H_{25}$	$-COOCH_2CHC_2H_5$ (CH$_3$)	C 37/28 I
7-4	*n*-$C_{11}H_{23}$	$-COOC_6H_{13}^n$	C 48 S_A 12 43 I
7-5	*n*-$C_{10}H_{21}$	$-CH=CH-COOCH_2CHC_2H_5$ (CH$_3$)	C 35/−50 S_A 71/71 I
7-6	*n*-$C_{11}H_{23}$	$-CH=CH-COOCH_2CHC_2H_5$ (CH$_3$)	C 50/−19 S_A 74/74 I

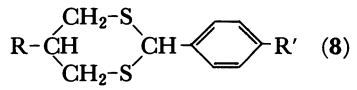

(**8**)

8-1	*n*-$C_{10}H_{21}$	$-COOCH_2CHC_2H_5$ (CH$_3$)	C 46 S_A −15 23 I
8-2	*n*-$C_{11}H_{23}$	$-COOCH_2CHC_2H_5$ (CH$_3$)	C 44 S_A 18 28 I
8-3	*n*-$C_{12}H_{25}$	$-COOCH_2CHC_2H_5$ (CH$_3$)	C 48 S_A 27 39 I
8-4	*n*-$C_{12}H_{25}$	$-COOC_6H_{13}^n$	C 56 S_A 16 54 I
8-5	*n*-$C_{10}H_{21}$	$-CH=CH-COOCH_2CHC_2H_5$ (CH$_3$)	C 53/16 S_A 88/88 I
8-6	*n*-$C_{11}H_{23}$	$-CH=CH-COOCH_2CHC_2H_5$ (CH$_3$)	C 54/18 S_A 82/82 I

a) C: crystal; S: smectic; I: isotropic.

liquid-crystal phases. However, the corresponding 1,3-dithiane compounds (**8-1**, **8-2**, and **8-3**) exhibited a smectic phase. Also, compound **7-4** having a normal alkyl chain in substituent R′ exhibited a smectic phase. From these results, the main factor for the formation of the mesophase must be the molecular width; thus, compounds **7-1**, **7-2**, and **7-3**, having wider molecular widths, can not exhibit any mesophases. That is, the bend at the 1,3-oxathiane ring due to a difference in the atomic size between sulfur and oxygen and the side chain included in R′ increase the molecular width of compounds **7-1**, **7-2**, and **7-3**; this must weaken interactions among the molecules.

Though compounds **7-5**, **7-6**, **8-5**, and **8-6** exhibited an enantiotropic-type behavior, corresponding benzoate compounds (**7-1**, **7-2**, **8-1**, **8-2**) did not. The existence of the CH=CH part implies an increase in molecular length and the length of the conjugated system. These two factors must contribute to the appearance on the enantiotropic behavior.

The transition temperatures of isotropic to smectic for 1,3-oxathiane compounds (**7-5**, **7-6**) were lower than those for the corresponding 1,3-dithianes (**8-5**, **8-6**). Generally, in a smectic liquid crystal, the temperature of isotropic to smectic is affected by two factors: the molecular width and interactions of side substituents.[11] In this case, a wider molecular width caused by a bend at the oxathiane ring seems to be the cause.

All of compounds **7** and **8** exhibited supercooling states, especially **7-5** and **7-6** have a wide range.

$\Delta H_{C\text{-}I}$ of compounds **7-1**, **7-5**, **8-1**, and **8-5** are 24.64, 21.25, 23.78, and 26.07 kJ mol^{-1} and $\Delta S_{C\text{-}I}$ of them are 79.9, 68.99, 79.96, and 75.77 $JK^{-1}mol^{-1}$, respectively. These values are somewhat smaller than those of other common liquid-crystal materials.[12]

Experimental

IR, ^{1}H NMR, and mass spectra were obtained with a Hitachi 215 spectrophotometer, a JNM-PMX 60 spectrometer, and a Hitachi M-80B spectrometer, respectively. Elemental analyses were carried out with a Perkin-Elmer 250 instrument. Transition temperatures and mesomorphic phases were determined by means of both a Mitamura Riken micro melting-point aparatus equipped with polarizers and a Rigaku Denki DSC CN8059L1, CN8208A2. The rate of cooling was fixed to 1 °C min^{-1}.

Mixture of 2-Alkyl-3-bromo-1-propanol (2) and 2-Alkyl-1,3-dibromopropane (2). To a solution of 48% HBr (50 g) and concd H_2SO_4 (15 g) cooled in an ice bath were added, successively, compound **1** (0.1 mol) and concd H_2SO_4 (25 g). The solution was kept at 80—85 °C for 15 h. The reaction mixture was then poured into ice water (200 g), stirred and extracted twice with ether (each 400 ml). The extract was washed with cold 10% aq $NaHCO_3$ (100 ml), dried over anhyd Na_2SO_4, and concentrated on an evaporator at 30 °C. The residue was distilled in vacuo to afford a transparent liquid in a 50—60% yield.

2-Alkyl-3-mercapto-1-propanol (4) and 2-Alkyl-1,3-propanedithiol (5). To a solution of thiourea (0.2 mol) in triethylene glycol (15 ml) kept at 75 °C was added a mixture of compounds **2** and **3** in a nitrogen atmosphere, followed by stirring at 75 °C for 18 h. Tetraethylenepentamine (0.05 mol) was then added, and the mixture was stirred at 75 °C for 2 h under a nitrogen atmosphere. The reaction mixture was distilled in vacuo to afford a transparent liquid. The separation of compounds **4** and **5** was carried out by column chromatography (Wakogel C-300). Compounds **5** effused in a hexane fraction and **4** in an ether fraction. Compound **4** was a colorless transparent liquid and **5** was a yellow transparent liquid.

IR ($CHCl_3$) Compounds **4**: 3600 (OH), 2800—3000 (alkyl) cm^{-1}. Compounds **5**: 2800—3000 (alkyl).

^{1}H NMR ($CDCl_3$) Compounds **4**: δ=0.6—2.0 (m, R-CH, SH), 2.5—2.8 (m, 2H, CH_2S), 3.3—3.9 (m, 3H, CH_2OH). Compounds **5**: δ=0.6—2.0 (m, R-CH, SH), 2.5—2.9 (m, 4H, $-CH_2S$).

(+)-2-Methylbutyl *p*-Formylcinnamate (6-1). A solution of *p*-formylcinnamic acid (0.03 mol) and 1,8-diazabicyclo-[5.4.0] undec-7-ene (0.03 mol) and (+)-2-methylbutyl bromide (0.03 mol) in anhyd DMF (60 ml) was stirred at 80—90 °C for 18 h under a nitrogen atmosphere. The solution was poured into ice water and extracted twice with ether (each 200 ml). The extract was washed with cold 2% aq HCl, dried over anhyd Na_2SO_4, and evaporated in vacuo at 30 °C. The residue was dissolved in hexane (30 ml) and filtered. The filtrate was evaporated in vacuo at 40 °C. A transparent liquid was obtained in 70—80% yields.

IR ($CHCl_3$) 2800—3000 (alkyl), 2730 (CHO), 1680—1720 (C=O) cm^{-1}. ^{1}H NMR ($CDCl_3$) δ=0.5—2.0 (m, 9H, OCH_2R''), 4.1 (d, 2H, OCH_2), 6.6 (d, 1H, =CH), 7.5—8.1 (q, 5H, CH=, ArH), 10.1 (s, 1H, CHO).

(+)-2-Methylbutyl *p*-Formylbenzoate (6-2). IR ($CHCl_3$) 2800—3000 (alkyl), 2730 (CHO), 1680—1720 (C=O) cm^{-1}. ^{1}H NMR ($CDCl_3$) δ=0.6—2.1 (m, 9H, $OCH_2\underline{R}''$), 4.25 (d, 2H, OCH_2), 8.2 (q, 4H, ArH), 10.2 (s, 1H, CHO).

Hexyl *p*-Formylbenzoate (6-3). IR ($CHCl_3$) 2800—3000 (alkyl), 2730 (CHO), 1680—1720 (C=O) cm^{-1}. ^{1}H NMR ($CDCl_3$) δ=0.7—2.1 (m, 11H, $OCH_2C_5\underline{H}_{11}$), 4.4 (t, 2H, OCH_2), 8.1 (q, 4H, ArH), 10.2 (s, 1H, CHO).

Alkyl *p*-(5-Alkyl-1,3-oxathian-2-yl)benzoate or -cinnamate (7). To a solution of compound **4** (0.04 mol) and *p*-substituted benzaldehyde **6** (0.04 mol) in anhyd $CHCl_3$ (200 ml) cooled in an ice bath were added $BF_3\cdot(C_2H_5)_2O$ (0.5 g) and molecular sieves (3A, 1/15; 3g). The mixture was stirred at 0—5 °C for 8h and then at 20 °C for 15h. The solution was first washed with 10% aq $NaHCO_3$ (400 ml), then with water (400 ml), dried over anhyd Na_2SO_4, and evaporated in vacuo at 40 °C. The crude product was purified by column chromatography and recrystallizations from hexane; then, several compounds which could not be isolated as trans isomers were subjected to separative TLC (hexane:ether= 5 : 2) to isolate trans isomers.

IR ($CHCl_3$) 2800—3000 (alkyl), 1710 (C=O), 1605 (Ar) cm^{-1}. ^{1}H NMR ($CDCl_3$).

(+)-2-Methylbutyl *p*-(5-Alkyl-1,3-oxathian-2-yl)benzoate. δ=0.7—2.1 (m, R-CH, OCH_2R''), 2.8 (d, 2H, CH_2S), 3.3, 4.3 (m, 2H, CH_2O), 4.2 (d, 2H, OCH_2R''), 5.75 (s, 1H, $\overset{S}{O}\!>\!CH$), 7.8 (q, 4H, ArH).

Hexyl *p*-(5-Undecyl-1,3-oxathian-2-yl)benzoate: δ=0.5—2.1 (m, 35H, R-CH, $OCH_2C_5H_{11}$), 2.8 (d, 2H, CH_2S), 3.3, 4.3 (m, 2H, CH_2O), 4.3 (t, 2H, $OC\underline{H}_2C_5H_{11}$), 5.75 (s, 1H, $\overset{S}{O}\!>\!CH$), 7.8 (q, 4H, ArH).

(+) 2-Methylbutyl *p*-(5-Alkyl-1,3-oxathian-2-yl)cinnamate: δ=0.5—2.2 (m, R-CH, OCH_2R''), 2.8 (d, 2H, CH_2S), 3.3, 4.2 (m, 4H, CH_2O), 5.7 (s, 1H, $\overset{S}{O}\!>\!CH$), 6.4 (d, 1H, =CH), 7.5 (s, 4H, ArH), 8.0 (d, 1H, CH=).

Alkyl *p*-(5-Alkyl-1,3-dithian-2-yl)benzoate or -cinnamate (8). Compounds **8** were synthesized according to the same ptocedure as that for compounds **7**.

IR ($CHCl_3$) 2800—3000 (alkyl), 1705 (C=O), 1600 (Ar) cm^{-1}. ^{1}H NMR ($CDCl_3$).

(+)-2-Methylbutyl *p*-(5-Alkyl-1,3-dithian-2-yl)benzoate: δ=0.5—2.1 (m, R-CH, $OCH_2\underline{R}''$), 2.6—2.9 (m, 4H, CH_2S), 4.2 (d, 2H, CH_2O), 5.2 (s, 1H, $\overset{S}{S}\!>\!CH$), 7.8 (q, 4H, ArH).

Hexyl *p*-(5-Dodecyl-1,3-dithian-2-yl)benzoate: δ=0.6—2.1 (m, 37H, R-CH, $OCH_2C_5\underline{H}_{11}$), 2.6—2.9 (d, 4H, CH_2S), 4.3 (t, 2H, CH_2O), 5.2 (s, 1H, $\overset{S}{S}\!>\!CH$), 7.8 (q, 4H, ArH).

(+)-2-Methylbutyl *p*-(5-Alkyl-1,3-dithian-2-yl)cinnamate: δ=0.5—2.2 (m, R-CH, OCH_2R''), 2.6—2.9 (m, 4H, CH_2S), 4.05 (d, 2H, OCH_2), 5.15 (s, 1H, $\overset{S}{S}\!>\!CH$), 6.4 (d, 1H, =CH), 7.5 (s, 4H, ArH), 8.05 (d, 1H, CH=).

7-1: Yield 29%. Found: C, 71.59; H, 9.82%. Calcd for $C_{26}H_{42}O_3S$: C, 71.84; H, 9.74%. (*m/z*) 434 (M^+).
7-2: Yield 28%. Found: C, 71.91; H, 9.92%. Calcd for $C_{27}H_{44}O_3S$: C, 72.27; H, 9.88%. MS (*m/z*) 448 (M^+).
7-3: Yield 32%. Found: C, 72.88; H, 9.99%. Calcd for $C_{28}H_{46}O_3S$: C, 72.68; H, 10.02%. MS (*m/z*) 462 (M^+).
7-4: Yield 26%. Found: C, 72.71; H, 10.02%. Calcd for $C_{28}H_{46}O_3S$: C, 72.68; H, 10.02%. MS (*m/z*) 462 (M^+).
7-5: Yield 28%. Found: C, 72.90; H, 9.70%. Calcd for $C_{28}H_{44}O_3S$: C, 72.99; H, 9.63%. MS (*m/z*) 460 (M^+).
7-6: Yield 37%. Found: C, 72.99; H, 9.82%. Calcd for $C_{29}H_{46}O_3S$: C, 73.37; H, 9.77%. MS (*m/z*) 474 (M^+).
8-1: Yield 28%. Found: C, 68.91; H, 9.44%. Calcd for $C_{26}H_{42}O_2S_2$: C, 69.28; H, 9.39%. MS (*m/z*) 450 (M^+).
8-2: Yield 32%. Found: C, 69.00; H, 9.65%. Calcd for $C_{27}H_{44}O_2S_2$: C, 69.77; H, 9.54%. MS (*m/z*) 464 (M^+).
8-3: Yield 21%. Found: C, 69.83; H, 9.75%. Calcd for $C_{28}H_{46}O_2S_2$: C, 70.24; H, 9.68%. MS (*m/z*) 478 (M^+).
8-4: Yield 30%. Found: C, 70.62; H, 9.83%. Calcd for $C_{29}H_{48}O_2S_2$: C, 70.68; H, 9.82%. MS (*m/z*) 492 (M^+).
8-5: Yield 32%. Found: C, 70.63; H, 9.51%. Calcd for $C_{28}H_{44}O_2S_2$: C, 70.53; H, 9.30%. MS (*m/z*) 476 (M^+).
8-6: Yield 30%. Found: C, 71.28; H, 9.42%. Calcd for $C_{29}H_{46}O_2S_2$: C, 70.97; H, 9.45%. MS (*m/z*) 490 (M^+).

References

1) Y. Haramoto and H. Kamogawa, *J. Chem. Soc., Chem. Commun.*, **1983**, 75.
2) Y. Haramoto, A. Nobe, and H. Kamogawa, *Bull. Chem. Soc. Jpn.*, **57**, 1966 (1984).
3) Y. Haramoto, K. Akazawa, and H. Kamogawa, *Bull. Chem. Soc. Jpn.*, **57**, 3173 (1984).
4) Y. Haramoto and H. Kamogawa, *Bull. Chem. Soc. Jpn.*, **58**, 477 (1985).
5) Y. Haramoto and H. Kamogawa, *Chem. Lett.*, **1985**, 79.
6) Y. Haramoto and H. Kamogawa, *Bull. Chem. Soc. Jpn.*, **58**, 1821 (1985).
7) Y. Haramoto and H. Kamogawa, *Mol. Cryst. Liq. Cryst.*, **131**, 101 (1985).
8) Y. Haramoto and H. Kamogawa, *Mol. Cryst. Liq. Cryst.*, **131**, 201 (1985).
9) Y. Haramoto, M. Sano, and H. Kamogawa, *Bull. Chem. Soc. Jpn.*, **59**, 1337 (1986).
10) D. Demus and L. Richter, "Textures of Liquid Crystals," Verlag Chemie, Weinheim, New York (1978).
11) G.W. Gray and B.M. Worrall, *J. Chem. Soc.*, **1959**, 1545.
12) G.W. Gray and P.A. Winsor, "Liquid Crystals & Plastic Crystals," Wiley, New York (1978), Vol. 2, p. 254.

 © 1986 The Chemical Society of Japan Bull. Chem. Soc. Jpn., 59, 3881—3884 (1986)

Synthetic Studies of Diels-Alder Adduct of Furan. Formal Total Synthesis of (±)-Avenaciolide

Hiyoshizo KOTSUKI,* Hiroyuki OHNISHI, Yasuhiro AKITOMO, Masamitsu OCHI
Department of Chemistry, Faculty of Science, Kochi University, Akebono-cho, Kochi 780
(Received May 30, 1986)

The *endo*-Diels-Alder adduct of furan with methyl acrylate was transformed into a bis-γ-lactone derivative which is a well-known precursor for the synthesis of (±)-avenaciolide. The route involves 13 steps and the overall yield was 17.9%.

The 7-oxabicyclo[2.2.1]heptene derivatives, which can be prepared by Diels-Alder reaction of furan with appropriate dienophiles, are versatile precursors for the synthesis of various important natural products.[1] However, mainly due to the sluggish reactivity of furan itself, such derivatives have remained difficult to access.

Recently, we demonstrated a practical method for the preparation of the Diels-Alder adduct (**1**) between furan and methyl acrylate under $BF_3 \cdot OEt_2$-catalyzed conditions (Eq. 1).[2] Herein, we wish to report on the

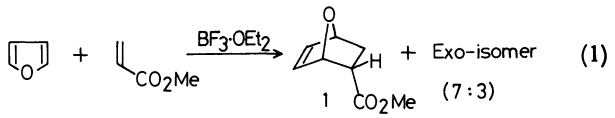

(1)

stereoselective synthesis of the antifungal metabolite (±)-avenaciolide (**2**).[3] The strategy of the synthesis

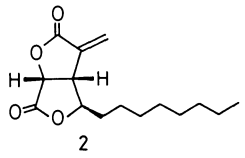

2

relies on the advantageous structure of adduct (**1**) which has two of three stereocenters in the target system and the stereoselective iodolactonization for the preparation of the remaining one (Scheme 1).

The *endo*-ester (**1**) was transformed into the alcohol (**5**) via the triol (**4**) in 77.8% overall yield. Swern oxidation[4] of this alcohol under carefully controlled conditions gave cleanly aldehyde (**6**) without epimerization,[5] this was treated with Wittig reagent to give **7** as the sole product. The structure of the olefin was determined as having a cis-configuration by ^1H NMR measurement (J=11 Hz). Deprotection of acetonide, $NaIO_4$ cleavage, and Jones oxidation provided dicarboxylic acid (**9**). Since this product was rather unstable, presumably due to its sterically congested structure, the crude sample was used directly for the further experiment.

For the construction of the remained stereocenter we applied the well-known chemistry of iodolactonization.[6] Thus, by treatment with KI-I_2 **9** was smoothly converted into the iodo lactone carboxylic acid (**10**). The relative stereochemistry of this product could not be determined at this stage, but we expected the reaction to yield predominantly compound (**10**) with the

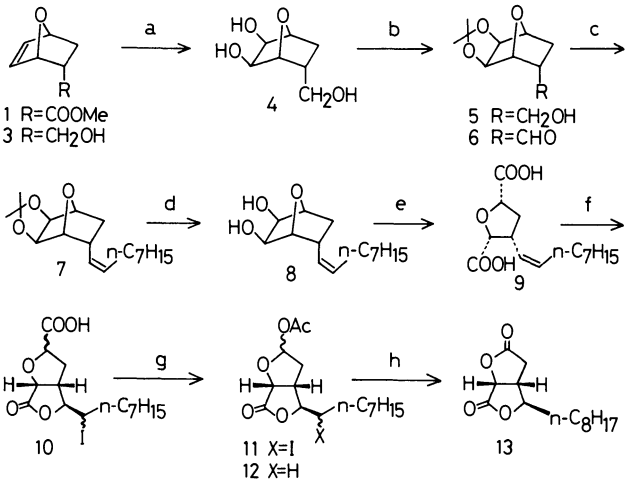

Scheme 1. Reagents and Conditions.
(a): 1) $LiAlH_4$, Et_2O, 2) OsO_4, 30% H_2O_2, RT, (b): 1) 2,2-dimethoxypropane, MeOH, pyridinium *p*-toluenesulfonate, RT, 2) $(COCl)_2$, DMSO, Et_3N, −78°C, (c): Ph_3P^+-*n*-$C_8H_{17}Br^-$, *n*-BuLi, THF, RT, overnight, (d): 2M HCl, MeOH, (e): 1) $NaIO_4$, THF-H_2O, 2) CrO_3-H_2SO_4, acetone, (f): KI-I_2, $NaHCO_3$, THF-H_2O, RT, overnight, (g): 1) $Pb(OAc)_4$, C_6H_6, reflux, 2 h, 2) *n*-Bu_3SnH, AIBN(cat.), C_6H_6, reflux, 20 h, (h): 1) K_2CO_3, MeOH-H_2O, 2) CrO_3-H_2SO_4, acetone.

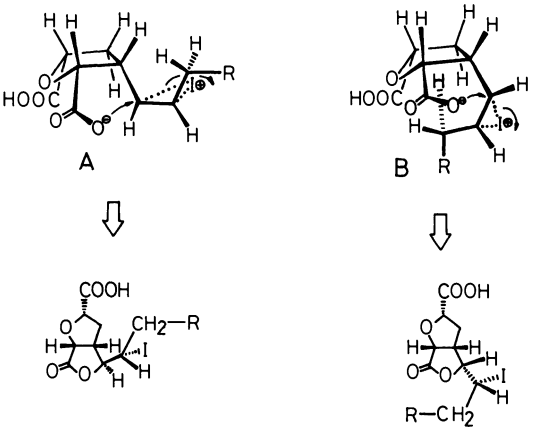

Fig. 1.

desired stereochemistry based on the consideration of molecular models. As illustrated in Fig. 1, there are two stereoselections for this cyclization process in which the ring closure should take a favored *5-Exo-Trig* path[7] and the nucleophile should cleave the iod-

onium ring by rear-side attack. When the reaction takes place through an intermediate **A**, the desired product will be obtained. While the intermediate **B** will give the undesired one which possesses an isoavenaciolide skeleton. The obvious relative steric comfort will favor the intermediate **A** over **B**. We recognized that this expectation is correct after completion of our work (vide infra).

In analogy with Masamune's earlier work,[8] bis-γ-lactone formation was performed by a 4-step process; decarboxylative acetylation with lead tetraacetate, deiodination with tributyltin hydride, hydrolysis of acetate, and Jones oxidation. Purification by silica-gel column chromatography gave the desired bis-γ-lactone (**13**) as a single product in 32.3% overall yield from **8** and the structure was confirmed by the comparison with an authentic sample.[9] This result means that as expected the iodolactonization proceeded in a desired fashion.[10] Introduction of the α-methylene group on **13** was reported previously,[3] so this work constitutes a formal total synthesis of (±)-avenaciolide.

By using optically pure starting material[11] it will be possible to synthesize avenaciolide in the natural form.

Experimental

General. All boiling and melting points are uncorrected. ^{1}H NMR spectra were obtained on a JEOL-MH-100 spectrometer using TMS as the internal standard. ^{13}C NMR spectra were obtained at 25.05 MHz on a JEOL-FX-100 spectrometer. The IR spectra were measured with a JASCO infrared spectrophotometer Model IRA-1 or A-302 and the high resolution mass spectra on a JEOL-HX-100 spectrometer.

TLC was conducted using Merck's precoated Kieselgel 60 F-254 plates (0.25 mm) and for column chromatography, Wakogel C-200 was employed.

Ether and THF were distilled from sodium benzophenone ketyl. Benzene was distilled from sodium metal. Dichloromethane, triethylamine and DMSO were distilled over CaH_2. Acetone was distilled once from CrO_3 and stored over molecular sieves 3A.

Reduction of 1: To a stirred suspension of 360 mg (9.5 mmol) of $LiAlH_4$ in 36 ml of dry Et_2O at 0 °C was added a solution of **1** (1.68 g, 11 mmol) in 12 ml of dry Et_2O. After being stirred at room temperature for 5 h, the reaction mixture was diluted with Et_2O (20 ml) and quenched at 0 °C by addition of a minimum amount of water. After drying with anhydrous $MgSO_4$ the mixture was filtered through Celite and the solid washed well with AcOEt. Evaporation of the solvent gave 1.38 g (100%) of almost pure alcohol (**3**).

3: TLC R_f=0.34 (Et_2O); Bp 110 °C/5 mmHg (1 mmHg =133.322 Pa; bath temperature); IR (neat) 3400 and 1035 cm^{-1}; ^{1}H NMR ($CDCl_3$) δ=0.64 (1H, dd, J=12, 4 Hz), 1.96 (1H, ddd, J=12, 9, 4.5 Hz), 2.2—2.6 (1H, m), 3.10 (1H, t, J=10 Hz), 3.4—3.7 (2H, m), 4.90, 4.98 (each 1H, dd, J=4.5, 1.5 Hz), 6.26, 6.37 (each 1H, dd, J=6, 1.5 Hz). Found: C, 66.47; H, 8.03%. Calcd for $C_7H_{10}O_2$: C, 66.64; H, 7.99%.

Formation of Triol (4) with OsO_4: To a solution of **3** (1.19 g, 9.4 mmol) in 35 ml of acetone and 9 ml of Et_2O were successively added 11.5 ml aqueous solution of OsO_4 (0.055 mmol) and 3.8 ml of 30% H_2O_2 at 0 °C and the resulting brownish solution was stirred at room temperature overnight. At the end of the reaction the solution color disappeared. After evaporation of the solvent, finally azeotropically with toluene, the residue was purified by silica-gel column chromatography, elution with AcOEt–MeOH (9 : 1), and recrystallized from AcOEt–MeOH to give 1.22 g (80.7%) of triol (**4**) as colorless needles.

4: TLC R_f=0.34 (AcOEt–MeOH, 9:1); Mp 101.0—101.5 °C; IR (nujol) 3400 and 1075 cm^{-1}; ^{1}H NMR (DMSO-d^6–$CDCl_3$) δ=0.93 (1H, dd, J=12.5, 5 Hz), 1.82 (1H, ddd, J=12.5, 12, 6 Hz), 2.0—2.4 (1H, br m), 2.7 (1H, br), 3.3—4.0 (4H, m), 4.0—4.4 (4H, m). Found: C, 52.47; H, 7.59%. Calcd for $C_7H_{12}O_4$: C, 52.49; H, 7.55%.

Formation of Acetonide (5): A mixture of **4** (1.22 g, 7.63 mmol) and 2,2-dimethoxypropane (5.6 ml) in 2.4 ml of dry MeOH containing a catalytic amount of pyridinium *p*-toluenesulfonate was stirred at room temperature overnight. After evaporation of most of the organic solvent the residue was poured into CH_2Cl_2 and washed successively with water, satd $NaHCO_3$, and satd NaCl, dried with $MgSO_4$, and evaporated. Recrystallization from hexane–Et_2O gave 1.47 g (96.4 %) of the acetonide (**5**).

5: TLC R_f=0.63 (AcOEt–MeOH, 9 : 1); Mp 104.5—107 °C; IR (nujol) 3460 and 1055 cm^{-1}; ^{1}H NMR ($CDCl_3$) δ=0.89 (1H, dd, J=12.5, 5.5 Hz), 1.29, 1.48 (each 3H, s), 1.89 (1H, ddd, J=12.5, 12, 6 Hz), 2.1—2.5 (1H, m), 2.6 (1H, br), 3.51 (1H, dd, J=11, 8.5 Hz), 3.72 (1H, dd, J=11, 7 Hz), 4.15 (1H, d, J=6 Hz), 4.33 (1H, d, J=2 Hz), 4.39 (1H, br s), 4.55 (1H, d, J=6 Hz). Found: C, 59.76; H, 7.97%. Calcd for $C_{10}H_{16}O_4$: C, 59.98; H, 8.05%.

Swern Oxidation of the Alcohol (5): To a stirred suspension of 0.39 ml (4.5 mmol) of oxalyl dichloride in 7 ml of dry CH_2Cl_2 at −78 °C was added 0.64 ml (9.0 mmol) of dry DMSO. After being stirred at −78 °C for 10 min, to the suspension was added a solution of **5** (500 mg, 2.5 mmol) in 3 ml of dry CH_2Cl_2 at the same temperature. After being stirred at −78 °C for 1 h,[12] to the reaction mixture was added 2.44 ml (17.5 mmol) of dry Et_3N. The reaction mixture was diluted with 120 ml of AcOEt and quickly washed with cold satd $NaHCO_3$ and satd NaCl, dried with $MgSO_4$, and evaporated. The crude product was purified by silica-gel column chromatography and elution with hexane–AcOEt (1 : 2), to give 395 mg (80%) of pure aldehyde (**6**) as colorless crystals.

6: TLC R_f=0.25 (Et_2O); Mp 93—94.5 °C (from hexane–acetone); IR (nujol) 1710, 1210, and 1065 cm^{-1}; ^{1}H NMR ($CDCl_3$) δ=1.26, 1.46 (each 3H, s), 1.71—1.88 (2H, m), 3.08 (1H, m), 4.19 (2H, s), 4.45 (1H, dd, J=4, 2 Hz), 4.69 (1H, dd, J=6, 1.5 Hz), 9.17 (1H, d, J=1.5 Hz); MS (30 eV) m/z (rel intensity) 183 (M^+-CH_3, 100), 111 (8), 95 (3), 83 (31), 66 (20), 59 (22), 55 (7), 43 (27). Found: m/z 198.0871. Calcd for $C_{10}H_{14}O_4$: M, m/z 198.0892.

Wittig Reaction of the Aldehyde (6): To 22 ml of dry THF solution of Ph_3P^+n-$C_8H_{17}Br^-$ (4.1 g, 9.0 mmol)[13] was added 4.9 ml (8.0 mmol) of butyllithium at 0 °C under N_2 and the resultant reddish solution was stirred at room temperature for 1 h. To this solution 395 mg (2.0 mmol) of **6** in 4.4 ml of dry THF was introduced at −20 °C by using cannula and the mixture was stirred at room temperature overnight under N_2. After quenching by careful addition of satd NaCl at 0 °C, the insoluble substance which formed was filtered through Celite and washed with AcOEt. After evaporation of most of the organic solvent, the residue was

extracted with AcOEt. The combined extracts were washed with satd NaCl, dried with $MgSO_4$, and evaporated. The crude product was purified by silica-gel column chromatography, elution with hexane-AcOEt (9:1), to give 586 mg (100%) of **7** as a colorless oil.

7: TLC R_f=0.18 (hexane-AcOEt, 9:1); IR (neat) 1455, 1370, 1210, and 1070 cm^{-1}; ^1H NMR (CCl_4) δ=0.90 (3H, t, J=6 Hz), 1.18, 1.37 (each 3H, s), 1.31 (10H, br s), 2.2—1.6 (4H, m), 2.83 (1H, m), 4.04, 4.08 (each 1H, d, J=3 Hz), 4.21, 4.33 (each 1H, d, J=6 Hz), 5.09 (1H, dd, J=11, 9.5 Hz), 5.43 (1H, dt, J=11, 7.5 Hz).

Formation of Diol (8): A mixture of **7** (610 mg, 2.07 mmol) and 8.7 ml of 2M HCl (1M=1 mol dm^{-3}) in 8.7 ml of MeOH was refluxed overnight under N_2. After evaporation of MeOH, the aqueous layer was extracted with AcOEt. The combined extracts were washed with satd $NaHCO_3$ and satd NaCl, dried with $MgSO_4$, and evaporated. Recrystallization from hexane-AcOEt gave 470 mg (89.2%) of diol (**8**).

8: TLC R_f=0.63 (AcOEt); Mp 77.5—78.5 °C; IR (nujol) 3400, 1460, 1205, 1080, 990, and 910 cm^{-1}; ^1H NMR ($CDCl_3$) δ=0.88 (3H, t, J=6 Hz), 1.27 (10H, br s), 1.6—2.2 (4H, m), 2.93 (1H, m), 3.2—3.6 (2H, m), 3.7—3.9 (1H, m), 4.0—4.2 (1H, m), 4.18, 4.33 (each 1H, d, J=6 Hz), 5.08 (1H, dd, J=10, 8 Hz), 5.50 (1H, dt, J=10, 8 Hz). Found: C, 70.90; H, 10.31%. Calcd for $C_{15}H_{26}O_3$: C, 70.83; H, 10.30%.

Formation of Dicarboxylic Acid (9): To a stirred solution of 660 mg (2.6 mmol) of **8** in 12 ml of THF was added at 0 °C 830 mg (3.88 mmol) of $NaIO_4$ in 3.5 ml of water. The resulting white creamy mixture was stirred at room temperature overnight. After evaporation of THF, the aqueous layer was saturated with NaCl and extracted with AcOEt. The combined extracts were washed with satd NaCl, dried with $MgSO_4$, and evaporated to give 700 mg of product: TLC R_f=0.33 ($CHCl_3$-AcOEt, 1:1).[14]

The product so obtained was dissolved in 15 ml of acetone and to this solution was added at −20 °C 5.2 ml of Jones reagent (1.25 M) and the mixture stirred at 0 °C for 20 min. After quenching by addition of MeOH, the mixture was diluted with 6M H_2SO_4. After evaporation of most of the organic solvent, the aqueous layer was extracted with AcOEt. The combined extracts were washed with satd NaCl, dried with $MgSO_4$, and evaporated to give 700 mg (94.9% crude overall yield from **8**) of dicarboxylic acid (**9**) as an oil: IR (neat) 3400—2800, 1730, 1365, and 1230 cm^{-1}. This sample was sufficiently pure judging from its TLC and ^1H NMR result and was used immediately for the next reaction.[15]

Formation of Iodo Lactone Acetate (11): To a stirred solution of 700 mg (2.47 mmol) of **9** in 30 ml of THF were successively added 2 ml aqueous solution of $NaHCO_3$ (2.07 g) and 4 ml aqueous solution of KI (2.05 g) and I_2 (1.81 g). Then the resulting black solution was stirred at room temperature overnight. After quenching the excess of I_2 by addition of aq $Na_2S_2O_3$ solution and evaporation of THF, the aqueous phase was saturated with NaCl and extracted thoroughly with AcOEt. The combined extracts were washed with satd NaCl, dried with $MgSO_4$, and evaporated to give 948 mg of iodo lactone carboxylic acid (**10**): IR (neat) 1785 and 1740 cm^{-1}.

The product (175 mg, 0.43 mmol) so obtained was dried azeotropically with toluene, and then dissolved in 4 ml of dry C_6H_6 and treated with 210 mg (0.47 mmol) of freshly recrystallized $Pb(OAc)_4$ under reflux for 2 h. After cooling the mixture was filtered through Celite and washed well with Et_2O. Evaporation of the solvent gave another crop of precipitate. From the Et_2O soluble fraction 190 mg of iodo lactone acetate (**11**) was obtained as almost 1:1 mixture of acetate.

11: R_f=0.60 (Et_2O); IR (neat) 1790, 1750, and 1230 cm^{-1}; ^1H NMR ($CDCl_3$) δ=0.90 (3H, t, J=6 Hz), 1.31 (12H, br s), 1.95, 2.01 (total 3H, each s), 1.8—2.6 (3H, m), 2.8—3.2 (1H, m), 4.15 (1H, m), 4.75, 4.87 (total 1H, each d, J=8 Hz), 6.34 (1H, d, J=8 Hz). Found: m/z 424.0733. Calcd for $C_{16}H_{25}O_5I$: M, m/z 424.0747.

Fomation of Bis-γ-Lactone (13): A mixture of 190 mg of **11**, 0.15 ml of n-Bu_3SnH, and a catalytic amount of α,α′-azobisisobutyronitrile in 4 ml of dry C_6H_6 was refluxed under N_2 for 20 h. Evaporation of the solvent gave 230 mg of crude product (**12**). This sample was used for the next reaction without further purification. In a separate experiment **12** was prepared in 43.3% overall yield from **8** as crystalline solid after purification by silica-gel column chromatography (elution with Et_2O).

12: R_f=0.48 and 0.44 (Et_2O); Mp 131—134 °C (from hexane-Et_2O); IR ($CHCl_3$) 1785, 1240, and 1185 cm^{-1}; ^1H NMR ($CDCl_3$) δ=0.90 (3H, t, J=6 Hz), 1.31 (12H, br s), 1.98, 2.04 (total 3H, each s), 1.8—2.6 (3H, m), 2.8—3.3 (1H, m), 4.2 (1H, m), 4.85, 4.97 (total 1H, each d, J=8 Hz), 5.75 (0.4H, m), 6.48 (0.6H, d, J=5 Hz). Found: m/z 255.1617. Calcd for $C_{16}H_{26}O_5$-$COCH_3$: M, m/z 255.1596.

The crude product so obtained was dissolved in 3 ml of MeOH and then treated with 0.8 ml aqueous solution of K_2CO_3 (270 mg). After stirring for 4 h, the mixture was acidified with 2M HCl and extracted with Et_2O. After evaporation of the solvent, the residue was dissolved in 3 ml of acetone and to this solution at 0 °C Jones reagent was added until the solution showed an orange color. After being stirred for 20 min at 0 °C, the excess reagent was decomposed with MeOH and the mixture extracted with AcOEt. The combined extracts were washed with water and satd NaCl, dried with $MgSO_4$, and evaporated to give the crude product. Purification by silica-gel column chromatography, elution with hexane-Et_2O (1:1), afforded 40 mg (32.3% overall yield from **8**) of **13** as a colorless oil.

13: R_f=0.43 (Et_2O); IR (neat) 1790, 1460, 1240, 1210, 1140, 1070, and 970 cm^{-1}; ^1H NMR ($CDCl_3$) δ=0.89 (3H, t, J=6 Hz), 1.29 (12H, br s), 1.71 (2H, m), 2.4—3.2 (3H, m), 4.25—4.45 (1H, m), 5.00 (1H, d, J=7.5 Hz); ^{13}C NMR ($CDCl_3$) δ=14.0, 22.7, 25.0, 29.1 (×2), 29.3, 31.8, 32.8, 35.5, 40.2, 77.1, 85.0, 170.0, 173.8. Found: m/z 254.1493. Calcd for $C_{14}H_{22}O_4$: M, m/z 254.1518.

All these spectral data were in good agreement with those reported in the literature.[3,9]

The authors are grateful to Professor Takashi Tokoroyama of Osaka City University for his helpful suggestions. We are indebted to Dr. Takashi Sakai of Okayama University for spectral data of (±)-avenaciolide and bis-γ-lactone (**13**), and we also thank Dr. Ayumi Ohsaki of Kinki University for performing the high-resolution mass spectra measurements.

References

1) See for recent examples: a) L. C. Garver and E. E. van Tamelen, *J. Am. Chem. Soc.*, **104**, 867 (1982); b) M. E. Jung and L. J. Street, *ibid.*, **106**, 8327 (1984); c) S. Ogawa, Y. Iwasawa,

and T. Suami, *Chem. Lett.*, **1984**, 355; d) M. Ohno, Y. Ito, M. Arita, T. Shibata, K. Adachi, and H. Sawai, *Tetrahedron*, **40**, 145 (1984); e) M. M. Campbell, A. D. Kaye, M. Sainsbury, and R. Yavarzadeh, *ibid.*, **40**, 2461 (1984); f) P. J. De Clercq, *ibid.*, **40**, 3729 (1984); g) M. M. Campbell, M. Sainsbury, and R. Yavarzadeh, *ibid.*, **40**, 5063 (1984); h) A. B. Holmes, C. L. D. Jennings-White, and D. A. Kendrick, *J. Chem. Soc., Chem. Commun.*, **1984**, 1594; i) Y. Shizuri, S. Nishiyama, H. Shigemori, and S. Yamamura, *ibid.*, **1985**, 292; j) A. B. Smith, III, N. J. Liverton, N. J. Hrib, H. Sivaramakrishnan, and K. Winzenberg, *J. Org. Chem.*, **50**, 3239 (1985); k) A. Warm and P. Vogel, *Tetrahedon Lett.*, **26**, 5128 (1985); l) W. M. Grootaer and P. J. De Clercq, *ibid.*, **27**, 1731 (1986).

2) H. Kotsuki, K. Asao, and H. Ohnishi, *Bull. Chem. Soc. Jpn.*, **57**, 3339 (1984).

3) For recent work, see S. L. Schreiber and A. H. Hoveyda, *J. Am. Chem. Soc.*, **106**, 7200 (1984); R. C. Anderson and B. Fraser-Reid, *J. Org. Chem.*, **50**, 4781 (1985); J. Kallmerten and T. J. Gould, *ibid.*, **50**, 1128 (1985); S. D. Burke and G. J. Pacofsky, *Tetrahedron Lett.*, **27**, 445 (1986). See also Johann Wolfgang Goethe-Universitaet, *Synform*, **3**, 134 (1985).

4) K. Omura, A. K. Sharma, and D. Swern, *J. Org. Chem.*, **41**, 957 (1976); S. L. Huang, K. Omura, and D. Swern, *ibid.*, **41**, 3329 (1976); A. J. Mancuso, S. L. Huang, and D. Swern, *ibid.*, **43**, 2480 (1978); K. Omura and D. Swern, *Tetrahedron*, **34**, 1651 (1978).

5) The use of pyridinium chlorochromate or pyridinium dichromate as oxidizing agent gave 3 : 1 or 8 : 1 of *endo*/*exo* mixture in 94 or 66% respective yield. Unfortunately these isomers were indistinguishable on TLC. See also Ref. 12.

6) M. D. Dowle and D. I. Davies, *Chem. Soc. Rev.*, **8**, 171 (1979); S. Kobayashi, *Yuki Gosei Kagaku Kyokai Shi*, **41**, 745 (1983); P. A. Bartlett, *Tetrahedron*, **36**, 2 (1980); Idem, "Asymmetric Synthesis," ed by J. D. Morrison, Academic Press, New York (1984), Vol. 3, Chap. 6.

7) J. E. Baldwin, *J. Chem. Soc., Chem. Commun*, **1976**, 734.

8) A. Murai, K. Takahashi, H. Taketsuru, and T. Masamune, *J. Chem. Soc., Chem. Commun.*, **1981**, 221.

9) T. Sakai, H. Horikawa, and A. Takeda, *J. Org. Chem.*, **45**, 2039 (1980).

10) Although we could not detect an isomer in the reaction mixture of **13**, the possibility of the formation of this one, which would be derived from the intermediate **B** as shown in Fig. 1, can not be excluded completely. Unfortunately, however, at no stage we could clarify this problem because of the complexity of the ^{1}H NMR spectra. So the conclusion relies on the result of the last stage composition.

11) Optical resolution of the corresponding carboxylic acid is reported: see Ref. 1c.

12) When Et_3N was introduced after 30 min stirring, exclusive formation of the *exo*-aldehyde was observed. Data for *exo*-isomer: Mp 61—63 °C (from hexane-acetone); IR (nujol) 1725, 1215, 1165, 1095, 1075, and 1055 cm^{-1}; ^{1}H NMR ($CDCl_3$) δ=1.28, 1.47 (each 3H, s), 1.39—1.62 (1H, m), 2.05 (1H, ddd, J=13.5, 6, 4.5 Hz), 2.31 (1H, ddd, δ=9, 4.5, 2 Hz), 4.19 (2H, s), 4.49 (1H, d, J=6 Hz), 4.62 (1H, s), 9.57 (1H, d, J=2 Hz). Found: m/z 198.0896.

13) This reagent was prepared by refluxing 1-bromooctane with triphenylphosphine in dry C_6H_6 and washed well with C_6H_6. The product was a highly viscous oil. It was hard to purify, so was used as obtained.

14) This compound would exist in the hydrated form from ^{1}H NMR measurement.

15) The use of stored or chromatographed samples gave poor results.

 © 1986 The Chemical Society of Japan Bull. Chem. Soc. Jpn., 59, 3885—3892 (1986)

Syntheses of (−)-8-*epi*-Swainsonine and (−)-1,8-Di-*epi*-swainsonine, Stereoisomers of Physiologically Interesting Indolizidine Alkaloid, Swainsonine

Kin-ichi TADANO,* Youichi IIMURA, Yukinori HOTTA, Chiyoko FUKABORI, and Tetsuo SUAMI*
Department of Applied Chemistry, Faculty of Science and Technology, Keio University, Hiyoshi, Kohoku-ku, Yokohama 223
(Received June 10, 1986)

Two stereoisomers of the indolizidine alkaloid swainsonine, (−)-8-*epi*-swainsonine (**2**) and (−)-1,8-di-*epi*-swainsonine (**3**), have been synthesized from the known methyl 3-acetamido-2-*O*-acetyl-4,6-*O*-benzylidene-3-deoxy-α-D-glucopyranoside and methyl 3-acetamido-2-*O*-acetyl-3-deoxy-4,6-di-*O*-mesyl-α-D-glucopyranoside (**14**), respectively. The key pyrrolidine ring formation was achieved by intramolecular cyclization of a 6-*O*-tosyl derivative or a di-*O*-mesyl derivative **14** efficiently. The α-mannosidase inhibitory activity of the synthetic **2** and **3** was also evaluated.

(−)-Swainsonine (**1**), (1*S*, 2*R*, 8*R*, 8a*R*)-octahydro-1,2,8-indolizinetriol, is one of the indolizidine alkaloids isolated from *Swainsona canescens*,[1] *Astragalus lentiginosus*,[2] *Rhizoctonia leguminicola*,[3] and *Metarhizium anisopline*[4] (Fig. 1). The structure of **1** was established by chemical and spectral means,[1,3] and the rarely known trihydroxylated octahydroindolizine structure of **1** prompted us to achieve the total synthesis. We have completed the total synthesis of **1** in the natural form from 3-amino-3-deoxy-D-mannose derivative.[5] The total synthesis of **1** has also been achieved by Richardson et al.,[6] Fleet et al.,[7] Takaya et al.,[8] Sharpless et al.,[9] and Hashimoto et al.[10] Meanwhile, the alkaloid **1** was found to exhibit a remarkable physiological effects such as an α-mannosidase inhibitory activity[3] and an immunoregulating activity.[4,11] In order to elucidate a relationship between structure and physiological activity, the synthesis of stereoisomers of **1** is another interesting problem.[12] Recently, we have finished the syntheses of 8-*epi*-swainsonine **2** and 1,8-di-*epi*-swainsonine **3** from readily available 3-amino-3-deoxy-D-glucose derivatives.[13] Herein, we wish to describe details of these syntheses, and the α-mannosidase inhibitory activity of **2** and **3** is also reported.

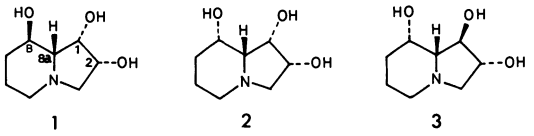

1 2 3

Fig. 1.

Results and Discussion

The synthesis of **2** was commenced with the known methyl 3-acetamido-2-*O*-acetyl-4,6-*O*-benzylidene-3-deoxy-α-D-glucopyranoside (**4**)[14] (Fig. 2). The compound **4** possesses all the chiral centers in **2** with correct configurations (the configurations at C-2, 3, 4, and 5 in **4** are corresponding to C-8, 8a, 1, and 2 in **2**, respectively). Hydrolysis of **4** in 50% aqueous acetic acid under reflux, and successive preferential *O*-tosylation of the primary hydroxyl group provided a compound **5** in 83% yield. Intramolecular *N*-alkylation at *N*-3 in **5** (a pyrrolidine ring formation) was achieved smoothly by treatment of **5** with sodium hydride in DMF at 100 °C, and the product was acetylated in the usual manner to afford a bicyclic compound, methyl 2,4-di-*O*-acetyl-3,6-acetylimino-3,6-dideoxy-α-D-glucopyranoside (**6**) in 68% yield. *O*-Deacetylation of **6** with sodium methoxide in methanol, dithioacetal formation with ethanethiol in concd HCl, and successive *O*-benzylation of the diethyl dithioacetal with benzyl bromide in the presence of sodium hydride, furnished a trisubstituted pyrrolidine (**7**) in 59% yield. A two-carbon elongation of **7** for construction of the octahydroindolizine skeleton was accomplished as follows. Dethioacetalization of **7** with mercury(II) chloride in aqueous acetonitrile followed by the Horner-Emmons olefination of the resulting aldehyde with diethyl ethoxycarbonylmethylphosphonate in the presence of sodium hydride provided an (*E*)-α,β-unsaturated ester (**8**) in 82% yield. The (*E*) geometry of the double bond in **8** was established by the ^{1}H NMR spectrum, in which the α-vinyl proton of the α,β-unsaturated ester appeared at δ 6.10 as a double-doublet with J=2 and 15 Hz. No (*Z*)-isomer was detected in the reaction mixture. In the ^{1}H NMR spectrum of **8**, two singlets with totally three protons appeared at δ 1.95 and 2.10 (approximately 3 to 1 ratio) and these signals are attributable to methyl protons of the *N*-acetyl group. This spectral phenomenon is explained by the exsistence of both endo and exo stereoisomers on the trisubstituted nitrogen atom. Some of other trisubstituted pyrrolidine derivatives exhibited the same property in the ^{1}H NMR spectra (see the spectral data of each compound in the Experimental). Catalytic hydrogenation of **8** in the presence of Raney nickel T-4 in ethanol gave a saturated ester (**9**) in 86% yield. Intramolecular cyclization (δ-lactam formation) of the compound **9** to an octahydro-5-indolizinone (**10**) was best accomplished by heating **9** in a mixture of 15 mol dm^{-3} aqueous KOH and ethanol at 120 °C (sealed tube) for 14 d. Under these conditions, the compound **10** was obtained in 40% yield along with an uncyclized carboxylic acid (**11**) in 51% yield. Although a pro-

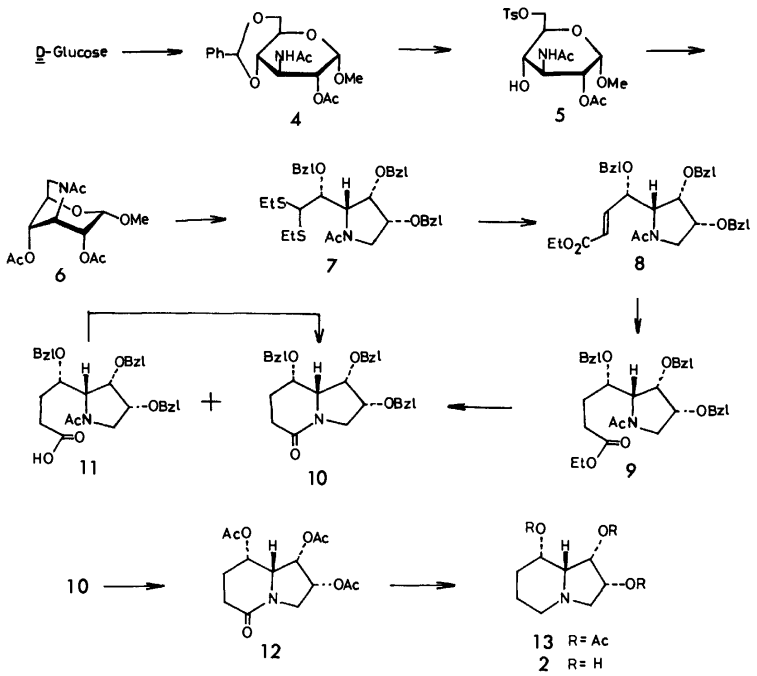

Fig. 2.

longed heating of **9** in the basic solution decreased the yield **10**, the isolated carboxylic acid **11** was converted to **10** in 43% yield by the same conditions. Reduction of the compound **10** to the corresponding octahydroindolizine was a troublesome step. In the case of swainsonine synthesis,[5] the corresponding octahydro-5-indolizinone derivative was smoothly converted to tribenzyloxyswainsonine by lithium aluminium hydride reduction in a high yield. On the contrary, lithium aluminium hydride reduction of **10** in THF gave a complex mixture. The other conditions (BH_3-THF and $NaBH_4$-pyridine-reflux) gave the same disappointing results. We have no rational explanation for this complex reaction. Next, reduction of the *O*-acetyl derivative (**12**) was examined. The compound **12** was prepared by *O*-debenzylation of **10** with cyclohexene in refluxing ethanol in the presence of 20% $Pd(OH)_2$ on charcoal[15] followed by acetylation in 84% yield. Reduction of **12** with borane-dimethyl sulfide complex in THF followed by aqueous $NaHCO_3$ treatment provided 8-*epi*-swainsonine triacetate (**13**) in 64% yield. To convert an intermediate amine-borane complex to **13**, the work-up with $NaHCO_3$ solution was necessary. Deprotection of **13** with K_2CO_3 in methanol, the same conditions employed for *O*-deacetylation of swainsonine triacetate,[5] gave an uncharacterized complex mixture. On the contrary, hydrolysis of **13** in refluxing 1 mol dm^{-3} aqueous HCl followed by deionization with Amberlite IRA-400 (OH^-) afforded 8-*epi*-swainsonine **2** as crystals in 86% yield. The synthetic **2** was fully characterized by the correlation of the ^1H and ^{13}C NMR spectra with those of swainsonine **1**. The optical rotation value of **2** ($[\alpha]_D^{21}=-24.8°$) was somewhat different from the reported value ($[\alpha]_D^{21}=-3.4°$).[12] The $[\alpha]_D^{21}$ of our synthetic compound was determined with a pure crystalline sample, while the reported value[12] was taken with a syrupy compound. Therefore, we believe that our measurement gave the correct $[\alpha]_D^{21}$ value of the compound **2**.

The synthesis of the other stereoisomer **3** was started from the known methyl 3-acetamido-2-*O*-acetyl-3-deoxy-4,6-di-*O*-mesyl-α-D-glucopyranoside (**14**)[16] (Fig. 3). Solvolysis of the compound **14** in refluxing 90% aqueous 2-methoxyethanol in the presence of sodium acetate followed by acetylation, according to the literature,[16] furnished methyl 2,4-di-*O*-acetyl-3,6-acetylimino-3,6-dideoxy-α-D-galactopyranoside (**15**, 68%) accompanied by methyl 3-acetamido-2,4,6-tri-*O*-acetyl-3-deoxy-α-D-galactopyranoside (**16**, 27%), which was readily separated by silica-gel chromatography. In contrast to our result, Guthrie and Mutter[16] did not show the isolation of the 3,6-imino compound **15** in their literature. After acetolysis of the solvolytic product, *O*-deacetylation and successive acid hydrolysis, they isolated 3-amino-3-deoxy-D-galactose hydrochloride as a sole product (no yield was given). In our opinions, they would miss accidentally the presence of the compound **15** in the reaction mixture. The D-galacto configuration of **16** was confirmed in the following way. Hydrolysis of **16** in refluxing 2 mol dm^{-3} HCl followed by acetylation gave an anomeric mixture of 3-acetamido-1,2,4,6-tetra-*O*-acetyl-3-deoxy-α-D-galactopyranose (**17**-α) and (**17**-β), which were readily separated by silica-gel chromatography (**17**-α, 41%; **17**-β, 43%). The α-anomer **17**-α was the known compound,[17] and the melting point and $[\alpha]_D$ value of **17**-α were in accordance with the reported ones. The 3,6-imino structure of the bicyclic compound **15** pos-

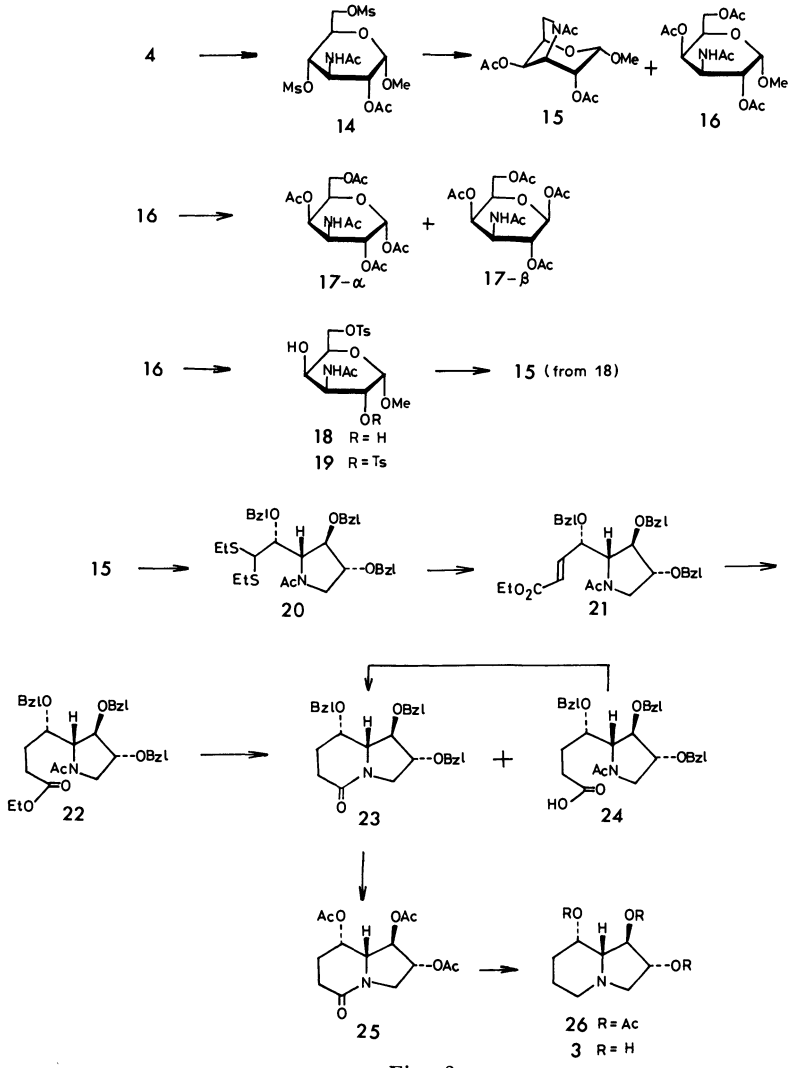

Fig. 3.

sessing D-galacto configuration was established as follows. *O*-Deacetylation of **16** with sodium methoxide in methanol and preferential *O*-tosylation of the primary hydroxyl group in the 2,4,6-triol afforded a 6-*O*-tosyl derivative (**18**) in 32% yield [a 2,6-di-*O*-tosyl derivative (**19**, 12% yield) was accompanied, and 28% of the 2,4,6-triol was recovered]. Treatment of the compound **18** with sodium hydride in DMF at 100 °C for 3,6-imino formation and successive acetylation provided the compound **15** in 56% yield as a sole product. The compound **15** is equipped with the correct configuration of all chiral centers in **3**, and the route from **15** to **3** was virtually the same as in the synthesis of **2** from **6**. *O*-Deacetylation of the compound **15** with sodium methoxide in methanol, diethyl dithioacetal formation with ethanethiol in concd HCl and successive *O*-benzylation afforded a trisubstituted pyrrolidine (**20**) in 56% yield. Dethioacetalization of **20** with mercury(II) chloride in aqueous acetonitrile followed by Horner-Emmons reaction of the aldehyde with diethyl ethoxycarbonylmethylphosphonate gave an (*E*)-α,β-unsaturated ester (**21**) as a sole product in 52% yield. Hydrogenation of **21** in the presence of Raney nickel T-4 provided a saturated ester (**22**) in 86% yield. Intramolecular cyclization of **22** by the treatment with a mixture of 15 mol dm^{-3} aqueous KOH and ethanol in a sealed tube at 120 °C for 10 d furnished a compound (**23**, 34%) and an uncyclized carboxylic acid (**24**, 62%). The compound **24** was converted to **23** in 75% yield by the same base treatment. *O*-Debenzylation of **23** by the Hanessian's condition[15] and successive acetylation afforded compound (**25**) in 83% yield. Reduction of **25** with borane-dimethyl sulfide complex, aqueous $NaHCO_3$ treatment and successive acetylation gave 1,8-di-*epi*-swainsonine triacetate (**26**) in 67% yield. Finally, deprotection of **26** with potassium carbonate in methanol afforded 1,8-di-*epi*-swainsonine **3** in 98% yield. In this case, methanolysis of the *O*-acetyl groups proceeded cleanly under the basic conditions. This newly synthesized compound **3** was fully characterized by the spectral methods (^{13}C and ^{1}H NMR spectra).

The α-mannosidase inhibitory effect of the compounds **2** and **3** was examined at pH 4. Under the conditions, in which swainsonine **1** exhibits a 92%

inhibition, the compounds **2** and **3** exhibit 15 and 20% inhibition, respectively. So the inhibitory effect of **2** and **3** against the enzyme is approximately one-fifth of that of swainsonine.

Experimental

General. Evaporations were performed under diminished pressure at below 40 °C (bath). Melting points were determined with a Mitamura Riken micro apparatus and are uncorrected. Specific rotations were measured in a 1-dm tube with a Jasco DIP-4 polarimeter. Column chromatography was performed on Kieselgel 60 (Merck), and TLC was performed on Kieselgel 60 GF_{254} (Merck) with detection by UV light and charring with sulfuric acid. Preparative TLC was performed on Kieselgel 60 PF_{254} (Merck). IR spectra were recorded with Hitachi Model 225 (KBr) and Jasco A-202 ($CHCl_3$) spectrometers. ^1H NMR spectra were recorded with a Varian EM-390 spectrometer for solutions in $CDCl_3$ (internal standard Me_4Si). ^{13}C NMR spectra were recorded with a JEOL FX-200 spectrometer for solutions in CD_3OD (internal standard Me_4Si). High resolution mass spectra were obtained using a Hitachi M-80 mass spectrometer. Elemental analyses were performed by Mr. Saburo Nakada to whom our thanks are due.

Methyl 3-Acetamido-2-*O*-acetyl-3-deoxy-6-*O*-tosyl-α-D-glucopyranoside (5). A suspension of methyl 3-acetamido-2-*O*-acetyl-4,6-*O*-benzylidene-3-deoxy-α-D-glucopyranoside (**4**)[14] (10.20 g, 27.9 mmol) in 50% aqueous acetic acid (250 ml) was heated under reflux for 30 min and evaporated. The residue was dissolved in water (400 ml) and the aqueous solution was washed with ethyl acetate (300 ml). After evaporation of the aqueous layer, the residual white solid was dissolved in pyridine (70 ml). To the solution was added *p*-toluenesulfonyl chloride (10.66 g, 55.9 mmol), and the mixture was stirred at 0 °C for 18 h. After evaporation of the mixture, the residue was partitioned between chloroform (200 ml) and water (200 ml). The aqueous layer was extracted with chloroform (200 ml×2), and the combined extracts were dried (Na_2SO_4). After evaporation of the extracts, the residue was chromatographed on SiO_2 (300 g, ethanol: toluene=1 : 20). Fractions corresponding to R_f 0.58 (ethanol: toluene=1 : 3) were evaporated to afford **5** (9.93 g, 83%) as a colorless foam, $[\alpha]_D^{24}$+88.7° (*c* 1.10, $CHCl_3$); IR $\nu_{max}^{CHCl_3}$ 3010, 1740, 1660, 1520, 1370 cm^{-1}; ^1H NMR ($CDCl_3$) δ=1.97 (3H, s, $NCOCH_3$), 2.10 (3H, s, $OCOCH_3$), 2.47 (3H, s, $OSO_2C_6H_4C\underline{H}_3$), 3.36 (3H, s, OCH_3), 3.40—5.00 (8H, m, H-1, 2, 3, 4, 5, 6, 6′, OH), 6.60 (1H, d, *J*=8 Hz, NH), 7.59 (4H, ABq, *J*=10 Hz, $SO_2C_6\underline{H}_4CH_3$). Found: C, 50.14; H, 5.82; N, 3.09; S, 7.31%. Calcd for $C_{18}H_{25}NO_9S_2$: C, 50.11; H, 5.84; N, 3.25; S, 7.43%.

Methyl 2,4-Di-*O*-acetyl-3,6-acetylimino-3,6-dideoxy-α-D-glucopyranoside (6). To a stirred suspension of sodium hydride (60% emulsion in mineral oil, 1.88 g, 47.0 mmol, washed with hexane; 10 ml×3) in DMF (25 ml) was added a DMF (60 ml) solution of **5** (5.80 g, 13.4 mmol). The mixture was heated at 100 °C for 30 min with stirring, and ethanol (10 ml) was added. After evaporation of the resulting solution, the residue was triturated with methanol (50 ml). The resulting insoluble materials were removed by filtration, and the filtrate was evaporated. The residue was acetylated with acetic anhydride (50 ml) in pyridine (60 ml) for 12 h and the solution was evaporated. The residue was partitioned between chloroform (250 ml) and water (400 ml), and the aqueous layer was extracted with chloroform (250 ml×1, 100 ml×1). The combined extracts were washed with saturated aqueous NaCl (300 ml), dried (Na_2SO_4) and evaporated. The residue was chromatographed on SiO_2 (100 g, ethyl acetate: toluene=1 : 1), and fractions corresponding to R_f 0.50 (ethanol: toluene=1 : 3) were evaporated to afford **6** (2.75 g, 68%), mp 166—168 °C; $[\alpha]_D^{22}$+89.0° (*c* 1.00, $CHCl_3$); IR ν_{max}^{KBr} 2940, 1750, 1650, 1410, 1390, 1300 cm^{-1}; ^1H NMR ($CDCl_3$) δ=2.10 (3H, s, $NCOCH_3$), 2.20, 2.21 (3H×2, each s, 2×$OCOCH_3$), 3.56 (3H, s, OCH_3), 3.40—3.91 (2H, m, H-6, 6′), 4.42—5.32 (5H, m, H-1, 2, 3, 4, 5). Found: C, 52.10; H, 6.25; N, 4.38%. Calcd for $C_{13}H_{19}NO_7$: C, 51.82; H, 6.36; N, 4.65%.

(2*S*,3*S*,4*R*)-1-Acetyl-3,4-bis(benzyloxy)-2-[(1*R*)-1-benzyloxy-2,2-bis(ethylthio)ethyl]pyrrolidine (7). To a stirred solution of **6** (4.30 g, 14.3 mmol) in dichloromethane (15 ml) was added sodium methoxide in methanol (1 mol dm^{-3}, 34.3 ml, 34.3 mmol). After stirring for 30 min, the solution was neutralized with Amberlite IR-120 B (H^+). The resin was removed by filtration and the filtrate was evaporated. The residue was dissolved in concd HCl (10.0 ml) and ethanethiol (10.0 ml) was added at 0 °C. After stirring for 18 h at the temperature, the mixture was diluted with water (50 ml) and neutralized with lead(II) carbonate hydroxide. The resulting insoluble materials were removed through Celite-pad, and the filtrate was evaporated. The residue was triturated with methanol (70 ml) and insoluble materials were removed. After evaporation of the filtrate, the residue was benzylated without purification. To a suspension of sodium hydride (60%, 2.05 g, 51.4 mmol, washed with hexane; 10 ml×3) in DMF (15 ml) was added a DMF (40 ml) solution of the above residue. After stirring for 20 min at ambient temperature, benzyl bromide (6.1 ml, 51.4 mmol) was added to the mixture. The mixture was stirred for 1.5 h and ethanol (15 ml) was added. The solution was evaporated and the residue was partitioned between dichloromethane (300 ml) and water (400 ml). After extraction of the aqueous layer with dichloromethane (300 ml×2), the combined extracts were dried (Na_2SO_4) and evaporated. The residue was chromatographed on SiO_2 (200 g, ethyl acetate: hexane=1 : 1), and fractions corresponding to R_f 0.52 (ethanol: toluene=1 : 6) were evaporated to afford **7** (4.88 g, 59%) as a colorless syrup, $[\alpha]_D^{22}$+8.5° (*c* 1.10, $CHCl_3$); IR $\nu_{max}^{CHCl_3}$ 3000, 2920, 1630, 1450, 1360 cm^{-1}; ^1H NMR ($CDCl_3$) δ=0.98, 1.18 (3H×2, each t, *J*=8 Hz, 2×$SCH_2C\underline{H}_3$), 2.10 (3H, s, $NCOCH_3$), 2.38, 2.70 (2H×2, each q, *J*=8 Hz, 2×$SC\underline{H}_2CH_3$), 3.40—4.75 (13H, m, H-2,3,4,5,5′, H-1,2 of the side chain, 3×$OC\underline{H}_2C_6H_5$), 7.26, 7.33, 7.34 (total 15H, each s, 3×$OCH_2C_6\underline{H}_5$). High resolution mass spectrum, calcd for $C_{33}H_{42}NO_4S_2$: *m/z* 580.2553, found: M+H, 580.2563.

(2*R*,3*S*,4*R*)-1-Acetyl-3,4-bis(benzyloxy)-2-[(1*S*,2*E*)-1-benzyloxy-3-ethoxycarbonyl-2-propenyl]pyrrolidine (8). To a stirred solution of **7** (1.00 g, 1.72 mmol) in a mixture of acetonitrile (8 ml) and water (2 ml) were added mercury(II) chloride (2.34 g, 8.62 mmol) and calcium carbonate (0.95 g, 9.49 mmol). After stirring for 4 h, an insoluble material was removed through Celite-pad. The filtrate was diluted with dichloromethane (200 ml), washed with 1 mol dm^{-3} aqueous KI (100 ml×3), dried (Na_2SO_2), and evaporated. The residue was subjected to the Horner–Emmons reaction directly. To a suspension of sodium hydride (60%, 0.24 g, 6.04 mmol, washed with hexane; 2 ml×3) in THF (5 ml) was added diethyl ethoxycarbonylmethylphosphonate (1.20 ml, 6.04

mmol) at 0 °C. After stirring for 20 min, a solution of the above residue in THF (10 ml) was added. The mixture was stirred for 3 h at ambient temperature and diluted with water (100 ml). The aqueous solution was extracted with dichloromethane (150 ml×2, 100 ml×1), and the combined extracts were dried (Na_2SO_4) and evaporated. The residue was chromatographed on SiO_2 (60 g, ethyl acetate : hexane=2 : 5), and fractions corresponding to R_f 0.28 (ethyl acetate : hexane=1 : 2) were evaporated to afford **8** (0.77 g, 82%) as a colorless syrup, $[\alpha]_D^{23}$+71.5° (*c* 1.10, $CHCl_3$); IR $\nu_{max}^{CHCl_3}$ 2990, 2930, 2860, 1730, 1630, 1450, 1420, 1360, 1260, 1150 cm^{-1}; ^1H NMR ($CDCl_3$) δ=1.24 (3H, t, *J*=7 Hz, $COOCH_2C\underline{H}_3$), 1.95, 2.10 (total 3H, each s, $NCOCH_3$), 3.36 (1H, d, *J*=13 Hz, H-5), 3.72 (1H, d, *J*=7 Hz, H-5′), 3.76—5.00 (12H, m, H-2, 3, 4, H-1 of the side chain, $COOC\underline{H}_2CH_3$, 3×$OC\underline{H}_2C_6H_5$), 6.10 (1H, dd, *J*=2 and 15 Hz, H-3 of the side chain), 7.00—7.05 (16H, m, H-2 of the side chain, 3×$OCH_2C_6\underline{H}_5$). High resolution mass spectrum, calcd for $C_{33}H_{38}NO_6$: *m/z* 544.2696, found: M+H, 544.2677.

(2*R*,3*S*,4*R*)-1-Acetyl-3,4-bis(benzyloxy)-2-[(1*S*)-1-benzyloxy-3-(ethoxycarbonyl)propyl]pyrrolidine (9). A solution of **8** (2.45 g, 4.51 mmol) in ethanol (20 ml) was hydrogenated in the presence of Raney nickel T-4 under atmospheric hydrogen pressure for 5 h. After removal of the catalyst through Celite-pad, the filtrate was evaporated. The residue was chromatographed on SiO_2 (200 g, ethyl acetate : hexane =1 : 1), and fractions corresponding to R_f 0.19 (ethyl acetate : hexane=2 : 1) were evaporated to afford **9** (2.11 g, 86%) as a colorless syrup, $[\alpha]_D^{22}$+0.9° (*c* 1.10, $CHCl_3$); IR $\nu_{max}^{CHCl_3}$ 2990, 2930, 2860, 1730, 1630, 1450, 1420, 1360, 1260, 1150, 1090 cm^{-1}; ^1H NMR ($CDCl_3$) δ=1.13, 1.16 (total 3H, each t, *J*=7 Hz, $COOCH_2C\underline{H}_3$), 1.50—2.50 (7H, m, $C\underline{H}_2C\underline{H}_2COOEt$, $NCOCH_3$), 3.45—4.80 (14H, m, H-2, 3, 4, 5, 5′, H-1 of the side chain, $COOC\underline{H}_2CH_3$, 3×$OC\underline{H}_2C_6H_5$), 7.23, 7.33 (total 15H, each s, 3×$OCH_2C_6\underline{H}_5$). High resolution mass spectrum, calcd for $C_{33}H_{40}NO_6$: *m/z* 546.2853, found: M+H, 546.2853.

(1*S*,2*R*,8*S*,8*aR*)-1,2,8-Tris(benzyloxy)-octahydro-5-indolizinone (10) and (2*R*,3*S*,4*R*)-1-Acetyl-3,4-bis(benzyloxy)-2-[(1*S*)-1-benzyloxy-3-carboxypropyl]pyrrolidine (11). A solution of **9** (240 mg, 0.44 mmol) in a mixture of ethanol (8 ml) and 15 mol dm^{-3} aqueous KOH (2 ml) was heated at 120 °C (Pyrex-glass sealed tube) for 14 d. After neutralization with 1 mol dm^{-3} aqueous HCl, the resulting solution was evaporated. The residue was diluted with water (25 ml) and extracted with dichloromethane (20 ml×3). The extracts were dried (Na_2SO_4) and evaporated. The residual brown syrup was chromatographed on SiO_2 (20 g, ethanol : toluene =1 : 30). Fractions corresponding to R_f 0.46 (ethanol : toluene =1 : 5) were evaporated to afford **10** (80 mg, 40%), and fractions corresponding to R_f 0.43 were evaporated to afford **11** (115 mg, 51%) as a colorless syrup. **10**: Mp 98—99 °C; $[\alpha]_D^{22}$—28.2 (*c* 1.00, $CHCl_3$); IR ν_{max}^{KBr} 3420, 2920, 2860, 1640, 1450, 1410, 1370, 1200, 1140 cm^{-1}; ^1H NMR ($CDCl_3$) δ=1.56—2.68 (4H, m, H-6,6′,7,7′), 3.30—4.84 (12H, m, H-1, 2, 3, 3′, 8, 8a, 3×$OC\underline{H}_2C_6H_5$), 7.27, 7.29 (total 15H, each s, 3×$OCH_2C_6\underline{H}_5$). Found: C, 76.27; H, 6.85; N, 3.08%. Calcd for $C_{29}H_{31}NO_4$: C, 76.12; H, 6.83; N, 3.06%. **11**: $[\alpha]_D^{23}$—4.0° (*c* 1.05, $CHCl_3$); IR $\nu_{max}^{CHCl_3}$ 3670, 3500, 3020, 2400, 1710, 1630, 1450, 1420, 1360, 1260, 1210, 1170 cm^{-1}; ^1H NMR ($CDCl_3$) δ=1.57—2.60 (7H, m, H-2, 2′, 3, 3′ of the side chain, $NCOCH_3$), 3.43—4.76 (12H, m, H-2, 3, 4, 5, 5′, H-1 of the side chain, 3×$OC\underline{H}_2C_6H_5$), 7.00—7.50 (15H, m, 3×$OCH_2C_6\underline{H}_5$).

Conversion of 11 to 10. A solution of **11** (219 mg, 0.42 mmol) in a mixture of ethanol (4 ml) and 15 mol dm^{-3} aqueous KOH (1 ml) was heated at 120 °C for 14 d. After the analogous work-up described above, the crude mixture was chromatographed on SiO_2 to afford **10** (80 mg, 43%) [95 mg (46%) of **11** was recovered].

(1*S*,2*R*,8*S*,8*aR*)-1,2,8-Triacetoxyoctahydro-5-indolizinone (12). To a solution of **10** (80 mg, 0.175 mmol) in ethanol (1.5 ml) were added cyclohexene (1.5 ml) and 20% $Pd(OH)_2$ on charcoal (40 mg). The mixture was heated under reflux for 4 h, and the catalyst was removed through Celite-pad. The filtrate was evaporated, and the residue was acetylated with acetic anhydride (1 ml) in pyridine (1 ml) for 4 h. After evaporation of the mixture, the residue was chromatographed on SiO_2 (5 g, ethanol : toluene=1 : 20). Fractions corresponding to R_f 0.51 (ethanol : toluene=1 : 3) were evaporated to afford **12** (46 mg, 84%), mp 126—127 °C; $[\alpha]_D^{21}$ −21.8° (*c* 0.90, $CHCl_3$); IR ν_{max}^{KBr} 3450, 2960, 1730, 1640, 1470, 1420, 1380, 1270, 1230, 1110 cm^{-1}; ^1H NMR ($CDCl_3$) δ=1.47—2.83 (13H, m, H-6, 6′, 7, 7′, 3×$OCOCH_3$), 3.50—4.30 (3H, m, H-3, 3′, 8a), 5.20—5.77 (3H, m, H-1, 2, 8). Found: C, 53.52; H, 6.05; N, 4.47%. Calcd for $C_{14}H_{19}NO_7$: C, 53.67; H, 6.11; N, 4.47%.

(1*S*,2*R*,8*S*,8*aR*)-1,2,8-Triacetoxyoctahydroindolizine, 8-*epi*-Swainsonine Triacetate (13). To a stirred solution of **12** (26 mg, 0.08 mmol) in THF (1 ml) was added borane-dimethyl sulfide complex (Aldrich, 10.0 mol dm^{-3} in BH_3, 0.04 ml, 0.42 mmol) at 0 °C under argon atmosphere. After stirring at ambient temperature for 2 h, the mixture was diluted with water (10 ml) and stirred for 15 min. The aqueous solution was extracted with dichloromethane (10 ml×3). The extracts were dried (Na_2SO_4) and evaporated. The residue was dissolved in dioxane (1.5 ml) and saturated aqueous $NaHCO_3$ solution (0.5 ml) was added. After stirring for 5 h at ambient temperature, the solution was diluted with water (10 ml), extracted with dichloromethane (10 ml×3). The extracts were dried (Na_2SO_4) and evaporated. The residue was purified by PTLC (ethanol : toluene=1 : 15) to afford **13** (R_f= 0.44; ethanol : toluene=1 : 5) (16 mg, 64%), mp 79—80 °C; $[\alpha]_D^{19}$—17.1° (*c* 0.35, $CHCl_3$); IR ν_{max}^{KBr} 3450, 2940, 1730, 1380, 1270, 1250, 1160, 1130 cm^{-1}; ^1H NMR ($CDCl_3$) δ= 1.14—2.30 (6H, m, H-5, 6, 6′, 7, 7′, 8a), 2.00, 2.03, 2.11 (3H×3, each s, 3×$OCOCH_3$), 2.42 (1H, dd, *J*=7 and 12 Hz, H-3), 3.10—3.35 (2H, m, H-3′, 5′), 5.13—5.50 (3H, m, H-1, 2, 8). High resolution mass spectrum, calcd for $C_{14}H_{22}NO_6$: *m/z* 300.1446, found: M+H, 300.1447.

(1*S*,2*R*,8*S*,8*aR*)-Octahydro-1,2,8-indolizinetriol, 8-*epi*-Swainsonine (2). A solution of **13** (27.0 mg, 0.09 mmol) in 1 mol dm^{-3} aqueous HCl (1 ml) was heated under reflux for 3 h and evaporated. The residue was dissolved in a minimum volume of water and charged on a column of Amberlite IRA-400 (OH^-) (2 ml). The column was eluted with water, and the ninhydrin-positive fractions (R_f 0.35, aqueous ammonia : 1-butanol : chloroform : ethanol=1 : 4 : 4 : 4) were evaporated to afford **2** (13.4 mg, 86%), mp 93—95 °C; $[\alpha]_D^{21}$—24.8° (*c* 0.67, MeOH); IR ν_{max}^{KBr} 3600—3000 (br), 2940, 2850, 2820, 1440, 1150, 1100 cm^{-1}; ^1H NMR (D_2O) δ=1.40—2.30 (6H, m, H-5, 6, 6′, 7, 7′, 8a), 2.50 (1H, dd, *J*=7 and 11 Hz, H-3), 2.86—3.20 (2H, m, H-3′, 5′), 4.20—4.46 (3H, m, H-1,2,8); ^{13}C NMR (CD_3OD) δ=20.63, 32.09, 54.27, 62.98, 67.53, 69.40, 69.96, 74.29. High resolution mass spectrum, calcd for $C_8H_{15}NO_3$: *m/z* 173.1051, found: M, 173.1056.

Methyl 2,4-Di-*O*-acetyl-3,6-acetylimino-3,6-dideoxy-α-D-

galactopyranoside (15) and Methyl 3-Acetamido-2,4,6-tri-*O*-acetyl-3-deoxy-α-D-galactopyranoside (16). A solution of methyl 3-acetamido-2-*O*-acetyl-3-deoxy-4,6-di-*O*-mesyl-α-D-glucopyranoside (**14**)[16] (7.80 g, 18.0 mmol) in a mixture of 2-methoxyethanol (180 ml) and water (20 ml) containing sodium acetate (7.82 g, 95.0 mmol) was heated under reflux for 6 h, and evaporated. The residue was triturated with boiling acetone (400 ml) and insoluble materials were removed by filtration. After evaporation of the filtrate, the residue was acetylated with acetic anhydride (65 ml) in pyridine (65 ml) for 14 h. The mixture was evaporated with toluene and the residue was chromatographed on SiO_2 (300 g, ethanol : toluene=1 : 30). Fractions corresponding to R_f 0.32 (ethanol : toluene=1 : 5) were evaporated to afford **15** (3.67 g, 68%) as a foam, and fractions corresponding to R_f 0.27 were evaporated to afford **16** (1.72 g, 27%) as crystals. **15**: $[\alpha]_D^{26}$+25.3° (*c* 1.36, $CHCl_3$); IR $\nu_{max}^{CHCl_3}$ 3660, 3020, 2400, 1750, 1650, 1410, 1370, 1260, 1220, 1170 cm^{-1}; ^1H NMR ($CDCl_3$) δ=2.03 (3H, s, $NCOCH_3$), 2.09, 2.12, 2.15, 2.19 (total 6H, each s, 2×$OCOCH_3$), 3.45, 3.49 (total 3H, each s, OCH_3), 3.60—3.76 (2H, m, H-6, 6′), 4.23—4.68 (2H, m, H-3, 5), 4.71, 4.73 (total 1H, each d, *J*=2 Hz, H-1), 5.02—5.49 (2H, m, H-2, 4). High resolution mass spectrum, calcd for $C_{13}H_{19}NO_7$: *m/z* 301.1160, found: M, 301.1133. **16**: Mp 107—108 °C; $[\alpha]_D^{21}$+117.8° (*c* 1.48, $CHCl_3$); IR ν_{max}^{KBr} 3340, 3240, 2930, 1735, 1655, 1540, 1440, 1370, 1230 cm^{-1}; ^1H NMR ($CDCl_3$) δ=1.90 (3H, s, $NCOCH_3$), 2.06, 2.10, 2.17 (3H×3, each s, 3×$OCOCH_3$), 3.45 (3H, s, OCH_3), 3.95—4.32 (3H, m, H-5, 6, 6′), 4.66 (1H, ddd, *J*=3, 8, and 12 Hz, H-3), 4.84 (1H, d, *J*=4 Hz, H-1), 5.10 (1H, dd, *J*=4 and 12 Hz, H-2), 5.40 (1H, dd, *J*=1 and 3 Hz, H-4), 5.72 (1H, d, *J*=8 Hz, NH). Found: C, 50.14; H, 6.50; N, 3.93%. Calcd for $C_{15}H_{23}NO_9$: C, 49.86; H, 6.41; N, 3.88%.

3-Acetamido-1,2,4,6-tetra-*O*-acetyl-3-deoxy-α- and -β-D-galactopyranose (17-α and 17-β). A solution of **16** (45 mg, 0.12 mmol) in 2 mol dm^{-3} aqueous HCl (2 ml) was heated under reflux for 13 h and evaporated. The residue was acetylated with acetic anhydride (0.5 ml) in pyridine (0.5 ml) for 4 h. After evaporation of the mixture, the residue was chromatographed on SiO_2 (5 g, ethanol : toluene=1 : 20). Fractions corresponding to R_f 0.49 (ethanol : toluene=1 : 5) were evaporated to afford **17-β** (21 mg, 43%), and fractions corresponding to R_f 0.45 were evaporated to afford **17-α** (20 mg, 41%). **17-α**: Mp 178—179 °C, lit,[17] mp 181—182 °C; $[\alpha]_D^{26}$+123.8° (*c* 1.00, $CHCl_3$), lit,[17] $[\alpha]_D^{23}$+119° (*c* 1.00, $CHCl_3$); IR ν_{max}^{KBr} 3440, 1760, 1740, 1680, 1530, 1435, 1375 cm^{-1}; ^1H NMR ($CDCl_3$) δ=1.93 (3H, s, $NCOCH_3$), 2.03, 2.19 (6H×2, each s, 4×$OCOCH_3$), 3.85—4.25 (2H, m, H-6, 6′), 4.38 (1H, dt, *J*=1 and 7 Hz, H-5), 4.68 (1H, ddd, *J*=3, 9, and 11 Hz, H-3), 5.25 (1H, dd, *J*=4 and 11 Hz, H-2), 5.48 (1H, dd, *J*=1 and 3 Hz, H-4), 6.01 (1H, d, *J*=9 Hz, NH), 6.31 (1H, d, *J*=4 Hz, H-1). **17-β**: Mp 117—118 °C; $[\alpha]_D^{24}$+36.0° (*c*, 1.06, $CHCl_3$); IR ν_{max}^{KBr} 3370, 1740, 1650, 1520, 1370, 1220 cm^{-1}; ^1H NMR ($CDCl_3$) δ=1.89 (3H, s, $NCOCH_3$), 2.02, 2.04, 2.10, 2.15 (3H×4, each s, 4×$OCOCH_3$), 3.97—4.23 (3H, m, H-5, 6, 6′), 4.44 (1H, ddd, *J*=4, 8, and 9 Hz, H-3), 5.06 (1H, dd, *J*=9 and 12 Hz, H-2), *5.40 (1H, d, J=4Hz, H-4), 5.80 (1H, d, J=9 Hz, H-1), 6.04* (1H, d, *J*=8 Hz, NH). Found: C, 49.09; H, 5.91; N, 3.66%. Calcd for $C_{16}H_{23}NO_{10}$: C, 49.36; H, 5.95; N, 3.60%.

Methyl 3-Acetamido-3-deoxy-6-*O*-tosyl-α-D-galactopyranoside (18) and Methyl 3-Acetamido-3-deoxy-2,6-di-*O*-tosyl-α-D-galactopyranoside (19). To a stirred solution of **16** (350 mg, 0.97 mmol) in methanol (3 ml) was added sodium methoxide in methanol (1 mol dm^{-3} solution, 3.8 ml, 3.8 mmol) at 0 °C. After stirring at the temperature for 30 min, the solution was neutralized with Amberlite 120B (H^+). The resin was removed by filtration and the filtrate was evaporated to afford a colorless syrup. To a solution of the syrup in pyridine (4 ml) was added *p*-toluenesulfonyl chloride (184 mg, 0.97 mmol). The mixture was stirred for 10 h at −17 to −10 °C and evaporated. The residue was chromatographed on SiO_2 (60 g, chloroform : methanol=40 : 1). Fractions corresponding to R_f 0.58 (ethanol : toluene=1 : 3) were evaporated to afford **19** (64 mg, 12%), fractions corresponding to R_f 0.31 were evaporated to afford **18** (120 mg, 32%), and fractions corresponding to R_f 0.10 were evaporated to recover the 2,4,6-triol (64 mg, 28%). **18**: Mp 146—147 °C; $[\alpha]_D^{23}$+136.1° (*c* 1.09, MeOH); IR ν_{max}^{KBr} 3340, 2920, 1630, 1600, 1570, 1445, 1370, 1190 cm^{-1}; ^1H NMR ($CDCl_3$) δ=2.04 (3H, s, $NCOCH_3$), 2.45 (3H, s, $OSO_2C_6H_4C\underline{H}_3$), 2.56—2.98 (2H, m, 2×OH), 3.36 (3H, s, OCH_3), 3.62—4.33 (6H, m, H-2, 3, 4, 5, 6, 6′), 4.71 (1H, d, *J*=4 Hz, H-1), 6.54 (1H, d, *J*=8 Hz, NH), 7.58 (4H, ABq, $OSO_2C_6\underline{H}_4CH_3$). High resolution mass spectrum, calcd for $C_{16}H_{24}NO_8S$: *m/z* 390.1220, found: M+H, 390.1214. **19**: Mp 194—195 °C; $[\alpha]_D^{24}$+75.2° (*c* 1.00, DMF); IR ν_{max}^{KBr} 3330, 3200, 1640, 1590, 1540, 1360, 1190, 1175 cm^{-1}; ^1H NMR (DMSO-d_6) δ=1.69 (3H, s, $NCOCH_3$), 2.42 (6H, s, 2×$OSO_2C_6H_4C\underline{H}_3$), 3.12 (3H, s, OCH_3), 3.53—4.62 (7H, m, H-1, 2, 3, 4, 5, 6, 6′), 5.34 (1H, d, *J*=6 Hz, NH), 7.61, 7.63 (total 8H, 2×$OSO_2C_6\underline{H}_4CH_3$). Found: C, 51.08; H, 5.43; N, 2.77; S, 11.50%. Calcd for $C_{23}H_{29}NO_{10}S_2$: C, 50.82; H, 5.38; N, 2.58; S, 11.80%.

Compound 15 from Compound 18. To a suspension of sodium hydride (60%, 31 mg, 1.28 mmol, washed with hexane; 1 ml×3) in DMF (0.5 ml) was added a solution of **18** (86 mg, 0.22 mmol) in DMF (1 ml). The mixture was heated at 100 °C for 3 h and ethanol (0.5 ml) was added. After evaporation of the mixture, the residue was acetylated with acetic anhydride (2 ml) in pyridine (2 ml) for 16 h. The mixture was evaporated and the residue was partitioned between chloroform (30 ml) and water (30 ml). The aqueous layer was extracted with chloroform (30 ml). The combined extracts were dried (Na_2SO_4) and evaporated. The residue was chromatographed on SiO_2 (5 g, ethanol : toluene=1 : 10), and fractions corresponding to R_f 0.32 (ethanol : toluene= 1 : 5) were evaporated to afford **15** (37 mg, 56%) which was identical in all respects with that prepared by the solvolysis of **14**.

(2*S*,3*R*,4*R*)-1-Acetyl-3,4-bis(benzyloxy)-2-[(1*R*)-1-benzyloxy-2,2-bis(ethylthio)ethyl]pyrrolidine (20). Compound **15** (1.43 g, 4.75 mmol) was *O*-deacetylated with 1 mol dm^{-3} sodium methoxide in methanol (14.2 ml) at 0 °C for 30 min. After neutralization of the mixture with Amberlite IR-120B (H^+), the crude product was treated with ethanethiol (5 ml) in concd HCl (3 ml) at 0 °C for 1 h. Work-up as described in preparation of **7** gave the dithioacetal derivative (R_f=0.51, ethanol : toluene=1 : 2) which was directly benzylated with benzyl bromide (1.72 ml) in DMF (25 ml) in the presence of sodium hydride (580 mg) for 12 h. Extractive work-up *($CHCl_3$)* and *chromatography of the product on SiO_2 (100* g, ethyl acetate : toluene=1 : 10) afforded **20** (R_f=0.36, ethyl acetate : hexane=1 : 1) (1.55 g, 56%) as a colorless syrup; $[\alpha]_D^{27}$+9.6° (*c* 1.17, $CHCl_3$); IR $\nu_{max}^{CHCl_3}$ 3000, 1620, 1450, 1420, 1360, 1260, 1210, 1170 cm^{-1}; ^1H NMR ($CDCl_3$) δ=1.13, 1.20 (3H×2, each t, *J*=8 Hz, 2×$SCH_2C\underline{H}_3$), 2.09 (3H, s, $NCOCH_3$), 2.50, 2.66 (2H×2, each q, *J*=8 Hz, 2×$SC\underline{H}_2CH_3$),

3.20—4.70 (13H, m, H-2, 3, 4, 5, 5′, H-1, 2 of the side chain, 3×OC$\underline{H}_2$C$_6$H$_5$), 7.25, 7.30, 7.35 (total 15H, each s, 3×OCH$_2$C$_6\underline{H}_5$). High resolution mass spectrum, calcd for $C_{33}H_{41}NO_4S_2$: *m/z* 579.2475, found: M, 579.2503.

(2*R*,3*R*,4*R*)-1-Acetyl-3,4-bis(benzyloxy)-2-[(1*S*,2*E*)-1-benzyloxy-3-ethoxycarbonyl-2-propenyl]pyrrolidine (21). Compound **20** (2.66 g, 4.6 mmol) in a mixture of acetonitrile (40 ml) and water (10 ml) was treated with mercury(II) chloride (3.99 g) and calcium carbonate (1.61 g). Work-up as described in preparation of **8** gave the dethioacetal derivative (R_f 0.54, ethyl acetate : hexane=1 : 2), which was subjected to Horner-Emmons reaction with diethyl ethoxycarbonylmethylphosphonate (3.19 ml) in THF in the presence of sodium hydride (0.64 g) for 90 min at ambient temperature. Extractive work-up (CH_2Cl_2) and repeated chromatography on SiO_2 (2-butanone : toluene=1 : 14, then ethyl acetate : toluene=1 : 2) of the reaction mixture afforded **21** (R_f 0.47, ethyl acetate : toluene=1 : 2) (1.29 g, 52%) as a colorless syrup, $[\alpha]_D^{27}$+9.9° (*c* 0.91, $CHCl_3$); IR $\nu_{max}^{CHCl_3}$ 2990, 2960, 2930, 1710, 1630, 1450, 1410, 1370, 1300, 1270, 1175, 1095 cm^{-1}; ^{1}H NMR ($CDCl_3$) δ=1.22, 1.31 (total 3H, each t, *J*=7 Hz, COOCH$_2$C$\underline{H}_3$), 2.00, 2.05 (total 3H, each s, NCOCH$_3$), 3.06—4.90 (14H, m, H-2, 3, 4, 5, 5′, H-1 of the side chain, COOC$\underline{H}_2$CH$_3$, 3×OC$\underline{H}_2$C$_6$H$_5$), 5.91, 6.01 (total 1H, d and dd, *J*=15 Hz and *J*=2 and 15 Hz, CH=C$\underline{H}$COOEt), 6.60—7.02 (1H, m, C$\underline{H}$=CHCOOEt), 7.30, 7.34 (total 15H, each s, 3×OCH$_2$C$_6\underline{H}_5$). High resolution mass spectrum, calcd for $C_{33}H_{37}NO_6$: *m/z* 543.2618, found: *m/z* 543.2589.

(2*R*,3*R*,4*R*)-1-Acetyl-3,4-bis(benzyloxy)-2-[(1*S*)-1-benzyloxy-3-(ethoxycarbonyl)propyl]pyrrolidine (22). Compound **21** (668 mg, 1.23 mmol) in ethanol (9 ml) was hydrogenated in the presence of Raney nickel T-4 for 3 h. Work-up as described in preparation of **9** and chromatography of the product on SiO_2 (2-butanone : toluene=1 : 10) afforded **22** (R_f=0.46, ethyl acetate : toluene1=1 : 1) (577 mg, 86%) as a colorless syrup, $[\alpha]_D^{20}$−28.1° (*c* 1.34, $CHCl_3$); IR $\nu_{max}^{CHCl_3}$ 3660, 3570, 3480, 3010, 1725, 1630, 1420, 1270, 1170 cm^{-1}; ^{1}H NMR ($CDCl_3$) δ=1.18, 1.20 (total 3H, each t, *J*=7 Hz, COOCH$_2$C$\underline{H}_3$), 1.57—1.93 (2H, m, H-2, 2′ of the side chain), 2.00, 2.04 (total 3H, each s, NCOCH$_3$), 2.30, 2.32 (total 2H, each t, *J*=7 Hz, H-3, 3′ of the side chain), 3.27—4.73 (13H, m, H-2, 3, 4, 5, 5′, COOC$\underline{H}_2$CH$_3$, 3×OC$\underline{H}_2$C$_6$H$_5$), 7.27, 7.30 (total 15H, each s, 3×OCH$_2$C$_6\underline{H}_5$). High resolution mass spectrum, calcd for $C_{33}H_{39}NO_6$: *m/z* 545.2775, found: M, 545.2786.

(1*R*,2*R*,8*S*,8*aR*)-1,2,8-Tris(benzyloxy)-octahydro-5-indolizinone (23) and (2*R*,3*R*,4*R*)-1-Acetyl-3,4-bis(benzyloxy)-2-[(1*S*)-1-benzyloxy-3-carboxypropyl]pyrrolidine (24). A solution of **22** (577 mg, 1.1 mmol) in a mixture of ethanol (20 ml) and 15 mol dm^{-3} aqueous KOH (20 ml) in sealed tubes (100—120 mg of **22**/tube) was heated at 120 °C for 10 d. The soluble part was collected, and the unsoluble material was washed with ethanol several times. The ethanolic soluble part and washing were combined, diluted with water (20 ml), neutralized with acetic acid and evaporated. The residue was partitioned between chloroform (50 ml) and water (50 ml), and the aqueous layer was extracted with chloroform (50 ml×2). The extracts were dried (Na_2SO_4) and evaporated. The residue was chromatographed on SiO_2 (50 g, ethanol : toluene=1 : 35). Fractions corresponding to R_f 0.38 (ethanol : toluene=1 : 10, acidified with acetic acid) were evaporated to afford **23** (166 mg, 34%) as a colorless syrup which crystallized gradually from ether and petroleum ether. Fractions corresponding to R_f 0.35 were evaporated to afford **24** (340 mg, 62%) as a colorless syrup. **23**: Mp 52—54 °C; $[\alpha]_D^{20}$+15.1° (*c* 1.18, $CHCl_3$); IR ν_{max}^{KBr} 3420, 3020, 2880, 1640, 1490, 1410 cm^{-1}; ^{1}H NMR ($CDCl_3$) δ=1.43—2.54 (4H, m, H-6, 6′, 7, 7′), 3.40—4.85 (12H, m, H-1, 2, 3, 3′, 8, 8a, 3×OC$\underline{H}_2$C$_6$H$_5$), 7.27, 7.29, 7.33 (total 15H, each s, 3×OCH$_2$C$_6\underline{H}_5$). High resolution mass spectrum, calcd for $C_{29}H_{31}NO_4$: *m/z* 457.2251, found: M, 457.2226. **24**: $[\alpha]_D^{20}$−21.5° (*c* 0.93, $CHCl_3$); IR ν_{max}^{KBr} 3660, 3020, 2880, 1720, 1650, 1450, 1420, 1360, 1260, 1170 cm^{-1}; ^{1}H NMR ($CDCl_3$) δ=1.42—1.92 (2H, m, H-2, 2′ of the side chain), 1.98, 2.03 (total 3H, each s, NCOCH$_3$), 2.13—2.58 (2H, m, H-3, 3′ of the side chain), 3.23—4.70 (12H, m, H-2, 3, 4, 5, 5′, H-1 of the side chain, 3×OC$\underline{H}_2$C$_6$H$_5$), 7.27, 7.29, 7.32 (total 15H, each s, 3×OCH$_2$C$_6\underline{H}_5$).

Compound 23 from 24. Compound **24** (66 mg) was cyclized under the same conditions employed above. After SiO_2 chromatography, 44 mg (75%) of **23** was obtained and 13 mg (20%) of **24** was recovered.

(1*R*,2*R*,8*S*,8*aR*)-1,2,8-Triacetoxy-octahydro-5-indolizinone (25). *O*-Debenzylation of **23** (103 mg, 0.23 mmol) and successive acetylation under the same conditions and work-up described in preparation of **12** provided **25** (59 mg, 83%) after SiO_2 chromatography (ethanol : toluene=1 : 20, **25**: R_f=0.39, ethanol : toluene=1 : 8). **25**: Mp 118—119 °C; $[\alpha]_D^{24}$−20.9° (*c* 1.04, $CHCl_3$); IR ν_{max}^{KBr} 3440, 1740, 1635, 1460, 1380, 1260, 1230 cm^{-1}; ^{1}H NMR ($CDCl_3$) δ=1.58—2.75 (4H, m, H-6, 6′, 7, 7′), 2.09, 2.10, 2.13 (3H×3, each s, 3×OCOCH$_3$), 3.60—4.04 (3H, m, H-3, 3′, 8a), 5.10—5.53 (3H, m, H-1, 2, 8). Found: C, 53.38; H, 5.90; N, 4.43%. Calcd for $C_{14}H_{19}NO_7$: C, 53.67; H, 6.11; N, 4.47%.

(1*R*,2*R*,8*S*,8*aR*)-1,2,8-Triacetoxyoctahydroindolizine (26). Reduction of compound **25** (33 mg, 0.11 mmol) with borane-dimethyl sulfide (0.03 ml) at 0 °C, extractive work-up, saturated aqueous $NaHCO_3$ treatment, and successive acetylation as described in preparation of **13** afforded **26** (21 mg, 67%) after PTLC purification (ethanol : toluene=1 : 10). **26** (R_f=0.38, ethanol : toluene=1 : 10): Mp 124—125 °C; $[\alpha]_D^{20}$ −20.8° (*c* 1.00, $CHCl_3$), IR ν_{max}^{KBr} 3440, 2950, 2800, 1730, 1240, 1170 cm^{-1}; ^{1}H NMR δ=1.20—2.32 (6H, m, H-5, 6, 6′, 7, 7′, 8a), 2.07, 2.10, 2.17 (3H×3, each s, 3×OCOCH$_3$), 2.64 (1H, dd, *J*=8 and 11 Hz, H-3), 2.99—3.23 (2H, m, H-3′, 5′), 4.96—5.25 (3H, m, H-1, 2, 8). High resolution mass spectrum, calcd for $C_{14}H_{21}NO_6$: *m/z* 299.1367, found: M, 299.1344.

(1*R*,2*R*,8*S*,8*aR*)-Octahydro-1,2,8-indolizinetriol, 1,8-Di-*epi*-swainsonine (3). To a stirred solution of **26** (21 mg, 0.07 mmol) in methanol (1.5 ml) was added potassium carbonate (29 mg, 0.21 mmol). After stirring for 3 h at ambient temperature, the mixture was evaporated. The residue was purified by PTLC (aqueous ammonia : acetone : chloroform : water=1 : 30 : 5 : 4, the edge of the plate was colorized with ninhydrin and iodine) to afford a crystalline **3** (12 mg, 98%, R_f=0.28), which was recrystallized from chloroform, mp 138—140 °C (decomp); $[\alpha]_D^{21}$−35.6° (*c* 0.59, MeOH); IR ν_{max}^{KBr} 3600—3000 (br), 2920, 2810, 1330, 1240, 1210, 1150, 1135, 1100 cm^{-1}; ^{1}H NMR (D_2O) δ=1.22—2.27 (6H, m, H-5, 6, 6′, 7, 7′, 8a), 2.60 (1H, dd, *J*=6 and 11 Hz, H-3), 2.75—3.10 (2H, m, H-3′, 5′), 3.83—4.30 (3H, m, H-1, 2, 8); ^{13}C NMR (CD_3OD) δ=20.39, 32.19, 54.08, 62.74, 64.66, 75.05, 77.89, 80.23. High resolution mass spectrum, calcd for $C_8H_{15}NO_3$: *m/z* 173.1051, found: M, 173.1052.

The authors wish to express their thanks to Professor Anthony C. Richardson and Dr. Brian Winchester of the University of London for the mannosidase

inhibitory assay of the compound **2** and **3**. ^{13}C NMR spectral measurements were kindly performed by Dr. Yoshimasa Fukuda (Meiji Seika Co. Ltd) to whom our thanks are due. The financial support by the Kawakami Memorial Foundation is also acknowledged.

References

1) S. M. Colegate, P. R. Dorling, and C. R. Huxtable, *Aust. J. Chem.*, **32**, 2257 (1979).

2) R. J. Molyneux and L. F. James, *Science*, **216**, 190 (1982).

3) M. J. Schneider, F. S. Ungemach, H. P. Broquist, and T. M. Harris, *Tetrahedron*, **39**, 29 (1983).

4) M. Hino, O. Nakayama, Y. Tsurumi, K. Adachi, T. Shibata, H. Terano, M. Kohsaka, H. Aoki, and H. Imanaka, *J. Antibiot.*, **38**, 926 (1985).

5) T. Suami, K. Tadano, and Ŷ. Iimura, *Chem. Lett.*, **1984**, 513; *Carbohydr. Res.*, **136**, 67 (1985).

6) M. H. Ali, L. Hough, and A. C. Richardson, *J. Chem. Soc., Chem. Commun.*, **1984**, 447; *Carbohydr. Res.*, **136**, 225 (1985).

7) G. W. J. Fleet, M. J. Gough, and P. W. Smith, *Tetrahedron Lett.*, **25**, 1853 (1984).

8) N. Yasuda, H. Tsutsumi, and T. Takaya, *Chem. Lett.*, **1984**, 1201.

9) C. E. Adams, F. J. Walker, and K. B. Sharpless, *J. Org. Chem.*, **50**, 422 (1985).

10) H. Setoi, H. Takeno, and M. Hashimoto, *J. Org. Chem.*, **50**, 3948 (1985)

11) T. Kino, N. Inamura, K. Nakahara, S. Kiyoto, T. Goto, H. Terana, M. Kohsaka, H. Aoki, and H. Imanaka, *J. Antibiot.*, **38**, 936 (1985).

12) The syntheses of 8-*epi*-swainsonine and 2,8-di-*epi*-swainsonine were reported recently: N. Yasuda, H. Tsutsumi, and T. Takaya, *Chem. Lett.*, **1985**, 31. The overall yield of 8-*epi*-swainsonine in the literature seems to be unpractical.

13) The preliminary communication of the synthesis: Y. Iimura, Y. Hotta, C. Fukabori, K. Tadano, and T. Suami, *J. Carbohydr. Chem.*, **5**, 147 (1986).

14) R. D. Guthrie and L. F. Johnson, *J. Chem. Soc.*, **1961**, 4166.

15) S. Hanessian, T. J. Liak, and B. Vanasse, *Synthesis*, **1981**, 398.

16) R. D. Guthrie and G. P. B. Mutter, *J. Chem. Soc.*, **1964**, 1614.

17) F. W. Lichtenthaler, G. Bambach, and U. Scheidegger, *Chem. Ber.*, **102**, 986 (1969).

Pyrolyse und Massenspektren von 5-(Hydroxyphenoxymethyl)-2-oxazolidinon und *p*- oder *m*-Bis(2-oxooxazolidin-5-ylmethoxy)benzol[1)]

Choichiro SHIMASAKI,* Mariko WAKABAYASHI, und Shizuo YOSHIDA
Fakultät für Ingenieurwissenschaften, Universität Toyama, Gofuku, Toyama 930
(Eingangsdatum: 12. Juni, 1986)

5-(Hydroxyphenoxymethyl)-2-oxazolidinone (**1**) and *p*- or *m*-bis(2-oxooxazolidin-5-ylmethoxy)benzene (**2** or **3**) were prepared by the reaction of tris(2,3-epoxypropyl)-1,3,5-triazin-2,4,6(1*H*,3*H*,5*H*)-trione with hydroquinone and resorcinol. These compounds were found by the thermal analysis to be thermally stable. The activation energies of the pyrolysis for **1**, **2**, and **3** were calculated from the DTA curves to be 142.7, 158.8, and 130.0 kJ mol^{-1}, respectively. The mechanism of the main fragmentation of the linkages between the benzene and oxazolidinone rings by electron impact was found to consist of two processes; a simple cleavage and a rearrangement reaction. Further, each process had the three cleavage modes. In mass spectra of **2** and **3**, the fragment ion which corresponded to the molecular ion peak for **1** was detected. High resolution mass spectrometry established the composition of many peaks in the low resolution spectra of the compounds studied.

5-(Hydroxyphenoxymethyl)-2-oxazolidinon (**1**) und *p*- oder *m*-Bis(2-oxooxazolidin-5-ylmethoxy)benzol (**2** oder **3**) wurden aus Tris(2,3-epoxypropyl)-1,3,5-triazin-2,4,6(1*H*,3*H*,5*H*)-trion und Hydrochinon oder Resorcin hergestellt. Durch die thermischen Analysen wurden es gefunden daß diese Verbindungen der Hitze gegenüber relativ stabil waren. Beide, **1** und **2**, haben die dimorphischen Kristalle gegeben. Eine kinetische Berechnung der thermischen Zersetzungsreaktion auf Grund von DTA Kurven hat gezeigt, daß die Aktivierungsenergien der Zersetzungsreaktionen von **1**, **2**, und **3** jeweils 142.7, 158.8, und 130.0 kJ mol^{-1} sind. Der Hauptspaltungsmechanismus der Bindung zwischen Benzolring und Oxazolidinonring bei dem Elektronenschlag besteht aus den zwei Prozesse; die einfache Spaltungsreaktion und die Wasserstoff-Umlagerungsreaktion. Außerdem besteht jeder Prozeß aus der drei Spaltungsstilen. Bei der Spaltung von **2** und **3** wurden Spitze M^+ von **1** gemessen. Die hochauflösende Massen-spektrometrie bestätigte die Zusammensetzung einer grossen Anzahl von Spitzen in niederauflösenden Massenstrahlenspektren.

Einige Forschungen[2)] wurde über die Synthese von Poly(2-oxazolidinon) ausgeführt, aber die thermischen Eigenschaften von Poly(2-oxazolidinon) im Festzustand sind noch nicht vollständig erforscht. In der vorliegenden Abhandlung wurden die thermische Zersetzungsreaktion mit Differenz-Thermo-Analyse (DTA), Differential-Scanning-Kalorimetrie (DSC), und Thermogravimetrische Analyse (TG) und Zersetzung mit dem Elektronenschlag zusammengefaßt. Außerdem wurde die dimorphischen Kristalle von Poly(2-oxazolidinon) diskutiert.

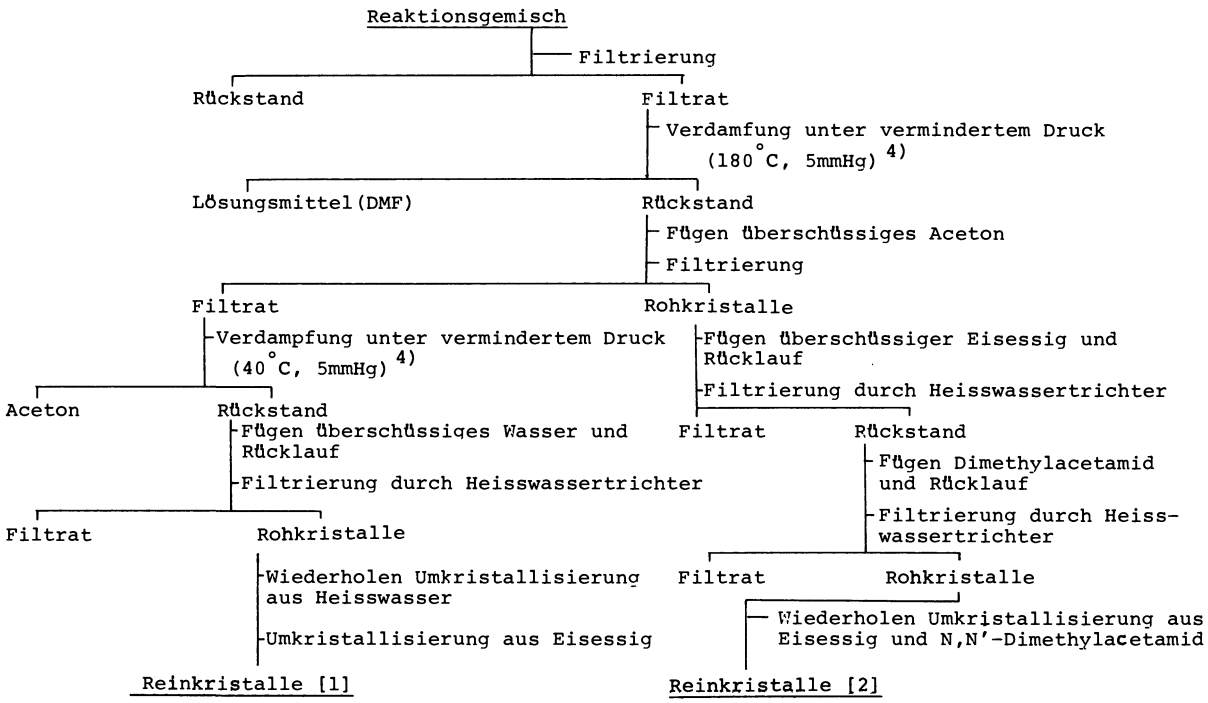

Schema 1. Typisches Isolationsverfahren von **1** und **2** aus Reaktionsgemisch.

Tabelle 1. Physikalische Eigenschaften von **1**, **2**, und **3**

Verbindung	Elementaranalyse Gef. (Ber.)/%			Schmp. θ_m/°C	IR Spektrum (KBr) cm^{-1}	M^+ / m/z	R_f Wert
	C	H	O				
1	56.82	5.50	6.82	175.9	1720	209	0.49
	(57.41)	(5.30)	(6.70)	178.3—182.3	3280		
2	54.26	5.27	9.18	265.2—266.6	1722, 1760	308	0.37
	(54.54)	(5.23)	(9.09)	267.3—268.0	3250		
3	54.20	5.10	8.96	170.6	1729, 1759	308	0.53
	(54.54)	(5.23)	(9.09)	173.7—179.0	3285		

Durchführung der Experimente

Materialien. 5-(Hydroxyphenoxymethyl)-2-oxazolidinon (**1**) und *p*- oder *m*-Bis(2-oxooxazolidin-5-ylmethoxy)benzol (**2** oder **3**) wurden nach Ishikawa et al.[3] hergestellt. Die Trennung von **1** und **2** wurde nach der Method in Schema 1 ausgeführt. **3** wurde aus Tris(2,3-epoxypropyl)-1,3,5-triazin-2,4,6(1*H*, 3*H*, 5*H*)-trion und Resorcin mit Natriumhydroxid als Katalysator synthetisiert. Die Ergebnisse der physikochemischen Eigenschaften von **1**, **2**, und **3** sind in Tabelle 1 zusammengestellt.

Messapparatur und Verfahren. Die DTA, DSC, und TG Kurven wurden in der Luft mit einer Aufheizgeschwindigkeit von 5 °C min^{-1} mit einem Rigaku TG-DTA, TG-DSC Thermoflex aufgenommen. Für DTA und DSC α-Al_2O_3 als Bezugsmittel gebraucht. Die IR Spektren wurden mittels Präparat von KBr-Presslingen mit einem Beugungsgitter IR Spektrometer der JASCO aufgenommen. ^1H und ^{13}C NMR-Spektren wurden mit einem JEOL JNM-FX 90 QET Spektrometer aufgenommen. Tetramethylsilan wurde als innere Standardsubstanz verwendet. Die Massenspektren wurden durch einen JMS-D300 Massenspektrometer mit direkten Probeinjektionen registriert.

Die Schmelzpunkte wurden durch einen Mitamura-Mikroschmelzpunkt-Apparat bestimmt und nicht korrigiert. Für Dünnschicht-Chromatographie wurden Platten mit Kiselgel G nach Stahl (typ 60) von Merck gebraucht. Die Elementaranalysen wurden bei der Analysen-Zentrale in der Medizinischen-Pharmazeutischen Universität Toyama durchgeführt.

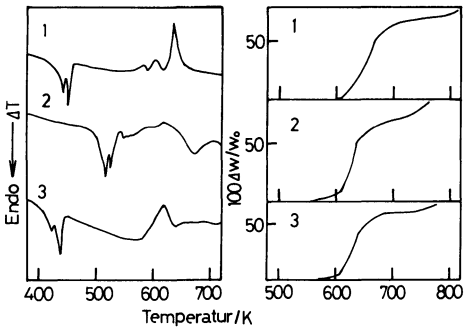

Abb. 1. DSC-TG Kurven von **1**, **2**, und **3**.

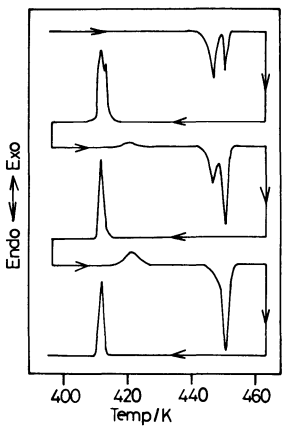

Abb. 2. Effekt des Heiz-Abkühlungsprozesses auf DTA von **1**.

Ergebnisse und Diskussionen

Thermische Analyse. Die DSC und TG Kurven der Probe (**1**, **2**, und **3**) sind in Abb. 1 dargestellt. Die DSC Kurven ergeben in allen drei Proben durch den Schmelzprozeß eine endotherme Spitze, die in zwei Teile geteilt ist. Die TG Kurven zeigen, daß der Prozeß der Zersetzung zwischen 10—50% vom Gewichtverlust bei allen drei Proben in einer Stufe geschieht. Es gibt keine deutliche Hochebene an der TG Kurven bei allen Fällen. Beim Heiz-Abkühlungskreisprozeß der DTA Kurven von **1** und **2** war das thermische Benehmen[3] gleich wie von 5-Phenoxymethyl-2-oxazoldinon. Abbildung 2 zeigt den Effekt des Heiz-Abkühlungskreisprozesses auf DTA von **1**. Bei erstem Kreisprozeß wird jeweils eine endotherme oder eine exotherme Spitze angezeigt, die in zwei Teile geteilt ist. Wenn der Kreisprozeß über dreimal wiederholt wurde, erschien deutlich eine schwache exotherme Spitze vor der Spitze des Schmelzpunktes. Diese Spitze hat ihren Ursprung in der Kristallisationswärme. Durch das Mikroskop wurde der Zustand der Veränderung von Amorphe zu Kristalle erkannt. Bei der Untersuchung der Kristalle durch das Mikroskop wurde beim Kreisprozeß einmal die Zweiform des Gemisches von Blätter- und Nadelkristalle festgestellt, aber danach nur Nadelkristalle.

IR Spektren. Abbildung 3 zeigt den Heizeffekt auf IR Spektren unter vermindertem Druck (10^{-3} mmHg)[4] bei 3 Proben. Die Kurven von **1** und **2** sind nach Erwärmung gleich. Die $\nu_{C=O}$ Bänder von **2** und **3**, die in zwei Teile geteilt sind, zeigen nach der Erwärmung eine Spitze. Die Benzolkern Bänder (1505 cm^{-1}) von **1**, **2**, und **3**, die in schmalen großen Spitze erscheinen, zeigen am Anfang und am Ende der Erwärmung auf

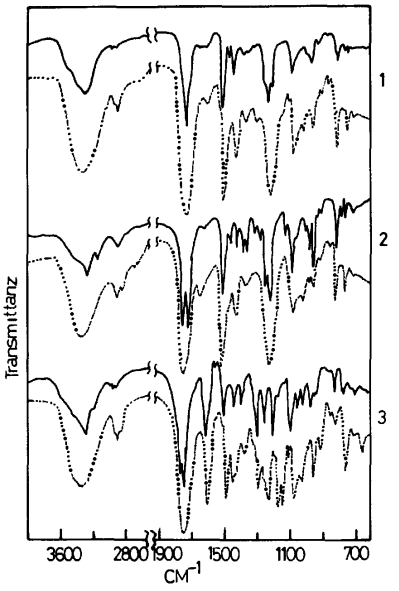

Abb. 3. Heizeffekt auf IR Spektren unter vermindertem Druck (10^{-3} mmHg) bei **1**, **2**, und **3**. Eine durchgehende Linie: vor Erwärmung. Eine punktierte Linie: nach Erwärmung bei 250°C.

alle Fälle eine gleiche Spitze. Aus den Veränderungen der IR Spektren von **1**, **2**, und **3** mit zunehmender Laufzeit der Erwärmung läßt sich schließen, daß gemäß der Erwärmung einige CH_2O-Bindung zwischen Benzolring und Oxazolidinonring zerreißt wird. Durch die Erwärmung wurde alle 3 Proben in 2-Imidazolidinon und Hydrochinon oder Resorcin zersetzt.

Massenspektren. Der Zersetzungsverlauf kann mittels der entsprechenden Massenspektroskopie direkt verfolgt werden. Die Veränderung der Massenspektren von den 3 Proben wurde im Bereich der Ionisierungsspannung 10—75 eV untersucht. Die niederauflösenden Massenspektren von **1**, **2**, und **3** sind in Abb. 4 dargestellt. Wie in Abb. 4 ersichtlich ist, ergibt sich in allen drei Proben eine Molekulionspitze. Die Basisionenspitze von **1**, **2**, und **3** ist m/z 110 ($C_6H_6O_2^+$, Unsättigungsgrad=4.0). Diese Spitze entspricht einer Spaltungstücksion von Hydrochinon und Resorcin. Aus den Resultate der niederauflösenden Massenspektren wurde vorausberechnet, daß der durch Elektronenschläge erregte Hauptspaltungsmechanismus von allen 3 Proben über der Spaltung der Bindung zwischen Benzolring und oxazolidinonring in sechs Spaltungsstilen besteht. Die hierbei auftretenden Spaltungsstile lassen sich in zwei Gruppen gliedern:

— Einfache Spaltungsreaktionen (3 Stile)

— Wasserstoff-Umlagerungsreaktionen (3 Stile)

In Abb. 5 sind sechs Spaltungsstile dargestellt. Die Spaltstücksionen, $RC_6H_4^+$, $RC_6H_5^+$, die durch den Prozeß(I) in Abb. 5 bei niederauflösenden Massenspektren festgestellt wurden, konnten - vom Gesichtspunkt der hochauflösenden Massenspektren aus - nicht

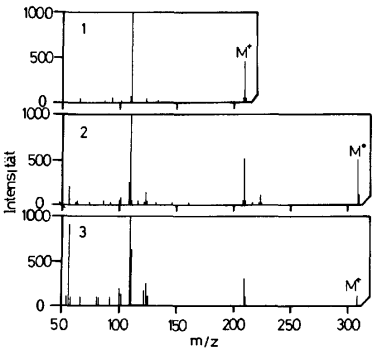

Abb. 4. Massenspektren von **1**, **2**, und **3**.

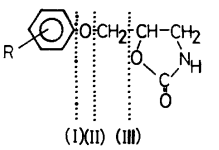

R: OH 1
$C_4H_6NO_3$ 2 und 3

Einfache Spaltungsreaktionen

(I)	$RC_6H_4^+$	$C_4H_6NO_3^+$
(II)	$RC_6H_4O^+$	$C_4H_6NO_2^+$
(III)	$RC_7H_6O^+$	$C_3H_4NO_2^+$

Wasserstoff-Umlagerungsreaktionen

(I)	$RC_6H_5^+$	$C_4H_5NO_3^+$
(II)	$RC_6H_5O^+$	$C_4H_5NO_2^+$
(III)	$RC_7H_7O^+$	$C_3H_3NO_2^+$

Abb. 5. Hauptspaltungsmechanismus des Elektronenschlages von **1**, **2**, und **3**.

erfaßt werden. Das war dasselbe Result wie bei der früheren Untersuchung über Phenol.[5] Die Spaltstücksionen bei den Hauptspaltungsmechanismen des Elektronschlages zwischen Benzolring und Oxazolidinonring von **1**, **2**, und **3** zeigten, daß die Benzolring enthaltende Spaltstückionen in überwiegender Mehrheit existierten. Die hochauflösende Massenspektroskopie wurde ausgeführt, um den Spaltungsmechanismus bis in Details zu untersuchen. Die Ergebnisse der Messung von **2** sind in Tabelle 2 zusammengestellt.

Kinetik vom thermischen Zersetzungsvorgang. Die Kinetik der thermischen Zersetzung wurde an der DTA Kurves untersucht. Am Anfang wurde die Abhängigkeit der Temperatur des DTA-Maximums von der Aufheizgeschwindigkeit bei der thermischen Zersetzung von **1**, **2**, und **3** untersucht. Kissinger[6] leitete die einer thermischen Zersetzungsreaktion entsprechende Gleichung ab

$$\frac{d\ln(\phi/T_m^2)}{d(1/T_m)} = E/R \qquad (1)$$

wo ϕ für Aufheizgeschwindigkeit steht, T_m für Temperatur des DTA-Maximums, und E für Aktivierungsenergie, und R für Gaskonstant. Aus Gl. 1 ersieht man, daß bei kleinen Aktivierungsenergien eine starke Verschiebung des Temperaturmaximums der DTA-Kurve zu erwarten ist. In Abb. 6 ist das $\ln(\phi/T_m^2)-1/T_m$

Tabelle 2. Massenstrahlenspektren von **2**

m/z[a]	Relative Intensität[b]	Sigma/%[c]	Gefunden Molekulargewicht	U.S.[e]	Wahrscheinliche Ionenzusammensetzung
56.0	21.88	5.94	56.0126(56.0135)[d]	2.5	C_2H_2NO
			56.0501(56.0498)	1.5	C_3H_6N
100.0	7.21	1.95	100.0421(100.0396)	2.5	$C_4H_6NO_2$
109.0	25.21	6.84	109.0288(109.0288)	4.5	$C_6H_5O_2$
110.0	100.00	27.15	110.0358(110.0366)	4.0	$C_6H_6O_2$
123.0	11.14	3.02	123.0464(123.0444)	4.5	$C_7H_7O_2$
124.0	4.48	1.21	124.0574(124.0522)	4.0	$C_7H_8O_2$
208.0	5.33	1.45	208.0646(208.0606)	6.5	$C_{10}H_{10}NO_4$
209.0	53.09	14.41	209.0680(209.0684)	6.0	$C_{10}H_{11}NO_4$
210.0	6.88	1.84	210.0752(210.0762)	5.5	$C_{10}H_{12}NO_4$
223.0	8.12	2.20	223.0826(223.0840)	6.0	$C_{11}H_{13}NO_4$
308.0	52.29	14.20	308.0978(308.1002)	8.0	$C_{14}H_{16}N_2O_6$

a) Molekular-Ion, unterstrichen. b) Relative Intensität gegenüber der Basisionenspitze der Spektren als 100. c) Spitzenhöhe im Prozent der Gesamtionization. d) Berechnete Werte. e) U.S.=Unsättigungsgrad.

Tabelle 3. Zusammenfassung der Kinetischen Daten der Thermischen Zersetzung von **1**, **2**, und **3**

Verbindungen	Schmelzwärme	Aktivierungsenergie	Kristallisationswärme[a]
	kJ mol^{-1}	kJ mol^{-1}	kJ mol^{-1}
1	30.5	142.7	—
2	42.7	158.8	3.8
3	48.1	130.0	—

a) Berechnete Wert von einer exothermen Spitze, die nach dreimaliger Wiederholung des Kreisprozess in Abb. 2 erschien.

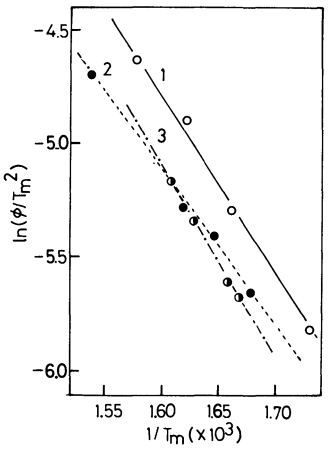

Abb. 6. $\ln(\phi/T_m^2)-1/T_m$ Diagram zur Berechnung der Aktivierungsenergie nach der Kissingerschen-Gleichung.

Diagram zur Berechnug der Aktivierungsenergie dargestellt. In Tabelle 3 sind die, aus dem Flächengröße der DSC Kurve berechneten, Schmelzwärme, Kristallisationswärme, und die aus DTA Kurven nach der Kissingerschen Gleichung berechneten Aktivierungsenergien der Zersetzungsreaktionen bei den 3 Proben zusammengestellt. Aus Tabelle 3 ist ersichtlich, daß der Wert der Schmelzwärmen nach der Reihe **3>2>1** zunahm und der Wert der Aktivierungsenergien nach der Reihe **2>1>3**. Aus diese Resultate wurde bestätigt, daß die thermischen Zersetzung von **2** oder **3** über den Prozeß der Bildung von **1** oder 4-(Hydroxyphenoxymethyl)-2-oxazolidinon verlaufe. Die Aktivierungsenergie nimmt mit der Zahl der Bindungen zwischen Benzolring und Oxazolidinonring ab.

Die Materialien in der vorliegenden Arbeit wurden von Nissankagaku A.G. angeboten. Für die Bedienung der Apparatur zur Anfertigung der Mass und NMR Spektren haben sich in dankenwerterweise Fräulein M. Shinoda und Herr K. Yoneyama zur Verfügung gestellt. Herrn Prof. S. Takeuchi danken wir bestens für wertvolle Hinweise.

Literaturen

1) Nachricht XI von "Untersuchung über Zersetzung und Bildung von Triazinserien Verbindungen." Nachricht X von dieser Serien: C. Shimasaki, M. Takeuchi, J. Tsutuguchi, K. Shimizu, und H. Yamakawa, *Bull. Chem. Soc. Jpn.*, **58**, 2197 (1985).

2) G. P. Spranza und W. J. Pepel, *J. Org. Chem.*, **23**, 1922 (1958); S. R. Sandler, *J. Polym. Sci., A-1*, **5**, 1481 (1967); J. E. Herweh und W. Y. Whitmore, *ibid.*, **8**, 2759 (1970); T. Ishikawa und N. Watanabe, *Nippon Kagaku Kaishi*, **1980**, 852.

3) C. Shimasaki, Y. Iino, und M. Saito, *Nippon Kagaku Kaishi*, **1979**, 1739.

4) In SI Einheit entspricht 1 mmHg 133.3 N m^{-2}.

5) T. Aczel und H. H. Lumpkin, *Anal. Chem.*, **32**, 1819 (1960).

6) H. E. Kissinger, *Anal. Chem.*, **29**, 1702 (1957).

The Lithium Diisopropylamide-Induced Fragmentation of 2,2-Diphenyl-1,3-dithiolane *S*-Oxide and Several 2,2-Diaryl-1,3-dithiolane *S,S'*-Dioxides

Yoshihiko INOUE, Shigeo TANIMOTO,* and Tatsuo OIDA
Institute for Chemical Research, Kyoto University, Uji, Kyoto 611
(Received June 12, 1986)

The reaction of 2,2-diphenyl-1,3-dithiolane *S*-oxide with lithium diisopropylamide results in fragmentation to thiobenzophenone followed by further conversion leading to alkyl diphenylmethyl sulfide on trapping with alkyl halide. The reaction of 2,2-diaryl-1,3-dithiolane *S,S'*-dioxides with lithium diisopropylamide proceeded smoothly to afford 1,1-diaryl-*N,N*-diisopropylmethanesulfinamides in moderate yields via the intermediate diaryl thioketone *S*-oxides.

It is well-known that 2-lithio-1,3-dithiolanes undergo facile elimination to form ethylene and dithiocarbonates.[1,2] On the other hand, 4-lithio-1,3-dithiolanes, as unstable intermediates occurring in the reaction of 1,3-dithiolanes with butyllithium, undergo facile fragmentation to the corresponding thiocarbonyl compounds followed by further reaction such as reduction, *S*-addition, *C*-addition, or double addition with butyllithium.[3,4] 4-Lithio-1,3-dithiolanes bearing two aromatic substituents at *C*-2 are also formed by the reaction of 2,2-diaryl-1,3-dithiolanes with less nucleophilic lithium diisopropylamide (LDA), and diaryl thioketones arising from these 4-lithio-1,3-dithiolanes afforded alkyl diarylmethyl sulfides or their α-alkyl derivatives by quenching the reaction mixture with alkyl halides.[2] The same fragmentation-alkylation sequence using LDA has also been applied to several 2-alkyl-2-aryl-1,3-dithiolanes.[5] Moreover, it has been reported[6] that 1,3-dithiolane *S,S*-dioxides derived from benzophenone and camphor undergo facile metalation with LDA or potassium *t*-butoxide followed by fragmentation to the corresponding thiobenzophenone and thiocamphor, respectively. These thioketones have been isolated[6] without any conversion by the bases used in the reaction systems. With these considerations in mind, we have studied the reaction of 2,2-diphenyl-1,3-dithiolane *S*-oxide (**1**) and several 2,2-diaryl-1,3-dithiolane *S,S'*-dioxides (**7**) with LDA in tetrahydrofuran.

Results and Discussion

A noteworthy observation[7] on the stereoselectivity in oxidation of 2-substituted 1,3-dithiolanes with *m*-chloroperbenzoic acid is recorded in the literature. Also, the oxidation of a few 2,2-disubstituted 1,3-dithiolanes such as 2,2-diphenyl-1,3-dithiolane with H_2O_2 providing the corresponding *S*-oxides or *S,S'*-dioxides has been reported.[8] However, no report thus far appears in which the oxidation of 2,2-diaryl-1,3-dithiolanes with *m*-chloroperbenzoic acid is described. Although not proved, almost all of **1** and **7** used in this research will probably be a mixture of two or more stereoisomers. Compound **1** is a racemic mixture, and both 2,2-diphenyl-1,3-dithiolane *S,S'*-dioxide (**7a**) and spiro[1,3-dithiolane-2,9'-[9*H*]fluorene] *S,S'*-dioxide (**7i**) are mixtures of cis and trans-forms.[9] Other 2,2-diaryl-1,3-dithiolane *S,S'*-dioxides (**7b—h**) are constituted of four stereoisomers. This may be evidenced by the fact that most of **7** melt over a relatively broad range of temperature, especially 2-(2-naphthyl)-2-phenyl-1,3-dithiolane *S,S'*-dioxide (**7h**) melts abnormally.[10] Alo, according to Henbest and his coworker,[11] the competitive formation of 2,2-diaryl-1,3-dithiolane *S,S*-dioxides in the oxidative process of 2,2-diaryl-1,3-dithiolanes with *m*-chloroperbenzoic acid giving **7** seems to be negligible. Thus, **1** and **7** have been prepared using *m*-chloroperbenzoic acid and submitted to the action of LDA in tetrahydrofuran.

The reaction of **1** with an excess of LDA proceeded smoothly via proton abstraction at *C*-5 followed by cyclo-elimination affording thiobenzophenone (**3**) and an ethylenesulfinate anion. The resulting **3** is labile in this reaction system, and hence **3** is converted to alkyl diphenylmethyl sulfides (**6**) via a process involving a one-electron transfer from LDA, the charge neutralization by the added alkyl iodide (methyl iodide or butyl iodide), and the abstraction of a hydrogen radical from tetrahydrofuran. Thus, we have obtained excellent yields of diphenylmethyl methyl sulfide (**6a**) and butyl diphenylmethyl sulfide (**6b**), which are identical with those obtained[2] by the reaction of 2,2-diphenyl-1,3-dithiolane itself and LDA followed by trapping with methyl iodide and butyl iodide, respectively.

Next, 2,2-diaryl-1,3-dithiolane *S,S'*-dioxides (**7a—i**) were submitted to fragmentation with an excess of LDA in tetrahydrofuran at low temperature. These, without any trapping with alkyl halide, led to the corresponding 1,1-diaryl-*N,N*-diisopropylmethanesulfinamides (**11a—i**) via a successive attack of 2 molar equivalents of LDA to **7a—i**. Though the exact mechanism is still in doubt, it is certain that the deprotonation at *C*-4 of the ring affording **8** is the first step. Probably, the intermediate **8** undergoes cyclo-elimination leading to diaryl thioketone *S*-oxides (**9**) and an ethylenesulfinate anion. The former is converted to an anionic species (**10**) by the nucleophilic attack of a second LDA molecule. In another experiment with **7a**,

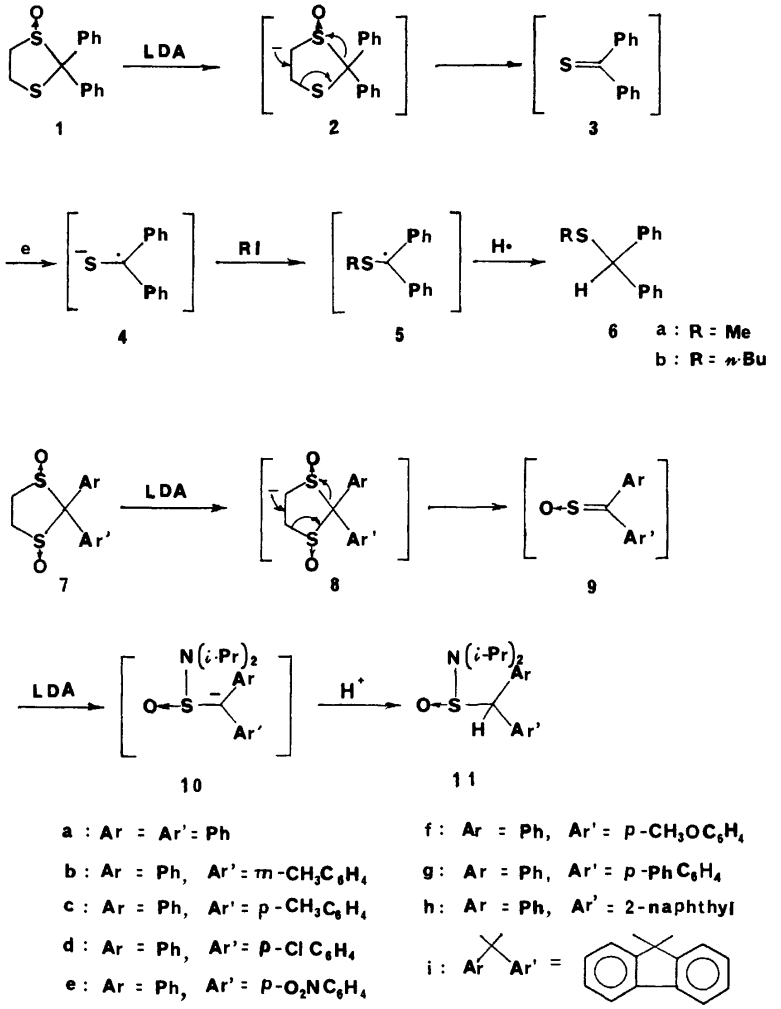

in which only a 1.2-fold excess of LDA was used, *N,N*-diisopropyl-1,1-diphenylmethanesulfinamide (**11a**) was obtained in 28% yield. This result indicates that the nucleophilic attack of a second LDA molecule to thiobenzophenone *S*-oxide (**9a**) takes place very rapidly. When D_2O was used in the quenching step of the experiment, which was conducted with **7a** and a 2.5-fold excess of LDA, 1-deuterio-*N,N*-diisopropyl-1,1-diphenylmethanesulfinamide was obtained in almost the same yield as **11a**. These experimental facts substantiate the proposed mechanical assignment of the present reaction. The results with **1** and **7a—i** are summarized in Table 1. The physical and analytical data of the products obtained are listed in Table 2.

Except **11a** and *N,N*-diisopropyl-9*H*-fluorene-9-sulfinamide (**11i**), the 1,1-diaryl-*N,N*-diisopropylmethanesulfinamides (**11b—h**) obtained possess two dissimilar asymmetric centers, and hence four stereoisomers are possible. Each of the two products, 1-(4-chlorophenyl)-*N,N*-diisopropyl-1-phenylmethanesulfinamide (**11d**) and *N,N*-diisopropyl-1-(4-nitrophenyl)-1-phenylmethanesulfinamide (**11e**), was chromatographically separated into two kinds of racemates distinguishable from each other by a difference in melting point. Each of **11a** and **11i** is a racemic mixture; the former was isolated as crystals with relatively sharp melting point and the latter was an oily substance.

Experimental

Preparation of 2,2-Diphenyl-1,3-dithiolane *S*-Oxide (1). To a stirred, cooled (0 °C) solution of 2,2-diphenyl-1,3-dithiolane (5.2 g, 20 mmol) in dichloromethane (50 ml) a solution of *m*-chloroperbenzoic acid (3.4 g, 20 mmol) in dichloromethane (40 ml) was added during 2 h, followed by stirring at reflux temperature for 3 h. The reaction mixture was cooled overnight in an ice bath. The precipitated benzoic acid was filtered off and the filtrate was washed with 10% aqueous $NaHCO_3$ (3×50 ml). The washings were extracted with dichloromethane (3×50 ml) and the dichloromethane extract obtained was combined with the above filtrate. It was dried over $MgSO_4$ and the solvent was removed in vacuo to give a residue which was recrystallized from ethanol, yield 3.7 g (65%), mp 127—129 °C (lit,[8] mp of 2,2-diphenyl-1,3-dithiolane *S*-oxide prepared from 2,2-diphenyl-1,3-dithiolane and H_2O_2 is 131—132 °C). Found: C, 65.67; H, 5.22%. Calcd for $C_{15}H_{14}OS_2$: C, 65.66; H, 5.14%. ^{1}H-NMR ($CDCl_3$) δ=2.9—4.0 (m, 4H), 7.0—8.1 (m, 10H).

Preparation of 2,2-Diaryl-1,3-dithiolane *S,S'*-Dioxides (7a—i). 2,2-Diphenyl-1,3-dithiolane *S,S'*-Dioxide (7a): To a stirred, cooled (0 °C) solution of 2,2-diphenyl-1,3-dithiolane

Table 1. The Reaction of 2,2-Diphenyl-1,3-dithiolane S-Oxide (**1**) and 2,2-Diaryl-1,3-dithiolane S,S'-Dioxides (**7a—i**) with Lithium Diisopropylamide (LDA)

Entry	Starting substrate (**1** or **7**)	Molar ratio (LDA/**1** or **7**)	Trapping agent	Eluent used in chromatographic purification	Product	
					Abbreviation	Yield/%
1	**1**	2.5	MeI	CH_3CO_2Et/Hexane (1:1)	**6a**	90
2	**1**	2.5	*n*-BuI	CH_3CO_2Et/Hexane (1:1)	**6b**	92
3	**7a**	2.5	H_2O	CH_3CO_2Et	**11a**	60
4	**7a**	2.5	*n*-BuI	CH_3CO_2Et	**11a**	59
5	**7b**	2.5	H_2O	CH_3CO_2Et/Hexane (3:1)	**11b**	69
6	**7c**	2.5	H_2O	CH_3CO_2Et/Hexane (1:4)	**11c**	67
7	**7d**	2.5	H_2O	CH_3CO_2Et/Hexane (3:2)	**11d**(I)[a]	27
					11d(II)[a]	37
8	**7e**	2.5	H_2O	CH_3CO_2Et/Hexane (5:2)	**11e**(I)[b]	31
					11e(II)[b]	28
9	**7f**	2.5	H_2O	CH_2Cl_2/Hexane (1:1)	**11f**	17
10	**7g**	2.5	H_2O	CH_2Cl_2/Hexane (1:1)	**11g**	50
11	**7h**	2.5	H_2O	CH_2Cl_2/Hexane (1:1)	**11h**	65
12	**7i**	2.5	H_2O	CH_3CO_2Et	**11i**	36

a) Column chromatography afforded two products **11d**(I) and **11d**(II), which are diastereoisomeric with each other. b) Similarly, two diastereoisomers **11e**(I) and **11e**(II) were obtained.

Table 2. Physical Properties and Analytical Data of the Products

Product	Mp or Bp θ_m/°C θ_b/°C (Torr)	^{1}H NMR Spectra (δ, in $CDCl_3$)	Found (Calcd) (%)		
			C	H	N
6a	140(2) [Lit,[12] 108—111(1)]	1.89(s, 3H), 5.00(s, 1H), 7.1—7.6(m, 10H)	78.47 (78.45)	6.88 (6.58)	
6b	164—166(1—2)	0.6—1.9(m, 7H), 2.19(t, 2H), 4.98(s, 1H), 6.8—7.4 (m, 10H)	79.53 (79.63)	7.80 (7.86)	
11a[a]	102—104 (Hexane)	0.58(d, 6H), 1.26(d, 6H), 3.63(m, 2H), 5.04(s, 1H), 7.0—7.6(m, 10H)	72.57 (72.34)	7.90 (7.99)	4.22 (4.44)
11b[b]	Oil	0.73(d, 6H), 1.25(d, 6H), 2.22(s, 3H), 3.56(m, 2H), 4.90(s, 1H), 6.7—7.4(m, 9H)	73.11 (72.90)	8.47 (8.26)	4.21 (4.25)
11c[b]	Oil	0.72(d, 6H), 1.24(d, 6H), 2.17(s, 3H), 3.55(m, 2H), 4.90(s, 1H), 6.7—7.4(m, 9H)	73.13 (72.90)	8.28 (8.26)	4.01 (4.25)
11d(I)	55—57 (Hexane)	0.74(d, 6H), 1.25(d, 6H), 3.57(m, 2H), 4.88(s, 1H), 6.9—7.3(m, 9H)	65.23 (65.22)	6.89 (6.91)	3.86 (4.00)
11d(II)	121—124 (Hexane)	0.78(d, 6H), 1.26(d, 6H), 3.57(m, 2H), 4.87(s, 1H), 6.9—7.4(m, 9H)	65.34 (65.22)	6.79 (6.91)	3.90 (4.00)
11e(I)	133—134 (Hexane)	0.77(d, 6H), 1.27(d, 6H), 3.62(m, 2H), 5.08(s, 1H), 7.0—7.6(m, 7H), 7.8—8.1 (m, 2H)	63.60 (63.31)	6.91 (6.71)	7.49 (7.77)
11e(II)	48—49 (Hexane)	0.77(d, 6H), 1.28(d, 6H), 3.60(s, 2H), 5.07(s, 1H), 7.0—7.6(m, 7H), 7.8—8.1(m, 2H)	63.26 (63.31)	6.95 (6.71)	7.80 (7.77)
11f[b]	Oil	0.76 and 0.80(d and d, 6H), 1.29(d, 6H), 3.67(m, 2H), 3.74(s, 3H), 4.94(s, 1H), 6.7—7.0(m, 2H), 7.1—7.6(m, 7H)	69.35 (69.53)	8.00 (7.88)	3.81 (4.05)
11g[b]	Oil	0.76(d, 6H), 1.62(d, 6H), 3.67(m, 2H), 5.09(s, 1H), 7.0—7.8(m, 14H)	76.43 (76.68)	7.33 (7.47)	3.54 (3.58)
11h[b]	Oil	0.65 and 0.75(d and d, 6H), 1.26(d, 6H), 3.27 and 3.30(m and m, 2H), 5.19(s, 1H), 7.0—7.9(m, 12H)	75.66 (75.57)	7.35 (7.45)	3.92 (3.83)
11i[a]	Oil	0.79(d, 6H), 1.34(d, 6H), 3.56(m, 2H), 4.99(s, 1H), 6.9—7.9(m, 8H)	72.56 (72.80)	7.15 (7.40)	4.30 (4.47)

a) Racemic mixture. b) Mixture composed of four stereoisomers unseparable from each other by column chromatography. 1 Torr = 133.322 Pa.

(5.2 g, 20 mmol) in dichloromethane (50 ml) a solution of *m*-chloroperbenzoic acid (6.9 g, 40 mmol) in dichloromethane (50 ml) was added during 3 h, followed by stirring at reflux temperature for 3 h. The reaction mixture was conducted as above. The crude product obtained was recrystallized from ethanol. If necessary, the crude product was purified by column chromatography on silica gel, using ethyl acetate as eluent, prior to the recrystallization, yield 6.51 g (56%), mp 186—189 °C. Found: C, 61.98; H, 4.95%. Calcd for $C_{15}H_{14}O_2S_2$: C, 62.04; H, 4.86%. ^{1}H-NMR ($CDCl_3$)

δ=3.42 (ddd, 2H), 3.93 (ddd, 2H), 6.9—7.6 (m, 10H).

In a similar manner, other 2,2-diaryl-1,3-dithiolane *S,S'*-dioxides (**7b—i**) were prepared from the corresponding 2,2-diaryl-1,3-dithiolanes.

2-(3-Methylphenyl)-2-phenyl-1,3-dithiolane *S,S'*-Dioxide (7b): 97%, mp 167—171 °C (from ethanol). Found: C, 63.01; H, 5.14%. Calcd for $C_{16}H_{16}O_2S_2$: C, 63.13; H, 5.30%. ^{1}H-NMR ($CDCl_3$) δ=3.44 (d, 2H), 3.80 (d, 2H), 6.9—7.6 (m, 9H).

2-(4-Methylphenyl)-2-phenyl-1,3-dithiolane *S,S'*-Dioxide (7c): 80%, mp 177—180 °C (from ethanol). Found: C, 62.88; H, 5.09%. Calcd for $C_{16}H_{16}O_2S_2$: C, 63.13; H, 5.30%. ^{1}H-NMR ($CDCl_3$) δ=3.31 (s, 3H), 3.3—4.1 (m, 4H), 6.9—7.5 (m, 9H).

2-(4-Chlorophenyl)-2-phenyl-1,3-dithiolane *S,S'*-Dioxide (7d): 61%, mp was not measured. Found: C, 55.24; H, 4.06%. Calcd for $C_{15}H_{13}ClO_2S_2$: C, 55.46; H. 4.03%. ^{1}H-NMR ($CDCl_3$) δ=3.2—4.1 (m, 4H), 6.8—7.6 (m, 9H).

2-(4-Nitrophenyl)-2-phenyl-1,3-dithiolane *S,S'*-Dioxide (7e): 83%, mp was not measured. Found: C, 53.65; H, 4.05; N, 4.11%. Calcd for $C_{15}H_{13}NO_4S_2$: C, 53.72; H, 3.91; N, 4.18%. ^{1}H-NMR ($CDCl_3$) δ=3.5—4.3 (m, 4H), 7.0—7.5 (m, 7H), 8.11 (s, 1H), 8.26 (s, 1H).

2-(4-Methoxyphenyl)-2-phenyl-1,3-dithiolane *S,S'*-Dioxide (7f): 84%, mp 180—183 °C (from ethanol). Found: C, 59.95; H, 5.07%. Calcd for $C_{16}H_{16}O_3S_2$: C, 59.97; H, 5.03%. ^{1}H-NMR ($CDCl_3$) δ=3.71 (s, 3H), 3.3—4.0 (m, 4H), 6.70 and 6.86 (s and s, 2H), 7.1—7.6 (m, 7H).

2-(1,1'-Biphenyl-4-yl)-2-phenyl-1,3-dithiolane *S,S'*-Dioxide (7g): 48%, mp 186—189 °C (from ethanol). Found: C, 68.70; H, 4.68%. Calcd for $C_{21}H_{18}O_2S_2$: C, 68.82; H, 4.95%. ^{1}H-NMR ($CDCl_3$) δ=3.2—4.1 (m, 4H), 7.0—7.8 (m, 14H).

2-(2-Naphthyl)-2-phenyl-1,3-dithiolane *S,S'*-Dioxide (7h): 59%, mp 163— °C (from ethanol). Found: C, 67.68; H, 5.05%. Calcd for $C_{19}H_{16}O_2S_2$: C, 67.03; H, 4.74%. ^{1}H-NMR ($CDCl_3$) δ=3.2—4.5 (m, 4H), 7.0—8.0 (m, 12H).

Spiro[1,3-dithiolane-2,9'-[9*H*]fluorene] *S,S'*-Dioxide (7i): 74%, mp 176—181 °C (from ethanol). Found: C, 62.22; H, 4.06%. Calcd for $C_{15}H_{12}O_2S_2$: C, 62.47; H, 4.19%. ^{1}H-NMR ($CDCl_3$) δ=3.69 (dd, 2H), 4.27 (dd, 2H), 7.1—7.9 (m, 8H).

The Reaction of 2,2-Diphenyl-1,3-dithiolane *S*-Oxide (1) with Lithium Diisopropylamide (LDA) (Entries 1 and 2 of Table 1). To a stirred, cooled (−78 °C) solution of diisopropylamine (0.35 g, 3.5 mmol) in tetrahydrofuran (7 ml) was added a 1.56 molar solution (2.1 ml, 3.3 mmol) of butyllithium in hexane under nitrogen, followed by stirring at the same temperature for 30 min and further stirring at −15 °C for 10 min. The solution of LDA thus prepared was maintained at −15 °C. It was slowly added to a stirred, cooled (−78 °C) solution of **1** (0.35 g, 1.3 mmol) in tetrahydrofuran (4 ml) under nitrogen. The reaction mixture was warmed to room temperature and the stirring was continued for 1 h. The mixture was cooled again to −78 °C, and 3.3 mmol of an alkyl halide (0.47 g of methyl iodide or 0.61 g of butyl iodide) was added with stirring. The mixture was stirred for 1 h at 0 °C, warmed to room temperature, stirred an additional 24 h, quenched with 20 ml of a saturated aqueous solution of NH_4Cl, and extracted with ether (3×60 ml). The ethereal extract was dried over $MgSO_4$ and concentrated in vacuo to give a residue, which was subjected to purification by column chromatography on silica gel.

The Reaction of 2,2-Diaryl-1,3-dithiolane *S,S'*-Dioxides (7a—i) with Lithium Diisopropylamide (LDA) (Entries 3—12 of Table 1). The LDA solution prepared in the same way as above was slowly added with stirring to a cooled (−78 °C) solution of the appropriate **7a—i** (1.3 mmol) in tetrahydrofuran (4 ml) under nitrogen. Stirring was continued for 2 h at −78 °C, and the reaction mixture was quenched with 100 ml of H_2O and 20 ml of a saturated aqueous solution of NH_4Cl. It was extracted with ether (3×60 ml). The ethereal extract was dried over $MgSO_4$, filtered, and concentrated in vacuo to give a residue, which was purified by column chromatography on silica gel. Only in the case of Entry 4 in Table 1, an excess of butyl iodide was added to the reaction mixture prior to the quenching with H_2O. However, the yield of the objective **11a** was not altered by the addition, suggesting that the anionic species **10** is unreactive to butyl iodide and hence the true trapping agent is H_2O.

References

1) D. Seebach and E. J. Corey, *J. Org. Chem.*, **40**, 231 (1975).

2) H. Ikehira, S. Tanimoto, T. Oida, and M. Okano, *J. Org. Chem.*, **48**, 1120 (1983), and references cited therein.

3) S. R. Wilson, G. M. Georgiadis, H. N. Khatri, and J. E. Bartmess, *J. Am. Chem. Soc.*, **102**, 3577 (1980).

4) S. R. Wilson, P. Caldera, and M. A. Jester, *J. Org. Chem.*, **47**, 3319 (1982).

5) H. Ikehira, S. Tanimoto, and T. Oida, *Bull. Chem. Soc. Jpn.*, **56**, 2537 (1983).

6) E. Schaumann, U. Wriede, and G. Rühter, *Angew. Chem., Int. Ed. Engl.*, **22**, 55 (1983).

7) F. A. Carey, O. D. Dailey, Jr., and T. E. Fromuth, *Phosphorus Sulfur*, **10**, 163 (1981).

8) R. Kuhn and F. A. Neugebauer, *Chem. Ber.*, **94**, 2629 (1961).

9) The melting point of *cis*-**7a** and that of *trans*-**7a** are reported to be 190—191 and 205—206 °C, respectively: W. Otting and F. A. Neugebauer, *Chem. Ber.*, **95**, 540 (1962).

10) The compound **7h** melts in too broad range of temperature to determine the upper limit of melting point.

11) H. B. Henbest and S. A. Khan, *J. Chem. Soc., Chem. Commun.*, **1968**, 1036.

12) M. M. Klenk, C. M. Suter, and S. Archer, *J. Am. Chem. Soc.*, **70**, 3846 (1948).

 © 1986 The Chemical Society of Japan Bull. Chem. Soc. Jpn., 59, 3901—3904 (1986)

Exo/Endo Stereoselectivity in 1,3-Dipolar Cycloaddition of Trifluoroacetonitrile Oxide and -nitrilimine with Bicyclic Olefins[1)]

Kiyoshi TANAKA,* Hideyuki MASUDA, and Keiryo MITSUHASHI
Department of Industrial Chemistry, College of Technology, Seikei University, Musashino, Tokyo 180
(Received June 13, 1986)

Trifluoroacetonitrile oxide and *N*-phenyl-*C*-(trifluoromethyl)nitrilimine cycloadded with norbornenes, resulting in the exclusive formation of the exo-adducts, while the concomitant formation of the endo-adducts was observed in their cycloadditions with norbornadienes. The nitrile oxide was subjected to the cycloaddition with 2,3-disubstituted norbornadienes to evaluate the effect of the substituents on the exo/endo stereoselectivity. The electron-withdrawing substituents tend to favor the formation of the exo-adducts.

Remarkable stereoselectivity has been observed in 1,3-dipolar cycloadditions with bicyclic systems,[2)] and indeed, that with norbornenes proceeds exclusively on the exo face.[3)] In norbornadiene system, however, the stereospecificity is released. Cycloadditions of benzonitrile oxide and *C,N*-diphenylnitrilimine with norbornadiene itself, for example, afford a small amount of the endo-adducts together with the exo-adducts as the major products.[4,5)] Imoto and his coworkers have reported that the substituents attached to the unsaturated carbon in norbornadiene system affect the exo/endo product ratios. The amount of the endo-adduct, in the cycloadditions of phenylglyoxylonitrile oxide, increases with the electron-withdrawing substituents.[5)] These interesting results prompted us to investigate the exo/endo stereoselectivity in 1,3-dipolar cycloadditions of trifluoroacetonitrile oxide (**2**), which could be comparable to phenylglyoxylonitrile oxide in point of its electronic effect, with norbornenes and norbornadienes. The stereoselectivity of *N*-phenyl-*C*-(trifluoromethyl)nitrilimine (**10**) is also described.

The nitrile oxide **2**, generated in situ from trifluoroacetohydroximoyl bromide etherate (**1**) with triethylamine, cycloadded with norbornene in toluene, resulting in the exclusive formation of the exo-adduct, 5-trifluoromethyl-3-oxa-4-azatricyclo[5.2.1.$0^{2,6exo}$]dec-4-ene (**3a**), in a good yield (Table 1). Its configuration was determined on the basis of the absence of the coupling between the 2-proton and the vicinal bridgehead

Table 1. Preparation of 5-Trifluoromethyl-3-oxa-4-azatricyclo[5.2.1.0]dec-4-enes and -deca-4,8-dienes

Compound	Yield %	Mp(θ_m/°C)[a)] [Bp(θ_b/°C/mmHg)]	Formula	Calcd(Found)/% C	H	N	IR ν/cm^{-1}
3a	68	[88—89/9]	$C_9H_{10}F_3NO$	52.69 (52.40)	4.91 (4.83)	6.83 (6.75)	1618(C=N)
3b	31	203—204[b)]	$C_{11}H_8F_3N_3O$	51.77 (52.08)	3.16 (3.15)	16.47 (16.43)	1614(C=N), 2215(C≡N)
4	56	183—184[c)]	$C_{11}H_8F_3NO_4$	48.01 (48.01)	2.93 (2.72)	5.09 (5.19)	1621(C=N), 1851, 1776(C=O)
5	72	[108—110/4][d)]	$C_{12}H_{12}F_3NO$	59.26 (59.21)	4.97 (4.93)	5.76 (5.93)	—
6	78[e)]	[100—101/4]	$C_{12}H_{14}F_3NO$	58.77 (58.71)	5.75 (5.82)	5.71 (5.85)	1617(C=N)
7a	77	Colorless oil	$C_9H_8F_3NO$	53.21 (53.05)	3.97 (3.93)	6.89 (6.86)	1617(C=N)
7'a		Colorless oil[f)]	$C_9H_8F_3NO$			6.89 (6.86)	1612(C=N)
7b	82	[140—141/3]	$C_{13}H_{12}F_3NO_5$	48.91 (48.76)	3.79 (3.98)	4.39 (4.25)	1620(C=N, C=C), 1730(C=O)
7'b		101—102	$C_{13}H_{12}F_3NO_5$	48.91 (48.91)	3.79 (3.84)	4.39 (4.44)	1615(C=N), 1635(C=C), 1740, 1718(C=O)
7c	75	115—116	$C_{11}H_6F_3N_3O$	52.18 (52.22)	2.39 (2.29)	16.60 (16.61)	1615(C=N), 2218(C≡N)
7'c		94—95	$C_{11}H_6F_3N_3O$	52.18 (52.22)	2.39 (2.35)	16.60 (16.58)	1610(C=N), 2225(C≡N)
7d	42	60—61	$C_{11}H_6F_9NO$			4.13 (3.90)	1616(C=N), 1681(C=C)

a) Recrystallized from hexane–chloroform unless otherwise noted. b) Recrystallized from ethanol. c) Recrystallized from chloroform–methanol. d) Boiling range. e) Yield from **5**. f) MS (CI, m/z) 204(M+1)$^+$, 138(M+1−C_5H_6)$^+$, 67(C_5H_6+1)$^+$. 1 mmHg=133.322 Pa.

proton and that between the 6- and 7-protons in ^{1}H NMR spectrum.[6] In the cycloaddition with 2,3-dicyanonorbornene, the product was isolated as the sole exo-adduct **3b** and, however, its absolute configuration around the carbon atom bearing the cyano group was ambiguous. The similar high stereospecificity was observed in the cases with endo-bicyclo-[2.2.1]hept-5-ene-2,3-dicarboxylic anhydride and dicyclopentadiene to afford the exo-adducts **4** and **5**, respectively. The adduct **5** was a mixture consisting of two isomers, having the carbon-carbon double bond at different position. And their double bonds were selectively saturated by hydrogen using palladium-carbon catalyst to give the same product **6**.

In the cases with norbornadienes, the high stereospecificity was relaxed. The nitrile oxide **2** was first subjected to the reaction with norbornadiene in toluene at room temperature to afford a mixture of the exo-adduct, 5-trifluoromethyl-3-oxa-4-azatricyclo-[5.2.1.$0^{2,6\text{exo}}$]deca-4,8-diene (**7a**), and its endo-isomer **7'a** in the ratio of 79/21 (Scheme 2). In ^{1}H NMR spectrum of the latter, both 2- and 6-protons couple with their adjacent bridgehead protons in 4 Hz (Table 2).[5] Although being stable at room temperature, both isomers were found to undergo the retro Diels-Alder reaction into 3-trifluoromethylisoxazole (**8**) under more drastic conditions.[7] ^{1}H NMR analysis of their breakdown with lapse of time reveals that the exo-adduct **7a** is much more stable than the endo-adduct **7'a**. After heating at 130 °C for 1 h, **7'a** was completely disappeared to form **8** in a 93% yield, whereas 33% of **7a** was found to survive even after 4 h, accompanied by the formation of 65% of **8**. These results support that **7'a** does not isomerize to the stable isomer **7a** on heating, indicating **7a** and **7'a** to be both primary products of the cycloaddition. The effect of the substituents, attached to the unsaturated carbon atom in the norbornadiene system, on the exo/endo stereoselectivity was next investigated. The reactions were carried out in toluene at room temperature and the results are summarized in Table 3. The electron-withdrawing substituents such as methoxycarbonyl and cyano groups

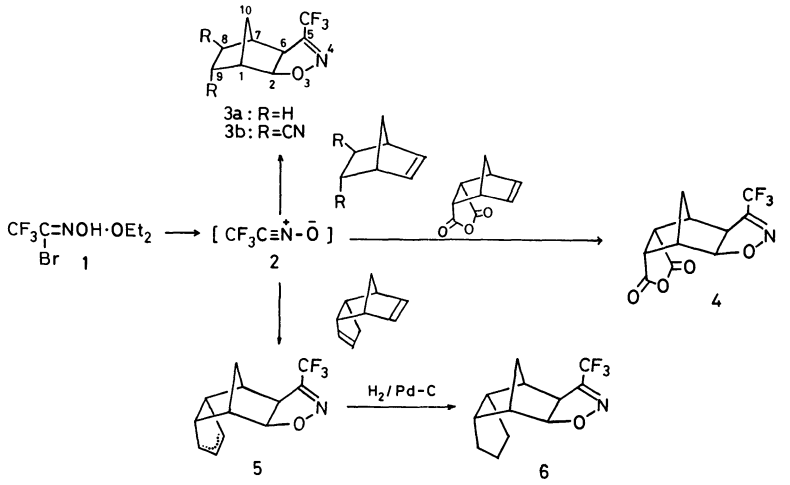

Scheme 1.

Table 2. ^{1}H NMR Data of 5-Trifluoromethyl-3-oxa-4-azatricyclo[5.2.1.0]dec-4-enes and -deca-4,8-dienes

Compound	Chemical Shift/δ[a]	Coupling Constant/Hz		
		$J_{2,6}$	$J_{1,2}$	$J_{6,7}$
3a	1.0—1.8(m, 6H), 2.4—2.7(m, 2H), 3.19(d, 1H), 4.64(d, 1H)	9	—	—
3b	1.3—1.9(m, 2H), 2.8—3.8(m, 4H), 4.02(d, 1H), 5.12(d, 1H)[b]	8	—	—
4	1.4—2.0(m, 2H), 2.9—3.2(m, 2H), 3.6—3.8(m, 2H), 4.0—4.5(m, 1H), 4.94(d, 1H)[b]	9	—	—
6	1.4—1.8(m, 8H), 2.3—2.7(m, 4H), 3.48(d, 1H), 4.85(d, 1H)	8	—	—
7a	1.5—1.9(m, 2H), 3.1—3.3(m, 2H), 3.46(d, 1H), 5.00(d, 1H), 6.05(dd, 1H), 6.30(dd, 1H)[c]	8	—	—
7'a	1.2—1.7(m, 2H), 3.1—3.5(m, 2H), 3.81(dd, 1H), 5.41(dd, 1H), 5.9—6.2 (m, 2H)[c]	10	4	4
7b	1.5—2.1(m, 2H), 3.5—3.9(m, 3H), 3.80(s, 6H), 5.27(d, 1H)	8	—	—
7'b	1.5—2.1(m, 2H), 3.6—4.2(m, 3H), 3.80(s, 6H), 5.72(dd, 1H)	10	4	—[d]
7c	1.8—2.3(m, 2H), 3.6—4.0(m, 3H), 5.33(d, 1H)	8	—	—
7'c	1.6—2.2(m, 2H), 3.6—4.0(m, 2H), 4.20(dd, 1H), 5.80(dd, 1H)	10	4	4
7d	1.6—2.3(m, 2H), 3.5—4.0(m, 3H), 5.33(d, 1H)	8	—	—

a) Measured in $CDCl_3$ unless otherwise noted. b) Measured in $CDCl_3$-DMSO-d_6. c) Measured in CCl_4. d) Could not be evaluated because of the joint of the peaks of 6-H with other complex multiplet.

Table 3. Exo/Endo Stereoselectivity in the Cycloadditions of Trifluoroacetonitrile Oxide to Norbornadienes

2,3-Disubstituted (R) Norbornadiene	Exo/Endo Ratio[a]	Reaction Conditions (Solvent, Temp.)
R=H	79/21	(Toluene, r.t.)
	72/28	(THF, r.t.)
	71/29	(THF, 0°C) [81/19 (THF, 0°C)][b]
R=CO_2Me	88/12	(Toluene, r.t.)
	88/12	(THF, r.t.)
	92/8	(THF, 0°C) [75/25 (THF, 0°C)][b]
R=CN	83/17	(Toluene, r.t.)
	92/8	(THF, r.t.) [68/32 (THF, 0°C)][b]
R=CF_3	100/0	(Toluene, r.t.)

a) Determined by ^{1}H NMR analysis of the reaction mixture. b) Outcome from the cycloaddition of phenylglyoxylonitrile oxide; see Ref. 5.

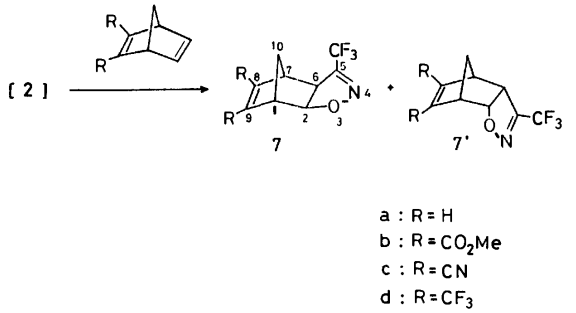

Scheme 2.

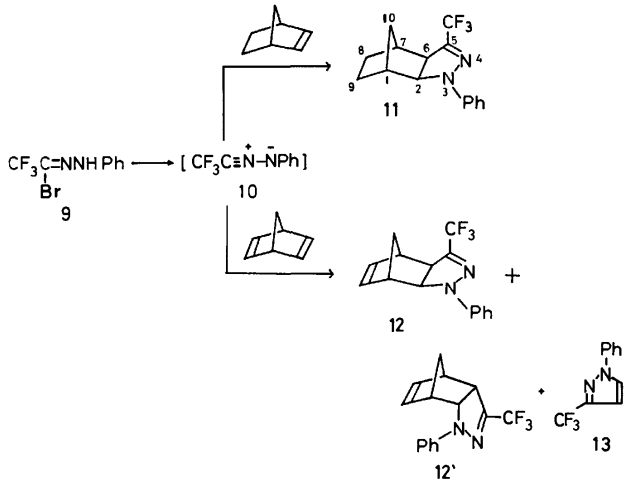

Scheme 3.

were found to favor slightly the formation of the exo-adducts, compared with that in unsubstituted norbornadiene itself. And, in the case of trifluoromethyl group as the substituent, the exo-adduct was exclusively formed, accompanying no endo-adduct any longer. The temperature dependence of the exo/endo stereoselectivity is not apparently observed whereas the appreciable solvent effect between toluene and tetrahydrofuran is detected in the cases of norbornadiene and 2,3-dicyanonorbornadiene, as shown in Table 3.[8] However, in any case, the tendency of the electron-withdrawing substituents in favor of the exo-adducts is always consistent. This tendency is in sharp contrast to that of phenylglyoxylonitrile oxide, where the electron-withdrawing substituents increase the formation of the endo-adducts reversely (Table 3).[5] Although the reason why the tendency of **2** in the exo/endo stereoselectivity is different from that of phenylglyoxylonitrile oxide is not definite, it is suggested that the selectivity could be controlled by not only the electronic status of the substituted norbornadienes but also the interactions between the norbornadienes and the 1,3-dipolar compounds.

The stereoselectivity was next investigated with regard to the nitrilimine **10**, derived in situ from *N*-phenyltrifluoroacetohydrazonoyl bromide (**9**) in the presence of triethylamine. It was allowed to cycloadd with norbornene in toluene, giving rise to only the exo-adduct, 3-phenyl-5-trifluoromethyl-3,4-diazatricyclo-[5.2.1.$0^{2,6exo}$]dec-4-ene (**11**), in a moderate yield. With norbornadiene, the concomitant formation of the endo-adduct was again observed. 3-Phenyl-5-trifluoromethyl-3,4-diazatricyclo[5.2.1.$0^{2,6exo}$]deca-4,8-diene (**12**) and its endo-isomer **12'** as well as 1-phenyl-3-trifluoromethylpyrazole (**13**) were obtained in 45, 18, and 7% yields, respectively. The endo-adduct **12'** was found to undergo the breakdown rather easily even at room temperature into the pyrazole **13**.[9]

Experimental

All melting and boiling points are uncorrected. The IR spectra were recorded on a JASCO A-100 spectrometer. Samples were run as potassium bromide pellets for crystals or as film for oil. The ^{1}H NMR spectra were measured with a JEOL JNM-PMX 60 spectrometer using tetramethylsilane as an internal standard, the chemical shifts being given in δ ppm downfield. The MS spectra were obtained on a Finnigan 4023 GC-MS DS spectrometer. The bromides **1** and **9** were prepared by the methods reported in our previous papers.[10]

Cycloaddition of 2 with Norbornenes. General Procedures. A solution of triethylamine (20.0 mmol) in 10 cm^3 of toluene was added dropwise to a solution of **1** (10.0 mmol) and the corresponding norbornene derivative (30.0 mmol) in

20 cm^3 of toluene. After stirring at room temperature for 3 h, excess of hexane was added to the reaction mixture. The formed solid was filtered off and the filtrate was washed with water and brine, dried over magnesium sulfate, and evaporated to leave a residue. The resulting residue was (a) distilled under reduced pressure to give **3a** and **5**, respectively, (b) recrystallized from ethanol to give **3b**. On the other hand, **4** was isolated from the formed solid as follows. The solid consisting of **4** and triethylammonium bromide was extracted with acetone. Removal of the solvent left a solid which was recrystallized from chloroform–methanol to give **4**.

Hydrogenation of 5. A mixture of **5** (0.70 g, 2.88 mmol) and 5% palladium-carbon (40 mg) in 20 cm^3 of methanol was stirred at room temperature under an atmosphere of hydrogen. When an equivalent of hydrogen was consumed, the reaction was stopped. The catalyst was filtered off and, after the solvent was removed, the resulting oil was distilled to give 0.55 g (78%) of **6**.

Cycloaddition of 2 with Norbornadienes. General Procedures. To a solution of **1** (13.0 mmol) and the corresponding norbornadiene derivative (39.0 mmol for norbornadiene itself or 13.0 mmol for other substituted norbornadienes) in 20 cm^3 of toluene or tetrahydrofuran was added dropwise a solution of triethylamine (16.9 mmol) in 10 cm^3 of toluene or tetrahydrofuran at the temperature shown in Table 3. After the reaction mixture was stirred at the same temperature for 2 h, excess diethyl ether was added to the mixture and the resulting triethylammonium bromide was removed by filtration. The filtrate was washed with water and brine, dried over magnesium sulfate, and evaporated to leave a residue. Thus obtained residue was chromatographed on silica gel to separate the corresponding exo- and endo-adducts, respectively. Each adduct was further purified by distillation or recrystallization.

Retro Diels–Alder Reaction of 7'a. The endo-adduct **7'a** (100 mg) was heated at 130 °C in a sealed tube. After 1 h of heating, the mixture was cooled. ^1H NMR analysis of the mixture showed **8** in a 93% yield and dicyclopentadiene. The isoxazole **8** was purified by preparative GLC, ^1H NMR ($CDCl_3$) δ=6.64 (d, J=2.3 Hz, 1H), 8.59 (br.s, 1H), IR 3160, 3140 (CH), 1190, 1150 cm^{-1} (CF_3).

Found: C, 34.83; H, 1.21; N, 10.18%. Calcd for $C_4H_2F_3NO$: C, 35.05; H; 1.47; N, 10.22%.

Cycloaddition of 10 with Norbornadiene. Triethylamine (4 ml) was added dropwise to a solution of **9** (2.00 g, 7.5 mmol) and norbornadiene (2.07 g, 22.5 mmol) in 20 cm^3 of toluene. After 20 h of stirring at room temperature, 100 cm^3 of diethyl ether was added. The mixture was washed with water and brine, dried over magnesium sulfate, and evaporated under reduced pressure to leave a residue which was placed on a column (silica gel) and eluted with hexane–chloroform (10:1) to give 0.94 g (45%) of **12**, 0.37 g (18%) of **12'**, and 0.11 g (7%) of **13**, respectively. The exo-adduct **12** was further purified by recrystallization from hexane, mp 75—77 °C, ^1H NMR (CCl_4) δ=1.61 (br.s, 2H), 3.2—3.8 (m, 3H), 4.47 (d, J=10 Hz, 1H), 6.14 (dd, 1H), 6.32 (dd, 1H), 6.5—7.5 (m, 5H), IR 1604 (C=N), 1180, 1165 cm^{-1} (CF_3).

Found: C, 64.87; H, 4.54; N, 10.33%. Calcd for $C_{15}H_{13}F_3N_2$: C, 64.74; H, 4.71; N, 10.07%.

12': Pale yellow oil, ^1H NMR (CCl_4) δ=1.2—1.7 (m, 2H), 3.2—3.7 (m, 2H), 3.85 (ddq, J=11, 4, and 2 Hz, 1H), 4.83 (dd, J=11 and 4 Hz, 1H), 5.83 (dd, 1H), 6.06 (dd, 1H), 6.5—7.5 (m, 5H). IR 1602 (C=N), 1180, 1150 cm^{-1} (CF_3). The reliable elemental analysis could not be performed because of its easy breakdown.

Spectral data of thus obtained pyrazole **13** are consistent with those of our authentic sample.[11]

The exo-adduct **11** was similarly obtained in a 67% yield from the reaction of **9** with norbornene, mp 78.5—79.5 °C (lit,[12] 78.5—79.5 °C).

References

1) Part X in "Applications of the fluorinated 1,3-dipolar compounds as the building blocks of the heterocycles with fluorine groups." Part IX: K. Tanaka, M. Kishida, S. Maeno, and K. Mitsuhashi, *Bull. Chem. Soc. Jpn.*, **59**, 2631 (1986).

2) "1,3-Dipolar Cycloaddition Chemistry," ed by A. Padwa, Wiley Interscience, New York (1984).

3) G. Bianchi, C. De Micheli, and R. Gandolfi, "1,3-Dipolar Cycloadditions Involving X=Y Groups," in "The Chemistry of Double-bonded Functional Groups," ed by S. Patai, Interscience, London (1977), Supplement A, Part 1, Chap. 6; R. Huisgen, R. Grashey, and J. Sauer, "Cycloaddition Reactions of Alkenes," in "The Chemistry of Alkenes," ed by S. Patai, Interscience, London (1964), Chap. 11.

4) R. Lazar, F. G. Cocu, and N. Barbulescu, *Rev. Roum. Chem.*, **20**, 3 (1969).

5) H. Taniguchi, T. Ikeda, Y. Yoshida, and E. Imoto, *Bull. Chem. Soc. Jpn.*, **50**, 2694 (1977); *Chem. Lett.*, **1976**, 1139.

6) P. Laszlo and P. von R. Schleyer, *J. Am. Chem. Soc.*, **86**, 1171 (1964).

7) For the retro Diels–Alder reaction of 3-oxa-4-azatricyclo[5.2.1.$0^{2,6exo}$]deca-4,8-diene, see R. Huisgen and M. Christl, *Chem. Ber.*, **106**, 3291 (1973).

8) For the solvent and temperature dependence of the exo/endo stereoselectivity in 1,3-dipolar cycloadditions, consult H. Taniguchi, Y. Yoshida, and E. Imoto, *Bull. Chem. Soc. Jpn.*, **50**, 3335 (1977); H. Taniguchi and E. Imoto, *ibid.*, **51**, 2405 (1978).

9) 3,5-Diphenyl-3,4-diazatricyclo[5.2.1.$0^{2,6exo}$]deca-4,8-diene is also reported to undergo the retro Diels–Alder reaction at 135 °C into 1,3-diphenylpyrazole, R. Huisgen, M. Seidel, G. Wallbillich, and H. Knupfer, *Tetrahedron*, **17**, 3 (1962).

10) K. Tanaka, H. Masuda, and K. Mitsuhashi, *Bull. Chem. Soc. Jpn.*, **57**, 2184 (1984); K. Tanaka, S. Maeno, and K. Mitsuhashi, *J. Heterocyclic. Chem.*, **22**, 565 (1985).

11) K. Tanaka, S. Maeno, and K. Mitsuhashi, *Bull. Chem. Soc. Jpn.*, **58**, 1841 (1985).

12) K. Tanaka, T. Igarashi, S. Maeno, and K. Mitsuhashi, *Bull. Chem. Soc. Jpn.*, **57**, 2689 (1984).

 © 1986 The Chemical Society of Japan Bull. Chem. Soc. Jpn., 59, 3905—3909 (1986)

Radiation-Induced Alkylation of Quinoline Derivatives with Alcohol

Akira SUGIMORI,* Tetsuo YAMADA, Hiroaki ISHIDA, Masayuki NOSE, Keiko TERASHIMA, and Noriko OOHATA
Department of Chemistry, Faculty of Science and Technology, Sophia University, Kioi-cho 7-1, Chiyoda-ku, Tokyo 102
(Received June 16, 1986)

Gamma-irradiation of quinoline and its derivatives in alcohols brings about alkylation at the 2- or 4-position of pyridine ring. Hydroxyalkyl radicals play important roles in the radiation-induced alkylation with alcohol. The radiation-induced substitution of CF_3CH_2- and $CF_3CH(OH)$- for H in pyridine and pyrimidine rings occurs in low yields.

The introduction of substituents in aromatic rings can be effectively done by the use of electrophilic reagents. However, electophilic substitution is not effective for the electron-deficient heteroaromatic rings such as pyridine nucleus.

The method utilizing anionic species such as Grignard reagents and organolithium compounds have been developed for the introduction of alkyl groups in the pyridine ring.[1] Free radical species have also been used for the substitution in the pyridine ring. Alkylation and hydroxyalkylation initiated by peroxodisulfate have been studied extensively by Minisci et al.[2,3] Ultraviolet irradiation causes the alkylation of pyridine ring with alcohols[4] or alkanoic acids.[5]

The irradiation of ionizing radiation can generate free radical species but it has not been used effectively for the introduction of substituents in the electron-deficient heteroaromatic ring. We have reported the radiation-induced alkylation and hydroxyalkylation of pyridinecarboxylic esters,[6] pyridinecarboxamides,[7] and pyridinecarbonitriles[8] in alcohols.

In this paper, we describe the radiation-induced alkylation and hydroxyalkylation by alcohols using quinoline derivatives as fundamental pyridine derivatives. The method of γ-irradiation is compared with other methods generating free radical species.

Results and Discussion

Radiation-Induced Alkylation with Alcohol. The γ-irradiation of the alcoholic solutions of 4-methylquinoline (**1a**) in the presence of sulfuric acid brings about the alkylation at the 4-position in good radiation chemical yields (*G*-values) (Table 1). The alkyl groups introduced have mainly the same skeletal structures as those of the alcohols. However, with higher alcohols, especially with secondary alcohol (2-propanol), the alkyl groups of the smaller carbon numbers than those of the original alcohols are introduced.

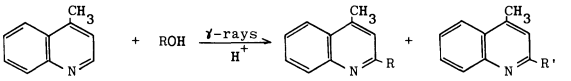

R': Alkyl group with smaller carbon number than R.

The radiation-induced alkylation in the pyridine ring occurs efficiently in the γ-irradiation of the quinolinium salt in alcohol in the presence and absence of sulfuric acid (Table 1).

The main reactive species formed in the radiolysis of alcohols are solvated electron, hydrogen atom, and 1-hydroxyalkyl radical. The *G*-values of e_{solv}^-, $\cdot H$, $\cdot OH$, $\cdot CH_2OH$, and $\cdot CH_3$ in the radiolysis of methanol have been reported to be 2.0, 1.1, 0.2, 2.7, and 0.2, respectively.[9]

Methyl radical can bring about methylation of the pyridine ring.[10,11] However, the methyl radical formed in the radiolysis of methanol can explain only a part of the radiation-induced methylation of **1a** with methanol, because the *G*(methylation) is larger than $G(\cdot CH_3)$. Thus, hydroxymethyl radical should play more important roles than methyl radical.

Hydroxymethyl radical can be produced by the hydrogen abstraction from methanol by free radicals pro-

Table 1. Radiation-Induced Alkylation of 4-Methylquinoline (**1a**) and 1,4-Dimethylquinolinium Methyl Sulfate (**1b**) in Alcohol

Substrate	Alcohol	Atmosphere	$[H_2SO_4]$ / mol dm^{-3}	Dose / 10^7 rad	Alkyl group introduced at the 2-position: Me G-value	Me Yield / %	Et G-value	Et Yield / %	*n*-Pr G-value	*n*-Pr Yield / %	*i*-Pr G-value	*i*-Pr Yield / %
1a	MeOH	Ar	0.10	1.0	2.05	(66)						
1b	MeOH	Ar	0.00	5.0	1.27	(80)						
1b	MeOH	Ar	0.50	5.0	2.38	(94)						
1b	MeOH	N_2O	0.00	5.0	1.15	(41)						
1a	EtOH	Ar	0.10	1.0	0.04	(2)	1.02	(41)				
1a	*n*-PrOH	Ar	0.10	1.0	0.05	(2)	0.43	(16)	0.68	(25)		
1a	*i*-PrOH	Ar	0.10	1.0	0.06	(3)	0.06	(3)			0.02	(1)

[**1a**]=0.06 mol dm^{-3}; [**1b**]=0.15 mol dm^{-3}. Yield=Amount of product/Amount of substrate reacted.

Table 2. Methylation of Quinoline and Isoquinoline by Hydroxymethyl Radicals

Substrate	Method for generating $\cdot CH_2OH$	Methylation product					
		1-Me		2-Me		4-Me	
		Yield %	(G-value)	Yield %	(G-value)	Yield %	(G-value)
Quinoline	Gamma-irradiation[a)]			8.6	(0.51)	15.6	(0.92)
	Thermal decomposition of *t*-BuCOOO-*t*-Bu at 65 °C[b)]			17.5		14.7	
	UV-irradiation in the presence of acetone[c)]			3.2		2.9	
Isoquinoline	Gamma-irradiation[a)]	9.4	(0.47)				
	Thermal decomposition of *t*-BuCOOO-*t*-Bu at 65 °C[b)]	10.1					
	UV-irradiation in the presence of acetone[c)]	1.8					

Yield=Amount of product/Amount of substrate reacted. a) [Substrate]=0.06 mol dm^{-3}; [H_2SO_4]=0.10 mol dm^{-3}; Dose, 1.0×10^7 rad. b) [Substrate]=0.06 mol dm^{-3}; [H_2SO_4]=0.10 mol dm^{-3}; [*t*-BuCOOO-*t*-Bu]=0.06 mol dm^{-3}; Heated at 64 or 65 °C for 4 h under Ar. c) [Substrate]=0.01 mol dm^{-3}; [H_2SO_4]=0.02 mol dm^{-3}; [Acetone]=2.0 mol dm^{-3}; Irradiated in a Pyrex vessel with a high-pressure mercury lamp for 16 h under Ar.

duced in the thermal decomposition of peroxides such as *t*-butyl peroxypivalate. The UV-irradiation of acetone in methanol can also produce hydroxymethyl radical via hydrogen abstraction of excited acetone from methanol.

$$CH_3COCH_3 \xrightarrow{h\nu} {}^1(CH_3COCH_3)^* \longrightarrow {}^3(CH_3COCH_3)^*$$

$${}^3(CH_3COCH_3)^* + CH_3OH \longrightarrow CH_3\dot{C}(OH)CH_3 + \cdot CH_2OH$$

As is shown in Table 2, quinoline and isoquinoline are methylated similarily in radiation-induced reaction and in the reaction initiated by the thermolysis of *t*-butyl peroxypivalate. When the solution of quinoline or isoquinoline was irradiated in methanol in the presence of acetone with a high-pressure mercury lamp, the light from which is absorbed selectively by acetone, methylation of the pyridine rings occurs actually.

In the radiolysis of alcohol in the presence of sulfuric acid, solvated electron is converted to hydrogen atom.

$$e^-_{solv} + H^+ \longrightarrow \cdot H$$

Hydrogen atom can react either with methanol to give $\cdot CH_2OH$ radical or with quinolinium. The rate constants of $\cdot H$ with methanol (in acidified aqueous solutions) and with pyridinium ion are reported to be 2.4×10^6 [12] and 2.2×10^8 dm^{3}mol^{-1} s^{-1},[13] respectively. Considering that the concentrations of methanol and quinolinium under our reaction conditions are 25 and 0.06 mol dm^{-3}, respectively, we can postulate that hydrogen abstraction from methanol is the more favorable process for hydrogen atom than the reaction with pyridinium.

As a mechanism for alkylation by hydroxyalkyl radical, the reaction path in Scheme 1 can be postulated.

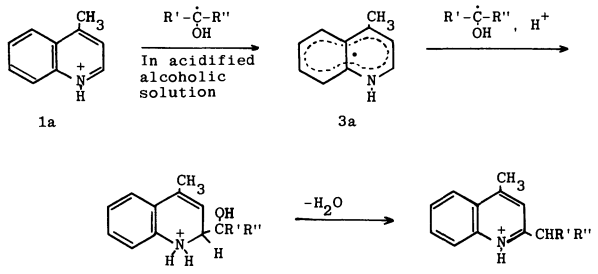

Scheme 1.

In the radiation-induced reaction of 1,4-dimethylquinolinium (**1b**) in neutral methanol, solvated electron would contribute to the methylation.

The radiation-induced methylation of **1b** is slightly affected by N_2O which converts solvated electron to hydroxymethyl radical via hydroxyl radical.

$$e^-_{solv} + N_2O \xrightarrow{H^+} \cdot OH + N_2$$

$$\cdot OH + CH_3OH \longrightarrow \cdot CH_2OH + H_2O$$

If the solvated electron does not contribute to the methylation, the *G*-value for methylation under Ar should be lower (about a half) than that under N_2O. The experimental results indicate that solvated electron and hydroxymethyl radical participate equivalently in the methylation. The lower chemical yield of methylation under N_2O than under Ar can not be explained at present.

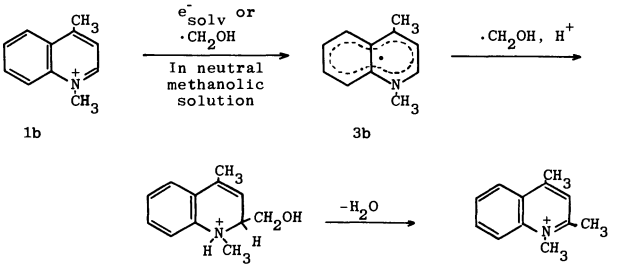

Scheme 2.

Table 3. Radiation-Induced Reactions of Quinoline Derivatives and 4-Methylpyrimidine in CF_3CH_2OH. Dose rate, 1.0×10^6 rad h^{-1}; Dose, 5.0×10^7 rad

Substrate	[Substrate] / mol dm^{-3}	[H_2SO_4] / mol dm^{-3}	Substituent introduced	G-value	Yield / %
4-Methylquinoline	0.15	0.25	2-CF_3CH_2-	0.08	6.7
			2-CF_3CH(OH)-	0.07	5.6
2-Methylquinoline	0.15	0.25	4-CF_3CH_2-	0.13	8.3
Quinoline	0.30	0.50	2-CF_3CH(OH)-	0.02	1.1
			4-CF_3CH_2-	0.09	5.5
4-Methylpyrimidine	0.50	1.00	2-CF_3CH(OH)-	0.09	0.3
			6-CF_3CH(OH)-	0.48	1.3

Yield=Amount of product/Amount of substrate reacted.

As a mechanism in which solvated electron and hydroxymethyl radical participate equivalently, the reaction paths in Scheme 2 can be postulated.

According to the mechanism in Schemes 1 and 2, the efficiency for alkylation should depend both on the efficiency for the formation of the radical **3** via the attack of electron or the electron transfer from hydroxyalkyl radical to the substrate and on the efficiency for the coupling of **3** with hydroxyalkyl radical. If the two efficiencies of the hydroxyalkyl radicals are in good balance, the alkylation should proceed efficiently. 1-Hydroxy-1-methylethyl radical which is formed in the radiolysis of 2-propanol is a good electron donor but is not a reactive free radical. The inefficiency of the second step would result in the low *G*-value for isopropylation by 2-propanol. Instead, in the radiation-induced reaction in 2-propanol ethylation occurs in greater *G*-value than isopropylation. Ethylation in 2-propanol is brought about probably by 1-hydroxyethyl radical which is formed by the cleavage of a C-C bond of 2-propanol.

Radiation-Induced Reaction in 2,2,2-Trifluoroethanol. As an extension of the radiation-induced alkylation with alcohols, we examined the radiation-induced reaction of 4-methylquinoline, 2-methylquinoline, quinoline, and 4-methylpyrimidine in 2,2,2-trifluoroethanol in the presence of sulfuric acid, aiming at the introduction of fluorinated alkyl groups in the pyridine and pyrimidine rings (Table 3). Although the trifluoroethylated quinolines are formed, their chemical yields (and their *G*-values) are low. Another difference between the reactions in CH_3CH_2OH and in CF_3CH_2OH is the substitution of the 2,2,2-trifluoro-1-hydroxyethyl group in the reaction in CF_3CH_2OH.

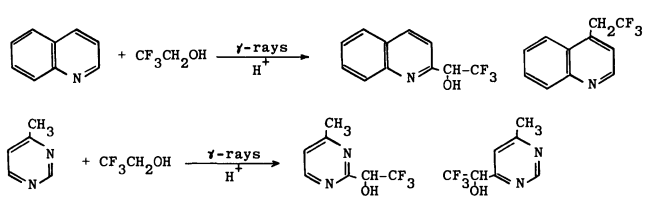

One of the reasons for the low *G*-values of trifluoroethylation is due to the low efficiency of the electron transfer from $CF_3\dot{C}HOH$ to the electron-deficient hetroaromatic molecules, because of the high electronegativity of fluorine in the radical. In the radiation-induced reaction of **1a** in a mixed solvent of CF_3CH_2OH, CH_3OH, and H_2O (6:3:1 by volume), 4-methyl-2-(2,2,2-trifluoroethyl)quinoline (**4**) and 4-methyl-2-(2,2,2-trifluoro-1-hydroxyethyl)quinoline (**5**) are formed in equal or greater *G*-values (G(**4**)=0.07 and G(**5**)=0.09) than in the reaction in a mixed solvent of CF_3CH_2OH and H_2O (9:1 by volume)(G(**4**)=0.07 and G(**5**)=0.07) in spite of the lower formation of $CF_3\dot{C}HOH$ because of the lower concentration of CF_3CH_2OH. The fact can be explained by the contribution of $\cdot CH_2OH$ radical from methanol to the formation of **4** and **5** by the electron transfer to the protonated **1** to give the radical **3**.

The fact that the radical reaction initiated by *t*-butyl hydroperoxide and iron(II) sulfate in CF_3CH_2OH brings about neither trifluoroethylation nor trifluorohydroxyethylation, suggests that the formation of $CF_3\dot{C}HOH$ radical is not a favorable process. (In this case quinoline is methylated by the methyl radical formed by the decomposition of *t*-BuO· radical). The unfavorable formation of $CF_3\dot{C}HOH$ radical is supported by the observation that the UV-irradiation of 4-methylquinoline in CF_3CH_2OH in the presence of sulfuric acid gives no trifluoroethylation nor trifluorohydroxyethylation products. The low efficiency of the formation of $CF_3\dot{C}HOH$ is another reason for the low yields of the introduction of CF_3CH_2- and CF_3CH(OH)- groups. Only the high energy radiation enables the reaction which is not realized by free radical or photochemical processes, although the efficiencies are not high.

The formation of a trifluorohydroxyethylated products can partly be explained by the low basicity of O atom to which H^+ attack to cause dehydration.

Experimental

Materials. Commercial quinoline (GR grade reagent of Wako Junyaku Co.), isoquinoline (EP grade reagent of

Wako Junyaku Co.), 4-methylquinoline(GR grade reagent of Tokyo Kasei Co.), 2-methylquinoline (EP grade reagent of Tokyo Kasei Co.), and 4-methylpyrimidine (made by Aldrich Co.; purity, 99.7%) were purified by vacuum distillation.

1,4-Dimethylquinolinium methyl sulfate was synthesized in the reaction of 4-methylquinoline with dimethyl sulfate.

Commercial methanol (GR grade reagent of Wako Junyaku Co.), ethanol (Nippon Alcohol Co.), 1-propanol (GR grade reagent of Wako Junyaku Co.), 2-propanol (EP grade reagent of Wako Junyaku Co.) were purified by distillation.

A solution of *t*-butyl hydroperoxide (70% of purity, supplied by Aldrich Co.) was used.

2,2,2-Trifluoroethanol and *t*-butyl peroxypivalate were kindly given by Japan Halon Co. and Nippon Oil and Fats Co., respectively.

Gamma-Irradiation. Solutions containing the substrate and sulfuric acid if necessary in alcohol were deaerated by bubbling Ar (in some cases by N_2O) for 45 min before irradiation.

The solution was irradiated by Co-60 γ-rays at the irradiation facility of Japan Atomic Energy Research Institute in Takasaki at the dose of 1.0×10^7 rad (at the dose rate of 5.0×10^5 rad h^{-1} for 20 h) or at the dose of 5.0×10^7 rad (at the dose rate of 1.0×10^6 rad h^{-1} for 50 h).

Reaction Initiated by Peroxides. A methanolic solution (100 cm^3) of quinoline or isoquinoline ([Substrate]=0.06 mol dm^{-3}), sulfuric acid (0.1 mol dm^{-3}), and *t*-butyl peroxypivalate (0.06 mol dm^{-3}) was deaerated by bubbling Ar and then heated at 64 or 65 °C for 4 h.

The free radical-initiated reaction in CF_3CH_2OH was carried out in the following procedure. To a solution of the substrate (0.01 mol), *t*-butyl hydroperoxide (0.02 mol), and sulfuric acid (0.5 cm^3) in trifluoroethanol (8.3 cm^3) kept below 10 °C, was added dropwise an aqueous solution of iron(II) sulfate (0.02 mol) and sulfuric acid under Ar. After the addition of the peroxide, the solution was kept at 10—20 °C for 80 min. The reaction mixture was treated in a similar manner to that for the radiation-induced reaction.

Photoreaction in the Presence of Acetone. Solutions of the substrate (0.01 mol dm^{-3}) in methanol or trifluoroethanol in the presence of acetone (2.0 mol dm^{-3}) and sulfuric acid (0.02 mol dm^{-3}) were irradiated with a high-pressure mercury lamp for 16 h. The work up of the reaction mixture was similar to that for the radiation-induced reaction.

Separation of Products. The products in the radiation-induced reactions in alcohol in the presence of sulfuric acid were separated by means of TLC (plate, GF_{254} Type 60 supplied by E. Merck Co.), after the removal of the most part of the solvent under reduced pressure, neutralization with sodium carbonate, and the extraction with dichloromethane.

The reaction mixture from the radiation-induced reactions in 2,2,2-trifluoroethanol in the presence of sulfuric acid was treated as follows. Most part of the solvent were removed under reduced pressure and the solution was neutralized with aqueous sodium carbonate solution. The products were extracted with dichloromethane and separated by TLC (plate, GF_{254} Type 60 of E. Merck Co.). The developing solvents for the separation of the products from quinoline, 2-methylquinoline, 4-methylquinoline, and 4-methylpyrimidine are dichloromethane, dichloromethane(90%)-ethyl acetate(10%), and dichlomethane(75%)-ethyl acetate(25%), respectively.

The products were further purified by preparative gas-chromatography (column, 2 m column of PEG 20M (5%)). The column temperatures for the separation of the products from quinoline, 2-methylquinoline, 4-methylquinoline, and 4-methylpyrimidine are 190, 180, 190, and 140 °C, respectively.

Identification of Products. The formation of 2,4-dimethyl-, 2-ethyl-4-methyl-, 4-methyl-2-propyl-, and 2-isopropyl-4-methylquinolines were identified by the agreement of the spectra and gas-chromatographic behavior with the authentic samples. Authentic 2,4-dimethylquinoline is commercially available. 2-Ethyl-4-methyl-, 4-methyl-2-propyl-, and 2-isopropyl-4-methylquinolines were prepared by the reaction of 4-methylquinoline with the alkanoic acids having the alkyl moiety to be introduced under the catalysis of ammonium peroxodisulfate and silver nitrate according to Minisci et al.[11]

2-Ethyl-4-methylquinoline: ^1H NMR ($CDCl_3$) δ=1.38 (3H, t, J=7.6 Hz, 2-$CH_2C\underline{H}_3$), 2.67 (3H, s, 4-CH_3), 2.95 (2H, q, J=7.6 Hz, 2-$C\underline{H}_2CH_3$), 7.15 (1H, s, ring H at the 3-position), and 7.45—8.07 (4H, m, H of benzene ring).

4-Methyl-2-propylquinoline: ^1H NMR δ=1.02 (3H, t, J=7.5 Hz, 2-$CH_2CH_2C\underline{H}_3$), 1.83 (2H, sextet, J=7.5 Hz, 2-$CH_2C\underline{H}_2CH_3$), 2.65 (3H, s, 4-CH_3), 2.89 (2H, t, J=7.5 Hz, 2-$C\underline{H}_2CH_2CH_3$), 7.12 (1H, s, ring H at the 3-position), and 7.44—8.07 (4H, m, H of benzene ring).

2-Isopropyl-4-methylquinoline: ^1H NMR δ=1.38 (6H, d, J=6.8 Hz, 2-$CH(C\underline{H}_3)_2$), 2.66 (3H, s, 4-CH_3), 3.21 (1H, septet, J=6.8 Hz, 2-$C\underline{H}(CH_3)_2$), 7.15 (1H, s, ring H at the 3-position), and 7.43—8.08 (4H, m, H of benzene ring).

The products from the radiation-induced reactions in 2,2,2-trifluoroethanol were identified on the basis of their spectral data.

4-Methyl-6-(1-hydroxy-2,2,2-trifluoroethyl)pyrimidine: White crystals; mp 75—76 °C (sublime); IR (KBr disk) 3120, 2870, 2730, 1600, 1540, 1470, 1380, 1360, 1340, 1320, 1280, 1260, 1170, 1140, 1130, 1110, 1045, 1000, 945, 900, 850, 810, 770, 740, 710, and 660 cm^{-1}; ^1H NMR δ=2.55 (3H, s, 4-CH_3), 5.10 (1H, q, J=6.8 Hz, 6-$C\underline{H}(OH)CF_3$), 7.60 (1H, s, ring H at the 5-position), and 8.98 (1H, s, ring H at the 2-position); MS (70 eV) m/z (rel intensity) 192 (M^+; 19), 124 (8), 123 (100), 95 (10), 94 (6), 93 (13), 68 (9), 67 (7), 66 (22), and 52 (6). Found: m/z 192.0507. Calcd for $C_7H_7F_3N_2O$: M, 192.0510.

2-(1-Hydroxy-2,2,2-trifluoroethyl)-4-methylpyrimidine: White crystals; mp 37—38 °C; IR (KBr disk) 3420, 3100, 1600, 1560, 1460, 1370, 1350, 1260, 1180, 1170, 1140, 1130, 1110, 1000, 930, 860, 840, 820, 790, 700, and 680 cm^{-1}; ^1H NMR (CD_3OD) δ=2.50 (3H, s, 4-CH_3), 5.10 (1H, q, J=6.7 Hz, 2-$C\underline{H}(OH)CF_3$), 7.33 (1H, d, J=7.2 Hz, ring H at the 5-position), and 8.61 (1H, d, J=7.2 Hz, ring H at the 6-position); MS (70 eV) m/z (rel intensity) 192 (M^+, 15), 125 (5), 124 (18), 123 (100), 95 (42), 94 (6), 93 (10), 68 (9), 66 (9), 53 (6), and 52 (6). Found: m/z 192.0508. Calcd for $C_7H_7F_3N_2O$: M, 192.0510.

4-(2,2,2-Trifluoroethyl)quinoline: IR (neat) 3450, 3080, 3050, 2970, 1600, 1580, 1520, 1430, 1400, 1360, 1320, 1280, 1260, 1240, 1170, 1140, 1100, 1040, 910, 830, 770, and 670 cm^{-1}; ^1H NMR ($CDCl_3$) δ=3.83 (2H, q, J=10 Hz, 4-CH_2CF_3), 7.26—8.19 (5H, m, ring H), and 8.85 (1H, d, J=4 Hz, ring H at the 2-position); MS (70 eV) m/z (rel intensity) 212 (13), 211 (M^+, 100), 143 (80), 142 (59), 116 (55), 115 (25). Found: m/z 211.0611. Calcd for $C_{11}H_8F_3N$: M, 211.0608.

2-(1-Hydroxy-2,2,2-trifluoroethyl)quinoline: White crys-

tals; mp 97—98 °C; IR (KBr disk) 3360, 3090, 2900, 2760, 1620, 1600, 1580, 1520, 1470, 1440, 1380, 1340, 1270, 1190, 1160, 1130, 1100, 1030, 980, 940, 860, 830, 805, 795, 770, 760, 710, and 630 cm^{-1}; ^1H NMR (CD_3OD) δ=5.22 (1H, q, J=7.8 Hz, 2-C<u>H</u>(OH)CF_3) and 7.50—8.40 (6H, m, ring H); MS (70 eV) m/z (rel intensity) 227 (M^+, 25), 207 (10), 159 (14), 158 (100), 156 (6), 130 (17), 129 (20), 128 (77), 103 (7), 102 (11), 101 (18), 77 (15), 76 (6), 75 (10), and 51 (8). Found: m/z 227.0558. Calcd for $C_{11}H_8F_3NO$: M, 227.0557.

2-Methyl-4-(2,2,2-trifluoroethyl)quinoline: White crystals; mp 47—48 °C; IR (KBr disk) 3450, 3370, 2990, 1600, 1560, 1520, 1380, 1370, 1330, 1280, 1260, 1230, 1200, 1150, 1140, 1100, 1050, 920, 910, 830, 770, 750, and 610 cm^{-1}; ^1H NMR ($CDCl_3$) δ=2.75 (3H, s, CH_3), 3.81 (2H, q, J=10.4 Hz, -CH_2CF_3), 7.27 (1H, s, ring H at the 3-position), and 7.50—8.10 (4H, m, H of benzene ring); MS (70 eV) m/z (rel intensity) 226 (14), 225 (M^+, 100), 205 (9), 156 (18), 129 (8), and 115 (5). Found: m/z 225.0763. Calcd for $C_{12}H_{10}F_3N$: M, 225.0765.

4-Methyl-2-(2,2,2-trifluoroethyl)quinoline: White crystals; mp 62—63 °C; IR (KBr disk) 3450, 3100, 3000, 2980, 2930, 1600, 1560, 1510, 1450, 1430, 1420, 1380, 1370, 1340, 1270, 1260, 1140, 1130, 1080, 1070, 970, 920, 860, 830, 770, and 760 cm^{-1}; ^1H NMR ($CDCl_3$) δ=2.66 (3H, s, CH_3), 3.70 (2H, q, J=10.8 Hz, -CH_2CF_3), 7.25 (1H, s, ring H at the 3-position), and 7.42—8.10 (4H, m, H of benzene ring); MS (70 eV) m/z (rel intensity) 226 (14), 225 (M^+, 100), 206 (13), 205 (57), 156 (16), 142 (6), 141 (5), 140 (6), 129 (6), 116 (9), and 115 (13). Found: m/z 225.0750. Calcd for $C_{12}H_{10}F_3N$: M, 225.0765.

4-Methyl-2-(2,2,2-trifluoro-1-hydroxyethyl)quinoline: White crystals; mp 117—118 °C; IR (KBr disk) 3100, 2870, 2700, 1600, 1570, 1510, 1450, 1420, 1370, 1270, 1260, 1190, 1180, 1140, 1130, 1120, 970, 900, 880, 860, 780, and 760 cm^{-1}; ^1H NMR (CD_3OD) δ=2.72 (3H, s, CH_3), 5.20 (1H, q, J=7.7 Hz, -C<u>H</u>(OH)CF_3), and 7.52—8.22 (5H, m, ring H); MS (70 eV) m/z (rel intensity) 241 (M^+, 24), 173 (13), 172 (100), 144 (10), 143 (14), 142 (28), 140 (5), 116 (9), and 115 (18). Found: m/z 241.0715. Calcd for $C_{12}H_{10}F_3NO$: M, 241.0714.

The products from the reaction of 1,4-dimethylquinolinium methyl sulfate (**1b**) in methanol could not be separated from the starting material by means of gel filtration (column, Sephadex G-10; eluent H_2O)

Quantitative Analyses. The irradiated alcoholic solutions were concentrated by distillation under reduced pressure and were neutralized with aqueous sodium hydrogencarbonate. The products were extracted several times with dichloromethane and were submitted to the GLC analyses (column, 2 or 3 m column of 5 or 10% PEG 20M; column temperature, 140 or 160 °C; internal standard, 3-pyridinecarbonitrile). The products from the peroxide-initiated and photochemical reactions were analyzed under similar conditions.

The work has been partially supported by a Grant-in-Aid for Scientific Research No. 60470028 from the Ministry of Education, Science and Culture and by the Inter-University Program for the Common Use of JAERI Facilities. The authors thank Japan Halon Co. and Nippon Oil and Fats Co. for kindly supplying 2,2,2-trifluoroethanol and *t*-butyl peroxypivalate, respectively.

References

1) G. R. Newkome and W. W. Paudler, "Contemporary Heterocyclic Chemistry. Syntheses, Reactions, and Applications" John Wiley and Sons (1982), pp. 271—274.

2) F. Minisci, *Synthesis*, **1973**, 1.

3) F. Minisci and O. Porta, *Adv. Heterocycl. Chem.*, **16**, 123 (1974).

4) F. R. Stermitz, C. C. Wei, and W. H. Huang, *Chem. Commun.*, **1968**, 482.

5) R. Noyori, M. Kato, M. Kawanisi, and H. Nozaki, *Tetrahedron*, **25**, 1125 (1969).

6) K. Nakamura, T. Sugiyama, T. Suzuki, and A. Sugimori, *Chem. Lett.*, **1977**, 1203; K. Nakamura, Y. Morita, T. Suzuki, T. Sugiyama, and A. Sugimori, *Bull. Chem. Soc. Jpn.*, **52**, 489 (1979).

7) A. Sugimori, M. Nishijima, and H. Itoh, *Bull. Chem. Soc. Jpn.*, **55**, 3055 (1982).

8) A. Sugimori, S. Mori, K. Maeda, and M. Nishijima, *Chem. Lett.*, **1984**, 769.

9) J. W. T. Spinks and R. J. Woods, "An Introduction to Radiation Chemistry," 2nd ed, John Wiley, New York (1976), p. 415.

10) A. Sugimori and T. Yamada, *Bull. Chem. Soc. Jpn.*, **59**, 3911 (1986).

11) F. Minisci, R. Bernardi, F. Bertini, R. Galli, and M. Perchinummo, *Tetrahedron*, **27**, 3578 (1971).

12) P. Neta, R. W. Fessenden, and R. H. Schuler, *J. Phys. Chem.*, **75**, 1654 (1971).

13) P. Neta and R. H. Schuler, *J. Am. Chem. Soc.*, **94**, 1056 (1972).

 © 1986 The Chemical Society of Japan Bull. Chem. Soc. Jpn., 59, 3911—3915 (1986)

Visible Light- and Radiation-Induced Alkylation of Pyridine Ring with Alkanoic Acid. Effective Alkylation in the Presence of Iron(III) Sulfate

Akira SUGIMORI* and Tetsuo YAMADA
Department of Chemistry, Faculty of Science and Technology, Sophia University, Kioi-cho 7-1, Chiyoda-ku, Tokyo 102
(Received June 16, 1986)

Quinoline and 4-methylquinoline are efficiently alkylated with alkanoic acid in the presence of iron(III) sulfate upon visible light-irradiation. Iron(III) sulfate not only accelerates the photoreaction but also increases the yield of alkylation. Gamma-irradiation also brings about the alkylation. In the photo- and radiation-induced alkylation with alkanoic acid, alkyl radicals play important roles.

The utilization of solar light for organic syntheses is one of the challenging problems in photochemistry. The catalyses by transition metal ions and transition metal complexes which absorb solar light effectively are one of the promising fields for the chemical utilization of the solar light.

Many types of photoreactions catalyzed by metal salts or metal complexes have been studied,[1] including $TiCl_4$-catalyzed photochemical addition of alcohol to ketone[2] and $FeCl_3$-catalyzed photooxidation of olefins.[3] Sato et al. proposed a long range electron-transfer mechanism for the transition metal ion-catalyzed photooxidation.[4]

However, there have been a few attempts to use solar light for the metal salt- (or metal complex-) catalyzed photoreactions. The examples of the recent studies which have been done in aiming the effective uses of solar light are photochemical carbon dioxide fixation catalyzed by metal porphyrins[5] and photo-reduction of methyl viologen under the catalysis by ferrocene derivatives.[6,7]

The generation of free radicals by solar light under the catalysis by transition metal salts and complexes is a useful reaction. Free radical species can play important roles in the chemistry of heteroaromatic compounds, because free radical species can attack electron-deficient heteroaromatic rings to give substitution products, while electrophiles which attack the normal aromatic rings to undergo substitution are not effective for the introduction of substituents in the electron-deficient heteroaromatic rings. One of the successful reactions of the category is the alkylation of the pyridine derivatives with alkanoic acids initiated by the thermal decomposition of peroxodisulfate under the catalysis by silver salt.[8]

The free radical species generated by gamma-irradiation, such as hydroxyalkyl radicals from alcohols, can be used for the alkylation of the pyridine ring.[9]

This paper describes the alkylation of the pyridine ring by alkyl radicals formed from alkanoic acids by the visible (or solar) light-irradiation under the catalysis by iron(III) sulfate or by γ-irradiation.[10] The iron(III)-catalyzed photoreaction is compared with the photoreactions catalyzed by TiO_2 and $EuCl_3$.

Results and Discussion

Visible Light-Induced Alkylation with Alkanoic Acid. The irradiation of 4-methylquinoline (**1**) in aqueous alkanoic acid solutions with a Xe lamp in the presence or absence of additives (sulfuric acid, metal salts, and titanium(IV) oxide) brings about alkylation at the 2-position of **1** (Table 1).

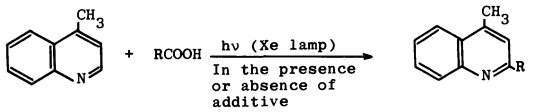

1 **2**

Although the photoalkylation with alkanoic acid occurs without any additives (the reaction in this case should be caused by the UV-light contained in the light emitted by a Xe lamp),[11] the reaction is the most effective in the acidic media in the presence of iron(III) sulfate. Iron(III) sulfate not only accelerates the photoreaction but also increases the yield of alkylation (yield=amount of product formed/amount of substrate reacted) either in the presence or absence of sulfuric acid. In particular, the effect of iron(III) sulfate is more remarkable in the presence of sulfuric acid than in its absence. In the reaction in the absence of iron(III), the addition of sulfuric acid inhibits the photoalkylation. The inhibition of photoreaction can be ascribed to the destruction of a hydrogen bond between quinoline and carboxylic acid. The addition of iron(III) sulfate in the acidic system results in the formation of the greater amount of the product than in the reaction in the absence of sulfuric acid and iron(III).

Europium chloride which has been reported to catalyze the photochemical hydroxymethylation of 1,3-dimethyluracil with methanol[12] inhibits the photoalkylation of 4-methylquinoline with alkanoic acid. Platinized titamium(IV) oxide promotes the photoalky-

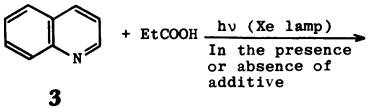

3

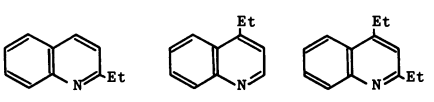

4 **5** **6**

Table 1. Visible Light-Induced Alkylation of 4-Methylquinoline (**1**) with Alkanoic Acid (RCOOH). Light Source, 500 W Xe Lamp; Irradiation Time, 20 h; Irradiated Solution, 50 cm^3 Solution (Solvent: H_2O 80%–RCOOH 20% v/v) containing 1.0 mmol of **1**

R	$[H_2SO_4]$ / mol dm^{-3}	Additive	Amount of additive / g	Atmosphere	Amount of **1** reacted / μmol	Amount of **2** formed / μmol	Yield of **2**[a] / %
Me	—	$Fe_2(SO_4)_3$	0.36	Ar	190	19	10
	0.033	—	—	Ar	157	1	1
	0.033	$Fe_2(SO_4)_3$	0.36	Ar	189	60	32
	0.033	TiO_2-Pt	0.5	Ar	80	9	11
Et	—	—	—	Ar	140	79	56
	—	—	—	O_2	41	38	91
	—	$Fe_2(SO_4)_3$	0.36	Ar	165	126	76
	—	$Fe_2(SO_4)_3$	0.36	O_2	81	1	1
	0.033	—	—	Ar	203	16	8
	0.033	$Fe_2(SO_4)_3$	0.36	Ar	619	458	74
	0.033	$Fe_2(SO_4)_3$	0.36	O_2	96	1	1
	0.033	$EuCl_3 \cdot 6H_2O$	0.5	Ar	Trace	Trace	—
	0.033	TiO_2-Pt	0.5	Ar	96	35	36
	0.033	TiO_2-Pt	0.5	O_2	67	2	3
	0.033	(TiO_2-Pt / $AgNO_3$)	(0.5 / 0.2)	Ar	82	78	95
	0.033	$AgNO_3$	0.2	Ar	13	8	62
n-Pr	0.033	—	—	Ar	101	21	21
	0.033	$Fe_2(SO_4)_3$	0.36	Ar	385	291	76
	0.033	TiO_2-Pt	0.5	Ar	117	17	15
i-Pr	0.033	—	—	Ar	147	20	14
	0.033	$Fe_2(SO_4)_3$	0.36	Ar	605	407	67
	0.033	TiO_2-Pt	0.2	Ar	159	52	32

a) Yield=Amount of product/Amount of substrate reacted.

Table 2. Visible Light-Induced Ethylation of Quinoline (**3**) with Propionic Acid. Reaction Conditions are the Same as Those for **1**

$[H_2SO_4]$ / mol dm^{-3}	Additive	Amount of additive / g	Amount of **3** reacted / μmol	Amount of Product / μmol and (Yield[a] / %) **4**	**5**	**6**	Amount of **5** / Amount of **4**
—	—		233	38 (16)	29 (12)	0 (0)	0.76
—	$Fe_2(SO_4)_3$	0.36	322	57 (18)	66 (20)	3 (1)	1.16
0.033	—		266	3 (1)	3 (1)	0 (0)	1
0.033	$Fe_2(SO_4)_3$	0.36	477	131 (27)	158 (33)	19 (4)	1.21
0.033	TiO_2-Pt	0.5	230	24 (11)	14 (6)	0 (0)	0.58
0.033	(TiO_2-Pt / $AgNO_3$)	(0.5 / 0.2)	234	35 (15)	40 (17)	0 (0)	1.14
0.033	$AgNO_3$	0.2	115	4 (4)	4 (4)	0 (0)	1

a) Yield=Amount of product/Amount of substrate reacted.

lation much less efficiently than iron(III) sulfate.

The irradiation of quinoline (**3**) with propionic acid with the light from a Xe lamp causes the ethylation at the 2- and 4-position (Table 2).

The effects of iron(III) on the photoreaction of the quinoline-propionic acid system are similar to those of the 4-methylquinoline-propionic acid system. In iron(III) sulfate-catalyzed photochemical alkylation, alkyl radicals should play important roles. The reaction is inhibited by oxygen. Alkyl radicals would be produced by the excitation of a sort of complex between iron(III) and alkanoic acid (or alkanoate) which has an absorption band spreading over near ultraviolet-visible region. Brownish yellow color appears, when iron(III) sulfate and propionic acid are mixed in an aqueous sulfuric acid solution. The appearance of color is ascribed to the formation of a complex between iron(III) and propionic acid. No color develops, when iron(III) sulfate and 4-methylquinoline are mixed in an aqueous sulfuric acid solution. The alkyl radicals thus formed attack the electron-deficient protonated quinoline derivative.

Another role of iron(III) would be as an oxidant of the intermediate (**7**) and the reduction products of alkylquinoline, which are formed by the disproportionation of **7**. This contributes to the improvement of

Table 3. Gamma-Ray-Induced Alkylation of 4-Methylquinoline (**1**) with Alkanoic Acid (RCOOH). Radiation Source, Co-60 γ-Rays; Dose Rate 1.0×10^6 rad h^{-1}; Dose, 5×10^7 rad; Irradiated Solution, 10 cm^3 RCOOH Solution Containing 3 mmol of **1**

R	Atmosphere	Amount of **1** reacted	Amount of **2** formed	Yield of **2**[a]	G(**2**)
		μmol	μmol	%	
Me	Ar	1220	447	37	0.82
Et	Ar	1500	489	33	0.95
	O_2	870	480	56	0.95
n-Pr	Ar	1440	372	26	0.74
i-Pr	Ar	1530	598	39	1.2

a) Yield=Amount of product/Amount of substrate reacted.

Table 4. Gamma-Ray-Induced Ethylation of Quinoline (**3**) with Propionic Acid. Reaction Conditions are the Same as Those for **1**

Atmosphere	Amount of **3** reacted	Amount of product, (Yield[a]), and [G-value]			Amount of **5** / Amount of **4**
	μmol	μmol			
		4	**5**	**6**	
Ar	1480	278 (19) [0.60]	102 (7) [0.22]	46 (3) [0.10]	0.37
O_2	1020	240 (23) [0.52]	88 (9) [0.19]	18 (2) [0.04]	0.37

a) Yield=Amount of product/Amount of substrate reacted.

the yield of the alkylation.

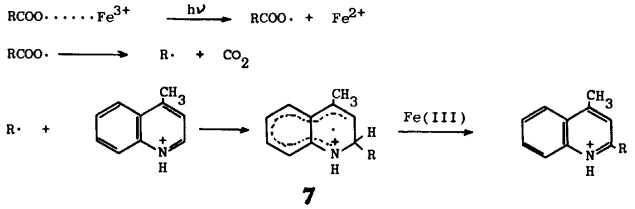

7

The excitation of the semiconducting titanium(IV) oxide generates electrons in the conduction band and holes. The holes undergo the oxidative decarboxylation of carboxylate to give an alkyl radical. The holes can also oxidize the intermediary formed radical **7** and/or the reduction products of quinoline and alkylquinolines. Therefore, the mechanism for the titanium(IV) oxide-catalyzed photoalkylation of the pyridine ring with alkanoic acid is similar to that for the iron(III)-catalyzed photoalkylation.

However, the TiO_2-catalyzed alkylation under the irradiation with a Xe lamp is inferior to the iron(III) sulfate-catalyzed reaction both with respect to the reaction rates and with respect to the yield of the alkylation. The low reaction rate is due to the low light absorption of titanium(IV) oxide in the visible region. The low yield for alkylation can be ascribed to the reduction of the substrate and the intermediate by the electron in the conduction band. The addition of Ag^+ which removes the electron in the conduction band of TiO_2 and/or oxidize the intermediate **7** improves the yield for alkylation (Table 1). In the semiconductor-catalyzed photo-cycloreversion and -valence isomerization, the promotion by oxygen has been reported.[13] The promoting effect of oxygen is ascribed to the acceleration of the charge separation of a hole-electron pair and the increase in the lifetime of a hole due to the removal of electron from depletion layer. However, in the titanium(IV) oxide-catalyzed photoalkylation of pyridine ring with alkanoic acid, oxygen inhibits the reaction. In this case, oxygen would inhibit the reaction by trapping the alkyl radicals.

Radiation-Induced Alkylation with Alkanoic Acid. Gamma-irradiation of **1** and **3** in alkanoic acid also brings about the substitution of alkyl group derived from the decarboxylation of alkanoic acid for the hydrogen of the pyridine ring (Tables 3 and 4).

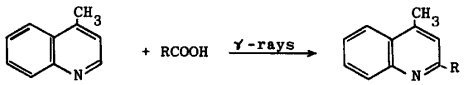

Methyl, ethyl, propyl, and isopropyl groups are introduced at the 2- and 4-positions of the pyridine ring in fairly good radiation-chemical yields (G-value=Number of molecules of product/100 eV of absorbed radiation energy).

Added sulfuric acid has only a small effect on the radiation-induced alkylation (Fig. 1). Oxygen retards the conversion of the substrate but increases the yield of the alkylation (Tables 3 and 4).

As it has been established that the main radiolysis product of alkanoic acid is carbon dioxide,[14] the formation of alkyl radicals by the radiolysis of the alkanoic acid can be safely postulated. The key step of radiolytic alkylation with alkanoic acid should be the attack of the alkyl radicals to the pyridine ring. The isopropylation with isobutyric acid (2-methylpropanoic acid) which has a large G-value for decarboxylation ($G(CO_2)$=14.4[15]) occurs in higher G-value than propyla-

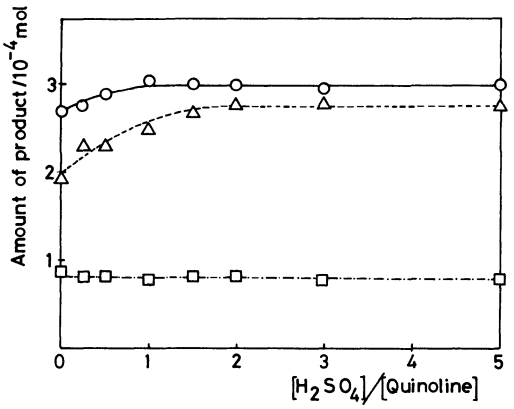

Fig. 1. Relation between yields of products and concentration of added sulfuric acid in radiation-induced alkylation of quinoline with propionic acid. [Quinoline]=0.18 mol dm^{-3}; Solvent, EtCOOH (60%)-H_2O (40%); Volume of irradiated solution, 15 cm^3; Dose rate, 1.0×10^6 rad h^{-1}; Dose, 5×10^7 rad. —○— **4**, ----△---- **5**, —·—□—·— **6**.

tion with butyric acid.

The radical species **7** would be converted to the alkylation product presumably via disproportionation. The fact that we observed the peak at m/z=161 in GC-MS of the mixture of the products in radiation-induced reaction of quinoline in propionic acid indicates the formation of the tetrahydro compound of **4** and/or **5**. The increase in the selectivity for **4** and **5** by oxygen can be explained by the oxidation of the intermediate **7** and/or reduction products.

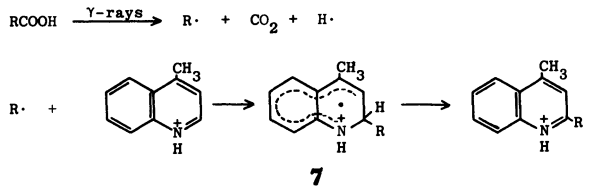

7

Experimental

Materials. Commercial quinoline (GR grade reagent of Tokyo Kasei Co.) and 4-methylquinoline (GR reagent of Wako Junyaku Co.) were used after the purification by distillation. Commercial GR grade reagents of acetic, propionic, butyric, and isobutyric acids (Wako Junyaku Co.) were used without further purification. Commercial europium(III) chloride 6 hydrate (made by Wako Junyaku Co.; 99.9% of purity), silver nitrate (EP grade reagent of Nisshin Kasei Co.), and iron(III) sulfate x hydrate (GR grade reagent of Wako Junyaku Co.) were used without further purification. The content of iron which was determined by the colorimetry with 1,10-phenanthroline was 72%.

Platinized titanium(IV) oxide was prepared by grinding 0.025 g of platinum black (Nippon Engelhard Co.) and 0.475 g of titanium(IV) oxide (P-25 made by Nippon Aerosil Co., a mixture of anatase and rutile) in a mortar according to Kawai and Sakata.[16]

Irradiation with a Xenon Lamp. Solutions (50 cm^3) of the substrate (0.02 mol dm^{-3}) and the additives in a mixed solvent of water and alkanoic acid (H_2O : RCOOH=4 : 1 v/v) were deaerated by bubbling Ar for 45 min before irradiation. The solutions were irradiated with a 500 W Xe lamp for 20 h under magnetical stirring.

For the irradiation under O_2 was bubbled oxygen gas through the solution for 45 min before irradiation.

Irradiation with γ-Rays. A solution containing the substrate (0.3 mol dm^{-3}) in alkanoic acid was deaerated by bubbling Ar (in some cases by oxygen) for 45 min before irradiation.

The solution was irradiated by Co-60 γ-rays at the irradiation facility of Japan Atomic Energy Research Institute in Takasaki at the dose of 5.0×10^7 rad (Dose rate, 1.0×10^6 rad h^{-1}).

For the dependence of the reaction on added sulfuric acid, solutions containing **3** (0.18 mol dm^{-3}) and sulfuric acid in a mixed solvent of H_2O (40%) and propionic acid (60%) were used.

Identification of Products. The identification of the alkylquinolines was described in our another paper.[9]

Quantitative Analysis of Photoproducts. The solution which was irradiated in the presence of sulfuric acid was neutralized with sodium carbonate. In the case of the irradiation in the presence of iron(III) sulfate, the formed precipitate of iron hydroxide was filtered off. The aqueous filtrate and the precipitate were extracted repeatedly with dichloromethane. After the removal of dichloromethane, the solvent was replaced by ethyl acetate and the solution was submitted to the gas-chromatographic analysis (column, 3 m column of PEG 20 M (10%); column temperature, 190 °C), using 3-pyridinecarbonitrile as an internal standard.

The work has been supported in part by a Grant-in-Aid for Scientific Research No. 60470028 from the Ministry of Education, Science and Culture. The γ-irradiation was done under the Inter-University Program for the Common Use of JAERI Facilities.

References

1) Reviews: T. Sato, *Yuki Gosei Kagaku Kyokai Shi*, **32**, 989 (1974); R. G. Salomon, *Tetrahedron*, **39**, 485 (1983).

2) T. Sato, H. Kaneko, and S. Yamaguchi, *J. Org. Chem.*, **45**, 3778 (1980).

3) T. Sato, T. Oikawa, and K. Kobayashi, *J. Org. Chem.*, **50**, 1646 (1985).

4) E. Murayama, A. Kohda, and T. Sato, *J. Chem, Soc., Perkin Trans. 1*, **1980**, 947.

5) S. Inoue, M. Nukui, and F. Kojima, *Chem. Lett.*, **1984**, 619.

6) T. Akiyama, A. Kondo, M. Omata, M. Kajitani, and A. Sugimori, *Chem. Lett.*, **1985**, 301.

7) T. Akiyama, A. Kondo, Y. Kawaharada, M. Kajitani, A. Endo, K. Shimizu, and A. Sugimori, *Chem. Lett.*, **1985**, 1071.

8) F. Minisci, R. Bernardi, F. Bertini, R. Galli, and M. Perchinummo, *Tetrahedron*, **27**, 3575 (1971).

9) A. Sugimori, T. Yamada, H. Ishida, M. Nose, K. Terashima, and N. Oohata, *Bull. Chem. Soc. Jpn.*, **59**, 3905 (1986).

10) Preliminary report, A. Sugimori and T. Yamada,

Chem. Lett., **1986**, 409.
11) R. Noyori, M. Kato, M. Kawanisi, and H. Nozaki, *Tetrahedron*, **25**, 1125 (1969).
12) A. Ishida, S. Toki, and S. Takamuku, *J. Chem. Soc., Chem. Commun.*, **1985**, 1481.
13) K. Okada, K. Hisamitsu, Y. Takahashi, T. Hanaoka, T. Miyashi, and T. Mukai, *Tetrahedron Lett.*, **25**, 5311 (1984).
14) J. W. T. Spinks and R. J. Woods, "An Introduction to Radiation Chemistry," 2nd ed, John-Wiley and Sons Co., NY (1976), pp. 427—430.
15) R. H. Johnsen, *J. Phys. Chem.*, **63**, 2041 (1959).
16) T. Kawai and T. Sakata, *J. Chem. Soc., Chem. Commun.*, **1980**, 694.

Convenient Synthesis of 3-Aminocoumarin Derivatives by the Condensation of 1,4-Diacetyl- or 3-Substituent-2,5-piperazinediones with Various Salicylaldehyde Derivatives

Chung-gi SHIN,* Yoshiharu NAKAJIMA, Toshiya HAGA, and Yoshiaki SATO
Laboratory of Organic Chemistry, Faculty of Technology, Kanagawa University, Rokkakubashi, Kanagawa-ku, Yokohama 221
(Received June 17, 1986)

The condensation of 1,4-diacetyl- or 3-substituted 2,5-piperazinediones (PDO) with various salicylaldehyde derivatives in the presence of a base, such as potassium *t*-butoxide or triethylamine, was found to give two extremely different kinds of products: 1-acetyl-3-arylmethylene-PDO and 3-(acylamino)coumarin derivatives. The former, which has a (*Z*)-geometric structure, was readily converted to the latter by irradiation. Furthermore, the conversion mechanism and the structural confirmation are discussed.

In a previous paper,[1] we briefly reported on the synthesis of a (*Z*)-3-salicylidene-2,5-piperazinedione derivative (**2a**; 2,5-piperazinedione=PDO), which was supposed to be the most promising precursor for the synthesis of spiro[benzofuran-2(3*H*), 2′-piperazine]-3′,6′-dione as the main skeleton of aspirochlorin.[2,3] In addition, interestingly enough, a similar reaction of 1,4-diacetyl-PDO (**1**) with salicylaldehyde gave an unexpected 3-aminocoumarin derivative **3a** along with **2a**, which was found to be further converted to **3a** upon irradiation. However, in regard to the synthesis of 3-(acylamino)coumarin from α-amino acid derivatives, at present only a few synthetic methods have been reported.[4-6]

In the present paper we wish to report on details regarding the facile and convenient syntheses of several kinds of 3-(acylamino)coumarin derivatives by the condensation of **1**, (3*S*)-1,4-diacetyl-3-alkyl-PDO (**4**) or 4-substituted (*Z*)-1-acetyl-3-alkylidene-PDO (**7**) with various salicylaldehyde derivatives, followed by the irradiation. Furthermore, the mechanism of the photochemical conversion and the structural confirmation of all the new compounds are also discussed.

Results and Discussion

Condensation of 1,4-Diacetyl-PDO with Salicylaldehydes. According to the Gallina and Liberatori method,[7] the condensation of equimolar **1** with salicylaldehyde in the presence of potassium *t*-butoxide was performed to give 1-acetyl-3-(2-hydroxybenzylidene)-PDO (**2a**) and 3-(*N*-acetylglycylamino)coumarin (**3a**) derivatives in a 53 and a 40% yields, respectively. As was previously reported,[1] the structure of **3a** could be readily determined by the conversion of **3a** with 1 M† HCl to the authentic 3-hydroxycoumarin; this was completely consistent with the product derived by the hydrolysis of known 3-(acetylamino)coumarin with 1 M HCl.

Furthermore, in order to generallize the synthesis of 3-(acylamino)coumarin (**3**) derivatives, first a similar condensation of **1** with several mono- and disubstituted 2-hydroxybenzaldehydes (**b**; X_1=5-Cl, **c**; X_1=5-Br, **d**; X_2=3,5-Cl_2, **e**; X_2=3,5-Br_2, **f**; X_1=3-OCH_3, **g**; X_1=4-$OCOCH_3$, **h**; X_1=4-OCH_2OCH_3) in *N*,*N*-dimethylformamide (DMF) at 10 °C was carried out, as shown in Scheme 1. As a result, both 1-acetyl-3-(2-hydroxyarylidene)-PDO (**2b—h**) as main products and 3-(*N*-acetylglycylamino)coumarin derivatives **3b—h** were also obtained in good yields. However, in the case of the reaction of **1** with 2-hydroxy-3-methoxybenzaldehyde (**f**), it was found that a similar condensation ultimately took place in the presence of two molar potassium *t*-butoxide to give only 3-(2-hydroxy-3-methoxybenzylidene)-PDO (**2f**) in a 30% yield not accompanied by the corresponding 3-aminocoumarin derivative **3f**. On the other hand, a similar reaction in the presence of equimolar triethylamine instead of potassium *t*-butoxide was found to give **2f** and **3f** in a 80 and a 16% yields, respectively. In addition, the analogous condensation of **1** with 2-hydroxy-4-(methoxymethoxy)benzaldehyde (**h**) was also carried out to give the corresponding 3-benzylidene-PDO (**2h**) and 3-aminocoumarin derivatives **3h** in a 43 and a 21% yields, respectively.

The reaction conditions of the above several condensations and the ratio of the yield of products **2** and **3** are summarized in Table 1.

Subsequently, compounds **2b—h** were irradiated in methanol with a high-pressure mercury lamp (500 W) under a stream of N_2 gas at room temperature to give **3b—h** in almost quantitative yields. In addition, it was found that the condensation products obtained as a mixture of **2** and **3** were in situ also irradiated to give only **3**. In both cases, the photochemical conversion of **2** to **3** was completed in less than 1 h.

Furthermore, in order to develop the above consecutive reaction and to investigate the asymmetric addition to the aminocoumarin derivatives containing a chiral α-amino acid residue, the other 1,4-diacetyl-PDO derivatives **4** and **7** as substrates were chosen and subjected to a similar condensation, followed by the irradiation. The optically active PDO (**4**: **a**; R=CH_3, **b**; R=*i*-C_3H_7, **c**; R=$C_6H_5CH_2$, **d**; R=CH_3-$COOCH_2$) were similarly condensed with salicylalde-

† 1 M=1 mol dm^{-3}.

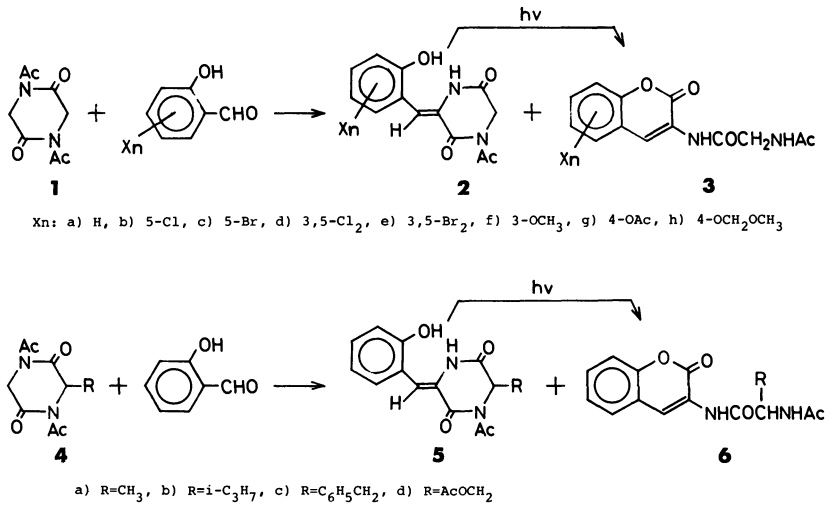

Scheme 1.

Table 1. Reaction Conditions of the Condensation and Yield Ratio of the Products **2** and **3**

(2-Hydroxy)arylaldehyde Substituent Xn	Base (equiv) *t*-BuOK (Et3N)	Yield/% 2	3	Ratio (2/3)
—	1	53	40	1.3
5-Cl	1	73	19	4.0
5-Br	1	80	20	4.0
3,5-Cl_2	1	70	18	4.0
3,5-Br_2	1	54	26	2.0
3-OMe	1	0	0	—
3-OMe	2	30	0	—
3-OMe	(1)	80	16	5.0
4-OAc	1	30	10	3.0
4-OCH_2OMe	(1)	43	21	2.0

hyde to give the desired 1-acetyl-6-alkyl-3-salicylidene-PDO (**5a—d**) and 3-[α-(acetylamino)acylamino]-coumarin derivatives **6a—d** in 49—64 and 16—25% yields, respectively. In an analogous manner as in the case of **2**, the subsequent irradiation of **5a—d** were also converted to **6a—d** within 1 h, as illustrated in Schemel.

On the other hand, in the case of 3-alkylidene-PDO derivatives **7**, for example, 1-acetyl-3-isobutylidene-(**7a**), 1,4-diacetyl-3-benzylidene-(**7b**), and 1-acetyl-3-benzylidene-4-methyl-PDO (**7c**) were found to not react at all when the Gallina and Liberatori method[7] was used. However, according to the Sasaki method,[8] compounds **7a—c** reacted with 2.5 mole of salicylaldehyde in the presence of 4 mole of anhydrous sodium acetate in acetic anhydride under reflux for 8 h to give the corresponding 3-alkylidene-6-salicylidene-PDO derivatives **8a—c** in 60—74% yields as the main products along with a very small amount of 3-(α-acetylamino-α-alkylideneacetylamino)coumarins **9a, c** in low yields. As shown in Scheme 2, in the case of **7b**, the by-product **9b** could not be obtained at all. Unfortunately, it was found that not only increasing the yield of **9** by even the modified Sasaki method but also the photochemical conversion of **8** to **9** was unsuccessful.

The yields, physical constants, and the spectral (IR and ^1H NMR) data of **2, 3, 5, 6, 8,** and **9** are summarized in Tables 2—5, and 6.

In order to further extend the above sequential reactions, another type of aromatic aldehyde was explored as an alternative to the salicylaldehyde derivatives. For example, the condensation of **1** with 2-hydroxy-1-naphthaldehyde in the presence of potassium *t*-butoxide was carried out in order to give the expected (*Z*)-1-acetyl-3-(2-hydroxy-1-naphthylmethylene)-2,5-piperazinedione (**10**) and 2-(*N*-acetylglycylamino)-3*H*-naphtho[2,1-*b*]pyran-3-one (**11**) in a 50 and a 20% yields, respectively. Subsequently, the former **10** was also converted in quantitative yield to **11** by irradiation. As a result, it could be concluded that the aromatic aldehyde having a vicinal hydroxyl group was applicable to the above successive condensation with PDO derivatives and irradiation.

Conversion Mechanism. For the purpose of the investigating the photochemical conversion mechanism of **2** to 3-aminocoumarin derivatives, in particular, (*Z*)-**2a** was subjected to geometric isomerization; this is because it was assumed that **2a** isomerized to (*E*)-isomer, followed immediately by a conversion to

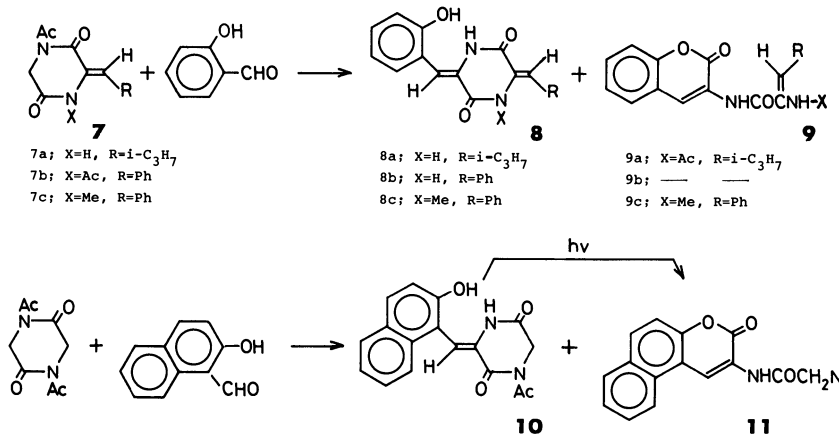

Scheme 2.

Table 2. The Yields and Physical Constants of **2**

Compd No.	Mp θ_m/°C[a)]	Formula	Found (Calcd) (%)			IR, ν/cm^{-1} in KBr		^{1}H NMR, δ in DMSO-d_6	
			C	H	N	NH (OH)	C=C	NH (OH)	-CH=
2a	200—201	$C_{13}H_{12}N_2O_4$	60.37 (59.99	4.60 4.65	10.82 10.77)	3070 (3380)	1630	10.00bs (10.56bs)	7.03s
2b	214—216	$C_{13}H_{11}N_2O_4Cl$	53.01 (52.97	3.70 3.74	9.49 9.52)	3100 (3400)	1630	8.60bs (9.80bs)	7.01s
2c	208—210	$C_{13}H_{11}N_2O_4Br$	46.05 (46.02	3.09 2.95	8.26 8.26)	3100 (3400)	1630	8.06bs (9.92bs)	7.08s
2d	221—222	$C_{13}H_{10}N_2O_4Cl_2$	47.61 (47.42	2.96 3.04	8.28 8.51)	3100 (3300)	1640	8.64bs (10.10bs)	7.00s
2e	255—256	$C_{13}H_{10}N_2O_4Br_2$	37.21 (37.34	2.31 2.40	6.48 6.70)	3050 (3300)	1635	8.54bs (9.90bs)	6.98s
2f	216—217	$C_{14}H_{14}N_2O_4$	57.82 (57.92	4.71 4.86	9.62 9.65)	3100 (3200)	1635	6.8—7.2m (Ph) (9.90b)	
2g	191—192	$C_{15}H_{14}N_2O_6$	56.19 (56.05	4.43 4.35	8.80 8.65)	3380	1630	6.6—7.6m (Ph)	6.72s
2h	192—193	$C_{15}H_{16}N_2O_6$	56.19 (56.04	4.86 4.75	8.71 8.98)	3400	1630	6.3—7.6m (Ph) (10.02bs)	

a) Colorless needles from methanol.

Table 3. The Yields and Physical Constants of **3**

Compd[a)] No.	Mp θ_m/°C[b)]	Formula	Found (Calcd) (%)			IR ν/cm^{-1} in KBr			^{1}H NMR, δ in $CDCl_3$		
			C	H	N	NH	NCO	C=C	-NHCO-	-CH_2NH- (J_{Hz})	-CH=
3a	213—214	$C_{13}H_{12}N_2O_4$	60.99 (60.98	4.64 4.68	10.77 10.88)	3315	1690 1535	1620	9.64bs	8.33t (5.5)	8.57s
3b	224—226	$C_{13}H_{11}N_2O_4Cl$	52.62 (52.97	3.44 3.74	9.35 9.52)	3300	1680 1530	1630	10.26bs	8.55t (5.5)	6.90s
3c	235—236	$C_{13}H_{11}N_2O_4Br$	46.04 (46.03	3.09 2.95	8.23 8.26)	3300	1680 1530	1630	9.69bs	8.32t (6.0)	7.00s
3d	232—233	$C_{13}H_{10}N_2O_4Cl_2$	47.32 (47.42	2.88 3.04	8.47 8.51)	3300	1680 1540	1630	9.96bs	8.36t (6.0)	7.46s

Table 3. (Continued)

Compd[a] No.	Mp θ_m/°C[b]	Formula	Found (Calcd) (%)			IR ν/cm^{-1} in KBr			^{1}H NMR, δ in $CDCl_3$		
			C	H	N	NH	NCO	C=C	-NHCO-	$-CH_2NH-$ (J_{Hz})	-CH=
3e	259—260	$C_{13}H_{10}N_2O_4Br_2$	37.52 (37.34	2.30 2.40	6.64 6.70)	3300	1680 1540	1630	10.02bs	8.26t (6.0)	6.94s
3f	248—249	$C_{14}H_{14}N_2O_5$	57.90 (57.92	4.77 4.86	9.65 9.65)	3300	1680 1540	1630	8.38bs	8.32t (6.0)	6.70—7.60 (Ph)
3g	223—224	$C_{15}H_{14}N_2O_6$	56.20 (56.04	4.43 4.35	8.80 8.65)	3375 3275	1690 1515	1630	9.69bs	8.32t (6.0)	7.28s
3h	199—200	$C_{15}H_{16}N_2O_6$	56.24 (56.04	4.73 4.43	8.74 8.67)	3370 3300	1680 1540	1630	9.64bs	8.36t (6.0)	7.10s

a) Almost quantitative yield from **2** by the irradiation. b) Colorless needles from methanol.

Table 4. The Yields and Melting Points of **5** and **6**

Compd No.	Yield %	Mp θ_m/°C	Formula	Found (Calcd) (%)		
				C	H	N
5a	64	135—136[a]	$C_{14}H_{14}N_2O_4$	60.99 (61.31	5.15 5.15	9.81 10.21)
5b	62	85—86[a]	$C_{17}H_{20}N_2O_4$	64.25 (64.54	6.79 6.37	8.81 8.86)
5c	54	syrup	$C_{20}H_{18}N_2O_4$	68.20 (68.56	5.00 5.18	7.74 8.00)
5d	49	syrup	$C_{16}H_{16}N_2O_6$	57.49 (57.83	4.58 4.85	8.11 8.43)
6a	22	195—196[b]	$C_{14}H_{14}N_2O_4$	61.02 (61.31	5.20 5.15	9.90 10.21)
6b	16	186—187[c]	$C_{17}H_{20}N_2O_4$	64.32 (64.54	6.25 6.37	8.61 8.86)
6c	25	241—242[d]	$C_{20}H_{18}N_2O_4$	68.20 (68.56	5.20 5.18	8.06 8.00)
6d	24	172—173[e]	$C_{16}H_{16}N_2O_6$	57.82 (57.83	4.85 4.85	8.63 8.43)

a) Colorless needles from cyclohexane. b) Colorless needles from benzene. c) Colorless needles from CCl_4. d) Colorless needles from methanol. e) Colorless needles from ethanol.

Table 5. The Spectral and Optical Data of **5** and **6**

Compd No.	IR, ν/cm^{-1} in KBr NH	C=C	-OH, -NHCH- (J_{Hz})	^{1}H NMR, δ in $CDCl_3$ -NHCO-	-CH= [Ph+H]	-CH-R (J_{Hz})	$[\alpha]_D^{25}$ (c 1.0) in MeOH
5a	3150	1630	10.56bs	7.14bs	[6.84—7.44m]	5.15q (7.3)	−154.4°
5b	3180	1635	10.75bs	7.16bs	[6.84—7.42m]	6.27t (6.0)	−31.6°
5c	3175	1630	10.76bs	10.56bs	[7.10—7.80m]	4.40t (5.0)	−120.0°
5d	3370	1630	10.46bs	7.16bs	[6.80—7.80m]	5.36t (4.0)	−80.4°

Table 5. (Continued)

Compd No.	IR, ν/cm^{-1} in KBr NH	C=C	^{1}H NMR, δ in CDCl$_3$ -OH, -NHCH- (J Hz)	-NHCO-	-CH= [Ph+H]	-CH-R (J Hz)	$[\alpha]_D^{25}$ (c 1.0) in MeOH
6a	3275	1630	8.32d (8.0)	9.60bs	8.56s	4.60t (8.0)	−120.7°
6b	3350	1635	6.67d (7.5)	8.90bs	8.64s	7.78t (8.0)	−92.5°
6c	3300	1635	8.36d (8.0)	9.84bs	8.60s	4.90m	−146.1°
6d	3325	1635	8.24d (8.0)	9.75bs	8.56s	4.92m	−105.5°

Table 6. The Yields and Physical Constants of **8** and **9**

Compd No.	Yield %	Mp[a] θ_m/°C	Formula	Found (Calcd) (%) C	H	N	IR, ν/cm^{-1} in KBr NH (OH)	C=C	^{1}H NMR, δ[b] -OH	-CH= (J Hz)
8a	60	176—177	$C_{15}H_{16}N_2O_3$	66.02 (66.16	6.21 5.92	10.08 10.29)	3080 (3400)	1630	10.18	5.66d (10.00)
8b	72	270—271	$C_{17}H_{14}N_2O_3$	69.31 (69.37)	4.92 4.80	9.39 9.52)	3160 (3400)	1630	10.10	6.6—7.6m (+Ph)
8c	74	175—176	$C_{19}H_{16}N_2O_3$	71.33 (71.24)	5.12 5.03	8.64 8.75)	3150 (3400)	1630	10.56	6.6—7.3m (+Ph)
9a	3	203—204	$C_{15}H_{16}N_2O_3$	65.98 (66.16	6.11 5.92	10.33 10.29)	3325	1630	—	?
9c	3	154—155	$C_{19}H_{16}N_2O_3$	71.22 (71.24	4.87 5.03	8.95 8.75)	3300 3325	1630	—	7.1—7.5m (+Ph)

a) Colorless needles from cyclohexane. b) Recorded in DMSO-d_6.

the coumarin derivative **3a**. Accordingly, firstly, in order to confirm the resulting isomerization and to prevent the transformation, *o*-hydroxyl group of 3-salicylidene in **2a** was protected with methoxymethyl (MOM) chloride by the usual method to give (*Z*)-1-acetyl-3-[(*O*-MOM)salicylidene]-PDO (**12**) in good yield. Subsequently, the photochemical conversion of **12** with a high-pressure Hg lamp (500 W) gave the expected (*E*)-1-acetyl-3-[(*O*-MOM)salicylidene]-PDO (**13**) in ca. a 40% yield. The configurational structure of **13**, thus obtained, was readily confirmed by a comparison with both chemical shifts of the olefin protons between the two geometric isomers. Generally, it is well-known that the olefin proton of α,β-unsaturated α-amino acid and its cyclic dipeptide of (*E*)-isomer shift at a higher magnetic field than that of (*Z*)-isomer.[9-11] In fact, it was found that the olefin proton of (*E*)-isomer **13** shifted at a higher magnetic field (δ 6.62) than that of (*Z*)-isomer **12** (δ 7.10) by ca. $\Delta\delta$ 0.48. The subsequent deprotection of **13** with a saturated HCl methanol solution at room temperature gave the desired **3a**, as illustrated in Scheme 3. From this result, it could by readily determined that, after the photochemical isomerization of **12** to **13** and subsequent deprotection of **13**, the PDO ring of the unstable intermediate (*E*)-1-acetyl-3-salicylidene-PDO [(*E*)-**2**], thus obtained, easily cleaved and a simultaneous nucleophilic addition of the resulting *o*-hydroxyl group to the neighboring carbonyl group took place to form **3**.

In conclusion, the conversion mechanism could be confirmed unambigously that the condensation of **1**, **4**, or **7** with salicylaldehyde derivatives yielded a mixture of (*Z*)- and (*E*)-isomers during the first step, the latter of which was immediately transformed by a successive ring cleavage and then recyclized to give **3**, **6**, **9**, and **11**.

Experimental

General. Melting points were determined with a Yamato micro melting-point apparatus model MP-21 and were uncorrected. The IR spectra were recorded with a Hitachi EPI-G2 grating spectrometer. The ^{1}H NMR spectra were measured with a JEOL JMN PS-100 spectrometer in a CDCl$_3$ solution with tetramethylsilane as the internal standard. The specific rotations were measured in a 0.5-dm tube using a JASCO DIP-4 polarimeter (Japan Spectroscopic Co. Ltd.).

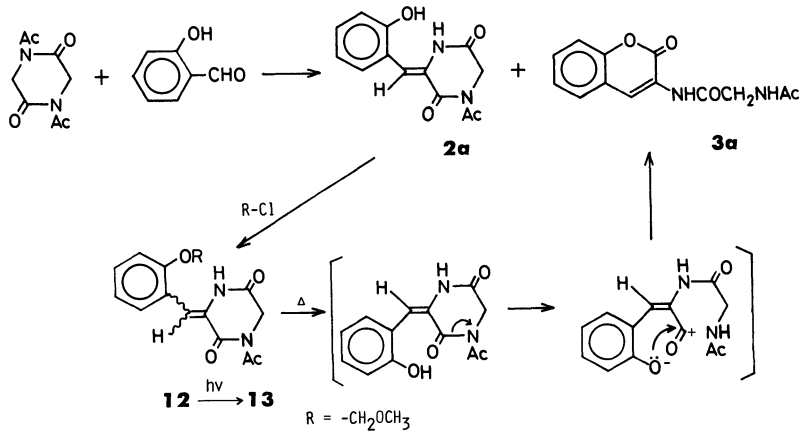

Scheme 3.

Condensation of 1 with Salicylaldehyde Derivatives. General Procedure. To a solution of **1** (19.8 g, 100 mmol) and an appropriate salicyladehyde (110 mmol) in DMF (260 ml) was added 1.1 mole of 0.5 M potassium *t*-butoxide, with stirring, drop-by-drop at 0 °C for 1 h. After the addition, the solution was continuously stirred at room temperature for 12 h and neutralized with acetic acid. It was then poured into ice-water (100 ml). A colorless crystalline deposited substance was collected and recrystallized from methanol to give two kinds of colorless needles. Repeated recrystallization from methanol gave pure **2** as colorless needles. On the other hand, after concentrating the mother liquor, the residual crystalline mixture was then chromatographed on a silica-gel column using a mixture of benzene and acetone (40 : 1 v/v) as the eluent to give two fractions. The main fraction was evaporated under reduced pressure to give residual crystals, which were also recrystallized from methanol to give **3** as colorless needles.

In the case of reactions with 3-methoxy- and 4-(*O*-MOM)-salicylaldehyde, a similar condensation was worked up in the presence of triethylamine, instead of potassium *t*-butoxide (See Table 1).

Irradiation of 2. A solution of **2** (0.1 mmol) in methanol (50 ml) was irradiated with a 500-W high-pressure mercury lamp under a N_2 gas stream at room temperature. The photochemical conversion of **2** was terminated within 1 h. The solution was concentrated under reduced pressure to give residual crystals which were subsequently recrystallized from methanol to give **3**.

Condensation of 4 with Salicylaldehyde. In a similar manner as in the case of **1**, the treatment of **4** (9.35 mmol) with 1.1 equivalent of salicylaldehyde (10.30 mmol) in the presence of 0.5 M potassium *t*-butoxide was worked up for 30 min to give **5** and **6** as colorless needles.

Irradiation of 5. A solution of **5** (0.1 mmol) in methanol (50 ml) was similarly irradiated to give **6**.

Condensation of 7 with Salicylaldehyde. A solution of **7** (20 mmol) and salicylaldehyde (6.1 g, 50 mmol) in acetic anhydride (29 ml) in the presence of anhydrous sodium acetate (6.5 g, 79 mmol) was refluxed for 8 h. After removing excess acetic anhydride under reduced pressure, the residue was dissolved in ethyl acetate (200 ml) and the solution was washed once with 1 M hydrochloric acid and once with a saturated sodium chloride aqueous solution and then dried over anhydrous magnesium sulfate. The removal of the solvent under reduced pressure gave colorless crystals which comprised two chemical species. Subsequent separation by chromatography on a silica-gel column using a mixture of chloroform and acetone (30 : 1 v/v) as the eluent afforded two fractions. The first fraction was concentrated under reduced pressure to give **8** and the second gave **9** as colorless needles (See Table 6).

Condensation of 1 with 2-Hydroxy-1-naphthaldehyde. To a mixture of **1** (5.0 g, 28.1 mmol) in DMF (80 ml) was slowly added triethylamine (3.4 g, 33.6 mmol), with stirring, at −10 °C. After stirring at room temperature for 16 h, the reaction solution was neutralized to pH 7 with 3 M HCl under cooling and then diluted with water (300 ml). The solution was extracted three times with ethyl acetate (300 ml) and the combined extracts were dried over anhydrous sodium sulfate. After removing the solvent under reduced pressure, the obtained residual syrup was gradually solidified to give crude crystals; these were collected after adding diisopropyl ether. Recrystallization from acetone gave yellowish fibrous solid as a mixture of **10** and **11**, which were did not separated. However, based on the ^{1}H NMR spectrum, the ratio of yield was found to be 4 : 1 (**10** : **11**).

Preparation of 11. The above mixture (300 mg) in methanol (70 ml) was irradiated with a 500-W high-pressure Hg lamp under a N_2 gas stream at room temperature for 3 h. The mixture gradually dissolved to give a homogeneous solution. The removal of methanol gave a crude crystalline substance, which was recrystallized from acetone to give **11** as a pale-yellow fibrous solid. Mp 250 °C (decomp). ν_{max}^{KBr} (cm^{-1}) 3200 (NH), 1685, 1530 (NHCO), 1650 (C=C); ^{1}H NMR (DMSO-d_6) δ=9.79 (bs, 1H, NH), 9.27 (s, 1H, -CH=), 8.35 (t, 1H, J=6.0 Hz, NH), 4.10 (d, 2H, J=6.0 Hz, -CH_2-). Found: C, 65.93; H, 4.41; N, 8.97%. Calcd for $C_{17}H_{14}N_2O_4$: C, 65.80; H, 4.55; N, 9.03%.

Preparation of 12. To a solution of **2a** (3 g, 11.5 mmol) in tetrahydrofuran (45 ml) in the presence of triethylamine (1.28 g, 12.6 mmol) was slowly added chloromethyl methyl ether (1.21 g, 15.0 mmol) with stirring at 0 °C for 1 h. The deposited salt was filtered off and the filtrate was concentrated under reduced pressure. The residual crystals, thus obtained, were collected and then recrystallized from ethyl acetate to give **12** as colorless needles. Yield 82%, mp 137—138 °C. ν_{max}^{KBr} (cm^{-1}) 1725, 1700 (C=O), 1620 (C=C); ^{1}H NMR δ=10.1 (bs, 1H, NH), 7.10 (s, 1H, -CH=), 4.35 (s, 2H, -CH_2-). Found: C, 59.15; H, 5.28; N, 9.16%. Calcd for $C_{15}H_{16}N_2O_5$: C,

59.20; H, 5.30; N, 9.21%.

Preparation of 13. A solution of **12** (1.49 g, 4.9 mmol) in methanol (70 ml) was irradiated with a 500-W high-pressure Hg lamp under a N_2 gas stream at room temperature for 8 h. Insoluble materials separeted out were filtered off and then the filtrate was concentrated under reduced pressure to give a crystalline residue. The crystals, thus obtained, were purified on a silica-gel column using a mixture of chloroform and acetone (20 : 1 v/v) as the eluent. After concentration of the fraction, the obtained crystals were recrystallized from carbon tetrachloride to give **13** as colorless needles. Yield 33%, mp 85—86 °C. ν_{max}^{KBr} (cm^{-1}) 3040 (NH), 1630 (C=C); ^1H NMR δ=10.62 (bs, 1H, NH), 4.30 (s, 2H, $-CH_2-$). Found: C, 58.99; H, 5.27; N, 9.17%. Calcd for $C_{15}H_{16}N_2O_5$: C, 59.20; H, 5.30; N, 9.21%.

Conversion of 13 to 3a. A solution of **13** (110 mg, 0.38 mmol) in methanol (10 ml) was stirred below 0 °C. To the solution was added a methanol solution (10 ml) saturated with hydrogen chloride gas. After stirring for 2 h and then removing the solvent, the obtained residue was purified on a silica-gel column using a mixture of chloroform and methanol (10 : 1 v/v) as the eluent to give **3a** in a 70% yield.

References

1) C. Shin, Y. Nakajima, and Y. Sato, *Chem. Lett.*, **1984**, 1301.

2) K. Sakata, H. Masago, A. Sakurai, and N. Takahashi, *Tetrahedron Lett.*, **23**, 2095 (1982).

3) D. Brewer, A. G. McInnes, D. G. Smith, A. Taylor, and J. A. Walter, *J. Chem. Soc., Perkin Trans. 1*, **1978**, 1248.

4) A. E. EL-Naggar, F. T. M. Ahmed, A. M. Abd El-Salam, M. A. Radi, and M. S. A. Latif, *J. Heterocycl. Chem.*, **18**, 1203 (1981).

5) L. Jurd, A. D. King. Jr., and K. Mihara, *Photochemistry*, **10**, 2965, 2971 (1971).

6) R. Walter, T. C. Purecelly, and H. Zimmer, *J. Heterocycl. Chem.*, **3**, 235 (1966).

7) C. Gallina and A. Liberatori, *Tetrahedron*, **1974**, 664.

8) T. Sasaki, *Chem. Ber.*, **54**, 163 (1921).

9) A. Srinivasan, K. D. Richards, and R. K. Olsen, *Tetrahedron Lett.*, **1976**, 891.

10) D. Hoppe and R. Follmann, *Chem. Ber.*, **109**, 3062 (1976).

11) C. Shin, M. Hayakawa, T. Suzuki, A. Ohtsuka, and J. Yoshimura, *Bull. Chem. Soc. Jpn.*, **51**, 550 (1978).

 © 1986 The Chemical Society of Japan Bull. Chem. Soc. Jpn., 59, 3925—3930 (1986)

Chemical Reactivities of Coordinatively Unsaturated Hydridotris(phosphonite)-cobalt(I) Species Photogenerated towards Allylic and Related Compounds

Masayoshi Onishi,* Shigero Oishi,†,†† Mitoshi Sakaguchi, Isato Takaki, and Katsuma Hiraki
Department of Industrial Chemistry, Faculty of Engineering, Nagasaki University, Bunkyo-machi, Nagasaki 852
†Sagami Chemical Research Center, Nishi-Ohnuma 4-4-1, Sagamihara, Kanagawa 229
(Received June 18, 1986)

Pyrex-filtered photoirradiation with a high-pressure Hg lamp was performed for a thermally inert hydridocobalt(I) $CoH[PPh(OEt)_2]_4$ in the presence of some allylic compounds. Allyl benzoate and allyl phenyl ether showed the cleavage of allylic-O bonds to give propene in a stoichiometric quantity to the complex charged. Photoassisted catalytic double-bond migration occurred for *N*-allylacetamide, *N*,*N*-diethylallylamine, and allylbenzene to afford the respective (*E*)- and (*Z*)-1-propenyl derivatives with kinetically controlled *E*, *Z* compositions, and the fractions of *Z* isomers at the initial stage of the reaction proceeding were near 79, 30, and 20%, respectively. Laser flash photolysis study revealed that the double-bond migration was initiated by the coordination of the substrates through C=C double bond rather than nitrogen or oxygen donor-atom to the coordinatively unsaturated species "$CoH[PPh(OEt)_2]_3$" photogenerated.

Pyrex-filtered photoirradiation of a thermally inert hydridocobalt(I) complex $CoH[PPh(OR)_2]_4$ caused dissociation of a $PPh(OR)_2$ ligand from cobalt efficiently without cleavage of the hydrido-cobalt bond, and produced a coordinatively unsaturated hydrido species "$CoH[PPh(OR)_2]_3$."[1,2] Nitrogen-laser pulse excitation was also found to generate the hydrido species with a quantum yield of almost 1.0, and absolute rate constants were determined for coordination of free $PPh(OR)_2$ and some olefins to the species.[3] Furthermore, high catalytic activities of the hydrido species were realized in hydrogen transfer from secondary alcohols to ketones and isomerization of olefins.[1,4,5]

In the present paper, chemical reactivities of the hydrido species "$CoH[PPh(OEt)_2]_3$" ($CoHP_3$) photogenerated from $CoH[PPh(OEt)_2]_4$ (**1**) were studied towards some allylic compounds linked to heteroatoms or aromatic rings, which included *N*-allylacetamide, *N*,*N*-diethylallylamine, allylbenzene, allyl benzoate, and allyl phenyl ether. Incentive for studies on these reactions was derived from the following; (i) competitive coordination through two coexisting ligating sites i.e. the olefinic moiety and the heteroatoms with lone pairs of electrons to $CoHP_3$, (ii) chemical reactivities of $CoHP_3$ with the allylic compounds to cleave bonds between the allylic carbon and the heteroatoms,[6] and (iii) potential synthetic utility of catalytic olefin isomerization.[7] One of the authors (S.O.)[8] communicated that photoreaction of **1** with allyl phenyl ether gave almost equimolar quantity of propene to **1** charged and a small amount of 1-propenyl phenyl ether, and excluded initial coordination to $CoHP_3$ via the ether oxygen. As for nitrogen donor-ligands with higher coordination ability than ether oxygen, there were a few papers on formation of their cobalt(I) complexes.[9] It seems worthwhile to compare two ligating sites of the olefinic nitrogen compounds on coordination towards the transient $CoHP_3$ species, by means of laser flash photolysis.

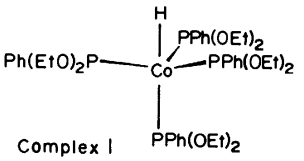

Complex I

Experimental

Materials. *N*,*N*-Diethyl-1-propenylamine,[10] *N*-(1-propenyl)acetamide,[11] and *N*-allylacetamide[12] were prepared by the literature methods, and other allylic compounds and their isomerized 1-propenyl derivatives were commercially available. The complex $CoH[PPh(OEt)_2]_4$ **1** was prepared according to the Gray's method.[13] Benzene was treated with concentrated sulfuric acid until thiophen-free. After water washing, it was dried over anhydrous magnesium sulfate, and distilled from sodium under nitrogen. Toluene was purified similarly.

General Procedures. ^1H NMR spectra were recorded on a JEOL FX-90Q and a BRUKER AM-400 spectrometers. The gas chromatographic (GLC) analyses were performed on a SHIMADZU GC-8AIT (TCD) and a GC-8APF (FID) instruments. For irradiation, a high-pressure mercury lamp (400 W) was used with a Pyrex filter, and reactant solutions were placed at about 45 mm from the lamp.

Olefin Isomerization and GLC Analyses of the Products. Benzene solutions (5 cm^3) of **1** (0.04 mmol) and allylic compounds (0.8 mmol) were degassed by freeze-pump-thaw cycles in a Pyrex Schlenk tube (18 mm^{ϕ}). After standing the solutions at 30 °C in the dark or under irradiation to proceed double-bond migration of the olefins, GLC analyses of gaseous products were performed using a Porapak Q or a molecular-sieve 5A column (3 m×3 mm^{ϕ}) with a TCD detector, and other organic compounds were determined with a similar PEG-20M column and a FID detector.

Cis-trans isomerization of 1-propenyl derivatives was carried out analogously.

In the case of *N*,*N*-diethylallylamine, toluene was used as solvent for better resolution of GLC signals to evaluate conversion of the double-bond migration. However, determination of the *E*, *Z* composition in *N*,*N*-diethyl-1-propenylamine made it necessary to adopt ^1H NMR product analyses,

††Present address: Radiation Laboratory, University of Notre Dame, Notre Dame, Indiana 46556, U.S.A.

as follows.

Reaction of *N,N*-Diethylallylamine or *N,N*-Diethyl-1-propenylamine and ^{1}H NMR Product Analyses. *N,N*-Diethylallylamine (0.8 mmol) was added to a C_6D_6 solution (0.6 cm^3) of **1** (0.04 mmol) and the mixture was degassed in a Schlenk tube (5 mm$^\phi$). After reaction at 10 °C, a small amount of tetramethylsilane was added to the mixture. Some quantity of the volatile components was separated from the nonvolatiles by trap-to-trap vacuum distillation without heating, and was sealed in NMR tubes under vacuum. The ^{1}H NMR spectrum of the distillate showed resonances for *E* and *Z* isomers of *N,N*-diethyl-1-propenylamine together with some unreacted *N,N*-diethylallylamine, and olefinic proton signals in the 1-propenylamines were useful for determination of the *E*/*Z* ratio.

Cis-trans isomerization of *N,N*-diethyl-1-propenylamine was performed similarly.

Laser Flash Photolysis. The apparatus of laser flash photolysis consists of a nitrogen laser (National Research Group, pulse width 5 ns, 4 mJ/pulse) for excitation at 337 nm, a 150 W xenon lamp (Ushio) for monitoring, a grating monochromator (Union Giken), a photomultiplier (Hamamatsu Photonics R446 or R212), a storage oscilloscope (Iwatsu TS-B123), and a personal computer (Sharp MZ-2000) for controlling the system, averaging the signal, and analyzing the data. A right-angle optical system was employed for the excitation-analysis set-up. An average of at least 9 shots, at each particular wavelength, was used for the determination of transient spectra or the investigation of reaction kinetics. The rate constants were determined according to the procedure of Ref. 16 and can be regarded as accurate to within ca. 10%. Solutions (5 cm^3) of **1** (≈0.6 mM†††) and *N,N*-diethylpropylamine (1.0—6.4 M), *N,N*-diethylallylamine (13—47 mM), *N*-propylacetamide (0.108—0.51 M), or *N*-allylacetamide (1.9—11.7 mM) were purged of oxygen by bubbling with argon and subjected to laser flash photolysis at 23 °C. Toluene and benzene were used as solvents for the amines and the amides, respectively.

Results and Discussion

Photoassisted Double-Bond Migration of Olefins with the Hydridocobalt(I) Complex. The complex $CoH[PPh(OEt)_2]_4$ (**1**) was mixed with 20-fold moles of allylic compounds in deaerated benzene or toluene solutions. In the cases of *N*-allylacetamide, *N,N*-diethylallylamine, and allylbenzene, photoirradiation of the solutions led to their catalytic double-bond migration, yielding the corresponding (*E*)- and (*Z*)-1-propenyl derivatives, which are thermodynamically stabilized through π-conjugation with a lone electron pair on nitrogen or a delocalized π-system. Figure 1

$$RCH_2CH{=}CH_2 \xrightarrow{Cat} RCH{=}CH{\sim}CH_3$$

$$R = -NHCOCH_3,\ -NEt_2,\ -C_6H_5$$

shows plots of the conversions versus time for the double-bond migration of these compounds at 30 °C. The double-bond migration of *N*-allylacetamide proceeded well and was completed within 20 min. On the other hand, photoreactions of allyl benzoate and allyl phenyl ether for 6 h gave 1-propenyl derivatives with the conversions of only ca. 1 and 5%, respectively, and large quantities of unreacted substrates were recovered. However, propene was formed in the yields of 71 and 76% based on **1**, respectively. In the photocatalytic reaction with *N,N*-diethylallylamine, we detected only small amount of propene (1.6% based on **1**) together with traces of ethylene and ethane, whereas the reaction with *N*-allylacetamide did not yield propene at all.

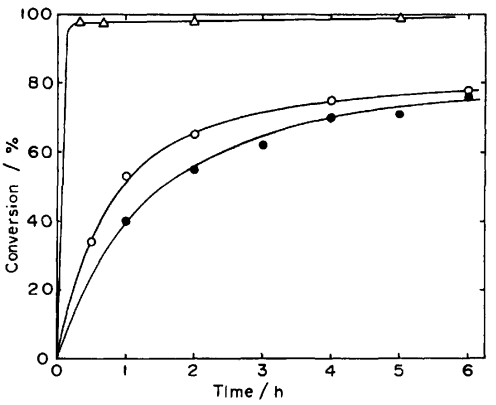

Fig. 1. Double-bond migration of allylic compounds to (*E*)- and (*Z*)-1-propenyl derivatives under irradiation with **1**.
At 30°C; Monitored by GLC; △: *N*-Allylacetamide, ○: *N,N*-Diethylallylamine, ●: Allylbenzene.

Allylic compounds did not afford propene or 1-propenyl derivatives under irradiation in the absence of **1**, and addition of free $PPh(OEt)_2$ did not change the situation either. Furthermore, neither double-bond migration nor propene formation occurred for the allylic compounds in the presence of **1** in the dark at 30 °C. These two types of reactions proceeded only in the presence of **1** under irradiation, and were attributed to operations of the photogenerated $CoHP_3$.

When irradiation of *N*-allylacetamide, *N,N*-diethylallylamine, and allylbenzene with **1** was stopped in the middle of the reaction proceeding, the double-bond migration ceased immediately. On restarting irradiation, the migration proceeded again. The double-bond migration of the present system was determined to be virtually "photoassisted" rather than "true photocatalytic."[14] The immediate cessation of the reaction proceeding upon interruption of irradiation was due to easy recombination of $CoHP_3$ with the photodissociated $PPh(OEt)_2$.[1,3] After incorporation of these allylic compounds with the photogenerated $CoHP_3$, insertion of their olefinic moieties into the hydridocobalt bond formed alkyl intermediates, which released (*E*)- and (*Z*)-1-propenyl derivatives through β-hydrogen abstraction by cobalt, and $CoHP_3$ was regenerated, as shown in Scheme.

Kurosawa[15] performed reactions of allylamines with some cationic platinum(II) hydrides, affording π-allyl

†††1 M=1 mol dm^{-3}.

complexes and amine products through replacement of the allylic group in the parent amines with hydrogen, and suggested that allylamines ligated to platinum via the nitrogen atoms rather than via the C=C double-bond at the first stage. On the other hand, laser flash photolysis (vide infra) of the present system with **1** revealed the initial π-coordination of the C=C bonds to cobalt, leading to the catalytic double-bond migration under continuous irradiation. Furthermore, photoassisted double-bond migration of *N*-allylacetamide with **1** showed a sharp contrast to the case with the platinum(II) hydrides, which formed a catalytically inactive [1-(acetylamino)propyl-C^1,O]platinum(II) complex.[15]

Photoirradiation of allyl benzoate and allyl phenyl ether in the presence of **1** would form alkyl intermediates similarly, but then alternative abstraction of β-benzoyloxy and β-phenoxy entities[8] by cobalt was presumed to occur as the major pathway, affording benzoato- and phenoxocobalt species with release of propene (Scheme). These cobalt species were not catalytically active, and the formation of propene was stoichiometric to **1** charged. Similar cleavage of allylic-O bonds in allylic carbonates and esters was observed by Yamamoto and his co-workers,[6h,6i] in reactions with some transition-metal hydrides without photoirradiation.

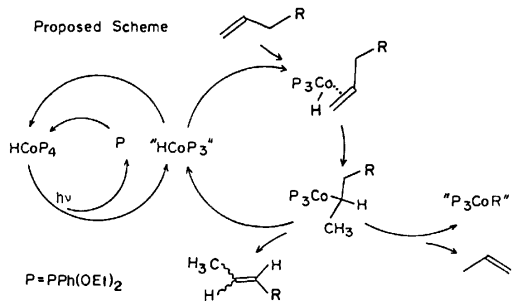

Coordination Process of Substrates to the CoHP$_3$ Species. Time-resolved absorption spectra were observed after laser flash photolysis of **1** in the presence of amides or amines, and second-order rate constants k' were determined for coordination of substrates to the transient CoHP$_3$ species photoproduced. Photoisomerization of *N*-allylacetamide and *N*,*N*-diethylallylamine observed in the present study was presumed to involve their coordination of CoHP$_3$ as one of key processes in catalytic cycles, similarly to that communicated for allylbenzene.[1]

Amides and amines may coordinate to CoHP$_3$ through a lone electron pair of an oxygen or nitrogen donor-atom. In the case of a nonolefinic amide or amine, the transient absorption spectra showed both peak-decay of the band at 580 nm and peak-growth of the band in the region of about 450 to 420 nm, with formation of an isosbestic point (Figs. 2 and 3). The peak of the latter band grew almost on the same rate as the peak at 580 nm decayed (Table 1). On the other hand, in the case of an olefinic amide or amine, we observed only the peak-decay at 580 nm (Figs. 4 and 5). The band at 580 nm is attributed to the living CoHP$_3$ species, and its peak-decay was caused by the coordination of the substrates and by the recombination of CoHP$_3$ with the photodissociated PPh(OEt)$_2$.[3,8,16]

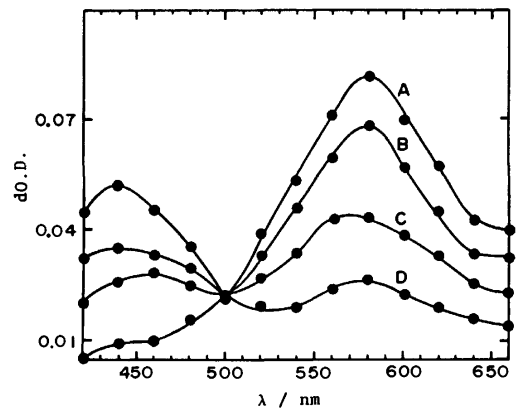

Fig. 2. Time-resolved absorption spectra for *N*-propylacetamide after pulsed laser photolysis. Substrate, 0.108 M (benzene); Complex **1**, 0.656 mM. A: 0.20 μs, B: 0.98 μs, C: 2.49 μs, D: 4.99 μs.

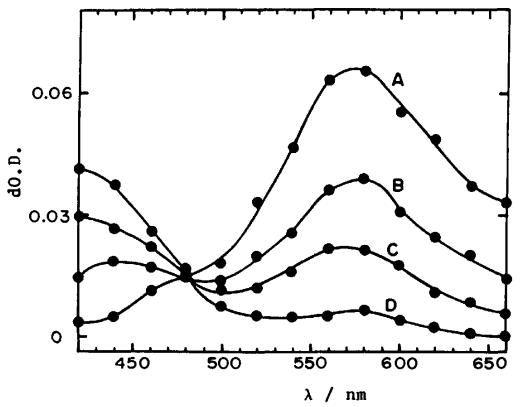

Fig. 3. Time-resolved absorption spectra for *N*,*N*-diethylpropylamine after pulsed laser photolysis. Substrate, 6.44 M (neat); Complex **1**, 0.656 mM. A: 0.82 μs, B: 4.49 μs, C: 8.79 μs, D: 20.0 μs.

Table 1. Second-Order Rate Constants k' for Coordination ($M^{-1}s^{-1}$)[a]

$(C_2H_5)_2N$	1.9×10^4 (1.9×10^4)	H_3C N H O	1.8×10^6 (2.1×10^6)
$(C_2H_5)_2N$	4.7×10^7	H_3C N H O	1.9×10^8

a) Values were determined from the peak-decay at 580 nm, and those in the parentheses were obtained from the peak-growth in the region of about 450 to 420 nm; The rate constants k' were evaluated from the following equation.[16]

$$-\frac{d[CoHP_3]}{dt} = k[CoHP_3][P] + k'[CoHP_3][Substrate]$$

The olefinic compounds, *N*-allylacetamide and *N,N*-diethylallylamine gave similar spectral change to that observed for 1-hexene or allylbenzene,[3,16] indicating the ligation to $CoHP_3$ via the double bond in a π-fashion, rather than via the oxygen or nitrogen donor-atom.

The peak-growth in the region of about 450 to 420 nm for the nonolefinic amide or amine was associated with formation of the new adducts of $CoHP_3$ with the substrates attached via the oxygen or nitrogen donor-atom. These donor-atoms have not empty low-lying orbitals appropriate for back donation bonding with metal, in contrast to $PPh(OEt)_2$ and the C=C double bond. Accordingly, absorption spectra of the hydridocobalt adducts with oxygen or nitrogen donor-ligands are expected to show red shifts of bands significantly from those of **1**.[17] On the other hand, absorption spectral change would be small on transformation from **1** to the adducts of $CoHP_3$ with olefins, and it is no wonder that we observed only the peak-decay of the band at 580 nm, attributable to $CoHP_3$, in the laser photolysis of **1** in the presence of the olefinic compounds.

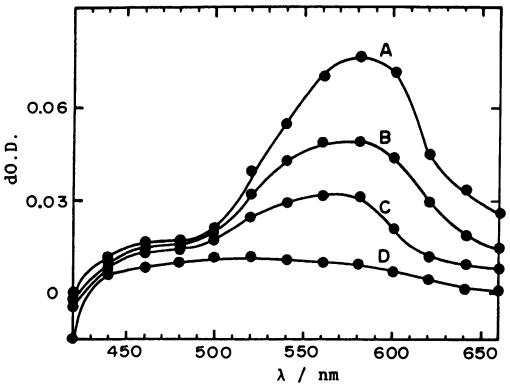

Fig. 4. Time-resolved absorption spectra for *N*-allylacetamide after pulsed laser photolysis. Substrate, 3.90 mM (benzene); Complex **1**, 0.656 mM. A: 0.29 μs, B: 0.98 μs, C: 1.76 μs, D: 4.39 μs.

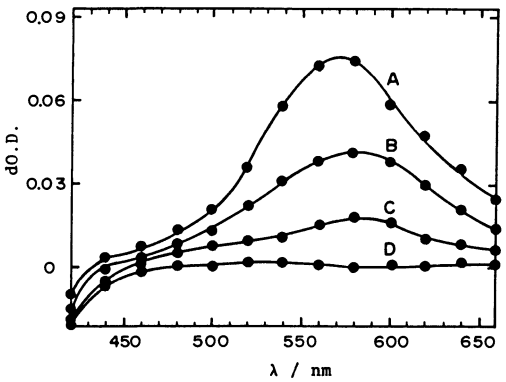

Fig. 5. Time-resolved absorption spectra for *N,N*-diethylallylamine after pulsed laser photolysis. Substrate, 20.1 mM (toluene); Complex **1**, 0.656 mM. A: 0.27 μs, B: 0.98 μs, C: 1.95 μs, D: 20.0 μs.

The rate constants k' of *N*-allylacetamide and *N,N*-diethylallylamine were comparable to those of 1-hexene and allylbenzene ($\approx 1.2\times10^8$ M^{-1} s^{-1}),[16] and were far larger than those of *N*-propylacetamide and *N,N*-diethylpropylamine, confirming the π-coordination of the allylic compounds via the C=C double bond.

***E,Z* Selectivity in 1-Propenyl Derivative Formation from Allylic Compounds.** 1-Propenyl compounds with several *E/Z* isomeric ratios were added in 20-fold molar quantities to deaerated solutions of the complex **1**, and their cis-trans isomerization was attempted. Table 2 summarizes the results of *N*-(1-propenyl)-acetamide, *N,N*-diethyl-1-propenylamine, and 1-propenylbenzene. Photoirradiation with **1** promoted the isomerization, and the fraction of *Z* isomer in each of the 1-propenyl compounds approached one equilibrium value at the photostationary state after prolonged irradiation. The *Z* fractions were 51±2, 2±2, and 2±1% for *N*-(1-propenyl)acetamide, *N,N*-diethyl-1-propenylamine, and 1-propenylbenzene, respectively. In several runs performed with the constant quantity of **1**, change of the amount of 1-propenyl compounds charged did not show any significant effect on the *Z* fractions at the photoassisted equilibrium.

Table 2. Cis-trans Isomerization of 1-Propenyl Derivatives[a]

R	Analysis	Reaction Time / h	Reaction Temp / °C	*Z* Fraction/% Before Reaction	*Z* Fraction/% After Reaction
$-NHCOCH_3$	GLC	6	30	72±2	51±2
		6	30	22±1	52±2
$-N(C_2H_5)_2$	^1H NMR	5	10	27±2	12±2
		24	10	26±2	2±2
		24	10	2±2	2±2
$-C_6H_5$	GLC	5	30	61±2	23±1
		5	30	15±1	2±1
		14	30	35±2	2±1
		5	30	2±1	3±1

a) The cobalt(I) complex **1** (0.04 mmol) was mixed with the 1-propenyl derivatives (0.8 mmol) in benzene, and the mixture was irradiated. See the experimental section.

Table 3. *Z* Fraction of 1-Propenyl Derivatives Formed during the Early Stage from Allylic Compounds[a)]

R	Analysis	Temp	*Z* Fraction/% (Conversion/%)	
		°C	Experimental Values	Extrapolated Value[b)]
-NHCOCH$_3$	GLC	30	75±2 (5.4), 68±2 (14)	~79 (0)
-N(C$_2$H$_5$)$_2$	^{1}H NMR	10	26±2 (20), 24±2 (30)	~30 (0)
-C$_6$H$_5$	GLC	30	20±4 (1.3), 26±2 (17), 24±2 (27)	~20 (0)

a) The cobalt(I) complex **1** (0.04 mmol) was mixed with the allylic compounds (0.8 mmol) in benzene, and the mixture was irradiated. See the experimental section. b) These values were obtained by extrapolating plots of the experimental value vs. conversion to the intercept at zero conversion.

In consideration of absorption spectra of **1** and the 1-propenyl compounds and of the radiation spectrum from the Hg lamp equipped with the Pyrex filter, the line at 366 nm and its trailing part were mainly responsible for the photoreactions with **1**, and incident photons in this wavelength region were absorbed almost completely by **1**. Thus, direct cis-trans photoisomerization of the 1-propenyl compounds without intervention of the CoHP$_3$ species, was presumed to make relatively small contribution to the photoassisted equilibrium states. Main contribution to the states was believed to be thermodynamically equilibrated interconversion between two isomers of the respective 1-propenyl compounds. For *N*-(1-propenyl)-acetamide and 1-propenylbenzene, the cis-trans isomerization was not observed in the presence of **1** in the dark at 30 °C, and hence the thermodynamic interconversion was assumed to occur actually only under assistance of CoHP$_3$ photogenerated. On the other hand, the *Z* isomer of *N*,*N*-diethyl-1-propenylamine is thermally labile, and prolonged standing at 10 °C converted it slowly to *E* isomer. Photoirradiation of the *Z* isomer in the presence of **1** enhanced the isomerization rate considerably.

As for the double-bond migration of allylic compounds, Table 3 shows the *Z* fractions in 1-propenyl derivatives formed during the early stage of the reaction proceeding. The *Z* fractions extrapolated back near zero conversions were approximately 79, 30, and 20% for the reactions of *N*-allylacetamide, *N*,*N*-diethylallylamine, and allylbenzene, respectively. These numerical values were considerably different from those of the above-described photoassisted equilibrium for the cis-trans isomerization of the 1-propenyl compounds. Accordingly, the present double-bond migration was determined to yield kinetically controlled products of the 1-propenyl derivatives.

In the course of the double-bond migration, allylic compounds were allowed to coordinate to CoHP$_3$ photoproduced, and insertion of the olefins into the hydrido-cobalt bond probably followed to form alkyl intermediates (Scheme). At the stage immediately before conversion of the intermediates to CoHP$_3$ and product olefins through β-hydogen elimination, steric interactions within the alkylmetal groups would favor an eclipsed transient conformation A (Fig. 6), which is

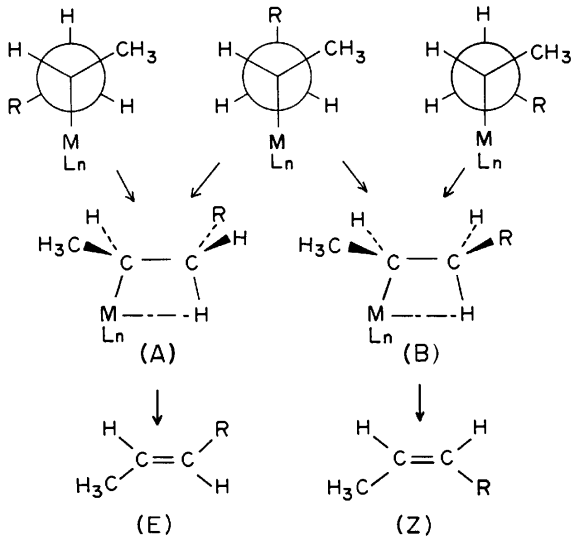

Fig. 6. β-Hydrogen elimination from the alkyl intermediates.

expected to yield *E* isomer of product olefins predominantly. This was probably the case for *N*,*N*-diethylallylamine and allylbenzene. However, in case of *N*-allylacetamide, we believed that probable additional weak interaction[18)] of the amide oxygen with cobalt in the alkyl intermediate enhanced steric interactions between the alkyl group and other coexisting ligands on cobalt significantly, causing preferential formation of the transient conformation B to release the *Z* isomer mainly.

Concluding Remarks

The CoHP$_3$ species, photogenerated from the thermally inert hydridocobalt(I) **1**, cleaved the allylic-O bonds in allyl benzoate and allyl phenyl ether with release of propene, whereas the species catalyzed the double-bond migration of *N*-allylacetamide, *N*,*N*-diethylallylamine, and allylbenzene to the respective 1-propenyl derivatives with kinetically controlled *E*, *Z* isomeric compositions. For the double-bond migration of the latter group of allylic compounds, π-coordination of the C=C double bond to CoHP$_3$ was found to occur at the first stage rather than via the nitrogen or oxygen donor-atom. The present study confirmed the utility of pulsed-laser photolysis in

observation of time-resolved absorption spectra of transient metal species and in determination of absolute rate constants for coordination, suggesting further application to other organometallic systems.

One of the authors (M. O.) wishes to acknowledge a Grant-in-Aid for Scientific Research No. 59550556 from the Ministry of Education, Science and Culture.

References

1) M. Onishi, K. Hiraki, M. Matsuda, and T. Fukunaga, *Chem. Lett.*, **1983**, 261.

2) Conder and his coworkers suggested formation of a "$CoH[P(OPh)_3]_3$" intermediate in photochemical phosphite-substitution reactions of $CoH[P(OPh)_3]_4$ with another ligands, such as CO; H. L. Conder, A. R. Courtney, and D. DeMarco, *J. Am. Chem. Soc.*, **101**, 1606 (1979).

3) S. Oishi, K. Tajime, A. Hosaka, and I. Shiojima, *J. Chem. Soc., Chem. Commun.*, **1984**, 607.

4) M. Onishi, M. Matsuda, and K. Hiraki, *Chem. Lett.*, **1984**, 1157.

5) M. Onishi, K. Hiraki, S. Kitamura, and Y. Ohama, *Nippon Kagaku Kaishi*, **1985**, 400.

6) a) B. M. Trost and E. Keinan, *Tetrahedron Lett.*, **21**, 2595 (1980); b) J. Godschalx and J. K. Stille, *Tetrahedron Lett.*, **21**, 2599 (1980); c) J. Tsuji and T. Yamakawa, *Tetrahedron Lett.*, **1979**, 613; d) T. Yamamoto, O. Saito, and A. Yamamoto, *J. Am. Chem. Soc.*, **103**, 5600 (1981); e) K. Osakada, K. Matsumoto, T. Yamamoto, and A. Yamamoto, *Organometallics*, **4**, 857 (1985); f) T. Yamamoto, J. Ishizu, and A. Yamamoto, *J. Am. Chem. Soc.*, **103**, 6863 (1981); g) H. Matsushita and E. Negishi, *J. Org. Chem.*, **47**, 4161 (1982); h) T. Yamamoto, S. Miyashita, Y. Naito, S. Komiya, T. Ito, and A. Yamamoto, *Organometallics*, **1**, 808 (1982); i) Y. Hayashi, S. Komiya, T. Yamamoto, and A. Yamamoto, *Chem. Lett.*, **1984**, 977.

7) H. Kumobayashi, S. Akutagawa, and S. Otsuka *J. Am. Chem. Soc.*, **100**, 3949 (1978).

8) S. Oishi, N. Kihara, and A. Hosaka, *Chem. Lett.*, **1985**, 621.

9) a) E. Mentasti, E. Pelizzetti, R. Rossetti, and P. L. Stanghellini, *Inorg. Chim. Acta*, **25**, 7 (1977); b) I. Wender, H. W. Sternberg, and M. Orchin, *J. Am. Chem. Soc.*, **74**, 1216 (1952); c) A. Yamamoto, S. Kitazume, L. S. Pu, and S. Ikeda, *J. Am. Chem. Soc.*, **93**, 371 (1971).

10) J. Sauer and H. Prahl, *Chem. Ber.*, **102**, 1917 (1969).

11) J. K. Stille and Y. Becker, *J. Org. Chem.*, **45**, 2139 (1980).

12) S. Sato, *Nippon Kagaku Zasshi*, **90**, 404 (1969).

13) D. Titus, A. A. Orio, and H. B. Gray, *Inorg. Synth.*, **13**, 117 (1977).

14) L. Moggi, A. Juris, D. Sandrini, and M. F. Manfrin, *Rev. Chem. Intermediates*, **4**, 171 (1981).

15) H. Kurosawa, *Inorg. Chem.*, **15**, 120 (1976).

16) S. Oishi, N. Kihara, and A. Hosaka, *J. Organomet. Chem.*, **276**, C33 (1984).

17) $CoH[PPh(OEt)_2]_4$; UV_{max} (CH_2Cl_2) 344 nm (ε 6400).

18) In reactions of *N*-allylacetamide with ruthenium(II) and rhodium(I) hydrides, Stille and Becker[11] proposed interaction of the amide oxygen with metal and formation of six-membered metallocycles for dominant production of *Z* isomer.

 © 1986 The Chemical Society of Japan Bull. Chem. Soc. Jpn., 59, 3931—3934 (1986)

Reactivity of (Porphinato)aluminum Phenoxide and Alkoxide as Active Initiators for Polymerization of Epoxide and Lactone

Tomokazu YASUDA, Takuzo AIDA, and Shohei INOUE*
Department of Synthetic Chemistry, Faculty of Engineering, University of Tokyo, Hongo, Bunkyo-ku, Tokyo 113
(Received June 18, 1986)

Reactivity of the axial aluminum-phenoxyl and -alkoxyl bond (Al-X) of aluminum porphyrin (**1**, (TPP)AlX, (TPP): (5,10,15,20-tetraphenylporphinato)) toward epoxide, β-lactone, and ε-lactone was examined in relation to the ring-opening polymerization of these cyclic compounds catalyzed by **1**. The reactivity of

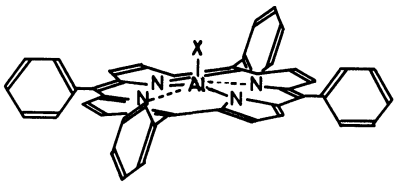

(TPP)AlX (1)

aluminum phenoxide was in the order, epoxide>β-lactone>ε-lactone, while that of the alkoxide, ε-lactone >β-lactone.

Control of molecular weight of polymer is a subject of primary importance for elaborate design of polymeric materials with desired function.[1] Recently, we found aluminum porphyrin such as (5,10,15,20-tetraphenylporphinato)aluminum chloride (**1**, X=Cl: (TPP)AlCl) to be an excellent initiator or catalyst for the ring-opening polymerization of epoxide[2] and β-lactone[3] to give polyether and polyester, respectively, of very narrow molecular-weight distribution.[4] This remarkable characteristics is due to unusually high reactivity of the aluminum-axial ligand bond (Al-X) of the aluminum porphyrin.[2-4] Typically, the reactivity of aluminum-chlorine bond in (TPP)AlCl is much higher than that expected for usual aluminum-chlorine bond, and (TPP)AlCl reacts readily with epoxide to initiate the polymerization which proceeds with a (porphinato)aluminum alkoxide as the growing species.[5]

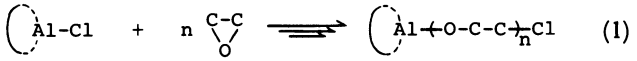

(1)

1 (X = Cl) **2**

The reactivity of (porphinato)aluminum chloride toward epoxide is considered higher than, or at least the same as, that of (porphinato)aluminum alkoxide, taking into account the narrow molecular-weight distribution of the polymer formed. If the reactivity of (porphinato)aluminum chloride were lower than that of the alkoxide, slower initiation followed by faster propagation should result in the broad molecular-weight distribution of polymer. The reactivity of (porphinato)aluminum carboxylate (**1**, X=O_2CR) toward epoxide is also considered not lower than that of the alkoxide, on the basis of the fact that the polymerization of epoxide initiated by (porphinato)aluminum carboxylate affords the polymer with narrow molecular-weight distribution.[6]

Polymerization of β-lactone initiated by (TPP)AlCl proceeds by the ring cleavage at alkyl-oxygen linkage, with a (porphinato)aluminum carboxylate as the growing species.[7]

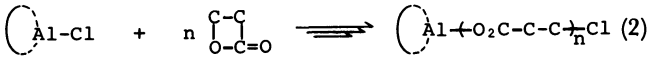

(2)

1 (X = Cl)

The narrow molecular-weight distribution of the polymer indicates that the reactivity of (porphinato)-aluminum chloride toward β-lactone is higher than, or the same as, that of the carboxylate, on the basis of the same consideration as described above.

Corresponding to the above findings, (porphinato)-aluminum alkoxide (**1**, (X=OR): **2**) and carboxylate (**1**, X=O_2CR) initiate the polymerization of epoxide[2,5] and β-lactone,[7] respectively. The latter can initiate also the polymerization of epoxide as mentioned above.[6] (Porphinato)aluminum phenoxide (**1**, X=OAr) was found to initiate the polymerization of epoxide and β-lactone to give the polymers with narrow molecular-weight distribution.[6]

These interesting findings prompted us to examine the reactivity of aluminum porphyrin in more detail by NMR analysis of the reaction system, which proved very useful to follow the reaction by virtue of the remarkable effect of the porphyrin ring current.[4-7] The present paper places emphasis on the reactivity of (porphinato)aluminum phenoxide, which is expected to exhibit an intermediate reactivity between the alkoxide and the carboxylate, toward epoxide, β-lactone, and ε-lactone.

Results and Discussion

Reaction of (Porphinato)aluminum Phenoxide. In the reaction of (tetraphenylporphinato)aluminum phenoxide (**1**, X=OPh: (TPP)AlOPh) with eight molar equivalents of β-propiolactone (PL) in $CDCl_3$ at

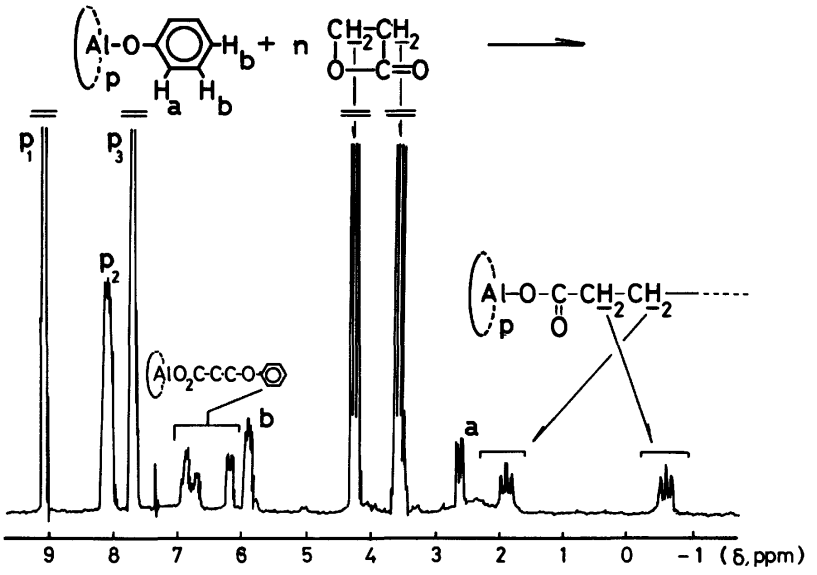

Fig. 1. ^{1}H NMR spectrum of the reaction mixture between (TPP)AlOPh (**1**, X=OPh) and β-propiolactone (PL) in $CDCl_3$. $[PL]_o/[(TPP)AlOPh]_o$=8.1; $[(TPP)AlOPh]_o$=130 mmol dm^{-3}; r.t.; 6 h.

room temperature (≈20 °C), the ^{1}H NMR spectrum of the reaction mixture (Fig. 1) showed that the signals at δ 2.6 (a, *o*-H) and δ 5.9 (b, *m*- and *p*-H) due to the phenoxyl group of (TPP)AlOPh[6] decreased in intensity. On the other hand, a new signal appeared at δ −0.66, which is assigned to a carboxylate (TPP)AlO_2C-$C\underline{H}_2$-CH_2-[7,8] formed by the ring opening of the β-lactone at alkyl-oxygen bond. Similarly, the formation of a (porphinato)aluminum alkoxide by the reaction of (TPP)AlOPh with an excess of 1,2-epoxypropane (PO) was confirmed by the ^{1}H NMR spectrum of the reaction mixture; (TPP)AlOCH($C\underline{H}_3$)-CH_2-, δ −1.86.[5]

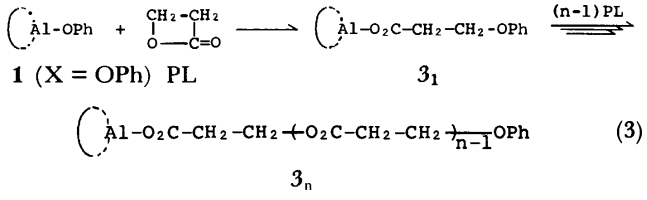

1 (X = OPh) PL 3_1

(3)

3_n

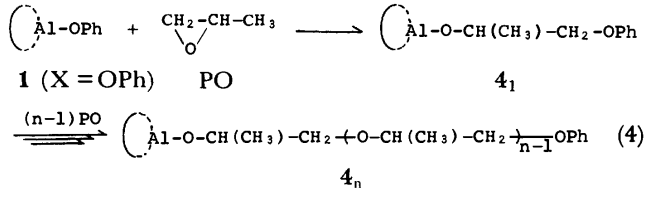

1 (X = OPh) PO 4_1

(4)

4_n

The reaction of (TPP)AlOPh with an excess (7—8 times) of β-lactone or epoxide at room temperature in $CDCl_3$ was followed by the change in the intensity of the signal for the phenoxyl group (δ 5.9 (b, 3H), *m*-, *p*-H) with respect to that due to the pyrrole β-proton of aluminum porphyrin (δ 9.1 (p_1, 8H)) as standard. In each case, the signal due to the corresponding polymeric unit[9] was hardly observed under the conditions examined, indicating that the observation made here can be related to the initiation step to give $\mathbf{3}_1$ and $\mathbf{4}_1$, respectively. As shown in Fig. 2, the reaction of (TPP)AlOPh with epoxide proceeded rapidly and was completed in about 4 h, while the reaction with β-lactone was rather slow to attain the complete consumption of (TPP)AlOPh after about 24 h. On the other hand, in the attempted reaction of (TPP)AlOPh with ε-caprolactone (6-hexanolide) under similar conditions, no change was observed in the ^{1}H NMR spectrum of the reaction mixture.

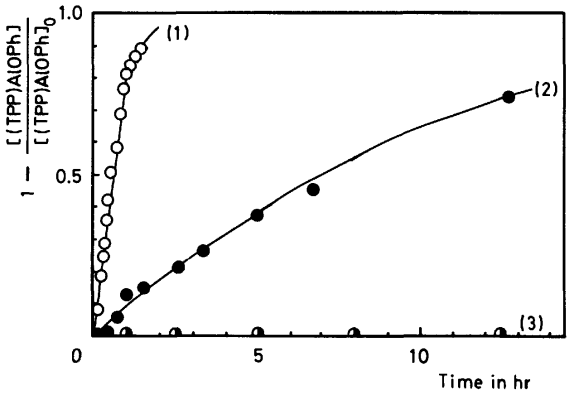

Fig. 2. Reaction of (TPP)AlOPh (**1**, X=OPh) with (1) 1,2-epoxypropane (PO), (2) β-propiolactone (PL), and (3) ε-caprolactone (CL). $[PO]_o/[(TPP)AlOPh]_o$=8.0, $[PL]_o/[(TPP)AlOPh]_o$=8.1, $[CL]_o/[(TPP)AlOPh]_o$=7.2; $[(TPP)AlOPh]_o$=130 mmol dm^{-3}; in $CDCl_3$; at r.t.

Reaction of (Porphinato)aluminum Alkoxide. The reaction of (tetraphenylporphinato)aluminum alkoxide (**1**, X=OR: (TPP)AlOR) with lactone was exam-

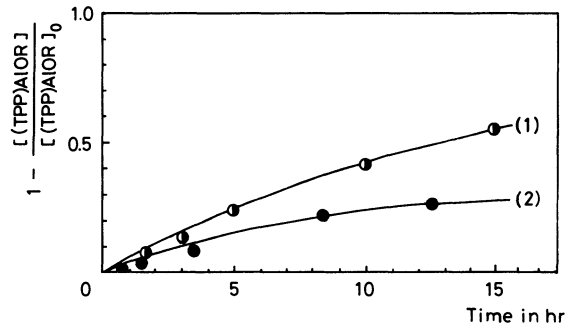

Fig. 3. Reaction of (TPP)AlOR (**2**) with (1) ε-caprolactone (CL), and (2) β-propiolactone (PL). $[CL]_0/[(TPP)AlOR]_0=8.2$, $[PL]_0/[(TPP)AlOR]_0=7.8$; $[(TPP)AlOR]_0=227$ mmol dm^{-3}; in $CDCl_3$; r.t.

ined by using an oligomeric alkoxide **2** prepared from 1,2-epoxypropane with (TPP)AlCl as initiator.[5,10] In contrast to (TPP)AlOPh, (TPP)AlOR exhibited a moderate reactivity toward ε-caprolactone (CL) (Fig. 3). In the ^{1}H NMR spectrum of the reaction mixture of (TPP)AlOR (**2**) with a large excess of the lactone, a new signal appeared at δ −1.09, at the expense of the signal at δ −1.86 due to (TPP)Al-OCH-($C\underline{H}_3$)-CH_2- of **2**. The former signal is assigned to an alkoxide (TPP)Al-O-$C\underline{H}_2(CH_2)_4$-CO-,[11] the product of ring opening at acyl-oxygen bond of ε-caprolactone.

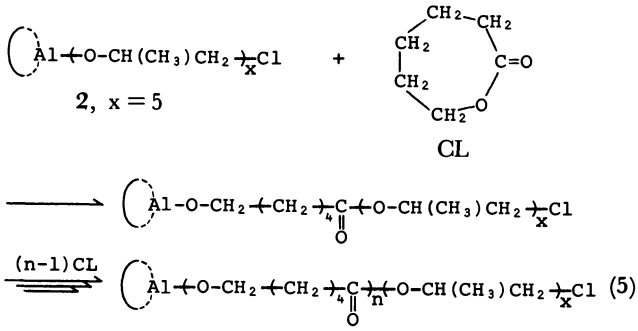

On the other hand, the reaction of (TPP)AlOR with β-propiolactone proceeded much slower. The main product as detected by the ^{1}H NMR spectrum was a (porphinato)aluminum carboxylate resulting from the ring cleavage at alkyl-oxygen bond, similarly to the reaction of (TPP)AlOPh.

Thus, the reactivity of (porphinato)aluminum phenoxide is much different from that of the alkoxide, but is rather similar to the reactivity of the carboxylate, which does not react with ε-caprolactone. Much lower reactivity with ε-lactone than with β-lactone is of particular interest, since in many cases the reactivity of the former has been reported to be higher than the latter.[12]

Experimental

Materials. 5,10,15,20-Tetraphenylporphine ($TPPH_2$) was synthesized by the reaction of pyrrole with benzaldehyde.[13] (Tetraphenylporphinato)aluminum phenoxide (**1**, X=OPh: (TPP)AlOPh) and 3-phenoxypropionate[8] (**1**, X=O_2C-CH_2CH_2-OPh: (TPP)$AlO_2CCH_2CH_2OPh$) were synthesized, respectively, by the reaction of phenol[6] and 3-phenoxypropionic acid with ethyl(tetraphenylporphinato)-aluminum (**1**, X=Et: (TPP)AlEt) which was obtained by the reaction of $TPPH_2$ and triethylaluminum.[14] Oligomeric (tetraphenylporphinato)aluminum alkoxide (**2**) was prepared by the reaction of (tetraphenylporphinato)aluminum chloride (**1**, X=Cl: (TPP)AlCl) with five molar equivalents of 1,2-epoxypropane.[5,10] 1,2-Epoxypropane was purified by refluxing over a mixture of potassium hydroxide and calcium hydride and then distilled twice under a nitrogen atmosphere. β-Propiolactone, dried by stirring with calcium hydride overnight at room temperature, was purified by fractional distillation under reduced pressure under a nitrogen atmosphere over calcium hydride. ε-Caprolactone was distilled over calcium hydride under reduced pressure. Deuterated chloroform ($CDCl_3$) was distilled after refluxing over calcium hydride under a nitrogen atmosphere.

Reaction. To a 50 cm^3 flask equipped with a three-way stop cock containing a $CDCl_3$ solution of an aluminum porphyrin, epoxide or lactone was added by syringe at room temperature under a nitrogen atmosphere with constant stirring. After an appropriate time, a portion of the reaction mixture was subjected to ^{1}H NMR spectroscopy with a JEOL JNM PS-100 spectrometer to follow the reaction. Chemical shift was separately determined with an improved accuracy by using a JEOL JNM GX-400 FT spectrometer operating at 399.7 MHz with $CHCl_3$ (δ 7.28) as standard.

References

1) a) M. Szwarc, *Adv. Polym. Sci.*, **49**, 1 (1983); b) O. W. Webster, W. R. Hertler, D. Y. Sogah, W. B. Farnham, and T. V. RajanBabu, *J. Am. Chem. Soc.*, **105**, 5706 (1983); c) T. Higashimura and M. Sawamoto, *Adv. Polym. Sci.*, **62**, 49 (1984); d) Y. Doi, S. Ueki, and T. Keii, *Macromolecules*, **12**, 814 (1979); e) T. Aida and S. Inoue, *Yuki Gosei Kagaku Kyokai Shi*, **43**, 300 (1985).

2) a) T. Aida and S. Inoue, *Makromol. Chem., Rapid Commun.*, **1**, 677 (1980); b) T. Aida and S. Inoue, *Macromolecules*, **14**, 1162 (1981).

3) a) T. Yasuda, T. Aida, and S. Inoue, *Makromol. Chem., Rapid Commun.*, **3**, 585 (1982); b) T. Yasuda, T. Aida, and S. Inoue, *Macromolecules*, **17**, 2217 (1984).

4) a) S. Inoue and T. Aida, *ACS Symp. Ser.*, **286**, 137 (1985); b) T. Aida and S. Inoue, *J. Am. Chem. Soc.*, **107**, 1358 (1985); c) T. Aida, K. Sanuki, and S. Inoue, *Macromolecules*, **18**, 1049 (1985); d) T. Aida, M. Ishikawa, and S. Inoue, *Macromolecules*, **19**, 8 (1986).

5) T. Aida and S. Inoue, *Macromolecules*, **14**, 1166 (1981).

6) T. Yasuda, T. Aida, and S. Inoue, *J. Macromol. Sci. Chem.*, **A21**, 1035 (1983).

7) T. Yasuda, T. Aida, and S. Inoue, *Macromolecules*, **16**, 1792 (1983). (TPP)$AlO_2CC\underline{H}_2CH_2$-$(O_2CCH_2CH_2)_x$X by the polymerization of β-propiolactone with **1**: δ=−0.55 in $CDCl_3$.

8) (TPP)$AlO_2CC\underline{H}_2CH_2OPh$ (see Experimental): δ=−0.66 in $CDCl_3$.

9) For $-O_2CC\underline{H}_2CH_2-_x$: δ=2.7 ($O_2CC\underline{H}_2$), δ=4.3 (CH_2); for $-OCH(CH_3)CH_2-_x$: δ=1.1 (CH_3), δ=3.5 (CH, CH_2), in $CDCl_3$.

10) T. Aida, R. Mizuta, Y. Yoshida, and S. Inoue, *Makromol.*

Chem., **182**, 1073 (1981).

11) The oligomeric alkoxide prepared from ethylene oxide with (TPP)AlCl (**1**, X=Cl) shows a similar triplet signal at δ=−1.13 due to (TPP)Al-O-C$\underline{H}_2$CH_2-: T. Aida and S. Inoue, *J. Am. Chem. Soc.*, **105**, 1304 (1983).

12) a) "Ring-Opening Polymerization," ed by K. C. Frisch, S. Reegen, Marcel Dekker, New York (1969), pp. 247—302; b) A. Hamitou, T. Ouhadi, R. Jerome, and P. Teyssié, *J. Polym. Sci., Polym. Chem. Ed.*, **15**, 865 (1977).

13) A. D. Adler, F. R. Longo, J. D. Finarelli, J. Goldmacher, J. Assour, and L. Korsakoff, *J. Org. Chem.*, **32**, 476 (1976).

14) S. Inoue and N. Takeda, *Bull. Chem. Soc. Jpn.*, **50**, 984 (1977).

 © 1986 The Chemical Society of Japan Bull. Chem. Soc. Jpn., 59, 3935—3939 (1986)

The Hydrogenation of 1,3-Butadiene over a Palladium Membrane

Hidetoshi NAGAMOTO* and Hakuai INOUE
Department of Chemical Engineering, The University of Tokyo, Hongo 7-3-1, Bunkyo-ku, Tokyo 113
(Received February 20, 1986)

The hydrogenation of 1,3-butadiene was carried out over a palladium membrane at 100 °C in two ways: (1) by hydrogen permeating the membrane, and (2) by hydrogen premixed in the gas phase. In the reactions using permeate hydrogen, hydrogenation at the higher pressures of butadiene was limited by the hydrogen permeation; namely, the rate was determined by the pressure of hydrogen upstream. The product composition was, at the same time, unchanged by the reaction rate. At the lower pressures of butadiene, the selectivity for butene formation was decreased with the decrease in the butadiene pressure, and the reaction rate was approximately equal to that when the premixed hydrogen was used over the β-phase membrane. The mechanism of the reaction using premixed hydrogen over the α-phase membrane was analyzed quantitatively by obtaining the dissolved hydrogen concentration from the measurement of the hydrogen-permeation rate from the reaction surface. It was elucidated that the reaction was limited by the hydrogen adsorption, the rate of which was affected by the presence of 1,3-butadiene, and that the reaction rate was much smaller than that when permeate hydrogen was used.

The catalytic hydrogenation of olefins is one of the reactions investigated most frequently. Palladium, among the metallic catalysts employed for hydrogenation, has the peculiar property of dissolving a large amount of hydrogen at room temperature and of making the hydrogen diffuse through it. It has been reported that the reaction of propylene by the hydrogen dissolved in palladium proceeds much faster than that by gaseous hydrogen.[1] The present authors have also observed that the hydrogen permeating the palladium membrane enhanced the hydrogenation of 1,3-butadiene.[2] For the hydrogenation of ethylene, however, no such enhancement could be observed.

The measurement of the hydrogen-permeation rate through the α-phase palladium membrane showed that the hydrogen permeation from the reaction surface was decreased by the reaction of 1,3-butadiene, not by the reaction of ethylene. It was considered, therefore, that the enhancement of olefin hydrogenation was related to the decrease in the hydrogen-permeation rate.[2]

In a previous study,[3] the present authors analyzed the kinetic mechanism of ethylene hydrogenation by means of permeate hydrogen. The hydrogen transport was considered to consist of three processes: (I) hydrogen adsorption or desorption on the membrane surface, (II) transfer into or out of the membrane through the interface, and (III) diffusion through the membrane. As for the hydrogenation of ethylene by means of permeate hydrogen, the reaction rate was found to be expressed by the mechanism assuming that the equilibrium was established for Processes (I) and (II) at the reaction surface of the membrane.[3] In the case of 1,3-butadiene hydrogenation, the results of the hydrogen-permeation-rate measurement suggested that the equilibrium was not established.

In the present paper, the concentration of dissolved hydrogen in the vicinity of the reaction surface of the membrane was calculated from the permeation rate and the hydrogen sorption equilibrium data. Using the concentration thus calculated, the kinetic mechanism of 1,3-butadiene hydrogenation was investigated quantitatively based on the mechanism of hydrogen transport memtioned above.

Experimental

Materials. The palladium membranes purchased from the Tanaka Kikinzoku Kogyo Co. were 99.95% pure and 50 μm thick. The membrane was pretreated before the reaction as follows: Primarily, the membrane degreased with acetone was polished electrolytically in 0.5 M† H_2SO_4 aqueous solution, and palladium black was electrodeposited on both the surfaces of the membrane in 0.05 M of a $PdCl_2$ aqueous solution. Secondly, the membrane was oxidized in air at 600 to 700 °C.[4] Then, the oxidized membrane which was set into the reactor was reduced by hydrogen at room temperature and heated in nitrogen stream to the reaction temperature in order to remove the hydrogen dissolved in the membrane.

The hydrogen contained in a cylinder was 99.99999% pure, and the other gases and reagents employed in the experiments were commercial-grade and were used without further purification.

Reactor and Procedure. The reactor, made of stainless steel, was separated into two compartments of equal volumes by the use of a palladium membrane pinched by reduced copper gaskets. Reactant gases were introduced into one compartment, called the reaction compartment, and hydrogen into the other, called the hydrogen compartment, for hydrogenation by means of permeate hydrogen. The effective area for hydrogen permeation was 4.9 cm^2. The details about the reactor was described elsewhere.[3]

The hydrogenation of 1,3-butadiene was carried out by two different methods: (I) by the use of hydrogen permeating the palladium membrane from the hydrogen compartment, and (II) by the use of premixed hydrogen. The reaction system by Method (I) was named the permeation system; here, a mixture of 1,3-butadiene and a diluent gas such as nitrogen passed through the reaction compartment. The system by Method (II) was named the mixture system; here, a mixture of hydrogen, 1,3-butadiene, and nitrogen was passed through the reaction compartment, with nitrogen filling the hydrogen compartment.

† 1 M=1 mol dm^{-3}.

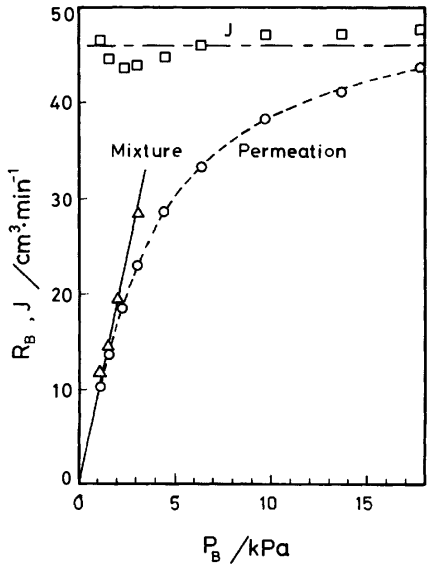

Fig. 1. Hydrogenation rates of 1,3-butadiene over a 0.005 cm palladium membrane and hydrogen permeation rate, J, at 100°C and at the upstream hydrogen pressure of 100 kPa. Triangles represent the rates of the reaction by premixed hydrogen of 47 kPa.

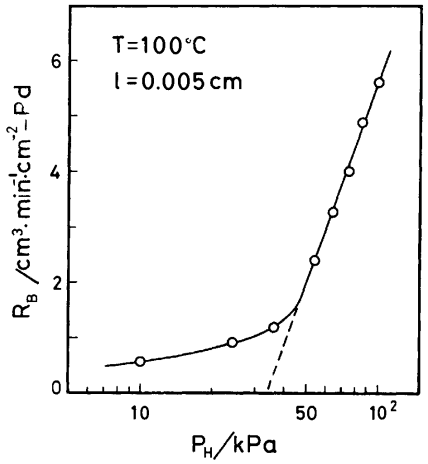

Fig. 2. Hydrogenation rate of 1,3-butadiene by permeate hydrogen through a 0.005 cm Pd membrane at the butadiene pressure of 40 kPa and at 100°C as a function of the upstream hydrogen pressure.

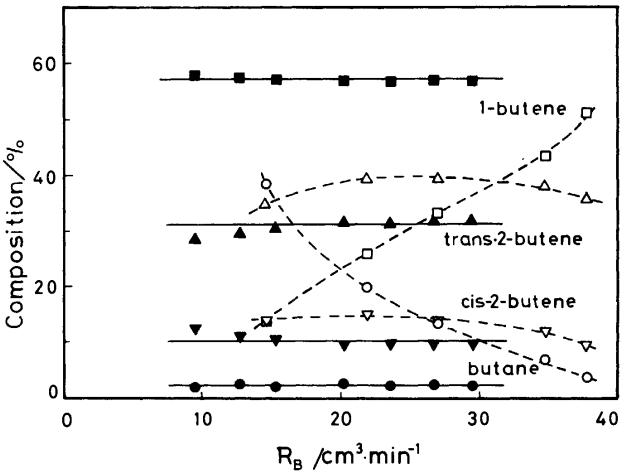

Fig. 3. Product distribution in the hydrogenation of 1,3-butadiene by permeate hydrogen at 100°C. Filled symbols represent the compositions under the hydrogen permeation limitation and open symbols otherwise.

The molar fractions of the component gases were determined with a gas chromatograph equipped with a TC detector. The column packings were VZ-7 for the analysis of hydrocarbons and Molecular Sieve 13X for hydrogen.

The reaction was carried out at 100 °C for both systems. The partial pressures of 1,3-butadiene ranged from 1 to 41 kPa. The hydrogen partial pressures ranged from 10 to 100 kPa for the permeation system and from 1 to 47 kPa for the mixture system. The flow rate in the reaction compartment was kept at 500—600 cm^3 min^{-1} in order to avoid limiting the reaction rate by mass transfer in the gas-boundary film.[5]

Results

Hydrogenation by Permeate Hydrogen. Figure 1 shows the hydrogenation rate and the hydrogen permeation rate as a function of the 1,3-butadiene pressure at the upstream hydrogen pressure of 100 kPa. The behavior of the reaction rate was different from that for ethylene hydrogenation, which showed that the dependence of the reaction rate on the ethylene pressure could be expressed approximately by two straight lines.[5]

At the butadiene pressures higher than 20 kPa, the hydrogenation rate was approximately constant and almost identical with the hydrogen-permeation rate. The hydrogenation rate at the butadiene pressure of 40 kPa is shown in Fig. 2 as a function of the upstream hydrogen pressure. The rate was varied linearly with ln P_H when the hydrogen pressure was higher than 35 kPa, which approximately corresponds to the minimum pressure for forming the β-phase at the reaction temperature.[6] While the reaction rate was changed by the upstream hydrogen pressure, the composition of the products was substantially unchanged, and the selectivity for butene formation was more than 0.98 (Fig. 3).

At the butadiene pressures lower than 20 kPa, the hydrogenation rate was dependent on the butadiene pressure. At a pressure as low as 1 kPa, the rate was very close to that obtained for the mixture system at the hydrogen pressure of 47 kPa, where the membrane formed the β-phase. However, the pressure of the unreacted hydrogen in the reaction compartment was much lower than the minimum pressure for forming the β-phase. Since the hydrogen-permeation rate under a reaction was approximately independent of the reaction rate or the butadiene pressure, the pressure of the unreacted hydrogen increased as the reaction rate decreased. With the increase in the unreacted hy-

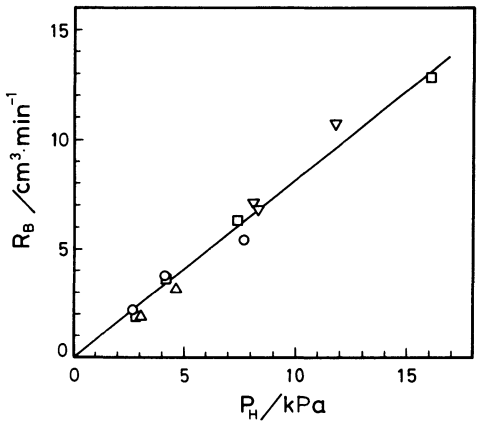

Fig. 4. Hydrogenation rate of 1,3-butadiene by premixed hydrogen over an α-phase Pd membrane of 0.005 cm at 100°C. 1,3-Butadiene pressure (kPa)----- ○: 1.0, □: 2.5, △: 5.0, ▽: 7.0.

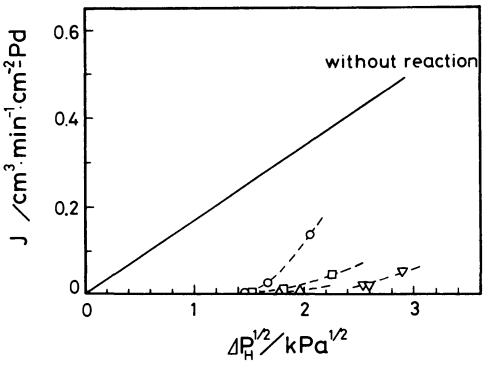

Fig. 5. Hydrogen permeation rate from the reaction surface of a 0.005 cm Pd membrane at 100°C. Keys are the same as in Fig. 4.

drogen pressure, the product composition was remarkably changed, as is shown in Fig. 3.

Hydrogenation by Premixed Hydrogen. The hydrogenation was performed over the palladium membrane of two different phases. When the membrane consisted of the β-phase, i.e., when the hydrogen pressure was over 30 kPa, the hydrogenation rate was proportional to the butadiene pressure, as is shown in Fig. 1. In the case of the α-phase membrane, the rate was proportional to the hydrogen pressure and independent of the butadiene pressure, as is shown in Fig. 4.

As for the latter case, the hydrogen-permeation rate from the reaction side to the other side of the membrane was also measured; it is shown in Fig. 5. The permeation rate was strongly dependent on the butadiene pressure. The hydrogen-permeation rate after the butadiene feed to the reactor had been stopped was well recovered to the initial permeation rate. The concentration of the dissolved hydrogen in the vicinity of the reaction surface, n, was calculated from the permeation rate by the use of Eq. 1:

$$n = \frac{P_H}{K_H} + \frac{J}{\kappa D_\alpha / l} \quad (1)$$

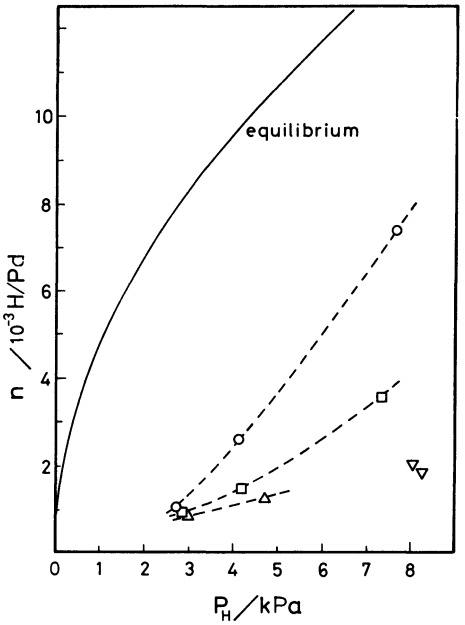

Fig. 6. Dissolved hydrogen concentration in the vicinity of the reaction surface under reaction at 100°C as a function of hydrogen pressure. Keys are the same as in Fig. 4.

P_H is the hydrogen pressure in the compartment to which hydrogen diffuses, and J is the hydrogen permeation rate. K_H is Sieverts' constant; l, the membrane thickness; κ, the hydrogen concentration at n=1, and D_α, the hydrogen-diffusion coefficient through the α-phase palladium. The calculated values of the hydrogen concentration under the reaction, shown in Fig. 6, were lower than those in equilibrium with the gaseous hydrogen and decreased as the butadiene pressure increased.

Discussion

Hydrogenation by Permeate Hydrogen. The previous kinetic analysis of reaction by permeate hydrogen[3] obtained the following results. When the adsorption constant of hydrogen is much larger than the value determined by the operational condition, the reaction rate increases in proportion to the olefin-surface coverage until the rate becomes equal to the hydrogen-diffusion rate, and thereafter the rate is limited by the diffusion rate. This case was observed in the hydrogenation of ethylene. When the hydrogen-adsorption constant is as large as the value determined by the operational condition, the reaction rate increases, but not in proportion to the olefin surface coverage.

Based on the analysis presented above, the behavior of the hydrogenation of 1,3-butadiene shown in Fig. 1 can be explained either by the small adsorption constant of hydrogen affected by butadiene, or by the nonlinear adsorption isotherm of butadiene and the large hydrogen-adsorption constant. The hydrogenation

rate by permeate hydrogen at a butadiene pressure of less than 3 kPa was found to be smaller than that by premixed hydrogen over the β-phase membrane, where the hydrogen surface coverage was considered to be unity. The adsorption constant of hydrogen under the reaction of 1,3-butadiene, therefore, was not so large as that under the reaction of ethylene. It was concluded that the presence of 1,3-butadiene affected the hydrogen adsorption. This conclusion was supported by the change in the butene selectivity caused by the butadiene pressure, as is shown in Fig. 3.

At a butadiene pressure as high as 40 kPa, it was observed that the hydrogenation rate for the permeation system was over ten times larger than that for the mixture system at the same hydrogen pressure as low as 0.2 kPa.[2] This suggested that the rate-determining step was different between the two systems. For the permeation system, the reaction rate was limited by the hydrogen permeation through the membrane, since the rate was varied linearly with ln P_H and since its slope was in good agreement with that predicted for the hydrogen permeation limitation.[6] Thus, it is reasonable to consider that the permeate hydrogen is ready to react with the adsorbed butadiene after reaching the reaction surface when butadiene is adsorbed in a sufficient amount.

Rate Process over α-Phase Membrane for the Mixture System. The hydrogenation rate equation over the α-phase membrane was expressed as:

$$R = kP_H^{1.0}P_B^{0}. \tag{2}$$

This equation for the α-phase is different from that for the α-phase, but is often met with in the hydrogenation of olefins. Sato et al.[7] analyzed the kinetic mechanism of ethylene hydrogenation over various metallic catalysts, including palladium, and reached the conclusion that the rate-determining step lies on the hydrogen adsorption. Since it was found that 1,3-butadiene affects the hydrogen adsorption, as has been discussed above, it is reasonable to assume that the hydrogenation of butadiene proceeds under the hydrogen-adsorption limitation.

It is generally difficult to determine the rate equation of the surface reaction under the adsorption limitation. In the 1,3-butadiene hydrogenation, however, there have been many studies which provide some knowledge about the reaction mechanism. The mechanism neglecting the conformations of the adsorbed butadiene and butenes can be described as follows[8]:

$$C_4H_6(\text{gas}) \rightleftharpoons C_4H_6(\text{ads}) \underset{2}{\overset{1}{\rightleftharpoons}} C_4H_7 \xrightarrow{3} C_4H_8(\text{ads}).$$

The half-hydrogenated species, C_4H_7 may change back to diene and to butene. Since it has been reported that the ratio of hydrogen to deuterium atoms on the palladium surface is low,[9] the reverse reaction of the half-hydrogenation (Step 2) can be considered to be a slow step. When the reaction of half-hydrogenated species with hydrogen (Step 3) proceeds faster than the reverse reaction, the rate equation is expressed as:

$$R = k_B\theta_H\theta_B. \tag{3}$$

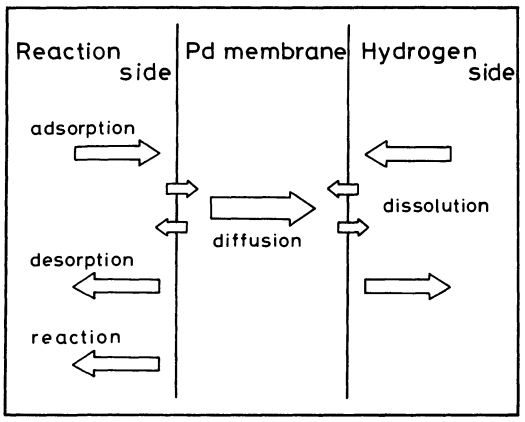

Fig. 7. Illustration of mass transfer process of hydrogen.

When the hydrogenation occurs on the palladium membrane, hydrogen is, at the same time, dissolved into the membrane and diffuses through the membrane. These processes are shown schematically in Fig. 7. The rate equations of these processes may be presented as:

$$\text{dissolution: } r_s = k_i\theta_H - k_o n \tag{4}$$

$$\text{diffusion : } r_d = k_d(n-n_o) \fallingdotseq k_d n \tag{5}$$

The hydrogen adsorption rate is:

$$\text{adsorption: } r_a = k_a P_H \tag{6}$$

Where k_i and k_o are the rate constants for hydrogen transfer into a membrane and out of a membrane respectively. k_d is equal to $\kappa D_\alpha/l$, as has been noted previously. k_a is the rate constant of hydrogen adsorption.

From Eqs. 4 and 5, the concentration of the dissolved hydrogen atom, n, in the steady-state is expressed as:

$$n = \frac{k_i}{k_o+k_d}\theta_H \tag{7}$$

and:

$$r_s = r_d = \frac{k_d k_i}{k_o+k_d}\theta_H. \tag{8}$$

Since the hydrogen-adsorption rate is equal to the sum of the reaction rate and the diffusion rate, then:

$$r_a = \left(k_B\theta_B + \frac{k_d k_i}{k_o+k_d}\right)\theta_H. \tag{9}$$

From Eqs. 6, 7, and 9, the following expression is obtained:

$$n = \frac{k_a P_H}{(k_o+k_d)k_B\theta_B/k_i + k_d}. \tag{10}$$

The reaction rate was much larger than the hydrogen-permeation rate, as is shown in Fig. 5, and the next expression can be derived:

$$k_B\theta_B \gg k_1k_d/(k_o+k_d). \quad (11)$$

Finally, n is expressed as:

$$n = \frac{k_1k_a}{k_B(k_o+k_d)}\frac{P_H}{\theta_B}. \quad (12)$$

Equation 12 shows that the concentration of the dissolved hydrogen is dependent on the butadiene surface coverage as well as the hydrogen pressure. It was found that the behavior of the hydrogen concentration shown in Fig. 6 can be qualitatively explained by Eq. 12.

From Eq. 12, the butadiene coverage is expressed by the following equation:

$$\theta_B = \frac{k_1k_a}{k_B(k_o+k_d)}\frac{P_H}{n} \quad (13)$$

Since the Langmuir-type adsorption isotherm has a wide applicability, it was assumed that the adsorption of butadiene obeys the Langmuir-type isotherm under the present experimental conditions; namely:

$$\frac{P_B}{\theta_B} = \frac{1}{K_B} + P_B \quad (14)$$

Therefore, a quantitative examination of Eq. 12 can be made by a cross plotting of nP_B/P_H against P_B, as is shown in Fig. 8. Since the relationship between nP_B/P_H and P_B was described fairly well by a straight line, Eq. 12 was considered to be reasonable. In addition, the result that the calculated value of the butadiene adsorption constant, 0.23 kPa^{-1}, was larger than that of 1-butene[3] at 100 °C was consistent with the result obtained by other investigators.[9] It was concluded that, for the present mixture system, the reaction was limited by the hydrogen adsorption and that the hydrogen adsorption was affected by the adsorption and/or the reaction of 1,3-butadiene.

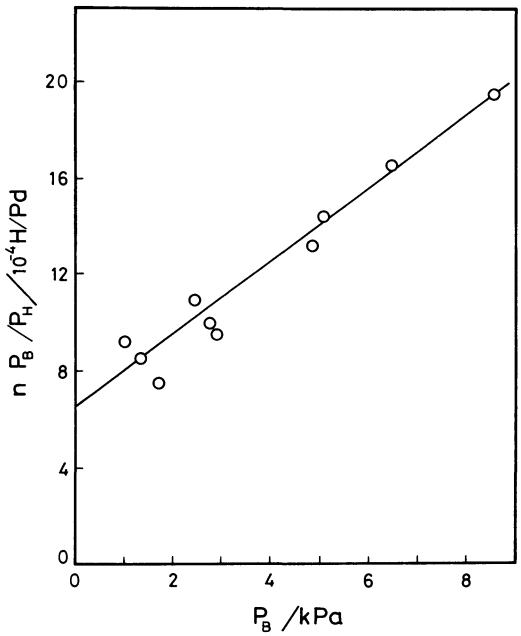

Fig. 8. Plot of nP_B/P_H against P_B for the hydrogenation of 1,3-butadiene at 100°C.

Comparison of Reaction Rates for the Mixture and Permeation Systems. Based on the above considerations, the reason for the difference in the reaction rates for the permeation and mixture systems at the same composition of reactant gases may be explained as follows.

For the mixture system, the concentration of hydrogen atoms on the catalyst surface is very small because the hydrogen adsorption is strongly affected by the butadiene adsorption and/or the reaction. For the permeation system, on the other hand, hydrogen atoms are supplied from the dissolved phase in palladium, and the hydrogen-transfer process through the interface is scarcely affected at all since the reaction was not limited by this process, but by the diffusion process in bulk. Therefore, the surface coverage of hydrogen for the permeation system can considerably exceed that for the mixture system, even at the same hydrogen pressure. Thus, the reaction proceeded much faster for the permeation system than for the mixture system.

References

1) R. J. Rennard, Jr., and R. J. Kokes, *J. Phys. Chem.*, **70**, 2543 (1966).
2) H. Nagamoto and H. Inoue, *Chem. Eng. Commun.*, **34**, 315 (1985).
3) H. Nagamoto and H. Inoue, *J. Chem. Eng. Jpn.*, **14**, 377 (1981).
4) H. Nagamoto and H. Inoue *Nippon Kagaku Kaishi*, **1977**, 1264.
5) H. Nagamoto and H. Inoue, *Nippon Kagaku Kaishi*, **1979**, 327.
6) E. Wicke and G. H. Nernst, *Ber. Bunsenges. Physik. Chem.*, **68**, 224 (1964).
7) S. Sato and K. Miyahara, *Shokubai*, **18**, 153 (1976).
8) E. F. Meyer and R. L. Burwell, Jr., *J. Am. Chem. Soc.*, **85**, 2881 (1963).
9) G. C. Bond and P. B. Wells, *Advances Catalysis*, **15**, 91 (1964).

Epoxidation of Fatty Acid Esters with Aqueous Hydrogen Peroxide in the Presence of Molybdenum Oxide-Tributyltin Chloride on Charcoal Catalyst

Yasushi Itoi, Masami Inoue,* and Saburo Enomoto
Faculty of Pharmaceutical Sciences, Toyama Medical and Pharmaceutical University, 2630 Sugitani, Toyama 930-01
(Received May 31, 1986)

The epoxidation of fatty acid esters was carried out with a 30% aqueous hydrogen peroxide in the presence of a molybdenum oxide-tributyltin chloride on a charcoal catalyst in 2-propanol at 50 °C. Such inner olefins as ethyl erucate and ethyl oleate gave good yields of 77 and 76%, respectively. Ethyl elaidate, a trans-form of ethyl oleate, was less reactive (40% yield). Several vegetable oils such as rapeseed oil, olive oil, soybean oil, cottonseed oil, corn oil, and linseed oil were oxidized with the oxirane oxygen contents of 5.3 to 3.5%.

Epoxy fatty acid esters have been used for the plasticizer of a poly(vinyl chloride) resin since it was found by Greenspan et al.[1] Among various oxidation processes, an in situ method using acetic acid and a highly-concentrated hydrogen peroxide is practical.[2] However, epoxidation with peracetic acid or performic acid tends to open the oxirane rings. Also, it has some difficulties to separate acid catalysts from the reaction products. Furthermore, hydrogen peroxide of a high concentration is dangerous to handle. Therefore, the use of 30% aqueous hydrogen peroxide in place of organic peroxy acids is favorable.

Hitherto, we have studied the epoxidation of C_5-C_8 alkenes using 30% aqueous hydrogen peroxide as an oxidizing agent. We used molybdenum oxide on charcoal under the presence of organotin compounds as cocatalysts.[3] The catalyst system was applied on several unsaturated fatty acid esters to give epoxides in good yields. The epoxidation was selectively carried out and the separation of the catalyst was easily performed by filtration.

Results and Discussion

Epoxidation of Various Unsaturated Fatty Acid Esters. Previously, we found that certain alkenes such as cyclopentene, cyclohexene, cyclooctene, 1-octene, and 2-octene were epoxidized selectively in high yields in the presence of molybdenum blue (MB), a type of mixed acids of Mo(V) and Mo(VI),[4] and tributyltin chloride on charcoal.[3] In this paper we applied the catalyst for the epoxidation of various unsaturated fatty acid esters. Then, the epoxidation of ethyl erucate, ethyl oleate, ethyl elaidate, ethyl linoleate, ethyl 2-hexenoate, and ethyl 3-hexenoate was carried out with 30% aqueous hydrogen peroxide in 2-propanol solvent for 15 h at 50 °C. Results are shown in Table 1. In all the substrates examined, products were the epoxidized fatty acid esters and recovered materials as was confirmed by the analyses of HPLC and flash chromatography. The epoxidation of unsaturated fatty acid esters of cis-form such as ethyl erucate, ethyl oleate, and ethyl linoleate afforded higher yields than those of the trans-form; it was considered that the activity to the cis-form was higher than that of the trans-form owing to a steric effect.

Table 1. Epoxidation of Various Unsaturated Fatty Acid Esters with 30% H_2O_2 in the Presence of Molybdenum Oxide-Bu_3SnCl-Charcoal (DMFBA) Catalyst[a]

Material	Epoxide yield/%
Ethyl erucate	77
Ethyl oleate	76
Ethyl elaidate	40
Ethyl 10-undecenoate	29
Ethyl linoleate	56
Ethyl 2-hexenoate	0
Ethyl 3-hexenoate	0

a) Substrate (3.0 mmol), 30% H_2O_2 (1.8 ml, 17.6 mmol), 1.25% MB-charcoal (0.4 g), Bu_3SnCl (50 mg, 0.15 mmol), and 2-propanol (12 ml) were used. The reaction was carried out at 50°C for 15 h. DMFBA; *N,N*-dimethylformamide dibutyl acetal.

Ethyl 10-undecenoate, an ester including a terminal double bond, gave a lower yield than those of inner ones. On the other hand, unsaturated fatty acids which included a double bond near the carbonyl group, such as ethyl 2-hexenoate or ethyl 3-hexenoate, did not epoxidized at all.

Recently, it has been reported that a pair of isomers, methyl oleate and methyl elaidate, were epoxidized using excess molar ratios of aqueous hydrogen peroxide in the presence of iron(III) acetylacetonate.[5] The epoxidation has took place to give trans-isomer in high yields either from methyl oleate or methyl elaidate. In our reaction system, a double bond was epoxidized by keeping its configuration. This tendency has also been reported in the epoxidation using *m*-chloroperbenzoic acid.[5]

In the epoxidation of ethyl linoleate, the oxidation rate of one double bond was faster than that of others. The monoepoxides were selectively separated from ethyl linoleate and the oxirane ring was confirmed by elemental analyses; NMR spectra though the epoxidized site could not be determined. The epoxidation of α,β-unsaturated acids has been carried out using hydrogen peroxide in the presence of tungstic acid in an alkaline media.[6] The active species for the reaction systems were suggested to be HOO^- which reacted at the electron-poor double bond of α,β-unsaturated

Table 2. Epoxidation of Various Vegatable Oils Using 30% H_2O_2 in the Presence of Molybdenum Oxide-Bu_3SnCl-Charcoal (BSA) Catalyst[a]

Oil (Iodine number)	Iodine number	Oxirane oxygen/%	Constitution[b] Erc[c]	Ole[d]	Li_2[e]	Li_3[f]
Rapeseed oil (104)	42	3.9	45—55	12—18	12—16	7— 9
Olive oil (81)	12	4.0	0	65—85	4—15	0
Soybean oil (139)	45	5.3	0	15—33	43—56	5—11
Cottonseed oil (121)	59	3.5	0	15—36	34—55	0
Corn oil (127)	57	3.6	0	19—49	34—62	0
Linseed oil (152)	75	4.6	0	13—38	5—29	26—58

a) Oil (3 g), 30% H_2O_2 (6 ml, 58.7 mmol), 1.25% MB-charcoal (0.8 g), Bu_3SnCl (100 mg, 0.3 mmol), and 2-propanol (24 ml) were used. The reaction was carried out at 50°C for 15 h. b) These constitutions were quoted from JP IX and Yushi Kagaku Binran (ed by Chemical Society of Oil and Fats, 1971). c) Erucic acid. d) Oleic acid. e) Linoleic acid. f) Linolenic acid. BSA; *N,O*-bis(trimethylsilyl)acetamide.

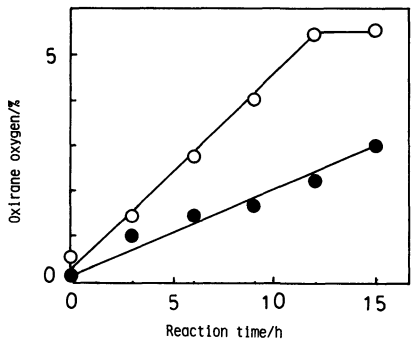

Fig. 1. Oxirane oxygen (%) vs. reaction time in the epoxidation of ethyl erucate and soybean oil with 30% H_2O_2 in the presence of molybdenum oxide-Bu_3SnCl-charcoal (DMFBA) catalyst.
○: Soybean oil, ●: ethyl erucate.
Substrate (2 g), 30% H_2O_2 (3 ml), 1.25% molybdenum oxide-charcoal (0.8 g), Bu_3SnCl (100 mg), and 2-propanol (19 ml) were used. DMFBA; *N, N*-dimethylformamide dibutyl acetal.

acids.

Epoxidation of Various Vegetable Oils. In the plastic industries, soybean oil and oleic acid derivatives are used as a plasticizer. Therefore, we epoxidized various vegetable oils such as rapeseed oil, olive oil, soybean oil, corn oil, cottonseed oil, and linseed oil with 30% aqueous hydrogen peroxide in the presence of molybdenum oxide-tributyltin chloride-charcoal catalyst.

In the oxidation of soybean oil and ethyl erucate, a linear increase of oxirane oxygen according to the reaction time to give the values of 5.6 and 3.0%, respectively (Fig. 1). Also, various vegetable oils were oxidized. Results are shown in Table 2. According to Japanese Pharmacopoeia IX, rapeseed oil contains an erucic acid ester as the main component, and was expected to give a high yield of epoxides since ethyl erucate gave the epoxide in good yield (Table 1). However, the oil gave a poor yield. For this result, it was supposed that the rapeseed oil used in our experiment did not contain erucic acid ester according to the history of the recent process.[7] On the other hand, olive oil which contains an oleic acid ester as a main component was epoxidized in high yield.

Vegetable oils which have linoleic or linolenic acid as a main component gave rather low yields. In our experiments, the epoxidized soybean oil contained 5.3% oxirane oxygen. Other epoxidized vegetable oils, such as olive oil or linseed oil, could also be used as a plasticizer.

Experimantal

Materials. Aqueous hydrogen peroxide (30%) (Hayashi Pure Chemicals), ethyl oleate, ethyl erucate, ethyl linoleate, 2-hexenoic acid, 3-hexenoic acid, tributyltin chloride (Tokyo Chemical Industry), elaidic acid, *N,N*-dimethylformamide dibutyl acetal (DMFBA), and *N,O*-bis(trimethylsilyl)acetamide (BSA)(Wako Pure Chemicals) were purchased. Charcoal (DC-5200w) was kindly provided by Dia Catalysts & Chemicals.

Esterification. 2-Hexenoic acid, 3-hexenoic acid, and elaidic acid (1 g) were respectively esterified with ethanol (10 ml) in the presence of two drops of concd H_2SO_4 at room temperature for 6 h. After the ethanol was evaporated off under reduced pressure, the reaction solution was diluted with water (20 ml). The product was extracted with ether and dried with anhydrous Na_2SO_4. The evaporation of ether gave an oily product.

Pretreatment of Charcoal. Charcoal powder (1 g) was treated with DMFBA or BSA (50 mg) in cyclohexane (20 ml) by stirring at 50 °C. After 2 h, the charcoal was filtered off, washed with hexane, and dried.

Preparation of Catalyst. The molybdenum oxide-charcoal catalyst was prepared by fixing MB which was prepared from molybdenum powder and H_2O_2[4,8] on pretreated charcoal (65 mesh) by stirring overnight at room temperature. The catalyst was separated by filtration and dried.

Epoxidation Procedure. Into the dispersed 2-propanol solution of the molybdenum oxide-charcoal catalyst (0.4 g), Bu_3SnCl (50 mg) was added. After 30 min, additional 2-propanol (10 ml), substrate (1 g), and 30% aqueous hydrogen peroxide (2 ml) were added. The reaction was carried out at 50±1 °C in an oil bath under magnetic stirring.

Analyses of Products. After the reaction, the catalyst was filtered off and 2-propanol was evaporated from the reaction solution. Then, the reaction mixture was extracted with ether and dried. After the removal of ether, the residue was subjected to flash chromatography by passing it through a

Kieselgel 60 column. Elution with benzene-hexane (9:1, v/v) and evaporation of the solvents gave epoxides.

The melting point was uncorrected. NMR spectra were recorded on a Varian XL-200 spectrometer with tetramethylsilane (TMS) as an internal standard. The chemical shifts and coupling constants (J) are given in δ and Hz, respectively.

***cis*-Ethyl 13,14-Epoxydocosanoate.** Colorless crystals (mp 26—27 °C). ^{1}H NMR ($CDCl_3$) 0.88 (3H, t, J=6 Hz, $C\underline{H}_3$), 1.00—1.72 (34H, m, $C\underline{H}_2$), 2.28 (3H, t, J=8 Hz, $C\underline{H}_3$), 2.90 (*cis*-2H, m, C<u>H</u>),[9] 4.13 (2H, q, J=8 Hz, $C\underline{H}_2$). Found: C, 75.55; H, 12.30%. Calcd for $C_{22}H_{44}O_3$: C, 75.33; H, 12.12%.

***cis*-Ethyl 9,10-Epoxyoctadecanoate.** Colorless oil. ^{1}H NMR ($CDCl_3$) 0.92 (3H, t, J=6 Hz, $C\underline{H}_3$), 1.12—1.76 (32H, m, $C\underline{H}_2$), 2.32 (3H, t, J=8 Hz, $C\underline{H}_3$), 2.95 (*cis*-2H, m, C<u>H</u>),[9] 4.18 (2H, q, J=8 Hz, $C\underline{H}_2$). Found: C, 73.53; H, 11.82%. Calcd for $C_{20}H_{42}O_3$: C, 73.57; H, 11.73%.

***trans*-Ethyl 9,10-Epoxyoctadecanoate.** Colorless oil. ^{1}H NMR ($CDCl_3$) 0.90 (3H, t, J=6Hz, $C\underline{H}_3$), 1.06—1.76 (32H, m, $C\underline{H}_2$), 2.31 (3H, t, J=8 Hz, $C\underline{H}_3$), 2.68 (*trans*-2H, m, C<u>H</u>),[9] 4.17 (2H, q, J=8 Hz, $C\underline{H}_2$). Found: C, 73.23; H, 11.74%. Calcd for $C_{20}H_{42}O_3$: C, 73.57; H, 11.73%.

Ethyl 10,11-Epoxyundecanoate. Colorless oil. ^{1}H NMR ($CDCl_3$) 1.12—1.90 (16H, m, $C\underline{H}_2$), 2.32 (3H, t, J=8 Hz, $C\underline{H}_3$), 2.42—2.60 (1H, m, C<u>H</u>), 2.72—3.02 (2H, m, $C\underline{H}_2$), 4.17 (2H, q, J=8 Hz, $C\underline{H}_2$). Found: C, 68.10; H, 10.75%. Calcd for $C_{13}H_{24}O_3$: C, 68.38; H, 10.59%.

Ethyl Epoxyoctadecenoate. Colorless oil. ^{1}H NMR ($CDCl_3$) 0.90 (3H, t, J=6 Hz, $C\underline{H}_3$), 1.08—1.73 (24H, m, $C\underline{H}_2$), 2.38 (3H, t, J=8 Hz, $C\underline{H}_3$), 2.93 (2H, m, C<u>H</u>), 4.13 (2H, q, J=8 Hz, $C\underline{H}_2$), 5.33—5.63 (2H, m, C<u>H</u>). Found: C, 73.77; H, 11.10%. Calcd for $C_{20}H_{37}O_3$: C, 74.03; H, 11.18%.

Iodine Numbers of Vegetable Oils. Iodine numbers of vegetable oils were obtained by the titration with 0.1 M† sodium thiosulfate after oils were treated with iodine trichloride.[10]

Oxirane Oxygens of Vegetable Oils. Oxirane oxygens of vegetable oils were estimated by titration with 0.1 M HBr/AcOH in benzene using 0.1% Crystal Violet as an indicator.[11]

† 1 M=1 mol dm^{-3}.

References

1) F. P. Greenspan and R. J. Gall, *Ind. Eng. Chem.*, **45**, 2722 (1953).

2) S. Nishimura, *Yuki Gosei Kagaku Kyokai Shi*, **23**, 612 (1965).

3) M. Inoue, Y. Itoi, S. Enomoto, and Y. Watanabe, *Chem. Lett.*, **1982**, 1375; Y. Itoi, M. Inoue, S. Enomoto, and Y. Watanabe, *Chem. Pharm. Bull.*, **32**, 418 (1984); Y. Itoi, M, Inoue, and S. Enomoto, *Chem. Pharm. Bull.*, **33**, 3583 (1985); Y. Itoi, M. Inoue, and S. Enomoto, *Bull. Chem. Soc. Jpn.*, **58**, 3193 (1985).

4) T. Chitani, "Muki Kagaku (Inorganic Chemistry)," Sangyo Tosho, (1959), p. 873.

5) T. Yamamoto and M. Kimura, *J. Chem. Soc., Chem. Commun.*, **1977**, 948.

6) G. B. Payne and P. H. Williams, *J. Org. Chem.*, **24**, 54 (1959); K. S. Kirshenbaum and K. B. Sharpless, *J. Org. Chem.*, **50**, 1979 (1985).

7) M. Mori, "Nippon Shokuhin Jiten," Ishiyaku, (1983), p. 122.

8) Y. Kurusu, *Bull. Chem. Soc. Jpn.*, **54**, 293 (1981).

9) L. M. Jackmann and S. Sterenhell, "Application of Nuclear Magnetic Resonance Spectroscopy in Organic Chemistry," Pergamon Press, (1969), p. 224.

10) Iodine number was determined according to Japan Pharmacopoeia IX.

11) A. J. Durbetaki, *Anal. Chem.*, **28**, 2000 (1956).

 © 1986 The Chemical Society of Japan Bull. Chem. Soc. Jpn., 59, 3945—3950 (1986)

Solvation of Carboxylic Acids in Nonaqueous Binaries. Solvation Models for Butyric and Trichloroacetic Acids in Nitrobenzene-Toluene Mixtures

Mohamed M. Fahmi Hegazi†
Kuwait Institute of Technology, Shuwaikh, Kuwait
(Received June 20, 1985)

The partitions of trichloroacetic and butyric acids between aqueous solutions and various nitrobenzene-toluene mixtures have been carried out at 25.0 and 30.0 °C, respectively. The observed nonlinearities for both acids of the monomer partition constants and the dimerization constants with the nitrobenzene mole fraction are interpreted in terms of the fractionation factors of effective exchangeable solvation sites of the involved species. Butyric acid monomer is concluded to have three sites for the solvation of the carboxylic hydrogen, carboxylate region, and alkyl chain. Desolvation of the former two sites is necessary for the formation of the dimer for which only two sites corresponding to its two alkyl chain are identified. The solvation sites of trichloroacetic acid monomer and dimer are identical and a singly hydrogen-bonded structure for the dimer is deduced. Dimerization of this acid in the organic phase proceeds by desolvation of what is equivalent to the sites of only one monomer.

Considerable attention has been devoted to solute-solvent interactions in binary solvent mixtures. The larger solute stabilization derived from one of the solvent components compared to that from the other is known to lead to the phenomenon of preferential solvation. This phenomenon is of paramount importance in interpretation of many kinetic data measured in these binaries.[1] Although several studies pertaining to this phenomenon have been reported,[1-3] a refined picture of various solute-solvent interactions has not as yet emerged.

Recently, partition data of acetic acid between aqueous solutions and various nitrobenzene-toluene mixtures have been interpreted in terms of Gross-Butler formalism to deduce various exchangeable sites involved in solvation of the monomer and the dimer in such binaries.[4] Although developed, long time ago, for studying reactions in H_2O-D_2O mixtures,[5-7] this formalism seems to provide a quantitative approach for elucidation of various interactions involved in solute solvation in these extracting binaries. Two assumptions are considered (i) the solvation number of a solute is the same in pure binary components and (ii) solvent exchange processes at various sites take place independently and on the basis of one by one replacement of solvent molecules.

In the present work, the applicability of the above aproach in studying the solvation of butyric and trichloroacetic acids in these binaries are confirmed. The results are compared with those reported for acetic acid in order to examine the effect of solute structural change on the observed solvation behavior.

Experimental

Materials. Nitrobenzene, toluene (Riedel De Haen AG), butyric and trichloroacetic acids (BDH) were used without additional purification.

Procedure. Extracting mixtures of nitrobenzene and toluene as well as aqueous solutions of butyric and trichloroacetic acids were prepared by weight. Appropriate amounts of sodium chloride and hydrochloric acid were added to butyric acid aqueous solution so that their final concentrations were 0.09 and 0.01 mol dm^{-3}, respectively. No sodium chloride was added to trichloroacetic acid solution and the concentration of hydrochloric acid was 0.8 mol dm^{-3}. Partition experiment was made by stirring equal volumes of aqueous and organic phases (20 cm^3 each) in a stoppered conical flask for 1 h with a magnetic stirrer. The contents were transferred into a test tube sealed tightly with a high quality rubber stopper and thermostated at the desired temperature where it is shaked several times before it is allowed to settle overnight for complete phase separation. Carboxylic acid content in the organic phase was determined by titrating a known volume of that phase with NaOH using phenolphthalein indicator. The corresponding concentration in the aqueous phase was determined by difference from initial aqueous phase acid concentration. Blank partition experiments using various extracting mixtures were carried out similarly in the absence of carboxylic acids and no acid (due to HCl) in organic phases was detected. For the determination of association constants of these acids with toluene and nitrobenzene similar partition experiments were carried out using organic phases composed of cyclohexane containing various concentrations of either toluene or nitrobenzene.

Results

The partition coefficient, $D^{(n)}$, of a carboxylic acid between an aqueous solution and a binary mixture of toluene and nitrobenzene (mole fraction n) is related to the partition constant of monomer, $K_d^{(n)}$, and the dimerization constant in the organic phase, $K_{dim}^{(n)}$, by Eq. 1[8]

$$D^{(n)} = (K_d^{(n)} + 2(K_d^{(n)})^2 K_{dim}^{(n)}[HA]_{aq})/(1+K_a/[H^+]), \quad (1)$$

where $[HA]_{aq}$ is the concentration of undissociated acid in the aqueous phase. The partition data of butyric acid were obtained under conditions where its ionization in the aqueous phase was negligible i.e. $[H^+] \gg K_a$. On the other hand, ionization of tri-

†Present address: P. O. Box 3318, Salmiyah 22034, Kuwait.

Table 1. Partition Coefficients of Butyric Acid between Various Binary Mixtures of Toluene and Nitrobenzene (Mole Fraction n) and 0.1 mol dm^{-3} (Na^+, H^+)Cl^- Aqueous Solutions Containing Various Butyric Acid Concentrations at 30.0 °C

n	$10D$ (10[Butyric Acid]$_{aq}$/mol dm^{-3})
0.000	4.51, 4.74 (0.37); 7.30, 7.09 (0.63); 9.23, 9.17 (0.85); 11.1, 11.1 (1.03); 12.2 (1.22); 13.4 (1.39); 14.9 (1.52).
0.040	5.00 (0.36); 7.55 (0.62), 9.31 (0.84); 9.93 (0.95); 12.2 (1.22).
0.081	5.34 (0.35); 7.48 (0.62); 9.36 (0.83); 10.5 (1.05); 11.7 (1.24).
0.142	5.60 (0.35); 7.62 (0.61); 9.13 (0.84); 10.7 (1.04); 12.3 (1.21).
0.151	7.60 (0.61); 9.34 (0.84); 10.9 (1.03); 13.5 (1.38); 14.5 (1.54).
0.299	5.51 (0.35); 7.51 (0.62); 9.29 (0.84); 10.5 (1.05); 11.7 (1.24).
0.369	7.83 (0.61); 9.41 (0.84), 11.0 (1.03); 12.0 (1.25); 13.1 (1.41); 13.8 (1.59).
0.499	8.18 (0.59); 9.45 (0.83); 11.1 (1.02); 13.2 (1.39); 14.0 (1.57).
0.500	6.06 (0.34); 8.06 (0.60); 9.76 (0.82); 10.2 (1.07); 12.1 (1.22).
0.698	6.81 (0.32); 8.06 (0.60); 9.18 (0.84); 10.3 (1.06); 11.5 (1.25).
0.806	8.42 (0.54); 9.32 (0.84); 11.0 (1.03); 11.9 (1.24); 12.5 (1.44); 13.6 (1.61).
0.900	6.81 (0.32); 8.21 (0.59); 9.00 (0.85); 9.88 (1.08); 11.2 (1.27).
1.00	8.59, 8.27 (0.58); 8.69, 9.07 (0.86); 10.3, 10.6 (1.05); 11.5 (1.20); 11.3 (1.27); 11.5, 11.9 (1.49); 12.4, 12.7 (1.67).

Table 2. Partition Coefficients of Trichloroacetic Acid between Various Binary Mixtures of Toluene and Nitrobenzene (Mole Fraction n) and 0.8 mol dm^{-3} HCl Aqueous Solutions Containing Various Trichloroacetic Acid Concentrations at 25.0 °C

n	$10D$ (10[Trichloroacetic Acid]$_{aq}$/mol dm^{-3})
0.000	1.08 (0.64); 1.12 (1.12); 1.27 (1.59); 1.34 (2.06); 1.41 (2.53); 1.58 (3.13).
0.101	1.97 (0.48); 2.19 (0.95); 2.24 (1.42); 2.43 (1.87); 2.64 (2.31).
0.249	3.43 (0.29); 3.63 (0.70); 3.71 (0.98); 3.95 (1.39); 4.21 (1.63).
0.369	4.73 (0.26); 4.90 (0.64); 5.25 (0.88); 5.50 (1.25); 5.77 (1.47).
0.500	6.59 (0.32); 6.92 (0.941); 7.73 (1.21); 7.94 (1.50).
0.598	7.53 (0.22); 8.01 (0.53); 8.38 (0.73); 8.46 (1.04); 8.99 (1.22).
0.798	10.0 (0.19); 10.6 (0.47); 11.17 (0.64); 11.2 (0.91); 11.8 (1.06).
1.00	13.8 (0.52); 13.6 (0.76); 14.6 (0.94); 15.2 (1.14); 15.7 (1.40).

Table 3. $K_d^{(n)}$ and $K_{dim}^{(n)}$ Data for Butyric Acid Transfer between 0.1 mol dm^{-3} (Na^+, H^+)Cl^- Aqueous Solutions and Various Binary Mixtures of Toluene and Nitrobenzene (Mole Fraction n) at 30.0 °C. A Comparision between the Calculated and Observed $K_{dim}^{(n)}(K_d^{(n)})^2$ Values

n	$K_d^{(n)}$	$K_{dim}^{(n)}$	$10K_{dim}^{(n)}(K_d^{(n)})^2$	$10K_{dim}^{(n)}(K_d^{(n)})^2_{calcd}$
		mol^{-1} dm^3	mol^{-1} dm^3	mol^{-1} dm^3
0.000	0.161±0.021	170±32	—	—
0.039	0.225±0.025	81±13	41±9	43
0.081	0.230±0.028	40± 6	36±7	42
0.142	0.288±0.021	47± 5	38±6	40
0.151	0.311±0.018	37± 3	37±4	40
0.299	0.322±0.019	34± 3	35±4	36
0.369	0.431±0.035	17± 2	31±5	34
0.499	0.456±0.031	15± 2	37±5	31
0.500	0.417±0.053	18± 4	31±9	31
0.698	0.511±0.018	9.5±0.6	25±2	26
0.806	0.544±0.034	8.5±0.9	25±4	24
0.900	0.544±0.026	7.3±0.7	22±3	22
1.00	0.604±0.039	5.4±0.6	—	—

Table 4. $K_d^{(n)}$ and $K_{dim}^{(n)}$ Data for Trichloroacetic Acid Transfer between 0.8 mol dm^{-3} Aqueous Solutions and Various Binary Mixtures of Toluene and Nitrobenzene (Mole Fraction n) at 25.0 C°

n	$10^3K_d^{(n)}$	$10^2K_{dim}^{(n)}$	$10^3K_d^{(n)}K_{dim(calcd)}^{(n)}$ [a]
		mol^{-1} dm^3	mol^{-1} dm^3
0.000	119± 4	923±73	—
0.101	235± 6	409±39	1099
0.249	424± 8	201±22	1099
0.369	582± 9	168±14	1098
0.500	798±36	124±27	1099
0.598	955±18	95±12	1096
0.798	1280±24	75±11	1098
1.00	1608±58	61±12	1101
			Av[b] 1099±2

a) Calculated on the basis of Eqs. 13 and 14. b) The observed $K_d^{TL}K_{dim}^{TL}$ is 1.10±0.9.

chloroacetic acid (pK_a=0.62)[8] was significant at 0.8 mol dm^{-3} HCl used for partition experiments and $[HA]_{aq}$ was accordingly calculated. Salting out effect by such concentration of electrolyte is reported to be insignificantly small.[9] The partition coefficients for butyric and trichloroacetic acids by various binary mixtures as a function of the concentration of undissociated acid in the aqueous phase are presented in Tables 1 and 2, respectively. The values of $K_d^{(n)}$ and $K_{dim}^{(n)}$ at

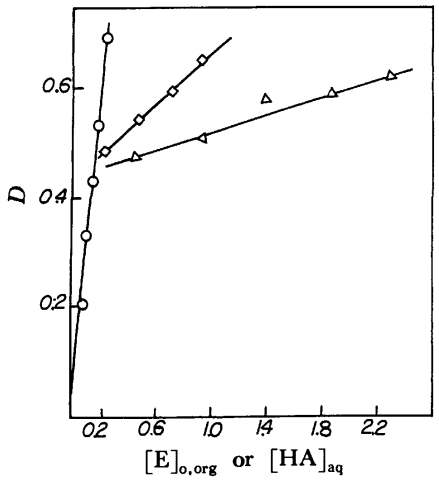

Fig. 1. Partition coefficient of butyric acid at 30°C between cyclohexane and 0.1 mol dm^{-3} (Na^+, H^+)Cl^- aqueous solution as a function of the concentration of undissociated acid in the aqueous phase; ○ and as a function of the concentration of free toluene; △ or free nitrobenzene; □ in the cyclohexane phase at a constant butyric acid concentration of 0.2 mol dm^{-3} in the aqueous phase.

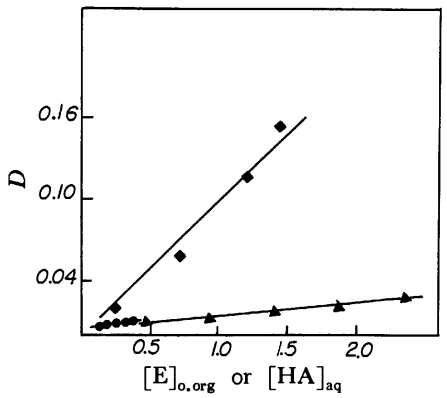

Fig. 2. Partition coefficient of trichloroacetic acid at 25°C between cyclohexane and 1.0 mol dm^{-3} HCl aqeous solution as a function of the concentration of undissociated acid in the aqueous phase; ● and as a function of the concentration of free toluene; ▲ or free nitrobenzene; ■ in the cyclohexane phase at a constant trichloroacetic acid concentration of 0.24 mol dm^{-3}.

various n were deduced from the intercepts and the slopes of linear least squares D-$[HA]_{aq}$ plots (not shown). These are listed in Tables 3 and 4.

The n dependencies of $K_d^{(n)}$ and $K_{dim}^{(n)}$ for butyric acid are portrayed in Figs. 3 and 4 while those of trichloroacetic acid are presented in Figs. 5 and 6, respectively.

Since nitrobenzene and toluene are hydrogen-bonding acceptors,[10] it is necessary in the present study to determine the association constants of each of these compounds with each of the individual acids used. These constants, determined in cyclohexane, as an inert solvent, were calculated from Figs. 1 and 2 using

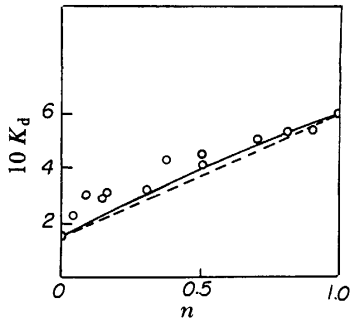

Fig. 3. Dependence of the partition constants of butyric acid monomer on the nitrobenzene mole fraction in the nitrobenzene-toluene mixture at 30°C. The solid curve is calculated based upon the three sites model represented by Eq. 7.†)

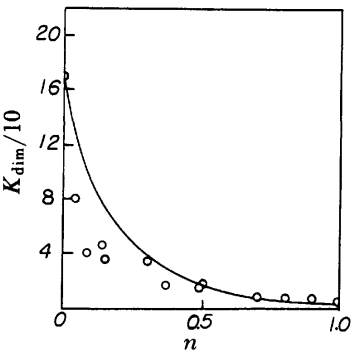

Fig. 4. Plot of the dimerization constant of butyric acid against the nitrobenzene mole fraction in the binary mixture at 30°C. The solid curve is generated from Eq. 11.

Eq. 2[11]

$$D = D_o + K_{ass}K_d[E]_{o,org}/(1+K_a/[H^+]), \quad (2)$$

where D_o is the partition coefficient in the absence of toluene or nitrobenzene and $[E]_{o,org}$ represents the concentration of free toluene or nitrobenzene in cyclohexane phase. The K_d values for both acids in cyclohexane were deduced from the intercepts of the corresponding D-$[HA]_{aq}$ plots shown in Figs. 1 and 2. The association constants for butyric acid with toluene and nitrobenzene are 3.3±0.4 and 9.4±0.1 mol^{-1} dm^3 at 30.0°C while those of trichloroacetic

†) The systematic deviation of the observed K_d values from the fitted ones obtained from Eq. 7 can be attributed to the fact that the fitted values are calculated on the basis of a solvation model for the unhydrated monomer only while the observed value at a given solvent composition represents infact the sum of contributions generated from the solvation of both monomer and its dihydrate. The smaller the extent of hydration the smaller the difference between the observed value and the predicted value will be. The extent of hydration would be expected to decrease as the nitrobenzene mole fraction in the binary increases (I. Kojima, M. Kako, and M. Tanaka, *J. Inorg. Nucl. Chem.*, **32**, 1651 (1970)). Accordingly, the predicted K_d values approach the observed ones at higher nitrobenzene mole fractions, as shown in Fig. 3.

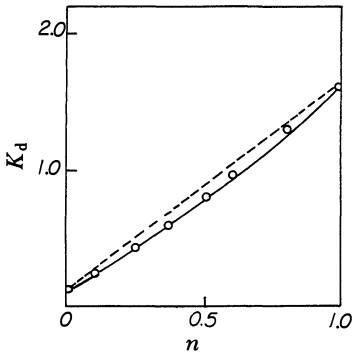

Fig. 5. Dependence of the partition constants of trichloroacetic acid monomer on the nitrobenzene mole fraction in the binary mixture at 25°C. The solid curve is calculated from Eq. 13 representing the two site model while the dashed line represents the one site model.

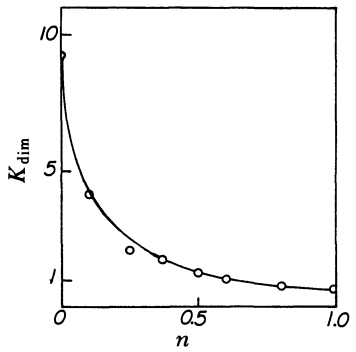

Fig. 6. Plot of the dimerization constant of trichloroacetic acid against the nitrobenzene mole fraction in the binary nitrobenzene-toluene mixture at 25°C. The drawn curve is generated from Eq. 14.

acid are 1.96±0.09 and 25.1±1.9 $mol^{-1}dm^3$, at 25.0°C respectively.

Discussion

Consider a single molecular solute partitioned between an aqueous solution and a binary mixture of nitrobenzene (mole fraction n) and toluene (mole fraction $1-n$). The solute partition constant, $K^{(n)}$, according to its additive constituent nature,[12] equals to the product of contributions $A_1^{(n)}$, $A_2^{(n)}$, $A_3^{(n)}$, ··· $A_m^{(n)}$ generated from stabilization or destabilization of various structural units a_1, a_2, a_3, ··· a_m of that solute in the organic phase. The contribution from mutual interactions among various structural units is assumed to be negligible,

$$K^{(n)} = A_1^{(n)} \cdot A_2^{(n)} \cdot A_3^{(n)} \cdots A_m^{(n)}, \quad (3)$$

where (n) is just a superscript refering to the binary solvent composition. If each of the solute structural units is assumed to have only one effective exchangeable solvation site, any single contribution $A_i^{(n)}$ will equal to the mole fraction weighted average of contributions of a_i in pure nitrobenzene, A_i^{NB} and in pure toluene, A_i^{TL}:

$$\begin{aligned} A_i^{(n)} &= (1-n)A_i^{TL} + n A_i^{NB} \\ &= A_i^{TL}(1-n+\Phi_i n), \end{aligned} \quad (4)$$

where $\Phi_i = A_i^{NB}/A_i^{TL}$ reflects the preference of structural unit a_i for solvation by nitrobenzene relative to that preference for solvation by toluene. It might be considered as a solvation fractionation factor for structural unit a_i. $K^{(n)}$ can thus be expressed in terms of all possible solvation sites as follows:

$$K^{(n)} = K^{TL} \prod_i^v (1-n+\Phi_i n), \quad (5)$$

where K^{TL} is the solute partition constant when pure toluene is used and v is the number of solvation sites, each contributing a $(1-n+\Phi_i n)$ term to the observed $K^{(n)}$. The magnitude of Φ_i is determined by the electronic and geometric factors involved in both the site under consideration and the exchangeable solvents as well.

In the present study, when Φ_i is greater than unity, the i-th site will be stabilized to a greater extent by nitrobenzene than by toluene and vice versa. As Φ_i approaches one, the site will be equally stable in both solvents and no contribution to $K^{(n)}$ will be seen.

It may be noted that Eq. 5 is a special form of the general Gross-Butler equation originally derived for studying chemical reactions in H_2O–D_2O mixtures and is currently used in the well known proton inventory technique.[5-7] Equation 5 predicts that $K^{(n)}$ will vary linearly with n if the partitioning solute has only one solvation site and nonlinearly if the solute have multisolvation sites.

When a solute dimerizes in such binary mixture, the extent of dimerization is governed by the contributions generated from solvation of various structural units composing the monomer and the dimer. It can be shown, in analogy with the above derivation that the dimerization constant, $K_{dim}^{(n)}$, in a given nitrobenzene-toluene mixture is related to the dimerization constant in pure toluene, K_{dim}^{TL}, by a series of correction factors,

$$K_{dim}^{(n)} = K_{dim}^{(n)} \prod_i^v (1-n+\Phi_j^D n) / \prod_i^v (1-n+\Phi_i^M n), \quad (6)$$

where each correction factor $(1-n+\Phi_i^D n)/(1-n+\Phi_i^M n)$ represents the contribution of i-th site in the dimer relative to that contribution in the monomer. The total number of sites v in mumerator and denominator is not necessary to be the same since any $(1-n+\Phi_i n)$ term may be either contributing if $\Phi_i \neq 1$ or not contributing if $\Phi_i = 1$.

Solvation of Butyric Acid. The nonlinear n dependence of partition constant of butyric acid monomer, $K_d^{(n)}$, portrayed in Fig. 3 suggests the involvement of two or more sites for monomer solvation. It is therefore, necessary to formulate a chemically reason-

Table 5. Comparison of Sum of Squared Residuals after Regressions Representing Various Mathematical Monomer Solvation Models

Proposed model	Values	Sum of squared residual
	Butyric acid[a]	
Two sites	Φ_2=1.30	6.5×10^{-2}
Three sites A	Φ_2=4.32; Φ_3=0.30	7.5×10^{-2}
Three sites B	Φ_2=2.16; Φ_3=0.60	3.9×10^{-2}
Three sites C	Φ_2=1.62; Φ_3=0.80	5.7×10^{-2}
	Trichloroacetic acid	
One site	Φ=13.48	2.2×10^{-2}
Two sites D	Φ_1=14.00; Φ_2=0.96	3.1×10^{-2}
Two sites E	Φ_1=12.85; Φ_2=1.05	1.2×10^{-2}
Two sites F	Φ_1=11.00; Φ_2=1.23	1.2×10^{-3}
Two sites G	Φ_1= 9.00; Φ_2=1.50	1.1×10^{-2}

a) A value of 2.90 is used for Φ_1 in all butyric acid models.

able solvation model capable of reproducing the experimental data. Possible models may include a site for the carboxylic hydrogen and one or two sites for the remainder of the molecule. A reasonable estimate for the fractionation factor of carboxylic hydrogen site, Φ_1, is obtained from the ratio of the association constants of butyric acid with nitrobenzene and toluene in the inert solvent cyclohexane. This ratio (2.9) is used for this site in all proposed models, listed in Table 5. The other fractionation factors Φ_2 and Φ_3 corresponding to the other sites are derived so that the product of all fractionation factors for any single model is equal to K_d^{NB}/K_d^{TL} ratio. In order to arrive at the most probable solvation model, the sums of squared residuals after various regressions were computed and compared. The minimum sum of squared residuals is exhibited by model B. Substitution of various values of n in Eq. 7 duplicates reasonably the experimental data, as illustrated in Fig. 3.

$$K_d^{(n)} = K_d^{TL}(1-n+2.90n)(1-n+2.16n)(1-n+0.6n) \quad (7)$$

It is of interest to compare this equation with that reported earlier for solvation of acetic acid monomer in the same binaries,[4] Eq. 8.

$$K_d^{(n)} = K_d^{TL}(1-n+2.85n)(1-n+1.91n) \quad (8)$$

The additional term in Eq. 7 with a fractionation factor of 0.6 must reflect the contribution generated from the solvation site of alkyl chain in butyric acid. A reasonable estimate for the fractionation factor of this site can be independently produced from the ratio of contributions of this alkyl chain to K_d's in nitrobenzene and toluene. These contributions can be obtained from the K_d's of acetic and butyric acids in both solvents using Hansch equation;[12]

$$\Phi_3^{calcd} = \frac{\text{Antilog}(\log K_{d.But}^{NB} - \log K_{d.Acet}^{NB})}{\text{Antilog}(\log K_{d.But}^{TL} - \log K_{d.Acet}^{TL})}. \quad (9)$$

The excellent agreement between the calculated value of 0.7±0.1 and the one obtained from model B, 0.6±0.1, offers a support for the proposed solvation model of butyric acid monomer in these binaries.

The similarity in the second terms of Eqs. 7 and 8 implies their contributing sites are nearly identical. These terms are more likely to arise from interactions of carboxylate region of the monomer with the exchangeable solvent molecules.

In order to deduce a suitable solvation model for butyric acid dimer, it is necessary to determine the various fractionation factors involved. The product of these factors obtained from Eq. 6 (n=1) equals 0.45±0.13. Because of the known cyclic and the nearly symmetrical nature of this dimer,[13] an even number of solvation sites might be anticipated. The value of 0.45 is more likely, therefore, to represent the product of at least two similar fractionation factors (0.67±0.14 each) corresponding to two identical sites. This predicted value for each site is very close to the fractionation factor for alkyl chain solvation site in the monomer obtained from both Eq. 9 and the above $K_d^{(n)}$–n analysis. It is not unreasonable, therefore, to assign this obtained fractionation factor product to solvation sites of the two alkyl groups present in the dimer. According to this picture, no contribution is seen from the other two sites involved in monomer solvation. This seems to be consistent with the conclusion drawn earlier for the dimerization of acetic acid in such binaries that desolvation of its two monomer sites is necessary for the formation of the dimer.[4] The n dependence of $K_{dim}^{(n)}$ may thus be represented by:

$$K_{dim}^{(n)} = K_{dim}^{TL}(1-n+0.67n)^2/ ((1-n+2.90n)(1-n+2.16n)(1-n+0.6n))^2, \quad (10)$$

where the denominator represents the contribution from solvation of two butyric acid monomers. Since the contribution of alkyl chain in both the dimer and monomer is nearly the same, the alkyl chain terms in Eq. 10 could be cancelled out and the n dependence of $K_d^{(n)}$ can be expressed by Eq. 11

$$K_{dim}^{(n)} = K_{dim}^{TL}/((1-n+2.90n)(1-n+2.16n))^2, \quad (11)$$

which duplicates reasonably the experimentally determined $K_{dim}^{(n)}$ data by substitution of various values of n, as shown in Fig. 4. The excellent agreement between $K_{dim}^{(n)}(K_d^{(n)})^2$ values, calculated from Eq. 12,

$$K_{dim}^{(n)}(K_d^{(n)})_{calcd}^2 = K_{dim}^{TL}(K_d^{TL})^2(1-n+0.67n)^2, \quad (12)$$

and the corresponding experimental ones, displayed in Table 3 lend another support to the proposed solva-

tion model of butyric acid dimer in these binaries.

Solvation of Trichloroacetic Acid. The curved $K_d^{(n)}$–n relationship, depicted in Fig. 5 implies the presence of more than one solvation sites for the monomer. It is therefore necessary to formulate a solvation model that is both statistically and chemically acceptable. The fractionation factors of carboxylic hydrogen solvation site for various two sites models, listed in Table 5, are derived either from the ratio of association constants of this acid with nitrobenzene and toluene or from other assumed value in the neighborhood of that ratio. It transpires form Table 5 that regression F represents the most probable model. The experimentally determined $K_d^{(n)}$ values fit nicely the curve generated from

$$K_d^{(n)} = K_d^{TL}(1-n+11.0n)(1-n+1.23n). \quad (13)$$

The product of fractionation factors for the dimer sites is predicted from Eq. 6 (n=1) to be ca. 12, a value very close to that obtained for the monomer sites. This speaks for the similarity in the solvation sites of both species and is consistent with a singly hydrogen-bonded structure for the dimer in nitrobenzene–toluene binaries. Formation of the two hydrogen bonds linking the two monomers is known to be favorable when the dimer has an eight membered cyclic structure.[14] The presence of nitrobenzene in such solvent binaries would tend, however, to form with the acid monomer a stronger hydrogen bond than those formed between the two monomeric entities. This occurs because of the higher hydrogen bonding acceptor basicity of nitrobenzene compared to that of trichloroacetic acid monomer itself.[10] Two effects are thus generated i) a dramatic decrease in the extent of dimerization as the nitrobenzene mole fraction increases in the binary and ii) formation of an open singly hydrogen-bonded dimer. According to this view dimerization proceeds by desolvation of what is equivalent to the sites of one monomer. The n dependence of $K_{dim}^{(n)}$ could thus be represented by:

$$K_{dim}^{(n)} = K_{dim}^{TL}/((1-n+11.0n)(1-n+1.23n)). \quad (14)$$

Substitution of n values in Eq. 14 duplicates reasonably the experimentally determined $K_{dim}^{(n)}$ values, as shown in Fig. 6. Equation 14 predicts that:

$$(K_{dim}^{(n)} K_d^{(n)})_{calcd} = K_{dim}^{TL} K_d^{TL} = \text{constant}.$$

This is born out to be true as illustrated in Table 4.

In summary, the present work offers an approach towards elucidation of various solute–solvent interactions involved in binary nonaqueous mixtures. The nonlinear n dependence of both $K_d^{(n)}$ and $K_{dim}^{(n)}$ for butyric and trichloroacetic acids has been quantitatively rationalized in terms of fractionation factors of various solvation sites of involved species using Gross-Butler formalism. The interactions of the studied species with nitrobenzene are certainly different from those with toluene and require reorientation of solvent molecules upon exchanges. This factor does not seem to materially affect the results reported here.

Rererences

1) Y. Kondo, K. Uosaki, and N. Tokura, *Bull. Chem. Soc. Jpn.*, **44**, 2548 (1971) and the papers cited therein.

2) K. Ramerie and J. B. F. N. Engberts, *J. Phys. Chem.*, **87**, 5449 (1983).

3) a) C. H. Langford and J. P. K. Tong, *Acc. Chem. Res.*, **10**, 258 (1977); b) M. wa Muanda, J. B. Nagy, and O. B. Nagy, *J. Chem. Soc., Faraday Trans. 1*, **74**, 2210 (1978); c) L. S. Frankel, T. R. Stengle, and C. H. Langford, *J. Phys. Chem.*, **74**, 1376 (1970).

4) M. F. Hegazi, *Gazz. Chim. Ital.*, **113**, 835 (1983).

5) M. Hegazi, J. Mata-Segreda, and R. L. Schowen, *J. Org. Chem.*, **45**, 307 (1980).

6) K. B. Schowen, "Transition States of Biochemical Processes," ed by R. D. Gandour and R. L. Schowen, Plenum Press, New York (1978). Chap. 6.

7) J. L. Hogg and W. P. Huskey, *J. Org. Chem.*, **46**, 53 (1981) and references therein.

8) N. Niitsu and T. Sekine, *Bull. Chem. Soc. Jpn.*, **51**, 705 (1978).

9) T. Sekine and Y. Hasegawa, "Solvent Extraction Chemistry," Marcel Dekker, New York (1977), p. 137.

10) M. J. Kamlet, J. -L. M. Abboud, M. H. Abraham, and R. W. Taft, *J. Org. Chem.*, **48**, 2877 (1983).

11) M. F. Hegazi, *J. Chem. Tech. Biotechnol.*, **34A**, 251 (1984).

12) A. Leo, C. Hansch, and D. Elkin, *Chem. Rev.*, **71**, 525 (1971).

13) J. T. Bulmer and H. F. Shurvell, *J. Phys. Chem.*, **77**, 256 (1973).

14) R. D. Gandour, *Tetrahedron Lett.*, **1974**, 295.

Titanium Determination under High-Sensitivity Conditions with 2-(5-Chloro-2-pyridylazo)-5-dimethylaminophenol. I

Héctor Jose MARINI, Rosa Isabel ANTÓN, Maria Susana BOERIS,† and Roberto Antonio OLSINA*
Departamento de Quimica Analitica "Dr. Carlos B. Marone," Universidad Nacional de San Luis, Argentina
†Universidad Nacional de La Pampa, Argentina
(Received August 16, 1985)

The optimum working conditions for the complexing reactions between Ti(IV) and 2-(5-chloro-2-pyridylazo)-5-dimethylaminophenol (5.ClDMPAP) in aqueous alcoholic solutions were studied. When an ethanol solution of 5.ClDMPAP is added to a Ti(IV) aqueous solution, complex species, whose spectral and stoichiometric characteristics depend on pH, develop rapidly. The complex selected for the analytical work forms between pH 4.7 and 5.8 and has a 3:1 ligand-metal molar ratio. The complex fulfils Beer's law up to a Ti(IV) concentration of 0.7 ppm, working at λ_{max}=580 nm. The optimum concentration range (Ringbom) was between 0.05 and 0.7 ppm of Ti(IV). The molar absorptivity at λ_{max}=580 nm and Sandell index are 4.39×10^4 dm^3 mol^{-1}cm^{-1} and 0.0011 μg cm^{-2}, respectively. An absorptiometric method to determine Ti(IV) was developed and the proper ways to reduce interferences produced by some anions and cations are described. The method developed was applied to Ti(IV) determination in optical glass and ceramic materials.

The determination of small quantities of titanium is a very important fact when analyzing diverse materials such as glass, frits, ceramics, paints, sands, and natural water from nearby vanadium mines.

The atomic absorption technique, using flame as an atomization means, has not the sensitivity necessary for many cases. So, the searching of chromogenic reagents and the perfecting of techniques having analytical procedures with the proper sensitivity and selectivity for Ti(IV), is interesting. Reagents derived from phenylfluorone[1] and the azo group (pyridylazo)[2] and thiazolylazo[3] yielded significant results. As to those reagents of the pyridylazo type, Shibata et al.[4] proved that the presence of a dialkylamino group in a *p*-position with respect to the azo group and the existence of one halogen atom in the pyridine nucleus are highly important to attain a larger sensitivity in chromatic reactions. The reagent selected, 2-(5-chloro-2-pyridylazo)-5-dimethylaminophenol, fulfils both requirements. The general characteristics of this reagent and its use in zinc and vanadium determination have already been studied.[5,6]

Experimental

Reagents. A 5.ClDMPAP solution was prepared by coupling *m*-dimethylaminophenol with sodium 5-chloro-2-pyridyldiazotate, according to the method described by Shibata et al.[7] Purification was carried out by means of repeated cycles of dissolution-reprecipitation starting from ethanol-water mixtures. A 0.25% (w/v) solution from the pure material was prepared. Lower concentration solutions from the above one by dilution with ethanol, were prepared. All solutions were kept away from light. A 5×10^{-4} mol dm^{-3} solution can be kept unaltered for at least 25 d. The Ti(IV) solution was prepared according to that described by Roseman and Thornton.[8] Its titer was determined by complexometric titration.[9] To obtain reproducible results, the solution must be prepared daily. All the other chemicals were also of an analytical-reagent grade.

Apparatus. A Varian 634 UV-vis. spectrophotometer with 10 mm optical path cell to obtain the absorption spectra and absorbance measures was used. An Orion 701-A pH meter for pH measurements was used. Volumes in Ti(IV) complexometric titrations were obtained by means of an automatic Metrohm Dosimat E412P buret.

Results and Discussion

Influence of pH, Stoichiometry, and Conditions for Ti(IV) Absorptiometric Determination. The reaction between aqueous solutions of Ti(IV) and 5.ClDMPAP dissolved in ethanol produces, almost instantaneously and at different pH values, diverse complex species (Fig. 1). Table 1 shows the most important characteristics of the complexes. For the analytical work, the complex selected is the one formed quantitatively between pH 4.7 and 5.8 as it shows larger values of absorptivity and bathochromatic shift. Its formation starts at pH 4.3 and its maximum development is at the above pH range. As shown by the application of the method of continuous variations (Fig. 2) stoichiometry of the complex was 3:1 (5.ClDMPAP:Ti(IV)). The order in which the reagents are added is very important. First, the reaction between Ti(IV) and 5.ClDMPAP is promoted at low pH values (<2), and then a 5.0 pH buffer is added, so it is possible to work with the selected complex. According to the

Table 1. Characteristics of the Ti(IV)-5.ClDMPAP Complexes in Aqueous Alcoholic Solutions (55% v/v of Ethanol)

pH range of formation	5.ClDMPAP/Ti(IV) ratio	λ_{max}/nm	Absorptivity dm^{3}mol^{-1}cm^{-1}
2.7—4.2	2/1	560	3.69×10^4
4.7—5.8	3/1	580	4.39×10^4
7.8—9.1	2/1	570	2.48×10^4

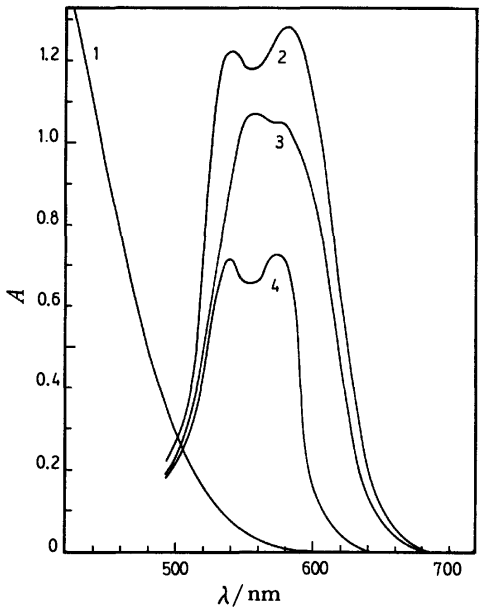

Fig. 1. Absorption spectra of the 5.CIDMPAP; Titanium-5.CIDMPAP complex in aqueous alcoholic solution.
C_{reag}=1.2×10^{-4}M; C_{Ti}=1.2×10^{-5}M; Ethanol-Water 55% (v/v). 1: 5.CIDMPAP vs. pure solvent as blank. 5.CIDMPAP-Ti(IV) complex vs. blank of reagent; 2: pH= 5.0; 3: pH=3.5; 4: pH=8.5.

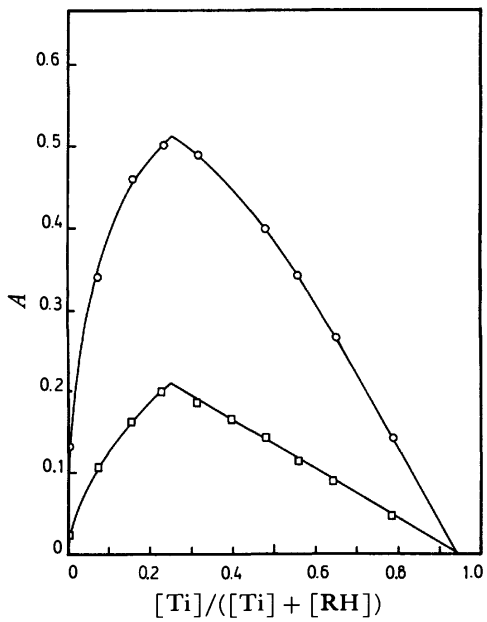

Fig. 2. Continuous variation method applied to the Ti(IV)-5.CIDMPAP complex.
C_{reag}=C_{Ti}=1×10^{-4}M; pH=5.0. Ethanol-Water 55% (v/v).
Wavelength: ○ 580 nm; □ 600 nm.

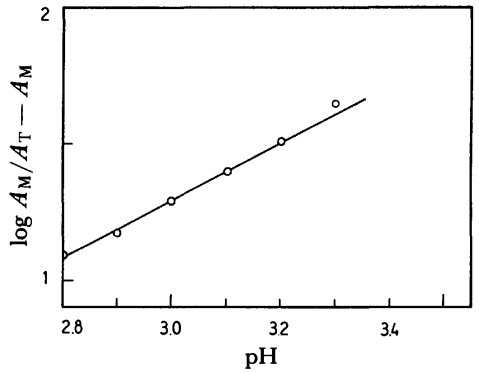

Fig. 3. Equilibrium shift method for determining hydrogen ions released during complexation.
C_{Ti}=1.7×10^{-5}M; C_{reag}=2.5×10^{-4}M; pH=variable; Wavelength 580 nm.
A_M=Absorbance read at unfavorable pH values for the complex formation.
A_T=Absorbance corresponding to a 3.4 pH solution and to a 1.7×10^{-5}M of the complex.

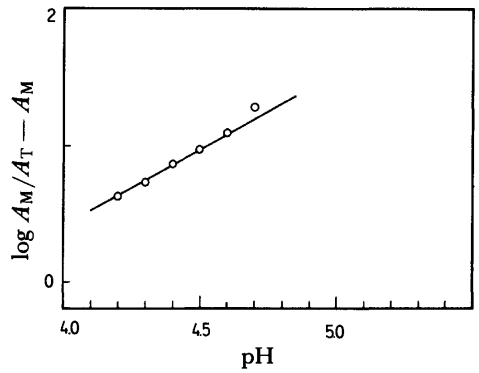

Fig. 4. Equilibrium shift method.
C_{Ti}=1.4×10^{-5}M; C_{reag}=2.2×10^{-4}M; pH=variable; Wavelength 580 nm.
A_M=Absorbance corresponding to a 4.8 pH solution and to a 1.4×10^{-5}M of the complex.
A_T=Absorbance read at unfavorable pH values for the complex formation.

electrophoretic migration studies and the extraction with different solvents (benzene, chloroform, 3-methyl-1-butanol, and nitromethane) which have demonstrated the ionic nature of the chelates formed, and also assuming that $(Ti(OH)_2)^{2+}$ is the predominant species of Ti(IV),[10] the following reactions can be written:

$$(Ti(OH_2))^{2+} + 2RH \rightleftharpoons (Ti(OH)R_2)^+ + H_2O + H^+$$

$$(Ti(OH)R_2)^+ + RH \rightleftharpoons (TiR_3)^+OH^- + H^+.$$

The results obtained by applying the equilibrium shift method[11] (Figs. 3 and 4) have shown a release of one hydrogen-ion for each complexed Ti(IV)-ion in every chelation reaction. The above results sustain the proposed reactions. The equilibrium constant of the chelation reaction was studied by means of absorptiometric measurements;[12] the value obtained was 4.41×10^{15} at 25 °C. Table 2 shows experimental variables of Ti(IV) absorptiometric determination.

Influence of the Nature and Concentration of the Organic Solvent. Considering the poor solubility in water of 5.ClDMPAP and its Ti(IV) complexes, the

Table 2. Experimental Variables of Ti(IV) Absorptiometric Determination

pH Range	4.7—5.8
Solvent	Ethanol-water 55% (v/v)
Stoichiometry	3:1 (Reagent:metal)
Maximum absorption of complex	580 nm
Maximum absorption of reagent	440 nm
$\Delta\lambda$	140 nm
Stability of complex	At least 5 min
Beer's law-sensitivity acidity (pH)	5.0
Molar absorptivity	4.39×10^4 dm^3 mol^{-1} cm^{-1} (s=1228; $Cl_{\alpha=0.05}^{42690-45270}$)
Optimum concentration range (Ringbom)	0.05—0.7 ppm
Sensitivity of sandell	0.0011 μg/cm^2
Beer's law fulfilment	Up to 0.7 ppm

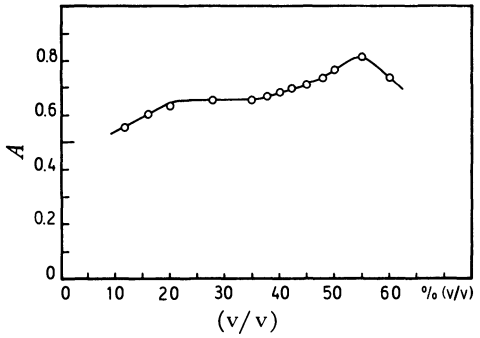

Fig. 5. Influence of the concentration of ethanol on the absorbance of Ti(IV)-5.ClDMPAP complex. pH=5.0; Wavelength 580 nm. Ethanol-Water % (v/v): variable.

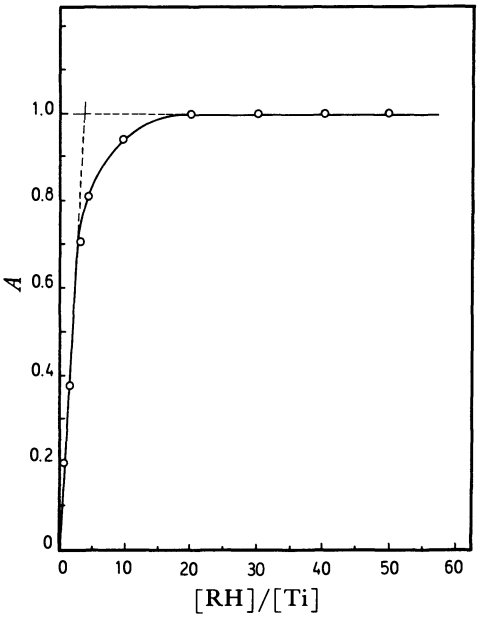

Fig. 6. Saturation curve. pH=5.0; Ethanol-Water 55% (v/v); C_{Ti}=constant=2.4×10^{-5} M. Wavelength 580 nm.

addition of an organic solvent miscible in water is necessary. The influence of different solvents (methanol, ethanol, dioxane, acetone, and pyridine) was studied. Experimental results show that there are no changes in λ_{max} of the complex whichever the solvent used, but a maximum absorptivity is obtained when methanol or ethanol are used. The latter was selected for the work. The minimum ethanol concentration necessary to produce a maximum absorbance was 55% (v/v). It is also possible to work with a lower sensitivity by reducing ethanol percentage up to 30% (v/v) (Fig. 5) and no variations in the spectral characteristics or in the stoichiometric of the complex are observed.

Reagent Concentration. To evaluate this variable, a saturation curve was plotted (Fig. 6) at pH 5.0. The Ti(IV) concentration was kept constant 2.4×10^{-5} mol dm^{-3} and the one belonging to 5.ClDMPAP was modified between 2.0×10^{-6} and 1.2×10^{-3} mol dm^{-3}. Absorbance was read at λ_{max}=580 nm and ethanol concentration remained in 55% (v/v). The absorbance of the complex's solutions reached a maximum value for a 15:1 ligand-metal ratio and they remained unaltered for proportions of up to 50:1. On the other hand, the graph shows that the complex formed has a relatively high stability and that, at the same time, proves stoichiometry already established. The complex's solutions at pH 5.0, keeping a 20:1 ligand: metal molar ratio, show no changes in their spectral curves and absorptivity at λ_{max}=580 nm for, at least, 5 minutes.

Effect of Foreign Ions. Under the experimental conditions required for the 5.ClDMPAP complexation with Ti(IV), the reagent also reacts with other metal ions. This is the case for other reagents of this type and thus there occur more or less severe spectral interferences that cannot be controlled by masking. Interferers are Fe(III), Cu(II), Ni(II), Co(II), W(VI), Nb(V), Ta(V), and V(V). The Zn(II), Mn(II), Mo(VI), and Cr(VI) ions are tolerated in a 10:1 molar ratio (foreign ion:Ti(IV)). For Al(III) and Mg(II), the ratio tolerated is 50:1; for Na(I) and K(I), it is 1000:1. Besides, the tolerances for different anions, especially those from strong acids used to dissolve samples and other anions and compounds added as possible masking agents, were delimited. If a maximum 2% error is admitted, the hydrogen phtalate, bromide, perchlorate, sulfate, thiosulfate, and iodide ions may be present in a 2000:1 ratio in front of Ti(IV), whereas thiourea and sulfamic

Table 3. Tolerances for Some Common Cations

Ion	Ion-Ti(IV) tolerated molar ratio	Ion-Ti(IV) tolerated mass ratio	Notes[a)]
Cd(II)	10	26	b)
Co(II)	10	13	b)
Ni(II)	10	13	b)
Mn(II)	20	25	b)
Pb(II)	25	119	b)
Zn(II)	50	75	b)
Mo(VI)	100	220	b)
Cr(VI)	100	119	b)
UO_2(II)	10	58	b)
Fe(III)	5	6	c)
Zr(IV)	10	21	d)
Hf(IV)	10	41	d)

a) Ti(IV) taken: 0.55 ppm. b) Previous extraction with 8-quinolinol 0.1 mol dm^{-3} in chloroform with no masking agents present. (V_o=V_w), at pH 1.5. Probable interferences by Ca(II), Sr(II), Ba(II), La(III), Na(I), and K(I) are also solvent by this method. c) Previous double extraction with 8-quinolinol 0.1 mol dm^{-3} in chloroform with EDTA 0.1 mol dm^{-3} present as masking agent. (V_o=V_w), at pH 8.2. This method is also useful to solve interferences by Co(II) and Ni(II) and it increases the tolerances for Zn(II), Mn(II), Mo(II), Al(III), and Mg(II). d) Previous extraction with 8-quinolinol 0.1 mol dm^{-3} in chloroform with oxalate 0.1 mol dm^{-3} present as masking agent. (V_o=V_w), at pH 8.2.

Table 4. Results in the Determination of TiO_2 in Samples

Sample	Found % (w/w) in this method	Found % (w/w) in standard method[17)]	Error/%
Optical glass type Athermal-50	0.66 (s=0.019), Cl 0.64—0.68, α=0.05	0.67 (s=0.018), Cl 0.65—0.69, α=0.05	1.5

Table 5. Results in the Determination of TiO_2 in Samples

Sample	Composition % (w/w)		Found % (w/w)	Error/%
Glass soda-lime flat (NBS N° 621)	SiO_2	80.800	0.0118 (s=0.002; $Cl_{\alpha=0.05}^{0.010-0.014}$)	1.6
	Al_2O_3	2.300		
	Fe_2O_3	0.029		
	TiO_2	0.012		
	ZrO_2	0.030		
	CaO	0.020		
	MgO	0.020		
Ceramic material soda-feldspar (BCS N° 375)	SiO_2	67.10	0.375 (s=0.016; $Cl_{\alpha=0.05}^{0.358-0.392}$)	1.3
	Al_2O_3	19.80		
	Fe_2O_3	0.12		
	CaO	0.89		
	TiO_2	0.38		
	MgO	0.05		
	K_2O	0.79		
	Na_2O	10.40		

acid may exist in a 5000:1 molar ratio. The acetate ion may be present in a 10000:1 molar ratio. The tolerance for oxalate and fluoride were 10:1; for ascorbic acid, 50:1. Tartrate, phosphate, citrate, EDTA, and CDTA also interfere. In order to attain a larger selectivity, the behavior of several reagents (cupferron,[13)] 8-quinolinol,[14)] diethyldithiocarbamate[15)]) that allow Ti(IV) separation by means of liquid-liquid extraction was studied. The extraction procedure using 8-quinolinol and chloroform as solvent, together with pH regulation and the presence of complexing agents, proved to be the most efficient method to separate several interferes.

Method Using 8-Quinolinol and Chloroform. Into a decanting flask, pour 5 cm^3 of solution having between 0.25 and 3.5 ppm of Ti(IV) and the foreign ion under analysis. Then add 5 cm^3 of 8-quinolinol 0.1 mol dm^{-3} in chloroform and stir it vigorously during 5 min; separate the organic phase, put it dry into a porcelain crucible on sand bath and melt it with 0.4 g of potassium hydrogensulfate. Cool it, take it with water and pour it into a 25 cm^3 flask; then add 2 cm^3 of reagent, 6 cm^3 of ethanol, 1 cm^3 of sodium hydroxide 1 mol dm^{-3}, 4 cm^3 of buffer (acetic/acetate) of pH 5.0 and bring it to gauging. Read the solution absorbance at λ_{max}=580 nm against a reference prepared as usual. By the above method, tolerances shown in Table 3 are attained (the maximum admissible error was set in 2%).

The characteristics of interferences by Nb(V), Ta(V), V(V), and Cu(II) made it necessary a new methodology, still under development, which yielded significant results.

Applications. The methodology developed was applied to two kinds of samples:

1. Optical glass: samples: Athermal 50 and Soda-Lime Flat (NBS N° 620). The method applied is as follows: In a platinum crucible, weigh one amount of crushed glass sample having no more than 1 mg of TiO_2. Then add 10 cm^3 of sulfuric acid 1:1 and 15 cm^3 of hydrofluoric acid. Evaporate on sand bath until sulfuric acid white fumes appear. Let it get cold and take with 15—20 cm^3 of distilled water. Pour it into a 150 cm^3 flask and heat it until salt dissolution. Pour it into a 100 cm^3 flask (filter in case barium sulfate is present) and bring it up to gauging. Take 2 cm^3 of the filtrate; add 1 cm^3 of solution 0.2 mol dm^{-3} of sodium oxalate and adjust pH at 3.9 in 5 cm^3 as final volume; proceed with the method as above described. Results obtained for Athermal 50 optical glass contrasted against the hydrogen peroxide method[16,17] (Table 4).

2. Ceramic material:sample: Soda Feldspar (BCS N° 375). The method was the same as the one described for glass samples. Results are shown in Table 5.

The autors are gratefully indebted to CONICET for financial assistance.

References

1) S. Chen, Q. Rong, and Q. Pan, *Zh. Daxue Xeubao, Ziran Kexueban*, **1983**, 51; *Chem. Abstr.*, **100**, 29035j (1984).
2) T. Ozawa, *Bunseki Kagaku*, **16**, 435 (1967).
3) C. Tsurumi and K. Furuya, *Bunseki Kagaku*, **26**, 149 (1977).
4) S. Shibata and M. Furukawa, *Bunseki Kagaku*, **23**, 1420 (1974).
5) E. Marchevsky, R. Olsina, and C. Marone, *An. Quím.*, **80**, 101 (1984).
6) E. Marchevsky, R. Olsina, and C. Marone, *Talanta*, **32**, 54 (1985).
7) S. Shibata, M. Furukawa, and K. Toei, *Anal. Chim. Acta*, **66**, 397 (1973).
8) R. Roseman and W. M. Thornton, *Am. J. Sci.*, **20**, 14 (1930).
9) D. H. Wilkins, *Anal. Chim. Acta*, **20**, 113 (1959).
10) J. Kragten, "Atlas of Metal-ligand Equilibria in Aqueous Solution," John Wiley & Sons, N.Y. (1978).
11) Yu. A. Zolotov, "Extraction of Chelate Compounds," Ann Arbor-Humphrey Science Publishers Inc., London (1970).
12) L. Meites and H. C. Thomas, "Advanced Analytical Chemistry," McGraw-Hill, N.Y. (1958).
13) I. P. Alimarin and I. M. Gibalo, *Dokl. Akad. Nauk SSSR*, **109**, 1137 (1956).
14) J. Starý, *Anal. Chim. Acta*, **28**, 132 (1963).
15) H. Bode, Z. *Anal. Chem.*, **144**, 165 (1955).
16) M. Mori, M. Shibata, E. Kyuno, and S. Ito, *Bull. Chem. Soc. Jpn.*, **29**, 904 (1956).
17) "Standard Methods of Chemical Analysis," 6th ed, ed by F. J. Welcher, N.Y. (1975), Vol. 2.

Structural Study of the Methylnaphthazarins. X-Ray Structure of the Tetramethylnaphthazarin, a Charge Transfer Complex

José-Gonzalo Rodriguez,* Alfonso De Pablo, Pilar Smith-Verdier,† Feliciana Florencio,† and Severino Garcia-Blanco†

Departamento de Química Orgánica, Universidad Autónoma de Madrid, Canto Blanco, 28049 Madrid, Spain
†Department de Rayos X, Instituto Rocasolano, Serrano 119, 28006 Madrid, Spain

(Received December 17, 1984)

The synthesis and analysis by ^{1}H NMR of the methyl substituted naphthazarins were attempted. The chemical shifts of the substituents and of the ring protons were compared with those in their diacetates and were then correlated with the quinonoid or benzenoid nature of the rings. X-Ray diffraction analysis of tetramethylnaphthazarin, 2,3,6,7-tetramethyl-5,8-dihydroxy-1,4-naphthoquinone, has shown that this exists, in solid state, as a centrosymmetric charge-transfer complex with itself. The compound crystallizes in the *Ibam* space group, with an orthorhombic cell of dimensions a=17.479(1), b=9.983(1), c=6.752(1) Å, and four molecules in the unit cell. The crystal is built from molecules stacked up the c-axis and the interplanar distance between two overlapping molecules is 3.38 Å.

The naphthazarin nucleus 5,8-dihydroxy-1,4-naphthoquinone exists in nature in the spinochromes of the echinoderms,[1] and some derivatives can be used as the starting products in the synthesis of the tetracyclic antibiotics.[2]

Various investigations in the solid state of each of the three naphthazarin crystalline forms,[3] designated A, B, and C, have led to the conclusion that the molecule is centrosymmetric.

"Magic angle" spinning techniques, in ^{13}C NMR analysis, have provided evidence for dynamic disordered structures of naphthazarin (B form) in the solid state at −160 °C.[4]

On the other hand, NMR studies in solutions[5] indicates that a fast tautomeric equilibrium among **1⇄2a⇄2b⇄3** (Scheme 1) is present until −75 °C. From IR analysis,[6] it is observed that naphthazarin exists as 5,8-dihydroxy-1,4-naphthoquinone.

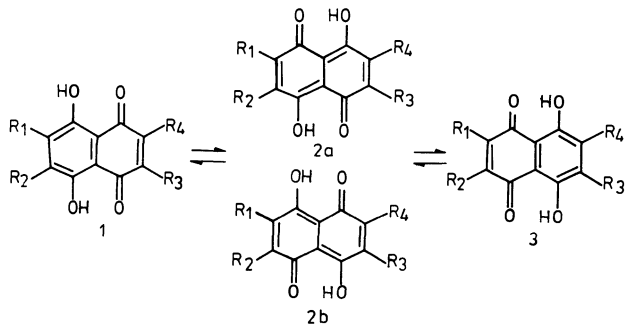

Scheme 1.

In a previous paper[7] we reported a structural study of dimethylnaphthazarin as a charge-transfer complex. This compound is present in the solid state as 2,3-dimethyl-1,5-dihydroxynaphthoquinone whilst a tautomeric equilibrium is observed in chloroform solution. The molecular structure of the tetramethylnaphthazarin in solid state has now been investigated and compared with that in chloroform solution. In a continuing study of the tautomerism of the naphthazarin system, the structural behavior in solution of the methylnaphthazarins with the substitution has now been analyzed. This structural elucidation can be applicable to the polyhydroxyanthraquinones and other related systems.

Synthesis

According to the known procedures,[8] methyl substituted naphthazarins were obtained by Diels–Alder cycloaddition of appropriate 1,3-butadiene and *p*-benzoquinone, followed by acetylation and chromium trioxide oxidation of the adducts and hydrolysis of the corresponding diacetate of naphthazarin (Scheme 2).

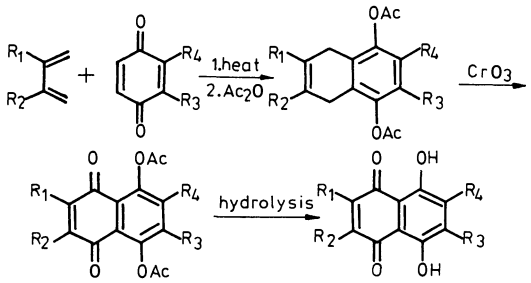

Scheme 2.

Experimental

For the preparation of unknown compounds, the synthesis of the methyl substituted naphthazarins which were not reported in the previous paper,[8] are now described in this section.

All melting points were taken in a hot plate microscope and are uncorrected. ^{1}H NMR spectra were obtained in $CDCl_3$, with TMS as an internal reference, at 60 MHz with a Hitachi Perkin Elmer R 24 A or at 100 MHz with a Varian XL 100 spectrometers. The elemental analysis were made in a Perkin Elmer Model 240 Elemental Analyzer. X-Ray analysis were carried out with an automatic Philips 1100 diffractometer. IR spectra were obtained with a Pye Unicam SP-1100 spectrophotometer.

Dimethylnaphthazarin (General Procedure). 2,3-Dimethyl-*p*-benzoquinone. 2,3-Dimethyl-*p*-benzoquinone was obtained by oxidation of 2,3-dimethylphenol (6 g) with Fremy's salt (1440 ml aqueous solution composed by 30 g of Fremy's salt and 3 g of sodium acetate); ethereal extraction was washed with aqueous sodium hydroxide, dried with sodium

sulfate and finally recrystallized from heptane, yielding 75% of pure quinone, mp 54—55 °C. Found: C, 70.51; H, 5.82%. Calcd for $C_8H_8O_2$: C, 70.57; H, 5.92%.

2,3-Dimethyl-4a,5,8,8a-tetrahydro-1,4-naphthoquinone. A benzene solution of 2,3-dimethyl-*p*-benzoquinone (5 g) and 1,3-butadiene (3.5 g) was heated at 100 °C in a glass sealed tube for 4 h. The adduct was recrystallized from heptane, yielding 81% of the title compound, mp 74—75 °C. IR 1685 cm^{-1} (C=O). ^1H NMR (60 MHz) δ=5.6 (s, 2H), 3.2 (m, 2H), 2.3 (m, 4H), 2.0 (s, 6H). Found: C, 75.58; H, 7.36%. Calcd for $C_{12}H_{14}O_2$: C, 75.76; H, 7.42%.

Diacetate of the 2,3-Dimethyl-5,8-dihydro-1,4-naphthalenediol. A solution of 2,3-dimethyl-4a,5,8,8a-tetrahydro-1,4-naphthoquinone (3 g) in 20 ml of acetic anhydride and 2 ml of acetic acid were refluxed for 3 h. The mixture was added over 500 ml of ice-water. Precipitate was filtered off and the white crystalline product recrystallized from ethanol, yielding 80% of the diol, mp 186 °C. IR 1750 cm^{-1} (C=O). ^1H NMR (60 MHz) δ=5.7 (s, 2H), 3.1 (s, 4H), 2.3 (s, 6H), 2.1 (s, 6H). Found: C, 70.12; H, 6.56%. Calcd for $C_{16}H_{18}O_4$: C, 70.06; H, 6.61%.

Diacetate of the 2,3-Dimethylnaphthazarin. To a saturated solution of chromium trioxide (4.5 g) in acetic acid (80%), was added a solution of the diacetate of the adduct (3 g) in glacial acetic acid, while the reaction temperature was kept at 0—5 °C. The mixture was stirred at room temperature overnight and finally added on 500 ml of ice-water with continuous stirring. By filtration was obtained a yellow solid which was recrystallized from ethanol, yielding 35% of the diacetate, mp 184—186 °C. ^1H NMR at 100 MHz of this solid indicates that it was a mixture of the diacetates of 2,3- and 6,7-dimethylnaphthazarin. Integration of the ^1H NMR signals shows that the ratio of 2,3- to 6,7-dimethyl compounds is 97:3. Found: C, 63.39; H, 4.58%. Calcd for $C_{16}H_{14}O_6$: C, 63.57; H, 4.67%.

Dimethylnaphthazarin. An aqueous solution of sodium hydroxide (10%) was stirred with the diacetate of 2,3-dimethylnaphthazarin for 2 h until a dark blue homogeneous solution was formed. Neutralization was carried out with aqueous hydrochloric acid (10%) and a red precipitate was formed. Then, it was extracted with chloroform and purified by silica-gel column chromatography eluting with chloroform, to give the dimethylnaphthazarin, in nearly quantitative yield, as the sole product, mp 165 °C (subl.). Found: C, 66.20; H, 4.53%. Calcd for $C_{12}H_{10}O_4$: C, 66.05; H, 4.62%.

Trimethylnaphthazarin. 2,3,6-Trimethyl-4a,5,8,8a-tetrahydro-1,4-naphthoquinone. This compound was obtained according to the method described above for 2,3-dimethylnaphthazarin.

2,3-Dimethyl-*p*-benzoquinone (5 g) and isoprene (3 g) in benzene, were refluxed for 4 h. The adduct was recrystallized from heptane, yielding 83% of the title compound, mp 71—72 °C. IR 1680 cm^{-1} (C=O). ^1H NMR (60 MHz) δ=5.3 (s, 1H), 3.2 (m, 2H), 2.3 (m, 4H), 2.0 (two s, 6H), 1.7 (s, 3H). Found: C, 76.47; H, 7.72%. Calcd for $C_{13}H_{16}O_2$: C, 76.44; H, 7.90%.

Diacetate of 2,3,6-Trimethyl-5,8-dihydro-1,4-naphthalenediol. 2,3,6-Trimethyl-4a,5,8,8a-tetrahydro-1,4-naphthoquinone was acetylated in a similar manner as described above, yielding 82% of the title compound, mp 137—138 °C. IR 1750 cm^{-1} (C=O). ^1H NMR (60 MHz) δ=5.5 (m, 1H), 3.0 (s, 4H), 2.3 (two s, 6H), 2.1 (s, 6H), 1.8 (s, 3H). Found: C, 70.91; H, 6.84%. Calcd for $C_{17}H_{20}O_4$: C, 70.81; H, 6.99%.

Diacetate of 2,3,6-Trimethylnaphthazarin. Oxidation of the diacetate of the adduct with chromium trioxide provides a yellow solid, in 35% yield, mp 164—167 °C. ^1H NMR at 100 MHz of this solid, indicates that it was a mixture of the diacetates of 2,3,6- and 2,6,7-trimethylnaphthazarins. Integration of the ^1H NMR signals indicates the ratio of 2,3,6- to 2,6,7-trimethyl compounds is 88:12. Found: C, 64.47; H, 5.29%. Calcd for $C_{17}H_{16}O_6$: C, 64.55; H, 5.10%.

Trimethylnaphthazarin. Hydrolysis of the diacetates of 2,3,6- and 2,6,7-trimethylnaphthazarin gave the trimethylnaphthazarin in quantitative yield, as the sole product, mp 165 °C (subl.). Found: C, 67.20; H, 5.27%. Calcd for $C_{13}H_{12}O_4$: C, 67.23; H, 5.21%.

Tetramethylnaphthazarin. 2,3,6,7-Tetramethyl-4a,5,8,8a-tetrahydro-1,4-naphthoquinone. 2,3-Dimethyl-*p*-benzoquinone (12 g) and 2,3-dimethyl-1,3-butadiene (7.2 g), in benzene, were refluxed for 4 h. The adduct was recrystallized from heptane, yielding 80% of the title compound, 100—101 °C. IR 1680 cm^{-1} (C=O). ^1H NMR (60 MHz) δ=3.2 (m, 2H), 2.2 (m, 4H), 2.0 (s, 6H), 1.6 (s, 6H). Found: C, 76.87,; H, 8.26%. Calcd for $C_{14}H_{18}O_2$: C, 77.03; H, 8.31%.

Diacetate of the 2,3,6,7-Tetramethyl-5,8-dihydro-1,4-naphthalenediol. 2,3,6,7-Tetramethyl-4a,5,8,8a-tetrahydro-1,4-naphthoquinone was acetylated in a similar manner as described above, yielding 75% of the title compound, mp 205—207 °C. IR 1760 cm^{-1} (C=O). ^1H MNR (60 MHz) δ=3.0 (s, 4H), 2.3 (s, 6H), 2.0 (s, 6H), 1.7 (s, 6H). Found: C, 71.36; H, 7.19%. Calcd for $C_{18}H_{22}O_4$: C, 71.50; H, 7.33%.

Diacetate of 2,3,6,7-Tetramethylnaphthazarin. Oxidation of the diacetate of the adduct with chromium trioxide provided 50% of a yellow solid, mp 219—220 °C. Found: C, 65.46,; H, 5.38%. Calcd for $C_{18}H_{18}O_6$: C, 65.45; H, 5.49%.

2,3,6,7-Tetramethylnaphthazarin. Hydrolysis of the diacetate of 2,3,6,7-tetramethylnaphthazarin gave 2,3,6,7-tetramethylnaphthazarin in nearly quantitative yield, mp 186—187 °C (subl.). Found: C, 68.19; H, 5.79%. Calcd for $C_{14}H_{14}O_4$: C, 68.28; H, 5.73%.

X-Ray Structure Determination

Good crystals of 2,3,6,7-tetramethylnaphthazarin for X-ray study were formed by evaporation from an ethyl acetate solution at low temperature.

Space group and preliminary cell dimensions were determined from oscillation and Weissenberg photographs. Accurate lattice constants and intensities were measured on an automatic Philips 1100 diffractometer with Mo $K\alpha$ radiation (0.71069 Å) monochromatized by a graphite crystal. Refined cell parameters were calculated by a least-squares fit of the θ angles of 25 reflections.

The crystal data are: $C_{14}H_{14}O_4$, M=246.3, space group *Ibam* with a=17.479(1), b=9.983(1), c=6.752(1) Å, V=1178.2 Å^3, Z=4, density (calcd)=1.388 g cm^{-3}, absorption coefficient μ=0.9507 cm^{-1}.

The intensities were collected within the range $2<2\theta<60°$ by the $\omega/2\theta$ scan technique. Of the 1386 reflections measured, 1023 were considered observed, $I>2\sigma(I)$. Two standard reflections monitored every 61, remained essentially constants, showing no X-ray damage. Lorentz and polarization factors but no

Table 1. ^{1}H NMR (100 MHz) of the Methyl-Substituted Naphthazarins

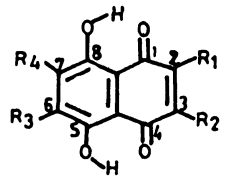	OH	H_2 H_3	H_6 H_7	Me_2 Me_3	Me_6 Me_7
R_1=R_2=R_3=R_4=H	12.40	7.15	7.15	—	—
R_1=Me, R_2=R_3=R_4=H	12.86	—			
	12.54	6.99 (q)	7.30	2.34 (d)	—
		J=1.38 Hz		J=1.38 Hz	
R_1=R_2=Me, R_3=R_4=H	12.60		7.18	2.18	
R_1=R_3=R_4=Me, R_2=H	12.97	—	—	2.23 (d)	2.12
	12.64	6.89 (q)	—	J=1.02 Hz	
		J=1.02 Hz		—	
R_1=R_2=R_3=R_4=Me	13.37	—	—	2.23	2.23

Table 2. ^{1}H NMR (100 MHz) of the Diacetates of the Methyl-Substituted Naphthazarins

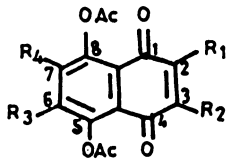	OAc	H_2 H_3	H_6 H_7	Me_2 Me_3	Me_6 Me_7
R_1=R_2=R_3=R_4=H	2.40	6.86	7.31	—	—
R_1=Me, R_2=R_3=R_4=H	2.43	—		2.09 (d)	
	2.41	6.66 (q)	7.35	J=1.6 Hz	—
		J=1.6 Hz		—	
R_1=R_2=Me, R_3=R_4=H	2.43	—	7.30	2.07	—
R_1=R_2=H, R_3=R_4=Me	2.43	6.66	—	—	2.36
R_1=R_2=R_3=Me, R_4=H	2.46	—	—	2.07	2.27
	2.42		7.19		
R_1=R_3=R_4=Me, R_2=H	2.46	6.56	—	—	2.22
	2.42	—		2.07	
R_1=R_2=R_3=R_4=Me	2.47	—	—	2.20	2.39

absorption corrections were applied.

Results and Discussion

^{1}H NMR analysis of the methyl substituted naphthazarins (see Tables 1 and 2).

Naphthazarin. The 100 MHz ^{1}H NMR spectrum of the naphthazarin in solution of $CDCl_3$ shows only one signal for both, the benzenoid and the quinonoid protons, at δ 7.15. This averaged chemical shift of the signals for the benzenoid and the quinonoid protons of the naphthazarin, can be observed as a fast prototropic tautomerism among **1**⇄**2**⇄**3** forms (Scheme 1). This equilibrium is blocked by acetylation of the hydroxyl groups of the naphthazarin and thus, their diacetate shows two different signals for the benzenoid and the quinonoid protons at δ 7.31 and 6.86 respectively (7.09 as averaged value for both protons).

Methylnaphthazarin. ^{1}H NMR spectrum of the methylnaphthazarin shows a quartet signal centered at δ 6.99 (J= 1.38 Hz) for a quinonoid proton, a doublet signal at δ 2.34 (J=1.38 Hz) for a quinonoid methyl and two benzenoid protons at δ 7.30 vs. 6.66 q (J=1.6 Hz), 2.09 d (J=1.6 Hz), and δ=7.35 for their diacetate.

From those spectral data it can be deduced that methylnaphthazarin in $CDCl_3$ solution is mainly as 2-methyl-5,8-dihydroxy-1,4-naphthoquinone (Scheme 1).

Dimethylnaphthazarin. ^{1}H NMR spectrum of the dimethylnaphthazarin shows two protons at δ 7.18 and two methyl groups at 2.18 as singlet signals (vs. 7.30 and 2.07 for their diacetate). Those averaged chemical shift of the signals for annular and methyl protons can be rationalized by the above referred prototropic tautomerism (Scheme 1). In solid state this molecule is mainly present as the tautomer 2,3-dimethyl-5,8-dihydroxy-1,4-naphthoquinone.[7]

Trimethylnaphthazarin. ^{1}H NMR spectrum of the trimethylnaphthazarin shows a quartet signal centered at δ 6.89 (J=1.02 Hz) for a quinonoid type proton, a doublet signal at 2.23 (J=1.02 Hz) for a quinonoid methyl and a singlet signal at δ 2.12 for two methyl

groups (vs. 6.56 q (J=1.4 Hz), 2.07 d (J=1.4 Hz), and 2.22 for the diacetate of 2,6,7-trimethylnaphthazarin). The quadruplet signal indicates that this proton have an appreciable quinonoid character and the averaged chemical shift of the signals can be rationalized by the above referred prototropic tautomerism (Scheme 1) for this compound.

Tetramethylnaphthazarin. ^{1}H NMR spectrum of the tetramethylnaphthazarin shows a singlet at δ=2.23 for all the methyl groups, while their diacetate shows two different signals at δ 2.39 and 2.20 for the methyl groups attached to the benzenoid or to the quinonoid ring respectively (δ 2.30 as averaged value for both methyl groups type). This spectral data indicates that a tautomeric equilibrium among **1**⇄**2**⇄**3** is present, in solution, at room temperature.

Hydroxyl Groups. Hydroxyl groups in these methyl substituted naphthazarins show an important intramolecular chelation of the hydroxyl group in ^{1}H NMR as a bridge hydrogen bonding between phenolic and quinonoid oxygens. The effect of the methyl substituents on the chemical shift of the peri-hydroxyl protons is summarized in Table 1. The signal of the hydroxyl protons in the ^{1}H NMR spectrum is shifted further to downfield when the methyl substituent is nearer to this hydroxyl group. Of the steric and electrical substituent effect, the former is predominant.

X-Ray Analysis of the Tetramethylnaphthazarin

Structure Solution and Refinement. Assuming the centrosymmetric space group *Ibam* (vs. *Iba*2) as it was evidenced by refinement techniques and suggested by the normalized structure factor statistics, the molecule must occupy a special position at the intersection of a twofold axis with a mirror plane or at the intersection of three twofold axes. The first position is the only possible accordingly to the symmetry of the molecule. From an analysis of the Patterson function, it was deduced the position of the molecule. The atomic positions were refined by full-matrix least-square methods, first isotropically and finally anisotropically. The minimized function was $\sum\omega(|F_o|-|F_c|)^2$ with ω= 1.00.

A difference synthesis showed all the hydrogen atoms. These were included in the refinement with an isotropic B value equal to that of the carried carbon atoms and they were allowed to vary. Refinement was stopped when the parameter shifts were $<0.1\sigma$. The adequacy of the weight was checked by inspection of the mean of $\omega|F_o^2|$ as a function of the F_o and sin δ/λ ranges. In both cases the function was nearly constant. The final R and R_ω are 0.087 and 0.068 respectively for all observed reflections. Scattering factors were taken from International Tables for X-Ray Crystallography.[9] Positional and thermal parameters are in Table 3.

The X-ray diffraction study in the solid state of the tetramethylnaphthazarin showed that the molecule is completely planar and centrosymmetric since it is situated in the intersection of a symmetry mirror plane and a twofold axis. Both, the bond distances C(2)–O(1)=1.293(3) and C(4)–O(2)=1.304(4) Å (Fig. 1) and the important intramolecular chelation of the hydroxyl group observed in solution, indicates that the H(O2) should occupy a mid-way position between the two oxygen atoms. A peak was experimentally observed in this position by difference synthesis (Fig. 2); bond distances O(2)–H(O2)=1.24(5) and O(1)···H(O2)= 1.37(5) Å. When the H(O2) was refined, however, its position moved closer to the O(2) atom which may indicate a double-minimum potential energy surface. What should be taken into account is that the temperature factor value of the H(O2) atom was perceptibly decreased. The refined bond length resulted to be O(2)–H(O2)=1.01(5) and the nonbonded intramolecular distance was O(1)···H(O2)=1.63(5) Å.

In addition, the bond lengths C(1)–C(2)=1.444(4) and C(4)–C(5)=1.451(5) indicates a considerable single bond character.

Moreover, C(1)–C(5′)=C(5)–C(1′) has a value of 1.357(4) slightly larger than the corresponding double bond of diacetate of naphthazarin,[10] whilst the corresponding double bond of 2,3-dimethylnaphthazarin[7] and diacetate of tetramethylnaphthazarin[11] reach a similar value. Then, it is assumed that this lengthening is due to the steric hindrance between the two methyl groups bearing in those carbon atoms (see also bond angles in Fig. 1).

Final position and thermal parameters for the tetramethylnaphthazarin are listed in Table 3.

The structural molecular disorder can be considered as a frequent fact in the crystalline solid state of the compounds forming CT complexes. Molecular disorder was analyzed around C_6–C_7, which are more affected by thermal vibrations, in tetramethylnaphthazarin but all the attempts in this way does result unsuccessful and thus molecular disorder was not detected.

Table 3. Tetramethylnaphthazarin Atomic Cordinates and B_{eq}

Atom	x/a	y/b	z/c	B_{eq}
C_1	0.6315(2)	0.6165(3)	0.0000	3.2899
C_2	0.6064(1)	0.4787(3)	0.0000	3.3688
C_3	0.5271(1)	0.4474(2)	0.0000	2.6056
C_4	0.5014(2)	0.3131(3)	0.0000	3.3425
C_5	0.4204(2)	0.2821(3)	0.0000	3.3951
C_6	0.7170(2)	0.6384(5)	0.0000	5.1322
C_7	0.3986(3)	0.1365(4)	0.0000	5.7112
O_1	0.6574(1)	0.3847(3)	0.0000	5.0532
O_2	0.5496(2)	0.2135(3)	0.0000	5.1585
H_{02}	0.6030(3)	0.2560(5)	0.0000	8.5273
H_{61}	0.7420(2)	0.5970(3)	0.1120(5)	7.8117
H_{63}	0.7310(3)	0.7260(6)	0.0000	8.5273
H_{71}	0.3730(2)	0.1090(3)	0.0990(6)	8.5273
H_{73}	0.4420(3)	0.0750(5)	0.0000	8.5273

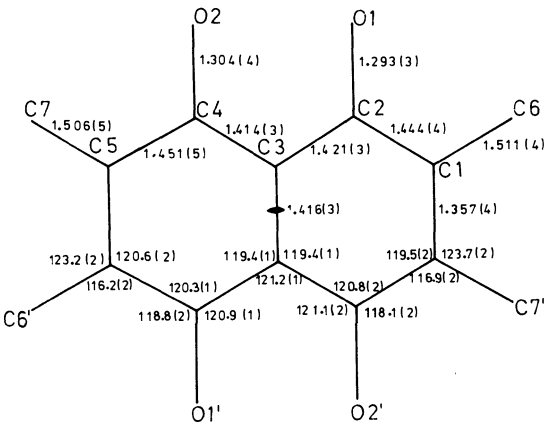

Fig. 1. Bond distances and angles of tetramethylnaphthazarin.

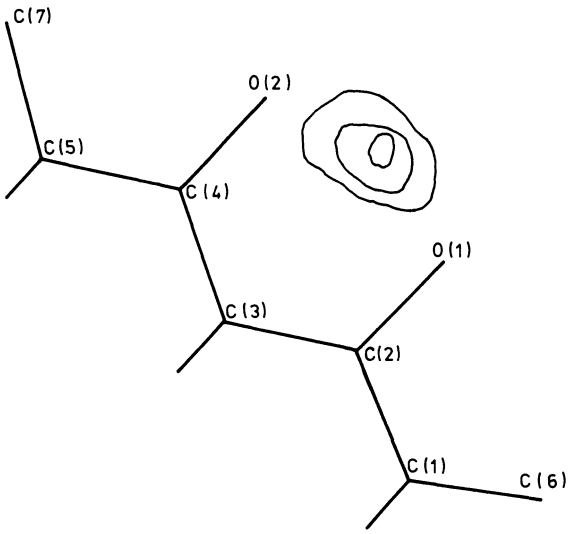

Fig. 2. Density map showing the hydroxyl hydrogen position before refinement.

There could be distortion in the bond distances of the naphthazarin nucleus (Fig. 1) arising from the fact that a molecular charge-transfer complex is formed between two molecules of the tetramethylnaphthazarin. The molecular overlap is shown in Fig. 3 and the interplanar distance, C/2, is 3.38 Å.

Finally, according to bond distances in tetramethylnaphthazarin, the molecular structure of this compound, in solid state, could be represented as a resonance hybrid between molecular forms of the type **2a**. **2b** and **1** and **3** contributing in minor extent, Scheme 1, better than a tautomerism because of the absence of molecular disorder.

Ring substitution seems to affect the tautomerism of the naphthazarin system in chloroform solution. Thus, while methylnaphthazarin is present as the tautomer

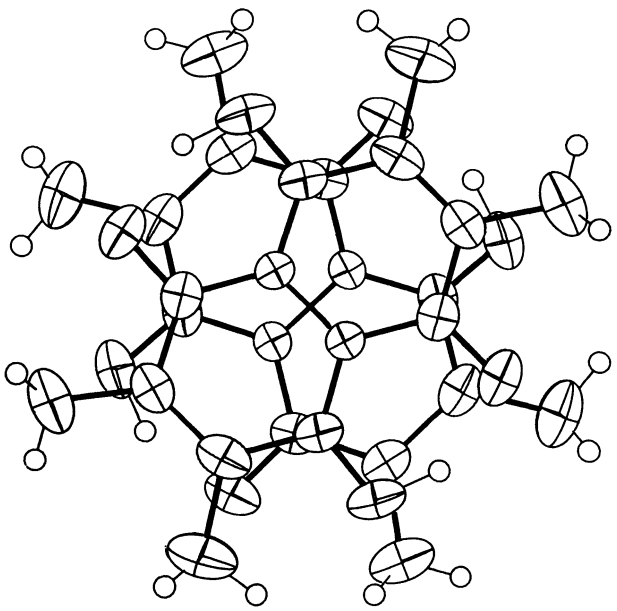

Fig. 3. Molecular overlapping of tetramethylnaphthazarin being 3.38 Å the interplanar distance.

with the substituent on the quinonoid ring, dimethyl-, trimethyl-, and tetramethylnaphthazarins, which have two methyl groups attached on the same ring show averaged structures according to the prototropic equilibrium pointed out in Scheme 1. This effect agrees with the observed increase of the C_2–C_3 bond length in solid state.

References

1) J. S. Grossert, *Chem. Soc. Rev.*, **1**, 1 (1972).

2) T. Kametani and K. Fukumoto, *Med. Res. Rev.*, **1**, 23 (1981).

3) a) C. Pascard-Billy, *Bull. Soc. Chim. Fr.*, **1962**, 2282; *Acta Crystallogr.*, **15**, 519 (1962). b) P. D. Cradwick and D. Hall, *ibid.*, *Sect B*, **27**, 1990 (1971).

4) W. Shiau, E. N. Duesler, I. C. Paul, D. Y. Curtin, W. G. Blann, and C. A. Fyfe, *J. Am. Chem. Soc.*, **102**, 4546 (1980).

5) H. Brockmann and A. Zeek, *Chem. Ber.*, **101**, 4221 (1968).

6) H. L. K. Schmand and P. Boldt, *J. Am. Chem. Soc.*, **97**, 447 (1975).

7) J. G. Rodriguez, P. Smith-Verdier, F. Florencio, and S. Garcia-Blanco, *J. Mol. Struct.*, **112**, 101 (1984).

8) F. Fariña, M. Lora-Tamayo, and C. Suarez, *Tetrahedron Lett.*, **1959**, 9.

9) A list of F_o—F_c can be obtained from the authors on request.

10) J. G. Rodriguez, F. H. Cano, and S. Garcia-Blanco, *Acta Crystallogr., Sect B*, **23**, 491 (1979).

11) J. G. Rodriguez, F. H. Cano, and S. Garcia-Blanco, *Cryst. Struct. Commun.*, **8**, 93 (1979).

Balance in Forces Acting on Electrons in Molecules

Makoto ISIHARA
Department of General Education, Shotoku-Gakuen Women's Junior College, Nakauzura 1-38, Gifu 500
(Received April 2, 1986)

Synopsis. The force theorem is generalized by using the spin-specified momentum operator in the hypervirial theorem. A theorem consequent on this concerns a balance in forces acting on up- and down- spin electrons. The theorem is expected to be useful for examining accuracy of approximate wave functions for open-shell molecules.

In the previous paper[1] the author has shown the spin virial theorem as a consequence of a generalization of the virial theorem, suggesting a natural way of deriving various spin-related theorems from the hypervirial theorem.[2] Amongst such theorems, fundamental and significant in molecular electronic structure theory is a theorem obtained through a generalization of the force theorem.[3,4] The theorem has lucid physical meaning, describing a balance in forces acting on up- and down-spin electrons.[5] Although the derivation is rather straightforward, the explicit expression will be worth communicating with some remarks.

Let $\phi_{i\sigma}(\boldsymbol{r})$ be the σ-spin component of the electron field operator. The spin index σ is allowed to take $\uparrow$ (up) or $\downarrow$ (down), $\boldsymbol{r}$ stading for spatial coordinates. We use the notation $\overline{\sigma}$ for the spin state opposite to σ in what follows. Suppose the electronic Hamiltonian consisting of the kinetic energy of electrons, the nuclear attraction potential, and the electronic repulsion potential. It is suitable for our purpose to retain the spin index; we put

$$H = \sum_{\sigma} (T_{\sigma} + V_{\sigma} + W_{\sigma\sigma} + W_{\sigma\overline{\sigma}}) \tag{1}$$

with

$$T_{\sigma} = \int \phi_{\sigma}^{\dagger}(\boldsymbol{r})(-\nabla^2/2)\phi_{\sigma}(\boldsymbol{r})\mathrm{d}\boldsymbol{r}, \tag{2}$$

$$V_{\sigma} = \int \phi_{\sigma}^{\dagger}(\boldsymbol{r}) \sum_{\alpha} (-Z_{\alpha}|\boldsymbol{r}-\boldsymbol{R}_{\alpha}|^{-1})\phi_{\sigma}(\boldsymbol{r})\mathrm{d}\boldsymbol{r}, \tag{3}$$

and

$$W_{\sigma\tau} = \frac{1}{2}\iint \phi_{\sigma}^{\dagger}(\boldsymbol{r})\phi_{\tau}^{\dagger}(\boldsymbol{q})|\boldsymbol{r}-\boldsymbol{q}|^{-1}\phi_{\tau}(\boldsymbol{q})\phi_{\sigma}(\boldsymbol{r})\mathrm{d}\boldsymbol{q}\mathrm{d}\boldsymbol{r}, \tag{4}$$

where Z_{α} and $\boldsymbol{R}_{\alpha}$ are the atomic number and the position of the α-th nucleus, respectively. Of course, we have

$$W_{\uparrow\downarrow} = W_{\downarrow\uparrow}. \tag{5}$$

On the other hand, we define the momentum operator as

$$\boldsymbol{P}_{\sigma} = \int \phi_{\sigma}^{\dagger}(\boldsymbol{r})(-\mathrm{i}\nabla)\phi_{\sigma}(\boldsymbol{r})\mathrm{d}\boldsymbol{r} \quad (\sigma=\uparrow,\downarrow), \tag{6}$$

specifying the spin state. What is to be done is to work out the commutator between $\boldsymbol{P}_{\sigma}$ and H.

Among the commutators of $\boldsymbol{P}_{\sigma}$ with the constituents of H, only the two kinds are nonvanishing:

$$[V_{\sigma}, \boldsymbol{P}_{\sigma}] = -\mathrm{i}\boldsymbol{F}_{\sigma} \tag{7}$$

and

$$[W_{\sigma\overline{\sigma}}, \boldsymbol{P}_{\sigma}] = -\mathrm{i}\boldsymbol{B}_{\sigma\overline{\sigma}}/2, \tag{8}$$

where

$$\boldsymbol{F}_{\sigma} = \int \phi_{\sigma}^{\dagger}(\boldsymbol{r}) \sum_{\alpha} (-Z_{\alpha}(\boldsymbol{r}-\boldsymbol{R}_{\alpha})|\boldsymbol{r}-\boldsymbol{R}_{\alpha}|^{-3})\phi_{\sigma}(\boldsymbol{r})\mathrm{d}\boldsymbol{r} \tag{9}$$

and

$$\boldsymbol{B}_{\sigma\overline{\sigma}} = \iint \phi_{\sigma}^{\dagger}(\boldsymbol{r})\phi_{\overline{\sigma}}^{\dagger}(\boldsymbol{q})(\boldsymbol{r}-\boldsymbol{q})|\boldsymbol{r}-\boldsymbol{q}|^{-3}\phi_{\overline{\sigma}}(\boldsymbol{q})\phi_{\sigma}(\boldsymbol{r})\mathrm{d}\boldsymbol{q}\mathrm{d}\boldsymbol{r}. \tag{10}$$

We can regard $\boldsymbol{F}_{\sigma}$ and $\boldsymbol{B}_{\sigma\overline{\sigma}}$ as representing the forces exerted on σ-spin electrons by nuclei and by $\overline{\sigma}$-spin electrons, respectively. After all, since H contains $W_{\sigma\overline{\sigma}}$ twice, we obtain

$$[H, \boldsymbol{P}_{\sigma}] = -\mathrm{i}(\boldsymbol{F}_{\sigma} + \boldsymbol{B}_{\sigma\overline{\sigma}}). \tag{11}$$

It should be noted that

$$\boldsymbol{B}_{\uparrow\downarrow} = -\boldsymbol{B}_{\downarrow\uparrow}. \tag{12}$$

We often abbreviate $\boldsymbol{B}_{\uparrow\downarrow}$ to $\boldsymbol{B}$ below, $\boldsymbol{B}_{\downarrow\uparrow}$ being identically equal to $-\boldsymbol{B}$.

The hypervirial theorem asserts that an arbitrary stationary state of a system of the Hamiltonian H fulfils

$$\langle [H, A] \rangle = 0 \tag{13}$$

for any operator A of the system, the bracket standing for the stationary state expectation value. Now we adopt $\boldsymbol{P}_{\uparrow} \pm \boldsymbol{P}_{\downarrow}$ as A. A new result, to which we will refer tentatively as the spin force theorem, immediately follows besides the force theorem;

$$\begin{cases} \langle \boldsymbol{F} \rangle = 0 & (14) \\ \langle \Delta\boldsymbol{F} \rangle + \langle \Delta\boldsymbol{B} \rangle = 0 & (15) \end{cases}$$

with

$$\boldsymbol{F} = \boldsymbol{F}_{\uparrow} + \boldsymbol{F}_{\downarrow}, \tag{16}$$

$$\Delta\boldsymbol{F} = \boldsymbol{F}_{\uparrow} - \boldsymbol{F}_{\downarrow} \tag{17}$$

and

$$\Delta\boldsymbol{B} = \boldsymbol{B}_{\uparrow\downarrow} - \boldsymbol{B}_{\downarrow\uparrow} = 2\boldsymbol{B}. \tag{18}$$

From now on, we abbreviate the force theorem to FT and the spin force theorem to SFT. Whereas FT is derivable also from the electrostatic theorem,[6] SFT is not. The latter has no classical counterpart in a strict sense, being inherently quantum-mechanical. If $\boldsymbol{P}_{\uparrow}$ and $\boldsymbol{P}_{\downarrow}$ are taken as A, we have the set of equations tantamount to the set of FT and SFT;

$$\begin{cases} \langle \boldsymbol{F}_{\uparrow} \rangle + \langle \boldsymbol{B} \rangle = 0 & (19) \\ \langle \boldsymbol{F}_{\downarrow} \rangle - \langle \boldsymbol{B} \rangle = 0, & (20) \end{cases}$$

where FT is implicit. Here note that each of the above two equations is equivalent to SFT under FT because of

$$\langle \Delta F \rangle = 2\langle F_{\uparrow} \rangle = -2\langle F_{\downarrow} \rangle. \quad (21)$$

An important point is that SFT directly concerns the interelectronic interaction in sharp contrast to FT.

The molecular symmetry sometimes makes FT trivial.[4] The same is true for SFT, the simplest example being atoms and homonuclear diatomic molecules. In particular, the symmetry in distributions of up- and down-spin electrons is enough for SFT (aside from FT). For most of molecular open-shell systems SFT is obviously meaningful. One can thus utilize SFT together with FT for examining accuracy of approximate wave functions for such systems. The fulfillment of these theorems is a necessary condition for sound approximate wave functions.[7] Surely it is interesting to see how far the theorems hold for elaborate approximate wave functions obtained with various advanced methods; this will be entrusted to computational chemists. Finally we add that SFT lets the spin virial theorem be origin-independent as FT does the virial theorem.[4]

References

1) M. Isihara, *Bull Chem. Soc. Jpn.*, **58**, 2472 (1985).
2) J. O. Hirschfelder, *J. Chem. Phys.*, **33**, 1462 (1960).
3) One should not confuse the force theorem with the Hellmann–Feynman theorem or the electrostatic theorem.
4) S. T. Epstein, "The Variation Method in Quantum Chemistry," Academic Press, New York (1974), Section 18.
5) Strictly speaking, we should say "electrons in the up-spin state" instead of "up-spin electrons" which is used throughout for convenience.
6) R. P. Feynman, *Phys. Rev.*, **56**, 340 (1939); A. C. Hurley, *Proc. R. Soc. London A*, **226**, 170 (1954).
7) The unrestricted Hartree-Fock function fulfills SFT as well as FT (in the exact limit of approximation). For this point, see Ref. 1.

The Preparation and Thermal Properties of Terminal Disubstituted *N*-(4-Benzoyloxybenzylidene)anilines

Shunsuke TAKENAKA,* Tetsuya IKEMOTO, and Shigekazu KUSABAYASHI
Department of Applied Chemistry, Faculty of Engineering, Osaka University, Suita, Osaka 565
(Received May 6, 1986)

Synopsis. The homologous series of *N*-[4-(4-*n*-alkoxybenzoyloxy)benzylidene]-4-(2-methylbutoxy)aniline (**1**), and *N*-[4-[4-(2-methylbutoxy)benzoyloxy]benzylidene]-4-*n*-alkoxyaniline (**2**), and *N*-[4-(4-*n*-alkoxybenzoyloxy)-3-hydroxybenzylidene]-4-(2-methylbutoxy)aniline (**3**) where the 2-methylbutoxyl group has an S-configuration, have been prepared. Series **1** and **2** form a chiral smectic C (S_C^*) phase in addition to a cholesteric (Ch) and a chiral smetic G (S_G^*) phases, and series **3** form (S_C^*) and Ch phases.

It has been known that three-ring compounds incorporating ester **4** or azomethine **5** linkages display highly stable liquid crystalline phases.[1,2]

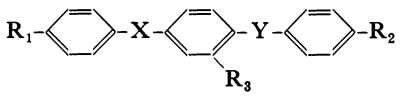

1 X = -COO-, Y = -CH=N-, R_1=*n*-$C_nH_{2n+1}O$-, R_2 = 2MBO-, R_3 = H-

2 X = -COO-, Y = -CH=N-, R^1 = 2MBO-, R_2 = *n*-$C_nH_{2n+1}O$-, R_3 = H-

3 X = -COO-, Y = -CH=N-, R_1 = *n*-$C_nH_{2n+1}O$-, R_2 = 2MBO-, R_3 = HO-

4 X = -COO-, Y = -OOC-, R_1, R_2 = *n*-$C_nH_{2n+1}O$-, R_3 = H-

5 X = -N=CH-, Y = -CH=N-, R_1, R_2 = *n*-$C_nH_{2n+1}O$-, R_3 = H-

(2MBO- = (*S*)-2-methylbutoxy)

Series **4** in which the linkages are relatively polar, and flexible, display stable nematic (N), smectic A and C phases (S_A and S_C, respectively). Series **5** in which the linkages are less polar and more rigid than those of series **4**, display some tilt smectic phases in addition to an N phase, and undergo complicating smectic-smectic transitions.[2] On the other hand, the series of **1—3**, which incorporate both ester and azomethine linkages, are expected to display mesomorphic properties between those two series.

In this paper, we have examined the thermal properties of series **1—3**, where a chiral group is introduced at one of the terminal positions, in order to examine the applicability to ferroelectric liquid crystals.

Experimental

Materials. 4-[(*S*)-2-Methylbutoxy]aniline was obtained by the reaction of *p*-nitrophenol and (*S*)-2-methyl-1-bromobutane, followed by catalytic hydrogenation with palladium-carbon. 4-[(*S*)-2-Methylbutoxy]benzoic acid was obtained by the reaction of methyl 4-hydroxybenzoate and (*S*)-2-methyl-1-bromobutane, followed by hydrolysis. 4-(4-*n*-Alkoxybenzoyloxy) and 4-[4-(2-methylbutoxy)benzoyloxy]-benzaldehydes and 4-(4-*n*-alkoxybenzoyloxy)-3-hydroxybenzaldehydes were obtained by the reaction of corresponding acid chlorides and 4-hydroxybenzaldehyde or 2,4-dihydroxybenzaldehyde in dry pyridine. Series **1—3** were obtained by the condensation of the corresponding benzaldehydes with the substituted anilines in absolute ethanol. Purification was carried out by recrystallization from absolute ethanol. The purity of the products was confirmed by elementary analysis.

Method: The transition temperatures were determined by using a Nikon POH polarizing microscope fitted with a Mettler FP-5 heating stage, and also a Daini-seikosha SSC-560 differential scanning calorimeter.

Results and Discussion

The transition temperatures and latent heats for series **1—3**, are summarized in Tables 1—3.

The S_G^* phase was identified by an examination of the miscibility diagram with *p*-bis(4-*n*-hexylphenyliminomethyl)benzene.[3]

The series **1** and **2** fundamentally have a similar mesomorphic sequence, i.e., S_G^*-S_C^*-Ch-I, while the

Table 1. Transition Temperatures (°C) and Latent Heats (kJ mol^{-1}) of Series **1**

n	C	S_G^*	S_C^*	Ch	I	$\Delta H_{S_C^*-Ch}$
3[a]	122.7	—	—	222.6	—	
4[b]	122.2	—	—	216.2	—	
5	104.5	—	—	114.2	209.1	~0
6	102.2	(82.9)		126.5	205.3	2.4
7	85.0	(75.5)		131.7	193.2	1.8
8	94.0	(78.2)		144.8	197.3	2.2
9	97.0	(74.5)		145.2	185.6	1.7

a) This compound underwent a crystal-crystal transition at 116.5°C. b) This compound underwent a crystal-crystal transition at 119.6°C. Refer to footnote in Table 2.

Table 2. Transition Temperatures (°C) and Latent Heats (kJ mol^{-1}) of Series **2**

n	C	S_G^*	S_C^*	Ch	I	$\Delta H_{S_C^*-Ch}$
1	101.0	—			233.3	—
2	118.6	(110.1)	—		237.4	—
3	119.5	(118.5)	—		218.3	—
4	113.4	116.0	—		215.9	—
5	102.7	(101.0)	—		205.5	—
6	92.6	(83.5)		99.8	202.3	1.4
7	94.5	(75.0)		111.3	196.1	1.6
8	81.6	(76.7)		115.9	193.6	1.4
9	91.1	(73.5)		119.8	187.7	1.4
10	88.6	(73.1)		122.7	184.7	1.3

C, S_G^*, S_C^*, Ch, and I represent crystal, smectic G* smectic C*, cholesteric, and isotropic phases, respectively. Parentheses indicate monotropic transitions.

Table 3. Transition Temperatures (°C) and Latent Heats (kJ mol^{-1}) of Series **3**

n	C	S_G^*	S_C^*	Ch	I	$\Delta H_{S_C^*-Ch}$
3	. 133.0	—	—	. 223.6	.	—
4	. 129.8	—	—	. 221.7	.	—
5	. 119.1	—	(. 99.0)	. 208.1	.	~0
6	. 120.5	—	(. 112.4)	. 213.4	.	1.0
7	. 121.9	—	. 122.5	. 210.0	.	2.2
8	. 112.7	—	. 131.3	. 205.2	.	2.2
9	. 113.1	—	. 135.6	. 198.6	.	2.5

thermal stabilities of the mesophases are slightly different. The phase sequence is simpler than those of *p*-bis(4-*n*-alkoxyphenyliminomethyl)benzenes (**5**),[2] and the thermal stability of the S_C^* phase is higher than those of *p*-bis(4-*n*-alkoxyphenoxycarbonyl)benzenes (**4**).[1] The difference in the smectic properties must be concerned with the difference in the geometrical and electrostatic structure, i.e., the cores of **1** and **2** are more rigid but less polar than those of **4**, and more polar but less rigid than **5**.

A noteworthy fact in the two series is that series **1** display a more stable S_C^* phase than **2**. A similar trend has been observed in the thermal properties of some liquid crystals. For example, 4-*n*-alkoxyphenyl 4-[(*S*)-2-methylbutoxy]benzoates do not display an S_C^* phase, while 4-[(*S*)-2-methylbutoxy]phenyl 4-*n*-alkoxybenzoates display it.[4] From these facts, we can assume that a relative orientation of the 2-methylbutoxyl group, a relatively bulky substituent, with respect to the carboxyl group, a polar linkage, is important in determining the thermal stability of the S_C^* phase.

In series **3**, a lateral hydroxy group was introduced in order to increase the chemical stability of the azomethine linkage. Although the mesophase stabilities of **3** are lower than those of series **1** and **2**, probably due to the increased molecular breadth, these appear to have similar mesomorphic properties, while no S_G^* phase could be observed in series **3**.

It is concluded that series **1**—**3** having one ester and one azomethine linkages have simpler smectic polymesomorphism than the corresponding azomethine compounds **5**, and display a higher stable S_C^* phase than the corresponding ester compounds **4**, so that the present series are more useful for dopant liquid crystals for devices employing a ferroelectric mode.

References

1) D. Demus, H. Demus, H. Zaschke, "Flüssig Kristalle im Tabellen', VEB Deutscher Verlag für Grundstoff Industrie," Leipzig (1974).

2) M. E. Neubert and L. J. Maurer, *Mol. Cryst. Liq. Cryst.*, **43**, 313 (1977).

3) A. Wiegelegen, L. Richter, J. Deresch, and D. Demus, *Mol. Cryst. Liq. Cryst.*, **59**, 329 (1980).

4) J. W. Goodby and T. M. Leslie, "Liquid Crystals and Ordered Fluids," ed by A. C. Griffin and J. F. Johnson, Plenum Press, New York (1984), Vol. 4, p. 1.

Photoinduced Hydrogen Evolution with Viologen Linked Porphyrin in a Micellar System

Ichiro OKURA,* Naruhiko KAJI, Shigetoshi AONO, and Tsuyoshi NISHISAKA†
Department of Chemical Engineering, Tokyo Institute of Technology, Meguro-ku, Tokyo 152
†Health Science Center, Tokyo Noh-Koh University, Nakamachi, Koganei, Tokyo 184
(Received May 28, 1986)

Synopsis. Viologen linked porphyrins, $ZnP(C_nV)_4$, with various methylene chain lengths (n=2—5) between the porphyrin and the viologen have been synthesized. These compounds were applied to photoinduced hydrogen evolution in a system containing NADPH-$ZnP(C_nV)_4$-hydrogenase under steady state irradiation. On the addition of surfactant to the system, a remarkable rate increase of hydrogen evolution was observed in the case of $ZnP(C_5V)_4$.

Photoinduced hydrogen evolution systems containing an electron donor, a photosensitizer, an electron carrier, and a catalyst have been studied extensively. As photosensitizers metallo-porphyrins have been widely used and methyl viologen has been a popular electron carrier. Recently we synthesized viologen linked water-soluble zinc porphyrins and found that they took part as both a photosensitizer and an electron carrier in the same molecule for photoinduced hydrogen evolution.[1,2] To improve the rate of photoinduced hydrogen evolution, effective charge separation between the photoexcited sensitizer and the quencher is needed. As electrostatic field, such as a micellar surface, has been widely applied to separate the charges effectively.[3] Only in a few of the micellar systems, however, has the hydrogen evolution been studied. In this paper we describe the effect of micelles on the photoinduced hydrogen evolution in a system containing NADPH, $ZnP(C_nV)_4$ and hydrogenase.

Experimental

The structure of the viologen linked water soluble zinc porphyrins, $ZnP(C_nV)_4$, is illustrated in Fig. 1. These compounds were synthesized as described elsewhere.[1,2] Hydrogenase was obtained from Desulfovibrio vulgaris (Miyazaki type, IAM 12604) and purified by Yagi's method.[4] The concentration of hydrogenase is not known, but 1.48×10^{-6} mol of hydrogen was generated by the following reaction system: hydrogenase (0.5 cm^3)-$Na_2S_2O_4$ (5.7×10^{-3} mol dm^{-3})-methylviologen (4.1×10^{-5} mol dm^{-3}) in 5.0 cm^3 of 0.02 mol dm^{-3} Tris-HCl buffer (pH 7.0) at 30 °C for 10 min.

Laser flash photolysis was carried out by using a Nd-YAG laser, model DCR-2A-10 from Quanta-Ray Inc., generating the second harmonic (532 nm). Pulses of 10 ns duration, energy of 200 mJ per pulse, and a repetion rate 10 Hz were used for excitation of the sample solution throughout this study. The light beam, after passage through a sample cell, was collimated into the entrance slit of a monochromator (model BM 50/50 from B & M Spectronik Co.). The output signal from the photomultiplier (Hamamatsu Photonics, R 446) attached to the slit of the monochromator was displayed

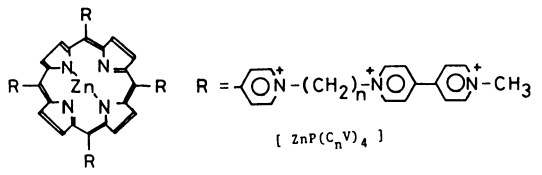

Fig. 1. Illustration of the structure of $ZnP(C_nV)_4$.

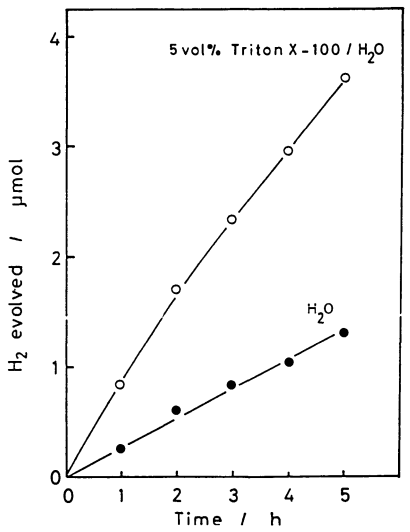

Fig. 2. Time dependence of hydrogen evolution. Sample solution (6.5 cm^3) containing $ZnP(C_5V)_4$ (2.0×10^{-6} mol dm^{-3}), NADPH (1.0×10^{-3} mol dm^{-3}) and hydrogenase (0.5 cm^3) was irradiated at 30°C.

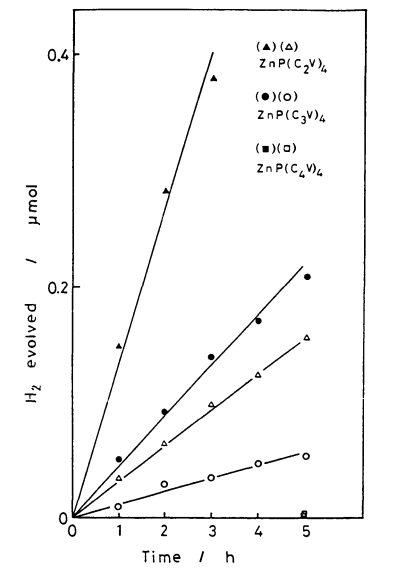

Fig. 3. Time dependence of hydrogen evolution. Sample solution (6.5 cm^3) containing $ZnP(C_nV)_4$ (2.0×10^{-6} mol dm^{-3}), NADPH (1.0×10^{-3} mol dm^{-3}) and hydrogenase (0.5 cm^3) was irradiated at 30°C. (△), (○), (□): 5 vol% Triton X-100/H_2O. (▲), (●), (■): H_2O.

Table 1. Lifetimes of Excited Triplet State of $ZnP(C_nV)_4$

Solvent	$ZnP(C_2V)_4$	$ZnP(C_3V)_4$	$ZnP(C_4V)_4$	$ZnP(C_5V)_4$
H_2O τ_T/s	190	510	640	470
10% Triton X-100 τ_T/s	150	400	890	2000

on a Hitachi oscilloscope, model V-1050F.

For steady state irradiation a 200 W tungsten lamp was used as a light source. The light of wavelength less than 390 nm was removed by a Toshiba L-39 filter.

Photoinduced hydrogen evolution was carried out with $ZnP(C_nV)_4$ with n=2—5 under steady state irradiation at 30 °C. A sample solution containing nicotineamide-adenine dinucleotide phosphate (reduced form, NADPH), $ZnP(C_nV)_4$, hydrogenase and Triton X-100 was deaerated by repeated freeze-pump-thaw cycles.

Results and Discussion

When an aqueous solution containing $ZnP(C_nV)_4$, NADPH and hydrogenase was irradiated, hydrogen evolution was observed as added in Figs. 2 and 3. When surfactant, Triton X-100, was added to the above three component system, remarkable increase of hydrogen evolution rate was observed in the case of $ZnP(C_nV)_4$. On the contrary, the hydrogen evolution rates decreased in the cases of $ZnP(C_2V)_4$ and $ZnP(C_3V)_4$.

The photoexcited lifetimes of these compounds in the presence and in the absence of Triton X-100 were investigated by using laser flash photolysis technique (Table 1). The triplet lifetime of viologen linked porphyrin, $ZnP(C_5V)_4$, increased in the case of the system showing a rise of hydrogen evolution rate by the addition of Triton X-100. On the contrary the triplet lifetimes of $ZnP(C_2V)_4$ and $ZnP(C_3V)_4$ slightly decreased in the case of the systems showing a decrease of hydrogen evolution rate with Triton X-100.

The fact that hydrogen evolution rate increases in the case of $ZnP(C_5V)_4$ in spite of the increase of the triplet state lifetime indicates that the intramolecular quenching between the photoexcited porphyrin and viologen occurs only with difficulty. Accordingly, the reductive quenching of the photoexcited triplet state of porphyrin by NADPH will be predominant, and the following reaction mechanism is proposed.

$$^3P^*\text{-}V + D \longrightarrow P^-\text{-}V + D^+$$

$$P^-\text{-}V \longrightarrow P\text{-}V^-$$

At the first stage of the reaction the photoexcited triplet state ($^3P^*$-V) is reductively quenched by NADPH (D) and the reduced form of porphyrin (P^--V) is formed after which the electron transfers from the porphyrin to the viologen.

The cause of the remarkable increase of hydrogen evolution rate in micelles in the case of $ZnP(C_5V)_4$ has not been clarified completely. As the absorption spectrum of $ZnP(C_5V)_4$ in water is broad, there are some intra- or inter-molecular interactions. When the surfactant, Triton X-100, was added to the system, a sharp absorption spectrum of $ZnP(C_5V)_4$ was obtained. The result indicates that the intra- or inter-molecular interactions disappear and that the suppression of the interaction extends the lifetime of the excited $ZnP(C_5V)_4$ in the micelles.

References

1) I. Okura, S. Aono, and N. Kaji, *J. Chem. Soc., Chem. Commun.*, **1986**, 170.

2) N. Kaji, S. Aono, and I. Okura, *J. Mol. Catal.*, **36**, 201 (1986).

3) a) N. J. Turro, M. Gratzel, and A. M. Braun, *Angew. Chem., Int. Ed. Engl.*, **19**, 675 (1980); b) K. Kano, K. Takuma, T. Ikeda, M. Nakajima, Y. Tsutsui, and T. Matsuo, *Photochem. Photobiol.*, **27**, 695 (1978); c) J. R. Escabi-perez, F. Nome, and J. H. Fendler, *J. Am. Chem. Soc.*, **99**, 7749 (1977); d) U. Lachish, M. Ottolenghi, and J. Rabani, *J. Am. Chem. Soc.*, **99**, 8062 (1977).

4) T. Yagi, *J. Biochem.*, **68**, 694 (1970).

Temperature Dependences of ^{69}Ga and ^{81}Br NQR Frequencies in $[R_4N]_2Ga_2Br_6$ ($R=CH_3$ and C_2H_5)

Hideta ISHIHARA,* Koji YAMADA,† and Tsutomu OKUDA†
Department of Chemistry, Faculty of Education, Saga University, Honjo-machi, Saga 840
†Department of Chemistry, Faculty of Science, Hiroshima University, Higashisenda-machi, Naka-ku, Hiroshima 730
(Received June 7, 1986)

Synopsis. Temperature dependences of ^{69}Ga and ^{81}Br NQR frequencies showed that phase transitions take place at 98 and 137 K in $[(CH_3)_4N]_2Ga_2Br_6$ and that the C_3 reorientation of the $GaBr_3$ group occurs in $[(C_2H_5)_4N]_2Ga_2Br_6$ around room temperature.

Unusual temperature dependences of ^{69}Ga and ^{81}Br nuclear quadrupole resonance (NQR) frequencies were observed for $[R_4N]_2Ga_2Br_6$ ($R=CH_3$ and C_2H_5) in a study of bond character in Ga(II) compounds.[1] Although no crystal structure analysis of these two compounds has been reported as yet, we expect that the ethane-like $Ga_2Br_6^{2-}$ ions exist in both crystals, and that the cations are situated on the extension of the Ga-Ga bond of the $Ga_2Br_6^{2-}$ ion in a similar manner to the crystal of $[(CH_3)_4N]_2Ga_2Cl_6$.[2] On the basis of these expected crystal structures, we examined a possibility that unusual temperature dependences of ^{69}Ga and ^{81}Br NQR frequencies can be attributed to reorientations of the cation and/or anion.

Experimental

The compounds were prepared according to Ref. 3. NQR spectra of ^{81}Br and ^{69}Ga were recorded on a pen-recorder using a superregenerative oscillator with Zeeman modulation. The temperature dependence of the NQR frequencies was measured in the temperature range between 77 and ca. 300 K by immersing the sample into a bath of cooled petroleum-ether or heated silicone oil. The sample-temperature was measured using a copper-constantan thermocouple whose e.m.f. was displayed on a digital multimeter. Broad-line ^1H NMR spectra were observed at 60 MHz using a JEOL JNM-FW 60 spectrometer in a temperature range between 300 and 110 K and at 77 K.

Results and Discussion

Figure 1 shows the temperature dependence of ^{69}Ga NQR frequencies in $[(CH_3)_4N]_2Ga_2Br_6$. Three weak ^{69}Ga NQR lines were observed at 77 K and intensities of these lines increased on raising the temperature to 83 K. Another resonance line appeared at 83 K. The discontinuous change of the temperature dependence took place at 98 K and four NQR lines reduced to three. On further increasing the temperature, three lines reduced to two at 137 K. Accordingly we infer that phase transitions take place at 98 and 137 K. Figure 2 shows the temperature dependence of ^{81}Br NQR frequencies. The ^{81}Br NQR lines observed between 77 and 137 K were too weak to measure accurately the frequency variation especially above 98 K. Five NQR lines were observed above 137 K. A differential thermal analysis (DTA) experiment was carried out above 100 K using a homemade apparatus. On heating, an endothermic peak with a small shoulder at

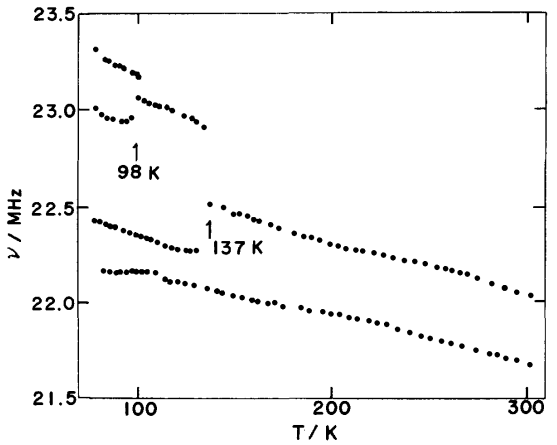

Fig. 1. Temperature dependence of ^{69}Ga NQR frequencies in $[(CH_3)_4N]_2Ga_2Br_6$.

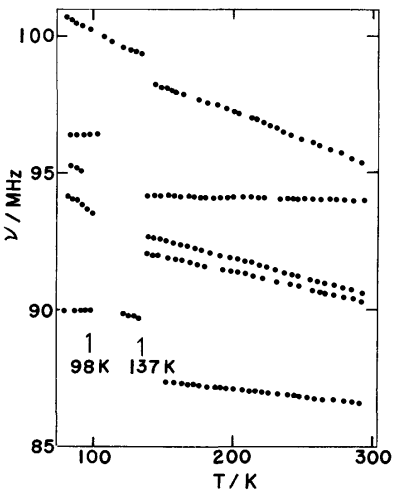

Fig. 2. Temperature dependence of ^{81}Br NQR frequencies in $[(CH_3)_4N]_2Ga_2Br_6$.

ca. 135 K appeared at 137 K. Unsymmetrical DTA peaks with a long tail on the low-temperature side were reported for $(CH_3NH_3)_2PtX_6$ (X=Cl, Br, and I) and attributed to the structural phase transitions related to the rearrangement of the octahedral anions PtX_6^{2-}.[5] In $[(CH_3)_4N]_2Ga_2Br_6$, it can be considered that the phase transitions at 98 and 137 K are related to motions of the $(CH_3)_4N^+$ ion.

The temperature dependence of the second moment M_2 of ^1H NMR spectra is shown in Fig. 3. On cooling, M_2 showed a constant value of ca. 0.5×10^{-8} T^2 down to ca. 140 K, while it increased rapidly below ca. 140 K and reached 20.1×10^{-8} T^2 at 77 K. According to the M_2

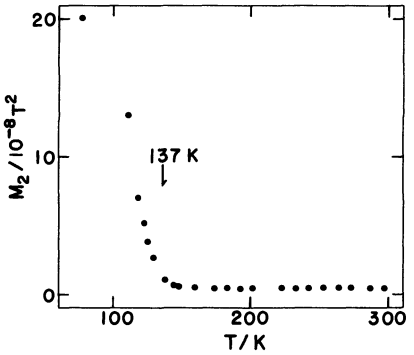

Fig. 3. Temperature dependence of the ^{1}H NMR second moment in $[(CH_3)_4N]_2Ga_2Br_6$.

calculation for $(CH_3)_4NX$(X=Cl, Br, and I),[4] the theoretical M_2 values in these halides are as follows: ca. 30×10^{-8} T^2 for the rigid lattice; ca. 11×10^{-8} T^2 for the rotaion of all methyl groups about C_3 axes; ca. 1×10^{-8} T^2 for the isotropic reorientation of $(CH_3)_4N^+$ ion. Accordingly, motions of the cation in $[(CH_3)_4N]_2Ga_2Br_6$ freeze for the most part at 77 K and the isotropic reorientation takes place above 140 K. On the other hand, a single ^{69}Ga NQR line was observed in $[(CH_3)_4N]_2Ga_2Cl_6$ and its frequency decreased monotonously from 23.37 MHz at 77 K to 22.68 MHz at 293 K with increasing temperature. The M_2 values of ^{1}H NMR spectra were 0.5×10^{-8} T^2 above 110 K and 11.3×10^{-8} T^2 at 77 K. Accordingly the rotation of the methyl group takes place even at 77 K for the chloro-complex. We predict that the phase transitions in $[(CH_3)_4N]_2Ga_2Br_6$ at 98 and 137 K can be ascribed to the onset of the isotropic reorientation of the $(CH_3)_4N^+$ ion and/or the rotation of the methyl groups. The occurence of these motions leads to the highly symmetric structure of the crystal being consistent with the fact that the number of the ^{69}Ga NQR lines decreased above these transition temperatures.

Figure 4 shows the temperature dependence of the ^{81}Br and ^{69}Ga NQR frequencies in $[(C_2H_5)_4N]_2Ga_2Br_6$. The single ^{69}Ga NQR line observed was so weak and broad between 77 and 118 K that we could not determine the resonance frequency accurately. A similar phenomenon was also observed for the above-mentioned $[(CH_3)_4N]_2Ga_2Br_6$, although the reason of the broadening is unknown. On heating, the resonance line became sharp and could be observed from 118 K up to 308 K, above which the resonance line disappeared. Three ^{81}Br lines which could be seen at low temperatures disappeared at ca. 275 K when the temperature was increased. The disappearance of the NQR lines can be attributed to the onset of the C_3 reorientation of the $GaBr_3$ group about the Ga-Ga bond for the following reasons. If the $Ga_2Br_6^{2-}$ ion has

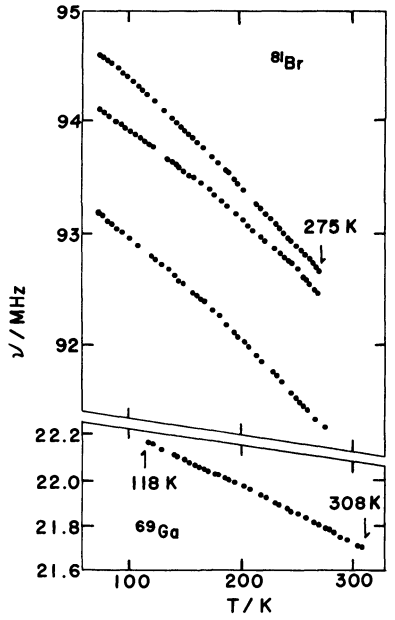

Fig. 4. Temperature dependences ^{81}Br and ^{69}Ga NQR frequencies in $[(C_2H_5)_4N]_2Ga_2Br_6$.

a structure of D_{3d} symmetry, the C_3 reorientation of the $GaBr_3$ group about the C_3 axis must not affect the ^{69}Ga NQR line.[6,7] The $Ga_2Br_6^{2-}$ ion in $[(C_2H_5)_4N]_2Ga_2Br_6$, however, has no D_{3d} symmetry because three ^{81}Br NQR lines were observed. Therefore, we can expect that the asymmetry parameter of the ^{69}Ga EFG is not zero and the principal z-axis of the EFG tensor is not parallel to the Ga-Ga bond. In addition, two bulky $GaBr_3$ groups should have a high barrier for rotation about the C_3 axis. Accordingly, the onset of the C_3 reorientation gives so drastic change of the EFG's at both ^{81}Br and ^{69}Ga nuclei that it is probable that this motion causes the disappearance of the NQR lines.

References

1) T. Okuda, N. Yoshida, M. Hiura, H. Ishihara, K. Yamada, and H. Negita, *J. Mol. Struct.*, **96**, 169 (1982).
2) K. L. Brown and D. Hall, *J. Chem. Soc., Dalton Trans.*, **1973**, 1843.
3) C. A. Evans and M. J. Taylor, *J. Chem. Soc., Chem. Commun.*, **1969**, 1201.
4) M. Mahajan and B. D. Nageswara Rao, *J. Phys. Chem. Solids*, **33**, 2191 (1972).
5) Y. Kume, R. Ikeda, and D. Nakamura, *J. Magn. Reson.*, **33**, 331 (1979).
6) R. Sh. Lotfulin and G. K. Semin, *Phys. Status Solidi*, **35**, 133 (1969).
7) J. L. Ragle, *J. Phys. Chem.*, **63**, 1395 (1959).

Comparison of Reactivities of Dibromide Anion Radical and Dichloride Anion Radical in Neutral Aqueous Solution

Yuusuke KATSURAGI, Osamu NEDA, Kotaro YAMAUCHI, and Takahiro MASUDA*
Department of Chemistry, Faculty of Science, Tokyo Metropolitan University, Fukasawa, Setagaya-ku, Tokyo 158
(Received June 11, 1986)

Synopsis. Rate constants of reactions of dibromide anion radical with some aliphatic dipeptides or unsaturated compounds including pyrimidine bases have been determined by flash photolysis. Difference in activation energy between dibromide and dichloride anion radicals has been estimated by comparing rate constants obtained for common substrates.

Dibromide anion radical ($Br_2^{\cdot-}$ as well as dichloride anion radical ($Cl_2^{\cdot-}$) has often been used as a probe for the oxidation of biomolecules.[1-6] The reactivities of both the anion radicals appear to be somewhat different from each other, in particular, with respect to specificity. No detailed investigation, however, has been found in literatures on the difference of their reactivities, because radiation-chemical determination of rate constants for $Cl_2^{\cdot-}$ is restricted to acid solution. Recently, we found a convenient system to be used to determine rate constants for $Cl_2^{\cdot-}$ in neutral aqueous solutions.[7-10] Thus, a quantitative comparison of reactivity between $Br_2^{\cdot-}$ and $Cl_2^{\cdot-}$ was attempted by determining rate constants for $Br_2^{\cdot-}$ with some common substrates, with which rate constants had already been obtained for $Cl_2^{\cdot-}$ in neutral aqueous solutions. Since at least two kinds of reactions, hydrogen atom abstraction and one-electron oxidation, are expected to take place with these anion radicals, a series of aliphatic dipeptides and some unsaturated compounds including several pyrimidine bases were adopted as common substrates. From the results obtained, some difference in activation energy could roughly be evaluated between $Br_2^{\cdot-}$ and $Cl_2^{\cdot-}$.

Experimental

Dipeptides were obtained from Nutritional Biochemical Corp. and pyrimidine bases from Sigma Chemical Corp. The other chemicals were of reagent grade.

Solutions for irradiation were prepared by dissolving 10^{-2} mol dm^{-3} KBr, 10^{-4} mol dm^{-3} $K_2S_2O_8$, and a desired amount of substrate in triply distilled water and adjusting pH to 7. The solutions were bubbled with N_2 for 20 min immediately before flash photolysis. Experimental conditions, the apparatus used for flash photolysis, and the procedure of kinetic analysis were described in detail elsewhere.[10,11]

Results and Discussion

During flash photolysis of N_2-saturated solutions containing 10^{-2} mol dm^{-3} KBr and 10^{-4} mol dm^{-3} $K_2S_2O_8$, the following reactions are expected to take place:

$$Br^- + h\nu \longrightarrow Br\cdot + e_{aq}^-, \quad (1)$$

$$S_2O_8^{2-} + h\nu' \longrightarrow 2SO_4^{\cdot-}, \quad (2)$$

$$e_{aq}^- + S_2O_8^{2-} \longrightarrow SO_4^{\cdot-} + SO_4^{2-}, \quad (3)$$

$$Br^- + SO_4^{\cdot-} \longrightarrow Br\cdot + SO_4^{2-}, \quad (4)$$

$$Br\cdot + Br^- \longrightarrow Br_2^{\cdot-}. \quad (5)$$

Since the rate constant of Reaction 3 was reported to be 1.1×10^{10} dm^3 mol^{-1} s^{-1} and the concentration of $S_2O_8^{2-}$ is 10^{-4} mol dm^{-3}, the lifetime of hydrated electrons is calculated as 9.1×10^{-7} s. If it is assumed that the rate constant k_4 is equal to that of the reaction of $SO_4^{\cdot-}$ with Cl^-, the lifetime $SO_4^{\cdot-}$ with respect to Reaction 4 is 3.2×10^{-7} s. Therefore, the decay rate of $SO_4^{\cdot-}$ due to Reaction 4 is faster than its formation by Reaction 3. Hence the lifetime of $SO_4^{\cdot-}$ can be estimated to be of the order of 10^{-6} s. The lifetime with respect to Reaction 5 may be taken to be of the order of nanosecond because the rate constant of the analogous reaction, $Cl\cdot + Cl^- \rightarrow Cl_2^{\cdot-}$, is known to be 2.1×10^{10} dm^3 mol^{-1} s^{-1}.[12] Since the rate constant of the reaction of $Br_2^{\cdot-}$ with e_{aq}^- is 1.3×10^{10} dm^3 mol^{-1} s^{-1} [13] and $Br_2^{\cdot-}$ of approximately 10^{-5} mol dm^{-3} has been observed to exist at the initial stage, a few percent portions of e_{aq}^- will be consumed by Reaction 6 in competition with Reaction 3:

$$e_{aq}^- + Br_2^{\cdot-} \longrightarrow 2Br^-. \quad (6)$$

The above discussion leads to a conclusion that the majority of reactive species found in the system 50 μs after start of flash are $Br_2^{\cdot-}$. Since the kinetic analysis is based on the data obtained during the period 50—100 μs, the following reactions are conceivable to take place in the presence of substrate, S:

$$Br_2^{\cdot-} + Br_2^{\cdot-} \longrightarrow Br_2 + 2Br^-, \quad (7)$$

$$Br_2^{\cdot-} + S \longrightarrow 2Br^- + \text{product(s)}. \quad (8)$$

From these reactions a rate equation is derived as follows:

$$\ln\frac{[Br_2^{\cdot-}]_0(2k[Br_2^{\cdot-}]+k_{ob})}{[Br_2^{\cdot-}](2k[Br_2^{\cdot-}]_0+k_{ob})} - k_{ob}t = 0, \quad (9)$$

where k_{ob} is equal to k_8 [S], $[Br_2^{\cdot-}]_0$ and $[Br_2^{\cdot-}]$ are the concentrations of $Br_2^{\cdot-}$ at times zero and t, respectively, and $2k$ is the rate constant of Reaction 7. Equation 9 can be solved numerically for k_{ob} with the aid of microcomputer. The second order rate constant, k_8, is obtained by plotting k_{ob} vs. [S]. In Fig. 1, rate constants for $Cl_2^{\cdot-}$ are plotted against those for $Br_2^{\cdot-}$ for several aliphatic dipeptides, which are known to undergo hydrogen atom abstraction reaction with these anion radicals.[14] A linear relation can be seen between the reactivities of both the anion radicals, although there is left a small intercept, -6.4×10^6 dm^3 mol^{-1} s^{-1}. The slope is obtained as 9.9 with a correlation coefficient of 0.944. Similarly, a linear relation was found for some unsaturated compounds including pyrimidine bases, as shown in Fig. 2. A slope of 2.64 and an intercept of 2.9×10^7 dm^3 mol^{-1} s^{-1} are obtained with a correlation coefficient of 0.938. An addition

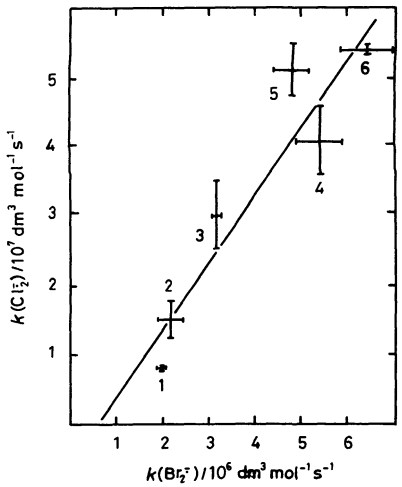

Fig. 1. $k(Cl_2^-)$ vs. $k(Br_2^-)$ for dipeptides.
1: Glycylglycine, 2: glycylalanine, 3: *N*-glycyl-2-aminobutyric acid, 4: glycylvaline, 5: glycylnorvaline, 6: glycylleucine. $k(Cl_2^-)$, see Ref. 7.

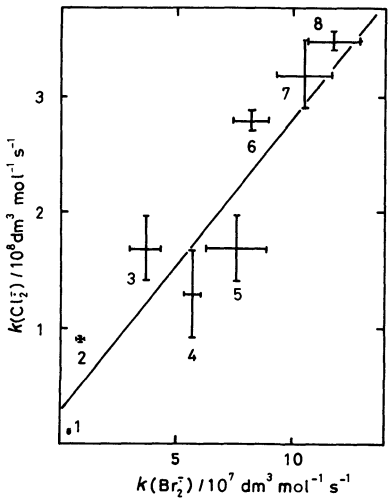

Fig. 2. $k(Cl_2^-)$ vs. $k(Br_2^-)$ for unsaturated compounds.
1: Pyrimidine, 2: acrylate, 3: maleate, 4: orotic acid, 5: isoorotic acid, 6: uracil, 7: thymine, 8: cytosine. $k(Cl_2^-)$, see Refs. 8 and 9.

reaction of Cl_2^- was reported for some unsaturated compounds.[14,15] If maleate and acrylate are excluded from the calculation, a slope of 3.1 and an intercept of -2.1×10^7 dm^3 mol^{-1} s^{-1} are obtained with a correlation coefficient of 0.968. Since ESR studies have shown that with pyrimidine bases one-electron oxidation takes place to yield their cation radicals,[16] the slope obtained above must correspond to the difference in reactivity of one-electron oxidation between Br_2^- and Cl_2^-.

If the Arrhenius equation is applied, the apparent difference in activation energy between Br_2^- snd Cl_2^- for hydrogen atom abstraction or one-electron oxidation may be estimated from the slopes of the straight lines shown in Figs. 1 and 2, because each slope corresponds to a ratio of rate constants. For the estimation, the ratio of frequency factors is required. If the ratio is taken as unity, the differences in activation energy are 5.7 kJ mol^{-1} for hydrogen atom abstraction reaction and 2.4 kJ mol^{-1} for one-electron oxidation reaction. If the value 1.4, which is estimated from $2k$, is adopted as the ratio, they are 4.8 and 1.6 kJ mol^{-1} respectively. These values are smaller than the differences in heat of reaction obtainable from thermodynamic data, which satisfies the Horiuchi-Polanyi rule. Furthermore, these differences in activation energy indicate that Br_2^- is more appropriate to unsaturated compounds as a one-electron oxidation probe than Cl_2^-.

References

1) G. E. Adams, J. E. Aldrich, R. H. Bisby, R. B. Cundall, J. L. Redpath, and R. L. Willson, *Radiat. Res.*, **49**, 278 (1972).
2) G. E. Adams, R. H. Bisby, R. B. Cundall, J. L. Redpath, and R. L. Willson, *Radiat. Res.*, **49**, 290 (1972).
3) P. W. Roberts, *Int. J. Radiat. Biol. Relat. Stud. Phys. Chem. Med.*, **24**, 143 (1973).
4) G. E. Adams, J. L. Redpath, R. H. Bisby, and R. B. Cundall, *J. Chem. Soc., Faraday Trans. 1*, **69**, 1608 (1973).
5) S. Hashimoto, A. Kira, M. Imamura, and T. Masuda, *Int. J. Radiat. Biol. Relat. Stud. Phys. Chem. Med.*, **41**, 303 (1982).
6) W. A. Prütz, J. Butler, and E. J. Land, *Int. J. Radiat. Biol. Relat. Stud. Phys. Chem. Med.*, **47**, 149 (1985).
7) T. Masuda, T. Hayashi, and M. Kondo, *J. Radiat. Res.*, **23**, 298 (1982).
8) T. Masuda, T. Kimura, E. Kadoi, T. Takahashi, K. Yamauchi, and M. Kondo, *J. Radiat. Res.*, **24**, 165 (1983).
9) T. Masuda, R. Gunji, T. Kimura, and K. Yamauchi, *Bull. Chem. Soc. Jpn.*, **56**, 3595 (1983).
10) O. Neda, K. Yamauchi, and T. Masuda, *Bull. Chem. Soc. Jpn.*, **58**, 227 (1985).
11) T. Takahashi, K. Yamauchi, and T. Masuda, *Bull. Chem. Soc. Jpn.*, **58**, 223 (1985).
12) G. G. Jayson, B. J. Parsons, and A. J. Swallow, *J. Chem. Soc., Faraday Trans. 1*, **69**, 1597 (1973).
13) M. S. Matheson, W. A. Mulac, J. L. Weeks, and J. Rabani, *J. Phys. Chem.*, **70**, 2092 (1966).
14) K. Hasegawa and P. Neta, *J. Phys. Chem.*, **82**, 854 (1978).
15) M. J. Davies and B. C. Gilbert, *J. Chem. Soc., Perkin Trans. 2*, **1984**, 1809.
16) M. D. Sevilla, D. Suryanarayana, and K. M. Morehouse, *J. Phys. Chem.*, **85**, 1027 (1981).

Size Effects of Small Platinum Particles on the Electrocatalytic Oxidation of Methanol

Yoshio TAKASU,* Yuichi FUJII, and Yoshiharu MATSUDA
Department of Industrial Chemistry, Faculty of Engineering, Yamaguchi University, 2557 Tokiwadai, Ube 755
(Received March 22, 1986)

Synopsis. A cyclic voltammetry study of a platinum-glassy carbon model catalyst-electrode (Pt/GC) in an aqueous solution of H_2SO_4 revealed that the peak potentials for the anodic oxidation of methanol shifted a little to the negative potential and that the current densities decreased greatly with the decrease in the size of the platinum particles.

A model catalyst, consisting of metal particles embedded on a flat and electric conducting substrate by means of vacuum evaporation, enables us to examine precisely the effects of metal-particle size on the catalytic properties of supported metal catalyst-electrodes.[1] Since the substrate is flat, not only is the observation of the shape of the particles by transmission electron microscopy (TEM) easy, but also any effect of the pore structure of the substrate on the catalytic properties can be neglected. This study will discuss the effect of the particle size of Pt/GC catalyst-electrode on the electrocatalytic oxidation of methanol in an aqueous solution of H_2SO_4.

Experimental

The support for the electrode was a glassy carbon rod (Tokai Carbon, GC-10, 0.53 cm in diam.). The base of the rod was polished with a cloth and alumina powder (ca. 0.3μm in diam.). The amount of platinum evaporated onto the base of the glassy carbon rod was determined with a quartz thickness monitor (Anelva, EVM-32B); i.e.,the amount of incident platinum was determined as the mass. The platinum particles were observed by means of a TEM (JEOL, JEM-200 CX). The electrochemical measurements were carried out by using a glass beaker cell filled with 0.2 dm^3 of a 1.0 mol dm^{-3} H_2SO_4 solution at 25 °C containing 1.0 mol dm^{-3} CH_3OH. The counter and reference electrodes were a platinum plate (3×3 cm^2) and a saturated calomel electrode (SCE) respectively.

Results and Discussion

Figure 1 shows same typical cyclic voltammograms for a platinum-wire, a galssy-carbon, and three Pt/GC model catalyst-electrodes under a steady state. Prior to the measurements of these voltammograms, the electrodes were treated by means of electrochemical aging; i.e., the electrode potential was swept repeatedly between −0.190 V and +0.920 V (vs. SCE) at a sweep rate of 300 mV s^{-1} for 10 min. By this treatment, the numerical mean diameter of the platinum particles, $\bar{d}$, increased a little; e.g., the $\bar{d}$ of a specimen evaporated with 3.8×10^{15} Pt atoms cm^{-2} increased 20% after the treatment. The anodic peak which appeared around 0.65 V (vs. SCE) during the anodic sweep and that around 0.5 V during the cathodic sweep are termed P_{a1}, and P_{a2} respectively. The first noticeable feature in Fig. 1 is that the anodic peak potential, $E_{P_{a1}}$, for the platinum-wire electrode (0.665 V) was higher than that

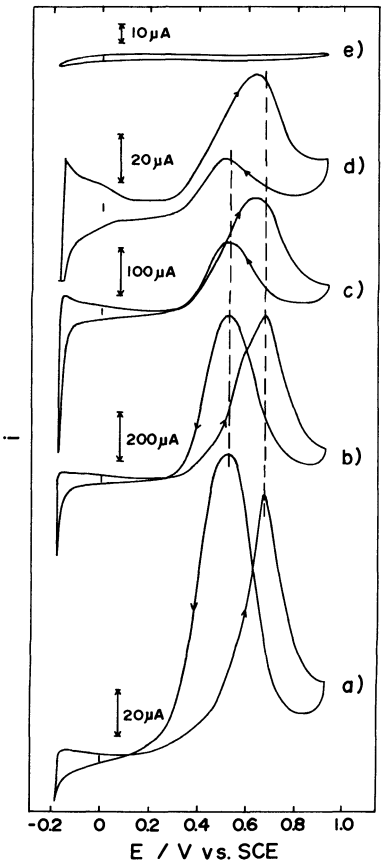

Fig. 1. Steady-state cyclic voltammograms for platinum wire, glassy carbon, and Pt/GC model catalyst electrodes in an aqueous solution of H_2SO_4 containing CH_3OH. Electrolyte: 1.0 mol dm^{-3} H_2SO_4, 1.0 mol dm^{-3} CH_3OH, 25°C. Sweep rate: 100 mV s^{-1}. Working electrode: a) platinum wire (geometric surface area; S_g=0.019 cm^2, real surface area determined by a cyclic voltammetry in 1.0 mol dm^{-3} H_2SO_4; S_r=0.093 cm^2), b) Pt/GC (S_r= 0.393 cm^2, the amount of the incident platinum atoms on the substrate; $M=7.6\times10^{15}$ Pt atoms cm^{-2}, mean diameter of platinum particles determined by TEM; $\bar{d}$=2.3 nm), c) Pt/GC (S_r=0.190 cm^2, $M=2.3\times10^{15}$ Pt atoms cm^{-2}, $\bar{d}$=1.9 nm), d) Pt/GC (S_r=0.067 cm^2, $M=7.6\times10^{14}$ Pt atoms cm^{-2}, $\bar{d}$= 1.5 nm), e) glassy carbon (S_g=0.22 cm^2).

for the Pt/GC electrodes which consisted of smaller platinum particles (0.622 V). A shoulder peak was found for the Pt/GC electrode with larger platinum particles (voltammogram b)), as had also been observed by Sobokowsky and his co-workers.[2] Similar shifts of the peak potential can also be observed for $E_{P_{a2}}$, although the potential shift is only about 0.02 V. The second noticeable feature is that the ratio of the

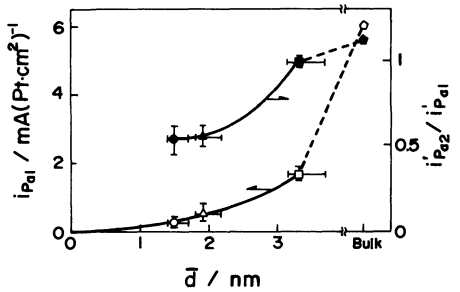

Fig. 2. The ratio of the peak current for P_{a1} and P_{a2} and the peak current density of P_{a1} for the oxidation of CH_3OH, as a function of mean diameter of platimum particles. The experimental conditions: see in Fig. 1. Amount of platinum evaporated. ○, ●: (M=7.6×10¹⁴ Pt atoms cm⁻²), △, ▲: (M=2.3×10¹⁵ Pt atoms cm⁻²), □, ■: (M=7.6×10¹⁵ Pt atoms cm⁻²), ◇, ◆: (Platinum wire).

peak currents for P_{a1} and P_{a2}, $i'_{P_{a2}}/i'_{P_{a1}}$, decreased with a decrease in the platinum particle size, $\bar{d}$, as is illustrated in Fig. 2. In order to determine the current density per surface area of the platinum particles, the real surface area of the platinum particles, S_r, was estimated from the total amount of electricity used for the anodic desorption of adsorbed hydrogen on the platinum particles in a 1.0 mol dm^{-3} H_2SO_4 solution after the electrochemical aging of the electrodes.[3,4] The current density for P_{a1} is shown in Fig. 2. It is worth noting that the peak current density, $i_{P_{a1}}$, abruptly decreased with a decrease in the size of the platinum particles.

As regards the size effects on the catalytic properties of supported platinum particles, the following aspects must be considered: a) the geometry of surface atoms,[5] b) the electronic state of the surface,[6] and c) the interaction with the substrate. The anodic oxidation of methanol on platinum is a typical structure-sensitive reaction;[7-9] i.e., Clavilier et al. found that the (110) plane of a single crystal was the most active in the initial stage, but that it became less active during continuous cycling, while the Pt(100) plane was the most electroactive plane under steady state conditions.[7] Contrary to their results, we observed that the ratio of the peak current due to the desorption of hydrogen from Pt(110) to that from Pt(100), $i'_{Pt(110)}/i'_{Pt(100)}$, decreased with a decrease in the size of the platinum particles [Ref. 1 Fig. 2, 2-a, b)].[1] However, the peak potential for the Pt(100) plane decreased with a decrease in the particle size, while that for the Pt(110) increased a little.[1] In order to explain the size effects, therefore, we must consider the contribution of each of the crystal planes of the small metal particles, which have rather different properties from those of the single crystals, to the electrocatalytic properties. Moreover, it has been suggested that methanol requires three adjacent sites for the adsorption, viz;[9,10]

$$CH_3OH + 3Pt = \underset{\displaystyle Pt \diagup \underset{Pt}{\diagup\!\diagdown} Pt}{\overset{COH}{\overset{|}{C}}} + 3H^+ + 3e^-.$$

It may not be easy for small platinum particles to provide such suitable sites with respect to the adsorption of methanol. The shifts of the anodic-peak potentials [Fig. 1] and the change in the peak-current ratio [Fig. 2], $i'_{P_{a2}}/i'_{P_{a1}}$, with the particle size must be caused by the ease of the formation of either the oxide layer of platinum or the oxidized adsorbed species of methanol, which interfere with the methanol oxidation, on the smaller rather than on the larger platinum particles. This speculation can be supported by the fact that the peak potentials for the reduction of the surface-oxide layer of platinum particles, as measured by a cyclic voltammetry in an aqueous solution of H_2SO_4, shifted to the negative potential with a decrease in the platinum-particle size.[1,11]

The authors are grateful to Dr. Akiko Aramata, of the Research Institute for Catalysis of Hokkaido University, for sending us useful literature.

References

1) Y. Takasu, Y. Fujii, and Y. Matsuda, *Chem. Lett.*, **1986**,445.
2) J. Sobokowski and A. Wiekowski, *J. Electroanal. Chem.*, **34**, 185 (1972).
3) T. Biegler, D. A. Rand, and R. Woods, *J. Electroanal. Chem.*, **29**, 169 (1971).
4) J. Bett, J. Lundquist, E. Washington, and P. Stonehart, *Electrochim. Acta*, **18**, 343 (1973).
5) R. J. Anderson, "Structure of Metallic Catalysts," Academic Press, New York, N. Y. (1975), p. 244.
6) Y. Takasu, Y. Matsuda, and I. Toyoshima, *Chem. Phys. Lett.*, **108**, 384 (1984).
7) J. Clavilier, C. Lamy, and J. M. Leger, *J. Electroanal. Chem.*, **125**, 249 (1981).
8) B. D. McNicol, *J. Electroanal. Chem.*, **118**, 71 (1981).
9) B. D. McNicol, P. Attwood, and R. T. Short, *J. Chem. Soc., Faraday Trans. 1*, **77**, 2017 (1981).
10) V. S. Bagotzky and Yu. B. Vassiliev, *Electrochim. Acta*, **12**, 1323 (1967).
11) Y. Takasu, Y. Fujii, K. Yasuda, and Y. Matsuda (to be submitted).

Penicillin-Cephalosporin Conversion. XII.[1] Electroreductive Dechlorination of 3′-Chlorocephalosporins into 3-Methylenecephams

Sigeru TORII,* Hideo TANAKA, Toshiyuki OHSHIMA, and Michio SASAOKA
Department of Industrial Chemistry, School of Engineering, Okayama University, Tsushima Naka 3-1, Okayama 700
(Received May 29, 1986)

Synopsis. An efficient electroreductive conversion of 3′-chlorocephalosporins and their analogues into the corresponding 3-methylenecephams has been performed in an aqueous THF-$LiClO_4$-(Pb cathode) and/or aqueous MeCN-EtOH-$LiClO_4$-NH_4ClO_4 (Pb cathode) system.

3-Methylenecephams (**5**) are useful precursors of 3-norcephalosporins (**6**), unnatural β-lactam antibiotics, where the C(3)-position directly combines with a heteroatom (Y), e.g., chlorine and methoxy groups.[2] Recently, we have succeeded in exploring a simple and efficient synthetic scheme of 3′-chlorocephalosporins (**4**), which comprises the ene-type chlorination of azetidinone (**2**) derived from natural penicillins and subsequent cyclization of **3** with ammonia (Scheme 1).[3] Consequently, our next efforts were focused on reductive elimination of the chlorine atom at C(3′)- position of **4** as a straightforward access to the 3-methylenecephams. We investigated this possibility by use of electroreductive procedure.

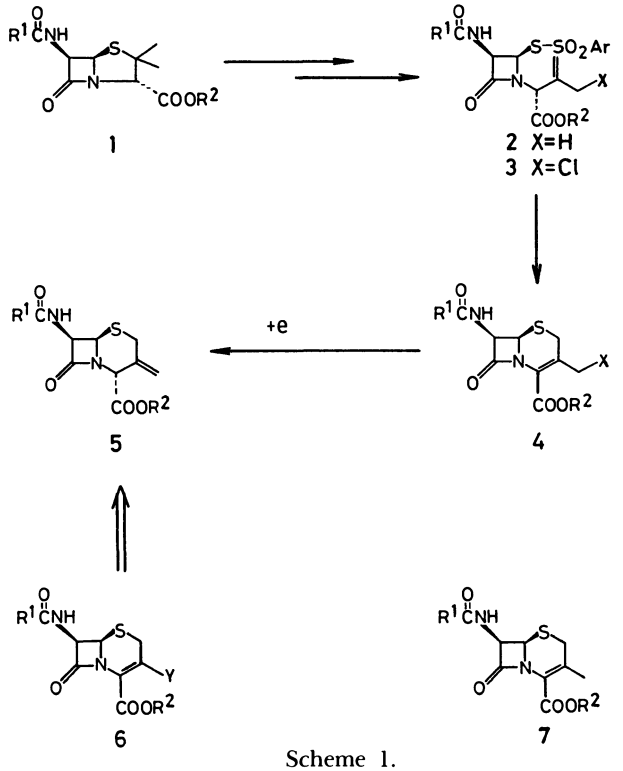

Scheme 1.

Electroreductive elimination of C(3′)-substituents of cephalosporins **4** (X=OAc, SAc, $^+NC_5H_5$, etc.) has been extensively investigated in buffer solution with Hg cathode under controled potential electrolysis conditions.[4] To our knowledge, however, electroreductive conversion of 3′-chlorocephalosporins (**4**) (X=Cl) into the corresponding 3-methylenecephams (**5**) has not been realized. In this paper, we wish to describe an efficient electroreductive elimination of C(3′)-substituents of 3′-chlorocephalosporins (**4**) (X=Cl) and their analogues **4** (X=I and SBT) in a slightly modified electroreductive system, wherein Hg cathode was replaced with Pb cathode and electrolysis was conducted under regulated current density without strict control of the electrode potential.

Electrolysis was carried out in a divided cell fitted with Pt anode and Pb cathode (3 cm^2 each). A mixture of tetrahydrofuran (THF) and H_2O (4/1) containing $LiClO_4$ and NH_4ClO_4 was charged into both compartments of the cell. The cephalosporins **4** (X=Cl, I, SBT, and OAc) were added into the cathode compartment and regulated d.c. power at 3.3 mA cm^{-2} was supplied at room temperature, until most of the starting materials **4** were consumed.

Typical results of electroreductive removal of the C(3′)-substituents of **4** are summarized in Table 1. Electroreduction of 3′-chlorocephalosporins (**4**) (X=Cl) proceeded smoothly and, after passage of 3.5 F mol^{-1} of electricity, afforded the corresponding 3-methylenecephams (**5**), which contained less than 2% of their endo isomers **7** (Entries 1 and 2). Electroreduction of **4a** (R^1, R^2=$PhCH_2$; X=Cl) into **5** was also performed in MeCN-H_2O-EtOH (4/1/0.07) with the same supporting electrolytes (Entry 3), while the electrolysis of **4a** in the absence of ethanol (Entry 4) provided no reduction product. Proper choice of the cathode material is significant. Thus, Pb cathode was indispensable for the successful conversion of **4** into **5**, since the yields of **5** varied depending on the choice of cathode materials in the order: Pb (87%)>C(58%)>Cu (51%)>Pt(19%).

Next, the electroreductive procedure was applied to 3′-iodo-, 3′-(2-benzothiazolylthio)- and 3′-acetoxycephalosporins (**4**) (X=I, SBT, and OAc). Iodide **4c** (X=I) was less effective than chloride **4a** (X=Cl), affording only 64% yield of **5** (Entry 5). It is likely that considerable portion of **4c** would suffer from decomposition in the aqueous electrolysis media prior to the electroreduction. 3′-(2-Benzothiazolylthio)cephalosporin (**4d**) (X=SBT)[5] was smoothly converted to the corresponding 3-methylenecepham (**5**) in 78—90% yields (Entries 6 and 7). On the other hand, 3′-acetoxycephalosporin **4e** (X=OAc) could not be reduced in the present electroreductive media (Entry 8). The almost complete recovery of **4e** was somewhat surprising in comparison with the successful conversion of **4** (X=OAc) to **5** in a buffer solution-(Hg cathode) system, reported by Ochiai, et al.[4a,b] Although scope and limitation of the present electroreductive procedure are still unclear, it is evident that a combination of the electroreductive dechlorination of 3′-chlorocephalosporins **4** (X=Cl)

Table 1. Electroreductive Removal of C(3′)-Substituents of Cephalosporins[a)]

Entry	Compound 4[b)]	R^1	R^2	X	Solvent	Electricity[c)] F/mol	Yield/%[d)] 5	7
1	**4a**	$PhCH_2$	PMB	Cl	THF-H_2O(4/1)	3.5	87	—
2	**4b**	$PhCH_2$	$PhCH_2$	Cl	THF-H_2O(4/1)	3.5	84	2
3	**4b**				MeCN-H_2O-EtOH (4/1/0.07)	7	79	—
4	**4b**				MeCN-H_2O(4/1)	7	—	—
5	**4c**	$PhCH_2$	PMB	I	THF-H_2O(4/1)	3.5	64	2
6	**4d**	$PhOCH_2$	$PhCH_2$	SBT	THF-H_2O(4/1)	4.5	78	2
7	**4d**				MeCN-H_2O-EtOH (4/1/0.07)	7	90	3
8	**4e**	$PhCH_2$	PMB	OAc	MeCN-H_2O-EtOH (4/1/0.07)	7	—[e)]	—

a) Carried out at 3.3 mA cm^{-2} with Pb plate (3 cm^2) cathode at room temperature. b) PMB: *p*-methoxybenzyl; SBT: 2-benzothiazolylthio. c) Unless otherwise noted, d.c. current was supplied until most of the starting materials **4** were consumed. d) Isolated yields after column chromatography. e) **4e** was recovered (96%).

and previous "Penicillin-Cephalosporin Conversion"[3)] (Scheme 1) provides a new convenient route for synthesis of **5**.

Experimental

IR spectra were obtained on a JASCO IRA-1 grating infrared spectrophotometer. ^1H NMR spectra were recorded with a Hitachi R-24 spectrometer and chemical shifts are reported in part per million (δ) relative to tetramethylsilane (δ=0.0 ppm) as an internal standard in a $CDCl_3$ solution. C(3′)-Substituted cephalosporins **4a**, **4b** (X=Cl),[3)] **4d** (X=SBT)[5)] and **4e** (X=OAc)[5)] were prepared by the reported procedure. Iodide **4c** (X=I) was prepared by treatment of **4a** with KI (1.2 equiv) and $NaHCO_3$ in refluxing acetone for 1 h.

General Procedure for Electrochemical Reductions. The electroreduction was carried out at room temperature in a H-shaped cell separated by fritted glass, which was fitted with lead cathode (3 cm^2) and platinum anode (3 cm^2). Regulated d.c. power was supplied by Metronix Galvanostat Model 543B. When the starting materials were almost consumed (3.5—7.0 F mol^{-1}), the electrolysis was terminated and the catholytes were worked up in the usual manner. The structual assignment of the products **5** and **6** were performed by comparison of the IR and ^1H NMR spectra with those of authentic samples.[2d)] The conditions and results are summarized in Table 1. A typical electrolysis procedure is as follows.

Electroreduction of 4a (R^1=$PhCH_2$; R^2=*p*-CH_3O-$C_6H_4CH_2$; X=Cl) (Entry 1). A mixture of THF (12 ml) and H_2O (3 ml) containing $LiClO_4$ (330 mg) and NH_4ClO_4 (460 mg) was added into both the cathode and anode compartments (7.5 ml each) and **4a** (101 mg, 0.21 mmol) was added into the catholytes. The mixture was electrolyzed under stirring at 3.3 mA cm^{-2} for 1.4 h. The catholytes were concentrated in vacuo to ca. 2 ml and the residue was extracted with AcOEt. The extracts were combined, washed with brine, and dried (Na_2SO_4). Evaporation of the solvents followed by column chromatography on SiO_2 with hexane/AcOEt (5 : 1) afforded 2-methylenecepham **5a** (=**5c**) (R^1=$PhCH_2$; R^2=*p*-CH_3O-$C_5H_4CH_2$, 82 mg, 87%)[2d)]: IR ($CDCl_3$) 3398, 3010, 1779, 1745, 1689, 1620, 1597, 1519, 1251 cm^{-1}; ^1H NMR ($CDCl_3$) δ=3.01, 3.43 (2H, AB q, *J*=14 Hz, CH_2S), 3.57 (3H, s, OCH_3), 3.76 (2H, s, CH_2), 5.04 (2H, s, CH_2), 5.12 (2H, s, H_2C=C), 5.21 (1H, d, *J*=4 Hz, CH (6)), 5.57 (1H, dd, *J*=4 Hz and 10 Hz, CH (7)), 6.80 (1H, d, *J*=10 Hz, NH), 7.10—7.41 (9H, m).

2-Methylenecepham **5b** (R^1=$PhCH_2$; R^2=$PhCH_2$)[2d)]: IR ($CDCl_3$) 3398, 3000, 1768, 1742, 1680, 1510, 1220 cm^{-1}; ^1H NMR ($CDCl_3$) δ=3.07, 3.56 (2H, AB q, *J*=14 Hz, CH_2S), 3.48 (2H, s, CH_2), 5.03 (2H, s, CH_2), 5.12 (2H, s, H_2C=C), 5.20 (1H, d, *J*=4 Hz, CH (6)), 5.12 (1H, dd, *J*=4 Hz and 8 Hz, CH (7)), 6.78 (1H, d, *J*=8 Hz, NH), 7.10—7.41 (10H, m).

2-Methylenecepham **5d** (R^1=$PhOCH_2$; R^2=$PhCH_2$): IR ($CDCl_3$) 3390, 3010, 1775, 1744, 1681, 1610, 1590, 1220 cm^{-1}; ^1H NMR ($CDCl_3$) δ=3.06, 3.51 (2H, AB q, *J*=14 Hz, CH_2S), 4.50 (2H, s, CH_2), 5.14 (2H, s, CH_2O), 5.22 (2H, s, H_2C=C), 5.36 (1H, d, *J*=4 Hz, CH (6)), 5.66 (1H, dd, *J*=4 Hz and 10 Hz, CH (7)), 6.85 (1H, d, *J*=10 Hz, NH), 7.00—8.75 (10H, m).

References

1) Part XI: S. Torii, H. Tanaka, T. Siroi, and M. Sasaoka, *Tetrahedron Lett.*, **25**, 1801 (1984).

2) a) Y. Hamashina, T. Kubota, K. Ishikura, K. Minami, K. Tokuda, and W. Nagata, *Heterocycles*, **5**, 419 (1976); b) S. Kukolja, M. R. Gleissner, A. I. Ellis, D. E. Dorman, and J. W. Paschal, *J. Org. Chem.*, **41**, 2276 (1976); c) R. R. Chauvette and P. A. Pennington, *J. Am. Chem. Soc.*, **96**, 1986 (1974); Various synthetic schemes of **5** have been explored; d) S. Torii, H. Tanaka, T. Siroi, T. Madono, N. Saitoh, M. Sasaoka, and J. Nokami, *Bull. Chem. Soc. Jpn.*, **56**, 1567 (1983); e) F. A. Jung, W. R. Pilgrim, J. P. Poyser, and P. J. Siret, "Topics in Anibiotics," ed by P. G. Sammes, Ellis Horwood, Chichester (1980), Vol. 4, p. 159, and references cited therein.

3) S. Torii, H. Tanaka, N. Saitoh, T. Siroi, M. Sasaoka, and J. Nokami, *Tetrahedron Lett.*, **23**, 2187 (1982).

4) a) M. Ochiai, O. Aki, A. Morimoto, T. Okada, K. Shinozaki, and Y. Asahi, *Tetrahedron Lett.*, **1972**, 2341; b) *J. Chem. Soc., Perkin Trans. 1*, **1974**, 258; c) D. A. Hall, D. M. Berry, and C. J. Schnerder, *J. Electroanal. Chem.*, **80**, 155 (1977).

5) S. Torii, H. Tanaka, T. Siroi, and M. Sasaoka, *Tetrahedron Lett.*, **25**, 2017 (1984).

Novel Synthesis of Enol Ethers from β-Alkoxy Alcohols through *t*-BuOK-Promoted Elimination Reaction

Junzo OTERA* and Yoshihisa NIIBO
Department of Applied Chemistry, Okayama University of Science, Ridai-cho, Okayama 700
(Received June 3, 1986)

Synopsis. A new synthesis of enol ethers from β-alkoxy alcohols was achieved through a *t*-BuOK-promoted elimination reaction.

It was not until recently that enol ethers proved to be synthetically useful intermediates and accordingly so much attention has not been paid for their efficient synthetic methods.[1] Previously, we have demonstrated a new route via *t*-BuOK-promoted elimination of a phenylsulfinyl or phenylsulfonyl group from α-methoxy sulfoxides or sulfones.[2] Here we wish to describe another route starting from β-substituted alcohols.

We have already disclosed the practical ring opening of epoxides by alcohols with the aid of organotin phosphate condensate catalysts (Eq. 1).[3] The reaction

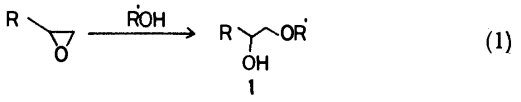

1 (1)

proceeds under neutral conditions with an excellent regioselectivity so that a wide variety of the β-alkoxy alcohols **1** are now accessible. In the development of synthetic applications of these compounds, we have achieved an effective route to enol ethers which has recourse to a *t*-BuOK-promoted elimination reaction of the corresponding mesylates **2** (Eq. 2).

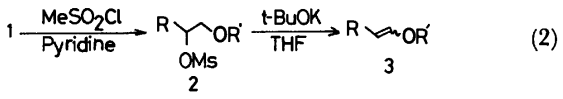

2 3 (2)

Treatment of **1**[4] with methanesulfonyl chloride in pyridine at room temperature delivered **2** in quantitative yields. β-Alkoxy mesylates thus obtained were exposed to five equiv of *t*-BuOK in THF at room temperature or under reflux. The reaction proceeded smoothly to give various types of enol ethers **3** in good yields. The results are summarized in Table 1. It should be noted that the allyloxy derivative suffered from substantial contamination of 1-propenyl ether **4** under analogous reaction conditions due to the base-catalyzed isomerization of the allyl ether. The difficulty, however, was overcome by decreasing the amount of employed *t*-BuOK (1 equiv) along with employment of one equiv of 18-crown-6. As a whole, the present procedure has established a new method for transformation of epoxides to enol ethers.

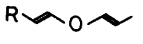

4

Experimental

Preparation of β-Alkoxy Mesylates 2 (Typical Procedure). A pyridine solution (10 cm³) of 2-hydroxypropyl octyl ether[3] (1.24 g, 6.60 mmol) and methanesulfonyl chloride (903 mg, 7.90 mmol) was stirred at room temperature for 12 h. The reaction mixture was extracted with ether-water and the ethereal layer was washed with water repeatedly. Drying ($MgSO_4$), evaporation, and column chromatography (silica gel, 50:1 hexane-ethyl acetate) gave 2-(methylsulfonyloxy)-propyl octyl ether (1.58 g, 90%): ^{1}H NMR (CCl_4) δ=0.87 (br t, 3H), 1.07—1.77 (m, 15H), 2.88 (s, 3H), 3.20—3.53 (m, 4H), and 4.47—4.97 (m, 1H).

Synthesis of Enol Ethers 3 (Typical Procedure). A THF solution (10 cm³) of 2-(methylsulfonyloxy)propyl octyl ether (266 mg, 1 mmol) and *t*-BuOK (561 mg, 5 mmol) was heated at reflux for 2 h. The reaction mixture was extracted with ether-water. The organic layer was dried ($MgSO_4$) and evaporated. The residual oil was distilled (120 °C/4660 Pa, Kugelrohr bath temperature) to give 1-octyloxy-1-propene (128 mg, 75%, *E*/*Z*= 62:38): ^{1}H NMR ($CDCl_3$) δ=0.89 (t, 3H, *J*=7.1 Hz), 1.14—1.44 (m, 12H), 1.54 (dd, 1.86H, *J*=6.7 and 1.7 Hz), 1.57 (dd, 1.14H, *J*=6.7 and 1.7 Hz), 3.47—3.77 (m, 2H), 4.34 (dq, 0.38H, *J*=6.4 and 6.7 Hz), 4.73 (dq, 0.62H, *J*=12.6 and 6.7 Hz), 5.89 (dq, 0.38H, *J*=6.4 and 1.7 Hz), and 6.18 (dq, 0.62H, *J*=12.6 and 1.7 Hz); MS *m*/*z* 170 (M^+) and

Table 1. Conversion of the Mesylates **2** into Enol Ethers **3**[a]

R	R′	Reaction		Product	
		Temp	Time/h	Yield/%	E:Z[b]
CH_3	C_8H_{17}	Reflux	2	75[c]	62:38
	$PhCH_2$	Reflux	12	74[c]	63:37
C_6H_{13}	CH_3	Reflux	1	74[d]	79:21
	$PhCH_2$	Rt	1	70[d]	71:29
$C_{10}H_{21}$	CH_3	Reflux	1	75[d]	67:33
	$PhCH_2$	Reflux	1	68[d]	63:37
	CH_2=$CHCH_2$	Rt	12[e]	66[d]	73:27
$(CH_3)_2C$=$CH(CH_2)_2$	$PhCH_2$	Reflux	2	69[d]	71:29

a) Five equiv of *t*-BuOK was employed unless otherwise noted. b) Determined on the basis of ^{1}H NMR spectra. c) Purified by means of distillation. d) Purified by means of column chromatography on silica gel. e) Each one equiv of *t*-BuOK and 18-crown-6 was added.

171 (M^++1). Found: C, 77.44; H, 13.09. Calcd for $C_{11}H_{22}O$: C, 77.58; H, 13.02.

1-Benzyloxy-1-propene (E/Z=63:37): ^1H NMR ($CDCl_3$) δ=1.44—1.71 (m, 3H), 4.31-5.01 (m, 3H), 5.98 (dt, 0.37H, J=7.1 and 1.4 Hz), 6.28 (dt, 0.63H, J=12.8 and 1.6 Hz), and 7.27 (br s, 5H); MS m/z 148 (M^+). Found: C, 81.35; H, 8.01. Calcd for $C_{10}H_{12}O$: C, 81.04; H, 8.16.

1-Methoxy-1-octene (E/Z=79:21): ^1H NMR ($CDCl_3$) δ= 0.89 (t, 3H, J=7.1 Hz), 1.07—1.46 (m, 8H), 1.71—2.09 (m, 2H), 3.46 (s, 2.37H), 3.54 (s, 0.63H), 4.31 (dt, 0.21H, J=7.1 and 6.3 Hz), 4.70 (dt, 0.79H, J=12.6 and 7.1 Hz), 5.80 (dt, 0.21H, J=6.3 and 1.4 Hz), and 6.23 (dt, 0.79H, 12.6 and 1.3 Hz); MS m/z 142 (M^+). Found: C, 75.85; H, 12.98. Calcd for $C_9H_{18}O$: C, 76.00; H, 12.75.

1-Benzyloxy-1-octene (E/Z=71:29): ^1H NMR ($CDCl_3$) δ=0.86 (t, 3H, J=7.1 Hz), 1.00—1.45 (m, 8H), 1.63—2.26 (m, 2H), 4.20—4.97 (m, 3H), 5.94 (dt, 0.29H, J=6.3 and 1.6 Hz), 6.27 (dt, 0.71H, J=12.6 and 1.2 Hz), and 7.30 (br s, 5H); MS m/z 218 (M^+). Found: C, 81.53; H, 10.65. Calcd for $C_{14}H_{22}O$: C, 81.50; H, 10.75.

1-Methoxy-1-dodecene (E/Z=67:33): ^1H NMR ($CDCl_3$) δ=0.87 (t, 3H, J=7.1 Hz), 1.01—1.54 (m, 16H), 1.69—2.17 (m, 2H), 3.46 (s, 2.0H), 3.54 (s, 1.0H), 4.31 (dt, 0.33H, J=7.4 and 6.9 Hz), 4.70 (dt, 0.67H, J=12.6 and 7.1 Hz), 5.83 (dt, 0.33H, J=6.9 and 1.7 Hz), and 6.23 (dt, 0.67H, J=12.6 and 1.5H); MS m/z 198 (M^+). Found: C, 78.46; H, 13.50. Calcd for $C_{13}H_{26}O$: C, 78.72; H, 13.21.

1-Benzyloxy-1-dodecene (E/Z=63:37): ^1H NMR ($CDCl_3$) δ=0.87 (t, 3H, J=6.3 Hz), 1.09—1.40 (m, 16H), 1.75—2.20 (m, 2H), 4.20—5.00 (m, 3H), 5.94 (dt, 0.37H, J=6.3 and 1.4 Hz), 6.27 (dt, 0.63H, J=12.6 and 1.4 Hz), and 7.31 (br s, 5H); MS m/z 274 (M^+). Found: C, 83.00; H, 11.22. Calcd for $C_{19}H_{30}O$: C, 83.15, H, 11.02.

1-Allyloxy-1-dodecene (E/Z=73:27): ^1H NMR ($CDCl_3$) δ=0.88 (t, 3H, J=7.1 Hz), 1.14—1.43 (m, 16H), 1.74—2.17 (m, 2H), 4.19 (m, 2H), 4.34 (dt, 0.27H, J=7.1 and 6.6 Hz), 4.79 (dt, 0.73H, J=12.6 and 7.4 Hz), 5.06—5.41 (m, 2H), 5.67—6.07 (m, 1.27H), and 6.17 (dt, 0.73H, J=12.6 and 1.3 Hz); MS m/z 224 (M^+). Found: C, 80.51; H, 12.44. Calcd for $C_{15}H_{28}O$: C, 80.29; H, 12.58.

1-Benzyloxy-6-methyl-1,5-heptadiene (EE/ZE=71:29): ^1H NMR ($CDCl_3$) δ=1.58 (s, 3H), 1.67 (s, 3H), 1.81—2.23 (m, 4H), 4.26—5.23 (m, 4H), 5.95 (dt, 0.29H, J=6.1 and 1.4 Hz), 6.30 (dt, 0.71H, J=13.0 and 1.1 Hz), and 7.27 (br s, 5H); MS m/z 216 (M^+). Found: C, 83.54; H, 9.22. Calcd for $C_{15}H_{20}O$: C, 83.29; H, 9.32.

References

1) For the most recent studies on this subject: J.-M. Vatele, *Tetrahedron Lett.*, **25**, 5997 (1984); G. M. McGarvey, M. Kimura, and A. Kucerovy, *ibid.*, **26**, 1419 (1985).

2) T. Mandai, K. Hara, T. Nakajima, M. Kawada, and J. Otera, *Tetrahedron Lett.*, **24**, 4993 (1983).

3) J. Otera, Y. Yoshinaga, and K. Hirakawa, *Tetrahedron Lett.*, **26**, 3219 (1985).

4) In the case where the regioisomer is contaminated, **1** can be separated easily by means of column chromatography.

Synthesis of Substituted Crown Ether Acetals

Takumi OSHIMA* and Toshikazu NAGAI
Institute of Chemistry, College of General Education, Osaka University, Toyonaka, Osaka 560
(Received July 11, 1986)

Synopsis. Reactions of phenyldiazomethane with chloranil and of 1-phenyldiazoethane and 9-diazofluorene with 2,3-dichloro-5,6-dicyano-*p*-benzoquinone in the presence of oligoethylene glycols and its monomethyl ethers gave the corresponding substituted crown ether acetals and open-chain analogues.

Crown ether acetals (**1**) which involve one (or more) $-OCR^1R^2O-$ function in the crown rings, are interesting compounds as they exhibit cation-binding properties[1] and also undergo polymerization[2] and hydrolysis.[1b,3] A few varieties in which R^1 and/or R^2 are hydrogen were hitherto available by conventional methods using acid catalysts[2a,4] ion-exchange resins[5] from aldehydes and oligoethylene glycols. However, the formation of disubstituted acetals is noticeably difficult by the traditional methods.[6] Therefore, a new type of method is required to synthesize various disubstituted acetals.

We have recently reported a new method for the synthesis of diphenyl-substituted crown ether acetals ($Ph_2\overline{C(OCH_2CH_2)_nO}$, n=1—6) by way of the redoxical acetalization caused by three reactants, i.e., diphenyldiazomethane (DDM), 2,3-dichloro-5,6-dicyanobenzoquinone (DDQ), and oligoethylene glycols.[7]

We have found that this technique is conveniently applicable for the preparation of several new substituted crown ether acetals (**1a—c**, **e**, and **f**) and open-chain analogues (**2a**, **b**) when adapted to other diazoalkanes like phenyldiazomethane (**3**), 1-phenyldiazoethane (**4**), and 9-diazofluorene (**5**). In a reaction with **3**, DDQ provided significant amounts of bicyclic dione derivatives[8] formed from the dipolar addition to the C=C bond, so that chloranil was utilized for this diazoalkane as an alternative quinone. As previously described,[7] this promising acetalization proceeds via a reaction sequence involving the formation of 1:1 betaines from diazoalkanes and quinones, subsequent nucleophilic attack of glycols, and final splitting into acetals and hydroquinones (Scheme).

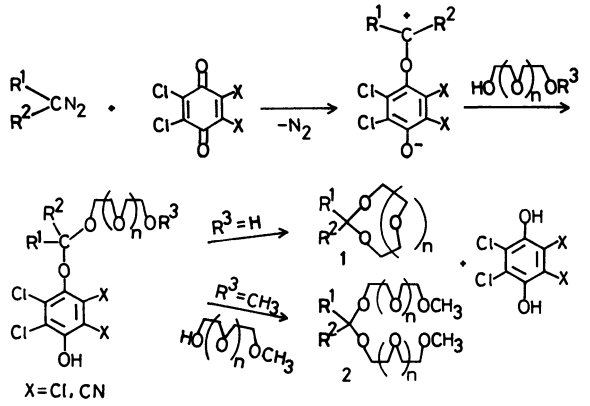

The present diazoalkanes provided only about half yields of acetals compared to DDM as tested for the fourteen-membered crown acetals (Table). The drop in the yields may be due to two reasons. First, diazoalkanes, **3** and **4**, tended to thermally decompose to azines and further reacted with the generated hydroquinones giving hydroquinone diethers. However, stable **5** provided 9,9′-bifluorenylidene and oxirane[9] as

Table 1. Crown Ether Acetals (**1a—f**) or Open Acetals (**2a**, **b**) from Reactions of Diazoalkanes, Quinones, and Oligoethylene Glycols or Its Monomethyl Ethers

Diazoalkanes	Quinones	Reaction times/h[a]	Acetal **1**(n) and **2**(n)	Substituents R^1	Substituents R^2	Yield[b] %
Phenyldiazomethane (**3**)	Chloranil	0.5	**1a**(3)	Ph	H	21
1-Phenyldiazoethane (**4**)	DDQ	1	**1b**(1)	Ph	CH_3	30
4	DDQ	1	**1c**(3)	Ph	CH_3	16
Diphenyldiazomethane (DDM)	DDQ	2	**1d**(3)	Ph	Ph	38[c]
9-Diazofluorene (**5**)	DDQ	6	**1e**(3)	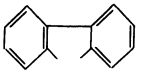		19
5	DDQ	6	**1f**(4)	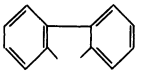		16
5	DDQ	3	**2a**(1)	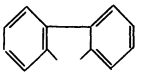		33
5	DDQ	3	**2b**(2)	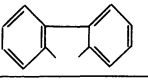		27

a) Chosen depending on the relative reactivities of diazoalkanes. b) Isolated yields by chromatography on alumina. c) Cited from Ref. 7.

by-products. Second, newly prepared crown acetals are appreciably sensitive to water as is evidenced by their complete degradation into carbonyl components and alcohols even after standing one week in a stoppered NMR tube(in $CDCl_3$). This observation, combined with the presence of fairly amounts of benzaldehyde, acetophenone, and 9-fluorenone in the crude reaction mixtures, implies that some parts of acetals were lost during such work-up treatments as washing with aqueous alkaline solution and separation by column chromatography.

However, our technique is expected to play a role in the preparation of many-membered disubstituted crown ether acetals for which no other efficient method has been found in a literature search.

Experimental

Infrared spectra were recorded on a Hitachi 260-10 and on a Perkin Elmer 983G spectrometer. ^1H NMR spectra were taken at 90 MHz on a Varian EM 390 spectrometer. Mass spectral data were obtained with a Hitachi RMU 6E mass spectrometer.

Materials. DDQ was of commercial origin (98%, Aldrich Chemical Co. Inc.) and was used without further purification. Chloranil was recrystallized from benzene. Phenyldiazomethane (**3**),[10] 1-phenyldiazoethane (**4**),[11] and 9-diazofluorene (**5**)[12] were prepared according to the procedure described in the literatures. Oily **3** and **4** were contaminated with 10—30% azines, but were used without purification because of their thermal instability. The **5** was recrystallized from ether; mp 94—95 °C. Benzene was refluxed over lithium aluminum hydride and was fractionated.

General Procedure. To a stirred solution of DDQ (1.2 g, 5.0 mmol) in benzene (20 ml) was added dropwise over 10 min at 20—25 °C a benzene solution (10 ml) of an 1 equiv mixture of diazoalkane and oligoethylene glycol (3 equiv for oligoethylene glycol monomethyl ether). After the mixture was stirred for the requisite times, the precipitated hydroquinone was filtered off and was washed with benzene (10 ml×3). The filtrate and washing parts were combined and were treated according to the previous manner.[7] The crude acetals containing such by-products as azines, hydrolyzed carbonyl compounds, hydroquinone diethers, and 9,9′-bifluorenylidene were column chromatographed on alumina. After a complete elution of these by-products, the acetals were eluted with benzene (**1b**), ether (**1a, c**), ether–ethanol (50:1) (**2a, b**), and ether–methanol (4:1) (**1e, f**). The structures of these acetals were established by following analytical data.

2-Phenyl-1,3,6,9,12-pentaoxacyclotetradecane (1a): Colorless viscous oil; IR (film) 2867, 1116 cm^{-1}; ^1H NMR ($CDCl_3$) δ=3.6—3.9 (16H, m), 5.72 (1H, s), 7.2—7.6 (5H, m); MS m/z 282 (M^+). Found: C, 63.66; H, 7.76%. Calcd for $C_{15}H_{22}O_5$: C, 63.81; H, 7.85%.

2-Methyl-2-phenyl-1,3,6-trioxacyclooctane (1b): Colorless viscous oil; IR(film) 2914, 1145 cm^{-1}; ^1H NMR ($CDCl_3$) δ=1.60 (3H, s), 3.5—4.0 (8H, m), 7.3—7.7 (5H, m); MS m/z 208 (M^+). Found: C, 69.27; H, 7.80%. Calcd for $C_{12}H_{16}O_3$: C, 69.21; H, 7.74%.

2-Methyl-2-phenyl-1,3,6,9,12-pentaoxacyclotetradecane (1c): Colorless viscous oil; IR (film) 2869, 1126 cm^{-1}; ^1H NMR ($CDCl_3$) δ=1.53 (3H, s), 3.4—3.7 (16H, m), 7.1—7.5 (5H, m); MS m/z 296 (M^+). Found: C, 64.79; H, 8.18%. Calcd for $C_{16}H_{24}O_5$: C, 64.84; H, 8.16%.

2,2-(Biphenyl-2,2′-diyl)-1,3,6,9,12-pentaoxacyclotetradecane (1e): Mp 128—129 °C, colorless prisms (from ether); IR (KBr) 2870, 1115 cm^{-1}; ^1H NMR ($CDCl_3$) δ=3.5—4.2 (16H, m), 7.2—7.7 (8H, m), MS m/z 356 (M^+). Found: C, 70.56; H, 6.81%. Calcd for $C_{21}H_{24}O_5$: C, 70.76; H, 6.79%.

2,2-(Biphenyl-2,2′-diyl)-1,3,6,9,12,15-hexaoxacycloheptadecane (1f): Mp 97—98 °C, colorless prisms (from ether); IR (KBr) 2860, 1072 cm^{-1}; ^1H NMR ($CDCl_3$) δ=3.5—4.0 (20H, m), 7.2—7.6 (8H, m), MS m/z 400 (M^+). Found: C, 69.88; H, 7.18%. Calcd for $C_{23}H_{28}O_6$: C, 69.98; H, 7.05%.

Fluorenone Bis(3,6-dioxaheptyl) Acetal (2a): Colorless viscous oil; IR (film) 2877, 1111 cm^{-1}; ^1H NMR($CDCl_3$) δ=3.30 (6H, s), 3.3—3.7 (16H, m), 7.2—7.7 (8H, m); MS m/z 402 (M^+). Found: C, 68.44; H, 7.47%. Calcd for $C_{23}H_{30}O_6$: C, 68.63; H, 7.51%.

Fluorenone Bis(3,6,9-trioxadecyl) Acetal (2b): Colorless viscous oil; IR (film) 2875, 1111 cm^{-1}; ^1H NMR δ=3.30 (6H, s), 3.4—3.7 (24H, m), 7.2—7.6 (8H, m); MS m/z 490 (M^+). Found: C, 66.40; H, 7.72%. Calcd for $C_{27}H_{38}O_8$: C, 66.10; H, 7.81%.

References

1) a) C. J. Pedersen, *J. Am. Chem. Soc.*, **92**, 7017 (1970); b) V. Gold and C. M. Sghibartz, *J. Chem. Soc., Chem. Commun.*, **1978**, 507; c) Y. Kawakami, T. Sugiura, and Y. Yamashita, *Bull. Chem. Soc. Jpn.*, **51**, 3053 (1978).

2) a) Y. Kawakami, J. Suzuki, and Y. Yamashita, *Polym. J.*, **9**, 519 (1977); b) C. Rentsch and R. C. Scheltz, *Makromol. Chem.*, **178**, 2535 (1977).

3) D. S. Baker, V. Gold, and C. M. Sghibartz, *J. Chem. Soc., Perkin Trans. 2*, **1983**, 1121.

4) J. M. Hill and W. H. Carothers, *J. Am. Chem. Soc.*, **57**, 925 (1935).

5) a) M. J. Astle, J. A. Zaslowsky, and P. G. Lafyatis, *Ind. Eng. Chem.*, **46**, 787 (1954); b) V. Gold and C. M. Sghibartz, *J. Chem. Soc., Perkin Trans. 1*, **1983**, 453.

6) Dimethyl-substituted(eleven-membered) and methyl, phenyl-substituted(eight-membered) crown ether acetals were synthesized in very low yields(5—8%) by J. Einhorn et al. in acetal-exchange reaction using orthoesters; *J. Heterocyclic Chem.*, **17**, 1345 (1980).

7) T. Oshima, R. Nishioka, S. Ueno, and T. Nagai, *J. Org. Chem.*, **47**, 2114 (1982).

8) T. Oshima and T. Nagai, *Bull. Chem. Soc. Jpn.*, **59**, 3865 (1986).

9) T. Shingaki, M. Tsujita, and T. Nagai, *Chem. Lett.*, **1986**, 1639.

10) G. L. Closs and R. A. Moss, *J. Am. Chem. Soc.*, **86**, 4042 (1964).

11) G. L. Closs and J. J. Coyle, *J. Org. Chem.*, **31**, 2759 (1966).

12) H. Staudinger and O. Kupfer, *Ber.*, **44**, 2197 (1911).

The Structure of Isoaplysin, a Brominated Rearranged Cuparane-Type Sesquiterpenoid from the Red Alga *Laurencia okamurai* Yamada[1]

Minoru SUZUKI,* Kazuya KURATA,† and Etsuro KUROSAWA
Department of Chemistry, Faculty of Science, Hokkaido University, Sapporo 060
†Department of Industrial Chemistry, Hakodate Technical College, Hakodate 042
(Received June 21, 1986)

Synopsis. The structure of isoaplysin isolated from the red alga *Laurencia okamurai* Yamada has been established by the spectral and chemical methods.

A number of halogenated and nonhalogenated sesquiterpenes with the cuparane or the rearranged cuparane skeleton have been isolated from the red alga *Laurencia* species and also from the sea hare *Aplysia* species.[2] In the course of our continuing studies on the constituents of the red alga *Laurencia okamurai* Yamada ("Mitsude-sozo"), we have reported, in the preliminary communication,[3] that the structure of isoaplysin has been shown by formula **1**. However, the possibility of an alternative formula **2** for isoaplysin could not be completely eliminated. In this note, we describe the structural determination of isoaplysin (**1**) in detail.

Isoaplysin (**1**) was isolated as a minor metabolite from the methanol extract of *L. okamurai* collected at various locations in Japan by a combination of column and thin-layer chromatography.[3,4]

Isoaplysin (**1**), colorless oil, $C_{15}H_{19}OBr$ (*m/z* 296 and 294; M^+), $[\alpha]_D^{24}$ −33° ($CHCl_3$), revealed in its ^1H NMR spectrum the presence of a secondary methyl group at δ=1.09 (3H, d, *J*=6 Hz), a tertiary methyl group at δ=1.50 (3H, s), an aromatic methyl group at δ=2.26 (3H, s), a methylene group with a heteroatom at δ=3.55 (2H, s), and a 1,2,4-trisubstituted phenyl moiety at δ=6.50 (1H, br s), 6.58 (1H, br d, *J*=8 Hz), and 6.82 (1H, d, *J*=8 Hz). The IR spectrum of **1** showed no hydroxyl and carbonyl absorptions, indicating that the oxygen atom in **1** was involved in a ether linkage. Since the ^{13}C NMR spectrum of **1** exhibits no signal due to a $-CH_2-O-$ grouping at near 70 ppm, the heteroatom above mentioned, which is adjacent to the methylene group at δ=3.55, must be bromine atom. The ^1H and ^{13}C NMR spectra of **1** were very similar to those of debromoaplysin (**3**), which has been obtained from this species[5] and also from the sea hare *Aplysia kurodai*.[6] However, in the ^1H NMR spectra, the distinct difference was observed in the higher magnetic field region as follows. As described above, the ^1H NMR spectrum of **1** indicates the presence of three methyl groups and one bromomethyl group, while the four methyl groups, including one secondary methyl and three tertiary methyls, are present in the spectrum of **3**. This fact suggested that one of the tertiary methyl groups in **3** is replaced by the bromomethyl group. Treatment of **1** with lithium aluminum hydride in tetrahydrofuran gave the debromo ether, $C_{15}H_{20}O$, $[\alpha]_D^{25}$ −53°, which was identical with debromoaplysin (**3**) in all respects. In view of the above-mentioned data, two possible formulae **1** and **2** could be proposed for isoaplysin.

Table 1. Selected ^{13}C NMR Chemical Shifts[a]

Carbon No	1	3	4	7	8	9[b]	10[b]
1	55.5	54.0	55.0	44.6	45.1	44.9	44.9
2	97.1	98.8	99.8	46.6	44.3	46.4	43.1
3	43.7	46.1	43.5	85.0	85.7	85.3	87.4
4	31.5	31.2	31.0	37.3	34.5	37.3	33.0
5	42.6	42.6	43.5	42.1	41.8	42.2	41.8

a) Measured at 25.0 MHz in $CDCl_3$ (TMS=0). b) Quoted from Ref. 9.

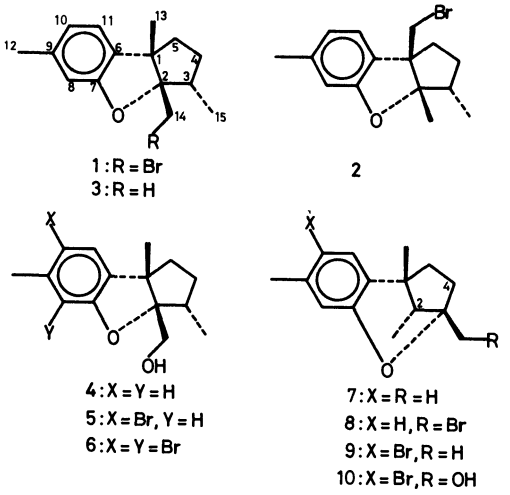

In the ^{13}C NMR spectra (Table 1), the signal for C-3 in **1** was shifted upfield by 2.4 ppm compared with that in **3**. The close upfield shift was seen in the spectrum of debromoaplysinol (**4**).[4] Furthermore, the comparative upfield shifts were also observed for the signals for C-2 and C-4 in the spectra of compounds **7**[7] and **8**[8] and also in those of filiformin (**9**)[9] and filiforminol (**10**).[9] The upfield shift of the signal for C-3 in isoaplysin is due to the γ-gauche interaction of this carbon with the bromomethyl carbon, whose situation is explicable well only by formula **1**. Confirmation of the structure **1** was obtained by the following chemical correlation.

In the previous paper,[4] the structure of debromoaplysinol (**4**) was deduced from the spectral properties. Debromoaplysinol (**4**), on treatment with bromine in acetic acid, yielded aplysinol (**5**)[5,6,10] in poor yield along with dibromo ether (**6**). On the other hand, treatment of **4** with carbon tetrabromide and triphenylphosphine in benzene gave a bromo ether, $C_{15}H_{19}OBr$, $[\alpha]_D^{18}$ −42°, which was identified as isoaplysin (**1**) by comparison of the spectral data. Accord-

ingly, the structure of isoaplysin is represented by formula **1**, including the absolute configuration.

Experimental

The melting points were uncorrected. The IR spectra were recorded on a JASCO A-102 or a JASCO IR-S spectrophotometer. The ^1H and ^{13}C NMR spectra were measured on a JEOL JNM-PS-100 or a JEOL JNM-FX 100 spectrometer, using tetramethylsilane as an internal standard. The low and high resolution mass spectra were taken with a JEOL JMS-D300 spectrometer. Specific rotations were measured on a JASCO DIP-140 or a Hitachi PO-B polarimeter, using $CHCl_3$ as solvent. Silica gel (Merck, Kieselgel 60, 70—230 mesh) was used for column chromatography. Silica gel (Merck, Kieselgel 60 GF_{254}) was used for preparative TLC. High-performance liquid chromatography was performed on a JASCO TRI ROTAR-III with a Finepak SIL-C_{18}column.

Isoaplysin (1): Colorless oil; $[\alpha]_D^{24}$ −33° (*c* 0.69); IR (film), ν_{max} 1620, 1597, 1501, 1275, 1265, 1255, 1135, 1001, 987, 960, 950, 855, and 802 cm^{-1}; ^1H NMR (CCl_4), in the text; ^{13}C NMR (25.0 MHz, $CDCl_3$), δ=158.7 (s; C-7), 138.2 (s; C-9), 132.9 (s; C-6), 122.1 (d; C-11), 121.4 (d; C-10), 109.3 (d; C-8), 97.1 (s; C-2), 55.5 (s; C-1), 43.7 (d; C-3), 42.6 (t; C-5), 34.5 (t; C-14), 31.5 (t; C-4), 22.9 (q; C-13), 21.5 (q; C-12), and 13.8 (q; C-15); MS (70 eV), *m/z* (rel intensity) 296, 294 (47 : 47; M^+) 281, 279 (7 : 7), 239, 237 (7 : 7), 215 (35), 201 (20), 199 (12), 173 (16), 159 (100), 145 (15), 135 (75), 121 (31), 115 (11), 107 (11), and 91 (12). Found: *m/z* 294.0607. Calcd for $C_{15}H_{19}O^{79}Br$: M, 294.0618.

Conversion of Isoaplysin (1) to Debromoaplysin (3). To a solution of **1** (13 mg) in dry tetrahydrofuran (7 ml) was added lithium aluminum hydride (50 mg), and the mixture was refluxed for 5 h, cooled, and mixed with water. After filtration and evaporation of the filtrate, the residue was extracted with ether. The ethereal solution was washed with saturated brine, dried over Na_2SO_4, and evaporated to leave an oily substance which was chromatographed on a silica-gel plate to give **3** (4 mg); oil; $[\alpha]_D^{25}$ −53° (*c* 0.15); The IR, ^1H NMR, and MS spectra were consistent with those of authentic debromoaplysin.

Conversion of Debromoaplysinol (4) to Aplysinol (5). To a solution of **4** (7 mg) in acetic acid (1 ml) was added a small excess of bromine in acetic acid, and the mixture was allowed to stand at room temperature for 30 min and then extracted with ether. The ethereal solution was successively washed with water, 5% aqueous $NaHCO_3$, and saturated brine. After drying over Na_2SO_4, the solvent was evaporated to give an oily residue which was subjected to high-performance liquid chromatography eluted with methanol/water (85 : 15) to afford **5** (2 mg) and **6** (6 mg): **5**: Mp 156—157 °C; $[\alpha]_D^{21}$ −53° (*c* 0.23); The IR and ^1H NMR spectra were identical with those of authentic aplysinol; **6**: Mp 91—93 °C; $[\alpha]_D^{19}$ −34° (*c*0.96); ^1H NMR ($CDCl_3$) δ=1.12 (3H, d, *J*=6 Hz), 1.50 (3H, s), 2.50 (3H, s), 3.86 (2H, m), and 7.14 (1H, s); MS (70 eV), *m/z* 392, 390, 388 (51 : 100 : 52; M^+).

Conversion of Debromoaplysinol (4) to Isoaplysin (1). A solution of **4** (8 mg) in dry benzene (1 ml) was refluxed with triphenylphosphine (35 mg) and carbon tetrabromide (40 mg) for 1 h in N_2 atmosphere. After removal of the solvent, the residual oil was chromatographed on silica-gel column to yield **1** (8 mg); oil; $[\alpha]_D^{18}$ −42° (*c* 0.77); The spectral properties were compatible with those of natural isoaplysin.

References

1) Part 66 of "Constituents of Marine Plants." Part 65; M. Suzuki, K. Kurata, T. Suzuki, and E. Kurosawa, *Bull. Chem. Soc. Jpn.*, in press.

2) In "Marine Natural Products," ed by P. J. Scheuer, Academic Press, New York; J. D. Martin and J. Darias, (1978), Vol. 1, pp. 152—161; K. L. Erickson, (1983), Vol. 5, pp. 155—164, p. 229, pp. 237—241.

3) M. Suzuki and E. Kurosawa, *Tetrahedron Lett.*, **1978**, 2503.

4) M. Suzuki and E. Kurosawa, *Bull. Chem. Soc. Jpn.*, **52**, 3352 (1979).

5) T. Irie, M. Suzuki, and Y. Hayakawa, *Bull. Chem. Soc. Jpn.*, **42**, 843 (1969).

6) S. Yamamura and Y. Hirata, *Tetrahedron*, **19**, 1485 (1963).

7) Compound **7** was synthesized in high yield from compound **8**[8] by treatment with W-7 Raney nickel in ethanol; **7**: $[\alpha]_D^{17}$ −12° (*c* 1.20; $CHCl_3$); ^1H NMR ($CDCl_3$), δ=0.77 (3H, d, *J*=7 Hz), 1.34 (3H, s), 1.39 (3H, s), 2.25 (3H, s), 6.54 (1H, br s), 6.63 (1H, br d, *J*=8 Hz), and 6.98 (1H, d, *J*=8 Hz); MS (70 eV), *m/z* 216 (44; M^+) and 201 (100; $M^+ - CH_3$).

8) M. Suzuki and E. Kurosawa, *Tetrahedron Lett.*, **1976**, 4817; T. Irie, A. Fukuzawa, M. Izawa, and E. Kurosawa, *ibid.*, **1969**, 1343.

9) R. Kazlauskas, P. T. Murphy, R. J. Quinn, and R. J. Wells, *Aust. J. Chem.*, **29**, 2533 (1976).

10) J. A. McMillan, I. C. Paul, S. Caccamese, and K. L. Rinehart, Jr., *Tetrahedron Lett.*, **1976**, 4219.

The Revised Structure of a Dihydrobenzofuran Derivative Isolated from *Lasiolaena morii*

Seiji YAMAGUCHI, Akihito SAITOH, and Yoshiyuki KAWASE*
Department of Chemistry, Faculty of Science, Toyama University, Gofuku 3190, Toyama 930
(Received March 24, 1986)

Synopsis. Two isopropenyldihydrobenzofuran derivatives are synthesized. By the comparison of ^{1}H NMR spectra, the proposed structure of a natural dihydrobenzofuran is revised to 4-acetyl-2-isopropenyl-2,3-dihydrobenzofuran-5-ol.

In 1982, F. Bohlmann et al. isolated a new dihydrobenzofuran from *Lasiolaena morii* and proposed a structure of 5-acetyl-2-isopropenyl-2,3-dihydrobenzofuran-4-ol (**1**).[1] We have already synthesized this compound by a demethylation of 5-acetyl-2-isopropenyl-4-methoxy-2,3-dihydrobenzofuran.[2] However, our synthetic compound showed a different ^{1}H NMR spectrum from that of the natural one. In the ^{1}H NMR spectra, the synthetic sample showed aromatic proton signals at δ=6.4 and 7.6 ppm, while the natural sample showed the corresponding signals at δ=6.81 and 6.99 ppm (Table 1). This fact indicates that the natural compound has another structure. Since the spectrum of the natural compound showed an intramolecular hydrogen-bonding (δ_{OH}=12.16 ppm) and no aromatic proton deshielded by an acetyl group in its ortho position, two structures, 7-acetyl-2-isopropenyl-2,3-dihydrobenzofuran-6-ol (**2**) and 4-acetyl-2-isopropenyl-2,3-dihydrobenzofuran-5-ol (**3**), are possible. In this paper, we describe the synthesis of these two dihydrobenzofurans and the structural reversion of the natural compound isolated from *Lasiolaena morii*.

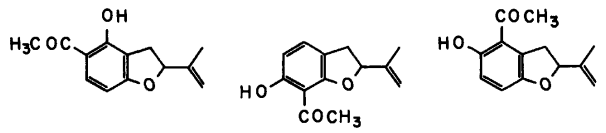

1 2 3

The compound **2** and **3** were synthesized by the procedure reported by F. Bigi et al.[3] After the similar treatment of 2′,6′-dihydroxyacetophenone with 1,4-dibromo-2-methyl-2-butene, **2** and 9-acetyl-3-methyl-2,5-dihydro-1-benzoxepin-8-ol (**4**)[4] were obtained as cyclized products. In this reaction, 1,4-bis(2-acetyl-3-hydroxyphenoxy)-2-methyl-2-butene was also isolated as non-cyclized product. Similarly, the treatment of 2′,5′-dihydroxyacetophenone with 1,4-dibromo-2-methyl-2-butene gave two dihydrobenzofurans, **3** and 4-acetyl-2-methyl-2-vinyl-2,3-dihydrobenzofuran-5-ol (**5**).

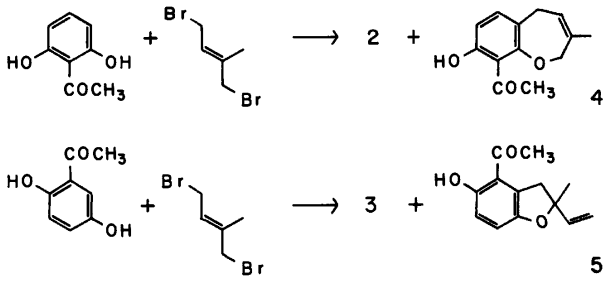

4

5

In the ^{1}H NMR spectra, two isopropenyldihydrobenzofuran derivatives **2** and **3** showed an ABX coupling pattern due to protons in the dihydrofuranring, and **5** showed signals due to a quarternary methyl and a vinyl proton. On the other hand, **4** gave another spectral mode of the oxepin ring part [a broad methyl singlet, a broad two-proton doublet (H-5), a broad two-proton singlet (H-2), and a broad one-proton triplet (H-4)], similar to those of some natural 3-methyl-2,5-dihydro-1-benzoxepin derivatives.[5]

In the cyclization of 2′,4′-dihydroxyacetophenone,[3] two 2-isopropenyl-2,3-dihydrobenzofurans, 5-acetyl-2-isopropenyl-2,3-dihydrobenzofuran-4-ol (major) and 5-acetyl-2-isopropenyl-2,3-dihydrobenzofuran-6-ol (minor), were obtained. However, in a similar cyclization of 2′,5′-dihydroxyacetophenone, all isolated products were formed via the alkylation at C-6, and no products derived from the C-4 alkylation were isolated.

Table 1. ^{1}H NMR Spectral Data of Isopropenyldihydrobenzofuran Derivatives [δ (ppm) and J(Hz) in $CDCl_3$]

	-CH_3	-$COCH_3$	3-CH_2		=CH_2		2-CH	Ar-H		-OH
Natural Compound	1.80 (s)	2.59 (s)	3.29 (dd, J=8.5, 16.5)	3.63 (dd, J=9.5, 16.5)	4.95 (broad s)	5.11 (broad s)	5.19 (dd, J=8.5, 9.5)	6.81 (d, J=8.5)	6.99 (d, J=8.5)	12.16[a] (s)
1	1.8 (s)	2.6 (s)	3.0 (dd, J=8, 16)	3.3 (dd, J=10, 16)	4.9 (broad s)	5.1 (broad s)	5.3 (dd, J=8, 10)	6.4 (d, J=9)	7.6 (d, J=9)	12.7[b] (s)
2	1.8 (s)	2.7 (s)	3.0 (dd, J=8, 15)	3.3 (dd, J=9.5, 15)	5.0 (broad s)	5.1 (broad s)	5.3 (dd, J=8, 9.5)	6.4 (d, J=8)	7.3 (d, J=8)	12.6 (s)
3	1.8 (s)	2.6 (s)	3.3 (dd, J=8, 16)	3.6 (dd, J=10, 16)	5.0 (broad s)	5.1 (broad s)	5.2 (dd, J=8, 10)	6.8 (d, J=9)	7.0 (d, J=9)	12.2 (s)

a) The data of natural compound from *Lasiolaena morii* provided by Bohlmann et al.[1] b) The data of our synthetic sample prepared by demethylation of 5-acetyl-2-isopropenyl-4-methoxy-2,3-dihydrobenzofuran.[2]

The ^{1}H NMR data of the three 2-isopropenyl-2,3-dihydrobenzofuran derivatives are summarized in Table 1. As shown in the table, the natural compound isolated from *Lasiolaena morii* was identical with 4-acetyl-2-isopropenyl-2,3-dihydrobenzofuran-5-ol (**3**).

Experimental

The melting points were uncorrected. The IR spectra were measured on a Hitachi EPI-S2 spectrophotometer in KBr disks, and the UV spectra were taken on a Hitachi 220A spectrophotometer in ethanol. The ^{1}H NMR spectra were recorded on a JEOL JNM-MH-60 NMR spectrometer or Varian XL-200 FT NMR spectrometer in CCl_4 or $CDCl_3$ and the mass spectra were determined on a JEOL JMS-OISG-2 mass spectrometer.

Cyclization of 2′,6′-Dihydroxyacetophenone with 1,4-Dibromo-2-methyl-2-butene. A suspension of the sodium salts was prepared by mixing 2′,6′-dihydroxyacetophenone (2.04 g, 13.4 mmol) and sodium hydride (52% mineral oil dispersion, 1.26 g, 27.8 mmol) in refluxing dry toluene (80 mL), and cooled to room temperature. To the suspension, 1,4-dibromo-2-methyl-2-butene (3.20 g, 14.0 mmol) was added and the mixture was refluxed for 24 h with stirring. After cooling, the mixture was treated with 10% hydrochloric acid and the toluene layer was collected. The toluene layer was washed with a 10% sodium carbonate solution and then extracted with a 5% sodium hydroxide solution. The sodium hydroxide solution was acidified with 10% hydrochloric acid and extracted with ether. The ethereal solution was dried over anhydrous sodium sulfate. After removing the ether, the oily residue was chromatographed on a silica-gel column to give two fractions as benzene eluents. One of the fractions (185 mg) showed three peaks (ratio **A**:**2**:**4**=1.4:4.1:1) in GLC. Pure samples of **2** and **4** were obtained after re-chromatography and recrystallization, but the component **A** could not be isolated as pure state.[6] From the other fraction (45 mg), 1,4-bis(2-acetyl-3-hydroxyphenoxy)-2-methyl-2-butene was isolated in pure crystals. The three compounds isolated showed the following data. **2**: mp 59—60 °C (from hexane); IR 1640 cm^{-1}; ^{1}H NMR cited in table 1; UV 230 (log ε 4.10), 268 (4.13), 356 nm (3.66); MS *m*/*z* 218 (M^+), 203, 185. Found: C, 71.78, H, 6.64%. Calcd for $C_{13}H_{14}O_3$: C, 71.54, H, 6.47%. **4**: mp 81—82 °C (from hexane); IR 1640 cm^{-1}; ^{1}H NMR ($CDCl_3$) δ=1.6 (3H, broad s), 2.8 (3H, s), 3.3 (2H, broad d, *J*=6 Hz), 4.5 (2H, broad s), 5.7 (1H, broad t, *J*=6 Hz), 6.7 (1H, d, *J*=8 Hz), 7.2 (1H, d, *J*=8 Hz), 12.8 ppm (1H, s); UV 221 (log ε 4.10), 260 (3.93), 341 nm (3.40); MS *m*/*z* 218 (M^+), 203, 185. Found: C, 71.49, H, 6.45%. Calcd for $C_{13}H_{14}O_3$: C, 71.54, H, 6.47%. 1,4-Bis(2-acetyl-3-hydroxyphenoxy)-2-methyl-2-butene; mp 133—135 °C (from benzene); IR 1630 cm^{-1}; ^{1}H NMR ($CDCl_3$) δ=1.9 (3H, s), 2.6 (3H, s), 2.7 (3H, s), 4.6 (2H, s), 4.7 (2H, d, *J*=7 Hz), 5.9 (1H, t, *J*=7 Hz), 6.4 (2H, d, *J*=8 Hz), 6.6 (2H, d, *J*=8 Hz), 7.4 (2H, t, *J*=8 Hz), 13.2 ppm (2H, s); MS *m*/*z* 370 (M^+), 259, 218. Found: C, 67.79, H, 6.04%. Calcd for $C_{21}H_{22}O_6$: C, 68.09, H, 5.99%. From the fraction soluble in a 10% sodium carbonate solution, ca. 20% of 2′,6′-dihydroxyacetophenone was recovered.

Similarly, cyclization of 2′,6′-dihydroxyacetophenone (20.0 mmol) with sodium hydride (23.3 mmol) and 1,4-dibromo-2-methyl-2-butene (21.6 mmol) gave **2** (1.85%), **4** (0.84%), and 1,4-bis(2-acetyl-3-hydroxyphenoxy)-2-methyl-2-butene (1.00%) and 40% of the starting material was recovered.

Cyclization of 2′,5′-Dihydroxyacetophenone with 1,4-Dibromo-2-methyl-2-butene. A similar treatment of 2′,5′-dihydroxyacetophenone (2.70 g, 17.8 mmol) with 1,4-dibromo-2-methyl-2-butene (4.30 g, 18.9 mmol) and sodium hydride (52% mineral oil dispersion, 0.84 g, 18.5 mmol) in dry toluene (90 mL) gave an oily product. This was purified on a silica-gel column and the fraction (total 282 mg) eluted by benzene showed two peaks (ratio **3**:**5**=2.2:1) in GLC. Some pure samples were obtained after re-chromatography and recrystallization. These two compounds showed the following data. **3**: mp 75—76 °C (from hexane); IR 1640 cm^{-1}; ^{1}H NMR cited in table 1; UV 233 (log ε 4.21), 261sh (3.90), 368 nm (3.65); MS *m*/*z* 218 (M^+), 203, 185, 177, 175. Found: C, 71.40, H, 6.67%. Calcd for $C_{13}H_{14}O_3$: C, 71.54, H, 6.47%. **5**: mp 96—98 °C (from hexane); IR 1640 cm^{-1}; ^{1}H NMR ($CDCl_3$) δ=1.6 (3H, s), 2.6 (3H, s), 3.4 (1H, d, *J*=18 Hz), 3.5 (1H, d, *J*=18 Hz), 5.2 (1H, dd, *J*=1 and 11 Hz), 5.4 (1H, dd, *J*=1 and 17 Hz), 6.1 (1H, dd, *J*=11 and 17 Hz), 6.8 (1H, d, *J*=9 Hz), 7.0 (1H, d, *J*=9 Hz), 12.2 ppm (1H, s); UV 232 (log ε 4.31), 261sh (4.08), 366 nm (3.80); MS *m*/*z* 218 (M^+), 205, 175. Found: C, 71.78, H, 6.59%. Calcd for $C_{13}H_{14}O_3$: C, 71.54, H, 6.47%. From the fraction soluble in 10% sodium carbonate solution, ca. 50% of 2′,5′-dihydroxyacetophenone was recovered.

Similarly, in a cyclization of 2′,5′-dihydroxyacetophenone (7.83 mmol) with sodium hydride (17.4 mmol) and 1,4-dibromo-2-methyl-2-butene (7.89 mmol), a mixture (105 mg) of **3** and **5** (ratio **3**:**5**=2.4:1 in GLC) was obtained.

We wish to thank Professor Dr. Ferdinand Bohlmann for providing a copy of the ^{1}H NMR spectrum of the natural compound.

References

1) F. Bohlmann, J. Jakupovic, A. Schuster, R.M. King, and H. Robinson, *Phytochemistry*, **21**, 161 (1982).

2) S. Yamaguchi, K. Sugiura, R. Fukuoka, K. Okazaki, M. Takeuchi, and Y. Kawase, *Bull. Chem. Soc. Jpn.*, **57**, 3067 (1984).

3) F. Bigi, G. Casiraghi, G. Casnati, and G. Sartori, *Tetrahedron*, **39**, 169 (1983).

4) The oxepin derivative **4** may be formed via a cyclopropane intermediate **6**, which would be derived by a double C-alkylation. Mechanistic studies on the formation of **4** is now in progress.

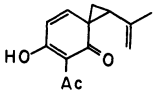

6

5) a) F.M. Dean and D. A. H. Taylor, *J. Chem. Soc. (C)*, **1966**, 114; b) P. H. McCabe, F. McCrindle, and R. D. H. Murray, *J. Chem. Soc. (C)*, **1967**, 145; c) Y. Asakawa, M. Toyota, and T. Takemoto, *Phytochemistry*, **17**, 2005 (1978).

6) The ^{1}H NMR spectrum of an impure sample showed that the compound **A** would be 7-acetyl-2-methyl-2-vinyl-2,3-dihydrobenzofuran-6-ol.

An Improved Method for Stereoselective Synthesis of (*E*)-Alkenes via Alkenyldialkylboranes

Masayuki HOSHI, Yuzuru MASUDA, and Akira ARASE*
Department of Industrial Chemistry, Kitami Institute of Technology, Kitami 090
(Received April 2, 1986)

Synopsis. Successive treatments of alkenyldialkylboranes, formed by the reaction of alkynes and sterically hindered dialkylboranes, with alkyllithium and benzenesulfenyl chloride afforded highly pure (*E*)-alkenes in good or excellent yields.

(*Z*)-[1] and (*E*)-[2] alkene syntheses reported by Zweifel and co-workers are some of the interesting reactions using alkenylboranes; it has a limitation that the available alkyl group is restricted to those derived from sterically hindered alkenes.[3] From a different point of view, the reactions provide a convenient method for the regio- and stereoselective synthesis of alkenes by the combination of the alkenyl group to the alkyl group on the boron moiety.

For a practical use of above (*E*)-alkene synthesis (Scheme 1), the reaction had two disadvantages: The use of very poisonous cyanogen bromide and contamination by the *Z* isomer. We wish to report here a modified method for the (*E*)-alkene synthesis using alkyllithium and benzenesulfenyl chloride instead of cyanogen bromide.

In the Zweifel's reactions, the combined yields of the (*E*)- and (*Z*)-alkenes seemed to be affected by the degree of the coordination of the anion (CN^-) to the boron atom; also, the ratio of the two isomers seemed to be affected by the ease of the elimination of the electrophile (Br^+), which once attacked the alkenyl double bond, from the carbon atom. Accordingly, we examined both nucleophilic reagents for the boron atom and electrophilic reagents for the double bond, using (*E*)-1-hexenyldicyclohexylborane. Thus, successive treatments of the 1-hexenylborane with alkyllithium and benzenesulfenyl chloride gave excellent results.

In preliminary examinations, where alkyllithium was absent, (*E*)-1-hexenyldicyclohexylborane was treated with an equimolar amount of benzenesulfenyl chloride in THF. The reaction mixture was then treated with hexane for an analysis. However, only a small amount of a mixture of (*E*)- and (*Z*)-1-cyclohexyl-1-hexene was obtained. In similar treatments of an ate-complex formed by the addition of an equimolar amount of methyllithium or butyllithium to the 1-hexenylborane, gave the mixture of the alkenes quantitatively. Essentially, the pure *E*-isomer was obtained at −78 °C. These results are shown in Table 1.

In a similar reaction, [(*E*)-1-hexenyl]bis(1,2-dimethylpropyl)borane also gave almost pure (*E*)-2,3-dimethyl-4-nonene in 92% yield. [(*E*)-1-Hexenyl]bis(*trans*-2-methylcyclohexyl)borane gave a mixture of (*E*)- and (*Z*)-(*trans*-2-methylcyclohexyl)-1-hexene (*E*/*Z*=90/10), while the *trans*-2-methylcyclohexyl group migrated with a retention of the configuration. A stereochemical consideration for the above facts suggested that the large steric hindrance between the 2-methylcyclohexyl group R, remaining on the boron atom, and the phenylthio group interfered somewhat with the favorable arrangement regarding to the cis-elimination; thus, it increased the chance for the trans-elimination which gave the *Z* isomer (Scheme 2). In a reaction of [(*E*)-3,3-dimethyl-1-butenyl]bis(*trans*-2-methylcyclohexyl)-borane or [(*E*)-2-phenylethenyl]bis(*trans*-2-methylcyclohexyl)borane, having such a bulkier group as *t*-butyl or phenyl group instead of *n*-butyl group on the β-carbon atom, exclusively gave the *E* isomer. In this case, a steric hindrance between the *trans*-2-methylcyclohexyl group R, migrated to the α-carbon, and the *t*-butyl or the phenyl group R' interfered with the arrangement favored with the trans-elimination and

Table 1. 1-Cyclohexyl-1-hexenes from 1-Hexenyldicyclohexylborane[a]

RLi	Temp °C	Alkene ratio *E*	Alkene ratio *Z*	Total alkene yield/%
None	0			trace
	−78	14	86	5
n-C_4H_9Li	0	92	8	≒100
	−78	>99	<1	≒100
CH_3Li	−78	>99	<1	≒100

a) The isomer distribution and the yield of alkenes were determined by GLC.

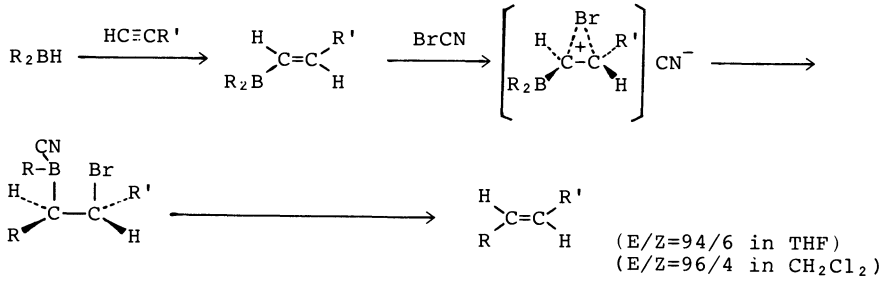

Scheme 1.

Table 2. (*E*)-1-Alkyl-1-alkenes from (*E*)-1-Alkenyldialkylboranes[a)]

R of R_2BH	Alkyne	R″ of R″Li	Yield of *E*-alkene/%	Isomeric purity/%
C_6H_{11}-*c*	HC≡CC_4H_9-*n*	*n*-C_4H_9	100[b)](91)[c)]	>99
	HC≡CC_6H_5	*n*-C_4H_9	85 (79)	≒100
	HC≡CC_4H_9-*t*	CH_3	76 (70)	≒100
$(CH_3)_2CH(CH_3)CH$	HC≡CC_4H_9-*n*	*n*-C_4H_9	92 (83)	>99
	HC≡CC_6H_5	*n*-C_4H_9	80 (75)	≒100
2-$CH_3C_6H_{10}$-*c*	HC≡CC_4H_9-*n*	CH_3	79 (72)	90
	HC≡CC_6H_5	CH_3	65 (60)	≒100
	HC≡CC_4H_9-*t*	CH_3	80 (75)	≒100

a) The alkenyldialkylborane was treated with equimolar amounts of alkyllithium (at 0°C, for 0.5 h) and benzenesulfenyl chloride (at −78°C, for 0.5 h) to the alkenyldialkylborane. b) Determined by GLC. c) The value in the parenthesis is isolated yield.

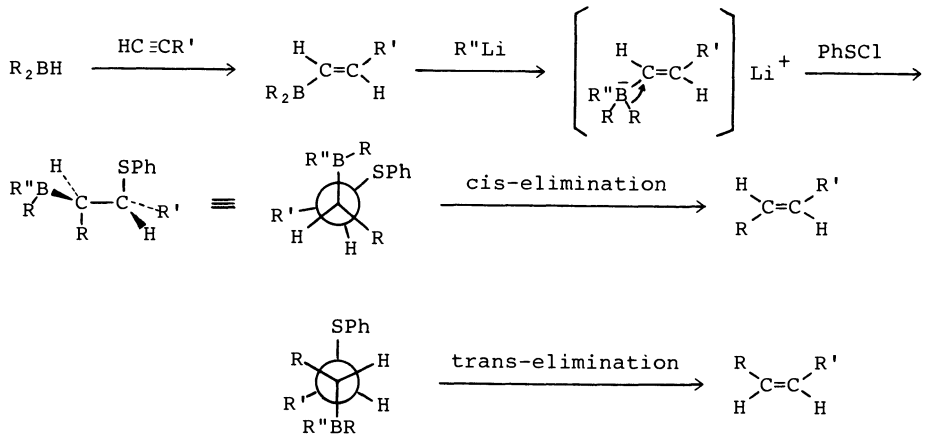

Scheme 2.

gave no chance for the formation of the *Z* isomer (Scheme 2). Similar alkenylboranes, having a *t*-butyl or a phenyl group on the β-carbon atom, gave almost pure (*E*)-alkenes. In all the cases examined, (*E*)-alkenes were isolated from the reaction mixtures by column chromatography.[4)] These results are shown in Table 2.

The high stereoselectivity and the ease of the reaction procedure, shown above, seem to make the present reaction of practically applicable to the synthesis of (*E*)-alkenes, especially having two bulky alkyl groups on the alkenyl carbon atoms.

Experimental

Instruments. IR spectra were recorded using a Hitachi 285 spectrometer. ^1H NMR and ^{13}C NMR (200 MHz) spectra ($CDCl_3$, TMS) were run on a JEOL FX-200 spectrometer. Mass spectra were recorded by a Hitachi M-52 mass spectrometer.

Reagents. Cyclohexene, 2-methyl-2-butene, 1-methyl-1-cyclohexene and THF were dried over lithium aluminium hydride and distilled under an argon stream. Commercial 1-hexyne and phenylacetylene were dried over Molecular Sieves-4A. 3,3-Dimethyl-1-butyne was prepared by a method described in the literature,[5)] and dried over Molecular Sieves-4A. Commercial alkyllithiums were used without any purification. Benzenesulfenyl chloride was prepared by the method described in the literature.[6)]

Reaction Procedure. A 50-ml round-bottomed flask, equipped with a gas inlet for argon, a sample inlet with a serum cap and a magnetic stirring bar, was flushed with argon. In the flask, alkenyldialkylborane was prepared by the addition of alkyne (10 mmol) to dialkylborane (10 mmol) in THF under appropriate conditions. Then, butyllithium (10 mmol) in hexane or methyllithium (10 mmol) in diethyl ether was added at 0 °C and the solution was stirred for 0.5 h, and then cooled to −78 °C. To this solution, benzenesulfenyl chloride (10 mmol) was slowly added and the reaction mixture was stirred for 0.5 h and then extracted three times with diethyl ether. The combined extracts were washed twice with NaCl-saturated water and dried over anhydrous magnesium sulfate. After evaporation of the solvent, the residue was put on a column packed with silica gel (Wako-gel Q-50) and eluted by pentane.

Spectral Data of the Products are as Follows. (*E*)-1-Cyclohexyl-1-hexene: ^1H NMR δ=0.88 (t, *J*=6.8Hz, 3H), 0.89—2.10 (m, 17H) and 5.30—5.40 (m, 2H); ^{13}C NMR δ=13.98, 22.18, 26.14 (-CH_2-, 2C), 26.27, 31.88, 32.55, 33.30 (-CH_2-, 2C), 40.69 (>CH-), 127.68 (-CH=) and 136.38 (-CH=); IR 970 cm^{-1} (⁀C=C⁀); MS *m/z* 166 (M^+).

(*E*)-1-Cyclohexyl-3,3-dimethyl-1-butene: ^1H NMR δ=0.97 (s, 9H), 0.97—1.97 (m, 11H), 5.22 (dd, *J*=15.6 and 6.3 Hz, 1H) and 5.39 (d, *J*=15.6 Hz, 1H); ^{13}C NMR δ=26.19 (-CH_2-, 2C), 26.27, 29.87 (-CH_3, 3C), 32.54 (-C-). 33.44 (-CH_2-, 2C), 40.69 (>CH-), 130.72 (-CH=) and 138.82 (-CH=); IR 1360 and 970 (⁀C=C⁀) cm^{-1}; MS *m/z* 166 (M^+).

(*E*)-1-Cyclohexyl-2-phenylethene: ^1H NMR δ=1.06—2.23 (m, 11H), 6.16 (dd, *J*=16.1 and 6.8 Hz, 1H), 6.34 (d, *J*=16.1 Hz, 1H) and 7.13—7.40 (m, 5H); ^{13}C NMR δ=26.02 (-CH_2-,

2C), 26.17, 32.93 (-CH_2-, 2C), 41.55 (>CH-), 125.90 (-CH=, 2C), 126.68 (-CH=), 127.19 (-CH=), 128.41(-CH=, 2C), 136.80 (-CH=) and 138.01 (>C=); IR 965 ($\diagdown$C=C$\diagup$), 745 and 690 cm^{-1}; MS m/z 186 (M^+).

(*E*)-2,3-Dimethyl-4-nonene: ^{1}H NMR δ=0.82 (d, J=6.8 Hz, 3H), 0.84 (d, J=6.8 Hz, 3H), 0.89 (t, J=6.8 Hz, 3H), 0.92 (d, J=6.8 Hz, 3H), 1.22—1.60 (m, 5H), 1.78—2.10 (m, 3H) and 5.26—5.36 (m, 2H); ^{13}C NMR δ=13.96, 17.68, 19.63, 19.89, 22.18, 31.93, 32.37, 33.05, 42.98, 129.35 (-CH=) and 134.49 (-CH=); IR 970 ($\diagdown$C=C$\diagup$) cm^{-1}; MS m/z 154 (M^+).

(*E*)-1-Phenyl-3,4-dimethyl-1-pentene: ^{1}H NMR δ=0.87 (d, J=7.3 Hz, 3H), 0.89 (d, J=6.8 Hz, 3H), 1.05 (d, J=6.3 Hz, 3H), 1.48—1.74 (m, 1H), 1.98—2.24 (m, 1H), 6.12 (dd, J=16.1 and 8.3 Hz, 1H), 6.23 (d, J=16.1 Hz, 1H) and 7.12—7.39 (m, 5H); ^{13}C NMR δ=17.44, 19.80, 19.97, 33.27, 43.54, 125.95 (-CH=, 2C), 126.70 (-CH=), 128.43 (-CH=, 2C), 128.82 (-CH=), 135.34 (-CH=) and 138.04 (>C=); IR 965 ($\diagdown$C=C$\diagup$), 745 and 690 cm^{-1}; MS m/z 172 (M^+).

(*E*)-1-(*trans*-2-Methylcyclohexyl)-3,3-dimethyl-1-butene: ^{1}H NMR δ=0.80 (d, J=5.8 Hz, 3H), 0.85—1.80 (m, 10H), 0.98 (s, 9H), 5.07 (dd, J=15.6 and 8.3 Hz, 1H) and 5.38 (d, J=15.6 Hz, 1H); ^{13}C NMR δ=20.82, 26.29, 26.63, 29.89 (-CH_3, 3C), 32.66 (-$\underset{|}{\overset{|}{C}}$-), 34.03, 35.31, 37.14 (>CH-), 48.91 (>CH-), 129.72 (-CH=) and 140.69 (-CH=); IR 1355 and 970 ($\diagdown$C=C$\diagup$) cm^{-1}; MS m/z 180 (M^+).

(*E*)-1-(*trans*-2-Methylcyclohexyl)-2-phenylethene: ^{1}H NMR δ=0.87 (d, J=6.3 Hz, 3H), 0.90—1.90 (m, 10H), 6.03 (dd, J=15.6 and 8.3 Hz, 1H) 6.34 (d, J=15.6 Hz, 1H) and 7.07—7.43 (m, 5H); ^{13}C NMR δ=21.01, 26.10 26.46, 33.59, 35.17, 37.11 (>CH-), 49.37 (>CH-), 125.90 (-CH=, 2C), 126.65 (-CH=), 128.41 (-CH=, 2C), 128.87 (-CH=), 136.04 (-CH=) and 138.04 (>C=); IR 960 ($\diagdown$C=C$\diagup$), 740 and 690 cm^{-1}; MS m/z 200 (M^+).

References

1) G. Zweifel, H. Arzoumanian, and C. C. Whitney, *J. Am. Chem. Soc.*, **89**, 3652 (1967).

2) G. Zweifel, R. P. Fischer, J. T. Snow, and C. C. Whitney, *J. Am. Chem. Soc.*, **94**, 6560 (1972).

3) See for example: a) H. C. Brown, "Hydroboration," W. A. Benjamin New York (1962); b) G. M. L. Cragg, "Organoboranes in Organic Synthesis," Marcel Dekker, New York (1973); c) H. C. Brown, "Organic Synthesis via Boranes," J. Wiley & Sons, New York (1975).

4) Spectral data of these alkenes coincided with those obtained by the method in Ref. 2.

5) W. L. Collier and R. S. Macomber, *J. Org. Chem.*, **38**, 1367 (1973)

6) D. N. Harpp, B. T. Friedlander, and R. A. Smith, *Synthesis*, **1979**, 181.

Stereoselectivity of Diels-Alder Reactions of 6,7-Dioxabicyclo[3.2.2]-nona-3,8-dien-2-one and 6,7-Diethoxycarbonyl-6,7-diazabicyclo[3.2.2]nona-3,8-dien-2-one

Hitoshi TAKESHITA,* Akira MORI, Shigeru SUGIYAMA, and Tohru TSUDA†
Research Institute of Industrial Science, 86, Kyushu University, Kasuga-koen, Kasuga, Fukuoka 816
†Graduate School of Engineering Sciences, 39, Kyushu University, Kasuga-koen, Kasuga, Fukuoka 816
(Received May 22, 1986)

Synopsis. A Diels-Alder reaction of 6,7-dioxabicyclo[3.2.2]-nona-3,8-dien-2-one (**2**) with cyclopentadiene gave the *cis-endo*-[4+2] adduct and the *trans-endo*-[4+2] adduct. Their yields were improved when the reaction was carried out under high-pressure conditions. The reaction of 6,7-diethoxycarbonyl-6,7-diazabicyclo[3.2.2]nona-3,8-dien-2-one (**3**) gave the *cis-endo*-[4+2] adduct. Reactions of **2** and **3** with isobenzofuran and its 1,3-diphenyl derivative gave the thermodynamically-controlled *exo*-[4+2] adducts.

Several years ago, we investigated the Diels-Alder reaction[1] of bicyclo[3.2.2]nona-3,6-dien-2-one (**1**),[2] to give stereospecific *cis-endo*-adducts[3] from several dienes. The bicyclic enone, **1**, is an interesting dienophile, whose structure possesses an ideal arrangement of a vinylene group having an intramolecular homoconjugation with the enone,[4] to evaluate the secondary stereoelectronic effect in the Diels-Alder reaction. An HMO calculation supported the results.[1] In this connection, it will be worthwhile to check the Diels-Alder reaction of the heterocyclic analogs of **1** as dienophiles. Herein, we wish to describe the reaction of 6,7-dioxabicyclo[3.2.2]nona-3,8-dien-2-one (**2**)[5] and 6,7-diethoxycarbonyl-6,7-diazabicyclo[3.2.2]nona-3,8-dien-2-one (**3**),[6] dioxa and diaza analogs of **1**, with dienes.

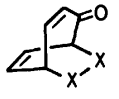

1 X=CH_2
2 X=O
3 X=NCO_2Et

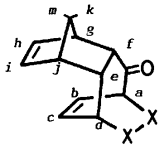

5 X=O
12 X=NCO_2Et

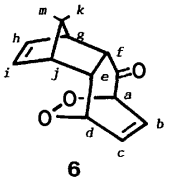

6

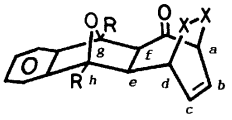

8 X=O, R=H
11 X=O, R=Ph
14 X=NCO_2Et, R=H

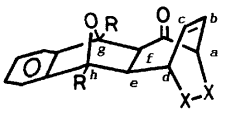

9 X=O, R=H
13 X=NCO_2Et, R=H
15 X=NCO_2Et, R=Ph

Heating of **2** in benzene with cyclopentadiene (**4**) and a catalytic amount of *p*-toluenesulfonic acid (TsOH) formed two products (**5** and **6**). Silica-gel column chromatography led to an isolation, from the less polar eluent, of colorless needles (**5**) in 2% yield. Its ^1H NMR spectrum revealed a broad vinylic proton signal at a somewhat higher field than expected, δ=5.93 (2H, m), ascribable for the norbornene part. In addition, mutually coupled two-proton signals appeared at 6.50 (dd, J=9, 7 Hz, Hc) and 5.77 (dd, J=9, 7 Hz, Hb). The coupling constant of the methine protons, J_{ej}=3 Hz, showed that the stereochemistry was an *endo*-attack to the enone part. These findings indicated that the stereochemistry of **5** is same to that of the Diels-Alder adducts of **1** with **4** and some cyclic dienes.[1] Subsequent elution afforded colorless needles (**6**) in 3% yield. Its NMR signals of vinylic protons revealed different stereochemistry with **5**; the characteristic signals ascribable to the norbornene part were at 6.06 and 6.35 as each dd; the other signals at 6.29 and 6.83 were those of the dioxacyclohexene moiety. Yet, the coupling constants of the methine protons, J_{ej}=3 Hz and J_{fg}=4 Hz, had the same magnitude as **5** and confirmed the *endo*-orientation. Thus, **6** is *trans-endo*-adduct.

Similarly, **2** with isobenzofuran (**7**),[7] afforded two products (**8**, 41% yield, and **9**, 18% yield) which were deduced to be both *exo*-adducts from a different magnitude of the spin-spin couplings; J_{ch}=J_{fg}=0 Hz for both **8** and **9**. A comparison of the chemical shifts ascribable to H_e and H_f determined the rest of the stereochemistry as depicted; **5** and **9** showed signals at a lower field than **6** and **8**. Moreover, the reaction of **2** with 1,3-diphenylisobenzofuran (**10**) also only yielded a *trans-exo*-adduct (**11**) in 31% yield.

These observations indicated: i) in the reaction of **2** with **4**, the secondary effect of the orbital interaction was still operative for an exclusive *endo*-adducts formation, ii) the secondary effect of the lone-pair electrons of dioxy oxygens is capable of determining the stereochemistry of the adducts to the same extent as the π-orbital of the vinylene group,[8] and iii) an exclusive formation of the thermodynamically stable *exo*-adducts from **7** is attributable to a facile cycloreversion of the kinetically controlled *proto*-adducts under the reaction conditions. The Diels-Alder adducts of furans fall into a category.[9]

When a reaction of **2** with **4** was carried out under high-pressure conditions, the yields were improved to a great extent; the best result was 45% for **5** and 38% for **6** (Table 1).

It is evident that the improved formation of **5** and **6** under high-pressure conditions showed them to be the kinetically controlled products; an inhibition of the *retro*-Diels-Alder process should favor a retention of the *proto*-adducts. It should be noted that a reaction of **2** and **4** under atmospheric pressure produced **5** and **6** only in the presence of TsOH at 80 °C. However, due to the instability of **2** under acidic conditions, an accel-

Table 1. The Reaction of **2** and **4** under Various Conditions

Runs	Solv.	Conditions Press./bar	Temp/°C	Consumption/% Additive	2	Yield/% 5	6
1	Benzene	1	80	TsOH	79	2	3
2	Cumene	2500	40	TsOH	66	36	28
3	Cumene	2500	40		64	45	38
4	Acetone	2000	40		49	27	8

eration of the product formation was compensated by the decomposition of **2**. This may be attributable to the lower yields for **5** and **6** with TsOH than without TsOH at 2500 bar.

In cases of reactions of **3**, the nitrogen analogs of **2**, a similar secondary orbital effect should also play a role in the stereochemistry of the adducts; however, at the same time, the inversion of unshared electron pairs of nitrogen and a steric hindrance due to bulky ethoxycarbonyl groups on the hydrazo linkage should minimize the effect of the secondary interaction. The reaction of **3** with **4** yielded a *cis-endo*-adduct (**12**, 96% yield) as the product only identified. The improved yield was due to the stability of the bicyclic dienophile under the conditions. The reaction of **3** with **7** gave two products, *cis-exo*-adduct (**13**, 54% yield) and *trans-exo*-adduct (**14**, 31% yield), while that of **3** with **10** gave the sole product, *cis-exo*-adduct (**15**, 46% yield).

In conclusion, the reactions of **2** and **3** with **4** verified the operation of an attractive secondary interaction between the dioxy group or the hydrazo group as well as the vinylene group and the diene chromophore of **4**, and the absence of a *trans-endo*-adduct from **3**, should be interpreted as a steric effect rather than a lack of the secondary orbital interaction. However, this could not be extended to the reactions with **7** and **10**, since the furans are known to preferably give the thermodynamically controlled cycloadducts.[9]

Experimental

Elemental analyses were performed at the Research Institute of Industrial Science, Kyushu University. The NMR spectra were measured by a JEOL FX 100 Spectrometer in a $CDCl_3$ solution, unless otherwise specified, and the chemical shifts were expressed in δ units (internal Me_4Si). The mass spectra were measured by a JEOL 01SG-2 Spectrometer. The IR spectra were taken either as KBr disks or as liquid films inserted between NaCl plates using a Jasco IR-A 102 Spectrometer.

Reaction of 2 and 4. **a)** A benzene solution (10 cm^3) of **2** (1.01 g) and **4** (5 cm^3) containing TsOH (200 mg) was refluxed for 1.5 h. The mixture was chromatographed on a silica-gel column to give colorless needles, mp 119—121 °C, 29 mg (2%), **5** [Found: M.W., 204.0786. Calcd for $C_{12}H_{12}O_3$: 204.0784. ^1H NMR δ=1.36 (d, J=8.5 Hz, Hm), 1.55 (dt, J=8.5, 2 Hz, Hk), 2.85 (m, Hj), 3.08 (dtd, J=11, 3, 1.5 Hz, He), 3.4 (m, Hf and Hg), 4.67 (dt, J=7, 3 Hz, Hd), 4.93 (dd, J=7, 2 Hz, Ha), 5.77 (dd, J=9, 7 Hz, Hb), 5.93 (m, Hh and Hi), and 6.50 (dd, J=9, 7 Hz, Hc). ^{13}C NMR δ=43.8, 44.8, 45.8, 49.0, 54.6, 80.4, 84.2, 118.4, 132.7, 134.8, 136.6, and 200.3. IR ν: 1700 cm^{-1}], and colorless needles, mp 104—105.5 °C, 37.2 mg (3%), **6** [Found: M.W., 204.0786. ^1H NMR δ=1.34 (dtt, J=8.5, 1.5, 0.5 Hz, Hm), 1.52 (dt, J=8.5, 2 Hz, Hk), 2.55 (dt, J=9.5, 3 Hz, He), 2.98 (m, Hj), 3.12 (dd, J=9.5, 4 Hz, Hf), 3.34 (m, Hg), 4.57 (ddd, J=7, 2, 1 Hz, Ha), 4.73 (dddt, J=7, 3, 2, 1 Hz, Hd), 6.06 (dd, J=5.5, 2.5 Hz, Hh), 6.29 (ddd, J=9, 7, 1 Hz, Hb), 6.35 (dd, J=5.5, 3 Hz, Hi), and 6.83 (ddd, J=9, 7, 1 Hz, Hc). ^{13}C NMR δ=45.2, 46.5, 48.4, 49.4, 51.1, 78.5, 83.4, 123.0, 132.9, 136.0, 136.5, and 204.3. IR ν: 1700 cm^{-1}], together with the recovered **2**, 207.3 mg (21%).

b) A cumene solution (3 cm^3) of **2** (ca. 0.5 mmol) and **4** (ca. 10 mmol), with or without TsOH (21 mg), was heated at 40 °C by means of the pressure vessel under the pressure as indicated in Table 1, for ca. 10 h. The mixture was chromatographed to obtain the products **5** and **6**, and the recovered **2**.

c) An acetone solution (3 cm^3) of **2** (102.6 mg) and **4** (551 mg) was similarly heated by use of the pressure vessel under 2000 bar at 40 °C for 10 h. The results are compiled in Table 1.

Reaction of 2 and 7. A CH_2Cl_2 solution (2 cm^3) of **2** (112.5 mg) was added at −70 °C to **7**, generated in situ by the pyrolysis of dihydro derivative of benzyne-furan adduct.[10] The mixture was kept at 4 °C for 2 d, and chromatographed on a silica-gel column to give colorless needles, mp 144—147 °C, 75.5 mg (41%), **8** [Found: C, 70.27; H, 4.65%. Calcd for $C_{15}H_{12}O_4$: C, 70.30; H, 4.73%. ^1H NMR δ=2.22 (dd, J=9, 4 Hz, He), 2.80 (d, J=9 Hz, Hf), 4.90 (ddd, J=7, 2, 1 Hz, Ha), 5.07 (ddd, J=7, 4, 2.5 Hz, Hd), 5.46 (s, Hh), 5.54 (s, Hg), 6.35 (ddd, J=9, 7, 1 Hz, Hb), 6.82 (ddd, J=9, 7, 1 Hz, Hc), and 7.1—7.4 (4H, m). ^{13}C NMR δ=46.2, 52.8, 78.4, 81.8, 83.6, 84.3, 119.0, 119.8, 123.0, 127.2, 127.4, 135.4, 144.8, 146.0, and 200.9. IR ν: 1695 cm^{-1}], and colorless needles, mp 137—140 °C, 34.1 mg (18%), **9** [Found: C, 70.45; H, 4.65%. ^1H NMR δ=2.69 (dd, J=8, 3 Hz, He), 2.92 (d, J=8 Hz, Hf), 5.0—5.15 (m, Ha and Hd), 5.16 (s, Hh), 5.70 (s, Hg), 6.23 (dd, J=9.5, 8 Hz, Hb), 6.87 (dd, J=9.5, 8 Hz, Hc), and 7.1—7.4 (4H, m). ^{13}C NMR δ=44.7, 54.7, 79.8, 80.9 (2C), 83.8, 119.0, 120.0, 121.4, 127.4, 127.5, 135.2, 143.9, 145.3, and 199.2. IR ν: 1710 cm^{-1}], together with the recovered **2**, 12.6 mg (11%).

Reaction of 2 and 10. A CH_2Cl_2 solution (2 cm^3) of **2** (102.2 mg) and **10**[11] (298.5 mg) was refluxed for 14 h. The mixture was then chromatographed on a silica-gel column to give colorless crystals, mp 139—141 °C, 94 mg (31%), **11** [Found: M.W., 408.1362. Calcd for $C_{27}H_{20}O_4$: 408.1360. ^1H NMR δ=3.30 (dd, J=8, 3 Hz, He), 3.48 (dd, J=8, 1 Hz, Hf), 4.55 (ddt, J=7, 2, 1 Hz, Ha), 4.76 (dddd, J=7, 3, 2, 1 Hz, Hd), 5.99 (ddd, J=9, 7, 1 Hz, Hb), 6.39 (ddd, J=9, 7, 1 Hz, Hc), and 7.1—7.8 (14H, m). ^{13}C NMR δ=48.9, 59.7, 79.2, 83.7, 88.9, 90.3, 118.7, 119.3, 119.7, 125.6 (2C), 126.8 (2C), 127.3, 127.7 (2C), 127.8 (2C), 128.6, 129.3 (2C), 135.1, 135.3, 136.5, 145.5, 148.7, and 195.0. IR ν: 1700 cm^{-1}].

Reaction of 3 and 4. A toluene solution (5 cm^3) of **3** (367.5 mg), and **4** (5.5 cm^3), TsOH (59 mg) was refluxed for 10 h. Silica-gel column chromatography of the mixture yielded colorless needles, mp 146.5—149.5 °C, 344.6 mg (96%), **12** [Found: C, 62.61; H, 6.41; N, 8.06%. Calcd for $C_{18}H_{22}O_5N_2$: C, 62.40; H, 6.41; N, 8.09%. ^1H NMR δ=1.25 (3H, t, J=7 Hz), 1.30 (3H, t, J=7 Hz), 1.15—1.4 (m, Hm, underneath the t), 1.48 (dt, J=8.5, 2 Hz, Hk), 2.75 (dt, J=9, 2.5 Hz, He), 2.8—2.9 (m, Hj, underneath the dd), 2.96 (dd, J=9, 3 Hz, Hf), 3.38 (m, Hg), 4.18 (2H, q, J=7 Hz), 4.25 (2H, q, J=7 Hz), 4.83 (2H, dm, J=7 Hz, Ha and Hd), 5.50 (ddd, J=9, 7, 3 Hz, Hb), 5.94 (2H, t, J=2 Hz, Hh and Hi), and 6.40 (ddd, J=9, 7, 1.5 Hz,

Hc). IR ν: 1700 cm^{-1}] together with the recovered **3**, 76.5 mg (21%).

Reaction of 3 and 7. A CH_2Cl_2 solution (2 cm^3) of **3** (293.6 mg) was added to similarly generated **7**. The mixture was then chromatographed on silica-gel column to give a colorless oil, 173 mg (54%), **13** [Found: M.W., 398.1477. Calcd for $C_{22}H_{22}O_2N_2$: 398.1476. ^1H NMR δ=1.18 (3H, t, J=7 Hz), 1.26 (3H, t, J=7 Hz), 2.49 (m, He and Hf), 4.17 (2H, q, J=7 Hz), 4.20 (2H, q, J=7 Hz), 4.98 (d, J=7 Hz, Ha), 5.26 (s, Hh), 5.29 (dm, J=6 Hz, Hd), 5.74 (s, Hg), 5.97 (dd, J=9, 7 Hz, Hb), 6.78 (dd, J=9, 6 Hz, Hc), and 7.1—7.4 (4H, m). IR ν: 1705 cm^{-1}], and a colorless oil, 100.2 mg (31%), **14** [Found: M. W., 398.1479. ^1H NMR δ=1.1—1.4 (6H, m), 2.30 (dd, J=8.5, 5.5 Hz, He), 2.75 (dd, J=8.5, 1.5 Hz, Hf), 4.0—4.4 (4H, m), 4.94 (dd, J=7, 2 Hz, Ha), 5.2—5.4 (m, Hd), 5.32 (s, Hh), 5.39 (s, Hg), 6.12 (ddd, J=9, 7, 1.5 Hz, Hb), 6.69 (dd, J=9, 6.5 Hz, Hc) and 7.1—7.4 (4H, m). IR ν: 1710 cm^{-1}] together with the recovered **3**, 66.5 mg (23%).

Reaction of 3 and 10. Similarly, a toluene solution (4 cm^3) of **3** (101.8 mg) and **10** (100.2 mg) was refluxed for 4 h. The mixture was then chromatographed on a silica-gel column to give colorless crystals, mp 182—184 °C, 63.6 mg (46%), **15** [Found: C, 71.74; H, 5.56; N, 5.57%. $C_{33}H_{30}O_6N_2$: C, 71.97; H, 5.50; N, 5.09%. ^1H NMR δ=1.14 (3H, t, J=7 Hz), 1.20 (3H, t, J=7 Hz), 3.09 (dd, J=8, 2 Hz, He), 3.20 (dd, J=8, 0.5 Hz, Hf), 3.9—4.2 (4H, m), 4.66 (d, J=7 Hz, Ha), 5.03 (ddd, J=6, 2, 1 Hz, Hd), 5.72 (ddd, J=9, 7, 1 Hz, Hb), 6.27 (ddd, J=9, 6, 1 Hz, Hc), and 7.1—7.8 (14H, m). ^{13}C NMR δ=14.2, 14.5, 48.4, 57.2, 62.8, 63.1, 63.5, 78.4, 89.4, 90.1, 119.2, 119.5, 120.0, 125.7, 126.8 (2C), 127.2, 127.6 (3C), 128.5 (3C), 129.2 (2C), 135.9, 136.7, 137.1, 145.9, 148.3, 155.4, 157.4, and 191.4. IR ν: 1710 cm^{-1}] together with the recovered **3**, 32 mg (31%).

References

1) H. Takeshita, T. Hatsui, I. Shimooda, and H. Mametsuka, *Bull. Chem. Soc. Jpn.*, **55**, 2291 (1982).

2) T. Uehara and Y. Kitahara, *Chem. & Ind.*, **1971**, 354.

3) The terms, cis and trans, define stereochemistries for the adducts derived by an attack of dienes from the sites of the vinylene and dioxy (or hydrazo) groups of the bicyclo[3.2.2] systems, respectively.

4) S. Itô, H. Takeshita, Y. Shoji, Y. Toyooka, and T. Nozoe, *Tetrahedron Lett.*, **1969**, 443.

5) M. Oda and Y. Kitahara, *Tetrahedron Lett.*, **1969**, 3295.

6) Y. Kitahara, I. Murata, and T. Nitta, *Tetrahedron Lett.*, **1967**, 3003.

7) The Diels-Alder reaction of **7** with tropone was reported earlier; it gave [2+4]-, [4+2]-, and [6+4] cycloadducts having mostly the *exo*-configuration. See H. Takeshita, Y. Wada, A. Mori, and T. Hatsui, *Chem. Lett.*, **1973**, 335.

8) By the photochemical reaction of **2**, we have obtained a photolysate whose mechanism of formation could be explained by an orbital interaction between the enone part and the dioxy group. This will be a matter of an independent paper (A. Mori and H. Takeshita).

9) C. K. Ingold, "Structure and Mechanism in Organic Chemistry," Cornell Univ. Press., Ithaca (1969), pp. 1090—1093; J. March, "Advanced Organic Chemistry: Reactions, Mechanisms, and Structure," McGraw Hill Book Co., New York (1968), p. 631; R. B. Woodward and H. Baer, *J. Am. Chem. Soc.*, **70**, 1161 (1948); J. A. Berson and R. Swilder, *ibid.*, **75**, 4366 (1953); J. Sauer, *Angew. Chem. Internl. Edit.*, **6**, 16 (1967).

10) U. E. Wiersum and W. J. Mijs, *J. Chem. Soc., Chem. Commun.*, **1972**, 347.

11) Commercially available from Tokyo Kasei Co., Ltd., Tokyo.

Conductometric Determination of the Association Constants of β-Cyclodextrin with Amphiphilic Ions

Iwao SATAKE,* Shoji YOSHIDA, Katumitu HAYAKAWA,
Tamaki MAEDA, and Yoshihumi KUSUMOTO†
Department of Chemistry, Faculty of Science, Kagoshima University, Korimoto, Kagoshima 890
†Chemical Institute, College of Liberal Arts, Kagoshima University, Korimoto, Kagoshima 890
(Received June 14, 1986)

Synopsis. The association constants (K) of β-cyclodextrin with 13 amphiphilic ions were determined. For a homologous series 1-alkanesulfonate ions, the saturation phenomenon of K occurred at the number of carbon atoms of 10. The values of K for amphiphilic ions with dodecyl chain were similar to one another.

It is well-known that the hydrophobic interaction between hydrophobic moieties of host and guest molecules plays an important role in the complexation of cyclodextrins.[1] In this connection, studies have been made for the associations of cyclodextrins with fatty acids[2] and amphiphilic ions[3-6] which have a long hydrocarbon chain of varying hydrophobicity. With a homologous series 1-alkanesulfonate ions, we found that the association constant of α-cyclodextrin (αCD) increases monotonously with increasing carbon atom (n) and become abruptly constant at n=10.[4] A similar saturation phenomenon of the association constant has also been observed for the complexation of fatty acid salts with α- and β-cyclodextrins.[7] We also found that the association constants of αCD for ionic surfactants with the same alkyl chain length are similar to one another regardless of the sign of ionic head group.[4]

In order to elucidate the effect of cavity size on the cyclodextrin-amphiphilic ion interactions, the conductometric investigation was made in this paper for the association constants (K) of β-cyclodextrin (βCD) with ionic surfactants and their homologs.

Experimental

Materials. Sodium 1-alkanesulfonates with n from 8 to 12 were synthesized from the corresponding alkyl bromides purified by vacuum distillation.[8] Dodecylammonium chloride (DAC) was prepared from dodecylamine (purity>99%, Nakarai Chemicals Ltd.).[9] Sodium dodecyl sulfate (SDS, Nakarai Chemicals Ltd.) and 1-dodecylpyridinium chloride (DPC, Tokyo Kasei Kogyo Co. Ltd.) were purified further by the procedures described elsewhere.[4] Sodium 1-alkanesulfonates with n from 5 to 7 (Tokyo Kasei Kogyo Co. Ltd., guaranteed grade), sodium p-dodecylbenzenesulfonate (SDBS, purity>99%, Wako Pure Chemical Industry Co. Ltd.), dodecyltrimethylammonium bromide (DTAB, purity>99%, Tokyo Kasei Kogyo Co. Ltd.), and β-cyclodextrin ($[\alpha]_D^{25}$=+162°, Seikagaku Kogyo Co. Ltd.) were used without further purifications. Deionized water was obtained by passing twice distilled water through the mixed ion bed (Bio-Rad AG501-X8).

Measurements. The conductivity was measured to a precision of 0.1 μS by using a TOA Electronics Ltd. Conductivity Meter model CM-50AT and the conductivity cell with cell constant of 1.000 cm^{-1} at 25 °C. The concentration of βCD was determined by drying aliquots of the stock solution over phosphorus pentaoxide in vacuo at 110 °C. The conductivity was followed as a function of βCD concentration, C_h, under the conditions of a constant amphiphile concentration, C.

The solution viscosities of α- and βCD were measured by a Ubbelohde's viscometer at 25 °C.

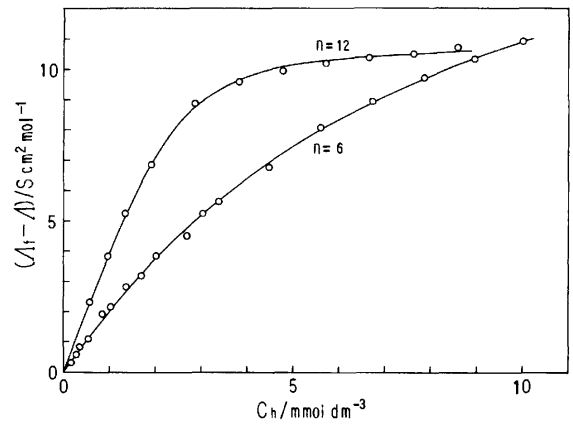

Fig. 1. Plots of $\Lambda_f-\Lambda$ vs. βCD concentration (C_h) for sodium 1-alkanesulfonates with n=6 and 12 at 25°C. C=2.584 mmol dm^{-3} (n=6), 2.434 mmol dm^{-3} (n=12) O, observed; solid line: calculated curve from Eq. 1 with parameters shown in Table 1.

Results and Discussion

On the basis of the assumption of a 1 : 1 reaction scheme, the change in the equivalent conductivity, Λ, with βCD concentration can be described as follows.[4]

$$\Lambda_f - \Lambda = \frac{\lambda_f-\lambda_a}{2KC}[K(C+C_h) + 1 - \sqrt{\{K(C+C_h) + 1\}^2 - 4K^2CC_h}] \quad (1)$$

Here, Λ_f refers to the equivalent conductivity in the absence of βCD, and λ_f and λ_a to the ionic equivalent conductivities of unassociated and associated amphiphilic ion, respectively. Thus the nonlinear least squares treatment of Λ_f—Λ vs. C_h plots permits the simultaneous determinations of K and λ_f—λ_a.[4]

In Flg. 1 is shown the typical plots of Λ_f—Λ vs. C_h for sodium 1-hexane- and 1-dodecanesulfonates at 25 °C, together with the calculated curves which give the best fit of the experimental data. An excellent agreement between observed and calculated conductivity curves supports the foregoing assumption of a 1 : 1 reaction scheme for βCD- amphiphilic ion interaction. This is also the case for whole systems studied. The association constants and the conductometric parameters thus determined are summarized in Table

Table 1. The Conductometric and Thermodynamic Parameters of βCD-Amphiphile Systems

Amphiphile	C	Temp	Λ_f	$\lambda_f-\lambda_a$	K	$-\Delta G^\circ$
	mmol dm^{-3}	°C	S cm^2 mol^{-1}	S cm^2 mol^{-1}	dm^3 mol^{-1}	kJ mol^{-1}
$C_nH_{2n+1}SO_3Na$						
n=5	2.947	10	52.5	12.2	66	19.3
	2.365	25	77.0	18.9	60	20.1
	1.539	40	104.7	26.9	52	20.7
n=6	2.886	10	50.8	11.8	191	21.8
	2.584	25	74.0	18.1	177	22.8
	1.936	40	100.4	24.7	150	23.5
n=7	2.665	25	73.6	16.7	436	25.0
n=8	2.838	10	49.8	9.8	1090	25.9
	2.409	25	73.1	15.0	1030	27.2
	1.841	40	99.2	20.2	914	28.2
n=9	2.512	10	49.0	8.9	2210	27.6
	2.501	25	71.2	13.5	2170	29.0
	1.761	40	96.5	17.0	2150	30.4
n=10	2.502	25	70.2	12.2	4090	30.6
n=11	2.567	25	69.4	11.8	4130	30.6
n=12	2.434	25	68.6	11.0	4340	30.7
SDS	2.597	25	68.8	12.0	3630	30.3
SDBS	0.740	25	69.1	8.7	7040	31.9
DAC	2.025	25	96.7	13.2	4760	30.9
DTAB	2.024	25	97.4	12.5	4880	31.0
DPC	1.991	25	89.7	10.8	4980	31.0

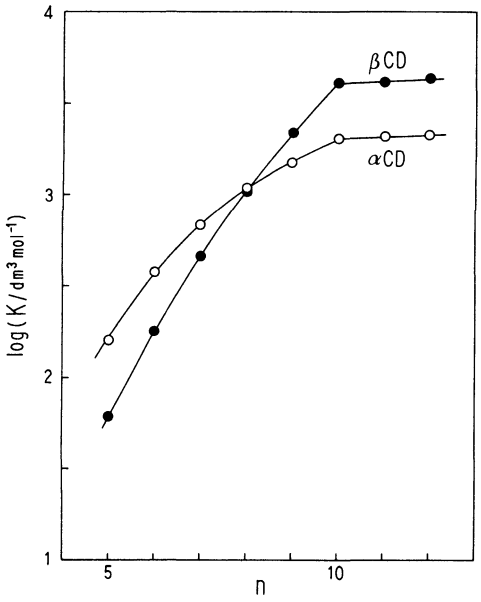

Fig. 2. The chain length dependence of K for sodium 1-alkanesulfonate at 25°C. ●, βCD; ○, αCD.[4]

1. In this table is also given the standard free energy change of complex formation, ΔG° ($=-RT$ ln $K_X=-RT$ ln $55.5K$). Figure 2 shows the chain length dependence of K for 1-alkanesulfonate ion. For the sake of comparison, the previous data for αCD[4] are also shown in this figure.

It can immediately be seen that the association constant of βCD increases more rapidly than that of αCD with increasing chain length but become also constant at n=10. In the complexation of homologous series amphiphilic ions, therefore, the hydrophobic cavity of βCD is supposed to accomodate the hydrocarbon tail in a similar manner to αCD, even though the degree of interaction is different from each other. However, it seems difficult to interpret the observed saturation phenomena at n=10 in terms of the hydrophobic interaction alone, since the hydrophobic cavities of α- and βCD molecules are of the order of 0.67—0.7 nm[1a] in depth and can accomodate at most 6 methylene groups of a fully extended chain. A tentative application of Einstein equation to the viscosity data for cyclodextrin solutions leads immediately to the hydrodynamic volumes of α- and βCD molecules of 1.40 and 1.90 nm^3, which correspond to the diameters of 1.40 and 1.54 nm respectively. On the other hand, the head-to-tail distance of 1-decanesulfonate ion with a fully extended chain can be estimated to be 1.55 nm on the basis of an assumption that the radius of hydrated sulfonate group is comparable to that of HSO_3^- ion (0.23 nm[10]). In connection with the saturation phenomena of K at n=10, it is interesting to note that the estimated size of 1-decanesulfonate ion is slightly larger than the diameter of hydrated αCD but almost identical with that of hydrated βCD. Moreover, the methylene group adjacent to head group has been recognized to make little or no contribution to the hydrophobic interaction.[11] With these observations in mind, α- and βCD molecules seem to include the successive 10 methylene groups of 1-alkanesulfonate ion with n larger than 10 in such a manner as the head group and first methylene group in hydration shell on one side of the cavity, succeeding 6 methylene groups in the hydrophobic cavity, and the residual 3 methylene groups in hydration shell on another side of the cavity. If this is really the case, the thermodynamic parameters such as the enthalpy and entropy of complexing will probably reflect the difference in the microscopic environment around hydrocarbon chain.

Table 2. The Thermodynamic Parameters of Complexing for Sodium 1-Alkanesulfonates with $n=5$, 6, 8, and 9 at 25 °C

n	ΔH°	ΔS°	$\Delta(\Delta H^\circ)$	$\Delta(\Delta S^\circ)$
	kJ mol^{-1}	J K^{-1} mol^{-1}	kJ mol^{-1}	J K^{-1} mol^{-1}
5	−5.87	47.7	≈0	9.1
6	−5.86	56.8		
8	−4.39	76.5	3.7	18.3
9	−0.74	94.8		

Table 2 shows the standard enthalpy and entropy changes estimated for 1-alkanesulfonate ions with $n=5$, 6, 8, and 9 from temperature dependence of K_X. In last two columns are given the increments of ΔH° and ΔS° per methylene group which correspond to the enthalpy and entropy changes for transferring one methylene group from an aqueous medium to the complex state respectively. It should be noted that the observed increment of ΔH° accompanying the increase in n from 5 to 6 is comparable to the enthalpy changes per methylene group characteristic of hydrophobic interaction. For example with heptane-βCD system, Wishnia and Lappi[12] obtained ΔH° of 0.84 kJ mol^{-1} at 20 °C, which corresponds roughly to 0.12 kJ mol^{-1} per methylene group. In the case of micellization process, the enthalpy change per methylene group has been found to be of the order of 0.2 kJ mol^{-1}.[13] On the contrary, the increments of ΔH° and ΔS° accompanying the change in n from 8 to 9 are quite different from those from 5 to 6. In a previous paper,[4] we assumed the partial breakdown of the hydration shell around lateral hydrophilic surface through which hydrocarbon tail penetrates. Apart from the plausible explanation of the effect of hydrocarbon tail on hydration shell, the thermodynamic data seem to support the foregoing geometric consideration on the inclusion mechanism of long-chain 1-alkanesulfonate ions. In their study of the complexation of homologous series fatty acid salts, Ono et al.[7] found that the saturation phenomenon of K occurs at $n=8$ for αCD and $n=12$ for βCD respectively. They assumed a trans to gauche conformational change of hydrocarbon chain in cavity of βCD.

The qualitative features of the association constants of βCD for surfactant ions with dodecyl chain are identical with those of αCD.[4] As was pointed out previously,[4] a marked resembrance in the values of K for sodium 1-dodecanesulfonate, DAC, DTAB, and DPC suggests that the interaction between βCD and surfactant ion does not depend appreciably on the chemical and electrical properties of ionic head group. A striking increase in K for SDBS can also be attributed to the presence of the aromatic ring which interacts strongly with βCD.[1]

References

1) See for example a) M. L. Bender and M. Komiyama, "Cyclodextrin Chemistry," Springer-Verlag, Berlin (1978); b) W. Saenger, *Angew. Chem. Int. Ed. Engl.*, **19**, 344 (1980).

2) H. Schlenk and D. M. Sand, *J. Am. Chem. Soc.*, **83**, 2312 (1961).

3) T. Okubo, H. Kitano, and N. Ise, *J. Phys. Chem.*, **80**, 2661 (1976).

4) I. Satake, T. Ikenoue, T. Takeshita, K. Hayakawa, and T. Maeda, *Bull. Chem. Soc. Jpn.*, **58**, 2746 (1985).

5) S. Hashimoto and J. K. Thomas, *J. Am. Chem. Soc.*, **107**, 4655 (1985).

6) Y. Kusumoto, M. Shizuka, and I. Satake, *Chem. Phys. Lett.*, **125**, 64 (1986).

7) K. Ono, M. Tokuda, and K. Murakami, *Polymer Preprints, Japan*, **28**, No. 7, 1302 (1979).

8) S. Zuffanti, *J. Am. Chem. Soc.*, **62**, 1044 (1940).

9) I. M. Kolthoff and W. Strickes, *J. Phys. Colloid Chem.*, **52**, 915 (1948).

10) J. Kielland, *J. Am. Chem. Soc.*, **59**, 1675 (1937).

11) C. Tanford, "The Hydrophobic Effect: Formation of Micelles and Biological Membranes," 2nd ed., John Wiley & Sons, New York (1980), p. 14.

12) A. Wishnia and S. J. Lappi, *J. Mol. Biol.*, **82**, 77 (1974).

13) K. Shinoda, T. Nakagawa, B. Tamamushi, and T. Isemura, "Colloidal Surfactants," Academic Press, New York (1963), p. 31.

The Crystal and Molecular Structure of Inner Triple-Layered Paracyclophanequinone

Toshihiro TOYODA, Hitoshi TATEMITSU, Yoshiteru SAKATA, Nobutami KASAI,*,† and Soichi MISUMI*
The Institute of Scientific and Industrial Research, Osaka University, Ibaraki, Osaka 567
†Department of Applied Chemistry, Faculty of Engineering, Osaka University, Suita, Osaka 565
(Received April 25, 1986)

Synopsis. The molecular structure of inner quinone isomer of two triple-layered paracyclophanequinones has been determined by means of X-ray diffraction. $C_{26}H_{24}O_2$, M 368.5, orthorhombic, space group $Pbcn$, a=12.923(1), b=11.507(1), c=12.550(1) Å, V=1866.2(3) Å^3, Z=4. The structure was solved by the direct method. Anisotropic refinement by the block-diagonal least-squares procedure gave R=0.042 for non-zero reflections. The molecule has a two-fold symmetry. The benzoquinone moiety is sandwiched by two donor benzene rings, and the two-fold axis passes through the O=C···C=O bonds of the twisted benzoquinone moiety. The outer benzene rings take a boat-form and the central benzoquinone ring is twisted.

Three isomeric triple-layered and two isomeric quadruple-layered charge-transfer cyclophanes containing benzoquinone and dimethoxybenzene moieties have been synthesized together with two quadruple-layered paracyclophanes and interesting charge-transfer spectra related to their structures, e.g. number of layers and relative donor-acceptor orientation, have been reported.[1] Two isomeric triple-layered paracyclophanequinones also showed a structural relationship corresponding to the position of quinone group in their CT spectra.[2]

Experimental

Yellow prismatic crystals were recrystallized from a solution of benzene-hexane mixed solvent. The crystal used had dimensions of ca. 0.15×0.23×0.20 mm. A Rigaku automated, four-circle diffractometer combined with rotating-anode X-ray generator was used at the Institute for Protein Research, Osaka University. Ni-filtered Cu$K\alpha$ radiation (λ=1.54178 Å) was used.

Intensity data were collected by the θ—2θ scan technique: the 2θ scan rate was 16° min^{-1} and the scan width from $\{2\theta(\alpha_1)-1.0\}$ to $\{2\theta(\alpha_2)+1.0\}$°. Backgrounds were measured ca. 1 s at both ends of a scan. Three standard reflections were measured after every 57 reflections, which showed no intensity decrease during the data collection. In total, 1307 reflections out of 1567(2θ<118°), were observed ($|F_o|>3\sigma(F_o)$). Usual Lorentz and polarization corrections were applied but absorption correction was ignored[μ(Cu)=6.3 cm^{-1}].

Structure Solution and Refinement

The structure was solved by the direct method (*MULTAN*),[4] and refined anisotropically by the block-diagonal least-squares procedure (*HBLS* V).[5] The function minimized was $\sum w(\Delta F)^2$. All the hydrogen atoms were located on a difference Fourier map, which were included in the refinement with isotropic temperature factors. The R value converged to 0.042. The weighting schemes used at the final stage were $w=\{\sigma^2(F_o)-0.096|F_o|+0.005|F_o|^2\}^{-1}$ for $|F_o|>0$ and w=0.667 for $|F_o|=0$, where σ is the standard deviation obtained by the counting statistics. The final atomic parameters are given in Table 1.††

Table 1. Final Atomic Coordinates of Non-Hydrogen Atoms with Equivalent Isotropic Temperature Factors[6]

Atom	x	y	z	B_{eq}/Å^2
O(1)	0.50000	0.44109(14)	0.25000	3.9
O(2)	0.50000	−0.01366(14)	0.25000	4.3
C(1)	0.59996(13)	0.33588(16)	0.42624(14)	3.7
C(2)	0.52320(14)	0.31909(16)	0.52302(13)	3.8
C(3)	0.42039(13)	0.27061(14)	0.48638(12)	3.0
C(4)	0.34967(12)	0.33880(14)	0.43081(13)	3.0
C(5)	0.27872(12)	0.28866(14)	0.36215(13)	3.1
C(6)	0.27561(11)	0.16862(14)	0.34701(13)	3.0
C(7)	0.33271(12)	0.10106(14)	0.41754(13)	3.2
C(8)	0.40369(13)	0.15099(14)	0.48626(13)	3.2
C(9)	0.23218(13)	0.11955(15)	0.24473(14)	3.7
C(10)	0.32077(13)	0.09249(16)	0.16281(13)	3.7
C(11)	0.41796(11)	0.15743(14)	0.19172(12)	2.7
C(12)	0.43766(11)	0.27001(14)	0.16987(12)	2.7
C(13)	0.50000	0.33463(19)	0.25000	2.7
C(14)	0.50000	0.09285(19)	0.25000	2.9

Atomic scattering factors were taken from International Tables for X-Ray Crystallography.[7] Computations were done mainly on an NEAC 2200—500 computer at the Computation Center, Osaka University, and at the final stage an ACOS 850 computer was used at the Crystallographic Research Center, Institute for Protein Research, Osaka University.

Results and Discussion

Figure 1 shows a perspective view[8] of the molecule. Selected bond distances and bond angles are given in Fig. 2.

The feature of the molecular structure is that the O(1), C(13), C(14), and O(2) atoms lie on a crystallographic two-fold axis, and the molecule has a two-fold symmetry. Three benzene rings are not in the exact eclipsed position. They are mutually rotated slightly in a helical way (Fig. 3): the C(5)-C(4) and C(12)-C(13) bonds projected onto the least-squares plane of the central benzoquinone ring make an angle of 5.5°, and similarly the C(12)-C(13) and C(3′)-C(4′) bonds form 4.3°. The corresponding angles in XD(Br)X[3] are 4.1 and 6.4°, respectively.

The outer benzene rings deformed to a boat form as in [2.2]paracyclophanes.[9-12] The bending angle P_1, i.e. the dihedral angle between the plane defined by the

††Tables of anisotropic thermal parameters, coordinates of hydrogen atoms, and observed and calculated structure factors are kept at the Chemical Society of Japan, Document No. 8703.

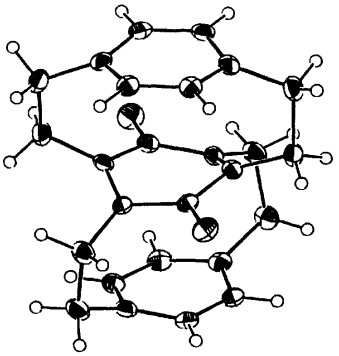

Fig. 1. A perspective view[8] of the molecule. Non-hydrogen atoms are represented as thermal ellipsoids with 30% probability level, and hydrogen atoms as spheres with B=1.0 Å^2.

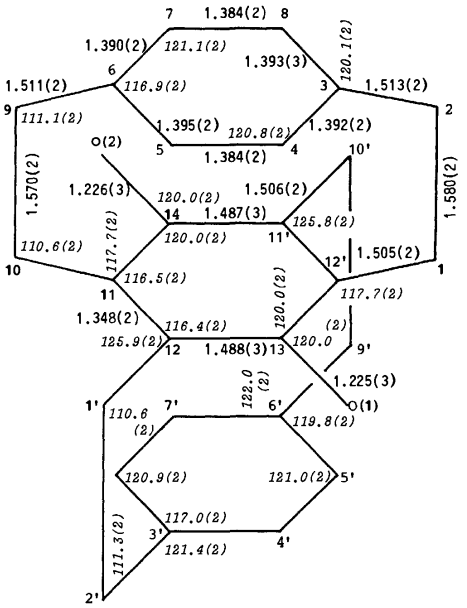

Fig. 2. Selected bond lengths [l/Å] and bond angles [ϕ/°] with estimated standard deviations in parentheses.

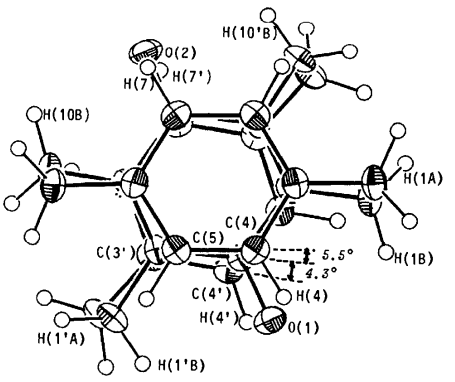

(a)

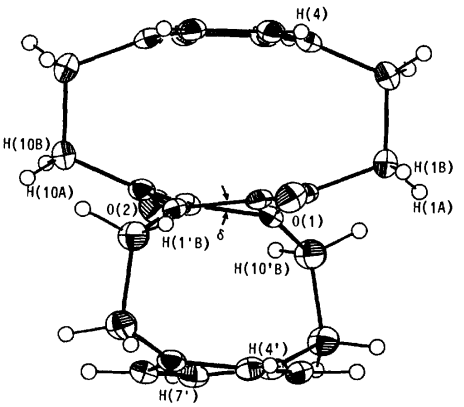

(b_1)

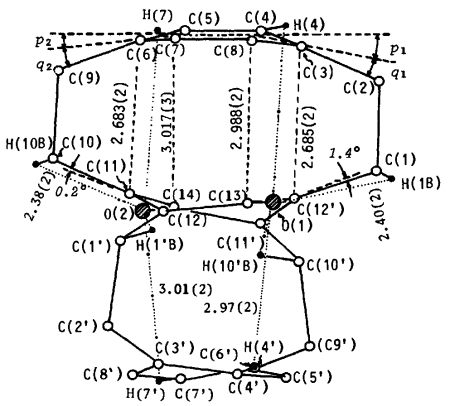

(b_2)

Fig. 3. Projections of the molecules.[8]
(a): Projected along the normal to the mean plane defined by the C(11), C(12), C(13), C(14), C(11'), and C(12') atoms.
(b_1): Projected along the normal to the plane defined by the C(6), C(11), and C(12') atoms.
(b_2): Schematic drawing of the (b_1) with nonbonded atomic distances between the outer benzene and central benzoquinone rings [l/Å]. p, q,[3] and other angles [ϕ/°] are also given.

C(4), C(5), C(7), and C(8) atoms (Plane 1) and that by the C(3), C(4), and C(8) (Plane 2) is 10.5°, and P_2, the dihedral angle between the Plane 1 and the Plane 3 (formed by the C(5), C(6), and C(7) atoms) is 9.9°. These are smaller than the corresponding angles in XD(Br)X [12.0 and 12.1°, respectively],[3] [2.2]paracyclophane [12.6°],[9] and other multi-layered paracyclophanes.[10-12] The C(2)-C(3) bond forms an angle q_1 of 11.9° with the Plane 2, and the C(6)-C(9) an angle q_2 of 11.5° with the Plane 3. These values are almost the same as those of the XD(Br)X and other [2.2]paracyclophanes.

Six C-C bond distances in the outer benzene rings are equal within a range of error [av. 1.390 Å]. The C(4)-C(3)-C(8) and C(5)-C(6)-C(7) angles [117.0(2) and 116.9(2)°], which are the bow and stern of the boat form, are smaller than the other four inner angles which have normal values [from 120.8(2) to 121.1(2)°].

The C_{sp^3}-C_{sp^3} bonds of ethylene bridges, C(1)-C(2) and C(9)-C(10), are 1.580(3) and 1.570(2) Å, which seem slightly shorter than that in [2.2]paracyclophane [1.593 Å].[8] Torsional angles around the C(1)-C(2) [15.5°] and C(9)-C(10) [18.8°] bonds can be compared with those in XD(Br)X [12.5 and 17.6°, respectively].

In the central benzoquinone moiety, the C(11)=C(12)

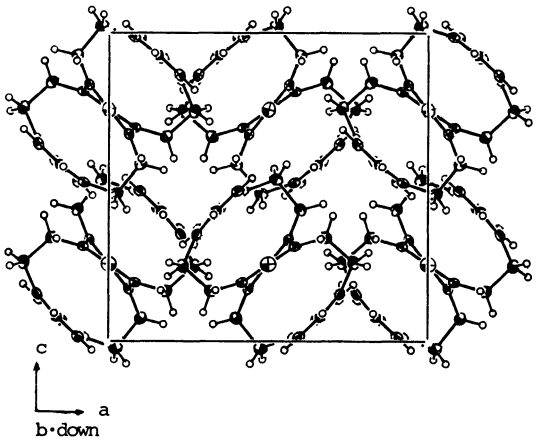

Fig. 4. Crystal structure projected along the b axis.[8]

double bond distance [1.348(2) Å] is slightly longer and the C(12)-C(13)-C(12′) bond angles[120.0(2)°] is smaller than the corresponding bond distances and bond angles in the free benzoquinone molecule,[13] and the rest has normal values. In the benzoquinone moiety, three bond angles around the C(13) and C(14) atoms are all equal [120.0(2)°]. The benzoquinone moiety consists of two planes, one defined by the O(1), C(12), C(13), and C(12′) atoms and the other formed by the rest of atoms. The dihedral angle made by these planes, i.e. the twisting angle δ (Fig. 3(b_1)) is 16.7°, which is much larger than the corresponding angles in triple- and quadruple-layered paracyclophanes [13.6 and 13.4°].[12] Closest nonbonded distances between the benzoquinone moiety and outer layer benzene ring are those observed between the C(6) and C(11) atoms [2.683(2) Å] and between the C(3) and C(12′) [2.685(2) Å], which are shorter than the corresponding distances in XD(Br)X [2.744(7) and 2.754(7) Å] (Fig. 3(b_2)). The C(1)-C(12′) bond bends by 1.4° away from the plane defined by the C(11′), C(12′), and C(13) atoms and the C(10)-C(11) bond by only 0.2° away from the plane made by the C(11), C(12), and C(14). These two angles are much smaller than the corresponding angles in XD(Br)X [6.6 and 4.7°, respectively]. Among the intramolecular nonbonded O···H distances, the O(1)···H(1B) [2.40(2) Å] and O(2)···H(10B) [2.38(2) Å] are closest. Next to these are O(1)···H(4) [2.97(2) Å] and O(2)···H(7) [3.09(2) Å].

The packing of molecules in the crystal is drawn in Fig. 4.[8] The structure of the present crystal is isomorphous with that of XD(Br)X. All of the intermolecular atomic contacts are longer than the van der Waals distances. The closest distance [3.637(2) Å] is observed between the O(1)(x, y, z) and C(9)(0.5−x, 0.5+y, z) atoms.

The authors wish to express their deep thanks to Miss Nobuko Kanehisa who helped them at the final stage of the refinement and *ORTEP* drawings.

References

1) H. Machida, H. Tatemitsu, T. Otsubo, Y. Sakata, and S. Misumi, *Bull. Chem. Soc. Jpn.*, **53**, 2943 (1980).
2) H. Tatemitsu, T. Otsubo, Y. Sakata, and S. Misumi, *Tetrahedron Lett.*, **1975**, 3059.
3) Y. Koizumi, T. Toyoda, K. Miki, N. Kasai, and S. Misumi, *Bull. Chem. Soc. Jpn.*, **59**, 239 (1986).
4) G. Germain. P. Main, and M. M. Woolfson, *Acta Crystallogr.*, **21**, 849 (1966).
5) T. Ashida, *HBLS* V, "The Universal Crystallographic Computing System-Osaka," The Computation Center, Osaka Univ. (1973), pp. 55—61.
6) W. C. Hamilton, *Acta Crystallogr.*, **12**, 609 (1959).
7) International Tables for X-Ray Crystallography, The Kynoch Press, Birmingham, Vol. IV (1974), p. 71.
8) C. K. Johnson, *ORTEP* II, Report ORNL-5138, Oakridge National Laboratory, Tennessee (1976).
9) H. Hope, J. Bernstein, and K. N. Trueblood, *Acta Crystallogr., Sect. B*, **28**, 1733 (1972).
10) H. Goto, Y. Kai, N. Yasuoka, and N. Kasai, Abst. 10th Symposium on Structural Organic Chemistry, Matsuyama (1977), p. 219.
11) Y. Kai, N. Yasuoka, and N. Kasai, *Acta Crystallogr., Sect. B*, **34**, 2840 (1978).
12) H. Mizuno, K. Nishiguchi, T. Toyoda, T. Otsubo, S. Misumi, and N. Morimoto, *Acta Crystallogr., Sect. B*, **33**, 329 (1977).

The Spectrophotometric Determination of Trace Vanadium with 3,4,5,6-Tetrachlorogallein

Itsuo MORI,* Yoshikazu FUJITA, Kinuko FUJITA, Yozo KOSHIYAMA, and Takeshi TANAKA
Osaka University of Pharmaceutical Sciences, 2-10-65, Kawai, Matsubara, Osaka 580
(Received April 21, 1986)

Synopsis. As a solution of 3,4,5,6-tetrachlorogallein (T.Cl.gall) in a weakly acidic medium was easily decomposed by vanadium(V), a simple and sensitive spectrophotometric determination of vanadium by using the difference in absorbance at 385 nm between T.Cl.gall and T.Cl.gall-vanadium(V) solutions in the presence of hexadecylpyridinium chloride (HPC) and poly (*N*-vinylpyrrolidone) (PVP) was established. Under optimum conditions, vanadium could be determined in the range of 0—0.8 μg/10 cm^3. The apparent molar absorptivity was calculated to be 7.0×10^5 $dm^3 mol^{-1} cm^{-1}$, with a Sandell sensitivity of 0.00006 μg cm^{-2}, by the use of a decomposed T. Cl. gall solution in the presence of vanadium(V) at 385 nm. The recovery tests of vanadium added to prepared artificial water were examined; the results were a good agreement with the certified values (98.6—102.8%).

We have already reported[1] the spectrophotometric determination of vanadium by using the color reaction system between vanadium and Gallein (gall) in the presence of sodium sulfite and sodium dodecyl sulfate.

On the other hand, Cabeza et al.[2,3] have reported the methods of the determination of vanadium utilizing the oxidation reaction of pyrogallolsulfophthalein= Pyrogallol Red (PR) by vanadium(V) or bromate ions. Also, we ourselves have recognized that 3,4,5,6-tetrachlorogallein (T.Cl.gall),[4] in the presence of hexadecylpyridinium chloride (HPC) and poly (*N*-vinylpyrrolidone) (PVP) as surfactants in a weakly acidic medium, was readily decomposed by the coexistence of vanadium(V) (=oxidation of T.Cl.gall), and that the difference in absorbance between the T.Cl.gall solution (Solution A) and the T.Cl.gall-vanadium(V) solution (Solution B) was proportional to the concentration of vanadium.

This paper describes a simple and sensitive spectrophotometric determination of micro amounts of vanadium using the oxidation and decomposition of a T. Cl. gall solution by the catalytic reaction of trace amounts of vanadium(V) in the presence of HPC and PVP.

Experimental

Apparatus and Reagents. The absorption spectra and absorbance were measured by the use of Shimadzu model UV-200 and Hitachi model 150-20 recording spectrophotometers, with 1.0-cm silica cells. Hitachi-Horiba model M-5 and F-7AD glass electrode pH meters were employed for the pH measurements.

A 1.0×10^{-3} mol dm^{-3} T. Cl. gall solution was prepared by dissolving T.Cl.gall[4] in methanol according to the method of a previous report.[5] 1.0×10^{-2} mol dm^{-3} HPC and 1.0% PVP (K-90) solutions were prepared by dissolving HPC and PVP respectively in water. A 5.0×10^{-4} mol dm^{-3} vanadium(V) solution was prepared according to the method of a previous report.[1] A 2.0×10^{-1} mol dm^{-3} sodium acetate-acetic acid buffer solution (Walpole buffer, pH 4.5) was used for the pH adjustments. The other reagents were of an analytical reagent grade, and twice-distilled or deionized water was used.

Standard Procedure. A solution containing up to 0.8 μg of vanadium(V) was placed in a 10-cm^3 volumetric flask. To this solution, 2.0 cm^3 of the buffer solution (pH 4.5), 1.5 cm^3 of a 1.0×10^{-2} mol dm^{-3} HPC solution, 1.0 cm^3 of a 1.0% PVP solution, and 1.4 cm^3 of a 1.0×10^{-3} mol dm^{-3} T.Cl.gall solution were added. This mixture was diluted to the mark with water and then heated at 60 °C for 30 min (Solution B). After the solution had then been cooled in water for 10 min, the absorbance of Solution B at 385 nm was measured against Solution A. The concentration of vanadium was determined by using a calibration curve.

Results and Discussion

Absorption Spectra and Analytical Wavelength. The T.Cl.gall solution, including vanadium as vanadium(V) in a weakly acidic medium (pH 4.5) (Solution B), was unstable and was gradually decomposed in proportion to the concentration of vanadium(V). Moreover, the use of T.Cl.gall was superior to the use of gall in terms of sensitivity and reproducibility. As is shown in Fig. 1, a large differences in absorbance between Solutions A and B were found at around 555 nm and 385 nm. The absorbance at 555 nm was unsa-

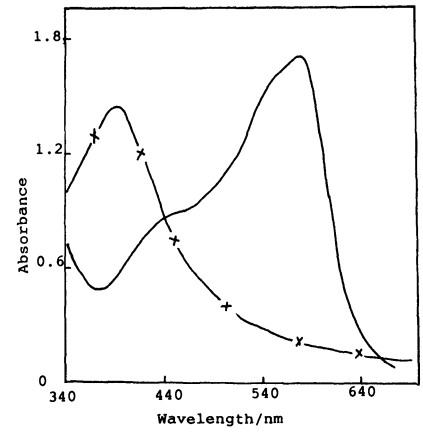

Fig. 1 Absorption spectra of T.Cl.gall and T.Cl.gall-vanadium(V) solutions in the presence of HPC and PVP at pH 4.5.
T.Cl.gall: 1.4×10^{-4} mol dm^{-3}; Vanadium(V): 1.0×10^{-6} mol dm^{-3}; HPC: 1.5×10^{-3} mol dm^{-3}; PVP: 1.0 cm^3 of 1.0% PVP solution/10 cm^3; Reference: Water.
—: T.Cl.gall solution; —X—: T.Cl.gall-vandium-(V) solution.

†Application of Xanthene Derivatives for Analytical Chemistry, Part LVIII. Part LVII: I. Mori, Y. Fujita, H. Kawabe, K. Fujita, T. Tanaka, and A. Kishimoto, *Analyst (London)*, **111**, printing (1986).

tisfactory in terms of reproducibility and the effect of foreign ions. On the other hand, the use of the difference in absorbance at 385 nm between Solutions A and B was satisfactory in reproducibility and the influence of foreign ions.

Consequently, the later measurements were carried out by measuring the absorbance of Solution B at 385 nm against Solution A.

Effect of pH. The maximum and constant absorbance was obtained in the pH range from 3.7 to 4.8 by using 2.0 cm^3 of a 2.0×10^{-1} mol dm^{-3} sodium acetate-acetic acid buffer solution (Walpole buffer) for the pH adjustments. Subsequent measurements were carried out at pH 4.5 for the determination of vanadium.

Effects of Surfactants. Among the various surfactants tested (HPC, hexadecyltrimethylammonium chloride (HTAC), and Zephiramine (Zp) as cationic surfactants, and PVP and poly (vinyl alcohol) (PVA) as nonionic surfactants), the combination of HPC and PVP had the effect of remarkably increasing the stabilization, reproducibility, and sensitivity. The effects of the concentrations of HPC and PVP were also studied. A maximum and almost constant absorbance was observed upon the addition of 0.5—2.0 cm^3 of a 1.0×10^{-2} mol dm^{-3} HPC solution, together with 1.0 cm^3 of a 1.0% PVP solution, to the final volume of 10 cm^3. Thus, all further measurements were made with 1.5×10^{-3} mol dm^{-3} HPC and 0.1% PVP as the final concentrations.

Effect of T.Cl.gall Concentration. The effect of the T.Cl.gall concentration on the standard procedure was examined by measuring the absorbance at 385 nm for 5.0×10^{-6} mol dm^{-3} vanadium(V). The absorbance at 385 nm was constant when the volume of the 1.0×10^{-3} mol dm^{-3} T.Cl.gall solution was varied between 1.25—1.5 cm^3 in the final 10 cm^3. Hence, 1.4 cm^3 of the 1.0×10^{-3} mol dm^{-3} T.Cl.gall solution was chosen for the determination of vanadium.

Effects of Temperature and Time. The absorbance at 385 nm of Solution B against Solution A was instantaneously unconstant at room temperature (15—25 °C) and was gradually decomposed. The effect of the temperature was examined by heating Solutions A and B at various temperatures (10, 20, 40, 60, and 80 °C). The most favorable results were obtained by heating Solutions A and B at 60 °C for 20—30 min and by then cooling these solutions to room temperature (15—25 °C) in water for 10 min. The solution B decomposed by the standard procedure was relatively stable, but further standing (for more than 60 min) caused a gradual and slight decrease in the absorbance.

Calibration Curve, Sensitivity, and Reproducibility. A good linear relationship was observed over the range of 0—0.8 μg of vanadium in the final volume of 10 cm^3 at 385 nm against a reagent blank (Solution A). The sensitivity on Sandell's scale and the apparent molar absorptivity were calculated for vanadium to be 0.00006 μg cm^{-2}, and 7.0×10^5 dm^3 mol^{-1} cm^{-1} at 385 nm, using a T.Cl.gall solution decompsed by the presence of vanadium(V) in the presence of HPC and PVP. Although a further investigation of the mechanism and the produced species of this reaction is necessary, this reason for the high sensitivity was assumed to be that the oxidation and decomposition of the T.Cl.gall solution in the presence of HPC and PVP was catalyzed by trace amounts of vanadium(V). The relative standard deviation was 1.7% at the concentration of 0.5 μg/10 cm^3 vanadium (n=5).

Table 1. Effect of Foreign Ions

Foreign ions	Added as	Added μg/10 cm^3	Absorbance at 385 nm
—	—	—	0.460
Cu(II)	Nitrate	12.7	0.375
Zn(II)	Nitrate	26.2	0.380
Fe(III)	Sulfate	11.2	0.378
Al(III)	Sulfate	1.1	0.365
Sn(IV)	Sulfate	4.8	0.380
MoO_4^{2-}	Sodium	64.0	0.320
CN^-	Potassium	156.0	0.440
$S_2O_3^{2-}$	Sodium	11.2	0.420
SO_3^{2-}	Sodium	80.1	0.415
Citrate	Sodium	75.0	0.410

Vanadium taken: 0.3 μg/10 ml; T.Cl.gall: 1.4×10^{-4} mol dm^{-3}; HPC: 1.0×10^{-3} mol dm^{-3}; PVP: 1.0 cm^3 of 1.0% PVP solution/10 cm^3; pH: 4.5; Reference: Reagent blank (Solution A).

Table 2. Analytical Results for Vanadium(V) Added to Artificial Water

Molar ratio Total metal/ Vanadium[a)]	Masking agents	Absorbance at 385 nm	Recovery %[b)]
—	—	0.460	100.0
1:1	—	0.460	100.5
5:1	—	0.458	99.6
10:1	—	0.440	95.6
25:1	—	0.430	93.2
	NaF[c)]	0.425	92.3
	NaF+KCN[c)]	0.462	100.4

Vanadium(V) taken: 0.3 μg/10 cm^3; T.Cl.gall: 1.4×10^{-4} mol dm^{-3}; HPC: 1.5×10^{-3} mol dm^{-3}; PVP: 1.0 cm^3 of 1.0% PVP solution/10 cm^3; pH: 4.5; Reference: Reagent blank. a): Fe(II)+Co(II)+Al(III)+Zn(II)+Co(II), b): Mean of 5 determinations, c): NaF, 6.0×10^{-4} mol dm^{-3}; KCN, 6.0×10^{-4} mol dm^{-3}; notice that a potassium cyanide solution is used in an acidic medium.

Effect of Foreign Ions. The interfering effects of various foreign ions on the determination of vanadium were examined. As is shown in Table 1, the presence of copper(II), aluminum(III), and iron(III) interfered with the determination of vanadium in forming a colored complex in a weakly acidic media. The interference from aluminum(III), copper(II), or iron(III) could, however, be overcome by the addition of sodium fluoride or a nitrilotriacetic acid (NTA) or potassium cyanide (KCN) solution as masking agents respectively. (Needless to say, it must be kept in mind that a slight amount of HCN gas is produced by the addition of the KCN solution in a weakly acidic medium as a masking agent.)

Moreover, the presence of molybdate, tungstate, thiosulfate, citrate, and such oxidizing agents as perman-

ganate, bromate and chlorate, seriously interfered. These interfering ions must be removed by a suitable procedure.

Application. The proposed methods were applicable for the recoveries of vanadium in prepared artificial water (involving various metal ions-iron(III), cobalt(II), aluminum(III), zinc(II), copper(II), etc.). The sample solution (as vanadium(V)) was treated with sodium carbonate solutions, and then filtered or centrifuged. The filtrated or centrifuged solution was adjusted to about pH 5 with hydrochloric acid and sodium hydroxide solutions. Also, sodium fluoride, potassium cyanide and NTA solutions were added to this sample solution as masking agents, and then the concentration of vanadium in the artificial water(molar ratio of total metal ions to vanadium=25 : 1) was determined by using the standard procedure, as is shown in Table 2. The experimental results were in a good agreement with the certified values (recovery test, 98.6—102.8%).

In conclusion, a rapid and sensitive spectrophotometric determination of trace amounts of vanadium (0—0.8 μg/10 cm^3 vanadium) was established by using the oxidation and decomposition of the T.Cl.gall solution by the catalytic reaction of vanadium(V) in the presence of HPC and PVP. The sensitivity of this proposed method was about 16 times greater than that of the method[6] using *N*-benzoyl-*N*-phenylhydroxylamine, and about 20—40 times greater than, that of the PR-oxidation method,[3] the 4-(2-pyridylazo) resorcinol (PAR) method,[7] or the gall-sodium sulfite method.[1] This proposed method should be useful for the determination of trace amounts of vanadium in air pollution, petroleum, steel, the sea, river and lake water, etc.

References

1) I. Mori, Y. Fujita, and K. Sakaguchi, *Bunseki Kagaku*, **31**, E193 (1982).
2) J. M. Escriche, A. S. Cabeza, M. G. Cirugeda, and F. B. Reig, *Analyst (London)*, **108**, 1402 (1983).
3) A. S. Cabeza, J. M. Escriche, and F. B. Reig, *Analyst (London)*, **109**, 1559 (1984).
4) W. R. Orndorff, *Cornell. Univ. Am. J.*, **42**, 183; *Chem. Abstr.*, **3**, 293 (1909).
5) I. Mori, Y. Fujita, M. Ida, and T. Enoki, *Bunseki Kagaku*, **25**, 239 (1976).
6) F. Einaga and H.Ishii, *Bunseki Kagaku*, **17**, 836 (1968).
7) Y. Shijo and T. Takeuchi, *Bunseki Kagaku*, **14**, 115 (1965).

Control of Product in the Reaction of Tributyltin ω-Haloalkoxide (n-$Bu_3SnO(CH_2)_nX$) with Diphenylketene

Ikuya SHIBATA,* Akio BABA, and Haruo MATSUDA
Department of Applied Chemistry, Faculty of Engineering, Osaka University, Yamadaoka 2-1, Suita, Osaka 565
(Received June 20, 1986)

Synopsis. The reaction of tributyltin ω-haloalkoxide with diphenylketene gave cyclic ketene acetals and/or lactones, and the ratio of these products were controled by the number of methylene groups and by the addition of Lewis base in the reaction system. Moreover, the direct cycloaddition of diphenylketene with cyclic ethers proceeded in high yields, catalyzed by organotin halide-Lewis base complexes.

We have recently reported the novel use of tributyltin ω-haloalkoxides (**1**) (n-$Bu_3SnO(CH_2)_nX$, X=Cl, Br, I, n=2, 3),[1,2] yielding a variety of five- and six-membered heterocycles in the reactions with heterocumulenes such as isocyanates, isothiocyanates and carbodiimides.[1,2] In particular, it has been pointed out that the addition of Lewis bases significantly stimulated the formation of heterocyclic compounds. Moreover, new effective catalysts, the complexes of organotin halides with bases, have been developed on the basis of investigations on this reaction mechanism, conducting the direct cycloaddition of oxiranes with heterocumulenes under very mild conditions.[3] In the course of the study on this type of reaction in terms of diphenylketene (**2**) with **1**, we recognized some different features from the reactions of other heterocumulenes which have been already reported.[1,2] Thus, the types of the products were drastically changed by the number of methylene (n) of **1**, and moreover the addition of bases completely changed the product in the reaction with n-$Bu_3SnO(CH_2)_3X$ (**1b**). In addition, the direct cycloadditions of oxiranes or oxetane with **2** were performed.

The results of the reactions between tributyltin β-haloethoxides (n-$Bu_3SnO(CH_2)_2X$) (**1a**) with **2** are summarized in Table 1 (Entries 1—8). The types of products and the reactivity varied with temperature, additives and the kind of halogen. γ-Butyrolactone (**4a**) was obtained in only the reactions with iodide derivative (**1aa**) (Entries 1—3), and the 1,3-dioxolane **3a** was exclusively produced from the bromide (**1ab**) (Entry 4). Moreover, the ratio of **4a** to **3a** was increased with lowering the reaction temperature, however the reaction proceeded very slowly below 60 °C. The presence of Lewis bases allowed the reaction to proceed in high yields under significantly milder conditions, in addition, giving **3a** exclusively (Entries 6—8).

The effect of the number of methylene groups was very definitive as shown in the reaction with tributyltin γ-halopropoxides (n-$Bu_3SnO(CH_2)_3X$) (**1b**). In sharp contrast to the 1,3-dioxolane formation from the reaction of **1a**, δ-valerolactone (**4b**) was selectively obtained with **1b** (Entries 9 and 10). Moreover, the effect of base was more remarkable than in the reaction of **1a**, and the product was completely changed from the lactone **4b** to the 1,3-dioxane **3b** (Entry 11). This drastic change is very characteristic of the reaction of diphenylketene. Thus, no change of products by the addition of bases was observed in the reaction of **1b** with isocyanates or isothiocyanates.[1,2]

As Bloodworth et al. have reported,[4] these reactions are thought to proceed via stannyl ester type of adduct (**A**) as shown in Scheme 1. Products, **3** and **4**, may be

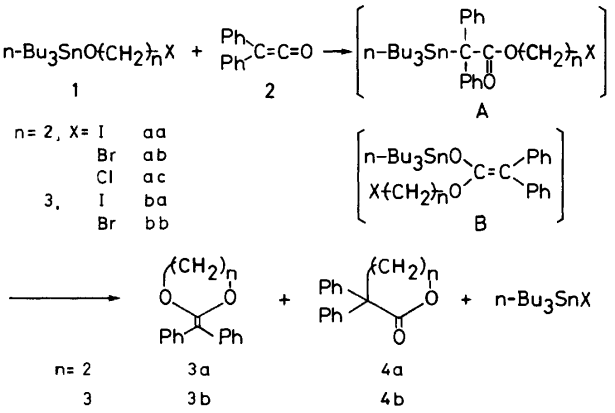

Scheme 1.

Table 1. Reactions of **1** with **2**[a]

Entry	1	Base	Temp °C	Product	Isolated Yield/%[b]
1	**1aa**	—	80	**3a**+**4a**	60 (40/60)[c]
2	**1aa**	—	100	**3a**+**4a**	52 (50/50)[c]
3	**1aa**	—	150	**3a**+**4a**	51 (85/15)[c]
4	**1ab**	—	100	**3a**	43
5	**1ac**	—	120	**3a**	12
6	**1aa**	HMPA[d]	60	**3a**	67
7	**1ab**	Et_3N[e]	40	**3a**	78
8	**1ab**	Ph_3P[e]	40	**3a**	93
9	**1ba**	—	120	**4b**	77
10	**1bb**	—	120	**4b**	57
11	**1ba**	HMPA[d]	100	**3b**	52

a) **1** 5 mmol, **2** 4 mmol, Time 1 h, b) Based on **2**, c) **3a**/**4a** ratio; determined by ^1H NMR, d) 3 ml, e) 5 mmol.

Table 2. Cycloaddition of Oxiranes with **2**[a]

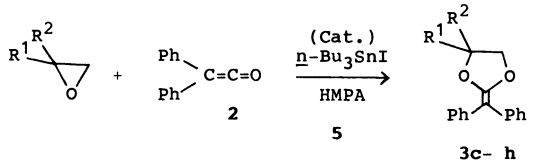

R^1	R^2	Product	Yield/%[b]
Me	H	**3c**	100
Et	H	**3d**	93
Me	Me	**3e**	73
CH_2Cl	H	**3f**	88
$PhOCH_2$	H	**3g**	82
Ph	H	**3h**	94

a) Oxirane 25 mmol, **2** 5 mmol, *n*-Bu_3SnI 1 mmol, HMPA 1 mmol, Temp 40°C, Time 1 h, b) Based on **2**.

formed by intramolecular *O*- and *C*-alkylations, respectively. As to the formation of **3**, stannyl enolate type of adduct (**B**) can be considered. However, IR spectrum showed the absorption at 1730 cm^{-1} (C=O) in the addition of **2** with **1a** or **1b**, where no cyclization occurred. And this absorption was also observed in the case using HMPA as a solvent. From these facts, we propose **A** as an intermediate rather than **B**.[5] While it is unclear exactly why the remarkable alternation of products occurred, the significant effect of the number of methylene group seems to suggest an important role of the intramolecular coordination of the terminal halide to the tin atom. The characteristic reaction mode of diphenylketene may be rationalized by the lower ability of an intermolecular coordination of **A** in comparison with the adducts of **1** with an isocyanate. Namely, the nitrogen atom in the adduct of isocyanates, *n*-$Bu_3SnN(R)COO(CH_2)_nX$, can bring an intermolecular coordination toward another tin atom,[4] whereas the carbon atom adjacent to Sn atom in **A** has no coordinative ability.

In the next stage, we tried to use *n*-Bu_3SnI-HMPA complex (**5**) as a catalyst for the cycloaddition of oxiranes with **2**. As shown in Table 2, cycloaddition proceeded under very mild conditions, and a variety of 1,3-dioxolanes, **3c—h**, were obtained in good to excellent yields. In this reaction system, the complex **5**, formally forms in situ, undergoes ring opening to give organotin β-iodoalkoxides.[6] The activated halogen by the coordination of base to a tin atom of *n*-Bu_3SnI is effective for ring opening. Next, these tin alkoxides react with diphenylketene, and the 1,3-dioxolanes are formed, accompanied by the regeneration of the Sn-I bond. While, oxetane showed a lower reactivity than oxiranes, and heterocycles were scarcely obtained by using **5**. However, $MeSnI_3$-HMPA complex showed higher catalytic activity in direct cycloaddition reaction using oxetane and **2**, and heterocycles **3b** and **4b** were obtained in 18 and 40% yields, respectively. Although the yields are not so good as the case of oxiranes, this result is interesting because cycloaddition of heterocumulenes with oxetanes has been scarcely reported.[7]

Experimental

Reaction of Tributyltin ω-Haloalkoxide (*n*-$Bu_3SnO(CH_2)_nX$) (1) with Diphenylketene (2). All reactions were carried out under dry nitrogen. A typical procedure is described for the reaction of **1aa** with **2**. **1aa** (2.30 g, 5 mmol) and **2** (0.78 g, 4 mmol) were stirred in a 50 ml round-bottomed flask, then heat was evolved about 40 °C. The infrared spectrum showed disappearance of the characteristic absorption band of ν_{CCO} at 2100 cm^{-1}, and the presence of the new band at 1730 cm^{-1}. After 1 h at 80 °C, addition of excess amounts of hexane on cooling induced 0.57 g (60%) of white precipitates immediately, which were collected by filtration, washed with hexane and dried in vacuo. The precipitates were turned out to 2-diphenylmethylene-1,3-dioxolane (**3a**) (24% yield) and α,α-diphenyl-γ-butyrolactone (**4a**) (36% yield). The **3a**/**4a** ratio was determined by ^1H NMR spectra. When the reaction was carried out in a solvent, **1**, **2**, and a solvent were charged in this turn.

2-Diphenylmethylene-1,3-dioxolane (3a): Mp 148—149 °C (lit,[8] mp 149—151 °C); IR (KBr) 1660 cm^{-1} (C=C); MS *m*/*z* 238 (M^+); ^1H NMR ($CDCl_3$) δ=4.20 (s, 4H, CH_2), 7.00—7.40 (m, 10H, Ph).

2-Diphenylmethylene-1,3-dioxane (3b): Mp 80—81 °C; IR (KBr) 1640 cm^{-1} (C=C); MS *m*/*z* 252 (M^+); ^1H NMR ($CDCl_3$) δ=1.95—2.25 (m, 2H, CH_2), 4.15 (t, 4H, OCH_2), 7.10—7.40 (s, 10H, Ph).

α,α-Diphenyl-γ-butyrolactone (4a): Pure sample was isolated by column chromatography (Silica-gel, $CHCl_3$); Mp 80—81 °C (lit,[9] mp 77—79 °C); IR (KBr) 1780 cm^{-1}; MS *m*/*z* 238 (M^+); ^1H NMR ($CDCl_3$) δ=2.98 (t, 2H, CH_2), 4.22 (t, 2H, CH_2O), 7.32 (s, 10H, Ph).

α,α-Diphenyl-δ-valerolatone (4b): Mp 116 °C (lit,[10] mp 112 °C); IR (KBr) 1730 cm^{-1}; MS *m*/*z* 252 (M^+); ^1H NMR ($CDCl_3$) δ=1.88 (m, 2H, CH_2), 2.62 (t, 2H, Ph_2CCH_2), 4.22 (t, 2H, CH_2O), 7.22 (s, 10H, Ph).

Cycloaddition of Diphenylketene (2) with Oxiranes or Oxetane: A typical procedure is described for the reaction of diphenylketene with 2-methyloxirane, catalyzed by *n*-Bu_3SnI-HMPA. To a solution of *n*-Bu_3SnI (0.42 g, 1 mmol) and HMPA (0.18 g, 1 mmol) in 2-methyloxirane (1.45 g, 25 mmol) was added **2** (0.97 g, 5 mmol) with stirring under dry nitrogen. The resulting mixture was stirred at 40 °C for 2 h and the yield was monitored by GLC. Diphenylketene was no longer detected, which was confirmed by the disappearance of IR absorption band of ketene (2100 cm^{-1}). Excess amounts of hexane was added on cooling to the reaction mixture, then 1.12 g (89%) of white precipitates were obtained immediately. This was collected by filtration, washed with hexane and dried in vacuo. The precipitates was 2-diphenylmethylene-4-methyl-1,3-dioxolane (**3c**). Compounds **3b**, **4b**, **3d**, and **3e** were isolated by a similar method. **3f**, **3g**, and **3h** were isolated by distillation from the reaction mixture.

2-Diphenylmethylene-4-methyl-1,3-dioxolane (3c): Mp 88—89 °C; IR (KBr) 1660 cm^{-1}; MS *m*/*z* 252 (M^+); ^1H NMR ($CDCl_3$) δ=1.42 (d, 1H, CH_3), 3.82 (t, 1H, one of CH_2O), 4.38 (dd, 1H, one of CH_2O), 4.70 (m, 1H, OCH), 7.00—7.40 (m, 10H, Ph).

2-Diphenylmethylene-4-ethyl-1,3-dioxolane (3d): Mp 57—58 °C; IR (KBr) 1660 cm^{-1} (C=C); MS *m*/*z* 266 (M^+); ^1H NMR ($CDCl_3$) δ=1.00 (t, 3H, CH_3), 1.50—1.90 (m, 2H, $MeCH_2$), 3.90 (t, 1H, one of OCH_2), 4.30 (t, 1H, one of OCH_2), 4.30—4.60 (m, 1H, OCH), 7.00—7.40 (m, 10H, Ph).

2-Diphenylmethylene-4,4-dimethyl-1,3-dioxolane (3e): Mp 98—100 °C; IR (KBr) 1660 cm^{-1} (C=C); MS *m*/*z* 266 (M^+); ^1H NMR ($CDCl_3$) δ=1.15 (s, 3H, CH_3), 1.45 (s, 3H, CH_3), 4.00 (d, 2H, CH_2O), 7.00—7.40 (m, 10H, Ph).

2-Diphenylmethylene-4-chloromethyl-1,3-dioxolane (3f): Bp 142 °C/10^{-3} mmHg (1 mmHg=133.322 Pa); IR (KBr) 1660 cm^{-1} (C=C); MS *m/z* 286.5 (M^+); ^1H NMR ($CDCl_3$) δ=3.60 (d, 2H, $ClCH_2$), 4.30 (t, 2H, CH_2O), 4.60—4.80 (m, 1H, OCH), 7.00—7.60 (m, 10H, Ph).

2-Diphenylmethylene-4-phenoxymethyl-1,3-dioxolane (3g): Bp 140 °C/10^{-3} mmHg (lit,[8] 220—260 °C/0.8 mmHg); IR (neat) 1660 cm^{-1} (C=C); MS *m/z* 344 (M^+); ^1H NMR ($CDCl_3$) δ=4.10 (d, 2H, $PhOCH_2$), 4.30 (dd, 2H, CH_2O), 4.70—5.00 (m, 1H, OCH), 6.70—7.40 (m, 15H, Ph).

2-Diphenylmethylene-4-phenyl-1,3-dioxolane (3h): Bp 132 °C/10^{-3} mmHg (lit,[8] bp 225—230 °C/0.8 mmHg); IR (neat) 1660 cm^{-1} (C=C); MS *m/z* 314 (M^+); ^1H NMR ($CDCl_3$) δ=4.10 (t, 1H, one of CH_2O), 4.60 (t, 1H, one of CH_2O), 5.50 (t, 1H, OCH), 7.00—7.40 (m, 15H, Ph).

References

1) A. Baba, H. Kishiki, I. Shibata, and H. Matsuda, *Organimetallics*, **4**, 1329 (1985).

2) A. Baba, I. Shibata, H. Kashiwagi, and H. Matsuda, *Bull. Chem. Soc. Jpn*, **59**, 341 (1986).

3) I. Shibata, A. Baba, H. Iwasaki, and H. Matsuda, *J. Org. Chem.*, **51**, 2177 (1986).

4) A. J. Bloodworth and A. G. Davies, *J. Chem. Soc.*, **1965**, 5238.

5) In the adduct of an organotin alkoxide with a ketene, it has been reported that an stannyl enolate type of adduct was labile and could exist only under −30 °C. (E. Shimada, K. Inomata and T. Mukaiyama, *Chem. Lett.*, **1974**, 689)

6) In the cycloaddition of oxiranes with isocyanates, we have confirmed that oxiranes are cleavaged at unhindered carbon-oxygen bond (β-cleavage) by this catalyst system. (Ref. 3)

7) S. H. Metzger, Jr., U. S. Patent 3, 479351; *Chem. Abstr.*, **72**, 21699 m (1970).

8) K. Gulbins and K. Hamann, *Chem. Ber.*, **94**, 3287 (1965).

9) M. M. Kayser, J. Salvador, and P. Morand, *Can. J. Chem.*, **61**, 439 (1983).

10) M. Utjes-Le Gall, F. Salmon-Legagneur, and H. Le Moal, *J. Chem. Res. (C)*, **1978**, 198.

Substance P Analogs Containing Homoglutamine at Position 5 and 6

Yoshiki UCHIDA, Miwako NISHIJIMA, Tadashi MORO, Naoki SAKURA, Kyoko HIROSE, Hitoshi KONTANI, and Tadashi HASHIMOTO*
School of Pharmacy, Hokuriku University, Ho-3, Kanagawa-machi, Kanazawa 920-11
(Received May 31, 1986)

Synopsis. Six substance P (SP) analogs, in which the glutaminyl residue(s) at the position(s) 5 or/and 6 were replaced by homoglutamine (Hgn), were prepared using a novel N^{α},N^{ca}-$(Boc)_2$-Hgn-OH by the solid phase method. The activity of the analogs was assayed on isolated guinea pig organs. Results indicate that the elongation of the methylene on glutaminyl residue(s) in SP enhances the activity on isolated guinea pig ileum.

Chang and Leeman[1] isolated in 1970 substance P (SP) from bovine hypothalami and the amino acid sequence was elucidated by Chang, et al.,[2] to be H-Arg-Pro-Lys-Pro-Gln-Gln-Phe-Phe-Gly-Leu-Met-NH_2.[3] Studies on the relationship between peptide chain length and activity[4] of SP revealed that the contractile activity of certain C-terminal fragments was as high as or even higher than that of SP itself on the smooth muscle of isolated guinea pig ileum. Although the C-terminal pentapeptide had much lower activity, addition of Gln residue(s) at the N-terminal of the pentapeptide leads to an enhancement of biological activity. The conformation analyses suggest a U shape for the C-terminal part of the molecule, providing an explanation for the observation that full biological activity is retained in SP hexapeptide, and that bioactive structures are stabilized by the formation of intramolecular hydrogen bond between the amide proton (or amino proton) of the glutamine residue at position 6 and the carbonyl group of the C-terminal amide.[5] These imply that the Gln residue(s) of SP is very important for inducing the activity.

This paper describes the first synthetic example of bioactive peptide analogs substituted with homoglutamine (Hgn; α-aminoadipamic acid). In order to examine the biological effect of the elongation of methylene group in the Gln residue(s) at positions of 5 or/and 6 by the displacement with Hgn, we synthesized six analogs and submitted them for biological assay to compare with our synthetic SP.

The SP analogs were synthesized by the solid phase technique[6] using an automated peptide synthesizer. Deprotection and dicyclohexylcarbodiimide (DCC) coupling were programed as given in Table 1. *t*-Butoxycarbonyl (Boc) protection was used for α-amino function and the amide nitrogen (N^{ca}) of Hgn. The Hgn residue was incorporated into peptide chains as usual manner using N^{α},N^{ca}-$(Boc)_2$-Hgn-OH,[7,8] which was derived from an ester of $(Boc)_2$-Lys-OH by ruthenium tetraoxide oxidation. This oxidative transformation[9,10] made it possible to produce quite conveniently the novel Hgn derivative which is applicable to synthetic studies (on the structure-activity relationships of peptides). The protecting group on the amide can be deblocked by the same reagents as those for the groups on α-amino function to yield Hgn residue.[8] Other side-chain protecting groups were Z for Lys and tosyl (Tos) for Arg. After the completion of the chain elongations, the peptide resin was treated with liquid hydrogen fluoride (HF)[11] in the presence of anisole to cleave the peptide from the resin with simultaneous removal of the protecting groups and formation of the carboxyl terminal amide. The crude product was purified by preparative reverse-phase high-performance liquid chromatography (HPLC) using 0.1% TFA in acetonitrile (CH_3CN) as eluent. Highly purified peptides were obtained after gel filtration on Sephadex G-10 column. The yield was sacrificed for the purity. Homogeneity of the peptides was demonstrated by analytical HPLC and thin-layer chromatography (TLC). When single peaks and single spots were observed for a peptide in all chromatographic systems, the sample

Table 1. Program for Solid Phase Peptide Synthesis

	Reagents	Operation	Mix time / min
1	CH_2Cl_2	3×Wash	1.5
2	TFA (25% in CH_2Cl_2)	Prewash	1.5
3	TFA (25% in CH_2Cl_2)	Deprotection	30
4	CH_2Cl_2	3×Wash	1.5
5	CH_2Cl_2	3×Wash	1.5
6	TEA (10% in CH_2Cl_2)	3×Neutralization	1.5
7	CH_2Cl_2	6×Wash	1.5
8	Boc-Amino Acid (in CH_2Cl_2 or DMF)	Mix	5
9	DCC	Mix	120
10	CH_2Cl_2	6×Wash	1.5

1	4	5	6	11		
H-Arg-Pro-Lys-Pro-Hgn-Gln-				Phe-Phe-Gly-Leu-Met-NH_2	[Hgn^5]-SP	**1**
H-Arg-Pro-Lys-Pro-Gln-			Hgn-	Phe-Phe-Gly-Leu-Met-NH_2	[Hgn^6]-SP	**2**
H-Arg-Pro-Lys-Pro-Hgn-		Hgn-		Phe-Phe-Gly-Leu-Met-NH_2	[$Hgn^{5,6}$]-SP	**3**
	H-Pro-Hgn-Gln-			Phe-Phe-Gly-Leu-Met-NH_2	[Hgn^5]-SP (4−11)	**4**
	H-Pro-Gln-	Hgn-		Phe-Phe-Gly-Leu-Met-NH_2	[Hgn^6]-SP (4−11)	**5**
	H-Pro-Hgn-	Hgn-		Phe-Phe-Gly-Leu-Met-NH_2	[$Hgn^{5,6}$]-SP (4−11)	**6**

Fig. 1. Synthetic SP analogs.

Table 2. Physical Properties and Yield of the Peptides

Analog	$[\alpha]_D^{25}$ (c 0.5, 3M AcOH)/°	Retention time[a] min	R_f^I	R_f^{II}	Yield %
1	−80.4	9.8	0.00	0.56	30.8
2	−86.2	10.2	0.00	0.57	18.2
3	−82.2	11.0	0.00	0.56	28.2
4	−54.0	13.2	0.13	0.68	24.7
5	−58.0	13.6	0.14	0.74	20.2
6	−52.8	15.0	0.13	0.69	25.5

a) Condition of analytical HPLC: column, NOVA-PAK C_{18}; flow rate, 1 ml min^{-1}; Detection, 210 nm; eluent system, linear gradient from 21% to 35% CH_3CN (15 min) in 20 mM phosphate buffer (pH 3.0).

Table 3. Amino Acid Analyses of the Peptides

Analog	Found (Calcd)									
	Lys	Arg	Glu	Pro	Gly	Hgu[a]	Met	Leu	Phe	NH_3
1	1.10 (1)	1.13 (1)	0.98 (1)	1.77 (2)	0.97 (1)	1.10 (1)	0.94 (1)	0.98 (1)	2.03 (2)	3.84 (3)
2	1.12 (1)	1.10 (1)	0.98 (1)	1.85 (2)	0.95 (1)	1.08 (1)	0.97 (1)	0.98 (1)	1.98 (2)	3.82 (3)
3	0.94 (1)	1.04 (1)	—	1.77 (2)	1.05 (1)	2.18 (2)	0.99 (1)	1.00 (1)	2.04 (2)	3.29 (3)
4	—	—	1.00 (1)	0.85 (1)	0.98 (1)	1.15 (1)	0.98 (1)	0.98 (1)	2.05 (2)	3.85 (3)
5	—	—	1.01 (1)	0.89 (1)	1.00 (1)	1.03 (1)	0.98 (1)	0.98 (1)	2.10 (2)	3.86 (3)
6	—	—	—	0.93 (1)	1.02 (1)	2.20 (2)	0.96 (1)	0.98 (1)	1.92 (2)	3.67 (3)

a) Homoglutamic acid; α-aminoadipic acid.

Table 4. Relative Potencies of SP Analogs on Guinea Pig Organs

Analog	Relative contractile activity to SP=1	
	Ileum	Trachea
1	1.81	2.09
2	1.25	1.20
3	3.41	2.09
4	3.41	4.36
5	1.97	1.00
6	1.50	2.75

was considered appropriately pure for bioassay. These chromatographic data were reinforced by the amino acid analytical data.

Biological properties of the synthetic SP analogs in this study were examined on isolated guinea pig organs and the contractile activities of the analogs were compared with that of synthetic SP. The results are shown in Table 4.

The elongation of the methylene group of Gln residue(s) at position 5 or/and 6 of SP enhanced the biological activity on isolated guinea pig ileum, and [$Hgn^{5,6}$]-SP **3** possessed the highest potency among the three analogs (**1**—**3**). Octapeptide analogs **4** and **5** showed about 340 and 200% of the activity of SP respectively and their potencies were higher than those of **1** and **2** replaced at the same position, while [$Hgn^{5,6}$]-SP (**4**—**11**) **6** had significant activity, but its potency was less than those of analogs **4** and **5**, and about a half of the undecapeptide **3**.

The analogs **1**, **3**, **4**, and **6** were also found to be highly active on the trachea assay, while **2** and **5** were as high as that of SP. Octapeptide analog **4** had the highest activity on the both bioassays. Thus the potencies of Hgn^5 analogs **1** and **4** were higher than the activities of Hgn^6 analogs **2** and **5** respectively. The potencies of all analogs prepared in the present investigation were as high as or higher than the activity of SP itself. This indicates probably that resistibility of the peptides to metabolic breakdown is increased by the introduction of Hgn residue(s) and the Hgn analogs may possess a U-shape conformation and hydrogen bond very similar to natural SP.

Experimental

Amino acid derivatives were purchased from Peptide Institute, Inc., Osaka, Japan and benzhydrylamine (BHA) resin (available amine of the resin: 0.6 mmol g^{-1} of support) from Beckman Inc., Palo Alto, Calif. Optical rotations were measured in a Nipponbunkoh DIP-4 Polarimeter. Amino acid analyses on samples previously hydrolyzed with 6M HCl (1 M=1 mol dm^{-3}) (110 °C, 24 h) were performed on a Hitachi KLA-5 Amino Acid Analyzer. TLC was carried out on silica-gel plates (Merck). The following solvent systems were used and allowed to ascend for 10 cm: R_f^I, *n*-BuOH : AcOH : H_2O (4 : 1 : 5, upper phase); R_f^{II}, *n*-BuOH: pyridine : AcOH : H_2O (30 : 20 : 6 : 24). Analytical HPLC was effected on the following systems: column, NOVA-PAK C_{18} (3.9×150 mm); flow rate, 1 ml min^{-1}, detection, 210 nm; eluent system, linear gradient of CH_3CN in 20 mM phosphate buffer (pH 3.0).

General Procedure for the Preparation of Analogs. The solid phase synthesis was carried out using a Beckman System 990C Peptide Synthesizer. Half gram of BHA-resin hydrochloride for each analog served as the solid support. For the incorporation of each N^{α}-Boc-protected amino acid, a program given in Table 1 was used. The amino acid derivatives were dissolved in dichloromethane, except Boc-Arg(Tos)-OH and Boc-Gln-OH which were dissolved in DMF, and employed for the coupling reaction. A 2.5 fold excess of the amino acid derivative was used for all couplings. One equivalent of HOBt was added as an additive to facilitate the repetitive coupling reaction, using the program

without step 1—4. In the case of Boc-Gln-OH, 2.5 equiv of HOBt was used for all couplings. The completion of the coupling reaction was assessed by a negative ninhydrin test. When the ninhydrin test was positive, even after repetition of the coupling two or three times, the unreacted amino groups were blocked completely by acetylation using an excess of Ac_2O (5 equiv of resin used) in the presence of pyridine (1 equiv) in dichloromethane for 20 min. The protected peptide resin was treated with anhydrous liquid HF containing 10% anisole. Approximately 5 ml of liquid HF was used for 0.25 g resin, and the reaction time was 1 h at 0 °C. After evaporation of HF in vacuo under ice-cooling, the peptide-resin mixture was washed with AcOEt. The peptide was extracted with three portions of 10% AcOH and the combined extracts were lyophilized.

Purification of the Peptides. The crude peptide was subjected to HPLC. The apparatus was composed of a model 590 pump and a U6K injector (Waters) connecting with a column (20×300 mm) of Chemcosorb ODS (Chemco). The eluates were monitored with a UV detector S-310A model-II (Soma) at 210 nm wavelength. CH_3CN–0.1% TFA solvent system was used as eluent at flow rate 10 ml min^{-1}. Each peptide was emerged at 40—60 min by isocratical elution with 21—23% CH_3CN contents of the solvent system. The desired fraction was passed through a Sephadex G-10 column (16×930 mm) eluted with 2M AcOH and the product was lyophilized. Homogeneity of the peptides was analyzed by analytical HPLC and TLC. The peptides on silica-gel plate were detected with ninhydrin and chlorine-*o*-tolidine reagents. When single peaks and single spots were observed for a peptide in all chromatographic systems and the amino acid compositions after hydrolysis of the peptides were consistent with the calculated values, the sample was submitted for bioassay.

Bioassay. Male guinea pig (weighing 200—250 g) was stunned by a blow to the back and exsanguinated. Ileum and trachea were rapidly isolated and kept for dissection in Tyrode's solution (137 mM NaCl, 2.7 mM KCl, 1.8 mM $CaCl_2$, 1.1 mM $MgCl_2$, 0.4 mM NaH_2PO_4, 12 mM $NaHCO_3$, 5.6 mM glucose) at room temperature. Both organs were suspended in a 30 ml organ bath containing Tyrode's solution thermostated at 30 °C and bubbled with 95% O_2 and 5% CO_2 gas for 1 h. The contraction was recorded by means of isotonic transducer (Nippon Kohden, TD-111T) with load of 1 or 2 g (for trachea and ileum respectively) on a Servocorder (Watanabe Instruments, SR6204). Trachea was transversely cut into pieces and six pieces were connected to make a trachea preparation. Concentration-response curves were obtained using a cumulative dose-assay, the time between two consecutive dose-response curves being longer than 10 min.

References

1) M. M. Chang and S. E. Leeman, *J. Biol. Chem.*, **245**, 4784 (1970).
2) M. M Chang, S. E. Leeman, and H. D. Niall, *Nature, New Biol.*, **232**, 86 (1971).
3) Amino acids, peptides and their derivatives mentioned in this paper are of L-configuration. The abbreviations for amino acids and peptides are in accordance with the rules of the IUPAC-IBU Commission on Biochemical Nomenclature in *Eur. J. Biochem.*, **138**, 9 (1984).
4) N. Yanaihara, C. Yanaihara, M. Hirohashi, H. Sato, Y. Iizuka, T. Hashimoto, and M. Sakagami, "Substance P," ed by U. S. von Euler and B. Pernow, Raven Press, New York (1977), p. 27.
5) F. Inagaki, T. Miyazawa, N. Yanaihara, and M. Otsuka, "Peptide Chemistry 1977," ed by T. Shiba, Protein Research Foundation (1978), p. 103.
6) R. B. Merrifield, *Adv. Enzymol.*, **32**, 221 (1969).
7) Y. Uchida, M. Nishijima, K. Hirose, T. Moro, N. Sakura, and T. Hashimoto, "Peptide Chemistry 1985," ed by Y. Kiso, Protein Research Foundation (1986), p. 125.
8) N. Sakura, K. Hirose, and T. Hashimoto, *Chem. Pharm. Bull.*, in press.
9) S. Yoshifuji, K. Tanaka, and Y. Nitta, *Chem. Pharm. Bull.*, **33**, 1749 (1985).
10) N. Sakura, K. Hirose, and T. Hashimoto, *Chem. Pharm. Bull.*, **33**, 1752 (1985).
11) S. Sakakibara, Y. Shimonishi, Y. Kishida, M. Okada, and H. Sugihara, *Bull. Chem. Soc. Jpn.*, **40**, 2164 (1967).

Neurokinin B Analogs Substituted with Glycine

Tadashi HASHIMOTO,* Tadashi MORO, and Yoshiki UCHIDA
School of Pharmacy, Hokuriku University, Ho-3, Kanagawa-machi, Kanazawa 920-11
(Received July 2, 1986)

Synopsis. Four Neurokinin B analogs substituted with glycine at position 4, 5, 6, or 7 were synthesized by Merrifield's solid phase method. Pharmacological property of the analogs is described. The results suggest that Phe[6] and Val[7] residues may be essential for intrinsic activity on smooth muscle.

Neurokinin B (NKB, also called neuromedin K) is a novel neuropeptide isolated from porcine spinal cord. Structure elucidation[1] revealed that NKB has close structural homologies with tachykinin such as substance P (SP), kassinin and physalaemin (Fig. 1). NKB, decapeptide amide, is very similar to the undecapeptide SP, particularly in the sequence between Phe[6] and Met[10] residues of NKB, and between Phe[7] and Met[11], and has the same C-terminal pentapeptide sequence of dodecapeptide kassinin.

The structural determination of NKB led us to undertake systematic studies on structure-activity relationship by means of highly purified synthetic peptides related to the neuropeptide. This paper describes synthesis and biological property of four kinds of NKB analogs.

In study[3] of the relationships between chain length and activity, it is revealed that the removal of the N-terminal two amino acids from NKB increases the contractile activity on rat vas deferens as the peptide chain is shortened and NKB (5—10) shows unequivocal loss of activity. In the present investigation, in order to examine the biological effect of the substitution of Gly moiety for Asp[4], Phe[5], Phe[6], and Val[7] residues, we synthesized [Gly[4]]-, [Gly[5]]-, [Gly[6]]-, and [Gly[7]]-NKB (3-10) (Fig. 2), and submitted them for biological assay to compare with our synthetic NKB.

Synthesis of NKB and the related peptides used in this study was performed on a Beckman System 990C Peptide Synthesizer by standard solid phase method[4] starting from *t*-butoxycarbonyl (Boc)-Met benzhydrylamine-resin. Boc protection was used for α-amino function. The side-chain protective groups used were cyclohexyl for Asp and *p*-toluenesulfonyl for His. Deprotection and dicyclohexylcarbodiimide (DCC) coupling were programed as given in Table 1. For second coupling, a program without steps 1—4 was used. A 2.5 fold excess of amino acid derivatives was used for all couplings. The second coupling was repeated with additive of one equivalent of 1-hydroxybenzotriazole (HOBt). The coupling reaction was monitored by the ninhydrin color test procedure of Kaiser et al.[5] A trace of unreacted amino group was acetylated. After the completion of the chain elongations, the peptide resin was treated with liquid hydrogen fluoride (HF)[6] in the presence of anisole for 1 h at 0 °C to cleave the peptide from the resin with simultaneous removal of the protecting groups and formation of the carboxyl terminal amide. The excess HF was removed in vacuo, and the resulting material was washed with ethyl acetate prior to extraction of the peptide with aq acetic acid (50%). The crude product was purified by preparative reverse-phase high-performance liquid chromatography (HPLC) using dil trifluoroacetic acid (0.1%) in acetonitrile as eluent. The desired fractions were collected and desalted on a column of Sephadex LH-20 eluted with aq *N,N*-dimethylformamide (90%), giving pure peptide. The yield was sacrificed for the purity of the fractions selected. Homogeneity of the peptides was demonstrated by analytical HPLC and thin-layer chromatography (TLC) (Table 2). When single peaks and single spots were observed for a peptide in all chromatographic systems, the sample was considered

	1									10
NKB	H-Asp-	Met-	His-	Asp-	Phe-	Phe-	Val-	Gly-	Leu-	Met-NH_2
	1									11
SP	H-Arg-	Pro-	Lys—	Pro-	Gln-	Gln-	Phe-	Phe-	Gly-	Leu-Met-NH_2
	1									12
Kassinin	H-Asp-	Val-	Pro-	Lys—	Ser-	Asp-	Gln-	Phe-	Val-	Gly-Leu-Met-NH_2
	1									11
Physalaemin	pGlu-	Ala-	Asp-	Pro-	Asn-	Lys-	Phe-	Tyr-	Gly-	Leu-Met-NH_2

Fig. 1. Amino acid sequences[2] of tachykinin peptides.

	3							10	
[Gly[4]]-NKB (3—10)	H-His-	Gly-	Phe-	Phe-	Val-	Gly-	Leu-	Met-NH_2	**1**
[Gly[5]]-NKB (3—10)	H-His-	Asp-	Gly-	Phe-	Val-	Gly-	Leu-	Met-NH_2	**2**
[Gly[6]]-NKB (3—10)	H-His-	Asp-	Phe-	Gly-	Val-	Gly-	Leu-	Met-NH_2	**3**
[Gly[7]]-NKB (3—10)	H-His-	Asp-	Phe-	Phe-	Gly-	Gly-	Leu-	Met-NH_2	**4**

Fig. 2. Synthetic NKB analogs.

Table 1. Program for Solid Phase Synthesis

Step	Reagent	Operation	Mix time/min
1	CH_2Cl_2	3×Wash	1.5
2	TFA (25% in CH_2Cl_2)	Prewash	1.5
3	TFA (25% in CH_2Cl_2)	Deprotection	30
4	CH_2Cl_2	3×Wash	1.5
5	CH_2Cl_2	3×Wash	1.5
6	TEA (10% in CH_2Cl_2)	3×Neutralization	1.5
7	CH_2Cl_2	6×Wash	1.5
8	Boc-Amino Acid (in CH_2Cl_2)	Mix	5
9	DCC	Mix	120
10	CH_2Cl_2	6×Wash	1.5

Table 2. Physical Properties and Yield of the Peptides

Analog	$[\alpha]_D^{22}$/° (*c* 0.1, DMF)	Retention time[a)]/min	R_f^I	R_f^{II}	Yield/%
1	−36.0	17.5	0.15	0.75	39.2
2	−33.0	15.1	0.10	0.68	6.3
3	−83.0	14.8	0.10	0.68	10.5
4	−47.0	16.9	0.10	0.68	38.0

a) Condition of analytical HPLC: column, NOVA-PAK C_{18}; flow rate, 1 ml min^{-1}; Detection, 210 nm; eluent system, linear gradient from 7% to 42% CH_3CN (15 min) in 20 mM phosphate buffer (pH 3.0).

Table 3. Amino Acid Analyses of the Peptides

Analog	Found (Calcd)							
	His	Asp	Gly	Val	Met	Leu	Phe	NH_3
1	0.93 (1)	—	2.04 (2)	1.16 (1)	0.98 (1)	0.94 (1)	1.90 (2)	1.79 (1)
2	1.04 (1)	1.19 (1)	1.87 (2)	1.03 (1)	0.89 (1)	1.09 (1)	0.84 (1)	1.27 (1)
3	1.33 (1)	1.21 (1)	1.80 (2)	0.94 (1)	0.84 (1)	0.90 (1)	1.03 (1)	1.67 (1)
4	1.08 (1)	1.23 (1)	1.95 (2)	—	0.93 (1)	1.00 (1)	1.82 (2)	1.57 (1)

Table 4. Relative Potencies of Synthetic NKB Analogs

Analog	GPI[a)]	RVD[a)]
1	0.28	0.63
2	2.0	1.58
3	0	0
4	0	0

a) Relative activity accepted NKB as 1.

appropriately pure for bioassay. These chromatographic data were reinforced by the amino acid analytical data (Table 3).

Biological properties of the synthetic NKB analogs in this study were examined on the isolated rat vas deferens (RVD) and the guinea pig ileum (GPI). The contractile activities of the analogs were compared with those of synthetic NKB. The results are shown in Table 4.

The potencies of analog **2** were higher than the activities of NKB itself on both assays. Analog **1** showed reduced potency, while the peptides **3** and **4** possessed no activity. Thus, these results suggest that Phe^6 and Val^7 residues of NKB may be essential for the intrinsic activity.

Experimental

Amino acid derivatives were purchased from Peptide Institute, Inc., Osaka, Japan and benzhydrylamine (BHA) resin (available amine of the resin: 0.6 mmol g^{-1} of support) from Beckman Inc., Palo Alto, Calif. Optical rotations were measured in a Nipponbunkoh DIP-4 Polarimeter. Amino acid analyses on samples previously hydrolyzed with 6 M HCl (1 M=1 mol dm^{-3}) (110 °C, 24 h) were performed on a Hitachi KLA-5 Amino Acid Analyzer. TLC was carried out on silica-gel plates (Merck). The following solvent systems were used and allowed to ascend for 10 cm: R_f^I, *n*-BuOH : AcOH : H_2O (4 : 1 : 5, upper phase); R_f^{II}, *n*-BuOH : pyridine : AcOH : H_2O (30 : 20 : 6 : 24). Analytical HPLC was effected on the following systems: column, NOVA-PAK C_{18} (3.9×150 mm); flow rate, 1 ml min^{-1}, detection, 210 nm; eluent system, linear gradient of CH_3CN in 20 mM phosphate buffer (pH 3.0).

General Procedure of Analog. The first Boc-amino acid was coupled as follows to the BHA-resin (0.60 mequiv N g^{-1}). The BHA-resin hydrochloride was treated with a solution of 10% (by volume) triethylamine (TEA) in dichloromethane (10 ml g^{-1} of resin) for 4.5 min. Then the resin was washed with 10 ml of dichloromethane per gram. For half gram of the resin, 2.5 equiv of Boc-Met-OH and DCC were used. The quantitation of coupling reaction was revealed by a negative ninhydrin color test. When the ninhydrin test was positive, even after second coupling, the unreacted amino

groups were blocked by acetylation using Ac_2O (5 equiv) and pyridine (1 equiv) in dichloromethane for 20 min. For the coupling reactions, using 2.5 equiv of DCC in dichloromethane, the amino acid derivatives were dissolved in dichloromethane. Deprotection and DCC coupling were programed as given in Table 1. For second coupling, a program without steps 1—4 was used. A 2.5 fold excess of the amino acid derivative was used for all couplings. One equivalent of HOBt was used only for the second DCC-coupling. The protected peptide resin was simultaneously cleaved and deblocked with anhydrous liquid HF containing 10% anisole. Approximately 5 ml of liquid HF was used for 0.25 g resin, and the reaction time was 1 h at 0 °C. After evaporation of HF, the peptide-resin mixture was washed with AcOEt. The peptide was extracted with three portions of 50% AcOH and the extracts combined were lyophilized.

Purification of the Peptides. The crude peptide was subjected to HPLC which is composed of a model 590 pump and a U6K injector (Waters) connecting with a column (20×300 mm) of Chemcosorb ODS (Chemco). The eluates were monitored with a UV detector S-310A model-II (Soma) at 210 nm wavelength. CH_3CN-0.1% TFA solvent system was used as eluent at flow rate 10 ml min^{-1}. Each peptide was emerged at 40—60 min by isocratical elution with 22—28% CH_3CN contents of the solvent system. The desired fraction was desalted on a Sephadex LH-20 column (15×500 mm) eluted with DMF-H_2O (9:1) and the product was lyophilized. Homogeneity of the peptides was analyzed by analytical HPLC on a column of NOVA-PAK C_{18} (3.9×150 mm) with gradient elution using 20 mM phosphate buffer (pH 3.0)/CH_3CN and by TLC on silica-gel plate. The peptides on silica- gel plate were detected with ninhydrin and chlorine-*o*-tolidine reagents. When single peaks and single spots were observed for a peptide in all chromatographic systems and amino acid composition after hydrolysis of the peptides were consistent with the calculated values, the sample was submitted for bioassay.

Bioassay. The bioactivities of NKB analogs were measured on the isolated rat vas deferens and guinea pig ileum. Male rat (weighing 250—300 g) and male guinea pig (weighing 200—250 g) were stunned by a blow to the neck and exsanguinated. Vas deferens and ileum were rapidly isolated and kept for dissection in Tyrode's solution (137 mM NaCl, 2.7 mM KCl, 1.8 mM $CaCl_2$, 1.1 mM $MgCl_2$, 0.4 mM NaH_2PO_4, 12 mM $NaHCO_3$, 5.6 mM glucose) at room temperature. Both organs were suspended in a 30 ml organ bath containing Tyrode's solution thermostated at 30 °C and bubbled with 95% O_2 and 5% CO_2 gas for 1 h. The contraction was recorded by means of an isotonic transducer (Nippon Kohden, TD-111T) with load of 1 or 2 g (for vas deferens and ileum respectively) on a Servocorder (Watanabe Instruments, SR6204). Concentration-response curves were obtained using a cumulative dose-assay, the time between two consecutive dose-response curves longer than 10 min.

References

1) S. Kimura, M. Okada, Y. Sugita, I. Kanazawa, and E. Munekata, *Proc. Jpn. Acad.*, **59B**, 101 (1983); H. Kangawa, N. Minamino, A. Fukuda, and H. Matsuo, *Biochem. Biophys. Res. Commun.*, **114**, 533 (1983).

2) Amino acids, peptides and their derivatives mentioned in this paper are of L-configuration. The abbreviations for amino acids and peptides are in accordance with the rules of the IUPAC-IBU Commission on Biochemical Nomenclature in *Eur. J. Biochem.*, **138**, 9 (1984).

3) F. Osakada, K. Kubo, K. Goto, I. Kanazawa, and E. Munekata, *Eur. J. Pharmacol.*, **120**, 201 (1986).

4) R. B. Merrifield, *Adv. Enzymol.*, **32**, 221 (1969).

5) E. Kaiser, R. L. Colescott, C. D. Bossinger, and P. I. Cook, *Anal. Biochem.*, **34**, 595 (1970).

6) S. Sakakibara, Y. Shimonishi, Y. Kishida, M. Okada, and H. Sugihara, *Bull. Chem. Soc. Jpn.*, **40**, 2164 (1967).